Available online at www.sciencedirect.com
SCIENCE DIRECT®
Polyhedron 25 (2006) 1–8
POLYHEDRON
www.elsevier.com/locate/poly

Syntheses and characterization of two novel heptanuclear trigonal prismatic $LnNi_6$ clusters with different terminal ligands

Jian-Jun Zhang, Sheng-Min Hu, Sheng-Chang Xiang, Xin-Tao Wu *, Long-Sheng Wang, Ya-Min Li

State Key Laboratory of Structural Chemistry, Fujian Institute of Research on the Structure of Matter, Chinese Academy of Sciences, Fuzhou, Fujian 350002, China

Received 25 February 2005; accepted 12 April 2005
Available online 2 December 2005

Abstract

Two novel heptanuclear trigonal prismatic $LnNi_6$ clusters, $[SmNi_6(Gly)_6(Ac)(\mu_3\text{-}OH)_3(\mu_2\text{-}H_2O)_2(im)_6]\cdot(ClO_4)_5\cdot(H_2O)_5$ (**1**) and $[GdNi_6(Gly)_6Cl_3(OH)_3(py)_6]\cdot Cl\cdot(ClO_4)_2\cdot(H_2O)_5$ (**2**), were synthesized through self-assembly, and were characterized by X-ray structure analyses. Complex **1** crystallizes in the monoclinic *Cc* space group ($a = 17.9722(3)$ Å, $b = 16.3906(2)$ Å, $c = 25.3463(3)$ Å, $\beta = 99.832(1)°$ and $Z = 4$). Complex **2** attributes to the monoclinic $P2(1)/c$ space group ($a = 15.5408(2)$ Å, $b = 20.0516(4)$ Å, $c = 23.8204(4)$ Å, $\beta = 100.096(1)°$ and $Z = 4$). **1** has six terminal imidazole ligands, while **2** has six terminal pyridine ligands. The two complexes both have a $[LnNi_6(Gly)_6(\mu_3\text{-}OH)_3]^{6+}$ core. The magnetic measurements reveal that **1** exhibits an overall antiferromagnetic interaction, while **2** exhibits a ferromagnetic interaction.
© 2005 Elsevier Ltd. All rights reserved.

Keywords: Nickel; Lanthanides; Heptanuclear trigonal prism; Substitution reaction; Cluster compounds; Terminal ligand

1. Introduction

Polynuclear mixed-metal clusters are of considerable interest owning to their special physicochemical properties arising from the close proximity of dissimilar metal ions. For about three decades, the design and characterization of molecular complexes comprising simultaneously of 3d and 4f metal ions have been one of the interesting research areas [1,2]. Up until now most of the studies were focused on low-nuclearity 3d–4f compounds [2], and similar research about high-nuclearity compounds is still very limited [3–7]. Therefore the design and syntheses of high-nuclearity 3d–4f clusters are still significant.

In order to synthesize 3d–4f heteronuclear compounds, it is necessary to find suitable ligands that can associate the two different metal ions. Many chelating ligands such as pyridones [8] , Schiff-base [9], oxalato [10], oximates [11] or oxamides [12], cyano groups [13] and carboxylic acids [14] have been used to construct heterometallic compounds. Recently we found amino acid, one of the most important biological ligands, is also a good candidate for such a purpose [3c,7]. The ligand can use its amino and carboxylate groups to coordinate to 3d and 4f metal ions simultaneously. But of course, during the synthetic process it is very necessary to choose a suitable pH window so that the unprotonated amino group can take part in coordination. As the ligand has a variety of coordinated modes, its use for the synthesis of 3d–4f heteronuclear compounds may lead to much more complex and intriguing structures than using a simple carboxylic acid [3c,7].

* Corresponding author. Tel.: +86 591 8371 9238/8379 2837; fax: +86 591 83714946.
E-mail address: wxt@ms.fjirsm.ac.cn (X.-T. Wu).

0277-5387/$ - see front matter © 2005 Elsevier Ltd. All rights reserved.
doi:10.1016/j.poly.2005.04.030

Up until now several heptanuclear 3d–4f clusters with the general formula of LnM_6 (M means transition metal) have been reported [3]. They have the structure motif of an octahedron ($LnNi_6$) [3a,b], trigonal prism ($LnNi_6$, $LnCu_6$) [3c,d] and wheel ($LnCu_6$) [3e]. We have reported a series of novel heptanuclear $LnNi_6$ trigonal prismatic clusters with different edge ligands [3c]. The complexes all have a $[LnNi_6(Gly)_6(\mu_3\text{-}OH)_3(H_2O)_6]^{6+}$ core, but different edge ligands. In this paper we report two new heptanuclear $LnNi_6$ clusters which have the same $[LnNi_6(Gly)_6(\mu_3\text{-}OH)_3]^{6+}$ core but different terminal ligands: $[SmNi_6(Gly)_6(Ac)(\mu_3\text{-}OH)_3(\mu_2\text{-}H_2O)_2(im)_6]\cdot(ClO_4)_5\cdot(H_2O)_6$ (**1**), with imidazole (im) as terminal ligands, and $[GdNi_6(Gly)_6Cl_3(OH)_3(py)_6]\cdot Cl\cdot(ClO_4)_2\cdot(H_2O)_5$ (**2**) with pyridine (py) as terminal ligands. The crystal structures of these clusters are reported and their magnetic properties are investigated.

2. Experimental

2.1. Materials and instrumentation

$Ln(ClO_4)_3\cdot 6H_2O$ was synthesized by dissolving Ln_2O_3 in an excess amount of perchloric acid. Other starting materials were of reagent grade and used without further purification. Elemental analyses were carried out by the Elemental Analysis Lab of our Institute. Magnetic measurements were carried out with a Quantum Design PPMS model 6000 magnetometer.

2.2. Synthesis of the complexes

2.2.1. $[SmNi_6(Gly)_6(Ac)(\mu_3\text{-}OH)_3(\mu_2\text{-}H_2O)_2(im)_6]\cdot(ClO_4)_5\cdot(H_2O)_5$ (**1**)

To an aqueous solution (10 ml) of $Sm(ClO_4)_3\cdot 6H_2O$ (0.556 g, 1 mmol), $Ni(Ac)_2\cdot 4H_2O$ (1.493 g, 6 mmol) and glycine (0.45 g, 6 mmol) were added. Then the pH value of the reaction mixture was carefully adjusted to about 6.6 by slow addition of 0.1 M NaOH solution. After 2 h of stirring, 6 mmol imidazole were added and the solution was stirred for half an hour. Then it was filtrated to remove the precipitate and placed in a desiccator filled with phosphorus pentaoxide. Green crystals were obtained about a month later. Yield: 0.41 g, 19.6%. *Anal.* Calc. for $C_{32}H_{68}Cl_5N_{18}Ni_6O_{44}Sm$: C, 18.40; H, 3.28; N, 12.07. Found: C, 18.16; H, 3.13; N, 11.88%.

2.2.2. $[GdNi_6(Gly)_6Cl_3(OH)_3(py)_6]\cdot Cl\cdot(ClO_4)_2\cdot(H_2O)_5$ (**2**)

The above procedure was repeated except that $Gd(ClO_4)_3\cdot 6H_2O$, $NiCl_2\cdot 6H_2O$ and pyridine were used. Yield: 0.37 g, 19.4%. *Anal.* Calc. for $C_{42}H_{67}Cl_6GdN_{12}Ni_6O_{28}$: C, 26.41; H, 3.54; N, 8.80. Found: C, 26.12; H, 3.24; N, 8.50%.

Table 1
Crystallographic and data collection parameters for **1** and **2**

	1	**2**
Formula	$C_{32}H_{68}Cl_5N_{18}Ni_6O_{44}Sm$	$C_{42}H_{67}Cl_6GdN_{12}Ni_6O_{28}$
M_r	2088.90	1910.29
Crystal system	monoclinic	monoclinic
Space group	*Cc*	*P*2(1)/*c*
a (Å)	17.9722(3)	15.5408(2)
b (Å)	16.3906(2)	20.0516(4)
c (Å)	25.3463(3)	23.8204(4)
β (°)	99.832(1)	100.096(1)
Volume (Å^3)	7356.7(2)	7307.9(2)
Z	4	4
$D_{calc.}$ (g/cm^3)	1.886	1.736
F(000)	4212	3844
Measured reflections	11025	23453
Independent reflections	8398	12824
R_{int}	0.0238	0.0448
Goodness-of-fit on F^2	1.236	1.140
R^a	0.0538	0.0759
$R_w{}^b$	0.1443	0.1951

1, *a* = 0.0857, *b* = 38.9450; **2**, *a* = 0.1034, *b* = 55.3219.

[a] $R = \sum(||F_o| - |F_c||)/\sum|F_o|$.

[b] $R_w = \{\sum w[(F_o^2 - F_c^2)^2]/\sum w[(F_o^2)^2]\}^{1/2}$, $w = 1/[\sigma^2(F_o^2) + (aP)^2 + bP]$, $P = (F_o^2 + F_c^2)/3]$.

2.3. X-ray crystallography

Intensity data for the complexes were collected at 293(2) K on a Siemens Smart/CCD area-detector diffractometer with Mo Kα radiation ($\lambda = 0.71073$ Å). Data reduction and unit cell refinement were performed with Smart-CCD software [15]. The structures were solved by direct methods using SHELXS-97 [16] and were refined by full-matrix least squares methods using SHELXL-97. Anisotropic displacement parameters were refined for all non-hydrogen atoms. Final $R\sum||F_o| - F_c||)/\sum|F_o|$, $R_w = \{\sum w[(F_o^2 - F_c^2)^2]/\sum w[(F_o^2)^2]\}^{1/2}$, with $w = 1/[\sigma^2(F_o^2) + (aP)^2 + bP]$ [where $P = (F_o^2 + F_c^2)/3$]. The crystallographic data are summarized in Table 1.

3. Results and discussion

3.1. Syntheses of the complexes

We have reported that the three μ_2-OH_2 edge ligands of the $[LnNi_6(Gly)_6(\mu_3\text{-}OH)_3(H_2O)_6(\mu_2\text{-}OH_2)_3]^{6+}$ species can be partly or wholly replaced by glycine or Cl^- and a series of novel heptanuclear $LnNi_6$ trigonal prismatic clusters can be obtained [3c]. In this paper, complex **1** has one acetate and two μ_2-OH_2 edge ligands, while **2** has three μ_2-Cl edge ligands.

Complexes **1** and **2** also have six im and py terminal ligands, respectively. Although further evidences is

lacking, the strong structural relationships between **1**, **2** and $[LnNi_6(Gly)_6(\mu_3\text{-}OH)_3(H_2O)_6(\mu_2\text{-}OH_2)_3]^{6+}$ suggests a possible terminal ligand substitution reaction, as shown in Scheme 1. This is reminiscent of other famous poly-nuclear clusters whose terminal sites are occupied by solvent molecules and could be substituted by pyridine, carboxylic acid or other ligands, such as trinuclear clusters of the type $[M_3(\mu_3\text{-}O)(\mu\text{-}RCO_2)_6L_3]^{n+}$ (L = neutral monodentate ligand) which widely occur in a variety of first-, second- and third-row transition-metal ions [17], and polynuclear manganese clusters [18]. However, we notice a similar reaction is still very rare in 3d–4f

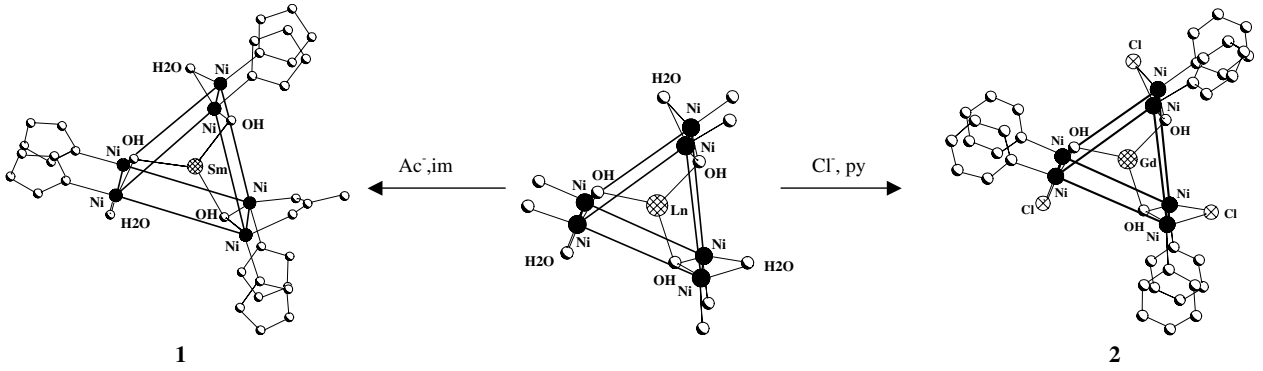

Scheme 1. The syntheses of **1** and **2** through the possible substitution reaction of the species $[LnNi_6(Gly)_6(\mu_3\text{-}OH)_3(H_2O)_6(\mu_2\text{-}OH_2)_3]^{6+}$.

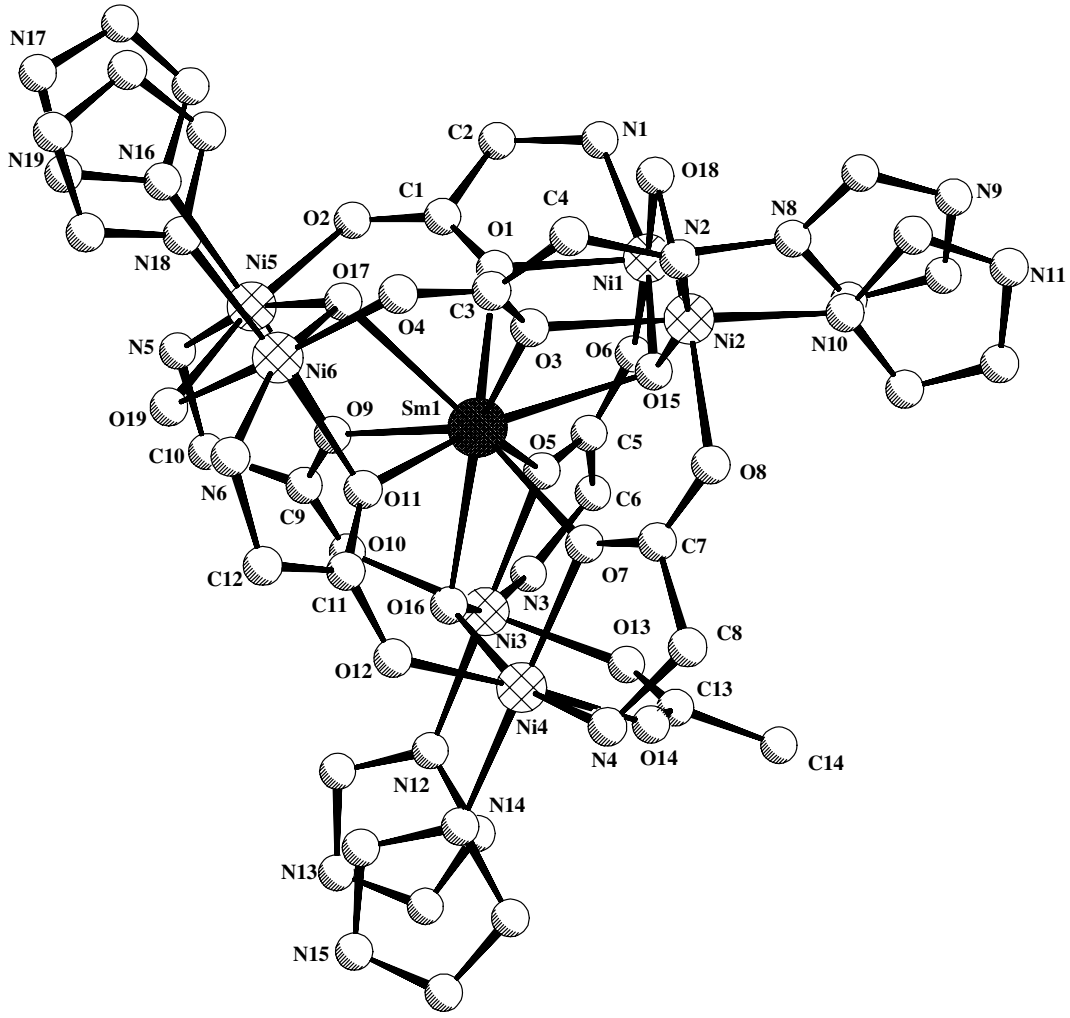

Fig. 1. A view of the cation of complex **1** with the atom numbering scheme.

heteronuclear clusters. This strategy may help us to design and synthesize a large variety of 3d–4f clusters.

3.2. The structure of complex *1*

The structure of the cation is shown in Fig. 1. Selected bond distances and bond angles are shown in Table 2. Fig. 1 shows that in **1** six Ni^{2+} ions form a large trigonal prism and a Sm^{3+} ion is situated at the center. The Sm···Ni distance is about 3.52 Å, longer than the Tb···Cu distance (3.45 Å) in another trigonal prismatic $TbCu_6$ cluster [12] with iminodiacetic acid as a ligand, and close to the Ln···Ni distances in the former reported series of trigonal prismatic $LnNi_6$ clusters [3c]. The six nickel ions belong to two bases (Ni1, Ni3, Ni5 and Ni2, Ni4, Ni6). In each base, with the help of three $[3.1_12_{23}1_3]$-coordinated glycinato ligands, the three Ni^{2+} ions are connected to form an equilateral triangle with a side distance of about 5.3 Å (Ni···Ni distance). The two bases are connected by one acetate (Ni3 and Ni4) and two μ_2-H_2O ligands (Ni1 and Ni2, Ni5 and Ni6). The Ni3···Ni4 distance is about 3.581 Å, while those of Ni1···Ni2, and Ni5···Ni6 are 3.345 and 3.335 Å, respectively. This causes a slight distortion of the metal skeleton. In other words, a 3.0° torsion angle may be formed between the two bases. This value is comparable with those (4.5°) in other heptanuclear trigonal prismatic $LnNi_6$ clusters [3c].

As shown in Fig. 2, the centered Sm^{3+} ion is nine-coordinated in a tricapped trigonal prismatic geometry and has an O_9 donor set. The six carboxyl oxygen atoms from six glycinato ligands form six apexes, and the three oxygen atoms from three μ_3-OH^- groups form three caps. The Sm–O bond lengths are all about 2.45 Å.

Ni(1), Ni(2), Ni(5) and Ni(6) all have N_2O_4 donor sets which consist of two nitrogen atoms from a glycinato and an im ligand, respectively, two carboxyl

Table 2
Selected bond lengths (Å) and bond angles (°) for **1**

Sm–Ni	3.513(2)–3.527(2)
Ni–Ni(different base)	3.335(1)–3.581(1)
Sm–O(carboxylate)	2.406(8)–2.462(8)
Ni–O(carboxylate)	2.05(1)–2.16(1)
Ni–N	1.98(1)–2.09(1)
Ni–Ni(same base)	5.291(1)–5.338(1)
Sm–O(OH)	2.437(9)–2.475(8)
Ni–O(OH)	1.991(8)–2.04(1)
Ni–O(H_2O)	2.29(1)–2.23(1)
O(15)–Ni(1)–N(1)	162.5(5)
N(8)–Ni(1)–O(1)	176.0(4)
O(6)–Ni(1)–O(18)	168.7(4)
N(10)–Ni(2)–O(3)	176.5(5)
O(15)–Ni(2)–N(2)	163.2(4)
O(8)–Ni(2)–O(18)	171.8(4)
N(12)–Ni(3)–O(5)	177.6(4)
O(16)–Ni(3)–N(3)	162.9(4)
O(13)–Ni(3)–O(10)	173.2(4)
N(14)–Ni(4)–O(7)	176.8(4)
O(16)–Ni(4)–N(4)	161.8(4)
O(14)–Ni(4)–O(12)	172.6(4)
N(16)–Ni(5)–O(9)	175.8(5)
O(17)–Ni(5)–N(5)	163.6(4)
O(2)–Ni(5)–O(19)	166.9(4)
O(17)–Ni(6)–N(6)	163.5(4)
N(18)–Ni(6)–O(11)	175.1(5)
O(4)–Ni(6)–O(19)	166.9(4)
Ni(1)–O(1)–Sm(1)	102.1(4)
Ni(2)–O(3)–Sm(1)	101.8(3)
Ni(3)–O(5)–Sm(1)	101.8(3)
Ni(4)–O(7)–Sm(1)	103.3(3)
Ni(5)–O(9)–Sm(1)	103.7(3)
Ni(6)–O(11)–Sm(1)	103.8(3)
Ni(1)–O(15)–Ni(2)	111.5(4)
Ni(1)–O(15)–Sm(1)	104.3(4)
Ni(2)–O(15)–Sm(1)	103.3(3)
Ni(3)–O(16)–Ni(4)	124.1(5)
Ni(3)–O(16)–Sm(1)	104.2(4)
Ni(4)–O(16)–Sm(1)	104.4(4)
Ni(5)–O(17)–Ni(6)	113.4(4)
Ni(5)–O(17)–Sm(1)	104.2(3)
Ni(6)–O(17)–Sm(1)	103.7(3)
Ni(2)–O(18)–Ni(1)	94.8(3)
Ni(6)–O(19)–Ni(5)	92.8(4)

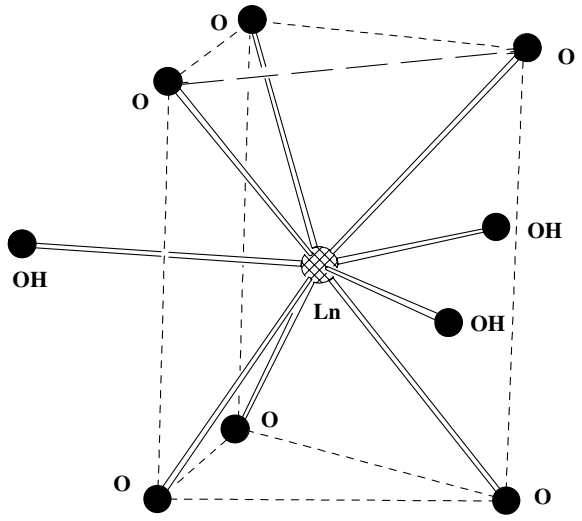

Fig. 2. Coordination polyhedron of the Ln^{3+} ion in the heptanuclear clusters.

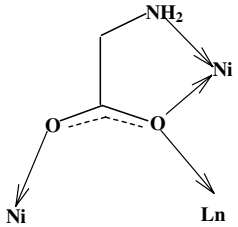

$[3.1_12_{23}1_3]$

Scheme 2. The $[3.1_12_{23}1_3]$-coordinate mode of the glycinato ligand indicated by the Harris notation [19].

oxygen atoms from two glycinato ligands, one μ_2-H_2O and one μ_3-OH^- group. The distances of Ni^{2+} to the μ_2-H_2O are about 2.3 Å, slightly longer than other Ni–O and Ni–N distances (all about 2.0 Å). To Ni(1), small deviations of bond angles from the value of 180° of the idealized octahedral geometry are found for angles N(8)–Ni(1)–O(1) [176.0(4)°], O(15)–Ni(1)–N(1) [162.5(5)°] and O(6)–Ni(1)–O(18) [168.7(4)°], implying it has a slightly distorted octahedral configuration. Ni(2), Ni(5) and Ni(6) show similar configurations. Ni(3) and Ni(4) also have N_2O_4 donor sets which are almost the same as the above-mentioned four Ni^{2+} ions, except a carboxylate oxygen atom was used instead the μ_2-H_2O. They also have slightly distorted octahedral configurations.

There are two μ_2-H_2O edge ligands (O18 and O19) in the cluster. Each of them coordinates to two corresponding Ni^{2+} ions from the two bases with a distance of about 2.3 Å. The ∠Ni(2)–O(18)–Ni(1) and ∠Ni(6)–O(19)–Ni(5) are about 94.8° and 92.8°, respectively. Each cation also has three μ_3-OH^- groups (O15, O16 and O17). They are located in almost the same plane with the Sm^{3+} ion. Each coordinates to the central Sm^{3+} ion and the two corresponding Ni^{2+} ions from different bases.

In the complex the glycinato ligand adopts a $[3.1_12_{23}1_3]$-coordinated mode, each coordinates to the central Sm^{3+} ion and two Ni^{2+} ions in the same base, as shown in Scheme 2. The five-membered chelate rings (N–Ni–O) formed in the $[3.1_12_{23}1_3]$-coordinated mode are all about 80°. The acetate edge ligand coordinates to Ni(3) and Ni(4), adopting a bidentate coordination mode. Six im terminal ligands, each coordinating to one Ni^{2+} ion, were used to construct the cluster. The five-membered rings of two neighboring im ligands are almost parallel, with a face-to-face distance of about 3.4 Å, which falls within the limit for strong offset π–π aromatic stacking interactions.

3.3. The structure of complex **2**

The structure of the cation of **2** is shown in Fig. 3. Selected bond distances and bond angles are shown in Table 3. The skeleton of **2** is almost the same as that

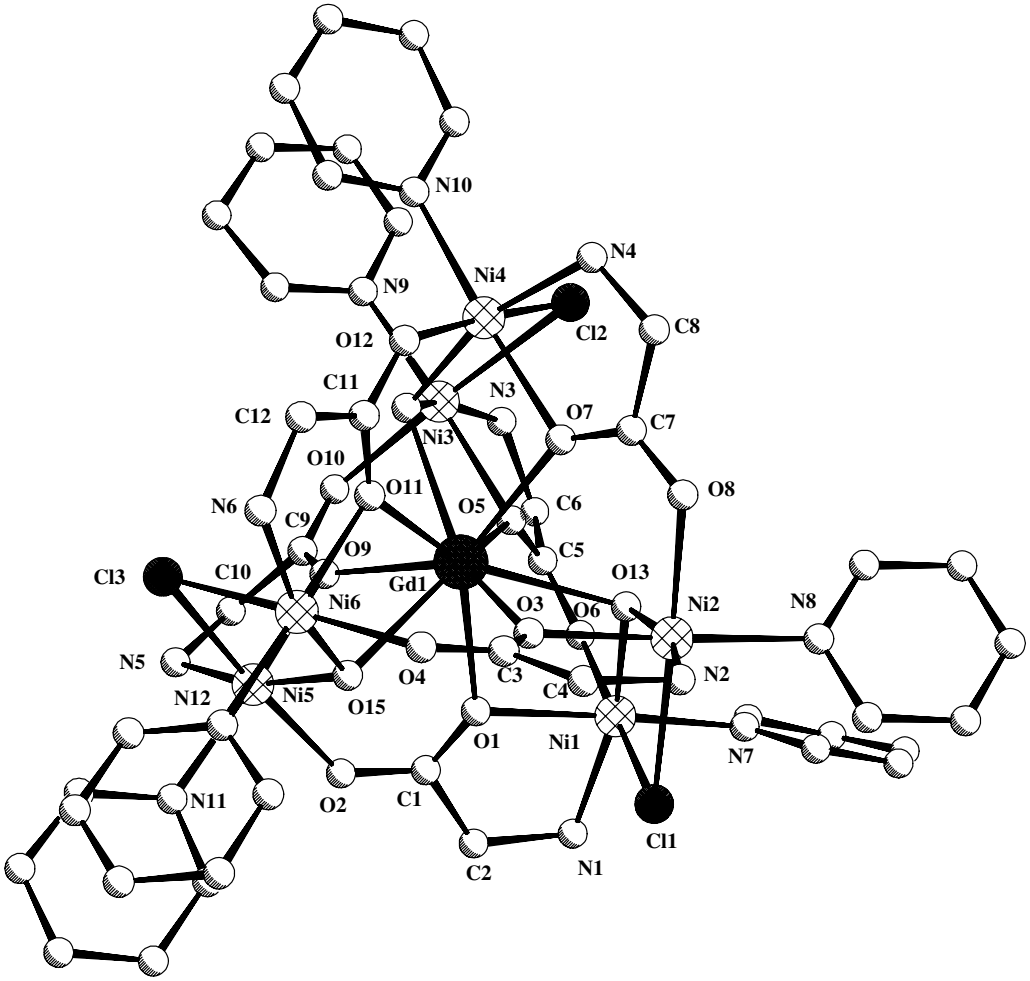

Fig. 3. A view of the cation of complex **2** with the atom numbering scheme.

Table 3
Selected bond lengths (Å) and bond angles (°) for **2**

Gd–Ni	3.513(2)–3.528(2)
Ni–Ni(different base)	3.341(1)–3.398(1)
Gd–O(carboxylate)	2.411(8)–2.425(7)
Ni–O(carboxylate)	2.061(7)–2.111(9)
Ni–N	2.04(1)–2.09(1)
Ni–Ni(same base)	5.371(1)–5.383(1)
Gd–O(OH)	2.451(7)–2.485(8)
Ni–O(OH)	2.002(7)–2.029(8)
Ni–Cl	2.519(4)–2.560(4)
O(13)–Ni(1)–N(1)	163.5(4)
O(1)–Ni(1)–N(7)	169.3(5)
O(6)–Ni(1)–Cl(1)	174.1(3)
O(13)–Ni(2)–N(2)	163.8(4)
O(3)–Ni(2)–N(8)	173.1(4)
O(8)–Ni(2)–Cl(1)	172.8(3)
O(14)–Ni(3)–N(3)	162.6(5)
N(9)–Ni(3)–O(5)	176.1(4)
O(10)–Ni(3)–Cl(2)	175.4(2)
O(14)–Ni(4)–N(4)	163.1(4)
N(10)–Ni(4)–O(7)	174.3(4)
O(12)–Ni(4)–Cl(2)	175.6(2)
O(15)–Ni(5)–N(5)	164.6(4)
O(9)–Ni(5)–N(11)	173.2(4)
O(2)–Ni(5)–Cl(3)	171.8(3)
O(15)–Ni(6)–N(6)	163.7(4)
O(11)–Ni(6)–N(12)	174.4(3)
O(4)–Ni(6)–Cl(3)	172.6(2)
Ni(1)–O(1)–Gd(1)	102.8(3)
Ni(2)–O(3)–Gd(1)	103.0(3)
Ni(3)–O(5)–Gd(1)	103.4(3)
Ni(4)–O(7)–Gd(1)	102.9(3)
Ni(5)–O(9)–Gd(1)	102.3(3)
Ni(6)–O(11)–Gd(1)	103.4(3)
Ni(1)–O(13)–Ni(2)	114.2(4)
Ni(1)–O(13)–Gd(1)	103.0(3)
Ni(2)–O(13)–Gd(1)	102.3(3)
Ni(3)–O(14)–Ni(4)	111.8(3)
Ni(3)–O(14)–Gd(1)	104.1(3)
Ni(4)–O(14)–Gd(1)	103.9(3)
Ni(5)–O(15)–Ni(6)	113.1(3)
Ni(5)–O(15)–Gd(1)	103.6(3)
Ni(6)–O(15)–Gd(1)	103.7(3)
Ni(1)–Cl(1)–Ni(2)	83.9(1)
Ni(4)–Cl(2)–Ni(3)	82.1(1)
Ni(5)–Cl(3)–Ni(6)	83.2(1)

of complex **1** except three μ_2-Cl edge ligands and six pyridine terminal ligands were used to construct the structure. The upper and down bases (Ni1, Ni3, Ni5 and Ni2, Ni4, Ni6) are almost parallel, which may be compared with that of **1** (3.0°).

Another interesting structural feature of **2** is the abnormal behavior of one of the py ligands. Four of the six py ligands, N9, N10 and N11, N12 are all stacked with strong offset aromatic stacking interactions, with a face-to-face distance of about 3.4 Å, just as the im ligands observed in **1**. The other two py ligands, N7 and N8, are not parallel, a 63.6° torsion angle is observed between the two six-membered rings. It is not suitable to say there is a face-to-face π–π stacking interaction, but a weak edge-to-face C–H···π interaction exists between the two py rings. This phenomenon is somewhat strange considering the behaviors of the other py ligands, as well as the im ligands of complex **1**.

In complex **2**, each Ni ion has a N_2O_3Cl slightly distorted octahedral configuration. The Ni–O and Ni–N distances are about 2.00–2.11 Å, while the Ni–Cl distances are much longer (2.52–2.56 Å). Two neighboring Ni^{2+} ions from different bases are bridged by one μ_3-OH^- and one Cl^- ion. The average value of ∠Ni–Cl–Ni is about 83.083, which is compared with the ∠Ni–H_2O–Ni (about 93°) in **1**. It is also an intermediate value between those found in polynuclear nickel complexes with Cl^- as bridge. (81.8–85.6°) [20].

3.4. Magnetic properties

Temperature dependent magnetic susceptibilities of complexes **1** and **2** were measured in the range 5–300 K at 10 kOe. Fig. 4 shows the $\chi_M T$ versus T curves for them. At 300 K, the $\chi_M T$ values per $GdNi_6$ unit are 14.68 $cm^3\,mol^{-1}\,K$ for **2**, slightly smaller than the expected values (15.33 $cm^3\,mol^{-1}\,K$) for one Gd^{III} with free-ion state and six spin only Ni^{II} ions ($S = 1$, $g = 2.23$). On decreasing the temperature, $\chi_M T$ remains almost constant down to ca. 90 K, where it begins to increase smoothly until it reaches a maximum of 20.89 $cm^3\,mol^{-1}\,K$ around 7 K and then it decreases. This phenomenon corresponds to an overall ferromagnetic interaction. This ferromagnetic interaction is also confirmed by the positive Weiss constants (3.87 K), determined by data in the temperature range 50–300 K.

The Gd^{3+} ion has an f^7 electron configuration. The contributions of spin-orbit coupling and zero-field splitting do not need to be taken into consideration, which makes it simple to interpret the nature of the Gd–M interaction (M = 3d metal ion). Up until now most of the studies on the magnetic properties of 3d–4f compounds have been limited to the Gd(III)–Cu(II) system and many attempts have been made to rationalize the relationship between the structure and the nature of the Gd···Cu interaction in Gd–Cu heterometallic compounds [2]. It has been suggested that the dihedral angle of the GdOOCu bridging network plays an important role in affecting the magnetic interaction between the metal ions [9a]. Generally the smaller the dihedral angle, the larger the magnitude of the ferromagnetic interaction, and a large dihedral angle means a small ferromagnetic or even an antiferromagnetic interaction. In **2**, a carboxylate oxygen atom and a μ_3-OH^- were used to bridge the central Gd^{3+} ion and Ni^{2+} ion. The average dihedral angle of 12.6° is an intermediate value between those found in the three Gd–Ni heterometallic compounds (4.2–62.6°) with Gd–Ni ferromagnetic interactions [21]. So we may deduce in this compound the Gd–Ni interaction is also ferromagnetic.

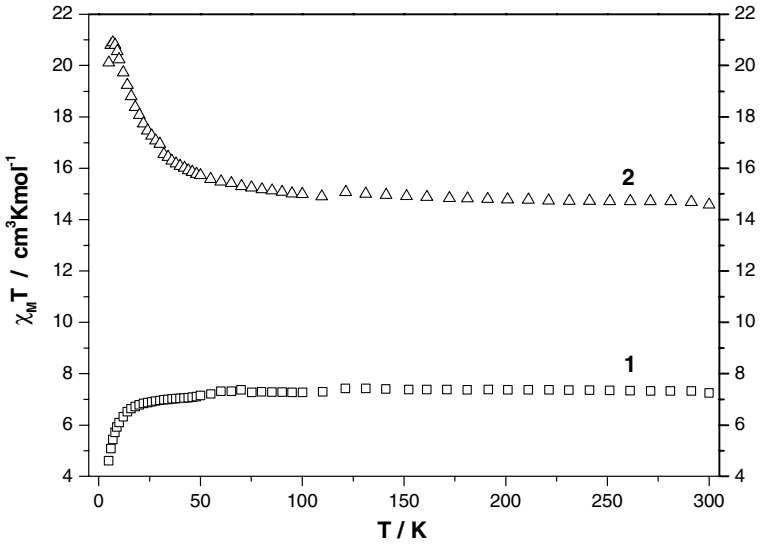

Fig. 4. Temperature dependence of the magnetic susceptibilities of **1** and **2** (5–300 K at 10000 G).

1 shows an overall antiferromagnetic interaction. The free-ion approximation for Sm(III) is not valid because of the presence of thermally populated excited states. The $\chi_M T$ value at room temperature is about 7.25 $cm^3\,mol^{-1}\,K$, which is compared with the calculated value 7.49 $cm^3\,mol^{-1}\,K$ (a $\chi_M T$ value of 0.32 $cm^3\,mol^{-1}\,K$ is used for the Sm^{3+} ion [22]).

4. Conclusion

Two novel heptanuclear trigonal prismatic $LnNi_6$ clusters with different terminal aromatic ligands were synthesized. The magnetic measurements reveal the Gd–Ni interaction is ferromagnetic in the $\{GdNi_6\}$ cluster. Future work will be aimed at using bifunctional bridging ligands containing O-donors or N-donors, such as bipyridine or polycarboxylates, to replace the edge or terminal ligands to synthesize polydimensional coordination polymers with the heptanuclear cluster as nodes.

5. Supplementary data

CCDC 262010–262011 contain the supplementary crystallographic data for this paper. These data can be obtained free of charge via www.ccdc.cam.ac.uk/conts/retrieving.html (or from the Cambridge Crystallographic Data Centre, 12 Union Road, Cambridge CB2 1EZ, UK, fax: +44 1223 336 033, or deposit@ccdc.cam.ac.uk.

Acknowledgments

This research was supported by grants from the State Key Laboratory of Structural Chemistry, Fujian Institute of Research on the Structure of Matter, Chinese Academy of Sciences, the Ministry of Science and Technology of China (001CB1089), the National Science Foundation (20333070, 20273073, 90206040) of China and Fujian Province (2004HZ01-1, 2003J042, 2004J041).

References

[1] A. Bencini, C. Benelli, A. Caneschi, R.L. Carlin, A. Dei, D. Gatteschi, J. Am. Chem. Soc. 107 (1985) 8128.
[2] (a) R.E.P. Winpenny, Chem. Soc. Rev. 27 (1998) 447;
(b) C. Benelli, D. Gatteschi, Chem. Rev. 102 (2002) 2369;
(c) M. Sakamoto, K. Manseki, H. Okawa, Coord. Chem. Rev. 219–221 (2001) 379.
[3] (a) Y. Yukawa, S. Igarashi, A. Yamano, S. Sato, Chem. Commun. (1997) 711;
(b) D.M.J. Doble, C.H. Benison, A.J. Blake, D. Fenska, M.S. Jackson, R.D. Kay, W.-S. Li, M. Schroder, Angew. Chem., Int. Ed. Engl. 38 (1999) 1915;
(c) J.-J. Zhang, S.-M. Hu, L.-M. Zheng, X.-T. Wu, Z.-Y. Fu, J.-C. Dai, W.-X. Du, H.-H. Zhang, R.-Q. Sun, Chem. – Eur. J. 8 (2002) 5742;
(d) Q.-D. Liu, S. Gao, J.-R. Li, Q.-Z. Zhou, K.-B. Yu, B.-Q. Ma, S.-W. Zhang, X.-X. Zhang, T.-Z. Jin, Inorg. Chem. 39 (2000) 2488;
(e) Y.-J. Zhang, B.-Q. Ma, S. Gao, J.-R. Li, Q.-D. Liu, J. Chem. Soc., Dalton Trans. (2000) 2249;
(f) A.J. Tasiopoulos, T.A. O'Brien, K.A. Abboud, G. Christou, Angew. Chem., Int. Ed. Engl. 43 (2004) 345.
[4] (a) J. Tasiopoulos, W. Wernsdorfer, B. Moulton, M.J. Zaworotko, G. Christou, J. Am. Chem. Soc. 125 (2003) 15274;
(b) R.A. Reynolds, D. Coucouvanis, J. Am. Chem. Soc. 120 (1998) 209;
(c) J.-K. Tang, Y.-Z. Li, Q.-L. Wang, E.-Q. Gao, D.-Z. Liao, Z.-H. Jiang, S.-P. Yan, P. Cheng, L.-F. Wang, G.-L. Wang, Inorg. Chem. 41 (2002) 2188;
(d) C.M. Zaleski, E.C. Depperman, J.W. Kampf, M.L. Kirk, V.L. Pecoraro, Angew. Chem. Int. Ed. 43 (2004) 3912.
[5] (a) S.N. Wang, Z. Pang, M.J. Wagner, Inorg. Chem. 31 (1992) 5381;

(b) X.-M. Chen, S.M.J. Aubin, Y.-L. Wu, Y.-S. Yang, T.C.W. Mak, D.N. Hendrickson, J. Am. Chem. Soc. 117 (1995) 9600.
[6] (a) A.J. Blake, R.O. Gould, C.M. Grant, P.E.Y. Milne, S. Parsons, R.E.P. Winpenny, J. Chem. Soc., Dalton Trans. (1997) 485;
(b) A.J. Blake, P.E.Y. Milne, P. Thornton, R.E.P. Winpenny, Angew. Chem., Int. Ed. Engl. 30 (1991) 1139.
[7] (a) S.-M. Hu, J.-C. Dai, X.-T. Wu, L.-M. Wu, C.-P. Cui, Z.-Y. Fu, M.-C. Hong, Y.-C. Liang, J. Cluster Sci. 13 (2002) 33;
(b) J.-J. Zhang, S.-Q. Xia, T.-L. Sheng, S.-M. Hu, G. Leibeling, F. Meyer, X.-T. Wu, S.-C. Xiang, R.-B. Fu, Chem. Commun. (2004) 1186;
(c) J.-J. Zhang, T.-L. Sheng, S.-Q. Xia, G. Leibeling, F. Meyer, S.-M. Hu, R.-B. Fu, S.-C. Xiang, X.-T. Wu, Inorg. Chem. 43 (2004) 5472;
(d) J.-J. Zhang, T.-L. Sheng, S.-M. Hu, S.-Q. Xia, G. Leibeling, F. Meyer, Z.-Y. Fu, L. Chen, X.-T. Wu, R.-B. Fu, Chem. – Eur. J. 10 (2004) 3963;
(e) W.-X. Du, J.-J. Zhang, S.-M. Hu, S.-Q. Xia, R.-B. Fu, S.-C. Xiang, Y.-M. Li, L.-S. Wang, X.-T. Wu, J. Mol. Struct. 701 (2004) 25;
(f) J.-J. Zhang, S.-C. Xiang, S.-M. Hu, S.-Q. Xia, R.-B. Fu, X.-T. Wu, Y.-M. Li, H.-S. Zhang, Polyhedron 23 (2004) 2265.
[8] A.J. Blake, R.O. Gould, C.M. Grant, P.E.Y. Milne, S. Parsons, R.E.P. Winpenny, J. Chem. Soc., Dalton Trans. (1997) 1665, and references therein.
[9] (a) J.-P. Costes, F. Dahan, A. Dupuis, Inorg. Chem. 39 (2000) 165;
(b) Q.-Y Chen, Q.-H. Luo, Z.-L. Wang, J.-T. Chen, Chem. Commun. (2000) 1033.
[10] S. Decurtins, M. Gross, H.W. Schmalle, S. Ferlay, Inorg. Chem. 37 (1998) 2443.
[11] (a) A.D. Cutland, R.G. Malkani, J.W. Kampf, V.L. Pecoraro, Angew. Chem., Int. Ed. Engl. 39 (2000) 2689;
(b) M.L. Kahn, C. Mathoniere, O. Kahn, Inorg. Chem. 38 (1999) 3692.
[12] T. Sanada, T. Suzuki, S Kaizaki, J. Chem. Soc., Dalton Trans. (1998) 959.
[13] (a) B.-Q. Ma, S. Gao, G. Su, G.-X. Xu, Angew. Chem., Int. Ed. Engl. 40 (2001) 434;
(b) S.-M. Liu, E.A. Merers, S.G. Shore, Angew. Chem., Int. Ed. Engl. 41 (2002) 3609.
[14] (a) X.-M. Chen, Y.-L. Wu, Y.-Y. Yang, S.M.J. Aubin, D.N. Hendrickson, Inorg. Chem. 37 (1998) 6186;
(b) Y.-C. Liang, R. Cao, W.-P. Su, M.-C. Hong, W.-J. Zhang, Angew. Chem., Int. Ed. Engl. 39 (2000) 3304.
[15] XSCANS (Version 2.1), Siemens Analytical X-Ray Instruments Inc., Madison, WI, 1994.
[16] G.M. Sheldrick, SHELXL-97, Program for X-ray Crystal Structure Refinement, University of Göttingen, Göttingen, Germany, 1997.
[17] M. Abe, Y. Sasaki, Y. Yamada, K. Tsukahara, S. Yano, T. Ito, Inorg. Chem. 34 (1995) 4490, and references therein.
[18] (a) A.R.E. Baikie, A.J. Howers, M.B. Hursthouse, A.B. Quick, P. Thornton, J. Chem. Soc., Chem. Commun. (1986) 1587;
(b) D.W. Boyd, Q. Li, J.B. Vincent, K. Folting, H.-R. Chang, W.E. Streib, J.C. Huffman, G. Christou, D.N. Hendrickson, J. Am. Chem. Soc. 110 (1988) 8537;
(c) D.W. Low, D.M. Eichhorn, A. Draganescu, W.H. Armstrong, Inorg. Chem. 30 (1991) 877.
[19] R.A. Coxall, S.G. Harris, D.K. Henderson, S. Parsons, P.A. Tasker, R.E.P. Winpenny, J. Chem. Soc., Dalton Trans. (2000) 2349.
[20] (a) E. Bouwman, P. Evans, H. Kooijman, J. Reedijk, A.L. Spek, J. Chem Soc., Chem. Commun. (1993) 1746;
(b) P. Dapporto, M. Formica, V. Fusi, M. Micheloni, P. Paoli, R. Pontellini, P. Romani, P. Rossi, Inorg. Chem 39 (2000) 2156;
(c) P. Dapporto, M. Formica, V. Fusi, M. Micheloni, P. Paoli, R. Pontellini, P. Rossi, Inorg.Chem. 39 (2000) 4663;
(d) E.R. Quijano, E.D. Stevens, C.J. O'Connor, Inorg. Chim. Acta 177 (1990) 267.
[21] (a) T. Yamaguchi, Y. Sunatsuki, M. Kojima, H. Akashi, M. Tsuchimoto, N. Re, S. Osa, N. Matsumoto, Chem. Commun. (2004) 1048;
(b) J.-P. Costes, F. Dahan, A. Dupuis, J.-P. Laurent, Inorg. Chem. 36 (1997) 4284;
(c) Q.-Y. Chen, Q.-H. Luo, L.-M. Zheng, Z.-L. Wang, J.-T. Chen, Inorg. Chem. 41 (2002) 605.
[22] B.N. Figgis, M.A. Hitchman, Ligand Field Theory and Its Applications, Wiley-VCH, Toronto, 2000 (Chapters 9 and 11).

Available online at www.sciencedirect.com
SCIENCE DIRECT®
Polyhedron 25 (2006) 9–16
POLYHEDRON
www.elsevier.com/locate/poly

The new $Ru(NBD)Cl_2$(substituted-2,2′-biquinoline) complexes. Synthesis and characterization

Juan Guerrero [a,b,*], Liliana Farías [a,b,*], Luis Lemus [a], Africa Quintanilla [a], Alex Mena [a], Luis Cortez [a], Ricardo F. Baggio [b], María T. Garland [c]

[a] *Departamento de Química de los Materiales, Facultad de Química y Biología, Universidad de Santiago de Chile, Santiago, Chile*
[b] *Departamento de Física, U. de A. Física (Lab. TANDAR), Comisión Nacional de Energía Atómica, Av. del Libertador 8250, 1429 Buenos Aires, Argentina*
[c] *Departamento de Física, Facultad de Ciencias Físicas y Matemáticas, Universidad de Chile, Santiago de Chile, Chile*

Received 4 November 2003; accepted 19 May 2005
Available online 14 November 2005

Abstract

A new ruthenium complex series of type $Ru(NBD)Cl_2L$ (with L = 2,2′-biquinoline derivative) was prepared. Their spectroscopic properties were analysed by RMN ^1H, UV–Vis and Infrared and their electrochemical potentials were obtained by cyclic voltammetry technique. The structure for a complex of this series was established by X-ray analysis. This structure shows a planarity distortion of biquinoline ligand on the complex. The coplanarity distortion degree through the complex series is modulated by the 3,3′-substitued position on the 2,2′-biquinoline ligand, and show correlation with the differences observed on their spectroscopic properties.
© 2005 Elsevier Ltd. All rights reserved.

Keywords: Ruthenium complexes; Heterocyclic nitrogen ligand; Biquinoline ligand

1. Introduction

The ruthenium compounds have been intensively used in different studies. For example, charge and energy transfer, excited state properties and catalyst in thermal and photochemical reaction [1]. Numerous thermal reactions of industrial interest [2], for example, hydrogenation and hydrogen transfer are actively catalyzed by ruthenium coordination compounds using polypyridine ligands [3]. In general, the mechanism for this thermally catalyzed reaction considers a generation of the free coordination site. The labile diolefin norbornadiene (NBD) ligand is a good precursor for catalyst in many reactions due to substitution may easily allow the coordination of the substrate to metal center in the $Ru^{(II)}$(diolefine)(polypyridine) compound. Consequently, we have reported the preparation of the $Ru(NBD)Cl_2L$ (L = bipyridine and substituted phenanthroline) and their application to hydrogen transfer reaction with adequate results [4].

The modulation of the complex properties through the electronic and conformational effect generated by the ligand constitutes an interesting route to prepare compounds with enhanced catalytic properties. In previous works [5], we observed that the distortion degree of biquinoline ligand induces variation on the spectroscopic and electrochemical properties of the rhenium and manganese complexes. The modulation of this

* Corresponding authors. Present address: Departamento de Química Aplicada, Facultad de Química y Biología, Universidad de Santiago de Chile, Casilla 307-Correo 2, Santiago, Chile. Tel.: +56 2 681 1542/2575; fax: +56 2 681 2108 (J. Guerrero), fax: +54 1 754 7121 (L. Farías).
E-mail addresses: jguerrer@lauca.usach.cl (J. Guerrero), lfarias@lauca.usach.cl (L. Farías), baggio@cnea.gov.ar (R.F. Baggio).

0277-5387/$ - see front matter © 2005 Elsevier Ltd. All rights reserved.
doi:10.1016/j.poly.2005.05.009

distortion may be defined through substitution on 3,3′-position of the biquinoline ligand.

Our main purpose is obtains biquinoline ruthenium complexes to evaluate the conformational effect on the catalytic properties. Consequently, we have prepared and analysed the spectroscopical properties of a new series of ruthenium complexes as a function of the conformational characteristics of the annealed 3,3′-substituted-2,2′-biquinoline ligand. The general formulation of complexes is $Ru^{(II)}(NBD)Cl_2L$, where NBD is norbornadiene and L is 2,2′-biquinoline (0,2N), 3,3′-dimethylene-2,2′-biquinoline (2,2N) or 3,3′-trimethylene-2,2′-biquinoline (3,2N).

2. Experimental

2.1. Physical measurements

Microanalyses were performed at the Departamento de Química Orgánica, Facultad de Química y Farmacia, Universidad de Chile. IR spectra were obtained in solid state (KBr cell of 0.2 mm) using a Bruker IFS-66 V FT-IR spectrophotometer. ^1H NMR and COSY spectra were recorded at 400.13 MHz in a Bruker Avance 400 NMR spectrometer gradient enhanced. Absorption spectra were recorded in quartz cells at room temperature in a Shimadzu UV-160 spectrophotometer, using solvents of different polarity previously purified. Molar conductivities were determined from 10^{-3} mol dm^{-3} solutions of complexes in CH_3CN at 25 °C using a conductivitymeter Cole-Parmer 01481.

Electrochemical data were acquired by cyclic voltammetry following the procedure already reported [6]. The measurements were carried out with a PAR 173 potentiostat coupled to a PAR 175 universal programmer. Deaerated solutions, 10^{-4} M complex and 10^{-2} M tetraethylammonium perchlorate in acetonitrile, were placed in a three-electrode cell with a glassy carbon working electrode, a Pt wire counter electrode, and a Ag/AgCl reference electrode. Solvents and supporting electrolyte for the electrochemical measurements were dried according to the literature procedures [7]. Potentials were reported as $E_{1/2}$ values versus SCE and they were determined from the following relationship $E_{1/2} = 1/2(E_{pa} + E_{pc})$, where E_{pa} and E_{pc} are the anodic and cathodic peak potentials, respectively. The cyclic voltammograms were recorded at a sweep rate of 250–1000 mV s^{-1} range for all the scans, at room temperature and in a nitrogen atmosphere.

For the crystalline structure determination, a highly redundant diffractometer data set was collected at room temperature ($T = 295$ K) up to 2θ maximum of ca. 58°, with a Bruker AXS SMART APEX CCD diffractometer using monochromatic Mo Kα radiation, $\lambda = 0.71069$ Å, and a 0.3° separation between frames. Integration was performed using SAINT, and a semi-empirical absorption correction was applied using SADABS, both programs being included in the diffractometer package. The structure resolution was achieved routinely by direct methods and difference Fourier. The structure was refined by least squares on F^2, with anisotropic displacement parameters for non-H atoms. Hydrogen atoms were placed at their calculated positions and allowed to ride onto their host carbons both in coordinates as well as in thermal parameters. The tetrahydrofurane (THF) solvato molecule appears riding onto a symmetry center, a place with a site of symmetry higher than the one of the molecule itself. The molecule is thus forced to split into two equally populated, centro-symmetrically related halves ($Z' = 0.5$), giving to the final local electron density map an intriguing S_6 look.

All calculations to solve the structures, refine the proposed models and obtain derived results were carried out with the computer programs SHELXS-97, SHELXL-97 [8], and SHELXTL/PC [9]. Full use of the CCDC package was also made for searching in the CSD Database [10]. Pertinent results are given in Tables 1–3 and Figs. 1 and 2, respectively.

2.2. Chemical

All the operations were carried out under purified nitrogen atmosphere by standard Schlenk and vacuum-line techniques using freshly distilled, dried and degassed solvents. The solvents used in preparations,

Table 1
Crystal and refinement data for **1**

Compound	**1**
Formula	$C_{25}H_{20}Cl_2N_2Ru \cdot 0.5(C_4H_8O)$
Formula weight	556.45
Crystal system	monoclinic
Space group	$P2_1/c$
Crystal shape, colour	prisms, bluish brown
a (Å)	8.2461(5)
b (Å)	15.7978(10)
c (Å)	17.7575(11)
β (°)	100.6750(10)
V (Å^3)	2273.2(2)
Z	4
D_{Calc} (g cm^{-3})	1.626
$F(000)$	1128
μ (mm^{-1})	0.946
θ Range (°)	1.74–28.09
Index range	$-8 \leqslant h \leqslant 10$; $-20 \leqslant k \leqslant 20$; $-23 \leqslant l \leqslant 16$
Data, parameters (R_{int})	5114 (0.0398)
R_1[a], wR_2[b] [$F^2 > 2\sigma(F^2)$]	$R_1 = 0.0415$, $wR_2 = 0.0726$
R_1[a], wR_2[b] (all data)	$R_1 = 0.0669$, $wR_2 = 0.0796$
Maximum and minimum peaks (e Å^{-3})	0.729 and −0.511

[a] R_1: $\sum\|F_o| - |F_c\|/\sum|F_o|$.
[b] wR_2 : $[\sum[w(F_o^2 - F_c^2)^2]/\sum[w(F_o^2)^2]]^{1/2}$.

Table 2
Selected bond lengths (Å) and angle (°) for **1**

Ru(1)–N(1A)	2.166(3)
Ru(1)–C(2B)	2.181(3)
Ru(1)–C(1B)	2.231(3)
Ru(1)–Cl(2)	2.4224(10)
Ru(1)–X(1)	2.0983(6)
Ru(1)–N(2A)	2.169(3)
Ru(1)–C(4B)	2.185(3)
Ru(1)–C(5B)	2.234(3)
Ru(1)–Cl(1)	2.4303(10)
Ru(1)–X(2)	2.1001(6)
X(1)–Ru(1)–X(2)	67.632(19)
X(1)–Ru(1)–N(1A)	172.92(17)
X(2)–Ru(1)–N(1A)	107.31(17)
X(1)–Ru(1)–N(2A)	107.51(17)
X(2)–Ru(1)–N(2A)	174.30(18)
N(1A)–Ru(1)–N(2A)	77.2(2)
X(1)–Ru(1)–Cl(2)	99.42(6)
X(2)–Ru(1)–Cl(2)	99.15(6)
N(1A)–Ru(1)–Cl(2)	86.13(18)
N(2A)–Ru(1)–Cl(2)	84.44(19)
X(1)–Ru(1)–Cl(1)	95.71(6)
X(2)–Ru(1)–Cl(1)	96.17(6)
N(1A)–Ru(1)–Cl(1)	79.69(18)
N(2A)–Ru(1)–Cl(1)	81.13(18)
Cl(2)–Ru(1)–Cl(1)	161.65(8)

X(1) and X(2) are the midpoints of the double bonds C(1)=C(2) and C(4)=C(5), respectively.

Table 3
Hydrogen bonds for **1** (Å and °)

D–H···A	*d*(D–H)	*d*(H···A)	*d*(D···A)	∠(DHA)
C(4A)–H(4A)···Cl(1)#1	0.93	2.83	3.679(4)	152.5
C(8A)–H(8A)···Cl(2)#2	0.93	2.77	3.649(4)	158.2

Symmetry transformations used to generate equivalent atoms: $^{\#1}x$, $-y+3/2$, $z-1/2$; $^{\#2}x-1$, y, z.

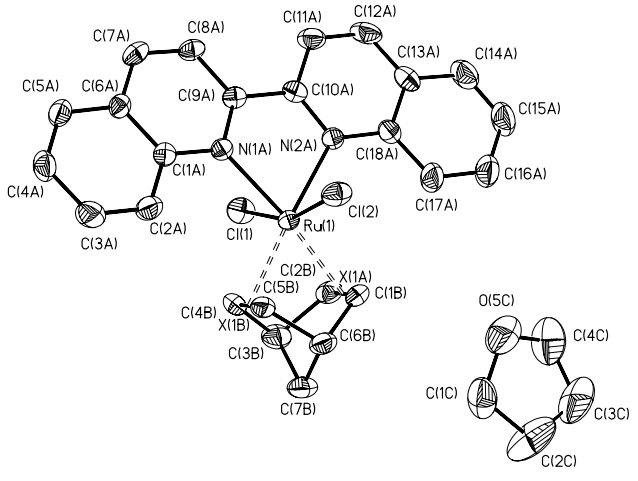

Fig. 1. Ellipsoid plot of the molecule showing the numbering scheme used. The π interaction between the Ru atom and the NBD ligand has been represented by double dashed lines joining the cation and the mid points (X(1), X(2)) of the corresponding double bonds involved (C(1B)=C(2B), C(4B)=C(5B), respectively). Only one out of the two disordered THF moieties is shown, for clarity.

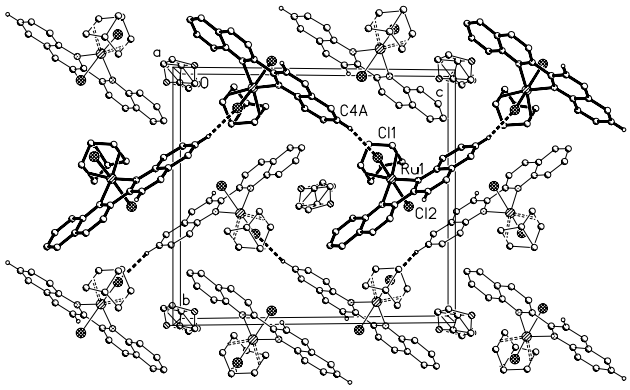

Fig. 2. Packing view of the structure along *a*, where the zig-zag chains formed by C(4A)–H(4A)···Cl(1) are clearly seen (one of them has been highlighted, for clarity). The second hydrogen bond (C(8A)–H(8A)···Cl(2)) linking chains together along the vertical a axis, is not drawn. The THF is shown in its two disordered parts.

crystallizations and spectroscopic analysis (Mallinckrodt, grade HPLC) were treated and distilled from the appropriate drying prior to use. In electrochemical studies, anhydrous acetonitrile was dried using CaH_2 under nitrogen atmosphere at reflux for a period of 2 h and freshly distilled prior to use. Commercially available 2,2′-biquinoline (0,2N), $AgCF_3SO_3$, $RuCl_3(H_2O)$ (Aldrich) compounds were used without further purification. The synthesis of the 3,3′-dimethylene-2,2′-biquinoline ligand (2,2N), 3,3′-trimethylene-2,2′-biquinoline ligand (3,2N) and precursor complexes $[Ru(NBD)Cl_2]_x$ has been previously described [11].

2.3. General synthesis procedure for the complexes

The new complexes were prepared at 60 °C under inert atmosphere. A stoichiometric amount of the biquinoline ligand was added to an emulsion of $[Ru(NBD)Cl_2]_x$ polymer in a THF/water (70:30) solvent mixture. The mixture was vigorous stirred for 6 h until the formation of a microcrystalline dark red precipitate that then was filtered. The product was purified dissolving the crystals in methylene chloride/THF solvent mixture and then it was filtered through celite. The resulting red solution was concentrated and the fine dark red crystals were isolated after crystallization. The mono crystal for a X-ray analysis, was obtained of the THF solution for the $[Ru(NBD)Cl_2(0,2N)]$ complex.

[Ru(NBD)Cl₂(0,2N)]. Yield: 60%. IR (KBr disk) NBD, 3004, 2928, 2854, 1551, 1310, 736 cm^{-1}; 0,2N: 1618, 1596, 1510 cm^{-1}. Molar conductivity ($CHCl_3$) 0.60 S cm^2 mol^{-1}; m.p. 198 °C (d). *Anal*. Calc.: C, 57.70; N, 5.38; H, 3.87. Found: C, 57.70; N, 5.35; H, 3.85%.

Ru(NBD)Cl₂(3,2N). Yield: 63%. IR (KBr disk) NBD: 2996, 2922, 2859, 1569, 1309, 753 cm^{-1}; 0,2N: 1621, 1597, 1496 cm^{-1}. Molar conductivity ($CHCl_3$)

0.66 S cm^2 mol^{-1}; m.p. 196 °C (d). *Anal.* Calc.: C, 60.00; N, 5.00; H, 4.32. Found: C, 59.71; N, 4.97; H, 4.29%.

Ru(NBD)Cl$_2$(2,2N). Yield: 63%. IR (KBr disk) NBD: 2996, 2922, 2859, 1569, 1309, 753 cm^{-1}; 0,2N: 1621, 1597, 1496 cm^{-1}. Molar conductivity ($CHCl_3$) 0.66 S cm^2 mol^{-1}; m.p. 196 °C (d). *Anal.* Calc.: C, 5.35; N, 5.13; H, 4.06. Found: C, 59.71; N, 4.97; H, 4.29%.

3. Results and discussion

The complexes are sparingly soluble in most common organic solvents, e.g., methyl alcohol, acetonitrile, acetone, methylenechloride. The elemental analysis, conductivity measurements and spectroscopic results are in accord with the Ru(NBD)Cl$_2$L formulation for all the complexes and with the X-ray analysis for a Ru(NBD)Cl$_2$(0,2N).

The structure for the Ru(NBD)Cl$_2$(0,2N) is conformed by the mononuclear complex units and disordered tetrahydrofurane molecules, in a (2:1) ratio. The ruthenium cation is octahedrally surrounded (Fig. 1). The basal plane of the polyhedron being defined by the two active nitrogen from a bidentate biquinoline ligand and a double π interaction mediated by the two parallel double bonds (C1B=C2B, C4B=C5B) of a NBD unit, to be represented in that follows (Tables 2 and 3) by their midpoints X(1) and X(2). The apical sites, in turn, are occupied by two chlorine anions, thus providing for the required charge balance.

The coordination geometry is basically a regular octahedral. The only exception is the restraint imposed by chelation, which turns the expected basal square into a rectangle-like form (opposite chelation angles: 77.4° and 67.6° for expected values of 90°). The main plane through the four basal atoms has an esd of 0.017Å, and leaves the ruthenium atom 0.07 Å away, towards the Cl(2) site.

The protruding hydrogens in the structure force numerous situations of steric hindrance which the system avoids through further departures from a regular geometry.

Thus, the hydrogen pairs H(2B), H(4B) and H(1B), H(5B) in NBD push Cl(1) and Cl(2) by 9.7° and 8.7° away from the apical line (Mean Cl(1)–H: 2.775 Å; mean Cl(2)–H: 2.893 Å) in such a way that the angle subtended by the chlorine atoms to the cation center is 161.6° [12].

The biquinoline group is in turn rotated some 20° away from the basal plane of the Ru coordination polyhedron by way of a couple of Cl$\cdots$H$_{biq}$ interactions (to be described below) to end up with its H(2A) and H(17A) hydrogens at a colliding distance from H(5B) and H(1B) in NBD, viz.: H(2A)$\cdots$H(5B): 2.016 Å; H(17A)$\cdots$H(1B): 1.921 Å. This fact forces a rotation of the NBD group in order to oppose the effect, with a concomitant lengthening of some C$_{NBD}$–Ru bond lengths and the shortening of some others. This fact renders the coordination to the cation notoriously asymmetric (Ru–C(2B): 2.188 Å; Ru–C(4B): 2.191 Å against Ru–C(1B): 2.237 Å; Ru–C5B): 2.238 Å).

As a consequence of this process the biquinoline ligand adopts a sort of "butterfly" look with the individual quinolinic moieties (planar to within 0.02 Å) subtending a dihedral angle of 8.3° to each other, which seems to be the main distortion of the ligand.

The monomers interact with each other through two mild C–H$\cdots$Cl hydrogen bonds involving both chlorine atoms (Table 3). The first one, in which Cl(1) takes part defines "zig-zag" chains running along *c*; the second, in which Cl(2) is involved, links these chains together along the *a*-axis into some sort of 2D "corrugated" structures expanding normal to (0 1 0) and fitting into each other in a zip-like fashion (Fig. 2).

The link of these 2D structures is mainly due to the π–π interaction arising between symmetry related biquinoline groups. The symmetry centers which relate contiguous 2D structures also end up positioning one of the lateral wings of the 0,2N ligand at a graphitic distance (ca. 3.30 Å) of its (parallel) symmetry related image, with an overlap of ca. 80% of a whole aromatic ring and a slippage of ca. 1.5 Å.

The structure is stabilized by the inclusion of half of a tetrahydrofurane molecule like a solvato, which appears disordered as it was described in Section 2.

The infrared spectra of the ruthenium complexes do not show a notorious effect of the metal–nitrogen coordination on the characteristic bands of the biquinoline or NBD ligands. The assignation of the Ru–Cl frequency values expected into IR distant region is difficult due to this appear overlapped with another ligand bands. Therefore, it is expected that the structural differences into biquinoline ligand produce only negligible changes in the ruthenium electronic density.

Proton NMR data for the ruthenium complexes and free ligands are shown in Table 4. The ^{1}H assignments for the both NBD and biquinoline free ligands are previously reported (Fig. 3) [11a].

The ^{1}H NMR spectra in solution of the complexes exhibit in the high field region, the characteristic set of signal for NBD ligand. The shielding of the H$_{1'}$ in the complexes related to uncoordinated NBD agrees with the electron density shifting towards the metal due to π coordination. However, the π coordination to Ru(II) causes a shift to upfield of the signal of the H$_{1'}$ with respect to this proton in the free NBD. The set of three signals observed for NBD indicates that this ligand has high symmetry in the complexes. This is only possible if the NBD is placed in the same plane than the biquinoline ligand (X-ray structure).

The ^{1}H NMR spectra in the aromatic region correspond to the expected biquinoline signals (Fig. 4). Due

Table 4
^{1}H NMR spectral data for the Ru(NBD)Cl_2L complexes and the free ligand[a]

Compound	Aromatic L proton						Bridged L proton		NBD		
	H_3	H_4	H_5	H_6	H_7	H_8	H_a	H_b	$H_{1'}$	$H_{2'}$	$H_{3'}$
NBD									6.70 t	3.55 m	2.0 t
Ru(NBD)Cl_2(0,2N)	8.28 d	8.41 d	7.90 dd	7.74 m	7.64 m	7.68 dd			5.68 dd	4.09 m	1.76 t
0,2N	8.85 d	8.30 d	7.86 d	7.58 t	7.75 t	8.25 d					
$\Delta\delta$		0.11				0.57			1.20		
Ru(NBD)Cl_2(2,2N)		8.16 s	7.82 dd	7.61 dd	7.61 dd	7.55 dd	3.30 s		5.71 dd	4.10 m	1.77 m
2,2N		8.03 s	7.77 d	7.52 t	7.68 t	8.43 d	3.20 s				
$\Delta\delta$		0.13				0.83			0.99		
Ru(NBD)Cl_2(3,2N)		8.19 s	7.87 dd	7.62 m	7.65 m	7.44 dd	2.83 t	2.35 q	5.48 dd	4.03 m	1.68 m
3,2N		8.00 s	7.81 d	7.54 t	7.69 t	8.35 d	2.70 t	2.20 q			
$\Delta\delta$		0.19				0.87			1.22		

[a] δ in ppm relative to $SiMe_4$ at 300 K in $CDCl_3$.

to the fact that all the biquinoline aromatic protons are coupled between themselves (similar J values), the assignation to each proton was made using COSY correlation and differences in their coupling pattern (Table 4).

The ^{1}H NMR spectra of the coordinated biquinoline exhibit same set of signals when compared to that of free biquinoline and coordinated biquinoline in other complexes [5]. However, the difference in the chemical shift with respect to the free biquinoline and coordinated biquinoline in other complexes reveals a marked effect of coordination and the complexes structure.

In general, all aromatic proton signals for the biquinoline ligand in the complex appear shifted toward lower field with respect to the free ligand. This deshielding effect is due to the electron density of the metal in the coordinated quinoline. However, the H_8 proton shifted to high field in all complexes. This could be due to the double bond diamagnetic effect of the NBD ligand placed in the same plane, which affords a more protected environment.

The shifting to high field of the H_3 proton in $RuCl_2$(NBD)(2,2′-biquinoline), relative to the uncoordinated 0,2N ligand, has been generally observed in 2,2′-biquinoline complexes [5]. This effect was explained for a "peri" interaction with nitrogen into *trans* preferential free ligand conformation [11a] (see Figs. 4 and 5).

The restriction to coplanarity of two halves of biquinoline ligand, due to 3,3′ substitution and coordinate

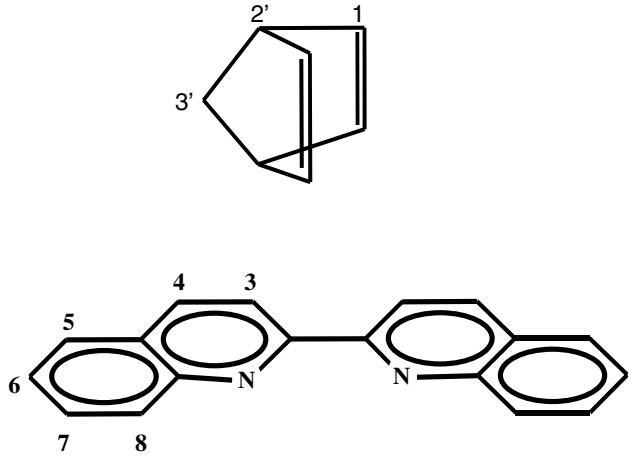

Fig. 3. Structure of the biquinoline and NBD ligands used in this study showing hydrogen positions for NMR considerations.

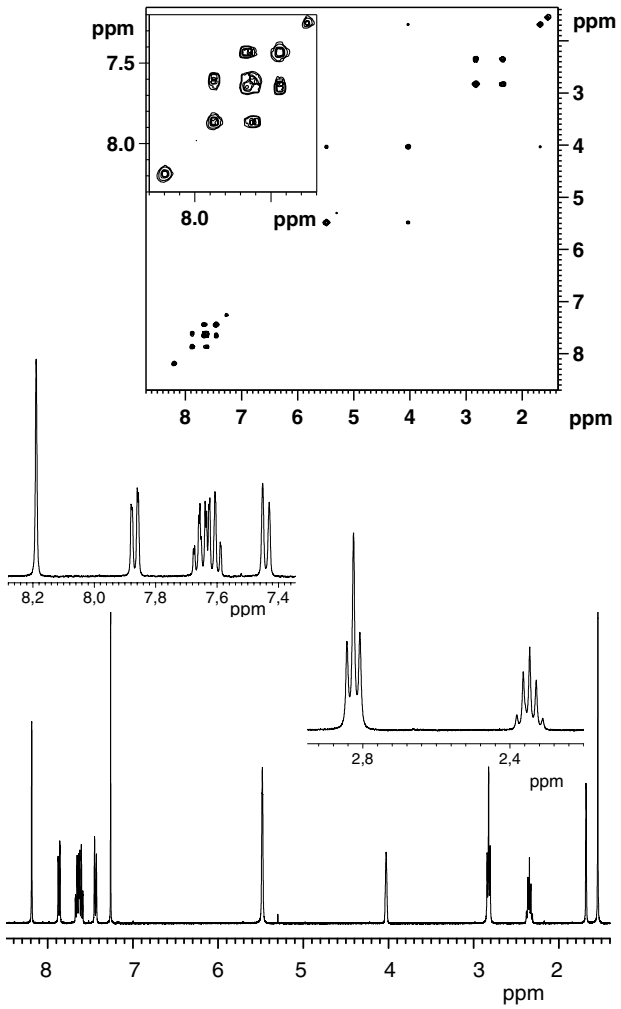

Fig. 4. ^{1}H NMR and COSY spectra for $RuCl_2$(NBD)(3,2N) complex.

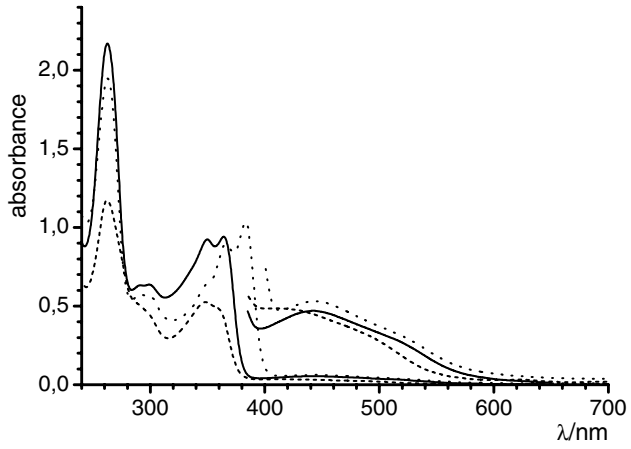

Fig. 5. UV-spectra of $Ru(NBD)Cl_2L$ complexes in CH_2Cl_2 solvent to 25 °C. Solid line: $Ru(NBD)Cl_2(0,2N)$; dot line: $Ru(NBD)Cl_2(2,2N)$; dash line: $Ru(NBD)Cl_2(3,2N)$.

requirement to metal for this ligand, determinates geometrical restriction on the complexes. Therefore, the geometric differences through the series of biquinoline complexes can be spectroscopically analyzed.

The proton shift differences for the analogous proton in different biquinoline ligand were observed in all complexes (Table 4). Mainly, ^1H NMR chemical shift data of H_4, H_8 and $H_{1'}$ protons are informative of the disposition of the ligand geometries in the complexes. The chemical shift difference between the complexes and the corresponding free ligand ($\Delta\delta$) of the H_4 and H_8 protons were greater. These $\Delta\delta$ values decrease in the next ligands order: (0,2N), (2,2N), (3,2N).

These chemical shift differences were also observed for the $H_{1'}$ in all series of complexes. However, correlation with biquinoline ligands was not observed.

In the structure of the complexes, the H_4 chemical shift is notoriously influenced by electronic effects associated with the coordination of nitrogen in *para*-position. On the other hand, the H_8 chemical shift is influenced by the diamagnetic effect of NBD. For $H_{1'}$, the chemical shifts are the result of the paramagnetic effect of aromatic ring of biquinoline. From the previous information, it appears that the chemical shifts of these protons are influenced by the non-planarity grade of substituted-biquinoline in the structure of complexes [5a,5j,11a].

The UV–Vis spectroscopical data for the complexes are shown in Table 5. The $Ru(NBD)Cl_2L$ complexes show one band placed up on 430 nm, that has been assigned to a ruthenium-to-biquinoline-charge-transfer (MLCT) transition, in accord with electron acceptor biquinoline ligand characteristic and assignments previously reported for related complexes [1,5]. Consequently, this band shows a slight solvent polarity dependence.

The energy for the MLCT band increases in the order of (0,2N), (2,2N), (3,2N) showing a slight dependence with the deviation of the quinoline halves from planarity in the coordinated biquinoline ligand. A similar trend is exhibited by the biquinoline rhenium and manganese complexes previously reported [5]. In previous work [5a], we explain the shift of the MLCT band through complex series with changes in the electronic repulsion between the d-orbital metal and the biquinoline orbitals. The HOMO stabilization and the LUMO destabilization usually result from the increase in this conformational distortion.

The most intense bands below 400 nm correspond to biquinoline intraligand transitions. These bands may overlap the Ru to NBD MLCT bands expected in this same region.

The electrochemical data were obtained with cyclic voltammetry in 250 and 1000 mV s^{-1} scan rates range. The voltammograms for the all complexes exhibited similar features, i.e., one oxidation pick and two reduction pick on the −2.0 to 2.0 V potential range (Table 6). The pick separation between the cathodic and anodic waves, of all the redox couples, increase with the scan rates increase, that suggest a quasireversible process.

The only oxidation wave is a quasireversible process, and it is found close to +1.12 V. This process has been observed in several related polypyridine Ru(II) com-

Table 5
UV–Vis spectral data to free ligand and derivatives $Ru(NBD)Cl_2L$ complexes

Compound	Solvent	λ_{max}, nm (ε, L cm^{-1} M^{-1})		
		TCML (Ru → biq)		IL ($\pi \rightarrow \pi^*$)
$Ru(NBD)Cl_2(2,2N)$	CH_2Cl_2	443 (1280)	384 (17104) 366 (14344)	299 (11624) 289 (11704)
	$CHCl_3$	439 (967)	384 (19814) 366 (15996) 302 (10484)	290 (10782) 264 (35065)
	$(CH_3)_2CO$	442 (1184)	382 (16168) 364 (13168)	
$Ru(NBD)Cl_2(0,2N)$	CH_2Cl_2	442 (1088)	366 (14088) 344 (18752)	299 (12088) 288 (11960) 256 (19592)
	$CHCl_3$	434 (1054)	367 (13699) 345 (18206)	288 (12669) 265 (48643)
	$(CH_3)_2CO$	442 (1216)	365 (14104) 344 (19904)	
$Ru(NBD)Cl_2(3,2N)$	CH_2Cl_2	412 (980)	360 (11032) 347 (14456)	255 (19528)
	$CHCl_3$	412 (1080)	361 (12120)	262 (31569)
	$(CH_3)_2CO$	418 (1000)	358 (10872) 344 (14352)	

ε = Molar extinction coefficient at 298 K.

Table 6
Electrochemical properties of Ru(II) complexes[a]

Complex	Redox potential (V)		
	Reduction		Oxidation[b]
$Ru(NBD)Cl_2(0,2N)$	−1.24[b]	−1.04[b] to −0.88[b]	1.12
$Ru(NBD)Cl_2(2,2N)$	−1.18	−0.95	1.11
$Ru(NBD)Cl_2(3,2N)$	−1.06[b]	−0.85[c]	1.13

[a] The experimental error in the potential measurements is ±0.01;V. Half-wave potentials relative to the SCE recorded with a scan rate of 1000 mV s^{-1}. The ΔE_p increase when the scan rate increase.
[b] Quasireversible wave.
[c] E_{pc}.

pounds [1b,1e,1f,13] and correspond to the typical one electron Ru(III)/Ru(II) couple.

The two electrochemical reductions on the first scan occur in the $E_{1/2} = -0.85$ to -1.04 V range and $E_{1/2} = -1.06$ to -1.24 V range, respectively. According to previous studies, the first reduction wave could be attributed to a ligand-centered process that involves the addition of an electron to the π* orbital on the biquinoline ligand. The another reduction peak may be assigned to the second reduction of the biquinoline ligand. This assumption is unclear due to the small difference between the two reduction peak is not consistent with the differences reported previously (roughly 500 mV) found for related complexes showing similar electrochemical behavior [1h,1e,5a,14].

4. Conclusions

The X-ray studies for a ruthenium complex revealed that the structure of the complexes is a quasi perfect octahedron. However, spectroscopic and electrochemical results already discussed showed differences through the series that only are attributed to conformational differences in the complexes. In previous works, we established that the structural restriction in the biquinoline derivative ligands remove to quinoline halves from a perfect plane in the octahedral complexes and also it influence their spectroscopical properties. Our presumption is that these differences may determinate interesting catalytic properties.

5. Supplementary materials

Crystallographic data (excluding structure factors) have been deposited in the Cambridge Crystallographic Data Centre like Supplementary Publication No. CCDC_212516. Copies of the data can be obtained free of charge on application to The Director, CCDC, 12 Union Road, Cambridge CB2 1EZ, UK (fax: +44 1233 336 033; e-mail: deposit@ccdc.cam.ac.uk or http://www.ccdc.cam.ac.uk).

Acknowledgments

We thank DICYT-USACH, for the financial support.

References

[1] (a) K. Kalyanasundaram, Photochemistry of Polypyridine and Porphyrin Complexes, Academic Press, London, 1992;
(b) A. Del Guerzo, S. Leroy, F. Fages, R.H. Schmehl, Inorg. Chem. 41 (2002) 359 (references therein);
(c) E. Holder, G. Shoetz, V. Schurig, E. Lindner, Tetrahedron: Assym 12 (2001) 2289;
(d) S. Encinas, A.M. Barthram, M.D. Ward, F. Barigelletti, S. Campagna, Chem. Commun. (2001) 277;
(e) A. Juris, S. Campagna, V. Balzani, G. Gremaud, A. Von, Zelewsky. Inorg. Chem. 27 (1998) 3652;
(f) J.P. Sauvage, J.P. Collin, J.C. Chambron, S. Guillerez, C. Coudret, V. Balzani, F. Barigelletti, L. De Cola, L. Flamigni, Chem. Rev. 94 (1994) 993;
(g) S.A. Moya, I. Azócar-Guzmán, J. Guerrero, P. Aguirre, Bol. Soc. Chil. Quim. 47 (2002) 393;
(h) K. Kalyanasundaram, M. Grätzel (Eds.), Photosensitization and Photocatalysis Using Inorganic and Organometallic, Kluwer Academic Publishers, Dordrecht, 1993;
(i) E. Baranoff, J.P. Collin, J. Furusho, Y. Furusho, A. CH. Laemmel, J.P. Sauvage, Inorg. Chem. 41 (2002) 1215.
[2] S. Bennett, S.M. Brown, G. Conole, M. Kessler, E. Sinn, S. Woodward, J. Chem. Soc., Dalton Trans. (1995) 367.
[3] (a) B.P. Sullivan, J.A. Baumann, T.L. Meyer, D.J. Salmon, H.E. Lehmann, A. Ludi, J. Am. Chem. Soc. 99 (1977) 7368;
(b) B.P. Sullivan, D.J. Salmon, T.J. Meyer, Inorg. Chem. 17 (1978) 3334;
(c) M.E. Marmion, K.J. Takeuchi, J. Am. Chem. Soc. 110 (1988) 1472;
(d) P.A. Chaloner, M.A. Esteruelas, F. Joó, L.A. Oro, Homogeneous Hidrogenation, Kluwer Academic Publishers, Dordrecht, 1993.
[4] R. Sariego, L. Farías, S.A. Moya, Polyhedron 16 (1997) 3847.
[5] (a) S.A. Moya, J. Guerrero, R. Pastene, R. Schmidt, R. Sariego, R. Sartori, J. Sans-Aparicio, I. Fonseca, M. Martinez-Ripoll, Inorg. Chem. 33 (1994) 2341;
(b) A. Terraza, J. Guerrero, S.A. Moya, F.M. Rabagliati, Polym. Bull. 41 (1998) 669;
(c) G. Ferraudi, M. Feliz, E. Wolcan, I. Hsu, S.A. Moya, J. Guerrero, J. Phys. Chem. 99 (1995) 4929;
(d) S.A. Moya, J. Guerrero, R. Pastene, A.J. Pardey, P. Baricelli, Polyhedron 17 (1998) 2289;
(e) J. Guerrero, O.E. Piro, E. Wolcan, M.R. Féliz, G. Ferraudi, S.A. Moya, Organometallics 20 (2001) 2842;
(f) S.A. Moya, J. Guerrero, R. Pastene, R. Sartori, R. Schmidt, R. Sariego, Bol. Soc. Chil. Quim. 37 (1992) 311;
(g) R.F. Baggio, S.A. Moya, R. Schmidt, M. Gulppi, J. Guerrero, R. Sartori, M.T. Garland, Acta Crystallogr., Sect. C 50 (1994) 1701;
(h) J. Guerrero, S.A. Moya, M.T. Garland, Acta Crystallogr., Sect. C 54 (1998) 1592;
(i) J. Guerrero, S.A. Moya, M.T. Garland, R.F. Baggio, Acta Crystallogr., Sect. C 55 (1999) 932;
(j) S.A. Moya, J. Guerrero, R. Pastene, I. Azocar-Guzman, A.J. Pardey, Polyhedron 21 (2002) 439.
[6] S.A. Moya, R. Pastene, R. Sariego, R. Sartori, P. Aguirre, H. Le Bozec, Polyhedron 15 (1996) 1823.
[7] (a) J.F. Coetzee, g.P. Cunningham, D.K. McGuire, G.R. Padmanabhan, Anal. Chem. 31 (1962) 1139;
(b) I.M. Kolhoff, J.F. Coetzee, J. Am. Chem. Soc. 79 (1957) 870.

[8] G.M. Sheldrick, SHELXS-97 and SHELXL-97: Programs for Structure Resolution and Refinement, University of Göttingen, Germany, 1997.
[9] G.M. Sheldrick, SHELXTL-PC, Version 5.0., Siemens Analytical X-ray Instruments, Inc., Madison, WI, USA, 1994.
[10] F.H. Allen, O. Kennard, Chem. Design Automation News 8 (1993) 131.
[11] (a) R.P. Thummel, F.J. Lefoulon, Org. Chem. 50 (1985) 666;
(b) E.W. Abel, M.A. Bennett, G. Wilkinson, J. Chem. Soc. (1959) 3178.
[12] C. Potvin, J.M. Manoli, G. Pannetier, R. Chevalier, N. Platzer, J. Organomet. Chem. 113 (1976) 273.
[13] (a) B. Galland, D. Limosin, H. Laguitton-Pasquier, A. Deronzier, Inorg. Chem. Commun. 5 (2002) 5;
(b) S.M. Scott, K.C. Gordon, A.K. Burrell, J. Chem. Soc., Dalton Trans. (1998) 2873.
[14] (a) M. Haukka, P. Hirva, s. Luukkanen, M. Kallinen, M. Ahlgrén, T. Pakkanen, Inorg. Chem. 38 (1999) 3182;
(b) S. Isiet, H. Taube, J. Am. Chem. Soc. 95 (1973) 8198;
(c) D.P. Rillema, K.B. Mack, Inorg. Chem. 21 (1982) 3849.

Available online at www.sciencedirect.com
SCIENCE DIRECT®
Polyhedron 25 (2006) 17–24
POLYHEDRON
www.elsevier.com/locate/poly

N-phthaloylglycinato complexes of cobalt, nickel, copper and zinc

Nilotpal Barooah [a,b], Rupam J. Sarma [a], Andrei S. Batsanov [b], Jubaraj B. Baruah [a,*]

[a] *Department of Chemistry, Indian Institute of Technology, North Guwahati, Assam 781 039, India*
[b] *Department of Chemistry, University of Durham, Durham DH1 3LE, United Kingdom*

Received 7 June 2005; accepted 14 June 2005
Available online 26 September 2005

Abstract

The cobalt(II), nickel(II), copper(II) and zinc(II) complexes of *N*-phthaloylglycinato (Nphgly) ligands have been synthesised and characterised. The cobalt and zinc complexes have the composition $[M(Nphgly)_2(H_2O)_4]2H_2O$ with an octahedral geometry around the metal ion. In these two complexes, the phthaloylglycinato groups are monodentate and have four coordinated water molecules and two molecules of lattice water. The lattice water molecules are held through hydrogen bonding with one carbonyl group of the phthalimide part and the carbonyl group of glycinato part. Such water molecules are further held by hydrogen bonding to two coordinated water molecules. There are also two other coordinated water molecules having a different hydrogen-bonding environment. These two water molecules attached to the metal are stabilised by hydrogen bonding through two carbonyl groups from the glycinato part and the phthalimide part. Distinctions of these two sets of water environment are reflected in thermogravimetry and DSC of the complexes. In the thermogram of these two complexes there is loss of four water molecules at a relatively lower temperature than the other two water molecules. The copper complex containing *N*-phthaloylglycinato and pyridine ligands, having the composition $[Cu(Nphgly)_2(py)_3]$, is prepared. This complex has a square pyramidal structure with one pyridine molecule at the axial position. The complex on thermal degradation leads to the formation of CuO at 380 °C. The similar nickel complex has the composition $[Ni(Nphgly)_2(py)_3 1.3H_2O]$, having a trimeric H-bonded structure with a distorted octahedral environment around nickel(II).
© 2005 Elsevier Ltd. All rights reserved.

Keywords: *N*-phthaloylglycine; First row transition metal complexes; Thermochemistry; Hydrogen bonding

1. Introduction

Amino acid complexes are important in biology [1,2]. The *N*-protected amino acids are used for the synthesis of peptide bonds in solid phase syntheses [3–5]. The phthalimide group acts as a protecting group for amines and amino acids [6–10]. The *N*-phthaloylamino acids undergo photochemical reactions to give rearranged products [11]. Several such phthalimide derivatives have importance in medicinal chemistry [12] and are used as antimicrobial reagents [13]. The silver(I) complex of *N*-phthaloylglycinato has an interesting three-dimensional network [14]. Several other studies on the transition metal complexes of *N*-phthaloylglycine are reported but these studies lack structural details [15–17]. *N*-hydroxyphthalimide along with the cobalt(II) complexes in the presence of oxygen acts as a catalyst for selective oxidation of primary alcohols to the corresponding aldehydes [18,19]. Palladium complexes are known to catalyses amido-carbonylation of *N*-phthalimide derivatives [20]. We have earlier discussed that in adducts of *N*-substituted phthalimide with polyhydroxy aromatics supramolecular features play an important role in the structure [21]. Thus, the structural features of these molecules are important and we report here characteristic features of *N*-phthaloylglycinato complexes of cobalt (II), zinc(II), copper(II) and nickel (II).

* Corresponding author. Tel.: +91 361 2582301; fax: +91 361 2690762.
E-mail address: juba@iitg.ernet.in (J.B. Baruah).

0277-5387/$ - see front matter © 2005 Elsevier Ltd. All rights reserved.
doi:10.1016/j.poly.2005.06.057

2. Experimental

2.1. Material and methodology

All the chemicals used in this study were analytical grade and used as procured. The solvents were distilled and dried prior to use. For example, acetonitrile was distilled over calcium hydride, pyridine was distilled over potassium hydroxide. The IR spectra were recorded as KBr pellets on a Nicolet Impact 410 FT-IR spectrometer. Magnetic moments were measured on a Sherwood Scientific Magnetic susceptibility balance. The conductance and pH were measured by a digital conductivity bridge and pH metre of Systronics. For molar conductance, the cell constants were determined by standard KCl, and for pH measurements the pH-metre was calibrated with a solution prepared from standard pH tablets. The thermal analyses were performed on a Metler Toledo TGA/SDTA 851^e and Metler Toledo 821^e thermal analyzer. Thermogravimetry studies were done in an aluminium crucible under pure nitrogen gas. DSCs were done under ordinary conditions in a platinum crucible. The visible spectra were recorded on a Hitachi U-2001 UV–Vis spectrometer.

X-ray diffraction data were collected on a Bruker 3-circle diffractometer with CCD area detectors ProteumM APEX or SMART 6000, using graphite monochromated Mo Kα radiation from a 60 W microfocus Bede Microsource® with glass polycapillary optics. The low temperature was maintained using an Oxford cryosystem open flow N_2 cryostat. The structures were solved by direct methods and refined by full-matrix least squares against F^2 of all data, using SHELXTL software.

2.2. Synthesis of tetra-aqua-bis-N-phthaloylglycinatocobalt(II) dihydrate

A finely ground mixture of phthalic anhydride (0.74 g, 5 mmol) and glycine (0.38 g, 5 mmol) was heated at 80 °C for 30 min; the solid mass was then dissolved in methanol (10 ml) and filtered; the filtrate was taken and evaporated. Water (10 ml) was added to the residue obtained from the filtrate after evaporation; this was followed by addition of a solution of cobalt(II)acetate tetrahydrate (0.5 g, 2 mmol, in 5 ml water). The reaction mixture was stirred at room temperature (4 h), which led to the precipitation of pink coloured tetra-aqua-bis-*N*-phthaloylglycinatocobalt(II) dehydrate (Yield: 0.32 g, 31%). Recrystallisation of the complex was done from an aqueous solution of the complex by diffusing acetone. Elemental *Anal*. Calc. for $C_{20}H_{24}CoN_2O_{14}$: C, 41.45; H, 4.15; N, 4.84. Found: C, 41.39; H, 4.12; N, 4.90%. IR (KBr, cm^{-1}): 3476(s), 3263(bs), 2925(m), 1772(w), 1701(s), 1598(s), 1470(w), 1429(s), 1383(s), 1312(s), 1194(w), 1117(s), 968(s), 743(s), 717(s), 630(s) cm^{-1}. Vis (λ_{max}, acetonitrile), 540 nm ($\varepsilon = 30\ mol^{-1}\ dm^3\ cm^{-1}$).

2.3. Synthesis of tetra-aqua-bis-N-phthaloylglycinatozinc(II) dihydrate

An aqueous solution of zinc acetate dihydrate (0.219 g, 1 mmol in 10 ml) was added dropwise to a well-stirred solution of *N*-phthaloylglycine (0.410 g, 2 mmol) in ethanol (10 ml) at room temperature. After half an hour of stirring a gelatinous precipitate was formed. The stirring was continued for another 3 h and the precipitate obtained was redissolved in water (10 ml). After redissolving the precipitate the solvent was slowly evaporated to give colourless crystals after three days (Yield: 0.36 g, 66%). Elemental *Anal*. Calc. for $C_{20}H_{24}N_2O_{14}Zn$: C, 41.25; H, 4.13; N, 4.81. Found: C, 41.30; H, 4.11; N, 4.78%. IR (KBr, cm^{-1}): 3486(b), 3288(b), 1776(s), 1706(s), 1610(b), 1428(s), 1390(s), 1314(s), 1120(s), 966(s), 750(s), 720(s).

2.4. Synthesis of tri-pyridine-di-phthaloylglycinato copper(II)

An ethanolic solution of copper acetate monohydrate (0.199 g, 1 mmol, 10 ml ethanol) was added dropwise to a well-stirred solution of *N*-phthaloylglycine (0.410 g, 2 mmol) in ethanol (10 ml) at room temperature. A light blue precipitate appeared instantaneously. The reaction was allowed to proceed for 3 h with constant stirring. The blue precipitate was collected through filtration and the residue obtained was washed with water followed by ethanol and dried in air. The precipitate was redissolved in pyridine (5 ml) and slow evaporation gave a complex having composition the $Cu(py)_3(Nphgly)_2$ (Yield: 0.24 g, 34%). Elemental *Anal*. Calc. for $C_{35}H_{27}CuN_5O_8$: C, 59.22; H, 3.81; N, 9.87. Found: C, 59.20; H, 3.79; N, 9.85%. Vis (λ_{max}, pyridine) 662 nm ($\varepsilon = 156\ dm^3\ mol^{-1}\ cm^{-1}$). IR (KBr, cm^{-1}): 3462(w), 3083(w), 2950(w), 1772(s), 1721(s), 1655(s), 1598(s), 1455(s), 1419(s), 1368(s), 1291(s), 1194(s), 1117(s), 963(s), 743(s), 712(s), 649(s).

2.5. Synthesis of the phthaloylglycinato complex of nickel(II)

An ethanolic solution (10 ml) of nickel(II)acetate tetrahydrate (0.248 g, 1 mmol) was added dropwise to a stirred solution of *N*-phthaloylglycine (0.410 g, 2 mmol) in ethanol (10 ml) at room temperature. The resulting light green solution was stirred at room temperature for 2 h and left undisturbed. A light green precipitate was obtained after seven days by slow evaporation of the solution. The precipitate was filtered, washed with ethanol and dried in air. Finally, it was dissolved in pyridine (10 ml) to obtain a light blue solution. Light blue crystals were obtained after three weeks by slow evaporation of the solvent (Yield: 0.25 g, 35%). Elemental *Anal*. Calc. for $C_{35}H_{27}NiN_5O_8 \cdot 1.3H_2O$: C, 57.03; H,

4.02; N, 9.31. Found: C, 57.09; H, 4.09; N, 9.52%. IR (KBr,cm^{-1}): 3568(bw), 3472(bw), 3260(w), 3106(w), 3072(w), 2948(w), 1770(s), 1711(s), 1602(b), 1418(s), 1376(s), 1314(s), 1113(s), 963(s), 744(s), 714(s). Vis (λ_{max}, pyridine)610 nm ($\varepsilon = 34\ dm^3\ mol^{-1}\ cm^{-1}$).

3. Results and discussion

A cobalt complex having the composition [Co(Nphgly)$_2$(H_2O)$_4$]2H_2O can be prepared by the reaction of *N*-phthaloylglycine (NphglyH) with cobalt(II)acetate tetrahydrate (Eq. (1)). This complex is prepared by reaction of cobalt(II)acetate tetrahydrate with in situ generated *N*-phthaloylglycine. The reaction is carried out in one pot by the condensation of phthalic anhydride and glycine followed by the reaction with cobalt(II)acetate. In this reaction, cobalt(II)acetate itself causes the deprotonation of *N*-phthalolylglycine to form the desired complex and thus no buffer or external reagent needs be added to maintain a pH for making a basic medium. It is also to be noted that the pK_a of *N*-phthalolylglycine is 3.48 whereas acetic acid has pK_a 4.76 at 25 °C, thus, the cobalt acetate can get protonated by *N*-phthalolylglycine to release acetic acid which allows the formation of the desired complex

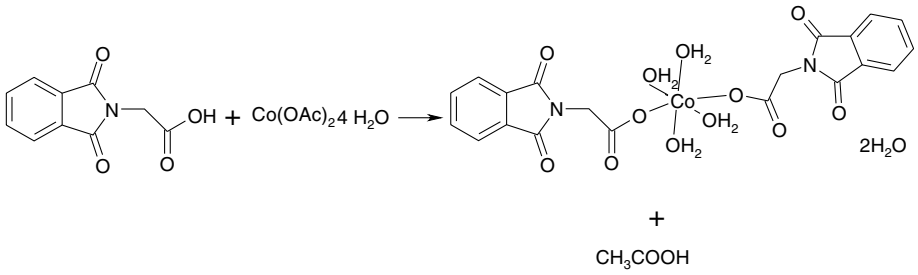

(1)

results are in accordance with a distorted octahedral geometry around cobalt(II). The structure of [Co(Nphgly$_2$)(H_2O)$_4$]2H_2O in the solid state shows that all the four coordinating water molecules have extensive hydrogen bonding. Two water molecules are linked to carbonyl groups of the carboxylato ligand through hydrogen bonding; this provides a chelate like structure. The other two coordinated water molecules are attached to the lattice water molecules by hydrogen bonding, which in turn are held in between the carbonyl groups of the phthalimide part. Thus, a cyclic structure including the cobalt centre and coordinated water molecules along with the lattice water through intermolecular hydrogen bonding is formed. The hydrogen atom of the coordinated water molecules are also associated with the carbonyl group (for example H11W···O5) of the phthalimide ring of another phthaloylglycinato ligand bound to another cobalt centre through intermolecular hydrogen bonding. All water molecules in the complex are involved in extensive hydrogen bonding to form a self assembled structure (Fig. 1). There are both intra- and intermolecular hydrogen bonds.

The structure of the complex has been determined by X-ray crystallography and it is observed that cobalt(II) has a distorted octahedral environment with four aqua ligands occupying one plane of the octahedron. There are two monodentate carboxylate groups at the axial positions (Fig. 1). In the coordination chemistry of cobalt(II), the monodentate carboxylato group is a common phenomenon, for example cobalt(II)acetate itself has monodentate carboxylate groups linked to the cobalt atom [22]. However, in the case of [Co(Nphgly)$_2$(H_2O)$_4$]2H_2O, we have observed interesting supramolecular features that are not present in ordinary cobalt(II)acetate. The bond distance between Co1–O3, Co1–O2 and Co1–O1 are 2.1165(14), 2.0833(16) and 2.0694(16) Å, respectively, whereas the O3–Co1–O2, O2–Co1–O1 and O1–Co1–O3 bond angles are 88.98(6)°, 88.04(7)° and 90.72(6)°, respectively. These

The intramolecular H-bonds are:

	D–H	H···A	D···A	DHA
O1–H12W···O4	0.84(3)	1.88(3)	2.640(2)	150(3)
O2–H22W···O7	0.83(4)	1.87(4)	2.663(3)	159(4)
O7–H71W···O6	0.873(10)	1.93(3)	2.732(3)	151(5)

There are also intermolecular H-bonds involving the remaining H atoms of the water molecules not involved in intramolecular H-bonds:

	D–H	H···A	D···A	DHA
O1 H11W O5B	0.75(3)	2.02(3)	2.772(2)	173(3)
O2AA H21W O4	0.88(3)	1.83(3)	2.710(2)	172(3)

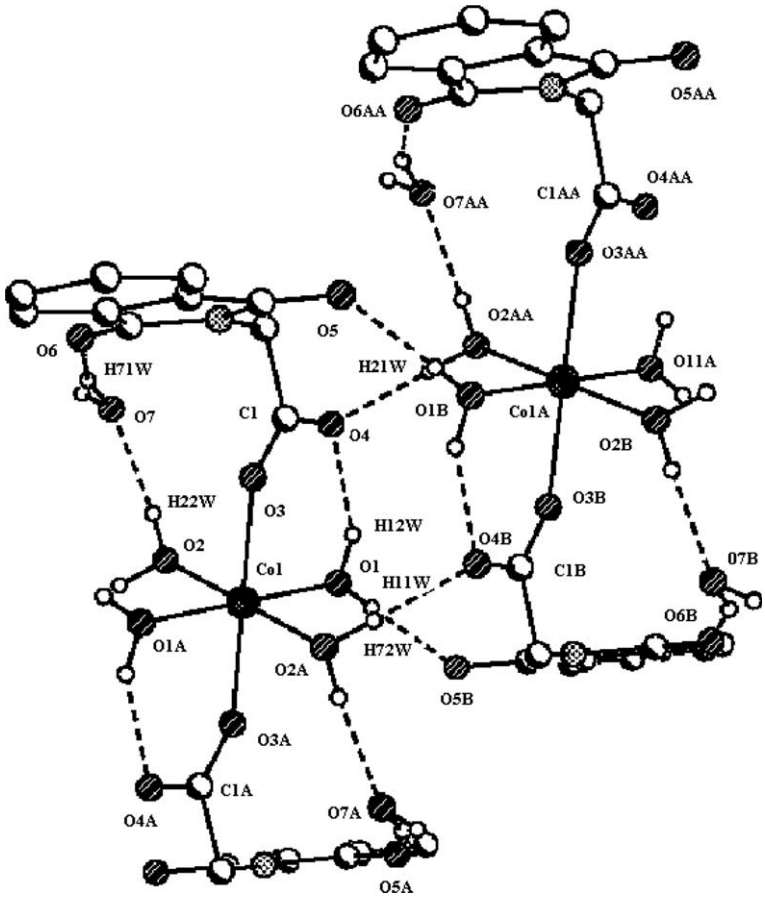

Fig. 1. Crystal structure showing two units of tetra-aqua-bis-*N*-phthaloylglycinato cobalt(II)dihydrate (the H-atoms of the phthaloyl part are not shown for clarity).

In the structure shown in Fig. 1 the hydrogen-bonds have a twofold effect on the crystal packing. Firstly, the hydrogen-bonds involving the coordinated molecules make a chain of molecular units. Secondly, the intermolecular H-bond involving the loose water molecule joins these chains along one direction, producing layers of molecular units on the plane containing the two directions of the chain linkages. This effect along with the bipolar arrangement of phthalimide makes two types of environments for water molecules. Two different environments around coordinated water molecules are represented in Fig. 2. Two types of environments around the coordinated water molecules are shown by taking segments from Fig. 1 (segment A and B in Fig. 2). These fragments are created by the H-bonding between the ligands that are bonded in an intermolecular fashion with the ligands that are associated to two cobalt centres. The two environments for the coordinated water molecules are also reflected in the bond lengths. Namely, there is a bond length difference of 0.0139 Å between the two types of Co–O bonds in the two types of coordinated water molecules as depicted in A and B of Fig. 2. Since the cobalt complex is coordinated through the carboxylate group, it's coordination may be compared with the supramolecular construction that is made from the analogous carboxy-phosphonate complex reported in the literature [23]. We have found that water molecules are involved in a tight packed structure in our cobalt complex, in contrast to the supramolecular assembly reported for the carboxylate phosphate that has interesting S-shaped voids filled with water molecules [23]. In their case they observed hexa coordinated cobalt with two water molecules occupying coordination sites and had observed it to be a cluster containing three cobalt centres. But in our case four water molecules are coordinated to cobalt(II), which are in two different environments with a three-dimensional network. The crystallographic parameters of the complex are listed in Table 1.

The two types of water environment, as shown in A and B (Fig. 2), are also reflected in the thermogravimetric study. The cobalt complex on heating shows that it loses four water molecules in the region 35–104 °C (experimental loss 11.82%, theoretical 12.5%). In the temperature range 104–146 °C the complex loses two molecules of water (experimental loss 18.16%, theoretical 18.76%). In DSC these two losses are also reflected as endothermic processes occurring at 104.37 and

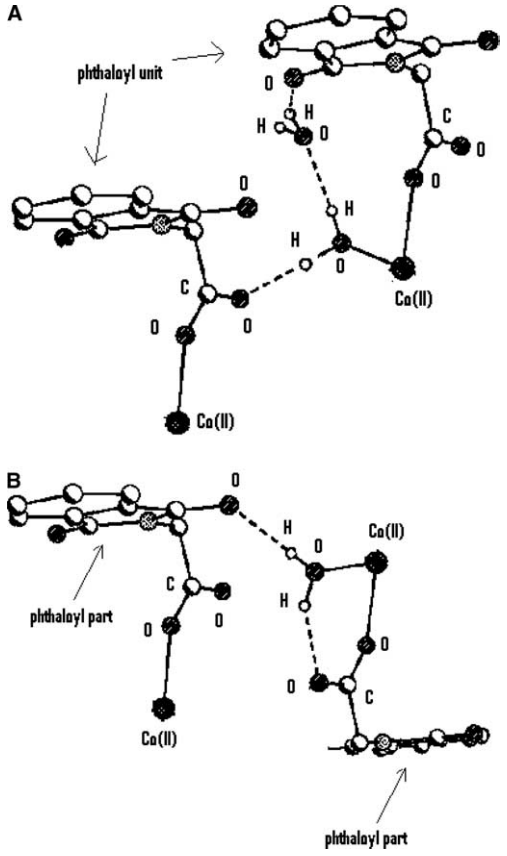

Fig. 2. Two different types of environment for coordinated water molecules in tetra-aqua-bis-*N*-phthaloylglycinato cobalt(II)dihydrate (segment from Fig. 1 is drawn omitting the H-atoms on the ring).

143.72 °C. This clearly indicates that the water molecules present in the complex are not in equivalent environments. Generally, a lattice water molecule is expected to be lost at a lower temperature and one would anticipate a loss of two water molecules of crystallisation at a lower temperature than the coordinated water molecules in our cobalt complex. But the experimental observation shows that there are four water molecules lost at a lower temperature. This can be interpreted in terms of the two different molecular environments around the coordinated water due to hydrogen-bonding. Thus, the loss of four water molecules at a low temperature relative to the two other molecules implies that these are water molecules that are held through weak hydrogen bonding between the metal and one carbonyl group of the phthalimide unit, providing the H-bonding scheme as shown in motif A of Fig. 2. The other two water molecules that are lost at 144 °C are tightly bound by coordination to the metal and held by the carbonyl group of the glycinato part as well as by a carbonyl group of the phthalimide part, as shown as motif B in Fig. 2. The molecule on further heating shows a third weight loss in the region of 302–680 °C, to form cobalt oxide (experimental loss 89.2%, theoretical 87.5%).

The cobalt complex is non-ionic and has a molar conductance of 4.6 S cm^2 mol^{-1} in acetonitrile. The magnetic moment of the complex is 5.22BM at room temperature, which is usual for high spin cobalt (II) octahedral complexes.

The reaction of zinc acetate with *N*-phthaloylglycine also results in the formation of a *N*-phthaloylglycinato complex, having the composition $[Zn(Nphgly)_2(H_2O)_4]$-$2H_2O$. In this complex, the zinc atom is held in a distorted octahedral environment with a similar coordination to that observed for the analogous cobalt(II) complex. The selected bond distances in the complex for Zn–O3, Zn–O5 and Zn–O6 are 2.095, 2.094 and 2.075 Å, respectively. The O6–Zn–O5, O6–Zn–O3 and O6–Zn–O3′ bond angles are 92.07°, 88.71° and 91.29°, respectively. The solid state structure of the complex is shown in Fig. 3. It is clear that the *N*-phthaloylglycinato complexes of cobalt(II) and zinc(II) are isostructural.

Table 1
Crystal data for the complexes

Complex	$[Co(Nphgly)_2(H_2O)_4]2H_2O$	$[Zn(Nphgly)_2(H_2O)_4]2H_2O$	$[Cu(Nphgly)_2(py)_3]$
Formula	$C_{20}H_{24}N_2O_{14}Co$	$C_{20}H_{24}N_2O_{14}Zn$	$C_{35}H_{27}Cu\ N_5O_8$
Formula weight	575.34	581.78	709.16
Crystal system	triclinic	triclinic	monoclinic
Temperature (K)	120	120	120
Space group	$P\bar{1}$	$P\bar{1}$	$C2/c$
a (Å)	6.2487(6)	6.2047(4)	14.911(2)
b (Å)	8.1580(7)	8.1266(6)	9.421(1)
c (Å)	12.0022(11)	12.022(1)	22.943(2)
α (°)	94.407(4)	94.56(1)	90.00
β (°)	104.562(3)	104.24(1)	107.77(1)
γ (°)	98.630(4)	98.41(1)	90.00
Z	1	1	4
V (Å^3)	581.26(9)	577.01(7)	3069.2(6)
μ (mm^{-1})	0.817	1.144	0.776
R	0.0424	0.0403	0.0304
WR	0.1087	0.1058	0.0723
Goodness-of-fit	1.063	1.080	1.044

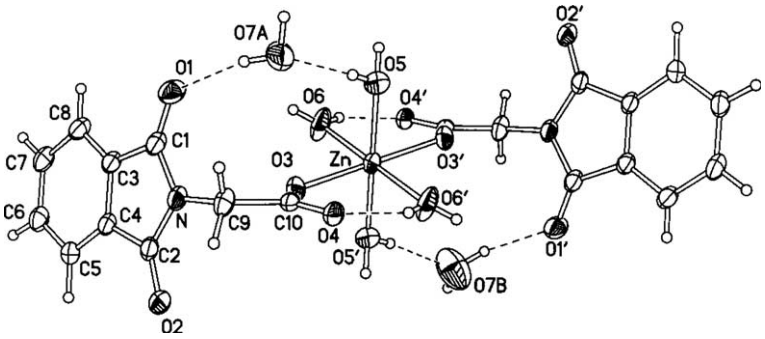

Fig. 3. Crystal structure of tetra-aqua-bis-*N*-phthaloylglycinato zinc(II)dihydrate.

Zinc complexes generally show six-coordination [21], however, due to the presence of extensive hydrogen bonding, this complex shows a distorted octahedral geometry around the zinc. The ^{1}H NMR of the complex shows signals from the aromatic protons (7.9 ppm, multiplet) and the CH_2– protons (4.25 ppm, singlet) only. Due to solubility problems, we have measured the ^{1}H NMR in deuterated dimethylsulfoxide. It is observed that in the solution state the two types of coordinated water molecules cannot be distinguished and their signals merges as one and appear with the signals of water present in DMSO-d^6 at 3.4 ppm. The complex formation is confirmed in solution from the fact that the carboxylic proton that is observed at 13.2 ppm for the ligand is not present in the complex.

In the thermogram of the zinc complex it is observed that heating at a rate of 5 °C/min, the complex loses weight in three steps. In the first step the loss occurs at 80–100 °C; which corresponds to15.5% of the total weight. This loss of weight can be accounted for by the loss of four water molecules; theoretically loss of four water molecules would amount to 13.2% weight loss. At 160–184 °C the molecule loses the other two coordinated water molecules, totaling to a loss of weight of 18.71%, for the loss of all the six water molecules, the calculated loss would be 18.75%. Our observations on the cobalt–phthaloylglycinato complex also tallies with this observation. Thus, a similar explanation can be put forward for the loss of weight from two types of environment around coordinated water, as already illustrated. The third weight loss occurs at 342–363 °C which corresponds to 44.0% and this is due to formation of Zn(Nphgly)(OAc). The calculated weight loss for this transformation is 43.54%. The TG-plot of the zinc-complex is shown in Fig. 4.

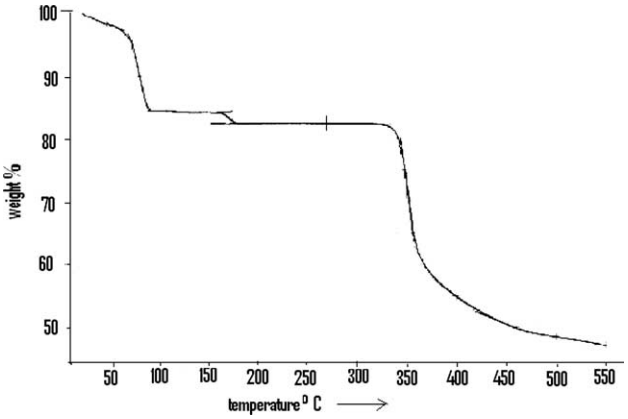

Fig. 4. Thermogram of tetra-aqua-bis-*N*-phthaloylglycinatozinc(II) dihydrate (heating rate 5 °C per minute).

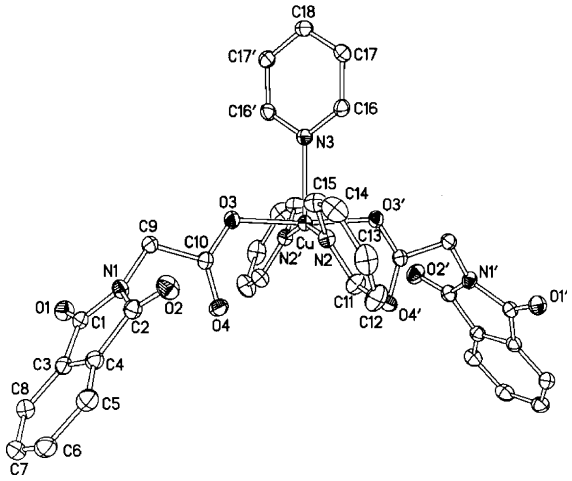

Fig. 5. Structure of $[Cu(py)_3(Nphgly)_2]$.

While attempting to crystallise analogous copper complex from various solvents such as methanol, acetonitrile, DMF, etc., was not successful. However, the compound could be crystallised from pyridine and the crystallised product has the composition $[Cu(py)_3(Nphgly)_2]$. The crystal structure, represented in Fig. 5, shows that this copper complex has a square pyramidal geometry around the copper atom. In this complex, the *N*-phthalolylglycinato ligand also coordinates to the copper in a monodentate fashion. Two of the pyridine ligands and two monodentate carboxylate ligands occupy the basal plane of the square pyramid in which the other pyridine occupies the axial position. In this arrangement, the carboxylate parts are *trans* to each

other and the two pyridines are also *trans* to each other. The bond angles between different atoms attached to the copper ion are N3–Cu–N2, 100.75°; N3–Cu–N2′, 100.75°; N3-Cu–O3, 87.25°; N3–Cu–O3′, 87.25°; N2–Cu–O3, 90.92°; N2′–Cu–O3, 90.10°. Selected bond distances are N2–Cu, 2.303 Å; O3–Cu, 1.956 Å; O3′–Cu, 1.956 Å; N2–Cu, 2.030 Å; N2′–Cu, 2.030 Å; N3–Cu, 2.235 Å. This shows that the molecule has a distorted square pyramidal geometry. It is also interesting to note that the pyridine molecules in the basal plane are twisted such that they are inclined at an angle of 27.51° from a common plane. This puckering brings the carbonyl group of the carboxylic acid group to the proximity of a hydrogen atom present at the 3-position of a coordinated pyridine molecule, resulting in a weak C–H···O interaction in the lattice. The copper(II) complex can be compared to the corresponding copper(II) acetate [21] rather than the bis-glycinato copper(II) complexes as the coordination is restricted to the carboxylate group of the glycine derivative [1f]. In the copper(II) acetate a dimeric structure through a bidentate carboxylate is observed, but in our case we have observed a monodentate carboxy linkage and it is obvious that the pyridine, being a strong ligand, occupies three coordination sites to complete the five coordination.

In the thermogram of the copper complex there is 20.49% weight loss at 90–150 °C corresponding to the weight of two pyridine molecules (theoretical loss 22.23%). These two pyridine molecules are positioned at the base of the square pyramid. As in the complex, the two pyridines have a slightly shorter bond length than the third pyridine ($\Delta R = 0.205$ Å). At 190–240 °C the molecule loses another molecule of pyridine, this amounts to 31.70% of loss (theoretical 33.35%). However, looking at the bond distances determined at 120 K there should have been a weight loss in the reverse manner, that is the loss of axial pyridine first rather than the loss of the other two pyridine ligands from the base of the square pyramid. However, a careful look at the structure suggests that loss of two pyridines would release the steric congestion, which is a thermodynamically favourable process. In fact due to steric crowding the two pyridines in the basal plane do not remain in one plane (Fig. 5). Thus, it may be possible that on heating the system adopts a triangular bipyramidal geometry to release the steric effect and there is loss of two axial pyridine ligands, leaving the equatorial one to be lost at a later stage. In the temperature range 270–380 °C, the molecule transforms to CuO by losing 88.8% of its weight (theoretical 88.39%).

The reaction of *N*-phthaloylglycine with nickel acetate tetrahydrate, followed by crystallisation of the complex from pyridine, gave a nickel complex having the composition $[Ni(py)_3(Nphgly)_2 1.3H_2O]$. Although, we could not refine the X-ray diffraction data for this complex to our satisfaction, we can predict that the molecule has octahedral geometry and remains as a trimeric cluster through involvement of coordinated water and the carbonyl groups of the glycinato and phthalolyl part. The evidence for the presence of water in the complex also comes from the IR absorptions at 3568 and 3472 cm^{-1}, as well as being reflected in the elemental analysis. Further quantification could be determined from the weight loss at low temperature in the thermogram. In the thermogram of this compound, we have found that on heating at a rate of 10 °C per minute it loses 16.13% of its weight between 83 and 140 °C. This corresponds to the loss of water and a pyridine molecule from the complex (theory 14.24%). There is a further loss of weight of 32.19% in the region 140–320 °C, corresponding to the formation of $Ni(Nphgly)_2$ (theoretical 36.09%). The compound loses a further 75.62% of its weight from the parent composition in the region of 340–487 °C. This weight loss corresponds to loss of the phthalimide units and formation of $Ni(OAc)_2$ (theoretical 75.66%).

4. Conclusion

In conclusion, the phthaloylglycinato complexes of Cu(II), Co(II), Zn(II), Ni(II) possess monodentate *N*-phthaloylglycinato ligand. The carbonyl groups in the phthaloyl moiety as well as in the glycinato part provide the anchor to form two distinguishable sets of hydrogen-bonded motifs in the cobalt and zinc complexes. From the crystallographic and thermal studies two hydrogen-bonded environments for coordinated water could be unambiguously established. A square pyramidal copper(II) complex having phthaloylglycinato and pyridine as ligands, has been synthesised and characterised.

5. Supplementary materials

Supplementary data on the crystal structures are available from The Director, CCDC, 12 Union Road, Cambridge, CB2 1EZ, UK (fax: +44 1223 336 033; e-mail: deposit@ccdc.cam.ac.uk or http://www.ccdc.cam.ac.uk) on request, quoting the Deposition Nos. 268833, 268834 and 204520. ^{1}H NMR spectra of tetra-aqua-bis-*N*-phthaloylglycinato zinc(II)dihydrate.

Acknowledgements

R.J.S. and N.B. thank the British Council for Commonwealth split-site fellowship. The authors thank Dr. A. Goeta for helping in structure solving and Dr. R. Kataky and Dr. R.K. Barman for their help. The financial assistance for this work was received from the Department of Science and Technology, New Delhi, India.

References

[1] (a) M.A. Halcrow, Angew Chem. Int. Ed. 40 (2001) 346;
(b) H.C. Freeman, in: E.L. Eichhorn (Ed.), Inorganic BioChemistry, Elsevier, Amsterdam, 1973;
(c) K. Severin, R. Bergs, W. Becks, Angew Chem., Int. Ed. Engl. 37 (1998) 1635;
(d) M. Manikandan, B. Epel, D. Goldfrab, Inorg. Chem. 40 (2001) 781;
(e) D.L. Stone, D.K. Smith, A.C. Whitwood, Polyhedron 23 (2004) 1709 (references therein);
(f) T. Chen, B. Liang, X. Xin, J. Phys. Chem. Solids 58 (1997) 951;
(g) K. Ucida, P. Mandebva, C.S. Ballard, C.J. Snften, M.P. Carter, Animal Feed Sci. Technol. 93 (2001) 193.
[2] R.W. Hay, K.B. Nolan, Amino Acid Peptide 22 (1991) 343.
[3] S. Chandrasekhar, M.B. Padmaja, A. Raza, Synlett (1999) 1597.
[4] J. Sebastian, G. Antonio, G. Joan, J. Chem. Soc., Chem. Commun. (1978) 742.
[5] V.M. Eugenio, D.M. Rothman, B. Imperiali, Org. Biomol. Chem. 2 (2004) 1965.
[6] R.O. Hutchins, J. Wei, S.J. Rao, J. Org. Chem. 59 (1994) 4007.
[7] C.J. McAdam, J.L. Morgan, R.E. Murray, B.H. Robinson, J. Simpson, Aust. J. Chem. 57 (2004) 525.
[8] S.E. Sen, S.L. Roach, Synthesis (1995) 756.
[9] M. North, Contemp. Org. Synth. 3 (1996) 323.
[10] T. Sakamoto, C. Pac, J. Org. Chem. 66 (2001) 94.
[11] A.G. Griesbeck, J. Hirt, K. Peters, E.-M. Peters, H.G. von Schnering, Chem. Eur. J. 2 (1996) 1388.
[12] R. Antunes, H. Batista, R.M. Srivastava, G. Thomas, C.C. Araujo, Bioorg. Med. Chem. Lett. 8 (1998) 3071.
[13] S.W. Ng, A.J. Kuthubutheen, V.G.K. Das, A. Linden, E.R.T. Tiekink, Appl. Organomet. Chem. 8 (1994) 37.
[14] F. Jaber, F. Charbonnier, R. Faure, Acta Crystallogr. C: Cryst. Struct. Commun. C51 (1995) 1765.
[15] G.K. Sandhu, S.S. Sandhu Jr., Synth. React. Inorg. Metal-Org. Chem. 25 (1995) 93.
[16] A.A. El-Asmy, M.A. Hafez, E.M. Saad, F.I. Taha, Trans. Metal Chem. 19 (1994) 603.
[17] L.H. Abdel-Rahman, Trans. Metal Chem. 26 (2001) 412.
[18] F. Minisci, C. Punta, F. Recupero, F. Fontana, G.F. Pedulli, Chem. Commun. (2002) 688.
[19] Y. Ishii, S. Sakaguchi, T. Iwahama, Adv. Syn. Catal. 343 (2001) 393.
[20] A. Enzmann, M. Eckert, W. Ponikwar, K. Polborn, S. Schneiderbauer, M. Beller, W. Beck, Eur. J. Inorg. Chem. (2004) 1330.
[21] N. Barooah, R.J. Sarma, J.B. Baruah, Cryst. Growth Des. 3 (2003) 639.
[22] A.F. Wells, Structural Inorganic Chemistry, 4th ed., Oxford University Press, Oxford, 1975.
[23] A. Distler, S.C. Sevov, Chem. Commun. (1998) 959.

Available online at www.sciencedirect.com
SCIENCE DIRECT®
Polyhedron 25 (2006) 25–30
POLYHEDRON
www.elsevier.com/locate/poly

Synthesis, structure and magnetic properties of two end-on double azido bridged nickel(II) dinuclear entities incorporating *N*,*N*,*N*-coordinating tridentate reduced Schiff base ligands

Sumana Sarkar [a], Amrita Mondal [a], Mohamed Salah El Fallah [b], Joan Ribas [b], Deepak Chopra [c], Helen Stoeckli-Evans [d], Kajal Krishna Rajak [a,*]

[a] *Inorganic Chemistry Section, Department of Chemistry, Jadavpur University, Kolkata 700 032, India*
[b] *Department de Química Inorgánica, Universitat de Barcelona, Diagonal 6487, 08028 Barcelona, Spain*
[c] *Solid State and Structural Chemistry Unit, Indian Institute of Science, Bangalore 560 012, India*
[d] *Institut de Chimie, Université de Neuchâtel, Av. de Bellevaux 51, 2000 Neuchâtel, Switzerland*

Received 25 May 2005; accepted 22 June 2005
Available online 26 August 2005

Abstract

Complexes of the general formula $[Ni_2L_2(\mu_{1,1}\text{-}N_3)_2(N_3)_2]$ have been synthesised in good yields by reacting $Ni(NO_3)_2 \cdot 6H_2O$ with L in the presence of excess of sodium azide in methanol at room temperature. Here L is *N*,*N*-bis(2-pyridylmethyl)amine (L^1) and *N*-(2-pyridylmethyl)-*N*′,*N*′-diethylethylenediamine (L^2). The X-ray structures of both compounds reveal that the *N*,*N*,*N* coordinating reduced Schiff bases are ligated facially. The Ni–N_{azido}–Ni angle is ∼100° and the Ni···Ni separation is ∼3.2 Å. The variable temperature magnetic susceptibility measurements of the two complexes show ferromagnetic behavior.
© 2005 Elsevier Ltd. All rights reserved.

Keywords: Reduced Schiff base; Nickel; Azide; Crystal structure; Ferromagnetic

1. Introduction

Nickel enzymes are involved in various biological reactions [1–4] and consequently the study of the coordination chemistry of nickel has been of significant interest in recent years [5–7]. It has been demonstrated that the azido group inhibits enzymatic reactions [8,9]. Thus, the investigation of nickel–azido complexes has become a field of recent interest to understand the role of the metal ion in biological reactions. In addition, the study of such complexes has also received great deal of attention in the context of enhancement of the knowledge about magnetic interactions as well as development of magnetic materials [10–12].

Although a sizeable number of azido-bridged nickel(II) complexes have so far been reported [13–15], such complexes with reduced Schiff base ligands are rare. Herein, we describe the synthesis and characterization of two neutral end-on diazido-bridged nickel(II) complexes incorporating conformationally labile *N*,*N*,*N*-coordinating reduced Schiff bases. The single crystal X-ray structures, IR and UV–Vis spectroscopic and redox properties are discussed. The variable temperature magnetic susceptibility measurements of the complexes confirm the ferromagnetic behavior in the solid state.

2. Experimental

Materials. All the starting chemicals were analytically pure and used without further purification. The ligands were prepared according to the literature procedure [16].

* Corresponding author. Tel.: +91 33 24146223; fax: +91 33 24146584.
E-mail address: kajalrajak@hotmail.com (K.K. Rajak).

0277-5387/$ - see front matter © 2005 Elsevier Ltd. All rights reserved.
doi:10.1016/j.poly.2005.06.059

Caution! Azido complexes of metal ions are potentially explosive, and should be handled with care and in small amounts.

2.1. Physical measurements

The UV–Vis spectra were recorded on a Perkin–Elmer LAMBDA EZ-301 spectrophotometer and IR spectra were measured with a Perkin–Elmer L-0100 spectrometer. Electrochemical measurements were performed (acetonitrile solution) on a CH 620A electrochemical analyzer using a platinum electrode. Tetraethylammonium perchlorate (TEAP) [17] was used as a supporting electrolyte and the potentials are referenced to the standard calomel electrode (SCE) without junction correction. Magnetic measurements were carried out on polycrystalline samples with a Quantum Design MPMS XL SQUID susceptometer operating at a magnetic field of 0.1 T between 2 and 300 K. The diamagnetic corrections were evaluated from Pascal's constants. Elemental analyses (C, H, N) were performed on a Perkin–Elmer 2400 Series II elemental analyzer.

2.2. Synthesis of the complexes

The complexes were prepared by the same general methods. Details are given here for a representative case.

$[Ni_2(L^1)_2(\mu_{1,1}\text{-}N_3)_2(N_3)_2]$ (**1**). To a methanolic solution (10 mL) of nickel(II) nitrate hexahydrate (0.146 g, 0.5 mmol) was added L^1 (0.100 g, 0.5 mmol), followed by an aqueous solution of sodium azide (0.065 g, 0.10 mmol). The resulting pale green solution was stirred for 0.5 h at room temperature. Slow evaporation of the solution yielded a light green coloured crystalline product. Yield: 0.09 g, 68%. *Anal*. Calc. for $C_{24}H_{26}N_{18}Ni_2$: C, 42.1; H, 3.8; N, 36.84. Found: C, 41.9; H, 3.6; N, 36.6%. UV–Vis (λ_{max}/nm (ε/M^{-1} cm^{-1}) CH_2Cl_2 solution): 625(12); 1010(32). IR (KBr)/cm^{-1}: ν(NH) 3010; $\nu(N_3^-)$ 2065, 2040. $E_{pa}(Ni^{III}/Ni^{II})$: 1.7 V.

$[Ni_2(L^2)_2(\mu_{1,1}\text{-}N_3)_2(N_3)_2]$ (**2**). Yield: 0.12 g, 68%. *Anal*. Calc. for $C_{24}H_{42}N_{18}Ni_2$: C, 41.1; H, 5.99; N, 35.99. Found: C, 41.4; H, 5.7; N, 36.2%. UV–Vis (λ_{max}/nm (ε/M^{-1} cm^{-1}) CH_2Cl_2 solution): 632(12); 1015(26). IR (KBr)/cm^{-1}: ν (NH) 3005; $\nu(N_3^-)$ 2070, 2045. $E_{pa}(Ni^{III}/Ni^{II})$: 1.6 V.

2.3. Crystallographic studies

Suitable crystals of complexes **1** and **2** were grown by slow evaporation of their methanolic solutions. In the case of **1**, the X-ray intensity data were measured at 293 K on a Bruker AXS SMART APEX CCD diffractometer (Mo Kα, $\lambda = 0.71073$ Å). The detector was placed at a distance of 6.03 cm from the crystal. A total 606 frames were collected with a scan width of 0.3° in different settings of φ. The data were reduced in SAINTPLUS [18] and empirical absorption correction was applied using the SADABS package [18]. It was found that there was limited resolution of X-ray data in the case of **1**. For complex **2**, the intensity data were collected at 153 K on a Stoe Mark II-Image Plate Diffraction System [19] equipped with a two-circle goniometer and using Mo Kα graphite monochromated radiation. The image plate distance was 135 mm, ω rotation scans 0–180° at ϕ 0°, and 0–42° at ϕ 90°, step $\Delta\omega = 1.0°$, 2θ range 2.7–51.2°, d_{min}–d_{max} = 15.03–0.82 Å. An empirical absorption correction was applied using the DELrefABS routine in PLATON [20]. The structures were solved by direct methods using the program SHELXS-97 [21]. The refinement and all further calculations were carried out using SHELXL97 [22]. In complex **1**, the N(8) and N(9) atoms of the terminal azide group are distorted and these two were refined isotropically. The remaining non-hydrogen atoms of **1** and all the non-hydrogen atoms of **2** were refined anisotropically, using full-matrix least-squares procedures on F^2. The hydrogen atoms were included in calculated positions. Molecular structure plots were drawn using ORTEP [23]. Relevant crystal data are given in Table 1.

Table 1
Crystallographic data for **1** and **2**

	1	**2**
Formula	$C_{24}H_{26}N_{18}Ni_2$	$C_{24}H_{42}N_{18}Ni_2$
Formula weight	684.04	700.18
Crystal system	monoclinic	orthorhombic
Space group	*C*2/*c*	*Pbca*
a (Å)	19.626(4)	13.8403(5)
b (Å)	11.100(2)	15.0279(5)
c (Å)	14.719(3)	45.367(2)
β (°)	101.27(3)	90.0
V (Å^3)	3144.6(11)	9435.9(6)
Z	4	12
D_{calcd} (Mg m^{-3})	1.445	1.479
μ (mm^{-1})	1.245	1.246
Measured reflections	6604	56329
Unique reflections/R_{int}	1642/0.0649	8582/0.0748
T (K)	293(2)	153(2)
R_1[a], wR_2[b] [$I > 2\sigma(I)$]	0.0809, 0.2304	0.0420, 0.0856
$R1$[a], $wR2$[b] [all data]	0.1086, 0.2461	0.0575, 0.0920
Goodness-of-fit on F^2	1.089	1.038

[a] $R_1 = \sum |F_o| - |F_c| / \sum |F_o|$.
[b] $wR_2 = [\sum w(F_o^2 - F_c^2)^2 / \sum w(F_o^2)^2]^{1/2}$.

3. Results and discussion

Two reduced Schiff bases L^1 and L^2 (general abbreviation L) are used in this present work and these are synthesized by $NaBH_4$ reduction of their respective Schiff bases [16].

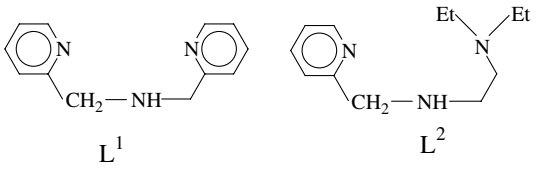

The stoichiometric reaction of $Ni(NO_3)_2 \cdot 6H_2O$ with L in methanol in the presence of excess of sodium azide at room temperature furnishing the pale green coloured

$$Ni(NO_3)_2 \cdot 6H_2O + L \xrightarrow[MeOH]{NaN_3} Ni_2L_2(\mu_{1,1} - N_3)_2(N_3)_2 \quad (1)$$

complexes of type $[Ni_2L_2(\mu_{1,1}\text{-}N_3)_2(N_3)_2]$ Eq. (1).

The complexes display asymmetric azide stretches near 2040 and 2070 cm^{-1}. The stretching frequency of NH group occurs as a broad band near 3000 cm^{-1}. The complexes display an irreversible peak near 1.6 V that may be assigned as a $Ni^{II} \rightarrow Ni^{III}$ oxidation couple.

Both the complexes show two bands in CH_2Cl_2 solution and the bands near 1000 and 630 nm are believed to be of ligand field origin [24].

4. Crystal structure

The crystal structures of $[Ni_2(L^1)_2(\mu_{1,1}\text{-}N_3)_2(N_3)_2]$ (**1**), and $[Ni_2(L^2)_2(\mu_{1,1}\text{-}N_3)_2(N_3)_2]$ (**2**) have been determined and the ORTEP diagrams are given in Figs. 1 and 2. Selected bond distances and angles are given in Tables 2 and 3. The asymmetric unit of **1** consists of one molecule while that of complex **2** contains one non-centrosymmetric and one half of a centrosymmetric molecule. In both cases, in each half of the dinuclear complexes, the tridentate ligand, L (L^1–L^2) is ligated facially and the other two equatorial sites are occupied by one terminal and one bridging azide group. The remaining axial site of one half of the molecule is fulfilled by the equatorially coordinated azide nitrogen atom of the other half and vice versa, thus, forming a double end-on azido-bridged entity.

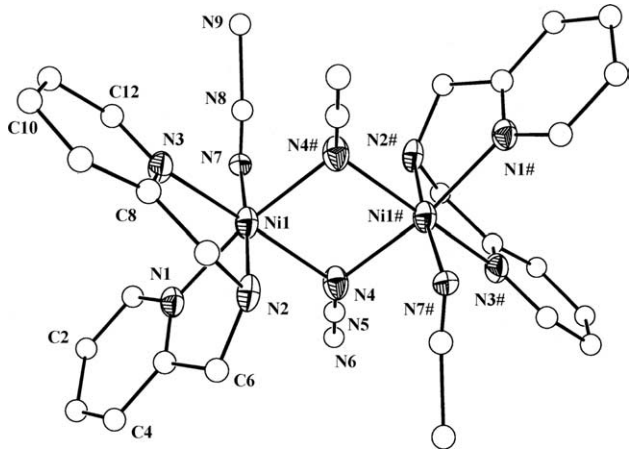

Fig. 1. Perspective view and atom labelling scheme of $[Ni_2(L^1)_2(\mu_{1,1}\text{-}N_3)_2(N_3)_2]$ (**1**).

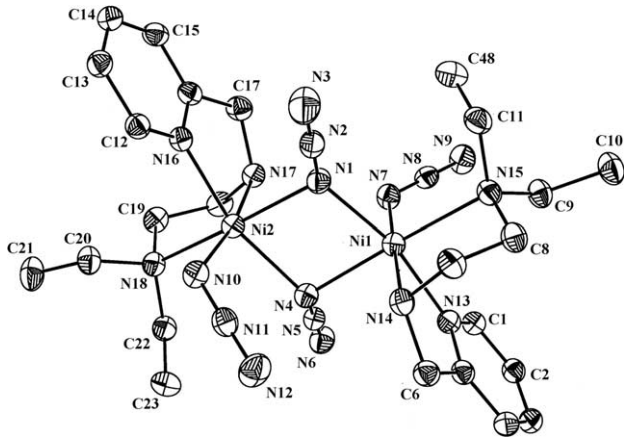

Fig. 2. Perspective view and atom labelling scheme of $[Ni_2(L^2)_2(\mu_{1,1}\text{-}N_3)_2(Ni_3)_2]$ (**2**) (of one molecule).

Table 2
Selected bond distances (Å) and angles (°) for **1**

Distances	
Ni(1)–N(1)	2.048(8)
Ni(1)–N(2)	2.080(8)
Ni(1)–N(3)	2.055(8)
Ni(1)–N(4)	2.086(8)
Ni(1)–N(4) #	2.088(9)
Ni(1)–N(7)	2.249(8)
Ni···Ni	3.191(4)
Angles	
N(1)–Ni(1)–N(2)	81.9(3)
N(1)–Ni(1)–N(3)	90.0(3)
N(1)–Ni(1)–N(4)	93.2(3)
N(1)–Ni(1)–N(4)#	170.5(4)
N(1)–Ni(1)–N(7)	93.5(3)
N(2)–Ni(1)–N(3)	80.6(4)
N(2)–Ni(1)–N(4)	88.5(3)
N(2)–Ni(1)–N(4)#	91.0(4)
N(2)–Ni(1)–N(7)	175.2(3)
N(3)–Ni(1)–N(4)	168.1(4)
N(3)–Ni(1)–N(4)#	95.1(3)
N(3)–Ni(1)–N(7)	101.0(3)
N(4)–Ni(1)–N(4)#	80.3(4)
N(4)–Ni(1)–N(7)	90.3(3)
N(7)–Ni(1)–N(4)#	93.4(3)
Ni(1)–N(4)–Ni(1)#	99.7(4)

In the distorted NiN_6 octahedral environment, the Ni–N bonds span the range 2.043(2)–2.264(2) Å. The Ni–N_{azido}(terminal) and the Ni–N_{azido}(end-on) bonds are usual [15a]. The Ni–N_{azido}–Ni–N_{azido} rings are planar [md < 0.05 Å] and the Ni–N_{azido}–Ni bond angles are ~99° and ~100° in complexes **1** and **2**, respectively. The dihedral angle between the two bridging azido groups is ~30° for **1** and ~25° for **2** and the $\mu_{1,1}$-N_3 groups form an angle of ~50° for **1** and ~40° for **2** with

Table 3
Selected bond distances (Å) and angles (°) for **2** (one molecule)

Distances	
Ni(1)–N(1)	2.085(2)
Ni(1)–N(4)	2.184(2)
Ni(1)–N(7)	2.077(3)
Ni(1)–N(13)	2.073(2)
Ni(1)–N(14)	2.095(3)
Ni(1)–N(15)	2.264(2)
Ni···Ni	3.222(3)
Ni(2)–N(1)	2.176(2)
Ni(2)–N(4)	2.117(2)
Ni(2)–N(10)	2.043(2)
Ni(2)–N(16)	2.072(2)
Ni(2)–N(17)	2.092(3)
Ni(2)–N(18)	2.242(2)
Angles	
N(1)–Ni(1)–N(4)	79.03(9)
N(1)–Ni(1)–N(7)	90.29(10)
N(1)–Ni(1)–N(13)	166.37(10)
N(1)–Ni(1)–N(14)	92.20(10)
N(1)–Ni(1)–N(15)	101.01(9)
N(4)–Ni(1)–N(7)	87.01(10)
N(4)–Ni(1)–N(13)	89.16(9)
N(4)–Ni(1)–N(14)	92.70(10)
N(4)–Ni(1)–N(15)	175.83(9)
N(7)–Ni(1)–N(13)	95.91(10)
N(7)–Ni(1)–N(14)	177.38(10)
N(7)–Ni(1)–N(15)	97.15(10)
N(13)–Ni(1)–N(14)	81.48(10)
N(13)–Ni(1)–N(15)	90.27(9)
N(14)–Ni(1)–N(15)	83.13(10)
Ni(1)–N(1)–Ni(2)	101.31(10)
N(1)–Ni(2)–N(4)	78.51(9)
N(1)–Ni(2)–N(10)	93.91(10)
N(1)–Ni(2)–N(16)	87.03(9)
N(1)–Ni(2)–N(17)	90.79(10)
N(1)–Ni(2)–N(18)	174.05(10)
N(4)–Ni(2)–N(10)	95.23(10)
N(4)–Ni(2)–N(16)	164.43(10)
N(4)–Ni(2)–N(17)	92.94(10)
N(4)–Ni(2)–N(18)	101.26(9)
N(10)–Ni(2)–N(16)	91.43(10)
N(10)–Ni(2)–N(17)	171.24(10)
N(10)–Ni(2)–N(18)	92.04(10)
N(16)–Ni(2)–N(17)	81.43(10)
N(16)–Ni(2)–N(18)	92.52(9)
N(17)–Ni(2)–N(18)	83.27(10)
Ni(1)–N(4)–Ni(2)	100.01(10)

the Ni–N_{azido}–Ni–N_{azido} plane. The terminal azide groups are quasilinear and coordinate *trans* to each other, the N–Ni···Ni–N torsion angles being 180° for **1** and 177.52(8)° and 179.47(9)° for **2**. The Ni···Ni distances in the dinuclear entities are 3.191(4) Å for complex **1** and 3.296(2) and 3.222(3) Å for **2**.

5. Magnetic studies

The variable temperature magnetic susceptibility measurements were carried out in the temperature range 2–300 K. The $\chi_M T$ versus T plot for complexes **1** and **2** are given in Figs. 3 and 4. The experimental $\chi_M T$ value is 2.6 $cm^3\ mol^{-1}$ K for **1** and 2.96 $cm^3\ mol^{-1}$ K for **2** at 300 K [a characteristic feature for a Ni^{II} ion with g close to 2.30]. This value increases to 3.4 $cm^3\ mol^{-1}$ K at 30 K and to 3.94 $cm^3\ mol^{-1}$ K at 10 K for complexes **1** and **2**, respectively. Below 30 K (for **1**) and 10 K (for **2**) the $\chi_M T$ values decreases abruptly to 2.4 and ~3 $cm^3\ mol^{-1}$ K at 2 K. The shape of the curve is typical of intramolecular ferromagnetic coupling with the presence of either zero-field splitting (D parameter) and/or intermolecular antiferromagnetic interactions (J'). Both D and J' are strongly correlated and show same results at low temperature. Thus, it was not possible to separate them in any attempt to fit the experimental data [25]. So two different approaches have been used to fit the experimental data for **1** and **2**: the first one was a full diagonalisation formalism introducing the single-ion D parameter employing, thus, the spin-Hamiltonian $H = -JS_1S_1 + D[S_z^2 - 1/3S(S+1)] + g\beta HS_z$, and the second one using the molecular field approximation, with the intermolecular J' parameter, according to the method given by Kahn with the Hamiltomian $H = -JS_1S_1 + g\beta HS_z - zJ'\langle S_z\rangle S_z$ [26]. In both the approaches, the best J values were obtained by minimizing the function $R = \sum(\chi_M^{calc} - \chi_M^{obs})^2 / \sum(\chi_M^{obs})^2$. By using the molecular field approach (neglecting the D parameter), the best-fit parameters obtained were as follows: complex **1**; $J = 34.19 \pm 0.7\ cm^{-1}$, $z'J' =$

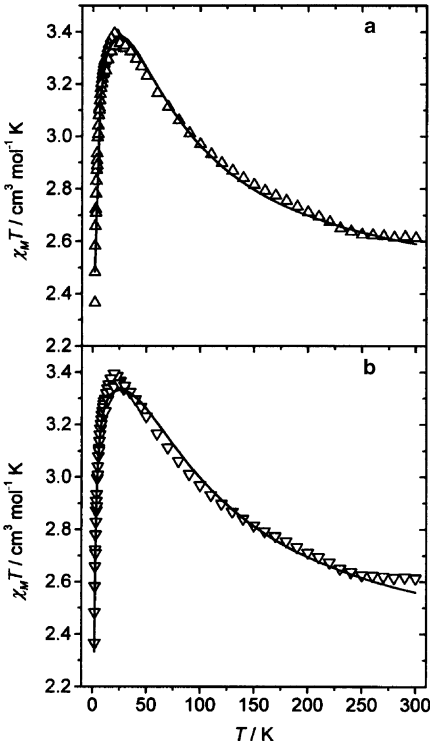

Fig. 3. Plot of $\chi_M T$ vs. T for complex **1** (a) assuming the J' parameter without the D parameter and (b) assuming the D parameter without the J' interaction. Solid line represents the best-fit curve.

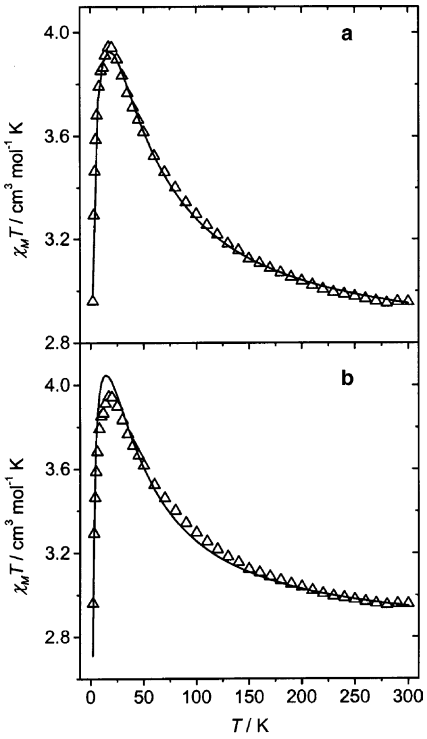

Fig. 4. Plot of $\chi_M T$ vs. T for complex **2** (a) without considering the D parameter and with the $z'J'$ parameter (intermolecular interactions) and (b) assuming the D parameter without the J' interaction. Solid line represents the best-fit curve.

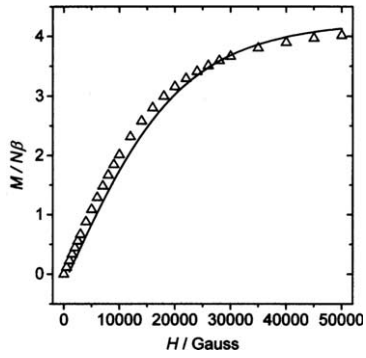

Fig. 5. Plot of the reduced magnetization (M/Nβ) vs. H at 2 K for **1**. Solid line represents the Brillouin function for two isolated Ni^{2+} ions with $g = 2.13$.

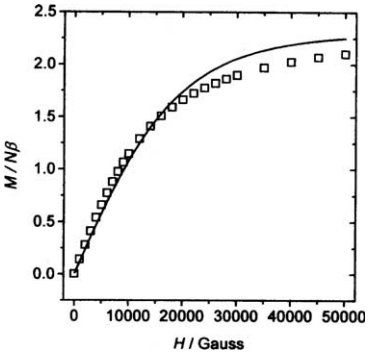

Fig. 6. Plot of the reduced magnetization (M/Nβ) vs. H at 2 K for **2**. Solid line represents the Brillouin formula for $g = 2.35$.

$-0.29\ cm^{-1}$, $g = 2.17 \pm 0.01$ and $R = 6 \times 10^{-4}$ and complex **2**; $J = 22.7\ cm^{-1}$, $z'J' = -0.27\ cm^{-1}$, $g = 2.35$ and $R = 1.5 \times 10^{-4}$ (Figs. 3(a) and 4(a)). By using a full diagonalization method with the D parameter (Figs. 3(b) and 4(b)), the best-fit was obtained with the following parameters: $J = 47.6 \pm 1\ cm^{-1}$, $D = 8.4 \pm 0.5\ cm^{-1}$, $g = 2.12 \pm 0.01$ and $R = 3 \times 10^{-3}$ for complex **1** and $J = 23.2\ cm^{-1}$, $D = 5.27\ cm^{-1}$, $g = 2.25$ and $R = 1.2 \times 10^{-3}$ for complex **2**. The zero-field splitting parameters of isolated Ni(II) ions are usually large and lie in the range 4–8 cm^{-1} [27]. The plot of the reduced magnetization (M/Nβ) is shown in Figs. 5 and 6 for complexes **1** and **2**, respectively. For complex **1**, this curve is in good agreement with the theoretical Brillouin function for two isolated nickel(II) ions assuming $g = 2.13$ (average of the two different fits). The coincidence of the curve can be attributed to the positive J value and the negative J' and D parameters having an opposite effect. The curve of reduced magnetization does not follow the Brillouin formula in the case of **2**. At low fields, the experimental points are above the theoretical ones but at high fields, the experimental points lie below the theoretical curve. This feature is indicative of the complication due to the D parameter and the presence of ferromagnetic and antiferromagnetic interactions.

It is stated in the literature [12,28] that for a bis ($\mu_{1,1}$-N_3) bridged dinuclear nickel(II) system the strength of ferromagnetic coupling between two paramagnetic centers mainly depends on the Ni–N_{azido}–Ni angle, the average angle being close to 101°. With this and similar angles the coupling is ferromagnetic. In **1**, this angle is ~99° and in **2** it is ~100°. The Ni–N_{azido} and Ni···Ni distances are ~2.085 and ~3.191 Å for **1** and ~2.12 and ~3.22 Å for **2**, respectively. Thus the structural parameters corroborate the observed ferromagnetic interactions in the two complexes.

In the solid state, in complex **2** the N(14)–H(14) and N(17)–H(17) groups are involved in intramolecular hydrogen bonding with N(12) and N(7) atoms, respectively. The intramolecular hydrogen bonding could originate a small but not negligible coupling into the magnetic exchange interaction. Hence, the weak coupling generated by such hydrogen bonding may modify the overall Ni–N_{azido}–Ni coupling in case of complex **2**.

6. Conclusion

Two new complexes of the formula $[Ni_2(L^1)_2(\mu_{1,1}\text{-}N_3)_2(N_3)_2]$ (**1**) and $[Ni_2(L^2)_2(\mu_{1,1}\text{-}N_3)_2(N_3)_2]$ (**2**) have been synthesized and characterized. These species represent the first examples of an end-on azido bridged dinuclear entity incorporating conformationally flexible reduced Schiff base ligands. Variable temperature magnetic

moment measurements of the two complexes confirm the ferromagnetic behavior in the solid state and in the case of **2**, the intramolecular hydrogen bonding modulates the overall Ni–N_{azido}–Ni coupling. Our search for new nickel(II) complexes with different reduced Schiff base ligands and the study of their solid state behavior is in progress.

7. Supporting Information

Crystallographic data for structural analysis have been deposited with the Cambridge Crystallographic Data Centre with CCDC numbers 272898 and 246819 for **1** and **2**, respectively. Copies of this information may be obtained free of charge from the Director, CCDC, 12 Union Road, Cambridge CB2 1EZ, UK, fax: +44 1223 336 033, or e-mail: deposite@ccdc.cam.ac.uk or www: http://www.ccdc.cam.ac.uk.

Acknowledgments

Financial support from the Council of Scientific and Industrial Research, New Delhi, India and from the Department of Science and Technology, New Delhi, India are gratefully acknowledged. We are also thankful to DST for the data collection on the CCD facility setup (Indian Institute of Science, Bangalore, India) under the IRHPA-DST program. Joan Ribas acknowledges the financial support from the Spanish Government (Grant BQU2000/0791).

References

[1] J.R. Lancaster, Jr. (Ed.), The Bioinorganic Chemistry of Nickel, VCH Publishers, New York, 1998.
[2] M.A Halcrow, G. Christou, Chem. Rev. 94 (1994) 2421.
[3] T.I. Doukov, T.M. Iverson, J. Seravalli, S.W. Ragsdab, C.L. Drenman, Science 298 (2002) 567.
[4] J. Wuerges, J.-W. Lee, Y.-I. Yim, H.-S. Yim, S.-O. Kang, K.D. Carugo, Proc. Natl. Acad. Sci. USA 101 (2004) 8569.
[5] S. Akine, T. Nabeshima, Inorg. Chem. 44 (2005) 1205.
[6] N. Sprutta, S.P. Rath, M.M. Olmstead, A.L. Balch, Inorg. Chem. 44 (2005) 1452.
[7] C.-M. Lee, C.-H. Chen, S.-C. Ke, G.-H. Lee, W.-F. Liaw, J. Am. Chem. Soc. 126 (2004) 8406.
[8] H.-D. Youn, E.-J. Kim, J.-H. Roe, Y.C. Hah, S.-O. Kang, Biochem. J. 318 (1996) 1452.
[9] R.K. Watt, P.W. Ludden, J. Bacteriol. 181 (1999) 4554.
[10] (a) A. Escuer, R. Vicente, J. Ribas, M.S. El Fallah, X. Solans, M. Font-Bardía, Inorg. Chem. 32 (1993) 3727;
(b) M. Monfort, I. Resino, J. Ribas, X. Solans, M. Font-Bardía, New J. Chem. 25 (2001) 1577.
[11] (a) M.-F. Charlot, O. Kahn, M. Chaillet, C. Larrieu, J. Am. Chem. Soc. 108 (1986) 2574;
(b) L.K. Thompson, S.S. Tandon, M.E. Manuel, Inorg. Chem. 34 (1995) 2356.
[12] E. Ruiz, J. Cano, S. Alvarez, P. Alemany, J. Am. Chem. Soc. 120 (1998) 11122.
[13] (a) R.J. Butcher, C.J. O'Connor, E. Sinn, Inorg. Chem. 21 (1982) 616;
(b) S. Sikorav, I. Bkouche-Waksman, O. Kahn, Inorg. Chem. 23 (1984) 490;
(c) R. Vicente, A. Escuer, J. Ribas, M.S. El Fallah, X. Solans, M. Font-Bardía, Inorg. Chem. 32 (1993) 1920.
[14] (a) M. Monfort, I. Resino, J. Ribas, H. Stoeckli-Evans, Angew. Chem., Int. Ed. Engl. 39 (2000) 191;
(b) M. Monfort, I. Resino, M.S. El Fallah, J. Ribas, X. Solans, M. Font-Bardía, H. Stoeckli-Evans, Chem. Eur. J. 7 (2001) 280;
(c) S. Martin, M.G. Barandika, L. Lezama, J.L. Pizzaro, Z.E. Serna, J.I.R. de Larramendi, M.I. Arriortua, T. Rojo, R. Cortes, Inorg. Chem. 40 (2001) 4109;
(d) A. Escuer, R. Vicente, F.A. Mautner, M.A.S. Goher, M.A.M. Abu-Youssef, Chem. Commun. (2002) 64.
[15] (a) S. Deoghoria, S. Sain, M. Soler, W.T. Wong, G. Christou, S.K. Bera, S.K. Chandra, Polyhedron 22 (2003) 257;
(b) S.K. Dey, N. Mondal, M.S. El Fallah, R. Vicente, A. Escuer, X. Solans, M. Font-Bardía, T. Matsushita, V. Gramlich, S. Mitra, Inorg. Chem. 43 (2004) 2427.
[16] S. Larsen, K. Michelsen, E. Pedersen, Acta Chem. Scand. Sect. A 40 (1986) 63.
[17] G.K. Lahiri, S. Bhattacharya, B.K. Ghosh, A. Chakravorty, Inorg. Chem. 26 (1987) 4324.
[18] SMART, SAINT, SADABS, XPREP, SHELXTL, Bruker AXS Inc., Madison, WI, 1998.
[19] X-AREA V1.17 & X-RED32 V1.04 Software, Stoe & Cie GmbH, Darmstadt, Germany, 2002.
[20] A.L. Spek, J. Appl. Crystallogr. 36 (2003) 7.
[21] G.M. Sheldrick, SHELXS97, Program for Crystal Structure Determination, Acta Crystallogr., Sect. A 46 (1990) 467.
[22] G. Sheldrick, SHELXL97, Universität Göttingen, Göttingen, Germany, 1999.
[23] C.K. Johnson, ORTEP, Report ORNL-5138, Oak Ridge National Laboratory, Oak Ridge, TN, 1976.
[24] (a) G. Zakrzewski, L. Sacconi, Inorg. Chem. 7 (1968) 1034;
(b) P. Bamfield, R. Price, R.G.J. Miller, J. Chem. Soc., Sect. A (1969) 1447.
[25] A.P. Ginsberg, R.L. Martin, R.W. Brookes, R.C. Sherwood, Inorg. Chem. 11 (1972) 2884.
[26] O. Kahn, Molecular Magnetism, VCH, New York, 1993.
[27] R. Boča, Coord. Chem. Rev. 248 (2004) 757.
[28] J. Ribas, A. Escuer, M. Monfort, R. Vicente, R. Cortes, L. Lezama, T. Rojo, Coord. Chem. Rev. 193–195 (1999) 1027.

Available online at www.sciencedirect.com
SCIENCE DIRECT®
Polyhedron 25 (2006) 31–38
POLYHEDRON
www.elsevier.com/locate/poly

Studies on cobalt(II) complexes with *N*,*N*,*N*′,*N*′-tetraethylpyridine-2,6-dicarboxamide(L^1) containing PF_6^-, BF_4^-, ClO_4^- and NO_3^- anions: X-ray crystal structures of $[Co(L^1)_2(CH_3CN)](PF_6)_2$ and $[Co(L^1)_2(H_2O)_2](X)_2 \cdot H_2O (X = PF_6^-, ClO_4^-)$

Ramesh Kapoor *, Anuradha Pathak, Pratibha Kapoor, Paloth Venugopalan

Department of Chemistry, Panjab University, Chandigarh 160014, India

Received 6 April 2005; accepted 23 June 2005
Available online 19 August 2005

Abstract

The ligand *N*,*N*,*N*′,*N*′-tetraethylpyridine-2,6-dicarboxamide (L^1 and abbreviated as deap) reacts with CoX_2 ($X = PF_6^-, BF_4^-, ClO_4^-$ and NO_3^-) salts to give the octahedral complexes, $[Co(L^1)_2(CH_3CN)](PF_6)_2$ (**1**) and $[Co(L^1)_2(H_2O)_2](X)_2 \cdot H_2O$ ($X = PF_6^-$ (**2**), BF_4^- (**3**), ClO_4^- (**4**) and NO_3^- (**5**). The compounds have been characterised by elemental analysis, IR spectroscopy and X-ray crystallography. The composition of the product is dependant upon the nature of the reaction medium. Compound **1** contains ON and ONO bonded deap ligands in bidentate and tridentate coordinating modes, in which the coordination sphere of the Co^{2+} ion is completed by attachment of an acetonitrile molecule. Compounds **2** and **4** have identical cationic species $[Co(L^1)_2(H_2O)]^{2+}$ in which Co^{2+} is bonded by deap ligands in a bidentate ON mode. As deap is coordinating in a bidentate mode, the two coordinating water molecules are placed *cis* to each other in the octahedral arrangement.

The similarity of the molecular structure of compounds **2** and **4** is, interestingly, also reflected in their crystal structures, both are structurally similar with a *C*2/*c* space group in the monoclinic crystal system. In the crystal lattice, due to the symmetrical disposition of the complex on a twofold axis, there is an interesting chain of molecules formed through hydrogen bonding. The lattice water has a crucial role in the formation of this chain, in fact it acts as a connecting link between the complex molecules running almost perpendicular to the '*ac*' plane.
© 2005 Elsevier Ltd. All rights reserved.

Keywords: Cobalt(II) complexes; *N*,*N*,*N*′,*N*′-tetraethylpyridine-2,6-dicarboxamide; X-ray crystal structures; IR spectra; UV–Vis spectra

1. Introduction

Pyridine-2,6-dicarboxamide ligands, like their precursor pyridine-2,6-dicarboxylic acid, are versatile ONO donors capable of forming stable chelates with metal ions [1–8]. These ligands have been widely used to prepare metal complexes exhibiting a range of coordination numbers, geometries and nuclearities. Complexes of divalent transition metal [1,5] and lanthanide ions [2] with these ligands have been investigated to study the effects of steric and electronic factors brought about by peripheral modifications in the tertiary amide side arms at the 2- and 6-positions of the central pyridine ring.

Apart from the general interest reported above, there has been a report on the preparation and spectral characterisation of bis-complexes of cobalt(II), nickel(II)

* Corresponding author. Tel.: +91 1722541435; fax: +91 1722545074.
E-mail address: rkapoor@pu.ac.in (R. Kapoor).

0277-5387/$ - see front matter © 2005 Elsevier Ltd. All rights reserved.
doi:10.1016/j.poly.2005.06.060

and copper(II) with *N*,*N*,*N*′,*N*′-tetraethylpyridinedicarboxamide (L^1, deap) with particular reference to the two cobalt compounds, $[Co(L^1)_2](X)_2 \cdot 3H_2O$ ($X = PF_6^-, ClO_4^-$) [3]. Based on IR and electronic spectral data, it was proposed that the cobalt ion had distorted octahedral stereochemistry bonded by the *N*,*N*,*N*′,*N*′-tetraethylpyridinedicarboxamide ligand in a tridentate mode and containing ionic PF_6^- and ClO_4^- groups [3]. Continuing our work on the ligational behaviour of a number of tridentate ligands containing ONO(L^1), [9,10] (L^2) [11,12] and *SNS*(L^3) [13,14] sets of donor atoms towards cobalt, nickel and copper, we have now synthesized cobalt complexes of deap (L^1) with PF_6^- (**1**) and (**2**), BF_4^- (**3**), ClO_4^- (**4**), and NO_3^- (**5**), and report the X-ray crystal structures of **1**, **2** and **4**. These anions have different coordinating abilities, i.e., from virtually 'non-coordinating' (PF_6^-, BF_4^- and ClO_4^-) to strongly coordinating (NO_3^-). The present work is also aimed at finding out the role of the counter ions in determining the flexibility of the network created by the arrangement of the cationic species.

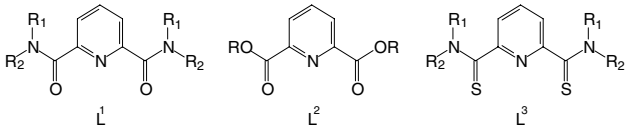

Interestingly, formulations of **2** and **4** are the same as had been reported earlier [3], but the compounds show significant structural differences to that which had been proposed on the basis of spectral data. Our crystallographic studies show that the deap ligands are coordinating in a bidentate mode and to the best of our knowledge these are the only examples of this structural type. Possibly, the nature of the anions and lattice effects may be responsible for the variation in coordination mode observed for deap in the complexes isolated.

2. Experimental

2.1. Preparation of complexes

N,*N*,*N*′,*N*′-tetraethylpyridinedicarboxamide (L^1) was prepared as reported [12]. Solvents were dried using standard techniques [15]. $Co(NO_3)_2 \cdot 6H_2O$ (s.d. fine chemicals) and $CoCl_2 \cdot 6H_2O$(BDH) were used as such.

2.1.1. Syntheses

$[Co(L^1)_2(CH_3CN)](PF_6)_2$ (1). To a dark blue coloured solution of $Co(NO_3)_2 \cdot 6H_2O$ (0.567 g, 1.95 mmol, in 10 mL) in acetonitrile was added, with stirring, a solution of deap (1.080 g, 3.90 mmol in 10 mL) in the same solvent. An aqueous solution of KPF_6 in a minimum amount of water (0.714 g, 3.90 mmol) was added to the dark purple solution. The solution was stirred for 24 h, which subsequently on cooling to 0 °C yielded a pink crystalline solid. It was filtered, washed with ether and dried in vacuo. *Anal.* Calc. for $C_{32}H_{49}CoO_4N_7P_2F_{12}$: C, 40.68; H, 5.19; N, 10.38. Found: C, 40.24; H, 4.98; N, 10.16%. M.p., 260 °C. Λ_M ($ohm^{-1}\,cm^2\,mol^{-1}$) = 210 (CH_3CN) and 136 (CH_3NO_2) [expected range for 1:1 and 1:2 electrolytes in these solvents are 120–160 and 220–380 (CH_3CN) and 75–95 and 150–180 (CH_3NO_2) $ohm^{-1}\,cm^2\,mol^{-1}$. ^{19}F NMR ($CDCl_3$/DMSO-d_6, ppm): δ, −70.93 and −73.45; J_{PF} 712 Hz. Absorption spectrum [λ_{max}, nm]: 506(sh), 530 (CH_3OH). Selected IR bands(cm^{-1}): 3586m, 3185m,br, 2324w, 1608s, 845s,br, 558m. Magnetic moment (BM, 300 K): 5.01.

$[Co(L^1)_2(H_2O)_2](PF_6)_2 \cdot H_2O$ (2). This was prepared by following the above procedure except that the reaction was now performed in an aqueous acetonitrile medium. It has been noted that irrespective of whether the metal–ligand ratio is 1:1 or 1:2 the product is always complex **2**. *Anal.* Calc. for $C_{30}H_{52}CoO_7N_6P_2F_{12}$: C, 37.62; H, 5.43; N, 8.78. Found: C, 37.26; H, 5.08; N, 8.60%. M.p., 162–165 °C. Λ_M ($ohm^{-1}\,cm^2\,mol^{-1}$) = 228 (CH_3CN) and 144 (CH_3NO_2). ^{19}F NMR ($CDCl_3$/DMSO-d_6, ppm):δ, −69.50 and −72.02; J_{PF} = 711 Hz. Absorption spectrum [λ_{max}, nm]: 490(sh), 534 (CH_3OH). Selected IR bands (cm^{-1}): 3584m, 3190m, br, 1614s, 845s,br, 558m. Magnetic moment (BM, 300 K): 4.68.

$[Co(L^1)_2(H_2O)_2](BF_4)_2 \cdot H_2O$ (3). This complex was prepared by the procedure described for **1** using $NaBF_4$ instead of KPF_6. A pink crystalline solid of **3** was obtained (ca. 78% yield based on L^1). *Anal.* Calc. for $C_{30}H_{52}CoO_7N_6B_2F_8$: C, 42.80; H, 6.18; N, 9.98. Found: C, 42.56; H, 5.88; N, 10.24%. M.p., 105 °C. Λ_M ($ohm^{-1}\,cm^2\,mol^{-1}$) = 208 (CH_3CN) and 165 (CH_3NO_2). Absorption spectrum [λ_{max}, nm]: 490(sh), 530 (CH_3OH). Selected IR bands (cm^{-1}): 3474m, 3190m,br, 1609s, 1080s. Magnetic moment (BM, 300 K): 4.68.

$[Co(L^1)_2(H_2O)_2](ClO_4)_2 \cdot H_2O$ (4). To a deep blue solution of $CoCl_2$ in ethanol (0.447 g, 3.44 mmol in 10 mL) was added an aqueous solution of $NaClO_4$ (0.842 g, 6.88 mmol). After stirring for 4 h at r.t., NaCl was removed by filtration. A solution of deap in ethanol (0.953 g, 3.44 mmol) was added with stirring to the solution of cobalt perchlorate. The contents were stirred for 8 h, and on vacuum drying yielded a purple solid. It was recrystallised from ethanol solution on keeping it at 0 °C. *Anal.* Calc. for $C_{30}H_{52}Cl_2CoO_{15}N_6$: C, 41.57; H, 6.00; N, 9.70. Found: C, 41.24; H, 6.38; N, 9.56%. M.p., 110 °C. Λ_M ($ohm^{-1}\,cm^2\,mol^{-1}$) = 184 (CH_3CN) and 160 (CH_3NO_2). Absorption spectrum [λ_{max}, nm]: 490(sh), 515 (CH_3OH). Selected IR bands (cm^{-1}): 3400m, 3189m,br, 1609s, 1112s,br, 624m. Magnetic moment (BM, 300 K): 4.75.

$[Co(L^1)_2(H_2O)_2](NO_3)_2 \cdot H_2O$ (5). A solution of $Co(NO_3)_2 \cdot 6H_2O$ in CH_3CN was stirred with a solution of deap in the same solvent for about 8 h. On addition of diethylether, a pink crystalline solid separated out of the solution. It was filtered, washed with diethylether and acetonitrile mixture and dried under vacuo. *Anal*. Calc. for $C_{30}H_{52}CoO_{13}N_8$: C, 45.51; H, 6.57; N, 14.15. Found: C, 45.14; H, 6.18; N, 14.01%. M.p., 140 °C. Λ_M ($ohm^{-1}\,cm^2\,mol^{-1}$) = 215 (CH_3CN) and 158 (CH_3NO_2). Absorption spectrum [λ_{max}, nm]: 490(sh), 515 (CH_3OH). Selected IR bands (cm^{-1}): 3400m, 3189m,br, 1609s, 1112s,br, 624m. Magnetic moment (BM, 300 K): 4.75.

Caution! Perchlorate salts of metal complexes with organic ligands are potentially explosive and should be handled with care.

2.2. Physical measurements

Elemental analyses (C, H, N) were carried out using a Perkin–Elmer model 2400 CHN elemental analyzer at the SAIF, Panjab University. Cobalt was determined gravimetrically as $[Co(C_5H_5N)_4](SCN)_2$. IR spectra were recorded as KBr pellets on a Perkin–Elmer RX-1 FTIR spectrophotometer. The UV–Vis spectra (200–1000 nm) were recorded on a JASCO V-530 UV–VIS spectrophotometer in 1 cm matched quartz cells. Molar conductances were measured using a Digital conductivity bridge, Model CC601. Magnetic susceptibilities were measured on a Gouy balance at 300 K using solid $Hg[Co(NCS)_4]$ as calibrant.

2.3. X-ray crystallography

Crystallization of **1**, **2** and **4** at room temperature by slow evaporation of their saturated solutions in CH_3CN, slightly aqueous CH_3CN and C_2H_5OH respectively yielded good single crystals. Intensity data were collected on a Siemens P4 single-crystal diffractometer equipped with a molybdenum sealed tube (λ = 0.7173 Å) and highly oriented graphite monochromator at 293(2) K. The lattice parameters and standard deviations were obtained by a least-squares fit to 40 reflections [$10.27 < 2\Theta < 28.08°$] for **1**. The data were collected by the $2\Theta-\Theta$ scan mode with a variable scan speed ranging from 2.0 to a maximum of $60° \,min^{-1}$. Three reflections were used to monitor the stability and orientation of the crystal and were measured after every 97 reflections. Their intensities showed only statistical fluctuations during 74.92 h of X-ray exposure time. The data were collected for Lorentz and polarisation factors and an empirical absorption correction based on the Psi scan method was applied. The structures were solved by direct methods using SHELX-97 [16] and also refined on F^2. All the non-hydrogen atoms were refined anisotropically. During the refinement, the difference Fourier clearly showed the twofold disordered positions of the PF_6^- anions in **1** and one of the ethyl moieties [C(14)–C(15)] of the side arms of **2** and **4**. These disordered atoms were refined with partial occupancy factors. Similarly, the twofold disordered oxygen atoms of ClO_4^- (in **4**) through the [Cl(1)–O(5)] axis were refined to a major occupancy factor of 0.89%. The minor

Table 1
Crystal data and structure refinement parameters for complexes **1**, **2** and **4**

	Complex **1**	Complex **2**	Complex **4**
Empirical formula	$C_{32}H_{49}CoF_{12}N_7O_4P_2$	$C_{30}H_{52}CoF_{12}N_6O_7P_2$	$C_{30}H_{52}Cl_2CoN_6O_{15}$
Formula weight	944.65	957.65	866.61
Crystal system	monoclinic	monoclinic	monoclinic
Space group	$P2_1/n$	$C2/c$	$C2/c$
Unit cell dimensions			
a (Å)	13.752(1)	27.617(2)	26.013(2)
b (Å)	14.279(1)	9.060(1)	9.046(1)
c (Å)	22.418(2)	21.133(2)	20.575(1)
α (°)	90	90	90
β (°)	97.69	124.08	123.32
γ (°)	90	90	90
V (Å^3)	4362.5(6)	4379.6(7)	4045.7(6)
Z	4	4	4
D_{calc} (Mg/m^3)	1.438	1.452	1.423
Absorption coefficient (mm^{-1})	0.561	0.564	0.628
Crystal size (mm)	$0.22 \times 0.19 \times 0.18$	$0.25 \times 0.21 \times 0.15$	$0.24 \times 0.19 \times 0.14$
Limiting indices	$-15 \leqslant h \leqslant 0$, $-16 \leqslant k \leqslant 0$, $-24 \leqslant l \leqslant 25$	$-31 \leqslant h \leqslant 0$, $0 \leqslant k \leqslant 10$, $-20 \leqslant l \leqslant 24$	$-29 \leqslant h \leqslant 0$, $0 \leqslant k \leqslant 10$, $-19 \leqslant l \leqslant 23$
Reflections collected/unique	6734/6415 [$R_{int} = 0.0187$]	3518/3439 [$R_{int} = 0.0228$]	3263/3183 [$R_{int} = 0.0230$]
Data/restraints/parameters	6415/43/597	3439/5/296	3183/4/269
Goodness-of-fit on F^2	1.012	1.013	1.057
Final R indices [$I > 2\sigma(I)$]	$R_1 = 0.0648$	$R_1 = 0.0555$	$R_1 = 0.0474$
R indices (all data)	$R_1 = 0.0880$, $wR_2 = 0.1855$	$R_1 = 0.0828$, $wR_2 = 0.1625$	$R_1 = 0.0607$, $wR_2 = 0.1392$
Largest different peak and hole (e Å^3)	0.621 and −0.628	0.379 and −0.405	0.488 and −0.296

positions of all these disordered atoms were assigned an occupancy of $1 - x$ (where $x =$ major occupancy). The hydrogen atoms were included in ideal positions with fixed isotropic U values and riding with their respective non-hydrogen atoms. A weighting scheme of the form $w = 1/[(\sigma 2F_o^2) + (ap)^2 + bp]$ with $a = 0.0980$ and $b = 5.60$ was used. The refinement converged to a final R value of 0.0648 ($wR_2 = 0.1723$ for 4823 reflections) [$I > 2\sigma(I)$]. The final difference map was featureless. The data collection procedure, structure solution and refinement for compounds **2** and **4** were essentially the same as for **1**. The parameters associated with their structures are as follows: **2**. 40 reflections ($10.13 < 2\theta < 28.27°$) for an accurate cell parameter determination, $R = 0.0555$ ($wR_2 = 0.1431$ for 2475 reflections) [$I > 2\sigma(I)$] with $a = 0.0934$ and $b = 3.89$ in the weighting scheme. **4** 40 reflections ($9.52 < 2\theta < 30.04°$) for an accurate cell parameter determination, $R = 0.0474$ ($wR_2 = 0.1285$ for 2551 reflections) [$I > 2\sigma(I)$] with $a = 0.0739$ and $b = 5.10$ in the above mentioned weighting scheme. A summary of the crystal parameters, experimental details and refinement results are listed in Table 1.

3. Results and discussion

Complexes **1**–**5** are isolated in good yield by stirring $Co(NO_3)_2 \cdot 6H_2O$ or $CoCl_2 \cdot 6H_2O$ with two equivalents of the alkali metal salt of the appropriate anion containing 2 moles of deap. The final composition of the product is dependant on the solvent used. The complexes are sensitive to moisture and were identified and characterised through melting points, elemental analyses, IR and visible spectral data, conductivity measurements, X-ray crystallography and magnetic measurements. The complexes are practically insoluble in CH_2Cl_2, $CHCl_3$, CCl_4 and C_6H_6 but easily dissolve in polar organic solvents such as CH_3OH, CH_3CN and CH_3NO_2. Their conductivities were measured in CH_3CN and/or CH_3NO_2 and the molar conductances are slightly below the expected ranges for 1:2 electrolytes in these solvents [17]. The magnetic moment of the complexes at room temperature falls in the range 4.60–4.80u_B, consistent with the presence of three unpaired d electrons, suggesting a high-spin octahedral structure [18]. The visible spectra of complexes **1**–**4** show a weak absorption band near 530 nm which is due to the $^4T_{1g}(F) \rightarrow {}^4T_{1g}(P)$ transition. The shoulder band on the high frequency side is attributed to spin–orbit coupling in the $^4T_{1g}(P)$ state [18]. The other two transitions, i.e., $^4T_{1g}(F) \rightarrow {}^4A_{2g}$ and $^4T_{1g}(F) \rightarrow {}^4T_{2g}$ expected for an octahedrally coordinated Co^{II} ion are not observed [18].

Vibrational spectroscopy is also in agreement with the present structures. The IR spectra of compounds **1**–**5** show absorptions characteristic of the coordinated ligand. In the free ligand, the carbonyl stretching frequency appears as a strong band at 1625 cm^{-1}, and this is lowered by about 15–20 cm^{-1} on coordination to the metal ion in the complexes. In these compounds, we were expecting two bands in this region, one band near 1625 cm^{-1} due to a free carbonyl group and the second peak near 1600 cm^{-1} due to a coordinated carbonyl group. In fact only a single broad peak was observed around 1600 cm^{-1}. Probably, due to strong hydrogen bonding between the free carbonyl oxygen and the lattice water, the $\nu_{C=O}$ peak is lowered to an extent that only a single peak is observed. Participation of the pyridine ring nitrogen in all the complexes is indicated by the upward movement in the absorption and ring breathing mode of pyridine. Compounds **2**–**5** show a broad band centred around 3200 cm^{-1} and a sharper absorption near 3460 cm^{-1}. These bands are indicative of the presence of hydrogen-bonded lattice water and coordinated water. The IR spectra of **2**–**5** are essentially similar to each other except for the vibrations of the respective counteranion (PF_6^-, 845 and 560 cm^{-1} in **1** and **2** [19]; BF_4^-, 1072 cm^{-1} in **3** [20]; ClO_4^-, 1090 and 630 cm^{-1} in **4** [21] and NO_3^-, 1390 cm^{-1} in **5**) [20].

In order to prepare mixed ligand complexes, **1**, **2** and **4** were treated with HMPA. However, deap was eliminated resulting in the isolation of $MX_2 \cdot 2$ HMPA ($X = PF_6^-$ and ClO_4^-). It suggests that HMPA is a stronger nucleophile than deap.

3.1. Crystal structure of $[Co(deap)_2CH_3CN](PF_6)_2$ (1)

Selected bond angles and bond distances for complex **1** are given in Table 2. A perspective view of complex **1** is depicted in Fig. 1. The complex consists of discrete $[Co(deap)_2CH_3CN]^{2+}$ cations and PF_6^- anions. The cobalt atom in the complex cation is hexacoordinated (CoN_3O_3 chromophore), one deap ligand is acting as a tridentate ligand [bonding through two carboxamide oxygen atoms O(1), O(2) and the pyridilic N(1) atom] while the second deap ligand is coordinated in a bidentate mode [bonding through O(3) and N(4) atoms]. The carboxamide oxygen O(4) of the other side arm moves away from the cobalt center, $Co(1)\cdots O(4) = 3.67$ Å, indicating no bonding interaction. The sixth coordination site is occupied by an acetonitrile molecule bonded to Co(1) through the N(7) atom. The bond angle involving the axial atoms, N(7)–Co(1)–N(4) is 161.37(17)°, giving a severely distorted octahedral arrangement. The four atoms O(2), O(1), N(1) and O(3) define a mean plane from which these atoms are deviated by −0.097, −0.117, +0.133 and +0.081 Å. The cobalt atom is displaced by +0.031 Å from the mean plane formed by these four atoms. The distortion exhibited by the complex may be attributed to the steric hindrance caused by the ethyl groups of the carboxamide moiety. Due

Table 2
Important bond lengths [Å] and angles [°] for complexes **1**, **2** and **4**

*Complex **1***	
Co(1)–O(3)	2.060(3)
Co(1)–O(2)	2.079(3)
Co(1)–O(1)	2.106(3)
Co(1)–N(7)	2.072(5)
Co(1)–N(1)	2.088(4)
Co(1)–N(4)	2.190(4)
O(3)–Co(1)–N(7)	86.25(18)
N(7)–Co(1)–O(2)	91.75(18)
N(7)–Co(1)–N(1)	90.34(18)
O(3)–Co(1)–O(1)	90.45(13)
O(2)–Co(1)–O(1)	148.97(13)
O(3)–Co(1)–N(4)	76.10(13)
O(2)–Co(1)–N(4)	91.90(12)
O(1)–Co(1)–N(4)	88.74(14)
O(3)–Co(1)–O(2)	119.80(12)
O(3)–Co(1)–N(1)	164.40(14)
O(2)–Co(1)–N(1)	75.47(13)
N(7)–Co(1)–O(1)	97.43(19)
N(1)–Co(1)–O(1)	74.89(14)
N(7)–Co(1)–N(4)	161.37(17)
N(1)–Co(1)–N(4)	108.26(13)
*Complex **2***	
Co(1)–O(1)#1	2.041(3)
Co(1)–O(3)	2.101(3)
Co(1)–N(1)	2.189(3)
Co(1)–O(1)	2.041(3)
Co(1)–O(3)#1	2.101(3)
Co(1)–N(1)#1	2.189(3)
O(1)#1–Co(1)–O(1)	177.51(16)
O(1)–Co(1)–O(3)	88.34(12)
O(1)–Co(1)–O(3)#1	89.85(13)
O(1)#1–Co(1)–N(1)	104.93(11)
O(3)–Co(1)–N(1)	164.82(12)
O(1)–Co(1)–N(1)#1	76.79(11)
O(3)–Co(1)–N(1)#1	90.63(10)
N(1)–Co(1)–N(1)#1	96.03(15)
O(1)#1–Co(1)–O(3)	89.85(13)
O(1)#1–Co(1)–O(3)#1	88.34(12)
O(3)–Co(1)–O(3)#1	86.29(15)
O(1)–Co(1)–N(1)	76.79(11)
O(3)#1–Co(1)–N(1)	90.63(11)
O(1)–Co(1)–N(1)#1	104.93(11)
O(3)#1–Co(1)–N(1)#1	164.82(12)
*Complex **4***	
Co–O(1)	2.035(2)
Co(1)–O(1)#2	2.035(2)
Co(1)–O(3)	2.094(2)
Co(1)–O(3)#2	2.094(2)
Co(1)–N(1)	2.198(2)
Co(1)–N(1)#2	2.198(2)
O(1)–C(6)	1.255(4)
O(1)–Co(1)–O(1)#2	178.25(13)
O(1)–Co(1)–O(3)	89.67(11)
O(1)#2–Co(1)–O(3)	89.05(11)
O(1)–Co(1)–O(3)#2	89.05(11)
O(1)#2–Co(1)–O(3)#2	89.67(11)
O(3)–Co(1)–O(3)#2	86.64(13)
O(1)–Co(1)–N(1)	76.84(9)
O(1)#2–Co(1)–N(1)	104.37(10)
O(3)–Co(1)–N(1)	166.20(11)
O(3)#2–Co(1)–N(1)	90.18(9)
O(1)–Co(1)–N(1)#2	104.37(10)
O(1)#2–Co(1)–N(1)#2	76.84(9)
O(3)–Co(1)–N(1)#2	90.18(9)
O(3)#2–Co(1)–N(1)#2	166.20(11)
N(1)–Co(1)–N(1)#2	95.93(12)

Symmetry transformations used to generate equivalent atoms #1 $-x+2, y, -z+3/2$; #2 $-x, y, -z+3/2$.

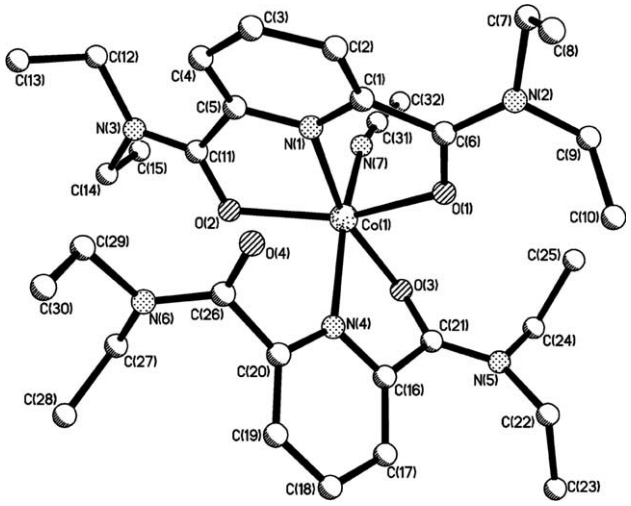

Fig. 1. A perspective view of complex **1** with the atom numbering scheme. The hydrogen atoms and anions are omitted for clarity.

to the difference in coordination mode, the conformation of the two deap ligands is also different in the crystal lattice. To maximize the electron donation through coordination, both the carbonyl moieties of the tridentate deap are almost in the meridional plane of the ligand, the torsion angle with respect to the C(1)–C(6) and C(5)–C(11) bonds being −18.4° and 22.0°, respectively. On the other hand, in the bidentate deap, as this restriction does not apply, the torsional angles are much more varied [at the C(16)–C(21) bond −28.8°, and at the C(20)–C(28) bond −65.7°]. In fact it is the non-coordinating carbonyl moiety [C(26)–O(4)], that is quite out of plane from the aromatic pyridyl ring [N(4)–C(20)–C(26)–O(4) = −65.7°]. In the crystal lattice both the PF_6^- anions are disordered and placed in the cavities formed by the metal ligand complex cations. Such disordered PF_6^- anions are common in other similar structures containing PF_6^- anions [22].

3.2. Crystal structures of $[Co(deap)_2(H_2O)_2](X)_2$ [X = PF_6^- (2); ClO_4^- (4)]

The crystal structures of **2** and **4** comprise of $[Co(deap)_2(H_2O)_2]^{2+}$ cations and PF_6^- or ClO_4^- anions. The structure of the cation involves a hexa-coordinated CoO_4N_2 chromophore with the metal center presenting a nearly perfect octahedral geometry. The molecules of **2** and **4**

occupy the twofold axis of the $C2/c$ space group, resulting in an interesting network of hydrogen bonds. The deap ligands are coordinated in a bidentate mode bonded by the pyridilic N atom and an oxygen atom of the carboxamide moiety. The oxygen atom of the non-coordinating part of the side arm moves away from the metal center [Co(1)···O(2) = 4.114 Å]. The fifth and sixth coordination sites are occupied by water molecules. The four atoms O(3), N(1), O(3)$^{\#}$ and N(1)$^{\#}$ (# = $-x$, $-y$, $1.5 - z$) define a mean plane from which these atoms are deviated by −0.284, −0.249, 0.284 and 0.249 Å for **2** and −0.257, −0.225, 0.257 and 0.225 Å for **4**, respectively. Interestingly, the cobalt atom resides exactly on this plane, deviation = 0.00 Å. The bite angles around the cobalt atom range from 76.89(9) to 104.37(10)°, summing up the in-plane angles to be 359.98°.

The similarity in the molecular structure of compounds **2** and **4** is, interestingly, reflected in their crystal structures also, both are structurally similar with a $C2/c$ space group in the monoclinic crystal system. However, to accommodate a larger PF_6^- anion (in **2**) than ClO_4^- (in **4**), the cell volume has increased by ca. 334 Å^3 in **2** compared to **4**. In effect, the monoclinic 'box' has enlarged significantly in the '*a*' and '*c*' directions (1.604 and 0.586 Å increase) and only slightly in the '*b*' direction (0.014 Å increase) to accommodate the larger counteranion, but the structural features are strikingly similar (vide infra). Firstly, both anions in these complexes are disordered in the lattice, probably due to their high symmetry, as the walls of the cavity from the cations have similar stabilizing interactions even if the anion is positioned in a different orientation. Secondly, even the disordered nature of one of the coordinating 'arms' is preserved in both the crystal lattices. Thus, this family of cations may adjust to the topological demand of the varying nature of the anions by showing larger flexibility in their cavity size for anion accommodation. Structure determination of a series of complexes with different counter ions may validate this point.

In the crystal lattice, the cobalt cation sits on a twofold axis, and two deap ligands and two water molecules together complete the octahedral geometry around the metal ion (due to the structural similarity between **2** and **4**, the structural description regarding **2** is equally valid for **4** and relevant parameters are recorded in brackets for **4**). As deap is only acting as a bidentate ligand, the two coordinating water molecules are placed *cis* to each other in the octahedral arrangement (Figs. 2 and 3). It is also interesting to note that deap is not utilizing all of its coordinating abilities (it can act as a tridentate ligand [12]) but only binds to the metal atom in a bidentate mode with one of its carbonyl oxygen atoms and its pyridyl nitrogen atom. The free carbonyl group is in fact strongly hydrogen bonded to the lattice water molecule (Fig. 4). As observed in **1** the non-coordinating

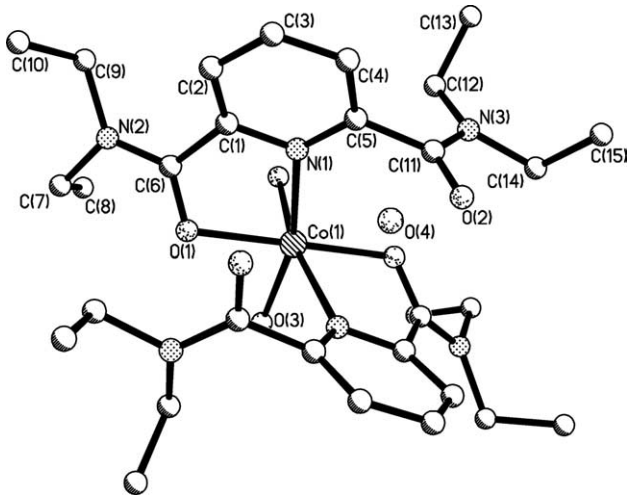

Fig. 2. A perspective view of complex **2** with the atom numbering scheme. The hydrogen atoms and anions are omitted for clarity.

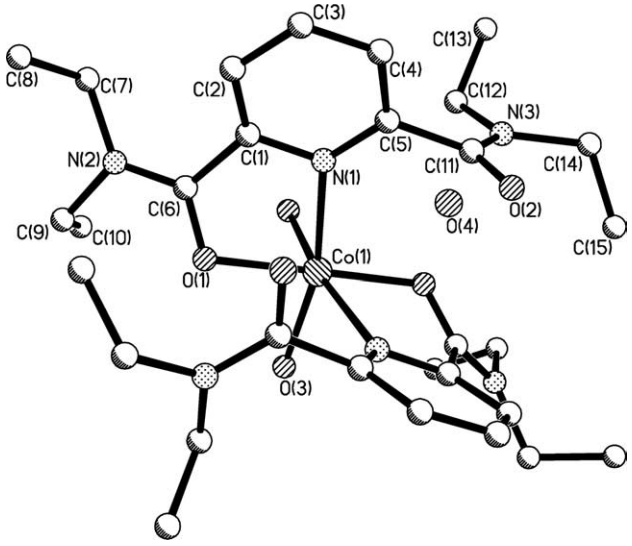

Fig. 3. A perspective view of complex **3** with the atom numbering scheme. The hydrogen atoms and anions are omitted for clarity.

carbonyl moiety is almost orthogonal to the pyridyl ring, the relevant torsional angle being −103.3° (**2**) and 99.8° (**4**). The coordinating carbonyl group is also deviated to an extent of 30.0° from the aromatic plane [N(1)–C(1)–C(6)–O(1)].

In the crystal lattice, due to the symmetrical disposition of the complex on the twofold axis, there is an interesting chain of molecules formed through hydrogen bonding (Fig. 4). The lattice water has a crucial role in the formation of this chain, in fact it acts as a connecting link between the complex molecules running almost perpendicular to the '*ac*' plane. The relevant hydrogen bonding parameters are given in Table 3. This water molecule is saturated in terms of its hydrogen bonding capabilities and, as expected, the four hydrogen bonds are almost tetrahedrally oriented and they are strong

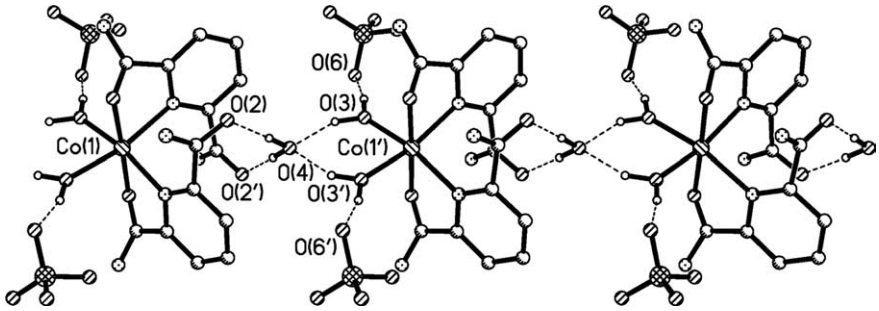

Fig. 4. Interlinkage of complex molecules of **4** through the lattice water leading to the formation of a molecular chain. Note that the water is saturated in its hydrogen bonding capability. Due to crystallographic symmetry O(2) and O(2′) are identical and similarly so are O(3) and O(3′).

O–H···O hydrogen bonds $d(H\cdots A < 1.9$ Å). Such a strong holding of the water molecule to the ligand moiety has its physical consequences. Our deliberate attempt to remove this water by warming the complex to 60 °C for 12 h or applying vacuum (10^{-3} Torr) for 12 h or both did not remove this water molecule. The IR spectra before and after these experiments remained virtually identical.

The hydrogen bonded chains of the complex generate flexible linear columns in which either PF_6^- (**2**) or ClO_4^- (**4**) reside and stabilize the lattice (Fig. 5). These anions are topologically locked in their place through either O–H···F (**2**) or O–H···O (**4**) hydrogen bonds (Table 3). It is noteworthy that it is the lattice water that anchors these anions through multiple interactions. Even the disordered positions of the anions are stabilized through hydrogen bonds. One such typical example is shown in Table 3. Thus, in this family of complexes, the columnar cavity is flexible to accommodate anions of different sizes and the cavity surface can also provide multiple interaction sites with the anions that can provide overall stability to the lattice. If these cavities are capable of exchanging the anions at different rates and stabilities, they can even act as specific receptors for these anions. A careful combination of kinetic and spectroscopic studies on these systems may validate this aspect. Preliminary experiments show anion exchange of $[Co(deap)_2(H_2O)_2](BF_4)_2 \cdot H_2O$ with PF_6^- in acetonitrile solution.

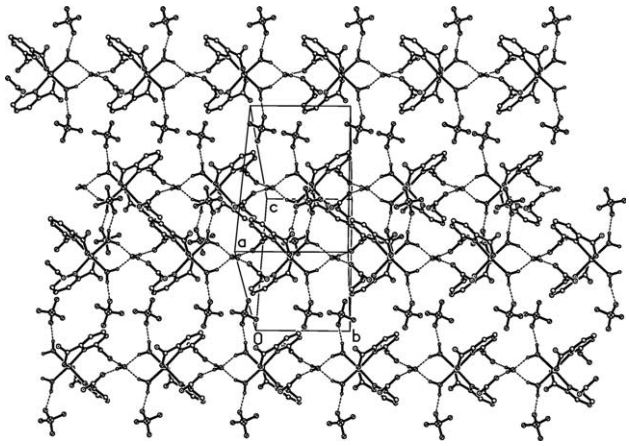

Fig. 5. Formation of channels out of the molecular chains shown in Fig. 4. The anions are disordered (only the major positions are shown here) and are stabilized through hydrogen bonding. Due to the similarity of structure, the packing of complex **2** is exactly the same as **4** except for a change of the counterion to PF_6^-.

Appendix A. Supplementary data

Crystallographic data for structural analysis have been deposited with the Cambridge Crystallographic Data Centre with CCDC numbers for **1**, **2** and **4** of 266713, 266714 and 266715, respectively. Copies of this information may be obtained free of charge from the Director, CCDC, 12 Union Road, Cambridge CB2 1EZ, U.K.

Table 3
Hydrogen bonding parameters of **2** and **4** (Angstroms and degrees)

D–H	*d*(D–H)	*d*(H···A)	<DHA	*d*(D···A)	*A*(symm.op.)
Complex ***2***					
O(3)–H(3A)	0.886	1.893	150.76	2.702	O4[x, $y-1$, z]
O(3)–H(3B)	0.891	2.096	157.60	2.940	F1[$-x+2$, y, $-z+3/2$]
O(4)–H(4A)	0.866	1.892	162.28	2.729	O2
O(3)–H(3B)	0.891	2.131	144.41	2.902	F6′[$-x+2$, y, $-z+3/2$]
Complex ***4***					
O(3)–H(3A)	0.971	1.785	156.12	2.702	O4[x, $y-1$, z]
O(3)–H(3B)	0.910	1.930	162.28	2.810	O6
O(4)–H(4A)	0.892	1.838	175.71	2.728	O2
O(3)–H(3B)	0.910	2.504	150.13	3.324	O8′

fax: +44 1223 336 033; or deposite@ccdc.cam.ac.ukor www: http://www.ccdc.cam.ac.uk. Supplementary data associated with this article can be found, in the online version at doi:10.1016/j.poly.2005.06.060.

References

[1] S.L. Jain, P. Bhattacharyya, H.L. Milton, A.M.Z. Slawin, J.A. Crayston, J.D. Woollins, J. Chem. Soc., Dalton Trans. (2004) 862.
[2] (a) T. Le Borgne, P. Altmann, N. Andre, J.-C.G. Bunzli, G. Bernardinelli, P. Morgantini, J. Weber, C. Piguet, J. Chem. Soc., Dalton Trans. (2004) 723;
(b) T. Le Borgne, J.-M. Benech, S. Floquet, G. Bernardinelli, C. Aliprandini, P. Bettens, C. Piguet, J. Chem. Soc., Dalton Trans. (2003) 3856;
(c) F. Renaud, C. Piguet, G. Bernardinelli, J.-C.G. Bunzli, G. Hopfgartner, Chem. Eur. J. (1997) 1646.
[3] J. Garcia-Lozano, M.A. Martinez-Lorente, E. Escriva, R. Ballesteros, Synth. React. Inorg. Met. Org. Chem. 24 (1994) 365.
[4] J. Garcia-Lozano, L. Soto, J.V. Folgado, E. Escriva, Polyhedron 15 (1996) 4003.
[5] J.G.H. Du Preez, B. van Brecht, Inorg. Chim. Acta 162 (1989) 49.
[6] J.G.H. Du Preez, B. van Brecht, J.F. de Wet, J. Koorts, Inorg. Nucl. Chem. Lett. 10 (1974) 935.
[7] A.K. Singh, V. Balamurugan, R.N. Mukherjee, Inorg. Chem. 42 (2003) 6497, and references therein.
[8] D.S. Marlin, P.K. Mascharak, Chem. Soc. Rev. 29 (2000) 69.
[9] R. Kapoor, A. Kataria, P. Kapoor, P. Venugopalan, Trans. Met. Chem. 29 (2004) 425.
[10] R. Kapoor, A. Kataria, A. Pathak, P. Venugopalan, G. Hundal, P. Kapoor, Polyhedron 24 (2005) 1221.
[11] R. Kapoor, A. Kataria, P. Venugopalan, P. Kapoor, M. Corbella, M. Rodriguez, M. Romero, M. Sola, A. Llobet, Inorg. Chem. 43 (2004) 6699.
[12] P. Kapoor, A. Kumar, J. Nistandra, P. Venugopalan, Trans. Met. Chem. 25 (2000) 465.
[13] P. Kapoor, A. Pathak, P. Kaur, P. Venugopalan, R. Kapoor, Trans. Met. Chem. 29 (2004) 251.
[14] P. Kapoor, A. Pathak, R. Kapoor, P. Venugopalan, M. Corbella, M. Rodriguez, J. Robles, A. Llobet, Inorg. Chem. 41 (2002) 6153.
[15] W.L.F. Armarego, D.D. Perrin, Purification of Laboratory Chemicals, fourth ed., Butterworth-Heinemann, Oxford, 1996.
[16] SHELX-97 G.M. Sheldric, Program for Solution and Refinement of Crystal Structures, University of Gottingen, Gottingen, Germany, 1997.
[17] W.J. Geary, Coord. Chem. Rev. 7 (1971) 81.
[18] F.A. Cotton, G. Wilkinson, Advanced Inorganic Chemistry, second ed., Wiley Eastern Pvt. Ltd., New Delhi, 1966, p. 870.
[19] K. Nakamoto, Infrared and Raman Spectra of Inorganic and Coordination Compounds, fourth ed., Wiley, NewYork, 1986.
[20] O.-S. Jung, Y.J. Kim, Y.-A. Lee, H.K. Chae, H.G. Jang, J. Hong, Inorg. Chem. 40 (2001) 2105.
[21] F.A. Cotton, D.L. Weaver, J. Am. Chem. Soc. 87 (1965) 4189.
[22] (a) J.A. Kaduk, A.T. Poulos, J. Organomet. Chem. 127 (1977) 245;
(b) R.J. Webb, M.D. Lowery, Y. Shiomi, M. Sorai, R.J. Wittebort, D.N. Hendrickson, Inorg. Chem. 31 (1992) 5211;
(c) D.A. McMorran, P.J. Steel, Angew. Chem. Int. Ed. 37 (1998) 3295.

Available online at www.sciencedirect.com
SCIENCE DIRECT®
Polyhedron 25 (2006) 39–42
POLYHEDRON
www.elsevier.com/locate/poly

Phthalocyanines with rigid carboxylic acid containing pendant arms

Ayfer Kalkan, Zehra Altuntaş Bayır *

Department of Chemistry, Technical University of Istanbul, TR34469 Maslak, Istanbul, Turkey

Received 6 June 2005; accepted 25 June 2005
Available online 18 August 2005

Abstract

Metal-free and metallophthalocyanines (Zn, Co) substituted with four carboxybiphenyloxy groups on the peripheral positions were prepared from 4-(4′-carboxybiphenyloxy)phthalonitrile. Esterification of all of the biphenylcarboxylic acid groups of metal-free phthalocyanine with hexanol afforded 2,9,16,23-tetrakis(4′-carbhexyloxybiphenyloxy) phthalocyanine. These new compounds have been characterised by ^{1}H NMR, ^{13}C NMR, FT-IR, UV–Vis and mass spectroscopies.
© 2005 Elsevier Ltd. All rights reserved.

Keywords: Phthalocyanine; Biphenylcarboxylic acid; Zinc; Cobalt

1. Introduction

Phthalocyanine is a close relative of the porphyrin macrocycle and is the parent compound of one of the most studied class of functional organic materials. The most important and extensive application of phthalocyanines is to be used as colorants. Furthermore, phthalocyanine and its derivatives displaying interesting photophysical properties, electron transfer ability and reduction–oxidation behaviour are studied for applications in electrophotography, photovoltaic cells, fuel cells and electrochromic displays [1,2].

Recent years, remarkable progress has been made in the use of phthalocyanine derivatives as sensitisers for photodynamic therapy (PDT) of cancer [3,4]. PDT employs the combination of light and photosensitiser. Photosensitiser is getting excited after the absorption of light of proper wavelength. It is followed by a singlet oxygen production by energy transfer from activated photosensitiser. Phthalocyanines display cytotoxic effects when activated by light. Especially, water soluble zinc and aluminium phthalocyanine complexes have good photosensitising properties for PDT [5–7].

The main restricting factor of phthalocyanines is a rather low solubility in organic solvents. Periferal substitution of phthalocyanines with alkyl, alkoxy, alkythio chains or bulky groups enhances their solubility drastically [8–18]. The introduction of carboxy or amino groups gives water-soluble products. The synthesis of soluble phthalocyanines should provide them new optical, electronic, redox and magnetic properties which could increase the field of possible applications [19–21].

Recently, we have reported on the synthesis, separation and characterisation of unsymmetrical and symmetrical phthalocyanines [22–25]. This paper describes metal-free and metallo phthalocyanines (Zn, Co) carrying biphenylcarboxylic acid substituents on the periphery. Also, all of the biphenylcarboxylic acid substituents of the metal-free phthalocyanine were esterified with hexanol.

2. Experimental

IR spectra were recorded on a Perkin–Elmer Spectrum One FT-IR (ATR sampling accessory)

* Corresponding author. Tel.: +90 212 285 32 23; fax: +90 212 285 63 86.
E-mail address: bayir@itu.edu.tr (Z.A. Bayır).

0277-5387/$ - see front matter © 2005 Elsevier Ltd. All rights reserved.
doi:10.1016/j.poly.2005.06.056

spectrophotometer, electronic spectra on a Unicam UV2 spectrophotometer. ^{1}H NMR spectra were recorded on Bruker 250 MHz and Inova 500 spectrometers using TMS as internal reference. Mass spectra were performed on Ultima Fourier Transform and Varian 711 mass spectrometer. All reagents and solvents were of reagent grade quality obtained from commercial suppliers. The homogeneity of the products was tested in each step by TLC. All solvents were dried and purified as described by Perrin and Armarego [26]. The solvents were stored over molecular sieves. 4-Nitrophthalonitrile (**1**) [27] was synthesised according to published methods.

2.1. 4-(4′-Carboxybiphenyloxy)phthalonitrile (*2*)

4-Nitrophthalonitrile (0.5, 2.89 mmol) and an excess of 4′-hydroxy-4-biphenylcarboxylic acid (1.24 g, 5.78 mmol) were dissolved in 10 ml dry DMF. Anhydrous K_2CO_3 (1.59 g, 11.56 mmol) was added portion wise over 2 h and the mixture was stirred vigorously at room temperature under N_2 for 48 h. The reaction mixture was poured into water (100 ml) and the pH of solution was adjusted to 1 by addition of aqueous hydrochloric acid. The precipitated solid was filtered, washed with water until the filtrate was neutral, and then dried. Finally, a pale beige product was crystallised from methanol–water. Yield: 0.54 g, 55%. M.p. >200 °C. IR $\nu_{max}/(cm^{-1})$: 3055 (Ar–H), 2238 (C≡N), 1681 (C=O), 1588, 1522, 1489, 1268, 1242 (C–O–C), 1183, 1007, 839, 776, ^{1}H NMR (*d*-DMSO): 13.03 (s, 1H, OH), 8.14 (d, 2H, Ar–H), 8.05 (d, 1H, Ar–H), 7.85 (m, 4H, Ar–H), 7.49 (d, 1H, Ar–H), 7.46 (d, 1H, Ar–H), 7.34 (d, 2H, Ar–H); ^{13}C NMR (*d*-DMSO, APT): 167.58 (C=O), 161.24 (aromatic C), 154.57 (biphenyl C), 143.66 (biphenyl C), 136.85 (biphenyl C), 136.81 (aromatic CH), 130.48 (biphenyl CH), 130.17 (biphenyl C), 129.66 (biphenyl CH), 127.22 (biphenyl CH), 123.45 (aromatic CH), 122.82 (aromatic CH), 121.26 (biphenyl CH), 117.22 (aromatic C), 116.37 (C≡N), 115.85 (C≡N), 108.93 (aromatic C); UV–Vis λ_{max} (nm) (log ε) in THF: 291 (4.63). *Anal.* Calc. for $C_{21}H_{12}N_2O_3$: C, 74.11; H, 3.55; N, 8.23. Found: C, 74.10; H, 3.52; N, 8.22%.

2.2. 2,9,16,23-Tetrakis(4′-carboxybiphenyloxy)-phthalocyanine (*3*)

4-(4′-Carboxybiphenyloxy)phthalonitrile (0.50 g, 1.47 mmol) was dissolved in 6 ml dry 1-pentanol and heated at 140 °C under N_2. After addition of elemental lithium (0.07 g, 10.3 mmol) a green colour appeared in a few seconds. The suspension was stirred under reflux for 1 h. Then, the mixture was cooled to room temperature. The reaction mixture was acidified with HCl and the resulting precipitate was centrifuged off. The precipitated blue-green coloured solid was filtered and washed first with water, then with ethanol and acetone finally dried in vacuo. Yield: 0.34 g, 17%. M.p. >200 °C. IR $\nu_{max}/(cm^{-1})$: 3310 (N–H), 3050 (Ar–H), 1683 (C=O), 1598, 1522, 1470, 1250, 1181, 1091, 1003, 926, 825, 771; ^{1}H NMR (*d*-DMSO): 8.01–7.38 (m, 44H, Ar–H); UV–Vis λ_{max} (nm) (log ε) in DMSO: 288 (4.77), 340 (4.36), 668 (4.41), 700 (4.40); MS (MALDI-TOF): *m*/*z* 1363.4 [M^+], 1317.4 [$M^+ - COOH - H$]. *Anal.* Calc. for $C_{84}H_{50}N_8O_{12}$: C, 74.01; H, 3.67; N, 8.22. Found: C, 73.99; H, 3.65; N, 8.19%.

2.3. 2,9,16,23-Tetrakis(4′-carboxybiphenyloxy)-phthalocyaninatozinc(II) (*4*)

The metal-free phthalocyanine **3** (0.20 g, 0.14 mmol) was dissolved in 20 ml dry DMF and anhydrous zinc acetate (0.27 g, 1.46 mmol) was added and the mixture was heated under stirring for 24 h at 80 °C. After cooling to room temperature, the suspension was added to diethyl ether (100 ml) and the precipitated green solid was filtered. The crude product was treated with CH_3COOH (10 ml) for 2 h then filtered off and washed with ethanol, acetone and then dried in vacuo. Yield: 0.10 g, 48%. M.p. >200 °C. IR $\nu_{max}/(cm^{-1})$: 3050 (Ar–H), 1688 (C=O), 1600, 1522, 1472, 1250, 1184, 1092, 1004, 928, 827, 773; ^{1}H NMR (*d*-DMSO): 12. 78 (br s, 4H, OH), 8.01–7.31 (m, 44H, Ar–H); UV–Vis λ_{max} (nm) (log ε) in DMSO: 289 (4.78), 347 (4.47), 679 (4.51); MS (FAB): *m*/*z* 1426.3 [M^+]. *Anal.* Calc. for $C_{84}H_{48}N_8O_{12}Zn$: C, 70.72; H, 3.37; N, 7.85. Found: C, 70.70; H, 3.34; N, 7.83%.

2.4. 2,9,16,23-Tetrakis(4′-carboxybiphenyloxy)-phthalocyaninatocobalt(II) (*5*)

A mixture of **3** (0.25 g, 0.18 mmol) and anhydrous cobalt(II)chloride (0.24 g, 1.84 mmol) was heated in dry DMF (20 ml) at 80 °C under N_2 with stirring for 18 h. The resulting green suspension was cooled and then added drop wise to diethyl ether (100 ml). The precipitate was stirred with CH_3COOH for 2 h and then filtered off. The green product was washed several times with hot ethanol and acetone to remove unreacted materials and then dried in vacuo. Yield: 0.13 g, 51%. M.p. >200 °C. IR $\nu_{max}/(cm^{-1})$: 3050 (Ar–H), 1687 (C=O), 1598, 1522, 1470, 1250, 1182, 1090, 1004, 927, 826, 771; UV–Vis λ_{max} (nm) (log ε) in DMSO: 289 (4.68), 343 (4.40), 664 (4.41); MS (MALDI-TOF): *m*/*z* 1420.3 [M^+]. *Anal.* Calc. for $C_{84}H_{48}N_8O_{12}Co$: C, 71.04; H, 3.38; N, 7.89. Found: C, 71.02; H, 3.37; N, 7.86%.

2.5. 2,9,16,23-Tetrakis(4′-carbhexyloxybiphenyloxy)-phthalocyanine (*6*)

A mixture of **3** (0.20 g, 0.14 mmol), dicyclohexylcarbodiimide (DCCI) (0.36 g, 1.76 mmol), toluene-*p*-sulfonic

acid (0.03 g, 0.14 mmol) and 1-hexanol (0.22 ml, 1.76 mmol) was stirred in dry pyridine (15 ml) under N_2 for 72 h. The suspension was filtered and the solvent was evaporated in vacuum. The residue was dissolved in chloroform (10 ml) and washed first with a solution of 10% Na_2CO_3 (50 ml) and then with water. The chloroform phase was dried over anhydrous Na_2SO_4 and finally the solvent was evaporated in vacuo. The green product was washed with 20 ml of ethanol–cyclohexane (1:1) mixture and then purified by column chromatography with silica gel using THF as eluent. Yield: 0.05 g, 21%. IR $\nu_{max}/(cm^{-1})$: 3310 (N–H), 3080 (Ar–H), 2927–2870 (alkyl CH), 1689 (C=O), 1599, 1522, 1470, 1250, 1180, 1091, 1004, 927, 825, 771; ^1H NMR (d-chloroform): 8.10–7.36 (m, 44H, Ar–H), 4.33 (t, 8H, OCH_2), 1.78–1.65 (m, 32H, CCH_2C), 0.93 (t, 12H, CH_3); UV–Vis λ_{max} (nm) (log ε): 287 (4.75), 338 (4.55), 668 (4.66), 699 (4.68); MS (FAB): *m*/*z* 1698.8 [M]. *Anal*. Calc. for $C_{108}H_{98}N_8O_{12}$: C, 76.34; H, 5.76; N, 6.59. Found: C, 76.31; H, 5.75; N, 6.59%.

3. Results and discussion

Scheme 1 shows the synthesis of the target phthalocyanines **3**–**6**. The first step in the synthetic procedure was to obtain 4-(4′-carboxybiphenyloxy)phthalonitrile (**2**). **2** was prepared from 4-nitrophthalonitrile and 4′-hydroxy-4-biphenylcarboxylic acid in DMF. K_2CO_3 was used as the base for this nucleophilic aromatic displacement [28].

The most usual method to prepare metal-free phthalocyanines is the cyclotetramerisation of a phthalic acid derivative such as phthalonitrile or diiminoisoindoline. A practical way of achieving this goal is the treatment of a phthalonitrile with lithium alkoxide, giving rise to the corresponding alkali metal phthalocyanine and it can be subsequently demetallated to the metal-free phthalocyanine with a mineral acid. In the present work, the latter was chosen for synthesising the metal-free phthalocyanine **3**; i.e., cyclisation of **2** by using lithium in 1-pentanol, and then acidification with HCl resulted with the formation of **3**.

The crude product obtained by metallation of metal-free phthalocyanine **3** with zinc acetate in dry DMF was insoluble in all common solvents. Such insoluble products were encountered frequently as a result of complexation between the COOH groups and the zinc(II) ions [4]. After treatment of the product with acetic acid, desired zinc phthalocyanine **4** with free carboxy groups are obtained. The same route was also applied for synthesising cobalt phthalocyanine **5**.

As expected, all the phthalocyanines synthesised during this work are a mixture of positional isomers starting with the phthalonitrile precursor **2** with a single substituent [2]. However, our attempts to separate these isomers by column chromatography and, also by HPLC methods using different solvents were not successful.

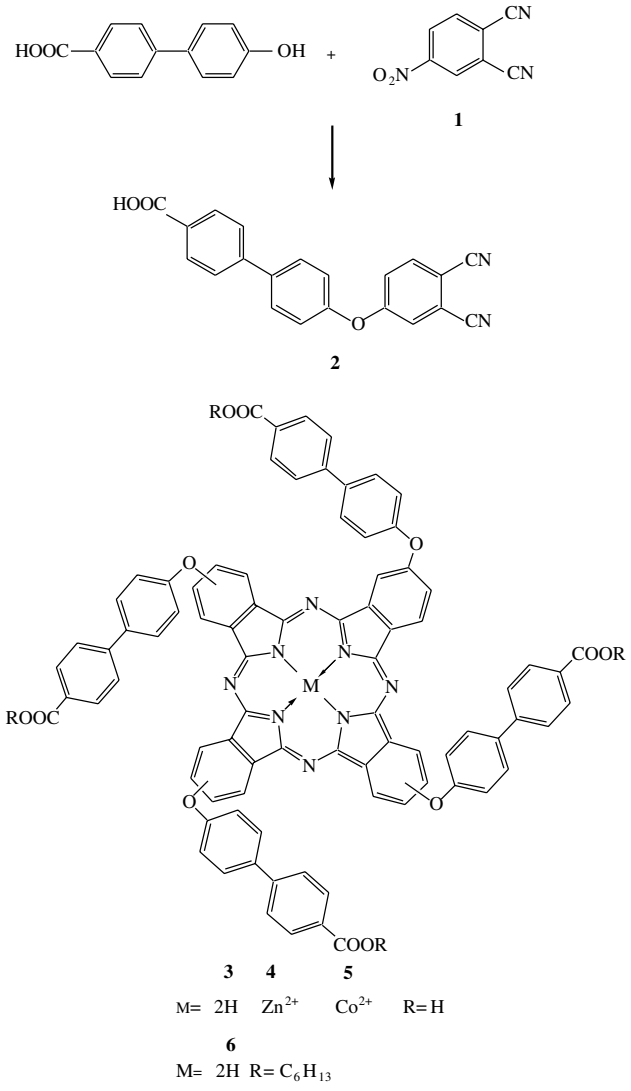

Scheme 1.

The phthalocyanines **3**–**5** are only soluble in DMSO and DMF. The biphenylcarboxylic acid substituents on the phthalocyanine core bring out a vast number of possibilities for binding with different groups. To achieve a better solubility of **3**, hexyl substituents were introduced into the biphenyl units. Esterification of all the COOH groups in **3** with hexanol to give tetrakis(4′-carbhexyloxybiphenyloxy)phthalocyanine **6** was accomplished in pyridine in the presence dicyclohexylcarbodiimide and 4-toluenesulfonic acid as catalyst for 72 h at room temperature. **6** shows good solubility in organic solvents such as $CHCl_3$, THF, $CHCl_2$.

Characterisation of the products involved a combination of methods including elemental analysis, ^1H and ^{13}C NMR, UV/Vis, IR and mass spectroscopy. The

spectroscopic data of the new compounds were in accordance with the structures. When IR spectrum of **1** is compared with that of **2**, a distinct difference is the disappearance of the aromatic $-NO_2$ band at 1548 cm^{-1} and the appearance of a new absorption at 1242 cm^{-1} attributable to aromatic (C–O–C) [29].

In the IR spectrum of **2** the presence of C≡N and C=O groups is indicated by the intense stretching bands at 2238 and 1681 cm^{-1}. ^1H NMR spectrum of **2** exhibited the aromatic protons around 7.34–8.14 ppm and the COOH proton at 13.03 ppm. The ^{13}C NMR spectral data are in accord with expected structure. The ^{13}C APT (Attached Proton Test) NMR spectrum of **2** indicated the nitrile carbons at 116.37 and 115.85 ppm as expected [30]. Protonated aromatic and unsaturated carbon atoms appeared in the range at δ 161.24–108.93 ppm. Also the carbon atom of carboxylic acid was observed at the lowest field at δ 167.58 ppm.

A diagnostic feature of the phthalocyanine formation from **2** is the disappearance of the C≡N peak of the reactant. The IR spectra of metal-free **3** and metallo phthalocyanines (**4**, **5**) are very similar. The significant difference is the presence of NH vibrations of the inner phthalocyanine core which are assigned to a weak band at 3310 cm^{-1} in the metal-free molecule. In the ^1H NMR spectrum of **3** aromatic protons appeared at 8.01–7.38 ppm. COOH protons and inner core NH protons could not be observed probably due to the broad nature of these peaks in the presence of intense resonances of phthalocyanine ring and the biphenyl group [31]. ^1H NMR spectrum of **4** showed the aromatic protons at 8.01–7.31 ppm and COOH protons at 12.78 ppm. In the IR spectrum of **6** indicated the presence of alkyl groups by the intense stretching bands at 2927–2870 cm^{-1}. Chemical shifts due to the alkyl protons of **6** were observed between 4.33 and 0.93 ppm as expected.

A close investigation of the mass spectra of the phthalocyanines confirmed the proposed structure. In the mass spectrum of **3** in addition to the $[M^+]$ peak at 1363.4 a fragment ion corresponding to the loss of COOH–H $[M^+ - 46]$ is easily identified.

The phthalocyanines show typical electronic spectra with two absorption regions, the Q band around 600–700 nm and the B band in the near UV region around 300–350 nm, both correlate to π–π* transitions [32–34]. The split form of Q band in **3**, which is characteristic for metal-free phthalocyanines, is observed at λ_{max} 700 and 668 nm. The presence of absorption band in **3** in the near UV region at λ_{max} 340 nm also show B band. The Q band absorption of metallophthalocyanines is observed as a single band of high intensity in the visible region. The metallophthalocyanines **4** and **5** showed the expected absorptions of the Q and B bands appearing at 679, 664 nm and 347, 343 nm, respectively.

Acknowledgements

This work was supported by the Research Fund of the Technical University of Istanbul and State Planning Organization (DPT).

References

[1] C.C. Leznoff, A.B.P. Lever (Eds.), Phthalocyanines Properties and Applications, vols. 1–4, VCH, Weinheim, 1989–1996.
[2] N.B. McKeown, Phthalocyanine Materials, Cambridge University Press, Cambridge, 1998.
[3] A. Ogunsipe, J.Y. Chen, T. Nyokong, New J. Chem. 28 (2004) 822.
[4] P. Zimcik, M. Miletin, J. Ponec, M. Kostka, Z. Fiedler, J. Photochem. Photobiol. A: Chem. 155 (2003) 127.
[5] S. Kudrevich, N. Brasseur, C. LaMadeleine, S. Gilbert, J.E. van Lier, J. Med. Chem. 40 (1997) 3897.
[6] H. Ali, J.E. van Lier, Chem. Rev. 99 (1999) 2379.
[7] W. Liu, T.J. Jensen, F.R. Fronczek, R.P. Hammer, K.M. Smith, M.G.H. Vicente, J. Med. Chem. 48 (2005) 1033.
[8] S. Vagin, M. Hanack, Eur. J. Org. Chem. (2003) 2661.
[9] Y. Gök, H. Kantekin, I. Degirmencioglu, Supramol. Chem. 15 (2003) 335.
[10] M. Kandaz, S.L.J. Michel, B.M. Hoffmann, J. Porphyr. Phthalocya. 7 (2003) 700.
[11] J.A. Duro, G. dela Torre, J. Barbera, J.L. Serrano, T. Torres, Chem. Mater. 8 (1996) 1061.
[12] E. Gonca, Y. Koseoglu, B. Aktas, A. Gul, Polyhedron 23 (2004) 1845.
[13] A. Kalkan, Z.A. Bayır, Monatsh. Chem. 134 (2003) 1555.
[14] M. Clarkson, G.J. Clarkson, M. Helliwell, A.M. Holder, N.B. McKeown, Chem. Eur. J. 6 (2000) 4630.
[15] E. Hamuryudan, Z.A. Bayır, Ö. Bekaroğlu, Dyes Pigments 43 (1999) 77.
[16] W. Liu, C.H. Lee, H.S. Chan, T.C.W. Mak, D.K.P. Ng, Eur. J. Inorg. Chem. (2004) 286.
[17] Z.A. Bayır, E. Hamuryudan, A.G. Gurek, Ö. Bekaroğlu, J. Porphyr. Phthalocya. 1 (1997) 349.
[18] A.W. Snow, N.L. Jarvis, J. Am. Chem. Soc. 106 (1984) 4706.
[19] M.J. Cook, J. Mater. Chem. 6 (1996) 677.
[20] A.R. Özkaya, E. Hamuryudan, Z.A. Bayır, Ö. Bekaroğlu, J. Porphyr. Phthalocya. 4 (2000) 689.
[21] J.C. Swarts, E.H.G. Langner, N. Kroeide-Hove, M.J. Cook, J. Mater. Chem. 11 (2001) 434.
[22] Z.A. Bayır, S. Merey, E. Hamuryudan, Monatsh. Chem. 134 (2003) 1027.
[23] E. Hamuryudan, S. Merey, Z.A. Bayir, Dyes Pigments 59 (2003) 263.
[24] A. Kalkan, A. Koca, Z.A. Bayir, Polyhedron 23 (2004) 3155.
[25] Z.A. Bayir, Dyes Pigments 65 (2005) 235.
[26] D.D. Perrin, W.L.F. Armarego, Purification of Laboratory Chemicals, second ed., Pergamon, Oxford, 1980.
[27] J.G. Young, W. Onyebuagu, J. Org. Chem. 55 (1990) 2155.
[28] M.D.K. Nazeeruddin, R.H. Baker, M. Gratzel, D. Wöhrle, G. Schnurpheil, G. Schneider, A. Hirth, N. Trombach, J. Porphyr. Phthalocya. 3 (1999) 230.
[29] T.M. Keller, T.R. Price, J.R. Griffith, Synthesis (1980) 613.
[30] I. Gurol, V. Ahsen, J. Porphyr. Phthalocya. 4 (2000) 621.
[31] P. Matlaba, T. Nyokong, Polyhedron 21 (2002) 2463.
[32] Z.A. Bayır, E. Hamuryudan, Ö. Bekaroğlu, J. Chem. Res. (S) (1999) 702.
[33] S. Gursoy, Z.A. Bayır, E. Hamuryudan, Ö. Bekaroğlu, Monatsh. Chem. 131 (2000) 287.
[34] M. Kocak, A. Cihan, A.I. Okur, A. Gul, Ö. Bekaroğlu, Dyes Pigments 45 (2000) 9.

Available online at www.sciencedirect.com
SCIENCE DIRECT®
Polyhedron 25 (2006) 43–51
POLYHEDRON
www.elsevier.com/locate/poly

The coordination behaviour of two structural isomeric ligands towards cadmium (II): Synthesis, spectroscopic characterization and crystal structures

F.J. Barros-García, F. Luna-Giles *, M.A. Maldonado-Rogado, E. Viñuelas-Zahínos

Departamento de Química Inorgánica, Facultad de Ciencias, Universidad de Extremadura, 06071 Badajoz, Spain

Received 6 June 2005; accepted 30 June 2005
Available online 19 August 2005

Abstract

Two new structural isomeric ligands, 2-(indazol-1-yl)-2-thiazoline (TnInA) (**1**) and 2-(indazol-2-yl)-2-thiazoline (TnInL) (**2**), have been prepared and characterized by a variety of physico-chemical techniques. Likewise, the cadmium (II) complexes $[Cd(NO_3)_2(TnInA)_2]$ (**3**) and $[Cd(NO_3)_2(TnInL)_2]$ (**4**) have been isolated and characterized through elemental analysis, IR and UV–Vis spectroscopy. Moreover, the structures have been determined by X-ray diffraction. Both ligands act as bidentate ligands through thiazoline nitrogen atom and indazole nitrogen atom, making a five-membered chelate ring. The environment around the cadmium (II) atom in both complexes may be described as a triangulated dodecahedral geometry.
© 2005 Elsevier Ltd. All rights reserved.

Keywords: Cadmium (II) complex; Crystal structures; Thiazoline; Indazole

1. Introduction

The indazole subunit is a frequently found motif in drug substances with important biological activities such as anti-inflammatory, anti-tumor and anti-HIV activities [1–3]. Moreover, several indazoles are found to exhibit significant levels of activity as serototonin 5-$HT_{1\alpha}$, 5-HT_2 and 5-HT_3 receptor antagonists and aldol reductase inhibitors [4–7]. On the other hand, some thiazoline derivatives are of interest due to their potential activity as antibiotic and antitumoral agents [8–10].

Interestingly, coordination makes bioactive ligands improve their bioactivity profiles, while inactive ligands may acquire pharmacological properties [11–13]. Thus, there is a ruthenium complex with indazole as ligand which has inhibitory activity against colon carcinomas and other tumor types [14]. In addition, metal coordination is one of the most efficient strategies in the design of repository, slow release or long-acting drugs [15].

Because of the importance of these heterocycles in pharmaceutical development, we are initiating a line of investigation on the coordination chemistry of compounds containing thiazoline and indazole rings. In this paper, we report the synthesis of two structural isomeric ligands 2-(indazol-1-yl)-2-thiazoline (TnInA) and 2-(indazol-2-yl)-2-thiazoline (TnInL). The characterization of these ligands has been carried out by means of ultraviolet and visible spectroscopy (UV–Vis), proton nuclear magnetic resonance (^{1}H NMR), carbon nuclear magnetic resonance (^{13}C NMR), single crystal X-ray diffraction, elemental analysis and infrared spectroscopy (IR). Likewise, two cadmium complexes were obtained through reaction of cadmium (II) nitrate with these ligands and their characterization has been carried out by means of ultraviolet and visible spectroscopy (UV–Vis), elemental analysis, single crystal X-ray diffraction and infrared spectroscopy (IR).

* Corresponding author. Tel.: +34924289397; fax: +34924289395.
E-mail address: pacoluna@unex.es (F. Luna-Giles).

0277-5387/$ - see front matter © 2005 Elsevier Ltd. All rights reserved.
doi:10.1016/j.poly.2005.06.058

2. Experimental

2.1. Preparation of 2-(indazol-1-yl)-2-thiazoline (TnInA) (1) and 2-(indazol-1-yl)-2-thiazoline (TnInL) (2)

TnInA (**1**) and TnInL (**2**) were prepared according to modifications of the procedure reported by Haugwitz et al. [16]. To a solution of 6.02 g (50 mmol) of indazole in dry glyme (500 mL) was added 4 g sodium hydride (100 mmol; 60%) and the mixture was stirred at room temperature for 6 h. Then a solution of 13.36 g of 3-chloroethylisothiocyanate [17] (110 mmol) in dry glyme (10 mL) was added and the reaction mixture was refluxed for 24 h and cooled. After the addition of methanol (5 mL), the solvent was removed in vacuo. Water was added to the residue and the resulting oily solid was extracted once with 25 mL of chloroform. The organic layer was dried over anhydrous magnesium sulfate and concentrated under reduced pressure to give an oil. This oil was flash chromatographed using 1:1 v/v ether/ether petroleum as eluent. The early fraction contained **1** and the last fraction contained **2**. Colourless crystals of **1** were obtained after a slow evaporation of the ethanol solution at room temperature (3.63 g, 25%). ^{1}H NMR ($CDCl_3$): δ 8.43 (d, $J = 8.14$ Hz, 1H), 8.12 (s, 1H), 7.71 (d, $J = 7.99$ Hz, 1H), 7.52 (t, $J = 7.49$ Hz, 1H), 7.29 (t, $J = 7.57$ Hz, 1H), 4.45 (t, $J = 8.07$ Hz, 2H), 3.45 (t, $J = 8.08$ Hz, 2H); ^{13}C NMR ($CDCl_3$): δ 158.84, 138.87, 137.99, 128.68, 125.89, 123.55, 120.87, 114.29, 62.02, 33.26. *Anal.* Calc. for $C_{10}H_9N_3S$: C, 59.09; H, 4.46; N, 20.67; S, 15.77. Found: C, 59.45; H, 4.83; N, 20.22; S, 15.43%. UV–Vis (EtOH): λ_{max}, nm; (ε, L mol^{-1} cm^{-1}) 232 (26 000), 295 (9248), 306 (9585). Colourless crystals of **2** were obtained after a slow evaporation of the acetone solution at room temperature (2.54 g, 25%). ^{1}H NMR ($CDCl_3$): δ 8.73 (s, 1H), 7.71 (d, $J = 8{,}84$ Hz, 1H), 7.64 (d, $J = 8.76$ Hz, 1H), 7.31 (t, $J = 6.52$ Hz, 1H), 7.10 (t, $J = 6.75$ Hz, 1H), 4.45 (t, $J = 4.12$ Hz, 2H), 3.59 (t, $J = 4.12$ Hz, 2H); ^{13}C NMR ($CDCl_3$): δ 159.99, 150.13, 128.14, 123.59, 122.16, 121.54, 120.86, 118.31, 61.50, 34.27. *Anal.* Calc. for $C_{10}H_9N_3S$: C, 59.09; H, 4.46; N, 20.67; S, 15.77. Found: C, 58.86; H, 4.69; N, 20.53; S, 15.53%. UV–Vis (EtOH): λ_{max}, nm; (ε, L mol^{-1} cm^{-1}) 225 (26 728), 293 (12 193), 300 (12 246).

2.2. Preparation of [Cd(NO$_3$)$_2$(TnInA)$_2$] (3)

This complex was prepared by reacting an ethanol solution (1 mL) of $Cd(NO_3)_2 \cdot 4H_2O$ (151.8 mg, 0.5 mmol) with an ethanol solution (15 mL) of TnInA (100 mg, 0.5 mmol). By means of slow evaporation of the solution at room temperature, colourless crystals were isolated (127.4 mg, 40.3%). The crystals were filtered and washed with cold ether and air-dried. *Anal.* Calc. for $C_{20}H_{18}CdN_8S_2O_6$: C, 37.36; H, 2.82; N, 17.43; S, 9.97. Found: C, 37.20; H, 2.97; N, 17.20; S, 10.21%. UV–Vis (EtOH): λ_{max}, nm; (ε, L mol^{-1} cm^{-1}) 232 (53 794), 295 (18 192), 306 (18 744).

2.3. Preparation of [Cd(NO$_3$)$_2$(TnInL)$_2$] (4)

This complex was prepared by reacting an ethanol solution (10 mL) of $Cd(NO_3)_2 \cdot 4H_2O$ (151.8 mg, 0.5 mmol) with an ethanol solution (15 mL) of TnInL (100 mg, 0.5 mmol), giving colourless crystals after a slow evaporation of the solution at room temperature (153.7 mg, 48.6%). The crystals were filtered and washed with cold ether and air-dried. *Anal.* Calc. for $C_{20}H_{18}CdN_8S_2O_6$: C, 37.36; H, 2.82; N, 17.43; S, 9.97. Found: C, 37.16; H, 2.74; N, 17.18; S, 9.85%. UV–Vis (EtOH): λ_{max}, nm; (ε, L mol^{-1} cm^{-1}) 224 (81 795), 292 (34 093), 301 (34 231).

2.4. Instrumental procedures

Chemical analyses of carbon, hydrogen, nitrogen and sulphur were performed by microanalytical methods using a Leco CHNS-932 microanalyser. IR spectra were recorded on a Perkin–Elmer FT-IR 1720 spectrophotometer, from KBr pellets in the 4000–370 cm^{-1} range and on a Perkin–Elmer FT-IR 1700X spectrophotometer, from polyethylene pellets in the 500–150 cm^{-1} range. Electronic spectra in solution were measured on a Shimadzu UV-3101 PC using a 10-mm quartz cell. ^{1}H and ^{13}C NMR spectra were obtained with a Bruker AM 400 instrument at 400 and 100 MHz, respectively, in $CDCl_3$ using Me_4Si as internal standard.

2.5. Crystal structure determinations

Experimental details of crystal structure determinations including crystal data, data collection, structure determinations and refinement parameters for **1**–**4** are listed in Table 1. X-ray diffraction measurements were performed at room temperature (298 K) using a Bruker SMART CCD diffractometer equipped with graphite-monochromated Mo Kα radiation ($\lambda = 0.71073$ Å) using the ϕ–ω scan technique. The first 50 frames were recollected at the end of data collection to monitor for decay. Empirical absorption corrections were applied using the program SADABS [18]. The structures of **1**, **2** and **4** were solved by direct methods and subsequent Fourier differences, whereas the structure of **3** was solved by Patterson methods and subsequent Fourier differences using, in all cases, the WINGX package [19] and refined by full-matrix least-squares on F^2. All non-hydrogen atoms were refined with anisotropic displacement parameters. Hydrogen atoms attached to carbon and nitrogen atoms were positioned geometrically, with U_{iso} values derived from U_{eq} values of the corresponding

Table 1
Crystal data, data collection and refinement details for TnInA (**1**), TnInL (**2**), $[Cd(NO_3)_2(TnInA)_2]$ (**3**) and $[Cd(NO_3)_2(TnInL)_2]$ (**4**)

	1	**2**	**3**	**4**
Crystal shape	prism	prism	prism	prism
Colour	colourless	colourless	colourless	colourless
Size (mm)	$0.56 \times 0.45 \times 0.45$	$0.77 \times 0.39 \times 0.36$	$0.31 \times 0.23 \times 0.20$	$0.43 \times 0.19 \times 0.12$
Chemical formula	$C_{10}H_9N_3S$	$C_{10}H_9N_3S$	$C_{20}H_{18}CdN_8O_6S_2$	$C_{20}H_{18}CdN_8O_6S_2$
Formula weight	203.3	203.3	643.0	643.0
Crystal system	monoclinic	trigonal	triclinic	monoclinic
Space group	$P21/n$	$R\bar{3}$	$P\bar{1}$	$C2/c$
Unit cell dimensions				
a (Å)	6.621(1)	29.928(1)	9.484(8)	23.220(6)
b (Å)	11.056(1)	29.928(1)	12.771(10)	7.293(2)
c (Å)	13.305(1)	5.639(1)	13.950(11)	16.402(4)
α (°)			101.079(13)	
β (°)	91.036(10)		107.856(13)	123.221(3)
γ (°)			111.459(12)	
Cell volume (Å^3)	973.8(1)	4373.9(3)	1405.6(19)	2323.7(10)
Z	4	18	2	4
D_{calc} (g cm^{-3})	1.386	1.389	1.519	1.838
μ (mm^{-1})	0.292	0.293	0.973	1.117
$F(000)$	424	1908	644	1288
2θ Range	4.8–56.7	2.7–56.5	3.3–53.5	4.2–52.8
Index ranges	$-8 \leqslant h \leqslant 8$, $-12 \leqslant k \leqslant 14$, $-17 \leqslant l \leqslant 14$	$-39 \leqslant h \leqslant 36$, $-38 \leqslant k \leqslant 33$, $-7 \leqslant l \leqslant 7$	$-12 \leqslant h \leqslant 11$, $-16 \leqslant k \leqslant 15$, $-17 \leqslant l \leqslant 17$	$-28 \leqslant h \leqslant 28$, $-8 \leqslant k \leqslant 9$, $-20 \leqslant l \leqslant 20$
Independent reflections	2201	2267	5926	2374
Observed reflections	1897 [$F > 4.0\sigma(F)$]	2062 [$F > 4.0\sigma(F)$]	4719 [$F > 4.0\sigma(F)$]	2120 [$F > 4.0\sigma(F)$]
Maximum/minimum transmission	0.880/0.854	0.902/0.806	0.829/0.753	0.872/0.632
Number of refined parameters	127	127	334	168
$R[F > 4.0\sigma(F)]$[a]	0.046	0.048	0.031	0.025
$wR[F > 4.0\sigma(F)]$[b]	0.127	0.158	0.072	0.062
Goodness-of-fit[c]	1.055	1.108	1.077	1.141
ρ_{max}, ρ_{min} (e Å^{-3})	0.217, −0.192	1.299, −0.187	0.391, −0.338	0.392, −0.719

[a] $R = \sum ||F_o| - |F_c|| / \sum |F_o|$.
[b] $R = \{\sum[w(F_o^2 - F_c^2)^2] / \sum[w(F_o^2)^2]\}^{1/2}$.
[c] The goodness-of-fit (GOF) equals $\{\sum[w(F_o^2 - F_c^2)^2] / (N_{rflns} - N_{params})\}^{1/2}$.

carbon and nitrogen atoms. The final electron density map for compound **3** contained various electron density peaks, clustered in one region of the unit cell. These could not sensibly be resolved into a molecule and presumably represent a severely disordered solvent molecule. Despite exhaustive attempts at modelling this severely disordered solvent molecule, satisfactory solutions were not obtained and a diffuse solvent correction was applied using the SQUEEZE routine in PLATON [20]. The unit cell contains a symmetry-unique cavity centered at (1, 1/10, 1/2), filled with disordered solvent, probably ethanol. The volume of cavity is 254.8 Å^3 with a total of 82 electrons calculated, compared to 78 electrons predicted for the presence three ethanol molecules.

3. Results and discussion

3.1. Crystal structures of the ligands

ORTEP diagrams of the molecular structure of **1** and **2** are shown in Figs. 1 and 2, respectively. Bond lengths and angles are listed in Table 2.

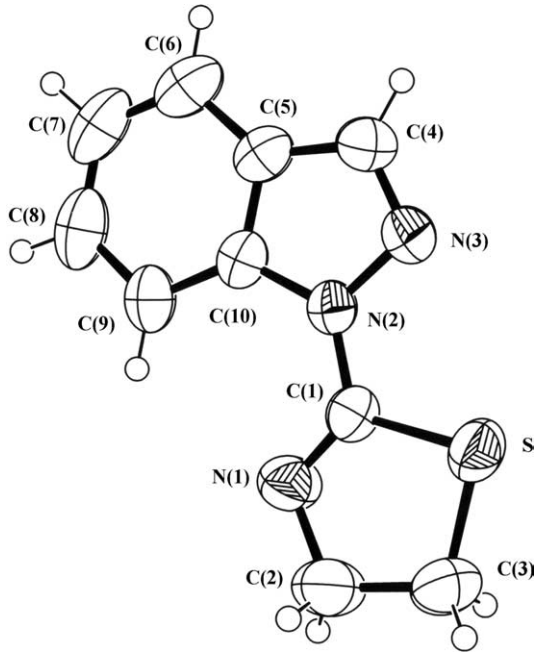

Fig. 1. Crystal structure of **1**, showing the atom-numbering scheme. The thermal ellipsoids are plotted at the 50% probability level.

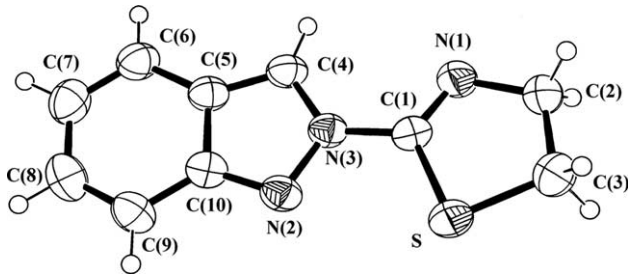

Fig. 2. Crystal structure of **2**, showing the atom-numbering scheme used for better comparison with **1**. The thermal ellipsoids are plotted at the 50% probability level.

Table 2
Selected bond lengths (Å) and angles (°) for TnInA (**1**) and TnInL (**2**)

	TnInA (**1**)	TnInL (**2**)
S–C(1)	1.764(2)	1.752(2)
S–C(3)	1.802(2)	1.810(2)
C(1)–N(1)	1.256(2)	1.252(2)
N(1)–C(2)	1.450(3)	1.463(3)
N(2)–N(3)	1.377(2)	1.362(2)
N(2)–C(10)	1.390(2)	1.343(3)
N(3)–C(4)	1.303(2)	1.356(2)
N(2)–C(1)	1.383(2)	
N(3)–C(1)		1.408(2)
C(1)–S–C(3)	88.2(1)	88.8(1)
C(1)–N(1)–C(2)	110.5(2)	111.0(2)
N(1)–C(1)–S	119.9(1)	121.4(2)
N(1)–C(1)–N(2)	123.1(2)	
N(1)–C(1)–N(3)		121.9(2)
N(2)–C(1)–S	117.0(1)	
N(3)–C(1)–S		116.6(1)
N(3)–N(2)–C(1)	119.0(1)	
N(2)–N(3)–C(1)		118.5(2)
N(3)–N(2)–C(10)	111.4(1)	102.9(2)
N(3)–C(4)–C(5)	112.4(2)	105.6(2)

In the S–C(1)–N(1)–C(2)–C(3) rings of the ligands, the short endocyclic C=N bonds [C(1)–N(1) = 1.256(2) Å for **1**; 1.252(2) Å for **2**] are accompanied by high N–C–S angles [N(1)–C(1)–S = 119.9(1)° for **1**; 121.4(2)° for **2**] and relatively long S^{II}–C(sp^2) bonds [S–C(1) = 1.764(2) Å for **1**; 1.752(2) Å for **2**], which are characteristic of a thiazoline ring [21]. Likewise, bond lengths and angles in indazole rings are in good accord with literature [22].

The thiazoline ring in **1** shows a conformation near to envelope with the C(3) atom deviating 0.309 Å above the plane formed by S, C(1), N(1) and C(2). This geometry is proved by the puckering parameters $q = 0.203$ Å and $\phi = 138.5°$, calculated according to Cremer and Pople [23]. However, the thiazoline ring in **2** is essentially planar [$q = 0.019$ Å, $\phi = 68.6°$].

As was to be expected, the indazole rings in both compounds are essentially planar with maximum least square plane deviations for C(9) [0.009 Å] in **1** and C(6) [0.007 Å] in **2**. Likewise, the planarity of indazole systems is shown by the dihedral angles between the mean planes of the six- and five-membered rings, being 0.4° in **1** and 0.6° in **2** (maximum least square plane deviation of N(2), N(3), C(4), C(5), C(10) for C(10) = 0.005 Å in **1** and C(10) = 0.003 Å in **2**).

3.2. Crystal structures of the cadmium complexes

The structure of the complex **3** consists of discrete neutral monomeric units in which the metal is eight-coordinate, being bound to four oxygen atoms from two bidentate nitrate ligands, two thiazoline nitrogen atoms and two indazole nitrogen atoms. A diagram of the molecular structure and the atom numbering system used is shown in Fig. 3. The most relevant bond lengths and angles are given in Table 3.

Eight-coordinate systems are found to adopt either a cube, a square antiprism or a triangulated dodecahedron (TD) arrangement [24]. On the basis of the observed angles, complex **3** adopts a slightly distorted TD geometry with N(3) as the lone capping atom whereas O(4) and O(5) are the shared capping atoms (see Fig. 4). Likewise, the two interpenetrating trapezoids, which characterize [25] the dodecahedron, are defined by the positions of the atoms O(1), O(2), N(6), N(4) and O(4), O(5), N(3), N(1). The angle between the mean planes of these trapezoidal planes is 89.1°, very close to the ideal one (90°). As indicated by Drew [26], the values of δ angles (δ_1, δ_2, δ_3 and δ_4), are too a good test for the determination of the shape of the coordination polyhedron. The δ angles calculated by using the hard sphere model (HSM) shape characteristics, are $\delta_1 = 29.5$, $\delta_2 = 29.5$, $\delta_3 = 29.5$ and $\delta_4 = 29.5$ for the ideal dodecahedron and $\delta_1 = 0.0$, $\delta_2 = 0.0$, $\delta_3 = 52.4$ and $\delta_4 = 52.4$ for the ideal squared antiprism. In this case, the δ values (Table 4) indicate that the coordination polyhedron is best described as a distorted TD geometry.

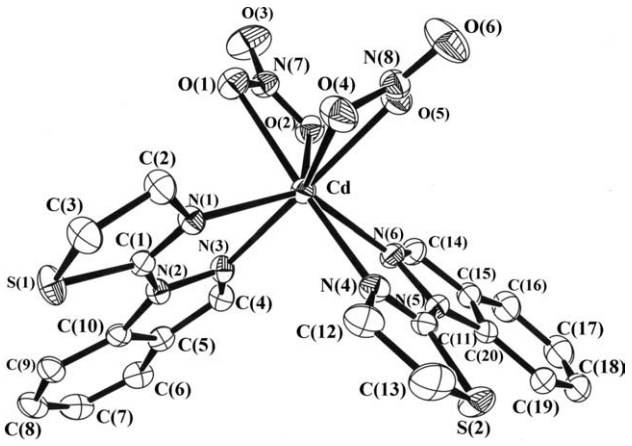

Fig. 3. Molecular structure of **3**, showing the atom-numbering scheme. The thermal ellipsoids are drawn at the 30% probability level.

Table 3
Selected bond lengths (Å) and angles (°) for $[Cd(NO_3)_2(TnInA)_2]$ (**3**) and $[Cd(NO_3)_2(TnInL)_2]$ (**4**)[a]

(**3**)				(**4**)[a]	
Cd–O(1)	2.479(3)	Cd–O(4)	2.684(3)	Cd–O(1)	2.528(2)
Cd–O(2)	2.504(2)	Cd–O(5)	2.332(3)	Cd–O(2)	2.436(2)
Cd–N(1)	2.325(2)	Cd–N(4)	2.394(3)	Cd–N(1)	2.318(2)
Cd–N(3)	2.416(3)	Cd–N(6)	2.441(3)	Cd–N(2)	2.554(2)
N(1)–C(1)	1.262(3)	N(4)–C(11)	1.249(4)	N(1)–C(1)	1.265(3)
N(2)–N(3)	1.379(3)	N(5)–N(6)	1.373(3)	N(2)–N(3)	1.369(3)
N(2)–C(10)	1.391(3)	N(5)–C(20)	1.391(3)	N(2)–C(10)	1.343(3)
N(3)–C(4)	1.297(3)	N(6)–C(14)	1.303(3)	N(3)–C(4)	1.355(3)
N(1)–Cd–N(3)	68.6(1)	N(4)–Cd–N(6)	66.5(1)	N(1)–Cd–N(2)	67.7(1)
N(1)–Cd–N(6)	137.8(1)	N(3)–Cd–N(4)	99.1(1)	N(1)–Cd–N(2A)	83.4(1)
N(1)–Cd–O(1)	85.9(1)	N(4)–Cd–O(4)	77.5(1)	N(1)–Cd–O(1)	82.9(1)
N(1)–Cd–O(4)	79.9(1)	N(4)–Cd–O(1)	168.3(1)	N(1)–Cd–O(1A)	145.2(1)
N(1)–Cd–O(2)	127.5(1)	N(4)–Cd–O(5)	91.5(1)	N(1)–Cd–O(2)	132.4(1)
N(1)–Cd–O(5)	127.4(1)	N(4)–Cd–O(2)	138.7(1)	N(1)–Cd–O(2A)	107.6(1)
N(3)–Cd–O(1)	89.3(1)	N(6)–Cd–O(4)	124.0(1)	N(2)–Cd–O(1)	129.4(1)
N(3)–Cd–O(4)	148.3(1)	N(6)–Cd–O(1)	123.3(1)	N(2)–Cd–O(1A)	79.5(1)
N(3)–Cd–O(2)	81.8(1)	N(6)–Cd–O(5)	89.2(1)	N(2)–Cd–O(2)	149.7(1)
N(3)–Cd–O(5)	161.1(1)	N(6)–Cd–O(2)	73.0(1)	N(2)–Cd–O(2A)	76.8(1)
O(1)–Cd–O(2)	50.4(1)	O(4)–Cd–O(5)	49.4(1)	O(1)–Cd–O(2)	51.4(1)
O(1)–Cd–O(5)	82.7(1)	O(4)–Cd–O(2)	121.7(1)	O(1)–Cd–O(2A)	74.2(1)
C(4)–N(3)–N(2)	106.7(2)	C(14)–N(6)–N(5)	106.0(2)	C(4)–N(3)–N(2)	113.4(2)
C(10)–N(2)–N(3)	110.4(2)	C(20)–N(5)–N(6)	110.4(2)	C(10)–N(2)–N(3)	103.5(2)
N(1)–Cd–N(4)	89.6(1)			N(1)–Cd–N(1A)	104.0(1)
N(3)–Cd–N(6)	80.9(1)			N(2)–Cd–N(2A)	132.7(1)
O(1)–Cd–O(4)	91.1(1)			O(1)–Cd–O(1A)	111.1(1)
O(2)–Cd–O(5)	79.9(1)			O(2)–Cd–O(2A)	75.2(1)

[a] This complex presents a C_2 symmetry, therefore only half angles and distances are shown.

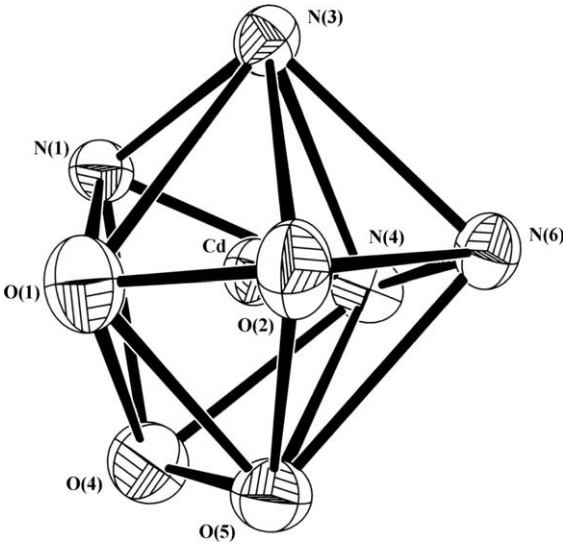

Fig. 4. View of the dodecahedral coordination polyhedron for **3**.

Table 4
Quantification of the geometry of the cadmium (II) polyhedra

	Triangulated dodecahedral	Square antiprism	**3**	**4**
δ_1	29.5	0.0	31.27	15.53
δ_2	29.5	0.0	21.71	19.89
δ_3	29.5	52.4	36.59	28.73
δ_4	29.5	52.4	35.83	15.53

One nitrate group may be considered as a symmetric one, while the other nitrate group presents a high asymmetry [{Cd–O(4)}–{Cd–O(5)} = δ = 0.352 Å], which is similar to those found in $[Cd(NO_3)_2L_2]$ (L = 1,6,7-trimethyllumazine) (δ = 0.395 Å) [27] and $[Cd(NO_3)_2L]$ (L = 1,4,7-tris(cyanomethyl)-1,4,7-triaza-10,13-dioxacyclopentadecane) (δ = 0.365 Å) [28].

The Cd–O distances for symmetric bidentate nitrate group (av. 2.492 Å) and asymmetric bidentate nitrate group (av. 2.508 Å) are comparable with the calculated mean value [2.482(144) Å] for 28 eight-coordinate cadmium (II) complexes obtained from CONQUEST software [29] from the Cambridge Structural Database (CSD) [30]. Finally, the Cd–$N_{thiazoline}$ bond lengths (av. 2.360 Å) are closer to that found in $[Cd(NO_3)_2(PyTT)(H_2O)]$ (2.351 Å) [31], but somewhat longer than that observed in $[CdCl_2\{(\mu\text{-}Cl)_2CdCl(\mu\text{-}Cl)(\mu\text{- PyTT})Cd\}_2]_n$ (2.271 Å) [31] and $[CdCl_2(HzTz)]\cdot H_2O$ (2.241 Å) [32].

The chelate rings Cd–N(1)–C(1)–N(2)–N(3) and Cd–N(4)–C(11)–N(5)–N(6) are essentially planar with maximum mean plane deviation for N(2) (0.024 Å) and N(6) (0.036 Å), respectively.

The thiazoline ring S(1)–C(1)–N(1)–C(2)–C(3) shows a conformation near to half-chair [q = 0.197 Å, ϕ = −45.2°] [23] with C(2) and C(3) deviating by −0.112 and 0.209 Å of the plane formed by S(1), C(1) and N(1). However, the other thiazoline ring S(2)–C(11)–N(4)–C(12)–C(13) shows a conformation near

to envelope [$q = 0.141$ Å, $\phi = -39.1°$] [23] with the apex at C(13). This atom is 0.222 Å out of the mean plane formed by S(2), C(11), N(4) and C(12).

The X-ray structure of **4** shows a eight-coordinated environment around cadmium (II) with four oxygen atoms from two bidentate nitrate ligands, two thiazoline nitrogen atoms and two indazole nitrogen atoms. The overall view and labelling of the atoms of complex are displayed in Fig. 5. Table 3 lists the selected bond lengths and angles.

The disposition of the eight donor atoms is adequately best described as a distorted triangulated dodecahedron (Fig. 6), with approximate C_2 symmetry, with the twofold axis placed at the bisector of the angle formed by the two four-membered chelate rings present in the molecule. In the dodecahedral geometry O(1) is the lone capping atom whereas N(1) and N(2) are the shared capping atoms (see Fig. 6). Likewise, the two interpenetrating trapezoids are defined by the positions

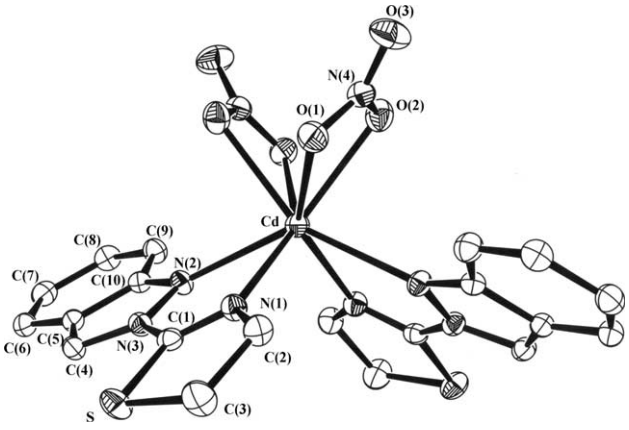

Fig. 5. Molecular structure of **4**, showing the atom-numbering scheme. The thermal ellipsoids are drawn at the 30% probability level.

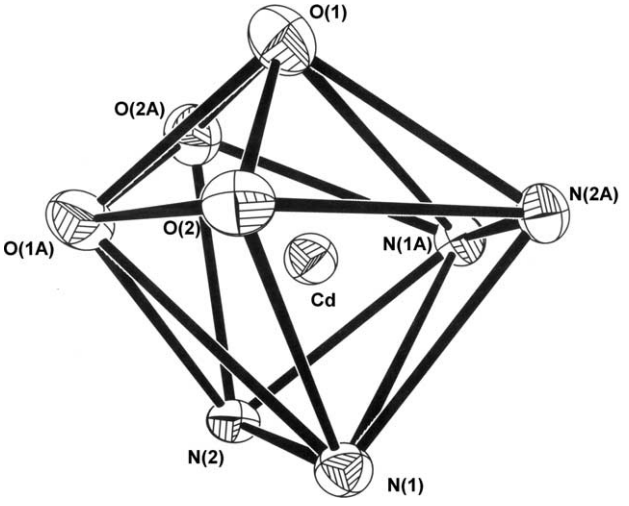

Fig. 6. View of the dodecahedral coordination polyhedron for **4**.

of the atoms O(1), O(2A), N(2), N(1) and O(1A), O(2), N(2A), N(1A). The angle between the mean planes of these trapezoidal planes is 79.9°, whereas the ideal one is 90°. The δ values for this complex (Table 4) indicates that the coordination polyhedron is best described as a distorted TD geometry.

The nitrate group show a slight but significant asymmetry [{Cd–O(2)}–{Cd–O(1)} = $\delta = 0.153$ Å], which is similar to those found in [$Cd(NO_3)_2(H_2O)_2$(μ-adeninium)$_2$] ($\delta = 0.155$ Å) [33] and [$Cd(NO_3)$L] (L = 1-aza-4,10-dithia-7-oxacyclododecane) ($\delta = 0.149$ Å) [34].

The Cd–O bond lengths are similar to those collected from the CSD used during discussion of complex **3**. The Cd–$N_{thiazoline}$ and the Cd–$N_{indazole}$ bond distances are similar, and slightly longer, respectively, than those observed in **3**.

The chelate ring Cd–N(1)–C(1)–N(3)–N(2) shows a conformation near to envelope [$q = 0.086$ Å, $\phi = -26.7°$] [23] with the apex at N(2), deviating 0.135 Å from the mean plane formed by Cd, N(1), C(1) and N(3).

For the thiazoline ring, the puckering parameters $q = 0.106$ Å, $\phi = -34.9°$ [23] indicate a conformation near to envelope with the C(3) atom deviating 0.173 Å above the mean plane formed by S, C(1), N(1) and C(2).

Finally, it should be pointed out that the main difference in both complexes with respect to the structure of free TnInA (**1**) and TnInL (**2**) is due to the different degree of rotation of the thiazoline ring around the C(1)–N(2) [or C(11)–N(5)] and C(1)–N(3) bond, respectively, which permits the coordination through N(1) (torsion angle N(1)–C(1)–N(2)–N(3) = −4.0° and [N(4)–C(11)–N(5)–N(6) = −4.4° in **3**; −176.9° in **1**; torsion angle N(1)–C(1)–N(3)–N(2) = 5.7° in **4**; 178.8° in **2**].

3.3. IR spectra

The IR spectra of **1** and **2** in the 4000–370 cm^{-1} region show the presence of bands due to thiazoline ring vibrations at 1632 (W_1), 921 (W_3), 752 (W_5), 671 (W_6), 586 (W_8), 553 (W_7), and 430 cm^{-1} (Γ_1) for **1**, and at 1641 (W_1), 985 (W_2), 919 (W_3), 785 (W_4), 757 (W_5), 676 (W_6), 586 (W_8), 555 (W_7) and 438 cm^{-1} (Γ_1) for **2** [35,36].

Likewise, the spectra of **1** and **2** exhibit bands assignable to the indazole ring vibrations at 1614, 1583, 1503, 1451, 1427, 1391, 1352, 1314, 1276 and 1250 cm^{-1} for stretching skeletal vibrations (ν); at 1004, 890, 768 and 624 cm^{-1} for bending skeletal in-plane vibrations (δ); and at 478 and 430 cm^{-1} for bending skeletal out-of-plane vibrations (τ), for compound **1**, and at 1637, 1652, 1517, 1455, 1441, 1387, 1376, 1361, 1338, 1270 and 1234 cm^{-1} for stretching skeletal vibrations (ν); at 1010, 945, 893, 640, 610 and 538 cm^{-1} for bending skeletal in-plane vibrations (δ); and at 573, 497 and

438 cm^{-1} for bending skeletal out-of-plane vibrations (τ), for compound **2** [37].

The IR spectra of **3** and **4** in the 4000–370 cm^{-1} region show the presence of bands due to the organic moiety ring vibrations as is shown in Table 5. On the other hand, bands due to nitrate ligands are registered at 689 and 709 (ν_4), 1386 and 1319 (ν_3), 818 (ν_2) and 1036 (ν_1) cm^{-1} for **3** and at 691 and 701 (ν_4), 1387 and 1321 (ν_3), 809 (ν_2) and 1057 (ν_1) cm^{-1} for **4** [38].

Methods to discriminate between bidentate and monodentate bonded nitrate groups have been reported and have been proved reliable. They are based on the ($\nu_1 + \nu_4$) combination bands pattern or on the splitting [39–42]. The bands registered at 1749 and 1718 cm^{-1} for **3** are assigned to ($\nu_1 + \nu_4$) combination bands. The value of the splitting ($\Delta = 31$ cm^{-1}) reveals the presence of a bidentate nitrate group in agreement with Lever's criteria [40]. In the same way, the bands observed at 1763 and 1736 cm^{-1} for (**4**) ($\Delta = 27$ cm^{-1}) can be assigned to one bidentate nitrate group.

In both complexes, the bands assigned to ν(C=N) vibration and the in-plane stretching vibrations corresponding to ν(C=N) skeletal vibrations of the heterocyclic rings (W_1), suffering a negative shift when compared with that for the uncoordinated respective ligand (Table 4). From all this can be deduced a coordination via these nitrogen atoms of the ligands [43–46].

Only three bands assignable to metal–ligand stretching vibrations are observed in the low frequency range for **3** and **4** spectra. Thus, in the **3** and **4** spectra, the bands at 227 and 232 cm^{-1}, respectively, are tentatively assigned to $\nu(Cd–N_{thiazoline})$ vibration in agreement with the values of complexes containing thiazoline derivative ligands [31,47]. The bands at 206 cm^{-1} for **3** and at 195 cm^{-1} for **4**, have been attributed to $\nu(Cd–ONO_2)$ vibration [31,38]. Finally, because of bibliography for cadmium–indazole unions has not been reported to the best of our knowledge, the bands at 176 cm^{-1}, in the case of **3** complex, and at 169 cm^{-1}, in the case of **4** complex, could be tentatively assigned to $\nu(Cd–N_{indazole})$, according to the consulted bibli-

Table 5
Infrared bands (cm^{-1}) assigned to ring vibrations of TnInA (**1**), TnInL (**2**), $[Cd(NO_3)_2(TnInA)_2]$ (**3**) and $[Cd(NO_3)_2(TnInL)_2]$ (**4**)

Assignment	(**1**)	(**2**)	(**3**)	(**4**)
Thiazoline				
W_1	1632 (vs)	1641 (vs)	1602 (s)	1636 (s)
W_2		985 (m)		986 (w)
W_3	921 (vs)	919 (s)	924 (w)	918 (m)
W_4		785 (m)	818 (m)	785 (w)
W_5	752 (s)	757 (s)	755 (m)	767 (m)
W_6	671 (m)	676 (m)	669 (w)	678 (w)
W_8	586 (m)	586 (w)	591 (m)	596 (w)
W_7	553 (m)	555 (w)	556 (w)	555 (w)
Γ_1	430 (m)	438 (m)	431 (w)	439 (m)
Indazole				
ν	1614 (s)	1637 (s)	1602 (s)	1625 (vs)
	1583 (m)	1562 (w)	1581 (s)	1560 (w)
	1503 (m)	1517 (m)	1509 (m)	1519 (m)
	1451 (s)	1455 (m)	1452 (s)	
	1427 (s)	1441 (w)	1437 (s)	1434 (sh)
	1391 (w)	1387 (s)	1386 (vs)	1387 (vs)
		1376 (s)		
	1352 (m)	1361 (s)	1354 (s)	1365 (sh)
	1314 (w)	1338 (m)	1319 (m)	1342 (m)
	1276 (m)	1270 (m)	1289 (s)	
	1250 (w)	1234 (m)		1242 (w)
δ	1004 (s)	1010 (s)	1016 (m)	1014 (m)
		945 (w)	954 (m)	
	890 (m)	893 (sh)	903 (m)	907 (w)
	768 (m)		777 (m)	
	624 (m)	640 (m)	624 (m)	634 (m)
		610 (m)		618 (m)
		538 (w)		540 (w)
τ		573 (m)		574 (w)
			520 (w)	
	478 (m)	497 (m)	486 (m)	506 (m)
	430 (m)	438 (m)	459 (w)	448 (m)

Abbreviations, (s) strong; (m) medium; (w) weak; (v) very.

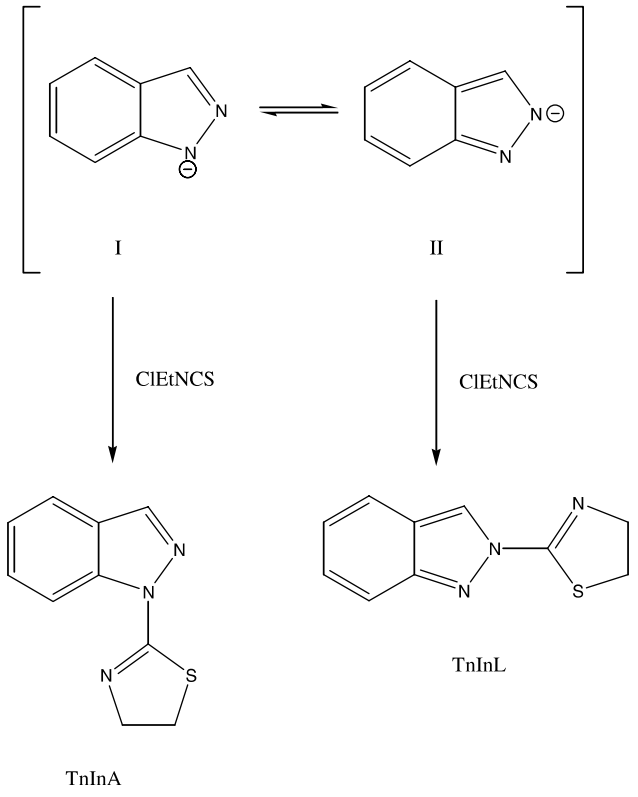

Scheme 1.

ographyforcadmiumcomplexescontainingpyrazolederivativeligands[48].

4. Conclusion

In summary, the reaction between indazole and 3-chloroethylisothiocyanate (ClEtNCS) produces two structural isomers: 2-(indazol-1-yl)-2-thiazoline (TnInA) and 2-(indazol-2-yl)-2-thiazoline (TnInL). This synthesis involves the generation of the anion I, in equilibrium with the resonant form II (Scheme 1). The reaction of the resonant forms I and II with 3-chloroethylisothiocyanate gives the isomers **1** and **2**. A comparison of cadmium (II) nitrate complexes containing TnInA and TnInL shows some similarities in the coordination behaviour of ligands. The structural studies reveals that both ligands act as bidentate. Likewise, cadmium complexes exhibits a triangulated dodecahedral geometry, however in case of complex **4** is a more distorted than in complex **3**. It can be due to packing effects on molecular geometry because of the different arrangement of heterocycles in ligands: angular in TnInA and linear in TnInL. Although this is notoriously difficult to estimate, a high percentage of molecules have imposed crystallographic symmetry where packing effects may well have tipped the balance towards one geometry rather than another.

Acknowledgements

We thank the Junta de Extremadura (Consejería de Educación, Ciencia y Tecnología) and the FEDER [Projects 2PR02A098 and 2PR04A011] for financial support. M.A. Maldonado-Rogado thanks the Spanish Ministerio de Ciencia y Tecnología and E. Viñuelas-Zahínos thanks the Junta de Extremadura (Consejería de Educación, Ciencia y Tecnología) and the FEDER for their Ph.D. fellowships.

Appendix A. Supplementary data

CCDC 274076, 274077, 274078 and 274079 corresponding to TnInA, TnInL, $[Cd(NO_3)_2(TnInA)_2]$ and $[Cd(NO_3)_2(TnInL)_2]$ contain the supplementary crystallographic data for this paper. These data can be obtained free of charge via www.ccdc.cam.ac.uk/conts/retrieving.html (or from the CCDC, 12 Union Road, Cambridge, CB2 1EZ, UK, fax: +44 1223 366 033, e-mail: deposit@ccdc.ac.uk or on the web www: http://www.ccdc.cam.ac.uk). Supplementary data associated with this article can be found, in the online version at doi:10.1016/j.poly.2005.06.058.

References

[1] S. Bräse, C. Gil, K. Knepper, Bioorg. Med. Chem. 10 (2002) 2415.
[2] G. Daidone, D. Raffa, B. Maggio, M.V. Raimondi, F. Plescia, D. Schillaci, Eur. J. Med. Chem. 39 (2004) 219.
[3] J.D. Rodgers, B.L. Johnson, H. Wang, R.A. Greenberg, S. Erickson-Viitanen, R.M. Klabe, B.C. Cordova, M.M. Rayner, G.N. Lam, C.-H. Chang, Bioorg. Med. Chem. Lett. 6 (1996) 2919.
[4] M.H. Norman, F. Navas III, J.B. Thompson, G.C. Rigdon, J. Med. Chem. 39 (1996) 4692.
[5] T. Yoshida, N. Matsuura, K. Yamamoto, M. Doi, K. Shimada, T. Morie, S. Kato, Heterocycles 43 (1996) 2701.
[6] D.W. Robertson, W. Bloomquist, M.L. Cohen, L.R. Reid, K. Schenck, D.T. Wong, J. Med. Chem. 33 (1990) 3176.
[7] B.L. Mylari, W.J. Zembrowski, T.A. Beyer, C.E. Aldinger, T.W. Siegel, J. Med. Chem. 35 (1992) 2155.
[8] C.G. Bonde, N.J. Gaikwad, Bioorg. Med. Chem. 12 (2004) 2151.
[9] S.H. Kim, H. Son, G. Nam, D.Y. Chi, J.H. Kim, Bioorg. Med. Chem. Lett. 10 (2000) 1143.
[10] L.M. Cañedo, J.A. de la Fuente, C. Gesto, M.J. Ferreiro, C. Jimenez, R. Riguera, Tetrahedron Lett. 40 (1999) 6841.
[11] R.A. Sánchez-Delgado, M. Navarro, H. Pérez, J.A. Urbina, J. Med. Chem. 39 (1996) 1095.
[12] M. Navarro, H. Pérez, R.A. Sánchez-Delgado, J. Med. Chem. 40 (1997) 1937.
[13] Z.H. Chohan, A. Rauf, J. Inorg. Biochem. 46 (1992) 41.
[14] A.P. Timerbaev, A.V. Rudnev, O. Semenova, C.G. Hartinger, B.K. Keppler, Anal. Biochem. 341 (2005) 326.
[15] N. Bharti, M.R. Maurya, F. Naqvi, A. Bhattacharya, S. Bhattacharya, A. Azam, Eur. J. Med. Chem. 35 (2000) 481.
[16] R.D. Haugwitz, V.L. Narayanan, US Patent 3, 1973, 759, 903
[17] R.J. Outcalt, J. Heterocycl. Chem. 24 (1987) 1425.
[18] Bruker AXS Inc., SADABS, version 2.03 Bruker AXS Inc., Madison, WI, 2001.
[19] L.J. Farrugia, J. Appl. Cryst. 32 (1999) 837.

[20] A.L. Spek, J. Appl. Cryst. 36 (2003) 7.
[21] C. Cohen-Addad, Acta Crystallogr. B 38 (1982) 1753.
[22] A. Escande, J. Lapasset, Acta Crystallogr. B 30 (1974) 2009.
[23] D. Cremer, J.A. Pople, J. Am. Chem. Soc. 97 (1975) 1354.
[24] J. Ribas Gispert, Quimica de Coordinacion, Omega, Barcelona, 2000.
[25] E.L. Muetterties, L.J. Guggenberger, J. Am. Chem. Soc. 96 (1974) 1748.
[26] M.G.B. Drew, Coordin. Chem. Rev. 24 (1977) 179.
[27] E.R. Acuña-Cueva, R. Faure, N.A. Illan-Cabeza, S.B. Jiménez-Pulido, M.N. Moreno-Carretero, M. Quirós-Olazabal, Inorg. Chim. Acta 342 (2003) 209.
[28] L. Tei, A.J. Blake, A. Bencini, B. Valtancoli, C. Wilson, M. Schroder, Inorg. Chim. Acta 337 (2002) 59.
[29] F.H. Allen, Acta Crystallogr. B 58 (2002) 380.
[30] I.J. Bruno, J.C. Cole, P.R. Edington, M. Kessler, C.F. Macrae, P. McCabe, J. Pearson, R. Taylor, Acta Crystallogr. B 58 (2002) 389.
[31] F.J. Barros García, A. Bernalte García, F.J. Higes Rolando, F. Luna Giles, R. Pedrero Marín, E. Viñuelas-Zahínos, Inorg. Chim. Acta 357 (2004) 1457.
[32] A. Bernalte-García, M.A. Díaz-Díez, F.J. García-Barros, F.J. Higes-Rolando, A.M. Pizarro-Galán, J.D. Martín-Ramos, C. Valenzuela-Calahorro, Polyhedron 16 (1997) 297.
[33] C.H. Wei, K.B. Jacobson, Inorg. Chem. 20 (1981) 356.
[34] C. Caltagirone, A. Bencini, F. Demartin, F.A. Devillanova, A. Garau, F. Isaia, V. Lippolis, P. Mariani, U. Papke, L. Tei, G. Verani, Dalton Trans. (2003) 901.
[35] G. Mille, J.L. Meyer, J. Chouteau, J. Mol. Struct. 50 (1978) 247.
[36] F.J. Barros-García, A. Bernalte-García, F.J. Higes-Rolando, F. Luna-Giles, M.A. Maldonado-Rogado, E. Viñuelas-Zahínos, Inorg. Chim. Acta 357 (2004) 3574.
[37] A. Bigotto, C. Zerbo, Spectrosc. Lett. 23 (1990) 65.
[38] J.R. Ferraro, Low-frequency Vibrations of Inorganic and Coordination Compounds, Plenum Press, New York, 1971.
[39] K. Nakamoto, Infrared and Raman Spectra of Inorganic and Coordination Compound, fifth ed., Wiley, New York, 1997.
[40] A.B.P. Lever, E. Mantovani, B.S. Ramaswamy, Can. J. Chem. 49 (1971) 1957.
[41] C.C. Addison, D. Suttom, Prog. Inorg. Chem. 8 (1967) 195.
[42] B.N. Gaterhouse, S.E. Livingstone, R.S. Nyholm, J. Chem. Soc. (1957) 4222.
[43] M. Shakir, S.P. Varkey, F. Firdaus, P.S. Hameed, Polyhedron 13 (1994) 2319.
[44] B. Singh, R.N. Singh, R.C. Aggarwal, Polyhedron 4 (1985) 401.
[45] M.M. Mostafa, M.A. Khattab, K.M. Ibrahim, Polyhedron 2 (1983) 583.
[46] J. Nelson, S. Martin Nelson, W.D. Perry, J. Chem. Soc., Dalton Trans. (1976) 1282.
[47] A. Bernalte-García, F.J. García-Barros, F.J. Higes-Rolando, A.M. Pizarro-Galán, C. Valenzuela-Calahorro, Thermochim. Acta 339 (1999) 95.
[48] J. Reedijk, Inorg. Chim. Acta 3 (1969) 517.

Available online at www.sciencedirect.com
SCIENCE DIRECT®
Polyhedron 25 (2006) 52–60
POLYHEDRON
www.elsevier.com/locate/poly

Synthesis, characterization and crystal structures of a bidentate indazole–thiazine derivative ligand and its cobalt (II) and cadmium (II) metal complexes

F.J. Barros-García, A. Bernalte-García *, F. Luna-Giles, M.A. Maldonado-Rogado, E. Viñuelas-Zahínos

Departamento de Química Inorgánica, Facultad de Ciencias, Universidad de Extremadura, Avda de Elvas sn, E06071 Badajoz, Spain

Received 23 May 2005; accepted 6 July 2005
Available online 11 August 2005

Abstract

A new ligand *N*-(5,6-dihydro-4H-1,3-thiazin-2-yl)indazole (InTz) and its metal complexes $[Co(NO_3)_2(InTz)_2]$ and $[Cd(NO_3)_2(InTz)_2]$ have been prepared and characterized by a variety of physico-chemical techniques. Likewise, the structures have been determined by X-ray diffraction. Metal complexes have C_2 symmetry. The environment around the cobalt atom may be described as a distorted octahedral geometry with the metallic atom coordinated to two oxygen atoms from two monodentate nitrate groups, two thiazine nitrogen atoms and two indazole nitrogen atoms. The cadmium complex consists of molecules in which the cadmium atom is eight coordinated, with two bidentate nitrate groups and two bidentate InTz ligands, each of the latter having one thiazine and one indazole nitrogen atom involved in coordination. The geometry around the cadmium atom is adequately described as a distorted dodecahedron.
© 2005 Elsevier Ltd. All rights reserved.

Keywords: Cobalt (II) complex; Cadmium (II) complex; Octahedral geometry; Dodecahedral geometry; Thiazine; Indazole

1. Introduction

Heterocycles containing nitrogen or sulphur atoms (or both) are common features incorporated in the structures of numerous natural products and pharmaceutical compounds. Besides, they form part of multidentate ligands extensively used in coordination chemistry with the aim of obtaining new frameworks having potential bioactivity [1]. Among these ligands are thiazine and indazol derivatives due to their biological importance as constituents of many biomolecules and drugs. Thiazines possess an N–C–S linkage that is believed to account for the anticonvulsant, fungicidal and antiviral activities [2,3]. Thus, some thiazine derivatives present antitumoral, antihistaminic, antiinflammatory, analgesic and antibiotic properties [4–9].

In the same way, indazole and its derivatives have gained considerable importance in recent year in view of their promising pharmacological properties [10]. Several indazoles are found to exhibit significant levels of activity as HIV protease inhibitors, serototonin $5\text{-}HT_{1\alpha}$, $5\text{-}HT_2$ and $5\text{-}HT_3$ receptor antagonists and aldol reductase inhibitors [11–16].

In some cases, the structural and biological properties of the organic ligands can be modified or even improved when coordinate to a metal ion [17].

Taking into account the aforementioned, recently we have been investigating the coordination chemistry of compounds containing these heterocycles [18–20]. As

* Corresponding author. Tel.: +34 924 289394; fax: +34 924 289395.
E-mail address: alberga@unex.es (A. Bernalte-García).

0277-5387/$ - see front matter © 2005 Elsevier Ltd. All rights reserved.
doi:10.1016/j.poly.2005.07.003

part of these investigations, we now report the synthesis and the characterization by elemental analysis, infrared spectra (IR), ultraviolet and visible spectra (UV–Vis), single crystal X-ray diffraction, proton nuclear magnetic resonance (^{1}H NMR) and carbon nuclear magnetic resonance (^{13}C NMR) of *N*-(5,6-dihydro-4H-1,3-thiazin-2-yl)indazole (InTz). The Cd(II) and Co(II) complexes have been isolated and their characterization has been carried out by means of elemental analysis, IR and X-ray diffraction. The cobalt complex has also been characterized through UV–Vis–NIR diffuse reflectance and magnetic susceptibility measurement.

2. Experimental

2.1. Preparation of N-(5,6-dihydro-4H-1,3-thiazin-2-yl)-indazole (InTz)

InTz was prepared according to a modifications of the procedure reported by Haugwitz and Narayanan [21]. To a solution of 1.20 g (10 mmol) of indazole in dry glyme (50 ml) was added 0.4 g sodium hydride (10 mmol; 60%) and the mixture was stirred at room temperature for 3 h. Then a solution of 1.49 g of 3-chloropropylisothiocyanate [22] (11 mmol) in dry glyme (3 ml) was added and the reaction mixture was refluxed for 4 h and cooled. After the addition of methanol (5 ml), the solvent was removed in vacuo. Water was added to the residue and the resulting oil solid was extracted with chloroform. The organic layer was dried over anhydrous magnesium sulfate and concentrated under reduced pressure to give an oil. This oil was flash chromatographed using 1:1 v/v ether/ether petroleum as eluent. Early fraction contained InTz. The resulting solution was allowed to evaporate slowly at room temperature and after a few days, colourless crystals were isolated from solution (1.00 g, 46%). ^{1}H NMR (CD_2Cl_2): δ 8.48 (d, $J = 8.52$ Hz, 1H), 8.06 (s, 1H), 7.68 (d, $J = 7.94$ Hz, 1H), 7.44 (t, $J = 7.37$ Hz, 1H), 7.23 (t, $J = 7.51$ Hz, 1H), 3.94 (t, $J = 5.62$ Hz, 2H), 3.15 (t, $J = 5.87$ Hz, 2H), 1.97 (m, 2H); ^{13}C NMR (CD_2Cl_2): δ 147.71, 138.20, 135.90, 128.10, 125.70, 122.90, 120.60, 114.94, 46.00, 26.70, 19.80. Found: C, 60.58; H, 5.09; N, 19.37; S, 14.45%. *Anal*. Calc. for $C_{11}H_{11}N_3S$: C, 60.81; H, 5.10; N, 19.33; S, 14.75%. UV–Vis (EtOH): λ_{max}, nm; (ε, L mol^{-1} cm^{-1}) 234 (22 100), 295 (8860), 306 (8118). FT-IR (cm^{-1}): 1632, 1610, 1578, 1497, 1373, 1350, 1314, 1288, 1250, 1005, 954, 907, 877, 768, 752, 624, 585, 552, 515, 467, 431, 405.

2.2. Preparation of $[Co(NO_3)_2(InTz)_2]$

This complex was prepared by reacting a methanol solution (1 mL) of $Co(NO_3)_2 \cdot 6H_2O$ (134 mg, 0.461 mmol) with a methanol solution (15 mL) of InTz (100 mg, 0.461 mmol). By means of liquid–vapor diffusion of ether over this solution, red crystals were isolated (123 mg, 43.3%). The crystals were filtered and washed with cold ether and air-dried. This complex is soluble in EtOH and MeOH, sparingly in acetonitrile and insoluble in H_2O, ether, acetone and $CHCl_3$. Found: C, 42.95; H, 3.89; N, 18.18; S, 10.04%. *Anal*. Calc. for $C_{22}H_{22}CoN_8S_2O_6$: C, 42.78; H, 3.59; N, 18.15; S, 10.39%. FT-IR (cm^{-1}): 1599, 1577, 1515, 1436, 1385, 1364, 1294, 1035, 1020, 958, 914, 900, 817, 782, 753, 729, 707, 629, 592, 558, 500, 491, 426, 298, 266, 227. $\mu_{eff} = 4.7$ BM. Diffuse reflectance spectrum (cm^{-1}): 9653, 11 211, 20 000, 32 895.

2.3. Preparation of $[Cd(NO_3)_2(InTz)_2]$

This complex was prepared by reacting an ethanol solution (1 mL) of $Cd(NO_3)_2 \cdot 4H_2O$ (142 mg, 0.461 mmol) with an ethanol solution (15 mL) of InTz (100 mg, 0.461 mmol), being obtained colourless crystals after a slow evaporation of the solution at room temperature (102 mg, 56.5%). The crystals were filtered and washed with cold ether and air-dried. This complex is soluble in EtOH and MeOH, sparingly in acetone and insoluble in H_2O, ether, acetonitrile and $CHCl_3$. Found: C, 39.32; H, 3.33; N, 16.50; S, 9.86%. *Anal*. Calc. for $C_{22}H_{22}CdN_8S_2O_6$: C, 39.38; H, 3.30; N, 16.70; S, 9.56%. FT-IR (cm^{-1}): 1607, 1577, 1514, 1434, 1385, 1363, 1299, 1034, 1017, 945, 911, 895, 820, 779, 753, 730, 707, 625, 587, 559, 499, 481, 423, 203, 193, 173.

2.4. Instrumental procedures

Chemical analyses of carbon, hydrogen, nitrogen and sulphur were performed by microanalytical methods using a Leco CHNS-932 microanalyser. IR spectra were recorded on a Perkin–Elmer FT-IR 1720 spectrophotometer, from KBr pellets in the 4000–370 cm^{-1} range and on a Perkin–Elmer FT-IR 1700X spectrophotometer, from polyethylene pellets in the 500–150 cm^{-1} range. Electronic spectra in solution of ligand were measured on a Shimadzu UV-3101 PC using a 10 mm quartz cell. The UV–Vis–NIR reflectance spectra for the cobalt complex in the 200–1600 nm range was registered from a pellet of the sample, using a Shimadzu UV-3101 PC spectrophotometer and $BaSO_4$ as a reference. Magnetic measurement was made at room temperature on a magnetometer with pendulum MANICS DSM8, equipped with helium continuous-flow cryostat and an electromagnetometer DRUSCH EAF 16 UE. Data were corrected for temperature-independent paramagnetism and diamagnetic contributions, which were estimated from the Pascal constants. ^{1}H and ^{13}C NMR spectra were obtained with a Bruker AM 400 instrument at 400 and 100 MHz, respectively, in CD_2Cl_2 using Me_4Si as internal standard.

2.5. Crystal structure determinations

Experimental details of crystal structure determinations including crystal data, data collection, structure determination and refinement parameters for InTz, $[Co(NO_3)_2(InTz)_2]$ and $[Cd(NO_3)_2(InTz)_2]$ are listed in Table 1. X-ray diffraction measurements were performed at room temperature (298 K) using a Bruker SMART CCD diffractometer equipped with graphite-monochromated Mo Kα radiation ($\lambda = 0.71073$ Å) using the ϕ–ω scan technique. The first fifty frames were recollected at the end of data collection to monitor for decay. Empirical absorption corrections were applied using program SADABS. The structures were solved by direct methods and subsequent Fourier differences using the WINGX package [23] and refined by full-matrix least-squares on F^2. All non-hydrogen atoms were refined with anisotropic displacement parameters, except C(3A) and C(14A) disordered atoms with isotropic displacement parameters. In the structure of InTz, the thiazine ring of both independent molecules show a disorder affecting C(3) and C(14) atoms, being the value of the refined occupancy 0.93(1) for C(3) and 0.07(1) for C(3A) in first independent molecule and 0.87(1) for C(14) and 0.13(1) for C(14A) in second one. Hydrogen atoms attached to carbon and nitrogen atoms were positioned geometrically, with U_{iso} values derived from U_{eq} values of the corresponding carbon and nitrogen atoms.

3. Results and discussion

3.1. Description of the structures

The single crystal X-ray diffraction analysis has revealed that InTz crystallizes in the triclinic system with two independent molecules in the asymmetric unit cell. The overall view and labelling of the atoms in two independent molecules are displayed in Fig. 1. Table 2 lists the selected bond lengths and angles.

In the S(1)–C(1)–N(1)–C(2)–C(3)–C(4) and S(2)–C(12)–N(4)–C(13)–C(14)–C(15) rings, the short endocyclic C=N bonds [C(1)–N(1) = 1.250(3) Å; C(12)–N(4) = 1.260(3) Å] are accompanied by high N–C–S

Table 1
Crystal data, data collection and refinement details for [InTz], $[Co(NO_3)_2(InTz)_2]$ and $[Cd(NO_3)_2(InTz)_2]$

	[InTz]	$[Co(NO_3)_2(InTz)_2]$	$[Cd(NO_3)_2(InTz)_2]$
Crystal shape	prism	prism	prism
Colour	colourless	red	colourless
Size (mm)	$0.44 \times 0.19 \times 0.10$	$0.37 \times 0.22 \times 0.12$	$0.37 \times 0.33 \times 0.30$
Chemical formula	$C_{11}H_{11}N_3S$	$C_{22}H_{22}CoN_8S_2O_6$	$C_{22}H_{22}CdN_8S_2O_6$
Formula weight	217.3	617.5	671.0
Crystal system	triclinic	orthorhombic	orthorhombic
Space group	$P\bar{1}$	*Pbcn*	*Pccn*
Unit cell dimensions			
a (Å)	6.456(1)	17.654(1)	22.760(1)
b (Å)	9.777(1)	8.787(1)	7.749(5)
c (Å)	16.952(2)	15.899(1)	14.77(9)
α (°)	93.614(3)		
β (°)	93.256(2)		
γ (°)	90.527(3)		
Cell volume (Å^3)	1066.1(3)	2466.3(3)	2606.4(3)
Z	4	4	4
D_{calc} (g cm^{-3})	1.354	1.663	1.710
μ (mm^{-1})	0.272	0.923	1.053
$F(000)$	456	1268	1352
2θ Range (°)	4.18–56.58	4.62–56.52	3.58–56.8
Index ranges	$-8 \leqslant h \leqslant 7$, $-13 \leqslant k \leqslant 10$, $-21 \leqslant l \leqslant 21$	$-23 \leqslant h \leqslant 17$, $-11 \leqslant k \leqslant 11$, $-20 \leqslant l \leqslant 19$	$-29 \leqslant h \leqslant 30$, $-10 \leqslant k \leqslant 10$, $-19 \leqslant l \leqslant 13$
Independent reflections	4794	2889	3091
Observed reflections [$F > 4.0\sigma(F)$]	3018	2426	2510
Maximum/minimum transmission	0.973/0.890	0.897/0.726	0.743/0.697
Number of refined parameters	289	177	177
$R[F > 4.0\sigma(F)]$[a]	0.047	0.046	0.040
$wR[F > 4.0\sigma(F)]$[b]	0.107	0.111	0.099
GOF[c]	1.025	1.078	1.068
ρ_{max}, ρ_{min} (e Å^{-3})	0.228/−0.253	0.503/−0.232	0.526/−0.298

[a] $R = \sum \| F_o | - | F_c \| / \sum | F_o |$.

[b] $R = \left\{ \sum [w(F_o^2 - F_c^2)^2] / \sum [w(F_o^2)^2] \right\}^{1/2}$.

[c] The goodness-of-fit (GOF) $= \left\{ \sum \left[w(F_o^2 - F_c^2)^2 \right] / (N_{rflns} - N_{params}) \right\}^{1/2}$.

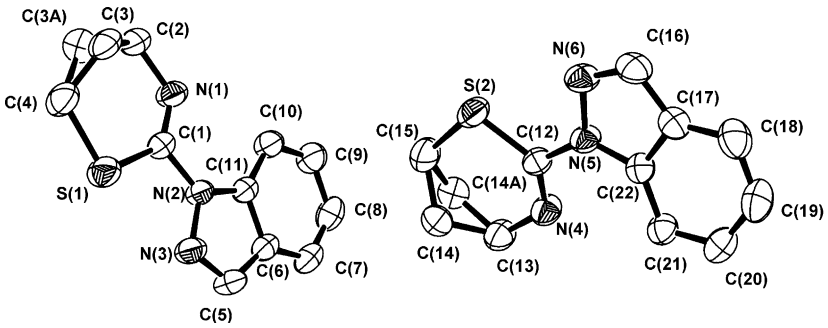

Fig. 1. The atom numbering scheme for two molecules on InTz constituting the asymmetric unit of the structure. The thermal ellipsoids are plotted at the 50% probability level.

angles [N(1)–C(1)–S(1) = 131.1(2)°; N(4)–C(12)–S(2) = 130.9(2)°] and relatively long S^{II}-C(sp^2) bonds [S(1)–C(1) = 1.753(2) Å; S(2)–C(12) = 1.757(2) Å], which are characteristic of a 5,6-dihydro-4-H-1,3-thiazine ring [24]. Likewise, bond lengths and angles in indazole rings are in good accord with the literature [25].

According to the X-ray results, the corresponding bond lengths in both independent molecules show small differences (±0.019 Å), except for bond lengths involving C(3A) and C(14A) atoms (±0.150 Å). In the same way, the corresponding bond angles are very similar (±1.4°), except for angles involving C(3A) and C(14A) atoms (±6.8°). These differences could be attributed to the disorder present in thiazine rings affecting C(3) and C(14) atoms. Finally, in first independent molecule, the thiazoline ring is in the same plane that indazole ring [torsion angle N(1)–C(1)–N(2)–N(3) = 179.7°], whereas, in second independent molecule, the thiazoline ring is slightly rotated with respect the indazole ring [torsion angle N(4)–C(12)–N(5)–N(6) = 167.2°].

In the first molecule of InTz, thiazine ring displays two conformations due to disorder. Both conformations show a half-boat form, with the C(3) and C(3A) atoms deviating −0.665 and 0.234 Å, respectively, from the plane formed by S(1), C(1), N(1), C(2) and C(4). These geometries are proved by the puckering parameters calculated according to Cremer and Pople [26], $Q = 0.492$ Å, $\phi = 66.9°$ and $\theta = 128.2°$ for S(1)–C(1)–N(1)–C(2)–C(3)–C(4) and $Q = 0.171$ Å, $\phi = 234.6°$ and $\theta = 53.2°$ for S(1)–C(1)–N(1)–C(2)–C(3A)–C(4). In the same way, the thiazine ring in second molecule of InTz presents two conformations near to half-boat form, with the C(14) and C(14A) atoms deviating 0.639 and −0.470 Å, respectively, from the plane formed by S(2), C(12), N(4), C(13) and C(15) [$Q = 0.453$ Å, $\phi = 232.8°$ and $\theta = 62.8°$ for S(2)–C(12)–N(4)–C(13)–C(14)–C(15) and $Q = 0.397$ Å, $\phi = 25.3°$ and $\theta = 122.8°$ for S(2)–C(12)–N(4)–C(13)–C(14A)–C(15)]. As was to be expected, the indazole rings are essentially planar with maximum least square plane deviations for C(8) [0.010 Å] and C(22) [0.026 Å].

The X-ray study of $[Co(NO_3)_2(InTz)_2]$ reveals that crystals are made up of orthorhombic cells, each one containing four complex molecules. A diagram of the molecular structure is shown in Fig. 2, and selected bond lengths and angles are given in Table 3.

The complex molecule possesses a crystallographic C_2 symmetry, with the twofold axis being coincident with the bisectrix of the O(1)–Co–O(1A) angle.

The environment around the cobalt (II) atom may be described as a distorted octahedral geometry with the metal coordinated to two oxygen atoms from two monodentate nitrate groups [Co–O(1) = 2.122(2) Å], two thiazine nitrogen atoms [Co–N(1) = 2.122(2) Å] and two indazole nitrogen atoms [Co–N(3) = 2.109(2) Å]. The ligand–metal–ligand bite angles differ from the ideal value of 90°, varying between 74.9(1)° and 101.2(1)°. This compound is the second structurally characterized compound having a 1,3-thiazine link to cobalt (II) [18], being, moreover, the first with an octahedral geometry.

The Co–O bond distance of monodentate nitrate group is comparable with the calculated average value [2.108(43) Å] for 46 six-coordinate cobalt (II) complexes obtained from CONQUEST software [27] from the Cambridge Structural Database (CSD) [28]. Likewise, the Co–$N_{indazole}$ bond length is similar to those found in bis(hydrotris(indazol-1-yl)borato)-cobalt (II) chloroform solvate (1/3.5) (average 2.116 Å) [29]. The Co–$N_{thiazine}$ bond distance is longer to this found in $[CoCl_2(TdTz)]$ (1.946 Å) [18].

The chelate ring Co–N(3)–N(2)–C(1)–N(1) shows a intermediate form between envelope and half-chair [$q = 0.213$ Å; $\phi = 12.4°$] [26] with the atoms Co and N(3) deviating by −0.293 and 0.128 Å, respectively, above the plane formed by N(2), C(1) and N(1).

The thiazine ring shows a conformation near to half-boat with the C(3) atom deviating 0.671 Å above the plane formed by S(1), C(1), N(1), C(2) and C(4). This geometry is proved by the puckering parameters $Q = 0.499$ Å, $\phi = 63.2°$ and $\theta = 121.9°$ [26].

The structure of the cadmium (II) complex consists of discrete neutral monomeric units in which the geometry

Table 2
Selected bond lengths (Å) and angles (°) for InTz

S(1)–C(1)	1.753(2)
S(1)–C(4)	1.809(2)
C(1)–N(1)	1.250(3)
N(1)–C(2)	1.466(3)
N(2)–N(3)	1.372(2)
N(2)–C(1)	1.423(2)
N(2)–C(11)	1.382(3)
N(3)–C(5)	1.310(3)
C(4)–C(3)	1.500(4)
C(4)–C(3A)	1.48(4)
C(2)–C(3)	1.495(4)
C(2)–C(3A)	1.35(4)
S(2)–C(12)	1.757(2)
S(2)–C(15)	1.809(3)
C(12)–N(4)	1.260(3)
N(4)–C(13)	1.447(3)
N(5)–N(6)	1.378(2)
N(5)–C(12)	1.417(3)
N(5)–C(22)	1.383(3)
N(6)–C(16)	1.299(3)
C(15)–C(14)	1.494(4)
C(15)–C(14A)	1.38(2)
C(13)–C(14)	1.487(4)
C(13)–C(14A)	1.50(2)
C(1)–S(1)–C(4)	99.4(1)
C(1)–N(1)–C(2)	120.9(2)
N(1)–C(1)–S(1)	131.1(2)
N(1)–C(2)–C(3)	114.9(2)
N(1)–C(1)–N(2)	117.2(2)
N(2)–C(1)–S(1)	111.7(1)
N(2)–C(11)–C(10)	132.6(2)
N(2)–C(11)–C(6)	105.7(2)
N(3)–N(2)–C(1)	119.6(2)
N(3)–N(2)–C(11)	111.6(2)
N(3)–C(5)–C(6)	112.7(2)
C(2)–C(3)–C(4)	111.8(3)
C(2)–C(3A)–C(4)	122(3)
C(3)–C(4)–S(1)	112.6(2)
C(3A)–C(4)–S(1)	119.0(2)
C(3A)–C(2)–N(1)	123.0(2)
C(5)–N(3)–N(2)	105.4(2)
C(12)–S(2)–C(15)	99.3(1)
C(12)–N(4)–C(13)	120.9(2)
N(4)–C(12)–S(2)	130.9(2)
N(4)–C(13)–C(14)	116.1(2)
N(4)–C(12)–N(5)	117.9(2)
N(5)–C(12)–S(2)	111.2(1)
N(5)–C(22)–C(21)	131.8(2)
N(5)–C(22)–C(17)	106.0(2)
N(6)–N(5)–C(12)	118.9(2)
N(6)–N(5)–C(22)	111.0(2)
N(6)–C(16)–C(17)	112.2(2)
C(13)–C(14)–C(15)	112.9(3)
C(15)–C(14A)–C(13)	119.4(2)
C(14)–C(15)–S(2)	113.6(2)
C(14A)–C(15)–S(2)	116.3(9)
N(4)–C(13)–C(14A)	116.2(8)
C(16)–N(6)–N(5)	106.1(2)

of the metal is eight coordinate, being bound to four oxygen atoms from two bidentate nitrate ligands [Cd–O(1) = 2.432(4) Å; Cd–O(2) = 2.585(3) Å], two thiazine nitrogen atom [Cd–N(1) = 2.385(3) Å] and two indazole nitrogen atom [Cd–N(3) = 2.332(2) Å]. To the best of our knowledge, this compound is the first structurally characterized compound having a 1,3-thiazine link to cadmium (II) and is, likewise, the first with indazole nitrogen bound to cadmium (II). A diagram of the molecular structure and the atom numbering system used is shown in Fig. 3. The most relevant bond lengths and angles are given in Table 4.

The disposition of the eight donor atoms is adequately best described as a distorted dodecahedron (Fig. 4), with approximate C_2 symmetry, with the two-fold axis placed at the bisector of the angle formed by the two four-membered chelate rings present in the molecule. In the dodecahedral geometry N(1) is the lone capping atom whereas O(1) and O(2) are the shared capping atoms (see Fig. 4). Likewise, the two interpenetrating trapezoids, which characterize [30] the dodecahedron, are defined by the positions of the atoms O(1), O(2), N(3), N(1) and O(1A), O(2A), N(3A), N(1A). The angle between the mean planes of these trapezoidal planes is 84.4°, very close to the ideal one (90°).

The Cd–O distances of bidentate nitrate groups are comparable with the calculated average value [2.476 (136) Å] for 26 eight-coordinate cadmium (II) complexes collected in CSD.

The nitrate group show a small asymmetry [{Cd–O(2)}–{Cd–O(1)} = δ = 0.153 Å], which is similar to those found in [$Cd(NO_3)_2(H_2O)_2$(μ-adeninium)$_2$] (δ = 0.155 Å) [31] and [$Cd(NO_3)$L] (L = 1-Aza-4,10-dithia-7-oxacyclododecane) (δ = 0.149 Å) [32].

The chelate ring Cd–N(3)–N(2)–C(1)–N(1) shows a conformation near to envelope [q = 0.200 Å; ϕ = 40.5°] [26] with the apex at Cd, deviating 0.415 Å from the plane formed by N(3), N(2), C(1) and N(1).

For the thiazine ring, the puckering parameters Q = 0.459 Å, ϕ = 234.0° and θ = 58.2° [26] indicate a conformation near to half-boat with the C(3) atom deviating by 0.614 Å above the plane formed by S(1), C(1), N(1), C(2) and C(4).

Finally, it should be pointed out that the aim difference in both complexes with respect to the structure of free InTz is due to the different degree of rotation of the thiazine ring around the C(1)–N(2) bond, which permit the coordination through N(1) [torsion angle N(1)–C(1)–N(2)–N(3) = −5.9° in [$Co(NO_3)_2$(InTz)$_2$]; 1.6° in [$Cd(NO_3)_2$(InTz)$_2$]; average value 173.5° in InTz].

3.2. Physical measurements

The observed molar magnetic susceptibility for [$Co(NO_3)_2$(InTz)$_2$] was corrected for diamagnetism and temperature-independent paramagnetism to provide the fully corrected magnetic moment at room temperature (μ_{eff} = 4.7 BM). This value is consistent with an octahedral environment around cobalt (II) [33].

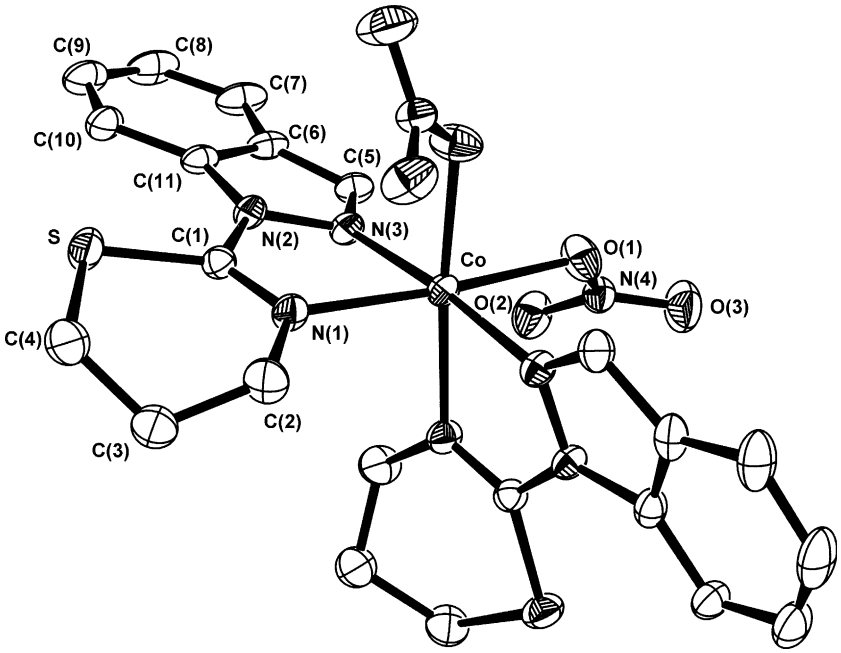

Fig. 2. Molecular structure of $[Co(NO_3)_2(InTz)_2]$, showing the atom-numbering scheme. The thermal ellipsoids are drawn at the 40% probability level.

Table 3
Selected bond lengths (Å) and angles (°) for $[Co(NO_3)_2(InTz)_2]$

Co–O(1)	2.122(2)
Co–N(3)	2.109(2)
C(1)–N(2)	1.403(3)
Co–N(1)	2.122(2)
N(1)–C(1)	1.272(3)
N(2)–N(3)	1.386(3)
N(1)–Co–N(1A)	89.3(1)
N(3)–Co–N(1A)	101.2(1)
N(3)–Co–O(1A)	85.5(1)
N(3)–Co–N(3A)	174.7(1)
O(1)–Co–N(1A)	93.2(1)
N(3)–Co–N(1)	74.9(1)
N(3)–Co–O(1)	98.4(1)
O(1)–Co–N(1)	173.2(1)
O(1)–Co–O(1A)	85.0(1)

The diffuse reflectance spectrum shows one intense band at 32 895 cm^{-1} (304 nm), which is assigned to transitions of the organic ligand. Moreover, the spectrum exhibits two main bands that have intensities consistent with spin-allowed d–d transitions. These bands may be assigned as: $\nu_1[^4T_{1g}(F) \rightarrow {}^4T_{2g}(F)]$ (10 361 cm^{-1}) and $\nu_3[^4T_{1g}(F) \rightarrow {}^4T_{1g}(P)]$ (20 000 cm^{-1}) transitions, in an idealized O_h symmetry. It must be pointed out that the ν_1 assignment has been made by calculating the baricenter of two bands (11 211, 9653 cm^{-1}) of approximately equal intensity in the solid-state spectrum [34]. The ligand field parameters, 10 Dq and B, were calculated using the following known relationships [35] for octahedral d^7 complexes:

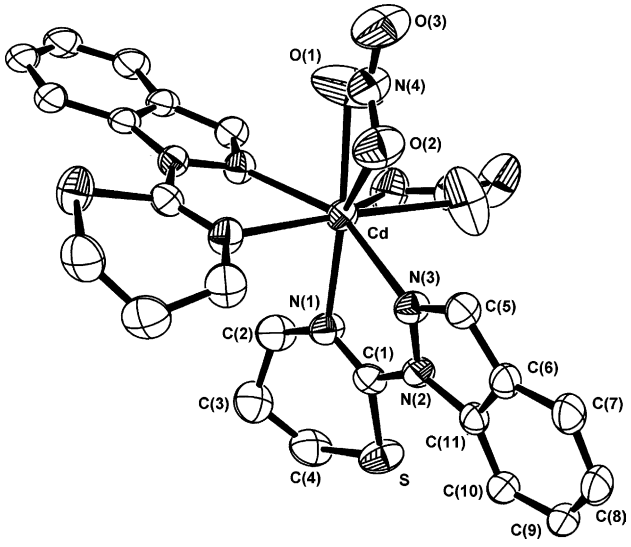

Fig. 3. Molecular structure of $[Cd(NO_3)_2(InTz)_2]$, showing the atom-numbering scheme. The thermal ellipsoids are drawn at the 40% probability level.

$$\nu_1[^4T_{1g}(F) \rightarrow {}^4T_{2g}(F)] = 1/2(10Dq - 15B) + 1/2[(10Dq + 15B)^2 - 12B \cdot 10Dq]^{1/2},$$

$$\nu_3[^4T_{1g}(F) \rightarrow {}^4T_{1g}(P)] = [(10Dq + 15B)^2 - 12B \cdot 10Dq]^{1/2}.$$

The calculated values of the ligand field parameters $10Dq = 12\,257\ cm^{-1}$ and $B = 769\ cm^{-1}$ are in fair agreement with the predicted values for octahedral complexes and are consistent with the presence of a cromophere group $[CoN_4O_2]$ [36–39].

Table 4
Selected bond lengths (Å) and angles (°) for $[Cd(NO_3)_2(InTz)_2]$

Cd–O(1)	2.432(4)
Cd–N(1)	2.385(3)
C(1)–N(2)	1.417(4)
N(2)–N(3)	1.382(3)
Cd–O(2)	2.585(3)
Cd–N(3)	2.332(2)
N(1)–C(1)	1.259(4)
N(1)–Cd–N(1A)	88.7(2)
N(1)–Cd–O(1A)	93.2(1)
N(1)–Cd–O(2A)	79.8(1)
N(3)–Cd–N(1A)	94.1(1)
N(3)–Cd–O(1)	122.4(1)
N(3)–Cd–O(2)	77.9(1)
O(1)–Cd–O(1A)	86.8(2)
O(1)–Cd–O(2A)	92.5(1)
N(1)–Cd–O(1)	169.3(1)
N(1)–Cd–O(2)	142.9(1)
N(3)–Cd–N(1)	67.9(1)
N(3)–Cd–N(3A)	155.3(1)
N(3)–Cd–O(1A)	77.0(1)
N(3)–Cd–O(2A)	113.4(1)
O(1)–Cd–O(2)	47.7(1)
O(2)–Cd–O(2A)	128.5(2)

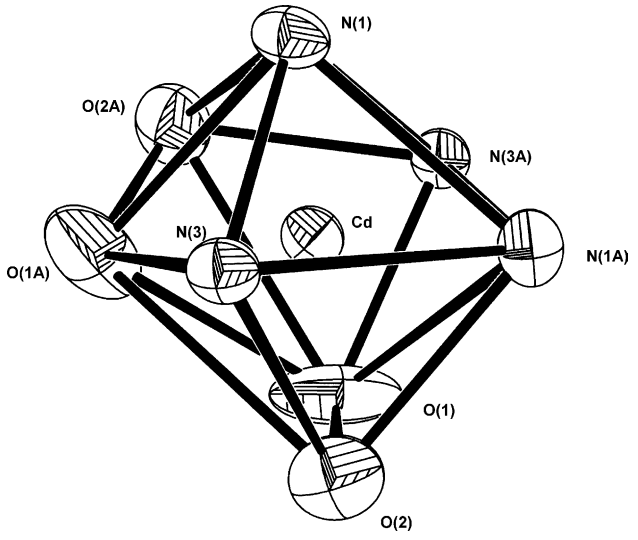

Fig. 4. View of the dodecahedral coordination polyhedron for $[Cd(NO_3)_2(InTz)_2]$.

The IR spectrum of InTz in the 4000–370 cm^{-1} region shows the presence of bands due to thiazine ring at 1632 (Ψ_1), 954 (Ψ_2), 907 (Ψ_3), 877 (Ψ_4), 768 (Ψ_5), 752 (Ψ_6), 624 (Ψ_7), 585 (Ψ_8), 515 (ϕ_1) and 467 (ϕ_2) cm^{-1} [18–20,40,41].

Likewise, the spectrum of InTz exhibits bands assignable to the indazole ring vibrations at 1610, 1578, 1497, 1373, 1350, 1314, 1288 and 1250 cm^{-1} for stretching skeletal vibrations (ν); at 1005, 954, 768 and 552 cm^{-1} for bending skeletal in-plane vibrations (δ); and at 431 and 405 cm^{-1} for bending skeletal out-of-plane vibrations (τ) [42].

The IR spectra of $[Co(NO_3)_2(InTz)_2]$ and $[Cd(NO_3)_2(InTz)_2]$ in the 4000–370 cm^{-1} region show the presence of bands due to the organic moiety ring vibrations as is shown in Table 5. On the other hand, bands due to nitrate ligands are registered at 729 and 707 (ν_4), 1436 and 1294 (ν_3), 817 (ν_2) and 1035 (ν_1) cm^{-1} for $[Co(NO_3)_2(InTz)_2]$ and at 730 and 707 (ν_4), 1435 and 1299 (ν_3), 820 (ν_2) and 1034 (ν_1) cm^{-1} for $[Cd(NO_3)_2(InTz)_2]$ [43].

Methods to discriminate between bidentate and monodentate bonded nitrate groups have been reported and have been proved reliable. They are based on the ($\nu_1 + \nu_4$) combination bands pattern or on the splitting [44–47]. The bands registered at 1748 and 1735 cm^{-1} for $[Co(NO_3)_2(InTz)_2]$ are assigned to ($\nu_1 + \nu_4$) combination bands. The value of the splitting ($\Delta = 13$ cm^{-1}) reveals the presence of one monodentate nitrate group in agreement with Lever's criteria [45]. In the same way, the bands observed at 1763 and 1737 cm^{-1} for $[Cd(NO_3)_2(InTz)_2]$ ($\Delta = 26$ cm^{-1}) can be assigned to one bidentate nitrate group.

Only three bands assignable to metal–ligand stretching vibrations are observed in the low frequency range for $[Co(NO_3)_2(InTz)_2]$ and $[Co(NO_3)_2(InTz)_2]$ spectra. Thus, the Co(II) spectrum shows the first band at 298 cm^{-1}, corresponding to ν(Co–ONO_2) vibration in

Table 5
Infrared bands (cm^{-1}) assigned to ring vibrations of InTz, $[Co(NO_3)_2(InTz)_2]$ and $[Cd(NO_3)_2(InTz)_2]$

Assignment	InTz	$[Co(NO_3)_2(InTz)_2]$	$[Cd(NO_3)_2(InTz)_2]$
Thiazine			
Ψ_1	1632 (vs)	1599 (vs)	1607 (vs)
Ψ_2	954 (s)	958 (m)	945 (m)
Ψ_3	907 (m)	914 (m)	911 (s)
Ψ_4	877 (m)	900 (m)	895 (m)
Ψ_5	768 (m)	782 (m)	779 (m)
Ψ_6	752 (m)	753 (s)	753 (s)
Ψ_7	624 (m)	629 (m)	625 (m)
Ψ_8	585 (w)	592 (m)	587 (m)
ϕ_1	515 (w)	500 (w)	499 (w)
ϕ_2	467 (w)	491 (w)	481 (w)
Indazole			
ν	1610 (m)	1599 (vs)	1607 (vs)
	1578 (w)	1577 (m)	1577 (m)
	1497 (m)	1515 (m)	1514 (m)
	1373 (s)	1385 (vs)	1385 (vs)
	1350 (s)	1364 (vs)	1363 (vs)
	1314 (w)		
	1288 (m)		
	1250 (w)		
δ	1005 (s)	1020 (m)	1017 (s)
	954 (s)	958 (m)	945 (m)
	768 (m)	782 (m)	779 (m)
	552 (w)	558 (w)	559 (w)
τ	431 (m)	426 (m)	423 (m)
	405 (w)		

Abbreviations. s, strong; m, medium; w, weak; v, very.

accord with the literature data for this type of bonds [39,48], whereas the band at 266 cm^{-1} is tentatively attributed to $\nu(Co–N_{indazole})$ vibration [49]. Finally, the band at 227 cm^{-1} is assigned to $\nu(Co–N_{thiazine})$ vibration [18]. In the Cd(II) spectrum, the band at 203 cm^{-1} is tentatively assigned to $\nu(Cd–N_{thiazine})$ vibration in agreement with the values of complexes containing thiazoline derivative ligands [50,51]. The second band at 193 cm^{-1} has been attributed to $\nu(Cd–ONO_2)$ vibration [43,50]. Finally, the band at 173 cm^{-1} could be tentatively assigned to $\nu(Cd–N_{indazole})$, according to the consulted bibliography for cadmium complexes containing pyrazole derivative ligands [52].

4. Supplementary material

CCDC 262540, 262541 and 262542 corresponding to InTz, $[Cd(NO_3)_2(InTz)_2]$ and $[Co(NO_3)_2(InTz)_2]$ contain the supplementary crystallographic data for this paper. These data can be obtained free of charge via www.ccdc.cam.ac.uk/conts/retrieving.html (or from the CCDC, 12 Union Road, Cambridge CB2 1EZ, UK; fax: +44 1223 336033; e-mail: deposit@ccdc.cam.ac.uk).

Acknowledgements

We would like to thank the Junta de Extremadura (Consejería de Educación, Ciencia y Tecnología) and the FEDER [Projects 2PR02A098 and 2PR04A011] for financial support. M.A. Maldonado-Rogado thanks the Spanish Ministerio de Ciencia y Tecnología and E. Viñuelas-Zahínos thanks the Junta de Extremadura (Consejería de Educación, Ciencia y Tecnología) and the FEDER for their Ph.D. fellowships.

References

[1] A.T. Chaviara, P.J. Cox, K.H. Repana, R.M. Papi, K.T. Papazisis, D. Zambouli, A.H. Kortsaris, D.A. Kyriakidis, C.A. Bolos, J. Inorg. Biochem. 98 (2004) 1271.
[2] H.D. Joshi, P.S. Upadhyay, A. Baxi, J. Indian J. Chem. 39B (2000) 967.
[3] H.A. Al-Khamees, S.M. Bayomi, H.A. Kandil, K.E.H. El-Tahir, Eur. J. Med. Chem. 25 (1990) 103.
[4] M. Koketsu, K. Tanaka, Y. Takenaka, C.D. Kwong, H. Ishihara, Eur. J. Pharm. Sci. 15 (2002) 307.
[5] B. Tozkoparan, G. Aktay, E. Yesilada, II Farmaco 57 (2002) 145.
[6] J.D. Bourzat, C. Cotrel, C. Guyon, Ph. Pitchen, US Patent 4994569, 1991.
[7] R.F. Schinazi, R.A. Floyd, PCT Int. Appl. WO 90 13,296 (Cl. A61K31/54), 1991.
[8] R.F. Schinazi, R.A. Floyd, Chem. Abstr. 115 (1991) 105989.
[9] J.F. Gonzales, P.A. Todd, Drugs 34 (1987) 298.
[10] S. Bräse, C. Gil, K. Knepper, Bioorgan. Med. Chem. 10 (2002) 2415.
[11] G. Daidone, D. Raffa, B. Maggio, M.V. Raimondi, F. Plescia, D. Schillaci, Eur. J. Med. Chem. 39 (2004) 219.
[12] J.D. Rodgers, B.L. Johnson, H. Wang, R.A. Greenberg, S. Erickson-Viitanen, R.M. Klabe, B.C. Cordova, M.M. Rayner, G.N. Lam, C.-H. Chang, Bioorg. Med. Chem. Lett. 6 (1996) 2919.
[13] M.H. Norman, F. Navas III, J.B. Thompson, G.C. Rigdon, J. Med. Chem. 39 (1996) 4692.
[14] T. Yoshida, N. Matsuura, K. Yamamoto, M. Doi, K. Shimada, T. Morie, S. Kato, Heterocycles 43 (1996) 2701.
[15] D.W. Robertson, W. Bloomquist, M.L. Cohen, L.R. Reid, K. Schenck, D.T. Wong, J. Med. Chem. 33 (1990) 3176.
[16] B.L. Mylari, W.J. Zembrowski, T.A. Beyer, C.E. Aldinger, T.W. Siegel, J. Med. Chem. 35 (1992) 2155.
[17] C.A. Bolos, K.T. Papazisis, A.H. Kortsaris, S. Voyatzi, D. Zambouli, D.A. Kyriakidis, J. Inorg. Biochem. 88 (2002) 25.
[18] F.J. Barros-García, A. Bernalte-García, A.M. Lozano-Vila, F. Luna-Giles, E. Viñuelas-Zahínos, Polyhedron 24 (2005) 129.
[19] A. Bernalte-García, F.J. García-Barros, F.J. Higes-Rolando, F. Luna-Giles, R. Pedrero-Marín, J. Inorg. Biochem. 98 (2004) 15.
[20] F.J. Barros-García, A. Bernalte-García, F.J. Higes-Rolando, F. Luna-Giles, R. Pedrero-Marín, Polyhedron 23 (2004) 1453.
[21] R.D. Haugwitz, V.L. Narayanan, US Patent 3 (1973) 759, 903.
[22] R.J. Outcalt, J. Heterocycl. Chem. 24 (1987) 1425.
[23] L.J. Farrugia, J. Appl. Cryst. 32 (1999) 837.
[24] G. Argay, A. Kalman, A. Kapor, B. Ribar, Acta Crystallogr. B36 (1980) 363.
[25] A. Escande, J. Lapasset, Acta Crystallogr. B30 (1974) 2009.
[26] D. Cremer, J.A. Pople, J. Am. Chem. Soc. 97 (1975) 1354.
[27] F.H. Allen, Acta Crystallogr. B58 (2002) 380.
[28] I.J. Bruno, J.C. Cole, P.R. Edington, M. Kessler, C.F. Macrae, P. McCabe, J. Pearson, R. Taylor, Acta Crystallogr. B58 (2002) 389.
[29] C. Janiak, S. Tenizdemir, S. Dechert, W. Deck, F. Girgsdies, J. Heinze, M.J. Kolm, T.G. Scharmann, O.M. Zipffel, Eur. J. Inorg. Chem. (2000) 1229.
[30] E.L. Muetterties, L.J. Guggenberger, J. Am. Chem. Soc. 96 (1974) 1748.
[31] C.H. Wei, K.B. Jacobson, Inorg. Chem. 20 (1981) 356.
[32] C. Caltagirone, A. Bencini, F. Demartin, F.A. Devillanova, A. Garau, F. Isaia, V. Lippolis, P. Mariani, U. Papke, L. Tei, G. Verani, Dalton Trans. (2003) 901.
[33] B.N. Figgis, J. Lewis, Prog. Inorg. Chem. 6 (1967) 185.
[34] F.A. Cotton, D.M.L. Goodgame, M. Goodgame, J. Am. Chem. Soc. 83 (1961) 4690.
[35] D.K. Rastogi, K.C. Sharma, S.K. Dua, M.P. Teotia, J. Inorg. Nucl. Chem. 37 (1975) 685.
[36] G. Alzuet, S. Ferrer, J. Borrás, A. Castiñeiras, X. Solans, M. Font-Bardía, Polyhedron 11 (1992) 2849.
[37] W.U. Malik, R. Bembi, R. Singh, Polyhedron 2 (1983) 369.
[38] J. Dillen, A.T.H. Lenstra, J.G. Haasnoot, J. Reedijk, Polyhedron 2 (1983) 195.
[39] A. Bernalte-García, F.J. García-Barros, F.J. Higes-Rolando, F. Luna-Giles, M.M. Pacheco-Rodriguez, E. Viñuelas-Zahínos, Bioinorg. Chem. Appl. 2 (2004) 307.
[40] A.I. Meyers, J. Org. Chem. 26 (1961) 218.
[41] A. Pastura, K. Thewalt, J. Prakt. Chem. 38 (1968) 177.
[42] A. Bigotto, C. Zerbo, Spectrosc. Lett. 23 (1990) 65.
[43] J.R. Ferraro, Low-Frequency Vibrations of Inorganic and Coordination Compounds, Plenum Press, New York, 1971.
[44] K. Nakamoto, Infrared and Raman Spectra of Inorganic and Coordination Compound, 5th ed., Wiley, New York, 1997.
[45] A.B.P. Lever, E. Mantovani, B.S. Ramaswamy, Can. J. Chem. 49 (1971) 1957.

[46] C.C. Addison, D. Sutton, Prog. Inorg. Chem. 8 (1967) 195.
[47] B.N. Gaterhouse, S.E. Livingstone, R.S. Nyholm, J. Chem. Soc. (1957) 4222.
[48] G. Kanagaraj, G.N. Rao, Polyhedron 12 (1993) 383.
[49] M. Hvastijová, R. Boča, J. Kohout, L. Jäger, I. Císařová, J. Kožíšek, Inorg. Chim. Acta 343 (2003) 217.
[50] F.J. Barros-García, A. Bernalte-García, F.J. Higes-Rolando, F. Luna-Giles, R. Pedrero-Marín, E. Viñuelas-Zahínos, Inorg. Chim. Acta 357 (2004) 1457.
[51] A. Bernalte-García, F.J. García-Barros, F.J. Higes-Rolando, A.M. Pizarro-Galán, C. Valenzuela-Calahorro, Thermochim. Acta 339 (1999) 95.
[52] J. Reedijk, Inorg. Chim. Acta 3 (1969) 517.

Available online at www.sciencedirect.com
SCIENCE DIRECT®
Polyhedron 25 (2006) 61–70
POLYHEDRON
www.elsevier.com/locate/poly

Structural, antimicrobial and spectral studies of copper(II) complexes of 2-benzoylpyridine *N*(4)-phenyl thiosemicarbazone

Marthakutty Joseph [a], Mini Kuriakose [a], M.R. Prathapachandra Kurup [a,*], E. Suresh [b], Archana Kishore [c], Sarita G. Bhat [c]

[a] *Department of Applied Chemistry, Cochin University of Science and Technology, Kochi 682022, Kerala, India*
[b] *Analytical Sciences Division, Central Salt and Marine Chemicals Research Institute, Bhavnagar, Gujarat 364 002, India*
[c] *Department of Biotechnology, Cochin University of Science and Technology, Kochi 682022, Kerala, India*

Received 9 May 2005; accepted 1 July 2005
Available online 15 August 2005

Abstract

Reaction of 2-benzoylpyridine *N*(4)-phenyl thiosemicarbazone (HL) with a variety of copper salts yielded a series of copper(II) complexes of the type [CuLX] where X = Cl (**1**), Br (**2**), NO_3 (**3**), NCS (**4**), N_3 (**5**) excluding the perchlorate complex. In the perchlorate complex (**6**), one molecule each of the neutral and deprotonated ligand is found to be coordinated to the metal. The complexes are characterized by molar conductivity measurements, magnetic studies, electronic, infrared and EPR spectral studies. The crystal structures of two copper complexes, **1** and **4** have been resolved using single crystal X-ray studies. The crystal structure of compound **1** revealed chlorine bridged dimer having monoclinic lattice with space group symmetry $P2_1/c$. The compound **4** adopts a distorted square planar geometry with N_3S core as the base. The antimicrobial activity of the ligand and the copper complexes were tested against five types of bacteria isolated from clinical samples. The ligand (HL) was found to be active against *Staphylococcus aureus*. The copper(II) complexes were found to be active against *Vibrio cholerae* O1 and *Salmonella paratyphi*.
© 2005 Elsevier Ltd. All rights reserved.

Keywords: Copper(II) complexes; 2-Benzoylpyridine; Thiosemicarbazone; EPR; Antimicrobial activity; Crystal structure

1. Introduction

Thiosemicarbazones and their metal complexes exhibit a wide range of medicinal applications. Owing to the interest they generate in pharmacology [1,2], thiosemicarbazones and their metal complexes have been extensively studied. The biological activity of thiosemicarbazones is related to its chelating ability with transition metal ions. Earlier studies on the biological properties of thiosemicarbazones and their metal complexes have concluded that the biologically active thiosemicarbazone molecules are planar and contain a pyridine ring or derivatives giving rise to NNS tridentate system [3]. In some cases, changing the point of attachment of the thiosemicarbazone chain from the 2-position in the pyridine ring to the 3- or 4-position causes a decrease in activity, presumably due to lower coordination ability but the presence of a bulky group at the terminal nitrogen considerably increases the activity. Earlier reports on *N*(4)-substituted thiosemicarbazones have concluded that, an additional potential bonding site together with the presence of bulky groups at the *N*(4) position of the thiosemicarbazone moiety greatly enhances biological activity [4–6]. Recently, we have reported diverse transition metal complexes of a variety of substituted thiosemicarbazones [7–13]. In the present work, our objective is to study the variation in

* Corresponding author. Tel.: +91 484 2575804; fax: +91 484 2577595.
E-mail addresses: mrp@cusat.ac.in, mrp_k@yahoo.com (M.R. Prathapachandra Kurup).

0277-5387/$ - see front matter © 2005 Elsevier Ltd. All rights reserved.
doi:10.1016/j.poly.2005.07.006

antimicrobial activity by changing the *N*(4) substituent from cyclohexyl [14] in 2-benzoylpyridine thiosemicarbazone to phenyl group. This paper describes the synthesis, UV–visible, infrared, EPR spectral studies and antimicrobial activities of Cu(II) complexes of 2-benzoylpyridine *N*(4)-phenyl thiosemicarbazone (HL).

2. Experimental

2.1. Materials

Phenyl isothiocyanate (Fluka), hydrazine hydrate (Lancaster), 2-benzoylpyridine (Lancaster), and the different Cu(II) salts were used as received. Solvents were purified by distillation.

2.2. Synthesis of ligand and complexes

The ligand 2-benzoylpyridine *N*(4)-phenyl thiosemicarbazone (HL) was prepared by adapting a reported method [15]. Phenyl isothiocyanate (6.759 g, 50 mmol) and hydrazine hydrate (2.4 ml, 50 mmol), each dissolved in 50 ml methanol were mixed with constant stirring. The stirring was continued for 30 min and the white product, *N*(4)-phenylthiosemicarbazide formed was washed with methanol and dried. A methanolic solution of 2-benzoylpyridine (9.16 g, 50 mmol) was added to a solution of *N*(4)-phenylthiosemicarbazide (8.35 g, 50 mmol) dissolved in 100 ml of methanol. The resulting solution was refluxed for 5 h after adding 2–3 drops of acetic acid. Yellow crystals separated on cooling were washed with methanol, recrystallised from ethanol and dried over P_4O_{10} in vacuo, m.p. 135 °C.

Complexes of copper(II) **1**, **2**, **3** and **6** were prepared by refluxing the respective methanolic solutions of the metal salts and the ligand HL in 1:1 molar ratio for 4–6 h. The resulting solution, on cooling yielded respective solids, which were filtered, washed with methanol and ether and dried over P_4O_{10} in vacuo. Compounds **4** and **5** were prepared by a metathetical displacement of the acetate anion of the copper acetate by the addition of 1 mmol each of the methanolic solutions of KSCN and NaN_3, respectively, to the reaction mixture of the ligand and copper acetate in methanol. The resulting solution was refluxed for 3 h and left overnight. The solids separated were filtered, washed with methanol and ether and dried over P_4O_{10} in vacuo. The colours, stoichiometries, elemental analyses, and magnetic moments of the copper(II) complexes are given in Table 1.

Caution! Azide and perchlorate salts of metal complexes with organic ligands are potentially explosive. So they should be prepared and handled carefully.

2.3. Physical measurements

Elemental analyses of the ligand and the complexes were done on a Heracus elemental analyzer at CDRI, Lucknow. The IR spectra were recorded on a Shimadzu DR 8001 series FTIR instrument using KBr pellets. The solid state reflectance spectra of the ligand and the complexes were recorded on Ocean Optics, Inc.SD2000 Fibre Optic Spectrometer. The EPR spectra of the complexes were recorded in a Varian E-112 Spectrometer using TCNE as the standard at SAIF, IIT, Bombay, India.

The magnetic susceptibility measurements were carried out at Indian Institute of Technology, Roorkee, at room temperature in the polycrystalline state on a PAR model 155 Vibrating sample magnetometer at 5 K Oersted field strength. The molar conductances of the complexes in dimethylformamide solutions (10^{-3}M) at room temperature were measured using a direct reading conductivity meter.

2.4. X-ray crystallography

Single crystals of compounds **1** and **4**, suitable for diffraction were grown by slow evaporation of 1:2 mixtures of methanol and DMF. Compound **1** crystallized with one molecule of water of crystallization. Selected crystal data and data collection parameters are presented in Table 2. Data were collected using a Bruker Smart Apex CCD diffractometer equipped with graphite monochromated Mo Kα ($\lambda = 0.71073$ Å) radiation at 273 K. The trial structure was solved using SHELXS-97 and refinement was carried out by full-matrix least squares on F^2 (SHELXTL) [16]. Molecular graphics employed was

Table 1
Colours and partial elemental analyses data of the complexes

Compound	Color	Found (Calc.)%			μ (B.M.)
		C	H	N	
$[CuLCl]\cdot CH_3OH$ **(1)**	Brown	51.45 (51.95)	4.01 (4.12)	12.16 (12.12)	1.54
$[CuLBr]\cdot 2H_2O$ **(2)**	Brown	44.79 (44.66)	3.42 (3.72)	10.60 (10.97)	1.67
$[CuLNO_3]\cdot H_2O$ **(3)**	Brown	48.61 (48.04)	3.31 (3.58)	14.87 (14.75)	1.84
$[CuLNCS]\cdot 2H_2O$ **(4)**	Brown	49.72 (49.12)	3.22 (3.88)	14.57 (14.32)	1.85
$[CuLN_3]$ **(5)**	Brown	51.23 (51.06)	3.44 (3.36)	22.41 (21.94)	1.47
$[Cu(HL)L](ClO_4)$ **(6)**	Brown	54.80 (55.20)	3.38 (3.75)	13.94 (13.55)	1.91

Table 2
Summary of crystal data and structure refinement for the compounds

Parameters	$[CuLCl]_2 \cdot H_2O$ **(1)**	[CuLNCS] **(2)**
Empirical formula	$C_{19}H_{17}ClCuN_4OS$	$C_{20}H_{15}CuN_5S_2$
Formula weight (M)	448.42	453.03
Temperature (T) (K)	273(2)	273(2)
Wavelength (Mo Kα) (Å)	0.71073	0.71073
Crystal system	monoclinic	monoclinic
Space group	$P2_1/c$	$P2_1/n$
Lattice constants		
a (Å)	14.842(2)	11.0066(10)
b (Å)	7.9517(12)	15.6762(14)
c (°)	16.313(3)	11.3128(11)
α (°)	90.00	90.00
β (°)	98.717(3)	94.623(2)
γ (°)	90.00	90.00
Volume (V) (Å^3)	1903.1(5)	1945.6(3)
Z	4	4
Calculated density (ρ) (Mg m^{-3})	1.565	1.547
Absorption coefficient (μ) (mm^{-1})	1.415	1.353
F(000)	916	924
Crystal size (mm)	$0.24 \times 0.12 \times 0.06$	$0.35 \times 0.26 \times 0.24$
Reflections collected	10802	11658
Unique reflections (R_{int})	4386 (0.0503)	4541 (0.0155)
Maximum and minimum transmission	0.919 and 0.816	none
Refinement method	full-matrix least-squares on F^2	full-matrix least-squares on F^2
Data/restraints/parameters	4386/0/248	4541/0/257
Goodness-of-fit on F^2	1.054	1.052
Final R indices [$I > 2\sigma(I)$]	$R_1 = 0.0460$, $wR_2 = 0.1255$	$R_1 = 0.0352$, $wR_2 = 0.0946$
R indices (all data)	$R_1 = 0.0554$, $wR_2 = 0.1298$	$R_1 = 0.0429$, $wR_2 = 0.0987$
Largest difference peak and hole (e Å^{-3})	0.667 and −0.326	0.536 and −0.193

PLATON [17]. The hkl ranges are $-19 \leqslant h \leqslant 18$, $-10 \leqslant k \leqslant 9$, $-20 \leqslant l \leqslant 17$ and $-13 \leqslant h \leqslant 14$, $-20 \leqslant k \leqslant 20$, $-14 \leqslant l \leqslant 9$ for compounds **1** and **4**, respectively.

2.5. Antimicrobial activity

The ligand and the complexes were tested for antimicrobial activity, at the Department of Biotechnology, Cochin University of Science and Technology. The test organisms chosen for antimicrobial activity were two Gram positive and three Gram negative bacteria. The MIC (minimum inhibitory concentration) determination and screening of antimicrobial property was done by the disc diffusion method.

3. Results and discussion

3.1. Synthesis of ligand and complexes

Reaction of methanolic solutions of the ligand and the corresponding copper salts in 1:1 molar ratio yielded compounds **1**, **2**, **3** and **6** whereas compounds **4** and **5** were prepared by the metathetical displacement of acetate in $Cu(OAc)_2 \cdot H_2O$ by either the thiocyanate or azide ion. The thiosemicarbazone deprotonates and chelates in thiolate form as evidenced by the IR spectra. The elemental analyses suggest the general formula as $[CuLX] \cdot xH_2O$ for complexes **1**–**5** but the perchlorate complex turned out to be $[Cu(HL)L]ClO_4$ with the perchlorate ion out of the coordination sphere. The complexes are appreciably soluble in alcohol and DMF. The molar conductance values of the compounds **1**, **2**, **3**, **4** and **5** in 10^{-3} M solution in DMF are found to be less than $20\ \Omega^{-1}\ mol^{-1}\ cm^{-1}$, showing that they are nonconductors [18] which indicate that the anion and the ligand are coordinated to the central copper(II). But the molar conductance value of compound **6** is $72\ \Omega^{-1}\ mol^{-1}\ cm^{-1}$ which is consistent with the value of 1:1 electrolyte as suggested by the formula. The effective magnetic moment values in the range 1.5–1.9 B.M. indicate a typical $S = 1/2$ Cu(II) system.

3.2. Crystal structures

The molecular structures of the compounds **1** and **4** along with atom numbering scheme are given in Figs. 1 and 2, respectively. Table 3 depicts a list of selected bond parameters of the ligand HL and complexes. While the present work was in progress, the molecular structure of HL was reported [19]. However we include here the various structural parameters of HL for comparison with the structures of the two complexes. Single crystal X-ray

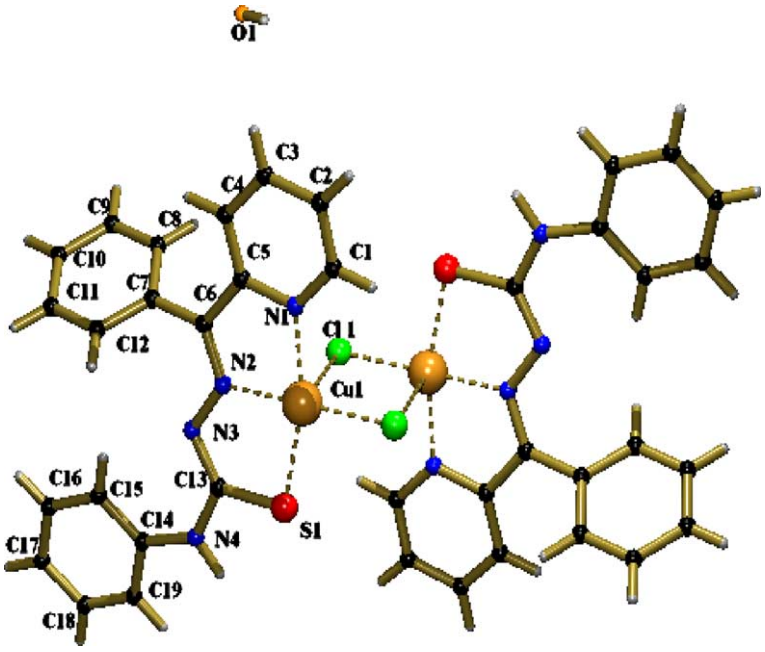

Fig. 1. Molecular structure for compound **1**.

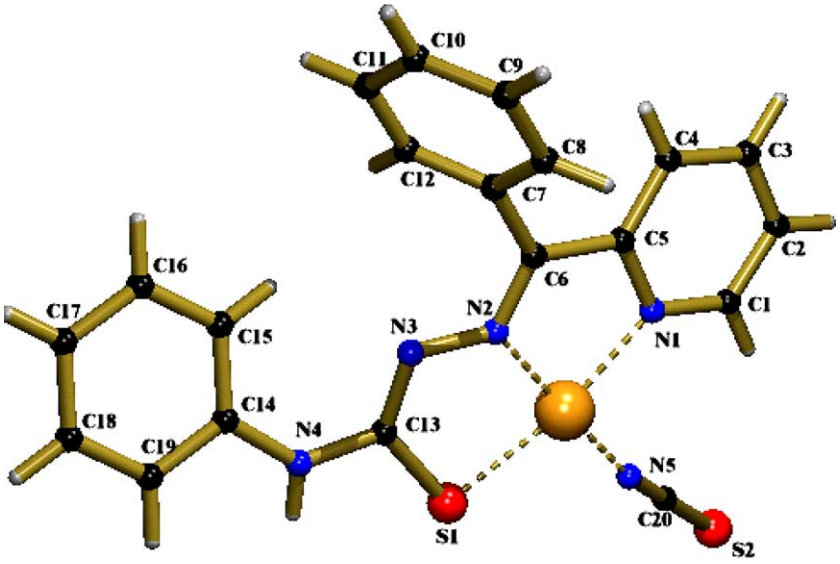

Fig. 2. Molecular structure for compound **4**.

studies of compound (**1**) show that the compound exists as a chlorine bridged dimer. The centrosymmetric nature of the molecule is revealed by a C_2 axis perpendicular to the Cu(1)–Cl(1)–Cu(2)–Cl(2) plane. The lattice nature is monoclinic with space group symmetry $P2_1/c$. Earlier, we have reported a similar chlorine bridged dimeric copper complex with the ligand 2-benzoylpyridine *N*(4), *N*(4)-(butane-1,4-diyl) thiosemicarbazone [20]. The thiosemicarbazone ligand coordinates in a tridentate manner with the metal atom using its azomethine nitrogen, thiolate sulfur and pyridyl nitrogen resulting in two five membered chelate rings. The compound exhibits a distorted square pyramidal geometry with the basal plane occupied by the thiosemicarbazone ligand and the chlorine atom. The chlorine atom of the adjacent monomer plugs into the axial position resulting in a dimer with a Cu–Cu separation of approximately 3.550 Å. The distortion from square pyramid geometry is evident from the bond angles Cl(1)–Cu(1)–S(1) 95.44(3), Cl(1)–Cu(1)–N(1) 98.70(7), N(2)–Cu(1)–N(1) 81.10(8) and N(2)–Cu(1)–S(1) 84.68(6). The basal plane defined by the atoms Cu(1), N(1), N(2), S(1), and Cl(1) deviates

Table 3
Comparison of selected bond lengths (Å) and bond angles (°) of HL, $[CuLCl]_2 \cdot H_2O$ and [CuLNCS]

	HL	$[CuLCl]_2 \cdot H_2O$	[CuLNCS]
C(6)–N(2)	1.3002(18)	1.299(3)	1.297(2)
N(2)–N(3)	1.3612(18)	1.368(3)	1.372(2)
N(3)–C(13)	1.3620(19)	1.316(3)	1.307(2)
S(1)–C(13)	1.6661(16)	1.741(2)	1.750(2)
C(13)–N(4)	1.334(2)	1.362(3)	1.364(2)
Cu(1)–S(1)		2.2318(8)	2.2600(6)
Cu(1)–N(1)		2.014(2)	2.0063(15)
Cu(1)–N(2)		1.963(2)	1.9524(15)
Cu(1)–Cl(1)		2.2459(7)	
Cu(1)–N(5)			1.9240(19)
N(2)–Cu(1)–N(1)		81.10(8)	81.06(6)
N(2)–Cu(1)–S(1)		84.68(6)	84.19(4)
N(1)–Cu(1)–S(1)		164.98(7)	165.13(5)
C(6)–N(2)–N(3)	119.41(14)	119.5(2)	119.02(15)
N(1)–C(5)–C(6)	118.01(13)	115.1(2)	114.51(15)
N(3)–C(13)–S(1)	117.72(13)	125.64(19)	125.41(15)
N(2)–Cu(1)–Cl(1)		178.94(6)	
N(5)–Cu(1)–N(2)			174.97(8)
N(1)–Cu(1)–Cl(1)		98.70(7)	
S(1)–Cu(1)–Cl (1)		95.44(3)	
N(5)–Cu(1)–N(1)			96.66(7)
N(5)–Cu(1)–S(1)			98.19(6)

significantly from planarity with a mean deviation of 0.0488 Å. A distance of 3.986 Å between the Cu(II) metal and the centroid Cg(6) defined by C(14),C(15),C(16), C(17),C(18) and C(19) leads to a ring metal interaction. The significant distance of 2.8613 Å between the centroids Cg(5) and Cg(2) consisting of Cu(1), N(1), C(5), C(6), N(2) and Cu(1), Cl(1), Cu(1a), Cl(1a) makes the crystal packing effective.

The compound **(4)** crystallizes into monoclinic lattice having $P2_1/n$ space symmetry with four molecules per unit cell. The ligand HL together with the thiocyanate group coordinate with Cu(II) resulting in a distorted square planar geometry. The bonding parameters agree with the coordinating pattern of thiosemicarbazone via the thiolate form. Upon complexation, the C(13)–S(1) bond and C(6)–N(2) bonds shift to 1.750(2) and 1.297(2) compared to 1.6661(16) and 1.3002(18), respectively in the ligand. There are also remarkable variations in C(13)–N(3) bond lengths of ligand and complex. The bond angles N(2)–Cu–N(1) 81.06(6), N(2)–Cu–S(1) 84.19(4), N(5)–Cu(1)–N(1) 96.66(7) and N(5)–Cu(1)–S(1) 98.19(6) illustrate that the complex is slightly distorted from the square planar geometry. Liu et al. [21] have synthesized a tetranuclear thiocyanato-copper complex from 2-benzoylpyridine thiosemicarbazone with *N*(4) position unsubstituted. The geometry of copper-ligand-thiocyanato moiety is distorted square planar as in the present complex. However, there is similarity in the N(2)–Cu(1)–N(5) bond angle, while the other bond angles and bond lengths differ significantly. Formation of the chelate ring Cu(1)–N(2)–N(3)–C(13)–S(1) is facilitated by change in configuration of C(13)–N(3) bond from Z in ligand to E in complex, the dihedral angle being 178.51(17) with respect to N(2) and N(4) substituents. Thus with Cu–N2 as the main frame, two chelate

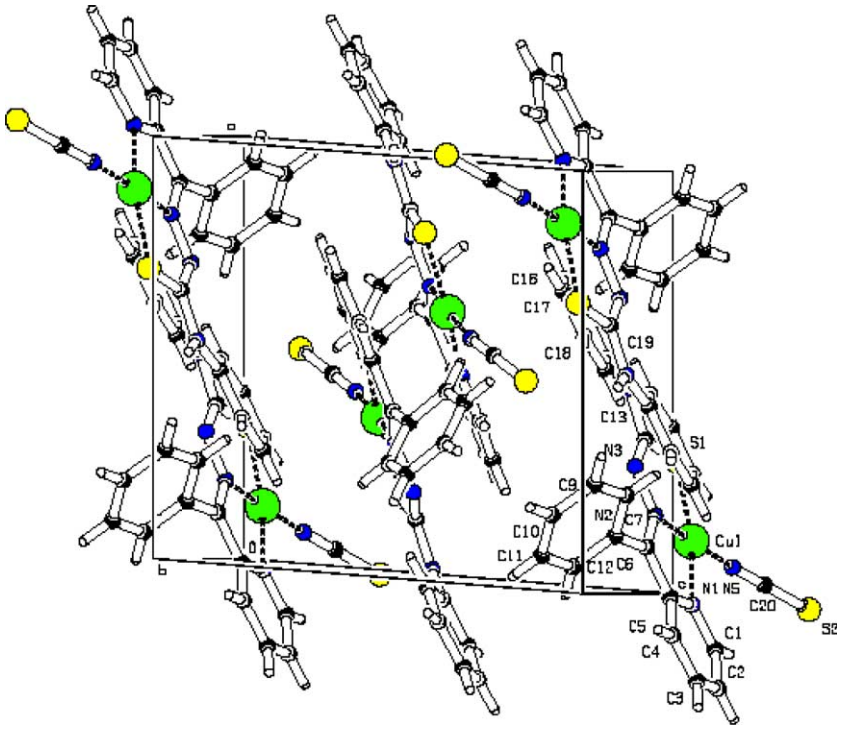

Fig. 3. Packing diagram of compound **4**.

rings are formed which are almost planar with a dihedral angle separation of 0.88°, the second chelate ring being Cu(1)–N(2)–C(6)–C(5)–N(1). Comparing compound **4** with a similar compound in which the *N*(4) substituent is cyclohexyl [12], there exists appreciable variation in C(13)–N(4) bond length. It is seen that in compound **4**, the C(13)–N(4) bond length, 1.364(2) is increased when compared to the value of 1.339(3) in the compound where the *N* (4) substituent is cyclohexyl. This may be due to the delocalization of lone pair electrons of *N*(4) with the phenyl ring. The bond angle C(20)–N(5)–Cu(1) 165.5(2) reveals that the Cu–NCS coordination is not linear while the linearity of N(5)–C(20)–S(2) bond angle, 179.5(2) is almost retained. In the unit cell, the molecules are arranged in a zig-zag manner, where the NCS tails on neighbouring molecules are pointing towards opposite sides (Fig. 3). Table 4 features the H-bonding interactions of HL and two complexes **1** and **4**.

Table 4
H-bonding parameters

D–H···A	D–H (Å)	H···A (Å)	D···A (Å)	D–H···A (°)
HL				
N(3)–H(1)···N(1)	0.888	1.940	2.621	132.3
N(4)–H(1)···N(2)	0.804	2.192	2.605	112.3
C(19)–H(19)···S(1)	0.930	2.638	3.216	120.84
Compound **(1)**				
C(12)–H(12)···N(4)[a]	0.930	2.745	3.470	135.48
C(12)–H(12)···O(1)[b]	0.930	2.948	3.849	163.64
C(19)–H(19)···O(1)[c]	0.930	2.606	3.356	135.75
N(4)–H(1)···O(1)[c]	0.937	1.951	2.875	168.74
O(1)–H(1)···Cl(1)[d]	0.983	2.393	3.348	163.64
O(1)–H(2)···Cl(1)[e]	0.914	2.784	3.492	135.04
Compound **(4)**				
C(16)–H(16)···S(2)[f]	0.930	2.955	3.833	157.91
N(4)–H(1)···S(1)[f]	0.811	2.840	3.604	158.07
C(3)–H(3)···S(2)[g]	0.930	2.867	3.723	153.59

D, donor; A, acceptor, Equivalent position codes: a = $x, -y+1/2+1, +z-1/2$; b = $x, -y+1/2+1, +z+1/2$; c = $x, +y, +z+1$; d = $-x+2, +y-1/2, -z+1/2+1$; e = $x, +y-1, +z-1$; f = $-x+1, -y, -z+2$; g = $-x-1/2, +y+1/2, -z+1/2+2$.

3.3. IR and electronic spectra

The tentative assignments of the significant IR spectral bands of HL and its copper(II) complexes are presented in Table 5. The *ν*(C=N) band of the thiosemicarbazone at 1591 cm^{-1} undergoes a negative shift of wavenumber in the complexes indicating coordination via the azomethine nitrogen. This is confirmed by the bands in the range 440–475 cm^{-1}, which have been assigned to the *ν*(Cu–N) band [22]. A strong band found at 1102 cm^{-1} is assigned to the *ν*(N–N) band of the thiosemicarbazone. The increase in the frequency of this band in the spectra of complexes is due to the increase in the bond strength, again confirms the coordination via the azomethine nitrogen. In the uncomplexed thiosemicarbazone the two bands appearing at the frequencies at 1369 and 835 cm^{-1} have been assigned to *ν*(C=S). In the complexes these two bands are found to be shifted to lower frequencies in the ranges 1280–1320 and 745–785 cm^{-1}, respectively. Thus due to coordination via the thiolate sulfur atom a negative shift occurs in the *ν*(C=S) band in all complexes [23]. In all the copper complexes, a strong band is observed in the region 270–295 cm^{-1}. This is consistent with the *ν*(Cu–N) of pyridine as suggested by Clark and Williams [24]. Based on the above spectral evidences, it is confirmed that the ligand HL is tridentate, coordinating via the azomethine nitrogen, the pyridyl nitrogen and thione/thiolate sulfur. In the chloro complex the strong band observed at 310 together with a band at 150 cm^{-1} has been assigned to the *ν*(Cu–Cl) which is in a bridging mode [20]. The *ν*(Cu–Br) frequency is observed at 255 cm^{-1} in the bromo complex. The *ν*(Cu–Br) frequency is consistent with the terminal bromo ligand. In the nitrato complex the three bands observed at 1431, 1302 and 1014 cm^{-1} indicates the ν_4, ν_1 and ν_2 modes of the nitrato group. The fact that the nitrato group is terminally bonded is understood from the separation of 129 cm^{-1} between the two highest frequency bands just mentioned above [22]. Besides, in the far IR spectrum of the complex, the band observed at 271 cm^{-1} can be assigned to *ν*(Cu–ONO_2)

Table 5
IR spectral assignments (cm^{-1}) of HL and the Cu(II) complexes

Compound	*ν*(C=N)	*ν*(N–N)	*ν*(C–S)	*ρ*(py)	*ν*(Cu–N)	*ν*(Cu–Npy)	*ν*(Cu–S)	(Cu–X)
HL	1591s	1102s	1369s, 835s	622m				
$[CuLCl]\cdot CH_3OH$	1554s	1123s	1318s, 784s	632w	460m	272s	349s	310s, 150m
$[CuLBr]\cdot 2H_2O$	1536s	1128s	1316s, 754s	640m	451s	296s	344s	255s
$[CuLNO_3]\cdot H_2O$	1545s	1128m	1280s, 788s	644s	446s	272s	345s	271s
$[CuLNCS]\cdot 2H_2O$	1534s	1124m	1314m, 748s	629s	452m	276s	346m	
$[CuLN_3]$	1529s	1123s	1322s, 788s	647m	463s	274s	352m	
$[CuL(HL)](ClO_4)$	1554s	1123s	1318s, 830, 785s	644m, 622sh	455s	278s	351s	

in consistence with the bands at 253–280 cm^{-1}, reported earlier for Cu–ONO_2 in metal complexes [25].

In the azido complex, the strong band observed at 2046 cm^{-1} is assigned to ν_a of the azide group indicative of azide coordination [26]. In the thiocyanato complex, a very strong band at 2098 cm^{-1}, a medium band at 869 cm^{-1} and a strong band at 480 cm^{-1} are assigned to ν(CN), ν(CS), and δ(NCS) modes of the NCS group, respectively. The intensity and position of these bands indicate the unidentate coordination of the thiocyanate group through the nitrogen [20,27]. For the perchlorate complex **6**, the bonding of the neutral ligand needs to be considered because the perchlorate group is not coordinated to the metal ion. The perchlorate complex contains a single broad band at 1123 cm^{-1} and an unsplit band at 644 cm^{-1}, indicating the presence of ionic perchlorate. The bands at 1123 and 644 cm^{-1} can be assigned to $\nu_3(ClO_4)$ and $\nu_4(ClO_4)$, respectively. The presence of these bands and the absence of a band near 930 cm^{-1} assignable to $\nu_1(ClO_4)$ suggest ionic perchlorate [28]. The IR spectrum of compound **6** contains a strong band at 785 cm^{-1} which has been assigned to ν(C–S) indicating coordination via the thiolate sulfur. In addition to this band, the spectrum also contains a band at 830 cm^{-1} indicating the presence of the ligand in the thione form. The presence of a weak shoulder at ~622 cm^{-1} indicates that the neutral ligand does not coordinate through pyridyl nitrogen. However, bands corresponding to azomethine groups of both HL and L are shifted indicating that the neutral ligand coordinates through azomethine nitrogen while the ligand in thiolate form coordinates via azomethine nitrogen, pyridyl nitrogen and thiolate sulfur resulting in a four coordinate structure. Based on the elemental analyses and IR spectral data a tentative structure is proposed for compound **6** and is given in Fig. 4. Attempts to isolate single crystals of compound **6** were unsuccessful.

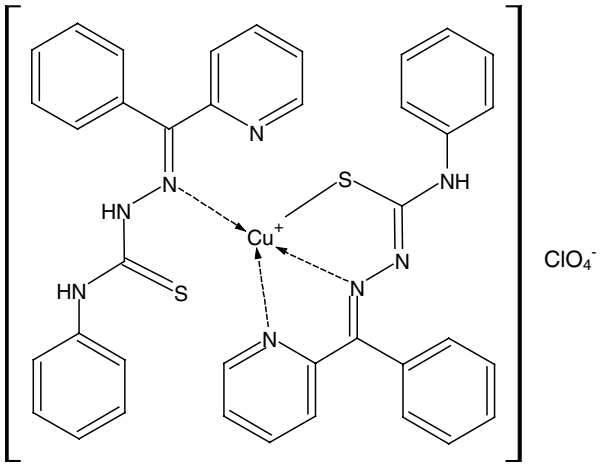

Fig. 4. Tentative structure for compound **6**.

The solid state electronic spectrum of HL consists of a broad band at ca. 29410 cm^{-1} which is n → π* band of the pyridine ring. An absorption band observed at ca. 37313 cm^{-1} in the solid state spectrum of the ligand may be due to π → π* transition. The electronic spectra of Cu(II) complexes (Table 6) consist of bands in the region 27000–33000 cm^{-1} which are assigned to n → π* band of pyridine ring. A strong band in the range 22500–24500 cm^{-1} observed in the spectra of all Cu(II) complexes which are assigned to S → Cu and py → Cu charge-transfer bands [29,30]. In the chloro complex a shoulder observed at 31446 cm^{-1} is assigned as Cl → Cu charge-transfer transitions. The solid state spectra of all compounds exhibit d → d bands in the range 19000–16000 cm^{-1} which are consistent with a broad structured band suggested for square planar complexes in the range 13000–20000 cm^{-1} [31]. In the electronic spectra of Cu(II) complexes in DMF, the bands corresponding to electronic transitions are found to be shifted from that of the solid state.

Table 6
Electronic spectral assignments (cm^{-1}) (logε in parentheses) of HL and the Cu(II) complexes

Compound	Mode	d → d	L → M	n → π*	π → π*
HL	Solid			29410	37313
	DMF			29810 (4.13)	38167
[CuLCl] · CH_3OH	Solid	16393	24154, 31446sh	31948	39215
	DMF	17452 (2.60)	22883 (4.14)	27624 (3.83)	39062 (4.41)
[CuLBr] · $2H_2O$	Solid	16920	242133	30303	36900sh
	DMF	18083 (2.41)	22075 (4.27)	28328 (4.61)	36496sh (4.15)
[CuLNO$_3$] · H_2O	Solid	16474	23980	30674	35460
	DMF	16025 (2.43)	24570 (4.27)	32154 (4.32)	38461sh (4.25)
[CuLNCS] · $2H_2O$	Solid	17825sh	23640	32573	35842
	DMF	16000 (2.5)	22573 (4.33)	32154 (4.25)	36101 (4.16)
[CuLN$_3$]	Solid	16949sh	23696	30959	36101
	DMF	18939 (2.41)	22624 (3.81)	28409 (4.71)	35714sh (4.15)
[CuL(HL)](ClO$_4$)	Solid	18691sh	24213	3236	37453sh
	DMF	17123sh (2.34)	22727 (4.35)	228409 (4.21)	37037sh (4.01)

3.4. EPR spectra

The EPR spectra of the complexes in the polycrystalline sample at 298 K, in solution at 298 and 77 K were recorded in the X band, using 100 kHz field modulation and the g factors were quoted relative to the standard marker TCNE ($g = 2.0277$). The EPR parameters of the copper(II) complexes obtained for the polycrystalline state at 298 K and in DMF at 298 and 77 K are presented in Table 7. In the case of a $3d^9$ copper(II) ion the appropriate spin Hamiltonian assuming a B_{1g} ground state is given by [32].

$$\hat{H} = \beta[g_{\parallel}H_zS_z + g_{\perp}(H_xS_x + H_yS_y)] + AI_zS_z + B(I_xS_x + I_yS_y).$$

The EPR spectrum of compound **5** in the polycrystalline state (298 K) show only one broad signal at $g = 2.07$. The spectra of the compounds **2**, **3** and **4** show typical axial spectra with well-defined $g_{\parallel}$ and $g_{\perp}$ values at ≈2.21 and 2.05, respectively. The spectra of compounds **1** and **6** give three g values viz. g_1, g_2 and g_3 which indicate rhombic distortions in their geometry. The geometric parameter G, which is a measure of the exchange interaction between the copper centres in the polycrystalline compound, is calculated using the equation:

$G = (g_{\parallel} - 2.0023)/(g_{\perp} - 2.0023)$ for axial spectra and for rhombic spectra, $g_{\perp} = (g_1 + g_2)/2$. If $G > 4$, exchange interaction is negligible and if it is less than 4, considerable exchange interaction is indicated in the solid complex [33,34]. In all the copper(II) complexes $g_{\parallel} > g_{\perp} > 2.0023$ and G value within the range 2.5–3.5 are consistent with a $d_{x^2-y^2}$ ground state. In the EPR spectra of the complexes in DMF solution at 298 K, four hyperfine lines are observed which arise from the coupling of the odd electron with the copper nuclei (^{65}Cu, $I = 3/2$). The spectrum of compound **1** at 77 K is a typical axial one with well-resolved hyperfine lines with no superhyperfine lines. However, the half field signal corresponding to the dimer was not observed for compound **1**. The spectrum of compound **2**, is isotropic without any hyperfine lines due to poor glass formation. The spectrum of compound **6** is a typical rhombic one without any hyperfine and superhyperfine lines.

The EPR parameters $g_{\parallel}$, $g_{\perp}$, g_{av}, $A_{\parallel}$(Cu) and $A_{\perp}$(Cu) and the energies of d–d transition were used to evaluate the bonding parameters α^2, β^2 and γ^2, which may be regarded as measures of the covalency of the in-plane σ bonds, in-plane π bonds, and out-of-plane π bonds, respectively. In all the copper(II) complexes, it is observed that $K_{\parallel} < K_{\perp}$ (Table 8) which indicates the presence of significant in-plane π bonding. This is further

Table 7
EPR parameters of the Cu(II) complexes of HL

Compound	Solid (298 K)		DMF solution (298 K)			DMF solution (77 K)		
	$g_{iso}/g_{\parallel}/g_3$	$g_{\perp}/g_2/g_1$	g_{iso}	$A_{iso(Cu)}$[a]	$g_{\parallel}/g_3$	$g_{\perp}/g_2/g_1$	g_{av}	$A_{\parallel}$[a]
$[CuLCl]CH_3 \cdot OH$	$g_3$2.1230	$g_2$2.0434 $g_1$1.9991	2.0698	84.13	$g_{\parallel}$2.1500	$g_{\perp}$2.0510	2.0840	158.91
$[CuLBr] \cdot 2H_2O$	$g_{\parallel}$2.2348	$g_{\perp}$2.0898	2.0749	112.13				
$[CuLNO_3] \cdot 2H_2O$	$g_{\parallel}$2.213	$g_{\perp}$2.0960	2.0560	84.00	$g_3$2.1274	$g_2$2.0498 $g_1$1.971	2.0494	154.23
$[CuLNCS] \cdot H_2O$	$g_{\parallel}$2.1168	$g_{\perp}$2.0433	2.1618	85.10	$g_3$2.2913	$g_2$2.169 $g_1$2.0593	2.1732	175.73
$[CuLN_3]$	g_{iso}2.0720		2.0750	102.90	$g_3$2.2052	$g_2$2.065 $g_1$1.972	2.0809	163.58
$[CuL(HL)]ClO_4$	$g_3$2.1274	$g_2$2.0649 $g_1$2.0306	2.0886	79.45	$g_3$2.1274 $g_1$2.0301	$g_2$2.0498	2.0691	168.26

[a] A values in 10^{-4} cm^{-1}.

Table 8
Bonding parameters and orbital reduction parameters of Cu(II) complexes of HL

Compound	α^2	β^2	γ^2	$K_{\parallel}$	$K_{\perp}$	K_o	f
$[CuLCl]CH_3OH$	0.6392	0.9877	0.9976	0.6315	0.6333	0.3168	135.2
$[CuLBr]2H_2O$	0.6423	0.9505	0.9582	0.6105	0.6155	0.4359	134.19
$[CuLNO_3]H_2O$	0.6479	0.9101	0.9793	0.5897	0.6345	0.3025	126.4
$[CuLNCS]H_2O$	0.660	0.8440	0.9224	0.5570	0.608	0.3532	130.38
$[CuLN_3]$	0.6741	0.9980	0.9877	0.6741	0.6677	0.3526	132.16
$[CuL(HL)]ClO_4$	0.6479	0.9101	0.9793	0.5696	0.6345	0.3513	126.4

Table 9
The antimicrobial activity of the complexes using the disc diffusion method

Compound	Conc.(Conc/Disc in μg)	Microbial activity inhibition zone				
		Bacillus sp.	*Vibrio cholerae* O1	*Escherichia coli*	*Staphylococcus aureus*	*Salmonella paratyphi*
HL	50				+12 mm	
$[CuLCl]CH_3OH$	50		+9 mm			
$[CuLBr]2H_2O$	50		+10 mm			
$[CuLNCS]H_2O$	50		+10 mm			
$[CuLN_3]$	50		+10 mm			+9 mm
$[CuL(HL)]ClO_4$	50		+9 mm			

Table 10
MIC of HL and Cu(II) complexes

Compound	MIC in μg			
	Bacillus sp.	*Vibrio cholerae* O1	*Salmonella paratyphi*	*Staphylococcus aureus*
HL				4
$[CuLCl]CH_3OH$ (**1**)		5		
$[CuLBr] \cdot 2H_2O$ (**2**)		5		
$[CuLNCS] \cdot H_2O$ (**4**)		5		
$[CuLN_3]$ (**5**)		5	4	
$[CuL(HL)](ClO_4)$ (**6**)		5		

confirmed by the bonding parameters α^2, β^2 and γ^2 which are less than 1.0, expected for 100% ionic character of the bonds, and decrease on increasing the covalent character of the bonding. This observation supports the argument that there is significant in-plane π bonding and in-plane σ bonding in the copper(II) complexes of HL.

3.5. Antimicrobial activity

The ligand and its five Cu(II) complexes were tested for their antimicrobial activity. Two Gram positive bacteria and three Gram negative bacteria were used as test organisms: (1) *Staphylococcus aureus*, (2) *Bacillus* sp. (Gram positive), (3) *Escherichia coli*, (4) *Salmonella paratyphi*, (5) *Vibrio cholerae* O1 (Gram negative). Table 9 depicts the antimicrobial activity of the complexes using the disc diffusion method [35]. The effectiveness of an antimicrobial agent in sensitivity testing is based on the size of the zones of inhibition. The diameter of the zone is measured to the nearest millimeter. Test substances which produce the zone of inhibition with diameters 9 mm or more are regarded as positive, i.e. having antimicrobial activity; while those cases where the diameter is below 9 mm, the bacteria are resistant to the sample tested and the sample is said to have no antimicrobial activity. The MIC (minimum inhibitory concentration) expressed in micrograms, of the compounds showing positive antimicrobial property was determined using the disc diffusion method and is given in Table 10.

It was observed that the ligand HL was active against *Staphylococcus aureus* while it was inactive against the other four test organisms. But all its Cu(II) complexes were found to be inactive against this particular bacteria. Out of the five Cu(II) complexes, four complexes were found to be active against only one type of microorganism under study, i.e. *Vibrio cholerae* O1. The complex $[CuLN_3]$ was found to be active against *Vibrio cholerae* and *Salmonella paratyphi*. The ligand and the Cu(II) complexes are found to be inactive against *Bacillus* sp. and *Escherichia coli*. It was surprising to find that *N*(4)-phenyl substituted thiosemicarbazone was active whereas the more bulky cyclohexyl substituted thiosemicarbazone ligand was inactive. But the activity of Cu(II) complexes were found to be reversed as expected, where the more bulky *N*(4) substituent leads to more activity.

Acknowledgements

The authors are thankful to Sophisticated Analytical Instruments Facilities at CDRI, Lucknow and IIT, Bombay, India for the elemental analyses and EPR spectral studies, respectively. M.R.P. Kurup would like to thank the Department of Science and Technology, New Delhi for financial assistance (SR/S1/IC-31/2002) and M. Joseph acknowledges Kerala State Council for Science, Technology and Environment, Govt. of Kerala for financial support.

Appendix A. Supplementary data

Crystallographic data for the structural analysis has been deposited with the Cambridge Crystallographic

Data center, CCDC reference numbers are 251896, 254305 and 254304 for HL, compounds **1** and **4**, respectively. Copies of this information may be obtained free of charge via www.ccdc.cam.ac.uk/conts/retrieving.html or from the Director, CCDC, 12 Union Road, Cambridge, CB2, IEZ, UK (fax: +44 1223 336 033; e-mail: deposit@ccdc.cam.ac.uk. Supplementary data associated with this article can be found, in the online version, at doi:10.1016/j.poly.2005.07.006.

References

[1] D.X. West, S.B. Padhye, P.S. Sonawane, Struct. Bond. 76 (1991) 1.
[2] D.X. West, A.E. Liberta, S.B. Padhye, R.C. Rajeev, P.B. Sonawane, A.S. Kumbhar, R.G. Yerande, Coord. Chem. Rev. 49 (1993) 123.
[3] J.G. Tojal, A.G. Orad, J.L. Serra, J.L. Pizarro, L. Lezama, M.I. Arriortua, T. Rojo, J. Inorg. Biochem. 75 (1999) 45.
[4] S.K. Jain, B.S. Garg, Y.K. Bhoon, Spectrochim. Acta A 42 (1986) 959.
[5] M.E. Hossain, M.N. Alam, J. Begum, M.A. Ali, M. Nazimudhin, F.E. Smith, R.C. Hynes, Inorg. Chim. Acta 249 (1996) 207.
[6] H. Beraldo, D. Gambino, Mini Rev. Med. Chem. 4 (2004) 159.
[7] A. Sreekanth, M.R.P. Kurup, Polyhedron 23 (2004) 969.
[8] V. Philip, V. Suni, M.R.P. Kurup, M. Nethaji, Polyhedron 23 (2004) 1225.
[9] M. Joseph, V. Suni, C.R. Nayar, M.R.P. Kurup, H.K. Fun, J. Mol. Struct. 705 (2004) 63.
[10] A. Sreekanth, H.-K. Fun, M.R.P. Kurup, Inorg. Chem. Commun. 7 (2004) 1250.
[11] A. Sreekanth, V. Rajakannan, T.A. Ajith, M.R.P. Kurup, Polyhedron 23 (2004) 2549.
[12] V. Philip, V. Suni, M.R.P. Kurup, Acta Crystallogr., Sect. C 60 (2004) o856.
[13] V. Philip, V. Suni, M.R.P. Kurup, M. Nethaji, Polyhedron 24 (2005) 1133.
[14] M. Joseph, V. Suni, M.R.P. Kurup, M. Nethaji, A. Kishore, S. Bhat, Polyhedron 23 (2004) 3069.
[15] D.L. Klayman, J.F. Bartosevich, T.S. Griffin, C.J. Mason, J.P. Scovill, J. Med. Chem. 22 (1979) 855.
[16] G.M. Sheldrick, SHELXS-97 Program for the Solution of Crystal Structures, University of Göttingen, Göttingen, Germany, 1997.
[17] A.L. Speck, PLATON, A Multipurpose Crystallographic Tool, Utrecht University, Utrecht, The Netherlands, 1999.
[18] W.J. Geary, Coord. Chem. Rev. 7 (1971) 81.
[19] A.P. Rebolledo, G.M. de Lima, L.N. Gambi, N.L. Speziali, D.F. Maia, C.B. Pinheiro, J.D. Ardisson, M.E. Cortes, H. Beraldo, Appl. Organometal. Chem. 17 (2003) 945.
[20] A. Sreekanth, M.R.P. Kurup, Polyhedron 22 (2003) 3321.
[21] Z.H. Liu, S.Y. Yang, C.Y. Duan, X.Z. You, Chem. Lett. (1999) 1063.
[22] K. Nakamoto, Infrared and Raman spectra of Inorganic and Coordination Compounds, 5th ed., Wiley, New York, 1997.
[23] R. Mayer, in: M. Jansen (Ed.), Organosulfur Chemistry, Interscience, New York, 1967.
[24] R.J. Clark, C.S. Williams, Inorg. Chem. 4 (1965) 350.
[25] S.K. Jain, B.S. Garg, Y.K. Bhoon, Spectrochim. Acta 42 (1986) 701.
[26] R. Raina, T.S. Srivastava, Indian J. Chem. A 22 (1983) 701.
[27] R.A. Bailey, S.L. Kozak, T.W. Michelson, W.N. Mills, Coord. Chem. Rev. 6 (1971) 407.
[28] B.S. Garg, M.R.P. Kurup, S.K. Jain, Y.K. Bhoon, Transit. Met. Chem. 13 (1988) 309.
[29] E. Ainscough, A.M. Brodie, N.G. Larsen, Inorg. Chim. Acta 60 (1982) 25.
[30] R.P. John, A. Sreekanth, M.R.P. Kurup, S.M. Mobin, Polyhedron 21 (2002) 2515.
[31] A.B.P. Lever, Inorganic Electronic Spectroscopy, second ed., Elsevier Science Publishing Company, Amsterdam, 1984.
[32] D. Kivelson, R. Neiman, J. Chem. Phys. 35 (1961) 149.
[33] I.M. Proctor, B.J. Hathaway, P. Nicholis, J. Chem. Soc. (1968) 1678.
[34] B.J. Hathaway, D.E. Billing, Coord. Chem. Rev. 5 (1970) 1949.
[35] A.W. Bauer, M.M. Kirby, J.C. Sherris, M. Turch, Am. J. Clin. Pathol. 36 (1966) 493.

Available online at www.sciencedirect.com
SCIENCE DIRECT®
Polyhedron 25 (2006) 71–80
POLYHEDRON
www.elsevier.com/locate/poly

Molecular architecture by means of interactions between Ag(I) and glycine derivatives

Miquel Barceló-Oliver [a], Andrés Tasada [a], Juan J. Fiol [a], Angel García-Raso [a], Angel Terrón [a,*], Elies Molins [b]

[a] *Departament de Química, Universitat de les Illes Balears, Campus UIB, Cta. Valldemossa km 7.5, Edifici Mateu Orfila, E-07122 Palma de Mallorca, Spain*
[b] *Institut de Ciència dels Materials de Barcelona (CSIC), Campus de la Universitat Autònoma, E-08193 Cerdanyola, Spain*

Received 6 June 2005; accepted 1 July 2005
Available online 19 August 2005

Abstract

The use of a ligand directed strategy in the assembly of discrete cluster, 2D layers and 3D networks, using *N*-substituted glycine derivatives with *o*-iodobenzoyl (a bulky substituent) or pyrimidyl, create a new possibility in the design of coordination networks. According to the nature of the substituent, 2D layers (with *o*-iodobenzoyl) or 3D networks (with pyrimidyl), with tubular cavities and Ag···Ag short contacts, are obtained. The synthesis and crystalline structure of the ligand *N*-(pyrimidyl)glycine (**1**), its silver derivative [Ag(pyr-gly)] · $0.5H_20$ (**2**) and the silver derivative of *o*-iodohippuric acid [Ag(I-hip)] · $1.25H_2O$ (**3**) are described. The structures of **2** and **3** present tubular cavities being, in complex **2** a 3D structure with cycles and clusters Ag_4O_4 that retains water inside the tubular channels. In the other hand, the compound 3 presents a 2D structure generated by macrocyclic rings formed between the ligand and the metal ion; these bi-dimensional networks are piled in the *c*-direction, and the different layers are detached by water molecules as an intercalation compound; in addition, each layer interacts with the others by stacking (distance, 3.38 Å) between series of two aryl rings inside of the channel and preserving it along the *c*-axis. Finally, short Ag···I contacts are also present as recognition factors in compound **3**.
© 2005 Elsevier Ltd. All rights reserved.

Keywords: Silver; Amino acids; Glycine; Coordination polymer; Supramolecular chemistry; Iodine interactions; X-ray structure; Stacking

1. Introduction

The control of the self-assembly process between labile metal ions and flexible polydentate ligands is a key objective in the development of supramolecular coordination chemistry [1]. Obviously, this process will be related with the number, type and spatial disposition of the binding sites of ligands, the steric plasticity of metal ions, the coordinative versatility of the ligands, the solvent effect and the nature of counter anions [2,3]. The combination of all of these factors leads to numerous metallosupramolecular complexes with various structural topologies [2–12].

In this context, Ag(I) is a profitable metal ion choice because of presents suitable coordination geometries such as linear, T-shaped, trigonal, distorted tetrahedral, or octahedral [7].

The aim to obtain highly specific materials can be tackled with the properties of Ag(I) to produce nanomaterials [8], porous open channels structures with properties like zeolites [5,9,10], polymers with controlled chirality [11], frameworks with luminescence and special conductivity properties [12].

The choice of particular ligands has generated different type of structures: 3D [3,13,14], 2D [15,16], 1D [11,17,18] or discrete polynuclear complexes [19]. The

* Corresponding author. Tel.: +34 971 173 249; fax: +34 971 173 426.
E-mail address: angel.terron@uib.es (A. Terrón).

0277-5387/$ - see front matter © 2005 Elsevier Ltd. All rights reserved.
doi:10.1016/j.poly.2005.07.014

ligands designed for self-assembly of silver are normally rigid or with a degree of preorganization as for example polypyridyl [20,21], diphosphine [22], pyridine substituted [23], pyrimidine derivatives [24], hexamethylenetetramine [25], aliphatic amines [26], aryl iodine or alkyl iodine derivatives [27–33] or [2,2]-paracyclophane (that produces a 2D polymer with reversible guest-driven solid state transformation) [34].

Recently the topic is boosting and a great number of references appear in the literature, between them the importance of Ag–Ag short contacts are emerging as a relevant factor to self-assembly [35–37].

Previously, we have studied the coordination chemistry of hippuric and *o*-iodohippuric acids [38,39] with 3d metals. Some aspects are of interest, the N peptide of these hippuric derivatives do not coordinate with the metal ions except for the case of Pd [40] whereas the terminal carboxylic group is the main target. Moreover, in the *o*-iodohippuric compound should be mentioned that the plane of the aryl group is strictly perpendicular to the peptide bond producing a steric restriction that could prevent the formation of well defined 3D structures. On the other hand, the coordination behaviour of pyrimidine-substituted derivatives was also known [41].

For these reason, we have obtained the ligand *N*-(pyrimidyl)glycine (pyr-gly), where this steric restriction of the bulky iodo-aryl is not present in order to compare the coordination chemistry of the two ligands whereas the ligands have a similar distance between the coordination atoms (Scheme 1). Due to the lack of coordination with metal ions of the N amide bond [38,39] the terminal carboxylic group and the O atom of the peptidic bond (I-hip) or the N atom of the pyrimidine ring (pyr-gly) were considered the coordination targets of silver.

In this study we report results related to the coordination chemistry of two *N*-substituted glycine derivatives, *o*-iodobenzoylglycine (*o*-iodohippuric acid; I-hipH) and pyr-gly (Scheme 1), with silver nitrate. We have prepared this last ligand, pyr-gly, by means of a modification of a previously described methodology [42]. In this context, the two ligands have an interesting angular geometry, which leads to build multidimensional architectures forming tri- (pyr-gly) and bi-dimensional (I-hip) macrocyclic open networks that could be added to previous examples. Also, the capability of iodine residues to form short interactions with metal ions is also of the maximum interest owing to the presence of this recognition factor in thyroid hormones, which are iodinated derivatives of the tyrosine residues from thyroglobin [43].

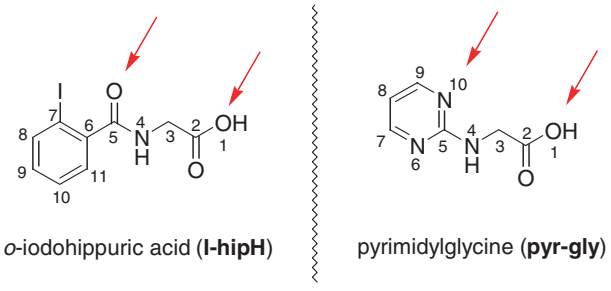

Scheme 1. Formulae and numeration of *o*-iodohippuric acid and *N*-(pyrimidyl)-glycine ligands (arrows indicate the coordination atom to the metal ion).

2. Experimental

Elemental microanalyses were carried out using a Carlo Erba model 1108 microanalyzer and a Thermo Finnigan model Flash 1112 microanalyzer. IR spectra in the solid state (KBr pellets) were measured in the 4000–400 cm^{-1} range on a Bruker IFS 66 spectrometer. ^1H NMR spectra were recorded at room temperature on a Bruker AMX 300 (300 MHz). Proton chemical shifts in deuterated dimethylsulfoxide ([D_6] DMSO) were referenced to [D_6] DMSO (δ[D_6] DMSO: 2.47 ppm). Thermogravimetric data in the temperature range from 30 to 900 °C were recorded in a flowing oxygen atmosphere (heating rate 2 °C/min) on a TA Instruments SDT 2960 Simultaneous DSC-TGA thermobalance.

Reagents were used as received from Sigma, Merck or Aldrich. *o*-Iodohippuric acid (*o*-iodobenzoylglycine) was prepared according to the literature procedure [44,45] or supplied by Aldrich. *N*-(pyrimidyl)glycine was synthesized by reaction between 2-chloropyrimidine and glycine (see below).

2.1. Synthesis of N-(pyrimidyl)glycine (pyr-gly) (1)

Glycine (16 mmol), 2-chloropyrimidine (8 mmol) and Na_2CO_3 (9 mmol) in water (20 ml) were refluxed during 3 h. The resulting solution was cooled. The pH was adjusted to 3.75 with formic acid and the product precipitates (55% yield). White crystals, suitable for X-ray studies, appeared by slow evaporation at room temperature of the filtered final solution (6–7 days). *Anal.* Calc. for $C_6H_7N_3O_2$: C, 47.06; H, 4.61; N, 27.44. Found: C, 46.87; H, 4.60; N, 27.00%. IR (cm^{-1}): 445w, 551w, 577w, 611w, 651m, 699m, 798m, 883m, 927m, 1050m, 1151m, 1326m, 1388m, 1457m, 1522s, 1540s, 1560s, 1576vs, 1601vs, 1718m, 3426vs. ^1H NMR ([D_6] DMSO): δ 8.24 [d, 2H, H(7), $J = 4.8$ Hz], 7.27 [t, 1H, N(4)–H, $J = 6.3$ Hz], 6.57 [t, 1H, H(8), $J = 4.8$ Hz], 3.86 [d, 2H, H(3), $J = 6.3$ Hz].

2.2. [Ag(pyr-gly)] · 0.5H_2O (2)

Ag(I) nitrate (1 mmol) in water (5 ml) was added dropwise to a solution of pyr-gly (1 mmol) in 30 ml of

HNO_3 0.16 M. These conditions were designed to ensure the lack of coordination of the NH moiety. The resulting colourless solution was refluxed during 2 h and left to cool. Small white crystals (75% yield), diamond type, suitable for X-ray diffraction studies, appeared on standing the final solution at room temperature (3–4 days). *Anal.* Calc. for $AgC_6H_6N_3O_2 \cdot 0.5H_2O$: C, 26.79; H, 2.62; N, 15.62. Found: C, 27.50; H, 2.62; N, 15.64%. TG: The decomposition of the complex takes place in two steps. The water was loosed smoothly between 100 and 180 °C [calc.: 3.3; found: 3.0%]. The first overall step takes place in the 100–250 °C temperature range implying a higher decomposition of the molecule at 200 °C, whereas the second overall step occurs in the 350–500 °C temperature range with a higher loss about 450 °C. The weight loss associated with these two steps is in accordance with the expected value for the total decomposition of the complex [calc.: 59.96; found: 60.54% (1st step 24.66; 2nd step 35.94)], leading to the final residue Ag [calc.: 40.04; found: 39.39%]. There is no loss of water molecules before 100 °C. IR (cm^{-1}): 416vw, 520w, 585m, 648m, 700m, 799s, 907w, 985w, 993w, 1005w, 1077w, 1136w, 1180w, 1237w, 1305s, 1360m, 1384s, 1414s, 1452m, 1583vs, 1596vs, 1684w, 3298vs, 3438vs. ^{1}H NMR: This product is insoluble in the most common NMR solvents ([D_6] DMSO, CD_3OD, D_2O and $CDCl_3$).

2.3. [Ag(I-hip)] · 1.25H_2O (3)

Ag(I) nitrate (1 mmol) in water (5 ml) was added dropwise to a solution at neutral pH obtained dissolving *o*-iodohippuric acid (1 mmol) in 30 ml of NaOH 0.03 M. The resulting solution was refluxed during 2 h, filtered off to eliminate white precipitate of silver hydroxide, and left to cool. White needles (60% yield), suitable for X-ray studies, were obtained by slow evaporation at room temperature of the final solution (4–5 days). *Anal.* Calc. for $AgC_9H_7INO_3 \cdot 1.25H_2O$: C, 24.88; H, 2.20; N, 3.22. Found: C, 24.90; H, 1.97; N, 3.15%. TG: The complex exhibits a weight loss between 50 and 150 °C corresponding to 1.25 water molecules per formula unit [calc.: 5.18; found: 4.93%]. A subsequent decomposition corresponding to one I-hip molecule occurs between 180 and 320 °C [calc. for $C_9H_7NO_3$:

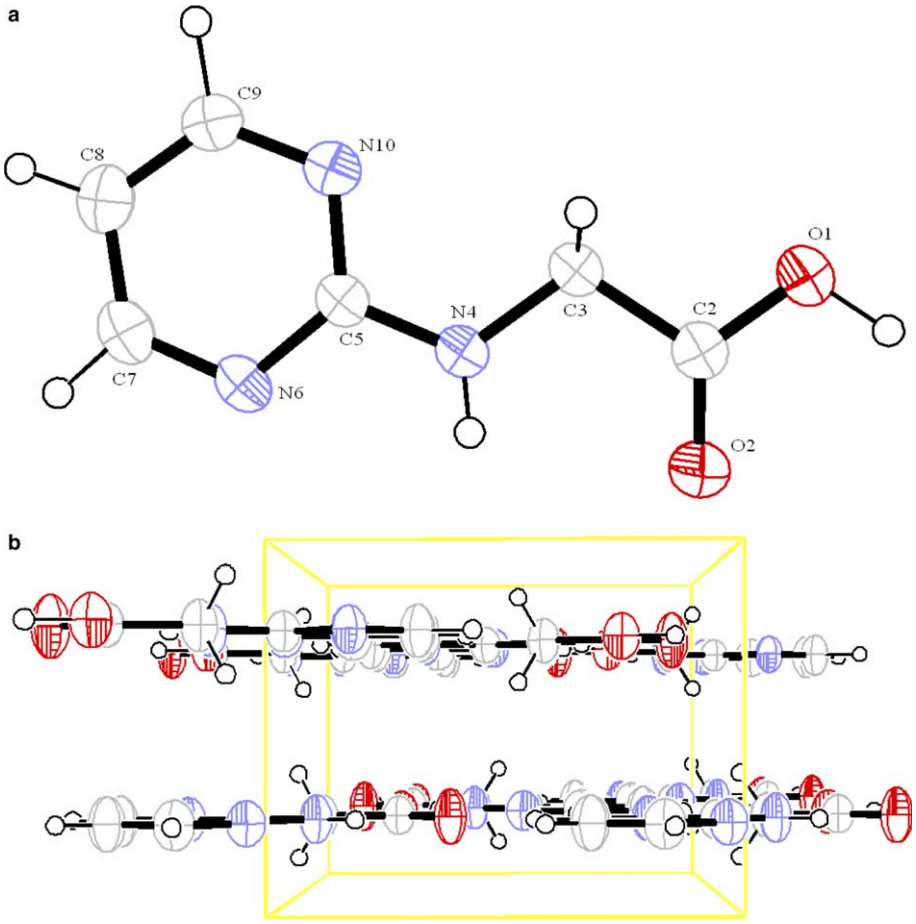

Fig. 1. ORTEP representation of the ligand *N*-(pyrimidyl)glycine (pyr-gly) (**1**). (a) Top: asymmetrical unit. (b) Bottom: view showing the planarity of the compound.

40.78; found: 40.01%] leading to AgI [calc.: 54.04; found: 55.00%] that decomposes at 556 °C in I_2 and metallic Ag, generally with projections of the analyzed material. The third weight loss takes place between 450 and 750 °C, leading to the final residue Ag. IR (cm^{-1}): 435w, 510w, 559w, 603w, 641w, 684w, 722m, 755m, 913vw, 947vw, 998m, 1016w, 1062vw, 1165vw, 1235w, 1258w, 1302m, 1328vw, 1392m, 1429m, 1460w, 1541m, 1597vs, 1642s, 3320m. ^{1}H NMR ([D_6] DMSO): δ 8.10 [t, 1H, N(4)–H, $J = 5.4$ Hz], 7.84 [d, 1 H, H(11), $J = 7.8$ Hz], 7.41 [t, 1H, H(9), $J = 7.2$ Hz], 7.35 [dd, 1H, H(8), $J = 7.4$ and 1.7 Hz], 7.13 [dt, 1H, H(10), $J = 7.5$ and 2.1 Hz], 3.73 [d, 2H, H(3), $J = 5.4$ Hz].

2.4. X-ray crystallographic study

Suitable crystals of **1**, **2** and **3** were selected for X-ray single crystal diffraction experiments and mounted at the tips of glass fibres on an Enraf-Nonius CAD4 diffractometer producing graphite monochromated Mo Kα radiation. After the random search of 25 reflections, the indexation procedure gave rise to the cell parameters (see Table 2 for a summary of the crystal data of the three compounds). Data were collected in the $\omega-2\vartheta$ scan mode. Absorption correction was performed following the PSI-scan semi-empirical (**1**) and the empirical DIFABS (**2**, **3**) methods. The structural resolution procedure was made using the WINGX package [46]. Solving for structure factor phases was performed by SIR2002 [47] and the full-matrix refinement, by SHELXL97 [48]. Noticeably, all the non-hydrogen atoms in **1** lay on m planes. Non-H atoms were refined anisotropically and H-atoms were introduced in calculated positions and refined riding on their parent atoms. A summary of the refinement parameters can be also seen in Table 2. The ORTEP [49] representations of the three complexes were made at 50% probability.

3. Results and discussion

3.1. Crystal structure of N-(pyrimidyl)glycine (*1*)

The molecular structure of *N*-(pyrimidyl)glycine (**1**) is depicted in Fig. 1(a). Selected bond lengths and angles are collected in Table 1. The bond lengths and angles are similar to pyrimidine related molecules [17,23,24,41] and hippuric acid derivatives in the glycine moiety [38,39]. This compound presents a perfectly planar disposition (Fig. 1(b)). The molecular structure is formed by different planes were molecules interact via intermolecular H-bonds (in the same plane) [dist. COO(1)···N(6), 2.62 Å; angle COO(1)–H···N(6), 173.5°] and via stacking (among parallel planes) [ca. 3.41 Å between N(4)–C(5)–N(6)–C(7) moieties; dihedral angle between planes, 180°].

Table 1
Selected bond lengths (Å) and angles (°) of the three compounds

	1	2	3
O1–C2	1.308(2)	1.25(7)	
C2–O2	1.208(2)	1.23(7)	
C2–C3	1.507(3)	1.52(9)	
C3–N4	1.440(2)	1.46(8)	
N4–C5	1.342(2)	1.34(8)	
C5–N6	1.343(2)	1.36(8)	
N6–C7	1.330(3)	1.34(8)	
C7–C8	1.380(3)	1.37(9)	
C8–C9	1.369(3)	1.36(9)	
C9–N10	1.327(3)	1.35(8)	
N10–C5	1.353(2)	1.34(8)	
Ag–O1		2.31(4)	
Ag–N6		2.19(5)	
Ag–Ag		3.099(11)	
Ag–O1		2.34(5)	
Ag1–O1			2.167(9)
Ag1–O2			2.222(8)
Ag1–O2′			2.490(8)
Ag1–Ag1			2.955(2)
Ag2–Ag2			3.047(3)
Ag1–I1′			3.1527(16)
Ag2–O1′			2.217(9)
N6–Ag–O1		142.9(18)	
N6-Ag–O1		134.5(17)	
O1–Ag–O1		81.8(14)	
N6–Ag–Ag		94.3(13)	
O1–Ag–Ag		98.1(12)	
O1–Ag–Ag		63.4(12)	
C7–N6–Ag		119(4)	
C5–N6–Ag		124(4)	
Cl–O1–Ag		130(4)	
Cl–O1–Ag		116(4)	
Ag–O1–Ag		111.4(19)	
O1–Ag1–O2			159.5(3)
O1–Ag1–O2′			113.0(3)
O1′–Ag2–O2′			147.8(3)
O2–Ag1–O2′			86.8(3)
O1–Ag1–Ag1			80.0(2)
O2–Ag1–Ag1			80.3(2)
O2′–Ag1–Ag1			147.4(2)
O1′–Ag2–Ag2			79.4(2)
O2′–Ag2–Ag2			75.4(2)
Ag2–O2′–Ag1			95.8(3)
Ag1–Ag1–I1′			125.05(6)
O1–Ag1–I1′			95.8(3)
O2–Ag1–I1′			90.9(2)
O2′–Ag1–I1′			84.7(2)
C7–I1′–Ag1			87.8(3)
C2–O1-Ag1			126.7(8)
C2′–O1′–Ag2			122.2(8)
C2–O2–Ag1			122.8(8)
C2′–O2′–Ag2			124.3(81)
C2′–O2′–Ag1			139.5(8)

3.2. Crystal structure of [Ag(pyr-gly)] · 0.5H_2O (*2*)

In this complex, [Ag(pyr-gly)] · 0.5H_2O (2), the metal ion present a very distorted tetragonal (3 + 1) coordination, nearly to trigonal pyramid, linked to two oxygen atoms of two carboxylato groups [Ag–O(1), 2.31(4)

Table 2
Crystal data and structure refinement for the three compounds

	1	2	3
Empirical formula	$C_3H_{3.50}N_{1.50}O$	$C_6H_7AgN_3O_{2.50}$	$C_{18}H_{14}Ag_2I_2N_2O_{8.50}$
Formula weight	76.57	269.02	863.85
Temperature (K)	294(2)	294(2)	293(2)
Wavelength (Å)	0.71073	0.71073	0.71073
Crystal system	orthorhombic	tetragonal	monoclinic
Space group	*Pmcn*	*I*41/*a*	*C*2/*c*
Unit cell dimensions			
a (Å)	6.487(2)	12.262(2)	19.951(5)
b (Å)	8.2545(9)	12.262(2)	7.656(2)
c (Å)	13.060(4)	20.338(3)	31.410(3)
α (°)	90	90	90
β (°)	90	90	94.240(10)
γ (°)	90	90	90
Volume (Å^3)	699.3(3)	3057.8(8)	4784.6(18)
Z	8	16	8
Density (calculated) (Mg m^{-3})	1.455	2.337	2.398
Absorption coefficient (mm^{-1})	0.113	2.602	4.266
F(000)	320	2096	3232
Crystal size (mm^3)	$0.65 \times 0.35 \times 0.27$	$0.15 \times 0.12 \times 0.12$	$0.47 \times 0.21 \times 0.08$
θ Range for data collection (°)	2.92–29.94	1.94–23.96	1.30–24.99
Index ranges	$0 \leqslant h \leqslant 9$; $0 \leqslant k \leqslant 11$; $0 \leqslant l \leqslant 18$	$-14 \leqslant h \leqslant 12$; $-12 \leqslant k \leqslant 14$; $-15 \leqslant l \leqslant 23$	$-23 \leqslant h \leqslant 23$; $0 \leqslant k \leqslant 9$; $-37 \leqslant l \leqslant 0$
Reflections collected	1101	4936	4353
Independent reflections [R_{int}]	1101	1195 [0.0806]	4196 [0.0616]
Completeness to $\theta = 24.99°$ (%)	100.0	100.0	99.7
Maximum and minimum transmission	0.9702 and 0.9303	0.6973 and 0.5352	0.7453 and 0.6962
Data/restraints/parameters	1101/0/87	1195/2/117	4196/0/299
Goodness-of-fit on F^2	1.067	1.095	1.041
Final *R* indices $I>2\sigma(I)$	$R_1 = 0.0509$, $wR_2 = 0.1367$	$R1 = 0.0340$, $wR_2 = 0.0635$	$R_1 = 0.0556$, $wR_2 = 0.1457$
R indices (all data)	$R_1 = 0.0790$, $wR_2 = 0.1606$	$R_1 = 0.0681$, $wR_2 = 0.0712$	$R_1 = 0.1081$, $wR_2 = 0.1777$
Extinction coefficient	0.016(6)		
Largest difference peak and hole (e Å^{-3})	0.486 and −0.188	0.439 and −0.592	1.448 and −1.877

and 2.34(5) Å] and a nitrogen atom of other pyr-gly molecule [Ag–N(6), 2.19(5) Å]. The coordination sphere is completed by means of a long Ag–Ag interaction [Ag–Ag, 3.099(11) Å], which must be considered, at least, as a short contact interaction. Thus, the value for distance Ag–Ag in metallic silver is 2.89 Å [35]. Short contacts present in coordination complexes are comprised between 2.86–3.07 Å in salicylic acid derivates [35]. Values of 2.85 are described for Ag–Ag metal bonds in di- and tetranuclear silver (I) saccharinate complexes [36]. In other tetranuclear silver units, values comprised between 2.93–3.13 Å are described [50,51]. In polymer structures, distances of 2.92–2.97 Å for 1D, and 2.89 Å and 2.88 Å for 2D polymers are presented [27,37]. Distances of 3.02, 3.12, 3.13 and 3.09 Å are described as short intermetallic contacts [7,26]. Finally a value of 3.30 Å is considered the upper limit for an Ag···Ag contact in coordination chemistry [52], whereas other authors stated that an actual Ag–Ag bond requires a distance of 2.89 Å or lower similar to the distance in metallic silver [35]. Between the five hundred references deposited in the CCDC, distances from 2.65 to 3.36 Å are considered Ag–Ag single bonds.

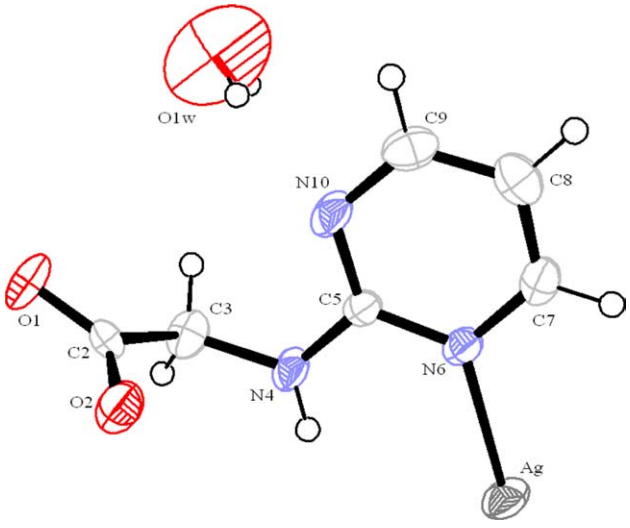

Fig. 2. ORTEP representation of [Ag(pyr-gly)] · 0.5H_2O (**2**).

A strong distortion in the coordination environment of the metal is indicated by the observed bond angles, which vary from 81.7° [O–Ag–O] to approximately 140.0° [O–Ag–N] in the basal plane, and from 63.4° to 98.1° with the apical Ag–Ag bond. The ORTEP

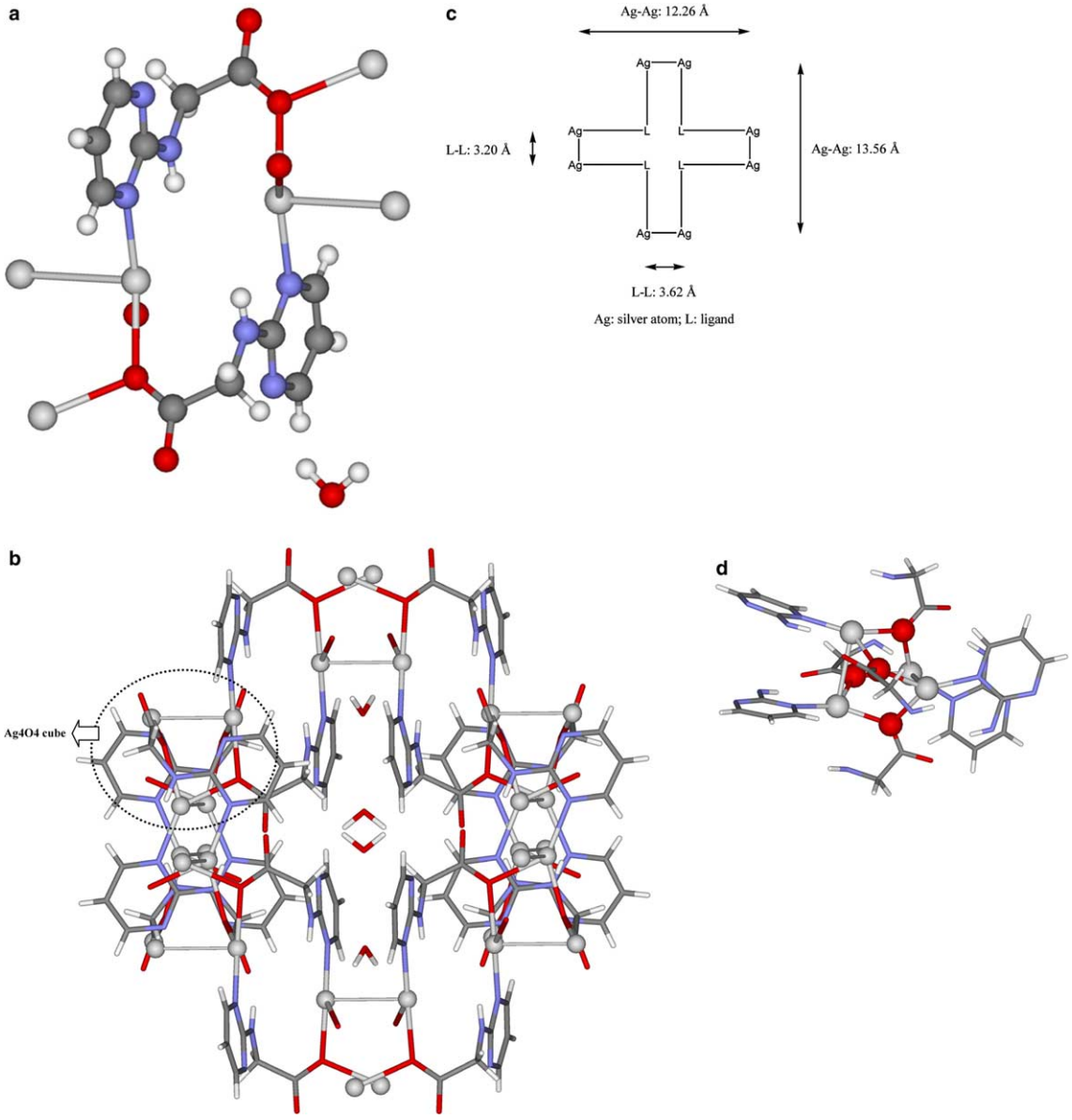

Fig. 3. Representation of the complex [Ag(pyr-gly)] · 0.5H_2O (**2**): (a) rectangular-shaped small holes; (b) bigger cross-type holes; (c) scheme of the hole; (d) cluster Ag_4O_4 very distorted cube.

representation of minimal asymmetric unit is depicted in Fig. 2. Selected bond lengths and angles are summarized in Table 1.

Two different holes, connecting among them are present in the structure (Fig. 3): (i) rectangular-shaped small holes, formed by two pyr-gly molecules and two silver atoms [C(2)–C(2′), 8.31; O(1)–C(3′), 6.92; Ag–N(6′), 3.74; Ag–N(4′), 2.91; and O(1)–C(3), 2.39 Å] (Fig. 3(a)), and (ii) bigger cross-type holes where several water molecules are present inside the channels, formed by four coplanar holes of the first type (Figs. 3(b) and 3(c)). Moreover, the water molecule present in the crystal structure is symmetrically distributed inside the hole, forming two hydrogen bonds with two non coordinated nitrogen of pyrimidine rings of two ligands [dist. N(10)···O(1w) and N(10′)···O(1w), 3.17 and 3.17 Å; angle N(10)···H–O(1w) and N(10′)···H–O(1w), 164.8 and 164.8°] forming a bridge between two pyr-gly molecules. In addition, the perfectly planar structure of the ligand changes to a quasi orthogonal disposition (dihedral angle between pyrimidine and –CH_2–COO– moieties, 80.4°). The three-dimensional network of this structure yields very distorted Ag_4O_4 cube (Fig. 3(d)).

A view of the three-dimensional network according to *a*-axis is depicted in Fig. 4. Four Ag_4O_4 cubes (with an Ag atom or an oxygen atom alternatively occupy the vertices of the distorted hexahedron) nucleate the 3D structure. The framework generates five tubular

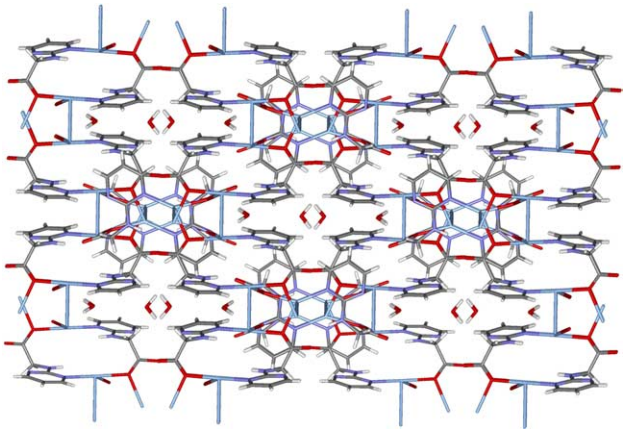

Fig. 4. View of the 3D network in [Ag(pyr-gly)] · 0.5H_2O (**2**) along the *a*-axis.

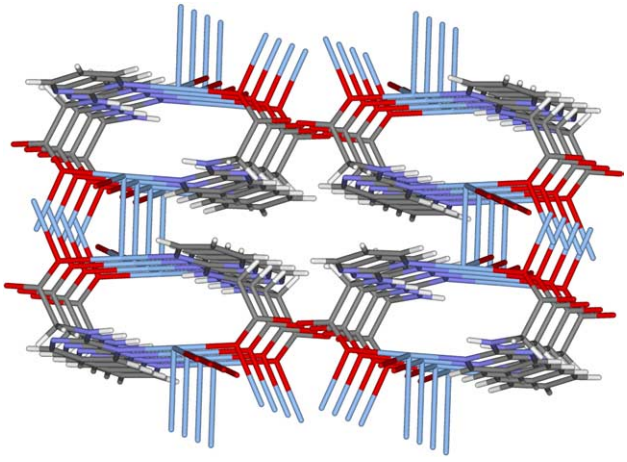

Fig. 5. Simplified structure of **2** showing the tubular cross holes. Different pseudo-layers are showed along the *a*-axis.

cross type holes were four water molecules are retained. One cross is showed in the centre of the figure, and four near the four corners of the picture. Interacting with this cross type holes, without any water molecule, four narrow channels encircled each cross type hole. The pseudo-layer depicted in Fig. 4 is repeated along the *a*-axis, being the Ag_4O_4 cubes the responsible of the 3D character of the structure connecting the apparent 2D planes formed by axis *b* and *c*. The connection between the cube unities is made with ligand cross-links. Each Ag atom is bound to an oxygen and a nitrogen atoms, another Ag atom and to an oxygen atom (from the carboxylic group) alternatively from upper or lower pseudo-layers.

A more clear vision of the channels is depicted in the Fig. 5, were the water molecules are not depicted for clarity. The pseudo layers are shown along the *a*-axis, perpendicular from the frontal *b*–*c* plane.

3.3. Crystal structure of [Ag(I-hip)] · 1.25H_2O (**3**)

The structure of [Ag(I-hip)] · 1.25H_2O (**3**), is shown in Fig. 6(a). This compound present two types of Ag(I) atoms, Ag1 and Ag2.[1] Thus, Ag1 corresponds to a distorted trigonal bipyramid geometry (3 + 2) [three shorter bond distances of Ag–O(carboxylate moiety): Ag–O(1), 2.167(9) Å, Ag–O(2), 2.222(8) Å and Ag–O(2′), 2.490(8) Å; a larger distance Ag1–Ag1, 2.955 Å; and a short contact Ag–I(7′), 3.15 Å]. Moreover, Ag2 possess a distorted octahedral environment (2 + 4) [shorter bond distances Ag–O(carboxylate): Ag–O(1′), 2.217(9) Å and Ag–O(2′), 2.253(9) Å, and larger distances Ag–O(2)(carboxylate), 2.688 Å, Ag–O(5′) (peptide moiety), 2.607 Å and Ag2–Ag2, 3.047 Å. The coordination sphere is completed with a short contact: Ag–I(7′), 3.36 Å].

These distance are in agreement with other carboxylato complexes, for instance [31] Powell refers values comprised between 2.22 and 2.51 Å for the short bonds. A typical value for longer coordination carboxylato bond is 2.757 Å [35]. As we have discussed in the previous complex distances for Ag–Ag are comprised between 2.72 and 3.36 Å [7,26,27,35–37,50–52]. Distances of magnitude like 2.955 and 3.047 Å, present in the compound **3**, are best described as short intermetallic contacts [7,26,50,51].

The number of references about silver–iodine bonds when the iodine is bound to an aryl or alkyl group is very limited in the literature [27–33]. Typical values are comprised between 2.812 and 3.309 Å [27–33]. The distances are longer for iodo-aryl derivatives, as for example 3.138 and 3.229 Å (aryl group: 1,2-diiodobenzene) and 3.309 Å (aryl group: iodobenzene) [31] or 3.053 Å (2,3,5-triiodobenzoato) [27]. Our distance values for Ag–I are 3.15 and 3.36 Å (aryl group: *o*-iodobenzoyl) which implies, in agreement with Powell and Ino [27,31], a weak interaction.

In the crystal packing it is possible to observe bi-dimensional networks build up by overlapped chains of 4 and 8 atoms links (Fig. 6(b)), which are connected between them through I-hip molecules bounded to Ag2 atoms across the peptide moieties. The lateral view of this network (Fig. 6(c)) shows the presence of rectangular-shaped holes along the *c*-axis [7.66 (vertically) and 11.31 Å (horizontally in the figure)], with an aryl ring of I-hip in the front and the top of every hole. The Fig. 6(c) depicts clearly one sheet perpendicular to the *c*-axis that is repeated along.

These bi-dimensional networks are piled in the *c*-direction. The interaction between two layers is made by van der Waals interactions and staking between aryl rings. Water molecules detach the different layers as an intercalation compound. In addition, each layer is

[1] In the crystallographic data we use Ag for Ag1 and Ag′ for Ag2.

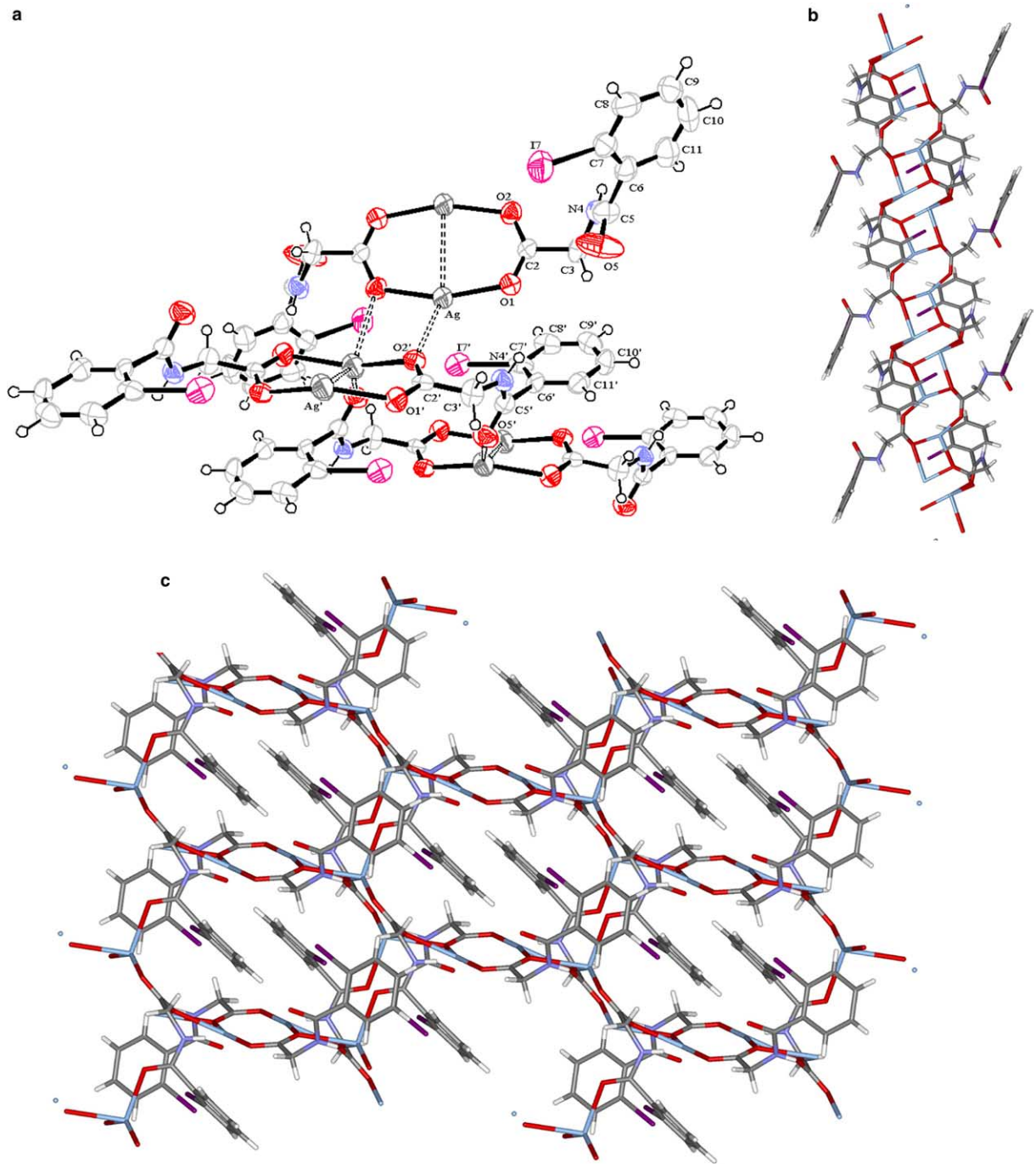

Fig. 6. Representation of the complex [Ag(I-hip)] · 1.25H_2O (**3**): (a) ORTEP; (b) bi-dimensional network builds up by overlapped chains of 4 and 8 atoms links; (c) macrocyclic holes along the *c*-axis.

connected with the next one by stacking (distance, 3.38 Å) [39,53] between series of two aryl rings inside of the channel and preserving it along the *c*-axis (Fig. 7). Selected bond lengths and angles are summarized in Table 1.

It must be mentioned other short contact interactions between iodine atoms and the entourage. Distances I(7)···H of 3.10 and 3.08 Å are distinctly shorter than the van der Waals distance of 3.18 Å determined by Bondi [54]. I(7′)···O(peptide) of 3.47 Å are also observed (van der Waals distance: 3.50 Å). The two interactions can be considered short contacts as it occurs in some described structures [43,55–57]. This ligand shows similar contacts that other related binary and ternary complexes previously described: Thus, binary complex $Zn(I\text{-}hip)_2$ shows a I···C(aromatic ring) contact of 3.56 Å (similar to a C–H···π interaction) shorter than the corresponding van der Waals distance (3.68 Å). On the other hand, ternary derivatives (Zn, Co or Ni)

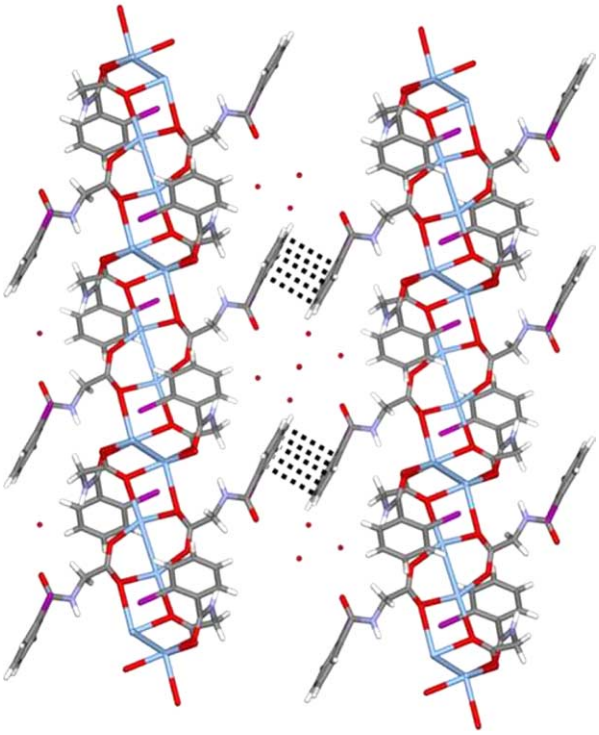

Fig. 7. Two bi-dimensional networks, in complex **3**, connected by stacking (dotted lines). The water molecules detach the different layers.

$(I\text{-hip})_2(ACV)$ with I···I distances of 3.80 and 3.79 Å (van der Waals distance: 3.96 Å) and I···H of 3.15 Å should be mentioned [39].

4. Conclusion

Using relatively flexible *N*-substituted glycine derivatives with *o*-iodobenzoyl or pyrimidyl substituents creates a new possibility in the design of coordination networks. The lack of reactivity of the nitrogen atom of the peptidic bond of I-Hip, the planarity of peptidic bond and the fact that the conformation of the iodo-aryl group is perpendicular to the peptidic group provides an unique ligand with a capability to produce 2D networks with silver(I). Comparison was made with a similar glycine derivative as ligand, with less steric restrictions of bulky susbstituents, but with the same "bite" for coordination (pyr-gly). This ligand instead produces 3D structures.

5. Supplementary material

CCDC Nos. 269071, 269072 and 269073 contains the supplementary crystallographic data for this paper, corresponding to the compounds **1**, **2** and **3**, respectively. These data can be obtained free of charge from The Director, CCDC, 12 Union Road, Cambridge, CB2 1EZ, UK, fax: +44 1223 366 033, e-mail: deposit@ccdc.ac.uk or www.ccdc.cam.ac.uk/conts/retrieving.html.

Acknowledgements

We are grateful to Dirección General de Investigación Científica y Técnica Project No. BQU0002-02546, and to COST D-20 WG-006 for financial support. We also thank Mr. lago López for his contribution to the preparation of *N*-(pyrimidyl)glycine.

References

[1] J.M. Lehn, Supramolecular Chemistry – Concepts and Perspectives, VCH, Weinheim, 1995.
[2] B.C. Constable, An Introduction to the Organic Chemistry of Metal Complexes, VCH, Weinheim, 1996.
[3] M. Munakata, L.P. Wu, G.L. Ning, Coord. Chem. Rev. 198 (2000) 171.
[4] R.-H. Wang, M.-C. Hong, W.-P. Su, Y.-C. Liang, R. Cao, Y.-J. Zhao, J.-B. Weng, Inorg. Chim. Acta 323 (2001) 139.
[5] C.V.K. Sharma, S.T. Griffin, R.D. Rogers, Chem. Commun. (1998) 215.
[6] C.V.K. Sharma, R.D. Rogers, Crystal Eng. 1 (1998) 19.
[7] J.A.R. Navarro, J.M. Salas, M.A. Romero, R. Faure, J. Chem. Soc., Dalton Trans. (1998) 901.
[8] I.W. Hamley, Angew. Chem., Int. Ed. Eng. 42 (1998) 1692.
[9] Y.H. Kiang, G.B. Gardner, S. Lee, Z. Xu, E.B. Lobkovsky, J. Am. Chem. Soc. 121 (1999) 8204.
[10] M. Bartelli, L. Carlucci, G. Ciani, D.M. Proserpio, A. Sironi, J. Mater. Chem. 7 (1997) 1271.
[11] O. Mamula, A. von Zelewsky, T. Bark, G. Bernardinelli, Angew. Chem., Int. Ed. Engl. 38 (1999) 2945.
[12] S.Q. Liu, T. Kuroda-Sowa, H. Konaka, Y. Suenaga, M. Maekawa, T. Mizutani, G.L. Ning, M. Munakata, Inorg. Chem. 44 (2005) 1031.
[13] L. Carlucci, G. Ciani, D.M. Proserpio, A. Sironi, J. Am. Chem. Soc. 117 (1995) 4562.
[14] M. Munakata, L.P. Wu, T. Kuroda-Sowa, Bull. Chem. Soc. Jpn. 70 (1997) 1727.
[15] G.L. Ning, L.P. Wu, K. Sugimoto, M. Munakata, T. Kuroda-Sowa, M. Maekawa, J. Chem. Soc., Dalton Trans. (1999) 2529.
[16] D.D. Wu, T.C.W. Mak, J. Chem. Soc., Dalton Trans. (1995) 2671.
[17] W. Su, R. Cao, M. Hong, W.-T. Wong, J. Lu, Inorg. Chem. Commun. 2 (1999) 241.
[18] Y. Kang, S.S. Lee, K.-M. Park, S.H. Lee, S.O. Kang, J. Ko, Inorg. Chem. 40 (2001) 7027.
[19] E.C. Constable, C.E. Housecroft, M. Neuburger, S. Reymann, S. Schaffner, Chem. Commun. (2004) 1056.
[20] M.-L. Tong, X.-M. Chen, B.-H. Ye, S.W. Ng, Inorg. Chem. 37 (1998) 5278.
[21] H.-L. Hu, C.-W. Yeh, J.-D. Chen, Eur. J. Inorg. Chem. (2004) 4696.
[22] M.C. Brandys, R.J. Puddephatt, J. Am. Chem. Soc. 124 (2002) 3946.
[23] G. Smith, B.A. Cloud, D.E. Lynch, K.A.L. Byriel, C.H.L. Kennard, Inorg. Chem. 37 (1998) 3236.
[24] H. Cai, H.-M. Hu, W.-Z. Chen, H.-G. Zhu, X.-Z. You, Chem. Lett. 28 (1999) 221.
[25] L. Carlucci, G. Ciani, D.M. Proserpio, S. Rizzato, J. Solid State Chem. 152 (2000) 211.

[26] A.L. Pickering, D.-L. Long, L. Cronin, Inorg. Chem. 43 (2004) 4953.
[27] I. Ino, L. Ping, M. Munakata, M. Maekawa, Y. Suenaga, T. Kuroda-Sowa, Y. Kitamori, Inorg. Chem. 39 (2000) 2146.
[28] I. Ino, J.C. Zhong, M. Munakata, T. Kuroda-Sowa, M. Maekawa, Y. Suenaga, Y. Kitamori, Inorg. Chem. 39 (2000) 4273.
[29] L.P. Wu, M. Munakata, T. Kuroda-Sowa, M. Maekawa, Y. Kitamori, Inorg. Chim. Acta 290 (1999) 251.
[30] J. Powell, M. Horvath, A. Lough, J. Organomet. Chem. 456 (1993) C27.
[31] J. Powell, M. Horvath, A. Lough, A. Phillips, J. Brunet, J. Chem. Soc., Dalton Trans. (1998) 637.
[32] J. Powell, M. Horvath, A. Lough, J. Chem. Soc., Chem. Commun. (1993) 733.
[33] J. Powell, M. Horvath, A. Lough, J. Chem. Soc., Dalton Trans. (1996) 1669.
[34] T. Kuroda-Sowa, S.Q. Liu, Y. Yamazaki, M. Munakata, M. Maekawa, Y. Suenaga, H. Konaka, H. Nakagawa, Inorg. Chem. 44 (2005) 1686.
[35] B. Coyle, M. McCann, K. Kavanagh, M. Devereux, V. Mckee, N. Kayal, D. Egan, C. Deagan, G.J. Finn, J. Inorg. Biochem. 98 (2004) 1361.
[36] V.T. Yilmaz, S. Hamamci, W.T.A. Harrison, C. Thöne, Polyhedron 24 (2005) 693.
[37] E. Bosch, C.L. Barnes, Inorg. Chem. 41 (2002) 2543.
[38] M.C. Capllonch, A. García-Raso, A. Terrón, M.C. Apellla, E. Espinosa, E. Molins, J. Inorg. Biochem. 85 (2001) 173.
[39] M. Barceló-Oliver, A. Terrón, A. García-Raso, J.J. Fiol, E. Molins, C. Miravitlles, J. Inorg. Biochem. 98 (2004) 1703, and references therein.
[40] Y.-Q. Gong, Y.-F. Cheng, J.-M. Gu, X.-R. Hu, Polyhedron 16 (1997) 3743.
[41] A. Terrón, A. García-Raso, J.J. Fiol, S. Amengual, M. Barceló-Oliver, R.M. Tótato, M.C. Apella, E. Molins, I. Mata, J. Inorg. Biochem. 98 (2004) 632.
[42] A. García-Raso, J.J. Fiol, F. Bádenas, A. Tasada, X. Solans, M. Font-Bardia, M.G. Basallote, M.A. Máñez, M.J. Fernández-Trujillo, D. Sańchez, J. Inorg. Biochem. 93 (2003) 141.
[43] F. Zhang, Y.-Z. Li, X. Gao, H.-L. Chen, Q.-T. Liu, A. Odani, O. Yamauchi, Chem. Lett. 33 (2004) 556.
[44] A.H. Blatt et al., Organic Synthesis Collective Volume 2, John Wiley & Sons, New York, 1943, p. 328.
[45] F. Wild, in: S.A. Gustavo Gili (Ed.), Identificación de Compuestos Orgánicos (Spanish translation of Characterization of Organic Compounds), Cambridge University Press, Spain, 1951, p. 186.
[46] L.J. Farrugia, J. Appl. Crystallogr. 32 (1999) 837.
[47] M.C. Burla, M. Camalli, B. Carrozzini, G.L. Cascarano, C. Giacovazzo, G. Polidori, R. Spagna, J. Appl. Crystallogr. 36 (2003) 1103.
[48] G.M. Sheldrick, Programs for Crystal Structure Analysis (Release 97-2), Institüt für Anorganische Chemie der Universität, Tammanstrasse 4, D-3400 Göttingen, Germany, 1998.
[49] L.J. Farrugia, J. Appl. Crystallogr. 30 (1997) 565.
[50] L.S. Ahmet, J.R. Dilworth, J.R. Miller, N. Wheatley, Inorg. Chim. Acta 278 (1998) 229.
[51] S.-P. Yang, H.-L. Zhu, X.-H. Yin, X.-M. Chen, L.-N. Ji, Polyhedron 19 (2000) 2237.
[52] M. Jansen, Angew. Chem., Int. Ed. Engl. 26 (1987) 1098.
[53] O. Yamauchi, A. Odani, M. Takani, J. Chem. Soc., Dalton Trans. (2002) 3411, and references therein.
[54] A. Bondi, J. Phys. Chem. 68 (1964) 441.
[55] F. Zhang, A. Odani, H. Masuda, O. Yamauchi, Inorg. Chem. 35 (1996) 7148.
[56] F. Zhang, T. Yajima, H. Masuda, A. Odani, O. Yamauchi, Inorg. Chem. 36 (1997) 5777.
[57] F. Zhang, T. Yajima, A. Odani, O. Yamauchi, Inorg. Chim. Acta 278 (1998) 136.

Available online at www.sciencedirect.com
SCIENCE DIRECT®
Polyhedron 25 (2006) 81–86
POLYHEDRON
www.elsevier.com/locate/poly

Crystal structure, magnetism and spectroscopy of a dinuclear Cu(II) compound with a chiral ligand; $Cu_2(SL)(\mu\text{-}Cl)(Cl)_2(CH_3OH)$ (HSL = *S*-1,2-bis(benzimidazol-2-yl)-1-hydroxyethane)

Gerard A. van Albada [a], Ilpo Mutikainen [b], Urho Turpeinen [b], Jan Reedijk [a,*]

[a] *Leiden Institute of Chemistry, Gorlaeus Laboratories, Leiden University, P.O. Box 9502, 2300 RA Leiden, The Netherlands*
[b] *Laboratory of Inorganic Chemistry, Department of Chemistry, P.O. Box 55 (A.I.Virtasen aukio 1), 00014 University of Helsinki, Finland*

Received 8 June 2005; accepted 3 July 2005
Available online 29 August 2005

Abstract

The dinuclear compound, $Cu_2(SL)(\mu\text{-}Cl)(Cl)_2(CH_3OH)$ (in which HSL is the chiral ligand *S*-1,2-bis(benzimidazol-2-yl)-1-hydroxyethane), has been synthesized and characterized by X-ray crystallography and infrared spectroscopy. In addition, EPR and magnetic measurements have been performed, and related to the dinuclear structural details. The compound crystallizes in the orthorhombic space group $P2_12_12_1$, with $a = 6.1240(12)$ Å, $b = 15.780(3)$ Å, $c = 20.316(4)$ Å, $V = 1963.3(7)$ Å^3 and $Z = 4$.

The Cu1 ion has a distorted square-pyramidal geometry with the basal plane consisting of a nitrogen atom from the ligand with a Cu–N distance of 1.995(8) Å, a bridging oxygen atom of the ligand with a Cu–O distance of 1.943(8) Å and two chloride anions (of which one is bridging to Cu2) with Cu–Cl distances of 2.259(3) and 2.351(3) Å. The apical position is occupied by a third chloride atom (Cl3), which is also connected to Cu2 from a neighbouring unit, at a semi-coordinating distance of 3.114(3) Å.

The second copper atom, Cu2, has also a distorted square-pyramidal geometry with the basal plane also consisting of a nitrogen atom from the ligand with a Cu–N distance of 1.960(8) Å, a bridging oxygen atom of the ligand with a Cu–O distance of 1.934(8) Å and two chloride atoms (of which one is bridging to Cu1) with Cu–Cl distances of 2.258(3) and 2.309(3) Å. The apical position is occupied by an oxygen atom of a coordinating methanol molecule at a distance of 2.392(3) Å. The bridging Cl3 atom, forms a zig-zag chain between Cu1 and Cu2 from different units forming an extended chain with a Cu···Cu distance of 4.2114(19) Å. The intramolecular Cu···Cu distance is 3.2301(18) Å.

At room temperature the title compound displays an EPR silent behaviour and magnetic susceptibility measurements, down to 5 K, agree with a strong overall antiferromagnetic interaction having a large singlet-triplet splitting ($J = -348$ cm^{-1}).
© 2005 Elsevier Ltd. All rights reserved.

Keywords: Copper; Structure; Magnetism; Dinuclear; EPR

1. Introduction

The coordination chemistry of azoles acting as ligands in copper(II) compounds in the context of modelling biological systems has gained much interest in the past decades [1–4]. In this respect bis(2-benzimidazoles) have received much attention for their wide-ranging antivirus activity [5,6], their importance in selective ion-exchange resins [7,8] and the possibility to form supramolecular aggregates with d^{10} metal ions [9].

Previously, spectroscopic and magnetic properties, as well as some structures of copper(II) coordination compounds with bis(2-benzimidazolyl)alkanes and

* Corresponding author.
E-mail address: reedijk@chem.leidenuniv.nl (J. Reedijk).

0277-5387/$ - see front matter © 2005 Elsevier Ltd. All rights reserved.
doi:10.1016/j.poly.2005.07.013

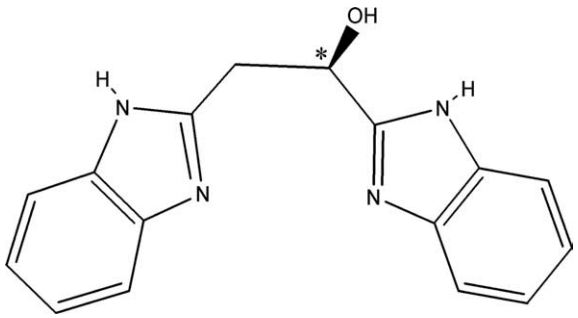

Scheme 1. 1,2-bis(benzimidazol-2-yl)-1-hydroxyethane (* = chiral atom).

zsome substituted bis(2-benzimidazolyl)alkanes have been reported [10–20] by others and us. In one of the earlier studies, we synthesized racemic mixture of a chiral, chelating ligand, i.e., 1,2-bis(benzimidazol-2-yl)-1-hydroxyethane (abbreviated HRSL) (see Scheme 1) [19]. The chiral centre is present at C*, allowing also the study of the (*R*) and (*S*) isomers of this ligand, apart from the (*RS*) mixture. In this earlier study, a number of transition metal compounds were synthesized from the racemic ligand. Also two X-ray crystal structures were reported, one of a tetranuclear copper(II) compound and one of a mononuclear Ni(II) compound. In both cases, the ligand acts as a tridentate chelating ligand with dehydronation of the alcohol oxygen.

The present study describes a new Cu(II) dinuclear compound, using the *S* isomer of the ligand. The compound $Cu_2(SL)(\mu\text{-}Cl)(Cl)_2(CH_3OH)$ contains a bridging chloride ion in addition to the trinuclear chelating ligand. This compound was characterised by X-ray structure analysis, ligand-field and EPR. Also the magnetic susceptibility was investigated and discussed.

2. Experimental

2.1. General

C,H,N determinations were performed on a Perkin–Elmer 2400 Series II analyzer. Ligand field spectra were obtained on a Perkin–Elmer Lambda900 spectrophotometer using the diffuse reflectance technique, with MgO as a reference. X-band powder EPR spectra were obtained on a Jeol RE2x electron spin resonance spectrometer using DPPH ($g = 2.0036$) as a standard. FTIR spectra were obtained on a Perkin–Elmer Paragon 1000 FTIR spectrophotometer equipped with a Golden Gate ATR device, using the reflectance technique (4000–300 cm^{-1}, res. 4 cm^{-1}). Magnetic susceptibility measurement (5–300 K) were carried out (at 0.1 T) using a Quantum Design MPMS-5S SQUID magnetometer. Data were corrected for the magnetisation of the sample holder and for diamagnetic contributions, which were estimated from Pascal constants.

2.2. Synthesis

The ligands HRSL and HSL (the racemic mixture and the *S* form, respectively, of 1,2-bis(benzimidazol-2-yl)-1-hydroxyethane) and the coordination compounds were synthesized as described in the literature [19]. After dehydronation the abbreviations RSL and SL, respectively, are being used. The Cu(II) chloride compound with the ligand HRSL (the racemic mixture) only provides a powder and no crystalline material could be obtained. Fortunately, very small green crystals were obtained when the ligand HSL and methanol as a solvent were used and these crystals were characterized by elemental analysis, Yield: 82%, Elemental *Anal*. Calc. for $C_{17}H_{17}Cl_3Cu_2N_4O_2$: C, 38.0; H, 3.1; N, 10.4. Found: C, 37.6; H, 3.2; N, 10.3%.

2.3. X-ray crystallography

A crystal was selected and mounted to the glass fiber using the oil-drop method; data were collected on a Nonius KappaCCD diffractometer (graphite-monochromated Mo Kα radiation). The intensity data were corrected for Lorentz and polarization effects, for absorption and extinction. The structures were solved by direct methods. The programs COLLECT [21], SHELXS-97 [22], SHELXL-97 [23] were used for data reduction, structure solution and structure refinement,

Table 1
Crystallographic data for $Cu_2(SL)(\mu\text{-}Cl)(Cl)_2(CH_3OH)$

Formula	$C_{17}H_{17}Cl_3Cu_2N_4O_2$
Molecular weight	542.80
Crystal system	orthorhombic
Space group	$P2_12_12_1$ (No. 19)
a (Å)	6.1240(12)
b (Å)	15.780(3)
c (Å)	20.316(4)
V (Å^3)	1963.3(7)
Z	4
D_{calc} (g cm^{-3})	1.836
$F(000)$	1088
μ (mm^{-1})	2.596
Crystal size (mm)	$0.17 \times 0.12 \times 0.07$
Temperature (K)	173(2)
θ_{min}, θ_{max} (°)	3.27, 27.53
Total reflections	39 158
Total unique reflections (R_{int})	4402 (0.092)
Observed reflections ($I > 2\sigma(I)$)	3802
Number of refined parameters	250
R[a], wR_2[b], S	0.0824, 0.2032, 1.13
Minimum and maximum residual densities (e/Å^3)	−0.95 and 3.24

[a] $R_1 = \sum||F_o| - |F_c||/\sum|F_o|$.
[b] $wR_2 = [\sum[w(F_o^2 - F_c^2)^2]/\sum[w(F_o^2)^2]]^{1/2}$.

respectively. Refinement of F^2 was done against all reflections. All non-hydrogen atoms were refined anisotropically. The H atoms were introduced in calculated positions and refined with fixed geometry with respect to their carrier atoms. Crystallographic data are presented in Table 1.

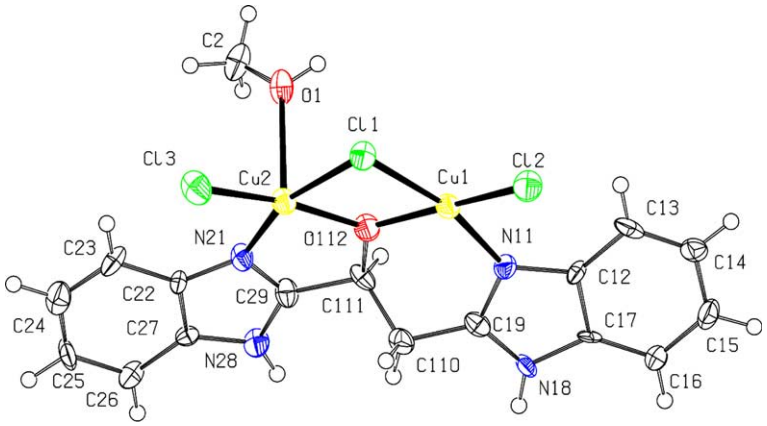

Fig. 1. Atomic displacement plot (50% probability level) of the molecular structure of $Cu_2(SL)(\mu\text{-}Cl)(Cl)_2(CH_3OH)$.

Table 2
Selected bond lengths (Å) and angles (°) for $Cu_2(SL)(\mu\text{-}Cl)(Cl)_2(CH_3OH)$

Cu1–Cl1	2.351(3)
Cu1–O112	1.943(8)
Cu1–Cl3A	3.114(3)
Cu2–Cl3	2.258(3)
Cu2–O112	1.934(8)
Cu1–Cu2	3.2301(18)
Cu1–Cl2	2.259(3)
Cu1–N11	1.995(8)
Cu2–Cl1	2.309(3)
Cu2–O1	2.3923
Cu2–N21	1.960(8)
Cu1–Cu2A	4.2114(19)
Cl1–Cu1–Cl2	91.51(10)
Cl1–Cu1–N11	167.1(2)
Cl2–Cu1–N11	96.6(2)
Cl1–Cu2–Cl3	93.67(11)
Cl1–Cu2–O112	80.1(2)
Cl3–Cu2–O1	97.58
Cl3–Cu2–N21	101.8(2)
O1–Cu2–N21	102.17
Cu1–Cl1–Cu2	87.75(9)
Cl1–Cu1–O112	78.9(2)
Cl2–Cu1–O112	167.8(2)
O112–Cu1–N11	91.7(3)
Cl1–Cu2–O1	85.06
Cl1–Cu2–N21	161.7(2)
Cl3–Cu2–O112	166.3(3)
O1–Cu2–O112	94.02
O112–Cu2–N21	82.7(3)
Cu1–O112–Cu2	112.8(4)

D–H···A	D–H (Å)	H···A (Å)	D···A (Å)	D–H···A (°)
Hydrogen-bonding parameters				
O1–H1A···Cl3 [−1 + *x*, *y*, *z*]	0.84	2.53	3.2518	144
N18–H18A···O1 [−*x*, 1/2 + *y*,1/2 − *z*]	0.88	2.04	2.8917	164
N28–H28A···Cl2 [−x, 1/2+y,1/2−z]	0.88	2.61	3.295(8)	135

A = −1 + *x*, *y*, *z*.

3. Results and discussion

3.1. Crystal structure of $Cu_2(SL)(\mu\text{-}Cl)(Cl)_2(CH_3OH)$

The structure of the title compound is depicted in Fig. 1, with relevant bond length and bond angle information given in Table 2. Both Cu ions have both a slightly different five-coordination geometry. The Cu1 atom has the basal plane consisting of a nitrogen atom from the ligand with a Cu–N distance of 1.995(8) Å, a bridging oxygen atom of the ligand with a Cu–O distance of 1.943(8) Å and two chloride atoms (of which one is bridging to Cu2) with Cu–Cl distances of 2.259(3) and 2.351(3) Å. The angles of the basal plane are 167.1(2)° and 167.8(2)°. The apical position is occupied by a third chloride atom (Cl3), which is also connected to Cu2 ion from a neighbouring unit, at a semi-coordinating distance of 3.114(3) Å. The intermolecular Cu···Cu distance is 4.2114(19), while the intramolecular Cu···Cu distance is 3.2301(18) Å.

The second copper atom, Cu2, has the basal plane also consisting of a nitrogen atom from the ligand with a Cu–N distance of 1.960(8) Å, a bridging oxygen atom of the ligand with a Cu–O distance of 1.934(8) Å and two chloride atoms (of which one is bridging to Cu1) with Cu–Cl distances of 2.258(3) and 2.309(3) Å. The trans angles of the basal plane are 161.7(2)° and 166.3(3)°. The apical position is occupied by an oxygen atom of a coordinating methanol molecule at a distance of 2.392(3) Å.

The degree of distortion in five-coordinated compounds can be described by the structural parameter τ (τ describes the relative amount of trigonality; $\tau = 0$ for square pyramidal and $\tau = 1$ for trigonal bipyramidal) [24]. This value is only 0.01 and 0.08 for Cu1 and Cu2, respectively, providing for both copper compounds almost a perfect square pyramidal geometry. The bridging Cl3 atom, forms a zig-zag chain between Cu1 and Cu2 from different units forming a extended chain (see Fig. 2).

The crystal lattice is further stabilised by an extensive H-bonding system between an imidazole nitrogen atom and the methoxo oxygen atom (N18···O1 2.8917 Å), between an imidazole nitrogen atom and a chloride anion (N26···Cl2 3.295(8) Å) and between the methoxo oxygen atom and a chloride anion (O1···Cl3 3.2518 Å). More details are given in Table 2.

3.2. Ligand field spectroscopy and EPR

The ligand-field transition band measured as a solid with the diffuse reflectance technique is not quite informative and is observed as a very broad tail-shaped band with a maximum at 14.1×10^3 cm^{-1}, which is a normal ligand field transition for distorted square pyramidal geometries [25].

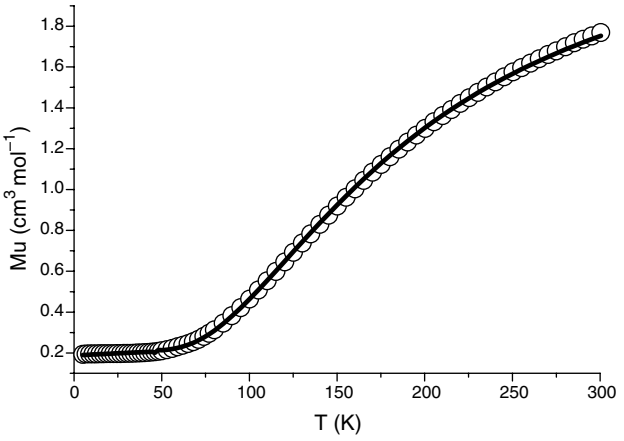

Fig. 3. A plot of the temperature dependence of μ_{eff} vs. T for $Cu_2(SL)(\mu\text{-}Cl)(Cl)_2(CH_3OH)$. The solid line represents the calculated curve for the parameters $J = -348$ cm^{-1}, $g = 2.04$, $zJ' = -0.015$ cm^{-1} (see text).

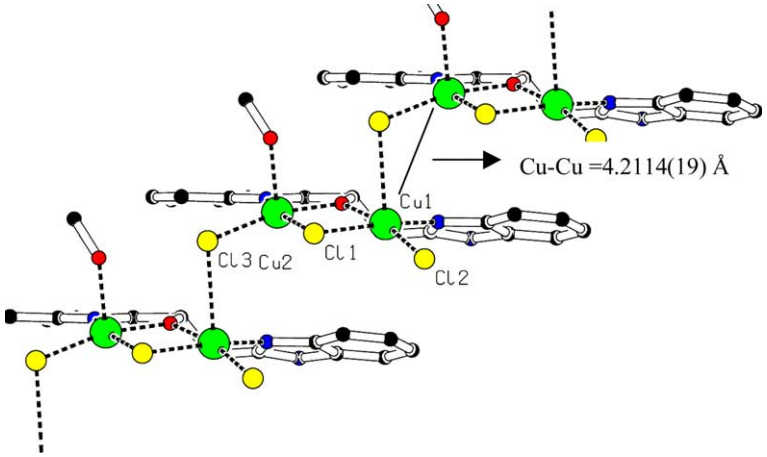

Fig. 2. The polymeric zig-zag chain formed by the bridging chloride anion in $Cu_2(SL)(\mu\text{-}Cl)(Cl)_2(CH_3OH)$. Hydrogen atoms are omitted for clarity.

Table 3
Relevant dinuclear Cu(II) oxygen/chloride bridged compounds

Compound[a]	Cu–O–Cu angle (°)	Cu–Cl–Cu angle (°)	Cu–Cu distance (Å)	J (cm^{-1})	References
$[Cu_2(L1)(\mu\text{-}Cl)](BPh_4)(C_2H_6O)$	111.4(3)	89.6(1)	3.265	−335	[37]
$[Cu_2(L2)(\mu\text{-}Cl)(Cl)_2](CH_3OH)$	113.4(2)	86.1(0)	3.255(1)	−443	[38]
$Cu_2(L3)(\mu\text{-}Cl)(Cl)_2$	116.23[b]	84.81[b]	3.293(5)[b]	−374	[39]
	115.18	84.84	3.272		
$Cu_2(SL)(\mu\text{-}Cl)(Cl)_2(CH_3OH)$	112.8(4)	87.75(9)	3.2301(18)	−348	this work

[a] *Abbreviations:* L1 = 2,6-bis(bis(2-pyridylethyl)aminomethyl)phenolate; BPh_4, tetraphenylborate; L2 = 2,6-bis(4-(2-benzimidazolyl)-2-thiabutyl)-4-methylphenolate; L3 = 2,6-bis(*N*-methyl-*N*-(2-pyridylethyl)aminomethyl)phenolate.
[b] Two crystallographic independent dinuclear units present in the unitcell.

The EPR of the title compound, measured as a polycrystalline powder at RT is weak and very broad and almost EPR silent, while at 77 K only a very weak mononuclear signal is observed with $g_\perp = 2.06$, $g_\parallel = 2.28$ and $A_\parallel = 12.7$ mT. The absence of an EPR signal indicates a strong AF interaction (vide infra), while the weak signal at 77 K most probably originates from a small mononuclear impurity, which is usually present in dinuclear compounds, as has been also observed earlier [19]. No triplet signals are visible, indicating that the zero-field splitting is larger then the EPR frequency.

3.3. Magnetic properties

The magnetic susceptibility of a powdered sample was measured from 5 to 300 K. The magnetic properties of the complex are depicted in Fig. 3 in the form of μ_{eff} versus T for two Cu(II) ions. At 300 K, the μ_{eff} starts at a value of about 1.76 BM (much below the spin only value for two Cu ions of 2.83 BM) and the μ_{eff} gradually decreases at 50 K to about 0.10 BM and stays then constant till 5 K. This behaviour agrees with a strong antiferromagnetic interaction.

The theoretical expression for the magnetic susceptibility for two interacting $S = 1/2$ centres, which is based on the general Hamiltonian [26] is: $H_{ex} = -JS_1S_2$, in which the exchange parameter J, is negative for antiferromagnetic and positive for ferromagnetic interaction. The magnetic data were fitted to the equation given in the literature for dinuclear copper compounds [26]:

$$\chi_m = (2N\mathrm{g}^2\beta^2)[kT - (2zJ'/(3 + \exp(-J/kT)))]^{-1} \times [3 + \exp(-J/kT)]^{-1}(1 - p) + \chi_p p,$$

in which N, g, β, k and T have their usual meanings [26]. The parameter p denotes the fraction of paramagnetic impurity in the sample and zJ' the interaction between neighbouring dinuclear identities. The fit was accomplished by minimisation of $R = (\chi_m T_{calc} - \chi_m T_{obs})^2/(\chi_m T_{obs})^2$ by a least-squares procedure. The best fit, depicted in Fig. 3 as a solid line, was obtained for $J = -348$ cm^{-1}, $g = 2.04$, $zJ' = -0.015$ cm^{-1}, $p = 0.006$, with a final R of 3.0×10^{-2}.

The magnitude of the antiferromagnetic interaction also corresponds very nicely with the preliminary results for the compound $Cu_2(RSL)Cl(Cl)_2(H_2O)$, a compound for which no X-ray crystal structure could be obtained in our earlier study [19].

4. Concluding remarks

A new dinuclear chloride-bridged Cu(II) compound prepared from the tridentate chelating ligand HSL is described. The dinuclear unit contains two Cu(II) ions with different geometries and a third chloride anion, which is bridging between two Cu ions from different units forming a polymeric zig-zag chain.

The magnetic interaction between the two Cu ions in the dinuclear unit is strongly antiferromagnetic ($J = -348$ cm^{-1}). In the literature much research has been undertaken to describe the relationship between the Cu–X–Cu (where X = OH, MeO, Cl, etc.) angle and the magnetic interaction [27–36]. A number of Cu(II) dinuclear compounds which have the same bridge and which are structurally and magnetically characterised are summarised in Table 3. As can be seen from Table 3 the Cu–Cl–Cu bridge is in all cases <90°, which contribution should be weakly ferromagnetic [36], while the Cu–O–Cu angle is in all cases >110° and this contribution should be the strongly antiferromagnetic [35]. In total the "overall" magnetic exchange interaction is then strong antiferromagnetic, which is in fact observed in all five compounds.

5. Supplementary material

Crystallographic data (excluding structure factors) for the structure reported in this paper have been deposited with the Cambridge Crystallographic Data Centre as Supplementary Publication No. CCDC-273762. Copies of available material can be obtained, free of charge, on application to the Director, CCDC, 12 Union Road, Cambridge, CB2 1EZ, UK, fax: +44 1223 366 033, e-mail: deposit@ccdc.ac.uk or on the web www: http://www.ccdc.cam.ac.uk.

Acknowledgements

The work described in this paper was supported by the Leiden University Study group WFMO (Werkgroep Fundamenteel Materialen Onderzoek) and the Council for Chemical Sciences of the Netherlands Organisation for Scientific Research (CW-NWO). Part of the was supported financially by the Graduate Research School Combination NRSC "Catalysis".

References

[1] J. Reedijk, in: G. Wilkinson, R.D. Gillard, J.A. McCleverty (Eds.), Comprehensive Coordination Chemistry, vol. 2, Pergamon Press, 1987, p. 73.
[2] E. Bouwman, W.L. Driessen, J. Reedijk, Coord. Chem. Rev. 104 (1990) 143.
[3] T.N. Sorrell, Tetrahedron 45 (1989) 3.
[4] P. Zanello, S. Tamburini, P.A. Vigato, G.A. Mazzocchin, Coord. Chem. Rev. 77 (1987) 165.
[5] B. Çakir, E. Büyükbingöl, Ü. Uçucu, U. Abbasoğlu, N. Noyanalpan, J. Fac. Pharm. Gazi 5 (1988) 71.
[6] W.R. Roderick, C.W. Nordeen Jr., A.M. von Esch, R.N. Appell, J. Med. Chem. 15 (1972) 655.
[7] H.J. Hoorn, P. de Joode, W.L. Driessen, J. Reedijk, React. Funct. Polym. 27 (1995) 223.
[8] P.M. van Berkel, D.J. Dijkstra, W.L. Driessen, J. Reedijk, D.C. Sherrington, React. Funct. Polym. 28 (1995) 39.
[9] C. Piquet, J.-C.G. Bünzli, G. Bernardinelli, G. Hopfgartner, A.F. Williams, J. Alloys Compd. 225 (1995) 324.
[10] G. Bernardinelli, A. Kübel-Pollak, S. Rüttimann, A.F. Williams, Chimia 46 (1992) 155.
[11] (a) G. Bernardinelli, A. Kübel-Pollak, S. Rüttimann, A.F. Williams, Zeitschrift Kristallogr. 203 (1993) 132;
(b) K. Isele, P. Franz, C. Ambrus, G. Bernardinelli, S. Decurtins, A.F. Williams, Inorg. Chem. 44 (2005) 3896.
[12] G.A. van Albada, M.T. Lakin, N. Veldman, A.L. Spek, J. Reedijk, Inorg. Chem. 34 (1995) 4910.
[13] G.A. van Albada, W.J.J. Smeets, A.L. Spek, J. Reedijk, Inorg. Chim. Acta 260 (1997) 151.
[14] G.A. van Albada, W.J.J. Smeets, A.L. Spek, J. Reedijk, Inorg. Chim. Acta 288 (1999) 220.
[15] G.A. van Albada, W.J.J. Smeets, N. Veldman, A.L. Spek, J. Reedijk, Inorg. Chim. Acta 290 (1999) 105.
[16] G.A. van Albada, W.J.J. Smeets, A.L. Spek, J. Reedijk, Inorg. Chim. Acta 299 (2000) 35.
[17] G.A. van Albada, N. Veldman, A.L. Spek, J. Reedijk, J. Chem. Crystallogr. 30 (2000) 69.
[18] G.A. van Albada, I. Riggio, I. Mutikainen, U. Turpeinen, J. Reedijk, J. Chem. Cryst. 30 (2000) 793.
[19] G.A. van Albada, J. Reedijk, R. Hämäläinen, U. Turpeinen, A.L. Spek, Inorg. Chim. Acta 163 (1989) 213.
[20] G.A. van Albada, I. Mutikainen, I. Riggio, U. Turpeinen, J. Reedijk, Polyhedron 21 (2002) 141.
[21] Nonius, COLLECT, Nonius BV, Delft, The Netherlands, 2002.
[22] G.M. Sheldrick, SHELXS-97, Program for Crystal Structure Determination, University of Göttingen, Germany, 1997.
[23] G.M. Sheldrick, SHELXL-97, Program for the Refinement of Crystal Structures, University of Göttingen, Germany, 1997.
[24] A.W. Addison, T.N. Rao, J. Reedijk, J. van Rijn, G.C. Verschoor, J. Chem. Soc., Dalton Trans. (1984) 1349.
[25] B.J. Hathaway, in: G. Wilkinson, R.D. Gill, J.A. McCleverty (Eds.), Comprehensive Coordination Chemistry, vol. 5, Pergamon Press, Oxford, 1995 (Chapter 53).
[26] O. Kahn, Molecular Magnetism, VCH Publ., NY, 1993.
[27] P.J. Hay, J.C. Thibault, R. Hoffmann, J. Am. Chem. Soc. 97 (1975) 4884.
[28] A. Bencini, D. Gatteschi, Inorg. Chim. Acta 31 (1978) 11.
[29] M. Handa, N. Koga, S. Kida, Bull. Chem. Soc. Jpn. 61 (1988) 3853.
[30] K.-S. Bürger, P. Chaudhuri, K. Wieghardt, J. Chem. Soc., Dalton Trans. (1996) 247.
[31] C.J. Boxwell, R. Bhalla, L. Cronin, S.S. Turner, P.H. Walton, J. Chem. Soc., Dalton Trans. (1998) 2449.
[32] H. Astheimer, W. Haase, J. Chem. Phys. 85 (1986) 1427.
[33] C.J. Cairns, D.H. Busch, Coord. Chem. Rev. 69 (1986) 1.
[34] S. Alvarez, A.A. Palacios, G. Aullón, Coord. Chem. Rev. 185–186 (1999) 431.
[35] V.H. Crawford, H.W. Richardson, J.R. Wasson, D.J. Hodgson, W.E. Hatfield, Inorg. Chem. 15 (1976) 2107.
[36] S.G.N. Roundhill, D.M. Roundhill, D.R. Bloomquist, C. Landee, R.D. Willett, D.N. Dooley, H.B. Gray, Inorg. Chem. 18 (1979) 831.
[37] K.D. Karlin, A. Farooq, J.C. Hayes, B.I. Cohen, T.M. Rowe, E. Sinn, J. Zubieta, Inorg. Chem. 26 (1987) 1271.
[38] A. Benzekri, P. Dubourdeaux, J.-M. Latour, J. Laugier, P. Rey, Inorg. Chem. 27 (1988) 3710.
[39] S.P. Foxon, D. Utz, J. Astner, S. Schindler, F. Thaler, F.W. Heinemann, G. Liehr, J. Mukherjee, V. Balamurugan, D. Ghosh, R. Mukherjee, J. Chem. Soc., Dalton Trans. (2004) 2321.

Available online at www.sciencedirect.com
SCIENCE DIRECT®
Polyhedron 25 (2006) 87–94
POLYHEDRON
www.elsevier.com/locate/poly

Synthesis, spectroscopy and structures of *o*-diphenylphosphinobenzoic acid complexes of diorganotin (IV), palladium (II) and platinum (II)

Prasad P. Phadnis [a], Sandip Dey [a], Vimal K. Jain [a,*], M. Nethaji [b], Ray J. Butcher [c]

[a] *Novel Materials and Structural Chemistry Division, Bhabha Atomic Research Centre, Trombay, Mumbai 400 085, Maharasthra, India*
[b] *Department of Inorganic & Physical Chemistry, Indian Institute of Science, Bangalore 560012, India*
[c] *Department of Chemistry, Howard University, Washington, DC 20059, USA*

Received 10 June 2005; accepted 6 July 2005
Available online 25 August 2005

Abstract

The reactions of diorganotin oxides with *o*-diphenylphosphinobenzoic acid ([PPh_2(*o*-C_6H_4COOH)], LH) in 1:1 stoichiometry afforded tetraorganodistannoxanes [{$R_2Sn(OOC\text{-}C_6H_4PPh_2)$}$_2O$]$_2$ (R = Me, Et, Pr^n, Bu^n). *o*-(Diphenylphosphino)benzoic acid complexes of palladium (II) and platinum (II) with the formulae [$MCl_2(LH)_2$], [$MCl_2(PR_3)(LH)$] (PR_3 = PEt_3, PBu_3, $PMePh_2$; M = Pd, Pt) have been prepared. Reactions of [{$Bu_2Sn(OOC\text{-}C_6H_4PPh_2)$}$_2O$]$_2$ with $PtCl_2(PhCN)_2$ in 1:1 and 1:2 ratio gave a complex mixture of products from which [$Pt(O_2CC_6H_4PPh_2)_2$] was isolated. All the complexes have been characterized by elemental analyses, IR, NMR (^{1}H, ^{13}C{^{1}H}, ^{31}P{^{1}H} and ^{119}Sn{^{1}H}) and UV–Vis spectroscopy. The stereochemistry of these complexes has been deduced from spectroscopic data. The structures of [{$Bu_2Sn(OOC\text{-}C_6H_4PPh_2)$}$_2O$]$_2$ and [$Pt(O_2CC_6H_4PPh_2)_2$] have been established by X-ray crystallography.
© 2005 Elsevier Ltd. All rights reserved.

Keywords: *o*-(Diphenylphosphino)benzoic acid; Tetraorganodistannoxanes; Palladium (II); Platinum (II); NMR; Crystal structures

1. Introduction

Functionalized phosphines, such as *o*-(diphenylphosphino)phenol [1–4], *o*-(diphenylphosphino)benzaldehyde [5–10], *o*-(diphenylphosphino)benzoic acid [11–16] and several other related molecules [17–21], represent a versatile family of ligands. They are capable of forming complexes of variable stoichiometries and in stabilizing hetero-metallic complexes containing metals of different reactivities. Classical and organometallic complexes derived from these ligands display several interesting and useful properties [22,23]. *o*-(Diphenylphosphino)benzoic acid (**1**) is of particular interest as the hydrophilic carboxylate group would give water soluble complexes which can be employed in phase-transfer catalysis. The mixed donor set would permit isolation of hetero-bi and -poly-nuclear complexes. Dicarboxylato tetraorganodistannoxanes, obtained readily by the reaction of R_2SnO with carboxylic acids in 1:1 ratio [24–26], as well as palladium phosphine complexes have been employed as homogeneous catalysts [27–30]. With this objective reactions of **1** with diorganotin oxides and palladium/platinum complexes have been investigated and the results are reported herein.

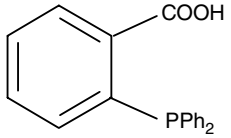

(1)

* Corresponding author. Tel.: +91 22 2559 5095; fax: +91 22 2550 5150/5.
E-mail address: jainvk@apsara.barc.ernet.in (V.K. Jain).

0277-5387/$ - see front matter © 2005 Elsevier Ltd. All rights reserved.
doi:10.1016/j.poly.2005.07.011

2. Experimental

2.1. Materials and methods

o-(Diphenylphosphino)benzoic acid [11], Na_2PdCl_4, $[PdCl_2(MeCN)_2]$, $[PtCl_2(PhCN)_2]$ were prepared by the literature procedures [31]. All the reactions were carried out under a nitrogen atmosphere in dry and distilled analytical grade solvents. Microanalyses were carried out in the Analytical Chemistry Division, BARC. The ^1H, $^{13}C\{^1H\}$ and $^{31}P\{^1H\}$ and $^{119}Sn\{^1H\}$ NMR spectra were recorded on a Bruker DPX-300 spectrometer operating at 300, 75.47, 121.49 and 111.82 MHz, respectively. Chemical shifts are relative to the internal chloroform peak ($\delta = 7.26$ ppm for ^1H; $\delta = 77.0$ ppm for ^{13}C) external Me_4Sn in C_6D_6 for $^{119}Sn\{^1H\}$ and external H_3PO_4 (85%) for $^{31}P\{^1H\}$ NMR. IR spectra were recorded as Nujol mulls using CsI plates on a Bomen-102 FT IR spectrometer in the range 200–4000 cm^{-1}. UV–Vis absorption spectra were recorded on a JASCO V-530 spectrophotometer.

2.2. Synthesis of ligand and complexes

2.2.1. *o*-(Diphenylphosphino)benzoic acid [$PPh_2(o\text{-}C_6H_4COOH)$] (**1**)

Sodium metal (6.02 g, 261.79 mmol) in a three necked round bottom flask was dissolved in liq. NH_3 resulting in a blue solution (~100 cm^3) and the solution was cooled to −78 °C. To this PPh_3 (34.3 g, 130.91 mmol) was added in portions with stirring resulting in the formation of orange-red $NaPPh_2$ solution. To this *o*-chlorobenzoic acid (20.65 g, 131.93 mmol) was added in portions followed by addition of dry THF (150 cm^3). The reaction mixture was brought to room temperature whereupon ammonia evaporates and the reaction mixture turned golden yellow. The solid residue was dissolved in distilled water (~500 cm^3) which was washed with diethylether (3×100 cm^3). pH of the aqueous phase was adjusted to 2 by addition of conc. HCl (~20 cm^3). From this, the desired compound was extracted with dichloromethane (4×75 cm^3), which was evaporated and from the residue **1** was precipitated by addition of methanol. The precipitate was filtered through G-3 filter and then dried in vacuo. This was recrystallized from hot methanol as pale yellow needle shaped crystals in 38% (15.26 g) yield [11]. Melting point 166 °C. *Anal.* Calc. for $C_{19}H_{15}O_2P$: C, 74.5; H, 4.9. Found: C, 75.1; H, 5.1%. UV–Vis λ_{max} (nm) (ε in $M^{-1}\,cm^{-1}$): 237 (10085), 257 (6228), 324 (1762). $^{13}C\{^1H\}$ NMR in $CDCl_3$: 128.3 (br, C-3, 5 (Ph), C-4, 6 (C_6H_4)), 131.6 (br, C-5, C_6H_4); 131.8 (d, 66 Hz, C-1, Ph); 133.8 (d, 21 Hz, C-2, 6 (Ph), C-3 (C_6H_4)); 134.1 (s, C-4, Ph); 141.4 (d, 28 Hz, C-2, C_6H_4); 170.3 (CO).

2.2.2. [{$R_2Sn(OOC\text{-}C_6H_4PPh_2)$}$_2O$]$_2$

To a benzene solution (50 cm^3) of $PPh_2(C_6H_4COOH)$ (1.057 g, 3.45 mmol), Bu^n_2SnO (869 mg, 3.49 mmol) was added and the whole was refluxed for 8 h on a Dean and Stark assembly. A clear pale yellow solution was obtained. The solvent was evaporated and the compound was recrystallized twice from CH_2Cl_2–hexane mixture to give a white cubic crystalline compound in 43% yield. Melting point 115 °C. *Anal.* Calc. for $C_{108}H_{128}O_{10}P_4Sn_4$: C, 59.2; H, 6.0. Found: C, 58.5; H, 5.8%. UV–Vis λ_{max} (nm) (ε in $M^{-1}\,cm^{-1}$): 238 (47388), 330 (10064), 378 (2975). $^{13}C\{^1H\}$ NMR in $CDCl_3$ δ: 13.6 (s, Sn–CCCMe); 26.7, 26.9 (each s, Sn–$CCCH_2$); 27.3, 27.7 (each s, Sn–CCH_2); 28.4, 30.1 ($SnCH_2$); 130.9 (d, 10 Hz); 133.8 (d, 20 Hz); 134.3 (s); 138.2 (2-C of C_6H_4); 139.5 (d, 12 Hz); 173.3 (s, CO).

2.2.3. [{$Pr^n_2Sn(OOC\text{-}C_6H_4PPh_2)$}$_2O$]$_2$

Prepared similar to Section 2.2.2 and recrystallized from CH_2Cl_2–hexane in 37% yield. Melting point 205 °C. *Anal.* Calc. for $C_{100}H_{112}O_{10}P_4Sn_4$: C, 57.8; H, 5.6. Found: C, 57.3; H, 5.6%. UV–Vis λ_{max} (nm) (ε in $M^{-1}\,cm^{-1}$): 237 (41479), 270 (sh), 322 (sh).

2.2.4. [{$Et_2Sn(OOC\text{-}C_6H_4PPh_2)$}$_2O$]$_2$

Prepared similar to Section 2.2.2 and recrystallized from toluene–hexane in 34% yield. Melting point 173 °C. *Anal.* Calc. for $C_{92}H_{96}O_{10}P_4Sn_4$: C, 56.2; H, 5.1. Found: C, 56.3; H, 5.5%. UV–Vis λ_{max} (nm) (ε in $M^{-1}\,cm^{-1}$): 236 (32230), 271 (sh), 334 (sh).

2.2.5. [{$Me_2Sn(OOC\text{-}C_6H_4PPh_2)$}$_2O$]$_2$

To facilitate dissociation of Me_2SnO, methanol (~5 cm^3) was also added in the reaction. Product was recrystallized twice from benzene–hexane as colorless crystals in 36% yield. Melting point 239 °C. *Anal.* Calc. for $C_{84}H_{80}O_{10}P_4Sn_4$: C, 54.5; H, 4.6. Found: C, 53.2; H, 4.9%. UV–Vis λ_{max} (nm) (ε in $M^{-1}\,cm^{-1}$): 236 (29644), 267 (sh), 324 (sh). $^{13}C\{^1H\}$ NMR in $CDCl_3$ δ: 6.6 (s, Sn–Me; $^1J(^{119/117}Sn–^{13}C) = 721$ Hz), 11.3 (s, Sn–Me; $^1J(^{119/117}Sn–^{13}C) = 846$ Hz); 128.2, 128.4, 131.2 (d, 27 Hz); 134.0 (d, 21 Hz); 137.2 (d, 12 Hz); 139.2 (d, 12 Hz); 140.1 (d, 24 Hz, C-2, C_6H_4); 173.5 (s, CO).

2.2.6. [$PdCl_2${$PPh_2(C_6H_4COOH)$}$_2$]

To a stirred acetone solution of $[PdCl_2(MeCN)_2]$ (342 mg, 1.32 mmol), a solution of $PPh_2(C_6H_4\text{-}COOH)$ (808 mg, 2.64 mmol) was added, whereupon a yellow precipitate formed. The whole was stirred for 3 h. The precipitate was filtered out using a G-3 fritz, washed with hexane and dried in vacuo. The product was recrystallized from DMF–ether mixture to give yellowish orange solid in 84% (879 mg) yield. Melting point 182 °C (dec). *Anal.* Calc. for $C_{38}H_{30}Cl_2O_4P_2Pd$: C, 57.8; H, 3.8. Found: C, 58.3; H, 4.3%. UV–Vis λ_{max} (nm) (ε in $M^{-1}\,cm^{-1}$): 240 (15929), 292 (sh), 349 (13590).

2.2.7. $[PtCl_2\{PPh_2(C_6H_4COOH)\}_2]$

Prepared from $PtCl_2(PhCN)_2$ and $Ph_2P(C_6H_4COOH)$ in 81% yield. Melting point 225 °C. *Anal.* Calc. for $C_{38}H_{30}Cl_2O_4P_2Pt$: C, 52.0; H, 3.4. Found: C, 52.3; H, 3.6%. UV–Vis λ_{max} (nm) (ε in $M^{-1}\,cm^{-1}$): 232 (6673), 290 (3575).

2.2.8. $[PdCl_2(PEt_3)\{PPh_2(C_6H_4COOH)\}]$

To a CH_2Cl_2 stirred solution of $[Pd_2Cl_2(\mu\text{-}Cl)_2(PEt_3)_2]$ (34 mg, 0.057 mmol), $PPh_2(C_6H_4\text{-}COOH)$ (36 mg, 0.12 mmol) was added with stirring. Orange solution changed instantly to yellow. The whole was stirred for 2 h. The solvent was evaporated in vacuo and the residue was recrystallized from CH_2Cl_2–hexane mixture in 87% (61 mg) yield. Melting point 148 °C (dec). *Anal.* Calc. for $C_{25}H_{30}Cl_2O_2P_2Pd$: C, 49.9; H, 5.0. Found: C, 50.5; H, 5.4%. UV–Vis λ_{max} (nm) (ε in $M^{-1}\,cm^{-1}$): 238 (21 616), 293 (sh), 320 (22 055), 337 (sh). $^{13}C\{^1H\}$ NMR in $CDCl_3$ δ: 8.0 (s, $PCCH_3$); 14.2 (d, 29 Hz, PCH_2); 128.0 (d, 10 Hz), 130.0 (d, 13 Hz); 131.1 (s); 131.2 (d, 5 Hz), 131.4 (br), 132.4 (d, 6 Hz); 133.2 (d, 7 Hz), 134.4 (s), 135.2 (d, 11 Hz); 170.0 (s, CO).

2.2.9. $[PdCl_2(PMePh_2)\{PPh_2(C_6H_4COOH)\}]$

Prepared similar to Section 2.2.8 in 80% yield as yellow powder. Melting point 128 °C (dec). *Anal.* Calc. for $C_{32}H_{28}Cl_2O_2P_2Pd$: C, 56.2; H, 4.1. Found: C, 55.5; H, 4.6%. UV–Vis λ_{max} (nm) (ε in $M^{-1}\,cm^{-1}$): 237 (18 798), 270 (10 244), 345 (8364).

2.2.10. $[PtCl_2(PBu_3)\{PPh_2(C_6H_4COOH)\}]$

Prepared similar to Section 2.2.8 in 85% yield as yellow powder. Melting point 168 °C (dec). *Anal.* Calc. for $C_{31}H_{42}Cl_2O_2P_2Pt$: C, 48.1; H, 5.5. Found: C, 48.8; H, 5.7%. UV–Vis λ_{max} (nm) (ε in $M^{-1}\,cm^{-1}$): 238 (14 678), 268 (13 365).

2.2.11. Reactions of $[\{Bu_2Sn(OOC\text{-}C_6H_4PPh_2)\}_2O]_2$ with $PtCl_2(PhCN)_2$

To a stirred CH_2Cl_2 solution (10 cm^3) of $PtCl_2(PhCN)_2$ (53 mg, 0.11 mmol), a solution of $[\{Bu_2Sn(OOC\text{-}C_6H_4PPh_2)\}_2O]_2$ (249 mg, 0.11 mmol) was added slowly at room temperature. The solvent was evaporated under vacuum and the pale yellow residue was investigated by NMR spectroscopy. After three recrystallizations, $[Pt(O_2CC_6H_4PPh_2)_2]$ was isolated, which was coordinated with two water molecules. Melting point 220 °C (dec). *Anal.* Calc. for $C_{38}H_{32}O_6P_2Pt$: C, 54.2; H, 3.8. Found: C, 52.1; H, 3.6%. $^{13}C\{^1H\}$ NMR: 125.2 (d, 70 Hz); 127.0 (d, 64 Hz); 128.8 (d, 5 Hz); 128.9 (d, 5 Hz), 130.6 (d, 82 Hz), 132.0 (s), 134.1 (m, three peeks); 166.9 (CO). Similarly reaction between $PtCl_2(PhCN)_2$ (63 mg, 0.13 mmol) and $[\{Bu_2Sn(OOC\text{-}C_6H_4PPh_2)\}_2O]_2$ (148 mg, 0.07 mmol) in 2:1 molar ratio was carried out.

2.3. Crystallography

X-ray data of a colorless single crystal of $[\{Bu_2Sn(O_2CC_6H_4PPh_2)\}_2O]_2\cdot 2CH_2Cl_2$ were collected on a Rigaku AFC-6S diffractometer (at 103(2) K) using graphite monochromated Mo-Kα radiation. The intensity data were corrected for Lorentz and polarization effects [32]. Semi-empirical absorptions correction was based on ψ scan of several reflections. The structure was solved by direct methods and refined by full-matrix least squares on F^2. All calculations were performed using the TEXSAN [33] crystallographic software package of the Molecular Structure Corporation.

The unit cell parameters and the intensity data for a colorless single crystal of $[Pt(O_2CC_6H_4PPh_2)_2]\cdot 2H_2O$ were collected at −170 °C on a Bruker Smart 1K CCD diffractometer using graphite-monochromated Mo Kα radiation ($\lambda = 0.71073$ Å), employing the ω scan technique. The intensity data were corrected for Lorentz, polarization and absorption effects. The structure was solved and refined with SHELX program [34]. The non-hydrogen atoms were refined anisotropically. One water molecule is disordered so the site occupancy was shared. Selected crystallographic data are given in Table 1.

3. Results and discussion

3.1. Synthesis and spectroscopy

Reactions of diorganotin oxides with *o*-(diphenylphosphino)benzoic acid in 1:1 stoichiometry afforded complexes of composition $[\{R_2Sn(O_2CC_6H_4PPh_2)\}_2O]_2$ as colorless crystalline solids. The IR spectra exhibited absorption due to $\nu_{C=O}$ in the region 1644–1590 cm^{-1}. Stretching vibrations associated with the Sn–O and Sn–C are tentatively assigned in the regions 490–650 and 570–650 cm^{-1}, respectively. The Et, Pr^n and Bu^n groups attached to the tin atom exhibited multiplet or broad resonances in their ^1H NMR spectra (Table 2). For the dimethyl tin derivative, two methyl tin resonances were observed both in the ^1H and $^{13}C\{^1H\}$ NMR spectra as expected for dicarboxylato tetraorganostannoxanes. The ^{119}Sn NMR spectra of $[\{R_2Sn(OOC\text{-}C_6H_4PPh_2)\}_2O]_2$ (R = Me; $\delta = -174$, -200 ppm; R = Bu; $\delta = -201$, -208 ppm) displayed two well separated resonances. The NMR data clearly favor the formation of familiar dicarboxylato tetraorganodistannoxanes [25,26,35] and was unambiguously established by X-ray diffraction analysis of $[\{Bu_2Sn(O_2CC_6H_4PPh_2)\}_2O]_2$ (see later).

Treatment of $[MCl_2(RCN)_2]$ (M = Pd or Pt; R = Me or Ph) with two equivalents of *o*-diphenylphosphinobenzoic acid readily yields poorly soluble $[MCl_2(PPh_2C_6H_4\text{-}COOH)_2]$. The IR spectrum of $[PtCl_2(PPh_2C_6H_4\text{-}COOH)_2]$ showed an absorption at 346 cm^{-1} attributable

Table 1
Crystallographic and structure refinement details for $[\{Bu_2Sn(O_2CC_6H_4PPh_2)\}_2O]_2$ and $[Pt(O_2CC_6H_4PPh_2)_2]$

	$[\{Bu_2Sn(O_2CC_6H_4PPh_2)\}_2O]_2 \cdot 2CH_2Cl_2$	$[Pt(O_2CC_6H_4PPh_2)_2] \cdot 2H_2O$
Chemical formula	$C_{110}H_{132}Cl_4O_{10}P_4Sn_4$	$C_{38}H_{32}O_6P_2Pt$
Formula weight	2354.60	841.7
Crystal size (mm^3)/color	$0.80 \times 0.35 \times 0.25$/colorless	$0.35 \times 0.33 \times 0.26$/colorless
Temperature (K)	103(2)	293(2)
λ (Å)	0.71073	0.71073
Crystal system	monoclinic	monoclinic
Space group	*C*2/*c*	$P2_1/n$
Unit cell dimensions		
a (Å)	23.936(6)	13.030(3)
b (Å)	17.434(5)	12.609(3)
c (Å)	27.467(7)	21.837(5)
β (°)	104.288(5)	95.809(4)
Volume ($Å^3$)	11108(5)	3569.3(15)
Density calcd. ($g\,cm^{-1}$)	1.408	1.566
Z	4	4
μ (mm^{-1})/*F*(000)	1.097/4800	4.065/1664
θ for data collection	1.75–28.31	1.75–28.01
Goodness of fit on F^2	1.020	1.082
Reflections collected/unique	42253/13480	8474/6595
Parameters	623	429
Structure solution	TEXSAN	SHELXS-97
Final R_1, wR_2 indices	0.0501, 0.1245	0.0347, 0.0953
R_1, wR_2 (all data)	0.0761, 0.1359	0.0514, 0.1017

Table 2
The ^1H and $^{31}P\{^1H\}$ NMR (in $CDCl_3$) and IR data of the *o*-diphenylphosphinobenzoic acid complexes

Complex	$^{31}P\{^1H\}$NMR data δ in ppm	^1H NMR data (chemical shift, δ in ppm)	IR data in cm^{-1}	
			υ(CO)	υ(M–Cl)
$Ph_2PC_6H_4COOH$[a]	−3.5	3.45 (s, OH); 6.96 (br), 7.33 (br) 7.40 (br), 8.16 (br) (Ph + C_6H_4)	1686 1273	
$[\{Me_2Sn(OOC\text{-}C_6H_4PPh_2)\}_2O]_2$	−4.2	0.41 (s, Sn*Me*, ^2J(Sn–H) = 87 Hz); 0.72 (s, Sn*Me*, ^2J(Sn–H) = 94 Hz); 6.81 (br), 7.11–7.25 (br), 8.10 (br)	1590 1283	
$[\{Et_2Sn(OOC\text{-}C_6H_4PPh_2)\}_2O]_2$	−3.1	1.30 (m), 3.01 (m), 7.11–7.79 (br, Ph), 8.15 (br) (Ph + C_6H_4)	1608	
$[\{Pr_2Sn(OOC\text{-}C_6H_4PPh_2)\}_2O]_2$		0.78–1.61 (br, m, *Pr*$_2$Sn); 6.83 (br), 7.16–7.37 (br), 8.00 (br) (Ph + C_6H_4)	1601 1281	
$[\{Bu_2Sn(OOC\text{-}C_6H_4PPh_2)\}_2O]_2$	−4.7	0.80 (br, $SnCH_2CH_2CH_2$*Me*); 1.22 (br, $SnCH_2CH_2CH_2$); 1.55 ($SnCH_2$); 6.87 (br), 7.30 (br), 8.09 (br), (Ph + C_6H_4)	1644 1284	
$[PdCl_2(PPh_2C_6H_4\text{-}COOH)_2]$[b]	21.2 25.7 (1:1)	3.50 (br, OH); 6.48–8.11 (m, Ph + C_6H_4)	1688 1267	352 (d) 358
$[PtCl_2(PPh_2C_6H_4\text{-}COOH)_2]$[b]	16.4 (^1J(Pt–P) = 2911 Hz)	3.36 (OH); 6.78 (m), 7.33–7.75 (m), 8.07 (m), (Ph + C_6H_4)	1692 1268	346
$[PdCl_2(PEt_3)(PPh_2C_6H_4\text{-}COOH)]$	18.3 (d) 27.1 (d) ^2J(PP) = 568 Hz	1.13 (dt, 7.1, 16 Hz, PCH_2CH_3); 1.89 (m, PCH_2); 3.88 (br, OH); 7.05 (t, 5.4 Hz), 7.32–7.54 (m), 7.76–7.81 (m), 8.23 (br) (Ph + C_6H_4)	1684 1275	354
$[PdCl_2(PMePh_2)(PPh_2C_6H_4\text{-}COOH)]$		1.94 (d, 10.8 Hz, PMe); 7.28–7.81 (m, Ph)	1687 1270	356
$[Pt(O_2C\text{-}C_6H_4PPh_2)_2]$	3.5 (^1J(Pt–P) = 3823 Hz)	6.64 (d, d, 3.6, 7.6 Hz, 1H; C_6H_4); 7.16–7.40 (m, 8H, 2Ph + C_6H_4); 7.55 (t, 7.6 Hz, 1H, C_6H_4); 8.40 (br, 1H, C_6H_4)		

[a] υ(OH) 3397 cm^{-1}.
[b] NMR in dmso-d_6.

to υ(Pt–Cl) indicating a *trans* configuration. This is further substantiated by the ^1J(Pt–P) coupling constant of 2911 Hz. It is worthnoting that the complex was isolated exclusively as the *trans* isomer. The reaction of $PtCl_2$(COD) with **1**, however, has been reported to afford *cis* isomer with an unusually small ^1J(Pt–P) of 3305 Hz as compared to other analogous derivatives (~3650 Hz) [16]. Isomerization of $MCl_2(PR_3)_2$ (M = Pd or Pt) in the presence of catalytic amounts of free phosphine is well established. Thus $^{31}P\{^1H\}$ NMR spectrum of

trans-[$PtCl_2(PPh_2C_6H_4$-$COOH)_2$] was monitored in the presence of catalytic amounts of $PPh_2C_6H_4$-COOH. The spectrum recorded immediately after mixing of phosphinobenzoic acid, besides parent complex and free phosphine, exhibited an additional resonance due to $Pt(O_2CC_6H_4PPh_2)_2$. An equilibrium was established after a few hours which did not change the concentration of the later complex on prolong standing (48 h) at room temperature. The palladium complex [$PdCl_2(Ph_2$-$PC_6H_4COOH)_2$] displayed three IR absorptions at $\sim$350 cm^{-1} due to ν_{Pd-Cl} suggesting the formation of a mixture of *cis* and *trans* isomers. The $^{31}P\{^1H\}$ NMR spectrum of [$PdCl_2(PPh_2C_6H_4$-$COOH)_2$] exhibited peaks at δ 21.2, 25.7 ppm substantiating the presence of *cis* and *trans* isomers. The ^1H NMR spectra in DMSO-d_6 exhibited multiplets for aromatic protons in the region 6.48–8.11 ppm (Table 2). The CO absorptions are little influenced as compared to the absorptions for free ligand.

The UV–Vis spectra in CH_2Cl_2 exhibited absorption due to π–π* charge transfer transitions in case of $PPh_2C_6H_4$-COOH and in the palladium and platinum complexes the mixed metal-to-ligand charge transfer (MLCT) and π–π* are observed. The representative spectra are shown in Fig. 1.

To assess suitability of $[\{Bu_2Sn(O_2CC_6H_4PPh_2)\}_2O]_2$ (**2**) as a metallo-ligand by coordinating dangling free phosphine, its reactions with $PtCl_2(PhCN)_2$ in different stoichiometries were investigated. The reactions of **2** with $PtCl_2(PhCN)_2$ in 1:1 and 1:2 molar ratios were monitored by NMR spectroscopy. $^{31}P\{^1H\}$ and $^{119}Sn\{^1H\}$ NMR spectra of both the reactions showed the formation of a complex mixture of products. In this mixture, at least three products are readily identifiable – $Pt(O_2CC_6H_4PPh_2)_2$, *trans*-$PtCl_2(PPh_2C_6H_4COOH)_2$ and a product showing ^{31}P resonance at δ 11.5 ppm (^1J(Pt–P) 2865 Hz) which can be assigned tentatively for *trans*-[$PtCl_2(\{Bu_2Sn(O_2CC_6H_4PPh_2)\}_2O)_2$]. The latter product dominates in the reaction carried out in 1:2 molar ratio. The former complex could be isolated by repeated recrystallization and its structure was established by X-ray crystallography (see later). The ^{119}Sn NMR spectra of these reactions did not show peaks due to **2**, but resonances attributable to asymmetric tetraorganodistannoxanes as well as for $[(Bu_2SnCl)_2O\}_2$-$O]_2$ (^{119}Sn −89, −138 ppm) can be identified. The ^{119}Sn resonances at −118 and −163 ppm may be assigned tentatively to $[Bu_2SnClOSn(O_2CC_6H_4PPh_2)Bu_2]_2$. From these reactions, it is evident that ligand scrambling from tetraorganodistannoxane (**2**) and "$PtCl_2$" fragment takes place. Ligand scrambling in tetraorganodistannoxanes has been reported by us earlier [36].

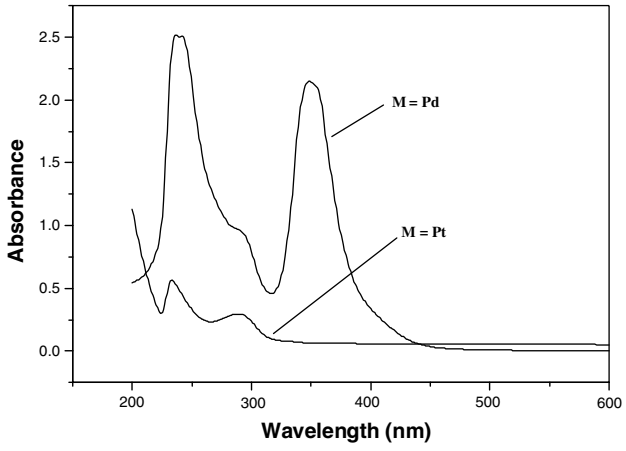

Fig. 1. UV–Vis spectra of $[MCl_2(Ph_2PC_6H_4$-$COOH)_2]$ in CH_2Cl_2.

3.2. X-ray crystallography

3.2.1. Crystal structure of $[\{Bu_2Sn(O_2CC_6H_4PPh_2)\}_2O]_2$

The X-ray structural analysis of [$\{Bu_2Sn(O_2CC_6H_4P$-$Ph_2)\}_2O]_2$ revealed the dicarboxylato tetraorganodistannoxane formulation. The structure, shown in Fig. 2 with crystallographic numbering scheme, is similar to related complexes [25,26,37–42]. The molecule consists of a centrosymmetric (crystallographically imposed) planar four-membered Sn_2O_2 ring with the bridging oxygens further bonded to two "$Bu_2Sn(O_2CC_6H_4PPh_2)$" fragments. There are two distinct carboxylate groups. One of the carboxylate ligands functions essentially in a monodentate fashion, i.e., bonded to exocyclic tin atom through O1B atom only. The second carboxylate ligand bridges both exo and endocyclic tin centers through O1A and O2A atoms.

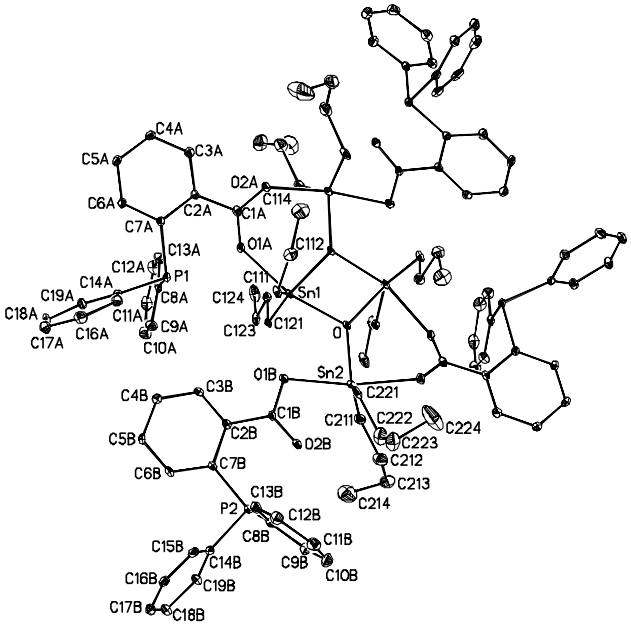

Fig. 2. Molecular structure of $[\{Bu_2Sn(O_2CC_6H_4PPh_2)\}_2O]_2 \cdot 2CH_2Cl_2$.

Both endo (Sn1) and exo (Sn2) cyclic tin atoms adopt a distorted trigonal bipyramidal geometry with each tin atom bonded two butyl groups and three oxygen atoms. The trigonal plane of *endo*-cyclic tin atom is defined by large C–Sn–C angle (139.01(12)°) and two compressed C–Sn–O#1 angles of 108.51(10)° and 112.25(10)° (Table 3). The apical angle, O–Sn–O(1A), of 162.88(8)° deviates significantly from linearity. A similar situation exists for exocyclic tin atom with apical angle O(1B)–Sn(2)–O(2A)# 169.72(8)° and trigonal angles, C(211)–Sn–C(221) 138.2(2)°; O–Sn(2)–C(211) 107.53(17)° and O–Sn(2)–C(221) 113.06(13)°. Various Sn–C and Sn–O distances are normal and can be compared with the distances reported in related complexes [37–42].

There is no significant contact between the tin atoms and P atom of the carboxylate ligand. The P–C (av. 1.84 Å) and C–P–C angles ranging from 99.36(14)° to 103.13(15)° are as expected for uncoordinated phosphines.

Table 3
Selected bond lengths (Å) and angles (°) for $[\{Bu_2Sn(O_2CC_6H_4PPh_2)\}_2O]_2$

Sn(1)–O	2.158(2)
Sn(1)–O#1	2.043(2)
Sn(2)–O	2.0320(19)
Sn(1)#–O	2.043(2)
Sn(1)–C(111)	2.124(3)
Sn(1)–C(121)	2.112(3)
Sn(2)–C(211)	2.152(7)
Sn(2)–C(221)	2.085(5)
P(1)–C(7A)	1.845(3)
P(1)–C(8A)	1.830(3)
P(1)–C(14A)	1.837(3)
Sn(1)–O(1A)	2.279(2)
Sn(2)–O(2A)#1	2.263(2)
Sn(2)#1–O(2A)	2.263(2)
Sn(2)–O(1B)	2.215(2)
O(1A)–C(1A)	1.262(4)
O(2A)–C(1A)	1.257(4)
O(1B)–C(1B)	1.285(4)
O(2B)–C(1B)	1.227(4)
P(2)–C(7B)	1.848(3)
P(2)–C(8B)	1.837(3)
P(2)–C(14B)	1.848(3)
O–Sn(1)–O#1	75.84(8)
Sn(1)–O–Sn(1)#1	103.47(8)
Sn(2)–O–Sn(1)	121.94(10)
Sn(2)–O–Sn(1)#1	134.50(11)
C(111)–Sn(1)–C(121)	139.01(12)
C(111)–Sn(1)–O	97.04(10)
C(121)–Sn(1)–O	96.81(10)
C(111)–Sn(1)–O#1	108.51(10)
C(121)–Sn(1)–O#1	112.25(10)
C(111)–Sn(1)–O(1A)	92.58(10)
C(121)–Sn(1)–O(1A)	84.95(10)
Sn(1)–O(1A)–C(1A)	129.9(2)
Sn(2)–O(1B)–C(1B)	101.77(18)
C(1A)–O(2A)–Sn(2)#1	128.0(2)
O(1B)–Sn(2)–O(2A)#1	169.72(8)
O(1A)–C(1A)–O(2A)	124.6(3)
O(1A)–Sn(1)–O#1	87.70(8)
O–Sn(1)–O(1A)	162.88(8)
O–Sn(2)–C(211)	107.53(17)
O–Sn(2)–C(221)	113.06(13)
C(211)–Sn(2)–C(221)	138.2(2)
O–Sn(2)–O(1B)	80.82(8)
C(211)–Sn(2)–O(1B)	100.8(2)
C(221)–Sn(2)–O(1B)	95.29(15)
O–Sn(2)–O(2A)#1	90.34(8)
C(211)–Sn(2)–O(2A)#1	86.8(2)
C(221)–Sn(2)–O(2A)#1	83.28(16)
O(2A)–C(1A)–C(2A)	117.4(3)
O(1A)–C(1A)–C(2A)	118.1(3)
O(1B)–C(1B)–O(2B)	121.7(3)
O(1B)–C(1B)–C(2B)	118.0(3)
O(2B)–C(1B)–C(2B)	120.3(3)

3.2.2. Crystal structure of $[Pt(O_2CC_6H_4PPh_2)_2]$

The structure of $[Pt(O_2CC_6H_4PPh_2)_2]$, which crystallizes with two water molecules, was unambiguously established by X-ray diffraction analysis. The structure (ORTEP [43], Fig. 3) consists of discrete molecule with the platinum atom acquiring distorted square planar geometry defined by two oxygen atoms of the carboxylate groups and two P atoms of the chelated phosphine ligand. The neutral P atoms are mutually *cis* disposed. The two Pt–O distances are essentially identical so are the two Pt–P distances (Table 4). These distances (Pt–O ~2.1 Å) [44,45] and Pt–P ~2.21 Å [46] are in agreement with the values reported for platinum complexes. The six-membered chelate rings, "PC_3O" are non-planar. The P(1)–Pt(1)–P(2) angle has opened up to 102.87° from the ideal value of 90° owing to relieve steric crowding of the phenyl groups on two P atoms. Consequently P(2)–Pt(1)–O(3), P(1)–Pt(1)–O(1) and O(1)–Pt(1)–O(3) angles are acute.

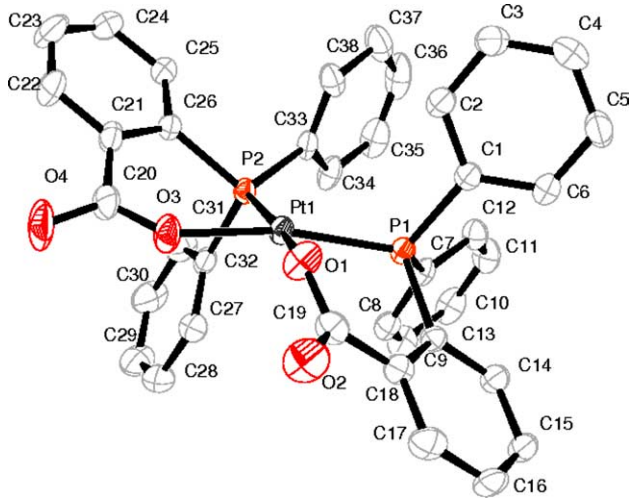

Fig. 3. Molecular structure $[Pt(O_2CC_6H_4PPh_2)_2]$.

Table 4
Selected bond lengths (Å) and angles (°) for $[Pt(O_2CC_6H_4PPh_2)_2]\cdot 2H_2O$

Pt(1)–O(1)	2.046(3)
Pt(1)–O(3)	2.048(3)
Pt(1)–P(1)	2.2054(10)
Pt(1)–P(2)	2.2147(11)
O(1)–C(19)	1.284(5)
O(2)–C(19)	1.229(5)
O(3)–C(20)	1.279(5)
O(4)–C(20)	1.221(6)
C(20)–C(21)	1.502(6)
C(18)–C(19)	1.504(6)
P(1)–C(1)	1.808(4)
P(1)–C(7)	1.807(4)
P(1)–C(13)	1.832(4)
P(2)–C(26)	1.829(4)
P(2)–C(32)	1.810(5)
P(2)–C(33)	1.810(4)
O(1)–Pt(1)–O(3)	83.87(12)
O(1)–Pt(1)–P(1)	86.22(9)
O(1)–Pt(1)–P(2)	170.10(9)
O(3)–Pt(1)–P(1)	166.69(9)
O(3)–Pt(1)–P(2)	87.72(9)
P(1)–Pt(1)–P(2)	102.87(4)
Pt(1)–O(1)–C(19)	129.1(3)
Pt(1)–O(3)–C(20)	136.3(3)
Pt(1)–P(1)–C(1)	115.48(13)
Pt(1)–P(1)–C(7)	116.27(13)
Pt(1)–P(1)–C(13)	108.40(12)
Pt(1)–P(2)–C(26)	108.36(14)
Pt(1)–P(2)–C(32)	112.17(14)
Pt(1)–P(2)–C(33)	118.45(13)
O(1)–C(19)–O(2)	120.3(4)
O(2)–C(19)–C(18)	118.6(4)
O(1)–C(19)–C(18)	121.2(4)
O(3)–C(20)–O(4)	120.2(4)
O(4)–C(20)–C(21)	118.5(4)
O(3)–C(20)–C(21)	121.3(4)

4. Supplementary materials

CCDC No. 266873 for $[Pt(O_2CC_6H_4PPh_2)_2]\cdot 2H_2O$ and 268183 for $[\{Bu_2Sn(O_2CC_6H_4PPh_2)\}_2O]_2$ contains the supplementary crystallographic data for this paper. These data can be obtained free of charge at www.ccdc.cam.ac.uk/conts/retrieving.html or from the Cambridge Crystallographic Data Centre, 12 Union Road, Cambridge CB2 1EZ, UK [Fax: (internat.) +44 1223/336 033; E-mail: deposit@ccdc.cam.ac.uk].

Acknowledgments

One of the authors (P.P.P.) is grateful to DAE for the award of a Senior Research Fellowship. The authors thank Drs. T. Mukherjee and S.K. Kulshreshtha for encouragement of this work. The facilities provided by Analytical Chemistry Division, BARC for microanalyses are gratefully acknowledged.

References

[1] T.B. Rauchfuss, Inorg. Chem. 16 (1977) 2966.
[2] H. Luo, I. Setyawati, S.J. Rettig, C. Orvig, Inorg. Chem. 34 (1995) 2287.
[3] C. Bolzati, F. Tisato, F. Refoco, G. Bandoli, A. Dolmella, Inorg. Chem. 35 (1996) 6221.
[4] J.S. Kim, A. Sen, I.A. Guzei, L.M. Liable-Sands, A.L. Rheingold, J. Chem. Soc., Dalton Trans. (2002) 4726.
[5] T.B. Rauchfuss, J. Am. Chem. Soc. 101 (1979) 1045.
[6] H.F. Klein, U. Lemke, M. Lemke, A. Brand, Organometallics 17 (1998) 4196.
[7] X. Chen, F.J. Femia, J.W. Babich, J. Zubieta, Inorg. Chim. Acta 315 (2001) 147.
[8] G. Brockaart, R.E. Mail, M.A. Garralda, P. Hernandez, L. Ibarlucea, J.I. Santos, Inorg. Chim. Acta 338 (2002) 249.
[9] R.E. Mail, M.A. Garralda, P. Hernandez, L. Ibarlucea, E. Pinilla, M.R. Torres, Helv. Chim. Acta 85 (2002) 1485.
[10] H. Mahalaxmi, P.P. Phadnis, V.K. Jain, E.R.T. Tiekink, Indian J. Chem. 43A (2004) 2287.
[11] J.E. Hoots, T.B. Rauchfuss, D.B. Wrobeeski, Inorg. Synth. 21 (1982) 175.
[12] J. Pietsch, L. Dahlenburg, A. Wolski, H. Berke, I.L. Eremenko, J. Organomet. Chem. 495 (1995) 113.
[13] W.-K. Wong, L. Zhang, W.-T. Wong, Chem. Commun. (1998) 673.
[14] J.D.G. Correia, A. Domingos, I. Santos, C. Bolzati, F. Refesco, F. Tisato, Inorg. Chim. Acta 315 (2001) 213.
[15] S.M. Kuang, P.E. Fanwick, R.A. Walton, Inorg. Chem. 41 (2002) 405.
[16] V. Ravindar, H. Schumann, H. Hemling, J. Blum, Inorg. Chim. Acta 240 (1995) 145.
[17] C.M. Thomas, R. Mafua, B. Therrien, E. Rusanov, H. Stoeckli-Evans, G. Suss-Fink, Chem. Eur. J. 8 (2002) 3343.
[18] D. Hedden, M. Roundhill, Inorg. Chem. 24 (1985) 4152.
[19] K. Tani, M. Yabuta, S. Nakamura, T. Yamagata, J. Chem. Soc., Dalton Trans. (1993) 2781.
[20] J.R. Dilworth, N. Wheatley, Coord. Chem. Rev. 199 (2000) 89.
[21] J.A. Cabezza, M. Martinez-Garcia, V. Riera, D. Ardura, S. Garcia-Granda, Eur. J. Inorg. Chem. (2000) 499.
[22] Y. Uozumi, H. Danjo, T. Hayashi, Tetrahed. Lett. 38 (1997) 3557.
[23] G.C. Lloyd-Jones, S.C. Stephen, Chem. Eur. J. 4 (1998) 2539.
[24] V.B. Mokal, V.K. Jain, J. Organomet. Chem. 441 (1992) 215.
[25] M. Boualam, R. Willem, M. Biesemans, B. Mahieu, J. Meunier-Piret, M. Gielen, Transition Met. Chem. 14 (1991) 41.
[26] M. Boualam, R. Willem, M. Biesemans, M. Gielen, Appl. Organomet. Chem. 5 (1991) 497.
[27] J. Otera, T. Yano, R. Ckawara, Organometallics 5 (1986) 1167.
[28] J. Otera, T. Yano, E. Kunimoto, T. Nakata, Organometallics 3 (1984) 426.
[29] J. Otera, N. Dan-oh, H. Nozaki, J. Org. Chem. 56 (1991) 5307.
[30] J. Tsuji, Palladium Reagents and Catalysis, Wiley, Chichester, 2004.
[31] F.R. Hartley, The Chemistry of Platinum and Palladium, Wiley, New York, 1972.
[32] J.A. Ibers, W.C. Hamilton, Acta Crystallogr. 17 (1964) 781.
[33] TEXSAN, Structure Analysis Package, Molecular Structure Corporation, 1985.
[34] G.-M. Sheldrick, SHELX-97, A Computer Program for Crystal Structure Solution and Refinement, Universitaet Gottingen, Gottingen, Germany, 1997.

[35] V.K. Jain, Proc. Indian Acad. Sci. 108 (1996) 165.
[36] V.K. Jain, V.B. Mokal, P. Sundar, Mag. Res. Chem. 30 (1992) 1158.
[37] C.S. Parulekar, V.K. Jain, T.K. Das, A.R. Gupta, B.F. Hoskins, E.R.T. Tiekink, J. Organomet. Chem. 372 (1989) 193.
[38] C. Vasta, V.K. Jain, T.K. Das, E.R.T. Tiekink, J. Organomet. Chem. 396 (1990) 9.
[39] C.S. Parulekar, V.K. Jain, T.K. Das, E.R.T. Tiekink, J. Organomet. Chem. 387 (1990) 163.
[40] R. Graziani, G. Bombieri, E. Forsellini, P. Furlan, V. Paruzzo, G. Tagliavini, J. Organomet. Chem. 125 (1977) 43.
[41] G. Valle, V. Peruzzo, G. Tagliavini, P. Ganis, J. Organomet. Chem. 276 (1984) 325.
[42] S.P. Narula, S.K. Bharadwaj, H.K. Sharma, G. Mairerse, P. Barbier, G. Nawogrocki, J. Chem. Soc., Dalton Trans. (1988) 1719.
[43] C.K. Johnson, ORTEP II-A FORTRAN Thermal Ellipsoid Plot Program for Crystal Structure Illustrations, ORNL-5138, 1976.
[44] V.K. Jain, R.J. Butcher, Polyhedron 17 (1998) 1317.
[45] I.I. Moisen, N.Yu. Kozitsyna, D.I. Kochubey, V.N. Kolomijchuk, K.I. Zamaraev, J. Organomet. Chem. 451 (1993) 231.
[46] S. Dey, V.K. Jain, A. Knoedler, A. Klein, W. Kaim, S. Zalis, Inorg. Chem. 41 (2002) 2864.

Available online at www.sciencedirect.com
SCIENCE DIRECT®
Polyhedron 25 (2006) 95–104
POLYHEDRON
www.elsevier.com/locate/poly

Reactions of $[(\mu\text{-H})Os_3(CO)_{10}(\mu\text{-OMe})]$ and $[(\mu\text{-H})Os_3(CO)_9(\mu\text{-OMe})(MeCN)]$ with dppm, dppe, dppp, and PPh_2H: X-ray crystal structures of $[(\mu\text{-H})Os_3(CO)_8(\mu\text{-OMe})\text{-}(\mu_2\text{-}\eta^2\text{-dppm})]$ and $[(\mu\text{-H})Os_3(CO)_9(\mu\text{-OMe})(PPh_2H)]$

Shariff E. Kabir [a,*], Md. Abdul Mottalib [a], G.M. Golzar Hossain [b], Ebbe Nordlander [c], Edward Rosenberg [d]

[a] Department of Chemistry, Jahangirnagar University, Savar, Dhaka-1342, Bangladesh
[b] Department of Chemistry, Cardiff University, P.O. Box 912, Park Place, Cardiff CF10 3TB, UK
[c] Inorganic Chemistry, Center for Chemistry and Chemical Engineering, Lund University, P.O. Box 124, SE-22100, Lund, Sweden
[d] Department of Chemistry, University of Montana, Missoula, MT 59812, USA

Received 31 March 2005; accepted 6 July 2005
Available online 18 August 2005

Abstract

Treatment of $[(\mu\text{-H})Os_3(CO)_{10}(\mu\text{-OMe})]$ (**1**) with dppm {dppm = bis(diphenylphosphino)methane} at 110 °C gave the known compound $[Os_3(CO)_{10}(\mu_2\text{-}\eta^2\text{-dppm})]$ (**2**) and the new compound $[(\mu\text{-H})Os_3(CO)_8(\mu\text{-OMe})(\mu_2\text{-}\eta^2\text{-dppm})]$ (**3**). A similar reaction of **1** with dppe {dppe = bis(diphenylphosphino)ethane} afforded two products, $[(\mu\text{-H})Os_3(CO)_8(\mu\text{-OMe})(\mu_1\text{-}\eta^2\text{-dppe})]$ (**5**) and $[(\mu\text{-H})Os_3(CO)_8(\mu\text{-OMe})(\mu_2\text{-}\eta^2\text{-dppe})]$ (**6**) which differ in the mode of bonding of the dppe ligand. The reaction of **1** with dppp {dppp = bis(diphenylphosphino)propane} at 110 °C gave exclusively $[(\mu\text{-H})Os_3(CO)_8(\mu\text{-OMe})(\mu_2\text{-}\eta^2\text{-dppp})]$ (**7**) which exists as two isomers in solution. Compounds **2**, **3**, and **5**–**7** are also obtained in almost similar yields from reactions of $[(\mu\text{-H})Os_3(CO)_9(\mu\text{-OMe})(MeCN)]$ (**4**) with the appropriate diphosphine at ambient temperature. The reaction of **1** with PPh_2H at 110 °C gave the new compounds $[(\mu\text{-H})Os_3(CO)_9(\mu\text{-OMe})(PPh_2H)]$ (**8**) and $[(\mu\text{-H})_2Os_3(CO)_7(\mu\text{-}PPh_2)_2(PPh_2H)]$ (**10**) and the previously reported compound $[(\mu\text{-H})_2Os_3(CO)_8(\mu\text{-}PPh_2)_2]$ (**9**). The molecular structures of **3** and **8** were determined by single crystal X-ray diffraction. In compound **3**, the dppm ligand bridges the same Os–Os edge as the hydride and the methoxide ligand. In **8**, the PPh_2H ligand occupies a 'pseudo' axial site on one of the osmium atoms bearing the bridging hydride and methoxide ligand.
© 2005 Elsevier Ltd. All rights reserved.

Keywords: Osmium carbonyl; Diphosphine; Diphenylphosphine; Methoxide; Crystal structures

1. Introduction

In recent years bridging diphosphine groups have been used in metal cluster chemistry because of their ability to maintain the integrity of the metal core during chemical reactions, to act as templates for the synthesis of metal–metal bonds by bridge assisted reactions [1–5] and in applications in homogeneous catalysis [6–8]. The chemistry of dodecacarbonyltriosmium with diphosphine ligands is well established [9–17]; $[Os_3(CO)_{12}]$ derivatives containing one and two diphosphine ligands have been synthesized and fully characterized. The structures of a substantial number of derivatives have been reported over the past two decades: $[Os_3(CO)_{10}(dppm)]$ [12], $[Os_3(CO)_9(dppm)(dppm)]$

* Corresponding author. Present address: Department of Chemistry, University of Montana, Missoula, MT 59812, USA. Tel.: +1 406 243 2592; fax: +1 406 243 4227.
E-mail address: skabir_ju@yahoo.com (S.E. Kabir).

0277-5387/$ - see front matter © 2005 Elsevier Ltd. All rights reserved.
doi:10.1016/j.poly.2005.07.004

[13], $[Os_3(CO)_8(dppm)_2]$ [15], $[Os_3(CO)_{10}(dppe)]$ [16,17], $[Os_3(CO)_{10}(dppp)]$ [15], and $[Os_3(CO)_{10}(dppb)]$ [15]. From these studies it has been found that the diphosphine groups adopt a variety of bonding modes on the cluster surface including monodentate, chelating and edge bridging.

In polynuclear complexes dppm can chelate but the four membered rings are strained and the ligand has a greater tendency to act either as a monodentate ligand or as a bridging bidentate ligand. Dppe has been widely used as a chelating ligand. Although less common, it is also known to bridge metal–metal bonds [18]. Both the chelating and bridging coordination modes have been structurally characterized in the cluster $[Os_3(CO)_{10}$-(dppe)] [16,17]. The chelating tendency decreases as the chain length increases, so for the ligand dppb {dppb = $Ph_2P(CH_2)_4PPh_2$} only the bridging isomer of $[Os_3(CO)_{10}(dppb)]$ was isolated and structurally characterized [15]. It is likely that steric effects will have a major influence on the bridging vs. chelating behaviour of these ligands.

Although a large number of diphosphine derivatives of $[Os_3(CO)_{12}]$ have been described, only a few examples of such derivatives of hydrido-triosmium compounds of the type $[(\mu\text{-H})Os_3(CO)_{10}(\mu\text{-X})]$ are known. Lewis et al. [19] investigated the reaction of $[(\mu\text{-H})Os_3(CO)_{10}(\mu$-OH)] with dppm at 80 °C and obtained the bridging dppm compound $[(\mu\text{-H})Os_3(CO)_8(\mu\text{-OH})(\mu_2\text{-}\eta^2\text{-dppm})]$. Recently, Leong and co-workers have reported reactions of $[(\mu\text{-H})Os_3(CO)_{10}(\mu\text{-OH})]$ with glycols and naphthol affording compounds of the type $[(\mu\text{-H})Os_3(CO)_{10}(\mu$-O-OH)] [20] and $[(\mu\text{-H})_2Os_3(CO)_9(\mu_3\text{-1-}C_{10}H_6)]$, [21], respectively. As a part of our ongoing studies of the reactivity of triosmium clusters with mono and diphosphine ligands, we have now investigated the chemistry of $[(\mu\text{-H})Os_3(CO)_{10}(\mu\text{-OMe})]$ (**1**) and its acetonitrile derivative $[(\mu\text{-H})Os_3(CO)_9(\mu\text{-OMe})(\mu\text{-MeCN})]$ (**4**) with dppm, dppe, and dppp, in order to make a comparison of the structural variation that can arise from lengthening of the methylene chain of the organic backbone of the diphosphine ligands. We have also investigated the reaction of **1** with PPh_2H in order to synthesize triosmium clusters containing bridging methoxy and phosphido ligands. These results are reported here.

2. Experimental

All reactions and manipulations were routinely performed under a nitrogen atmosphere by using standard Schlenk techniques. Reagent grade solvents were dried and distilled prior to use by standard methods. Infrared spectra were recorded on a Shimadzu FT-IR 8101 spectrophotometer. ^1H and $^{31}P\{^1H\}$ NMR spectra were recorded on a Varian Unity Plus 400 spectrometer. Chemical shifts for the $^{31}P\{^1H\}$ NMR spectra are relative to 85% H_3PO_4. Bis(diphenylphosphino)methane (dppm), bis(diphenylphosphino)ethane) (dppe) and bis(diphenylphosphino)propane) (dppp) were purchased from Strem and PPh_2H from Sigma–Aldrich Chemical Company and used as received. Reagent grade solvents were dried and distilled prior to use by standard procedures. The products were purified by thin-layer chromatography (TLC) on 20 × 20 cm glass plates coated with Merck GF254 silica gel. Fast atom bombardment mass spectra were obtained on a JEOL SX-102 spectrometer using 3-nitrobenzyl alcohol as matrix and CsI as calibrant. The starting clusters $[(\mu\text{-H})Os_3(CO)_{10}(\mu\text{-OMe})]$ (**1**) [22] and $[(\mu\text{-H})Os_3(CO)_9(\mu\text{-OMe})(MeCN)]$ (**4**) [23] were prepared according to the literature methods.

2.1. Reaction of $[(\mu\text{-H})Os_3(CO)_{10}(\mu\text{-OMe})]$ (1) with dppm

To a toluene solution (20 mL) of $[(\mu\text{-H})Os_3(CO)_{10}(\mu$-OMe)] (**1**) (0.100 g, 0.113 mmol) was added dppm (0.043 g, 0.113 mmol) and the reaction mixture was heated to reflux for 8 h. The solvent was removed under reduced pressure and the residue chromatographed by TLC on silica gel. Elution with hexane/CH_2Cl_2 (3:2, v/v) developed three bands. The first band gave a small quantity of an uncharacterized compound. The second band afforded $[Os_3(CO)_{10}(\mu_2\text{-}\eta^2\text{-dppm})]$ (**2**) (0.032 g, 23%) while the third band gave $[(\mu\text{-H})Os_3(CO)_8(\mu$-OMe)$(\mu_2\text{-}\eta^2\text{-dppm})]$ (**3**) (0.055 g, 40%) as yellow crystals after recrystallization from hexane/CH_2Cl_2 at −20 °C (*Anal*. Calc. for $C_{34}H_{26}O_9Os_3P_2$: C, 33.72; H, 2.17. Found: C, 33.95; H, 2.38%). IR [ν(CO), CH_2Cl_2]: 2070 s, 1998 vs, 1993 s, 1956 w, 1931 m cm^{-1}. ^1H NMR ($CDCl_3$): δ 7.37 (m, 20H), 3.41 (s, 3H), 3.07 (m, 1H), 2.86 (m, 1H), −11.2 (t, 1H, J = 12.0 Hz). $^{31}P\{^1H\}$ NMR ($CDCl_3$): δ −7.9 (s). Mass spectrum: m/z 1210 (M^+).

2.2. Reaction of $[(\mu\text{-H})Os_3(CO)_9(\mu\text{-OMe})(MeCN)]$ (4) with dppm

To a dichloromethane solution (15 mL) of **4** (0.086 g, 0.096 mmol) was added dppm (0.037 g, 0.096 mmol) and the reaction mixture was stirred for 1 h. Work up and chromatographic separation as above gave **2** (0.030 g, 25%) and **3** (0.053 g, 45%).

2.3. Reaction of 1 with dppe

A toluene solution (15 mL) of **1** (0.075 g, 0.085 mmol) and dppe (0.034 g, 0.085 mmol) was heated to reflux for 8 h. The solvent was rotary evaporated and the residue chromatographed by TLC on silica gel. Elution with hexane/CH_2Cl_2 (7:3, v/v) developed two bands. The faster moving band gave $[(\mu\text{-H})Os_3(CO)_8(\mu\text{-OMe})$-$(\mu_1\text{-}\eta^2\text{-dppe})]$ (**5**) (0.030 g, 29%) as yellow crystals after

recrystallization from hexane/CH_2Cl_2 at −20 °C (*Anal.* Calc. for $C_{35}H_{28}O_9Os_3P_2$: C, 34.31; H, 2.31. Found: C, 34.53; H, 2.56%). IR [ν(CO), CH_2Cl_2]: 2078 s, 2053 vs, 2005 vs, 1975 w, 1939 m cm^{-1}. ^1H NMR ($CDCl_3$): δ 7.35 (m, 20H), 2.93 (s, 3H), 2.86 (m, 1H), 2.71 (m, 1H), 2.62 (m, 1H), 2.52 (m, 1H), −11.91 (t, 1H, $J = 3.6$ Hz). $^{31}P\{^1H\}$ NMR ($CDCl_3$): δ 7.3 (s). Mass spectrum: m/z 1224 (M^+). The second band gave [(μ-H)$Os_3(CO)_8$(μ-OMe)(μ_2-η^2-dppe)] (**6**) (0.039 g, 38%) as yellow crystals after recrystallization from hexane/CH_2Cl_2 at 20 °C (*Anal.* Calc. for $C_{35}H_{28}O_9Os_3P_2$: C, 34.31; H, 2.31. Found: C, 34.65; H, 2.66%). IR [ν(CO), CH_2Cl_2]: 2067 vs, 2001 vs, 1984 s, 1950 w, 1932 m cm^{-1}. ^1H NMR ($CDCl_3$): δ 7.51 (m, 20H), 3.39 (s, 3H), 2.80 (m, 2H), 2.30 (m, 2H), −11.54 (t, 1H, $J = 10.4$ Hz). $^{31}P\{^1H\}$ NMR ($CDCl_3$): δ 8.0 (s). Mass spectrum: m/z 1224 (M^+).

2.4. Reaction of *4* with dppe

To a dichloromethane solution (15 mL) of **4** (0.085 g, 0.095 mmol) was added dppe (0.038 g, 0.095 mmol) and the reaction mixture was stirred for 1 h. The solvent was removed under reduced pressure and the residue chromatographed as above to give **5** (0.031 g, 30%) and **6** (0.046 g, 44%).

2.5. Reaction of *1* with dppp

To a toluene solution (15 mL) of **1** (0.098 g, 0.111 mmol) was added dppp (0.046 g, 0.112 mmol) and the reaction mixture was refluxed for 4 h. The solvent was removed in vacuo and the residue chromatographed by TLC on silica gel. Elution with hexane/CH_2Cl_2 (4:1, v/v) developed two bands. The faster moving band gave [(μ-H)$Os_3(CO)_8$(μ-OMe)(μ_2-η^2-dppp)] (**7**) (0.090 g, 66%) as yellow crystals after recrystallization from hexane/CH_2Cl_2 at 20 °C (*Anal.* Calc. for $C_{36}H_{30}O_9Os_3P_2$: C, 34.89; H, 2.44. Found: C, 35.25; H, 2.66%). IR [ν(CO), CH_2Cl_2]: 2072 s, 2065 m, 2005 vs, 2000 sh, 1996 s, 1986 w, 1965 sh, 1935 w cm^{-1}. ^1H NMR ($CDCl_3$): *major isomer*, δ 7.45 (m, 20H), 3.62 (s, 3H), 2.62 (m, 2H), 2.49 (m, 2H), 2.20 (m, 2H), −14.22 (t, $J = 10.0$ Hz, 1H); *minor isomer*, 7.45 (m, 20H), 3.26, (s, 3H), 2.75 (m, 2H), 2.35 (m, 2H), 2.05 (m, 2H), −10.94 (t, $J = 10.2$ Hz, 1H), $^{31}P\{^1H\}$ NMR ($CDCl_3$): *major isomer*, δ 7.0 (s); *minor isomer*, δ 11.0 (s). Mass spectrum: m/z 1238 (M^+).

2.6. Reaction of *4* with dppp

A dichloromethane solution (15 mL) of **4** (0.045 g, 0.051 mmol) and dppp (0.038 g, 0.092 mmol) was stirred at room temperature for 1 h. The solvent was removed under reduced pressure and the residue chromatographed as above to give **7** (0.034 g, 54%).

2.7. Reaction of *1* with PPh_2H

A toluene solution (20 mL) of **1** (0.100 g, 0.113 mmol) and PPh_2H (0.042 g, 0.224 mmol) was heated to reflux for 4 h. The solvent was removed under reduced pressure and the residue chromatographed by TLC on silica gel. Elution with hexane/CH_2Cl_2 (9:1, v/v) developed three bands. The first band gave [(μ-H)$Os_3(CO)_8$(μ-OMe)(PPh_2H)] (**8**) (0.046 g, 35%) as yellow crystals after recrystallization from hexane/CH_2Cl_2 at 20 °C (*Anal.* Calc. for $C_{22}H_{15}O_{10}Os_3P_2$: C, 25.38; H, 1.46. Found: C, 25.65; H, 1.63%). IR [ν(CO), CH_2Cl_2]: 2091 m, 2053 s, 2016 vs, 1991 m, 1968 m, 1946 m cm^{-1}. ^1H NMR ($CDCl_3$): δ 7.57 (m, 10H), 7.33(d, 1H, $J = 384.0$ Hz), 3.45(m, 3H), −12.51(d, 1H, $J = 34.8$ Hz). $^{31}P\{^1H\}$ NMR ($CDCl_3$): δ −38.5 (s). Mass spectrum: m/z 1040 (M^+). The second band gave the known compound [(μ-H)$_2Os_3(CO)_9$(μ-PPh_2)$_2$] (**9**) (0.036 g, 30%) while the third band afforded [(μ-H)$_2Os_3(CO)_7$(μ-PPh_2)$_2$($PHPh_2$)] (**10**) (0.021 g, 15%) as yellow crystals after recrystallization from hexane/CH_2Cl_2 at 20 °C (*Anal.* Calc. for $C_{43}H_{33}O_7Os_3P_3$: C, 38.97; H, 2.51. Found: C, 39.25; H, 2.70%). IR [ν(CO), C_6H_{12}]: 2054 vs, 2014 vs, 1999 m, 1991 m, 1979 m, 1954 w cm^{-1}. ^1H NMR ($CDCl_3$): δ 7.40 (m, 30H), 6.74 (d, 1H, $J = 74.8$ Hz), −16.23 (dd, 1H, $J = 7.5$, 5.0 Hz), −17.74 (ddd, 1H, $J = 3.5$, 7.5, 15.0 Hz); $^{31}P\{^1H\}$ NMR ($CDCl_3$): δ 99.5 (d, $J = 65.5$ Hz), 66.9 (dd, $J = 65.5$, 40.5 Hz), −14.27 (d, $J = 40.5$ Hz). Mass spectrum: m/z 1324 (M^+).

2.8. X-ray crystallography

Yellow crystals of compounds **3** and **8** were grown by slow diffusion of a layered hexane/methylene chloride solution at −4 °C. Crystallographic data were collected at 293 K, using a Bruker-Nonius CCD area detector diffractometer and Mo Kα radiation ($\lambda = 0.71073$ Å). The crystal-to detector distance was 32 mm, and ϕ and ω scans (1.2° increments, 15 s exposure time) were carried out to fill the Ewald sphere. Data collection and processing were carried out using the program COLLECT [24] and DENZO [25]. Empirical absorption corrections were applied to the data set using multiple and symmetry-related data measurements via the program SORTAV [26,27]. The unit cell was indexed on low angle reflections and refined from 25 reflections in a range of 12°–13°. The structure was solved by direct methods (SHELXS-96) [28] and refined on F^2 by full matrix lest squares (SHELXS-97) [29] using all unique data. All non-hydrogen atoms were refined anisotropically. Hydrogen atoms were included in calculated positions (riding model) with U_{iso} set at 1.2 times the U_{eq} of the parent atom. Atoms O(2) and C(12) C(22) in **3** were refined with an ISOR = 0.015 restraint and C(6) in **8** with an ISOR = 0.02 restraint. Details of crystal parameters,

Table 1
Crystallographic data and structure refinement parameters[a] for **3** and **8**

	3	**8**
Empirical formula	$C_{34}H_{26}O_9Os_3P_2$	$C_{22}H_{15}O_{10}Os_3P$
Formula weight	1211.09	1040.91
Crystal system	monoclinic	monoclinic
Space group	*P*2(1)/*c*	*P*2(1)/*c*
a (Å)	16.978(3)	7.589(2)
b (Å)	18.954(4)	20.382(4)
c (Å)	11.431(2)	17.308(3)
α (°)	90	90
β (°)	96.36(3)	91.29(2)
γ (°)	90	90
V (Å^3)	3655.9(12)	2726.5(10)
Z	4	4
D_{calc} (g cm^{-3})	2.200	1.596
Absorption coefficient (mm^{-1})	10.539	14.317
F(000)	2240	1880
Crystal size (mm)	0.25 × 0.22 × 0.18	0.30 × 0.12 × 0.08
θ Range (°)	2.09 to 25.06	2.00 to 25.02
Limiting indices	$-19 \leqslant h \leqslant 13$	$-6 \leqslant h \leqslant 8$
	$-21 \leqslant k \leqslant 22$	$-15 \leqslant k \leqslant 22$
	$-13 \leqslant l \leqslant 13$	$-18 \leqslant l \leqslant 18$
Reflections collected	13719	9151
Independent reflections	5246 ($R_{int} = 0.0900$)	3753 ($R_{int} = 0.0935$)
Maximum and minimum transmission factor	0.2528 and 0.1781	0.3938 and 0.0992
Data/restraints/parameters	5246/72/388	3753/6/303
Goodness-of-fit on F^2	0.747	0.924
Final *R* indices [$I > 2\sigma(I)$]	$R_1 = 0.0381$	$R_1 = 0.0531$
	$wR_2 = 0.0803$	$wR_2 = 0.1292$
R indices (all data)	$R_1 = 0.0689$	$R_1 = 0.700$
	$wR_2 = 0.1533$	$wR_2 = 0.1320$
Largest different peak and hole (e Å^{-3})	1.355 and −0.910	4.417 and −1.794

[a] Details in common: X-radiation, Mo Kα ($\lambda = 0.71073$ Å), temperature (K) 292(2), refinement method: full-matrix least-squares on F^2.

data collection parameters, and refinement data are summarized in Table 1. Selected bond lengths and angles for **3** and **8** are given in Tables 2 and 3, respectively.

3. Results and discussion

The reaction of [(μ-H)Os_3(CO)$_{10}$(μ-OMe)] (**1**) with dppm in refluxing toluene at 110 °C gives the new compound [(μ-H)Os_3(CO)$_8$(μ-OMe)(μ$_2$-η^2-dppm] (**3**) and the previously reported cluster [Os_3(CO)$_{10}$(μ$_2$-η^2-dppm] (**2**) in 40% and 23% yields, respectively (Scheme 1). Compound **2** has been characterized by a combination of elemental analysis, IR, ^{1}H, and ^{31}P{^{1}H} NMR spectroscopies, FAB mass spectrometry and a single crystal X-ray diffraction study. The pattern of the infrared spectrum of **2** is similar to that of [(μ-H)Os_3(CO)$_8$(μ-OH)-(μ$_2$-η^2-dppm] [19] indicating that they a have similar distribution of the carbonyl ligands. The hydride region of the ^{1}H NMR spectrum contains a triplet at δ −11.2 with an H–P coupling constant of 12.0 Hz indicating that the hydride is coupled to two equivalent phosphorus atoms. The aliphatic region of the spectrum exhibits two multiplets at δ 3.07 and 2.86 due to the methylene protons of the dppm ligand and a singlet at δ 3.41 attributed to the methoxy protons. The ^{31}P{^{1}H} NMR spectrum of **3** shows a singlet at δ −7.9 indicating that the phosphorus atoms of the dppm ligand are equivalent. The FAB mass spectrum of **3** confirms the formula [(μ-H)Os_3(CO)$_8$(μ-OMe)(μ$_2$-η^2-dppm)], exhibiting the molecular ion peak at *m*/*z* 1210 and peaks due to the sequential loss of eight carbonyl groups. In order to confirm the coordination mode of the dppm ligand, an X-ray diffraction study was undertaken on compound **3**. The molecular structure of **3** is shown in Fig. 1, crystallographic data are given in Table 1 and selected bond distances and angles are collected in Table 2. The molecule consists of an approximate isosceles triangle of osmium atoms with one bridging dppm ligand, one bridging methoxy ligand, a bridging hydride and eight terminal carbonyl ligands. The osmium–osmium distances in **3** {Os(1)–Os(2) = 2.8329(9) Å, Os(1)–Os(3) = 2.8365(10) Å, and Os(2)–Os(3) = 2.8143(9) Å}, are somewhat shorter than the average Os–Os distances of {2.877(3) Å} in [Os_3(CO)$_{12}$] {2.877(3)} [30]. Two CO ligands are bound to Os(2) and Os(3) atoms while Os(1) bears four CO groups. An interesting feature of the structure of **3** is that the OMe group and the hydride bridge the same Os–Os vector as the dppm ligand. The bridging hydride ligand was located along the Os(2)–

Table 2
Selected bond lengths (Å) and angles (°) for [(μ-H)Os_3(CO)$_8$-(μ-OMe)(μ$_2$-η^2-dppm)] (**3**)

Os(1)–C(2)	1.76(2)
Os(1)–C(4)	1.879(18)
Os(1)–Os(2)	2.8329(9)
Os(2)–C(5)	1.787(17)
Os(2)–O(9)	2.126(8)
Os(2)–Os(3)	2.8143(9)
Os(3)–C(7)	1.784(18)
Os(3)–O(9)	2.099(9)
P(2)–C(29)	1.825(8)
P(2)–C(23)	1.848(8)
P(2)–C(10)	1.838(13)
Os(1)–C(3)	1.869(16)
Os(1)–C(1)	1.896(19)
Os(1)–Os(3)	2.8365(10)
Os(2)–C(6)	1.884(16)
Os(2)–P(1)	2.382(4)
Os(3)–C(8)	1.823(17)
Os(3)–P(2)	2.362(3)
P(1)–C(11)	1.838(10)
P(1)–C(17)	1.814(10)
P(1)–C(10)	1.917(12)
O(9)–C(9)	1.453(15)
C(2)–Os(1)–Os(2)	83.2(4)
C(4)–Os(1)–Os(2)	83.0(4)
C(2)–Os(1)–Os(3)	87.8(5)
C(4)–Os(1)–Os(3)	82.1(4)
Os(2)–Os(1)–Os(3)	59.524(19)
C(4)–Os(1)–Os(3)	82.1(4)
Os(2)–Os(1)–Os(3)	59.524(19)
O(9)–Os(2)–P(1)	83.1(2)
C(6)–Os(2)–Os(1)	90.3(4)
P(1)–Os(2)–Os(1)	154.39(9)
C(7)–Os(2)–Os(3)	124.3(5)
O(9)–Os(3)–Os(2)	48.6(2)
C(7)–Os(3)–Os(1)	94.1(4)
Os(2)–Os(3)–Os(1)	60.18(2)
C(3)–Os(1)–Os(2)	104.7(5)
C(1)–Os(1)–Os(2)	154.4(5)
C(3)–Os(1)–Os(3)	164.1(5)
C(1)–Os(1)–Os(3)	94.9(5)
C(5)–Os(2)–Os(3)	139.8(5)
O(9)–Os(2)–Os(3)	47.8(2)
C(9)–Os(2)–Os(1)	82.5(2)
Os(3)–Os(2)–Os(1)	60.30(2)
O(9)–Os(3)–P(2)	81.9(5)
C(8)–Os(3)–Os(2)	140.3(6)
P(2)–Os(3)–Os(2)	94.31(9)
C(8)–Os(3)–Os(1)	99.4(5)
P(2)–Os(3)–Os(1)	154.27(9)
Os(3)–O(9)–Os(2)	83.5(3)

Table 3
Selected bond lengths (Å) and angles (°) for [(μ-H)Os_3(CO)$_8$-(μ-OMe)(PPh_2H)] (**8**)

Os(1)–C(3)	1.89(3)
Os(1)–C(1)	1.92(2)
Os(1)–Os(2)	2.8272(13)
Os(2)–C(6)	1.74(3)
Os(2)–C(7)	1.98(3)
Os(2)–Os(3)	2.7993(11)
P(1)–C(11)	1.812(11)
O(10)–C(10)	1.42(2)
Os(3)–C(9)	1.86(2)
Os(1)–C(2)	1.91(3)
Os(1)–C(4)	1.95(3)
Os(1)–Os(3)	2.8492(11)
Os(2)–C(5)	1.91(2)
Os(2)–O(10)	2.008(13)
Os(3)–C(8)	1.87(3)
Os(3)–P(1)	2.309(5)
P(1)–C(17)	1.802(12)
C(3)–Os(1)–Os(2)	159.8(7)
C(1)–Os(1)–Os(2)	83.0(5)
C(3)–Os(1)–Os(3)	100.8(7)
C(1)–Os(1)–Os(3)	83.2(5)
Os(2)–Os(1)–Os(3)	59.09(3)
C(5)–Os(2)–Os(3)	132.9(6)
O(10)–Os(2)–Os(3)	48.9(3)
C(5)–Os(2)–Os(1)	90.3(5)
O(10)–Os(2)–Os(1)	82.8(3)
O(10)–Os(3)–Os(2)	47.8(3)
C(9)–Os(3)–Os(1)	90.4(7)
O(10)–Os(3)–Os(1)	90.4(7)
Os(2)–Os(3)–Os(1)	60.06(3)
C(2)–Os(1)–Os(2)	101.3(6)
C(4)–Os(1)–Os(2)	87.1(6)
C(2)–Os(1)–Os(3)	160.4(6)
C(3)–Os(1)–Os(2)	159.8(7)
C(6)–Os(2)–Os(3)	120.7(6)
C(7)–Os(2)–Os(1)	172.9(7)
Os(3)–Os(2)–Os(1)	60.84(3)
C(8)–Os(2)–Os(2)	112.7(7)
P(1)–Os(3)–Os(2)	134.32(13)
C(8)–Os(3)–Os(1)	172.2(6)
P(1)–Os(3)–Os(1)	94.53(14)
Os(3)–O(10)–Os(3)	83.3(4)

Os(3) edge but not refined. The Os–O bond distances and angles associated with the bridging OMe unit {Os(2)–O(9) = 2.126(8), Os(3)–O(9) = 2.099(9) Å, Os(3)–O(9)–Os(2) = 83.5(3)°} are comparable to those found in **1** {Os–O = 2.112–2.093 Å, Os–O–Os = 83.9°} [31]. As expected the dppm ligand is equatorially coordinated; the Os–P bond distances {Os(2)–P(1) = 2.382(4), Os(3)–P(2) = 2.362(3) Å} are somewhat longer than those found in [Os_3(CO)$_{10}$(μ$_2$-η^2-dppm)] {2.332(3) and 2.312(3) Å} [32]. To synthesize compound **3** selectively in high yield and to stop the formation of the known compound **2** we decided to react the labile acetonitrile compound [(μ-H)Os_3(CO)$_9$(μ-OMe)(MeCN)] (**4**) with dppm at ambient temperature. However, compound **4** reacts with dppm at ambient temperature to give **2** and **3** in 25% and 45% yields, respectively.

In contrast, the reaction of **1** with dppe at 110 °C gives both the chelating and bridging isomers, [(μ-H)Os_3-(CO)$_8$(μ-OMe)(μ$_1$-η^2-dppe)] (**5**) and [(μ-H)Os_3(CO)$_8$-(μ-OMe)(μ$_2$-η^2-dppe)] (**6**) in 29% and 38% yields, respectively (Scheme 2). The two isomers have different colors (the chelating isomer **5** is pale yellow and the bridging isomer **6** is orange). This reaction can be compared to that of [Os_3(CO)$_{10}$(η^4-*cis*-C_4H_6)] which

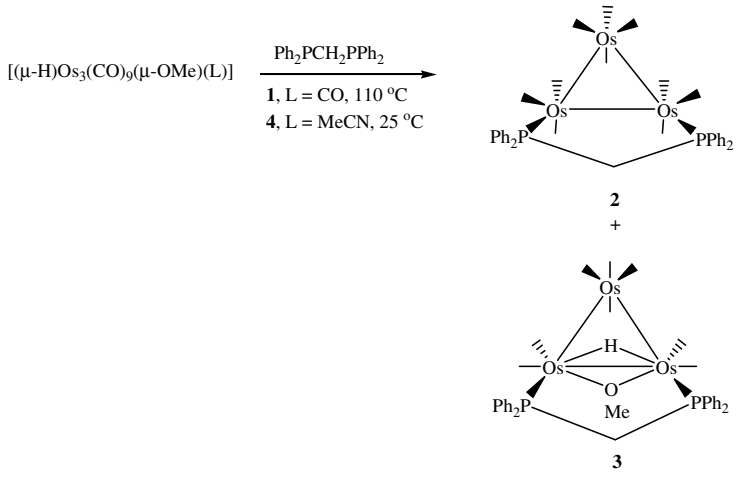

Scheme 1.

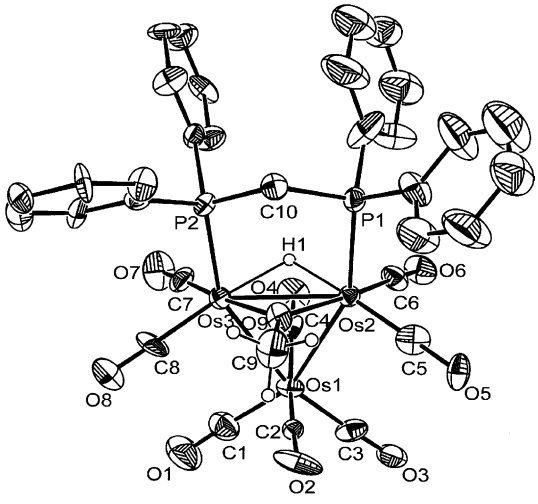

Fig. 1. Molecular structure of $[(\mu\text{-H})Os_3(CO)_8(\mu\text{-OMe})(\mu_2\text{-}\eta^2\text{-dppm})]$ (**3**) showing the atom-labeling scheme. Thermal ellipsoids are drawn at the 35% probability level.

led to the formation of $[Os_3(CO)_{10}(\mu_1\text{-}\eta^2\text{-dppe})]$ and $[Os_3(CO)_{10}(\mu_2\text{-}\eta^2\text{-dppe})]$ [10,16]. We were unable to obtain X-ray quality crystals of compounds **5** and **6**, therefore, their characterization was based on elemental analysis, infrared, ^{1}H NMR, ^{31}P{^{1}H} NMR and mass spectroscopic data. The mass spectra of both **5** and **6** exhibit the molecular ion peak at m/z 1224 corresponding to the formulation $[(\mu\text{-H})Os_3(CO)_8(\mu\text{-OMe})(dppe)]$ and fragment ions due to the sequential loss of eight carbonyl ligands. The infrared spectrum of **6** is similar to that of **3** but quite different from that of **5**, indicating that the distribution of the carbonyl groups in **5** is different from that of **3** and **6**. The hydride region of the ^{1}H NMR spectrum of **5** contains a triplet at δ −11.91 with a H–P coupling constant of 3.6 Hz. The phosphorus–hydrogen coupling constant observed in this spectrum is typical of a three bond P–H coupling [33] indicating that the dppe ligand is coordinated to the osmium atom not bridged by the hydride and the methoxide group. In addition to usual phenyl resonances, the aliphatic region of the spectrum exhibits four equally intense multiplets at δ 2.86, 2.71, 2.62 and 2.52 due to the methylene protons of the dppe ligand and a singlet at δ 2.93 attributable to the methy1 protons of OMe group. The ^{31}P{^{1}H} NMR spectrum of **5** shows a singlet at δ 7.3 indicating that the phosphorus nuclei are equivalent. The spectroscopic data of **5** are thus consistent with the structure with the hydride and the methoxide ligand bridging one edge of the Os_3 triangle and the dppe ligand coordinated to the third osmium atom. This is the only possible structure and conformation where the two phosphorus atoms are magnetically equivalent. The aliphatic region of the ^{1}H NMR spectrum of **6** exhibits two equally intense multiplets at δ 2.30 and 2.80 due to the methylene protons of dppe ligand and a singlet at δ 3.39 due to the methyl protons of the methoxide group. The hydride region of the spectrum contains a triplet at δ −11.54 with a phosphorus–hydrogen coupling constant of 10.4 Hz, which is consistent with the hydride being coupled to two equivalent phosphorus atoms. The ^{31}P{^{1}H} NMR spectrum of **5** exhibits a single peak at δ 8.0 for the two equivalent phosphorus atoms of the dppe ligand. The similarities of the spectroscopic data of **6** to those of **3** points to a structure for the former with the dppe, hydride and OMe group bridging the same Os–Os edge of the Os_3 triangle (Scheme 2). Compounds **5** and **6** have also been obtained in 30% and 44% yields, respectively from the room temperature reaction of **4** with dppe.

The reaction of **1** with dppp at 110 °C gave exclusively $[(\mu\text{-H})Os_3(CO)_8(\mu\text{-OMe})(\mu_2\text{-}\eta^2\text{-dppp}]$ (**7**) in 66% yield, which exists as a mixture of two isomers in a 3:2 ratio. These two isomers could not be separated by using either chromatography or crystallization techniques. The pattern of the infrared spectrum of **7**, in the carbonyl-stretching region, is similar to those of **3** and **6** but contains two additional bands at 2065 and

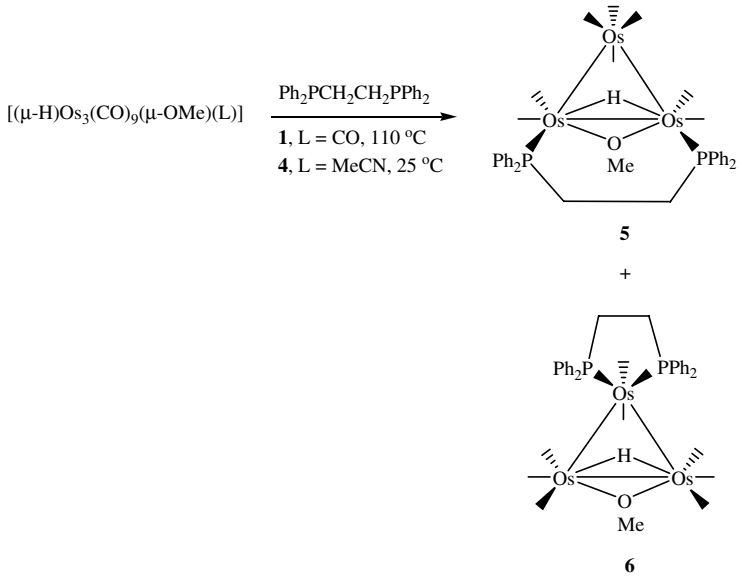

Scheme 2.

1996 cm^{-1}. The hydride region of the ^1H NMR spectrum of **7** exhibits two triplets at δ −14.22 and −10.94 with a relative intensity of 3:2 indicating that in each isomer the hydride is coupled to two equivalent ^{31}P nuclei. The aliphatic region of the spectrum shows two singlets at δ 3.62 and 3.26 for the methyl protons of the methoxide ligand and two sets of the three multiplets (see Section 2) for the methylene protons of the dppp ligand. The $^{31}P\{^1H\}$ NMR spectrum of **7** contains two singlets at δ 11.0 and 7.0 with a relative intensity of 3:2 (one singlet for each isomer). Thus the spectroscopic data clearly indicate that compound **7** exists as two isomers in solution in a 3:2 ratio. The probable structures for the two isomers are shown in Scheme 3. A comparison may be made between **7** and the previously reported compound $[(\mu\text{-H})Os_3(CO)_8(\mu\text{-OPh})P(OMe)_{32}]$ which also exists as two isomers in solution [33]. In the latter complex the major isomer has both the $P(OMe)_3$ ligands at equatorial sites on the bridgehead Os atoms whereas in the minor isomer one $P(OMe)_3$ ligand coordinated at equatorial site and the other at an axial site of the bridged Os atoms. The structure of **7** with one phosphorus atom coordinating at an axial position and another at an equatorial site can be ruled out since one would expect a hydride double doublet and two ^{31}P signals for such a structure. Therefore, in this case the second isomer must be one in which both phosphorous atoms occupy axial positions (Scheme 3). Due to lack of X-ray quality

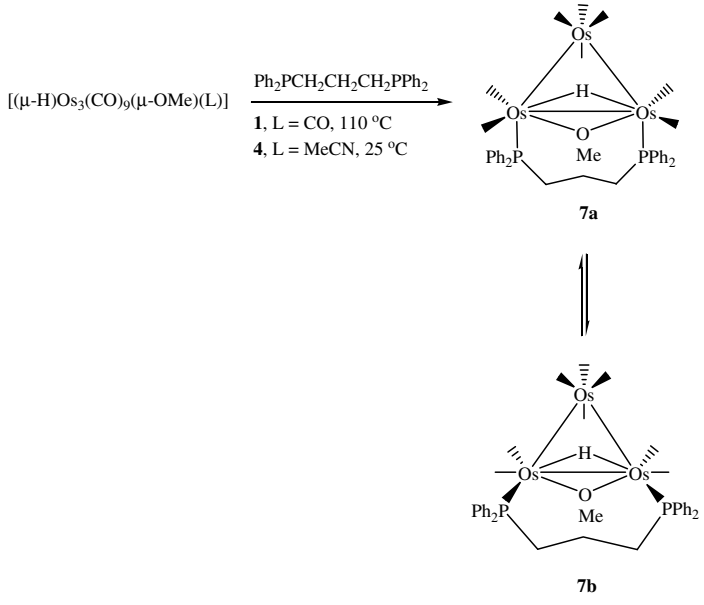

crystals and the similarity of the ratio of the two isomers we cannot be certain which of the two would be present in the solid state. However, the two isomers of **7** are the analogs of compounds **5** and **6**. Compound **4** also reacts with dppp at room temperature to give **7** (54%).

The reaction of **1** with $PHPh_2$ in refluxing toluene at 110 °C gave two new compounds $[(\mu\text{-H})Os_3(CO)_9(\mu\text{-OMe})(PHPh_2)]$ (**8**), and $[(\mu\text{-H})_2Os_3(CO)_7(\mu\text{-PPh}_2)_2(PHPh_2)]$ (**10**) in 35% and 15% yields, respectively together with the known compound $[(\mu\text{-H})_2\ Os_3(CO)_8(\mu\text{-PPh}_2)_2]$ (**9**) in 30% yield. Compound **9** was previously reported by Carty et al. [34] from the phosphine compound $[Os_3(CO)_{10}(\mu\text{-PPh}_2H)_2]$ via oxidative addition of P–H bond. Compound **8** has been characterized by a combination of spectroscopic data and single crystal X-ray diffraction studies. The pattern of the IR spectrum of **8** is similar to that of $[(\mu\text{-H})Os_3(CO)_9(\mu\text{-SPh})(PEt_3)]$ in which the PEt_3 ligand is coordinated to one of the bridgehead osmium atoms [33]. In addition to the usual phenyl resonances, the ^1H NMR spectrum of **8** shows a singlet at δ 3.45 due to the methyl protons of the OMe group and a strongly coupled doublet at δ 7.33 ($J = 384.0$ Hz) attributed to the P–H proton of the $PHPh_2$ ligand. The magnitude of the P–H coupling constant of the doublet at δ 7.33 is similar to those observed for other terminally coordinated PPh_2H compounds [35,36]. The hydride region of the spectrum contains a doublet at δ −12.51 with a P–H coupling constant of 34.8 Hz. The $^{31}P\{^1H\}$ NMR spectrum shows a singlet at δ −38.5. The mass spectrum of **8** exhibits a molecular ion peak at m/z 1040, which undergoes fragmentation by sequential loss of nine carbonyl groups. The spectroscopic data, therefore, suggest that **8** has a structure similar to that of $[(\mu\text{-H})Os_3(CO)_9(\mu\text{-SPh})(PEt_3)]$ [33] as shown in Scheme 4.

A single crystal X-ray diffraction analysis of compound **8** confirmed the proposed structure. The molecular structure of **8** is depicted in Fig. 2, crystallographic data are collected in Table 1 and selected bond distances and angles are listed in Table 3. The structure is derived from $[(\mu\text{-H})Os_3(CO)_{10}(\mu\text{-OMe})]$ by replacement of one CO group from one of the bridgehead osmium atoms. The overall structure is similar to that of $[(\mu\text{-H})Os_3(CO)_9(\mu\text{-SPh})(PEt_3)]$. The bridging hydride ligand was located along the Os(2)–Os(3) edge but not refined. This edge is also bridged by the methoxide ligand. The Os–O bond distances and angles associated with the bridging OMe unit {Os(2)–O(10) = 2.088 (13), Os(3)–O(10) = 2.125(12) Å, Os(3)–O(10)–Os(2) = 83.3(4)°} are comparable to those found in **3**. The nine carbonyl groups are in terminal positions with four bonded to Os(1), three bonded to Os (2) and two attached to Os(3). The doubly bridged Os(2)–Os(3) edge {2.7993(11) Å} is shorter than the two non-bridged Os–Os bonds {Os(1)–Os(2) = 2.8273(13), Os(1)–Os(3) = 2.8492(11) Å}. It is possible that the usual bond lengthening effect produced

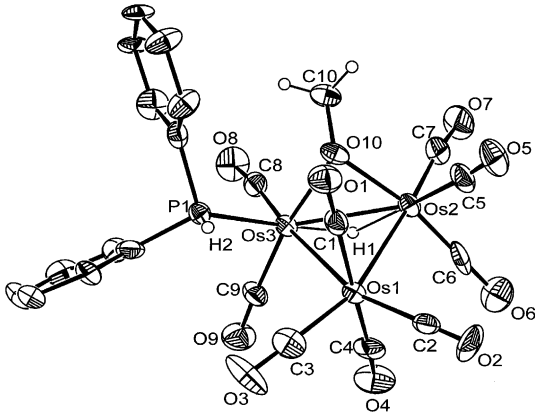

Fig. 2. Molecular structure of $[(\mu\text{-H})Os_3(CO)_9(\mu\text{-OMe})(PPh_2H)]$ (**8**) showing the atom-labeling scheme. Thermal ellipsoids are drawn at the 35% probability level.

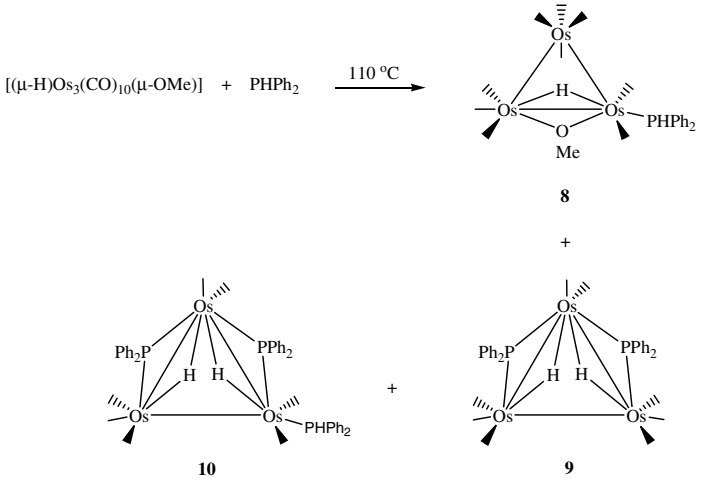

by the hydride ligand may be counterbalanced by the bridging methoxide ligand. The two unbridged Os–Os edges differ by ca. 0.002 Å, but the average value is somewhat shorter than the average Os–Os distance of 2.877(3) Å in $[Os_3(CO)_{12}]$ [30]. The longer Os(1)–Os(3) bond has the 'pseudo axial' phosphine *cis* to it and the increase in length may be consistent with the greater steric bulk of this group. The Os(3)–P(1) bond distance of 2.309(5) Å is comparable to that observed in $[(\mu\text{-H})Os_3(CO)_9(\mu\text{-OH})(PMe_2Ph)]$ (2.329(2) Å} [19].

The elemental analysis, infrared, ^{1}H NMR, $^{31}P\{^1H\}$ NMR and mass spectroscopic data for compound **10** are consistent with the proposed structure. The infrared spectrum of **10** indicates that the carbonyl groups are terminal. The mass spectrum shows molecular ion peak at *m/z* 1324, which is consistent with the proposed formulation. The $^{31}P\{^1H\}$ NMR spectrum of **10** shows two doublets at δ 99.5 ($J = 65.5$ Hz) and −14.3 ($J = 40.5$ Hz) and a double doublets at δ 66.9 ($J = 40.5$, 65.5 Hz) consistent with the proposed structure. The strongly deshielded resonances at δ 99.49 and 66.9 are due to the bridging phenylphosphido ligands while the doublet at δ −14.27 is attributed to the phosphorus atom of the terminal PPh_2H ligand. The hydride region of the ^{1}H NMR spectrum of **10** contains two equally intense signals, a doublet of doublets at δ −16.23 ($J = 7.5$, 15.0 Hz) and a doublet of a double doublets at δ −17.74 ($J = 3.5$, 7.5, 15.0 Hz) indicating that the compound has two non-equivalent bridging hydride ligands. The hydride and ^{31}P chemical shifts and coupling constants are in agreement with the proposed structure for **10** (Scheme 4).

4. Conclusions

In summary, the present work demonstrates that the reactivity of both $[(\mu\text{-H})Os_3(CO)_{10}(\mu\text{-OMe})]$ (**1**) and $[(\mu\text{-H})Os_3(CO)_9(\mu\text{-OMe})(MeCN)]$ (**4**) toward diphosphines depends on the methylene chain length of the organic back bone of the diphosphine ligands. Two compounds, $[Os_3(CO)_{10}(\mu_2\text{-}\eta^2\text{-dppm})]$ (**2**) and $[(\mu\text{-H})Os_3(CO)_8(\mu\text{-OMe})(\mu_2\text{-}\eta^2\text{-dppm})]$ (**3**) have been obtained from the reaction of dppm with **1**. Compound **2** results from reductive elimination of methanol followed by addition of dppm and **3** by substitution of one CO ligand from each of the bridgehead osmium atom by a PPh_2 group of the dppm ligand. The single crystal structure analysis of **3** reveals that the dppm ligand spans the same Os–Os vector as the methoxide and hydride ligands. In contrast, dppe reacts with both **1** giving two isomeric compounds, $[(\mu\text{-H})Os_3(CO)_8(\mu\text{-OMe})(\mu_1\text{-}\eta^2\text{-dppe})]$ (**5**) and $[(\mu\text{-H})Os_3(CO)_8(\mu\text{-OMe})(\mu_2\text{-}\eta^2\text{-dppe})]$ (**6**), which differ in the mode of bonding of the dppe ligand. In **5**, the dppe ligand is coordinated at the unbridged Os atom (chelating mode) whereas in **6** the ligand is coordinated at the bridgehead Os atoms (edge-bridging mode) as in **3**. Treatment of **1** with dppp produces only $[(\mu\text{-H})Os_3(CO)_8(\mu\text{-OMe})(\mu_2\text{-}\eta^2\text{-dppp})]$ (**7**) which exists as two isomers in solution (Scheme 3). Similar products were obtained from the reactions of dppm, dppe, and dppp with **4**. The attempted preparation of bridging methoxide and phosphido compounds from the reaction of **1** with PPh_2H at 110 °C gave the new compounds $[(\mu\text{-H})Os_3(CO)_9(\mu\text{-OMe})(PPh_2\mathit{H})]$ (**8**) and $[(\mu\text{-H})_2Os_3(CO)_7(\mu\text{-}PPh_2)_2$ $(PPh_2H)]$ (**10**) and previously reported compound $[(\mu\text{-H})_2Os_3(CO)_8(\mu\text{-}PPh_2)_2]$ (**9**). In **8**, the PPh_2H ligand occupies a 'pseudo' axial site on one of the osmium atoms bearing the bridging hydride and methoxide ligand. The formation of the μ-phosphido complexes is directly related to the elimination of methanol and points out the lability of this moiety as a cluster ligand. This may provide a general synthetic route, using **1**, for the formation of cluster derivatives with compounds containing active hydrogen atoms but where no additional hydride is desired in the final product.

Acknowledgements

The Swedish International Development Agency (SIDA) and the Swedish Research Council (VR) are gratefully acknowledged for supporting the collaboration between SEK and EN.

Appendix A. Supplementary data

Crystallographic data for the compounds have been deposited with the Cambridge Crystallographic Data-Centre, CCDC Nos. 267409 (**3**), and 267410 (**8**). Copies of this information may be obtained free of charge from the Director, CCDC, 12 Union Road, Cambridge, CB2 1EZ, UK (fax: +44 1223 3360333 or e-mail: deposit@ccdc.cam.ac.uk or www: http://www.ccdc.cam. ac.uk). Supplementary data associated with this article can be found, in the online version, at doi:10.1016/j.poly.2005.07.004.

References

[1] W. Fan, R. Zhang, W.K. Leong, Y.K. Yan, Inorg. Chim. Acta 357 (2004) 2441.
[2] M.P. Brown, P.A. Dolby, M.M. Harding, A. Mathews, A.K. Smith, J. Chem. Soc., Dalton Trans. (1993) 1671.
[3] T. Adatia, S.S.D. Brown, I.D. Salter, J. Chem. Soc., Dalton Trans. (1993) 559.
[4] D. Braga, U. Matteoli, P. Sabatino, A. Scrivanti, J. Chem. Soc., Dalton Trans. (1995) 419.
[5] T. Adatia, G. Conole, S.R. Drake, B.F.G. Johnson, M. Kessler, J. Lewis, M. McPartlin, J. Chem. Soc., Dalton Trans. (1997) 669.
[6] E.L. Diz, A. Neels, H. Stoeckli-Evans, G. Süss-Fink, Polyhedron 20 (2001) 2771.

[7] (a) J.N.L. Dennett, A.L. Gillon, K. Heslop, D.J. Hyett, J.S. Fleming, C.E. Lloyd-Jones, A.G. Orpen, P.G. Pringle, D.F. Wass, J.N. Scutt, R.H. Weatherhead, Organometallics 23 (2004) 6078;
(b) J.L. Kuiper, P.A. Shapley, C.M. Rayner, Organometallics 23 (2004) 3814.
[8] I. Albers, E. Álvarez, J. Cámpora, C.M. Maya, P. Palma, L.J. Sánchez, E. Passaglia, J. Organomet. Chem. 689 (2004) 833.
[9] A. Poe, V.C. Sekhar, J. Am. Chem. Soc. 106 (1984) 5034.
[10] A.J. Deeming, S. Donovan-Mtunzi, S.E. Kabir, J. Organomet. Chem. 276 (1984) C65.
[11] J.A. Clucas, D.F. Foster, M.M. Harding, A.K. Smith, J. Chem. Soc., Chem. Commun. (1984) 949.
[12] K.A. Azam, M.B. Hursthouse, S.E. Kabir, K.M.A. Malik, M.A. Mottalib, J. Chem. Crystallogr. 29 (1999) 813.
[13] S. Cartwright, J.A. Clucas, R.H. Dawson, D.F. Foster, M.M. Harding, A.J. Mathews, A.K. Smith, J. Organomet. Chem. 295 (1985) 99.
[14] A.J. Deeming, S. Donovan-Mtunzi, S.E. Kabir, J. Organomet. Chem. 333 (1987) 253.
[15] S.E. Kabir, A. Miah, L. Nesa, K. Uddin, K.I. Hardcastle, E. Rosenberg, A.J. Deeming, J. Organomet. Chem. 492 (1995) 41.
[16] A.J. Deeming, S. Donovan-Mtunzi, K.I. Hardcastle, S.E. Kabir, K. Henrick, M. McPartlin, J. Chem. Soc., Dalton Trans. (1988) 579.
[17] B.F.G. Johnson, J. Lewis, M. Monari, D. Braga, F. Grepioni, C. Gradella, J. Chem. Soc., Dalton Trans. (1990) 2863.
[18] R.J. Puddephatt, Chem. Soc. Rev. 12 (1983) 99.
[19] S.R. Hodge, B.F.G. Johnson, J. Lewis, P.R. Raithby, J. Chem. Soc., Dalton Trans. (1987) 931.
[20] M.W. Lum, W.K. Leong, J. Chem. Soc., Dalton Trans. (2001) 2476.
[21] M.W. Lum, W.K. Leong, J. Organomet. Chem. 687 (2003) 203.
[22] J.R. Shapley, M. Tackikawa, J. Organomet. Chem. 124 (1977) C19.
[23] R.D. Adams, M.P. Pompeo, J.T. Tanner, Organometallics 10 (1991) 1068.
[24] R. Hooft, COLLECT Data Collection Software, Nonius B V, Delft, The Netherlands, 1998.
[25] Z. Otwinowski, W. Minor, in: C.W. Carter Jr., R.M. Sweet (Eds.), Macromolecular Crystallography, Academic Press, New York, 1997, pp. 307–326.
[26] R.H. Blessing, Acta Crystallogr. A 51 (1995) 33.
[27] R.H. Blessing, J. Appl. Crystallogr. 30 (1997) 421.
[28] G.M. Sheldrick, Acta Crystallogr. A 61 (1990) 467.
[29] G.M. Sheldrick, SHELXL-97, Program for Crystal Structure Refinement, University of Göttingen, Germany, 1997.
[30] M.R. Churchill, B.G. DeBoer, Inorg. Chem. 16 (1977) 878.
[31] M.R. Churchill, H.J. Wasserman, Inorg. Chem. 19 (1990) 2391.
[32] K.A. Azam, M.B. Hursthouse, S.E. Kabir, K.M.A. Malik, M.A. Mottalib, J. Chem. Crystallogr. 29 (1999) 813.
[33] E.J. Ditzel, M.P.G. Sal, B.F.G. Johnson, J. Lewis, P.R. Raithby, J. Chem. Soc., Dalton Trans. (1987) 1623.
[34] V.D. Patel, A.A. Cherkas, D. Nucciarone, N.J. Taylor, A.J. Carty, Organometallics 4 (1985) 1792.
[35] K.A. Azam, M.B. Hursthouse, M.R. Islam, S.E. Kabir, K.M.A. Malik, R. Miah, C. Sudbrake, H. Vahrenkamp, J. Chem. Soc., Dalton Trans. (1998) 1097.
[36] S.S.M.C. Godinho, B. Royo, M.T. Lobato, E. Herdtweck, C.C. Romao, Polyhedron 23 (2004) 1263.

Available online at www.sciencedirect.com
SCIENCE DIRECT®
Polyhedron 25 (2006) 105–112
POLYHEDRON
www.elsevier.com/locate/poly

Synthesis and thermal decarbonylation of $W(CO)_5$ complexes supported by nitrile, pyridine or phosphine ligands to poly-spirophosphazene random copolymers carrying $O–C_6H_5–CO_2Pr$ groups

Gabino A. Carriedo [a,*], F.J. Garcia Alonso [a], Carlos Diaz Valenzuela [b], Maria Luisa Valenzuela [b]

[a] *Departamento de Química Orgánica e Inorgánica, Facultad de Química, Universidad de Oviedo, Oviedo 33071, Spain*
[b] *Departamento de Química, Facultad de Ciencias, Universidad de Chile, Casilla 653, Santiago, Chile*

Received 13 May 2005; accepted 8 July 2005
Available online 23 September 2005

Abstract

The phosphazene copolymers $\{[NP(O_2C_{12}H_8)]_{0.5}[NP(O–C_6H_4–CO_2Pr^n)(O–C_6H_4–L)]_{0.5}\}_n$ [L = CN (**1**), PPh_2 (**2**)] and $\{[NP(O_2C_{12}H_8)]_{0.6}[NP(O–C_6H_4–CO_2Pr^n)(O–C_5H_4N)]_{0.4}\}_n$ (**3**) have been synthesized by sequential substitution from $[NPCl_2]_n$. Their reactions with $[W(MeOH)(CO)_5]$ gives the corresponding tungsten carbonyl complexes $\{[NP(O_2C_{12}H_8)]_{0.5}[NP(O–C_6H_4–CO_2Pr^n)(O–C_6H_4–CN)(W(CO)_5)_{0.4}]_{0.5}\}_n$ (**4**), $\{[NP(O_2C_{12}H_8)]_{0.5}[NP(O\text{-}C_6H_4–CO_2Pr^n)(O–C_6H_4–PPh_2)(W(CO)_5)_{0.7}]_{0.5}\}_n$ (**5**), $\{[NP(O_2C_{12}H_8)]_{0.6}[NP(O–C_6H_4–CO_2Pr^n)(O–C_5H_4N–W(CO)_5)]_{0.4}\}_n$ (**6a**), and $\{[NP(O_2C_{12}H_8)]_{0.6}[NP(O–C_6H_4–CO_2Pr^n)(O–C_5H_4N)(W(CO)_5)_{0.4}]_{0.4}\}_n$ (**6b**), that have been fully characterized by IR and NMR spectroscopies. The thermal properties (TGA and DSC) of the polymeric complexes showed that they are high glass transition materials that undergo a complete decarbonylation below 300 °C forming metal containing species that have a stabilizing effect on the polymeric matrices. The final residues up to 800 °C are of the order of30–50%.
© 2005 Elsevier Ltd. All rights reserved.

Keywords: Polyphosphazenes; Tungsten; Carbonyl complexes

1. Introduction

The polyphosphazenes, that are inorganic–organic polymers with $[–N=PR_2–]$ repeating units, continue attracting a great deal of interest in both basic and applied material science [1]. In particular, they can be used to support a variety of transition metal carbonyl and organometallic complexes [2,3]. In earlier papers we reported [4] that the polydichlorophosphazene reacts directly first with 2,2′-(HO)–C_6H_4–C_6H_4(OH) and subsequently with para-substituted phenols OH–C_6H_4–R in THF in the in the presence of K_2CO_3, affording a new type of phosphazene copolymers $\{[NP(O_2C_{12}H_8)]_x[NP(O–C_6H_4–R)_2]_{1-x}\}_n$ with high thermal stability and elevated transition temperatures.

This sequential substitution, using also Cs_2CO_3 as proton abstractor, allowed the facile synthesis of a wide range of functionalized random copolymers systematically designed to carry chemical functions including ligands for transition metal fragments [3], useful in catalysis [5–7]. Therefore, we have extended this synthetic route to the preparation of new polyphosphazene random copolymers incorporating nitrile, phosphine or pyridine ligands in the vicinity of a carboxylate group

* Corresponding author. Tel.: +34 985 103462; fax: +34 985 103446.
E-mail address: fjga@fq.uniovi.es (G.A. Carriedo).

0277-5387/$ - see front matter © 2005 Elsevier Ltd. All rights reserved.
doi:10.1016/j.poly.2005.07.016

(CO_2Pr), that, as we have shown recently, are very helpful in determining the composition of the polymers, to modify their physical properties [8] and that may be easily transformed into other groups, including the useful carboxylic acids COOH [9].

In this paper we report the synthesis and the study of the thermal properties of new polymers of this type, and the formation of their complexes with $W(CO)_5$. We have found that these complexes undergo a fast decarbonylation below 300 °C that, depending on the electronic characteristics of the ligand, specially its labilizing effect to CO dissociation, may give carbide-oxide or metallic tungsten particles that, in the latter cases, appear to have an stabilizing effect on the polymeric matrices. Therefore, those observations could be useful to understand the characteristics of the residues generated by thermal treatments of polymeric complexes, and to the design of precursor complexes in order to control the nature of the metal containing particles resulting within the polymeric matrices, which is a topic of current interest [10].

2. Results and discussion

The reaction of $[NPCl_2]_n$ in THF first with 0.5 equivalents of 2,2′-dihydroxybiphenyl $(HO)_2(C_{12}H_8)$ and K_2CO_3, followed by 0.5 equivalents of $HO–C_6H_4–CO_2Pr_n$ and Cs_2CO_3, and finally with ca. 0.6 equivalents (see Section 3) of $HO–C_6H_4–L$ (L = CN or PPh_2), gave the random phosphazene copolymers $\{[NP(O_2C_{12}H_8)]_{0.5}[NP(O–C_6H_4–CO_2Pr^n)(O–C_6H_4–L)]_{0.5}\}_n$ [L = CN (**1**), PPh_2 (**2**)]. A similar sequential substitution but using 4-hydroxypyridine in the third step afforded the polymer $\{[NP(O_2C_{12}H_8)]_{0.6}[NP(O–C_6H_4–CO_2Pr^n)(O–C_5H_4N)]_{0.4}\}_n$ (**3**) (Scheme 1).

The average M_w (of the order of 1.210^6 with polydispersities in the range 2–5) and the glass transition temperatures (around 70 °C) were not far from the values observed for the related polymer $\{[NP(O_2C_{12}H_8)]_{0.5}[NP(O–C_6H_4\text{-}CO_2Pr^n)_2]_{0.5}\}_n$ published recently [8].

All the analytical and spectroscopic data (Section 3) were in accord with the chemical composition (calculated values are for the idealized formulas and some deviation from the experimental data is frequently found in polymers of this type) and the structure of the new polymers. Most significantly, the ^{31}P NMR spectra exhibited two broad signals, one for the $[NP(O_2C_{12}H_8)]$ units (ca. −4 ppm) and other for the $[NP(O–C_6H_4–CO_2Pr^n)(O–C_6H_4\text{-}L)]$ units (ca. −22 ppm). No signals of [NPCl(OR)] units were detected, indicating that the unreacted Cl is negligible. The relative intensities (that were more accurately measured in DMSO at 110 °C where the spectra were much sharper) indicated the actual composition of the copolymers, that also agreed with the calculated from the ^1H NMR spectra. In the ^{31}P NMR spectrum of **2** a singlet at −6.4 ppm (chloroform) or −4.5 ppm (DMSO) confirmed the presence of the PPh_2 ligands (in DMSO at 110 °C a conspicuous inversion of the relative positions of the

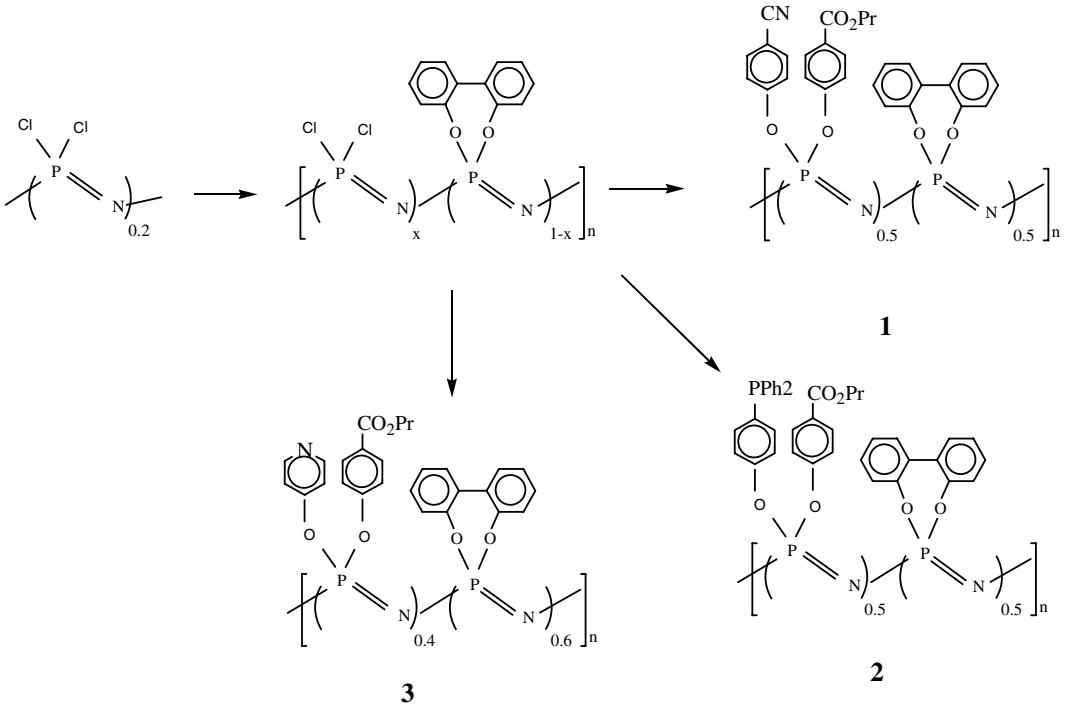

Scheme 1.

[$NP(O_2C_{12}H_8)$] and (PPh_2) signals were observed). However, another peak at 29 ppm (chloroform) indicated that some of the phosphines were oxidized to –P(O)Ph_2 groups. From the relative intensity of this signal (also measured in the spectrum in DMSO at 110 °C, where it appears at 24 ppm) the degree of oxidation was found to be ca. 8%.

Among other useful NMR spectral data were the small peak at 112 ppm in the ^{13}CNMR of **1** clearly attributable to the C_4 carbon of the O–C_6H_4–CN group (the expected very weak CN signal around 120 ppm was obscured by the abundant signals in that region).

The IR clearly evidenced the presence of the (O–C_6H_4–CO_2Pr^n) groups (carbonyl stretching at 1717 cm^{-1}), and the ligand supported in the lateral groups, namely: the *v*-CN stretching at 2228 cm^{-1} (polymer **1**) or the characteristic pyridine ring stretching band [3] at 1585 cm^{-1} (polymer **3**). The presence of the phosphine ligand is best detected in the IR spectrum of **2** by the medium intensity band at 696 cm^{-1}, typical of the mono-substituted arene ring [11] (in the spectrum of the related compound without phosphine {[$NP(O_2C_{12}H_8)]_{0.5}$[NP-($O–C_6H_4–CO_2Pr^n)_2]_{0.5}\}_n$, only a very weak absorption at 694 cm^{-1} could be observed).

Although it cannot be shown experimentally, it should be noted that, because of the essentially random nature [8] of the substitution reactions that lead to **1**, **2** and **3** from $[NPCl_2]_n$, only mixed units of the type [$NP(O–C_6H_4–CO_2Pr^n)$(O–R–L)] are present in the chains of the copolymers, and, therefore, most of the pendant ligands L are in the vicinity of the (O–C_6H_4–CO_2Pr^n) groups (see Scheme 1).

The reaction of the polymeric ligands **1**, **2** and **3** with the corresponding stoichiometric or substoichiometric amounts of [$W(MeOH)(CO)_5$] in a mixture of dichloromethane–methanol gave the complexes (Scheme 2) {[NP-($O_2C_{12}H_8$)]$_{0.5}$[NP(O–C_6H_4–CO_2Pr^n)(O–C_6H_4–CN)(W-$(CO)_5)_{0.4}]_{0.5}\}_n$ (**4**), {[$NP(O_2C_{12}H_8)]_{0.5}$[NP(O–C_6H_4–CO_2-Pr^n)(O–C_6H_4–PPh_2)($W(CO)_5)_{0.7}]_{0.5}\}_n$ (**5**), {[$NP(O_2C_{12}$-$H_8)]_{0.6}$[NP(O–C_6H_4–CO_2Pr^n)(O–C_5H_4N–$W(CO)_5)]_{0.4}\}_n$ (**6a**), and {[$NP(O_2C_{12}H_8)]_{0.6}$[NP(O–C_6H_4–CO_2Pr^n)(O–C_5H_4N)($W(CO)_5)_{0.4}]_{0.4}\}_n$ (**6b**). The relative quantities of the polymeric ligand and the precursor complex were calculated using the functionalization degree of the ligands FD (in mmol of ligating group per gram of polymer) given in the experimental part. In the case of the phosphine the calculation took into account the 8% of the oxidized PPh_2 groups.

All the analytical and spectroscopic data (Section 3) confirmed that the composition of the new complexes were not too far from the intended one (50–100% coordination of the available ligands).

Most significant were the changes in the IR spectra evidencing the incorporation of the $W(CO)_5$ fragment. The absence of $W(CO)_6$ was guaranteed by the constancy of the spectra after several purifications. Apart from the expected *v*(CO) stretching absorbances of the pentacarbonyl moiety, the spectrum of **6a** showed the absence of the strong absorption at 1585 cm^{-1} (present in the spectrum of the free ligand **3**, and with

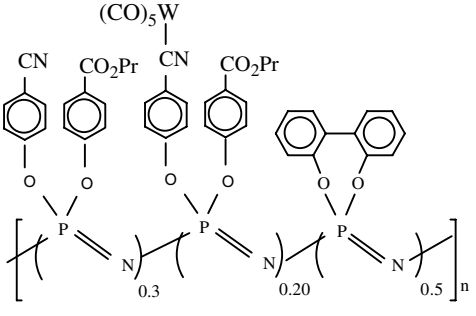

4

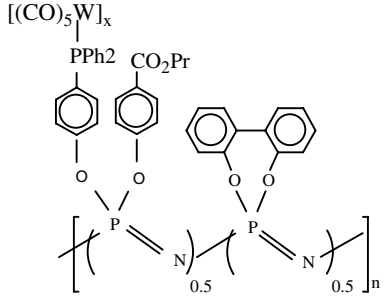

5. x=0.7

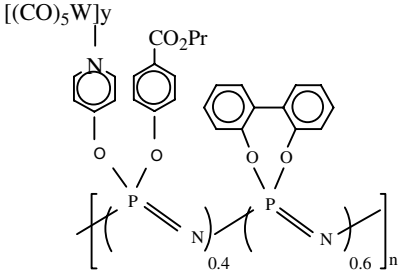

6a(y=1), **6b**(y=0.4)

Scheme 2.

less intensity also in the incompletely charged complex **6b**) that is a good diagnosis of the coordination of a MLn fragment to the pyridine [3]. In all cases, the carbonyl stretching frequency of the CO_2Pr group was unaffected by the presence of the tungsten carbonyl units, indicating that the electronic interaction between this group and the ligand attached to the vicinal aryloxy group is very small. The ^{31}P NMR spectrum (measured in NMP) showed the two phosphazene units at chemical shifts only 1 ppm lower than those of the free ligands. This limited sensibility of the PN groups to the coordination of metals to the ligands supported on them has been frequently observed [3].

In the case of the phosphine ligand **2** the composition of the products obtained in the reactions with $[W(HOMe)(CO)_5]$ were not reproducible and always contained ca. 70% of the maximum $W(CO)_5$ fragments. The isolated products were not completely soluble and gave rather cloudy solutions (the NMR spectral signals were extremely broad, preventing the observation of the ^{183}W satellites). This, and the presence of a shoulder at 1890 cm^{-1} in the IR spectrum, strongly suggest that, as found in similar reactions [12], some interchain substitution of CO by phosphine groups might take place during the formation of **5**. It should be noticed that a very few of such cross-linking points would transform the polymer into an insoluble gel-forming material [13].

The thermal properties of the new complexes were studied by TGA and DSC calorimetry (Tables 1 and 2). In all cases the TGA curves exhibited a distinct first weight loss step between 100 and 300 °C, and a main loss between 300 and 800 °C. It was clearly noted that the weight loss produced by further heating the complexes for 1/2 h at 800 °C were almost negligible, while the free polymeric ligands underwent another weight loss of the order of 7%. Therefore, unlike the precursor ligand, the residues left by the complexes are already stabilized at 800 °C.

The first weight loss could be unambiguously assigned to a decarbonylation process. Thus, the IR spectra of the samples heated in this range of temperatures under N_2 atmosphere (Fig. 1), evidenced the total disappearance of the initial ν(CO) absorptions (that changed gradually to lower CO frequency patterns clearly attributable to intermediate tetra, tri or dicarbonyls units [14] and the final spectra were identical to those of the free ligands. In the cases of **6a** and **6b**, the disappearance of the tungsten carbonyl complex was also noted by the re-appearance of the absorption at 1585 cm^{-1} of the free pyridine ligand. However, although in all the cases all the CO ligands had disappeared at 300 °C, the weight losses measured in the TGA thermograms below this temperature range (Table 1) were slightly lower than the expected from the $W(CO)_5$ contents in the original complexes (Table 2). The difference (C/O res. in Table 2) was small for the complexes **4**, **6a** and **6b** (ca. 2%), but more significant for **5** (3.4%). Although not very pronounced, this effect might be indicating that,

Table 1
Thermocalorimetric data for the polymers **1**, **2** and **3** and their complexes

Polym	Range (°C)	Weight loss (%)	Range (°C)	Weight loss (%)	Loss after 1/2 h at 800 °C (%)	Residue[a]	T_g (°C)[b]
1	50–200	3.5	300–800	72	7.3	17.2	64
2	50–200	2.0	300–800	71	6.6	20.4	70
3	50–200	3.4	250–800	71	7.3	18.3	75
4	50–250	5.1	250–800	61.7	0.8	32.4	69
5	50–250	4.9	250–800	57.0	1.1	37.1	ca. 90[c]
6a	50–280	12.4	300–800	33.8	1.0	52.8	87
6b	50–250	6.7	250–800	55.4	1.2	36.7	84

[a] The final residues were reproducible with uncertainties not greater than 2%.
[b] Measured between −50 and 250 °C, and in the second heating (3rd run).
[c] Changing with the sample (see text).

Table 2
Expected and found TGA residues for the complexes **4**, **5** and **6**

Polym	W content (% experimental)	CO content[a] (% experimental)	RL[b]	C/O res.[c]	Expected[d] residue (%)	Difference[e]
4	8.5	6.5	17.2	1.4	27.1	5.3
5	11.0	8.4	20.4	3.4	34.8	2.3
6a	19.2	14.6	18.3	2.2	39.7	13.1
6b	10.2	7.8	18.3	1.1	29.6	7.1

[a] Calculated from the experimental W content.
[b] Residue left by the free polymeric ligand (Table 1).
[c] Carbon and oxygen not lost in the decarbonylation (%CO content − weight loss below 350 °C).
[d] W content + RL + C/O res.
[e] Residue found (Table 1) – expected residue.

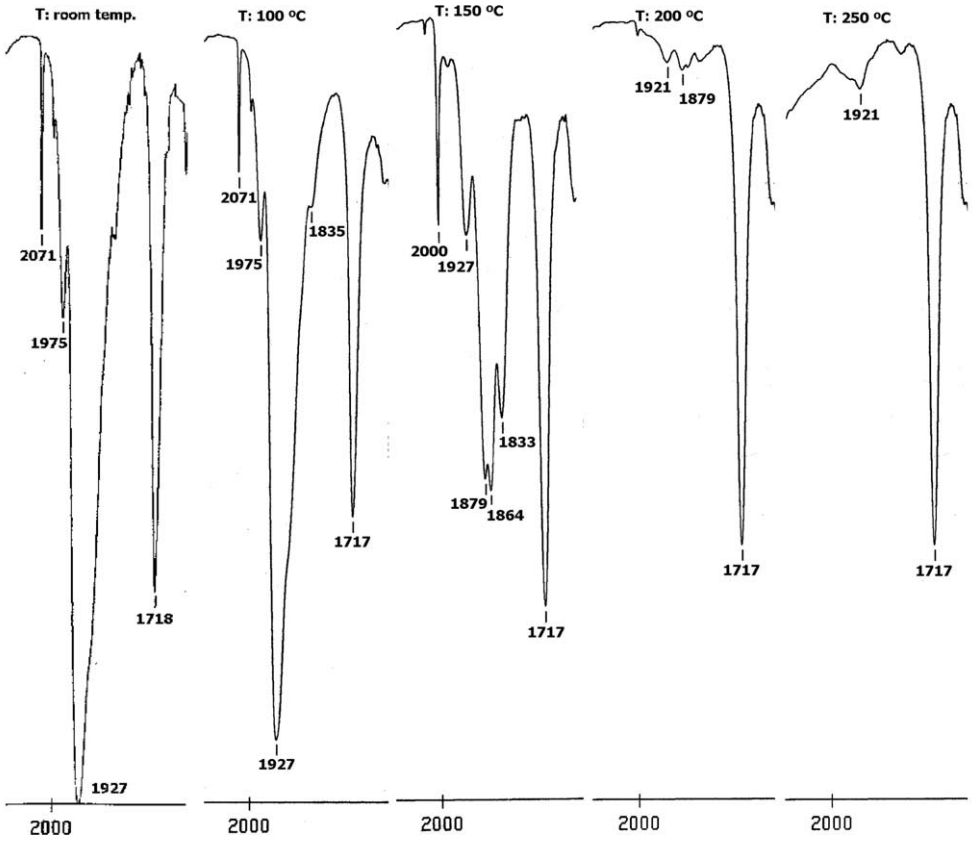

Fig. 1. Monitoring by IR spectrum (ν_{CO} region) of the decarbonylation of $\{[NP(O_2C_{12}H_8)]_{0.6}[NP(O–C_6H_4–CO_2Pr^n)(O–C_5H_4N)(W(CO)_5)_{0.4}]_{0.4}\}_n$ (**6b**), below 300 °C.

as it has been well established [15] the decarbonylation of tungsten carbonyls below 300 °C give residues that consist on tungsten oxide carbides, formed by the dissociation of a fraction of the CO ligands on the metal surface. Therefore, it is possible that, with the more *cis*-labilizing [16] N-donor ligands, the decarbonylation is more favoured minimizing the secondary CO scission process, forming mainly tungsten particles trapped in the residual polymeric matrix. This observation could be useful in designing polymeric complexes in order to control the nature of the metal containing particles resulting in the thermal decomposition.

On the other hand, the thermograms also indicated that, in the case of **4**, and **6b** and, even more conspicuously, in the case of **6a**, the final residues left by the complexes after an stabilization step at 800 °C for 1/2 hour, (Table 1) were higher than those expected by adding the metallic residues to the residues left (under the same conditions) by the free polymeric ligands (Table 1). For complex **5** the difference was much smaller. This suggests that the tungsten particles might have a greater stabilizing effect on the polymeric matrices (yielding less proportion of volatiles at higher temperatures) than the carbide-oxide richer particles.

The decarbonylation of the tungsten carbonyl fragments also accounted for the DSC thermograms of the complexes, that showed a distinct glass transition with a T_g that depended on the metal content and also on the temperature range chosen for the running cycles (Table 1). It has been established that the T_g of a polyphosphazene bearing a complex should be higher than that of the corresponding polyphosphazene free ligand [17]. Thus, although the T_g of the complex **4** is only 5 °C higher than that of the polymeric ligand **1**, the T_g observed for **5** and **6** (Table 1) were ca. 25 °C higher than those of **2** and **3**. However, taking into account that the complexes undergo a decarbonylation in this range of temperatures, the effect of the T_g must be due to the formation of the resulting metallic or metal-carbide-oxide residues rather than to the present of the original $W(CO)_5$ fragments. It was also noted that, in those cases were a heat capacity jump attributable to a glass transition could be detected in the first heating runs of the DSC experiments (i.e., before extensive decarbonylation had taken place) the measured T_g were approximately (but not well reproducible) 20–30 °C higher than the observed in the second heating run. It is to be expected that the final residues are heavily cross-linked polymeric matrices and it is known that, as found for polystyrene [18], the cross-linking increases the glass transition temperatures of the polymers.

3. Experimental part

K_2CO_3 and Cs_2CO_3 were dried at 140 °C prior to use. The THF was treated with KOH and distilled twice from Na in the presence of benzophenone. The 2,2′-dihydroxibiphenyl HO–C_6H_4–C_6H_4–OH, the phenols HO–C_6H_4–R (R = CO_2Pr or CN), and the pyridone HO–C_5H_4N were used as purchased (Aldrich). The phosphine HO–C_6H_4–R was obtained as described elsewhere [19]. The starting polymer $[NPCl_2]_n$ was prepared as described previously [20]. The complexes $[W(MeOH)(CO)_5]$ were obtained by the literature methods [21].

The IR spectra were recorded with a Perkin–Elmer FT Paragon 1000 spectrometer. NMR spectra were recorded on Bruker AC-200, AC-300 and Avance 300 instruments, using $CDCl_3$, DMSO (dimethylsulfoxide) or NMP (*N*-methyl-pyrrolidone) as solvents. ^1H and $^{13}C\{^1H\}$ NMR are given in δ relative to TMS. $^{31}P\{^1H\}$ NMR are given in δ relative to external 85% aqueous H_3PO_4. Coupling constants are in Hz. C, H, N analyses were performed with a Perkin–Elmer 240 microanalyzer. Chlorine analyses were performed by Galbraith Laboratories. GPC were measured with a Perkin–Elmer equipment with a Model LC 250 pump, a Model LC 290 UV, and a Model LC 30 refractive index detector. The samples were eluted with a 0.1% by weight solution of tetra-*n*-butylammonium bromide in THF through Perkin–Elmer PLGel (Guard, 10^5, 10^4 and 10^3 Å) at 30 °C. Approximate molecular weight calibration was obtained using narrow molecular weight distribution polystyrene standards. T_g values were measured with a Mettler DSC 300 differential scanning calorimeter equipped with a TA 1100 computer. Thermal gravimetric analyses were performed on a Mettler TA 4000 instrument. The polymer samples were heated at a rate of 10 °C/min from ambient temperature to 800 °C under constant flow of nitrogen, and further heated at 800 °C for 1/2 h for stabilization of the residue.

3.1. {[NP($O_2C_{12}H_8$)]$_{0.5}$[NP(O–C_6H_4–CO_2Pr^n)-(O–C_6H_4–CN)]$_{0.5}$}$_n$ (1)

To a THF solution of $[NPCl_2]_n$ (200 mL, 2.08 g, 17.9 mmol), 2,2′-(HO)–C_6H_4–C_6H_4(OH) (1.67 g, 8.97 mmol) and solid K_2CO_3(2.48 g, 17.9 mmol) were added and the mixture was refluxed with mechanical stirring for 15 h. Then, HO–C_6H_4–CO_2Pr (1.61 g, 8.97 mmol) and Cs_2CO_3 (8.8 g, 27 mmol) were added, and refluxing was continued for another 6.5 h. To the mixture HO–C_6H_4–CN (1.18 g, 9.9 mmol) were added, and refluxing was continued for another 24 h. The reaction mixture was poured into water (2 L) to give a precipitate that was filtered, washed with water (2 × 100 mL), isopropanol and hexane, and dried. The purification was performed by dissolving the product in THF (600 mL) to give a clear solution that was concentred at reduced pressure until the formation of a viscous liquid that was poured portion-wise (Pasteur pipette) into water (1 L), followed by two further reprecipitations from THF/isopropyl-alcohol and THF/hexane. The final white material was dried 72 h in vacuo at 50 °C. Yield: 3.67 g (71.7%). *Anal.* Calc. for $C_{14.5}H_{11.5}N_{1.5}O_3P$ (285.7): C, 60.9; H, 4.06; N, 7.35. Found: C, 58.0; H, 3.38; N, 6.37%. IR (KBr): ν = 3067w (ν-CH-arom.), 2965m (ν-CH-aliph.), 2228m (ν-CN), 1717s (ν-CO_2Pr), 1603s, 1505s, 1478m (ν-C=C-arom.), 1273vs (ν-C–OP), 1244vs 1196vs, br., 1162s (ν-PN), 1095s (ν-P–OC), 928vs, br. (δ-POC), 784s, 752m, 716m, 609w, 536s (other) cm^{-1}. $^{31}P\{^1H\}$ NMR ($CDCl_3$): δ = −4.8 ppm, br. [NP($O_2C_{12}H_8$)]; −22.2 ppm, br. [NP(O–C_6H_4–CO_2Pr^n)(O–C_6H_4–CN)]. ^1H NMR ($CDCl_3$): δ = 7.5–6.5m, br. ($C_{12}H_8$ and C_6H_4); 4.2m, br. (OCH_2); 1.73m, br. (–CH_2–); 0.94m, br. (CH_3). $^{13}C\{^1H\}$ NMR ($CDCl_3$): δ = 166 (CO), 154br (C_1–OC_6H_4–), 148 (C_2–$C_{12}H_8$), 133–118 ($C_{12}H_8$, OC_6H_4); 112 (C_4–OC_6H_4–CN), 66.4 (OCH_2); 22.1 (–CH_2); 10.5 (CH_3). M_w (GPC) : 1 300 000, M_w/M_n = 2.4. T_g (DSC from 0 to 250 °C) = 64 °C. ΔC_p = 0.16 J g^{-1} K^{-1}.

3.2. {[NP($O_2C_{12}H_8$)]$_{0.5}$[NP(O–C_6H_4–CO_2Pr^n)-(O–C_6H_4–PPh_2)]$_{0.5}$}$_n$ (2)

To a THF solution of $[NPCl_2]_n$ (200 mL, 1.5 g, 12.9 mmol), 2,2′-(HO)–C_6H_4–C_6H_4–(OH) (1.2 g, 6.44 mmol) and solid K_2CO_3 (1.78 g, 12.9 mmol) were added and the mixture was refluxed with mechanical stirring for 14 h. Then, HO–C_6H_4–CO_2Pr (1.16 g, 6.44 mmol) and Cs_2CO_3 (10.5 g, 32.2 mmol) were added, and refluxing was continued for another 9 h. To the mixture HO–C_6H_4–PPh_2 (2.5 g, 9.01 mmol) and more THF (80 mL) were added, and refluxing was continued for another 20 h. The reaction mixture was concentrated to half volume and poured into water (2 L) to give a precipitate that was filtered, washed with water (2 × 100 mL), isopropanol and hexane, and dried. The purification was performed as for polymer **1**. The final white material was dried 72 h in vacuo at 50 °C. Yield: 3.2 g (68%). *Anal.* Calc. for $C_{20}H_{16.5}NO_3P_{1.5}$ (365.2): C, 65.8; H, 4.55; N, 3.83. Found: C, 61.6; H, 5.07; N, 4.12%. IR (KBr): ν = 3068w (ν-CH-arom.), 2966 m (ν-CH-aliph.), 1717s (ν-CO_2Pr^n), 1603s, 1503s, 1477m (ν-C=C-arom.), 1272vs (ν-COP), 1245vs, 1198vs, br., 1165s (ν-PN), 1095m (ν-P–OC), 933vs, br. (δ-POC), 784s, 751s, 696m, 609w, 540s (other) cm^{-1}. $^{31}P\{^1H\}$ NMR ($CDCl_3$): δ = −4.8 ppm, broad [NP($O_2C_{12}H_8$)]; −22.2 ppm broad [NP(O–C_6H_4–CO_2Pr^n)(O–C_6H_4–PPh_2)]; −6.4 (PPh_2). In DMSO at 110° the values were −6.3, −23.5 and −4.5, respectively (with a conspicuous inversion of the relative position of the [NP($O_2C_{12}H_8$)]

and (PPh_2) signals. ^1H NMR ($CDCl_3$): $\delta = 7.4$–6.6m, br. ($C_{12}H_8$, C_6H_4 and C_6H_5); 4.13m, br. (OCH_2); 1.67m, br. (–CH_2–); 0.94m, br. (CH_3). $^{13}C\{^1H\}$ NMR ($CDCl_3$): $\delta = 166$(CO), 154(C_1–OC_6H_4–), 148.2(C_2–$C_{12}H_8$), 151, 137–120($C_{12}H_8$, OC_6H_4 and C_6H_5); 66.1(OCH_2); 22.0(–CH_2); 10.4(CH_3). M_w (GPC) = 1 350 000, $M_w/M_n = 4.3$. T_g (DSC from −50 to 200 °C) = 70 °C. $\Delta C_p = 0.20$ J g^{-1} K^{-1}.

3.3. {[NP(O$_2$C$_{12}$H$_8$)]$_{0.6}$[NP(O–C$_6$H$_4$–CO$_2$Pr^n)-(O–C$_5$H$_4$N)]$_{0.4}$}$_n$ (3)

To a THF solution of $[NPCl_2]_n$ (200 mL, 2.83 g, 24.4 mmol), 2,2′-(HO)–C_6H_4–C_6H_4–(OH) (2.27 g, 12.2 mmol) and solid K_2CO_3(6.74 g, 24.4 mmol) were added and the mixture was refluxed with mechanical stirring for 13 h. Then, HO–C_6H_4–CO_2Pr (1.48 g, 8.2 mmol) and Cs_2CO_3 (19.8 g, 60.9 mmol) were added, and refluxing was continued for another 9 h. To the mixture HOC_5H_4N (1.86 g, 19.6 mmol) and another 80 mL THF were added, and refluxing was continued for another 12 h. The reaction mixture was concentrated to half volume and poured into water (2 L) to give a precipitate that was filtered, washed with water (2 × 100 mL), isopropanol and hexane, and dried. The purification was performed as for polymer **1**. The final white material was dried for 72 h in vacuo at 50 °C. Yield: 2.2 g (34%). *Anal.* Calc. for $C_{13.2}H_{10.8}N_{1.4}O_{2.8}P$ (264.8): C, 59.8; H, 4.08; N, 7.4. Found: C, 58.1; H, 5.1; N, 7.1%. IR (KBr): $\nu = 3066$w (ν-CH-arom.), 3028w (ν-CH–C_5H_4N), 2966m (ν-CH-aliph.), 1717s (ν-CO), 1604s, 1503s, 1477m (ν-C=C-arom.), 1585m (CCN–C_5H_4N), (δ-CH-aliph), 1272s, (ν-COP), 1245m, 1194vs, br., 1163s (ν-PN), 1095s (νP-OC),928s, br. (ν-POC), 784s, 752m, 716m, 609w, 534s (other) cm^{-1}. $^{31}P\{^1H\}$ NMR ($CDCl_3$): $\delta = -4.3$ ppm, broad [NP($O_2C_{12}H_8$)]; −23 ppm broad [NP(O–C_6H_4–CO_2Pr^n)(O–C_5H_4N)]. In DMSO at 110 °C the values were −6.0, −24, respectively. ^1H NMR ($CDCl_3$): 7.8–6.6m, br. ($C_{12}H_8$, C_6H_4 and C_5H_4N); 4.16m, br. (OCH_2); 1.71m, br. (–CH_2–); 1.0m, br. (CH_3). $^{13}C\{^1H\}$ NMR ($CDCl_3$): $\delta = 166$ (CO), 157,5 (C_4–OC_5H_4N); 154 (C1O-C_6H_4); 151(C_2–OC_6H_4–), 148 (C_2–$C_{12}H_8$), 130–120 ($C_{12}H_8$, OC_6H_4 and C_5H_4N); 115,5 (C_3–OC_5H_4N); 66 (OCH_2); 22 (–CH_2); 10.3(CH_3). M_w (GPC) = 1 100 000, $M_w/M_n = 4.5$. T_g (DSC from 50 to 200 °C) = 75 °C. $\Delta C_p = 0.14$ Jg^{-1} K^{-1}.

3.4. Synthesis of the polymeric complexes 4, 5 and 6

The following preparation for complex **6a** is representative of all the other complexes using the data given below, calculated with the corresponding functionalization degrees of the polymeric ligands (FD in mmol(Ligand)/g (polymer)), and aiming to coordinate $W(CO)_5$ to ca. 50% or 100% of the available ligands.

3.4.1. {[NP(O$_2$C$_{12}$H$_8$)]$_{0.6}$[NP(O–C$_6$H$_4$–CO$_2$Pr^n)-(O–C$_5$H$_4$N–W(CO)$_5$)]$_{0.4}$}$_n$ (6a)

A solution of $[W(CO)_6]$ (0.06 g, 0.17 mmol) in methanol (75 mL) was stirred under UV irradiation until the disappearance of the 1977 cm^{-1} IR absorption (ca. 1 h), to give an orange solution of $[W(HOMe)(CO)_5]$ (IR: 2075w, 1932 s, 1887m,br.). To this solution, another solution of the polymeric ligand **3**(FD = 1.5) (0.09 g, 0.34 mmol ≡ 0.135 mmol OC_5H_4N) in CH_2Cl_2 (250 mL) was added and the mixture was stirred at room temperature for 2.5 h. The volatiles were evaporated and the resulting solid was washed with hexane (4 × 50 mL) and CH_2Cl_2, and dried in vacuum for 24 h to give complex **6a** as yellow solid. Yield: 0.114 g (85%). *Anal.* Calc. for $C_{15.2}H_{10.8}N_{1.4}O_{4.8}PW_{0.4}$ (394.4): C, 46.3; H, 2.76; N, 4.97; W, 18.65. Found: C, 41.7; H, 2.67; N, 4.5; W, 19.2%. IR (KBr): $\nu = 3068$m, br. (νCH, arom), 2966m (ν-CH-aliph.), 2071w, 1977m, 1922s, br. [ν(W–CO)], 1716s (ν-CO_2Pr), 1603m, 1501s, 1477s (νCC arom.), 1272s, (ν-COP), 1245s, 1193vs, 1160m, (νPN), 1096s (νP-OC), 928vs, br. (δPOC), 785m, 753m, 588m, 536m, br. (other) cm^{-1}. $^{31}P\{^1H\}$ NMR (NMP/D_2O) $\delta =$ −4.5br. [NP($O_2C_{12}H_8$], −23vbr. [NP(O–C_6H_4–CO_2Pr^n)-(OC_5H_4N–)$_2$]. T_g (DSC from −50 to 250 °C) = 87 °C. $\Delta C_p = 0.13$ J g^{-1} K^{-1}.

3.4.2. {[NP(O$_2$C$_{12}$H$_8$)]$_{0.5}$[NP(O–C$_6$H$_4$–CO$_2$Pr^n)-(O–C$_6$H$_4$CN)(W(CO)$_5$)$_{0.4}$]$_{0.5}$}$_n$ (4)

$[W(CO)_6]$ (0.062 g, 0.18 mmol), **1** (FD = 1.75) (0.2 g, 0.7 mmol ≡ 0.35 mmol of –CN), 30 min. Yellow solid. Yield: 0.193 g (75%). *Anal.* Calc. for $C_{15.5}H_{11.5}N_{1.5}O_4PW_{0.2}$ (350.5): C, 53.1; H, 3.31; N, 5.99; W, 10.5. Found: C, 51.5; H, 3.7; N, 5.3; W, 8.53%. IR (KBr): $\nu = 3067$m, br. (νCH, arom), 2966m (ν-CH-aliph.), 2228vw (νCN), 2074vw, 1982w, 1939vs, br. [ν(W–CO)], 1717s (ν-CO_2Pr), 1602m, 1502s, 1477s (νCC arom.), 1272s, (ν-COP), 1246s, 1195vs, 1163m (νPN), 1095s (ν-P–OC), 930vs, br. (δPOC), 784m, 752m (δCH-arom), 609m, 589m, 538m, br (other) cm^{-1}. $^{31}P\{^1H\}$ NMR (NMP/D_2O) δ: −4.2br. [NP($O_2C_{12}H_8$], −22br. [NP(O–C_6H_4–CO_2Pr^n) (OC_6H_4-CN–)]. T_g (DSC from −50 to 250 °C) = 69 °C. $\Delta C_p = 0.13$ J g^{-1} K^{-1}.

3.4.3. {[NP(O$_2$C$_{12}$H$_8$)]$_{0.5}$[NP(O–C$_6$H$_4$–CO$_2$Pr^n)-(O–C$_6$H$_4$–PPh$_2$)(W(CO)$_5$)$_{0.7}$]$_{0.5}$}$_n$ (5)

$[W(CO)_6]$ (0.1 g, 0.28 mmol), **2** (FD = 1.26) (0.2 g, 0.55 mmol ≡ 0.252 mmol –PPh_2), 30 min. Yellow solid. Yield: 0.19 g (72%). *Anal.* Calc. for $C_{21.75}H_{16.5}NO_{4.79}P_{1.5}W_{0.35}$ (479.3): C, 54.5; H, 3.47; N, 2.92; W, 13.4. Found: C, 50.8; H, 3.64; N, 3.42%. W 11. IR (KBr): $\nu = 3063$m, br. (νCH, arom), 2966m (ν-CH-aliph.), 2071vw, 1979vw, 1929vs, br. [ν(W–CO)], 1717s (ν-CO_2Pr), 1603m, 1501s 1478s (νCC arom.), 1273vs, (ν-COP), 1246s, 1196vs, 1165m (νPN), 1096s (νP-OC), 931vs, br. (δPOC), 784m, 752m (δCH-arom), 694m

(monosubstituted C_6H_5), 609m, 537m, br. (other) cm^{-1}. $^{31}P\{^1H\}$ NMR (NMP/D_2O) δ (ppm): −24 (W-PPh_2), −5 br. [$NP(O_2C_{12}H_8]$, −22vbr. [$NP(O–C_6H_4–CO_2Pr^n)$-$(OC_5H_4PPh_2)$]. T_g (DSC from −50 to 250 °C) = ca. 90 °C (it changes with the sample). $\Delta C_p = 0.10$ J g^{-1} K^{-1}.

*3.4.4. {[NP(O$_2$C$_{12}$H$_8$)]$_{0.6}$[NP(O–C$_6$H$_4$–CO$_2$Pr^n)-(O–C$_5$H$_4$N)(W(CO)$_5$)$_{0.4}$]$_{0.4}$}$_n$ (**6b**)*

[$W(CO)_6$] (0.1 g, 0.27 mmol), **3** (FD = 1.5) (0.28 g, 1.06 mmol ≡ 0.42 mmol –Py), 30 min. Yield: 0.178 g (53%). *Anal*. Calc. for $C_{14}H_{10.8}N_{1.4}O_{3.6}PW_{0.16}$ (316.6): C, 53.1; H, 3.44; N, 6.19; W, 9.29. Found: C, 51.2; H, 3.92; N, 5.27; W, 10.19%.

Spectroscopic data as **6a** except the weak band in the IR at 1585m (CCN–C_5H_4N). T_g (DSC from −50 to 250 °C) = 84 °C. $\Delta C_p = 0.08$ J g^{-1} K^{-1}.

Acknowledgements

We are grateful to the DGICYT (Project CTQ2004-01484/BQU), the CSIC, and the CONYCYT (Project 2003CL0027) and the FONDECYT (Project 1030515) for financial support.

References

[1] M. Gleria, R. De Jaeger (Eds.), Phosphazenes: a World Wide Insight, Nova Science Publishers, New York, 2004.
[2] H.R. Allcock, J.L. Desorcie, G.H. Riding, Polyhedron 6 (1987) 119–157.
[3] G.A. Carriedo, F.J. García Alonso, J.L. García Alvarez, C. Díaz Valenzuela, N. Yutronic Sáez, Polyhedron 21 (2002) 2587–2592, and references therein.
[4] G.A. Carriedo, L. Fernández-Catuxo, F.J. García Alonso, P. Gómez Elipe, P.A. González, Macromolecules 29 (1996) 5320–5325.
[5] G.A. Carriedo, F.J. García Alonso, A. Presa Soto, Eur. J. Inorg. Chem. (2003) 4341–4346.
[6] G.A. Carriedo, P. Crochet, F.J. García Alonso, J. Gimeno, A. Presa Soto, Eur. J. Inorg. Chem. (2004) 3668–3674.
[7] G.A. Carriedo, F.J. García Alonso, A. Presa Soto, J. Inorg. Organometal. Polym. 14 (2004) 29–37.
[8] G.A. Carriedo, J.I. Fidalgo, F.J. García Alonso, A. Presa Soto, C. Díaz Valenzuela, M.L. Valenzuela, Macromolecules 37 (2004) 9431–9437.
[9] (a) H.R. Allcock, S. Kwon, Macromolecules 22 (1989) 75–79;
(b) H.R. Allcock, C.T. Morrissey, W.K. Way, N. Winograd, Chem. Mater. 8 (1996) 2730–2738;
(c) A.K. Andrianov, J. Chen, M.P. LeGolvan, Macromolecules 37 (2004) 414–420;
(d) G.A. Carriedo, F.J. García Alonso, C. Díaz Valenzuela, M.L. Valenzuela, Macromolecules 38 (2005) 3255–3262.
[10] S. Kidambi, M.L. Bruening, Chem. Mater. 17 (2005) 301–307.
[11] L.J. Bellami, third ed. The Infrared Spectra of Complex Molecules, vol. I, Chapman-Hall, London, 1975, p. 86.
[12] G.A. Carriedo, F.J. García Alonso, P.A. González, P. Gómez Elipe, Polyhedron 18 (1999) 2853–2859.
[13] H.R. Allcock, K.D. Lavin, N.M. Tollefson, T.L. Evans, Organometallics 2 (1983) 267–275.
[14] (a) C.S. Kraihanzel, F.A. Cotton, Inorg. Chem. 2 (1963) 533–540;
(b) F.A. Cotton, Inorg. Chem. 3 (1964) 702–711.
[15] I.M. Watson, J.A. Connor, R. Whyman, Polyhedron 8 (1989) 1794–1796.
[16] (a) R.J. Angelici, J.R. Graham, J. Am. Chem. Soc. 87 (1965) 5586–5590;
(b) J.D. Atwood, T.L. Brown, J. Am. Chem. Soc. 98 (1976) 3160–3166.
[17] (a) H.R. Allcok, J.T. Connolly, S. Sisco, S. Al-Shali, Macromolecules 21 (1988) 323–334;
(b) H.R. Allcock, A.A. Dembek, E.H. Klingenberg, Macromolecules 24 (1991) 5208–5214;
(c) A.L. Crumbliss, D. Coobe, J. Castillo, P. Wisian-Neilson, Inorg. Chem. 32 (1993) 6088–6094.
[18] A.G. Theodoropoulos, I.C. Konstantakopoulos, in: J.C. Salamone (Ed.), Polymeric Materials Encyclopedia, CRS Press, London, 1996, p. 1546.
[19] G.A. Carriedo, F.J. García Alonso, P.A. González, C. Díaz Valenzuela, N. Yutronic Sáez, Polyhedron 21 (2002) 2579–2586.
[20] G.A. Carriedo, F.J. García Alonso, P. Gómez Elipe, J.I. Fidalgo, J.L. García Alvarez, A. Presa Soto, Chem. Eur. J. 9 (2003) 3833–3836.
[21] D.J. Darensbourg, C.J. Bischoff, J.H. Reibenspies, Inorg. Chem. 30 (1991) 1144–1147.

Available online at www.sciencedirect.com
SCIENCE DIRECT®
Polyhedron 25 (2006) 113–118
POLYHEDRON
www.elsevier.com/locate/poly

Investigations of the stability of $\{[(tacn)_6Fe_8(\mu_3\text{-}O)_2(\mu_2\text{-}OH)_{12}]Br_7(H_2O)\}Br \cdot 8H_2O$ (Fe_8) cluster in aqueous solution by spectroscopic and magnetic methods

Elisenda Rodríguez [a,*], Martí Gich [a], Anna Roig [a], Elies Molins [a], Nataliya Nedelko [b], Anna Ślawska-Waniewska [b], Andrzej Szewczyk [b]

[a] *Institut de Ciència de Materials de Barcelona-Consell d'Investigacions Cientfiques (ICMAB-CSIC), Campus UAB, 08193 Bellaterra, Spain*
[b] *Institute of Physics, Polish Academy of Sciences, Al. Lotnikow 32/46, 02-668, Warszawa, Poland*

Received 22 April 2005; accepted 8 July 2005
Available online 19 August 2005

Abstract

Studies of the known single-molecule magnet $\{[(tacn)_6Fe_8(\mu_3\text{-}O)_2(\mu_2\text{-}OH)_{12}]Br_7(H_2O)\}Br \cdot 8H_2O$ complex, tacn = 1,4,7-triazacyclononane, in an aqueous solution and in the powder state have been carried out with the aim of characterizing the stability of the Fe_8 cluster in an aqueous solution. The characterization involves IR, UV–Vis, NMR (Evans method) and Mössbauer spectroscopies, as well as dc-magnetic susceptibility and magnetization studies. Both spectroscopic and magnetic measurements clearly show the lack of stability of the Fe_8 cluster in an aqueous solution.
© 2005 Elsevier Ltd. All rights reserved.

Keywords: Fe_8; Single-molecule magnet; Aqueous solution

1. Introduction

Molecular chemistry is presently having a great impact on the field of nanoscale magnetism by providing new magnetic clusters based on either metallic ions or organic radicals [1–3]. Molecular clusters are unique objects, which are useful in studying the magnetic behaviour of organized matter of a few nanometres in size. In contrast to conventional metallic magnets, in which exchange interactions that couple localized magnetic moments are mediated by conduction electrons, magnetic interactions between metallic centres in molecular magnets occur via diamagnetic bridges, such as oxygen or carboxylate groups, i.e., by a mechanism known as superexchange.

Single-molecule magnets (SMM) are a broad, emerging class of magnetic nanomaterials based on metal ions bridged by O^{2-}, OH^-, OR^- and RCO_2^-. The main characteristics of SMM are a large-spin ground state and stepwise magnetization hysteresis loops at low temperatures resulting from transitions between quantized states of individual molecules rather than long-range order effects [4,5]. Molecular clusters containing metal ions, mostly $\{[(tacn)_6Fe_8(\mu_3\text{-}O)_2(\mu_2\text{-}OH)_{12}]Br_7(H_2O)\}Br \cdot 8H_2O$, Fe_8, and $[Mn_{12}O_{12}(O_2CCH_3)_{16}(H_2O)_4]$, Mn_{12}, have been widely studied and special emphasis has been given to the observation of quantum effects, such as tunnelling of the magnetic moment [6]. $\{[(tacn)_6Fe_8(\mu_3\text{-}O)_2(\mu_2\text{-}OH)_{12}]Br_7(H_2O)\}Br \cdot 8H_2O$ is characterized by an $S = 10$ spin ground state [7]. In fact, for this cluster pure quantum tunnelling relaxation of the magnetization

* Corresponding author. Tel.: +349 358 01853; fax: +349 358 05729.
E-mail address: elisenda@icmab.es (E. Rodríguez).

0277-5387/$ - see front matter © 2005 Elsevier Ltd. All rights reserved.
doi:10.1016/j.poly.2005.07.017

has been observed below 0.4 K, thanks to a relatively large transverse intrinsic magnetic field [8].

Potential medical applications of magnetic molecular clusters are nowadays of high interest in the fields of active targets for medical therapy [9,10]; aqueous solutions of $\{[(tacn)_6Fe_8(\mu_3\text{-}O)_2(\mu_2\text{-}OH)_{12}]Br_7(H_2O)\}Br \cdot 8H_2O$ have been checked as contrast agents in magnetic resonance imaging obtaining fruitful results [11]. From this point of view, their stability in biological solutions and their overall magnetic properties are basic features of these metallo-organic compounds.

Here, we have undertaken the study of the structural stability and magnetic properties of $[(tacn)_6Fe_8(\mu_3\text{-}O)_2(\mu_2\text{-}OH)_{12}]^{8+}$ clusters (where tacn = 1,4,7-triazacyclononane) in an aqueous solution, hereafter referred to as $Fe_{8(aq)}$. Water was chosen as the solvent mainly due to its importance as a biological medium. In fact, Fe_8 presents very low solubility in other solvents, with the exception of methanol in which it is slightly soluble. For the comparison study, the magnetic behaviour of a powder sample ($Fe_{8(s)}$) (the precursor for the aqueous solution) has also been examined. Considering that intermolecular interactions between Fe_8 clusters are negligible [12] in the solid, we believe possible to compare the magnetic results for the powder sample with those for the aqueous solution. The results obtained by all the techniques indicate a lack of stability of Fe_8 clusters in aqueous solution, although further studies should be undertaken to assess the kinetics of the hydrolisation process.

2. Results and discussion

2.1. Spectroscopic characterization

The crystal structure of $[(tacn)_6Fe_8(\mu_3\text{-}O)_2(\mu_2\text{-}OH)_{12}]^{8+}$, reported by Wieghardt et al. [7], is shown in Fig. 1. An octameric Fe^{III} cation is formed, in which six of the eight Fe^{III} atoms are bonded to an amine ligand. The iron ions are coupled by 12 hydroxo-bridges and by two oxo-bridges. The center of the cluster is formed by two central irons coupled by two μ_3-oxo bridges. The oxygens are bonded to two other irons completing a $\{Fe_4O_2\}^{8+}$ unit, known as 'butterfly core'.

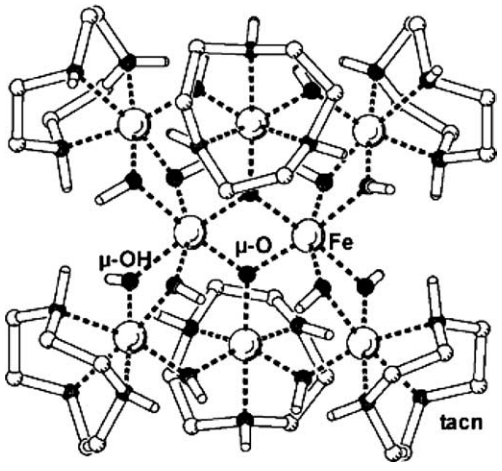

Fig. 1. Crystal structure of $[(tacn)_6Fe_8(\mu_3\text{-}O)_2(\mu_2\text{-}OH)_{12}]^{8+}$, tacn = 1,4,7-triazacyclononane molecule cluster.

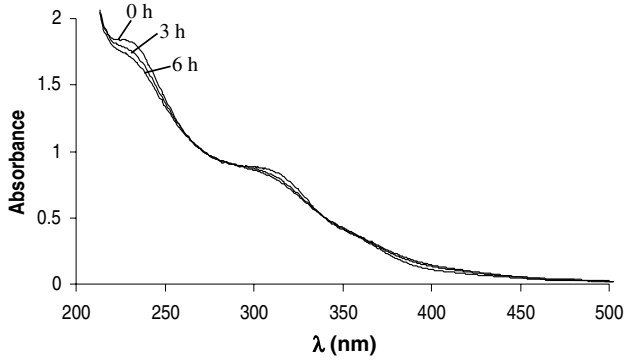

Fig. 2. Repetitive scan UV–Vis spectra of $Fe_{8(aq)}$ at 25 °C. Spectra were recorded at three-hourly intervals.

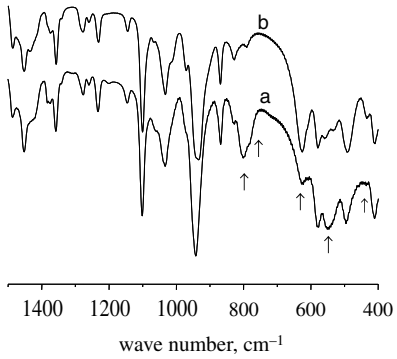

Fig. 3. Infrared absorption spectra: (a) $Fe_{8(aq)}$; and (b) $Fe_{8(s)}$, with arrows indicating significant differences between two spectra.

The UV–Vis spectra of $Fe_{8(aq)}$ are displayed in Fig. 2, they were recorded at different times: 0 h, 3 h and 6 h, where 0 h means right after the aqueous dissolution was made. The three spectra consist of three main weak bands at 230, 300 and 410 nm. Oxo-bridged Fe(III) complexes exhibit intense absorption in the visible and near-UV region, these include two very strong bands in the near-UV region (320–380 nm) and several less intense bands in the visible region (430–550 nm) [13]. Several related complexes present the $\{Fe_4(\mu\text{-}O)_2\}^{8+}$ unit [14–16]; these tetranuclear species may arise by dimerization of the $\{Fe_2O\}^{4+}$ binuclear species, which are very stable in solution due to Fe–O–Fe unit [17,18]. Gorun et al. [15] reported that the 'butterfly core' presents bands at ~465–475 and 565–575 nm, which provides a useful tool for discriminating between the $\{Fe_4O_2\}^{8+}$ unit and its $\{Fe_3O\}^{7+}$ and $\{Fe_2O\}^{4+}$ subsets. The UV–Vis spectrum of $Fe_{8(aq)}$ is similar to those obtained for other, already reported, complexes containing the 'butterfly core'. This

could indicate that the 'butterfly core' remains stable in solution. Nevertheless, a slight diminution of the intensity of the bands is detected for increasing times, better seen for $t = 6$ h, which would indicate the dissociation of the Fe_8 complex in an aqueous solution, even though no precipitate was observed.

Fig. 3 shows the infrared spectra (the region from 1500 to 400 cm^{-1}) of $Fe_{8(aq)}$ freeze-dried (spectrum a) and of $Fe_{8(s)}$ (spectrum b). Most of the peaks above 800 cm^{-1} are due to vibrations in the organic ligands. In this region, there is a strong similarity between the two spectra. However between 800 and 400 cm^{-1} there are some small differences. In this region the symmetric stretch of the Fe–O–Fe unit occurs between 540 and 340 cm^{-1} for (μ-oxo)diiron (III) complexes and the asymmetric stretch occurs between 885 and 725 cm^{-1} [17], but a clear band assignment for Fe_8 spectrum has not been done. Moreover, Spool et al. [19] have studied the integrity of the $[Fe_2(\mu\text{-}O)(\mu\text{-}O_2CCH_3)_2(tacn)_2]^{2+}$ core in water by comparing the infrared spectra of the as-prepared powder and the dry powder, after dissolution in water and removal of the solvent in vacuum, showing that both spectra were identical. However, after a few hours, the standing aqueous solution of $[Fe_2(\mu\text{-}O)(\mu\text{-}O_2CCH_3)_2(tacn)_2]^{2+}$ became cloudy and developed a precipitate if left overnight, which seems to indicate a lack of integrity of their complex. Drüke et al. [20] have interpreted such observations by pointing out that μ-carboxylate bridges are relatively labile, and that this lability depends on the cyclic amine attached to the core, since in the complex $[(L)_2Fe_2(\mu\text{-}O)(\mu\text{-}O_2CCH_3)_2](ClO_4)_2 \cdot H_2O$, where L = 1,4,7-trimethyl-1,4,7-triazacyclononane, no significant dissociation of the (μ-oxo)(μ-carboxylate)diiron occurs. They argued that the methylated capping ligand is sterically more demanding than its unmethylated analogue, thereby providing an increased stability of the methylated species in water. We propose then a hypothetic mechanism of the decomposition pathway of the Fe_8 cluster in aqueous solution based on the low sterically demand from the tacn which provide a poor protection to our iron-cluster.

2.2. Magnetic characterization

Room-temperature magnetic susceptibility of Fe_8 in an aqueous solution was obtained from NMR measurements with the Evans method, as described in the literature for similar compounds [21]. A value for μ_{Fe8} of $11.7 \pm 2\mu_B$ at 300 K was calculated for $Fe_{8(aq)}$, which is ~10% smaller than that for $Fe_{8(s)}$ complexes, as shown below.

In view of the non-conclusive findings obtained by the spectroscopic techniques and the Evans method, more in-depth magnetic studies were performed.

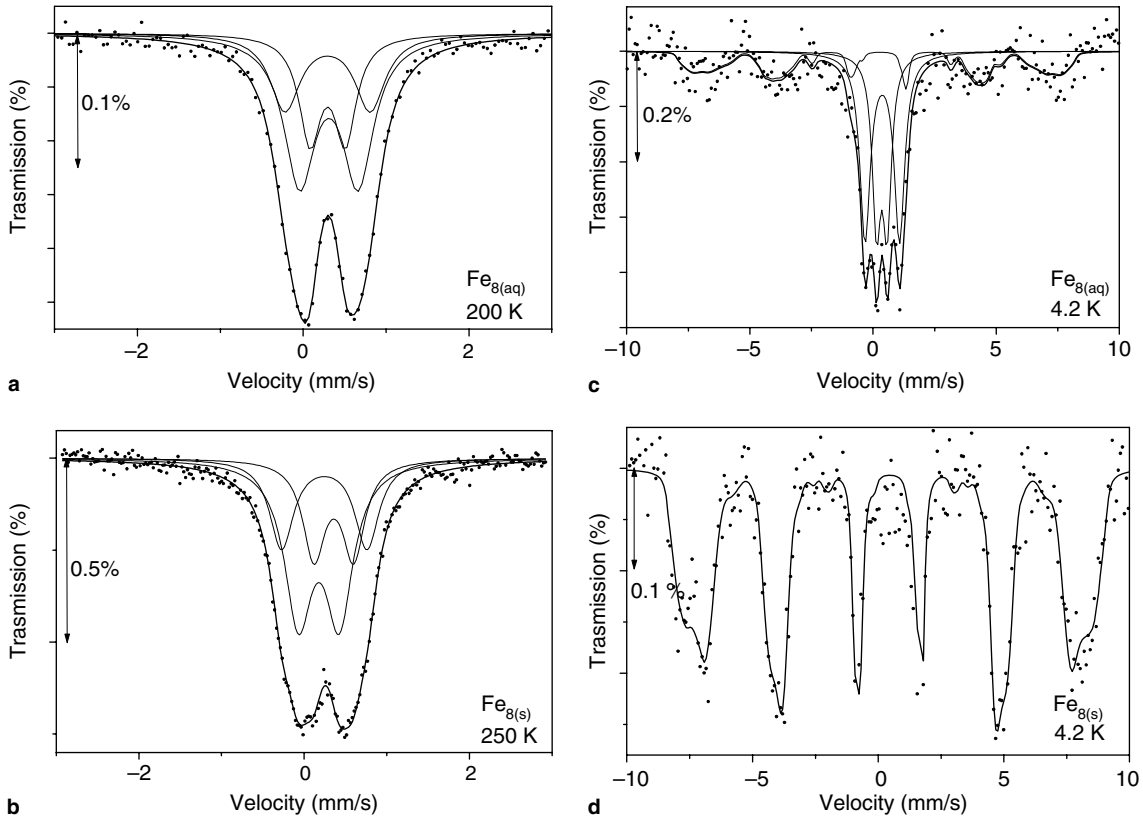

Fig. 4. Mössbauer spectra for $Fe_{8(aq)}$ and $Fe_{8(s)}$; (a) and (c) correspond to $Fe_{8(aq)}$ at 200 and 4.2 K, respectively; (b) and (d) correspond to $Fe_{8(s)}$ at 250 and 4.2 K, respectively.

Mössbauer spectra and the hyperfine parameters, resulting from the fitting of the spectra, for the powder sample (Fig. 4(b) and (d)) are the same to those previously reported [12]. The fit was done in the basis of the three different iron sites within the molecule, $[FeO_2(OH)_4]_2$, $[FeO(OH)_2N_3]_2$, $[Fe(OH)_3N_3]_4$ with area ratios of 1:1:2. The Mössbauer spectrum of $Fe_{8(aq)}$ at 200 K (see Fig. 4(a)) consists of a very broad, almost symmetrical, doublet that could be also fitted using three subspectra since its overall appearance is somehow similar to that of $Fe_{8(s)}$ at 250 K (see Fig. 4(b)). However, the hyperfine parameters of the three subspectra are very different (see Table 1). Only at 4 K the differences between $Fe_{8(aq)}$ (see Fig. 4(c)) and $Fe_{8(s)}$ (see Fig. 4(d)) are evident. The $Fe_{8(aq)}$ spectrum could be fit using three subspectra; two symmetric doublets and a magnetically split component accounting for a 25% of the total area (that sub-spectra was fitted using a distribution of hyperfine fields). On the other hand, the $Fe_{8(s)}$ spectrum shows a magnetically split broad sextet that was fit using three six-line subpectra with 1:1:2 area ratios. In this sample the spectrum is completely resolved indicating that all the spins are frozen in a collective state and no paramagnetic component are detected for the $Fe_{8(s)}$ sample which would lead to a central doublet or singlet. From the low temperature Mössbauer spectrum of the $Fe_{8(aq)}$ we can suggest the presence of several iron sites in the solution: (i) two very different paramagnetic Fe ion centres and (ii) and a minor phase, magnetically split, that we have tentatively assigned to iron hydroxide colloidal particles of the gel–type $Fe(OH)_3 \cdot 0.9H_2O$ [22]. Such phase shows superparamagnetic behaviour at higher temperature, namely at 250 K where the magnetically split component is not visible.

The substantial differences between $Fe_{8(s)}$ and $Fe_{8(aq)}$ are also seen in the dc magnetization results. The temperature dependence of $\chi_g T$ for $Fe_{8(aq)}$ and $Fe_{8(s)}$ samples obtained in a field of 90 kOe are shown in Fig. 5(a) and (b), respectively. For the powdered sample the $\chi_g T(T)$ curve measured at 10 kOe is also presented in Fig. 5(b). The $\chi_g T(T)$ dependence of the $Fe_{8(s)}$ sample exhibits a plateau at elevated temperatures, then a steady increase for decreasing temperatures, up to a certain maximum followed by a rapid decrease. The maximum strongly depends on the measuring field and corresponds to: (i) $\chi_g T = 0.029$ emu K g^{-1} Oe^{-1}, at 12.5 K for 10 kOe and (ii) $\chi_g T = 0.0175$ emu K g^{-1} Oe^{-1}, at 62 K for 90 kOe. The peak is stronger and better pronounced for 10 kOe, which is due to saturation effects in the field, and shows a much higher susceptibility at lower fields than that at high fields. The dependence obtained at 10 kOe is very similar to that published by Delfs et al. [23]. The $\chi_g T(T)$ curve obtained for powder $Fe_{8(s)}$ is indicative of the presence of ferrimagnetic interactions between the Fe ions. This is seen even better from the

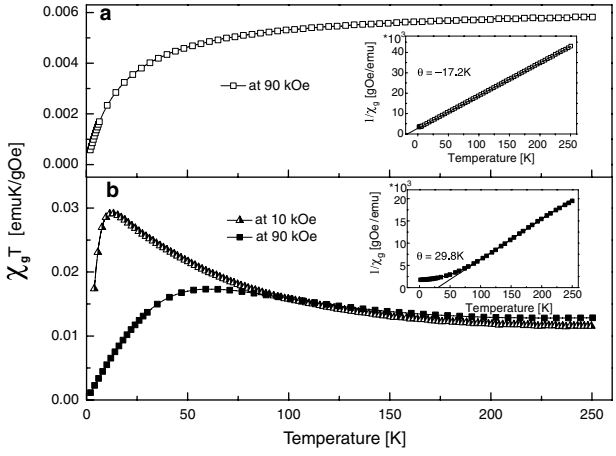

Fig. 5. Temperature dependence of the susceptibility measured at H = 90 kOe – $\chi_g T$ vs. T for: (a) $Fe_{8(aq)}$ and (b) $Fe_{8(s)}$. Inverse susceptibility vs. T is shown in the insets.

Table 1
Hyperfine parameters for the fitting of the Mössbauer spectra

Sample	Iron site	δ_{Fe} (mm/s)	ΔE (mm/s)	Γ (mm/s)	B_{HF} (T)	Area (%)
Fe_8(aq) 200 K	Site 1	0.39(2)	0.43(4)	0.32(4)		25
	Site 2	0.39(2)	1.03(8)	0.43(6)		25
	Site 3	0.41(2)	0.71(5)	0.45(6)		50
Fe_8(s) 250 K	$[FeO_2(OH)_4]_2$	0.46(1)	0.47(2)	0.32(4)		25
	$[FeO(OH)_2N_3]_2$	0.34(1)	1.05(2)	0.35(2)		25
	$[Fe(OH)_3N_3]_4$	0.28(1)	0.50(2)	0.40(2)		50
Fe_8(aq) 4.2 K	Site 1	0.48(2)	1.45(4)	0.41(6)		32
	Site 2	0.46(2)	0.48(4)	0.53(6)		43
	Site 3	0.38(8)			44 (2)	26
Fe_8(s) 4.2 K	$[FeO_2(OH)_4]_2$	0.49(2)		0.37(8)	46.3(1)	25
	$[FeO(OH)_2N_3]_2$	0.44(2)		0.34(4)	43.9(1)	25
	$[Fe(OH)_3N_3]_4$	0.40(2)		0.65(8)	50.1(1)	50

δ_{Fe}, ΔE and Γ are the isomer shift (relative to metallic iron), quadrupolar splitting and the full-width at half-maximum, respectively (in mm/s) $\langle B_{HF} \rangle$ is the mean hyperfine field in Tesla. The area represents the Mössbauer fraction of each sub-spectra in relative percentage. The errors are given within brackets and correspond to the last digit.

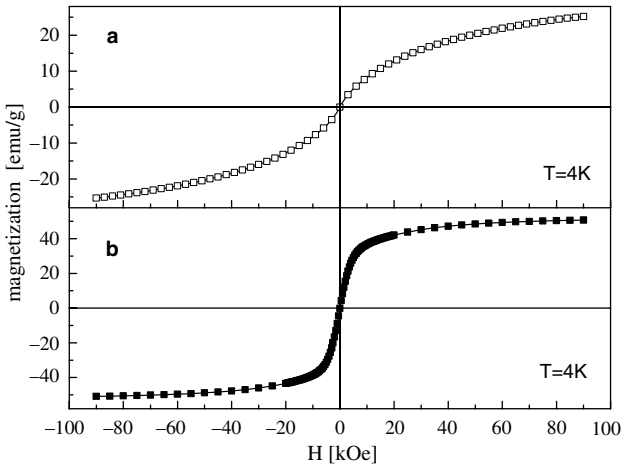

Fig. 6. Magnetization curves at 4 K: (a) for $Fe_{8(aq)}$; and (b) for $Fe_{8(s)}$.

temperature dependence of the inverse susceptibility, shown in the inset in Fig. 5(b), which reveals Curie–Weiss behaviour at $T > 100$ K with a positive Weiss constant $\theta = 29.8$ K and a magnetic moment of $13.5 \pm 0.5\mu_B$. For the $Fe_{8(aq)}$ sample, the $\chi_g T(T)$ dependence (Fig. 6(a)) presents completely different behaviour – $\chi_g T$ remains almost constant (at a value of $\sim$0.006 emu K g^{-1} Oe^{-1}) down to 100 K, and then decreases slowly with temperature, suggesting the presence of dominant antiferromagnetic coupling between Fe ions. The $\chi_g{}^{-1}(T)$ obeys the Curie–Weiss law (see the inset in Fig. 6(a)) with a negative Weiss constant $\theta = -17.2$ K and a magnetic moment of $10.6 \pm 0.5\ \mu_B$ (i.e., similar to that estimated from the Evans method).

The magnetization curves of $Fe_{8(aq)}$ and $Fe_{8(s)}$ samples are also very different, as shown in Fig. 6(a) and (b) in the loops recorded at 4 K. The $Fe_{8(s)}$ sample exhibit superparamagnetic behaviour at low temperatures, for the time scale used in the magnetic measures, and the magnetization curve at 4 K for $Fe_{8(s)}$ can be fitted to a Langevin function with a saturation magnetization of $\sim 20\ \mu_B$, which corresponds to an $S = 10$ ground state. On the other hand, the corresponding magnetization curve of the $Fe_{8(aq)}$ sample cannot be described by a simple Langevin function, which indicates a change in structure of the initially unisize iron clusters. Moreover, the saturation magnetization cannot be estimated. Thus, the magnetic results demonstrate that the Fe_8 clusters do not remain stable in the aqueous solution and this conclusion is additionally supported in [24], where NMR studies show indication of partial decomposition of Fe_8 in aqueous solution.

3. Conclusions

Studies of the large $\{[(tacn)_6Fe_8(\mu_3\text{-}O)_2(\mu_2\text{-}OH)_{12}]^{8+}$ cluster in the powder state and in the aqueous solution have been performed aimed at characterizing the stability of this 3d-metal magnetic cluster in solution. The IR spectra of the powder and aqueous samples do not show significant differences. The UV–Vis spectrum of $Fe_{8(aq)}$ shows bands that could be assigned to the $\{Fe_4O_2\}^{8+}$ core. However, these bands decrease with time which indicates a slow kinetic decomposition. The NMR Evans method, routinely used to assess the magnetic moment of complexes in solution, yielded a value for the magnetic moment only slightly lower than that found for the solid sample, although fluctuations of this value were observed. The clearest evidence for the decomposition of the core of the Fe_8 cluster in solution is provided by Mössbauer spectroscopy and dc magnetization studies.

At low temperatures, all the Fe ions are in a collective magnetic state in Fe_8 powder and are coupled by the predominantly ferrimagnetic interactions. In turn, when Fe_8 molecules are in an aqueous solution, most of the superexchange bonds between Fe ions are broken, a majority of Fe(III) ions appears in the paramagnetic state, whereas the remaining 30% of Fe(III) ions are coupled by preferential antiferromagnetic interactions, we suppose that are in a form of small iron oxide hydroxide colloidal clusters. The results presented in this paper are in agreement with those presented in previous studies [25], which suggested that tacn does not provide stability to the core and hydroxo and oxo bridges can be hydrolyzed in an aqueous solution.

4. Experimental

4.1. Synthesis of $\{[(tacn)_6Fe_8(\mu_3\text{-}O)_2(\mu_2\text{-}OH)_{12}]\text{-}Br_7(H_2O)\}Br \cdot 8H_2O$

Reagents were obtained from commercial sources and used as received without further purification. Fe_8 synthesis was performed in two steps, as described by Wieghardt et al. [7,26]; first, the complex (tacn)$FeCl_3$ was formed by mixing $FeCl_3$ and tacn in an ethanolic solution, then the complex (tacn)$FeCl_3$ was dissolved in H_2O/pyridine and NaBr was added. Brown crystals of Fe_8 appeared after 24 h. A special batch enriched with ^{57}Fe isotope was prepared to be used for Mössbauer characterization. The aqueous solution was prepared by mixing the Fe_8 powder with distilled water at a concentration of 5 mM of Fe_8; the pH of the solutions was not adjusted.

4.2. Physical methods

4.2.1. Spectroscopy measurements

UV–Vis spectral measurements for $Fe_{8(aq)}$ were performed using a Varian Cary 5 E Spectrophotometer. IR spectra (4000–400 cm^{-1}) from KBr discs of $Fe_{8(aq)}$ (after freeze-drying the aqueous solution) and $Fe_{8(s)}$

were recorded on a Fourier transform Perkin–Elmer spectrometer.

Evans susceptibility measurements, based on the Evan's method [20], were carried out using a Bruker AMX-400-WB spectrometer. 5-mm-diameter NMR tubes containing an aqueous solution of 5 mM Fe_8 and a capillary tube filled with deuterated water were used. 5% of *t*-BuOH was added to both solutions.

Mössbauer spectra of $Fe_{8(aq)}$ and $Fe_{8(s)}$ both enriched with Fe^{57} were recorded at 200 and 4.2 K with a conventional transmission spectrometer using a ^{57}Co source in a Rh matrix. The source was moved via triangular velocity wave and the γ-counts were collected in a 512 multichannel analyzer. The data were folded, plotted and fitted by a computer procedure NORMOS [27]. Velocity calibration was done using a 25 μm thick metallic Fe foil, and the Mössbauer spectral parameters are given relative to this standard at room temperature. $Fe_{8(aq)}$ spectra were obtained from a frozen solution in water.

4.2.2. Magnetic characterization

The dc magnetization temperature dependence for the powder and frozen aqueous Fe_8 samples were measured with a VSM (Oxford Instruments Ltd.) and a PPMS magnetometer (Quantum Design) over the temperature range 2–250 K in the applied field up to 90 KOe. Hysteresis loops for both samples were measured at selected temperatures. The experimental results were corrected for the holder contribution and for a temperature-independent diamagnetic contribution. All the magnetization data are presented in emu per gram of Fe_8. The measurements for $Fe_{8(aq)}$ were performed at high field since $Fe_{8(aq)}$ shows very large high field susceptibility. This allowed to enhance the signal (which is low because the content of the magnetic phase in the solution is small) even though this is associated with an increase of the diamagnetic contribution. For $Fe_{8(s)}$ sample, which saturates at lower fields the susceptibility measurements were performed both at high field, and low fields.

Acknowledgements

We gratefully acknowledge V. Lloveras (ICMAB-CSIC) for help in the UV–Vis measurements, Prof. Silvio Aime (Univ. Torino) for NMR measurements, Dr. Eliano Diana (Univ. Torino) for IR measurements and Dr. A. Wioniewski (IF-PAN) for PPMS measurements. Partial financial support from DURSI (AIRE-2003-5) of the Generalitat de Catalunya is also acknowledged.

References

[1] O. Kahn (Ed.), Molecular Magnetism, Wiley-VCH, New York, 1993.
[2] A. Caneschi, D. Gatteschi, C. Sangregorio, R. Sessoli, L. Sorace, A. Cornia, M.A. Novak, C. Paulsen, W. Wernsdorfer, J. Magnet. Magnet. Mater. 200 (1999) 182.
[3] J.M. Clemente-Juan, E. Coronado, Coord. Chem. Rev. 193–195 (1999) 361.
[4] (a) G. Christou, D. Gatteschi, D.N. Hendrickson, R. Sessoli, MRS Bull. 25 (2000) 66;
(b) D. Gatteschi, R. Sessoli, Angew. Chem. Int. Ed. 42 (2003) 268.
[5] N. Domingo, B.E. Williamson, J. Gómez-Segura, Ph. Gerbier, D. Ruiz-Molina, D.B. Amabilino, J. Veciana, J. Tejada, Phys. Rev. B. 69 (2004) 052405.
[6] (a) J.R. Friedman, M.P. Sarachik, J. Tejada, R. Ziolo, Phys. Rev. Lett. 76 (1996) 3830;
(b) L. Thomas, F. Lionti, R. Ballou, D. Gatteschi, R. Sessoli, B. Barbara, Nature 383 (1996) 145.
[7] K. Wieghardt, K. Pohl, I. Jibril, G. Huttner, Angew. Chem., Int. Ed. Engl. 1 (1984) 77.
[8] C. Sangregorio, T. Ohm, C. Paulsen, R. Sessoli, D. Gatteschi, Phys. Rev. Lett. 78 (24) (1997) 4645.
[9] Y. Gossuin, A. Roch, R.N. Muller, P. Gillis, Magnet. Reson. Med. 43 (2003) 237.
[10] S. Mornet, S. Vasseur, F. Grasset, E. Duguet, J. Mater. Chem. 14 (2004) 2161.
[11] E. Rodríguez, A. Roig, E. Molins, C. Arús, M.R. Quintero, M.E. Cabañas, S. Cerdán, P. Lopez-Larrubia, C. Sanfeliu, NMR Biomed. 18 (2005) 1.
[12] A.L. Barra, P. Debrunner, D. Gatteschi, E. Schultz, R. Sessoli, Europhys Lett. 35 (1996) 133.
[13] J. Sanders-Loehr, W.D. Wheeler, A.K. Shiemke, B.A. Averill, T.M. Loehr, J. Am. Chem. Soc. 111 (1989) 8084.
[14] J.K. McCusker, J.B. Vincent, E.A. Schmitt, M.L. Mino, K. Shin, D.K. Coggin, P.M. Hagen, J.C. Huffman, G. Christou, D.N. Hendrickson, J. Am. Chem. Soc. 113 (1991) 3012.
[15] S.M. Gorun, S.J. Lippard, Inorg. Chem. 27 (1988) 149.
[16] W.H. Armstrong, M.E. Roth, S.J. Lippard, J. Am. Chem. Soc. 109 (1987) 6318.
[17] D.M. Kurtz, Chem. Rev. 90 (1990) 585.
[18] S.J. Lippard, Angew. Chem., Int. Ed. Engl. 27 (1988) 344.
[19] A. Spool, I.D. Williams, S.J. Lippard, Inorg. Chem. 24 (1985) 2156.
[20] S. Drüke, K. Wieghardt, B. Nuber, J. Weiss, H.-P. Fleischlauer, S. Gehring, W. Haase, J. Am. Chem. Soc. 111 (1989) 8622.
[21] D.F. Evans, J. Chem. Soc. (1959) 2003.
[22] J.M.D. Coey, P.W. Readman, Earth Planet. Sci. Lett. 21 (1973) 45.
[23] C. Delfs, D. Gatteschi, L. Pardi, R. Sessoli, K. Wieghardt, D. Hanke, Inorg. Chem. 32 (1993) 3099.
[24] S. Isaacman, R. Kumar, E. del Barco, A.D. Kent, J.W. Canary, A. Jerschow, Polyhedron, in press.
[25] K. Wieghardt, P. Chaudhuri, in: S. Lippard (Ed.), Progress in Inorganic Chemistry, Wiley, New York, 1987, p. 329.
[26] K. Wieghardt, K. Pohl, W. Gebert, Angew. Chem. 95 (1983) 739.
[27] R.A. Brand, Nucl. Instrum. Methods B 28 (1987) 398.

Available online at www.sciencedirect.com
SCIENCE DIRECT®
Polyhedron 25 (2006) 119–123
POLYHEDRON
www.elsevier.com/locate/poly

Synthesis and X-ray structural characterization of M(3,5-^{t}Bu$_2$-salophen) (M = Cu, V=O)

Michael P. Weberski Jr., Craig C. McLauchlan *, Christopher G. Hamaker *

Department of Chemistry, Illinois State University, Campus Box 4160, Normal, IL 61790-4160, USA

Received 13 May 2005; accepted 8 July 2005
Available online 29 August 2005

Abstract

The synthesis and characterization of Cu(3,5-^{t}Bu$_2$-salophen) (**4**) and VO(3,5-^{t}Bu$_2$-salophen) (**5**) as well as the crystallographic elucidation of the structures are reported. X-ray analyses show the expected approximately square planar geometry of copper (II) and the square pyramidal geometry of vanadium in structures **4** and **5**, respectively. Both discrete molecular structures are well defined with no obvious hydrogen bonding present. The EPR spectra of **4** and **5** are typical of complexes of this type. 3,5-^{t}Bu$_2$-salophen = *N*,*N*′–phenylenebis(3,5-di-*tert*-butylsalicylideneimine).
© 2005 Elsevier Ltd. All rights reserved.

Keywords: Copper; Vanadium; Vanadyl; Crystal structures; EPR

1. Introduction

Schiff bases are common ligands in coordination chemistry because of their ease of preparation. Many Schiff base complexes are efficient catalysts for industrially important reactions. For example, chiral manganese (III) salen complexes have been shown by both Jacobsen and Katsuki and their co-workers to catalyze the asymmetric epoxidation of olefins [1–4]. Recently, Zolezzi et al. [5] have shown that copper (II) Schiff base complexes catalyze the epoxidation of styrene. Scheme 1 illustrates the Schiff bases H_2salen (**1**), H_2salophen (**2**), and H_2[3,5-^{t}Bu$_2$-salophen] (**3**).

Use of the Schiff base H_2[3,5-^{t}Bu$_2$-salophen] (**3**) as a ligand has been previously reported [6,7]. Crystal structures of **3** complexed with many elements including Sr, Sn, Ga, Mo, Al, Zn, In, and Rh have been reported [8–15]. The preparations of these complexes were, in many cases, quite straightforward and employed the reaction of metal salts with **3** that had been generated in situ. In our efforts to prepare a model complex to model a structurally more complex copper (II) porphyrin for EPR study [16], we synthesized the complex Cu(3,5-^{t}Bu$_2$-salophen) (**4**). Also prepared was vanadyl(3,5-^{t}Bu$_2$-salophen) (**5**), which is known to catalyze the electroreduction of O_2 to H_2O [17]. The metal–ligand bond distances of some of the previously reported [3,5-^{t}Bu$_2$-salophen] compounds are similar to the metrics for **4** and **5** [10,12,13,15].

The synthesis, characterization, and crystallographic elucidation of the structures of **4** and **5** are presented here.

2. Experimental

2.1. General considerations

All materials were obtained from commercial sources and used as received. Infrared spectra were collected on a Nicolet 5SXC FT-IR spectrometer as KBr mulls. Electronic absorption (UV–Vis) spectra were collected on a

* Corresponding authors. Tel.: +3094387019; fax: +3094385538.
E-mail addresses: ccmclau@ilstu.edu (C.C. McLauchlan), chamake@ilstu.edu (C.G. Hamaker).

0277-5387/$ - see front matter © 2005 Elsevier Ltd. All rights reserved.
doi:10.1016/j.poly.2005.07.018

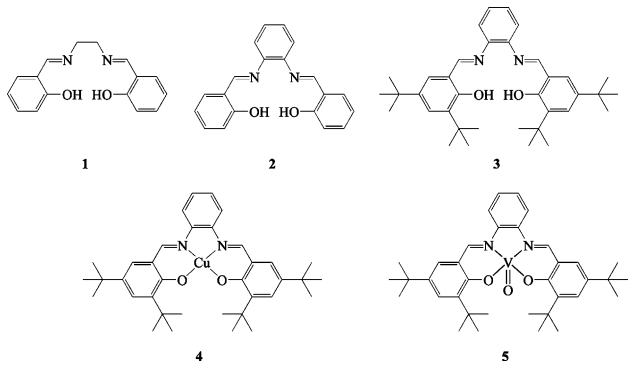

Scheme 1.

Cary 500 UV–Vis–NIR spectrophotometer. ^{1}H NMR spectra were collected on a 400-MHz Bruker spectrometer and were referenced to residual $CHCl_3$. EPR spectra were collected at 290 K on a Bruker EMX-080 spectrometer. Magnetic susceptibility measurements were carried out using a Johnson Matthey magnetic susceptibility balance. Microanalyses were conducted by the Microanalytical Laboratory, School of Chemical Sciences, University of Illinois, Urbana-Champaign.

2.2. Synthesis of H_2[3,5-^{t}Bu$_2$-salophen] (3)

This compound has been previously reported [6,7]. To a solution of 3,5-di-*tert*-butyl-2-hydroxybenzaldehyde (4.74 g, 20.2 mmol) in 100 ml of absolute ethanol was added 1.09 g (10.1 mmol) of 1,2-phenylenediamine. The resulting solution was refluxed for 2 h, cooled to room temperature, and then placed into a freezer at −40 °C for 16 h. The solution was filtered and the solid was washed with cold ethanol and air dried giving 1.04 g of **3** as a fluffy yellow solid. The volume of the filtrate liquid was reduced to approximately 50 ml and placed into the freezer. The resulting solid was filtered to produce an additional 2.95 g of product. Total yield was 3.99 g (7.38 mmol, 73%). IR (KBr cm^{-1}): 3125 (OH), 1617 (C=N). ^{1}H ($CDCl_3$, δ) 11.64 (s, 2H, O*H*); 8.66 (s, 2H, C*H*=N); 7.44 (d, 2H, $C_6H_2(^t$Bu$)_2$(OH)); 7.32 (m, 2H, *o*-$C_6H_4N_2$); 7.24 (m, 2H, *o*-$C_6H_4N_2$); 7.21 (d, 2H, $C_6H_2(^t$Bu$)_2$(OH)); 1.43 (s, 18H, C(CH_3)$_3$); 1.32 ppm (s, 18H, C(CH_3)$_3$).

2.3. Synthesis of Cu(3,5-^{t}Bu$_2$-salophen) (4)

To a solution of H_2[3,5-^{t}Bu$_2$-salophen] (**3**) (0.2024 g, 0.3740 mmol) in ethanol(15 ml) was added Cu$(NO_3)_2 \cdot 2.5H_2O$(0.0870 g, 0.374 mmol) in ethanol (8 ml). The reaction mixture was heated gently to 50 °C and 1.5 ml of 0.5 M NaOH was added. The resulting brown crystals were filtered off and washed with cold ethanol. Total yield was 0.1837 g (0.3050 mmol, 82%). IR (KBr cm^{-1}): 1601(C=N). UV–Vis (toluene λ, nm (ε, M^{-1} cm^{-1})): 317 (20 300), 334 (18 100), 352 (14 500), 408 (11 000), 453 (14 800), 711 (3011). Elemental *Anal.* Calc. for $C_{36}H_{46}N_2O_2Cu$: C, 71.79; H, 7.70; N, 4.65. Found: C, 70.20; H, 7.26; N, 4.56%. Magnetic susceptibility χ_m (erg G^{-2} mol^{-1}): 1.73×10^{-3} μ_{eff} (μ_B): 2.04 ($\chi_m T = 0.520$). This compound was further characterized by X-ray crystallography.

2.4. Synthesis of VO(3,5-^{t}Bu$_2$-salophen) (5)

Vanadyl sulphate dihydrate (0.421 g, 2.12 mmol) and H_2[3,5-^{t}Bu$_2$-salophen] **3** (1.084 g, 2.01 mmol) were dissolved in 50 ml of methanol. To the resulting solution was added 0.60 ml (4.3 mmol) of triethylamine and the reaction was refluxed for 45 min. The reaction was cooled to room temperature and placed into a freezer at −40 °C for 4 h. The resulting precipitate was filtered, washed with cold methanol and hexanes and air dried to yield 1.063 g (1.76 mmol, 88%) of the product as an olive green microcrystalline solid. IR (KBr cm^{-1}): 1609(C=N), 982(V=O). UV–Vis (toluene λ, nm (ε, M^{-1} cm^{-1})): 333 (24 678), 427 (17 386), 713 (3365). Elemental *Anal.* Calc. for $C_{36}H_{46}N_2O_3V$: C, 71.39; H, 7.65; N, 4.62. Found: C, 71.33; H, 7.70; N, 4.82%. Magnetic susceptibility χ_m (erg G^{-2} mol^{-1}): 1.99×10^{-3} μ_{eff} (μ_B): 2.18 ($\chi_m T =$ 0.594). This compound, as its ethanol solvate, was further characterized by X-ray crystallography.

2.5. X-ray structure determinations

Single crystals of **4** and **5** · EtOH suitable for X-ray were obtained by slow growth in ethanol. Intensity data were collected at Johns Hopkins University, Baltimore, MD at −173 °C on an Oxford Xcaliber3 diffractometer equipped with a CCD area detector. Graphite monochromated Mo Kα radiation from an Enhance source was used. Data were reduced and corrected for absorption using the Crysalis Software Suite [18]. Structure solutions were obtained by direct methods and were refined on F^2 with the use of full-matrix least-squares techniques [19]. Except where noted, all non-hydrogen atoms were refined anisotropically and hydrogen atoms were refined with a riding model. All compounds solved and refined routinely. The crystallographic results are summarized in Table 1. Further details are available in Supporting Information.

3. Results and discussion

3.1. Electronic and magnetic properties

Compound **4** has a calculated μ_{eff} value of 2.04μ_B ($\chi_m T = 0.520$) representative of a d^9 metal corresponding to the one unpaired electron of copper in the 2+

Table 1
Details of crystallographic results

	4	5 · EtOH
Formula	$C_{36}H_{46}CuN_2O_2$	$C_{36}H_{46}N_2O_3V \cdot C_2H_6O$
FW	602.32	651.76
Temperature (K)	100 (2)	100 (2)
λ (Å)	0.71073	0.71073
Crystal system	triclinic	monoclinic
Space group	$P\bar{1}$	$P2_1/c$
a (Å)	10.047(7)	14.610 (2)
b (Å)	12.069(8)	9.794 (1)
c (Å)	13.847(6)	27.14 (1)
α (°)	85.11 (4)	
β (°)	88.78 (5)	116.13 (1)
γ (°)	71.22 (6)	
V (Å^3)	1584 (2)	3486 (1)
Z	2	4
D_χ (Mg m^{-3})	1.263	1.242
$R_1(F)$[a]	0.048	0.077
$wR_2(F_o^2)$[b]	0.111	0.129

[a] $R_1(F) = \sum(||F_o| - |F_c||)/\sum|F_o|$.
[b] $wR_2(F_o^2) = [\sum[w(F_o^2 - F_c^2)^2]/\sum wF_o^4]^{1/2}$; $w_4 = 1/[\sigma^2(F_o^2)+(0.0487P)^2]$ where $P = (F_o^2 + 2F_c^2)/3$; $w_{5\cdot EtOH} = 1/[\sigma^2(F_o^2)+(0.0348P)^2 + 3.0757P]$ where $P = (F_o^2 + 2F_c^2)/3$.

oxidation state. Magnetic susceptibility measurements for **4** are consistent with published μ_{eff} values for copper (II) systems [20].

Compound **5** has a calculated μ_{eff} value of $1.30\mu_B$ ($\chi_m T = 0.594$). This value is lower than expected μ_b values for V^{4+} of 1.7–1.8 [20]. Other reported oxovanadium (IV) salen complexes have low magnetic susceptibilities [21,22].

The EPR spectrum for **4** was collected at room temperature in toluene and was consistent with previously reported copper (II) salen complexes [23,24]. Complex **4** is expected to have a single unpaired electron, consistent with a formulation of Cu(II), d^9 (vide supra). Four peaks centered around $g = 2.015$ are also consistent with the expected hyperfine splitting from the copper center ($I = 3/2$).

EPR spectral data for **5** have been previously reported by Liu and Anson [17]. The EPR spectrum for **5** collected at room temperature in acetonitrile showed an octet of peaks ($I_V = 7/2$) centered at $g = 1.988$. This study agrees with the previously reported g-factor value [17].

UV–Vis absorptions for **4** are also consistent with similar compounds that have been previously reported [24]. A similar copper (II) salen complex with a methyl in lieu of a *tert*-butyl gives visible absorptions (nm) at 405 and 444, whereas **4** gives absorptions 408 and 452. Similar electronic spectra were obtained for **5**. The character of the absorptions are similar to previously reported assignments [24], i.e., an intense absorption between 316 and 333 nm for both compounds is due to metal-to-ligand charge transfer; weak d–d transitions were observed around 711 nm.

3.2. X-ray structures

The crystal structure of Cu[3,5-^{t}Bu$_2$-salophen] (**4**) consists of one molecule in the asymmetric unit. The compound **4** crystallizes in the triclinic space group $P\bar{1}$. Selected geometric parameters are shown in Table 2. A displacement ellipsoid plot of **4** is shown in Fig. 1. The structure consists of discrete molecules with no obvious hydrogen bonding between adjacent molecules. The molecular structure is roughly planar with a curving of the plane of the Cu and 3 phenyl rings – the Cu atom sits 0.0266 Å below the mean O/O/N/N plane, but 0.2479 Å above the mean plane of the centroids of the three phenyl rings of the ligand. The Cu—N and Cu—O bond distances are typical of compounds of this type [24,25]. In the three-dimensional structure, the molecule packs in what appears to be dimers. The central phenyl ring of one molecule resides above the Cu atom of the adjacent molecule at a distance of 3.350 Å. The idealized H on a methyl group from the adjacent dimer forms a short contact (~2.78 Å) with Cu to "complete" a distorted octahedral geometry.

Table 2
Selected bond lengths (Å) and angles (°) for **4**

Cu–N(1)	1.940 (3)
Cu–N(2)	1.944 (2)
Cu–O(1)	1.896 (2)
Cu–O(2)	1.897 (2)
C(1)–O(1)–Cu	129.12 (17)
C(12)–O(2)–Cu	128.16 (17)
O(1)–Cu–O(2)	90.28 (9)
O(1)–Cu–N(1)	92.74 (10)
O(2)–Cu–N(1)	176.90 (8)
O(1)–Cu–N(2)	175.71 (9)
O(2)–Cu–N(2)	93.14 (10)
N(1)–Cu–N(2)	83.81 (10)

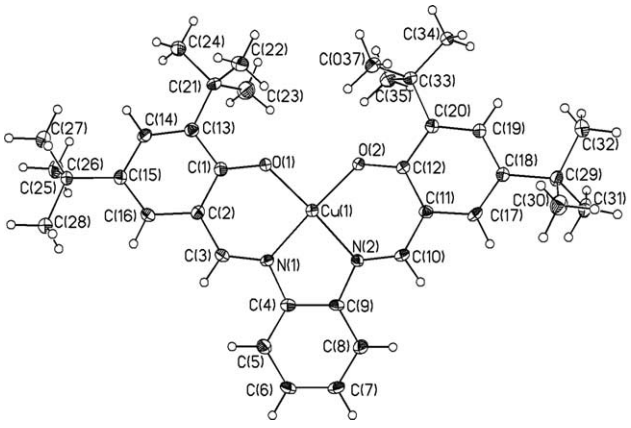

Fig. 1. Displacement ellipsoid plot of **4**. Here and in Fig. 2 displacement ellipsoids are drawn at the 50% probability level. Hydrogen atoms are drawn as arbitrarily small circles.

Compound **5** co-crystallizes with one equivalent of ethanol solvent molecule in the monoclinic space group $P2_1/c$. A displacement ellipsoid plot of **5** is shown in Fig. 2. Selected geometric parameters are shown in Table 3. Crystals of the compound effloresce when removed from the mother liquor. The molecular structure is well-defined and consists of a well-separated moiety and one solvent molecule per asymmetric unit, with four asymmetric units per unit cell. No hydrogen bonding is obvious in the molecular structure, however, π–π stacking of adjacent molecules is present. **5** packs in typical herringbone fashion when viewed along [1 0 0] with ethanol filling structural voids. The centroid of the central phenyl ring and the centroid of the π–π stacked outer phenyl ring of an adjacent molecule are separated by 3.832 Å (closest contact 3.52 Å C9···C11). The strength of π–π stacking interactions leads to several close contacts and disrupts any V=O···solvent hydrogen bonding that may have otherwise occurred. The metrics of the molecule are similar to the current 73 vanadyl salen complexes in the Cambridge Structural Database with V–N bonds of 2.051(2) Å, V–O bonds of 1.9133(18) Å, and a V=O bond of 1.5991(18) Å [26]. Average literature values for these types of bonds are 2.07, 1.88, and 1.60 Å, respectively [26]. The vanadium has the expected square pyramidal geometry and lies 0.611 Å above the O/O/N/N plane. A 21° angle exists between the *tert*-butyl substituted aromatic rings. This curvature of the salophen ligand is most likely due to steric hindrance between the *tert*-butyl groups in the 3 position.

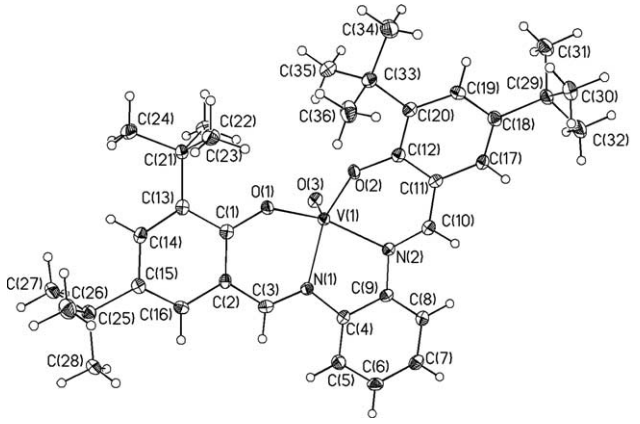

Fig. 2. Displacement ellipsoid plot of **5**. The O in V=O is projected into the plane of the page.

Table 3
Selected bond lengths (Å) and angles (°) for **5** · EtOH

V–N(1)	2.051 (2)
V–N(2)	2.053 (2)
V–O(1)	1.9106 (18)
V–O(2)	1.9133 (18)
V–O(3)	1.5991 (18)
C(9)–N(2)–V	113.42 (16)
C(1)–O(1)–V	131.38 (16)
C(12)–O(2)–V	131.96 (16)
O(3)–V–O(1)	108.00 (9)
O(3)–V–O(2)	111.74 (9)
O(1)–V–O(2)	86.25 (8)
O(3)–V–N(1)	108.68 (9)
O(1)–V–N(1)	87.42 (8)
O(2)–V–N(1)	139.07 (8)
O(3)–V–N(2)	103.31 (9)
O(1)–V–N(2)	148.42 (8)
O(2)–V–N(2)	86.06 (8)
N(1)–V–N(2)	78.66 (8)

3.3. Reactivity

Reactivity studies were also attempted on compound **4**. Initial attempts were made to bind pyridine to **4**. An amount of **4** was dissolved in toluene and titrated with pyridine while being monitored using UV–Vis spectroscopy. No changes in the UV–Vis spectrum were observed. An amount of **4** was also dissolved in neat pyridine, but again no change in the UV–Vis spectrum was observed. Initially it was believed that **4** existed as an ethanol solvated molecule, but X-ray structural information was not consistent with this theory, at least in the solid state. Pyridine may not bind to **4** due to the 18-electron rule. The central copper atom in **4** has an electron count of 17, so it is unlikely that the two electron donor pyridine could bind to the copper without the dissociation of a portion of the salophen ligand.

4. Supporting information available

Crystallographic data for the structural analyses have been deposited with the Cambridge Crystallographic Data Centre, CCDC Nos. 271743 and 271742 for **4** and **5**, respectively. Copies of this information maybe obtained free of charge from The Director, CCDC, 12 Union Road, Cambridge, CB2 1EZ, UK, fax: +44 1223 366 033, e-mail: deposit@ccdc.ac.uk or on the web www: http://www.ccdc.cam.ac.uk.

Acknowledgements

The authors thank Dr. Amy A. Narducci Sarjeant of Johns Hopkins University for collection of X-ray intensity data and Illinois State University for financial support (URG-NFIG and URG-PFIG Grants).

References

[1] W. Zhang, J.L. Loebach, S.R. Wilson, E.N. Jacobsen, J. Am. Chem. Soc. 112 (1990) 2801.
[2] E.N. Jacobsen, W. Zhang, A.R. Muci, J.R. Ecker, L. Deng, J. Am. Chem. Soc. 113 (1991) 7063.

[3] W. Zhang, E.N. Jacobsen, J. Org. Chem. 56 (1991) 2296.
[4] R. Irie, K. Noda, Y. Ito, N. Matsumoto, T. Katsuki, Tetrahedron Lett. 31 (1990) 7345.
[5] S. Zolezzi, E. Spodine, A. Decinti, Polyhedron 22 (2003) 1653.
[6] T. Kawato, H. Kanatomi, H. Koyama, T. Igarashi, J. Photochem. 33 (1986) 199.
[7] J. Wöltinger, J.-E. Bäckvall, Á. Zsigmond, Chem. Eur. J. 5 (1999) 1460.
[8] M. Sanchez, M.J. Harvey, F. Nordstrom, S. Parkin, D.A. Atwood, Inorg. Chem. 41 (2002) 5397.
[9] B. Yearwood, S. Parkin, D.A. Atwood, Inorg. Chim. Acta. 333 (2002) 124.
[10] M.S. Hill, D.A. Atwood, Eur. J. Inorg. Chem. (1998) 67.
[11] E. Solari, C. Maltese, M. Latronico, C. Floriani, A. Chiesi-Villa, C. Rizzoli, J. Chem. Soc., Dalton Trans. (1998) 2395.
[12] D.A. Atwood, M.S. Hill, J.A. Jegier, D. Rutherford, Organometallics 16 (1997) 2659.
[13] A.L. Singer, D.A. Atwood, Inorg. Chim. Acta. 277 (1998) 157.
[14] M.S. Hill, D.A. Atwood, Main Group Chem. 2 (1998) 191.
[15] D.J. Anderson, R. Eisenberg, Inorg. Chem. 33 (1994) 5378.
[16] D.A. Colby, G.M. Ferrence, T.D. Lash, Angew. Chem., Int. Ed. 43 (11) (2004) 1346.
[17] Z. Liu, F.C. Anson, Inorg. Chem. 40 (2001) 1329.
[18] Oxford Diffraction, Ltd., Xcalibur CCD System, Crysalis Software System, Oxford Diffraction, Ltd., Oxfordshire, UK, 2004.
[19] G.M. Sheldrick, SHELXS and SHELXL97, University of Göttingen, Germany, 1997.
[20] M.M. Singh, R.M. Pike, Z. Szafran, Microscale and Selected Macroscale Experiments For General Chemistry and Advanced General Chemistry, Wiley, New York, 1995.
[21] G. Asgedom, A. Sreedhara, J. Kivikoski, C.P. Rao, Polyhedron 16 (1996) 643.
[22] G.M. Klesova, V.V. Zelentsov, V.I. Spitsyn, Doklady Akademii Nauk SSSR 208 (3) (1973) 642.
[23] M. Valko, R. Klement, P. Pelikán, R. Boča, L. Dlháň, A. Bottcher, H. Elias, L. Müller, J. Phys. Chem. 99 (1995) 137.
[24] R. Klement, F. Stock, H. Elias, H. Paulus, P. Pelikán, M. Valko, M. Mazúr, Polyhedron 18 (1999) 3617.
[25] S. Bunce, R.J. Cross, L.J. Farrugia, S. Kunchandy, L.L. Meason, K.W. Muir, M. O'Donnell, R.D. Peacock, D. Stirling, S.J. Teat, Polyhedron 17 (23–24) (1998) 4179.
[26] The Cambridge Structural Database: a quarter of a million crystal structures and rising F.H. Allen, Acta Crystallogr. B 58 (2002) 380.

Available online at www.sciencedirect.com
SCIENCE DIRECT®
Polyhedron 25 (2006) 124–133
POLYHEDRON
www.elsevier.com/locate/poly

Copper(I) monophosphine complexes with functionalized acylpyrazolonate ligands: Syntheses of heterobimetallic Cu–Zn and Cu–Ru adducts

Augusto Cingolani [a], Fabio Marchetti [a,*], Claudio Pettinari [a], Riccardo Pettinari [a], Brian W. Skelton [b], Neil Somers [b], Allan H. White [b]

[a] *Dipartimento di Scienze Chimiche, Università degli Studi di Camerino, via S. Agostino 1, 62032 Camerino, Italy*
[b] *School of Biomolecular, Biomedical and Chemical Sciences, Chemistry M313, The University of Western Australia, Crawley, W. A. 6009, Australia*

Received 8 June 2005; accepted 12 July 2005
Available online 13 September 2005

Abstract

Copper(I) acylpyrazolonate derivatives of formula $[Cu(Q)(PPh_3)_2]$ (HQ = HQ^{C2F5} = 1-phenyl-3-methyl-4-pentafluoropropanoyl-pyrazol-5-one, $HQ^{CF3,CF3}$ = 1-(4-trifluoromethyl)phenyl-3-methyl-4-trifluoroacetylpyrazol-5-one, HQ^{naph} = 1-phenyl-3-methyl-4-(1-naphthoyl)pyrazol-5-one, HQ^{fur} = 1-phenyl-3-methyl-4-furylpyrazol-5-one, HQ^{thi} = 1-phenyl-3-methyl-4-thienoylpyrazol-5-one, $HQ^{CF3,py}$ = 1-(2-pyridyl)-3-methyl-4-trifluoromethylpyrazol-5-one) have been synthesized and characterized, both in the solid state and in solution. The isomorphous crystal structures of $[Cu(Q^{fur})(PPh_3)_2]$ and $[Cu(Q^{thi})(PPh_3)_2]$ and of $[Cu(Q^{C2F5})(PPh_3)_2]$ show their copper atoms in distorted tetrahedral environments. Apart from the derivative $[Cu(Q^{naph})(PPh_3)_2]$, they are fluxional in chloroform solution, dissociating partially to the $[Cu(Q)(PR_3)]$ fragment and free PR_3, or existing in solution as $[Cu(O_2–Q)(PR_3)_2]$ or $[Cu(O–Q)(PR_3)_2]$ species, with CuO_2P_2 or $CuOP_2$ metal environments, in equilibrium with each other. By contrast, in $[Cu(Q^{CF3,py})(PPh_3)_2]$ the $Q^{CF3,py}$ ligand is coordinated to copper through the nitrogen atoms of the pyrazole and pyridine rings. The latter compound reacts with $Zn(BF_4)_2 \cdot xH_2O$ and $[Ru(p\text{-cymene})Cl_2]_2$ affording ionic heterobimetallic adducts.
© 2005 Elsevier Ltd. All rights reserved.

Keywords: Copper; 4-Acyl-5-pyrazolones; Crystal structures; Heterobimetallic derivatives

1. Introduction

In the last decade we have been involved in elucidating the coordinative properties of a class of β-diketones, namely 4-acyl-5-pyrazolones [1], here indicated as HQ, having a pyrazole fused to the chelating moiety, well-known mainly for their selective extraction properties toward several metal ions [2,3]. They generally chelate metal centers in an unsymmetrical fashion because of the different donor capabilities of their oxygen atoms [4,5]. Furthermore they have been shown capable of binding also to soft metal acceptors through the nitrogen of the pyrazole [6]. These ligands can be easily functionalized in the acyl fragment and several examples can be found in the literature, in which the substituents range from electron-withdrawing groups to electron-donating ones [1].

We have also investigated the coordination chemistry of some acylpyrazolone-type ligands with copper(I) and copper(II) acceptors, due to potential applications in the microelectronic industry of some recent copper–β-diketonate compounds as promising molecular precursors for CVD techniques [7]. When heated in vacuo, copper(II) adducts of the type $Cu(Q)_2(L)$ (where L = dipy or phen

* Corresponding author. Tel.: +39 0737 402217; fax: +39 0737 637345.
E-mail address: fabio.marchetti@unicam.it (F. Marchetti).

0277-5387/$ - see front matter © 2005 Elsevier Ltd. All rights reserved.
doi:10.1016/j.poly.2005.07.020

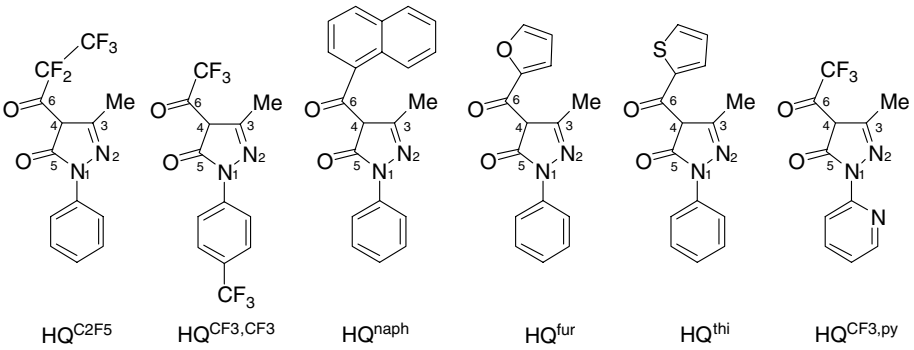

Fig. 1. Proligands HQ used in this work.

and Q = 1-phenyl-3-methyl-4-trifluoromethyl-pyrazolon-5-ato) eliminate the ancillary L ligand and convert into $Cu(Q)_2$, which have lower volatilities than their corresponding classical β-diketonato copper(II) complexes [8]. Cu(I) derivatives of the form $Cu(Q)(PR_3)_2$ (R = Ph, Cy, Bn, *p*-tolyl) show higher volatility, and during sublimation form a thin film of metallic copper, according to the disproportionation: $2\ Cu(Q)(PR_3)_2 \rightarrow Cu + Cu(Q)_2 + 4PR_3$ [8].

Here we extend previous studies on the interaction of copper(I) and silver(I) phosphino acceptors [6a,6b,9] with some selected acylpyrazolones, two containing fluorinated substituents, others with aromatic groups such as naphthyl, furanyl or thienyl in the acyl moiety and, finally, a ligand containing a pyridine ring bonded to N1 of the pyrazolone moiety (Fig. 1), recently reported as an N_2-chelating donor in the synthesis of new silver compounds [10]. A detailed structural and spectroscopic study of the derivatives obtained is reported, and comparison made with the features of the previously studied silver(I) phosphino acylpyrazolonates [6a,6b,9,10]. Possible further interactions through any additional N-, S- or O-donor atoms in $Q^{CF3,py}$, Q^{thi} or Q^{fur}, respectively, with additional metal acceptors, such as zinc(II) and (arene)ruthenium(II), have also been investigated.

2. Experimental section

2.1. General remarks

Solvents were used as supplied or distilled using standard methods. All chemicals were purchased from Aldrich (Milwaukee) and used as received. The samples for microanalyses were dried in vacuum to constant weight (20 °C, ca. 0.1 Torr). Elemental analyses (C, H, N, S) were performed in-house with Fisons Instruments 1108 CHNS–O Elemental Analyser. IR spectra were recorded from 4000 to 100 cm^{-1} using CsI pellets and a Perkin Elmer System 2000 FT-IT instrument. ^1H, ^{13}C, ^{19}F and ^{31}P NMR spectra were recorded on a VXR-300 Varian spectrometer operating at room temperature (300 MHz for ^1H, 75 MHz for ^{13}C, 282.3 MHz for ^{19}F and 121.4 MHz for ^{31}P) and are referred to TMS, 85% H_3PO_4 and $CFCl_3$, respectively; signals are indicated as s (singlet), d (doublet), t (triplet), q (quartet), m (multiplet). The electrical conductances of the acetonitrile solutions were measured with a Crison CDTM 522 conductimeter at room temperature.

2.2. Syntheses of the proligands

The proligands HQ^{C2F5}, $HQ^{CF3,CF3}$, HQ^{naph}, HQ^{fur}, HQ^{thi} and $HQ^{CF3,py}$ were synthesized according to the procedures previously described [6b,9–13].

2.3. Syntheses of the complexes

2.3.1. *[Cu(Q^{C2F5})(PPh$_3$)$_2$] (1)*

$CuNO_3(PPh_3)_2$ (650 mg, 1.0 mmol) was added to a toluene solution/suspension (30 ml) of HQ^{C2F5} (320 mg, 1.0 mmol) and $NaOCH_3$ (54 mg, 1.0 mmol). The clear solution was stirred for 1 h. Solvent was then removed on a rotary evaporator and chloroform (20 ml) was added to the crude of the mixture reaction. The solution was filtered and, after addition of light petroleum (20 ml), a yellow precipitate was afforded, which was filtered off, washed with light petroleum and shown to be compound **1**. Crystals suitable for the X-ray work were deposited from chloroform/diethyl ether solution. It is soluble in most organic solvents, except petroleum ether. Yield: 84%. M.p. 142–144 °C. *Anal.* Calc. for $C_{49}H_{38}CuF_5N_2O_2P_2$: C, 64.86; H, 4.22; N, 3.09. Found: C, 63.95; H, 4.09; N, 3.01%. IR (nujol, cm^{-1}): 1636vs, 1597s, 1584s and 1542m *ν*(C=O, C=N, N=N), 517vs, 503vs, 497vs, 443m, 430m and 426m *ν*(*y*- and *t*-mode of PPh_3), 397w and 345m *ν*(Cu–O). ^1H ($CDCl_3$) NMR: *δ* 2.25s (3H, C3–C*H*$_3$); 7.20–7.50m, 7.90d (35H, H_{arom} of Q^{C2F5} and PPh_3). $^{13}C\{^1H\}$ NMR ($CDCl_3$): *δ*, 17.4s (C3–*C*H$_3$), 120.0s, 124.2s, 128.5s, 148.1s (C_{arom} of Q^{C2F5}), 129.5d ($^3J_{(P-C)}$: 14.1 Hz, *m*-*C* of PPh_3), 129.9s (*p*-*C* of PPh_3), 133.2d ($^1J_{(P-C)}$: 36.1 Hz, *C*–P of PPh_3), 134.0d ($^2J_{(P-C)}$: 21.7 Hz, *o*-*C* of PPh_3), 104.6s (*C*4),

139.4s (*C*3), 165.8s (*C*5), 182.3s (*C*6), resonances of CF_2CF_3 not observed. $^{31}P\{^1H\}$ NMR ($CDCl_3$, $T = 293$ K): δ −2.42s. $^{31}P\{^1H\}$ NMR ($CDCl_3$, $T =$ 218 K): δ −0.46s [$Cu(O_2–Q^{C2F5})(PPh_3)$], −1.84s [$Cu(O_2–Q^{C2F5})(PPh_3)_2$], −3.63s [$PPh_3$]. $^{19}F\{^1H\}$ NMR ($CDCl_3$, $T = 293$ K): δ −81.7s (CF_2CF_3), −115.7s(CF_2CF_3).

2.3.2. [Cu($Q^{CF3,CF3}$)(PPh_3)$_2$] (2)

Compound **2** has been synthesized similarly to **1**. It is soluble in most organic solvents, except petroleum ether. Yield: 69%. M.p. 182–184 °C. *Anal.* Calc. for $C_{49}H_{37}CuF_6N_2O_2P_2$: C, 63.63; H, 4.03; N, 3.03. Found: C, 63.46; H, 4.25; N, 3.03%. IR (nujol, cm^{-1}): 1643vs, 1609s, 1586m, 1543m, 1518m and 1508s ν(C=O, C=N, N=N), 518vs, 504s, 488s, 461m, 447m and 434m ν(*y*- and *t*-mode of PPh_3), 416w and 344m ν(Cu–O). ^1H ($CDCl_3$) NMR: δ 2.45q (3H, $^6J_{(F–H)}$: 2.2. Hz, C3–CH_3), 7.15–7.40m, (30H, H_{arom} of PPh_3), 7.49d, 7.99d (4H, H_{arom} of $Q^{CF3,CF3}$). $^{13}C\{^1H\}$ NMR ($CDCl_3$): δ, 16.4s (C3–CH_3), 117.9q ($^1J_{(F–C)}$: 284.7 Hz, CF_3C=O), 118.9s, 125.5s, 128.7s, 148.2s (C_{arom} of $Q^{CF3,CF3}$), 128.7d ($^3J_{(P–C)}$: 13.5 Hz, *m*-*C* of PPh_3), 129.9s (*p*-*C* of PPh_3), 132.9d ($^1J_{(P–C)}$: 34.4 Hz, *C*–P of PPh_3), 133.9d ($^2J_{(P–C)}$: 20.2 Hz, *o*-*C* of PPh_3), 100.7s (*C*4), 142.1s (*C*3), 168.1s (*C*5), 183.9s (*C*6), resonances of N–C_6H_4–*p*-CF_3 not observed. $^{31}P\{^1H\}$ NMR ($CDCl_3$, $T = 293$ K): δ −2.49s. $^{31}P\{^1H\}$ NMR ($CDCl_3$, $T =$ 218K): δ −1.45s [$Cu(O–Q^{CF3,CF3})(PPh_3)_2$], −3.11s [$Cu(O_2–Q^{CF3,CF3})(PPh_3)_2$]. $^{19}F\{^1H\}$ NMR ($CDCl_3$, $T = 293$ K): δ −62.3s (N–C_6H_4–*p*-CF_3), −72.0s ((C=O)CF_3).

2.3.3. [Cu(Q^{naph})(PPh_3)$_2$] (3)

Compound **3** has been synthesized similarly to **1.** It is soluble in dmso, acetonitrile, acetone and chlorinated solvents. Yield: 88%. M.p. 204–207 °C. *Anal.* Calc. for $C_{57}H_{46}CuN_2O_2P_2$: C, 74.70; H, 5.06; N, 3.06. Found: C, 74.45; H, 5.10; N, 3.11%. IR (nujol, cm^{-1}): 1621vs, 1592s, 1578m, 1532m and 1500m ν(C=O), 528s, 515vs, 500vs, 437m and 420m ν(*y*- and *t*-mode of PPh_3), 343m ν(Cu–O). ^1H ($CDCl_3$) NMR: δ 1.21s (3H, C3–CH_3), 7.05–7.45m, 7.54d, 7.83dd, 7.97dd (37H, H_{arom} of Q^{naft} and PPh_3). $^{13}C\{^1H\}$ NMR ($CDCl_3$): δ, 16.1s (C3–CH_3), 119.5s, 123.5s, 123.9s, 125.3s, 125.9s, 126.1s, 126.6s, 128.1s, 130.4s, 140.0s (C_{arom} of Q^{naph}), 128.5d ($^3J_{(P–C)}$: 17.6 Hz, *m*-*C* of PPh_3), 129.6s (*p*-*C* of PPh_3), 133.4d ($^1J_{(P–C)}$: 34.4 Hz, *C*–P of PPh_3), 133.6d ($^2J_{(P–C)}$: 22.3 Hz, *o*-*C* of PPh_3), 106.3s (*C*4), 140.4s (*C*3), 165.9s (*C*5), 189.9s (*C*6). $^{31}P\{^1H\}$ NMR ($CDCl_3$, $T = 293$ K): δ −3.43s [$Cu(O_2–Q^{naph})(PPh_3)_2$]. $^{31}P\{^1H\}$ NMR ($CDCl_3$, $T = 218$ K): δ −4.15s.

2.3.4. [Cu(Q^{fur})(PPh_3)$_2$] (4)

Compound **4** has been synthesized similarly to **1**, crystals suitable for the X-ray work being deposited from chloroform/diethyl ether solution. Yield: 88%. M.p. 168–170 °C. *Anal.* Calc. for $C_{51}H_{41}CuN_2O_3P_2$: C, 71.70; H, 4.72; N, 3.28. Found: C, 71.53; H, 4.66; N, 3.24%. IR (nujol, cm^{-1}): 1610vs, 1592s, 1581s, 1557m and 1526m ν(C=O), 516s, 505vs, 494s, 440m and 426m ν(*y*- and *t*-mode of PPh_3), 408m and 356m ν(Cu–O). ^1H ($CDCl_3$) NMR: δ 2.61s (3H, C3–CH_3), 6.64m, 6.88m, 7.10–7.45m, 7.49dd, 7.65dd, 7.73d (38H, H_{arom} of Q^{fur} and PPh_3). $^{13}C\{^1H\}$ NMR ($CDCl_3$): δ, 16.7s (C3–CH_3), 111.4s, 114.4s, 119.9s, 123.5s, 143.6s, 154.0s (C_{arom} of Q^{fur}), 128.5d ($^3J_{(P–C)}$: 6.9 Hz, *m*-*C* of PPh_3), 129.6s (*p*-*C* of PPh_3), 132.4d ($^1J_{(P–C)}$: 27.1 Hz, *C*–P of PPh_3), 134.1d ($^2J_{(P–C)}$: 14.8 Hz, *o*-*C* of PPh_3), 104.8s (*C*4), 140.0s (*C*3), 167.2s (*C*5), 176.5s (*C*6). $^{31}P\{^1H\}$ NMR ($CDCl_3$, $T = 293$ K): δ −2.20s. $^{31}P\{^1H\}$ NMR ($CDCl_3$, $T = 218$ K): δ −2.68s [$Cu(O–Q^{fur})(PPh_3)_2$], −4.04s [$Cu(O_2–Q^{fur})(PPh_3)_2$].

2.3.5. [Cu(Q^{thi})(PPh_3)$_2$] (5)

Compound **5** has been synthesized similarly to **1**, crystals suitable for the X-ray work being deposited from chloroform/diethyl ether solution. Yield: 79%. M.p. 159–161 °C. *Anal.* Calc. for $C_{51}H_{41}CuN_2O_2P_2S$: C, 70.29; H, 4.74; N, 3.21; S, 3.68. Found: C, 69.87; H, 4.79; N, 3.22; S, 3.55%. IR (nujol, cm^{-1}): 1609vs, 1592s, 1579s, 1554m and 1516m ν(C=O), 515vs, 504vs, 498vs, 440m, 431m and 424m ν(*y*- and *t*-mode of PPh_3), 405w and 353m ν(Cu–O). ^1H ($CDCl_3$) NMR: δ 1.91s (3H, C3–CH_3); 6.97t, 7.05t, 7.15t, 7.22–7.40m, 7.88d (38H, H_{arom} of Q^{thi} and PPh_3). $^{13}C\{^1H\}$ NMR ($CDCl_3$): δ, 16.9s (C3–CH_3), 119.7s, 123.4s, 126.3s, 145.1s, 148.2s (C_{arom} of Q^{thi}), 128.2d ($^3J_{(P–C)}$: 7.1 Hz, *m*-*C* of PPh_3), 129.4s (*p*-*C* of PPh_3), 133.2d ($^1J_{(P–C)}$: 27.3 Hz, *C*–P of PPh_3), 133.8d ($^2J_{(P–C)}$: 14.1 Hz, *o*-*C* of PPh_3), 104.9s (*C*4), 139.9s (*C*3), 166.2s (*C*5), 181.4s (*C*6). $^{31}P\{^1H\}$ NMR ($CDCl_3$, $T = 293$ K): δ −2.62s. $^{31}P\{^1H\}$ NMR ($CDCl_3$, $T = 218$ K): δ −2.64s [$Cu(O–Q^{thi})(PPh_3)_2$], −4.17s [$Cu(O_2–Q^{thi})(PPh_3)_2$].

2.3.6. [Cu($Q^{CF3,py}$)(PPh_3)$_2$] (6)

Compound **6** has been synthesized similarly to **1**, but using a mixture of acetonitrile/methanol (1:1) because of the very low solubility of $HQ^{CF3,py}$ in toluene. Crystals suitable for the X-ray work were deposited from chloroform/diethyl ether solution. Yield: 67%. M.p. 180–183 °C. *Anal.* Calc. for $C_{47}H_{37}CuF_3N_3O_2P_2$: C, 65.77; H, 4.35; N, 4.90. Found: C, 65.43; H, 4.54; N, 4.88%. IR (nujol, cm^{-1}): 1667vs, 1636s, 1621s, 1596m and 1534m ν(C=O), 527s, 516vs, 512s, 494s, 446m, 422m and 412m ν(*y*- and *t*-mode of PPh_3), 310s and 244m ν(Cu–N). ^1H NMR ($CDCl_3$): δ 2.07s (3H, C3–CH_3), 7.19m, 7.34d, 7.50m, 7.62m, 8.83d (34H, H_{arom} of $Q^{CF3,py}$ and of PPh_3). $^{13}C\{^1H\}$ NMR ($CDCl_3$): δ 18.5s (C3–CH_3), 113.5s, 118.9s, 139.0s, 146.6s, 150.3s (C_{arom} of $Q^{CF3,py}$), 128.9d ($^3J_{(P–C)}$: 7.3 Hz, *m*-C of PPh_3), 132.6d ($^1J_{(P–C)}$: 38.7 Hz, C–P of PPh_3), 130.2s (*p*-*C* of

PPh_3), 133.4d ($^2J_{(P-C)}$: 33.1 Hz, *o-C* of PPh_3), 99.8s (*C*4), 155.8s (*C*3), 164.3s (*C*5), 173.5m (*C*6), $CF_3C{=}O$ not observed. $^{31}P\{^1H\}$ NMR ($CDCl_3$, $T = 293$ K): δ 1.1s. $^{31}P\{^1H\}$ NMR ($CDCl_3$, $T = 218$ K): δ 0.5s [$Cu(N_2$–$Q^{CF3,py})(PPh_3)_2$]. $^{19}F\{^1H\}$ NMR ($CDCl_3$, $T = 293$ K): δ −76.0s (CF_3).

2.3.7. [$Zn\{Cu(Q^{CF3,py})(PPh_3)_2\}_3(BF_4)_2$] · $2H_2O$ (7)

$Zn(BF_4)_2 \cdot xH_2O$ (80 mg, 0.3 mmol) was added to an acetonitrile solution (50 ml) of compound 6 (858 mg, 1 mmol). The clear violet solution was stirred at reflux for 4 h; solvent was then removed on a rotary evaporator and the crude product treated with chloroform/diethyl ether (1:1) (20 ml). A red-brown precipitate was afforded, which was filtered off, washed with diethyl ether (20 ml), dried to constant weight under reduced pressure and shown to be compound 7. It is soluble in dmso and acetonitrile. Yield: 85%. M.p. 156–158 °C. *Anal*. Calc. for $C_{141}H_{115}B_2Cu_3F_{17}N_9O_8P_6Zn$: C, 59.42; H, 4.07; N, 4.42. Found: C, 59.78; H, 4.14; N, 4.10%. Λ_m (MeCN, 10^{-3} M): 288 Ω^{-1} cm^2 mol^{-1}. IR (nujol, cm^{-1}): 3450br $\nu(H_2O)$, 1678m δ (H_2O), 1659vs, 1651vs, 1644vs, 1634s, 1601s, 1585s, 1557m, 1537m and 1519m ν(C=O), 1057vs and 966s $\nu(BF_4)$, 528s, 518vs, 503s, 492s, 432m, 423m ν(*y*- and *t*-mode of PPh_3), 441m ν(Zn–O), 253m ν(Cu–N). ^1H NMR (CD_3CN): δ 2.22s (9H, C3–CH_3), 7.23m, 7.39m, 7.44d, 7.48d, 8.10m (102H, H_{arom} of $Q^{CF3,py}$ and of PPh_3). $^{13}C\{^1H\}$ NMR (CD_3CN): δ 18.5s (C3–CH_3), 113.6s, 119.5s, 140.5s, 146.9s, 150.9s (C_{arom} of $Q^{CF3,py}$), 129.4d ($^3J_{(P-C)}$: 7.8 Hz, *m*-C of PPh_3), 132.8d ($^1J_{(P-C)}$: 38.9 Hz, C–P of PPh_3), 130.3s (*p*-C of PPh_3), 133.5d ($^2J_{(P-C)}$: 33.4 Hz, *o*-C of PPh_3), 101.0s (C4), 151.2s (C3), 165.8s (C5), 175.1m (C6), $CF_3C{=}O$ not observed. $^{31}P\{^1H\}$ NMR (CD_3CN, $T = 293$ K): δ 1.2s [$Zn\{Cu(Q^{CF3,py})(PPh_3)_2\}_3$]. $^{19}F\{^1H\}$ NMR (CD_3CN, $T = 293$ K): δ −76.1s (CF_3 in $Q^{CF3,py}$), −151.8s (BF_4).

2.3.8. [(*p*-cymene)Ru(Cl)(κ^4-O_2, N_2–$Q^{CF3,py}$)-$Cu(PPh_3)_2$]$PF_6 \cdot 3H_2O$ (8)

$[Ru(p\text{-cymene})Cl_2]_2$ (306 mg, 0.5 mmol) was added to an acetonitrile solution (50 ml) of compound 6 (858 mg, 1 mmol). The orange-red solution was stirred at reflux 24 h, and $AgPF_6$ (253 mg, 1.0 mmol) then added. A colourless precipitate immediately formed, which was removed by filtration. The volume of the filtrate was then removed on a rotary evaporator and the crude product treated with chloroform/petroleum ether (1:1) (20 ml). A red-brown precipitate resulted, which was filtered off, washed with petroleum ether (20 ml), dried to constant weight under reduced pressure and shown to be compound 8. It is soluble in dmso and acetonitrile. Yield: 85%. M.p. 143–145 °C. *Anal*. Calc. for $C_{57}H_{57}ClCuF_9N_3O_5P_3Ru$: C, 51.55; H, 4.33; N, 3.16. Found: C, 51.55; H, 4.42; N, 3.10%. Λ_m (MeCN, 10^{-3} M): 136 Ω^{-1} cm^2 mol^{-1}. IR (nujol, cm^{-1}): 3420br $\nu(H_2O)$, 1667m $\delta(H_2O)$, 1651vs, 1644vs, 1637vs, 1605s, 1568m, 1557m and 1531m ν(C=O), 840vs, 695s $\nu(PF_6)$, 527s, 512vs, 494s, 435m, 424m ν(*y*- and *t*-mode of PPh_3), 460m ν(Ru–O), 299m ν(Ru–Cl), 251m ν(Cu–N). ^1H NMR (CD_3CN): δ 1.12s, 1.15s, 1.34s, 1.36s, 1.37s, 1.39s (6H, CH_3–C_6H_4–$CH(CH_3)_3$), 1.73s, 1.88s, 1.94s (3H, CH_3–C_6H_4–$CH(CH_3)_3$), 1.99s, 2.27s, 2.31s (3H, C3–CH_3), 2.72m, 2.88m, 3.03m (1H, CH_3–C_6H_4–$CH(CH_3)_3$), 4.63d (AA′), 5.93d (BB′), 5.01d (AA′), 5.26d (BB′), 5.38d (AA′), 6.15d (BB′) (4H, CH_3–C_6H_4–$CH(CH_3)_3$), 7.18m, 7.38m, 7.55m, 7.61m, 7.81m 8.75m (34H, H_{arom} of Q^{py} and of PPh_3). $^{13}C\{^1H\}$ NMR (CD_3CN): δ 18.0s, 18.5s, 18.6s (C3–CH_3), 21.3s, 22.1s, 22.4s, 22.7s, 23.5s, 23.7s (CH_3–C_6H_4–$CH(CH_3)_3$), 30.6s, 31.4s, 34.0s (CH_3–C_6H_4–$CH(CH_3)_3$), 84.7s, 86.1s, 87.8s, 88.9s, 89.4s, 90.0s (CH_3–C_6H_4–$CH(CH_3)_3$), 113.8s, 119.6s, 140.8s, 147.0s, 151.7s (C_{arom} of Q^{py}), 128.2d ($^3J_{(P-C)}$: 9.8 Hz, *m*-C of PPh_3), 128.9d ($^3J_{(P-C)}$: 10.2 Hz, *m*-C of PPh_3), 130.6s (*p*-C of PPh_3), 131.7s (*p-C* of PPh_3), 132.2d ($^1J_{(P-C)}$: 36.1 Hz, C–P of PPh_3), 132.5d ($^1J_{(P-C)}$: 36.6 Hz, C–P of PPh_3), 134.5d ($^2J_{(P-C)}$: 29.8 Hz, *o*-C of PPh_3), 134.8d ($^2J_{(P-C)}$: 20.2 Hz, *o*-C of PPh_3), 96.5s (*C*4), 155.8s (*C*3), 165.3s (*C*5), 175.4m (*C*6), $CF_3C{=}O$ not observed. $^{31}P\{^1H\}$ NMR (CD_3CN, $T = 293$ K): δ 35.5s (PF_6), 1.5s [(*p*-cymene)Ru(Cl)(κ^4-O_2,N_2–$Q^{CF3,py}$) $Cu(PPh_3)_2$]. $^{19}F\{^1H\}$ NMR (CD_3CN, $T = 293$ K): δ −72.6d ($^2J_{(P-F)}$: 715.9 Hz, PF_6), −76.0s (CF_3 in $Q^{CF3,py}$).

2.4. Structure determinations

Full spheres of 'low-temperature' CCD diffractometer data were measured (Bruker AXS instrument, monochromatic Mo Kα radiation ($\lambda = 0.7107_3$ Å), ω-scans; T ca. 153 K), yielding $N_{t(otal)}$ reflections, merging to N unique after 'empirical'/multiscan absorption correction (proprietary software), N_o with $F > 4$ (F) considered 'observed' and used in the full matrix least squares refinements, refining anisotropic displacement parameter forms for the non-hydrogen atoms, $(x, y, z, U_{iso})_H$ being included constrained at estimates. Conventional residuals R, R_w (weights: $(\sigma^2(F) + 0.000n_wF^2)^{-1}$) are cited at convergence. Neutral atom complex scattering factors were employed, computation using the XTAL 3.4 program system [14]. Pertinent results are given below and in the Tables and Figures, the latter showing non-hydrogen atoms with 50% probability amplitude displacement ellipsoids, hydrogen atoms having arbitrary radii of 0.1 Å.

2.4.1. Crystal/refinement data

$[Cu(Q^{C2F5})(PPh_3)_2]$ (**1**). $C_{49}H_{38}CuF_5N_2O_2P_2$, $M = 907.4$. Triclinic, space group $P\bar{1}$ (C_i^1, No. 2), $a = 14.169(1)$, $b = 19.140(2)$, $c = 19.252(2)$ Å, $\alpha = 118.414(2)$, $\beta = 103.092(2)$, $\gamma = 99.222(2)°$, $V = 4248$ Å^3. D_c ($Z = 4$) $= 1.41_9$ g cm^{-3}. $\mu_{Mo} = 6.5$ cm^{-1}; specimen:

$0.26 \times 0.22 \times 0.18$ mm; $'T'_{min/max} = 0.65$. $2\theta_{max} = 60°$; $N_t = 87869$, $N = 24407$ ($R_{int} = 0.12$), $N_o = 14682$; $R = 0.075$; $R_w = 0.14$ ($n_w = 850$ (refinement on F^2)). $|\Delta\rho_{max}| = 2.2(2)$ eÅ^{-3}.

Variata. The ligand on molecule **2** was modelled as disordered over two sets of sites, occupancies refining to 0.680(1) and complement, the geometries of the two C_2F_5 components being constrained. P(22) and associated ring 223 were modelled as disordered over two sets of sites, occupancies refining to 0.743(3) and complement.

[Cu(Q^{fur})(PPh$_3$)$_2$] (**4**). $C_{51}H_{41}CuN_2O_3P_2$, $M = 855.4$. Orthorhombic, space group $P2_12_12_1$ (D_2^4, No. 19), $a = 10.778(1)$, $b = 18.872(2)$, $c = 20.829(2)$ Å, $V = 4237$ Å^3. D_c ($Z = 4$) $= 1.34_1$ g cm^{-3}. $\mu_{Mo} = 6.4$ cm^{-1}; specimen: $0.15 \times 0.12 \times 0.10$ mm; $'T'_{min/max} = 0.70$. $2\theta_{max} = 58°$; $N_t = 42477$, $N = 5987$ ($R_{int} = 0.071$), $N_o = 4264$; $R = 0.048$; $R_w = 0.052$ ($n_w = 4$). $|\Delta\rho_{max}| = 0.8(2)$ eÅ^{-3}. $x_{abs} = 0.02(2)$.

[Cu(Q^{thi})(PPh$_3$)$_2$] (**5**). $C_{51}H_{41}CuN_2O_2P_2S$, $M = 871.5$ is isomorphous with **4**, the specimen chosen being of opposite chirality. $a = 10.764(1)$, $b = 19.015(2)$, $c = 21.034(3)$ Å, $V = 4305$ Å^3. $D_c = 1.34_4$ g cm^{-3}. $\mu_{Mo} = 6.7$ cm^{-1}; specimen: $0.38 \times 0.35 \times 0.20$ mm; $'T'_{min/max} = 0.83$. $2\theta_{max} = 58°$; $N_t = 43413$, $N = 6148$ ($R_{int} = 0.051$), $N_o = 4722$; $R = 0.039$; $R_w = 0.037$ ($n_w = 4$). $|\Delta\rho_{max}| = 0.6(1)$ eÅ^{-3}. $x_{abs} = -0.03(1)$.

[Cu(Q^{CF3,py})(PPh$_3$)$_2$] (**6**). 1/4MeOH≡$C_{47}H_{38}CuF_3N_3O_2P_2$. 1/4 MeOH, $M = 867.3$. Monoclinic, space group $P2_1/n$ (C_{2h}^5, No. 14), $a = 23.771(2)$, $b = 15.797(2)$, $c = 24.585(3)$ Å, $\beta = 115.657(2)°$, $V = 8322$ Å^3. D_c ($Z = 8$) $= 1.38_4$ g cm^{-3}. $\mu_{Mo} = 0.66$ cm^{-1}; specimen: $0.33 \times 0.19 \times 0.16$ mm; $'T'_{min/max} = 0.89$. $2\theta_{max} = 55°$; $N_t = 119048$, $N = 19109$ ($R_{int} = 0.078$), $N_o = 13181$; $R = 0.052$; $R_w = 0.070$. $|\Delta\rho_{max}| = 0.70(5)$ eÅ^{-3}.

Variata. Difference map residues in a lattice void were modelled in terms of disordered methanol solvent C, O fragments (H not located), site occupancies set at 0.25 after trial refinement. Neighbouring ligand substituent residues also exhibit exalted displacement parameters, possibly encompassing unresolved (concerted?) disorder.

3. Results and discussion

3.1. Synthesis and spectroscopic characterization of the derivatives

The new copper(I) derivatives **1**–**6** have been obtained according to synthetic methods previously reported (Scheme 1) [7].

The choice of a mixture of acetonitrile/methanol in the synthesis of derivative **6** being dictated by the solubility of the proligand HQ^{CF3,py}. They are air-stable solid compounds with sharp melting points, very soluble in most organic solvents, as dmso, acetone, acetonitrile aromatic and chlorinated solvents, in which they are non-electrolytes.

The IR spectra of derivatives **1**–**5** show the typical strong bands in the range 1500–1650 cm^{-1}, due to the stretching modes of C=O, C=N and N=N of pyrazolo-

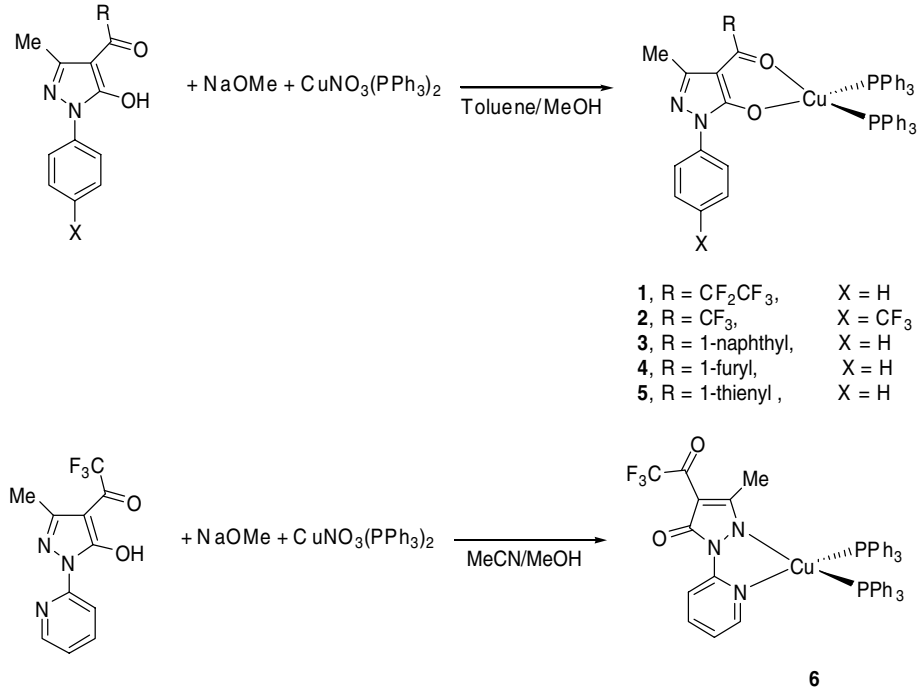

Scheme 1.

nate ligands, slightly shifted upon coordination to lower frequencies, the broad band between 2300 and 2800 cm^{-1} in free HQ donors due to the O–H···O moiety having disappeared, in accordance with deprotonation of the pyrazolonate [1,7]. In the low-frequency region the typical bands due to the *y*- and *t*-modes of vibration of triphenylphosphine have been detected at 400–530 cm^{-1} [15], partially overlapped with two medium Cu–O bands at ca 405 and 355 cm^{-1} [16]. The IR spectrum of **6** shows *ν*(C=O) to be unchanged, in accordance with coordination to copper through the two N atoms of the pyrazole and pyridine rings, with the Cu–N absorption bands at 310 and 244 cm^{-1} [17].

Proton, fluorine, phosphorus and carbon NMR spectra of **1**–**6** recorded at room temperature show a unique broad set of resonances. The integration of the signals in the proton spectra are in accordance with the formulation proposed, i.e. with a 1:2 Q:PPh_3 ratio. The low temperature (218 K) ^{31}P NMR spectrum of **1** exhibits three resonances, one of them being the free phosphine, the others, located at higher frequencies, being attributed to copper–phosphino species of the type $Cu(O_2–Q^{C2F5})(PPh_3)_2$ and $Cu(O_2–Q^{C2F5})(PPh_3)$, the latter arising from dissociation of one PPh_3 in solution, as previously found for similar copper derivatives [7a,7d].

The ^{31}P NMR spectra of **2**, **4** and **5** measured at low temperature (218 K), show two resonances, consistent with the presence of two different species, having CuO_2P_2 and a $CuOP_2$ metal environment, respectively, the latter containing a Q ligand which seemingly acts in an O-monodentate fashion [7c]. Finally the ^{31}P NMR spectra of **3** and **6** remains essentially unchanged with respect to cooling of the samples at 218 K.

The ^{13}C NMR spectra of **1**–**6** exhibit one set of carbon resonances, and the presence of further doublets due to C–P coupling assists in the assignment of signals arising from the C atoms of the phosphine ligand.

3.2. Structural studies

The results of structural characterisations by single crystal X-ray studies of **4** and **5** are consistent in terms of stoichiometry and connectivity with the above representations, unsolvated (Fig. 2). The two complexes are isomorphous with each other (single neutral molecules comprising their asymmetric units), but not with their silver(I) analogue [6b], the latter being modelled as a disordered array in which the pair of coordinated oxygen sites may be interchanged. In none of the three adducts is the substituent heterocycle chalcogen (O or S) found to interact with any metal component of the structure, and differences in the coordination environments of the two complexes are trivial. Because of the irrelevance of the substituent in this respect and the disorder in the immediate silver–furyl counterpart, we adopt the phenyl-substituted ligand analogue of the latter as a comparator. (The geometries of other relevant similar silver(I) systems are also tabulated comparatively in [9].) In that compound [6a], Ag–P are 2.475(3), 2.465(3) and Ag–O 2.498(6) and 2.349(7) Å; P–Ag–P is 120.9(1)°, O–Ag–O 73.0(2)° with O–Ag–P ranging between 92.1(2)–124.3(2)°, Ag–O exhibiting a much greater disparity (the Ag–pyrazolone–O distance being the longer) than the barely perceptible differences found in the present copper complexes (Table 1). In the latter, both P–M–P and O–M–O are enlarged relative to their silver counterpart. In **4**, **5**, the pair of PPh_3 ligands, of the quasi-3 conformation, are of opposite chiralities within each molecule, with the $Q^{fur,thi}$ non-hydrogen skeletons approximately planar, except for a slight twist

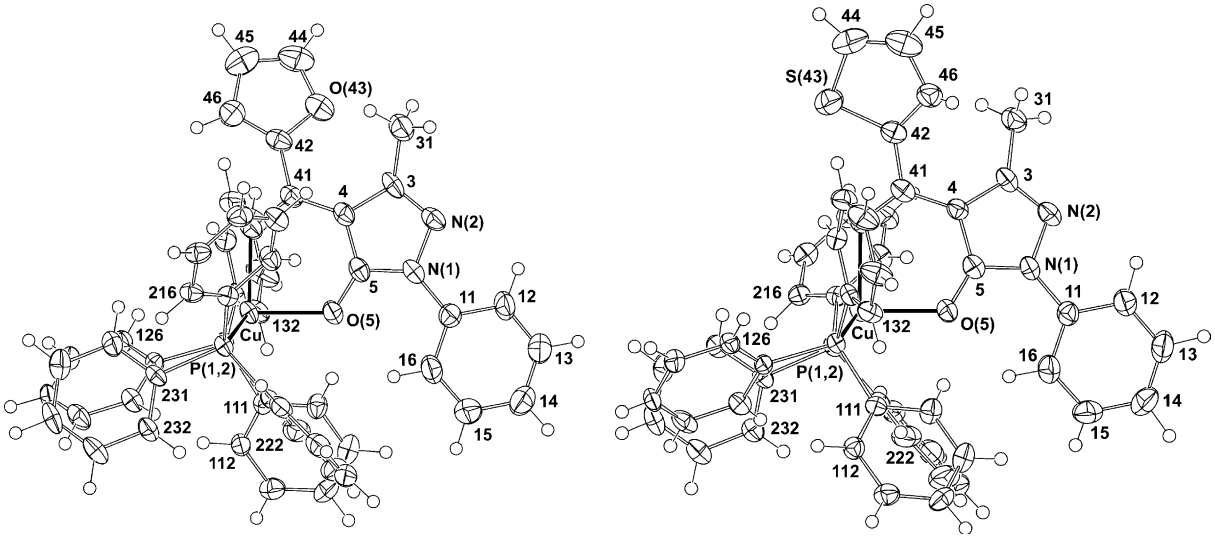

Fig. 2. Projections of **4** and **5**, normal to the Q skeletal planes, showing the reorientation of the heterocycle substituent within the pair of isomorphous structures.

Table 1
Selected geometries, **4**, **5**, **1** (mol. 1)

Atoms	Parameter
Distances (Å)	
Cu–P(1)	2.234(2), 2.246(1), 2.2597(9)
Cu–P(2)	2.235(2), 2.240(1), 2.2567(9)
Cu–O(4)	2.085(4), 2.098(3), 2.170(3)
Cu–O(5)	2.077(4), 2.082(3), 2.059(4)
Angles (°)	
P(1)–Cu–P(2)	127.16(6), 126.97(4), 125.02(4)
P(1)–Cu–O(4)	109.8(1), 110.26(8), 105.22(2)
P(1)–Cu–O(5)	105.4(1), 104.30(8), 100.96(7)
P(2)–Cu–O(4)	112.1(1), 112.36(8), 100.96(7)
P(2)–Cu–O(5)	106.2(1), 106.11(9), 116.76(7)
O(4)–Cu–O(5)	88.7(2), 89.5(1), 87.1(1)
Cu–P(C(nm1)–(ortho) torsion angles (°) (acute)	
nm = 11	−36.4(5), 32.4(5), −30.9(5)
nm = 12	−53.5(5), 54.4(3), −48.7(4)
nm = 13	−41.0(5), 40.5(4), −57.6(3)
nm = 21	−35.5(5), 35.0(4), −45.1(4)
nm = 22	−29.5(6), 31.7(4), −58.5(3)
nm = 23	−56.8(6), 47.8(4), −31.8(5)

of the fur/thi ring planes, presumably in consequence of the methyl proximity; interestingly, the substituent planes adopt alternate dispositions in the two complexes (Fig. 2): O(43)···C(31) is 2.83(1) Å, while in the Q^{thi} derivative C(46)···C(31) is 3.159(8) Å, the determinant of the twist presumably being the bulk of the sulphur atom. They are thus *not* isostructural.

Complex **1** is also of the above type (Fig. 3); the determination, although derivative of CCD data at low temperature, shows two molecules in the asymmetric unit, one having the ligand disordered by oxygen interchange in the manner described above for the previously disordered silver derivative [6b]. Nevertheless the non-disordered molecule provides useful data for a complex derivative of a ligand with a fluorinated substituent (Table 1), the Cu–O(4) distance adjoining the substituent being appreciably lengthened while Cu–O(5) is slightly shortened, in keeping with the expectations incumbent on the fluorinated substituent.

In **6**, although the formulation is again confirmed to be of the form $[CuQ(PPh_3)_2]$, the nature of the complex is quite different, presumably a consequence of the more potent donor capability of the py substituent. In $[Cu(Q^{CF3,py})(PPh_3)_2]$, **6**, two independent neutral molecules, accompanied by diverse solvent fragments in a lattice void, comprise the asymmetric unit of the structure; again the complex is not isomorphous with the recorded unsolvated structure of its silver(I) analogue [10] which is monoclinic, but with one independent molecule in the asymmetric unit. In both copper and silver complexes, the ligand $Q^{CF3,py}$ now behaves as an *N*,*N*′- rather than an *O*,*O*′-chelate, the *N*,*N*′-chelate ring being five-membered rather than six, with the extended ligand skeleton again quasi-planar (Fig. 4). In the silver(I) adduct Ag–P are 2.4585(7), 2.4494(7) Å, only slightly diminished cf. those of the Q^{fur} analogue; Ag–N are 2.400(2), 2.349(1) Å (the latter shorter distance associated with the py donor) and P–Ag–P and N–Ag–N are 119.36(2)° and 68.59(6)°, respectively. In **6** (Table 2), Cu–P are seen to be similar to the counterpart distances in **4**, **5**; Cu–N distances are inequivalent with Cu–N(py) the longer. The two molecules of **6** differ very significantly in terms of their P–Cu–P angles and in a manner which it is difficult to ascribe to anything other than a considerable and unexpected sensitivity to 'packing forces'. The other significant difference between the

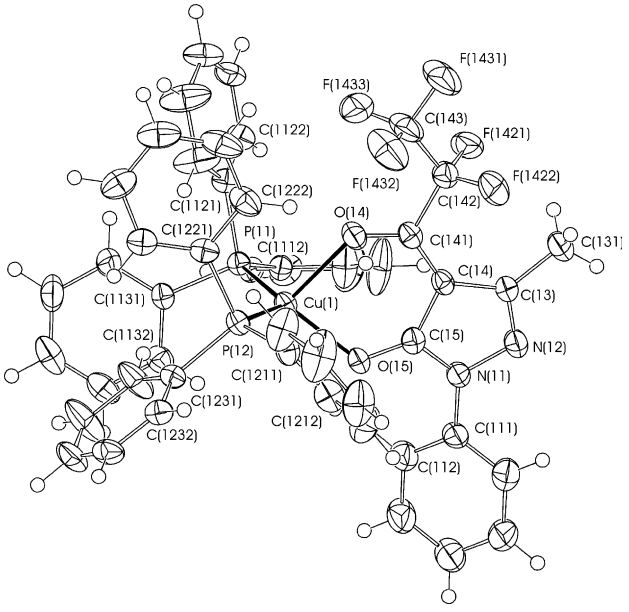

Fig. 3. Projection of derivative **1**.

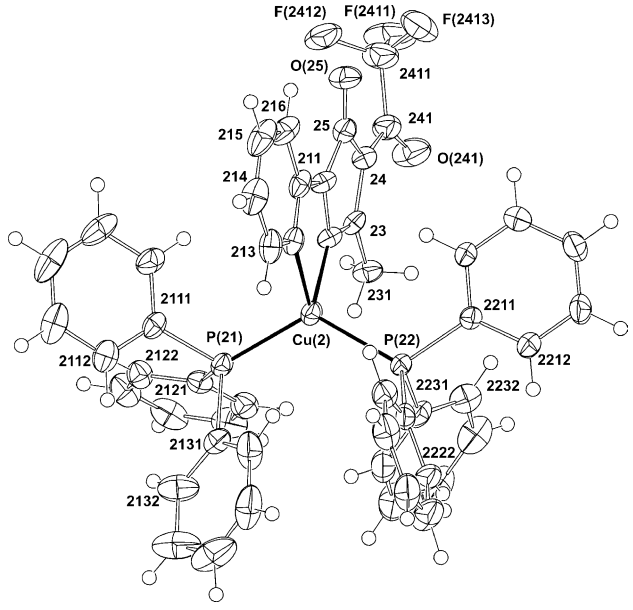

Fig. 4. Projection of **6** (molecule 1).

Table 2
Selected geometries, **6** (mols. 1,2)

Atoms	Parameter
Distances (Å)	
Cu–P(1)	2.249(1), 2.258(1)
Cu–P(2)	2.252(1), 2.263(1)
Cu–N(2)	2.045(3), 2.059(3)
Cu–N(12)	2.107(3), 2.091(3)
Angles (°)	
P(1)–Cu–P(2)	134.05(4), 120.89(4)
P(1)–Cu–N(2)	110.82(10), 117.94(10)
P(1)–Cu–N(12)	103.25(9), 107.73(8)
P(2)–Cu–N(2)	110.04(10), 108.36(10)
P(2)–Cu–N(12)	103.25(9), 115.30(10)
N(2)–Cu–N(12)	78.9(1), 79.2(1)
Cu–P(C(nm1)–C(ortho) torsion angles (°) (acute)	
nm = 11	50.1(3), 40.3(4)
nm = 12	7.4(3), 45,7(3)
nm = 13	62.3(3), 29.3(4)
nm = 21	−8.3(4), 7.6(3)
nm = 22	−53.5(4), −47.3(3)
nm = 23	−62.2(3), −69.1(5)

two molecules is found in the PPh_3 conformations – opposite chiralities are found within each molecule, but in only one PPh_3 group (molecule 2, ligand 1) is the symmetry at all a close approach to the usual three-fold norm.

3.3. Reactivity of derivative $[Cu(Q^{py})(PPh_3)_2]$

Because the Q ligands of derivatives **4**–**6** contain additional heterocyclic groups with different donor atoms, we planned to investigate their potential as multidentate donors by exploring their reactivity toward Lewis acids. Attempted reactions between derivatives **4** or **5** with a Lewis acid such as $Zn(BF_4)_2 \cdot xH_2O$ in acetonitrile were always unsuccessful, whereas with derivative **6** the same reaction takes place, affording the ionic adduct **7** in high yield (Scheme 2), the difference in behaviour being clearly due to the position of the additional heteroaromatic rings, in the acyl fragment for furyl and thienyl in derivatives **4** and **5**, and at N1 of the pyrazole for 2-pyridyl in derivative **6**, where the N_2-chelating face is involved in the coordination of the $\{Cu(PPh_3)_2\}$ fragment, leaving both the carbonyl arms un-coordinated and able to give additional interactions with new metal acceptors.

Adduct **7** is a yellow solid with a sharp melting point. The conductivity value of 288 Ω^{-1} cm^2 mol^{-1} in acetonitrile is typical of 2:1 ionic species [18]. Moreover the strong band at 1057 cm^{-1} and a sharp one at 966 cm^{-1} in the IR spectrum of **7**, due to ν_4 and ν_3 of BF_4, shows no splitting or fine structure of the degenerate asymmetric vibrations, consistent with an ionic BF_4 [19]. The most significant spectral feature in the IR of adduct **7** is related to the red shift of ν(C=O) with respect to that found in derivative **6**, in accordance with the coordination of $Q^{CF3,py}$ to the zinc through both carbonyl arms. Finally, the resonances in the proton and carbon NMR spectra of **7** show downfield shifts due to the electron density flow toward the zinc centre.

We decided to investigate also the reactivity of derivative **6** toward an organometallic Lewis acid such as $[Ru(p\text{-cymene})Cl_2]_2$. The reaction between **6** and $[Ru(p\text{-cymene})Cl_2]_2$ was performed in acetonitrile and, after 24 h refluxing, $AgPF_6$ was added to effect the chloride exchange, the ionic adduct **8** resulting (Scheme 3).

It is a brown solid with a sharp melting point. The conductivity value of 136 Ω^{-1} cm^2 mol^{-1} in acetonitrile is typical of 1:1 ionic species [18]. In the IR spectrum of **8** the strong bands at 840 and 695 cm^{-1} are typical of ν_{as} and ν_s of PF_6, typical of ionic PF_6 [20]. ν(C=O)

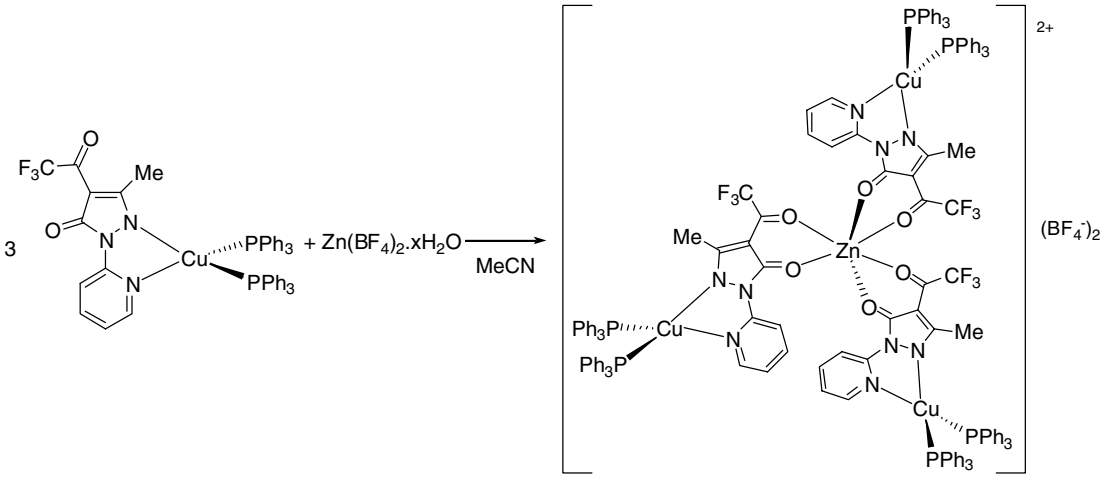

7

Scheme 2.

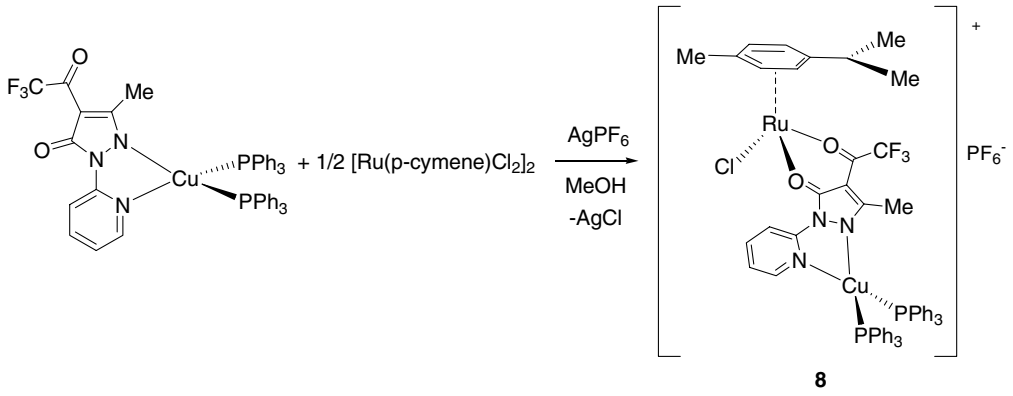

Scheme 3.

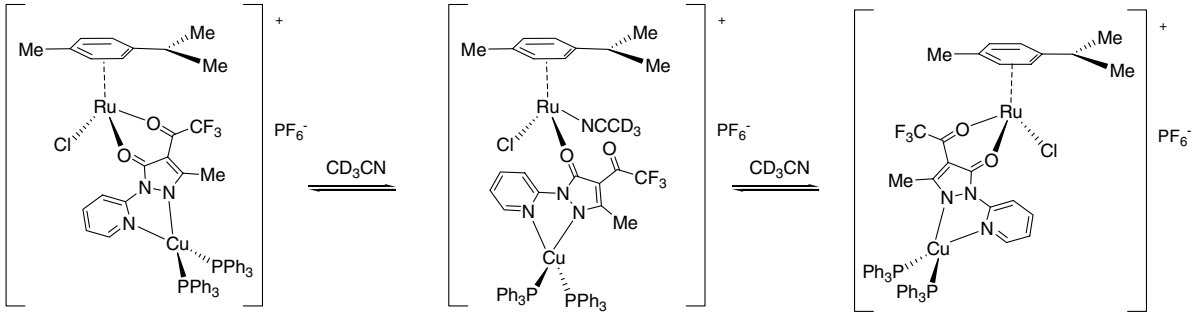

Fig. 5. Species in equilibrium with each other (hypothesized from NMR spectra of CD_3CN solution of derivative **8**).

is shifted to lower frequency with respect to that found in the IR of derivative **6**, in accordance with the coordination of $Q^{CF3,py}$ to the ruthenium through both carbonyl arms. In the far-IR region the bands due to PPh_3 [14] and to *ν*(Ru-Cl) have been detected [21]. The proton and carbon NMR spectra of **8** show three set of resonances for both the {Ru(*p*-cymene)} and $\{(Q^{CF3,py})Cu(PPh_3)_2\}$ fragments. This feature could be explained by the presence of three different species in equilibrium with each other, as suggested in Fig. 5.

The presence of two resonances in the ^{19}F NMR spectrum at −73 and −76 ppm, the former due to $CF_3C{=}O$ of a $Q^{CF3,py}$ coordinated through C=O and the second coincident with that found in the ^{19}F NMR spectrum of derivative **6**, further supports our previous hypothesis.

4. Supplementary material

X-ray crystallographic files, in *.cif* format, for the structure determinations of derivatives **1**, **4**, **5** and **6** have been deposited with the Cambridge Crystallographic Data Centre, CCDC 268466–268468, 269315. Copies of this information may be obtained free of charge from: The Director, CCDC, 12 Union Road, Cambridge, CB2 1EZ, UK (fax: +44-1223-336-033; e-mail: deposit@ccdc.cam.ac.uk or www: http://www.ccdc.cam. ac.uk).

Acknowledgement

Thanks are due to the University of Camerino (Italy) and Carima Foundation for financial support.

References

[1] F. Marchetti, C. Pettinari, R. Pettinari, Coord. Chem. Rev. (in press).
[2] See for example: Y.A. Zolotov, N.M. Kuzmin, Extraction of Metals by Acylpyrazolones, Nauka, Moscow, Russia, 1977.
[3] S. Nishihama, T. Hirai, I. Komasawa, Ind. Eng. Chem. Res. 40 (2001) 3085.
[4] See for example: C. Pettinari, F. Marchetti, A. Cingolani, D. Leonesi, E. Mundorff, M. Rossi, F. Caruso, J. Organomet. Chem. 557 (1998) 187.
[5] E.C. Okafor, A.B. Uzoukwu, P.B. Hitchcock, J.D. Smith, Inorg. Chim. Acta 172 (1990) 97.
[6] (a) A. Cingolani, Effendy, F. Marchetti, C. Pettinari, R. Pettinari, B.W. Skelton, A.H. White, Inorg. Chem. 41 (2002) 1151;
(b) A. Cingolani, Effendy, F. Marchetti, C. Pettinari, R. Pettinari, B.W. Skelton, A.H. White, Inorg. Chim. Acta 329 (2002) 100;
(c) B.A. Uzoukwu, P.U. Adiukwu, S.S. Al-Juaid, P.B. Hitchcock, J.D. Smith, Inorg. Chim. Acta 250 (1996) 173;
(d) A. Jain, S. Saxena, A.K. Rai, R. Bohra, H. Wang, Main Group Met. Chem. 26 (2003) 1;
(e) A. Cingolani, F. Marchetti, C. Pettinari, R. Pettinari, B.W. Skelton, A.H. White, Inorg. Chem. Commun. 7 (2004) 235.
[7] (a) F. Marchetti, C. Pettinari, A. Cingolani, D. Leonesi, A. Drozdov, S. Troyanov, J. Chem. Soc., Dalton Trans. (1998) 3325;

(b) A. Drozdov, V. Vertlib, I. Timokhin, S. Troyanov, C. Pettinari, F. Marchetti, Russ. J. Coord. Chem. 28 (2002) 259;
(c) F. Marchetti, C. Pettinari, A. Cingolani, D. Leonesi, M. Camalli, A. Pifferi, Polyhedron 15 (1996) 3835;
(d) F. Marchetti, C. Pettinari, R. Pettinari, A. Cingolani, M. Camalli, R. Spagna, Inorg. Chim. Acta 299 (2000) 65.

[8] (a) A. Drozdov, S. Troyanov, O. Fedorchenko, G. Battiston, C. Pettinari, F. Marchetti, A. Cingolani, J. Phys. IV 9 (1999) 929;
(b) C. Pettinari, F. Marchetti, C. Santini, R. Pettinari, A. Drozdov, S. Troyanov, G. Battiston, R. Gerbasi, Inorg. Chim. Acta 315 (2001) 88.

[9] A. Lorenzotti, F. Marchetti, C. Pettinari, R. Pettinari, B.W. Skelton, A.H. White, Inorg. Chim. Acta 358 (2005) 3190.

[10] A. Cingolani, Effendy, F. Marchetti, C. Pettinari, R. Pettinari, B.W. Skelton, A.H. White, Inorg. Chem. 43 (2004) 4387.

[11] (a) F. Caruso, M. Rossi, F. Marchetti, C. Pettinari, Organometallics 18 (1999) 2398;
(b) C. Pettinari, F. Marchetti, A. Cingolani, A. Gindulyte, L. Massa, M. Rossi, F. Caruso, Eur. J. Inorg. Chem. (2001) 2171.

[12] T. Ozaki, S. Miyazaki, S. Umetani, S. Kihara, M. Matsui, Anal. Chim. Acta 226 (1989) 187.

[13] (a) B. Chantegrel, A.I. Nadi, S. Gelin, Heterocycles 20 (1983) 1801;
(b) C. Pettinari, F. Marchetti, R. Pettinari, A. Pizzabiocca, A. Drozdov, S. Troyanov, V. Vertlib, J. Organomet. Chem. 688 (2003) 216.

[14] S.R. Hall, G.S.D. King, J.M. Stewart (Eds.), The XTAL-3.4. User's Manual, University of Western Australia, Perth, 1995.

[15] (a) K. Shobatake, C. Postmus, J.R. Ferraro, K. Nakamoto, Appl. Spectrosc. 23 (1969) 12;
(b) J. Bradbury, K.P. Forest, R.H. Nuttall, S.W.A. Sharp, Spectrochim. Acta 23 (1967) 2701.

[16] (a) K. Nakamoto, A.E. Martell, J. Chem. Phys. 32 (1960) 588;
(b) M. Mikami, I. Makagawa, T. Shimanouchi, Spectrochim. Acta 23A (1967) 1037;
(c) K. Nakamoto, C. Udovich, J. Takemoto, J. Am. Chem. Soc. 73 (1970) 3973.

[17] (a) R.E. Wilde, T.K.K. Srinivasan, J. Inorg. Nucl. Chem. 36 (1974) 323;
(b) Y. Saito, J. Takemoto, B. Hutchinson, K. Nakamoto, Inorg. Chem. 11 (1972) 2003.

[18] W.J. Geary, Coord. Chem. Rev. 7 (1971) 81.

[19] (a) J. Reedijk, J.C. Jansen, H. van Koningsveld, C.G. van Kralingen, Inorg. Chem. 17 (1978) 1990;
(b) R. Bozio, C. Pecile, J.C. Scott, E.M. Engler, Mol. Cryst. Liquid Cryst. 119 (1985) 211;
(c) M.J. Bew, B.J. Hathaway, R.J. Fereday, J. Chem. Soc., Dalton Trans. (1972) 1229;
(d) G. Marcotrigiano, R. Battistuzzi, G. Peyronel, Inorg. Nucl. Chem. Lett. 8 (1972) 399;
(e) J. Reedijk, Rec. Trav. Chim. Pays-Bas 89 (1970) 605.

[20] (a) E.R. Talaty, S. Raja, V.J. Storhaug, A. Dölle, W.R. Carper, J. Phys. Chem. B 108 (2004) 13177;
(b) J.E. Eldridge, C.C. Homes, F.E. Bates, G.S. Bates, Phys. Rev. B 32 (1985) 5156;
(c) R.M. Morrison, R.C. Thompson, Can. J. Chem. 56 (1978) 985.

[21] K. Nakamoto, Infrared and Raman Spectra of Inorganic and Coordination Compounds, 5th ed., Wiley, New York, 1997, Part B: p. 183.

Available online at www.sciencedirect.com
SCIENCE DIRECT®
Polyhedron 25 (2006) 134–194
POLYHEDRON
www.elsevier.com/locate/poly

The coordination chemistry of pyridyl oximes

Constantinos J. Milios, Theocharis C. Stamatatos, Spyros P. Perlepes *

Department of Chemistry, University of Patras, GR-265 04 Patras, Greece

Received 14 July 2005
Available online 24 August 2005

Abstract

The coordination chemistry of pyridyl oximes is reviewed. Simple pyridyl oximes have the general formula (py)C(R)NOH, where py is a pyridyl group (2-, 3- or 4-) attached to the oxime carbon atom and R can be a donor or a non-donor group. There are also ligands containing more pyridyl and/or oxime groups. The coordination chemistry of twenty-three such ligands is described, including 2-acetylpyridine *N*-oxide oxime (which strictly speaking is not a pyridyl oxime) and of four polydentate ligands containing pyridyl groups that are not directly attached to the oxime carbon. References are given to methods for the synthesis of the ligands that are not available in the market. The coordination chemistry of each ligand with all metals is detailed, with emphasis being placed on structural features and physical properties (mainly magnetic) of the resulting metal complexes. This report shows that the anions of pyridyl oximes are versatile ligands for a variety of objectives/advantages, including μ_2 and μ_3 behavior, preparation of polynuclear complexes (clusters) and coordination polymers, mixed-metal chemistry and interesting magnetic characteristics. The activation of 2-pyridyl oximes by 3d-metal centers towards further reactions seems to be an emergent area of synthetic chemistry.
© 2005 Elsevier Ltd. All rights reserved.

Keywords: Clusters; Coordination chemistry; Coordination polymers; Molecular magnetism; Oximate group; Oxime group; Pyridyl oximes

1. Introduction and information for the organization of this report

Simple pyridyl oximes have the general structures depicted in Fig. 1 and consist of a pyridyl group (2-, 3- or 4-) attached to the oxime carbon atom. R can be a donor or a non-donor group. There are also pyridyl oximes containing more pyridyl and/or oxime groups.

The anionic forms of these molecules are versatile ligands for a variety of objectives, including μ_2 and μ_3 behavior, formation of polynuclear complexes (clusters), isolation of coordination polymers, mixed-metal chemistry and significant magnetic characteristics. The activation of 2-pyridyl oximes by 3d-metal centers towards further reactions is also becoming a fruitful area of research. The majority of the metal complexes of these ligands have been prepared only in the last 15 years and much of their chemistry remains to be explored in more detail.

This report presents a review of the chemistry of pyridyl oxime ligands. It aims not to be comprehensive in terms of a discussion of every known complex containing a pyridyl oxime ligand (such a task would create a monograph for the complexes of di-2-pyridyl ketone oxime alone!); rather, it aims to provide the reader some idea of the range of chemistry that has been carried out (and indeed remains still to do) with these ligands. This review will also deal with the coordination chemistry of 2-acetylpyridine *N*-oxide oxime (which is not a pyridyl oxime) and of some polydentate oxime ligands containing pyridyl groups that are not directly attached to the oxime carbon (Sections 5.6 and 7.3, respectively).

The report contains 10 sections. The first four are introductory. Section 2 briefly describes the already published reviews on metal oxime and oximato complexes. In Sections 3 and 4, the reader can find information on the organic, supramolecular and coordination chem-

* Corresponding author. Tel.: +30 2610 997146; fax: +30 2610 997118.
E-mail address: perlepes@patreas.upatras.gr (S.P. Perlepes).

0277-5387/$ - see front matter © 2005 Elsevier Ltd. All rights reserved.
doi:10.1016/j.poly.2005.07.022

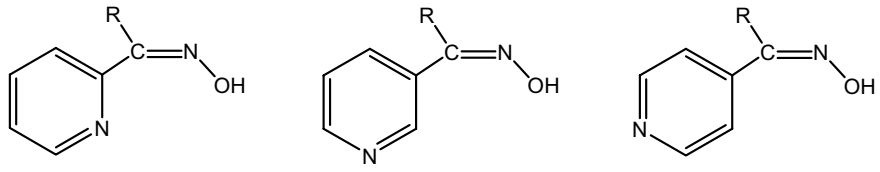

Fig. 1. General structures of simple pyridyl oximes.

istry of the simple oxime group. Sections 5–9 describe the chemistry of metal complexes that have neutral and anionic pyridyl oximes as ligands. The ligands' classification is based both on the nature of R and the number of pyridyl or oxime groups per molecule. Section 10 gives some conclusions and areas for further investigation. Most sections are divided into parts. Each part, devoted to the coordination chemistry of a particular pyridyl oxime, gives its structural formula, systematic name and abbreviation, details the synthesis of the free ligand, and discusses some of its important metal complexes, with particular emphasis being placed on structural aspects of these.

As in the case of many organic ligands, most pyridyl oxime ligands are known by an abbreviation, usually of three or four letters, nominally derived from the full name of the ligand. For example, the systematically named ligand pyridine-2-carbaldehyde oxime (Fig. 1, R = H; Section 5.2) is better known as paOH, the abbreviation being derived from the non-systematic names pyridine-2-aldoxime or 2-pyridinaldoxime; other abbreviations used for this ligand are HPOX and PyAH. The abbreviations of other pyridyl oximes are somewhat haphazard and confusing. Obviously, this is an unsatisfactory situation and ideally a systematic abbreviation system should be developed. In what follows, we adopt a common abbreviation system based on the use of the constituent py for a 2-pyridyl group, 3-py for a 3-pyridyl and 4-py for a 4-pyridyl group; the oxime group(s) and the nature of R (Fig. 1) will complete the abbreviation. For example, the abbreviation of pyridine-2-carbaldehyde oxime (Fig. 1, R = H; Section 5.2) will be (py)CHNOH, while the anionic ligand will be abbreviated as (py)CHNO. The abbreviation of 1-pyridine-2-yl-ethanone oxime (Fig. 1, $R = CH_3$; Section 5.4) will be (py)C(Me)NOH, etc. We hope that this abbreviation system is more convenient for the reader than abbreviations with letters derived from the name of the ligand.

2. Background

A review article on the coordination chemistry of pyridyl oximes has never appeared. However, metal complexes of pyridyl oximes have been incorporated into more general reviews on the chemistry of metal oxime/oximate complexes. This chemistry has been actively investigated since 1890, when Tschugaeff [1] first introduced dimethylglyoxime as a reagent for the gravimetric determination of Ni(II). Oximes as ligands have played a significant role in the development of transition metal chemistry. This development has been documented in a number of review articles and we refer the readers to some of these excellent treatises [2–9]. An early treatise by Chakravorty [2] is a comprehensive review on the structural chemistry of simple oximes, *vic*-dioximes, quinonemonoximes, and carbonyl-, imine-, pyridine-, azo-, hydroxy- and amidoximes. A review by Bertrand and Eller [3] covers oxime-bridged complexes of transition metals, while a concise review by Mehrotra [4] deals with the syntheses, structures and reactivity of complexes containing "simple" and *vic*-dioximes. In more recent years five excellent reviews have been published [5–9]. The survey by Tasker and co-workers [5] describes the rich coordination chemistry of phenolic oxime ligands. The strategy of using "metal oximate" building blocks as ligands to synthesize various homo- and heterometallic paramagnetic complexes has been reviewed by Chaudhuri [6]. This review is an important contribution to the field of Molecular Magnetism; the oximato groups ($>C{=}N{-}O^-$) can mediate exchange interactions of varying range, from moderate ferromagnetic to strong antiferromagnetic. Metal-ion mediated reactions of oximes, and reactivity of oxime-containing and oximate metal complexes have been described and classified by Kukushkin and Pombeiro [7–9]; the three reviews illustrate the fact that the chemistry of oxime/oximato metal complexes is rich since these species display an amazing variety of reactivity modes.

3. Brief information on the organic and supramolecular chemistry of the oxime group

3.1. Isomerism

The oxime group ($>C{=}N{-}OH$) is a well-explored group in organic chemistry. The type of isomerism about a C=C double bond [10] is also possible with the C=N bond, though in this case only three groups are connected to the double-bond atoms. The method, which can be applied, is based on the Cahn–Ingold–Prelog system [10]. The two groups at the carbon atom are ranked by the sequence rules. Then that isomer with the

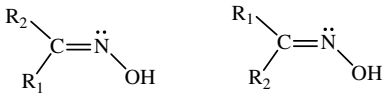

Z or *syn* *E* or *anti*

Fig. 2. The *Z*–*E* isomerism of the oxime group assuming that R_1 takes precedence over R_2 according to the Cahn–Ingold–Prelog system.

higher ranking group and the –OH group on the same side of the double bond is called *Z* (for the German word *zusammen* meaning *together*); the other is called *E* (for *entgegen* meaning *opposite*). In the case of oximes, the *Z* isomer may be called *syn* and the *E* isomer *anti* [11]. The isomerism of the oxime group is illustrated in Fig. 2 for the case in which the substituent R_1 is a higher ranking group than R_2. If there is more than one oxime group in a molecule, the number of isomers can be increased, e.g., *Z*, *Z*, *Z*, *E* and *E*, *E*.

3.2. Formation of the oxime group

Some synthetic schemes that lead to the oxime group may be useful for coordination chemists. These are briefly mentioned below [10].

3.2.1. Nitrosation at a carbon bearing an active hydrogen

Carbon atoms adjacent to a Z group (Z may be CO-OR′, CHO, COR′, $CONR'_2$, COO^-, CN, NO_2, SOR′, SO_2R', SO_2OR', $SO_2NR'_2$ or similar groups) can be nitrosated with nitrous acid or alkyl nitrates. The initial product is the C-nitroso compound, but these are stable only when there is no tautomerizable hydrogen. When there is, the product is the most stable oxime (Eq. (1)).

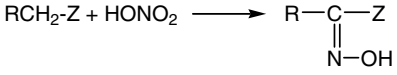

(1)

3.2.2. Addition of NOCl to olefins

The initial product is always the β-halo nitroso compound, but these are stable only if the carbon bearing the nitrogen has no hydrogen (Eq. (2a)). If it has, the nitroso compound tautomerizes to the oxime (Eq. (2b)).

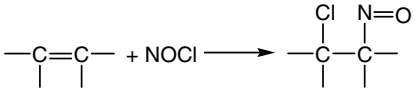

(2a)

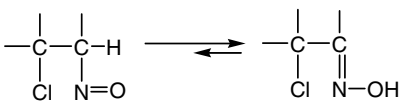

(2b)

3.2.3. Addition of hydroxylamine to aldehydes or ketones

This is the commonly used method for the synthesis of new oxime ligands by coordination chemists (Eq. 3). It has been shown that the rate of formation of oximes is maximum at a pH which depends on the substrate but is usually 4, and that the rate decreases as the pH is either raised or lowered from this point.

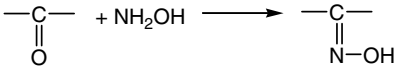

(3)

3.2.4. Addition of Grignard reagents to the conjugate bases of nitro compounds

The conjugate bases of nitro compounds (formed by treatment of the nitro compound with BuLi) react with Grignard reagents in the presence of $ClCH{=}NMe_2^+Cl^-$ to give oximes (Eq. (4)).

$$RCH{=}N(O)OLi + R'MgX \rightarrow RR'C{=}NOH \quad (4)$$

3.2.5. Oxidation of primary aliphatic amines

Primary aliphatic amines can be oxidized to nitroso compounds by Caro's acid (H_2SO_5) or with H_2O_2 in $MeCO_2H$. Hydroxylamines, which are probably intermediates in most cases, can sometimes be isolated, but under the reaction conditions are generally oxidized to the nitroso compounds. The nitroso compound is stable only if there is no α hydrogen; if there is an α hydrogen, the compound tautomerizes to the oxime.

3.2.6. Reduction of aliphatic nitro compounds

Nitro compounds that contain an α hydrogen can be reduced to oximes with Zn dust in acetic acid (Eq. (5)) or with other reagents, among them Co–Cu(II) salts in alkanediamines, CS_2–Et_3N and $CrCl_2$.

$$RCH_2NO_2 \xrightarrow[HOAc]{Zn} RCH{=}N\text{–}OH \quad (5)$$

3.3. The oxime group in supramolecular chemistry

In supramolecular chemistry a major goal is to control the aggregation of molecules via intermolecular interactions [12,13]. This is most readily achieved when such interactions are strong and directional. For this reason hydrogen bonds are often employed. More specifically, molecular building blocks can be designed to carry particular functional groups that are capable of recognition of other groups or self-recognition through the formation of one or more hydrogen bonds. By such a synthetic approach even quite complex molecular aggregates (supermolecules) can be prepared in a designed manner [14–16]. Where infinite assemblies are formed, the opportunity arises to construct crystalline solids in which 1D, 2D or 3D networks are propagated by hydrogen bonds [17,18].

Despite earlier studies establishing its capability to form hydrogen bonds [19–21], the oxime group has received far less attention in supramolecular chemistry and crystal engineering [22] than have other groups as carboxyl [23], amide [24] and alcohol [25]. Oximes are

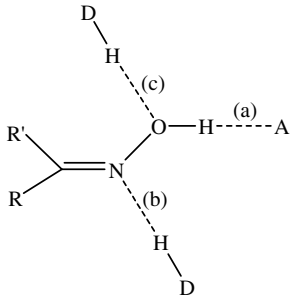

Fig. 3. Formation of hydrogen bonds by oxime groups [22]. A, hydrogen bond acceptor; D, hydrogen bond donor.

able to form three types of hydrogen bond (Fig. 3). Formation of only an O–H···A hydrogen bond is typical of the situation in which another strong hydrogen bond acceptor group is present, as is illustrated by the structures of pyridyl oximes [26]. The situation in which both O–H···A and D–H···N hydrogen bonds form is typified by the absence of other hydrogen bonding functional groups, or at least ones strong enough to compete with the oxime. Thus, O–H···N hydrogen bonds form between oxime groups, most often as either an $R_2^2(6)$ [27] dimeric arrangement (**I**) or a C(3) catemer (**II**) [22], resembling the $R_2^2(8)$ (**III**) and C(4) arrangements (**IV**,**V**) that are well established [13] for carboxyl groups (Fig. 4).

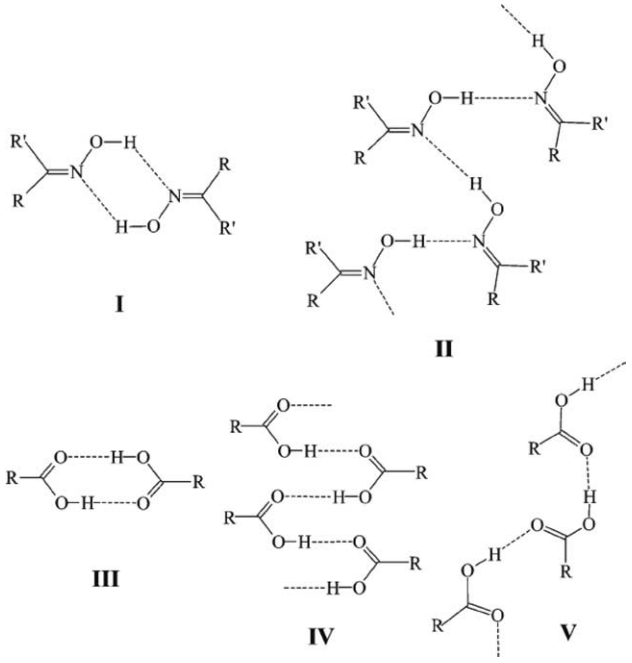

Fig. 4. Common hydrogen bonding arrangements [22] for oxime (**I**, **II**) and carboxyl (**III**–**V**) groups.

Less common, crystallographically established hydrogen bond patterns in oximes are presented in Fig. 5. One potential advantage [22] to the use of oximes is the possibility of greater tunability by facile variation of the substituent R′ (Fig. 3), which is not present in carboxylic acids or primary amides. Careful choice of this substituent also permits the solubility of the oxime ligand to be modified, facilitating supramolecular synthesis in a wider range of solvent systems.

4. The importance of oxime and oximate groups in coordination chemistry

4.1. General information

There is currently a renewed interest in the coordination chemistry of oximes [6,9]. The research efforts are driven by a number of considerations. These include the solution of pure chemical problems [28–34], the desire to provide useful bioinorganic models (oximes may be considered to be reasonable models for the biologically significant imidazole donor group of the amino acid histidine) [35], the design of Ca^{2+}- and Ba^{2+}-selective receptors based on site-selective transmetalation of multinuclear polyoxime–zinc(II) complexes [36], the development of new oxygen activation catalysis based on nickel(II)–polyoximate complexes [37], the application of metal ion/oxime systems as simple and efficient catalysts for the hydrolysis

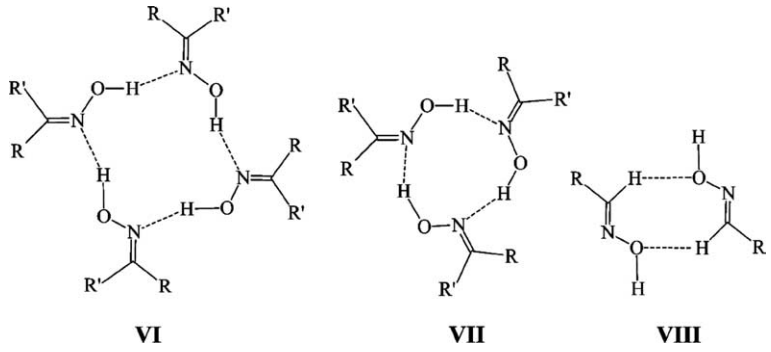

Fig. 5. Less common hydrogen bonding arrangements [22] for oxime groups: $R_4^4(12)$ oxime tetramer (**VI**), related $R_3^3(9)$ oxime trimer (**VII**) and aldoxime $R_2^2(8)$ C–H···O dimer (**VIII**).

of organonitriles [38] (metal ions can behave as extremely strong activators of RCN toward nucleophilic attack by OH^-/H_2O), the mechanistic study of corrosion inhibition by Acorga P5000 (a modern corrosion inhibitor comprising 5-nonylsalicylaldoxime as a mixture of carbon-chain isomers) on iron surfaces [39] and the employment of oximate ligands in the synthesis of homometallic [6,32,40,42] and heterometallic [6,29,41] clusters [6,29,32,40–42] and coordination polymers [43] with interesting magnetic properties including single-molecule magnetism [42] and single-chain magnetism [43] behaviors.

For example, the pure chemical interest in the coordination chemistry of oximes arises from the ability of the oximate(−1) group to stabilize higher oxidation states of metals, e.g., Ni(III) or Ni(IV) [33,34] and the fact that the activation of oximes by transition metal centers towards further reactions seems to be an emergent area of modern synthetic chemistry (Section 4.3). Another example of the importance of metal oximate complexes are the excellent studies on surface coordination chemistry by Collison, Garner, Tasker and co-workers; they have postulated (based on synthetic models) that the corrosion inhibition by P5000 on an iron surface is due to the generation of a tetranuclear iron(III) cluster complex [39]. Iron ions must be available for the formation of such species, and the efficiency of the inhibitor is therefore enhanced by treatment of an oxidized iron surface with a mild acid. The polyfunctional P5000 oxime ligand tends to produce compact polymetallic assemblies, and when formed at the surface of a metal, such species can form a protective barrier which inhibits further corrosion [39].

4.2. Coordination modes of oxime and oximato groups

Oxime and oximato groups can bind a metal ion in different modes [9]; these coordination modes are shown in Fig. 6. The numbers below each bonding mode refer to the Harris notation [44]. Harris notation describes the binding mode as $X{\cdot}Y_1Y_2Y_3{\cdots}Y_n$, where X is the overall number of metals bound by the whole ligand, and each value of Y refers to the number of metal atoms (ions) attached to the different donor atoms. The ordering of Y is listed by Cahn–Ingold–Prelog priority rules, hence (for most of the ligands included in this report) O before N. In the case of chelating/bridging ligands, to distinguish between several alternatives, a subscript number is included to show to which metal ion the donor is attached. In the following, the binding mode of the ligands will be often described using Harris notation. Since the reader will always have recourse to diagrams, we shall avoid using subscript numbers. Occasionally we shall use the currently approved notation based on Greek letters μ and η. We do believe that Harris notation

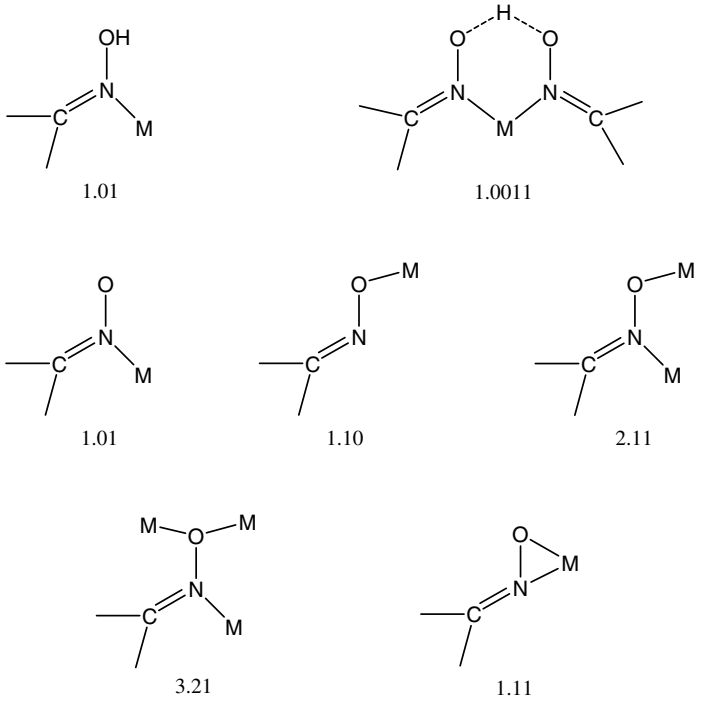

Fig. 6. The crystallographically established coordination modes of oxime and oximato groups, and the Harris notation [44] that describes these modes. Note that the upper right mode combines one formally neutral oxime group and one formally anionic oximato group.

is, at least for pyridyl oximes, more convenient than the notation based on Greek letters.

4.3. Reactivity of coordinated oximes

4.3.1. A brief introduction

As said in Section 2, oxime and oximato metal species exhibit versatile reactivity. Their reactions can be classified according to the extent of involvement of the {C=NO} moiety and to the bond at which the reaction is centered (see below). The reviews by Pombeiro and Kukushkin [7–9] are excellent sources on this topic.

The general modes of reactivity concerning nucleophilic or electrophilic additions to the polarized C=N bond are illustrated in Scheme 1. Nucleophilic reagents can add to the carbon atom of the azomethine linkage (a reaction that is promoted by coordination of the oxime, in particular via the N-atom), whereas electrophilic reagents can attack the O- or the N-sites.

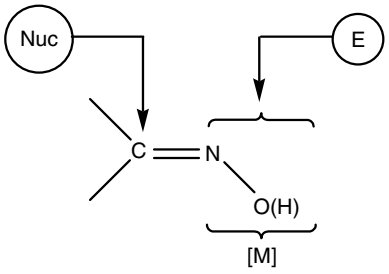

Scheme 1. General reactivity modes of the coordinated oxime group [9]. Nuc = nucleophile; E = electrophile.

4.3.2. Reactions with preservation of the {CNO} fragment [9]

The reactions can either be centered at any of the atoms of the {CNO} moiety, leading to oxime (or oximato), imine or other types of complexes, or occur at another part of the oxime molecule.

On account of the nucleophilic character of the oxime O-atom, the oximes can add, via this atom, to unsaturated species such as organonitriles, anhydrides, ketones, isocyanates, aldehydes, olefins and the olefinic group of an α,β-unsaturated oxime. Few examples of oxime coupling via the N-atom acting as the nucleophile, are known. These include reactions of oximes with allene-Pt^{II} complexes to produce metallacycles and reactions of Cu(II) or Ni(II) complexes of *o*-quinone monoxime with electrophilic acetylenes to give N-containing heterocycles. The electrophilicity of the C-atom of the NCO group of an oxime is expected to be promoted by oxidation and formal two-electron oxidations promote not only H^+ loss from the NOH group, but also addition of a nucleophile to that C-atom to yield nitrosoalkyl species.

4.3.3. Reactions with rupture of the {CNO} fragment

Several N–O bond rupture reactions are known (Fig. 7); these reactions usually involve the formation

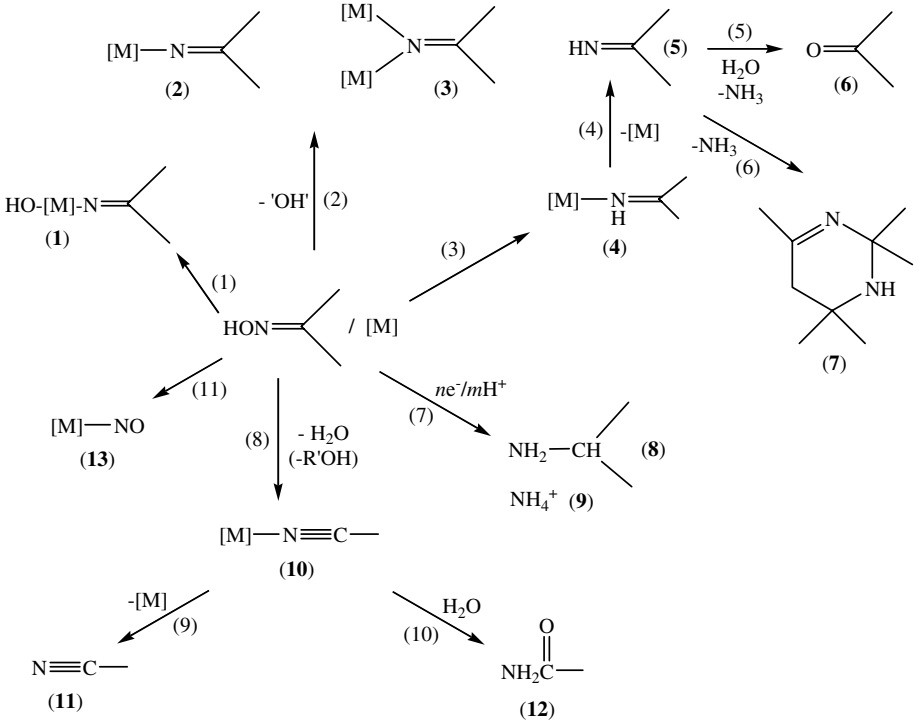

Fig. 7. Reactions of coordinated oximes that lead to N–O and N=C bond cleavage [9].

of an N–metal bond. The reactions include [9] oxidative addition of oximes to an electron-rich metal center (Reaction (1)), dehydroxygenation of oximes by a hydride metal center (Reaction (2)), deoxygenation of oximes (Reactions (3)–(7)), dehydration or alcohol elimination (Reactions (8) and (9)) and the Beckmann rearrangement of aldoximes into amides (Reactions (8) and (10)). Reactions with complete N=C bond cleavage are also known [9], for example, Reactions (3)–(5), (7) and (11) in Fig. 7.

5. Ligands containing one oxime group, one pyridyl group and no other donor atoms

5.1. Coordination modes

Ligands containing one oxime group, one pyridyl group and no other donor atoms are popular. Most of these ligands contain a 2-pyridyl group. The crystallographically established coordination modes of these 2-pyridyl oximes are shown in Fig. 8. Their anions can bridge two or three metal ions.

5.2. Pyridine-2-carbaldehyde oxime, (py)CHNOH

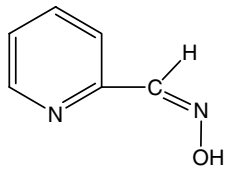

(py)CHNOH

The free ligand is commercially available. Its crystal structure has been determined [45]. There are two unique molecules in the asymmetric unit; the molecules related by a 2_1 screw axis, form infinite 1D chains held together by hydrogen bonds. The predominant hydrogen bond

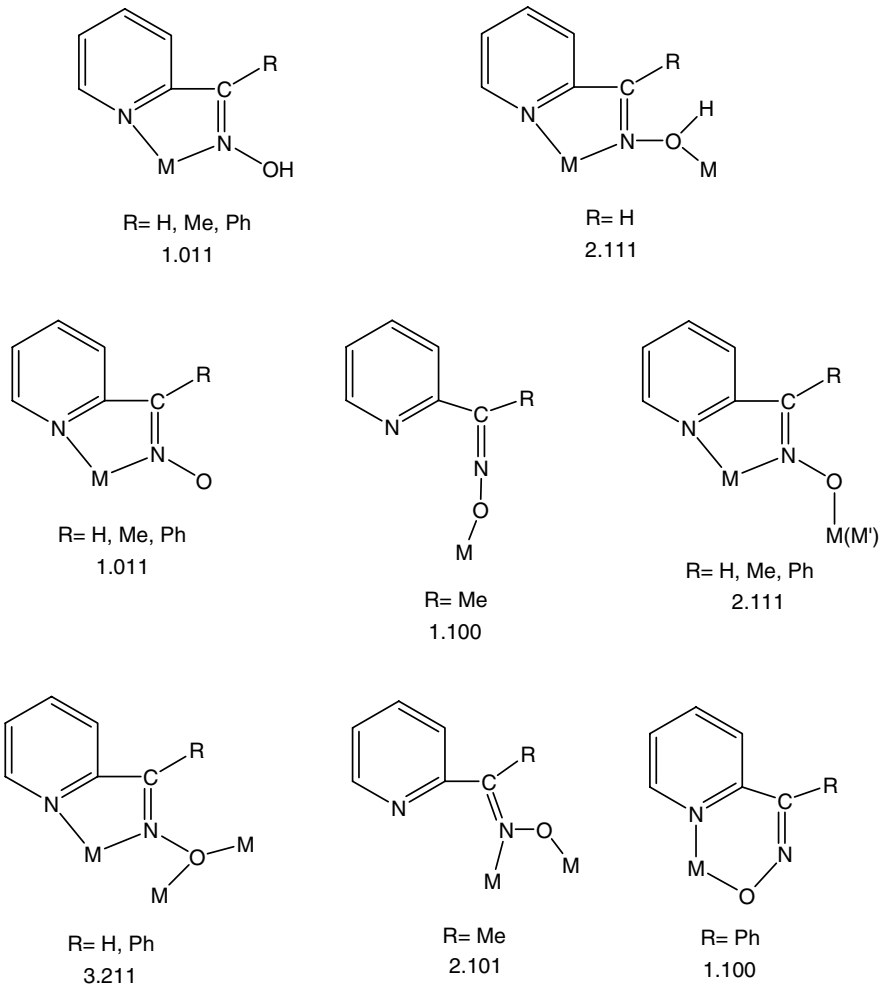

Fig. 8. The crystallographically established coordination modes of the neutral and anionic forms of simple 2-pyridyl oximes, and the Harris notation [44] that describes these modes.

interaction assembling the chains is a head-to-tail O–H···N hydrogen bond involving the oxime O–H and the 2-pyridyl nitrogen atom. There is also a C–H···N hydrogen bond involving the oxime C–H and the oxime nitrogen atom (C···N 3.274, 3.283 Å). The chains are arranged in an *anti*-parallel fashion and pack in a typical herringbone motif.

Potentiometric titrations at 25 °C in aqueous 0.1 M NaCl solution have provided the values of the logarithm of the protonation constant, $\log\beta$, of the 2-pyridyl nitrogen and the acid dissociation constant, pK_a, of the oxime group [46]; these values are 3.59 and 10.01, respectively.

The first studies on the coordination chemistry of (py)CHNOH were reported in the late 50s and early 60s [47–54]. No single-crystal X-ray structures were available at that time. Investigations based on physical and spectroscopic data showed [49,51,53] that square planar cationic complexes of divalent transition metals were capable of intramolecular hydrogen bonding in the type of structure shown in Fig. 9. However, this structural type has never been proven by crystallography. The groups of Busch [48] and Liu [50,54] were the first to suggest that the deprotonated oxygen atom of coordinated (py)CHNO$^-$ can act as donor giving homo- and heteropolynuclear complexes.

The first structurally characterized metal complex of pyridine-2-carbaldehyde oxime was $[Cu_3(OH)(SO_4)\{(py)CHNO\}_3]$ [55]. The Cu^{II} atoms fall at the corners of an exact equilateral triangle of side 3.22 Å due to the presence of a threefold crystallographic axis. The metal ions are held together by three distinct bridging systems: (i) the μ_3-hydroxo group, (ii) the sulfato group, lying on the threefold axis but below the plane containing the metal ions, and acting as a tripod bridge bonding to all three Cu^{II} atoms through three of its oxygen atoms ($\eta^1{:}\eta^1{:}\eta^1{:}\mu_3$), and (iii) the three symmetry-related (py)CHNO$^-$ ligands each of which functions as a bidentate chelate to one of the Cu^{II} atoms, through its two nitrogen atoms, and as a $Cu^{II}\cdots Cu^{II}$ bridging group through the nitrogen and oxygen atoms of the oximato moiety (Fig. 10). Thus, the (py)CHNO$^-$ ligands adopt

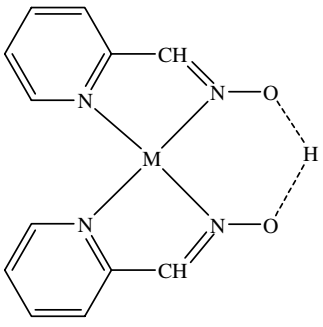

Fig. 9. The square planar structural type proposed [49,51,53] for the complex cations $[M\{(py)CHNO\}\{(py)CHNOH\}]^+$ (M = Ni, Cu, Pd).

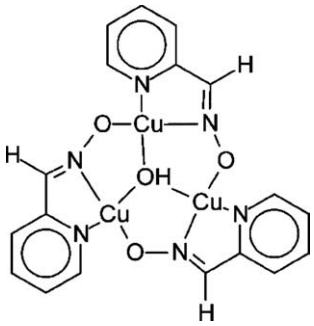

Fig. 10. A drawing of the trinuclear molecule $[Cu_3(OH)(SO_4)\{(py)CHNO\}_3]$ down its threefold axis; the SO_4^{2-} group has been omitted for clarity [6].

the coordination mode 2.111, see Fig. 8. Two of the three electrons of the Cu_3^{II} core are completely paired and only the doublet spin state ($S_T = 1/2$) is populated at room temperature ($\mu_{eff} = 1.0$ BM per Cu^{II} in the 80–300 K range) [6], which is evidence for strong antiferromagnetic coupling.

Addition of I^- to a solution of Cu^{2+} normally leads to reduction to CuI, but in the presence of nitrogen donors reduction is inhibited. Chaudhuri and co-workers [56] have synthesized the complex $[LCu^{II}\{(py)CHNO\}_2Cu^{II}I](ClO_4)$ [56], where L is the capping tridentate ligand 1,4,7-trimethyl-1,4,7-triazacyclononane. The molecular structure consists of dinuclear cations (Fig. 11). The Cu^{II} atoms are bridged by 2.111 oximato ligands. Both metal ions have a distorted square pyramidal (spy) geometry with a $Cu^{II}\cdots Cu^{II}$ separation of 3.45 Å; the Cu^{II}–I bond length is 2.74 Å. The chloro and acetato analogues of the iodo complex have also been prepared and structurally characterized [6]. The chloro complex has a very similar structure to that of the iodo compound. On the other hand, the acetate ion bridges the copper centers and, thus, one metal ion is five-coordinate and the other is six-coordinate. The magnitude of the exchange parameter J ($2J$ being the singlet-triplet splitting) depends on the nature of the axial ligand: $MeCO_2^-$ ($J = -358$ cm^{-1}), Cl^- ($J = -390$ cm^{-1}) and I^- ($J = -460$ cm^{-1}). Interestingly, the strength of the spin interaction is not related to the N–O and C=N bond distances, suggesting that a π exchange mechanism via the ring system is not the major pathway.

The coordination chemistry of (py)CHNOH with Fe and Co is practically unknown. Early aqueous solution studies by Hanania and Irvine [47,52] have shown that when Fe^{II} forms a complex with (py)CHNOH the acid strength of the oxime group increases considerably. The localized mixed-valence cation $[LFe^{III}\{(py)CHNO\}_3Fe^{II}]^{2+}$ (L = 1,4,7-trimethyl-1,4,7-triazacyclononane) contains a low-spin Fe^{II} atom [6], the complex behaves magnetically as a mononuclear high-spin Fe(III) species, with a μ_{eff} value of 5.83 ± 0.02 BM at 10–290 K.

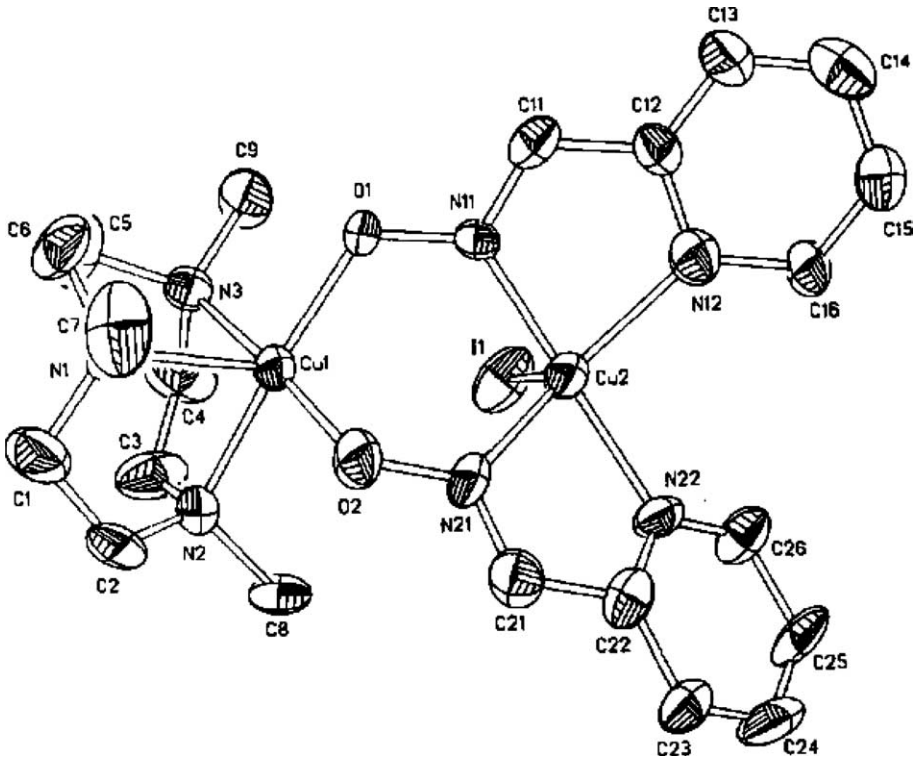

Fig. 11. X-ray molecular structure of the $[LCu^{II}\{(py)CHNO\}_2Cu^{II}I]^+$ cation [56].

A structurally impressive dodecanuclear Fe(III) cluster was recently reported by Christou's group [57]. The complex $[Fe_{12}(\mu_3\text{-}O)_8(\mu\text{-}OMe)_2(O_2CPh)_{12}\{(py)CHNO\}_6]$ was obtained from the reaction of $[Fe_3O(O_2CPh)_6(H_2O)_3](O_2CPh)$, (py)CHNOH and NaOMe in MeCN. The complicated core of the complex contains a central Fe_6 unit that can be described in various ways, one of which is as four edge-sharing $\{Fe_3(\mu_3\text{-}O)\}^{7+}$ triangular units and two additional $\{Fe_3(\mu_3\text{-}O)\}^{7+}$ units attached to the flanks. Variable-temperature solid-state susceptibility studies on the cluster in the temperature range 5.0–300 K reveal that this possesses an $S = 0$ ground state; this behavior is not suprising given the dominance of antiferromagnetic interactions in high-spin Fe(III) chemistry.

Blackmore and Magee [58a] reported a slow reaction between Co(II) and (py)CHNOH; their explanation was that the low rate is due to the slowness of the interconversion of the *syn* and *anti* forms of the ligand. A later photometric and pHmetric solution study by Beck's group [58b] showed that this reaction is complicated. The complex formation reaction itself is very fast, in contrast to the data by Blackmore and Magee [58a], and is followed by a slow redox process where the metal ion is oxidised by the ligand to yield an inert cobalt(III) complex. Recently, our group investigated the solid-state coordination chemistry of (py)CHNOH with Co [59]. The refluxing reaction mixtures $Co(O_2CMe)_2 \cdot 4H_2O$/(py)CHNOH/$NaClO_4$ (1:2:1) in MeOH, $CoCl_2 \cdot 6H_2O$/(py)CHNOH/LiOH/$NaClO_4$ (1:2:2:1) in H_2O or $Co(ClO_4)_2 \cdot 6H_2O$/(py)CHNOH/Me_4NOH (1:2:2) in MeOH led (under aerobic conditions) to the clean preparation of dark red complex $[Co_2^{III}Co^{II}\{(py)CHNO\}_6](ClO_4)_2$ (Fig. 12). The central Co^{II} atom, Co(2), which sits on a threefold axis of symmetry, is octahedrally coordinated by six oxygen atoms belonging to six crystallographically equivalent 2.111 $(py)CHNO^-$ ligands. The six sites on each of the distorted octahedral, terminal Co^{III} atoms, Co(1), which sit on a threefold axis of symmetry, are occupied by the nitrogen atoms that belong to the "chelating" part of three $(py)CHNO^-$ ligands, with the three oximato N atoms in the *fac* (or *cis*) configuration.

The fact that the two mononuclear neutral *fac*-$Co^{III}\{(py)CHNO\}_3$ units of the above mentioned mixed-valence, trinuclear cluster can be considered as acting as tridentate chelating "ligands" to the central Co^{II} center, Co(2), led us to suspect that the mononuclear 1:3 Co(III) complex would be capable of existence. Our suspicion was both correct and incorrect. It proved correct because the desired product has been, indeed, prepared and, simultaneously, it proved incorrect because the discrete mononuclear complex, $[Co^{III}\{(py)CHNO\}_3]$, that we managed to isolate and structurally characterize is the "wrong", i.e., the *mer* (or *trans*) isomer. The Co^{III} atom is coordinated by three *N*,*N*′-bidentate chelating (or 1.011 [44], Fig. 8) ligands.

The mononuclear distorted octahedral Co(III) complexes $[Co\{(py)CHNO\}_2(L\text{–}L)]Cl$ (L–L = bpy, phen) and $[Co(acac)_2\{(py)CHNO\}]$ have been recently

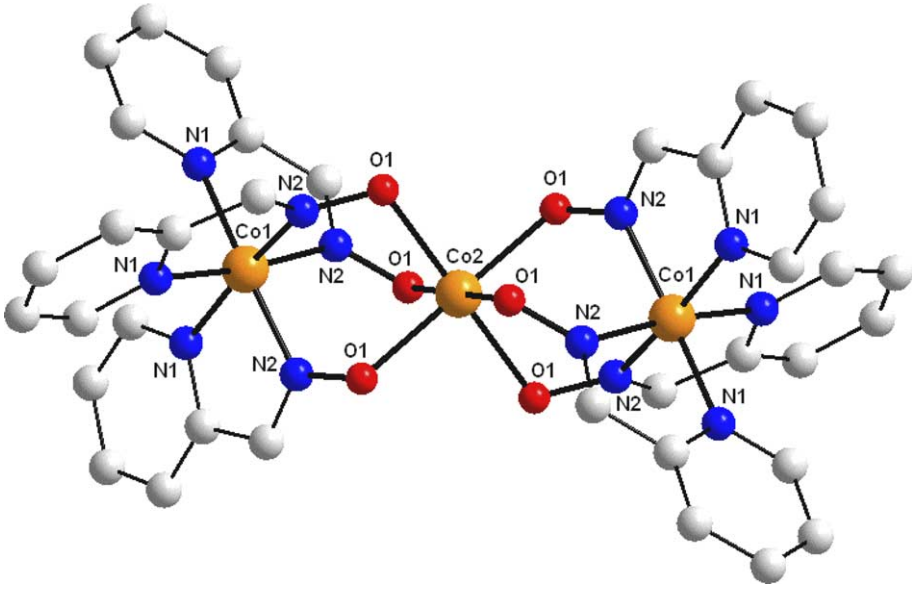

Fig. 12. The molecular structure of the mixed-valence (III/II/III) cation $[Co_3\{(py)CHNO\}_6]^{2+}$; identical atoms are used for atoms generated by symmetry [59].

prepared by our group; single-crystal X-ray crystallography revealed that $(py)CHNO^-$ behaves as an 1.011 ligand [60].

Few homometallic Ni(II) complexes containing the neutral and/or anionic ligand have been published [61–63]. All are mononuclear: $[Ni\{(py)CHNO\}_2\{(py)CHNOH\}]$ [61], $[Ni\{(py)CHNO\}_2L_2]$ (L = pyridine, 4-picoline, 4-ethylpyridine) [62] and $[Ni\{(py)CHNO\}_2(L–L)]$ (L–L = bpy, phen) [63]. Representative drawings are shown in Figs. 13 and 14. The deprotonated ligands are *N*,*N*′-bidentate (or 1.011). All compounds containing monodentate aromatic N-ligands have the same structural motif with *trans* coordination fashion for the identical donor groups [62], while those containing bpy or phen are racemic [63]. Polynuclear Ni(II) complexes comprise [64] several salts of the enneanuclear cation $[Ni_9(OH)_6\{(py)CHNO\}_{10}(H_2O)_6]^{2+}$ and $[Ni_3(acac)\{(py)CHNO\}_2\{(py)CHNOH\}_3](ClO_4)_3$.

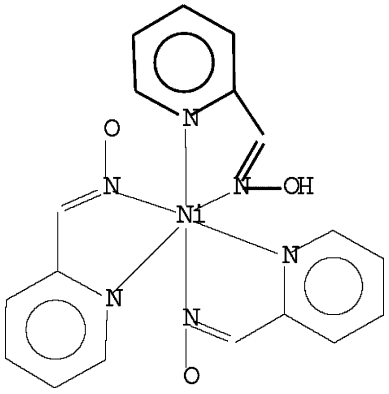

Fig. 13. A drawing of $[Ni\{(py)CHNO\}_2\{(py)CHNOH\}]$.

The latter (Fig. 15) contains two 2.111 neutral ligands, one 1.011 neutral ligand and two 3.211 deprotonated ligands (Fig. 8).

Although complex formation equilibria involving (py)CHNOH and Zn^{II} were studied [65], only one structurally characterized $Zn(II)/(py)CHNO^-$ complex has been reported [66]; this is $[Zn_4(OH)_2Cl_2\{(py)CHNO\}_4]$ (Fig. 16). The molecule of this complex features an inverse 12-metallacrown-4 motif [67] with the oximato ligand adopting the 2.111 coordination mode.

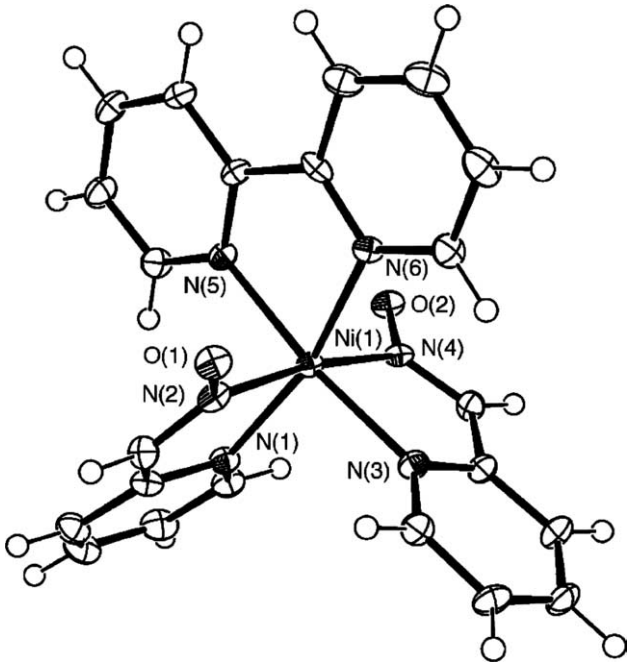

Fig. 14. The molecular structure of $[Ni\{(py)CHNO\}_2(bpy)]$ [63].

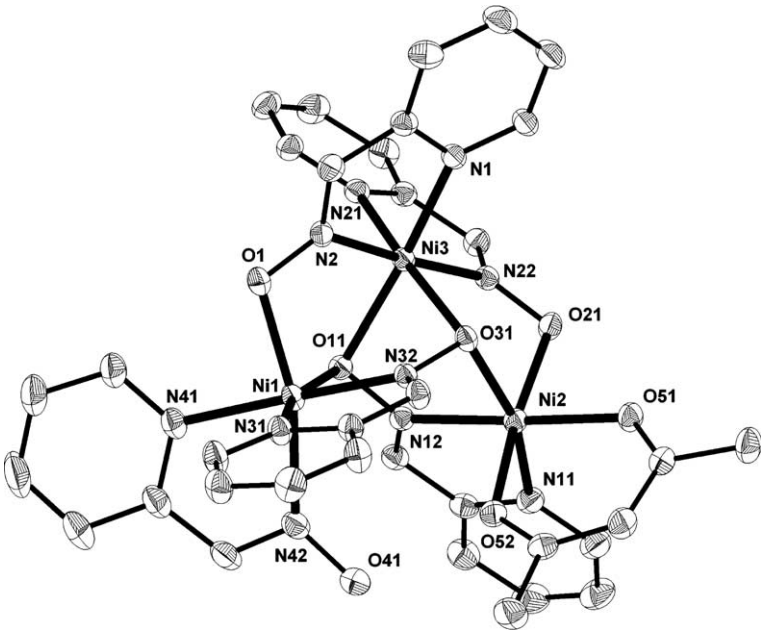

Fig. 15. The structure of the trinuclear cation $[Ni_3(acac)\{(py)CHNO\}_2\{(py)CHNOH\}_3]^{3+}$ [64].

A dinuclear mixed-valence d^3/d^4 complex $[LCr^{III}\{(py)CHNO\}_3Cr^{II}](ClO_4)_2$ has been prepared [68], in which the Cr^{III} and Cr^{II} centers are antiferromagnetically coupled ($J = -7.9$ cm^{-1}) [68]; L = 1,4,7-trimethyl-1,4,7-triazacyclononane. No structural data are available for this compound.

The Mn/(py)CHNOH chemistry is better developed. A modular approach (vide infra) using tris(pyridine-2-aldoximato)manganate(II), $[Mn^{II}\{(py)CHNO\}_3]^-$, and $[Mn^{III}L]$-units (L = 1,4,7-trimethyl-1,4,7-triazacyclononane) yielded the localized mixed-valence complex $[LMn^{III}\{(py)CHNO\}_3Mn^{II}]^{2+}$ [6]. The two manganese centers are bridged by the –NO oximato linkages of the three 2.111 $(py)CHNO^-$ ligands. The interaction between the two metal ions was found to be ferromagnetic ($J = +1.8$ cm^{-1}, $S_T = 9/2$).

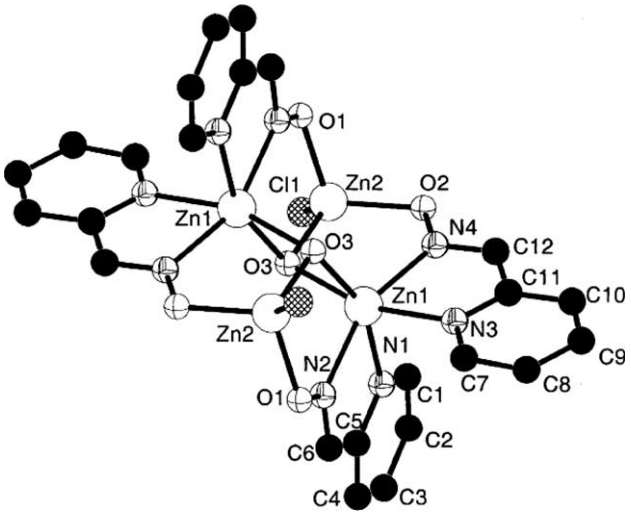

Fig. 16. X-ray structure of $[Zn_4(OH)_2Cl_2\{(py)CHNO\}_4]$; atoms O(3) are the hydroxo oxygen atoms [66].

The structure of the 1D polymer $[Mn(SO_4)\{(py)CHNOH\}(H_2O)]_n$ (Fig. 17) consists of double chains, in which the Mn^{II} ions are bridged by $\eta^1{:}\eta^1{:}\eta^1{:}\mu_3$ sulfato ligands [66]; the neutral oxime ligand behaves as *N*,*N*′-bidentate chelate (1.011, Fig. 8).

The preparation and crystal structures of four Mn(II) carboxylate complexes containing neutral (py)CHNOH were recently reported [69]. The 1:1 reaction between $Mn(O_2CPh)_2 \cdot 2H_2O$ and the ligand in MeCN led to isolation of $[Mn_4(O_2CPh)_6\{(py)CO_2\}_2\{(py)CHNOH\}_2]$ (Fig. 18). The most interesting synthetic feature of this reaction is the in situ formation of the picolinate(−1) ligand, $(py)CO_2^-$. The centrosymmetric tetranuclear cluster consists of an exactly planar zig-zag array of Mn^{II} atoms and is held together by four *syn*, *syn* $\eta^1{:}\eta^2{:}\mu_2$ and two $\eta^1{:}\eta^2{:}\mu_3$ $PhCO_2^-$ groups, two $\eta^1{:}\eta^2{:}\mu_2(py)CO_2^-$ ligands and two *N*,*N*′-bidentate chelating (py)CHNOH molecules.

The 1:4:7 $[Mn_3^{II,III,III}O(O_2CPh)_6(py)_2(H_2O)]$/$Me_3SiCl$/(py)CHNOH reaction mixture in MeCN (py = pyridine) yielded the 1D coordination polymer $[Mn(O_2CPh)\{(py)CO_2\}\{(py)CHNOH\}]_n$, in which the partial (py)CHNOH → $(py)CO_2^-$ transformation has again occurred. Its structure is shown in Fig. 19. The 1:3 reaction between $Mn(O_2CMe)_2 \cdot 4H_2O$ and (py)CHNOH in EtOH led to the isolation of the dinuclear complex $[Mn_2(O_2CMe)_2\{(py)CO_2\}_2\{(py)CHNO\}_2]$; crystallography again revealed the partial (py)CHNOH → $(py)CO_2^-$ transformation. A simplified scheme for this transformation was proposed (Fig. 20). Reaction of $Mn(hfac)_2 \cdot 3H_2O$ (hfacH = hexafluoroacet-

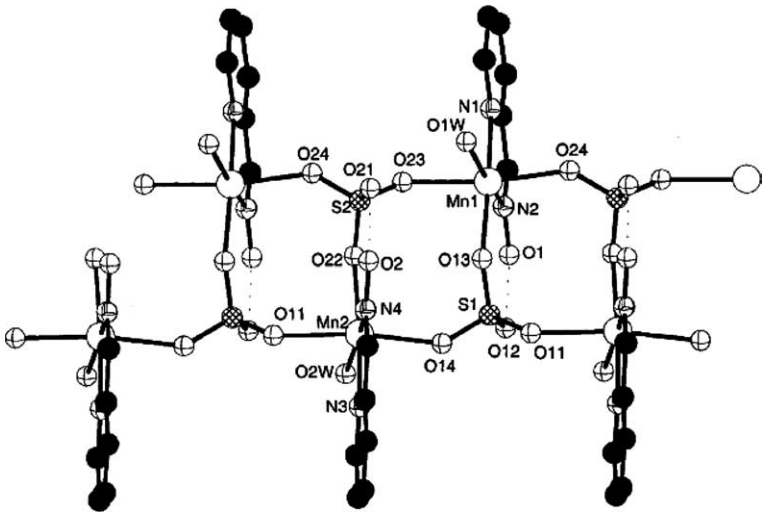

Fig. 17. A small portion of the 1D double chain present in complex $[Mn(SO_4)\{(py)CHNOH\}(H_2O)]_n$ [66].

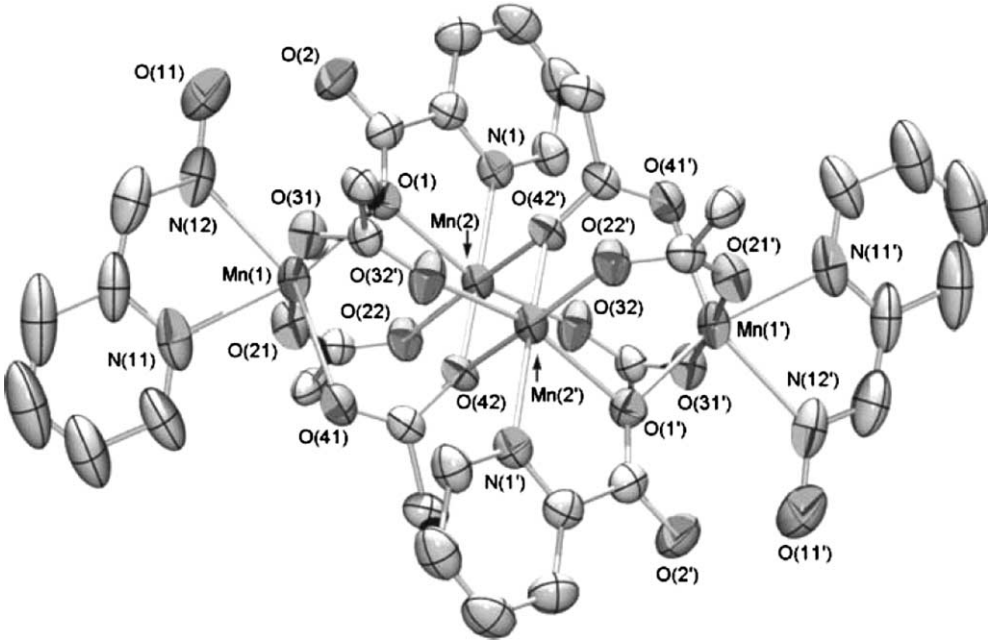

Fig. 18. The molecular structure [69] of the complex $[Mn_4(O_2CPh)_6\{(py)CO_2\}_2\{(py)CHNOH\}_2]$. Only the *ipso* carbon atoms of the phenyl groups of the benzoate ligands are shown.

ylacetone) with one equivalent of (py)CHNOH in CH_2Cl_2 yields complex $[Mn(O_2CCF_3)_2\{(py)CHNOH\}_2]$; the $CF_3CO_2^-$ ligand is one of the decomposition products of the hfac$^-$ ligand. The Mn^{II} ion is coordinated by two $CF_3CO_2^-$ groups and two 1.011 neutral oxime ligands.

$[Pt\{(py)CHNO\}_2]\cdot 2H_2O$ is the only structurally characterized (py)CHNOH- or (py)CHNO$^-$-based complex with 4d or 5d metals [70]. The coordination around the Pt^{II} center is roughly *trans* square planar, the ligating atoms being the two nitrogen atoms from each of two deprotonated ligands. The planar units form a chain parallel to the crystallographic *c*-axis (Pt$\cdots$Pt = 3.245 Å). A powdered sample of the complex shows enhanced electrical conductivity which is in the same range as that observed for Magnus's Green salt, $[Pt(NH_3)_4][PtCl_4]$.

The main-group metal chemistry of (py)CHNOH is virtually non-existent. The only exception is the organometallic complex $[In_2Me_4\{(py)CHNO\}_2]$ (Fig. 21), in which the In^{III} atoms are five-coordinate adopting a distorted trigonal bipyramidal geometry [71].

Up to now, we have discussed *homometal* complexes of (py)CHNOH/(py)CHNO$^-$. We now continue our discussion with the description of *heterometal* complexes that

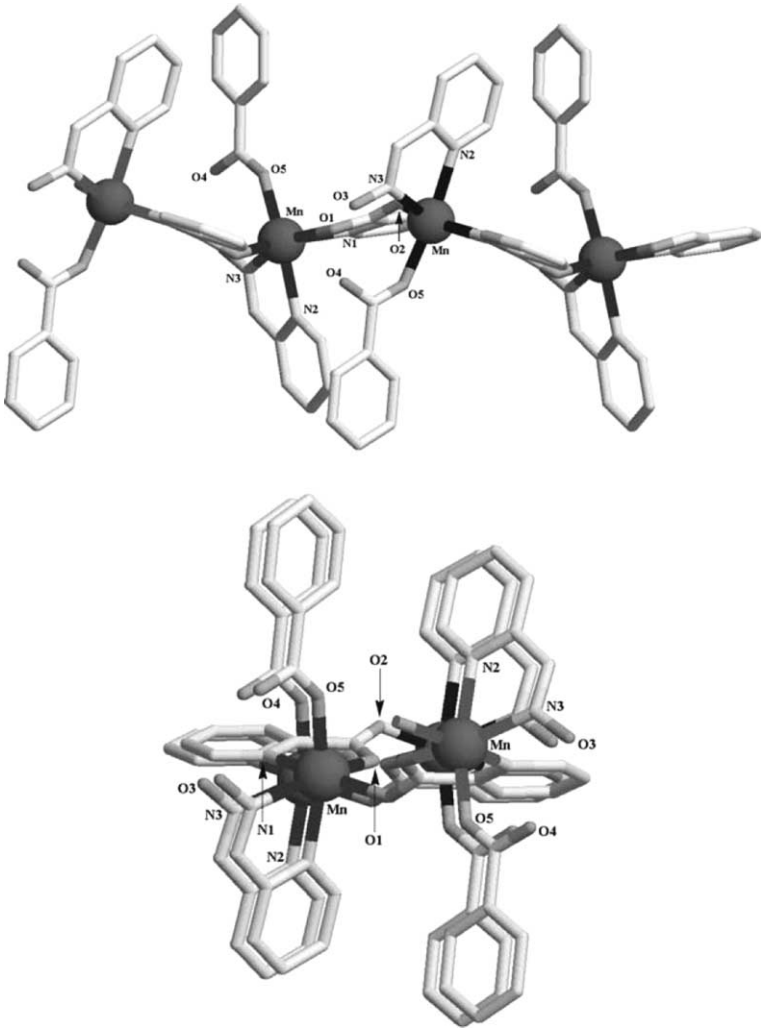

Fig. 19. Views of the complex $[Mn(O_2CPh)\{(py)CO_2\}\{(py)CHNOH\}]_n$ along *b*-axis (up) and *c*-axis (down) [69].

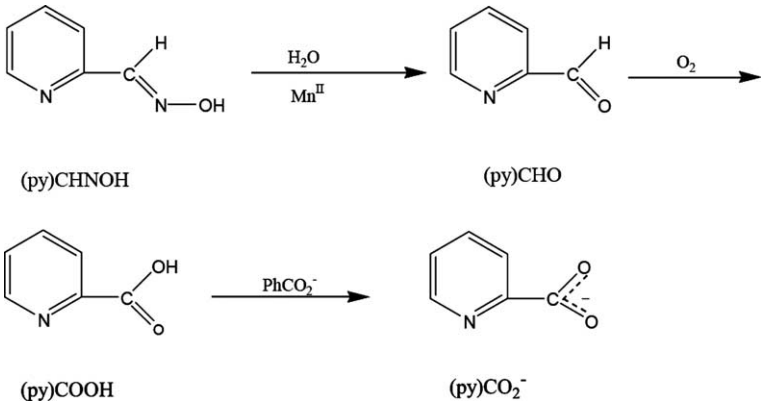

Fig. 20. A simplified view for the transformation of an account of (py)CHNOH to picolinate(−1) during the preparation of some Mn(II) carboxylate complexes.

are (exclusively or partially) based on bridging $(py)CHNO^-$ ligands. All these complexes have aesthetically beautiful structures, while some of them present interesting magnetic properties. Magnetic investigations of heteronuclear complexes are more informative than those of homonuclear complexes as new exchange pathways can be expected for two different spin carriers within a molecular unit, because unusual sets of magnetic orbitals are brought in close proximity [6]. Thus, oximato-bridged heterometal complexes are central players in the

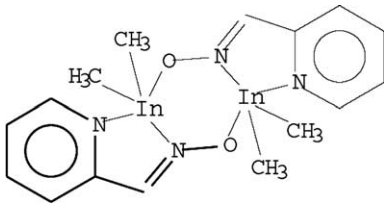

Fig. 21. A drawing of the molecule of $[In_2Me_4\{(py)CHNO\}_2]$.

field of molecular magnetism [72]. Most of these species are prepared by the so-named "modular" synthesis [6]; other names of this approach are "complexes as ligands" or "complexes as ligands and complexes as metals" strategies [73]. Different "modules", i.e., complexes containing one or more metal centers, are able to react further with other modules (different metal centers or metal complexes) through available appropriate donor atoms.

In an excellent paper [68], Chaudhuri, Wieghardt and co-workers reported that tris(pyridine-2-aldoximato)metalates(II), $[M^{II}\{(py)CHNO\}_3]^-$, are capable of acting as "ligands" reacting with $[LCr^{III}(MeOH)_3]^{3+}$ ("metals") to give various asymmetric dinuclear complexes of the general type $[LCr^{III}\{(py)CHNO\}_3M^{II}]^{2+}$ ($M^{II} = Mn^{II}$, Fe^{II}, Ni^{II}, Cu^{II}, Zn^{II}; L is the "end-cap" 1,4,7-trimethyl-1,4,7-triazacyclononane), see Scheme 2. In the case of cobalt(II), oxidation occurs and the resulting complex is $[LCr^{III}\{(py)CHNO\}_3Co^{III}](ClO_4)_3$. These compounds contain three 2.111 $(py)CHNO^-$ ions as bridging ligands. The complexes are isostructural in the sense that they all contain a terminal Cr^{III} atom in a distorted octahedral $Cr^{III}N_3O_3$ environment and a second six-coordinate metal ion M in a mostly trigonal prismatic MN_6 geometry. Analysis of the variable-temperature magnetic susceptibility data indicates the presence of weak ferro- or antiferromagnetic exchange interactions between the paramagnetic centers. A qualitative rationale on the basis of Goodenough–Kanamori rules [74,75] was provided to explain the differences in magnetic behavior.

Using the "complexes as ligands and complexes as metals" strategy Clérac, Miyasaka and co-workers [62] per-

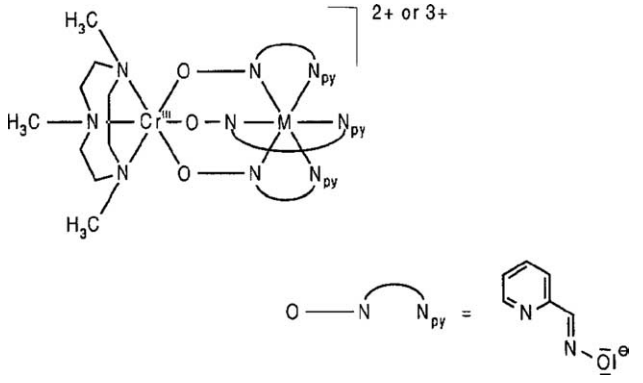

Scheme 2. General structural type of the $[LCr^{III}\{(py)CHNO\}_3M]^{2+\text{ or }3+}$ cations (L = 1,4,7-trimethyl-1,4,7-triazacyclononane); the metal ion M is Cr^{II}, Mn^{II}, Fe^{II}, Co^{III}, Ni^{II}, Cu^{II}, Zn^{II} [68].

formed the reaction between $[Mn_2^{III,III}(saltmen)_2(H_2O)_2](ClO_4)_2$ (the "metal") and $[Ni\{(py)CHNO\}_2(py)_2]$ (the "bridging ligand"), where saltmen^{2-} is *N*,*N*′-(1,1,2,2-tetramethylethylene)bis(salicylideneiminate), see Scheme 3. The product [43] consists of two fragments, the out-of-plane dimer $[Mn_2(saltmen)_2]^{2+}$ as a coordination acceptor building block and the neutral mononuclear unit $[Ni\{(py)CHNO\}_2(py)_2]$ as a coordination donor building block, forming an alternating chain having the $[-Mn^{III}-(O)_2-Mn^{III}-(ON)-Ni-(NO)-]$ repeating unit. The chains are well isolated and there are no interchain π–π overlaps between organic ligands; these features ensure a good magnetic isolation of the chains. The $Ni^{II}\cdots Mn^{III}$ exchange is antiferromagnetic ($J = -21$ K) and much stronger than the ferromagnetic intrachain $Mn^{III}\cdots Mn^{III}$ interaction ($J' = +0.67$ K). Hysteresis loops are observed below 3.5 K, indicating a magnet-type behavior. Combined ac (Fig. 22) and dc measurements show a slow relaxation of the magnetization. The material constitutes an elegant design of a heterometallic chain with $S_T = 3$ magnetic units showing a "single-chain magnet" behavior predicted in 1963 by Glauber [76] for an Ising 1D system and first experimentally documented by Gatteschi's group [77,78]. Complexes $\{[Mn_2^{III,III}(saltmen)_2Ni^{II}\{(py)CHNO\}_2(L)_2](A)_2\}_n$ (L = *N*-methylimidazole, A = ClO_4; L = py, A = PF_6; L = py, A = ReO_4) were also structurally characterized, and found to have similar structures and properties [79] with those of the L = py, A = ClO_4 archetype described above.

Employing $[Ni\{(py)CHNO\}(bpy)_2]^+$ as "terminal ligand", the groups of Miyasaka and Clérac characterized [80] the heterometallic linear tetramers $[Mn(5\text{-}R\text{-}saltmen)Ni\{(py)CHNO\}(bpy)_2]_2(ClO_4)_2$ (R = H, Cl, Br, MeO; Scheme 4). These tetramers can be seen as oligomeric units (components) of the aforementioned "single-chain magnets". Magnetic studies on the former [80] confirm the nature of the magnetic interactions reported for the latter [43,79]; a strong antiferromagnetic $Mn^{III}\cdots Ni^{II}$ coupling via the oximato bridge ($J_{Mn\cdots Ni}$ ranges from −23.7 to −26.1 K) and a weak ferromagnetic $Mn^{III}\cdots Mn^{III}$ coupling through the bis(phenolato) bridge ($J_{Mn\cdots Mn}$ ranges from +0.4 to +0.9 K). These magnetic interactions lead to tetramers with an $S = 2$ ground state.

5.3. 6-Methylpyridine-2-carbaldehyde oxime, (6-Mepy)CHNOH

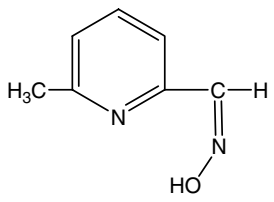

(6-Mepy)CHNOH

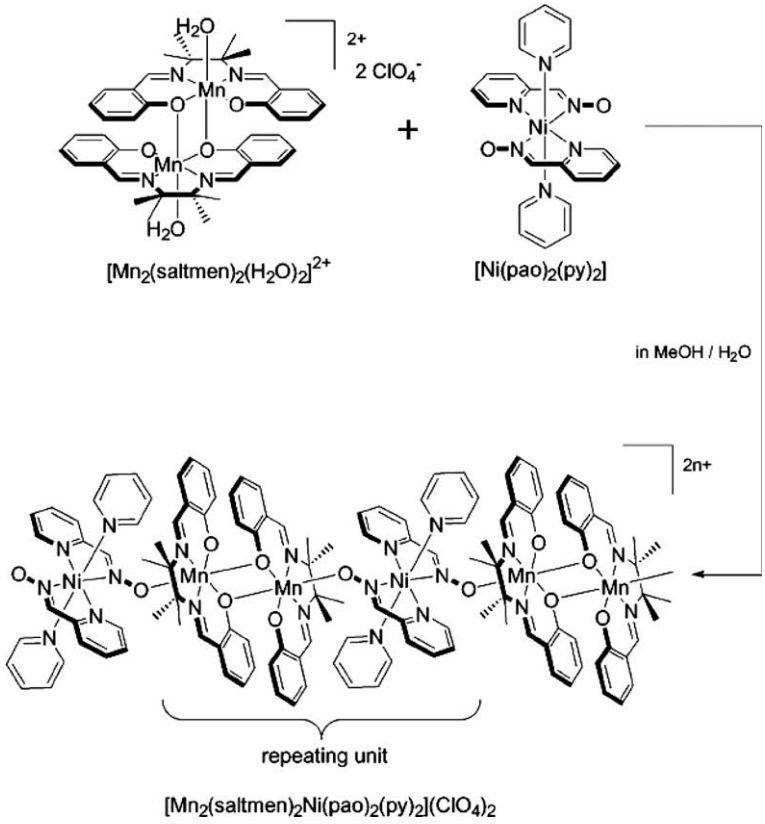

Scheme 3. Synthesis of the "single-chain magnet" $\{[Mn_2^{III,III}(saltmen)_2Ni^{II}\{(py)CHNO\}_2(py)_2](ClO_4)_2\}_n$; paO is another abbreviation for the anion of pyridine-2-carbaldehyde oxime (see Section 2).

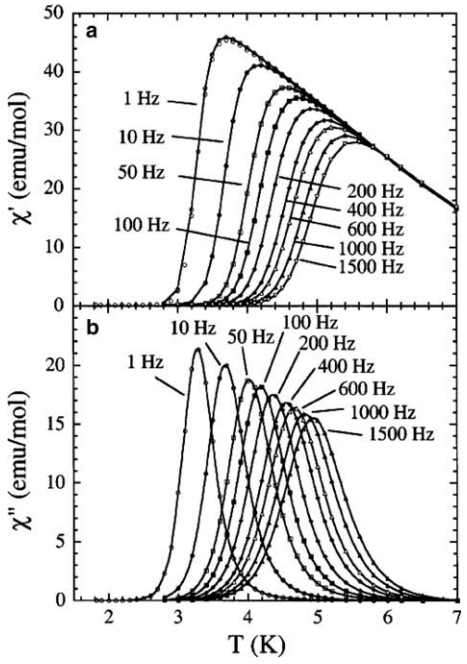

Fig. 22. Temperature and frequency dependence of (a) the real (χ') and (b) the imaginary (χ'') parts of the ac susceptibility; the solid lines are guides for the eye [43].

The free ligand is synthesized [46] by the reaction of 6-methylpyridine-2-carbaldehyde, (6-Mepy)CHO, with an equimolar amount of H_2NOH in MeOH under reflux. The values of the logarithm of the protonation constant of the 2-pyridyl nitrogen and pK_a of the oxime group are [46] 4.26 and 9.94, respectively. The coordination chemistry of this ligand is practically unknown. Complex formation equilibria involving (6-Mepy)CHNOH and Cu(II) [46], Zn(II) [65] and Cd(II) [65] have

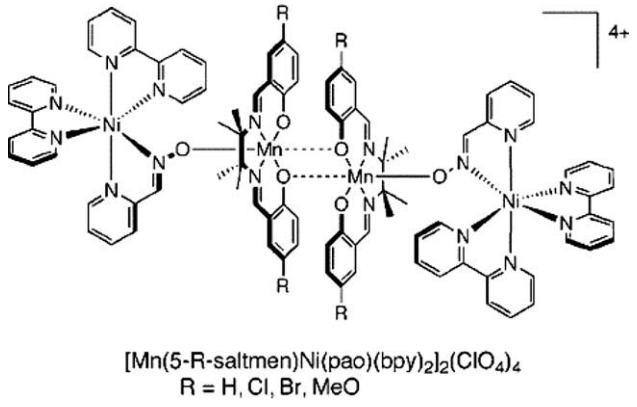

Scheme 4. A drawing of the cations $[Mn^{III}(5\text{-R-saltmen})Ni^{II}\{(py)CHNO\}(bpy)_2]_2^{4+}$ which are the tetrameric components of the "single-chain magnets" depicted in Scheme 3.

been studied by Saarinen's group. Only one complex has been structurally characterized [81]. This is the enneanuclear Ni(II) cluster $[Ni_9(\mu_3\text{-}OH)_2(\mu_2\text{-}OH)_4\{\mu_3\text{-}(6\text{-Mepy})CHNO\}_4\{\mu_2\text{-}(6\text{-Mepy})CHNO\}_6(H_2O)_6](ClO_4)_2$, prepared by the reaction between $NiCl_2 \cdot 6H_2O$ and the ligand in H_2O at pH 8 (Eq. (6)). The chromophores in the structure are NiO_6, NiN_2O_4 and NiN_4O_2. The nine Ni^{II} atoms are held together via $\mu_3\text{-}OH^-$, $\mu_2\text{-}OH^-$, 2.111 and 3.211 (6-Mepy)$CHNO^-$ ligands.

$$9NiCl_2 \cdot 6H_2O + 10(6\text{-Mepy})CHNOH + 16NaOH + 2NaClO_4 \xrightarrow[\text{pH 8}]{H_2O} [Ni_9(OH)_6\{(6\text{-Mepy})CHNO\}_{10}(H_2O)_6](ClO_4)_2 + 18NaCl + 58H_2O \quad (6)$$

5.4. 1-Pyridin-2-yl-ethanone oxime, (py)C(Me)NOH

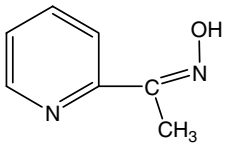

(py)C(Me)NOH

The free ligand can be synthesized [46] by the reaction of equimolar quantities of 1-pyridin-2-yl-ethanone (2-acetylpyridine), (py)C(Me)O, $H_2NOH \cdot HCl$ and NaOMe in EtOH. The values of $\log\beta$ of the 2-pyridyl nitrogen (β is the protonation constant) and pK_a of the oxime group are [46] 3.97 and 10.87, respectively. The acidity of the oxime group of (py)C(Me)NOH is lower than that of (py)CHNOH ($pK_a = 10.01$) due to the adjacent methyl group in the former. Complex formation equilibria involving the neutral and/or the deprotonated ligand and Cu(II) [46], Zn(II) [65] and Cd(II) [65] have been studied in aqueous solution by potentiometic methods.

The published coordination chemistry of (py)C(Me)NOH is limited compared with (py)CHNOH. The structurally characterized metal complexes of (py)C(Me)NOH and/or (py)C(Me)NO^- [82–91] are listed in Table 1, along with the coordination modes of the ligands and few structural details. Of particular note are the coordination modes 1.100 and 2.101 observed in organometallic compounds of Sb(V) and Sn(IV) [89–91], which are unique for the (py)C(R)NO^- ligands (R = H, Me, Ph).

Molecular structures of representative complexes are shown in Figs. 23–27. In general terms, the comparison of the coordination chemistry of (py)C(Me)NOH with that of (py)C(H)NOH is not possible because of the different nature of the reaction systems studied. However, three metal/(py)C(Me)NO^- complexes, i.e., $[Co\{(py)C(Me)NO\}_3]$ [59], $[Zn_4(OH)_2Cl_2\{(py)C(Me)NO\}_4]$ [84] and $[Pt\{(py)C(Me)NO\}_2]$ [88], have rather similar molecular structures to their (py)$CHNO^-$ counterparts, i.e., $[Co\{(py)CHNO\}_3]$ [59], $[Zn_4(OH)_2Cl_2\{(py)CHNO\}_4]$ [66] and $[Pt\{(py)CHNO\}_2]$ [70]. It should be mentioned that the Co(III)/(py)C(Me)NO^- complex is the *fac* isomer, whereas the Co(III)/(py)C(H)NO^- complex is the *mer* isomer. The nature of R affects the structural identity of the organometallic complexes $[R_8Sn_4O_2\{(py)C(Me)NO\}_4]$ [90,91], see Table 1.

The crystal structure of the free ligand consists of chains of molecules arising from intermolecular hydrogen bonding with the ring nitrogen atom as acceptor [90].

5.5. Phenyl-pyridin-2-yl-methanone oxime, (py)C(ph)NOH

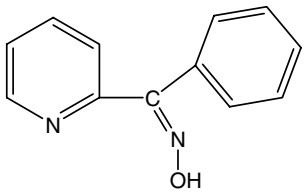

(py)C(ph)NOH

The free ligand can be synthesized [92] by the reaction of 2-benzoylpyridine, (py)C(ph)O, with an excess of NH_2OH ($NH_2OH \cdot HCl + NaOH$) in $EtOH/H_2O$. The first structurally characterized metal complexes of (py)C(ph)NOH were the carbonyl compounds [93] $[Os_3(CO)_8\{(py)C(ph)NO\}_2]$, $[Os_3(CO)_8\{(py)C(ph)NO\}\{(py)C(ph)HNH\}]$, $[Os_3H(CO)_9\{(py)C(ph)NO\}]$ and $[Os_3H(CO)_{11}\{(py)C(ph)NO\}]$, which exhibit interesting structural features. The structurally characterized, non-organometallic metal complexes of the neutral or anionic ligand are listed in Table 2.

The comproportionation reaction between $Mn(O_2CPh)_2 \cdot 2H_2O$ and $^nBu_4MnO_4$ (3:1) in the presence of (py)C(ph)NOH in $MeCN/EtOH/CH_2Cl_2$ leads to the isolation of the mixed-valent cluster $[Mn_4^{II}Mn_4^{III}O_2(OH)_2(O_2CPh)_{10}\{(py)C(ph)NO\}_4]$. The centrosymmetric octanuclear molecule (Fig. 28) contains four Mn^{II} and four Mn^{III} ions held together by two $\mu_4\text{-}O^{2-}$ ligands and two $\mu_3\text{-}OH^-$ ions to give the $\{Mn_8(\mu_4\text{-}O)_2(\mu_3\text{-}OH)_2\}^{14+}$ core (Fig. 29), with peripheral ligation provided by 10 $PhCO_2^-$ ligands that exhibit three different coordination modes and four 2.111 (py)C(ph)NO^- ions [94,95]. The molecular structure of this complex is very similar with that of $[Mn_4^{II}Mn_4^{III}O_2(OH)_2(O_2CPh)_{10}\{(py)C(Me)NO\}_4]$ [82].

Table 1
Structurally characterized metal complexes containing (py)C(Me)NOH and/or (py)C(Me)NO$^-$ ligands

Complex[a]	Coordination mode of the oxime/oximate ligand	Coordination spheres; coordination geometries	Reference
$[Mn(O_2CPh)_2\{(py)C(Me)NOH\}_2]$	1.011	*cis*,*cis*,*trans*-$Mn^{II}O_2(N_{py})_2(N_{ox})_2$; oct	[82]
$[Mn_3O(O_2CMe)_3\{(py)C(Me)NO\}_3](ClO_4)$	2.111	$Mn^{III}(\mu_3\text{-}O)(O_{carb})_2(O_{ox})N_2$; oct	[82]
$[Mn_4^{II}Mn_4^{III}O_2(OH)_2(O_2CPh)_{10}\{(py)C(Me)NO\}_4]$	2.111	$Mn^{II}(\mu_4\text{-}O)(\mu_3\text{-}OH)(O_{carb})_4$, $Mn^{II}(\mu_3\text{-}OH)(O_{carb})_3N_2$, $Mn^{III}(\mu_4\text{-}O)_2(O_{carb})_3(O_{ox})$, $Mn^{III}(\mu_4\text{-}O)(\mu_3\text{-}OH)(O_{carb})(O_{ox})N_2$; oct, oct, oct, oct	[82]
$[Co\{(py)C(Me)NO\}_3]$	1.011	*fac*-$Co^{III}N_6$; oct	[59]
$[NiBr_2\{(py)C(Me)NOH\}_2]$	1.011	*cis*,*cis*,*cis*-$Ni^{II}Br_2(N_{py})_2(N_{ox})_2$; oct	[83]
$[Ni\{(py)C(Me)NO\}\{(py)C(Me)NOH\}(H_2O)_2](NO_3)$	1.011, 1.011	*trans*,*cis*,*cis*-$Ni^{II}O_2(N_{py})_2(N_{ox})_2$; oct	[83]
$[Ni(SO_4)\{(py)C(Me)NOH\}(H_2O)_3]$	1.011	$Ni^{II}(O_{sulf})(O_{aqua})_3N_2$; oct	[84]
$[Ni(SO_4)\{(py)C(Me)NOH\}_2(H_2O)]$	1.011	$Ni^{II}(O_{sulf})(O_{aqua})N_4$; oct	[84]
$[Ni\{(py)C(Me)NO\}\}\{(py)C(Me)NOH\}(H_2O)_2](ClO_4)$	1.011, 1.011	*trans, cis, cis*-$Ni^{II}O_2(N_{py})_2(N_{ox})_2$; oct	[85]
$[ZnCl_2\{(py)C(Me)NOH\}_2]$	1.011	*cis*,*cis*,*trans*-$Zn^{II}Cl_2(N_{py})_2(N_{ox})_2$; oct	[84]
$[Zn(NO_3)_2\{(py)C(Me)NOH\}_2]$	1.011	all *trans*-$Zn^{II}O_2(N_{py})_2(N_{ox})_2$; oct	[86]
$[Zn(SO_4)\{(py)C(Me)NOH\}(H_2O)_3]$	1.011	$Zn^{II}(O_{sulf})(O_{aqua})_3N_2$; oct	[84]
$[Zn_4(OH)_2Cl_2\{(py)C(Me)NO\}_4]$	2.111	$Zn^{II}(\mu_3\text{-}OH)(O_{ox})_2Cl$, $Zn^{II}(\mu_3\text{-}OH)_2N_4$; tet, oct	[84]
$\{[Cd(SO_4)\{(py)C(Me)NOH\}(H_2O)]\cdot[Cd(SO_4)\{(py)C(Me)NOH\}(H_2O)_2]\}_n$[b]	1.011	$Cd^{II}(O_{sulf})_3(O_{aqua})N_2$, $Cd^{II}(O_{sulf})_2(O_{aqua})_2N_2$; oct, oct	[84]
$[RhCl_2\{(py)C(Me)NO\}\{(py)C(Me)NOH\}]$	1.011, 1.011	*trans*,*cis*,*cis*-$Rh^{III}Cl_2(N_{py})_2(N_{ox})_2$; oct	[87]
$[Pt\{(py)C(Me)NO\}_2]$	1.011	*trans*-$Pt^{II}N_4$; sp	[88]
$[Ph_3Sb\{(py)C(Me)NO\}_2]$	1.100	*trans*-$Sb^{V}C_3(O_{ox})_2$; tbp	[89]
$[^nBu_8Sn_4O_2\{(py)C(Me)NO\}_4]$	1.100, 2.101	$Sn^{IV}C_2(\mu_3\text{-}O)(O_{ox})(N_{ox})$, $Sn^{IV}C_2(\mu_3\text{-}O)_2(O_{ox})$; spy, tbp	[90]
$[Et_8Sn_4O_2\{(py)C(Me)NO\}_4]$	1.100, 2.101	$Sn^{IV}C_2(\mu_3\text{-}O)(O_{ox})_2$, $Sn^{IV}C_2(\mu_3\text{-}O)_2(N_{ox})$; tbp, spy	[90]
$[Me_8Sn_4O_2\{(py)C(Me)NO\}_4]$	1.100, 2.111	$Sn^{IV}C_2(\mu_3\text{-}O)(O_{ox})_2$, $Sn^{IV}C_2(\mu_3\text{-}O)_2(N_{py})(N_{ox})$; tbp, oct	[91]

Abbreviations: N_{ox}, oxime or oximato nitrogen; N_{py}, 2-pyridyl nitrogen; O_{carb}, carboxylate oxygen; O_{ox}, oximate oxygen; O_{sulf}, sulfate oxygen; oct, octahedral; sp, square planar; spy, square pyramidal; tbp, trigonal bipyramidal; tet, tetrahedral.

[a] Solvate and other lattice molecules have been omitted.

[b] The crystal structure of this coordination polymer consists of single and double chains.

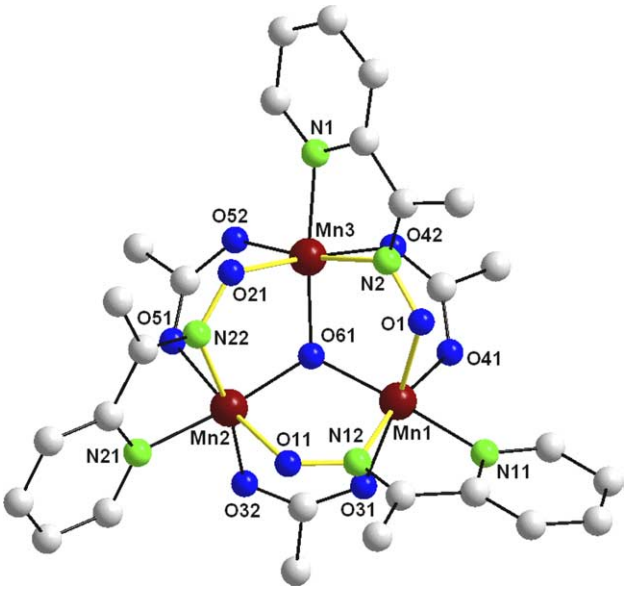

Fig. 23. X-ray structure of the $[Mn_3O(O_2CMe)_3\{(py)C(Me)NO\}_3]^+$ cation [82].

The reaction of $Mn(O_2CPh)_2 \cdot 2H_2O$ with the sodium salt of (py)C(ph)CNOH and NaN_3 in MeOH gives a tetranuclear cage (Fig. 30) with a $\{Mn_3^{II}Mn^{IV}(\mu_4\text{-}O)(\eta^1{:}\mu_2\text{-}N_3)\}^{7+}$ core; the four oximate anions behave as 2.111 ligands [96]. Magnetic and EPR (Fig. 31) studies show the cage has an $S = 6$ ground state.

Complexes $[Co_2^{III,III}Co^{II}\{(py)C(ph)NO\}_6](PF_6)_2$ and $[Co\{(py)C(ph)NO\}_3]$ are structurally similar to their $(py)CHNO^-$ partners. The use of $(py)C(ph)NO^-/MeCO_2^-$ and $(py)C(ph)NO^-/SO_4^{2-}$ "blends" in Ni(II) chemistry leads to a variety of structurally interesting clusters [84,97]. Of particular note are the complexes $[Ni_3\{(py)C(ph)NO\}_6]$ and $[Ni_6(OH)(SO_4)_4\{(py)C(ph)NO\}_3\{(py)C(ph)NOH\}_3(MeOH)_3]$; both complexes have been isolated from the $NiSO_4 \cdot 6H_2O/(py)C(ph)NOH/NaOMe$ reaction mixtures. In the former [84], the oximate ligands adopt four different coordination modes, including the unique 1.110 mode (Fig. 8) which gives rise to a six-membered chelating ring. The molecular structure of the latter consists of two parallel triangles (Fig. 32). The metal ions in the "small" triangle (defined by Ni(2), Ni(5) and Ni(6)) are held together by the μ_3-OH^-, the $\eta^1{:}\eta^1{:}\eta^1{:}\mu_3$-$SO_4^{2-}$ and the deprotonated oximate groups of the three 3.211 $(py)C(ph)NO^-$ ligands; this triangle can be viewed as an inverse 9-MC-3-subunit [67]. The metal ions in the "large" triangle (defined by Ni(1), Ni(3), Ni(4)) are held together by the three $\eta^1{:}\eta^2{:}\mu_3$-SO_4^{2-} groups. Monoatomic oxygen bridges from the

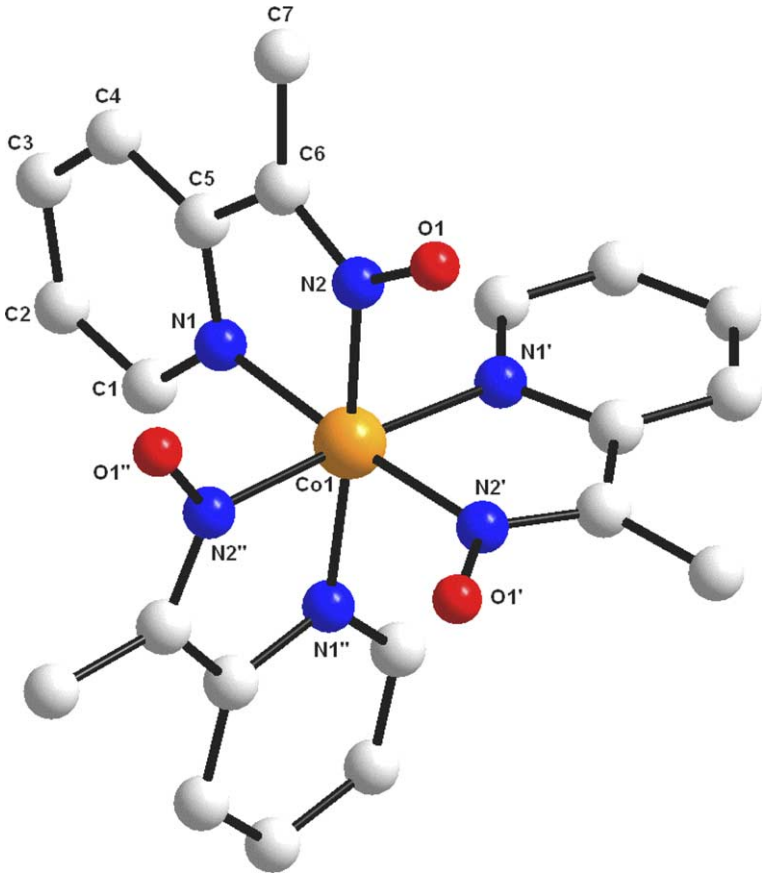

Fig. 24. Molecular structure of complex $[Co\{(py)C(Me)NO\}_3]$; the Co^{III} atom sits on a threefold axis of symmetry [59].

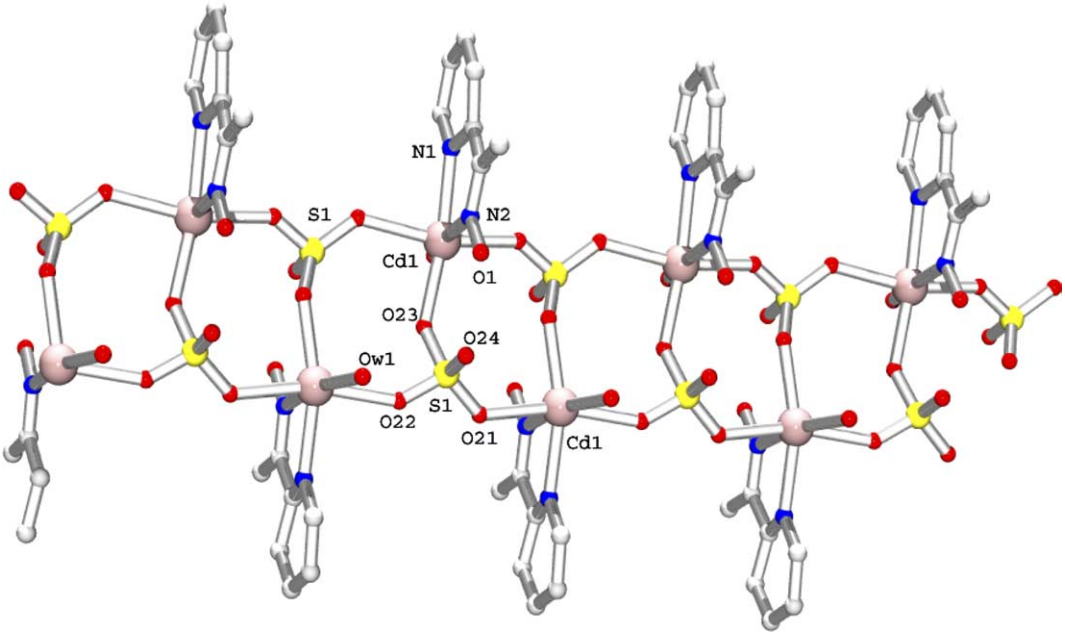

Fig. 25. A small portion of the double chain $[Cd(SO_4)\{(py)C(Me)NOH\}(H_2O)]_n$ present in the complex $\{[Cd(SO_4)\{(py)C(Me)NOH\}(H_2O)]\cdot[Cd(SO_4)\{(py)C(Me)NOH\}(H_2O)_2]\}_n$ [84].

$\eta^1:\eta^2:\mu_3$-SO_4^{2-} and the 3.211 (py)C(ph)NO$^-$ ligands link up the two triangles.

Despite the four complexes listed in Table 2, the Cu(II), Zn(II) and Cd(II) chemistry of (py)C(ph)NOH is virtually non-existent. In the dinuclear complex $[Cu_2(hfac)_2\{(py)C(ph)NO\}_2]$ (Fig. 33) [97], the two bridges are the oximato groups of the two 2.111 (py)C(ph)NO$^-$ ligands, whereas complexes $[M_2(SO_4)_2\{(py)C(ph)NOH\}_4]$ (M = Zn, Cd) contain neutral 1.011 oxime ligands and $\eta^1:\eta^1:\mu_2$ sulfato groups (Fig. 34) [84]. Complex $[Zn_4(OH)_2(N_3)_2\{(py)C(ph)NO\}_4]$ features [84] an inverse 12-metallacrown-4 motif,

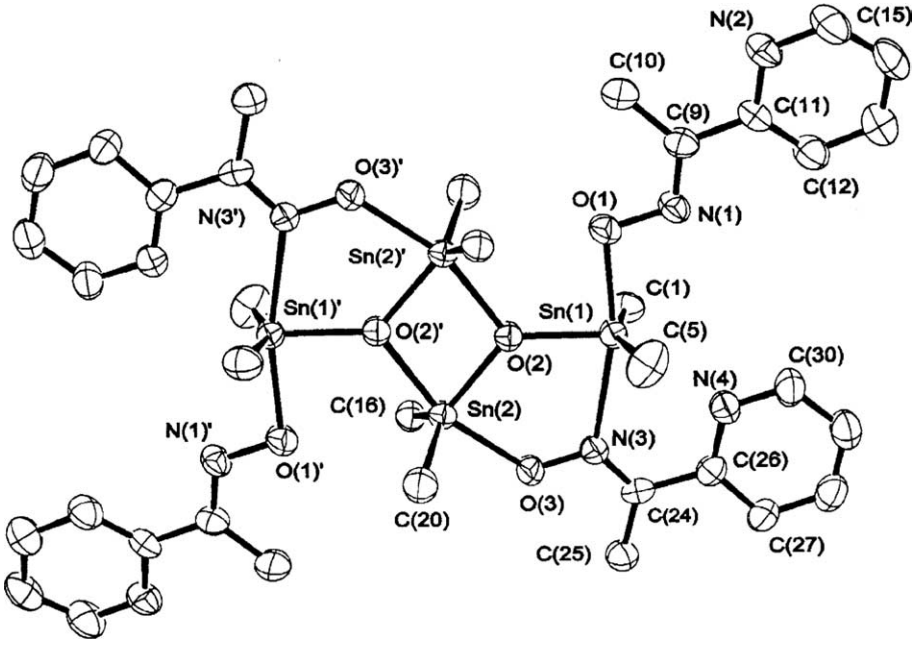

Fig. 26. X-ray structure of $[^nBu_8Sn_4O_2\{(py)C(Me)NO\}_4]$ [90].

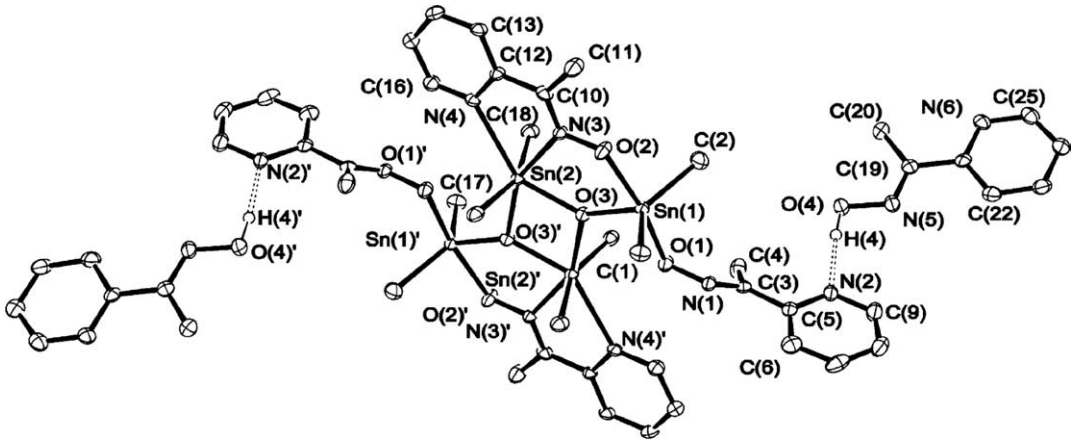

Fig. 27. X-ray structure of $[Me_8Sn_4O_2\{(py)C(Me)NO\}_4]\cdot 2(py)C(Me)CNOH$ [91].

like its $(py)CHNO^-$ [66] and $(py)C(Me)NO^-$ [84] chloro analogs.

5.6. Metal complexes of 2-acetylpyridine N-oxide oxime, (Opy)C(Me)NOH

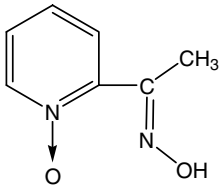

(Opy)C(Me)NOH

Strictly speaking this ligand is not a pyridyl oxime. The (Opy)C(Me)NOH ligand was first mentioned in the literature in 1977 in a paper describing Co(II) and Ni(II) complexes of 2-substituted pyridine *N*-oxides, although the synthesis of (Opy)C(Me)NOH was not detailed [98]. The detailed synthesis was reported in 1982 and involves the reaction of $NH_2OH\cdot HCl$ with 2-acetylpyridine *N*-oxide in warm H_2O in the presence of $NaO_2CMe\cdot 3H_2O$ [99].

The only metal complexes of (Opy)C(Me)NOH that have been structurally characterized are $[CoBr_2\{(Opy)C(Me)NOH\}_2]$ [100] and $[Co_2Cl_4\{(Opy)C(Me)NOH\}_2(MeOH)_2]$ [101]. The Co^{II} ion in the mononuclear complex is coordinated by two bromo ions and two $O_{N\text{-oxide}}$, N_{oxime}-bidentate chelating (Opy)C(Me)NOH ligands (1.101, Fig. 35) in a *cis–cis–trans* fashion (the *trans* donor atoms are the N_{oxime} atoms) [100]. The ligand adopts the 2.201 coordination mode (Fig. 35) in the centrosymmetric dinuclear complex [101]. Each Co^{II} ion has a six-coordinate O_3NCl_2 environment, produced by *O*,*N*-coordination from one ligand, bridging *N*-oxide bonding from the second ligand, two terminal chlorides and one coordinated MeOH.

5.7. Pyridine-3-carbaldehyde oxime, (3-py)CHNOH, and 1-pyridin-3-yl-ethanone oxime, (3-py)C(Me)NOH

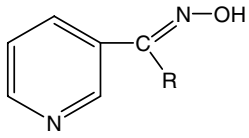

(3-py)CHNOH (R= H)

(3-py)C(Me)NOH (R= Me)

Compounds (3-py)CHNOH and (3-py)C(Me)NOH are the 3-pyridyl analogs (isomers) of (py)CHNOH (Section 5.2) and (py)C(Me)NOH (Section 5.4), respectively. The free ligand (3-py)CHNOH is commercially available. Its crystal structure has been determined [45]. Infinite 1D chains are assembled through a head-to-tail O–H···N hydrogen bond involving the oxime O–H and the pyridine nitrogen atom. Adjacent chains are related by a glide plane and the two chains are linked through a C–H···O hydrogen bond to form an 1D ribbon; the ribbons are arranged in a herringbone motif and are hydrogen bonded to neighboring ribbons via $C–H\cdots N_{oxime}$ interactions to produce an overall 3D hydrogen bonded structure. The free ligand (3-py)C(Me)NOH can be synthesized by the reaction of 3-acetylpyridine, (3-py)C(Me)O, with $NH_2OH\cdot HCl$ in $EtOH/H_2O$ under reflux in the presence of excess Na_2CO_3 [45]. In the crystal structure of this compound, the molecules form infinite 1D chains assembled through a head-to-tail $O–H\cdots N_{pyridine}$ hydrogen bond; additional $C–H\cdots N_{oxime}$ and C–H···O hydrogen bonds cross-link the 1D chains to produce a 3D hydrogen bonded infinite architecture [45]. In contrast to their 2-pyridyl analogs, the published coordination chemistry of (3-py)CHNOH and (3-py)C(Me)NOH is very limited.

Aakeröy and co-workers [102,103] have employed (3-py)CHNOH and (3-py)C(Me)NOH as versatile tools

Table 2
Structurally characterized metal complexes containing (py)C(ph)NOH and/or (py)C(ph)NO$^-$ligands

Complex[a]	Coordination mode of the oxime/oximate ligand	Coordination spheres; coordination geometries	Reference
$[Mn(O_2CPh)_2\{(py)C(ph)NOH\}_2]$	1.011	*cis*,*cis*,*trans*-$Mn^{II}O_2(N_{py})_2(N_{ox})_2$; oct	[82]
$[Mn_4{}^{II}Mn_4{}^{III}O_2(OH)_2(O_2CPh)_{10}\{(py)C(ph)NO\}_4]$	2.111	$Mn^{II}(\mu_4\text{-}O)(\mu_3\text{-}OH)(O_{carb})_4$, $Mn^{II}(\mu_3\text{-}OH)(O_{carb})_3N_2$, $Mn^{III}(\mu_4\text{-}O)_2(O_{carb})_3(O_{ox})$, $Mn^{III}(\mu_4\text{-}O)(\mu_3\text{-}OH)(O_{carb})(O_{ox})N_2$; oct, oct, oct, oct	[94,95]
$[Mn_3{}^{II}Mn^{IV}O(N_3)(O_2CPh)_3\{(py)C(ph)NO\}_4]$	2.111	$Mn^{II}(\mu_4\text{-}O)(O_{carb})_2(O_{ox})(N_{py})(N_{ox})$, $Mn^{II}(\mu_4\text{-}O)(O_{carb})_2(N_{azido})N_2$, $Mn^{IV}(\mu_4\text{-}O)(O_{ox})_3(N_{py})(N_{ox})$; oct, oct, oct	[96]
$[Co_2{}^{III}Co^{II}\{(py)C(ph)NO\}_6](PF_6)_2$	2.111	*fac*-$Co^{III}N_6$, $Co^{II}O_6$; oct	[59]
$[Co\{(py)C(ph)NO\}_3]$	1.011	*mer*-$Co^{III}N_6$; oct	[59]
$[Ni(O_2CPh)_2\{(py)C(ph)NOH\}_2]$	1.011	*cis*,*cis*,*trans*-$Ni^{II}O_2(N_{py})_2(N_{ox})_2$; oct	[97]
$[Ni_4(O_2CMe)_2(NCS)_2\{(py)C(ph)NO\}_4(PrOH)(H_2O)]$	3.211	$Ni^{II}(O_{carb})(O_{ox})_2(N_{isothiocyanato})(N_{py})(N_{ox})$, $Ni^{II}(O_{carb})(O_{aqua/PrOH})(O_{ox})_2(N_{py})(N_{ox})$; oct	[97]
$[Ni_4(O_2CMe)_4\{(py)C(ph)NO\}_4(MeOH)_2]$	3.211	$Ni^{II}(O_{carb})_2(O_{ox})_2N_2$, $Ni^{II}(O_{carb})(O_{ox})_2(O_{MeOH})N_2$; oct, oct	[97]
$[Ni_3\{(py)C(ph)NO\}_6]$	1.110, 1.011, 2.111, 3.211	$Ni^{II}O_2N_4$; oct	[84]
$[Ni\{(py)C(ph)NOH\}_3](SO_4)$	1.011	*fac*-$Ni^{II}N_6$; oct	[84]
$[Ni_2(SO_4)_2\{(py)C(ph)NOH\}_4]$	1.011	$Ni^{II}(O_{sulf})_2N_4$; oct	[84]
$[Ni_6(OH)(SO_4)_4\{(py)C(ph)NO\}_3\{(py)C(ph)NOH\}_3(MeOH)_3]$	3.211, 1.011	$Ni^{II}(\mu_3\text{-}OH)(O_{sulf})_2(O_{ox})N_2$, $Ni^{II}(O_{sulf})_2(O_{MeOH})(O_{ox})N_2$; oct, oct	[84]
$[Cu_2(hfac)_2\{(py)C(ph)NO\}_2]$	2.111	$Cu^{II}(O_{hfac})_2(O_{ox})N_2$; spy	[97]
$[Zn_4(OH)_2(N_3)_2\{(py)C(ph)NO\}_4]$	2.111	$Zn^{II}(\mu_3\text{-}OH)(O_{ox})_2(N_{azido})$, $Zn^{II}(\mu_3\text{-}OH)_2(N_{py})_2(N_{ox})_2$; tet, oct	[84]
$[Zn_2(SO_4)_2\{(py)C(ph)NOH\}_4]$	1.011	$Zn^{II}(O_{sulf})_2N_4$; oct	[84]
$[Cd_2(SO_4)_2\{(py)C(ph)NOH\}_4]$	1.011	$Cd^{II}(O_{sulf})_2N_4$; oct	[84]

Abbreviations: N_{ox}, oxime or oximate nitrogen; N_{py}, 2-pyridyl nitrogen; O_{carb}, carboxylate oxygen; O_{ox}, oximate oxygen; O_{sulf}, sulfate oxygen; oct, octahedral; spy, square pyramidal; tet, tetrahedral.

[a] Solvate molecules have been omitted.

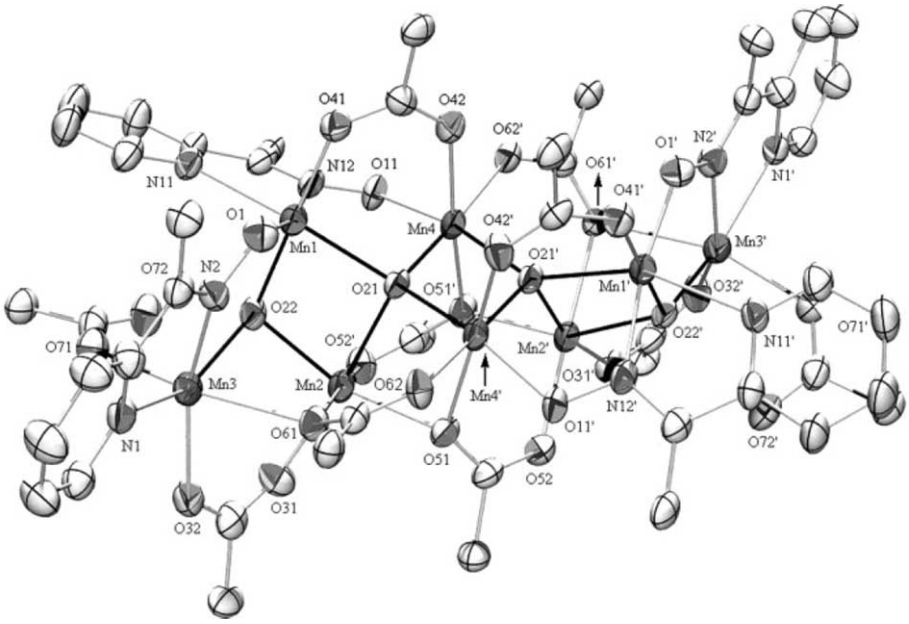

Fig. 28. X-ray structure of complex $[Mn_8O_2(OH)_2(O_2CPh)_{10}\{(py)C(ph)NO\}_4]$; only the *ipso* carbon atoms of the phenyl groups of the benzoato and oximato ligands are shown.

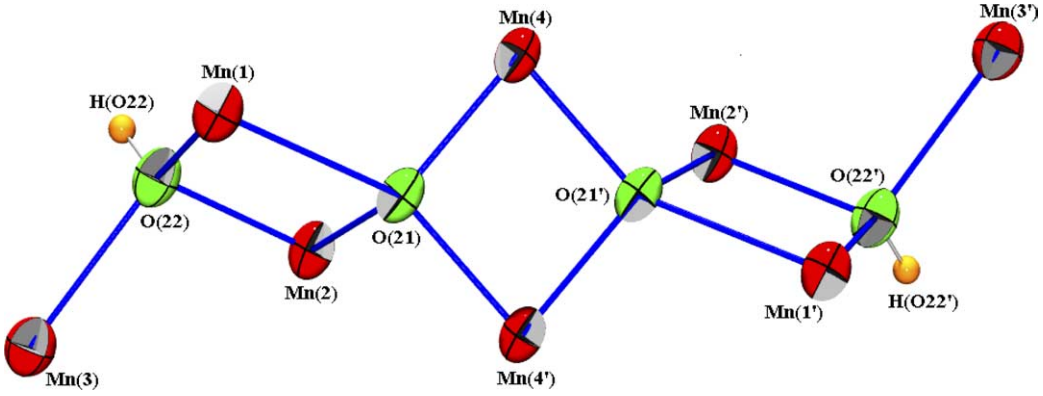

Fig. 29. ORTEP representation of the $\{Mn_8(\mu_4\text{-}O)_2(\mu_3\text{-}OH)_2\}^{14+}$ core. Mn(2), Mn(2′), Mn(3) and Mn(3′) are Mn^{II} atoms.

for supramolecular assembly of silver(I)- and copper(I)-containing hydrogen-bonded architectures. The crystal structure of $[Ag\{(3\text{-py})CHNOH\}_2](PF_6)$ [102] contains cations (Fig. 36) comprised of two ligands coordinated through the 3-pyridyl nitrogen atoms to a Ag^I ion (coordination mode 1.010, Fig. 37). The oxime moieties are *cis* with respect to each other, and cations are linked by complementary O–H···N hydrogen bonds between oxime moieties on neighboring ligands (**I** in Fig. 4), generating infinite 1D chains. Adjacent chains are linked by C–H···O hydrogen bonds, resulting in 2D cationic sheets, Fig. 36. The PF_6^- counterions occupy the resulting "holes" within the cationic sheet, and are held in position by several C–H···F hydrogen bonds. The result is an anisotropic, lamellar structure. The crystal structure of $[Ag\{(3\text{-py})CHNOH\}_2](ClO_4)$ [102] is very similar to that of the PF_6^- salt, even though the size of the anion has changed significantly from the PF_6^- to the ClO_4^- salt (molecular volumes of 72 and 55 $Å^3$, respectively).

The crystal structure of $[Ag\{(3\text{-py})C(Me)NOH\}_2](PF_6)$ [102] contains cations comprised of two 1.010 ligands. The oxime moieties are arranged *trans* with respect to each other and neighboring cations are linked by oxime O–H···N hydrogen bonds, $R_2^2(6)$, into 1D chains. The chains are arranged within well-defined 3D regions, connected by intermolecular hydrogen bonds. The anions, positioned *between* layers, act as "bridges", via C–H···F hydrogen bonds (Fig. 38). The crystal structure of $[Ag\{(3\text{-py})C(Me)NOH\}_2](ClO_4)$ [102] is very similar to that of the PF_6^- salt.

The persistence of the intermolecular $R_2^2(6)$ motif in the presence of different counterions and ligand substituents in the crystal structures of the above described Ag(I) complexes is testimony to the utility of the oxime

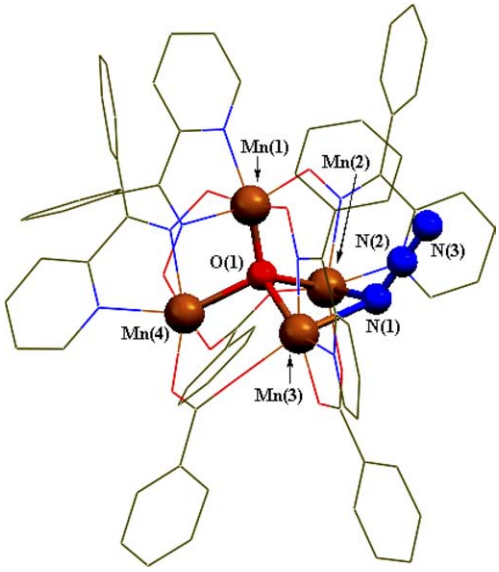

Fig. 30. The molecular structure of the complex $[Mn_3^{II}Mn^{IV}O(N_3)(O_2CPh)_3\{(py)C(ph)NO\}_4]$ emphasizing its core.

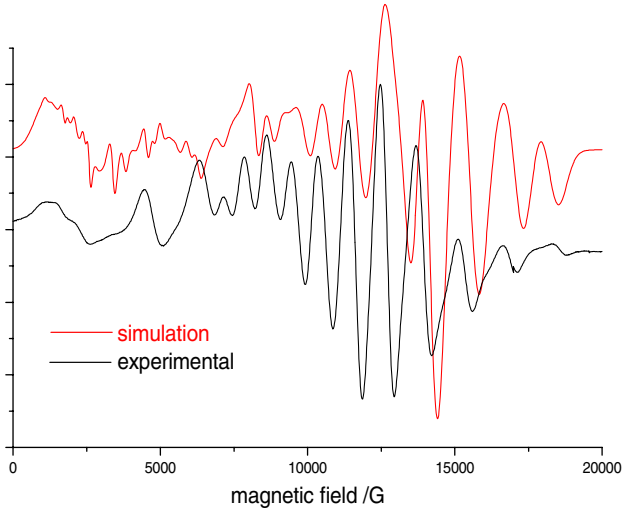

Fig. 31. The measured and simulated Q-band EPR spectra for the complex $[Mn_4O(N_3)(O_2CPh)_3\{(py)C(ph)NO\}_4]$.

moiety as a versatile intermolecular connector which can allow coordination complexes to be directed into ordered networks.

In the crystal structure of $[CuI\{(3\text{-py})CHNOH\}]_n$ [103] each tetrahedral Cu^I atom is coordinated to three μ_3-I^- ligands to generate an infinite 1D motif consisting of "staircases" of CuI; the (3-py)CHNOH ligand is

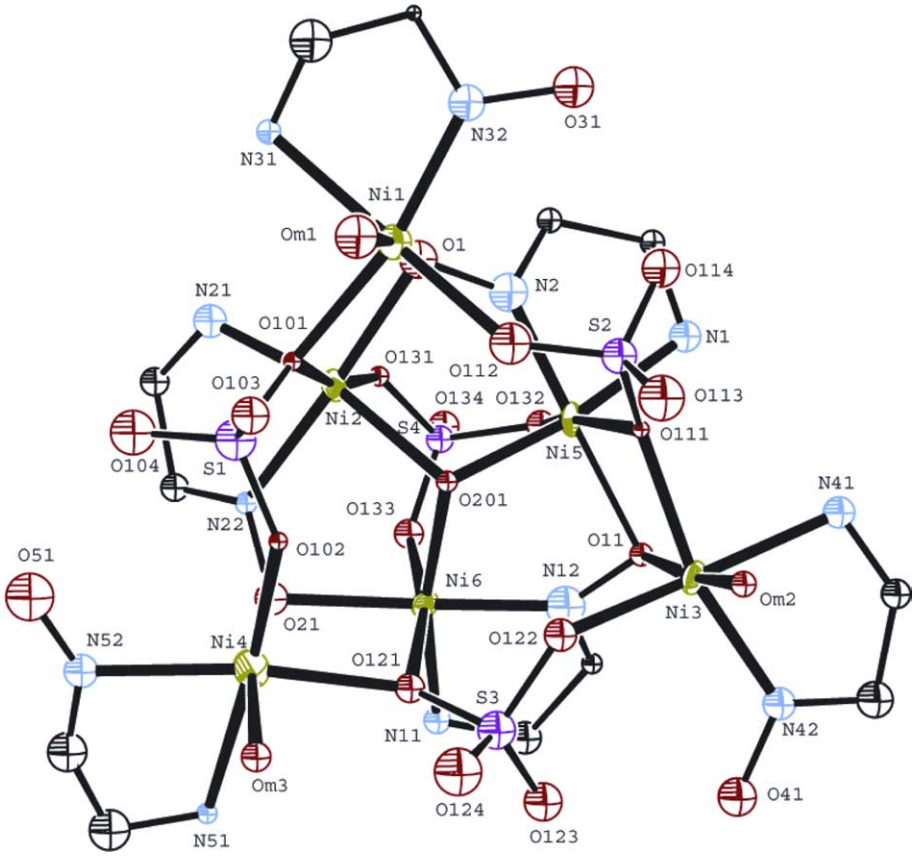

Fig. 32. X-ray structure of $[Ni_6(OH)(SO_4)_4\{(py)C(ph)NO\}_3\{(py)C(ph)NOH\}_3(MeOH)_3]$. Only the two carbon atoms that intervene between the nitrogen atoms of (py)C(ph)NOH and $(py)C(ph)NO^-$ are shown.

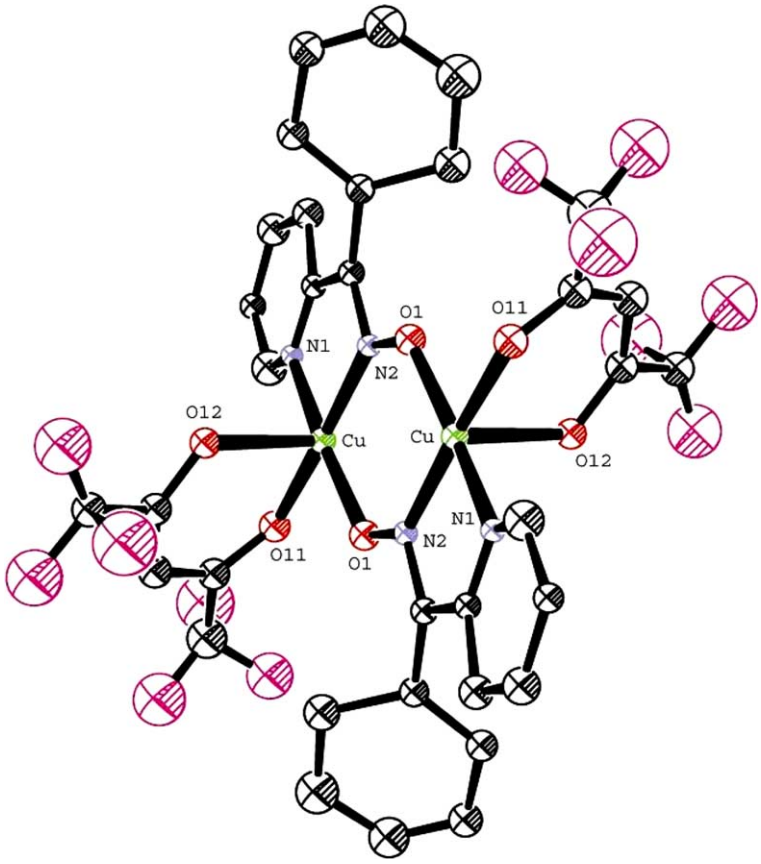

Fig. 33. X-ray structure of $[Cu_2(hfac)_2\{(py)C(ph)NO\}_2]$.

attached to each metal ion through the 3-pyridyl nitrogen atom, to complete the coordination sphere. Adjacent oxime moieties are connected via O–H···N hydrogen bonds, in a catemer-like fashion, to propagate the 1D polymeric chains into an infinite 2D sheet (Fig. 39).

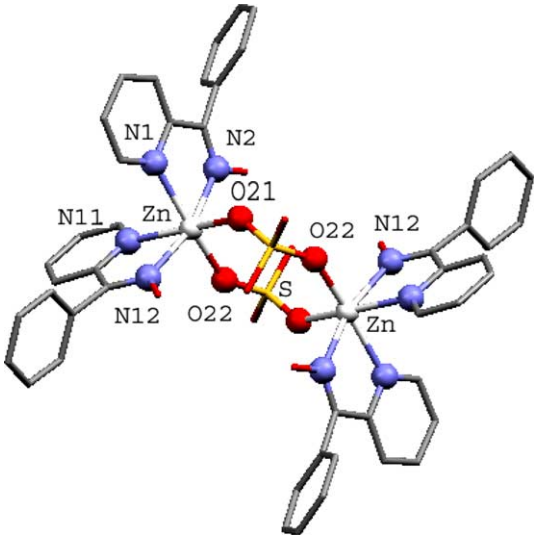

Fig. 34. Molecular structure of the complex $[Zn_2(SO_4)_2\{(py)C(ph)NOH\}_4]$.

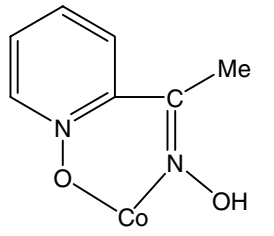

1.101

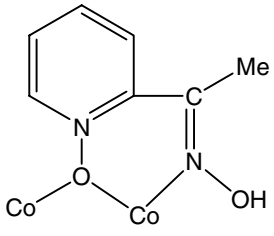

2.201

Fig. 35. The coordination modes of (Opy)C(Me)NOH in its structurally characterized Co(II) complexes.

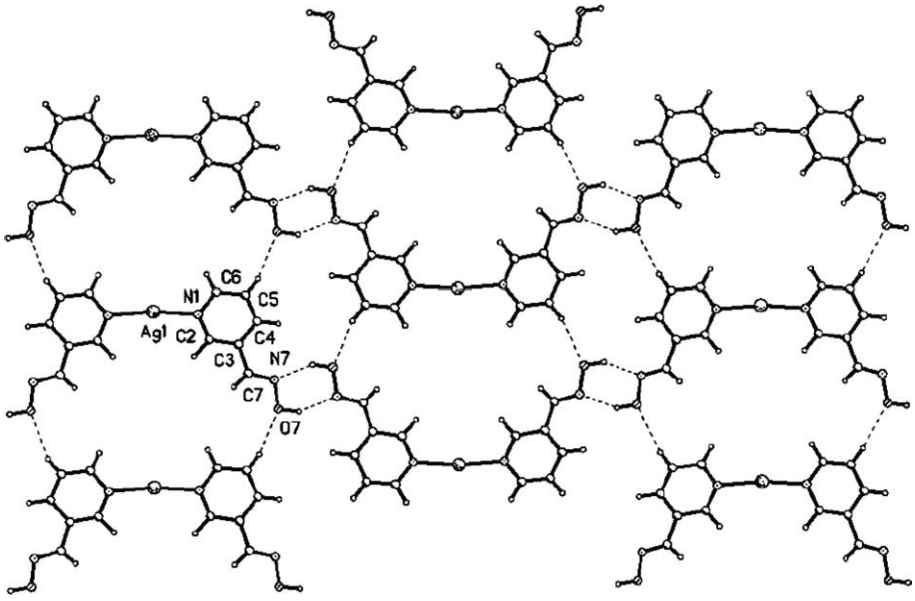

Fig. 36. Hydrogen-bonded cationic sheet in $[Ag\{(3\text{-py})CHNOH\}_2](PF_6)$ [102].

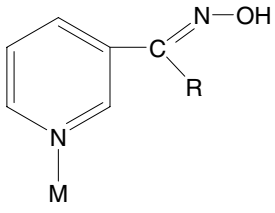

1.010; R= H, Me

Fig. 37. The crystallographically established coordination mode of the ligands (3-py)CHNOH and (3-py)C(Me)NOH in their Ag(I) and Cu(I) complexes.

5.8. Pyridine-4-carbaldehyde oxime, (4-py)CHNOH

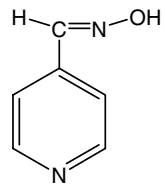

(4-py)CHNOH

The free ligand is commercially available. In a general project that is aimed at assembling metal complexes through hydrogen bonds to form porous molecular materials, Aakeröy and co-workers [104] synthesized the complex $[Ni\{(4\text{-py})CHNOH\}_4(H_2O)_2]Br_2 \cdot 6H_2O$2-(4-py)CHNOH. The ligand adopts the 1.010 coordination mode (see Fig. 40).

The oxime hydroxy groups link through complementary O–H···O hydrogen bonds to form sheets with large, hourglass-shaped holes. The sheets are cross-linked by hydrogen bonds between the axially coordinated H_2O molecules and the bromide counterions, forming a 3D network, where the large holes are aligned into channels. Twofold interpenetration of the 3D network blocks the center of the large hole, leaving two smaller channels at each end. A host–guest complex is formed, and the guest molecules, (4-py)CHNOH, are contained inside the channels, held in the lattice by hydrogen bonds to the bromide ion and the coordinated oxime ligands. The structure of this complex demonstrates that an octahedral system can generate a 3D network with holes large enough to hold relatively small organic molecules.

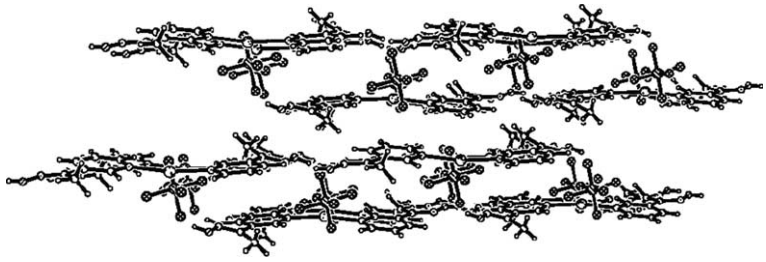

Fig. 38. Edge-on view of the packing in $[Ag\{(3\text{-py})C(Me)NOH\}_2](PF_6)$, with PF_6^- anions positioned between cationic sheets [102].

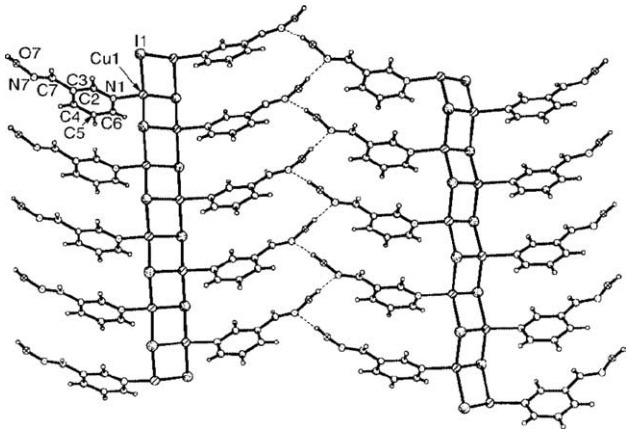

Fig. 39. Infinite 2D sheets of $[CuI\{(3\text{-py})CHNOH\}]_n$ [103].

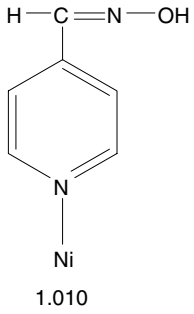

1.010

Fig. 40. The coordination mode of (4-py)CHNOH in the structurally characterized complex $[Ni\{(4\text{-py})CHNOH\}_4(H_2O)_2]Br_2 \cdot 2(4\text{-py})CHNOH$.

6. Ligands containing two oxime groups and one or two pyridyl groups, with no other donor atoms

6.1. 1-[6-(1-Hydroxyimino-ethyl)pyridin-2-yl]-ethanone oxime, (py){C(Me)NOH}$_2$

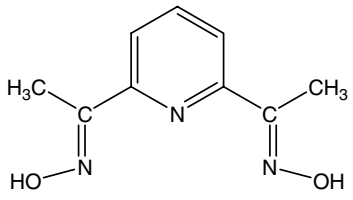

$(py)\{C(Me)NOH\}_2$

The free ligand can be synthesized [105,106] by the reaction of 2,6-diacetylpyridine, $(py)\{C(Me)O\}_2$, with 2 equiv. of $NH_2OH \cdot HCl$ and 2 equiv. of NaOH in $MeOH/H_2O$ under heating. The two oxime groups have strongly overlapping titration curves; the pK_{a1} and pK_{a2} values are ~10.1 and ~10.8, respectively [107]. The ligand was first investigated by Hartkamp [108], who reported that aqueous Ni(II) solutions of $(py)\{C(Me)NOH\}_2$ are oxidized by air. The ligand was also investigated by Irvine and co-workers [107], who studied Fe(II) complexes in solution. It was found that pK_a for the ligand dropped markedly upon coordination, an effect that was attributed to resonance stabilization of the anionic conjugate base.

Early solid-state coordination chemistry with this ligand involved nickel. Following Hartkamp's report [108], Baucom and Drago [105] isolated several complexes, including $[Ni\{(py)\{C(Me)NOH\}_2\}_2]^{2+}$, the deprotonated species $[Ni\{(py)\{C(Me)NO\}_2\}_2]^{2-}$ and the formally Ni(IV) complex $[Ni\{(py)\{C(Me)NO\}_2\}_2]$. Subsequently, Sproul and Stucky [109] reported the crystal structure of $[Ni\{(py)\{C(Me)NO\}_2\}_2]$ (Fig. 41), and showed that the ligand is planar with coordination through nitrogen (1.00111, Fig. 42) and that considerable strain is introduced into the $(py)\{C(Me)NO\}_2^{2-}$ moiety when it coordinates to Ni^{IV}. A comparison of the nickel-nitrogen bond distances with those found in analogous Ni(II) complexes suggests a shortening of 0.17 Å in the Ni^{IV}–N bond.

X-ray structures of cationic octahedral complexes of the general formula $[M\{(py)\{C(Me)NOH\}_2\}_2]X_2$, where M = Mn, X = ClO_4 [106], M = Fe, X = Cl [110] and M = Cu, X = ClO_4 (Fig. 43) [106] have been reported. X-ray diffraction studies of the 1:1 five-coordinate

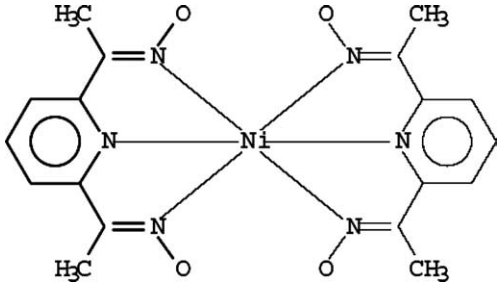

Fig. 41. A structural drawing of $[Ni^{IV}\{(py)\{C(Me)NO\}_2\}_2]$.

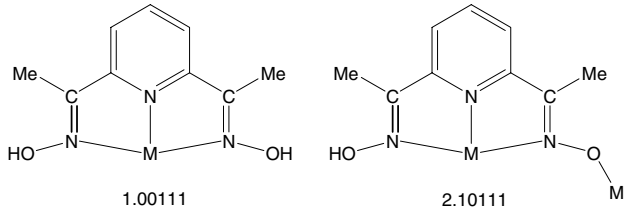

1.00111 2.10111

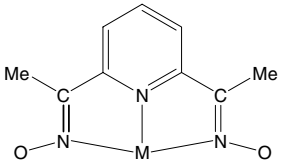

1.00111

Fig. 42. The crystallographically established coordination modes of $(py)\{C(Me)NOH\}_2$ and its mono- and dianionic forms.

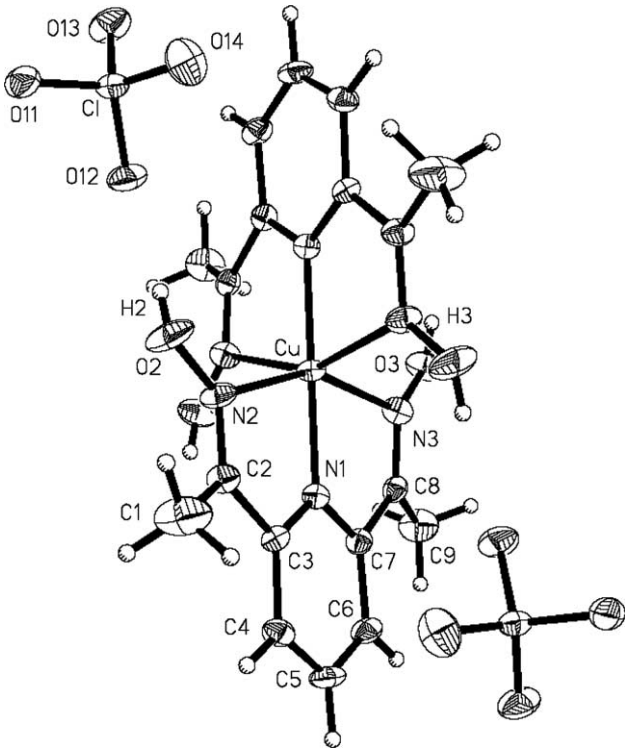

Fig. 43. X-ray structure of $[Cu\{(py)\{C(Me)NOH\}_2\}_2](ClO_4)_2$ [106].

complexes $[M\{(py)\{C(Me)NOH\}_2\}Cl_2]$, where M = Cu and Zn (Fig. 44), were also performed [111]. For the Cu(II) complex, the coordination environment about the metal center resembles a distorted square pyramid with a chloro ligand at the apex. For the Zn(II) complex, the environment about the metal ion can be viewed as a distorted trigonal bipyramid, with the equatorial positions occupied by the two chloro ligands and the pyridine nitrogen. A second form (monoclinic) of the Cu(II) complex was structurally characterized in 1994 [112]. The stoichiometrically similar Mn(II) complex [113,114], $[Mn\{(py)\{C(Me)NOH\}_2\}Cl_2]_n$, has an interesting polymeric structure. The metal ion coordinates to form pentagonal bipyramids $Mn^{II}(N_3Cl_2)Cl_2$ in which each chloro ligand occupies axial and equatorial sites on

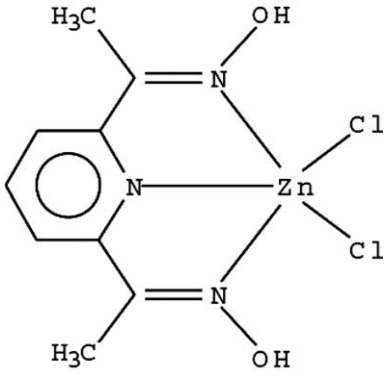

Fig. 44. A structural drawing of $[Zn\{(py)\{C(Me)NOH\}_2\}Cl_2]$.

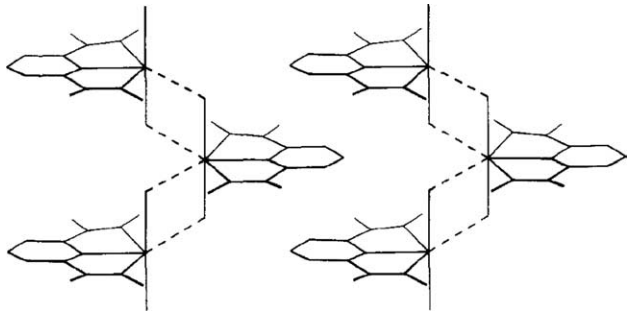

Fig. 45. View of small portions (three monomer units) of two chains in complex $[Mn\{(py)\{C(Me)NOH\}_2\}Cl_2]_n$ [113].

adjacent monomer units in the helical chains (Fig. 45). Variable-temperature magnetic susceptibility studies [112] indicate weak ferromagnetic coupling.

The (2,6-diacetylpyridine dioxime)copper(II) unit is also present in the trinuclear cluster $[Cu_3\{(py)\{C(Me)NOH\}_2\}_2Cl_6]$ [115]. The complex is a "sandwich" made of two $Cu\{(py)\{C(Me)NOH\}_2\}Cl^+$ cationic units (the "bread") and a $CuCl_4^{2-}$ anionic unit (the "filling"); the latter can be viewed as a bis(monodentate) "bridging" ligand, see Fig. 46. The three Cu^{II} centers are ferromagnetically coupled.

A series of monomeric In(III) complexes containing neutral 1.00111 $(py)\{C(Me)NOH\}_2$ ligands are also known. The ligand reacts with $InCl_3$ in MeOH to give the seven-coordinate complex $[InCl_3\{(py)\{C(Me)NOH\}_2\}(MeOH)]$ (Fig. 47) [116]. The MeOH ligand can be replaced by Cl^- or H_2O to give the complex anion $[InCl_4\{(py)\{C(Me)NOH\}_2\}]^-$ and $[InCl_3\{(py)\{C(Me)NOH\}_2\}(H_2O)]$, respectively. The pentagonal bipyramidal coordination environment of the metal is preserved during the substitution reactions [116]. The MeOH-containing complex can react with bidentate

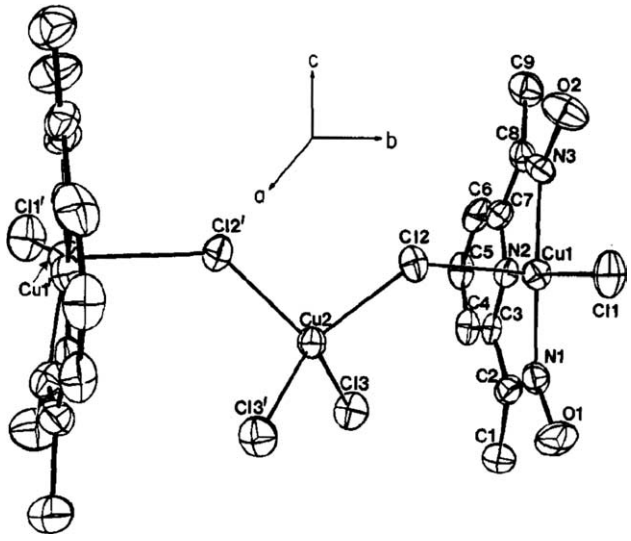

Fig. 46. The "sandwich" structure of $[Cu_3\{(py)\{C(Me)NOH\}_2\}_2Cl_6]$ [115].

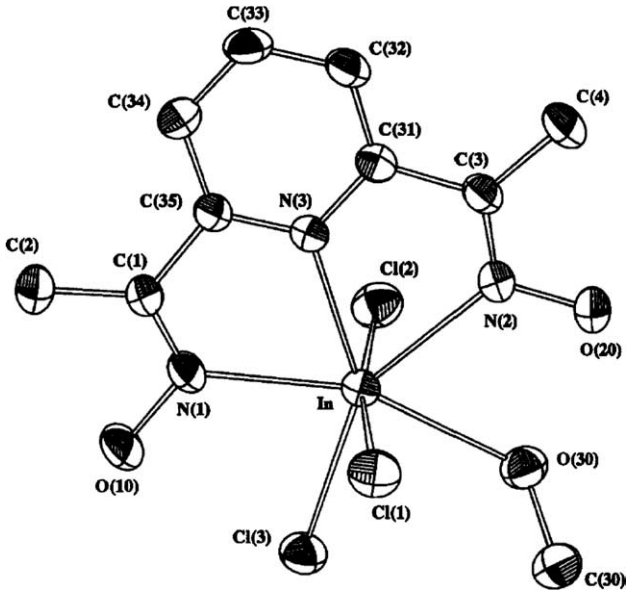

Fig. 47. X-ray structure of $[InCl_3\{(py)\{C(Me)NOH\}_2\}(MeOH)]$ [116].

ligands by ligand exchange [117]. A seven-coordinate complex of the composition $[InCl(ox)\{(py)\{C(Me)NOH\}_2\}(H_2O)]$ is formed with potassium oxalate (K_2ox); the oxalato(−2) ligand occupies the equatorial plane of a pentagonal bipyramid together with the tridentate chelating oxime. With sodium 1,2-dicyanoethene-1,2-dithiolate (Na_2mnt) the analogous reaction produces the six-coordinate, mixed-ligand complex $[InCl(mnt)\{(py)\{C(Me)NOH\}_2\}]$, which has a distorted octahedral coordination sphere (Fig. 48). Ligands which form four-membered chelate rings, like dialkyldithiocarbamates or pyridine-2-thiolate, are able to replace all ligands of $[InCl_3\{(py)\{C(Me)NOH\}_2\}(MeOH)]$ to form neutral tris chelates [117].

We have up to now discussed in this part metal complexes containing the neutral, $(py)\{C(Me)NOH\}_2$, or the dianionic, $(py)\{C(Me)NO\}_2^{2-}$, ligand. Two complexes containing the monoanionic ligand $(py)\{C(Me)NOH\}\{C(Me)NO\}^-$ have been also reported. Complex $[Cu\{(py)\{C(Me)NOH\}_2\}_2Cl_2]$ [111] is remarkably acidic [118], the value of pK_a being 2.8 at 25 °C. Deprotonation of this complex in alcoholic solution leads to the dinuclear dication $[Cu_2\{(py)\{C(Me)NOH\}\{C(Me)NO\}\}_2(H_2O)_2]^{2+}$ which has been isolated [118] as the chloride or tetrafluoroborate salt. The crystal structure of the latter has been determined [119] to establish the coordination mode of the monoanionic ligand, see Fig. 49. The structural analysis revealed that the nearly planar $(py)\{C(Me)NOH\}\{C(Me)NO\}^-$ ion behaves as a bridging tetradentate ligand adopting the 2.10111 coordination mode, see Fig. 42. The same coordination mode is adopted by the ligand in the mixed-valence trinuclear cluster $[Fe^{II}\{(py)\{C(Me)NOH\}\{C(Me)NO\}\}_2$-$Fe_2^{III}(\mu\text{-}O)Cl_4]$ [110].

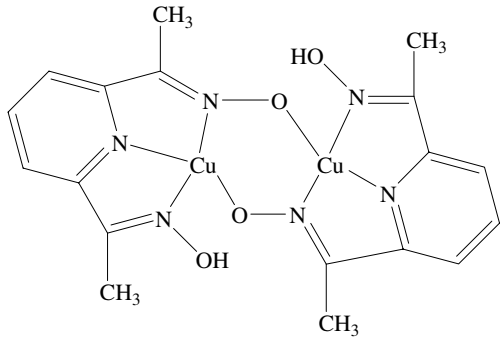

Fig. 49. A structural drawing of the dinuclear dication $[Cu_2\{(py)\{C(Me)NOH\}\{C(Me)NO\}\}_2(H_2O)_2]^{2+}$; the weakly bound aqua ligands have been omitted for clarity.

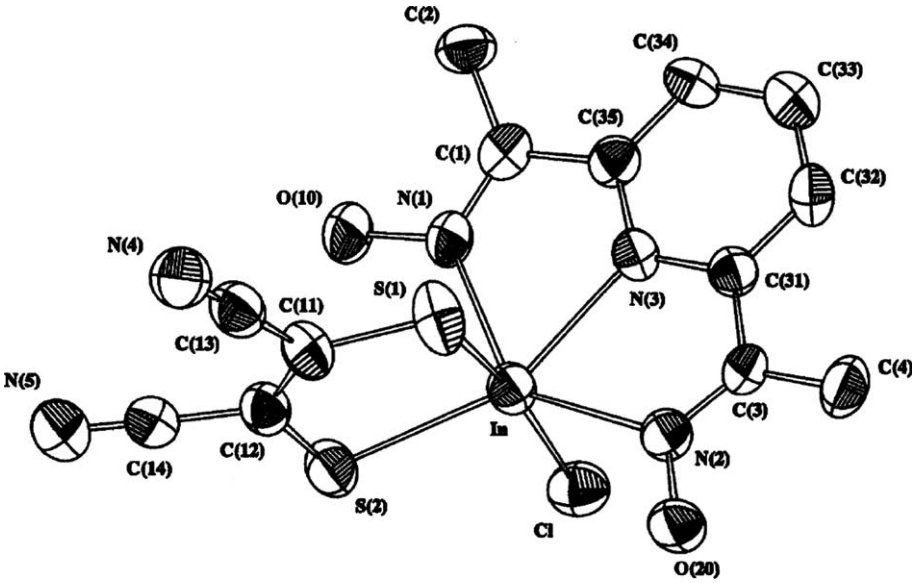

Fig. 48. X-ray structure of $[InCl(mnt)\{(py)\{C(Me)NOH\}_2\}]$ [117].

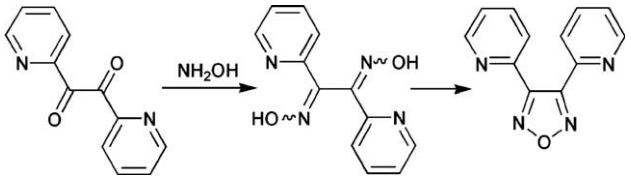

Scheme 5. Synthesis of (py)(CNOH)$_2$(py) and 3,4-di(2-pyridyl)-1,2,5-oxadiazole.

The kinetics and mechanism of ester hydrolysis by metal complexes of (py){C(Me)NOH}$_2$ and (py){C(Me)NOH} {C(Me)NO}$^-$ were studied by Yatsimirsky's group a few years ago [120,121]. The rate constants of the cleavage of 4-nitrophenyl acetate by the ligand over the pH interval 6–8 increase 10^3–10^4 times in the presence of Pb(II), Mn(II) and Cd(II), and 2–100 times in the presence of Ni(II), Hg(II), Pr(III) and Zn(II). The reactive species are monomeric complexes of the type M{(py){C(Me)NOH}{C(Me)NO}}$^+$.

6.2. Di-2-pyridylglyoxal dioxime, (py)(CNOH)$_2$(py)

The free ligand was first reported in 2002 as an intermediate in the synthesis of 3,4-di(2-pyridyl)-1,2,5-oxadiazole [122], see Scheme 5. The dioxime was prepared, in 52% yield, by reacting the commercially available diketone di-2-pyridylglyoxal (2,2′-pyridil) with an excess of aqueous NH_2OH. The compound was characterized by melting point, ^{1}H and ^{13}C NMR spectroscopy, positive-ion EI mass spectrometry and elemental analysis. Subsequent heating of the dioxime at 185 °C for 18 h in a sealed tube effected cyclodehydration to give the substituted oxadiazole [122].

7. Ligands containing one pyridyl group, one oxime group and a third donor group

7.1. Hydroxyimino-pyridin-2-yl-acetonitrile, (py)C(CN)NOH, and the 2-quinolyl analogue

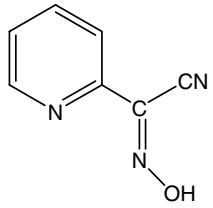

(py)C(CN)NOH

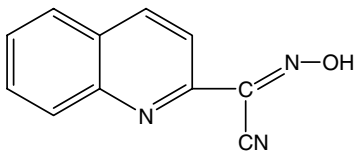

(qu)C(CN)NOH

These compounds belong to a relatively new class of ligands which have the general name cyanoximes. The coordination chemistry of cyanoximes first received detailed attention about two decades ago [123,124]. These ligands have the general formula RC(CN)NOH, where R is usually an electron withdrawing group such as an amide, ester or keto group [125]. The presence of the cyano group close to the oxime fragment makes the acidity of cyanoximes about 10^3–10^5 times greater than that of common oximes or dioximes. Thus, all currently known cyanoximes readily form yellow-colored conjugated anions in water or alcoholic solutions. The deprotonated cyanoximes form numerous complexes with different metal ions [126–131]. These anions demonstrate ambidentate properties participating in complex formation through different donor atoms in complexes with different metal ions. In addition, some cyanoximes and their metal complexes have demonstrated biological activities such as growth-regulating [132], antimicrobial [133], detoxifying agricultural pesticide [134] and antiproliferating [131] properties.

The free ligands (py)C(CN)NOH and (qu)C(CN)NOH are synthesized by the reaction of equimolar quantities of 2-pyridylacetonitrile and 2-quilonylacetonitrile, respectively, and KNO_2 in glacial CH_3COOH at −50 °C [135]. The structures of the two free ligands have been determined by single-crystal X-ray crystallography [135]. There are two planar fragments in the molecular structure of (py)C(CN)NOH, the 2-pyridyl group and the cyanoxime NCCNO group. The dihedral angle between these planes is 10.6(1)°. This compound exists in a *cis–anti* configuration with respect to the orientation of the CNO group and the nitrogen atom of the 2-pyridyl ring. The crystal structure of the monohydrate of (qu)C(CN)NOH, (qu)C(CN)NOH · H_2O, reveals that the molecule adopts a *trans–anti* configuration (see the structural formulae of the free ligands in the beginning of this part). Compound (qu)C(CN)NOH exhibits a nitroso-oxime equilibrium in polar solvents [136].

The crystal structure of [Tl{(py)C(CN)NO}]$_n$ reveals polymer formation (Fig. 50) [137]. The anionic ligand is planar, exists in its nitroso form and adopts the *cis–anti* conformation; it exhibits a simultaneously chelating and bridging behavior. Compound [Cs{(py)C(CN)NO}]$_n$ is also polymeric. The anionic ligand is planar, exists in its nitroso form and adopts the *trans–anti* configuration [138]. Complexes of the general composition

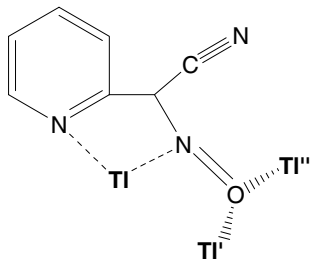

3.2110

Fig. 50. The basic unit in compound [Tl{(py)C(CN)NO}]$_n$.

$[M\{(py)C(CN)NO\}_2L_2]$, where M = Fe^{II}, Ni^{II}, Cu^{II} and L = pyridine, 3-picoline, have been prepared [139]. The authors used spectroscopic methods to propose the structures of the complexes. Based on such data the complexes appear to have monomeric, *trans*-octahedral structures in the solid state. The anionic ligand seems to adopt its nitroso form exhibiting the *N*(2-pyridyl), *N*(nitroso)-chelating mode. The anions $(py)C(CN)NO^-$ and $(qu)C(CN)NO^-$ have an important analytical application as reagents for the photometric determination of Fe^{2+}, because of the great stability and large molar absorptivities of the low-spin, 1:3 monoanionic Fe(II) complexes [135]. It has been established that the presence of other metal ions, such as Co^{2+}, Mn^{2+} and Ni^{2+}, does not affect the quantitative determination of Fe^{2+}.

7.2. *N*-Hydroxy-pyridine-2-carboxamidine, $(py)C(NH_2)NOH$

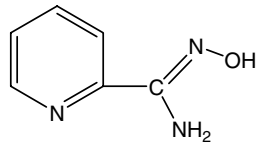

$(py)C(NH_2)NOH$

Amidoximes and their metal complexes find a wide range of applications in technology, medicinal chemistry and agriculture [140]. As a bidentate ligand, $(py)C(NH_2)NOH$ incorporates the structural features of pyridine-2-carbaldehyde oxime (Section 5.2) and 2-pyridylamine, $(py)CH_2NH_2$, in a single molecule. The experimental procedure for its synthesis [141] consists of liberating the hydroxylamine from its hydrochloride by means of sodium carbonate in water, adding an equivalent amount of 2-cyanopyridine and enough ethanol to obtain a clear solution, and finally keeping the mixture at 85 °C for 2 h; the yield of the crude product can reach 98%. The crystal structure of the free ligand [142] reveals that the molecule exists as the *syn* isomer (Fig. 51), with the N atom of the 2-pyridyl ring on the same side of the exocyclic C–C bond as the NH_2 group.

$(py)C(NH_2)NOH$ had been known to form stable complexes with various metal ions (characterized by spectroscopic methods) [143], some of which were exploited in analytical chemistry [144]. Few transition metal complexes containing the neutral ligand have been structurally characterized [142,145–147]. The X-ray structure of $[Cu\{(py)C(NH_2)NOH\}_2(H_2O)]Cl_2$ (Fig. 52) was reported independently by two groups in 1989 [142,145]. The structure of the complex shows the five-coordinate nature of the metal ion which is bound

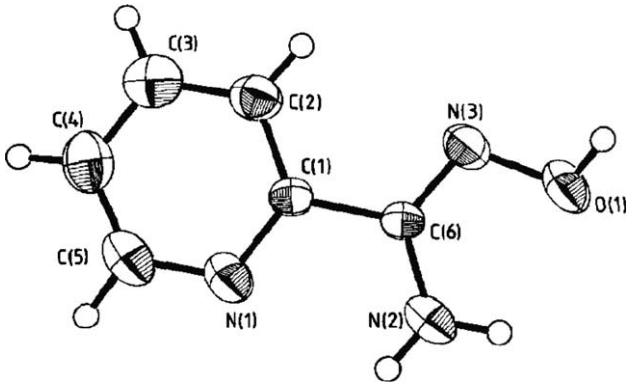

Fig. 51. Molecular structure of $(py)C(NH_2)NOH$ [142].

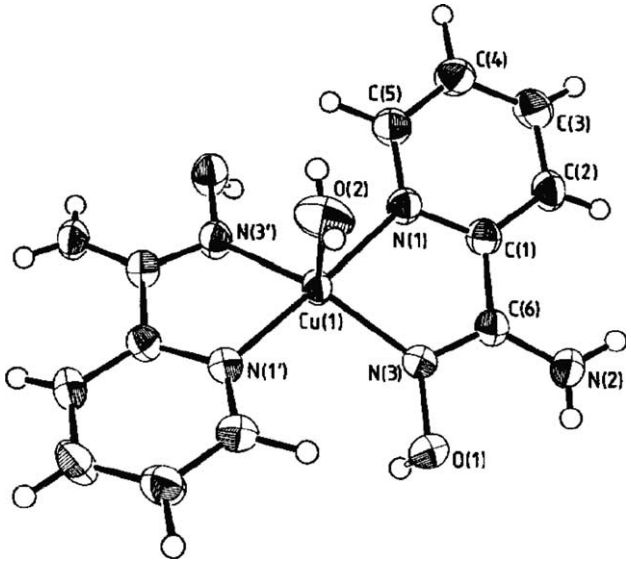

Fig. 52. Molecular structure of the cation present in complex $[Cu\{(py)C(NH_2)NOH\}_2(H_2O)]Cl_2$ [142].

through the heterocyclic and oxime nitrogen atoms (Fig. 53) of two *trans*-oriented bidentate ligands plus a H_2O molecule to give a square-based pyramidal chelate. When an ethanolic solution of $Ni(NO_3)_2 \cdot 6H_2O$ is treated with $(py)C(NH_2)NOH$, a dark blue solution results if the ratio of ligand to metal does not exceed 2:1. From this solution the blue complex $[Ni(NO_3)_2\{(py)C(NH_2)$-

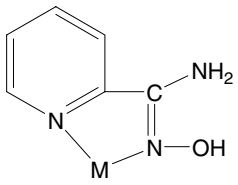

1.0110

Fig. 53. The coordination mode of $(py)C(NH_2)NOH$ in its structurally characterized transition metal complexes.

$NOH\}_2$] crystallizes [146]. If three equivalents of ligand are added to one equivalent of $Ni(NO_3)_2 \cdot 6H_2O$ in aqueous solution the initial color is blue, which changes to wine-red and the 1:3 complex $[Ni\{(py)C(NH_2)NOH\}_3](NO_3)_2$ is obtained as red-brown crystals. In both complexes the neutral ligand adopts the 1.0110 chelating mode (Fig. 53). The octahedral 1:2 complex (Fig. 54) has two coordinated nitrato groups in the equatorial plane which are *cis* to each other [146]. As $(py)C(NH_2)NOH$ is added, the two *cis* equatorial monodentate nitrato groups are replaced by the third ligand, resulting in the 1:3 cationic complex which has the structure [146] shown in Fig. 55. In the neutral 1:2 complex, the two heterocyclic nitrogens are in a *cis* arrangement. The three organic ligands in the cationic 1:3 complex have their heterocyclic nitrogens co-planar with one oxime nitrogen and the metal ion; this results in the two remaining oxime nitrogens being *trans* to each other.

In an attempt to deprotonate $(py)C(NH_2)NOH$, Jones and co-workers [147] performed the 1:2 reaction between $Ni(O_2CMe)_2 \cdot 4H_2O$ and the ligand in EtOH. The ligand is not deprotonated during complex formation, as was confirmed by the X-ray structure of the resulting mononuclear octahedral complex $[Ni(O_2CMe)_2\{(py)C(NH_2)NOH\}_2]$ (Fig. 56). It is possible [147] that the NH_2 group stabilizes the oxime group by delocalization of the lone pair at the N atom of the amino group; the ensuing reduced electron density is the probable reason for its low affinity for the metal ion, i.e., the non-participation of the NH_2 group in coordination, in all the structurally characterized complexes of this

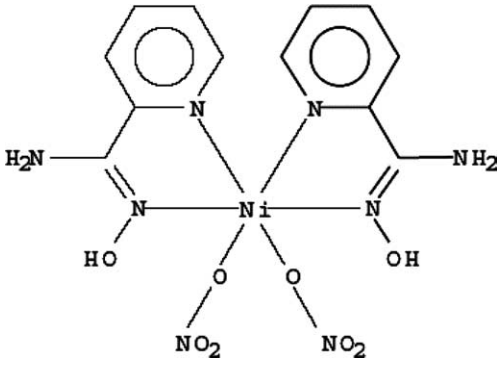

Fig. 54. Block diagram structure of $[Ni(NO_3)_2\{(py)C(NH_2)NOH\}_2]$.

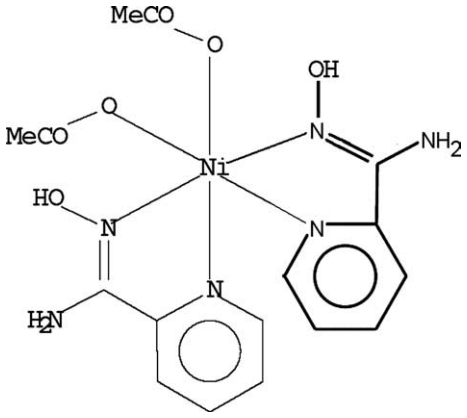

Fig. 56. Block diagram structure of $[Ni(O_2CMe)_2\{(py)C(NH_2)NOH\}_2]$.

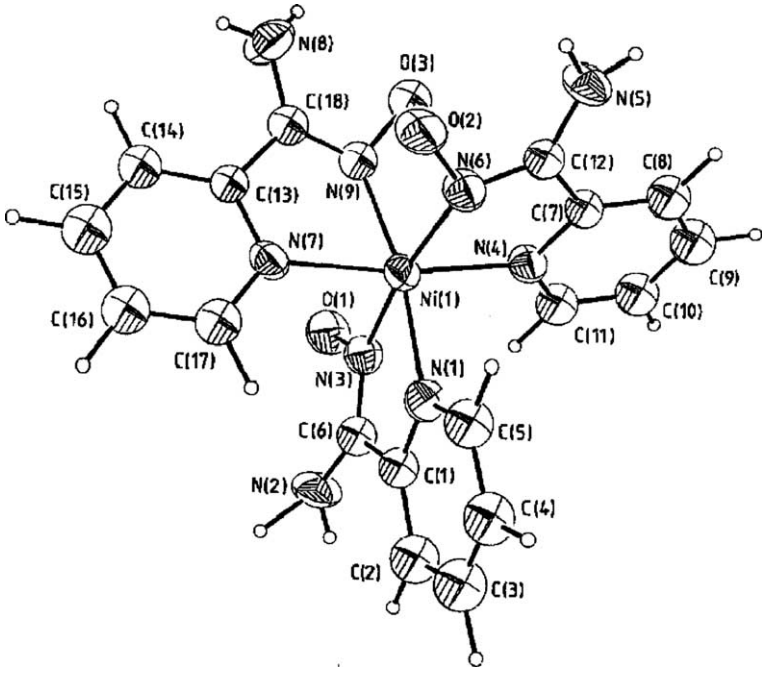

Fig. 55. X-ray structure of the octahedral cation present in complex $[Ni\{(py)C(NH_2)NOH\}_3](NO_3)_2$ [146].

ligand. Two mutually *cis* positions in the nickel(II) distorted octahedron are occupied by the O atoms of the two monodentate acetato ligands and the two other pairs by two 1.0110 (Fig. 53) ligands. The oxime nitrogens are mutually *trans* and the 2-pyridyl nitrogens mutually *cis*.

The coordination chemistry of the anionic ligand $(py)C(NH_2)NO^-$ remains to be studied.

Although the 3- and 4-pyridyl isomers of $(py)C(NH_2)NOH$ have been synthesized [141,148], their coordination chemistry has not been investigated.

7.3. 3-(2-Pyridin-2-yl-methylimino)-butan-2-one oxime (pmiboH), 3-(2-Pyridin-2-yl-ethylimino)-butan-2-one oxime (peiboH) and their reduced amino analogs (pmaboH, peaboH)

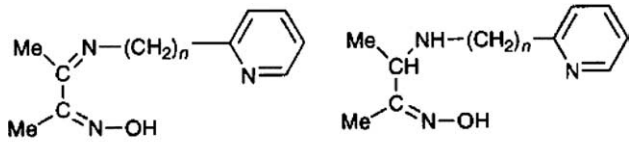

pmiboH (n= 1) pmaboH (n= 1)

peiboH (n= 2) peaboH (n= 2)

The above shown ligands contain 2-pyridyl groups that are not directly attached to the oxime carbon atom. The abbreviations of the ligands in this part derive [149] from the non-systematic names 2-[2-(α-pyridyl)methyl] imino-3-butanone oxime (pmiboH), 2-[2-(α-pyridyl)ethyl]imino-3-butanone oxime (peiboH), 2-[2-(α-pyridyl)methyl]amino-3-butanone oxime (pmaboH) and 2-[2-(α-pyridyl)ethyl]amino-3-butanone oxime (peaboH); H denotes the oximic hydrogen.

Detailed syntheses of the four free ligands were reported by Randacci and co-workers [150]. The compounds pmiboH and peiboH were synthesized starting from diacetyl monoxime and the appropriate aminopyridine following the usual procedure for the preparation of Schiff bases; the solvent used was diisopropyl ether. The compounds pmaboH and peaboH were prepared by treating pmiboH and peiboH, respectively, with $NaBH_4$ in methanol; the reactions involves hydrogenation of the $>C{=}N{-}CH_2{-}$ imino groups to $>CHNH{-}CH_2{-}$ amino groups. The crystal structure of pmiboH has been determined [151].

The crystallographically established coordination modes of the neutral and monoanionic ligands are shown in Fig. 57.

The first structurally characterized complex of these ligands was $[Cu_2(peibo)_2(MeCN)_2](ClO_4)_2$ [152]. The cation (Fig. 58) contains a six-membered ring formed by two Cu^{II} atoms and two oximate groups; the ring is distinctly non-planar with a twisted-boat conformation. Each $peibo^-$ ligand adopts the 2.1111 coordination mode (Fig. 57). Perchlorate and nitrate salts containing the structurally similar cations $[Cu_2(peibo)_2]^{2+}$, $[Cu_2(peibo)_2(H_2O)_2]^{2+}$ and $[Cu_2(pmibo)_2]^{2+}$ have been prepared [149]. The $-2J$ values ($H = -2JS_1S_2$) are in the 510–835 cm^{-1} range, indicative of strong antiferromagnetic coupling. The dinuclear complexes showed relatively narrow ^1H NMR signals in the −0.5–30 ppm range ($\Delta\nu_{1/2} = 60$–1500 Hz), indicating that the antiferromagnetic interaction is maintained in DMSO-d_6 [149]. The $-2J$ values roughly correlate with the ^1H NMR parameters; the larger the $-2J$ values, the smaller the chemical shifts and linewidths. The cation $[Cu_2(pmibo)_2]^{2+}$ was found to undergo an autoreduction reaction in DMSO, DMF and DMA. The triply-bridged dinuclear copper(II) complexes $[Cu_2(peibo)_2(pz)](ClO_4)$ and $[Cu_2(peibo)_2(phta)](ClO_4)_2$ (Fig. 59), where pz^- is the pyrazolate anion and phta is phthalazine, have been prepared [153]; a very strong antiferromagnetic interaction ($2J = -760$ cm^{-1}) between the metal ions was observed for the latter. In the dinuclear complexes $[Cu_2(OMe)(ClO_4)(peibo)(bpy)](ClO_4)$ and $[Cu_2(O_2CMe)_2(peibo)(bpy)](ClO_4)$ the two Cu^{II} atoms are bridged by one 2.1111 $peibo^-$, one methoxo and one perchlorato ligands, and one 2.1111 $peibo^-$ and two acetato ligands, respectively [154]. Matsumoto and co-workers [155] prepared and structurally characterized the dinuclear, end-on azido-bridged complexes $[Cu_2(N_3)(peibo)(bpy)](ClO_4)_2$ and $[Cu_2(N_3)(peibo)(pmdt)](ClO_4)_2$, where pmdt is the tridentate chelating ligand *N*,*N*′,*N*″,*N*″-pentamethyldiethylenetriamine. The $peibo^-$ ligand is in the 2.1111 (Fig. 57) coordination mode. For both complexes, the two Cu^{II} atoms are antiferromagnetically coupled with a singlet-triplet separation of $2J = -520$ and -296 cm^{-1} for the bpy and pmdt complexes, respectively. The complexes are EPR-silent in the solid state at room temperature. Two other $peibo^-$-containing Cu(II) complexes have been reported; these are $[Cu_3(N_3)_2(peibo)_2(NO_3)_2(H_2O)_2]$ [156] and $[Cu_2(peibo)_2(OClO_3)_2]_n$ [157], in which the ligand is in the 2.1111 mode. In the perchlorato coordination polymer, the dinuclear units are bridged by one inorganic anion which adopts an $\eta^1{:}\eta^1{:}\eta^1{:}\mu_3$ mode [157].

The Ni(II) coordination chemistry of pmiboH and peiboH is practically unknown. The crystal structure of the complex $[Ni(peiboH)_2](NO_3)_2$ has been reported [158]. In the all-*trans* mononuclear octahedral cation, the neutral ligand adopts the 1.0111 mode (Fig. 57).

Contrary to Ni chemistry, the Co coordination chemistry of pmiboH and peiboH is well developed; most of the known complexes are organometallic. The first reference to a Co complex of these ligands in the literature came in 1983 in the X-ray structure of $[Co^{III}(peibo)_2](ClO_4)$ (Fig. 60) [159]. The Co^{III} ion is coordinated to six N atoms from two tridentate chelating anionic

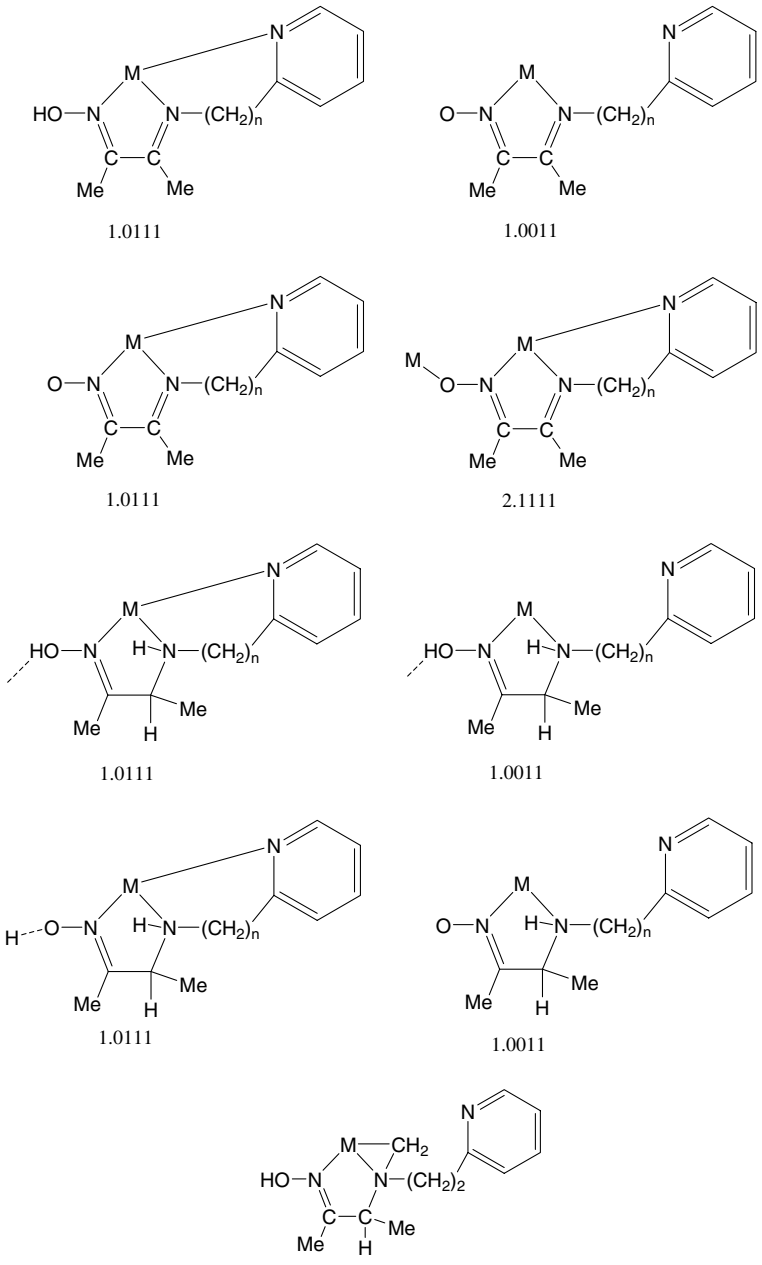

Fig. 57. The crystallographically established coordination modes of pmiboH, peiboH, pmaboH, peaboH and their monoanions, and the Harris notation [44] that describes these modes. The dashed lines indicate hydrogen bonds.

ligands (1.0111, Fig. 57) in a slightly distorted octahedral arrangement. Each peibo$^-$ ligand forms one five- and one six-membered chelating ring. The ligands are almost planar in a *mer* configuration around the metal. The molecular structure of the cation $[Co(pmibo)_2]^+$ is similar (Fig. 60) [150]. The decrease in the Co^{III}–N_{py} distances and N_{py}–Co–N_{im} angles from $[Co(peibo)_2]^+$ to $[Co(pmibo)_2]^+$ has been ascribed to the steric constraint imposed by the closure of the five-membered ring, containing the N_{py} atom in the latter [150]. The aminooximes pmaboH and peaboH react with $CoCl_2 \cdot 6H_2O$ in MeOH in the presence of ClO_4^- under atmospheric conditions to give the complexes $[Co(pmabo)(pmaboH)](ClO_4)_2$ and $[Co(peabo)(peaboH)](ClO_4)_2$ [150]. In both structures (Fig. 61), one protonated 1.0111 and one deprotonated 1.0111 ligand coordinate the Co^{III} ion through their N donors in a *fac* configuration, in such a way that the two 2-pyridyl rings are *trans* to each other. The two O atoms make a strong intramolecular hydrogen bond. The formation of the hydrogen bond serves further to stabilize the *fac* arrangement of the ligands.

The reduction of $[Co^{III}(peibo)_2](ClO_4)$ with $NaBH_4$ in alkaline media produces a nucleophilic Co(I) species

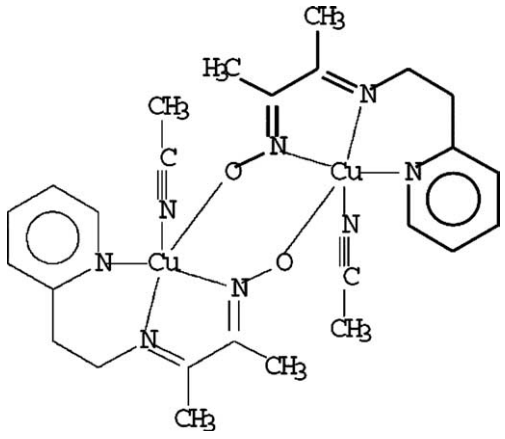

Fig. 58. Block diagram structure of the cation $[Cu_2(peibo)_2(MeCN)_2]^{2+}$.

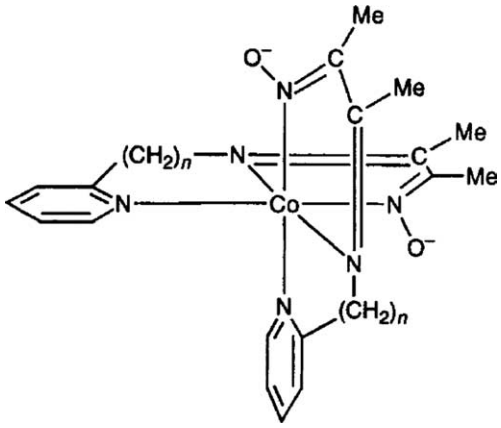

Fig. 60. Block diagram structure of the cations $[Co(pmibo)_2]^{+}$ and $[Co(peibo)_2]^{+}$.

which, upon reaction with alkyl halides, gives stable organocobalt dinuclear complexes (Scheme 6). This reactivity pattern parallels that observed for cobaloximes and other vitamin B_{12} models [160]. The molecular structure of the methyl complex [161] is shown in Fig. 62. The $R = CH_2CF_3$, Cy analogues have similar structures [162]. The peibo^{-} ligand adopts the 2.1111 mode. On the contrary, the reduction of $[Co^{III}(pmibo)_2](ClO_4)$ involves hydrogenation of the ligand from imino- to amino-oxime, with the formation of a stable Co(II) species; the latter can be oxidized to afford $[Co(pmabo)(pmaboH)](ClO_4)_2$, see Scheme 6. The different reactivity was attributed [150] to the more strained coordination in $[Co^{III}(pmibo)_2](ClO_4)$ with respect to that in $[Co^{III}(peibo)_2](ClO_4)$.

Addition of $NaBH_4$ to an alkaline solution of $[Co^{III}(peibo)_2](ClO_4)$ under a nitrogen atmosphere, followed by addition of benzyl chloride gave the mononuclear complex $[Co^{III}(C_6H_5CH_2)(peibo)L](ClO_4)$, where L is

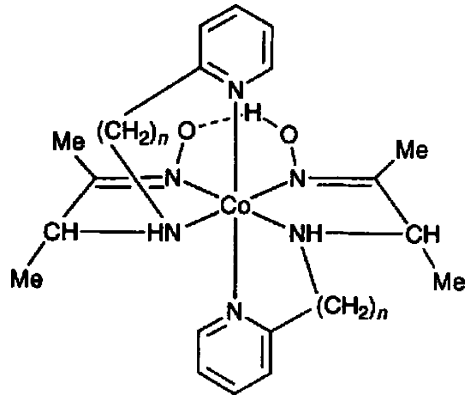

Fig. 61. Block diagram structure of the cations $[Co(pmabo)(pmaboH)]^{2+}$ $(n = 1)$ and $[Co(peabo)(peaboH)]^{2+}$ $(n = 2)$.

2-[(2-pyridylethyl)amino]-3-aminobutane [163]. The peibo^{-} tridentate ligand in a *mer* configuration coordinates Co^{III} through its *N*-donors (1.0111). The complex

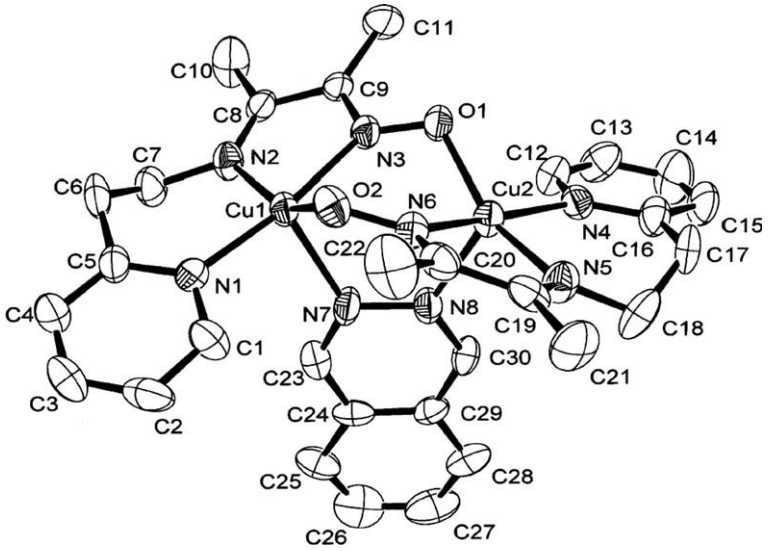

Fig. 59. X-ray structure of the cation present in complex $[Cu_2(peibo)_2(phta)](ClO_4)_2$ [153].

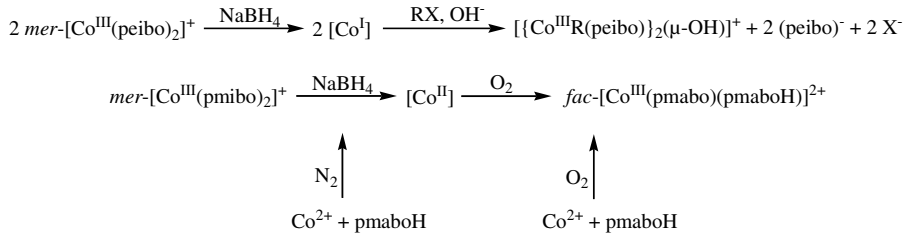

Scheme 6. Redox reactivity pattern of $[Co^{III}(peibo)_2]^+$ and $[Co^{III}(pmibo)_2]^+$.

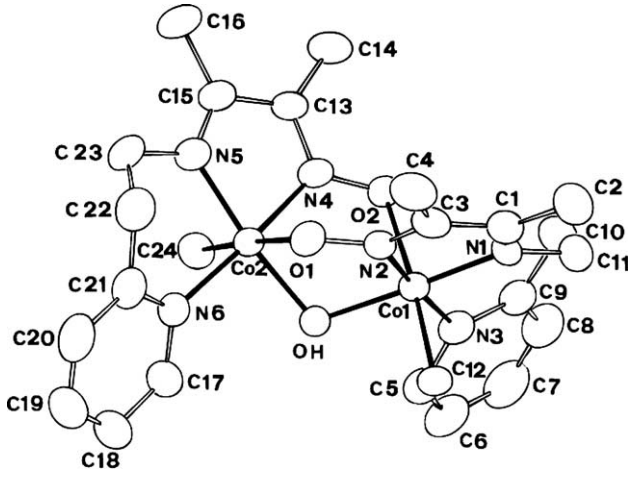

Fig. 62. The molecular structure of the dinuclear cation present in complex $[\{Co^{III}(Me)(peibo)\}_2(\mu\text{-}OH)](ClO_4)$ [161].

undergoes Co–C homolytic cleavage under acidic conditions, giving dibenzyl under a nitrogen atmosphere and benzaldehyde in the presence of air [163].

The oxidative addition of alkyl halides to the Co^I species generated by the reduction of $[Co^{III}(peabo)(peaboH)](ClO_4)_2$ (Fig. 61) [150], led to the formation of a new class of organocobalt complexes of general formula $[Co^{III}R(peabo)(peaboH)](ClO_4)$ [164], where R = Me, Et, CH_2CF_3, ^{n}Bu and CH_2Cl. The X-ray structures of the R = Me, Et (Fig. 63) and CH_2CF_3 compounds provide conclusive evidence for a distorted octahedral structure, where peaboH and $peabo^-$ act as 1.0011 (Fig. 57) and 1.0111 (Fig. 57) ligands, respectively. In fact, the non-organometallic ligand system about Co^{III} can be considered as $(peabo\cdots H\cdots peabo)^-$; adopting this formulation, the hydrogen bridged anion behaves as a pentadentate chelating ligand. The axial geometry in the R = Me compound is closer to that found in methylcobalamin than that reported for other models, suggesting steric and electronic *cis* influences of the equatorial ligands close to those of the corrin nucleus [164].

Treatment of the complexes $[Co^{III}R(peabo)(peaboH)](ClO_4)$ [164], where $R = CH_2X$ (X = halogen), with diluted NaOH afforded [165] the complex $[Co^{III}(peabo)L](ClO_4)$, where L is the monoanionic ligand whose coordination mode is shown on the bottom of Fig. 57. The three-membered ring is formed by a pathway involving intramolecular nucleophilic addition of an equatorial nitrogen donor to the axial carbon.

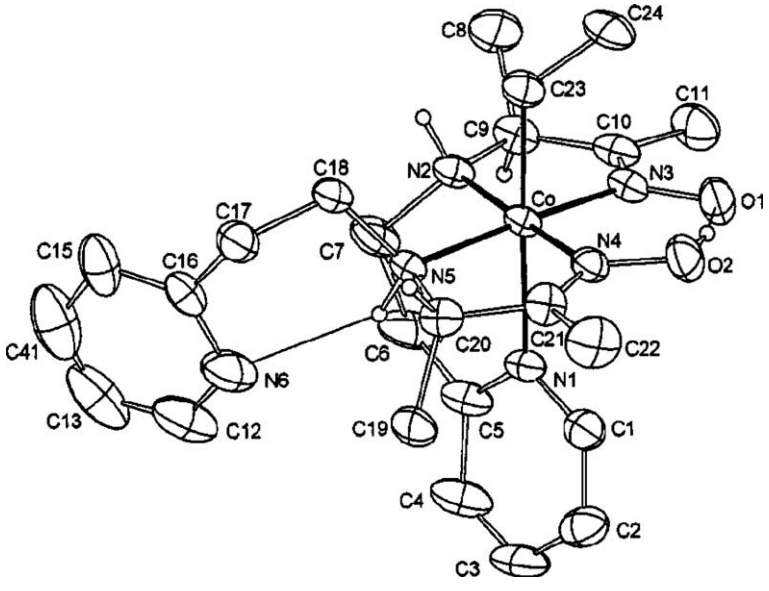

Fig. 63. X-ray structure of the cation present in the complex $[Co^{III}(Et)(peabo)(peaboH)](ClO_4)$ [164].

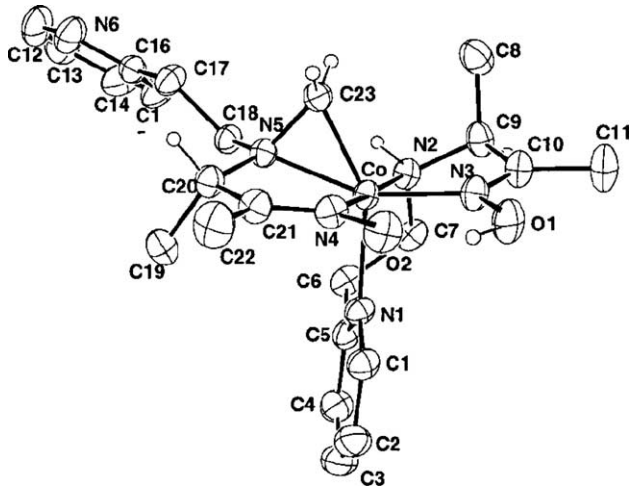

Fig. 64. X-ray structure of the cation present in complex $[Co^{III}(peabo)L](ClO_4)$ [165].

X-ray analysis reveals a highly distorted structure (Fig. 64). The C–Co–N angle is acute (42.8°). The $peabo^-$ ion behaves as 1.0111 ligand.

Complex *mer*-$[Co^{III}(pmibo)_2](ClO_4)$ (Fig. 60) [150] gives cobalt alkyl derivatives after reduction with $NaBH_4/Pd^{2+}$ to Co^I and alkylation [166]. The formation of the Co–C bond is accompanied by the reduction of the amino form of one or both imino ligands (depending on the experimental conditions) initially present in the starting material. In one series of experiments, complexes of the type *fac*-$[Co^{III}R(pmibo)(pmaboH)](ClO_4)$ (R = Me, *i*-Pr, CH_2Cl, CH_2Br, CH_2CF_3, Bz) were obtained, in which only one of the two ligands was reduced to the amino form (pmaboH). The molecular structures of two representative cations are shown in Fig. 65. The anion of the unmodified imino ligand acts as a bidentate N_{imino}, $N_{oximate}$-ligand (1.0011, Fig. 57), whereas the neutral amino-oxime molecule (pmaboH) acts as a tridentate ligand (1.0111, Fig. 57). The saturation of one azomethine group causes the product to assume a *fac*-configuration and induces the formation of one asymmetric carbon and one asymmetric nitrogen center in the chelating system. When an excess of reducing agent was used, both azomethine groups were saturated, causing the introduction of one pair of chiral carbons and one pair of chiral nitrogens. Two isomers of the methyl derivative $[Co^{III}(Me)(pmabo)(pmaboH)]^+$ were isolated (Fig. 66) [166]. The $pmabo^-$ and pmaboH ligands adopt the 1.0011 and 1.0111 modes, respectively. One isomer differs from the other in the opposite configuration of the C and N centers located on the bidentate ligand. One isomer closely resembles the $peabo^-$/peaboH analog [164]. Similarities and differences in the reactivity exhibited by $[Co^{III}(pmibo)_2]^+$ and $[Co^{III}(peibo)_2]^+$ were discussed [166].

7.4. Other ligands

Ligands featuring a 6-alkylaminomethyl-2-pyridinealdoxime moiety (alkyl = CH_3, *n*-$C_{12}H_{25}$) have been synthesized as outlined in Scheme 7 [167]. The reactivity of their Ni(II), see Fig. 67, and Zn(II) complexes in the cleavage of *p*-nitrophenylacetate and *p*-nitrophenylhexanoate has been investigated in the absence (R = CH_3) or in the presence (R = *n*-$C_{12}H_{25}$)

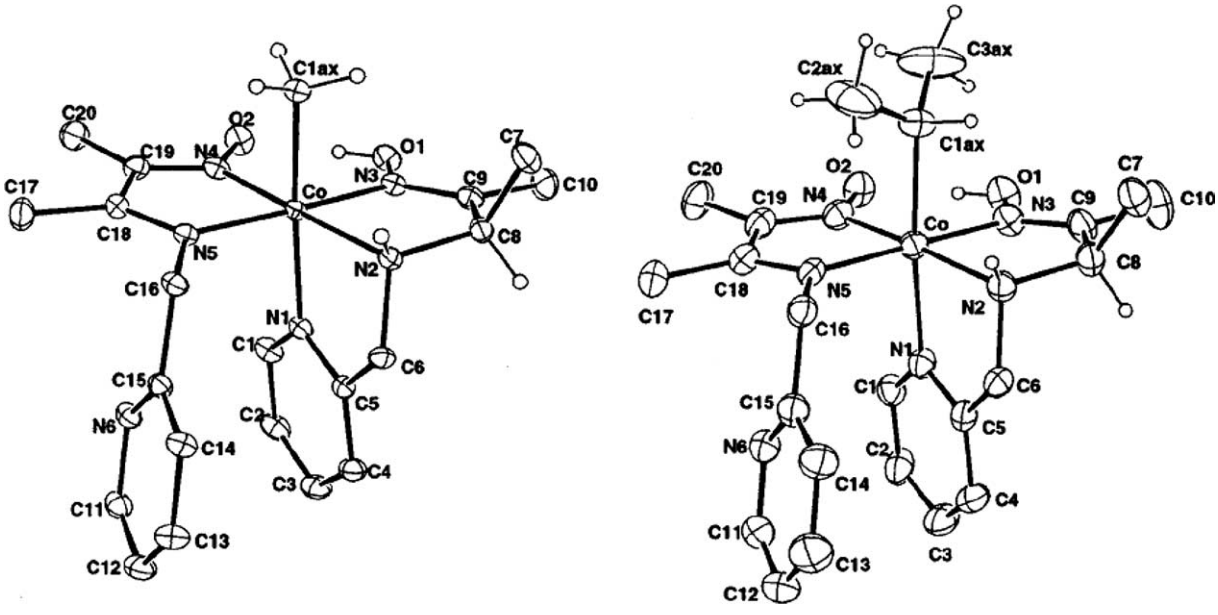

Fig. 65. Molecular structures [166] of the cations present in complexes *fac*-$[Co^{III}(Me)(pmibo)(pmaboH)](ClO_4)$ (left) and *fac*-$[Co^{III}$-(*i*-Pr)(pmibo)(pmaboH)$](ClO_4)$ (right).

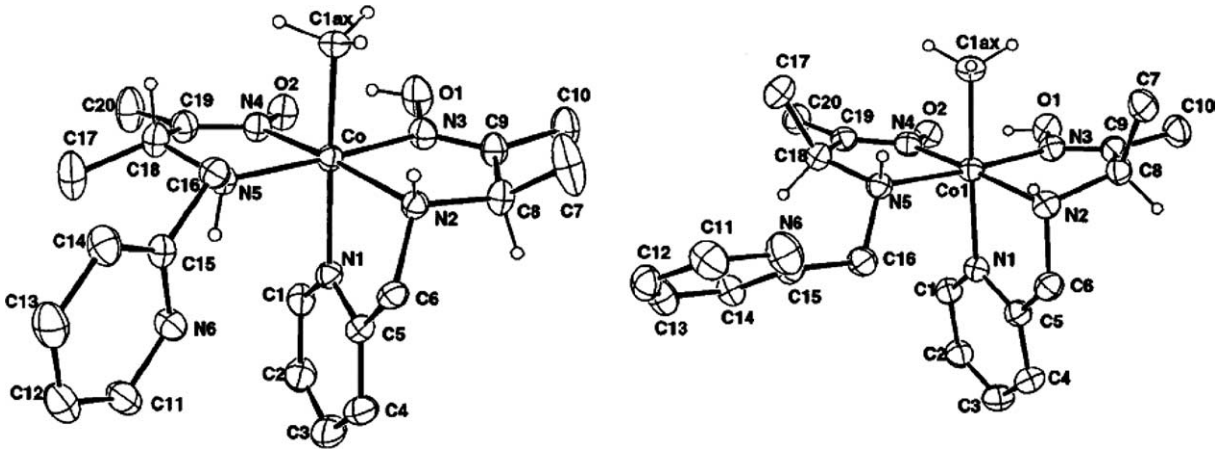

Fig. 66. The two $[Co^{III}(Me)(pmabo)(pmaboH)]^{+}$ isomers [166].

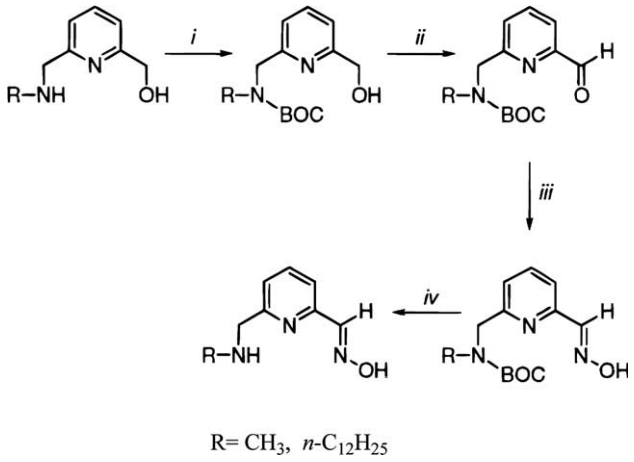

Scheme 7. Synthesis of ligands featuring a 6-alkylaminomethyl-2-pyridinealdoxime moiety. Conditions: (i) di-*tert*-butyl dicarbonate, triethylamine, dioxane, 20 °C; (ii) selenium dioxide, dioxane, reflux; (iii) hydroxylamine hydrochloride, Na_2CO_3, EtOH, 60 °C; (iv) trifluoroacetic acid, 20 °C.

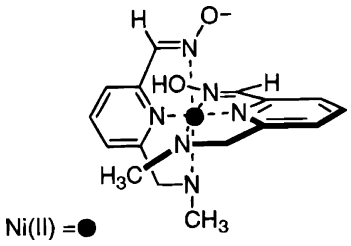

Fig. 67. Proposed structure of the 1:2 nickel(II)/6-methylaminomethyl-2-pyridinealdoximate complex.

of hexadecyltrimethylammonium bromide micelles. The micellar complexes are effective in promoting the cleavage of the substrate with accelerations strongly dependent on pH, being larger in moderately acidic than in neutral solutions. The coordination chemistry of these 2-pyridyl oximes remains completely unexplored.

8. The rich coordination chemistry of di-pyridin-2-yl-methanone oxime (di-2-pyridyl ketone oxime), $(py)_2CNOH$

8.1. Introduction

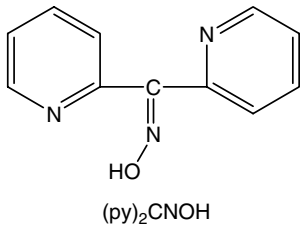

Di-pyridin-2-yl-methanone oxime (di-2-pyridyl ketone oxime), $(py)_2CNOH$, occupies a special position amongst the 2-pyridyl oximes. One area to which the anionic ligand $(py)_2CNO^-$ is relevant is the chemistry of metallamacrocycles. Another attractive aspect of $(py)_2CNO^-$ is its great coordinative flexibility and versatility, characteristics that have led to polynuclear 3d-metal complexes with impressive structures and interesting magnetic properties. A third interesting feature is the activation of $(py)_2CNOH$ by 3d-metal centers, which appears to be a fruitful area of synthetic inorganic chemistry; examples of this activation will be described below.

The published coordination chemistry of $(py)_2$-CNOH is rich [168–188]. The free ligand is commercially available. Since several complexes of $(py)_2CNO^-$ can be considered as metallamacrocycles, and especially as metallacrowns, we feel obliged to give brief information about these compounds. Metallamacrocycles have gained increasing attention over the past decade due to their potentially unique properties. These molecules have already been used in applications as diverse as catalysts [189], sensors [190] or as chiral building

blocks for 2D and 3D solids [191,192]. Metallamacrocycles include complexes such as metallacrowns [67,193], metallacrowns containing carbon in the macrocycle [194,195], metallacrown ethers [196], azametallacrowns [197,198], anticrowns [199], metallahelicates [200], metallacalixarenes [201], metallacryptates [202], molecular squares and boxes [203], and the aesthetically pleasant polynuclear fluoro, alkoxo or oxo metal complexes [204–206]. Metallacrowns (MCs) [67], the inorganic structural and functional analogs of crown ethers [207], are usually formed when a transition metal ion and a nitrogen replace the methylene carbon atoms. MCs exhibit selective recognition of cations and anions, and can display intramolecular magnetic exchange interactions. The isolation of metallacrowns requires the employment of tri- and tetradentate ligands containing hydroxamate or oximate functionalities to provide a scaffolding within which the desired metal-containing core can be realized. One example of such a ligand is $(py)_2CNO^-$. This approach yields clusters with M–N–O–M networks. Metallacrown nomenclature has been given in refs. [67,181] and [193]. There are nine metals in four oxidation states (II–IV) that have been incorporated into the MC ring, while more than 20 metal ions, i.e., lanthanide, actinide, alkali, alkaline earth and transition metal ions have been captured in the central cavity of MCs. For 12-MC-4 complexes, two structural motifs have been reported: classical or regular [67,181,193,208] and inverse [66,67,172,179,184,185]. In the regular motif,

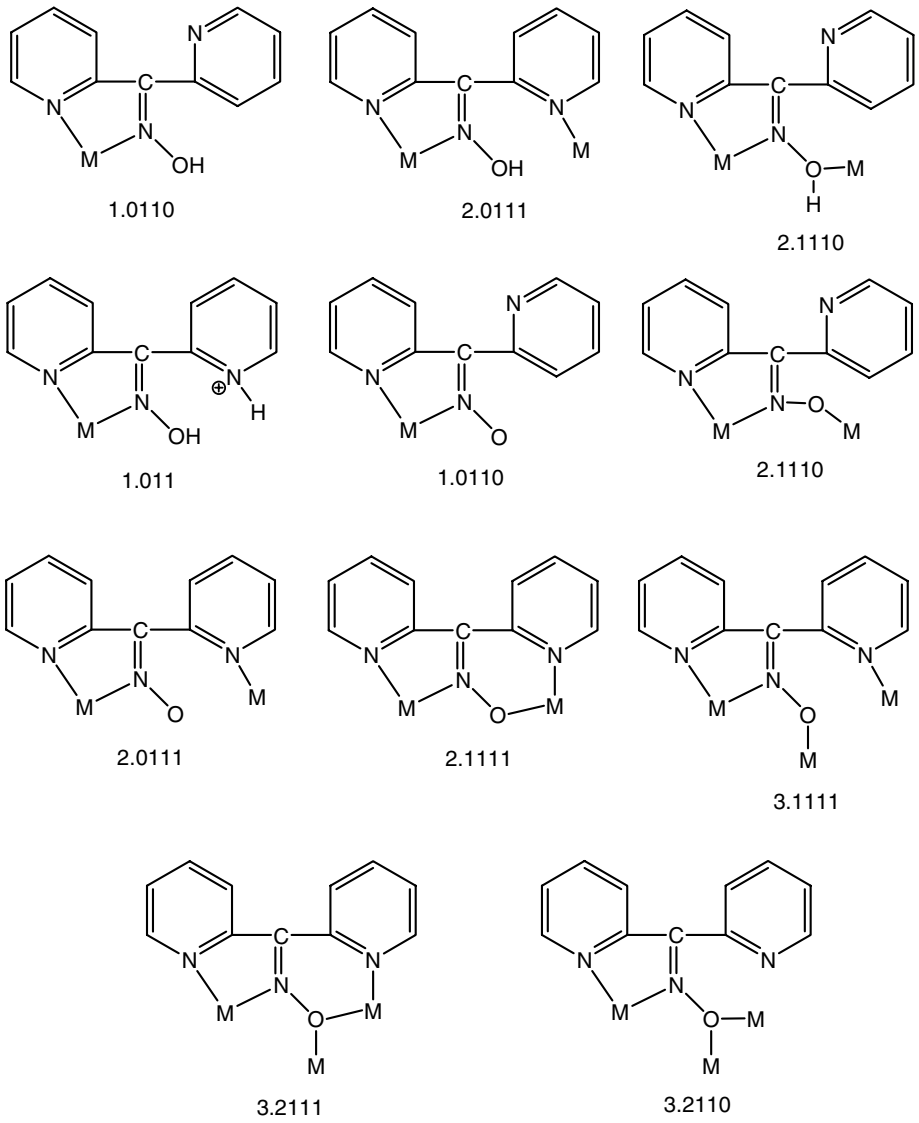

Fig. 68. The crystallographically established coordination modes of $(py)_2CNOH$ and $(py)_2CNO^-$, and the Harris notation [44] that describes these modes.

there is an N–O–M–N–O–M linkage, i.e., an [M–N–O]$_n$ repeat unit, with the oxygen atoms oriented towards the center of the cavity and capable of binding cations. In the inverse motif, which has been realized only for Zn and Co, the ring metal ions are oriented towards the center of the cavity which is now capable of encapsulating anions, whereas the connectivity is transposed to N–O–M–O–N–M. It should be mentioned at this point that some researchers prefer to consider MCs simply as one sub-area of metal wheel (ring) chemistry, avoiding the use of their specialized nomenclature.

The crystallographically established coordination modes of (py)$_2$CNOH and (py)$_2$CNO$^-$ are shown in Fig. 68.

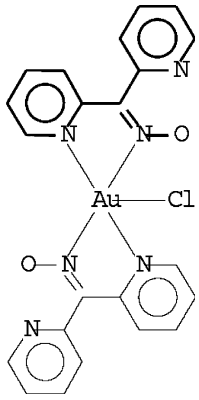

Fig. 69. Block diagram structure of the square pyramidal complex [AuCl{(py)$_2$CNO}$_2$].

8.2. Metal complexes containing terminal (py)$_2$CNOH and/or (py)$_2$CNO$^-$ ligands

These complexes are listed in Table 3. Molecular structures of representative complexes are shown in Figs. 69–71. Six out of the eight complexes listed in Table 3 are mononuclear and present no special structural interest. In the trinuclear complex [Ni$_3$(shi)$_2${(py)$_2$CNOH}$_2$(py)$_2$], the Ni^{II} ions are bridged by the shi^{3-} ligands [169]; two metal ions have a square planar geometry while the third one is in an octahedral environment. The open array of the three metal ions is angular, with an Ni···Ni···Ni dihedral angle of 46.5°. The structure of [Cu(NCS){(py)$_2$CNOH}]$_n$ features tetrahedral geometry around Cu^I atoms (Fig. 70) with a *N*,*S*-bridging thiocyanate group creating zig-zag chains along the *c*-axis of the unit cell [171].

Complex [Cu$_2^{II}$(μ-Cl)$_2$Cl$_2${(py)(pyH)CNOH}$_2$-(H$_2$O)$_2$]Cl$_2$ (Fig. 71), not listed in Table 3, is unique, because it contains the monocation of di-2-pyridyl ketone oxime as a ligand [186b]. The cation (py)(pyH)CNOH behaves as a terminal 1.011 ligand, see Fig. 68.

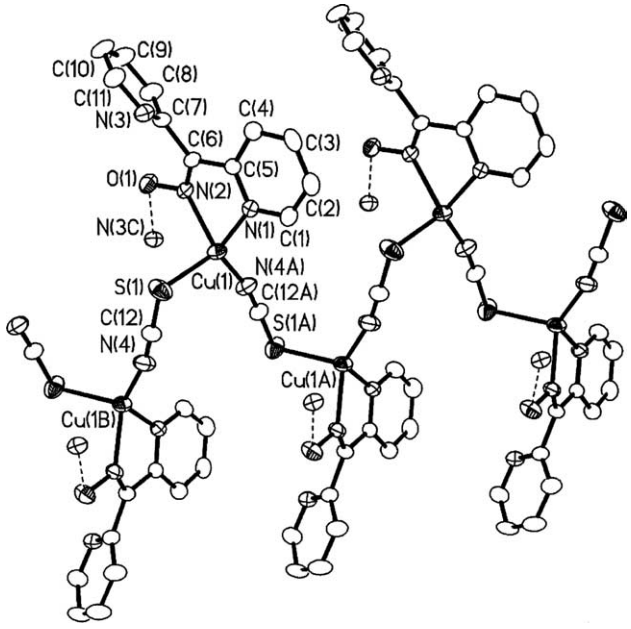

Fig. 70. A small portion of one of the zig-zag chains present in the complex [Cu(NCS){(py)$_2$CNOH}]$_n$ [171].

Table 3
Structurally characterized metal complexes containing *exclusively* terminal (py)$_2$CNOH and/or (py)$_2$CNO$^-$ ligands

Complex[a]	Coordination mode	Coordination sphere; coordination geometry	Reference
[Mn(O$_2$CPh)$_2${(py)$_2$CNOH}$_2$]	1.0110	*cis*,*cis*,*trans*-Mn^{II}O$_2$(N$_{py}$)$_2$(N$_{ox}$)$_2$; oct	[168]
[Ni$_3$(shi)$_2${(py)$_2$CNOH}$_2$(py)$_2$]	1.0110	Ni^{II}O$_3$N, NiO$_4$N$_2$; sp, oct	[169]
[Co(NO$_2$){(py)$_2$C(OH)O}{(py)$_2$CNO}][b]	1.0110	Co^{III}ON$_5$; oct	[170]
[Ni(O$_2$CPh)$_2${(py)$_2$CNOH}$_2$]	1.0110	*cis*,*cis*,*trans*-Ni^{II}O$_2$(N$_{py}$)$_2$(N$_{ox}$)$_2$; oct	[97]
[CuCl{(py)$_2$CNO}{(py)$_2$CNOH}][c]	1.0110, 1.0110	Cu^{II}N$_4$Cl; spy	[97]
[Cu(NCS){(py)$_2$CNOH}]$_n$	1.0110	Cu^{I}N$_3$S; tet	[171]
[ZnCl$_2${(py)$_2$CNOH}$_2$]	1.0110	Zn^{II}N$_2$Cl$_2$; tet	[172]
[AuCl{(py)$_2$CNO}$_2$]	1.0110	Au^{III}N$_4$Cl; spy	[173]

Abbreviations: N$_{ox}$, oxime or oximate nitrogen; N$_{py}$, 2-pyridyl nitrogen; oct, octahedral; (py)$_2$C(OH)O$^-$, the mononanion of the *gem*-diol derivative of di-2-pyridyl ketone; shi^{3-}, the fully deprotonated form of salicylhydroxamic acid; sp, square planar; spy, square pyramidal; tet, tetrahedral.

[a] Solvate molecules have been omitted.

[b] The NO$_2^-$ ligand is in its nitro form.

[c] In fact, the ligand system about Cu^{II} can be considered as {(py)$_2$CNO···H···ONC(py)$_2$}$^-$; adopting this formulation, the hydrogen-bridged anion behaves as a tetradentate chelating ligand.

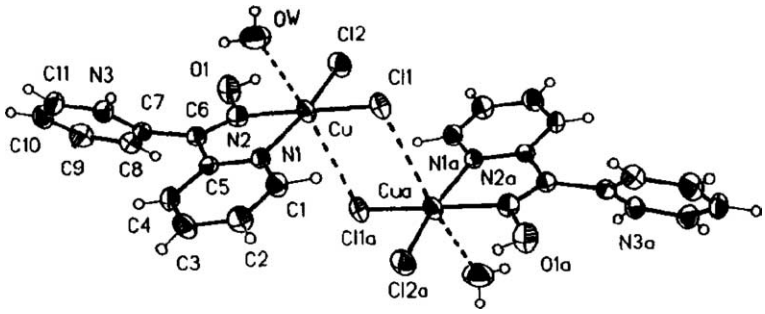

Fig. 71. X-ray structure of the dinuclear cation present in the complex $[Cu_2Cl_4\{(py)(pyH)CNOH\}_2(H_2O)_2]Cl_2$, which contains the monocation of $(py)_2CNOH$ as a ligand [186b].

8.3. Metal complexes containing bridging $(py)_2CNOH$ and/or $(py)_2CNO^-$ ligands

These complexes are listed in Table 4. Molecular structures of representative complexes are shown in Figs. 73–95. The majority of the listed complexes are dinuclear and polynuclear (clusters).

The Mn/$(py)_2CNO^-$ chemistry is interesting [168,174–178]. Using a variety of synthetic routes the complexes $[Mn_2^{II}Mn_2^{III}(O_2CR)_2\{(py)_2CO_2\}_2\{(py)_2CNO\}_2X_2]$, where R = Me, Ph and X = Cl, Br, NO_3, etc. have been isolated in good yields [168,176]. Remarkable features of the reactions are the in situ transformation of an amount of $(py)_2CNOH$ to yield the coordinated dianion, $(py)_2CO_2^{2-}$, of the *gem*-diol derivative of di-2-pyridyl ketone, $(py)_2CO$ (Fig. 72) and the coordination of nitrate ligands in the $X^- = NO_3^-$ cluster (Fig. 73) although the starting materials were nitrate-free (Scheme 8). It is noteworthy that a similar transformation of $(py)_2CNOH$ to the monoanion (and not to the dianion as observed in the $Mn_2^{II}Mn_2^{III}$ clusters) of the *gem*-diol derivative of di-2-pyridyl ketone, $(py)_2C(OH)O^-$ (Fig. 72), was also reported by Jensen and co-workers [170]. The 1:2 reaction between $[Co^{III}(CO_3)(NH_3)_4](NO_3)$ and $(py)_2CNOH$ in H_2O yielded the complex $[Co^{III}(NO_2)\{(py)_2C(OH)O\}\{(py)_2CNO\}]$, see Table 3. The authors avoided mechanistic discussions and it is not clear whether the nitro ligand present in the product resulted from oxidation of the oxime or from reduction of the NO_3^- counterion of the starting material. The tetranuclear clusters have completely analogous molecular structures [168,176]. The centrosymmetric tetranuclear molecule contains two Mn^{II} and two Mn^{III} six-coordinate ions (the Mn^{II} ions are seven-coordinate in the nitrato cluster because of the chelating behavior of the NO_3^- ions) held together by four μ-oxygen atoms from the two 3.2211 $(py)_2CO_2^{2-}$ ligands to give the $\{Mn^{II}(\mu\text{-}OR'')Mn^{III}(\mu\text{-}OR'')_2Mn^{III}(\mu\text{-}OR'')Mn^{II}\}^{6+}$ core consisting of a planar zig-zag array of the four metal ions (R″ = $(py)_2C(OH)$–). Peripheral ligation is provided by two 2.1110 $(py)_2CNO^-$, two 2.11 RCO_2^- and two terminal X^- ligands. Variable-temperature magnetic susceptibility studies in the 2–300 K range reveal weak antiferromagnetic exchange interactions, leading to non-magnetic $S = 0$ ground states.

Reaction of $Mn(hfac)_2 \cdot 3H_2O$ ($hfac^-$ = hexafluoroacetylacetonate) with one equivalent of $(py)_2CNOH$ in CH_2Cl_2 gives the dinuclear complex $[Mn_2(O_2CCF_3)_2(hfac)_2\{(py)_2CNOH\}_2]$ in 70% yield. The $CF_3CO_2^-$ ligand is one of the decomposition products of the $hfac^-$ ligand [168]. The two Mn^{II} ions are bridged by two neutral $(py)_2CNOH$ ligands which adopt the 2.0111 coordination mode.

The trinuclear complexes $[Mn_2^{II}Mn^{IV}(OMe)_2X_2\{(py)_2CNO\}_4]$ are rare examples of complexes simultaneously containing Mn^{II} and Mn^{IV} ions ($X^- = Cl^-$, NCO^-, NCS^-) [174,175]. The molecular structure of the $X^- = NCS^-$ cluster is shown in Fig. 74. X-ray crystallography and XANES spectroscopy clearly distinguish the $Mn_2^{II}Mn^{IV}$ valence isomer from the more commonly observed $Mn_2^{III}Mn^{II}$ formulation. There is a central six-coordinate Mn^{IV} ion in an MnO_6 coordination environment and two terminal six-coordinate Mn^{II} ions having an $MnO\Psi N_4$ chromophore. Fits to variable-temperature magnetic susceptibility data (Fig. 75) indicate that the Mn^{II} and Mn^{IV} ions are ferromagnetically coupled and that the compounds have an $S = 13/2$ ground state.

Complex $[Mn_3^{II}Mn^{IV}O(3,4\text{-}D)_4\{(py)_2CNO\}_4]$, where $3,4\text{-}D^-$ is the anion of 3,4-dichlorophenoxyacetic acid, has the $\{Mn_3^{II}Mn^{IV}(\mu_4\text{-}O)(\eta^1:\mu_2\text{-}O_2CR)\}^{7+}$ core [177]; its molecular structure (Fig. 76) is very similar to that (Fig. 30) of the complex $[Mn_3^{II}Mn^{IV}O(N_3)(O_2CPh)_3\{(py)C(ph)NO\}_4]$ [96], the only essential difference being the presence of one η^1:μ_2 carboxylate group instead of one η^1:μ_2 azido group. Magnetization measurements (Fig. 77) support an $S = 6$ ground state.

Reaction of $Mn(ClO_4)_2 \cdot 6H_2O$ with $(py)_2CNOH$ in MeOH in the presence of NaOH gives the mixed-valent cluster $[Mn_4^{II}Mn_6^{III}Mn_2^{IV}(\mu_3\text{-}OH)_4(\mu_3\text{-}O)_4(\mu_4\text{-}O)_2(\mu\text{-}OMe)_2\{(py)_2CNO\}_{12}](OH)(ClO_4)_3$. The cluster contains a 24-MC-8 ring which wraps a 16-membered, star-shaped ring containing four metal ions [178]. This

Table 4
Structurally characterized metal complexes containing bridging $(py)_2CNOH$ and/or $(py)_2CNO^-$ ligands

Complex[a]	Coordination mode	Coordination sphere; coordination geometry	Reference
$[Mn_2(O_2CCF_3)_2(hfac)_2\{(py)_2CNOH\}_2]$	2.0111	$Mn^{II}(O_{hfac-})_2(O_{CF3CO2-})(N_{py})_2(N_{ox})$; oct	[168]
$[Mn_2^{II}Mn^{IV}(OMe)_2\Psi_2\{(py)_2CNO\}_4]$	2.1110	$Mn^{II}(O_{methoxo})(N_{py})_2(N_{ox})_2\Psi$, $Mn^{IV}(O_{methoxo})_2(O_{ox})_4$; oct, oct	[174,175]
$[Mn_2^{II}Mn_2^{III}(O_2CR)_2\{(py)_2CO_2\}_2\{(py)_2CNO\}_2X_2]$	2.1110	$Mn^{II}O_2N_3X$, $Mn^{III}O_5N$; oct, oct	[168,176]
$[Mn_2^{II}Mn_2^{III}(O_2CMe)_2\{(py)_2CO_2\}_2\{(py)_2CNO\}_2(NO_3)_2]$	2.1110	$Mn^{II}O_4N_3$, $Mn^{III}O_5N$; pbp, oct	[168]
$[Mn_3^{II}Mn^{IV}O(3,4\text{-}D)_4\{(py)_2CNO\}_4]$	2.1110	$Mn^{II}(\mu_4\text{-}O)(O_{carb})_3(N_{py})(N_{ox})$, $Mn^{II}(\mu_4\text{-}O)(O_{carb})_2(O_{ox})(N_{py})(N_{ox})$, $Mn^{IV}(\mu_4\text{-}O)(O_{ox})_3(N_{py})(N_{ox})$; oct, oct, oct	[177]
$[Mn_{12}(OH)_4O_6(OMe)_2\{(py)_2CNO\}_{12}](ClO_4)_3(OH)$	2.1110	$Mn^{II}(\mu_3\text{-}OH)(\mu_3\text{-}O)(N_{ox})_4$, $Mn^{II}(\mu_3\text{-}OH)(\mu_3\text{-}O)_2(\mu_4\text{-}O)_2(O_{ox})$, $Mn^{III}(\mu_3\text{-}OH)(\mu_3\text{-}O)(\mu_4\text{-}O)(O_{ox})(N_{ox})_2$, $Mn^{III}(\mu_3\text{-}OH)(\mu_3\text{-}O)(O_{ox})_2(N_{ox})_2$, $Mn^{III}(\mu_3\text{-}OH)(\mu_4\text{-}O)(O_{methoxo})(N_{ox})_2$, $Mn^{IV}(\mu_3\text{-}OH)(\mu_3\text{-}O)(O_{ox})_2(N_{ox})_2$; oct, oct, oct, tbp, oct	[178]
$[Co_2^{II}Co_2^{III}(OR')_2(O_2CR)_2\{(py)_2CNO\}_4S_2](ClO_4)_2$	2.1110, 2.1111	$Co^{II}(O_{R'O-})(O_{carb})(O_{ox})_2(O_S)(N_{py})$, $Co^{III}(O_{R'O-})(O_{carb})(N_{py})_2(N_{ox})_2$; oct, oct	[179]
$[Ni_4\{(py)_2CNO\}_6(MeOH)_2](ClO_4)(OH)$	2.1110, 2.1111	*fac*-$Ni^{II}(N_{py})_3(N_{ox})_3$, $Ni^{II}(O_{ox})_4(O_{MeOH})(N_{py})$; oct, oct	[180]
$[Ni_4(NCS)_2(Hshi)_2\{(py)_2CNO\}_2(DMF)(H_2O)]$	2.1111	$Ni^{II}O_3N_3$, $Ni^{II}N_3O$; oct, sp	[181]
$[Ni_4Na_2(acac)_4\{(py)_2CNO\}_4](ClO_4)_2$	2.1111[b]	$Ni^{II}(O_{acac-})_2(N_{py})_2(N_{ox})_2$, $Ni^{II}(O_{acac-})_2(N_{py})_2(O_{ox})_2$; oct, oct	[97]
$[Ni_4(O_2CMe)_2\{(py)_2CNO\}_4](SCN)(OH)$	3.2111	$Ni^{II}(O_{carb})(O_{ox})_2(N_{py})_2(N_{ox})$; oct	[97]
$[Ni_4\{(py)_2CNO\}_4\{(py)_2CNOH\}_2(H_2O)_2](ClO_4)_4$	2.1110, 3.2111, 2.1110	*fac*-$Ni^{II}(N_{py})_3(N_{ox})_3$, $Ni^{II}(O_{aqua})(O_{ox})_4(N_{py})$; oct, oct	[97]
$[Ni_5(O_2CMe)_2(shi)_2\{(py)_2CNO\}_2]$	3.2111	$Ni^{II}O_4N_2$, $Ni^{II}O_6$, $Ni^{II}O_2N_2$; oct, oct, sp	[181]
$[Ni_5(acac)_2\{(py)_2CNO\}_6(H_2O)(MeOH)](ClO_4)_2$	2.1110, 3.1111, 3.2111	$Ni^{II}(O_{solvent})(O_{ox})_2(N_{py})_2(N_{ox})$, $Ni^{II}(O_{ox})_2(N_{py})_2(N_{ox})_2$, $Ni^{II}(O_{acac-})_2(O_{ox})(N_{py})_2(N_{ox})$	[97]
$[Ni_5(O_2CMe)_7\{(py)_2CNO\}_3(H_2O)]$	2.1111, 3.2110, 3.2111	$Ni^{II}(O_{aqua})(O_{carb})_2(O_{ox})(N_{py})(N_{ox})$, $Ni^{II}(O_{carb})_3(O_{ox})_2(N_{py})$, $Ni^{II}(O_{aqua})(O_{carb})_3(N_{py})(N_{ox})$, $Ni^{II}(O_{carb})_4(N_{py})(N_{ox})$, $Ni^{II}(O_{carb})_2(O_{ox})_3(N_{py})$; oct, oct, oct, oct, oct	[97]
$[Ni_5\{(py)_2CNO\}_5(H_2O)_7](NO_3)_5$	2.1110, 3.2111	$Ni^{II}(O_{aqua})_2(O_{ox})_2(N_{py})_2$, $Ni^{II}(O_{aqua})(O_{ox})_5$, $Ni^{II}(O_{aqua})_2(O_{ox})(N_{py})_2(N_{ox})$, $Ni^{II}(O_{aqua})_2(N_{py})_2(N_{ox})_2$, $Ni^{II}(O_{ox})(N_{py})_3(N_{ox})_2$; oct, oct, oct, oct, oct	[97]
$[Ni_7(O_2CMe)_6(N_3)_2\{(py)_2CNO\}_6(H_2O)_2]$[c]	1.0110, 3.2111	$Ni^{II}(O_{carb})_2(O_{ox})_2(N_{py})_2$, $Ni^{II}(O_{aqua})(O_{carb})_2(O_{ox})_2(N_{py})$, $Ni^{II}(O_{carb})(N_{azido})(N_{py})_2(N_{ox})_2$, $Ni^{II}(O_{carb})_2(O_{ox})(N_{azido})(N_{py})(N_{ox})$; oct, oct, oct, oct	[97]
$[Ni_{10}(MCPA)_2(shi)_5\{(py)_2CNO\}_3(MeOH)_3(H_2O)]$	3.2111	Various chromophores; 8 Ni^{II} ions oct, two Ni^{II} ions sp	[181]

$[Mn_2Ni_2(O_2CMe)_2(shi)_2\{(py)_2CNO\}_2(DMF)_5]$	2.1110	$Mn^{III}O_5N$, $Ni^{II}O_4N_2$; oct, oct	[181]
$[Cu_2Cl_2\{(py)_2CNOH\}_2]$	2.0111	$Cu^{I}Cl(N_{py})_2(N_{ox})$	[171]
$[Cu_2\{(py)_2CNO\}_4]$[c]	1.0110, 2.1110	$Cu^{II}(O_{ox})(N_{py})_2(N_{ox})_2$; tbp	[182]
$[Cu_2(hfac)_2\{(py)_2CNO\}_2]$	2.1110	$Cu^{II}(O_{hfac-})_2(O_{ox})(N_{py})_2(N_{ox})$; tbp	[97]
$[Cu_3(OH)(O_2CR)_2\{(py)_2CNO\}_3]$	2.1110	$Cu^{II}(\mu_3\text{-}OH)(O_{carb})(O_{ox})(N_{py})(N_{ox})$; spy	[183]
$[Zn_4(OH)_2X'_2\{(py)_2CNO\}_4]$	2.1110	$Zn^{II}(\mu_3\text{-}OH)(O_{ox})_2X'$, $Zn^{II}(\mu_3\text{-}OH)_2(N_{py})_2(N_{ox})_2$; tet, oct	[172,184]
$[Zn_4(OH)_2Z_2\{(py)_2CNO\}_4]$	2.1110	$Zn^{II}(\mu_3\text{-}OH)(O_Z)_2(O_{ox})_2$, $Zn^{II}(\mu_3\text{-}OH)_2(N_{py})_2(N_{ox})_2$; tbp, oct	[184,185]
$[Zn_5Cl_2\{(py)_2CNO\}_6][ZnCl(NCS)_3]$	2.1110, 3.1111, 3.2111	*cis*,*cis*,*trans*-$Zn^{II}(O_{ox})_2(N_{py})_2(N_{ox})_2$, $Zn^{II}(O_{ox})_2(N_{py})_2(N_{ox})$, $Zn^{II}(O_{ox})(N_{py})_2(N_{ox})Cl$; oct, tbp, spy	[184]
$[Zn_5(NCS)_2\{(py)_2CNO\}_6(MeOH)][Zn(NCS)_4]$	2.1110, 3.1111, 3.2111	*cis*,*cis*,*trans*-$Zn^{II}(O_{ox})_2(N_{py})_2(N_{ox})_2$, $Zn^{II}(O_{ox})_2(N_{py})_2(N_{ox})$, $Zn^{II}(O_{ox})(N_{isothiocyanato})(N_{py})_2(N_{ox})$, $Zn^{II}(O_{MeOH})(O_{ox})(N_{isothiocyanato})(N_{py})_2(N_{ox})$; oct, tbp, tbp, oct	[184]
$[Zn_8(shi)_4\{(py)_2CNO\}_4(MeOH)_2]$	2.1110, 3.1111	$Zn^{II}O_6$, $Zn^{II}O_3N_3$, $Zn^{II}O_3N_2$, $Zn^{II}O_4$; oct, oct, tbp, tet	[172]
$[Ru_3\{(py)_2CNO\}_2(CO)_8]$[d]	2.1110	$RuC_2(O_{ox})(N_{py})(N_{ox})Ru$, RuC_4Ru_2	[186a]
$[Ru_2\{(py)_2CNO\}_2(CO)_4]$[d]	2.1110	$RuC_2(O_{ox})(N_{py})(N_{ox})Ru$	[186a]
$[Os_3(\mu\text{-}H)\{(py)_2CNO\}(CO)_9]$[d]	2.1110	OsC_4Os_2, $OsHC_2(N_{py})(N_{ox})Os_2$, $OsHC_3(O_{ox})Os_2$	[186a]
$[Ag_2(NO_3)_2\{(py)_2CNOH\}_2]$	2.0111	$Ag^{I}(O_{nitrato})(O_{ox})(N_{py})_2(N_{ox})$; tet	[186b]
$[Cd_2(O_2CR)_4\{(py)_2CNOH\}_2]$	2.0111	$Cd^{II}(O_{carb})_3(N_{py})_2(N_{ox})$; oct	[187]
$[Cd(O_2CMe)(SCN)\{(py)_2CNOH\}]_n$	2.0111	$Cd^{II}(O_{carb})(N_{SCN-})(N_{py})_2(N_{ox})S$; oct	[187]
$[Hg_2(O_2CMe)_4\{(py)_2CNOH\}_2]$	2.0111	$Hg^{II}(O_{carb})_3(N_{py})_2(N_{ox})$; oct	[97]
$[Hg_2(O_2CPh)_3\{(py)_2CNO\}\{(py)_2CNOH\}_2(MeOH)]$	2.0111, 2.0111	$Hg^{II}(O_{carb})_3(N_{py})_2(N_{ox})$, $Hg^{II}(O_{MeOH})(O_{carb})_2(N_{py})_2(N_{ox})$; oct, oct	[97]
$[HgCl(O_2CPh)\{(py)_2CNOH\}]_n$	2.0111	$Hg^{II}Cl_2(O_{carb})(N_{py})_2(N_{ox})$; oct	[97]
$[Tb_3Zn_3\{(py)_2CNO\}_6(NO_3)_9]$	3.2111	$Tb^{III}(O_{nitrato})_6(O_{ox})_2(N_{py})_2$, $Zn^{II}(N_{py})_3(N_{ox})_3$, $Zn^{II}(O_{ox})_6$; sph, oct	[187]
$[Ln_2Ni(hfac)_6\{(py)_2CNO\}_2(py)_2]$	2.1111	No details available	[188]
$[LnNi_2(hfac)_2\{(py)_2CNO\}_4(MeOH)][Ln(hfac)_4(MeOH)]$	2.1110, 3.2111	No details available	[188]

Abbreviations: $acac^-$, acetylacetonate; 3,4-D^-, 3,4-dichlorophenoxyacetate(−1); $hfac^-$, hexafluoroacetylacetonate; $Hshi^{2-}$, the dianion of salicylhydroxamic acid; M = Ru, Os; $MCPA^-$, 2-methyl-4-chlorophenoxyacetate(−1); N_{ox}, oxime or oximate nitrogen; N_{py}, 2-pyridyl nitrogen; O_{carb}, carboxylate oxygen; O_{ox}, oximate oxygen; oct, octahedral; pbp, pentagonal bipyramidal; $(py)_2CO_2^{2-}$, the dianion of the *gem*-diol derivative of di-2-pyridyl ketone; R = Me, Ph; R′ = H, Me; S, solvate molecule; shi^{3-}, the trianion of salicylhydroxamic acid; sp, square planar; sph, sphenocorona; spy, square pyramidal; tbp, trigonal bipyramidal; tet, tetrahedral; $X^- = Cl^-$, Br^-, NO_3^-, $X'^- = Cl^-$, N_3^-, OCN^-, SCN^-, $Z^- = acac^-$, $MeCO_2^-$.

[a] Solvate molecules have been omitted.

[b] Considering only the Ni^{II}; the O atom of $(py)_2CNO^-$ interacts with Na^+ ions.

[c] These complexes contain simultaneously terminal and bridging $(py)_2CNO^-$ ligands.

[d] These molecules have metal–metal bonds.

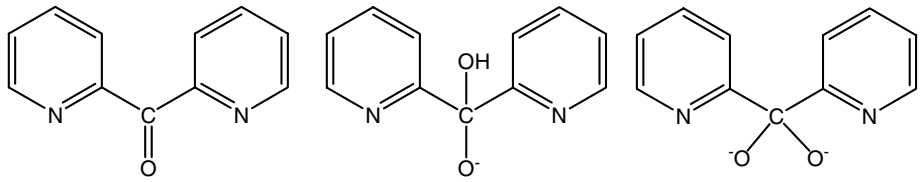

$(py)_2CO$ $(py)_2C(OH)O^-$ $(py)_2CO_2^{2-}$

Fig. 72. The formulae of the $(py)_2CO$-based ligands discussed in the text; note that $(py)_2C(OH)O^-$ and $(py)_2CO_2^{2-}$ do not exist as free species but exist only in their respective metal complexes.

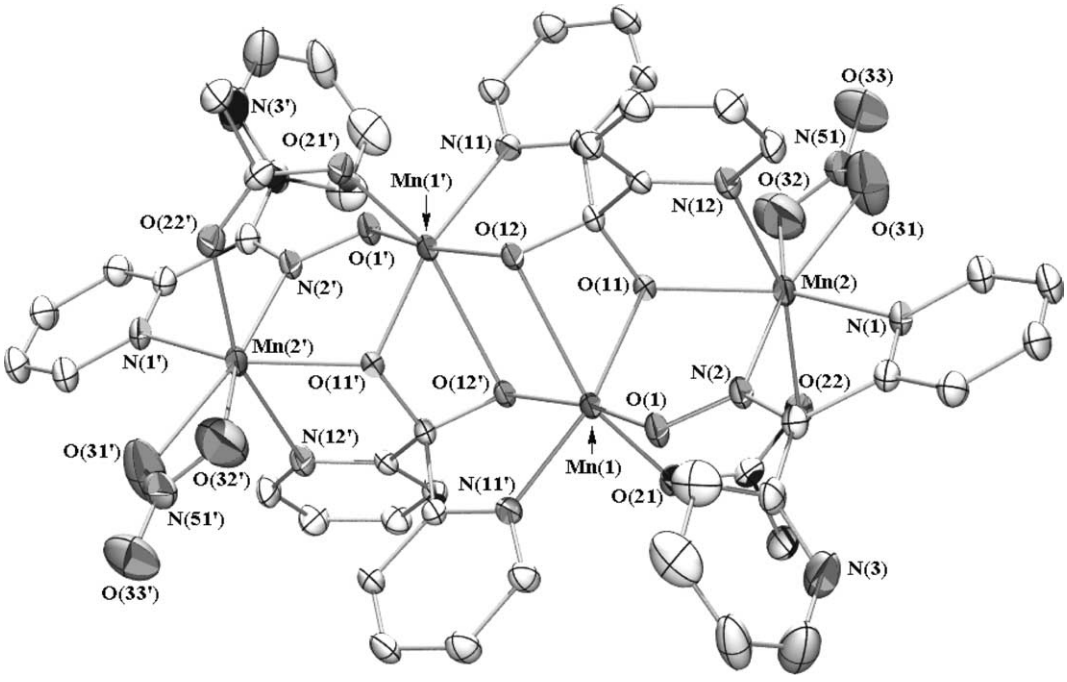

Fig. 73. X-ray structure of $[Mn_2^{II}Mn_2^{III}(O_2CMe)_2\{(py)_2CO_2\}_2\{(py)_2CNO\}_2(NO_3)_2]$. Mn(1) and Mn(1′) are assigned as the Mn^{III} ions [168].

complex is the first metallacrown with ring metal ions in three different oxidation states.

Aerobic reactions of $Co(O_2CR)_2 \cdot 4H_2O$ with $(py)_2$-CNOH, in the presence of counterions (ClO_4^-, PF_6^-), give complexes [179] containing the tetranuclear, mixed-valence cobalt(II/III) cations $[Co_2^{II}Co_2^{III}(OR')_2$-$(O_2CR)_2\{(py)_2CNO\}_4S_2]^{2+}$ (R = Me, Ph; R′ = H, Me; S = MeOH, EtOH) depending on the solvent mixture [179]. These complexes are the first Co members in the family of metallacrowns adopting the extremely rare inverse 12-MC-4 motif (Fig. 78). The $(py)_2CNO^-$ ligands comprise two pairs arranged along the edges and the sides of the Co_4 rectangle. Edge $(py)_2CNO^-$ ions function as 2.1110 ligands, whereas long side $(py)_2CNO^-$ ions adopt the 2.1111 coordination mode.

All known polynuclear Ni(II)/$(py)_2CNO^-$ complexes come from Pecoraro's, Kessissoglou's and our groups. Complex $[Ni_4\{(py)_2CNO\}_6(MeOH)_2](ClO_4)(OH)$ [180], containing both 2.1110 and 2.1111 $(py)_2CNO^-$ ligands, is a rare example of an $\{Ni_4(OR)_2\}^{6+}$ core based on a chair or butterfly "out-of-face" topology (Fig. 79). The complex is characterized by the presence of both ferromagnetic and antiferromagnetic exchange interactions.

The "monomeric", vacant mixed-ligand metallacrown $[Ni_4(NCS)_2(Hshi)_2\{(py)_2CNO\}_2(DMF)(H_2O)]$ shows [181] the connectivity pattern [–O–Ni–O–N–Ni–N–]$_2$. Two Ni^{II} ions are bound only to nitrogen atoms along the metallacrown core and are in a square planar arrangement. The other two Ni^{II} ions are coordinated only to oxygen atoms along the metallacrown ring and are in an octahedral environment. This complex can be described as the acid form of metallacrown, i.e., $H_2$12MC4 [181]. The refinement of $[Ni_4Na_2(acac)_4\{(py)_2CNO\}_4](ClO_4)_2$ has not been completed yet [97]; the MC ring encapsulates two Na^+ ions.

Complex $[Ni_5(O_2CMe)_2(shi)_2\{(py)_2CNO\}_2]$ has an interesting structure [181]. The two shi^{3-} and two $(py)_2CNO^-$ (in the 3.2111 mode) ligands are arranged in a *trans* configuration to construct a 12-MC-4 core

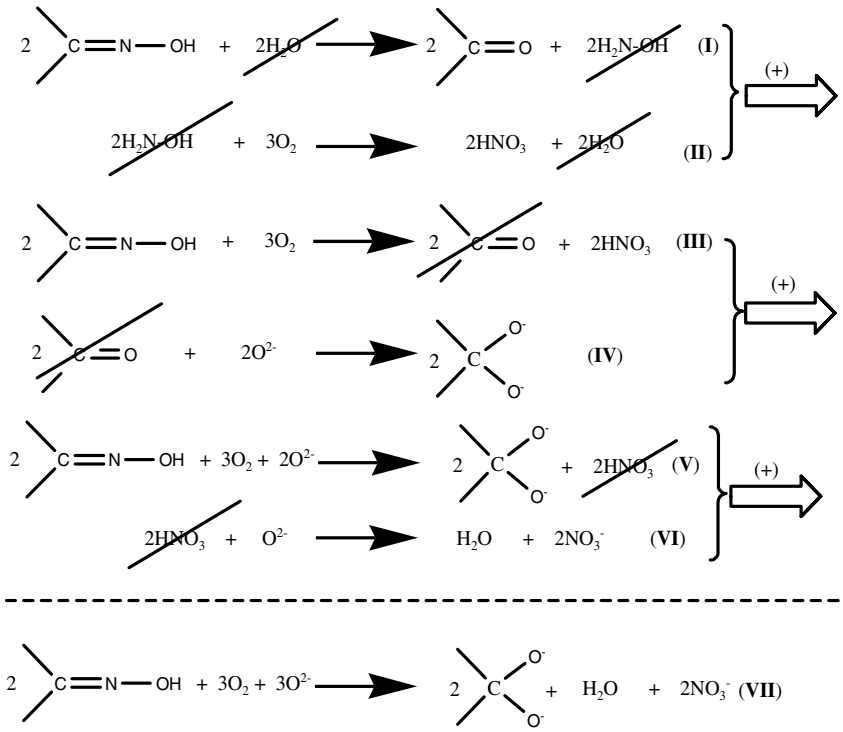

Scheme 8. A proposed simplified reaction scheme for the metal-mediated, partial transformation of di-2-pyridyl ketone oxime, $(py)_2CNOH$, towards the dianion of the *gem*-diol form of di-2-pyridyl ketone, $(py)_2CO_2^{2-}$, involving NO_3^- generation. The O^{2-} species can be derived from H_2O and/or the oxidation of Mn^{II} by atmospheric dioxygen. The 2-pyridyl rings have been omitted for clarity.

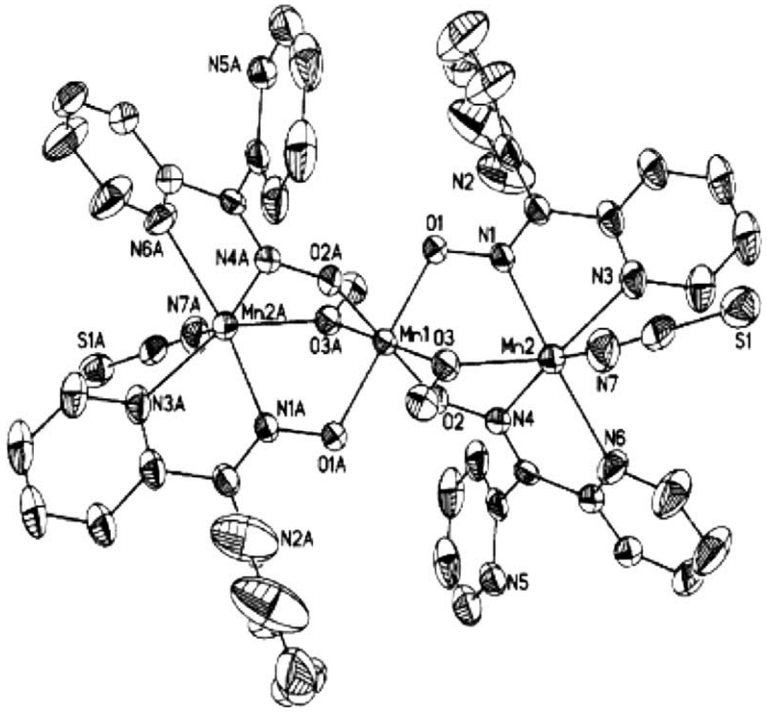

Fig. 74. X-ray structure of $[Mn_2^{II}Mn^{IV}(OMe)_2(NCS)_2\{(py)_2CNO\}_4]$ [174].

with a fifth Ni^{II} encapsulated ion (Fig. 80). The two $MeCO_2^-$ ions bridge the encapsulated metal ion to two ring metal ions giving an overall neutral charge to the molecule. The $(py)_2CNO^-$ ligand is nonplanar due to steric hindrance between the two pyridyl rings; this confers a nonplanar conformation to the metallacrown

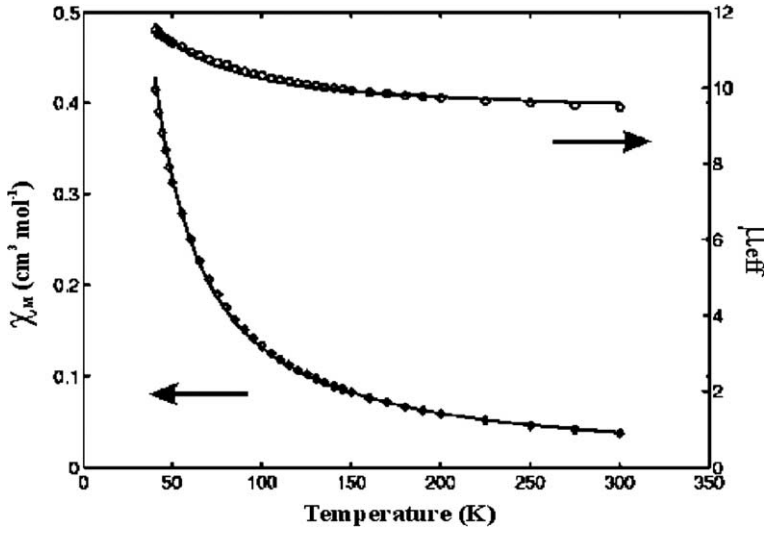

Fig. 75. Variable-temperature magnetic susceptibility for $[Mn_2^{II}Mn^{IV}(OMe)_2(NCS)_2\{(py)_2CNO\}_4]$ [174].

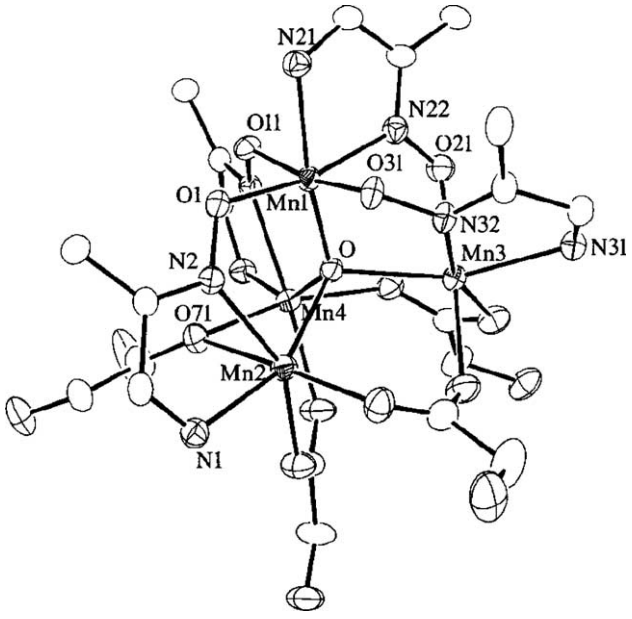

Fig. 76. X-ray structure of $[Mn_3^{II}Mn^{IV}O(3,4\text{-}D)_4\{(py)_2CNO\}_4]$ [177].

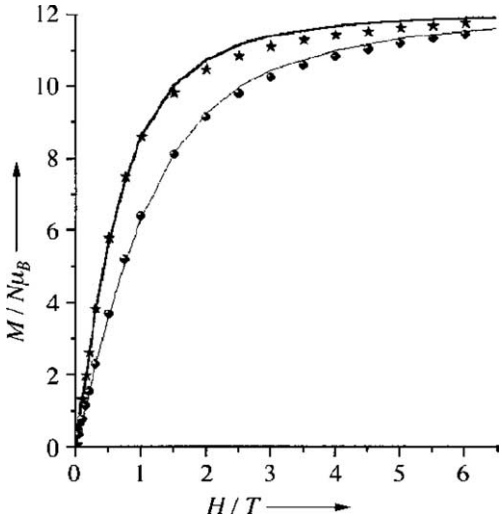

Fig. 77. Magnetization measurements for $[Mn_3^{II}Mn^{IV}O(3,4\text{-}D)_4\{(py)_2CNO\}_4]$ in the field range 0–6.5 T at 2.5 K (∗) and 4.5 K (•). The solid lines represent the simulations according to the Brillouin function of a system with an $S = 6$ ground state and $D = 0.025$ cm^{-1} [177].

ring or a "saddle" shape. Two Ni^{II} ions in the ring are octahedral and two are square planar; the encapsulated metal ion is also in an octahedral oxygen environment with four oxygens coming from the MC cavity and two from the bridging *syn*, *anti* $MeCO_2^-$ ligands. The relationship between the bridging acetates and the MC ring requires that stereoisomers are present. Magnetically the compound is characterized by weak antiferromagnetic exchange interactions. Our group have also isolated a series of pentanuclear Ni(II) clusters [97] based on $(py)_2CNO^-$, see Table 4 and Figs. 81–83. Their magnetic properties are being studied.

The molecular structure of the azido-bridged heptanuclear cluster $[Ni_7(O_2CMe)_6(N_3)_2\{(py)_2CNO\}_6(H_2O)_2]$ is based on the fusion (at a central metal ion) of two tetranuclear fragments [97].

The X-ray structure of $[Ni_{10}(MCPA)_2(shi)_5\{(py)_2CNO\}_3(MeOH)(H_2O)]$ (Fig. 84), where $MCPA^-$ is the anion of 2-methyl-4-chlorophenoxyacetic acid, consists of two 12-MC-4 units with charges of +1 and −1 [181]. Each tetranuclear unit has one additional encapsulated Ni^{II} ion. The cationic unit is bound to the anionic unit via O bridges. The ground state of this cluster is $S = 0$, with $S = 1$, 2 low-lying excited states [193]; this leads to a non-Brillouin behavior of the magnetization.

Complex $[Mn_2Ni_2(O_2CMe)_2(shi)_2\{(py)_2CNO\}_2(DMF)_5]$ consists of a mixed metal/mixed ligand "collapsed" 12-MC-4 motif (Fig. 85) [181]. The oxophilic

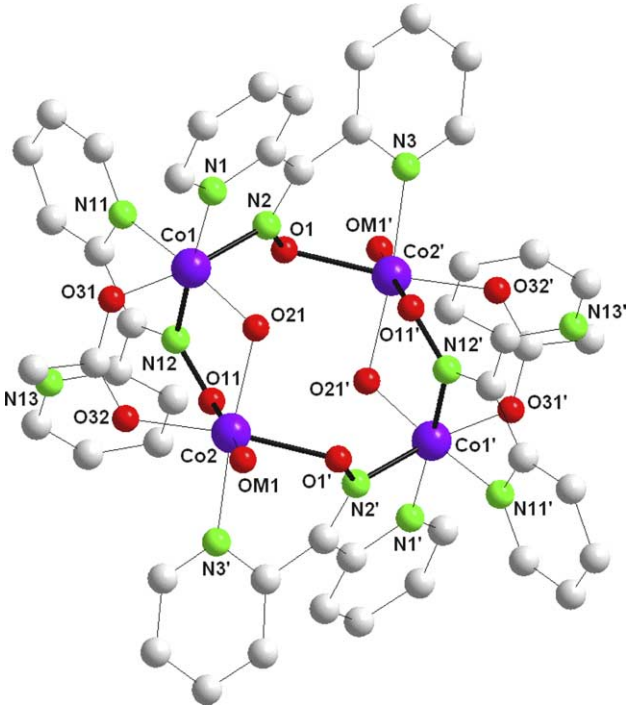

Fig. 78. X-ray structure of the cation of $[Co_2^{II}Co_2^{III}(OH)_2(O_2CMe)_2\{(py)_2CNO\}_4(MeOH)_2](ClO_4)_2$. O(21) and O(21′) are the hydroxo oxygen atoms, while OM(1) and OM(1′) are the oxygen atoms of the methanol ligands. The metallacrown ring is outlined in bold [179].

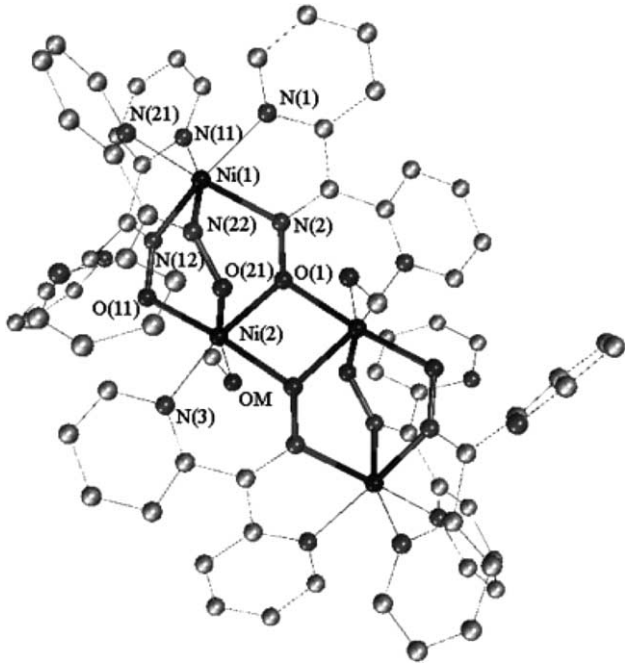

Fig. 79. X-ray structure of $[Ni_4\{(py)_2CNO\}_6(MeOH)_2]^{2+}$ [180].

Mn^{III} ions are bound to the O, N chelating part of the shi^{3-} ligand and then bind across the core to the oxime oxygens instead of the pyridyl nitrogens of the 2.1110

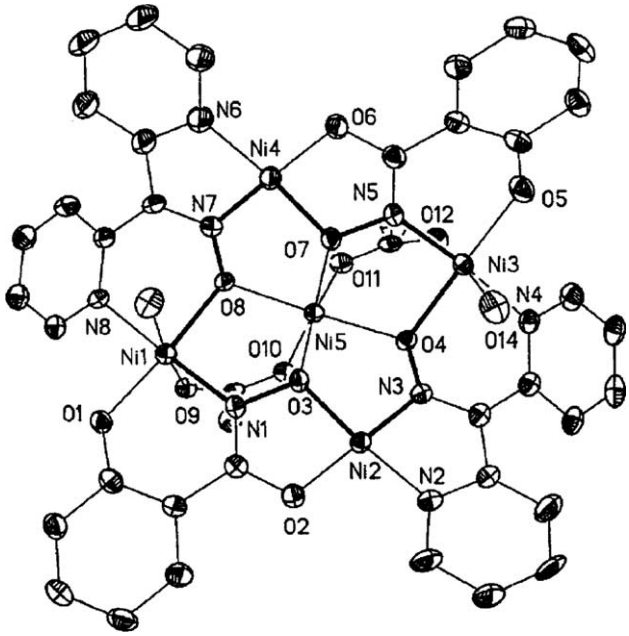

Fig. 80. X-ray structure of $[Ni_5(O_2CMe)_2(shi)_2\{(py)_2CNO\}_2]$; the molecule shown here is the Λ isomer as defined by the screw axis oriented along the C_2-axis [181].

$(py)_2CNO^-$ ligands. Paramagnetic ^1H NMR studies demonstrate that the mixed metallacrown retains its structure in solution [181].

The only copper(I) complex containing bridging $(py)_2CNOH$ or $(py)_2CNO^-$ ligands is [171] the dimer $[Cu_2Cl_2\{(py)_2CNO\}_2]$, in which each Cu^I ion is coordinated by one chloride and three nitrogen atoms in a distorted tetrahedral environment.

Copper(II) complexes possessing bridging $(py)_2CNOH$ or $(py)_2CNO^-$ ligands have not been studied extensively. The crystal structure of $[Cu_2\{(py)_2CNO\}_4]\cdot 2H_2O$ [182,183] consists of dinuclear molecules containing both 1.0110 and 2.1110 $(py)_2CNO^-$ ligands (Fig. 86); the Cu^{II} coordination geometry is slightly distorted trigonal bipyramidal. Employment of carboxylates in the reaction mixtures gives trinuclear complexes of the general formula $[Cu_3(OH)(O_2CR)_2\{(py)_2CNO\}_3]$; the molecular structure of the acetate complex is shown in Fig. 87. The trinuclear cluster, which has an inverse 9-MC-3 motif, is held together by one μ_3-OH group, one $\eta^1:\eta^1:\mu_2$-$MeCO_2^{2-}$ ligand and three 2.1110 $(py)_2CNO^-$ ions [183]; a monodentate acetate completes five coordination at one Cu^{II} center. Two trinuclear molecules are "dimerized" in the crystal lattice through weak interactions between two Cu^{II} ions and "free" 2-pyridyl nitrogen atoms creating a hexamer. The benzoate analogue consists of well-isolated trinuclear molecules [183]. In the dinuclear complex $[Cu_2(hfac)_2\{(py)_2CNO\}_2]$, the two five-coordinate Cu^{II} ions are bridged by two 2.1110 $(py)_2CNO^-$ ligands.

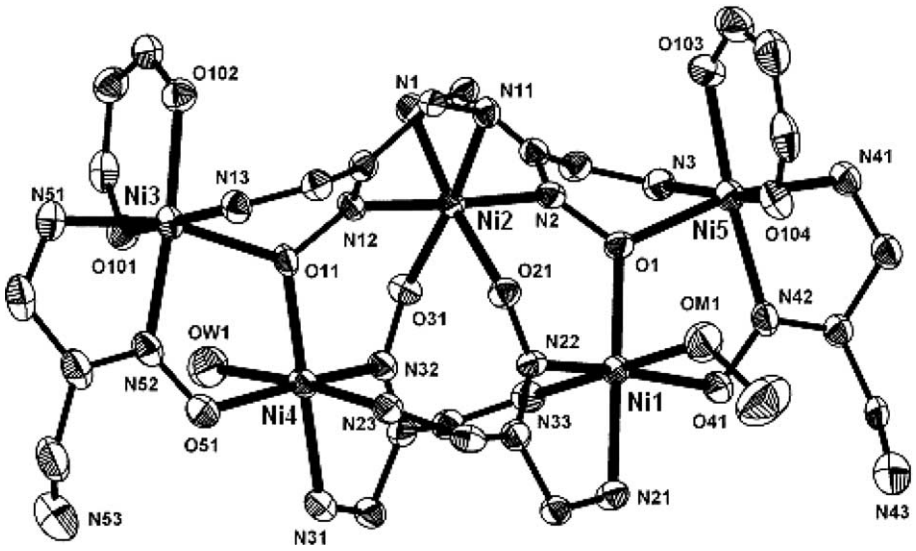

Fig. 81. X-ray structure of the cation present in the complex $[Ni_5(acac)_2\{(py)_2CNO\}_6(H_2O)(MeOH)][ClO_4)_2$; many carbon atoms have been omitted for clarity [97].

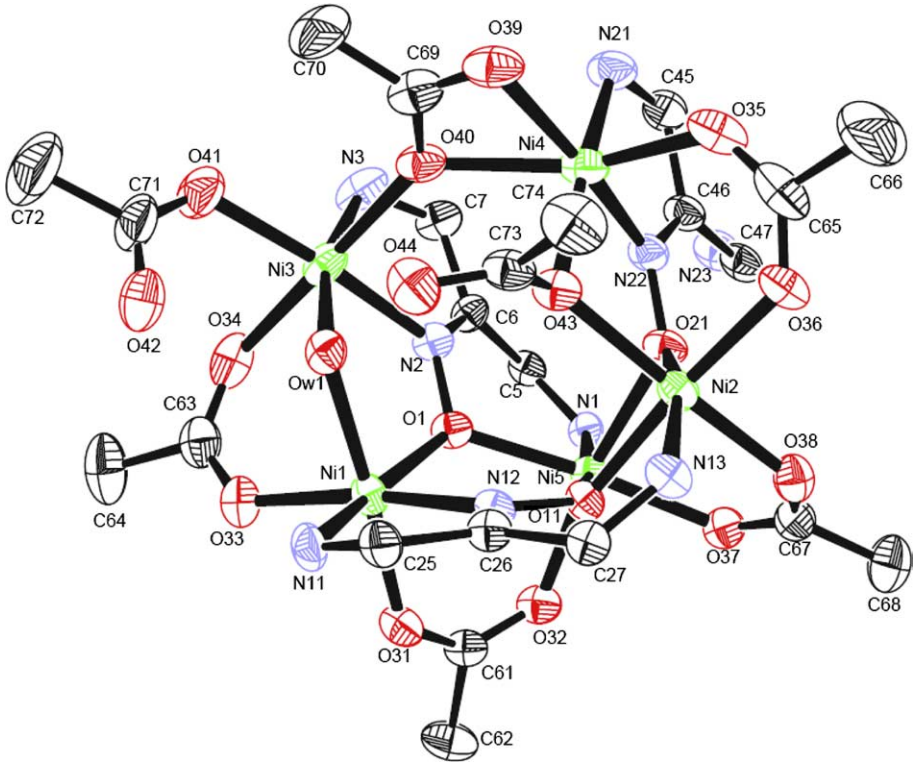

Fig. 82. X-ray structure of $[Ni_5(O_2CMe)_7\{(py)_2CNO\}_3(H_2O)]$; many carbon atoms of the $(py)_2CNO^-$ ligands have been omitted [97].

The use of $(py)_2CNO^-/X^-$ "blends" ($X^- = MeCO_2^-$, $PhCO_2^-$, Cl^-, N_3^-, NCO^-, $acac^-$, NCS^-, Cl^-/NCS^-) in Zn^{II} chemistry yields neutral tetranuclear and cationic pentanuclear clusters [172,184,185], see Scheme 9. Various synthetic procedures have led to the synthesis of compounds $[Zn_4(OH)_2X'_2\{(py)_2CNO\}_4]$ ($X'^- = Cl^-, N_3^-$, NCO^-), $[Zn_4(OH)_2Z_2\{(py)_2CNO\}_4]$ ($Z^- = MeCO_2^-, acac^-$), $[Zn_5Cl_2\{(py)_2CNO\}_6][ZnCl(NCS)_3]$ and $[Zn_5(NCS)_2\{(py)_2CNO\}_6(MeOH)][Zn(NCS)_4]$; representative structures are shown in Figs. 88 and 89. The tetranuclear molecules have an inverse 12-MC-4 topology. The triply bridging hydroxides are accommodated in the center of the metallacrown ring. The $(py)_2CNO^-$ ligands form a propeller configuration that imposes absolute stereoisomerism with Λ and Δ chirality. Two metal ions are in distorted O_2N_4 octahedral environments,

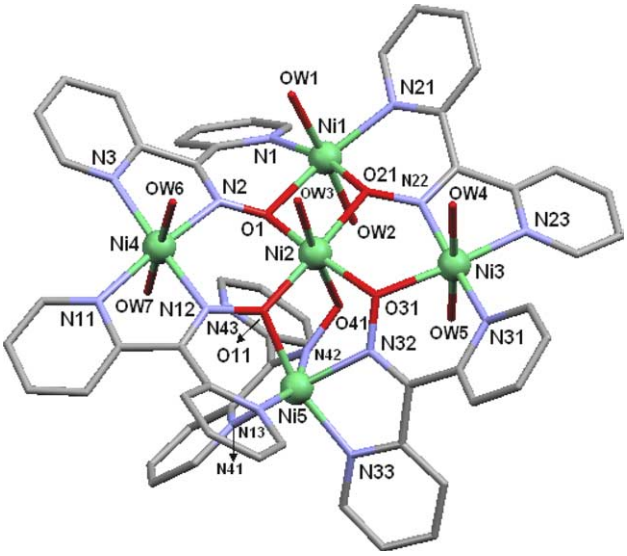

Fig. 83. X-ray structure of the cation present in complex $[Ni_5\{(py)_2CNO\}_5(H_2O)_7](NO_3)_5$ [97].

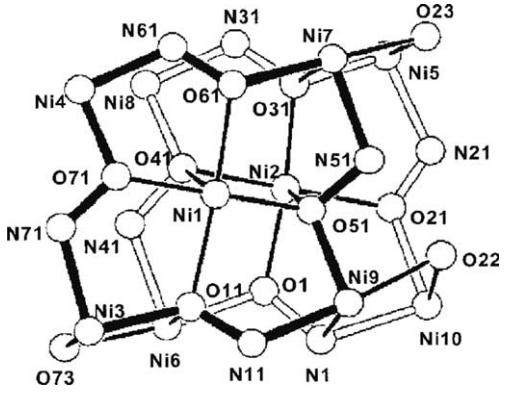

Fig. 84. A view of $[Ni_{10}(MCPA)_2(shi)_5\{(py)_2CNO\}_3(MeOH)(H_2O)]$; many atoms have been omitted for clarity [181].

whereas the rest are in severely distorted tetrahedral ($X'^{-} = Cl^-, N_3^-, NCO^-, PhCO_2^-$) or tbp ($Z^- = MeCO_2^-, acac^-$) environments. The five Zn^{II} ions of the pentanuclear cations are held together by six $(py)_2CNO^-$ ligands which adopt three different coordination modes (2.1110, 3.1111, 3.2111); the chloro and isothiocyanato ligands in these cluster cations are terminal. The five Zn^{II} ions define two nearly equilateral triangles sharing a common apex, and the novel Zn_5 topology can be described as two "collapsed" 9-MC-3 structures sharing a common metal apex.

Employment of shi^{3-} in $ZnCl_2/(py)_2CNO^-$ chemistry yields [172] the octanuclear cluster $[Zn_8(shi)_4\{(py)_2CNO\}_4(MeOH)_2]$. The molecule contains a 12-MC-4 core constructed by four metal ions, i.e., Zn(3), Zn(5), Zn(7) and Zn(8) in Fig. 90, and four shi^{3-} ligands. The MC core accommodates a dinuclear $Zn_2\{(py)_2CNO\}_4$ component (Zn(1), Zn(4)), while the ring metal ions Zn(3) and Zn(5) create dinuclear units with Zn(2) and Zn(6), respectively, through oxygen bridges.

There also exist $(py)_2CNO^-$-based complexes of 4d- and 5d-metals, including organometallic compounds. Treatment of $[Ru_3(CO)_{12}]$ with $(py)_2CNOH$ in refluxing THF leads [186a] to a separable mixture of $[Ru_3\{(py)_2CNO\}_2(CO)_8]$ (Fig. 91) and $[Ru_2\{(py)_2CNO\}_2(CO)_4]$. Compounds $[M_3(CO)_{10}(MeCN)_2]$ (M = Ru, Os) react with $(py)_2CNOH$ in THF at room temperature to give $[M_3(\mu\text{-}H)\{(py)_2CNO\}(CO)_9]$ [186a]. The thermal reaction of $[Os_3(\mu\text{-}H)\{(py)_2CNO\}(CO)_9]$ with $(py)_2CNOH$ gives [186a] $[Os_3\{(py)_2CNO\}_2(CO)_8]$, which is isostructural with the Ru analogue. These complexes display low activity as DNA cleavage agents. The crystals of $[Ag_2(NO_3)_2\{(py)_2CNOH\}_2]$ were found [186b] to contains neutral dinuclear molecules (Fig. 92). The $(py)_2CNOH$ ligands bridge the two Ag^I ions in a 2.0111 fashion, see Fig. 68. The nitrato ligands are monodentate

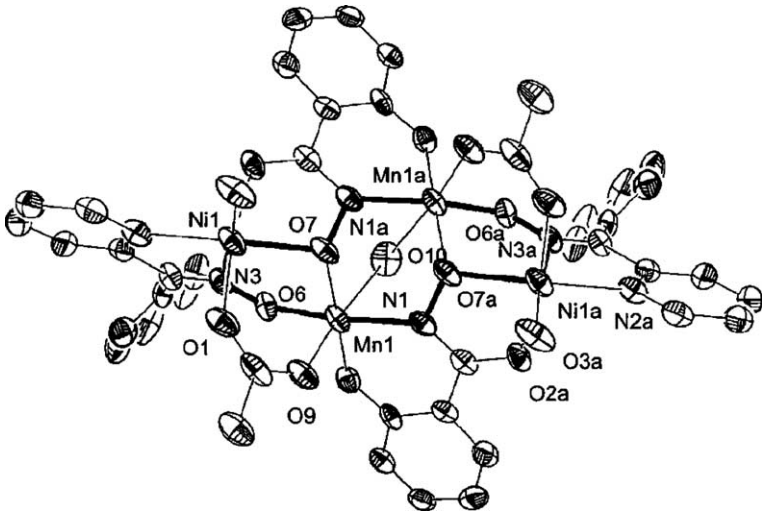

Fig. 85. X-ray of the mixed metal/mixed ligand "collapsed" 12-MC-4 complex $[Mn_2Ni_2(O_2CMe)_2(shi)_2\{(py)_2CNO\}_2(DMF)_5]$ [181].

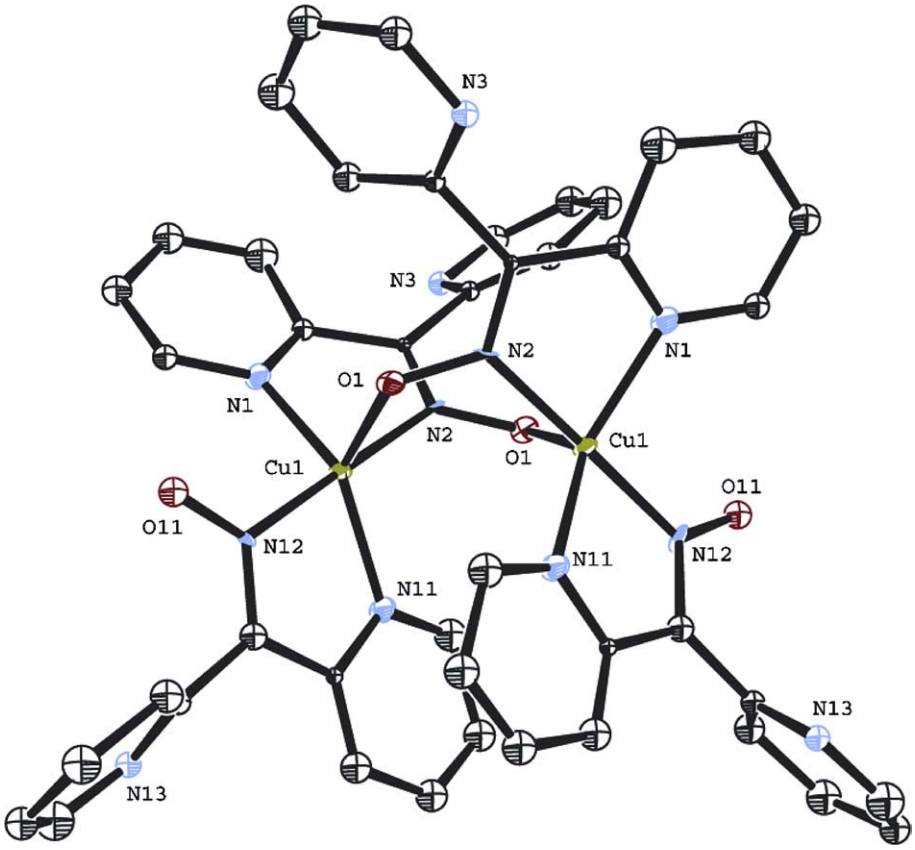

Fig. 86. X-ray structure of $[Cu_2\{(py)_2CNO\}_4]$ [183].

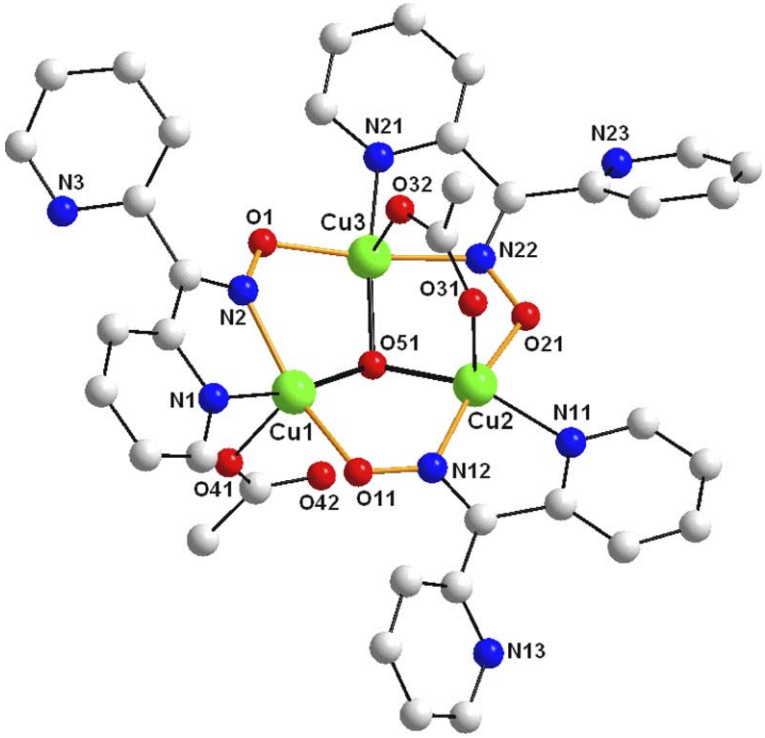

Fig. 87. X-ray structure of $[Cu_3(OH)(O_2CR)_2\{(py)_2CNO\}_3]$; the ''dimerization'' of the trinuclear molecules is not shown [183].

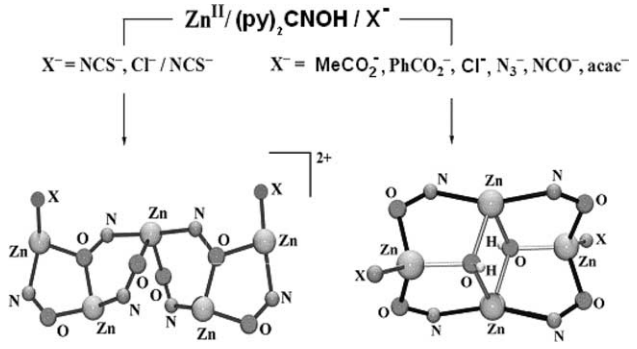

Scheme 9. The $Zn^{II}/(py)_2CNOH/X^-$ reaction scheme that leads to neutral tetranuclear and cationic pentanuclear clusters.

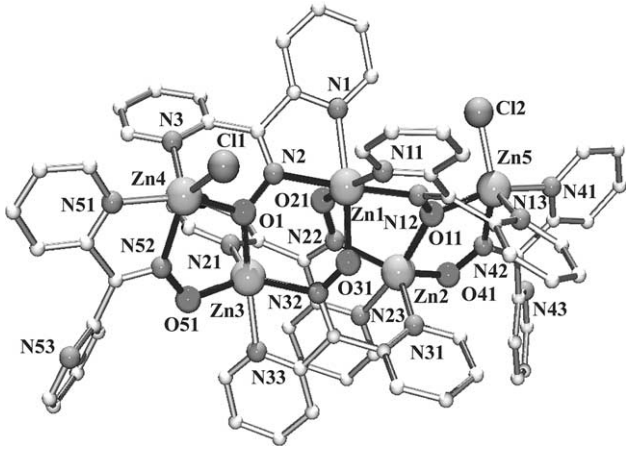

Fig. 89. X-ray structure of the pentanuclear cation present in the complex $[Zn_5Cl_2\{(py)_2CNO\}_6][ZnCl(NCS)_3]$.

and the geometry around the metal centers can be described as distorted tetrahedral. The 2.0111 ligation mode is also adopted by the neutral ligand in the dinuclear complexes $[Cd_2(O_2CR)_4\{(py)_2CNOH\}_2]$ (R = Me, Ph) and the coordination polymer $[Cd(O_2CMe)(SCN)\{(py)_2CNOH\}]_n$ [187]. The structurally characterized mercury(II) complexes are [97] $[Hg_2(O_2CMe)_4\{(py)_2CNOH\}_2]$, $[Hg_2(O_2CPh)_3\{(py)_2CNO\}\{(py)_2CNOH\}(MeOH)]$ (Fig. 93) and $[HgCl(O_2CPh)\{(py)_2CNOH\}]_n$; details are given in Table 4. The three complexes contain 2.0111 ligands.

Working with $(py)_2CNOH$, we have been able to apply the "metal complexes as ligands" strategy [73,209] to isolate mixed-metal 3d/4f complexes [187]. Complexes $[M\{(py)_2CNOH\}_2(H_2O)_2](NO_3)_2$ [187], which have yet to be structurally characterized, most probably contain 1.0110 neutral oxime ligands. Since these species contain two potentially free (the oxime oxygen, the second 2-pyridyl nitrogen) coordination sites, they can be regarded as "ligands". Reactions between equimolar quantities of $[M\{(py)_2CNOH\}_2(H_2O)_2](NO_3)_2$, where M = Mn, Ni, Cu, Zn, and $Ln(NO_3)_3 \cdot xH_2O$ (Ln = lanthanide) in various solvents lead to hexanuclear clusters of the general formula $[M_3Ln_3\{(py)_2CNO\}_6(NO_3)_9]$ (Eq. (7)).

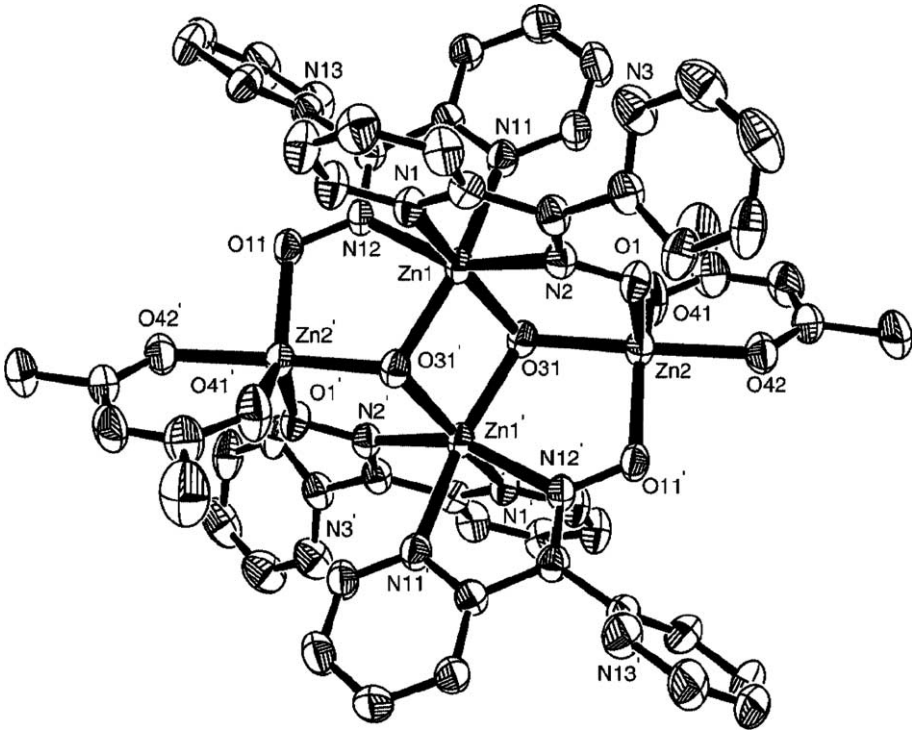

Fig. 88. X-ray structure of $[Zn_4(OH)_2(acac)_2\{(py)_2CNO\}_4]$ [184].

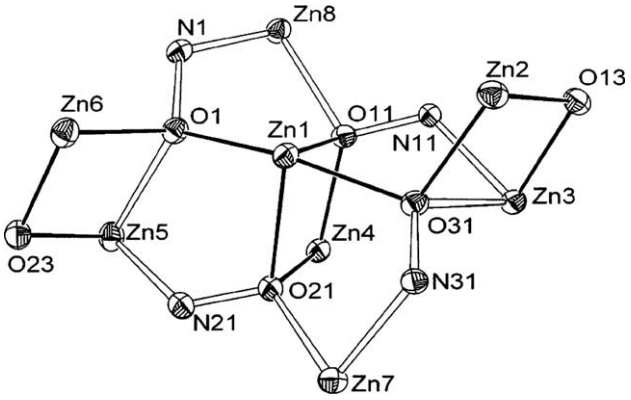

Fig. 90. The connectivity pattern of the complex $[Zn_8(shi)_4\{(py)_2CNO\}_4(MeOH)_2]$ [172].

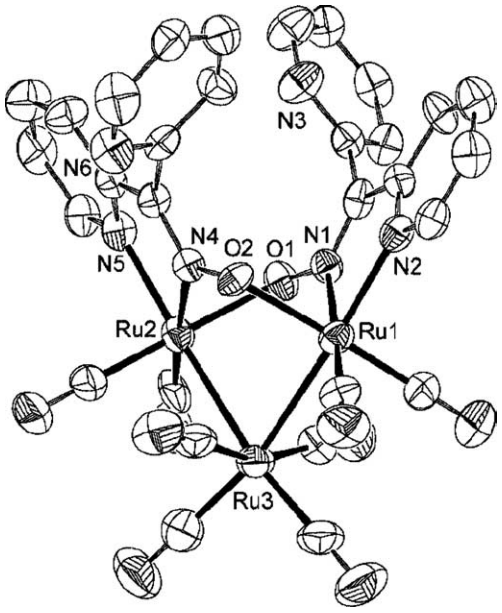

Fig. 91. X-ray structure of $[Ru_3\{(py)_2CNO\}_2(CO)_8]$ [186a].

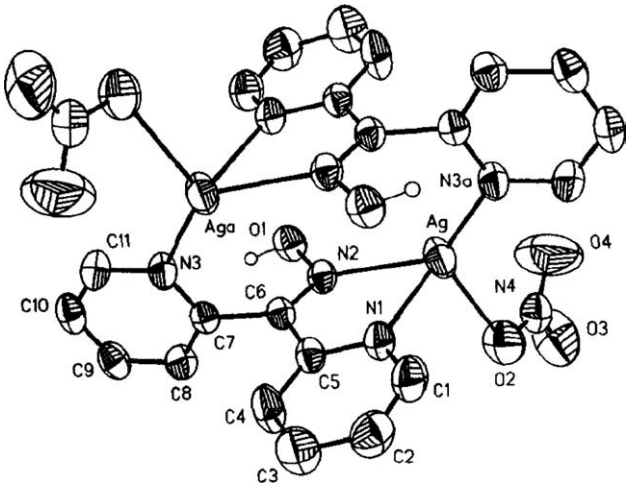

Fig. 92. X-ray structure of $[Ag_2(NO_3)_2\{(py)_2CNOH\}_2]$ [186b].

$$3[M\{(py)_2CNOH\}_2(H_2O)_2](NO_3)_2 + 3Ln(NO_3)_3 \cdot xH_2O + 6LiOH \rightarrow [M_3Ln_3\{(py)_2CNO\}_6(NO_3)_9] + 6LiNO_3 + 3(4+x)H_2O$$

The molecular structure of the M = Zn, Ln = Tb complex is shown in Fig. 94. The $(py)_2CNO^-$ ligands adopt the 3.2111 coordination mode, each bridging two Zn^{II} ions and one Tb^{III} center; three chelating nitrates are bound to each Tb^{III} ion. The two donor atoms, that were free in the mononuclear "ligand" 3d-metal complex, are indeed coordinated to terbium(III), as anticipated; however, the deprotonated oximate oxygen is bound to a second Zn^{II} ions and this does not permit a full synthetic control of the reaction. Five, out of the six, metal ions define a trigonal bipyramid (Fig. 95). The Tb^{III} ions occupy the equatorial positions, while the third Zn^{II} ion lies in the middle of the equatorial plane. Trinuclear Ni^{II}/Ln^{III} clusters based on $(py)_2CNO^-$ and containing chelating $hfac^-$ as ancillary ligand have also been communicated at a conference [188].

8.4. Metal-ion assisted transformations of $(py)_2CNOH$

We have already mentioned the in situ transformations of $(py)_2CNOH$ to give the coordination dianion and monoanion of the *gem*-diol derivative of di-2-pyridyl ketone (Fig. 72) during the preparation of $[Mn_2^{II}Mn_2^{III}(O_2CR)_2\{(py)_2CO_2\}_2\{(py)_2CNO\}_2X_2]$ (Fig. 73, Scheme 8) [168,176] and $[Co(NO_2)\{(py)_2C(OH)O\}\{(py)_2CNO\}]$ (Table 3) [170], respectively. In these complexes, an amount of the oximate ligand still remains coordinated in the product. We shall briefly discuss here the few cases in which the initially $(py)_2CNOH$ ligand employed does not appear in the products.

The synthetic utility of the metal-mediated organic transformations and the reactions of coordinated ligands is an important subject [210]. It is based on the enhancement in reactivity of organic ligands as a consequence of metal coordination. For example, the metal can act as a 'super acid' and cause enhanced nucleophilic attack on coordinated carbonyl and imine ligands. The metal ion can also enable the ligand itself to act as a nucleophile, sometimes by direct activation, sometimes by protecting other parts of the ligand and sometimes by a combination of both. The ligands which undergo reaction can be bound to the metal ion in the transition state or in relatively stable, isolable complexes.

The reaction between $[VCl_3(THF)_3]$ and $(py)_2CNOH$ is solvent dependent (Scheme 10) [211]. In THF, the product is $[VOCl_2\{(py)_2CNH\}(THF)]$, where $(py)_2CNH$ is di-2-pyridylimine. The molecular structure of this

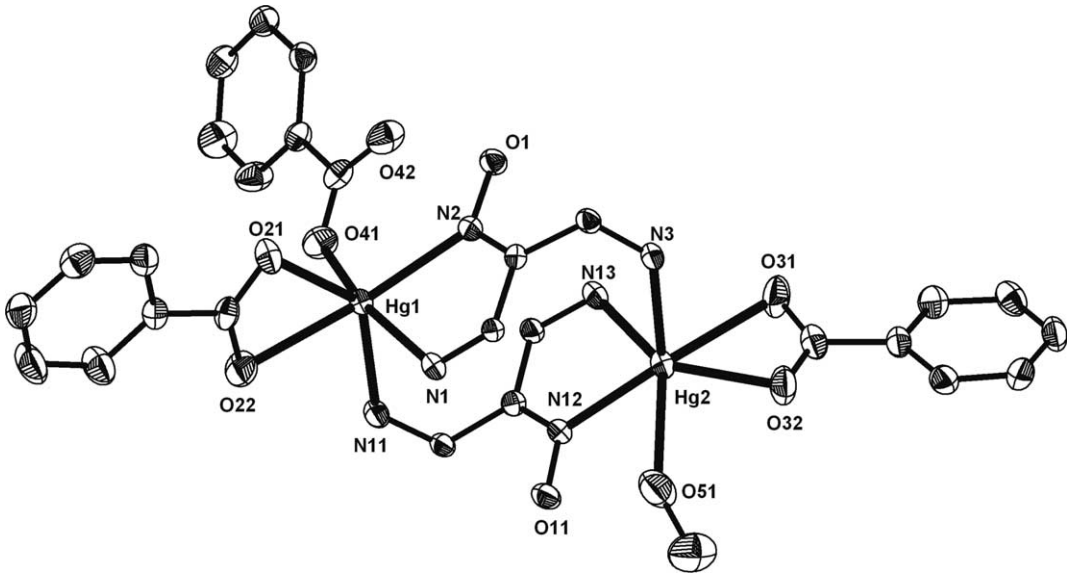

Fig. 93. X-ray structure of $[Hg_2(O_2CPh)_3\{(py)_2CNO\}\{(py)_2CNOH\}(MeOH)]$; many carbon atoms of the oxime and oximate ligands have been omitted for clarity [97].

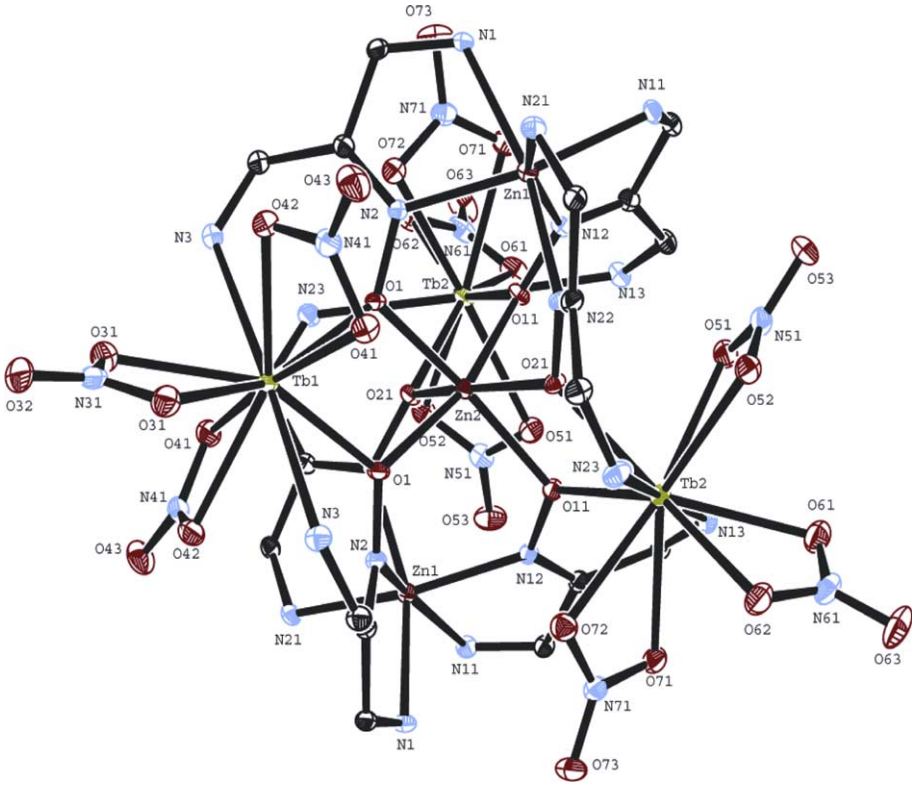

Fig. 94. X-ray structure of $[Zn_3Tb_3\{(py)_2CNO\}_6(NO_3)_9]$ [187].

compound is shown in Fig. 96. The structure reveals two important features: (a) the oxidation of the initially V^{III} ion to the oxovanadium(IV) ion, $V^{IV}O^{2+}$ and (b) the transformation of the oxime group to an imino group. In EtOH the product is $[VOCl_2\{(py)_2C(OEt)(NH_2)\}]$, where $(py)_2C(OEt)(NH_2)$ is amino-di-2-pyridyl-methyl ethyl ether. The new ligand exhibits an $(N_{py})_2(N_{amino})$ chelating behavior (Fig. 97). The reaction in MeOH gives a mixture of two-coordination isomers of $[VOCl_2\{(py)_2C(OMe)(NH_2)\}]$, where $(py)_2C(OMe)$-

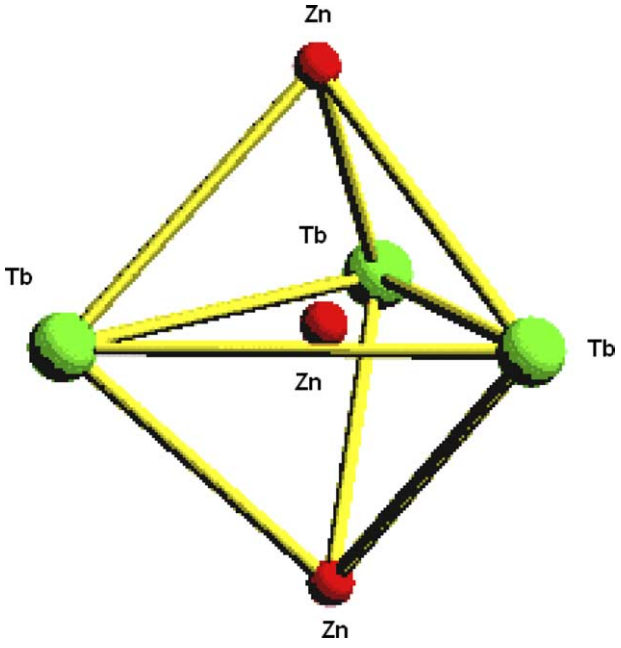

Fig. 95. The topological arrangement of the six metal ions in the 3d/4f cluster $[Zn_3Tb_3\{(py)_2CNO\}_6(NO_3)_9]$ [187].

(NH_2) is amino-di-2-pyridyl-methyl methyl ether. One isomer bears striking structural resemblance to $[VOCl_2\{(py)_2C(OEt)(NH_2)\}]$ (Fig. 97), while in the other isomer an $(N_{py})_2(O_{ether})$ chelating behavior of the ligand is realized (Fig. 98). One pyridyl nitrogen atom exhibits no interaction with V^{IV} in $[VOCl_2\{(py)_2CNH\}(THF)]$ due to the sp^2 character of the central carbon atom (C(6)), whereas the coordination of both pyridyl nitrogen atoms has been observed in the rest of the complexes as a result of flexibility of C(6) due to sp^3 hybridization [211]. It was concluded that the vanadyl oxygen comes from N–O bond cleavage.

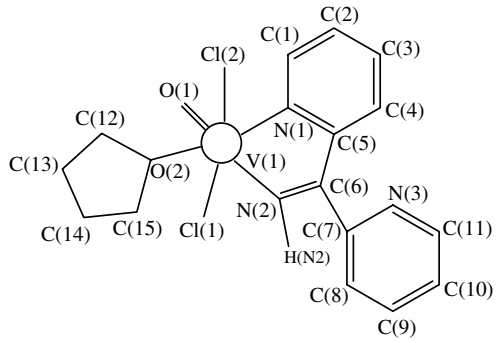

Fig. 96. X-ray structure of $[VOCl_2\{(py)_2CNH\}(THF)]$.

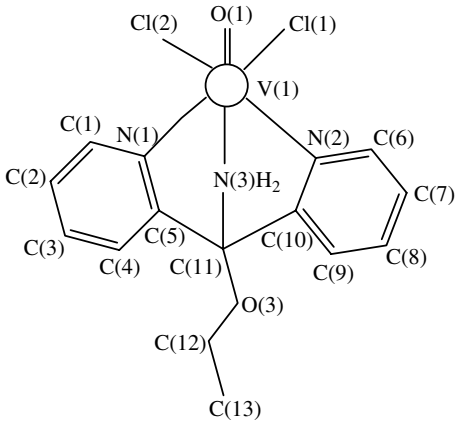

Fig. 97. X-ray structure of $[VOCl_2\{(py)_2C(OEt)(NH_2)\}]$.

Recent results [97] reveal that the $Co(O_2CMe)_2 \cdot 4H_2O/(py)_2CNOH/NaN_3$ reaction mixture in MeCN gives the complex $[Co_4(N_3)_2(O_2CMe)_2\{(py)_2C(OH)O\}_4]$. The remarkable feature of the reaction is the in situ transformation of $(py)_2CNOH$ to yield the triply-

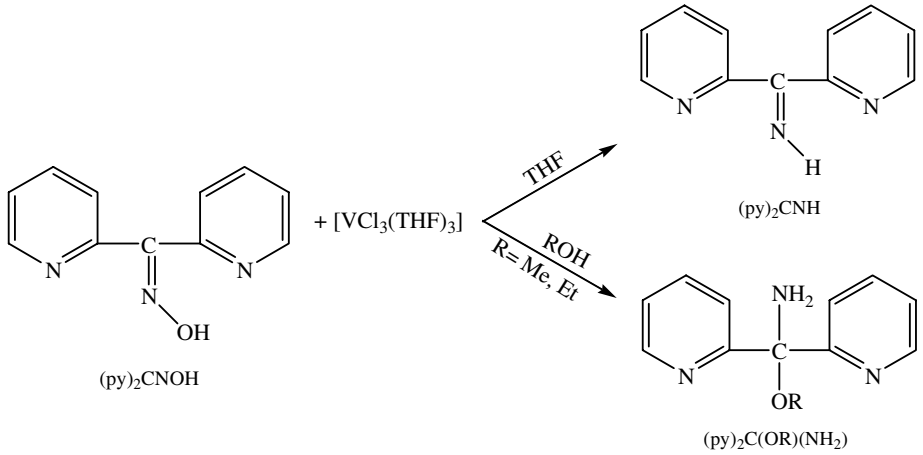

Scheme 10. The $[VCl_3(THF)_3]/(py)_2CNOH$ reaction system [211].

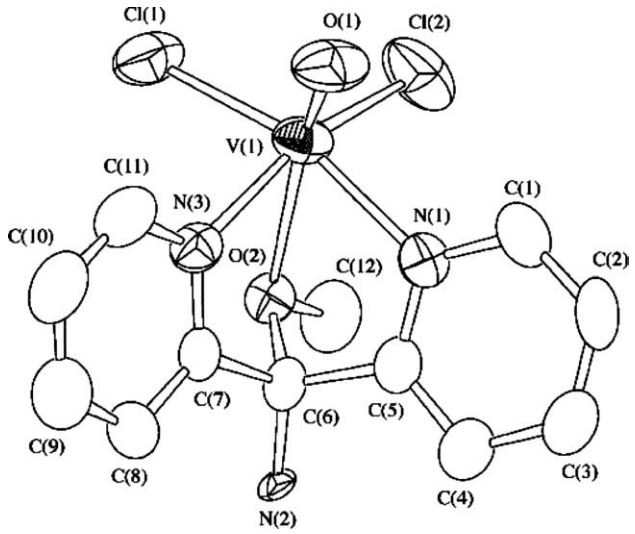

Fig. 98. X-ray structure of the second coordination isomer of $[VOCl_2\{(py)_2C(OMe)(NH_2)\}]$.

bridging monoanion, $(py)_2C(OH)O^-$, of the *gem*-diol derivative of di-2-pyridyl ketone, $(py)_2CO$, see Fig. 72. The X-ray diffraction analysis shows (Fig. 99) a defective double-cubane, tetranuclear entity in which the Co^{II} ions are linked by end-on (2.100) azido ligands and two kinds of O-bridges from two 3.3011 and two 2.2011 $(py)_2C(OH)O^-$ ligands. Magnetic susceptibility studies of this compound in the 2–300 K range indicate bulk ferromagnetic coupling. Efforts are in progress to elucidate the mechanism of this transformation.

9. The coordination chemistry of tris(2-aldoximo-6-pyridyl)phosphine, P{(py-H)CHNOH}$_3$, and of the related clathro-chelates

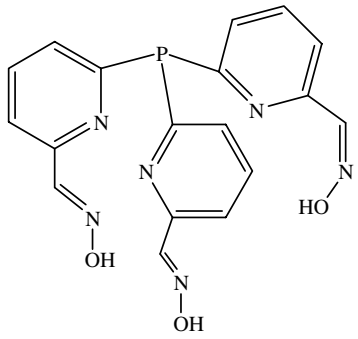

$P\{(py\text{-}H)CHNOH\}_3$

The ligand was synthesized by Holm's group some 35 years ago [212,213] during his successful project for the design of complexes containing encapsulated metal ions with trigonal prismatic coordination. As shown in Scheme 11, $P\{(py\text{-}H)CHNOH\}_3$ can be obtained in ~20% overall yield from 2,6-dibromopyridine in a six-step process.

Reaction of Fe^{II}, Co^{II}, Ni^{II}, Cu^{II} and Zn^{II} salt with $P\{(py\text{-}H)CHNOH\}_3$ in MeCN yields the cations $[M(P\{(py\text{-}H)CHNOH\}_2\{(py\text{-}H)CHNO\})]^+$, which can be isolated as analytically pure perchlorate salts; the

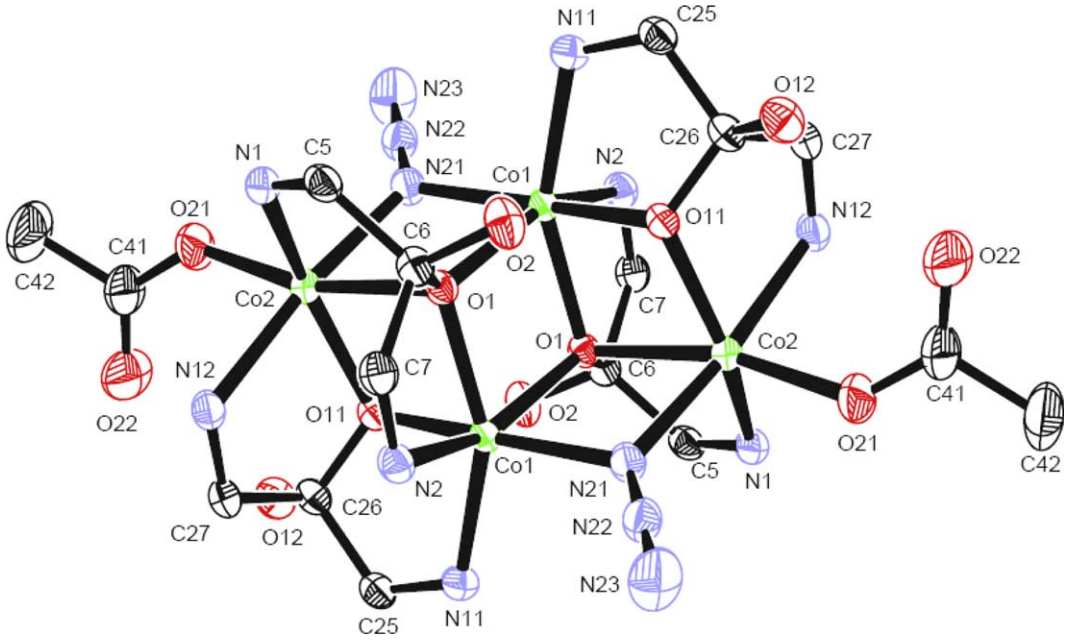

Fig. 99. X-ray structure of $[Co_4(N_3)_2(O_2CMe)_2\{(py)_2C(OH)O\}_4]$; this $(py)_2CNO^-$-free complex is prepared by the reaction of $Co(O_2CMe)_2 \cdot 4H_2O$, $(py)_2CNOH$ and NaN_3 in MeCN.

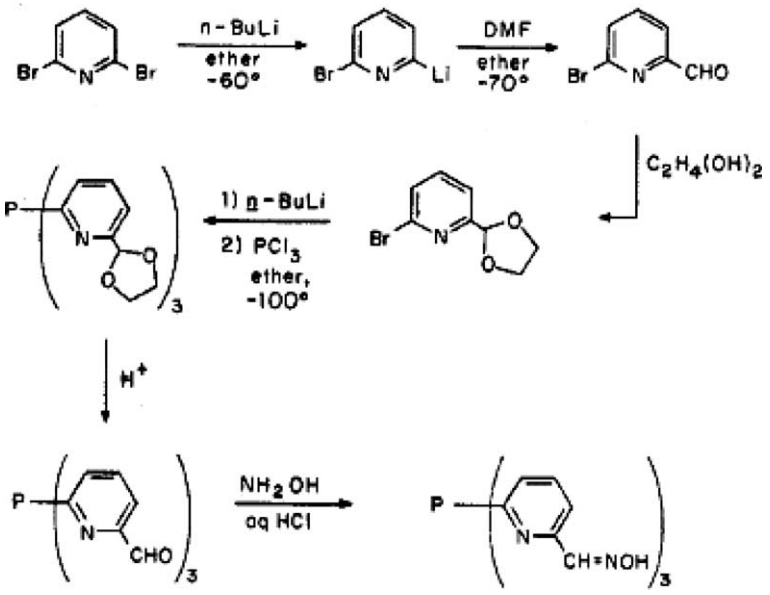

Scheme 11. Synthesis of P{(py-H)CHNOH}$_3$.

formation of these cations and their proposed structures (based on physical and spectroscopic data) [213] are shown in Scheme 12.

The chlathro-chelate fluoroborotris(2-aldoximo-6-pyridyl)phosphinemetal(II) cations, [M(P{(py-H)CHNO}$_3$BF)]$^+$, containing Fe(II), Co(II), Ni(II) and Zn(II), were prepared by closure reactions of [M(P{(py-H)CHNOH}$_2${(py-H)CHNO})]$^+$ with boron trifluoride etherate or tetrafluoroborate ion and isolated as BF_4^- salts (Scheme 12). X-ray results have shown [214] that the desired trigonal prismatic coordination has been very closely approached in [Ni(P{(py-H)CHNO}$_3$BF)](BF_4), and that the Co(II) and Zn(II) salts are isomorphous with the Ni^{II} compound. The general synthetic procedure shown in Scheme 12 failed when applied to the synthesis of the Cu^{II} clathro-chelate.

In a synthetically smart and magnetically elegant paper [68], Chaudhuri and co-workers used the metal-containing fragment $\{Cr^{III}L\}^{3+}$, instead of the B-capping unit, for encapsulation of the [Ni(P{(py-H)CHNO}$_3$)]$^-$ unit to yield the bicyclic chlathro-chelate (L = 1,4,7-trimethyl-1,4,7-triazacyclononane). The molecular structure of the resulting cation [LCr^{III}(P{(py-H)CHNO}$_3$)Ni^{II}]$^{2+}$ is shown in Fig. 100. The Cr^{III} and Ni^{II} coordination geometries are distorted octahedral and trigonal prismatic, respectively. The effective magnetic moment, μ_{eff}, for this complex exhibits an essentially temperature-independent behavior in the range 290–30 K (Fig. 101). Below 30 K the μ_{eff} decreases reaching a value of 3.82 BM at 2 K. The solid line in Fig. 4 represents the best fit with the parameters $J = 0$, $g_{Cr} = 1.98$, $g_{Ni} = 2.16$, $\theta = -1.42$ K. The isoelectronic

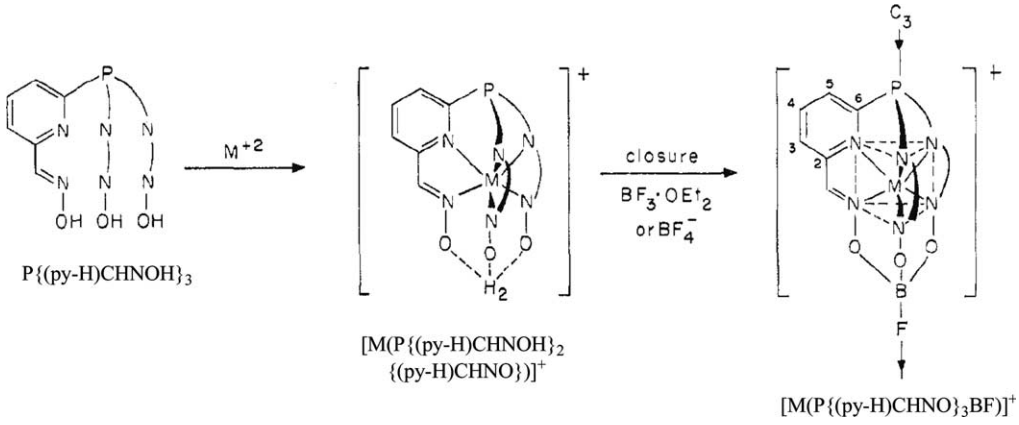

Scheme 12. Synthesis of [M(P{(py-H)CHNO}$_3$BF)]$^+$ complexes from P{(py-H)CHNOH}$_3$ using boron trifluoride etherate or tetrafluoroborate ion as ring-closure reagents. No specific stereochemistry of the intermediate six-coordinate complexes is implied. For purposes of clarity only one chelate ring structure is shown in each species (M = Fe, Co, Ni, Zn) [213].

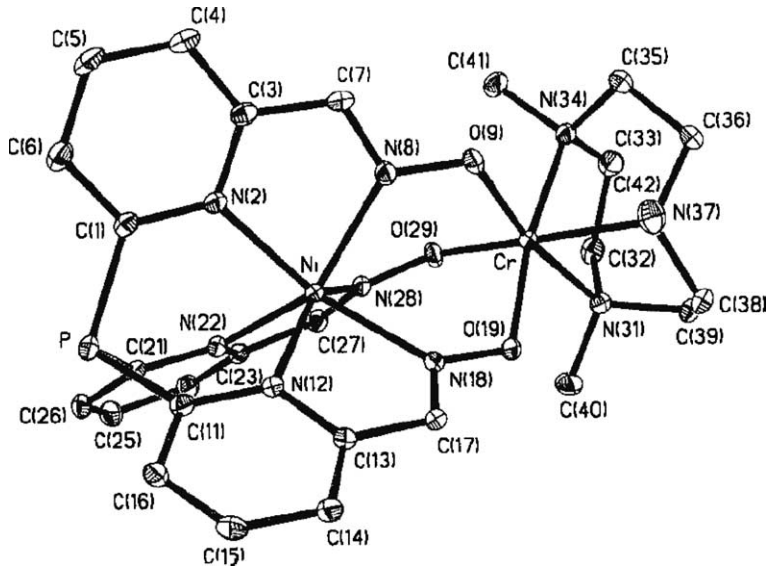

Fig. 100. X-ray structure of the cation $[LCr^{III}(P\{(py\text{-}H)CHNO\}_3)Ni^{II}]^{2+}$ in its perchlorate salt [68].

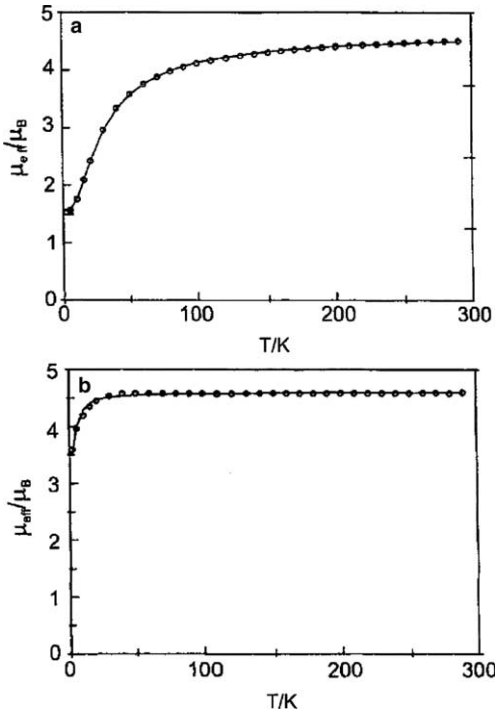

Fig. 101. Plots of μ_{eff} vs. T for solid $[LCr^{III}\{(py\text{-}H)CHNO\}_3Ni^{II}](ClO_4)_2$ (a) and $[LCr^{III}(P\{(py\text{-}H)CHNO\}_3)Ni^{II}](ClO_4)_2$ (b). The solid lines represent the best fit of the data to the Heisenberg-Dirac-van Vleck model.

analogue $[LCr^{III}\{(py\text{-}H)CHNO\}_3Ni^{II}](ClO_4)_2$ exhibits (Fig. 101) a weak antiferromagnetic exchange interaction between the Cr^{III} and Ni^{II} ions ($J = -9.2$ cm^{-1}, $g_{Cr} = 2.0$, $g_{Ni} = 2.19$) and has an $S_t = 1/2$ ground state [68]. These two complexes are rare examples of weak antiferromagnetic or no coupling at all between Cr^{III} and Ni^{II}. Interestingly, most of the known Cr^{III}–Ni^{II} interactions in the literature are in accord with the predictions made nearly 35 years ago [215], namely ferromagnetic in nature.

10. Conclusions and perspectives

It is obvious from the preceding pages that, just over a half century since the first preparations of metal complexes of pyridyl oximes, the coordination chemistry of such ligands is an expanding field of great current interest. This chemistry is an area that has something for everyone: from smart synthetic inorganic chemistry to complexes (both polynuclear and polymeric) with aesthetically pleasant structures, and from high-spin molecules to single-chain magnets. For example, in the area of homo- and heterometallic polynuclear transition metal complexes we hope that this report illustrates what is possible through very simple coordination chemistry. The monoanions of simple 2-pyridyl oximes have fulfilled their promise as a source of polynuclear 3d-metal complexes with interesting structures and properties. The immense structural diversity of the complexes described here stems from the ability of the $(py)C(R)NO^-$ ligands to exhibit many distinct coordination modes (Figs. 8 and 68). Presumably, the presence of dissimilar donor atoms within these anionic ligands leads to this coordinative flexibility; however, their versatility was unexpected. Employment of carboxylates, β-diketonates and sulfates in the $(py)C(R)NO^-$ metal chemistry gives an extraordinary structural flexibility in the resulting mixed-ligand systems (“blends” [216]). The remarkable diversity of structures has prevented any guiding structural principles from being proposed. It is clear that the

pyridyloximato clusters do not correspond in a straightforward manner to fragments of common minerals or to polyhedral archetypes, but rather, display a richness of topology and nuclearity that is unpredictable but intriguing. In the area of molecular magnetism, the oximato group of the anionic pyridyl oximes can mediate exchange interactions of varying range, from weak and moderate ferromagnetic to strong antiferromagnetic. Although almost all of the complexes discussed in this report have been structurally characterized, our current knowledge of magnetostructural correlations is still poor. As also emphasized by Chaudhuri [6], the "irregular spin-state structure" approach, resulting from a particular spin topology, is more effective in obtaining high-spin molecules than the more rational approach of obtaining ferromagnetically coupled systems through the approach of the strict orthogonality of the magnetical orbitals of the interacting metal centers. An additional important chemical lesson of this report is that the activation of the oxime group of 2-pyridyl oximes by 3d-metal ions towards further reactions seems to be an emergent area of synthetic inorganic chemistry.

This area of research will undoubtedly continue to expand, given the relatively recent nature of the majority of references in this paper, and the numerous synthetic routes now documented for the isolation of pyridyloximato metal complexes. Obvious areas for further investigation include:

1. The chemistry of other 3d-metals, and second and third row transition metals with such ligands. The reactions of V, Cr and Fe sources with pyridyl oximes should be studied in detail, considering how interesting the magnetic properties of the products could be. For example, it is surprising that iron(II) and iron(III) pyridyloximato complexes have little been investigated; high-spin Fe^{III} ($S = 5/2$) complexes are promising candidates to obtain large S values in the ground state.
2. Studies of the chemistry of pyridyl oximes with the generally oxophilic lanthanide ions. Such studies are completely lacking.
3. Further studies of the chemistry of heterometallic pyridyloximato complexes. For example, 3d/4f clusters are extremely rare, and in the context of the recent discovery that such complexes can be single-molecule magnets [217–220], could be very interesting.
4. The use of pyridyl oximes in supramolecular systems; the published studies are interesting but, simultaneously, limited in number. Several pyridyl oximes can be proven versatile tools for supramolecular assembly of metal-containing supramolecular architectures and interesting building blocks for crystal engineering.
5. Studies of the reactivity of some known pyridyloximato complexes; such studies are lacking. The paramagnetism of many known compounds makes NMR a method of limited applicability, especially in case where some ligands are weakly bound, creating additional problems of fluxionality. Therefore, solution studies have been limited. The growing use of electrospray mass spectrometry suggests more may be done. According to our experience, there are several systems in which several clusters can be crystallized from very similar reaction mixtures, and an examination of which of these clusters is present in solution would be a step toward understanding how, and when, these complexes form.
6. The use of new pyridyl oximes in metal chemistry. Synthesizing new ligands will be challenging and may lead to novel properties. A characteristic example is provided by the polydentate ligand 1,10-phenanthroline-2,9-dicarbaldehyde dioxime (L), synthesized [221] as illustrated in Scheme 13. The attachment of two oxime groups to a metal-chelating, pyridyl-based ligand is an attractive way of developing the design of small metal complexes which are potentially able to hydrolyze the phosphodiester backbone of nucleic acids (chemical nucleases). The oximate group has been chosen because it can effectively act as a nucleophile endowed with nucleolytic activity [221]. The complexes of the monoanion of L are designed to interact with the initial negatively charged phosphate, and to promote hydrolysis of the phosphodiester P–O bond through nucleophilic attack on the P atom by one oximate group, the other oxime group stabilizing the leaving oxygen atom (Fig. 102).

Scheme 13. Synthesis of 1,10-phenanthroline-2,9-dicarbaldehyde dioxime (L) [221].

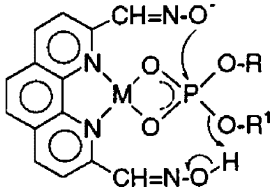

Fig. 102. Schematic representation of a model ternary metal ion/monoanion of L/phosphodiester system [221].

The results of the above proposed future investigations will be probably described in another polyhedron report.

Acknowledgments

The described work from our group is in the main based on the Ph.D. work of two of us (C.J.M., Th.C.S.) and eight talented scientists: Dr. Eugenia Katsoulakou, Dr. Eleanna Diamantopoulou, Dr. Elena Kefalloniti, Dr. Athanassios Boudalis, Constantina Papatriantafyllopoulou-Efthymiou, Gina Vlahopoulou, Konstantina Priggouri and Constantinos Stoumpos. We also acknowledge our longstanding collaboration with Dr. Aris Terzis, Dr. Catherine P. Raptopoulou and Dr. Vassilis Psycharis (NCSR "Demokritos", Athens) for X-ray crystallography, Dr. Vassilis Tangoulis and Dr. Nikolia Lalioti (University of Patras, Greece), Dr. Yiannis Sanakis (NCSR "Demokritos", Athens), Professors Albert Escuer and Ramon Vicente (University of Barcelona, Spain) for performing magnetic and EPR studies, Lecturer Panagiotis Kyritsis (University of Athens, Greece) for electrochemistry and Professor Evangelos G. Bakalbassis (University of Thessaloniki, Greece) for quantum-chemical calculations. We thank Professors George Christou (University of Florida, USA), Richard E.P. Winpenny (University of Manchester, UK), Dimitris Kessissoglou (University of Thessaloniki, Greece), and Lecturers Euan Brechin (University of Edinburgh, UK), Sarah L. Heath (University of Manchester, UK), Anastasios Tasiopoulos (University of Cyprus, Cyprus) for helpful discussions. Th.C.S. and S.P.P. are grateful to the European Social Fund (ESF), Operational Program for Educational and Vocational Training II (EPEAEK II), and particularly the Program PYTHAGORAS (Grant b.365.037), for funding our research efforts in the area of the pyridyloximato clusters. S.P.P. also thanks the Research Committee of the University of Patras (K. Caratheodory Program No. 03016) for support of our work on the coordination polymers of pyridyl oximes.

References

[1] L. Tschugaeff, Chem. Ber. 23 (1890) 1.
[2] A. Chakravorty, Coord. Chem. Rev. 13 (1974) 1.
[3] J.A. Bertrand, P.G. Eller, Prog. Inorg. Chem. 21 (1976) 29.
[4] R.C. Mehrotra, in: G. Wilkinson, R.D. Gillard, J.A. McCleverty (Eds.), Comprehensive Coordination Chemistry, vol. 2, Pergamon Press, Oxford, 1987, p. 269.
[5] A.G. Smith, P.A. Tasker, D.J. White, Coord. Chem. Rev. 241 (2003) 61.
[6] P. Chaudhuri, Coord. Chem. Rev. 243 (2003) 143.
[7] V.Yu. Kukushkin, D. Tudela, A.J.L. Pombeiro, Coord. Chem. Rev. 156 (1996) 333.
[8] V.Yu. Kukushkin, A.J.L. Pombeiro, Coord. Chem. Rev. 181 (1999) 147.
[9] A.J.L. Pombeiro, V.Yu. Kukushkin, in: J.A. McCleverty, T.C. Meyer (Eds.), Comprehensive Coordination Chemistry II, vol. 1, Elsevier, Amsterdam, 2004, p. 631.
[10] J. March, Advanced Organic Chemistry, 4th ed., Wiley, New York, 1992, pp. 109, 110, 127, 128, 592, 593, 818, 906, 907, 934, 935, 1198, 1223.
[11] For reviews on isomerizations about C=N bonds, see: S. Patai (Ed.), The Chemistry of the Carbon–Nitrogen Double Bond, Wiley, New York, 1970.
[12] J.-M. Lehn, Supramolecular Chemistry, VCH, Weinheim, 1995.
[13] S. Subramanian, M.J. Zaworotko, Coord. Chem. Rev. 137 (1994) 357.
[14] B.M. O'Leary, T. Szabo, N. Svenstrup, C.A. Schalley, A. Lützen, M. Schäfer, J. Rebek Jr., J. Am. Chem. Soc. 123 (2001) 11519.
[15] L.J. Prins, P. Timmermann, D.N. Reinhoudt, J. Am. Chem. Soc. 123 (2001) 10153.
[16] J.L. Atwood, A. Szumma, J. Am. Chem. Soc. 124 (2002) 10646.
[17] G.R. Desiraju, Crystal Engineering: The Design of Organic Solids, Elsevier, Amsterdam, 1989.
[18] C.B. Aakeröy, Acta Crystallogr., Sect. B 53 (1997) 569.
[19] V. Bertalosi, G. Gilli, A. Veronese, Acta Crystallogr., Sect. B 38 (1982) 502.
[20] F. Bachechi, L. Zambonelli, Acta Crystallogr., Sect. B 29 (1973) 2598.
[21] T.K. Bierlein, E.C. Lingafelter, Acta Crystallogr. 4 (1951) 450.
[22] E.A. Burton, L. Brammer, F.C. Pigge, C.B. Aakeröy, D.S. Leinen, New J. Chem. 27 (2003) 1084.
[23] D. Braga, L. Maini, M. Polito, L. Scaccianoce, G. Cojazzi, F. Grepioni, Coord. Chem. Rev. 216–217 (2001) 225.
[24] S.S. Kudüva, D. Bläser, R. Boese, G.R. Desiraju, J. Org. Chem. 66 (2001) 1621.
[25] M. Tremayne, C. Glidewell, Chem. Commun. (2000) 2425.
[26] C.B. Aakeröy, A.M. Beatty, D.S. Leinen, CrystEngComm. 4 (2002) 310.
[27] For a description of graph set notation for classifying hydrogen bonding patterns, see: M.C. Etter, Acc. Chem. Res. 23 (1990) 120.
[28] P. Chaudhuri, M. Hess, T. Weyhermüller, E. Bill, H.-J. Haupt, U. Flörke, Inorg. Chem. Commun. 1 (1998) 39.
[29] D. Burdinski, F. Birkelbach, T. Weyhermüller, U. Flörke, H.-J. Haupt, M. Lengen, A.X. Trautwein, E. Bill, K. Wieghardt, P. Chaudhuri, Inorg. Chem. 37 (1998) 1009.
[30] Y. Gök, U. Ocak, H.B. Sentürk, New J. Chem. 25 (2001) 364.
[31] N.A. Bokach, M. Haukka, A.J.L. Pombeiro, S.N. Morozkina, V.Yu. Kukushkin, Inorg. Chim. Acta 336 (2002) 95.
[32] V.V. Pavlishchuk, S.V. Kolotilov, A.W. Addison, M.J. Prushan, D. Schollmeyer, L.K. Thompson, T. Weyhermüller, E.A. Goreshnik, Dalton Trans. (2003) 1587.
[33] A.N. Singh, A. Chakravorty, Inorg. Chem. 19 (1980) 969.
[34] H.-J. Krüger, G. Peng, R.H. Holm, Inorg. Chem. 30 (1991) 734.
[35] D.T. Rosa, J.A. Krause Bauer, M.J. Baldwin, Inorg. Chem. 40 (2001) 1606.
[36] S. Akine, T. Taniguchi, T. Saiki, T. Nabeshima, J. Am. Chem. Soc. 127 (2005) 540.
[37] M.J. Goldcamp, S.E. Robison, J.A. Krause Bauer, M.J. Baldwin, Inorg. Chem. 41 (2002) 2307.
[38] M.N. Kopylovich, V.Yu. Kukushkin, M. Haukka, J.J.R.F. da Silva, A.J.L. Pombeiro, Inorg. Chem. 41 (2002) 4798.
[39] J.M. Thorpe, R.L. Beddoes, D. Collison, C.D. Garner, M. Helliwell, J.M. Holmes, P.A. Tasker, Angew. Chem. Int. Ed. 38 (1999) 1119.
[40] R.J. Butcher, C.J. O'Connor, E. Sinn, Inorg. Chem. 20 (1981) 537.
[41] P. Chaudhuri, M. Winter, F. Birkelbach, P. Fleischhauer, W. Haase, U. Flörke, H.-J. Haupt, Inorg. Chem. 30 (1991) 4291.

[42] C.J. Milios, C.P. Raptopoulou, A. Terzis, F. Lloret, R. Vicente, S.P. Perlepes, A. Escuer, Angew. Chem. Int. Ed. 43 (2004) 210.
[43] See, for example: R. Clérac, H. Miyasaka, M. Yamashita, C. Coulon, J. Am. Chem. Soc. 124 (2002) 12837.
[44] R.A. Coxall, S.G. Harris, D.K. Henderson, S. Parsons, P.A. Tasker, R.E.P. Winpenny, J. Chem. Soc., Dalton Trans. (2000) 2349.
[45] C.B. Aakeröy, A.M. Beatty, D.S. Leinen, CrystEngComm. 27 (2000) 1.
[46] M. Orama, H. Saarinen, J. Korvenranta, J. Coord. Chem. 22 (1990) 183.
[47] G.I.H. Hanania, D.H. Irvine, Nature 183 (1959) 40.
[48] R.A. Krause, D.H. Busch, J. Am. Chem. Soc. 82 (1960) 4830.
[49] C.H. Liu, C.F. Liu, J. Am. Chem. Soc. 83 (1961) 2615.
[50] C.H. Liu, C.F. Liu, J. Am. Chem. Soc. 83 (1961) 4167.
[51] C.H. Liu, C.F. Liu, J. Am. Chem. Soc. 83 (1961) 4169.
[52] G.I.H. Hanania, D.H. Irvine, J. Chem. Soc. (1962) 2745.
[53] C.F. Liu, C.H. Liu, Inorg. Chem. 2 (1963) 706.
[54] C.F. Liu, C.H. Liu, Inorg. Chem. 3 (1964) 678.
[55] R. Beckett, B.F. Hoskins, J. Chem. Soc., Dalton Trans. (1972) 291.
[56] P. Chaudhuri, M. Winter, U. Flörke, H.-J. Haupt, Inorg. Chim. Acta 232 (1995) 125.
[57] M. Murugesu, K.A. Abboud, G. Christou, Polyhedron 23 (2004) 2779.
[58] (a) M.W. Blackmore, R.J. Magee, J. Inorg. Nucl. Chem. 31 (1969) 2859;
(b) G. Bazsa, H.G. Shinouda, M.T. Beck, J. Inorg. Nucl. Chem. 40 (1978) 1665.
[59] T.C. Stamatatos, A. Bell, P. Cooper, A. Terzis, C.P. Raptopoulou, S.L. Heath, R.E.P. Winpenny, S.P. Perlepes, Inorg. Chem. Commun. 8 (2005) 533.
[60] Th.C. Stamatatos, I. Katsoulis, C.P. Raptopoulou, A. Terzis, S.P. Perlepes, unpublished results.
[61] M. Orama, H. Soarinen, J. Korvenranta, Acta Chem. Scand. 43 (1989) 407.
[62] H. Miyasaka, K. Mizushima, K. Sugiura, M. Yamashita, Synth. Met. 137 (2003) 1245.
[63] H. Miyasaka, S. Furukawa, S. Yanagida, K. Sugiura, M. Yamashita, Inorg. Chim. Acta 357 (2004) 1619.
[64] Th.C. Stamatatos, E. Diamantopoulou, C.P. Raptopoulou, A. Terzis, S.P. Perlepes, unpublished results.
[65] M. Salonen, H. Saarinen, M. Orama, J. Coord. Chem. 56 (2003) 1041.
[66] J.-L. Song, J.-G. Mao, H.-Y. Zeng, R.K. Kremer, Z.-C. Dong, Inorg. Chem. Commun. 6 (2003) 891.
[67] V.L. Pecoraro, A.J. Stemmler, B.R. Gibney, J.J. Bodwin, H. Wang, J.W. Kampf, A. Barwinski, Prog. Inorg. Chem. 45 (1997) 83.
[68] S. Ross, T. Weyhermüller, E. Bill, K. Wieghardt, P. Chaudhuri, Inorg. Chem. 40 (2001) 6656.
[69] C.J. Milios, E. Kefalloniti, C.P. Raptopoulou, A. Terzis, A. Escuer, R. Vicente, S.P. Perlepes, Polyhedron 23 (2004) 83.
[70] K.W. Nordquest, D.W. Phelps, W.F. Little, D.J. Hodgson, J. Am. Chem. Soc. 98 (1976) 1104.
[71] H.M.M. Shearer, J. Twiss, K. Wade, J. Organomet. Chem. 184 (1980) 309.
[72] O. Kahn, Molecular Magnetism, VCH, Weinheim, 1993.
[73] G. Denti, S. Serroni, S. Campagna, A. Juris, M. Ciano, V. Balzani, in: A.F. Williams, C. Floriani, A.E. Merbach (Eds.), Perspectives in Coordination Chemistry, VCH, Weinheim, 1992, p. 153.
[74] J.B. Goodenough, Magnetism and the Chemical Bond, Wiley, New York, 1963.
[75] J. Kanamori, J. Phys. Chem. Solids 10 (1959) 87.
[76] R.J. Glauber, J. Math. Phys. 4 (1963) 294.
[77] A. Caneschi, D. Gatteschi, N. Lalioti, C. Sangregorio, R. Sessoli, G. Venturi, A. Vindigni, A. Rettori, M.G. Pini, M.A. Novak, Angew. Chem., Int. Ed. 40 (2001) 1760.
[78] A. Caneschi, D. Gatteschi, N. Lalioti, R. Sessoli, L. Sorace, V. Tangoulis, A. Vindigni, Chem. Eur. J. 8 (2002) 286.
[79] H. Miyasaka, R. Clérac, K. Mizushima, K. Sugiura, M. Yamashita, W. Wernsdorfer, C. Coulon, Inorg. Chem. 42 (2003) 8203.
[80] H. Miyasaka, T. Nezu, K. Sugimoto, K. Sugiura, M. Yamashita, R. Clerac, Inorg. Chem. 43 (2004) 5486.
[81] A. Pajunen, I. Mutikainen, H. Saarinen, M. Orama, Z. Kristallogr. 214 (1999) 217.
[82] Th.C. Stamatatos, C. Stoumpos, C.P. Raptopoulou, A. Terzis, S.P. Perlepes, G. Christou, unpublished results.
[83] K. Riggle, T. Lynde-Kernell, E.O. Schlemper, J. Coord. Chem. 25 (1992) 117.
[84] C. Papatriantafillopoulou, Ph. D. Thesis, University of Patras, 2005.
[85] A. Pajunen, M. Orama, H. Saarinen, Acta Crystallogr., Sect. C 55 (1999) 2075.
[86] R. Cibulka, I. Cisarova, J. Ondracek, F. Liska, J. Ludvik, Collect. Czech. Chem. Commun. 66 (2001) 170.
[87] T. Lynde-Kernell, E.O. Schlemper, J. Coord. Chem. 16 (1988) 347.
[88] D.W. Phelps, W.F. Little, D.J. Hodgson, Inorg. Chem. 15 (1976) 2263.
[89] A. Gupta, R.K. Sharma, R. Bohra, V.K. Jain, J.E. Drake, M.B. Hursthouse, M.E. Light, Polyhedron 21 (2002) 2387.
[90] V. Sharma, R.K. Sharma, R. Bohra, R. Ratnani, V.K. Jain, J.E. Drake, M.B. Hursthouse, M.E. Light, J. Organomet. Chem. 651 (2002) 98.
[91] V. Sharma, R.K. Sharma, R. Bohra, V.K. Jain, J.E. Drake, M.E. Light, M.B. Hursthouse, J. Organomet. Chem. 664 (2002) 66.
[92] A.B. Zaitsev, A.M. Vasil'tsov, E.Yu. Schmidt, A.I. Mikhaleva, L.V. Morozova, A.V. Afonin, I.A. Uskakov, B.A. Trofimov, Tetrahedron 58 (2002) 10043.
[93] J. Shuk-Yee Wong, W.T. Wong, New J. Chem. 26 (2002) 94.
[94] C.J. Milios, E. Kefalloniti, C.P. Raptopoulou, A. Terzis, R. Vicente, N. Lalioti, A. Escuer, S.P. Perlepes, Chem. Commun. (2003) 819.
[95] C.J. Milios, Th.C. Stamatatos, P. Kyritsis, A. Terzis, C.P. Raptopoulou, R. Vicente, A. Escuer, S.P. Perlepes, Eur. J. Inorg. Chem. (2004) 2885.
[96] C.J. Milios, S. Piligkos, A.R. Bell, R.H. Laye, S.J. Teat, A. Escuer, R. Vicente, E. Mclnnes, S.P. Perlepes, R.E.P. Winpenny, unpublished.
[97] Th.C. Stamatatos, Ph.D. Thesis, University of Patras, 2005.
[98] A.E. Landers, D.J. Phillips, Inorg. Chim. Acta 25 (1977) L39.
[99] A.E. Landers, D.J. Phillips, Inorg. Chim. Acta 59 (1982) 41.
[100] G.C. Chiumia, D.C. Craig, I.D.J. Phillips, Inorg. Chim. Acta 209 (1993) 213.
[101] G.C. Chiumia, D.J. Phillips, A.D. Rae, Inorg. Chim. Acta 238 (1995) 197.
[102] C.B. Aakeröy, A.M. Beatty, D.S. Leinen, J. Am. Chem. Soc. 120 (1998) 7383.
[103] C.B. Aakeröy, A.M. Beatty, D.S. Leinen, K.P. Lorimer, Chem. Commun. (2000) 935.
[104] C.B. Aakeröy, A.M. Beatty, D.S. Leinen, Angew. Chem., Int. Ed. 38 (1999) 1815.
[105] E.I. Baucom, R.S. Drago, J. Am. Chem. Soc. 93 (1971) 6469.
[106] C.W. Glynn, M.M. Turnbull, Transition Met. Chem. 27 (2002) 822.
[107] G.I.H. Hanania, D.H. Irvine, F. Shurayh, J. Chem. Soc. (1965) 1149.
[108] H. Hartkamp, Fresen. Z. Anal. Chem. 178 (1960) 19.
[109] G. Sproul, G.D. Stucky, Inorg. Chem. 12 (1973) 2898.

[110] I. Vasilevsky, R.E. Stenkamp, E.C. Lingafelter, N.J. Rose, J. Coord. Chem. 19 (1988) 171.
[111] G.A Nicholson, J.L. Petersen, B.J. McCormick, Inorg. Chem. 21 (1982) 3274.
[112] K.A. Abboud, R.C. Palenik, G.J. Palenik, Acta Crystallogr., Sect. C 50 (1994) 525.
[113] B.C. Unni Nair, J.E. Sheats, R. Ponteciello, D. Van Engen, V. Petrouleas, G.C. Dismukes, Inorg. Chem. 28 (1989) 1582.
[114] R.E. Marsh, Inorg. Chem. 29 (1990) 572.
[115] I.V. Vasilevsky, R.E. Stenkamp, E.C. Lingafelter, V. Schomaker, R.D. Willet, N.J. Rose, Inorg. Chem. 28 (1989) 2619.
[116] S. Abram, C. Maichle-Mössmer, U. Abram, Polyhedron 16 (1997) 2183.
[117] S. Abram, C. Maichle-Mössmer, U. Abram, Polyhedron 16 (1997) 2291.
[118] G.A. Nicholson, C.R. Lazarus, B.J. McCormick, Inorg. Chem. 19 (1980) 192.
[119] G.A. Nicholson, J.L. Petersen, B.J. McCormick, Inorg. Chem. 19 (1980) 195.
[120] A.K. Yatsimirsky, P. Gómez-Tagle, S. Escalante-Tovar, L. Ruiz-Ramírez, Inorg. Chim. Acta 273 (1998) 167.
[121] P.G. Tagle, A.K. Yatsimirsky, Polyhedron 16 (1997) 877.
[122] C. Richardson, P.J. Steel, D.M. D'Alessandro, P.C. Junk, F.R. Keene, J. Chem. Soc., Dalton Trans. (2002) 2775.
[123] V.V. Skopenko, N.N. Gerasimchuk, S.I. Tyukhtenko, H. Kohler, Z. Anorg. Allg. Chem. 542 (1986) 65.
[124] T.V. Guskova, M.S. Tchernoviants, K.N. Bagdasarov, Ukrainskii Khim. Zhurn. 50 (1984) 982.
[125] N. Gerasimchuk, E. Kuzmann, A. Buki, L. Nagy, K. Burger, Inorg. Chim. Acta 188 (1991) 45.
[126] N.N. Gerasimchuk, Yu.A. Simonov, A.A. Dvorkin, N. Rebrova, Russ. J. Inorg. Chem. 38 (1993) 247.
[127] V.V. Skopenko, V.V. Ponomareva, Yu.A. Simonov, K.V. Domasevich, Russ. J. Inorg. Chem. 39 (1994) 1332.
[128] N.N. Gerasimchuk, V.V. Skopenko, V.V. Ponomareva, K.V. Domasevich, Russ. J. Inorg. Chem. 38 (1993) 964.
[129] V.V. Ponomareva, N.K. Dalley, X. Kou, N.N. Gerasimchuk, K.V. Domasevitch, J. Chem. Soc., Dalton Trans. (1996) 2351.
[130] K.V. Domasevitch, N.N. Gerasimchuk, A. Mokhir, Inorg. Chem. 39 (2000) 1227.
[131] D. Eddings, C. Barnes, N. Gerasimchuk, P. Durham, K. Domasevich, Inorg. Chem. 43 (2004) 3894.
[132] A. Kuhne, A. Hubele, USA Patent, 4,063,921, 1978.
[133] S.H. Davidson, USA Patent, 3,957,847, 1978.
[134] Ciba-Geigy, Austria Patent, 367,268, 1982.
[135] A.A. Mokhir, K.V. Domasevich, N.K. Dalley, X. Kou, N.N. Gerasimchuk, O.A. Gerasimchuk, Inorg. Chim. Acta 284 (1999) 85.
[136] S.I. Tyukhtenko, N.P. Bernik, A.T. Pilipenko, Yu.M. Volovenka, N.N. Gerasimchuk, Dokl. Akad. Nauk USSR B (1) (1986) 58.
[137] N. Gerasimchuk, L. Nagy, H.G. Schmidt, M. Notlemeyer, R. Bohra, H. Roesky, Z. Naturforsch. B 47 (1992) 1741.
[138] K.V. Domasevich, N.N. Gerasimchuk, E.V. Rusanov, O.A. Gerasimchuk, Russ. J. Gen. Chem. 66 (1996) 635.
[139] N.N. Gerasimchuk, O.A. Zhmurko, S.I. Tykhtenko, Russ. J. Inorg. Chem. 38 (1993) 282.
[140] D.N. Nicolaides, E.A. Varella, in: S. Patai (Ed.), The Chemistry of Acid Derivatives, vol. 2, Wiley, Chichester, 1992, p. 875 (Chapter 16).
[141] E. Bernasek, J. Org. Chem. 22 (1957) 1263.
[142] G.A. Pearse, P.R. Raithby, J. Lewis, Polyhedron 8 (1989) 301.
[143] G.S. Sanyal, A.B. Modak, A.K. Mudi, Indian J. Chem. A 22 (1983) 307.
[144] J. Losada del Bario, E.L. Abad, S. Vicente-Perez, An. Quim. Ser. B 82 (1986) 66.
[145] M. Näsäkkälä, H. Saarinen, J. Korvenranta, M. Orama, Acta Crystallogr., Sect. C 45 (1989) 1514.
[146] G.A. Pearse, P.R. Raithby, C.M. Hay, J. Lewis, Polyhedron 8 (1989) 305.
[147] M. Werner, J. Berner, P.G. Jones, Acta Crystallogr., Sect. C 52 (1996) 72.
[148] L. Michaelis, Ber. 24 (1891) 3439.
[149] M. Maekawa, S. Kitagawa, Y. Nakao, S. Sakamoto, A. Yatani, W. Mori, S. Kashino, M. Munakata, Inorg. Chim. Acta 293 (1999) 20.
[150] L. Catalano, R. Dreos, G. Nardin, L. Randaccio, G. Tauzher, S. Vuano, J. Chem. Soc., Dalton Trans. (1996) 4269.
[151] J. Iulek, J. Zukerman-Schpector, C.C. Stradler, A. Tozetto, M. Vega, Z. Kristallogr. 216 (2001) 585.
[152] J.A. Bertrand, J.H. Smith, D.G. Van Derveer, Inorg. Chem. 16 (1977) 1477.
[153] A. Yatani, M. Fujii, Y. Nakao, S. Kashino, M. Kinoshita, W. Mori, S. Suzuki, Inorg. Chim. Acta 316 (2001) 127.
[154] S. Sakamoto, A. Yatani, K. Kimura, M. Fujii, Y. Nakao, S. Kashino, M. Kinoshita, W. Mori, Bull. Chem. Soc. Jpn. 74 (2001) 2375.
[155] K. Matsumoto, S. Ooi, W. Mori, Y. Nakao, J. Chem. Soc., Dalton Trans. (1990) 3117.
[156] F. Akagi, Y. Nakao, K. Matsumoto, S. Takamizawa, W. Mori, S. Suzuki, Chem. Lett. (1997) 181.
[157] A. Pajunen, S. Pajunen, Z. Kristallogr. 213 (1998) 439.
[158] N.M. Levy, A. Neves, C.V. Franco, A. Cota, E. Castellano, Y. Primerano Mascarenhas, J. Braz. Chem. Soc. 2 (1991) 66.
[159] A. Pajunen, S. Pajunen, Acta Crystallogr. Sect. C 39 (1983) 852.
[160] L. Randaccio, N. Bresciani Pahor, E. Zangrando, L.G. Marzilli, Chem. Soc. Rev. 18 (1989) 225.
[161] R. Dreos, G. Tauzher, D.H. Trendafilova, G. Nardin, L. Randaccio, Inorg. Chem. 35 (1996) 2715.
[162] A. Bigotto, A. Felluga, R. Dreos, G. Nardin, L. Randaccio, G. Tauzher, S. Peressini, C. Tavagnacco, J. Chem. Soc., Dalton Trans. (2002) 99.
[163] R. Dreos, E. Herlinger, G. Tauzher, S. Vuano, G. Nardin, L. Randaccio, Organometallics 17 (1998) 2366.
[164] R. Dreos, A. Felluga, G. Nardin, L. Randaccio, P. Siega, G. Tauzher, Eur. J. Inorg. Chem. (2001) 267.
[165] R. Dreos, A. Felluga, G. Nardin, L. Randaccio, P. Siega, G. Tauzher, Inorg. Chem. 40 (2001) 5541.
[166] R. Dreos, A. Felluga, G. Nardin, L. Randaccio, M. Sandri, G. Tauzher, Inorg. Chem. 41 (2002) 4548.
[167] F. Mancin, P. Tecilla, U. Tonellato, Langmuir 16 (2000) 227.
[168] C.J. Milios, P. Kyritsis, C.P. Raptopoulou, A. Terzis, R. Vicente, A. Escuer, S.P. Perlepes, Dalton Trans. (2005) 501.
[169] M. Alexiou, I. Tsivikas, C. Dendrinou-Samara, A.A. Pantazaki, P. Trikalitis, N. Lalioti, D.A. Kyriakidis, D.P. Kessissoglou, J. Inorg. Biochem. 93 (2003) 256.
[170] W.P. Jensen, A.I. Hamza, Il-Hwan Suh, R.A. Jacobson, S.O. Sommerer, Inorg. Chim. Acta 254 (1997) 367.
[171] M.A.S. Goher, F.A. Mautner, Polyhedron 18 (1999) 3425.
[172] M. Alexiou, C. Dendrinou-Samara, C.P. Raptopoulou, A. Terzis, D.P. Kessissoglou, Inorg. Chem. 41 (2002) 4732.
[173] S.O. Sommer, C.E. MacBeth, A.J. Jircitano, K.A. Abboud, Acta Crystallogr., Sect. C 53 (1997) 1551.
[174] M. Alexiou, C. Dendrinou-Samara, A. Karagianni, S. Biswas, C.M. Zaleski, J. Kampf, D. Yoder, J.E. Penner-Hahn, V.L. Pecoraro, D.P. Kessissoglou, Inorg. Chem. 42 (2003) 2185.
[175] M. Alexiou, C.M. Zaleski, C. Dendrinou-Samara, J. Kampf, D.P. Kessissoglou, V.L. Pecoraro, Z. Anorg. Allg. Chem. 629 (2003) 2348.
[176] C.J. Milios, C.P. Raptopoulou, A. Terzis, R. Vicente, A. Escuer, S.P. Perlepes, Inorg. Chem. Commun. 6 (2003) 1056.

[177] T. Afrati, C. Dendrinou-Samara, C.P. Raptopoulou, A. Terzis, V. Tangoulis, D.P. Kessissoglou, Angew. Chem. Int. Ed. 41 (2002) 2148.
[178] C. Dendrinou-Samara, C.M. Zaleski, A. Evagorou, J.W. Kampf, V.L. Pecoraro, D.P. Kessissoglou, Chem. Commun. (2003) 2668.
[179] Th.C. Stamatatos, S. Dionyssopoulou, G. Efthymiou, P. Kyritsis, C.P. Raptopoulou, A. Terzis, R. Vicente, A. Escuer, S.P. Perlepes, Inorg. Chem. 44 (2005) 3374.
[180] M. Alexiou, C. Dendrinou-Samara, C.P. Raptopoulou, A. Terzis, V. Tangoulis, D.P. Kessissoglou, Eur. J. Inorg. Chem. (2004) 3822.
[181] G. Psomas, A.J. Stemmler, C. Dendrinou-Samara, J.J. Bodwin, M. Schneider, M. Alexiou, J.W. Kampf, D.P. Kessissoglou, V.L. Pecoraro, Inorg. Chem. 40 (2001) 1562.
[182] E.O. Schlemper, J. Stunkel, C. Patterson, Acta Crystallogr., Sect. C 46 (1990) 1226.
[183] Th.C. Stamatatos, G. Vlahopoulou, A. Terzis, C.P. Raptopoulou, S.P. Perlepes, unpublished results.
[184] M. Alexiou, E. Katsoulakou, C. Dendrinou-Samara, C.P. Raptopoulou, V. Psycharis, E. Manessi-Zoupa, S.P. Perlepes, D.P. Kessissoglou, Eur. J. Inorg. Chem. (2005) 1964.
[185] A.J. Stemmler, J.W. Kampf, V.L. Pecoraro, Inorg. Chem. 34 (1995) 2271.
[186] (a) J.A. Cabeza, I. del Rio, V. Riera, M. Suárez, C. Álvarez-Rúa, S. Garcia-Granda, S.H. Chuang, J.R. Hwu, Eur. J. Inorg. Chem. (2003) 4159;
(b) S.O. Sommerer, B.L. Westcott, A.J. Jircitano, K.A. Abboud, Inorg. Chim. Acta 238 (1995) 149.
[187] E. Katsoulakou, Ph.D. Thesis, University of Patras, 2004.
[188] F. Mori, T. Ishida, N. Takashi, in: Book of Abstracts of the IXth International Conference on Molecule-based Magnets (ICMM 2004), Tsukuba, Japan, October 4–8, 2004, PA-112.
[189] M. Fujita, J.Y. Kwon, S. Washizu, K. Ogura, J. Am. Chem. Soc. 116 (1994) 1151.
[190] H. Piotrowski, K. Polborn, G. Hilt, K. Severin, J. Am. Chem. Soc. 123 (2001) 2699.
[191] J.J. Bodwin, V.L. Pecoraro, Inorg. Chem. 39 (2000) 3434.
[192] M. Moon, I. Kim, M.S. Lah, Inorg. Chem. 39 (2000) 2710.
[193] C. Dendrinou-Samara, G. Psomas, L. Iordanidis, V. Tangoulis, D.P. Kessissoglou, Chem. Eur. J. 7 (2001) 5041.
[194] A.J. Blake, R.O. Gould, P.E.Y. Milne, R.E.P. Winpenny, J. Chem. Soc., Chem. Commun. (1991) 1453.
[195] A.J. Blake, R.O. Gould, G.M. Grant, P.E.Y. Milne, D. Reed, R.E.P. Winpenny, Angew. Chem., Int. Ed. Engl. 33 (1994) 195.
[196] R.W. Saalfrank, N. Löw, F. Hampel, H.-D. Stachel, Angew. Chem., Int. Ed. Engl. 35 (1996) 2209.
[197] S.-X. Liu, S. Lin, B.-Z. Lin, C.-C. Lin, J.-Q. Huang, Angew. Chem. Int. Ed. 40 (2001) 1084.
[198] B. Kwak, H. Rhee, S. Park, M.S. Lah, Inorg. Chem. 37 (1998) 3599.
[199] X. Yang, C.B. Knobler, Z. Zheng, M.F. Hawthorne, J. Am. Chem. Soc. 116 (1994) 7142.
[200] E.C. Constable, Prog. Inorg. Chem. 42 (1994) 67.
[201] H. Rauter, E.C. Hillgeries, A. Erxleben, B. Lippert, J. Am. Chem. Soc. 116 (1994) 616.
[202] C. Dendrinou-Samara, M. Alexiou, C.M. Zaleski, J.W. Kampf, M.L. Kirk, D.P. Kessissoglou, V.L. Pecoraro, Angew. Chem. Int. Ed. 42 (2003) 3763.
[203] P.J. Stang, K. Chen, J. Am. Chem. Soc. 117 (1995) 1667.
[204] For example, see: R.W. Saalfrank, C. Deutscher, H. Maid, A.M. Ako, S. Sperner, T. Nakajima, W. Bauer, F. Hampel, B.A. Hess, N.J.R. van Eikema Hommes, R. Puchta, F.W. Heinemann, Chem. Eur. J. 10 (2004) 1899.
[205] For example, see: A. Caneschi, A. Cornia, S.J. Lippard, Angew. Chem., Int. Ed. Engl. 34 (1995) 467.
[206] For example, see: R.H. Laye, F.K. Larsen, J. Overgaard, C.A. Muryn, E.J.L. McInnes, E. Rentschler, V. Sanchez, S.J. Teat, H.U. Güdel, O. Waldmann, G.A. Timco, R.E.P. Winpenny, Chem. Commun. (2005) 1125.
[207] C.J. Pedersen, Angew. Chem., Int. Ed. Engl. 27 (1988) 1021.
[208] B.R. Gibney, H. Wang, J.W. Kampf, V.L. Pecoraro, Inorg. Chem. 35 (1996) 6184.
[209] O. Kahn, Acc. Chem. Res. 33 (2000) 647.
[210] A.J.L. Pombeiro, V. Yu. Kukushkin, in: J.A. McCleverty, T.C. Meyer (Eds.), Comprehensive Coordination Chemistry II, vol.1, Elsevier, Amsterdam, 2004, p. 585.
[211] H. Kumagai, M. Endo, M. Kondo, S. Kawata, S. Kitagawa, Coord. Chem. Rev. 237 (2003) 197.
[212] J.E. Parks, B.E. Wagner, R.H. Holm, J. Am. Chem. Soc. 92 (1970) 3500.
[213] J.E. Parks, B.E. Wagner, R.H. Holm, Inorg. Chem. 10 (1971) 2472.
[214] M.R. Churchill, A.H. Reis Jr., Chem. Commun. (1970) 879.
[215] A.P. Ginsberg, Inorg. Chim. Acta Rev. 5 (1971) 45.
[216] C. Benelli, A.J. Blake, E.K. Brechin, S.J. Coles, A. Graham, S.G. Harris, S. Meier, A. Parkin, S. Parsons, A.M. Seddon, R.E.P. Winpenny, Chem. Eur. J. 6 (2000) 883.
[217] A. Mishra, W. Wernsdorfer, S. Parsons, G. Christou, E.K. Brechin, Chem. Commun. (2005) 2086.
[218] S. Osa, T. Kido, N. Matsumoto, N. Re, A. Pochaba, J. Mrozinski, J. Am. Chem. Soc. 126 (2004) 420.
[219] C.M. Zaleski, E.C. Depperman, J.W. Kampf, M.L. Kirk, V.L. Pecoraro, Angew. Chem., Int. Ed. 43 (2004) 3912.
[220] A. Mishra, W. Wernsdorfer, K.A. Abboud, G. Christou, J. Am. Chem. Soc. 126 (2004) 15648.
[221] A. Angeloff, J.-C. Daran, J. Bernadou, B. Meunier, Eur. J. Inorg. Chem. (2000) 1985.

Available online at www.sciencedirect.com
SCIENCE DIRECT®
Polyhedron 25 (2006) 195–202
POLYHEDRON
www.elsevier.com/locate/poly

A novel ligand *N*,*N*′-di(2-pyridyl)-2,4-diamino-6-phenyl-1,3,5-triazine (dpdapt) and its complexes: [Cu(dpdapt)Cl_2] and [Cu(dpdapt)(NO_3)(H_2O)] · NO_3 · H_2O

Cui-Juan Wang [a], Yao-Yu Wang [a,*], Hai-Rui Ma [a], Hui Wang [a], Qi-Zhen Shi [a], Shie-Ming Peng [b]

[a] *Department of Chemistry, Shaanxi Key Laboratory of Physico-inorganic Chemistry, Northwest University, Xi'an 710069, PR China*
[b] *Department of Chemistry, National Taiwan University, Taipei, Taiwan*

Received 30 March 2005; accepted 23 June 2005
Available online 22 August 2005

Abstract

The novel ligand *N*,*N*′-di(2-pyridyl)-2,4-diamino-6-phenyl-1,3,5-triazine (dpdapt) has been synthesized and the reactions of $CuCl_2 \cdot 2H_2O$ and $Cu(NO_3)_2 \cdot 8H_2O$ with the new ligand afforded two crystalline forms [Cu(dpdapt)Cl_2] (**1**) and [Cu(dpdapt)-(NO_3)(H_2O)] · NO_3 · H_2O (**2**), respectively. The molecular structures of **1** and **2** were established by single-crystal X-ray diffraction studies. The copper(II) atoms in complexes **1** and **2** are both five-coordinated in trigonal bipyramidal environments. In **1**, antiparallel dimers construct a two-dimensional supramolecular architecture by π–π stacking and hydrogen bonding, whereas **2** is connected by the same interactions to form a three-dimensional supramolecular framework. Quantum chemical calculations have been performed using Density Functional Theory (DFT) in order to gain some insight about the coordination behavior of dpdapt and complex **1**.
© 2005 Elsevier Ltd. All rights reserved.

Keywords: Novel ligand; Copper(II) complexes; Crystal structure; Supramolecular compounds; DFT studies

1. Introduction

The crystal engineering of coordination polymers and supramolecular compounds has attracted considerable current attention, not only because of their fascinating structural diversities [1], but also for their potential applications in optical, electrical, magnetic and biological materials [2]. The design of suitable organic ligands is one of the important roles in the synthetic strategies for these polymers and supramolecular compounds [3]. The modified 1,3,5-triazine ligand 2,4,6-tris(2-pyridyl)-1,3,5-triazine (tpt) [4] and several transition-metal complexes using the ligand tpt have been reported [5,6]. We have synthesized a novel modified 1,3,5-triazine ligand, *N*,*N*′-di(2-pyridyl)-2,4-diamino-6-phenyl-1,3,5-triazine (dpdapt). The ligand dpdapt is a versatile ligand like tpt, but with more diversity than 2,2,:6′,2″-terpyridine (tpy). Dpdapt, which functions as a tridentate or a bis-bidentate ligand, has gained our interest because of its use as a spacer for designing supramolecular complexes. Thus, dpdapt has its own coordination feature and functions primarily as a tridentate ligand (Scheme 1(a); *anti–anti–anti–anti*) forming complexes of the general type ($[Cu(dpdapt)]^{2+}$), as we described in this paper.

* Corresponding author. Tel.: +86 29 88303097; fax: +86 29 88373398.
E-mail address: wyaoyu@nwu.edu.cn (Y.-Y. Wang).

0277-5387/$ - see front matter © 2005 Elsevier Ltd. All rights reserved.
doi:10.1016/j.poly.2005.06.061

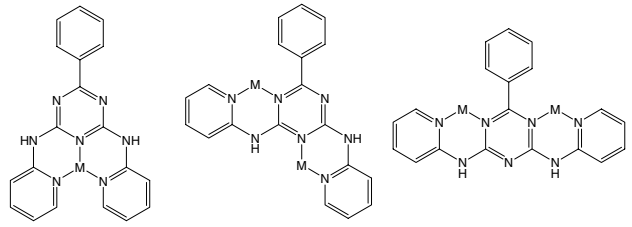

a. anti-anti-anti-anti b. syn-syn-anti-anti c. syn-syn-syn-syn

Scheme 1. Coordination modes of the ligand dpdapt.

The second coordination mode as a bis-bidentate ligand, including *syn–syn–anti–anti* (b) and *syn–syn–syn–syn* (c), is shown in Scheme 1. DFT studies have been applied to dpdapt. Theoretical calculations illuminate the coordination modes of the ligand.

Herein, we report the copper(II) complexes with dpdapt as a tridentate ligand. The crystal structures of the copper(II) complexes with the all-*anti* conformation of the chelating ligand are presented. Complex **1** consists of dimeric units, doubly bridged by π–π stacking and hydrogen bonding, thus forming an unusual 1-D ladder structure. Complex **2** self-assembles into a 1-D chain by hydrogen bonding and π–π stacking, and a 3-D layer structure which is sustained via hydrogen bonds. We also employed DFT studies to **1** and explained its coordination behavior.

2. Experimental

2.1. Materials and physical measurements

Commercially available chemicals were reagent grade and were used without further purification. Infrared spectra on KBr pellets were recorded on a Nicolet 170SX FT-IR spectrophotometer in the range 4000–400 cm^{-1}. Elemental analyses were determined with a Perkin–Elmer model 240C instrument. Electronic spectra were recorded on a Cary 300 Bio UV–Vis spectrophotometer. FAB-MS mass spectra were obtained with a JEOL HX-110 HF double focusing spectrometer operating in the positive ion detection mode. Fluorescence experiments used a HITACHI F-4500 Fluorescence Spectrophotometer and were measured in methanol.

2.2. Synthesis of N,N′-di(2-pyridyl)-2,4-diamino-6-phenyl-1,3,5-triazine (dpdapt)

2,4-Diamino-6-phenyl-1,3,5-triazine (5.0 g, 26.7 mmol), BuOK (14.3 g, 127.7 mmol) and tris(dibenzylideneacetone)dipalladium ($Pd_2(dba)_3$) (2.0 g, 2.2 mmol) were added to a 200 ml flask under nitrogen. Then 100 ml dry benzene and 2-bromopyridine (14 g, 13.5 ml, 88.6 mmol) were injected into the former solid sequentially also under nitrogen. The resulting solution was stirred for 148 h under reflux. The product was filtered and washed three times each with methanol and water.

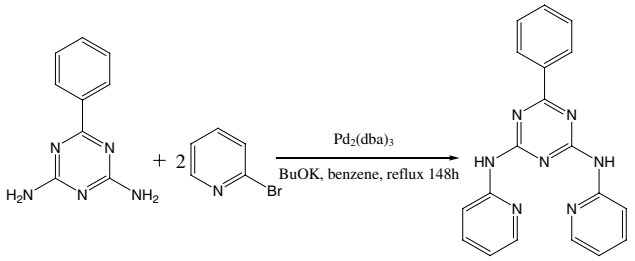

Dpdapt was obtained as a white powder in 64% yield (5.8 g). *Anal*. Calc. for $C_{19}H_{15}N_7$: C, 66.86; H, 4.399; N, 28.74. Found: C, 66.87; H, 4.328; N, 28.56%. IR (KBr, cm^{-1}): $v = 3025$(w), 2952(w), 1604(m), 1563(w), 1496(s), 1425(s), 1364(m), 1307(m), 1244(w), 1194(w), 1047(w), 989(m), 934(w), 770(s), 729(m), 693(w). MS (FAB) *m*/*z* (%) 342.1 (dpdapt).

2.3. Synthesis of [Cu(dpdapt)Cl_2] (1)

A green solution was obtained by adding a methanol solution (10 ml) of $CuCl_2 \cdot 2H_2O$ (34.1 mg, 0.20 mmol) to a methanol suspension (15 ml) of dpdapt (75.0 mg, 0.22 mmol) and stirring for 4 h. Diffused in Et_2O, after filtering green needle-shaped crystals of **1** were produced. Yield: 56%. *Anal*. Calc. for $[Cu(C_{19}H_{15}N_7)Cl_2]$:C, 47.92; H, 3.152; N, 20.60. Found: C, 47.86; H, 3.185; N, 20.52%.

2.4. Synthesis of [Cu(dpdapt)(NO_3)(H_2O)] · NO_3 · H_2O (2)

A suspension of $Cu(NO_3)_2 \cdot 8H_2O$ (53.9 mg, 0.2 mmol) in 10 ml water was allowed to react with dpdapt (75.0 mg, 0.22 mmol) dissolved in 20 ml methanol. The resulting mixture was stirred for 3 h and the product was removed by filtration. After a few days, dark green crystals were obtained by diffusion in Et_2O. Yield: 48%. *Anal*. Calc. for $[Cu(dpdapt)(NO_3)(H_2O)] \cdot NO_3 \cdot H_2O$: C, 40.36; H, 3.363; N, 22.30. Found: C, 40.46; H, 3.385; N, 22.52%.

2.5. Crystal structures determination

X-ray diffraction data were collected on a BRUKER SMART APEX-II diffractometer using graphite-monochromated Mo Kα radiation ($\lambda = 0.71073$ Å) for complexes **1** and **2**. The structures were solved by direct methods [7]. Then the structures were refined by the least-squares method using SHELXL-97 [8] with anisotropic temperature factors for all non-H atoms. Crystal data and structure refinement details are summarized in

Table 1
Data collection and processing parameters for [Cu(dpdapt)Cl_2] (**1**) and [Cu(dpdapt)(NO_3)(H_2O)] · NO_3 · H_2O (**2**)

Complex	**1**	**2**
Empirical formula	$C_{19}H_{15}Cl_2CuN_7$	$C_{19}H_{19}CuN_9O_8$
Formula weight	475.82	564.97
T (K)	273(2)	273(2)
λ (Å)	0.71073	0.71073
Crystal system	monoclinic	monoclinic
Space group	$P2_1/c$	$P2_1/c$
a (Å)	8.374(2)	12.156(5)
b (Å)	17.789(5)	8.708(3)
c (Å)	12.647(4)	21.327(8)
β (°)	95.226(4)	92.847(6)
V (Å^3)	1876.3(9)	2255(1)
Z	4	4
D_{calc} (g/cm^3)	1.684	1.664
Absorption coefficient (nm^{-1})	1.471	1.037
$F(000)$	964	1156
Crystal size (mm^3)	$0.37 \times 0.11 \times 0.07$	$0.29 \times 0.13 \times 0.08$
θ Range for data collection (°)	1.98–29.22	1.91–29.17
Limiting indices	$-11 \leqslant h \leqslant 10$, $-23 \leqslant k \leqslant 17$, $-17 \leqslant l \leqslant 13$	$-16 \leqslant h \leqslant 13$, $-11 \leqslant k \leqslant 11$, $-27 \leqslant l \leqslant 27$
Reflections collected	11 889	13 865
Independent reflections	4671	5559
Absorption correction	semi-empirical	semi-empirical
Maximum and minimum transmission	0.9040 and 0.6121	0.9244 and 0.7557
Refinement method	full-matrix least-squares on F^2	full-matrix least-squares on F^2
Data/restraints/parameters	4671/0/262	5559/0/364
Goodness-of-fit on F^2	1.114	1.005
R_1[a], wR_2[b] [$I > 2\sigma(I)$]	0.0321, 0.0859	0.0378, 0.1007
R_1[a], wR_2[b] (all data)	0.0483, 0.0898	0.0605, 0.1082
Largest difference in peak and hole (e Å^{-3})	0.334 and −0.505	0.400 and −0.614

[a] $R_1 = \sum\|F_o| - |F_c\|/\sum|F_o|$.
[b] $wR_2 = [\sum[w(F_o^2 - F_c^2)^2]/\sum[(F_o^2)^2]]^{1/2}$.

Table 1. Selected bond lengths and bond angles are given in Table 2.

2.6. Computational details

The calculations were carried out using the GAUSSIAN-03 program suite [9], including optimized geometries, and calculation of vibrational frequencies were carried out at the B3LYP [10,11] level of theory. Mulliken population analysis was also performed under this method. We employed the 6-31G(d) basis set for H, C, N and Cl, and the LANL2DZ effective core potential (ECP) set of Hay and Wadt [12] for Cu. All of the results (structures and energies) from the DFT calculations are available as electronic supplementary information.

3. Results and discussion

3.1. Description of structures

The crystal structure of complex **1** reveals that the coordination geometry around the copper(II) atom is a distorted trigonal bipyramid with the dpdapt ligand existing in an all-*anti* configuration. The Cu(1) atom is coordinated by three nitrogen atoms (N(3) of triazine and N(5), N(1) of different pyridyls) with two additional chloride atoms resulting in five-coordinated geometry (Fig. 1). The Cu(1)–N(3) distance is 2.024(2) Å and the distance to the pyridyl donors N(5) and N(1) are 2.079(2) and 2.066(2) Å, respectively. The distance of Cu(1)–Cl(2) is 2.288(1) Å whereas Cu(1)–Cl(1) forms a long bond with a distance of 2.424(1) Å. The average Cu–N bond length is observed to be 2.056 Å while the average Cu–Cl bond length is 2.356 Å. The bond angles N(1)–Cu(1)–N(5) (124.53(7)°), N(5)–Cu(1)–Cl(1) (113.66(5)°) and N(1)–Cu(1)–Cl(1) (120.32(5)°) sum up approximately to 360° and the angle N(3)–Cu(1)–Cl(2) (177.41(5)°) is approximately 180°, so the coordinated geometry of Cu(II) may be described as distorted trigonal bipyramidal with Cu(1), N(1), N(5) and Cl(1) forming the equatorial plane and Cl(2), N(3) occupying the axial positions. The dihedral angle between the plane (Cu(1), N(1), N(5), Cl(1)) and the triazine plane is 86.7°.

Two molecules of **1** form an antiparallel dimer structure as a result of two N–H···Cl hydrogen bonds (Cl(1A)···N(4B) 3.258 Å, N(4A)···Cl(1B) 3.258 Å) which are symmetry related, then each dimer is linked

Table 2
Selected bond lengths (Å) and bond angles (°) of Cu(dpdapt)Cl_2 (**1**) and [Cu(dpdapt)(NO_3)(H_2O)] · NO_3 · H_2O (**2**)

Cu(dpdapt)Cl_2 (**1**)			[Cu(dpdapt)(NO_3)(H_2O)] · NO_3 · H_2O (**2**)	
	Experimental	Optimized		Experimental
Bond lengths				
Cu(1)–N(3)	2.024(2)	2.095	Cu(1)–N(3)	2.018(2)
Cu(1)–N(1)	2.066(2)	2.175	Cu(1)–N(1)	1.974(2)
Cu(1)–N(5)	2.079(2)	2.246	Cu(1)–N(5)	1.980(2)
Cu(1)–Cl(1)	2.4243(8)	2.363	Cu(1)–O(5)	2.114(3)
Cu(1)–Cl(2)	2.2878(7)	2.333	Cu(1)–O(7)	2.225(2)
N(1)–C(1)	1.351(3)	1.360	N(9)–O(5)	1.197(4)
N(1)–C(5)	1.335(3)	1.351	N(8)–O(1)	1.250(3)
N(3)–C(8)	1.364(2)	1.362	N(1)–C(1)	1.358(3)
N(3)–C(6)	1.346(2)	1.358	N(1)–C(5)	1.337(3)
N(5)–C(15)	1.331(2)	1.348	N(3)–C(6)	1.359(3)
N(5)–C(19)	1.351(3)	1.359	N(3)–C(8)	1.364(3)
N(6)–C(7)	1.346(2)	1.355	N(5)–C(9)	1.341(3)
N(7)–C(8)	1.326(2)	1.352	N(5)–C(13)	1.365(3)
Bond angles				
N(3)–Cu(1)–N(1)	86.93(7)	84.74	N(1)–Cu(1)–N(5)	170.03(7)
N(3)–Cu(1)–N(5)	87.79(7)	84.33	N(1)–Cu(1)–N(3)	92.90(7)
N(1)–Cu(1)–N(5)	124.53(7)	122.56	N(5)–Cu(1)–N(3)	93.63(7)
N(1)–Cu(1)–Cl(1)	120.32(5)	123.77	N(1)–Cu(1)–O(5)	88.40(9)
N(5)–Cu(1)–Cl(1)	113.66(5)	111.44	N(5)–Cu(1)–O(5)	89.65(9)
N(5)–Cu(1)–Cl(2)	94.13(5)	94.28	N(3)–Cu(1)–O(5)	150.3(1)
N(1)–Cu(1)–Cl(2)	93.39(5)	92.41	N(1)–Cu(1)–O(7)	83.58(8)
N(3)–Cu(1)–Cl(2)	177.41(5)	180.0	N(3)–Cu(1)–O(7)	116.54(7)
N(3)–Cu(1)–Cl(1)	82.94(5)	86.16	N(5)–Cu(1)–O(7)	86.76(8)
Cl(2)–Cu(1)–Cl(1)	94.69(3)	98.05	O(5)–Cu(1)–O(7)	93.10(1)
Hydrogen bonds				
N(2)–H(2A)···Cl(2)#1	3.588		N(2)–H(2)···O(4)#4	3.051
N(4)–H(4A)···Cl(1)#2	3.258		O(7)–H(7A)···O(1)	2.815
C(4)–H(4)···Cl(1)#3	3.405		C(12)–H(12)···O(2)#4	3.205

Symmetry codes: #1: $1/2 + x$, $1/2 - y$, $-1/2 + z$; #2: $-x$, $1 - y$, $-z$; #3: $1 + x$, y, z; #4: x, $-1 + y$, z.

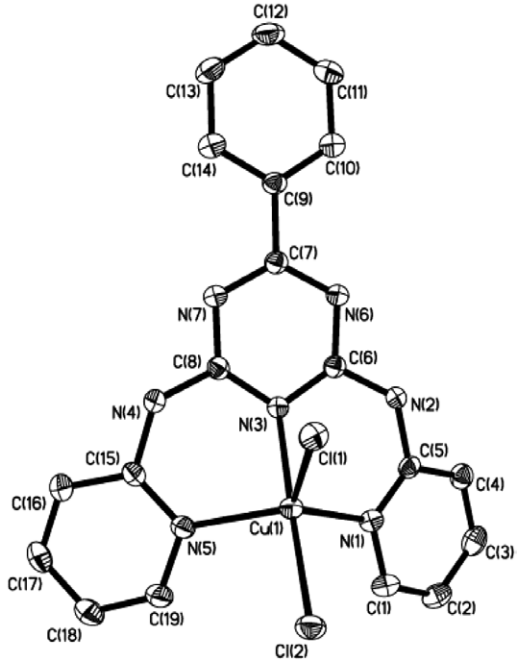

Fig. 1. The ORTEP drawing of Cu(dpdapt)Cl_2 (**2**). Thermal ellipsoids are drawn at the 50% probability level. Hydrogen atoms are omitted for clarity.

by face to face π–π stacking (3.461 Å) (between the triazine rings of two neighboring dimers) and two weak hydrogen bonds interactions (Cl···H–C 3.405 Å) forming a 1-D supramolecular ladder structure along the *c*-axis (Fig. 2). The structural characterization of such hydrogen-bonded dimeric structures linked by self-complementary donor/accepter groups is scarce for metal organic framework [13]. On the other hand, the 1-D supramolecular stacking in the *ab*-plane using N(2)–H···Cl(2) hydrogen bonds, thereby gives rise to a 2-D layer structure (Fig. 3).

Complex **2** has the same coordination configuration as **1**. The Cu(1) atom sits in a five-coordinated environment composed of three nitrogen donors (N(3) of triazine and N(5), N(1) of different pyridyls) with two different oxygen atoms, one (O(7)) from a water molecule, the other (O(5)) from a nitrate anion (Fig. 4). The bond distance to the terminal triazine N(3), (Cu(1)–N(3)) is 2.018(2) Å and the distance to the pyridyl donors N(5) (Cu(1)–N(5)) and N(1) (Cu(1)–N(1)) are 1.980(2) and 1.974(2) Å, respectively. The average Cu–N bond length is observed to be 1.990 Å, which is shorter than that of **1**. Both Cu–N bond lengths are typical of those found for the five–coordinate Cu(II)-μ-

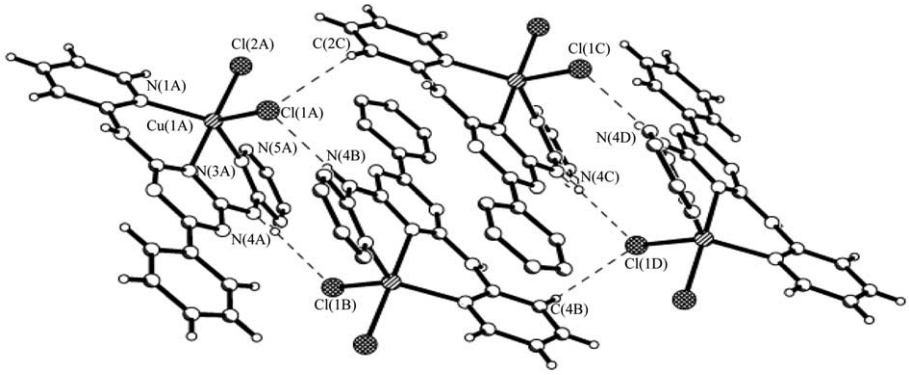

Fig. 2. The one-dimensional ladder structure of $[Cu(dpdapt)Cl_2]$ (**1**) formed by hydrogen-bonding interactions (dashed lines) and π–π stacking along the *c*-axis. Some hydrogen atoms are omitted for clarity.

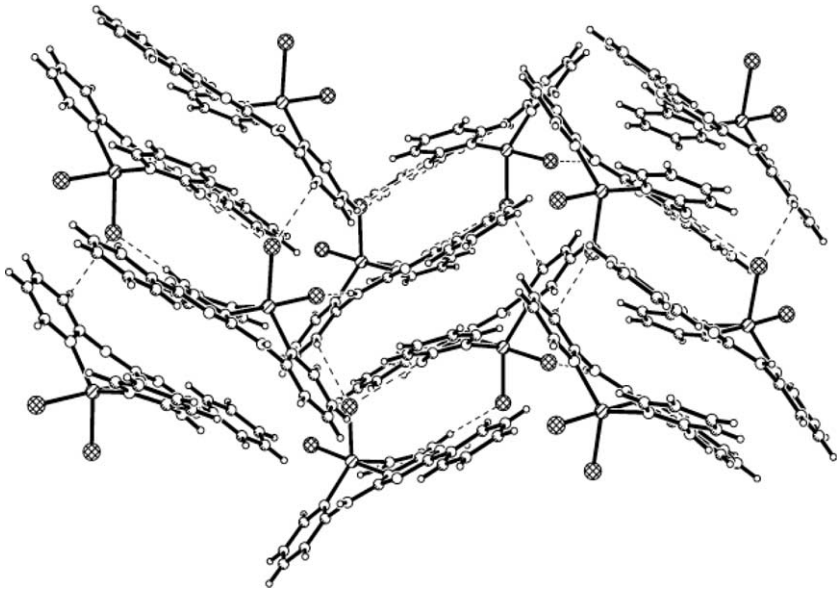

Fig. 3. The layer structure of $[Cu(dpdapt)Cl_2]$ (**1**).

pmea analogues [14]. The Cu(1)–O(7) distance is 2.225(2) Å and Cu(1)–O(5) is 2.114(3) Å. The coordination geometry of Cu(1) is also distorted trigonal bipyramidal with O(7), N(3), Cu(1) and O(5) in the equatorial plane and the apical sites are occupied by the N(1) and N(5) atoms of the pyridyl rings. The dihedral angle between the plane (Cu(1), O(5), O(7), N(3)) and the triazine ring plane is 85.8°.

The crystal framework testifies a one-dimensional chain along the *b*-axis with hydrogen bonds and π–π stacking interactions. As depicted in Fig. 5, the one-dimensional chains along the *b*-axis are formed by three different types of hydrogen bonds involving the coordinated molecular water, the coordinated nitrate anion and the non-coordinated nitrate anion (N(2A)–H···O(4B), 3.051 Å; O(7A)–H···O(1A), 2.815 Å; C(12B)–H···O(2A), 3.201 Å) as well as π–π stacking (3.345 Å) between the phenyl and pyridyl rings of two neighboring molecules. Moreover, the crystal structure consists of alternate layers with an antiparallel alignment of the molecules, and each layer is built up via solvent molecular interactions and hydrogen bonds in the *ac*-plane as shown in Fig. 6. The adjacent layers are interconnected by solvent molecules, resulting in a 3-D structure.

Although the structures of **1** and **2** exhibit the coordination character of dpdapt in part, the framework structures of **1** and **2** are scarce for inorganic triazine compounds. To the best of our knowledge, only one dimeric unit of a transition-metal complex based on tpt has been reported [6a], but no π–π interactions were discussed. Additionally, the ladder and layer frameworks of **1** and **2** are exclusive and structures of this type containing tpt have not been reported to date. The coordination of one metal ion, especially Cu(II), to tpt induces the hydrolysis of tpt [5,6]. Dinuclear metal complexes of tpt have also been described [6]. Although tpt has a more versatile coordination ability [6b] than

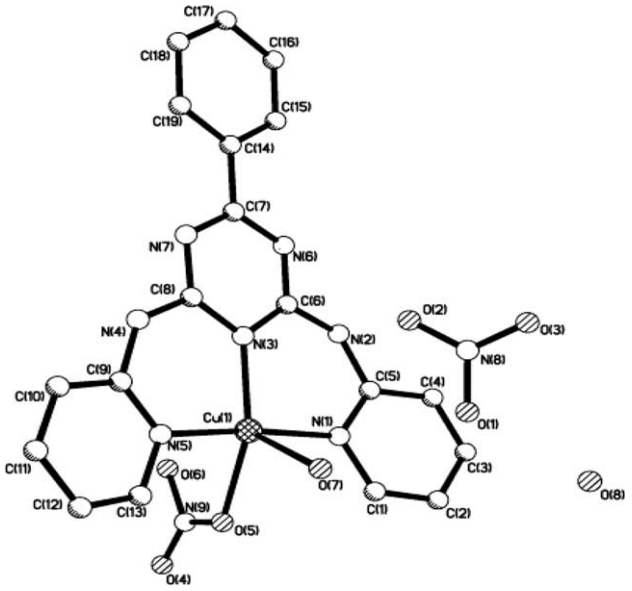

Fig. 4. Molecular structure of $[Cu(dpdapt)(NO_3)(H_2O)] \cdot NO_3 \cdot H_2O$ (**2**) Thermal ellipsoids represent the 50% probability surfaces. Hydrogen atoms are omitted for clarity.

dpdapt, in theory, the dpdapt ligand has its intriguing character revealed in this article.

3.2. Spectroscopic properties

The IR spectra of the complexes exhibit several characteristic strong bands. In complex **1**, the bands around 1425 and 1496 cm^{-1} in the ligand dpdapt, attributed to the C=N groups, are shifted to 1464 and 1570 cm^{-1}, respectively, confirming the involvement of dpdapt in the copper complexation. In complex **2**, the corresponding bands are shifted to 1580 and 1640 cm^{-1}. The bands corresponding to NO_3^- are at 1421, 1382, 1022 and 775 cm^{-1} and the broad band at 3290–3421 cm^{-1} represents the existence of $\nu(H_2O)$ in complex **2**.

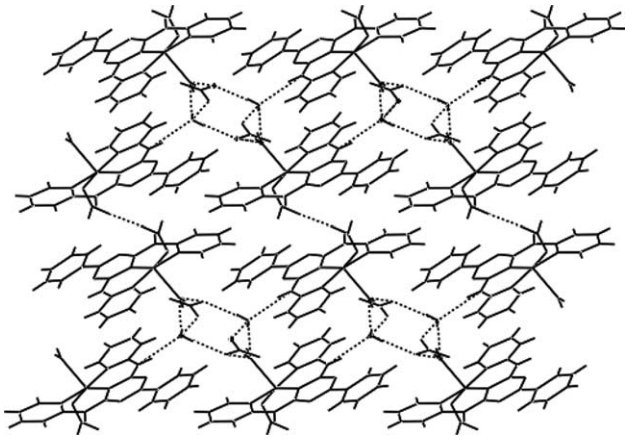

Fig. 6. Layer framework of $[Cu(dpdapt)(NO_3)(H_2O)] \cdot NO_3 \cdot H_2O$ (**2**) in the *ac*-plane.

The UV–Vis spectra of the complexes are recorded in methanol and are characterised by several spectral regions. The absorption bands in the region of 260 and 285 nm for the ligand dpdapt are ligand-centered (LC) due to π–π* transitions [15,16]. The shoulder at 300 nm for complexes **1** and **2** is due to a d–d transition and the low-energy bands at 341, 384 and 389 nm are assigned to metal-to-ligand charge transfer (MLCT) transitions [17,18].

The luminescence data were recorded in methanol at room temperature. The excitation–emission spectrum of dpdapt shows the strongest emission peak at 375.4 nm with the excitation peak at 330.0 nm. The emission band of dpdapt is attributed to the π*–n transitions. The strongest excitation peak for complex **1** is at 310.0 nm and for complex **2** at 300.0 nm, and their emission spectra show a main strong peak at 413.6 and 438.0 nm, respectively. These shoulder peaks of the emission spectra are probably due to the ligand-to-metal charge-transfer (LMCT) bands [19]. The strong fluorescent emissions of the dpdapt supramolecular complexes **1**

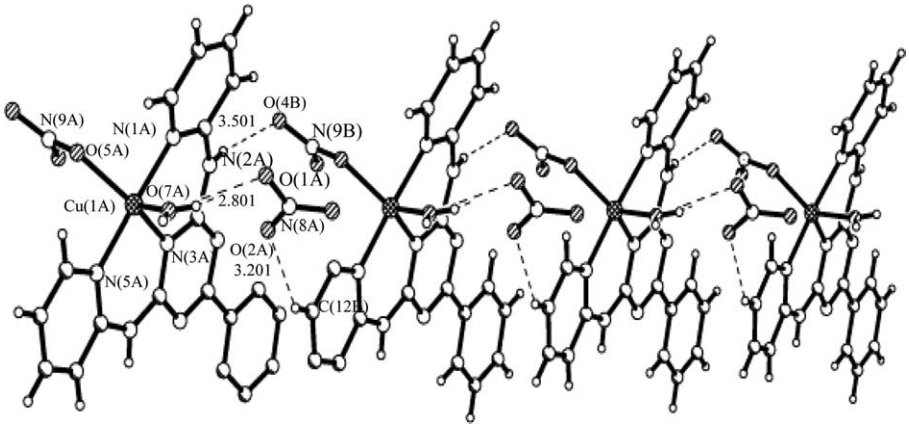

Fig. 5. The one-dimensional chain structure of $[Cu(dpdapt)(NO_3)(H_2O)] \cdot NO_3 \cdot H_2O$ (**2**) formed by hydrogen-bonding interactions (dashed lines) and π–π stacking along the *b*-axis. Some hydrogen atoms are omitted for clarity.

and **2** make them potentially useful photoactive materials.

3.3. Computational results and discussion

DFT calculations (B3LYP/6-31G(d)) have been carried out for the coordination conformations of dpdapt, and the optimized structures (verified by calculating the vibrational frequencies that result in the absence of imaginary eigenvalues) are shown in Fig. 7. The relative energies of each conformation given in this article include zero-point corrections (ZPE). $E_{anti\text{–}anti\text{–}anti\text{–}anti}$, $E_{syn\text{–}syn\text{–}anti\text{–}anti}$ and $E_{syn\text{–}syn\text{–}syn\text{–}syn}$ equal −1115.698749, −1115.700689 and −1115.699802 hartree, respectively. It is found that the energies of the conformers are similar, while the *syn–syn–anti–anti* conformer is the most stable by 5.09–2.33 kJ mol^{-1}. Complexes **1** and **2** exist with the ligand in the all-*anti* conformation. Clearly the free ligand, with its preferred *syn–syn–anti–anti* conformation, does not effect the conformation change in **1** and **2** because of its minimal energy difference.

Optimized geometries for **1** were verified by performing a frequency calculation. The optimized bond lengths and angles are presented in Table 2. In general, the calculated bond lengths and angles are in agreement with experimental crystal data and the large differences (∼0.2 Å, ∼3°) may be noticed for deviations around the central copper atoms. The deviations come mainly from two factors: one is that the theoretical calculations do not consider the effects of chemical environment (the complex is treated as a free molecule), and basis sets are still approximate to a certain extent. However, the coordination geometry of Cu(II) is also a distorted trigonal bipyramid. The bond angles N(1)–Cu(1)–N(5) (121.56°), N(5)–Cu(1)–Cl(1) (111.44°) and N(1)–Cu(1)–Cl(1) (124.77°) sum up approximately to 360° and the angle N(3)–Cu(1)–Cl(2) is 180°. So the results should be significant in computations of this large system.

The overlap populations (Table 3) between Cu(1) and Cl(1) (0.2663) is stronger than that of Cu(1)–Cl(2) (0.2275), which is consistent with the experimental result that the bond length of Cu(1)–Cl(2) is clearly longer than that of Cu(1)–Cl(1). The bond intensity order is Cu(1)–N(3) > Cu(1)–N(1) > Cu(1)–N(5) in accord with that in the experimental results (Cu(1)–N(5) > Cu(1)–N(1) > Cu(1)–N(3)). Because N(3) is coordinated to the center Cu atom, the populations of N(3)–C(6) and N(3)–C(8) are less than that of N(6)–C(7) and N(7)–C(8).

Table 3
Population analysis of **1**

Bond	
Cu(1)–Cl(1)	0.2663
Cu(1)–Cl(2)	0.2275
Cu(1)–N(3)	0.1236
Cu(1)–N(1)	0.1123
Cu(1)–N(5)	0.1065
N(3)–C(6)	0.2716
N(3)–C(8)	0.2790
N(6)–C(7)	0.3589
N(7)–C(8)	0.4484

The Mulliken charge of the central Cu metal (Table 4) changes from +2 to 0.275. Obviously, Cu has been coordinated by the ligand and its charge transfers to the ligand. The net atomic charge of the coordinated Cl(1), Cl(2), N(1), N(3) and N(5) atoms are negative. Compared to the dpdapt ligand (N(1), −0.259; N(3) and N(5), −0.438; N(6) and N(7), −0.353), the change in the charge distribution value of the donor nitrogen atoms (N(1), N(3), N(5)) are more than that of the non-coordinated nitrogen atoms (N(6), N(7)) in triazine.

Table 4
Mulliken atomic charges (e) for **1**

Atom	Charge
Cu(1)	0.275
Cl(1)	−0.397
Cl(2)	−0.383
N(3)	−0.498
N(5)	−0.518
N(1)	−0.545
N(6)	−0.432
N(7)	−0.437

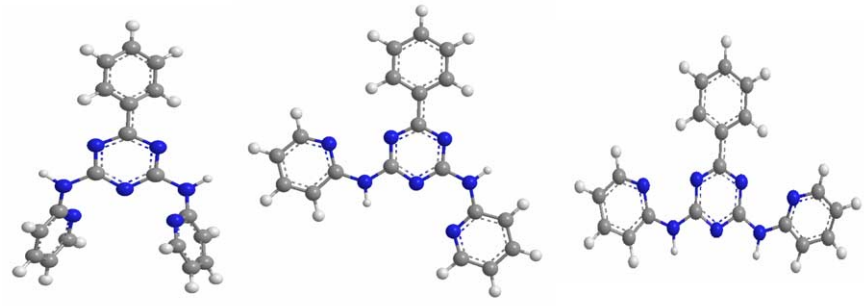

a. anti-anti-anti-anti b. syn-syn-anti-anti c. syn-syn-syn-syn

Fig. 7. Optimized structures of dpdapt's coordination conformations.

Table 5
The energy (eV) and character of the selected molecular orbitals with α spins for **1**

Orbital	Energy	Character
HOMO − 3	−6.126	π(Cu–Cl), π(Cl)
HOMO − 2	−5.711	d_{xz}(Cu), π(Cl)
HOMO − 1	−5.472	d_{yz}(Cu), π(Cl)
HOMO	−5.364	d_{xy}(Cu), π(Cl)
LUMO	−3.096	π*(dpdapt), d_{xy}(Cu)
LUMO + 1	−1.989	π*(dpdapt)
LUMO + 2	−1.686	π*(dpdapt), d_{xy}(Cu)
LUMO + 3	−1.600	d_{z^2}(Cu)–σ(Cl)

All this data show strong complexation between Cu and its coordinated atoms.

The energies and characters of the selected MOs for **1** are presented in Table 5. According to molecular orbital theory, the frontier orbital and nearby molecular orbitals are the most important factors to the activity. The highest occupied molecular orbital (HOMO) and the nearby occupied molecular orbitals are prone to donate electrons, but the lowest unoccupied molecular orbital (LUMO) and the nearby unoccupied orbitals are prone to accept electrons. The more different the frontier orbitals are, the more stable the molecular structure is [20]. The copper d_π atomic orbitals (d_{xz},d_{yz} and d_{xy}) and π orbitals of the chlorine atoms make the main contributions into the HOMO − 2 , HOMO − 1 and HOMO. The LUMO orbital has predominantly π*(dpdapt) character. The results approved its coordination behavior and the value of ΔE ($\Delta E = E_{LUMO} - E_{HOMO}$) is 2.268 eV, which shows that the complex **1** can exist stably.

Appendix A. Supplementary data

Crystallographic data for the structural analysis have been deposited with the Cambridge Crystallographic Data Centre, CCDC No. 260645 for compound **1** and 260646 for compound **2.** Copies of this information may be obtained free of charge on application to CCDC, 12 Union Road, Cambridge CB2 1EZ, UK (fax: +44 1223 336 033; e-mail: deposit@ccdc.cam.ac.uk or www: http://www.ccdc.cam.ac.uk). Supplementary data associated with this article can be found, in the online version at doi:10.1016/j.poly.2005.06.061.

References

[1] (a) Y.-Q. Sun, J. Zhang, G.-Y. Yang, J. Chem Soc., Dalton Trans. (2003) 3634;
(b) B. Moulton, M.J. Zaworotko, Chem. Rev. 101 (2001) 1629;
(c) Y.B. Dong, P. Wang, R.Q. Huang, Inorg. Chem. 43 (2004) 4727;
(d) D.N. Dybtsev, H. Chun, K. Kim, Chem. Commun. (2004) 1594.
[2] (a) S. Koner, S. Saha, K.L. Okamoto, J.P. Tuchagues, Inorg. Chem. 42 (2003) 4668;
(b) Y.Q. Zheng, J.L. Lin, Z.P. Kong, Inorg. Chem. 43 (2004) 2590;
(c) C.D. Wu, H.L. Ngo, W. Lin, Chem. Commun. (2004) 1588;
(d) I.G. Filippova, V.K. Kravtsov, M.R.J. Gdanec, Coord. Chem. 39 (2000) 1363.
[3] (a) Z. Huang, H.B. Song, M. Du, S.T. Chen, X.H. Bu, Inorg. Chem. 43 (2004) 932;
(b) C. Janiak, J. Chem Soc., Dalton Trans. (2003) 2781.
[4] F.H. Case, E.J. Koft, J. Am. Chem. Soc. 81 (1959) 905.
[5] (a) A. Cantarero, J.M. Amigo, J. Faus, M. Julve, T. Debaerdemaeker, J. Chem. Soc., Dalton Trans. (1988) 2033;
(b) E.I. Lerner, S.J. Lippard, Inorg. Chem. 16 (1977) 1546;
(c) J. Faus, M. Julve, J.M. Amigo, T. Debaerdemaeker, J. Chem. Soc., Dalton Trans. (1989) 1681;
(d) N.C. Thomas, B.L. Foley, A.L. Rheingold, Inorg. Chem. 27 (1977) 1546;
(e) X.Y. Chen, F.J. Femia, J.W. Babich, J.A. Zubieta, Inorg. Chem. 40 (2001) 2769.
[6] (a) G. Thorsten, L. Thomas, F. Roland, Eur. J. Inorg. Chem. (2004) 394;
(b) N.C. Thomas, B.L. Foley, A.L. Rheingold, Inorg. Chem. 27 (1988) 3427.
[7] G.M. Sheldrick, SHELXL-97: Program for Crystal Structure Determination, University of Göttingen, Göttingen, Germany, 1997.
[8] G.M. Sheldrick, SHELXL-97: Program for Crystal Structure Refinement, University of Göttingen, Göttingen, Germany, 1997.
[9] M.J. Frisch, G.W. Trucks, H.B. Schlegel, G.E. Scuseria, M.A. Robb, J.R. Cheeseman, J.A. Montgomery Jr., T. Vreven, K.N. Kudin, J.C. Burant, J.M. Millam, S.S. Iyengar, J. Tomasi, V. Barone, B. Mennucci, M. Cossi, G. Scalmani, N. Rega, G.A. Petersson, H. Nakatsuji, M. Hada, M. Ehara, K. Toyota, R. Fukuda, J. Hasegawa, M. Ishida, T. Nakajima, Y. Honda, O. Kitao, H. Nakai, M. Klene, X. Li, J.E. Knox, H.P. Hratchian, J.B. Cross, C. Adamo, J. Jaramillo, R. Gomperts, R.E. Stratmann, O. Yazyev, A.J. Austin, R. Cammi, C. Pomelli, J.W. Ochterski, P.Y. Ayala, K. Morokuma, G.A. Voth, P. Salvador, J.J. Dannenberg, V.G. Zakrzewski, S. Dapprich, A.D. Daniels, M.C. Strain, O. Frakas, D.K. Malick, A.D. Rabuck, K. Raghavachari, J.B. Foresman, J.V. Ortiz, Q. Cui, A.G. Baboul, S. Clifford, J. Cioslowski, B.B. Stefanov, G. Liu, A. Liashenko, P. Piskorz, I. Komaromi, R.L. Martin, D.J. Fox, T. Keith, K.A. Allaham, C.Y. Peng, A. Nanayakkara, M. Challacombe, P.M.W. Gill, B. Johson, W. Chen, M.W. Wong, C. Gonzalez, J.A. Pople, GAUSSIAN-03. Revision B.03, Gaussian, Inc., Pittsburgh, PA, 2003.
[10] A.D. Becke, J. Chem. Phys. 98 (1993) 5648.
[11] C.L.W. Yang, R.G. Parr, Phys. Rev. 37 (1988) 785.
[12] A.K. Vrkic, T. Taverner, J. Chem Soc., Dalton Trans. (2004) 197.
[13] H.-R. Ma, Y.-Y. Wang, P. Liu, D.-S. Li, G.-H. Lee, S.-M. Peng, Polyhedron 24 (2005) 215.
[14] K.-Y. Choi, Y.-M. Jeon, H. Ryu, J.-J. Oh, H.-H. Lim, M.-W. Kim, Polyhedron 23 (2004) 903.
[15] D.B. MacQueen, J.D. Petersen, Inorg. Chem. 29 (1990) 2313.
[16] R.M. Berger, J.R. Holcombe, Inorg. Chim. Acta (1995) 232.
[17] A. Juris, V. Balzani, F. Barigelletti, S. Campagna, P. Belser, A.V. Zelewsky, Coord. Chem. Rev. (1998) 8485.
[18] R.M. Berger, D.D. Ellis, Inorg. Chim. Acta (1996) 241.
[19] Q.R. Fang, G.S. Zhu, M. Xue, J. Chem Soc., Dalton Trans. (2004) 2205.
[20] K.C. Zheng, Z.N. Chen, Acta Phys. Chim. Sinica (Chinese) 15 (1999) 204.

Available online at www.sciencedirect.com
SCIENCE DIRECT®
Polyhedron 25 (2006) 203–204
POLYHEDRON
www.elsevier.com/locate/poly

Preface

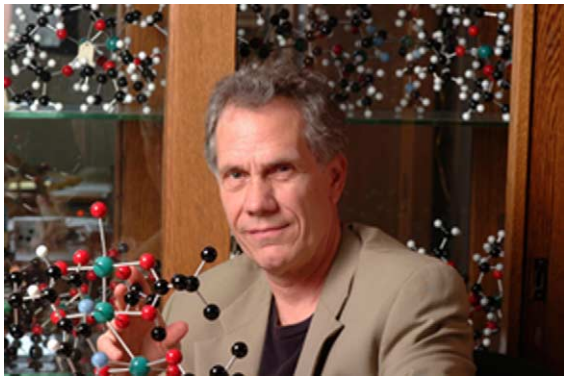

Professor Malcolm H. Chisholm

It gives me great personal pleasure to edit this special issue of *Polyhedron* dedicated to Professor Malcolm H. Chisholm on the occasion of his 60th birthday. Malcolm and I were inorganic chemistry colleagues at Indiana University for 17 years from 1983 to 2000, when he moved to Ohio State University. Those years in Indiana were extremely enjoyable for me and for everyone else associated with what by the late 1990s had become a top 10 inorganic division in the USA. A major reason for this was the presence there of Malcolm Chisholm and his research program. My memories of those years will always be of a very exciting, stimulating and intellectual environment with which it was a pleasure to be associated, and it had a great impact on the scientific education and training of a whole host of graduate students and postdoctoral associates from around the world.

Malcolm Chisholm has worked in transition metal chemistry his whole research career, which has been characterized by outstanding levels of creativity, innovation, and sheer quality over some four decades. But then what else could one expect from a scientist whose first paper as a young student, 'Iron Enneacarbonyl' was in *Nature* [1], and who has since been the author of 600 or so first-class publications. His Ph.D. advisor at Queen Mary College, London, was Professor Don Bradley, who recalls those early days:

"Malcolm joined my research group at Queen Mary as a Ph.D. student in the late 1960s when we were studying the dialkylamido compounds of the early transition metals, and he quickly provided a tremendous impetus to the programme. He obtained the tungsten hexadimethylamide and gave a sample to a (nameless!) crystallographer friend who accidentally dropped the flask spilling the precious contents on the bench. Seeing that the compound had not disappeared in a puff of smoke, Malcolm quickly scooped it up, fished out the fragments of glass, redissolved and recrystallized it, and grew a single crystal for the X-ray structure! Interestingly, a few years later when he was a faculty member at Princeton where he brilliantly developed the triple metal–metal bonded compounds, he showed that our hexadimethylamide was in fact a solid solution containing both tungsten hexadimethylamide and the ditungsten hexadimethylamide, which were remarkably close in structure due to the short W≡W triple bond. Malcolm had the ability to inspire everyone else in the lab to greater efforts and it became perceptibly quiet when he left to do postdoctoral research with Howard Clark in Canada. In addition to being a brilliant chemist, Malcolm is also a most friendly and generous spirited person with whom it was a privilege to be associated closely for a few exciting years".

Malcolm Chisholm has made great contributions to numerous areas of transition metal chemistry, and will always be particularly associated with the properties and reactivity of the Mo≡Mo and W≡W triple bonded compounds with dialkylamide or alkoxide ligands, truly seminal work that he began in the mid-1970s and which has greatly influenced the research of subsequent generations

0277-5387/$ - see front matter © 2005 Elsevier Ltd. All rights reserved.
doi:10.1016/j.poly.2005.11.003

of workers. However, his impact on the scientific community goes far beyond just his publication list. He has also given so much of himself to the selfless service of chemistry and to the cause of higher education through his numerous organizational and other activities for the American Chemical Society and the Royal Society of Chemistry, as well as for many other societies and individual universities around the world. His well-deserved awards are too numerous to list here, but include the prestigious Royal Society of Chemistry Ludwig-Mond Lectureship for the year 2000, and election as both Fellow of the Royal Society of the UK, and member of the National Academy of Sciences of the USA.

One issue of a journal is a sadly limited forum, but nevertheless I have attempted as far as possible to have this special issue of *Polyhedron* reflect the great respect that Malcolm commands throughout the world. This issue certainly contains contributions from some of his many ex-students, and from ex-colleagues such as myself, but there are also many others who gladly and indeed eagerly accepted my invitation to participate as a means to show their great admiration for the man and his chemistry. There is no unifying scientific theme to the issue, other than that the papers are all dedicated to Malcolm Chisholm, who was also Executive Editor for the Americas/Symposia-in-Print Editor of Polyhedron from 1983 to 1997. On behalf of all of these authors, and indeed the scientific community as a whole, I wish him a Happy 60th Birthday, and many more years of success in his future scientific endeavors.

Reference

[1] M.H. Chisholm, A.G. Massey, N.R. Thompson, Nature 211 (1966) 67.

George Christou
Department of Chemistry,
University of Florida,
Gainesville, FL 32611-7200, USA
E-mail address: christou@chem.ufl.edu

Available online at www.sciencedirect.com
SCIENCE DIRECT®
Polyhedron 25 (2006) 205–210
POLYHEDRON
www.elsevier.com/locate/poly

Syntheses and X-ray structures of cerium amide complexes

Sherrika D. Daniel, Jean-Sébastien M. Lehn, James D. Korp, David M. Hoffman *

Department of Chemistry and Center for Materials Chemistry, 136 Fleming Building, University of Houston, Houston, TX 77204-5003, USA

Received 8 February 2005; accepted 24 June 2005
Available online 10 August 2005

Abstract

Reaction of $CeCl_3$ with an excess of LiTMP (TMP-H = 2,2,6,6-tetramethylpiperidine) gave $[Ce(\mu\text{-}OCH{=}CH_2)(TMP)_2]_2$. The alkoxide ligand originated from THF, which was used as the solvent in the reaction. $CeCl_3$ reacted with 3 equiv. of LiTMP in THF to produce, after crystallization, a 3:2 crystalline mixture of $Ce(TMP)_3$ and $[Ce(\mu\text{-}OCH{=}CH_2)(TMP)_2]_2$. $Ce(TMP)_3$ could not be isolated cleanly or separated from the mixture except by handpicking the crystals under a microscope. The homoleptic amide complex $Ce[N\text{-}t\text{-}Bu(SiMe_3)]_3$ was obtained by reacting $CeCl_3(THF)_2$ with 3 equivalents of $LiN\text{-}t\text{-}Bu(SiMe_3)$. In the solid state, $[Ce(\mu\text{-}OCH{=}CH_2)(TMP)_2]_2$ is a dimer with a $Ce(\mu\text{-}OR)_2Ce$ four-member ring, while $Ce(TMP)_3$ and $Ce[N\text{-}t\text{-}Bu(SiMe_3)]_3$ are trigonal planar monomers. There is structural evidence to suggest the presence of a Ce–vinyl group interaction in $[Ce(\mu\text{-}OCH{=}CH_2)(TMP)_2]_2$.
© 2005 Elsevier Ltd. All rights reserved.

Keywords: Cerium; Amide; Alkoxide

1. Introduction

The dialkyl amide complexes $Si(NMe_2)_4$, $Sn(NMe_2)_4$, $Zr(NEt_2)_4$, $Ta(NMe_2)_5$, and $Zn(TMP)_2$ (TMP-H = 2,2,-6,6-tetramethylpiperidine) have been used as precursors to silicon, tin, zirconium, tantalum, and zinc oxide thin films, respectively [1–4]. We were interested in synthesizing cerium alkyl amide complexes for possible use as precursors to cerium oxide films. In this paper, we describe the syntheses and X-ray crystal structures of two homoleptic cerium alkylamide complexes and $[Ce(\mu\text{-}OCH{=}CH_2)(TMP)_2]_2$, a complex derived from the decomposition of THF solvent.

A limited number of neutral lanthanide tris(alkylamide) derivatives have been reported previously. The first report appears to be from 1976 when Bradley and co-workers [5] described the synthesis of $Yb(N\text{-}i\text{-}Pr_2)_3$ and $Nd(N\text{-}i\text{-}Pr_2)_3(THF)$. Almost 20 years later, $Nd(N\text{-}i\text{-}Pr_2)_3(THF)$ was prepared as part of mixture with the related lithium "ate" complex, and the neutral complex was partially structurally characterized [6]. Aspinall and Tillotson [7] reported the preparation of the analogous Yb complex, $Yb(N\text{-}i\text{-}Pr_2)_3(THF)$, and Gambarotta and co-workers [8] synthesized and structurally characterized $Sm(NCy_2)_3(THF)$. Finally, Lappert and co-workers [9] described the preparation of $Ce(TMP)_3(THF)$. In the same paper, they also reported the preparation of $[Ce(\mu\text{-}OEt)(TMP)_2]_2$ from the apparent decomposition of diethyl ether solvent, which is an observation relevant to this study.

2. Results and discussion

2.1. Synthetic studies

The reaction of $CeCl_3$ with 5 equiv. of LiTMP (TMP-H = 2,2,6,6-tetramethylpiperidine) in THF produced $[Ce(\mu\text{-}OCH{=}CH_2)(TMP)_2]_2$ in high yield.

* Corresponding author. Tel.: +1 7137433255; fax: +1 7137432787.
E-mail address: hoffman@uh.edu (D.M. Hoffman).

0277-5387/$ - see front matter © 2005 Elsevier Ltd. All rights reserved.
doi:10.1016/j.poly.2005.06.029

Proposed mechanisms for the formation of $[Ce(\mu\text{-}OCH{=}CH_2)(TMP)_2]_2$ involving fragmentation of the solvent THF are presented in Scheme 1. Evans et al. [10] prepared similar lanthanide complexes $[Ln(\mu\text{-}OCH{=}CH_2)(C_5H_4R)_2]_2$ (R = H, CH_3; Ln = Lu, Yb) by reacting $LiOCH{=}CH_2$ with $[(C_5H_4R)_2LnCl]_2$. They also prepared $[Yb(\mu\text{-}OCH{=}CH_2)(C_5H_5)_2]_2$ by thermolysis of $[(C_5H_5)_2YbCH_3]_2$ in the presence of LiCl and THF. In the latter case, they proposed a mechanism for formation of the alkoxide complexes involving metallation of THF. More recently, Lappert et al. [9] prepared $[Ce(\mu\text{-}OEt)(TMP)_2]_2$ by stirring $Ce(TMP)_3(THF)$ with diethyl ether. In this case, the ethoxide ligand was proposed to result from cleavage of diethyl ether with formation of TMP-Et. Alternative plausible mechanistic routes for the cleavage of diethyl ether could involve deprotonation of coordinated ether (at the γ position, $EtOCH_2CH_3$) with formation of TMP-H, ethylene, and an ethoxide ligand (i.e., mechanistic routes analogous to those in Scheme 1).

The reaction of $CeCl_3$ with 3 equiv. of LiTMP (rather than 5 equiv.) in THF produced a mixture of $Ce(TMP)_3$ and $[Ce(\mu\text{-}OCH{=}CH_2)(TMP)_2]_2$ in an approximate ratio of 3:2, as determined by examination of the crystalline mixture under a microscope. The use of $CeCl_3(THF)_2$ in place of $CeCl_3$ in this reaction failed to produce $Ce(TMP)_3$, $[Ce(\mu\text{-}OCH{=}CH_2)(TMP)_2]_2$, or any other crystalline products. Attempts to prepare $Ce(TMP)_3$ cleanly by using less than 3 equiv. LiTMP per Ce ion in the reaction, decreasing the reaction temperature, or letting the reactants stir for one week failed. The closely related complex $Ce(TMP)_3(THF)$ was obtained by Lappert et al. [9] by reacting $Ce(OTf)_3$ (TfO-H = triflic acid) with KTMP and crystallizing from hexane/THF.

Yellow crystalline needles of $Ce[N\text{-}t\text{-}Bu(SiMe_3)]_3$ were obtained by reacting $CeCl_3(THF)_2$ with 3 equiv. of $LiN\text{-}t\text{-}Bu(SiMe_3)$ in THF (Eq. (1)). The analogous samarium complex $Sm[N\text{-}t\text{-}Bu(SiMe_3)]_3$ was prepared previously by following a similar procedure [11]. A problem with the cerium preparation was the presence of an unidentified amorphous brown solid that always accompanied the yellow crystals of the product. Despite repeated purification attempts, $Ce[N\text{-}t\text{-}Bu(SiMe_3)]_3$ could not be isolated free of these contaminants and, consequently, a satisfactory carbon elemental analysis was not obtained for $Ce[N\text{-}t\text{-}Bu(SiMe_3)]_3$. Attempts to prepare $Ce[N\text{-}t\text{-}Bu(SiMe_3)]_3$ in better yield or more cleanly by varying the reaction temperature or using fewer or more equivalents of $LiN\text{-}t\text{-}Bu(SiMe_3)$ per Ce ion in the reaction were also not successful. An attempt to carry out the reaction in diethyl ether at 70 °C in a pressure flask resulted in the isolation of an unidentified waxy red solid and yellow crystalline needles of $[Ce(\mu\text{-}OEt)\{N\text{-}t\text{-}Bu(SiMe_3)\}_2]_2$ (as identified by X-ray crystallography).

$$CeCl_3(THF)_2 + 3LiN\text{-}t\text{-}Bu(SiMe_3) \rightarrow Ce[N\text{-}t\text{-}Bu(SiMe_3)]_3 + 3LiCl + 2THF \quad (1)$$

The complexes $[Ce(\mu\text{-}OCH{=}CH_2)(TMP)_2]_2$, $Ce(TMP)_3$, and $Ce[N\text{-}t\text{-}Bu(SiMe_3)]_3$ are soluble in hexanes and toluene. They decomposed rapidly with formation of brown solids during attempted sublimations.

2.2. X-ray crystallographic studies

The X-ray structures of $[Ce(\mu\text{-}OCH{=}CH_2)(TMP)_2]_2$ and $Ce(TMP)_3$ were determined (Figs. 1 and 2, respec-

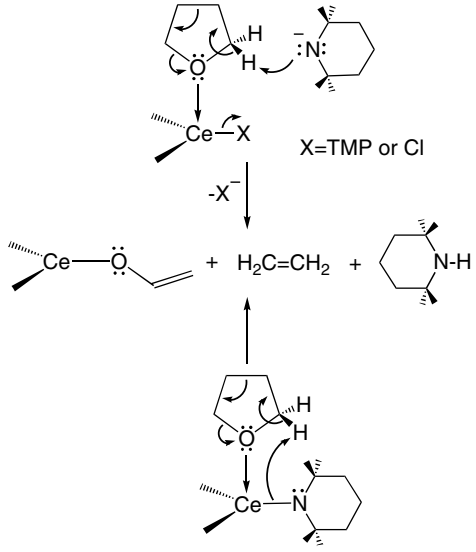

Scheme 1. Possible mechanisms to explain the formation of the alkoxide ligand in $[Ce(\mu\text{-}OCH{=}CH_2)(TMP)_2]_2$ from THF.

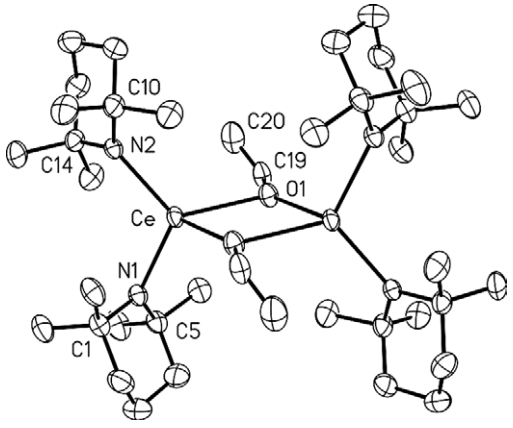

Fig. 1. View of the $[Ce(\mu\text{-}OCH{=}CH_2)(TMP)_2]_2$ molecule showing the atom-numbering scheme. Thermal ellipsoids are 40% equiprobability envelopes, with hydrogen atoms omitted.

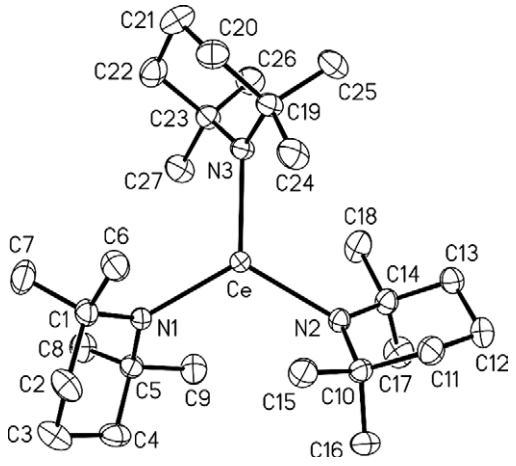

Fig. 2. View of the $Ce(TMP)_3$ molecule showing the atom-numbering scheme. Thermal ellipsoids are 40% equiprobability envelopes, with hydrogen atoms omitted. One position of the disordered Ce atom is shown.

tively). Selected bond distances and angles are presented in Table 1. The $Ce(TMP)_3$ complex is isostructural with $La(TMP)_3$ [12]. Preliminary data indicated that $Ce[N\text{-}t\text{-}Bu(SiMe_3)]_3$ was isostructural with $Sm[N\text{-}t\text{-}Bu(SiMe_3)]_3$ [13]; therefore, a full data collection and refinement were not performed for $Ce[N\text{-}t\text{-}Bu(SiMe_3)]_3$.

The asymmetric unit of $[Ce(\mu\text{-}OCH{=}CH_2)(TMP)_2]_2$ consists of one-half of a dimer situated about an inversion center. The coordination geometry around Ce can be described as trigonal pyramidal with O1′ in the apical position and N1, N2, and O1 defining the trigonal plane (Ce is displaced 0.28 Å from the plane; see Drawing I). The $Ce–O_{bridge}–C$ angles are significantly different (Ce′–O1–C19 = 147.9(2)° versus Ce–O1–C19 = 100.7(2)°). The wide Ce′–O1–C19 angle allows the vinyl group (C19 and C20) to approach Ce trans to the O1′ position, resulting in Ce–C19 and Ce–C20 distances of 3.03 and 3.27 Å, respectively. These distances, along with the distorted Ce coordination geometry, suggest the possibility of a weak vinyl group to cerium donor–acceptor interaction. The Ce–C19 and Ce–C20 distances are long, however, compared to Ce–C bonds such as those in cerium cyclopentadienyl complexes ($Ce–C_{Cp} = 2.74–2.84$ Å) [14,15], and the C19–C20 distance (1.309(6) Å) in $[Ce(\mu\text{-}OCH{=}CH_2)(TMP)_2]_2$ is not lengthened compared to a normal C–C double bond as might be expected if there were an interaction with cerium. Conversely, the Ce–C19 and Ce–C20 distances may be as short as the geometric constraints of the bridging ligand will allow, and the vinyl C–C distance may appear shortened because a libration correction was not applied [16].

Relevant to the question of whether there is an interaction between the Ce and vinyl group are the structures of $[Ce(\mu\text{-}OEt)(TMP)_2]_2$ [9], a molecule that differs only slightly in composition from $[Ce(\mu\text{-}OCH{=}CH_2)(TMP)_2]_2$, and $[Ce(\mu\text{-}OSiPh_3)(OSiPh_3)_2]_2$ (Drawing II) [17]. The complex $[Ce(\mu\text{-}OEt)(TMP)_2]_2$ shows none of the distortions discussed for $[Ce(\mu\text{-}OCH{=}CH_2)(TMP)_2]_2$ (i.e., $[Ce(\mu\text{-}OEt)(TMP)_2]_2$ has a normal edge-shared tetrahedral geometry and the ethyl substituent on oxygen does not approach Ce). By contrast, in $[Ce(\mu\text{-}OSiPh_3)(OSiPh_3)_2]_2$ one of the phenyl substituents on Si bends towards Ce to allow for the interaction of three phenyl carbon atoms with Ce ($Ce–C_{phenyl} = 2.97–3.26$ Å and O1–Si1–C13 = 102°). The apparent interaction between the Ce and the phenyl group results in structural distortions analogous to those discussed for $[Ce(\mu\text{-}OCH{=}CH_2)(TMP)_2]_2$ (e.g., in $[Ce(\mu\text{-}OSiPh_3)(OSiPh_3)_2]_2$ the atoms Ce, O1, O2, and O3 lie in a plane and the Ce–O1–Si angles are significantly different, 110° versus 144°, to accommodate the cerium–phenyl group interaction). In both $[Ce(\mu\text{-}OCH{=}CH_2)(TMP)_2]_2$ and $[Ce(\mu\text{-}OSiPh_3)(OSiPh_3)_2]_2$ there are two short and two long (shown as open rods in I and II) Ce–O bonds, whereas in $[Ce(\mu\text{-}OEt)(TMP)_2]_2$ the ethoxide ligands are symmetrically bonded between the Ce atoms. The asymmetry in Ce–O bond distances in $[Ce(\mu\text{-}OCH{=}CH_2)(TMP)_2]_2$ and $[Ce(\mu\text{-}OSiPh_3)(OSiPh_3)_2]_2$ allow the vinyl and phenyl substituents, respectively, to approach the Ce atom at a more favorable angle. The undistorted structure of $[Ce(\mu\text{-}OEt)(TMP)_2]_2$ and the similar pattern of distortions observed for both $[Ce(\mu\text{-}OSiPh_3)(OSiPh_3)_2]_2$ and $[Ce(\mu\text{-}OCH{=}CH_2)(TMP)_2]_2$ support the notion of a cerium–vinyl interaction in $[Ce(\mu\text{-}OCH{=}CH_2)(TMP)_2]_2$.

Table 1
Selected bond distances (Å) and angles (°) for $[Ce(\mu\text{-}OCH{=}CH_2)(TMP)_2]_2$ and $Ce(TMP)_3$

	$[Ce(\mu\text{-}OCH{=}CH_2)(TMP)_2]_2$	$Ce(TMP)_3$
Ce–N1	2.298(3)	2.332(7)
Ce–N2	2.309(3)	2.346(7)
Ce–N3		2.291(7)
Ce–O1	2.482(2)	
Ce–O1′	2.400(2)	
C19–C20	1.309(6)	
N1–Ce–N2	113.48(9)	119.3(3)
N3–Ce–N1		120.6(3)
N3–Ce–N2		119.3(3)
N1–Ce–O1	122.94(9)	
N1–Ce–O1′	102.79(8)	
N2–Ce–O1	119.36(8)	
N2–Ce–O1′	119.70(8)	
O1–Ce–O1′	68.57(9)	
Ce–O1–Ce′	111.43(9)	
C19–O1–Ce	100.7(2)	
C19–O1–Ce′	147.9(2)	

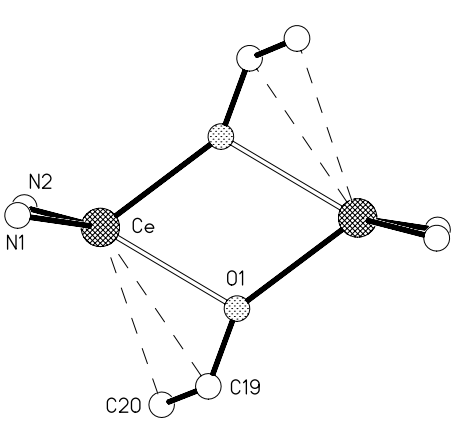

I

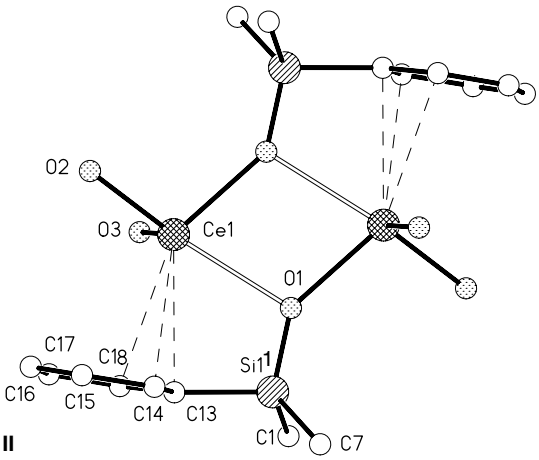

II

The three-coordinate amide complexes $Ce(TMP)_3$, and $Ce[N\text{-}t\text{-}Bu(SiMe_3)]_3$ are trigonal planar, resembling closely the structures of $Ln[N(SiMe_3)_2]_3$ (Ln = Ce, Nd, Eu, Dy, Er, and Yb) [18–22]. The Ce–N distances in $[Ce(\mu\text{-}OCH{=}CH_2)(TMP)_2]_2$ and $Ce(TMP)_3$ range from 2.298(3) to 2.346(7) Å, with the longest distance found in the sterically congested monomer $Ce(TMP)_3$. These Ce–N distances are similar to those found in $[Ce(\mu\text{-}OEt)(TMP)_2]_2$ (average 2.333(2) Å) and $Ce(TMP)_3(THF)$ (average 2.361(2) Å) [9].

3. Summary

The cerium amide complexes $[Ce(\mu\text{-}OCH{=}CH_2)(TMP)_2]_2$, $Ce(TMP)_3$, and $Ce(N\text{-}t\text{-}BuSiMe_3)_3$ were synthesized. The alkoxide ligand in $[Ce(\mu\text{-}OCH{=}CH_2)(TMP)_2]_2$ was derived from the THF solvent used in the synthesis. $Ce(TMP)_3$ could not be separated from $[Ce(\mu\text{-}OCH{=}CH_2)(TMP)_2]_2$. The motivation for this study was the possible use of cerium amide complexes as chemical vapor deposition precursors to cerium oxide films. None of the new compounds were found to be suitable precursors: $Ce(TMP)_3$ was not isolated cleanly, and upon heating, all of the compounds decompose before they are vaporized.

4. Experimental

4.1. Synthesis

4.1.1. General considerations

All manipulations were carried out in a glove box or by using Schlenk techniques. The solvents were purified according to standard methods and stored until needed in the glove box over molecular sieves. The amines were purchased from Aldrich and distilled over CaH_2 before use. $CeCl_3$ was purchased from Strem and used as received. The preparation of $CeCl_3(THF)_2$ was based on the literature method [23]. Midwest Microlab, LLC, Indianapolis, IN USA performed the chemical analyses.

4.1.2. Synthesis of complexes

4.1.2.1. $[Ce(\mu\text{-}OCH{=}CH_2)(TMP)_2]_2$. To a milky white slurry of $CeCl_3$ (0.20 g, 0.76 mmol) in THF (15 mL), LiTMP (0.57 g, 3.9 mmol) was added slowly. The mixture turned yellow immediately after the addition began. After 12 h of stirring, the mixture was dark red. The THF was removed under vacuum to yield a yellow solid. The solid was extracted with hexanes (3×15 mL) and the extracts were filtered over Celite. The yellow filtrates were combined and the solution was concentrated under vacuum to 4 mL. The flask was placed in the freezer (−35 °C). After 16 h, yellow crystalline plates had formed, which were isolated and dried under vacuum (Yield: 0.28 g, 0.30 mmol, 79%). *Anal.* Calc. for $C_{40}H_{78}N_4O_2Ce_2$: C, 51.77; H, 8.48; N, 6.04. Found: C, 51.42; H, 8.34; N, 5.94%. IR (Nujol, NaCl, cm^{-1}): 1591 s, 1396 w, 1356 m, 1336 m, 1307 s, 1284 s, 1228 m, 1191 w, 1170 m, 1120 m, 1070 w, 1043 s, 1002 s, 973 m, 956 w, 935 w, 875 m, 850 s, 825 s.

4.1.2.2. $Ce(TMP)_3$. To a milky white slurry of $CeCl_3$ (0.20 g, 0.8 mmol) in THF (15 mL), LiTMP (0.36 g, 2.4 mmol) was added slowly. The mixture turned yellow immediately after the addition began. After 12 h of stirring, the mixture was dark red. The THF was removed under vacuum to yield an orange-red solid. The solid was extracted with hexanes (3×15 mL), and the extracts were filtered over Celite. The orange filtrates were combined and concentrated under vacuum to 4 mL, and the flask was placed in the freezer (−35 °C). After 16 h, a mixture of crystalline orange-red columns and yellow plates had formed, which were isolated and dried under vacuum (Yield 0.36 g). The orange-red columns and yellow plates were determined to be $Ce(TMP)_3$ and

$[Ce(TMP)_2(\mu\text{-}OCH{=}CH_2)]_2$, respectively, by X-ray crystallographic analysis. A ratio of approximately 3:2, $Ce(TMP)_3$ to $[Ce(TMP)_2(\mu\text{-}OCH{=}CH_2)]_2$, was determined from an examination of the crystalline mixture under a microscope. IR (Nujol, NaCl, cm^{-1}): 1591 s, 1556 w, 1396 m, 1350 s, 1305 s, 1284 s, 1232 s, 1184 s, 1170 s, 1128 s, 1070 m, 1054 s, 1010 s, 974 s, 954 m, 937 m, 908 m, 883 s, 848 s, 825 s.

4.1.2.3. Ce[N-t-Bu(SiMe$_3$)]$_3$. To a solution of $CeCl_3(THF)_2$ (0.30 g, 0.77 mmol) in THF (20 mL), LiN-*t*-Bu($SiMe_3$) (0.36 g, 2.4 mmol) was added slowly. The mixture was stirred for 14 h after the addition was completed. The THF was removed under vacuum from the reaction mixture to yield a yellow solid. The solid was extracted with hexanes (2 × 15 mL), and the extracts were filtered over Celite. The filtrates were combined and concentrated under vacuum to 4 mL, and the flask was placed in the freezer (−35 °C). After 14 h yellow crystalline needles had formed, which were isolated and dried under vacuum (Yield: 0.34 g, 0.59 mmol, 77%). A satisfactory carbon analysis was not obtained despite repeated attempts to do so. The best analysis is reported here. *Anal.* Calc. for $C_{21}H_{54}N_3Si_3Ce$: C, 44.01; H, 9.50; N, 7.33. Found: C, 44.98; H, 9.30; N, 7.29%. IR (Nujol, NaCl, cm^{-1}): 1356 s, 1240 s, 1190 s, 1037 s, 1012 s, 916 m, 890 m, 856 m, 820 m, 759 s, 692 s, 661 m, 646 m, 613 s.

Table 2
Crystal data for $[Ce(\mu\text{-}OCH{=}CH_2)(TMP)_2]_2$ and $Ce(TMP)_3$

Complex	$[Ce(\mu\text{-}OCH{=}CH_2)(TMP)_2]_2$	$Ce(TMP)_3$
Formula	$C_{40}H_{78}N_4O_2Ce_2$	$C_{27}H_{54}N_3Ce$
M	927.30	560.85
Crystal dimensions (mm)	0.30 × 0.15 × 0.05	0.32 × 0.20 × 0.10
Space group (crystal system)	$P2_1/n$ (monoclinic)	$P2_1/n$ (monoclinic)
a (Å)	11.1955(6)	7.7530(4)
b (Å)	17.3392(9)	18.5188(10)
c (Å)	11.5226(6)	20.1527(11)
β (°)	95.394(1)	94.163(1)
U (Å^3)	2226.9(2)	2885.8(3)
T (°C)	−50(2)	−50(2)
Z	2	4
μ (Mo Kα) (mm^{-1})	2.052	1.594
Total number of reflections (unique)	10374(3437)	13973(4689)
R_{int}	0.0439	0.0361
Observed data [$I > 4\sigma(I)$] (number of parameters)	2377(220)	3711(290)
R_1 [$I > 4\sigma(I)$]	0.0196	0.0202
R_1 (all data)	0.0375	0.0277
wR_2 [$I > 4\sigma(I)$]	0.0455	0.0510
wR_2 (all data)	0.0509	0.0540

$R_1 = \sum ||F_o| - |F_c|| / \sum |F_o|; wR_2 = [\sum w(F_o^2 - F_c^2)^2 / \sum w(F_o^2)^2]^{1/2}$.

4.2. X-ray crystallography studies

X-ray crystallographic data were collected for yellow plates of $[Ce(\mu\text{-}OCH{=}CH_2)(TMP)_2]_2$ and orange-red columns of $Ce(TMP)_3$ that were hand picked from a crystalline mixture grown from a cold (−35 °C) hexanes solution. All measurements were made with a Siemens SMART platform diffractometer equipped with a 1 K CCD area detector. Crystal data are presented in Table 2. In $Ce(TMP)_3$, the Ce atom is disordered 50:50 over two positions separated by 0.23 Å along a virtual C_3 axis.

5. Supplementary material

Crystallographic data for $[Ce(\mu\text{-}OCH{=}CH_2)(TMP)_2]_2$ and $Ce(TMP)_3$ have been deposited with the Cambridge Crystallographic Data Center as CCDC-242597 and 242598, respectively. These data can be obtained free of charge by contacting The Cambridge Crystallographic Data Centre, 12 Union Road, Cambridge CB2 1EZ, UK [fax: + 44 1223 336033, e-mail: deposit@ccdc.cam.ac.uk, or www at http://www.ccdc.cam.ac.uk].

Acknowledgement

The Robert A. Welch Foundation supported this research.

References

[1] L.M. Atagi, D.M. Hoffman, J.-R. Liu, Z. Zheng, W.-K. Chu, R.R. Rubiano, R.W. Springer, D.C. Smith, Chem. Mater. 6 (1994) 360.
[2] A. Bastianini, G.A. Battiston, R. Gerbasi, M. Porchia, S. Daolio, J. de Physique IV 5 (1995) C5-525.
[3] T. Tabuchi, Y. Sawado, K. Uematsu, S. Koshiba, Jpn. J. Appl. Phys. 30 (1991) L1974.
[4] S. Suh, L.A. Míinea, D.M. Hoffman, Z. Zhang, W.-K. Chu, J. Mat. Sci. Lett. 20 (2001) 115.
[5] D.C. Bradley, J.S. Ghotra, F.A. Hart, Inorg. Nucl. Chem. Lett. 12 (1976) 735.
[6] W.J. Evans, R. Anwander, J.W. Ziller, Inorg. Chem. 34 (1995) 5927.
[7] H.C. Aspinall, M.R. Tillotson, Polyhedron 13 (1994) 3229.
[8] R.K. Minhas, Y. Ma, J.-I. Song, S. Gambarotta, Inorg. Chem. 35 (1996) 1866.
[9] P.B. Hitchcock, Q.-G. Huang, M.F. Lappert, X.-H. Wei, J. Mater. Chem. 14 (2004) 3266.
[10] W.J. Evans, R. Dominguez, T.P. Hanusa, Organometallics 5 (1986) 1291.
[11] S. Suh, D.M. Hoffman, unpublished results.
[12] B.S. Lim, A. Rahtu, J.-S. Park, R.G. Gordon, Inorg. Chem. 42 (2003) 7951.
[13] S. Suh, D.M. Hoffman, private communication, Cambridge Crystallographic Data Center 262003.
[14] H.J. Heeres, J.H. Teuben, R.D. Rogers, J. Organomet. Chem. 364 (1989) 87.

[15] W.J. Evans, T.J. Deming, J.W. Ziller, Organometallics 8 (1989) 1581.
[16] V. Schomaker, K.N. Trueblood, Acta Cryst. B 24 (1968) 63.
[17] W.J. Evans, R.E. Golden, J.W. Ziller, Inorg. Chem. 30 (1991) 4963.
[18] J.S. Ghotra, M.B. Hursthouse, A.J. Welch, J. Chem. Soc., Chem. Comm. (1973) 669.
[19] R.A. Andersen, D.H. Templeton, A. Zalkin, Inorg. Chem. 17 (1978) 2317.
[20] W.A. Herrmann, R. Anwander, F.C. Munck, W. Scherer, V. Dufaud, N.W. Huber, G.R.J. Artus, Z. Naturforsch., Teil B 49 (1994) 1789.
[21] W.S. Rees Jr., O. Just, D.S. Van Derveer, J. Mater. Chem. 9 (1999) 249.
[22] M. Niemeyer, Z. Anorg. Allg. Chem. 628 (2002) 647.
[23] G.B. Deacon, T. Feng, S. Nickel, B.W. Skelton, A.H. White, J. Chem. Soc., Chem. Comm. (1993) 1328.

Available online at www.sciencedirect.com
SCIENCE DIRECT®
Polyhedron 25 (2006) 211–218
POLYHEDRON
www.elsevier.com/locate/poly

Synthesis and molecular structure of mixed alkyne-cyclopentadienyl clusters via the ionic coupling of $[Os_3(CO)_9(R_2C_2)]^{2-}$ with $[Ru(\eta^5\text{-}C_5H_5)(MeCN)_3]^+$ and the reaction $[Os_3RuH(\eta^5\text{-}C_5H_5)(CO)_{10}(MeCN)]$ with alkynes (R_2C_2) (R = Me, Ph)

Andrew J. Edwards [a], Jack Lewis [a], Chi-Keung Li [a], Catherine A. Morewood [a], Paul R. Raithby [b,*], Gregory P. Shields [a]

[a] *Department of Chemistry, Lensfield Road, Cambridge CB2 1EW, UK*
[b] *Department of Chemsitry, University of Bath, Claverton Down, Bath BA2 7AY, UK*

Received 27 March 2005; accepted 24 June 2005
Available online 10 August 2005

Dedicated to Professor Malcolm Chisholm in recognition of this outstanding contribution to inorganic chemistry.

Abstract

The ionic coupling reaction of the dianion $[Os_3(CO)_9(R_2C_2)]^{2-}$ (R = Me, Ph) with two equivalents of the monocation $[Ru(\eta^5\text{-}C_5H_5)(CH_3CN)_3]^+$ affords the neutral clusters $[Os_3Ru_2(CO)_9(R_2C_2)(\eta^5\text{-}C_5H_5)_2]$ [R = Me, **1** and R = Ph, **2**] in ca. 80% yield. An X-ray crystallographic study of **1** confirms that these clusters exhibit a capped pseudo-octahedral $Os_3Ru_2C_2$ core, with the alkyne bonded parallel to the hinge bond of the capped butterfly metal geometry in a μ_4–η^2 manner, the Ru atoms adopting the wing-tip and capping positions. Reaction of the activated cluster $[Os_3RuH(\eta^5\text{-}C_5H_5)(CO)_{10}(MeCN)]$ (**3**) with RCCR (R = Me, Ph) affords the related clusters $[Os_3RuH(CO)_9(\eta^5\text{-}C_5H_5)(R_2C_2)]$ (R = Me, **4** and R = Ph, **5**) in ca. 35% yield. The reaction with PhCCPh also produces $[Os_3Ru(CO)_8(\eta^5\text{-}C_5H_5)(PhCCPh)(PhCC(H)Ph)]$ (**6**) in ca. 15% yield. An X-ray crystallographic study shows that this cluster has a pseudo-octahedral Os_3RuC_2 core, with the $Ru(\eta^5\text{-}C_5H_5)$ unit adopting the wing-tip position, the alkyne bonded in a μ_4–η^2 arrangement and the ethenyl ligand bridging an Os–Os edge in a μ_2–η^1:η^2 configuration.
© 2005 Elsevier Ltd. All rights reserved.

Keywords: Osmium; Ruthenium; Cluster carbonyl; Alkyne; X-ray crystal structure

1. Introduction

The chemistry of alkyne-substituted metal clusters has developed extensively over the last four decades and remains a central theme of cluster chemistry [1,2]. The earliest studies were concentrated in the area of late transition metal cluster carbonyls, but Chisholm, in an elegant series of studies, has been responsible for extending the chemistry to include earlier transition elements to form polynuclear complexes stabilised by π-donor ligands [3]. Now, for both early and late alkyne-substituted polynuclear metal complexes there is an interest in generating mixed-metal species, and this paper provides an example of the synthesis and characterisation of mixed-osmium and ruthenium alkyne-substituted clusters.

* Corresponding author. Tel.: +44 1225 383183; fax: +44 1225 386231.
E-mail address: p.r.raithby@bath.ac.uk (P.R. Raithby).

0277-5387/$ - see front matter © 2005 Elsevier Ltd. All rights reserved.
doi:10.1016/j.poly.2005.06.030

Studies have shown that osmium and mixed osmium/ruthenium clusters with both arene and alkyne ligands may be synthesised via two principal routes, either ionic coupling of an Os-alkyne cluster dianion with a mononuclear Ru or Os arene cation [4,5] or reaction of an acetonitrile-activated Os arene cluster with an alkyne [5]. The ionic coupling method provides a high-yield route to the sythesis of the butterfly clusters $[Os_3M(C_6H_6)(RCCR')(CO)_9]$ from the dianions $[Os_3(CO)_9(RCCR')]^{2-}$ with $[M(\eta^6\text{-}C_6H_6)(CH_3CN)_3]^{2+}$, where M = Ru or Os, R, R′ = Me or Ph [4,5]. In these clusters, the Os_3MC_2 unit adopts a quasi-octahedral arrangment with a formal valence electron count of 66, and the arene ligand is η^6-coordinated in the wing-tip position. The Os clusters $[Os_4(C_6H_6)(RCCR')(CO)_9]$ (R = R′ = Me; R = Me, R′ = Ph) may also be prepared in lower yield via the reaction of $[Os_4H_2(CO)_9(\eta^6\text{-}C_6H_6)(CH_3CN)]$ with the respective alkyne RCCR′ [5]. However, with Ph_2C_2, the arene ligand is displaced and the major product is the alkyne cluster $[Os_4H_2(CO)_9(PhCCPh)_2]$ [5,6].

Similarly, heating the cyclopentadiene complexes $[PPh_4][MRu_3(CO)_{12}(\eta^5\text{-}C_5H_5)]$ (where M = W or Mo) with the alkynes, MeCCMe or PhCCH, under reflux in THF gave products of the type $[PPh_4][MRu_3(CO)_{10}(\eta^5\text{-}C_5H_5)(RCCR')]$ (where M = W or Mo) in which the MRu_3C_2 unit forms the same quasi-octahedral arrangement [7]. However, in these structures the $M(\eta^5\text{-}C_5H_5)$ unit was found in the hinge position of the butterfly regardless of the alkyne employed. More recently, it has been shown that the mixed-metal cluster $[Os_3Rh(\mu_3\text{-}H)_3(CO)_9(COD)]$ (COD = cycloocta-1,5-diene) reacts with Ph_2C_2 at 60 °C with the loss of the COD ligand and insertion of a diphenylacetylene ligand into an Os–Rh bond to generate the cluster $[Os_3Rh(CO)_{10}(\mu_4\text{–}\eta^2\text{-}Ph_2C_2)(\mu_2\text{–}\eta^1\text{:}\eta^2\text{-}PhCC(H)Ph)]$ [8] with a pseudo-octahedral Os_3RhC_2 core and the Rh atom in the wing-tip position.

We have shown recently that either one or two $Ru(\eta^5\text{-}C_5H_5)$ units may be added to Os cluster anions via ionic coupling with $[Ru(\eta^5\text{-}C_5H_5)(CH_3CN)_3]^+$ [9–13]. In this paper, we extend these studies to include a discussion of the ionic coupling reaction of $[Os_3(CO)_9(RCCR')]^{2-}$ with the monocation $[Ru(\eta^5\text{-}C_5H_5)(CH_3CN)_3]^+$. The reactivity of $[HOs_3Ru(\eta^5\text{-}C_5H_5)(CO)_{10}(MeCN)]$ with alkynes, as an alternative route to mixed alkyne/cyclopentadienyl clusters, is also investigated.

2. Results and discussion

2.1. Reaction of alkyne-substituted triosmium cluster anions with $[Ru(\eta^5\text{-}C_5H_5)(CH_3CN)_3][PF_6]$

The ionic coupling reaction between the dianion $[Os_3(CO)_9(R_2C_2)]^{2-}$ (where R = Me or Ph) and two equivalents of the monocation $[Ru(\eta^5\text{-}C_5H_5)(CH_3CN)_3]^+$ (as its PF_6^- salt) affords the neutral clusters $[Os_3Ru_2(CO)_9(R_2C_2)(\eta^5\text{-}C_5H_5)_2]$ [R = Me, **1** and R = Ph, **2**] in high yield (ca. 80%) upon separation by TLC using dichloromethane/hexane (1:1) as eluent (Scheme 1). Compounds **1** and **2** were characterised initially by spectroscopic methods (Table 1). The IR spectra of **1** and **2** are very similar, indicating that the structures are closely related. The singlets observed in the ^1H NMR spectrum

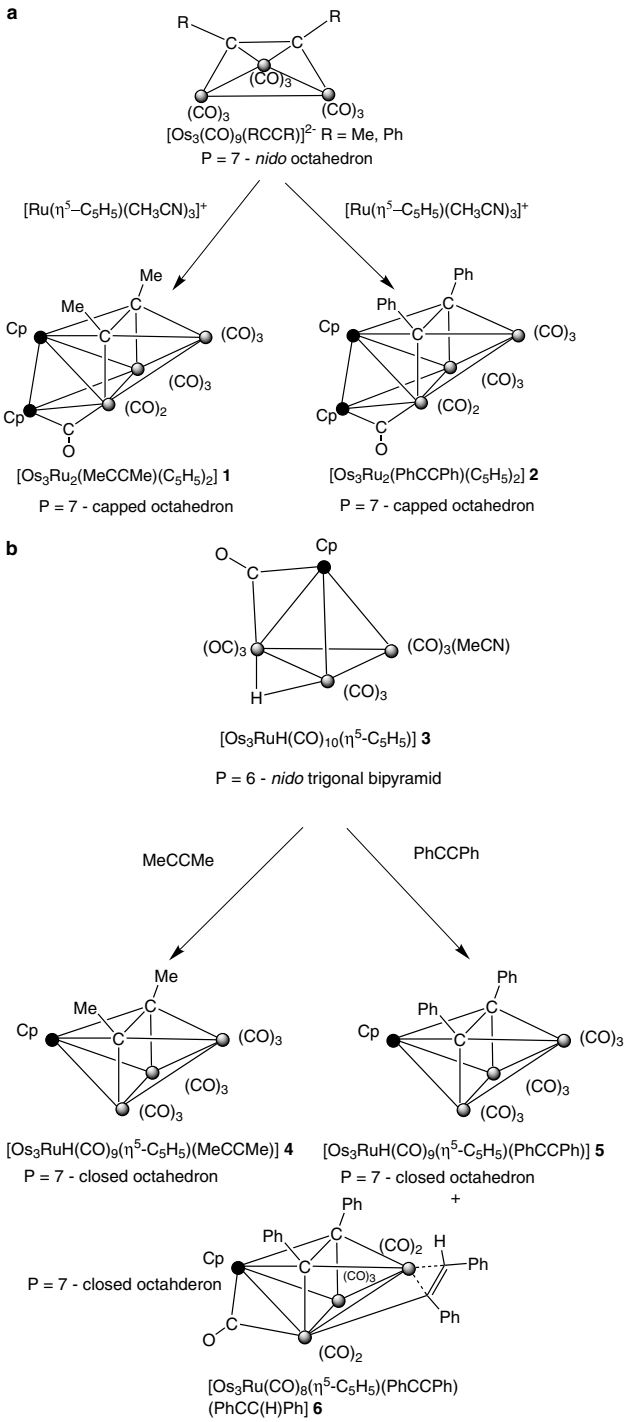

Scheme 1.

Table 1
Spectroscopic data for the new compounds **1–6**

Compound	IR (υ_{CO}/cm^{-1}) (CH_2Cl_2)	^{1}H NMR (δ) ($CDCl_3$)	MS Obs. (Calc. ^{190}Os, ^{101}Ru)
$[Os_3Ru_2(Me_2C_2)(CO)_9(\eta^5\text{-}C_5H_5)_2]$ (**1**)	2063vs, 2016sh, 2006vs, 1988s, 1933m,br	4.87 (s,5H), 4.44 (s,5H), 3.61 (s,6H)	1210 (1208)
$[Os_3Ru_2(Ph_2C_2)(CO)_9(\eta^5\text{-}C_5H_5)_2]$ (**2**)	2066vs, 2019sh, 2009vs, 1996s, 1940m,br	7.12 (m,10H), 4.92 (s,5H), 4.41 (s,5H)	1333 (1332)
$[Os_3RuH(CO)_{10}(\eta^5\text{-}C_5H_5)(MeCN)]$ (**3**)	2071m, 2041s, 1997vs, 1957s,br, 1942s,br		
$[Os_3RuH(Me_2C_2)(CO)_9(\eta^5\text{-}C_5H_5)]$ (**4**)	2079m, 2052m, 2032vs, 2004s, 1966w,br	4.55 (s,5H), 3.39 (s,6H), −22.69 (s)	990 (989)
$[Os_3RuH(Ph_2C_2)(CO)_9(\eta^5\text{-}C_5H_5)]$ (**5**)	2080m, 2055s, 2038vs, 1996s, 1960w,br	7.5 (m,10H), 4.49 (s,5H), −20.33 (s)	1175 (1180)
$[Os_3Ru(CO)_8(Ph_2C_2)(PhCC(H)Ph)(\eta^5\text{-}C_5H_5)]$ (**6**)	2068m, 2046vs, 2013m,sh, 1991vs, 1963m, 1930m, 1606s	7.5 (m,10H), 6.9 (m,10H) 5.05 (s,5H) 4.1 (s, br,1H)	1325 (1322)

of complex **1** at δ 4.87 and 4.44 and of **2** at 4.92 and 4.41 may be assigned to two inequivalent η^5-coordinated cyclopentadienyl ligands. Similar chemical shifts have been observed for the cyclopentadienyl protons in other mixed Ru/Os clusters [9–13]. The singlet peak at δ 3.61 corresponds to the two methyl groups of the acetylene in cluster **1**, similarly the multiplet at δ 7.12 for **2** results from the resonance of the 10 phenyl protons. The molecular ion peak is observed in the mass spectra for both **1** and **2**, and the sequential loss of nine carbonyls is evident.

Slow evaporation from a dichloromethane/hexane solution of **1** gave single crystals suitable for a crystal structure determination (Table 2). The molecular structure is shown in Fig. 1, and relevant bond parameters are listed in Table 3. The metal framework in cluster **1** may be described as being based on a quasi-octahedral $RuOs_3C_2$ unit, the alkyne being σ-bonded to the hinge atoms Os(1) and Os(3) and π-bonded to Ru(1) and Os(2), with the Os_2Ru face capped by a second ruthenium atom Ru(2). A similar capped butterfly arrangement is exhibited by the alkyne cluster $[Ru_5(CO)_{11}(\mu_2\text{-}PPh_2)_2$-(cyclohex-1-yne-4-ene)] [14]. The dihedral angle of the metal butterfly (113°) is comparable to that in $[Os_3Ru$-$(C_6H_6)(MeCCMe)(CO)_9]$ (111°) [4], and the hinge Os(1)–Os(3) edge is longer than the hinge-tip Os(1)–Os(2) and Os(2)–Os(3) edges, as in the benzene cluster.

One of the cyclopentadiene ligands is symmetrically η^5-bound to the ruthenium atom in the ''wing-tip'' position, Ru(1), while the second is η^5-coordinated to the other ruthenium atom which is in the ''capping'' position, Ru(2). There are eight terminal carbonyls, three of which are coordinated to the Os(2) and Os(3) atoms, while two are associated with Os(1). A bridging carbonyl spans the Os(1)–Ru(2) edge, which is significantly shorter [2.634(3) Å] than the corresponding Os(3)–Ru(2) edge [2.877(4) Å]. It is thought that this bridging carbonyl assists the redistribution of electron density to the formally electron-deficient Ru(2) centre.

The structure is related formally to that of the trigonal bi-pyramidal cluster $[Os_3Ru_2(\eta^5\text{-}C_5H_5)(CO)_9(\mu_3$-$CO)_2]$ [10] by the loss of two carbonyl ligands and insertion of the alkyne into a Ru–Os bond. In both $[Os_3$-$Ru_2(\eta^5\text{-}C_5H_5)(CO)_9(\mu_3\text{-}CO)_2]$ [10] and $[Os_6Ru_2$-$(\eta^5\text{-}C_5H_5)(CO)_{15}(\mu_3\text{-}CO)_2(Au_2dppm)_2]$ [11], the μ_3-CO ligands can be rationalised on the basis of both Ru atoms being formally electron-deficient. In cluster **1**, Ru(2) is electron-precise and thus a different arrangement of carbonyl ligands is observed.

In terms of electron counting, an appropriate way to consider alkyne-substituted clusters is to include both the metals and the acetylenic carbons as the ''cluster core''. Using this approach polyhedral skeletal electron pair theory (PSEPT) [15] can be used to rationalise the cluster geometries. The initial cluster dianion $[Os_3(CO)_9$-$(RCCR)]^{2-}$ (R = Me, Ph) has 54 valence electrons and

Table 2
Crystal data for **1** and **6**

Complex	**1**	**6**
Molecular formula	$C_{23}H_{16}O_9Os_3Ru_2$	$C_{41}H_{25}O_8Os_3Ru$
Molecular weight	1209.10	1317.28
Crystal system	orthorhombic	monoclinic
a (Å)	15.500(7)	12.124(2)
b (Å)	15.675(4)	20.427(4)
c (Å)	20.832(6)	15.821(3)
α (°)	90	90
β (°)	90	107.02(3)
γ (°)	90	90
U (Å^3)	5061.4(30)	3746.6(12)
Space group	*Pbca*	$P2_1/n$
Z	8	4
D_{calc} (Mg m^3)	3.173	2.335
Crystal size (mm)	$0.34 \times 0.28 \times 0.18$	$0.30 \times 0.26 \times 0.15$
Crystal habit	black prism	red lamina
$F(000)$	4336	2428
Radiation	Mo Kα	Mo Kα
Wavelength (Å)	0.71073	0.71073
μ (mm^{-1})	16.224	10.590
Transmission	0.026–0.082	0.240–0.766
Temperature (K)	293(2)	293(2)
Diffractometer	Siemens R3mV	Siemens R3mV
Scan type	$\omega/2\theta$	$\omega/2\theta$
Data collection range (°)	$5.20 < 2\theta < 45.08°$	$5.02 < 2\theta < 47.10°$
Index ranges	$0 \leqslant h \leqslant 16$, $0 \leqslant k \leqslant 16$, $0 \leqslant l \leqslant 22$	$-3 \leqslant h \leqslant 13$, $-5 \leqslant k \leqslant 22$, $-17 \leqslant l \leqslant 17$
Reflections measured	3447	5649
Independent reflections (R_{int})	3327 (0.017)	5178 (0.051)
Parameters, restraints	220, 49	273, 0
wR_2 (all data)[a]	0.227	0.156
x, y[a]	0.1063, 0.0	0.0393, 153.29
R_1 [$I > 2\sigma(I)$][a]	0.072	0.066
Observed reflections	1995	3010
Goodness-of-fit on F^2 (all data)[b]	1.089	1.035
Maximum shift/σ	0.004	0.001
Highest residual peak (e Å^{-3})	2.086	2.280

[a] $R_1 = \sum ||F_o| - |F_c|| / \sum |F_o|$, $wR_2 = [\sum w(F_o^2 - F_c^2)^2 / \sum wF_o^4]^{1/2}$, $w = 1/[\sigma^2(F_o)^2 + (xP)^2 + yP]$, $P = (F_o^2 + 2F_c^2)/3$, where x and y are parameters adjusted by the program.
[b] Goodness-of-fit $= [\sum [w(F_o^2 - F_c^2)^2]/(n-p)]^{1/2}$, where n is the number of reflections and p the number of parameters.

7 skeletal electron pairs for Os_3C_2 core bonding that is consistent with the *nido*-octahedral (square-based pyramidal) geometry. Similarly, clusters **1** and **2** have 78 valence electrons and 7 skeletal electron pairs for bonding in the $Os_3Ru_2C_2$ core. Thus, the seven core atoms are held by seven electron pairs consistent with the observed capped octahedral framework geometry.

2.2. Reaction of $Os_3RuH(CO)_{11}(\eta^5\text{-}C_5H_5)$ with alkynes

To activate $[Os_3RuH(CO)_{11}(\eta^5\text{-}C_5H_5)]$ [10] towards nucleophilic substitution, the acetonitrile derivative $[Os_3RuH(CO)_{10}(\eta^5\text{-}C_5H_5)(CH_3CN)]$ (**3**) was prepared by adding one equivalent of Me_3NO to an acetonitrile solution of $[Os_3RuH(CO)_{11}(\eta^5\text{-}C_5H_5)]$ [10]. After stirring for 0.5 h the solution was filtered and taken to dryness. The orange-red product was unstable in oxygen, and was therefore not isolated, but was formulated as the acetonitrile derivative **3** on the basis of IR spectroscopy (Table 1). An excess of the alkynes Me_2C_2 and Ph_2C_2, respectively, were added to a dichloromethane solution of the activated complex and the resultant mixture was stirred at room temperature for 24 h, after which an IR spectrum indicated total consumption of the starting material. Separation by TLC, using a dichloromethane/hexane (1:1) mixture as eluent, gave an orange-brown compound [R = Me, **4**; R = Ph, **5**] in approximately 35% yield for both reactions (Scheme 1). A second orange compound **6** was isolated, in 15% yield, in the Ph_2C_2 reaction. Other trace products in both reactions, could not be characterised because of their low abundance. The three new clusters **4**, **5** and **6** were fully characterised by IR and NMR spectroscopy (Table 1), and the complex **6** was also characterised by X-ray diffraction.

The molecular ion peaks in the mass spectra of **4** and **5** are consistent with the formulation $[Os_3RuH(CO)_9(\eta^5\text{-}C_5H_5)(R_2C_2)]$ (R = Me, **4** or R = Ph, **5**). The ^{1}H NMR spectra of **4** and **5** are similar, with a singlet peak in the region typical for η^5-coordinated cyclopentadiene

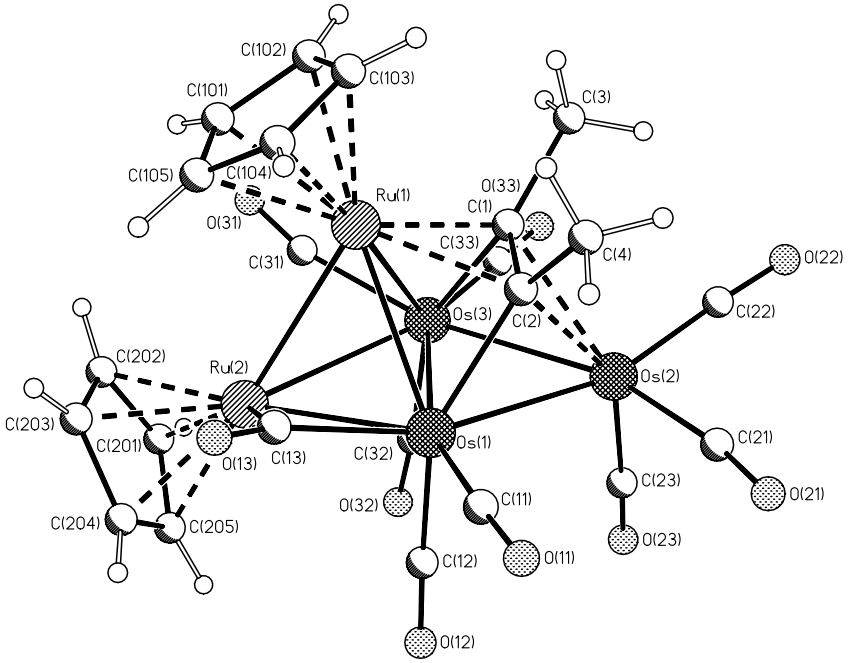

Fig. 1. The molecular structure of $[Os_3Ru_2(Me_2C_2)(CO)_9(\eta^5\text{-}C_5H_5)_2]$ (**1**).

ligands (δ 4.55 and 4.49, respectively) and a high-field hydride resonance (δ −22.69 and −20.33, respectively). In addition, the ^{1}H NMR spectrum of **4** shows a singlet at δ 3.39 for the methyl protons, while that of **5** displays a phenyl multiplet centred at δ 7.5. Although attempts to obtain single crystals of **4** and **5** were unsuccessful this indicates that the alkyne substituents are in chemically equivalent environments, suggesting that the Ru(η^5-C_5H_5) unit occupies the wing-tip position of a quasi-octahedral Os_3RuC_2 structure, as is observed in the solid-state structure of **6** (vide infra). Thus, in the synthesis of **4** and **5**, the CH_3CN and one carbonyl ligand are substituted by the alkyne which inserts into a Ru–Os edge of the tetrahedral metal core of the starting cluster $[Os_3RuH(CO)_{10}(\eta^5\text{-}C_5H_5)(MeCN)]$ (**3**).

This interpretation of the structures of **4** and **5** is consistent with an analysis using PSEPT [15]. From the formulation both clusters have 66 valence electrons, and the observed, closed-octahedral Os_3RuC_2 core is consistent with the presence of seven electron pairs for framework bonding.

The molecular ion peak (1325) in the mass spectrum of compound **6** corresponds to a formulation of $[Os_3RuH(CO)_8(Ph_2C_2)_2(C_5H_5)]$. In the ^{1}H NMR spectrum of **6**, the peak at δ 5.05 gives evidence for the η^5-coordination of the cyclopentadiene group and the phenyl resonances occur in two distinct regions, δ 7.5 and 6.9, which suggests that the two diphenylacetylene ligands are coordinated in different environments. To confirm the molecular structure of **6**, single crystals were grown by slow evaporation from dichloromethane/hexane solution. The molecular structure is presented in Fig. 2 and relevant bond parameters are listed in Table 4. As in the structure of **1**, the Ru and three Os atoms adopt a butterfly framework geometry with the Ru atom occupying the wing-tip position. One diphenylacetylene ligand spans the Os(2)–Os(3) hinge, forming two σ-bonds with the hinge osmium atoms and two π-bonds with the wing-tip atoms to make up a quasi-octahedral Os_3RuC_2 unit. The metal–carbon bond distances within the Os_3RuC_2 core are closely similar to those in **1**. The cluster is formally derived from the tetrahedral structure of $[Os_3RuH(CO)_{11}(\eta^5\text{-}C_5H_5)]$ [10] by insertion of the alkyne into an Ru–Os edge, the cyclopentadiene ligand remaining symmetrically η^5-coordinated to the Ru atom. The second diphenylacetylene has transformed into a 1,2 diphenylethenyl ligand by hydride transfer from the cluster core, and is μ_2–η^1:η^2-coordinated across the Os(1)–Os(3) edge, with the σ bond to Os(3), thus acting as a 3-electron donor. This type of transformation of a diphenylacetylene ligand on osmium and ruthenium hydrido clusters is well established, with similar bond distances in the resulting 1,2-diphenylethenyl unit to those in $[Os_3Ru(\mu\text{-}CO)(CO)_7(\eta^5\text{-}C_5H_5)(PhCCPh)(PhC(H)CPh)]$ (**6**) being found in previous studies [16].

There are seven terminal carbonyl ligands which are pseudo-linearly coordinated, two each to Os(1) and Os(3) and three to Os(2). Os(3) also has a bridging carbonyl ligand associated with it which spans the Os(3)–Ru edge, which is ca. 0.2 Å longer than the unbridged Os(2)–Ru edge. As in cluster **1**, this arrangement allows redistribution of electron density to the otherwise formally electron-deficient Ru(η^5-C_5H_5) unit. The structure

Table 3
Selected bond and angle parameters for $[Os_3Ru_2(Me_2C_2)(CO)_9(\eta^5\text{-}C_5H_5)_2]$ (**1**)

Lengths	(Å)
Os(1)–Ru(1)	2.710(3)
Os(1)–Os(2)	2.713(2)
Os(2)–Os(3)	2.765(2)
Os(3)–Ru(2)	2.877(4)
Ru(1)–Ru(2)	2.831(4)
Os(2)–C(1)	2.36(4)
Os(3)–C(1)	2.17(4)
Ru(1)–C(1)	2.06(4)
Ru(1)–C(2)	2.20(4)
C(1)–C(2)	1.48(5)
C(1)–C(3)	1.63(5)
C(2)–C(4)	1.57(5)
Os(1)–Ru(2)	2.634(3)
Os(1)–Os(3)	2.814(2)
Os(3)–Ru(1)	2.722(4)
Os(1)–C(2)	2.08(4)
Os(2)–C(2)	2.22(4)
Ru(1)–C(101)	2.16(4)
Ru(1)–C(102)	2.15(4)
Ru(1)–C(103)	2.13(4)
Ru(1)–C(104)	2.24(5)
Ru(1)–C(105)	2.18(5)
Ru(2)–C(13)	2.12(4)
Os(1)–C(13)	2.07(4)
Ru(2)–C(201)	2.15(4)
Ru(2)–C(202)	2.15(3)
Ru(2)–C(203)	2.12(4)
Ru(2)–C(204)	2.13(4)
Ru(2)–C(205)	2.14(4)
Angles	**(°)**
O(13)–C(13)–Os(1)	149(3)
O(13)–C(13)–Ru(2)	133(3)
Os(1)–C(13)–Ru(2)	78(2)
C(2)–C(1)–C(3)	128(4)
C(1)–C(2)–C(4)	120(3)

is closely related to that of $[Os_3Rh(\mu\text{-}CO)(CO)_9(PhCCPh)(PhC(H)CPh)]$ [8], in which $Rh(CO)_2$ occupies an equivalent site to the $Ru(\eta^5\text{-}C_5H_5)$ unit in **6** and the remaining ligands adopt essentially the same arrangement. As in the Rh complex, the hinge Os(2)–Os(3) bond is substantially longer than the other Os–Os bonds in **6**, and the alkenyl-bridged Os(1)–Os(3) bond is shorter than the unbridged Os(1)–Os(2) edge.

As with clusters **4** and **5**, cluster **6** has 66 valence electrons and 7 skeletal electron pairs for bonding in the Os_3RuC_2 cluster core. This is consistent with the observed distorted octahedral geometry for the Os_3RuC_2 core.

The minor product $[Os_3Ru(CO)_8(\eta^5\text{-}C_5H_5)(PhCCPh)(PhC(H)CPh)]$ (**6**) is related to the major insertion product $[Os_3RuH(CO)_9(\eta^5\text{-}C_5H_5)(PhCCPh)]$ (**5**) by the substitution of a further CO ligand with diphenylacetylene and hydride transfer to this alkyne. Conversely, it would seem that the dimethylacetylene analogue **4** is not susceptible to further reaction with dimethylacetylene at room temperature.

3. Experimental

All manipulations were performed under an atmosphere of dry, oxygen-free nitrogen using standard Schlenk and vacuum-line techniques, at room temperature, unless otherwise stated. Solvents were distilled over appropriate drying agents, under an inert nitrogen atmosphere, prior to use. Routine separation of products was performed by thin layer chromatography (TLC), using commercially prepared glass plates, precoated to 0.25 mm thickness with Merck Kieselgel 60 F_{254}, as supplied by Merck; or using laboratory prepared glass plates, coated to 1 mm thickness with Merck Kieselgel 60 F_{254}. IR spectra were recorded as solution spectra on a Perkin–Elmer 1710 Fourier Transform infra-red spectrophotometer using 0.5 mm NaCl or CaF_2 cells. NMR spectra were recorded on a Bruker WM250 or WM400 FT-NMR spectrometer. FAB mass spectra were recorded on a Kratos AEI MS 902 instrument.

The reagents $[Ru(C_5H_5)(MeCN)_3][PF_6]$ [16], $[Os_3(CO)_9(R_2C_2)]^{2-}$ (where R = Ph or Me) [4] and $[Os_3RuH(CO)_{11}(\eta^5\text{-}C_5H_5)]$ [10] were prepared and purified according to literature methods. Other chemicals were used as purchased without further purification.

3.1. Preparation of $[Os_3Ru_2(R_2C_2)(CO)_9(\eta^5\text{-}C_5H_5)_2]$ where R = Me 1 or Ph 2

A solution of $[Os_3(CO)_9(R_2C_2)]^{2-}$ [R = Me or Ph] (prepared from 11.5×10^{-5} mol of $[Os_3(CO)_9(R_2C_2)]$ as described previously [4]) in dichloromethane was cooled to −78 °C and 2 molar equivalents of $[Ru(C_5H_5)(CH_3CN)_3][PF_6]_2$ (100 mg, 23.1×10^{-5} mol) were added. The brown solution darkened immediately and was allowed to warm to room temperature, with stirring, over a period of 30 min. After removal of solvent, the solid residue was chromatographed by TLC using 1:1 CH_2Cl_2/hexane as eluent. $[Os_3Ru_2(CO)_9(\eta^5\text{-}C_5H_5)_2(R_2C_2)]$ [R = Me **1** or Ph **2**] was isolated as an orange-brown solid in 82% yield for **1** (109 mg, 9.0×10^{-5} mol) and 80% yield for **2** (117 mg, 8.8×10^{-5} mol). Calc. for $C_{23}H_{16}O_9Os_3Ru_2$ (**1**): C, 26.85; H, 1.32. Found: C, 26.07; H, 1.27%.

3.2. Preparation of $[Os_3RuH(CO)_{10}(\eta^5\text{-}C_5H_5)(CH_3CN)]$ (3)

To an acetonitrile solution (20 ml) of $[Os_3RuH(CO)_{11}(\eta^5\text{-}C_5H_5)]$ (100 mg, 9.6×10^{-5} mol) one equivalent of Me_3NO (8 mg, 10.5×10^{-5} mol) in CH_3CN (5 ml) was added dropwise at room temperature and the mixture stirred for 45 min. The IR spectrum showed complete consumption the starting material and the newly formed species was tentatively formulated as $[Os_3RuH(CO)_{10}(\eta^5\text{-}C_5H_5)(CH_3CN)]$ (**3**). The solvent was

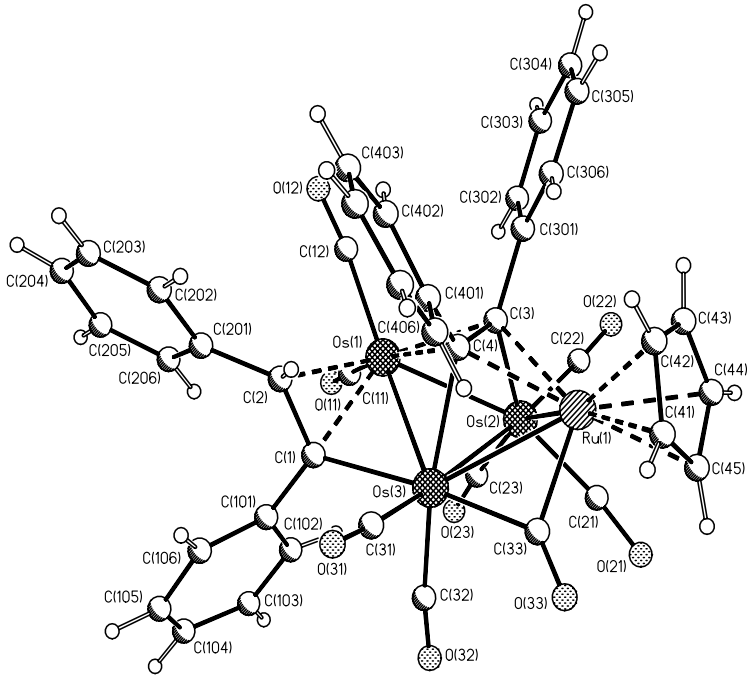

Fig. 2. The molecular structure of $[Os_3Ru(CO)_8(Ph_2C_2)(PhCC(H)Ph)(\eta^5\text{-}C_5H_5)]$ (**6**).

Table 4
Selected bond and angle parameters for $[Os_3Ru(CO)_8(Ph_2C_2)(PhCC(H)Ph)(\eta^5\text{-}C_5H_5)]$ (**6**)

Lengths	(Å)
Os(1)–Os(2)	2.703(2)
Os(2)–Os(3)	2.896(2)
Os(1)–Os(3)	2.686(2)
Os(3)–Ru(1)	2.757(3)
Os(2)–Ru(1)	2.736(2)
Os(1)–C(1)	2.12(3)
Os(1)–C(2)	2.25(3)
Os(1)–C(3)	2.14(3)
Os(1)–C(4)	2.35(3)
Os(2)–C(3)	2.13(2)
Os(3)–C(1)	2.17(3)
Os(3)–C(4)	2.26(3)
Ru(1)–C(3)	2.29(3)
Ru(1)–C(4)	2.21(3)
Os(3)–C(33)	2.07(3)
Ru(1)–C(33)	2.02(3)
Ru(1)–C(41)	2.18(3)
Ru(1)–C(42)	2.21(3)
Ru(1)–C(43)	2.22(3)
Ru(1)–C(44)	2.25(3)
Ru(1)–C(45)	2.17(3)
C(1)–C(2)	1.42(3)
C(3)–C(4)	1.49(4)
Angles	**(°)**
O(33)–C(33)–Os(3)	139(2)
O(33)–C(33)–Ru(1)	137(2)
Ru(1)–C(33)–Os(3)	84.8(10)
C(2)–C(1)–C(101)	122(2)
C(1)–C(2)–C(201)	124(2)
C(4)–C(3)–C(301)	117(2)
C(3)–C(4)–C(401)	132(2)

removed in vacuo and the resulting orange-red solid was used for reactions without further purification.

3.3. Reaction of $[Os_3RuH(CO)_{10}(\eta^5\text{-}C_5H_5)(CH_3CN)]$ (**3**) with Ph_2C_2 and Me_2C_2

Freshly prepared $[Os_3RuH(CO)_{10}(\eta^5\text{-}C_5H_5)(CH_3CN)]$ (**3**) (from 100 mg, 9.6×10^{-5} mol $[Os_3RuH(CO)_{11}(\eta^5\text{-}C_5H_5)]$) was dissolved in CH_2Cl_2 and an excess of R_2C_2 (where R = Me or Ph) was added to the solution and the reaction followed by IR spectroscopy. The reaction mixture was stirred for 24 h at room temperature, the solvent subsequently evaporated and the residue separated by TLC using 1:1 CH_2Cl_2/hexane as eluent. With Me_2C_2, the complex $[Os_3RuH(Me_2C_2)(CO)_9(\eta^5\text{-}C_5H_5)]$ (**4**) was isolated as the major product in 35% yield (35 mg, 3.4×10^{-5} mol). With Ph_2C_2, two complexes $[Os_3RuH(Ph_2C_2)(CO)_9(\eta^5\text{-}C_5H_5)]$ (**5**) (35% yield, 40 mg, 3.4×10^{-5} mol) and $[Os_3Ru(CO)_8(Ph_2C_2)(PhCC(H)Ph)(\eta^5\text{-}C_5H_5)]$ (**6**) (15% yield, 19 mg, 1.4×10^{-5} mol). Calc. for $C_{28}H_{16}O_9Os_3Ru$ (**5**): C, 28.79; H, 1.37. Found: C, 29.32; H, 1.46%. Calc. for $C_{41}H_{26}O_8Os_3Ru$ (**6**): C, 37.36; H, 1.97. Found: C, 36.68; H, 2.45%.

3.4. Crystallography

Poor quality crystals of clusters **1** and **6** were obtained by recrystallisation from dichloromethane/hexane. These crystals were irregular blocks (**1**) and plates (**6**) that precluded face indexing and, therefore, the application of numerical absorption corrections. The materials were

also relatively weakly diffracting. Details of crystal data, data collection and structure refinement are summarised in Table 2. Structures were solved via direct methods [17] and refined by full-matrix least squares on F^2 [18]. Because of the poor quality of the crystals and low resolution of the data only the heavier atoms were refined with anisotropic displacement parameters. Hydrogen atoms were included in geometrically idealised positions.

4. Conclusions

In this paper, we have shown that the coupling reaction between cluster anions and mononuclear metal cations such as the labile, cyclopentadiene-substituted complex $[Ru(\eta^5\text{-}C_5H_5)(CH_3CN)_3]^+$, leading to controlled cluster build up, can be extended to include the alkyne-substituted cluster anion $[Os_3(CO)_9(R_2C_2)]^{2-}$ (R = Me, Ph). The resultant, neutral cluster $[Os_3Ru_2(CO)_9(R_2C_2)(\eta^5\text{-}C_5H_5)_2]$ [R = Me, **1** and R = Ph, **2**] is obtained in high yield as the single product. An alternative approach to the synthesis of mixed alkyne, cyclopentadienyl-substituted clusters has also been exploited in which the alkyne is added directly to a labilised cyclopentidenyl-cluster, such as $[Os_3RuH(\eta^5\text{-}C_5H_5)(CO)_{10}(MeCN)]$, but here the reaction is less controllable, and more than one cluster product is obtained.

5. Supplementary data

Crystallographic data for **1** and **6** have been deposited in CIF format at the Cambridge Crystallographic Data Centre. CCDC 208283–208284 contain the supplementary crystallographic data for this paper. These data can be obtained free of charge via http://www.ccdc.cam.ac.uk/conts/retrieving.html (or from the Cambridge Crystallographic Data Centre, 12, Union Road, Cambridge CB2 1EZ, UK; fax: +44 1223 336 033; or deposit@ccdc.cam.ac.uk).

Acknowledgements

We are grateful for financial support from the Croucher Foundation (C.-K.L.), the Overseas Research Scheme, Cambridge Overseas Trust and ICI plc (C.A.M), EPSRC and the Cambridge Crystallographic Data Centre (G.P.S.), and Johnson Matthey plc for the generous loan of Os and Ru salts.

References

[1] P.R. Raithby, M. Rosales, Adv. Inorg. Radio Chem. 29 (1985) 169.
[2] P. Braunstein, L.A. Oro, P.R. Raithby (Eds.), Metal Clusters in Chemistry, vol. 1, Wiley-VCH, Weinheim, 1999.
[3] (a) M.J. Byrnes, M.H. Chisholm, J. Gallucci, P.J. Wilson, Organometallics 21 (2002) 2240;
(b) M.H. Chisholm, E.R. Davidson, M. Pink, K.B. Quinlan, Chem. Commun. (2002) 2770;
(c) M.H. Chisholm, D.R. Click, J.C. Gallucci, C.M. Hadad, P.J. Wilson, J. Am. Chem. Soc. 124 (2002) 14518;
(d) M.H. Chisholm, E.R. Davidson, K.B. Quinlan, J. Am. Chem. Soc. 124 (2002) 1531;
(e) M.H. Chisholm, D.R. Click, J.C. Gallucci, C.M. Hadad, P.J. Wilson, Organometallics 22 (2003) 4725.
[4] A.T. Brooker, P.A. Jackson, B.F.G. Johnson, J. Lewis, P.R. Raithby, J. Chem. Soc., Dalton Trans. (1991) 707.
[5] H. Chen, B.F.G. Johnson, J. Lewis, Chi-Keung Li, C.A. Morewood, P.R. Raithby, M.C. RamirezdeArellano, W.-T. Wong, Inorg. Chim. Acta 213 (1993) 177.
[6] H. Chen, B.F.G. Johnson, J. Lewis, D. Braga, F. Grepioni, P. Sabatino, J. Organomet. Chem. 405 (1991) C22.
[7] M. Cazanoue, N. Lugan, J.-J. Bonnet, R. Mathieu, Organometallics 7 (1988) 2480.
[8] W.-T. Wong, Organometallics 18 (1999) 3474.
[9] J. Lewis, C.A. Morewood, P.R. Raithby, M.C. Ramirez de Arellano, J. Chem. Soc., Dalton Trans. (1996) 4509.
[10] R. Buntem, J. Lewis, C.A. Morewood, P.R. Raithby, M.C. Ramirez de Arellano, G.P. Shields, J. Chem. Soc., Dalton Trans. (1998) 1091.
[11] Z. Akhter, A.J. Edwards, J.F. Gallagher, J. Lewis, P.R. Raithby, G.P. Shields, J. Organomet. Chem. 596 (2000) 204.
[12] R. Buntem, J.F. Gallagher, J. Lewis, P.R. Raithby, M.-A. Rennie, G.P. Shields, J. Chem. Soc., Dalton Trans. (2000) 4297.
[13] (a) N.L. Cromhout, J.F. Gallagher, J. Lewis, P.R. Raithby, Inorg. Chem. Comm. 2 (1999) 389;
(b) M.R.A. Al-Mandhary, R. Buntem, C. Cathey, J. Lewis, M.C. Ramirez de Arellano, G.P. Shields, C.L. Doherty, P.R. Raithby, Inorg. Chim. Acta 350 (2003) 299;
(c) M.R.A. Al-Mandhary, R. Buntem, C.L. Doherty, A.J. Edwards, J.F. Gallagher, J. Lewis, C.-K. Li, P.R. Raithby, M.C. Ramirez de Arellano, G.P. Shields, J. Cluster. Sci. (in press).
[14] C.J. Adams, M.I. Bruce, B.W. Skelton, A.H. White, J. Organomet. Chem. 430 (1992) 181.
[15] K. Wade, Adv. Inorg. Chem. Radiochem. 18 (1976) 1.
[16] (a) H. Chen, B.F.G. Johnson, J. Lewis, P.R. Raithby, J. Organomet Chem. 376 (1989) C7;
(b) A.D Clauss, M. Tachikawa, J.R. Shapley, C.G. Pierpont, Inorg. Chem. 20 (1991) 1528;
(c) R.D. Adams, G. Chen, Organometallics 10 (1991) 3028;
(d) R.D. Adams, G. Chen, Organometallics 11 (1992) 837;
(e) R.D. Adams, G. Chen, X. Qu, W. Wu, Organometallics 12 (1993) 3426;
(f) J.A. Cabeza, S. Garcia-Granda, A. Llamazares, V. Riera, J.F. van derMaelen, Organometallics 12 (1993) 157;
(g) S.E. Kabir, E. Rosenberg, L. Milone, R. Gobetto, D. Osella, M. Ravera, J. McPhillips, M.W. Day, D. Carlot, S. Hajela, E. Wolf, K. Hardcastle, Organometallics 16 (1997) 2674.
[17] G.M. Sheldrick, SHELXS-86: Program for Crystal Structure Solution, University of Göttingen, 1990.
[18] G.M. Sheldrick, SHELXL-97: Program for Crystal Structure Refinement, University of Göttingen, 1997.

Available online at www.sciencedirect.com
SCIENCE DIRECT®
Polyhedron 25 (2006) 219–223
POLYHEDRON
www.elsevier.com/locate/poly

Trishomobarrelenedicarboxylate dianion as a bridge between dimolybdenum units: Comparison to similar compounds

F. Albert Cotton [a,*], Armin de Meijere [b,*], Carlos A. Murillo [a,*], Karsten Rauch [b], Rongmin Yu [a]

[a] Department of Chemistry and Laboratory for Molecular Structure and Bonding, P.O. Box 30012, Texas A&M University, College Station, TX 77842-3012, USA
[b] Institut für Organische und Biomolekulare Chemie der Georg-August-Universität Göttingen, Tammannstr. 2, 37077 Göttingen, Germany

Received 25 February 2005; accepted 23 May 2005
Available online 11 August 2005

Dedicated to Prof. Malcolm H. Chisholm for his contributions to the chemistry of metal–metal bonded compounds.

Abstract

A new molecular pair composed of two quadruply bonded $Mo_2(DAniF)_3^+$ units (DAniF = (*p*-$MeOC_6H_4$)NC(H)N-(*p*-$MeOC_6H_4$)) linked by a trishomobarrelene-1,5-dicarboxylate dianion has been prepared. This compound, $[Mo_2(DAniF)_3]_2(O_2CC_{11}H_{12}CO_2)$ (**1**), has been characterized by X-ray crystallography and by ^1H NMR and UV–Vis spectroscopy. There is only weak electronic coupling between the two Mo_2 units according to electrochemical measurements. A comparison with other dicarboxylate-linked molecular pairs is presented.
© 2005 Elsevier Ltd. All rights reserved.

Keywords: Quadruple bond; Dimolybdenum compounds; Trishomobarrelene-1,5-dicarboxylate; Electronic coupling

1. Introduction

It has been known that metal–metal bonded Mo_2^{n+} and Rh_2^{4+} units may be linked into pairs, loops, triangles, squares and a few other types of assembly by employing the dianions of dicarboxylic acids [1–3]. Although products containing more than 25 such dianions have already been reported, the work described here was prompted by several questions that were still not fully answered by the earlier work. With regard to compounds of the type $(DAniF)_3Mo_2O_2CXCO_2Mo_2(DAniF)_3$, the use of the bridge with trishomobarrelene as X, namely, the title dianion (Scheme 1) provides a compound in which the bridge has very little flexibility and consists entirely of C–C single bonds. This means that the distance between the Mo_2 units as determined in the crystal structure may be assumed with confidence to pertain to the molecule in solution. Given the "insulating" character of the trishomobarrelene unit and the rather large separation between the two Mo_2 units electronic coupling between these Mo_2 units should be negligible. Therefore, the difference between the potentials for the first and second oxidations should be of essentially electrostatic origin and should be small.

We report here the preparation of $(DAniF)_3Mo_2(O_2CC_{11}H_{12}CO_2)Mo_2(DAniF)_3$ (**1**) where $C_{11}H_{12}$ is the trishomobarrelene diradical. Also reported are the structure of **1** and some of its spectroscopic properties.

* Corresponding authors. Tel.: +1 9798454432; fax: +1 9798459351.
E-mail addresses: cotton@tamu.edu (F.A. Cotton), ameijer1@gwdg.de (A.de Meijere), murillo@tamu.edu (C.A. Murillo).

0277-5387/$ - see front matter © 2005 Elsevier Ltd. All rights reserved.
doi:10.1016/j.poly.2005.05.027

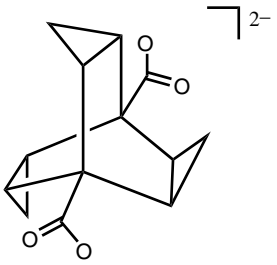

Scheme 1. Trishomobarrelenedicarboxylate dianion.

2. Experimental

2.1. Materials and methods

All manipulations and procedures were conducted under N_2 using either an N_2 drybox or standard Schlenk line techniques. Solvents were distilled and degassed prior to use: MeCN was twice distilled under N_2, first from activated molecular sieves and then from CaH_2. Dichloromethane was dried and distilled from P_2O_5, and ethyl ether was dried and distilled from Na/K-benzophenone. The compound $Mo_2(DAniF)_3Cl_2$ was prepared by the literature method [4]. The salt $(Bu_4N)_2(O_2CC_{11}H_{12}CO_2)$ was prepared and isolated as a colorless solid by neutralizing the corresponding diacid with 2 equiv. of Bu_4NOH. It was then carefully dried in vacuum. All other reagents were purchased from commercial sources and used as received.

Elemental analysis was performed by Canadian Microanalytical Service, Delta, British Columbia. The ^1H NMR spectrum was recorded on a Mercury 300 System NMR spectrometer, with chemical shifts (δ) referenced to CD_2Cl_2. The differential pulse voltammogram and cyclic voltammogram were recorded on a CH Instruments electrochemical analyzer in 0.1 M Bu_4NPF_6 solution (CH_2Cl_2) with Pt working and auxiliary electrodes, an Ag/AgCl reference electrode. The scan rate for the CV was 100 mV/s. The oxidation potentials are referenced to the Ag/AgCl electrode, and under the present experimental conditions, the $E_{1/2}(Fc^+/Fc)$ was measured at 440 mV.

2.2. Preparation of trishomobarrelene-1,5-dicarboxylic acid

This linker was prepared from 1,5-dichlorotrishomobarrelene according to a modified protocol from a previously published one [5]: to a solution of 1,5-dichlorotrishomobarrelene (214 mg, 1 mmol) in anhydrous dichloromethane (2 ml) cooled to −78 °C (dry ice/acetone) was added under an inert atmosphere (N_2) within 10 min a 1 M solution of antimony pentachloride in anhydrous dichloromethane (Aldrich, 4 ml, 4 mmol). After stirring for an additional 1 h at the same temperature, dry carbon monoxide was bubbled through the suspension at −78 °C. The suspension was then transferred under N_2 via a cannula to a cold solution (−78 °C) of sodium methoxide (5 g, 217 mmol) in methanol (65 ml). The mixture was warmed up to ambient temperature, water (20 ml) was added, and the resulting mixture stirred for 6 h at 70 °C. The precipitate was filtered off, the filtrate was extracted with pentane (4 × 40 ml). The aqueous phase was evaporated to dryness, and the residue dissolved in a minimum of water so that the resulting solution was completely clear. Under cooling in an ice-water bath, conc. hydrochloric acid was added to pH 1–2. After extraction with ether (6 × 50 ml) and evaporation to dryness, the residue weighed 164 mg and was crude trishomobarrelenedicarboxylic acid containing a little sodium chloride. Pure diacid was obtained by dissolving the crude material in saturated aqueous sodium hydrogencarbonate (5 ml), extracting the solution with ether (5 ml) and acidifying the aqueous phase with conc. hydrochloric acid under cooling in an ice-water bath to pH 1–2. The resulting colorless precipitate was filtered off and dissolved in ether (150 ml). The ether solution was filtered through a 2 cm pad of Celite, and the Celite was washed with an additional 100 ml of ether. The solvent was evaporated and the crystalline residue dried in vacuum to yield 106 mg (45%) of pure trishomobarrelene-1,5-dicarboxylic acid (m.p. 230 °C, dec). ^1H NMR (600 MHz, [d_6]-DMSO): $\delta = 0.15$ (dt, $^3J = 7.5$ Hz, $^2J = 5.5$ Hz, 3H), 0.78 (dd, $^3J = 7.5$ Hz, $^3J = 4.0$ Hz, 6H), 0.87 (dt, $^2J = 5.5$ Hz, $^3J = 4.0$ Hz, 3H), 12.33 ppm (s, 2H, COOH). ^{13}C NMR (62.9 MHz, [d_6]-DMSO, additional DEPT): $\delta = 0.6$ (−, 3C, CH_2), 12.7 (+, 6C, CH), 38.4 (quat, 2C), 177.8 ppm (quat, 2C, COOH). MS (EI, 70 eV), m/z (5): 234.1 (52) [M^+], 189.1 (46) [$M^+ - COOH$], 171.1 (47), 143.1 (99), 128.1 (100), 115.1 (77), 111.1 (56), 105.1 (29), 91.1 (87), 77.0 (76), 65.0 (38), 51.0 (30), 41.0 (35).

2.3. Preparation of $[Mo_2(DAniF)_3]_2(O_2CC_{11}H_{12}CO_2)$ (1)

A solution of $Mo_2(DAniF)_3Cl_2$ (0.450 g, 0.441 mmol) in 50 ml of MeCN was treated with Zn dust (4.5 g). The resulting suspension was stirred vigorously for 1.5 h. The yellow filtrate was transferred to a flask containing $(Bu_4N)_2(O_2CC_{11}H_{12}CO_2)$ (0.142 g, 0.200 mmol). Within a few minutes of stirring, a yellow precipitate appeared. Stirring was continued for 2 h. The mixture was concentrated to about 5 ml, and 30 ml of methanol was added. The precipitate was isolated by filtration, washed with methanol (2 × 20 ml) and ether (1 × 30 ml), dried in vacuum, and then extracted with 20 ml of dichloromethane. The extract was layered with 40 ml of ether, and allowed to stand undisturbed for two days. A yellow crystalline product was isolated and dried for 24 h in vacuum.

Yield, 210 mg (49%). *Anal.* Calc. for (**1**), $C_{103}H_{102}Mo_4N_{12}O_{16}\cdot 0.5CH_2Cl_2$: C, 56.55; H, 4.73; N, 7.65. Found: C, 56.34; H, 4.85; N, 7.47%. ^{1}H NMR δ (ppm in CD_2Cl_2): 8.509 (s, 2H, –NCHN–), 8.385 (s, 4H, –NCHN–), 6.617 (m, 32H, aromatic), 6.471 (d, 8H, aromatic), 6.254 (d, 8H, aromatic), 3.692 (s, 24H, $-OCH_3$), 3.650(s, 12H, $-OCH_3$), 1.261 (s, 9H,), 0.395 (q, 3H).

2.4. X-ray structure determination

Single crystals suitable for X-ray diffraction analysis were grown by diffusion of ether into a CH_2Cl_2 solution of the compound. The data were collected on a Bruker SMART 100 CCD area detector system. Cell parameters were determined using the program SMART [6]. Data reduction and integration were performed with the software package SAINT [7], while absorption corrections were applied by using the program SADABS [8]. The positions of the Mo atoms were found by direct methods using the program package SHELXTL [9]. Subsequent cycles of least-squares refinement followed by difference Fourier syntheses revealed the positions of the remaining non-hydrogen atoms. Hydrogen atoms were added in idealized positions. Non-hydrogen atoms were refined with anisotropic displacement parameters. All hydrogen atoms were included in the calculation of the structure factors.

The bridging dicarboxylate ligand has two rotational orientations in a ratio of 0.6–0.4 in the crystallographic structure. Some methoxyl groups of DAniF ligands are disordered in two positions. Disorder in the interstitial solvent molecules was also found. Cell parameters and refinement results are summarized in Table 1. Selected bond distances and angles are listed in Table 2.

Table 1
Crystallographic data and refinement for $\mathbf{1}\cdot 2CH_2Cl_2$

Chemical formula	$C_{105}H_{106}Cl_4Mo_4N_{12}O_{16}$
Molecular weight	2317.58
Crystal system	monoclinic
Space group	$P2_1/n$
a (Å)	21.342(1)
b (Å)	19.239(1)
c (Å)	25.513(2)
β (°)	91.764(1)
V (Å^3)	10471(1)
Z	4
$D_{calc.}$ (Mg m^{-3})	1.470
λ (Å)	0.71073
μ (mm^{-1})	0.640
Crystal size (mm)	$0.40\times 0.33\times 0.23$
T (K)	213(2)
R_1, wR_2 [$I>2\sigma(I)$]	0.0545, 0.1234

$R_1=\left[\sum w(F_o-F_c)^2/\sum wF_o^2\right]^{1/2}$, $wR_2=\left[\sum\left[w(F_o^2-F_c^2)^2\right]/\sum w(F_o^2)^2\right]^{1/2}$, $w=1/\left[\sigma^2(F_o^2)+(aP)^2+bP\right]$, where $P=\left[\max(F_o^2,0)+2(F_c^2)\right]/3$.

Table 2
Selected bond distances (Å) and bond angles (°) for $\mathbf{1}\cdot 2CH_2Cl_2$

Mo(1)–Mo(2)	2.0916(7)
Mo(3)–Mo(4)	2.0920(6)
Mo(1)–N(1)	2.158(4)
Mo(1)–N(3)	2.109(4)
Mo(1)–N(5)	2.155(4)
Mo(2)–N(2)	2.132(4)
Mo(2)–N(4)	2.142(5)
Mo(2)–N(6)	2.143(4)
Mo(3)–N(7)	2.172(4)
Mo(3)–N(9)	2.135(4)
Mo(3)–N(11)	2.144(4)
Mo(4)–N(8)	2.130(4)
Mo(4)–N(10)	2.129(4)
Mo(4)–N(12)	2.145(4)
Mo(1)–O(13)	2.153(4)
Mo(2)–O(14)	2.143(4)
Mo(3)–O(15)	2.142(3)
Mo(4)–O(16)	2.147(3)
N(1)–Mo(1)–N(3)	91.1(2)
N(3)–Mo(1)–N(5)	92.7(2)
N(5)–Mo(1)–O(13)	90.2(2)
O(13)–Mo(1)–N(1)	85.7(2)
N(2)–Mo(2)–N(4)	91.4(2)
N(4)–Mo(2)–N(6)	94.2(2)
N(6)–Mo(2)– O(14)	89.5(2)
O(14)–Mo(2)–N(2)	84.5(2)
N(9)–Mo(3)–N(7)	96.7(2)
N(9)–Mo(3)–N(11)	92.1(2)
N(11)–Mo(3)–O(15)	85.1(2)
O(15)–Mo(3)–N(7)	85.7(2)
N(8)–Mo(4)–N(10)	94.4(2)
N(10)–Mo(4)–N(12)	93.4(2)
N(12)–Mo(4)–O(16)	85.3(2)
O(16)–Mo(4)– N(8)	86.4(2)

3. Results

3.1. Structure

The structure of $[Mo_2(DAniF)_3]_2(O_2CC_{11}H_{12}CO_2)$ is presented in Fig. 1, where the formamidinate ligands are shown as N–C–N chains and hydrogen atoms are omitted for clarity. In this compound, two $[Mo_2(DAniF)_3]^+$ units are linked by the trishomobarrelene-1,5-dicarboxylate dianion. The twist angle between Mo_2 axes is 22.8°. The dimensions of the $[Mo_2]$ units retain the characteristics of quadruply bonded dimolybdenum

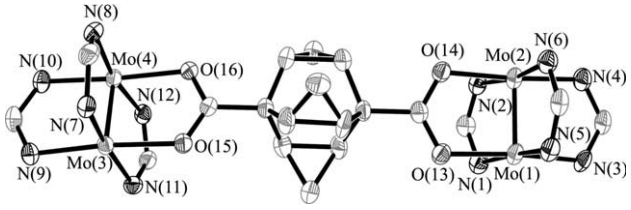

Fig. 1. Core structure of **1** in $\mathbf{1}\cdot 2CH_2Cl_2$ drawn with 50% probability ellipsoids. All *p*-anisyl groups and hydrogen atoms have been omitted for clarity.

compounds. The Mo–Mo distances are 2.0916(7) Å for Mo(1)–Mo(2) and 2.0920(6) Å for Mo(3)–Mo(4). The Mo–O and Mo–N distances fall in narrow ranges, 2.142(3)–2.153(4) Å for Mo–O and 2.109(4)–2.172(4) Å for Mo–N, respectively. The distance between the centers of the two Mo_2 units is 11.06 Å. The structure of the dicarboxylate ligand is first studied here even though the trishomobarrelene core has been known for decades [10]. Within the error limits all structural parameters of this dicarboxylate ligand are in agreement with the ones for the parent hydrocarbon [11]. The single C–C bond distances are close to 1.52 Å. The distances in the cyclopropyl rings do not significantly differ from others. However, the C–C–C angles vary considerably. The bicyclo[2.2.2]octane moiety in the trishomobarrelene-1,5-dicarboxylate ligand is similar to that of the bicyclo[2.2.2]octane-1,4-dicarboxylic acid with bond angles close to 109.5° [12]. In contrast, the angles inside the cyclopropyl groups are very close to 60°. The dihedral angles between the planes of the cyclopropyl groups and the plane defined by the axis of the propeller and two atoms from the cyclopropyl group are in the range of 62.0–66.6°. A more detailed listing of bond angles and distances is available as supplementary material.

3.2. Electrochemistry

The CV and DPV of $[Mo_2(DAniF)_3]_2(O_2CC_{11}H_{12}CO_2)$ in CH_2Cl_2 have the shape and current of a single step charge transfer of 2 electrons. This is not surprising because the coupling capability between the two Mo_2 dimers is weak due to the large distances between them and the properties of the linker. The $\Delta E_{1/2}$ between the two successive one-electron oxidations was calculated to be 66 mV from the differential pulse voltammogram by the method of Richardson and Taube [13].

3.3. Electronic spectrum

The only absorption band observed between 380 and 600 nm was a shoulder on the absorption rising into the shorter wave length region. This had a maximum at 430 ± 10 nm and a molar extinction of about 800 $mol^{-1}\,cm^{-1}$. It is very similar to a band found in $(DAniF)_3Mo_2O_2CCH_3$ [14] at 430 nm and $\varepsilon = 1000$, and assignment to the $\delta \rightarrow \delta^*$ transition is indicated.

4. Discussion

The mere existence of compound **1** is not particularly interesting, but several features of interest arise when it is compared with other compounds of the type $(DAniF)_3Mo_2O_2CXCO_2Mo_2(DAniF)_3$ [15,16]. These features are evident in the data plot of $\Delta E_{1/2}$ versus d (the distance between centers of Mo_2 units) shown in Fig. 2. Points 1–4 shown by circles are for compounds with "insulating" bridges in which the connector X is a rigid unit that does not provide a π-orbital pathway, except point 1 which is for oxalate where there is no X. The lack of a π-orbital pathway is obvious for 3 and 4, but it is also true of 2, which has π electrons but the adjacent double bonds are orthogonal to each other.

We first note that compound **1**, as represented by point 4, provides a significant extension to the line through points 1, 2 and 3. However, Fig. 2 also shows that there is a dearth of data for compounds with "insulating" bridges. There are none for distances between 7 and 9 Å, and none beyond about 11 Å. While there is little likelihood of filling the 7–9 Å gap, one or more compounds in the region beyond 11 Å should be affordable. For example, if the dicarboxylic acid with two trishomobarrelenes instead of only one could be made, a point at about 15 Å would be possible.

Also shown in Fig. 2 are points for compounds in which X is one of five $(CH{=}CH)_n$ ($n = 1$–4) groups as well as C≡C. For details see the figure caption. Apart from some scatter among points 5, 6 and 7, there is a smooth (though not linear) downward trend in $\Delta E_{1/2}$ values. This presumably means that the presence of a π bond, or an extended sequence of conjugated π bonds, allows electronic coupling in addition to electrostatic coupling.

In connection with Fig. 2, it must be noted that regardless of the nature of the coupling mechanism, as $d \rightarrow \infty$, the value of $\Delta E_{1/2}$ should drop to 35.6 mV,

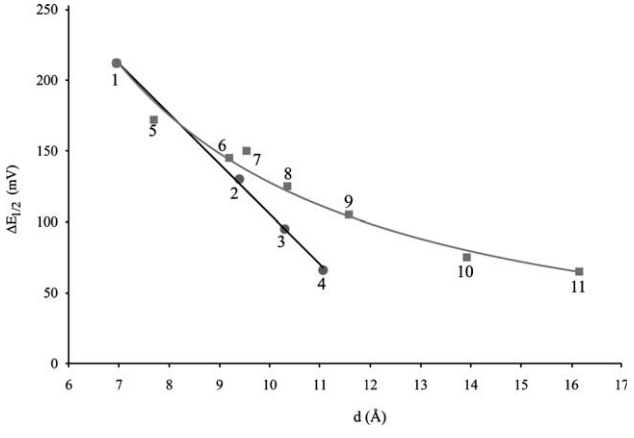

Fig. 2. The $\Delta E_{1/2}$ values for two classes of $(DAniF)_3Mo_2O_2CXCO_2Mo_2(DAniF)_3$ compounds, plotted against the distance between the two Mo_2 units. Points 2–4 are for those in which there is little or no electronic coupling between them. Points 5–11 are for those in which π electrons are present. The X for point 1 is simply the C–C bond. For the others the X groups are as follows: 2 – C=C=C; 3 – C(μ–CH_2)$_3$C; 4 – trishomobarrelene; 5 – *cis*-CH=CH; 6 – *trans*-CH=CH; 7 – C≡C; 8 – *cis*,*cis*-CH=CH–CH=CH; 9 – *trans*,*trans*-CH=CH–CH=CH; 10 – all *trans*-$(CH{=}CH)_3$; 11 – all *trans*-$(CH{=}CH)_4$.

which corresponds to the purely statistical value for K_C (the comproportionation constant) of 4. On this basis, the linear trend in the points for compounds with "insulating" connection cannot continue; instead, the $\Delta E_{1/2}$ values for longer distances (d) must asymptotically approach 35.6 mV. Thus, data for one or two more compounds in the range above $d = 11$ Å would be very desirable.

It is also interesting that the points for the compounds with conjugated polyene connectors appear to approach an asymptote of about 60 mV instead of 35.6 mV. This observation makes it even more interesting to extend the range of d for compounds with "insulating" connectors, and we shall seek to do so. It is known that $\Delta E_{1/2}$ values may have a "significant – and sometimes unpredictable – dependence" on the solvents and counter ions [17].

5. Supplementary material

Crystallographic data (excluding structure factors) have been deposited with the Cambridge Crystallographic Data Center as supplementary publication No. CCDC 259665. These data can be obtained free of charge from The Cambridge Crystallographic Data Centre, 12 Union Road, Cambridge CB2 1EZ, UK, fax: +44 1223 336 033, e-mail: deposit@ccdc.cam.ac.ukvia, www.ccdc.cam.ac.uk/data_request/cif.

Acknowledgments

Support for this work was provided by the Welch Foundation and National Science Foundation at TAMU and the State of Niedersachsen at GAU, Göttingen.

References

[1] F.A. Cotton, C. Lin, C.A. Murillo, Acc. Chem. Res. 34 (2001) 759.
[2] F.A. Cotton, C. Lin, C.A. Murillo, Proc. Natl. Acad. Sci. USA 99 (2002) 4810.
[3] F.A. Cotton, C.A. Murillo, R.A. Walton (Eds.), Multiple Bonds between Metal Atoms, third ed., Springer Science and Media, Inc., New York, 2005.
[4] F.A. Cotton, L.M. Daniels, G.T. Jordan IV, C. Lin, C.A. Murillo, J. Am. Chem. Soc. 120 (1998) 3398.
[5] A. de Meijere, O. Schallner, G.D. Mateescu, P. Gölitz, P. Bischof, Helv. Chim. Acta 68 (1985) 1114.
[6] SMART for Windows NT, Version 5.618, Bruker Advanced X-ray Solutions, Inc., Madison, WI, 2001.
[7] SAINT. Data Reduction Software. Version 6.36A, Bruker Advanced X-ray Solutions, Inc., Madison, WI, 2001.
[8] SADABS. Area Detector Absorption and other Corrections Software, Version 2.05, Bruker Advanced X-ray Solutions, Inc., Madison, WI, 2000.
[9] G.M. Sheldrick, SHELXTL, Version 6.12, Advanced X-ray Solutions, Inc., Madison, WI, 2002.
[10] A. de Meijere, C. Weitemeyer, Angew. Chem., Int. Ed. Engl. 9 (1970) 376.
[11] B. Anderson, O. Schallner, A. de Meijere, J. Am. Chem. Soc. 97 (1975) 3351.
[12] O. Ermer, J.D. Dunitz, J. Chem. Soc., Chem. Commun. (1968) 567.
[13] D.E. Richardson, H. Taube, Inorg. Chem. 20 (1981) 1278.
[14] F.A. Cotton, C.Y. Liu, C.A. Murillo, Inorg. Chem. 43 (2004) 2267.
[15] F.A. Cotton, J.P. Donahue, C. Lin, C.A. Murillo, Inorg. Chem. 40 (2001) 1234.
[16] F.A. Cotton, J.P. Donahue, C.A. Murillo, J. Am. Chem. Soc. 125 (2003) 5436.
[17] D.M. D'Alessandro, F.R. Keene, Dalton Trans. (2004) 3950.

Available online at www.sciencedirect.com
SCIENCE DIRECT®
Polyhedron 25 (2006) 224–234
POLYHEDRON
www.elsevier.com/locate/poly

Complexes of the heavier alkaline earth metals containing β-diketiminato and iodide ligand sets

Hani M. El-Kaderi, Mary Jane Heeg, Charles H. Winter *

Department of Chemistry, Wayne State University, 5101 Cass Avenue, Detroit, MI 48202, USA

Received 5 April 2005; accepted 30 June 2005
Available online 11 August 2005

Abstract

Treatment of $[(2,6\text{-}i\mathrm{Pr}_2\mathrm{C}_6\mathrm{H}_3)\mathrm{NC}(t\mathrm{Bu})\mathrm{CH}_2\mathrm{C}(t\mathrm{Bu})\mathrm{N}(2,6\text{-}i\mathrm{Pr}_2\mathrm{C}_6\mathrm{H}_3)](\mathrm{L}^{\mathrm{Ar}'}\mathrm{H})$ with potassium hydride in tetrahydrofuran afforded $\mathrm{K}(\eta^1\text{-}\mathrm{L}^{\mathrm{Ar}'})(\mathrm{THF})_3$ (89%) as a yellow crystalline solid after workup. The crystal structure of $\mathrm{K}(\eta^1\text{-}\mathrm{L}^{\mathrm{Ar}'})(\mathrm{THF})_3$ revealed an open monomeric molecule in which the potassium ion is bonded to three tetrahydrofuran ligands and one η^1-β-diketiminato ligand through one of the nitrogen atoms. Treatment of $\mathrm{K}(\eta^1\text{-}\mathrm{L}^{\mathrm{Ar}'})(\mathrm{THF})_3$ with equimolar amounts of MI_2 (M = Ca, Ba) afforded $[\mathrm{Ca}(\eta^5\text{-}\mathrm{L}^{\mathrm{Ar}'})(\mu\text{-I})(\mathrm{THF})]_2$ (62%) and $[\mathrm{Ba}(\eta^2\text{-}\mathrm{L}^{\mathrm{Ar}'})(\mu\text{-I})]_2$ (27%) as yellow crystalline solids. Treatment of $\mathrm{M}(\eta^5\text{-}\mathrm{L}^{t\mathrm{Bu}})_2$ (M = Ca, Sr, Ba, $\mathrm{L}^{t\mathrm{Bu}} = t\mathrm{BuNC}(\mathrm{CH}_3)\mathrm{CHC}(\mathrm{CH}_3)\mathrm{N}t\mathrm{Bu}^-$) with the corresponding metal iodide in tetrahydrofuran afforded $[\mathrm{Ca}(\eta^5\text{-}\mathrm{L}^{t\mathrm{Bu}})(\mu\text{-I})(\mathrm{THF})]_2$ (68%), $[\mathrm{Sr}(\eta^5\text{-}\mathrm{L}^{t\mathrm{Bu}})(\mu\text{-I})(\mathrm{THF})]_2$ (53%), and $[(\eta^5\text{-}\mathrm{L}^{t\mathrm{Bu}})\mathrm{Ba}(\mu\text{-I})(\mu\text{-}\eta^2\text{:}\eta^5\text{-}\mathrm{L}^{t\mathrm{Bu}})\mathrm{Ba}(\eta^5\text{-}\mathrm{L}^{t\mathrm{Bu}})]_2$(24%). Structural assignments for these complexes were based on spectral and analytical data as well as X-ray crystallography. $[\mathrm{Ca}(\eta^5\text{-}\mathrm{L}^{t\mathrm{Bu}})(\mu\text{-I})(\mathrm{THF})]_2$ and $[\mathrm{Sr}(\eta^5\text{-}\mathrm{L}^{t\mathrm{Bu}})(\mu\text{-I})(\mathrm{THF})]_2$ are dimers that are held together by bridging iodide ligands, while $[\mathrm{Ba}(\eta^5\text{-}\mathrm{L}^{t\mathrm{Bu}})(\mu\text{-I})(\mu\text{-}\eta^2\text{:}\eta^5\text{-}\mathrm{L}^{t\mathrm{Bu}})\mathrm{Ba}(\eta^5\text{-}\mathrm{L}^{t\mathrm{Bu}})]_2$ is a tetramer containing two symmetrical dimeric units that are linked by two bridging iodide ligands. In benzene-d_6 solution, $[\mathrm{Ca}(\eta^5\text{-}\mathrm{L}^{\mathrm{Ar}'})(\mu\text{-I})(\mathrm{THF})]_2$ and $[\mathrm{Ba}(\eta^2\text{-}\mathrm{L}^{\mathrm{Ar}'})(\mu\text{-I})]_2$ are stable toward ligand redistribution. $[\mathrm{Ca}(\eta^5\text{-}\mathrm{L}^{t\mathrm{Bu}})(\mu\text{-I})(\mathrm{THF})]_2$ exists as mixtures of three species in toluene-d_8, but the mixed ligand complex is strongly favored under the conditions studied. At 31.3 °C, the equilibrium constant for ligand redistribution of $[\mathrm{Sr}(\eta^5\text{-}\mathrm{L}^{t\mathrm{Bu}})(\mu\text{-I})(\mathrm{THF})]_2$ to $\mathrm{Sr}(\eta^5\text{-}\mathrm{L}^{t\mathrm{Bu}})_2$ and $\mathrm{SrI}_2(\mathrm{THF})_2$ in toluene-d_8 was 5.3×10^{-5} M.
© 2005 Elsevier Ltd. All rights reserved.

Keywords: N-ligands; Group 2 elements; Calcium; Strontium; Barium

1. Introduction

Recent efforts in the coordination chemistry of calcium, strontium, and barium have been driven by applications in film growth by chemical vapor deposition (CVD) and related techniques [1], as well as organic synthesis and polymerization catalysis [2–4]. In polymerization reactions, unsymmetrical LMX complexes are the desired precatalysts, since X^- possesses the needed nucleophilic properties to initiate catalysis and the steric properties of L can be designed to promote stereoselectivity in the growing polymer [2–4]. As part of the development of group 2-based polymerization catalysis, there is a growing need to understand the redistribution equilibria of LMX, since ML_2 is unlikely to initiate catalysis efficiently and MX_2 may not promote stereoselective polymerization. Most calcium, strontium, and barium complexes containing mixed ligand sets are of the formula $[\mathrm{M}(\mathrm{C}_5\mathrm{R}_5)(\mathrm{X})(\mathrm{L})_n]_y$, where $\mathrm{C}_5\mathrm{R}_5$ is a bulky substituted cyclopentadienyl ligand, X is a halide ligand, and L is a neutral oxygen donor ligand [5–10]. Bulky cyclopentadienyl ligands appear to stabilize these mixed ligand complexes toward ligand redistribution through steric inhibition of dimerization

* Corresponding author. Tel.: +1 313 577 5224; fax: +1 313 577 8289.
E-mail address: chw@chem.wayne.edu (C.H. Winter).

0277-5387/$ - see front matter © 2005 Elsevier Ltd. All rights reserved.
doi:10.1016/j.poly.2005.06.042

[11]. Strongly coordinating oxygen ligands such as tetrahydrofuran also contribute to the stability of the mixed ligand complexes toward ligand redistribution [11a]. However, complexes of the formula $[M(C_5R_5)(X)(L)_n]_y$ are difficult to handle in aromatic solvents in the absence of coordinating ligands, due to the appearance of facile redistribution equilibria (e.g., $2M(C_5R_5)(X) \leftrightarrow M(C_5R_5)_2 + MX_2$) [10,11a]. Furthermore, replacement of the halide ligand in $[M(C_5R_5)(X)(L)_n]_y$ by salt metathesis routes can be problematic. For example, treatment of $MN(SiMe_3)_2$ (M = Li, Na, K) with $(C_5H_2(SiMe_3)_3)$-CaI(THF) resulted in the formation of $M(C_5H_2$-$(SiMe_3)_3)$ and $Ca(N(SiMe_3)_2)(I)(THF)_n$ [6].

Recently we [12] and others [3,4] have been exploring the use of β-diketiminato ligands as ancillary ligands for the stabilization of the heavier group 2 metal complexes. The β-diketiminato ligand is isoelectronic with cyclopentadienyl and β-diketonato ligands, and its steric profile is easily adjusted at both the core nitrogen and carbon atoms [13]. Such steric manipulations can have a profound effect on the bonding modes of the β-diketiminato ligands, especially with barium [12b,14,15]. For example, the complex $Ba_2(L^{Cy})_3(N(SiMe_3)_2)$ ($L^{Cy} = C_6H_{11}NC(CH_3)CHC(CH_3)N(C_6H_{11})^-$) contains η^5-, μ-η^2:η^5-, and μ-η^2:η^3-β-diketiminato ligands [14], $Ba_2(L^{iPr})_4$ ($L^{iPr} = i$PrNC(CH$_3$)CHC(CH$_3$)NiPr$^-$) features η^5-, μ-η^5:η^5-, and μ-η^1:η^1-β-diketiminato ligands [12b], and $Ba(L^{Ar})_2$ ($L^{Ar} = (2,6\text{-}i\text{Pr}_2C_6H_3)NC(CH_3)$-$CHC(CH_3)N(2,6\text{-}i\text{Pr}_2C_6H_3)^-$) possesses η^2-β-diketiminato ligands [15]. We have recently reported that homoleptic calcium, strontium, and barium complexes containing η^5-β-diketiminato ligands have many similarities to the analogous metallocenes [12b]. In view of the increasing importance of mixed ligand group 2 complexes in polymerization reactions [3,4], we set out to explore the synthesis and ligand redistribution reactions of calcium, strontium, and barium complexes that contain both halide and β-diketiminato ligands. Herein, we describe the synthesis, structure, and properties of a series of calcium, strontium, and barium complexes that contain $L^{Ar'}$ ($L^{Ar'} = (2,6\text{-}i\text{Pr}_2C_6H_3)$-$NC(C(CH_3)_3)CHC(C(CH_3)_3)N(2,6\text{-}i\text{Pr}_2C_6H_3)^-$) or L^{tBu} ($L^{tBu} = t$BuNC(CH$_3$)CH-C(CH$_3$)NtBu$^-$) and iodide ligand sets. Depending on the nature of the β-diketiminato ligand nitrogen atom substituents and the group 2 ion, iodide-bridged tetrahydrofuran-coordinated dimers, iodide-bridged solvent-free dimers, and a unique tetramer are obtained. In addition, the tendency of these complexes to undergo redistribution reactions in solution is described. $[Ca(\eta^5\text{-}L^{Ar'})(\mu\text{-}I)(THF)]_2$ and $[Ba(\eta^2\text{-}L^{Ar'})(\mu\text{-}I)]_2$ show no evidence for redistribution equilibria in benzene, while $[Ca(\eta^5\text{-}L^{tBu})(\mu\text{-}I)(THF)]_2$ and $[Sr(\eta^5\text{-}L^{tBu})(\mu\text{-}I)(THF)]_2$ exist as equilibrium mixtures of two or more species. Estimated equilibrium constants, however, suggest that the mixed ligand species are strongly favored at ambient temperature.

2. Results

2.1. Synthetic aspects

Treatment of $L^{Ar'}H$ with KH (1 equiv.) in tetrahydrofuran afforded $K(\eta^1\text{-}L^{Ar'})(THF)_3$ (**1**, 89%) as a yellow crystalline solid after workup (Eq. (1)). Complex **1** is soluble in toluene, easily crystallized, can be stored for several months under argon without decomposition, and is thus a very useful reagent. Treatment of **1** with MI_2 (M = Ca, Ba) (1 equiv.) in anhydrous tetrahydrofuran afforded $[Ca(\eta^5\text{-}L^{Ar'})(\mu\text{-}I)(THF)]_2$ (**2**, 62%), and $[Ba(\eta^2\text{-}L^{Ar'})(\mu\text{-}I)]_2$ (**3**, 27%) as yellow crystalline solids after workup (Eq. (1)). The structural assignments for **1**–**3** were based upon spectral and analytical data as well as X-ray structure determinations. In the solid state, **1** exists as a monomeric molecule in which the β-diketiminato ligand is bonded to the potassium center through one nitrogen atom with an η^1-coordination mode. The potassium ion is also coordinated to three tetrahydrofuran ligands. The structural determination for **1** was of low precision, and is not discussed further herein. The solid state structures of **2** and **3** revealed dimeric molecules that are held together by bridging iodide ligands. Further details of the ligand bonding modes are described below. Several attempts were made to prepare the analogous strontium complex, however, this complex did not crystallize well and was very difficult to isolate in a pure state in good yields. In one case, a few crystals of the strontium complex were obtained, and analysis of the diffraction data revealed a molecular structure similar to that of **3**.

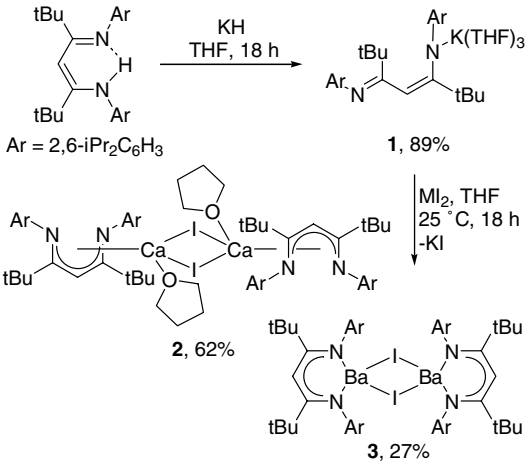

(1)

The ^{1}H NMR spectrum of **1** in toluene-d_8 at 25 °C showed one type of 2,6-diisopropylphenyl group, one type of *tert*-butyl group, and one type of tetrahydrofuran ligand. The β-C*H* resonance of the β-diketiminato ligand appeared as a singlet at δ 4.89. These resonances are inconsistent with the solid state structure, where the potassium ion is coordinated to only one of the

nitrogen atoms. It is very likely that the potassium ion exchanges with the two nitrogen atoms very rapidly on the NMR timescale, and thus an averaged spectrum is obtained. Alternatively, both nitrogen atoms could be coordinated to the potassium ion in solution, thus affording a species with a plane of symmetry. There were two doublets for the isopropyl methyl groups (δ 0.96, 1.33), and one septet for the isopropyl methine groups at δ 3.27. The observation of only one methine septet demonstrates that the isopropyl methyl groups are diastereotopic. There were no major changes in the ^{1}H NMR spectra of **1** between −60 and +80 °C. The lability of the tetrahydrofuran ligands in **1** was probed by drying a sample for 18 h at 0.1 Torr in a drying tube heated with refluxing acetone (56 °C). A ^{1}H NMR spectrum of the dried material showed free $L^{Ar'}H$ and unidentified resonances, demonstrating facile loss of tetrahydrofuran and concomitant decomposition.

The ^{1}H NMR spectrum of **2** in benzene-d_6 at 25 °C showed a single species, with the β-diketiminato ligand β-C*H* resonance at δ 5.52, isopropyl methyl resonances at δ 1.34 and 1.17, and a *tert*-butyl resonance at δ 1.24. The isopropyl methine resonance ($\sim\delta$ 3.2) overlapped with the α-CH_2 resonance of the tetrahydrofuran ligand. The ^{1}H NMR spectrum of **2** at 75 °C was very similar, except for small chemical shift changes.

The ^{1}H NMR spectrum of **3** in benzene-d_6 at 25 °C shows a single species. The β-diketiminato ligand β-C*H* proton resonance appeared at δ 5.24, which is δ 0.28 upfield of the same resonance in **2**. The difference in the positions of this resonance for **2** and **3** may be related to the η^5-β-diketiminato coordination mode in **2** and the η^2-β-diketiminato coordination mode in **3**. The isopropyl methyl group resonances appeared at δ 1.24 and 1.21, while the isopropyl methine resonance was observed at δ 2.99. The latter resonance is upfield compared to that of **2** (δ 3.27). The *tert*-butyl protons resonated at δ 1.19.

The synthesis of mixed ligand complexes containing L^{tBu} proceeded by a different route than was used for **2** and **3**. Treatment of M(η^5-L^{tBu})$_2$ (M = Ca, Sr, Ba) [12b] and MI_2 in refluxing tetrahydrofuran as indicated in Eq. (2) afforded [Ca(η^5-L^{tBu})(μ-I)(THF)]$_2$ (**4**, 68%), [Sr(η^5-L^{tBu})(μ-I)(THF)]$_2$ (**5**, 53%), and [Ba(η^5-L^{tBu})-(μ-I)(μ-η^2:η^5-L^{tBu})Ba(η^5-L^{tBu})]$_2$ (**6**, 24%) as colorless (**4**, **5**) or yellow crystals (**6**) after workup. The structural assignments for **4**–**6** were based upon spectral and analytical data, as well as X-ray structure determinations as described below. In the solid state, **4** and **5** exist as iodide-bridged dimers with molecular structures analogous to that of **2**. In contrast to **2**–**5**, the molecule of **6** is a tetramer which consists of two dimeric units that are bridged by two iodide ligands. Further details of the ligand bonding modes are described below.

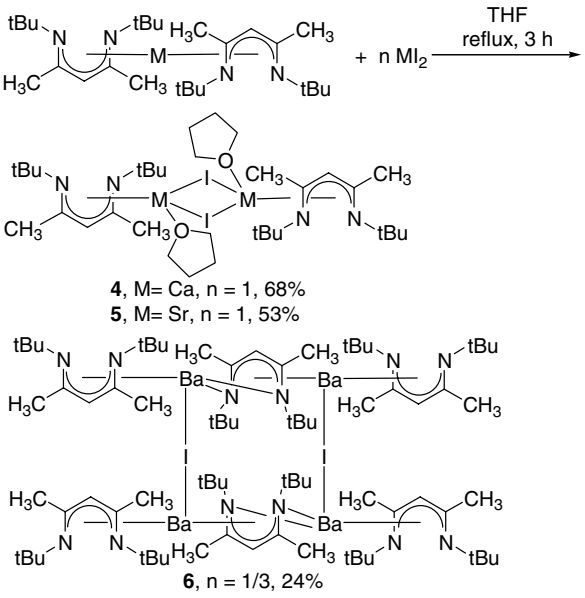

(2)

The ^{1}H NMR spectrum of **4** in toluene-d_8 at 25 °C showed three β-diketiminato ligand β-C*H* resonances at δ 4.45, 4.30, and 4.21 in a 26:61:13 ratio. The resonance at δ 4.21 corresponds exactly to the resonance for Ca(η^5-L^{tBu})$_2$ [12b]. Presumably, one of the other two resonances corresponds to **4**. However, the presence of three β-diketiminato ligand β-C*H* resonances suggests that **4** is engaged in multiple equilibria in solution. Unlike **4**, the ^{1}H NMR spectrum of **5** in toluene-d_8 at 25 °C showed two β-diketiminato ligand β-C*H* resonances at δ 4.34 and 4.21 in a 94:6 ratio. The resonance at δ 4.21 corresponds exactly to the resonance for Sr(η^5-L^{tBu})$_2$ [12b]. The observation of a major species with resonances consistent with **5**, along with Sr(η^5-L^{tBu})$_2$, suggests the equilibrium process that is outlined in Eq. (3). The ^{1}H NMR spectra of **5** were recorded between 30 and 85 °C in toluene-d_8 to assess how the equilibrium was affected by temperature. Above 60 °C, the resonances for Sr(η^5-L^{tBu})$_2$ disappeared, and only one species was observed. Cooling the sample of **5** to −50 °C did not change the ratio of the major species to Sr(η^5-L^{tBu})$_2$, within experimental error. Due to the small amount of Sr(η^5-L^{tBu})$_2$ and the inherent errors associated with measuring the concentrations by integration, we did not carry out a van't Hoff analysis to obtain the equilibrium thermodynamic parameters. However, at 31.4 °C, K_{eq} was calculated to be 5.3×10^{-5} M for a 0.0134 M solution of **5** in toluene-d_8. Thus, the equilibrium strongly favors the mixed ligand species **5** at all of the temperatures that we examined. We note that the assignment of $SrI_2(THF)_2$ is uncertain, and is offered for convenience to allow correct stoichiometry. $SrI_2(THF)_5$ has been crystallographically characterized,

but rapidly loses tetrahydrofuran in the solid state [16]. The number of coordinated tetrahydrofuran ligands in solution is thus unclear.

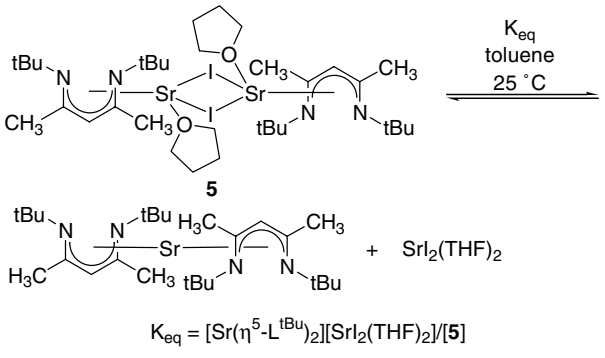

(3)

The ^{1}H NMR spectrum of **6** in toluene-d_8 at 25 °C consisted of very broad singlets centered at δ 4.26, 2.07, and 1.39 for the β-diketiminato ligand β-C*H*, backbone methyl, and *tert*-butyl resonances, respectively. Further studies were hampered by the low solubility of **6** in toluene. The broad resonances suggest that the β-diketiminato ligands undergo site exchange in solution.

2.2. Structural aspects

The X-ray crystal structures of **2**–**6** were determined to establish the geometries about the metal centers and the bonding modes of the β-diketiminato ligands. Experimental crystallographic data are summarized in Table 1, selected bond lengths and angles are given in Tables 2–6, and perspective views are presented in Figs. 1–5.

Table 2
Selected bond lengths (Å) and bond angles (°) for **2**[a]

Ca–I(1)	3.210(1)
Ca–I(1)′	3.273(1)
Ca(1)–N(1)	2.416(2)
Ca(1)–N(2)	2.386(2)
Ca(1)–O(1)	2.407(2)
Ca–C(13)	2.955(3)
Ca–C(14)	2.748(3)
Ca–C(15)	2.723(3)
N(1)–C(13)	1.297(3)
N(2)–C(15)	1.351(3)
C(13)–C(14)	1.453(4)
C(14)–C(15)	1.399(4)
Ca–I(1)–Ca′	104.62(1)
N(1)–Ca–N(2)	79.16(7)
C(13)–C(14)–C(15)	130.9(2)

[a] Primes indicate symmetry equivalent positions.

Table 3
Selected bond lengths (Å) and bond angles (°) for **3**[a]

Ba–I(2)	3.362(2)
Ba–I(2)′	3.523(2)
Ba–N(1)	2.680(7)
Ba–N(2)	2.695(7)
Ba–C(4)	3.029(8)
Ba–C(5)	3.656(8)
Ba–C(9)	3.367(8)
Ba–C(24)	2.940(8)
Ba–C(25)	3.436(8)
Ba–C(29)	3.311(8)
N(1)–C(1)	1.339(10)
N(2)–C(3)	1.332(10)
C(1)–C(2)	1.404(12)
C(2)–C(3)	1.398(12)
N(2)–Ba–N(1)	66.0(2)
I(2)–Ba–I(2)′	81.97(3)
C(1)–C(2)–C(3)	131.6(8)

[a] Primes indicate symmetry equivalent positions.

Table 1
Crystal data and data collection parameters for **2**–**6**

	2	**3**	**4**	**5**	**6**
Formula	$C_{84}H_{136}Ca_2I_2N_4O_2$	$C_{70}H_{106}Ba_2I_2N_4$	$C_{34}H_{66}Ca_2I_2N_4O_2$	$C_{34}H_{66}Sr_2I_2N_4O_2$	$C_{78}H_{150}Ba_4I_2N_{12}$
F_W	1567.93	1532.07	896.87	991.95	2059.26
Space group	$P\bar{1}$	$P\bar{1}$	C_2/c	C_2/c	$P\bar{1}$
a (Å)	10.2916(10)	9.778(5)	23.314(4)	24.39(2)	10.7357(13)
b (Å)	13.7305(15)	13.174(7)	13.413(2)	13.428(13)	15.581(2)
c (Å)	16.3599(18)	15.984(9)	13.695(2)	13.813(14)	15.801(2)
α (°)	82.157(2)	96.488(11)			106.921(3)
β (°)	78.079(2)	106.886(12)	97.303(4)	97.681(17)	104.216(3)
γ (°)	70.133(2)	108.736(12)			100.502(3)
V (Å^3)	2121.8(4)	1816.8(16)	4248.0(11)	4483.0(8)	2357.68
Z	1	1	4	4	1
T (K)	295(2)	295(2)	212(2)	295(2)	295(2)
λ (Å)	0.71073	0.71073	0.71073	0.71073	0.71073
Density calculated (g cm^{-3})	1.227	1.400	1.402	1.470	1.450
μ (mm^{-1})	0.907	1.965	1.753	3.786	2.345
$R(F)$[a] (%)	4.01	7.62	3.43	3.33	6.00
$R_w(F)$[b] (%)	9.25	14.85	7.74	6.69	11.95

[a] $R(F) = \sum ||F_o| - |F_c|| / \sum |F_o|$.
[b] $R_w(F) = [\sum w(F_o^2 - F_c^2)^2 / \sum w(F_o^2)^2]^{1/2}$.

Table 4
Selected bond lengths (Å) and bond angles (°) for **4**[a]

Ca–I(1)	3.131(1)
Ca–I(2)	3.157(1)
Ca–O(1)	2.390(2)
Ca–N(1)	2.332(2)
Ca–N(2)	2.333(3)
Ca–C(1)	2.779(3)
Ca–C(3)	2.695(3)
Ca–C(4)	2.759(3)
N(1)–C(1)	1.306(4)
N(2)–C(4)	1.309(4)
C(1)–C(3)	1.427(4)
C(3)–C(4)	1.428(4)
Ca–I(1)–Ca′	90.91(3)
Ca–I(2)–Ca′	89.96(2)
I(1)–Ca–I(2)	89.56(2)
N(1)–Ca(1)–N(2)	76.75(9)

[a] Primes indicate symmetry equivalent positions.

Table 5
Selected bond lengths (Å) and bond angles (°) for **5**[a]

Sr–I(1)	3.275(2)
Sr–I(2)	3.289(2)
Sr–O(1)	2.538(3)
Sr–N(1)	2.473(3)
Sr–N(2)	2.466(3)
Sr–C(1)	2.921(4)
Sr–C(3)	2.845(4)
Sr–C(4)	2.916(4)
N(1)–C(1)	1.287(4)
N(2)–C(4)	1.307(5)
C(1)–C(3)	1.427(5)
C(3)–C(4)	1.422(5)
Sr–I(1)–Sr′	91.45(7)
Sr–I(2)–Sr′	90.97(7)
I(1)–Sr–I(2)	88.79(7)
N(1)–Sr–N(2)	72.79(11)

[a] Primes indicate symmetry equivalent positions.

A perspective view of **2** is shown in Fig. 1. The overall molecular structure consists of a dimer connected by two bridging iodide ligands, with one tetrahydrofuran and one η^5-$L^{Ar'}$ ligand bonded to each calcium ion. The calcium–iodine bond lengths are 3.210(1) and 3.273(1) Å. The calcium–iodine–calcium angle is 104.62(1)°. The calcium–oxygen bond distance is 2.407(2) Å. The calcium–nitrogen bond lengths are 2.386(2) and 2.416(2) Å, while the calcium–carbon distances are 2.748(3) and 2.723(3) Å for C(14) and C(15) and 2.955(3) Å for C(13). The longer Ca–C(13) bond length appears to arise from steric interactions associated with accommodation of the tetrahydrofuran ligand on the same side of the calcium ion as C(13). For comparison, the calcium–nitrogen and calcium–carbon bond lengths in $Ca(\eta^5\text{-}L^{tBu})_2$ range from 2.34 to 2.36 and 2.84 to 2.90 Å, respectively [12b]. The calcium–carbon distance in $Ca(C_5(CH_3)_5)_2$ is 2.64(2) Å [17]. The nitrogen–calcium–nitrogen bite angle is 79.16(7)°.

Table 6
Selected bond lengths (Å) and bond angles (°) for **6**[a]

Ba(1)–I(1)	3.362(1)
Ba(2)–I(1)′	3.454(1)
Ba(1)–N(1)	2.644(8)
Ba(1)–N(2)	2.680(8)
Ba(1)–N(3)	3.070(8)
Ba(1)–N(4)	3.032(7)
Ba(2)–N(3)	2.837(7)
Ba(2)–N(4)	2.860(8)
Ba(2)–N(5)	2.638(8)
Ba(2)–N(6)	2.648(7)
Ba(1)–C(1)	3.105(11)
Ba(1)–C(3)	2.989(10)
Ba(1)–C(4)	3.088(11)
Ba(1)–C(14)	3.185(10)
Ba(1)–C(16)	3.139(11)
Ba(1)–C(17)	3.181(10)
Ba(2)–C(14)	3.56(1)
Ba(2)–C(16)	3.78(1)
Ba(2)–C(17)	3.54(1)
Ba(2)–C(27)	3.118(11)
Ba(2)–C(29)	3.039(10)
Ba(2)–C(30)	3.114(10)
Ba(1)–Ba(2)	4.7725(10)
Ba(1)–I(1)–Ba(2)′	173.88(4)
Ba(2)–Ba(1)–I(1)	75.64(2)
Ba(1)–Ba(2)–I(1)′	99.49(2)
N(1)–Ba(1)–N(2)	68.5(3)
N(3)–Ba(1)–N(4)	61.5(2)
N(3)–Ba(2)–N(4)	66.4(2)
N(5)–Ba(2)–N(6)	67.7(2)

[a] Primes indicate symmetry equivalent positions.

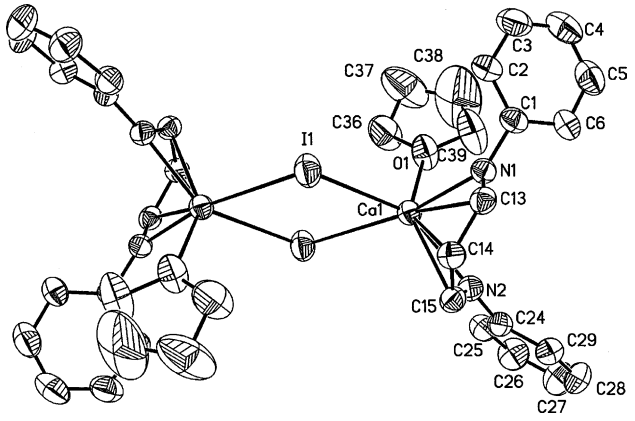

Fig. 1. Perspective view of **2** with probability ellipsoids at the 50% level. The isopropyl and *tert*-butyl groups have been removed for clarity.

A perspective view of **3** is shown in Fig. 2. The overall structure of **3** consists of two barium ions that are bridged by two iodide ligands. Each barium ion is also coordinated to one $L^{Ar'}$ ligand. Unlike the η^5-$L^{Ar'}$ ligands in **2**, the $L^{Ar'}$ ligand core in **3** is bonded to the barium atoms with the η^2-coordination mode. The barium–iodine distances are 3.362(2) and 3.523(2) Å, which indicate some asymmetry in the Ba_2I_2 core. The barium–nitrogen bond distances are 2.680(7) and 2.695(7) Å.

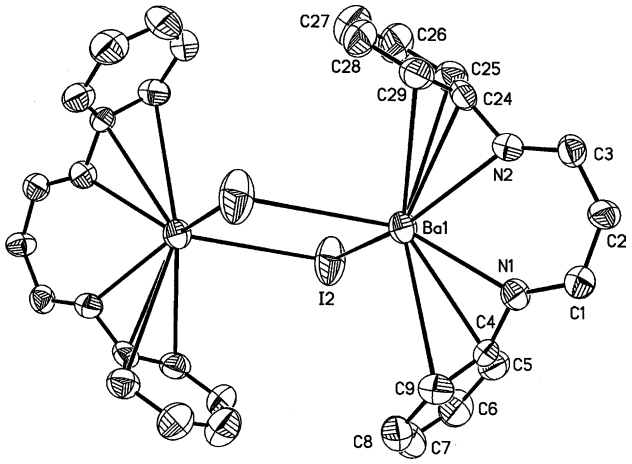

Fig. 2. Perspective view of **3** with probability ellipsoids at the 50% level. The isopropyl and *tert*-butyl groups have been removed for clarity.

The Ba–C(1,2,3) distances range from 3.79–4.14 Å, and are consistent with the η^2-β-diketiminato ligand coordination mode. Several of the aryl group carbon atoms have short contacts to the barium ion. In particular, the Ba–C(4) and Ba–C(24) distances are 3.029(8) and 2.940(8) Å, respectively. Distances from barium to the *ortho*-carbon atoms of the aryl rings range from 3.31 to 3.66 Å. For comparison, the barium– carbon distances in Ba(η^5-L$^{t\mathrm{Bu}}$)$_2$ range from 3.06 to 3.16 Å [12b], while the barium–carbon distances in Ba($C_5(CH_3)_5$)$_2$ are 2.98–2.99 Å [16]. Thus the barium–carbon distances to the *ipso*-carbon atoms of the aryl groups are comparable to those of metallocenes, and must constitute strong interactions. The fact that **3** is isolated as a solvent free complex is probably related to the saturation of the coordination sphere about the barium atoms by bonding to the bulky aryl groups.

A perspective view of **4** is shown in Fig. 3. The molecular structure of **4** is similar overall to that of **2**. The calcium–iodine bond lengths are 3.131(1) and 3.157(1) Å, and the angles associated with the Ca_2I_2 core are very close to 90°. The calcium–oxygen bond length is 2.390(2) Å, which is identical to that of **2** within experimental error. The calcium–nitrogen bond distances are 2.332(2) and 2.333(3) Å, while the calcium–carbon distances range from 2.695(3) to 2.779(3) Å. The calcium–nitrogen bond distances in **4** are shorter than those of **2**, possibly due to accommodation of the very bulky aryl groups in **2**. The calcium–carbon distances are similar in **2** and **4**, except that there is no asymmetry in the bond distances to L$^{t\mathrm{Bu}}$ in **4**. The lack of asymmetry in the calcium–carbon distances is probably due to the lower steric profile of L$^{t\mathrm{Bu}}$ compared to L$^{\mathrm{Ar'}}$. The nitrogen–calcium–nitrogen bite angle is 76.75(9)°.

A perspective view of **5** is shown in Fig. 4. The molecular structure of **5** consists of a dimer that is held together by two bridging iodide ligands. Each strontium ion is additionally coordinated to one η^5-L$^{t\mathrm{Bu}}$ and one tetrahydrofuran ligand. The overall molecular structure is similar to those of **2** and **4**. The strontium–iodine bond distances are 3.275(2) and 3.289(2) Å. The angles associated with the Sr_2I_2 core are close to 90°, and the equivalent strontium–iodine bond lengths make this core nearly a perfect square. The strontium–nitrogen bond distances are 2.466(3) and 2.473(3) Å, while the strontium–carbon distances range from 2.845(4) to 2.921(4) Å. For comparison, the strontium–nitrogen and strontium–carbon bond lengths in Sr(η^5-L$^{t\mathrm{Bu}}$)$_2$ range from 2.49 to 2.52 and 2.96 to 3.02 Å, respectively [12b]. Thus, the strontium–nitrogen and strontium–carbon bond lengths in **5** are slightly shorter than those of Sr(η^5-L$^{t\mathrm{Bu}}$)$_2$, and support the assignment of η^5-L$^{t\mathrm{Bu}}$ ligands in **5**. Unlike in **2**, there is only a small bond length asymmetry on the side of the L$^{t\mathrm{Bu}}$ ligand that is closest to the tetrahydrofuran ligand. The larger size of the

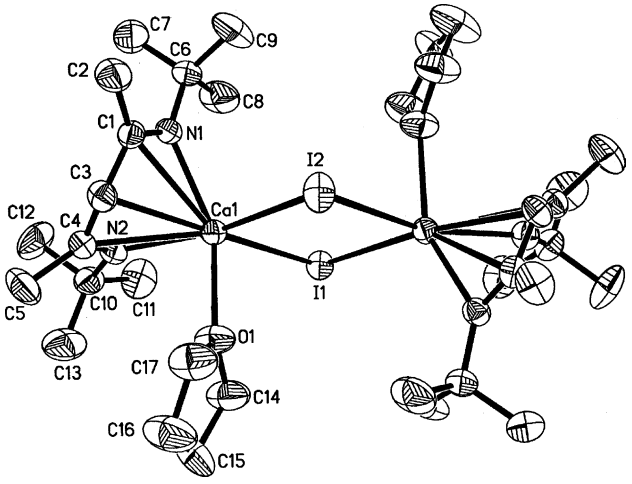

Fig. 3. Perspective view of **4** with probability ellipsoids at the 50% level.

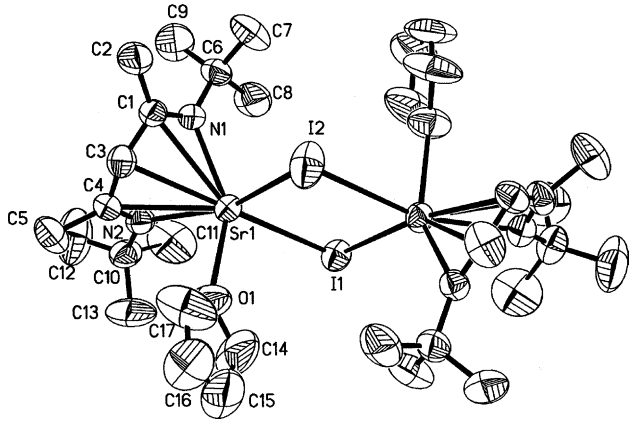

Fig. 4. Perspective view of **5** with probability ellipsoids at the 50% level.

strontium ion, compared to the calcium ion, lessens the steric interactions between the β-diketiminato and tetrahydrofuran ligands. The nitrogen–strontium–nitrogen bite angle is 72.79(11)°.

Perspective views of **6** are shown in Fig. 5. Fig. 5(a) shows one half of the tetrameric structure, while Fig. 5(b) presents the complete tetrameric molecule. Complex **6** is located on an inversion center, which makes the two halves of the molecule identical by symmetry. The overall structure consists of two $Ba_2(L^{tBu})_3I$ units that are connected through two essentially linear bridging iodide ligands. Each barium ion within the $Ba_2(L^{tBu})_3I$ unit bonds to one iodide and one terminal η^5-L^{tBu} ligand, and is connected to an adjacent barium ion through a μ-η^2:η^5-β-diketiminato ligand. The barium–iodine bond lengths are 3.362(1) and 3.454(1) Å, and are thus slightly asymmetric. These bond lengths and degree of asymmetry are very similar to those of **3**. The barium–nitrogen and barium–carbon distances associated with the terminal η^5-L^{tBu} ligands range from 2.638(8) to 2.680(8) and 2.989(10) to 3.114(10) Å, respectively. These barium–nitrogen distances are very similar to those of **3**. These values for **6** can also be compared to those of Ba(η^5-L^{tBu})$_2$, for which the barium nitrogen and barium–carbon distances were 2.62–2.68 and 3.08–3.16 Å, respectively [12b]. These bond lengths for Ba(η^5-L^{tBu})$_2$ are essentially identical to the values for the terminal η^5-L^{tBu} ligands in **6**. The barium–nitrogen distances associated with the μ-η^2:η^5-L^{tBu} ligands are 3.032(7) and 3.070(8) Å for the η^5-interaction with Ba(1) and 2.837(7) and 2.860(8) Å for the η^2-interaction with Ba(2). These values are longer than those of the terminal η^5-L^{tBu} ligands, the related values in **3**, and those of Ba(η^5-L^{tBu})$_2$ [12b], as expected for a bridging β-diketiminato ligand. The barium–carbon distances for the bridging η^5-interaction with Ba(1) range from 3.14 to 3.18 Å, which are slightly longer than those of the terminal η^5-L^{tBu} ligands in **6** and **3** and are comparable to the related distances in Ba(η^5-L^{tBu})$_2$ [12b]. The barium–carbon distances to Ba(2) ranged from 3.54 to 3.76 Å, supporting the assignment of an η^2-interaction to the nitrogen atoms. The bite angles of the terminal η^5-L^{tBu} ligands were 67.7(2)° and 68.5(3)°, while the values for the μ-η^2:η^5-L^{tBu} ligand were 66.4(2)° and 61.5(2)°.

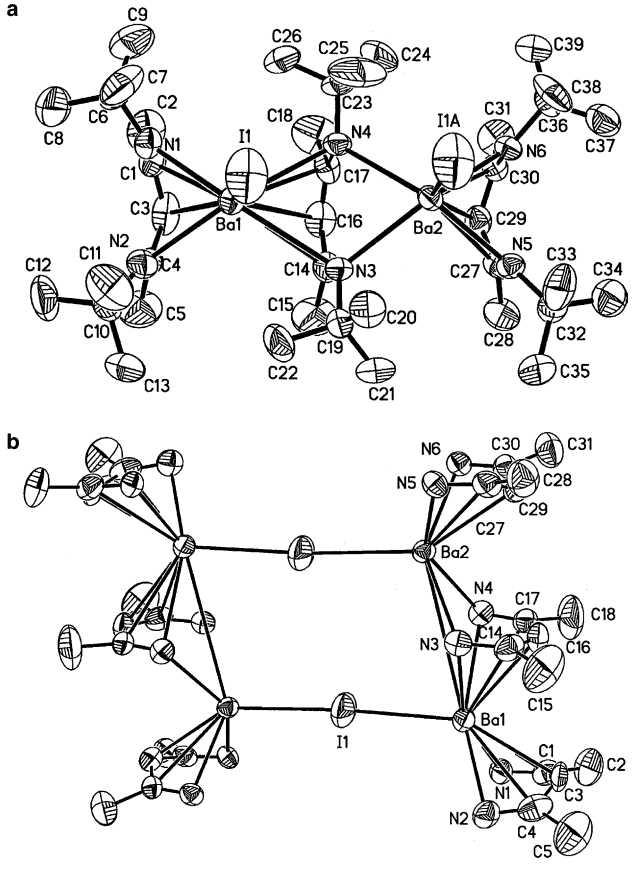

Fig. 5. Perspective views of **6** with probability ellipsoids at the 50% level: (a) one-half molecule with atom labels, (b) overall tetrameric molecule, with *tert*-butyl groups removed for clarity.

3. Discussion

3.1. Characterization of the η^5-bonding

The η^5-coordination of the β-diketiminato ligands is a prominent structural feature of **2** and **4**–**6**. We have recently reported that group 2 complexes adopt sandwich-like structures with η^5-L^{tBu} ligands [12]. In our paper on M(η^5-L^{tBu})$_2$ (M = Ca, Sr, Ba) [12b], the η^5-L^{tBu} bonding was analyzed in terms of the planes incorporating the atoms MN_2 (a), $N_2(C_\alpha)_2$ (b), and $(C_\alpha)_2C_\beta$ (c). For these complexes, the *a*/*b* angles were between 70° and 72°, the *b*/*c* angles were between 25° and 26°, and these metrical parameters were used to support the η^5-coordination mode and differentiate it from the more common η^2-form (which has much smaller *a*/*b* and *b*/*c* values [12b,13]). The corresponding metrical parameters for **2**–**5** are as follows: **2**, $a/b = 74.0(1)°$ and $b/c = 30.0(2)°$; **3**, $a/b = 172.0(4)°$ and $b/c = 4.6(1.4)°$; **4**, $a/b = 77.7(1)°$ and $b/c = 28.4(2)°$; **5**, $a/b = 75.5(1)°$ and 28.3(3)°. For **2**, **4** and **5**, these values are close to those of M(η^5-L^{tBu})$_2$, and are consistent with similar η^5-bonding of the L^{tBu} ligands. For **6**, the terminal η^5-L^{tBu} ligands have *a*/*b* values of 73.3(3)° and 75.3(4)° and *b*/*c* values of 31(2)° and 31.5(8)°, which are similar to those of M(η^5-L^{tBu})$_2$, **2**, **4**, and **5**. For the μ-η^2:η^5-β-diketiminato ligand, the side with the η^5-interaction has $a/b = 89.4(4)°$ and $b/c = 5(2)°$, while the side with the η^2-interaction has $a/b = 54.2(5)°$ and $b/c = 5(2)°$. The a/b angle associated with η^5-interaction in **6** is larger than the related angles in M(η^5-L^{tBu})$_2$, **2**, **4**, **5**, and the η^5-L^{tBu} terminal ligands in **6**, possibly to maximize bonding to C(16) (which is essentially coplanar with the other μ-η^2:η^5-β-diketiminato ligand core atoms). In **3**, the assignment of the

η^2-coordination mode is clearly warranted by the large *a*/*b* and small *b*/*c* angles.

3.2. Comparison with previously reported group 2 β-diketiminato complexes

All of the other heavier group 2 β-diketiminato complexes described to date feature 2,6-diisopropylphenyl [3,4b,4c,4d,15], 2-methoxyphenyl [4a], or cyclohexyl [14] moieties as the nitrogen atom substituents and methyl groups on the α-carbon atoms of the ligand core. Calcium, strontium, and barium complexes containing L^{Ar} exhibit the η^2-coordination mode, through the nitrogen atoms of L^{Ar}. Adoption of the η^2-coordination mode in complexes containing L^{Ar} is presumably a steric effect that is driven by the bulky aromatic isopropyl substituents. Use of the *N*-cyclohexyl-substituted diketiminato ligand L^{Cy} afforded the dimeric barium complex $Ba_2(L^{Cy})_3(N(SiMe_3)_2)$, which contains η^5-, μ-η^2:η^5-, and μ-η^2:η^3−β-diketiminato ligands [14]. The various coordination modes of β-diketiminato ligands have been recently reviewed [13]. The terminal η^5-β-diketiminato ligand has been structurally documented in a few main group, lanthanide, and early transition metal complexes, but still remains rare [12b,13,18]. In the present work, **2** and **4**–**6** possess the terminal η^5-β-diketiminato ligand coordination mode. In particular, **2** is the first group 2 complex that contains an η^5-$L^{Ar'}$ ligand. In **3**, the η^2-coordination mode appears to be stabilized through several close Ba–C_{aryl} contacts. With the smaller calcium ion in **2**, such contacts may be too long to afford much stabilization, and instead tetrahydrofuran and η^5-$L^{Ar'}$ coordination ensue. The present results, our previous report on $M(\eta^5\text{-}L^{tBu})_2$ [12b], and $Ba_2(L^{Cy})_3(N(SiMe_3)_2)$ [14] suggest that the η^5-β-diketiminato coordination mode should be common in the heavier group 2 complexes when alkyl groups or less bulky aromatic rings are present on the nitrogen atoms. Adoption of the η^5-β-diketiminato coordination mode with $L^{Ar'}$ and related ligands containing bulky aryl groups will depend upon the size of the group 2 metal ion, the degree of coordinative unsaturation at the metal center, and the possibility of aryl group interactions with the metal center.

3.3. Redistribution equilibria in solution

The redistribution equilibria of **2**–**6** are of relevance to recent reports of lactide polymerization catalysis by unsymmetrical group 2 complexes (LMX) containing β-diketiminato ligands (L) [3,4]. A recent report by Hill has explored the stability of β-diketiminato complexes of the formula $L^{Ar}M(N(SiMe_3)_2)(THF)$ toward ligand redistribution in solution [3c]. Interestingly, $L^{Ar}Ca(N(SiMe_3)_2)(THF)$ was found to be inert toward ligand redistribution in toluene-d_8 solution at ambient temperature, while $L^{Ar}Ba(N(SiMe_3)_2)(THF)$ was in equilibrium with $Ba(L^{Ar})_2$ and $Ba(N(SiMe_3)_2)(THF)_x$ under the same conditions. It was proposed that the larger size and lower Lewis acidity of the barium ion makes it more susceptible toward ligand redistribution, compared to $L^{Ar}Ca(N(SiMe_3)_2)(THF)$ [3c]. In the present work, **2** and **3** did not show any evidence for ligand redistribution in solution. The lack of ligand redistribution in **3** is probably related to the coordination of both aryl ligands to the barium ion, which creates a more rigid, very large ligand. Harder has reported the synthesis and structure of $Ba(L^{Ar})_2$, which contains no Ba–C_{aryl} interactions and only η^2-L^{Ar} ligands [15]. The $L^{Ar'}$ ligand employed in the present work is bulkier than L^{Ar}, due to the presence of the *tert*-butyl groups on the α-carbon atoms of the ligand core. These *tert*-butyl groups may provide enough steric bulk to destabilize $Ba(L^{Ar'})_2$, and thus remove low energy ligand redistribution paths for **3**. The lack of redistribution equilibria for **2** may also be related to destabilization of $Ca(L^{Ar'})_2$. In solution, **4** showed multiple equilibria, and as a result, it was not possible to carry out equilibrium constant determinations. However, the amount of products other than the unsymmetrical starting materials was small and the equilibrium constants are thus small. For **5**, NMR spectra suggested the equilibrium process depicted in Eq. (3), and an equilibrium constant of 5.3×10^{-5} M was determined at 31.3 °C. Thus, the equilibrium lies far toward the unsymmetrical starting material **5**. These experiments demonstrate that the unsymmetrical complexes **2**–**5** are strongly favored thermodynamically in solution. There are few other equilibrium constant data with which the behavior of **2**–**5** can be compared. $Cp^*CaI(THF)_2$ is reported to dissociate in tetrahydrofuran-d_8 to afford $Cp^*_2Ca(THF)_2$ and $CaI_2(THF)_2$ with $K_{eq} = 4$ [5]. $(C_5HiPr_4)CaI(OEt_2)_n$ dissociates in diethyl ether to $Ca(C_5HiPr_4)_2$ and $CaI_2(OEt_2)_n$ with $K_{eq} = 2$ [6]. Mixtures of $Ba(CH_2C_6H_5)_2(THF)_2$ and $Ba(C_5Me_4SiMe_2C_6H_5)_2$ favor the heteroleptic complex $Ba(C_5Me_4SiMe_2C_6H_5)(CH_2C_6\ H_5)(THF)$ with K_{eq} values that are much greater than one [19]. The complex $[Ba(C_5HiPr_4)(I)(THF)_2]_2$ resists ligand redistribution in tetrahydrofuran, but does scramble ligands in less coordinating solvents such as benzene [8]. We have recently reported that $[Sr(\mu\text{-}\eta^5\text{:}\eta^2\text{-}tBu_2pz)(\eta^5\text{-}L^{tBu})]_2$ exists in equilibrium with $Sr(\eta^5\text{-}L^{tBu})_2$ and $Sr_4(tBu_2pz)_8$ (tBu_2pz = 3,5-di-*tert*-butylpyrazolato) [12c]. A van't Hoff analysis of this equilibrium between 46 and 104 °C afforded $\Delta H^0 = 22.2 \pm 0.7$ kcal/mol, $\Delta S^0 = 43.7 \pm 1.9$ cal/mol · K, and $\Delta G^0(298K) = 9.2 \pm 0.9$ kcal/mol. The equilibrium constant at 46.0 °C was 2.17×10^{-6} M. Thus, the mixed ligand complex $[Sr(\mu\text{-}\eta^5\text{:}\eta^2\text{-}tBu_2pz)(\eta^5\text{-}L^{tBu})]_2$ is strongly favored thermodynamically. Redistribution equilibria are also important for the heavier group 2 Grignard analogs [20].

3.4. Conclusions

We have prepared and characterized a series of mixed ligand complexes containing β-diketiminato and iodide ligands. Observation of tetrahydrofuran coordination depended on the nature of the β-diketiminato ligand and the metal ion. $[Ca(\eta^5\text{-}L^{Ar'})(\mu\text{-}I)(THF)]_2$, $[M(\eta^5\text{-}L^{tBu})(\mu\text{-}I)(THF)]_2$ (M = Ca, Sr), and $Ba_4(L^{tBu})_6(I)_2$ contain terminal η^5-β-diketiminato ligands, which is a novel coordination mode for this class of ligands. In addition, $Ba_4(L^{tBu})_6(I)_2$ contains novel $\mu\text{-}\eta^2\text{:}\eta^5$-β-diketiminato ligands. The complex $[Ba(\eta^2\text{-}L^{Ar'})(\mu\text{-}I)]_2$ contains η^2-β-diketiminato ligands, and this coordination mode appears to be stabilized by close Ba–C_{aryl} contacts to the *ipso*- and *ortho*-carbon atoms of the aryl rings. $[M(\eta^5\text{-}L^{tBu})(\mu\text{-}I)(THF)]_2$ (M = Ca, Sr) undergo ligand redistribution in solution, although the position of the equilibrium strongly favors the mixed ligand complexes under the conditions studied. $[Ca(\eta^5\text{-}L^{Ar'})(\mu\text{-}I)(THF)]_2$ and $[Ba(\eta^2\text{-}L^{Ar'})(\mu\text{-}I)]_2$ show no evidence for ligand redistribution equilbria in solution. The combined results suggest that $L^{Ar'}$ and L^{tBu} are strongly coordinating ligands for group 2 metal ions, and are effective at stabilizing mixed ligand complexes toward redistribution equilibria.

4. Experimental

4.1. General considerations

All reactions were performed under an inert atmosphere of argon using either glove box or Schlenk line techniques. Tetrahydrofuran and toluene were distilled from sodium. $M(\eta^5\text{-}L^{tBu})_2$ [12b], $L^{tBu}H$ [21], and $L^{Ar'}H$ [22] were prepared according to literature methods. Anhydrous metal iodides were purchased from Aldrich Chemical and were used as received. ^1H and $^{13}C\{^1H\}$ NMR were obtained at 300 and 75 MHz in the indicated solvents. Infrared spectra were obtained using Nujol as the medium. Elemental analyses were performed by Midwest Microlab, Indianapolis, IN. Melting points were obtained on a Haake-Buchler HBI digital melting point apparatus and are uncorrected.

4.2. Preparation of $K(L^{Ar'})(THF)_3$ (**1**)

A 100-mL Schlenk flask was charged with $L^{Ar'}H$ (5.00 g, 9.96 mmol) and tetrahydrofuran (60 mL). To this solution was added potassium hydride (0.80 g, 19.9 mmol), and the resultant solution was stirred at ambient temperature for 24 h. During this time a deep-yellow solution was observed. The resulting solution was filtered through a 2-cm pad of Celite on a coarse glass frit to afford a clear yellow solution. The volume of the filtrate was reduced to 20 mL, and then this solution was layered with hexane (40 mL). Equilibration at ambient temperature for 48 h gave yellow crystals. Removal of the solvent with a cannula, followed by vacuum drying, afforded **1** as a yellow crystalline solid (6.70 g, 89%): m.p. 332–334 °C (dec); IR (Nujol, cm^{-1}) 1547 (w), 1311 (s), 1254 (s), 1165 (s), 1082 (s), 1018 (s), 921 (w), 798 (s); ^1H NMR (toluene-d_8, 23 °C, δ) 6.77–6.99 (m, 6H, aryl-*H*), 4.89 (s, 1 H, β-C*H*), 3.54 (m, 12H, OCH_2CH_2), 3.27 (septet, $J = 6.3$ Hz, 4H, $CH(CH_3)_2$), 1.46 (m, 12H, OCH_2CH_2), 1.34 (s, 18H, $C(CH_3)_3$), 1.33 (d, $J = 6.3$ Hz, 12H, $CH(CH_3)_2$), 0.96 (d, $J = 6.3$ Hz, 12H, $CH(CH_3)_2$); $^{13}C\{^1H\}$ NMR (toluene-d_8, 23 °C, ppm) 166.13 (s, $CC(CH_3)_3$), 151.69 (s, C_{ipso}), 135.96 (s, C_{ortho}), 123.5 (s, C_{para}), 118.43 (s, C_{meta}), 89.83 (s, β-*C*H), 67.57 (s, OCH_2CH_2), 44.22 (s, $C(CH_3)_3$), 32.74 (s, $C(CH_3)_3$), 27.21 (s, $CH(CH_3)_2$), 25.67 (s, OCH_2CH_2), 25.00 (s, $CH(CH_3)_2$), 23.47 (s, $CH(CH_3)_2$).

Anal. Calc. for $C_{47}H_{77}KN_2O_3$: C, 74.55; H, 10.25; N, 3.70. Found: C, 75.46; H, 10.32; N, 4.06%.

4.3. Preparation of $[Ca(L^{Ar'})(THF)(\mu\text{-}I)]_2$ (**2**)

A 100-mL Schlenk flask was charged with **1** (0.553 g, 0.731 mmol), CaI_2(0.215 g, 0.731 mmol), and tetrahydrofuran (40 mL). The resultant solution was stirred for 18 h at ambient temperature to afford a yellow solution. The volatile components were removed under reduced pressure and the residue was extracted with toluene (40 mL). This mixture was filtered through a 2-cm pad of Celite on a medium glass frit to afford a clear yellow solution. The filtrate was concentrated to a volume of 15 mL, hexane (10 mL) was mixed with the toluene solution, and this solution was stored at −25 °C for 7 days to afford **2** as yellow crystals (0.35 g, 62%): m.p. 340–347 °C (dec); IR (Nujol, cm^{-1}) 1546 (s), 1399 (s), 1259 (s), 1211 (w), 1185 (w), 1097 (w), 1024 (s), 930 (w), 871 (s), 798 (s), 687 (w); ^1H NMR (benzene-d_6, 23 °C, δ) 7.00–7.06 (m, 12H, aryl-*H*), 5.52 (s, 2H, β-C*H*), 3.24 (septet, $J = 7.2$ Hz, 8H, $CH(CH_3)_2$), 3.12 (m, 8H, OCH_2CH_2), 1.34 (d, $J = 7.2$ Hz, 24H, $CH(CH_3)_2$), 1.24 (s, 36H, $C(CH_3)_3$), 1.17 (d, $J = 7.2$ Hz, 24H, $CH(CH_3)_2$), 0.89 (m, 8H, OCH_2CH_2); $^{13}C\{^1H\}$ NMR (benzene-d_6, 23 °C, ppm) 174.63 (s, $CC(CH_3)_3$), 145.69 (s, C_{ipso}), 139.25 (s, C_{ortho}), 123.64 (s, C_{meta}), 123.33 (s, C_{para}), 90.25 (s, β-*C*H), 69.65 (s, OCH_2CH_2), 44.77 (s, $C(CH_3)_3$), 32.46 (s, $CH(CH_3)_3$), 28.63 (s, $CH(CH_3)_2$), 26.44 (s, $CH(CH_3)_2$), 24.52 (s, OCH_2CH_2), 23.46 (s, $CH(CH_3)_2$).

Anal. Calc. for $C_{78}H_{122}Ca_2I_2N_4O_4$: C, 63.22; H, 8.30; N, 3.78. Found: C, 62.98; H, 8.15; N; 3.31%. The X-ray crystal structure was solved as $\mathbf{2}\cdot(C_6H_{14})_{1.0}$, but the crystals lose hexane rapidly at ambient temperature and the bulk material was isolated as hexane-free crystals (*Anal.* Calc. for $C_{78}H_{122}Ca_2I_2N_4O_4\cdot C_6H_{14}$: C, 64.35; H, 8.74; N, 3.57%).

4.4. Preparation of $[(L^{Ar'})Ba(\mu\text{-}I)]_2$ (3)

In a fashion similar to the preparation of **2**, treatment of **1** (0.553 g, 0.731 mmol) with BaI_2 (0.288 g, 0.731 mmol) afforded **3** as yellow crystals (0.150 g, 27%): m.p. 310–314 °C (dec); IR (Nujol, cm^{-1}) 1614 (w), 1544 (s), 1404 (s), 1260 (s), 1214 (w), 1139 (w), 1092 (s), 1020 (m), 872 (w), 798 (s); ^1H NMR (benzene-d_6, 23 °C, δ) 7.03–7.17 (m, 12H, aryl-*H*), 5.24 (s, 2H, β-C*H*), 2.99 (septet, $J = 6.9$ Hz, 8H, C*H*$(CH_3)_2$), 1.24 (d, $J = 6.9$ Hz, 24H, CH(C*H*$_3)_2$), 1.21 (d, $J = 6.9$ Hz, 24H, CH(C*H*$_3)_2$), 1.19 (s, 36 H, C(C*H*$_3)_3$); ^{13}C $\{^1H\}$ NMR (benzene-d_6, 23 °C, ppm) 169.77 (s, *C*C$(CH_3)_3$), 146.68 (s, C_{ipso}), 137.67 (s, C_{ortho}), 126.43 (s, C_{meta}), 123.76 (s, C_{para}), 94.55 (s, β-*C*H), 43.83 (s, *C*$(CH_3)_3$), 32.41 (s, C(*C*$H_3)_3$), 28.19 (s, *C*H$(CH_3)_2$), 24.47 (s, CH(*C*$H_3)_2$), 23.37 (s, CH(*C*$H_3)_2$).

Anal. Calc. for $C_{70}H_{106}Ba_2I_2N_4$: C, 54.88; H, 6.97; N, 3.66. Found: C, 53.86; H, 6.83; N, 3.54%.

4.5. Preparation of $[Ca(L^{tBu})(\mu\text{-}I)(THF)]_2$ (4)

A 100-mL Schlenk flask was charged with $Ca(\eta^5\text{-}L^{tBu})_2$ (0.40 g, 0.87 mmol), CaI_2 (0.255 g, 0.87 mmol), a stir bar, and tetrahydrofuran (30 mL). The resultant solution was refluxed for 3 h, and then the volatile components were removed under reduced pressure. The residue was dissolved in hot toluene (40 mL) and the resultant solution was filtered through a 2-cm pad of Celite on a medium glass frit. The clear, colorless solution was then concentrated to a volume of 30 mL and was stored at −25 °C for 7 days to afford **4** as a colorless solid (0.53 g, 68%): m.p. 202–204 °C (dec); IR (Nujol, cm^{-1}) 1631 (w), 1548 (s), 1519 (m), 1496 (s), 1359 (s), 1256 (s), 1210 (s), 1093 (w), 1032 (s), 1002 (m), 975 (w), 917 (w), 879 (m), 799 (m), 725 (m); ^1H NMR (toluene-d_8, 23 °C, δ) 4.30 (s, 2H, β-C*H*), 3.85 (m, 8H, OCH_2CH_2), 2.05 (s, 12H, C-CH_3), 1.47 (s, 8H + 36H, overlapped OCH_2CH_2 and C(C$H_3)_3$); ^{13}C $\{^1H\}$ NMR (toluene-d_8, 23 °C, ppm) 161.18 (s, *C*-CH_3), 90.07 (s, β-*C*H), 69.66 (O*C*H_2CH$_2$), 54.38 (s, *C*$(CH_3)_3$), 32.89 (s, C(*C*$H_3)_3$), 25.39 (OCH$_2$*C*H$_2$), 24.81 (s, C-*C*H_3). NMR data are reported only for the major isomer (61% of total integration). In addition, $Ca(\eta^5\text{-}L^{tBu})_2$ (13% of total integration) and an unidentified species (26% of total integration) were observed.

Anal. Calc. for $C_{34}H_{66}Ca_2I_2N_4O_2$: C, 45.53; H, 7.42; N, 6.25. Found: C, 46.18; H, 7.45; N, 5.88%.

4.6. Preparation of $[Sr(L^{tBu})(\mu\text{-}I)(THF)]_2$ (5)

In a fashion similar to the preparation of **4**, treatment of $Sr(\eta^5\text{-}L^{tBu})_2$ (0.80 g, 1.58 mmol) with SrI_2 (0.60 g, 1.58 mmol) in tetrahydrofuran afforded **5** as colorless crystals (0.83 g, 53%): m.p. 250–255 °C (dec); IR (Nujol, cm^{-1}) 1630 (w), 1548 (m), 1459 (s), 1379 (s), 1358 (s), 1260 (s), 1210 (m), 1093 (m), 1025 (m), 878 (w), 800 (s); ^1H NMR (toluene-d_8, 23 °C, δ) 4.32 (s, 2H, β-C*H*), 3.69 (m, 8H, OCH_2CH_2), 2.05 (s, 12H, C-CH_3), 1.46 (s, 8H + 36H, overlapped OCH_2CH_2 and C(C$H_3)_3$); ^{13}C $\{^1H\}$ NMR (toluene-d_8, 23 °C, ppm) 160.55 (s, *C*-CH_3), 89.73 (s, β-*C*H), 68.74 (O*C*H_2CH$_2$), 54.49 (s, *C*$(CH_3)_3$), 32.98 (s, C(*C*$H_3)_3$), 25.60 (OCH$_2$*C*H$_2$), 24.79 (s, C-*C*H_3).

Anal. Calc. for $C_{34}H_{66}Sr_2I_2N_4O_2$: C, 41.17; H, 6.71; N, 5.65. Found: C, 39.79; H, 6.63; N, 5.63%.

4.7. Preparation of $Ba_4(L^{tBu})_6(I)_2$ (6)

In a fashion similar to the preparation of **4**, treatment of $Ba(\eta^5\text{-}L^{tBu})_2$ (0.20 g, 0.359 mmol) with BaI_2 (0.047 g, 0.112 mmol) in tetrahydrofuran afforded **6** as yellow crystals (0.06 g, 24%): m.p. 244–248 °C (dec); IR (Nujol, cm^{-1}) 1529 (s), 1406 (s), 1248 (s), 1092 (w), 1023 (s), 996 (w), 963 (m), 799 (m), 773 (w), 751 (w), 693 (w); ^1H NMR (toluene-d_8, 23 °C, δ) 4.31 (broad s, 6H, β-C*H*), 1.99 (broad s, 36H, C-CH_3), 1.39 (broad s, 108H, C(C$H_3)_3$); the low solubility in toluene-d_8 precluded collection of the ^{13}C $\{^1H\}$ NMR spectrum.

Anal. Calc. for $C_{78}H_{150}Ba_4I_2N_{12}$: C, 45.49; H, 7.34; N, 8.16. Found: C, 46.84; H, 7.36; N, 7.45%.

4.8. X-ray crystallographic structure determinations for 2–6

Diffraction data for **2**–**6** were collected on a Bruker *P4/CCD* diffractometer equipped with Mo radiation and a graphite monochromator. Complexes **2**, **3**, **5**, and **6** were mounted in thin walled glass capillaries. Data collections were conducted at ambient temperature. The data collection for **4** was carried out at −61 °C. In all cases, a sphere of data was measured at 10–20 s/frames and 0.2° between frames. The frame data were indexed and integrated with the manufacturer's SMART, SAINT, and SADABS software [23]. The models were refined and reported using Sheldrick's SHELX-97 software [24].

Complex **2** crystallized as yellow flat fragments. The hydrogen atoms were placed in calculated positions. One equivalent of hexane solvate was disordered near an inversion center and was modeled with partial atoms and refined isotropically. All other non-hydrogen atoms were refined anisotropically. There is a tetrahydrofuran ligand on the calcium atom that exhibits unreliable bond lengths and angles due to disorder. The overall molecule occupies a crystallographic inversion center.

Complex **3** crystallized as yellow rods. Hydrogen atoms were placed in calculated positions. All non-hydrogen atoms were refined anisotropically. The molecule occupies a crystallographic inversion center with no solvent present.

Complex **4** crystallized as colorless flat rods. The dimer occupies a crystallographic 2-fold rotation axis with

both bridging iodine atoms on the 2-fold axis. Hydrogen atoms were placed in observed or calculated positions. Partial occupancy positions were used to describe the disorder in the *tert*-butyl group on C(10) and the disordered tetrahydrofuran carbon atoms. All non-hydrogen atoms were nevertheless refined anisotropically. Complex **5** crystallized as colorless cubes, is isostructural with **4**, and shows similar disorder.

Complex **6** crystallized as yellow rhomboids. The molecule is a tetramer occupying a crystallographic inversion center. Hydrogen atoms were placed in calculated positions, and all non-hydrogen atoms were refined anisotropically.

5. Supplementary material

Crystallographic data for the structural analyses have been deposited with the Cambridge Crystallographic Data Centre, quoting No. 267402 for **2**, No. 267403 for **3**, No. 267404 for **4**, No. 267405 for **5**, and No. 267406 for **6**. Copies of this information may be obtained free of charge from The Director, CCDC, 12 Union Road, Cambridge CB2 1EZ, UK (fax: +44 1233 336 033; e-mail: deposit@ccdc.cam.ac.uk or www: http://www.ccdc.cam.ac.uk).

Acknowledgments

We thank the Army Research Office (grants no. DAAD19-01-1-0575 and W911NF-04-1-0332) for generous support of this research.

References

[1] For reviews, see:
(a) J.S. Matthews, W.S. Rees Jr., Adv. Inorg. Chem. 50 (2000) 173;
(b) D.J. Otway, W.S. Rees Jr., Coord. Chem. Rev. 210 (2000) 279;
(c) W.A. Wojtczak, P.F. Fleig, M.J. Hampden-Smith, Adv. Organomet. Chem. 40 (1996) 215;
(d) D. Schulz, T.J. Marks, Adv. Mater. 6 (1994) 719;
(e) A.R. Barron, W.S. Rees Jr., Adv. Mater. Opt. Electron. 2 (1993) 271.

[2] For selected, leading references, see:
(a) S. Harder, S. Müller, E. Hübner, Organometallics 23 (2004) 178;
(b) F. Feil, S. Harder, Macromolecules 36 (2003) 3446;
(c) F. Feil, S. Harder, Eur. J. Inorg. Chem. (2003) 3401;
(d) S. Harder, F. Feil, Organometallics 21 (2002) 2268;
(e) S. Harder, Angew. Chem. Int. Ed. 42 (2003) 3430;
(f) S. Harder, F. Feil, A. Weeber, Organometallics 20 (2001) 1044;
(g) F. Feil, S. Harder, Organometallics 19 (2000) 5010.

[3] (a) M.R. Crimmin, I.J. Casely, M.S. Hill, J. Am. Chem. Soc. 127 (2005) 2042;
(b) A.G. Avent, M.R. Crimmin, M.S. Hill, P.B. Hitchcock, Dalton Trans. (2005) 278;
(c) A.G. Avent, M.R. Crimmin, M.S. Hill, P.B. Hitchcock, Dalton Trans. (2004) 3166;
(d) M.S. Hill, P.B. Hitchcock, Chem. Commun. (2003) 1758;
(e) A.G. Avent, M.R. Crimmin, M.S. Hill, P.B. Hitchcock, Organometallics 24 (2005) 1184.

[4] (a) M.H. Chisholm, J. Galucci, K. Phomphrai, Inorg. Chem. 43 (2004) 6717;
(b) M.H. Chisholm, Z.P. Zhou, J. Mater. Chem. 14 (2004) 3081;
(c) M.H. Chisholm, J. Gallucci, K. Phomphrai, Chem. Commun. (2003) 48;
(d) M.H. Chisholm, J.C. Huffman, K. Phomphrai, J. Chem. Soc., Dalton Trans. (2001) 222.

[5] M.J. McCormick, S.C. Sockwell, C.E.H. Davies, T.P. Hanusa, J.C. Huffman, Organometallics 8 (1989) 2044.

[6] D.J. Burkey, E.K. Alexander, T.P. Hanusa, Organometallics 13 (1994) 2773.

[7] M.J. Harvey, T.P. Hanusa, Organometallics 19 (2000) 1556.

[8] H. Sitzmann, F. Weber, M.D. Walter, G. Wolmershäuser, Organometallics 22 (2003) 1931.

[9] M.J. Harvey, T.P. Hanusa, V.G. Young, J. Organomet. Chem. 626 (2001) 43.

[10] M. Westerhausen, M.H. Digeser, C. Guckel, H. Noth, J. Knizek, W. Ponikwar, Organometallics 18 (1999) 2491.

[11] For recent reviews see: (a) T.P. Hanusa, Organometallics 21 (2002) 2559;
(b) P. Jutzi, N. Burford, Chem. Rev. 99 (1999) 969.

[12] (a) H.M. El-Kaderi, A. Xia, M.J. Heeg, C.H. Winter, Organometallics 23 (2004) 3488;
(b) H.M. El-Kaderi, M.J. Heeg, C.H. Winter, Organometallics 23 (2004) 4995;
(c) H.M. El-Kaderi, M.J. Heeg, C.H. Winter, Eur. J. Inorg. Chem. (2005) 2081.

[13] L. Bourget-Merle, M.F. Lappert, J.R. Severn, Chem. Rev. 102 (2002) 3031.

[14] W. Clegg, S.J. Coles, E.K. Cope, F.S. Mair, Angew. Chem. Int. Ed. 37 (1998) 769.

[15] S. Harder, Organometallics 21 (2002) 3782.

[16] K. Ruhlandt-Senge, K. Davis, S. Dalal, U. Englich, M.O. Senge, Inorg. Chem. 34 (1995) 2587.

[17] R.A. Williams, T.P. Hanusa, J.C. Huffman, Organometallics 9 (1990) 1128.

[18] (a) G.B. Nikiforov, H.W. Roesky, D. Vidovic, J. Magull, J. Mol. Struct. 656 (2003) 155;
(b) P.B. Hitchcock, M.F. Lappert, D.-S. Liu, J. Chem. Soc., Chem. Commun. (1994) 2637;
(c) M. Rahim, M.J. Taylor, S. Xin, S. Collins, Organometallics 17 (1998) 1315;
(d) L. Kakaliou, W.J. Scanlon, B. Qian, S.W. Baek, M.R. Smith III, D.H. Motry, Inorg. Chem. 38 (1999) 5964;
(e) R. Vollmerhaus, M. Rahim, R. Tomaszewski, S. Xin, N.J. Taylor, S. Collins, Organometallics 19 (2000) 2161.

[19] A. Weeber, S. Harder, H.H. Brintzinger, K. Knoll, Organometallics 19 (2000) 1325.

[20] (a) J.S. Alexander, K. Ruhlandt-Senge, Eur. J. Inorg. Chem. (2002) 2761;
(b) M. Westerhausen, Angew. Chem. Int. Ed. 40 (2002) 2975.

[21] N. Kuhn, H. Lanfermann, P. Schmitz, Liebigs Ann. Chem. (1987) 727.

[22] P.H.M. Budzelaar, A.B. van Oort, A.G. Orpen, Eur. J. Inorg. Chem. (1998) 1485.

[23] SMART, SAINT, and SADABS are collection and processing programs distributed by the manufacturer: Bruker AXS Inc., Madison, WI, USA.

[24] G. Sheldrick, SHELX-97, University of Göttingen, Germany, 1997.

Available online at www.sciencedirect.com
SCIENCE DIRECT®
Polyhedron 25 (2006) 235–240
POLYHEDRON
www.elsevier.com/locate/poly

An iron(II) complex of 2,6-di(pyrazol-1-yl)pyrazine that crystallises in three forms, two of which exhibit an unusual angular Jahn–Teller distortion

Colin A. Kilner, Malcolm A. Halcrow *

School of Chemistry, University of Leeds, Woodhouse Lane, Leeds LS2 9JT, UK

Received 30 March 2005; accepted 24 June 2005
Available online 10 August 2005

Dedicated to Malcolm Chisholm on the occasion of his 60th birthday.

Abstract

Treatment of hydrated $FeCl_2$ with 2 equiv. of 2,6-di(pyrazol-1-yl)pyrazine (L^1H) and $AgSbF_6$ in refluxing $MeNO_2$ yields $[Fe(L^1H)_2][SbF_6]_2$ (**1**[**SbF$_6$**]$_2$). This compound is fully high-spin as a powder between 5 and 300 K, and exhibits a small zero-field splitting consistent with it adopting an unusual angularly distorted six-coordinate coordination geometry. Slow diffusion of Et_2O into a $MeNO_2$ solution of the compound gives varying proportions of three different crystal forms. Solvent-free **1**[**SbF$_6$**]$_2$ and solvated **1**[**SbF$_6$**]$_2 \cdot 2CH_3NO_2$ are both high-spin at 150 K, and have undergone the proposed angular Jahn–Teller distortion to differing extents. This is the first time that this structural distortion has been observed in an iron(II) complex of a 2,6-di(pyrazol-1-yl)pyrazine derivative. In contrast **1**[**SbF$_6$**]$_2 \cdot 3CH_3NO_2$ is low-spin at room temperature and has a regular six-coordinate geometry.
© 2005 Elsevier Ltd. All rights reserved.

Keywords: Iron; Magnetic measurements; Crystal structure

1. Introduction

We have been studying the spin-crossover [1] properties of iron(II) complexes of ligands from the 2,6-di(pyrazol-1-yl)pyrazine (L^1R) [2–6] and 2,6-di(pyrazol-1-yl)pyridine (L^2R) series [2,6–13]. A wide range of L^1R and L^2R derivatives with different 'R' groups are synthetically accessible, yielding homoleptic iron(II) complexes whose spin states depend on the steric and inductive properties of 'R' in a qualitatively predictable way [2,10]. A complication of this chemistry, however, is the existence of an unusual angular Jahn–Teller distorted structure in some of our high-spin $[Fe(L^2R)_2]^{2+}$ compounds, which traps them in a high-spin state [8,12,13]. Similar structures have also been observed in some iron(II) complexes of 6,6″-disubstituted 2,2′:6′,2″-terpyridines [14]. As a part of this work, we have described two iron(II) complex salts of the unsubstituted 2,6-di(pyrazol-1-yl)pyrazine ligand, $[Fe(L^1H)_2][BF_4]_2$ (**1**[**BF$_4$**]$_2$) and $[Fe(L^1H)_2][ClO_4]_2$ (**1**[**ClO$_4$**]$_2$) [3,4,6]. Both these solids undergo abrupt high → low spin transitions upon cooling, at 223 and 206 K, respectively. Although neither compound is crystalline, powder diffraction studies showed that they are not isostructural, that both spin transitions were accompanied by a crystallographic phase change [3,4], and that the high-spin phase of **1**[**ClO$_4$**]$_2$ (but *not* **1**[**BF$_4$**]$_2$) was isostructural with the chemically very similar compound $[Fe(L^2H)_2][BF_4]_2$ (**2**[**BF$_4$**]$_2$) [4]. Interestingly, a solvated crystal phase **1**[**BF$_4$**]$_2 \cdot 3CH_3NO_2$ was also characterised which undergoes abrupt spin-crossover at 198 K, a very similar temperature to the unsolvated material [3]. We

* Corresponding author. Tel.: +44 113 343 6506; fax: +44 113 343 6565.
E-mail address: m.a.halcrow@leeds.ac.uk (M.A. Halcrow).

0277-5387/$ - see front matter © 2005 Elsevier Ltd. All rights reserved.
doi:10.1016/j.poly.2005.06.034

report here a new compound, [Fe-(L^1H)$_2$][**SbF$_6$**]$_2$ (**1**[**SbF$_6$**]$_2$), whose crystallographic and magnetochemical behaviour is very different from the other two salts of the same complex dication.

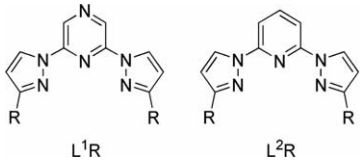

2. Experimental

All manipulations were carried out in air, using distilled water or reagent-grade solvents. Ligand L^1H was prepared by the literature procedure [15], while all other organic and inorganic reagents were used as supplied.

2.1. Synthesis of [Fe(L^1H)$_2$][SbF$_6$]$_2$(1[SbF$_6$]$_2$)

A mixture of L^1H (0.25 g, 1.2 mmol), $FeCl_2 \cdot 4H_2O$ (0.12 g, 0.59 mmol) and $AgSbF_6$ (0.45 g, 1.2 mmol) in CH_3NO_2 (50 cm^3) was heated at 80 °C for 1 h, yielding a brown solution with a white suspension. The solution was filtered and concentrated in vacuo to ca. 5 cm^3 volume. Addition of excess Et_2O to this solution yielded a yellow precipitate which was stored overnight at −30 °C, then collected, washed with Et_2O and dried in vacuo. Yield: 0.39 g, 68%. Calc. for $C_{20}H_{16}F_{12}FeN_{12}Sb_2$: C, 25.2; H, 1.7; N, 17.7. Found C, 25.3; H, 1.8; N, 17.8%.

2.2. Single crystal X-ray structure determinations

Slow diffusion of Et_2O vapour into a CH_3NO_2 solution of the compound at room temperature yielded a mixture of three different forms: yellow cubic prisms of solvent-free **1**[**SbF$_6$**]$_2$; yellow plates of formula **1**[**SbF$_6$**]$_2 \cdot 2CH_3NO_2$; and brown needles of **1**[**SbF$_6$**]$_2 \cdot 3CH_3NO_2$. Experimental details for all the structure determinations are given in Table 1. X-ray data for **1**[**SbF$_6$**]$_2$ and **1**[**SbF$_6$**]$_2 \cdot 2CH_3NO_2$ were collected on a Nonius KappaCCD area-detector diffractometer, using graphite-monochromated Mo Kα radiation. Data for **1**[**SbF$_6$**]$_2 \cdot 3CH_3NO_2$ were obtained using a Bruker X8

Table 1
Experimental details for the crystal structure determinations in this study

	1[**SbF$_6$**]$_2$	**1**[**SbF$_6$**]$_2 \cdot 2CH_3NO_2$	**1**[**SbF$_6$**]$_2 \cdot CH_3NO_2$ (3/2.7)
Formula	$C_{20}H_{16}F_{12}FeN_{12}Sb_2$	$C_{22}H_{22}F_{12}FeN_{14}O_4Sb_2$	$C_{22.7}H_{24.1}F_{12}FeN_{14.7}O_{5.4}Sb_2$
M_r	951.80	1073.89	1116.62
Crystal size (mm)	0.10 × 0.10 × 0.10	0.18 × 0.13 × 0.02	0.15 × 0.14 × 0.02
Crystal class	monoclinic	triclinic	monoclinic
Space group	*C*2/*c*	$P\bar{1}$	$P2_1/n$
a (Å)	14.7630(3)	8.3371(2)	8.8934(4)
b (Å)	9.4278(2)	9.1052(2)	16.8452(8)
c (Å)	20.9049(6)	23.8819(6)	25.1352(13)
α (°)	–	81.0665(8)	–
β (°)	99.3336(9)	83.3689(9)	97.775(2)
γ (°)	–	83.8740(14)	–
V (Å^3)	2871.07(12)	1771.63(7)	3730.9(3)
Z	4	2	4
μ (Mo Kα) (mm^{-1})	2.483	2.034	1.939
T (K)	150(2)	150(2)	100(2)
Radiation λ (Å)	0.71073	0.71073	0.71073
Absorption correction	multi-scan	multi-scan	multi-scan
Minimum/maximum transmission	0.68/0.87	0.60/0.97	0.76/0.96
Measured reflections	20092	30803	36317
Independent reflections	3291	8030	8964
R_{int}	0.081	0.103	0.031
Observed reflections [$I > 2\sigma(I)$]	2580	5734	7545
Range in 2θ (°)	$5.6 \leqslant 2\theta \leqslant 55.0$	$4.5 \leqslant 2\theta \leqslant 55.0$	$3.0 \leqslant 2\theta \leqslant 56.0$
Parameters/restraints	214/0	599/45	599/18
$R(F)$[a], w$R(F^2)$[b]	0.035, 0.087	0.051, 0.147	0.044, 0.116
Goodness-of-fit	1.033	1.045	1.117
Weighting scheme[c]	$w = 1/[\sigma^2(F_0^2) + (0.0441P)^2]$	$w = 1/[\sigma^2(F_0^2) + (0.0797P)^2 + (0.5230P)]$	$w = 1/[\sigma^2(F_0^2) + (0.0445P)^2 + (13.9651P)]$
Δρ (maximum/minimum) (e Å^{-3})	0.81/−1.67	0.90/−1.43	1.13/−0.98

[a] $R = \Sigma[|F_o| - |F_c|]/\Sigma|F_o|$.
[b] $wR = [\Sigma w(F_o^2 - F_c^2)/\Sigma wF_o^4]^{1/2}$.
[c] $P = (F_o^2 + 2F_c^2)/3$.

Apex diffractometer, with graphite-monochromated Mo Kα radiation generated by a rotating anode. All the structures were solved by direct methods (SHELXS 97 [16]) and refined by full matrix least-squares on F^2 (SHELXL 97 [17]).

2.2.1. Single crystal X-ray structure of ***1[SbF$_6$]$_2$***

The asymmetric unit contains half a formula unit, with Fe(1) lying on the crystallographic C_2 axis $-x$, y, $1/2 - z$. No disorder was detected during refinement, and no restraints were applied. All non-H atoms were refined anisotropically, while all H atoms were placed in calculated positions and refined using a riding model. The deepest residual Fourier hole of -1.7 e Å^{-3} is 0.9 Å from Sb(18).

2.2.2. Single crystal X-ray structure of ***1[SbF$_6$]$_2$ · 2CH$_3$-NO$_2$***

Both SbF_6^- anions in the asymmetric unit are disordered: one over two equally-occupied orientations, and the other over three sites with a 0.4:0.4:0.2 occupancy ratio. All Sb–F bonds were restrained to 1.86(2) Å, and *trans*-F···F distances within each SbF_6 octahedron to 3.72(2) Å. All non-H atoms except for F atoms with occupancy <0.5 were refined anisotropically. All H atoms were placed in calculated positions and refined using a riding model. The deepest Fourier hole of -1.4 e Å^{-3} lies within one of the disordered anions.

2.2.3. Single crystal X-ray structure of ***1[SbF$_6$]$_2$ · CH$_3$-NO$_2$ (3/2.7)***

Two of the three CH_3NO_2 sites in the asymmetric unit are wholly occupied, while the third was modelled with an occupancy of 0.7. This makes a total solvent content of 2.7 mole equivalents of CH_3NO_2 in the crystal examined. One of the two SbF_6^- anions is disordered over two equally occupied sites, and was modelled with the restraints Sb–F = 1.87(2) Å, and *trans*-F···F = 3.74(2) Å. All non-H atoms were refined anisotropically. All H atoms were placed in calculated positions and refined using a riding model. The highest residual Fourier peak of 1.1 e Å^{-3} lies 0.8 Å from the wholly occupied Sb atom.

2.3. Other measurements

CHN microanalyses were performed by the University of Leeds, Department of Chemistry microanalytical service. Variable temperature magnetic susceptibility measurements were obtained in the solid state using a Quantum Design SQUID magnetometer in an applied field of 1000 G. Diamagnetic corrections for the sample (from Pascal's constants [18]) and the sample holder were applied to the data. Theoretical fits of the susceptibility data to the equation for the zero-field splitting of a high-spin d^6 transition ion [18] were carried out using SIGMAPLOT [19].

3. Results and discussion

The title compound was prepared by reaction of hydrated $FeCl_2$, L^1H and $AgSbF_6$ in a 1:2:2 molar ratio in refluxing CH_3NO_2. The resultant brown solution was filtered to remove an off-white AgCl precipitate and concentrated in vacuo. Addition of a excess Et_2O to the solution yielded a yellow microcrystalline product which analysed cleanly as solvent-free $[Fe(L^1H)_2][SbF_6]_2$ (**1[SbF$_6$]$_2$**). Variable temperature susceptibility data from a powder sample produced by grinding these microcrystals showed that, in contrast to **1[BF$_4$]$_2$** and **1[ClO$_4$]$_2$**, **1[SbF$_6$]$_2$** is fully high-spin over this temperature range (Fig. 1). The small decrease in $\chi_M T$ below 30 K arises from zero-field splitting of the high-spin d^6 ^5E ground term (in the D_{2d} symmetry shown by undistorted compounds of this type). These data were modelled to derive the zero-field splitting parameter [18], yielding $g = 2.18 \pm 0.01$ and $|D| = 5.6 \pm 0.1$ cm^{-1}. This value of $|D|$ is at the low end of the range exhibited by high-spin $[Fe(L^2R)_2]^{2+}$ derivatives ($3 \leqslant |D| \leqslant 13$ cm^{-1} [8,10,13]), which we have suggested might be characteristic of an unusual angular Jahn–Teller distortion in these compounds [13]. The crystallographic study of **1[SbF$_6$]$_2$** described below confirms that this complex does adopt such a distorted structure in the crystal.

Slow diffusion of Et_2O vapour into solutions of **1[SbF$_6$]$_2$** in acetone or CH_3CN afforded homogeneous solvate crystals that suffered from twinning. However, similar crystallisations of **1[SbF$_6$]$_2$** from CH_3NO_2 yielded three different single crystalline phases which were all crystallographically characterised. Two of these were the same yellow colour at room temperature, but had distinct prismatic and plate morphologies. They were, respectively, formulated as solvent-free **1[SbF$_6$]$_2$** and as solvated **1[SbF$_6$]$_2$** · $2CH_3NO_2$. The third crystal form

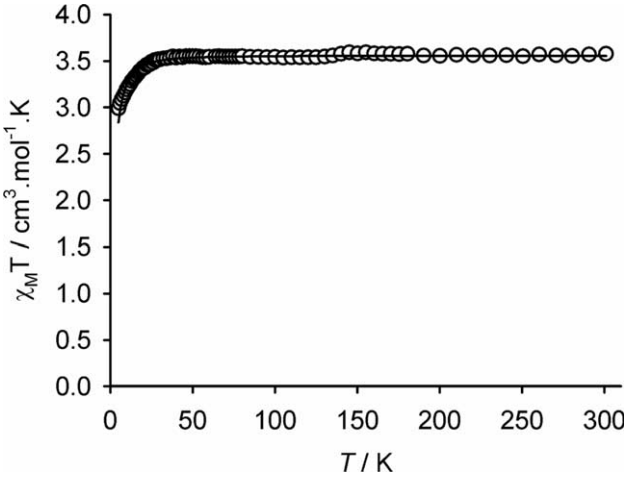

Fig. 1. Variable temperature magnetic susceptibility data for powdered **1[SbF$_6$]$_2$** (○). The line shows the theoretical fit of these data to the equation deriving the zero-field splitting parameter $|D|$. See text for more details.

existed as layered brown needles, from which single crystalline fragments could be separated. These had the formulation **1**[SbF_6]$_2$ · $3CH_3NO_2$ (although one of the three CH_3NO_2 sites was only ca. 70% occupied in the crystal examined). Both solvates rapidly decompose to a yellow powder upon exposure to air. The yellow and brown colours of these crystals are characteristic of high- and low-spin iron centres, respectively, in this series of complexes [3,7–13]. The distribution of the three crystal types in different crystallisation vials appeared to be essentially random. So, different batches of crystals each contained at least two of the three crystal types, with a different one predominating in each case.

The complex dication in unsolvated **1**[SbF_6]$_2$ is six-coordinate, with Fe–N bond lengths that are typical of a high-spin iron centre in this ligand environment [3–5, 7–13] (Table 2, Fig. 2). The coordination geometry about the iron centre is strongly distorted away from octahedral, however. This unusual structure is also exhibited by several $[Fe(L^2R)_2]^{2+}$ complex salts [8,12, 13], including $[Fe(L^2H)_2][SbF_6]_2$ (**2**[SbF_6]$_2$) which is isostructural with **1**[SbF_6]$_2$ [13]. This is the first time it has been observed in a complex from the $[Fe(L^1R)_2]^{2+}$ series, however. The distortion results from a Jahn–Teller splitting of the high-spin iron(II) centre and has two components, which can occur independently of each other [13]. These are a twisting of the plane of one ligand relative to the other about the N{pyridine}–Fe–N{pyridine} vector (so that $\theta < 90°$, Scheme 1); and, a rotation of one ligand about the Fe ion ($\phi < 180°$, Scheme 1). Examples of $[Fe(L^2R)_2]^{2+}$ complexes showing $61.2 \leqslant \theta \leqslant 90°$ and $154.4 \leqslant \phi \leqslant 180°$ have been previously characterised. In **1**[SbF_6]$_2$, θ (the dihedral angle between the least squares planes of the two symmetry-related ligands in the molecule) is 59.84(3)° and ϕ (the angle N(2)–Fe(1)–N(2^i), related by $-x$, y, $1/2 - z$) is 154.52(14)°. So, the structural distortion in **1**[SbF_6]$_2$ is the most pronounced yet observed. In order to accommodate this geometry, Fe(1) also protrudes out of the least-squares planes of the symmetry-related L^1H ligands by 0.4814 (15) Å (Fig. 3).

Table 2
Selected bond lengths (Å) and angles (°) in the crystal structure of **1**[SbF_6]$_2$

Fe(1)–N(2)	2.158(3)
Fe(1)–N(9)	2.191(3)
Fe(1)–N(14)	2.228(3)
N(2)–Fe(1)–N(2^i) (ϕ)	154.52(14)
N(2)–Fe(1)–N(9)	72.05(10)
N(2)–Fe(1)–N(9^i)	129.38(11)
N(2)–Fe(1)–N(14)	71.65(10)
N(2)–Fe(1)–N(14^i)	89.24(10)
N(9)–Fe(1)–N(9′)	84.59(15)
N(9)–Fe(1)–N(14)	141.27(10)
N(9)–Fe(1)–N(14^i)	108.70(11)
N(14)–Fe(1)–N(14^i)	83.85(14)
θ	59.84(3)

The parameters ϕ and θ are those defined in Scheme 1. Symmetry code (i): $-x$, y, $1/2 - z$.

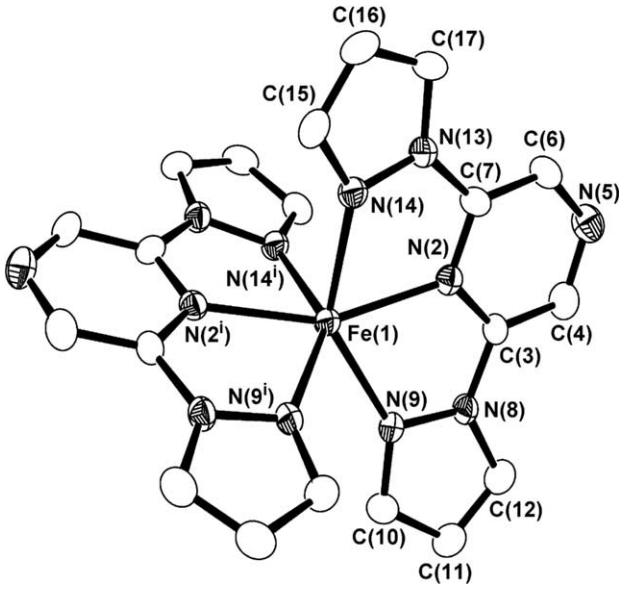

Fig. 2. View of the $[Fe(L^1H)_2]^{2+}$ dication in the crystal structure of **1**[SbF_6]$_2$, showing the atom numbering scheme employed. All H atoms have been omitted for clarity, and thermal ellipsoids are at the 50% probability level. Symmetry code (i): $-x$, y, $1/2 - z$.

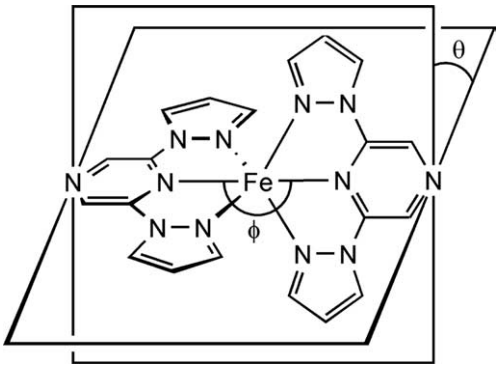

Scheme 1. The angles referred to in the discussion of the angular Jahn–Teller distortion in high-spin $[Fe(L^1H)_2]^{2+}$.

There is an intermolecular π–π interaction between pyrazole rings N(13)–C(17) and N(8)–C(12^{ii}) (related by $1/2 + x$, $-1/2 + y$, z), which are 3.356(5) Å apart at closest approach with a dihedral angle of 14.6(2)° between them. This gives rise to a four-way 'terpyridine embrace' packing motif [20], forming 2-D layers of π-stacked complex centres running parallel to the (110) crystal plane. While the X-ray analysis of **1**[SbF_6]$_2$ was performed at 150 K, further cooling of the crystal to 90 K did not cause it to darken in colour. That implies that the crystalline compound does not undergo a high → low spin-transition within this temperature range. The magnetic properties of **1**[SbF_6]$_2$ as a powder are consistent with that observation, and are what would be expected for a compound with this distorted coordina-

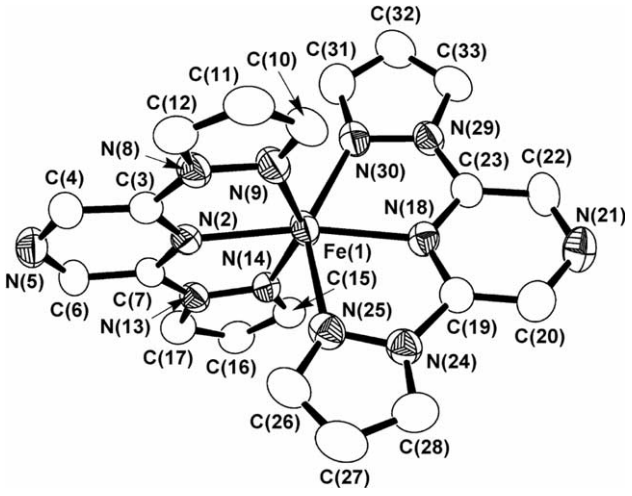

Fig. 3. View of the $[Fe(L^1H)_2]^{2+}$ dication in the crystal structure of $\mathbf{1}[\mathbf{SbF_6}]_2 \cdot 2CH_3NO_2$, showing the atom numbering scheme employed. All H atoms have been omitted for clarity, and thermal ellipsoids are at the 50% probability level. The complex dication in $\mathbf{1}[\mathbf{SbF_6}]_2 \cdot 3CH_3NO_2$ is visually similar to the one here, and uses the same atom numbering scheme.

tion geometry (see above). Hence, rapidly precipitated bulk samples of $\mathbf{1}[\mathbf{SbF_6}]_2$ also probably have this structure.

The iron centre in $\mathbf{1}[\mathbf{SbF_6}]_2 \cdot 2CH_3NO_2$ is also six-coordinate, and high-spin from its Fe–N bond distances (Table 3, Fig. 3). However, the coordination geometry about Fe(1) in this crystal is more regular (Fig. 4). The two ligands in the molecule are nearly perpendicular [$\theta = 84.66(4)°$], ϕ is closer to its ideal value at

Table 3
Selected bond lengths (Å) and angles (°) in the crystal structures of the two solvates of $\mathbf{1}[\mathbf{SbF_6}]_2$

	$\mathbf{1}[\mathbf{SbF_6}]_2 \cdot 2CH_3NO_2$	$\mathbf{1}[\mathbf{SbF_6}]_2 \cdot 3CH_3NO_2$
Fe(1)–N(2)	2.138(3)	1.884(3)
Fe(1)–N(9)	2.194(4)	1.976(4)
Fe(1)–N(14)	2.198(4)	1.982(4)
Fe(1)–N(18)	2.146(3)	1.889(3)
Fe(1)–N(25)	2.240(4)	1.978(4)
Fe(1)–N(30)	2.185(4)	1.975(4)
N(2)–Fe(1)–N(9)	73.46(13)	80.09(15)
N(2)–Fe(1)–N(14)	72.99(12)	80.32(15)
N(2)–Fe(1)–N(18) (ϕ)	163.23(13)	178.59(15)
N(2)–Fe(1)–N(25)	92.03(13)	100.47(15)
N(2)–Fe(1)–N(30)	122.64(13)	99.35(15)
N(9)–Fe(1)–N(14)	146.35(13)	160.41(15)
N(9)–Fe(1)–N(18)	100.41(13)	98.70(15)
N(9)–Fe(1)–N(25)	92.03(13)	91.49(15)
N(9)–Fe(1)–N(30)	96.89(14)	92.41(15)
N(14)–Fe(1)–N(18)	112.56(12)	100.89(15)
N(14)–Fe(1)–N(25)	96.38(13)	92.05(15)
N(14)–Fe(1)–N(30)	98.86(14)	90.76(15)
N(18)–Fe(1)–N(25)	71.88(13)	80.25(15)
N(18)–Fe(1)–N(30)	73.09(14)	79.95(15)
N(25)–Fe(1)–N(30)	144.91(14)	160.17(15)
θ	84.66(4)	88.59(4)

The parameters ϕ and θ are those defined in Scheme 1.

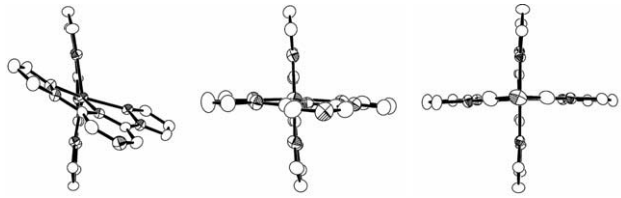

Fig. 4. Comparative views of the $[Fe(L^1H)_2]^{2+}$ dications in the crystal structures of $\mathbf{1}[\mathbf{SbF_6}]_2$ (left), $\mathbf{1}[\mathbf{SbF_6}]_2 \cdot 2CH_3NO_2$ (centre) and $\mathbf{1}[\mathbf{SbF_6}]_2 \cdot 3CH_3NO_2$ (right), emphasising the structural differences between them. The view in each case is parallel to the Fe(1)–N(2) bond with the ligand N(2)–C(17) vertical. All H atoms have been omitted for clarity, and thermal ellipsoids are at the 50% probability level.

163.23(13)°, and the Fe(1) site protrudes from the planes of each L^1H ligand by <0.1 Å. The complex dications in the structure again pack in the crystal through a four-way terpyridine embrace [20] with two unique intermolecular π–π interactions. These are between pyrazole rings N(8)–C(12) and $N(13^{iii})$–$C(17^{iii})$ (related by $1 + x$, y, z), which are 3.301(8) Å apart at closest approach with a dihedral angle of 4.4(3)° between them; and, between N(24)–C(28) and $N(29^{iv})$–$C(33^{iv})$ (related by x, $1 + y$, z), which are separated by 3.530(7) Å with a dihedral angle of 6.1(2)°. The resultant sheets of π-stacked complex molecules are aligned parallel to the (0 0 1) crystal plane and are separated by layers of CH_3NO_2 solvent molecules. While the full X-ray dataset was collected at 150 K, the crystal did not darken in colour upon further cooling to 90 K (the lowest temperature accessible with our N_2 cryostat). This strongly implies that $\mathbf{1}[\mathbf{SbF_6}]_2 \cdot 2CH_3NO_2$ also remains fully high-spin at this temperature and above.

In contrast to the other two crystal forms, the Fe–N bond lengths in $\mathbf{1}[\mathbf{SbF_6}]_2 \cdot 3CH_3NO_2$ are characteristic of a fully low-spin iron(II) centre [3–5,7–11] (Table 3). That is consistent with the dark brown colouration of this phase. As expected, the six-coordinate geometry about this low-spin iron(II) centre is more regular than for the two high-spin phases, with distortion angles θ [88.59(4)°] and ϕ [178.59(15)°] that are very close to their ideal values (Fig. 4). In contrast to the other two structures, there are no π–π interactions between neighbouring complex molecules in $\mathbf{1}[\mathbf{SbF_6}]_2 \cdot 3CH_3NO_2$, which does not exhibit the 'terpyridine embrace' packing motif. Rather, adjacent molecules in the crystal are linked through weak C–H···F and C–H···O hydrogen bonding interactions and van der Waals contacts only.

4. Conclusion

The polymorphism shown by $\mathbf{1}[\mathbf{SbF_6}]_2$ is consistent with several other $[Fe(L^1R)_2]^{2+}$ and $[Fe(L^2R)_2]^{2+}$ compounds we have studied, which also crystallise as mixtures of phases [3,8,12,13]. Interestingly unsolvated

1[SbF_6]$_2$ and **2**[SbF_6]$_2$ are the first pair of otherwise identical complex salts we have found from the [Fe(L^1R)$_2$]$^{2+}$ and [Fe(L^2R)$_2$]$^{2+}$ series that are isostructural. Importantly, **1**[SbF_6]$_2$ is the first known compound from the [Fe(L^1R)$_2$]$^{2+}$ series to undergo the angular Jahn–Teller distortion, which is quite common in [Fe(L^2R)$_2$]$^{2+}$ compounds [8,12,13]. Rapidly precipitated **1**[SbF_6]$_2$ also probably adopts this coordination geometry according to its susceptibility data. The now-proven existence of the angular distortion in [Fe(L^1R)$_2$]$^{2+}$ complexes emphasises that the magnetic properties of future compounds from this series will have to be interpreted with care if crystallographic data are not available. Structurally, **1**[SbF_6]$_2$ also represents the most severe example of this angular distortion yet discovered.

It is also notable that **1**[SbF_6]$_2 \cdot 2CH_3NO_2$ also remains high-spin at 90 K and above, despite showing a greatly reduced structural distortion. In comparison, **1**[BF_4]$_2 \cdot 3CH_3NO_2$ (which is not isostructural with **1**[SbF_6]$_2 \cdot 3CH_3NO_2$) does undergo an abrupt high $\rightarrow$ low spin-transition at 198 K and shows $\phi =$ 173.18(11)° in its high-spin form (Scheme 1) [3]. Clearly, the contraction of ϕ by an extra 9.95(17)° in **1**[SbF_6]$_2 \cdot 2CH_3NO_2$ compared to **1**[BF_4]$_2 \cdot 3CH_3NO_2$ is sufficient to prohibit a thermal spin-transition at accessible temperatures.

5. Supplementary data

Full crystallographic data for the compounds in this study are available on request from The Director, CCDC, 12 Union Road, Cambridge, CB2 1EZ, UK, fax: +44 1223 366 033, e-mail: deposit@ccdc.ac.uk or on the web www: http://www.ccdc.cam.ac.uk. The CCDC deposition numbers are 266335 (**1**[SbF_6]$_2$), 266336 (**1**[SbF_6]$_2 \cdot 2CH_3NO_2$) and 266337 (**1**[SbF_6]$_2 \cdot 3CH_3NO_2$).

Acknowledgements

The authors thank Dr. M. J. Hardie (University of Leeds) for the X-ray data collection of **1**[SbF_6]$_2 \cdot 3CH_3NO_2$ and Dr. H.J. Blythe (University of Sheffield) for the solid state susceptibility measurements. This work was funded by the EPSRC and the University of Leeds.

References

[1] (a) P. Gütlich, A. Hauser, H. Spiering, Angew. Chem. Int. Ed. 33 (1994) 2024;
(b) P. Gütlich, Y. Garcia, H.A. Goodwin, Chem. Soc. Rev. 29 (2000) 419;
(c) J.A. Real, A.B. Gaspar, V. Niel, M.C. Muñoz, Coord. Chem. Rev. 236 (2003) 121.
[2] M.A. Halcrow, Coord. Chem. Rev. (in press).
[3] J. Elhaïk, V.A. Money, S.A. Barrett, C.A. Kilner, I. Radosavljevic Evans, M.A. Halcrow, Dalton Trans. (2003) 2053.
[4] V.A. Money, I. Radosavljevic Evans, J. Elhaïk, M.A. Halcrow, J.A.K. Howard, Acta Crystallogr., Sect. B 60 (2004) 41.
[5] V.A. Money, J. Elhaïk, I. Radosavljevic Evans, M.A. Halcrow, J.A.K. Howard, Dalton Trans. (2004) 65.
[6] V.A. Money, J. Sánchez Costa, S. Marcén, G. Chastanet, J. Elhaïk, M.A. Halcrow, J.A.K. Howard, J.-F. Létard, Chem. Phys. Lett. 391 (2004) 273.
[7] J.M. Holland, J.A. McAllister, Z. Lu, C.A. Kilner, M. Thornton-Pett, M.A. Halcrow, Chem. Commun. (2001) 577.
[8] J.M. Holland, J.A. McAllister, C.A. Kilner, M. Thornton-Pett, A.J. Bridgeman, M.A. Halcrow, J. Chem. Soc., Dalton Trans. (2002) 548.
[9] V.A. Money, I. Radosavljevic Evans, M.A. Halcrow, A.E. Goeta, J.A.K. Howard, Chem. Commun. (2003) 158.
[10] J.M. Holland, C.A. Kilner, M.A. Halcrow, Inorg. Chem. Commun. 5 (2002) 328.
[11] V.A. Money, J. Elhaïk, M.A. Halcrow, J.A.K. Howard, Dalton Trans. (2004) 1516.
[12] J. Elhaïk, C.A. Kilner, M.A. Halcrow, Cryst. Eng. Commun. 7 (2005) 151.
[13] J. Elhaïk, D.J. Evans, C.A. Kilner, M.A. Halcrow, Dalton Trans. (2005) 1693.
[14] (a) E.C. Constable, G. Baum, E. Bill, R. Dyson, R. van Eldik, D. Fenske, S. Kaderli, D. Morris, A. Neubrand, M. Neuberger, D.R. Smith, K. Wieghardt, M. Zehnder, A.D. Zuberbühler, Chem. Eur. J. 5 (1999) 498;
(b) F. Pelascini, M. Wesolek, F. Peruch, A. De Cian, N. Kyritsakas, P.J. Lutz, J. Kress, Polyhedron 23 (2004) 3193.
[15] M. Loï, M.W. Hosseini, A. Jouaiti, A. De Cian, J. Fischer, Eur. J. Inorg. Chem. (1999) 1981.
[16] G.M. Sheldrick, Acta Crystallogr. A46 (1990) 467.
[17] G.M. Sheldrick, SHELXL 97, Program for the Refinement of Crystal Structures, University of Göttingen, Germany, 1997.
[18] C.J. O'Connor, Prog. Inorg. Chem. 29 (1982) 203.
[19] SIGMAPLOT, v. 8.02, Program for Tabulating, Modelling and Displaying Data, SPSS Scientific Inc., Chicago IL, USA, 2002.
[20] (a) M.L. Scudder, H.A. Goodwin, I.G. Dance, New J. Chem. 23 (1999) 695;
(b) J. McMurtrie, I. Dance, Cryst. Eng. Commun. 7 (2005) 216;
(c) J. McMurtrie, I. Dance, Cryst. Eng. Commun. 7 (2005) 230.

Available online at www.sciencedirect.com
SCIENCE DIRECT®
Polyhedron 25 (2006) 241–250
POLYHEDRON
www.elsevier.com/locate/poly

The adoption of the beryllium acetate structural motif in zinc oxycarbamates, oxythiocarbamates and oxythiophosphinates

Mohammad Azad Malik [a], Paul O'Brien [a,*], Majid Motevalli [b], Isaac Abrahams [b]

[a] School of Materials and School of Chemistry, The University of Manchester, Oxford Road, Manchester, M13 9PL, UK
[b] Centre for Materials Research, Department of Chemistry, Queen Mary, University of London, Mile End Road, London E1 4NS, UK

Received 30 March 2005; accepted 24 June 2005
Available online 15 August 2005

Abstract

Zn_4OL_6 (L = S_2CNEt_2, S_2PEt_2 and $OCNEt_2$) complexes are readily formed by hydrolysis of the mixed alkylzinc-carbamato, thiophophinato or thiocabamato (RZnL) compounds. These oxyzinc complexes all adapt a basic beryllium-acetate-like tetrahedral (μ_4-O)Zn_4 core. The coordination of each zinc atom is completed by bridging carbamato, thiocarbamato or thiophosphinato groups. Disorder is observed in the zinc positions for the two sulfur-containing compounds, with zinc atoms disordered over the eight corners of a cube. The geometry of the core (μ_4-O)Zn_4 moiety is compared with ZnO and a number of related complexes.
© 2005 Elsevier Ltd. All rights reserved.

Keywords: Zinc; Carbamato; Thiocarbamato; Thiophosphinato; Zinc oxide; Crystal structure

1. Introduction

Dithiocarbamates are used in rubber chemistry and technology, inorganic analysis and in agriculture as fungicides. Bis(diethyldithiocarbamato)zinc(II) and alkyl-(dialkyldithiocarbamato)zinc(II) have successfully been used to grow thin films and nanoparticles of ZnS using MOCVD and colloidal methods, respectively [1–4]. The structures of bis(diethyldithiocarbamato)zinc(II) [5] bis(dimethyldithiocarbamato)zinc(II) [6] asymmetric bis(dialkyldithiocarbamato)zinc(II) [7] and alkyl(dialkyldithiocarbamato)zinc(II) [8] have been reported.

Dialkylcarbamato complexes have been prepared by various methods including the reaction of metal chlorides with carbon dioxide and a secondary amine [9], the elemental metal with carbon dioxide and a secondary amine [10] and the insertion of carbon dioxide into a M-NR_2 (R = alkyl, M = metal) bond [11]. We have reported the synthesis of a series of diseleno- and dithiocarbamato complexes ($[RME_2CNR'_2]_2$, E = S, Se) [8,12–17] via insertion reaction with CS_2 or CSe_2. The structural chemistry of these compounds is dominated by the formation of dimeric species. The reaction of CO_2 with alkylzincdiethylamides ($RZnNEt_2$) gave unusual tetrameric species such as $[(CH_3)_2Zn_4(O_2CN(C_2H_5)_2)_6]$ [18] and $[(CH_3)_4Zn_4(O_2CN(C_2H_5)_2)_4]$ [19] which on further reaction with tetramethylethylenediamine or pyridine gave monomeric $[(Me_2NCH_2)_2Zn(O_2CN(C_2H_5)_2)_2]$ and dimeric $[C_5H_5NZn_2Me(O_2CN–(C_2H_5)_2)_3]$ species, respectively [20,21]. $Zn_4O(O_2CN\text{-}(C_2H_5)_2)_6]$ [10] was obtained when elemental zinc was reacted with CO_2/$HNEt_2$. This structure was found to exhibit the beryllium acetate structural motif [22], with a (μ_4-O)Zn_4 tetrahedron at the core of the molecule.

Dithiophosphinates have many important industrial and agricultural applications, including solvent extraction reagents for metals [23], insecticides and pesticides, flotation agents for mineral ores, and additives to lubricant oils [24]. Metal complexes of such ligands have the

* Corresponding author. Tel.: +44 161 275 4652; fax: +44 161 275 4616.
E-mail addresses: azad.malik@man.ac.uk (M.A. Malik), paul.obrien@manchester.ac.uk (P. O'Brien).

0277-5387/$ - see front matter © 2005 Elsevier Ltd. All rights reserved.
doi:10.1016/j.poly.2005.06.033

potential to be new precursors for use in LP-MOCVD. The deposition of II/VI semiconductors had been previously achieved with zinc and cadmium dimethyldithiophosphinates by Takahashi et al. [25]. They grew good quality ZnS and CdS films on silver-plated glass substrates between 400 and 500 °C.

In continuation of our studies on carbamato, thiophophinatio and thiocarbamato complexes, here we report the synthesis and the X-ray single crystal structures of the zinc complexes: $[Zn_4(\mu_4\text{-}O)(O_2CNEt_2)_6]$ (**1**), $[Zn_4(\mu_4\text{-}O)(S_2PEt_2)_6]$ (**2**) and $[Zn_4(\mu_4\text{-}O)(S_2CNEt_2)_6]$ (**3**) which all exhibit the beryllium acetate structural motif.

2. Experimental

2.1. Chemicals

All operations were carried out under air sensitive conditions using a standard Schlenck line. Diethylzinc, carbon dioxide and diethylamine were supplied by Aldrich Chemical Co. Ltd, dimethylzinc from Epichem Ltd. Sulfur, zinc sulfate (99%) and solvents were obtained from BDH.

2.2. Synthesis

2.2.1. $[Zn_4(\mu_4\text{-}O)(O_2CNEt_2)_6]$ (1)

This compound was first prepared serendipitously by the reaction of carbon dioxide with Et_2NZnMe in toluene containing traces of water. The expected product $MeZnO_2CNEt_2$was later prepared using dry toluene [19]. $[Zn_4(\mu_4\text{-}O)(O_2CNEt_2)_6]$ (**1**) was subsequently reproducibly prepared by the reaction of dimethylzinc (4.64 g, 48.6 mmol) with diethylamine (3.55 g, 48.6 mmol) in toluene at 70 °C for 2 h and then bubbling carbon dioxide through this product solution after addition of 2 ml of wet toluene (prepared by adding a drop of water in 50 ml of dry toluene) at 0 °C. The solvent was evaporated completely and the solid crystallised from hot toluene. The product was identified as $Zn_4O(O_2CNEt_2)_6$ (**1**) (2.9 g, yield: 60%). Elemental *Anal*. Calc.: C, 36.97; H, 6.16; N, 8.63. Found: C, 37.12; H, 6.20; N, 8.69%. I.R. spectrum Nujol (cm^{-1}): 2975–2580 s, 1566 vs, 1425 s, 1220 s, 518 s. ^1H NMR (ppm): 1.01 (t, CH_3), 3.53 (q, CH_2).

2.2.2. $[Zn_4(\mu_4\text{-}O)(S_2PEt_2)_6]$ (2)

Compound (**2**) was isolated by first preparing sodium diethyldithiophosphinate using the method of Kuchen et al. [26]. An aqueous solution of sodium diethyldithiophosphinate (3.5 g, 20 mmol) was then reacted with zinc sulfate (1.6 g, 10 mmol) to produce diethyldithiophophinatozinc(II) [9]. The product was recrystallised from acetone at room temperature. Diethyldithiophophinatozinc(II) (2.6 g, 7 mmol) was then reacted with diethylzinc (0.4 g, 3 mmol) in wet toluene to give $Zn_4O(S_2PEt_2)_6$. X-ray quality crystals were obtained from the toluene solution (yield: 2.4 g, 87%). Elemental *Anal*. Calc.: C, 24.07; H, 5.05; S, 32.13. Found: C, 24.21; H, 5.11; S, 32.34%. I.R spectrum major bands (nujol (cm^{-1})): 2980–2840 s, 1555, 1510 vs, 987 s, 560 s. ^1H NMR (ppm): 1.03 (t, CH_3), 3.67 (q, CH_2).

2.2.3. $[Zn_4(\mu_4\text{-}O)(S_2CNEt_2)_6]$ (3)

The preparation of compound (**3**) was carried out by first preparing diethyldithiocarbamatozinc(II) using a slight modification of the method of Bernard and Woodbrige [27]. The ammonium salt of thiocarbamic acid was prepared by the reaction of carbon disulfide and diethylamine in 1:2 mole ratio at room temperature in methanol. A solution of zinc dichloride in water was then added to this mixture dropwise at 10 °C to give diethyldithiocarbamatozinc(II). A white precipitate was separated by filtration and dried under vacuum. Diethyl zinc (0.9 g, 7.3 mmol) was added to the solution of diethyldithiocarbamatozinc(II) (8.0 g, 22.0 mmol) in toluene in the presence of 2 ml of wet toluene (Eq. (10)) to give $Zn_4O(S_2CNEt_2)_6$ as a white crystalline solid (3.7 g, yield: 44%). Elemental *Anal*. Calc.: C, 30.88; H, 5.18; N, 7.20; S, 32.98. Found: C, 31.07; H, 5.21; N, 7.28; S, 33.36%. I.R. spectrum Nujol (cm^{-1}): 2977–2834 s, 1558 vs, 1433 s, 1211 s, 975 vs. ^1H NMR (ppm) 1.01 (t, CH_3), 3.41 (q, CH_2).

2.3. Physical measurements

^1H NMR spectra were recorded using a Bruker AM250 pulsed Fourier transform spectrometer. Infrared spectra were measured on a Matteson Polaris FT-IR spectrometer as nujol mulls.

2.4. X-ray crystallography

X-ray diffraction data were collected on selected crystals of compounds (**1**), (**2**) and (**3**). The intensity data for (**1**) were collected using a FAST area detector at 120(2) K. Data collection, reduction and cell refinement procedures are described elsewhere [28]. Intensity data for (**2**) and (**3**) were collected on an Enraf Nonius CAD-4 diffractometer using Mo Kα radiation ($\lambda = 0.71069$ Å) with ω–2θ scans at 293(2) K. Data for were corrected for absorption using the program SORTAV [29] for (**1**) and DIFABS [30] for (**2**) and (**3**). All structures were solved by direct methods using SHELXS-97 [31–33] and refined on F^2 using SHELXL-97 [31–33]. Anisotropic parameters were refined for all non-hydrogen atoms. The H atoms were calculated geometrically and refined using a riding model. Molecular graphics were obtained using ORTEP3 for Windows [34]. Data collection and structure refinement details are summarised in Table 1. CCDC reference numbers 264145–264147.

Table 1
Crystal data and structure refinement for $[Zn_4(\mu_4\text{-}O)(O_2CNEt_2)_6]$ (**1**), $[Zn_4(\mu_4\text{-}O)(S_2PEt_2)_6]\cdot C_7H_8$ **2** and $[Zn_4(\mu_4\text{-}O)(S_2CNEt_2)_6]\cdot C_7H_8$ **3**

Compound	**1**	**2**	**3**
Formula	$C_{30}H_{60}N_6O_{13}Zn_4$	$C_{31}H_{68}OP_6S_{12}Zn_4$	$C_{37}H_{68}N_6OS_{12}Zn_4$
M	974.32	1288.87	1259.17
T (K)	150(2)	293(2)	293(2)
Crystal system	monoclinic	monoclinic	orthorhombic
Space group	$P2_1/a$	$P2_1/n$	*Pcab*
Unit cell dimensions			
a (Å)	21.825(1)	11.986(6)	14.942(2)
b (Å)	36.879(1)	20.242(16)	18.468(4)
c (Å)	21.213(1)	11.656(9)	20.387(7)
β (°)	98.21(1)	97.53(5)	
U (Å^3)	17457(1)	2804(3)	5626(2)
Z	16	2	4
μ (Mo Kα) (mm^{-1})	2.233	2.334	2.164
Reflections collected	150995	5173	4351
Independent reflections	39144	4919	3883
R_{int}	0.1151	0.0235	0.0164
Final *R* indices [$I > 2\sigma(I)$]	$R_1 = 0.0665$	$R_1 = 0.0371$	$R_1 = 0.0472$
	$wR_2 = 0.1067$	$wR_2 = 0.0854$	$wR_2 = 0.1088$
R indices (all data)	$R_1 = 0.2094$	$R_1 = 0.0892$	$R_1 = 0.1489$
	$wR_2 = 0.1386$	$wR_2 = 0.0992$	$wR_2 = 0.1311$

3. Results and discussion

$[Zn_4(\mu_4\text{-}O)(O_2CNEt_2)_6]$ (**1**) was first prepared serendipitously instead of an expected product $MeZnO_2CNEt_2$ during the insertion reaction of carbon dioxide into the Zn–N bond of Et_2NZnMe. The insertion of the oxide into the expected product was believed to have derived from poorly dried toluene which was used as a solvent in the reaction. The expected product $MeZnO_2CNEt_2$ was then successfully prepared by using dry toluene [19] and the serendipitous product was reproducibly prepared using wet toluene (Eq. (1)) and then bubbling carbon dioxide through this product solution after addition of 2 ml of wet toluene (prepared by adding a drop of water in 50 ml of dry toluene) at 0 °C (Eq. (2)).

$$Me_2Zn + Et_2NH \xrightarrow[70^\circ C]{\text{toluene}} Et_2NZnMe + CH_4 \quad (1)$$

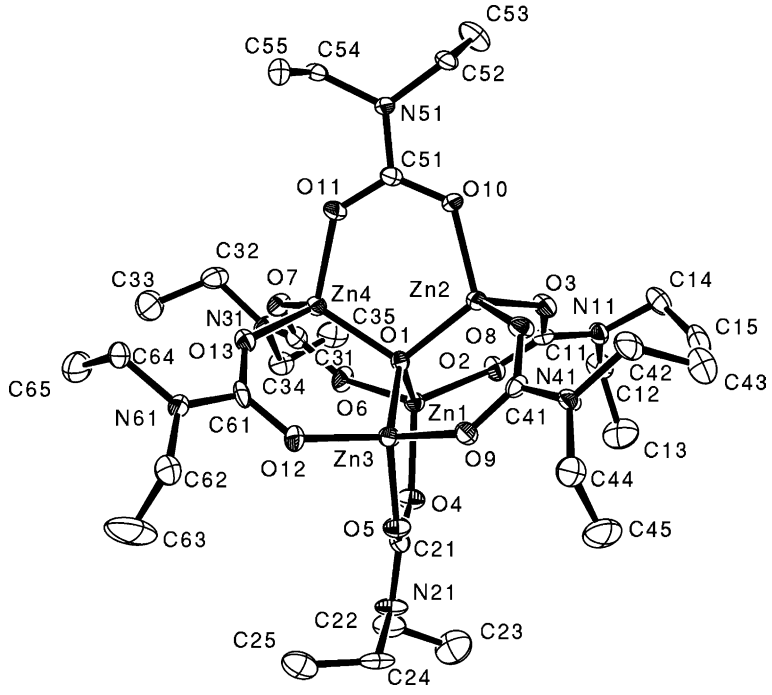

Fig. 1. Thermal ellipsoid plot (50% probability) showing structure of $[Zn_4(\mu_4\text{-}O)(O_2CNEt_2)_6]$ (**1**). Molecule a is only shown.

$$6Et_2NZnMe + 6CO_2 + 3H_2O \xrightarrow[0^\circ C]{\text{toluene}} Zn_4O(O_2CNEt_2)_6 + 2ZnO + 6CH_4 \quad (2)$$

Compound (**2**) was isolated by first preparing sodium diethyldithiophosphinate using the method of Kuchen et al. [26] (Eqs. (3)–(5)).

$$4EtMgBr + 2PSCl_3 \rightarrow Et_2PSSPEt_2 + 4MgBrCl + Cl_2 \quad (3)$$

$$Et_2PSSPEt_2 + Na_2S + S \rightarrow 2NaS_2PEt_2 \quad (4)$$

$$2NaS_2PEt_2(aq) + ZnSO_4(aq) \rightarrow Zn(S_2PEt)_2 + Na_2SO_4(aq) \quad (5)$$

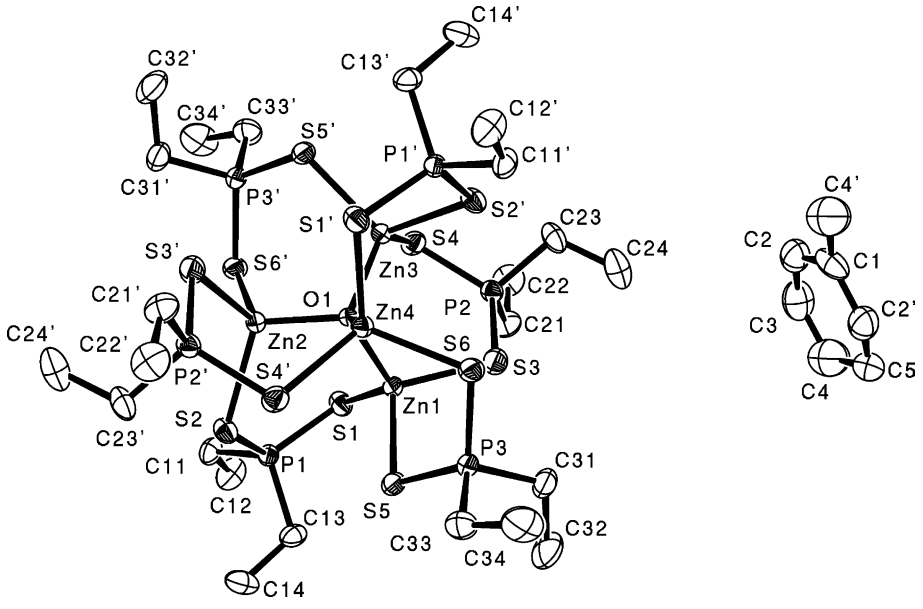

Fig. 2. Thermal ellipsoid plot (50% probability) showing structure of $[Zn_4(\mu_4\text{-}O)(S_2PEt_2)_6]\cdot C_7H_8$ (**2**). Disorder in Zn positions and solvent molecule not shown for clarity.

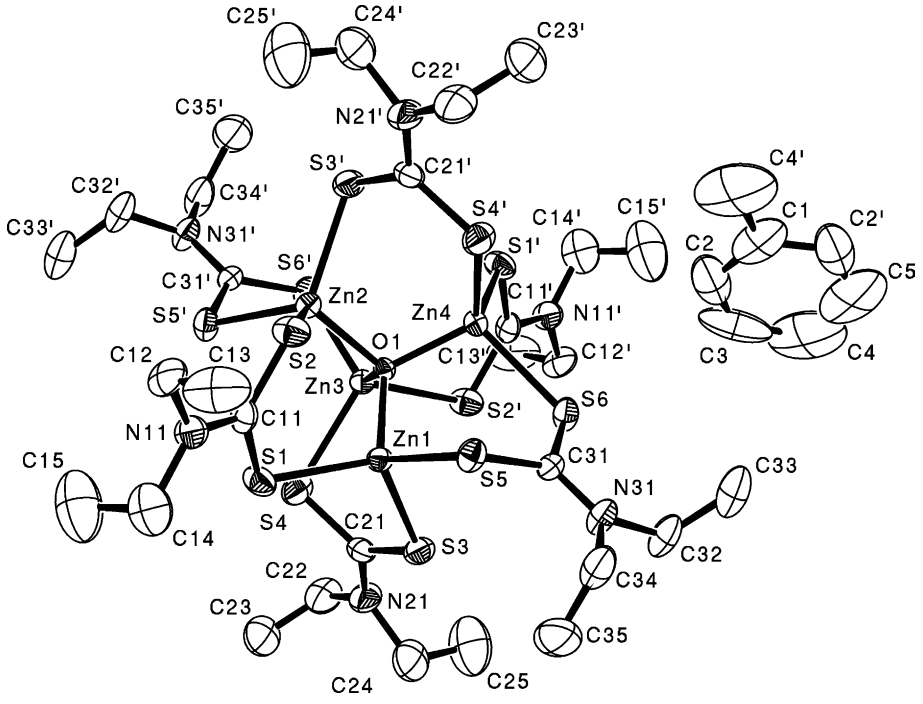

Fig. 3. Thermal ellipsoid plot (50% probability) showing structure of $[Zn_4(\mu_4\text{-}O)(S_2CNEt_2)_6]\cdot C_7H_8$ (**3**). Disorder in Zn positions and solvent molecule not shown for clarity.

Table 2
Selected bond distances (Å) and angles (°) in $[Zn_4(\mu_4\text{-}O)(O_2CNEt_2)_6]$ (**1**)

	a	b	c	d
μ_4O–Zn				
O(1)–Zn(1)	1.955(3)	1.950(3)	1.950(3)	1.946(4)
O(1)–Zn(2)	1.934(3)	1.945(3)	1.948(3)	1.943(3)
O(1)–Zn(3)	1.947(3)	1.938(3)	1.947(3)	1.945(3)
O(1)–Zn(4)	1.951(3)	1.949(3)	1.944(3)	1.948(3)
Zn(1)–O(1)–Zn(2)	110.9(2)	110.1(2)	108.2(2)	108.5(2)
Zn(1)–O(1)–Zn(3)	108.1(2)	108.1(2)	109.6(2)	111.3(2)
Zn(1)–O(1)–Zn(4)	109.5(2)	108.1(2)	109.3(2)	109.5(2)
Zn(2)–O(1)–Zn(3)	111.4(2)	109.6(2)	108.0(2)	107.8(2)
Zn(2)–O(1)–Zn(4)	107.7(2)	109.2(2)	112.1(2)	111.5(2)
Zn(3)–O(1)–Zn(4)	109.3(2)	111.8(2)	109.7(2)	108.3(2)
Zn-μ_2O				
Zn(1)–O(2)	1.933(4)	1.930(4)	1.933(4)	1.949(4)
Zn(1)–O(4)	1.942(3)	1.926(4)	1.928(4)	1.946(3)
Zn(1)–O(6)	1.925(4)	1.930(4)	1.933(4)	1.934(4)
Zn(2)–O(3)	1.938(4)	1.931(4)	1.932(4)	1.925(5)
Zn(2)–O(8)	1.944(3)	1.951(4)	1.934(4)	1.931(4)
Zn(2)–O(10)	1.937(3)	1.929(4)	1.948(4)	1.926(4)
Zn(3)–O(5)	1.940(4)	1.937(4)	1.940(4)	1.935(4)
Zn(3)–O(9)	1.950(4)	1.944(4)	1.946(4)	1.945(4)
Zn(3)–O(12)	1.935(4)	1.936(4)	1.931(4)	1.936(4)
Zn(4)–O(7)	1.938(4)	1.946(4)	1.941(4)	1.944(4)
Zn(4)–O(11)	1.938(3)	1.933(3)	1.953(3)	1.952(4)
Zn(4)–O(13)	1.924(4)	1.930(4)	1.941(4)	1.938(4)
O(1)–Zn(1)–O(2)	110.2(2)	109.2(2)	111.7(2)	112.5(2)
O(1)–Zn(1)–O(4)	112.9(2)	112.6(2)	111.1(2)	109.9(2)
O(1)–Zn(1)–O(6)	109.8(2)	110.9(2)	110.2(2)	110.0(2)
O(2)–Zn(1)–O(4)	112.6(2)	108.6(2)	111.9(2)	111.1(2)
O(2)–Zn(1)–O(6)	108.0(2)	109.3(2)	108.2(2)	106.6(2)
O(4)–Zn(1)–O(6)	103.0(2)	106.2(2)	103.2(2)	106.4(2)
O(1)–Zn(2)–O(3)	110.5(2)	111.0(2)	111.5(2)	111.5(2)
O(1)–Zn(2)–O(8)	110.2(1)	111.0(1)	113.4(2)	114.8(2)
O(1)–Zn(2)–O(10)	115.5(2)	112.0(2)	108.4(1)	108.1(2)
O(3)–Zn(2)–O(8)	108.3(2)	104.9(2)	108.9(2)	105.0(2)
O(3)–Zn(2)–O(10)	107.0(2)	111.1(2)	106.5(2)	108.2(2)
O(8)–Zn(2)–O(10)	105.1(2)	106.7(2)	107.7(2)	108.9(2)
O(1)–Zn(3)–O(5)	112.5(2)	112.9(2)	111.1(2)	110.1(2)
O(1)–Zn(3)–O(9)	109.9(1)	110.7(1)	111.5(2)	111.2(2)
O(1)–Zn(3)–O(12)	112.5(2)	110.5(2)	108.6(2)	110.9(2)
O(5)–Zn(3)–O(9)	105.8(2)	107.6(2)	109.0(2)	107.2(2)
O(5)–Zn(3)–O(12)	103.8(2)	106.5(2)	112.2(2)	110.4(2)
O(9)–Zn(3)–O(12)	112.1(2)	108.5(2)	104.4(2)	106.8(2)
O(1)–Zn(4)–O(7)	112.5(2)	113.8(2)	112.5(2)	111.9(2)
O(1)–Zn(4)–O(11)	110.4(2)	110.9(2)	110.4(2)	110.0(2)
O(1)–Zn(4)–O(13)	110.9(1)	108.9(1)	113.5(2)	113.6(2)
O(7)–Zn(4)–O(11)	108.6(2)	103.9(2)	112.0(2)	110.1(2)
O(7)–Zn(4)–O(13)	108.0(2)	104.7(2)	102.4(2)	104.0(2)
O(11)–Zn(4)–O(13)	106.2(2)	114.5(2)	105.7(2)	107.0(2)
μ_2O–C				
O(2)–C(11)	1.272(6)	1.274(7)	1.266(7)	1.271(7)
O(3)–C(11)	1.276(7)	1.286(7)	1.272(7)	1.282(8)
O(4)–C(21)	1.277(6)	1.274(7)	1.266(7)	1.283(7)
O(5)–C(21)	1.276(7)	1.276(7)	1.266(7)	1.268(7)
O(6)–C(31)	1.279(7)	1.249(7)	1.285(6)	1.290(6)
O(7)–C(31)	1.264(7)	1.270(7)	1.264(7)	1.270(7)
O(8)–C(41)	1.267(6)	1.270(6)	1.276(7)	1.283(7)
O(9)–C(41)	1.273(6)	1.275(6)	1.281(7)	1.284(6)
O(10)–C(51)	1.270(6)	1.282(7)	1.271(6)	1.260(7)
O(11)–C(51)	1.276(6)	1.267(6)	1.270(6)	1.262(7)
O(12)–C(61)	1.287(7)	1.291(7)	1.278(7)	1.282(6)
O(13)–C(61)	1.272(6)	1.263(6)	1.273(7)	1.272(6)
Zn(1)–O(2)–C(11)	130.3(4)	129.5(4)	129.0(4)	129.7(5)
Zn(2)–O(3)–C(11)	130.9(4)	128.0(4)	128.0(4)	131.6(4)
Zn(1)–O(4)–C(21)	129.8(4)	130.7(4)	131.2(4)	130.9(4)
Zn(3)–O(5)–C(21)	130.3(3)	129.9(4)	130.2(4)	131.5(4)
Zn(1)–O(6)–C(31)	132.6(4)	132.7(4)	132.1(4)	132.0(4)
Zn(4)–O(7)–C(31)	129.0(4)	127.6(4)	129.2(4)	129.2(4)
Zn(2)–O(8)–C(41)	130.0(3)	129.1(4)	128.5(4)	128.7(4)
Zn(3)–O(9)–C(41)	130.5(3)	130.7(4)	130.7(4)	132.9(4)
Zn(2)–O(10)–C(51)	126.9(3)	130.3(4)	132.0(4)	132.5(4)
Zn(4)–O(11)–C(51)	133.0(4)	131.6(4)	129.6(3)	129.2(4)
Zn(3)–O(12)–C(61)	129.7(4)	129.4(4)	133.2(4)	132.8(4)
Zn(4)–O(13)–C(61)	132.8(4)	132.9(4)	127.2(4)	128.8(4)
O(2)–C(11)–O(3)	125.5(6)	125.5(6)	125.9(7)	124.1(7)
O(4)–C(21)–O(5)	125.5(5)	125.6(5)	125.6(5)	125.2(5)
O(6)–C(31)–O(7)	125.5(5)	126.3(6)	125.6(6)	124.6(6)
O(8)–C(41)–O(9)	125.8(5)	125.1(5)	124.8(6)	124.3(5)
O(10)–C(51)–O(11)	125.5(5)	124.8(5)	125.4(5)	125.1(5)
O(12)–C(61)–O(13)	124.8(6)	125.0(6)	124.6(7)	124.9(6)

Individual molecules in the asymmetric unit are designated **a**–**d**. Estimated standard deviations are given in parentheses.

The reaction of diethyldithiophophinatozinc(II) with diethylzinc in wet toluene (Eqs. (6) and (7)) gave $Zn_4O(S_2PEt_2)_6$.

$$Zn(S_2PEt_2)_2 + Et_2Zn \rightarrow 2EtZnS_2PEt_2 \quad (6)$$

$$6EtZnS_2PEt_2 + 3H_2O \rightarrow Zn_4O(S_2PEt_2)_6 + 6C_2H_6 + 2ZnO \quad (7)$$

Compound (**3**) was similarly prepared from diethyldithiocarbamatozinc(II) using a slight modification of the method of Bernard and Woodbrige (Eq. (8)) [27].

$$CS_2 + 2Et_2NH \rightarrow (S_2CNEt_2)^-(Et_2NH_2)^+ \quad (8)$$

A solution of zinc dichloride in water was then added to this mixture dropwise at 10 °C (Eq. (9)) to give diethyldithiocarbamatozinc(II)

$$2(S_2CNEt_2)^-(Et_2NH_2)^+ + ZnCl_2 \rightarrow Zn(S_2CNEt_2)_2 + 2Et_2NH_2^+Cl^- \quad (9)$$

A white precipitate was separated by filtration and dried under vacuum. Diethyl zinc was added to the solution of diethyldithiocarbamatozinc(II) in toluene in the presence of 2 ml of wet toluene (Eqs. (10) and (11)) to give $Zn_4O(S_2CNEt_2)_6$ as a white crystalline solid.

$$Zn(S_2CNEt_2)_2 + Et_2Zn \rightarrow 2EtZnS_2CNEt_2 \quad (10)$$

$$6EtZnS_2CNEt_2 + 3H_2O \rightarrow Zn_4O(S_2CNEt_2)_6 + 6C_2H_6 + 2ZnO \quad (11)$$

All three compounds are soluble in most organic solvents and can readily be crystallised from toluene to give good quality transparent cubic crystals. These complexes are stable at room temperature under nitrogen

for a period of several months but on exposure to air, they slowly decompose to give ZnO powder.

The structures of (**1**), (**2**) and (**3**) were determined by X-ray single crystal methods. All three structures are closely related to each other (Figs. 1–3). The structures of (**2**) and (**3**) show a degree of disorder and in order to describe them it is helpful to start with a description of the ordered structure of (**1**). Significant contact distances and angles in the structure of (**1**) are given in Table 2. The crystal structure of (**1**) has four unique molecules in the asymmetric unit that are closely related. Small differences are observed in the bond lengths and angles between the four unique molecules, particularly in the alkyl moieties. Each molecule consists of a beryllium acetate like (μ_4-O)Zn_4 core, with zinc atoms located at four corners of a cube of average edge length 2.25 Å, resulting in a tetrahedral coordination of the central oxygen atom, with an average Zn–O bond length of 1.946 Å. The zinc atoms are also tetrahedrally coordinated (Fig. 4(a)), with oxygen atoms of the bridging carbamato ligands making up the Zn coordination sphere. Each carbamato group bridges two zinc atoms on the central unit, i.e., one edge of the (μ_4-O)Zn_4 tetrahedron, giving an overall molecular formula of $[Zn_4(\mu_4O)(O_2CNEt_2)_6]$.

Significant distances and angles in the crystal structure of (**2**) are given in Table 3. The structure of (**2**) is very similar to that of (**1**), however, the zinc atoms of

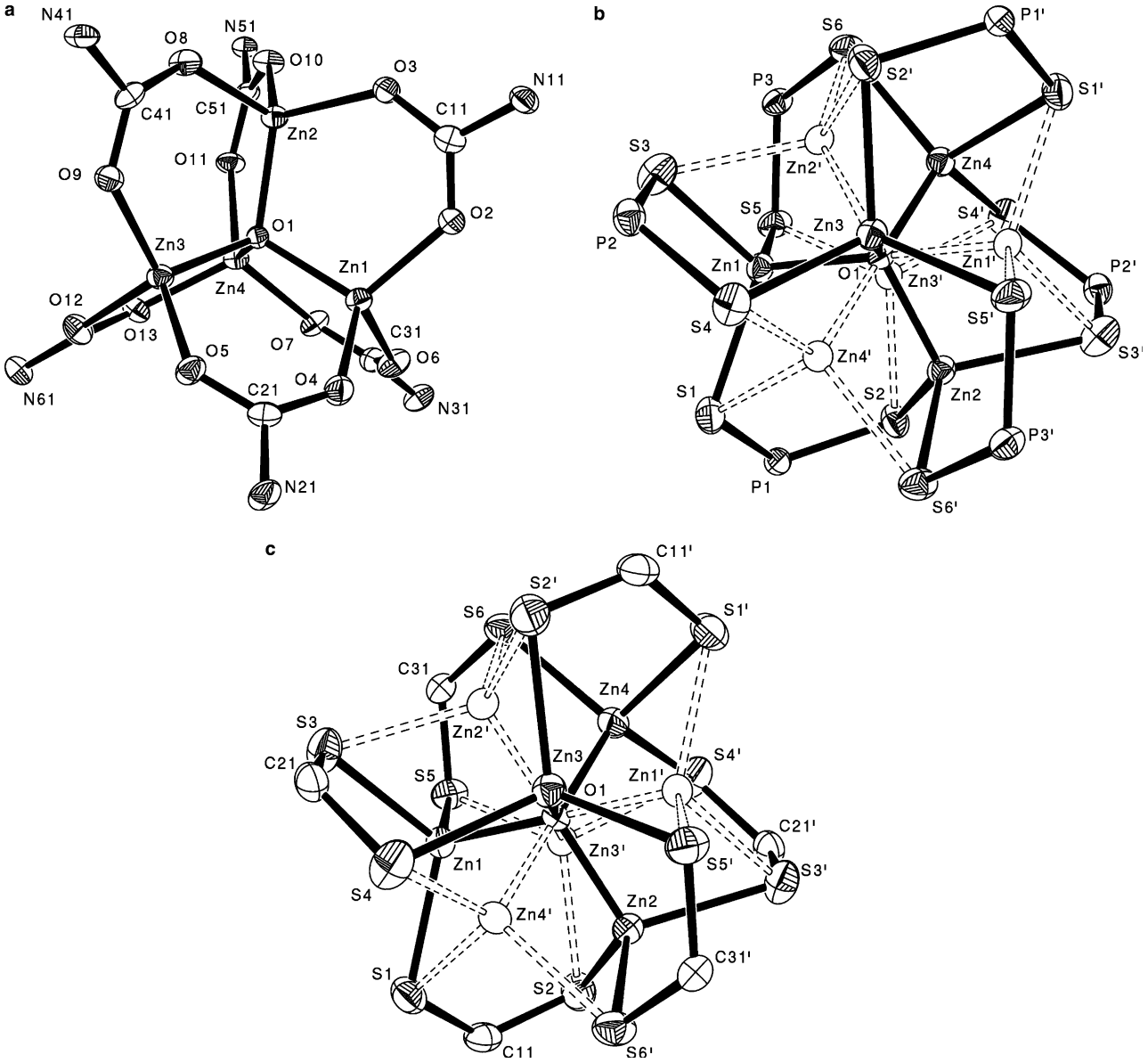

Fig. 4. (μ_4O)Zn_4 core in (a) **1**, (b) **2** and (c) **3** showing disorder of Zn positions in **2** and **3**. Molecule a shown only in **1**.

Table 3
Selected bond distances (Å) and angles (°) in $[Zn_4(\mu_4\text{-}O)(S_2PEt_2)_6]\cdot C_7H_8$ (**2**)

μ_4O–Zn	
O(1)–Zn(1)	2.002(2)
O(1)–Zn(3)	1.994(1)
O(1)–Zn(2)	1.982(2)
O(1)–Zn(4)	1.941(2)
Zn(1)–O(1)–Zn(2)	107.54(5)
Zn(1)–O(1)–Zn(4)	110.02(6)
Zn(2)–O(1)–Zn(4)	111.77(4)
Zn(1)–O(1)–Zn(3)	108.05(6)
Zn(2)–O(1)–Zn(3)	107.97(5)
Zn(3)–O(1)–Zn(4)	111.33(6)
Zn–S	
Zn(1)–S(1)	2.388(2)
Zn(1)–S(5)	2.451(2)
Zn(2)–S(3)′	2.462(2)
Zn(3)–S(2)′	2.394(2)
Zn(3)–S(5)′	2.340(2)
Zn(4)–S(4)′	2.422(2)
Zn(1)–S(3)	2.288(2)
Zn(2)–S(2)	2.369(2)
Zn(2)–S(6)′	2.341(2)
Zn(3)–S(4)	2.320(2)
Zn(4)–S(1)′	2.378(2)
Zn(4)–S(6)	2.378(2)
O(1)–Zn(1)–S(1)	109.77(6)
O(1)–Zn(1)–S(5)	106.33(6)
S(1)–Zn(1)–S(5)	112.56(7)
O(1)–Zn(2)–S(2)	109.68(6)
O(1)–Zn(2)–S(6)′	112.68(5)
S(2)–Zn(2)–S(6)′	109.65(7)
O(1)–Zn(3)–S(2)′	108.28(6)
O(1)–Zn(3)–S(5)′	110.88(7)
S(2)′–Zn(3)–S(5)′	108.22(7)
O(1)–Zn(4)–S(1)′	112.47(7)
O(1)–Zn(4)–S(6)	112.74(6)
S(1)′–Zn(4)–S(6)	105.02(6)
O(1)–Zn(1)–S(3)	111.92(6)
S(1)–Zn(1)–S(3)	108.97(6)
S(3)–Zn(1)–S(5)	107.28(6)
O(1)–Zn(2)–S(3)′	105.90(6)
S(2)–Zn(2)–S(3)′	110.39(7)
S(3)′–Zn(2)–S(6)′	108.47(7)
O(1)–Zn(3)–S(4)	112.20(6)
S(2)′–Zn(3)–S(4)	108.16(7)
S(4)–Zn(3)–S(5)′	108.99(7)
O(1)–Zn(4)–S(4)′	110.04(6)
S(1)′–Zn(4)–S(4)′	106.50(6)
S(4)′–Zn(4)–S(6)	109.79(8)
S–P	
S(1)–P(1)	2.007(2)
S(3)–P(2)	2.004(2)
S(5)–P(3)	2.013(2)
S(2)–P(1)	2.013(2)
S(4)–P(2)	2.007(2)
S(5)–P(3)	2.011(2)
Zn(1)–S(1)–P(1)	100.30(7)
Zn(2)–S(2)–P(1)	104.78(7)
Zn(1)–S(3)–P(2)	106.80(7)
Zn(3)–S(4)–P(2)	103.09(7)
Zn(1)–S(5)–P(3)	102.28(7)
Zn(2)–S(6)′–P(3)′	101.89(8)
Zn(4)–S(1)′–P(1)′	106.27(7)
Zn(3)–S(2)′–P(1)′	103.94(8)
Zn(2)–S(3)′–P(2)′	100.37(8)
Zn(4)–S(4)′–P(2)′	105.31(9)
Zn(3)–S(5)′–P(3)′	107.54(7)
Zn(4)–S(6)–P(3)	104.87(7)
S(1)–P(1)–S(2)	115.83(7)
S(5)–P(3)–S(6)	115.46(8)
S(3)–P(2)–S(4)	116.27(8)

Estimated standard deviations are given in parentheses.

Table 4
Selected bond distances (Å) and angles (°) in $[Zn_4(\mu_4\text{-}O)(S_2CNEt_2)_6]\cdot C_7H_8$ (**3**)

μ_4O–Zn	
O(1)–Zn(1)	1.934(2)
O(1)–Zn(3)	1.922(1)
O(1)–Zn(2)	1.988(1)
O(1)–Zn(4)	1.919(2)
Zn(1)–O(1)–Zn(2)	106.17(6)
Zn(1)–O(1)–Zn(4)	111.89(6)
Zn(2)–O(1)–Zn(4)	108.91(6)
Zn(1)–O(1)–Zn(3)	111.61(6)
Zn(2)–O(1)–Zn(3)	107.35(6)
Zn(3)–O(1)–Zn(4)	110.67(6)
Zn–S	
Zn(1)–S(1)	2.351(2)
Zn(1)–S(5)	2.438(2)
Zn(2)–S(3)′	2.406(2)
Zn(3)–S(2)′	2.424(2)
Zn(3)–S(5)′	2.294(2)
Zn(4)–S(4)′	2.313(2)
Zn(1)–S(3)	2.395(2)
Zn(2)–S(2)	2.354(2)
Zn(2)–S(6)′	2.363(2)
Zn(3)–S(4)	2.458(2)
Zn(4)–S(1)′	2.389(2)
Zn(4)–S(6)	2.394(2)
O(1)–Zn(1)–S(1)	110.62(8)
O(1)–Zn(1)–S(5)	107.31(8)
S(1)–Zn(1)–S(5)	111.02(8)
O(1)–Zn(2)–S(2)	108.71(8)
O(1)–Zn(2)–S(6)′	107.08(8)
S(2)–Zn(2)–S(6)′	114.01(9)
O(1)–Zn(3)–S(2)′	108.30(8)
O(1)–Zn(3)–S(5)′	113.62(8)
S(2)′–Zn(3)–S(5)′	109.99(8)
O(1)–Zn(4)–S(1)′	109.61(8)
O(1)–Zn(4)–S(6)	108.30(8)
S(1)′–Zn(4)–S(6)	106.82(9)
O(1)–Zn(1)–S(3)	108.82(8)
S(1)–Zn(1)–S(3)	112.88(9)
S(3)–Zn(1)–S(5)	105.93(8)
O(1)–Zn(2)–S(3)′	106.53(8)
S(2)–Zn(2)–S(3)′	111.80(8)
S(3)′–Zn(2)–S(6)′	108.34(8)
O(1)–Zn(3)–S(4)	105.43(7)
S(2)′–Zn(3)–S(4)	105.89(8)

(*continued on next page*)

Table 4 (*continued*)

S(4)–Zn(3)–S(5)′	113.17(9)
O(1)–Zn(4)–S(4)′	111.21(8)
S(1)′–Zn(4)–S(4)′	109.28(9)
S(4)′–Zn(4)–S(6)	111.52(9)
S–C	
S(1)–C(11)	1.724(7)
S(3)–C(21)	1.714(7)
S(5)–C(31)	1.730(6)
S(2)–C(11)	1.704(7)
S(4)–C(21)	1.721(7)
S(5)–C(31)	1.717(6)
Zn(1)–S(1)–C(11)	105.4(2)
Zn(2)–S(2)–C(11)	103.2(2)
Zn(1)–S(3)–C(21)	106.4(2)
Zn(3)–S(4)–C(21)	101.4(2)
Zn(1)–S(5)–C(31)	99.7(2)
Zn(2)–S(6)′–C(31)′	100.5(2)
Zn(4)–S(1)′–C(11)′	106.9(2)
Zn(3)–S(2)′–C(11)′	105.2(2)
Zn(2)–S(3)′–C(21)′	97.7(2)
Zn(4)–S(4)′–C(21)′	110.2(2)
Zn(3)–S(5)′–C(31)′	107.6(2)
Zn(4)–S(6)–C(31)	109.3(2)
S(1)–C(11)–S(2)	123.4(4)
S(5)–C(31)–S(6)	122.3(4)
S(3)–C(21)–S(4)	122.3(4)

Estimated standard deviations are given in parentheses.

the central (μ_4-O)Zn_4 unit are disordered over the eight corners of a cube of approximate edge length 2.29 Å (Fig. 4(b)), with an average Zn–O bond length of 1.980 Å. Each Zn site is half occupied and therefore it is likely that in any one particular molecule a tetrahedral coordination exists around the central oxygen atom as in Fig. 4(a). Bridging sulfur atoms from the thiocarbamato groups complete the tetrahedral coordination geometry around each of the Zn atoms. There is no disorder observed in the atomic positions of the thiocarbamato ligands. As in the structure of (**1**), each ligand effectively bridges two zinc atoms, which are distributed over four sites (i.e., four half occupied Zn sites in the disordered central unit). This again results in all edges of the central tetrahedral (μ_4-O)Zn_4 unit being shared with a ligand.

The structure of (**3**) also shows disorder of the zinc atoms of the central (μ_4-O)Zn_4 core (Fig. 4(c)), with ordered positions for the thiophosphinato ligands. Significant distances and angles in the crystal structure of (**3**) are presented in Table 4. The Zn atoms are disordered over the eight corners of a cube of average edge length 2.240 Å, with an average Zn–O bond length of 1.941 Å. As in the structure of (**2**), bridging ligands occupy the edges of the μ_4O-Zn_4 central tetrahedral unit, with each thiophosphinato ligand bridging two Zn atoms disordered over four sites.

Table 5
Average distances (Å), tetrahedral volume (Å^3) and distortion indices[a] for structures containing the (μ_4-O)(ZnX_3)$_4$ moiety (X = O, S)

Compound	Average distances			(μ_4-O)Zn_4	Distortion indices (μ_4-O)Zn_4			References
	μ_4O-Zn	Zn-X	Zn···Zn	Volume	D_b	D_e	D_a	
ZnO	1.978	1.978	3.230	3.969	0.003	0.006	0.013	[36]
[Zn_4(μ_4-O)($O_2CMe)_6$]	1.936	1.944	3.162	3.724	0.000	0.000	0.000	[37,38]
[Zn_4(μ_4-O) ($O_2CBu^t)_6$]	1.938	1.945	3.163	3.729	0.003	0.008	0.014	[39]
[Zn_4(μ_4-O) ($O_2CNEt_2)_6$]	1.938	1.920	3.163	3.730	0.024	0.003	0.013	[10]
[Zn_4(μ_4-O) ($O_2CNMe_2)_6$]	1.938	1.939	3.164	3.733	0.003	0.005	0.010	[40]
[Zn_4(μ_4-O) ($O_2CPh)_6$]	1.939	1.946	3.166	3.738	0.002	0.007	0.012	[39]
[Zn_4(μ_4-O) ($O_2CNC_5H_{10})_6$]	1.942	1.943	3.171	3.757	0.000	0.005	0.008	[41]
[Zn_4(μ_4-O) ($O_2CPh)_6$]	1.943	1.942	3.172	3.760	0.004	0.006	0.009	[42]
[Zn_4(μ_4-O) ($O_2CNBu^n_2)_6$]	1.943	1.952	3.173	3.759	0.000	0.011	0.016	[43]
[Zn_4(μ_4-O) ($O_2CNEt_2)_6$] (**1**)	1.946	1.940	3.178	3.779	0.002	0.007	0.010	This work
[Zn_4(μ_4-O) ($O_2CC(Co(CO)_3)_3)_6$]	1.946	1.927	3.175	3.771	0.033	0.002	0.029	[44]
[Zn_4(μ_4-O) ($O_2CNC_4H_8)_6$]	1.948	1.941	3.181	3.791	0.002	0.003	0.005	[41]
[Zn_4(μ_4-O) ($O_2CCpFeCp)_6$]	1.978	2.004	3.222	3.938	0.033	0.011	0.039	[45]
[Zn_4(μ_4-O) ($O_2P(OBu^t)_2)_6$]	1.996	1.946	3.259	4.078	0.007	0.004	0.008	[46]
[Zn_9(μ_4-O)$(Et)_6$(thf)$_2$($O_3PBu^t)_4$($O_2PBu^t_2)_4$]	2.013	2.028	3.274	4.126	0.030	0.018	0.041	[47]
[Zn_4(μ_4-O) (($S(CH_2)_2NHCH_2)_3N)Co)_4]^{6+}$	1.937	2.243	3.163	3.727	0.004	0.004	0.006	[48]
[Zn_4(μ_4-O) ($S_2CNEt_2)_6$] (**3**)	1.941	2.271	3.168	3.747	0.012	0.006	0.018	This work
[Zn_4(μ_4-O) (($S(CH_2)_2NH_2)_3Co)_4]^{6+}$	1.947	2.244	3.180	3.790	0.004	0.002	0.001	[49]
[Zn_4(μ_4-O) (($S(CH_2)_2NH_2)_3Rh)_4]^{6+}$	1.960	2.248	3.201	3.863	0.003	0.001	0.001	[50]
[Zn_4(μ_4-O) (($S(CH_2)_2N)_3Ir)_4]^{6+}$	1.965	2.249	3.208	3.892	0.004	0.002	0.004	[51]
[Zn_4(μ_4-O) ($S_2P(OCH_2Pr^i)_2)_6$]	1.966	2.252	3.211	3.900	0.002	0.002	0.004	[52]
[Zn_4(μ_4-O) (($S(CH_2)_2NH_2)_3Rh)_4]^{6+}$	1.966	2.256	3.211	3.901	0.007	0.001	0.006	[51]
[Zn_4(μ_4-O) (($S(CH_2)_2NH_2)_3Rh)_4]^{6+}$	1.966	2.256	3.211	3.901	0.006	0.000	0.006	[50]
[Zn_4(μ_4-O) (($S(CH_2)_2NH_2)_3Cr)_4]^{6+}$	1.970	2.250	3.216	3.919	0.011	0.001	0.009	[53]
[Zn_4(μ_4-O) ($S_2PEt_2)_6$] (**2**)	1.980	2.278	3.232	3.978	0.010	0.004	0.015	This work
[Zn_4(μ_4-O) ($S_2P(OBu^n)_2)_6$]	1.984	2.280	3.239	4.005	0.012	0.002	0.013	[54,55]

[a] $D_b = \frac{\sum |l_i - \bar{l}|}{4\bar{l}}$; $D_e = \frac{\sum |s_i - \bar{s}|}{6\bar{s}}$; $D_a = \frac{\sum |\theta_i - \bar{\theta}|}{6\bar{\theta}}$; where l_i is the central atom to vertex distance for vertex i and $\bar{l}$ is the mean value; s_i is the ith vertex to vertex distance and $\bar{s}$ is the mean value and θ_i is the ith angle and $\bar{\theta}$ is the mean value.

The crystal structure of (**1**) was determined previously by Belforte et al. [10] and refined in the tetragonal space group $I4_1/a$, with cell dimensions $a = 21.928$ Å and $c = 37.86$ Å. These cell dimensions are similar to the monoclinic dimensions presented here and the structures are in reasonable agreement. These authors, reported problems with low intensity data and consequently a low reflection/parameter ratio that prevented an anisotropic refinement or location of H atoms. It is therefore doubtful that the structure reported here and that by Belforte et al. represent different polymorphs.

Table 5 shows a comparison of geometrical parameters for structures containing the $(\mu_4\text{-O})(ZnX_3)_4$ moiety (X = O, S). These are compared with those for ZnO. Tetrahedral volumes have been calculated using the determinant method and vary from 3.72 Å^3 in $[Zn_4(\mu_4\text{-O})(O_2CMe)_6]$ to 4.13 Å^3 in $[Zn_9(\mu_4\text{-O})(Et)_6(thf)_2(O_3PBu^t)_4(O_2PBu^t_2)_4]$ and compare with a value of 3.97 Å^3 in ZnO. The secondary coordination sphere of the Zn atoms appears to have little affect on the volume of the $(\mu_4\text{-O})Zn_4$ core, despite the increase in average Zn–X bond length in the sulfur containing compounds. The distortion away from regular tetrahedral geometry has been characterised by Bauer in terms of three characteristic distortion indices reflecting distortions in bond length, edge length and angle (defined here as D_b, D_e and D_a, respectively) [35]. The structure of (**1**) shows average distortion indices ($D_b = 0.002$, $D_e = 0.007$, D_a 0.010) close to those of pure ZnO ($D_b = 0.003$, $D_e =$ 0.006, D_a 0.013), but with a significantly smaller average Zn–O distance. Structure **2** has a significantly larger bond distortion index ($D_b = 0.010$), which reflects the large Zn–O bond length range seen in this structure (Table 2), while D_e and D_a values (0.004 and 0.015, respectively) are close to those seen in ZnO. Interestingly, structure (**2**) show an average Zn–O bond length (1.980 Å) and a tetrahedral volume (3.978 Å^3) close to that in the pure oxide. Structure (**3**) has significantly larger values for D_b and D_a (0.012 and 0.018, respectively). The tetrahedral volume (3.75 Å^3) and average Zn–O bond length (1.941 Å) are similar to the values seen in structure (**1**).

4. Conclusions

The complexes (**1**), (**2**) and (**3**) are readily formed through the reaction of the appropriate alkyl zinc carbamate, thiocarbamates or thiophosphinates with water. The crystal structures of these complexes all exhibit a beryllium acetate like $(\mu_4\text{-O})Zn_4$ core. This structural motif appears to be relatively common in oxyzinc complexes, with the central $(\mu_4\text{-O})Zn_4$ tetrahedron showing geometrical parameters close to that of pure ZnO. These parameters are relatively unaffected by the secondary coordination sphere of the Zn atoms.

Acknowledgements

This work was funded by various EPSRC Grants to POB. We are indebted to the EPSRC National Crystallography Service at the University of Southampton, UK for X-ray data collection on structure (**1**). We gratefully acknowledge use of the EPSRC Chemical Databank Service at the Daresbury Laboratory UK.

References

[1] D.M. Frigo, O.F.Z. Khan, P. O'Brien, J. Cryst. Growth 96 (1989) 989.
[2] A. Saunders, A.Vecht, G. Yrell, Proceedings 7th International Conference on Ternary Multinary Compounds, 1986, 213 (published 1987) (Chem. Abstr., 1988, 108, 66226h).
[3] M.B. Hursthouse, M. Malik, M. Motevalli, P. O'Brien, Organometallics 10 (1991) 730.
[4] M.A. Malik, N. Revaprasadu, P. O'Brien, J. Mater. Chem. 11 (2001) 2382.
[5] M. Bonamico, G. Mazzone, A. Vaciago, L. Zambonelli, Acta Crystallogr. 19 (1965) 898.
[6] H.P. Klug, Acta Crystallogr. 21 (1966) 536.
[7] M. Motevalli, P. O'Brien, J.R. Walsh, I.M. Watson, Polyhedron 15 (1996) 2801.
[8] M.B. Hursthouse, M.A. Malik, M. Motevalli, P. O'Brien, Organometallics 10 (1991) 730.
[9] A. Belforte, F. Calderazzo, P.F. Zanazzi, J. Chem. Soc., Dalton Trans. (1988) 2921.
[10] A. Belforte, F. Calderazzo, U. Englert, J. Strahle, Inorg. Chem. (30) (1991) 3778.
[11] M.H. Chisholm, M.W. Extine, J. Am. Chem. Soc. (99) (1977) 792.
[12] M.A. Malik, P. O'Brien, J. Mater. Chem. 3 (1991) 999.
[13] M.B. Hursthouse, M.A. Malik, M. Motevalli, P. O'Brien, J. Mater. Chem 2 (1992) 949.
[14] M.A. Malik, M. Motevalli, J.R. Walsh, P. O'Brien, Organometallics 11 (1992) 3136.
[15] I. Abrahams, M.A. Malik, M. Motevalli, P. O'Brien, J. Organomet. Chem. 465 (1994) 73.
[16] M.A. Malik, T. Saeed, P. O'Brien, Polyhedron 12 (1993) 1533.
[17] M.A. Malik, M. Motevalli, T. Saeed, P. O'Brien, Adv. Mater. 5 (1993) 653.
[18] M.B. Hursthouse, M.A. Malik, M. Motevalli, P. O'Brien, J. Chem. Soc., Chem. Commun. (1991) 1690.
[19] I. Abrahams, M.A. Malik, M. Motevalli, P. O'Brien, J. Chem. Soc., Dalton Trans. (1995) 1043.
[20] M.A. Malik, M. Motevalli, P. O'Brien, Inorg. Chem. 34 (1995) 6223.
[21] M.A. Malik, P. O'Brien, Inorg. Chim. Acta 24 (1998) 239.
[22] A. Tulinsky, C.R. Worthington, E. Pignataro, Acta Crystallogr. 12 (1959) 623.
[23] W. Rickelton, R. Boyle, Solvent Extr. Ion Exc. 8 (1990) 783.
[24] I. Haiduc, D. Bryan-Sowerby, L. Shao-Fang, Polyhedron 14 (1995) 3389.
[25] Y. Takahashi, R. Yuki, M. Sugiura, S. Motojima, K. Sugiyama, J. Cryst. Growth 50 (1980) 491.
[26] W. Kuchen, J. Metten, A. Judat, Chem. Ber. 97 (1964) 2306.
[27] D. Barnard, D.T. Woodbridge, J. Chem. Soc. (1961) 2922.
[28] J.A. Darr, S.R. Drake, M.B. Hurstouse, K.M.A. Malik, Inorg. Chem. 32 (1993) 5704.
[29] R.H. Blessing, Acta Crystallogr., Sect. A 51 (1995) 33.
[30] N. Walker, D. Stuart, Acta Crystallogr., Sect. A 39 (1983) 158.

[31] G.M. Sheldrick, Programs for Crystal Structure Analysis (Release 97-2), Insitüt für Anorganische Chemie der Universität, Tammanstrasse 4, D-3400 Göttingen, Germany, 1998.
[32] G.M. Sheldrick, Acta Crystallogr., Sect. A 46 (1990) 467.
[33] G.M. Sheldrick, SHELXL-93, University of Göttingen, 1993.
[34] L.J. Farrugia, J. Appl. Crystallogr. 30 (1997) 565.
[35] W.H. Bauer, Acta Crystallogr., Sect. B 30 (1974) 1195.
[36] S.C. Abrahams, J.L. Bernstein, Acta Crystallogr. 25 (1969) 1233.
[37] H. Kovama, Y. Saito, Bull. Chem. Soc. Jpn. 27 (1954) 112.
[38] L. Hiltunen, M. Leskela, M. Makela, L. Niinisto, Acta Chem. Scand. A 41 (1987) 548.
[39] W. Clegg, D.R. Harbron, C.D. Homan, P.A. Hunt, I.R. Little, B.P. Straughan, Inorg. Chim. Acta 186 (1991) 51.
[40] D.B. Dell'Amico, F. Calderazzo, L. Labella, F. Marchetti, Inorg. Chim. Acta 350 (2003) 661.
[41] C.S. McCowan, T.L. Groy, M.T. Caudle, Inorg. Chem. 41 (2002) 1120.
[42] M.C. Yin, C.W. Wang, J.T. Sun, Cambridge Structural Database, Cambridge Crystallographic Data Centre, Cambridge, UK, 2004, Reference code XADJOC.
[43] D.B. Dell'Amico, F. Calderazzo, S. Farnocchi, L. Labella, F. Marchetti, Inorg. Chem. Commun. 5 (2002) 848.
[44] W. Cen, K.J. Haller, T.P. Fehlner, R.E. Marsh, Inorg. Chem. 31 (1992) 2672.
[45] H. Hou, L. Li, G. Li, Y. Fan, Y. Zhu, Inorg. Chem. 42 (2003) 3501.
[46] C.G. Lugmair, T.D. Tilley, A.L. Rheingold, Chem. Mater. 9 (1997) 339.
[47] Y. Yang, J. Pinkas, M. Noltemeyer, H.-G. Schmidt, H.W. Roesky, Angew. Chem., Int. Ed. Engl. 38 (1999) 664.
[48] K. Tokuda, K. Okamoto, T. Konno, Inorg. Chem. 39 (2000) 333.
[49] T. Konno, T. Nagashio, K. Okamoto, J. Hidaka, Inorg. Chem. 31 (1992) 1160.
[50] T. Konno, K. Okamoto, J. Hidaka, Inorg. Chem. 33 (1994) 538.
[51] T. Konno, K. Okamoto, J. Hidaka, Inorg. Chem. 30 (1991) 2253.
[52] S. Menzer, J.R. Phillips, A.M.Z. Slawin, D.J. Williams, J.D. Woollins, J. Chem. Soc., Dalton Trans. (2000) 3269.
[53] K. Okamoto, M. Matsumoto, Y. Miyashita, N. Sakagami, J. Hidaka, T. Konno, Inorg. Chim. Acta 260 (1997) 17.
[54] W. Qiguang, M. Yimin, J. Yaoxiu, C. Zhide, Lanzhou dax. xuebao, Zir. Kex. (Chin.) (J. Lanzhou. U. (Nat. Sci.)) 26 (1990) 24.
[55] S.-Z. Hu, Jiegou Huaxue (Chin.) (J. Struct. Chem.) 18 (1999) 470.

Available online at www.sciencedirect.com
SCIENCE DIRECT®
Polyhedron 25 (2006) 251–258
POLYHEDRON
www.elsevier.com/locate/poly

Synthesis and reactivity of $(silox)_2R_2WO$ (R = Cl, Me, Et, ^{n}Pr and ^{n}Bu; silox = OSi^tBu_3) and $(silox)_2MO_2$ (M = Mo and W)

Devon C. Rosenfeld, David S. Kuiper, Emil B. Lobkovsky, Peter T. Wolczanski *

Department of Chemistry and Chemical Biology, Baker Laboratory, Cornell University, Ithaca, NY 14853, United States

Received 30 March 2005; accepted 24 June 2005
Available online 24 August 2005

Dedicated to Prof. Malcolm H. Chisholm, whose mastery of group 6 helped inspire this and related research.

Abstract

Addition of Na(silox) (silox = OSi^tBu_3) to Cl_4WO afforded $(silox)_2Cl_2WO$ (**3**), and subsequent alkylation with appropriate Grignard reagents yielded $(silox)_2R_2WO$ (**4**-R; R = Me, Et, ^{n}Pr, ^{n}Bu). **4**-R adopt distorted trigonal bipyramidal structures with axial silox groups, as implied by the X-ray crystal structure of **4**-^{n}Bu. New metathetical procedures were utilized in the preparation of $(silox)_2M(O)_2$ (M = Mo, **6**; W, **7**); the addition of Na(silox) to $(DME)Cl_2M(O)_2$ (M = Mo, W) in THF afforded the dioxo species. None of the oxo complexes exhibited oxygen atom transfer (OAT) to PMe_3. The thermolysis of **4**-Et and **4**-^{n}Bu afforded olefin derivatives $(silox)_2$(ole)WO (**5**-ole; ole = C_2H_4, C_4H_8) as the primary products. Thermal degradation of $(silox)_2(CD_3CH_2)_2WO$ (**4**-CH_2CD_3) revealed H/D-scrambling among α- and β-positions indicative of reversible β-H-elimination prior to alkane loss. A brief discussion of the lack of OAT is presented.
© 2005 Elsevier Ltd. All rights reserved.

Keywords: Tungsten; Oxo; Atom transfer; Alkyl

1. Introduction

Recent investigations of oxygen atom transfer (OAT) [1] to $(silox)_3M$ (**1**-M, M = V, Nb, Ta; silox = OSi^tBu_3) from EO (EO = OPR_3, R = Me, Ph, ^{t}Bu; $(silox)_3WNO$ (**2**)) revealed that a linear reaction coordinate was symmetry (orbitally) forbidden, as shown in Fig. 1 [2]. Where EO = OPR_3 and R = Me and Ph, OAT to **1**-M (M = Nb, Ta) was facile because a bent transition state (or intermediate) was sterically feasible. When R = ^{t}Bu, no atom transfer was observed, and the X-ray crystal structure of (silox)V-O-P^{t}Bu$_3$ ($\angle$V–O–P = 180°) suggested that a similar bent transition state was sterically implausible. In corroboration, deoxygenations of $(silox)_3W$-NO (**2**) by $(silox)_3M$ (**1**-M, M = NbL (L = py, PMe_3), Ta) were extremely slow, although the free energy of reaction for each deoxygenation was calculated to be roughly −100 kcal/mol. A bent L_nM-O-E geometry allowed mixing of σ- and π-type orbitals in the lower symmetry environment, thereby rendering each step orbitally allowed. As a consequence, intersystem crossing events necessary for OAT occurred at lower energies. While the orbital symmetry arguments are compelling for the examples at hand, whether the bent versus linear transition state differences are general is still in question.

In search of additional examples of OAT, group 6 was an attractive target, especially tungsten and molybdenum [1]. For these metals, a published thermodynamic scale [3] of OAT suggested that the transfer might occur from the metal to a substrate such as a

* Corresponding author. Tel.: +1 607 255 7220; fax: +1 607 255 4137.
E-mail address: ptw2@cornell.edu (P.T. Wolczanski).

0277-5387/$ - see front matter © 2005 Elsevier Ltd. All rights reserved.
doi:10.1016/j.poly.2005.06.050

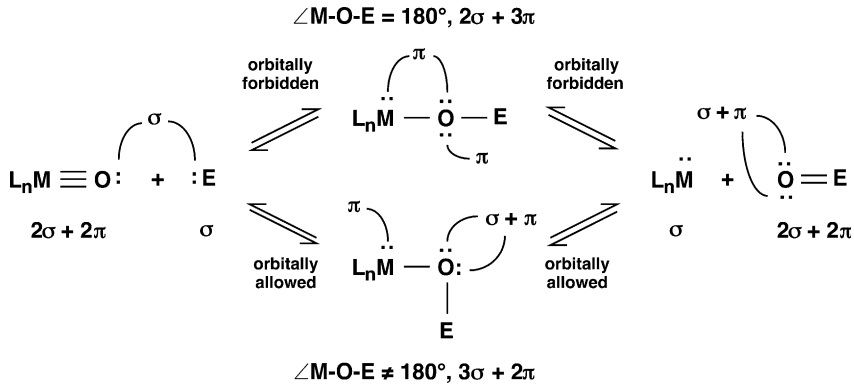

Fig. 1. Consequences of orbital symmetry upon oxygen atom transfer (OAT).

phosphine, since the bond dissociation energies of Cl_4WO and Ph_3PO were purported to be roughly 127 and 133 kcal/mol, respectively. Drew et al. [4] provided literature corroboration of the crude thermodynamics for OAT because exposure of Cl_4WO to PPh_3 yielded $Cl_4W(PPh_3)_2$, $Cl_4WO(OPPh_3)(PPh_3)$ and $OPPh_3$. It was postulated that OAT from $(silox)_2Cl_2WO$ would lead to $(silox)_2WCl_2$, a much sought after d^2 square planar compound whose reactivity could be compared with that of the trigonal group 5 d^2 species [2]. Cummins et al. have recently investigated the electronic differences between Mo and W [5], and have concluded that for tungsten, the torus of $5d_{z^2}$ is severely attenuated due to mixing with the 6s. A similar electronic origin to second versus third row reactivity differences has been proposed for Nb versus Ta [2]. As a consequence, a focus on the second and third row of group 6 seemed particularly appealing.

2. Results and discussion

2.1. Oxo-dichloride $(silox)_2Cl_2WO$ (3)

2.1.1. Synthesis

Exploratory NMR tube experiments prompted a simple metathesis approach, wherein treatment of Cl_4WO with 2 equiv of $NaOSi^tBu_3$ in

$$Cl_4WO + 2Na(silox) \xrightarrow[4\,h,\,25\,^\circ C]{Et_2O} (silox)_2Cl_2WO + 2NaCl \quad (1)$$

diethyl ether afforded yellow $(silox)_2Cl_2WO$ (**3**) in 73% yield according to Eq. (1). ^1H and $^{13}C\{^1H\}$ NMR spectral data for all compounds are listed in Table 1.

2.1.2. Oxygen atom abstraction attempts

Given precedent [4], initial OAT experiments were conducted with $(silox)_2Cl_2WO$ (**3**) and Ph_3P (cone angle = 145°) [6] in benzene-d_6. Even under thermolysis conditions (100 °C, 45 h), there was no evidence of a reaction. The combined sterics of the two chlorides and two siloxides might have been a greater factor than anticipated, hence the smaller PMe_3 (cone angle = 118°) [6] was employed. Varying amounts of phosphine (1, 3 and 5 equiv) were utilized, but while a reaction occurred, there was no evidence of $OPMe_3$ formation (δ 0.88, d, $J_{PH} = 13$) amidst the eventual degradation of **3**. Attempts to induce OAT using $P(OMe)_3$ (cone angle = 107°) [6] also failed under increasingly harsh conditions (5 d, 25 °C; 38 h, 60 °C; 47 h, 100 °C).

2.2. Oxo-dialkyls $(silox)_2R_2WO$ (R = Me, Et, ^{n}Pr, ^{n}Bu)

2.2.1. Synthesis

It seemed plausible that the substitution of silox for chloride rendered the OAT from $(silox)_2Cl_2WO$ (**3**) endoergic relative to Cl_4WO. Substitution of the remaining chlorides by less electronegative groups such as alkyls was considered to enable OAT, hence the alkylation of **3** was attempted. The addition of a slight excess (typically 2.05 equiv) of the appropriate Grignard reagent to **3** in diethyl ether provided the yellow to yellow/orange dialkyl compounds $(silox)_2R_2WO$ (**4**-R; R = Me, Et, ^{n}Pr, ^{n}Bu) in decent yield ($\geqslant$64%), as indicated by Eq. (2). The ^1H NMR spectrum of **4**-Me revealed a singlet at δ 1.65, accompanied by ^{183}W (14.40%) satellites ($J_{WH} = 12$ Hz), that was assigned to the tungsten-methyl groups. In $^{13}C\{^1H\}$ NMR spectra of **4**-R, tungsten satellites enabled ready identification of the Me resonance of **4**-Me (δ 47.01, $J_{WC} = 90$ Hz) and the α-CH_2

$$(silox)_2Cl_2WO + \underset{\substack{R = Me, Et; X = Br\\ R = {}^n Pr, {}^n Bu; X = Cl}}{2RMgX} \xrightarrow[4\,h,\,25\,^\circ C]{Et_2O} \underset{\substack{\mathbf{4}\text{-R, R = Me(64\%), Et(85\%),}\\ {}^n\text{Pr(68\%), }{}^n\text{Bu(67\%)}}}{(silox)_2R_2WO} \quad (2)$$

resonances (**4**-Et, δ 56.21, $J_{WC} = 88$ Hz; **4**-^{n}Pr, δ 66.93, $J_{WC} = 86$ Hz; **4**-^{n}Bu, δ 64.10, $J_{WC} = 87$ Hz) of the remaining dialkyls. Use of alkyllithiums typically generated mixtures that hinted at problems related to reduction.

Table 1
^{1}H and ^{13}C{^{1}H} NMR data[a] of (silox)$_2$Cl$_2$WO (**3**), (silox)$_2$R$_2$WO (**4**-R; R = Me, Et, ^{n}Pr, ^{n}Bu), (silox)$_2$(olefin)WO (**5**-ole; ole = C_2H_4, C_4H_8), (silox)$_2$M(O)$_2$ (M = Mo, **6**; W, **7**)

Compound	^{1}H NMR (δ (J (Hz)), ass'm't)		^{13}C{^{1}H} NMR (δ, (ass'm't))		
	^{t}Bu	ole/R	$SiCMe_3$	$SiC(CH_3)_3$	ole/R
(silox)$_2$Cl$_2$WO (**3**)	1.26		25.36	30.44	
(silox)$_2$Me$_2$WO (**4**-Me)	1.19	1.65, s, J_{WH} = 12, Me	24.13	30.07	47.01, J_{WC} = 90, Me
(silox)$_2$Et$_2$WO (**4**-Et)	1.22	2.11, t, 8, CH_3	24.39	30.48	13.57, CH_3
		2.45, q, 8, CH_2			56.21, J_{WC} = 88, CH_2
(silox)$_2$(^{n}Pr)$_2$WO (**4**-^{n}Pr)	1.24	1.18, t, 7, CH_3	24.41	30.47	20.06, Me
		2.23, m, 8, 2, CH_2			22.52, CH_2
		2.49, m, WCH_2			66.93, J_{WC} = 86, WCH_2
(silox)$_2$(^{n}Bu)$_2$WO (**4**-^{n}Bu)	1.25	1.02, t, 8, CH_3	24.30	30.70	14.24, Me
		1.52, m, 8, CH_2Me			28.74, CH_2Me
		2.26, m, 8, 2, CH_2			30.77, CH_2
		2.54, m, WCH_2			64.10, J_{WC} = 87, WCH_2
(silox)$_2$(C_2H_4)WO (**5**-C_2H_4)	1.17	2.05,[b] br s, H*H*C=	23.78	30.31	54.46, J_{WC} = 33, H_2C=
		2.95,[b] br s, *H*HC=			
(silox)$_2$(C_4H_8)WO (**5**-C_4H_8)[c]	1.16	1.25, t, 7, CH_3			
	1.21	2.15, m, 6, CH*H*			
		2.40, m, 6, C*H*H			
		2.70, m, –HC=CH–			
		2.88, m, =C*H*H			
(silox)$_2$Mo(O)$_2$ (**6**)	1.14		24.05	29.73	
(silox)$_2$W(O)$_2$ (**7**)	1.14		24.13	30.03	

[a] Benzene-d_6 unless otherwise noted.
[b] At the coalescence temperature of 62 °C, $k_{rot} = 997\ s^{-1}$ and $\Delta G^{\ddagger} = 15.1(1)$ kcal/mol.
[c] Assignments tentative.

Attempts to synthesize secondary and tertiary dialkyl derivatives (i.e., R = ^{i}Pr, ^{t}Bu) led to intractable mixtures.

The stability of the diethyl, di-*n*-propyl and di-*n*-butyl complexes with respect to β-H-elimination is unusual, but not without precedent. Boncella et al. reported the synthesis and isolation of stable [C_6H_4-1,2-($NSiMe_3$)$_2$]R_2W=NPh (R = Et, ^{n}Pr, ^{i}Bu, C_2H_3Ph) compounds, and showed that β-H-abstraction chemistry was induced by the addition of 2 equiv of PMe_3 to afford alkane and [C_6H_4-1,2-($NSiMe_3$)$_2$](PMe_3)$_2$(olefin)W=NPh [7]. It must be noted that (silox)$_2$R$_2$WO (**4**-R) and [C_6H_4-1,2-($NSiMe_3$)$_2$]R_2W=NPh can be considered 18e$^-$ species, which undoubtedly contributes to their stability. Nonetheless, the vacant site in these complexes and the limited donor capacity of the siloxide entities suggests that β-H-elimination or -abstraction should be facile.

2.2.2. Structure of (silox)$_2$(^{n}Bu)$_2$WO (**4**-^{n}Bu)

The most plausible limiting structures for (silox)$_2$R$_2$-WO (**4**-R; R = Me, Et, ^{n}Pr, ^{n}Bu) are a trigonal bipyramid (tbp) with diaxial siloxides and a square pyramid with *trans*-basal siloxides and an apical oxo group. The structure of (silox)$_2$(^{n}Bu)$_2$WO (**4**-^{n}Bu) was determined by X-ray crystallography; structural details are given in Table 2 and selected bond distances and angles are listed in Table 3. As Fig. 2 illustrates, its geometry is best described as distorted tbp [8]. Aside from a modest disorder in one *n*-butyl group, structure solution in $P2_1/n$ proved to be routine. The axial siloxides possess 1.880(2) and 1.878(2) Å tungsten–oxygen distances and are bent away from the oxo (∠O1–W1–O3 = 98.74(11)°, ∠O2–W1–O3 = 98.83(11)°, ∠O1–W1–O2 =

Table 2
Crystallographic data for (silox)$_2$(^{n}Bu)$_2$WO (**4**-^{n}Bu)

Formula	$C_{32}H_{72}O_3Si_2W$
Formula weight	744.93
Space group	$P2_1/n$
λ (Å)	0.71073
a (Å)	12.3862(9)
b (Å)	12.8741(9)
c (Å)	24.2455(18)
β (°)	97.998(1)
Vol (Å^3)	3828.6(5)
D(calc) (g cm^{-3})	1.292
T (K)	173(2)
Z	4
Absolute coefficients (mm^{-1})	3.106
$R_1[I > 2\sigma(I)]$[a]	0.0511
$wR_2[I > 2\sigma(I)]$[b]	0.1162
R_1 (all data)[a]	0.0824
wR_2 (all data)[b]	0.1287
Goodness-of-Fit[c]	1.050
Largest difference peak (e Å^{-3})	3.176
Largest difference hole (e Å^{-3})	−2.723

n = number of independent reflections (9497 of 39390, R_{int} = 0.0478), p = number of parameters (333).
[a] $R_1 = \sum||F_o| - |F_c||/\sum|F_o|$.
[b] $wR_2 = [\sum w(|F_o| - |F_c|)^2/\sum F_o^2]^{1/2}$.
[c] GOF = $[\sum w(|F_o| - |F_c|)^2/(n-p)]^{1/2}$.

Table 3
Selected bond distances (Å) and angles (°) pertaining to $(silox)_2$-$(^nBu)_2WO$ (**4**-^{n}Bu)

W1–O1	1.880(2)
W1–C1	2.102(4)
Si2–O2	1.666(2)
Si–C(av)	1.929(5)
W1–O2	1.878(2)
W1–C5	2.151(3)
C1–C2	1.512(5)
C–C(av)	1.538(11)
W1–O3	1.705(2)
Si1–O1	1.664(2)
C5–C6	1.519(6)
O1–W1–O2	162.31(10)
O1–W1–C1	86.46(13)
O2–W1–C5	85.51(13)
C1–W1–C5	128.35(14)
W1–C1–C2	117.4(3)
C–Si–C	112.5(9)
O1–W1–O3	98.74(11)
O1–W1–C5	85.89(13)
O3–W1–C1	114.96(13)
W1–O1–Si1	160.09(15)
W1–C5–C6	111.6(3)
Si–C–C(av)	111.4(9)
O2–W1–O3	98.93(11)
O2–W1–C1	86.81(13)
O3–W1–C5	116.68(14)
W1–O2–Si2	159.44(14)
O–Si–C(av)	106.3(12)
C–C–C(av)	107.5(10)

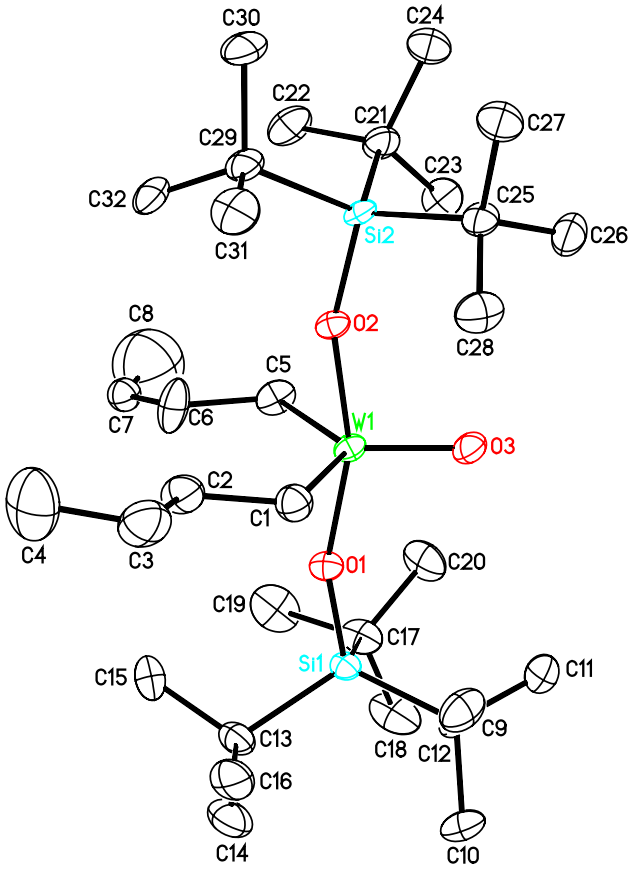

Fig. 2. Molecular view of $(silox)_2(^nBu)_2WO$ (**4**-^{n}Bu).

162.31(10)°), and toward the *n*-butyls (∠O1–W1–C1 = 86.46(13)°, ∠O2–W1–C5 = 85.89(13)°). The oxo has a normal *d*(WO) of 1.705(2) Å [2,8,9], and the tungsten–carbon distances are also standard (2.102(4), 2.151(3) Å). In the equatorial plane, the C1–W1–C5 angle is splayed slightly (128.35(14)°), and is compensated by the O3–W1–C1 and O3–W1–C5 angles of 114.96(13)° and 116.68(14)°, respectively. While the siloxides might be expected to occupy the sterically less demanding equatorial sites in a tbp, their high ionic character relative to the alkyls renders them axial, while the greater covalent bonding inherent in the equatorial plane better suits the *n*-butyl ligands [8,10].

2.2.3. Reactivity of $(silox)_2R_2WO$

Attempts at oxygen atom transfer to PMe_3 from $(silox)_2R_2WO$ (**4**-R; R = Me, Et) met with failure. No reaction was noted when **4**-Me was heated with 3 equiv PMe_3 in THF-d_8 for 33 h at 60 °C, and **4**-Et was stable to prolonged exposure of 2 equiv PMe_3 at 25 °C in benzene-d_6.

In the absence of any evidence of OAT, some thermolysis studies were undertaken. When **4**-Et was heated in benzene-d_6 for 27 h at 60 °C, the predominant product was the ethylene complex, $(silox)_2(C_2H_4)WO$ (**5**-C_2H_4) along with ethane and some ethylene according to Eq. (3). While the reaction

$$\underset{\textbf{4}\text{-Et}}{(silox)_2Et_2WO} \xrightarrow[3\text{ d, }60\text{ °C}]{\text{benzene-}d_6} \underset{\textbf{5}\text{-}C_2H_4}{(silox)_2(C_2H_4)WO} + EtH + C_2H_4 + \cdots \quad (3)$$

was not completely clean, it was scaled up to yield **5**-C_2H_4 in 89% yield upon precipitation from hexanes. The ethylene complex was not analyzed due to persistent 5–10% impurities, but its spectral characteristics in comparison to $(silox)_2(C_2H_4)W{=}N^tBu$ [11] leave little doubt as to its composition. Telltale broad singlets corresponding to two different ethylene resonances (δ 2.04, 2.95) in the ^{1}H NMR spectrum are accompanied by a singlet at δ 54.46 (J_{WC} = 33 Hz) in the $^{13}C\{^1H\}$ NMR spectrum, indicating that the ethylene in **5**-C_2H_4 is roughly perpendicular to the W=O linkage. Variable temperature ^{1}H NMR experiments placed the barrier for ethylene rotation at $\Delta G^{\ddagger}$(62 °C) = 15.1(1) kcal/mol in comparison to 15.3(5) kcal/mol at 69 °C for $(silox)_2(C_2H_4)W{=}N^tBu$ [11]. Thermolysis of the products at 90 °C for 24 h effected total degradation, with a roughly 1:1 ratio of ethane and ethylene

$$\underset{\textbf{4}\text{-}^n\text{Bu}}{(silox)_2{}^nBu_2WO} \xrightarrow[3\text{ d, }60\text{ °C}]{\text{benzene-}d_6} \underset{\textbf{5}\text{-}C_4H_8\text{(1-butene)}}{(silox)_2(C_4H_8)WO} + {}^nBuH + \text{1-butene} + \cdots \quad (4)$$

Thermolysis of $(silox)_2{}^nBu_2WO$ (**4**-^{n}Bu) for 4 h at 90 °C in benzene-d_6 afforded an appreciable amount (>50%) of the 1-butene adduct $(silox)_2(C_4H_8)WO$ (**5**-C_4H_8), but extended thermolysis effected decomposition, and no attempt was made to scale up this reaction. The 1-butene complex was tentatively identified via ^{1}H NMR spectral comparisons with $(silox)_3M(C_4H_8)$ (M = Nb, **1**-Nb(C_4H_8); Ta, **1**-Ta(C_4H_8)) [12] in addition to the observation of inequivalent silox groups, consistent with its lack of any symmetry element.

The thermolysis of **4**-Et was also conducted under excess dihydrogen (~400 Torr) for 15 h at 90 °C, but a side-by-side comparison with a reaction without added hydrogen revealed no difference. Similarly, when $(silox)_2Me_2WO$ (**4**-Me) was treated with 510 Torr dihydrogen, a minute amount of methane was seen after 6 h at 25 °C, and full degradation, accompanied by release of methane, was seen after 7 d at 90 °C.

β-Abstraction chemistry similar to that of $[C_6H_4$-1,2-$(NSiMe_3)_2]R_2W{=}NPh$ [7] was not observed for $(silox)_2R_2WO$ (**4**-R; R = Me, Et) in the presence of PMe_3, so labeling experiments were conducted to obtain further information about their thermal degradation. The synthesis of $(silox)_2(D_3CCH_2)_2WO$ (**4**-CH_2CD_3) was effected according to Eq. (2) via use of D_3CCH_2MgBr, and a thermolysis was conducted at 90 °C and crudely analyzed. H/D-Scrambling was revealed in the major product, $(silox)_2(H_{2-x}D_xC{=}CH_{2-y}D_y)WO$ (**5**-$H_{2-x}D_xC{=}CH_{2-y}D_y$) and in the trace of ethylene released as noted by NMR isotope-shifted resonances in the ^{1}H NMR spectrum. Scrambling is unlikely to occur concomitant with β-H-abstraction – assuming it is not induced by any of the minor products – hence the results point toward the standard mechanism of reversible β-H-elimination followed by EtH reductive elimination. The crude relative degradation rates of **4**-Et and **4**-CH_2CD_3 were similar, hence no large KIE for the process was evident, consistent with scrambling. If the β-H-abstraction mechanism were operational, there would be a large kinetic isotope effect: $k_H/k_D = 6.1(5)$ for $[C_6H_4$-1,2-$(NSiMe_3)_2]R_2W{=}NPh$ [7] and 5.2(2) for $Cp_2Zr(SCH_2Ph)(Me)$ [13]. No further investigation was undertaken.

2.3. $(silox)_2M(O)_2$ (M = Mo (**6**), W (**7**))

2.3.1. Synthesis

In a last effort to observe OAT, $(silox)_2M(O)_2$ (M = Mo, **6**; W, **7**) were considered attractive targets due to their lower coordination number, which would presumably allow access by an abstracting agent. A previously reported synthesis consisted of the thermolysis of MoO_3 and 2 equiv of $HOSi^tBu_3$ at 160 °C for 48 h, followed by pentane extraction of **6** [14], but this procedure failed in these laboratories. Given the unknown providence of the extended solid "MoO_3" in either instance, an alternative synthesis was sought. Treatment of $(DME)_2Cl_2M(O)_2$ (M = Mo, W) [15,16] with 2 equiv of Na(silox) in THF afforded the off-white dioxo derivatives, $(silox)_2M(O)_2$ (M = Mo, **6** (60%); W, **7** (52%)) in reasonable yield according to the following equation:

$$(DME)_2Cl_2M(O)_2 + 2Na(silox) \xrightarrow[12\ h,\ 25\ ^\circ C]{THF} \underset{M=Mo,\mathbf{6};W,\mathbf{7}}{(silox)_2M(O)_2} + 2NaCl \quad (5)$$

2.3.2. Attempted OAT

The first deoxygenation attempt was conducted by exposing $(silox)_2MoO_2$ (**6**) to 1 equiv of PPh_3. After 7 d at 25 °C there was no reaction, and thermolysis of the mixture at 60 °C for 4 d, followed by 49 h at 100 °C, resulted in no reaction. When **6** was treated to 2 or 4 equiv of PMe_3 in d_6-benzene or d_8-THF there was also no reaction even after extended thermolysis, and exposure of $(silox)_2WO_2$ (**7**) to 2 equiv of PMe_3 in d_6-benzene also resulted in no reaction, even after extended heating.

3. Conclusions

3.1. General

The syntheses of $(silox)_2Cl_2WO$ (**3**) and $(silox)_2R_2WO$ (**4**-R, R = Me, Et, ^{n}Pr, ^{n}Bu) were readily accomplished by metathetical procedures, and the structure of **4**-R implicated a distorted trigonal bipyramidal geometry for these five coordinate complexes. The dialkyls that contain β-hydrogens (e.g., **4**-Et, **4**-^{n}Bu) proved to be remarkably stable, and appeared to ultimately decompose via standard β-H-elimination and reductive elimination paths to afford $(silox)_2$(olefin)WO (**5**-ole; ole = ethylene, 1-butene).

3.2. Oxygen atom transfer attempts

The original premise for this study was to investigate OAT in group 6 compounds. The general lack of OAT by these compounds is difficult to interpret, simply because the absence of reactivity – in most cases thermal degradation was eventually noted – provides few hints about the transformation of interest! One obvious possibility is that OAT from the M(VI) derivatives to the various phosphines is endoergic. One could make the argument that the estimated thermochemistry is off [3], or that substitution of chloride, etc. by the silox anion renders these metal centers more oxophilic and more stable in their higher oxidation states. This might be convincing except that $(silox)_2Mo(O)_2$, the second row derivative, does not lose its oxygen either, and here it is doubtful that the thermodynamics are unfavorable.

It is plausible that a combination of kinetics and thermodynamics is responsible for the lack of OAT chemistry. Previously, it has been noted that OAT to $(silox)_3M$ (**1**-M, M = Nb, Ta) is extremely slow, even in instances where ΔG° is roughly −100 kcal/mol according to calculations [2]. It can be concluded that symmetry forbidden OAT reactions may be observed if the driving force is large. If the kinetic barrier is not partially offset by a large favorable free energy change, the barrier may be exceedingly difficult to overcome, even when the symmetry of the transition state can be lowered. An apparent exception to this statement is the ability of d^0 group 6 *cis*-dioxo derivatives to transfer oxygen under relatively mild conditions [1,17–19]. In these cases, the *cis*-dioxo disposition is unique in that of the four pπ-pairs of electrons, only three have the symmetry to interact with the metal; the fourth pair is asymmetric and delocalized on the two oxygens as non-bonding. It is this orbital – through extensive mixing as E: attacks at $\theta \neq 180°$ (see Fig. 1) – that helps facilitate the transfer of electron density from the σ-orbital on E to the ultimate π-receptor orbital on the metal [20].

In the mono-oxo and tetrahedral dioxo derivatives above, all pπ-pairs of electrons are involved in π-bonding, yet one pair must be transferred to the metal in the OAT process. Without a non-bonding π-orbital to facilitate the transfer via additional mixing at lower symmetry, this is quite difficult. Reduction of L_nM is also likely to place two electrons in d_{z^2} in both $(silox)_2X_2W$ and $(silox)_2M{=}O$, therefore the second orbitally forbidden process (i.e., L_nM: + OE is $3\sigma + 2\pi$ in Fig. 1), which does not really exist for the *cis*-dioxo cases because the pair of electrons resides in an orbital of π-symmetry (i.e., L_nM: +OE is $2\sigma + 3\pi$), can present a major kinetic barrier [20].

4. Experimental

4.1. General considerations

All manipulations were performed using either glovebox or high vacuum techniques. Hydrocarbon or ethereal solvents were refluxed over sodium, then vacuum transferred from sodium benzophenone ketyl (with 3–6 mL tetraglyme/L added to hydrocarbons). Benzene-d_6 was sequentially dried over sodium, then 4 Å molecular sieves and vacuum transferred from 4 Å molecular sieves. All glassware was oven dried for a minimum of 4 h and NMR tubes were flame dried under dynamic vacuum prior to use. Tungsten (VI) tetrachloride oxide was used as received from Aldrich and molybdenum (VI) dichloride dioxide was used as received from Strem chemicals. $(DME)Cl_2MO_2$ (M = Mo, W) were prepared according to the published procedures [15,16].

NMR spectra were obtained on Varian XL-200, XL-400, VXR-400S and Unity 500 spectrometers, and chemical shifts are reported relative to C_6D_6 (^1H, δ 7.15; $^{13}C\{^1H\}$, δ 128.00) and d_8-THF (^1H, δ 1.75). Infrared spectra were recorded using a Nicolet Impact 410 spectrophotometer interfaced to an IBM PC. Combustion analyses were performed by Robertson Microlit Laboratories, Madison, NJ.

4.2. Procedures

4.2.1. $(silox)_2Cl_2WO$ (**3**)

Into a round bottom flask containing $OWCl_4$ (0.200 g, 0.585 mmol) and Na(silox) (0.279 g, 1.17 mmol) was distilled 25 mL diethyl ether. The solution was allowed to warm to 25 °C and stirred for 4 h. The resulting yellow/green solution was filtered with 20 mL diethyl ether until there was no yellow color left in the filter cake. The filtrate volume was reduced to 8 mL and cooled to −78 °C for 1 h. Filtration yielded 0.302 g **3** as a yellow solid (74%). IR (Nujol Mull, cm^{-1}): 1477 (s), 1360 (s), 1188 (w), 1009 (s), 940 (s), 850 (br, s), 684 (w), 623 (s), 590 (s). *Anal.* Calc. for $H_{54}C_{24}O_3Si_2W$: C, 41.09; H, 7.76. Found: C, 41.06; H, 7.66%.

4.2.2. $(silox)_2Me_2WO$ (**4**-Me)

To slurry of **3** (0.344 g, 0.491 mmol) in 10 mL diethyl ether was syringed 0.36 mL (2.15 equiv, 1.056 mmol) MeMgBr (3.0 M in diethyl ether) at −78 °C under an argon counterflow. The mixture was allowed to warm to 25 °C and stirred for 4 h. The volatiles were removed in vacuo and the yellow residue was triturated with hexanes (3 × 10 mL). A 10-mL slurry in hexanes was filtered and washed until the filter cake was no longer yellow. The filtrate was reduced to 3 mL and cooled to −78 °C for 30 min to afford **4**-Me, which was collected as a dark yellow solid by filtration (0.208 g, 64%). IR (Nujol Mull, cm^{-1}): 1387 (m), 1003 (w), 944 (m), 857 (s), 818 (s), 731 (w), 625 (m). *Anal.* Calc. for $H_{60}C_{26}O_3Si_2W$: C, 47.30; H, 9.19. Found: C, 45.79; H; 8.88%.

4.2.3. $(silox)_2Et_2WO$ (**4**-Et)

To slurry of **3** (0.604 g, 0.861 mmol) in 18 mL diethyl ether was syringed 0.59 mL (2.05 equiv, 1.756 mmol) EtMgBr (3.0 M in diethyl ether) at −78 °C under an argon counterflow. The mixture was allowed to warm to 25 °C and stirred for 6 h. The volatiles were removed in vacuo and the yellow residue was triturated with hexanes (2 × 154 mL). A 15-mL slurry in hexanes was filtered and washed until the filter cake was no longer yellow. The filtrate was reduced to 5 mL and cooled to −78 °C for 30 min to yield **4**-Et as a yellow microcrystalline solid (0.504 g, 85%). IR (Nujol Mull, cm^{-1}): 1414 (w), 1367 (s), 1176 (w), 967 (s), 917 (m), 900 (br,s), 811 (s), 625 (s).

4.2.4. (silox)$_2$(^{n}Pr)$_2$WO (4-^{n}Pr)

To slurry of **3** (0.249 g, 0.355 mmol) in 12 mL diethyl ether was syringed 0.36 mL (2.05 equiv, 0.728 mmol) ^{n}PrMgCl (2.0 M in diethyl ether) at −78 °C under an argon counterflow. The mixture was allowed to warm to 25 °C and stirred for 3 h. The volatiles were removed in vacuo and the yellow residue triturated with hexanes (2 × 8 mL). A 10-mL slurry in hexanes was filtered and washed until the filter cake was no longer yellow. The filtrate was reduced to 2 mL and cooled to −78 °C for 20 min to afford **4**-^{n}Pr as a yellow-orange solid (0.172 g, 68%). IR (Nujol Mull, cm^{-1}): 1381 (m), 983 (m), 930 (m), 900 (m), 838 (s), 811 (s), 784 (s), 625 (s).

4.2.5. (silox)$_2$(^{n}Bu)$_2$WO (4-^{n}Bu)

To slurry of **3** (0.501 g, 0.714 mmol) in 18 mL diethyl ether was syringed 0.75 mL (2.05 equiv, 1.464 mmol) ^{n}BuMgCl (2.0 M in diethyl ether) at −78 °C under an argon counterflow. The mixture was allowed to warm to 25 °C and stirred for 4 h. The volatiles were removed in vacuo and the yellow residue was triturated with pentane (3 × 10 mL). A 10-mL slurry in hexanes was filtered and washed until the filter cake was no longer yellow. The filtrate was reduced to 5 mL and cooled to −78 °C for 2 h to yield **4**-^{n}Bu as a yellow-orange solid (0.355 g, 67.1%). IR (Nujol Mull, cm^{-1}): 1388 (s), 1368 (s), 1017 (w), 976 (s), 910 (m), 860 (br,s), 811 (s), 672 (w), 625 (s). *Anal.* Calc. for $H_{72}C_{32}O_3Si_2W$: C, 51.60; H, 9.74. Found: C, 51.60; H; 9.81%.

4.2.6. (silox)$_2$(C_2H_4)WO (5-C_2H_4)

To a 150-mL bomb reactor was added 0.330 g (0.479 mmol) of **4**-Et and 8 mL benzene. The reactor was freeze–pump–thaw degassed, sealed and heated to 90 °C for 24 h. All volatiles were removed and the residue was triturated with hexanes (3 × 5 mL) and filtered. Removal of solvent afforded 0.281 g of red-brown **5**-C_2H_4 (89%; 5–10% impurity resonances, as assayed by silox groups, were typically present).

4.2.7. (silox)$_2$$MoO_2$ (6)

Into a flask containing (DME)Cl_2MoO_2 (0.418 g, 1.446 mmol) and Na(silox) (0.688 g, 2.89 mmol) was distilled 15 mL tetrahydrofuran. The solution was warmed to 25 °C with stirring. After 12 h of stirring, the volatiles were removed in vacuo and the resulting off-white residue was triturated with pentane (3 × 10 mL). Filtration using pentane (10 mL), reduction of the solvent to 3 mL, cooling to −78 °C for 45 min and filtration yielded 0.482 g **6** as an off-white microcrystalline solid (60%). *Anal.* Calc. for $H_{54}C_{24}O_4Si_2Mo$: C, 51.60; H, 9.74. Found: C, 51.33; H; 10.03%.

4.2.8. (silox)$_2$$WO_2$ (7)

Into a flask containing (DME)Cl_2WO_2 (0.287 g, 0.762 mmol) and Na(silox) (0.362 g, 1.52 mmol) was distilled 13 mL tetrahydrofuran. The solution was allowed to warm to 25 °C with stirring. After 12 h of stirring, the volatiles were removed in vacuo, the resulting off-white residue was triturated with hexanes (3 × 10 mL) and filtered (8 mL). Reduction of the solvent to 3 mL, cooling to −78 °C for 1 h and filtration yielded 0.257 g **7** as an off-white microcrystalline solid (52%).

4.3. NMR tube reactions

Flame dried NMR tubes, sealed with 14/20 ground glass joints, were charged with the metal reagent (e.g., 0.012–0.025 g) in the dry box, and removed to the vacuum line on needle valve adapters. The NMR tubes were degassed, and after transfer of deuterated solvent, a calibrated gas bulb was used to introduce volatile reagents (e.g., PMe_3) at 77 K. The tubes were sealed with a torch. Solid substrates (e.g., PPh_3) were loaded along with the metal complex followed by solvent transfer on the vacuum line and flame sealing. Freshly distilled deuterated solvent was added to NMR tubes containing substrate and metal complex while in the dry box. The mixture was then degassed on the vacuum line and the tube flame sealed.

4.4. Single crystal X-ray structure determination of (silox)$_2$(^{n}Bu)$_2$WO (4-^{n}Bu)

Slow evaporation at 25 °C of a saturated benzene solution of (silox)$_2$(^{n}Bu)$_2$WO (**4**-^{n}Bu) yielded dark yellow block crystals suitable for X-ray analysis. A few crystals were immersed in polyisobutylene, and one with dimensions 0.30 × 0.20 × 0.10 mm was extracted with a glass fiber, and placed under a 173 K nitrogen stream on the gonimeter head of a Siemens SMART CCD area detector system equipped with a fine-focus molybdenum X-ray tube ($\lambda = 0.71073$ Å). Preliminary diffraction revealed a monoclinic crystal system. A hemisphere routine was used to determine the space group as $P2_1/n$, obtain precise lattice constants and for data collection (θ limits were 1.79–28.28°, the limiting indices were $-16 \leqslant h \leqslant 16$, $-17 \leqslant k \leqslant 17$, $-32 \leqslant l \leqslant 32$). The data was processed with the Bruker SAINT program to yield 39 390 reflections with 9497 of the reflections being symmetry independent ($R_{int} = 0.0478$). The data were corrected for absorption by SADABS. The structure was solved by direct methods (SHELXS), completed by subsequent difference Fourier syntheses, and refined by full-matrix least squares procedures (SHELXL, on F^2). A disordered *n*-butyl group was modeled with partial occupancies. All non-hydrogen atoms were refined using anisotropic displacement parameters and hydrogen atoms were included at calculated positions.[1]

[1] Cambridge Crystallographic Data Centre deposition number: CCDC 267411.

5. Supplementary material

Crystallographic data reported in this paper have been deposited with Cambridge Crystallographic Data Centre. These data can be obtained free of charge via www.ccdc.cam.ac.uk/conts/retrieving.html (or from the Cambridge Crystallographic Data Centre, 12, Union Road, Cambridge CB2 1EZ, UK; fax: +44 1223 336 033; or deposit@ccdc.cam.ac.uk).

Acknowledgments

We thank the National Science Foundation (CHE-9528914) and Cornell University for support.

References

[1] (a) A.E. Shilov, A.A. Shteinman, Acc. Chem. Res. 32 (1999) 763;
(b) L.K. Woo, Chem. Rev. 93 (1993) 1125;
(c) R.H. Holm, Coord. Chem. Rev. 100 (1990) 183;
(d) R.H. Holm, Chem. Rev. 87 (1987) 1401.
[2] (a) A.S. Veige, L.M. Slaughter, E.B. Lobkovsky, P.T. Wolczanski, N. Matsunaga, S.A. Decker, T.R. Cundari, Inorg. Chem. 42 (2003) 6204;
(b) A.S. Veige, L.M. Slaughter, P.T. Wolczanski, S.A. Decker, T.R. Cundari, J. Am. Chem. Soc. 123 (2001) 6419.
[3] H. Holm, J.P. Donahue, Polyhedron 12 (1993) 571.
[4] M.G.B. Drew, E.M. Page, D.A. Rice, J. Chem. Soc., Dalton Trans. (1983) 61.
[5] H.S. Soo, J.S. Figueroa, C.C. Cummins, J. Am. Chem. Soc. 126 (2004) 11370.
[6] (a) C.A. Tolman, Chem. Rev. 77 (1977) 313;
(b) K.A. Bunten, L. Chen, A.L. Fernandez, A.J. Poë, Coord. Chem. Rev. 233–234 (2002) 41.
[7] S.S. Wang, K.A. Abboud, J.M. Boncella, J. Am. Chem. Soc. 119 (1997) 11990.
[8] S.A. Strazisar, P.T. Wolczanski, J. Am. Chem. Soc. 123 (2001) 4728.
[9] W.A. Nugent, J.M. Mayer, Metal-Ligand Multiple Bonds, Wiley, New York, 1988.
[10] (a) A.R. Rossi, R. Hoffmann, Inorg. Chem. 14 (1975) 365;
(b) R. Hoffmann, J.M. Howell, E.L. Muetterties, J. Am. Chem. Soc. 94 (1972) 3047.
[11] D.F. Eppley, P.T. Wolczanski, G.D. Van Duyne, Angew. Chem. Int., Ed. Engl. 30 (1991) 584.
[12] K.F. Hirsekorn, A.S. Veige, M.P. Marshak, Y. Koldobskaya, P.T. Wolczanski, T.R. Cundari, E.B. Lobkovsky, J. Am. Chem. Soc. 127 (2005) 0000.
[13] S.L. Buchwald, R.B. Nielsen, J. Am. Chem. Soc. 110 (1988) 3171.
[14] M. Weidenbruch, C. Pierrard, H. Pesel, Z. Naturforsch. B 338 (1978) 1468.
[15] B. Kamenar, M. Penavic, B. Korpar-Colig, B. Markovic, Inorg. Chim. Acta 65 (1982) L245.
[16] K. Dreisch, C. Andersson, C. Stålhandske, Polyhedron 10 (1991) 2417.
[17] (a) M.S. Reynolds, J.M. Berg, R.H. Holm, Inorg. Chem. 23 (1984) 3057;
(b) J.M. Berg, R.H. Holm, J. Am. Chem. Soc. 107 (1985) 925;
(c) E.W. Harlan, J.M. Berg, R.H. Holm, J. Am. Chem. Soc. 108 (1986) 6992.
[18] (a) G.J.-J. Chen, J.W. McDonald, W.E. Newton, Inorg. Chem. 15 (1976) 2612;
(b) G.J.-J. Chen, J.W. McDonald, D.C. Bravard, W.E. Newton, Inorg. Chem. 24 (1985) 2327;
(c) J. Topich, J.T. Lyon III, Polyhedron 3 (1984) 61;
(d) J. Topich, J.T. Lyon III, Inorg. Chem. 23 (1984) 3202.
[19] (a) K.-M. Sung, R.H. Holm, Inorg. Chem. 39 (2000) 1275;
(b) K.M. Sung, R.H. Holm, J. Am. Chem. Soc. 123 (2001) 1931;
(c) K.M. Sung, R.H. Holm, Inorg. Chem. 40 (2001) 4518.
[20] (a) M.A. Pietsch, M.B. Hall, Inorg. Chem. 35 (1996) 1273;
(b) M.A. Pietsch, M. Couty, M.B. Hall, J. Phys. Chem. 99 (1995) 16315;
(c) L.M. Thomson, M.B. Hall, J. Am. Chem. Soc. 123 (2001) 3995.

Available online at www.sciencedirect.com
SCIENCE DIRECT®
Polyhedron 25 (2006) 259–265
POLYHEDRON
www.elsevier.com/locate/poly

Titanium(IV) complexes with amidinate and/or hydrazido ligands

Jeffrey M. Pietryga, Jamie N. Jones, Charles L.B. Macdonald, Jennifer A. Moore, Alan H. Cowley *

Department of Chemistry and Biochemistry, The University of Texas at Austin, 1 University Station A5300, Austin, TX 78712-0165, USA

Received 8 April 2005; accepted 24 June 2005
Available online 11 August 2005

Dedicated to Professor Malcolm H. Chisholm on the occasion of his 60th birthday.

Abstract

The complex $[Ti_2Cl_4(NNMe_2)_2(py)_3]$ (**1**) has been prepared via the reaction of $TiCl_4$ with $LiN(H)NMe_2$, followed by treatment with pyridine. Preparation of the complex $[TiCl(PhC\{N(SiMe_3)_2\}_2)_2(MeNNMe_2)]$ (**2**) was carried out by treatment of $TiCl_4$ with $Li[PhC\{N(SiMe_3)_2\}]$tmeda, followed by reaction with $LiN(Me)NMe_2$. The structures of **1** and **2** were determined by single crystal X-ray diffraction. The single crystal X-ray structure of $Li[PhC\{N(SiMe_3)_2\}]$tmeda (**3**) has also been determined.
© 2005 Elsevier Ltd. All rights reserved.

Keywords: Titanium; Amidinate; Hydrazido; Complexes; X-ray structures

1. Introduction

Several single-source precursors to titanium nitride have been reported over the past 15 years, including homoleptic titanium amides and mixed titanium amide/alkyl compounds [1], amides such as $[CpTiCl_2\{N(SiMe_3)_2\}]$ [2] and $[TiCl_2(NH\text{-}t\text{-}Bu)_2(NH_2\text{-}t\text{-}Bu)_2]_n$ [3], several imides [4], adducts of the type $[TiCl_4(NH_3)_2]$ [5] and azides such as $[Cp_2Ti(N_3)_2]$ [6] and $[Ti(NMe_2)_2(N_3)_2(py)_2]$ [7]. Ideally, the TiN single source precursor should possess reasonable volatility in order to facilitate vapor transport. In turn, this implies the avoidance of oligomerization. A second desirable precursor feature is an all-nitrogen coordination environment around the titanium atom since the presence of, e.g., titanium–chlorine or titanium–carbon bonds can result in the presence of chlorine or carbon impurities in the TiN films or particles.

In the present work, two strategies were employed in an effort to prepare monomeric titanium nitride precursors with all-nitrogen coordination spheres. The first approach featured the use of alkylhydrazido ligands; the second involved the use of alkylhydrazido ligands in conjunction with amidinate ligands. A major potential advantage of hydrazido ligands stems from the expectation that N–N bond cleavage will be more facile than N–C bond cleavage owing to the order of bond enthalpies N–C > N–N. In principle, this should result in lower deposition temperatures and less carbon incorporation for titanium hydrazides than for precursors with Ti–N–C linkages. Such a view is supported by the observation [8] that the decomposition of methylhydrazine on a titanium surface is initiated by N–N bond cleavage at modest temperatures (~200 °C). Moreover, Winter et al. [9,10] have demonstrated that alkylhydrazide ligands can be employed for the deposition of high quality TiN films; however, the inclusion of chloride ligands in these precursors led to chloride incorporation in the films that were grown at lower temperatures. A second potential advantage of the use of hydrazido ligands is

* Corresponding author. Tel.: +1 512 471 7484; fax: +1 512 471 6822.
E-mail address: cowley@mail.utexas.edu (A.H. Cowley).

0277-5387/$ - see front matter © 2005 Elsevier Ltd. All rights reserved.
doi:10.1016/j.poly.2005.06.035

that they are capable of binding to titanium in an η^2-fashion, thus facilitating the achievement of an all-nitrogen coordination environment. A similar comment applies to the use of amidinate ligands which also are capable of exhibiting an η^2-binding mode.

In the present contribution, we describe the reaction of $TiCl_4$ with $LiN(H)NMe_2$, followed by treatment with pyridine and the reaction of $TiCl_4$ with Li[PhC{N-$(SiMe_3)_2$}]tmeda, followed by treatment with LiN-$(Me)NMe_2$. Both products were characterized by single-crystal X-ray diffraction. We also report the X-ray crystal structure of Li[PhC{$N(SiMe_3)_2$}]tmeda. Although the latter is a known compound [11], it has not been structurally characterized previously.

2. Experimental

2.1. General procedures

All manipulations and reactions were performed under catalyst-scrubbed Ar, using a combination of glove box and standard Schlenk techniques. Dichloromethane was purified by distillation under N_2 from calcium hydride, and all other solvents were distilled under N_2 from sodium/benzophenone ketyl. Additional degassing of solvents was performed using either vigorous Ar bubbling, or freeze/pump/thaw cycling.

A 1.6 M hexane solution of *n*-BuLi was purchased from a commercial source, and used without further purification. Titanium(IV) chloride was purchased from a commercial source, and purified as necessary by vacuum distillation. 1,1,-Dimethylhydrazine was purchased from a commercial source, and purified by distillation. Trimethylhydrazine [12] and Li[PhC{$N(SiMe_3)_2$}]tmeda [11] were prepared and purified using literature methods.

2.2. Spectroscopic measurements

All CI mass spectra were recorded on a Finnigan MAT TSQ-700 instrument; the samples were sealed in glass capillaries under Ar in a glove box. NMR spectra were recorded at 295 K on a GE QE-300 spectrometer. The CD_2Cl_2 used in these measurements was purchased in sealed vials, either pure or with 1% (v/v) tetramethylsilane. The THF-d_8 was purchased from a commercial source and vacuum distilled under Ar prior to use. The ^1H NMR chemical shifts are reported relative to tetramethylsilane and are referenced either directly or to solvent.

2.3. Single crystal X-ray structure determinations

Crystals of $[Ti_2Cl_4(NNMe_2)_2(py)_3]$ (**1**), [TiCl(PhC{N-$(SiMe_3)_2$}$_2)_2(MeNNMe_2)$] (**2**) and Li[PhC{$N(SiMe_3)_2$}]-tmeda (**3**) of suitable quality were collected directly from Schlenk-type flasks under Ar pressure, and covered immediately with degassed perfluorinated polyether oil. The data for **1** were collected at 293(2) K on a Siemens P 4 diffractometer and the data for **2** and **3** were collected at 153(2) K on a Nonius Kappa CCD diffractometer. Each data set was corrected for Lorentz and polarization effects. All three structures were solved by direct methods, and refined by full-matrix least-squares on F^2 using the SHELXTL PLUS software package [13]. All non-hydrogen atoms were allowed anisotropic thermal motion and hydrogen atoms, which were included at calculated positions, were refined using a riding model and a general isotropic thermal parameter. The total number of reflections, collection ranges, and final *R* values are listed in Table 1.

2.4. Synthesis of $[Ti_2Cl_4(NNMe_2)_2(py)_3]$ (**1**)

A solution of NH_2NMe_2 (3.8 g, 63 mmol) in 40 mL of tetrahydrofuran was chilled to −78 °C and 25 mL of an *n*-BuLi solution (1.6 M in hexane) was added over a period of 10 min. The reaction mixture was allowed to warm to room temperature over several hours, then stirred overnight. Titanium tetrachloride (5.2 mL, 16 mmol) was added via syringe to 80 mL of tetrahydrofuran at −10 °C, to which was added the solution of $LiN(H)NMe_2$ over a period of 10 min. The reaction mixture was allowed to warm to room temperature overnight, following which the solvent was removed under reduced pressure and the resulting solids extracted with CH_2Cl_2 (3×75 mL). Filtration through a glass frit covered with diatomaceous earth resulted in a red colored filtrate. The volume of the latter solution was reduced to 100 mL, and pyridine (0.5 mL, 6 mmol) was added to a 30 mL aliquot. Cooling of this mixture to −20 °C for a period of days produced large red crystals of **1** in 40% yield.

^1H NMR (300 MHz, 298 K, CD_2Cl_2): δ 8.83 (m, 6H, *m*-py), 7.79 (t, 3H, *p*-py), 7.35 (t, 6H, *o*-py), 3.47 (s, 12H, Me_2N). MS (CI^+, CH_4): *m/e* 556 $[Ti_2Cl_3(NNMe_2)_2(py)_3]^+$ (5%), 475 $[Ti_2Cl_3(NNMe_2)_2(py)_2]^+$ (24%), 434 $[Ti_2Cl_3N_3C_2H_7(py)_2]^+$ (27%), 396 $[Ti_2Cl_3(NNMe_2)_2(py)]^+$ (49%), 355 $[Ti_2Cl_3N_3C_2H_7(py)]^+$ (100%), 317 $[Ti_2Cl_3(NNMe_2)_2]^+$ (23%).

2.5. Synthesis of $[TiCl(PhC\{N(SiMe_3)_2\}_2)_2(MeNNMe_2)]$ (**2**)

Titanium tetrachloride (2.0 mL, 18 mmol) was added via syringe to a solution of Li[PhC{$N(TMS)\}_2$]tmeda (13.9 g, 36 mmol) in 100 mL of tetrahydrofuran. The reaction mixture was stirred overnight, after which the volatiles were removed under reduced pressure and the resulting orange-red solid was extracted with diethyl ether (2×70 mL). After filtration through a glass frit covered with diatomaceous earth, the red filtrate was concentrated and maintained at −20 °C overnight. The intermediate, $TiCl_2(PhC\{N(SiMe_3)_2\}_2)_2$, was isolated as

Table 1
Selected crystal data and data collection refinement parameters for **1**–**3**

	1	**2**	**3**
Empirical formula	$C_{21}H_{31}Cl_8N_7Ti_2$	$C_{33}H_{65}ClN_6OSi_4Ti$	$C_{19}H_{39}LiN_4Si_2$
Formula weight	760.93	757.62	386.66
Crystal size (mm)	$0.15 \times 0.09 \times 0.07$	$0.13 \times 0.11 \times 0.04$	$0.40 \times 0.30 \times 0.21$
Crystal class	monoclinic	monoclinic	monoclinic
Space group	$P2_1/n$	$P2_1/c$	$P2_1/n$
a (Å)	16.9961(7)	11.664(2)	10.584(5)
b (Å)	11.1852(5)	21.175(4)	13.234(5)
c (Å)	18.3199(7)	17.730(4)	18.147(5)
β (°)	106.343(1)	100.42(3)	91.535(5)
U (Å^3)	3342.0(2)	4307.0(1)	2540.9(2)
Z	4	4	4
μ (Mo-Kα, mm^{-1})	1.142	0.404	0.149
T (K)	293(2)	153(2)	153(2)
Diffractometer	Siemens P4	Nonius Kappa CCD	Nonius Kappa CCD
Radiation		Graphite-monochromated Mo-Kα	
λ (Å)		0.71073	
Measured reflections	17961	14627	33850
Independent reflections	5891	7560	5816
R_{int}	0.0478	0.0708	0.0713
Range in 2θ (°)	$2.86 \leqslant 2\theta \leqslant 50.00$	$5.98 \leqslant 2\theta \leqslant 50.00$	$6.56 \leqslant 2\theta \leqslant 54.98$
Range in h	$-20 \leqslant h \leqslant 18$	$-13 \leqslant h \leqslant 13$	$-13 \leqslant h \leqslant 13$
Range in k	$-13 \leqslant k \leqslant 11$	$-25 \leqslant k \leqslant 25$	$-16 \leqslant k \leqslant 17$
Range in l	$-11 \leqslant l \leqslant 21$	$-21 \leqslant l \leqslant 21$	$-23 \leqslant l \leqslant 19$
Data/restraints/parameters	5891/0/347	7560/0/430	5816/150/245
R_1 [$I > 2\sigma(I)$]	0.0567	0.0539	0.0710
wR_2	0.1477	0.0979	0.1699

red crystals in 45% yield. This is a slight variation of the literature methods [11,14,15]. [^{1}H NMR (300 MHz, 298 K, CD_2Cl_2): δ 7.41 (m, 3H, *o*,*p*-Ph), 7.28 (m, 2H, *m*-Ph), 0.05 (s, 18H, Me_3Si)]. Trimethylhydrazine (0.23 g, 3 mmol) in 30 mL of diethyl ether was lithiated by treatment with 1.9 mL of a solution of *n*-BuLi (1.6 M in hexane) at −78 °C. The reaction mixture was allowed to assume room temperature and stirring was continued overnight. A solution of $TiCl_2(PhC\{N(SiMe_3)_2\}_2)_2$ (1.0 g, 1.5 mmol) in 50 mL of diethyl ether was then added, and the reaction mixture was stirred overnight. Following filtration through a glass frit covered with diatomaceous earth, the resulting orange filtrate was concentrated and chilled to −78 °C, affording an orange oil. A crop of orange-red crystals of **2** (0.22 g (0.33 mmol, 22% yield)) formed upon storage of the oil at ambient temperature. ^{1}H NMR (300 MHz, 298 K, THF-d_8): δ 7.44 (m, 6H, Ph), 7.31 (m, 4H, Ph), 2.74 (s, 3H, MeN), 2.36 (s, 6H, Me_2N), 0.07 (s, 18H, Me_3Si); MS (CI^+, CH_4) m/e 683 [M + 1, 14%], 647 [M-Cl^-, 15%], 609 [$TiCl_2(PhC\{N(SiMe_3)_2\}_2)_2$, 100%].

3. Results and discussion

3.1. Synthesis and preliminary identification of $[Ti_2Cl_4(NNMe_2)_2(py)_3]$ (**1**)

The initial phase of the synthesis was monolithiation of H_2NNMe_2 to form $LiN(H)NMe_2$. This lithium reagent was allowed to react with $TiCl_4$ in a 4:1 mole ratio in THF solution. The synthesis of **1** was completed by the addition of pyridine in an effort to prevent oligomerization (Scheme 1). ^{1}H NMR spectroscopic assay provided two clues to the structure of **1**, namely (i) no N–H signal was evident thus suggesting that the hydrazido ligand is attached to titanium in an η^1 or η^2 fashion, and (ii) the hydrazido and pyridine ligands are present in a 2:3 mole ratio. However, it was necessary to appeal to X-ray crystallography to provide more definitive structural information.

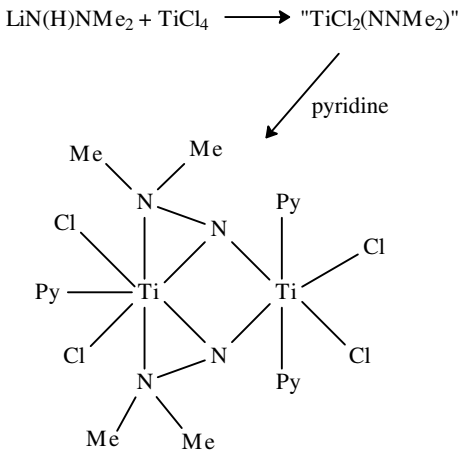

1

Scheme 1.

3.2. Single crystal X-ray structure of $[Ti_2Cl_4(NNMe_2)_2(py)_3]$ (1)

The X-ray analysis reveals a dititanium structure in which the two coordination environments are quite distinct (Fig. 1 and Table 2). One titanium atom [Ti(1)] is seven coordinate and features a pyridine molecule, two chlorides, and two η^2-attached $[Me_2NN]^{2-}$ ligands.

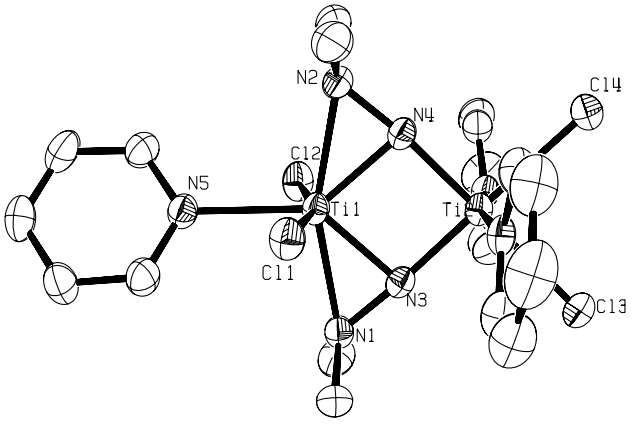

Fig. 1. Molecular structure of $[Ti_2Cl_4(NNMe_2)_2(py)_3]$ (**1**) showing the atom numbering scheme. Thermal ellipsoids are set to 30% probability. All hydrogen atoms and two molecules of CH_2Cl_2 of crystallization have been omitted for clarity.

The overall geometry at Ti(1) can be described as pentagonal bipyramidal. Thus, the sum of bond angles in the pentagonal plane described by the five nitrogen atoms is 360.0(1)°. Note, however, that the angles in this plane are very distorted and range from 38.1(1)° to 101.0(1)°. The departures from the ideal bond angle of 72° are caused by the very small bite angles of the η^2-hydrazide ligands. If, however, a pseudo-trigonal bipyramidal geometry is considered by defining the midpoints of the N–N moieties as "ligands" the "bond angles" in the equatorial plane would be 120.3°, 118.1°, and 121.6°. The axial ligands at N(1) are distorted from linearity as reflected by the Cl–Ti–Cl bond angle of 160.99(6)°. Note that both of these chloride ligands are inclined away from the more "crowded" side of the molecule.

The geometry at Ti(2) is octahedral. Two pyridine molecules are arranged in a *trans* fashion while the two chlorides and the two imido nitrogens [N(3) and N(4)] each possess a mutually *cis* arrangement. The departures from the ideal angle of 90° are modest and of the order of 5–6° (see Table 2). The view down the Ti(1)–Ti(2) vector shows that the C(13)–C(14)–N(3)–N(4)–N(1)–N(2) and N(6)–N(7)–C(11)–C(12) planes are close to orthogonal (Fig. 2).

The two hydrazides feature an imido nitrogen [N(3) and N(4)], each of which is formally σ-bonded to Ti(1)

Table 2
Selected bond lengths (Å) and angles (°) for **1**–**3**

1		**2**		**3**	
Bond lengths					
Ti(1)–N(1)	2.224(2)	Ti–N(1)	2.221(3)	Li–N(1)	2.021(6)
Ti(1)–N(2)	2.208(4)	Ti–N(2)	2.124(3)	Li–N(2)	2.035(6)
Ti(1)–N(3)	1.941(4)	Ti–N(3)	2.211(3)	N(1)–C(1)	1.330(3)
Ti(1)–N(4)	1.956(4)	Ti–N(4)	2.126(3)	N(2)–C(1)	1.329(3)
Ti(1)–N(5)	2.272(4)	Ti–N(5)	1.897(3)		
Ti(1)–Cl(1)	2.366(1)	Ti–N(6)	2.196(3)		
Ti(1)–Cl(2)	2.375(1)	Ti–Cl	2.375(1)		
Ti(2)–N(3)	1.853(4)				
Ti(2)–N(4)	1.859(4)				
Ti(2)–N(6)	2.223(4)				
Ti(2)–N(7)	2.230(4)				
Ti(2)–Cl(3)	2.461(1)				
Ti(2)–Cl(4)	2.465(1)				
Bond angles					
N(2)–Ti(1)–N(4)	38.6(1)	Ti–N(1)–C(1)	88.5(2)	N(1)–Li–N(2)	69.1(2)
Ti(1)–N(2)–N(4)	60.9(2)	N(1)–C(1)–N(2)	116.1(3)	Li–N(1)–C(1)	85.5(2)
Ti(1)–N(4)–N(2)	80.5(2)	C(1)–N(2)–Ti(1)	92.3(2)	N(1)–C(1)–N(2)	119.8(2)
N(1)–Ti(1)–N(3)	38.1(1)	N(1)–Ti(1)–N(2)	62.7(1)	C(1)–N(2)–Li	85.0(2)
Ti(1)–N(1)–N(3)	59.8(2)	Ti(1)–N(3)–C(14)	89.3(2)		
N(1)–N(3)–Ti(1)	82.1(2)	N(3)–C(14)–N(4)	115.4(3)		
Cl(1)–Ti(1)–Cl(2)	170.0(2)	C(14)–N(4)–Ti	92.5(2)		
Ti(1)–N(3)–Ti(2)	94.4(2)	N(3)–Ti(1)–N(4)	62.5(1)		
Ti(1)–N(4)–Ti(2)	93.7(2)	Ti(1)–N(5)–N(6)	81.8(2)		
N(3)–Ti(2)–N(4)	88.5(2)	N(5)–N(6)–Ti(1)	58.8(2)		
Cl(3)–Ti(2)–Cl(4)	87.8(1)	N(5)–Ti(1)–N(6)	39.4(1)		
		N(2)–Ti(1)–Cl	158.08(8)		

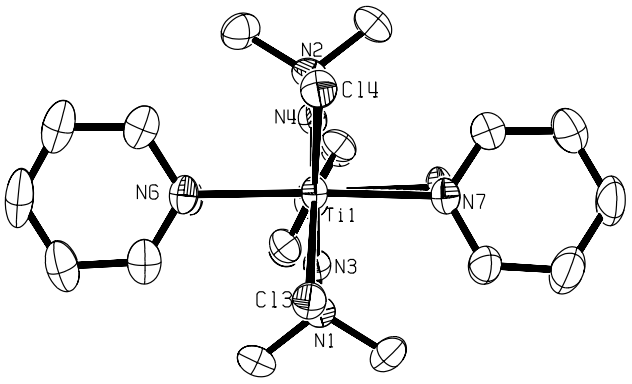

Fig. 2. View of the structure of $[Ti_2Cl_4(NNMe_2)_2(py)_3]$ (**1**) along the Ti–Ti vector. All hydrogen atoms and two molecules of CH_2Cl_2 of crystallization have been omitted for clarity.

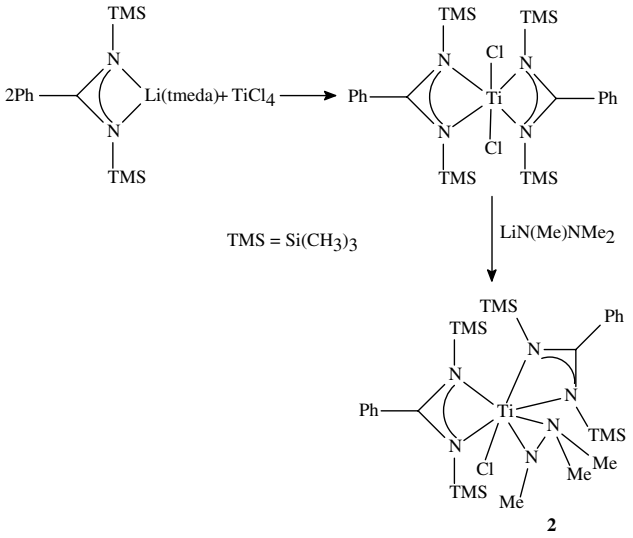

Scheme 2.

and coordinated to Ti(2). The geometries at N(3) and N(4) are close to trigonal planar as reflected by the sums of bond angles, 352.9(3)° and 348.3(3)°, respectively. The remaining nitrogens [N(1) and N(2)] are of the amido type and form donor–acceptor bonds to Ti(1). As expected, the average Ti–N bond distance for the imido nitrogens (1.948(4) Å) is considerably shorter than that for the amido nitrogens (2.216(4) Å). The Ti(1)–N(3)–Ti(2)–N(4) core is close to planar (sum of bond angles = 346.8(2)°); however, the average Ti–N bond distance to Ti(1) (1.948(4) Å) is longer than that to Ti(2) (1.856(4) Å). As anticipated on the basis of the higher coordination number of Ti(1), the N(3)–Ti(1)–N(4) bond angle (83.3(1)°) is more acute than the N(3)–Ti(2)–N(4) bond angle (88.5(2)°). Overall, the close-to-planar Ti_2N_2 core is similar to those reported for other dinuclear imido-bridged titanium complexes [16].

3.3. Synthesis and preliminary identification of $[TiCl(PhC\{N(SiMe_3)_2\}_2)_2(MeNNMe_2)]$ (2)

The initial phase of the synthesis involved the lithiation of trimethylhydrazine to form $LiN(Me)NMe_2$. The latter was allowed to react in Et_2O solution with 0.5 equiv. of $TiCl_2(PhC\{N(SiMe_3)_2\}_2)_2$ which was prepared by a slight variation of the literature methods [11,16]. The overall process is summarized in Scheme 2. The reason for selecting the trimethylhydrazide ligand was to minimize the chance of dimerization by imido bridge formation (as happens in the case of **1**). ^1H NMR spectroscopic examination of the product revealed the presence of amidinate and hydrazide resonances in a 2:1 mole ratio. The CI^+ mass spectrum of **2** evidenced low intensity peaks attributable to $[Ti(PhC\{N(SiMe_3)_2\}_2)_2(MeNNMe_2)]^+$ and $[TiCl(PhC\{N(SiMe_3)_2\}_2)_2(MeNNMe_2)]^+$ suggesting that the identity of the product is $[TiCl(PhC\{N(SiMe_3)_2\}_2)_2(MeNNMe_2)]$. This suggestion was confirmed by X-ray crystallography.

3.4. Single crystal X-ray structure of $[TiCl(PhC\{N(SiMe_3)_2\}_2)_2(MeNNMe_2)]$ (2)

The X-ray crystal structure confirms the presence of one chloride ligand in the product. Thus, even though there is sufficient space around the titanium atom (Fig. 3 and Table 2), the second equivalent of $LiN(Me)NMe_2$ fails to react. The coordination sphere comprises two η^2-bonded amidinate ligands, one chloride, and one η^2-bonded trimethylhydrazide. The titanium(IV) center is therefore heptacoordinate. The

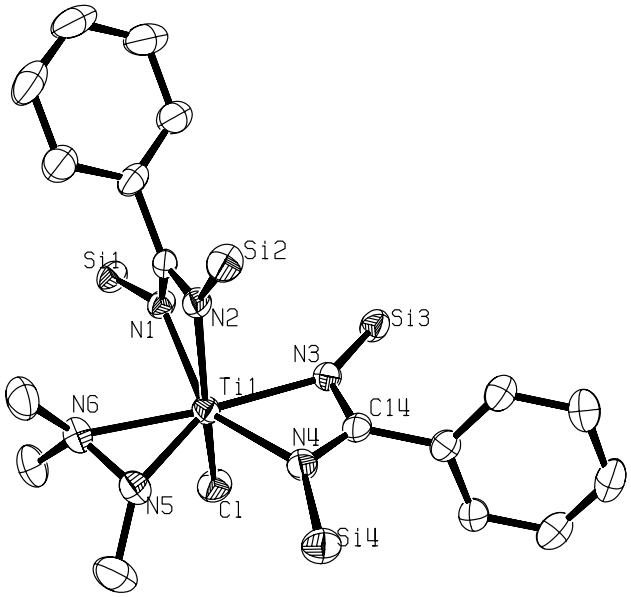

Fig. 3. Molecular structure of $[TiCl(PhC\{N(SiMe_3)_2\}_2)_2(MeNNMe_2)]$ (**2**) showing the atom numbering scheme. Thermal ellipsoids are set to 30% probability. All hydrogen atoms and the methyl groups on the silicon atoms have been omitted for clarity.

geometry of **2** does not fall in an easily described category. Nitrogen N(2) and the chloride ligand possess a mutually *trans* relationship with a Cl–Ti–N(2) bond angle of 158.08(8)° and, together with N(1) these atoms roughly describe a trigonal plane. Likewise, nitrogen atoms N(3) and N(6) are almost directly opposite each other (∠N(6)–Ti–N(3) = 171.6(1)°) and, in turn, nitrogen atoms N(3), N(4), N(5) and N(6) are close to planar. The maximum deviation from said plane is 0.185 Å for N(5). The N(1)–N(2)–Cl and N(3)–N(4)–N(5)–N(6) planes are roughly orthogonal, e.g., N(2) forms angles of 88.9(1)° and 91.4(1)° with N(3) and N(6), respectively.

As in the case of **1**, the N–Ti bond distance for the σ-bonded nitrogen of the hydrazide ligand, N(5) (1.897(3) Å) is shorter than that for the donor nitrogen, N(6) (2.196(3) Å). Although the two amidinate ligands are, as expected, bonded in an η^2-fashion, the two Ti–N bond distances are unequal. For example, the N(3)–Ti bond distance is 0.085(3) Å longer than that for the N(4)–Ti bond and the N(2)–Ti bond distance exceeds the N(1)–Ti bond distance by 0.097(3) Å. The average bite angle of the amidinate ligands in **2** is 62.6(1)° and thus considerably larger than that of the trimethylhydrazide ligand (39.4(1)°).

3.5. Single crystal X-ray structure of Li[PhC{N(SiMe$_3$)$_2$}]tmeda (3)

The structure of **3** (Fig. 4 and Table 2) is similar to those of other lithium amidinates [17]. In contrast to the structure of the titanium compound **2**, the C–N bond distances in the lithio derivative **3** are equal within experimental error and shorter than the average C–N bond distance in **2**.

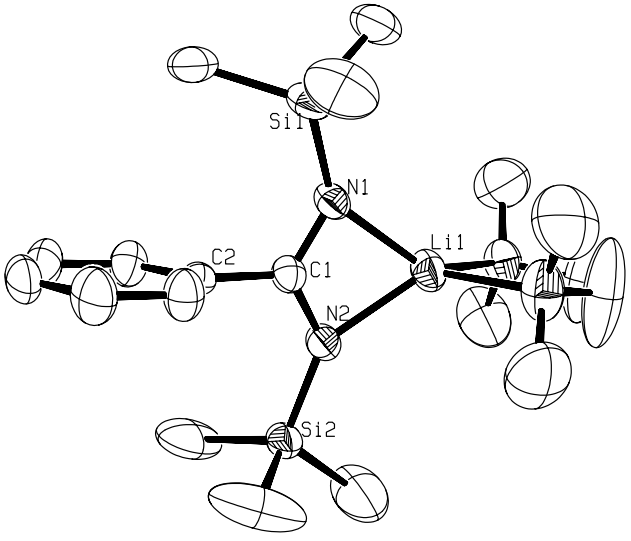

Fig. 4. Molecular structure of Li[PhC{N(SiMe$_3$)$_2$}]tmeda (**3**) showing the atom numbering scheme. Thermal ellipsoids are set to 30% probability.

4. Concluding remarks

Although LiN(H)NMe$_2$ is sufficiently reactive toward TiCl$_4$ to cause both LiCl and HCl elimination reactions, only two of the four chloride ligands are displaced. Repetition of this reaction with higher lithium hydrazide/TiCl$_4$ mole ratios did not change the outcome and **1** was the sole isolated product. Furthermore, the pronounced tendency of the hydrazide (2-) ligand to adopt a bridging position resulted in a dinuclear structure. The use of pyridine ligands to saturate the titanium centers, and thus preclude dimerization, was unsuccessful. In the case of **2**, despite the increase of size in going from hydrazide to amidinate ligands, again it was not possible to eliminate all the chloride ligands of TiCl$_4$.

Acknowledgments

The authors are grateful to the National Science Foundation (CHE-024008) and the Robert A. Welch Foundation (F-135) for financial support.

Appendix A. Supplementary data

Full crystallographic data for the structural analyses have been deposited with the Cambridge Crystallographic Data Centre, CCDC Nos. 268289 (**1**), 268290 (**2**) and 268291 (**3**). Copies of this information may be obtained free of charge from the Director, CCDC, 12 Union Road, Cambridge CB2 1EZ, UK (fax: +44 1223 336 033; e-mail:deposit@ccdc.cam.ac.uk or http://www.ccdc.cam.ac.uk). Supplementary data associated with this article can be found, in the online version, at doi:10.1016/j.poly.2005.06.035.

References

[1] R.M. Fix, R.G. Gordon, D.M. Hoffman, Chem. Mater. 2 (1990) 235.
[2] F. Laurent, J.S. Zhao, L. Valade, R. Choukron, P.J. Cassoux, J. Anal. Appl. Pyrolysis 24 (1992) 39.
[3] C.H. Winter, P.H. Sheridan, T.S. Lewkebandara, T.S. Heeg, J.W. Proscia, J. Am. Chem. Soc. 114 (1992) 1095.
[4] C.J. Carmalt, S.R. Whaley, P.S. Lall, A.H. Cowley, R.A. Jones, B.G. McBurnett, J.G. Ekerdt, J. Chem. Soc., Dalton Trans. (1998) 553.
[5] C.H. Winter, T.S. Lewkebandara, J.W. Proscia, A.L. Rheingold, Inorg. Chem. 33 (1994) 1227.
[6] K. Ikeda, M. Maeda, Y. Arita, Jpn. J. Appl. Phys. 32 (1993) 3085.
[7] C.J. Carmalt, A.H. Cowley, R.D. Culp, R.A. Jones, Y.-M. Sun, B. Fitts, S. Whaley, H.W. Roesky, Inorg. Chem. 36 (1997) 3108.
[8] T. Ohba, T. Suzuki, H. Yagi, Y. Furumura, T. Hatano, J. Electrochem. Soc. 142 (1995) 934.
[9] C.H. Winter, P.J. McKarns, J.T. Scheper, Mater. Res. Soc. Symp. Proc. 495 (1998) 95.

[10] J.T. Scheper, P.J. McKarns, T.S. Lewkebandara, C.H. Winter, Mater. Sci. Semicon. Proc. 2 (1999) 149.
[11] D.G. Dick, R. Duchateau, J.J.H. Edema, S. Gambarotta, Inorg. Chem. 32 (1993) 1959.
[12] J.B. Class, J.G. Aston, T.S. Oakwood, J. Am. Chem. Soc. 75 (1953) 2937.
[13] G.M. Sheldrick, SHELXTL/PC (Version 5.03), Siemens Analytical X-ray Instruments, Inc., Madison, WI, USA, 1994.
[14] See, for example, D.L. Thorn, W.A. Nugent, R.L. Harlow, J. Am. Chem. Soc. 103 (1981) 357.
[15] P.J. Stewart, A.J. Blake, P. Mountford, J. Organomet. Chem. 564 (1998) 209.
[16] H.W. Roesky, B. Meller, M. Noltemeyer, H.-G. Schmidt, U. Scholz, G.M. Sheldrick, Chem. Ber. 121 (1988) 1403.
[17] See, for example, C. Knapp, E. Lork, P.G. Watson, R. Mews, Inorg. Chem. 41 (2002) 2014.

Available online at www.sciencedirect.com
SCIENCE DIRECT®
Polyhedron 25 (2006) 266–270
POLYHEDRON
www.elsevier.com/locate/poly

Self-assembly of organometallic polymers through hydrogen bonding: A diplatinum(IV) complex with a single bridging halide ligand

Christopher S.A. Fraser, Dana J. Eisler, Richard J. Puddephatt *

Department of Chemistry, University of Western Ontario, Richmond Street, London, Canada N6A 5B7

Received 8 April 2005; accepted 15 August 2005
Available online 7 October 2005

Dedicated to Professor Malcolm Chisholm, master of molecular architecture, in recognition of his outstanding contributions to inorganic chemistry.

Abstract

The reaction of $[PtMe_2(bu_2bipy)]$, $bu_2bipy = 4,4'$-di-*t*-butyl-2,2′-bipyridine (**1**) with RCH_2Br occurs by *trans* oxidative addition to give the platinum(IV) complexes $[PtBrMe_2(CH_2R)(bu_2bipy)]$, $R = C_6H_4CO_2H$ (**2**); $R = C_6H_4CH_2CO_2H$ (**3**) and these reacted with half an equivalent of $Ag[PF_6]$ to give the unusual diplatinum(IV) complexes $[\{PtMe_2(CH_2R)(bu_2bipy)\}_2(\mu\text{-}Br)][PF_6]$, $R = C_6H_4CO_2H$ (**4**); $R = C_6H_4CH_2CO_2H$ (**5**). These diplatinum(IV) complexes, each of which contains a hydrogen bonding carboxylic acid group, are connected only by an unsupported bridging bromide ligand. In the solid state, complex **4** forms a self-assembled zig-zag polymer through intermolecular hydrogen bonding between pairs of carboxylic acid groups.
© 2005 Elsevier Ltd. All rights reserved.

Keywords: Platinum; Self-assembly; Polymer; Hydrogen bond

1. Introduction

Hydrogen bonding is widely used in supramolecular chemistry, such as in crystal engineering and in the design of molecular materials [1–3]. However, this approach has natural limitations in organometallic chemistry, since many alkyl-metal bonds react with the functional groups (e.g. OH or NH bonds) typically used as hydrogen bond donors [4]. Although methylplatinum(II) bonds can be cleaved by carboxylic acids [5], the reactions of $[PtMe_2(bu_2bipy)]$, $bu_2bipy = 4,4'$-di-*t*-butyl-2,2′-bipyridine (**1**) with $BrCH_2C_6H_4CO_2H$ and $BrCH_2C_6H_4CH_2CO_2H$ occur selectively by *trans* oxidative addition of the C–Br bond to give the platinum(IV) complexes **2** and **3**, rather than by protonolysis of a methylplatinum bond, as shown in Scheme 1 [6–8]. Since methyl-platinum(IV) bonds are typically inert towards protonolysis [4,5], with the notable exception of tetramethylplatinum(IV) compounds [9], the organoplatinum(IV) products, **2** and **3** of Scheme 1, that contain a carboxylic acid functional group are stable compounds. In the solid state, they form dimers by self-assembly as illustrated for complex **2** in Scheme 1 [6].

In order to form polymers by self-assembly, it is necessary to have at least two hydrogen-bonding donor/acceptor pairs per molecule. One way to prepare such "building block" molecules is to abstract the bromide ligand from **2** or **3** in the presence of an assembling ligand such as 4,4′-bipyridine, and the diplatinum(IV) complexes formed in this way have been shown to self-assemble to give unusual supramolecular polymers [6–8]. This paper reports a simpler way to prepare diplatinum(IV) complexes by formation of a bridging halide linking group, and shows that self-assembly can then give a supramolecular polymer.

2. Experimental

All reactions were performed under a nitrogen atmosphere by using standard Schlenk techniques. NMR and

* Corresponding author. Tel.: +1 519 661 2111/679 2111; fax: +1 519 661 3022.
E-mail address: pudd@uwo.ca (R.J. Puddephatt).

0277-5387/$ - see front matter © 2005 Elsevier Ltd. All rights reserved.
doi:10.1016/j.poly.2005.08.020

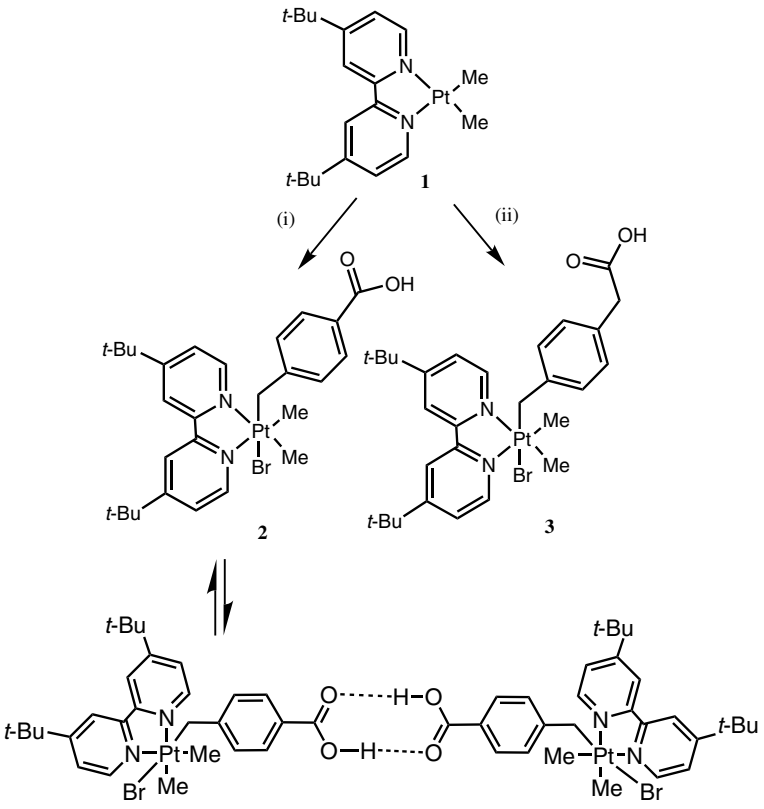

Scheme 1. Reagents are: (i) $BrCH_2C_6H_4CO_2H$ and (ii) $BrCH_2C_6H_4CH_2CO_2H$.

IR spectra were recorded by using a Varian Gemini 400 NMR and a Perkin-Elmer FT-IR 2000 spectrometer, respectively. Compound **1** was prepared using a method reported in the literature [10].

2.1. [{$PtMe_2(bu_2bipy)(CH_2C_6H_4CO_2H)$}$_2(\mu$-Br)][$PF_6$] (**4**[$PF_6$])

To a solution of [$PtMe_2(bu_2bipy)$] (100 mg) in acetone (30 mL) was added bromotoluic acid (44 mg), and the solution was stirred for 30 min., after which time a solution of $AgPF_6$ (26 mg) in acetone (5 mL) was added. After stirring for further 30 min, the mixture was filtered through Celite and evaporated under vacuum to give a white solid. Yield: 86%. *Anal.* Calc. for $C_{56}H_{74}BrF_6N_4O_4PPt_2$: C, 45.38; H, 5.03; N, 3.78. Found: C, 45.07; H, 5.21; N, 3.55%. NMR in acetone-d_6: $\delta(^1H) = 1.04$ [s, 12H, $^2J(PtH) = 70$ Hz, PtMe]; 1.44 [s, 36H, bu]; 2.82 [s, 4H, $^2J(PtH) = 90$ Hz, $PtCH_2$]; 6.35 [m, 4H, C_6H_4 H^2]; 7.25 [m, 4H, C_6H_4 H^3]; 7.70 [m, 4H, bipy H^5]; 8.45 [m, 4H, bipy H^3]; 8.60 [m, 4H, bipy H^6]. IR (Nujol mull): $\nu(CO) = 1697$ cm^{-1}, $\nu(OH) = 2624$, 2548 cm^{-1}.

2.2. [{$PtMe_2(bu_2bipy)(CH_2C_6H_4CH_2CO_2H)$}$_2(\mu$-Br)][$PF_6$] (**5**[$PF_6$])

This was prepared similarly from [$PtMe_2(bu_2bipy)$] (100 mg), bromomethylphenylacetic acid (46 mg) and $AgPF_6$ (26 mg). Yield: 87%. *Anal.* Calc. for $C_{58}H_{78}BrF_6N_4O_4PPt_2$: C, 46.13; H, 5.20; N, 3.71. Found: C, 45.71; H, 5.21; N, 3.58%. NMR in acetone-d_6: $\delta(^1H) = 1.02$ [s, 12H, $^2J(PtH) = 70$ Hz, PtMe]; 1.48 [s, 36H, bu]; 2.75 [s, 4H, $^2J(PtH) = 90$ Hz, $PtCH_2$]; 6.15 [m, 4H, C_6H_4 H^2]; 7.45 [m, 4H, C_6H_4 H^3]; 7.70 [m, 4H, bipy H^5]; 8.3–8.6 [m, br, 8H, bipy H^3 + bipy H^6]. IR (Nujol mull): $\nu(CO) = 1696$ cm^{-1}, $\nu(OH) = 2652$, 2516 cm^{-1}.

2.3. X-ray structure determination

Crystals of **4**[PF_6]$\cdot 4C_6H_6$ were grown by slow diffusion of benzene into an acetonitrile solution. A colorless plate was mounted on a glass fiber. Data were collected at 200 K using a Nonius Kappa CCD diffractometer with COLLECT (Nonius, B.V., 1998) software. The unit cell parameters were calculated and refined from the full data set. Crystal cell refinement and data reduction were carried out using the Nonius DENZO package. After data reduction, the data were scaled based on equivalent reflections using SCALEPACK (Nonius, B.V. 1998). The crystal data and refinement parameters are listed in Table 1. The SHELX-TL 5.1 (Sheldrick, G.M., Madison, WI) program package was used to solve the structure by direct methods. There was some disorder in the hexafluorophosphate anion, which was modeled as a mixture of two 50:50 occupancy groups, with the phosphorus fluorine bond lengths restrained to be equal and allowed to refine. Several of the solvent molecules were disordered and were modeled as isotropic 50:50 mixtures.

Table 1
Crystal data and structure refinement for complex $4[PF_6]\cdot 4C_6H_6$

Empirical formula	$C_{80}H_{98}BrF_6N_4O_4PPt_2$
Formula weight	1794.68
Temperature (K)	200(2)
Wavelength (Å)	0.71073
Crystal system	monoclinic
Space group	$P2(1)/n$
Unit cell dimensions	
a (Å)	14.57770(10)
b (Å)	32.5272(3)
c (Å)	19.4740(2)
β (°)	101.894(1)
Volume (Å^3)	9035.8(4)
Z	4
Density (calculated) (Mg/m^3)	1.319
Absorption coefficient (mm^{-1})	3.608
$F(000)$	3592
Reflections collected	51 358
Independent reflections	20 503 [$R_{int} = 0.048$]
Completeness to $\theta = 27.48°$ (%)	99.0
Absorption correction	integration
Final R indices [$I > 2\sigma(I)$]	$R_1 = 0.0707$, $wR_2 = 0.2073$
R indices (all data)	$R_1 = 0.1083$, $wR_2 = 0.2361$

All other non-hydrogen atoms were refined with anisotropic thermal parameters. The hydrogen atoms were calculated geometrically and were riding on their respective carbon atoms.

3. Results and discussion

The synthesis of the building blocks for self-assembly was achieved according to Scheme 2. The organoplatinum(IV) complexes **2** and **3**, each of which contains a single carboxylic acid substituent, were prepared in situ by reaction of $[PtMe_2(bu_2bipy)]$ with the corresponding benzyl bromide derivative according to Scheme 1. Reaction of these complexes with silver hexafluorophosphate in a 2:1 molar ratio occurred by bromide abstraction, to give insoluble AgBr, and then by formation of a bridging bromide group to give the cationic diplatinum(IV) complexes **4** and **5**, which were isolated as the hexafluorophosphate salts. In these reactions, it can be considered that the bromo ligand of one platinum(IV) center acts as a ligand at the

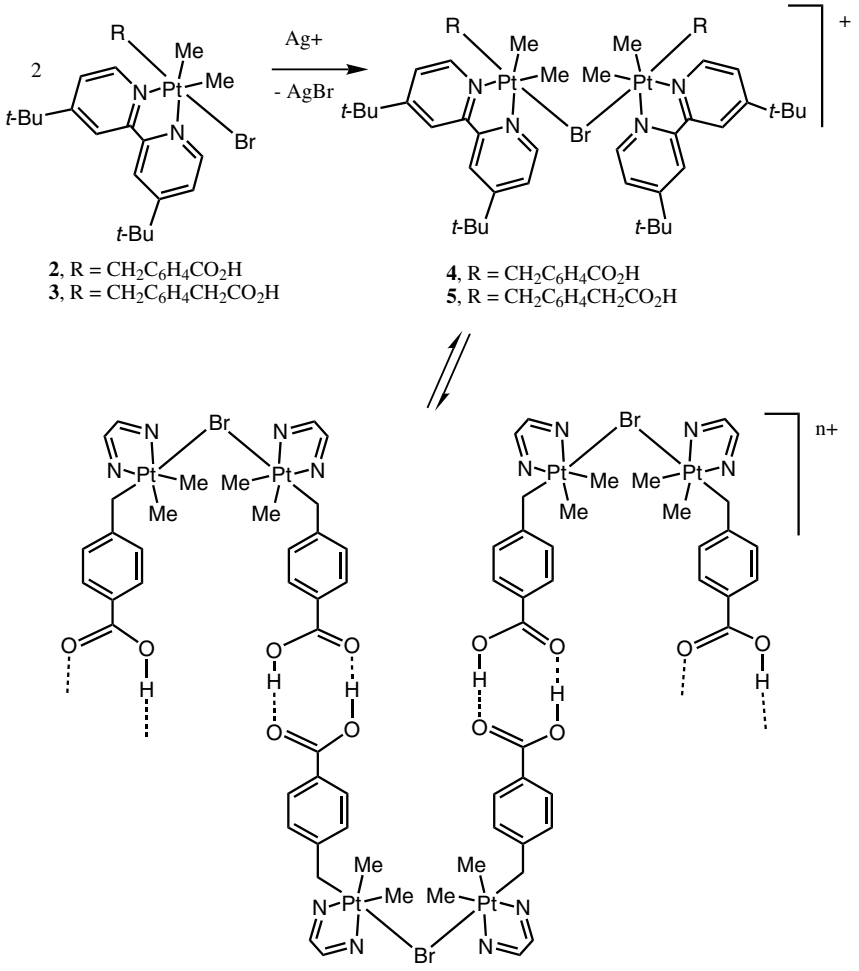

2, R = $CH_2C_6H_4CO_2H$
3, R = $CH_2C_6H_4CH_2CO_2H$

4, R = $CH_2C_6H_4CO_2H$
5, R = $CH_2C_6H_4CH_2CO_2H$

Scheme 2. In the self-assembled polymer only the core atoms of the bu_2bipy ligands are shown.

second platinum(IV) center by occupying the coordination site which is opened up by the bromide abstraction step.

The complexes **4** and **5** are air-stable complexes which are soluble in organic solvents such as acetone and dichloromethane. In acetone-d_6 solution, the ^{1}H NMR spectrum of complex **4** contained a single methylplatinum resonance at $\delta(^1H) = 1.04$, with coupling constant $^2J(PtH) = 70$ Hz, showing that all methylplatinum(IV) groups are equivalent. The benzylic protons also occurred as a singlet resonance at $\delta = 2.82$, with coupling constant $^2J(PtH) = 90$ Hz. The infrared spectrum of complex **4** as a Nujol mull contained a band due to ν(C=O) at 1697 cm^{-1} and bands due to ν(OH) at 2624 and 2548 cm^{-1}. The NMR data are fully consistent with the proposed structure of **4** in solution (Scheme 2), while the IR data indicate the presence of hydrogen-bonded carboxylic acid groups in the solid state [8,9]. Complex **5** was characterized spectroscopically in a similar way.

The molecular structure of complex **4** is shown in Fig. 1. It confirms the overall stereochemistry deduced from the spectroscopic data, with the methylplatinum groups *trans* to the bipyridine ligand and the substituted benzyl group *trans* to bromide. The bromide ligand bridges the two platinum atoms with roughly equal distances Pt(1)–Br(1) = 2.560(2) Å and Pt(2)–Br(1) = 2.565(2) Å. The large angle Pt(1)–Br(1)–Pt(2) = 127.88(8)° and correspondingly long distance Pt···Pt = 4.60 Å are clear indications that there is no platinum-platinum bonding interaction [10]. Thus, the natural bond angle M–X–M is close to 90° for complexes containing a bridging halide and no other bridging halides [10]. An M–X–M angle much less than 90° then indicates the presence of a metal–metal bonding interaction, while an M–X–M angle much greater than 90° indicates both the lack of an attractive force between the metals and the presence of steric interactions around the bridging halide [10–15].

The molecules of complex **4** associate through complementary hydrogen bonding between carboxylic acid

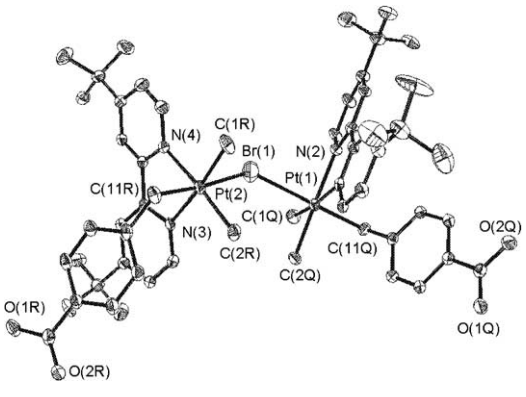

Fig. 1. A view of the structure of the cationic diplatinum(IV) complex **4**. Selected bond parameters: Pt(1)–C(2Q) 2.044(9) Å, Pt(1)–C(11Q) 2.074(9) Å, Pt(1)–C(1Q) 2.075(10) Å, Pt(1)–N(2) 2.145(7) Å, Pt(1)–N(1) 2.161(7) Å, Pt(1)–Br(1) 2.560(2) Å, Pt(2)–C(2R) 2.058(10) Å, Pt(2)–C(11R) 2.077(10) Å, Pt(2)–C(1R) 2.107(11) Å, Pt(2)–N(4) 2.136(8) Å, Pt(2)–N(3) 2.159(7) Å, Pt(2)–Br(1) 2.565(2) Å, C(11Q)–Pt(1)–Br(1) 175.0(3)°, C(11R)–Pt(2)–Br(1) 174.3(3)°, Pt(1)–Br(1)–Pt(2) 127.88(8)°.

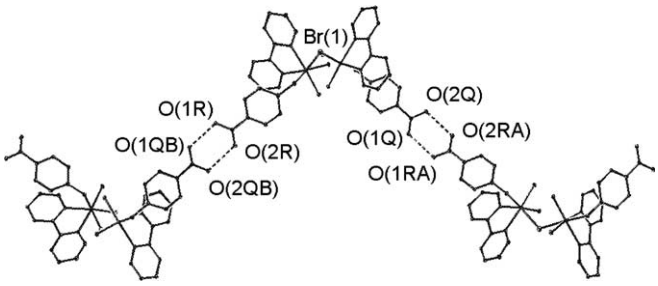

Fig. 2. Part of the zig-zag polymeric chain structure formed by self-assembly through hydrogen bonding between units of complex **4**.

substituents, as shown in Fig. 2. The intermolecular hydrogen bonding between the V-shaped building blocks **4** naturally leads to formation of a zig-zag polymeric structure. The O···O distances O(1Q)···O(1R) = 2.62(2) Å and O(2Q)···O(2R) = 2.71(2) Å are in the expected range for hydrogen bonds in carboxylic acids [5–7,9].

There are very few diplatinum complexes that have been characterized to contain a single unsupported halide bridge, and particularly few organoplatinum(IV) examples [11–14], so the characterization of the molecular structure of complex **4** is significant. More noteworthy is the observation that this is the first time that a complex of this type has been used in the self-assembly of supramolecular polymeric structures. Since the oxidative addition of alkyl halides to platinum(II) is a versatile method for the synthesis of alkyl(halogeno)platinum(IV) complexes containing functionally substituted alkyl groups [5–7], the finding that these monoplatinum(IV) complexes can easily be converted to the diplatinum(IV) complexes with bridging halide provides a valuable new method for the synthesis of bifunctional organodiplatinum(IV) complexes for use in the self-assembly of molecular materials.

Acknowledgments

We thank the NSERC (Canada) for financial support. R.J.P. thanks the Government of Canada for a Canada Research Chair.

Appendix A. Supplementary data

Supplementary data associated with this article can be found, in the online version, at doi:10.1016/j.poly.2005.08.020.

References

[1] J.W. Steed, J.L. Atwood, Supramolecular Chemistry, Wiley, New York, 2000.
[2] D.P. Gallasch, E.R.T. Tiekink, L.M. Rendina, Organometallics 16 (2001) 3373.
[3] M.H. Chisholm, Acc. Chem. Res. 33 (2000) 53.
[4] M.H. Chisholm, H.C. Clark, Acc. Chem. Res. 6 (1973) 202.
[5] C.S.A. Fraser, H.A. Jenkins, M.C. Jennings, R.J. Puddephatt, Organometallics 19 (2000) 1635.

[6] C.S.A. Fraser, H.A. Jenkins, M.C. Jennings, R.J. Puddephatt, Chem. Commun. (2000) 1310.
[7] C.S.A. Fraser, D.J. Eisler, M.C. Jennings, R.J. Puddephatt, Chem. Commun. (2002) 1224.
[8] J.B. Lambert, H.F. Shurvell, D. Lightner, R.G. Cooks, Structural Spectroscopy, Prentice-Hall, Englewood Cliffs, NJ, 1998.
[9] G.A. Jeffrey, An Introduction to Hydrogen Bonding, Oxford University Press, Oxford, UK, 1997.
[10] J. Watcher, F. Jeanneaux, G. LeBorgne, J.G. Riess, Organometallics 3 (1984) 1034.
[11] J. Terheijden, G. van Koten, D.M. Grove, K. Vrieze, A.L. Spek, J. Chem. Soc., Dalton Trans. (1987) 1359.
[12] C.R. Baar, L.P. Carbray, M.C. Jennings, R.J. Puddephatt, Organometallics 19 (2000) 2482.
[13] C.R. Baar, H.A. Jenkins, M.C. Jennings, G.P.A. Yap, R.J. Puddephatt, Organometallics 19 (2000) 4870.
[14] V.G. Albano, M. Di Serio, M. Monari, I. Orabona, A. Panunzi, F. Ruffo, Inorg. Chem. 41 (2002) 2672.
[15] F.A. Cotton, B.A. Frenz, A.J. White, J. Organomet. Chem. 60 (1973) 147.

Available online at www.sciencedirect.com
SCIENCE DIRECT®
Polyhedron 25 (2006) 271–278
POLYHEDRON
www.elsevier.com/locate/poly

Synthesis, crystal structures and antenna-like sensitization of visible and near infrared emission in heterobimetallic Zn–Eu and Zn–Nd Schiff base compounds

Xiaoping Yang [a], Richard A. Jones [a,*], Qiaoyin Wu [a], Michael M. Oye [b], Wing-Kit Lo [c], Wai-Kwok Wong [c,*], Archie L. Holmes [b]

[a] *Department of Chemistry and Biochemistry, The University of Texas at Austin, 1 University Station A 5300, Austin, TX 78712-0165, USA*
[b] *Microelectronics Research Center and Texas Materials Institute, The University of Texas at Austin, 1 University Station Stop R9900, Austin, TX 78712-0165, USA*
[c] *Department of Chemistry and Centre for Advanced Luminescence Materials, Hong Kong Baptist University, Waterloo Road, Kowloon Tong, Hong Kong, PR China*

Received 12 April 2005; accepted 24 June 2005
Available online 12 September 2005

Dedicated with admiration to Professor Malcolm H. Chisholm on the occasion of his 60th birthday.

Abstract

Visible and near infrared (NIR) luminescence are observed in heterobimetallic 3d–4f Schiff base complexes $[ZnLEu(OAc)(NO_3)_2]\cdot EtOH\cdot H_2O$ (**2**) and $[ZnLNd(OAc)(NO_3)_2(H_2O)]\cdot EtOH$ (**3**), respectively (H_2L = *N*,*N*′-bis(5-bromo-3-methoxysalicylidene)phenylene-1,2-diamine, OAc = acetate).
© 2005 Elsevier Ltd. All rights reserved.

Keywords: 3d–4f Complex; X-ray crystallography; Zinc-lanthanide; Luminescence; Schiff base

1. Introduction

Luminescent lanthanide (Ln) complexes have attracted a great deal of attention for many years due to their potential use in numerous analytical applications, ranging from proton relaxation agents for NMR imaging to luminescent probes in time-resolved fluoroimmunoassays [1]. Most trivalent lanthanide ions exhibit long-lived and linelike emission bands at characteristic wavelengths ranging from green (Tb^{3+}) to near-infrared (NIR) light (Nd^{3+}, Er^{3+}). However, for lanthanide ions, because the f–f transitions are parity forbidden, the absorption coefficients are normally very low and the emissive rates are slow. In order to overcome this, well-designed organic chromophores have been used to excite lanthanide ions as sensitizers (antenna effect) [2]. Over the past two decades, many studies have focused on complexes of Eu^{3+} and Tb^{3+}, which emit in the visible region of the spectrum. Currently, much interest is also devoted to lanthanide ions emitting in the NIR region because of potential applications in bioassays and laser systems [3]. Several recent investigations, by Bünzli and others, of sensitizers for NIR luminescence have focused on organic dyes and d-block metal complexes (i.e., $M = Pt^{II}$, Ru^{II} and Cr^{III}) [4], which display absorption bands in the near-UV or visible ranges.

There are several reports which describe the use of modified "salen" type of Schiff-base ligands for the

* Corresponding authors. Tel.: +1 512 471 1706; fax: +1 512 471 6822 (R.A. Jones).
E-mail address: rajones@mail.utexas.edu (R.A. Jones).

0277-5387/$ - see front matter © 2005 Elsevier Ltd. All rights reserved.
doi:10.1016/j.poly.2005.06.055

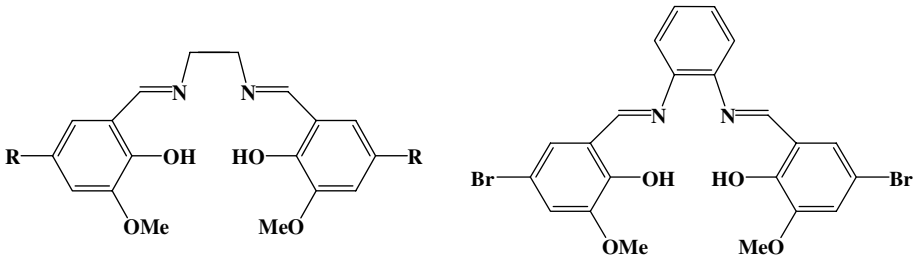

H_2L^1: R = H
H_2L^2: R = *p*-$C_6H_4CH_3$

H_2L

Scheme 1.

stabilization of heteronuclear 3d–4f complexes. Many of these studies have focused on magnetic behaviour while relatively few have described the photophysical properties of the compounds [5]. Recently, Wong and co-workers [6] described the room temperature NIR luminescence of a series of heteronuclear Zn–Ln Schiff-base complexes formed with ligands that are based on 1,2-diaminoethane (Scheme 1; H_2L^1, H_2L^2). Conjugated organic ligands, with absorption bands generally at longer wavelengths compared to non-conjugated systems, should function as improved sensitizers for the NIR luminescence of lanthanide ions compared to their non-conjugated counterparts. As part of our interest in luminescent lanthanide complexes [7–9], we describe here the synthesis, structures and photophysical properties of two heterobimetallic Zn–Ln complexes based on the Schiff base ligand $\mathbf{H_2L}$, which features an aromatic (phenylene) backbone. In addition the X-ray crystal structure of the ligand $\mathbf{H_2L}$ and the related dinuclear zinc complex [Zn_2LCl_2MeOH] (**1**) are also described.

2. Results and discussion

2.1. Free Schiff base ligand H_2L

The bright-red Schiff base ligand $\mathbf{H_2L}$ was prepared according to well established procedures [10]. The solid state structure of this compound was determined by an X-ray crystallographic study (Table 1) and two views

Table 1
Crystal data and structure refinement for $\mathbf{H_2L}$, **1**, **2** and **3**

Complex	$\mathbf{H_2L}\cdot$MeCN	**1**	**2**	**3**
Formula	$C_{24}H_{21}Br_2N_3O_4$	$C_{26}H_{30}Br_2Cl_2N_2O_7Zn_2$	$C_{26}H_{27}Br_2EuN_4O_{14}Zn$	$C_{26}H_{27}Br_2N_4NdO_{14}Zn$
Formula weight	575.23	844.00	996.63	988.94
Crystal system	triclinic	triclinic	monoclinic	triclinic
Space group	$P\bar{1}$	$P\bar{1}$	$C2/c$	$P\bar{1}$
a (Å)	7.9312(16)	11.504(2)	21.630(4)	11.002(2)
b (Å)	12.429(3)	11.857(2)	10.911(2)	11.655(2)
c (Å)	13.345(3)	13.937(3)	27.591(6)	14.447(3)
α (°)	64.83(3)	96.69(3)	90	84.23(3)
β (°)	76.76(3)	113.13(3)	91.16(3)	74.96(3)
γ (°)	83.18(3)	111.37(3)	90	66.08(3)
V (Å^3)	1158.6(4)	1551.5(5)	6510(2)	1635.3(6)
Z	2	2	8	2
D_{calc} (g cm^{-3})	1.640	1.774	2.026	2.006
T (K)	153(1)	153(1)	153(1)	153(1)
$F(000)$	570	818	3856	964
μ (mm^{-1})	3.535	4.336	5.174	4.820
θ Range (°)	2.97–27.51	2.98–27.53	3.03–27.35	2.92–27.52
Number of reflections measured	8235	12360	13212	12077
Number of reflections used	5234	7081	6766	7367
Parameters	298	342	413	433
$R^{a,b}$ [$I > 2\sigma(I)$]	$R_1 = 0.0597$, $wR_2 = 0.1224$	$R_1 = 0.0575$, $wR_2 = 0.1325$	$R_1 = 0.0945$, $wR_2 = 0.1650$	$R_1 = 0.0482$, $wR_2 = 0.0772$
$R^{a,b}$ (all data)	$R_1 = 0.1166$, $wR_2 = 0.1450$	$R_1 = 0.1105$, $wR_2 = 0.1518$	$R_1 = 0.2389$, $wR_2 = 0.2107$	$R_1 = 0.0965$, $wR_2 = 0937$
Goodness-of–fit, S	1.008	1.035	1.014	1.081

[a] $R_1 = \sum|F_o| - |F_c|/\sum|F_o|$.
[b] $wR_2 = [\sum w[(F_o^2 - F_c^2)^2]/\sum|[w(F_o^2)^2]]^{1/2}$. $w = 1/[\sigma^2(F_o^2) + (0.075P)^2]$, where $P = [\max(F_o^2, 0) + 2F_c^2]/3$.

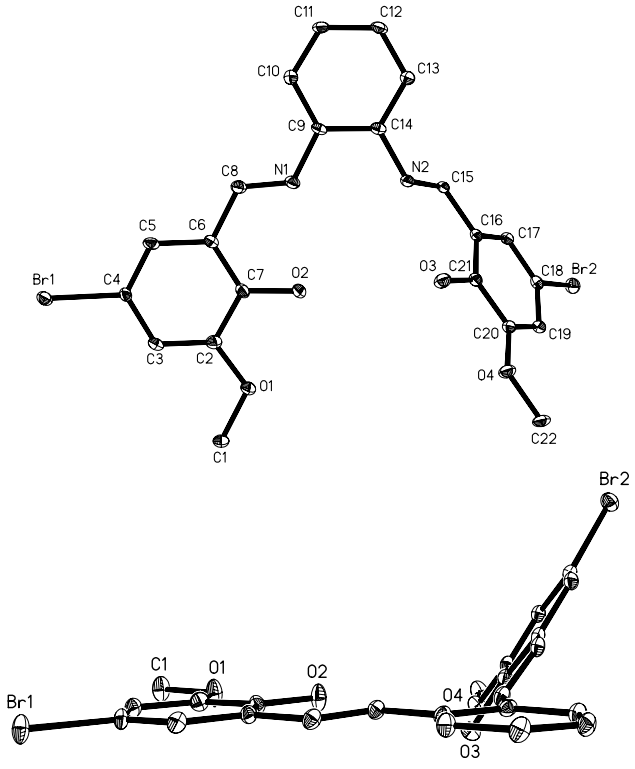

Fig. 1. Views of the crystal structure of the free ligand $\mathbf{H_2L}$. Thermal ellipsoids are drawn at the 25% probability level. Hydrogen atoms are omitted for clarity.

of the molecule are shown in Fig. 1. The compound crystallizes in the $P\bar{1}$ space group with two molecules per unit cell. There are no short intermolecular contacts and the metrical parameters fall within normal limits (Table 2). A noteworthy feature of the structure is the non-planarity of the molecule. This is caused by a twist of one of the "sal" rings which creates an angle of 56.2° with the rest of the molecule. It seems reasonable to assume that this occurs in order to minimize steric interactions between the two phenolic OH protons which would otherwise be directed at each other.

2.2. Metal complexes

Reaction of $\mathbf{H_2L}$ with $ZnCl_2$ (1:2) in MeOH/EtOH produces a yellow solution from which the dinuclear complex $[Zn_2LCl_2MeOH]$ (**1**) may be isolated in 30% yield as a yellow crystalline solid. A view of the molecule is shown in Fig. 2. In **1**, the deprotonated Schiff base ligand now adopts the expected planar configuration. One zinc atom (Zn(1)) is located slightly above the central N_2O_2 plane by 0.669 Å and has a square based pyramidal geometry via the coordination of a chlorine atom in the axial position. The other zinc atom (Zn(2)) has a pseudotetrahedral geometry formed by coordination to the two phenolic oxygen atoms, a chlorine atom and a molecule of MeOH. The Zn–Zn separation is 3.113 Å. It is interesting to note that neither of the two OMe

Table 2
Selected bond lengths (Å) and angles (°) for $\mathbf{H_2L}$

C(1)–O(1)	1.431(6)
C(2)–O(1)	1.376(6)
C(4)–Br(1)	1.910(5)
C(6)–C(8)	1.455(7)
C(7)–O(2)	1.340(6)
C(8)–N(1)	1.274(7)
C(9)–N(1)	1.424(6)
C(14)–N(2)	1.430(6)
C(15)–N(2)	1.285(7)
C(18)–Br(2)	1.900(5)
C(20)–O(4)	1.365(6)
C(20)–C(21)	1.412(7)
C(21)–O(3)	1.359(6)
C(22)–O(4)	1.446(6)
C(23)–C(24)	1.435(9)
C(24)–N(3)	1.113(8)
O(1)–C(2)–C(7)	114.8(5)
O(2)–C(7)–C(6)	122.3(4)
O(2)–C(7)–C(2)	118.7(5)
N(1)–C(8)–C(6)	121.6(5)
C(14)–C(9)–N(1)	116.8(4)
C(10)–C(9)–N(1)	124.8(5)
C(13)–C(14)–N(2)	121.1(5)
C(9)–C(14)–N(2)	118.7(4)
N(2)–C(15)–C(16)	122.6(5)
C(17)–C(18)–Br(2)	119.4(4)
C(19)–C(18)–Br(2)	118.7(4)
O(4)–C(20)–C(19)	124.5(4)
O(4)–C(20)–C(21)	115.3(5)
O(3)–C(21)–C(16)	122.4(4)
O(3)–C(21)–C(20)	117.8(4)
N(3)–C(24)–C(23)	178.2(8)
C(8)–N(1)–C(9)	121.5(4)
C(15)–N(2)–C(14)	117.8(4)
C(2)–O(1)–C(1)	116.7(4)
C(20)–O(4)–C(22)	115.7(4)

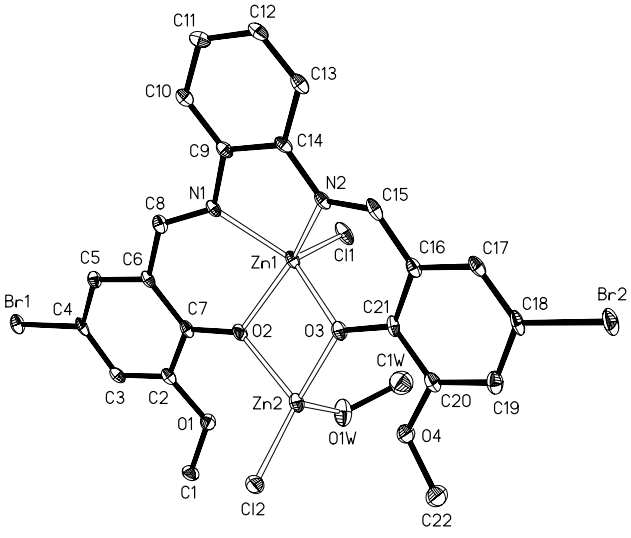

Fig. 2. X-ray structure of $[Zn_2LCl_2MeOH]$ (**1**). Thermal ellipsoids are drawn at the 25% probability level. Hydrogen atoms are omitted for clarity.

groups participate in bonding to Zn(2) with an average O–Zn separation of 2.702 Å.

Compound **1** may be regarded as a combination of a mononuclear Zn Schiff base complex "ZnL" and one mole of $ZnCl_2$. Since the presence of the second Zn moiety might hinder the subsequent formation of heterodinuclear Zn–Ln complexes, we chose $Zn(OAc)_2 \cdot 2H_2O$ as an alternative starting material. Reaction of $\mathbf{H_2L}$ with $Zn(OAc)_2 \cdot 2H_2O$ (1:1) in EtOH produces yellow solutions but we have been unable to isolate a pure compound from these reaction mixtures. We assume that a zinc Schiff base complex is formed under these conditions since further addition of $Ln(NO_3)_3 \cdot 6H_2O$ (Ln = Eu, Nd) in EtOH produces the heterodinuclear complexes $[ZnLEu(OAc)(NO_3)_2]$ (**2**) and $[ZnLNd(OAc)(NO_3)_2(H_2O)]$ (**3**). The X-ray structures of **2** and **3** are shown in Figs. 3 and 4, respectively. The compounds have similar structures with the Zn^{2+} and Ln^{3+} ions located in the N_2O_2 and O_2O_2 ligand binding sites, respectively. In both compounds the metal centers are bridged by a single bidentate acetate (OAc) ligand in addition to the phenolic oxygen atoms of the Schiff base ligand. The Zn–Eu and Zn–Nd separations are 3.369 and 3.400 Å in **2** and **3**, respectively. The oxygen atom of the μ-OAc group coordinated to Zn gives the metal center a distorted square pyramidal geometry. In both compounds the zinc atoms lie slightly above the N_2O_2 plane (0.586 Å (**2**), 0.558 Å (**3**)). In **2**, the Eu^{3+} ion is nine coordinate with an inner coordination environment provided by nine oxygen atoms, four from the Schiff base ligand, four from two bidentate nitrates and one from the μ-OAc group. In **3** the larger Nd^{3+} ion is 10 coordinate and has an additional bound H_2O molecule. In both **2** and **3**, the average distances for Zn–O(phenolic) (2.009 Å (**2**), 2.007 Å (**3**)), Zn–N (2.020 Å (**2**), 2.038 Å (**3**)), Ln–O(phenolic) (2.330 Å (**2**), 2.429 Å (**3**)) and Ln–O(methoxy) (2.600 Å (**2**), 2.735 Å (**3**)) are comparable to those found in the literature [6].

The UV–Vis absorption spectra of $\mathbf{H_2L}$, **2** and **3** in MeCN solution are shown in Fig. 5. The free ligand $\mathbf{H_2L}$ exhibits absorption bands at 235, 280 and 335 nm, which become red-shifted upon coordination to the metals in **2** and **3**. Complexes **2** and **3** exhibit similar solution absorption spectra and are stable in MeCN at room temperature as shown by the lack of changes over one week. Molar conductivity studies for **2** and **3** have also confirmed the presence of neutral, undissociated species in MeCN solutions. The visible emission spectra of the free ligand $\mathbf{H_2L}$, **2** and **3** in CH_3CN are shown in Fig. 6, and the NIR luminescence of **3** in Fig. 7. Excitation of the absorption band at 279 nm of $\mathbf{H_2L}$ produces a broad emission band at $\lambda_{max} = 468$ nm. Excitation of the ligand-centered absorption bands of **2** and **3** produces typical visible emission bands of the Eu^{3+} ion ($^5D_0 \rightarrow {}^7F_J$ transitions, $J = 1, 2, 3$ and 4) and NIR luminescence of Nd^{3+} ion ($^4F_{3/2} \rightarrow {}^4I_J$ transitions, $J = 9/2$, 11/2 and 13/2), respectively. It is noticeable that, the

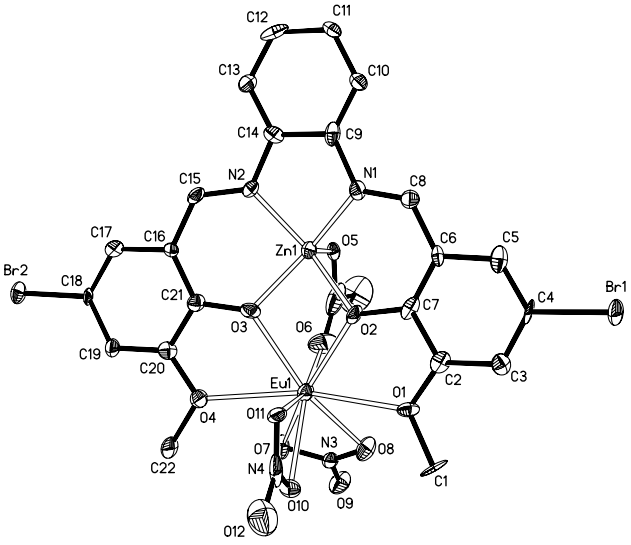

Fig. 3. X-ray structure of **2**. Thermal ellipsoids are drawn at the 25% probability level. Hydrogen atoms are omitted for clarity.

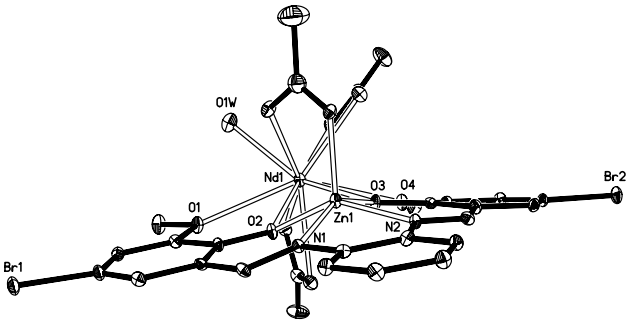

Fig. 4. X-ray structure of **3**. Thermal ellipsoids are drawn at the 25% probability level. Hydrogen atoms are omitted for clarity.

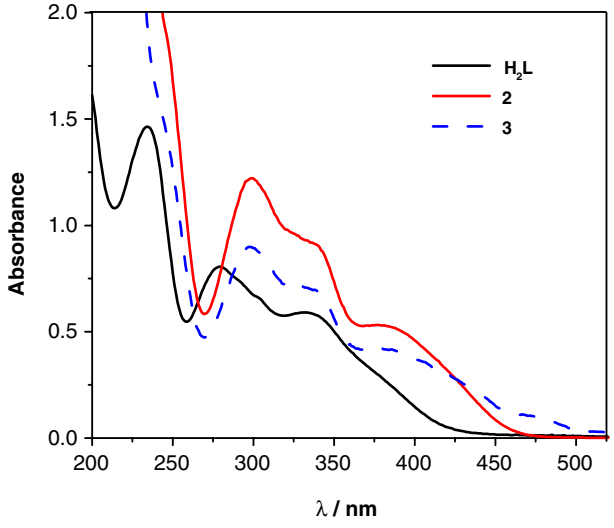

Fig. 5. Absorption spectra of the free ligand $\mathbf{H_2L}$, complexes **1** and **2** in CH_3CN at 298 K.

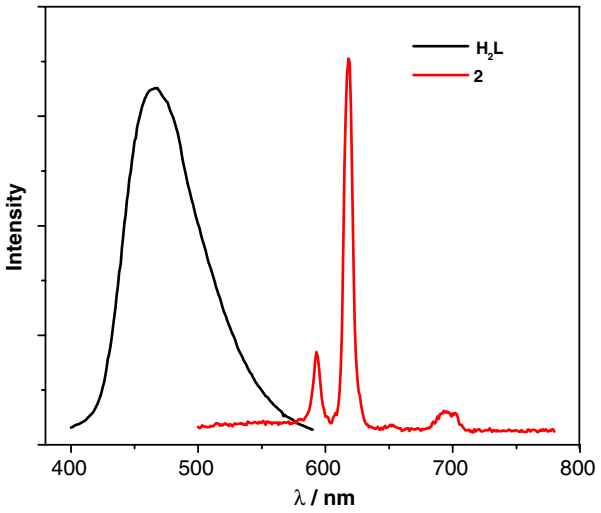

Fig. 6. Visible emission spectra of the free ligand $\mathbf{H_2L}$, complexes **2**, **3** and Zn–GdL in CH_3CN (10^{-4}–10^{-5} M). $\lambda_{ex} = 275$ nm.

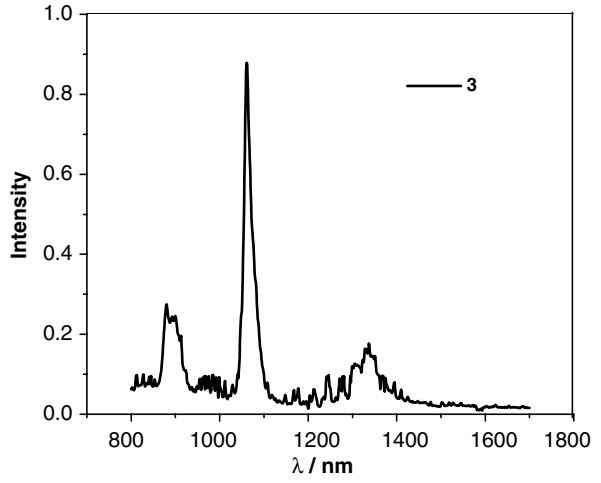

Fig. 7. Sensitized NIR emission spectrum of **3** in MeCN (6.31×10^{-4} M). The excitation was provided by an argon ion laser using either the UV multiline optics (333.6–363.8 nm range) or the 275.4 nm laser line.

fluorescence of ligand-centered (antenna) in visible region is almost quenched in both **2** and **3**, which suggests that the energy transfer from the antenna to lanthanide ion takes place efficiently [11]. The fluorescence quantum yields (Φ_{em}) of **2** in CH_3CN is 0.067 [12], while the NIR luminescence quantum yield of **3** could not be measured directly due to limitations with our instrumentation. However, its maximum possible quantum yield was estimated to be 0.082 using comparative methods as described by van Veggel et al. [4c].

In conclusion, we have shown that the aromatic salen-type ligand $\mathbf{H_2L}$ may be used for the preparation of 3d–4f bi-metallic Schiff base complexes, and it can act as an antenna for Eu^{3+} and Nd^{3+} luminescence while its emission in the visible region is effectively suppressed.

3. Experimental

3.1. Synthesis

3.1.1. Preparation of ligand H_2L

A solution of *o*-phenylenediamine (1.08 g, 0.01 mol) in ethanol (20 ml) was added to a solution of 5-bromo-2-hydroxy-3-methoxybenzaldehyde (4.62 g, 0.02 mol) in ethanol (60 ml). The mixture was stirred at room temperature (12 h) and the product filtered and washed with ethanol (20 ml). The material was recrystallized from ethanol. Yield: 3.373 g, 70%. m.p. = 170 °C. ESI-MS (CH_3CN) *m*/*z*: 535 $[M + H]^+$. ^1H NMR (400 MHz, DMSO-d_6): δ (ppm) 3.848 (s, 6H), 7.263 (s, 2H), 7.446 (m, 4H), 7.487 (s, 2H), 8.907 (s, 2H). IR (CH_3CN, cm^{-1}): 3385, 2971, 1644, 1636, 1558, 1487, 1458, 1245, 1060, 746, 618. Single crystals for X-ray crystallographic analysis were obtained by vapor diffusion of diethyl ether into solutions of $\mathbf{H_2L}$ in MeCN.

3.1.2. Preparation of $[Zn_2LCl_2MeOH] \cdot EtOH \cdot MeOH$ (**1**)

A solution of $ZnCl_2$ (0.068 g, 0.5 mmol) in 10 ml MeOH was added to a solution of $\mathbf{H_2L}$ (0.134 g, 0.25 mmol) in 5 ml EtOH. The mixture was stirred and refluxed for 10 min, cooled to room temperature, and filtered. Diethylether was allowed to diffuse slowly into the filtrate at room temperature and yellow single crystals were obtained in one month. Yield: 0.063 g, 30%. ESI-MS (CH_3CN) *m*/*z*: 730 $[M - Cl^- - EtOH - MeOH]^+$. m.p. >270 °C (dec). IR (CH_3CN, cm^{-1}): 3456.05, 1658.25, 1551.56, 1448.54, 1411.34, 1341.88, 1234.95, 1188.33, 1048.54, 1029.13, 681.25, 679.61.

3.1.3. Preparation of $[ZnLEu(OAc)(NO_3)_2] \cdot EtOH \cdot H_2O$ (**2**)

A mixture of $\mathbf{H_2L}$ (0.054 g, 0.10 mmol) and $Zn(OAc)_2 \cdot 2H_2O$ (0.022 g, 0.10 mmol) in EtOH (20 ml) was stirred and heated under reflux for 20 min. A solution of $Eu(NO_3)_3 \cdot 6H_2O$ (0.045 g, 0.10 mmol) in EtOH (10 ml) was added and the mixture was stirred and refluxed for 30 min. The mixture was allowed to cool to room temperature and filtered. The filtrate was allowed to evaporate in the air. Yellow single crystals of **2** were formed (3 weeks). Yield: 0.055 g, 56%, m.p. >310 °C (dec). ESI-MS (CH_3CN) *m*/*z*: 871 $[M - NO_3^- - EtOH - H_2O]^+$. IR ($CH_3CN$, cm^{-1}): 3382.52, 1611.65, 1541.75, 1440.78, 1355.34, 1231.07, 1188.35, 1048.54, 1013.59, 947.57, 831.07, 788.35, 741.75, 664.08.

3.1.4. Preparation of $[ZnLNd(OAc)(NO_3)_2(H_2O)] \cdot EtOH$ (**3**)

The method was similar to that used for **2** (above). $\mathbf{H_2L}$ (0.054 g, 0.10 mmol), $Zn(OAc)_2 \cdot 2H_2O$ (0.022 g, 0.10 mmol) and $Nd(NO_3)_3 \cdot 6H_2O$ (0.044 g, 0.10 mmol) were employed. Yield: 0.069 g, 70%, yellow crystals,

m.p. >308 °C (dec). ESI-MS (CH_3CN) *m/z*: 881 $[M - NO_3^- - EtOH]^+$. IR (CH_3CN, cm^{-1}): 3375.50, 1613.89, 1550.91, 1443.01, 1352.55, 1230.23, 1040.32, 1020.41, 948.08, 835.62, 789.57, 744.80, 660.11.

3.2. Photophysical measurements

Solvents for the photophysical investigations were dried over molecular sieves and freshly distilled under dry nitrogen before use. Absorption spectra were obtained on a BECKMAN DU 640 spectrophotometer, excitation and visible emission spectra on a QuantaMaster PTI fluorimeter. Near-infrared (NIR) emission spectra were measured with a one-meter SPEX 1704 spectrometer and a liquid-nitrogen cooled Ge detector, using an argon ion laser as excitation source. The fluorescence quantum yield of **2** was determined by using $[Ru(bipy)_3]Cl_2$ (bipy = 2,2′-bipyridine; $\Phi = 0.028$ in water) as a standard [12,13].

3.3. X-ray crystallographic studies

Details of crystallographic parameters, data collection and refinements are listed in Table 1. Selected bond lengths (Å) and angles (°) for H_2L, **1**, **2** and **3** are listed in Tables 2–5, respectively. Intensities were collected on a Nonius Kappa CCD diffractometer with graphite monochromated Mo Kα radiation ($\lambda = 0.71073$ Å) at 153 K. Absorption corrections were applied using GAUSSIAN. The structures were solved by direct methods and refined anisotropically using full-matrix least-squares methods with the SHELX-97 program package [14]. The coordinates of the non-hydrogen atoms were

Table 3
Selected bond lengths (Å) and angles (°) for **1**

Zn(1)–O(3)	2.024(4)
Zn(1)–O(2)	2.027(4)
Zn(1)–N(1)	2.041(5)
Zn(1)–N(2)	2.048(5)
Zn(1)–Cl(1)	2.2691(19)
Zn(2)–O(1W)	1.996(5)
Zn(2)–O(3)	1.998(4)
Zn(2)–O(2)	2.029(4)
Zn(2)–Cl(2)	2.174(2)
O(3)–Zn(1)–O(2)	77.47(16)
O(3)–Zn(1)–N(1)	139.17(17)
O(2)–Zn(1)–N(1)	88.97(17)
O(3)–Zn(1)–N(2)	87.96(18)
O(2)–Zn(1)–N(2)	143.96(17)
N(1)–Zn(1)–N(2)	80.79(19)
O(3)–Zn(1)–Cl(1)	108.48(14)
O(2)–Zn(1)–Cl(1)	109.41(13)
N(1)–Zn(1)–Cl(1)	112.35(14)
N(2)–Zn(1)–Cl(1)	106.44(13)
O(1W)–Zn(2)–O(3)	104.2(2)
O(1W)–Zn(2)–O(2)	103.3(2)
O(3)–Zn(2)–O(2)	77.99(16)
O(1W)–Zn(2)–Cl(2)	121.25(18)
O(3)–Zn(2)–Cl(2)	124.01(14)
O(2)–Zn(2)–Cl(2)	116.84(13)

Table 4
Selected bond lengths (Å) and angles (°) for **2**

Eu(1)–O(6)	2.315(4)
Eu(1)–O(2)	2.320(3)
Eu(1)–O(3)	2.343(3)
Eu(1)–O(7)	2.397(3)
Eu(1)–O(8)	2.423(3)
Eu(1)–O(10)	2.505(4)
Eu(1)–O(11)	2.517(3)
Eu(1)–O(4)	2.584(3)
Eu(1)–O(1)	2.620(3)
Zn(1)–O(5)	1.994(3)
Zn(1)–O(3)	2.007(3)
Zn(1)–N(2)	2.009(4)
Zn(1)–O(2)	2.012(3)
Zn(1)–N(1)	2.030(4)
O(6)–Eu(1)–O(2)	78.54(13)
O(6)–Eu(1)–O(3)	76.96(13)
O(2)–Eu(1)–O(3)	65.43(11)
O(6)–Eu(1)–O(7)	145.61(13)
O(2)–Eu(1)–O(7)	130.33(11)
O(3)–Eu(1)–O(7)	128.33(11)
O(6)–Eu(1)–O(8)	158.97(12)
O(2)–Eu(1)–O(8)	85.63(11)
O(3)–Eu(1)–O(8)	83.93(11)
O(7)–Eu(1)–O(8)	55.07(11)
O(6)–Eu(1)–O(10)	73.23(13)
O(2)–Eu(1)–O(10)	111.83(12)
O(3)–Eu(1)–O(10)	149.87(11)
O(7)–Eu(1)–O(10)	77.74(12)
O(8)–Eu(1)–O(10)	126.19(11)
O(6)–Eu(1)–O(11)	71.56(13)
O(2)–Eu(1)–O(11)	148.67(11)
O(3)–Eu(1)–O(11)	115.02(11)
O(7)–Eu(1)–O(11)	75.91(12)
O(8)–Eu(1)–O(11)	125.63(12)
O(10)–Eu(1)–O(11)	50.65(11)
O(6)–Eu(1)–O(4)	97.04(13)
O(2)–Eu(1)–O(4)	125.71(11)
O(3)–Eu(1)–O(4)	60.97(11)
O(7)–Eu(1)–O(4)	80.86(11)
O(8)–Eu(1)–O(4)	80.98(11)
O(10)–Eu(1)–O(4)	118.47(11)
O(11)–Eu(1)–O(4)	68.38(11)
O(6)–Eu(1)–O(1)	103.05(13)
O(2)–Eu(1)–O(1)	61.06(10)
O(3)–Eu(1)–O(1)	125.09(10)
O(7)–Eu(1)–O(1)	81.74(11)
O(8)–Eu(1)–O(1)	80.78(10)
O(10)–Eu(1)–O(1)	67.09(10)
O(11)–Eu(1)–O(1)	116.72(10)
O(4)–Eu(1)–O(1)	159.86(10)
O(5)–Zn(1)–O(3)	108.20(13)
O(5)–Zn(1)–N(2)	109.66(14)
O(3)–Zn(1)–N(2)	91.05(15)
O(5)–Zn(1)–O(2)	102.45(13)
O(3)–Zn(1)–O(2)	77.70(13)
N(2)–Zn(1)–O(2)	147.87(15)
O(5)–Zn(1)–N(1)	107.27(14)
O(3)–Zn(1)–N(1)	144.29(14)
N(2)–Zn(1)–N(1)	80.93(16)
O(2)–Zn(1)–N(1)	90.79(14)

Table 5
Selected bond lengths (Å) and angles (°) for **3**

Nd(1)–O(3)	2.385(4)
Nd(1)–O(6)	2.451(4)
Nd(1)–O(1W)	2.469(4)
Nd(1)–O(2)	2.471(4)
Nd(1)–O(11)	2.517(4)
Nd(1)–O(7)	2.532(4)
Nd(1)–O(10)	2.574(4)
Nd(1)–O(8)	2.584(4)
Nd(1)–O(1)	2.711(4)
Nd(1)–O(4)	2.758(4)
Nd(1)–N(4)	2.982(6)
Nd(1)–N(3)	2.989(5)
Zn(1)–O(5)	1.991(4)
Zn(1)–O(3)	2.007(4)
Zn(1)–O(2)	2.009(4)
Zn(1)–N(1)	2.032(5)
Zn(1)–N(2)	2.039(5)
O(3)–Nd(1)–O(6)	86.36(14)
O(3)–Nd(1)–O(1W)	155.77(15)
O(6)–Nd(1)–O(1W)	71.46(15)
O(3)–Nd(1)–O(2)	63.53(13)
O(6)–Nd(1)–O(2)	70.99(14)
O(1W)–Nd(1)–O(2)	115.59(14)
O(3)–Nd(1)–O(11)	123.19(14)
O(6)–Nd(1)–O(11)	150.20(14)
O(1W)–Nd(1)–O(11)	79.91(15)
O(2)–Nd(1)–O(11)	116.27(14)
O(3)–Nd(1)–O(7)	77.34(14)
O(6)–Nd(1)–O(7)	69.32(14)
O(1W)–Nd(1)–O(7)	85.56(15)
O(2)–Nd(1)–O(7)	124.96(14)
O(11)–Nd(1)–O(7)	117.26(14)
O(3)–Nd(1)–O(10)	80.76(14)
O(6)–Nd(1)–O(10)	145.39(14)
O(1W)–Nd(1)–O(10)	123.15(15)
O(2)–Nd(1)–O(10)	74.51(14)
O(11)–Nd(1)–O(10)	50.19(14)
O(7)–Nd(1)–O(10)	136.90(13)
O(3)–Nd(1)–O(8)	113.14(13)
O(6)–Nd(1)–O(8)	105.45(14)
O(1W)–Nd(1)–O(8)	65.67(14)
O(2)–Nd(1)–O(8)	174.94(13)
O(11)–Nd(1)–O(8)	68.63(14)
O(7)–Nd(1)–O(8)	49.98(13)
O(10)–Nd(1)–O(8)	109.16(14)
O(3)–Nd(1)–O(1)	121.36(13)
O(6)–Nd(1)–O(1)	85.78(13)
O(1W)–Nd(1)–O(1)	67.88(14)
O(2)–Nd(1)–O(1)	59.00(12)
O(11)–Nd(1)–O(1)	75.75(13)
O(7)–Nd(1)–O(1)	148.49(13)
O(10)–Nd(1)–O(1)	74.14(13)
O(8)–Nd(1)–O(1)	124.96(13)
O(3)–Nd(1)–O(4)	59.33(12)
O(6)–Nd(1)–O(4)	129.48(13)
O(1W)–Nd(1)–O(4)	128.99(13)
O(2)–Nd(1)–O(4)	115.34(13)
O(11)–Nd(1)–O(4)	75.67(13)
O(7)–Nd(1)–O(4)	67.79(13)
O(10)–Nd(1)–O(4)	69.11(13)
O(8)–Nd(1)–O(4)	63.86(13)
O(1)–Nd(1)–O(4)	142.60(12)
O(5)–Zn(1)–O(3)	97.10(17)
O(5)–Zn(1)–O(2)	110.11(17)
O(3)–Zn(1)–O(2)	79.11(16)
O(5)–Zn(1)–N(1)	112.56(18)
O(3)–Zn(1)–N(1)	150.34(18)
O(2)–Zn(1)–N(1)	90.32(17)
O(5)–Zn(1)–N(2)	103.92(18)
O(3)–Zn(1)–N(2)	91.32(17)
O(2)–Zn(1)–N(2)	145.48(18)
N(1)–Zn(1)–N(2)	81.79(1)

refined anisotropically, while hydrogen atoms were included in the calculation isotropically but not refined. Neutral atom scattering factors were taken from Cromer and Waber [15]. Full details are available in Supplementary material.

4. Supplementary material

Crystallographic data for the complexes have been deposited with the Cambridge Crystallographic Data Centre, CCDC Nos. 267241–267244, for $\mathbf{H_2L}$, **1**, **2** and **3**, respectively. Copies of this information may be obtained free of charge from the Director, CCDC, 12 Union Road, Cambridge CB2 1EZ, UK (fax: +44 1223 336 033; e-mail: deposit@ccdc.cam.ac.uk or www: http://www.ccdc.cam.ac.uk).

Acknowledgements

We thank the Robert A. Welch Foundation (Great F-816) for financial support. WKM thanks the Hong Kong Research Grants Council (HKBU 2038/02P) for financial support.

References

[1] (a) P. Caravan, J.J. Ellison, T.J. McMurry, R.B. Lauffer, Chem. Rev. 99 (1999) 2293;
(b) C. Piguet, J.-C.G. Bünzli, Chem. Soc. Rev. 28 (1999) 347.
[2] N. Sabbatini, M. Guardigli, J.M. Lehn, Coord. Chem. Rev. 123 (1993) 201.
[3] M.H.V. Werts, R.H. Woudenberg, P.G. Emmerink, R. van Gassel, J.W. Hofstraat, J.W. Verhoeven, Angew. Chem. Int. Ed. 39 (2000) 4542, and references therein.
[4] (a) D. Imbert, M. Cantuel, J.-C.G. Bünzli, G. Bemardinelli, C. Piguet, J. Am. Chem. Soc. 125 (2003) 15698;
(b) N.M. Shavaleev, L.P. Moorcraft, S.J.A. Pope, Z.R. Bell, S. Faulkner, M.D. Ward, Chem. Commun. (2003) 1134;
(c) S.I. Klink, H. Keizer, F.C.J.M. van Veggel, Angew. Chem. Int. Ed. 39 (2000) 4319;
(d) M.A. Subhan, H. Nakata, T. Suzuki, J.-H. Choi, S. Kaizaki, J. Lumin. 101 (2003) 307.
[5] M.P. Hogerheide, J. Boersma, G.V. Konten, Coord. Chem. Rev. 155 (1996) 87.

[6] (a) W.-K. Wong, H. Liang, W.-Y. Wong, Z.-W. Cai, K.-F. Li, K.-W. Cheah, New J. Chem. 26 (2002) 275;
(b) W.-K. Lo, W.-K. Wong, J.-P. Guo, W.-Y. Wang, K.-F. Li, K.-W. Cheah, Inorg. Chim. Acta 357 (2004) 4510.
[7] X.-P. Yang, B.-S. Kang, W.-K. Wong, C.-Y. Su, H.-Q. Liu, Inorg. Chem. 42 (2003) 169.
[8] X.-P. Yang, R.A. Jones, V. Lynch, M.M. Oye, A.L. Holmes, Dalton Trans. (2005) 849.
[9] X.-P. Yang, R.A. Jones, J. Amer. Chem. Soc. 125 (2005) 7686.
[10] (a) F. Lam, J.-X. Xu, K.S. Chan, J. Org. Chem. 61 (1996) 8414;
(b) P.G. Lacroix, S.D. Bella, I. Ledoux, Chem. Mater. 8 (1996) 541.
[11] S. Petoud, S.M. Cohen, J.-C.G. Bünzli, K.N. Raymond, J. Am. Chem. Soc. 125 (2003) 13324.
[12] K. Nakamaru, Bull. Soc. Chem. Jpn. 5 (1982) 2697.
[13] Quantum yield was determined relative to quinine sulfate in 0.5 M H_2SO_4 ($\Phi_{em} = 0.546$). S.R. Meech, D.J. Philips, J. Photochem. 23 (1983) 193.
[14] G.M. Sheldrick, SHELX-97: A Software Package for the Solution and Refinement of X-ray Data, University of Göttingen, Göttingen, Germany, 1997.
[15] D.T. Cromer, J.T. WaberInternational Tables for X-ray Crystallography, vol. 4, Kynoch Press, Birmingham, 1974, Table 2.2A.

Available online at www.sciencedirect.com
SCIENCE DIRECT®
Polyhedron 25 (2006) 279–285
POLYHEDRON
www.elsevier.com/locate/poly

Syntheses and X-ray crystal structures of zinc complexes with an amido-diamine ligand

Bing Luo, Benjamin E. Kucera, Wayne L. Gladfelter *

Department of Chemistry, University of Minnesota, 207 Pleasant Street, SE, Minneapolis, MN 55455, United States

Received 12 April 2005; accepted 29 June 2005
Available online 18 August 2005

Dedicated to Malcolm Chrisholm on the occasion of his 60th birthday

Abstract

The synthesis and characterization of complexes with a tridentate amido-diamine ligand $-N(CH_2CH_2NMe_2)_2$, $[ClZnN(CH_2CH_2NMe_2)_2]_2$ (**1**), $[EtZnN(CH_2CH_2NMe_2)_2]_2$ (**2**), $\{Zn[N(CH_2CH_2NMe_2)_2]_2\}_2$ (**3**) and $[^tBu_2NZnN(CH_2CH_2NMe_2)_2]_2$ (**4**), are described. Compounds **1** (57% yield) and **2** (49% yield) were obtained from the reactions of $ZnCl_2$ with 1 equiv. of $LiN(CH_2CH_2NMe_2)_2$ and $ZnEt_2$ with excess $HN(CH_2CH_2NMe_2)_2$, respectively. Compounds **3** (52% yield) and **4** (75% yield) were isolated from the reactions of $[Zn(N^tBu_2)_2]_2$ with $HN(CH_2CH_2NMe_2)_2$ in 1:4 and 1:2 molar ratios, respectively. Mass spectral data and NMR analyses suggested that all four compounds were dimeric. The solid-state structures of compounds **2** and **3** were determined via X-ray crystallography. Both compounds were centrosymmetric containing a four-membered Zn_2N_2 ring with bridging amido ligands. In both structures, one NMe_2 group in each bridging ligand bonded to a Zn center forming a five-membered ring. The ethyl groups in **2** and the second $-N(CH_2CH_2NMe_2)_2$ ligand in **3** occupied the terminal positions.
© 2005 Elsevier Ltd. All rights reserved.

Keywords: Zinc; Tridentate; Amide; Amido; Structure; Dimer

1. Introduction

Zinc coordination chemistry, involving a variety of nitrogen ligands, is of fundamental importance in chemistry, biology and materials science [1]. Structurally characterized diamido zinc compounds, $Zn(NR_2)_2$, where R is a bulky alkyl, silyl or aryl group, are typically monomeric with dicoordinate zinc [2–7] or dimeric with tricoordinate zinc atoms [4,6,8–10] (Scheme 1, **i** and **ii**).

Compounds with less sterically demanding ligands, such as bis(dimethylamido)zinc [11] and bis(diethylamido)-zinc [12], are polymeric. The coordinative saturation of zinc amido complexes can also be achieved with addition of Lewis base ligands. Examples include monomeric $Zn(NPh_2)_2(THF)_2$ [8] and dimeric $[MeN(SiMe_2NEt)_2$-$Zn(pyridine)]_2$ [13]. For less bulky bidentate amido-amine ligands, only hydrido and alkyl zinc derivatives are known. Examples are $[HZnNMe(CH_2)_2NMe_2]_2$ [14] and $[RZnNMe(CH_2)_nNMe_2]_2$ ($n = 2$ or 3 and R = Me or Et) [15] (Scheme 1, **iii**).

We are interested in preparing the volatile zinc complexes for the chemical vapor deposition of zinc-containing films. This led us to investigate the chemistry of a tridentate amido-diamine ligand, $-N(CH_2CH_2NMe_2)_2$. The lithium salt of $[N(CH_2CH_2NMe_2)_2]^-$ has been reported [16,17], and a volatile five-coordinate gallium dihydride has been characterized [18]. In this paper, we report the synthesis and characterization of several zinc complexes bearing a $-N(CH_2CH_2NMe_2)_2$ ligand.

* Corresponding author. Tel.: +1 612 624 4391; fax: +1 612 626 8659.
E-mail address: gladfelt@chem.umn.edu (W.L. Gladfelter).

0277-5387/$ - see front matter © 2005 Elsevier Ltd. All rights reserved.
doi:10.1016/j.poly.2005.06.041

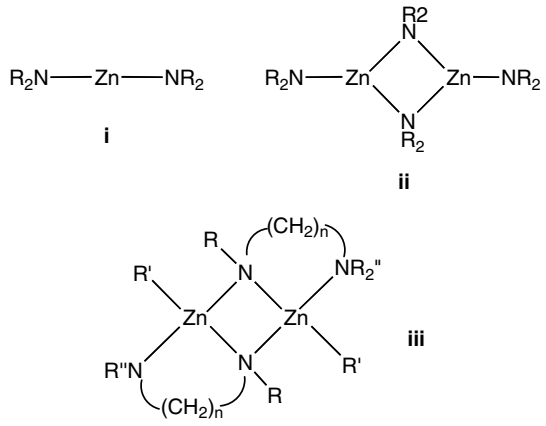

Scheme 1.

2. Experimental

2.1. Materials and general procedures

Zinc chloride (Aldrich) was heated under vacuum prior to use to remove trace moistures. $ZnEt_2$ (Aldrich) was used as received. Toluene was dried with alumina using an MBraun solvent purification system. Diethyl ether and pentane were dried over calcium hydride under nitrogen. All solvents were vigorously degassed. Diisobutylamine and benzene-d_6 were distilled over CaH_2 under nitrogen. $[Zn(N^iBu_2)_2]_2$ [4], $LiN(CH_2CH_2NMe_2)_2$ [19] and $HN(CH_2CH_2NMe_2)_2$ [19] were prepared according to the literature procedures. All experiments were conducted under an oxygen-free, dry-nitrogen atmosphere using standard Schlenk and glovebox techniques.

NMR spectra were obtained in benzene-d_6 solutions at room temperature on a Varian INOVA 300 spectrometer. The residual proton at 7.15 ppm and the carbon resonance at 128.39 ppm in benzene-d_6 were used as the internal standards for ^1H and ^{13}C NMR, respectively. Chemical-ionization mass spectra were acquired on a Finnigan Mat 95 spectrometer using a direct insertion probe. The samples were evaporated at 150 °C and the ionization gas mixture was methane with 4% ammonia. Melting points were measured in sealed glass capillaries and were uncorrected. The elemental analyses were performed by Desert Analytics, Tucson, AZ.

2.2. Synthesis of $[ClZnN(CH_2CH_2NMe_2)_2]_2$ (1)

To a stirred slurry of $ZnCl_2$ (3.00 g, 22.0 mmol) in 50 mL of toluene was added a solution of $LiN(CH_2CH_2NMe_2)_2$ (3.64 g, 22.0 mmol) in 50 mL of toluene. The mixture was refluxed for 28 h and then filtered to separate a white precipitate (LiCl) and a clear solution. After the solution was concentrated to ca. 20 mL and stored at −10 °C for a few days, colorless crystalline compound **1** precipitated and was isolated (3.22 g, 57% yield). Mp: 178 °C, decomp. ^1H NMR: δ 2.04 (24H, s, NMe_2), 2.30 (8H, t, $CH_2CH_2NMe_2$), 2.92 (8H, t, $CH_2CH_2NMe_2$). ^{13}C NMR: δ 46.5 (NMe_2), 52.7 ($CH_2CH_2NMe_2$), 62.2 ($CH_2CH_2NMe_2$). CI MS (assignment, % relative intensity): 519 ($\{[ClZnN(CH_2CH_2NMe_2)_2]_2 + H\}^+$, 5.6), 258 ($[ClZnN(CH_2CH_2NMe_2)_2 + H]^+$, 64), 160 ($[H_2N(CH_2CH_2NMe_2)_2]^+$, 100). *Anal.* calc. for $C_{16}H_{40}N_6Cl_2Zn_2$: C, 37.08; H, 7.78; N, 16.22. Found: C, 36.84; H, 7.45; N, 16.10%.

2.3. Reaction of $ZnCl_2$ with 2 equiv. of $LiN(CH_2CH_2NMe_2)_2$

To a stirred slurry of $ZnCl_2$ (0.400 g, 2.94 mmol) in 30 mL of toluene was added a solution of $LiN(CH_2CH_2NMe_2)_2$ (0.970 g, 5.87 mmol) in 50 mL of toluene. The mixture was refluxed for 5 h and then filtered to separate a white precipitate and a clear solution. After the solution was concentrated to ca. 40 mL and stored at −10 °C for several days, colorless small blocks precipitated. When isolated from the solution, the crystals lost solvent toluene molecules that had been co-crystallized in the lattice, and a white powder was obtained after drying under vacuum (0.72 g). Mp: 173 °C, decomp. ^1H NMR: δ 2.37 (s, NMe_2), 2.94 (br s, $CH_2CH_2N\ Me_2$), 3.23 (br s, $CH_2CH_2NMe_2$). ^{13}C NMR: δ 46.5 (NMe_2), 53.4 ($CH_2CH_2NMe_2$), 63.0 ($CH_2CH_2NMe_2$). This compound did not sublime under vacuum below its decomposition temperature.

The above reaction was also carried out in refluxing toluene for 16 h, and a partial decomposition leading to a gray solid (presumably zinc metal) was observed. After filtration and recrystallization, the same compound as described above was isolated.

2.4. Synthesis of $[EtZnN(CH_2CH_2NMe_2)_2]_2$ (2)

A mixture of neat $ZnEt_2$ (0.400 g, 3.24 mmol) and $HN(CH_2CH_2NMe_2)_2$ (1.03 g, 6.48 mmol) was heated at 100 °C for 2 h. During this period, gas evolution (C_2H_6) was observed. Unreacted $HN(CH_2CH_2NMe_2)_2$ was removed under vacuum leaving a wet, white solid, which was dissolved in pentane (4 mL). The resulting solution was cooled at −60 °C to precipitate a white solid. Vacuum sublimation of the solid at 90 °C afforded colorless, crystalline compound **2** (0.40 g, 49% yield). Mp: 83.0–84.0 °C. ^1H NMR: δ 0.42 (4H, q, CH_2CH_3), 1.71 (6H, t, CH_2CH_3), 2.08 (24H, s, NMe_2), 2.37 (8H, t, $CH_2CH_2NMe_2$), 3.00 (8H, t, $CH_2CH_2NMe_2$). ^{13}C NMR: δ −2.61 (CH_2CH_3), 15.4 (CH_2CH_3), 46.5 (NMe_2), 54.4 ($CH_2CH_2NMe_2$), 62.8 ($CH_2CH_2NMe_2$). CI MS (assignment, % relative intensity): 506 ($\{[EtZnN(CH_2CH_2NMe_2)_2]_2 + H\}^+$, 0.8), 475 ($\{[EtZnN(CH_2CH_2NMe_2)_2]_2 - Et\}^+$, 1.0), 346 ($\{[EtZnN(CH_2CH_2NMe_2)_2]_2 - N(CH_2CH_2NMe_2)_2\}^+$, 4.8), 256 ($[EtZnN(CH_2CH_2NMe_2)_2 + H]^+$, 100), 239 ($[EtZnN\ (CH_2CH_2NMe_2)_2 - Et + NH_3]^+$, 5.3), 222 ($[EtZnN(CH_2CH_2NMe_2)_2 - Et]^+$, 1.8), 193 ([EtZnN(CH$_2$-

$CH_2NMe_2)_2 - CH_2NMe_2]^+$, 6.3), 160 ($[H_2N(CH_2CH_2NMe_2)_2]^+$, 52). *Anal.* calc. for $C_{20}H_{50}N_6Zn_2$: C, 47.52; H, 9.97; N, 16.63. Found: C, 47.03; H, 10.16; N, 16.44%.

2.5. Synthesis of $\{Zn[N(CH_2CH_2NMe_2)_2]_2\}_2$ (3)

To a stirred solution of $[Zn(N^iBu_2)_2]_2$ (8.00 g, 12.5 mmol) in 40 mL of Et_2O was added a solution of $HN(CH_2CH_2NMe_2)_2$ (8.20 g, 51.5 mmol) in 30 mL of Et_2O. The mixture was refluxed for 20 h resulting in a clear solution. Volatiles were removed under vacuum affording a white solid. Colorless, crystalline compound **3** (4.90 g, 52% yield) was isolated after repeated recrystallization from toluene. Mp: 102.0–104.0 °C. ^{1}H NMR: δ 2.14 (24H, s, NMe_2), 2.17 (12H, s, NMe_2), 2.32 (12H, s, NMe_2), 2.47 partially overlapped with 2.45 (total 12H, t, $CH_2CH_2NMe_2$), 2.55 (4H, t, $CH_2CH_2NMe_2$), 3.01 (4H, t, $CH_2CH_2NMe_2$), 3.32 partially overlapped with 3.34 (12H, t, $CH_2CH_2NMe_2$). ^{13}C NMR: δ 46.0, 46.5 and 47.1 (NMe_2), 54.4, 54.8 and 55.3 ($CH_2CH_2NMe_2$), 62.7, 63.2 and 65.0 ($CH_2CH_2NMe_2$). CI MS (assignment, % relative intensity): 606 ($[\{Zn[N(CH_2CH_2NMe_2)_2]_2\}_2 - N(CH_2CH_2NMe_2)_2]^+$, 1.7), 381 ($[Zn[N(CH_2CH_2NMe_2)_2]_2 + H]^+$, 100), 322 ($[Zn[N(CH_2CH_2NMe_2)_2]_2 - CH_2NMe_2]^+$, 18), 160 ($[H_2N(CH_2CH_2NMe_2)_2]^+$, 34). *Anal.* calc. for $C_{32}H_{80}N_{12}Zn_2$: C, 50.31; H, 10.56; N, 22.00. Found: C, 50.06; H, 10.13; N, 21.74%.

2.6. Synthesis of $[^iBu_2NZnN(CH_2CH_2NMe_2)_2]_2$ (4)

To a stirred solution of $[Zn(N^iBu_2)_2]_2$ (3.00 g, 4.66 mmol) in 40 mL of Et_2O at room temperature was added a solution of $HN(CH_2CH_2NMe_2)_2$ (1.49 g, 9.32 mmol) in 20 mL of Et_2O. The mixture was stirred for 1 h and a clear solution was obtained. After the solution was cooled at −10 °C overnight, colorless blocks of compound **4** precipitated and were isolated (2.45 g, 75% yield). Mp: 134.5–136.0 °C. ^{1}H NMR: δ 1.15 (24H, d, $CHMe_2$), 2.03 (4H, m, CH), 2.15 (24H, s, NMe_2), 2.75 (8H, br s, $CH_2CH_2NMe_2$), 2.96 (8H, br s, CH_2CHMe_2), 3.20 (8H, br s, $CH_2CH_2NMe_2$). ^{13}C NMR: δ 21.9 ($CHMe_2$), 29.3 ($CHMe_2$), 46.5 (NMe_2), 55.2 ($CH_2CH_2NMe_2$), 62.8 ($CH_2CH_2NMe_2$), 65.0 (CH_2CHMe_2). CI MS (assignment, % relative intensity): 576 ($\{[^iBu_2NZnN(CH_2CH_2NMe_2)_2]_2 - N^iBu_2\}^+$, 2.8), 546 ($\{[^iBu_2NZnN(CH_2CH_2NMe_2)_2]_2 - N(CH_2CH_2NMe_2)_2\}^+$, 2.7), 351 ($[^iBu_2NZnN(CH_2CH_2NMe_2)_2 + H]^+$, 100), 160 ($[H_2N(CH_2CH_2NMe_2)_2]^+$, 18). *Anal.* calc. for $C_{32}H_{76}N_8Zn_2$: C, 54.61; H, 10.88; N, 15.92. Found: C, 54.30; H, 11.16; N, 15.74%.

2.7. X-ray data collection, structure solution and refinement

The detailed experimental procedure and structure solution method were previously described [20]. A Bruker SMART system and a Siemens SMART system were used for compounds **2** and **3**, respectively. The final cell constants were calculated from 2748 strong reflections for **2** and 3665 strong reflections for **3**. For both structures, all non-hydrogen atoms were refined with anisotropic displacement parameters. All hydrogen atoms were placed in ideal positions and refined as riding atoms with relative isotropic displacement parameters. The experimental conditions and unit cell information are summarized in Table 1.

Table 1
Crystallographic data of compounds **2** and **3**

Complex	**2**	**3**
Chemical formula	$C_{20}H_{50}N_6Zn_2$	$C_{32}H_{80}N_{12}Zn_2$
Formula weight	505.40	763.82
Color, morphology	colorless, plate	colorless, block
Size (mm)	$0.25\times0.15\times0.10$	$0.25\times0.20\times0.10$
Crystal system	triclinic	triclinic
Space group	$P\bar{1}$	$P\bar{1}$
a (Å)	9.0904(13)	9.5890(13)
b (Å)	10.4542(15)	9.5921(13)
c (Å)	16.052(2)	12.0741(16)
α (°)	76.797(3)	76.021(2)
β (°)	75.606(2)	86.183(2)
γ (°)	65.601(2)	84.893(2)
V (Å^3)	1331.9(3)	1072.2(3)
Z	2	1
T (°C)	−100	−100
λ (Å)	0.71073	0.71073
Total reflections	13909	12508
Unique reflections (R_{int})	5402 (0.0394)	4867 (0.0404)
Observed reflections	4316	4110
Completeness to theta	26.39°, 99.2%	27.53°, 98.2%
Absorption correction	multi-scan	multi-scan
$R_1[I>2\sigma(I)]$, wR_2 (all data)[a]	0.0393, 0.1080	0.0431, 0.1048

[a] $R_1 = \sum ||F_o| - |F_c|| / \sum |F_o|$ and $wR_2 = \{\sum[w(F_o^2 - F_c^2)^2] / \sum[w(F_o^2)^2]\}^{1/2}$, where $w = q/[\sigma^2(F_o^2) + (a^*P)^2 + b^*P + d + e^*\sin(\theta)]$, $P = (F_o^2 + 2F_c^2)/3$.

3. Results and discussion

3.1. Syntheses and characterizations of compounds 1–4

Several diamido zinc complexes have been synthesized from the metathesis reactions of $ZnCl_2$ with Li or Na amide compounds [2–9,12,13,21]. In this study, however, the mono-substituted complex, $[ClZnN(CH_2CH_2NMe_2)_2]_2$ (**1**), was obtained in 57% yield from the reaction of $ZnCl_2$ with 1 equiv. of $LiN(CH_2CH_2NMe_2)_2$ in refluxing toluene (Eq. (1))

$$ZnCl_2 + LiN(CH_2CH_2NMe_2)_2 \rightarrow 1/2[ClZnN(CH_2CH_2NMe_2)_2]_2 + LiCl \quad (1)$$

The reaction of $ZnCl_2$ with 2 equiv. of $LiN(CH_2CH_2NMe_2)_2$ in refluxing toluene for 5 h led to a white solid, in which the presence of the $-N(CH_2CH_2NMe_2)$ ligand was indicated by ^{1}H and ^{13}C NMR spectroscopy. Full

characterization, however, was not achieved due to its involatility and our inability in obtaining a single crystal. It is possible that it was a lithium zincate compound resulted from an incomplete elimination of LiCl. Zincate complexes including $LiZn[N(SiMe_3)_2]_3(THF)_4$ are known [22]. Increasing the reaction time to 16 h did not facilitate further LiCl elimination, rather this led to a partial decomposition.

After a mixture of $ZnEt_2$ and $HN(CH_2CH_2NMe_2)_2$ in 1:2 molar ratio was heated at 100 °C for 2 h, the mono-substituted compound, $[EtZnN(CH_2CH_2NMe_2)_2]_2$ (**2**), was isolated in 49% yield (based on Zn) according to the reaction shown in Scheme 2. This result was not particularly surprising. In the literature, incomplete Et elimination was observed from the reaction of $ZnEt_2$ with excess amines [12], and even with more acidic alcohols, the reactions of dialkyl zinc usually led to mono-substituted $(RZnOR')_n$ compounds [11,23–25].

An alternative route was sought for preparing the diamido zinc compound. It was reported that reactions of $Zn[N(SiMe_3)_2]_2$ with alcohols led to a variety of zinc dialkoxides [25,26]. This process avoided the use of $ZnCl_2$ and alkaline metal alkoxides. Recently, Armstrong et al. [10] adopted this strategy to prepare $[ZnN(CH_2Ph)_2]_2$ in the reaction of $Zn[N(SiMe_3)_2]_2$ with $HN(CH_2Ph)_2$. Recognizing that $HN(CH_2Ph)_2$ is a weaker acid than $HN(SiMe_3)_2$, they rationalized that the driving force of this transamination was obtained from the increased coordination number of Zn, e.g. three in $[ZnN(CH_2Ph)_2]_2$ and two in $Zn[N(SiMe_3)_2]_2$. As an extension of these synthetic methods, we started with a different diamido zinc, $[Zn(N^iBu_2)_2]_2$, and isolated bis-[bis(2-dimethylaminoethyl)amido] zinc dimer $\{Zn[N(CH_2CH_2N\text{-}Me_2)_2]_2\}_2$ (**3**), in 52% yield (Scheme 3).

The reaction proceeded via two transaminations as depicted in Eqs. (2) and (3). In contrast to earlier work, where the proposed intermediate $(Me_3Si)_2NZnN(CH_2Ph)_2$ was not isolable, the intermediate, $[^iBu_2NZnN(CH_2CH_2NMe_2)_2]_2$ (**4**), was readily isolated in 75% yield from a separate reaction according to the stoichiometry in Eq. (2)

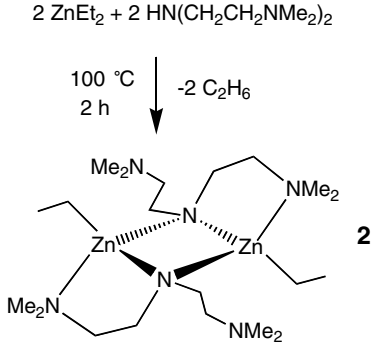

Scheme 2.

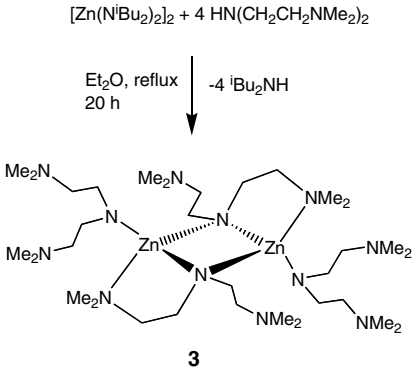

Scheme 3.

$$[Zn(N^iBu_2)_2]_2 + 2HN(CH_2CH_2NMe_2)_2 \rightarrow [^iBu_2NZnN(CH_2CH_2NMe_2)_2]_2 + 2HN^iBu_2 \quad (2)$$

$$[^iBu_2NZnN(CH_2CH_2NMe_2)_2]_2 + 2HN(CH_2CH_2NMe_2)_2 \rightarrow \{Zn[N(CH_2CH_2NMe_2)_2]_2\}_2 + 2HN^iBu_2 \quad (3)$$

Compounds **1**–**4** were colorless, crystalline solids. Except for **1** that decomposed when melted at 178 °C, all compounds exhibited sharp melting points. Compounds **1**, **3** and **4** were soluble in Et_2O, THF and aromatic solvents, and compound **2** was soluble in all common organic solvents. Compounds **2** and **3** sublimed at 90 °C under vacuum.

All compounds were characterized analytically and spectroscopically, and the dimeric structures of compounds **2** and **3** were determined using single crystal X-ray crystallography. In chemical ionization mass spectra, the highest observed masses were for the dimer ions (plus 1) for compounds **1** and **2** or for the ions closely related to the dimer ions, e.g. $[\{Zn[N(CH_2CH_2NMe_2)_2]_2\}_2 - N(CH_2CH_2NMe_2)_2]^+$ for **3** and $[(^iBu_2NZnN(CH_2CH_2NMe_2)_2)_2 - N^iBu_2]^+$ for **4**, suggesting that compounds **1** and **4** were also dimeric.

The ^1H NMR spectrum of compound **3** exhibited resonances attributable to three different dimethylaminoethyl groups, and the ^{13}C NMR showed clearly nine carbon resonances, also consistent with the dimeric structure in Scheme 3. Compound **2** would be expected to display spectroscopic differences between the two arms of the amido ligand, however, only one set of resonances were observed in the ^1H and ^{13}C NMR spectra. The ^1H NMR peaks were somewhat broad. We suggest that a fast exchange of the coordination to Zn between the two $-NMe_2$ groups in each bridging $-N(CH_2CH_2NMe_2)_2$ ligand was present in solution.

The ^1H and ^{13}C NMR spectra of compound **1** gave a set of sharp resonances for the $N(CH_2CH_2NMe_2)_2$ ligand. Based on the mass spectral data, a monomeric structure, which would give this NMR result, is ruled

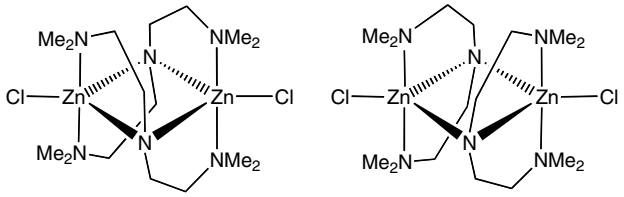

Fig. 1. Proposed structures for compound **1**.

out. A dimeric structure similar to those for compounds **2** and **3** combined with a fast exchange as suggested for compound **2** could explain the NMR results. Alternatively, the smaller size and higher electronegativity of the chloro ligand in compound **1** might favor a five-coordinate zinc as seen in some of the other chloro-containing zinc complexes [27,28]. Two structures are proposed in Fig. 1. However, despite of the equivalence of the $CH_2CH_2NMe_2$ moieties in each structure due to the D_2 symmetry for **a** and the C_{2h} symmetry for **b**, in each $CH_2CH_2NMe_2$ group the two methyls are not magnetically equivalent and neither are the two protons on each carbon atom. Thus, to account for the NMR results, a fast coordination exchange of each CH_2-CH_2NMe_2 between the two zinc centers would also be proposed for either structure.

The ^1H and ^{13}C NMR spectra of compound **4** each showed one set of sharp resonances for the $-N^iBu_2$ groups and one set of broad resonances for the $-N(CH_2CH_2NMe_2)_2$ groups. A dimeric structure similar to compounds **2** and **3** coupled with ligand exchange as suggested above is consistent with the NMR results. It should be noted that a dimer–monomer equilibrium in solution is less likely present for either compound **4** or **2**, otherwise, at least two sets of resonances for the N^iBu_2 or Et groups should be observed, as in the case for $[Zn(N^iBu_2)_2]_2$ where this type of equilibrium was present in solution [12].

3.2. Structures of compounds 2 and 3

Both **2** and **3** crystallized in space group $P\bar{1}$. For **2**, two chemically identical, but slightly structurally different molecules were determined. For **3**, half of a molecule acts as the asymmetric unit and each unit cell consists of one molecule. Selected bond lengths and angles for compounds **2** and **3** are given in Tables 2 and 3, respectively. One molecular structure of **2** and the molecular structure of **3** are shown in Figs. 2 and 3, respectively.

Both compounds **2** and **3** are dimeric containing a crystallographically imposed inversion symmetry and a four-membered Zn_2N_2 ring with bridging $-N(CH_2$-$CH_2NMe_2)_2$ ligands. In both structures, one NMe_2 group in each bridging ligand is bonded to a zinc center forming a five-membered ring. The Et group in compound **2** and one $-N(CH_2CH_2NMe_2)_2$ ligand in **3** occupy terminal positions. Reflective of the strains produced by the four- and five-membered rings, the zinc centers in both structures are distorted from ideal tetrahedral geometry. As a result, substantially larger bond angles are obtained between the other ligands and the terminal $-N(CH_2CH_2NMe_2)_2$ or ethyl ligand. For example, in **2**,

Table 2
Selected bond lengths (Å) and angles (°) for **2**

Zn(1)–N(1)	2.224(2)
Zn(1)–N(2)	2.057(2)
Zn(1)–N(2A)	2.093(2)
Zn(1)–C(9)	2.000(3)
Zn(2)–N(4)	2.210(2)
Zn(2)–N(5)	2.060(2)
Zn(2)–N(5A)	2.066(2)
Zn(2)–C(19)	1.987(3)
N(1)–Zn(1)–N(2)	83.84(8)
N(1)–Zn(1)–N(2A)	108.51(8)
N(1)–Zn(1)–C(9)	110.43(11)
N(2)–Zn(1)–N(2A)	90.19(8)
N(2)–Zn(1)–C(9)	135.70(11)
N(2A)–Zn(1)–C(9)	121.28(11)
Zn(1)–N(2)–Zn(1A)	89.82(8)
Zn(1)–N(2)–C(4)	110.90(17)
Zn(1)–N(1)–C(3)	101.03(15)
N(4)–Zn(2)–N(5)	83.72(9)
N(4)–Zn(2)–N(5A)	109.87(9)
N(4)–Zn(2)–C(19)	113.57(12)
N(5)–Zn(2)–N(5A)	91.66(8)
N(5)–Zn(2)–C(19)	129.46(11)
N(5A)–Zn(2)–C(19)	121.63(11)
Zn(2)–N(5)–Zn(2A)	88.34(8)
Zn(2)–N(5)–C(14)	111.04(17)
Zn(2)–N(4)–C(13)	101.42(17)

Table 3
Selected bond lengths (Å) and angles (°) for **3**

Zn(1)–N(2)	1.895(2)
Zn(1)–N(5)	2.0467(19)
Zn(1)–N(6)	2.176(2)
Zn(1)–N(5A)	2.0673(19)
N(2)–Zn(1)–N(5)	122.02(9)
N(2)–Zn(1)–N(5A)	124.56(8)
N(2)–Zn(1)–N(6)	114.97(9)
N(5)–Zn(1)–N(5A)	93.23(7)
N(5)–Zn(1)–N(6)	110.21(8)
N(5A)–Zn(1)–N(6)	84.76(8)
C(4)–N(2)–Zn(1)	122.35(17)
C(5)–N(2)–Zn(1)	123.45(16)
C(4)–N(2)–C(5)	114.0(2)
Zn(1)–N(5)–Zn(1A)	86.77(7)
C(12)–N(5)–C(13)	110.64(19)
C(12)–N(5)–Zn(1)	118.38(15)
C(12)–N(5)–Zn(1A)	116.61(14)
C(13)–N(5)–Zn(1)	112.83(14)
C(13)–N(5)–Zn(1A)	109.58(14)
C(14)–N(6)–Zn(1)	101.71(14)
C(15)–N(6)–Zn(1)	121.24(16)
C(16)–N(6)–Zn(1)	105.05(16)

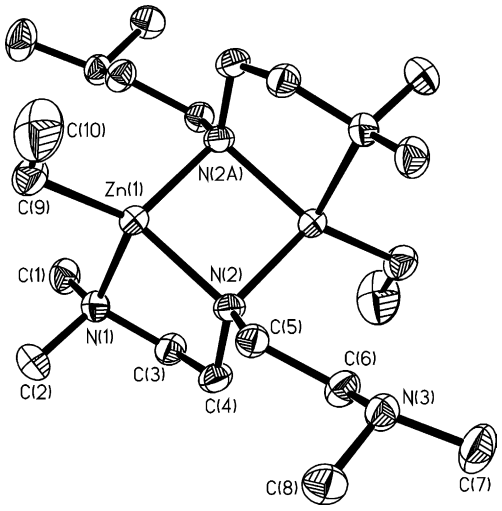

Fig. 2. Structure of **2** showing 50% thermal ellipsoids. The hydrogen atoms are omitted for clarity.

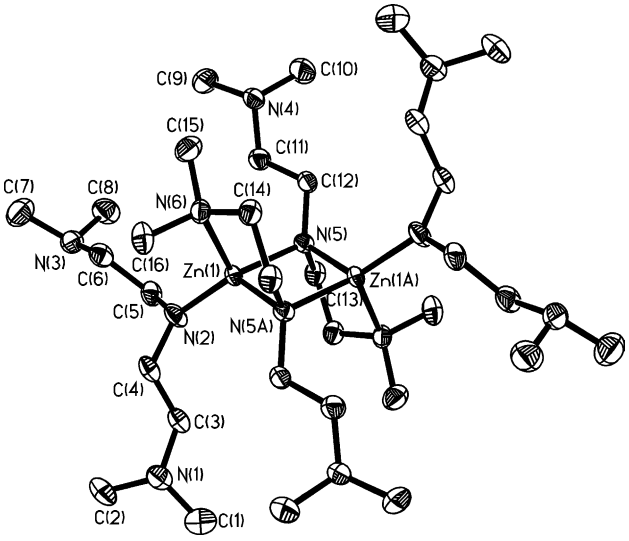

Fig. 3. Structure of **3** showing 50% thermal ellipsoids. The hydrogen atoms are omitted for clarity.

the N(2)–Zn(1)–C(9) bond angle is 135.70(11)° and in **3** the N(2)–Zn(1)–N(5) and N(2)–Zn(1)–N(5A) bond angles are 122.02(9)° and 124.56(8)°, respectively. This type of distortion on tetrahedral Zn was previously observed in compounds containing similar ring structures such as $[RZnMeN(CH_2)_nNMe_2]_2$ ($n = 2$ or 3 and R = Me or Et) [15].

The four Zn–N bonds in **3** are representative of three types of bondings. The terminal Zn(1)–N(2) bond length (1.895(2) Å) is slightly shorter than those in the four-coordinate zinc complexes, $Zn(NPh_2)_2(THF)_2$ (1.919(4)–1.927(5) Å) and $[MeN(SiMe_2NEt)_2Zn(pyridine)]_2$ (1.940(4) Å). The three-coordinate zinc compounds exhibit Zn–N bond lengths in the range of 1.844(2)–1.902(2) Å [4,6,8–10,26] while those in two-coordinate amido zinc complexes are still shorter (1.813(2)–1.850(3) Å) [2–7]. In **3**, the terminal N(2) adopts a trigonal planar geometry with the sum of the angles around it being 359.8(5)°. This is also seen in $[Zn(N^iBu_2)_2]_2$ [4], $Zn(N^tBu_2)_2$ [4] and $Zn[N(CMe_2(CH_2)_3CMe_2)]_2$ [5]. The dative Zn(1)–N(6) bond length (2.176(2) Å) in compound **3** is shorter than those in **2** (2.210(2) and 2.224(2) Å). This is because the Zn atoms in compound **3** are bonded to more electronegative N atoms on the terminal positions. The dative Zn–N bond lengths in **2** are comparable to those in compounds $[RZnMeN(CH_2)_nNMe_2]_2$ ($n = 2$ or 3 and R = Me or Et) (2.192(3)–2.226(5) Å) [15]. The geometries of the Zn_2N_2 rings in both structures are typical for dimeric zinc amido complexes [4,6,8–10].

Acknowledgment

We thank the National Science Foundation for the financial support through a Grant CHE-03159540.

Appendix A. Supplementary data

Crystallographic data in CIF format for the structures of compounds **2** and **3** have been deposited with the Cambridge Crystallographic Data Center as supplementary publication no. CCDC-268398 and -268399. Copies of the data can be obtained free of charge on application to CCDC, 12 Union Road, Cambridge CB2 1EZ, UK (fax: +44 1223 336 033; e-mail: deposit@ccdc.cam.ac.uk, and http://www.ccdc.cam.ac.uk). Supplementary data associated with this article can be found, in the online version, at doi:10.1016/j.poly.2005.06.041.

References

[1] S.J. Archibald, Comprehensive Coordination Chem II 6 (2004) 1147.
[2] P.P. Power, K. Ruhlandt-Senge, S.C. Shoner, Inorg. Chem. 30 (1991) 5013.
[3] W.S. Rees Jr., D.M. Green, W. Hesse, Polyhedron 11 (1992) 1697.
[4] H. Schumann, J. Gottfriedsen, F. Girgsdies, Z. Anorg. Allg. Chem. 623 (1997) 1881.
[5] W.S. Rees Jr., O. Just, H. Schumann, R. Weimann, Polyhedron 17 (1998) 1001.
[6] H. Schumann, J. Gottfriedsen, S. Dechert, F. Girgsdies, Z. Anorg. Allg. Chem. 626 (2000) 747.
[7] G. Margraf, H.W. Lerner, M. Bolte, M. Wagner, Z. Anorg. Allg. Chem. 630 (2004) 217.
[8] M.A. Putzer, A. Dashti-Mommertz, B. Neumueller, K. Dehnicke, Z. Anorg. Allg. Chem. 624 (1998) 263.
[9] O. Just, D.A. Gaul, W.S. Rees, Polyhedron 20 (2001) 815.
[10] D.R. Armstrong, G.C. Forbes, R.E. Mulvey, W. Clegg, D.M. Tooke, J. Chem. Soc., Dalton Trans. (2002) 1656.
[11] G.E. Coates, D. Ridley, J. Chem. Soc. (1965) 1870.

[12] M.A. Malik, P. O'Brien, Polyhedron 16 (1997) 3593.
[13] A.J. Elias, H.G. Schmidt, M. Noltemeyer, H.W. Roesky, Organometallics 11 (1992) 462.
[14] N.A. Bell, P.T. Moseley, H.M.M. Shearer, C.B. Spencer, Acta Crystallogr. Sect. B 36 (1980) 2950.
[15] M.A. Malik, P. O'Brien, M. Motevali, A.C. Jones, Inorg. Chem. 36 (1997) 5076.
[16] G.L.J. Van Vliet, F.J.J. De Kanter, M. Schakel, G.W. Klumpp, A.L. Spek, M. Lutz, Chem. Eur. J. 5 (1999) 1091.
[17] G.L.J. Van Vliet, H. Luitjes, M. Schakel, G.W. Klumpp, Angew. Chem. Int. Ed. 39 (2000) 1643.
[18] B. Luo, B.E. Kucera, W.L. Gladfelter, J. Chem. Soc., Chem. Commun. (2005) 3463.
[19] H. Luitjes, M. Schakel, G.W. Klumpp, Syn. Comm. 24 (1994) 2257.
[20] B. Luo, W.L. Gladfelter, Inorg. Chem. 41 (2002) 6249.
[21] D.A. Gaul, O. Just, W.S. Rees Jr., Inorg. Chem. 39 (2000) 5648.
[22] M. Westerhausen, Z. Anorg. Allg. Chem. 618 (1992) 131.
[23] G. Allen, J.M. Bruce, D.W. Farren, F.G. Hutchinson, J. Chem. Soc. B (1966) 799.
[24] J.M. Bruce, B.C. Cutsforth, D.W. Farren, F.G. Hutchinson, F.M. Rabagliati, D.R. Reed, J. Chem. Soc. B (1966) 1020.
[25] R.L. Geerts, J.C. Huffman, K.G. Caulton, Inorg. Chem. 25 (1986) 1803.
[26] S.C. Goel, M.Y. Chiang, W.E. Buhro, Inorg. Chem. 29 (1990) 4646.
[27] M.A. Goher, M.A.M. Abu-Youssef, F.A. Mautner, Polyhedron 15 (1996) 453.
[28] T. Darbre, C. Dubs, E. Rusanov, H. Stoeckli-Evans, Eur. J. Inorg. Chem. (2002) 3284.

Available online at www.sciencedirect.com
SCIENCE DIRECT®
Polyhedron 25 (2006) 286–292
POLYHEDRON
www.elsevier.com/locate/poly

Allyl complexes of heavy group 13 elements: Structure and bonding in $[1,3\text{-}(SiMe_3)_2C_3H_3]_3Ga$

Cameron K. Gren [a], Timothy P. Hanusa [a,*], William W. Brennessel [b]

[a] Department of Chemistry, Vanderbilt University, Box 1822B, Nashville, TN 37235, United States
[b] X-ray Crystallography Facility, Department of Chemistry, University of Minnesota, Minneapolis, MN 55455, United States

Received 13 April 2005; accepted 29 June 2005
Available online 22 August 2005

Dedicated to Malcolm Chisholm, a colleague and friend, on the occasion of his 60th birthday.

Abstract

With the exception of triallylboron compounds, allyl derivatives of the group 13 elements are uncommon and none have been structurally authenticated. A substituted allyl complex of gallium, tris(1,3-bis(trimethylsilyl)allyl)gallium, $[1,3\text{-}(SiMe_3)_2C_3H_3]_3Ga$, has been synthesized from the reaction of $K[1,3\text{-}(SiMe_3)_2C_3H_3]$ and $GaCl_3$ in THF and characterized with X-ray crystallography and NMR spectroscopy. In the solid state, the complex displays σ-bound ligands in a trigonal planar arrangement around the metal, with an average Ga–C distance of 1.980(5) Å. In solution at room temperature, the molecule is fluxional and the ligands appear as if symmetrically bound in a π-type fashion. The fluxionality is observed even at −75 °C. Density functional theory calculations indicate that the structure found in the solid state, with one allyl ligand antiparallel to the other two, is the lowest in energy, but an alternate arrangement with all three ligands parallel (C_3 symmetry) is less than 3 kcal mol^{-1} higher in energy.
© 2005 Elsevier Ltd. All rights reserved.

Keywords: Gallium; Allyl; p-Block; Group 13; Computational study

1. Introduction

In the years since Wilke synthesized the first homoleptic allyl complex, $(C_3H_5)_2Ni$ [1], allyl complexes of the transition metals have become well-known fixtures of organometallic chemistry, widely studied for their use in organic synthesis [2–5] and catalysis [6–8]. In contrast, interest in allyl complexes of the main-group elements varies considerably. Compounds of lithium and magnesium (e.g., $Li(C_3H_5)$, $(C_3H_5)MgX$) are commonly used to prepare transition metal derivatives, and among homoleptic allyl complexes of the p-block elements, attention has been focused on those of silicon [9–16], germanium [17–21], boron [22–29], and tin [30–41], the latter two being used predominantly as allylation reagents in organic reactions. Allyl complexes with other posttransition metals have received far less attention. For example, only a single report describes the use of triallylgallium and -indium reagents (of the form $(allyl')_3M$ and $(allyl')_3M_2X_3$; X = Br, I) as regioselective allylation reagents with α,β-unsaturated nitrile and carbonyl compounds [42]. The gallium and indium allyl complexes were prepared from the metal halides and Grignard reagents, and were used without isolation or further characterization. Gallium nitride film formation has been described from triallylgallium and ammonia under CVD conditions [43,44].

Just as sterically bulky cyclopentadienyl rings (e.g., C_5Me_5) and indenyl ligands have been used for several decades to alter the properties of their associated organometallic complexes, the same modifications could be

* Corresponding author. Tel.: +1 615 3224667; fax: +1 615 3431234.
E-mail address: t.hanusa@vanderbilt.edu (T.P. Hanusa).

0277-5387/$ - see front matter © 2005 Elsevier Ltd. All rights reserved.
doi:10.1016/j.poly.2005.06.044

made to other organic anions that are used as ligands. Only in the last few years has this approach been applied to the allyl anion, $C_3H_5^-$. Not only have new classes of metal complexes been prepared with the use of this methodology (e.g., $[1,3\text{-}(SiMe_3)_2C_3H_3]_2M$ (M = Cr, 12-e$^-$ [45]; Fe, 14-e$^-$ [46]; Co, 15-e$^-$ [47])), but allyl compounds with ligands substituted by trimethylsilyl and dimethyl(*tert*-butyl)silyl [48] groups have also provided versions of known compounds that are more robust and easily studied than the unsubstituted species. The nickel compound $[\eta^3\text{-}1,3\text{-}(SiMe_3)_2C_3H_3]_2Ni$, for example, is stable in water for several hours and in air for several days, unlike $(C_3H_5)_2Ni$, which inflames on contact with air [49]. Similarly, in contrast to $(C_3H_5)_4Th$, which decomposes at 0 °C, the trimethylsilylated derivatives $[(SiMe_3)_nC_3H_{5-n}]_4Th$ ($n = 1$, 2) are stable up to 90 °C [50]. Despite the kinetic stabilization provided by the bulky ligands, the geometries of the compounds are often similar to their parent counterparts (e.g., the Ni–C bond lengths in $[1,3\text{-}(SiMe_3)_2C_3H_3]_2Ni$ and $(C_3H_5)_2Ni$ differ by an average of only 0.02 Å).

It seemed reasonable that p-block allyl compounds could be stabilized by trimethylsilylated ligands, and we describe here the synthesis and characterization of the first gallium complex to benefit from such substitution. Density functional theory (DFT) calculations have been used to probe the preferences for particular metal–ligand bonding conformations in $(allyl')_3Ga$ compounds.

2. Results and discussion

2.1. Synthesis and solution behavior of $[1,3\text{-}(SiMe_3)_2C_3H_3]_3Ga$

The synthesis of a trimethylsilyl-substituted triallylgallium complex was achieved by a halide metathesis reaction performed under an inert atmosphere at −78 °C,

$$3K[1,3\text{-}(SiMe_3)_2C_3H_3] + GaCl_3 \xrightarrow[-78^\circ C]{THF} [1,3\text{-}(SiMe_3)_2C_3H_3]_3Ga + 3KCl \quad (1)$$

The triallylgallium compound was recovered in good yield as air- and moisture-sensitive pale yellow crystals, soluble in ethers and both aromatic and aliphatic hydrocarbons. It is stable indefinitely under an inert atmosphere at room temperature and can survive brief (minutes) exposure to air before substantial decomposition occurs.

The complex is diamagnetic and ^1H NMR spectra at room temperature have the appearance of a structure with symmetrically bound (“π-type”) allyl ligands; e.g., the resonance for the $SiMe_3$ groups appears as a sharp singlet, and the central hydrogen atom on the allyl ligands appears as a triplet. Such a structure differs from that found in the solid state, and is unlikely from theoretical considerations (see below); a variable temperature ^1H NMR study (Fig. 1) confirmed the fluxionality of the molecule in solution. The central doublet resonance at δ 3.91 broadens and coalesces to a single peak at −40 °C, and nearly disappears into the baseline by −75 °C. The triplet resonance at δ 6.35 and the trimethylsilyl peak at δ 0.16, however, only shift slightly downfield and broaden on cooling to −75 °C. Most notably, the $SiMe_3$ signal shows no sign of splitting into a more complex set of resonances. Obviously, a limiting spectrum is not reached, which is in contrast to the behavior of the related Group 13 allyl compound triallylboron, $(C_3H_5)_3B$. The latter exhibits a symmetric AX_4 NMR pattern at room temperature, but displays a static A_2BX_2 spectrum at −40 °C [51]; the activation barrier for the 1,3-sigmatropic shifts involved is estimated at 10 ± 1 kcal mol^{-1}. Evidently, the rearrangements represented in the spectra of $[1,3\text{-}(SiMe_3)_2C_3H_3]_3Ga$ must have a lower activation barrier.

2.2. X-ray crystal structure of $[1,3\text{-}(SiMe_3)_2C_3H_3]_3Ga$

The complex crystallizes from hexanes as a well-separated monomer with the gallium atom σ-bound to

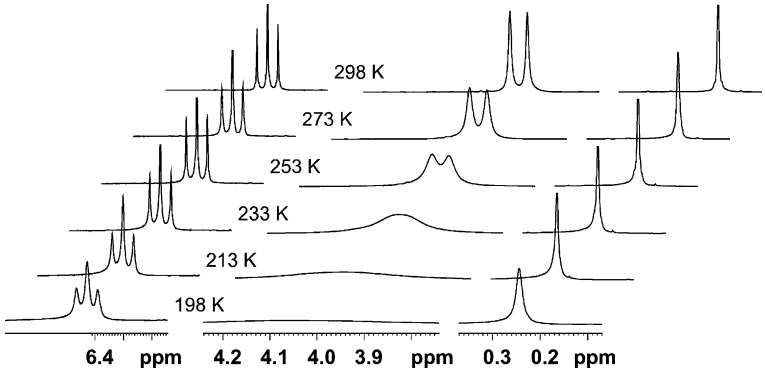

Fig. 1. Variable temperature ^1H-NMR spectra of $[1,3\text{-}(SiMe_3)_2C_3H_3]_3Ga$ (tol-d_8). Resonances (left to right) represent protons on the central carbon ($C_{(2)}$), the outer carbons ($C_{(1,3)}$), and the trimethylsilyl carbons. The peak heights of the three resonances are not to scale.

the bis(trimethylsilyl)allyl ligands in a trigonal planar manner. All three ligands are roughly perpendicular to the GaC_3 plane, with one antiparallel to the other two. The terminal trimethylsilyl groups are *syn* to the central hydrogen atoms of the allyl ligands. A summary of bond distances and angles for $[1,3\text{-}(SiMe_3)_2C_3H_3]_3Ga$ is given in Table 1 and an ORTEP view of the complex is displayed in Fig. 2.

The average Ga–C distance of 1.980(5) Å is typical for gallium–carbon single bonds; cf. those of trimethylgallium (1.957(3) Å) [52], trimesitylgallium (1.968(4) Å) [53], and triethylgallium (1.966(3)–1.996(3) Å) [52]. The Ga–C bonds in $(\sigma\text{-Cp})_3Ga$ are slightly longer (2.05(3) Å) [54]. The near perfect planarity of the central GaC_3 unit in $[1,3\text{-}(SiMe_3)_2C_3H_3]_3Ga$ is indicated by the sum of the C–Ga–C′ angles of 359.7°; the gallium atom lies only 0.058 Å from the C_3 plane. The fully localized C–C bonding in the allyl ligands is indicated by the average C=C bond distance of 1.329(7) Å and the average C–C bond length of 1.497(6) Å. The Ga–C–C angles average 106.6°, far less than the values observed in $GaEt_3$ (113.2–118.8°); in the latter compound, hyperconjugative effects between the gallium p-orbital and C–H bond orbitals may be operative [52] (see Table 2).

2.3. Computational modeling of $(R_2C_3H_3)_3Ga$ ($R = H$, SiH_3, $SiMe_3$)

The occurrence in the solid state of the antiparallel "2 up, 1 down" arrangement of the allyl ligands, and the evidently low energy required for rearrangements in solution, prompted a computational study on the relative energies of possible configurations of the complex. Structures of triallylgallium complexes using $C_3H_5^-$, $1,3\text{-}(SiH_3)_2C_3H_3^-$, and $1,3\text{-}(SiMe_3)_2C_3H_3^-$ ligands were calculated at the B3PW91/cc-pVDZ level (Fig. 3). Two all σ-bound geometries were examined, one of which had one ligand initially antiparallel to the other two ("2 up, 1 down"), similar to the asymmetric conformation

Table 1
Crystallographic summary of $[C_3(SiMe_3)_2H_3]_3Ga$

Empirical formula	$C_{27}H_{63}GaSi_6$
Formula weight	626.03
Temperature (K)	173(2)
Wavelength (Å)	0.71073
Crystal system	triclinic
Space group	$P\bar{1}$
Unit cell dimensions	
a (Å)	10.253(2)
b (Å)	12.840(2)
c (Å)	16.054(3)
α (°)	76.797(2)
β (°)	88.265(2)
γ (°)	81.855(2)
Volume (Å^3)	2036.9(5)
Z	2
D_{calc} (Mg/m^3)	1.021
Absorption coefficient (mm^{-1})	0.865
Independent reflections	8225 [$R_{int} = 0.0362$]
Data/restraints/parameters	8225/0/361
Goodness-of-fit on F^2	1.033
Final R indices [$I > 2\sigma(I)$]	$R1 = 0.0396$, $wR2 = 0.0956$
R indices (all data)	$R1 = 0.0615$, $wR2 = 0.1068$

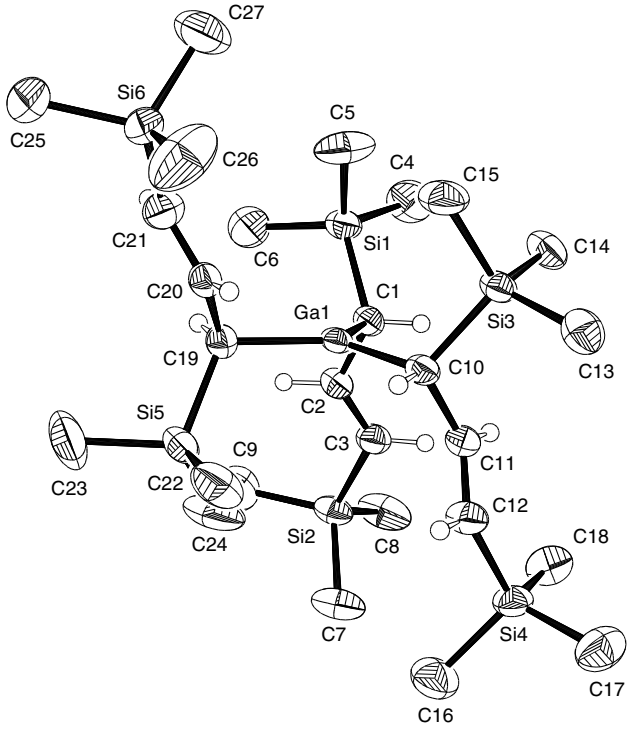

Fig. 2. ORTEP diagram of $[1,3\text{-}(SiMe_3)_2C_3H_3]_3Ga$, giving the numbering scheme used in the text. Displacement ellipsoids are displayed at the 50% probability level, and for clarity, only the allylic hydrogen atoms (drawn with arbitrary radii) are shown.

Table 2
Selected bond distances (Å) and angles (°) for $[C_3(SiMe_3)_2H_3]_3Ga$

Distance (Å)	
Ga(1)–C(19)	1.975(3)
Ga(1)–C(10)	1.981(3)
Ga(1)–C(1)	1.983(3)
C(1)–C(2)	1.499(3)
C(2)–C(3)	1.326(4)
C(10)–C(11)	1.499(3)
C(11)–C(12)	1.330(4)
C(19)–C(20)	1.493(4)
C(20)–C(21)	1.330(4)
Angles (°)	
C(19)–Ga(1)–C(10)	121.46(11)
C(19)–Ga(1)–C(1)	120.39(11)
C(10)–Ga(1)–C(1)	117.89(11)
C(3)–C(2)–C(1)	127.5(3)
C(12)–C(11)–C(10)	127.8(3)
C(21)–C(20)–C(19)	127.5(3)
C(2)–C(1)–Ga(1)	107.26(17)
C(11)–C(10)–Ga(1)	104.40(17)
C(20)–C(19)–Ga(1)	108.43(17)

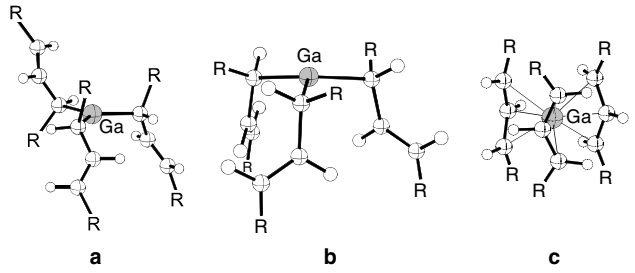

Fig. 3. Schematics of the three structural types examined for (1,3-$R_2C_3H_3)_3$ Ga (R = H, SiH_3, $SiMe_3$): all σ-bound (“2 up, 1 down”, C_1 symmetry); all σ-bound (“3 up”, C_3 symmetry); all π-bound (C_{3h} symmetry).

(C_1 symmetry) found in the crystal structure. In the second all σ conformation, the ligands were grouped together (“3 up”), with C_3 symmetry. Although it was not found to be an energetically realistic alternative, a π-bound geometry with C_{3h} symmetry was also computed for all three ligand types; such a structure would match the symmetry observed in the room temperature NMR spectra.

Key features of the geometry calculated for [1,3-($SiMe_3)_2C_3H_3]_3$Ga (Fig. 4) agree well with those observed in the crystal structure. These include the Ga–C bond distances (2.012 Å (av)), the C_α–C_β single bond distance (1.495 Å (av)), and the C_β=C_γ double bond distance (1.351 Å (av)). The calculated distances change relatively little as the $SiMe_3$ groups are replaced with SiH_3 and then H substituents. In $(C_3H_5)_3$Ga, for example, the Ga–C bond length is 2.007 Å, and the average C–C and C=C distances are 1.490 and 1.341 Å, respectively, all of which differ by less than 0.01 Å from the $SiMe_3$ version. The major change on substitution of SiH_3 and then H for $SiMe_3$ is a rotation of one of the allyl ligands so that the C_β atom is closer to the plane defined by the gallium and three C_α atoms. In the experimental and calculated structures of [1,3-($SiMe_3)_2C_3H_3]_3$Ga, the C_β atoms are >1.1 Å from the GaC_3 plane; in the SiH_3-substituted model, C(2) is 0.51 Å from the plane; in $(C_3H_5)_3$Ga, C(2) is 0.38 Å from the plane. Apparently the bulk of the substituents serve to keep the allyl ligands roughly perpendicular to the central GaC_3 plane.

Regardless of the identity of the allyl substituents, ΔG° of the C_1 form is the lowest, although that of the “3 up” C_3 form is at most only 2.6 kcal mol^{-1} higher in energy (Table 3). This difference is on the edge of being computationally significant, so that the two forms are nearly equienergetic. The “2 up, 1 down” form found for [1,3-($SiMe_3)_2C_3H_3]_3$Ga in the solid state is possibly reinforced by packing forces.

That the two σ-bound forms are close in energy is significant in the context of the solution fluxionality of the complex, as they are reasonable limiting structures in the rearrangement process. The energy of transition structures that involve delocalized allyl ligands depends critically on the identity of all the ligands in a complex. Correlated ab initio calculations have been used to find that the energy of (π-$C_3H_5)BH_2$ (C_s) is only 1.8 kcal mol^{-1} above that of (σ-$C_3H_5)BH_2$ (C_1), for example, but that (π-$C_3H_5)BMe_2$ is 9.2 kcal mol^{-1} above (σ-$C_3H_5)BMe_2$ (C_1) [55]. Considering that the vacant p orbital on the metal is involved in stabilizing a “π-bound” ligand, it is not surprising that threefold π-bound geometries (C_{3h} symmetry) can play no role in the fluxional process. They represent high-order transition structures ($N_{imag} = 4$) that are more than

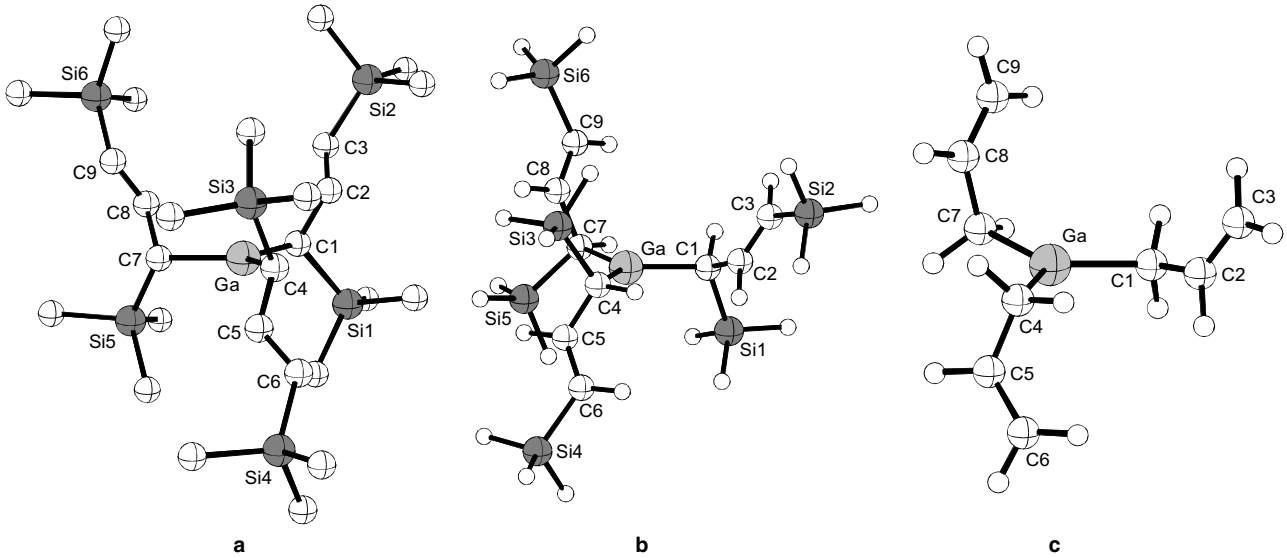

Fig. 4. Optimized lowest energy structures of [1,3-($SiMe_3)_2C_3H_3]_3$Ga (a), [1,3-($SiH_3)_2C_3H_3]_3$Ga (b), and $(C_3H_5)_3$Ga (c). For clarity, the hydrogen atoms (open circles in b and c) have been omitted from the drawing of [1,3-($SiMe_3)_2C_3H_3]_3$Ga.

Table 3
Energies of (allyl′)$_3$Ga conformations[a]

Ligand type		$\pi(C_{3h}$ symmetry)	σ (C_3 symmetry)	σ (C_1 symmetry)
C_3H_5	ΔH°	−2276.288137 (+81.4)	−2276.416999 (+0.5)	−2276.417834 (0.0)
	ΔG°	−2276.335697 (+90.4)	−2276.476641 (+2.0)	−2276.479762 (0.0)
1,3-$(SiH_3)_2C_3H_3$	ΔH°	−4020.156916 (+75.3)	−4020.276907 (0.0)	−4020.276101 (+0.5)
	ΔG°	−4020.237254 (+85.4)	−4020.372047 (+0.8)	−4020.373333 (0.0)
1,3-$(SiMe_3)_2C_3H_3$	ΔH°	−4727.225657 (+97.7)	−4727.37849 (0.0)	−4727.381309 (+1.8)
	ΔG°	−4727.374070 (+108.2)	−4727.54244 (+2.6)	−4727.546544 (0.0)

[a] The energies in parenthesis are calculated relative to the most stable form of each molecule (listed as "0.0"). All the π-bound forms had 4 imaginary frequencies; the σ-bound forms had none.

85 kcal mol^{-1} above the lowest energy σ-bonded configurations (Table 3). Structures with only one π-bound ligand are more reasonable and a preliminary search of the potential energy surface using the parent allyl ligand has identified a (π-C_3H_5)(σ-C_3H_5)$_2$Ga configuration (C_s symmetry) that is 7.3 kcal mol^{-1} above the lowest energy σ-bound form. It is a second order saddle point ($N_{imag} = 2$), but may be close to a transition structure of slightly lower symmetry. Similar structures may exist for the SiH_3 and $SiMe_3$ complexes, although these have not yet been investigated.

3. Conclusion

The use of trimethylsilyl substituents has afforded the first isolated example of a thermally stable, heavy Group 13 allyl complex. The allyl ligands are σ-bound in an asymmetric fashion, but DFT calculations indicate that a more symmetrical C_3 form is only a few kcal mol^{-1} higher in energy. This result is consistent with variable temperature NMR measurements, which suggest that the molecule has a low energy of activation for rearrangement.

The successful use of trimethylsilylated allyl ligands with gallium suggests that other substituents could be equally successful in stabilizing additional gallium species. Heavier members of the Group 13 metals could also be incorporated into new allyl complexes and we are examining this possibility.

4. Experimental

4.1. General considerations

All manipulations were performed with the rigorous exclusion of air and moisture using high vacuum, Schlenk, or glovebox techniques. Proton (^{1}H) and carbon (^{13}C) NMR experiments were obtained on a Bruker DPX-300 spectrometer at 300 and 75.5 MHz, respectively, or on a Bruker DPX-400 at 400 MHz (^{1}H), and were referenced to residual proton and ^{13}C resonances of toluene-d_8 (δ 2.09 and 20.4) and C_6D_6 (δ 7.15 and 128.1). Elemental analysis was performed at the Micro-Mass Facility, University of California, Berkeley (Berkeley, CA). Hexanes and diethyl ether were distilled under nitrogen from potassium benzophenone ketyl. Anhydrous tetrahydrofuran (THF) was purchased from Aldrich and used as received. Anhydrous gallium trichloride was purchased from Strem Chemicals and used as received. C_6D_6 and toluene-d_8 were vacuum-distilled from Na/K (22/78) alloy and stored over Type 4 molecular sieves prior to use. K[1,3-$(SiMe_3)_2C_3H_3$] was prepared following the literature procedure [8].

4.2. Preparation of [1,3-$(SiMe_3)_2C_3H_3$]$_3$Ga

A 125-mL Schlenk flask was charged with $GaCl_3$ (0.500 g; 2.84 mmol) in 20 mL THF. K[1,3-$(SiMe_3)_2C_3H_3$] (1.90 g; 8.52 mmol) in 20 mL THF was added to the dropping funnel. The apparatus was cooled to −78 °C. The THF solution of K[1,3-$(SiMe_3)_2C_3H_3$] was added dropwise with stirring over the course of 15 min. The solution was allowed to warm to room temperature overnight. Removal of solvent under vacuum, followed by extraction of the residue with hexanes, filtration of the extract over a medium-porosity glass frit, and removal of hexanes under vacuum, afforded air- and moisture-sensitive colorless to pale-yellow crystals (1.67 g, 94%), m.p. 44–46 °C. *Anal.* Calc. for $C_{27}H_{63}GaSi_6$: C, 51.80; H, 10.14. Found: C, 51.49; H, 10.55%. ^{1}H NMR (C_6D_6, 298 K): δ 6.38 (t, $J = 14.8$ Hz, 3H), 3.94 (d, $J = 14.8$ Hz, 6H), 0.18 (s, 54H, $SiMe_3$); (tol-d_8, 298 K, 300 MHz): δ 6.35 (t, $J = 14.8$ Hz, 3H), 3.91 (d $J = 14.8$ Hz, 6 H), 0.16 (s, 54H, $SiMe_3$). ^{13}C NMR (C_6D_6, 298 K): δ 145.31 ($C_{(2)}$, central), 83.72 ($C_{(1,3)}$, outer), 0.15 ($SiMe_3$). Variable temperature ^{1}H (tol-d_8, 400 MHz, δ): (198 K) 6.43 (t, $J = 14.8$, 3H), 3.7-4.3 (v br s, 2H), 0.24 (s, 54 H, $SiMe_3$); (213 K) 6.41 (t, $J = 14.8$ Hz, 3H), 4.01 (broad singlet, 6H), 0.23 (s, 54H, $SiMe_3$); (233 K) 6.40 (t, $J = 14.8$ Hz, 3H), 3.96 (broad singlet, 6H), 0.21 (s, 54H, $SiMe_3$); (253 K) 6.38 (t, $J = 14.8$ Hz, 3H), 3.94 (br d, $J = 14.2$ Hz, 6H), 0.20 (s, 54H, $SiMe_3$); (273 K) 6.37 (t, $J = 14.8$ Hz, 3H), 3.93 (d, $J = 14.8$ Hz, 6H), 0.18 (s, 54H, $SiMe_3$).

4.3. X-ray crystallography of [1,3-(SiMe$_3$)$_2$C$_3$H$_3$]$_3$Ga

Crystals of [1,3-(SiMe$_3$)$_2$C$_3$H$_3$]$_3$Ga were obtained as pale yellow plates upon removal of hexanes. A suitable crystal was located, placed onto the tip of a 0.1-mm diameter glass capillary and mounted on a Bruker SMART Platform CCD diffractometer for a data collection at 173(2) K. The intensity data were corrected for absorption (SADABS) [56], and the structure was solved using SIR97 and refined using SHELXL-97. The triclinic space group $P\bar{1}$ was indicated from intensity statistics and the lack of systematic absences. A direct-methods solution was calculated that provided most non-hydrogen atoms from the E-map. Full-matrix least squares/difference Fourier cycles were performed that located the remaining non-hydrogen atoms. All non-hydrogen atoms were refined with anisotropic displacement parameters. All methyl hydrogen atoms were placed in ideal positions and refined as riding atoms with relative isotropic displacement parameters. The allylic hydrogen atoms were found from the difference map and refined with individual isotropic displacement parameters. Additional crystal and data collection parameters are given in Table 1.

4.4. Computational details

Calculations were performed using the GAUSSIAN 03W suite of programs [57]. The B3PW91 functional, which incorporates Becke's three-parameter exchange functional [58] with the 1991 gradient-corrected correlation functional of Perdew and Wang [59], was used. This hybrid functional has previously been shown to provide realistic geometries for organometallic species [60]. The correlation consistent double zeta basis set cc-pVDZ was used for geometry optimization and final energy calculations [61]. Zero-point corrections were applied to the energies of the final geometries.

5. Supplementary material

Crystallographic data for the structural analysis have been deposited with the Cambridge Crystallographic Data Centre, CCDC 268307. Copies of this information may be obtained free of charge from The Director CCDC, 12 Union Road, Cambridge, CB2 1EZ, UK (fax: +44 1223 336033; e-mail: deposit@ccdc.cam.ac.uk or at www.ccdc.cam.ac.uk/index.html).

Acknowledgements

We thank the Petroleum Research Fund, administered by the American Chemical Society, for support of this research.

References

[1] G. Wilke, B. Bogdanovic, Angew. Chem. 73 (1961) 756.
[2] J.M. Chance, D.L. Linebarrier, T.A. Nile, Transition Met. Chem. (London) 12 (1987) 276.
[3] B. Alonso, I. Cuadrado, M. Moran, J. Losada, J. Chem. Soc., Chem. Commun. (1994) 2575.
[4] R.J. Franks, K.M. Nicholas, Organometallics 19 (2000) 1458.
[5] T. Hirashita, Y. Hayashi, K. Mitsui, S. Araki, J. Org. Chem. 68 (2003) 1309.
[6] F.J. Karol, R.N. Johnson, J. Polym. Sci. Polym. Chem. Ed. 13 (1975) 1607.
[7] P.P. Novakov, D. Kuckling, L. Fedorova, H.J.P. Adler, Macromol. Symp. 128 (1998) 195.
[8] C.K. Simpson, R.E. White, C.N. Carlson, D.A. Wrobleski, C.J. Kuehl, T.A. Croce, I.M. Steele, B.L. Scott, T.P. Hanusa, A.P. Sattelberger, K.D. John, Organometallics 24 (2005) 3685.
[9] M.G.H. Wallbridge, M. Fishwick, J. Chem. Soc. A (1971) 57.
[10] R. Meijboom, J.R. Moss, A.T. Hutton, T.-A. Makaluza, S.F. Mapolie, F. Waggie, M.R. Domingo, J. Organomet. Chem. 689 (2004) 1876.
[11] R.A. Fernandes, Y. Yamamoto, J. Org. Chem. 69 (2004) 735.
[12] D.C. Braddock, A. Matsuno, Synlett (2004) 2521.
[13] R. Meijboom, A.T. Hutton, J.R. Moss, Organometallics 22 (2003) 1811.
[14] M.F. Gozzi, M.D.C. Goncalves, I.V.P. Yoshida, J. Mater. Sci. 34 (1999) 155.
[15] A.W. Van der Made, P.W.N.M. Van Leeuwen, J. Chem. Soc., Chem. Commun. (1992) 1400.
[16] K. Nakanishi, K. Mizuno, Y. Otsuji, J. Chem. Soc., Chem. Commun. (1991) 90.
[17] V. Dejean, H. Gornitzka, G. Oba, M. Koenig, G. Manuel, Organometallics 19 (2000) 711.
[18] T. Akiyama, J. Iwai, M. Sugano, Tetrahedron 55 (1999) 7499.
[19] G. Cerveau, C. Chuit, R.J.P. Corriu, C. Reye, Organometallics 10 (1991) 1510.
[20] P. Mazerolles, F. Gregoire, R. Morancho, A. Reynes, N. Sefiani, J. Organomet. Chem. 328 (1987) 49.
[21] P.J. Rogers, J.I. Selco, F.S. Rowland, Chem. Phys. Lett. 97 (1983) 313.
[22] C.E. Wagner, K.J. Shea, Org. Lett. 6 (2004) 313.
[23] F.V. Pastukhov, I.V. Yampolsky, Y.N. Bubnov, J. Organomet. Chem. 657 (2002) 123.
[24] Y.N. Bubnov, I.V. Zhun, E.V. Klimkina, A.V. Ignatenko, Z.A. Starikova, Eur. J. Org. Chem. (2000) 3323.
[25] B. Wrackmeyer, O.L. Tok, E. Klimkina, Y.N. Bubnov, Inorg. Chim. Acta 300–302 (2000) 169.
[26] B. Wrackmeyer, O.L. Tok, Y.N. Bubnov, Angew. Chem., Int. Ed. 38 (1999) 124.
[27] H.C. Brown, U.S. Racherla, P.J. Pellechia, J. Org. Chem. 55 (1990) 1868.
[28] H.C. Brown, U.S. Racherla, Tetrahedron Lett. 26 (1985) 4311.
[29] B.M. Mikhailov, Pure Appl. Chem. 39 (1974) 505.
[30] A. Yanagisawa, Y. Nakamura, T. Arai, Tetrahedron – Asymmetry 15 (2004) 1909.
[31] J.S. Yadav, B.V.S. Reddy, T. Swamy, Tetrahedron Lett. 44 (2003) 4861.
[32] S. Kii, K. Maruoka, Chirality 15 (2003) 68.
[33] Y.Z. Jin, N. Yasuda, H. Furuno, J. Inanaga, Tetrahedron Lett. 44 (2003) 8765.
[34] K.M. Waltz, J. Gavenonis, P.J. Walsh, Angew. Chem., Int. Ed. 41 (2002) 3697.
[35] C.M. Gordon, C. Ritchie, Green Chem. 4 (2002) 124.
[36] A. Cunningham, S. Woodward, Synlett (2002) 43.
[37] A. McCluskey, J. Garner, D.J. Young, S. Caballero, Tetrahedron Lett. 41 (2000) 8147.

[38] T.M. Cokley, P.J. Harvey, R.L. Marshall, A. McCluskey, D.J. Young, J. Org. Chem. 62 (1997) 1961.
[39] M. Shi, K.M. Nicholas, J. Am. Chem. Soc. 119 (1997) 5057.
[40] A. Yanagisawa, H. Inoue, M. Morodome, H. Yamamoto, J. Am. Chem. Soc. 115 (1993) 10356.
[41] M. Fishwick, M.G.H. Wallbridge, J. Organomet. Chem. 25 (1970) 69.
[42] S. Araki, T. Horie, M. Kato, T. Hirashita, H. Yamamura, M. Kawai, Tetrahedron Lett. 40 (1999) 2331.
[43] K. Sato, T. Sukegawa, T. Sasaki, T. Matsuoka, A. Katsui. Jpn. Kokai Tokkyo Koho 01319927
[44] K. Sato, T. Sukegawa, T. Sasaki, T. Matsuoka, A. Katsui, Chem. Abst. 113 (1989) 50386.
[45] C.N. Carlson, J.D. Smith, T.P. Hanusa, W.W. Brennessel, V.G. Young Jr., J. Organomet. Chem. 683 (2003) 191.
[46] J.D. Smith, T.P. Hanusa, V.G. Young Jr., J. Am. Chem. Soc. 123 (2001) 6455.
[47] J.D. Smith, K.T. Quisenberry, T.P. Hanusa, W.W. Brennessel, Acta Crystallogr. C. 60 (2004) m507.
[48] B. Ray, T.G. Neyroud, M. Kapon, Y. Eichen, M.S. Eisen, Organometallics 20 (2001) 3044.
[49] K.T. Quisenberry, J.D. Smith, M. Voehler, D.F. Stec, T.P. Hanusa, W.W. Brennessel, J. Am. Chem. Soc. 127 (2005) 4376.
[50] C.N. Carlson, T.P. Hanusa, W.W. Brennessel, J. Am. Chem. Soc. 126 (2004) 10550.
[51] Y.N. Bubnov, M.E. Gurskii, I.D. Gridnev, A.V. Ignatenko, Y.A. Ustynyuk, V.I. Mstislavskii, J. Organomet. Chem. 424 (1992) 127.
[52] N.W. Mitzel, C. Lustig, R.J.F. Berger, N. Runeberg, Angew. Chem., Int. Ed. 41 (2002) 2519.
[53] O.T. Beachley Jr., M.R. Churchill, J.C. Pazik, J.W. Ziller, Organometallics 6 (1986) 1814.
[54] O.T. Beachley Jr., T.D. Getman, R.U. Kirss, R.B. Hallock, W.E. Hunter, J.L. Atwood, Organometallics 4 (1985) 751.
[55] M. Buehl, P.v.R. Schleyer, M.A. Ibrahim, T. Clark, J. Am. Chem. Soc. 113 (1991) 2466.
[56] R.H. Blessing, Acta Crystallogr. A 51 (1995) 33.
[57] M.J. Frisch, G.W. Trucks, H.B. Schlegel, G.E. Scuseria, M.A. Robb, J.R. Cheeseman, J.A. Montgomery Jr., T. Vreven, K.N. Kudin, J.C. Burant, J.M. Millam, S.S. Iyengar, J. Tomasi, V. Barone, B. Mennucci, M. Cossi, G. Scalmani, N. Rega, G.A. Petersson, H. Nakatsuji, M. Hada, M. Ehara, K. Toyota, R. Fukuda, J. Hasegawa, M. Ishida, T. Nakajima, Y. Honda, O. Kitao, H. Nakai, M. Klene, X. Li, J.E. Knox, H.P. Hratchian, J.B. Cross, V. Bakken, C. Adamo, J. Jaramillo, R. Gomperts, R.E. Stratmann, O. Yazyev, A.J. Austin, R. Cammi, C. Pomelli, J.W. Ochterski, P.Y. Ayala, K. Morokuma, G.A. Voth, P. Salvador, J.J. Dannenberg, V.G. Zakrzewski, S. Dapprich, A.D. Daniels, M.C. Strain, O. Farkas, D.K. Malick, A.D. Rabuck, K. Raghavachari, J.B. Foresman, J.V. Ortiz, Q. Cui, A.G. Baboul, S. Clifford, J. Cioslowski, B.B. Stefanov, G. Liu, A. Liashenko, P. Piskorz, I. Komaromi, R.L. Martin, D.J. Fox, T. Keith, M.A. Al-Laham, C.Y. Peng, A. Nanayakkara, M. Challacombe, P.M.W. Gill, B. Johnson, W. Chen, M.W. Wong, C. Gonzalez,, J.A. Pople, GAUSSIAN 03, Revision C.02, Gaussian, Inc., Wallingford, CT, 2004.
[58] A.D. Becke, J. Chem. Phys. 98 (1993) 5648.
[59] J.P. Perdew, Y. Wang, Phys. Rev. B 45 (1992) 13244.
[60] J.D. Smith, T.P. Hanusa, Organometallics 20 (2001) 3056.
[61] D.E. Woon, T.H. Dunning Jr., J. Chem. Phys. 98 (1993) 1358.

Available online at www.sciencedirect.com
SCIENCE DIRECT®
Polyhedron 25 (2006) 293–299
POLYHEDRON
www.elsevier.com/locate/poly

Synthesis and characterization of Hf–Al heterometallic aminoalkoxides as single-source MOCVD precursors for hafnium aluminate films

Liliane G. Hubert-Pfalzgraf [a,*], Adulfas Abrutis [*,b], Sergej Pasko [a,b], Nadia Touati [a], Dominique Luneau [c]

[a] Université Claude Bernard Lyon 1, IRC, 2 avenue A. Einstein, 69626 Villeurbanne Cedex, France
[b] Department of Chemistry, Vilnius University, Naugarduko 24, 03225, Vilnius, Lithuania
[c] Université Claude Bernard Lyon 1, Centre de diffractométrie, 69626 Villeurbanne Cedex, France

Received 16 April 2005; accepted 29 June 2005
Available online 10 August 2005

Dedicated to Professor Malcolm H. Chisholm for his 60th birthday.

Abstract

Alcohol exchange reactions applied to $HfAl_2(OPr^i)_{10}$ (**1**) afforded heterometallic Hf–Al aminoalkoxides namely $HfAl_2(OPr^i)_8(dmae)_2$ (dmae = *N*,*N*-dimethylaminoethoxide) (**2**) and $HfAl_2(OPr^i)_8(dmap)_2$ (dmap = dimethylaminopropoxide) (**3**). They were characterized by elemental analysis, FT-IR, ^1H NMR, mass spectrometry and TGA. The molecular structure of **2**, as established by single-crystal X-ray diffraction, $HfAl_2(\mu\text{-}OPr^i)_2(\mu,\eta^2\text{-}OC_2H_4NMe_2)_2(OPr^i)_6$, is based on an open-shell trinuclear unit with a central 6-coordinate Hf atom and 5-coordinate Al centres. Compound **2** was tested as a single-source precursor for the deposition of hafnium aluminate films by liquid-injection MOCVD. The films growth rate, composition and morphology were studied in relation with the deposition temperature. The as-deposited at 500–800 °C films (both on sapphire and silicon) were amorphous; partial crystallization occurred after 1 h annealing at 900 °C. The bulk of the films was Al-rich (Al/Hf = 1.2–1.6) and contained small amounts of carbon (2–4%) and nitrogen (4–5%).
© 2005 Elsevier Ltd. All rights reserved.

Keywords: Hafnium; Aluminate; Heterometallic alkoxide; Structure; MOCVD, High κ dielectrics

1. Introduction

Amorphous silicon oxide has been used for many years as dielectric layer in the microelectronic industry due to its dielectric properties and high stability interface with silicon. However, the increase in the circuit density and scaling down in the dimensions of field effect transistors in CMOS (complementary metal oxide semiconductor) technologies forces the thinning of the oxide layer down to a thickness where leakage current is an obstacle for device reliability [1,2]. A solution is to use as gate dielectric oxide materials with higher dielectric constants (κ) than SiO_2 ($\kappa = 3.9$). Various oxides were considered among which HfO_2 was the most investigated due to the high quality dielectric properties of its polycrystalline films [2]. However, in order to stabilize the interface between metal oxide and silicon it is desirable that the gate dielectric remains amorphous during CMOS processing [1]. Unfortunately, HfO_2 films crystallize during MOCVD deposition at ~500 °C

* Corresponding author. Tel.: +33 4 72 44 53 22; fax: +33 4 72 44 53 99.
E-mail address: hubert@univ-lyon1.fr (L.G. Hubert-Pfalzgraf).

0277-5387/$ - see front matter © 2005 Elsevier Ltd. All rights reserved.
doi:10.1016/j.poly.2005.06.037

(monoclinic phase) independently of the precursor used [3–5]. Grain boundaries in polycrystalline films can result in high leakage current. Hafnium silicate [1] or other binary alloys remaining amorphous up to 800–900 °C on silicon were considered as alternatives. Hafnium aluminate, actually an alloy $(HfO_2)_x(Al_2O_3)_{1-x}$, is especially attractive, it remains amorphous at 900 °C ($x = 0.75$) and even at 1050 °C ($x = 0.25$) [6] and has a higher dielectric constant ($\kappa \sim 15$) than hafnium silicate ($\kappa \sim 7$) [1].

$(HfO_2)_x(Al_2O_3)_{1-x}$ films have been deposited on Si(1 0 0) by physical (sputtering [7], pulsed laser deposition [8,9]) and chemical methods such as atomic layer deposition (ALD) and metal-organic chemical vapor deposition (MOCVD). Among chemical techniques ALD mainly has been applied for deposition of hafnium aluminate films [6,10] using combinations of various Hf and Al precursors. Major advantages of ALD are good control of the growth at a monolayer level and excellent step coverage [11]. MOCVD also has many advantages since it allows the growth of uniform layers on large, even non-planar substrates, good step coverage and composition control, but much higher growth rates than ALD. This technique is thus highly desirable for bulk production. Only few studies have been reported on the growth of hafnium aluminate films by MOCVD [12–14]. Two separate sources namely $Hf(mmp)_4$ ($mmp = OCMe_2CH_2OMe$) and $[Al(OiPr)_3]_4$ have been used for vapor generation [13,14]. Another alternative for the MOCVD growth of $(HfO_2)_x(Al_2O_3)_{1-x}$ films is the use of an heterometallic precursor containing both metals in a single molecule. Such an approach offers a good control of the composition of multimetallic oxides films and thus high homogeneity [15]. Recently, Joo et al. [12] reported about the use of the single cocktail liquid source $HfAl(mmp)_2(OiPr)_5$ for MOCVD of $(HfO_2)_x(Al_2O_3)_{1-x}$ films. However, no information on the origin, properties and structure of this precursor was given, it remains thus unclear if this source was an heterometalic precursor or a mixture of two alkoxides.

We report herein the synthesis and characterization of the first mixed-metal Hf–Al aminoalkoxides namely $HfAl_2(OPr^i)_8(dmae)_2$ (**2**) and $HfAl_2(OPr^i)_8(dmap)_2$ (**3**) (dmae = *N*,*N*-dimethylaminoethoxide, dmap = $OCHMeCH_2NMe_2$ = dimethylaminopropoxide). Compound **2** was tested as single-source heterometallic precursor for the deposition of $(HfO_2)_x(Al_2O_3)_{1-x}$ films by pulsed liquid-injection MOCVD.

2. Experimental

2.1. Synthesis

All reactions were performed under argon using Schlenk tubes and vacuum line techniques. Solvents were purified by standard methods. dmaeH (2-dimethylaminoethanol) and dmapH (1-dimethylamino-2-propanol) were distilled and stored over molecular sieves. FT-IR spectra were recorded with a Perkin–Elmer Paragon 500 Spectrometer as Nujol mulls. NMR spectra were recorded on an AM250 Bruker spectrometer, the peak of the solvent was used as reference. Mass spectra were obtained with a Thermofinnigan Mat95XL spectrometer under standard electron ionization conditions ($E_1 = 70$ eV). Elemental analyses were done at the Centre de microanalyses du CNRS.

$Al_2Hf(OPr^i)_{10}$ (**1**) was prepared by a slightly modified procedure [16]. $Hf_2(OPr^i)_8(Pr^iOH)_2$ (2.46 g, 5.01 mmol) and $[Al(OPr^i)_3]_4$ (2.05 g, 1.28 mmol) were mixed in 25 ml of toluene and refluxed for 6 h. Evaporation to dryness gave a white powder (4.00 g, 95%). IR (cm^{-1}): 594 m, 553 s, 540 s, 475 m, 450 m (νM-OR). ^1H NMR ($CDCl_3$, 20 °C): 4.8 sept ($J = 6$ Hz, 4H, CH), 4.64 sept ($J = 6$ Hz, 2H, CH), 4.58 sept ($J = 6$ Hz, 4H, CH), 1.57 d ($J = 6$ Hz, 12H, Me), 1.52 d ($J = 6$ Hz, 24H, Me), 1.48 d ($J = 6$ Hz, 24H, Me).

Synthesis of $Al_2Hf(OPr^i)_8(OR)_2$. R = $C_2H_4NMe_2$ (**2**), $CHMeCH_2NMe_2$ (**3**) dimethylaminoethanol (0.25 g, 2.82 mmol) was added to a solution of $Al_2Hf(OPr^i)_{10}$ (1.164 g, 1.41 mmol) in 20 ml of toluene. After refluxing for 3 h and filtration, the filtrate was evaporated to dryness. The crude powder was recrystallized in pentane. Crystals of **2** (0.96 g, 77%) were obtained at −20 °C. *Anal.* Calc. for $C_{32}H_{76}N_2O_{10}Al_2Hf$: C, 43.61; H, 8.69; N, 3.18. Found: C, 43.82; H, 8.75; N, 3.40%. IR (cm^{-1}): 632 m, 581 m, 545 s, 467 s (νM-OR). ^1H NMR ($CDCl_3$, 20 °C): 4.48 sept ($J = 6$ Hz, 4H, CH), 4.20 sept ($J = 6$ Hz, 2H, CH), 4.08 sept ($J = 6$ Hz, 2H, CH); 3.7 m (4H, CH_2), 2.7–2.22 m (4H, NCH_2); 2.35 s (12 H, NMe_2), 1.47–1.08 (overlapping of d, $J = 6$ Hz, 48H, Me). MS (m/z^+, I): M − $OC_2H_4NMe_2$ (3), M − OPr^i − Pr^iOH (3), M − $Al(OPr^i)_3$ − CH_4 (8), M − $Al(OPr^i)_3$ − Pr^iOH (18), M − $Al(OPr^i)_3$ − OH- $C_2H_4NMe_2$ (58), M − $Al(OPr^i)_3$ − OHC_2H_4-NMe_2 − C_2H_4 (25), M − $Al_2(OPr^i)_4(OC_2H_4NMe_2)$-$(OCH_2)$ 488 (10), $Al_2(OPr^i)_3(OC_2H_4N)$ (8), M − Hf $(OPr^i)_2$- $(OC_2H_4NMe_2)_2$ (1 0 0), $Hf(OPr^i)_4$ − C_2H_4 − 1/2 O_2 (20), $Al_2(OPr^i)_3$ − 3/2 H_2 (35), $Al(OPr^i)_3$ − C_3H_4 (50), $AlO(OPr^i)_2$ − 1/2 H_2 (30), $CH_2{=}NMe_2$ (64).

The same procedure applied to 1.14 g (1.38 mmol) of $Al_2Hf(OPr^i)_{10}$, 0.28 g (2.76 mmol) of $OCHMeCH_2NMe_2$ gave **3** after extraction of the crude product with petroleum ether and evaporation to dryness (1.14 g, 80%). *Anal.* Calc. for $C_{34}H_{80}N_2O_{10}Al_2Hf$: C, 44.90; H, 8.87; N, 3.08. Found: C, 44.60; H, 8.75; N, 3.10%. IR (cm^{-1}): 596 w, 546 s, 530 sh, 498 w, 444 m (νM-OR); ^1H NMR ($CDCl_3$, 20 °C): 4.45 sept, 4.47 sept ($J = 6$ Hz, 4H, 1:1, CH), 4.1 m (2H, CH), 4.0 m (2H, CH), 3.80–3.75 m (OCH, 2H), 2.15–2.6 (m, 4H, NCH_2), 2.2 (s, 12H, NMe_2), 1.1–1.35 overlapping of d ($J = 6$ Hz, 54H, Me(Pr^i) and CHMe).

The compounds were poorly soluble in aliphatic hydrocarbons and more soluble in toluene, THF, DME.

2.2. Crystallography of $HfAl_2(OPr^i)_8(dmae)_2$

Crystal data for **2**: $C_{32}H_{76}Al_2N_2O_{10}Hf$, FW 881.40, triclinic, $P\bar{1}$, $a = 9.5552(2)$, $b = 12.2673(2)$, $c = 19.9092(5)$ Å, $\alpha = 79.540(1)°$, $\beta = 82.661(1)°$, $\gamma = 82.661(1)°$, $V = 2262.99(8)$ Å^3, $Z = 2$, $T = 160(2)$ K, μ(Mo Kα) = 2.390 mm^{-1}.

Suitable crystals of **2** were grown by recrystallization in petroleum ether as colorless plates. 42 348 Reflections of which 10 057 were unique were measured with a Nonius CCD diffractometer. The data were collected using the COLLECT software they were processed through the DENZO reduction software [17]. The structure was solved and refined on F^2 using the SHELXTL software [18]. All non-hydrogen atoms were refined with anisotropic thermal parameters. Final data R_1 (all data) = 0.0743, $wR_2 = 0.1315$ for 424 parameters, GOF = 1.060. The hydrogen atoms were included in the final refinement in calculated positions with isotropic thermal parameters.

2.3. CVD experiments and films characterization

Pulsed liquid-injection MOCVD (PI-MOCVD) [19,20] was used for testing **2** as precursor for aluminate film deposition. This technique is based on repetitive injections of microdoses of solution of a metal-organic precursor, flash evaporation, vapor transport by a carrier gas ($Ar + O_2$) and decomposition on a hot substrate. Its advantages over classical MOCVD are better reproducibility of precursor feeding rate and easy control of film thickness and growth rate by changing injection parameters (injection frequency and injected drop size, concentration of solution). The deposition conditions are presented in Table 1. The substrates, Si(1 0 0) and R-plane sapphire, were cleaned in boiling toluene before use (sapphire was cleaned in an ultrasound bath in toluene for 15 min before; silicon was dipped in ~8% HF for 10 s to remove oxide). After deposition, films were cooled down to rt in an O_2 atmosphere (~760 Torr).

Table 1
Deposition conditions of $(HfO_2)_x(Al_2O_3)_{1-x}$ films

Evaporator temperature (°C)	280
Substrate temperature (°C)	500–800
Ar flow (l/h)	54
O_2 flow (l/h)	36
Total pressure (Torr)	5
Solvent	toluene
Precursor concentration (M)	0.01
Injection duration (ms)	2.5
Injection frequency (Hz)	2
Microdose mass (mg)	~3.5

Films were studied by X-ray diffraction (XRD) with a Bruker D8 diffractometer (Cu Kα radiation). X-ray photoelectron spectroscopy (XPS; RIBER LAS-3000, Mg Kα radiation) was used for composition analysis (precision of about ±10%) on film surface and in the depth (after the removal of surface layer by sputtering for 30 min with 1.5 keV Ar^+). The data were referenced to the peak of carbon (284.6 eV) for charge effects correction. The morphology of the film surface was examined by atomic force microscopy (AFM) (Digital Instruments Multimode Scanning Probe Microscope, tapping mode). Thickness of the films on Si(1 0 0) was determined by profilometry (Taylor–Hobson) on the steps formed by lithography and wet etching. The determined thickness was used for the calculation of the film growth rate.

3. Results and discussion

3.1. Synthesis, characterization and molecular structure

The reactions between $HfAl_2(OPr^i)_{10}$ (**1**) and aminoalcohols, namely dimethylaminoethanol (dmaeH) and dimethylaminopropanol (dmapH) in 1:2 stoichiometry in toluene at reflux give access to heteroleptic mixed-metal species, $HfAl_2(OPr^i)_8(OR)_2$ (R = dmae) (**2**), dmap (**3**), respectively. The compounds were characterized by elemental analysis, FT-IR, ^{1}H NMR and mass spectrometry. FT-IR spectra confirmed the absence of vOH absorption bands and thus formation of non-solvated species. The compounds were also characterized by vM-OR absorption bands in the 600–450 cm^{-1} range different from those of $HfAl_2(OPr^i)_{10}$. ^{1}H NMR data confirm the integration ratio between the isopropoxide and the aminoalkoxide ligands. As for the homoleptic $HfAl_2$ alkoxide, the various isopropoxide groups appear magnetically inequivalent even at rt in $CDCl_3$ solutions. Indeed, the spectra of **2** for instance show three type of methine CH groups at 4.48, 4.20, 4.08 ppm in a 4:2:2 integration ratio. According to the mass spectrometry data, compound **2** is also present in the vapor phase. However, the fragmentation pattern indicates quite an easy loss of aluminium fragments. Although moisture sensitive, **2** and **3** were more stable than the homoleptic derivative **1**.

Single crystal X-ray diffraction of **2** confirmed it to be a heterometallic species of formula $HfAl_2(\mu\text{-}OPr^i)_2(\mu,\eta^2\text{-}OC_2H_4NMe_2)_2(OPr^i)_6$. The structure (Fig. 1) is derived from that of $HfAl_2(\mu\text{-}OPr^i)_2(OPr^i)_8$ the bridging-chelating aminoalkoxide leading to fivefold coordination of the aluminium centres and a less symmetrical structure [16].The central hafnium is six-coordinate with a quite distorted surrounding due to the acute O–Hf–O angles of the bridge [65.4(1)° and 70.6(1)°] (Table 2). The Al

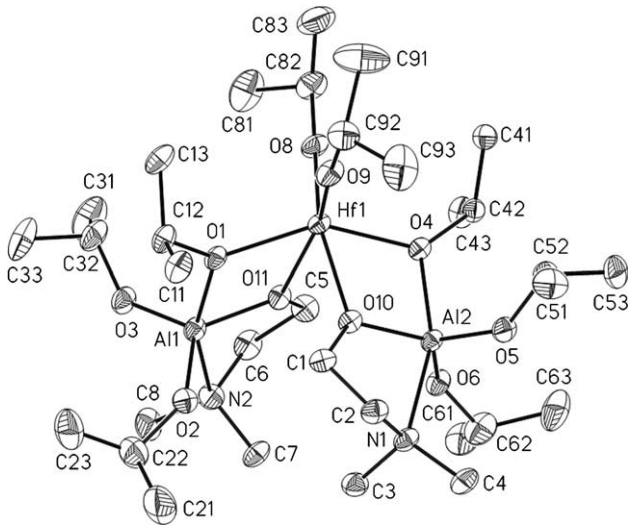

Fig. 1. Molecular structure of $HfAl_2(OPr^i)_8(dmae)_2$ showing the atom numbering scheme (thermal ellipsoids at 30% probability).

coordination geometry can be described as a trigonal bipyramid with the bridging μ-O(Pr^i) and μ-N(dmae) at the axial positions thus leading to significant distortions. The bite angles of the aminoethoxide ligand are quite small (77.5° av.) but comparable to the literature body [21]. The ranking of bond distances is Al–OR < Al–μOR < Hf–OR < Hf–μOR < Al–N. The bridges are thus asymmetrical. The terminal Hf–OR bond lengths are quite different (1.829(4) and 2.016(4) Å) although they have similar large Hf–O–C angles (175.5° av.) accounting for π-bonding. The increase of the coordination number of aluminium, by comparison to **1**, reflects in the Al–OPr^i bond distances [1.682(4)–1.932(4) Å versus 1.667(6)–1.803(5) Å], the Al–O–C angle being similar (136.7° av.) [22]. The Al–N coordination bonds are quite different for the two Al centres 2.143(5) and 2.380(5) Å, the longest one being *trans* to the longest Al-μOPr^i, 2.011(4) Å this suggesting the aminoethoxide ligand exerts a quite strong *trans* effect. The Al–N bond distances are quite long is comparison with the literature body [23]. The Hf–Al distances of 3.246(2) Å are longer than those of $HfAl_2(OPr^i)_{10}$ [3.125(2) Å] [16]. The modification of **1** by functional aminoalkoxide ligands giving **2** and **3** proceeds with retention of the initial Hf:Al stoichiometry since the increase in coordination of the Al centres allows to use the additional coordination site of the aminoalkoxide ligands with respect to the OPr^i one.

3.2. MOCVD deposition and properties of the films

Amorphous $(HfO_2)_x(Al_2O_3)_{1-x}$ films (50–120 nm thick) were deposited with **2** on Si(100) and R-plane sapphire substrates at 500–800 °C. In order to study the stability of the films toward crystallization, those

Table 2
Selected bond lengths (Å) and angles (°) for **2**

Bond lengths	
Hf1–O9	1.829(4)
Hf1–O8	2.016(4)
Hf1–O11	2.132(3)
Hf1–O4	2.154(4)
Al1–O3	1.682(4)
Al1–O2	1.846(4)
Al1–O1	1.864(4)
Al1–O11	1.932(4)
Al1–N2	2.143(5)
Hf1–O1	2.228(4)
Hf1–O10	2.274(4)
Hf1–Al2	3.246(2)
Al2–O6	1.663(4)
Al2–O5	1.676(4)
Al2–O10	1.856(4)
Al2–O4	2.011(4)
Al2–N1	2.380(5)
Angles	
O9–Hf1–O8	95.6(2)
O9–Hf1–O11	160.3(2)
O8–Hf1–O11	96.6(2)
O9–Hf1–O4	104.1(2)
O8–Hf1–O4	92.6(2)
O11–Hf1–O4	90.8(1)
O9–Hf1–O1	95.9(2)
O8–Hf1–O1	109.4(2)
O3–Al1–O2	115.5(2)
O3–Al1–O1	100.2(2)
O2–Al1–O1	103.5(2)
O3–Al1–O11	118.8(2)
O2–Al1–O11	124.7(2)
O1–Al1–O11	76.7(2)
O3–Al1–N2	91.9(2)
O2–Al1–N2	90.1(2)
O1–Al1–N2	155.5(2)
O11–Al1–N2	78.8(2)
Al1–O1–Hf1	107.8(2)
Al2–O4–Hf1	102.4(2)
Al1–O11–Hf1	109.2(2)
Al2–O10–Hf1	103.1(2)
O11–Hf1–O1	65.4(1)
O4–Hf1–O1	148.6(1)
O9–Hf1–O10	94.4(2)
O8–Hf1–O10	162.1(2)
O11–Hf1–O10	78.1(1)
O4–Hf1–O10	70.6(1)
O1–Hf1–O10	84.1(1)
O6–Al2–O10	122.7(2)
O5–Al2–O10	121.2(2)
O6–Al2–O4	97.2(2)
O5–Al2–O4	100.4(2)
O10–Al2–O4	82.2(2)
O6–Al2–N1	92.1(2)
O5–Al2–N1	92.6(2)
O10–Al2–N1	76.2(2)
O4–Al2–N1	159.0(2)
Al1–O2–C22	138.9(4)
Al2–O6–C62	136.8(4)
Al1–O3–C32	136.5(4)
Al2–O5–C52	136.8(4)
C92–O9–Hf1	174.8(5)
C82–O8–Hf1	175.9(4)

deposited at 700 °C were annealed for 1 h at 900 °C (under vacuum for the films on silicon; in air for those on sapphire). The signs of crystallization can be seen in Fig. 2, indicating partial separation of a monoclinic HfO_2 phase in films during the long time annealing. This demonstrates that despite the significantly higher resistance to crystallization compared to HfO_2 films, MOCVD grown hafnium aluminate films do not remain completely amorphous during annealing for 1 h. Nevertheless, this result can be considered as promising since it suggests that films might still remain amorphous during a rapid high-temperature annealing step (~20 s) in the CMOS process. For comparison, hafnium aluminate films grown by MOCVD from $HfAl(mmp)_2(O^iPr)_5$ became already crystalline after 30 s annealing at 900 °C [12].

The Arrhenius type plot of growth rate versus deposition temperature is presented in Fig. 3. The growth enters a diffusion controlled range at ~650 °C. The activation energy of the reaction was ~38 kJ/mol, thus, less than for completely kinetically limited growth ($E_a > 70$ kJ/mol). The growth rates of $(HfO_2)_x(Al_2O_3)_{1-x}$ films in the range of 500–800 °C (1.6–3.8 nm/min or 330–780 nm/mmol of injected precursor) were sufficiently high for the growth of thin dielectric films. Our growth rates were similar to those achieved with the $HfAl(mmp)_2(OPr^i)_5$ source [12]. It is worth noting that although this liquid precursor was injected continuously in a vaporizer chamber, we obtained similar growth rates through a pulsed injection of very diluted (0.01 M) solutions. This can be considered as an advantage of our new precursor and our deposition technique.

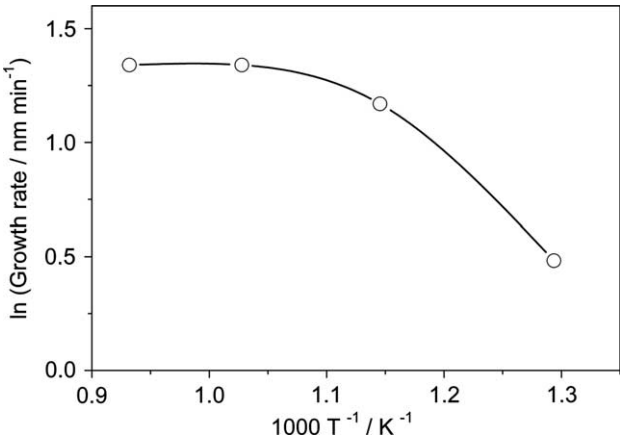

Fig. 3. Growth rate of $(HfO_2)_x(Al_2O_3)_{1-x}$ films vs. deposition temperature.

The films deposited at different temperatures were studied by AFM (Fig. 4). The relative roughness (ratio R_a/thickness, where R_a is an average roughness) was small (~2%) at low temperatures (500–600 °C) and significantly higher (~5%) at 800 °C where film growth vas diffusion controlled. This result is in agreement with previous observations that the grain size and roughness of HfO_2 [4,5] and Al_2O_3 [24] films increased with the deposition temperature.

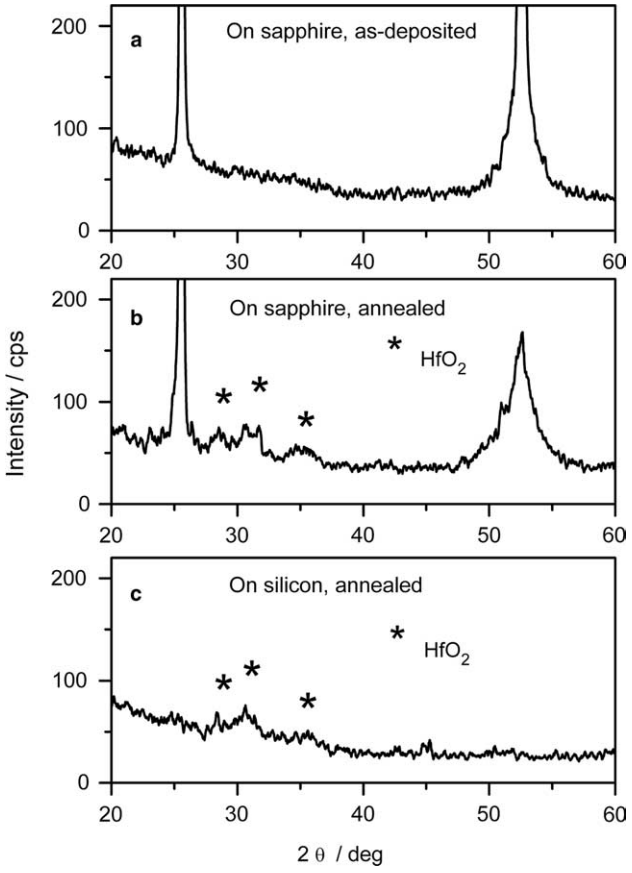

Fig. 2. XRD patterns of as-deposited and annealed at 900 °C $(HfO_2)_x(Al_2O_3)_{1-x}$ films, grown on sapphire (a, b) and (c) silicon at 700 °C. The thickness of as-deposited films is 105 nm.

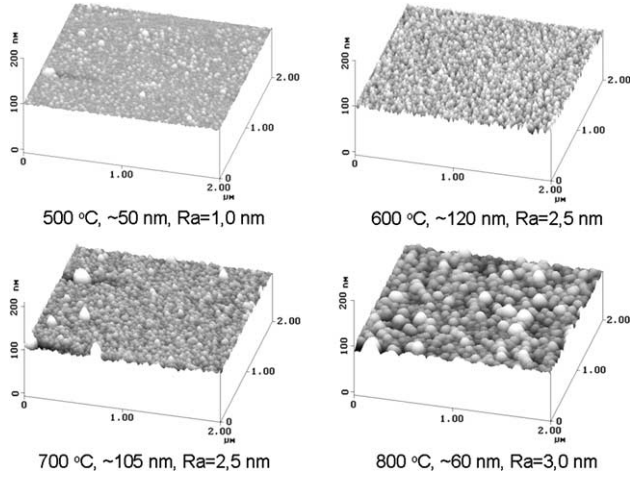

Fig. 4. AFM images of $(HfO_2)_x(Al_2O_3)_{1-x}$ films deposited on silicon at 500–800 °C. Deposition temperature, film thickness and roughness average (R_a) are indicated.

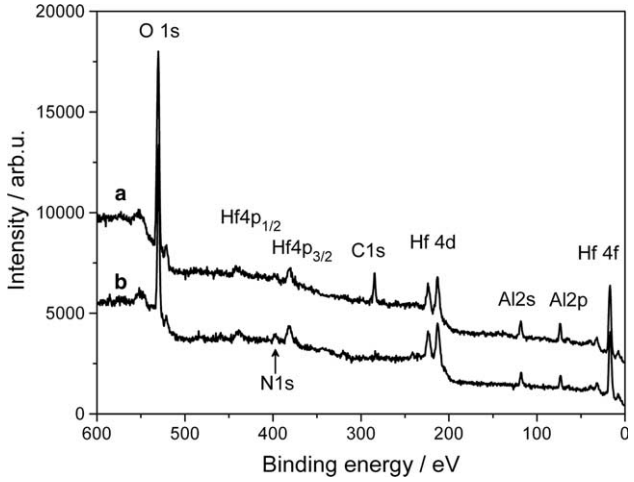

Fig. 5. XPS spectra of an $(HfO_2)_x(Al_2O_3)_{1-x}$ film deposited at 700 °C: (a) surface, (b) after 30 min of sputtering with Ar^+ at 1.5 keV.

The composition of the films on silicon was studied by XPS (Fig. 5). The XPS study revealed films that the Al/Hf ratios were 1.65–1.8 on the surface and 1.2–1.6 in the bulk of the films depending on deposition temperatures (Fig. 6(a)). Higher Al/Hf ratios compared to the bulk were also found with $HfAl(mmp)_2(OPr^i)_5$ [12]. The carbon content decreased after removal of the surface layer (by sputtering with 1.5 keV Ar^+ for 30 min) from ~10–14 to 2–4 at.% (Fig. 6(b)), while the nitrogen amount remained in the range ~4–5% (Fig. 6(c)). The presence of nitrogen (as nitride) in the films may be seen as an advantage since N dopants were reported to improve carrier mobility at the interface [1]. The Al/Hf ratio in films is lower than in the heterometallic precursor (Al/Hf = 2). The difference between the Al/Hf ratio on the surface and in the film depth suggests that the depth profile is not very homogeneous. TGA data of **2** (N_2, 1 atm) indicate loss of an $Al(OiPr)_3$ moiety as the first step of decomposition (~200 °C). Mass spectrometry data of **2** are also in agreement with an easy loss of Al-fragments. It is thus possible, that partial precursor segregation occurs in the gas phase near the substrate causing the deviation of the Al/Hf ratio between the films and the precursor. Partial desorption of Al-containing fragments of the precursor from the surface can also play a role. However, it is worth to note that the film growth from our heterometallic precursor is much less influenced by such secondary processes than the growth from $HfAl(mmp)_2(OPr^i)_5$ [12]. Indeed, the later led to films in which the Al/Hf ratio varied in a large range namely from 0.4 to 2.4 and the film composition was only poorly related with that of the source used (Hf/Al = 1). These results on the Hf/Al ratio are similar to those obtained by using a mixture of two homometallic precursors with variable ratio [13]. The deposition temperature appeared as the main factor of variation with $HfAl(mmp)_2(OPr^i)_5$, higher deposition temperatures reducing the incorporation of Al_2O_3 into HfO_2.

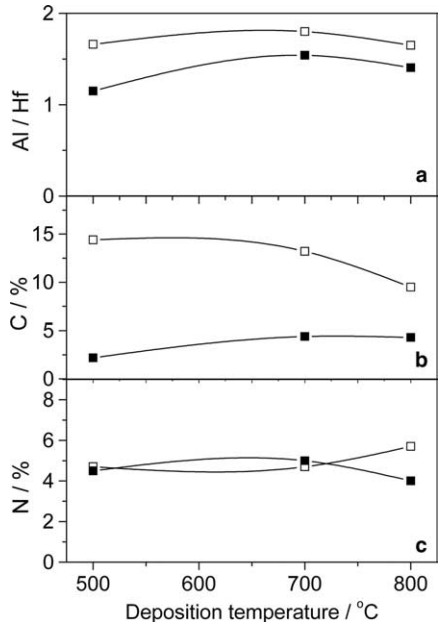

Fig. 6. The dependence of film composition on deposition temperature: (a) Al/Hf ratio, (b) carbon contamination, (c) nitrogen contamination. Composition determined by XPS on film surface (□) and after sputtering with 1.5 keV Ar^+ for 30 min (■).

Our preliminary results show that the use of an Hf/Al heterometallic precursor does not ensure exactly the same Hf/Al ratio in the hafnium aluminate alloy film than in the precursor. However, the new heterometallic precursor **2** is suitable for the deposition of amorphous $(HfO_2)_x(Al_2O_3)_{1-x}$ films with a controllable Al/Hf ratio in a quite narrow range namely 1.2–1.6.

4. Conclusions

The first Hf–Al heterometallic aminoalkoxides $HfAl_2(OPr^i)_8(dmae)_2$ (**2**) and $HfAl_2(OPr^i)_8(dmap)_2$ (**3**) were synthesized and characterized by elemental analysis, FT-IR, ^1H NMR, mass spectrometry and by single crystal X-ray diffraction for **2**. To the best of our knowledge**, 2** represents the first example of a well-defined, structurally characterized Hf–Al heterometallic species used for MOCVD of hafnium aluminate films. It gives amorphous hafnium aluminate $(HfO_2)_x(Al_2O_3)_{1-x}$ films in the 500–800 °C temperature range. Long time (1 h) annealing at 900 °C led to crystallization of some monoclinic HfO_2. Films contamination by carbon was rather low (2–4% by XPS). The films were rich in Al compared to Hf, however, the Al/Hf ratio (1.2–1.6) was lower than in the initial precursor **2** and was function of the deposition temperature. This shows that the use of an heterometallic precursor is less able to control the metal stoichiometry in alloys than in multimetallic oxides

having a definite formula. However, the composition of the $(HfO_2)_x(Al_2O_3)_{1-x}$ films is mainly defined by that of the heterometallic precursor used, 2, and can be controlled in a rather narrow range. The presence of N-donor ligands results in the presence of nitrogen as nitride in the films and might improve the properties of the films, further studies are in progress.

5. Supplementary material

Crystallographic data (tables of coordinates, of thermal parameters, of bond lengths and angles) have been deposited at the Cambridge Crystallographic Data Base Centre. CCDC reference number for **2** is 227405. Copies of this information may be obtained free of charge from The Director, CCDC, 12 Union Road, Cambridge, CB2 1EZ, UK (fax: +44 1223 336 033; e-mail: deposit@ccdc.cam.ac.uk or http://www.ccdc.cam.ac.uk).

Acknowledgments

L.H.P. and S.P. are grateful for financial support by MINEFI (Crolles 03) and for a fellowship by CNOUS (Centre National des Oeuvres Universitaires et Scolaires), respectively.

References

[1] (a) A.I. Kingon, J-P. Maria, S.K. Streiffer, Nature 406 (2000) 1032;
(b) R.G. Gordon, J. Becker, D. Hausmann, S. Suh, Chem. Mater. 13 (2001) 2463.
[2] G.D. Wilk, R.M. Wallace, J.M. Anthony, J. Appl. Phys. 89 (2001) 5243.
[3] S.V. Pasko, L.G. Hubert-Pfalzgraf, A. Abrutis, P. Richard, A. Bartasyte, V. Kazlauskiene, J. Mater. Chem. 14 (2004) 1245.
[4] A. Abrutis, L.G. Hubert-Pfalzgraf, S.V. Pasko, A. Bartasyte, F. Weiss, V. Janickis, J. Cryst. Growth 267 (2004) 529.
[5] S.V. Pasko, A. Abrutis, L.G. Hubert-Pfalzgraf, Mater. Lett. 59 (2005) 261.
[6] M.Y. Ho, H. Gong, G.D. Wilk, B.W. Busch, M.L. Green, W.H. Lin, A. See, S.K. Lahiri, M.E. Loomans, P.I. Räisänen, T. Gustaffson, Appl. Phys. Lett. 81 (2002) 4218.
[7] L. Manchanda, M.D. Morris, M.L. Green, R.B. van Dover, F. Klemens, T.W. Sorsch, P.J. Silverman, G. Wilk, B. Busch, S. Aravamudhan, Microelectron. Eng. 59 (2001) 351.
[8] P.F. Lee, J.Y. Dai, K.H. Wong, H.L.W. Chan, C.L. Choy, J. Appl. Phys. 93 (2003) 3665.
[9] P.F. Lee, J.Y. Dai, H.L.W. Chan, C.L. Choy, Integr. Ferroel. 57 (2003) 1213.
[10] (a) T. Kawahara, K. Torii, R. Mitsuhashi, A. Muto, A. Horiuchi, H. Ito, H. Kitajima, Jpn. J. Appl. Phys. P1 43 (A7) (2004) 4129;
(b) M.S. Joo, B.J. Cho, C.C. Yeo, N. Wu, H.Y. Yu, C.X. Zhu, M.F. Li, D.L. Kwong, N. Balasubramanian, Jpn. J. Appl. Phys. P2 42 (3A) (2003) L220;
(c) K. Kukli, M. Ritala, M. Leskelä, T. Sajavaara, J. Keinonen, J. Mater. Sci. Mater. Electron. 14 (2003) 361;
(d) Y. Yang, W.J. Zhu, T.P. Ma, S. Stemmer, J. Appl. Phys. 95 (2004) 3772;
(e) H.S. Chang, H. Hwang, M.H. Cho, H.K. Kim, D.W. Moon, J. Vacuum Sci. Technol. A 22 (2004) 165;
(f) H. Jin, H.J. Kang, S.W. Lee, Y.S. Lee, S.K. Rha, H.S. Lee, K.Y. Lim, J. Korean Phys. Soc. 45 (2004) 1292;
(g) M.H. Cho, H.S. Chang, Y.J. Cho, D.W. Moon, K.H. Min, R. Sinclair, S.K. Kang, D.H. Ko, J.H. Lee, J.H. Gu, N.I. Lee, Surf. Sci. 554 (2004) L75, and references therein.
[11] M. Ritala, M. Leskelä, in: Handbook of Thin Film Materials, Academic Press, San Diego, 2002, p. 103.
[12] M.S. Joo, B.J. Cho, C.C. Yeo, D.S.H. Chan, S.J. Whoang, S. Mathew, L.K. Bera, N. Balasubramanian, D.L. Kwong, IEEE Trans. Electron. Dev. 50 (2003) 2088.
[13] P.A. Marshall, R.J. Potter, A.C. Jones, P.R. Chalker, S. Taylor, G.W. Critchlow, S.A. Rushworth, Chem. Vap. Dep. 10 (2004) 275.
[14] R.J. Potter, P.A. Marshall, P.R. Chalker, S. Taylor, A.C. Jones, T.C.Q. Noakes, P. Bailey, Appl. Phys. Lett. 84 (2004) 4119.
[15] L.G. Hubert-Pfalzgraf, Inorg. Chem. Commun. 6 (2003) 102, Dalton 2004, 3113 and references therein.
[16] E.P. Turevskaya, D.V. Berdyev, N.Ya. Turova, Z.A. Starikova, A.I. Yanovsky, Yu.T. Struchkov, A.I. Belokon, Polyhedron 16 (1997) 663.
[17] Nonius COLLECT, DENZO, SCALEPACK, SORTAV: Kappa CCD Program Package, Nonius B.V., Delft, The Netherlands, 1999.
[18] G.M. Sheldrick, Program for the Refinement of Crystal Structures, University of Göttingen, Germany (Bruker-AXS, Madison, WI, USA), 1997.
[19] J.P. Senateur, F. Weiss, O. Thomas, R. Madar, A. Abrutis, Patent 93/08838 PCT FR94/00858, Europe, USA.
[20] J.P. Senateur, C. Dubourdieu, V. Galindo, F. Weiss, A. Abrutis, in: K.L. Choy (Ed.), Innovative Processing of Films and Nanocrystalline Powders, Imperial College Press, London, 2002, p. 71.
[21] (a) A.C. Jones, J. Mater. Chem. 12 (2002) 2576;
(b) H. Guillon, L.G. Hubert-Pfalzgraf, J. Vaissermann, Eur. J. Inorg. Chem. (2000) 1243;
(c) B.F.G. Johnson, M.C. Klunduk, T.J. O'Connell, C. McIntosh, J. Ridland, Dalton Trans. (2001) 1553.
[22] R.H. Cayton, M.H. Chisholm, E.R. Davidson, V.F. Disatsi, P. Du, J.C. Huffman, Inorg. Chem. 30 (1991) 1020.
[23] (a) K.M. Waggoner, M.M. Olmstead, P.P. Power, Polyhedron 9 (1990) 257;
(b) C.M. Means, S.G. Bott, J.L. Atwood, Polyhedron 9 (1990) 312;
(c) E. Hecht, T. Gelbrich, K.H. Thiele, J. Sieler, Z. Anorg. Allgem. Chem. 624 (1998) 315;
(d) S. Wang, Coord. Chem. Rev. 215 (2001) 79;
(e) A. Cottone III, D. Morales, J.F. Lecuivre, M.J. Scott, Organometallics 21 (2002) 418;
(f) K. Folting, W.E. Streib, K.G. Caulton, O. Poncelet, L.G. Hubert-Pfalzgraf, Polyhedron 10 (1991) 1639.
[24] Abrutis, A. Bartasyte, V. Kubilius, A. Teiserskis, P. Baumann, J. Lindner, M. Schumacher, C. Dubourdieu, Electrochem. Soc. Proc. 8 (2003) 771.

Available online at www.sciencedirect.com
SCIENCE DIRECT®
Polyhedron 25 (2006) 300–306
POLYHEDRON
www.elsevier.com/locate/poly

Preparative and structural studies on sulfur-linked carborane icosahedra: 2-Phenyl-*ortho*-carboranyl-sulfur systems (2-Ph-1,2-$C_2B_{10}H_{10}$)$_2$X (X = S, S_2 or SO), and *ortho*-carboran-di-yl systems (1,2-$C_2B_{10}H_{10}Y)_2$ (Y = S or SO)

Andrei S. Batsanov [a], William Clegg [b], Royston C.B. Copley [a], Mark A. Fox [a,*], Wendy R. Gill [a], Rachel S. Grimditch [a], Thomas G. Hibbert [a], Judith A.K. Howard [a], J.A. Hugh MacBride [a], Kenneth Wade [a]

[a] *Chemistry Department, Durham University Science Laboratories, South Road, Durham, DH1 3LE, UK*
[b] *School of Natural Sciences (Chemistry), University of Newcastle, Newcastle upon Tyne, NE1 7RU, UK*

Received 20 April 2005; accepted 30 June 2005
Available online 24 August 2005

Dedicated to Malcolm Chisholm on the occasion of his 60th birthday.

Abstract

Details are reported of the preparation and X-ray structural characterisation of the new compounds (PhCb^o)$_2$X, where PhCb^o = 2-Ph-1,2-$C_2B_{10}H_{10}$ and X = S (**1**) or SO (**3**), prepared from PhCb^{o}Li and SCl_2 or $SOCl_2$ respectively, as well as the known compound with X = S_2 (**2**). Hydrogen in the presence of palladium/carbon reduced (**3**) to (**1**). Features of their structures (*exo* C–S and cage C–C distances and substituent orientations) are consistent with significant *exo* S=C dative π-bonding from their sulfur atoms to the cage hypercarbon atoms and weak *exo* π-bonding from the phenyl groups. Attempts to prepare systems (Cb^{o}Y)$_2$, in which two *ortho*-carboran-di-yl residues Cb^o are linked through two bridging units Y (S, SO) are also reported, as are their calculated structures.
© 2005 Elsevier Ltd. All rights reserved.

Keywords: Carborane; Sulfur; Thionyl chloride; Cycles; Crystal structure

1. Introduction

Researches into carboranes with cage C–sulfur substituents were originally developed in the 1960s [1–4] and after a quiet period have acquired renewed momentum recently. Reactions between alkali metal (normally lithium) carborane derivatives and elemental sulfur or sulfur halides were used primarily to prepare derivatives of formula types $HCB_{10}H_{10}CSR$, $RCB_{10}H_{10}CSR'$ or $RSCB_{10}H_{10}CSR'$, where R and R′ = H, alkyl or aryl [1–8]. Derivatives Cb^o(SR)$_2$ of *ortho* carborane have attracted particular interest, in part in connection with their ligand potential, whether as bidentate chelating ligands, or as components of macrocycles when the substituents R are linked through successive ether or thioether units [9,10]. Where SR is SH they can be used as precursors to form [*closo*-$RC_2B_{10}H_{10}S]^-$ or [*closo*-$C_2B_{10}H_{10}S_2]^{2-}$ anionic residues [11–18]. They have also

* Corresponding author. Tel.: +0191 374 3138; fax: +0191 384 4734.
E-mail address: m.a.fox@durham.ac.uk (M.A. Fox).

0277-5387/$ - see front matter © 2005 Elsevier Ltd. All rights reserved.
doi:10.1016/j.poly.2005.06.046

been used as precursors from which [*nido*-$C_2B_9H_9(SR)_2]^{2-}$ anionic residues, offering yet further ligand potential, can be prepared [19–22].

Although many C–sulfur *ortho*-carboranes are now listed in the Cambridge Structural Database [23], it is perhaps surprising to find that there is only one reported compound, [$Cb^oSCb^oSiMe_2$] [24], in which two *ortho*-carboran-di-yl residues are linked through their carbon atoms by a single sulfur atom. This compound also contains a dimethylsilyl bridge between the two carboran-di-yl residues [24]. One other compound, $(MeCb^o)_2S$, with a sulfur bridge between *ortho*-carboranyl residues has been reported [4] but it was not structurally characterised.

In previous studies of the derivative chemistry of icosahedral carboranes, we have explored the effect on the 2-phenyl-*ortho*-carborane cage of the attachment of more strongly π-donor substituents to the cage hypercarbon atom C1 and found that the cage opens up from a *closo* to a near *nido* geometry as the *exo* bond order increases [25–27]. Our own published work so far has concentrated on one-cage systems and here we extend our investigation to the effect of one π-donating atom connected to *two ortho*-carborane cages. We prepared systems $(PhCb^o)_2X$ (X = S (**1**), S_2 (**2**) or SO (**3**)) in which the second cage carbon atom bore a phenyl substituent [26,28], choosing 2-phenyl-*ortho*-carborane derivatives because they generally form suitable crystals for X-ray crystallographic studies (over fifty such compounds have been structurally characterised) [29–34]. We also explored the synthesis of heterocyclic systems $(Cb^oY)_2$ (Y = S (**4**) or SO (**5**)) in which two C–S–C or C–S(O)–C bridges link pairs of *ortho* carborane icosahedra, and report calculated structures of (**4**) and (**5**). (See Fig. 1 for representative structures of (**1**)–(**5**).)

A very recent paper [35] by Viñas, Teixidor et al. on synthesis and structural characterisation of carborane mono- and di-sulfides appeared during submission of this work. While our synthetic route to the monosulfide differed from theirs, their structural findings and interpretations broadly agree with ours.

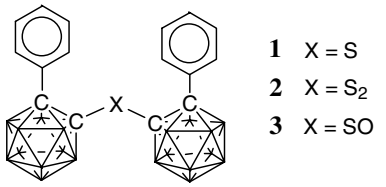

1 X = S
2 X = S_2
3 X = SO

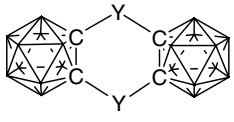

4 Y = S
5 Y = SO

Fig. 1. Representative structures of the title compounds (**1**)–(**5**).

2. Results and discussion

2.1. Preparative aspects

The new compounds (**1**) and (**3**) prepared in the present work were made from the lithio-carborane $PhCb^oLi$ with SCl_2 and $SOCl_2$, respectively, and characterised by NMR spectroscopic, elemental analytical and X-ray crystallographic study. To our knowledge, thionyl chloride has not been used to make carboranyl sulfur compounds previously. Compound **3** represents the first example containing an SO link between two *ortho*-carboranyl residues. It is easily reduced to compound **1** with hydrogen in the presence of palladium-carbon. It is, however, quite susceptible to deboronation. While compound **1** is stable in wet DMSO, compound **3** in wet DMSO gave a mixture of derivatives with *nido*-$C_2B_9H_{12}^-$ residues detected by NMR spectroscopy, and C–S cleavage was also evident. Some carboranyl derivatives are known to be susceptible to deboronation with mild solvents such as DMSO and alcohols [36–38]. Here, carboranes with C–S(O)R substituents were found to be much more susceptible to C–S bond cleavage and deboronation than those with C–SR substituents, as expected because the S(O)R residue is more electron-withdrawing than SR, facilitating nucleophilic attack on the most positive boron atom at B3 (or B6). The known compound **2** was made from $PhCb^oLi$ with sulfur and then oxidised with iodine [4].

Attempts to prepare and characterise (**4**) and (**5**), from reactions between dilithio-*ortho*-carborane and sulfur dichloride and thionyl chloride, respectively, were less successful in that, although the reactions appeared to proceed to formation of lithium chloride and the intended products (**4**) and (**5**) (obtained as colourless microcrystalline materials analysing correctly for the expected products), attempts to grow crystals suitable for X-ray characterisation were unsuccessful. Unlike **4**, compound **5** could not be purified further due to its facile deboronation and C–S bond cleavage with certain solvents.

2.2. Structural aspects

2.2.1. Systems $(PhCb^o)_2S$, $(PhCb^oS_2$, $(PhCb^oS)_2S$ and $(PhCb^o)_2SO$

Compounds **1**–**3**, like the related trisulfide $(PhCb^oS)_2S$ we have described elsewhere [27], all adopt orientations of their *exo*-SR units, and have cage C–C and *exo* C–S distances, consistent with significant dative S⇌C π-bonding from their *exo*-sulfur atoms to their cage hypercarbon atoms (see Figs. 2–4 and Table 1, which lists selected bond distances and angles for compounds **1**–**3** and the trisulfide $(PhCb^oS)_2S$). For compound **1** the *exo* bonds C–S–C lie in a plane roughly perpendicular to the C(2)–C(1)–S plane whereas for **2**,

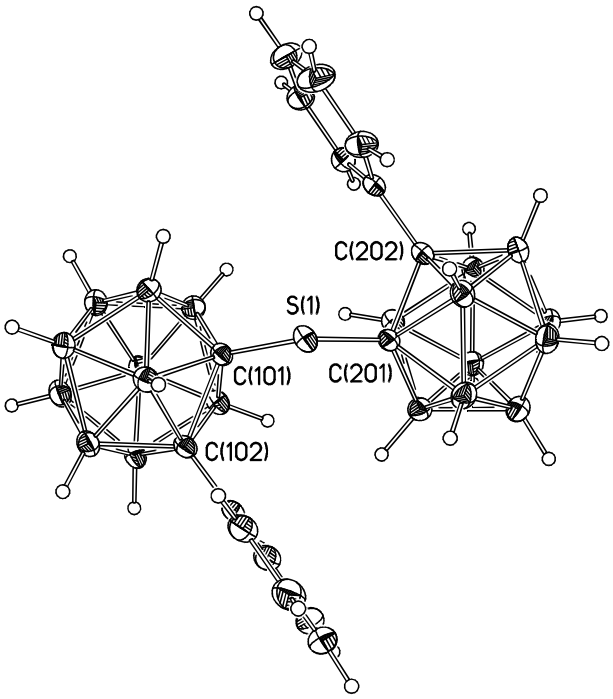

Fig. 2. Molecular structure of **1**, showing thermal ellipsoids at 50% probability level.

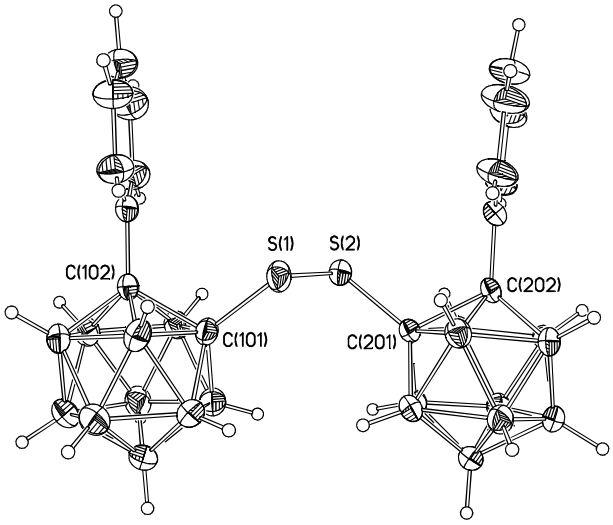

Fig. 3. Molecular structure of **2**.

3 and the trisulfide these bond orientations depart more from perpendicular (see torsion angle C–S–C/S in Table 1). We recently showed, in our discussion of a series of systems PhCb^{o}Z showing *exo* C⇐Z π-bonding (including the trisulfide (PhCb^{o}S)$_2$S), that such a perpendicular orientation optimised *exo* π-bonding [27].

The phenyl substituent on C(2) in compounds **2** and **3** also lies in a plane roughly perpendicular to the plane C(2)–C(1)–S, whereas in **1** and the trisulfide the orientations depart more from perpendicular. A perpendicular orientation minimises non-bonding repulsions with the

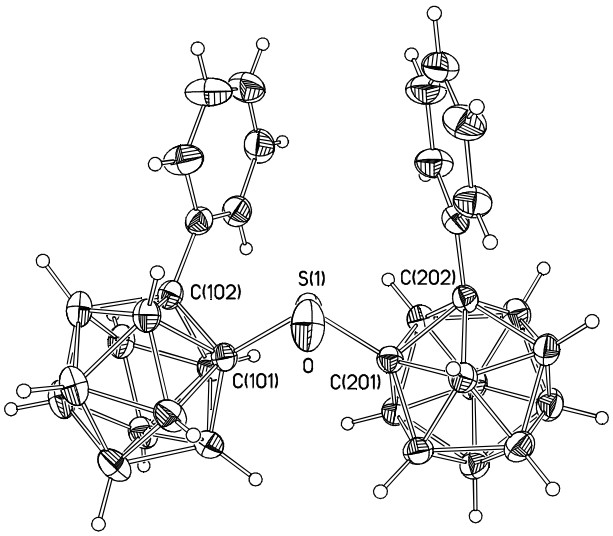

Fig. 4. Molecular structure of **3**.

other substituent on C(1), and maximises the opportunity for dative π-bonding from the π-system of the phenyl group to the carborane cage [39,40].

The cage carbon–carbon distance, C(1)–C(2), of *ortho* carborane is the cage edge link known to be most sensitive to the presence of π-bonding substituents on the cage hypercarbon atoms [27,41–43]. Its length increases as *exo* π-bonding increases. Steric effects have previously been invoked to explain the lengthening of the cage C–C bond in various disubstituted-*ortho*-carboranes [29–34]. In *ortho* carborane itself, HCb^{o}H, the C(1)–C(2) distance has been shown to be 1.62 Å by both X-ray studies of crystalline hydrogen-bonded adducts [44–47] and by gas-phase electron diffraction and calculational studies [48]. Attachment of a phenyl substituent to one carbon atom, oriented (as here) so that its ring plane is roughly perpendicular to the C(1)–C(2)–C(phenyl) plane, increases the cage C(1)–C(2) distance by some 0.04 Å to 1.66 Å [49]. In compound **2** (Table 1), where the orientations of the sulfur and phenyl substituents offer greater *exo* π-bonding effects compared to the trisulfide, the C(1)–C(2) distance is 1.755(4) Å. The sulfur atom lengthens the C(1)–C(2) bond distance by some 0.1 Å. The trisulfide has a shorter C(1)–C(2) bond distance of 1.735(3) Å, as expected for orientations of the substituents which lead to less effective *exo* π-bonding.

Surprisingly, compounds **1** and **2** have similar C(1)–C(2) and C(1)–S distances, suggesting a similar degree of S⇌C π-bonding in these two compounds. We had expected there to be weaker S⇌C π-bonding in **1**, where both carborane cages are attached to the same sulfur atom, and so competing for π-electron density from the same source. The C–S–C angle in **1** (112.8(1)°) is significantly greater than the C–S–S angle in **2** (105.5(2)°) which is due to steric repulsion between the two cages. Intramolecular B–H···H–B distances between the two

Table 1
Selected bond distances (Å) and angles (°) (averaged where variations are statistically insignificant) in X-ray structures of C–sulfur *ortho*-carboranes

Compound	$(PhCb^oS)_2S$ (**1**)[a]	$(PhCb^oS)_2S_2$ (**2**)[a]	$(PhCb^oS)_2S$[b]	$(PhCb^oS)_2SO$ (**3**)[a]	$PyCb^oSH$[c]	$PhCb^oSH$[b,d]
C(1)–C(2)	1.751(3)	1.755(4)	1.735(3)	1.729(3)	1.730(3)	1.729
C(1)–S	1.789(2)	1.796(3)	1.788(3)	1.859(2)	1.775(2)	1.782
C(2)–C(Ph)	1.510(3)	1.499(5)	1.499(3)	1.505(3)	1.507(3)[e]	1.495
C(1)–B(3)/(6)	1.725(10)[g]	1.709(5)	1.716(4)	1.722(10)[g]	1.720(3)	1.705
C(1)–B(4)/(5)	1.714(11)[g]	1.698(5)	1.702(7)[g]	1.700(3)	1.709(3)	1.700
C(2)–C(1)–S	116.1(2)	114.6(2)	115.9(2)	110.7(1)	117.7(1)	117.5
			117.6(2)	106.0(1)		
C(1)–S–E[f]	112.8(1)	105.5(1)	105.4(1)	106.2(1)	96(1)	95.1
C(2)–C(1)–S–E[f]	99.1(2)	108.0(2)	123.3(2)	−124.2(1)	99(2)	96.8
	97.1(2)	113.1(2)	−96.1(2)	160.4(1)		
C(1)–C(2)/Ph[h]	74.5(3)	81.7(3)	73.7(2)	87.6(1)	84.3(2)[e]	88.7
		88.9(3)		89.0(1)		

[a] This work.
[b] Ref. [27].
[c] Ref. [50], low-temperature structure.
[d] MP2/6-31G* calculation.
[e] Py for Ph.
[f] E = C (**1**, **3**), S (**2**).
[g] Shows statistically significant variations, individual e.s.d.'s 0.003–0.004 Å, which relate to the orientation of the group at sulfur.
[h] Calculated as the angle between the Ph (Py) ring and the C1–C2–C(Ph/Py) moiety.

cages are 2.27, 2.40 and 2.49 Å. Interestingly, the C(1)–C(2) bond in **2** is some 0.03 Å longer than in $PyCb^oSH$ (X-ray [50]) and $PhCb^oSH$ (calc [27]) which suggests that the disulfur bridge (S–S) is a more effective π-bond donor to the *ortho*-carborane cage than is a thiol (S–H) group.

The C(1)–C(2) and C(1)–S distances in compound **3**, $(PhCb^o)_2SO$ (Table 1), differ from those in **1** and **2**, though less than expected. The electron-withdrawing oxygen atom on the bridging sulfur atom in **3** was expected to reduce its capacity for S⇌C *exo* π-bonding relative to the lower oxidation state bridging sulfur atoms in **1** and **2**. Compound **3** appears to be affected (though to a lesser extent than **1**) by repulsive interactions between the cages; shortest intramolecular B–H···H–B contacts in **3** are 2.25 and 2.37 Å, and the C–S–C angle is 106.2(1). The *exo*-C–S bond distance in **3** is some 0.07 Å longer (less π-bonding) than that in **1**. Interestingly, **1** and **3** differ in their conformations, **1** is *trans* and **3** is *cis*. Besides our derivatives and those in the very recent report [35], only two neutral RCb^oSR' systems have been structurally characterised: HCb^oSpy [51] (Py = 2′-pyridyl) and $MeCb^oSPh$ [52] with C–S distances of 1.78 Å and cage C(1)–C(2) distances of 1.64 and 1.71 Å, respectively.

2.2.2. Systems $(Cb^oS)_2$ and $(Cb^oSO)_2$

Although our attempts to prepare crystalline samples of these species suitable for X-ray characterisation were unsuccessful, we carried out calculations to determine their likely structures, encouraged by our previous experience of the reliability of such calculations for calculating the structures of derivatives of *ortho*-carborane containing dative π-bonding substituents for which structures had separately been determined by X-ray studies [27]. Selected bond distances and angles are listed in Table 2, which also gives comparable bond distances and angles determined crystallographically for the compound $(Cb^oSCb^oSiMe_2)$ [24].

The C–C bond length of 1.62 Å in the calculated structure of **4** (see Fig. 5) is identical to that of parent *ortho*-carborane [48]. This may reflect both ring strain in the C_4S_2 heterocycle and inappropriate orientations of the bonds at sulfur for *exo* dative π-bonding to the cage C–C bond. The reported crystal structure of a related heterocycle, $Cb^oS_2C{=}S$, has a cage C–C bond length of 1.632(3) Å [53]. These lengths contrast with long cage C(1)–C(2) distances of 1.80 Å reported for neutral $Cb^o(SR)_2$ systems (R = Me or Ph) [43,54]. In **5**, the two SO moieties may exist in *trans* or the more stable *cis* configuration. The *cis*-configuration is lower by only 0.1 kcal mol^{-1}. As expected, the C–S distance in the sulfoxy compound is longer than that in the sulfide.

Table 2
Selected bond distances (Å) and angles for the compounds $(Cb^oSCb^oSiMe_2)$, $(Cb^oS)_2$ and $(Cb^oSO)_2$

Compound	$(Cb^oSCb^oSiMe_2)$[a]	$(Cb^oS)_2$ (**4**)[b]	$(Cb^oSO)_2$ (**5**)[b]	HCb^oH[c]
C(1)–C(2)	1.652(4)	1.621	1.637	1.62
C(1)–S	1.794(3)	1.800	1.873	
C(1)–B(3)/(6)	1.721(6)	1.734	1.716	1.71
C–S–C	111.2(2)	106.9	101.5	
C–C–S	126.2(3)	126.6	129.2	

[a] Ref. [24].
[b] This work, calculated at MP2/6-31G*.
[c] Refs. [44–48].

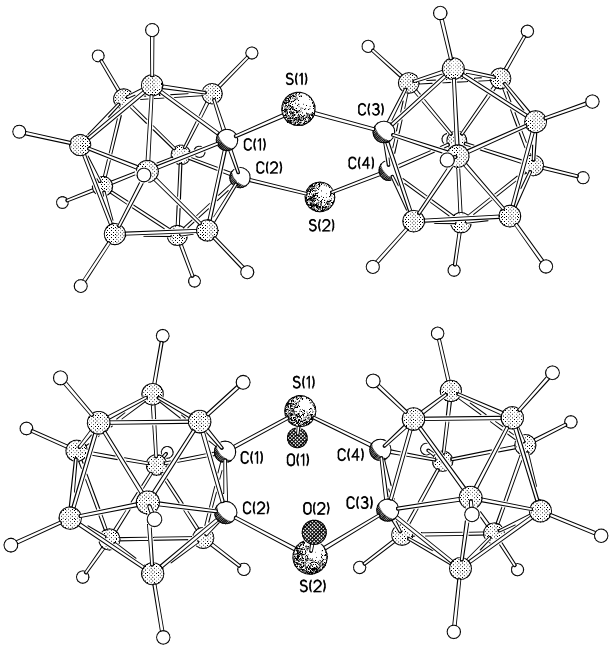

Fig. 5. MP2-optimised geometries for **4** and **5**.

3. Conclusions

The monosulfide $(PhCb^{o})_2S$ and sulfoxide $(PhCb^{o})_2SO$ in which two phenyl-*ortho*-carborane residues are linked at the cage carbon through a sulfur atom were synthesised simply by reactions of the lithio-*ortho*-carborane $PhCb^{o}Li$ with sulfur dichloride or thionyl chloride, respectively. Their structures show significant cage C(1)–C(2) bond lengthening relative to the parent carborane, an effect attributable mainly to π-bonding from the sulfur atom and to a lesser extent to π-bonding from the phenyl substituent. By contrast, the C(1)–C(2) bond lengths in the heterocyclic system $(Cb^{o}S)_2$, in which two C–S–C bridges link pairs of *ortho* carborane icosahedra, are calculated to be similar to the parent *ortho* carborane.

4. Experimental

4.1. General

All manipulations were carried out under dry, oxygen-free N_2. Commercial grade acetic acid, 10% palladium on carbon, SCl_2, $SOCl_2$ and *n*-butyllithium in hexanes were used without further purification. Dry Et_2O was obtained by reflux and distillation over Na wire. Demineralised water was used in the aqueous stages of syntheses. Compound **2** was prepared by the literature method [4].

Elemental analyses were performed using Exeter Analytical CE-440 apparatus. ^{1}H, ^{11}B, ^{13}C NMR spectra were recorded from room-temperature solutions on a Varian Unity 300 MHz spectrometer equipped with the appropriate decoupling accessories. Chemical shift values for ^{11}B NMR spectra were referenced to external $BF_3 \cdot OEt_2$, those for ^{1}H- and $^{13}C\{^{1}H\}$ NMR spectra were referenced to $SiMe_4$. ^{1}H NMR spectra were referenced to residual protio impurity in the solvent ($CDCl_3$, 7.26 ppm). ^{13}C NMR spectra were referenced to the solvent resonance ($CDCl_3$, 77.0 ppm). Chemical shifts are reported in units of parts per million downfield from reference. Mass spectra (MS) were recorded on a VG Micromass 7070E instrument under E.I conditions (EI) at 70 eV.

4.2. Preparation of *1*

Phenyl-*ortho*-carborane (0.71 g, 3.2 mmol) was dissolved in diethyl ether (20 ml) and BuLi (2.4 ml of 1.6 M solution in hexane, 3.8 mmol) was added under a nitrogen atmosphere at 0 °C. Sulfur dichloride (0.1 ml, 1.6 mmol) in diethyl ether (5 ml) was added. The solution was stirred at ambient temperature for 2 h. The solution was diluted with ether (60 ml). A white precipitate (0.22 g) was filtered off. The solution was washed with water (3×50 ml) and dried over $MgSO_4$. The solvent was removed under reduced pressure to yield white crystals. The crystals were washed with 60–80° petroleum ether to remove unreacted carborane, then recrystallised from a 50:50 benzene–hexane mixture (0.36 g, 49%). M.p. 237 °C. *Anal*. Calc. for $C_{16}H_{30}B_{20}S$: C, 40.8; H, 6.4. Found: C, 41.0; H, 6.5%. EI-MS 452–476 (with characteristic carborane isotope pattern). δ_H 7.6–7.2 (phenyl), 3.8–0.8 (BH). δ_B −1.3 (1B), −3.2 (1B), −9.8 (6B), −12.0 (2B).

4.3. Preparation of *3*

To a solution of 1-phenyl-*ortho*-carborane (925 mg, 4.2 mmol) in dry ether (40 ml) at 0 °C was added *n*BuLi in hexanes (1.6 ml, 2.7 M, 4.2 mmol), and this was stirred under N_2 for 1 h. $SOCl_2$ (0.19 ml, 2.1 mmol) was added, forming a white precipitate (LiCl). After warming to room temperature, the solid was removed by filtration, and the ether evaporated, leaving a white solid. Pure **3** was obtained by recrystallisation from a mixture of ethyl acetate and cyclohexane (1:9), affording colourless crystals. (0.35 g, 34%). M.p. 262 °C. *Anal*. Calc. for $C_{16}H_{30}B_{20}SO$: C, 39.5; H, 6.2. Found: C, 39.7; H, 6.3%. EI-MS 484-489 (with characteristic carborane isotope pattern). δ_H 7.4–7.2 (phenyl), 3.8–0.8 (BH). δ_B 1.5 (1B), −3.1 (1B), −8.6 (6B), −11.7 (2B). δ_C 131.9, 131.3, 128.8, 128.5, 92.3, 87.3.

4.4. Reduction of *3*

Hydrogen gas was slowly bubbled through a stirred suspension of **3** (84 mg, 0.17 mmol) and 10% palladium

on carbon (15 mg) in acetic acid (10 ml) for 15 h. Removal of the solvent from the filtered solution gave crystalline **1** (54 mg, 66%).

4.5. Preparation of **4**

ortho-Carborane (1.11 g, 7.72 mol) was dissolved at 0 °C in dry ether (30 ml) under N_2 and *n*BuLi in hexanes (6.4 ml, 2.42 M, 15.4 mmol) was added, precipitating white 1,2-dilithio-*ortho*-carborane. After 15 min stirring, SCl_2 (0.50 ml, 811 mg, 7.9 mmol) was added and the reaction was left to warm to room temperature over 1 h. Water (30 ml) was added and the ether layer was further washed before being isolated and dried over $MgSO_4$. Filtration and removal of the solvent gave a white solid which was sublimed in vacuo at 40 °C to remove unreacted *ortho*-carborane, then at 100 °C to give a white powder identified as pure **4**. 73.6 mg (5%). M.p. 122 °C. *Anal*. Calc. for $C_4H_{20}B_{20}S_2$: C, 13.8; H, 5.8. Found: C, 14.0; H, 5.9%. EI-MS, 346–352 (typical carborane isotope pattern).

4.6. Attempted synthesis of **5**

Ortho-carborane (0.723 g, 5.02 mmol), was dissolved at 0 °C under N_2 in dry ether (30 ml) and *n*BuLi in hexanes (4.3 ml, 2.42 M, 10.4 mmol) was added, precipitating white 1,2-dilithio-*ortho*-carborane. After 15 min stirring, $SOCl_2$ (0.37 ml, 5.07 mmol) was added and the reaction was left to warm to room temperature overnight. Water (30 ml) was added, dissolving the nascent LiCl, and the ether layer was washed with further water (2×30 ml) before being isolated and dried over $MgSO_4$. Removal of the solvent in vacuo gave a white solid. This was sublimed in vacuo at 50 °C to remove unreacted *ortho*-carborane. The unsublimed material contained **5**, based on mass spectroscopy with a carborane peak pattern observed at 375–381 (EI-MS). Purification attempts of the white powder (458 mg) were unsuccessful – several solvents were shown by boron NMR spectroscopy to degrade the carborane cages.

4.7. Crystallography

Single-crystal diffraction experiments (Table 3) for **1** and **3** were carried out on a Rigaku AFC6S 4-circle diffractometer, for **2** on a Stoe STADI4 4-circle diffractometer using graphite-monochromated Mo Kα (**1**) and Cu Kα (**2**, **3**) radiation. The structures were solved by direct methods and refined by full-matrix least-squares methods with F^2 of all unique data, using SHELXTL software. Hydrogen atoms positions were freely refined (except for the phenyl groups in **3**, in which they were constrained with a riding model). Structure **2** has been reported elsewhere [35]. The non-standard unit cell setting used in that report can be transformed by the operation $(001, \bar{1}00, 0\bar{1}0)$ to give the reduced cell $a = 10.511(5)$ Å, $b = 11.579(3)$ Å, $c = 12.917(4)$ Å, $\alpha = 85.09(3)°$, $\beta = 69.05(3)°$, $\gamma = 77.72(3)°$. The volume of this cell (1434.5(9) Å^3) is ca. 0.8% larger than found by us, although both experiments were carried out at room temperature. Our data gave rather lower residual electron density peaks near the sulfur atoms, but these can be successfully refined also as part of a very minor disorder component, with an occupancy of 0.059(3), similar to that recently reported. This disorder has no significant effect on the geometry of the molecule. Overall our results are of greater precision. Full crystallographic data, excluding structure factors, have been deposited at the Cambridge Crystallographic Data Centre, CCDC Nos. 269295, 269296 and 269297.

Table 3
Crystallographic data

	1	**2**	**3**
Chemical formula	$C_{16}H_{30}B_{20}S$	$C_{16}H_{30}B_{20}S_2$	$C_{16}H_{30}B_{20}OS$
Formula weight	470.7	502.7	486.7
T (K)	150	293	296
λ (Å)	0.71073	1.54184	1.54178
Crystal system	monoclinic	triclinic	triclinic
Space group	$P2_1/n$	$P\bar{1}$	$P\bar{1}$
Unit cell dimensions			
a (Å)	10.806(2)	10.475(1)	9.783(1)
b (Å)	17.727(4)	11.549(1)	10.360(1)
c (Å)	13.916(3)	12.900(1)	15.167(1)
α (°)	90	85.070(5)	91.94(1)
β (°)	97.81(3)	69.041(6)	95.61(1)
γ (°)	90	77.637(5)	116.10(1)
V, (Å^3)	2641(1)	1423.5(2)	1368.7(2)
Z	4	2	2
D_{calc} (g cm^{-3})	1.184	1.173	1.181
μ (mm^{-1})	0.13	1.72	1.11
Reflections collected	6644	3569	5900
Independent reflections	6325	3569	4999
R_{int}	0.030		0.018
R (F, $F^2 > 2\sigma$)	0.060	0.046	0.049
R_w (F^2, all data)	0.234	0.132	0.131
Goodness-of-fit on F^2	1.05	1.06	1.08
El. density extremes (e Å^{-3})	0.60, −0.49	0.18, −0.27	0.31, −0.42

4.8. Computational section

The ab initio computations were carried out with the GAUSSIAN 03 package [55]. The geometries of **4** and **5** (*cis* and *trans*) were optimised at the HF/6-31G* level with no symmetry constraints. Frequency calculations were computed on these optimised geometries at the HF/6-31G* level and revealed no imaginary frequencies. Optimisation of these geometries were then carried out at the MP2/6-31G* level. Total energies at MP2/6-31G* are −1454.57589 a.u. for **4** and −1604.55461 (*trans*) and −1604.55479 (*cis*) for **5**. The C_4S_2 rings in these geometries are planar.

Appendix A. Supplementary data

Supplementary data associated with this article can be found, in the online version at doi:10.1016/j.poly.2005.06.046.

References

[1] H.D. Smith Jr., C.O. Obenland, S. Papetti, Inorg. Chem. 5 (1966) 1013.
[2] N.S. Semenuk, S. Papetti, H. Schroeder, Inorg. Chem. 8 (1969) 2441.
[3] L.I. Zakharkin, G.G. Zhigareva, Zh. Obshch. Khim. 37 (1967) 2781.
[4] L.I. Zakharkin, G.G. Zhigareva, Izv. Akad. Nauk SSSR, Ser. Khim. (1967) 1358.
[5] J. Plešek, S. Heřmanek, Coll. Czech. Chem. Commun. 46 (1981) 687.
[6] C. Viñas, R. Benakki, F. Teixidor, J. Casabó, Inorg. Chem. 34 (1995) 3844.
[7] F. Teixidor, C. Viñas, R. Benakki, R. Kivekäs, R. Sillanpää, Inorg. Chem. 36 (1997) 1719.
[8] F. Teixidor, C. Viñas, J. Casabó, A.M. Romerosa, J. Rius, C. Miravitlles, Organometallics 13 (1994) 914.
[9] F. Teixidor, C. Viñas, J. Rius, C. Miravitlles, J. Casabó, Inorg. Chem. 29 (1990) 149.
[10] F. Teixidor, A.M. Romerosa, J. Rius, C. Miravitlles, J. Casabó, C. Viñas, E. Sanchez, J. Chem. Soc., Dalton Trans. (1990) 525.
[11] For examples, see M. Herberhold, H. Yan, W. Milius, B. Wrackmeyer, Chem. Eur. J. 8 (2002) 388.
[12] D.-H. Kim, J. Ko, K. Park, S. Cho, S.O. Kang, Organometallics 18 (1999) 2738.
[13] X.-Y. Yu, G.-X. Jin, N.-H. Hu, L.-H. Weng, Organometallics 21 (2002) 5540.
[14] O. Crespo, M.C. Gimeno, P.G. Jones, A. Laguna, J. Chem. Soc., Chem. Commun. (1993) 1696.
[15] J.-H. Won, H.-G. Lim, B.Y. Kim, J.-D. Lee, C. Lee, Y.-J. Lee, S. Cho, J. Ko, S.O. Kang, Organometallics 21 (2002) 5703.
[16] O. Crespo, M.C. Gimeno, P.G. Jones, A. Laguna, J. Chem. Soc., Dalton Trans. (1997) 1099.
[17] J.D. McKinney, H. Chen, T.A. Hamor, K. Paxton, C.J. Jones, J. Chem. Soc., Dalton Trans. (1998) 2163.
[18] M. Herberhold, H. Yan, W. Milius, B. Wrackmeyer, Angew. Chem., Int. Ed. Engl. 38 (1999) 3689.
[19] F. Teixidor, J.A. Ayllon, C. Viñas, J. Rius, C. Miravitlles, J. Casabó, J. Chem. Soc., Chem. Commun. (1992) 1279.
[20] F. Teixidor, J. Casabó, C. Viñas, E. Sanchez, R. Kivekäs, L. Escriche, Inorg. Chem. 30 (1991) 3053.
[21] F. Teixidor, J.A. Ayllon, C. Viñas, R. Sillanpää, R. Kivekäs, J. Casabó, Inorg. Chem. 33 (1994) 4815.
[22] F. Teixidor, J.A. Ayllon, C. Viñas, R. Kivekäs, R. Sillanpää, J. Casabó, Inorg. Chem. 33 (1994) 1756.
[23] Search on the Cambridge Structural Database (CSD Version 5.26) February 2005. See F.H. Allen, Acta Crystallogr., Sect. B 58 (2002) 380.
[24] L.I. Zakharkin, N.F. Shemyakin, A.V. Polyakov, A.I. Yanovskii, Y.T. Struchkov, Zh. Obshch. Khim. 57 (1987) 611.
[25] D.A. Brown, W. Clegg, H.M. Colquhoun, J.A. Daniels, I.R. Stephenson, K. Wade, J. Chem. Soc., Chem. Commun. (1987) 889.
[26] R. Coult, M.A. Fox, W.R. Gill, K. Wade, W. Clegg, Polyhedron 11 (1992) 2717.
[27] L.A. Boyd, W. Clegg, R.C.B. Copley, M.G. Davidson, M.A. Fox, T.G. Hibbert, J.A.K. Howard, A. Mackinnon, R.J. Peace, K. Wade, Dalton Trans. (2004) 2786.
[28] W. Clegg, H.M. Colquhoun, R. Coult, M.A. Fox, W.R. Gill, P.L. Herbertson, J.A.H. MacBride, K. Wade, Spec. Publ. – R. Soc. Chem. 143 (1994) 232.
[29] Z.G. Lewis, A.J. Welch, Acta Cryst. C 49 (1993) 705.
[30] T.D. McGrath, A.J. Welch, Acta Cryst. C 51 (1995) 646.
[31] T.D. McGrath, A.J. Welch, Acta Cryst. C 51 (1995) 651.
[32] T.D. McGrath, A.J. Welch, Acta Cryst. C 51 (1995) 654.
[33] T.D. McGrath, A.J. Welch, Acta Cryst. C 51 (1995) 649.
[34] R.L. Thomas, A.J. Welch, Polyhedron 18 (1999) 1961.
[35] A. Laromaine, F. Teixidor, R. Kivekäs, R. Sillanpää, R. Benakki, B. Grüner, C. Viñas, Dalton Trans. (2005) 1785.
[36] F. Teixidor, P. Angles, C. Viñas, Inorg. Chem. 38 (1999) 3605.
[37] J.J. Schaeck, S.B. Kahl, Inorg. Chem. 38 (1999) 204.
[38] Y.-J. Lee, J.-D. Lee, J. Ko, S.-H. Kim, S.O. Kang, Chem. Commun. (2003) 1364.
[39] W. Clegg, R. Coult, M.A. Fox, W.R. Gill, J.A.H. MacBride, K. Wade, Polyhedron 12 (1993) 2711.
[40] R. Kivekas, R. Sillanpaa, F. Teixidor, C. Viñas, R. Nuñez, Acta Cryst. Sect. C C50 (1994) 2027.
[41] L.A. Boyd, H.M. Colquhoun, M.G. Davidson, M.A. Fox, W.R. Gill, P.L. Herbertson, T.G. Hibbert, J.A.H. MacBride, R.J. Peace, G.P. Rivers, K. Wade, Spec. Publ. – R. Soc. Chem. 201 (1997) 289.
[42] F. Teixidor, C. Viñas, A. Demonceau, R. Nuñez, Pure Appl. Chem. 75 (2003) 1305.
[43] J. Llop, C. Viñas, J.M. Oliva, F. Teixidor, M.A. Flores, R. Kivekäs, R. Sillanpää, J. Organomet. Chem. 657 (2002) 232.
[44] M.G. Davidson, T.G. Hibbert, J.A.K. Howard, A. Mackinnon, K. Wade, Chem. Commun. (1996) 2285.
[45] R.J. Blanch, M. Williams, G.D. Fallon, M.G. Gardiner, R. Kaddour, C.L. Raston, Angew. Chem., Int. Ed. Engl. 36 (1997) 504.
[46] M.J. Hardie, C.L. Raston, Cryst. Eng. Commun. 3 (2001) 162.
[47] M.A. Fox, A.K. Hughes, Coord. Chem. Rev. 248 (2004) 457.
[48] A.R. Turner, H.E. Robertson, K.B. Borisenko, D.W.H. Rankin, M.A. Fox, Dalton Trans. (2005) 1310.
[49] E.S. Alekseyeva, M.A. Fox, J.A.K. Howard, J.A.H. MacBride, K. Wade, Appl. Organomet. Chem. 17 (2003) 499.
[50] A.S. Batsanov, M.A. Fox, T.G. Hibbert, J.A.K. Howard, R. Kivekäs, A. Laromaine, R. Sillanpää, C. Viñas, K. Wade, Dalton Trans. (2004) 3822.
[51] O. Crespo, M.C. Gimeno, A. Laguna, Polyhedron 18 (1999) 1279.
[52] R. Kivekäs, M.A. Flores, C. Viñas, R. Sillanpää, Acta Cryst. Sect. C58 (2002) o570.
[53] J.D. McKinney, T.A. Hamor, C.J. Jones, K. Paxton, Polyhedron 16 (1997) 1819.
[54] A. Laromaine, C. Viñas, R. Sillanpää, R. Kivekäs, Acta Cryst., Sect. C60 (2004) o524.
[55] M.J. Frisch, G.W. Trucks, H.B. Schlegel, G.E. Scuseria, M.A. Robb, J.R. Cheeseman, J.A. Montgomery Jr., T. Vreven, K.N. Kudin, J.C. Burant, J.M. Millam, S.S. Iyengar, J. Tomasi, V. Barone, B. Mennucci, M. Cossi, G. Scalmani, N. Rega, G.A. Petersson, H. Nakatsuji, M. Hada, M. Ehara, K. Toyota, R. Fukuda, J. Hasegawa, M. Ishida, T. Nakajima, Y. Honda, O. Kitao, H. Nakai, M. Klene, X. Li, J.E. Knox, H.P. Hratchian, J.B. Cross, C. Adamo, J. Jaramillo, R. Gomperts, R.E. Stratmann, O. Yazyev, A.J. Austin, R. Cammi, C. Pomelli, J.W. Ochterski, P.Y. Ayala, K. Morokuma, G.A. Voth, P. Salvador, J.J. Dannenberg, V.G. Zakrzewski, S. Dapprich, A.D. Daniels, M.C. Strain, O. Farkas, D.K. Malick, A.D. Rabuck, K. Raghavachari, J.B. Foresman, J.V. Ortiz, Q. Cui, A.G. Baboul, S. Clifford, J. Cioslowski, B.B. Stefanov, G. Liu, A. Liashenko, P. Piskorz, I. Komaromi, R.L. Martin, D.J. Fox, T. Keith, M.A. Al-Laham, C.Y. Peng, A. Nanayakkara, M. Challacombe, P.M.W. Gill, B. Johnson, W. Chen, M.W. Wong, C. Gonzalez, J.A. Pople, GAUSSIAN 03, Revision C.02, Gaussian, Inc., Wallingford, CT, 2004.

Available online at www.sciencedirect.com
SCIENCE DIRECT®
Polyhedron 25 (2006) 307–324
POLYHEDRON
www.elsevier.com/locate/poly

Mesomorphic silver(I) complexes of polycatenar 2′- and 3′-stilbazoles. Crystal and molecular structure of 3,4-dimethoxy-3′-stilbazole and of two silver triflate complexes

Deborah M. Huck [b,d], H. Loc Nguyen [d], Peter N. Horton [c], Michael B. Hursthouse [c], Daniel Guillon [b], Bertrand Donnio [*,b], Duncan W. Bruce [a,*]

[a] Department of Chemistry, University of York, Heslington, York Y10 5DD, UK
[b] IPCMS-GMO, 23, Rue de Loess UMR7504 (CNRS-ULP), 67037 Strasbourg Cedex, France
[c] EPSRC Crystallographic Service, Department of Chemistry, University of Southampton, Highfield, Southampton SO17 1BJ, UK
[d] Department of Chemistry, University of Exeter, Stocker Road, Exeter EX4 4QD, UK

Received 14 June 2005; accepted 12 July 2005
Available online 12 September 2005

Dedicated to Malcolm Chisholm on the occasion of his sixtieth birthday.

Abstract

The synthesis of 3,4-dialkoxy and 3,4,5-trialkoxy derivatives of 2- and 3-stilbazole are reported along with their related complexes with silver dodecylsulphate and silver triflate. The single crystal structures of one ligand and two complexes are reported. While none of the complexes of the 2-stilbazoles is liquid-crystalline, several complexes of the 3-stilbazoles show columnar mesophases as characterised by polarised optical microscopy and X-ray diffraction. The liquid crystal phase behaviour is compared with that of the parent 4-stilbazole derivatives.
© 2005 Elsevier Ltd. All rights reserved.

Keywords: Metallomesogen; Silver; Stilbazole; Polycatenar; Liquid crystal

1. Introduction

The study of metallomesogens [1,2] represents a major subject within liquid crystals that has developed strongly within the last twenty years or so. Large swathes of the periodic table have been investigated and a very large number of different elements have been incorporated into mesomorphic systems in one way or another. In a developing area such as this, there is a simultaneous need constantly to discover new systems, perhaps targeted because of particular properties, and to undertake systematic structure/function studies in order to determine how the properties of the new systems may be compared with and understood in relation to the existing literature. Both approaches have been adopted in the study of metallomesogens, and one feature of the latter has been the extra structural flexibility offered on account of the coordination around the metal under study.

Our own work has contributed to both approaches to the subject, but in particular regard to the latter, systematic approach, we have engaged extensively with the liquid crystal behaviour of stilbazoles in areas such as hydrogen- [3] and halogen- [4] bonding as well in combination with metals [5]. In particular, we have looked at both calamitic and polycatenar *bis*(ligand) metal complexes of Pd, Pt [6] and Ag [7] and have looked at how

* Corresponding author. Tel.: +44 1904 264188; fax: +44 1904 432516.
E-mail addresses: db519@york.ac.uk, d.bruce@exeter.ac.uk (D.W. Bruce).

0277-5387/$ - see front matter © 2005 Elsevier Ltd. All rights reserved.
doi:10.1016/j.poly.2005.07.023

control may be exercised over the nature of the phase formed, particularly in relation to the formation of the cubic phase [8], and the lamellar-to-columnar transition in polycatenar systems [9].

Within these studies, silver(I) complexes have offered the greatest opportunity for systematic evaluation due both to the availability of a range of stilbazoles and to the fact that the complexes are formally ionic making different anions available. In our initial work with 4-alkoxy-4′-stilbazoles (**1**, Fig. 1) we examined a range of counter-anions, but as the work progressed to complexes of di- and tri-alkoxy stilbazoles (**2**, **3** and **4**, Fig. 1), we settled on studies using triflate and alkyl sulphates (mainly dodecylsulphate).

Having investigated the effect of ligand chain substitution on these systems, more recently we turned our attention to varying the structure of the core by synthesising silver(I) complexes of a range of 4-alkoxy-2′- and 3′-stilbazoles (**5** and **6**, Fig. 2) [10]. Whereas with complexes of the 4-stilbazoles we had found polymorphism that included nematic and cubic phases, these isomeric systems showed a much more limited mesomorphism and only the SmA phase was seen.

In order to complete this study, we then turned our attention to polycatenar [11,12] systems. Our previous investigations had shown that the 3,4-tetracatenar complexes with DOS anions (**2a**) showed a progression from cubic to columnar (Col_h) phase as *n* increased, as did the related triflate complexes (**2b**) but at longer chain lengths. These results are consistent with arguments that invoke surface curvature as a driving force for this transition by analogy with the behaviour of lyotropic materials [9,13]. The mesomorphism of the 3,5-tetracatenar complexes (**3a**,**b**) and the hexacatenar complexes (**4a,b**) was dominated by the formation of columnar phases [14]. We have, therefore, undertaken the synthesis of 3,4-dialkoxy and 3,4,5-trialkoxy derivatives of 3′- and 2′-stilbazole, and have synthesised their complexes with silver(I). This work, along with the characterisation of the mesomorphism by optical microscopy and X-ray diffraction, is now described.

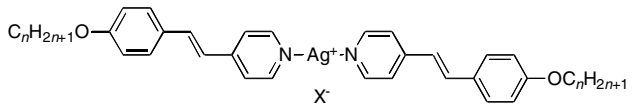

1a: X = BF_4
1b: X = NO_3
1c: X = CF_3SO_3 (OTf)
1d: X = $C_8H_{17}OSO_3$ (OS)
1e: X = $C_{12}H_{25}OSO_3$ (DOS)

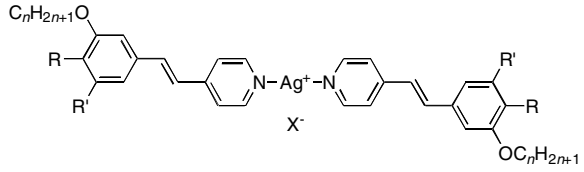

2a: R = $C_nH_{2n+1}O$, R' = H, X = $C_{12}H_{25}OSO_3$ (DOS)
2b: R = $C_nH_{2n+1}O$, R' = H, X = CF_3SO_3 (OTf)
3a: R = H, R' = $C_nH_{2n+1}O$, X = $C_{12}H_{25}OSO_3$ (DOS)
3b: R = H, R' = $C_nH_{2n+1}O$, X = CF_3SO_3 (OTf)
4a: R = R' = $C_nH_{2n+1}O$, X = $C_{12}H_{25}OSO_3$ (DOS)
4b: R = R' = $C_nH_{2n+1}O$, X = CF_3SO_3 (OTf)

Fig. 1. Calamitic (**1**) and polycatenar (**2**, **3** and **4**) silver(I) complexes of 4-stilbazoles.

2. Synthesis

In previous studies where stilbazoles had been used, we had employed either Heck coupling methodologies [15] or condensation reactions [3b], but in the present case, neither was particularly effective. Thus, here we employed a Siegrist methodology [16,17] in which a benzylidene group (derived from an imine) is transferred to an aromatic aldehyde function leading to a 1,2-diarylethene with high stereoselectivity. The approach, which we have used recently in the construction of prototypical dendrimers [18], and has been used in the synthesis of related stilbazole systems [19], is very effective and allowed access to the desired materials in good yield as indicated in Scheme 1.

Thus, 3,4-dialkoxybenzaldehyde (from 3,4-dihydroxybenzaldehyde and the appropriate 1-bromoalkane) [13] was reacted with aniline in ethanol to give *N*-phenyl-3,4-dialkoxybenzaldimine in isolated yields of 89–97%. The imine, which was used without further purification, was then treated with either 3- or 2-picoline in dimethylformamide in the presence of an excess of potassium *tert*-butoxide to yield 3,4-dialkoxy-3′-stilbazole (**7**) or 3,4-dialkoxy-2′-stilbazole (**8**), respectively, as colourless solids

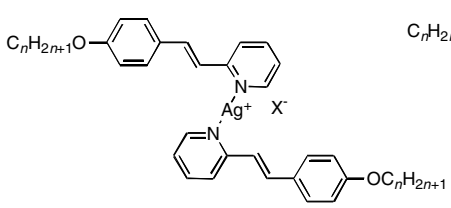

5: X = $C_{12}H_{25}OSO_3$ (DOS)

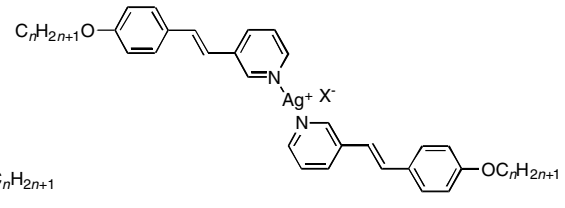

6a: X = $C_{12}H_{25}OSO_3$ (DOS)
6b X = CF_3SO_3 (OTf)

Fig. 2. Structure of calamitic silver(I) complexes of 2- and 3-stilbazoles.

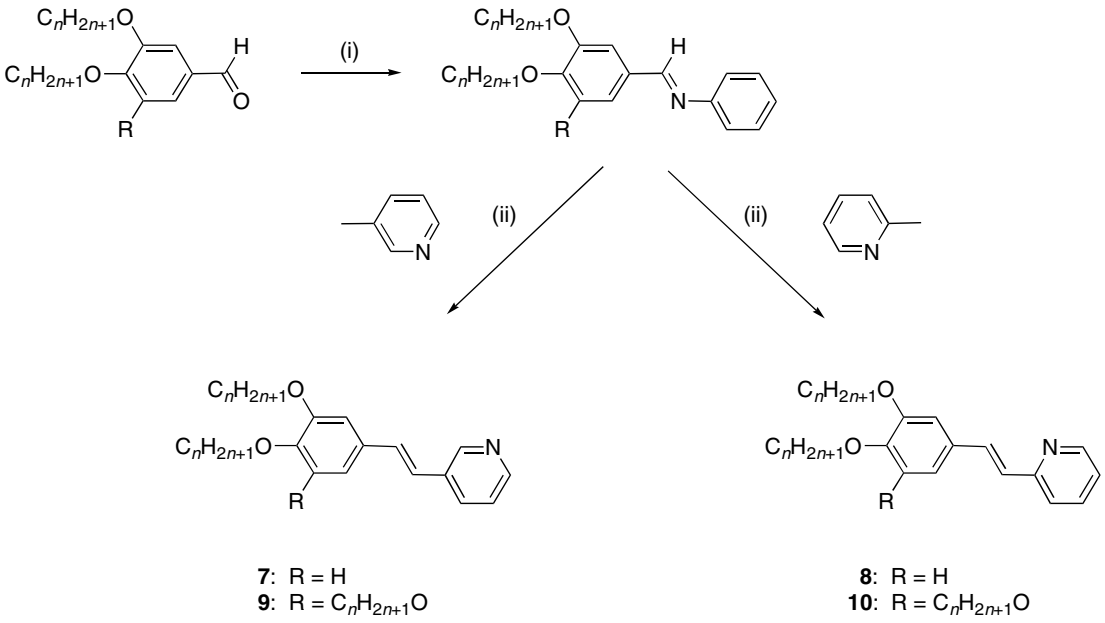

Scheme 1. Synthesis of the new stilbazole ligands: (i) Ph–NH_2/EtOH/TsOH (cat); (ii) KO^{t}Bu/DMF (ligands are identified in the text as, e.g., **8**-*n*, where *n* refers to the number of carbons in the alkoxy chain).

in moderate-to-good yields (over 53–88%) after purification by column chromatography on silica gel and crystallisation from hot hexane. The *trans* nature of the two isomeric compounds was confirmed by the ^{1}H NMR spectra with coupling constants of the AB systems of around 16 Hz. 3,4,5-Trialkoxystilbazoles (**9** and **10**) were prepared similarly from 3,4,5-trialkoxybenzaldehyde [14].

The silver(I) dodecylsulfate complexes of all four ligands were prepared by stirring the appropriate stilbazole with silver(I) dodecylsulfate in dichloromethane at room temperature in the dark for 4 h, yielding complexes **11a**, **12a**, **13a** and **14a**, respectively (Fig. 3). The silver(I) triflate complexes were similarly accessed using acetone as solvent to give complexes **11b**, **12b**, **13b** and **14b** (Fig. 3) in good yield.

2.1. Crystal and molecular structure of 3,4-dimethoxy-3′-stilbazole and of complexes *11b-1* and *11b-4*

In order to obtain more detailed information about the conformation of these new polycatenar stilbazoles and some of their complexes, 3,4-dimethoxy-3′-stilbazole was prepared and single crystals grown successfully by crystallisation from hexane. Single crystals of the silver triflate complex of this ligand (**11b-1**) and of the related 3,4-butyloxy-3′-stilbazole (**11b-4**) were also obtained from dichloromethane/methanol and from hot hexane, respectively. Crystallographic data are collected in Table 1.

2.1.1. 3,4-Dimethoxy-3′-stilbazole (7-1)

Two views of the structure are shown in Fig. 4. The molecular structure consists of two essentially planar moieties, namely, the pyridine ring (N1, C1 to C5) bonded *trans* across a C=C double bond to a 3,4-dimethoxystyryl group (C8 to C13, O1, C14, O2, C15). The planar fragments are related by a dihedral angle of 20.9(3)°. Although there are four possible 'planar' conformations about the trans double bond (180° rotations of the pyridyl and dimethoxyphenyl rings), only one is observed in the crystal structure.

2.1.2. Bis(3,4-dimethoxy-3′-stilbazole)silver(I) triflate (*11b-1*)

Two views of the structure are shown in Fig. 5. The molecular structure is quite complex, with two conformationally differing silver complexes in the asymmetric unit. Here three of the 3,4-dimethoxy-3′-stilbazole ligands (labelled **A**, **B** and **C**) adopt the same basic conformation as observed for **7-1**, but with slightly varying degrees of twist (16.1(4)°, 13.2(4)°, 14.7(5)°). The fourth (labelled **D**) has the pyridyl group rotated by 180° about the C64–C66 bond with respect to the other ligands. It still has adopts a similar twist (15.5(4)°). Although there are no Ag–Ag close contacts, there are Ag–$O_{triflate}$ contacts ranging from 2.84(1)–3.13(1) Å. These are similar, if a touch longer, than those found in known silver triflate complexes. In fact the triflate anions act as bridges between the two differing silver complexes with the third oxygen of each triflate co-ordinating towards the disordered water molecule. This results in an infinite slipped stack (Fig. 6).

2.1.3. Bis(3,4-dibutyloxy-3′-stilbazole)silver(I) triflate (*11b-4*)

Two views of the structure are shown in Fig. 7 and structural refinement parameters and crystal data are

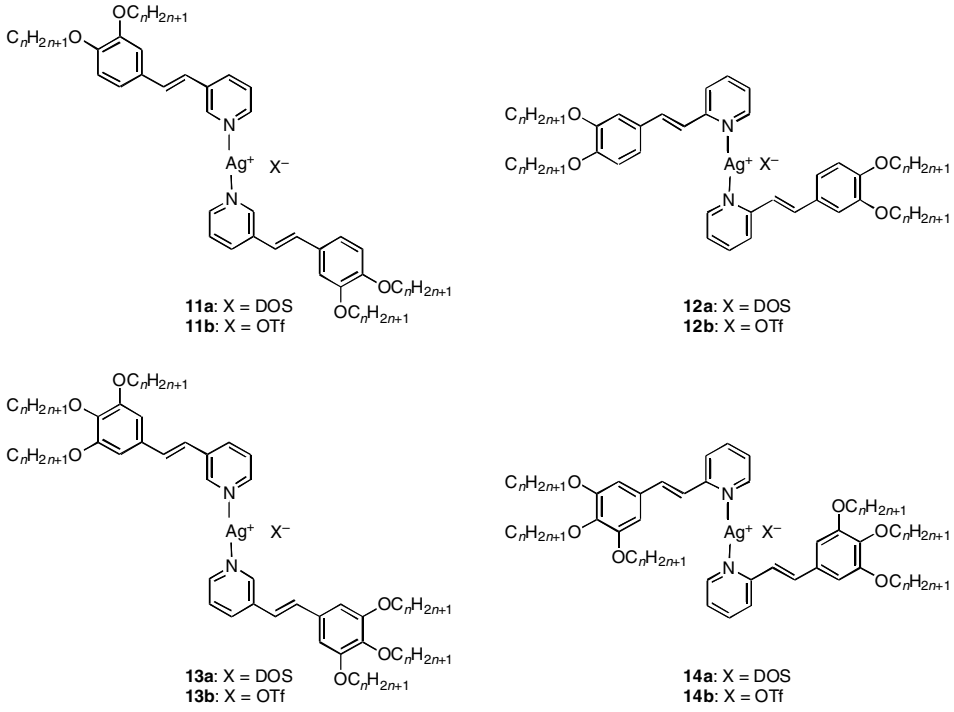

Fig. 3. Structure of the new silver stilbazole complexes (complexes are identified in the text as, e.g., **14a**-*n*, where *n* refers to the number of carbons in the alkoxy chain).

Table 1
Crystallographic data for **7**-1, **11b**-1 and **11b**-4

	Compound **7**-1	Compound **11b**-1	Compound **11b**-4
Empirical formula	$C_{15}H_{15}NO_2$	$C_{62}H_{61}Ag_2F_6N_4O_{15}S_2$	$C_{86}H_{108}Ag_2F_6N_4O_{14}S_2$
Formula weight (g mol^{-1})	241.28	1496.01	1815.62
Temperature (K)	298(2)	120(2)	120(2)
Crystal system	orthorhombic	monoclinic	triclinic
Space group	*Pbca*	*Cc*	$P\bar{1}$
Unit cell dimensions			
a (Å)	17.0538(8)	22.6036(4)	10.3538(2)
b (Å)	6.7808(3)	12.0562(2)	16.3472(2)
c (Å)	22.2685(10)	24.8145(5)	26.6281(5)
α (°)			93.408(1)
β (°)		113.549(1)	99.849(1)
γ (°)			102.717(1)
Volume (Å^3)	2575.1(2)	6199.1(2)	4309.44(13)
Z	8	4	2
D_{calc} (Mg m^{-3})	1.245	1.603	1.399
Absorption coefficient (mm^{-1})	0.083	0.788	0.579
F(000)	1024	3044	1888
Crystal	block; colourless	slab; colourless	plate; colourless
Crystal size (mm^3)	$0.10 \times 0.08 \times 0.07$	$0.35 \times 0.26 \times 0.06$	$0.40 \times 0.16 \times 0.03$
θ Range for data collection	6.74–27.48°	2.99–27.48°	2.96–27.48°
Reflections collected	13309	39248	81933
Independent reflections	2887 [$R_{int} = 0.1661$]	13877 [$R_{int} = 0.0482$]	19556 [$R_{int} = 0.0681$]
Completeness to $\theta = 27.48°$	97.6%	99.7%	98.8%
Absorption correction	semi-empirical from equivalents	semi-empirical from equivalents	semi-empirical from equivalents
Goodness-of-fit on F^2	0.989	1.031	1.006
Final *R* indices [$F^2 > 2\sigma(F^2)$]	$R_1 = 0.0830$, $wR_2 = 0.2249$	$R_1 = 0.0587$, $wR_2 = 0.1423$	$R_1 = 0.0412$, $wR_2 = 0.0792$
R indices (all data)	$R_1 = 0.2641$, $wR_2 = 0.3227$	$R_1 = 0.0869$, $wR_2 = 0.1586$	$R_1 = 0.0774$, $wR_2 = 0.0897$
Largest differential peak and hole (e Å^{-3})	0.461 and −0.118	1.572 and −0.604	0.863 and −0.607

summarised in Table 1. The molecular structure is dimeric and as such is broadly the same as that found for the silver(I) octylsulfate and silver(I) perchlorate complexes described by, for example, Adams et al. [20] and Gallardo et al. [21], respectively. It consists of two essentially planar bis(3,4-dibutoxy-3′-stilbazole)silver(I)

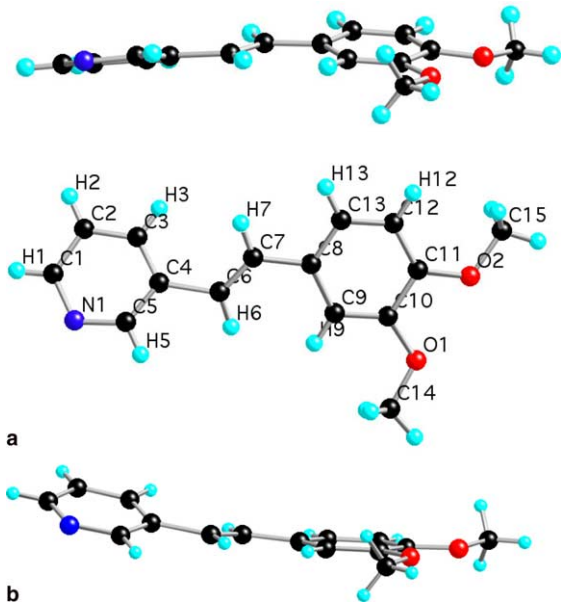

Fig. 4. Molecular structure of the 3,4-dimethoxy-3′-stilbazole.

cations that are arranged parallel to one another, supported by the two triflate anions. The Ag–Ag distance is 3.136(1) Å which is very similar to the equivalent distance in the octylsulfate (ca. 3.2 Å) and perchlorate (ca. 3.35 Å) salts. The triflate anions effectively bridge the dimeric structure and there are three, ionic Ag–O contacts at about 2.8 Å with a fourth Ag–O distance of 3.4 Å. This is slightly different from the octylsulfate and perchlorate structures where all four Ag–O distances are in the range 2.7–2.9 Å. Here, there are no strong interactions beyond the dimer and its pair of triflate anions. Also, and as can be seen clearly in Fig. 7, the stilbazoles exist in two differing conformations. Thus, two of the stilbazoles adopt the same conformation as **7-1**, while the other two adopt its 'inverse' (i.e. both rings rotated by 180° with respect to the *trans* double bond). Interestingly the stilbazoles that adopt the same conformation as **7-1** exhibit a greater twist (19.4(1)° and 33.6(1)°) compared to the two that adopt the inverse (13.9(1)° and 10.7(1)°).

Of course, one thing that is not known in relation to both silver complexes is the nature of the species present in the mesophase. Previously, structural arguments have suggested [13] that the dimeric structure is maintained in the columnar phase of mesomorphic, polycatenar DOS salts and this may be the case here, too, but in the absence of hard information, the discussion of the mesomorphism found below will make no assumptions about the state of aggregation.

2.2. Mesomorphism of the new silver(I) complexes

The mesomorphic behaviour of the new complexes was studied by polarised optical microscopy, differential scanning calorimetry (DSC), X-ray diffraction and miscibility studies. The thermal behaviour of the new complexes is collected in Table 2 and we found that the compounds behaved reproducibly over the lifetime of the DSC and microscopy experiments carried out.

Neither of the new 3,4-dialkoxy-2′-stilbazole ligands (**8**) was mesomorphic, rather melting to an isotropic liquid at 55.2 °C for $n = 8$ and at 68.7 °C for $n = 12$, and complexation of these two ligands to AgDOS (**12a**) or AgOTf (**12b**) did not lead to mesomorphic materials.

However, complexation of the non-mesomorphic 3,4-dialkoxy-3′-stilbazoles (**7**) with the two silver complexes did lead to mesomorphic, materials providing the alkoxy chain was long enough. Whilst the un-complexed ligand was not mesomorphic, melting straight to the isotropic phase between 54.2 °C for $n = 4$ and 68.0 °C for $n = 12$, complex **11a** was mesomorphic for $6 \leqslant n \leqslant 12$, with all homologues displaying a columnar hexagonal phase, characterised by its optical texture (Fig. 8).

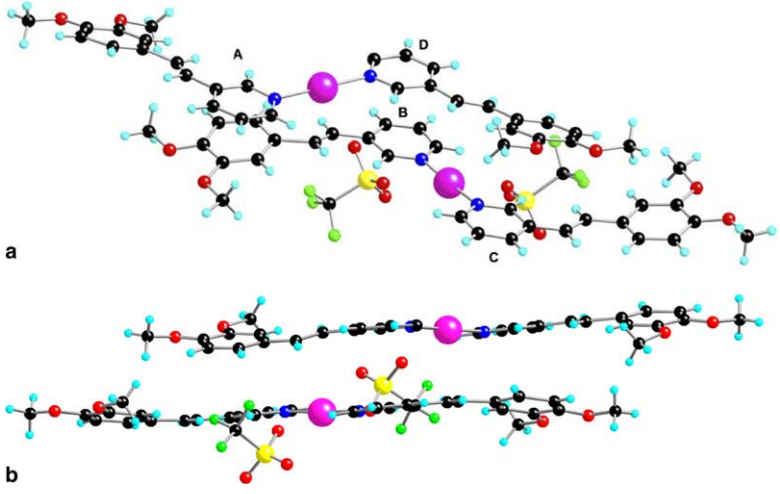

Fig. 5. Two views of the structure of the silver(I) triflate complex of 3,4-dimethoxy-3′-stilbazole.

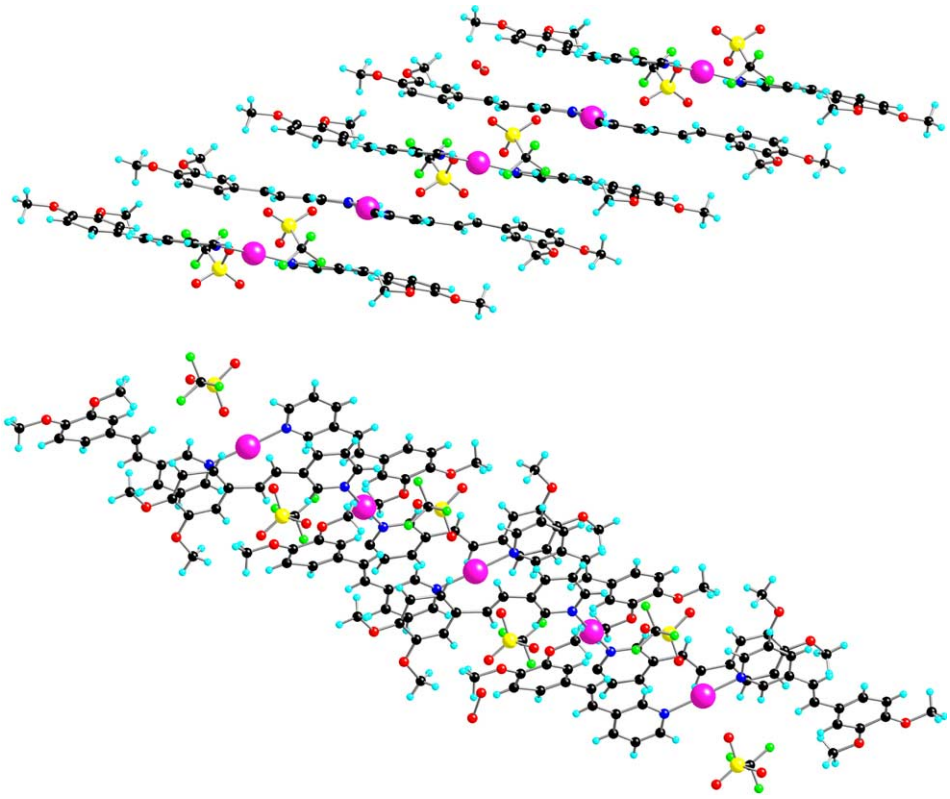

Fig. 6. Two views of the slipped-stack arrangement of **11b**-1.

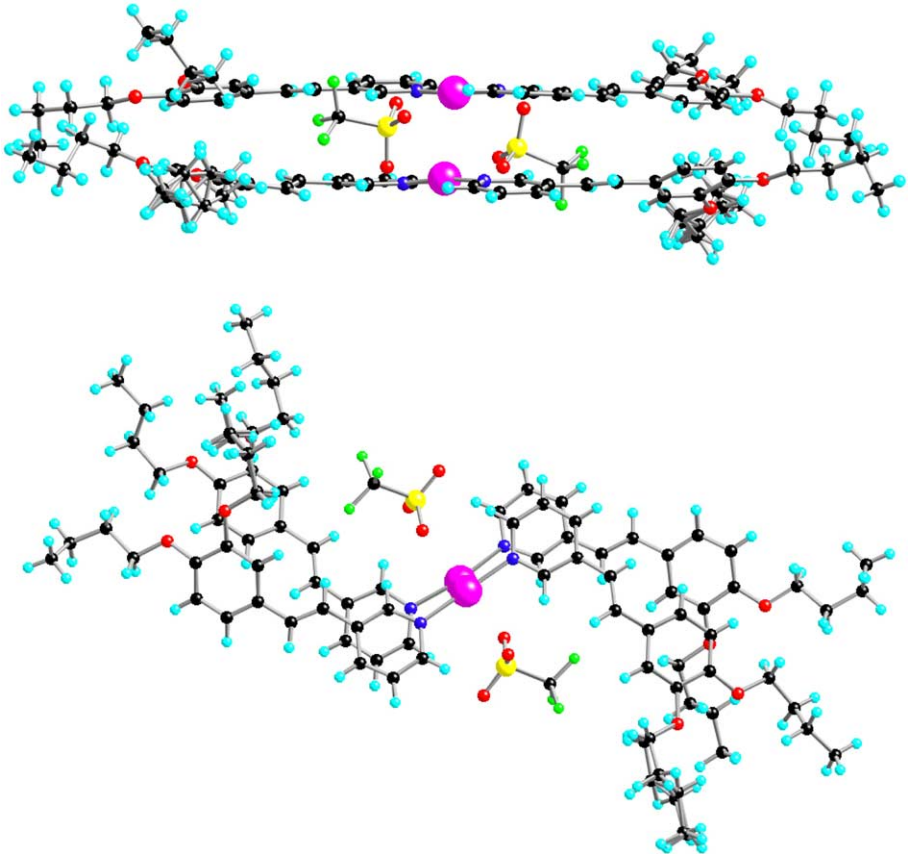

Fig. 7. Two views of the structure of the silver(I) triflate complex of 3,4-dibutyloxy-3′-stilbazole.

Table 2
Thermal data for the new complexes

Complex	n	Transition	T (°C)	ΔH (kJ mol^{-1})	ΔS (J K^{-1} mol^{-1})
11a	4	$Cr_1 \rightarrow Cr_2$	93.6	28.8	79
		$Cr_2 \rightarrow I$	99.8	10.3	28
	6	$Cr \rightarrow Col_h$	36.5	44.5	144
		$Col_h \rightarrow I$	60.0	0.5	2
	8	$Cr \rightarrow Col_h$	57.6	84.1	254
		$Col_h \rightarrow I$	80.9	1.3	3
	10	$Cr \rightarrow Col_h$	75.2	72.3	208
		$Col_h \rightarrow I$	94.9	1.5	4
	12	$Cr_1 \rightarrow Cr_2$	48.7	1.2	4
		$Cr_2 \rightarrow Cr_3$	65.4	26.0	77
		$Cr_3 \rightarrow Col_h$	75.7	39.1	112
		$Col_h \rightarrow I$	95.7	1.4	4
11b	4	$Cr_1 \rightarrow Cr_2$	152.7	1.6	4
		$Cr_2 \rightarrow I$	167.5	43.1	98
	6	$Cr \rightarrow I$	141.2	31.3	76
	8	$Cr_1 \rightarrow Cr_2$	103.3	16.9	45
		$Cr_2 \rightarrow I$	114.2	22.4	58
	10	$Cr_1 \rightarrow Cr_2$	54.9	29.4	90
		$Cr_2 \rightarrow Cr_3$	69.4	1.5	4
		$Cr_3 \rightarrow I$	101.4	44.6	118
		$(I \rightarrow Col_h)$	(93.2)	(−1.4)	(−4)
	12	$Cr_1 \rightarrow Cr_2$	63.5	51.8	154
		$Cr_2 \rightarrow Col_h$	107.0	49.5	130
		$Col_h \rightarrow I$	114.0	1.6	4
12a	8	$Cr_1 \rightarrow Cr_2$	52.9	20.3	62
		$Cr_2 \rightarrow I$	104.9	60.3	160
	12	$Cr_1 \rightarrow Cr_2$	52.0	10.2	31
		$Cr_2 \rightarrow Cr_3$	68.3	66.7	196
		$Cr_3 \rightarrow I$	80.5	17.8	50
12b	8	$Cr_1 \rightarrow Cr_2$	66.8	20.3	60
		$Cr_2 \rightarrow I$	107.5	33.7	88
	12	$Cr_1 \rightarrow Cr_2$	54.8	99.5	304
		$Cr_2 \rightarrow I$	81.2	11.9	34
13a	8	$Col_h \rightarrow I$[a]	86.8	2.2	6
	12	$Cr \rightarrow Col_h$	37.1	101.1	326
		$Col_h \rightarrow I$	81.2	3.2	9
13b	4	$Cr \rightarrow I$	189.0	35.6	77
	8	$Cr \rightarrow Col_h$	39.8	49.5	158
		$Col_h \rightarrow I$	105.3	2.3	6
	12	$Cr_1 \rightarrow Cr_2$	42.2	70.2	227
		$Cr_2 \rightarrow Col_h$	50.0	13.0	40
		$Col_h \rightarrow I$	119.8	1.5	4
14a	8	$Cr_1 \rightarrow Cr_2$	47.5	15.5	48
		$Cr_2 \rightarrow I$	67.7	29.5	87
	12	$Cr_1 \rightarrow Cr_2$	47.2	22.7	71
		$Cr_2 \rightarrow I$	57.7	68.1	206
14b	12	$Cr_1 \rightarrow I$	55.4	93.2	284

[a] Complex was in the mesophase at room temperature.

Two of the complexes **11b** were mesomorphic showing a columnar hexagonal phase over a narrow temperature range, monotropic for $n = 10$ and enantiotropic for $n = 12$.

None of the new 3,4,5-trialkoxystilbazole ligands (**9** or **10**) was mesomorphic and all melted directly into the isotropic phase. However, complexation of 3,4,5-trialkoxy-3′-stilbazoles to silver(I) dodecylsulfate or silver(I) triflate resulted in complexes (**13a** and **13b**) that were mesomorphic. The octyloxy homologue of complex **13a** was already in a columnar hexagonal mesophase at room temperature and cleared to the isotropic phase on heating to 86.8 °C. The dodecyloxy homologue also showed a columnar hexagonal phase from 37.1 to 81.2 °C, a smaller temperature range than for $n = 8$. These mesophases were characterised by optical microscopy.

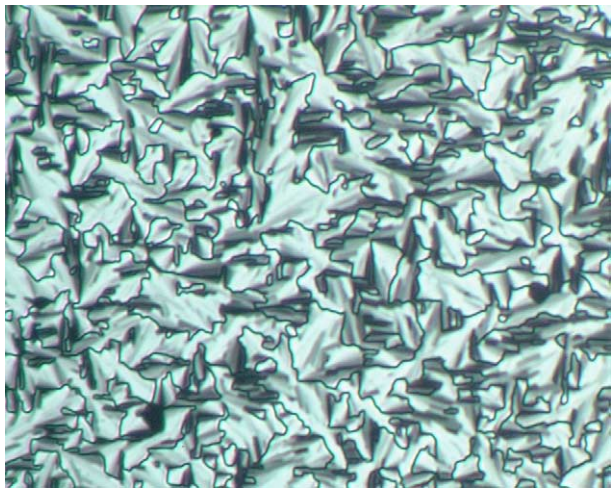

Fig. 8. The optical texture of the columnar hexagonal phase of **11a**-12 on cooling from the isotropic phase at 93.4 °C.

Bis(3,4,5-trioctyloxy-3′-stilbazole)silver(I) triflate was a pasty solid that melted at 39.8 °C to a columnar hexagonal phase which cleared to the isotropic at 105.3 °C. The mesophase was characterised by polarised optical microscopy from its optical texture. The dodecyloxy homologue of complex **13b** showed two crystal phases before melting to a columnar hexagonal phase at 50.0 °C and clearing at 119.8 °C. On cooling, the mesophase reappeared at 117 °C and remained until crystallisation at 21.8 °C. On second heating, the complex melted straight into the mesophase at 30.4 °C but cleared at the same temperature as the first heating. Subsequent cooling and heating repeated the behaviour of the second cycle so crystallisation from a solvent must result in a crystalline form that needs to rearrange on heating before it can melt into the mesophase. The columnar hexagonal phase was characterised from its optical texture (Fig. 9).

2.3. X-ray diffraction

X-ray diffractions studies were carried out on complexes **11a**, **11b**, **13a** and **13b**, and the results for complex **11a**, **13a** and **13b** are collected in Table 3, which contains both experimental and, in parentheses for cases with >1 observed reflection, calculated lattice parameters; the lattice parameter, a, and columnar cross-sectional area,

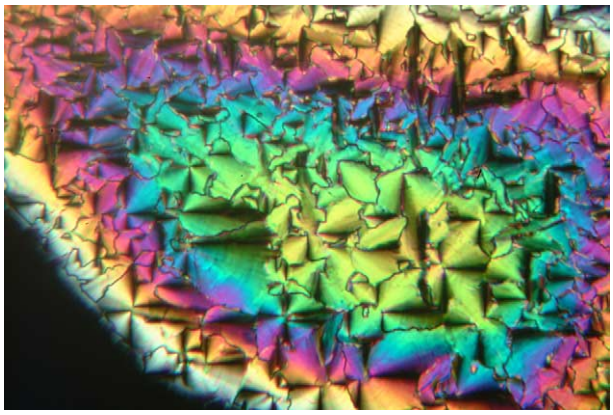

Fig. 9. The optical texture of the columnar hexagonal phase of **13b**-12 on cooling from the isotropic phase at 41.9 °C.

S, are derived from calculated data where these are available. Due to the small temperature range of the mesophases of **11b**, no conclusive results were obtained by X-ray diffraction studies so the mesophase remains assigned from its optical texture alone.

For **11a**-12 the X-ray diffraction studies confirmed the assignment of the mesophase as columnar hexagonal since two, sharp, small-angle reflections were observed in the patterns corresponding to the squared spacing ratios 1:3, and to the indexation $(h\,k) = (1\,0)$ and $(1\,1)$, as shown in Fig. 10. Diffuse reflections were also recorded for all complexes at around 4.5 Å, which corresponds to the liquid-like order of the molten alkoxy chains, and at around 10 Å, which may be due to loose interactions between dimeric species formed by these silver complexes [10].

The lattice parameter *a*, for the dodecyloxy homologue was found to be ca. 42 Å, which is around 12 Å smaller than the estimated length of the complex in its most extended form (53.8 Å). It is possible that this is due to the way the molecules may pack together in the repeat unit with the chains curled round in order to fill space efficiently (Fig. 11). However, another possibility is that in common with the generalised model for the packing of polycatenar mesogens that some of us advanced recently [22], the complexes can tilt at some angle within the column or otherwise organise to give a circular cross-section normal to the column direction that then allows formation of a columnar phase of hexagonal symmetry. The model in Fig. 11 would be one possible expression of this general approach.

Table 3
X-ray diffraction data for complexes **11a**, **13a** and **13b**

Complex	*n*	*T* (°C)	d_{10} (Å)	d_{11} (Å)	d_{20} (Å)	d_{21} (Å)	*a* (Å)	*S* (Å^2)
11a	6	60	31.3	–	–	–	36.1	1131
		50	31.4	–	–	–	36.3	1138
		40	31.6	–	–	–	36.4	1153
	8	80	33.2	–	–	–	38.3	1272
		75	33.6	–	–	–	38.8	1303
		70	33.9	–	–	–	39.1	1327
		65	34.2	–	–	–	39.5	1351
	10	90	34.0	–	–	–	39.3	1334
		85	34.4	–	–	–	39.7	1366
		80	34.8	–	–	–	40.2	1398
	12	95	34.5	19.9	–	–		
			(34.5)	(19.9)			39.8	1374
		90	36.2	20.9	–	–		
			(36.2)	(20.9)			41.8	1513
		85	36.5	21.1	–	–		
			(36.5)	(21.1)			42.15	1538
13a	12	80	32.15	18.6	15.6	12.5		
			(32.15)	(18.6)	(16.1)	(12.15)	37.1	1197
		70	32.7	19.0	16.1	12.5		
			(32.7)	(18.9)	(16.35)	(12.35)	37.75	1235
		60	33.25	19.2	16.7	12.5		
			(33.25)	(19.2)	(16.6)	(12.6)	38.4	1276
		50	33.9	19.6	16.9	12.8		
			(33.9)	(19.6)	(16.95)	(12.8)	39.15	1327
13b	12	80	35.0	20.2	–	–		
			(35.0)	(20.2)			40.4	1415
		50	36.4	21.0	–	–		
			(36.4)	(21.0)			42.0	1530

The calculated value of the reflections is deduced from the mathematical expression: $\langle d_{10}\rangle = \frac{1}{N_{hk}}(\sum_{hk} d_{hk}.\sqrt{h^2+k^2+hk})$, where N_{hk} is the number of $h\,k$ reflections for the Col_h phase; *a* is the lattice parameter of the Col_h phase $(a = \frac{2}{\sqrt{3}}\langle d_{10}\rangle)$, *S* is the lattice area $(S = a\langle d_{10}\rangle)$.

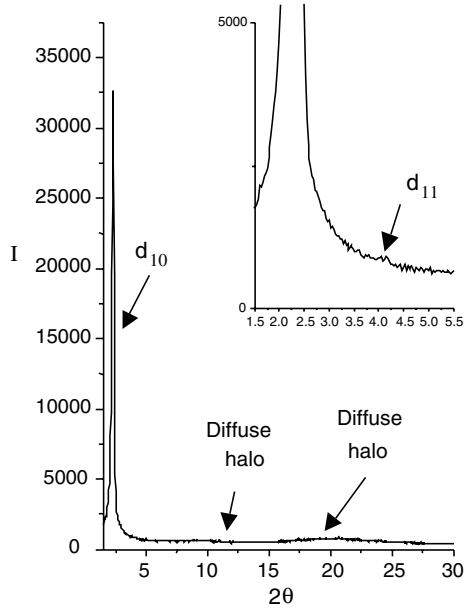

Fig. 10. X-ray diffraction pattern of **11a**-12 at 90 °C.

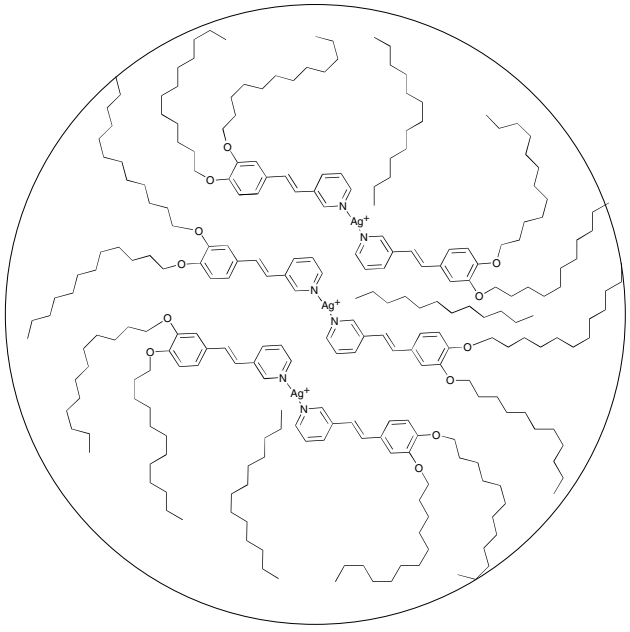

Fig. 11. Schematic of the possible packing of molecules in a columnar repeat unit.

For complexes **11a** with $n = 6$, 8 and 10, only one reflection was observed and so it was impossible to make an unequivocal assignment of the mesophase symmetry on this basis. Thus, to try to confirm the identity of the phase they form, contact preparations were carried out. Contact preparations between compound **11a**-12 and either compound **11a**-8 or **11a**-10 failed to show any miscibility as shown for **11a**-10 and **11a**-8 in Fig. 12; the same experiment for **11a**-6 was impossible due to incompatible temperature ranges. Such immiscibility does not preclude assignment of the phase of the shorter chain homologues of **11a** as Col_h and indeed, given the comparison of the d(10) data within the homologous series (Table 3), this is our assignment, which we believe to be sound.

X-ray diffraction studies of **13a**-12 confirmed the columnar hexagonal nature of the mesophase displayed (Table 3) since four, sharp, small-angle reflections were observed (Fig. 13), corresponding to the squared spacing ratios 1, 3, 4 and 7 with indexation $(h\,k) = (1\,0)$, (1 1), (2 0) and (2 1). In the case of **13b**-12, two, sharp, small-angle reflections were observed in the diffraction pattern corresponding to the squared spacing ratios 1 and 3 with indexation $(h\,k) = (1\,0)$ and (1 1). For **13a**-12 and **13b**-12, the lattice parameter, a, was around 14 and 11 Å shorter, respectively, than the estimated length of the complexes in their most extended form (53.8 Å). This behaviour was discussed above. Shorter-chain homologues of both triflate and DOS salts were characterised by optical microscopy alone since no satisfactory X-ray results were obtained.

3. Discussion

Fig. 14 summarises the thermal behaviour of complexes **11a** and **12a** and compares it with the behaviour of the 'parent' complexes bis(3,4-dialkoxy-4′-stilbazole)silver(I) dodecylsulfate (**2a**) (see Fig. 15).

The most noticeable difference in the mesomorphism of these three complexes is in the number of mesophases displayed. Thus, the parent complex (**2a**) is polymorphic and shows a cubic phase for $4 \leqslant n \leqslant 10$ and a Col_h phase for $6 \leqslant n \leqslant 12$. Complex **11a**, however, shows only one mesophase, namely a columnar hexagonal phase for $n \geqslant 6$. Thus, the melting point drops steeply from $n = 4$ (99.8 °C) to $n = 6$ (36.5 °C) and at the latter chain length a Col_h phase is introduced. The temperature range of the mesophase stays roughly constant with chain length (between 23 and 20 °C), but the temperature at which the phase is seen does increase with chain length ($T_{Col\text{-}I} = 60.0$, 80.9, 94.9 and 95.7 °C for $n = 6$, 8, 10 and 12, respectively). Combined with the very limited mesomorphism of the triflate analogues (**11b**) and the absence of mesomorphism in all the tetracatenar complexes of the 2-stilbazoles, the observations once more suggest a profound effect consequent on the reduction in anisotropy associated with the isomeric ligands.

In these complexes, the dodecylsulfate anion acts as a flexible lateral substituent and, therefore, prevents efficient packing of the molecules so the transition temperatures are lowered. Since the core length of these silver(I) complexes of the 3-stilbazole ligand is shorter than that of the complexes of the 4-stilbazole ligand, the dodecylsulfate alkyl chain is expected to extend beyond the length of the silver(I) core as it does in the case of the 'parent' [7].

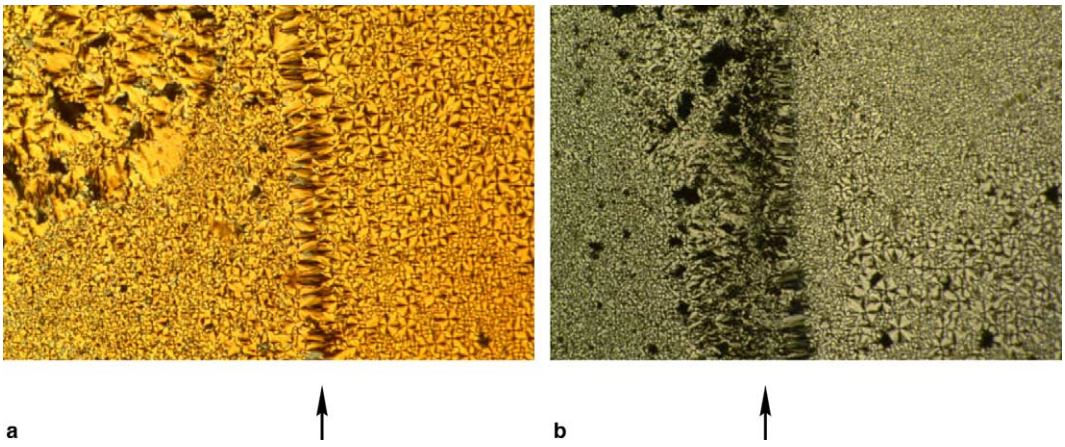

Fig. 12. Contact preparation (a) at 88.7 °C between the Col_h phase of complex **11a**-12 (left) and the unidentified mesophase of complex **11a**-10 (right), and (b) at 79.9 °C between **11a**-12 (left) and **11a**-8 (right). Lines of immiscibility are indicated by arrows.

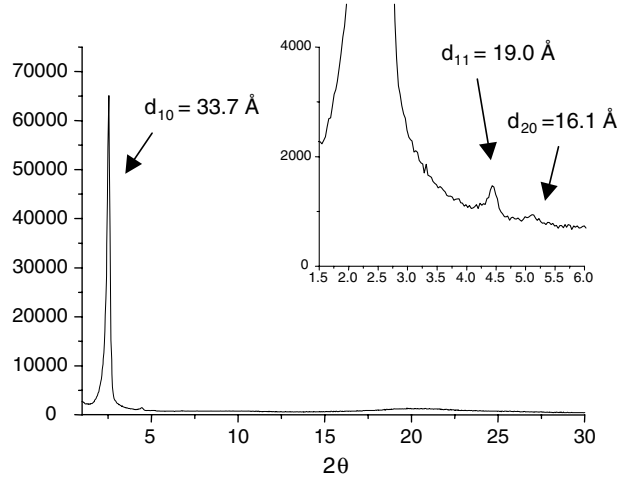

Fig. 13. X-ray diffraction pattern for **13a**-12 at 70 °C.

This affects the balance between the relative volumes of the core and the chain, a factor known to be important in determining the mesomorphism of polycatenar systems [7,9]. On this basis, the absence of a cubic phase in these isomeric materials may be rationalised. Further, it appears true that cubic phase formation requires the presence of discrete molecular aggregates [8,9,23], and the increased steric congestion caused by the reduction in ligand and complex anisotropy, as evidenced in the figures above from the crystal structures, may be the cause.

Because, in general, the mesomorphism of 3,4,5-hexacatenar complexes is restricted to a columnar phase, few examples were synthesised. In common with the preceding materials, none of the 2-stilbazole derivatives was mesomorphic and they melted between 55 and 67 °C with little apparent dependence on the anion.

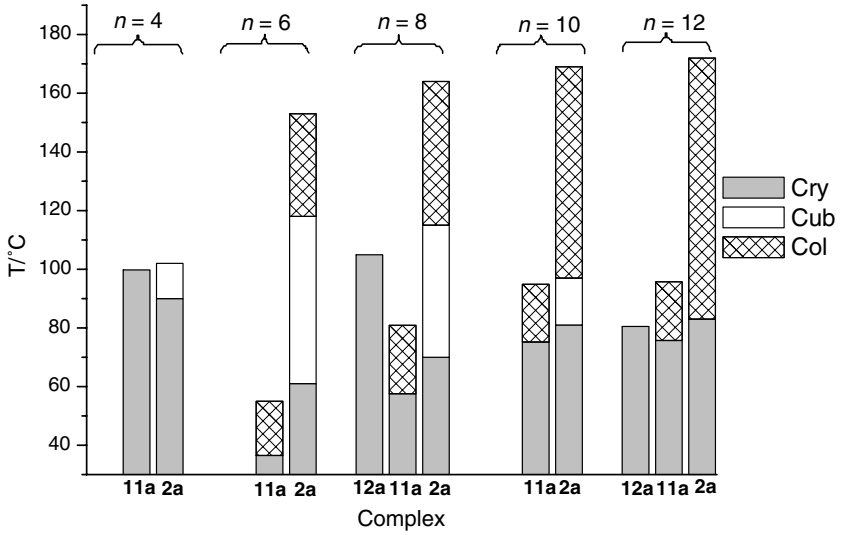

Fig. 14. Comparison of the thermal behaviour of complexes **11a** and **12a** with their 'parent' complex **2a**.

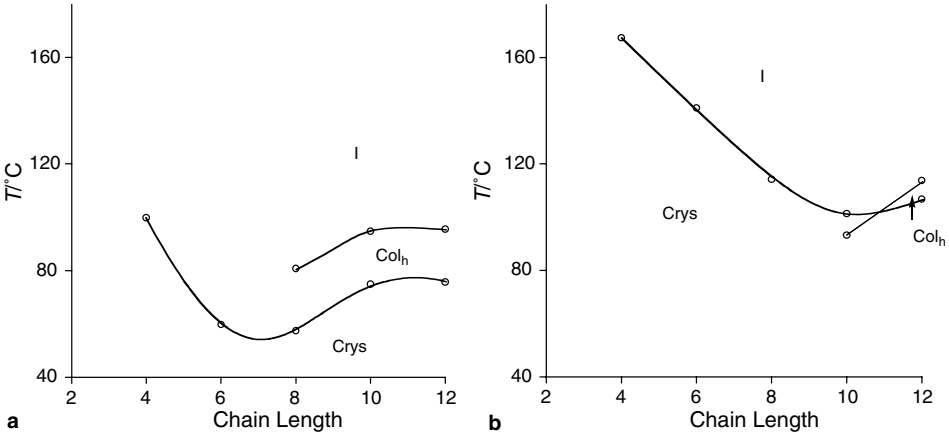

Fig. 15. Phase diagrams of complexes **11a** (a) and **11b** (b) plotted on the same scale.

4. Experimental

All solvents and chemicals were used as received, apart from THF which was dried by distillation over sodium and benzophenone immediately prior to use under an atmosphere of oxygen-free nitrogen. NMR spectra were recorded on a Bruker DRX-400, ACF 300 or ACF-200, operating at 400, 300 or 200 MHz, respectively, for protons and 100.6, 75.4 or 50.3 MHz, respectively, for carbon. Analysis by hot stage microscopy was carried out using an Olympus BX50 microscope equipped with a Link-Am HFS91 hot stage, and TMS92 controller and LNP2 cooling unit. Analysis by DSC was carried out on a Perkin–Elmer DSC7 instrument using heating and cooling rates of 10 and 5 K min^{-1}. All analytical data are collected in Table 4.

The XRD patterns were obtained with two different experimental set-ups. In the first, a linear monochromatic Cu Kα_1 beam ($\lambda = 1.5405$ Å) was obtained using a Guinier camera with a sealed-tube generator (900 W). In the second, a Debye–Scherrer camera equipped with a bent quartz monochromator and an electric oven was used. In both cases, the crude powder was filled in Lindemann capillaries of 1 mm diameter. An initial set of diffraction patterns was recorded with a curved Inel CPS 120 counter gas-filled detector linked to a data acquisition computer; periodicities up to 60 Å can be measured, and the sample temperature controlled to within ±0.05 °C. The second set of diffraction patterns was recorded on an image plate; cell parameters were calculated from the position of the sharp reflections at the smallest Bragg angle, which were in all cases the most intense. Periodicities up to 90 Å can be measured, and the sample temperature controlled to within ±0.3 °C. In each case, exposure times were varied from 1 to 24 h depending on the mesophase being observed and upon the specific reflections being sought (weaker reflections obviously taking longer exposure times).

Suitable single crystals were selected and data collected on a Bruker Nonius KappaCCD Area Detector at the window of a Bruker Nonius FR591 rotating anode ($\lambda_{Mo K\alpha} = 0.71073$ Å) driven by COLLECT [24] and DENZO [25] software at 120 K. The structure was determined in SHELXS-97 [26] and refined using SHELXL-97 [27].

4.1. Preparation of 3,4-dialkoxybenzylideneaniline

All homologues were made in the same way as 3,4-dioctyloxybenzylidene aniline described.

3,4-Dioctyloxybenzaldehyde (1.09 g, 3.0 mmol) was dissolved in ethanol (60 cm^3) and aniline (0.39 g, 4.2 mmol) was added. A few crystals of *para*-toluene sulfonic acid were added and the solution became yellow. It was stirred at room temperature for 2 h after which time there was no precipitate, so the mixture was placed in the freezer for 15 h. A white fluffy solid precipitated and was filtered off and used without further purification (1.27 g, 97%). For the longer-chain homologues, heating was required to dissolve the starting benzaldehyde and the product precipitated upon cooling the solution to room temperature.

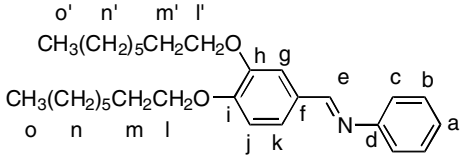

^{1}H NMR (400 MHz, CD_2Cl_2): $\delta = 8.39$ (1H, s, H**e**), 7.60 (1H, d, H**g**, $^4J_{HH} = 1.4$ Hz), 7.42 (2H, m, H**b**), 7.35 (1H, dd, H**k**, $^3J_{HH} = 8.2$ Hz, $^4J_{HH} = 1.4$ Hz), 7.24 (1H, m, H**a**), 7.23 (2H, m, H**c**), 6.97 (1H, d, H**j**, $^3J_{HH} = 8.2$ Hz) 4.11 (2H, t, H**l′**, $^3J_{HH} = 6.6$ Hz), 4.09 (2H, t, H**1**, $^3J_{HH} = 6.6$ Hz), 1.87 (2H, m, H**m′**), 1.84 (2H, m, H**m**), 1.44 (20H, m, H**n**, H**n′**), 0.92 (6H, 2 × t, H**o**, H**o′**, $^3J_{HH} = 6.7$ Hz).

^{13}C NMR (100.61 MHz, CD_2Cl_2): $\delta = 160.1$ (**e**), 152.8, 152.7 (**i**,**d**), 149.9 (**h**), 129.9 (**f**), 129.5 (**b**), 125.8

Table 4
Yields and analytical data for the new compounds

Compound	*n*	Yield (%)	MPt (°C)	Elemental analysis calculated (found) (%)		
				C	H	N
6	6	89	42.4	78.7 (78.6)	9.3 (9.2)	3.5 (3.6)
	8	97	51.6	79.6 (79.5)	9.9 (9.9)	3.2 (3.1)
	10	91	61.0	80.3 (80.1)	10.4 (10.4)	2.8 (2.9)
	12	91	68.8	80.8 (80.8)	10.8 (10.9)	2.6 (2.7)
7	4	53	54.2	77.5 (77.5)	8.4 (8.4)	4.3 (4.4)
	6	73	50.6	78.7 (78.6)	9.3 (9.3)	3.7 (3.8)
	8	55	46.3	79.6 (79.4)	9.9 (9.9)	3.2 (3.3)
	10	73	55.0	80.3 (80.2)	10.4 (10.5)	2.8 (2.9)
	12	64	68.0	80.8 (80.6)	10.8 (10.7)	2.6 (2.7)
8	8	88	55.2	79.6 (79.5)	9.9 (9.9)	3.2 (3.3)
	12	59	68.7	80.8 (80.8)	10.8 (10.9)	2.6 (2.7)
	12	88	39.8	80.2 (80.0)	11.4 (11.3)	1.9 (1.9)
9	8	93	oil	78.5 (78.3)	10.5 (10.6)	2.5 (2.7)
	12	88	42.6	80.2 (80.0)	11.4 (11.6)	1.9 (2.0)
10	8	78	oil	78.5 (78.1)	10.5 (10.6)	2.5 (2.6)
	12	53	41.2	80.2 (79.9)	11.4 (11.6)	1.9 (2.0)
11a	4	66	95.9	63.3 (63.2)	7.8 (8.0)	2.7 (2.6)
	6	39	30.6	65.5 (65.5)	8.4 (8.5)	2.5 (2.6)
	8	89	56.5	67.3 (67.1)	9.0 (9.0)	2.2 (2.4)
	10	60	75.4	68.9 (69.0)	9.4 (9.5)	2.1 (2.2)
	12	88	73.4	70.1 (70.2)	9.8 (9.9)	1.9 (2.0)
11b	4	86	167.5	56.9 (56.7)	6.0 (6.0)	3.1 (2.9)
	6	71	141.2	60.1 (59.8)	6.9 (7.0)	2.8 (3.0)
	8	60	114.2	62.6 (62.6)	7.7 (7.7)	2.5 (2.6)
	10	89	101.4	64.7 (64.5)	8.3 (8.5)	2.3 (2.4)
	12	86	107.0	66.4 (66.4)	8.8 (9.1)	2.1 (2.2)
12a	8	62	103.4	67.3 (67.5)	9.0 (8.9)	2.2 (2.4)
	12	59	68.0	70.1 (73.6)	9.8 (10.1)	1.9 (2.1)
12b	8	74	107.5	62.6 (62.7)	7.7 (7.7)	2.5 (2.5)
	12	85	81.2	66.4 (65.9)	8.8 (8.8)	2.1 (2.1)
13a	8	54	Below rt	68.6 (68.7)	9.6 (9.7)	1.9 (1.9)
	12	56	37.1	71.7 (71.6)	10.5 (10.5)	1.5 (1.1)
13b	4	53	189.0	58.2 (57.9)	6.7 (6.7)	2.7 (2.7)
	8	56	39.8	64.9 (64.6)	8.6 (8.6)	2.0 (2.0)
	12	89	50.0	68.9 (68.6)	9.7 (9.6)	1.7 (1.7)
14a	8	57	67.7	68.6 (68.8)	9.6 (9.6)	1.9 (1.9)
	12	67	57.7	71.7 (71.7)	10.5 (10.5)	1.5 (1.6)
14b	12	84	55.4	68.9 (68.4)	9.7 (9.7)	10.6 (1.0)

(**a**), 124.4 (**k**), 121.2 (**c**), 112.9 (**j**), 111.8 (**g**), 69.5 (**l**, **l′**), 32.3, 30.1, 30.0, 29.8, 29.7, 29.6, 26.4, 23.1 (**m**, **m′**, **n**, **n′**), 14.3 (**o**, **o′**).

*4.2. Preparation of 3,4-dialkoxy-3′-stilbazole (**7**) and 3,4-dialkoxy-2′-stilbazole (**8**)*

The preparation of 3,4-dodecyloxy-3′-stilbazole will be described; the same method was used for the other homologues. The series of 3,4-didecyloxy-2′-stilbazoles were made in the same way except that 3-picoline was replaced by 2-picoline. The reaction was carried out in an atmosphere of argon.

3,4-Didodecyloxybenzylidene aniline (5.00 g, 10.1 mmol) was dissolved with heating in DMF (50 cm^3). 3-Picoline (0.82 g, 8.8 mmol) was added with stirring, followed by potassium *tert*-butoxide (4.40 g, 36.0 mmol) in fractions. The solution immediately turned dark red. The system was heated to 80 °C and was stirred for 2.5 h. After cooling, HCl solution (10%) was added dropwise until the pH of the mixture was neutral. Water (100 cm^3) was added and the solution became yellow. The product was extracted into DCM (2×75 cm^3) and was washed with $NaHCO_3$ solution (200 cm^3 saturated) and water (200 cm^3). The organic phase was dried over magnesium sulfate and the DCM was removed. The

residue was then taken into toluene (100 cm^3) and washed repeatedly with water (4×100 cm^3) to remove the DMF. The toluene was then removed in vacuo to leave a light brown solid. This was purified by column chromatography on silica gel using DCM:methanol, 100:1 as eluant. A few drops of triethylamine were added to prevent the stilbazole sticking to the column. The product was then crystallised from hot hexane to give a colourless powder (3.17 g, 73%).

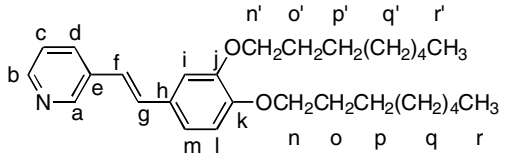

(7)

^{1}H NMR (400 MHz, $CDCl_3$): $\delta = 8.70$ (1H, d, H**a**, $^4J_{HH} = 1.8$ Hz), 8.46 (1H, dd, H**b**, $^3J_{HH} = 4.7$ Hz, $^4J_{HH} = 1.8$ Hz), 7.81 (1H, dt, H**d**, $^3J_{HH} = 7.9$ Hz, $2 \times {}^4J_{HH} = 1.8$ Hz), 7.28 (1H, dd, H**c**, $^3J_{HH} = 7.9$ Hz, $^3J_{HH} = 4.7$ Hz), 7.10 (1H, AB, H**g**, $J_{AB} = 16.4$ Hz), 7.09 (1H, d, H**i**, $^4J_{HH} = 1.9$ Hz), 7.06 (1H, dd, H**m**, $^3J_{rm\ HH}$ 8.3 Hz, $^4J_{HH} = 1.9$ Hz), 6.92 (1H, AB, H**f**, $J_{AB} = 16.4$ Hz), 6.87 (1H, d, H**l**, $^3J_{HH} = 8.3$ Hz), 4.06 (2H, t, H**n**′, $^3J_{HH} = 6.7$ Hz), 4.02 (2H, t, H**n**, $^3J_{HH} = 6.8$ Hz), 1.84 (4H, m, H**o**, H**o**′), 1.50 (4H, m, H**p**, H**p**′), 1.33 (16H, m, H**q**, H**q**′), 0.90 (6H, $2 \times$ t, H**r**, H**r**′, $^3J_{HH} = 6.9$ Hz).

^{13}C NMR (100.61 MHz, $CDCl_3$): $\delta = 149.6$ (**j**), 149.2 (**k**), 148.2 (**b**), 148.0 (**a**), 133.3 (**e**), 132.4 (**d**), 130.8 (**g**), 129.6 (**h**), 123.5 (**f**), 122.6 (**c**), 120.3 (**m**), 113.5 (**l**), 111.4 (**i**), 69.3 (**n**), 69.2 (**n**′), 31.8, 29.4, 29.3, 29.2, 26.0, 22.7 (**o**, **o**′, **p**, **p**′ **q**, **q**′), 14.1 (**r**, **r**′).

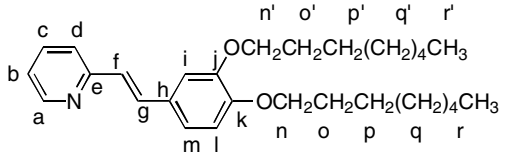

(8)

^{1}H NMR (400 MHz, $CDCl_3$): $\delta = 8.59$ (1H, dd, H**a**, $^3J_{HH} = 4.8$ Hz, $^4J_{HH} = 1.8$ Hz), 7.65 (1H, dt, H**c**, $2 \times {}^3J_{HH} = 7.7$ Hz, $^4J_{HH} = 1.8$ Hz), 7.55 (1H, AB, H**g**, $J_{AB} = 16.1$ Hz), 7.38 (1H, d, H**d**, $^3J_{HH} = 7.9$ Hz), 7.16 (1H, d, H**i**, $^4J_m = 1.8$ Hz), 7.11 (2H, m, H**b**, H**m**), 7.04 (1H, AB, H**f**, $J_{AB} = 16.1$ Hz), 6.87 (1H, d, H**l**, $^3J_{HH} = 8.3$ Hz), 4.05 (2H, t, H**n**′, $^3J_{HH} = 6.7$ Hz), 4.02 (2H, t, H**n**, $^3J_{HH} = 6.6$ Hz), 1.85 (2H, m, H**o**′), 1.83 (2H, m, H**o**), 1.49 (4H, m, H**p**, H**p**′), 1.32 (16H, m, H**q**, H**q**′), 0.89 (6H, $2 \times$ t, H**r**, H**r**′, $^3J_{HH} = 6.9$ Hz).

^{13}C NMR (100.61 MHz, $CDCl_3$): $\delta = 155.9$ (**e**), 149.8 (**j**), 149.5 (**a**), 149.2 (**k**), 136.5 (**g**), 132.8 (**g**), 129.6 (**h**), 125.8 (**f**), 121.7 (**b**), 121.6 (**d**), 120.9 (**m**), 113.4 (**l**), 111.7 (**i**), 69.3 (**n**), 69.2 (**n**′), 31.8, 29.4, 29.3, 29.2, 26.0, 22.7 (**o**, **o**′, **p**, **p**′, **q**, **q**′), 14.1 (**r**, **r**′).

4.3. Preparation of 3,4,5-trialkoxybenzylideneaniline

3,4,5-Trioctyloxybenzylidene aniline was prepared in the same way as 3,4,5-tridodecyloxybenzylidene aniline, which is described.

3,4,5-Tridodecyloxybenzaldehyde (7.90 g, 12.0 mmol) was heated with stirring in ethanol (150 cm^3) until it dissolved. Aniline (1.58 g, 17.0 mmol) was then added followed by a few crystals of toluene sulphonic acid. The mixture was stirred and was allowed to cool to room temperature, as it did so a thick, white precipitate formed. The mixture was stirred for a further 2 h and the colourless precipitate was then filtered off and dried in a dessicator (7.67 g, 10.5 mmol, 88% yield). It was used without further purification.

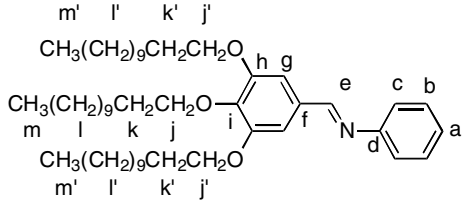

^{1}H NMR (400 MHz, CD_2Cl_2): $\delta = 8.36$ (1H, s, H**e**), 7.43 (2H, m, H**b**), 7.26 (1H, m, H**a**), 7.22 (2H, m, H**c**), 7.17 (2H, s, H**g**) 4.08 (4H, t, H**j**′, $^3J_{HH} = 6.5$ Hz), 4.04 (2H, t, H**j**, $^3J_{HH} = 6.5$ Hz), 1.86 (4H, m, H**k**′), 1.77 (2H, m, H**k**), 1.44 (52H, m, H**l**, H**l**′), 0.91 (9H, $2 \times$ t, H**m**, H**m**′, $^3J_{HH} = 7.0$ Hz).

^{13}C NMR (100.61 MHz, CD_2Cl_2): $\delta = 160.3$ (**e**), 153.8 (**h**), 152.6 (**d**), 141.5 (**i**), 131.79 (**f**), 129.5 (**b**), 126.0 (**a**), 121.1 (**c**), 107.2 (**g**), 73.8 (**j**), 69.5 (**j**′), 32.3, 30.8, 30.2, 30.1, 30.1, 30.0, 29.8, 29.7, 26.5, 23.1 (**k**, **k**′, **l**, **l**′), 14.3 (**m**, **m**).

4.4. Preparation of 3,4,5-trialkoxy-3′-stilbazole (*9*) and 3,4,5-trialkoxy-2′-stilbazole (*10*)

The preparation of 3,4,5-tridodecyloxy-3′-stilbazole will be described; 3,4,5-trioctyloxy-3′-stilbazole was made in the same way. The isomeric 3,4,5-trialkoxy-2′-stilbazoles were made in the same way except that the 3-picoline was replaced with 2-picoline.

3,4,5-Tridodecyloxybenzylidene aniline (3.50 g, 4.8 mmol) was dissolved with heating in DMF (30 cm^3). 3-Picoline (0.82 g, 8.8 mmol) was added with stirring, followed by potassium *tert*-butoxide (4.40 g, 36.0 mmol) in fractions. The solution immediately

turned dark red. The system was heated to 80 °C and was stirred for 2.5 h. After cooling HCl solution (10%) was added dropwise until the pH of the mixture was neutral. Water (100 cm^3) was added and the solution became yellow. The product was extracted into DCM (2×75 cm^3) and was washed with $NaHCO_3$ solution (200 cm^3 saturated) and H_2O (200 cm^3). The organic phase was dried over magnesium sulfate and the DCM was removed. The residue was then taken into toluene (100 cm^3) and was repeatedly with water (4×100 cm^3) to remove the DMF. The toluene was then removed in vacuo to leave a light brown solid. This was purified by column chromatography on silica gel. The solvent system was ethyl acetate:hexane, 1:4. A few drops of triethylamine were added to prevent the stilbazole sticking to the column. The product was then crystallised from hot hexane to give a colourless powder (2.59 g, 88%).

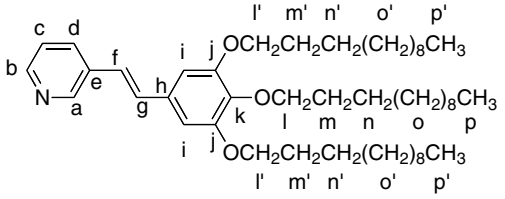

(9)

^{1}H NMR (400 MHz, $CDCl_3$): $\delta = 8.71$ (1H, d, H**a**, $^4J_m = 1.7$ Hz), 8.48 (1H, dd, H**b**, $^3J_{HH} = 4.7$ Hz, $^4J_{HH} = 1.7$ Hz), 7.82 (1H, dt, H**d**, $^3J_{HH} = 8.0$ Hz, $^4J_{HH} = 1.7$ Hz), 7.29 (1H, dd, H**c**, $^3J_{HH} = 8.0$ Hz, $^3J_{HH} = 4.7$ Hz), 7.07 (1H, AB, H**g**, $J_{AB} = 16.4$ Hz), 6.94 (1H, AB, H**f**, $J_{AB} = 16.4$ Hz), 6.73 (2H, s, H**i**), 4.03 (4H, t, H**l**′, $^3J_{HH} = 6.4$ Hz), 3.99 (2H, t, H**l**, $^3J_{HH} = 6.6$ Hz), 1.84 (4H, m, H**m**′), 1.76 (2H, m, H**m**), 1.48 (6H, m, H**n**, H**n**′), 1.27 (48H, m, H**o**, H**o**′), 0.87 (9H, t, H**p**, H**p**′, $^3J_{HH} = 6.8$ Hz).

^{13}C NMR (100.61 MHz, $CDCl_3$): $\delta = 153.4$ (**j**), 148.2 (**b**), 148.1 (**a**), 138.7 (**e**), 133.2 (**k**), 132.6 (**d**), 131.8 (**h**), 131.3 (**g**), 123.7 (**f**), 123.6 (**c**), 105.2 (**i**), 73.6 (**l**), 69.2 (**l**′), 32.0, 31.9, 30.3, 29.8, 29.7, 29.6, 29.4, 26.1, 22.7 (**m**, **m**′, **n**, **n**′, **o**, **o**′), 14.1 (**p**, **p**′).

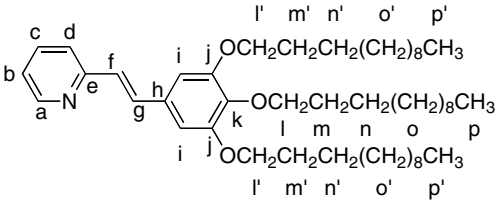

(10)

^{1}H NMR (400 MHz, $CDCl_3$): $\delta = 8.59$ (1H, dd, H**a**, $^3J_{HH} = 5.0$ Hz, $^4J_{HH} = 1.5$ Hz), 7.67 (1H, dt, H**c**, $^3J_{HH} = 7.6$ Hz, $^4J_{HH} = 1.5$ Hz), 7.52 (1H, AB, H**g**, $J_{AB} = 16.0$ Hz), 7.41 (1H, d, H**d**, $^3J_{HH} = 7.6$ Hz), 7.15 (1H, dd, H**b**, $^3J_{HH} = 7.6$ Hz, $^3J_{HH} = 5.0$ Hz), 7.06 (1H, AB, H**f**, $J_{AB} = 16.0$ Hz), 6.80 (2H, s, H**i**), 4.02 (4H, t, H**l**′, $^3J_{HH} = 6.7$ Hz), 3.98 (2H, t, H**l**, $^3J_{HH} = 6.8$), 1.83 (4H, m, H**m**′), 1.76 (2H, m, H**m**), 1.48 (6H, m, H**n**, H**n**′), 1.27 (40H, m, H**o**, H**o**′), 0.89 (9H, t, H**p**, H**p**′, $^3J_{HH} = 6.8$ Hz).

^{13}C NMR (100.61 MHz, $CDCl_3$): $\delta = 155.6$ (**e**), 153.3 (**j**), 149.4 (**a**), 138.9 (**k**), 136.7 (**c**), 133.2 (**g**), 131.6 (**h**), 126.6 (**f**), 121.9 (**b**), 121.7 (**d**), 105.7 (**i**), 73.6 (**l**), 69.1 (**l**′), 31.9, 30.3, 29.8, 29.7, 29.6, 29.4, 26.1, 22.7 (**m**, **m**′, **n**, **n**′, **o**, **o**′), 14.1 (**p**, **p**′).

*4.5. Preparation of bis(3,4-dialkoxy-3′-stilbazole)-silver(I) dodecylsulfate (**11a**) and bis(3,4-dialkoxy-2′-stilbazole)silver(I) dodecylsulfate (**12a**)*

All homologues were made by the same method as for bis(3,4-dioctyloxy-2′-stilbazole)silver(I) dodecylsulfate which is described. Bis(3,4-dialkoxy-3′-stilbazole) silver(I) dodecylsulfates were made in the same way.

In a vessel protected from light, silver(I) dodecylsulfate (97 mg, 0.26 mmol) was stirred as a suspension in DCM (10 cm^3). 3,4-Dioctyloxy-2′-stilbazole (250 mg, 0.27 mmol) dissolved in DCM (10 cm^3) was added slowly. The mixture was stirred at room temperature for 4 h. It was then filtered through celite, to remove any unreacted silver(I) dodecylsulfate, and the solvent was removed in vacuo to leave a yellow residue, which was crystallised from hot acetone and recrystallised from hot methanol to give a colourless, crystalline solid (199 mg, 62%).

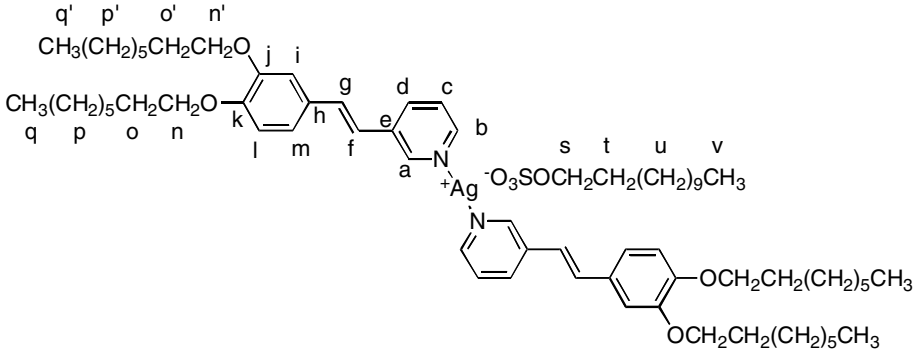

(11a)

^{1}H NMR (400 MHz, $CDCl_3$): $\delta = 8.92$ (2H, d, H**a**, $^4J_{HH} = 1.8$ Hz), 8.60 (2H, dd, H**b** $^3J_{HH} = 5.5$ Hz, $^4J_{HH} = 1.8$ Hz), 7.78 (2H, dt, H**d**, $^3J_{HH} = 8.0$ Hz, $^4J_{HH} = 1.8$ Hz), 7.29 (2H, dd, H**c**, $^3J_{HH} = 5.5$ Hz, $^3J_{HH} = 8.0$ Hz), 7.17 (2H, AB, H**g**, $J_{AB} = 16.3$ Hz), 7.07 (2H, d, H**i**, $^4J_{HH} = 1.8$ Hz), 7.03 (2H, dd, H**m**, $^3J_{HH} = 8.4$ Hz, $^4J_{HH} = 1.8$ Hz), 6.81 (2H, d, H**l**, $^3J_{HH} = 8.4$ Hz), 6.81 (2H, AB, H**f**, $J_{AB} = 16.3$ Hz), 4.14 (2H, t, Hs, $^3J_{HH} = 6.9$ Hz), 4.04 (4H, t, H**n**′, $^3J_{HH} = 6.6$ Hz), 4.02 (4H, t, H**n**, $^3J_{HH} = 6.3$ Hz), 1.83 (8H, m, H**o**, H**o**′), 1.65 (2H, m, H**t**), 1.54 (58H, m, H**p**, H**p**′, H**u**), 0.89 (15H, m, H**q**, H**q**′, H**v**).

4.6. Preparation of bis(3,4-dialkoxy-3′-stilbazole)silver(I) triflate (**11b**) and bis(3,4-dialkoxy-2′-stilbazole)silver(I) triflate (**12b**)

All homologues were made by the same method as for bis(3,4-dibutyloxy-3′-stilbazole) silver(I) triflate which is described. Bis(3,4-alkoxy-2′-stilbazole) silver(I) triflate was made in the same way.

4-Dibutyloxy-3′-stilbazole (0.300 g, 0.92 mmol) and silver(I) triflate (0.113 g, 0.044 mmol) were placed in a flask protected from light. Acetone (5 cm^3) was added and the mixture was stirred at room temperature for 4 h. After cooling in ice the colourless precipitate was filtered off and was washed with cold acetone giving a colourless solid of analytical purity (0.350 g, 86%).

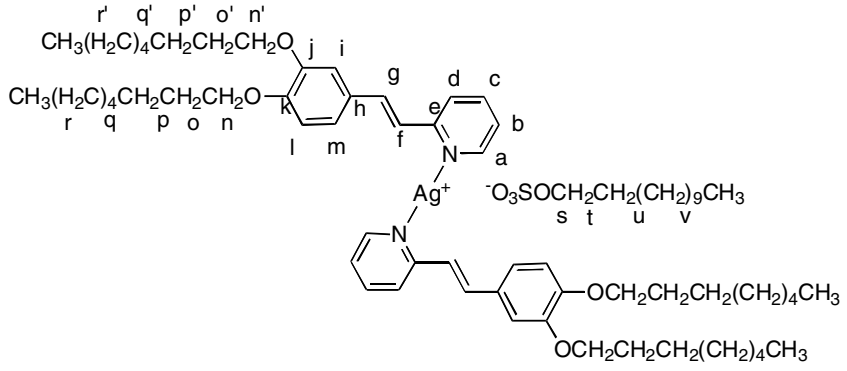

(12a)

^{1}H NMR (400 MHz, $CDCl_3$): $\delta = 8.95$ (2H, dd, H**a**, $^3J_{HH} = 4.5$ Hz, $^4J_{HH} = 1.5$ Hz), 7.80 (2H, dt, H**c**, $^3J_{HH} = 7.8$ Hz, $^4J_{HH} = 1.5$ Hz), 7.66 (2H, d, H**d**, $^3J_{HH} = 8.2$ Hz), (2H, dd, H**b**, $^3J_{HH} = 7.8$ Hz, $^3J_{HH} = 4.5$ Hz), 7.21 (2H, AB, H**g**, $J_{AB} = 16.2$ Hz), 7.06 (1H, AB, H**f**, $J_{AB} = 16.2$ Hz), 7.88 (2H, d, H**i**, $^4J_m = 1.8$ Hz), 6.84 (2H, d, H**m**, $^3J_{HH} = 8.2$ Hz, $^4J_{HH} = 1.8$ Hz), 6.68 (2H, d, H**l**, $^3J_{HH} = 8.2$ Hz), 4.09 (2H, t, H**s**, $^3J_{HH} = 6.7$ Hz), 3.96 (4H, t, H**n**′, $^3J_{HH} = 6.7$ Hz), 3.79 (4H, t, H**n**, $^3J_{HH} = 6.6$ Hz), 1.80 (4H, m, H**o**′), 1.73 (4H, m, H**o**), 1.63 (2H, m, H**t**), 1.52 (8H, m, H**p**, H**p**′), 1.34 (50H, m, H**q**, H**q**′, H**u**), 089 (15H, 2 × t, H**r**, H**r**′, $^3J_{HH} = 6.6$ Hz).

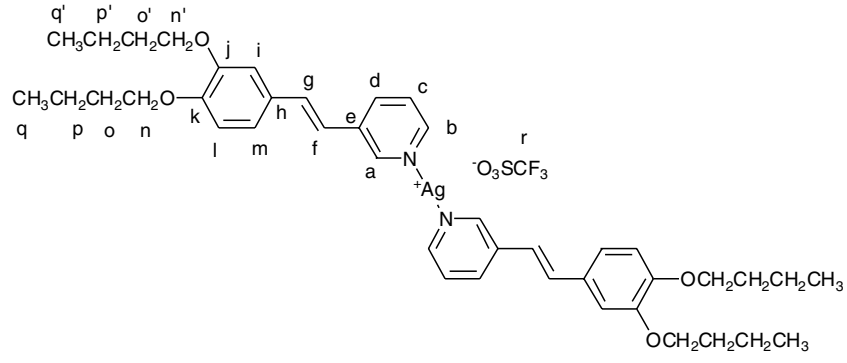

(11b)

^{1}H NMR (400 MHz, $CDCl_3$): $\delta = 8.84$ (2H, d, H**a**, $^4J_{HH} = 1.8$ Hz), 8.51 (2H, dd, H**b** $^3J_{HH} = 5.2$ Hz, $^4J_{HH} = 1.8$ Hz), 7.72 (2H, dt, H**d**, $^3J_{HH} = 8.1$ Hz, $^4J_{HH} = 1.8$ Hz), 7.24 (2H, dd, H**c**, $^3J_{HH} = 5.2$ Hz, $^3J_{HH} = 8.1$ Hz), 7.13 (2H, AB, H**g**, $J_{AB} = 16.4$ Hz), 7.05 (2H, d, H**i**, $^4J_{HH} = 1.8$ Hz), 6.99 (2H, d, H**m**, $^3J_{HH} = 8.3$ Hz, $^4J_{HH} = 1.8$ Hz), 6.80 (2H, d, H**l**, $J = 8.3$ Hz), 6.74 (2H, AB, H**f**, $J_{AB} = 16.4$ Hz), 4.03 (4H, t, H**n**′, $^3J_{HH} = 6.6$ Hz), 4.02 (4H, t, H**n**, $^3J_{HH} = 6.6$ Hz), 1.83 (8H, m, H**o**, H**o**′), 1.53 (8H, m, H**p**, H**p**′), 1.00 (12H, m, H**q**, H**q**′).

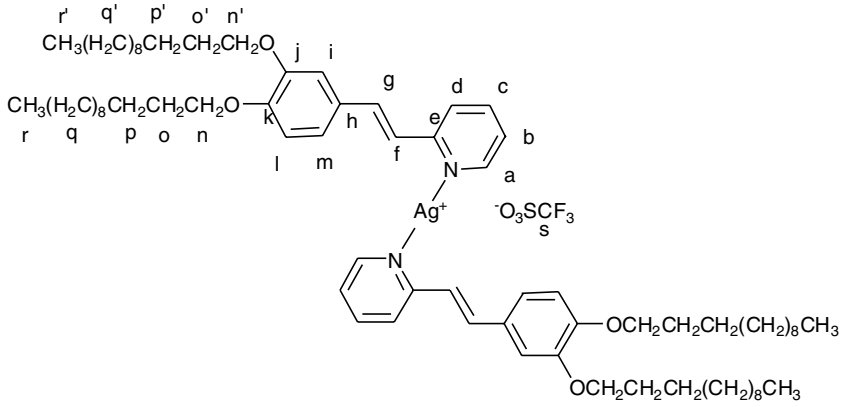

(12b)

^{1}H NMR (400 MHz, $CDCl_3$): $\delta = 8.95$ (2H, dd, H**a**, $^3J_{HH} = 4.5$ Hz, $^4J_{HH} = 1.5$ Hz), 7.80 (2H, dt, H**c**, $^3J_{HH} = 7.8$ Hz, $^4J_{HH} = 1.5$ Hz), 7.66 (2H, d, H**d**, $^3J_{HH} = 8.2$ Hz), (2H, dd, H**b**, $^3J_{HH} = 7.8$ Hz, $^3J_{HH} = 4.5$ Hz), 7.21 (2H, AB, H**g**, $J_{AB} = 16.2$ Hz), 7.06 (1H, AB, H**f**, $J_{AB} = 16.2$ Hz), 7.88 (2H, d, H**i**, $^4J_m = 1.8$ Hz), 6.84 (2H, d, H**m**, $^3J_{HH} = 8.2$ Hz, $^4J_{HH} = 1.8$ Hz), 6.68 (2H, d, H**l**, $^3J_{HH} = 8.2$ Hz), 3.96 (4H, t, H**n**′, $^3J_{HH} = 6.7$ Hz), 3.79 (4H, t, H**n**, $^3J_{HH} = 6.6$), 1.80 (4H, m, H**o**′), 1.73 (4H, m, H**o**), 1 (8H, m, H**p**, H**p**′), 1.34 (64H, m, H**q**, H**q**′), 089 (12H, 2 × t, H**r**, H**r**′, $^3J_{HH} = 6.6$ Hz).

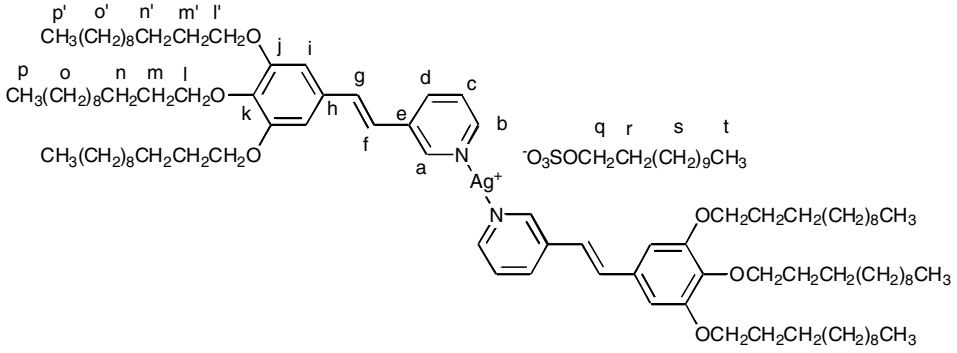

(13a)

*4.7. Preparation of bis(3,4,5-trialkoxy-3′-stilbazole)-silver(I) dodecylsulfate (**13a**) and bis(3,4,5-trialkoxy-2′-stilbazole)silver(I) dodecylsulfate (**14a**)*

The preparation of bis(3,4,5-dodecyloxy-2′-stilbazole)silver(I) dodecylsulfate is described and the octyloxy homologue was made in the same way. Bis(3,4,5-alkoxy-3′-stilbazole)silver(I) dodecylsulfates were prepared in the same way as is described for bis(3,4,5-alkoxy-2′-stilbazole)silver(I) dodecylsulfates except that the 2′-stilbazole was replaced by 3′-stilbazole.

In a vessel protected from light, silver(I) dodecylsulfate (56 mg, 0.15 mmol) was stirred as a suspension in DCM (10 cm^3). 3,4,5-Tridodecyloxy-2′-stilbazole (250 mg, 0.14 mmol) dissolved in DCM (10 cm^3) was added slowly. The mixture was stirred at room temperature for 4 h. It was then filtered over celite, to remove any unreacted silver(I) dodecylsulfate, and the solvent was removed in vacuo to leave a yellow residue. This was crystallised from hot acetone and recrystallised from hot methanol to give a colourless crystalline solid (189 mg, 67%).

^{1}H NMR (200 MHz, $CDCl_3$): $\delta = 8.90$ (2H, d, H**a**, $^4J_{HH} = 1.6$ Hz), 8.59 (2H, dd, H**b** $^3J_{HH} = 5.1$ Hz, $^4J_{HH} = 2.0$ Hz), 7.82 (2H, dt, H**d**, $^3J_{HH} = 8.07$ Hz, $^4J_{HH} = 2.0$ Hz), 7.29 (2H, dd, H**c**, $^3J_{HH} = 5.1$ Hz, $^3J_{HH} = 8.0$ Hz), 7.16 (2H, AB, H**g**, $J_{AB} = 16.3$ Hz), 6.90 (2H, AB, H**f**, $J_{AB} = 16.3$ Hz), 6.74 (4H, s, H**i**), 4.09 (2H, t, H**q**, $^3J_{HH} = 6.77$ Hz), 4.06 (8H, t, H**l**′, $^3J_{HH} = 6.8$ Hz), 3.99 (4H, t, H**l**, $^3J_{HH} = 6.8$ Hz), 1.80 (14H, m, H**m**, H**m**′, H**r**), 1.36

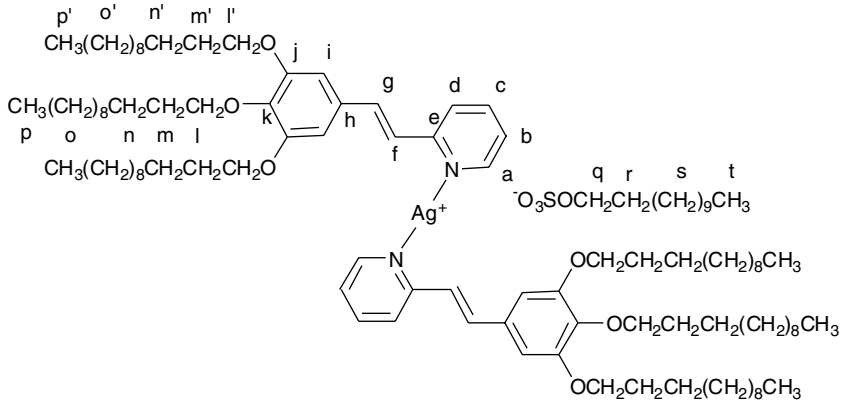

(14a)

(126H, m, H**n**, H**n**′, H**o**, H**o**′, H**s**), 0.88 (21H, m, H**p**, H**p**′, H**t**).

^{1}H NMR (400 MHz, $CDCl_3$): $\delta = 8.97$ (2H, dd, H**a**, $^3J_{HH} = 4.8$ Hz, $^4J_{HH} = 1.5$ Hz), 7.82 (2H, dt, H**c**, $^3J_{HH} = 7.7$ Hz, $^4J_{HH} = 1.5$ Hz), 7.65 (2H, d, H**d**, $^3J_{HH} = 7.7$ Hz), 7.33 (2H, dd, H**b**, $^3J_{HH} = 4.8$ Hz, $^3J_{HH} = 7.7$ Hz), 7.16 (2H, AB, H**g**, $J_{AB} = 15.8$ Hz), 7.06 (2H, AB, H**f**, $J_{AB} = 15.8$ Hz), 6.44 (4H, s, H**i**), 4.11 (2H, t, H**q**, $^3J_{HH} = 6.7$ Hz), 3.92 (4H, t, H**l**, $^3J_{HH} = 6.6$ Hz), 3.76 (8H, t, H**l**′ $^3J_{HH} = 6.0$), 1.69 (12H, m, H**m**′, H**m**), 1.34 (128H, m, H**n**, H**n**′, H**o**, H**o**′, H**r**, H**s**), 0.89 (21H, 2 × t, H**r**, H**r**′, H**t**, $^3J_{HH} = 6.4$ Hz).

*4.8. Preparation of bis(3,4,5-trialkoxy-3′-stilbazole) silver-(I) triflate (**13b**) and bis(3,4,5-trialkoxy-2′-stilbazole)-silver(I) triflate (**14b**)*

Bis(3,4,5-tridodecyloxy-3′-stilbazole)silver(I) triflate is described and the other homologues were prepared in the same way. Bis(3,4,5-dodecyloxy-2′-stilbazole)silver(I) triflate was also prepared in the same way except that the 3′-stilbazole was replaced by 2′-stilbazole.

3,4,5-Tridodecyloxy-3′-stilbazole (200 mg, 0.27 mmol) and silver(I) triflate (20 mg, 0.19 mmol) were placed in a flask protected from light. Acetone (5 cm^3) was added and the mixture was stirred at room temperature for 4 h. The mixture was then cooled in ice before being

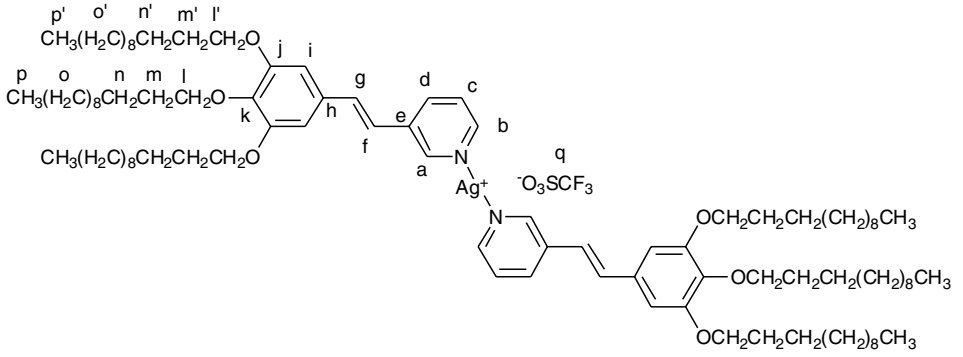

(13b)

filtered and washed with cold acetone giving a colourless solid (190 mg, 84%).

^{1}H NMR (400 MHz, $CDCl_3$): $\delta = 8.87$ (2H, d, H**a**, $^4J_{HH} = 1.6$ Hz), 8.50 (2H, dd, H**b** $^3J_{HH} = 5.2$ Hz, $^4J_{HH} = 1.8$ Hz), 7.82 (2H, dt, H**d**, $^3J_{HH} = 8.1$ Hz, $^4J_{HH} = 1.6$ Hz), 7.29 (2H, dd, H**c**, $^3J_{HH} = 5.2$ Hz, $^3J_{HH} = 8.1$ Hz), 7.14 (2H, AB, H**g**, $J_{AB} = 16.4$ Hz), 6.81 (2H, AB, H**f**, $J_{AB} = 16.4$ Hz), 6.73 (4H, s, H**i**), 4.01 (8H, t, H**l**′, $^3J_{HH} = 6.3$ Hz), 3.98 (4H, t, H**l**, $^3J_{HH} = 6.7$ Hz), 1.79 (12H, m, H**m**, H**m**′), 1.36 (108H, m, H**n**, H**n**′, H**o**, H**o**′), 0.88 (18H, m, H**p**, H**p**′).

^{1}H NMR (400 MHz, $CDCl_3$): $\delta = 8.91$ (2H, dd, H**a**, $^3J_{HH} = 5.1$ Hz, $^4J_{HH} = 1.5$ Hz), 7.85 (2H, dt, H**c**,

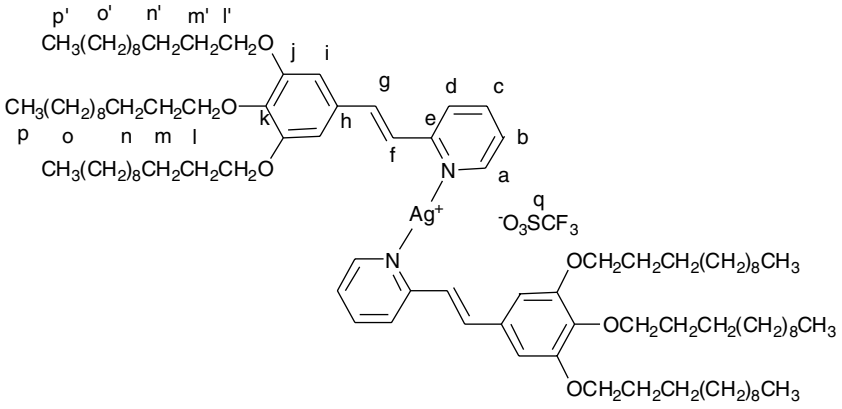

(14b)

$^3J_{HH} = 7.7$ Hz, $^4J_{HH} = 1.46$ Hz), 7.66 (2H, d, H**d**, $^3J_{HH} = 7.7$ Hz), 7.36 (2H, dd, H**b**, $^3J_{HH} = 5.1$ Hz, $^3J_{HH} = 7.7$ Hz), 7.15 (2H, AB, H**g**, $J_{AB} = 16.2$ Hz), 7.08 (2H, AB, H**f**, $J_{AB} = 16.2$ Hz), 6.41 (4H, s, H**i**), 3.91 (4H, t, H**l**, $^3J_{HH} = 6.5$ Hz), 3.73 (8H, t, H**l**′, $^3J_{HH} = 6.4$), 1.86 (12H, m, H**m**′, H**m**), 1.30 (108H, m, H**n**, H**n**′, H**o**, H**o**′), 0.81 (18H, 2 × t, H**r**, H**r**′, H**t**, $^3J_{HH} = 6.4$ Hz).

5. Supplementary material

Crystallographic data (excluding structure factors) for the structures in this paper, has been deposited with the Cambridge Crystallographic Data Centre as supplementary publication numbers CCDC 267944, 267945 and 267946. Copies of the data can be obtained, free of charge, on application to CCDC, 12 Union Road, Cambridge CB2 1EZ, UK (Fax: +44(0) 1223 336033 or e-mail: deposit@ccdc.cam.ac.uk).

Acknowledgements

We thank the EPSRC and the Collège Doctoral Européen de Strasbourg for support.

References

[1] B. Donnio, D. Guillon, R. Deschenaux, D.W. Bruce, in: J.A. McCleverty, T.J. Meyer (Eds.), Comprehensive Coordination Chemistry II, vol. 7, Elsevier, Oxford, UK, 2003, p. 357 (Chapter 7.9).
[2] R. Giménez, D.P. Lydon, J.L. Serrano, Curr. Opn. Solid State Mat. Sci. 6 (2002) 527.
[3] (a) See e.g. K. Willis, D.J. Price, H. Adams, G. Ungar, D.W. Bruce, J. Mater. Chem. 5 (1995) 2195;
(b) D.J. Price, K. Willis, T. Richardson, G. Ungar, D.W. Bruce, J. Mater. Chem. 7 (1997) 883.
[4] H.L. Nguyen, P.N. Horton, M.B. Hursthouse, A.C. Legon, D.W. Bruce, J. Am. Chem. Soc. 126 (2004) 16.
[5] D.W. Bruce, Adv. Inorg. Chem. 52 (2001) 151.
[6] B. Donnio, D.W. Bruce, J. Chem. Soc., Dalton Trans. (1997) 2745.
[7] D.W. Bruce, Acc. Chem. Res. 33 (2000) 831.
[8] C. Mongin, B. Donnio, D.W. Bruce, J. Am Chem. Soc. 123 (2001) 8426.
[9] D. Fazio, C. Mongin, B. Donnio, Y. Galerne, D. Guillon, D.W. Bruce, J. Mater. Chem. 11 (2001) 2852.
[10] D.M. Huck, H.L. Nguyen, S.J. Coles, M.B. Hursthouse, B. Donnio, D.W. Bruce, J. Mater. Chem. 12 (2002) 2879.
[11] J. Malthête, H.-T. Nguyen, C. Destrade, Liq. Cryst. 13 (1993) 171.
[12] H.-T. Nguyen, C. Destrade, J. Malthête, Adv. Mater. 9 (1997) 375.
[13] B. Donnio, D.W. Bruce, B. Heinrich, D. Guillon, H. Delacroix, T. Gulik-Krzywicki, Chem. Mater. 9 (1997) 2951.
[14] B. Donnio, D.W. Bruce, New J. Chem. 23 (1999) 275.
[15] (a) C.B. Ziegler Jr., R.F. Heck, J. Org. Chem. 43 (1978) 2941;
(b) W.C. Frank, Y.C. Kim, R.F. Heck, J. Org. Chem. 43 (1978) 2947;
(c) C.B. Ziegler Jr., R.F. Heck, J. Org. Chem. 43 (1978) 2949;
(d) N.A. Cortese, C.B. Ziegler Jr., R.F. Heck, J. Org. Chem. 43 (1978) 2952.
[16] A.E. Siegrist, Helv. Chim. Acta 50 (1967) 906.
[17] H. Meier, Angew. Chem. Int. Ed. Engl. 31 (1992) 1399.
[18] D.M. Huck, H.L. Nguyen, B. Donnio, D.W. Bruce, Liq. Cryst. 31 (2004) 503.
[19] J.F. Eckert, U. Maciejczuk, D. Guillon, J.F. Nierengarten, Chem. Commun. (2001) 1278.
[20] H. Adams, N.A. Bailey, D.W. Bruce, D.A. Dunmur, S.C. Davies, P.M. Maitlis, P.D. Hempstead, S.A. Hudson, S.J. Thorpe, J. Mater. Chem. 2 (1992) 395.
[21] H. Gallardo, R. Magnaco, A.J. Bortoluzzi, Liq. Cryst. 28 (2001) 1343.
[22] B. Donnio, B. Heinrich, H. Allouchi, J. Kain, S. Diele, D. Guillon, D.W. Bruce, J. Am. Chem. Soc. 126 (2004) 15258.
[23] S. Diele, P. Göring, in: D. Demus, J. Goodby, G.W. Gray, H.-W. Spiess, V. Vill (Eds.), Handbook of Liquid Crystals, vol. 2B, Wiley-VCH, Weinheim, 1998 (Chapter XIII).
[24] Collect: Data collection software, R. Hooft, Nonius B.V., 1998.
[25] Z. Otwinowski, W. Minor, in: C.W. Carter, R.M. Sweet Jr. (Eds.), Methods in Enzymology: Macromolecular Crystallography, part A, vol. 276, Academic Press, New York, 1997, pp. 307–326.
[26] G.M. Sheldrick, Acta Cryst. A46 (1990) 467.
[27] G.M. Sheldrick, University of Göttingen, Germany, 1977.

Available online at www.sciencedirect.com
SCIENCE DIRECT®
Polyhedron 25 (2006) 325–333
POLYHEDRON
www.elsevier.com/locate/poly

Fe(III) clusters built with tripodal alcohol ligands

Leigh F. Jones [a], David M. Low [a], Madeleine Helliwell [a], James Raftery [a], David Collison [a], Guillem Aromí [b], Joan Cano [b,c], Talal Mallah [c], Wolfgang Wernsdorfer [d], Euan K. Brechin [a,e,*], Eric J.L. Mcinnes [*,a]

[a] School of Chemistry, The University of Manchester, Oxford Road, Manchester M13 9PL, UK
[b] Departament de Química Inorgànica, Facultat de Química, Universitat de Barcelona, Diagonal 647, E-08028 Barcelona, Spain
[c] Laboratoire de Chimie Inorganique, UMR CNRS 8613, Université Paris-Sud, F-91405, Orsay, France
[d] Laboratoire Louis Néel -CNRS, 38042 Grenoble, Cedex 9, France
[e] School of Chemistry, The University of Edinburgh, West Mains Road, Edinburgh EH9 3JJ, UK

Received 21 April 2005; accepted 3 August 2005
Available online 29 September 2005

Dedicated to Prof. Malcolm Chisholm on the occasion of his 60th birthday.

Abstract

Reaction of the tripodal ligand 1,1,1-tris(hydroxymethyl)ethane (H_3thme) with a variety of Fe(III) precursors under both ambient and solvothermal conditions has led to the isolation of a number of new complexes ranging in nuclearity from 4 to 16. These include the rhomb or diamond-like clusters $[Fe_4(thme)_2Cl_4(O_2CR)_2(R'OH)_2]$ (**1**, R = Me, R′ = Et; **2**, R = Ph, R′ = Me; **3**, R = CMe_3, R′ = Me); the related nonanuclear and undecanuclear clusters $[Fe_9O_4(O_2CCMe_3)_{13}(thme)_2]$ (**4**) and $[NEt_4][Fe_{11}O_4(O_2CPh)_{10}(thme)_4(dmhp)_2Cl_4]$ (**5**) (dmhp = 4,6-dimethyl-2-hydroxypyrimidine) and the octametallic and hexadecametallic wheels $[Fe_8(O_2CR)_{12}(thme)_4]$ (**6**, R = Ph; **7**, R = CMe_3) and $[Fe_{16}(EtO)_4(O_2CPh)_{16}(Hthme)_{12}](NO_3)_4$ (**8**). Magnetic studies reveal the presence of dominant antiferromagnetic interactions between the Fe centres in all eight complexes which results in the presence of small spin ground states for complexes **1**–**4** and **6**–**8**. For **5** however, these stabilise an $S = 11/2$ spin ground state with an axial zero-field splitting parameter of $D = -0.46\ cm^{-1}$. Single crystal hysteresis loops in magnetisation versus external magnetic field measurements show the temperature and sweep rate dependence indicative of single-molecule magnetism behaviour.
© 2005 Elsevier Ltd. All rights reserved.

Keywords: Iron; Clusters; Single-molecule magnets

1. Introduction

Polymetallic cluster complexes of paramagnetic transition metal ions have attracted intense study since the discovery that such molecules can display the phenomenon of single-molecule magnetism (SMM) [1]. There is a barrier to relaxation of magnetisation in SMMs due to the combination of a large ground state spin multiplicity and a significant negative zero-field splitting of that ground state and this imparts a molecular magnetic memory effect that can be observed as hysteresis loops in M versus H studies. All SMMs made to date only exhibit this memory effect at very low temperatures and there is therefore an intense effort in synthesizing larger clusters in an attempt to generate larger spin ground states and higher energy barriers to loss of magnetization [2]. Here, we describe the synthesis of some new Fe^{III} clusters with the tripodal ligand 1,1,1-tris(hydroxymethl)ethane (H_3thme). Tripodal ligands such as H_3thme have previously been used in the solvothermal synthesis of oxo-vanadium and oxo-molybdenum clusters but until recently, very rarely in the synthesis of paramagnetic 3d transition metal clusters [3]. To date most cluster

* Corresponding author. Tel.: +44 131 650 7545; fax: +44 131 650 4743.
E-mail addresses: ebrechin@staffmail.ed.ac.uk (E.K. Brechin), eric.mcinnes@manchester.ac.uk (E.J.L. Mcinnes).

0277-5387/$ - see front matter © 2005 Elsevier Ltd. All rights reserved.
doi:10.1016/j.poly.2005.08.034

synthesis has involved "conventional" coordination chemistry techniques, i.e., solution chemistry under atmospheric pressure and at temperatures limited to the boiling points of common solvents. Solvothermal techniques allow the application of high temperatures to reactions in low boiling solvents and are also an excellent method for the preparation of pure, crystalline products [4]. In this work, we have explored reactions of Fe^{III} precursors with H_3thme under both ambient and solvothermal conditions and we observe a very wide range of cluster topologies and nuclearities depending on subtle changes in the reaction conditions.

2. Experimental

2.1. Synthesis

The complexes $[Fe_3O(O_2CR)_6(H_2O)_3]X$ (R = Me, CMe_3, Ph; X = Cl, NO_3, O_2CMe_3) and $[NEt_4]_2[Fe_2OCl_6]$ were made as previously described [5].

2.1.1. $[Fe_4(thme)_2Cl_4(O_2CMe)_2(EtOH)_2]$ (**1**)

$FeCl_3 \cdot 6H_2O$ (2.0 g, 7.39 mmol), H_3thme (0.30 g, 2.46 mmol) and NaO_2CMe (0.61 g, 7.39 mmol) were dissolved in acetonitrile (30 ml) with stirring. The resultant yellow solution was stirred for 8 h, filtered and taken to dryness under reduced pressure. The resulting residue was then re-dissolved in MeOH (15 ml) and filtered. Yellow crystals grew upon diffusion of ethanol during three weeks. Yield: ~17%. Elemental *Anal*. Calc. for **1**: C, 45.86; H, 7.60; Fe, 15.99. Found: C, 45.91; H, 7.68; Fe, 16.02%. IR (KBr; ν/cm^{-1}): 2997 (w), 2953 (m), 2912 (w), 2862 (w), 1527 (s), 1461 (w), 1433 (s), 1399 (w), 1321 (m), 1208 (w), 1119 (m), 1016 (s), 979 (s), 917 (w), 866 (m), 722 (w), 663 (m), 608 (m), 551 (w), 502 (s), 413 (w).

2.1.2. $[Fe_4(thme)_2Cl_4(O_2CPh)_2(MeOH)_2]$ (**2**)

$FeCl_3 \cdot 6H_2O$ (2.0 g, 7.39 mmol), H_3thme (0.30 g, 2.46 mmol) and NaO_2CPh (1.06 g, 7.39 mmol) were dissolved in methanol (30 ml) with stirring. The yellow solution was stirred for 8 h, filtered and taken to dryness under reduced pressure. The resulting residue was re-dissolved in methanol (15 ml) and filtered. Yellow-brown crystals grew upon diffusion of diethyl ether during three weeks. Yield: ~20 %. Elemental *Anal*. Calc. for **2**: C, 37.00; H, 4.14; Cl, 14.56; Fe, 22.94. Found: C, 37.69; H, 3.61; Cl, 14.59; Fe, 22.25%. IR (KBr; ν/cm^{-1}): 2976 (w), 2934 (w), 2867 (w), 1600 (m), 1562 (m), 1519 (m), 1493 (w), 1406 (s), 1178 (m), 1121 (m), 1070 (m), 1017 (s), 918 (w), 834 (w), 790 (w), 721 (m), 676 (w), 607 (w), 488 (s), 406 (w).

2.1.3. $[Fe_4(thme)_2Cl_4(O_2CCMe_3)_2(MeOH)_2]$ (**3**)

$FeCl_3 \cdot 6H_2O$ (2.0 g, 7.39 mmol), H_3thme (0.30 g, 2.46 mmol) and NaO_2CCMe_3 (0.92 g, 7.39 mmol) were dissolved in methanol (30 ml) with stirring. The yellow solution was stirred for 8 h, filtered and taken to dryness under reduced pressure. The resulting residue was re-dissolved in methanol (15 ml) and filtered. Yellow-brown crystals grew upon diffusion of diethyl ether after 2–3 weeks. Yield: ~17 %. Elemental *Anal*. Calc. for **3**: C, 32.47; H, 4.77; Cl, 15.97; Fe, 25.16. Found: C, 31.89; H, 4.46; Cl, 16.50; Fe, 24.39%. IR (KBr) ν/cm^{-1}): 2932 (w), 2863 (w), 1587 (m), 1561 (w), 1514 (s), 1445 (w), 1401 (s), 1177 (w), 1119 (m), 1037 (m), 1017 (s), 985 (w), 913 (w), 723 (s), 677 (m), 607 (m), 487 (s).

2.1.4. $[Fe_9O_4(O_2CCMe_3)_{13}(thme)_2]$ (**4**)

$[Fe_3O(O_2CCMe_3)_6(H_2O)_3](O_2CCMe_3)$ (0.30 g, 0.32 mmol) and H_3thme (0.038 g, 0.32 mmol) were dissolved in acetonitrile (6 ml) and placed in a 23 ml Teflon-lined autoclave. This was then heated at a rate of 1.0 °C min^{-1} to 150 °C and maintained at this temperature for 12 h. Cooling to room temperature at a rate of 0.05 °C min^{-1} resulted in the formation of large orange/brown crystals. These were washed with several portions of fresh acetonitrile and air dried. Yield: ~50 %. Elemental *Anal*. Calc. for **4**: C, 44.75; H, 6.63; Fe, 20.80. Found: C, 45.13; H, 7.26; Fe, 20.93%. IR (KBr ν/cm^{-1}): 29.62 (s), 2931 (m), 2903 (m), 2873 (m), 1567 (s), 1538 (s), 1484 (s),1459 (m) 1428 (s), 1393 (w), 1379 (s), 1362 (m), 1230 (s), 1153 (m), 1073 (s), 1015 (s), 966 (w), 939 (w), 919 (w), 896 (w), 788 (m), 608 (s), 441 (s).

2.1.5. $[NEt_4][Fe_{11}O_4(O_2CPh)_{10}(thme)_4(dmhp)_2Cl_4]$ (**5**)

$[NEt_4][Fe_2OCl_6]$ (0.5 g, 0.83 mmol), NaO_2CPh (0.24 g, 1.66 mmol) dmhp (0.103 g, 0.83 mmol) and H_3thme (0.1 g, 0.83 mmol) were added to MeCN (30 ml) and stirred for 12 h and then filtered. The resulting orange solution was allowed to evaporate yielding complex **5** in approximately 20% yield after one week. Elemental *Anal*. Calc. for **5**: C, 45.86; H, 4.24; N, 2.43. Found: C, 45.15; H, 4.23; N, 2.57%. IR (KBr ν/cm^{-1}): 1590 (w), 1533 (s), 1480 (m), 1447 (w), 1394 (s), 1171 (w), 1123 (w) , 1047 (m), 1021 (m), 996 (m), 778 (w), 721 (m), 677 (w), 608 (w), 477 (m).

2.1.6. $[Fe_8(O_2CPh)_{12}(thme)_4]$ (**6**)

(a) $[Fe_3O(O_2CPh)_6(H_2O)_3]Cl$ (0.30 g, 0.30 mmol) and H_3thme (0.036 g, 0.30 mmol) were dissolved in acetonitrile and placed in a 23 ml Teflon-lined autoclave. This was then heated at a rate of 1.0 °C min^{-1} to 150 °C and maintained at this temperature for 12 h. Cooling to room temperature at a rate of 0.05 °C min^{-1} resulted in the formation of large orange/brown crystals. These were washed with several portions of fresh acetonitrile and air dried. Yield: ~50%. (b) $[Fe_3O(O_2CPh)_6(H_2O)_3](NO_3)$ (0.5 g 0.49 mmol) and H_3thme (0.06 g, 0.49 mmol) were stirred in MeCN (30 ml) for 12 h. The resulting precipitate was filtered, air-dried and re-dissolved in CH_2Cl_2. Crystals formed in two days after diffusion of diethyl ether into the solution in approximately 30% yield.

Elemental *Anal*. Calc. for **6**: C, 52.74; H, 4.09; Fe, 18.75. Found: C, 52.73; H, 4.10; Fe, 18.86%. IR (KBr ν/cm^{-1}): 3055 (w), 1598 (m), 1555 (m), 1530 (m), 1521 (m), 1429

(s), 1307 (w), 1177 (m), 1152 w), 1065 (m), 1023 (w), 1011 (m), 838 (w), 718 (s), 676 (m), 623 (m), 588 (m), 477 (s), 442 (w).

2.1.7. $[Fe_8(O_2CCMe_3)_{12}(thme)_4]$ (7)

$[Fe_3O(O_2CCMe_3)_6(H_2O)_3]Cl$ (0.30 g, 0.34 mmol) and H_3thme (0.041 g, 0.34 mmol) were dissolved in acetonitrile and placed in a 23 ml Teflon-lined autoclave. This was then heated at a rate of 1.0 °C min^{-1} to 150 °C and maintained at this temperature for 12 h. Cooling to room temperature at a rate of 0.05 °C min^{-1} resulted in the formation of large orange/brown crystals. These were washed with several portions of fresh acetonitrile and air dried. Yield: ~50 %. Elemental *Anal*. Calc. C, 45.15; H, 6.82; Fe, 20.95. Found: C, 45.13; H, 7.07; Fe, 20.99%. IR (KBr) ν/cm^{-1}: 2962 (m), 2931 (w), 1567 (s), 1536 (s), 1484 (s), 1427 (s), 1379 (m), 1362 (m), 1231 (s), 1153 (w), 1071 (s), 1015 (m), 897 (w), 789 (w), 606 (m), 442 (s).

2.1.8. $[Fe_{16}(EtO)_4(O_2CPh)_{16}(Hthme)_{12}](NO_3)_4$ (8)

$[Fe_3O(O_2CPh)_6(H_2O)_3](NO_3)$ (0.5 g, 0.49 mmol) and H_3thme (0.06 g, 0.49 mmol) were stirred in MeCN (30 ml) for 12 h. The resulting precipitate was filtered, air-dried and re-dissolved in a 1:1 mixture of CH_2Cl_2 and EtOH. Crystals formed after two days in approximately 15% yield. Elemental *Anal*. Calc. C, 46.22; H, 4.74; N, 1.20. Found: C, 46.08; H, 4.41; N, 1.14%. Selected IR data (KBr pellet, cm^{-1}): 1554 (s), 1528 (s) 1493 (m), 1409 (s), 1307 (w), 1176 (m), 1158 (w), 1069 (w), 1045 (m), 1025 (m), 877 (w), 717 (s).

2.2. X-ray crystallography and structure solution

All structures were solved by direct methods. The data are summarised in Table 1.

For complexes **1**, **2**, and **6** all the non-hydrogen atoms were refined anisotropically and the H atoms were included in calculated positions. **3**: the asymmetric unit contains half a molecule and two disordered MeOH molecules. The CMe_3 group of the pivalates was disordered. All non-H atoms were refined anisotropically except those of the disordered atoms of the solvent at lower occupancy. H atoms were included in calculated positions except those bonded to C1T and C2T which were omitted. **4**: a number of the CMe_3 groups were disordered over two sites whose occupancies were constrained to sum to 1.0 with restraints on the geometric parameters. All non-H atoms were refined anisotropically except the disordered atoms. H atoms were included in calculated positions. **5**: the asymmetric unit contains half the molecule together with a number of solvent fragments; there are two CH_2Cl_2 molecules and three highly disordered fragments which were not recognisable so the atoms were all defined as C with some at occupancy 0.5. The non-H atoms were refined anisotropically. H atoms were included in calculated positions except those of the disordered solvent. **7**: the atoms C23–C25 and C42, C43, C45 were disordered over two sites each whose

Table 1
Crystallographic details for complexes **1**-**8**

	1[Fe_4]	**2**[Fe_4]	**3**[Fe_4]	**4**[Fe_9]	**5**[Fe_{11}]	**6**[Fe_8]	**7**[Fe_8]	**8**[Fe_{16}]
Formula	$C_{18}H_{36}Cl_4Fe_4O_{12}$	$C_{34}H_{44}Cl_4Fe_4O_{14}$	$C_{26}H_{58}Cl_4Fe_4O_{16}$	$C_{75}H_{135}Fe_9O_{36}$	$C_{131}H_{130}Cl_4Fe_{11}N_{14}O_{38}$	$C_{117}H_{96}Fe_8O_{38}$	$C_{81}H_{145.5}Fe_8N_{0.50}O_{36}$	$C_{196}H_{204}Cl_8Fe_{16}O_{82}$
M (g mol^{-1})	809.67	1041.89	991.92	2115.48	3264.64	2556.74	2149.28	5048.81
Crystal system	monoclinic	orthorhombic	monoclinic	monoclinic	monoclinic	monoclinic	monoclinic	tetragonal
Space group	$P2(1)/n$	$Pbca$	$P2(1)/c$	$P2(1)/c$	$P2(1)/c$	$P2(1)$	$C2/c$	$P4(2)/n$
a (Å)	8.3469(11)	9.6283(10)	12.583(7)	15.350(3)	13.9889(9)	16.490(15)	27.147(2)	24.7413(16)
b (Å)	16.265(2)	16.8943(18)	16.947(12)	28.114(3)	21.5807(15)	22.51(2)	17.3115(12)	24.7413(16)
c (Å)	10.6978(15)	27.275(3)	9.820(10)	24.484(2)	23.9145(16)	18.531(7)	44.931(3)	20.6068(19)
α (°)	90.00	90.00	90.00	90.00	90.00	90.00	90.00	90.00
β (°)	96.873(2)	90.00	96.41(7)	108.025(11)	94.753(1)	115.563(1)	91.6430(10)	90.00
γ (°)	90.00	90.00	90.00	90.00	90.00	90.00	90.00	90.00
V (Å^3)	1441.9(3)	4436.7(8)	2081(3)	10047(2)	7194.7(8)	6204(10)	21107(3)	12614.1(16)
T (K)	100(2)	100(2)	100(2)	100(2)	100(2)	100(2)	100(2)	100(2)
Z	2	4	2	4	2	2	8	2
P_{calc} (g cm^{-3})	1.865	1.560	1.583	1.398	1.507	1.369	1.353	1.358
Crystal shape/colour	yellow prism	brown cuboid	brown block	brown plate	brown prism	yellow plate	yellow plate	yellow plate
μ (mm^{-1})	2.398	1.582	1.685	1.335	1.229	0.985	1.142	1.057
Unique data	3405	5366	4224	20458	14643	21439	21549	11123
Unique data ($I > 2\sigma(I)$)	2838	4705	3855	13963	11583	14358	15951	8547
R_1, wR_2	0.0401, 0.0755	0.0422, 0.0957	0.0417, 0.1072	0.0920, 0.1449	0.040, 0.1105	0.097, 0.2369	0.0565, 0.1375	0.0952, 0.2717

occupancies were constrained to sum to 1.0. There were two partially occupied MeCN solvent molecules one of which was incomplete. All non-H atoms were refined anisotropically except the disordered atoms and those of the solvent. H atoms were included in calculated positions except those of the solvent. **8**: initially, the *R* value was very high and twinning was suspected. A twin matrix which exchanges the *h* and *k* axes was applied (01010000−1), and the twin fraction was found to be 0.44788. Accounting for the twinning reduced the *R* value from over 30% to under 10%. The asymmetric unit contains one quarter of the molecule together with a nitrate and a disordered solvent fragment, assumed to be CH_2Cl_2, and some water molecules. The phenyl rings were constrained to ideal geometry. Most of the non-H atoms were refined anisotropically except those of the solvent fragments, using restraints. H atoms were included in calculated positions except for the solvent H atoms.

3. Crystal structure description

3.1. Structure of $[Fe_4(thme)_2Cl_4(O_2CR)_2(R'OH)_2]$ (**1**, R = Me, R′ = Et; **2**, R = Ph, R′ = Me; **3**, R = CMe_3, R′ = Me)

The core structures of complexes **1**–**3** (Fig. 1) are isostructural and consist of a central $[Fe_4O_6]^{6+}$ planar rhomb or diamond in which each of the oxygen atoms is derived from bridging $[thme]^{3-}$ ligands. These sit one-above and one-below the $[Fe_4]$ plane and each provide one μ_3-oxygen arm that bridges between the two central Fe^{III} ions and one outer Fe^{III} ion, and two μ_2-oxygen arms that each bridge between an outer and central Fe^{III} ion. These ions are also bridged by the two carboxylates which adopt their common *syn*, *syn* μ-mode. Each of the four Fe^{III} ions contains a terminal chloride ion, while the coordination spheres of each of the two terminal Fe ions is completed by one R′OH molecule. The Fe centres are in distorted octahedral geometries and all are in the +3 oxidation state as confirmed by a combination of charge balance and bond length considerations and BVS calculations.

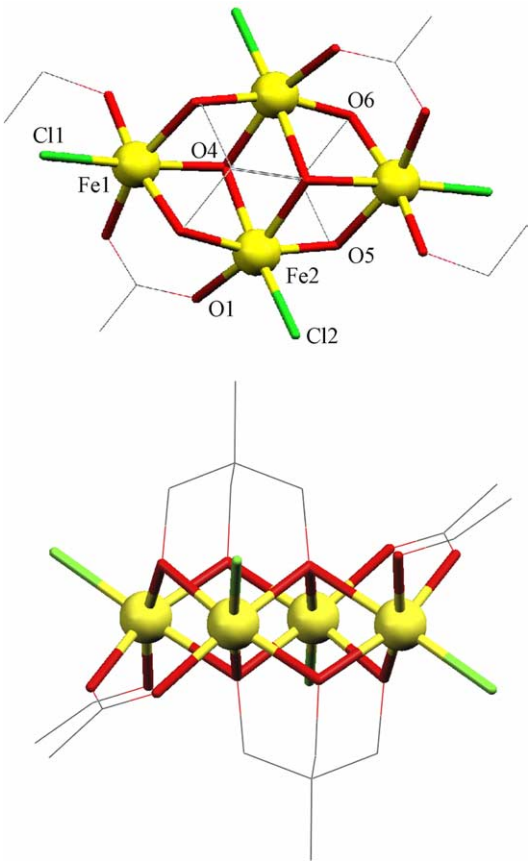

Fig. 1. The structure of complex **1** viewed perpendicular (top) and parallel (bottom) to the $[Fe_4]$ plane.

3.2. Structure of $[Fe_9O_4(O_2CCMe_3)_{13}(thme)_2]$ (**4**)

Complex **4** (Fig. 2) has a near planar rhomb-like array of nine Fe^{III} ions linked via a combination of oxide and alkoxide ions to give a $[Fe_9(O^{2-})_4(RO^{1-})_6]^{13+}$ core. Closer inspection reveals that the complex contains the identical $[Fe_4O_6]^{6+}$ rhomb (Fe6–Fe9, O25–O30) seen in complexes **1**–**3**. To this rhomb are now attached four $[Fe_3O]^{7+}$ triangular units which each share one Fe ion (Fe8, Fe9 or Fe6) with the $[Fe_4O_6]^{6+}$ rhomb. The two central $[Fe_3O]^{7+}$ triangular units (containing Fe2, Fe3, Fe9 and O6 and Fe3, Fe4, Fe9 and O11) edge share to form a $[Fe_4O_2]^{8+}$ rhomb. The two peripheral $[Fe_3O]^{7+}$ triangles (containing Fe4, Fe5, Fe6 and O16, and Fe1, Fe2, Fe8 and O1) each share one vertex with the $[Fe_4O_2]^{8+}$ rhomb and one vertex with the $[Fe_4O_6]^{6+}$ rhomb. The $[Fe_4O_6]^{6+}$ unit and the $[Fe_3O]^{7+}$ triangles are linked to each other through the thirteen carboxylate ligands that bind in three different modes: the usual μ, η_1, η_1, mode, the less common μ, η_2, η_1 mode

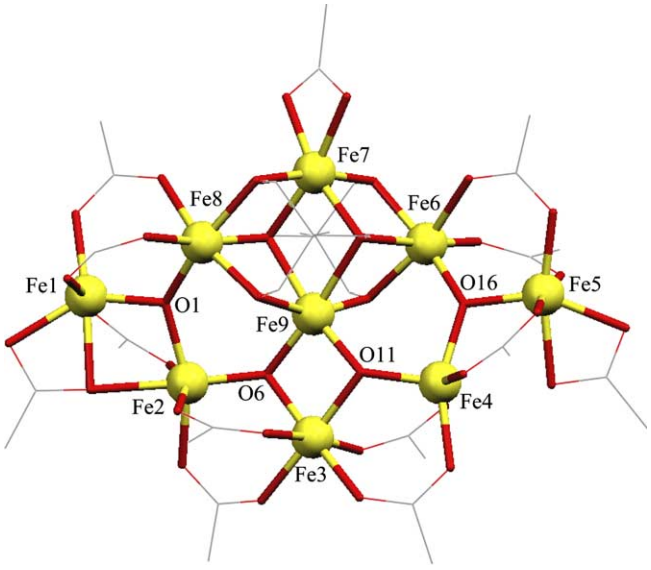

Fig. 2. The structure of complex **4** viewed perpendicular to the $[Fe_9]$ 'plane'.

(e.g., between Fe1 and Fe2), and as simple chelates (completing the coordination geometries of Fe(5) and Fe(7)).

All the Fe ions are in the +3 oxidation state and exhibit distorted octahedral geometries, with the exception of Fe(4), which is five-coordinate and in a distorted square based pyramidal geometry.

3.3. Structure of $[NEt_4][Fe_{11}O_4(O_2CPh)_{10}(thme)_4(dmhp)_2Cl_4]$ (5)

The structure of complex **5** (Fig. 3) closely resembles that observed in **1**–**3** and **4**. This time the structure contains two identical $[Fe_4O_6]^{6+}$ rhombs (containing Fe2, Fe4, Fe5 and Fe6 and symmetry equivalents), one at each 'end' of the molecule, linked to a central linear $[Fe_3O_4]^{1+}$ unit (containing Fe1, Fe3 and Fe1A). Alternatively the core can be thought of as four vertex sharing $[Fe_4]^{n+}$ units in which the two peripheral $[Fe_4O_6]^{6+}$ rhombs are connected to two central $[Fe_4O_2]^{8+}$ rhombs (comprising Fe1, Fe2 and symmetry equivalents) which themselves share one vertex (Fe3) forming a $[M_7O_4]^{13+}$ sub-unit. The 10 $PhCO_2^-$ ligands bridge in their familiar *syn*, *syn* μ-mode both within and between the various $[Fe_4]$ units. The coordination geometries of Fe2 and Fe4 are completed by a combination of terminal Cl^- ions and neutral dmhp ligands. These latter ligands are protonated with the nitrogen atom hydrogen bonding to a μ_2-oxygen of a $thme^{3-}$ ligand. The $[M_4]$ units seen in all of the above complexes are common building blocks in the structures of Fe^{III} and Mn^{III} clusters and the $[M_7O_4]^{13+}$ sub-unit is also a common feature in larger clusters, including $[Fe_{17}]$/$[Fe_{19}]$ [6], $[Mn_8]$ [7], and $[Fe_{11}]$ clusters [8]. In fact the $[Fe_{11}]$ core is similar to a $[Mn_{11}]$ cluster reported by Christou and co-workers [9], but in this case the peripheral units are $[Mn_4]$ cubes not rhombs.

While there are many examples of tetranuclear Fe aggregates, complex **4** is only the fifth nonanuclear Fe cluster reported [10] and complex **5** is only the second undecanuclear Fe complex reported. The original $[Fe_{11}]$ has no structural resemblance to **5** being based on a penta-capped trigonal prism [5].

3.4. Structure of $[Fe_8(O_2CR)_{12}(thme)_4]$ (6, R = Ph; 7, R = CMe_3)

The structure of both complex **6** and complex **7** (Fig. 4) can be described as a wheel of eight Fe^{III} ions bridged by a combination of RCO_2^- and $thme^{3-}$ ligands. The RCO_2^- ligands bridge neighbouring Fe^{III} ions in the usual *syn*, *syn* μ-manner while the triply-deprotonated $thme^{3-}$ ligands show much greater flexibility in each bridging four iron centres – each arm providing a μ_2-oxygen for adjacent metals. The iron ions all lie in distorted octahedral geometries and are of four types: Fe1, Fe3, Fe5 and Fe7 are bridged to three RCO_2^- and two $thme^{3-}$ ligands; Fe2 and Fe6 are bound to four RCO_2^- and two $thme^{3-}$ ligands; and Fe4 and Fe8 bond to two RCO_2^- and two $thme^{3-}$ ligands. The "Fe_8" wheel is non-planar and perhaps best described as ladle-shaped with a diameter of approximately 8 Å.

3.5. Structure of $[Fe_{16}(EtO)_4(O_2CPh)_{16}(Hthme)_{12}](NO_3)_4$ (8)

The size of the wheel seen in complex **7** is doubled by the addition of a coordinating alcohol in the crystallisation step – use of EtOH produces the hexadecametallic wheel $[Fe_{16}(EtO)_4(O_2CPh)_{16}(Hthme)_{12}](NO_3)_4$. Complex **8** (Fig. 5) can be described as a wheel of sixteen Fe^{III} ions bridged by $PhCO_2^-$, $Hthme^{2-}$ and EtO^- ligands. The

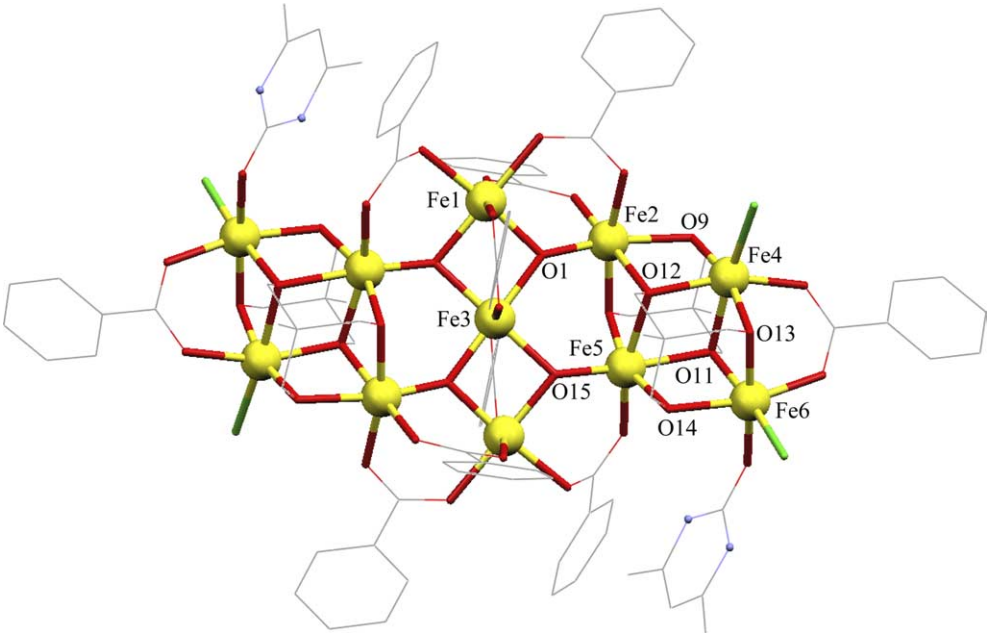

Fig. 3. The structure of complex **5** viewed perpendicular to the $[Fe_{11}]$ 'plane'.

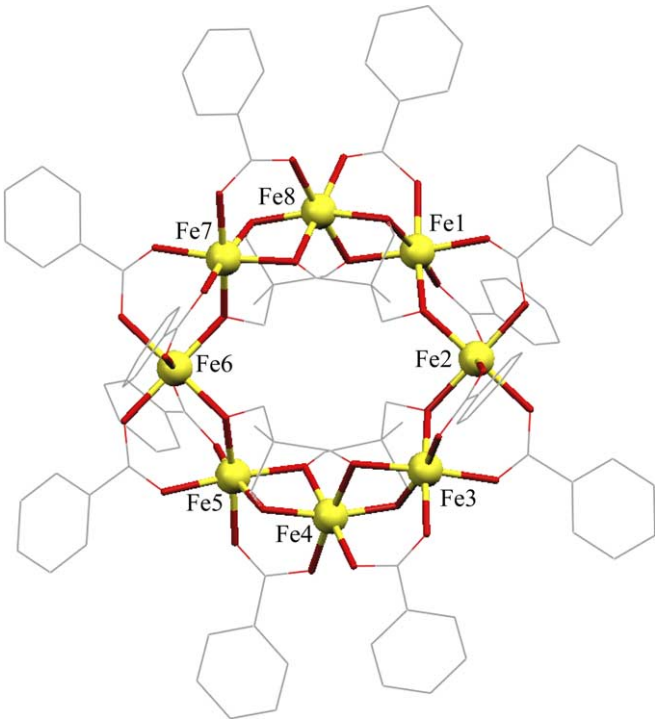

Fig. 4. The structure of complex **6** viewed parallel to the [Fe8] 'plane'.

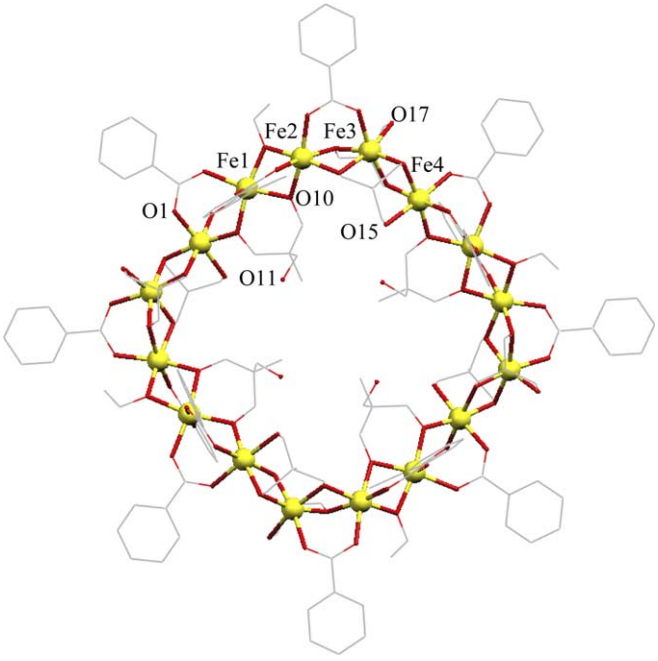

Fig. 5. The structure of complex **8** viewed perpendicular to the [Fe_{16}] 'plane'.

$PhCO_2^-$ ligands again bridge in their familiar μ-mode: above, below and in the 'plane' of the [Fe_{16}] wheel. The $Hthme^{2-}$ ligands are of two types. Eight ligands use their two deprotonated arms as μ_2-bridges forming a nearly linear chain of three metals, with the third protonated arm bonded only to the central iron center. Four $Hthme^{2-}$ ligands occupy the central cavity of the wheel: the deprotonated arms again acting as μ_2-bridges, with the protonated arm hydrogen bonding to the monodentate arm of an adjacent $Hthme^{2-}$ ligand (for example, O11–O15B 2.591(6) Å) and to a water molecule above the central cavity of the wheel (O11–O1S, 2.804(6)) Å. The four EtO^- ligands each bridge two iron centres on the outside edge of the wheel. The iron ions are all in distorted octahedral geometries and bound to six oxygen atoms. For Fe(1) these are derived from three $PhCO_2^-$, two $Hthme^{2-}$ ligands and one EtO^-. For Fe(2) from two $PhCO_2^-$, three $Hthme^{2-}$ ligands and one EtO^-. For Fe(3) from one $PhCO_2^-$ and five $Hthme^{2-}$ ligands, and for Fe(4) from two $PhCO_2^-$ and four $Hthme^{2-}$ ligands. Again the wheel is non-planar and best described as bowl-shaped with an approximate diameter of 16 Å.

4. Magnetic measurements

4.1. Magnetism of $[Fe_4(thme)_2Cl_4(O_2CR)_2(R'OH)_2]$ (1–3)

Solid state DC susceptibility measurements of complexes **1**–**3** were taken in the range of 2–300 K in a field of 3 kG. The data for all three complexes is essentially identical and here we limit our discussion to complex **1**. The $\chi_m T$ value of 10.61 $cm^3\,mol^{-1}$ K at 300 K gradually decreases with decreasing temperature to a minimum of 1.24 $cm^3\,mol^{-1}$ K at 6 K before increasing slightly to 1.52 $cm^3\,mol^{-1}$ K at 2 K. The spin only ($g = 2$) value expected for four non-interacting Fe^{III} centres is approximately 17.5 $cm^3\,mol^{-1}$ K. This behaviour is indicative of antiferromagnetic exchange between the Fe^{III} centres with the $\chi_m T$ value at low temperature consistent with a ground state spin of $S = 0$ or $S = 1$. Magnetisation data were collected in the range of 0–5.0 T at 2 K. The magnetisation increases beyond the expected saturation value for $S = 1$, most likely because higher multiplicity states become more stable as the magnetic field is increased due to the close proximity of these states to the ground state. Because of this no fit of the data was attempted.

4.2. Magnetism of $[Fe_9O_4(O_2CCMe_3)_{13}(thme)_2]$ (4)

Solid state DC susceptibility measurements of complex **4** were taken in the range 2–300 K in a field of 5 kG. The $\chi_m T$ value of 28.3 $cm^3\,mol^{-1}$ K at 300 K gradually decreases with decreasing temperature approaching a value of approximately 0.40 $cm^3\,mol^{-1}$ K at 2 K. The room temperature $\chi_m T$ value is smaller than the spin only value for nine non-interacting high spin Fe^{III} centres (39.38 $cm^3\,mol^{-1}$ K) indicating the presence of antiferromagnetic interactions. The low temperature value is close to that expected for a complex exhibiting a $S = 1/2$ spin ground state. Magnetisation data collected in the range of 0–5.0 T at 2 K are consistent with a small spin ground state with the presence of low-lying excited states of larger multiplicity that become

populated with increasing field – as indicated by an inflexion point (at ca. 2.2 T) and the continual rise in magnetization with applied field.

4.3. Magnetism of $[NEt_4][Fe_{11}O_4(O_2CPh)_{10}(thme)_4(dmhp)_2Cl_4]$ (5)

Solid state dc magnetization measurements were performed on **5** in the range 2–300 K in a field of 0.2 T between 300 and 50 K and 0.05 T between 50 and 2.0 K. (Fig. 6). The room temperature $\chi_m T$ value of approximately 18.7 $cm^3\,mol^{-1}\,K$ decreases to a minimum of 12.4 $cm^3\,mol^{-1}\,K$ at 70 K and then rises to a maximum of 15.4 $cm^3\,mol^{-1}\,K$ at 12 K. This indicates that **5** has a non-zero spin ground state and that the ground spin state is higher than $S = 9/2$. In order to obtain the ground state spin value magnetization data were collected in the ranges of 2.0–6.0 K and 0.01–5.5 T (Fig. 6). The fits were made simultaneously on the four different temperatures (2, 3, 4 and 6 K), assuming only the ground state is populated, giving a best fit of $S = 11/2$, $g = 2.03$ and $D = -0.46\ cm^{-1}$. The maximum value of $\chi_m T$ at low temperature (15.4 $cm^3\,mol^{-1}\,K$) and the fact that the magnetization data at 2 and 6 K can be fit with one set of parameters is a strong indication that the ground state is indeed $S = 11/2$ and that the first excited state is rather high in energy. The previously reported $[Fe_{11}]$ complex has an $S = 1/2$ spin ground state [5]. Given the nature of S and sign of D, measurements were taken to see if **5** acts as a SMM. Low-temperature (1.2–0.04 K) single crystal magnetic measurements were performed on **5** using a micro-SQUID instrument equipped with three orthogonal field that allow the magnetic field to be scanned in all directions [11]. Below 1.2 K hysteresis loops are seen in magnetization versus field studies whose coercivities increase with decreasing temperature (Fig. 7). A detailed study of the field sweep rate dependence of the hysteresis loops showed that the hysteresis at non-zero fields is not due to a phonon bottleneck but due to slow relaxation because of the anisotropy barrier. Slow relaxation is seen at $H = 0$ but the presence of strong tunnelling does not allow for a reliable Arrhenius plot. For all SMMs the barrier is reduced at $H = 0$ because of the presence of tunnelling. Even for half-integer spin systems which in theory should not tunnel do so because of coupling with the environment – dipolar coupling between molecules, hyperfine coupling, spin–spin cross relaxation, and other multibody quantum processes. For a system with $S = 11/2$ and $D = -0.46\ cm^{-1}$ for example, and assuming an internal transverse field of approximately 10 mT, one can estimate a tunnel splitting of ca. 2.8×10^{-6} K and thus a tunnel probability of $P = 0.68$ for a sweep rate of 0.1 $T\,s^{-1}$ in good agreement with our

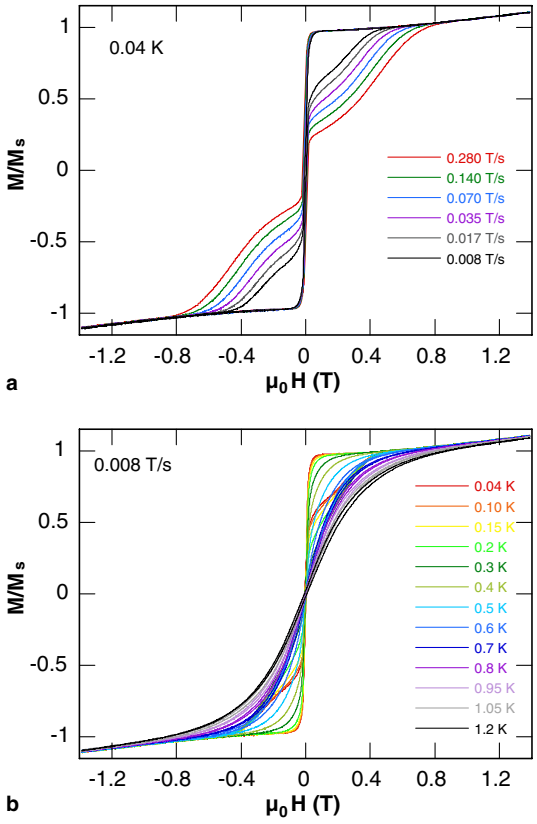

Fig. 7. Magnetisation (M) of **5** plotted as a fraction of maximum M_s vs. applied magnetic field ($\mu_0 H$). The loops are shown at different field sweep rates (top) and different temperatures (bottom).

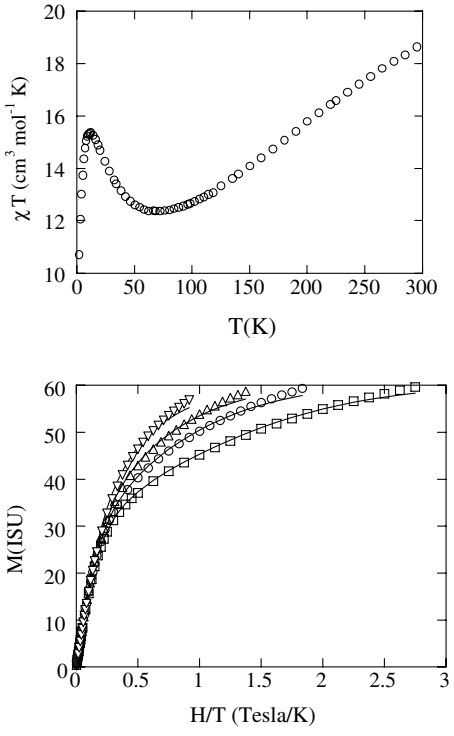

Fig. 6. Thermal variation of $\chi_m T$ in ranges 300–50 K at 0.2 T and 50–2 K at 0.05 T (top) and magnetization vs. H/T plot at 2 (□), 3 (○), 4 (△) and 6 (▽) K (bottom) for complex **5**.

measurements. This has also been observed in a $[Mn_4]$ cluster with $S = 9/2$ [7].

4.4. Magnetism of $[Fe_8(O_2CR)_{12}(thme)_4]$ (**6**, R = Ph; **7**, R = CMe_3) and $[Fe_{16}(EtO)_4(O_2CPh)_{16}(Hthme)_{12}](NO_3)_4$ (**8**)

The magnetic behaviour of compounds **6** and **7** are essentially identical and thus here we limit the discussion to complex **6**. Magnetic studies of both **6** and **8** indicate antiferromagnetic exchange between the metal centres. For both **6** and **8** the value of $\chi_m T$ declines rapidly from room temperature (~19, ~28 cm^3 K mol^{-1}, respectively) to a value approaching 0 cm^3 K mol^{-1} at 1.8 K indicative of $S = 0$ ground states for both complexes. The room temperature $\chi_m T$ value is approximately half the expected value for 8 (~35 cm^3 K mol^{-1}) and 16 (~70 cm^3 K mol^{-1}) non-interacting iron centres, indicating the existence of strong antiferromagnetic interactions even at room temperature. This is commonly found for iron-oxo clusters with Fe–O–Fe angles between 100° and 120° [12]. Both **6** and **8** can be broken down into simple units of two metal ions and the bridging ligands that connect them (Scheme 1). In this scheme, J_1, J_2 and J_3 are the magnetic coupling constants between two Fe^{III} ions for each of the three different bonding interactions found. These are: one alkoxo and two carboxylate bridging ligands (J_1); two alkoxo and one carboxylate bridging ligands (J_2); and two alkoxo bridging ligands (J_3). In order to analyse the magnetic behaviour of **6** and **8** we have found exact analytical equations for the χT product as a function of the temperature using the interaction topologies shown in Scheme 1. These equations have been developed following the classical spin approach and the methodology previously described by Fischer for one-dimensional systems [13]. This methodology can be applied since the spin correlation paths generated by the interaction schemes shown in Scheme 1 are large enough to neglect spin auto-correlation contributions through an entire loop [14]. The obtained analytical law is:

$$\chi T = \chi T_{\text{freeion}} \sum_{i,j,k} c_{i,j,k} u^i v^j w^k, \quad (1)$$

where u,v and w are the Langevin functions for J_1, J_2 and J_3, respectively, and $c_{i,j,k}$ are the coefficients of each term.

The best fits of the χ versus T curves (Fig. 8) in the 300–10 K temperature range are obtained with the following parameters: $g = 2.0$, $J_1 = -22.2$ cm^{-1} and $J_2 = -8.5$ cm^{-1} for **6**; and $g = 2.0$, $J_1 = -16.0$ cm^{-1}, $J_2 = -9.1$ cm^{-1} and $J_3 = -74.4$ cm^{-1} for **8**.

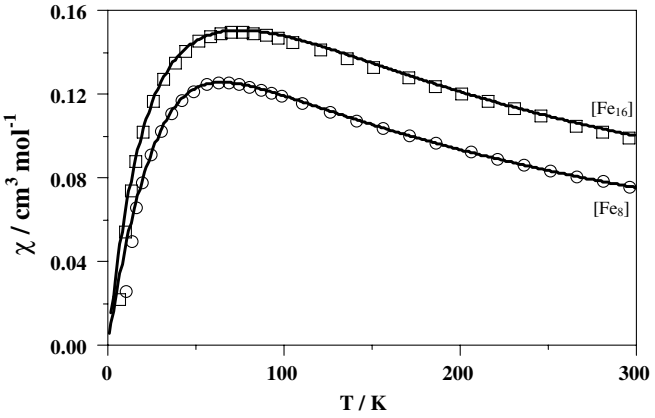

Fig. 8. Experimental and theoretical (solid lines) χ vs. T curves for [**Fe**$_{16}$] (squares) and [**Fe**$_8$] (circles).

5. Conclusions

The tripodal ligand H_3thme has led to the isolation of a series of new Fe^{III} clusters. A simple combination of $FeCl_3$, NaO_2CR and H_3thme in a mixture of MeCN and MeOH under ambient temperature and pressure gives rise to a series of rhomb- or diamond-like $[Fe_4]$ clusters. The identical $[Fe_4]$ units are seen as building blocks in the formation of related $[Fe_9]$ and $[Fe_{11}]$ clusters, appearing once in the $[Fe_9]$ cluster and twice in the $[Fe_{11}]$ cluster. The $[Fe_9]$ cluster was made via the solvothermal reaction of $[Fe_3O(O_2CR)(H_2O)_3]O_2CR$ with H_3thme in MeCN – the same reaction at room temperature produces no isolable products. Repeating this reaction but simply replacing the RCO_2^- counter ion with NO_3^- or Cl^- under the same conditions produces dramatically different compounds with the formation of octametallic wheel-like clusters. The benzoate (R = Ph) form of this cluster can also be made under ambient conditions, albeit in much lower yields and in lower purity due to a tendency to co-crystallise with unreacted starting material $[Fe_3O(O_2CPh)_6(H_2O)_3]NO_3$. The solvothermal reaction gives much higher yield and pure crystalline product directly. The pivalate analogue (R = CMe_3) could only be isolated by a solvothermal route. The size of the wheel formed can be doubled via the introduction of alcohol to the reaction mixture to give a $[Fe_{16}]$ wheel.

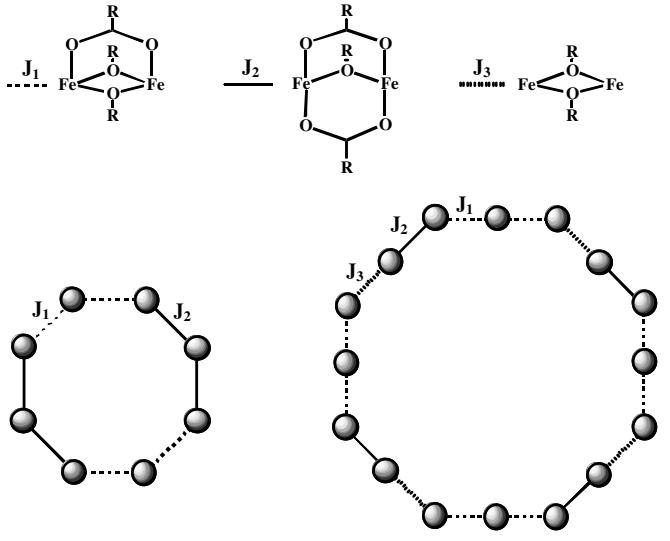

Scheme 1. The different bonding interactions (J_1, J_2, J_3) present in complexes **6**–**8**.

Previously reported cyclic [Fe_8] compounds have contained alkali metal ions within the central cavity of the wheel and the [Fe_{16}] complex is unprecedented. The above reactions highlight the very wide range of product cluster nuclearities and topologies that can result from subtle changes in reaction conditions – for example, changes in counter-ion, or solvothermal versus lower temperature routes.

All of the Fe species display dominant antiferromagnetic exchange interactions, but in the case of [Fe_{11}] this stabilises a rather large $S = 11/2$ spin ground state. Negative zero-field splitting within this ground state gives rise to single-molecule magnetism behaviour that is manifested in the presence of temperature and sweep rate dependent hysteresis loops.

Acknowledgements

The authors thank Lloyds of London Tercentenary Foundation, The Leverhulme Trust and the EPSRC.

References

[1] R. Sessoli, D. Gatteschi, D.N. Hendrickson, G. Christou, MRS Bull. 25 (2000) 66.
[2] (a) See for example D.N. Hendrickson, G. Christou, H. Ishimoto, J. Yoo, E.K. Brechin, A. Yamaguchi, E.M. Rumberger, S.M.J. Aubin, Z. Sun, G. Aromí, Polyhedron 20 (2001) 1479;
(b) C.J. Milios, C.P. Raptopoulou, A. Terzis, F. Lloret, R. Vicente, S.P. Perlepes, A. Escuer, Angew. Chem. Int. Ed. 43 (2003) 210;
(c) L.M. Wittick, K.S. Murray, B. Moubaraki, S.R. Batten, L. Spiccia, K.J. Berry, Dalton. Trans. (2004) 1003;
(d) M. Murugesu, M. Habrych, W. Wernsdorfer, K.A. Abboud, G. Christou, J. Am. Chem. Soc. 126 (2004) 4766;
(e) D.M. Low, L.F. Jones, A. Bell, E.K. Brechin, T. Mallah, E. Riviere, S.J. Teat, E.J.L. McInnes, Angew. Chem., Int. Ed. 42 (2003) 3781;
(f) A.J. Tasiopoulos, A. Vinslava, W. Wernsdorfer, K.A. Abboud, G. Christou, Angew. Chem., Int. Ed. 43 (2004) 2117.
[3] (a) See for example S. Piligkos, G. Rajaraman, M. Soler, N. Kirchner, J. van Slageren, R. Bircher, S. Parsons, H.-U. Güdel, J. Kortus, W. Wernsdorfer, G. Christou, E.K. Brechin, J. Am. Chem. Soc. 127 (2005) 5572;
(b) G. Rajaraman, M. Murugesu, M. Soler, W. Wernsdorfer, M. Helliwell, S.J. Teat, G. Christou, E.K. Brechin, J. Am. Chem. Soc. 126 (2004) 15445;
(c) M. Moragues-Cánovas, E. Rivière, L. Ricard, C. Paulsen, W. Wernsdorfer, E.K. Brechin, T. Mallah, Adv. Mater. 13 (2004) 1101;
(d) R. Shaw, I.S. Tidmarsh, R.H. Laye, B. Breeze, M. Helliwell, E.K. Brechin, S.L. Heath, M. Murrie, S. Ochsenbein, H.-U. Güdel, E.J.L. McInnes, Chem. Commun. (2004) 1418;
(e) M.I. Khan, J. Zubieta, Prog. Inorg. Chem. 43 (1995) 1;
(f) R.C. Finn, J. Zubieta, J. Cluster Sci. 11 (2000) 4;
(g) K. Hegetschweiler, H. Schmalle, H.M. Streit, W. Schneider, Inorg. Chem. 29 (1990) 3625;
(h) K. Hegetschweiler, H. Schmalle, H.M. Streit, V. Gramllicj, H.U. Hund, I. Erni, Inorg. Chem. 31 (1992) 1299;
(i) K. Hegetschweiler, D. Gatteschi, A. Cornia, L. Hausherr-Primo, V. Gramlich, Inorg. Chem. 33 (1996) 4414;
(j) C. Boskovic, H.U. Güdel, G. Labat, A. Neels, W. Wernsdorfer, B. Moubaraki, K.S. Murray, Inorg. Chem. 44 (2005) 3181;
(k) A. Cornia, A.C. Fabretti, P. Garrisi, C. Mortalo, D. Bonacchi, D. Gatteschi, R. Sessoli, L. Sorace, W. Wernsdorfer, A.L. Barra, Angew. Chem., Int. Ed. 43 (2004) 1136.
[4] R.H. Laye, E.L.L. McInnes, Eur. J. Inorg. Chem. (2004) 2811, and references therein.
[5] (a) R.D. Cannon, R.P. White, Prog. Inorg. Chem. 36 (1988) 195;
(b) W.H. Armstrong, S.J. Lippard, Inorg. Chem. 24 (1985) 981.
[6] J.C. Goodwin, R. Sessoli, D. Gatteschi, W. Wernsdorfer, A.K. Powell, S.L. Heath, J. Chem. Soc., Dalton Trans. (2000) 1835.
[7] (a) W. Wernsdorfer, S. Bhaduri, C. Boskovic, G. Christou, D.N. Hendrickson, Phys. Rev. B. 65 (2002) 180403;
(b) W. Wernsdorfer, S. Bhaduri, R. Tiron, D.N. Hendrickson, G. Christou, Phys. Rev. Lett. 89 (2002) 197201.
[8] S.M. Gorun, G.C. Papaefthymiou, R.B. Frankel, S.J. Lippard, J. Am. Chem. Soc. 109 (1987) 3337.
[9] S. Perlepes, J.C. Huffman, G. Christou, Chem. Commun. (1991) 1657.
[10] (a) A. Bino, I. Shweky, S. Cohen, E.R. Banninger, S.J. Lippard, Inorg. Chem. 37 (1998) 5168;
(b) W. Schmitt, C.E. Anson, B. Pilawa, A.K. Powell, Z. Anorg. Allg. Chem. 628 (2002) 2443;
(c) M. Veith, F. Grätz, V. Huch, Eur. J. Inorg. Chem. (2001) 367;
(d) A.K. Boudalis, B. Donnadieu, V. Nastopoulos, J.M. Clemente-Juan, A. Mari, Y. Sanakis, J.-P. Tuchagues, S.P. Perlepes, Angew. Chem., Int. Ed. 43 (2004) 2266.
[11] W. Wernsdorfer, Adv. Chem. Phys. 118 (2001) 99.
[12] (a) See for example K.L. Taft, S.J. Lippard, J. Am. Chem. Soc. 112 (1990) 9629;
(b) J. van Slageren, R. Sessoli, D. Gatteschi, A.A. Smith, M. Helliwell, R.E.P. Winpenny, A. Cornia, A.-L. Barra, A.G.M. Jansen, E. Rentscheler, G.A. Timco, Chem. Eur. J. 8 (2002) 277;
(c) O. Waldmann, R. Kock, S. Schromm, J. Schülein, P. Müller, I. Bernt, R.W. Saalfrank, F. Hampel, E. Balthes, Inorg. Chem. 40 (2001) 2986;
(d) A. Cornia, M. Affronte, A.G.M. Jansen, G.L. Abbati, D. Gatteschi, Angew. Chem., Int. Ed. 38 (1999) 2264.
[13] M.E. Fisher, Am. J. Phys. 32 (1964) 343.
[14] J. Cano, Y. Journaux, Monte Carlo simulation: a tool to analyse the magnetic properties, in: J.S. Miller, M. Drillon (Eds.), Magnetism: Molecules to Materials V, Wiley-VCH, Weinheim, Germany, 2005, p. 189.

Available online at www.sciencedirect.com
SCIENCE DIRECT®
Polyhedron 25 (2006) 334–338
POLYHEDRON
www.elsevier.com/locate/poly

Composite thermochromic thin films: (TiO_2)–(VO_2) prepared from titanium isopropoxide, $VOCl_3$ and water

Uzma Qureshi, Troy D. Manning, Christopher Blackman, Ivan P. Parkin *

Department of Chemistry, University College London, 20 Gordon Street, London WC1H OAJ, United Kingdom

Received 28 April 2005; accepted 12 August 2005
Available online 6 October 2005

Abstract

Atmospheric chemical vapour deposition (APCVD) was used to deposit composite TiO_2–VO_2 films on glass. The films were characterised by X-ray photoelectron spectroscopy, X-ray diffraction, Raman, energy dispersive X-ray analysis and scanning electron microscopy. These composite films exhibited photo-induced hydrophilicity, photocatalysis and a thermochromic switching temperature of 54 °C.
© 2005 Elsevier Ltd. All rights reserved.

Keyword: CVD

1. Introduction

Thermochromic coatings change their reflectance – transmission properties with temperature. Thermochromic materials are usually characterised by a semiconductor to metal transition occurring from a reversible change in their crystalline structure as a function of temperature [1]. They could find application in commercial and domestic windows in climates where there are significant fluctuations in temperature during the day and year (Northern Europe, Asia, North America, Near East). At temperatures below the thermochromic transition temperature (T_c) the material is largely transparent to sunlight and enables solar gain through a window. Above T_c the material increases its reflectivity and a reduction in solar gain occurs. The thermochromic material could thus make an 'intelligent glazing' as it responds to the external environment.

The thermochromic change has been observed in transition metal oxides such as Ti_2O_3, Fe_3O_4, Mo_9O_{26} [1,2] and in several forms of vanadium oxide, V_nO_{2n-1}. Among them, VO_2 has received the most attention because of the large reversible change of electric, magnetic and optical properties at temperatures around 70 °C [3]. Indeed of all of the transition metal oxides studied this material has its switching temperature closest to room temperature.

The thermochromic phase transition in vanadium dioxide was first demonstrated in 1959 [4]. This transition is due to a structural transformation from monoclinic to tetragonal. The optical properties of vanadium oxide through the transition temperature are characterised by a sharp decrease in transmission in the infrared spectrum. This is coupled with a concomitant increase in its IR reflectivity and electrical conductivity. Essentially in the monoclinic phase electrons are localised in V^{4+}–V^{4+} homopolar bonds and the material is a semiconductor. Above the transition temperature, the tetragonal phase is metallic and the V^{4+}–V^{4+} homopolar bonds are broken and the electrons free to enter the conduction band. Because of this unusual behaviour, VO_2 thin films have attractive applications as window coatings, electrical or optical switches, optical storage, laser protection and energy control for space satellites.

We have shown that substitutional doping of tungsten into the VO_2 lattice leads to a significant reduction in the thermochromic switching temperature – with a linear

* Corresponding author. Tel.: +44 0 207 679 4669; fax: +44 0 207 679 7463.
E-mail address: i.p.parkin@ucl.ac.uk (I.P. Parkin).

0277-5387/$ - see front matter © 2005 Elsevier Ltd. All rights reserved.
doi:10.1016/j.poly.2005.08.018

decrease in T_c with tungsten content (a reduction in T_c of 20 °C is seen per atom% W) [5,6]. Such a reduction in switching temperature offers a potentially useful commercial application because the T_c is now down below that desired for window applications (25–30 °C).

This paper details the reaction of $Ti(OiPr)_4$, $VOCl_3$ and water. The initial aim was to produce Ti-doped VO_2 thin films. However, we found that the reaction produced a TiO_2–VO_2 composite thin films – notably these films showed a reduction in switching temperature, photocatalytic activity and photoinduced superhydrophilicity. They also showed a sharp thermochromic transition with minimal hysteresis.

2. Experimental

All APCVD experiments were performed on a custom built apparatus consisting of a horizontal-bed cold-wall reactor connected to an arrangement of stainless-steel heated pipes, valves and bubblers [5,6]. A syringe driver was attached to the plain-line gas-flow for the introduction of water. A schematic of the APCVD rig has been published previously [5,6]. All heaters were regulated by Eurotherm controllers and RS type k thermocouples.

2.1. APCVD procedure

$VOCl_3$ (Aldrich UK, 99%) was transferred to bubbler 2 and titanium isopropoxide to bubbler 1 [5,6]. Distilled water was injected into the plain-line gas-flow using a fixed rate syringe driver (0.473 cm min^{-1}). The amount of water introduced was controlled via the size of the syringe. The substrate was SiO_2-precoated standard float glass (Pilkington, UK) 15 cm × 4.5 cm × 0.3 cm. The glass substrate was cleaned before use by being wiped with a tissue soaked in water, then with a tissue soaked in propan-2-ol and finally rinsed with propan-2-ol. The glass was allowed to dry in air prior to it being mounted in the CVD chamber.

A flow of nitrogen (BOC, 99.9%) was passed through the apparatus during all operations of the APCVD rig. The amount of $VOCl_3$ introduced into the system was calculated from

$$a = (\mathrm{VP} \times F)/((760 - \mathrm{VP}) \times 24.4),$$

where a is the amount of material introduced (mol min^{-1}), VP is the vapour pressure of the material at the temperature of the bubbler (mmHg), and F is the carrier-gas flow-rate through the bubbler (L min^{-1}).

The plain line and $VOCl_3$ bubbler-line flow-rates were set to 0.5 L min^{-1}. Once all the temperatures had been stabilised, the syringe driver valve was opened and distilled water was introduced into the plain-line gas-flow. Nitrogen was passed through the bubbler and the bypass valve was closed. $VOCl_3$ chloride was seen to pass through the exhaust. After allowing the flow to stabilise for approximately 10–20 s the three-way valve was switched to allow the precursor to pass into the mixing chamber and on to the reactor. Once the allotted reaction time was complete (60 s), the three-way valve was switched to the exhaust, the bypass valve opened and the nitrogen flow through the bubbler closed. The reactor heater was turned off and the substrate was allowed to cool under an atmosphere of nitrogen. The substrate was removed from the reactor below 200 °C. All samples were handled and stored in air.

The conditions for introducing titanium isopropoxide as a reactant involved setting the inert N_2 gas flow rate at 0.2 L min^{-1} for the bubbler containing the titanium isopropoxide, and the $VOCl_3$ flow rate was constant at 0.5 L min^{-1}. The substrate temperatures were 550, 600 and 650 °C – these temperatures were measured by an external thermocouple directly on the surface of the glass substrate. To achieve these temperatures on the substrate the control thermocouple within the graphite susceptor was set at between 8 and 10 °C higher (i.e., 560 °C rather than 550 °C).

2.2. Film analysis

Analysis of the resulting films consisted of UV/Vis absorption spectroscopy, contact angle measurements, scratch tests, solubility tests, photocatalysis measurements, Vis/IR reflectance–transmittance, Raman spectroscopy, SEM/EDAX and glancing angle X-ray diffraction. X-ray analysis of the films was determined using glancing angle incidence (1.5°) on a Siemens D5000 machine using primary monochromated Cu $K_{\alpha 1}$ radiation (1.5406 Å). SEM/EDAX was determined on a JEOL 35-CF instrument using ISIS software (Oxford Instruments). Electronic absorption measurements were obtained using a Thermospectronic Helios-α spectrometer from 300 to 1100 nm. Reflectance/transmittance measurements were made on a Zeiss miniature monolithic spectrometer (range 380–1150 nm) connected to a PC. Sheet resistance measurements were determined on a four-probe instrument. Raman measurements were carried out using a Renishaw System 1000 Raman spectrometer with a HeNe (632.8 nm) laser excitation source. Contact angles of selected glass samples were determined by measuring the spread of a 1.0 μL droplet of water. Scratch tests were determined with a paper towel, brass stylus and stainless steel scalpel. Solubility tests were achieved by immersion of small pieces of the coated glass in a range of solvents (toluene, acetone, methanol, hexane, water, 2 M NaOH, 2 M HCl and 2 M HNO_3). The adhesion of the films to the substrate was determined by the Scotch tape test (removal of an X shaped piece of sticking tape).

2.3. Photocatalytic analysis

Photocatalytic activity of the samples was assessed by the destruction of an overlayer of a test organic – stearic acid, on a 3 cm × 3 cm portion of coated glass. This coated glass had been irradiated at 254 nm for 1 h prior to measurement. The stearic acid was applied by dropping

7.5 μL of a 0.4 mmol methanol solution onto the glass surface, which was spun at 1500 revolutions a minute during the dropping procedure. The infrared spectra of the stearic acid overlayer was measured over the range 2950–2800 cm^{-1}. The glass coated with stearic acid was irradiated with 254 nm radiation provided by BDH germicidal lamps (2×8 W). The IR spectra of the stearic acid were measured after 30 min intervals for up to 2 h and the areas of the bands attributed to the C–H stretches quantified.

2.4. Thermochromic analysis

The thermochromic switching temperature was determined by measuring the absorption of the film at 4000 cm^{-1} at different temperatures using a Nicholet FT-IR spectrometer.

3. Results and discussion

The APCVD reaction of titanium isopropoxide, $VOCl_3$ and water at substrate temperatures of 650, 600 and 550 °C deposited composite TiO_2–VO_2 films. It was found with all samples that the films had a uniform composition across the substrate. The films were light brown, passed the scotch tape test, were not removed by a tissue or felt but were scratched with both brass and steel. All films were insoluble in water and common organic solvents (methanol, ethanol, acetone), but they did dissolve in both acid (HCl, 2 M) and alkali (NaOH, 2 M). The films showed no change in optical properties on storage in air for one year.

Glancing angle X-ray diffraction confirmed the presence of both crystalline anatase TiO_2 and VO_2 in the composite films as shown in Fig. 1. A strong signal at approximately 27.8° 2θ can be seen in the XRD data, this strong signal corresponds to the (0 1 1) reflection of monoclinic VO_2, and indicates the films are preferentially orientated on the substrate. The additional weaker reflections at 38°, 54° and 56° 2θ are as expected for the anatase phase of titania [7]. The X-ray data confirms that a composite film is formed and furthermore no shift in the main (0 1 1) diffraction peak of VO_2 is seen indicating that very little if any titanium is actually present within the VO_2 lattice as in a solid solution.

Raman spectroscopy of the films showed a pattern consistent with that for a composite film and showed the expected bands for both anatase TiO_2 and monoclinic VO_2, Fig. 2. The Raman pattern showed monoclinic VO_2 with bands at 144, 190, 315, 389, 498 and 611 cm^{-1}. These are comparable to reference values identified by Parker [8] and Aronov [9,10]. No bands due to VO_2(B), the metastable form of VO_2 were observed [11]. There are also peaks present that indicate the presence of anatase TiO_2 at 143, 396 and 612 cm^{-1}. There are no shifts in the Raman peaks that would indicate the incorporation of Ti into the VO_2 network as in a solid solution.

SEM imaging confirmed that the films are composed of two distinct types of particle – the majority where 'rectangle like' particles of size ca. 3 μm by 200 nm at a deposition temperature of 650 °C and 2 μm by 200 nm at both 600 and 500 °C. The second particle type were approximately spherical aggregates of varying diameter across the film surface at all substrate temperatures and flow rates, averaging ca. (1 μm, Fig. 3). Side on SEM analysis indicated a growth rate of ca. 400 nm min^{-1}.

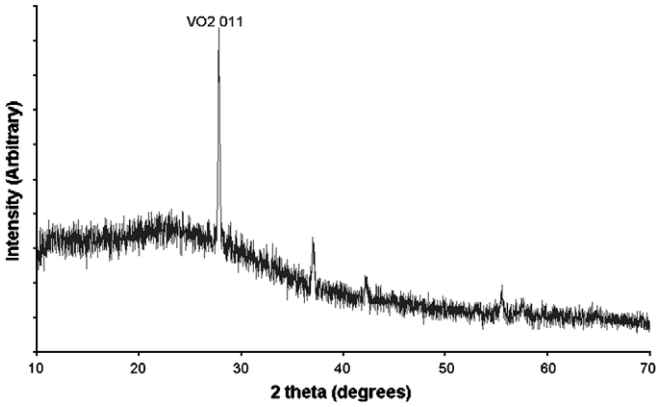

Fig. 1. X-ray diffraction pattern of the film formed by the APCVD reaction of $VOCl_3$, $Ti(O^iPr)_4$ and water at 650 °C.

Spot EDAX (wavelength dispersive detector) analysis showed that the 'rectangle-like' particles contained only vanadium and oxygen in a 1:2 ratio and the non-uniform 'blob' like particles contained only titanium and oxygen in a 1:2 ratio. The wide area EDAX analysis showed that the films were composed of 1 part TiO_2 to 10 parts VO_2. Notably carbon was not detected by EDAX (less than 1 atom%). The elemental analysis gave results that were comparable to the gas-phase concentration of the precursors used – a constant ratio was used in the reactions. Therefore, there was a good transferability from the solution to the deposited films. Spot analysis on all the rectangle particles and aggregated particles from all films yielded similar results which suggests a homogeneous distribution of the TiO_2 on the surface of the film at a ratio of ca. 1 part TiO_2 to 10 parts VO_2.

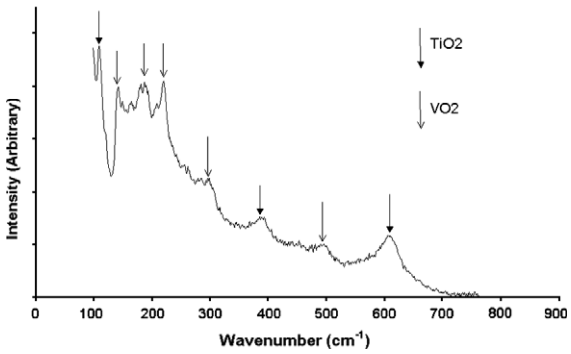

Fig. 2. Raman pattern obtained from the film formed by the APCVD reaction of $VOCl_3$, $Ti(O^iPr)_4$ and water at 650 °C.

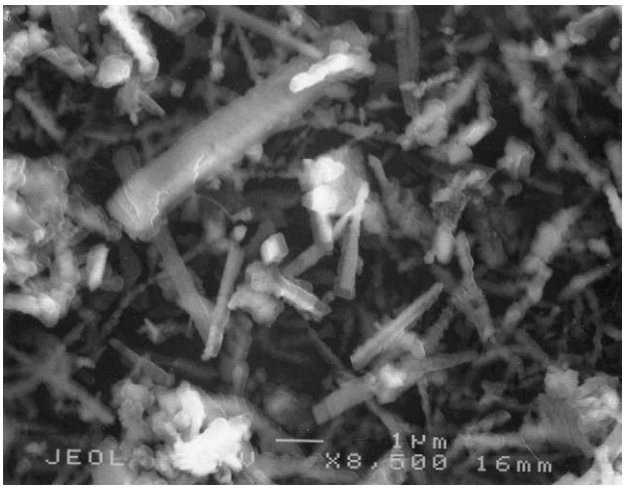

Fig. 3. SEM image obtained from the film formed by the APCVD reaction of $VOCl_3$, $Ti(O^iPr)_4$ and water at 650 °C.

All of the composite films exhibited a band gap of 0.7 eV by the Tauc method. This value is directly comparable to reference values for VO_2 [12]. All of this data ties in well with the formation of a composite film that is in effect a matrix of interlocked TiO_2 and VO_2 particles with no evidence for the formation of a solid solution of $Ti_xV_yO_2$.

3.1. Functional properties

The thermochromic transition temperature was measured for the TiO_2–VO_2 films at 54 °C. This was determined by measuring the transmission through the film at a fixed wavelength of 2.5 μm, Fig. 4.

The thermochromic switching temperatures did not alter with reaction conditions such as flow rate or substrate temperature. There is a clear decrease in switching temperature from that of pure VO_2 films and is most probably related to the morphology of the VO_2 films which all have one axis that is ca. 200 nm in dimension and this is likely to have induced some strain [13]. Physical vapour deposited VO_2 films that have one dimension less than 300 nm have been reported as causing a reduction in up to 20 °C in the thermochromic switch. Notably as all of the VO_2 films were made up of the same morphology of crystallite, with the same restricted length axis, it is probably not too surprising that they all had similar reductions in T_c. Beteille et al. [14], prepared $Ti_xV_yO_2$ solid solutions via the sol gel process and found that the T_c increases and the hysteresis width lowers with increasing Ti dopant. This lends further evidence to the formation of a composite film in this APCVD study as a reduction in T_c was observed – the opposite to what would be expected for solid solution formation.

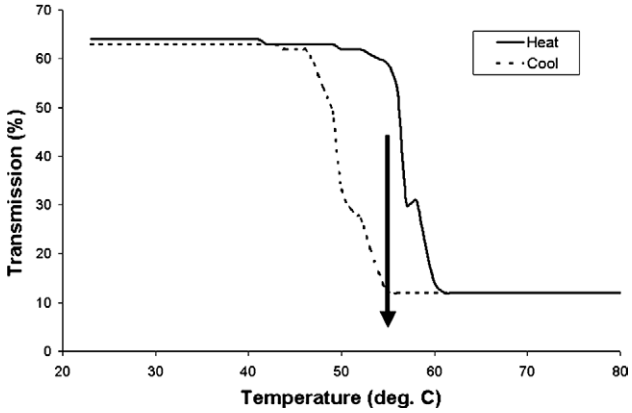

Fig. 4. Variable temperature transmission plot at 2.5 μm for the film formed by the APCVD reaction of $VOCl_3$, $Ti(O^iPr)_4$ and water at 650 °C.

The composite TiO_2–VO_2 films displayed photocatalytic activity and exhibited photo-induced hydrophilicity. The initial contact angles for water droplets were in the range 85–105° prior to irradiation, this reduced to 31–48° on exposure to 254 nm radiation for 1 h and decreased further to values of 16–20° after 12 h exposure to sunlight. Leaving the films in the dark for 24 h lead to an increase in contact angles to ca. 60–69°. The system could be multiply light–dark cycled and the same variation in contact angle was noted. The variations in contact angle are readily explained by the TiO_2 component of the films. Anatase is an excellent photocatalyst that also exhibits photo-induced superhydrophilicity [15] and water contact angles of less than 5° are often observed for pure anatase films. The composite films formed contain ca. 10% TiO_2 that is sufficient to allow part of the surface to show low contact angles. The photocatalytic results are also indicative of small amounts of titania incorporated into the film.

We have investigated the formation of VO_2–TiO_2 films previously from a different precursor set – $TiCl_4$ and $VOCl_3$ and water [5,6]. The morphology of the films formed is quite different – the VO_2 component was made from 'worm-like' particles as opposed to the straight edged crystalline materials seen here from the APCVD of $VOCl_3$, titanium tetraisopropoxide and water. The proportion of titanium to vanadium in both sets of films was quite surprising at 1:10. Furthermore, both sets of films showed a similar reduction in T_c values 54 °C measured in this study and 51 °C previously. The films formed in this work were more robust and importantly the hysteresis width of the transition was narrower – ca. 6–8 °C here compared to ca. 10–15 °C previously. This is significant because for a commercial application the minimum possible hysteresis is required to maximise solar reflection at a specific temperature.

3.2. Solid solution versus composite film

The films produced in this study were composite mixtures of TiO_2 and VO_2 rather than a solid solution $Ti_xV_yO_2$. Solid solutions are readily formed from a sol–gel approach so the fact that it is not formed here is not related to atomic incompatibility [14]. Furthermore, the heat treatments used in making sol–gel $Ti_xV_yO_2$ are

comparable to the temperatures used in this CVD reaction (albeit for a longer duration). The most likely determining factor in the formation of composite films is reaction kinetics. The titanium tetraisopropoxide used as a titanium precursor reacts much faster under CVD conditions with water than $VOCl_3$. Hence, the titanium dioxide particles found in the films have a rounded morphology that strongly suggest that they have arisen from gas phase nucleation – reaction between titanium isopropoxide and water and become trapped within a vanadium dioxide matrix. The fact that the vanadium dioxide has a well-defined crystalline morphology indicates that it is predominantly formed from surface reactions – that is conventional CVD growth. This hypothesis would readily explain why a solid solution is not formed because the titanium tetraisopropoxide has effectively already reacted before it hits the surface and hence few if any titanium species are available for incorporation into the vanadium dioxide lattice.

3.3. Multifunctional coatings

The composite films formed in this study show photocatalysis, hydrophilicity and a thermochromic switch. The photocatalysis is less than a pure CVD prepared anatase TiO_2 thin film – about 10% of the activity. This level of activity scales exactly with the titania content of the film. Although this photoactivity is relatively low it still sufficient for self-cleaning action. The reduction in water contact angle of the TiO_2/VO_2 thin film when exposed to sunlight again is less than what would be expected for a CVD prepared anatase film – however, it does render the surface hydrophilic. The reduction in thermochromic switching temperature observed for the films is a result of induced strain. The reduction of 16 °C from pure VO_2 is noteworthy and somewhat larger than that seen for pure VO_2 formed by CVD (where a reduction of ca. 10 °C is common). Furthermore, the hysteresis width of the transition is significantly lowered in the films formed in this study. It is possible that the co-location of titania particles within the VO_2 matrix improves marginally the thermochromic performance.

4. Conclusion

Composite TiO_2–VO_2 films were deposited via the APCVD reaction of $VOCl_3$, titanium isopropoxide and water. The composite films formed show three useful functional properties – photocatalysis, low contact angles and some significant reduction in thermochromic switching temperature, 54 °C. It also shows that composite films of this kind do not interfere with the functionality of each individual component and that solid solutions are not formed.

Acknowledgements

Pilkington Glass are thanked for supply glass substrates. EPSRC/Pilkington are thanked for a CASE award to U.Q. I.P.P. thanks the EPSRC for support of the Raman spectrometer. This paper is dedicated to M.H. Chisholm who has been an inspiration. His forceful presence – especially on the squash court – followed by fatherly chats have redirected more than one research career.

References

[1] N.F. Mott, Rev. Mod. Phys. 40 (1968) 677.
[2] D. Adler, Rev. Mod. Phys. 40 (1968) 714.
[3] F.J. Morin, Phys. Rev. Lett. 3 (1959) 34.
[4] F.J. Morin, Phys. Rev. Lett. 14 (1959) 34.
[5] T.D. Manning, I.P. Parkin, J. Mater. Chem. 14 (2004) 2463.
[6] U. Qureshi, T.D. Manning, I.P. Parkin, J. Mater. Chem. 14 (2004) 1190.
[7] Y.H. Chee, R.P. Cooney, R.F. Howe, P.A.W. van der Heide, J. Raman Spectrosc. 23 (1992) 243.
[8] J.C. Parker, Phys. Rev. B 42 (1990) 3164.
[9] A.G. Aronov, D.N. Mirlin, I.I. Reshina, F.A. Chudrovski, Fiz Tverd Tela (Leningrad) 19 (1977) 193.
[10] A.G. Aronov, D.N. Mirlin, I.I. Reshina, F.A. Chudrovski, Sov. Phys. Solid State (English translation) 19 (1977) 110.
[11] F. Theobold, R. Cabala, J. Bernard, J. Solid State Chem. 17 (1976) 431.
[12] F. Beiteille, L. Mazerolles, J. Livage, Mater. Res. Bull. 34 (1999) 2177.
[13] T. Maruyama, Y. Ikuta, J. Mater. Sci. 28 (1990) 5073.
[14] F. Beteille, J. Livage, J. Sol, J. Sol. Gel Sci. Tech. 13 (1998) 915.
[15] A. Fujishima, T.N. Rao, D. Tryk, J. Photochem. Photobiol. 1 (2000) 1.

Available online at www.sciencedirect.com
SCIENCE DIRECT®
Polyhedron 25 (2006) 339–348
POLYHEDRON
www.elsevier.com/locate/poly

DFT calculations of NMR J_{C-H} coupling constants: An additional tool to characterize the α-agostic interaction in high oxidation state M-alkylidene complexes (M = Re, Mo and Ta)

Xavier Solans-Monfort, Odile Eisenstein *

Laboratoire de Structure et Dynamique des Systèmes Moléculaires et Solides (UMR 5636, CNRS), cc14, Institut Gerhardt, Université Montpellier II, F-34095 Montpellier Cedex 05, France

Received 27 April 2005; accepted 11 August 2005
Available online 23 September 2005

Abstract

NMR spin–spin J_{C-H} coupling constants have been calculated for the α-alkylidene C–H bond in several high oxidation state d^0 transition metal-alkylidene complexes (M = Re, Mo, Ta). The DFT(B3PW91) calculations have been carried out using the GIAO method for the isolated molecules, with no solvent effect or thermal corrections. The experimental systems have been modeled either by replacing all large size ligands by ligands of smaller size with similar electronic properties or by calculating the full chemical entities. It is shown that the calculations are able to reproduce well the trends in the J_{C-H} values over a range of 75–150 Hz when the IGLO basis sets are used. In addition, the calculated J_{C-H} values differ from the experimental ones by about 10% in the case of weak α-C–H agostic interactions (pseudotetrahedral Re and Mo complexes) and by 15% in the case of strong α-C–H agostic interactions (pseudooctahedral Ta complexes). This shows that the electronic environment of the alkylidene C–H bonds, associated with the α-agostic interaction, is properly evaluated at this level of calculations for transition metal complexes of rather large size.
© 2005 Elsevier Ltd. All rights reserved.

Keywords: NMR spin–spin J_{C-H} coupling constant; DFT; GIAO; IGLO; Transition metal complexes; Re; Mo; Ta; Alkylidene complexes; α-Agostic interactions

1. Introduction

High oxidation state (d^0) transition metal-alkylidene complexes were discovered 30 years ago, and since this time, a large variety of them have been synthesized, in part because they are potential olefin metathesis catalysts [1–7]. In several of these complexes, the J_{C-H} NMR spin–spin coupling constant of the α-alkylidene C–H bond is low. This has been attributed to a weakening of the C–H bond due to the presence of an α-C–H agostic interaction, i.e., an intramolecular interaction between the C–H bond, acting as a Lewis base, and the electron deficient metal center acting as a Lewis acid [8–11].

The NMR spin–spin coupling constant is a key tool to characterize the C–H···M agostic interactions because the J_{C-H} varies over a rather large range of values whereas the C–H bond length varies little. The J_{C-H} value of a non-agostic $C(sp^2)$–H bond is around 160 Hz [12] whereas values as low as about 75 Hz have been observed in some complexes (see later). In contrast, the C–H bond is lengthened by 0.05 Å at most [13]. Furthermore, the C–H bond length cannot be determined experimentally with high accuracy by other techniques than the expensive and difficult neutron diffraction method. Vibrational stretching frequencies of the agostic C–H bond may be hard to identify because the band can be weak and broad [13]; computational studies are therefore very useful. The geometrical optimizations give C–H values, which usually compare very well with

* Corresponding author. Tel.: +33 467143306; fax: +33 467144839.
E-mail address: odile.eisenstein@univ-montp2.fr (O. Eisenstein).

0277-5387/$ - see front matter © 2005 Elsevier Ltd. All rights reserved.
doi:10.1016/j.poly.2005.08.015

experiment in the few complexes whose structure has been studied by neutron diffraction [10]. Associated with the lengthening of the C–H bond, the stretching frequency is lower than that of a non-agostic C–H bond. However, direct comparison between the calculations and the experiment requires the calculations of J_{C-H}.

In general, calculations of NMR chemical shifts and spin–spin coupling constants require considerable computational effort [14–18]. However computations of NMR parameters for transition metal complexes have been made possible because of the successful development of the DFT methods as described in the recent review by Autschbach [17]. The key point is that calculations using the GIAO [19,20] or IGLO [21,22] methods, along with extended basis sets, give NMR chemical shifts and spin–spin coupling constants that can be reasonably compared with experiment. In the case of the spin–spin coupling constant, the calculated values differ from the experimental ones by 10–20% [17,23]. Because of the computational effort involved, spin–spin C–H coupling constants have so far only been calculated for various relatively small organic molecules [23–26] and few metal complexes [27–29]. In the case of transition metal complexes, NMR spin–spin coupling constant calculations have been focused on ligand–ligand, metal–ligand and metal–metal coupling constants [30–37].

It has been shown that the spin–spin coupling constant is influenced both by the solvent and by vibrational effects [23,38,39] and that the solvent effect is especially important in the case of electron deficient complexes [33,34,40]. In the case of transition metal complexes, the solvent effect has been shown to be due in large part to the coordination of molecule of solvent, which changes the coordination number of the metal center. Anharmonicity and vibrational effects have been shown to be most important in the case of two atoms with distance that are far from usual distance. For instance these effects will be more important in the case of compressed dihydride and stretched dihydride complexes than in the case of regular dihydrogen or dihydride complexes [30,37]. In such cases, a temperature effect is expected [41].

These limitations being known, it should be possible to calculate J_{C-H} for agostic C–H bonds. An agostic interaction requires an electron deficient metal but is usually observed in weakly or non-coordinating solvent. The C–H bond is only very slightly elongated by the agostic interaction so that the vibrational effect should be negligible since temperature effects have never been reported. We can thus study if the calculations reproduce, with reasonable computational effort (DFT with electronic core potential on heavy atoms and limited basis sets), the changes in the J_{C-H} values in systems where it should be acceptable to neglect the temperature and solvent effects. To better test the validity of the computational method, we have studied two sets of complexes. One set is the pseudotetrahedral series, Re(≡C*t*Bu)(=CH*t*Bu)(X)(Y) (X = Y = CH_2*t*Bu; X = Y = O*t*Bu; X = CH_2*t*Bu, Y = $OSiPh_3$) [42–46] and Mo(=NR)(=CH*t*Bu)(X)(Y) (R = 2,6-*i*Pr_2-(C_6H_3) or CPh_3; X = Y = CH_2*t*Bu; X = Y = O*t*Bu) [47–51] where the agostic interaction is weak and has been observed only in one of the two isomers. The second set is the pseudooctahedral cyclopentadienyl tantalum alkylidene series, Ta(C_5R_5)(=CH*t*Bu)(X)(Y) (R = H (Cp) or CH_3(Cp*), X = Y = Cl; X = Y = CH_2*t*Bu) where the alkylidene C–H α-agostic interaction is strong [52]. The alkylidene group has a relatively high barrier for rotation in all these complexes [1,27,44,48,53,54], which avoids averaging problems. The following pattern emerges from the experimental results. Changing the metal and the coordination number changes J_{C-H} significantly but changes of only a few hertz result from a substitution of ligands in a given complex. Experimentalists consider, nevertheless, these small changes as meaningful and it is therefore of interest to establish if the computations are able to reproduce the detailed changes in J_{C-H} as well as the absolute values in a quantitative way.

The GIAO method with basis sets including functions with large exponents for accurate representation of the core electrons such as the IGLO-II and IGLO-III basis sets, elaborated by Kutzelnigg et al. [55] give very good results for NMR properties including spin–spin coupling constants. Good results have been also obtained with aug-cc-pXVZ basis sets after addition of supplementary core functions [14,23]. However, the vast number of calculations of transition metal complexes have been carried out with 6-31G(d,p) Pople type basis set on the organic ligand [56]. We will thus compare the results obtained with the Pople basis set and the IGLO basis set in the case the rhenium complexes. Only the IGLO basis sets will be used for the other systems.

2. Computational details

In one set of calculations, the experimental rhenium Re(≡C*t*Bu)(=CH*t*Bu)(X)(Y) (X = Y = CH_2*t*Bu, Re-1; X = CH_2*t*Bu, Y = $OSiPh_3$, Re-2; X = Y = O*t*Bu, Re-3) complexes, the molybdenum Mo(=NR)(=CH*t*Bu)(X)(Y) (R = 2,6-*i*Pr_2-(C_6H_3), X = Y = CH_2*t*Bu, Mo-1; R = CPh_3, X = Y = CH_2*t*Bu, Mo-2; R = 2,6-*i*Pr_2-(C_6H_3),X = Y = O*t*Bu, Mo-3) complexes and the tantalum Ta(C_5R_5)(=CH*t*Bu)(X)(Y) (R = CH_3, X = Y = CH_2*t*Bu, Ta-1; R = CH_3, X = Y = Cl, Ta-2 and R = H, X = Y = CH_2*t*Bu, Ta-3; R = H, X = Y = Cl, Ta-4) complexes have been represented by small models, constructed by substitution of *t*Bu by Me, *i*Pr groups by H and Ph by H. The calculated small systems are labeled with a subscript q (i.e., Re-1_q, Re-2_q, Re-3_q, etc.) by analogy with our previous contribution [27]. In another

set of calculations, the full experimental systems have been calculated only for the rhenium and selected tantalum complexes in order to evaluate the influence of the bulk of the substituents in the pseudotetrahedral and pseudooctahedral coordination spheres. All systems are shown in Scheme 1.

Geometry optimizations are performed, without any geometrical constraint, with the hybrid B3PW91 density functional [57,58], as implemented in the GAUSSIAN03 package [59] for the small systems and with the ONIOM (B3PW91:UFF) approach [60,61] for the full systems. In the ONIOM scheme the inner layer is equal to the small model. The Re, Mo, Ta and Si atoms are represented with the quasi relativistic effective core pseudopotentials (RECP) of the Stuttgart group and the associated basis set augmented with a polarization function [62,63]. The remaining atoms (C, H, and O) are represented with 6-31G(d,p) basis sets [64].

NMR J_{C-H} coupling constants are computed using the GIAO method [19,20] with a full DFT (B3PW91) calculation at the previous optimized (B3PW91 or ONIOM) geometries. To test the dependence of J_{C-H} on the basis set level, the J_{C-H} coupling constants have been calculated using six different basis sets for the rhenium complexes within the small model approximation. In all systems, Si and the metal atoms are represented with the previously described basis sets and only the representation of C, O and H has been varied. The Pople's double-ζ 6-31G(d,p) (BS1) and 6-31+G(d,p) [64] (BS2) and triple-ζ 6-311+G(d,p) (BS3) and 6-311++G(2df, 2pd) [65] (BS4) basis sets have been chosen to test the effect of valence electron representation on computing J_{C-H}. These basis sets have been previously used for computation of J_{C-H} coupling constants involving agostic interactions [27,29]. The Kutzelnigg's IGLO-II (BS5) and IGLO-III [55] (BS6) basis sets have been used. These basis sets are derived from Huzinaga's basis sets [66] and adapted to reproduce NMR properties [22,67]. They have been shown to give good results for NMR chemical shifts and coupling constants especially for organic molecules [14,15,23,28]. Finally the J_{C-H} coupling constants have been calculated at the optimized B3PW91/IGLO-II geometry.

The J_{C-H} values for Mo and Ta complexes are only calculated with IGLO-II basis set, which is found to give the best results at a competing level.

As mentioned in the introduction, the solvent effect was not included because agostic interaction is only observed in weakly or non-coordinating solvent. The anharmonicity, vibrational and thermal effects have been neglected because the C–H bond is relatively close to its usual length.

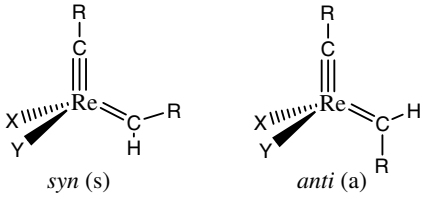

Re-1$_q$ R = CH_3, X = Y = CH_2CH_3
Re-2$_q$ R = CH_3, X = $OSiH_3$ Y = CH_2CH_3
Re-3$_q$ R = CH_3, X = Y = OCH_3
Re-1 R = *t*Bu, X = Y = CH_2*t*Bu
Re-2 R = *t*Bu, X = $OSiPh_3$ Y = CH_2*t*Bu
Re-3 R = *t*Bu, X = Y = O*t*Bu

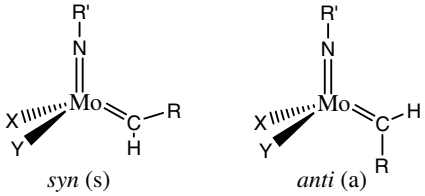

Mo-1$_q$ R = CH_3, R' = Ph, X = Y = CH_2CH_3
Mo-2$_q$ R = CH_3, R' = CH_3, X = Y = CH_2CH_3
Mo-3$_q$ R = CH_3, R' = Ph, X = Y = OCH_3

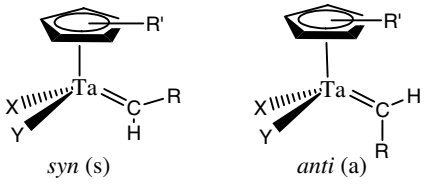

Ta-1$_q$ R = CH_3, R' = CH_3, X = Y = CH_2CH_3
Ta-2$_q$ R = CH_3, R' = CH_3, X = Y = Cl
Ta-3$_q$ R = CH_3, R' = H, X = Y = CH_2CH_3
Ta-4$_q$ R = CH_3, R' = H, X = Y = Cl
Ta-1 R = *t*Bu, R' = CH_3, X = Y = CH_2*t*Bu
Ta-2 R = *t*Bu, R' = CH_3, X = Y = Cl
Ta-3 R = *t*Bu, R' = H, X = Y = CH_2*t*Bu
Ta-4 R = *t*Bu, R' = H, X = Y = Cl

Scheme 1.

3. Results and discussion

3.1. The Re(≡CtBu)(=CHtBu)(X)(Y) complexes: methodology and calibration

The geometries of Re complexes, presented in Fig. 1, have been discussed at length in our previous contribution [27]. Thus, only key points will be mentioned here when needed. The overall geometries of the complexes for the small models are in good agreement with the available experimental data. The presence of the full ligands introduced only minor changes in the structures, the main difference residing in a slight change in the difference in the energy between the *syn* and *anti* isomers, the two isomers being always close in energy. The *syn* isomer is more stable than the *anti* isomer for the small and full models for Re-1 and Re-2. The situation is different for complex Re-3: the *syn* isomer is more stable

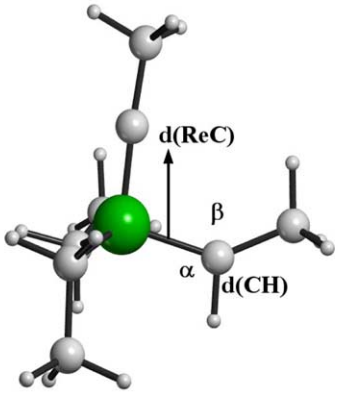

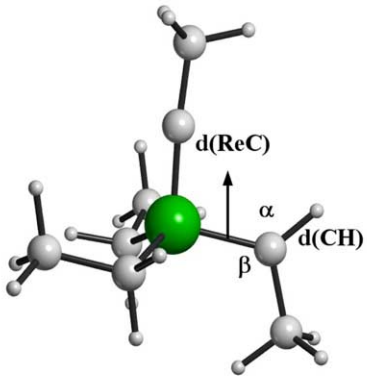

Re-1s$_q$ d(ReC) = 1.861, d(CH) = 1.112, α = 104.2, β = 140.3
Re-2s$_q$ d(ReC) = 1.873, d(CH) = 1.110, α = 107.2, β = 138.8
Re-3s$_q$ d(ReC) = 1.876, d(CH) = 1.108, α = 108.3, β = 137.8
Re-1s d(ReC) = 1.860, d(CH) = 1.119, α = 97.5, β = 148.1
Re-2s d(ReC) = 1.867, d(CH) = 1.117, α = 99.3, β = 147.3
Re-3s d(ReC) = 1.874, d(CH) = 1.114, α = 101.6, β = 145.6

Re-1a$_q$ d(ReC) = 1.872, d(CH) = 1.090, α = 128.5, β = 115.7
Re-2a$_q$ d(ReC) = 1.882, d(CH) = 1.091, α = 127.9, β = 117.4
Re-3a$_q$ d(ReC) = 1.884, d(CH) = 1.090, α = 127.8, β = 117.1
Re-1a d(ReC) = 1.897, d(CH) = 1.094, α = 118.0, β = 130.3
Re-2a d(ReC) = 1.890, d(CH) = 1.093, α = 122.6, β = 123.0
Re-3a d(ReC) = 1.891, d(CH) = 1.092, α = 123.7, β = 122.6

Fig. 1. Optimized geometries of *syn* and *anti* Re(≡CCH$_3$)(=CHCH$_3$)(CH$_2$CH$_3$)$_2$ isomers and a selected list of geometrical parameters for all Re(≡CR)(=CHR)(X)(Y) complexes [12]. Distances in Å and angles in degrees.

for the small model and the *anti* isomer is more stable for the full model. The changes in the geometries of the Re–alkylidene–alkylidyne moiety from Re-1 to Re-3 are small. Focusing on the C–H alkylidene bond, the geometrical parameters suggest that the C–H bond is weaker in the *syn* isomer than in the *anti* isomer and support the presence of an α-agostic interaction in the *syn* isomer. However, the small magnitude of the geometrical changes, which furthermore are spread over several bond distances and bond angles, makes the structural analysis difficult. The analysis of the wave function shows that, among the five empty metal d orbitals, three of them are used for Re–C multiple bonds with the alkylidene and alkylidyne groups provided that the two groups are coplanar (best conformation). Another empty metal orbital, at relatively low energy, is well adapted to overlap with the σ_{C-H} of the alkylidene group, hence giving rise to the stabilizing agostic interaction only in the *syn* isomer [27].

The J_{C-H} coupling constants calculated with 6-31G(d,p) basis set for the small (Re-1$_q$ to Re-3$_q$) and large systems (Re-1 and Re-3) are shown in Table 1. As shown in our previous article, DFT calculations with 6-31G(d,p) basis sets on C and H overestimate J_{C-H} by about 20 Hz [27]. However, the J_{C-H} for the *syn* isomer is smaller than for the *anti* isomer by 30–40 Hz in good agreement with experiment [42,44,46]. This suggests that the different environment for the alkylidene C–H bond in the *syn* and *anti* isomer is well reproduced, consistent with the presence of an α-agostic bond in the *syn* isomer only. Enlarging the system by inclusion of the real substituents decreases J_{C-H} by only 3–8 Hz. This is rationalized by the fact that the geometries of the small and full complexes are similar with the exception of the C–H bond which is slightly elongated in the full system. This

Table 1
Calculated C_{ene}–H NMR coupling constants, J_{C-H}, (Hz) for Re(≡CR)(=CHR)(CH$_2$R)$_2$, Re(≡CR)(=CHR)(CH$_2$R)(OSiR$'_3$) and Re(≡CR)(=CHR) (OR)$_2$ *syn* (s) and *anti* (a) isomers

Structure[a]	BS1[b]	Structure[a]	BS1[b]	Exp.
Re-1s$_q$	138	Re-1s	132	115[c]
Re-1a$_q$	175	Re-1a	167	N.A.
Re-2s$_q$	140	Re-2s	133	116[d]
Re-2a$_q$	180	Re-2a	166	159[d]
Re-3s$_q$	144	Re-3s	141	120[e]
Re-3a$_q$	176	Re-3a	171	157[e]

Experimental J_{C-H} values are added. Optimized B3PW91/6-31G(d,p) structures are shown in Fig. 1.
[a] See Scheme 1 for definition.
[b] BS1 = 6-31G(d,p).
[c] This J_{C-H} coupling constant has been measured directly in the ^{1}H NMR of the ^{13}C labeled compound [46], and differs from the 121 Hz reported in [42].
[d] Ref. [46].
[e] Ref. [44].

suggests that the small structural changes, associated with the bulky ligands, do not much affect the local electronic environment of the alkylidene C–H bond. It also shows that there are no long range electronic effects of the *t*Bu groups on the alkylidene J_{C-H}. Therefore, even if the chemical identity of the whole complexes are taken into account, the calculated J_{C-H} values are still significantly larger than the observed values. The influence of X and Y on J_{C-H} is small although a slight increase in J_{C-H} from Re-1s to Re-3s suggests a weakening of the agostic interaction. A similar trend is seen in the experimental data [42,44,46]. The same conclusion was reached from the analysis of the wave functions [27]. We conclude that the calculations also reproduce the small variations in J_{C-H} between isomers and the effect of the ancillary ligands (X and Y). However, further calculations with the aim of better reproducing the absolute values of J_{C-H} should be done. Thus, we tested the influence of the basis set on the small systems.

Calculations of J_{C-H} coupling constants in organic molecules have shown an important influence of the basis set [23,24]. We decided to stay within the DFT methodology, which has been recognized as appropriate for a wide variety of systems and which allows the calculations of large species and in particular of transition metal complexes. Therefore, we have studied the variation of J_{C-H} with the basis set level, within the DFT-(B3PW91) method (Table 2).

In a first set of calculations we have improved mostly the representation of the valence electrons, without significantly changing the representation of the inner shells. The values for J_{C-H} vary little between BS1 and BS2 showing little influence of the diffuse orbital. The coupling constants become closer to the experimental values with BS3 and BS4 and the biggest change is obtained when going from BS2 to BS3. The change from a double-ζ type basis set to a triple-ζ improves the results although the calculated J_{C-H} values are lower than the experimental values. Furthermore, the lack of convergence in the results shows that these basis sets are inappropriate. It is should be mentioned that a continuous decrease of the J_{C-H} value with the basis set up to convergence is not necessarily expected [14,17]. The changes in J_{C-H} should not be attributed entirely to the improvement in the representation of the valence shell because the inner shell is different for (BS3- BS4) and for (BS1-BS2).

The single point calculations with the IGLO-II and IGLO-III basis sets at the BS1 optimized geometries give very good results. The results are similar for the two basis sets, showing, as already known, that the good performance of the IGLO basis sets comes most probably from a better representation of the orbitals near the nucleus. The influence of X and Y is fairly reproduced

Table 3
C_{ene}–H NMR coupling constants, J_{C-H}, (Hz) for Re(≡CCH_3)(=$CHCH_3$)(CH_2CH_3)$_2$(1), Re(≡CCH_3)(=$CHCH_3$)(CH_2CH_3)(OSiH_3) (2) and Re(≡CCH_3)(=$CHCH_3$)(OCH_3)$_2$(3) *syn* (s) and *anti* (a) isomers using IGLO-II functions for geometries optimized with 6-31G(d,p) and IGLO-II basis sets

Structure[a]	Geometry	
	B3PW91/6-31G(d,p)	B3PW91/IGLO-II
Re-1s_q	113	113
Re-1a_q	154	154
Re-2s_q	113	113
Re-2a_q	151	151
Re-3s_q	118	117
Re-3a_q	154	154

[a] See Scheme 1 for definition.

Table 2
Basis set dependence of the calculated C_{ene}–H NMR coupling constants, J_{C-H}, (Hz) for Re(≡CCH_3)(=$CHCH_3$)(CH_2CH_3)$_2$(1), Re(≡CCH_3)(=$CHCH_3$)(CH_2CH_3)(OSiH_3) (2) and Re(≡CCH_3)(=$CHCH_3$)(OCH_3)$_2$(3) *syn* (s) and *anti* (a) isomers

Structure[a]	BS1[b]	BS2[c]	BS3[d]	BS4[e]	IGLO-II	IGLO-III	Exp.	Structure[a]	IGLO-II	Exp.
Re-1s_q	138	138	109		113	112	115[f]	Re-1s	104	115[f]
Re-1a_q	175	176	149		154	152	N. A.	Re-1a	142	N.A.
Re-2s_q	140	139	109		113	112	116[g]	Re-2s		116[g]
Re-2a_q	180	174	146		151	148	159[g]	Re-2a		159[g]
Re-3s_q	144	144	114	103	118	116	120[h]	Re-3s	111	120[h]
Re-3a_q	176	176	149	138	154	151	157[h]	Re-3a	147	157[h]

Experimental J_{C-H} values are added. Optimized B3PW91/6-31G(d,p) structures are shown in Fig. 1.
[a] See Scheme 1 for definition.
[b] BS1 = 6-31G(d,p).
[c] BS2 = 6-31+G(d,p).
[d] BS3 = 6-311+G(d,p).
[e] BS4 = 6-311++G(2df,2pd).
[f] This J_{C-H} coupling constant has been measured directly in the ^{1}H NMR of the ^{13}C labeled compound [46], which differs from 121 Hz reported in [42].
[g] Ref. [46].
[h] Ref. [44].

for the *syn* isomers. Thus, J_{C-H} is higher for Re-3s$_q$ than for Re-1s$_q$ and Re-2s$_q$, which have almost equal J_{C-H}. The accuracy of the calculations for the *anti* isomers can only come from the comparison between Re-2a and Re-3a because no *anti* isomer has been observed for X = Y = alkyl. The calculations do not reproduce the lower value for Re-2a$_q$ compared to Re-3a$_q$ with the exception of the non satisfying BS1 basis set. A difference of 2 Hz is probably challenging to reproduce in the absence of the steric effect of the bulky groups. No further studies can be carried because no other anti isomers have been identified experimentally.

The geometry of the complexes was re-optimized with the IGLO-II basis sets. The geometries are essentially unchanged and accordingly the values for the coupling constants are equal to those obtained with the 6-31G(d,p) basis set geometry optimization (Table 3). In total, the calculated values for the small model differ from the experimental ones by less than 4 Hz.

Additional calculations for the full system have been carried out for Re-1 and Re-3 (Re-2 J_{C-H} calculation is not feasible). As already noted for the calculations with 6-31G(d,p) basis set, the J_{C-H} is always lower by around 10 Hz for the full systems compared with the small systems, which is consistent with a slightly increase of the α-agostic interaction in the presence of the bulky groups. The calculated J_{C-H} values for the best level of calculation (large model and IGLO-II basis sets) are always lower than the experimental values by about 10 Hz, giving a relative error of about 10%.

3.2. The Mo(=NR)(=CHtBu)(X)(Y) complexes

The molybdenum complexes, isolobal to the rhenium complexes, have been studied. They have been represented only with the small models at the B3PW91 level and the NMR J_{C-H} values have been computed with the IGLO-II basis sets (Table 4 and Fig. 2). The geometries of the Mo complexes are similar to those of the small rhenium complexes and close to the X-ray structures of similar complexes [68–70]. In particular, the C–H bond length is almost equal in the Re and Mo complexes, which should lead to a similar J_{C-H} value. However, the calculated J_{C-H} values are lower for the molybdenum complexes than that for rhenium complexes by about 4-6 Hz in agreement with experiment [47–49,51]. The J_{C-H} values of around 105 Hz found for the *syn* Mo complexes have been considered as indicative of an α-agostic interaction [53] whereas no such suggestion have been done for the Re complexes where the J_{C-H} values are 10 Hz higher. However, the calculations show that the difference between the J_{C-H} of the *syn* isomer and that of the *anti* isomer is similar for all Re and Mo complexes suggesting an α-agostic interaction of the same strength. Further studies are needed to clarify this point. It is worth pointing out that the calculated and experimental J_{C-H} values differ by less than 2–3 Hz. Although such agreement may be somewhat fortuitous because it is obtained for the small model, these results show that the present methodology is appropriate to reproduce trends (metal and ligand effects) for weak α-C–H agostic interactions.

3.3. The Ta(C$_5$R$_5$)(=CHtBu)(X)(Y) complexes

These 16 electron Ta(C$_5$R$_5$)(=CH*t*Bu)(X)(Y) (C$_5$H$_5$ = Cp; C$_5$Me$_5$ = Cp*) complexes, shown in Fig. 3, are pseudooctahedral and display a strong α-agostic interaction with coupling constants less than 84 Hz [52]. Molecular orbital (MO) analysis have rationalized the strength of the α-agostic interaction in electron deficient tantalum complexes [71]. Another MO study has provided an interpretation for the stronger α-agostic interaction in the octahedral field relative to the tetrahedral coordination [72]. Thus, the present calculations are only concerned with the ability of the present computational methodology to reproduce quantitatively the J_{C-H} values for strong α-agostic interactions.

Table 4
Calculated C$_{ene}$–H NMR coupling constants (J_{C-H}) in Hz for Mo(=NR)(=CHCH$_3$)(X)(Y) and Ta(C$_5$R′$_5$)(=CHR)(X)(Y) *syn* (s) and *anti* (a) isomers

Structure[a]	IGLO-II	Exp.	Structure[a]	IGLO-II	Structure[a]	IGLO-II	Exp.
Mo-1s$_q$	107	108[b]	Ta-1s$_q$	79	Ta-1s	N.A.	76[e]
Mo-1a$_q$	150		Ta-1a$_q$	136	Ta-1a	N.A.	
Mo-2s$_q$	106	108.5[c]	Ta-2s$_q$	82	Ta-2s	72	83[e]
Mo-2a$_q$	150		Ta-2a$_q$	145	Ta-2a	N.A.	
Mo-3s$_q$	114	115[d]	Ta-3s$_q$	82	Ta-3s	79	80[e]
Mo-3a$_q$	147		Ta-3a$_q$	141	Ta-3a	N.A.	
			Ta-4s$_q$	91	Ta-4s	77	84[e]
			Ta-4a$_q$	149	Ta-4a	N.A.	

Experimental J_{C-H} values are added. Optimized B3PW91/6-31G(d,p) structures are shown in Figs. 2 and 3.
[a] See Scheme 1 for definition.
[b] Ref. [51].
[c] Ref. [49].
[d] Ref. [47].
[e] Ref. [52].

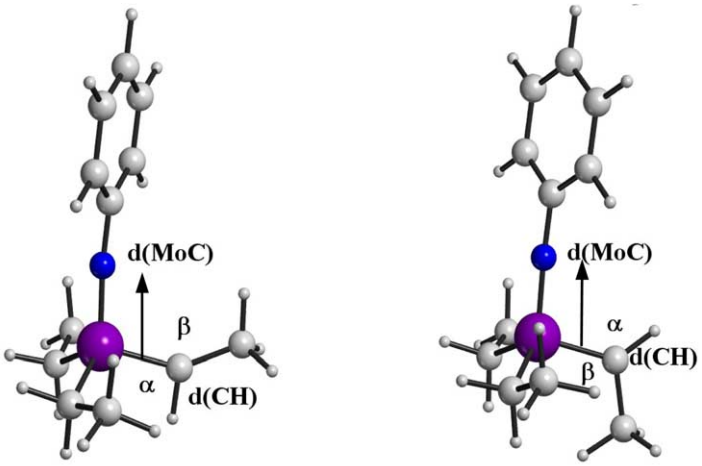

Mo-1s$_q$ d(MoC) = 1.857, d(CH) = 1.115, α = 98.3, β = 145.2
Mo-2s$_q$ d(MoC) = 1.861, d(CH) = 1.115, α = 97.9, β = 145.6
Mo-3s$_q$ d(MoC) = 1.875, d(CH) = 1.109, α = 106.6, β = 138.4
Mo-1a$_q$ d(MoC) = 1.876, d(CH) = 1.091, α = 129.3, β = 114.5
Mo-2a$_q$ d(MoC) = 1.878, d(CH) = 1.090, α = 130.3, β = 113.4
Mo-3a$_q$ d(MoC) = 1.887, d(CH) = 1.092, α = 124.4, β = 120.5

Fig. 2. Optimized geometry of *syn* and *anti* Mo(=NPh)(=CHCH$_3$)(CH$_2$CH$_3$)$_2$ isomers and selected list of geometrical parameters for all Mo(=NR′)(=CHR)(X)(Y) complexes. Distances in Å and angles in degrees.

The optimized geometries of *syn* isomer agree well with the experimental parameters of available similar complexes (Fig. 3) [73,74]. In particular the optimized Ta=C bond length is around 1.91 Å for all complexes, which is within the range of the experimental values (1.883–1.925 Å). The Ta=C–C angle is remarkably open and reaches values up to 155–175°, which is also close to the experimental values of 165°. The hydrogen atom cannot be located by X-ray diffraction spectroscopy and its position can only come from the calculations. The C–H bond length is found to be between 1.125 and 1.150 Å, which corresponds to a strong elongation. The Ta=C–H angle is always less than 90°, which leads to a short nonbonding Ta···H distance (ranging between 1.972 and 2.207 Å). These geometrical features, quite different from those of the Re and Mo complexes, are indicative of a significantly weakened C–H bond and maybe even of a direct, albeit very weak, Ta···H interaction. These geometries support the proposal of a strong α-agostic interaction.

The geometrical parameters are consistent with a weaker α-agostic interaction for X = Y = Cl than X = Y = alkyl. A similar trend was found for the Re complexes where the α-agostic interaction is weaker for X = Y = OR than for X = Y = alkyl. The interpretation given in our previous work [27] applies also for the tantalum complexes: π-donor groups disfavor the agostic interaction by raising the energy of the empty metal d orbital responsible of the agostic interaction.

Calculations for the full systems with the ONIOM method, give similar geometries. As in the case of Re, the structural parameters associated with the C–H alkylidene bond suggest that the α-agostic interaction becomes stronger in the full system due to the steric repulsion between the *t*Bu of the alkylidene and the cyclopentadienyl ring; in particular, the α-agostic interaction is stronger for Cp* than for Cp. The strengthening of an α-agostic interaction caused by steric factors has been observed before and has been rationalized by QM/MM calculations [75,76].

The *anti* isomer, which has never been observed experimentally for these complexes, has geometrical features notably different from the *syn* isomer. In particular, the Ta=C bond is considerably longer (around 1.95 Å) than in the *syn* isomer, the Ta=C–C angle 105–115° is close to what is expected for a sp^2 carbon and no C–H elongation is observed (the C–H bond length is around 1.09 Å). Inclusion of the real substituents leads to similar geometries. Therefore, no α-agostic interaction is present in the *anti* isomer. The *anti* isomer is always less stable than the corresponding *syn* complexes in line with the sole observation of the latter.

The calculated NMR J_{C-H} coupling constants for tantalum complexes are shown in Table 4. The J_{C-H} values for the *syn* isomer within the small model are higher than the experimental data [52], in contrast to what was obtained for Re and Mo complexes. Although the difference between experimental and calculated values is larger than for Re and Mo (the largest difference being

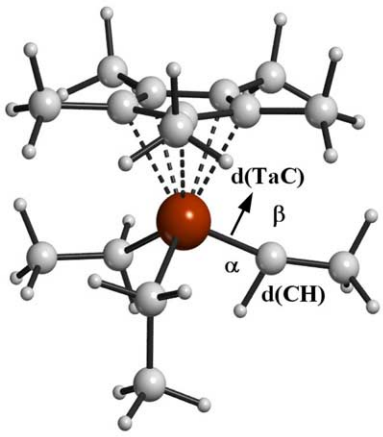

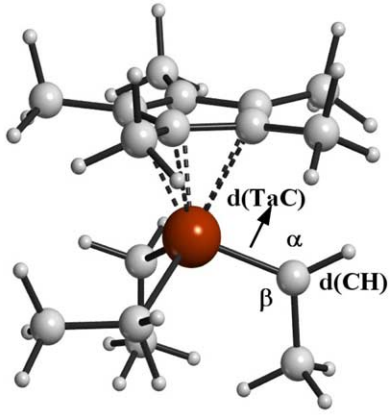

Ta-1s$_q$ d(TaC) = 1.911, d(CH) = 1.136, α = 81.6, β = 165.4
Ta-2s$_q$ d(TaC) = 1.906, d(CH) = 1.135, α = 83.4, β = 164.2
Ta-3s$_q$ d(TaC) = 1.909, d(CH) = 1.134, α = 84.1, β = 161.0
Ta-4s$_q$ d(TaC) = 1.910, d(CH) = 1.125, α = 89.4, β = 156.2
Ta-1s d(TaC) = 1.915, d(CH) = 1.147, α = 75.5, β = 171.1
Ta-2s d(TaC) = 1.906, d(CH) = 1.150, α = 75.9, β = 174.1
Ta-3s d(TaC) = 1.909, d(CH) = 1.139, α = 79.5, β = 164.3
Ta-4s d(TaC) = 1.902, d(CH) = 1.144, α = 79.4, β = 168.7

Ta-1a$_q$ d(TaC) = 1.957, d(CH) = 1.091, α = 133.3, b = 114.0
Ta-2a$_q$ d(TaC) = 1.940, d(CH) = 1.088, α = 136.9, β = 108.9
Ta-3a$_q$ d(TaC) = 1.957, d(CH) = 1.091, α = 133.8, β = 112.9
Ta-4a$_q$ d(TaC) = 1.944, d(CH) = 1.089, α = 135.6, β = 109.6
Ta-1a Not available
Ta-2a d(TaC) = 1.967, d(CH) = 1.091, α = 122.2, β = 126.6
Ta-3a Not available
Ta-4a d(TaC) = 1.972, d(CH) = 1.092, α = 122.3, β = 126.1

Fig. 3. Optimized geometry of *syn* and *anti* $Ta(C_5Me_5)(=CHCH_3)(CH_2CH_3)_2$ isomers and selected list of geometrical parameters for all $Ta(C_5R'_5)(=CHR)(X)(Y)$ complexes. Distances in Å and angles in degrees.

7 Hz), the present methodology leads to reasonable agreement with experiment. In addition, the influence of X and Y on the J_{C-H} coupling constant is reasonably represented with the small model. However, these results must be considered with caution because the agreement between calculations and experiment is slightly worse for the full system than for the small systems (see next).

The calculations for the full systems are carried out only for the *syn* isomer and for Ta-2s, Ta-3s and Ta-4s due to computational limitations. The J_{C-H} values are significantly lower than those computed with the small models when X = Y = Cl, the difference between the two models ranging from 10 to 15 Hz (15–20%). In contrast, for Ta-3s (X = Y = alkyl), very little variation is obtained in J_{C-H} value between small and full models (3 Hz). Overall, the present level of theory gives fair results for the J_{C-H} in the case where the C–H bond is engaged in a strong agostic interaction and the largest difference between computed and experimental values is 11 Hz for a coupling constant of around 80 Hz, i.e., 14% error. Furthermore, the influence of X and Y on J_{C-H} being rather small (<10 Hz), is thus rather difficult to reproduce. With the full models, the changes in J_{C-H} observed by replacing Cp by Cp* are well reproduced but not that for replacing X = Y = alkyl by X = Y = Cl. This poorer agreement between calculated and experimental values for the Ta complexes compared to the Re and Mo cases, is most probably associated with the approximations done in the calculations of the coupling constant: the neglect of the thermal effect and of the anharmonicity is probably less valid in the case of a flat potential energy surface associated with a strongly weakened C–H bond and a possible weak direct Ta···H interaction (distance around 2 Å).

The J_{C-H} values calculated for the *anti* isomer are lower than those for Mo and Re. Although comparison with experiment is not possible because the *anti* isomer has not been characterised for this set of substituents in the Ta complexes, the overall quality of the agreement between the calculations and experiments suggests that the values found for Ta are reasonable. Since the C–H bond length for all *anti* isomers in the Re, Mo and Ta complexes is around 1.09 Å, the differences in J_{C-H} is not due to differences in the C–H distances but in the change of the metal center. Thus, the nature of the metal influence the absolute NMR J_{C-H} value and these results

open the question of the J_{C-H} value to take as reference to define the α-agostic interaction strength; an unique reference independent of the metal center may not be entirely justified.

4. Conclusion and perspective

This study shows that NMR J_{C-H} coupling constants can be calculated accurately without excessive computational effort. B3PW91 NMR calculations with IGLO-II basis sets for main group atoms on geometries optimized with the same functional and 6-31G(d,p) basis sets is accurate enough to reproduce the experimental J_{C-H} values associated with either weak or strong α-C–H agostic interactions in d^0 metal–alkylidene complexes (Re, Mo and Ta). It appears that the computed values with the full systems are always lower than experimental J_{C-H}, the average error being 10–15%. In addition, the influence of the isomer (*syn* versus *anti*), of the metal and of the ligands are overall well reproduced by the calculations, the agreement for the later being better for Re and Mo. However, for a given metal, J_{C-H} is only slightly influenced by the nature of X and Y. The values computed for the pseudooctahedral Ta complexes, where the α-agostic C–H interaction is strong, are overall in less good agreement with experiment than for the pseudotetrahedral Re and Mo complexes where the α-agostic interaction is weak. This may be attributed to the neglect of the vibrational and anharmonic effects in the calculations in the case of a significantly weakened C–H bond. It should be pointed out that the complexes selected for this study are good benchmark species because of the absence of interconversion between the *syn* and *anti* isomers, which could have averaged the J_{C-H} values.

The ability to compute with fair to good accuracy a magnetic J_{C-H} spin–spin coupling constant opens interesting perspectives in the computational analysis of organometallic complexes and in particular in that of the agostic interactions. Similar calculations of J_{C-H} can therefore be carried out for a wide variety of transition metal complexes, which will allow a more direct comparison between calculations and experiments.

Acknowledgements

It is my great pleasure to thank Malcolm Chisholm, an old friend, who initially attracted me to Indiana University as visiting professor. He has always been an enthusiastic supporter of the dialogue between experimental and computational chemists. The present work is far removed from the simple MO pictures that we used to draw over a cup of tea in his office while looking out at the autumn foliage turning red during an Indian summer.

X.S.M. thanks the CNRS for a post-doctoral fellowship. We are indebted to IDRIS for a generous donation of computing time through Grant 041744.

References

[1] R.R. Schrock, Chem. Rev. 102 (2002) 145.
[2] R.R. Schrock, J. Chem. Soc., Dalton Trans. (2001) 2541.
[3] D. Astruc, New J. Chem. 29 (2005) 42.
[4] A. Fürstner, Angew. Chem. Int. Ed. 39 (2000) 3012.
[5] R.R. Schrock, Top. Organomet. Chem. 1 (1998) 1.
[6] R. Buchmeiser, Chem. Rev. 100 (2000) 1565.
[7] C. Copéret, New J. Chem. 28 (2004) 1.
[8] M. Brookhart, M.L.H. Green, J. Organomet. Chem. 250 (1983) 395.
[9] M. Brookhart, M.L.H. Green, L.-L. Wong, Prog. Inorg. Chem. 36 (1988) 1.
[10] E. Clot, O. Eisenstein, in: N. Kaltsoyannis, J.E. McGrady (Eds.), Principles and Applications of Density Functional Theory in Inorganic Chemistry II, Springer-Verlag, Heidelberg, 2004, p. 1.
[11] W. Scherer, G.S. McGrady, Angew. Chem. Int. Ed. 43 (2004) 1782.
[12] R.H. Crabtree, The Organometallic Chemistry of the Transition Metals, John Wiley and Sons, New York, 2001.
[13] G.J. Kubas, Metal Dihydrogen and σ-Bond Complexes: Structure, Theory and Reactivity, Kluwer Academic Publishers, New York, 2001.
[14] T. Helgaker, M. Jaszuński, K. Ruud, Chem. Rev. 99 (1999) 293.
[15] J. Vaara, J. Jokisaari, R.E. Wasylishen, D.L. Bryce, Prog. Nucl. Magn. Res. Spectrosc. 41 (2002) 233.
[16] T. Ziegler, J. Autschbach, Chem. Rev. 105 (2005) 2695.
[17] J. Autschbach, Struct. Bond. 112 (2004) 1.
[18] M. Kaupp, V.G. Malkin, O.L. Malkina, in: P. von Ragué-Schleyer (Ed.), Encyclopedia of Computational Chemistry, John Wiley and Sons, Chichester, 1998, p. 1857.
[19] A.M. Lee, N.C. Handy, S.M. Colwell, J. Chem. Phys. 103 (1995) 10095.
[20] R. Ditchfield, J. Chem. Phys. 56 (1972) 5688.
[21] M. Schindler, W. Kutzelnigg, J. Chem. Phys. 76 (1982) 1919.
[22] M. Schindler, W. Kutzelnigg, J. Am. Chem. Soc. 105 (1983) 1360.
[23] O.B. Lutnæs, T.A. Ruden, T. Helgaker, Magn. Reson. Chem. 42 (2004) S117.
[24] J.E. Peralta, G.E. Scuseria, J.R. Cheeseman, M.J. Frisch, Chem. Phys. Lett. 375 (2003) 452.
[25] S.N. Maximoff, J.E. Peralta, V. Barone, G.E. Scuseria, J. Chem. Theory Comput. 1 (2005) 541.
[26] F. Cloran, I. Carmichael, A.S. Serianni, J. Am. Chem. Soc. 123 (2001) 4781.
[27] X. Solans-Monfort, E. Clot, C. Copéret, O. Eisenstein, Organometallics 24 (2005) 1586.
[28] P.D. Bolton, E. Clot, A.R. Cowley, P. Mountford, Chem. Commun. (2005) 3313.
[29] A.B. Chaplin, J.A. Harrison, A.J. Nielson, C. Shen, J.M. Waters, Dalton Trans. (2004) 2643.
[30] R. Gelabert, M. Moreno, J.M. Lluch, A. Lledós, D.M. Heinekey, J. Am. Chem. Soc. 127 (2005) 5632.
[31] G.B. Bacskay, I. Bytheway, N.S. Hush, J. Am. Chem. Soc. 118 (1996) 3753.
[32] D.L. Lichtenberger, Organometallics 22 (2003) 1599.
[33] J. Autschbach, T. Ziegler, J. Am. Chem. Soc. 123 (2001) 5320.
[34] J. Autschbach, B. Le Guennic, J. Am. Chem. Soc. 125 (2003) 13585.
[35] J. Autschbach, C.D. Igna, T. Ziegler, J. Am. Chem. Soc. 125 (2003) 4937.

[36] B. Wrackmeyer, O.L. Tok, A.A. Koridze, Magn. Reson. Chem. 42 (2004) 750.
[37] B. Le Guennic, S. Patchkovskii, J. Autschbach, J. Chem. Theory Comput. 1 (2005) 601.
[38] J. Oddershede, J. Geertsen, G.E. Scuseria, J. Phys. Chem. 92 (1988) 3056.
[39] T.A. Ruden, O.B. Lutnæs, T. Helgaker, K. Ruud, J. Chem. Phys. 118 (2003) 9572.
[40] J. Autschbach, T. Ziegler, J. Am. Chem. Soc. 123 (2001) 3341.
[41] R. Gelabert, M. Moreno, J.M. Lluch, A. Lledós, V. Pons, D.M. Heinekey, J. Am. Chem. Soc. 126 (2004) 8813.
[42] D.S. Edwards, L. Vollaro Biondi, J.W. Ziller, M.R. Churchill, R.R. Schrock, Organometallics 2 (1983) 1505.
[43] A.M. LaPointe, R.R. Schrock, Organometallics 14 (1995) 1875.
[44] R. Toreki, R.R. Schrock, W.M. Davis, J. Am. Chem. Soc. 114 (1992) 3367.
[45] R. Toreki, G.A. Vaughan, R.R. Schrock, W.M. Davis, J. Am. Chem. Soc. 115 (1993) 127.
[46] M. Chabanas, A. Baudouin, C. Copéret, J.-M. Basset, W. Lukens, A. Lesage, S. Hediger, L. Emsley, J. Am. Chem. Soc. 125 (2003) 492.
[47] J.H. Oskam, H.H. Fox, K.B. Yap, D.H. McConville, R. O'Dell, B.J. Lichtenstein, R.R. Schrock, J. Organomet. Chem. 459 (1993) 185.
[48] J.H. Oskam, R.R. Schrock, J. Am. Chem. Soc. 115 (1993) 11831.
[49] T.S. Pilyugina, R.R. Schrock, A.S. Hock, P. Müller, Organometallics 24 (2005) 1929.
[50] R.R. Schrock, W.E. Crowe, G.C. Bazan, M. DiMare, M.B. O'Regan, M.H. Schofield, Organometallics 10 (1991) 1832.
[51] A. Sinha, R.R. Schrock, Organometallics 23 (2004) 1643.
[52] C.D. Wood, S.J. McLain, R.R. Schrock, J. Am. Chem. Soc. 101 (1979) 3210.
[53] H.H. Fox, M.H. Schofield, R.R. Schrock, Organometallics 13 (1994) 2804.
[54] L.J. Guggenberger, R.R. Schrock, J. Am. Chem. Soc. 97 (1975) 6578.
[55] W. Kutzelnigg, U. Fleischer, M. Schindler, NMR Basic Principles and Progress, Springer-Verlag, Berlin, 1990, p. 165.
[56] E.R. Davidson, Chem. Rev. 100 (2000) 351, and all articles included in this issue.
[57] A.D. Becke, J. Chem. Phys. 98 (1993) 5648.
[58] J.P. Perdew, Y. Wang, Phys. Rev. B 45 (1992) 13244.
[59] M.J. Frisch, G.W. Trucks, H.B. Sclegel, G.E. Scuseria, M.A. Robb, J.R. Cheeseman, J.A.J. Montgomery, T. Vreven, K.N. Kudin, J.C. Burant, J.M. Millam, S.S. Iyengar, J. Tomasi, V. Barone, B. Mennucci, M. Cossi, G. Scalmani, N. Rega, G.A. Petersson, H. Nakatsuji, M. Hada, M. Ehara, K. Toyota, R. Fukuda, J. Hasegawa, M. Ishida, T. Nakajima, Y. Honda, O. Kitao, H. Nakai, M. Klene, X. Li, J.E. Knox, H.P. Hratchian, J.B. Cross, C. Adamo, J. Jaramillo, R. Gomperts, R.E. Stratmann, O. Yazyev, A.J. Austin, R. Cammi, C. Pomelli, J.W. Ochterski, P.Y. Ayala, K. Morokuma, G.A. Voth, P. Salvador, J.J. Dannenberg, V.G. Zakrzewski, S. Dapprich, A.D. Daniels, M.C. Strain, O. Farkas, D.K. Malick, A.D. Rabuck, K. Raghavachari, J.B. Foresman, J.V. Ortiz, Q. Cui, A.G. Baboul, S. Clifford, J. Cioslowski, B.B. Stefanov, G. Liu, A. Liashenko, P. Piskorz, I. Komaromi, R.L. Martin, D.J. Fox, T. Keith, M.A. Al-Laham, C.Y. Peng, A. Nanayakkara, M. Challacombe, P.M.W. Gill, B. Johnson, W. Chen, M.W. Wong, C. Gonzalez, J.A. Pople, GAUSSIAN03, Gaussian Inc., Wallingford, CT, 2004.
[60] M. Svensson, S. Humbel, R.D.J. Froese, T. Matsubara, S. Sieber, K. Morokuma, J. Phys. Chem. 100 (1996) 19357.
[61] A.K. Rappé, C.J. Casewit, K.S. Colwell, W.A. Goddard III, W.M. Skiff, J. Am. Chem. Soc. 114 (1992) 10024.
[62] D. Andrae, U. Häussermann, M. Dolg, H. Stoll, H. Preuss, Theor. Chim. Acta 77 (1990) 123.
[63] A. Bergner, M. Dolg, W. Küchle, H. Stoll, H. Preuss, Mol. Phys. 80 (1993) 1431.
[64] W.J. Hehre, R. Ditchfield, J.A. Pople, J. Chem. Phys. 56 (1972) 2257.
[65] R. Krishnan, J.S. Binkley, R. Seeger, J.A. Pople, J. Chem. Phys. 72 (1980) 650.
[66] S. Huzinaga, J. Chem. Phys. 42 (1965) 1293.
[67] U. Fleischer, W. Kutzelnigg, A. Bleiber, J. Sauer, J. Am. Chem. Soc. 115 (1993) 7833.
[68] J.B. Alexander, D.S. La, D.R. Cefalo, A.H. Hoveyda, R.R. Schrock, J. Am. Chem. Soc. 120 (1998) 4041.
[69] J.Y. Jamieson, R.R. Schrock, W.M. Davis, P.J. Bonitatebus, S.S. Zhu, A.H. Hoveyda, Organometallics 19 (2000) 925.
[70] U. Anders, O. Nuyken, M.R. Buchmeiser, K. Wurst, Angew. Chem. Int. Ed. 41 (2002) 4044.
[71] R.J. Goddard, R. Hoffmann, E.D. Jemmis, J. Am. Chem. Soc. 102 (1980) 7667.
[72] O. Eisenstein, Y. Jean, J. Am. Chem. Soc. 107 (1985) 1177.
[73] K. Mashima, M. Kaidzu, Y. Tanaka, Y. Nakayama, A. Nakamura, J.G. Hamilton, J.J. Rooney, Organometallics 17 (1998) 4183.
[74] L.W. Messerle, P. Jennische, R.R. Schrock, G. Stucky, J. Am. Chem. Soc. 102 (1980) 6744.
[75] A.C. Cooper, E. Clot, J.C. Huffman, W.E. Streib, F. Maseras, O. Eisenstein, K.G. Caulton, J. Am. Chem. Soc. 121 (1999) 97.
[76] G. Ujaque, A.C. Cooper, F. Maseras, O. Eisenstein, K.G. Caulton, J. Am. Chem. Soc. 120 (1998) 361.

Available online at www.sciencedirect.com
SCIENCE DIRECT®
Polyhedron 25 (2006) 349–359
POLYHEDRON
www.elsevier.com/locate/poly

Benzene and ethylene binding to copper(I)–ziconium(IV) chloride materials: The crystal structure and solid-state reactivity of $((bz)_2Cu)_2Zr_2Cl_{10} \cdot bz$

Andrew M. Dattelbaum, James D. Martin *

Department of Chemistry, North Carolina State University, Box 8204, Raleigh, NC 27695-8204, United States

Received 29 April 2005; accepted 9 August 2005
Available online 5 October 2005

In dedication to Malcolm H. Chisholm on the occasion of his 60th birthday. Professor Chisholm's work describing metal alkoxides as models of metal oxides planted the seed for JDM's work designing metal halide analogs of metal oxides and the exploration of their reactivity.

Abstract

The solvothermal reaction of Cu_2ZrCl_6 and $ZrCl_4$ in benzene is shown to yield the molecular species $((bz)_2Cu)_2Zr_2Cl_{10} \cdot bz$ (**1**), which is characterized by single crystal X-ray diffraction. The structure consists of edge-shared dimers of zirconium chloride octahedra whose axial chlorides are bridged by bis-benzene chlorocuprate fragments. The Cu_2Zr_2 tetramers are linked in the crystal lattice by edge-to-face π-stacking of the coordinated and lattice benzene molecules, as well as benzene-to-chloride hydrogen bonding. Benzene is lost from this material in a stepwise fashion resulting in what are described to be chain, $((bz)Cu)_2Zr_2Cl_{10}$ (**2**) and layered clay-type materials, $Cu_2Zr_2Cl_{10}$ (**3**). The desolvated materials, **2** and **3**, reversibly sorb ethylene, as characterized by sorption isotherms, in situ pressure-resolved synchrotron X-ray diffraction and UV/Vis diffuse reflectance spectroscopy.
© 2005 Elsevier Ltd. All rights reserved.

Keywords: Metal halides; Olefin; Aromatic; Pressure resolved XRD; Copper(I); Zirconium(IV); Chemisorption; Sorptive reconstruction

1. Introduction

The reactivity of small molecules with crystalline materials is of significant importance for separations and heterogeneous catalysis applications [1,2]. In spite of this, structural and mechanistic aspects of such heterogeneous reactions are not well understood on the molecular scale. We recently articulated the mechanism of sorptive reconstruction of the $CuAlCl_4$ framework upon ethylene sorption [3]. In that system, the reactivity of Cu(I) toward ethylene was dramatically enhanced by the strong Lewis acid, Al(III), which is a co-building block of the framework. The binding of neutral ligands, L = benzene, ethylene, CO, to the copper(I) center in these metal–halide frameworks suggested to us a potential structural analogy between phosphonates, RPO_3^{2-}, and chlorocuprates, $LCuCl_3^{2-}$ [4]. In the latter, the neutral ligand L bound to copper(I) is more labile than the R group that is bound to P in a phosphonate. Nevertheless, the ligands L may provide a similar pillaring-type function that open galleries of molecular dimension in the inorganic framework. The pillaring structural motif and the lability of the Cu–L bond, specifically when L is an olefin, aromatic, or carbonyl, makes such structures of considerable interest for separations and catalysis applications. In an effort to create clay-type architectures (i.e., patterned after aluminosilicate clays with octahedral Al(III) and tetrahedral Si(IV)) we have

* Corresponding author. Tel.: +1 91 9515 3402; fax: +1 91 9515 8909.
E-mail address: jdmartin@ncsu.edu (J.D. Martin).

0277-5387/$ - see front matter © 2005 Elsevier Ltd. All rights reserved.
doi:10.1016/j.poly.2005.08.011

prepared several materials which employ the octahedral Lewis acidic metal zirconium(IV) as a co-building block with copper(I). The parent network compound Cu_2ZrCl_6 [5] was previously shown to react with benzene under solvothermal conditions to form the linear chain compound $((bz)CuCl_3)_2Zr$ [4]. In the present work we demonstrate that under more zirconium rich conditions, solvothermal reaction in benzene yields the molecular species $((bz)_2Cu)_2Zr_2Cl_{10}\cdot bz$ (**1**). Strong aromatic π-stacking and hydrogen bonding orients the crystal lattice of these molecules such that framework condensation is proposed to occur during the step-wise loss of benzene to yield the chain $((bz)Cu)_2Zr_2Cl_{10}$ (**2**) and a layered clay-type material, $Cu_2Zr_2Cl_{10}$ (**3**). The lattice of **2** is sufficiently rigid to support a long-lived excited state such that it is a brilliant yellow phosphor under UV illumination. Both **2** and **3** are further shown to reversibly sorb ethylene under modest pressures.

2. Experimental

2.1. General information

All reactions were performed under an inert atmosphere of dry N_2 in a glove box or using Schlenk techniques. $ZrCl_4$ (99.99%) was used as received from Aldrich. CuCl was prepared from Cu metal and $CuCl_2$ (Aldrich) according to literature methods and further purified by sublimation [6]. The syntheses of Cu_2ZrCl_6 is reported elsewhere [5]. Benzene (99.9%, Fisher) was distilled from Na/benzophenone, and stored under nitrogen over 4 Å molecular sieves. Elemental analyses were performed by Atlantic Microlab, Inc. Routine powder X-ray diffraction characterization was obtained using an Enraf-Nonius Guinier camera and an Inel diffractometer with a CPS-120 detector, using monocromated Cu Kα radiation.

2.2. Preparation of $((bz)_2Cu)_2Zr_2Cl_{10}\cdot bz$ (*1*)

Cu_2ZrCl_6 (0.100 g, 0.232 mmol) and $ZrCl_4$ (0.0540 g, 0.232 mmol) were ground together in a mortar and pestle and transferred to a thick walled fused silica tube (10 mm o.d. × 6 mm i.d.). On a Schlenk line, 1.0 mL of benzene was added to the reaction vessel. The reaction mixture was frozen with liquid N_2 and sealed using a torch such that the fused silica vessel was filled to 25% volume. The reaction mixture was heated to 125 °C for one week then slow cooled to ambient temperature at a rate of 0.05 °C/min. (*Note of caution*. Significant pressures are generated upon heating the sealed reaction vessel, which can lead to vessel rupture. Appropriate shielding should be utilized such as placing the reaction vessels in a capped iron pipe during heating.) Upon standing at room temperature for two days, colorless crystals of **1** grew from which a single crystal was isolated for an X-ray structure determination. The crystalline material rapidly looses solvent when removed from the benzene yielding a pale yellow powder, $((bz)Cu)_2Zr_2Cl_{10}$ (**2**) precluding reliable elemental analysis.

2.3. Desolvation of *1* to prepare $((bz)Cu)_2Zr_2Cl_{10}$ (*2*) and $Cu_2Zr_2Cl_{10}$ (*3*)

To prepare bulk quantities of $((bz)Cu)_2Zr_2Cl_{10}$ (**2**) Cu_2ZrCl_6 (1.00 g, 2.32 mmol), and $ZrCl_4$ (0.541 g, 2.32 mmol) were placed in a 100 mL Schlenk flask to which 30 mL of benzene was added. The reaction mixture was heated to reflux with stirring under a passive flow of N_2 for 15 h., during which time about half the solids dissolved. The solid residue, a combination of an as yet unidentified phase and unreacted starting material, was separated from the supernatant using a medium porosity glass frit. Shock exposure to liquid N_2 or a dry ice/acetone bath stimulated the crystallization of **1**. The benzene was removed from **1** in vacuo to yield **2** with approximately a 50% yield based on the initial starting material concentration. Elemental analysis for $((C_6H_6)Cu)_2Zr_2Cl_{10}$ Calc.: C, 17.56; H, 1.48. Found: C, 16.96; H, 1.70%. The remaining benzene is slowly lost over a period of weeks when stored in a glove box under a nitrogen atmosphere, or, it can be removed over the course of several hours under dynamic vacuum to yield a yellow solid, $Cu_2Zr_2Cl_{10}$ (**3**). However, **2** can be stored in a capped vial, which significantly reduces the amount of benzene loss.

2.4. $((et)Cu)_2Zr_2Cl_{10}$ (*4*)

A sample of **2** (300 mg) was distributed across the base of a 25 mL Pyrex vessel so as to maximize reactant surface area. The reaction vessel was then affixed to a gas line (<10 mTorr) and evacuated for 6 h. as appropriate for the in situ synthesis of **3**. The sample was then exposed to ethylene at a pressure of 1500 Torr for 3 h. The resulting product was also pale yellow in color, though qualitative observation suggested that a reaction had occurred. Elemental analysis of the product is consistent with the displacement of the benzene by ethylene to yield $((et)Cu)_2Zr_2Cl_{10}$ (**4**). Elemental analysis for $((C_2H_4)Cu)_2Zr_2Cl_{10}$ Calc.: C, 6.66; H, 1.11. Found: C, 6.04; H, 1.51%. As was the case for the benzene adduct, **2**, ethylene is slowly lost from **4** over a period of weeks. However, desorption can be significantly reduced by storing the sample in a sealed container.

2.5. X-ray structure determination of $((C_6H_6)_2Cu)_2Zr_2Cl_{10}\cdot C_6H_6$ (*1*)

Under a flow of argon a single crystal (0.3 × 0.2 × 0.14 mm) covered in silicone grease was mounted on

the end of a glass fiber, and immediately transferred to the diffractometer where it was cooled to −116 °C under a stream of dry nitrogen. Data were then collected on an Enraf-Nonius CAD4-Mach diffractometer with monochromated Mo(Kα), $\lambda = 0.71073$ Å, radiation. Lattice constants were determined by a symmetry-constrained fit of 24 well centered reflections between $32° < 2\theta < 36°$ and their Friedel pairs to yield $a = 21.144(2)$ Å, $b = 7.4987(5)$ Å, $c = 24.170(2)$ Å, and $\beta = 90.365(6)°$. A unique quadrant, h, $\pm k$, l, was collected with 4144 independent reflections by ω-scans with $0° < 2\theta < 54°$. The data were scaled to three intensity check reflections using a five point smoothing routine. An empirical absorption correction was applied using psi scan data. Systematic absences were found to be consistent with the space group $I2/a$ (No. 15), which was confirmed in the subsequent refinement. The structure of $((C_6H_6)_2Cu)_2Zr_2Cl_{10} \cdot C_6H_6$, $Z = 4$, was refined using the NRCVAX suite of programs [7]. All non-hydrogen atoms were located by direct methods using the SIR92 program [8] and refined anisotropically in the final refinement. Hydrogen atoms bound to the benzene rings were then added in calculated positions (idealized to C–H = 0.96 Å) and assigned fixed temperature factors. A full matrix least squares calculation using the 2989 unique reflections ($I > 1.0\sigma(I)$) gave a final refinement with R factors of $R_f = 0.058$ and $R_w = 0.060$.

A room temperature data set was also collected, $a = 21.616(3)$ Å, $b = 7.658(1)$ Å, $c = 24.308(5)$ Å, and $\beta = 90.95(2)°$. However, structural disorder, due in part to solvent loss, prevented a quality structural refinement.

2.6. Adsorption isotherm measurements

A stainless steel volumetric gas line, described previously [3], was utilized for the measurement of sorption isotherms. Powdered samples were dispersed across the 7 cm^2 base of a 16 mL fused silica sample holder. The dead-volume of the sample holder was measured by an N_2 isotherm prior to each experiment. In a typical sorption experiment $((bz)Cu)_2Zr_2Cl_{10}$ (**2**) (0.026 g, 0.032 mmol) was weighed out in the sample holder, which was just enough to cover the sample holder base. The calibrated volume of the gas line was filled to the dosing pressure of 100 Torr, then the valve to the sample holder was opened and the gas was allowed to expand into the sample volume. The amount of ethylene sorbed by the sample was determined using the ideal gas law and the difference between the pressure expected from Boyle's law, based on expansion to the line + sample volume, and the equilibrated pressure. In subsequent steps, 100 Torr of ethylene above the equilibrated pressure was added to the line and then opened to the sample volume until an equilibrated pressure of 1500 Torr was achieved. Equilibration times of one hour were used before final pressure readings were recorded. Greater than 99.9% of the gas was sorbed within the first 5 min after exposure. Therefore, subsequent experiments, including the spectroscopic and diffraction investigations described below, were performed with 10-min equilibration times.

2.7. Spectroscopy

In situ Diffuse Reflectance Spectra were taken using a Cary 3e UV–Vis spectrometer equipped with an integrating sphere. Spectra were measured with respect to a pressed polytetrafluoroethylene (Teflon) powder standard. Reflectance spectra were collected as $R_\infty = R_{sample}/R_{reference}$, then plotted as the remission function, $F(R_\infty) = (1 - R_\infty)^2/2\,R_\infty$, based on the Kubelka–Munk theory of diffuse reflectance [9]. A quartz diffuse reflectance cell ($1.0 \times 10 \times 40$ mm) was affixed to a gas line to measure spectra as a function of ethylene pressure. The gas pressure was monitored from 1×10^{-3} to 760 Torr using a Varian Ba2C SenTorr Gauge Controller and a ConvecTorr vacuum tube gauge transducer. Pressures greater than 760 Torr were controlled using the regulator attached directly to the gas tank.

In a typical experiment $((C_6H_6)Cu)_2Zr_2Cl_{10}$ (**2**) (0.200 g, 0.243 mmol) was diluted into 2.0 g of fused silica (ground and passed through 60 mesh (0.1 mm) sieve and dried at 160 °C for at least 24 h.) and ground together in a mortar and pestle. A portion of that mixture was used to completely fill the quartz sample holder. The sample was evacuated, then dosed with ethylene. Diffuse reflectance spectra were recorded at 100 Torr intervals up to 1500 Torr. Spectra were recorded after approximately 10 min of equilibration at each pressure. The sample was then exposed to vacuum and the ethylene was removed under reduced pressure. Sorption and desorption experiments were also performed with $Cu_2Zr_2Cl_{10}$ (**3**) diluted in ground fused silica. In this case the sample was directly exposed to 1500–1800 Torr of ethylene and the sorption monitored periodically by diffuse reflectance spectroscopy.

Steady-state fluorescence spectra were measured with an ISS PC-1 fluorometer equipped with a Xenon arc lamp and using a front-face detection geometry to orient the sample face at an angle of 22.5° with respect to the incident beam. A low band-pass UG-11 filter was placed after the excitation monochromator. Excitation spectra were corrected with respect to a standard quinine sulfate solution and the NIST spectrum. Emission spectra were plotted using the relative emitted energy per constant interval ($\Phi_E = \Phi_\lambda \lambda^2/hc$) [10].

2.8. Time/pressure resolved powder X-ray diffraction

Time and pressure resolved powder X-ray diffraction experiments were performed at the X7B beamline of the National Synchrotron Light Source at Brookhaven National Laboratories with a wavelength of approximately

0.93 Å, in a Debye–Scherrer collection geometry using either a translating image plate (TIP) detector mounted on a four circle Huber diffractometer [11], or a MAR345 image plate detector system. The wavelength, sample to detector distance, tilting angle of the IP and zero shift position of the IP for the data collection were determined using full Debye–Scherrer rings of LaB_6. Data reduction of the full rings was done using Fit2d [12,13]. Powdered samples placed in 0.7 mm fused silica capillaries, were affixed to a gas line with Swagelok fittings and aligned on a goniometer head [14]. Samples were exposed to ethylene pressures of 100–1500 Torr, or vacuum.

3. Results

3.1. Structure of $((bz)_2Cu)_2Zr_2Cl_{10} \cdot (bz)$ (1)

A summary of crystallographic data for $((bz)_2Cu)_2Zr_2Cl_{10} \cdot (bz)$ (**1**) is available in cif format as supplementary information. An ORTEP drawing of the $((bz)_2Cu)_2Zr_2Cl_{10}$ molecule is shown in Fig. 1. Selected bond distances and angles are reported in Table 1. This molecule sits on a C_2 axis of symmetry. The core of the molecule consists of an edged-shared zirconium bioctahedron with two slightly asymmetric chloride bridges Zr–Cl(1) = 2.607(2) Å and Zr–Cl(2) = 2.582(2) Å. As expected, the four terminal Zr–Cl bonds in the equatorial plane are about 0.2 Å shorter than the corresponding equatorial bridges, Zr–Cl(5) = 2.371(2) Å × 2 and Zr–Cl(6) = 2.358(2) Å × 2. The axial chlorides, Cl(3) and Cl(4), bound to zirconium at an intermediate distance (Zr–Cl(3) = 2.463(2) Å and Zr–Cl(4) 2.475(2) Å), form bridges to Cu(I) cations (Cu–Cl(3) 2.372(2) Å and Cu–Cl(4) = 2.417(2) Å) such that a boat-like geometry is observed for the $Cu_2Zr_2Cl_4$ tetrameric ring with the two copper bridges both bent to the same side of the axial plane of the bioctahedron. The Cl(3)–Cu–Cl(4) plane is bent about 31° out of the Cl(3)–Zr′–Cl(4)′–Cl(3)′–Zr–Cl(4) molecular plane. The pseudo-tetrahedral coordination sphere of the copper cations is completed with

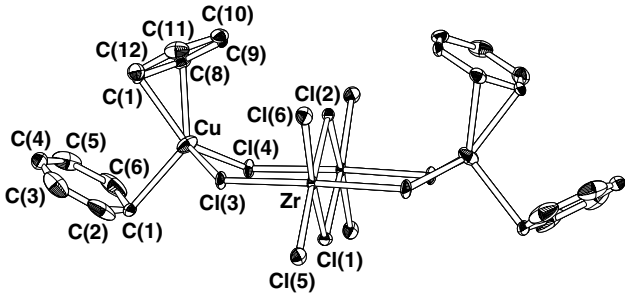

Fig. 1. ORTEP drawing of $((bz)_2Cu)_2Zr_2Cls_{10}$ showing the atom labeling scheme. Thermal ellipsoids are shown at the 50% confidence level.

Table 1
Selected bond distances (Å) and angles (°) for $((bz)_2Cu)_2Zr_2Cl_{10} \cdot bz$ (**1**)

Zr–Zr	4.007(1)
Zr–Cl(1)	2.607(2)
Zr–Cl(2)	2.582(2)
Zr–Cl(3)	2.463(2)
Zr–Cl(4)	2.475(2)
Zr–Cl(5)	2.371(2)
Zr–Cl(6)	2.358(2)
Cu–C(1)	2.385(8)
Cu–C(7)	2.237(7)
Cu–C(8)	2.235(8)
Cu–Cl(3)	2.372(2)
Cu–Cl(4)	2.417(2)
Cl(1)–Zr–Cl(2)	78.89(6)
Cl(1)–Zr–Cl(3)	87.16(5)
Cl(1)–Zr–Cl(4)	86.04(5)
Cl(1)–Zr–Cl(5)	91.68(7)
Cl(1)–Zr–Cl(6)	167.01(7)
Cl(2)–Zr–Cl(3)	88.54(4)
Cl(2)–Zr–Cl(4)	88.03(5)
Cl(2)–Zr–Cl(5)	170.57(7)
Cl(2)–Zr–Cl(6)	88.13(7)
Cl(3)–Zr–Cl(4)	172.87(6)
Cl(3)–Zr–Cl(5)	90.74(6)
Cl(3)–Zr–Cl(6)	93.05(7)
Cl(4)–Zr–Cl(5)	91.62(6)
Cl(4)–Zr–Cl(6)	93.08(7)
Cl(5)–Zr–Cl(6)	101.30(7)
Cl(3)–Cu–Cl(4)	102.01(7)
Zr–Cl(1)–Zr	100.45(8)
Zr–Cl(2)–Zr	101.77(9)
Zr–Cl(3)–Cu	125.79(7)
Zr–Cl(4)–Cu	125.61(7)

two equivalents of benzene; one bound in an η^2-fashion, Cu–C(7) = 2.237(7) Å and Cu–C(8) = 2.235(8) Å, and the other is weakly coordinated in an η^1-fashion with a Cu–C(1) = 2.385(8) Å. The coordination to Cu(I) does not dramatically distort the C–C bond distances in the benzene ligands. The quality of the crystal structure demands that care must be taken to not over interpret C–C distances, nevertheless, it is worth noting that the longest C–C contact is observed for the C(7)–C(8) bond, 1.41(1) Å, which also corresponds to the site of the η^2-coordination. Greater variation between C–C bond distances is observed for both types of coordinated benzene ligands, 1.35(1) to 1.41(1) Å ($\Delta = 0.06$ Å), compared to the lattice solvated molecule, 1.38(1) to 1.40(1) Å ($\Delta = 0.02$ Å), presumably a result of charge transfer upon coordination to the Cu(I). The thermal parameters are notably larger for the carbon atoms of the η^1-bound benzene ligand consistent with its weaker coordination as opposed to the η^2-coordinated ligand and the strong hydrogen bonding of the solvated benzene molecules.

3.2. Excitation and emission spectroscopy

The partially desolvated material $((bz)Cu)_2Zr_2Cl_{10}$ (**2**) exhibits brilliant yellow photoluminescence at room temperature under UV excitation. The excitation and

emission maxima for **2**, shown in Fig. 2, were observed at 26 110 cm^{-1} (383 nm) and 17 390 cm^{-1} (575 nm), respectively. The emission intensity is approximately 25% the intensity of anthracene [15]. Desorption of the benzene from **2** to form **3** results in a loss of the observed room temperature luminescence.

3.3. Ethylene sorption isotherms

Room temperature ethylene sorption isotherms were measured to demonstrate both ligand exchange and olefin sorption capacity of these materials. The luminescent, partially desolvated material **2**, was used as the starting sorbate for the sorption, desorption and resorption measurements for which the data are presented in Fig. 3. Monitoring the luminescence of the sample using a hand held mercury lamp (350 nm), confirmed that the initial evacuation of the sample prior to the sorption isotherm did not significantly convert compound **2** to compound **3**. To interpret this sorption data, we further recognize that the vapor pressure of benzene is low at room temperature with respect to ethylene. Thus, as the benzene is displaced by ethylene, it does not significantly contribute to the measured gas pressure in the line. Significant sorption is observed immediately upon exposure of **2** to ethylene at a pressure of 100 Torr. An inflection in the initial sorption isotherm is observed at approximately 0.5 equivalents of ethylene per mole of copper. Additional sorption is observed as the equilibrated pressure of ethylene exceeds about 400 Torr. At an equilibrated pressure of 1500 Torr approximately 1.5 equivalents of ethylene are sorbed per equivalent of copper. Upon desorption, there is a plateau in the isotherm at a 1:1 stoichiometric ratio of ethylene to copper, consistent with the formation of **4**. Ethylene is not lost from the one equivalent adduct until pressures well below 50 Torr are achieved. To achieve full desorption, the sample was exposed to dynamic vacuum overnight resulting in the formation of **3** prior to resorption. While the one-equivalent ethylene adduct is not luminescent, compound **3** is a significantly deeper shade of yellow than are the adduct phases providing a visual indication of its formation. Upon resorption starting with the darker yellow material **3**, ethylene up-take is not initially as facile as low-pressure sorption into **2**. However, at equilibrium pressures above about 400 Torr the sorption isotherms for the initial sorption into **2** and resorption into **3** are nearly equivalent. The sorption and desorption of ethylene is reversible without any appreciable loss of activity, having been repeated for five cycles in our laboratory.

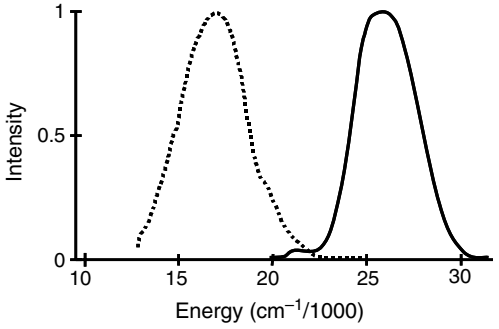

Fig. 2. Excitation (dotted line) ($\lambda_{em} = 575$ nm) and emission (solid line) ($\lambda_{ex} = 383$ nm) spectra for $((bz)Cu)_2Zr_2Cl_{10}$ (**2**).

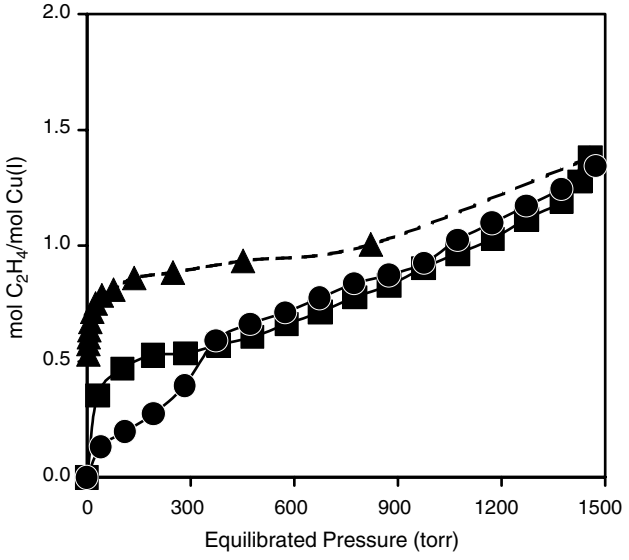

Fig. 3. Ethylene sorption/desorption isotherms. Initial sorption (■) into **2**, desorption (▲), and resorption (●) into **3**.

3.4. Diffuse reflectance spectroscopy

Diffuse reflectance data collected during the sorption and desorption of ethylene into $((bz)Cu)_2Zr_2Cl_{10}$ (**2**) are shown in Fig. 4. The initial spectrum of **2** exhibits a

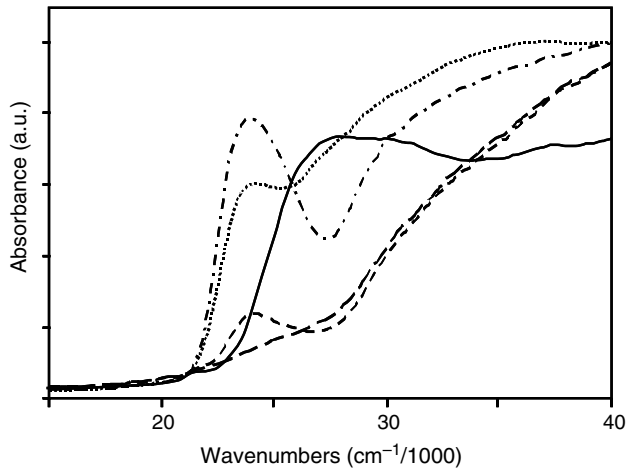

Fig. 4. Diffuse reflectance UV/Vis spectra of $((bz)Cu)_2Zr_2Cl_{10}$ (**2**) (—); **2** exposed to ethylene in 100 Torr steps, shown at 300 Torr (– – –), $(et)Cu_2Zr_2Cl_6$ (**5**) and at 1000 Torr (- - - -), $((et)Cu)_2Zr_2Cl_{10}$ (**4**); $Cu_2Zr_2Cl_{10}$ (**3**) from desorbtion of ethylene adducts (· · ·); and high pressure ethylene adduct at ~1500 Torr (–·–·–).

broad band-edge at ca. 24 900 cm^{-1} (416 nm, 3.09 eV). As a point of reference, this band edge is red shifted from that of CuCl (3.2 eV) and that of $ZrCl_4$, which is in the vacuum ultraviolet, but is very similar to the diffuse reflectance spectrum of Cu_2ZrCl_6 [5]. Exposure to 100 and 200 Torr of ethylene appeared to have little effect on the position of the band edge, although a slight increase in absorption intensity is observed at higher energy. At 300 Torr of ethylene, the band edge shifts abruptly to ca. 30 000 cm^{-1} (333 nm, 3.72 eV) with a much less intense broad shoulder at ~25 000 cm^{-1}. A well-defined peak with a maximum at 24 038 cm^{-1} (416 nm, 2.98 eV) is observed to gradually grow upon increasing ethylene pressure from 300 to 1000 Torr, with a clear isosbestic point at 26 200 cm^{-1}. The spectrum at 1000 Torr of ethylene corresponds to the formation of the one equivalent adduct, **4**. Evacuation of the sample results in the appearance of the spectrum of **3** with a significantly red-shifted band edge, 24 400 cm^{-1}, consistent with the deeper yellow color observed for **3**. Allowing the sample to stand overnight under a pressure of 1500 Torr of ethylene results primarily in the increasing intensity of a well-resolved peak at 24 000 cm^{-1}.

3.5. Variable pressure X-ray diffraction

In situ synchrotron powder X-ray diffraction experiments as a function of ethylene pressure were preformed to monitor the structural changes taking place during the sorption of ethylene by $((bz)Cu)_2Zr_2Cl_{10}$ (**2**). For the experiment shown in Fig. 5, the sample was evacuated then the ethylene pressure was increased in 100 or 200 Torr increments to 1500 Torr. Diffractograms shown are those taken after 10 min equilibration at each given ethylene pressure. Under these conditions, the incremental addition of ethylene to **2** results in the gradual formation of the ethylene adduct phase, **4**. Subtraction of diffractogram Fig. 5(b) from Fig. 5(c) shows only trace formation of **4** and loss of **2**. Principal component analysis of this pressure resolved diffraction data finds that 99.898% of the total variance is explained by the first two principal components. After rotating these two components by −37° the diffraction patterns of **2** and **4** are reproduced. Existence curves, determined by normalization of the first two eigenvectors (rotated by 37°) of the principle component analysis, shown in Fig. 6, provide no evidence for a crystalline 0.5 equivalent intermediate. The curves for the loss of crystalline **2** and appearance of crystalline **4** cross at 50% transformation confirming that no amorphous intermediate exists either. However, a similar analysis looking only at the intensity of the major reflections shows that beyond 500 Torr the diffraction intensity of the major peaks gradually increases to a maximum at about 1100 Torr, and then slightly decreases with increased pressure. Diffraction data of the desorption of ethylene from **4** was not obtained because the seal of the sample capillary to the goniometer gas line was insufficient to obtain adequate vacuum to remove the ethylene without decomposing the sample due to exposure to atmospheric moisture.

Lattice constants for the one equivalent benzene and ethylene adduct phases, **2** and **4**, were refined from the diffractograms of Fig. 5(b) and (k), respectively (Table 2). Monoclinic symmetry is apparently retained upon loss of benzene from **1**, and upon ethylene for benzene substitution. The most dramatic effect of the solvent loss is a significant collapse by 5.5 and 7.0 Å along the *a* and *c* lattice directions, respectively. Only modest collapse by 0.3 Å is observed along the *b* direction. Exchange of ethylene for benzene results in further collapse of the *a* and

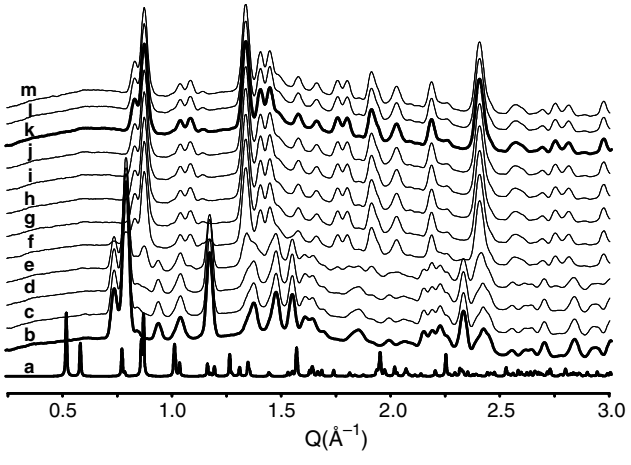

Fig. 5. In situ X-ray diffraction of ethylene sorption. a, calculated powder pattern of $((bz)_2Cu)_2Zr_2\ Cl_{10} \cdot bz$ (**1**); b, $((bz)Cu)_2Zr_2Cl_{10}$ (**2**); sample equilibrated for 10 min under ethylene pressures of c, 100 Torr; d, 200 Torr; e, 300 Torr; f, 400 Torr; g, 500 Torr; h, 600 Torr; i, 700 Torr; j, 900 Torr; k, 1100 Torr; l, 1300 Torr and m, 1500 Torr. Diffractogram k is that of $((et)Cu)_2Zr_2Cl_{10}$ (**4**).

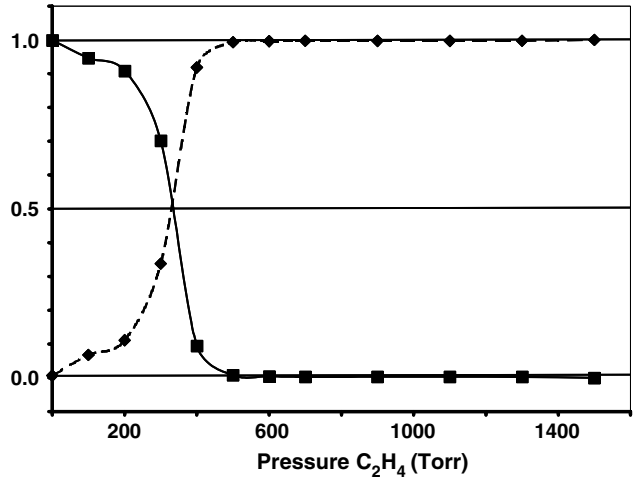

Fig. 6. Existence curves as determined by normalization of the first two eigenvectors (rotated by −37°) of the principal component analysis of the variable pressure diffraction. Squares correspond to the existence of **2** and diamonds to the existence of **4**.

Table 2
Room temperature lattice constants for compounds **1**, **2**, and **4**

	a (Å)	b (Å)	c (Å)	β (°)	V (Å^3)
1	21.616(3)	7.658(1)	24.308(5)	90.95(2)	4023
2	15.92(2)	7.35(1)	17.16(1)	94.3(1)	2000
4	14.53(1)	6.66(1)	15.15(1)	100.9(2)	1438

c lattice constants by 1.4 and 2.0 Å, respectively, and b by about 0.7 Å.

4. Discussion

A complex pattern of reactivity of crystalline copper zirconium chloride materials with benzene and ethylene is indicated by the diffraction, absorption isotherm and diffuse reflectance data presented here. The reaction pathways are summarized in Scheme 1. The reactivity of this gas/solid system, similar to that previously reported for the ethylene/$CuAlCl_4$ system [3], is significantly correlated to the structure of these materials. To understand these structure/reactivity correlations, we begin with a discussion of the crystal structure of the solvothermally synthesized molecular adduct **1**. Spectroscopic and diffraction data provide insight into the structural transformation upon loss of benzene and mechanistic insight regarding the sorption of ethylene by this system.

4.1. Molecular versus extended structure of *1*

The binding of aromatic molecules to Cu(I) centers has significant precedent in the literature [16], although a search of the Cambridge Structural Database finds only three other examples of benzene coordinated to chlorocuprates [4,17,18]. Furthermore, there are no previously reported crystal structures with more than one aromatic ligand coordinated to Cu(I). The filled π- and empty π*-orbitals of benzene can participate in bonding to transition metals, however, the benzene π*-orbitals do not effectively compete with the Lewis acidity of the Zr(IV) chloride also coordinated to copper. Therefore, the benzene–Cu bonding is almost exclusively of a non-classical type (i.e., donation into the empty s/p-hybrid orbitals of Cu(I) with no back-bonding into the benzene π*-orbitals) [19]. The strong Lewis acidity of Zr(IV) coordinated to Cu(I) through the chloride bridges enhances the σ-acceptor nature of Cu(I) making the coordination of multiple benzene ligands possible. Nevertheless, the d^{10}-copper center is not significantly electron deficient, and thus exhibits modest bonding to one benzene ligand in an η^2-fashion, but only very weak binding to the second benzene ligand in an η^1-fashion.

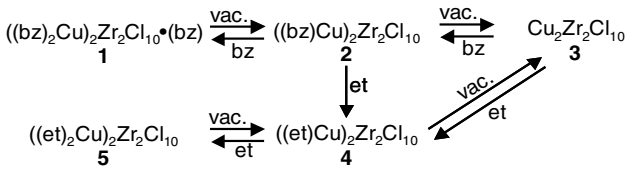

Scheme 1.

The local geometry of the pseudo-tetrahedral Cu(I) and octahedral Zr(IV) is consistent with that expected for these ions. The local geometry of these cations, however, gives no hint as to the reason for the unusual distortion of both copper tetrahedra to the same side of the zirconium chloride bioctahedron, seen in the molecular structure, Fig. 1. Rather, this unusual boat-type configuration is a result of a complex pattern of inter- and intra-molecular π-stacking and benzene–chloride hydrogen bonding. Numerous short contacts between the edge ($\delta+$) of one benzene molecule and the face ($\delta-$) of a neighboring molecule, and between chloride atoms and the edges of benzene molecules are observed, as shown in Fig. 7, with distances tabulated in Table 3. As a point

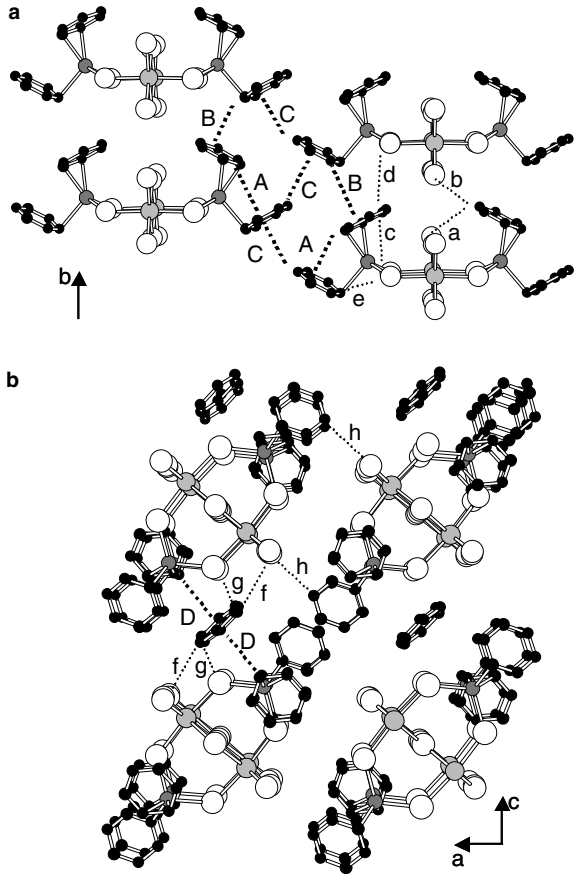

Fig. 7. Ball and stick drawings of **1** describing the intra- and intermolecular π-stacking and hydrogen bonding interactions. (Capital letters represent benzene–benzene π-stacking contacts and lower case letters represent benzene–Cl hydrogen bonding.) The view in (a) is a slice parallel to the (1,0,1) plane and (b) is a projection looking down the [0 1 0] direction.

Table 3
Hydrogen bonded and edge-to-face π-interactions in the crystal structure of $((C_6H_6)_2Cu)_2Zr_2Cl_{10} \cdot C_6H_6$ (**1**)

A	
η^2-edge–η^1-face	C(7)–B_1 = 3.36
B	
η^2-face–η^1-edge	B_2–C(1) = 3.67
C	
η^1-edge–η^1-face	C(4)–B_1 = 3.61
D	
η^2-edge–sol. face	C(8)–B_s = 3.55
a	
η^2-edge–intra Cl	C(9)–Cl(2) = 3.43 C(10)–Cl(2) = 3.67
b	
η^2-edge–inter Cl	C(9)–Cl(1) = 3.73 C(10)–Cl(1) = 3.70
c	
η^2-face–intra Cl	C(11)–Cl(3) = 3.63 C(12)–Cl(3) = 3.63 C(8)–Cl(4) = 3.63
d	
η^2-face–inter Cl	C(10)–Cl(3) = 3.78
e	
η^1-edge–intra Cl	C(6)–Cl(3) = 3.56 C(1)–Cl(3) = 3.62 C(1)–Cl(4) = 3.52 C(2)–Cl(4) = 3.66
f	
sol. edge–Cl	C(15)–Cl(6) = 3.68
g	
sol. edge–Cl	C(15)–Cl(4) = 3.59
h	
η^1-edge–inter Cl	C(5)–Cl(6) = 3.63

The center of the lattice solvate, η^1- and η^2-benzene molecules is represented by B_s, B_1, and B_2, respectively. Distances are reported in Å.

of reference, the edge-to-face contact in crystalline benzene is 3.6 Å [20,21]. The shortest of these contacts are the intra-molecular contacts between the edge of the η^2-benzene ligand and the face of the η^1-benzene ligand, 3.36 Å (A), and between the edge of the η^2-benzene and the equatorial chlorides of the Zr_2Cl_{10} bioctahedron, 3.43 and 3.67 Å (a). The contacts between the edge of the η^1-benzene ligand and the axial-chloride ligands, 3.52–3.66 Å (e), are only slightly longer. While a majority of these inter-ligand contacts are best described as the edge-to-face motif, the contacts c and d (Cl–η^2-benzene–Cl) are similar to a classical π-stack where the center of the benzene molecules are slipped off the axis of the stack. These π-to-π and hydrogen bond contacts cause the unusual boat-shape distortion, and stabilize the crystalline lattice of **1**. However, these interactions are not sufficient to stabilize this material in the absence of excess benzene. When removed from its mother liquor, three equivalents of benzene are readily lost from this crystalline lattice.

4.2. Solvent loss/framework construction

Three equivalents of benzene per formula unit are readily lost from the crystalline structure of **1**, as confirmed by elemental analysis. Diffraction and spectroscopic measurements confirm that the material formed, **2**, retains the remaining one equivalent of benzene/copper even under modest vacuum. It is likely that the lattice solvated- and weakly bound η^1-benzene ligands are those that are most readily lost. A model for the structure of the desolvated material can be constructed by removal of all but the η^2-benzene ligands, and consideration of the nearest intermolecular Cu···Cl contacts; an inverse of the sorptive reconstruction described for ethylene sorption by $CuAlCl_4$ [3]. The shortest intermolecular Cu···Cl contact is only 5.55 Å, along the direction of the η^1-edge to Cl(6) hydrogen bonded contact of the parent structure (described as contact h in Fig. 7). Several other intermolecular contacts between 6.4 and 7 Å exist, each of which link molecules within the *ab* plane. By collapsing the unit cell of **1**, with the lattice solvated and η^1-benzene ligands removed but otherwise maintaining the $((\eta^2\text{-bz})Cu)_2Zr_2Cl_{10}$ molecular geometry, to the lattice dimensions indexed from the X-ray powder pattern of **2** (Table 2), the model structure shown in Fig. 8 is achieved. These metrical parameters bring the

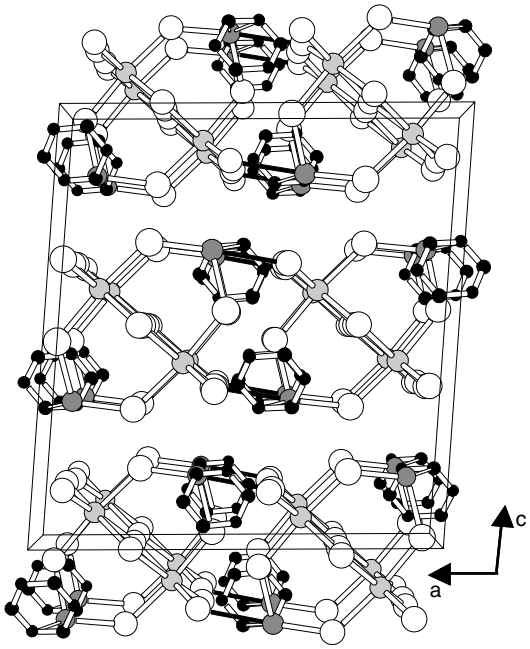

Fig. 8. Model for the structure of **2** based on the collapse of **1** to the observed unit cell dimensions after loss of the lattice solvated and η^1-benzene ligands. The bold, black lines represent the likely bonds formed between Cu and Cl(6) upon framework construction.

copper and Cl(6) atoms into bonding distance, well below the sum of their van der Waals radii (3.2 Å). This model structure is not the correct structure, since the peak intensities of the calculated powder pattern do not match the observed intensities. This is not surprising given that with the loss of the π-stacking interactions, the boat-geometry of the Cu_2Zr_2 core is likely to be lost, and the molecular orientations would need to be rotated to optimize crystal packing. Nevertheless, this model is a helpful starting point for consideration of the chemistry. Here, the large collapse along the *a* direction is consistent with the formation of covalent chains. The $(\eta^2\text{-bz})CuCl_3$ unit is reminiscent of bridging phosphonate-type ligands, as previously demonstrated for another copper zirconium halide chain [4]. The *b* lattice direction decreases the least upon solvent loss, consistent with this being the lattice direction in which the coordinated benzene remains. Solvent loss from the clay-like gallery between layers of these chains accounts for the 7 Å collapse along *c*.

The UV/Vis spectrum of **2**, exhibits a characteristic band structure similar to that observed for $[H_2NMe_2]$-$CuZrCl_6$ and Cu_2ZrCl_6 [5], which supports the proposal of a condensed framework rather than isolated molecules. However, it is challenging to fully decipher this absorption spectrum. While the d^{10}-copper M–Lσ* orbitals are the HOMO in this system, unoccupied benzene-π*, Zr-d and Cu-s/p states all provide relatively low energy acceptor states. Comparison of the excitation spectrum, Fig. 2, with the absorption spectrum, Fig. 4, clearly demonstrates that absorption at the band edge is responsible for the luminescence. Previously we showed that the higher energy blue luminescence of $CuAlCl_4$ was due to a copper centered d ← s/p transition [22]. Because of its higher energy this copper centered mechanism can likely be ruled out in the present case. Cu_2ZrCl_6, for which the LUMO was shown to be Zr-4d states [5], does not exhibit luminescence at room temperature. Furthermore, when the benzene is replaced with ethylene, which we propose to be isostructural (see below), the luminescence is also lost. Therefore we propose that a metal to ligand charge transfer between Cu and benzene is responsible for the luminescence of **2**. This assignment is consistent with that recently reported for the $Cu_2(CF_3SO_3)_2(bz)$ complex [23]. The benzene ligands in **2** must be held in a fairly rigid orientation so as not to quench the room temperature luminescence. If the Cl–bz–Cl π-to-anion stacking along the *b* lattice direction (represented as c and d in Fig. 7) persists as proposed in the model structure of **2**, this could in part account for such lattice rigidity.

The final equivalents of benzene are only lost when the sample is evacuated for several hours under dynamic vacuum forming $Cu_2Zr_2Cl_{10}$ (**3**). As the benzene is removed from the lattice, a significant structural rearrangement occurs such that the copper to zirconium charge transfer in **3** is at a lower energy than either the copper–benzene or copper–ethylene charge transfer in **2** or **4**, respectively, Fig. 4. This lower energy Cu → Zr charge transfer is responsible for the darker shade of yellow of this desolvated material. We have not yet been able to index a powder pattern for **3**, however, we speculate that loss of the η^2-benzene ligands results in further collapse along the *b* axis to yield a layered structure that may be related to a smectite-clay. We further suggest that retention of a layered structure is the most consistent model to accommodate the reversible sorption of ethylene, described below.

4.3. Ethylene sorption

Compounds **2** and **3** readily react with ethylene at room temperature, and at a pressure well below one atmosphere of ethylene. The general feature of the enhanced reactivity of copper(I) chlorides toward olefins and aromatics when associated with a strong Lewis acid shows considerable parallel between this copper(I) zirconium(IV) system and that previously reported for the copper(I) aluminum(III) system [3]; although higher ethylene pressure is required for the present system to achieve the comparable sorption capacity. Copper chloride itself does not sorb ethylene until pressure of >60 atm of ethylene is achieved [24]. Comparison of the powder diffraction patterns of **2** and **4** (Fig. 5) suggests that these two materials have a similar structural topology. Their diffraction patterns exhibit a similar peak profile, albeit at higher values of reciprocal space for the ethylene adduct because of the lattice contraction upon replacement of the benzene molecules with the smaller ethylene. Compound **4** is formed either by the replacement of benzene in **2** by ethylene, or by the addition of ethylene to the completely desolvated **3**.

Interestingly, a parallel comparison of the sorption isotherm and pressure resolved X-ray diffraction and diffuse reflectance spectroscopy data suggest a significant variation in the mechanisms of sorptive reconstruction between this copper zirconium system and the $CuAlCl_4$ system. The sorption isotherm, Fig. 3, clearly demonstrates that ethylene is immediately sorbed into the framework of **2**, with nearly 0.5 equivalents sorbed by an equilibrium pressure of 100 Torr. By contrast, the diffuse reflectance spectrum at 100 Torr of ethylene pressure shows little change from that of the parent material **2**. No significant change is observed in the diffuse reflectance spectra until the ethylene pressure is increased to 300 Torr (Fig. 4); an equilibrium pressure that corresponds to a plateau in the sorption isotherm. Similarly, only a trace of the diffraction signature for the ethylene adduct, **4**, is observed at ethylene pressures below 300 Torr. This seemingly contradictory behavior is highlighted by comparison of the existence curve determined by diffraction for the formation of **4** from

2, Fig. 6, with the corresponding sorption isotherm measured with the calibrated gas line, Fig. 3. By contrast, for the sorption of ethylene into the condensed framework of $CuAlCl_4$, the analogous sorption isotherm, diffuse reflectance and X-ray diffraction data are nearly superimposable. We suggest that the model with a rigid clay-like structure of the copper zirconium chloride inorganic framework, in which a significant range of benzene or ethylene solid solubility is possible, provides the most consistent explanation to the observed data. Whereas sorption of ethylene into $CuAlCl_4$ required a drastic framework transformation, sorption into the pseudo lamellar structure of **2** need not drastically restructure the framework because "galleries" for ligand exchange are held open by pillars of the remaining benzene ligands. Thus, no major structural change is required until all the benzene is displaced, apparently at approximately 0.5 equivalents of ethylene/copper site that occurs at an equilibrium ethylene pressure of around 300 Torr. Above 300 Torr, the sorption isotherm, diffraction and diffuse reflectance data provide parallel evidence of continued ethylene sorption. The diffraction data suggest that complete structural transformation occurs over the narrow pressure range between 300 and 500 Torr of ethylene. By contrast, the diffuse reflectance and sorption isotherm data imply a continued increase in the sorption of ethylene with increasing pressure. These data suggest that **4** in fact exists over a range of ethylene stoichiometry, $((et)_{1-x}Cu)_2Zr_2Cl_{10}$, where $x = 0$–0.5. This interpretation is further consistent with the slightly different profile of the sorption isotherm for sorption into 3. If 3 has the collapsed clay-type structure, as proposed, then initial sorption must open the "galleries" within the framework, rather than simply exchanging ethylene for benzene ligands. Once the "galleries" are opened with 0.5 equivalents of ethylene (>400 Torr), there is no discernable difference in the ethylene sorption starting from 2 or 3. The sorption isotherm, spectroscopic and diffraction data imply that the full stoichiometric loading of one equivalent of ethylene/copper site is achieved at around 1000 Torr of ethylene pressure.

Increasing the ethylene pressure beyond 1000 Torr demonstrates further sorption capacity of this material. Diffraction data at these higher pressures begin to show a slight decrease in the diffraction intensity although no evidence of a new crystalline phase is observed. However, the diffuse reflectance spectra show a dramatic growth of the copper → ethylene charge transfer band at 24 000 cm^{-1} (Fig. 4). This sharp MLCT band is most consistent with a further deconstruction of an extended framework, and the formation of a molecular species; likely $((et)_2Cu)_2Zr_2Cl_{10}$ (**5**) the bis-ethylene analog to the molecular structure of **1**.

The ethylene desorption isotherm (Fig. 3) demonstrates no significant hysteresis for the higher ethylene adduct, **5**, consistent with the facile loss of benzene from **1**. However, like the mono-benzene adduct **2**, the mono-ethylene adduct **4** only begins to exhibits ethylene loss at pressures less than 20 Torr.

5. Conclusion

The reactivity of a family of copper zirconium chloride materials toward benzene and ethylene has been characterized by single crystal and powder X-ray diffraction, diffuse reflectance spectroscopy and by volumetric adsorption analysis. Adduct phases with one and two equivalents of benzene or ethylene per equivalent of copper have been identified, as well as the ligand free inorganic host. The single crystal structure of **1** provides the first crystallographically characterized example of multiple aromatic ligands coordinated to a copper(I) center. Significant π-stacking of the benzene ligands and benzene–chloride hydrogen bonding cause a unique molecular distortion to **1** as well as providing the basis for organization of the crystalline lattice. The benzene ligands of **1** can be lost under relatively mild conditions resulting in the construction of a clay-type inorganic framework, or be exchanged for ethylene under modest pressures.

Like the previously reported reactivity of $CuAlCl_4$ toward ethylene, the Lewis acidic zirconium(IV) chloride dramatically enhances the reactivity of copper chloride toward olefins and aromatics by lowering the energy of copper(I)'s empty s/p orbitals to make it a more effective electron acceptor. Both $CuAlCl_4$ and $Cu_2Zr_2Cl_{10}$ undergo solid state, sorptive reconstruction reactions by a classic mechanism of nucleophilic substitution/addition. However, the framework of $CuAlCl_4$ is more flexible exhibiting a mechanism for the reaction with ethylene that was described as a 'rat-snake' model in which there is a continuous structural transition at the reacting phase boundary. The more rigid framework of $Cu_2Zr_2Cl_{10}$ appears to undergo an abrupt transformation where structural plates are separated by a given concentration of ethylene. The remaining coordination sites, opened by the pillaring of the initially sorbed ligands, can then sorb additional small molecules up to a stoichiometric loading.

Acknowledgements

The authors gratefully acknowledge Dr. Paul Boyle for collection of the single crystal data for **1**, and Dr. Jaap Folmer for assistance with the principal component analysis of the pressure resolved diffraction data. Dr. Jonathan C. Hanson provided invaluable support on line X7B through the general users program of the National Synchrotron Light Soruce supported by the

division of materials sciences of DOE. Funding for this work was provided by the National Science Foundation, DMR-0072828, and DMR-0305086

References

[1] National Research Council (US), Separation Technologies for the Industries of the Future, National Academy Press, Washington DC, 1998.
[2] R. Coontz, J. Fahrenkamp-Uppenbrink, P. Szuromi, Science 299 (2003) 1683, and special section p. 1684.
[3] R.M. Sullivan, H. Liu, D.S. Smith, J.C. Hanson, D. Osterhout, M. Ciraolo, C.P. Grey, J.D. Martin, J. Am. Chem. Soc. 125 (2003) 11065.
[4] A.M. Dattelbaum, J.D. Martin, Inorg. Chem. 38 (1999) 6200.
[5] A.M. Dattelbaum, L. He, F. Tsui, J.D. Martin, J. Alloys Compd. 338 (2002) 173.
[6] G.B. Kauffman, L.Y. Fang, Inorg. Syn. 22 (1983) 101.
[7] E.J. Gabe, Y. Le Page, J.-P. Charland, F.L. Lee, P.S. White, J. Appl. Crystallogr. 22 (1989) 384.
[8] A. Altomare, M.C. Burla, G. Camulli, G. Cascarano, C. Giacovazzo, A. Guagliardi, G. Polidori, J. Appl. Crystallogr. 27 (1994) 435.
[9] W.W. Wendlandt, H.G. Hecht, Reflectance Spectroscopy, Interscience, New York, 1966 (Chapter 3).
[10] G. Blasse, B.C. Grabmaier, Luminescent Materials, Sprinter-Verlag, Berlin, 1994, p. A4.
[11] P. Norby, J. Appl. Crystallogr. 30 (1997) 21.
[12] A.P. Hammersley, FIT2D: An Introduction and Overview, ESRF Internal Report, ESRF97HA02T, European Synchrotron Radiation Facility, Grenoble Cedex, France, 1997.
[13] A.P. Hammersley, FIT2D V9.129 Reference Manual V3.1, ESRF Internal Report, ESRF98HA01T, European Synchrotron Radiation Facility, Grenoble Cedex, France, 1998.
[14] P. Norby, In situ time-resolved synchrotron powder diffraction studies of syntheses and chemical reactions, in: R.J. Cernik, R. Delhec, E.J. Mittenmeijer (Eds.), European Powder Diffraction, Materials Science Forum, vol. 228–232, Trans Tech Publications, Zürich, Switzerland, 1996, p. 147.
[15] G.T. Wright, Proc. Phys. Soc., Lond. B68 (1955) 701.
[16] S.M. Hubig, S.V. Linderman, J.K. Kochi, Coord. Chem. Rev. 200–202 (2000) 831.
[17] R.W. Turner, E.L. Amma, J. Am. Chem. Soc. 88 (1966) 1877.
[18] H. Schmidmaur, W. Bublak, B. Huber, G. Reber, G. Muller, Angew. Chem. Int. Ed. 25 (1986) 1089.
[19] S.H. Strauss, J. Chem. Soc., Dalton Trans. (2000) 1.
[20] E.G. Cox, W.J. Cruickshank, J.A. Smith, Proc. R. Soc. Lond., Ser. A 247 (1958) 1.
[21] G.E. Bacon, N.A. Curry, S.A. Wilson, Proc. R. Soc. Lond., Ser. A 279 (1964) 98.
[22] R.M. Sullivan, J.D. Martin, J. Am. Chem. Soc. 121 (1999) 10092.
[23] H. Kunkely, A. Volger, Chem. Phys. Lett. 368 (2003) 49.
[24] E.R. Gilliland, J.E. Seebold, J.R. Fitzhugh, P.S.J. Morgan, Am. Chem. Soc. 61 (1939) 1960.

Available online at www.sciencedirect.com
SCIENCE DIRECT®
Polyhedron 25 (2006) 360–372
POLYHEDRON
www.elsevier.com/locate/poly

Benzotriazole based 1-D, 2-D and 3-D metal dicyanamide and tricyanomethanide coordination networks

Leigh F. Jones *, Laura O'Dea, Daniel A. Offermann, Paul Jensen, Boujemaa Moubaraki, Keith S. Murray *

School of Chemistry, Clayton Campus, Building 23, Monash University, Clayton, Victoria, 3800, Australia

Received 3 May 2005; accepted 2 August 2005
Available online 9 September 2005

This paper is dedicated to Professor Malcolm Chisholm on the occasion of his 60th birthday.

Abstract

The 1-methylbenzotriazole ligand (1-Mebta) has been successfully incorporated into four new 1-D coordination polymers of general formula $[M^{II}(dca)_2(1\text{-Mebta})_2]$ (M = Mn (**1**), Fe (**2**) and Cu (**3**)) and $[Cu^{II}(tcm)_2(1\text{-Mebta})_2]$ (**4**) containing the dicyanamide $(N(CN)_2^-, dca^-)$ or tricyanamide $(C(CN)_3^-, tcm^-)$ $\mu_{1,5}$-bridging ligands. Magnetic susceptibility measurements reveal weak antiferromagnetic interactions between the M^{II} centres without any long-range order. Spin-Hamiltonian parameters ($g = \pm 0.01$, $J = \pm 0.01$) were obtained using a chain model; $[M^{II}(dca)_2(1\text{-Mebta})_2]$ (Mn (**1**): $g = 1.94$, $J = -0.15\ cm^{-1}$, Fe (**2**): $g = 2.17$, $J = -0.38\ cm^{-1}$, and $g = 2.18$, $J = -0.01\ cm^{-1}$) in $[Cu^{II}(tcm)_2(1\text{-Mebta})_2]$ (**4**). To increase the dimensionality of these benzotriazole-based networks, two benzotriazole molecules were linked together via alkyl chains in the form of the 1,3-di(benzotriazol-1-yl)propane (dbtp) and 1,4-di(benzotriazol-1-yl)butane (dbtb) ligands and these have produced 1-D, 2-D and 3-D networks. The dbtp ligand yields a 1-D 'step-like' chain coordination polymer in $[Cu^{II}(dca)_2(dbtp)]$(**5**), where the dbtp ligands propagate the 1-D chains; a role normally carried out by bridging dca^- ions. Reaction of the dbtp ligand with Co^{II} increases the dimensionality by producing the α-Po related 3-D $[Co^{II}(dca)_2(dbtp)]$ (**7**) network. Compound **7** consists of 2-D (4,4) connecting sheets, linked together by the bridging dbtp ligand. The Ni^{II} analogue $[Ni^{II}(dca)_2(dbtp)]$ (**8**) has also been synthesized in polycrystalline form and characterized by powder X-ray diffraction. Magnetic measurements on **7** indicate extremely weak antiferromagnetic exchange interactions between the Co^{II} ions while $[Ni^{II}(dca)_2(dbtp)]$ (**8**) exhibits short range ferromagnetic coupling with best-fit parameters $g = 2.13$ and $J = +0.24\ cm^{-1}$. The synthesis of a 2-D (4,4) connected sheet $[Cu^{II}(dca)_2(dbtb)]$ (**9**) (where dbtb is 1,4-di(benzotriazol-1-yl)butane) illustrates how increasing the alkyl chain by one carbon length has dramatically changed the topology and dimensionality of the network. Magnetic susceptibility measurements reveal weak antiferromagnetic exchange coupling.
© 2005 Elsevier Ltd. All rights reserved.

Keywords: Benzotriazole; Coordination networks; Dicyanamide; Tricyanomethanide; Crystal structures; Magnetism

1. Introduction

The design and synthesis of 1-, 2- and 3-D coordinated networks containing the dicyanamide $(N(CN)_2^-, dca)$ and tricyanamide $(C(CN)_3^-, tcm)$ bridging ligands has grown significantly over the past decade. Interest in these networks intensified with the discovery of interesting magnetic properties such as long-range magnetic ordering in the rutile-like 3-D α-$M(dca)_2$ compounds (M = Cr, Mn, Fe, Co, Ni and Cu) [1–4]. The introduction of N-based bridging and terminal co-ligands into M/dca/tcm systems has led to many interesting architectures in all three dimensions. 1-D topologies include the zigzag chains in *cis*-$[M^{II}(dca)_2(2,2'\text{-bipy})]$, M = Mn [5] or Cd

* Corresponding author. Tel.: +61 3 99054577; fax: +61 3 9905 4597.
E-mail addresses: leigh.jones@sci.monash.edu.au (L.F. Jones), keith.murray@sci.monash.edu.au (K.S. Murray).

0277-5387/$ - see front matter © 2005 Elsevier Ltd. All rights reserved.
doi:10.1016/j.poly.2005.08.005

[6] and the 1-D infinite tubes of $[M^{II}(dca)_2(2\text{-aminopyrimidine})]$ ($M = Co^{II}$, Ni^{II}) [7] while examples of 2-D systems include the (4,4) sheets in $[Mn^{II}(dca)_2(H_2O)] \cdot phz$ (where phz is the phenazine ligand) [8]. The structures in $[M^{II}(dca)_2(pyrimidine)] \cdot EtOH$ ($M = Fe^{II}$, Co^{II}, Ni^{II} and Cu^{II}) are isostructural, consisting of M^{II}/dca (4,4) sheets bridged by the pyrimidine co-ligands, resulting in the 3-D networks of α-Po geometry with magnetic ordering at very low temperatures [9]. More recently, the incorporation of countercations while increasing the dca/M^{II} ratios has resulted in numerous novel cation templated 2-D and 3-D networks exhibiting interesting topological features. Examples include the 2-D sheets: $[M(2,2'\text{-bipy})_3][M'(dca)_3]_2$ ($M = Fe^{III}$, $M' = Mn^{II}$ or Fe^{II}; $M = Ni^{II}$, $M' = Mn^{II}$) [10] and $(Ph_4X)[Mn^{II}(dca)_3]$ ($X = P$ [11] or As [12]). Previously reported 3-D cation templated systems include the α-polonium type network $[Cp^*_2M][M'(dca)_3]$ (where $M = Fe^{III}$, Co^{III}; $M' = Mn^{II}$, Fe^{II}, Co^{II}, Ni^{II} and Cd^{II}) [13] and the spin-canted $(SPh_3)[Mn(dca)_3]$ system [14]. It has also been noted that slight variations in the size and shape of the countercations significantly changes the topologies of the anionic metal dicyanamide networks [15]. One such example is the move from 2-D topology in $(Ph_4P)[Mn^{II}(dca)_3]$ to 3-D in $(MePh_3P)[Mn^{II}(dca)_3]$; simply by substitution of one phenyl group in PPh_4^+ with a methyl substituent [15].

The series of 1-D, 2-D and 3-D networks described in this work contains derivatives of the benzotriazole pro-ligand (btaH). The coordination chemistry of benzotriazole (btaH) and its analogues has been an area of intense research over recent years due to their ability to inhibit corrosion of copper and its alloys [16]. Valuable insights into the bonding modes observed between benzotriazole and the oxygen rich $Cu^{I/II}$ surfaces in corrosion inhibition processes resulted in numerous pentametallic Cu^{II} clusters of general formula $[Cu_5^{II}(bta)_6(L)_4]$ (L includes the tropolonate [17], acetylacetonate [18] and tert-butyl isocyanate ligands [19]). In the case of these pentametallic Cu^{II} complexes, the bta^- anion bonds via all three nitrogen atoms (μ_3). However, bidentate bonding via adjacent [20] and non-adjacent [21] nitrogen atoms has been observed, along with terminal unidentate μ_1-bonding [22]. Furthermore, the important area of single-molecule magnetism (SMM) has benefited from the btaH pro-ligand through the synthesis of numerous high nuclearity $M^{III/IV}$ clusters, including the high-spin $S \geqslant 23$ Fe_{14} [23] and the $S = 4$ hexaicosametallic Mn_{26} SMM [24]. The flexibility in bonding, their neutral charge and their reactivity with first row transition metals made benzotriazole derivatives ideal ligands for the synthesis of 1-D, 2-D and 3-D networks.

2. Experimental

Sodium dicyanamide (Na(dca)) was supplied by Fluka chemicals and the 1-methylbenzotriazole (1-Mebta) ligand was supplied by Lancaster chemicals. The K(dca) [25] and K(tcm) salts [26], 1,3-di(benzotiazol-1-yl)propane (dbtp) and 1,4-di(benzotriazol-1-yl)butane (dbtb) were prepared using methods previously described in the literature [27].

2.1. Synthesis

2.1.1. $[Mn^{II}(dca)_2(1\text{-Mebta})_2]$ (1)

An aqueous solution (7.0 ml) of $Mn^{II}(ClO_4)_2 \cdot 6H_2O$ (25.0 mg, 0.07 mmol) and Na(dca) (12.4 mg, 0.14 mmol) was stirred at room temperature for 5 min and then filtered. A methanolic solution (10.0 ml) of 2 equivalents 1-methylbenzotriaozle (18.0 mg, 0.14 mmol) was carefully layered on top of the aqueous Mn^{II}/dca solution. Clear needle-like crystals of **1** crystallised in the $P\bar{1}$ triclinic space group in moderate yield (⩽30%) after 4 weeks. *Anal.* Calc. for $C_{18}H_{14}N_{12}Mn \cdot H_2O$: C, 45.85; H, 3.39; N, 35.67. Found: C, 45.59; H, 3.05; N, 35.39%. Selected IR data (KBr): 3578(m), 3450(b), 2297(s), 2241(s), 2177(vs), 1454(m), 1346(s), 1216 (m), 779(m), 739(vs).

2.1.2. $[Fe^{II}(dca)_2(1\text{-Mebta})_2]$ (2)

An aqueous solution (7.0 ml) of $Fe^{II}(ClO_4)_2 \cdot xH_2O$ (25.0 mg, 0.1 mmol) and Na(dca) (18.0 mg, 0.2 mmol) was stirred at room temperature for 5 min and then filtered. A methanolic solution (10.0 ml) of 2 equivalents 1-methylbenzotriaozle (26.0 mg, 0.2 mmol) was carefully layered on top of the aqueous Fe/dca solution. Yellow plate-like crystals of **2** formed in the $P\bar{1}$ triclinic space group in good yield (⩽45%) after 2 weeks. Elemental analysis: Calc.for $C_{18}H_{14}N_{12}Fe \cdot 2H_2O$: C, 45.76; H, 3.38; N, 35.55. Found: C, 45.56; H, 3.06; N, 35.05%. Selected IR data (KBr): 3449(b), 2294(m), 2244(m), 2181(vs), 1341(m), 1218(m), 779(m), 740(s).

2.1.3. $[Cu^{II}(dca)_2(1\text{-Mebta})_2]$ (3)

An aqueous solution (7.0 ml) of $Cu^{II}(ClO_4)_2 \cdot 6H_2O$ (25.0 mg, 0.07 mmol) and Na(dca) (12.4 mg, 0.14 mmol) was stirred at room temperature for 5 min and then filtered. A methanolic solution (10.0 ml) of 2 equivalents of 1-methylbenzotriaozle (18.0 mg, 0.14 mmol) was carefully layered on top of the aqueous Cu/dca solution. Blue thin plate-like crystals of **3** formed in the $P\bar{1}$ triclinic space group in good yield (⩽40%) after 1 week. *Anal.* Calc. for $C_{18}H_{16}N_{12}Cu.2H_2O$: C, 43.42; H, 3.62; N, 33.77. Found: C, 43.13; H, 3.35; N, 34.05%. Selected IR data (KBr): 3425(b), 2297(s), 2248(s), 2182(vs), 1351(m), 780(m), 744(s).

Pure microcrystalline bulk quantities of **1**–**3** were synthesised using the following method.

A 1:2 stoichiometric ratio of $M^{II}(ClO_4)_2 \cdot xH_2O$ and K(dca) was dissolved in a minimum quantity of methanol (5.0 ml). A methanolic solution of 1-methylbenzotriazole (2 equivalents in 5.0 ml) was then added dropwise into the methanolic M^{II}/dca solution yielding

microcrystalline powders of **1**–**3** after 10 min. IR spectral and Elemental analysis confirmed these powders to be compounds **1**–**3**.

*2.1.4. [$Cu^{II}(tcm)_2(1\text{-}Mebta)_2$] (**4**)*

An aqueous solution (10 ml) of $Cu^{II}(ClO_4)_2 \cdot 6H_2O$ (25.0 mg, 0.07 mmol) and K(tcm) (17.55 mg, 0.14 mmol) was stirred for 5 min and then filtered. A methanolic solution (10 ml) containing two equivalents of 1-methylbenzotriazole (17.92 mg, 0.14 mmol) was then carefully layered on top of the aqueous Cu/tcm solution. Thin brown irregular block crystals of **4** crystallised in the $P\bar{1}$ triclinic space group after four weeks in moderate yield (⩽30%). Elemental *Anal*. Calc. for $C_{22}H_{14}N_{12}Cu$: C, 51.81; H, 2.75; N, 32.97. Found: C, 51.80; H, 2.77; N, 33.17%. Selected IR data (KBr): 3423(b), 2239(m), 2188(vs), 1226(m), 780(m), 748(s).

*2.1.5. [$Cu^{II}(dca)_2(dbtp)$] (**5**)*

An aqueous solution (7.0 ml) of $Cu^{II}(ClO_4)_2 \cdot 6H_2O$ (25.0 mg, 0.07 mmol) and Na(dca) (12.0 mg, 0.14 mmol) was stirred for 5 min and then filtered. A 50:50 MeOH/H_2O solution (5.0 ml) was then layered on top of the Cu/dca solution. This was then layered with a methanolic solution (10.0 ml) containing 1 equivalent of 1, 1-dbtp (18.0 mg, 0.07 mmol). Thin blue plates of **5** were obtained overnight in adequate yield (⩽20%), crystallising in the monoclinic *C*2/*c* space group. *Anal*. Calc. for $C_{19}H_{14}N_{12}Cu$: C, 47.59; H, 2.91; N, 35.26. Found: C, 48.15; H, 2.96; N, 35.46%. Selected IR data (KBr): 3449(b), 2960(w), 2297(s), 2236(s), 2169(vs), 1363(m), 780(w), 756(m).

*2.1.6. [$Cu_2^{II}(tcm)_2(dbtp)_4](ClO_4)_2$ (**6**)*

An aqueous solution (7.0 ml) of $Cu^{II}(ClO_4)_2 \cdot 6H_2O$ (25.0 mg, 0.07 mmol) and K(tcm) (17.55 mg, 0.14 mmol) was stirred for 5 min and then filtered. Two equivalents of 1,1-dbtp (36.0 mg, 0.14 mmol) in methanolic solution (10.0 ml) was then carefully layered on top of the aqueous Cu/tcm solution. Dark green plate-like crystals of **6** were obtained overnight in moderate yield (⩽30%), crystallising in the *I*4/*m* tetragonal space group. *Anal*. Calc. for $C_{68}H_{56}N_{30}O_8Cl_2Cu_2$: C, 50.43; H, 3.46; N, 25.95; Cl, 4.38. Found: C, 50.89; H, 3.46; N, 26.66; Cl, 4.68%. Selected IR data (KBr); 3422(b), 2371(m), 2344(m), 2169 (vs), 1092(m), 780(s), 756(s).

*2.1.7. [$Co^{II}(dca)_2(dbtp)$] (**7**)*

$Co^{II}(NO_3)_2 \cdot 6H_2O$ (25.0 mg, 0.086 mmol) and Nadca (15.3 mg, 0.172 mmol) were dissolved in 5 ml distilled water. This aqueous solution was then carefully layered with a methanolic (10 ml) solution of the dbtp ligand (23.0 mg, 0.086 mmol). Thin lilac needles of **7** were obtained in 20% yield after 24 h. Compound **7** crystallized in the triclinic $P\bar{1}$ space group. Calc.for $C_{19}H_{14}N_{12}Co \cdot H_2O$: C, 46.84; H, 3.41; N, 34.49. Found: C, 46.88; H, 3.12; N, 33.10%. Selected IR data (KBr); 3487(b), 2318(m), 2245(m), 2172(s), 1720(m), 1638(m), 1544(m), 1525(m), 1385(m), 781(m), 746(s).

*2.1.8. [$Ni^{II}(dca)_2(dbtp)$] (**8**)*

$Ni^{II}(NO_3)_2 \cdot 6H_2O$ (30.0 mg, 0.103 mmol) and Nadca (18.6 mg, 0.206 mmol) were dissolved in 5 ml distilled water. This aqueous solution was then carefully layered with a methanolic (10 ml) solution of the dbtp ligand (28.6 mg, 0.103 mmol). Blue plates of **8** were obtained in 20% yield after 24 h. Compound **8** crystallized in the triclinic $P\bar{1}$ space group. Calc.for $C_{19}H_{14}N_{12}Ni$: C, 48.65; H, 2.99; N, 35.85. Found: C, 48.85; H, 3.07; N, 35.61%. Selected IR data (KBr); 3449(b), 2291(m), 2269(m), 2178(s), 1775(w), 1720(w), 1655(m), 1544(m), 1452(m), 1424(m), 1383(m), 1321(m), 1298(m), 1223(m), 1173(m), 782(m), 746(s).

*2.1.9. [$Cu^{II}(dca)_2(dbtb)$] (**9**)*

An aqueous solution (7.0 ml) of $Cu^{II}(ClO_4)_2 \cdot 6H_2O$ (25.0 mg, 0.07 mmol) and Na(dca) (12.0 mg, 0.14 mmol) was stirred for 5 min and then filtered. One equivalent of 1,1-dbtb (20.0 mg, 0.07 mmol) was dissolved with warming in *iso*-propanol (10.0 ml) and carefully layered on top of the aqueous Cu^{II}/dca solution. Light green needle-like crystals of **9** were obtained after 2 days in 30% yield. Compound **9** crystallised in the monoclinic $P2_1/c$ space group. Calc.for $C_{20}H_{16}N_{12}Cu$: C, 49.23; H, 3.28; N, 34.46. Found: C, 49.09; H, 3.38; N, 34.20%. Selected IR data (KBr); 3419(b), 2933(w), 2367(w), 2296(s), 2181(s), 1637(m), 1494(w), 1458(m), 1359(m), 1234(m), 1168(w), 780(m), 742(s), 668(w), 516(m).

2.2. Physical measurements

Elemental analyses (CHN) were carried out by Campbell Microanalytical laboratory, University of Otago, Dunedin, New Zealand. IR spectra were recorded on a Perkin–Elmer 1600 Series Spectrometer with the samples prepared as KBr discs.

2.3. Magnetic susceptibilities

DC magnetic susceptibility measurements were carried out on a Quantum Design MPMS 5 SQUID magnetometer calibrated by use of a standard palladium sample (Quantum Design) of accurately known magentisation or by use of magnetic calibrants such as $CuSO_4 \cdot 5H_2O$. A powder sample of ~30 mg was contained in a calibrated gelatine capsule held at the centre of a drinking straw at the end of the sample rod. Samples of Co^{II} and Fe^{II} were dispersed in Vaseline to avoid torquing of the crystallites at low temperatures and high fields. A 1 T field was generally used, but in a number of cases fields of 0.01 and 0.1 T (2–100 K) were used to check for evidence of long-range

order. Magnetisation isotherm measurements were made in fields of between 0 and 5 T.

2.4. X-ray crystallographic studies

Data were collected using a Nonius KappaCCD diffractometer with graphite monochromated Mo Kα radiation ($\lambda = 0.71073$ Å). Integration was carried out by the program DENZO-SMN [28] and data were corrected for Lorentz polarization effects and for absorption using the program SCALEPACK [28]. Solutions were obtained by direct methods (SHELXS-97) [29] followed by successive fourier difference methods, and refined by full-matrix least-squares on F^2obs (SHELXL-97) [29].

All structures were solved using direct methods and their corresponding data summarized in Table 1.

The crystal structure of $[Cu_2^{II}(dbtp)_4(tcm)_2](ClO_4)_2$ (**6**) crystallized in space group $I4/m$ and was found to be merohedrally twinned with two domain orientations related by twofold rotation about the 110 direction. The twin component refined to 0.44, which was consistent with the disparity between the R_{int}'s for the $4/m$ (0.042) and $4/mmm$ (0.071) Laue groups. The structure also exhibited disorder within the tcm^- ligands and perchlorate counter ions. The tcm^- ligands are disordered over four positions, related by a fourfold rotation. Steric effects dictate that the tcm^- ligands on adjacent dimers within the structure must be related by inversion and are relatively close together (C10···C10* ~ 3.38 Å) resulting in moderate π–π overlap, however, the structure solution shows that the four tcm positions on each Cu(II) relate to their neighbours by mirror plane symmetry. Suitable geometry for the tcm^- anions was obtained using distance restraints (SADI) with rigid bond restraints (DELU) applied to the anisotropic displacement parameters (ADP's). The perchlorate counter ions in **6** were also disordered over four close positions related by inversion and mirror plane symmetry. Restraints were applied to the Cl–O and O···O distances and oxygen atoms were constrained to have the same ADP's.

The crystal structure of $[Cu^{II}(dca)_2(dbtb)]$ (**9**) contained a 90:10 disorder of the Cu^{II} atom and dbtb ligand positions. These positions are related by non-crystallographic mirror plane symmetry perpendicular to the *b*-axis. The two Cu^{II} positions are 0.64 Å apart. The minor component of the dbtb ligand was restrained to be the same as the major component using SAME. Additionally, the dca ligands are disordered due to disorder of the Jahn–Teller distorted Cu^{II} ions which involve elongation of two of the four bonds to dca ligands. The dca ligands for the major component were refined with 50:50 disorder (i.e., 0.45 occupancy each), while only single dca positions were modeled for the minor component. The refinement required numerous

Table 1
Crystallographic data for networks **1**–**7** and **9**

Complex	**1**	**2**	**3**	**4**	**5**	**6**	**7**	**9**
Formula	$C_{18}H_{14}N_{12}Mn$	$C_{18}H_{14}N_{12}Fe$	$C_{18}H_{14}N_{12}Cu$	$C_{22}H_{14}N_{12}Cu$	$C_{19}H_{14}N_{12}Cu$	$C_{68}H_{56}N_{30}Cl_2O_8Cu_2$	$C_{19}H_{14}N_{12}Co$	$C_{20}H_{16}N_{12}Cu$
Molecular weight (g mol^{-1})	453.35	454.26	461.95	509.99	473.96	1619.39	469.35	487.99
Crystal system	triclinic	triclinic	triclinic	triclinic	monoclinic	tetragonal	triclinic	monoclinic
Space group	$P\bar{1}$	$P\bar{1}$	$P\bar{1}$	$P\bar{1}$	$C2/c$	$I4/m$	$P\bar{1}$	$P2_1/n$
a (Å)	7.4682(2)	7.3932(2)	7.3355(3)	7.2605(7)	16.350(3)	14.506	9.2311(2)	9.0955(2)
b (Å)	8.0849(2)	8.09260(10)	8.1008(5)	9.1105(11)	8.1462(16)	14.506	9.6677(2)	15.5302(3)
c (Å)	9.6306(3)	9.5947(3)	9.3443(10)	9.5071(12)	14.453(3)	17.9617	12.2370(5)	14.9825(3)
α (°)	66.0960(10)	65.6610(10)	66.649(2)	62.311(4)	90.0	90.0	91.836(10)	90.0
β (°)	68.8100(10)	67.9440(10)	68.451(2)	80.547(3)	90.03(3)	90.0	93.632(10)	103.421(10)
γ (°)	75.0920(10)	74.531(2)	76.274(5)	88.110(4)	90.00	90.0	116.656(10)	90.0
V (Å^3)	491.47(2)	480.48(2)	471.42(6)	548.61(11)	1925.0(7)	3779.57	971.80(5)	2058.56(7)
T (K)	123(2)	123(2)	123(2)	123(2)	123(2)	123(2)	123(2)	123(2)
Z	1	1	1	1	4	2	2	4
ρ_{calc} (g cm^{-3})	1.532	1.570	1.627	1.544	1.635	1.423	1.604	1.575
Crystal shape	plate	needle	plate	plate	plate	plate	plate	plate
Colour	colourless	yellow	blue	blue	blue	blue/green	pink	blue
μ (mm^{-1})	0.706	0.820	1.194	1.035	1.172	0.708	0.920	1.099
Unique data	2367	2275	2211	2611	2265	2402	3415	4958
Unique data [$I > 2\sigma(I)$] (R_{int})	1987 (0.0346)	1990 (0.0447)	1370 (0.1066)	1453 (0.1167)	1148 (0.1741)	2078 (0.0405)	2570 (0.0762)	3926 (0.0514)
R_1, wR_2 [$I > 2\sigma(I)$]	0.0286, 0.0679	0.0302, 0.0671	0.0839, 0.1918	0.0676, 0.1010	0.0777, 0.1392	0.0437, 0.1011	0.0779, 0.2321	0.0444, 0.0871

constraints and restraints. Only the major component and the Cu^{II} atom of the minor component were refined anisotropically.

2.5. Powder X-ray diffraction studies

A Scintag high-resolution automated powder diffractometer was employed using Cu Kα radiation ($\lambda = 1.54059$ Å).

3. Results and discussion

3.1. Structures of $[M^{II}(dca)_2(1\text{-}Mebta)_2]$ (M = Mn (**1**), Fe (**2**), Cu (**3**)) and $[Cu^{II}(tcm)_2(1\text{-}Mebta)_2]$ (**4**)

We report here the synthesis, structures and magnetic properties of a family of dca (**1**, **2** and **3**) or tcm (**4**) based 1-D coordination polymers where the 1-methylbenzotrioazole (1-Mebta) ligand acts as the co-ligand. The structures of **1**–**4** are closely related and so are described together. Structures **1**–**3** ($[M^{II}(dca)_2(1\text{-}Mebta)_2]$ (M = Mn (**1**), Fe (**2**), Cu (**3**))) consist of 1-D linear chains, in which each M^{II} centre is bridged by two $\mu_{1,5}$-dca^- ligands via the nitrile nitrogen atoms (N1). The coordination sphere at each M^{II} centre is completed by two 1-methylbenzotriazole ligands occupying the axial sites. In each case the coordination geometry around the M^{II} ion is distorted octahedral, with M1–N1(dca) bond lengths of 2.1973(12) (**1**), 2.1364(13) (**2**) and 2.157(10) (**3**) Å and M–N4(1-Mebta) distances of 2.289(11) (**1**), 2.2086(13) (**2**) and 2.042(5) Å (**3**) respectively (Table 2). Each M^{II} lies on a centre of inversion resulting in N4–M1–N4′ angles of 180° in all cases (Fig. 1). The d^9 electronic configuration at the Cu^{II} centres in **3** gives rise to a Jahn–Teller contraction about the N(1-Mebta)–Cu–N(1-Mebta) *z*-axis. Each chain propagates parallel along the *a*-axis, with the M···M distance corresponding to their unit cell lengths *a* of 7.4682(2) (**1**), 7.3932(2) (**2**) and 7.3355(3) (**3**) Å respectively. These angles and distances are comparable to other related coordinated polymers of general formula $[M^{II}(dca)_2(L)_2]$ (M = Mn, Fe, Co, Ni, Cu and L includes H_2O [30], pyridazine [31], 2,2′-bipy [32] and solvents such as DMF, pyridine and MeOH [33]). The structures of **1**–**3** consist of interdigitated linear chains, where each 1-Mebta ligand lies between two 1-Mebta ligands of an adjacent chain. The 1-Mebta ligands are crystallographically related via a centre of inversion and have centroid-centroid distances at the higher limit of π–π stacking classification (3.766 (**1**), 4.034 (**2**) and 3.797 (**3**) Å respectively) (see Fig. 1) [34].

Attempts in increasing the dimensionality of these linear chains led to the use of the tricyanomethanide (tcm) tridentate bridging ligand in complex $[Cu^{II}(tcm)_2(1\text{-}Mebta)_2]$ (**4**) (Fig. 2). However, just as observed in the 1-D chains **1**–**3**, the tcm^- ligands bridge via only two of its three available nitrile nitrogen atoms (N1), resulting in a 1-D linear chain, analogous to those observed in complexes **1**–**3**. The tcm^- ligands bridge the Cu^{II} metal centres in the $\mu_{1,5}$-tcm^- coordination mode, each disordered over two sites (half occupancy) at the equatorial positions (Fig 2). Each Cu^{II} lies on an inversion centre (N5–Cu–N5#3 = 180°) and exhibits distorted octahedral geometry. The coordination sphere at each Cu^{II} centre is completed by two axial 1-methylbenzotriazole terminal ligands. Like complexes **1**–**3**, the 1-D linear chains in **4** propagate parallel to the *a*-axis, giving rise to an M···M distance equal to that of the unit cell length *a* (7.2605(7) Å). The linear chains pack in the customary interdigitated fashion and the 1-methylbenzotriazole ligands are 3.719 Å apart. All Cu^{II}–N(1-Mebta) and Cu^{II}–N(tcm) bond lengths are comparable to those observed in **1**–**3** except for the long in-chain Cu(1)–N(1) of 2.454(4) (Table 2).

3.2. Magnetism on networks 1–4

Solid-state dc magnetic susceptibility studies were carried out on samples **1** to **4** in a field of 1 T over a temperature field range of 300–2 K. Plots of $\chi_m T$ versus *T* for samples **1**, **2** and **4** are shown in Fig. 3, and these are indicative of very weak antiferromagnetic interactions occuring between the M^{II} centres. The data were fitted using the Fisher chain model [35] giving the following Spin Hamiltonian parameters: $[M^{II}(dca)_2(1\text{-}Mebta)_2]$ ($M = Mn^{II}$(**1**): $S = 5/2$, $g = 1.94$, $J = -0.15\ cm^{-1}$, $M = Fe^{II}$(**2**): $S = 2$, $g = 2.17$, $J = -0.38\ cm^{-1}$, $M = Cu^{II}$(**4**) $S = 1/2$, $g = 2.18$, $J = -0.01\ cm^{-1}$ in $[Cu^{II}(tcm)_2(1\text{-}Mebta)_2]$ (**4**). Such *J* values are typical of $\mu_{1,5}$-dca^- and $\mu_{1,5}$-tcm^- bridging modes [15]. The tiny value for **4** implies essentially zero-coupling and this is because the unpaired spin on each Cu^{II} centre is in the $d_{x^2-y^2}$ orbital, at 90° to the chain direction. The small decrease in χT below 5 K could also be due to Zeeman level depopulation effects in the 1 T field. Complex **3** showed a somewhat unusual (almost linear) decrease of $\chi_m T$, from 0.38 $cm^3\ mol^{-1}\ K$ (1.74 μ_B) to 0.29 $cm^3\ mol^{-1}\ K$ (1.52 μ_B) at 4.2 K. This could not be simulated well using a chain model and we have no obvious explanation for this behaviour. In the case of **2**, the spin–orbit effects are included in the high value of *g*. The shape of the χT curve shows that the orbital degeneracy of the $^5T_{2g}$ single-ion state is largely removed and thus use of the Fisher model is a reasonable approximation.

3.3. Structures of networks 5–7

The results in **1**–**4** strongly suggest that the 1-Mebta ligand inevitably leads to linear chains due to its preference for terminal bonding via N4. It was anticipated that one way to increase the directionality of these systems would be to extent the methyl group in the

Table 2
Selected bond lengths (Å) and angles (°) observed in networks **1**–**4**

1		**2**		**3**		**4**	
M–L bonds (Å)							
Mn(1)–N(1)	2.1973(12)	Fe(1)–N(1)	2.1364(13)	Cu(1)–N(1)	2.157(10)	Cu(1)–N(1)	2.454(4)
Mn(1)–N(4)	2.289(11)	Fe(1)–N(4)	2.2086(13)	Cu(1)–N(4)	2.042(5)	Cu(1)–N(4)	1.988(3)
						Cu(1)–N(5)	2.024(3)
L–M–L angles (°)							
N(4)–Mn(1)–N(4′)	180.0	N(4)–Fe(1)–N(4′)	180.0	N(4)–Cu(1)–N(4′)	180.0	N(1)–Cu(1)–N(5)	90.27(14)
N(1)–Mn(1)–N(4)	91.35(4)	N(1)–Fe(1)–N(4)	89.46(5)	N(1)–Cu(1)–N(4)	90.9(2)	N(5)–Cu(1)–N(5′)	180.0
M···M	7.468	M···M	7.393	M···M	7.355	M···M	7.261

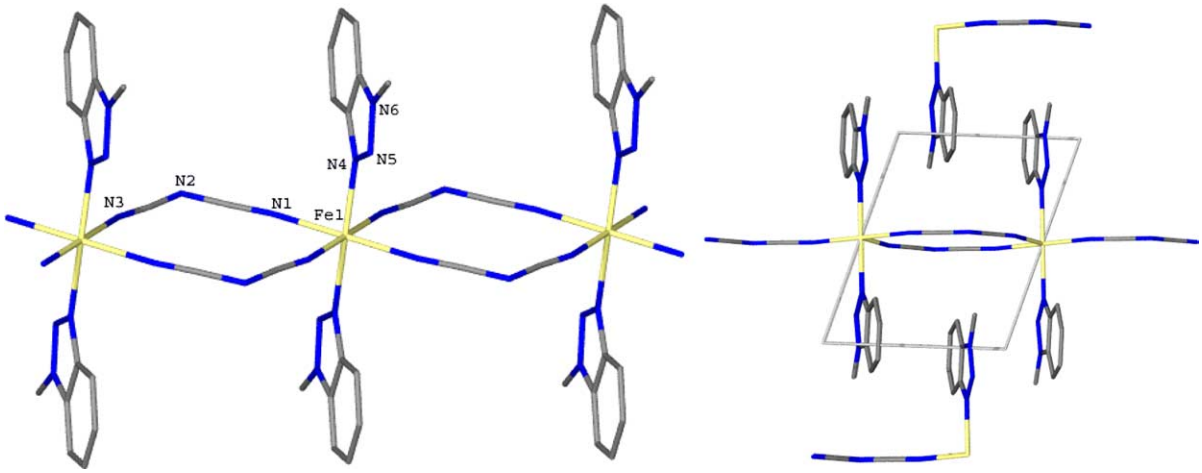

Fig. 1. (Left) The structure of $[Fe(dca)_2(1\text{-Mebta})_2]$ (**2**). The above 1-D motif is the same in $[M^{II}(dca)_2(1\text{-Mebta})_2]$, where M = Mn, Cu (compounds **1** and **3**). H atoms are omitted for clarity. Selected inter-atomic bond distances of **2** (Å): Fe1–N1 = 2.1364(13), Fe1–N3 = 2.1464(13), Fe1–N4 = 2.2086(13), Fe1–Fe1 = 7.393. (Right) The crystal packing in $[Fe^{II}(dca)_2(1\text{-Mebta})_2]$ (**2**), propagating along the *a*-plane.

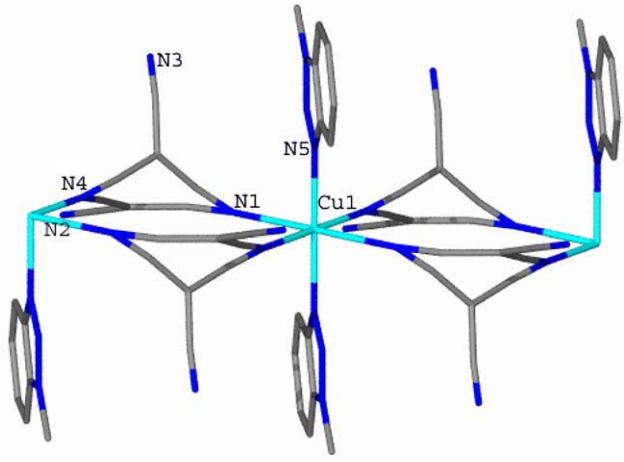

Fig. 2. The structure of $[Cu^{II}(tcm)_2(1\text{-Mebta})_2]$ (**4**), showing the disordered positioning of the tcm^- ligands over two sites. H atoms are omitted for clarity. Selected inter-atomic bond distances of **4** (Å): Cu1–N1 = 2.454(4), Cu1–N4 = 1.998(3), Cu1–N5 = 2.023(3), Cu1–Cu1′ of ~7.261.

1-Mebta ligand by linking two benzotriazole groups together via alkyl chains of various lengths, the premise being that these dibenzotriazole type ligands would link M^{II} centres in one direction while the anionic dca/tcm bridging ligands (Fig. 4) would propagate the system in the 2-D or 3-D modes. Extensive research by Katritzky et al. in 1996 produced a large family of these dibenzotriazol(alkane) molecules, the synthetic strategies for which were employed here. The first such ligand synthesised was 1,3-dibenzotriazol-1-yl)propane ($n = 3$ in Fig. 4) (abbreviated as dbtp) which, upon reaction with a Cu^{II}/dca solution, afforded a rather novel 1-D linear chain complex **5**. Unexpectedly, the dbtp ligands propagate the chains in **5**, while the dca^- ligands bond terminally (Fig. 5).

Each distorted square planar Cu^{II} centre in **5** is bridged by one dbtp ligand (Cu1–N4 = 2.014(5) Å) and is terminally bonded in the *trans* positions by two nitrile bonded dca^- ligands (Cu1–N1 = 1.966(6) Å). The twisting of the alkyl links of the dbtp ligands allow the propagation of the chains, resulting in 'step-like' 1-D polymer chains (Fig. 5). The terminal dca^- ligands are situated away from the linear dbtp-Cu-dbtp plane (N1–Cu1–N4 = 180.00°) at an angle of ~36.1°. Each square-planar $\{Cu(dca)_2(dbtp)\}$ moiety along an individual chain is related to its neighbour by a twist of approximately 90°, resulting in alternating criss-crossing

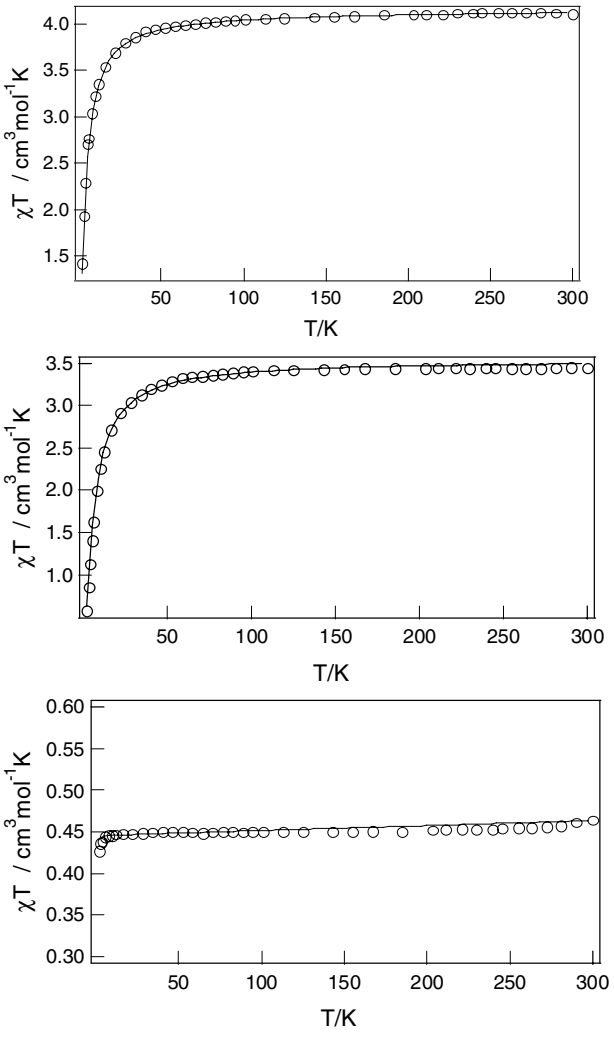

Fig. 3. Magnetic susceptibility ($\chi_m T$) vs. temperature, T, for complexes **1** (top), **2** and **4** (bottom). The solid lines are the best fits described in the text. Fitting of these data using the Fisher model ($g \pm 0.01$, $J \pm 0.01$) results in the following parameters: (**1**) $g = 1.94$, $N\alpha$ (temperature independent paramagnetic susceptibility) $= 50 \times 10^{-6}$ cm^3 mol^{-1}, $J = -0.15$ cm^{-1} (**2**) $g = 2.17$, $J = -0.38$ cm^{-1} and (**4**) $g = 2.18$, $N\alpha = 60 \times 10^{-6}$ cm^3 mol^{-1}, $J = -0.01$ cm^{-1}.

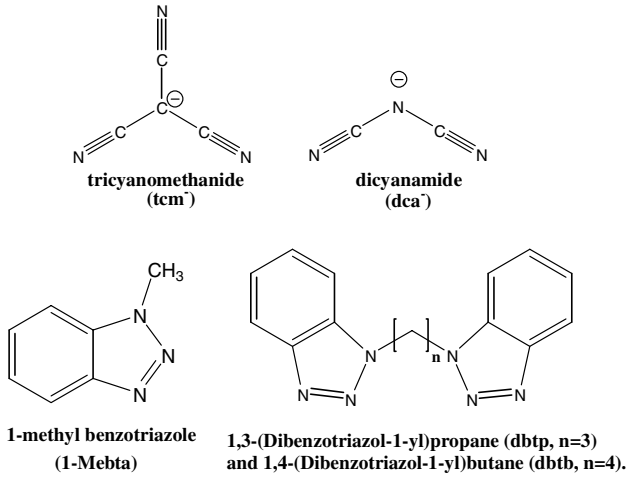

Fig. 4. Molecular structures of tricyanomethanide (tcm), dicyanamide (dca), 1-methylbenzotriazole (1-Mebta) and the 1,ω-(dibenzotriazol-1-yl)alkane (dbtp ($\omega = 3$), dbtb; ($\omega = 4$)) ligands.

when viewed along the plane of each 1-D chain. The chains in **5** pack in an efficient 'brickwork' formation.

Substitution of dca$^-$ with the potentially tridentate tcm$^-$ bridging ligand in the above reaction does not afford the analogous 1-D 'step-like' polymer in **5**, or even a 2-D or 3-D network, instead choosing to form a porous dimeric complex $[Cu_2^{II}(tcm)_2(dbtp)_4](ClO_4)_2$ (**6**) (Fig. 6). Compound **6** crystallises in the tetragonal I4/m space group, exhibiting a fourfold rotation axis along the Cu–Cu plane (along *c*-axis). The five-coordinate Cu^{II} centres in **6** exhibit distorted square based pyramidal geometry and are linked by four dbtp bridging ligands resulting in a Cu···Cu distance of 8.397 Å. The coordination sphere at each metal centre is completed by one tcm$^-$ ligand which is disordered over four sites (Fig. 7(left)). Each tcm$^-$ ligand is relatively close in proximity to an adjacent tcm$^-$ ligand, resulting in moderate π–π overlap (~3.38 Å). These relatively weak interactions form chains of dimers along the *c*-axis (Fig. 7(right)). The Cu^{II}–N(tcm) and Cu^{II}–N(dbtp) bond lengths are comparable to previously reported structures and are documented in Table 3. The perchlorate counter ions are disordered over four close positions (Section 2.1.3) and occupy the edges of the *ab* face and centres of the *ac* and *bc* faces.

This unexpected result can perhaps be attributed to the added steric effects the introduction of a tridentate tcm$^-$ ligand brings when competing with the already rather bulky dbtp ligand. This competition leads to the tcm$^-$ ligands bonding terminally at the apices of each $Cu^{(II)}$ centre, with the four bridging dbtp ligands occupying the basal plane positions. This view is supported by the general observation that tcm-based networks incorporating co-ligands are rare and the co-ligands are relatively small in size in relation to the dbtp ligand used here. Examples include the 2-D sheet structures $[Ag^{(II)}(tcm)_2(phenazine)_{1/2}]$, and $[Ag^{(II)}(tcm)_2(pyrazine)]$ [36] and the 3-D network $[M^{(II)}(tcm)_2(Me_4pyrazine)]$ (M = Co, Ni) [37].

The coordination geometries around the Cu^{II} centres in **5** and **6** are distorted square planar and distorted square based pyramidal respectively, and can be attributed to partial (square-based pyramidal) and extreme (square-planar) Jahn–Teller elongations along the *z*-direction. The question which arose from these findings was whether the extra coordinating node(s) of a six-coordinate metal centre would encourage 2-D and 3-D networks to form. This proved to be the case when the reaction of $Co^{II}(NO_3)_2 \cdot 6H_2O$ and Na(dca) in H_2O, followed by careful layering of a methanolic solution of the dbtp ligand resulted in the formation of the novel α-Po related 3-D network in $[Co^{II}(dca)_2(dbtp)]$ (**7**). Each

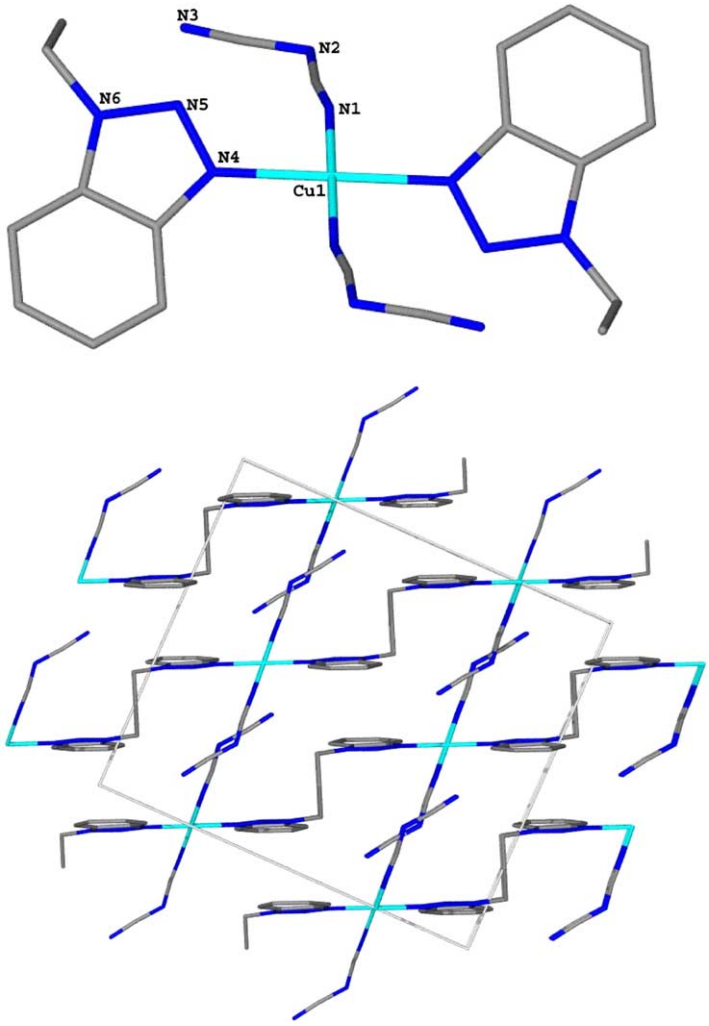

Fig. 5. (Top) The crystal structure of $[Cu^{II}(dca)_2(dbtp)]$ (**5**). H atoms are omitted for clarity. Selected inter-atomic bond distances of **5** (Å): Cu1–N1 = 1.966(6), Cu1–N4 = 2.014(5), Cu1···Cu1′ = 10.909. (Bottom) The crystal packing in $[Cu^{II}(dca)_2(dbtp)]$ (**5**) propagating along the *ac* plane. H atoms omitted for clarity.

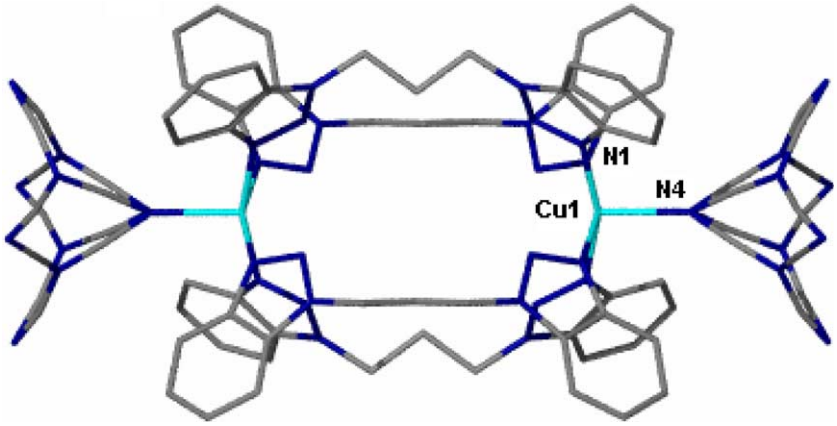

Fig. 6. The molecular structure of $[Cu_2^{II}(tcm)_2(dbtp)_4]$ (**6**), showing the disordered positioning of the tcm^- ligands over four sites. H atoms are omitted for clarity. Selected inter-atomic bond distances of **6** (Å): Cu1–N1 = 1.999(2), Cu1–N4 = 2.179(4), Cu1···Cu1′ = 8.397 Å.

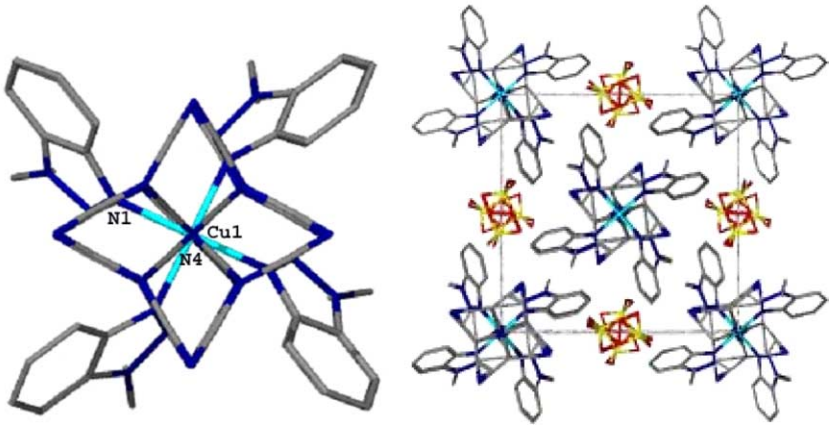

Fig. 7. (Left) "End on" structure of **6** showing the disorder of the tcm^- anions over four positions. Viewed along the *c*-axis, the H atoms have been omitted for clarity. (Right) Packing diagram showing the disordered perchlorates within **6** (H atoms omitted for clarity), viewed along the *c*-axis.

Table 3
Selected bond lengths (Å) and angles (°) observed in networks **5**–**7** and **9**

5		**6**		**7**		**9**	
M–L bonds (Å)							
Cu(1)–N(1)	1.966(6)	Cu(1)–N(1)	1.999(2)	Co(1)–N(1)	2.153(7)	Cu(1A)–N(1A)	1.951(7)
Cu(1)–N(4)	2.014(5)	Cu(1)–N(4)	2.179(4)	Co(1)–N(4)	2.087(7)	Cu(1′)–N(1′)	2.248(16)
				Co(1′)–N(6)	2.087(7)	Cu(1A)–N(4A)	2.457(8)
				Co(1)–N(7)	2.136(7)	Cu(1′)–N(4′)	2.091(17)
						Cu(1A)–N(7)	2.020(2)
						Cu(1′)–N(7′)	2.102(3)
L–M–L angles (°)							
N(4)–Cu(1)–N(4′)	180.0	N(1)–Cu(1)–N(4)	93.2(2)	N(4)–Co(1)–N(4′)	180.0	N(1A)–Cu(1A)–N(7)	90.4(3)
N(1)–Cu(1)–N(4)	89.7(2)	N(1)–Cu(1)–N(1′)	88.31(2)	N(1)–Co(1)–N(7)	89.8(3)	N(1′)–Cu(1′)–N(7′)	85.6(6)
				N(4)–Co(1)–N(7)	91.2(3)	N(1A)–Cu(1A)–N(4A)	85.0(5)
		M···M	8.397	N(7)–Co(1)–N(7′)	180.0	N(1′)–Cu(1′)–N(4′)	88.9(8)
						N(7)–Cu(1A)–N(10A)	177.87(10)
						N(7′)–Cu(1′)–N(10′)	171.4(6)

of the octahedral Co^{II} centres in **7** is bonded to four others by four equatorial $\mu_{1,5}$-dca^- bridging ions, resulting in distorted square grid-like (4,4) sheets of $\{Co^{II}(dca)_2\}$ (Fig. 8). The axial positions are occupied by two different dbtp ligands, each twisting away and bridging to opposite and adjacent (4,4) sheets to produce the 3-D array in **7** (Fig. 9). Selected bond angles and distances observed in **7** are given in Table 3. The analogous $[Ni^{II}(dca)_2(dbtp)]$ (**8**) 3-D network was synthesised using the same general method (Section 2.1), giving crystals of poor quality and so powder X-ray diffraction studies were employed to confirm its identity. Thus, the powder XRD pattern of **8** obtained at ambient temperature compares well to the generated powder XRD pattern using the crystal data from **7** (see Supplementary information).

3.4. Magnetic susceptibility measurements on 7 and 8

Magnetic susceptibility measurements were carried out on $[Co^{II}(dca)_2(dbtp)]$ (**7**) and $[Ni^{II}(dca)_2(dbtp)]$ (**8**) in a field of 1 T, giving room temperature μ_{eff} ($=2.83\sqrt{\chi_m T}$) values (per M^{II}) of 4.62 and 3.02 μ_B respectively, which are typical of such octahedrally coordinated ions having $^4T_{1g}$ and $^3A_{2g}$ single-ion ligand field states, respectively. The μ_{eff} values obtained from **7** then decreases gradually before becoming steeper at temperature of 150 K ($\mu_{eff} = 4.6\ \mu_B$), reaching a value at 4 K of 3.16 μ_B (Fig. 10(top)). This is the plot expected for a very weakly antiferromagnetically exchange coupled Co^{II} system. Similar curves have been observed in other Co^{II}–dca or tcm^- network systems [15]. The μ_{eff} values are independent of field when varied between 0.01 and 1 T in the 4–100 K region, thus ruling out any long-range magnetic ordering.

The plot in $[Ni^{II}(dca)_2(dbtp)]$ (**8**) differs greatly to that observed in $[Co^{II}(dca)_2(dbtp)]$ (**7**). The μ_{eff} value at 300 K of 3.02 μ_B remains almost constant with decreasing temperature, before increasing sharply below 40 K. A maximum is then reached at 4 K, giving a μ_{eff} value of 3.28 μ_B, before decreasing sharply (Fig. 10(bottom)). The shape of this curve strongly indicates the presence

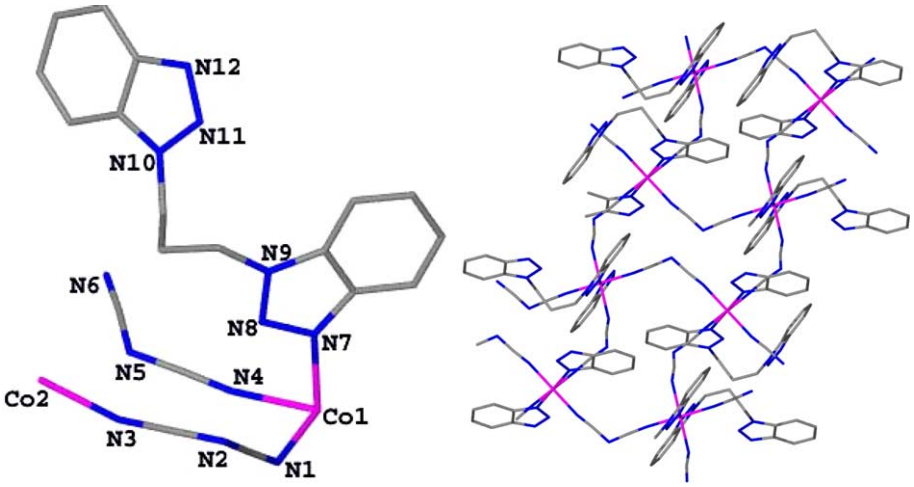

Fig. 8. (Left) The asymmetric unit in **7**. Selected inter-atomic bond distances (Å): Co1–N1 = 2.153(7), Co1–N4 = 2.087(7), Co2–N3 = 2.109(7), Co1–N7 = 2.136(7) Å. (Right) The 2-D (4,4) connecting distorted square-like $Co^{II}(dca)_2$ grids observed in **7**. H atoms omitted for clarity. Co···Co intrasheet distances = 7.918(2) Å.

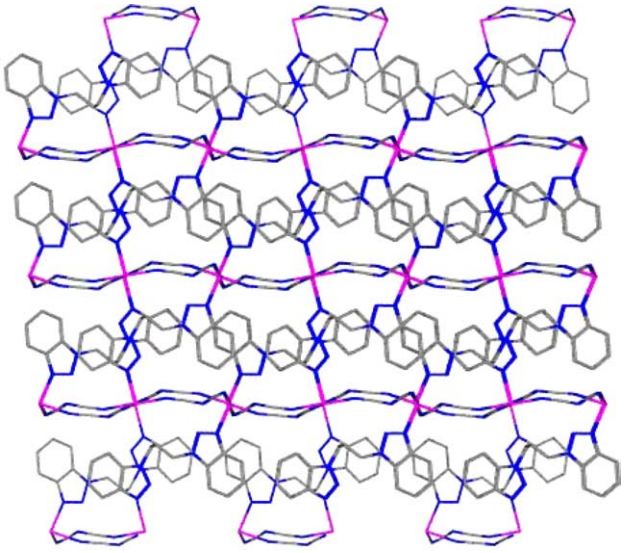

Fig. 9. The 3-D structure in **7**, illustrating the linking of adjacent 2-D (4,4) $Co^{II}(dca)_2$ sheets via the dbtp ligands. H atoms omitted for clarity. Intersheet $Co^{II}\cdots Co^{II}$ distance of ~8.22 Å.

of weak ferromagnetic coupling between the neighbouring Ni^{II} ions. As in the Co^{II} analogue, the μ_{eff} data in fields of 0.01 and 0.1 T (4–100 K) showed the same values as those observed in the 1 T field, thus indicating a lack of long-range magnetic ordering. The common observation [15] of traces of ferromagnetic α-$[Ni^{II}(dca)_2]$ showing a rapid increase in μ_{eff}, in the lower fields, at 21 K, did not occur here. The magnetic susceptibility data obtained from **8** were fitted using an $S = 1$ Fisher chain model. The best fit resulted in Spin-Hamiltonian parameters of $g = 2.13$ and $J = +0.24\ cm^{-1}$ (Fig. 11). Magnetizations isotherms were measured on the same sample of **8** at temperatures of 2, 3, 4, 5.5, 10 and 20 K. The plots in Fig. 12 show that magnetization saturation is not achieved even at $H = 5$ T and $T = 2$ K.

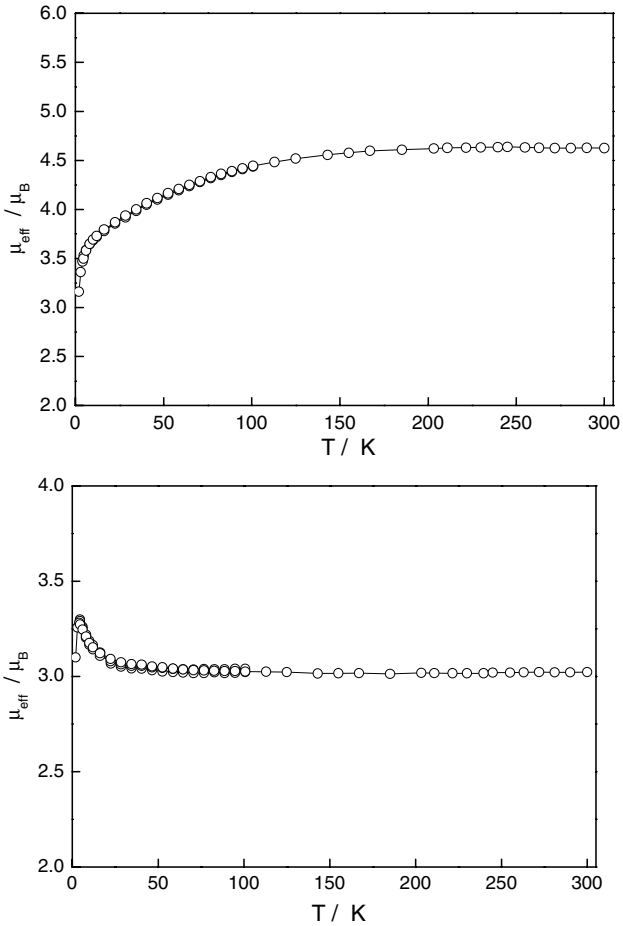

Fig. 10. Plot of μ_{eff} (per M^{II} ion) vs. temperature for **7** (top) and **8** (bottom) in a field of 1 T. (The solid lines just join the experimental points.)

The M value at this point (2.14 $N\beta$) and the shapes of the isotherms support very weak ferromagnetic coupling within $[Ni^{II}(dca)_2(dbtp)]$ (**8**) (Fig. 12).

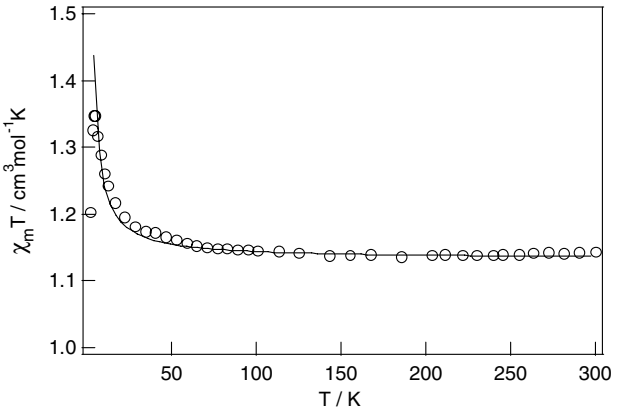

Fig. 11. $\chi_m T$ (○) vs. temperature plot for **8**. The solid line is best fit using a Fisher chain model, resulting in parameters of $S = 1$, $g = 2.13$ and $J = +0.24\ cm^{-1}$. The model cannot account for the decrease in $\chi_m T$ at very low temperatures due to zero-field splitting or inter-chain coupling.

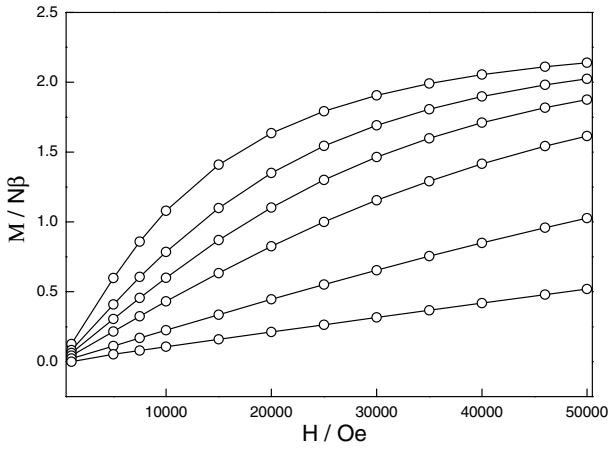

Fig. 12. Plots of magnetization ($M/N\beta$) vs. field (H) for [Ni^{II}(dca)$_2$-(dbtp)] (**8**) at temperatures: 2 (top), 3, 4, 5.5, 10 and 20 K (bottom). (The solid lines just join the experimental points.)

The reason for weak ferromagnetic coupling being observed in **8** while weak antiferromagnetic coupling occurs in **7** is not immediately obvious. There is precedence for such differences in other weakly coupled Co^{II} and Ni^{II}-dca networks [15]. Even in 3-D systems of the present kind, a fine balance in the sign of the M(dca)M coupling, around zero-coupling, is apparent.

3.5. Structure and magnetism of [Cu^{II}(dca)$_2$(dbtb)] (**9**)

The type of 3-D connectivity in **7** and **8** has been observed previously in 3-D networks including those of the pyrazine based family α-[M^{II}(dca)$_2$(pyz)] (M = Mn, Fe, Co, Ni and Zn) [38], in which two such 3-D networks interpenetrate, [Mn(dca)$_2$(C_2H_5OH)$_2$]·(CH_3)$_2$CO [33] and the [M(dca)$_2$(pyrimidine)] · EtOH (M = Fe^{II}, Co^{II}), [Ni(dca)$_2$(pyrimidine)] · H_2O and [Cu(dca)$_2$(pyrimidine)] · MeCN families [9]. In order to investigate the effect of increasing the alkyl chain length between the benzotriazole molecules, the butyl bridged ligand 1,4-di(benzotriazol-1-yl)butane (dbtb) was synthesized. Careful layering of a propan-2-ol solution of dbtb on top of an aqueous Cu^{II}/dca solution resulted in the formation of the 2-D [4,4] connected sheet system [Cu^{II}(dca)$_2$(dbtb)] (**9**). The Cu^{II} centres in **9** are distorted octahedral in geometry and are linked together by two dca$^-$ bridging ligands in the equatorial positions, each exhibiting the familiar $\mu_{1,5}$-dca$^-$ bonding modes. Two individual dbtb ligands occupy the axial sites at each Cu^{II} centre, which then twist away through the alkyl chain, thus linking the neighbouring Cu^{II}/dca rows together, forming the 2-D [4,4] sheet (Fig. 13(bottom)). Another way of rationalising the topology in **9** is by considering that the {Cu^{II}(dca)$_2$} chains are not only interdigitating (as observed in structures **1**–**4**) but are also covalently bound through the interdigitating moieties (Fig. 13(bottom)). The 2-D sheets in **9** then pack in parallel rows in a spatially efficient staggered arrangement (Fig. 14).

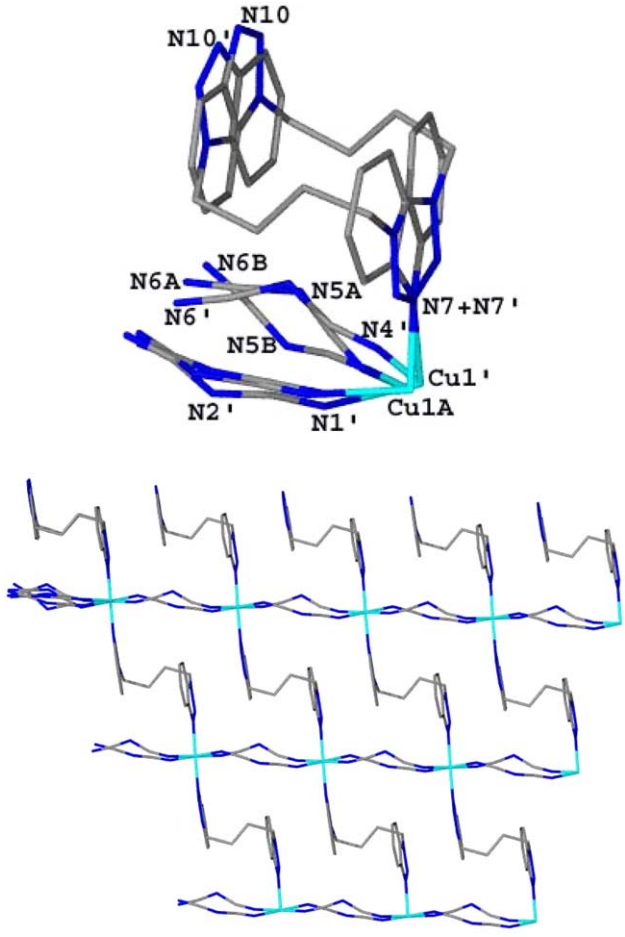

Fig. 13. (Top) The asymmetric unit in **9** showing high disorder of both the dbtb and dca$^-$ ligands. H atoms omitted for clarity. (Bottom) Observed linking of the interdigitating (Cu^{II}(dca)$_2$) chain rows in **9**, propagating along the *c*-axis. H atoms have been omitted for clarity.

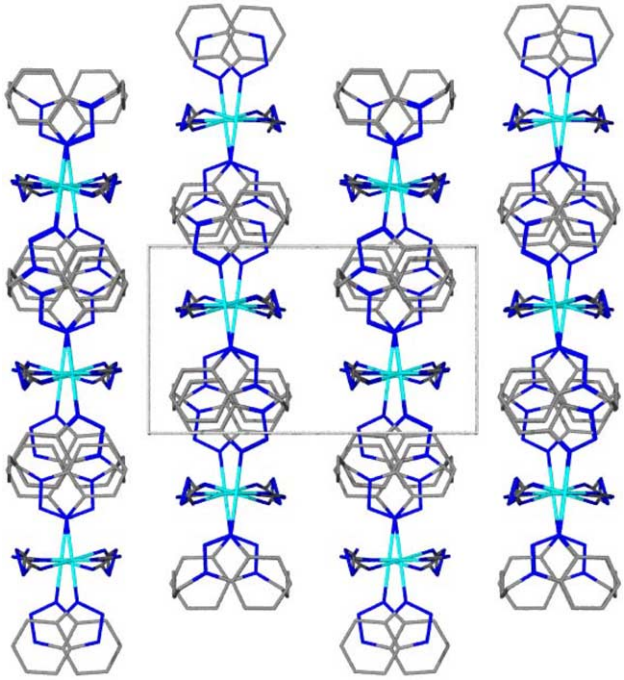

Fig. 14. Observed crystal packing in **9**. Viewed along the *c*-axis, H atoms have been omitted for clarity.

$[Cu^{II}(dca)_2(dbtb)]$ (**9**) contains a 90:10 disorder of the Cu^{II} atom and dbtb ligand position which are related by non-crystallographic mirror plane symmetry. The dca^- ligands are highly disordered due to disorder of the Jahn–Teller distorted Cu^{II} ions which involve elongation of two of the four bonds to dca ligands. As a result of this disorder, equivalent Cu–N(dca) bonds were restrained to be the same length, however, due to the nature of the disorder these lengths are not particularly reliable (Table 3).

The magnetic moment for **9** of 1.87 μ_B at 300 K (Fig. 15) is typical of that displayed by an isolated or very weakly coupled Cu^{II} ion. The susceptibilities are Curie-like, with μ_{eff} values largely independent of temperature, a small decrease below 10 K being due to very weak antiferromagnetic coupling or to Zeeman depopulation effects. These findings can be rationalized by looking at the structure in **9**. It is made up of individual $\{Cu^{II}(dca)_2\}$ chains linked in the second dimension by the dbtb ligands. The dbtb ligands separate these chains considerably and so it can be assumed that the Cu^{II} ions separated by the dbtb ligands are too far apart to exhibit magnetic exchange (interchain Cu1A···Cu1A distance ~8.8 Å) and any exchange will be between the Cu^{II} ions within the $\{Cu^{II}(dca)_2\}$ chains. Indeed, the data obtained from **9** are similar to those of the chain systems $[Cu^{II}(dca)_2(1\text{-Mebta})_2]$ (**3**) and $[Cu^{II}(tcm)_2(1\text{-Mebta})_2]$ (**4**) and those in previously reported $[Cu^{II}(dca)_2(L)_2]$ systems [39,40]. The spin coupling is extremely weak and there is, consequently, no evidence of long range magnetic ordering.

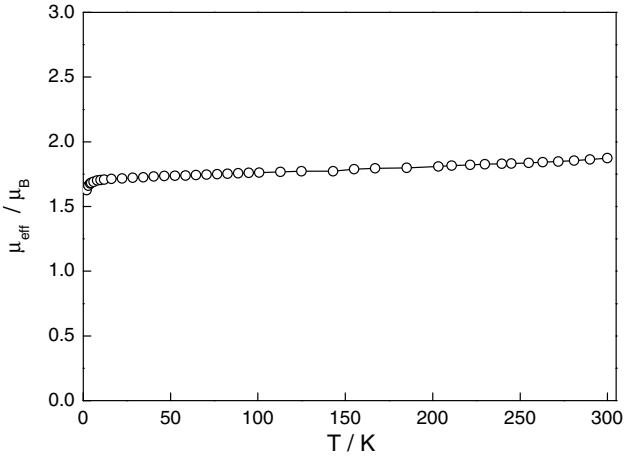

Fig. 15. Plot of μ_{eff} (per Cu^{II}) vs. *T* observed in **9** in a field of 1 T. (The solid lines just join the experimental points.)

4. Conclusions

In this work, we have expanded the coordination chemistry of benzotriazole and its derivatives into the area of metal coordination design and synthesis. The 1-D, 2-D and 3-D networks presented in this paper further illustrate the bonding affinity and flexibility that benzotriazole and its derivatives have with first row transition metal ions. The 1-methylbenzotriazole (1-Mebta) ligand has been shown to be a good terminal ligand in the synthesis of 1-D coordination polymers of general formula $[M^{II}(dca)_2(1\text{-Mebta})_2]$ (**1**–**3**) and $[M^{II}(tcm)_2(1\text{-Mebta})_2]$ (**4**). In an attempt to produce benzotriazole based bridging ligands, the 1,3-dibenzotriazol-1-yl(propane) (dbtp) and 1,4-dibenzotriazol-1-yl(butane) (dbtb) ligands have been synthesized and utilized in conjunction with the dicyanamide (dca^-) and tricyanomethanide (tcm^-) bridging ligands to good effect. The dbtp ligand has produced both the 1-D polymer $[Cu^{II}(dca)_2(dbtp)]$ (**5**) and the α-Po related $[Co^{II}(dca)_2(dbtp)]$ (**7**) and $[Ni^{II}(dca)_2(dbtp)]$ (**8**) 3-D networks. Magnetic susceptibility measurements on the 3-D networks **7** and **8** reveal weak to zero antiferromagnetic coupling in the former and weak ferromagnetic coupling in the latter.

In rationalizing the change in structural dimensionality, the transition from the 1-D chains in $[Cu^{II}(dca)_2(dbtp)]$ (**5**) to the 3-D networks in $[M^{II}(dca)_2(dbtp)]$ ($M = Co^{II}$ (**7**) and $M = Ni^{II}$ (**8**)) is largely due to the preference of cobalt and Nickel for octahedral geometries, whereas Cu^{II} can adopt other topologies because of Jahn–Teller distortion. Pseudo-octahedral geometries at the Cu^{II} centres are observed in the 2-D sheet in $[Cu^{II}(dca)_2(dbtb)]$ (**9**). Here, the slightly longer and more flexible butyl bridged dbtb ligand links the $Cu^{II}(dca)_2$ chains via the axial positions to form the 2-D (4,4) connecting sheets. Magnetic susceptibility measurements on

9 nevertheless, show that very weak coupling is occurring, a feature of all the present Cu^{II} network species.

Acknowledgements

This work was supported by a Discovery grant from the Australian Research Council (ARC) (to K.S.M.) and a Research Fellowship (to L.F.J.) from the Royal Society, London. The help of Mr. R. Mackie of the Physics Department, Monash University, with powder X-ray diffraction measurements is gratefully acknowledged.

Appendix A. Supplementary information

Crystallographic data have been deposited with the Cambridge Crystallographic Data Centre, CCDC Nos. 278066–278073 for structures **1**–**7** and **9** respectively. Copies of this information may be obtained from The Director, CCDC, 12 Union Road, Cambridge CB2 1EZ, UK (fax: +44 1223 336 033; e-mail: deposit@ccdc.cam.ac.uk or www: http://www.ccdc.cam.ac.uk). Supplementary data associated with this article can be found, in the online version, at doi:10.1016/j.poly.2005.08.005.

References

[1] S.R. Batten, P. Jensen, B. Moubaraki, K.S. Murray, R. Robson, Chem. Commun. (1998) 439.
[2] M. Kurmoo, C.J. Kepert, New J. Chem. 22 (1998) 1515.
[3] J.L. Manson, C.R. Kmety, Q.–Z. Huang, J.W. Lynn, G.M. Bendele, S. Pagola, P.W. Stephens, L.M. Liable-Sands, A.L. Rheingold, A.J. Epstein, J.S. Miller, Chem. Mater. 10 (1998) 2552.
[4] C.R. Kmety, Q. Huang, J.W. Flynn, R.W. Erwin, J.L. Manson, S. McCall, J.E. Crow, K.L. Stevenson, J.S. Miller, A.J. Epstein, Phys. Rev. B 62 (2000) 5576.
[5] J.L. Manson, A.M. Arif, C.D. Incarvito, L.M. Liable-Sands, A.L. Rheingold, J.S. Miller, J. Solid State Chem. 145 (1999) 369.
[6] J.-H. Luo, M.–C. Hong, R. Cao, Y.–C. Liang, Y.–J. Zhao, R.–H. Wang, J.–B. Weng, Polyhedron 21 (2002) 893.
[7] S.R. Batten, P. Jensen, B. Moubaraki, K.S. Murray, Chem. Commun. (2000) 793.
[8] A. Kutasi, S.R. Batten, B. Moubaraki, K.S. Murray, J. Chem. Soc., Dalton. Trans. (2002) 819.
[9] (a) T. Kusaka, T. Ishida, D. Hashizume, F. Iwasaki, T. Nogami, Chem. Lett. (2000) 1146;
(b) T. Kusaka, T. Ishida, D. Hashizume, F. Iwasaki, T. Nogami, Mol. Cryst. Liq. Cryst. 376 (2002) 463;
(c) I. Riggio, G.A. Albada, D.D. Ellis, A.L. Spek, J. Reedjik, Inorg. Chim. Acta 313 (2001) 120.
[10] S.R. Batten, P. Jensen, B. Moubaraki, K.S. Murray, Chem. Commun. (2000) 2331.
[11] P.M. van der Werff, S.R. Batten, P. Jensen, B. Moubaraki, K.S. Murray, Inorg. Chem. 40 (2001) 1718.
[12] J.W. Raebiger, J.L. Manson, R.D. Sommer, U. Geiser, A.L. Rheingold, J.S. Miller, Inorg. Chem. 40 (2001) 2578.
[13] P.M. van der Werff, E. Martinez-Ferrero, S.R. Batten, P. Jensen, C. Ruiz-Perez, M. Almeida, J.C. Waerenborgh, J.D. Cashion, B. Moubaraki, J.R. Galán-Mascarós, J.M. Martinez-Agudo, E. Coronado, K.S. Murray, Dalton Trans. 2 (2005) 285.
[14] J.A. Schlueter, J.L. Manson, K.A. Hyzer, U. Geiser, Inorg. Chem. 43 (2004) 4100.
[15] S.R. Batten, K.S. Murray, Coord. Chem. Rev. 246 (2003) 103.
[16] I. Dugdale, J.B. Cotton, Corros. Sci. 3 (1963) 39.
[17] M. Murrie, D. Collison, C.D. Garner, M. Helliwell, P.A. Tasker, S.S. Turner, Polyhedron 17 (1998) 3031.
[18] (a) J.H. Marshall, Inorg. Chem. 17 (1978) 3711;
(b) J. Handley, D. Collison, C.D. Garner, M. Helliwell, R. Docherty, J.R. Lawson, P.A. Tasker, Angew. Chem., Int. Ed. Engl. 32 (1993) 1036.
[19] V.L. Himes, A.D. Mighell, A.R. Siedle, J. Am. Chem. Soc. 103 (1981) 211.
[20] I. Søftofte, K. Nielsen, Acta Chem. Scand. A 38 (1984) 253.
[21] H.M.J. Hendricks, P.J.M.W.L. Birker, G.C. Vershoor, J. Reedjik, J. Chem. Soc., Dalton. Trans. 3 (1982) 623.
[22] I. Søftofte, K. Nielsen, Acta Chem. Scand. A 35 (1981) 733.
[23] D.M. Low, L.F. Jones, A.R. Bell, E.K. Brechin, T. Mallah, E. Riviere, S.J. Teat, E.J.L. McInnes, Angew. Chem. Int. Ed. 42 (2003) 3781.
[24] L.F. Jones, E.K. Brechin, D. Collison, A. Harrison, S.J. Teat, W. Wernsdorfer, Chem. Commun. (2002) 2974.
[25] P.M. Van der Werff, S.R. Batten, P. Jensen, B. Moubaraki, K.S. Murray, E.H.-K. Tan, Polyhedron 20 (2001) 1129.
[26] S. Trofimenko, E.L. Little Jr., H.F. Mower, J. Org. Chem. 27 (1962) 433.
[27] A. Katritzky, A. Jersorka, J. Wang, B. Yang, J. Wu, P.J. Steel, Liebigs Ann. (1996) 745.
[28] Z. Otwinowski, W. Minor, Methods Enzymol. 276 (1997) 307.
[29] G.M. Sheldrick, SHELX-97: Program for Crystal Structure Refinement, University of Göttingen, Göttingen, Germany, 1997.
[30] A. Kutasi, S.R. Batten, A.R. Harris, B. Moubaraki, K.S. Murray, Aust. J. Chem. 55 (2002) 311.
[31] A. Escuer, F.A. Mautner, N. Sanz, R. Vicente, Inorg. Chim. Acta 340 (2000) 163.
[32] (a) J.L. Manson, A.M. Arif, C.D. Incarvito, L.M. Liable-Sands, A.L. Rheingold, J.S. Miller, J. Solid State Chem. 145 (1999) 369;
(b) A. Escuer, F.A. Mautner, M. Sanz, R. Vicente, Inorg. Chem. 39 (2000) 72;
(c) J.L. Manson, C.D. Incarvito, A.M. Arif, J.S. Miller, Mol. Cryst. Liq. Cryst. 334 (1999) 605.
[33] S.R. Batten, P. Jensen, C.J. Kepert, M. Kurmoo, B. Moubaraki, K.S. Murray, Dalton Trans. (1999) 2987.
[34] C.J. Janiak, J. Chem. Soc., Dalton Trans. (2000) 3885.
[35] (a) M.E. Fisher, Am. J. Phys. 32 (1964) 343;
(b) R. Georges, R.J.J. Borras-Almenar, E. Coronado, J. Curley, M. Drillon, in: J.S. Miller, M. Drillon (Eds.), Magnetism: Molecules and Materials, Wiley–VCH, Weinheim, 2001, p. 49;
(c) O. Kahn, Molecular Magnetism, VCH, New York, 1993, p. 258.
[36] S.R. Batten, B.F. Hoskins, R. Robson, New J. Chem. (1998) 173.
[37] S.R. Batten, B.F. Hoskins, B. Moubaraki, K.S. Murray, R. Robson, CrystEngComm 8 (2001) 1.
[38] P. Jensen, S.R. Batten, B. Moubaraki, K.S. Murray, J. Solid State Chem. 159 (2001) 352.
[39] G.A. Albada, M.E. Quiroz-Castro, I. Mutikainen, U. Turpeinen, J. Reedjik, Inorg. Chim. Acta 298 (2000) 221.
[40] J. Mroziński, J. Kohout, M. Hvastijová, Polyhedron 8 (1989) 157.

Available online at www.sciencedirect.com
SCIENCE DIRECT®
Polyhedron 25 (2006) 373–378
POLYHEDRON
www.elsevier.com/locate/poly

Synthesis and Co(III) complexes of the new tetradentate mixed-donor tetraamine ligand *N*-{2-[(2-pyridin-2-ylethyl)amino]ethyl}ethane-1,2-diamine (peda)

Andrea J. Clarkson, Allan G. Blackman *

Department of Chemistry, University of Otago, P.O. Box 56, Dunedin, New Zealand

Received 2 May 2005; accepted 28 June 2005
Available online 10 August 2005

Dedicated to Professor Malcolm H. Chisholm, a Chemist who appreciates all kinds of Chemistry, on the happy occasion of his 60th birthday.

Abstract

Reaction of 2,2′-diphthalimidodiethylamine with 2-vinylpyridine in H_2O/MeOH and deprotection with HCl(aq) does not give the anticipated tripodal ligand *N*-2-(2-pyridylethyl)-*N*,*N*-bis(2-aminoethyl)amine. Instead, the new linear tetradentate tetraamine ligand *N*-{2-[(2-pyridin-2-ylethyl)amino]ethyl}ethane-1,2-diamine (peda) is formed. The synthesis and characterisation of the Co(III) complexes $[Co(peda)O_2CO]X \cdot H_2O$ (X = ClO_4, I), *trans*-$[Co(peda)Cl_2]ClO_4$ and *trans*-$[Co(peda)Br_2]Br$ is reported, and an X-ray crystal structure of $[Co(peda)O_2CO]I \cdot H_2O$ shows the presence of the *fm*$_s$ isomer only. Rate data for the acid hydrolysis of $[Co(peda)O_2CO]ClO_4 \cdot H_2O$ over the $[H_3O^+]$ range 0.2–1.0 M (I = 1.0, $NaClO_4$) are reported. Strict first-order kinetics are observed and the data are consistent with the currently accepted mechanism for the hydrolysis of bidentate carbonate complexes.
© 2005 Elsevier Ltd. All rights reserved.

Keywords: Tetraamine; Ligand; Co(III); Kinetics; Carbonate; Hydrolysis

1. Introduction

Multidentate amine ligands have played an important role in the development of synthetic, structural and stereochemical aspects of coordination chemistry. An enormous number of such ligands are now known, ranging from simple bidentate ethylenediamine to complex multidentate tripodal [1] polypyridine [2], macrocyclic [3] and azacryptand [4] ligands. Of the many methods available for the synthesis of multidentate amine ligands, one of the most widely used is the functionalisation of a preexisting amine ligand by alkylation with an amine-containing fragment. 2-Vinylpyridine has proven particularly useful in this respect as a reagent for the introduction of a 2-pyridylethyl group at either a primary or secondary amine centre [5–8]. However, 2-vinylpyridine tends to react with all available primary and secondary amine centres in a molecule and this means that protecting groups are usually necessary in cases where specific alkylation of a multidentate amine ligand is required. The phthaloyl group is often used in order to specifically protect primary amine centres, and it may be easily introduced by reaction of the polyamine with phthalic anhydride. Phthaloyl-protected diethylenetriamine and dipropylenetriamine have been used in the synthesis of the tripodal amine ligands baep (baep = 3-aminopropylbis(2-aminoethyl)amine) [9] and abap (abap = 2-aminoethylbis(3-aminopropyl)amine) [10], where alkylation at the secondary nitrogen atom using the appropriate bromoalkylphthalimide is followed by deprotection with HCl to give the ligand hydrochloride.

* Corresponding author. Tel.: +64 3 479 7931; fax: +64 3 479 7906.
E-mail address: blackman@alkali.otago.ac.nz (A.G. Blackman).

0277-5387/$ - see front matter © 2005 Elsevier Ltd. All rights reserved.
doi:10.1016/j.poly.2005.06.039

As part of our studies into the synthesis of new tripodal tetraamine ligands [1], we were interested in investigating the reaction of phthaloyl-protected triamines with 2-vinylpyridine in an attempt to prepare tripodal ligands containing mixed amine and pyridine donor atoms through pyridylethylation at the secondary N atom. However, the reaction of phthaloyl-protected diethylenetriamine with 2-vinylpyridine did not proceed as expected and in this paper we describe the serendipitous synthesis of the new *linear* tetradentate ligand *N*-{2-[(2-pyridin-2-ylethyl)amino]ethyl}ethane-1,2-diamine (peda, **1**) from a reaction designed to prepare the new tripodal ligand *N*-2-(2-pyridylethyl)-*N*,*N*-bis(2-aminoethyl)amine (**2**). We detail the synthesis of several Co(III) complexes of this ligand, as well as the X-ray structure of $[Co(peda)(O_2CO)]I \cdot H_2O$ and the acid-hydrolysis kinetics of $[Co(peda)(O_2CO)]ClO_4 \cdot H_2O$.

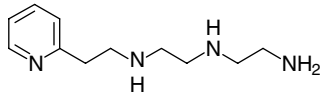

(1)

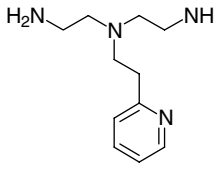

(2)

2. Experimental

All syntheses were carried out under aerobic conditions. ^{13}C and ^{1}H NMR spectra were recorded using either a Gemini 200 MHz or a UNITYInova 300 MHz spectrometer operating at (25 ± 1) °C. UV/Vis spectra and kinetic data were recorded using a Cary 219 Spectrophotometer thermostated at (25.0 ± 0.1) °C. Elemental analyses were carried out by the Campbell Microanalytical Laboratory at the University of Otago. 2,2′-Diphthalimidodiethylamine was synthesised according to the literature methods [11,12].

2.1. N-{2-[(2-Pyridin-2-ylethyl)amino]ethyl}ethane-1,2-diamine tetrahydrochloride dihydrate ($peda \cdot 4HCl \cdot 2H_2O$)

2,2′-Diphthalimidodiethylamine (22.1 g, 0.0608 mol) and 2-vinylpyridine (13.2 ml, 0.122 mol) were refluxed for 6 days in an H_2O/methanol mixture (550:220 ml). The solution was then cooled and evaporated under reduced pressure (rotavap) and the resulting residue was dissolved in chloroform (100 ml) and added dropwise to ether (600 ml). The white precipitate which formed was removed by filtration and refluxed overnight in HCl (8 M, 100 ml). The solution was cooled on ice for 3 h and a small amount of phthalic acid was filtered off. The filtrate was evaporated under reduced pressure to give a yellow residue which was dissolved in water and loaded onto a Dowex 50W × 2 cation exchange column. The column was washed with 1 M HCl and the product was eluted using 4 M HCl. Removal of solvent (rotavap) gave the product as a yellow oil (17.3 g, 73 %). Although ^{1}H NMR showed this to contain impurities, it was sufficiently pure for use in the synthesis of metal complexes. Analytically pure material can be obtained by repeated trituration with ethanol to give a solid which can then be crystallised from hot methanol to give the product as a white powder, although this decreases the yield significantly. *Anal*. Calc. for $C_{11}H_{24}N_4Cl_4 \cdot 2H_2O$: C, 33.86; H, 7.23; N, 14.36. Found: C, 33.94; H, 7.61; N, 14.43%. ^{1}H NMR (D_2O, 25 °C): δ 8.76–8.73 (d, 1H); 8.59–8.53 (t, 1H); 8.04–7.96 (m, 2H); 3.59–3.42 (m, 12H). ^{13}C NMR (D_2O, 25 °C): δ 151.9, 148.4, 143.4, 128.9, 127.3, 50.1, 45.9 45.8, 44.7, 44.6, 36.6 ppm.

2.2. $[Co(peda)(O_2CO)]ClO_4 \cdot H_2O$

Solid $Na_3[Co(O_2CO)_3] \cdot 3H_2O$ (6.63 g, 0.0183 mol) was added to a solution of $peda \cdot 4HCl \cdot 2H_2O$ (6.82 g, 0.0175 mol) in water (50 ml). The solution was stirred for 5 days then evaporated to low volume to give a maroon solid which was filtered off. Crystallisation as the ClO_4^- salt was effected by dissolution in the minimum volume of hot water, addition of $NaClO_4$(s) and cooling on ice. Yield: 3.01 g (38%). *Anal*. Calc. for $CoC_{12}H_{22}N_4O_8Cl$: C, 32.41; H, 4.99; N, 12.60; Cl, 7.97. Found: C, 32.31; H, 5.12; N, 12.56; Cl, 7.92%. ^{1}H NMR (D_2O, 25 °C): δ = 8.72–8.71 (d, 1H, 5.7); 8.04–7.99 (t, 1H, 6); 7.59–7.54 (m, 2H); 3.5–2.62 (m, 12H). ^{13}C NMR (D_2O, 25 °C): δ = 167.6, 162.8, 152.8, 141.5, 127.5, 125.4, 54.7, 53.9, 48.3, 47.6, 42.3, 35.4 ppm. UV/Vis (λ_{max}/nm (ε/mol^{-1} L cm^{-1})): 518 (187); 364 (157).

X-ray quality crystals of $[Co(peda)(O_2CO)]I \cdot H_2O$ were obtained by slow cooling of a hot concentrated solution of the Cl^- salt of the complex (above) to which NaI had been added.

2.3. trans-$[Co(peda)Cl_2]ClO_4$

$[Co(peda)O_2CO]ClO_4 \cdot H_2O$ (0.132 g, 3×10^{-4} mol) was added to aqueous HCl (5 M, 2 ml). Green crystals of the product formed on standing overnight, and these were filtered off and air dried. Yield: 0.10 g (72%). *Anal*. Calc. for $CoC_{11}H_{20}N_4O_4Cl_3$: C, 30.19; H, 4.61; N, 12.81; Cl, 24.31. Found: C, 30.30; H, 4.59; N, 12.72; Cl, 24.34%. ^{1}H NMR (DMSO, 25 °C): δ 8.94–8.92 (d, 1H, 5.1); 8.11–8.05 (t, 1H, 8); 7.68–7.59 (m, 2H); 7.23 (br s, 1H); 6.86 (br s, 1H); 6.61 (br s, 1H); 6.46–6.43 (br d, 1H); 3.75–2.99 (m, 12H). ^{13}C NMR (DMSO, 25 °C): δ 164.4, 157.9, 142.9, 131.4, 127.4, 60.1, 55.2, 53.0, 49.7, 48.7, 39.9 ppm.

2.4. trans-[Co(peda)Br$_2$]Br

[Co(peda)O_2CO]$ClO_4 \cdot H_2O$ (0.120 g, 2.70×10^{-4} mol) was added to aqueous HBr (5 M, 2 ml). Olive-green crystals of the product formed on standing overnight, and these were filtered off, washed with acetone, and air-dried. Yield: 0.105 g (77%). *Anal.* Calc. for $CoC_{11}H_{20}N_4Br_3$: C, 26.06; H, 3.98; N, 11.05; Br, 47.28. Found: C, 25.98; H, 4.06; N, 10.95; Br, 47.23%. The complex decomposed rapidly on dissolution in either d^6-Me_2SO or 5 M DBr to give a brown solution, the ^{1}H NMR spectrum of which showed the presence of more than one species.

2.5. X-ray data collection and refinement

X-ray structural data for *fm*$_s$-[Co(peda)O_2CO]I $\cdot H_2O$ were collected at −120 °C on a Siemens Smart system using graphite-monochromated Mo Kα radiation with exposures over 0.3°. Data were corrected for Lorentz and polarisation effects using SAINT [13]. The structure was solved using SHELXS-97 [14] with the resulting Fourier map revealing the locations of all non-hydrogen atoms. Weighted full matrix refinements on F^2 were carried out using SHELXL-97 [15] with all non-hydrogen atoms being refined anisotropically. All hydrogen atoms except those on the water of crystallisation (H41 and H42) were included in calculated positions and were refined as riding atoms with individual (or group, if appropriate) isotropic displacement parameters. H41 and H42 were located in a search of the Fourier map and were included in the final refinement cycles. Crystal data and collection parameters are given in Table 1.

Table 1
Crystal data and structure refinement for [Co(peda)(O_2CO)]I $\cdot H_2O$

Empirical formula	$C_{12}H_{22}CoIN_4O_4$
Formula weight	472.17
T (K)	153(2)
λ (Å)	0.71073
Crystal system	monoclinic
Space group	$P2_1/n$
Unit cell dimensions	
a (Å)	7.70720(10)
b (Å)	13.7724(3)
c (Å)	16.0599(3)
α (°)	90
β (°)	97.3930(10)
γ (°)	90
V (Å^3)	1690.53(5)
Z	4
D_{calc} (Mg/m^3)	1.855
Absorption coefficient (mm^{-1})	2.863
F(000)	936
Crystal size (mm^3)	$0.5 \times 0.33 \times 0.18$
θ Range for data collection (°)	1.95–30.57
Index ranges	$-6 \leqslant h \leqslant 10$, $-19 \leqslant k \leqslant 8$, $-22 \leqslant l \leqslant 20$
Reflections collected	10869
Independent reflections (R_{int})	4685 (0.0236)
Completeness to $\theta = 25.00°$ (%)	99.4
Absorption correction	semi-empirical from equivalents
Maximum and minimum transmission	1 and 0.752629
Refinement method	full-matrix least-squares on F^2
Data/restraints/parameters	4685/0/201
Goodness-of-fit on F^2	1.052
Final R indices [$I > 2\sigma(I)$]	$R_1 = 0.0202$, $wR_2 = 0.0492$
R indices (all data)	$R_1 = 0.0239$, $wR_2 = 0.0501$
Largest difference in peak and hole (e Å^{-3})	0.742 and −0.910

2.6. Acid hydrolysis of [Co(peda)O_2CO]$ClO_4 \cdot H_2O$

Rate data for acid hydrolysis of [Co(peda)O_2CO]-$ClO_4 \cdot H_2O$ in acidic aqueous solution were collected over the [H_3O^+] range 0.2–1.0 M at 25.0 ± 0.1 °C (I = 1.0 M, $NaClO_4$). Reactions were carried out under pseudo first-order conditions with $[H_3O^+] \gg [Co]_T$ ($[Co]_T$ typically 2.5×10^{-3} mol L^{-1}), and were monitored over at least six half lives by following the decrease in absorbance at 360 nm. The absorbance infinity values (A_∞) were evaluated at the end of each run and k_{obs} values were obtained from plots of $\ln(A_t - A_\infty)$ versus t.

3. Results and discussion

3.1. Synthesis of peda · 4HCl · 2H_2O

The reaction of 2,2′-diphthalimidodiethylamine with excess 2-vinylpyridine followed by deprotection in 8 M HCl was expected to give the tripodal ligand *N*-2-(2-pyridylethyl)-*N*,*N*-bis(2-aminoethyl)amine (**2**) as the hydrochloride salt. However, observation of 11 signals in the ^{13}C NMR spectrum of the product showed it to be of lower symmetry than expected and all analytical data were consistent with the formation of the asymmetric linear tetradentate tetraamine ligand peda · 4HCl · 2H_2O (**1**, Scheme 1). Pyridylethylation at a secondary N atom using 2-vinylpyridine has substantial precedent in the literature [16] and the secondary N atom of 2,2′-diphthalimidodiethylamine has significant nucleophilic character, as evidenced by its relatively facile alkylation in reactions to form tripodal tetraamine ligands [9,10]. Thus, it was expected that pyridylethylation of the secondary amine N atom would occur in this case. However, it appears that partial deprotection of 2,2′-diphthalimidodiethylamine occurs during the reaction with 2-vinylpyridine, and this then allows pyridylethylation at a primary N atom to give the monophthaloylated linear tetraamine ligand. Alkaline media (40% aqueous methylamine solution) have been used previously to effect deprotection of phthaloyl-protected amines [17] and similar reactivity is proposed to occur in this case, through either base- or 2-vinylpyridine-catalysed hydrolysis of a single phthaloyl group.

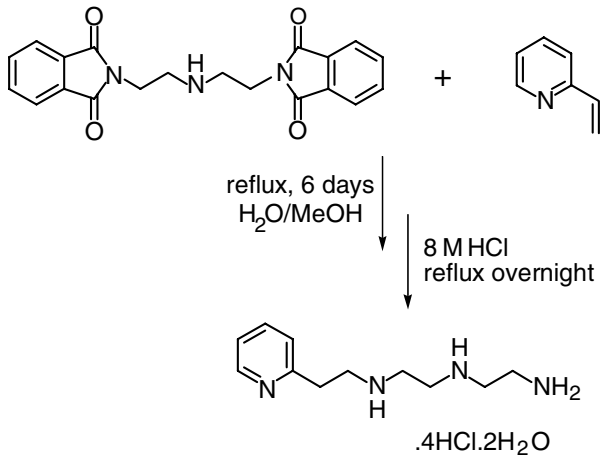

Scheme 1. Synthesis of peda.

Although peda has been mentioned previously in the patent literature as a possible corrosion inhibitor, a detailed synthesis was not given [18] and peda now joins the known asymmetric linear polyamine ligands containing terminal 2-pyridyl and aliphatic amine substituents outlined in Fig. 1.

3.2. Synthesis and X-ray structure of $[Co(peda)(O_2CO)]X \cdot H_2O$ ($X = ClO_4$, 1)

The maroon complex $[Co(peda)(O_2CO)]^+$ was prepared by reaction of peda $\cdot$ 4HCl $\cdot$ $2H_2O$ with $Na_3[Co(O_2CO)_3] \cdot 3H_2O$ in aqueous solution over 5 days. The product was initially isolated as the Cl^- salt following evaporation of the reaction mixture to low volume, and was crystallised as the ClO_4^- and I^- salts, with the latter giving X-ray quality crystals. There are numerous possible isomers of the complex which arise from the different possible foldings of the ligand, but both ^{13}C NMR and X-ray crystallographic data are consistent with the presence of only one isomer in both the solid state and solution. The X-ray structure of $[Co(peda)(O_2CO)]I \cdot H_2O$ (Fig. 2) shows the Co(III) ion coordinated to all four N atoms of the peda ligand, with the remaining two *cis* coordination sites occupied by a chelating carbonate ligand. The angle subtended by the chelated carbonate ligand (68.87°) is typical of those found in other structurally characterised Co(III) carbonate complexes.[1] The complex crystallises as the fm_s isomer [19] in which the two five membered chelate rings adopt δ conformations while the six-membered chelate ring exists in a distorted boat conformation. The *exo* oxygen atom of the chelated carbonate ligand is hydrogen-bonded to the water of crystallisation ($d_{O-O} = 2.739$ Å, O–H–O = 160.34°), while it also displays a close contact with N12 of a neighbouring cation ($d_{O-N} = 2.896$ Å).

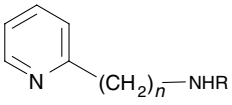

Ligand	Reference
n=1, R = $(CH_2)_2NH_2$	[22]
n=1, R = $(CH_2)_3NH_2$	[22]
n=1, R = $(CH_2)_2NH(CH_2)_2NH_2$	[23]
n=1, R = $(CH_2)_2NH(CH_2)_2NH(CH_2)_2NH_2$	[24]
n=1, R = $(CH_2)_2NH(CH_2)_2NH(CH_2)_2NH(CH_2)_2NH_2$	[25]
n=2, R = $(CH_2)_2NH_2$	[26]
n=2, R = $(CH_2)_3NH_2$	[22]
n=2, R = $(CH_2)_2NH(CH_2)_2NH_2$	[18], this work.
n=2, R = $(CH_2)_2NH(CH_2)_2NH(CH_2)_2NH_2$	[18]
n=3, R = $(CH_2)_2NH_2$	[27]

Fig. 1. Previously prepared asymmetric ligands containing terminal 2-pyridyl and aliphatic amine substituents (see [22–27]).

3.3. Acid hydrolysis of $[Co(peda)(O_2CO)]ClO_4 \cdot H_2O$

The $[Co(peda)(O_2CO)]^+$ cation undergoes acid-catalysed hydrolysis to give dechelation of the carbonate ligand with the final product dependent on the nature of the acid used. Reaction in 5 M aqueous HCl or HBr gives *trans*-$[Co(peda)Cl_2]ClO_4$ and *trans*-$[Co(peda)Br_2]Br$, respectively, as green crystalline solids. These complexes are assigned the *trans* configuration on the basis of their colour[2] and, in the case of the dibromo complex, a poor quality crystal structure. Reaction of $[Co(peda)(O_2CO)]^+$ in $HClO_4$ medium gives absorbance decreases at λ_{max} (518 and 364 nm) and results in formation of the diaqua complex $[Co(peda)(OH_2)_2]^{3+}$.[3] Rate data for this reaction were collected by monitoring the absorbance decrease at 360 nm and resulting values of k_{obs} versus $[H_3O^+]$ are given in Table 2. Strict first-order kinetics were observed under all conditions of $[H_3O^+]$ studied with no evidence of biphasic kinetics that obtain for more reactive $[(L)Co(O_2CO)]^+$ complexes. The data are consistent with the mechanism that has been proposed previously for the acid-catalysed hydrolysis of a number of Co(III) chelated carbonate complexes outlined in Scheme 2, with chelate ring-opening (k_1) being rate-determining [20]. Fitting of the observed data to the rate law derived for this mechanism

$$k_{obs} = \frac{Kk_1[H_3O^+]}{1 + K[H_3O^+]}$$

gives $K = 0.36 \pm 0.14$ M^{-1} and $k_1 = 0.043 \pm 0.013$ s^{-1} (Fig. 3). This corresponds to a half life of approximately 1 min in 1 M $HClO_4$, meaning that $[Co(peda)(O_2CO)]^+$

[1] The mean value for the O–Co–O bond angle in 49 structures from the Cambridge Structural Database is 68.80 (standard deviation = 0.61).

[2] Both *trans*-$[Co(en)_2Cl_2]^+$ and *trans*-$[Co(en)_2Br_2]^+$ are green, while the respective *cis* isomers are violet.

[3] We have thus far been unable to assign this as either the *cis* or *trans* isomer.

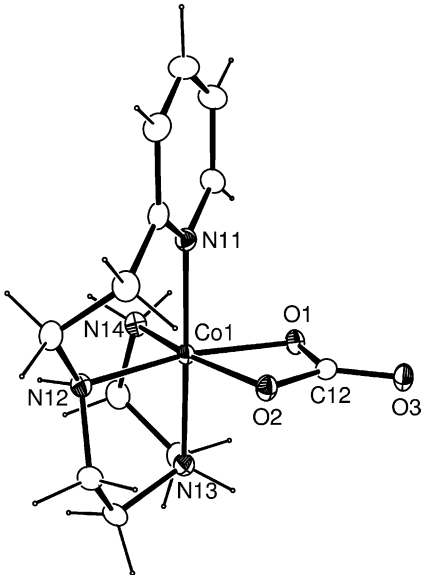

Fig. 2. ORTEP diagram of the cation of $[Co(peda)(O_2CO)]I \cdot H_2O$ with thermal ellipsoids drawn at the 50% level.

Table 2
Rate data for the acid-catalysed hydrolysis of $[Co(peda)(O_2CO)]^+$

$[H_3O]^+$ (M)	$10^3 k_{obs}$ (s^{-1})
0.2	3.20
0.4	5.43
0.6	7.79
0.8	9.16
1.0	11.8

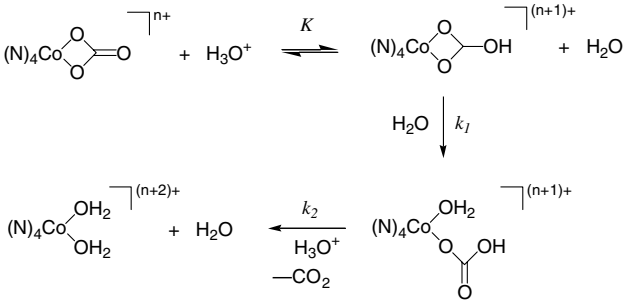

Scheme 2. Mechanism for the acid-catalysed hydrolysis of chelated carbonate complexes.

undergoes chelate ring opening significantly more slowly than complexes such as $[Co(NH_3)_4(O_2CO)]^+$ and $[Co(en)_2(O_2CO)]^+$ (k_1 values of 1.68 and 0.85 s^{-1}, respectively). Inspection of a space-filling model of $[Co(peda)(O_2CO)]I \cdot H_2O$ shows that methylene protons H6B and H8B of the peda ligand create significant steric hindrance at O2, one of the coordinated *endo* oxygen atoms of the chelated carbonate ligand (Fig. 4). Given that protonation at an *endo* O atom has been proposed to be the mechanistically important process which leads to chelate ring opening [20], this provides a possible

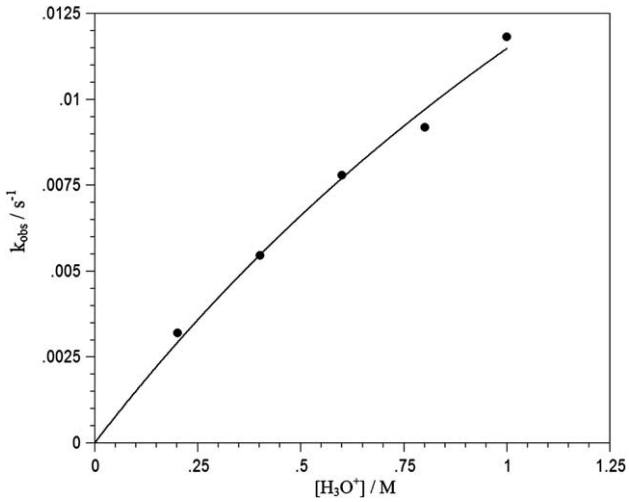

Fig. 3. Plot of k_{obs} vs. $[H_3O]^+$ for the acid-catalysed hydrolysis of $[Co(peda)(O_2CO)]^+$. Points depict observed data while the solid line is drawn using the equation $k_{obs} = \frac{Kk_1[H_3O^+]}{1+K[H_3O^+]}$ with $K = 0.36$ M^{-1} and $k_1 = 0.043$ s^{-1}.

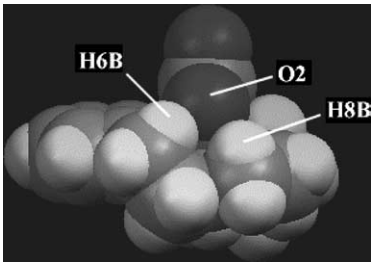

Fig. 4. Space filling diagram of the $[Co(peda)(O_2CO)]^+$ cation showing the steric hindrance of the *endo* oxygen atom O2.

rationalisation of the relatively low reactivity of this complex. Similar arguments have been advanced previously to explain the range of reactivities of a number of $[(L)Co(O_2CO)]^{n+}$ complexes [21].

4. Conclusions

We have shown that the phthaloyl protecting group is susceptible to hydrolysis in predominantly aqueous solutions containing 2-vinylpyridine and that the reaction of 2-vinylpyridine with phthaloyl-protected triamines is thus not a viable method by which to prepare tripodal tetraamine ligands. We are currently investigating alternative routes to the synthesis of the still-unknown ligand **2**.

Acknowledgements

We thank Professor Ward Robinson and Dr. Jan Wikaira (University of Canterbury) for X-ray data

collection. We also thank Dr. Charles Clark for his significant contribution to this work.

Appendix A. Supplementary material

CCDC 270932 contains the supplementary crystallographic data for this paper. These data can be obtained free of charge via www.ccdc.cam.ac.uk/data_request/cif, by emailing data_request@ccdc.cam.ac.uk, or by contacting the Cambridge Crystallographic Data Centre, 12, Union Road, Cambridge CB2 1EZ, UK; fax: +44 1223 3360333. Supplementary data associated with this article can be found, in the online version, at doi:10.1016/j.poly.2005.06.039.

References

[1] A.G. Blackman, Polyhedron 24 (2005) 1.
[2] R.P. Thummel, in: J.A. McCleverty, T.J. Meyer (Eds.), Comprehensive Coordination Chemistry II, vol. 1, Elsevier Pergamon, Amsterdam, 2004, p. 41.
[3] D. Parker (Ed.), Macrocycle Synthesis: A Practical Approach, Oxford University Press, Oxford, 1996.
[4] J. Nelson, V. Mckee, G. Morgan, Prog. Inorg. Chem. 47 (1998) 167.
[5] J. Dietrich, F.W. Heinemann, A. Schrodt, S. Schindler, Inorg. Chim. Acta 288 (1999) 206.
[6] K.D. Karlin, J.C. Hayes, J.P. Hutchinson, J.R. Hyde, J. Zubieta, Inorg. Chim. Acta 64 (1982) L219.
[7] N.N. Murthy, M. Mahroof-Tahir, K.D. Karlin, Inorg. Chem. 40 (2001) 628.
[8] H-C. Liang, M.J. Henson, L.Q. Hatcher, M.A. Vance, C.X. Zhang, D. Lahti, S. Kaderli, R.D. Sommer, A.L. Rheingold, A.D. Zuberbühler, E.I. Solomon, K.D. Karlin, Inorg. Chem. 43 (2004) 4115.
[9] R.J. Geue, A.M. Sargeson, R. Wijesekera, Aust. J. Chem. 46 (1993) 1021.
[10] R.L. Fanshawe, A.G. Blackman, Inorg. Chem. 34 (1995) 421.
[11] G.H. Searle, S.F. Lincoln, S.G. Teague, D.G. Rowe, Aust. J. Chem. 32 (1979) 519.
[12] D.A. Buckingham, J.D. Edwards, G.M. McLaughlin, Inorg. Chem. 21 (1982) 2770.
[13] SAINT, Version 4, Siemens Analytical X-ray Systems, Inc., Madison, WI, 1996.
[14] G.M. Sheldrick, SHELXS-97: A Program for the Solution of Crystal Structures from Diffraction Data, University of Göttingen, Göttingen, Germany, 1997.
[15] G.M. Sheldrick, T.R. Schneider, Methods Enzymol. 277 (1997) 319.
[16] H.E. Reich, R. Levine, J. Am. Chem. Soc. 77 (1955) 4913.
[17] S. Wolfe, S.K. Hasan, Can. J. Chem. 48 (1970) 3572.
[18] J.A. Haslegrave, D.S. Sullivan, Corrosion inhibitors, Brit. UK Pat. Appl. GB 2131785, 1984.
[19] R.M. Hartshorn, D.A. House, J. Chem. Soc., Dalton Trans. (1998) 2577.
[20] D.A. Buckingham, C.R. Clark, Inorg. Chem. 33 (1994) 6171.
[21] P.M. Jaffray, L.F. McClintock, K.E. Baxter, A.G. Blackman, Inorg. Chem. 44 (2005) 4215.
[22] J.K. Romary, R.D. Zachariasen, J.D. Barger, H. Schiesser, J. Chem. Soc. C. (1968) 2884.
[23] S. Tamburini, P.A. Vigato, U. Casellato, R. Graziani, J. Chem. Soc., Dalton Trans. (1989) 1993.
[24] A.L. Chaparro, R.W. Vachet, J. Mass Spectrom. 38 (2003) 333.
[25] S-D. Kim, J-K. Kim, W-S. Jung, Bull. Korean Chem. Soc. 18 (1997) 653.
[26] E. Profft, S. Lojack, Rev. Chim., Acad. Rep. Populaire Roumaine 7 (1962) 405.
[27] G.A. Gettys, C.D. Gutsche, Bioorg. Chem. 7 (1978) 141.

Available online at www.sciencedirect.com
SCIENCE DIRECT®
Polyhedron 25 (2006) 379–386
POLYHEDRON
www.elsevier.com/locate/poly

Synthesis and structural diversity of rare earth anthranilate complexes

Glen B. Deacon [a,c,*], Maria Forsyth [b,c], Peter C. Junk [a,c], Stuart G. Leary [a,c], Graeme J. Moxey [a,c]

[a] School of Chemistry, Box 23, Monash University, Clayton, Vic. 3800, Australia
[b] School of Physics and Materials Engineering, Monash University, Clayton, Vic. 3800, Australia
[c] ARC Special Research Centre for Green Chemistry, Monash University, Clayton, Vic. 3800, Australia

Received 3 May 2005; accepted 6 July 2005
Available online 15 August 2005

Dedicated to Professor Malcolm Chisholm F.R.S. on the occasion of his 60th birthday.

Abstract

Four structural classes have been established for rare earth anthranilates, which have been prepared from the lanthanoid chloride or triflate and anthranilic acid (anthH) followed by pH adjustment to 4. $[La(anth)_3]_n$ is a polymeric complex with nine coordinate lanthanum and bridging tridentate (O,O,O′) anthranilate ligands, whereas $[Nd(anth)_3(H_2O)_3] \cdot 3H_2O$ is monomeric with nine coordinate neodymium and solely chelating (O,O) anthranilate groups. Both chelating (O,O) and bridging bidentate (O,O′) ligands are observed in dimeric $[Er_2(anth)_6(H_2O)_4] \cdot 2H_2O$, in which erbium is eight coordinate and the water ligands are in a *trans* arrangement. A polymer is observed for $[Yb(anth)_3(H_2O)]_n$ with solely bridging bidentate (O,O′) ligands and seven coordination for ytterbium. The NH_2 groups of the anthranilate ligands are not coordinated to the metal but is unusually involved in hydrogen-bond networks with water molecules for Ln = Er, Yb.
© 2005 Elsevier Ltd. All rights reserved.

Keywords: Rare earths; Anthranilates; X-ray crystal structures; Amino acids

1. Introduction

Although there have been widespread studies of complexes of rare earth ions with amino acids [1], there are only two structurally characterised complexes with anthranilate ions (anth) (Fig. 1), viz. $[Y(anth)_3(H_2O)]_n$ [2] and $[Eu_2(anth)_6(bpy)_2]$ (bpy = 2,2′-bipyridine) [3]. This contrasts the extensive structural chemistry of anthranilate ions with alkali metals [4,5], alkaline earth metals [6,7], and transition metals [8–12].

Structural proposals have been made for rare earth anthranilates $Ln(anth)_3 \cdot nH_2O$ ($n = 0$, Ln = La, Ce, Pr, Nd, Sm; $n = 2$, Ln = Y, Tb–Lu; and $n = 1$, Ln = Eu, Gd) on the basis of analytical, IR, and X-ray powder data [13,14]. It was suggested that the lighter rare earth anthranilates form two isostructural groups, (i) La–Sm, and (ii) Y, Eu, Gd [13]. A subsequent study found Tb–Lu to be isostructural [14]. IR data suggested coordination of both carboxylate and amino groups.

The insoluble nature of lanthanoid anthranilates makes growing crystals suitable for X-ray diffraction difficult. However because of our interest in lanthanoid anthranilates as possible "green" corrosion inhibitors [15], we have undertaken a study of the structures of representative lanthanoid anthranilates to assist in understanding the structural basis of corrosion inhibitors.

* Corresponding author. Tel.: +61 3 9905 4568/4570; fax: +61 3 9905 4597.
E-mail addresses: glen.deacon@sci.monash.edu.au (G.B. Deacon), peter.junk@sci.monash.edu.au (P.C. Junk).

0277-5387/$ - see front matter © 2005 Elsevier Ltd. All rights reserved.
doi:10.1016/j.poly.2005.07.005

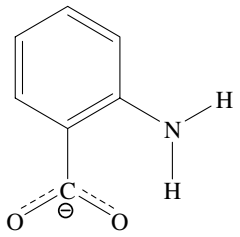

Fig. 1. A line drawing of the anthranilate anion.

2. Experimental

2.1. Materials and instrumentation

Lanthanoid oxides (Nd_2O_3 and Yb_2O_3) were obtained from Honeywell. Er_2O_3 was supplied by Aldrich. Lanthanoid chlorides (other than $LaCl_3$) were prepared by dissolving lanthanoid oxides in hydrochloric acid. $Er(OTf)_3$ was prepared by dissolving Er_2O_3 in trifluoromethanesulfonic acid (HOTf). The resulting solutions were diluted, and the concentrations of the prepared solutions were accurately determined by complexometric titration with standardised 0.01 M Na_2H_2–EDTA. $LaCl_3 \cdot 7H_2O$ was obtained from Chempur. Reagent grade anthranilic acid was obtained from Merck, and used without further purification. All other starting materials were used as received. Microanalyses were performed in duplicate by the Campbell Microanalytical Laboratory of the University of Otago, Dunedin, New Zealand. Rare earth analyses were carried out by digesting accurately weighed samples in concentrated nitric and sulphuric acid and boiling the solutions to dryness. The resulting residues were diluted with water, and aliquots were buffered with hexamethylenetetramine and titrated against standardised 0.01 M Na_2H_2–EDTA with Xylenol Orange as the indicator. Infrared spectra were recorded as Nujol mulls sandwiched between NaCl plates using a Perkin Elmer 1600 FTIR instrument in the range 4000–500 cm^{-1}. ^{19}F NMR spectra were recorded on a Bruker DPX 300 spectrometer, using $CFCl_3$ in d_6-acetone as an external reference. Thermogravimetric analysis (TGA) was performed using a Perkin Elmer Pyris 1 instrument at a heating rate of 10 °C min^{-1}, using a platinum sample pan.

2.2. Synthesis

2.2.1. $[La(anth)_3]_n$ (**1**)

Anthranilic acid (0.35 g, 2.6 mmol) was dissolved in 2 mL of MeOH, and the solution added to a stirred aqueous solution of $LaCl_3$ (5.0 mL, 5.0 mmol) heated to 70 °C. The pH of the reaction mixture was raised by the dropwise addition of 0.5 M NaOH. At a pH of approximately 4, a faint permanent precipitate formed. The reaction mixture was then cooled, and the precipitate filtered off. Crystals appeared following the slow evaporation of the reaction mixture at room temperature.

Yield: 0.21 g (45%). *Anal.* Calc. for $C_{21}H_{18}N_3O_6La$: C, 46.09; H, 3.32; N, 7.68; La, 25.38. Found: C, 46.23; H, 3.40; N, 7.83; La, 25.40%. Infrared (cm^{-1}): 3467 m, 3421 m, 3356 m, 3324 m, 1615 s, 1574 m, 1505 s, 1456 s, 1385 s, 1338 m, 1309 m, 1258 m, 1156 m, 1133 m, 1027 w, 978 w, 946 w, 875 m, 853 w, 811 m, 753 m, 707 m, 669 m.

2.2.2. $[Nd(anth)_3(H_2O)_3] \cdot 3H_2O$ (**2**)

The compound was synthesised using the above procedure except that $NdCl_3$ (4.0 mL, 3.3 mmol) and anthranilic acid (0.21 g, 1.5 mmol) were used.

Yield: 0.12 g (36%). *Anal.* Calc. for $C_{21}H_{30}N_3O_{12}Nd$: C, 38.18; H, 4.58; N, 6.36; Nd, 21.83. Found: C, 38.17; H, 4.43; N, 6.16; Nd, 22.65%. Infrared (cm^{-1}): 3593 m, 3431 s, 1656 m, 1614 s, 1574 m, 1506 s, 1446 m, 1398 s, 1331 m, 1308 m, 1256 m, 1158 m, 1128 w, 1030 w, 981 w, 959 w, 875 m, 821 m, 770 s, 707 m, 672 m.

2.2.3. $[Er_2(anth)_6(H_2O)_4] \cdot 2H_2O$ (**3**)

The compound was synthesised using the above procedure except that $Er(OTf)_3$ (4.0 mL, 3.5 mmol) and anthranilic acid (0.21 g, 1.5 mmol) were used. Single crystals of **3** were separated by hand picking. The bulk product analysed as $[Er_2(anth)_6(H_2O)_4] \cdot HO_3SCF_3 \cdot 2H_2O$, ($\mathbf{3} \cdot HO_3SCF_3$).

Yield: 0.18 g. *Anal.* Calc. for $C_{43}H_{49}F_3N_6O_{21}SEr_2$ ($\mathbf{3} \cdot HO_3SCF_3$): C, 36.64; H, 3.50; N, 5.96; Er, 23.73. Found: C, 36.23; H, 3.54; N, 5.25; Er, 24.30%. Infrared (cm^{-1}): 3627 m, 3478 s, 3361 m, 3343 s, 3312 m, 1614 m, 1574 m, 1538 m, 1514 m, 1506 m, 1485 s, 1421 s, 1340 m, 1302 m, 1262 m, 1260 m, 1159 m, 1156 m, 1032 m, 960 w, 879 m, 820 m, 770 m, 750 m, 704 m, 673 m, 641 m. ^{19}F NMR (d_6-acetone) $\delta = -37.66$ ppm.

2.2.4. $[Yb(anth)_3(H_2O)]_n$ (**4**)

The compound was synthesised using the above procedure except that $YbCl_3$ (9.5 mL, 7.6 mmol) and anthranilic acid (0.52 g, 3.8 mmol) were used. Single crystals of **4** were separated but the bulk crystalline product analysed as $\mathbf{4} \cdot 2H_2O$ after prolonged desiccation at room temperature.

Yield: 0.22 g. *Anal.* Calc. for $C_{21}H_{24}N_3O_9Yb$ ($\mathbf{4} \cdot 2H_2O$): C, 39.69; H, 3.81; N, 6.61; Yb, 27.23. Found: C, 39.91; H, 4.10; N, 6.49; Yb, 27.26%. Infrared (cm^{-1}): 3479 m, 3394 m, 3343 m, 3278 m, 3178 m, 1682 m, 1613 m, 1572 m, 1542 m, 1521 m, 1506 m, 1483 m, 1416 s, 1339 w, 1303 m, 1272 w, 1260 m, 1155 m, 1024 w, 880 m, 820 w, 767 w, 750 m, 704 w, 674 w. TGA: % mass loss 50–200 °C: 8.2%. Calculated mass loss of three H_2O molecules: 8.5%.

2.3. X-ray crystallography

Intensity data for complexes **1**–**4** were collected using an Enraf–Nonius KAPPA CCD at 123 °K with Mo Kα

radiation ($\lambda = 0.7170$ Å). Suitable crystals were immersed in viscous hydrocarbon oil, mounted on a glass fibre which was mounted on the diffractometer. Using psi and omega scans N_t (total) reflections were measured, which were reduced to N_o unique reflections, with $F_o > 2\sigma(F_o)$ being considered observed. Data were corrected for absorption with a SORTAV multi-scan absorption correction [16]. The structures were solved using direct methods, and observed reflections were used in least squares refinement on F^2, with anisotropic thermal parameters refined for non-hydrogen atoms. Aromatic hydrogen atoms were constrained in calculated positions and refined with a riding model. All other hydrogen atoms were found directly from the difference Fourier map and refined isotropically. Structure solutions and refinements were performed using the programs SHELXS-97 [17] and SHELXL-97 [18] through the graphical interface X-Seed [19]. Crystal data and structural refinement data for complexes **1**–**4** are given in Table 1. Selected bond lengths for complexes **1**–**4** are listed in Table 2, and hydrogen bond lengths and angles for complexes **2**–**4** are given in Table 3.

Bond angles and other crystallographic data (excluding structure factors) for the structures reported in this paper have been deposited with the Cambridge Crystallographic Data Centre as supplementary Publication No. CCDC-270607 for compound **1**, CCDC-270608 for compound **2**, CCDC-270609 for compound **3** and CCDC-270610 for compound **4**. Copies of the data can be obtained free of charge on application to the CCDC, 12 Union Road, Cambridge, CB2 1EZ, UK (fax: (+44) 1223 336 033; deposit@ccdc.cam.ac.uk).

3. Results and discussion

3.1. Synthesis of the complexes

Lanthanoid carboxylate complexes are typically synthesised by adding the carboxylate salt to a solution of the lanthanoid salt. An alternative procedure is to add the carboxylic acid to precipitated lanthanoid hydroxides, a method utilised by Brzyska and Rzaczynska [13,14] during their study of lanthanoid anthranilates. The insolubility of lanthanoid anthranilates limits the usefulness of these two methods to grow crystals suitable for single crystal X-ray analysis. The use of a diffusion apparatus yielded crystals of the complex $[Y(anth)_3(H_2O)]_n$ [2]. We have found that the use of a simpler method can yield suitable crystals. The addition of anthranilic acid to lanthanoid chloride solutions followed by the addition of NaOH dropwise to the reaction mixture to form the Na anthranilate salt led to the isolation of La, Nd, Er and Yb anthranilates after slow evaporation of the reaction mixture (pH ca. 4) at room temperature. This approach has been previously employed using higher pH conditions in the synthesis of lanthanoid hydroxo clusters [20].

Both the La and Nd anthranilates crystallise as large (diameter greater than 2 mm) single crystals, and the micro and metal analysis results of the La and Nd anthranilates confirm the stoichiometry obtained from the X-ray crystallography results. The Er and Yb anthranilates crystallise as clusters of thin needles, the clusters partially decomposing into watery solution as they are broken apart with a needle. Consequently, suitable crystals

Table 1
Crystallographic and data collection parameters for complexes **1**–**4**

Complex	**1**	**2**	**3**	**4**
Formula	$C_{42}H_{36}La_2N_6O_{12}$	$C_{21}H_{30}N_3NdO_{12}$	$C_{21}H_{24}ErN_3O_9$	$C_{21}H_{20}N_3O_7Yb$
Formula weight	1094.59	660.72	629.69	599.44
Colour, habit	brown block	dark brown block	light brown needle	light brown needle
Crystal size (mm)	$0.20 \times 0.20 \times 0.10$	$0.30 \times 0.25 \times 0.20$	$0.25 \times 0.25 \times 0.20$	$0.20 \times 0.10 \times 0.10$
Crystal system	monoclinic	hexagonal	orthorhombic	monoclinic
Space group	$P2_1/c$	$R3c$	$Pbca$	$C2/c$
Unit cell dimensions				
a (Å)	24.760(5)	18.566(3)	8.4910(17)	31.234(6)
b (Å)	7.4954(15)	18.566(3)	19.645(4)	9.0441(18)
c (Å)	24.485(5)	12.282(3)	28.129(6)	15.596(3)
α (°)	90	90	90	90
β (°)	119.29(3)	90	90	108.44(3)
γ (°)	90	120	90	90
Volume (Å^3)	3963.1(14)	3666.4(10)	4692.0(16)	4179.2(14)
Z	4	6	8	8
D_{calc} (g/cm^3)	1.835	1.795	1.783	1.905
$F(000)$	2160	1998	2488	2344
Measured reflections	25192	12462	43956	30452
Independent reflections	9027	1871	4612	4094
$R_{(int)}$	0.0272	0.0502	0.0804	0.0544
Goodness-of-fit on F^2	1.084	1.064	1.006	1.065
R	0.0264	0.0195	0.0378	0.0247
R_w	0.0582	0.0428	0.0929	0.0577

Table 2
Selected bond lengths (Å) for complexes **1**–**4**

Complex ***1***	
La(1)–O(1)	2.635(2)
La(1)–O(1)#1	2.473(2)
La(1)–O(2)	2.567(2)
La(1)–O(3)	2.634(2)
La(1)–O(3)#2	2.507(2)
La(1)–O(4)	2.530(2)
La(1)–O(5)	2.636(2)
La(1)–O(5)#1	2.475(2)
La(1)–O(6)	2.548(2)
La(2)–O(7)	2.634(2)
La(2)–O(7)#3	2.473(2)
La(2)–O(8)	2.566(2)
La(2)–O(9)	2.683(2)
La(2)–O(9)#3	2.475(2)
La(2)–O(10)	2.543(2)
La(2)–O(11)	2.655(2)
La(2)–O(11)#4	2.487(2)
La(2)–O(12)	2.524(2)
Complex ***2***	
Nd(1)–O(1)	2.464(2)
Nd(1)–O(2)	2.549(2)
Nd(1)–O(3)	2.492(2)
Complex ***3***	
Er(1)–O(1)	2.397(4)
Er(1)–O(2)	2.400(4)
Er(1)–O(3)	2.369(4)
Er(1)–O(4)	2.356(4)
Er(1)–O(5)	2.272(4)
Er(1)–O(6)#1	2.241(4)
Er(1)–O(7)	2.354(4)
Er(1)–O(8)	2.360(4)
Complex ***4***	
Yb(1)–O(1)	2.285(3)
Yb(1)–O(2)	2.276(2)
Yb(1)–O(3)#1	2.317(3)
Yb(1)–O(4)	2.301(3)
Yb(1)–O(5)#1	2.274(2)
Yb(1)–O(6)#1	2.199(3)
Yb(1)–O(7)	2.213(3)

Symmetry transformations used to generate equivalent atoms for:
Complex (**1**): #1 $-x, y+1/2, -z+1/2$; #2 $-x, y-1/2, -z+1/2$; #3 $-x+1, y-1/2, -z+1/2$; #4 $-x+1, y+1/2, -z+1/2$.
Complex (**3**): #1 $-x+1, -y, -z+1$.
Complex (**4**): #1 $-x+3/2, y+1/2, -z+1/2$.

Table 3
Hydrogen bond lengths (Å) and bond angles (°) for complexes **2**–**4**

D–H···A	*d*(D–H)	*d*(H···A)	*d*(D···A)	∠(DHA)
Complex ***2***				
O(3)–H(3A)···O(2)#3	0.971(19)	1.796(19)	2.765(3)	176(4)
O(3)–H(3B)···O(4)#1	0.955(18)	1.840(19)	2.794(3)	177(3)
Complex ***3***				
O(7)–H(7A)···O(9)#3	0.99(2)	1.67(3)	2.644(6)	166(8)
O(7)–H(7B)···N(1)#3	0.99(2)	1.89(3)	2.864(6)	166(6)
O(8)–H(8B)···O(1)#2	0.98(2)	2.01(6)	2.825(6)	138(6)
O(9)–H(9A)···O(3)	0.99(2)	1.76(2)	2.748(6)	171(6)
Complex ***4***				
O(1)–H(4A)···N(3)#3	0.79(5)	2.07(5)	2.845(5)	171(5)
O(1)–H(4B)···N(1)#4	0.85(5)	2.01(5)	2.845(5)	170(4)

Symmetry transformations used to generate equivalent atoms for:
Complex (**2**): #1 $-x+y, -x+1, z$; #3 $x, x-y+1, z+1/2$.
Complex (**3**): #2 $-x+2, -y, -z+1$; #3 $x-1/2, -y+1/2, -z+1$.
Complex (**4**): #3 $-x+3/2, -y+3/2, -z+1$; #4 $x, -y+2, z+1/2$.

of Er and Yb anthranilates for X-ray analysis were handpicked from the bulk product. The unit cells of several crystals obtained from the Yb anthranilate reaction mixture were in agreement with that of the crystal of the solved structure. The discrepancy between the X-ray determined composition and the observed micro and metal analysis values is likely to be due to the presence of additional water molecules trapped within the clusters of crystals. Microanalyses of bulk products from two preparations and a metal analysis were all consistent with $[Yb(anth)_3(H_2O)] \cdot 2H_2O$, i.e., $\mathbf{4} \cdot 2H_2O$, as was the TGA weight loss over 60–200 °C. Prior to analysis, the samples were dried in a desiccator to constant weight and they remained at constant weight for 2 days after removal from the desiccator. No disordered water was evident in the crystal structure but it is possible that highly disordered waters could be present in holes in the lattice. The issue of hydration in lanthanoid anthranilates is also observed in comparing the anhydrous $Nd(anth)_3$ composition proposed by Brzyska and Rzaczynska [13] from a synthesis in water with the composition of **2**, which contains six water molecules. Possibly small differences in reaction conditions and drying techniques have a major effect on hydration and structure.

An even more marked difference between single crystal structure and bulk composition is observed with **3**, where the bulk composition corresponds more closely to $\mathbf{3} \cdot HO_3SCF_3$, and the ^{19}F NMR spectrum shows clear evidence of a CF_3 resonance, somewhat paramagnetically shifted (by Er^{3+}) from the free acid value ($\delta = -77.9$ ppm). Plausibly, isolation at pH 4 leads to protonation of one amino group of **3** giving $\mathbf{3}H^+(OTf^-)$.

3.2. Crystal structure descriptions

Complexes **1**–**3** represent new structural classes of lanthanoid anthranilates, while complex **4** is isostructural with the previously reported Y anthranilate [2]. In all four structures, the anthranilate ligand is bound to the lanthanoid solely through the carboxylate group, in contrast to carboxylate and NH_2 coordination found in transition metal anthranilates and proposed for rare earth anthranilates [13,14]. Although the amino group is not bound to the lanthanoid cation, the amino group participates in hydrogen bonding in complexes **3** and **4**, stabilising the crystal structures. The results of this study demonstrate that lanthanoid anthranilates exhibit a range of structural classes, even more diverse than the closely related lanthanoid *p*-aminobenzoates [21].

Complex **1** crystallises as an anhydrous species in the monoclinic space group $P2_1/c$. Selected bond lengths are given in Table 2. The structure consists of two crystallographically distinct polymer chains. The bonding in the two chains is almost identical with only negligible differences in bond lengths (Table 2). Only bridging tridentate (O,O,O′) ligands are present. The asymmetric unit consists of two independent La mononuclear units, each bound to three anthranilate ligands. Each polymer strand (Fig. 2) is built up from the monomeric units by links to two adjacent La cations, through bridging tridentate anthranilate ligands. Overall, each lanthanum is surrounded by six bridging tridentate ligands, three of which chelate (O,O) to a given lanthanum, and three are unidentate (O). Consequently, each La ion displays a coordination number of nine. In chain 1 the average La(1)–O (carboxylate) bond distance is 2.556 Å, and the distances between adjacent La ions is 3.901 Å. In chain 2, the average La(2)–O carboxylate distance is 2.560 Å and the distance between adjacent La ions is 3.893 Å. The coordination environment around La(1) is best described as a doubled trigonal prism [22], while for La(2) the coordination environment most closely resembles a capped cube [22]. The presence of two independent polymer chains with the same composition but slightly different structures in the same crystal is uncommon, but it has been previously reported in a praseodymium β-alanine complex [23].

Complex **2** crystallises in the hexagonal space group *R3c* and is monomeric. Selected bond lengths are listed in Table 2. As displayed in Fig. 3, the Nd cation is surrounded by three chelating anthranilate ligands, and three water O atoms giving a coordination number of nine. The coordination environment around the Nd most closely resembles a doubled trigonal prism [22]. The Nd–O (carboxylate) distances are markedly different, being 2.464 (2) Å (Nd–O(1)) and 2.549 (2) Å (Nd–O(2)), indicating asymmetric chelation of the anthranilate ligands. The carboxylate angles (O(1)–C(1)–O(2)) are 119.1 (3)°. The angle between the Nd cation and centroids generated between the carboxylate oxygens of the anthranilate ligands is 99.36°, indicating that the anthranilate ligands adopt a *cisoid* geometry around the Nd cation. The Nd–O (water) distances are 2.492 (2) Å, comparable with the Nd–O carboxylate distances. The angle between the O atoms of coordinated water molecules and the Nd is 74.25 (10)°, indicating the coordinated water molecules are also arranged in a *cisoid* geometry. Three water molecules (two are symmetry generated) reside in the lattice and hydrogen bonding links coordinated water and lattice water molecules. Hydrogen bonding also occurs between the coordinated water and the carboxylate oxygen of the anthranilate ligand. Hydrogen bond lengths and angles are given in Table 3. Surprisingly, the structure is isostructural with the closely related lanthanoid *m*-aminobenzoate hydrate structures, despite the different positions of the NH_2 substituent. Lanthanoid complexes of *m*-aminobenzoates have been shown to be isostructural from La to Lu including Y [24], unlike the anthranilates.

Complex **3** crystallises in the orthorhombic space group *Pbca* and is a dimer. Selected bond lengths are listed in Table 2. In addition to two bound water molecules, each Er cation is encircled by four anthranilate ligands which exhibit two different binding modes (Fig. 4). Two chelating anthranilate ligands and two bridging bidentate anthranilate ligands give an overall

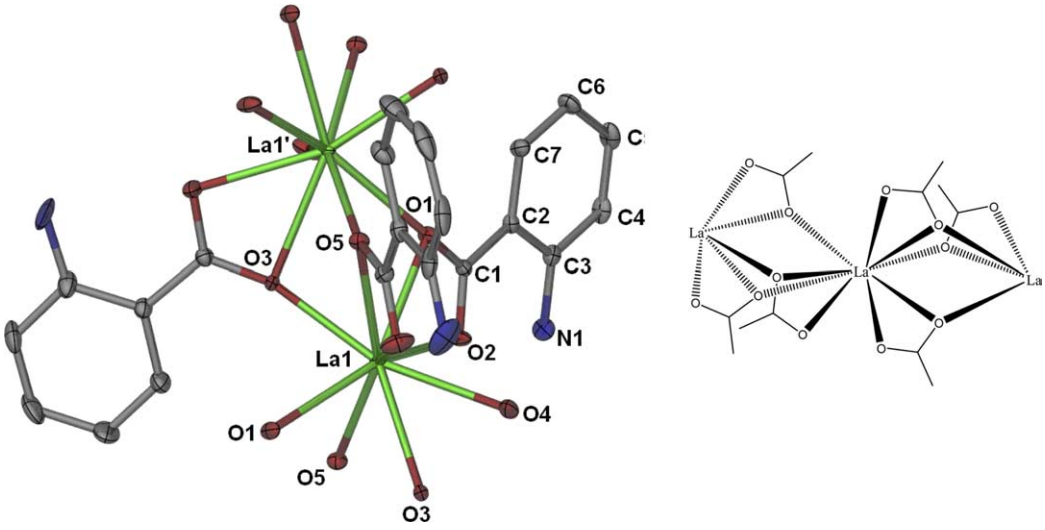

Fig. 2. An ORTEP representation of one of the unique polymer strands of **1**, displaying the bridging tridentate anthranilate ligands present in polymer strands. The second polymer strand is very similar to the pictured polymer strand. Hydrogen atoms have been omitted for clarity (ellipsoids at 50% probability). Inset – stylised diagram showing the ligand connectivity in both polymer strands (aromatic groups omitted for clarity).

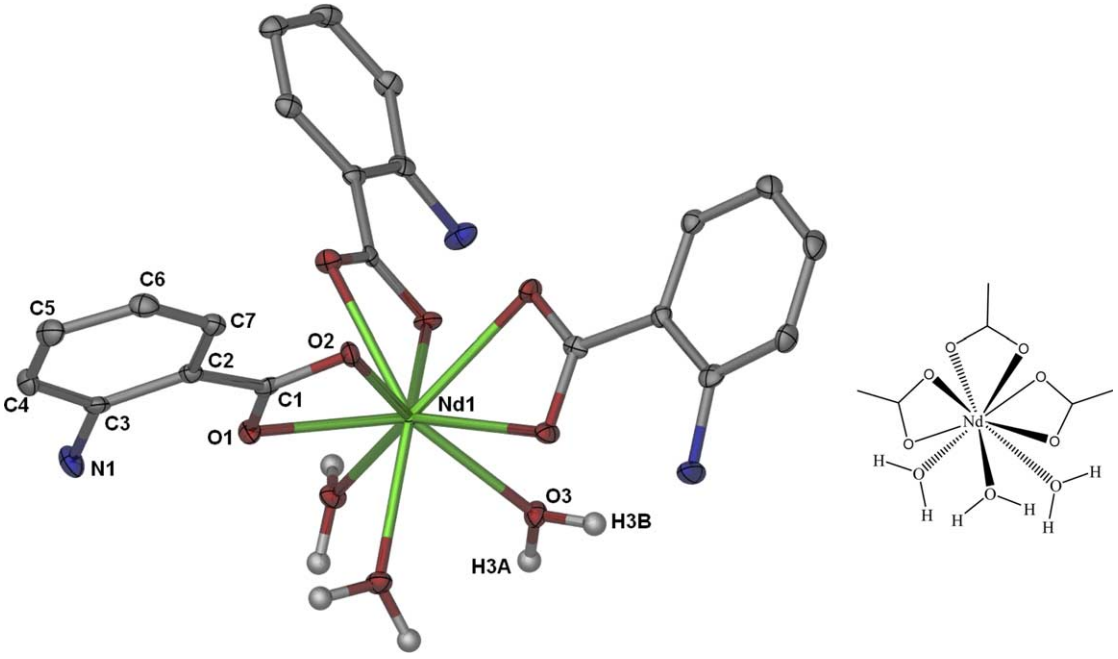

Fig. 3. An ORTEP representation of **2**, exhibiting the chelating anthranilate ligands. Lattice water molecules and hydrogen atoms on anthranilate ligands have been omitted for clarity (ellipsoids at 50% probability). Inset – stylised diagram displaying the ligand connectivity (aromatic groups omitted for clarity).

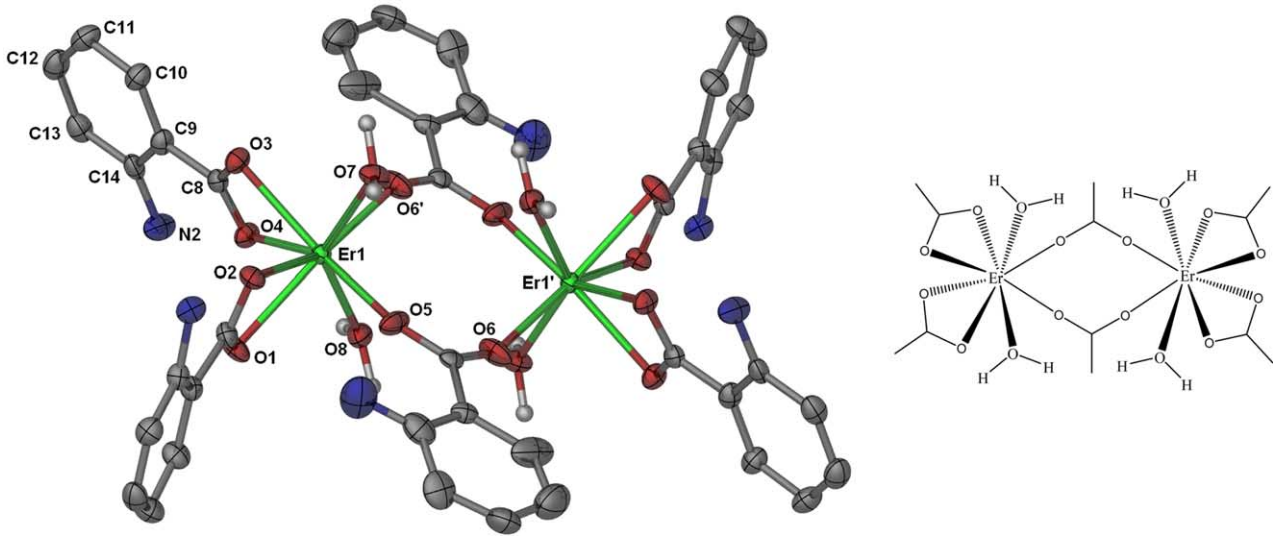

Fig. 4. An ORTEP representation of **3**, displaying the dimeric structure. Lattice water molecules and hydrogen atoms on anthranilate ligands have been omitted for clarity (ellipsoids at 50% probability). Inset – stylised diagram showing the ligand connectivity (aromatic groups omitted for clarity).

coordination number of eight for each Er cation. The coordination geometry around each Er centre most closely resembles a square antiprism [22]. The average carboxylate bite angle for the chelating anthranilate ligands is 118.95°, while for the bridging anthranilate ligands it is 122.82°. The chelating anthranilate ligands adopt a *cisoid* geometry around the Er cation, while the coordinated water molecules are arranged in a *transoid* geometry. The average Er–O distance for chelating anthranilate ligands is 2.381 Å, and for bridging anthranilate ligands is 2.257 Å. The average Er–O (water) distance is 2.357 Å. Two water molecules reside in the lattice. Hydrogen bonding links the lattice water molecule to the carboxylate group of the anthranilate ligand. The coordinated water molecules also participate in hydrogen bonding, and are linked to lattice water molecules and additionally to the amino groups of anthranilate ligands bound to neighbouring Er cations, therefore generating a polymeric supramolecular structure. Hydrogen bond lengths and angles are given in

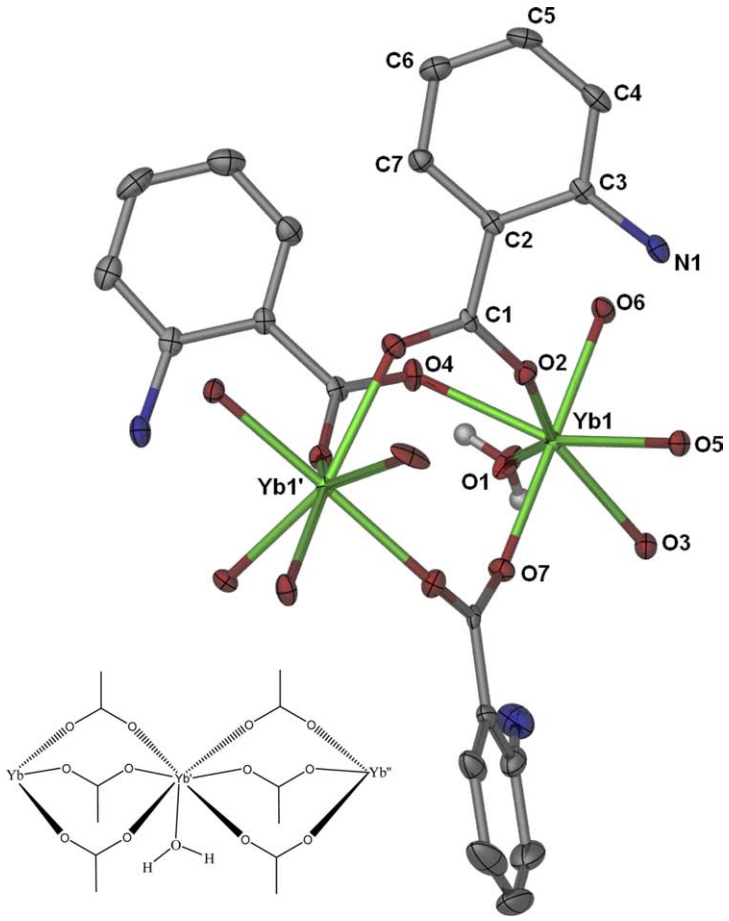

Fig. 5. An ORTEP representation of **4**, illustrating the bridging bidentate anthranilate ligands present in the polymeric structure. Hydrogen atoms on anthranilate ligands have been omitted for clarity (ellipsoids at 50% probability). Inset – stylised diagram displaying the ligand connectivity (aromatic groups omitted for clarity).

Table 3. The structure of complex **3** is similar to that of the related Er salicylate [25].

Complex **4** crystallises in the monoclinic space group *C2/c*. Selected bond lengths are listed in Table 2. The polymeric structure consists of Yb cations linked by six bridging bidentate anthranilate ligands, resulting in the formation of linear polymer chains (Fig. 5). In addition to one O atom from each of six anthranilate ligands, each Yb cation is also bound to one water molecule giving a coordination number of seven. The coordination environment around the Yb cation is best described as a pentagonal bipyramid [22]. The average Yb–O carboxylate distance is 2.263 Å, while the Yb–O (water) distance corresponds closely (2.285 Å). The Yb···Yb distance is 4.714 Å. Hydrogen bonding links the coordinated water molecule to the amino groups of two anthranilate ligands in an adjacent polymer chain. Hydrogen bond lengths and angles are given in Table 3. The complex is isostructural with the reported Y anthranilate [2]. Significant differences in the C–O distances of the carboxylate groups were reported for the Y anthranilate, but in the Yb anthranilate structure the C–O carboxylate distances are comparable. The Y–O (water) distance (2.301 Å) and the Y···Y distance (4.742 Å), are comparable with analogous values for complex **4** allowing for ionic radius differences.

Selected rare earth anthranilate complexes have been tested as potential "green" corrosion inhibitors. The results of these tests indicate that rare earth anthranilates do act as corrosion inhibitors; however they are less effective inhibitors than the closely related rare earth salicylates [15].

4. Conclusions

By employing an alternative synthetic route we have synthesised and crystallised a range of lanthanoid anthranilates, and probed the solid state structures using X-ray crystallography. The results reveal a diverse range of structural classes exhibited by lanthanoid anthranilates. In all cases, the amino group of the anthranilate ligand is not coordinated to the lanthanoid cation. The carboxylate groups of the anthranilate ligand exhibited three different binding modes, chelating, bridging bidentate and bridging tridentate. The variations in structural

class can be related to the lanthanoid contraction, with a decline from nine coordination (La) to seven (Yb). However other factors such as slight variations in reaction conditions including pH may influence the structural class isolated. Further investigation is required to unravel completely the origin of the structural diversity.

Acknowledgements

We are grateful to the ARC Centre for Green Chemistry for support, and to Monash University for a Monash Graduate Scholarship awarded to S.G.L. We also acknowledge Honeywell Specialty Chemicals, Seelze GmbH for a gift of rare earth oxides.

References

[1] C. Kremer, J. Torres, S. Dominguez, A. Mederos, Coord. Chem. Rev. 249 (2005) 567.
[2] S.M. Boudreau, H.M. Haendler, J. Solid State Chem. 36 (1981) 190.
[3] L. Jin, S. Lu, S. Lu, Polyhedron 15 (1996) 4069.
[4] F. Weisbrock, H. Schmidbaur, J. Chem. Soc., Dalton Trans. (2002) 4703.
[5] F. Weisbrock, H. Schmidbaur, Inorg. Chem. 42 (2003) 7283.
[6] R. Murugavel, V.V. Karambelkar, G. Anantharaman, M.G. Walawalkar, Inorg. Chem. 39 (2000) 1381.
[7] F. Weisbrock, A. Schier, H. Schmidbaur, Z. Naturforsch. B: Chem. Sci. 57 (2002) 251.
[8] M. Vithal, T.G. Narendra Babu, B. Narsimha Murthy, Indian J. Chem., Sect. A 28 (1989) 689.
[9] B.A. Lange, H.M. Haendler, J. Solid State Chem. 15 (1975) 325.
[10] S.M. Boudreau, R.A. Boudreau, H.M. Haendler, J. Solid State Chem. 49 (1983) 379.
[11] G. Smith, K.A. Byriel, C.H.L. Kennard, Aust. J. Chem. 52 (1999) 325.
[12] M. Hernandez-Molina, P.A. Lorenzo-Luis, P. Gili, C. Ruiz-Perez, Cryst. Growth Des. 3 (2003) 273.
[13] W. Brzyska, Z. Rzaczynska, Pol. J. Chem. 60 (1986) 27.
[14] W. Brzyska, Z. Rzaczynska, Monatsh. Chem. 119 (1988) 147.
[15] M. Forsyth, K. Wilson, T. Behrsing, C. Forsyth, G.B. Deacon, A. Phanasgoankar, Corrosion 58 (2002) 953.
[16] R.H. Blessing, Acta Cryst. A 51 (1995) 33.
[17] G.M. Sheldrick, SHELXS-97 Program for Crystal Structure Solution, University of Göttingen, Göttingen, Germany, 1997.
[18] G.M. Sheldrick, SHELXL-97 Program for Crystal Structure Refinement, University of Göttingen, Göttingen, Germany, 1997.
[19] L. Barbour, J. Supramol. Chem 1 (2001) 189.
[20] Z. Zheng, Chem. Commun. (2001) 2521.
[21] H.-L. Sun, C.-H. Ye, X.-Y. Wang, J.-R. Li, S. Gao, K.-B. Yu, J. Mol. Struct. 702 (2004) 77.
[22] M. Johnson, J.C. Taylor, G.W. Cox, J. Appl. Crystallogr. 13 (1980) 188.
[23] X. Wang, Y. Xie, J. Sun, Polyhedron 15 (1996) 3569.
[24] A.E. Koziol, B. Klimek, K. Stepniak, Z. Rzaczynska, W. Brzyska, O.I. Bodak, L.G. Aksel'rud, V.V. Pavlyuk, V.A. Tafeenko, Z. Kristallogr. 200 (1992) 25.
[25] J.P. Costes, J.M. Clemente-Juan, F. Dahan, F. Nicodeme, M. Verelst, Angew. Chem. Int., Eng. Ed. 41 (2002) 323.

Available online at www.sciencedirect.com
SCIENCE DIRECT®
Polyhedron 25 (2006) 387–396
POLYHEDRON
www.elsevier.com/locate/poly

Synthesis and structures of ferrocenyl-substituted salicylaldiminato complexes of magnesium, titanium and zirconium

Robyn K.J. Bott, Mark Schormann, David L. Hughes, Simon J. Lancaster *, Manfred Bochmann *

Wolfson Materials and Catalysis Centre, School of Chemical Sciences and Pharmacy, University of East Anglia, Norwich NR4 7TJ, UK

Received 6 July 2005; accepted 6 July 2005
Available online 18 August 2005

Dedicated to Professor Malcolm Chisholm on the occasion of his 60th birthday

Abstract

N-ferrocenyl salicylaldimine (FcPI)H, readily accessible from aminoferrocene and salicylaldehyde, reacts with dibutylmagnesium in THF to afford a red crystalline $(FcPI)_2Mg(THF)_2$ (**2**). The reactions of the Li(FcPI) with $CpTiCl_3$ gave $CpTiCl_2(FcPI) \cdot CH_2Cl_2$ (**4**), whereas with $CpZrCl_3 \cdot DME$ a mixture of three products is formed: $CpZrCl(FcPI)_2$ (**5**), $CpZrCl_2(FcPI)$ (**6**), and $(FcPI)_2ZrCl_2 \cdot CH_2Cl_2$ (**3** $\cdot CH_2Cl_2$). The crystal structures of compounds **2**–**6** are reported. Typically, the N–O chelates are oriented such that O donors are mutually *trans*, while N donors prefer to be *trans* to Cl ligands. The redox potentials of these complexes are very similar to ferrocene. On activation with methylaluminoxane, the Ti complex **4** shows moderate activity for ethylene polymerisation, while $(FcPI)_2ZrCl_2$ is highly active for the oligomerisation of ethylene, to give products with average degrees of polymerisation of 12–16.
© 2005 Elsevier Ltd. All rights reserved.

Keywords: Titanium; Zirconium; Magnesium; Chelate ligands; Ferrocene; Polymerisation catalysis

1. Introduction

Complexes based on ferrocenyl-substituted Schiff-base ligands have been widely explored, mainly based on the facile condensation reactions of amines with acyl- or formylferrocenes [1–3]. Alternatively, ligands derived from amino- and 1,1′-diaminoferrocene [4] can be employed. For example, Arnold et al. [5,6] reported a number of amido and tetradentate salen-type ligands in which the 1,1′ferrocenediyl unit is incorporated into the ligand backbone. A similar family of ligands were reported by Gibson et al. [7,8], including iminopyridines with pendant ferrocenyl substituents. Applied to group 4 complexes suitable for polymerisation catalysis, such ligands offer the possibility, at least in principle, of activating metal alkyl catalyst precursors electrochemically, taking advantage of redox active ferrocenyl substituent in the immediate vicinity of the active metal centre. In the course of a programme investigating the potential of new heteroatom chelates in olefin polymerisation catalysis [9], especially based on N–O ligands of the salicylaldiminato type [10], we became interested in ferrocenyl-substituted derivatives and report here the syntheses and structures of magnesium, titanium and zirconium complexes.

2. Results and discussion

2.1. Syntheses

The ferrocenyl salicylaldimine (FcPI)H (**1**-H) was prepared by reaction of 3-*tert*-butyl salicylaldehyde with

* Corresponding author. Tel.: +44 1603 502044.
E-mail address: m.bochmann@uea.ac.uk (M. Bochmann).

0277-5387/$ - see front matter © 2005 Elsevier Ltd. All rights reserved.
doi:10.1016/j.poly.2005.07.012

aminoferrocene in ethanol over molecular sieves (Eq. (1)). On concentrating the solution, **1**-H was obtained as a pale-red, microcrystalline powder in 65% yield.

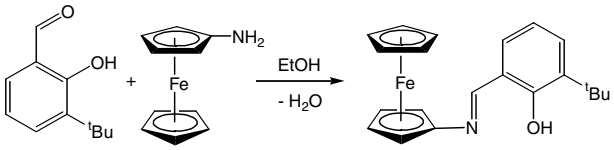

(1)

The reaction of **1**-H with dibutylmagnesium in tetrahydrofuran afforded a red crystalline compound, which was identified as $(FcPI)_2Mg(THF)_2$ (**2**). It had been the intention to use this magnesium reagent in reactions with $TiCl_4$ and $ZrCl_4$; however, no clean products could be isolated from these reactions under a variety of conditions. The treatment of group 4 metal halides with the lithium salt of **1** proved similarly unsatisfactory, whereas mixtures of the sodium salt **1**-Na with $ZrCl_4$ in tetrahydrofuran afforded the bis(*N*-ferrocenylsalicyliminato)-zirconium dichloride **3** (Scheme 1).

By contrast, the reaction of **1**-Li with $CpTiCl_3$ in THF proceeded as expected. Extraction of the crude product with dichloromethane and layering the concentrated dichloromethane solution with light petroleum afforded dark red-brown cubic crystals of $CpTiCl_2(FcPI) \cdot CH_2Cl_2$ (**4**).

In a similar manner, **1**-Li was reacted with $CpZrCl_3 \cdot DME$. However, this reaction led to several products which co-crystallised from dichloromethane solution: red-brown cubic crystals of $CpZrCl_2(FcPI)$ (**5**), clusters of dark red-brown needles of $CpZrCl(FcPI)_2$ (**6**), and dark red-brown cubic crystals of $(FcPI)_2ZrCl_2$

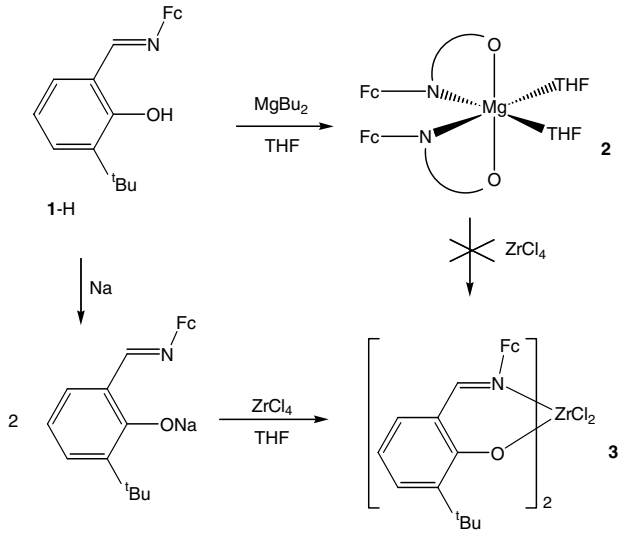

Scheme 1.

$(3 \cdot CH_2Cl_2)$ (Scheme 2). The latter is identical to the product from **1**-Na and $ZrCl_4$ but was obtained in this case as the dichloromethane solvate. The formation of **3** evidently results from Cp ligand exchange. The three products were separated manually and identified by single-crystal X-ray diffraction.

2.2. Structural studies

The magnesium complex **2** has octahedral geometry, with the salicylato-O atoms in *trans* and two THF ligands in *cis*-positions (Fig. 1). Selected bond lengths and angles are collected in Table 1. This contrasts with

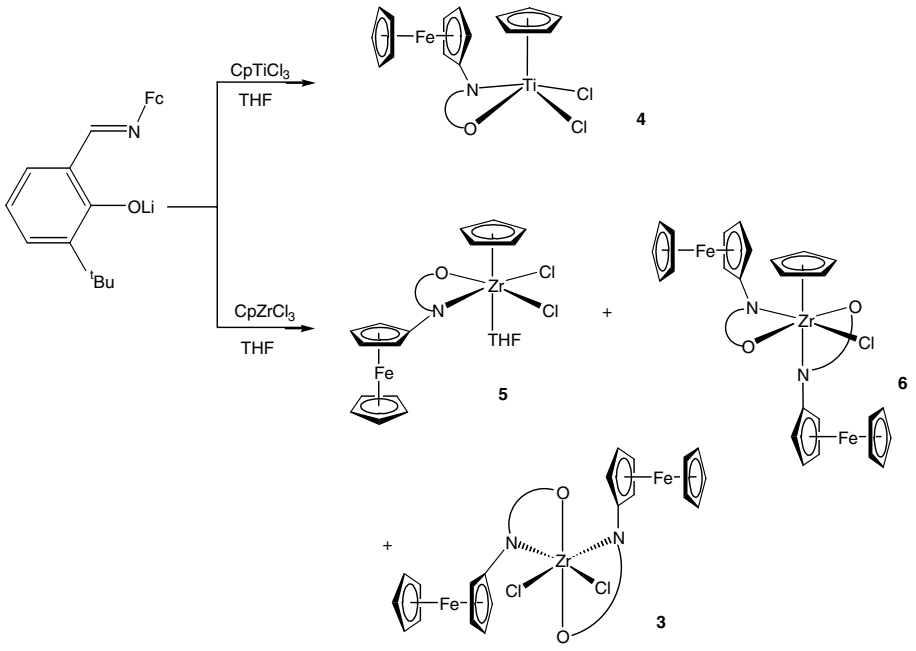

Scheme 2.

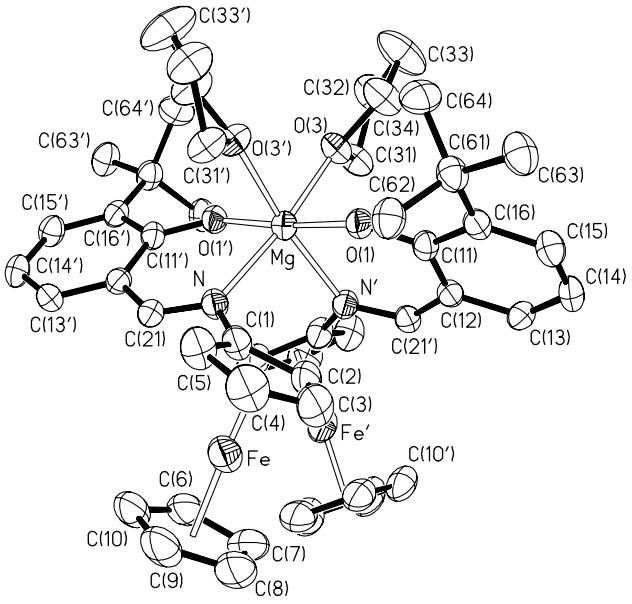

Fig. 1. Molecular structure of $(FcPI)_2Mg(THF)_2$ (**2**), showing the atomic numbering scheme with thermal ellipsoids at 30% probability.

a related complex of a tetradentate ferrocenediyl ligand reported by Arnold et al. [6] (compound **A**) where the salicylic O and N atoms are *cis* to one another in equatorial positions, while the THF ligands are *trans* [∠O(3)–Mg–O(4) = 169.3(2)°]. The bond distances from the THF–O atom to magnesium are similar in both complexes, 2.161(5) and 2.141(4) Å in **A** and 2.136(5) Å in **2**, as are the Mg–O(anionic) distances (1.974(5) and 1.984(5) Å, compared to 1.982(4) Å). The Mg–N bonds in **2** are 2.175(6) Å, significantly shorter than in **A**.

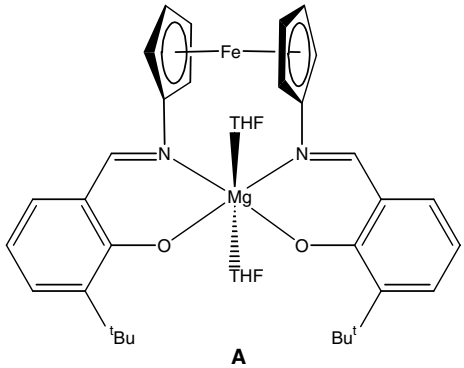

A

The titanium complex $CpTiCl_2(FcPI)$ (**4**), crystallises with one molecule of dichloromethane (Fig. 2). Selected bond lengths (Å) and angles (°) are collected in Table 2. The five-coordinate titanium resides in a distorted square-based pyramidal environment, with the cyclopentadienyl ring at the apex and the chlorides *cis* to each other. The N–O chelating ligand forms a plane which includes the phenoxide ring and the –C=N group. This pattern is similar to that seen in the previously published

Table 1
Selected bond lengths (Å) and angles (°) for $(FcPI)_2Mg(THF)_2$ (**2**)

Mg–O1	1.982(4)
Mg–N	2.174(6)
Fe–Cp1	1.632
Mg–O3	2.136(5)
Fe–Cp2	1.638
O(1)–Mg–O(1′)	175.5(3)
O1–Mg–N′	85.8(2)
O1–Mg–N	97.3(2)
O(1)–Mg–O(3)	90.6(2)
O1′–Mg–N′	97.3(2)
N–Mg–O1′	85.8(2)
O(3)–Mg–O(3′)	87.7(3)
N–Mg–N′	93.3(3)
O(3)–Mg–N	171.64(19)
Cp1–Fe–Cp2	177.9

The prime signifies a symmetry operation about a twofold symmetry axis. Here, and in all the complexes, the centroid of the substituted Cp ring of the Fc group is labelled as Cp1, and that of the outer Cp ring as Cp2.

structure of (trimethylphenyl)phenoxyimine titanium monocyclopentadienyl dichloride [10b]. The Ti–Cl bond length of the chlorine ligand *trans* to N is significantly longer than that *trans* to O. The Ti–Cp (centroid) distance is 2.053 Å, typical for Ti(IV) Cp complexes.

Complex **5** is the zirconium analogue of **4**. However, the larger zirconium also coordinates to one tetrahydrofuran molecule, to give a complex with a distorted octahedral geometry (Fig. 3). Selected bond lengths and angles are given in Table 3. Crystals of **5** were of limited quality ($R_1 = 0.127$). The chlorides are in *cis* positions [Cl(1)–Zr–Cl(2) angle 88.5(2)°] and in the same plane as the ferrocenyl phenoxyimine, with the cyclopentadienyl ring *trans* to the tetrahydrofuran [Cp(centroid)–Zr–O(2) angle 174.2°]. As was the case with the Ti complex **4**, the Zr–Cl(1) bond *trans* to N is slightly longer than Zr–Cl(2), although this difference is less pronounced than in the titanium example.

The mono-chloro complex **6** is also octahedral (Fig. 4), analogous to but slightly more distorted than the previously reported bis(*N*-ethylsalicyliminato) complex $CpZrCl(EtPI)_2$ [10d]. Selected bond lengths and angles are shown in Table 4. One N–O chelate is equatorially bound, while the Cp ring and the N atom of the second N–O ligands occupy axial positions. The oxygen atoms are approximately *trans* to one another [∠O(1)–Zr–O(2) = 156.1(2)°]. Steric pressures force the *cis*-nitrogen donors closer together, viz. ∠N(1)–Zr–N(2) = 74.2(3)°. This is similar to structures previously reported and is the expected structural trend for the favoured geometry of zirconium complexes containing two phenoxy-imine ligands [10,11]. As was the case in $CpZrCl(EtPI)_2$, the plane of one of the phenoxy-imine ligands, C(31)–O(2)–Zr–N(2), in complex **6** is almost parallel to the Cp plane, while the plane of the second phenoxy-imine, C(17)–N(1)–Zr–O(1), is nearly perpen-

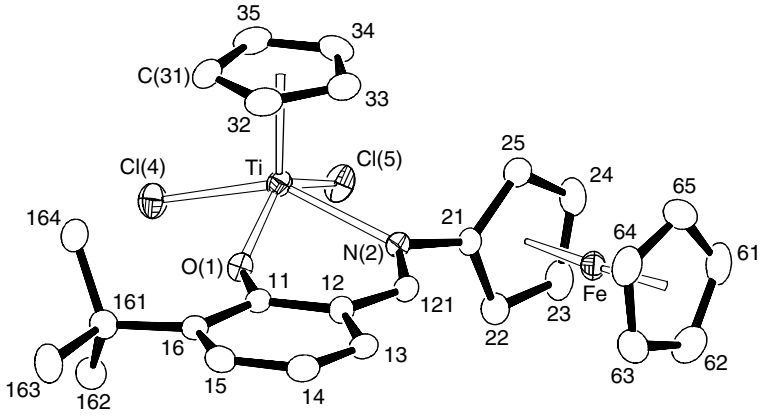

Fig. 2. Molecular structure of $CpTiCl_2(FcPI)$ (**4**), showing the atomic numbering scheme. Ellipsoids are drawn at the 50% probability level.

Table 2
Selected bond lengths (Å) and angles (°) for $(FcPI)TiCpCl_2 \cdot CH_2Cl_2$ (**4** · CH_2Cl_2)

Ti–Cp	2.052
Ti–N(2)	2.267(2)
Ti–O(1)	1.873(2)
Fe–Cp1	1.659
Ti–Cl(4)	2.3837(8)
Ti–Cl(5)	2.3217(7)
Fe–Cp2	1.663
O(1)–Ti–N(2)	78.76(8)
O(1)–Ti–Cl(4)	84.83(6)
O(1)–Ti–Cl(5)	132.95(6)
N(2)–Ti–Cl(4)	145.13(6)
N(2)–Ti–Cl(5)	83.44(5)
Cp1–Fe–Cp2	174.7
Cp–Ti–O(1)	113.9
Cp–Ti–N(2)	105.6
Cp–Ti–Cl(4)	109.2
Cp–Ti–Cl(5)	112.7
Cl(4)–Ti–Cl(5)	85.69(3)

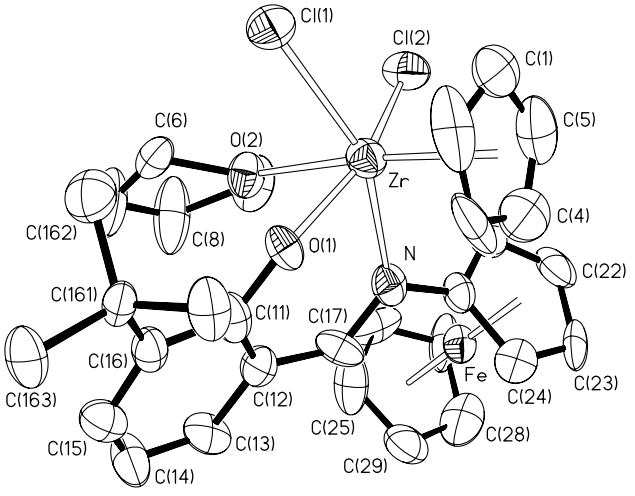

Fig. 3. Molecular structure of $CpZrCl_2(FcPI)(THF)$ (**5**), showing the atomic numbering scheme. Thermal ellipsoids at drawn 50% probability.

Table 3
Selected bond lengths (Å) and angles (°) for $(FcPI)CpZrCl_2 \cdot THF$ (**5**)

Zr–O(1)	2.025(13)
Zr–N	2.382(17)
Zr–Cl(1)	2.496(6)
Zr–Cl(2)	2.486(6)
Zr–Cp	2.262
Zr–O(2)	2.391(13)
Fe–Cp1	1.653
Fe1–Cp2	1.667
O(1)–Zr–N	79.4(6)
O(1)–Zr–Cl(1)	90.4(4)
O(1)–Zr–Cl(2)	154.3(4)
N–Zr–Cl(1)	153.8(4)
N–Zr–Cl(2)	90.5(4)
O(1)–Zr–O(2)	76.9(5)
Cp1–Fe–Cp2	175.6
Cl(1)–Zr–Cl(2)	88.5(2)
Cp–Zr–O(1)	102.6
Cp–Zr–O(2)	174.2
Cp–Zr–Cl(1)	104.3
Cp–Zr–Cl(2)	102.6
Cl(1)–Zr–O(2)	81.5(4)
Cl(2)–Zr–O(2)	77.5(4)

dicular to the Cp plane. The zirconium–chloride bond distances in **6**, 2.509(3) Å, is slightly longer than in **5**. Other geometric parameters resemble previous examples [5–12].

The last product isolated from the reaction of **1**-Li with $CpZrCl_3$ was the bis(ferrocenyl phenoxyimine) zirconium dichloride complex **3**, crystallised as CH_2Cl_2 solvate. The structure is shown in Fig. 5, with selected bond lengths and angles collected in Table 5. The complex possesses distorted octahedral goemetry. The phenoxy-oxygen atoms occupy *trans* positions [∠O(1)–Zr–O(2) 166.5(2)°], similar to Fujita's bis(*N*-phenyl phenoxyimine) zirconium complex, $ZrCl_2(Ph–PI)_2$ [13]. This leaves the nitrogen atoms in *cis* positions [∠N(1)–Zr–N(2) 75.3(2)°] and *trans* to the chlorine ligands. The bond lengths in **3** are very similar to Fujita's complex. The

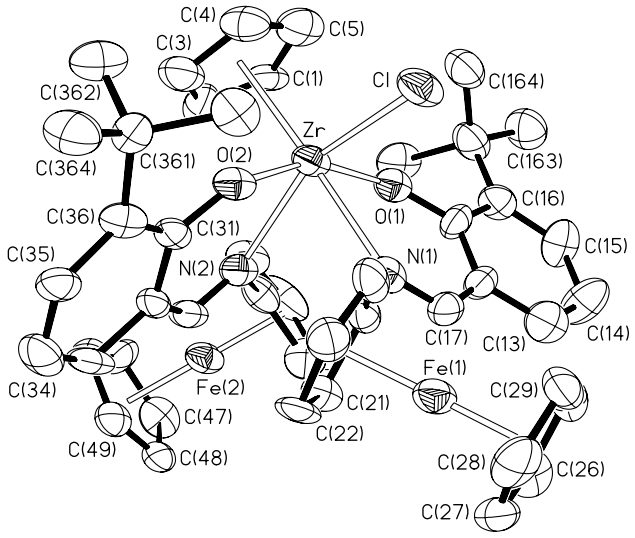

Fig. 4. Molecular structure of CpZrCl(FcPI)$_2$ (**6**) showing the atomic numbering scheme. Thermal ellipsoids at drawn at 50% probability.

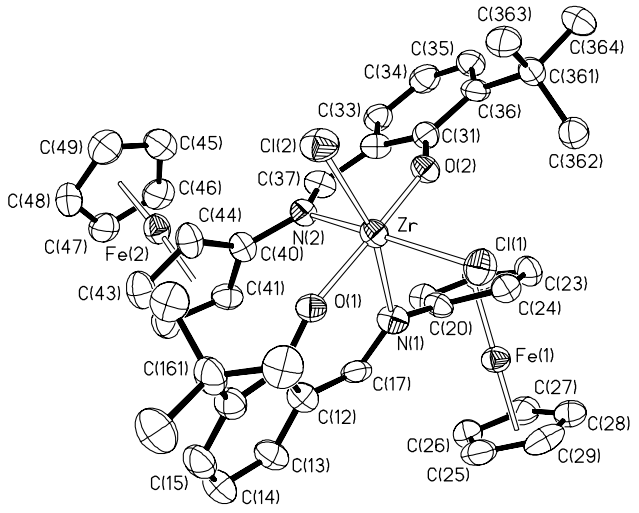

Fig. 5. Molecular structure of $ZrCl_2(FcPI)_2 \cdot CH_2Cl_2$ (**3** $\cdot CH_2Cl_2$), showing the atomic numbering scheme. Thermal ellipsoids are drawn at 50% probability.

Table 4
Selected bond lengths (Å) and angles (°) for $(FcPI)_2ZrCpCl$ (**6**)

Zr–N(1)	2.434(8)
Zr–O(1)	2.064(7)
Zr–N(2)	2.375(9)
Zr–O(2)	2.030(7)
Zr–Cl	2.509(3)
Zr–Cp	2.289
Fe(1)–Cp11	1.647
Fe(1)–Cp12	1.663
Fe(2)–Cp21	1.665
Fe(2)–Cp22	1.660
O(1)–Zr–N(1)	75.6(3)
N(2)–Zr–N(1)	74.2(3)
O(2)–Zr–N(1)	82.2(3)
N(1)–Zr–Cl	80.6(2)
Cp–Zr–N(1)	177.6
O(1)–Zr–N(2)	87.8(3)
O(2)–Zr–O(1)	156.1(2)
O(1)–Zr–Cl	92.1(2)
Cp–Zr–O(1)	103.8
O(2)–Zr–N(2)	77.7(3)
N(2)–Zr–Cl	154.0(2)
Cp–Zr–N(2)	103.5
O(2)–Zr–Cl	92.96(19)
Cp–Zr–O(2)	98.0
Cp–Zr–Cl	101.8
Cp11–Fe(1)–Cp12	177.6
Cp21–Fe(2)–Cp22	177.4

Table 5
Selected bond lengths (Å) and angles (°) for $(FcPI)_2ZrCl_2 \cdot CH_2Cl_2$ (**3** $\cdot CH_2Cl_2$)

Zr–N(1)	2.341(5)
Zr–O(1)	1.988(4)
Zr–Cl(1)	2.4394(14)
Zr–N(2)	2.367(4)
Zr–O(2)	1.984(4)
Zr–Cl(2)	2.4202(16)
Fe(1)–Cp11	1.654
Fe(1)–Cp12	1.661
Fe(2)–Cp21	1.656
Fe(2)–Cp22	1.651
O(1)–Zr–N(1)	76.65(16)
N(1)–Zr–N(2)	75.29(16)
O(2)–Zr–N(1)	93.66(16)
N(1)–Zr–Cl(1)	90.52(13)
N(1)–Zr–Cl(2)	164.63(13)
O(1)–Zr–N(2)	91.75(17)
O(2)–Zr–O(1)	166.51(18)
O(1)–Zr–Cl(1)	96.59(12)
O(1)–Zr–Cl(2)	92.63(12)
N(2)–Zr–Cl(1)	161.45(11)
O(2)–Zr–Cl(1)	92.82(12)
Cl(2)–Zr–Cl(1)	101.77(6)
O(2)–Zr–N(2)	76.55(17)
N(2)–Zr–Cl(2)	94.35(11)
O(2)–Zr–Cl(2)	94.91(12)
Cp11–Fe(1)–Cp12	177.0
Cp21–Fe(2)–Cp22	177.6

Zr–Cl distances in **3**, 2.4394(14) and 2.420(2) Å, are significantly shorter than those found in **6** [2.509(3) Å].

2.3. Electrochemistry

Cyclic voltammetry (CV) of the ligand **1** and zirconium complex **3** show that in each case quasi-reversible (electron transfer is slow relative to scan rate) one-electron transfers for the Fe^{II}–Fe^{III} redox couple of the ferrocenyl species are observed (Table 6). The dominant species recorded in the CV for **1** has a ΔE_p of 77 mV (Fig. 6), a good correspondence to that for a reversible reaction where $n = 1$ (for a fully reversible "Nernstian"

Table 6
Cyclic voltammetry of **1** and **3**

Compound	E_p^c (mV)	E_p^a (mV)	$E_{1/2}$ (mV)	ΔE_p
Ferrocene (Fc)	446	560	503	104
(FcPI)H (**1**)	505	582	543	77
$(FcPI)_2ZrCl_2$ (**3**)	455	568	511	113

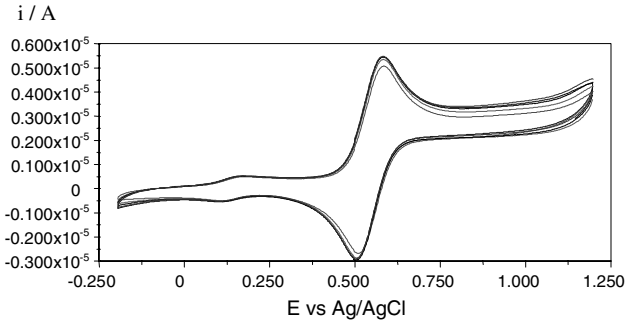

Fig. 6. Cyclic voltammogram of **1** in dry dichloromethane with 0.1 M in $[^nBu_4N]^+[PF_6]^-$ as supporting electrolyte.

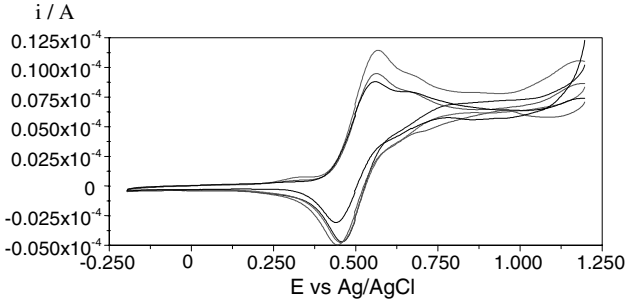

Fig. 7. Cyclic voltammogram of **3** (CH_2Cl_2, 0.1 M $[^nBu_4N]^+[PF_6]^-$).

type redox couple, $\Delta E_p = 60$ mV for $n = 1$). For **3**, the major species couple has $\Delta E_p = 113$ mV (Fig. 7); although a lot larger than 60 mV, it is in line with the ΔE_p of ferrocene (104 mV, $n = 1$). The difference is probably due to different electron transfer kinetics. The CV for **1** also shows a minor signal, $E_{1/2} = 134$–503 mV $= -369$ mV, similar to one reported by Gibson et al. [8]. These authors assigned this signal to an irreversible electrochemical reduction of C=N to an amine group, although in the case of **1** this process appears to be reversible. $\Delta E_p = 44$ mV for this signal ($E_{1/2} = 116$ mV) suggests $n = 2$, or the compound is adsorbed onto the electrode ($\Delta E_p = 0$ mV).

On coordination of the ligand to the zirconium metal centre, the Fe^{II}/Fe^{III} oxidation shifts to a lower potential, which is unexpected [8]. The two ferrocene moieties show independent behaviour, resulting in identical potentials. A shoulder appearing on the flank of the major signal for **3**, $E_{1/2} = 644$ mV, may be due to a redox active oxidation product or an impurity. In a similar cyclic voltammetry study over a wider potential range, this shoulder became more prominent after irreversible electrochemical oxidation took place, while the peaks of the major species assigned to **3** were unchanged by this process.

2.4. Polymerisation studies

The ethylene polymerisation of two representative examples of ferrocenyl-substituted phenoxyimine complexes, **3** and **4**, was investigated using MAO as the activator.

Complex **4**/MAO (Al:Ti = 4000) readily polymerises ethene (1 bar) at room temperature with a productivity of 1×10^4 g PE $(mol^{-1}$ Ti$) \cdot h^{-1} \cdot bar^{-1}$ (Table 7) (PE = polyethylene). This activity is quite similar to that exhibited by the mesityl-substituted analogue, $CpTiCl_2$(MesPI) (1.3×10^4 g PE $(mol^{-1}$ Ti$) \cdot h^{-1} \cdot bar^{-1}$) [10b].

By contrast, the bis(ferrocene phenoxyimine)zirconium dichloride, **3**, when activated with MAO, shows very high activity at 23 °C, 2×10^6 g PE $(mol^{-1}$ Zr$) \cdot h^{-1} \cdot bar^{-1}$, which increased further on cooling to 0 °C and on reducing the catalyst concentration. This activity is less than that reported by Fujita for $(PhPI)_2ZrCl_2$/MAO, although those results were obtained with a substantially higher Al/Zr ratio of 62 500:1. The catalyst based on **3** is thermally unstable, however, and conducting the polymerisation at 60 °C afforded only traces of polymer; again this is in line with the known behaviour of phenoxyimine catalysts which are prone to deactivation by C=N double bond reduction [10d,13–15]. Interestingly, complex **3** differs from the titanium complex **4** as well as comparable alkyl and aryl-substituted zirconium catalysts in producing ethene oligomers with excellent productivities, with average degrees of polymerisation of 12–16.

Table 7
Ethylene polymerisation data

Complex (μmol)	T (°C)	Time (min)	MAO (mmol)	Toluene (mL)	Activity (g mol^{-1} h^{-1} bar^{-1})	M_w	M_w/M_n	Ref.
4 (5)	23	15	2	50	1.6×10^4	350 000	13	this work
4 (5)	60	15	2	50	2.1×10^4	164 000	9.3	this work
$CpTiCl_2$(MesPI) (40)	25	15	8	50	1.3×10^4	328 000	1.5	[10b]
3 (10)	0	5	10	50	0.4×10^7	640	1.7	this work
3 (10)	23	5	10	50	0.2×10^7	600	1.7	this work
3 (1)	23	1	10	50	2.6×10^7	750	1.7	this work
2 I (0.02)	25	5	1.25	250	5.5×10^8	90 000 (M_v)	2.06	[13]

3. Experimental

Unless otherwise stated, syntheses were performed with exclusion of oxygen and moisture under nitrogen using standard Schlenk techniques in flame-dried glassware. Solvents were distilled over sodium benzophenone (diethyl ether, tetrahydrofuran), sodium (toluene), sodium–potassium alloy (petroleum ether, bp 40–60 °C), or CaH_2 (dichloromethane). NMR solvents were dried over activated 4 Å molecular sieves and degassed by several freeze–thaw cycles. NMR spectra were recorded using a Bruker DPX300 spectrometer. Chemical shifts are reported in ppm and referenced to residual solvent resonances (^{1}H, ^{13}C), ^{19}F is relative to $CFCl_3$. Nitrogen, argon and ethene (BOC, 99.5%) were purified by passing through columns of supported P_2O_5 with moisture indicator, and activated 4 Å molecular sieves. Aminoferrocene was prepared according to the literature procedures [16].

3.1. Preparation of 2-tert-butyl-6-(N-ferrocenylaldimino)phenol, (FcPI)H (1-H)

3-*tert*-Butylsalicylaldehyde (2.1 g, 12 mmol) was added dropwise to a stirred mixture of aminoferrocene (2.3 g, 11.4 mmol) with molecular sieves 4 Å (2 g) in ethanol (50 mL), at room temperature. The mixture was stirred for 18 h, filtered and the molecular sieves washed with diethyl ether (20 mL). Crystallisation from the concentrated solution gave **1**-H as a red microcrystalline powder (2.7 g, 7.5 mmol, 65%). ^{1}H NMR (300 MHz, 298 K, $CDCl_3$): δ 8.61 (s, 1H, C*H*=N), 7.34 (d, 1H, $J = 7.8$ Hz, ar-*H*), 7.14 (d, 1H, $J = 7.8$ Hz, ar-*H*), 6.82 (t, 1H, $J = 7.8$ Hz, ar-*H*), 4.57 (m, 2H, C_5H_4N), 4.25 (m, 2H, C_5H_4N), 4.17 (s, 5H, C_5H_5), 1.45 (s, 9H, ^{t}Bu). ^{13}C NMR (75.5 MHz, 298 K, $CDCl_3$): δ 161.1 (*C*H=N), 137.5 (ar-*C*), 129.5 (ar-*C*H), 129.3 (ar-*C*H), 119.5 (ar-*C*), 118.2 (ar-*C*H), 102.4 (ar-*C*), 69.8 (C_5H_5), 67.4 (C_5H_4N), 62.4 (C_5H_4N), 34.9 ($C(CH_3)_3$), 29.4 ($C(CH_3)_3$). *Anal.* Calc. for $C_{21}H_{23}NOFe$: C, 69.82; H, 6.42; N, 3.88. Found: C, 69.72; H, 6.56; N, 3.85%.

3.2. Preparation of (FcPI)$_2$Mg(THF)$_2$ (2)

Dibutylmagnesium (1.0 M in hexanes, 1 mL, 1 mmol) was added dropwise to a stirred solution of **1**-H (0.72 g, 2 mmol) in THF at −78 °C. The mixture was allowed to reach room temperature and stirred for 15 h. The solution was then concentrated, carefully layered with light petroleum and cooled to 5 °C to afford the title compound as red crystals in 51% yield (0.45 g, 0.5 mmol). ^{1}H NMR (C_6D_6): δ 8.63 (s, 1H, C*H*=N), 7.54 (dd, 1H, $J = 7.4$, 1.7 Hz, ar-*H*), 7.09 (dd, 1H, $J = 7.8$, 1.5 Hz, ar-*H*), 6.70 (t, 1H, $J = 7.6$ Hz, ar-*H*), 4.30 (m, 2H, N–Cp), 3.89 (s, 5H, Cp), 3.73 (m, 2H, N–Cp), 3.56 (m, 8H, THF), 1.70 (s, 9H, ^{t}Bu), 1.40 (m, 8H, THF). ^{13}C NMR (C_6D_6) δ 169.8 (*C*=N), 142.1 (ar-C), 134.6 (ar-C), 132.5 (ar-C), 122.0 (ar-C), 114.5 (ar-C), 105.8 (ar-C), 70.0 (Cp), 67.8 (N–Cp), 66.9 (THF), 62.9 (N–Cp), 35.6 (N–Cp), 35.6 ($C(CH_3)_3$), 29.9 ($C(CH_3)_3$), 25.7 (THF). *Anal.* Calc. for $C_{42}H_{44}N_2O_2Fe_2Mg.OC_4H_8$: C, 61.98; H, 6.24; N, 2.89. Found: C, 61.62; H, 7.29; N, 2.90%.

3.3. Preparation of (FcPI)$_2$ZrCl$_2$ (3)

Sodium hydride (0.07 g, 3.0 mmol) was added to a solution of **1**-H (1.00 g, 2.8 mmol) in tetrahydrofuran (50 mL). The dark red solution was stirred for 3 h at room temperature, cooled to −78 °C. Zirconium tetrachloride was added (0.32 g, 1.4 mmol), the mixture was allowed to reach room temperature and stirred for 18 h. The volatiles were removed in vacuo, and the resulting dark red solid was extracted with dichloromethane (50 mL), concentrated and layered with light petroleum. The title compound was obtained as dark red micro-crystals (0.51 g, 0.6 mmol, 42%) at −20 °C. This sample recovered did not contain dichloromethane of crystallisation. ^{1}H NMR (CCl_2D_2): δ 9.10 (s, 1H, CH=N), 7.50 (d, 1H, $J = 6.2$ Hz, ar-H), 7.19 (d, 1H, $J = 6.3$ Hz, ar-H), 6.87 (d, 1H, $J = 7.1$ Hz, ar-H), 4.49 (br, 1H, Cp–H), 4.17 (br, 5H, Cp–H), 3.84 (br, 1H, Cp–H), 3.68 (br, 1H, Cp–H), 1.46 (s, 9H, ^{t}Bu). ^{13}C NMR (CCl_2D_2): δ 172.9 (CH=N), 159.7 (ar-C), 134.4 (ar-C), 133.3 (ar-C), 123.9 (ar-C), 120.0 (ar-C), 69.7 (FcCH, C_5H_5), 66.9 (FcCH, C_5H_4), 64.9 (FcCH, C_5H_4), 35.2 ($C(CH_3)_3$), 29.9 ($C(CH_3)_3$). *Anal.* Calc. for $C_{42}H_{44}N_2O_2Cl_2Fe_2Zr$: C, 57.15;H, 5.02; N, 3.17; Cl, 8.03. Found: C, 56.82; H,5.28; N, 3.05; Cl, 9.42.

3.4. Preparation of CpTiCl$_2$(FcPI) · CH$_2$Cl$_2$ (4)

The lithium salt **1**-Li, prepared from **1**-H (0.5 g, 1.38 mmol) and ^{n}BuLi (0.9 mL, 1.6 M in hexanes, 1.38 mmol), was treated with $CpTiCl_3$ (0.30 g, 1.38 mmol) in THF (50 mL), stirred at −78 °C for 20 min, allowed to reach room temperature and stirred overnight. The volatiles were removed under vacuum and the product extracted with CH_2Cl_2 (20 mL). The solution was concentrated, layered with light petroleum and cooled to −20 °C to give **4** as dark red/brown, cubic crystals (0.28 g, 0.4 mmol, 32%). ^{1}H NMR (C_6D_6): δ 9.54 (s, 1H, C*H*=N), 8.35 (d, 1H, $J = 7.4$ Hz, ar-*H*), 7.43 (d, 1H, $J = 7.5$ Hz, ar-*H*), 6.80 (t, 1H, $J = 7.6$ Hz, ar-*H*), 6.31 (s, 5H, Cp), 4.28 (m, 4H, NC_5H_4), 3.95 (m, 5H, Cp), 1.56 (s, 9H, ^{t}Bu). ^{13}C NMR (C_6D_6) δ 129.8 (ar-*C*), 128.3 (ar-*C*), 124.3 (ar-*C*), 124.0 (ar-*C*), 122.1 (ar-*C*), 121.9 (Cp), 70.1 (FeC_5H_4), 69.9 (FeC_5H_4), 53.3 (FeC_5H_5), 35.2 ($C(CH_3)_3$), 29.7 ($C(CH_3)_3$). *Anal.* Calc. for $C_{26}H_{27}NOCl_2TiFe \cdot CH_2Cl_2$: C, 51.55; H, 4.65; N, 2.23; Cl, 22.54. Found: C, 51.70; H, 4.63; N, 2.07; Cl, 21.78%.

Table 8
Crystal data and collection parameters for complexes **2**–**6**

	$(FcPI)_2Mg(THF)_2$ (**2**)	$CpTiCl_2(FcPI) \cdot CH_2Cl_2$ (**4** · CH_2Cl_2)	$CpZrCl_2(FcPI)(THF)$ (**5**)	$CpZrCl(FcPI)_2$ (**6**)	$(FcPI)_2ZrCl_2 \cdot CH_2Cl_2$ (**3** · CH_2Cl_2)
Empirical formula	$C_{50}H_{60}Fe_2MgN_2O_4$	$C_{26}H_{27}Cl_2FeNOTi \cdot CH_2Cl_2$	$C_{30}H_{35}Cl_2FeNO_2Zr$	$C_{47}H_{49}ClFe_2N_2O_2Zr$	$C_{42}H_{44}Cl_2Fe_2N_2O_2Zr \cdot CH_2Cl_2$
Formula weight	889.01	629.1	659.56	912.25	967.54
Crystal size (mm)	$0.30 \times 0.25 \times 0.10$	$0.65 \times 0.20 \times 0.10$	$0.25 \times 0.05 \times 0.05$	$0.40 \times 0.15 \times 0.02$	$0.35 \times 0.30 \times 0.15$
Crystal system	hexagonal	orthorhombic	monoclinic	monoclinic	orthorhombic
Space group	$P\bar{3}c1$ (No. 165)	$P2_12_12_1$ (No. 19)	$P2_1/c$ (No. 14)	$C2/c$ (No. 15)	$Pna2_1$ (No. 33)
T (K)	140(1)	140(1)	140(1)	140(1)	140(1)
a (Å)	19.043(3)	7.797(1)	17.236(3)	32.212(6)	16.547(3)
b (Å)	19.043(3)	13.525(1)	9.527(2)	17.876(4)	16.543(3)
c (Å)	22.970(5)	25.894(1)	18.743(4)	17.339(4)	15.227(3)
α (°)	90	90	90	90	90
β (°)	90	90	113.04(3)	116.76(3)	90
γ (°)	120	90	90	90	90
V (Å^3)	7214(2)	2730.6(4)	2832.2(10)	8915(3)	4168.2(14)
Z	6	4	4	8	4
μ (mm^{-1})	0.659	1.237	1.097	0.969	1.227
$F(000)$	2820	1288	1352	3760	1976
Reflections collected	5848	13422	6888	11033	7216
Independent reflections (R_{int})	3141 (0.040)	4556 (0.036)	3673 (0.097)	5822 (0.110)	7216
Number of 'unobserved' reflections	1863	4430	2123	2666	5711
Final R indices	$R_1 = 0.084$, $wR_2 = 0.258$	$R_1 = 0.028$, $wR_2 = 0.070$	$R_1 = 0.127$, $wR_2 = 0.346$	$R_1 = 0.060$, $wR_2 = 0.164$	$R_1 = 0.045$, $wR_2 = 0.112$
R indices (all data)	$R_1 = 0.123$, $wR_2 = 0.279$	$R_1 = 0.029$, $wR_2 = 0.071$	$R_1 = 0.176$, $wR_2 = 0.369$	$R_1 = 0.138$, $wR_2 = 0.187$	$R_1 = 0.060$, $wR_2 = 0.119$
Goodness-of-fit	1.045	1.075	1.115	0.895	0.991

3.5. Isolation of $(FcPI)_2ZrCl_2 \cdot CH_2Cl_2$ (3), $CpZrCl_2(FcPI)$ (5) and $CpZrCl(FcPI)_2$ (6)

Following the procedure given for **4**, to a solution of **1**-Li (1.38 mmol) in THF (50 mL) was added $CpZrCl_3 \cdot DME$ (0.49 g, 1.38 mmol). The volatiles were removed and the products extracted with CH_2Cl_2. The solution was concentrated and layered with light petroleum. Dark red-brown cubic crystals of $(FcPI)_2ZrCl_2 \cdot CH_2Cl_2$ (**3** · CH_2Cl_2) dark red-brown needle clusters of $CpZrCl(FcPI)_2$ (**6**) and red-brown cubic crystals of $CpZrCl_2(FcPI)(THF)$ (**5**), which were isolated from the same Schlenk flask and picked out manually. The compounds were identified by X-ray crystallography. Unlike the preparation of **3** from **1**-Na, this crystallisation produced the dichloromethane solvate, **3** · CH_2Cl_2. No further characterisation has been undertaken.

3.6. Ethylene polymerisations

Ethylene polymerisation was carried out under 1 bar ethene in toluene. Toluene (total volume 50 mL including MAO) and co-catalyst (MAO) were introduced into the ethylene-purged reactor and stirred. After ethylene saturation and temperature equilibration, polymerisation was initiated by addition of a toluene solution of pre-catalyst into the reactor under vigorous stirring (1000 rpm). After the required amount of time, methanol (5 mL) was added to terminate the polymerisation, and the ethene gas flow halted. The polymer was precipitated, washed with a mixture of methanol (~300 mL) and 15% HCl (~5 mL), filtered, washed with methanol and dried in an oven at 80 °C to constant mass.

3.7. Electrochemistry

Electrochemical data were obtained at 298 K using a glassy-carbon working electrode, a platinum-wire auxiliary electrode and a silver wire (coated with AgCl by anodising in KCl solution) pseudo-reference electrode. Voltammetry was run at 20 mV s^{-1} on ca. 10^{-4}–10^{-3} M solutions in deoxygenated, dry dichloromethane with 0.1 M in $[^nBu_4N]PF_6$ as supporting electrolyte. The error in the reported potentials is estimated from comparison of successive scans to be ca. ±10 mV [17].

3.8. X-ray crystallography

Crystals coated with dry nujol or perfluoropolyether were mounted on a glass fibre and fixed in the cold nitrogen steam ($T = 140(1)$ K). Intensity data were collected on a Rigaku R-Axis IIc image plate diffractometer equipped with a rotating anode X-ray source (Mo Kα radiation) and graphite monochromator (Mo Kα, $\lambda = 0.71073$ Å). Data were processed using the DENZO/SCALEPACK programs [18] and absorption corrections applied in SORTAV [19]. The structures were determined by direct methods in the SHELXS programs and refined by full-matrix least-squares methods, on F^2 values, in SHELXL [20]. Crystal and refinement data are given in Table 8. Hydrogen atoms were included in idealized positions, and their U_{iso} values set to ride on the U_{eq} values of the parent carbon atoms. Scattering factors for neutral atoms were taken from the literature [21]. Computer programs were run on a DEC-AlphaStation 200 4/100 in the Biological Chemistry Department, John Innes Centre.

4. Supplementary material

Full tables of bond lengths and angles, tables of non-hydrogen and hydrogen atomic coordinates and anisotropic thermal parameters for non-hydrogen atoms are available from the Cambridge Crystallographic Data Centre, quoting CCDC deposition numbers 269489 (compound **2**), 269490 (**4**), 269491 (**3**), 269492 (**6**) and 269493 (**5**). Copies of the information may be obtained free of charge from The Director, CCDC, 12 Union Road, Cambridge CB2 1EZ, UK (fax: +44 1223 336 033; e-mail: deposit@ccdc.cam.ac.uk or www: http://www.ccdc.cam.ac.uk).

Acknowledgements

This work was supported by the Engineering and Physical Sciences Research Council and the European Commission (Contract HPRN-CT-2000-00004). We thank Dr. J.N. Butt (UEA) for assistance with electrochemical measurements.

References

[1] A. Togni, T. Hayashi (Eds.), Ferrocenes: Homogeneous Catalysis – Organic Synthesis – Materials Science, VCH, Weinheim, 1995.
[2] A. Togni, R. Halterman (Eds.), Metallocenes, Wiley–VCH, Weinheim, 1998.
[3] E. Bullita, U. Casellato, F. Ossola, P. Tomasin, P.A. Vigato, U. Russo, Inorg. Chim. Acta 287 (1999) 117, and references cited therein.
[4] A. Shafir, M.P. Power, G.D. Whitener, J. Arnold, Organometallics 19 (2000) 3978.
[5] A. Shafir, J. Arnold, Organometallics 22 (2003) 567.
[6] A. Shafir, D. Fiedler, J. Arnold, J. Chem. Soc., Dalton Trans. (2002) 555.
[7] V.C. Gibson, N.J. Long, E.I. Marshall, P.J. Oxford, A.J.P. White, D.J. Williams, J. Chem. Soc., Dalton Trans. (2001) 1162.
[8] V.C. Gibson, C.M. Halliwell, N.J. Long, P.J. Oxford, A.M. Smith, A.J.P. White, D.J. Williams, Dalton Trans. (2003) 918.
[9] (a) N.A.H. Male, M. Thornton-Pett, M. Bochmann, J. Chem. Soc., Dalton Trans. (1997) 2487;
(b) M.J. Sarsfield, M. Thornton-Pett, M. Bochmann, J. Chem. Soc., Dalton Trans. (1999) 3329;

(c) S. Al-Benna, M.J. Sarsfield, M. Thornton-Pett, D.L. Ormsby, P.J. Maddox, P. Brès, M. Bochmann, J. Chem. Soc., Dalton Trans. (2000) 4247;
(d) D.M. Dawson, D.A. Walker, M. Thornton-Pett, M. Bochmann, J. Chem. Soc., Dalton Trans. (2000) 459;
(e) M.D. Hannant, M. Schormann, M. Bochmann, J. Chem. Soc., Dalton Trans. (2002) 4071;
(f) M. Said, D.L. Hughes, M. Bochmann, Dalton Trans. (2004) 359;
(g) M.D. Hannant, M. Schormann, D.L. Hughes, M. Bochmann, Inorg. Chim. Acta 358 (2005) 1683.

[10] (a) A. Lara-Sanchez, A. Rodriguez, D.L. Hughes, M. Schormann, M. Bochmann, J. Organomet. Chem. 663 (2002) 63;
(b) R.K.J. Bott, D.L. Hughes, M. Schormann, M. Bochmann, S.J. Lancaster, J. Organomet. Chem. 665 (2003) 135;
(c) D.A. Pennington, D.L. Hughes, M. Bochmann, S.J. Lancaster, Dalton Trans. (2003) 3480;
(d) M. Sanz, T. Cuenca, Mikhail Galakhov, A. Grassi, R.K.J. Bott, D.L. Hughes, S.J. Lancaster, M. Bochmann, Organometallics 23 (2004) 5324.

[11] M. Mitani, J. Mohri, Y. Yoshida, J. Saito, S. Ishii, K. Tsuru, S. Matsui, R. Furuyama, T. Nakano, H. Tanaka, S. Kojoh, T. Matsugi, N. Kashiwa, T. Fujita, J. Am. Chem. Soc. 124 (2002) 3327.

[12] E.V. Salo, Z. Guan, Organometallics 22 (2003) 5033.

[13] S. Matsui, M. Mitani, J. Saito, H. Makio, N. Matsukawa, Y. Takagi, K. Tsuru, M. Nitabaru, T. Nakano, H. Tanaka, N. Kashiwa, T. Fujita, J. Am. Chem. Soc. 123 (2001) 6847.

[14] J. Saito, M. Mitani, S. Matsui, Y. Tohi, H. Makio, T. Nakano, H. Tanaka, N. Kashiwa, T. Fujita, Macromol. Chem. Phys. 203 (2002) 59.

[15] P.D. Knight, A.J. Clarke, B.S. Kimberley, R.A. Jackson, P. Scott, Chem. Commun. (2002) 352.

[16] (a) N. Montserrat, A.W. Parkins, J. Chem. Res. (S) (1995) 336;
(b) S. Bradley, P.C. McGowan, K.A. Oughton, M. Thornton-Pett, M.E. Walsh, Chem. Commun. (1999) 77;
(c) A. Shafir, M.P. Power, G.D. Whitener, J. Arnold, Organometallics 19 (2000) 3978;
(d) D. van Leusen, B. Hessen, Organometallics 20 (2001) 224.

[17] T.J. Brunker, C. Arisandy, A.R. Cowley, L.H. Rees, S. Barlow, D. O'Hare, J. Organomet. Chem. 689 (2004) 252.

[18] Z. Otwinowski, W. Minor, Methods Enzymol. 276 (1997) 307.

[19] R.H. Blessing, J. Appl. Crystallogr. 30 (1997) 421.

[20] G.M. Sheldrick, SHELX-97: Programs for Crystal Structure Determination (SHELXS) and Refinement (SHELXS), University of Göttingen, Göttingen, Germany, 1997.

[21] International Tables for X-ray Crystallography, Kluwer Academic Publishers, Dordrecht, The Netherlands, vol. C, 1992, pp. 193, 219, 500.

Available online at www.sciencedirect.com
SCIENCE DIRECT®
Polyhedron 25 (2006) 397–405
POLYHEDRON
www.elsevier.com/locate/poly

Studies on 1,2-phenylenedioxoborylcyclopentadienes and some of their metal (Ti, Zr, Fe) complexes

Michael J. Davies, Michael F. Lappert *

Department of Chemistry, University of Sussex, Falmer, Brighton BN1 9QJ, UK

Received 4 May 2005; accepted 29 June 2005
Available online 18 August 2005

Dedicated to Professor M.H. Chisholm, F.R.S., as a mark of friendship and esteem.

Abstract

Various properties of 1,2-phenylenedioxoborylcyclopentadienes $C_5H_4BO_2C_6H_4$-1,2 (≡C_5H_5BCAT), its 4-^{t}Bu (≡$C_5H_5BCAT^t$) and 3,5-^{t}Bu$_2$ (≡$C_5H_5BCAT^{tt}$) analogues are reported. Under ambient conditions [Zr(η^5-$C_5H_4BCAT)_2Cl_2$] (**3a**) in PhMe was unreactive towards ethene, but in the presence of a large excess of methylaluminoxane (MAO) it catalysed the conversion of propene into a low average molecular weight atactic polypropylene. Whereas various Ti(IV) complexes [Ti(η^5-$C_5H_4BX)Cl_3$] [BX = BCAT (**2a**), BCAT^t (**2b**), BCAT^{tt} (**2c**)] did not react under these conditions with C_2H_4, a number of corresponding Zr and Hf analogues, as well as the related metallocene dichlorides, afforded polyethylene of moderate polydispersity and average molecular weight, but were less active than [$ZrCp_2Cl_2$]. From ^{11}B NMR spectral data, it is concluded that the product of treating **3a** with MAO is possibly [Zr(η^5-$C_5H_4BMe_2)_2Cl_2$]. ^{11}B NMR chemical shifts on the three series of compounds Cl-BX (**10a**–**10c**), $Me_3SiC_5H_4$–BX (**1a**–**1c**) and **2a**–**2c** fall within the narrow range 27.2 (**2a**) to 29.5 (**1a**) with **10a** at 29.0. Cyclic voltammetry on a number of the metal complexes, including **2a**–**2c**, [Zr(η^5-$C_5H_4BCAT^t)_2Cl_2$] (**3c**) and [Fe(η^5-$C_5H_4BCAT^t)_2$] (**9**), showed three reduction waves, but only the first of these was reversible for **3c**. For **2a**–**2c** there was evidence for formation of successively [**2**]$^-$ and solvated $TiCl_3$ (together with oxidation of the anion [C_5H_4BCAT]$^-$); support for these Ti(III) species came from the EPR spectra of the in situ generated species obtained by the controlled potential electrolysis of **2a** and comparison with similar data derived from [Ti{η^5-$C_5H_3(SiMe_3)_2$-1,3}$_2Cl_2$]; while from **3c**, the formation of [**3c**]$^-$ is inferred.
© 2005 Elsevier Ltd. All rights reserved.

Keywords: 1,2-Phenylenedioxoborylcyclopentadienes; Boron; Titanium; Zirconium; Electrochemistry

1. Introduction

Recently, we described the synthesis and characterisation of a series of 1,2-phenylenedioxoborylcyclopentadienes of formulae **1a**–**1e** [1] and of some of their metal complexes **2**–**9** [2].

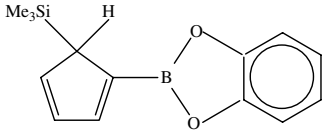

1a = $C_5H_4(BCAT)(SiMe_3)$

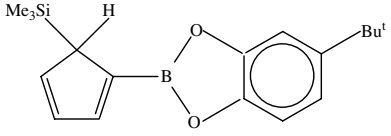

1b = $C_5H_4(BCAT^t)(SiMe_3)$

* Corresponding author. Tel.: +44 1273 678316; fax: +44 1273 677196.
E-mail address: m.f.lappert@sussex.ac.uk (M.F. Lappert).

0277-5387/$ - see front matter © 2005 Elsevier Ltd. All rights reserved.
doi:10.1016/j.poly.2005.06.051

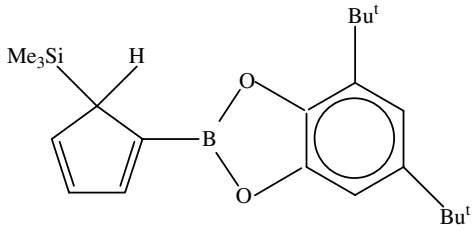

1c = $C_5H_4(BCAT^{tt})(SiMe_3)$

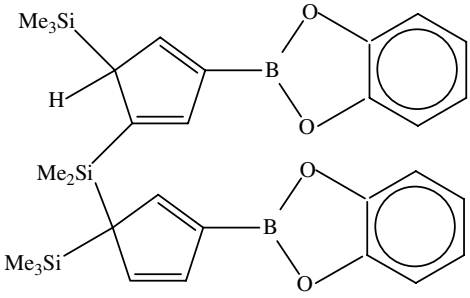

1d = $Me_2Si[C_5H_3(BCAT)(SiMe_3)]_2$

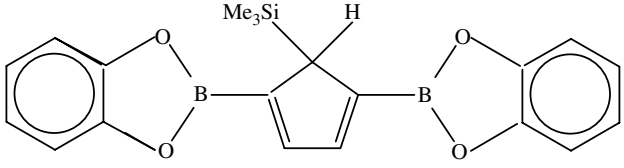

1e = $C_5H_3(SiMe_3)(1,4\text{-}BCAT)_2$

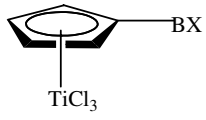

2a X = CAT
2b X = CAT^t
2c X = CAT^{tt}

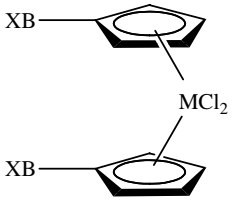

3a M = Zr, X = CAT
3b M = Hf, X = CAT
3c M = Zr, X = CAT^t
3d M = Hf, X = CAT^t

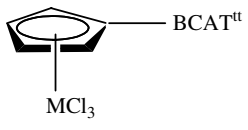

4a M = Zr
4b M = Hf

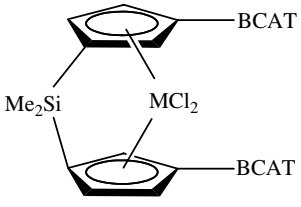

5a M = Zr
5b M = Hf

6a M = Zr
6b M = Hf

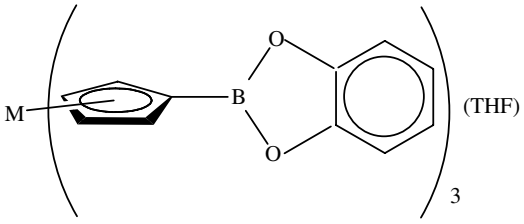

7a M = La
7b M = Ce
7c M = Yb

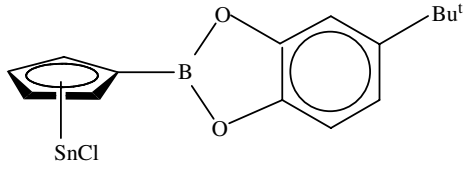

8

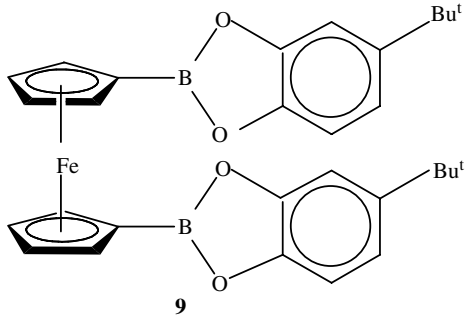

9

As previously noted [2], these studies were planned as a prelude to examining the potential of some of the organometallic compounds **2**–**9** as pro-catalysts for α-olefin polymerisation. The conceptual basis for undertaking this challenge lay in the knowledge that several mono-or bis-cyclopentadienylmetal complexes or of related ligands, particularly of Ti or Zr, were established as being effective in such catalysis when used with an excess of methylaluminoxane (MAO), or a similar Lewis acid metal alkyl, as cocatalyst [3].

We considered that a BX_2 substituent in the spectator ligand, such as the conjugate base of **1a**–**1e**, might serve a dual role by virtue of its readily available vacant p-orbital on the boron atom: in increasing the electrophilicity of the transition metal (M) active site compared

with its BX_2-free analogue and also in enhancing the prospect of an intramolecular M → B shift of Cl^-. Various X(X′)B-*ansa*-bridged-bis(cyclopentadienyl)-or -bis (indenyl)zirconium(IV) complexes have been reported, including salts containing the anion $[X(X')B(\eta^5\text{-}C_5H_4)_2ZrY_2]^-$ (X = Ph, X′ = Me, Y = Cl [4]; X = Ph, X′ = C_6F_5 = Y, or X = C_6F_5 = X′ = Y [5]), and the zwitterionic complexes $[Ph(Ph_3P^+CH_2)B^-(\eta^5\text{-}C_5H_4)_2\text{-}ZrCl_2]$ or two bis(η^5-indenyl) analogues [6]. Some of these with MAO were active catalysts for the polymerisation of ethene [5,6], as was $[Zr(\eta^5\text{-}C_5H_4BPh_2)_2Cl_2]$ with $AlEt_3$ [7]; while the above bis(η^5-indenyl) compounds with MAO were effective for propene polymerisation [6].

The objectives of the present work were to examine the effect of the BX_2 substituent in a selection of the compounds **1**–**9** by comparing their catalytic activity, as well as appropriate NMR, CV and E_{red} data, with those for BX_2-free analogues.

2. Results and discussion

An initial aim of these studies was to test the notion that 1,2-phenylenedioxoborylcyclopentadienylmetal complexes, particularly those of the group 4 metals, might be single site homogenous α-olefin polymerisation catalysts without recourse to a cocatalyst such as MAO. This objective was abandoned when it became clear that, at any rate in toluene under ambient conditions, $[Zr(\eta^5\text{-}C_5H_4BCAT)_2Cl_2]$ (**3a**) did not react with C_2H_4.

Accordingly, we then chose to focus on the following themes: (i) the polymerisation of ethene or propene, using some of the new [2] Ti(IV), Zr(IV) and Hf(IV) compounds as procatalysts with MAO, and the nature of the reaction between such a group 4 metal compound and MAO (Section 2.1); probing the electronic effect of the boryl substituent on some of the compounds **1**–**9** by means of (a) ^{11}B NMR spectroscopy (Section 2.2), (b) cyclic voltammetry (Section 2.3) and (c) EPR spectroscopy on controlled potential electrolysis products of some of the Ti or Zr complexes (**2**–**6**) (Section 2.4), and comparing for (b) and (c) the data with similar values for boryl-free analogous metal complexes.

2.1. Polymerisation of ethene and propene

The general conditions used to test the activity of various potential catalysts for the polymerisation of ethene or propene were as follows. A solution of toluene (ca. 50 ml), containing the appropriate catecholborylcyclopentadienylmetal complex (ca. 16 μmol) and MAO (ca. 3.2 mol) was placed under an atmosphere of ethene or propene (1.4 bar) at ambient temperature; after ca. 1 h, the mixture was quenched with a solution of HCl in methanol.

Under these conditions $[Zr(\eta^5\text{-}C_5H_4BCAT)_2Cl_2]$ (**3a**) and propene afforded a viscous oil. The ^1H NMR spectrum in $CDCl_3$ (Fig. 1) showed it to be low molecular weight atactic polypropylene (PP). In the light of the low activity of this catalytic system, producing ca. 50 kg PP mol^{-1} Zr^{-1} bar^{-1}, as well as the low average molecular weight (M_w) of the PP (M_w: 3360, GPC), no further catalytic experiments with C_3H_6 were carried out.

Several of the metal complexes **2**–**7** were next examined as procatalysts for the polymerisation of ethene in the presence of an excess of MAO in toluene, using the mild conditions indicated above. Surprisingly, the titanium complexes $[Ti(\eta^5\text{-}C_5H_4BX)Cl_3]$ [BX = BCAT

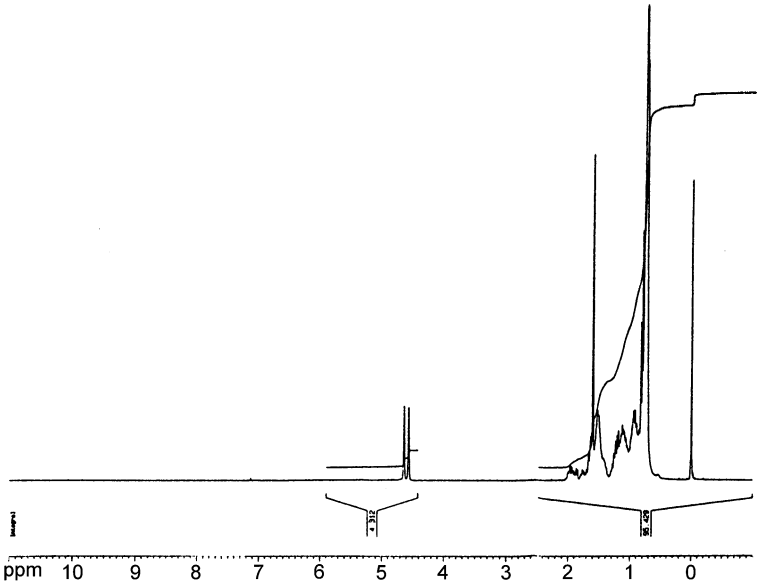

Fig. 1. The ^1H NMR spectrum of the produced polypropylene from $[Zr(C_5H_4BCAT)_2Cl_2]$ (**3a**) with MAO in $CDCl_3$ at 298 K and 300 MHz.

Table 1
Experiments on C_2H_4 polymerisation

Complex	Activity (kg PE mol^{-1} h^{-1} bar^{-1})	ETA[a] (dl g^{-1})	M_w[b] (g mol^{-1})	M_n[c] (g mol^{-1})	Q[d]
$[ZrCp_2Cl_2]$	600				
$[Zr\{\eta^5\text{-}C_5H_4(BCAT)\}_2Cl_2]$ (**3a**)	146	3.50	367260	20080	18.3
$[Hf\{\eta^5\text{-}C_5H_4(BCAT)\}_2Cl_2]$ (**3b**)	24	2.55	196930	18230	10.8
$[Zr\{\eta^5\text{-}C_5H_4(BCAT^t)\}_2Cl_2]$ (**3c**)	419	1.62	61890	7560	8.2
$[Hf\{\eta^5\text{-}C_5H_4(BCAT^t)\}_2Cl_2]$ (**3d**)	126	1.22	47220	6995	6.75
$[Zr\{\eta^5\text{-}C_5H_4(BCAT^{tt})\}Cl_3]$ (**4a**)	224	1.74	72440	8910	8.1
$[Hf\{\eta^5\text{-}C_5H_4(BCAT^{tt})\}Cl_3]$ (**4b**)	98	1.14	41170	6410	6.4
$[Zr\{(\mu,\eta^5\text{-}C_5H_3BCAT)_2SiMe_2\}Cl_2]$ (**5a**)	87	1.55	90970	16665	5.5
$[Hf\{(\mu,\eta^5\text{-}C_5H_3BCAT)_2SiMe_2\}Cl_2]$ (**5b**)	Inactive				
$[Zr\{\eta^5\text{-}C_5H_4(BCAT)\}Cl_3]$ (**6a**)	129	1.19	98280	13830	7.1

[a] ETA is the viscosity index.
[b] M_w is the weight-average molecular weight.
[c] M_n is the number average molecular weight.
[d] Q is the polydispersity, M_w/M_n.

(**2a**), BCAT^t (**2b**), BCAT^{tt} (**2c**)], as well as the 4f element analogues **7a**–**7c**, proved to be inactive. However, the majority of the zirconium and hafnium complexes **3**–**6** afforded polyethylene of moderate average molecular weight (M_w) and fairly high polydispersity (Q), somewhat typical of Ziegler Natta systems. The results are summarised in Table 1; comparison with zirconocene chloride under the same conditions reveals that the new complexes are slightly less active than $[ZrCp_2Cl_2]$.

The data of Table 1 raised the possibility that the catecholboryl moiety in each of the metal complexes there cited had been cleaved by treatment with MAO. In further support for this hypothesis were the following observations from the literature: (i) treatment of $C_5H_5BEt_2$ with Li^{n}Bu in hexane or Na[HBEt] in Et_2O under mild conditions caused the fission of the B–Cp bond, yielding LiCp or NaCp, respectively [8]; (ii) the B–O bond of borates $B(OR)_3$ is readily ruptured by organometallic reagents, as in the formation of BMe_3 from $B(OMe)_3$ and $AlMe_3$ [9]. Hence, a large excess of MAO was added to a solution of $[Zr(\eta^5\text{-}C_5H_4\text{-}BCAT^t)_2Cl_2]$ (**3c**) in toluene and the ^{11}B NMR spectrum recorded. Whereas the spectrum of **3c** in toluene showed the ^{11}B chemical shift at $\delta = 29.9$, the above experiment revealed a single ^{11}B resonance at $\delta = 84$. We conclude that the reaction of **3c** with MAO may have yielded $[Zr(\eta^5\text{-}C_5H_4BMe_2)_2Cl_2]$. Furthermore, it was shown, by using the same technique, that B(CAT)Cl reacted with MAO in toluene.

2.2. Trends in ^{11}B NMR spectral chemical shifts

^{11}B NMR spectroscopy of organic boron compounds provides a method of studying the environment at the boron atom. There is no direct link between the ^{11}B NMR spectral chemical shift $\delta[^{11}B]$ and the electron density at the corresponding boron atom. Nevertheless, in related series of compounds there is at least a qualitative correlation. For example, the trend in $\delta[^{11}B]$ (shown in parenthesis [10]) for $B(Me)_{3-n}(OMe)_n$ [BMe_3(86.3) > $BMe_2(OMe)$(53.1) > $BMe(OMe)_2$ (31.1) > $B(OMe)_3$(18.1)] corresponds to the progressive decrease of Lewis acidity of the four compounds.

The ^{11}B NMR spectral chemical shifts for the compounds **2**–**7a**, **8** and **9** in $CDCl_3$ at 298 K were in the range δ 26–30 [1,2]. Although these signals were broad, typically $\omega_{1/2} = 400$ Hz, they were reproducible to $\delta \pm 0.25$. Table 2 shows such data for the three related series: 1,2-phenylenedioxoboryl chlorides (Cl-BX) (**10a**–**10c**), trimethylsilylcyclopentadienes ($Me_3SiC_5H_4$–BX) (**1a**–**1c**), and trichlorotitanium η^5-cyclopentadienyls $[Cl_3Ti(\eta^5\text{-}C_5H_4\text{–}BX)]$ (**2a**–**2c**) [BX = BCAT (**a**), BCAT^t (**b**), BCAT^{tt} (**c**)].

The chemical shifts shown in Table 2 fall within a narrow range. Nevertheless, some minor trends are discernible, Fig. 2. (i) The *tert*-butyl substituents in the aromatic ring cause a shift in $\delta[^{11}B]$ to lower frequency (**a** > **b** > **c**) for the metal-free compounds **1** and **10**, consistent with the electron-releasing property of the ^{t}Bu groups being transmitted to the boron atom. (ii) A small frequency increase is noted by replacing the Cl atom of **10** by $Me_3SiC_5H_4$ in **1**. (iii) The π-electron acceptance by the Cl_3Ti moiety of **2** is reflected not only in a small low frequency shift ($\delta[^{11}B]$ for **2** < **1** or **10**), but also in neutralising the effect of the ^{t}Bu groups ($\delta[^{11}B]$ for **2a**–**2c** = 27.6 ± 0.4).

Table 2
^{11}B NMR spectral chemical shifts (δ, relative to $BF_3 \cdot OEt_2$) for compounds **1a**–**1c**, **2a**–**2c** and **10a**–**10c** in $CDCl_3$ at 298 K and 80.3 MHz

Compound	BX		
	BCAT	BCAT^t	BCAT^{tt}
Cl-BX (**10**)	29.0 (**10a**)	28.2 (**10b**)	26.4 (**10c**)
$Me_3SiC_5H_4$–BX (**1**)	29.5 (**1a**)	29.3 (**1b**)	28.1 (**1c**)
$Cl_3Ti(\eta^5\text{-}C_5H_4\text{–}BX)$ (**2**)	27.2 (**2a**)	27.9 (**2b**)	27.6 (**2c**)

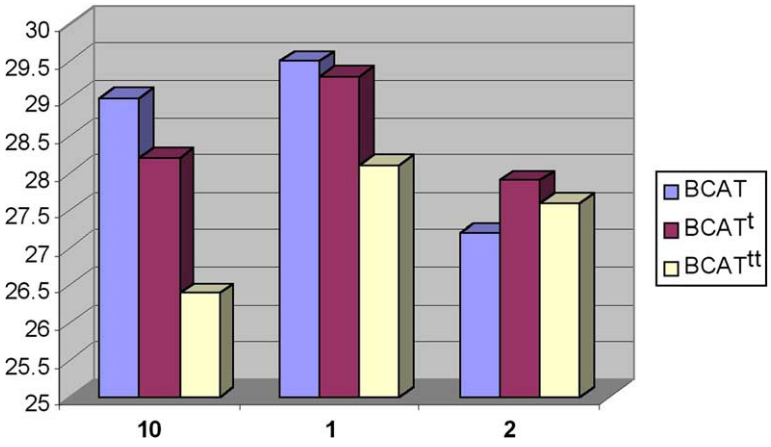

Fig. 2. Variation of $\delta[^{11}B]$ as a function of complex type (**10**, **1**, or **2**) and 1,2-phenylenedioxoboryl [BCAT (**a**), BCAT^{t} (**b**), or BCAT^{tt} (**c**)].

It is noted that the $\delta[^{11}B]$ value for the boron product of the reaction of **3c** with MAO, $\delta = 84$, is consistent with our assignment (Section 2.1) as due to $[Zr(\eta^5\text{-}C_5H_4BMe_2)_2Cl_2]$ (cf. the close correspondence to $\delta[^{11}B] = 86.3$ for BMe_3 [10]).

2.3. Cyclic voltammetry for a selection of 1,2-phenylenedioxoboryl compounds

Measurements were recorded in THF with $[N^nBu_4][PF_6]$ as supporting electrolyte at a platinum working electrode. Potentials were internally referenced to the ferrocene–ferrocenium redox couple. Results are summarised in Table 3.

Bis(4-*tert*-butylbenzene-1,2-dioxoborylcyclopentadienyl)zirconium(IV) chloride (**3c**) exhibited three, one-electron reductions in the range 0 to −2 V, Fig. 3. Both of the first two reductions showed peak-reverse to peak-forward current, i_p^f/i_p^r, equal to unity; and ΔE_{pp}, the difference between the potentials at peak-cathodic and peak-anodic potentials, for each of the first two was close to the 59 mV expected for thermodynamic reversibility. The final reduction waveform was, however, quasi-reversible, indicated by i_p^f/i_p^r being greater than unity and $\Delta E_{pp} = 180$ mV.

Likewise, bis(4-*tert*-butylbenzene-1,2-dioxoborylcyclopentadienyl)hafnium(IV) chloride (**3d**) exhibited three one-electron reductions in the range 0 to −2.5 V. In this case, the first reduction was quasi-reversible, with i_p^f/i_p^r being less than unity and $\Delta E_{pp} = 130$ mV. The latter reductions were irreversible with little reverse current being observed.

The ferrocene derivative **9** exhibited a partially reversible waveform in the oxidation sweep due to the Fe^{2+}/Fe^{3+} couple. Although the peak-reverse to peak-forward current i_p^f/i_p^r, was equal to unity, ΔE_{pp} was much greater than the required 59 mV for reversibility. Two quasi-reversible one-electron reductions were also

Table 3
Cyclic voltammetry data for a range of boryl substituted species[a]

Compound	E_o (V)[b]	ΔE_{pp}[c] (mV)	i^r:i^f[d]
$[Zr(\eta^5\text{-}C_5H_4BCAT^t)_2Cl_2]$ (**3c**)	−1.37	60	1.0
	−1.56	60	1.0
	−1.89	180	1.4
$[Hf(\eta^5\text{-}C_5H_4BCAT^t)_2Cl_2]$ (**3d**)	−1.79	130	0.78
	−2.11	[e]	0
	−2.40	[e]	0
$[Fe(\eta^5\text{-}C_5H_4BCAT^t)_2]$ (**9**)	+0.75	219	1.0
	−1.18	138	0.72
	−1.59	113	1.85
$C_5H_4(BCAT)(SiMe_3)$ (**1a**)	−2.31	[e]	0
B(CAT)Ph (**11**)	−0.22	[e]	0
	−1.37	[e]	0
$[Zr(\eta^5\text{-}C_5H_4BCAT^t)_2Cl_2(py)_2]$ (**12**)	−1.4	[e]	0
$[Ti(\eta^5\text{-}C_5H_4BCAT)Cl_3]$ (**2a**)	−1.07	[e]	0
	−1.59	[e]	0
	−0.27[f]	[e]	0
$[Ti(\eta^5\text{-}C_5H_4BCAT^t)Cl_3]$ (**2b**)	−1.20	[e]	0
	−1.69	[e]	0
	−0.25[f]	[e]	0
$[Ti(\eta^5\text{-}C_5H_4BCAT^{tt})Cl_3]$ (**2c**)	−1.25	[e]	0
	−1.72	[e]	0
	−0.25[f]	[e]	0

[a] A 2×10^{-3} solution in THF, containing 0.2 mol dm^{-3} $[N^nBu_4][PF_6]$ as supporting electrolyte, at a platinum working electrode. Potentials were internally referenced to the ferrocene–ferrocenium redox couple (+0.535 V with respect to s.c.e.). Values quoted were obtained at 200 mV s^{-1}.

[b] E_o is the potential measured halfway between the potentials of peak-cathodic and -anodic currents where the signal is reversible, or the potential of the peak-anodic current in the case of the irreversible signals.

[c] ΔE_{pp} is the difference between the potentials at peak-anodic and peak-cathodic potentials.

[d] The ratio of peak-forward to peak-reverse currents.

[e] Not measured, as signal was irreversible.

[f] Waveform due to oxidation of free anionic cyclopentadienyl ligand.

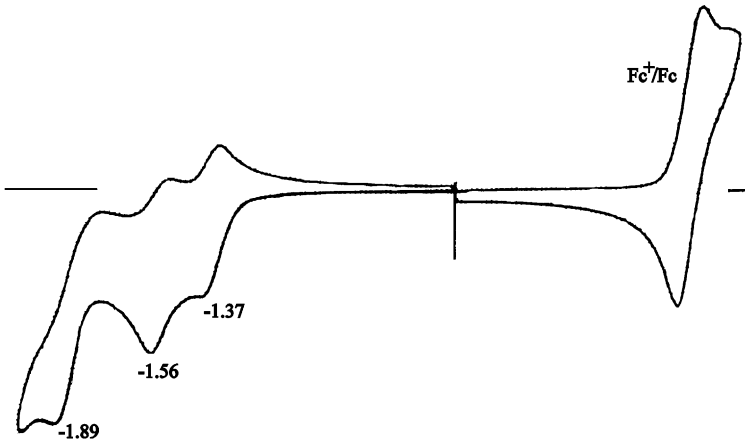

Fig. 3. The cyclic voltammogram of $[Zr\{\eta^5\text{-}C_5H_4(BCAT^t)\}_2Cl_2]$ (**3c**) in THF, at a vitreous carbon electrode, 200 mV/s sweep rate.

observed in the reverse sweep in the range 0 to −1.6 V. In both cases, i_p^f/i_p^r was not equal to unity and ΔE_{pp} was greater than 59 mV.

The only obvious difference between these complexes and other previously reported related species, such as $[Zr(\eta^5\text{-}C_5H_4SiMe_3)_2Cl_2]$ (E° −1.60 V, ΔE_{pp} 0.22 V, i_p^f/i_p^r 1.0 [11]) is the substituent. It is proposed, therefore, that the further unexpected reductions were due to the 1,2-phenylenedioxoboryl substituent. In that context, it is noteworthy not only that triarylboranes BAr_3 are well known to form one- or two-electron reduction products by treatment with sodium: $[BAr_3]^-$, $[Ar_3B\text{–}BAr_3]^{2-}$ or $[BAr_3]^{2-}$ [12], but also that ferrocenyldi(chloro)borane displayed partially reversible reduction waves at −0.16 and −0.33 V (as well as the reversible one-electron oxidation at $E_{1/2}$ 0.45 V, a similar value to that found for ferrocene) [13].

In an effort to discover whether these further reductions were boron-centred, the precursors to the borylcyclopentadienyl ligands were examined. Thus, 4-*tert*-butylbenzene-1,2-dioxo(chloro)borane (**10a**) was therefore studied; it did not show a reduction product in the range 0 to −3 V, but displayed a single waveform in the oxidation sweep due to Cl^- oxidation. The inertness to reduction is attributed to the lack of a stabilising aryl substituent.

The parent borylcyclopentadiene $C_5H_4(BCAT)(SiMe_3)$ (**1a**) displayed a single, irreversible reduction in the range 0 to −2.5 V. To study further whether the presence of an aromatic substituent favoured reduction under cyclic voltammetric conditions, 1,2-phenylenedioxo(phenyl)borane (**11**) was examined; it underwent two one-electron reductions. Although both were irreversible, it appeared that at higher scan rates the waveforms became more reversible.

If it is assumed that reduction at boron is possible due to the availability of a formally vacant p-orbital, it may prove possible to hinder this by coordination of a Lewis base to the Lewis acidic boron. Thus, the pyridine adduct $[Zr\{\eta^5\text{-}C_5H_4(BCAT^t)\}_2Cl_2(py)_2]$ (**12**) was studied. The reduction sweep in the range 0 to −2.5 V showed that a single, irreversible reduction was observed, which occurred at the same potential as the first (reversible) reduction of $[Zr\{\eta^5\text{-}C_5H_4(BCAT^t)\}_2Cl_2]$ (**3c**). Thus, the coordinated pyridine did not prevent the reduction at boron occurring; the second and third (boron-centred) reductions were observed, but were poorly defined.

The collected data from these experiments leads to several conclusions. The presence of two extra reduction waves in the cyclic voltammograms of the metal complexes studied is attributed to two sequential one-electron reductions at boron. The first of these appears to be more reversible than the second, which is consistent with previous experimental results on a borylferrocene [13]. The reduction potentials for **3c** and **3d** are significantly lower than in the appropriate $[M(\eta^5\text{-}C_5H_4SiMe_3)_2Cl_2]$ (M = Zr or Hf) [11], which is consistent with the view that the borylcyclopentadienyl ligands are removing electron density from the metal centre. A slightly greater oxidation potential for the iron complex **9** compared with ferrocene is in agreement with this conclusion.

The trichlorotitanium complex **2a** exhibited complex electrochemistry at ambient temperature, displaying several irreversible reduction waveforms in the range 0 to −2.2 V, Fig. 4. Three irreversible reduction products were observed, the first at −1.07 V. In the reverse sweep, an irreversible oxidation process was seen at −0.27 V, consistent with the oxidation of a free anionic cyclopentadienyl ligand [11]. The forward sweep exhibited a strong irreversible oxidation process, due to chloride oxidation. This oxidation [14] process hindered internal referencing to the Fc^+/Fc redox couple. Cooling the sample to 0 °C greatly simplified the electrochemistry, Fig. 5. A single irreversible reduction was now apparent

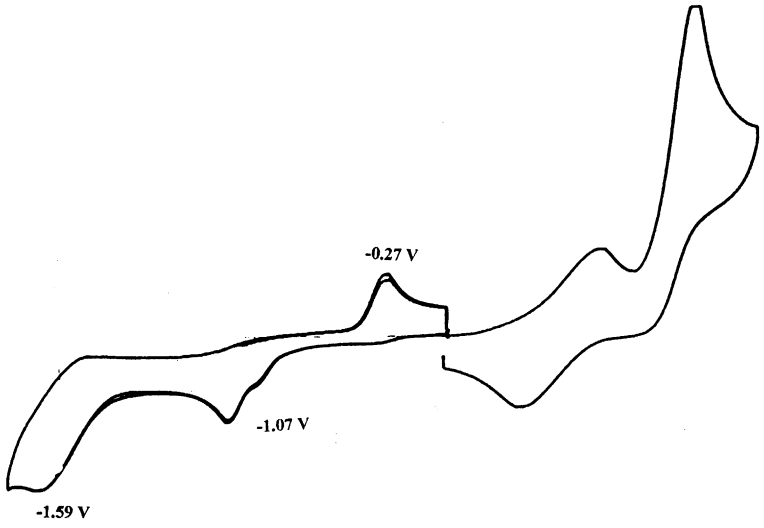

Fig. 4. The cyclic voltammogram of $[Ti\{\eta^5\text{-}C_5H_4(BCAT)\}Cl_3]$ (**2a**) at 20 °C in THF, at a vitreous carbon electrode, 200 mV/s sweep rate.

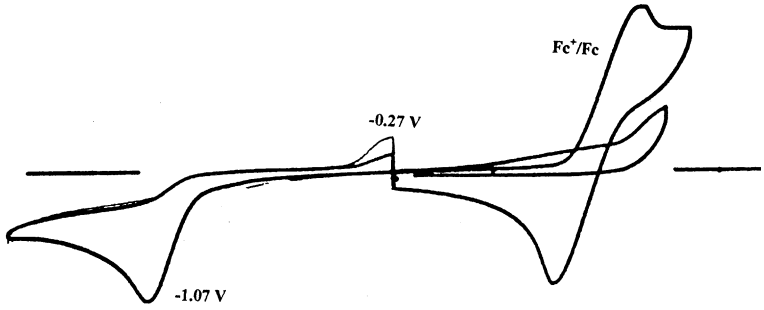

Fig. 5. The cyclic voltammogram of $[Ti\{\eta^5\text{-}C_5H_4(BCAT)\}Cl_3]$ (**2a**) at 0 °C in THF, at a vitreous carbon electrode, 200 mV/s sweep rate.

in the reverse sweep at −1.07 V. An irreversible oxidation process at −0.27 V, due to cyclopentadienyl oxidation, was still observed. The forward sweep was also simplified at lower temperature. Chloride oxidation became less prevalent, allowing internal referencing to the Fc^+/Fc redox couple. Broadening of the reference waveform was observed due to partial precipitation of the $[N^nBu_4][PF_6]$ electrolyte. The analogous complexes **2b** and **2c** behaved similarly.

2.4. EPR spectral studies on electrochemically generated radicals

We had earlier collected EPR spectroscopic data on Ti(III) [15a] and Zr(III) [15b] complexes, electrochemically generated from corresponding metallocene precursors $[MCp^x_2Cl_2]$ $[Cp^x = C_5H_5,\ C_5H_4SiMe_3,$ or $C_5H_3(SiMe_3)_2$-1,3, abbreviated as Cp, Cp′, or Cp″, respectively]. We now present for comparison similar data on the Ti(IV) compound **2a** and the Zr(IV) metallocene **3c**, as summarised in Table 4. The spectra were obtained by controlled potential electrolysis of the appropriate sample in THF with $[N^nBu_4][PF_6]$ as supporting electrolyte at −40 °C; the potential employed was only slightly greater than that at which the first reduction was observed for **2a**, **3c** and $[TiCp''_2Cl_2]$ [15a]; for $[ZrCp''_2Cl_2]$ only a single reversible reduction had been found [15b].

Electrolysis of $[Zr\{\eta^5\text{-}C_5H_4(BCAT^t)\}_2Cl_2]$ (**3c**) under these conditions gave rise to the EPR spectrum

Table 4
EPR spectroscopic data for M(III) (Ti or Zr) complexes, generated by in situ electrolysis

M(IV) starting material	A_{iso} (G)	g_{av}	Reference
$[Ti\{\eta^5\text{-}C_5H_4(BCAT)\}Cl_3]$ (**2a**)	Not observed	1.967 1.974	
$[Zr\{\eta^5\text{-}C_5H_4(BCAT^t)\}_2Cl_2]$ (**3c**)	28	1.983	
$[TiCp''_2Cl_2]$[a]	8.0[b] 12.0[c]	1.962[b] 1.980[c]	[15a]
$[ZrCp_2Cl_2]$[b]	28.9	1.971	[15b]
$[ZrCp'_2Cl_2]$[b]	28.0	1.975	[15b]
$[ZrCp''_2Cl_2]$[b]	25.9	1.979	[15b]

[a] Not observed.
[b] Assigned to $[TiCp''_2Cl_2]^-$.
[c] Assigned to $TiCp''Cl_2$.

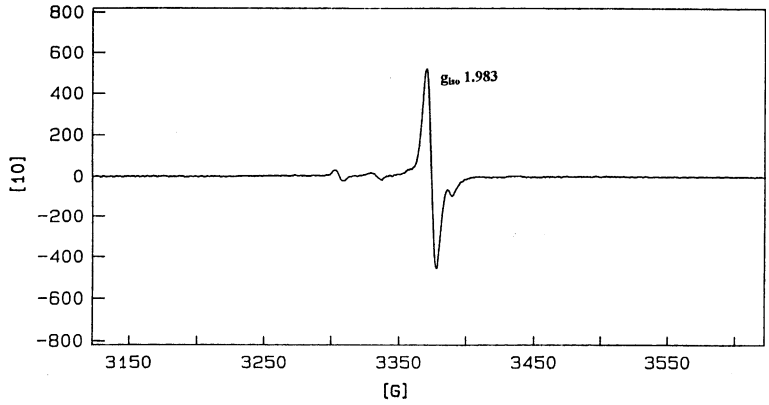

Fig. 6. The EPR spectrum of the electrochemically reduced $[Zr\{\eta^5\text{-}C_5H_4(BCAT^t)\}_2Cl_2]$ (**3c**) in THF at 223 K.

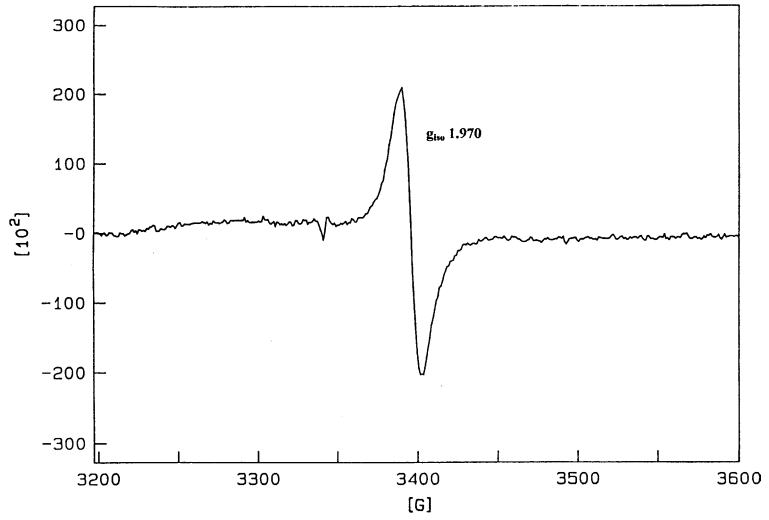

Fig. 7. The EPR spectrum of the electrochemically reduced $[Ti\{\eta^5\text{-}C_5H_4(BCAT^t)\}Cl_3]$ (**2a**) in THF at 223 K.

shown in Fig. 6, attributed to the d^1 reduction product $[Zr\{\eta^5\text{-}C_5H_4(BCAT^t)\}_2Cl_2]^-$. Increasing the applied potential to a greater negative voltage did not give rise to a further signal. A similar study of $[Ti\{\eta^5\text{-}C_5H_4(BCAT^t)\}Cl_3]$ (**2a**) gave a broad signal (Fig. 7), which by recording the second harmonic spectrum (Fig. 8) was shown to be derived from overlapping signals assigned to $[Ti\{\eta^5\text{-}C_5H_4(BCAT^t)\}Cl_3]^-$ and $[Ti\{\eta^5\text{-}C_5H_4(BCAT^t)\}Cl_2]$, respectively. The evidence is based on analogy with the $[TiCp''_2Cl_2]$ system, a detailed study of which concluded that the electrolysis products were $[TiCp''_2Cl_2]^-$ and $[TiCp''Cl_2]$, the latter formed by the decay of the former (Section 2.3).

3. Experimental

The 1,2-phenylenedioxoborylcyclopentadienes [1] and their metal complexes [2] were prepared and characterised as described in our two earlier papers.

3.1. Polymerisation experiments

In a typical experiment, $[Zr\{\eta^5\text{-}C_5H_4(BCAT)\}_2Cl_2]$ (**3a**) (8.5 mg, 16.1 mol) in toluene (50 cm^3) at room temperature was activated with MAO (approximately 200 molar excess, 10% by weight solution in toluene). The catalytic mixture was placed under an ethene atmosphere of 1.4 bar pressure for 1 h at room temperature. The mixture was then quenched with MeOH/HCl, filtered and the collected PE dried at 50 °C.

For the homogeneous polymerisation of propene with **3a**, the reaction conditions were identical to those described above. The PP produced was isolated by standard organic procedures, producing a viscous oil which was analysed by ^1H NMR spectroscopy.

3.2. Electrochemistry

Cyclic voltammetry measurements were initially carried out using a vitreous carbon electrode, and then

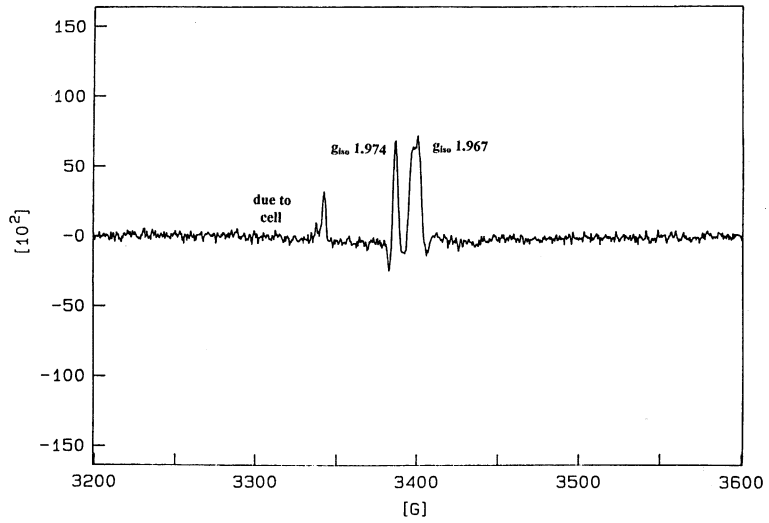

Fig. 8. The second harmonic EPR spectrum of the electrochemically reduced [Ti{η^5-C_5H_4(BCAT^t)}Cl_3] (**2a**) in THF at 223 K.

repeated at a platinum electrode, using a three electrode system. A Hi-Tek Instruments DT2101 potentiostat and waveform generator, connected to a Philips PM8042 X-Y recorder were utilised. All potentials were internally referenced to the potential for the one-electron oxidation of ferrocene (+0.535 V with respect to the standard calomel electrode = 0 V). The supporting electrolyte in all cases was tetra-*n*-butylammonium hexafluorophosphate; electrolysed solutions were 0.2 mol dm^{-3} in supporting electrolyte and approximately 2 mmol dm^{-3} in metal complex. The general experimental procedure was based upon that described in the literature [16].

3.3. EPR spectra

X-band EPR spectra were recorded with a Bruker ESP-300 spectrometer. The electrochemically produced species were generated in situ at a platinum electrode by a controlled potential electrolysis using a three electrode configuration at potentials slightly greater than the measured reduction potential of the complex. The apparatus used was a modification of that previously described [17]. Electrolyses were carried out at −40 °C using the Varian variable-temperature attachment.

Acknowledgements

We are grateful to BASF (and Dr. Marc Kristen) for the award of a studentship to M.J.D. and for facilitating the characterisation of the PE samples.

References

[1] A.G. Avent, M.J. Davies, P.B. Hitchcock, M.F. Lappert, Z. Anorg. Allg. Chem. 629 (2003) 1358.
[2] M.C. Cassani, M.J. Davies, P.B. Hitchcock, M.F. Lappert, Inorg. Chim. Acta 358 (2005) 1595.
[3] (a) A.L. McKnight, A.L. Waymouth, Chem. Rev. 98 (1998) 2587;
(b) H.H. Brintzinger, D. Fischer, R. Mülhaupt, B. Rieger, R.M. Waymouth, Angew. Chem. Int. Ed. 34 (1995) 1143;
(c) G.W. Coates, Chem. Rev. 100 (2000) 1223.
[4] C.T. Burns, D.S. Stelck, P.J. Shapiro, A. Vij, K. Kunz, G. Kehr, T. Concolino, A.L. Rheingold, Organometallics 18 (1999) 5432.
[5] S.J. Lancaster, M. Bochmann, Organometallics 20 (2001) 2093.
[6] P.J. Shapiro, F. Jiang, X. Jin, B. Twamley, J.T. Patton, A.L. Rheingold, Eur. J. Inorg. Chem. (2004) 3370.
[7] M.T. Reetz, H. Brümmer, M. Kessler, J. Kuhnigk, Chimia 49 (1995) 501.
[8] H. Grundke, P.I. Paetzold, Chem. Ber. 104 (1971) 1136.
[9] (a) J. Casanova, H.R. Kiefer, R.E. Williams, Org. Prep. Proced. 1 (1969) 57;
(b) T.P. Onak, in: Organoborane Chemistry, Academic Press, New York, 1975, pp. 19–20.
[10] cf. L.J. Todd, A.R. Siedle, Prog. NMR Spectrosc. 13 (1978) 87.
[11] A. Antiñolo, G.S. Bristow, G.K. Campbell, A.W. Duff, P.B. Hitchcock, R.A. Kamarudin, M.F. Lappert, R.J. Norton, N. Sarjudeen, D.J.W. Winterborn, J.L. Atwood, W.E. Hunter, H. Zhang, Polyhedron 8 (1989) 1601.
[12] cf. T.P. Onak, in: Organoborane Chemistry, Accademic Press, New York, 1975, pp. 131–132.
[13] J.C. Kotz, E.W. Post, Inorg. Chem. 9 (1970) 1661.
[14] N. El Murr, A. Chaloyard, E. Laviron, Nouv. J. Chim. (1978) 15.
[15] (a) G.K. Campbell, M.F. Lappert, D.J.W. Winterborn, unpublished work.;
(b) G.K. Campbell, M.F. Lappert, D.J.W. Winterborn, in: D.J. Cardin, M.F. Lappert, C.L. Raston (Eds.), Chemistry of Organo-zirconium and Hafnium Compounds, Ellis Horwood and Wiley, Chichester, 1980, p. 282.
[16] C.J. Pickett, D. Pletcher, J. Chem. Soc., Dalton Trans. (1975) 879.
[17] G.A. Bowmaker, P.D.W. Boyd, G.K. Campbell, J.M. Hope, R.L. Martin, Inorg. Chem. 21 (1982) 1152.

Available online at www.sciencedirect.com
SCIENCE DIRECT®
Polyhedron 25 (2006) 406–420
POLYHEDRON
www.elsevier.com/locate/poly

Structure–reactivity correlations in new W(IV) and Nb(IV) silicon-bridged *ansa*-metallocene hydrides

Stephen L.J. Conway, Malcolm L.H. Green *, Sofia I. Pascu *, Henry O. Peake

Inorganic Chemistry Laboratory, University of Oxford, South Parks Road, Oxford OX1 3QR, UK

Received 5 May 2005; accepted 19 August 2005
Available online 3 October 2005

Abstract

W(IV) and Nb(IV) derivatives: [W(L1)MeI] (**1**), [W(L1)MeH] (**2**) and [W(L1)O] (**3**), [W(L2)Cl_2] (**4**), [W(L2)H_2] (**5**), [W(L2)H_3][BF_4] (**6**), [Nb(L2)Cl_2] (**7**) and [Nb(L2)(η^2-BH_4)] (**8**), where L1 = [(η-C_5H_4)$_2$$SiMe_2$]$^{2-}$ and L2 = [(η-C_5H_3TMS)$_2$$SiMe_2$]$^{2-}$, have been prepared and characterised. The crystal structures of compounds **5** and **8** have been determined. Thermodynamic parameters for the elimination of methane from compound **2** have been evaluated based on ^{1}H NMR studies in C_6D_6. Trimethylsilyl substituents on the cyclopentadienyl rings appear to moderate the structural and dynamic properties of the silicon-bridged *ansa*-tungstenocenes.
© 2005 Elsevier Ltd. All rights reserved.

Keywords: *Ansa*-metallocenes; Methane elimination; Organometallics

1. Introduction

Early transition metals complexes incorporating *ansa*-metallocenes are of widespread interest as catalytic precursors in organic synthesis [1–4]. We and others have shown that the presence of an *ansa*-bridge induces a significant modification of the electronic properties and hence reactivity of metallocene compounds, compared to the analogous non-bridged compounds [5–25,15,26–50]. These developments have led to considerable growth in the study of bridged- or '*ansa*'-metallocenes. We have undertaken to study the relationship between structure and reactivity in *ansa*-metallocenes. Earlier work on silicon-bridged metallocenes of Groups 5–7 [19,25,30] has highlighted the changes in reactivity that the *ansa*-bridge brings to the chemistry of the dihydride compound [W{(η-C_5H_4)$SiMe_2$(η-C_5H_4)}H_2] with respect to that of [W(η-C_5H_5)$_2$$H_2$] and [W{($\eta$-$C_5H_4$)$CMe_2$($\eta$-$C_5H_4$)}$H_2$]. This work includes ^{1}H NMR studies of the corresponding trihydride cations and the reactivity of the dihydride compounds towards photolysis in benzene [19,25,51,52].

Here, we report new synthetic and spectroscopic studies of silicon-bridged W(IV) and Nb(IV) *ansa*-metallocenes with both unsubstituted and substituted cyclopentadienyl rings. Also, the thermodynamic parameters for the elimination of methane from a silicon-bridged *ansa*-tungstenocene are discussed.

2. Results and discussion

2.1. Syntheses

The preparation of [Li_2{(C_5H_4)$SiMe_2$(C_5H_4)}] (**Li_2L1**) has been reported elsewhere [25]. $WCl_4 \cdot DME$ and **Li_2L1** were stirred together in the absence of solvent. Diethyl ether was then added at −78 °C and after stirring for 3 days the compound [W{(η-C_5H_4)$SiMe_2$(η-C_5H_4)}Cl_2] was isolated as a brown solid [25]. The compound [W{(η-C_5H_4)$SiMe_2$(η-C_5H_4)}Me_2] was subsequently prepared via a procedure analogous to that described earlier [25]. Reaction of [W{(η-C_5H_4)$SiMe_2$(η-C_5H_4)}Me_2] with NH_4I (in THF at 65 °C) gave [W{(η-C_5H_4)$SiMe_2$(η-C_5H_4)}MeI]

* Corresponding author. Present address: Department of Chemistry, University of Cambridge, Lensfield Road, CB2 1EW, UK. Tel.: +1223 336317; fax: +1223 3363017.
E-mail address: sip22@cam.ac.uk (S.I. Pascu).

0277-5387/$ - see front matter © 2005 Elsevier Ltd. All rights reserved.
doi:10.1016/j.poly.2005.08.025

(**1**) as a green powder in 19% yield. The treatment of [W(η-$C_5H_5)_2$MeI] with sodium *bis*(2-methoxyethoxy)aluminium hydride, [Na{$AlH_2(OCH_2CH_2OCH_3)_2$}], gave the corresponding metal hydride has been reported [53] and has been successfully applied to give *ansa*-tungstenocenes such as [W{(η-C_5H_4)CMe_2(η-C_5H_4)}{$(CH_2)_nCH_3$}(I)] ($n = 2$, 1, 0) [14,53].

In an analogous procedure, compound **1** was treated with [Na{$AlH_2(OCH_2CH_2OCH_3)_2$}] in toluene at −78 °C to give, after cautious hydrolysis of excess [Na{$AlH_2(OCH_2CH_2OCH_3)_2$}], the compound [W{(η-C_5H_4)$SiMe_2$(η-C_5H_4)}Me(H)] (**2**) as a yellow crystalline solid in 63% yield.

The action of NaOH on the dichloride [W(η-$C_5H_5)_2Cl_2$] yields the oxo complex [W(η-$C_5H_5)_2$O] [54,55]. We have prepared [W{(η-C_5H_4)$SiMe_2$(η-C_5H_4)}O] (**3**) by applying a similar method (Scheme 1). The compound [W{(η-C_5H_4)$SiMe_2$(η-C_5H_4)}Cl_2] was treated with excess KOH in a 1:1 mixture of H_2O and ethanol. A colour change from brown/green to blue was observed, and subsequent removal of volatiles gave **3** as a red/blue crystalline solid in 46% yield.

For the preparation of [Li_2{(C_5H_3TMS)$SiMe_2$(C_5H_3TMS)}] (**Li_2L2**), [Na(C_5H_5)] was reacted with Me_3SiCl in THF, to give C_5H_5TMS, which was further purified by distillation under reduced pressure. Addition of ^{n}BuLi to C_5H_5TMS in petroleum ether (b.p. 40–60 °C) at −78 °C resulted in the formation of [Li(C_5H_4TMS)]. Me_2SiCl_2 was added to a suspension of this air- and moisture-sensitive solid in THF and the resulting ligand [(C_5H_4TMS)$SiMe_2$(C_5H_4TMS)] (**H_2L2**) was isolated. Addition of ^{n}BuLi at −78 °C resulted in the formation of **Li_2L2** as an air- and moisture-sensitive solid in 64% yield (Scheme 1). (*N.B.* Synthesis of [K_2{(C_5H_3TMS)$SiMe_2$(C_5H_3TMS)}] (**K_2L2**) has been reported previously in the preparation of *ansa*-zirconocenes [56]).

The compound [W{(η-C_5H_3TMS)$SiMe_2$(η-C_5H_3TMS)}-Cl_2] (**4**) was prepared by an analogous method with [W{(η-C_5H_4)$SiMe_2$(η-C_5H_4)}Cl_2] [25]. For the synthesis of [W{(η-C_5H_3TMS)$SiMe_2$(η-C_5H_3TMS)}H_2] (**5**), addition of an excess of $LiAlH_4$ as a suspension in diethyl ether to a suspension of **4** in diethyl ether at −78 °C resulted in a gradual colour change from dark brown to orange as the reaction mixture warmed to room temperature. The orange suspension was stirred overnight before the excess $LiAlH_4$ was hydrolysed with distilled water. Compound **5** was isolated as yellow crystals in 22% yield. Protonation of *ansa*-tungstenocene dihydrides to form the corresponding trihydride species [14,25] was carried out by the addition of a solution of HBF_4 in diethyl ether to a suspension of compound **5** in diethyl ether. As a result, the cationic trihydride species [W{(η-C_5H_3TMS)$SiMe_2$(η-C_5H_3TMS)}H_3][BF_4] (**6**) [14,25] was obtained as a flocculent, air-sensitive white solid in 59% crude yield and was used in ^{1}H VT NMR experiments without further purification.

The TMS-substituted compound [Nb{(η-C_5H_3TMS)-$SiMe_2$(η-C_5H_3TMS)}Cl_2] (**7**) was prepared via a method similar to that used to synthesise [Nb{(η-C_5H_4)$SiMe_2$-(η-C_5H_4)}Cl_2] [30]. A suspension of [Li_2{(C_5H_3TMS)-$SiMe_2$(C_5H_3TMS)}] in THF was added slowly to a suspension of $NbCl_4 \cdot 2THF$ in THF at room temperature. After work-up, complex **7** was obtained as a dark brown solid, in 50% yield (Scheme 2). Reaction between [Nb{(η-C_5H_3TMS)$SiMe_2$(η-C_5H_3TMS)}Cl_2] and $LiBH_4$ was performed [30] to yield the corresponding tetrahydroborate derivative [Nb{(η-C_5H_3TMS)$SiMe_2$(η-C_5H_3TMS)}(η^2-BH_4)] (**8**). Treatment of **7** with excess $LiBH_4$ in DME at room temperature gave green, extremely air-sensitive, crystals of **8** in 58% yield (Scheme 2).

The complexes **1**–**8** have been characterised by elemental analysis, mass spectrometry (FAB^+), infrared, ^{1}H and $^{13}C\{^1H\}$ NMR spectroscopy and selected data are given in Table 1. Structure–relationship correlations in the series of metal-hydrides **5**, **6**, and **8** have been investigated by ^{1}H NMR and IR spectroscopies and are discussed below. In case of compounds **5** and **8**, the structures were confirmed by single crystal X-ray diffraction.

2.2. ^{1}H NMR studies

The ^{1}H NMR spectrum of **5** (in C_6D_6, Fig. 1) contains partial triplets at δ 4.99, 4.32 and 4.24 corresponding to the cyclopentadienyl protons. A singlet at δ 0.34 arising from the 18 protons of the two TMS groups on the cyclopentadienyl rings is also observed, as well as two singlets at δ 0.25 and −0.16 corresponding to the protons on the inequivalent methyl groups on the $SiMe_2$ bridge. Two further doublets at δ −10.31 and −10.68

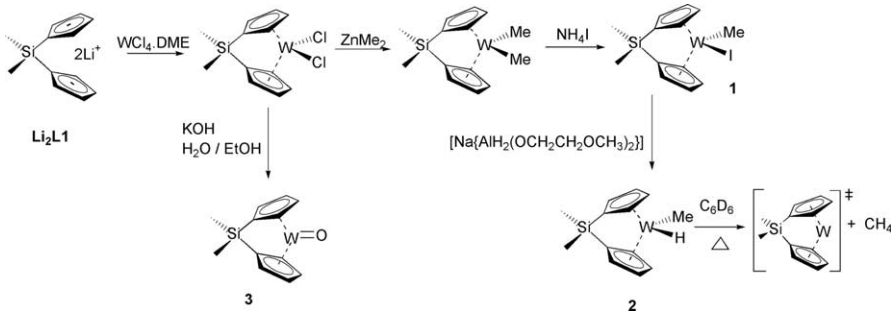

Scheme 1. Syntheses of silicon-bridged W(IV) *ansa*-metallocenes with unsubstituted cyclopentadienyl rings.

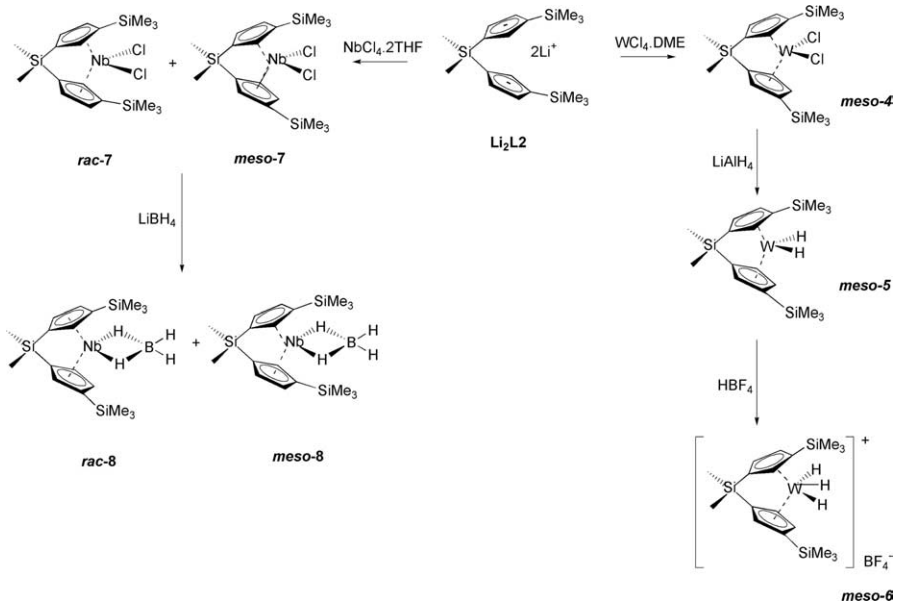

Scheme 2. Syntheses of silicon-bridged W(IV) and Nb(IV) *ansa*-metallocenes with TMS-substituted cyclopentadienyl rings.

were assigned to the two inequivalent hydride protons. Associated with these doublets were the characteristic ^{183}W satellites with $^{1}J_{WH} = 83.8$ and 80.0 Hz respectively. $^{1}J_{WH}$ of **5** is similar to that for the unsubstituted silicon- and ethylene-bridged analogues (Table 2) and this value is also mid-way between that of the unbridged and Me_2C-bridged compounds. It appears that a silicon-bridge does not constrain the rings as much as a Me_2C-bridge.

The $[W(\eta\text{-}C_5H_5)_2H_3]^+$ cation shows a H_A–H_B coupling constant, J_{AB}, of 8.5 Hz at all temperatures [52]. However when an *ansa*-bridge is introduced between the cyclopentadienyl rings the J_{AB} varies with temperature by several orders of magnitude [14,25]. For $[W\{(\eta\text{-}C_5H_4)SiMe_2(\eta\text{-}C_5H_4)\}H_3][BF_4]$, J_{AB} varies from 8 Hz at 133 K to 75 Hz at 273 K, while for $[W\{(\eta\text{-}C_5H_4)C_2Me_4(\eta\text{-}C_5H_4)\}H_3][Cl]$, J_{AB} is found to vary from 8 Hz at 193 K to 35 Hz at 293 K [25]. The compound $[W\{(\eta\text{-}C_5H_4)CMe_2(\eta\text{-}C_5H_4)\}H_3][PF_6]$ shows more extreme behaviour with J_{AB} varying from 2900 Hz at 133 K to 16 000 Hz at 203 K [14]. The main change in this series is that the inter-ring angle α increases (i.e. the bending angle β decreases, see Table 3 for details) as the bridge becomes more sterically constraining. This has been explained in terms of the ability of the hydride ligands to undergo quantum mechanical exchange coupling [57]. J_{AB} has two distinct contributors: $J_{AB} = -2J_{ex} + J_m$, where J_m is the *classical component* (i.e. the result of conventional Fermi contact interaction, temperature-independent and typically between 2 and 28 Hz) and J_{ex} is the *quantum mechanical exchange coupling*. The coupling J_{ex} arises from the quantum mechanical exchange of a pair of identical hydrogens, H_1 and H_2 between two chemically inequivalent sites, **A** and **B**. There are two possible configurations, which can be associated with two potential energy wells separated by an energy barrier (a ''double-well'' model). Tunnelling through this energy barrier gives rise to the quantum mechanical exchange coupling, as rationalised by Sabo-Etienne and Chaudret [58]:

(1) A soft bending vibration allows close approach of the two exchanging hydrogens.
(2) This vibration initiates a chemical pathway which brings the exchanging hydrogens closer together than the sum of their van der Waals radii.
(3) The barrier to chemical (classical) exchange must be between 35 and 75 kJ mol^{-1} to allow quantum mechanical exchange coupling to be observed by ^{1}H NMR spectroscopy.
(4) There is vibrational and rotational tunnelling through the energy barrier.
(5) The observed temperature dependence of J_{ex} is a consequence of thermal population of excited vibrational states.

The variable temperature ^{1}H NMR experiment on compound **6** showed temperature-independent behaviour. At room temperature the high field region was found to have a pair of triplets at δ −6.19 and −6.32 ppm (corresponding to a single proton) and a pair of doublets at δ −6.55 and −6.69 ppm (corresponding to two protons). The J_{AB} coupling constant was found to be 8.20 Hz at all temperatures, hence no evidence of quantum mechanical exchange coupling can be assumed in case of **6**. This behaviour is similar to that of the non-bridged trihydride $[W(\eta\text{-}C_5H_5)_2H_3]^+$ which exhibits a temperature-independent ^{1}H NMR spectrum with J_{AB} of 8.5 Hz [59]. This experiment suggests that the presence of bulky

Table 1
Data characterising new compounds **1**–**5** and **7**–**8**

Compound data		NMR data
1	[W{(η-C_5H_4)$SiMe_2$(η-C_5H_4)}Me(I)] $C_{13}H_{17}ISiW$ Mw 512.12 Green powder Elemental analysis: Found (Calc.) C % 30.5 (30.5) H % 3.7 (3.4)	^{1}H NMR (C_6D_6 500 MHz): 5.84 (m, 4H, C_5H_4), 4.87 (m, 4H, C_5H_4), 4.74 (m, 4H, C_5H_4), 4.00 (m, 4H, C_5H_4), 0.85 (s, 3H, WMe), −0.50 (s, 3H, $SiMe_2$), −0.57 (s, 3H, $SiMe_2$) ^{13}C{^{1}H} NMR (C_6D_6 126 MHz): 114.4 (s, C_5H_4), 113.8 (s, C_5H_4), 76.1 (s, C_5H_4), 73.5 (s, C_5H_4) 53.3 (s, $C_{ipso}C_5H_4$), −6.0 (s, $SiMe_2$), −6.8 (s, $SiMe_2$), −32.4 (s, WMe)
2	[W{(η-C_5H_4)$SiMe_2$(η-C_5H_4)}MeH] $C_{13}H_{18}SiW$ Mw Yellow crystalline solid	^{1}H NMR (C_6D_6 500 MHz): 4.93 (m, 2H, C_5H_4), 4.62 (m, 2H, C_5H_4), 3.63 (m, 2H, C_5H_4), 3.55 ppm (m, 2H, C_5H_4), 0.30 (s, 3H, $SiMe_2$), 0.22 ppm (s, 3H, $SiMe_2$), −0.05 ppm (s, 3H, WMe), −10.26 ppm (s, 1H, WH, $^1J_{WH} = 80.82$ Hz.)
3	[W{(η-C_5H_4)$SiMe_2$(η-C_5H_4)}O] $C_{12}H_{14}SiWO$ Mw 386.18 Red/blue crystalline solid Elemental Analysis: Found (Calc.) C % 37.18 (37.32) H % 4.14 (3.65) FAB$^+$ Mass Spectrometry: $m/z = 387$ (40%) [M]$^+$ IR (Nujol): ν(W=O) 869 cm^{-1}	[a]
4	[W{(η-C_5H_3TMS)$SiMe_2$(η-C_5H_3TMS)}Cl_2] $C_{18}H_{30}Cl_2Si_3W$ Mw = 585.45 Dark green powder Elemental Analysis: Found (Calc.) C % 37.82 (36.93) H %5.19 (5.16) FAB$^+$ Mass spectrometry: $m/z = 386$ (100%) [M]$^+$, 549 (45%) [M − Cl]$^+$	^{1}H NMR (C_6D_6 500 MHz): 5.22 (m, 2H, C_5H_3), 5.40 (m, 2H, C_5H_3), 6.60 (m, 2H, C_5H_3), 0.40 (s, 18H, $SiMe_3$), 0.32 (s, 3H, $SiMe_2$), 0.19 (s, 3H, $SiMe_2$) ^{13}C{^{1}H} NMR ($C_6D_6$126 MHz): 129.0 (s, C_5H_3), 84.3 (s, C_5H_3), 83.7 (s, C_5H_3), 82.9 (s, C_5SiMe_3), 71.5 (s, C_{ipso}), 1.2 (m, $SiMe_3$), −3.8 (s, $SiMe_2$), −4.2 (s, $SiMe_2$)
5	[W{(η-C_5H_3TMS)$SiMe_2$(η-C_5H_3TMS)}H_2] $C_{18}H_{32}Si_3W$ Mw 516.56 Yellow crystals Elemental Analysis: Found (Calc.) C % 38.30 (41.85), H % 5.97 (6.24) IR (Nujol) 1871 cm^{-1} ν(W–H)	^{1}H NMR (C_6D_6 500 MHz) 4.99 (m, 2H, C_5H_3), 4.32 (m, 2H, C_5H_3), 4.24 (m, 2H, C_5H_3), 0.34 (s, 18H, $SiMe_3$), 0.25 (s, 3H, $SiMe_2$), −0.16 (s, 3H, $SiMe_2$), −10.31 (s, $^1J_{WH} = 83.8$, 1H, WH_2), −10.68 (s, $^1J_{WH} = 83.0$, 1H, WH_2)
7	[Nb{(η-C_5H_3TMS)$SiMe_2$(η-C_5H_3TMS)}Cl_2] (*rac* + *meso*-mixture) $C_{18}H_{30}Cl_2Si_3Nb$ Mw = 494.51 Brown powder Elemental Analysis: Found (Calc.) C % 42.85 (43.72) H % 5.98 (6.11) FAB$^+$ Mass spectrometry: $m/z = 493$ (40%) [M]$^+$, 458 (80%) [M − Cl]$^+$, 424 (83%) [M − 2Cl]$^+$ ESR: CH_2Cl_2, 10 lines, $g_{iso} = 1.988$, $\lvert a^{93}\text{Nb}\rvert_{iso} = 106$ G	
8	[Nb{(η-C_5H_3TMS)$SiMe_2$(η-C_5H_3TMS)}(η^2-BH_4)] (*rac* + *meso*-mixture) $C_{18}H_{34}BNbSi_3$ Green crystals Mw = 438.44 Elemental Analysis: Found (Calc.) C % 48.19 (49.31) H % 7.57 (7.82) B % 2.23 (2.47) IR (Nujol) 2462, 2422, 2362, 2336 ν(B–$H_{terminal}$) 1728, 1715, 1642, 1631 ν(B–$H_{bridging}$)	^{1}H NMR (d^8-toluene 300 MHz) *rac*-isomer: 6.10 (m, 2H, C_5H_3), 5.43 (m, 2H, C_5H_3), 5.39 (m, 2H, C_5H_3), 0.28 (s, 18H, $SiMe_3$), −0.52 (s, 6H, $SiMe_2$), −0.47 (s, 6H, $SiMe_2$) *meso*-isomer: 5.83 (m, 2H, C_5H_3), 5.67 (m, 2H, C_5H_3), 4.97 (m, 2H, C_5H_3), 0.29 (s, 18H, $SiMe_3$), 0.55 (s, 6H, $SiMe_2$) ^{11}B NMR $C_6D_5CD_3$ 96.27 MHz, 38.6 (m, BH_4)

NMR data are given as chemical shift (δ) [multiplicity, relative intensity, assignment, coupling] at 298 K unless otherwise stated.
All IR data are expressed in wavenumbers (cm^{-1}). For the FAB mass spectrometry data, the characteristic isotope patterns were observed.
[a] Low solubility in common solvents prevented reliable NMR measurements.

TMS groups in *ansa*-metallocenes could induce changes in the structural properties such that these species' behaviour resembles more closely that of their non-bridged analogues.

The room temperature ^{1}H NMR spectra of compound **8** showed the presence of both *rac*- and *meso*-isomers, in the ratio of 1:2. In order to investigate the exchange between bridging and terminal hydrogens in the BH_4 ligand in compound **8**, a variable temperature ^{1}H NMR study was undertaken. Partial variable temperature ^{1}H NMR ($C_6D_5CD_3$) spectra between 193 and 363 K are shown in Fig. 2. At high temperature, exchange is fast on the NMR timescale and a single broad resonance is observed at δ −5.1 ppm. As temperature is decreased this resonance

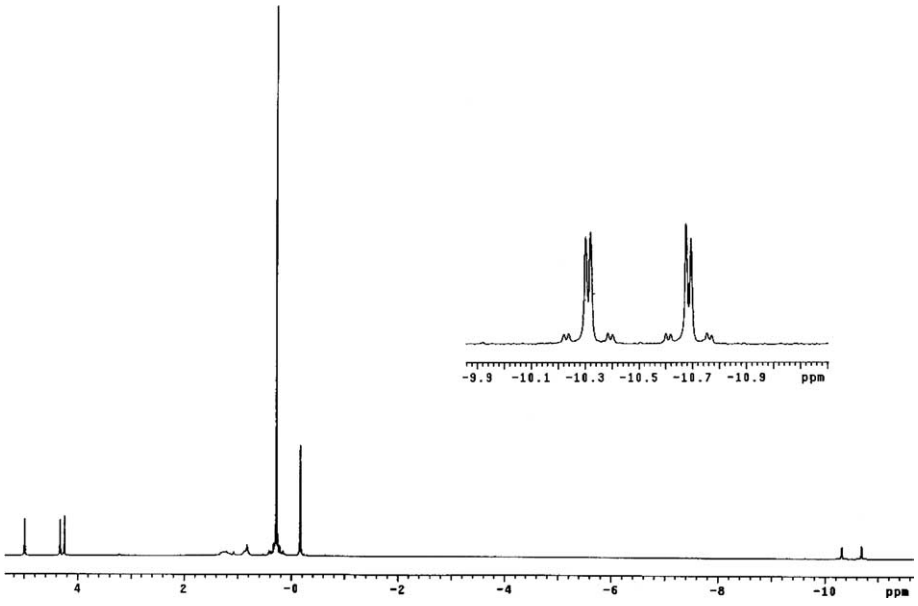

Fig. 1. ^{1}H NMR spectrum of [W{(η-C_5H_3TMS)$SiMe_2$(η-C_5H_3TMS)}H_2] (**5**) (the high field region is magnified).

Table 2
$^1J_{WH}$ and selected infrared data for selected tungstenocene dihydrides

Compound	$^1J_{WH}$ (Hz)	ν(W–H) (cm^{-1})	Ref.
[W(η-C_5H_5)$_2H_2$]	73	1896[a]	[52,78]
[W{(η-C_5H_3TMS)$SiMe_2$(η-C_5H_3TMS)}H_2] (**5**)	84, 80	1895, 1871[a]	
[W{(η-C_5H_4)$SiMe_2$(η-C_5H_4)}H_2]	79	1865[a]	[25]
[W{(η-C_5H_4)C_2Me_4(η-C_5H_4)}H_2]	80	1875, 1860[b]	[25]
[W{(η-C_5H_4)CMe_2(η-C_5H_4)}H_2]	92	1833, 1823[a]	[19]

[a] Nujol mull.
[b] KBr disc.

broadens until coalescence occurs at $T_c = 291 \pm 3$ K. Below the coalescence temperature T_c a broad resonance is observed centred at δ 5.65 ppm, corresponding to the bridging M–H–B protons. There are also three singlets, at δ −14.79, −14.91 and −15.31 ppm, corresponding to the terminal B–H protons of the *rac*- and *meso*-isomers. The free energy barrier $\Delta G^{\ddagger}$ at the coalescence temperature to bridge-terminal hydrogen exchange (calculated according to equation: $\Delta G^{\ddagger}$ (kJ mol^{-1}) $= 10^{-3}[RT_c(22.96 + \ln(T_c/\Delta v))]$) was evaluated from a variable temperature ^{1}H NMR study to be $\Delta G^{\ddagger} = 48.1 \pm 1$ kJ mol^{-1}. This is within the same range with the values found for related niobium metallocene tetrahydroborate complexes (Table 4). Here we assumed that $\Delta S^{\ddagger}$ for the exchange process is essentially the same for all species, and exchange proceeds via the same mechanism in all cases. The presence of an *ansa*-bridge reduces $\Delta G^{\ddagger}$ for the exchange process for the niobium complexes. The effect is most pronounced when the bending angle β is reduced the most, as in the case of the methylene-bridged compound. A silicon- or ethylene-bridge has a less marked effect both in the reduction of $\Delta G^{\ddagger}$ and the reduction of β (Tables 3 and 4). The barrier to exchange of the TMS substituted compound is similar to that for the unsubstituted silicon-bridged compound, and is consistent with the similarity in structural properties between compound **8** and the unsubstituted silicon-bridged compound. Density functional theoretical calculations (DFT) rationalised the changes in structure and reactivity of metallocenes upon introduction of an *ansa*-bridge and provided an explanation for the dynamic properties of related tetrahydroborate complexes [28,32,60,61]. A mechanism proposed for bridge-terminal hydrogen exchange is shown in Fig. 3. Based on the analogy between **8** and our earlier systems (described by NMR experiments and DFT modelling [28,32,60,61]), we assumed that at the mid-point of the exchange reaction the interchanging hydrogens are in equivalent positions. In the mechanism proposed, this equivalence is ensured by the presence of a mirror plane over *xz*. As a result H_a stays in the same position throughout the exchange process. The energy difference between the ground and transition states for the compounds studied was found to be in good agreement with the experimental values of $\Delta G^{\ddagger}$, making the proposed mechanism a good candidate for the exchange process. The introduction of an *ansa*-bridge increases the angle between the rings, α, and decreases the bending angle, β. This is manifested most

Table 3
Structural parameters for relevant *ansa*-metallocenes

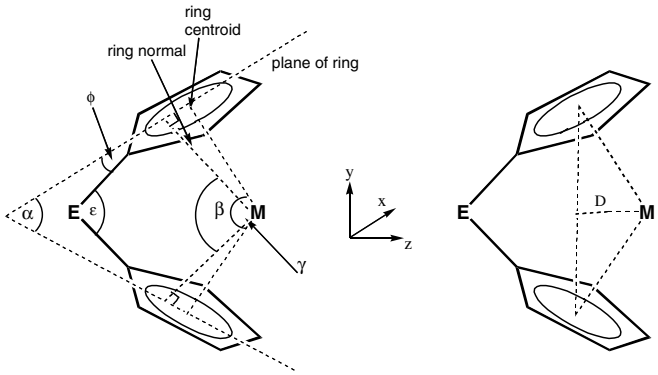

Compound	α (°)	β (°)	C_{ipso}–C_{ipso} (Å)	Ref.
(a) *Ansa*-tungstenocenes				
[W{(η-C_5H_3TMS)$SiMe_2$(η-C_5H_3TMS)}H_2] (**5**)	44.9	135.1	2.728	
[W{(η-C_5H_4)$SiMe_2$(η-C_5H_4)}Me_2]	50.4	129.6	2.660	[25]
[W{(η-C_5H_4)C_2Me_4(η-C_5H_4)}Me_2]	50.9	129.1	2.606	[25]
[W{(η-C_5H_4)CMe_2(η-C_5H_4)}Me_2]	60.9	119.1	2.273	[14]

Compound	α (°)	β (°)	γ (°)	ϕ (°)	C_{ipso}–C_{ipso} (Å)	Ref.
(b) *Ansa*-niobocene tetrahydroborate complexes						
[Nb(η-C_5H_5)$_2$(η^2-BH_4)]	50.2	129.8	130.0			[79,80]
[Nb{(η-C_5H_4)C_2Me_4(η-C_5H_4)}(η^2-BH_4)]	52.2	127.8	134.8	−2.5	2.685	[30]
[Nb{(η-C_5H_4)$SiMe_2$(η-C_5H_4)}(η^2-BH_4)]	52.8	127.2	135.7	20.6	2.699	[30]
meso-[Nb{(η-C_5H_3TMS)$SiMe_2$(η-C_5H_3TMS)}(η^2-BH_4)] (**8**)	53.0	127.0	135.1	19.8	2.704	
[Nb{(η-C_5H_4)CMe_2(η-C_5H_4)}(η^2-BH_4)]	65.9	114.1	125.0	17.0	2.266	[9,30]

N.B. Average value of ϕ used.

in the case of the methyl-bridged compound. This structural change reduces the covalent M–BH_4 interaction in the groundstate, while increasing the binding in the proposed transition state. This as a result facilitates the interchanging of the terminal and bridging hydrogens in the η^2-BH_4 unit [32]. In the case of the compound **8**, these factors are shown to reflect those found in the unsubstituted silicon- and ethyl-bridged compounds.

2.3. IR spectra

Compound [W{(η-C_5H_4)$SiMe_2$(η-C_5H_4)}O] (**3**) was characterised by elemental analysis, FAB mass spectrometry and infrared spectrometry (Table 1). The infrared stretching frequency was observed at 869 cm^{-1}. This is comparable to the values observed for *v*(W=O) in the related *oxo*-tungsten complexes [W{(η-C_5H_5)$_2$}O] of 799–879 cm^{-1}, and [W{(η-C_5H_4Me)$_2$}O], of 850 cm^{-1} [54,55].

The infrared spectrum of **5** (Nujol) showed two strong bands at 1895 and 1871 cm^{-1}, attributed to W–H stretching modes. Table 4 gives a comparison of *v*(W–H) stretching frequencies within the series. The values of *v*(W–H) show that the presence of an *ansa*-bridge reduces the stretching frequency, suggestive of a weakened W–H bond. This is most striking in the case of the methylene-bridged dihydride [W{(η-C_5H_4)CMe_2(η-C_5H_4)}H_2]. Compound **5** shows *v*(W–H) values between those of the unsubstituted silicon-bridged and the non-bridged analogue; this indicates that the trimethylsilyl groups have the effect of reducing the strain on the bridged system. DFT calculations have shown that, as the angle between the rings α is increased and thus the corresponding bending angle β is decreased, additional ligands at the metal centre of a metallocene become more weakly bound [32]. Compound **5** has a bending angle β of 135.13°, compared to 129.6° for [W{(η-C_5H_4)$SiMe_2$(η-C_5H_4)}H_2] [25]. It can be seen that the TMS groups have the effect of increasing the bending angle β relative to the unsubstituted silicon-bridged *ansa*-tungstenocene. As a result the stretching frequency of W–H is increased, suggesting a relatively stronger bond.

The IR spectrum of the compound **8** shows four bands in the terminal B–H region at 2462, 2422, 2362, and 2336 cm^{-1} and four bands in the bridging H–B region at 1728, 1715, 1642, and 1631 cm^{-1}. This is consistent with the existence of both *rac*- and *meso*-isomers. The bands were assigned by analogy to [Nb(η-C_5H_5)$_2$(η^2-BH_4)] and are consistent with a bidentate η^2-BH_4 binding mode [62]. Covalent interaction between the metal and the BH_4 unit is shown by the difference in energy between the terminal B–H and bridging B–H stretches, with the terminal B–H bond stretches being higher in energy. These stretching frequencies are compared to other selected Group 5 metallocene tetrahydroborate complexes (Table 5). The relationship between the average symmetric and asymmetric

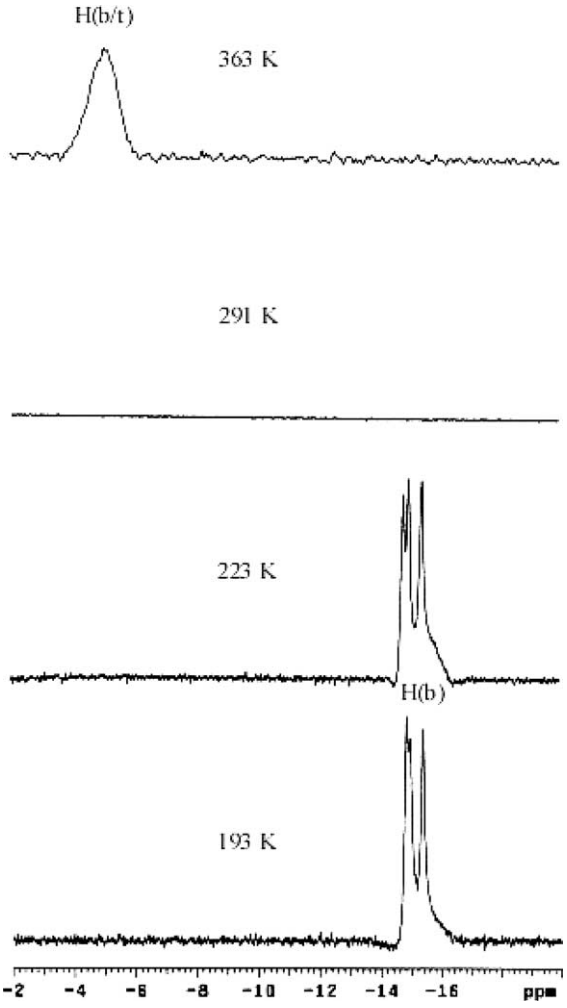

Fig. 2. Partial variable temperature ^{1}H NMR spectra of the compound [Nb{(η-C_5H_3TMS)$SiMe_2$(η-C_5H_3TMS)}(η^2-BH_4)] (**8**).

stretching frequencies for the B–H_t and B–H_b bonds has been used as a gauge of the M–BH_4 covalent interaction [63]. The data suggest there is a strengthening of the B–H_b bonds and weakening of the B–H_t bonds in the methylene-bridged species ***B*** relative to the non-bridged analogue, suggesting a reduced M–BH_4 covalent interaction. The average stretching frequencies for the silicon- and ethylene-bridged complexes, ***C*** and ***D***, are similar to the non-bridged analogue ***A***. Earlier DFT studies have shown that as the bending angle β is reduced, two of the metal d-orbitals become more involved in metal-ring bonding and are less available for binding other ligands [32]. Complex **8** shows an average B–H_b stretching frequency expected for a silicon-bridged compound. The B–H_t stretching frequency is however lower than expected, indicating an increased B–H_t bond strength compared to the non-substituted silicon-bridged compound ***D***.

2.4. X-ray diffraction studies

A search of the Cambridge Structural Database revealed that a total of 239 *ansa*-metallocenes containing $SiMe_2$ as the bridging unit have been reported so far. However, only 7 of these are niobocenes [9–13,20,30] and 6 are tungstenocenes [17,25]. Tungsten- and niobium-hydrides of this family are still rare examples, probably on the account of their extremely high reactivity and particularly their air- and moisture-sensitivity. Crystals suitable for single crystal X-ray structural determination were obtained for the hydrides [W(L2)H_2] (**5**) and [Nb(L2)(η^2-BH_4)] (**8**), where L2 = [(η-C_5H_3TMS)$_2SiMe_2$]$^{2-}$. ORTEP diagrams for these compounds are presented in Figs. 4(a) and (b) and Fig. 5, and relevant molecular parameters are listed in Table 6. In all cases, molecular structural determinations are consis-

Table 4
Free energy barrier, $\Delta G^{\ddagger}$ (at T_c) to bridge-terminal hydrogen exchange and bending angle β for niobium metallocene tetrahydroborate complexes

Compound	$\Delta G^{\ddagger}$ (kJ mol^{-1})	β (°)	Ref.
[Nb(η-C_5H_5)$_2$(η^2-BH_4)]	61.1 ± 1	129.8	[79,80]
[Nb{(η-C_5H_4)CEt_2(η-C_5H_4)}(η^2-BH_4)]	35.8 ± 1	115.6	[30]
[Nb{(η-C_5H_4)C_2Me_4(η-C_5H_4)}(η^2-BH_4)]	49.9 ± 1	127.8	[30]
[Nb{(η-C_5H_4)$SiMe_2$(η-C_5H_4)}(η^2-BH_4)]	49.3 ± 1	127.2	[30]
[Nb{(η-C_5H_3TMS)$SiMe_2$(η-C_5H_3TMS)}(η^2-BH_4)] (8)	48.1 ± 1	127.0	

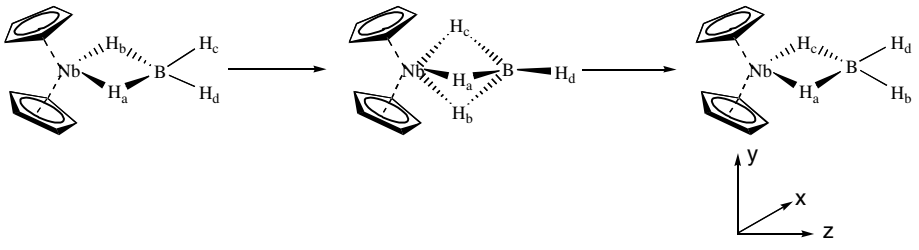

Fig. 3. Proposed mechanism for bridge-terminal hydrogen exchange in niobocene tetrahydroborate complexes.

Table 5
Selected IR stretching frequencies for niobium metallocene tetrahydroborate complexes

Compound	ν(B–H$_t$) (cm^{-1})	ν(B–H$_b$) (cm^{-1})	Ref.
[Nb(η-C_5H_5)$_2$(η^2-BH_4)] (**A**)	2460, 2423	1745, 1650	[81]
[Nb{(η-C_5H_4)CEt_2(η-C_5H_4)}(η^2-BH_4)] (**B**)	2442, 2395	1715, 1703	[30]
[Nb{(η-C_5H_4)C_2Me_4(η-C_5H_4)}(η^2-BH_4)] (**C**)	2465, 2427	1712, 1661	[30]
[Nb{(η-C_5H_4)$SiMe_2$(η-C_5H_4)}(η^2-BH_4)] (**D**)	2460, 2410	1703, 1652	[30]
[Nb{(η-C_5H_3TMS)$SiMe_2$(η-C_5H_3TMS)}(η^2-BH_4)] (**8**)	2462, 2422	1728, 1715	
	2362, 2336	1642, 1631	

tent with the observations made by elemental analysis and NMR spectroscopy. The slow cooling of a concentrated solution of compound **5** in pentane to −80 °C gave single crystals suitable for X-ray molecular structure determination, which proved to be those of the *meso*-isomer. The asymmetric unit contains two (crystallographically unique) identical molecules. The structural parameters of **5** are similar to those of the silicon- and ethyl-bridged compounds but the rings are far more constrained in the case of the methyl-bridged compounds. The increased bending of the rings in the single-carbon bridged compounds corresponds to a significant decrease in the C_{ipso}–C_{ipso} distance. It is also noted that the angles ϕ are large in the case of single atom bridges; for compound **5**, ϕ were found to be 24.8° and 25.1°, i.e. somewhat larger than the ϕ values observed for the unsubstituted silicon-bridged analogue (of 21.9° and 20.7°) [25]. Note that the ϕ values found for the ethylene-bridged analogous compound were 3.8° and 3.3° [25].

Slow cooling of a concentrated solution of compound **8** in toluene to −80 °C afforded single crystals of the *meso*-isomer suitable for X-ray molecular structure determination, however the quality of these deteriorated rapidly during the data collection despite being handled under inert atmosphere and at low temperature. This accounts for the low data quality and the structure assignment is supported by evidence from other spectroscopic investigations. Selected interatomic distances and angles and other structural information are shown in Table 6. The molecular structure is shown in Fig. 5 and details of the structure determination are given in Table 7. Selected structural parameters for compound **8** are compared to other bridged and non-bridged niobocene tetrahydroborate compounds in Table 3b. The greatest influence on the structure is exerted by a single carbon-bridge. The bending angle β is reduced ca. 16° in the compound with the CMe_2 bridging unit. This compares to a reduction of ca. 2–3° in the case of the silicon- and ethylene-bridged compounds and compound **8**. There is a large deviation from planarity at the *ipso*-carbon atoms, with an average value of ϕ of ca. 17–20° for the single atom-bridged compounds, whereas for the ethylene-bridged compound $\phi = -2.5°$. Compound **8** shows similar structural properties to the unsubstituted silicon- and ethylene-bridged, and the non-bridged analogue.

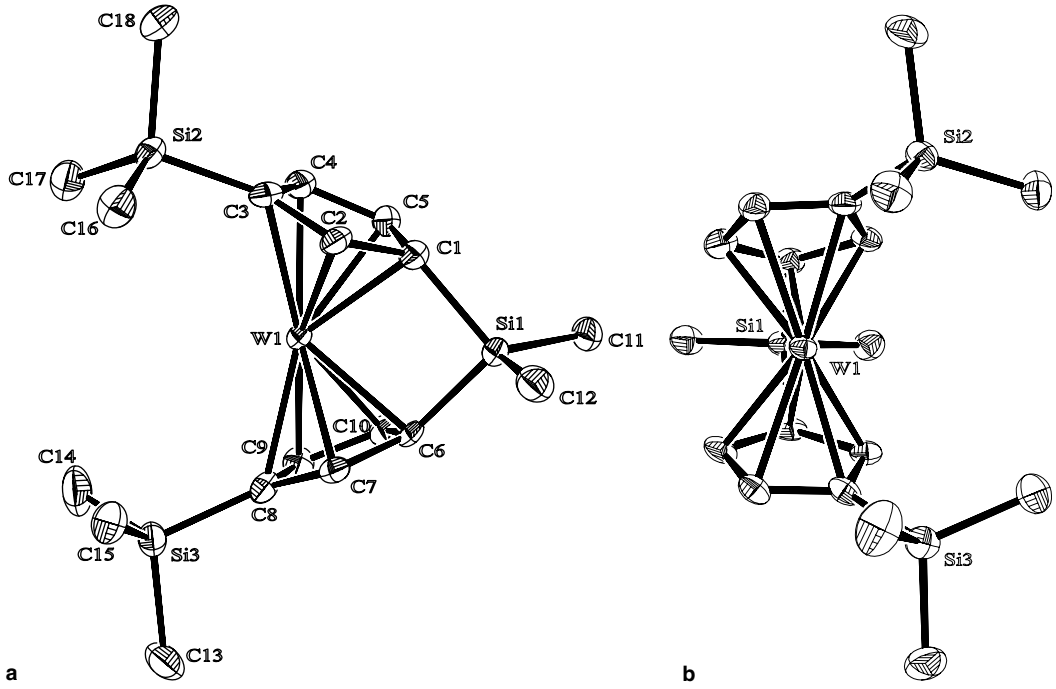

Fig. 4. (a) Molecular structure of *meso*-[W{(η-C_5H_3TMS)$SiMe_2$(η-C_5H_3TMS)}H_2] (**5**). (b) Alternative view of the molecular structure of *meso*-[W{(η-C_5H_3TMS)$SiMe_2$(η-C_5H_3TMS)}H_2] (**5**). Organic hydrogens are omitted for clarity and metal-bound hydrogens could not be located with precision.

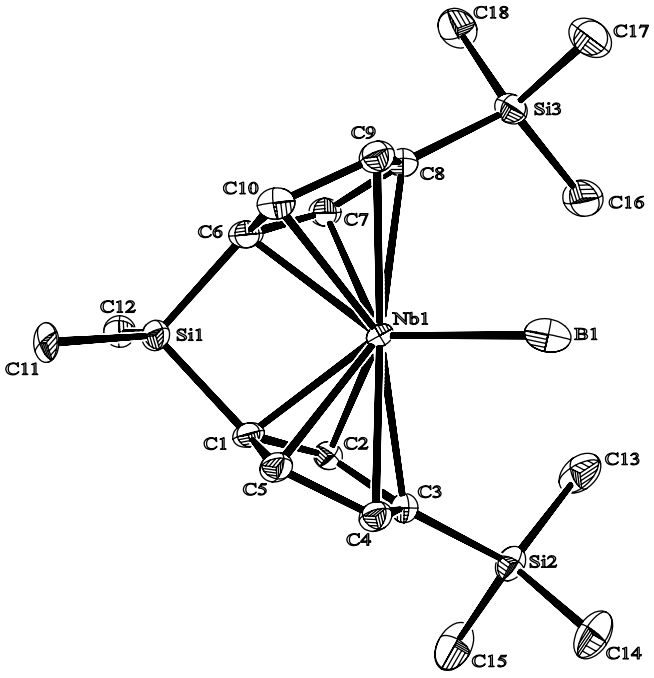

Fig. 5. Molecular structure of *meso*-[Nb{(η-C_5H_3TMS)$SiMe_2$(η-C_5H_3TMS)}(η^2-BH_4)] (**8**). Organic hydrogens are omitted for clarity and metal-bound hydrogens could not be located with precision.

Table 6
Selected interatomic distances and angles for *meso*-[W{(η-C_5H_3TMS)-$SiMe_2$(η-C_5H_3TMS)}H_2] (**5**) and *meso*-[Nb{(η-C_5H_3TMS)$SiMe_2$(η-C_5H_3TMS)}(η^2-BH_4)] (**8**)

	Length (Å)		Angle (°)
Compound **5**			
W–Cp^1_{cent}	1.928	Between Cp planes, α	44.87
W–Cp^1_{ave}	2.281	Cp^1_{norm}–W–Cp^2_{norm}, β	135.13
W–Cp^2_{cent}	1.928	C_{ipso}–Si(1)–C_{ipso}, ε	93.61
W–Cp^2_{ave}	2.282	C_{ipso}–Cp plane, φ	24.84, 25.06
C_{ipso}–C_{ipso}	2.728	Cp^1_{cent}–W–Cp^2_{cent}, γ	142.42
Compound **8**			
Nb–Cp^1_{cent}	2.040	Between Cp planes, α	53.0
Nb–Cp^1_{ave}	2.372	Cp^1_{norm}–Nb–Cp^2_{norm}, β	127.0
Nb–Cp^2_{cent}	2.042	Cp_{ipso}–Si(1)–Cp_{ipso}, ε	92.4
Nb–Cp^2_{ave}	2.378	C_{ipso}–Cp plane, φ	20.7, 18.9
C_{ipso}–C_{ipso}	2.704	Cp^1_{cent}–Nb–Cp^2_{cent}, γ	135.1

Cp^1 = Ring C(1)–C(5), Cp^2 = Ring C(6)–C(10).

3. Study of the methane elimination from [W{(η-C_5H_4)-$SiMe_2$(η-C_5H_4)}MeH] (2)

Studies have previously been made into the thermal stability of non-bridged alkyl-hydride tungstenoces and their *ansa*-bridged analogues [64,65]. For [W{(η-C_5H_4)CMe_2-

Table 7
Crystallographic data for compounds **5** and **8**

Compound	**5**	**8**
Empirical formula	$2C_{18}H_{30}Si_3W$	$C_{18}H_{30}BNbSi_3$
Formula weight	1029.09	434.41
Temperature (K)	150	150
Wavelength (Å)	0.71069	0.71069
Crystal system	triclinic	monoclinic
Space group	$P\bar{1}$	$P2_1/c$
Unit cell dimensions		
a (Å)	11.1170(5)	10.5300(9)
b (Å)	14.6840(7)	17.3810(14)
c (Å)	14.9170(7)	13.2200(8)
α (°)	97.991(3)	90
β (°)	110.571(3)	110.375(4)
γ (°)	104.806(3)	90
Volume (Å^3)	2132.5	2268.2
Z	2 ($Z' = 2$)	4
Density (calculated) (Mg m^{-3})	1.60	1.27
Absorption coefficient (mm^{-1})	5.58	0.69
F(000)	1011.44	895.97
Crystal size (mm)	$0.60 \times 0.20 \times 0.20$	$0.10 \times 0.10 \times 0.10$
Theta range for data collection (°)	1–25	0.00–26.57
Index ranges	$0 \leqslant h \leqslant 13$, $-18 \leqslant k \leqslant 17$, $-18 \leqslant l \leqslant 16$	$0 \leqslant h \leqslant 13$, $0 \leqslant k \leqslant 21$, $-16 \leqslant l \leqslant 15$
Reflections collected	12365	18752
Independent reflections	6881 [$R_{int} = 0.04$]	4496 [$R_{int} = 0.13$]
Absorption correction	semi-empirical from equivalents	semi-empirical from equivalents
Maximum and minimum transmission	0.27 and 0.33	0.93 and 0.93
Refinement method	full-matrix least-squares on *F*	full-matrix least-squares on *F*
Data/parameters	5512/397 [$I > 3\sigma(I)$]	2831/163 [$I > 4\sigma(I)$]
Goodness-of-fit	1.08	1.0785
R indices	$R_1 = 0.034$, $wR_2 = 0.038$	$R_1 = 0.127$, $wR_2 = 0.071$
Largest difference peak and hole (e Å^{-3})	2.37 and −2.25	2.72 and −2.69

(η-C_5H_4)}MeH] [19,14,60], the presence of the CMe_2 *ansa*-bridge was shown to induce a substantially increased thermal stability.

For [W(η-C_5Me_5)$_2$MeH] and [W{(η-C_5Me_4)$SiMe_2$(η-C_5Me_4)}MeH] [65] the *ansa*-bridge also *inhibits* the reductive elimination of CH_4, however, the same bridge was found to significantly *promote* reductive elimination in the related tantalum systems [21]. The investigation of the thermal stability of [W{(η-C_5H_4)$SiMe_2$(η-C_5H_4)}MeH] discussed here provides further information regarding the changes imparted on the reactivity of tungstenocene compounds upon the introduction of an *ansa*-bridge.

When the reductive elimination of methane from [W(η-C_5H_5)$_2$Me(H)] is performed at sufficiently low concentrations to avoid bimolecular reaction pathways, the elimination proceeds via an intramolecular mechanism supported by the first-order kinetics of the reaction [64,65]. The methyl-bridged *ansa*-tungstenocene was observed to have increased thermal stability relative to the non-bridged compound. This is of particular significance since both complexes display intramolecular hydrogen exchange between alkyl ligand and hydride sites [64,65]. The increased thermal stability in the CMe_2 *ansa*-compound is supported by a DFT study into hydrogen exchange and methane elimination from [W(η-C_5H_5)$_2$MeH] and [W{(η-C_5H_5)-CH_2(η-C_5H_5)}-MeH]. This showed that the tungstenocene [W(η-C_5H_5)$_2$] has a lowest energy structure in the triplet state; geometry optimisation predicts the non-bridged tungstenocene to have a ring angle of 172.1° due to a Jahn–Teller distortion [60]. This compares to a ring angle (β) of 127° in [W{(η-C_5H_4)CMe_2(η-C_5H_4)}Me_2] [14] and 136° in [W{(η-C_5H_4)-$SiMe_2$(η-C_5H_4)}Me_2] [25]. This explains the differences in reaction enthalpies, both calculated and experimental, that enable the thermal elimination of methane to occur at much lower temperature for [W{(η-C_5H_5)$_2$}Me(H)] than for the CMe_2-bridged analogue.

First-order plots for the elimination of methane from **2** over the temperature range 55–80 °C are shown in Fig. 6. Reactions were followed by monitoring the decrease in intensity of a selected resonance (i.e. the hydride resonance, at δ −10.26) of the starting complex in C_6D_6. Reaction temperatures were maintained by using constant temperature baths (±1 °C). The high-field ^{1}H NMR spectra recorded at different times at 65 °C are shown in Fig. 7. The NMR tubes were sealed and total submersion in the

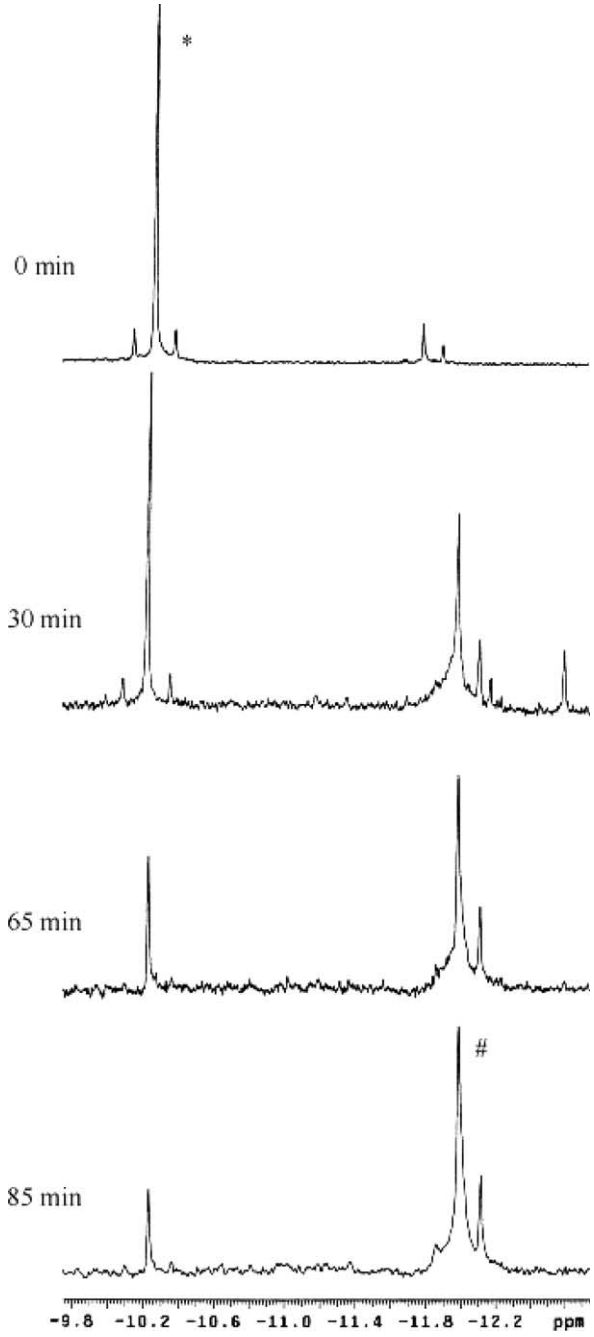

Fig. 7. Selected high field ^{1}H NMR spectra of elimination of methane from [W{(η-C_5H_5)$SiMe_2$(η-C_5H_5)}MeH] **(2)** at 65 °C (* denotes hydride peak in compound **2**, # denotes hydride peaks appearing in the high field region).

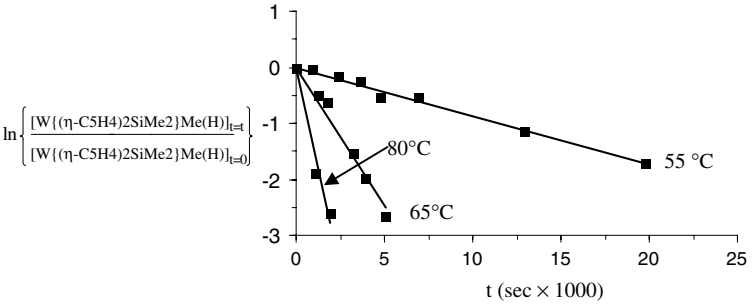

Fig. 6. First-order plots for the elimination of methane from [W{(η-C_5H_4)$SiMe_2$(η-C_5H_4)}Me(H)] (**2**) at 55, 65 and 80 °C.

baths prevented the deuterated benzene from refluxing at elevated temperatures. The rate of elimination can be calculated at each temperature, and are shown in Table 8, and activation parameters $\Delta H^{\ddagger}$ and $\Delta S^{\ddagger}$ have been calculated from an Eyring plot (Fig. 8). Table 9 shows a comparison of the activation parameters in related bridged- and non-bridged tungstenocene systems. It is believed that the alkane elimination from this type of alkyl hydride proceeds via a σ-complex intermediate [66,67]. The symmetry of the exchange pathway implies at some stage a η^2-H, H structure **I**, where both hydrogens are equidistant from the metal, as shown in Fig. 9. Elimination can occur through the η^2-H, C structure **II** or η^1-H structure **III**. Alkane elimination from an alkyl-hydride complex generates a highly reactive intermediate, which can undergo oxidative addition to other C–H bonds. Species capable of reacting with aromatic and aliphatic C–H bonds can occur upon thermolysis [53,68] or photolysis [69] of [W(η-C_5H_5)$_2$MeH]. In the absence of any suitably reactive C–H substrates, dinuclear compounds can be formed. The proposed mechanism involves the 16 electron tungstenocene intermediate [W(η-C_5H_5)$_2$] reacting with the C-H bonds in the cyclopentadienyl rings of [W{(η-C_5H_5)$_2$}MeH]. A similar reaction appears to have happened in the case of **2** even though the solution is dilute, since new peaks appear in the ^{1}H NMR spectrum, two singlets appear at δ −11.99 and −12.73 suggesting two new hydride sites (Fig. 7). The possible dinuclear compounds formed are shown in Fig. 10.

It appears that, under the conditions studied, the activation parameters at the methane elimination from [W{(η-C_5H_4)SiMe$_2$(η-C_5H_4)}Me$_2$] are similar to those found for

Table 8
Rates of methane elimination from [W{(η-C_5H_4)SiMe$_2$(η-C_5H_4)}Me(H)] (**2**)

Temperature (°C)	k, rate of elimination (10^{-4} s^{-1})
55	0.87
65	4.98
80	14.46

Estimated uncertainty on rate constants ±20%.

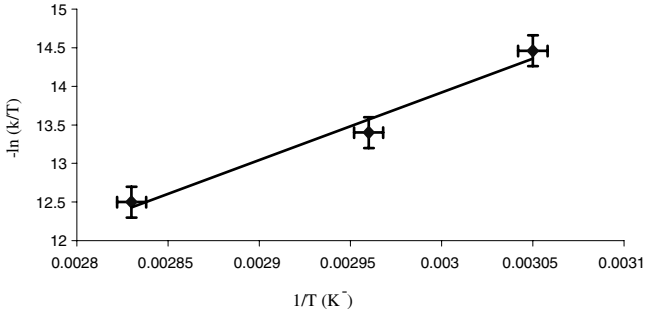

Fig. 8. Estimation of the barrier at the elimination of methane from [W{(η-C_5H_4)SiMe$_2$(η-C_5H_4)}MeH] (**2**) by the Eyring plot $y = 12389x - 22.85$ with estimated $R^2 = 0.9437$. (Eyring plot: $\ln(k/T) = -\Delta H^{\ddagger}/RT + \Delta S^{\ddagger}/R + 23.76$.) Estimated uncertainty on $k \pm 20\%$. In C_6D_6: $\Delta H^{\ddagger} = 24.6(5)$ kcal mol^{-1}, $\Delta S^{\ddagger} = -1.8(2) \times 10^{-3}$ kcal mol^{-1} and $\Delta G^{\ddagger}(273\ \text{K}) = 25.1(5)$ kcal mol^{-1}.

Table 9
Comparison of kinetic data for alkyl-hydride elimination reactions in selected tungstenoces

Compound	$\Delta H^{\ddagger}$ (kcal mol^{-1})	$\Delta S^{\ddagger}$ (kcal mol^{-1})	Selected *alkyl-H* elimination rate constants (s^{-1})	Experimental temperature interval (°C)	Solvent	Ref.
[W{(η-C_5H_4)$_2$}MeH][(a)]	25.1(3)	−4(1)	k(70.3 °C) = 0.97(20) × 10^{-4} k(80.5 °C) = 4.1(2) × 10^{-4} k(100 °C) = 18(1) × 10^{-4} (E_a = 26.4)	70–100[(b)]	10% CH_3CN 90% C_6D_6	[64]
[W{(η-C_5Me_4)$_2$}MeH]	N/A	N/A	k(100 °C) = 1.20(6) × 10^{-4}	65–112	C_6D_6	[65]
[W{(η-C_5Me_4)$_2$}($CH_2C_6H_5$)H]	29.3(8)	1.2(2)	k(100 °C) = 1.13(6) × 10^{-4}			
Ansa-[W{(η-C_5H_4)SiMe$_2$(η-C_5H_4)}MeH]	24.6(5)	−1.8(2)	k(80 °C) = 14.46(1) × 10^{-4}	55–80	C_6D_6	This work
Ansa-[W{(η-C_5Me_4)SiMe$_2$(η-C_5Me_4)}MeH]	27.3(2.6)	10(6)	k(100 °C) = 3.74(2) × 10^{-6}	100–159	C_6D_6	[17]

N.B. [(a)]For [W{(η-C_5H_4)$_2$}MeH], DFT calculated activation energy E_a = 19.12 kcal mol^{-1} (80 kJ mol^{-1}) and overall reaction energy = 19.6 kJ mol^{-1}; for *ansa*-[W{(η-C_5H_4)CH_2(η-C_5H_4)}MeH], DFT calculated E_a = 20.31 kcal mol^{-1} (85 kJ mol^{-1}) and overall reaction energy = 78.3 kJ mol^{-1} [60]. In C_6D_6 solutions, *ansa*-[W{(η-C_5H_4)CMe_2(η-C_5H_4)}MeH] and *ansa*-[W{(η-C_5H_4)CMe_2(η-C_5H_4)}EtH] are stable with respect to reductive elimination of alkane up to 120 °C; [14].
[(b)]Slow decomposition above 48 °C [64].

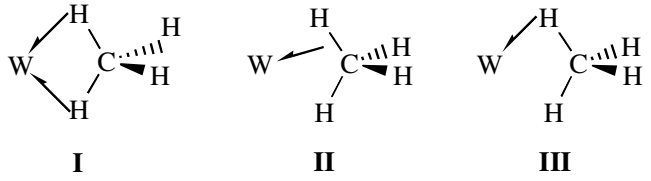

Fig. 9. Intermediates formed at the elimination of methane from alkyl-hydride tungstenocenes.

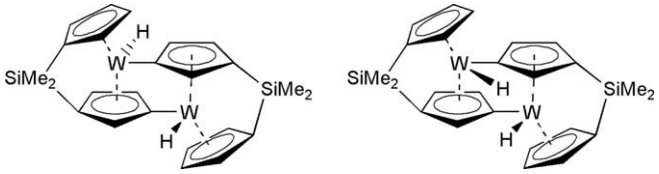

Fig. 10. Proposed species formed at the thermolysis of [W{(η-C_5H_4)$SiMe_2$(η-C_5H_4)}MeH] (**2**).

[W{(η-C_5H_5)$_2$}RH] (where R = Me, C_6H_5) [64,65]. The effect on the thermal stability is most pronounced in the case of a methylene-bridge [60], and it decreases as the *ansa*-bridge becomes less constraining (i.e. as the bending angle β is increased).

4. Conclusion

Studies of the synthesis of neutral W(IV) and Nb(V) complexes have led to the isolation and characterisation of [W(L1)MeI] (**1**), [W(L1)MeH] (**2**) and [W(L1)O] (**3**), [W(L2)Cl_2] (**4**), [W(L2)H_2] (**5**), [W(L2)H_3][BF_4] (**6**), [Nb(L2)Cl_2] (**7**) and [Nb(L2)(η^2-BH_4)] (**8**), where L1 = [(η-C_5H_4)$_2SiMe_2$]$^{2-}$ and L2 = [(η-C_5H_3TMS)$_2SiMe_2$]$^{2-}$. These have been characterised spectroscopically and for **5** and **8** structures were confirmed by X-ray diffraction.

We have shown that the silicon-bridged trimethylsilylsubstituted compounds have properties that are intermediate between the unsubstituted silicon-bridged *ansa*-compounds and the corresponding non-bridged compounds.

5. Experimental

5.1. General

All preparations and manipulations of air- and/or moisture-sensitive materials were carried out under an inert atmosphere of dinitrogen, using standard Schlenk line techniques, or in an inert atmosphere dry box containing dinitrogen. For the dry box dinitrogen was purified by passage through columns filled with molecular sieves (4 Å) and BASF catalyst. Solvents and solutions were transferred through stainless steel cannulae, using a positive pressure of inert gas. Filtrations were similarly performed using modified stainless steel cannulae fitted with glass fibre filter discs. All glassware and cannulae were thoroughly cleaned and then dried at 150 °C before use. All solvents were deoxygenated before use, either by repeated evacuation followed by admission of dinitrogen, or by bubbling dinitrogen through the solvent for approximately 15 min. Solvents were pre-dried over activated 4 Å molecular sieves and distilled over sodium (toluene, petroleum ether b.p. 100–120 °C), sodium/potassium alloy (diethyl ether, *n*-pentane, light petroleum ether b.p. 40–60 °C), potassium (THF, benzene), calcium hydride (acetonitrile, CH_2Cl_2) under a slow continuous stream of dinitrogen. Deionised H_2O was deoxygenated before use by bubbling dinitrogen through the solvent for approximately 15 min. Deuterated solvents for NMR spectroscopy were deoxygenated and dried over calcium hydride (d_2-dichloromethane) or potassium (d_6-benzene and d_8-toluene) and then distilled before use. NMR spectra were recorded on either a Varian Unit Plus 500: (^{1}H and ^{13}C NMR spectra were recorded at 499.868 and 125.704 MHz, respectively), or Bruker AM300 (^{1}H and ^{11}B NMR spectra were recorded at 300.1 and 96.3 MHz). The spectra were referenced internally using the residual protio solvent (^{1}H) and carbon solvent (^{13}C) resonances and measured relative to TMS (^{1}H and ^{13}C; $\delta = 0$ ppm) and $BF_3 \cdot Et_2O$ (^{11}B; $\delta = 0$ ppm).

Mass spectra (FAB) were obtained by the EPSRC Mass Spectrometry Service, Swansea. The characteristic isotope pattern was observed for all spectra. IR spectra were recorded on a Perkin–Elmer 1710 FTIR spectrometer. Samples were prepared as a Nujol mull between NaCl plates. Elemental analyses were performed by the Microanalytical Department of the Inorganic Chemistry Laboratory, Oxford.

WCl_6 (99%), $LiAlH_4$ (95%), $ZnMe_2$ (2.0 M solution in toluene), NH_4I, $NaBH_4$, $NbCl_5$, ^{n}BuLi (2.5 M solution in light petroleum ether (b.p. 40–60 °C)), HBF_4 (54 + wt% solution in diethyl ether), [Na{AlH_2($OCH_2CH_2OCH_3$)$_2$}] (3.3 M solution in toluene) and dichlorodimethylsilane (99%) were purchased from Aldrich and used as received. The following compounds were prepared by standard literature methods: [WCl_4(DME)] [70], TMSCp [71], [W{(η-C_5H_4)$SiMe_2$(η-C_5H_4)}Cl_2] [25] and $NbCl_4 \cdot 2THF$ [72]. Li_2[{(C_5H_4)$SiMe_2$(C_5H_4)}] (**Li_2L1**) was prepared by the literature method via the reaction between Na(C_5H_5) and Me_2SiCl_2, followed by deprotonation by ^{n}BuLi [25].

5.2. Preparation of [W{(η-C_5H_4)$SiMe_2$(η-C_5H_4)}Me_2]

A variation of the previously reported synthesis was used [25].

To a suspension of [W{(η-C_5H_4)$SiMe_2$(η-C_5H_4)}Cl_2] (1.04 g, 2.27 mmol) in toluene (150 cm^3) at −78 °C, a solution of $ZnMe_2$ (2.0 M solution in toluene, 12 cm^3, 6 mmol) was added dropwise. The resulting mixture was allowed to slowly warm to room temperature and then stirred overnight. The orange/brown solution was pumped to dryness under reduced pressure to remove any excess of $ZnMe_2$. The residual solid was then extracted with pentane (3×20 cm^3). The extracts were combined, concentrated

and cooled to −80 °C to yield orange crystals of [W{(η-C_5H_4)$SiMe_2$(η-C_5H_4)}Me_2]. Yield: 0.16 g, 17%.

5.3. Preparation of [W{(η-C_5H_4)$SiMe_2$(η-C_5H_4)}MeI] (1)

A solution of [W{(η-C_5H_4)$SiMe_2$(η-C_5H_4)}Me_2] (0.16 g, 0.38 mmol) in THF (50 cm^3) was added to NH_4I (0.20 g, 1.38 mmol) in a small ampoule. The orange solution was refluxed for 18 h in a constant temperature oil bath at 66 °C. The resulting green solution was pumped to dryness under reduced pressure to leave a green solid. The solid was extracted with toluene (3 × 10 cm^3). The extracts were combined and concentrated to 10 cm^3, 10 cm^3 of pentane was then added and the solution cooled to −80 °C to yield a green powder of [W{(η-C_5H_4)$SiMe_2$(η-C_5H_4)}Me(I)] (**1**). Yield: 0.038 g, 19%.

5.4. Preparation of [W{(η-C_5H_4)$SiMe_2$(η-C_5H_4)}MeH] (2)

To a green solution of compound 1 (0.038 g, 0.07 mmol) in toluene (30 cm^3) at −78 °C, a solution of [Na{AlH_2($OCH_2CH_2OCH_3$)$_2$}] in toluene (3.3 M, 0.75 cm^3, 2.5 mmol) was added. The solution was allowed to slowly warm to room temperature and stir overnight. The resulting yellow solution was cooled to 0 °C and unreacted [Na{AlH_2($OCH_2CH_2OCH_3$)$_2$}] was hydrolysed by the cautious addition of a few drops of distilled H_2O. After stirring for 30 min the reaction mixture was pumped to dryness under reduced pressure. The resulting yellow solid was extracted into pentane (3 × 10 cm^3). The extracts were combined, concentrated and cooled to −80 °C, to yield a yellow crystalline solid of [W{(η-C_5H_4)$SiMe_2$(η-C_5H_4)}Me(H)] (**2**). Yield: 0.017 g, 63%.

5.5. Preparation of [W{(η-C_5H_4)$SiMe_2$(η-C_5H_4)}O] (3)

To a solution of [W{(η-C_5H_4)$SiMe_2$(η-C_5H_4)}Cl_2] (0.075 g, 0.17 mmol) in 1/1H_2O/EtOH (40 cm^3), a few drops of saturated KOH solution in 1/1H_2O/EtOH was added with vigorous stirring. The solution changed colour from brown/green to blue. After stirring for 2 h the product was extracted into CH_2Cl_2 (3 × 25 cm^3). The CH_2Cl_2 extracts were combined and pumped to dryness under reduced pressure. The solid was extracted with toluene (3 × 5 cm^3) to give a red solution. The extracts were combined and concentrated to 5 cm^3, 5 cm^3 of pentane was then added and the solution cooled to −20 °C and then to −80 °C to yield a red/blue crystalline solid of [W{(η-C_5H_4)$SiMe_2$(η-C_5H_4)}O] (**3**). Yield: 0.030 g, 46%.

5.6. Preparation of [Li_2{(C_5H_3TMS)$SiMe_2$(C_5H_3TMS)}] (**Li_2L2**)

To a solution of LiCpTMS (3.5 g, 24.3 mmol) in THF (60 cm^3) at −78 °C, dichlorodimethylsilane (1.463 cm^3, $d = 1.07$ g cm^{-3}, 12.13 mmol) was added with vigorous stirring. The reaction mixture was allowed to slowly warm to room temperature and stirred overnight to yield a deep red solution. The solvent was removed under reduced pressure to yield a deep red oil. The oil was taken up in light petroleum ether b.p. 40–60 °C (60 cm^3). The solution was cooled to −78 °C and ^{n}BuLi (1.6 M solution in hexane, 15.5 cm^3, 24 mmol) was slowly added. A flocculent white solid was immediately formed. The mixture was allowed to warm to room temperature and stirred overnight. The air- and moisture-sensitive solid of [Li_2{(C_5H_3TMS)$SiMe_2$-(C_5H_3TMS)}] (**Li_2L2**) was washed with light petroleum ether b.p. 40–60 °C and dried under reduced pressure. Yield: 2.61 g, 63%.

5.7. Preparation of [W{(η-C_5H_3TMS)$SiMe_2$-(η-C_5H_3TMS)}Cl_2] (4)

A mixture of the two solids [WCl_4(DME)] (2.678 g, 6.44 mmol) and [Li_2{(C_5H_3TMS)$SiMe_2$(C_5H_3TMS)}] (2.678 g, 6.4 mmol) was stirred in the absence of solvent until a homogeneous mixture was formed. Diethyl ether (100 cm^3) was added at −78 °C, the resulting brown solution was allowed to warm to room temperature and stirred for 4 days. The mixture was pumped to dryness under reduced pressure. The resulting solid was extracted into pentane (3 × 20 cm^3). The pentane extracts were combined, concentrated and cooled to −80 °C to yield dark green crystals of [W{(η-C_5H_3TMS)$SiMe_2$(η-C_5H_3TMS)}Cl_2] (**4**). Yield: 0.61 g, 16%.

5.8. Preparation of [W{(η-C_5H_3TMS)$SiMe_2$-(η-C_5H_3TMS)}H_2] (5)

A suspension of $LiAlH_4$ (0.30 g, 7.9 mmol) in diethyl ether (20 cm^3) at −78 °C was added dropwise to a suspension of compound 4 (0.42 g, 0.72 mmol) in diethyl ether (30 cm^3) at −78 °C. The resulting yellow suspension was allowed to slowly warm to room temperature and stirred overnight. The suspension was filtered and the residual solid extracted into diethyl ether (3 × 40 cm^3). The diethyl ether extracts were combined and unreacted $LiAlH_4$ was hydrolysed by cautious addition of diethyl ether saturated with deionised H_2O (20 cm^3) and then deionised H_2O (10 cm^3) at 0 °C. After stirring for 30 min the organic phase was decanted off and the aqueous phase extracted with diethyl ether (3 × 20 cm^3). The yellow diethyl ether extracts were combined, washed with distilled water (10 cm^3) and pumped to dryness under reduced pressure to leave a yellow/orange oily solid. The solid was extracted into pentane (3 × 15 cm^3). The pentane extracts were combined, concentrated and cooled to −80 °C to yield yellow crystals of [W{(η-C_5H_3TMS)$SiMe_2$(η-C_5H_3TMS)}H_2] (**5**). Yield: 0.080 g, 22%.

5.9. Preparation of [W{(η-C_5H_3TMS)$SiMe_2$-(η-C_5H_3TMS)}H_3][BF_4] (6)

A dark yellow solution of compound **5** (0.025 g, 0.05 mmol) in diethyl ether (10 cm^3) was treated with a solution of HBF_4 in diethyl ether (0.066 mol dm^{-3}, 1.0 cm^3, 0.66 mmol). The resulting pale grey suspension was stirred for 30 min. The complex [W{(η-C_5H_3TMS)Si-Me_2(η-C_5H_3TMS)}H_3][BF_4] (**6**) was isolated as a white powder by filtration and washing with diethyl ether (2×10 cm^3) and then dried under reduced pressure. Yield: 0.018 g, 59%.

5.10. Preparation of [Nb{(η-C_5H_3TMS)$SiMe_2$-(η-C_5H_3TMS)}Cl_2] (7)

A mixture of the two solids $NbCl_4 \cdot 2THF$ (1.0 g, 2.64 mmol) and [Li_2\{(C_5H_3TMS)$SiMe_2$(C_5H_3TMS)\}] (0.908 g, 2.64 mmol) was stirred in the absence of solvent until a homogeneous mixture was formed. Diethyl ether (50 cm^3) was added at −78 °C, the resulting brown solution was allowed to warm to room temperature and stirred for 4 days. The mixture was pumped to dryness under reduced pressure. The resulting solid was extracted into CH_2Cl_2 (3×20 cm^3). The CH_2Cl_2 extracts were combined and pumped to dryness to yield an oily solid. The solid was washed with pentane (2×20 cm^3) at −78 °C and dried under reduced pressure to give a brown powder of [Nb{(η-C_5H_3TMS)$SiMe_2$(η-C_5H_3TMS)}Cl_2] (**7**). Yield: 0.67 g, 50%.

5.11. Preparation of [Nb{(η-C_5H_3TMS)$SiMe_2$-(η-C_5H_3TMS)}(η^2-BH_4)] (8)

A mixture of the compound **7** (0.35 g, 0.708 mmol) and $LiBH_4$ (0.17 g, 7.9 mmol) was suspended in DME (40 cm^3) at room temperature. Effervescence was observed on addition of the solvent. The brown reaction mixture was stirred overnight and then the volatiles were removed under reduced pressure. The resulting solid was extracted into petroleum ether b.p. 100–120 °C (2×30 cm^3). The petroleum ether b.p. 100–120 °C extracts were combined, concentrated and cooled to −80 °C, yielding the compound [Nb{(η-C_5H_3TMS)$SiMe_2$(η-C_5H_3TMS)}(η^2-BH_4)] (**8**) as dark green crystals. Yield: 0.18 g, 58%.

5.12. X-ray crystallography

In each case, a single crystal was selected under an inert atmosphere, encased in perfluoro-polyether oil, and mounted on the end of a glass fibre. The fibre, secured in a goniometer head was then placed under a stream of cold nitrogen maintained at 150 K and data collected on an Enraf-Nonius DIP2000 image plate diffractometer with graphite monochromated Mo Kα radiation ($\lambda =$ 0.71069 Å) The images were processed with the DENZO and SCALEPACK programs [73] and corrections for Lorentz and polarisation effects were performed. All solution, refinement, and graphical calculations were performed using the CRYSTALS and CAMERON [74,75] software packages.

The structures of were solved by direct methods using the SIR92 [76] program and refined by full-matrix least-squares procedure on F. The crystallographic data are summarised in Table 8. In each case, all non-hydrogen atoms were refined with anisotropic displacement parameters and hydrogen atoms were generated and allowed to ride on their corresponding carbon atoms with fixed thermal parameters. Empirical absorption corrections were applied [77], as well as the 3-term Chebychev polynomial weighting scheme.

The crystal structures have been deposited at the Cambridge Crystallographic Data Centre, CCDC Nos. 271121 and 271122.

Appendix A. Supplementary data

Supplementary data associated with this article can be found, in the online version, at doi:10.1016/j.poly.2005.08.025.

References

[1] F.R.W.P. Wild, L. Zsolnai, G. Huttner, H.H. Brintzinger, J. Organomet. Chem. 232 (1982) 233.
[2] F.R.W.P. Wild, M. Wasiucionek, G. Huttner, H.H. Brintzinger, J. Organomet. Chem. 288 (1985) 63.
[3] W. Kaminsky, K. Kulper, H.H. Brintzinger, F.R.W.P. Wild, Angew. Chem., Int. Ed. Engl. 24 (1985) 507.
[4] J.A. Ewen, J. Am. Chem. Soc. 106 (1984) 6355.
[5] J.A. Smith, J.V. Seyerl, G. Huttner, H.H. Brintzinger, J. Organomet. Chem. 173 (1979) 175.
[6] T.J. Katz, N. Acton, Tetrahedron Lett. 28 (1970) 2497.
[7] M. Hillman, A.J. Weiss, J. Organomet. Chem. 42 (1973) 123128.
[8] W. Mengele, J. Diebold, C. Troll, W. Roll, H.H. Brintzinger, Organometallics 12 (1993) 1931.
[9] N.J. Bailey, M.L.H. Green, M.A. Leech, J.F. Saunders, H.M. Tidswell, J. Organomet. Chem. 538 (1997) 111.
[10] N.J. Bailey, J.A. Cooper, H. Gailus, M.L.H. Green, J.T. James, M.A. Leech, J. Chem. Soc., Dalton Trans. (1997) 3579.
[11] A. Antinolo, M. Martinez-Ripoll, Y. Mugnier, A. Otero, S. Prashar, A.M. Rodriguez, Organometallics 15 (1996) 3241.
[12] A. Antinolo, A. Otero, S. Prashar, A.M. Rodriguez, Organometallics 17 (1998) 5454.
[13] A. Antinolo, I. Lopez-Solera, I. Orive, A. Otero, S. Prashar, A.M. Rodriguez, E. Villasenor, Organometallics 20 (2001) 71.
[14] A. Chernega, J. Cook, M.L.H. Green, L. Labella, S.J. Simpson, J. Souter, A.H.H. Stephens, J. Chem. Soc., Dalton Trans. (1997) 3225.
[15] D. Churchill, J.H. Shin, T. Hascall, J.M. Hahn, B.M. Bridgewater, G. Parkin, Organometallics 18 (1999) 2403.
[16] D.G. Churchill, B.M. Bridgewater, G. Parkin, J. Am. Chem. Soc. 122 (2000) 178.
[17] D.G. Churchill, K.E. Janak, J.S. Wittenberg, G. Parkin, J. Am. Chem. Soc. 125 (2003) 1403.
[18] I.V. Jourdain, M. Fourmigue, F. Guyon, J. Amaudrut, Organometallics 18 (1999) 1834.
[19] L. Labella, A. Chernega, M.L.H. Green, J. Chem. Soc., Dalton Trans. (1995) 395.

[20] P.J. Chirik, D.L. Zubris, L.J. Ackerman, L.M. Henling, M.W. Day, J.E. Bercaw, Organometallics 22 (2003) 172.
[21] J.H. Shin, G. Parkin, Chem. Commun. (1999) 887.
[22] V. Comte, O. Blacque, M.M. Kubicki, C. Moise, Organometallics 16 (1997) 5763.
[23] W.A. Herrmann, W. Baratta, E. Herdtweck, J. Organomet. Chem. 541 (1997) 445.
[24] C.E. Zachmanoglou, J.G. Melnick, B.M. Bridgewater, D.G. Churchill, G. Parkin, Organometallics 24 (2005) 603.
[25] S.L.J. Conway, T. Dijkstra, L.H. Doerrer, J.C. Green, M.L.H. Green, A.H.H. Stephens, J. Chem. Soc., Dalton Trans. (1998) 2689.
[26] D.M. Heinekey, C.E. Radzewich, Organometallics 18 (1999) 3070.
[27] F. Maseras, A. Lledos, E. Clot, O. Eisenstein, Chem. Rev. 100 (2000) 601.
[28] S.L.J. Conway, L.H. Doerrer, J.C. Green, M.L.H. Green, A. Scottow, A.H.H. Stephens, J. Chem. Soc., Dalton Trans. (2000) 329.
[29] J.C. Green, M.L.H. Green, G.C. Taylor, J. Saunders, J. Chem. Soc., Dalton Trans. (2000) 317.
[30] S.L.J. Conway, L.H. Doerrer, M.L.H. Green, M.A. Leech, Organometallics 19 (2000) 630.
[31] C.J. Matare, D.M. Foo, K.M. Kane, R. Zehnder, M. Wagener, P.J. Shapiro, T. Concolino, A.L. Rheingold, Organometallics 19 (2000) 1534.
[32] N.J. Ashworth, S.L.J. Conway, J.C. Green, M.L.H. Green, J. Organomet. Chem. 609 (2000) 83.
[33] H. Lee, B.M. Bridgewater, G. Parkin, J. Chem. Soc., Dalton Trans. (2000) 4490.
[34] M.D. Su, S.Y. Chu, J. Phys. Chem. A 105 (2001) 3591.
[35] T.M. Trnka, J.B. Bonanno, B.M. Bridgewater, G. Parkin, Organometallics 20 (2001) 3255.
[36] M.G.B. Drew, V. Felix, C.C. Romao, B. Royo, J. Chem. Soc., Dalton Trans. (2002) 584.
[37] D.M.J. Foo, P.J. Sinnema, B. Twamley, P.J. Shapiro, Organometallics 21 (2002) 1005.
[38] A. Antinolo, I. Lopez-Solera, A. Otero, S. Prashar, A.M. Rodriguez, E. Villasenor, Organometallics 21 (2002) 2460.
[39] A. Antinolo, T. Exposito, I. del Hierro, D. Lucas, Y. Mugnier, I. Orive, A. Otero, S. Prashar, J. Organomet. Chem. 655 (2002) 63.
[40] C.E. Zachmanoglou, A. Docrat, B.M. Bridgewater, G. Parkin, C.G. Brandow, J.E. Bercaw, C.N. Jardine, M. Lyall, J.C. Green, J.B. Keister, J. Am. Chem. Soc. 124 (2002) 9525.
[41] C. Alonso-Moreno, A. Antinolo, I. Lopez-Solera, A. Otero, S. Prashar, A.M. Rodriguez, E. Villasenor, J. Organomet. Chem. 656 (2002) 129.
[42] A. Antinolo, R. Fernandez-Galan, I. Orive, A. Otero, S. Prashar, Eur. J. Inorg. Chem. (2002) 2470.
[43] A.J. Hoskin, D.W. Stephan, Coord. Chem. Rev. 233 (2002) 107.
[44] A. Antinolo, R. Fernandez-Galan, B. Gallego, A. Otero, S. Prashar, A.M. Rodriguez, Eur. J. Inorg. Chem. (2003) 2626.
[45] A. Antinolo, M. Fajardo, S. Gomez-Ruiz, I. Lopez-Solera, A. Otero, S. Prashar, A.M. Rodriguez, J. Organomet. Chem. 683 (2003) 11.
[46] J.R. Ascenso, A.R. Dias, A.P. Ferreira, A.C. Galvao, M.S. Salema, L.F. Veiros, Inorg. Chim. Acta 356 (2003) 249.
[47] V. Pons, S.L.J. Conway, M.L.H. Green, J.C. Green, B.J. Herbert, D.M. Heinekey, Inorg. Chem. 43 (2004) 3475.
[48] N. Cabon, F.Y. Petillon, P. Schollhammer, J. Talarmin, K.W. Muir, Dalton Trans. (2004) 2708.
[49] A. Antinolo, M. Fajardo, S. Gomez-Ruiz, I. Lopez-Solera, A. Otero, S. Prashar, Organometallics 23 (2004) 4062.
[50] K.E. Janak, J.H. Shin, G. Parkin, J. Am. Chem. Soc. 126 (2004) 13054.
[51] M.L.H. Green, Pure Appl. Chem. 56 (1984) 47.
[52] M.L.H. Green, J.A. McCleverty, L. Pratt, G. Wilkinson, J. Chem. Soc (1961) 4854.
[53] N.J. Cooper, M.L.H. Green, R. Mahtab, J. Chem. Soc., Dalton Trans. (1979) 1557.
[54] M.L.H. Green, A.H. Lynch, M.G. Swanwick, J. Chem. Soc., Dalton Trans. (1972) 1445.
[55] L. Luo, I. Lanza, L. Fragala, C.L. Stern, T.J. Marks, J. Am. Chem Soc. 120 (1998) 3111.
[56] H. Weisenfeldt, A. Reinmuth, E. Barsties, K. Evertz, H. Britzinger, J. Organomet. Chem. 369 (1989) 359.
[57] D.M. Heinekey, A.S. Hinkle, J.D. Close, J. Am. Chem. Soc. 118 (1996) 5353.
[58] S. Sabo-Etienne, B. Chaudret, Chem. Rev. 98 (1998) 2077.
[59] D.M. Heinekey, J. Am. Chem. Soc. 113 (1991) 6074.
[60] J.C. Green, C.N. Jardine, J. Chem. Soc., Dalton Trans. (1998) 1057.
[61] J.C. Green, A. Scottow, N. J. Chem. 23 (1999) 651.
[62] T.J. Marks, W.J. Kennely, J. Am. Chem. Soc. 97 (1975) 1439.
[63] J.A. Jensen, G.S. Girolami, Inorg. Chem. 28 (1989) 2107.
[64] R.M. Bullock, C.E.L. Headford, K.M. Hennessy, S.E. Kegley, J.R. Norton, J. Am. Chem. Soc. 111 (1989) 3897.
[65] G. Parkin, J.E. Bercaw, Organometallics 8 (1989) 1172.
[66] C. Hall, R.N. Perutz, Chem. Rev. 96 (1996) 3125.
[67] R.H. Crabtree, Angew. Chem., Int. Ed. Engl. 32 (1993) 789.
[68] M. Berry, N.J. Cooper, M.L.H. Green, S.J. Simpson, J. Chem. Soc., Dalton Trans. (1980) 29.
[69] P. Grebenik, A.J. Downs, M.L.H. Green, R.N. Perutz, Chem. Commun. (1979) 742.
[70] C. Persson, C. Andersson, Inorg. Chim. Acta. 203 (1993) 235.
[71] C.S. Kraihanzel, M.L. Losee, J. Am. Chem. Soc. 90 (1968) 4701.
[72] L.E. Manzer, Inorg. Chem. 16 (1977) 525.
[73] Z. Otwinowski, W. Minor, Methods Enzymol. (1996) 276.
[74] D.J. Watkin, C.K. Prout, J.R. Carruthers, P.W. Betteridge, Issue 10 ed., Chemical Crystallography Laboratory, Oxford, UK, Oxford, 1996.
[75] P.W. Betteridge, J.R. Carruthers, R.I. Cooper, K. Prout, D.J. Watkin, J. Appl. Cryst. 36 (2003) 1487.
[76] A. Altomare, G. Carascano, C. Giacovazzo, A. Guagliardi, J. Appl. Crystallogr. 26 (1993) 343.
[77] N. Walker, D. Stuart, Acta Crystallogr., Sect. A 39 (1983) 158.
[78] R.B. Girling, P. Grebenik, R.N. Perutz, Inorg. Chem. 25 (1986) 31.
[79] R.A. Bell, S.A. Cohen, N.M. Doherty, R.S. Threlkel, J.E. Bercaw, Organometallics 5 (1986) 972.
[80] N.I. Kurillova, A.I. Gusev, Y.T. Struchkov, Zh. Strukt. Khim. 15 (1974) 718.
[81] T.J. Marks, J.R. Kolb, Chem. Rev. 77 (1977) 263.

Available online at www.sciencedirect.com
SCIENCE DIRECT®
Polyhedron 25 (2006) 421–428
POLYHEDRON
www.elsevier.com/locate/poly

Cobalt decorated metallostars and metallodendrimers: Synthetic strategies and spectroscopic correlations

Edwin C. Constable *, Deborah Gusmeroli, Catherine E. Housecroft *, Markus Neuburger, Silvia Schaffner

Department of Chemistry, University of Basel, Spitalstrasse 51, 4056-Basel, Switzerland

Received 4 May 2005; accepted 12 July 2005
Available online 24 August 2005

This paper is dedicated to our friend and colleague Malcolm Chisholm on the occasion of his 60th birthday, and recognizes his scientific achievements and his long association with Polyhedron.

Abstract

A series of compounds containing polyalkyne frameworks decorated with dicobalt carbonyl clusters and containing up to 10 Co atoms has been prepared and characterized; spectroscopic data for new compounds are analyzed to provide correlations to assist in the characterization of cobaltadendrimers.
© 2005 Elsevier Ltd. All rights reserved.

Keywords: Alkyne; Polyalkyne; Dendrimer; Cobalt carbonyl

1. Introduction

Among the potential applications of metallostars and metallodendrimers [1] are those in electrochemistry and photochemistry [2–4], liquid crystals [5], artificial photosynthetic systems [6–9], catalysis [10,11], molecular electronics [12,13] and in the development of new materials. In contrast to stars and dendrimers with flexible arms, those with rigid frameworks possess well-defined structures. We have previously reported the synthesis of high nuclearity stars and dendrimers containing alkyne functionalities that react with $Co_2(CO)_8$ to give cluster-containing species [14–16]. While we have been able to structurally characterize representative alkyne frameworks [16], characterization of the cobaltadendrimers has relied on MALDI-TOF mass spectrometry and ^{1}H and ^{13}C NMR spectroscopies. In a system such as that shown in Scheme 1, the reaction of each C≡C group with $Co_2(CO)_8$ can easily be monitored by a shift in the ^{1}H NMR spectrum from δ 3.06 to 6.37 ppm for the signal assigned to the terminal CH group [14,16]. This diagnostic spectroscopic signature is a powerful tool for the characterization, not only in the first generation star shown in Scheme 1, but also for the outer generations of related stars and dendrimers [14–16]. However, characterization of the inner generations and the concomitant confirmation of the extent to which all C≡C functionalities in polyalkynes such as $C\{(C_6H_4C{\equiv}C)_nH\}_4$ [14–16] have reacted with $Co_2(CO)_8$, is not straightforward. Furthermore, in the case of non-terminal alkynes, there is no convenient ^{1}H NMR spectroscopic spectator group for monitoring the cluster-formation reaction. Before extending our studies of this type of dendrimer, we have therefore carried out a systematic study of the reactions of a series of smaller alkynes with $Co_2(CO)_8$, in order to correlate

* Corresponding author. Tel.: +41 61 267 1008; fax: +41 61 267 1018.
E-mail address: catherine.housecroft@unibas.ch (C.E. Housecroft).

0277-5387/$ - see front matter © 2005 Elsevier Ltd. All rights reserved.
doi:10.1016/j.poly.2005.07.008

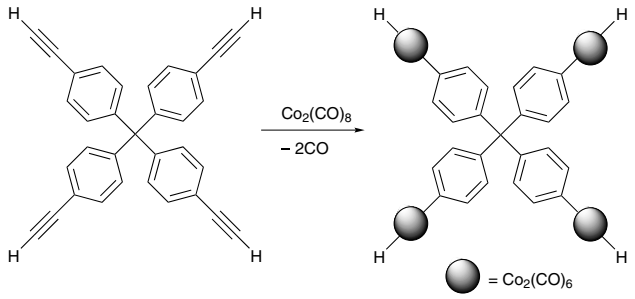

Scheme 1.

^{13}C NMR shift changes as the alkyne units (which will form the central cores of more extended systems) react with $Co_2(CO)_8$. These relatively small alkynes represent the cores from which we aim to synthesize cobaltadendrimers by a divergent strategy.

2. Experimental

2.1. General procedures

Commercially available chemicals were reagent grade and were used without further purification. ^1H and ^{13}C NMR spectra were recorded on a Bruker 400 MHz spectrometer; chemical shifts are defined with TMS δ 0 ppm for ^1H and ^{13}C spectra and are measured relative to residual $CHCl_3$. Infrared spectra were recorded on a Shimadzu FTIR-8400S spectrophotometer with neat samples on a Golden Gate diamond ATR accessory. FAB mass spectra were recorded on a Finnigan MAT95Q mass spectrometer; MALDI-TOF mass spectra were recorded on a Voyager-DE PRO spectrometer, in positive mode with α-cyano-4-hydroxycinnamic acid matrix. The microanalyses were performed with a LECO CHN-900 apparatus. Compounds **1** [17], **3** [18,19] and **14** [20] were prepared according to the literature, but using CuCl as catalyst in place of CuI. All solvents were freshly distilled and degassed; all reactions were carried out under argon. *Abbreviations*. TMS, trimethylsilyl; TIPS, triisopropylsilyl.

2.2. Compound 2

Compound **1** (100 mg, 0.37 mmol) was dissolved in CH_2Cl_2 (50 cm^3). $Co_2(CO)_8$ (557 mg, 1.63 mmol) was added and the mixture stirred at room temperature for 6 h. The solvent was removed and the residue purified by chromatography (silica, hexane:CH_2Cl_2/10:1) to give **2** as a dark red solid (290 mg, 93.0%). ^1H NMR (400 MHz, $CDCl_3$, δ/ppm): 7.44 (s, 4H, H^{Ar}) 0.42 (s, 18H, Me); ^{13}C NMR (100 MHz, $CDCl_3$, δ/ppm): 200.4 (CO), 138.5 (C^{Ar}), 130.8 (HC^{Ar}), 104.9 (C≡C), 79.9 (C≡C), 1.3 (Me). IR (cm^{-1}): 2075 m, 2023 s, 2005 vs (CO). FAB-MS, *m/z* 815 $[M + H - CO]^+$ with sequential loss of 12 CO and 4 Co to *m/z* 271 $[M + H - 12CO - 4Co]^+$.

2.3. Compound 4

Compound **3** (335 mg, 0.915 mmol) was dissolved in CH_2Cl_2 (50 cm^3). $Co_2(CO)_8$ (2.06 g, 6.02 mmol) was added and the mixture stirred at room temperature for 2 h. The solvent was removed and the residue purified by chromatography (silica, hexane) to give **4** as a dark red solid (815 mg, 72.8%). ^1H NMR (400 MHz, $CDCl_3$, δ/ppm): 7.52 (s, 3H, H^{Ar}) 0.40 (s, 27H, Me); ^{13}C NMR (100 MHz, $CDCl_3$, δ/ppm): 200.2 (CO), 140.5 (C^{Ar}), 130.8 (HC^{Ar}), 104.5 ($C_{cluster}$), 81.2 ($C_{cluster}$), 1.3 (Me). IR (cm^{-1}): 2083 m, 2044 s, 1983 vs (CO). FAB-MS *m/z* 1140 $[M + H - 3CO]^+$.

2.4. Compound 5

The method described by Stang was used [21]. ^{13}C NMR spectroscopic data in $CDCl_3$ were as reported [22]. ^1H NMR (400 MHz, $CDCl_3$): δ/ppm 7.64 (s, 2H, CH), 0.25 (s, 36H, Me). FAB-MS: *m/z* 462 M^+, 447 $[M - Me]^+$, 390 $[M - SiMe_3]^+$.

2.5. Compound 6

Compound **5** (200 mg, 0.433 mmol) was dissolved in CH_2Cl_2 (50 cm^3). $Co_2(CO)_8$ (1.30 g, 3.80 mmol) was added and the mixture stirred at room temperature for 4 h. The solvent was removed and the residue purified with chromatography (silica, hexane) to give **6** as a black solid (484.0 mg, 69.6%). ^1H NMR (400 MHz, $CDCl_3$, δ/ppm): 7.56 (s, 2H, H^{Ar}), 0.24 (s, 27 H, Me); ^{13}C NMR (100 MHz, $CDCl_3$, δ/ppm): 200.5 (CO), 136.4 (C^{Ar}), 125.7 (C^{Ar}), 102.4 ($CC_{cluster}$), 101.3 ($CC_{cluster}$), 0.3 (Me). IR (cm^{-1}): 2083 m, 2044 s, 1998 vs (CO). FAB-MS *m/z* 1630 $[M + Na]^+$ with sequential loss of 28 CO ligands.

2.6. Compound 7

1,2-Di(4-bromophenyl)ethyne (500 mg, 1.49 mmol) was dissolved in Et_3N (50 cm^3) and CuCl (21.8 mg, 0.22 mmol) and $[Pd(PPh_3)_2Cl_2]$ (154.4 mg, 0.22 mmol) were added. After the addition of HC≡CTMS (0.64 ml, 4.46 mmol), the reaction mixture was stirred for 6 h at 70° C. The solvent was removed and the residue extracted with hexane (150 cm^3). The solvent was evaporated and the crude product purified by chromatography (alumina, hexane/CH_2Cl_2, initially 1:0, gradually changing to 3:1) to give **7** as a white solid (546 mg, 99.0%). The ^1H and ^{13}C NMR spectroscopic data in $CDCl_3$ were as reported [23].

2.7. Compound 8

Compound **7** (500 mg, 1.35 mmol) was dissolved in THF (25 cm^3) and aqueous NaOH (25 cm^3 1 M) was added to the solution. The reaction mixture was stirred at room temperature for 20 h, after which time water (25 cm^3) was added until a precipitate began to form. The mixture was extracted with chloroform (100 cm^3), the solvent evaporated and the residue was purified by chromatography (alumina, hexane/CH_2Cl_2, initially 1:0, gradually changing to 2:1) to give **8** (282 mg, 92.4%). Characterization data were consistent with those reported [23].

2.8. Compound 9

Compound **8** (100 mg, 0.44 mmol) was dissolved in CH_2Cl_2 (50 cm^3). $Co_2(CO)_8$ (1.36 g, 3.98 mmol) was added and the mixture stirred at room temperature for 4 h. The solvent was removed and the residue purified by chromatography (silica, hexane) to give **9** as a black solid (305 mg, 63.9%). ^1H NMR (400 MHz, $CDCl_3$, δ/ppm): 7.62 (s, 8H, H^{Ar}), 6.72 (s, 2H, $C_{cluster}H$); ^{13}C NMR (100 MHz, $CDCl_3$, δ/ppm): 199.7 (CO), 138.7 (C^{Ar}), 137.9 (C^{Ar}), 131.1 (HC^{Ar}), 130.0 (HC^{Ar}), 91.7 ($CC_{cluster}$), 89.5 ($CCH_{cluster}$), 73.3 ($CCH_{cluster}$). IR (cm^{-1}): 2083 m, 2041 s, 1985 vs FAB-MS, *m/z* 1084 M^+, 1056 $[M - CO]^+$, 1028 $[M - 2CO]^+$, sequential loss of CO to 719 $[M - 13CO]^+$, 663 $[M - 15CO]^+$, 226 $[M - 6Co - 18CO]^+$.

2.9. Compound 10

Compound **10** was prepared by a route adapted from that reported by Bunz and coworkers [24]. 1,3-Dibromo-5-iodobenzene (1.00 g, 2.76 mmol) was dissolved in Et_3N (75 cm^3), and then CuCl (41 mg, 0.42 mmol) and $[Pd(PPh_3)_2Cl_2]$ (291 mg, 0.42 mmol) were added. After the addition of 1,3-dibromo-5-ethynylbenzene (718 mg, 2.76 mmol), the reaction mixture was stirred for 6 h at 60 °C. The solvent was then removed, and the residue extracted with hexane (150 cm^3). The mixture was filtered, the solvent removed and the crude product purified by chromatography (alumina, hexane:CH_2Cl_2, 3:1) to yield **10** as a yellow solid (1.10 g, 80.8%). The spectroscopic properties of **10** were consistent with those published [23].

2.10. Compound 11

Compound **10** (550 mg, 1.11 mmol) was dissolved in Et_3N (50 cm^3) and CuCl (11.0 mg, 0.11 mmol) and $[Pd(PPh_3)_2Cl_2]$ (77.9 mg, 0.11 mmol) were added. After the addition of HC≡CTMS (0.65 ml, 4.55 mmol), the mixture was stirred for 6 h at 60 °C. Then solvent was removed and the residue extracted with hexane (100 cm^3). The mixture was filtered, the solvent removed, and the product was purified by chromatography (alumina, hexane) to yield **11** as a light brown solid (490 mg, 78%). ^1H NMR (400 MHz, $CDCl_3$, δ/ppm): 7.52 (s, 6H, H^{Ar}), 0.24 (s, 32H, Me); ^{13}C NMR (100 MHz, $CDCl_3$, δ/ppm): 135.1 (HC^{Ar}), 134.6, (HC^{Ar}), 123.9 (C^{Ar}), 123.3 (C^{Ar}), 103.0 (C≡CTMS), 95.3 (C≡CTMS), 88.7 (central C≡C), –0.2 (Me).

2.11. Compound 12

Compound **11** (440 mg, 0.78 mmol) was dissolved in THF (35 cm^3) and after the addition of aqueous NaOH (30 cm^3 1 M), the mixture was stirred at room temperature for 4 h. Then water (100 cm^3) was added until a precipitate began to form. The mixture was extracted with CH_2Cl_2, the solvent evaporated and the residue purified by chromatography (silica, hexane) to give **12** as a light yellow solid (205 mg, 95.9%). ^1H NMR (400 MHz, $CDCl_3$, δ/ppm): 7.597 AB (d, $J = 1.5$ Hz, 4H, H^{Ar}), 7.573 AB (t, $J = 1.5$ Hz, 2H, H^{Ar}), 3.12 (s, 4H, C≡CH); ^{13}C NMR (100 MHz, $CDCl_3$, δ/ppm): 135.4 (HC^{Ar}), 135.1 (HC^{Ar}), 123.4 (C^{Ar}), 123.3 (C^{Ar}), 88.6 (central C≡C), 81.6 (*C*≡CH), 78.7 (C≡*C*H). FAB-MS *m/z* 274 M^+.

2.12. Compound 13

Compound **12** (25 mg, 0.091 mmol) was dissolved in CH_2Cl_2 (25 cm^3). $Co_2(CO)_8$ (343 mg, 1.00 mmol) was added and the reaction mixture was stirred at room temperature for 4 h. The solvent was removed and the product purified by chromatography (silica, hexane) to give **13** as a black solid (110 mg, 70.8%). ^1H NMR (400 MHz, $CDCl_3$, δ/ppm): 7.58 (overlapping multiplets, 6H, H^{Ar}), 6.36 (s, 4H, $C_{cluster}$ H); ^{13}C NMR (100 MHz, $CDCl_3$, δ/ppm): 199.0 (CO), 139.7 (C^{Ar}), 139.4 (C^{Ar}), 130.8 (C^{Ar}), 129.4 (C^{Ar}), 91.4 ($CC_{cluster}$), 88.4 ($CCH_{cluster}$), 72.8 ($CCH_{cluster}$). IR (cm^{-1}): 2091 m, 2044 s, 2006 vs MALDI-TOF MS *m/z* 1745 $[M + K]^+$ with 30 CO losses followed by 10 Co losses.

2.13. Crystal structure determination

Data were collected on an Enraf Nonius Kappa CCD instrument; data reduction, solution and refinement used the programmes COLLECT [25], SIR-92 [26] and CRYSTALS [27]. Crystal data: $C_{14}H_6Br_4$, $M = 493.82$, monoclinic, space group $P2_1/n$, $a = 13.336(2)$ Å, $b = 3.9189(7)$ Å, $c = 14.222(2)$ Å, $\beta = 110.74(1)°$; $U = 695.1(2)$ $Å^3$, $Z = 2$, $D_c = 2.359$ Mg m^{-3}, μ(Mo Kα) = 11.557 mm^{-1}, $T = 173$ K, 1560 reflections collected. Refinement of 1048 reflections (95 parameters) with $I > 3.0\sigma(I)$ converged at final $R_1 = 0.0376$, $wR_2 = 0.0454$, Gof = 1.11.

3. Results and discussion

As part of a wider investigation of star and dendrimer molecules in which alkyne frameworks are decorated with cobalt carbonyl clusters, we have undertaken a systematic study of the basic building blocks in order to provide a database of NMR spectroscopic chemical shifts which will aid characterization of larger systems. Two series of compounds were chosen for the study and these are shown in Schemes 2 and 3. The alkynes in Scheme 2 are of type $C_6H_{6-n}(C{\equiv}CTMS)_n$ ($n = 2$, 3 or 4) with the substituents providing representative *para*, *meta* and *ortho*-substitution patterns. Compounds **1**, **3** and **5** have previously been reported [17–19,21,22]. Each reacts with an excess of $Co_2(CO)_8$ to give compounds **2**, **4** and **6**, respectively, in high yield. The IR spectrum of each cobalt carbonyl derivative shows a diagnostic pattern of absorptions around 2000 cm^{-1}. The simplicity of the ^1H NMR spectrum of each of compounds **2**, **4** and **6** provides evidence that all alkyne functionalities have reacted with $Co_2(CO)_8$, and that mixtures of less symmetrical products containing clusters and unreacted C≡C units have not been obtained. For compounds **2** and **4**, FAB mass spectra showed sequential loss of CO and loss of Co, and relatively intense fragment peaks corresponding to the alkynes **1** and **3**, respectively. For the higher molecular mass cobalt carbonyl derivative **6**, we were not able to obtain satisfactory mass spectrometric data using the FAB technique. However, using MALDI-TOF MS with α-cyano-4-hydroxycinnamic acid as matrix, excellent mass spectra were obtained which provided unambiguous evidence for the formulation of **6** shown in Scheme 2. A peak at *m/z* 1630 was assigned to $[M + Na]^+$. A series of intense fragment peaks from *m/z* 1630 to 1048 were consistent with sequential loss of 12 CO and 4 Co. Less intense peaks are observed for fragments arising from the loss of the remaining cluster fragments.

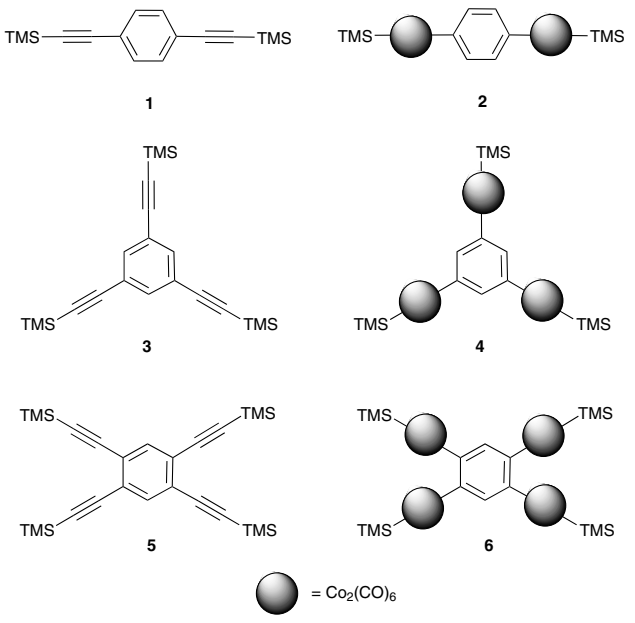

Scheme 2.

We mentioned earlier that on going from a HC≡C to $HC_2Co_2(CO)_6$ unit, a diagnostic shift in the ^1H NMR spectrum for the signal assigned to the alkyne proton from $\approx\delta$ 3.1 to 6.4 ppm is a clear indication that the alkyne has reacted to give the cobalt carbonyl derivative. However, in TMS or TIPS protected derivatives (which are favored for reasons of stability), no such ^1H NMR spectroscopic spectator is available. A similar situation occurs when we are investigating the reactions of inner generation alkynes with $Co_2(CO)_8$ in multigeneration stars and dendrimers. In these cases, ^{13}C NMR spectroscopy is diagnostic. Table 1 shows the changes in ^{13}C NMR shifts for the alkyne carbon atoms on going from compounds **1** to **2**, **3** to **4** and **5** to **6**. When the TMS-protected alkyne or cluster groups are mutually *meta* or *para*, the ^{13}C NMR spectroscopic signatures are similar, with a pair of signals at δ 96 and 104 ppm shifting to δ 80 and 105 upon reaction of the alkyne unit with $Co_2(CO)_8$. The same trend is observed on going from $C(C_6H_4\text{-}4\text{-}C{\equiv}CTMS)_4$ (**14**, Scheme 4) with δ 94.8 and 104.7 ppm for C_{alkyne} [20] to the cluster derivative **15** (δ 80.4 and 105.2 ppm for $C_{cluster}$) [28]. When two of the TMS-protected alkyne or cluster groups are *ortho* to each other, steric crowding leads to a deshielding effect; the pair of signals at δ 100.8 and 102.0 ppm in **5** shift only slightly to δ 101.3 and 102.4 ppm in the cobalt derivative **6**. Attempts to prepare the hexacluster derivative $C_6\{C_2Co_2(CO)_6TMS\}_6$ to complete this series of derivatives have not yet been successful.

The second set of model compounds, **7**–**9** and **11**–**13**, was designed so that we could investigate the effects of the alkyne to cobalt carbonyl cluster conversion on an internal alkyne group as well as peripheral deprotected alkyne functionalities. In compounds **7**–**9**, the alkyne or cluster groups are mutually *para* to one another, while in compounds **11**–**13**, they are *meta*. Compound **7** was prepared by a standard procedure, and deprotection with base leads to compound **8**. The ^1H and ^{13}C NMR spectroscopic properties of **7** and **8** were in accord with literature data [23]. Alkyne **8** reacted with $Co_2(CO)_8$ under ambient conditions to give **9** in 64% yield. The IR spectrum of **9** exhibited absorptions close to 2000 cm^{-1} indicative of the $C_2Co_2(CO)_6$ cluster unit, although these data alone do not provide evidence that all three alkynes have undergone reaction. On going from **8** to **9**, the retention of a simple spectrum indicated that **9** possessed the expected symmetry, and a shift in the ^1H NMR spectroscopic signal assigned to the terminal proton from δ 3.17 to 6.72 ppm confirmed that the both terminal C≡C groups had been converted to

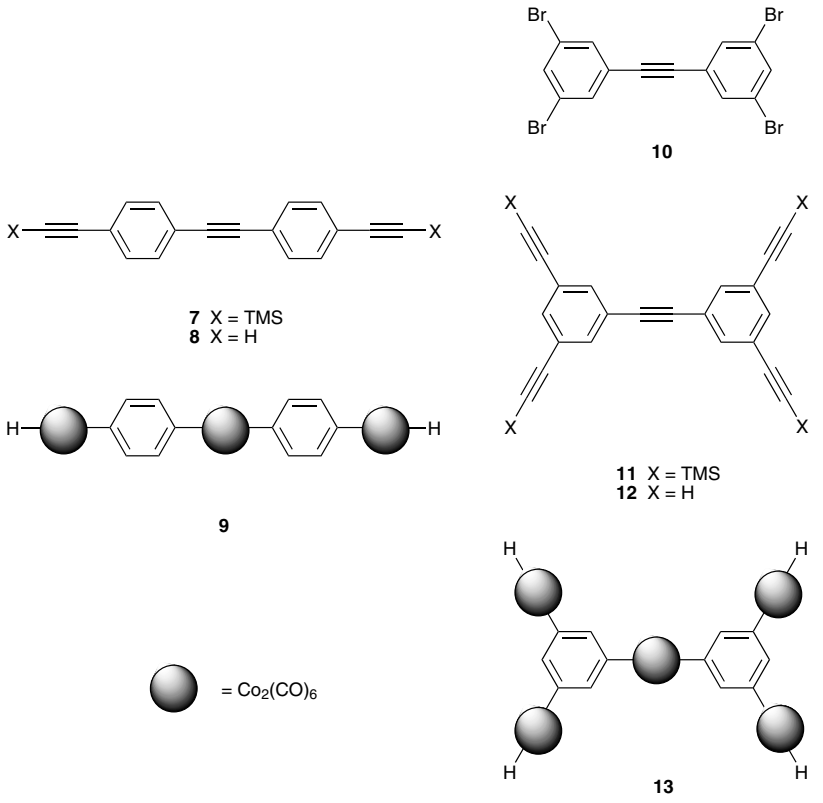

Scheme 3.

Table 1
Summary of ^{13}C NMR spectroscopic data for alkyne and cluster carbon atoms; all data were recorded in $CDCl_3$ (see Section 2 or text for references)

Compound (identity of terminal group X)	δ/ppm C≡C–X	δ/ppm $C_{cluster}$–$C_{cluster}$–X	δ/ppm C≡C (central alkyne)	δ/ppm $C_{cluster}$–$C_{cluster}$ (central unit)
1 (X = TMS)	96.6, 104.8			
2 (X = TMS)		79.9, 104.9		
3 (X = TMS)	95.9, 103.5			
4 (X = TMS)		81.2, 104.5		
14 (X = TMS)	94.8, 104.7			
15 (X = TMS)		80.4, 105.2		
5 (X = TMS)	100.8, 102.0			
6 (X = TMS)		101.3, 102.4		
7 (X = TMS)	96.5, 104.7		91.0	
8 (X = H)	79.5, 83.7		91.3	
9 (X = H)		73.3, 89.5		91.7
11 (X = TMS)	95.3, 103.0		88.7	
12 (X = H)	78.7, 81.6		88.6	
13 (X = H)		72.8, 88.4		91.4
16 (X = H)	77.6, 83.2			
17 (X = H)		73.0, 89.5		
18 (X = H)	78.9, 83.3		89.3, 90.9	
19 (X = H)		72.8, 89.1		91.3, 91.7
20 (X = H)	79.0, 83.3		89.6, 90.7, 90.9, 91.0	
21 (X = H)		72.9, 89.1		91.3, 91.4, 91.6, 91.7
22 (X = H)	79.2, 83.4		89.2, 91.5	
23 (X = H)		73.6, 89.7		91.5, 92.2

$C_2Co_2(CO)_6$ clusters. The FAB mass spectrum of **9** showed a parent ion at *m*/*z* 1084 with fragment peaks arising from sequential loss of CO followed by Co, leading to a peak at *m*/*z* 226 assigned to $[M - 6Co - 18CO]^+$, i.e., to the free alkyne **8**. We return to the ^{13}C NMR characterization of **8** and **9** later.

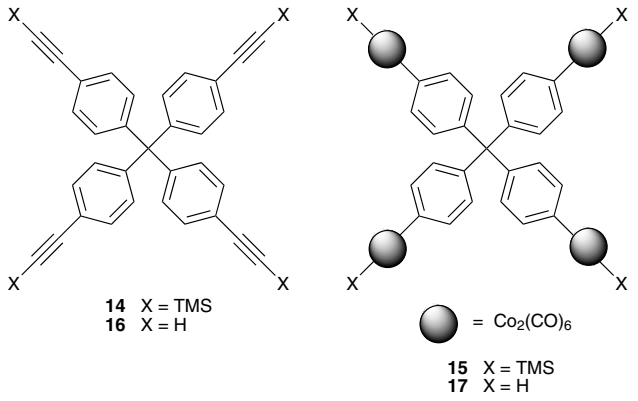

Scheme 4.

The precursor for compounds **11–13** was the tetrabromo derivative **10** which was prepared by a route adapted from that reported by Bunz and coworkers [24]. X-ray quality crystals of **10** were grown from a $CDCl_3$ solution and the molecular structure is shown in Fig. 1(a). The molecule is planar, and selected bond parameters are given in the figure caption. The molecules stack along the crystallographic *b*-axis (central stack in Fig. 1(b)) with distance between the molecular planes of 3.578 Å. The angle at which the plane containing a molecule is tilted with respect to the *b*-axis is 24°, and the centroid-to-centroid distance between adjacent molecules is 3.191 Å. It follows that both the shortest Br···Br and C···C contacts are both 3.191 Å, i.e., twice the van der Waals radius of Br (1.95 Å), but shorter than the optimum distance for π–π stacking between aromatic rings. A search of the Cambridge Structural Database [29] revealed the Br···Br interaction was common and present in 1274 bromobenzene derivatives in the data base. More interestingly, only 94 hits were obtained in which the aromatic rings were oriented approximately coplanar in a face-to-face manner. The interplanar distance depends upon the mutual rotation of the two rings, and is best described by the pseudotorsion angle Br–C···C–Br. At 0°, the two C–Br bonds lie above each other in an eclipsed conformation with the interplanar distance dictated by the van der Waals radius of the Br atom. The greater the pseudorotation angle, the closer the planes can come together, until the staggered conformation is reached at 60°. In compound **10**, the pseudorotation angle is 0°.

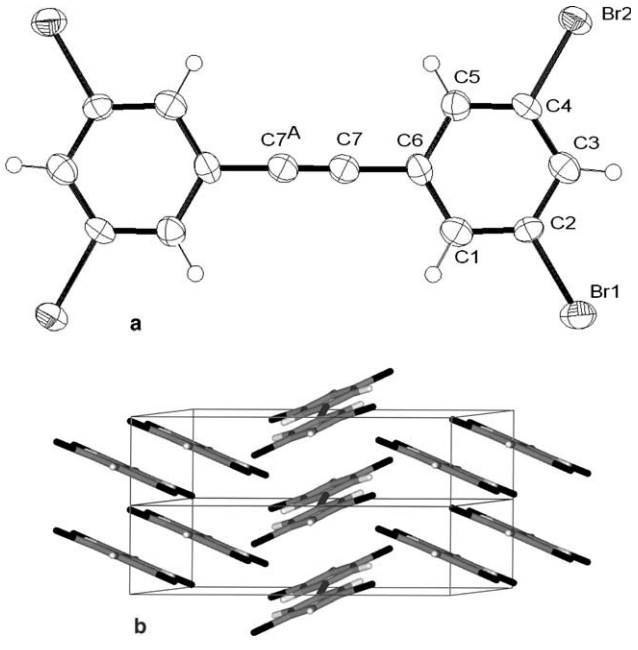

Fig. 1. (a) Molecular structure of compound **10**. Selected bond lengths and angles: C(7)–C(7A) = 1.17(1), C(6)–C(7) = 1.444(8), C(2)–Br(1) = 1.890(5), C(4)–Br(2) = 1.899(5) Å; C(5)–C(6)–C(7) = 119.3(5), C(1)–C(6)–C(7) = 121.0(5), C(6)–C(7)–C(7A) = 179.3(8)°. (b) Packing diagram of **10** showing two unit cells stacked along the crystallographic *b*-axis.

The reaction of **10** with four equivalents of HC≡CTMS under standard coupling conditions led to the formation of **11** in 78% yield. Subsequent deprotection with base gave the tetraalkyne **12** in almost quantitative yield. The FAB mass spectrum of **12** gave a parent ion at *m/z* 274, and ^1H and ^{13}C NMR spectra were fully consistent with the structure shown in Scheme 3. Compound **12** reacted with an excess of $Co_2(CO)_8$ at room temperature, and the black solid product **13** was isolated in 71% yield. In the ^1H NMR spectrum, a shift from δ 3.12 ppm for the C≡CH protons to δ 6.36 ppm is consistent with the conversion of all four peripheral alkyne groups to $C_2Co_2(CO)_6$ clusters. However, this gives no insight into the fate of the inner alkyne functionality. The highest mass region of the MALDI-TOF mass spectrum of **13** is shown in Fig. 2 and provides evidence for the fact that compound **13** contains five $C_2Co_2(CO)_6$ cluster units. The highest mass peak at *m/z* 1745 can be assigned to $[M + K]^+$, and the loss of 30 CO (28 of which are shown in the figure) followed by loss of 10 Co are observed.

We now look at correlations in ^{13}C NMR spectroscopic data on going across the series of compounds **7–9** and **11–13**. Data for the alkyne carbon atoms are summarized in Table 1. Deprotection on the terminal alkyne on going from **7** to **8**, and from **11** to **12**, shifts the ^{13}C NMR signals for the C≡C carbon atoms to lower frequencies as expected. On reaction of the terminal C≡CH units with $Co_2(CO)_8$, the two ^{13}C NMR signals for the alkyne C atoms move apart: $\Delta\delta$ = 4.2 ppm in **8** and 16.2 ppm in **9**, and $\Delta\delta = 2.9$ ppm in **12** and 15.6 ppm in **13**. We have also observed this trend on going from compound **16** ($\Delta\delta = 5.6$ ppm [20]) to **17** ($\Delta\delta = 16.5$ ppm [16]) (Scheme 4), from **18** ($\Delta\delta = 4.4$ ppm) to **19** ($\Delta\delta = 16.3$ ppm), from **20** ($\Delta\delta = 4.3$ ppm) to **21** ($\Delta\delta = 16.2$ ppm), and from **22** ($\Delta\delta = 4.2$ ppm) to **23** ($\Delta\delta = 16.1$ ppm) (Scheme 5) [16]. While changes in ^{13}C NMR shifts are diagnostic for the characterization

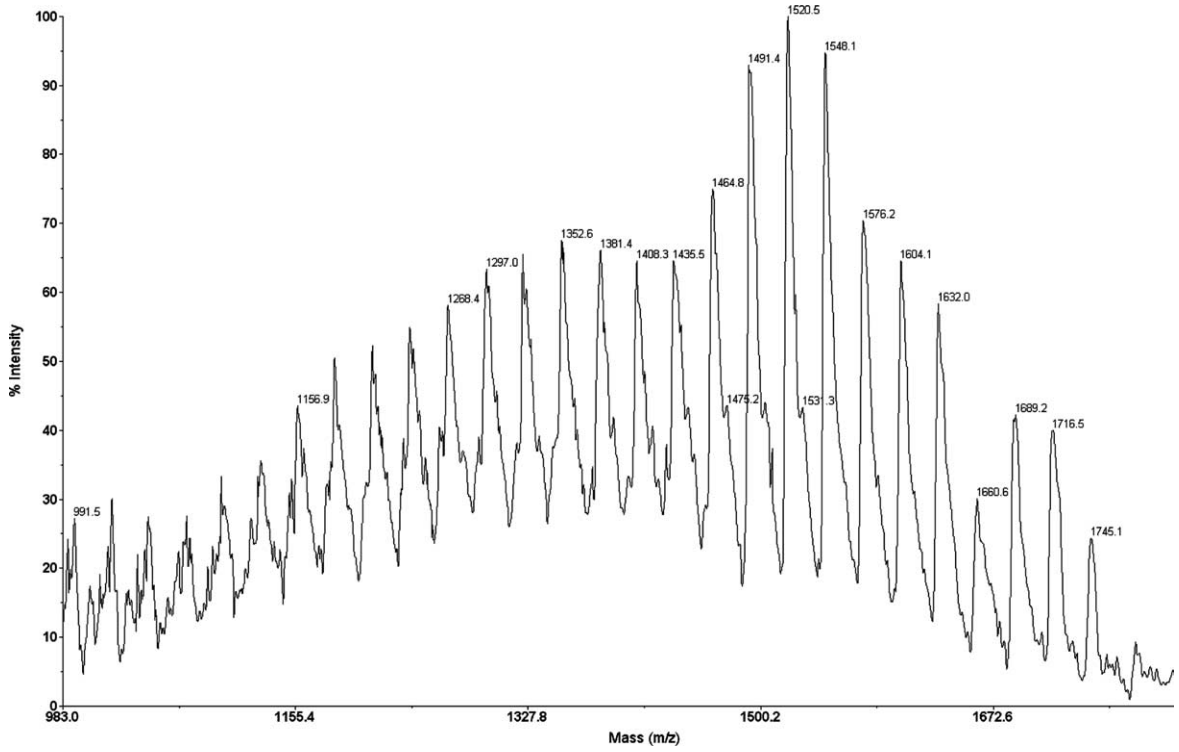

Fig. 2. The highest mass region of the MALDI-TOF mass spectrum of compound **13**. The highest mass peak is *m/z* 1745 assigned to $[M + K]^+$.

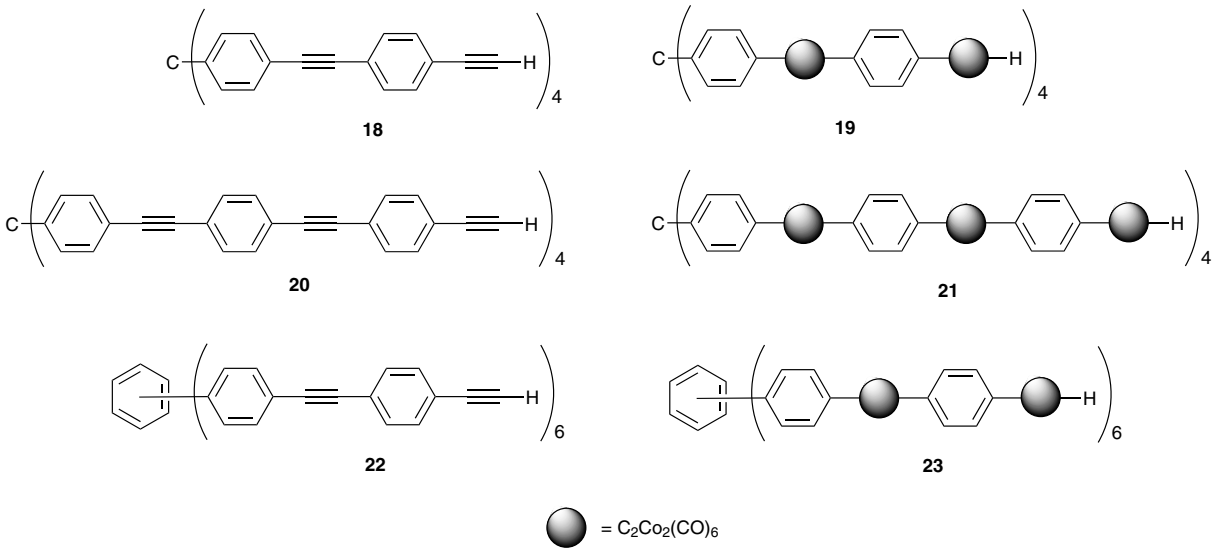

Scheme 5.

of the outer generation of alkynes/clusters, the results in Table 1 for the inner alkyne units are less clear cut. On going from compound **8** to **9**, or from **12** to **13**, only a small shift to higher frequency accompanies the transformation from C_{alkyne} to $C_{cluster}$. However, while the shift in δ values are indeed small, the trends are reproducible for the reactions of the inner alkynes with $Co_2(CO)_8$, for example on going from **8** to **9**, **12** to **13** (Scheme 3), **18** to **19**, **20** to **21** and **22** to **23** (Scheme 5).

4. Conclusions

Previous investigations of cobaltadendrimers have illustrated some of the problems associated with the characterization of such species. Our present studies of reactions between $Co_2(CO)_8$ and model alkynes (chosen so as to represent the core units for the divergent growth of stars and dendrimers) taken along with our past results [14–16] have allowed us to construct a database

of NMR chemical shift data which will invaluable for future work in this area. In addition, we have noted the limitations of FAB mass spectrometry in characterizing multicluster-containing species of the types shown in Schemes 2 and 3, and the power of the MALDI-TOF technique for analysing the cluster content of high molecular weight compounds.

5. Supplementary data

Crystallographic data including atomic coordinates, bond distances and angles for **10** have been deposited with the CCDC (Cambridge Crystallographic Data Centre, 12 Union Road, Cambridge CB2 1EZ, UK; fax +44 1223 336 033; e-mail: deposit@ccdc.cam.ac.uk or www: http://www.ccdc.cam.ac.uk) and may be obtained free of charge on quoting the deposition number CCDC 270614.

Acknowledgments

We thank the Swiss National Science Foundation and the University of Basel for financial support. Lukas J. Scherer is acknowledged for recording the MALDI-TOF mass spectra.

References

[1] E.C. Constable, in: J.A. McCleverty, T.J. Meyer (Eds.), Comprehensive Coordination Chemistry II, vol. 7, Elsevier, Oxford, 2004, p. 263.
[2] M. Venturi, S. Serroni, A. Juris, S. Campagna, V. Balzani, in: F. Vögtle (Ed.), Dendrimers, vol. 197, Springer-Verlag, Berlin, 1998, p. 193.
[3] V. Balzani, A. Juris, M. Venturi, S. Campagna, S. Serroni, Chem. Rev. 96 (1996) 759.
[4] M. Venturi, A. Credi, V. Balzani, Coord. Chem. Rev. 186 (1999) 233.
[5] B. Donnio, D. Guillon, R. Deschenaux, D.W. Bruce, in: J.A. McCleverty, T.J. Meyer (Eds.), Comprehensive Coordination Chemistry II, vol. 7, Elsevier, Oxford, 2004, p. 357.
[6] B.W. Jiang, S.W. Yang, S.L. Bailey, L.G. Hermans, R.A. Niver, M.A. Bolcar, W.E. Jones, Coord. Chem. Rev. 171 (1998) 365.
[7] A. Adronov, J.M. Fréchet, Chem. Commun. (2000) 1701.
[8] V. Balzani, S. Campagna, G. Denti, A. Juris, S. Serroni, M. Venturi, Sol. Energy Mater. Sol. Cells 38 (1995) 159.
[9] V. Balzani, S. Campagna, G. Denti, A. Juris, S. Serroni, M. Venturi, Acc. Chem. Res. 31 (1998) 26.
[10] R. Kreiter, A.W. Kleij, R. Gebbink, G. van Koten, in: F. Vögtle, C.A. Schalley (Eds.), Dendrimers IV, vol. 217, Springer-Verlag, Berlin, 2001, p. 163.
[11] D. Astruc, Pure Appl. Chem. 75 (2003) 461.
[12] D. Astruc, J.-C. Blais, M.-C. Daniel, S. Gatard, S. Nlate, J. Ruiz, CR Chim. 6 (2003) 1117.
[13] R.M. Crooks, B.I. Lemon, L. Sun, L.K. Yeung, M.Q. Zhao, in: F. Vögtle, C.A. Schalley (Eds.), Dendrimers III, vol. 212, Springer-Verlag, Berlin, 2001, p. 81.
[14] E.C. Constable, O. Eich, C.E. Housecroft, L.A. Johnston, Chem. Commun. (1998) 2661.
[15] E.C. Constable, O. Eich, C.E. Housecroft, J. Chem. Soc., Dalton Trans. (1999) 1363.
[16] E.C. Constable, O. Eich, D. Fenske, C.E. Housecroft, L.A. Johnston, Chem. Eur. J. 6 (2000) 4364.
[17] D.W. Price Jr., S.M. Dirk, F. Maya, J.M. Tour, Tetrahedron 59 (2003) 2497, and references therein.
[18] E. Weber, M. Hecker, E. Koepp, W. Orlia, M. Czugler, I. Csoregh, J. Chem. Soc., Perkin Trans. 2 (1988) 1251.
[19] D. Gelman, D. Tsvelikhovsky, G.A. Molander, J. Blum, J. Org. Chem. 67 (2002) 6287.
[20] O. Mongin, A. Gossauer, Tetrahdron 53 (1997) 6835.
[21] S. Leininger, P.J. Stang, S. Huang, Organometallics 17 (1998) 3981.
[22] B.C. Berris, G.H. Hovakeemian, Y.-H. Lai, H. Mestdagh, K.P.C. Vollhardt, J. Am. Chem. Soc. 107 (1985) 5670.
[23] C.D. Simpson, J.D. Brand, A.J. Berresheim, L. Przybilla, H.J. Räder, K. Müllen, Chem. Eur. J. 8 (2002) 1424.
[24] S.M. Waybright, K. McAlpine, M. Laskoski, M.D. Smith, U.H.F. Bunz, J. Am. Chem. Soc. 124 (2002) 8661.
[25] COLLECT Software, Nonius BV, 1997–2001.
[26] A. Altomare, G. Cascarano, G. Giacovazzo, A. Guagliardi, M.C. Burla, G. Polidori, M. Camalli, J. Appl. Crystallogr. 27 (1994) 435.
[27] P.W. Betteridge, J.R. Carruthers, R.I. Cooper, K. Prout, D.J. Watkin, J. Appl. Crystallogr. 36 (2003) 1487.
[28] O. Eich, Ph.D. Thesis, University of Basel, 2000.
[29] The Cambridge Structural Database: F.H. Allen, Acta Crystallogr., Sect. B 58 (2002) 380.

Available online at www.sciencedirect.com
SCIENCE DIRECT®
Polyhedron 25 (2006) 429–436
POLYHEDRON
www.elsevier.com/locate/poly

Synthesis and reactivity of [2]ferrocenophanes containing C–Pb and C–Zr bridges

Alexandra Bartole-Scott, Alan J. Lough, Ian Manners *

Department of Chemistry, University of Toronto, 80 St. George Street, Toronto, Ont., Canada, M5S 3H6

Received 4 May 2005; accepted 8 July 2005
Available online 1 September 2005

Dedicated to Professor Malcolm Chisholm for his outstanding and scholarly contributions to chemistry.

Abstract

The synthesis, characterization and reactivity of novel carbometalla[2]ferrocenophanes (η-C_5Me_4)Fe(η-C_5H_4)CH_2ER_2 (**14**) and (**15**) (E = Pb, R = Ph or E = Zr, R = (η-C_5H_5)) are reported. Compounds **14** and **15** were prepared by the reaction of the dilithiated species (η-C_5Me_4)Fe(η-C_5H_4Li)$CH_2Li \cdot x$TMEDA with the appropriate dichlorodiorganoplumbane or dichlorozirconocene in low yields (ca. 20%). The Pb species **14** was characterized by ^1H and ^{13}C NMR, and MS, however it could not be cleanly separated from pentamethylferrocene. Moreover, it was found that the C–Pb bonds of **14** underwent facile cleavage, and under ambient light or at room temperature, **14** decomposed to Pb_2Ph_6 and pentamethylferrocene. Compound **15**, on the other hand, was stable and readily purified; this species was characterized by ^1H and ^{13}C NMR, UV–Vis, MS, and elemental analysis. Single crystal X-ray diffraction studies of this compound revealed the presence of a moderate degree of ring-tilt with a value of $\alpha = -5.5(2)°$ (a negative value is used to denote tilting away from the bridging elements), and a potentially moderate degree of strain due to a large β(Zr) of 31.6(1)° (angle between Cp′(Fe) plane and *ipso*-Cp′–Zr bond). Attempted thermal ring-opening polymerization (ROP) of **15** resulted only in decomposition and attempted transition metal-catalyzed and photolytic ROP were also unsuccessful. The reaction of **15** with $HCl \cdot Et_2O$ resulted in cleavage of the C–Zr bonds, and led to the formation of pentamethylferrocene.
© 2005 Elsevier Ltd. All rights reserved.

Keywords: Ring-strain; Ferrocenophane; Plumbane; Zirconocene; Ring-opening polymerization

1. Introduction

[1]Ferrocenophanes have been the focus of much recent research due to the ring-strain imposed upon these organometallic species by the bridging of the cyclopentadienyl (Cp) rings by one atom [1–7]. This ring-strain leads to interesting reactivity for these compounds, and has led to their use in surface derivatization methods [8] and ring-opening polymerization (ROP) reactions [3,4]. Since the initial report of the thermal ROP of silicon-bridged [1]ferrocenophanes such as **1** ($(ER_x)_y$ = $SiMe_2$) to yield high molecular weight polymer **2** [3], the polymerization methods have been successfully expanded to include transition metal-catalyzed ROP [9,10], living anionic ROP [11], and photolytic ROP [12]. In addition, the ROP protocol has been extended to include other atoms in the bridge (E = B, P, Ge, Sn, S) [5–7], different metals (e.g., Ru, Cr and Ti) and also alternative π hydrocarbon ligands [6,7]. The resulting ring-opened polymers are attracting considerable attention due to their interesting physical and preceramic properties [13–20], and copolymers incorporating a ferrocene-containing block have intriguing applications in supramolecular chemistry [21,22]. In addition,

* Corresponding author. Tel./fax: +4169786157.
E-mail addresses: abartole@chem.utoronto.ca (A. Bartole-Scott), imanners@chem.utoronto.ca (I. Manners).

0277-5387/$ - see front matter © 2005 Elsevier Ltd. All rights reserved.
doi:10.1016/j.poly.2005.07.019

polyferrocenylsilanes have recently been used in the area of redox-responsive photonic crystals [23], as etch resists for the nanopatterning of substrates [24] and as precursors to patterned metal catalysts for the growth of carbon nanotubes [25].

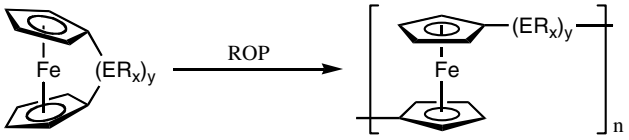

1 2

Examples of [1]ferrocenophanes with transition metals in the bridge have also been explored. Broussier et al. [26] reported the synthesis and reactivity of [1]ferrocenophanes (**3**) containing group 4 bridges. Analogues containing titanium, zirconium and hafnium bridges were prepared and single crystal X-ray diffraction of **3b** (L = *t*-BuCp) determined the tilting of the cyclopentadienyl rings to be moderate ($\alpha = 6.0°$). These [1]ferrocenophanes were shown to be reactive towards water and oxygen, in addition to heavier chalcogens leading to insertion of the chalcogen into the *ipso*-Cp–Zr bond [26]. In addition, we recently reported the synthesis of a zirconium-bridged [1]ruthenocenophane (**4**) with a larger tilt angle of the metallocene fragment ($\alpha = 10.4°$) [27].

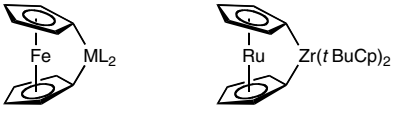

3a: M = Ti, L =Cp, *t*-BuCp
3b: M = Zr, L = Cp, *t*-BuCp
3c: M = Hf, L = Cp, *t*-BuCp

4

Attempts have also been made to introduce heavy atoms into ferrocenophane structures. Ferrocene was reacted with *n*-BuLi in hexanes to yield a mixture of $(\eta\text{-}C_5H_5)Fe(\eta\text{-}C_5H_4Li)$ and $(\eta\text{-}C_5H_4Li)_2Fe$ to which Ph_3PbCl and Ph_2PbCl_2 were added in situ [28]. The products isolated were a mixture of the plumbylferrocene (**5**), and the [1,1′]diplumbylferrocenophane (**6**). These products were characterized by NMR, MS and elemental analysis; however single crystals were not obtained, and no evidence for the formation of a [1]plumbaferrocenophane was reported [28].

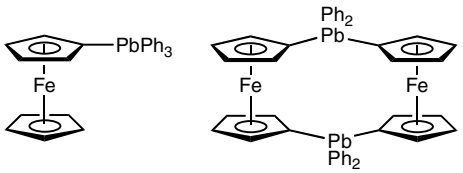

5 **6**

The preparation and reactivity of [1]ferrocenophanes have been well explored over the past few decades, however until recently the area of [2]ferrocenophanes has received comparatively less attention. Previous work has shown that highly strained hydrocarbon-bridged monomers **7** (M = Fe, R = H, Me, $E_2 = CH_2CH_2$) and the analogous [2]ruthenocenophane (**7**) (M = Ru, R = H, $E_2 = CH_2CH_2$), undergo thermal ROP [29,30], whereas ring-opening metathesis polymerization of [2]ferrocenophane (**7**) (M = Fe, R = H, $E_2 = CH{=}CH$) has also been described [31]. In contrast, [2]metallocenophanes with Si–Si bridges such as **7** (M = Fe or Ru, $E_2 = SiMe_2SiMe_2$), are relatively unstrained and resist ROP [32], whereas an analogue with a Ge–Ge bridge (**7**: M = Fe, $E_2 = GeMe_2GeMe_2$) has been successfully polymerized [33].

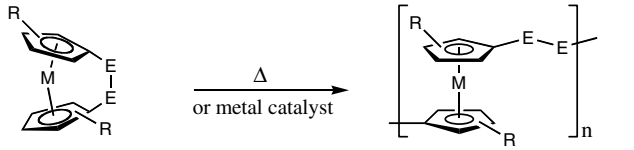

7: M = Fe or Ru,
R = H or Me,
$E_2 = CH_2CH_2$ or CH=CH
$E_2 = SiMe_2SiMe_2$ or $GeMe_2GeMe_2$

8: M = Fe or Ru,
R = H or Me,
$E_2 = CH_2CH_2$ or CH=CH
$E_2 = GeMe_2GeMe_2$

Recently, our group has studied the synthesis and ROP behaviour of [2]ferrocenophanes with unsymmetrical C–E bridges **9**–**13** [34,35]. It was shown for compounds **9**–**11** (E = Si, P, S) as the covalent radius of E was varied, the ring-strain was varied accordingly [34]. The least strained of these species (**9**, $\alpha = 11.8(1)°$) was found to be completely resistant to polymerization under all conditions studied, whereas the more strained species **10** ($\alpha_{avg} = 16.5°$) and **11** ($\alpha = 18.5(1)°$) were found to undergo successful ROP. This work recently prompted us to explore the synthesis and ROP behaviour of the [2]ferrocenophanes **12** and **13**. The presence of weak C–Ge and C–Sn bonds were expected to increase reactivity of group 14 carbo[2]ferrocenophanes, despite the decrease in tilt angle between the cyclopentadienyl rings. It was found however that the C–E bonds of **12** and **13** were insufficiently weak to permit ring-opening polymerization [35].

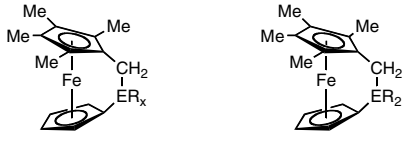

9 : $ER_x = SiMe_2$
10 : E = P, R = Ph, Mes
11 : $ER_x = S$

12 : E = Ge, R = Me, Ph
13 : E = Sn, R = Me, *t*-Bu, Mes

In this paper, we report on our attempts to further explore the area of carbon-heteroatom bridged [2]ferrocenophanes via the introduction of heavy main group elements and transition metals into the bridge. We report the synthesis and reactivity of the novel carboplumba[2]ferrocenophane (**14**) and carbozircona[2]ferrocenophane (**15**).

2. Results and discussion

2.1. Attempted synthesis of lead-bridged [2]ferrocenophanes

We attempted to prepare the C–Pb bridged [2]ferrocenophane (**14**) from the reaction of (η-C_5Me_4)Fe(η-C_5H_4Li)$CH_2Li \cdot x$TMEDA with Ph_2PbCl_2. This regenerated the precursor pentamethylferrocene as the major isolated product in addition to the desired C–Pb bridged [2]ferrocenophane (**14**). The mixture was isolated as an orange gummy material in 17% total yield. ^{1}H NMR characterization demonstrated the fraction of **14** in the reaction solution to be approximately 25%. One feature of the ^{1}H NMR spectrum of **14** is the methylene resonance observed at 3.23 ppm which is significantly more downfield than in compounds **9**–**13**, and the ^{1}H–^{207}Pb coupling observed for these protons ($J(^{207}Pb/^1H) = 54$ Hz). The structure of **14** was also confirmed by ^{13}C NMR analysis and mass spectrometry. The impetus for preparing compound **14** was to further weaken the C–E bond of group 14-containing carbo[2]ferrocenophanes (E = Si, Ge, Sn) which do not undergo ring-opening polymerization under thermal, transition metal-catalyzed, anionic or photolytic conditions [34,35]. Indeed, compound **14** possesses weak C–Pb bonds such that this species is both sensitive to light and temperature; attempts to recrystallize **14** from a concentrated hexanes solution under an inert atmosphere at room temperature led to the deposition of a black precipitate, the formation of $Ph_3PbPbPh_3$ and an increase in the amount of (η-C_5Me_5)Fe(η-C_5H_5) as detected by ^{1}H NMR and X-ray diffraction. At low temperature (−30 °C), decomposition did not occur as readily, however **14** could still not be successfully isolated in pure form from mixtures containing (η-C_5Me_5)Fe(η-C_5H_5).

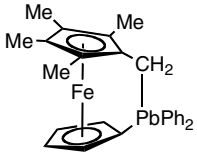

14

2.2. Synthesis and characterization of C–Zr bridged [2]ferrocenophane (*15*)

We attempted to prepare the C–Zr bridged [2]ferrocenophane (**15**) by the reaction of (η-C_5Me_4)Fe(η-C_5H_4Li)$CH_2Li \cdot x$TMEDA with (η-C_5H_5)$_2ZrCl_2$. A yellow product precipitated from THF/toluene, and ^{1}H and ^{13}C NMR analysis confirmed the structure of the product was **15**, which was isolated in 19% yield. In the ^{13}C NMR spectrum (in C_6D_6), however, it was difficult to assign the *ipso*-Cp′ and *ipso*-Cp* (Cp* = C_5Me_4) resonances due to low solubility of **16** in C_6D_6 and apparent overlapping with the Cp′ and Cp* resonances. In the solid state CP-MAS ^{13}C NMR, a peak was observed for the *ipso*-Cp′ at 156 ppm which is consistent with the *ipso*-Cp′ resonances of **3b** observed at 159 ppm [26]. The *ipso*-Cp* resonance was observed as a shoulder at 80 ppm of the broad peak at 86 ppm corresponding to Cp* carbon resonances. In moderately strained [1]ferrocenophanes [5–7] and C–E bridged [2]ferrocenophanes [34,35], the resonances for the *ipso*-Cp′ and/or *ipso*-Cp* carbons are shifted upfield which is consistent with a deviation from planar sp^2 hybridization imposed by the bridging of the rings. By comparison with NMR characterization of **3b** [26], **9** [34], **12** [35], it appears that **15** is relatively unstrained.

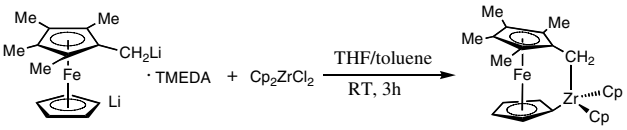

15

2.3. X-ray structural analysis of [2]ferrocenophane (*15*)

Suitable single crystals of **15** were obtained through low temperature (−30 °C) recrystallization from a concentrated toluene solution. Only one type of species was found in the unit cell. The molecular structure of **15** is shown in Fig. 1, and selected bond angles are given in Table 1. Of note in the molecular structure of **15** is the "bowtie" configuration of the Cp′Cp*Fe and Cp_2Zr rings and the relatively small α angle (−5.5(2)°) found between the planes of the Cp′ and Cp* rings. (*Note*. The negative α angle denotes tilting of the cyclopentadienyl rings away from the C–Zr bridge.) The tilt angle is expected to be moderate due to the large size of the zirconium atom ($r_{cov} = 1.55$ Å) [36] in comparison with other heteroatom-bridged [2]ferrocenophanes (cf. **12b**, $\alpha = 7.1(1)°$, Sn: $r_{cov} = 1.40$ Å) [35]. Due to the presence of two bridging atoms, it was expected that **15** would exhibit a smaller α angle relative to the corresponding [1]ferrocenophane (**3b**) ($\alpha = 6.0°$) [26], however the tilting of the cyclopentadienyl rings away from the bridge was unanticipated. This structure represents a rare case of [*n*]ferrocenophanes that contain "negative" tilt angles [37], and the first example for a [2]ferrocenophane that we are aware of. Since the tilt angle of the pentamethylferrocene fragment is small, other structural parameters may be of importance when discussing the strain of this compound. For example, the zirconium atom is found in an approximate tetrahedral environment (i.e., C(6)–Zr–C(15) = 109.0(1)°, Cp-centroid–Zr–Cp-centroid = 126.6(2)°) which may indicate moderate strain at the bridging atom, the staggering angle is relatively small (σ = 1.3(5)°) (σ = angle with which the Cp(Fe) rings deviate from an eclipsed conformation) and the torsional

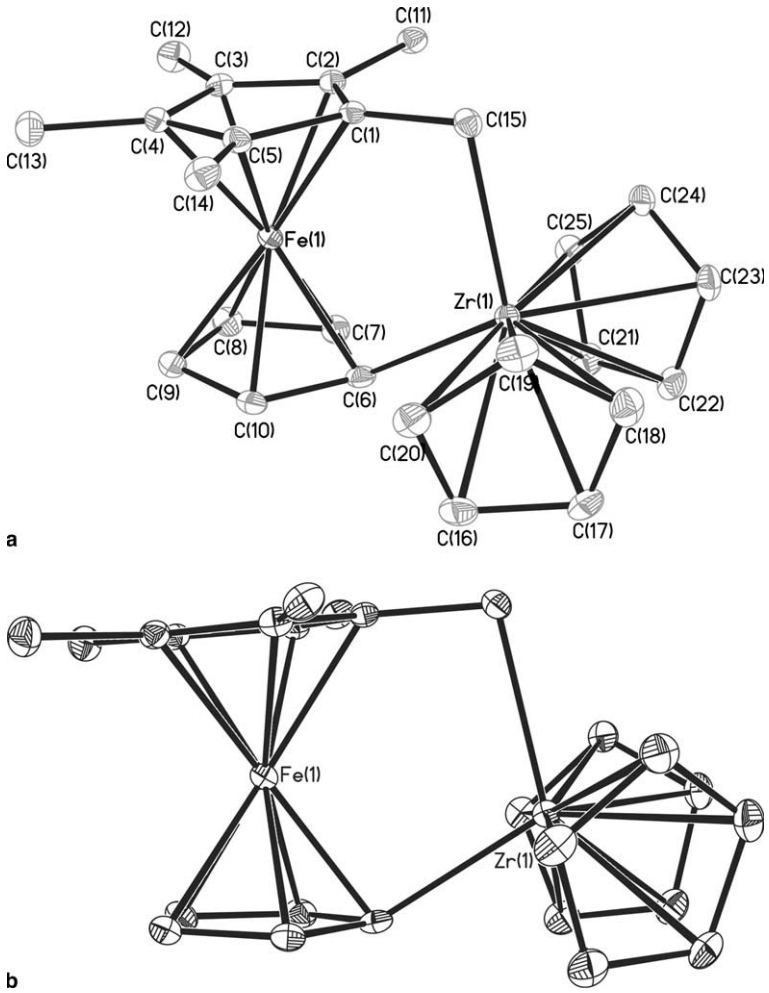

Fig. 1. Molecular structure of **15** showing 30% thermal ellipsoids. Hydrogen atoms are omitted for clarity. (a) View depicting $ZrCp_2$ environment. (b) Side view displaying tilt of Cp*FeCp′ fragment.

Table 1
Comparison of structural data for **9**, **11**–**13**, and **15**[a]

	Bridging moiety	α (°)	β^1 (°)	β^2 (°)	σ (°)	τ (°)	λ_{max}[d] (nm) (ε, M^{-1} cm^{-1})
9[b]	CH_2–$SiMe_2$	11.8(1)	7.3(3)	17.9(3)	0.1(2)	0.5(2)	458 (120)
11[b]	CH_2–S	18.5(1)	9.3(2)	10.6(2)	10.0(2)	17.9(3)	475 (243)
12a[c]	CH_2–$GePh_2$	11.81(5)	7.2(3)	17.6(2)	11.5(8)	16.5(3)	462 (173)
13b[c]	CH_2–$SnMes_2$	7.1(1)	3.8(2)	17.3(1)	2.8(3)	3.9(2)	454 (131)
15	CH_2–$ZrCp_2$	−5.5(2)	1.9(3)	31.6(1)	1.3(5)	1.5(2)	366 (299)[e]

[a] $\beta^1 = \beta(CH_2)$, $\beta^2 = \beta(E)$, where E = Si, S, Ge, Sn, Zr.
[b] See Ref. [34].
[c] See Ref. [35].
[d] In hexanes.
[e] In THF.

angle (τ) is 1.5(2)° (τ = angle between the CH_2–$ZrCp_2$ bond and the plane containing the Cp*/Cp′(Fe) centroids and iron atom) which would suggest that **15** may possess a small degree of strain. In addition, the structure revealed a β(CH_2) of 1.9(3)° (angle between Cp* plane and *ipso*-Cp*–CH_2 bond) and a β(Zr) of 31.6(1)° (angle between Cp′(Fe) plane and the *ipso*-Cp′–Zr bond). These results suggest that **15** possesses some degree of strain, since in non-bridged ferrocenes these angles would be expected to approach zero [38]. In addition, in comparison with other carbon-heteroatom bridged [2]ferrocenophanes **9**–**13** [34,35], compound **15**

contains the largest β(E) (where E = Si, P, S, Ge, Sn, Zr).

2.4. Attempted ROP of [2]ferrocenophane (15)

The thermal polymerization behaviour of **15** was initially investigated by heating a sample in an evacuated tube at temperatures up to 300 °C for up to 48 h. Alternatively, a sample was heated in solution (C_6D_6) in an NMR tube at 50 °C for up to 96 h. In each case, ^{1}H NMR analysis displayed peaks corresponding to unreacted **15** as well as amounts of (η-C_5Me_5)Fe(η-C_5H_5).

Transition metal-catalyzed ROP, which is a very useful method for preparing high molecular weight polyferrocenylsilanes and for achieving molecular weight control of these polymers [39], was also explored as a means to polymerize **15**. Karstedt's catalyst was added to a sample of **15** in solution in an NMR tube at 25 °C. However, after 48 h ^{1}H NMR characterization of this solution revealed the presence only of unreacted **15**. This sample was then heated to 40 °C for 96 h. The conversion of **15** to (η-C_5Me_5)Fe(η-C_5H_5) in 40% yield after 96 h, was most probably a result of the heating of the sample.

Photolytic ROP is a novel polymerization method for ferrocenophanes, and is expected to become an important technique for the preparation of polyferrocenylsilanes [12]. Photolytic treatment in the presence of phosphines has also been recently shown to induce ring-opening reactions of [2]ferrocenophanes **7** (M = Fe or Ru, $E_2 = CH_2CH_2$) [12d]. In order to probe the reactivity of **15**, photolytic ring-opening reactions were attempted. Samples of **15** in the presence of catalytic and equimolar amounts of Na[η-C_5H_5], equimolar amounts of the stronger donor Li[C_5H_4Me], and equimolar amounts of bis(diphenylphosphino)ethane were irradiated for several hours. In each case, only unreacted **15** was detected by ^{1}H NMR characterization.

2.5. Reaction of 15 in the presence of a strong protic acid

A sample of **15** was treated with an equimolar amount of HCl (2.0 M in Et_2O) at room temperature. The solution immediately changed colour to a deep red. After solvent was removed, ^{1}H NMR showed the presence of two products. One of the products was identified as pentamethylferrocene, however the fate of the {$ZrCp_2$} fragment could not be conclusively identified. Reaction with HCl seems to successfully ring-open **15**, however the reaction is not limited to breaking only one C–Zr bond.

3. Summary

The synthesis of carboplumba[2]ferrocenophane (**14**) and carbozircona[2]ferrocenophane (**15**) was achieved through the reaction of (η-C_5Me_4)Fe(η-C_5H_4Li)-CH_2Li · *x*TMEDA and dichlorodiphenylplumbane or dichlorozirconocene. Species **14** could not be isolated in pure form from pentamethylferrocene (η-C_5Me_5)-Fe(η-C_5H_5), however it was found that this compound possessed weaker C–E bonds (E = Si, Ge, Sn, Pb) than the analogous group 14-containing carbo[2]ferrocenophanes **9**, **12** and **13** since it decomposed under ambient light and room temperature conditions. By contrast, compound **15** which is the first example of a carbo[2]-ferrocenophane containing a transition metal as the bridging heteroatom, was isolated as yellow crystals with a moderate ring-tilt ($\alpha = -5.5(2)°$). Attempts to induce ring-opening polymerization under thermal, transition metal-catalyzed or photolytic conditions were unsuccessful; however the C–M bonds underwent cleavage in the presence of a strong protic acid.

4. Experimental

4.1. Materials

All reagents, unless otherwise specified, were purchased from Aldrich Chemical Co. and were used as received. Solvents were dried by standard procedures and distilled immediately prior to use. Cp_2ZrCl_2 was recrystallized from a concentrated $CHCl_3$ solution prior to use. Karstedt's catalyst (2.1–2.4% Pt in xylenes) was purchased from Gelest and used as received. Ph_2PbCl_2 was purchased from Strem Chemical Co. and was used as received. (η-C_5Me_4)Fe(η-C_5H_4Li)CH_2Li · *x*TMEDA was prepared according to the literature procedures [35].

4.2. Equipment

All reactions and manipulations were performed under an inert atmosphere (prepurified N_2) using either standard Schlenk techniques or an inert atmosphere glovebox (Mbraun). ^{1}H NMR (400 or 300 MHz) and ^{13}C NMR (100.5 MHz) spectra were recorded on Varian Unity 400 or Varian Mercury 300 spectrometers. All solution ^{1}H and ^{13}C NMR spectra were referenced internally to residual protonated solvent shifts. Solid state CP-MAS ^{13}C spectra were obtained on a Bruker DSX200 instrument with a spin rate of 8 KHz. UV–Vis spectra were obtained using a Perkin–Elmer Lambda 900 UV–Vis–near-IR spectrophotometer in THF at concentrations of 3.6 mmol L^{-1}. Mass spectra were obtained with the use of a VG 70-250S mass spectrometer operating in electron impact (EI) mode. The calculated isotopic distribution for each ion was in agreement with experimental values. The photoirradiation experiments were performed by placing the reaction flask next to a 125-W high

pressure Hg arc lamp (Philips). The emission was filtered by Pyrex glass ($\lambda >$ ca. 300 nm). Elemental analyses were obtained using a Perkin–Elmer Series II 2400 CHNS analyzer maintained by the Analest facility at the University of Toronto.

4.3. Synthesis of (η-C_5Me_4)Fe(η-C_5H_4)CH_2PbPh_2 (**14**)

To a suspension of (η-C_5Me_4)Fe(η-C_5H_4Li)-$CH_2Li \cdot x$TMEDA ($x = 0.66$) (2.0 g, 5.8 mmol) in Et_2O (150 mL) kept at −78 °C was added slowly with stirring a solution of Cl_2PbPh_2 (3.0 g, 6.9 mmol) in 150 mL Et_2O also kept at −78 °C. The resulting solution was allowed to stir for 2.5 h at −78 °C in the absence of light. The orange solution was then allowed to warm to room temperature and was filtered cold to remove LiCl. Solvent was removed under vacuum for approximately 5 h after which time the product was extracted from hexanes, filtered cold once more and solvent was removed completely to yield a light orange gummy material. The product contained quantities of (η-C_5Me_5)Fe(η-C_5H_5) and attempts to isolate **14** were unsuccessful. The product is light and temperature sensitive as attempts to recrystallize at room temperature under inert atmosphere led to a black precipitate on the side of the vial, formation of crystals of $Ph_3PbPbPh_3$ confirmed by single crystal X-ray diffraction; (see [40]) and an increase in the amount of (η-C_5Me_5)Fe(η-C_5H_5) as observed by ^{1}H NMR analysis. Purification of **14** from a concentrated hexanes solution at −30 °C proved unsuccessful. Crude yield: 0.61 g (17%). ^{1}H NMR (400 MHz, C_6D_6, 25 °C): $\delta = 7.77$–7.75 (m/m, $J(^{207}Pb/H) = 72$ Hz, 4H, *o*-C_6H_5), 7.31–7.27 (m/m, $J(^{207}Pb/H) = 38.4$ Hz, 4H, *m*-C_6H_5), 7.15 (m, 2H, *p*-C_6H_5), 4.46 (ps t/m, $J(^{207}Pb/H) = 12.4$ Hz, 2H, C_5H_4), 3.80 (ps t/m, $J(^{207}Pb/H) = 12.4$ Hz, 2H, C_5H_4), 3.23 (s/d, $J(^{207}Pb/H) = 54$ Hz, 2H, CH_2-Pb), 2.24 (s, 6H, C_5Me_4), 1.77 (s, 6H, C_5Me_4) ppm. ^{13}C NMR (100 MHz, C_6D_6, 25 °C): $\delta = 155.5$ ($J(^{207}Pb/^{13}C) = 30$ Hz, *ipso*-C_6H_5), 137.1 ($J(^{207}Pb/^{13}C) = 15$ Hz, *o*-C_6H_5), 131.1 (*p*-C_6H_5), 128.2 ($J(^{207}Pb/^{13}C) = 11$ Hz, *m*-C_6H_5), 107.2 ($J(^{207}Pb/^{13}C) = 35$ Hz, *ipso*-C_5Me_4), 92.4 ($J(^{207}Pb/^{13}C) = 10$ Hz, C_5Me_4), 82.6 ($J(^{207}Pb/^{13}C) = 9$ Hz, C_5Me_4), 80.1 (C_5H_4), 79.5 (C_5H_4), 71.8 ($J(^{207}Pb/^{13}C) = 16$ Hz, *ipso*-C_5H_4), 29.3 ($J(^{207}Pb/^{13}C) = 430$ Hz, CH_2-Pb), 11.9 (C_5Me_4), 11.7 (C_5Me_4) ppm. MS (70 eV, EI): *m*/*z* (%) 616 (27) [M^+], 439 (43) [M^+] − Fe − C_5Me_4, 254 (100) [M^+] − $PbPh_2$.

4.4. Synthesis of (η-C_5Me_4)Fe(η-C_5H_4)CH_2ZrCp_2 (**15**)

To a solution of (η-C_5Me_4)Fe(η-C_5H_4Li)$CH_2Li \cdot x$TMEDA ($x = 0.66$) (5.0 g, 14.5 mmol) in a THF/toluene mixture (50/50 v/v, 15 mL/15 mL) was added very slowly with stirring a solution of Cp_2ZrCl_2 (4.23 g, 14.5 mmol) in a THF/toluene mixture (50/50 v/v, 15 mL/15 mL) at room temperature. After the addition was complete, the deep purple solution was allowed to stir at room temperature for 2 additional hours. The resulting solution was filtered under N_2 resulting in the collection of a light yellow precipitate. This powder was washed with cold toluene (5–10 mL) and residual solvent was removed under vacuum overnight. The product is stable in air for several hours in the solid state. Recrystallization of this material at −30 °C from a concentrated solution in hot toluene afforded **15** as yellow crystals. Yield: 1.31 g (19%). ^{1}H NMR (C_6D_6, 400 MHz, 25 °C): $\delta = 5.61$ (s, 10H, Zr(η-C_5H_5)$_2$), 3.81 (ps t, 2H, C_5H_4), 3.21 (ps t, 2H, C_5H_4), 1.82 (s, 6H, C_5Me_4), 1.08 (s, 2H, CH_2-Zr), 1.01 (s, 6H, C_5Me_4) ppm. ^{13}C NMR (C_6D_6, 100 MHz, 25 °C): $\delta = 105.6$ (Zr(η-C_5H_5)$_2$), 85.6 (C_5Me_4), 84.6 (C_5Me_4), 76.9 (C_5H_4), 76.5 (C_5H_4), 12.7 (C_5Me_4), 12.3 (C_5Me_4), -2.7 (CH_2-Zr) ppm. Cp-MAS ^{13}C NMR (100.6 MHz, $k = 8$ KHz, 25 °C) $\delta = 156$ (*ipso*-Cp′), 106 (Zr(η-C_5H_5)$_2$), 86 (C_5Me_4), 80 (*ipso*-Cp*), 77 (C_5H_4), 76 (C_5H_4), 15 (C_5Me_4), 14 (C_5Me_4), −3 (CH_2-Zr) ppm. UV–Vis (THF): $\lambda_{max} = 366$ nm ($\varepsilon = 299$ M^{-1} cm^{-1}). MS (70 eV, EI): *m*/*z* (%) 474 (100) [M^+], 338 (49) [M^+] − $C_5Me_4CH_2$, 254 (35) [M^+] − $ZrCp_2$. *Anal*. Calc. for $C_{25}H_{28}ZrFe$ (475): C, 63.16; H, 5.93. Found: C, 63.32; H, 6.25%.

4.5. Attempted thermal polymerization of **15**

A sample of **15** (0.5 g) was sealed in an evacuated Pyrex tube and heated up to 300 °C for 48 h, however there was no observable increase in viscosity. The resulting material was characterized by ^{1}H NMR and contained unreacted **15** as well as (η-C_5Me_5)Fe(η-C_5H_5).

Alternatively, a solution of **15** (25 mg) in C_6D_6 (1.5 mL) was heated in an NMR tube under inert atmosphere at 50 °C for a period up to 96 h. After approximately 12 h, ^{1}H NMR characterization revealed 15% conversion to (η-C_5Me_5)Fe(η-C_5H_5). After 96 h, ^{1}H NMR characterization displayed very broad peaks and 70% conversion to (η-C_5Me_5)Fe(η-C_5H_5). No other products could be isolated.

4.6. Attempted platinum-catalyzed ring-opening reactions of **15**

To a solution of **15** (25 mg) in C_6D_6 (1.5 mL) was added Karstedt's catalyst (0.5% wt, 6.46 μL) in an NMR tube. The mixture was allowed to react under inert atmosphere for 48 h, after which time ^{1}H NMR characterization displayed only the presence of **15**. This solution was then heated to 40 °C for a period up to 96 h. After approximately 48 h, no change was observed in the ^{1}H NMR spectrum. At 96 h, ^{1}H NMR characterization revealed approximately 40% conversion to (η-C_5Me_5)Fe(η-C_5H_5).

4.7. Attempted photolytic ring-opening reactions of **15**

A solution of **15** (50 mg, 105 μmol) in THF (1 mL) in a Schlenk flask was treated with: (i) 10% $Na(C_5H_5)$ (2.0 M in THF, 5.25 μL), (ii) 1 equivalent of $Na(C_5H_5)$ (2.0 M in THF), 52.5 μL), (iii) 1 equivalent of $Li(C_5H_4CH_3)$ (9.0 mg), and (iv) 1 equivalent of bis(diphenylphosphino)ethane (41.9 mg). Solutions were placed in a 5 °C bath and irradiated for approximately 3–5 h. In each case, only unreacted **15** could be detected by ^{1}H NMR.

4.8. Reaction of **15** in the presence of a strong protic acid

One equivalent of $HCl \cdot Et_2O$ (2 M in Et_2O, 31.5 μL) was added dropwise to a yellow solution of **15** (30 mg, 63.1 μmol) in Et_2O (2 mL) at room temperature. Upon addition of $HCl \cdot Et_2O$, the solution immediately changed colour to deep red. The mixture was allowed to stir for an additional hour and remained a deep red colour, after which time solvent was removed under vacuum. Initial ^{1}H NMR characterization revealed a mixture of products, however after the product was kept under an inert atmosphere for 12 h, orange crystals were obtained which were identified as $(\eta\text{-}C_5Me_5)Fe(\eta\text{-}C_5H_5)$ by ^{1}H NMR.

4.9. X-ray crystallography

Selected crystal, data collection, and refinement parameters for **15** are given below. Selected angles are given in Table 1. Single-crystal X-ray diffraction data of air-sensitive yellow needles of **15** (approximate size: $0.15 \times 0.14 \times 0.07\ mm^3$) were collected at 150 K using a Nonius Kappa-CCD diffractometer and monochromated Mo Kα radiation ($\lambda = 0.71073$ Å). The chemical formula of the compound is $C_{25}H_{28}FeZr$ and **15** crystallized in the monoclinic crystal system and $P2_1/c$ space group containing four chemical units per cell. The unit cell parameters were determined to be: $a = 14.1433(5)$ Å, $b = 8.2367(2)$ Å, $c = 16.4805(6)$ Å, $\alpha = 90°$, $\beta = 90.467(2)°$, $\gamma = 90°$. The number of reflections collected were 15612, the number of independent reflections were 4385 [$R_{int} = 0.047$] and completeness to $\theta = 27.50°$ was 99.3%. The data were integrated and scaled using the DENZO-SMN package [41]. The SHELXTL/PC package was used to solve and refine the structures [42]. Refinement was by full-matrix least-squares on F^2 using all data (negative intensities included). The $R_1[I > 2(I)] = 0.0438$ and wR_2(all data) $= 0.1003$, where $R_1 = \sum||F| - |F_o|/\sum|F_o|$. $wR_2 = \{\sum[\omega(F_o^2 - F_c^2)^2]/\sum[\omega(F_o^2)^2]\}^{1/2}$. Hydrogen atoms were placed in calculated positions and included in the refinement in riding motion.

5. Supplementary material

CCDC 270933 contains the supplementary crystallographic data for this paper. These data can be obtained free of charge from The Cambridge Crystallographic Data Centre via www.ccdc.cam.ac.uk/data_request/cif.

Acknowledgements

We thank the Natural Science and Engineering Research Council of Canada (NSERC) for funding this research. In addition, A. Bartole-Scott would like to thank the Ontario Government for an O.G.S. scholarship (2004–2005) and I. Manners is grateful to the Government of Canada for a CRC award (2001–2008). We also thank Dr. Andrew Baer from the Solid State NMR facility at the University of Toronto for help performing CP-MAS experiments.

References

[1] A.G. Osborne, R.J. Whiteley, J. Organomet. Chem. 101 (1975) C27.
[2] A.B. Fischer, J.B. Kinney, R.H. Staley, M.S. Wrighton, J. Am. Chem. Soc. 101 (1979) 6501.
[3] D.A. Foucher, B.-Z. Tang, I. Manners, J. Am. Chem. Soc. 114 (1992) 6246.
[4] (a) I. Manners, Chem. Commun. (1999) 857;
(b) I. Manners, Science 294 (2001) 1664.
[5] (a) R. Rulkens, D.P. Gates, D. Balaishis, J.K. Pudelski, D.F. McIntosh, A.J. Lough, I. Manners, J. Am. Chem. Soc. 119 (1997) 10976;
(b) A. Berenbaum, H. Braunschweig, R. Dirk, U. Englert, J.C. Green, F. Jäkle, A.J. Lough, I. Manners, J. Am. Chem. Soc. 122 (2000) 5765;
(c) A. Berenbaum, A.J. Lough, I. Manners, Organometallics 21 (2002) 4415.
[6] (a) A. Bucaille, T. Le Borgne, M. Ephritikhine, J.-C. Daran, Organometallics 19 (2000) 4912;
(b) M. Herberhold, Angew. Chem., Int. Ed. Engl. 34 (1995) 1837;
(c) S. Zürcher, V. Gramlich, A. Togni, Inorg. Chim. Acta 291 (1999) 355;
(d) H. Brunner, J. Klankermayer, M. Zabel, J. Organomet. Chem. 601 (2000) 211;
(e) M. Herberhold, F. Hertel, W. Milius, B. Wrackmeyer, J. Organomet. Chem. 582 (1999) 352;
(f) M. Tamm, A. Kunst, T. Bannenberg, E. Herdtweck, P. Sirsch, C.J. Elsevier, J.M. Ernsting, Angew. Chem., Int. Ed. Engl. 43 (2004) 5530;
(g) M. Tamm, A. Kunst, E. Herdtweck, Chem. Commun. (2005) 1729;
(h) H. Braunschweig, M. Homberger, C. Hu, X. Zheng, E. Gullo, G. Clentsmith, M. Lutz, Organometallics 23 (2004) 1968.
[7] (a) D. Seyferth, H.P. Withers, Organometallics 1 (1982) 1275;
(b) C.H. Honeyman, D.A. Foucher, F.Y. Dahmen, R. Rulkens, A.J. Lough, I. Manners, Organometallics 14 (1995) 5503;
(c) T. Mizuta, M. Onishi, K. Miyoshi, Organometallics 19 (2000) 5005;
(d) T.J. Peckham, J.A. Massey, C.H. Honeyman, I. Manners, Macromolecules 32 (1999) 2830;

(e) D.A. Durfey, R.U. Kirss, C. Frommen, W. Feighery, Inorg. Chem. 39 (2000) 3506;
(f) H.K. Sharma, F. Cervantes-Lee, J.S. Mahmoud, K.H. Pannell, Organometallics 18 (1999) 399.
[8] A.B. Bocarsly, E.G. Walton, M.G. Bradley, M.S. Wrighton, J. Electroanal. Chem. Interfacial. Electrochem. 100 (1979) 283.
[9] (a) Y. Ni, R. Rulkens, J.K. Pudelski, I. Manners, I. Macromol. Rapid Commun. 16 (1995) 637;
(b) N.P. Reddy, H. Yamashita, M. Tanaka, J. Chem. Soc., Chem. Commun. (1995) 2263.
[10] (a) T.J. Peckham, J.A. Massey, M. Edwards, D.A. Foucher, I. Manners, Macromolecules 29 (1996) 2396;
(b) J.B. Sheridan, P. Gómez-Elipe, I. Manners, Macromol. Rapid Commun. 17 (1996) 319.
[11] Y. Ni, R. Rulkens, I. Manners, J. Am. Chem. Soc. 118 (1996) 4102.
[12] (a) T. Mizuta, Y. Imamura, K. Miyoshi, J. Am. Chem. Soc. 125 (2003) 2068;
(b) T. Mizuta, Y. Imamura, K. Miyoshi, Organometallics 24 (2005) 990;
(c) M. Tanabe, I. Manners, J. Am. Chem. Soc. 126 (2004) 11434;
(d) M. Tanabe, S.C. Bourke, A.J. Lough, I. Manners, D.E. Herbert, Angew. Chem. Int. Ed. 44 (2005), in press.
[13] K. Kulbaba, I. Manners, Macromol. Rapid. Comm. 22 (2001) 711.
[14] M. Ginzburg, J. Galloro, F. Jäkle, K.N. Power-Billard, S. Yang, I. Sokolov, C.N.C. Lam, A.W. Neumann, I. Manners, G.A. Ozin, Langmuir 16 (2000) 9609.
[15] M.J. MacLachlan, M. Ginzburg, N. Coombs, T.W. Coyle, N.P. Raju, J.E. Greedan, G.A. Ozin, I. Manners, Science 287 (2000) 1460.
[16] M. Hmyene, A. Yassar, M. Escorne, A. Percheronguegan, F. Garnier, Adv. Mater. 6 (1994) 564.
[17] S. Barlow, A.L. Rohl, S. Shi, C.M. Freeman, D. O'Hare, J. Am. Chem. Soc. 118 (1996) 7578.
[18] V.S. Papkov, M.V. Gerasimov, I.I. Dubovik, S. Sharma, V.V. Dementiev, K.H. Pannell, Macromolecules 33 (2000) 7107.
[19] L.I. Espada, M. Shadaram, J. Robillard, K.H. Pannell, J. Inorg. Organometall. Polym. 10 (2000) 169.
[20] Z. Wang, A. Lough, I. Manners, Macromolecules 35 (2002) 7669.
[21] (a) J.A. Massey, M.A. Winnik, I. Manners, V.Z.-H. Chan, J.M. Ostermann, R. Enchelmaier, J.P. Spatz, M. Möller, J. Am. Chem. Soc. 123 (2001) 3147;
(b) X. Wang, H. Wang, M.A. Winnik, I. Manners, J. Am. Chem. Soc. 127 (2005) 8924.
[22] X.-S. Wang, A. Arsenault, G.A. Ozin, M.A. Winnik, I. Manners, J. Am. Chem. Soc. 125 (2003) 12686.
[23] A. Arsenault, H. Miguez, V. Kitaev, G.A. Ozin, I. Manners, Adv. Mater. 15 (2003) 503.
[24] (a) S.B. Clendenning, S. Han, N. Coombs, C. Paquet, M.S. Rayat, D. Grozea, P.M. Broderson, R.N.S. Sodhi, C.M. Yip, Z.-H. Lu, I. Manners, Adv. Mater. 16 (2004) 291;
(b) A.Y. Cheng, S.B. Clendenning, G. Yang, Z.-H. Lu, C.M. Yip, I. Manners, Chem. Commun. (2004) 780;
(c) I. Korczagin, S. Golze, M.A. Hempenius, G.J. Vancso, Chem. Mater. 15 (2003) 3663;
(d) M.A. Hempenius, R.G.H. Lammertink, M. Peter, G.J. Vancso, Macromol. Symposia 196 (2003) 45.
[25] (a) S. Lastella, Y.J. Jung, H.C. Yang, R. Vajtai, P.M. Ajayan, C.Y. Ryu, D.A. Rider, I. Manners, J. Mater. Chem. 14 (2004) 1791;
(b) C. Hinderling, Y. Keles, T. Stöckli, H.F. Knapp, T. de los Arcos, P. Oelhafen, I. Korczagin, M.A. Hempenius, G.J. Vancso, R. Pugin, H. Heinzelmann, Adv. Mater. 16 (2004) 876;
(c) J.Q. Lu, T.E. Kopley, D. Roitman, N. Moll, D. Chamberlin, G. Girolami, Q. Fu, J. Liu, T.P. Russell, D.A. Rider, I. Manners, M.A. Winnik, Chem. Mater. 17 (2005) 2227.
[26] (a) R. Broussier, A. Da Rold, B. Gautheron, Y. Dromzee, Y. Jeannin, Inorg. Chem. 29 (1990) 1817;
(b) R. Broussier, A. Da Rold, M. Kubicki, B. Gautheron, Bull. Soc. Chim. Fr. 131 (1994) 951.
[27] U. Vogel, A.J. Lough, I. Manners, Angew. Chem., Int. Ed. Engl. 43 (2004) 3321.
[28] G. Utri, K.-E. Schwarzhans, G.M. Allmaier, Z. Naturforsch., B: 45 (1990) 755.
[29] J.M. Nelson, H. Rengel, I. Manners, J. Am. Chem. Soc. 115 (1993) 7035.
[30] J.M. Nelson, P. Nguyen, R. Petersen, H. Rengel, P.M. Macdonald, A.J. Lough, I. Manners, N.P. Raju, J.E. Greedan, S. Barlow, D. O'Hare, Chem. Eur. J. 3 (1997) 573.
[31] M.A. Buretea, T.D. Tilley, Organometallics 16 (1997) 1507.
[32] (a) W. Finckh, B.-Z. Tang, D.A. Foucher, D.B. Zamble, R. Ziembinski, A.J. Lough, I. Manners, Organometallics 12 (1993) 823;
(b) T.J. Peckham, D.A. Foucher, A.J. Lough, I. Manners, Can. J. Chem. 73 (1995) 2069.
[33] K. Mochida, N. Shiboyama, M. Goto, Chem. Lett. (1998) 339.
[34] R. Resendes, J.M. Nelson, A.B. Fischer, F. Jäkle, A. Bartole, A.J. Lough, I. Manners, J. Am. Chem. Soc. 123 (2001) 2116.
[35] A. Bartole-Scott, R. Resendes, F. Jäkle, A.J. Lough, I. Manners, Organometallics 23 (2004) 6116.
[36] A.F. Wells, Structural Inorganic Chemistry, fifth ed., Oxford University Press, New York, 1984.
[37] (a) For some examples of [*n*]ferrocenophanes containing cyclopentadienyl ring planes tilting away from bridge (negative tilt). Ref. [6c];
(b) M. Hisatome, M. Yoshihashi, K. Masuzoe, K. Yamakawa, Y. Iitaka, Organometallics 6 (1987) 1498;
(c) M. Herberhold, H.-D. Brendel, U. Thewalt, Angew. Chem., Int. Ed. Engl. 30 (1991) 1652;
(d) M. Herberhold, U. Steffl, W. Milius, B. Wrackmeyer, J. Organomet. Chem. 533 (1997) 109.
[38] M. Wedler, H.W. Roesky, F.T. Edelmann, U. Behrens, Z. Naturforsch., B: Chem. Sci. 43 (1988) 1461.
[39] (a) P. Gómez-Elipe, R. Resendes, P.M. Macdonald, I. Manners, J. Am. Chem. Soc. 120 (1998) 8348;
(b) A. Bartole-Scott, R. Resendes, I. Manners, Macromol. Chem. Phys. 204 (2003) 1259.
[40] H. Preut, F. Huber, Z. Anorg. Allg. Chem. 419 (1976) 92.
[41] Z. Otwinowski, W. Minor, Methods Enzymol. 276 (1997) 307.
[42] G.M. Sheldrick, SHELXTL/PC V5.1; Bruker Analytical X-ray Systems, Madison, WI, 1997.

Available online at www.sciencedirect.com
SCIENCE DIRECT®
Polyhedron 25 (2006) 437–458
POLYHEDRON
www.elsevier.com/locate/poly

Conventional and metal-directed synthesis of homodinuclear and heterotrinuclear complexes of homoditopic and heteroditopic ligands incorporating bpy and tpy metal-binding domains

Edwin C. Constable [a,*], Peter Harverson [a], Catherine E. Housecroft [a], Ebbe Nordlander [b], Jerry Olsson [a,b,c]

[a] Department of Chemistry, University of Basel, Spitalstrasse 51, CH 4056 Basel, Switzerland
[b] Lund University, Inorganic Chemistry 1, Chemical Center, Box 124, S-221 00 Lund, Sweden
[c] School of Chemistry, University of Birmingham, Edgbaston, Birmingham BN5 2TT, UK

Received 11 May 2005; accepted 5 July 2005
Available online 22 September 2005

This paper is dedicated to our friend and colleague Malcolm Chisholm on the occasion of his 60th birthday, and in recognition of his contributions to chemistry in general and to this journal in particular.

Abstract

Strategies for the preparation of multinuclear complexes containing homoditopic and heteroditopic ligands based upon 2,2′-bipyridine (bpy) and 2,2′:6′,2″-terpyridine metal binding domains are presented. Both conventional approaches based upon preparation of a free ligand and subsequent coordination and metal-directed reactions of coordinated ligands are utilized in the various strategies. A representative series of complexes of these ligands has been prepared.
© 2005 Elsevier Ltd. All rights reserved.

Keywords: Oligopyridine; Ruthenium; Polynuclear; Coordination; Metal-directed reactivity

1. Introduction

Multinuclear metal complexes are of interest in areas as disparate as bioinorganic chemistry, materials science, photophysics and artificial photosynthetic systems, redox and photoactive polymers, dendrimer chemistry and nanoscience, catalysis and sensors [1,2]. A useful concept for the design of such systems is that of a "metal-binding domain" – in other words a part of a polyfunctional molecule that is recognized as a ligand in its own right and which will bind metal centres in a predictable way, based upon knowledge of the coordination chemistry of the parent systems. We and others have developed synthetic approaches to metallodendrimers, metallostars, metallopolymers and metallooligomers based upon 2,2′-bipyridine (bpy) and 2,2′:6′,2″-terpyridine (tpy) metal-binding domains [3–14]. A variety of synthetic strategies have been adopted, most of which rely upon the initial synthesis of the desired free ligands with the metal-binding domains of choice. An increasingly commonly adopted synthetic strategy relies upon the generation of the new polytopic ligands within the coordination sphere of one or more metals by the reaction of electrophilic and nucleophilic components, either or both of which might be a mono- or multinuclear oligopyridine-metal complex [15–30]. Strategies involving preformed ligands or in situ ligand syntheses may be divergent, starting from a single metal centre and building outwards, or convergent, in which the final reaction

* Corresponding author. Tel.: +41 61 267 1001; fax: +41 61 267 1015.
E-mail address: edwin.constable@unibas.ch (E.C. Constable).

0277-5387/$ - see front matter © 2005 Elsevier Ltd. All rights reserved.
doi:10.1016/j.poly.2005.07.007

step involves the combination of metal-containing units with the total desired number of metal centres.

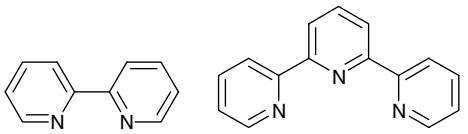

bpy tpy

An attractive metal-binding domain for incorporation into such systems is bpy which has an exceptionally well-understood coordination chemistry and which forms complexes with most elements in the periodic table [31,32]. Much of the interest in bpy-based systems relates to the useful photochemical and photophysical properties of $\{Ru(bpy)_3\}^{2+}$ and related coordination units which can readily be incorporated into polynuclear compounds [33–35]. Our original motivation for studying tpy-containing systems developed from the major disadvantage of compounds containing multiple $\{M(bpy)_3\}$ units – each $\{M(bpy)_3\}$ motif is chiral and may possess a Δ or Λ configuration, and whilst this presents no significant difficulties if a single such moiety is present, compounds containing multiple $\{M(bpy)_3\}$ motifs will exist as diastereoisomers with different spatial relationships between metal centres and hence, at least in principle, different energy and electron-transfer characteristics [36,37]. In contrast, the $\{M(tpy)_2\}$ motif is achiral provided that the substitution of the tpy ligand is symmetrical and multinuclear complexes will exist as single stereoisomers. Unfortunately, the photophysical properties of $\{Ru(tpy)_2\}$ units are seriously inferior to those of $\{Ru(bpy)_3\}^{2+}$ (short-lived ^{3}MLCT state, non-emittive in fluid solution) and we have extended our studies to heteropolytopic ligands containing both bpy and tpy metal binding domains. In this paper, we describe approaches to a series of homo- and heteroditopic ligands incorporating bpy and tpy metal-binding domains and describe a series of homo- and heteronuclear complexes.

2. Experimental

2.1. General experimental

Commercially available chemicals were reagent grade and were used without further purification; the compounds 2,2′-bipyridine *N*-oxide [38–51], 4-nitro-2,2′-bipyridine *N*-oxide [40,45,47,50,51], 4-bromo-2,2′-bipyridine (Brbpy) [40,51–53], 4-chloro-2,2′-bipyridine (Clbpy) [44,49,52,54,55], 2,2′-bipyridin-4(1H)-one (HObpy) [56], 4-amino-2,2′-bipyridine [47,56,57], 4′-chloro-2,2′:6′,2″-terpyridine (Cltpy) [58] and 4′-hydroxy-2,2′:6′,2″-terpyridine (HOtpy) [58] were prepared by minor modifications of the literature methods. ^{1}H and ^{13}C NMR spectra were recorded on Bruker 250, 400, 500 or 600 MHz; chemical shifts are defined with TMS $\delta = 0$ ppm and are measured relative to residual $CHCl_3$ or CHD_2CN. Infrared spectra were recorded on Shimadzu FTIR-8400S or Mattson Genesis FTIR spectrophotometers with neat samples on a Golden Gate diamond ATR accessory or in compressed KBr pellets. UV/VIS measurements were performed using a Varian Cary 5000 UV–Vis–NIR spectrophotometer; spectra were recorded for $\approx 10^{-5}$ M solutions in $CHCl_3$ (ligands) or MeCN (coordination compounds). FAB mass spectra were recorded on Jeol SX102, VG70-250 or a Finnigan MAT312 instruments. EI mass spectra were recorded on VG 70 SE or Kratos MS-50 mass spectrometers and electrospray (ES) mass spectra on a Finnigan MAT LCQ mass spectrometer. Maldi TOF mass spectra were recorded using a PerSeptive Biosystems Voyager-RP or a PerSeptive Biosystems Voyager-DE TM PRO Biospectrometry workstation. All electrochemical data were measured with a EG&G potentiostat/galvanostat model 263 or a BAS 100 B/W electrochemical workstation and a three electrode cell consisting of $Ag/AgNO_3$ reference, a glassy carbon disk as the working and a platinum wire as counter electrode was used. Tetra-*n*-butylammonium hexafluorophosphate acted as the electrolyte. All solutions were degassed thoroughly for at least 15 min with argon and during the measurement an inert gas blanket was maintained over the solution. After obtaining a full set of voltammograms, ferrocene was added in order to determine the exact position of the signals within the potential window.

2.2. Synthesis

2.2.1. 1,4-bis(2,2′:6′,2″-terpyridin-4′-yloxy)benzene (9)

A mixture of HOtpy (416 mg, 1.67 mmol) and K_2CO_3 (690 mg, 4.94 mmol, dried overnight at 180 °C) was added to DMF (25 mL, dried over molecular sieves) and stirred at 60 °C for 20 min, after which period 1,4-$BrCH_2C_6H_4CH_2Br$ (200 mg, 0.758 mmol) was added and the reaction mixture kept at 60 °C for 3 h. The mixture was then cooled to room temperature and water (50 mL) added to give a white precipitate that was collected by filtration. The filtrate was washed with water and recrystallized from ethanol/DMF to give **9** as a white solid (410 mg, 82%). ^{1}H NMR (300 MHz, $CDCl_3$): δ/ppm 8.71 (H_{A6}, m, 4H), 8.63 (H_{A3}, d, 4H, J 7.8 Hz), 8.14 (H_{B3}, s, 4H), 7.86 (H_{A4}, t, 4H, J 7.8 Hz), 7.55 (H_C, s, 4H), 7.34 (H_{A5}, m, 4H), 5.36 ($H_{methylene}$, s, 4H); ^{13}C NMR (100 MHz, $CDCl_3$): δ 164.4 (B4), 156.9 (A2/B2), 156.8 (A2/B2), 148.8 (A6), 137.8 (C1,4), 135.6 (A4), 127.8 (C2,3), 123.9 (A5), 121.5 (A3), 107.9 (B3), 69.8 (CH_2) *m*/*z*: (EI MS): 601 (M), 352 (M-Otpy). *Anal*. Calc. for $C_{38}H_{28}N_6O_2$: C, 76.0; H, 4.7; N, 14.0. Found: C 75.9; H, 4.6; N, 13.8%. IR $\bar{\nu}$/cm^{-1} (KBr): 3063w, 2993w, 2939w, 2877w, 1600s, 1558s, 1466m, 1442m, 1404m, 1350m, 1249w, 1188s, 1095m, 1026m,

993m, 925m, 856m, 823m, 787s, 732s, 690m, 656m, 625s; mp: 269–271 °C.

2.2.2. 1,4-bis(2,2′bipyridin-4-yloxy)benzene (7)

A mixture of HObpy (882 mg, 5.12 mmol) and K_2CO_3 (2.134 g, 15.26 mol, dried overnight at 170 °C) was added to DMF (20 mL, dried over molecular sieves) and heated to 60 °C. After 30 min 1,4-$BrCH_2C_6H_4CH_2Br$ (615 mg, 2.33 mmol) was added and the mixture was kept at 60 °C for 5 h after which time it was cooled to room temperature and water (50 mL) added to give an off-white precipitate. This was collected by filtration and washed with water to give **7** as a white solid (943 mg, 90.6%). ^{1}H NMR (300 MHz, $CDCl_3$): δ/ppm 8.69 (H_{A6}, m, 2H), 8.51 (H_{B6}, d, 2H, J 6.0 Hz), 8.41 (H_{A3}, d, 2H, J 7.8 Hz), 8.10 (H_{B3}, s, 2H), 7.83 (H_{A4}, t, 2H, J 7.8 Hz), 7.52 (H_C, s, 4H), 7.33 (H_{A5}, m, 2H), 6.93 (H_{B5}, m, 2H), 5.26 ($H_{methylene}$, s, 4H); ^{13}C NMR (100 MHz, $CDCl_3$): δ/ppm 165.8 (B4), 158.2 (A2/B2), 156.0 (A2/B2), 150.4 (B6), 149.1 (A6), 136.9 (C1,4), 136.0 (A4), 127.9 (C2,3), 123.8 (A3), 121.3 (A5), 111.4 (B3), 106.9 (B5), 69.5 (CH_2); m/z: (FAB MS) 447 (M). *Anal*. Calc. for $C_{25}H_{17}N_4O_2$: C, 77.5; H, 4.4; N, 18.1. Found: C, 77.6; H, 4.7; N, 17.7%. IR $\bar{\nu}$/cm^{-1} (KBr): 3340w, 2980m, 1736s, 1704s, 1624w, 1576m, 1448m, 1416m, 1368m, 1255s, 1160s, 1096w, 1032w, 984m, 904w, 840m, 760m, 664m, 584w; mp: 175–178 °C.

2.2.3. [Ru(bpy)$_2$(Brbpy)][PF$_6$]$_2$

Brbpy (30 mg, 0.13 mmol) and [Ru(bpy)$_2$Cl$_2$] (62 mg, 0.13 mmol) were added to $HOCH_2CH_2OH$ (4 mL) and the mixture was refluxed in a microwave oven for two 5 min periods. The red-brown solution was allowed to cool to room temperature and the complex precipitated with aqueous ammonium hexafluorophosphate. The crude red solid was purified by chromatography (SiO_2, MeCN-saturated aqueous KNO_3–H_2O 7:1:0.5) to give [Ru(bpy)$_2$(Brbpy)][PF$_6$]$_2$ as a red solid (90 mg, 75%). ^{1}H NMR (250 MHz, CD_3CN): δ/ppm 8.70 (H_{B3}, d, 1H, J 2.4 Hz), 8.46 ($H_{A3,C3,D3,E3,F3}$, d, 5H, J 7.5 Hz), 8.04 ($H_{A4,C4,D4,E4,F4}$, m, 5H), 7.74–7.68 ($H_{A6,C6,D6,E6,F6}$, m, 5H), 7.54 (H_{B6}, d, 1H), 7.37 ($H_{A5,B5,C5,D5,E5,F5}$, m, 6H); m/z: (ES–MS): 792/794 ([M−PF$_6$]$^+$); IR $\bar{\nu}$/cm^{-1} (KBr): 3600–3300w, 3100m, 3080m, 1590m, 1470m, 1450m, 1430m, 1380w, 850w, 760m, 700m; UV/VIS (CH_3CN): λ_{max}/nm (ε/dm^3 mol^{-1} cm^{-1}): 235 (22 600), 287 (65 400), 454 (11 100); Fluorescence (CH_3CN): λ_{em}/nm (λ_{ex}/nm): 620 (451). *Anal*. Calc. for $C_{30}H_{23}N_6BrRuP_2F_{12}\cdot 1.5H_2O$: C, 37.3; H, 2.7; N 8.7. Found: C, 37.3; H, 2.9; N, 8.8%. E^0/V vs. Fc: +0.92, −1.68, −1.90, −2.12.

2.2.4. [Ru(bpy)$_2$(Clbpy)][PF$_6$]$_2$

Clbpy (100.0 mg, 0.522 mmol) and [Ru(bpy)$_2$Cl$_2$] (253 mg, 0.522 mmol) were added to a 25 ml round bottom flask containing $HOCH_2CH_2OH$ (3 mL) and the mixture refluxed for two 5 min periods in a microwave oven. Aqueous ammonium hexafluorophosphate was then added and the red precipitate was collected and purified by chromatography (SiO_2, MeCN-saturated aqueous KNO_3–H_2O 7:1:0.5) to give [Ru(bpy)$_2$(Clbpy)][PF$_6$]$_2$ as a red solid (404 mg, 87%). ^{1}H NMR (300 MHz, $CDCl_3$): δ/ppm 8.55 (H_{B3}, d, 1H, J 2.4 Hz), 8.47 ($H_{A3,C3,D3,E3,F3}$, br d, 5H), 8.10–8.00 ($H_{A4,C4,D4,E4,F4}$, m, 5H), 7.77–7.67 ($H_{A6,C6,D6,E6,F6}$, m, 5H), 7.63 (H_{B6}, d, 1H, J 6.3 Hz), 7.37 ($H_{A5,B5,C5,D5,E5,F5}$, m, 6H); m/z: (ES–MS): 749/751 ([M−PF$_6$]$^+$), 302/303 ([M−2PF$_6$]$^{2+}$); IR $\bar{\nu}$/cm^{-1} (KBr): 3117w, 1605m, 1558m, 1463m, 1443m, 1430m, 1311m, 1242m, 1165m, 1128m, 1041m, 964w, 818s, 764m, 725m, 648m; UV/VIS (CH_3CN): λ_{max}/nm (ε/dm^3 mol^{-1} cm^{-1}) 241 (35 000), 284 (57 000), 448 (10 200); Fluorescence (CH_3CN): λ_{em}/nm (λ_{ex}/nm) 628 (445); E^0/V vs. Fc: +0.90, −1.78, −1.97, −2.19.

2.2.5. [Ru(bpy)$_2$(**16**)][PF$_6$]$_2$

16 (70 mg, 0.41 mmol) and [Ru(bpy)$_2$Cl$_2$] (197 mg, 0.410 mmol) were added to methanol–water (20 mL, 3:1) and the solution refluxed for 5 h, after which period the reaction mixture was allowed to cool to room temperature and the methanol was removed in vacuo to give a red precipitate which was purified by chromatography (SiO_2, MeCN-saturated aqueous KNO_3–H_2O 7:1:0.5) to give [Ru(bpy)$_2$(**16**)][PF$_6$]$_2$ as a red solid (100 mg, 42.0%). ^{1}H NMR (250 MHz, CD_3CN): δ/ppm 8.48 ($H_{C3,D3,E3}$, m, 4H), 8.25 (H_{A3}, d, 1H, J 7.8 Hz), 8.06–7.94 ($H_{A4,C4,D4,E4,F4}$, m, 5H), 7.89 (H_{A6}, m, 1H) 7.78–7.65 ($H_{BC6,D6,E6,F6}$, m, 4H) 7.62 (H_{B3}, d, 1H, J 2.4 Hz), 7.43–7.32 ($H_{A5,C5,D5,E5,F5}$, m, 5H), 7.02 (H_{B6}, d, 1H, J 6.0 Hz), 6.56 (H_{B5}, dd, 1H, J 6.0, 2.4 Hz); m/z: (ES–MS): 584.1 (584.6[M−2PF$_6$]$^+$), 292.5 (292.3 [M−2PF$_6$]$^{2+}$); IR $\bar{\nu}$/cm^{-1} (KBr): 3409w, 3240w, 3116w, 1635m, 1334m, 1164w, 1103w, 1049w, 964w, 818s, 784s, 656m, 625m;UV/VIS (CH_3CN): λ_{max}/nm (ε/dm^3 mol^{-1} cm^{-1}) 241 (41 000), 288 (68 500), 458 (12 500); Fluorescence (CH_3CN): λ_{em}/nm (λ_{ex}/nm) 645 (455); E^0/V vs. Fc: +0.70, −1.78, −1.97.

2.2.6. [Ru(bpy)$_2$(HObpy)][PF$_6$]$_2$

[Ru(bpy)$_2$(Clbpy)][PF$_6$]$_2$ (100 mg, 1.00 mmol) was added to 2 M aqueous sodium hydroxide solution (20 mL) and the mixture refluxed overnight. The reaction mixture was cooled to give an orange precipitate of [Ru(bpy)$_2$(Obpy)][PF$_6$] (60 mg). This was dissolved in hot water and re-precipitated by the addition of HPF_6 to give red crystals of [Ru(bpy)$_2$(HObpy)][PF$_6$]$_2$. ^{1}H NMR (300 MHz, CD_3CN): δ/ppm 8.51–8.40 ($H_{C3,D3,E3,F3}$, m, 4H), 8.18 (H_{A3}, d, 1H, J 8.1 Hz), 8.05 (H_{A6}, m, 1H), 8.01–7.92 ($H_{A4–D4}$, m, 4H), 7.86 (H_{E4}, H_{D6}, m, 2H), 7.75 (H_{B6}, d, 1H, $J = 4.8$ Hz), 7.69 (H_{C6}, d, 1H, $J = 6.0$ Hz), 7.57 (H_{E6}, d, 1H, $J = 6.0$ Hz), 7.47 (H_{A5}, m, 1H), 7.40 (H_{D5}, m, 1H), 7.29 ($H_{B5,C5}$, m,

2H), 7.17 (H_{A5}, m, 1H), 7.12 (H_{B3}, d, 1H, *J* 2.7 Hz), 6.51 (H_{B6}, d, 1H, *J* 6.9 Hz), 6.01 (H_{B5}, dd, 1H, *J* 6.9, 2.7 Hz); *m/z*: (ES–MS): 585.1($[M-PF_6]^+$). *Anal*. Calc. for $C_{30}H_{24}N_6ORuP_2F_{12}$: C, 41.2; H, 2.8; N, 9.6. Found: C, 41.0; H 2.6; N 9.6%. IR $\bar{\nu}/cm^{-1}$ (KBr): 3641m, 3572m, 3116w, 2970w, 1630m, 1604m, 1463m, 1442m, 1423m, 1358m, 1242m, 1165m, 1126w, 1026m, 818s, 764s, 656m; UV/VIS (CH_3CN): λ_{max}/nm (ε/$dm^3\,mol^{-1}\,cm^{-1}$) 242 (22 700), 287 (36 900), 446 (6500); Fluorescence (CH_3CN): λ_{em}/nm (λ_{ex}/nm) 627 (443); E^0/V vs. Fc: +0.84, −1.82, −2.05, −2.15.

2.2.7. *[Ru(HOtpy)Cl$_3$]*

Commercial ruthenium trichloride trihydrate (250 mg, 0.946 mmol) and HOtpy (233 mg, 0.946 mmol) were added to ethanol (10 mL) and the mixture refluxed for 2 h. The mixture was then cooled to room temperature and the brown precipitate was filtered off and washed with cold ethanol, water and diethyl ether to give [Ru(HOtpy)Cl_3] (360 mg, 75%). The compound was used without any further purification.

2.2.8. *[Ru(tpy)(Cltpy)][PF$_6$]$_2$*

[Ru(tpy)Cl_3] (327 mg, 0.750 mmol) and Cltpy (200 mg, 0.75 mmol) were dissolved in methanol (50 mL), a few drops of *N*-ethylmorpholine were added and the mixture heated to reflux. After 4 h the mixture was cooled to room temperature, most of the solvent removed and aqueous ammonium hexafluorophosphate added to give a red precipitate. Purification by chromatography (SiO_2, MeCN-saturated aqueous KNO_3–H_2O 7:1:0.5) gave a major red fraction from which [Ru(tpy)(Cltpy)][PF_6]$_2$ was obtained as a red solid (301 mg, 45%). ^{1}H NMR (300 MHz, CD_3CN): δ/ppm 8.84 (H_{B3}, s, 2H), 8.74 (H_{D3}, d, 2H, *J* 8.1 Hz), 8.48 ($H_{A3,C3}$, d, 2H, *J* 8.1 Hz), 8.42 (H_{D4}, t, 1H, *J* 8.1 Hz), 7.91 ($H_{A4,C4}$, m, 4H), 7.36 ($H_{C6,A5}$, m, 4H), 7.16 ($H_{C5,A6}$, m, 4H); *m/z*: (ES–MS): 747/749 ($[M-PF_6]^+$), 301/302 ($[M-2PF_6]^{2+}$); IR $\bar{\nu}/cm^{-1}$ (KBr): 3124m, 3100w, 1597m, 1550m, 1477m, 1427m, 1388m, 1288m, 1424m, 1157m, 1118m, 903m, 818s, 793s, 764s, 648m; UV/VIS (CH_3CN): λ_{max}/nm (ε/$dm^3\,mol^{-1}\,cm^{-1}$) 237 (19 900), 271 (26 300), 307 (43 100), 478 (10 700); E^0/V vs. Fc: +0.91, −1.58, −1.87, −2.19.

2.2.9. *[Ru(tpy)(HOtpy)][PF$_6$]$_2$*

[Ru(HOtpy)Cl_3] (100 mg, 0.195 mmol) and tpy (45.0 mg, 0.195 mmol) were added to methanol (10 mL) containing a few drops of *N*-ethylmorpholine and the mixture refluxed for 2 h, after which it was cooled, filtered and the solvent removed in vacuo. The red/brown solid was dissolved in acetonitrile and an aqueous ammonium hexafluorophosphate was added to give a red/brown precipitate that was purified by chromatography (SiO_2, MeCN-saturated aqueous KNO_3–H_2O 7:1:0.5) yielding [Ru(tpy)(Cltpy)][PF_6]$_2$ (72 mg, 39.8%). ^{1}H NMR (300 MHz, CD_3CN): δ/ppm 8.70 (H_{D3}, d, 2H, *J* 8.1 Hz), 8.47 (H_{C3}, d, 2H, *J* 8.1 Hz), 8.38 (H_{A3}, d, 2H, *J* 8.1 Hz), 8.35 (H_{C4}, t, 1H, *J* 8.1 Hz), 8.22 (H_{B3}, s, 2H), 7.89 ($H_{A4,C4}$, m, 4H), 7.45 (H_{A6}, d, 2H, *J* 5.1 Hz), 7.27 (H_{C6}, d, 2H, *J* 5.7 Hz), 7.18 (H_{A5}, m, 2H), 7.10 (H_{C5}, m, 2H); *m/z*: (ES–MS): 729 ($[M-PF_6]^+$), 292 ($[M-2PF_6]^{2+}$); IR $\bar{\nu}/cm^{-1}$ (KBr): 3487m, 3109m, 1620m, 1590m, 1552m, 1450m, 1423m, 1399m, 1342m, 1288m, 1211m, 1165m, 1111w, 1049w, 941m, 810s, 764s, 655m; UV/VIS (CH_3CN): λ_{max}/nm (ε/$dm^3\,mol^{-1}\,cm^{-1}$) 237 (45 000), 269 (43 400), 304 (57 500), 481 (15 100); E^0/V vs. Fc: +0.78, −1.77 (quasi reversible).

2.2.10. *[Ru(tpy)(N,N′-HOtpy)Cl][PF$_6$]*

[Ru(tpy)Cl_3] (35 mg, 8.0×10^{-2} mmol) and HOtpy (20 mg, 8.0×10^{-2} mmol) were dissolved in methanol (10 mL) containing a few drops of *N*-ethylmorpholine. The mixture was refluxed for 3 h. After cooling to room temperature, the solvent was removed and the residue was redissolved in a small amount of acetonitrile to give a purple solution. Aqueous ammonium hexafluorophosphate was added and a purple precipitate was collected. Purification by chromatography (SiO_2, MeCN-saturated aqueous KNO_3–H_2O 7:1:0.5) gave red [Ru(tpy)(HOtpy)][PF_6]$_2$ (50%) and purple [Ru(tpy)(*N*,*N*′-HOtpy)Cl][PF_6] (15 mg, 21%). ^{1}H NMR (300 MHz, acetone-d_6): δ/ppm 10.31 (H_{A6}, d, 1H, *J* 4.8 Hz), 9.17 (H_{B3}, bs, 1H), 9.00 (H_{A3}, d, 1H, *J* 7.8 Hz), 8.69 (H_{D3}, d, 2H, *J* 8.1 Hz), 8.63 ($H_{C3,E6}$, m, 3H), 8.40 (H_{A4}, dt, 1H, *J* 1.2, 7.2 Hz), 8.32 (H_{E3}, d, 1H, *J* 8.1 Hz), 8.22 (H_{A5}, dt, 1H, *J* 1.5, 7.0 Hz), 8.08 (H_{D4}, t, 1H, *J* 8.1 Hz), 8.03–7.97 ($H_{C4,C6,E4}$, m, 5H), 7.57 (H_{E5}, ddd, 1H, *J* 1.2, 4.8, 7.8 Hz), 7.49 (H_{C5}, dt, 2H, *J* 0.9, 5.4 Hz), 7.18 (H_{B5}, bs, 1H); IR $\bar{\nu}/cm^{-1}$ (KBr): 3734w, 3633w, 3418w, 3294w, 3070w, 2924w, 2854w, 2360m, 1705w, 1597w, 1543m, 1443m, 1442m, 1350m, 1288m, 1249m, 1157w, 1095w, 1010w, 833s, 764s, 648m, 548s; UV/VIS (CH_3CN): λ_{max}/nm (ε/$dm^3\,mol^{-1}\,cm^{-1}$) 324 (37 500), 352 (32 000), 389 (28 000), 596 (17 000).

2.2.11. *[Ru(tpy)(**20**)][PF$_6$]$_2$*

1,4-$BrCH_2C_6H_4CH_2Br$ (415 mg, 1.57 mmol) was added to a suspension of [Ru(tpy)(HOtpy)][PF_6]$_2$ (275 mg, 0.315 mmol) and potassium carbonate (175 mg, 1.26 mmol) in acetonitrile (35 mL) and the reaction mixture heated at 80 °C for 3 h. After this time, the resulting red solution was cooled to room temperature and aqueous ammonium hexafluorophosphate was added to give a red precipitate which was collected on celite by filtration, redissolved in the minimum volume of acetonitrile and purified by chromatography (SiO_2, MeCN-saturated aqueous KNO_3–H_2O 7:1:0.5). The main red fraction was collected and aqueous ammonium hexafluorophosphate was added. The mixture was reduced in volume in vacuo to precipitate the complex, which was

then collected by filtration and washed with ether. Recrystallization from 1:1 acetonitrile–water afforded [Ru(tpy)(**20**)][PF_6]$_2$ as a red solid (246 mg, 74%). ^{1}H NMR (300 MHz, CD_3CN): δ/ppm 8.70 (H_{E3}, d, 2H, J 8.1 Hz), 8.48 (H_{A3}, d, 2H, J 8.1 Hz), 8.46 (H_{D3}, d, 2H, J 8.1 Hz), 8.39 (H_{B3}, s, 2H), 8.34 (H_{E4}, t, 1H, J 8.1 Hz), 7.93 (H_{D4}, td, 2H), 7.89 (H_{A4}, td, 2H), 7.65 (H_{C2}, d, 2H, J 8.1 Hz), 7.58 (H_{C3}, d, 2H, J 8.1 Hz), 7.39 (H_{A6}, d, 2H, J 5.4 Hz), 7.27 (H_{D6}, d, 2H, J 5.4 Hz), 7.19 (H_{D5}, m, 2H), 7.13 (H_{A5}, m, 2H), 5.60 (CH_2O, s, 2H), 4.66 (CH_2Br, s, 2H); m/z: (ES–MS): 912/914 ([M−PF_6]$^+$), 383/384 ([M−2PF_6]$^{2+}$); IR $\bar{\nu}$/cm^{-1} (KBr): 3090w, 1705m, 1666s, 1562m, 1466s, 1443s, 1423w, 1354m, 1323m, 1303w, 1219m, 1165s, 1092m, 1065m, 1026m, 995w, 960w, 826w, 760m, 683w, 656w, 617w; UV/VIS (CH_3CN): λ_{max}/nm (ε/dm^3 mol^{-1} cm^{-1}) 242 (69 300), 304 (31 000), 481 (7600); E^0/V vs. Fc: +0.80, −1.71 (quasi reversible).

2.2.12. [Ru(bpy)$_2$(**22**)][PF_6]$_2$

A suspension of [Ru(bpy)$_2$(Obpy)][PF_6] (55 mg, 0.0063 mol) and K_2CO_3 (34.2 mg, 0.245 mmol, dried at 170 °C) in acetonitrile (10 mL) was heated to reflux for 30 min after which the reaction mixture was cooled and 1,4-Br$CH_2C_6H_4CH_2$Br (81.2 mg, 0.310 mmol) was added and the mixture brought back to reflux. After 3 h the reaction mixture was cooled to room temperature. The solvent was removed in vacuo and the red compound was redissolved in acetonitrile, aqueous ammonium hexafluorophosphate added and a red precipitate was collected and purified by chromatography (SiO_2, MeCN-saturated aqueous KNO_3–H_2O 7:1:0.5). The major red fraction was collected to give [Ru(bpy)$_2$(**22**)][PF_6]$_2$ (17.5 mg, 26.4%). ^{1}H NMR (300 MHz, $CDCl_3$): δ/ppm 8.50 ($H_{F3,E3,D3,A3,G3}$, d, 5H, J 7.9 Hz), 8.11 (H_{B3}, s, 1H), 8.03 ($H_{G4,F4,E4,D4,A4}$, m, 5H), 7.75 ($H_{G6,F6,E6,D6,A6}$, m, 5H), 7.49 (H_{B6}, d, 1H, J 4.1 Hz), 7.45 (H_{C2}, dd, 2H, J 6.0, 2.4 Hz), 7.42–7.34 ($H_{G5,F5,E5,D5,A5,C3}$, m, 7H), 7.00 (H_{B5}, dd, 1H, J 7.5, 2.5 Hz), 5.28 (OCH_2, s, 2H), 4.58 (CH_2Br, s, 2H); m/z: (ES–MS): 916/918 ([M−PF_6]$^+$). *Anal*. Calc. for $C_{38}H_{31}N_6OBrRuP_2F_{12}$: C, 43.2; H, 2.9; N, 8.0. Found: C, 43.1; H, 2.9; N, 7.9%. IR $\bar{\nu}$/cm^{-1} (KBr): 3649w, 3325w, 3085w, 1621m, 1429m, 1417m, 1390m, 1366m, 1222m, 1190m, 1081m, 987m, 835sm, 792m, 745s, 656m; UV/VIS (CH_3CN): λ_{max}/nm (ε/dm^3 mol^{-1} cm^{-1}) 286 (60 400), 456 (11 300); E^0/V vs. Fc: +0.86, −1.73, −1.89, −2.01, −2.14, −2.40.

2.2.13. [Ru(tpy)(**21**)][PF_6]$_2$

[Ru(tpy)(**20**)][PF_6]$_2$ (85 mg, 0.080 mmol) was added to a suspension of HOtpy (60 mg, 0.24 mmol) and potassium carbonate (100 mg, 0.72 mmol) in acetonitrile (15 mL), and the reaction mixture heated at 80 °C for 3 h. The resulting red solution was allowed to cool, and water (30 mL) along with excess methanolic [NH_4][PF_6] were added to precipitate the complex mixture. This was collected by filtration, washed well with water and then redissolved in the minimum volume of acetonitrile and purified by chromatography (SiO_2, MeCN-saturated aqueous KNO_3–H_2O 7:1:0.5) to give a major orange band. Recrystallization from 1:1 acetonitrile–water yielded [Ru(tpy)(**21**)][PF_6]$_2$ as a fine orange solid (61 mg, 74%). ^{1}H NMR (300 MHz, CD_3CN): δ/ppm 8.72 (H_{E3}, d, 2H, J 8.1 Hz), 8.48 (H_{A3}, d, 2H, J 8.1 Hz), 8.46 (H_{D3}, d, 2H, J 8.1 Hz), 8.41 (H_{B3}, s, 2H), 8.36 (H_{E4}, t, 1H, J 8.1 Hz), 7.93 (H_{D4}, td, 2H), 7.89 (H_{A4}, td, 2H), 7.69 (H_{C2}, d, 2H, J 8.1 Hz), 7.54 (H_{C3}, d, 2H, J 8.1 Hz), 7.42 (H_{A6}, d, 2H, J 5.4 Hz), 7.30 (H_{D6}, d, 2H, J 5.4 Hz), 7.19 (H_{D5}, m, 2H), 7.13 (H_{A5}, m, 2H), 5.62 (CH_2Otpy, s, 2H), 5.18 (CH_2OAc, s, 2H), 2.09 (CH_3CO, s, 3H). *Anal*. Calc. for $RuC_{40}H_{32}N_6O_3P_2F_{12}$: C, 46.4; H, 3.1; N, 8.1. Found: C, 44.9; H, 3.1; N, 8.1%. IR $\bar{\nu}$/cm^{-1} (KBr): 1736m, 1617m, 1449m, 1419m, 1387m, 1222m, 838s; m/z(MALDI-TOF) 746 ({M−2PF_6}$^+$), 687 ({M−OAc−2PF_6}$^+$). E^0/V vs. Fc: +0.80.

2.2.14. [(tpy)Ru(**9**)][PF_6]$_2$

A suspension of [Ru(tpy)Cl_3] (88 mg, 0.20 mmol) and $AgBF_4$ (117 mg, 0.600 mmol) were heated to reflux in acetone (25 mL) for 2 h. After this time the resulting blue suspension was filtered through celite to remove silver chloride, reduced to dryness and then redissolved in DMF (20 mL). This solution was added dropwise over 40 min to a solution of **9** in DMF (20 mL) at 110 °C, and the mixture then heated to reflux for a further 2 h. The resulting red suspension was then allowed to cool, before water (80 mL) and excess methanolic [NH_4][PF_6] were added to precipitate the complex mixture. This was collected on celite by filtration, and then redissolved in the minimum volume of acetonitrile and purified by chromatography (SiO_2, MeCN-saturated aqueous KNO_3–H_2O 7:1:0.5). Recrystallization from 1:1 acetonitrile–water afforded [(tpy)Ru(**9**)][PF_6]$_2$ as an orange powder (104 mg, 42%) and [(tpy)Ru(**9**)Ru(tpy)][PF_6]$_4$ as a brown solid (26 mg, 14%). ^{1}H NMR (300 MHz, CD_3CN): δ/ppm 8.94 (H_{F6}, m, 2H), 8.72 (H_{E3}, d, 2H, J 8.1 Hz), 8.61 (H_{F3}, d, 2H, J 8.7 Hz), 8.47 ($H_{D3,A3}$, m, 4H), 8.42 (H_{B3}, s, 2H), 8.37 (H_{E4}, t, 2H, J 8.1 Hz), 8.17 (H_{G3}, s, 2H), 7.92 ($H_{D4,A4}$, m, 4H), 7.81–7.72 ($H_{F4,C}$, m, 6H), 7.43 (H_{A6}, d, 2H, J 5.4 Hz), 7.30 (H_{D6}, d, 2H, J 6.3 Hz), 7.21–7.09 ($H_{D5,A5,F5}$, m, 6H), 5.65 (CH_2, s, 2H), 5.60 (CH_2, s, 2H); IR $\bar{\nu}$/cm^{-1} (KBr): 3649w, 3078w, 1604m, 1576m, 1558m, 1450m, 1411m, 1350m, 1203m, 1018m, 825s, 787m, 655w, 625w; m/z (MALDI-TOF): 1080 ({M−PF_6}$^+$), 935 ({M−2PF_6}$^+$), 687 ({M−Otpy−2PF_6}$^+$); UV/VIS (CH_3CN): λ_{max}/nm (ε/dm^3 mol^{-1} cm^{-1}) 237 (37 700), 273 (11 500), 305 (38 000), 479 (10 000); E^0/V vs. Fc: +0.79, −1.69, −1.81, −2.15.

2.2.15. [(bpy)$_2$Ru(7)][PF$_6$]$_2$

[Ru(bpy)$_2$Cl$_2$] (32.5 mg, 6.73×10^{-5} mol) and silver tetrafluoroborate (58.2 mg, 2.99 mmol) were added to acetone (25 mL) and the mixture refluxed for 2 h. Silver chloride was then filtered off and the solvent removed in vacuo. The compound was redissolved in DMF (20 mL) and the solution added dropwise to a solution of **7** (30 mg, 6.7×10^{-2} mmol) in DMF (20 mL) maintained at 110 °C over 40 min. After stirring the mixture for 3 h at 110 °C the mixture was cooled to room temperature and the solvent removed in vacuo. The red compound was redissolved in acetonitrile and aqueous ammonium hexafluorophosphate added to give a red precipitate that was collected by filtration and purified by chromatography (SiO_2, MeCN-saturated aqueous KNO_3–H_2O 7:1:0.5) to give [Ru(bpy)$_2$(**7**)][PF$_6$]$_2$ (21.3 mg, 37%). ^{1}H NMR (300 MHz, CD_3CN): δ/ppm 8.55–8.45($H_{A3,D3,E3,F3,G3,H3,H6,I6}$, m, 8H), 8.09 ($H_{B3}$, d, 1H, *J* 2.8 Hz), 8.08–7.93 ($H_{A4,D4,E4,F4,G4,H4}$, m, 6H), 7.80–7.72 ($H_{A6,D6,E6,F6,G6}$, m, 5H) 7.55 (H_{I3}, s, 1H) 7.53 (H_C, s, 4H) 7.48 (H_{B6}, dd, 1H, *J* 6.6, 2.6 Hz) 7.44–7.36 ($H_{A5,D5,E5,F5,G5,H5,I5}$, m, 7H), 7.01 (H_{B5}, dd, 1H, *J* 6.6, 2.6 Hz) 5.37 (CH_2OB_{ring}, s, 2H) 5.31 (CH_2OI_{ring}, s, 2H); *m*/*z* (ES–MS): 1005.3 ([M−PF$_6$]$^+$), 430.2 ([M−2PF$_6$]$^{2+}$). *Anal*. Calc. for $C_{48}H_{38}N_8O_2RuP_2F_{12}K$: C, 48.5; H, 3.2; N, 9.4. Found: C, 48.3; H, 2.7; N, 9.2%. IR $\bar{\nu}$/cm^{-1} (KBr): 3657w, 3587w, 3085w, 1604m, 1463m, 1442m, 1421m, 1327m, 1226m, 1164m, 1010m, 826s, 764m, 656m; UV/VIS (CH_3CN): λ_{max}/nm (ε/dm^3 mol^{-1} cm^{-1}) 285 (90 600), 453 (14 600); Fluorescence (CH_3CN): λ_{em}/nm (λ_{ex}/nm) 623 (450); E^0/V vs. Fc: +0.83, −1.77, −1.94, −2.18, −2.58.

*2.2.16. [Ru(bpy)$_2$(**5**)][PF$_6$]$_2$*

HOtpy (20.8 mg, 0.0840 mmol) and K_2CO_3 (34.7 mg, 0.250 mmol, dried overnight at 180 °C) were added to acetonitrile (20 mL) and stirred at room temperature, after 20 min [Ru(bpy)$_2$(4Clbpy)][PF$_6$]$_2$ (50 mg, 0.056 mmol) or [Ru(bpy)$_2$(Brbpy)][PF$_6$]$_2$ (52.5 mg, 0.0560 mmol) was added and the red mixture taken to reflux. After 3 h the reaction mixture was cooled to room temperature and filtered, and most of the solvent removed. Aqueous ammonium hexafluorophosphate was added and a red precipitate was collected and purified by chromatography (SiO_2, MeCN-saturated aqueous KNO_3–H_2O 7:1:0.5) to give [Ru(bpy)$_2$(**5**)][PF$_6$]$_2$ as a red solid (25.0 mg, 41%). ^{1}H NMR (300 MHz, CD_3CN): δ/ppm 8.77 (H_{D6}, dm, 2H, *J* 5.1 Hz), 8.68 (H_{D3}, d, 2H, *J* 8.1 Hz), 8.49 ($H_{E3,B3,G3,H3}$, m, 4H), 8.41 (H_{A3}, d, 1H, *J* 7.8 Hz), 8.31 (H_{D4}, t, 2H, *J* 8.0 Hz), 8.26 (H_{C3}, s, 2H), 8.23 (H_{B3}, s, 1H), 8.11–7.95 ($H_{A4,E4,F4,G4,H4}$, m, 5H), 7.87 (H_{E6}, d, 1H, *J* 5.4 Hz), 7.78–7.65 ($H_{D5,F6,H6,G6,A6,B6}$, m, 7H), 7.49–7.30 ($H_{A5,E5,F5,G5,H5}$, m, 5H), 7.16 (H_{B5}, dd, 1H, *J* 6.6, 2.4 Hz); *m*/*z*: (ES–MS): 961.8 ([M−PF$_6$]$^+$), 408.4 ([M−2PF$_6$]$^{2+}$). *Anal*. Calc. for $C_{45}H_{33}N_{10}O_4RuP_2F_{12} \cdot 0.5HPF_6$: C, 43.5; H, 2.7; N, 11.3. Found: C, 43.5; H, 2.7; N, 11.8%, IR $\bar{\nu}$/cm^{-1} (KBr): 3090, 1705, 1666, 1562, 1466, 1443, 1423, 1354, 1323, 1303, 1219, 1165, 1092, 1065, 1026, 995, 960, 826, 760, 683, 656, 617; UV/VIS (CH_3CN): λ_{max}/nm (ε/dm^3 mol^{-1} cm^{-1}) 245 (36 500), 292 (69 600), 460 (9400); Fluorescence (CH_3CN): λ_{em}/nm (λ_{ex}/nm) 620 (457); E^0/V vs. Fc: 0.88, −1.69, −1.89, −2.13, −2.49, −2.64.

*2.2.17. [Ru(bpy)$_2$(**2**)][PF$_6$]$_2 \cdot 3H_2O$*

[Ru(bpy)$_2$Cl$_2$] (95 mg, 0.29 mmol) and **2** (70 mg, 0.18 mmol) together with 4 drops of *N*-ethylmorpholine were added to ethanol (80 mL) and the mixture refluxed for 13 h. After cooling to room temperature the solvent was removed in vacuo and an orange solid was collected and purified by chromatography (SiO_2, MeCN-saturated aqueous KNO_3–H_2O 7:1:0.5) to give [Ru(bpy)$_2$(**2**)][PF$_6$]$_2$ as an orange solid (74 mg, 55%). ^{1}H NMR (250 MHz, CD_3CN): δ/ppm 8.92 (H_{B3}, s, 1H), 8.85 (H_{C3}, s, 2H), 8.72 ($H_{A3,D3,D6}$, d overlapping, 5H), 8.51 ($H_{E3,F3,G3,H3}$, dd, 4H), 8.15–7.98 ($H_{A4,D4E4,F4,G4,H4}$, m, 7H), 7.88 (H_{B5}, d, 1H, *J* 5.9 Hz), 7.85–7.72 ($H_{A6,B6,E6,F6,G6,H6}$, m, 6H), 7.61 (H_{HD}, dd, 2H, *J* 7.3, 5.8 Hz), 7.48–7.38 ($H_{A5,E5,F5,G5,H5}$, m, 5H); *m*/*z*: (ES–MS): 946.1 ([M−PF$_6$]$^+$) 400.6 ([M−2PF$_6$]$^{2+}$). *Anal*. Calc. for $C_{45}H_{33}N_9RuP_2F_{12} \cdot 3H_2O$: C, 47.2; H, 3.4; N, 11.0. Found: C, 47.2; H, 3.5; N, 11.2%. IR $\bar{\nu}$/cm^{-1} (KBr): 3430m, 1617m, 1475w, 1446w, 1423w, 842s, 793w, 765m, 558s; UV/VIS (CH_3CN): λ_{max}/nm (ε/dm^3 mol^{-1} cm^{-1}) 243 (59 400), 287 (82 500), 461 (14 500). Fluorescence (CH_3CN): λ_{em}/nm (λ_{ex}/nm) 628 (454); E^0/V vs. Fc: +0.93, −1.61, −1.87, −2.10, −2.57, −2.82.

*2.2.18. [(bpy)$_2$Ru(**7**)Ru(bpy)$_2$][PF$_6$]$_4$*

7 (40.0 mg, 8.93×10^{-2} mmol), [Ru(bpy)$_2$Cl$_2$] (93.5 mg, 1.80×10^{-3}) and 2 drops of *N*-ethylmorpholine were added to methanol (10 mL) and taken to reflux for 3 h after which period aqueous ammonium hexafluorophosphate was added and a dark red precipitate collected. The precipitate was purified by column chromatography (SiO_2, MeCN-saturated aqueous KNO_3–H_2O 7:1:0.5). The major red fraction was collected to give [(bpy)$_2$Ru(**7**)Ru(bpy)$_2$][PF$_6$]$_4$ as a red solid (31 mg, 18.7%). ^{1}H NMR (300 MHz, CD_3CN): δ/ppm 8.51–8.46(H_{A3-E3}, d, 10 H, *J* 8.1 Hz), 8.09 (H_{F3}, s, 2H), 8.08–7.93 (H_{A4-E4}, m, 10H) 7.80–7.72 (H_{A6-E6}, m, 10H) 7.54 (H_G, s, 4H) 7.48 (H_{F6}, d, 2H, *J* 6.6 Hz) 7.44–7.36 (H_{A5-E5}, m, 10H), 7.03 (H_{F5}, m, 2H), 5.29 (CH_2, s, 4H); *m*/*z* (ES–MS) 1709.1([M−PF$_6$]$^+$), 781.6 ([M−PF$_6$]$^{2+}$). *Anal*. Calc. for $C_{68}H_{54}N_{12}O_2Ru_2P_4F_{24}$: C, 44.1; H, 2.9; N, 9.1. Found: C, 44.3; H, 3.0; N, 9.2%. IR $\bar{\nu}$/cm^{-1} (KBr) 3656w, 3587w, 3333w, 3085w, 2924w, 1612m, 1558w, 1463m, 1442m, 1421m, 1327m, 1227m, 1165m, 1126w, 1034m, 995m, 818s, 756s, 656m; UV/VIS (CH_3CN): λ_{max}/nm (ε/dm^3 mol^{-1} cm^{-1}) 229 (73 000), 286 (127 700), 455 (22 600); Fluorescence

(CH_3CN): λ_{em}/nm (λ_{ex}/nm) 623 (452); E^0/V vs. Fc: +0.81, −1.75, −1.93, −2.16.

2.2.19. *[(bpy)$_2$Ru(**2**)Ru(tpy)][PF$_6$]$_4$ · 4H$_2$O*

A solution of [(bpy)$_2$Ru(**2**)][PF$_6$]$_2$ (30.0 mg, 0.0270 mmol) and [Ru(tpy)Cl$_3$] (12.0 mg, 0.0270 mmol) in ethanol (50 mL) together with two drops of *N*-ethylmorpholine was heated to reflux for 2 h. The solvent was then evaporated in vacuo and the residue was purified by column chromatography (SiO_2, MeCN-saturated aqueous KNO_3–H_2O 7:1:0.5). To the major red-orange fraction an excess of ammonium hexafluorophosphate was added and the solution reduced in volume. The precipitate was collected by filtration over celite, dissolved in acetonitrile and evaporated to dryness to give [(bpy)$_2$Ru(**2**)Ru(tpy)][PF$_6$]$_4$ as a red-orange powder (30.0 mg, 64%). ^{1}H NMR (250 MHz, CD_3CN): δ/ppm 9.18 (H_{F3}, m, 1H), 9.10 (H_{G3}, s, 2H), 8.92 (H_{E3}, d, 1H, *J* 8.1 Hz), 8.76 (H_{J3}, d, 2H, *J* 8.0 Hz), 8.67 (H_{H3}, d, 2H, *J* 7.9 Hz), 8.58–8.53 ($H_{A3–D3}$, m, 4H), 8.49 (H_{I3}, d, 2H, *J* 8.4 Hz), 8.44 (H_{J4}, t, 1H, *J* 8.0 Hz), 8.19 (H_{E4}, dt, 1H, *J* 8.0, 2.2 Hz), 8.14–8.04 ($H_{F5,F6,A4–D4}$, m, 6H), 7.99–7.88 ($H_{I4,H4}$, m, 4H), 7.85–7.70 ($H_{A6–E6}$, m, 5H), 7.53–7.41 ($H_{A5–E5}$, m, 5H), 7.39–7.33 ($H_{H6,I6}$, m, 4H), 7.23–7.11 ($H_{H5,I5}$, m, 4H); *m*/*z*: (ES–MS): 1570.0 ([M−PF$_6$]$^+$), 712.5 ([M−2PF$_6$]$^{2+}$). *Anal.* Calc. for $C_{60}H_{44}N_{12}Ru_2P_4F_{24} \cdot 4H_2O$: C, 40.3; H, 3.0; N, 9.4. Found: C, 40.3; H, 3.2; N, 9.4%. IR $\bar{\nu}$/cm^{-1} (KBr): 3443m, 3060w, 1605m, 1466m, 1448m, 1421w, 1388m, 1243w, 1029w, 840s, 788m, 765m, 732w, 558s; UV/VIS (CH_3CN): λ_{max}/nm (ε/dm^3 mol^{-1} cm^{-1}) 242 (54900), 287 (104200), 500 (37400); Fluorescence (CH_3CN): λ_{em}/nm (λ_{ex}/nm) 689 (460), 691 (500); E^0/V vs. Fc: 0.93, −1.34, −1.68, −1.84, −1.90, −2.23.

2.2.20. *[(bpy)$_2$Ru(**5**)Ru(tpy)][PF$_6$]$_4$ · 2H$_2$O*

[Ru(bpy)$_2$(**5**)][PF$_6$]$_2$ (22.0 mg, 1.99×10^{-2} mmol) and [Ru(tpy)Cl$_3$] (8.8 mg, 2.0×10^{-2} mmol) were dissolved in ethanol (10 mL) and a few drops of *N*-ethylmorpholine added. The mixture was refluxed for 4 h and then cooled to room temperature and the solvent removed. The red/brown compound was redissolved in acetonitrile and aqueous ammonium hexafluorophosphate was added. A brownish precipitate was collected by filtration. The precipitate was purified by column chromatography (SiO_2, MeCN-saturated aqueous KNO_3–H_2O 7:1:0.5). The second red fraction was collected and the solvent removed. The red residue was redissolved in acetonitrile and precipitated by the addition of aqueous ammonium hexafluorophosphate to give [(bpy)$_2$Ru(**5**)Ru(tpy)][PF$_6$]$_4$ (15.0 mg, 43.6%). ^{1}H NMR (300 MHz, CD_3CN): δ 8.72 (H_{H3}, d, 2H, *J* 8.1 Hz), 8.54 (H_{G3}, s, 2H), 8.53–8.44 ($H_{A3–F3,J3}$, m, 8H), 8.37 ($H_{I3,J4}$, d, 3H, *J* 9.0 Hz), 8.15–8.00 (H_{A4}–H_{E4}, m, 5H), 7.97 (H_{A6}, d, 1H, *J* 5.9 Hz), 7.89 ($H_{H4–I4}$, dd, 4H, *J* 8.1, 7.7 Hz), 7.84–7.70 ($H_{B6–F6}$, m, 5H), 7.50 (H_{A5}, dd, 1H, *J* 5.9 Hz), 7.47–7.35 ($H_{B5–F5,H6–I6}$, m, 9H), 7.16 (H_{H5}–H_{I5}, m, 4H); *m*/*z*: (ES–MS): 1587.3 ([M−PF$_6$]$^+$), 721.1 ([M−2PF$_6$]$^{2+}$). *Anal.* Calc. for $C_{60}H_{44}N_{12}ORu_2P_4F_{24} \cdot 2H_2O$: C, 40.8; H, 2.7; N, 9.5. Found: C, 40.8; H, 2.5; N, 9.3%. IR $\bar{\nu}$/cm^{-1} (KBr): 3649w, 3587w, 3325w, 3085w, 1605m, 1463m, 1442m, 1421m, 1404m, 1327m, 1219m, 1165m, 1118w, 1026m, 957m, 818s, 764s, 656m; UV/VIS (CH_3CN): λ_{max}/nm (ε/dm^3 mol^{-1} cm^{-1}) 241 (50300), 288 (87000), 304 (59000), 467 (23000); Fluorescence (CH_3CN): λ_{em}/nm (λ_{ex}/nm) 626 (464); E^0/V vs. Fc: +0.89, −1.54, −1.67, −1.85, −2.18, −2.33.

2.2.21. *[(tpy)Ru(**9**)Fe(**9**)Ru(tpy)][PF$_6$]$_6$ · 11H$_2$O*

[Ru(tpy)(**9**)][PF$_6$]$_2$ (35 mg, 0.032 mmol) was dissolved in methanol (3 mL) and a few drops of acetonitrile. A solution of Fe(BF$_4$)$_2$ · 4H$_2$O (4.47 mg, 0.0190 mmol) in methanol (2.8 mL) was added and the mixture heated to reflux with a heat gun. The dark red-purple solution was filtered through a cotton–wool plug and methanolic ammonium hexafluorophosphate was added dropwise. A dark red-purple precipitate was collected and dried to give [(tpy)Ru(**9**)Fe(**9**)Ru(tpy)][PF$_6$]$_6$ as a red solid (36.8 mg, 69.3%). ^{1}H NMR (300 MHz, CD_3CN): δ/ppm 8.73 (H_{A3}, d, 4H, *J* 8.1 Hz), 8.62 (H_{F3}, s, 4H), 8.52–8.48 ($H_{B3,C3,G3}$, m, 12H), 8.47 (H_{D3}, s, 4H), 8.38 (H_{A4}, t, 2H, *J* 8.1 Hz), 7.97–7.90 ($H_{B4,C4,G4}$, m, 12H), 7.90 (H_E, s, 8H), 7.45 (H_{C6}, d, 4H, *J* 6.2 Hz), 7.32 (H_{B6}, d, 4H, *J* 6.2 Hz), 7.23–7.13 ($H_{B5,C5,G5,G6}$, m, 16H) 5.78 (H_{E2}, s, 4H), 5.71 (H_{E3}, s, 4H); *m*/*z*: (ES–MS): 1253.3 ([M−2PF$_6$]$^{2+}$). *Anal.* Calc. for $C_{106}H_{78}N_{18}O_4Ru_2FeP_6F_{36} \cdot 11H_2O$: C, 42.5; H, 3.4; N, 8.4. Found: C, 42.7; H, 3.5; N, 8.4%. IR $\bar{\nu}$/cm^{-1} (KBr): 3649w, 3587w, 3093w, 2931w, 2160w, 1975w, 1604m, 1550m, 1501m, 1452m, 1412m, 1373m, 1357m, 1203m, 1148m, 1118w, 995m, 825s, 783m, 764m, 655m, 625m; UV/VIS (CH_3CN): λ_{max}/nm (ε/dm^3 mol^{-1} cm^{-1}) 242 (100100), 271 (126400), 304 (111700), 482 (30300), 553 (13400); E^0/V vs. Fc: +0.80, +0.55, −1.65, −1.90, −2.23.

2.2.22. *[(tpy)Ru(**9**)Co(**9**)Ru(tpy)][PF$_6$]$_6$ · 6H$_2$O*

[Ru(tpy)(**9**)][PF$_6$]$_2$ (35 mg, 0.032 mmol) was dissolved in methanol (3 mL) and a few drops of acetonitrile. A solution of Co(OAc)$_2$ · 4H$_2$O (4.47 mg, 0.0190 mmol) in methanol (3.7 mL) was added and the mixture heated to reflux with a heat-gun. The dark red solution was filtered through a cotton–wool plug and methanolic ammonium hexafluorophosphate was added dropwise. A dark red precipitate was collected and dried to give [(tpy)Ru(**9**)Co(**9**)Ru(tpy)][PF$_6$]$_6$ as a red solid (17.3 mg, 28.6%). ^{1}H NMR (300 MHz, CD_3CN): δ/ppm 75.8 (H_D, s, 4H), 71.8 (H_D, s, 4H), 35.0 (H_D, s, 4H), 16.1 (H_D, s, 4H), 12.9 (H_D, s, 4H), 10.3 (H_C, s, 8H), 10.1 (H_A, s, 2H), 9.38–7.16 ($H_{A–B}$, m, 50H), 6.39 (CH_2, s,

4H), 4.15 (CH_2, s, 4H); *m/z*: (ES–MS): 1254.7 ($[M-2PF_6]^{2+}$). *Anal.* Calc. for $C_{106}H_{78}N_{18}O_4Ru_2CoP_6F_{36}\cdot 6H_2O$: C, 43.8; H, 3.1; N, 8.7. Found: C, 44.0; H, 3.2; N, 8.3%. IR $\bar{\nu}/cm^{-1}$ (KBr): 3649w, 3595w, 3326w, 3085w, 1620m, 1566m, 1493m, 1419m, 1358m, 1203m, 1164m, 1103w, 1041m, 995m, 818s, 787m, 663m, 625m; UV/VIS (CH_3CN): λ_{max}/nm (ε/$dm^3\,mol^{-1}\,cm^{-1}$) 242 (91600), 268 (113800), 305.3 (106300), 480 (27400); E^0/V vs. Fc: +0.81, −0.15, −1.65, −1.87.

2.2.23. *[(tpy)Ru(9)Mn(9)Ru(tpy)][PF6]6*

[Ru(tpy)(**9**)][PF_6]$_2$ (24.5 mg, 0.0200 mmol) was dissolved in methanol (3 mL) and a few drops of acetonitrile. A methanol (2 ml) solution of $Mn(OAc)_2\cdot 4H_2O$ (1.73 mg, 0.0100 mmol) was added and the mixture heated to reflux with a heat-gun. The dark red solution was filtered through a cotton plug and methanolic ammonium hexafluorophosphate was added dropwise. A dark red precipitate was collected and dried to give [(tpy)Ru(**9**)Mn(**9**)Ru(tpy)][PF_6]$_6$ as a red solid (38.5 mg, 68.9%). ^{1}H NMR (300 MHz, CD_3CN): δ/ppm all peaks broadened due to paramagnetism; *m/z*: (ES–MS): 1252.5 ($[M-2PF_6]^{2+}$); IR $\bar{\nu}/cm^{-1}$ (KBr): 3326m, 1614m, 1554w, 1421m, 1361m, 1201m, 1155m, 1062m, 1014m, 828s; UV/VIS (CH_3CN): λ_{max}/nm (ε/$dm^3\,mol^{-1}\,cm^{-1}$) 241 (97900), 271 (103500), 304 (87400), 478 (28000); E^0/V vs. Fc: +0.81, −1.49 (irreversible), −1.72. −1.90, −2.20.

2.2.24. *[(tpy)Ru(3)Mn(3)Ru(tpy)][PF6]6*

[Ru(tpy)(**3**)][PF_6]$_2$ (22.1 mg, 0.0200 mmol) was dissolved in methanol (3 mL) and a few drops of acetonitrile. A methanol (2 ml) solution of $Mn(OAc)_2\cdot 4H_2O$ (1.73 mg, 0.0100 mmol) was added and the mixture heated to reflux with a heat gun. The dark red solution was filtered through a cotton plug and methanolic ammonium hexafluorophosphate was added dropwise. A dark red precipitate was collected and dried to give [(tpy)Ru(**3**)Mn(**3**)Ru(tpy)][PF_6]$_6$ as a red solid (31.8 mg, 61.9%) ^{1}H NMR (300 MHz, CD_3CN): δ/ppm all peaks broadened due to paramagnetism; *m/z*: (ES–MS): 1132.4 ($[M-2PF_6]^{2+}$); IR $\bar{\nu}/cm^{-1}$ (KBr): 3325m, 1596m, 1427m, 1372m, 1211m, 1164w, 1018m, 972m, 810s; UV/VIS (CH_3CN): λ_{max}/nm (ε/$dm^3\,mol^{-1}\,cm^{-1}$) 239 (83500), 279 (67600), 287 (68200), 305 (90800), 481 (23400); E^0/V vs. Fc: +0.88, −1.56. −1.76, −2.26.

2.2.25. *[(bpy)2Ru(5)Fe(5)Ru(bpy)2][PF6]6*

[Ru(bpy)$_2$(**5**)][PF_6]$_2$ (30.0 mg, 2.71×10^{-2} mmol) was dissolved in methanol (3 mL) and a few drops of acetonitrile. A methanol (2.9 mL) solution of $Fe(BF_4)_2\cdot 4H_2O$ (4.58 mg, 1.36×10^{-5} mol) was added and the mixture heated to reflux with a heat-gun. The dark red-purple solution was filtered through a cotton plug and methanolic ammonium hexafluorophosphate was added dropwise. The dark red-purple precipitate was collected and dried to give [(bpy)$_2$Ru(**5**)Fe(**5**)Ru(bpy)$_2$][PF_6]$_6$ as a red solid (30.8 mg, 88.5%). ^{1}H NMR (300 MHz, CD_3CN): δ/ppm 8.74 (H_{G3}, s, 4H), 8.66 ($H_{E3,\ F3}$, m, 4H), 8.58–8.51 (H_{A3-D3}, m, 8H), 8.41 (H_{H3}, d, 4H, *J* 8.1 Hz), 8.16–8.05 ($H_{A4-E4,F6}$, m, 12H), 7.91–7.80 ($H_{A6-D6,H4}$, m, 12H), 7.75 (H_{E6}, d, 2H, *J* 5.5 Hz), 7.58–7.40 (H_{A5-F5}, m, 12H), 7.28 (H_{H6}, d, 4H, *J* 6.0 Hz), 7.14 (H_{H5}, t, 4H, *J* 6.0 Hz); *m/z*: (ES–MS) 1135.1 ($[M-2PF_6]^{2+}$). *Anal.* Calc. for $C_{90}H_{66}N_{18}O_2Ru_2FeP_6F_{36}\cdot 4H_2O$: C, 41.1; H, 2.8; N, 9.6. Found: C, 40.8; H, 2.7; N, 9.5%. IR $\bar{\nu}/cm^{-1}$ (KBr): 3325m, 3093w, 2924w, 1605m, 1463m, 1427m, 1219m, 1018m, 956m, 825s, 751s, 725s; UV/VIS (CH_3CN): λ_{max}/nm (ε/$dm^3\,mol^{-1}\,cm^{-1}$) 244 (120000), 286 (260000), 314 (86000), 458 (40000), 559 (25700); Fluorescence (CH_3CN): λ_{em}/nm (λ_{ex}/nm) 625 (455), 639 (556); E^0/V vs. Fc: +0.86, +0.68.

2.2.26. *[(bpy)2Ru(5)Co(5)Ru(bpy)2][PF6]6*

[Ru(bpy)$_2$(**5**)][PF_6]$_2$ (35 mg, 0.032 mmol) was dissolved in acetonitrile (8 mL) and $Co(OAc)_2\cdot 4H_2O$ (4.47 mg, 0.0190 mmol), dissolved in 2 ml water, was added. The mixture was refluxed. After 3 h, the red mixture was cooled to room temperature and aqueous ammonium hexafluorophosphate was added. A red precipitate was collected and purified by preparative TLC (SiO_2, MeCN-saturated aqueous KNO_3–H_2O 7:1:0.5) followed by reprecipitation with ammonium hexafluorophosphate to give [(bpy)$_2$Ru(**5**)Co(**5**)Ru(bpy)$_2$][PF_6]$_6$ as a dark red solid (30 mg, 31.4%). ^{1}H NMR (300 MHz, CD_3CN): δ/ppm 67.9 (H_E, s, 4H), 65.9 (H_E, s, 4H), 37.0 (H_E, s, 4H), 13.8 (H_E, s, 4H), 13.1 (H_E, s, 4H), 10.6 (H_D, s, 2H), 10.1 (H_D, s, 2H), 9.8 (H_D, s, 2H), 9.2–7.7 (H_{A-C}, m, 40H); *m/z*: (ES–MS) 1136.6 ($[M-2PF_6]^{2+}$). *Anal.* Calc. for $C_{90}H_{66}N_{18}O_2Ru_2CoP_6F_{36}\cdot 1.25KPF_6$: C, 38.7; H, 2.4; N, 9.0. Found: C, 38.8; H, 2.2; N, 8.6%. IR $\bar{\nu}/cm^{-1}$ (KBr): 3641w, 3409w, 3085w, 2924w, 1705m, 1605m, 1485m, 1450m, 1420m, 1365m, 1319w, 1219m, 1165m, 1095w, 1064w, 1026w, 964w, 825s, 793m, 764s, 663m; UV/VIS (CH_3CN): λ_{max}/nm (ε/$dm^3\,mol^{-1}\,cm^{-1}$) 239 (93300), 286 (196500), 455 (28900); Fluorescence (CH_3CN): λ_{em}/nm (λ_{ex}/nm) 625 (453); E^0/V vs. Fc: +0.90, −0.02, −1.66, −1.84, −2.21, −2.30.

2.2.27. *[(bpy)2Ru(5)Mn(5)Ru(bpy)2][PF6]6*

[Ru(bpy)$_2$(**5**)][PF_6]$_2$ (22.1 mg, 0.0200 mmol) was dissolved in methanol (3 mL) and a few drops of acetonitrile. A methanol (2 mL) solution of $Mn(OAc)_2\cdot 4H_2O$ (1.73 mg, 0.0100 mmol) was added and the mixture heated to reflux with a heat gun. The dark red solution was filtered through a cotton plug and methanolic ammonium hexafluorophosphate was added dropwise. A dark red precipitate was collected and dried to

give $[(bpy)_2Ru(\mathbf{5})Mn(\mathbf{5})Ru(bpy)_2][PF_6]_6$ as a red solid (31.8 mg, 61.9%). ^{1}H NMR (300 MHz, CD_3CN): δ/ppm all peaks broadened due to paramagnetism; *m/z*: (ES–MS): 1134.5 ($[M-2PF_6]^{2+}$); IR $\bar{\nu}/cm^{-1}$ (KBr): 3660w, 3326m, 3085w, 1594m, 1460m, 1420m, 1359m, 1301w, 1223m, 1163w, 1053w, 1018w, 964w, 815s, 763s, 656m, 640m; UV/VIS (CH_3CN): λ_{max}/nm (ε/$dm^3\,mol^{-1}\,cm^{-1}$) 240 (83800), 287 (140800), 455 (22900); Fluorescence (CH_3CN): λ_{em}/nm (λ_{ex}/nm) 622 (453); E^0/V vs. Fc: +0.87, −1.69, −1.89, −2.13.

2.2.28. *[(bpy)$_2$Ru(**2**)Ru(**2**)Ru(bpy)$_2$][PF$_6$]$_6$ · 6H$_2$O*

A solution of $[(bpy)_2Ru(\mathbf{2})][PF_6]_2$ (10 mg, 0.009 mmol) and commercial $RuCl_3 \cdot 3H_2O$ (1 mg, 0.004 mmol) in $HOCH_2CH_2OH$ (4 mL) together with two drops of *N*-ethylmorpholine was heated to reflux in a microwave oven (800 W) for 6 min. A solution of saturated aqueous ammonium hexafluorophosphate (25 mL) was then added to the orange solution, the precipitate was collected by filtration over celite and dissolved in acetonitrile. The solvent was evaporated in vacuo and the residue was purified by column chromatography (SiO_2, MeCN-saturated aqueous KNO_3–H_2O 7:1:0.5). To the major red fraction, an excess of ammonium hexafluorophosphate was added and the solution reduced in volume. The precipitate was collected by filtration over celite, washed with acetonitrile and evaporated to dryness to give $[(bpy)_2Ru(\mathbf{2})Ru(\mathbf{2})Ru(bpy)_2][PF_6]_6$ as a red-orange powder (6.0 mg, 51%). ^{1}H NMR (250 MHz, CD_3CN): δ/ppm 9.25 (H_{F3}, d, 2H, *J* 2.4 Hz), 9.17 (H_{G3}, s, 4H), 8.98 (H_{E3}, d, 2H, *J* 7.9 Hz), 8.73 (H_{H3}, d, 4H, *J* 7.9 Hz), 8.59–8.54 (H_{A3-D3}, m, 8H), 8.23–8.08 ($H_{F5,F6,A4-E4}$, m, 14H), 8.01–7.92 ($H_{E6,H4}$, m, 6H), 7.86–7.78 (H_{A6-D6}, m, 8H), 7.53–7.40 ($H_{A5-E5,\ H6}$, m, 14H), 7.25–7.18 (H_{H5}, m, 4H); ES–MS: *m/z* 1141.6 ($[M-2PF_6]^{2+}$), 713.0 ($[M-3PF_6]^{3+}$), 498.3 ($[M-4PF_6]^{4+}$), 369.9 ($[M-5PF_6]^{5+}$), 283.9 ($[M-6PF_6]^{6+}$). *Anal*. Calc. for $C_{90}H_{66}N_{18}Ru_3P_6F_{36} \cdot 6H_2O$: C, 40.3; H, 2.9; N, 9.4. Found: C, 40.0; H, 3.2; N, 9.2%. IR $\bar{\nu}/cm^{-1}$ (KBr): 3650w, 3443m, 3091w, 2924w, 1617m, 1607m, 1466m, 1447m, 1421m, 1383m, 1244w, 1027w, 837s, 787m, 763m, 731w, 558s; UV/VIS (CH_3CN): λ_{max}/nm (ε/$dm^3\,mol^{-1}\,cm^{-1}$) 242 (51100), 286 (118300), 460 (17600), 512 (38700); Fluorescence (CH_3CN): λ_{em}/nm (λ_{ex}/nm) 670 (460), 681 (513); E^0/V vs. Fc: +0.91,+0.98, −1.31, −1.43, −1.73, −1.85, −2.23.

2.2.29. *[(bpy)$_2$Ru(**2**)Fe(**2**)Ru(bpy)$_2$][PF$_6$]$_6$ · 6H$_2$O*

A solution of $[(bpy)_2Ru(\mathbf{2})][PF_6]_2$ (25 mg, 0.023 mmol) and iron(II) tetrafluoroborate (6.0 mg, 0.017 mmol) in ethanol (50 mL) was heated to reflux for 1 h. After this period the solvent was evaporated in vacuo and the residue was purified by column chromatography (SiO_2, MeCN-saturated aqueous KNO_3–H_2O 7:1:0.5). To the major green-brown fraction, an excess of ammonium hexafluorophosphate was added and the solution reduced in volume. The precipitate was collected by filtration over celite, dissolved in acetonitrile and evaporated to dryness to give $[(bpy)_2Ru(\mathbf{2})Fe(\mathbf{2})Ru(bpy)_2][PF_6]_6$ as a red-brown powder (23.0 mg, 80%). ^{1}H NMR (250 MHz, CD_3CN): δ/ppm 9.34 (H_{F3}, d, 2H, *J* 2.4 Hz), 9.32 (H_{G3}, s, 4H), 8.98 (H_{E3}, d, 2H, *J* 7.9 Hz), 8.68 (H_{H3}, d, 4H, *J* 7.9 Hz), 8.60–8.54 (H_{A3-D3}, m, 8H), 8.24–8.10 ($H_{A4-E4,F5,F6}$, m, 14H), 7.96–7.90 ($H_{E6,H4}$, m, 6H), 7.86–7.79 (H_{A6-D6}, m, 8H), 7.55–7.42 (H_{A5-E5}, m, 10H), 7.18–7.08 ($H_{H5,H6}$, m, 8H); ES–MS: *m/z* 1119.1 ($[M-2PF_6]^{2+}$), 697.8 ($[M-3PF_6]^{3+}$), 487.1 ($[M-4PF_6]^{4+}$), 276.4 ($[M-6PF_6]^{6+}$). *Anal*. Calc. for $C_{90}H_{66}N_{18}FeRu_2P_6F_{36} \cdot 6H_2O$: C, 40.9; H, 3.0; N, 9.6. Found: C, 40.3; H, 3.3; N, 9.4%. IR $\bar{\nu}/cm^{-1}$ (KBr): 3650w, 3450m, 3088w, 2924w, 1720w, 1616m, 1606m, 1533w, 1466m, 1446m, 1423m, 1401m, 1243w, 1027w, 839s, 788m, 732w, 558s; UV/VIS (CH_3CN): λ_{max}/nm (ε/$dm^3\,mol^{-1}\,cm^{-1}$) 244 (78800), 287 (155700), 462 (27000), 591 (34700); Fluorescence (CH_3CN): λ_{em}/nm (λ_{ex}/nm) 628 (460); E^0/V vs. Fc: +0.92,+0.79, −1.30, −1.41, −1.73, −1.88, −2.22.

2.2.30. *[(bpy)$_2$Ru(**2**)Co(**2**)Ru(bpy)$_2$][PF$_6$]$_6$ · 10H$_2$O*

A solution of $[(bpy)_2Ru(\mathbf{2})][PF_6]_2$ (16.0 mg, 0.0150 mmol) and cobalt(II) tetrafluoroborate (3.0 mg, 0.0080 mmol) in ethanol (10 mL) was stirred at room temperature for 1 h. The solvent was then evaporated in vacuo and the residue was purified by column chromatography (SiO_2, MeCN-saturated aqueous KNO_3–H_2O 7:1:0.5). To the major orange fraction an excess of ammonium hexafluorophosphate was added and the solution reduced in volume. The precipitate was collected by filtration over celite, dissolved in acetonitrile and evaporated to dryness to give $[(bpy)_2Ru(\mathbf{2})Co(\mathbf{2})Ru(bpy)_2][PF_6]_6$ as an orange powder (15.0 mg, 81%). ^{1}H NMR (250 MHz, CD_3CN): δ/ppm 91.5 (H_H, bs, 4H), 52.5 (H_H, s, 4H), 36.9 (H_H, s, 4H), 32.9 (H_H, s, 4H), 13.9 (H_H, s, 2H), 12.7 (H_F, s, 2H), 10.2 (H_F, 2H, s, H_b), 9.8 (H_F, s, 2H), 9.2–7.7 (H_{A-E}, m, 40H); ES–MS: *m/z* 1120.1 ($[M-2PF_6]^{2+}$), 698.4 ($[M-3PF_6]^{3+}$), 487.6 ($[M-4PF_6]^{4+}$), 361.3 ($[M-5PF_6]^{5+}$), 276.7 ($[M-6PF_6]^{6+}$). *Anal*. Calc. for $C_{90}H_{66}N_{18}CoRu_2P_6F_{36} \cdot 10H_2O$: C, 39.8; H, 3.2; N, 9.3. Found: C, 39.8; H, 3.5; N, 9.4%. IR $\bar{\nu}/cm^{-1}$ (KBr): 3446m, 2924w, 1618m, 1604m, 1561w, 1534w, 1509w, 1467m, 1446m, 1422m, 1384s, 1274w, 1245w, 1028w, 1016w, 839s, 790m, 763m, 731w, 662w, 557s; UV/VIS (CH_3CN): λ_{max}/nm (ε/$dm^3\,mol^{-1}\,cm^{-1}$) 243 (87900), 287 (162000), 470 (30500); Fluorescence (CH_3CN): λ_{em}/nm (λ_{ex}/nm) 628 (454); E^0/V vs. Fc: 0.95, −0.07, −1.43, −1.60, −1.83, −1.91, −2.27.

2.2.31. *[(bpy)$_2$Ru(**2**)Mn(**2**)Ru(bpy)$_2$][PF$_6$]$_6$*

$[Ru(bpy)_2(\mathbf{2})][PF_6]_2$ (21.8 mg, 0.0200 mmol) was dissolved in methanol (3 mL) and a few drops of acetonitrile. A methanol (2 mL) solution of $Mn(OAc)_2 \cdot 4H_2O$ (1.73 mg, 0.0100 mmol) was added and the mixture heated to reflux with a heat gun. The dark red solution

was filtered through a cotton plug and methanolic ammonium hexafluorophosphate was added dropwise. A dark red precipitate was collected and dried to give $[(bpy)_2Ru(\mathbf{2})Mn(\mathbf{2})Ru(bpy)_2][PF_6]_6$ as a red solid (20.0 mg, 39.6%). ^{1}H NMR (300 MHz, CD_3CN): δ/ppm all peaks broadened due to paramagnetism; m/z: (ES–MS): 1118.4 ($[M-2PF_6]^{2+}$); IR $\bar{\nu}$/cm^{-1} (KBr): 3649w, 3325w, 3085w, 1604m, 1535w, 1463m, 1427m, 1311w, 1242m, 1165m, 1018m, 818s, 764s, 663m; UV/VIS (CH_3CN): λ_{max}/nm (ε/dm^3 mol^{-1} cm^{-1}) 244 (80 300), 293 (153 100), 460 (20 700); Fluorescence (CH_3CN): λ_{em}/nm (λ_{ex}/nm) 636 (457); E^0/V vs. Fc: +0.95, −1.28, −1.51, −1.70, −1.87, −2.20.

3. Results and discussion

3.1. Strategy and ligand design

A large number of ligands incorporating two (or more) bpy or tpy metal-binding domains have been described. In this paper, we concentrate upon three classes of ditopic ligands (Scheme 1). In the first class, metal-binding domains are directly linked through a C–C single bond which, in principle, allows free rotation and leads to potentially maximum conjugation of the two components; the bpy–bpy compound **1** is well known [55,59–64] and our initial report of the tpy–tpy analogue

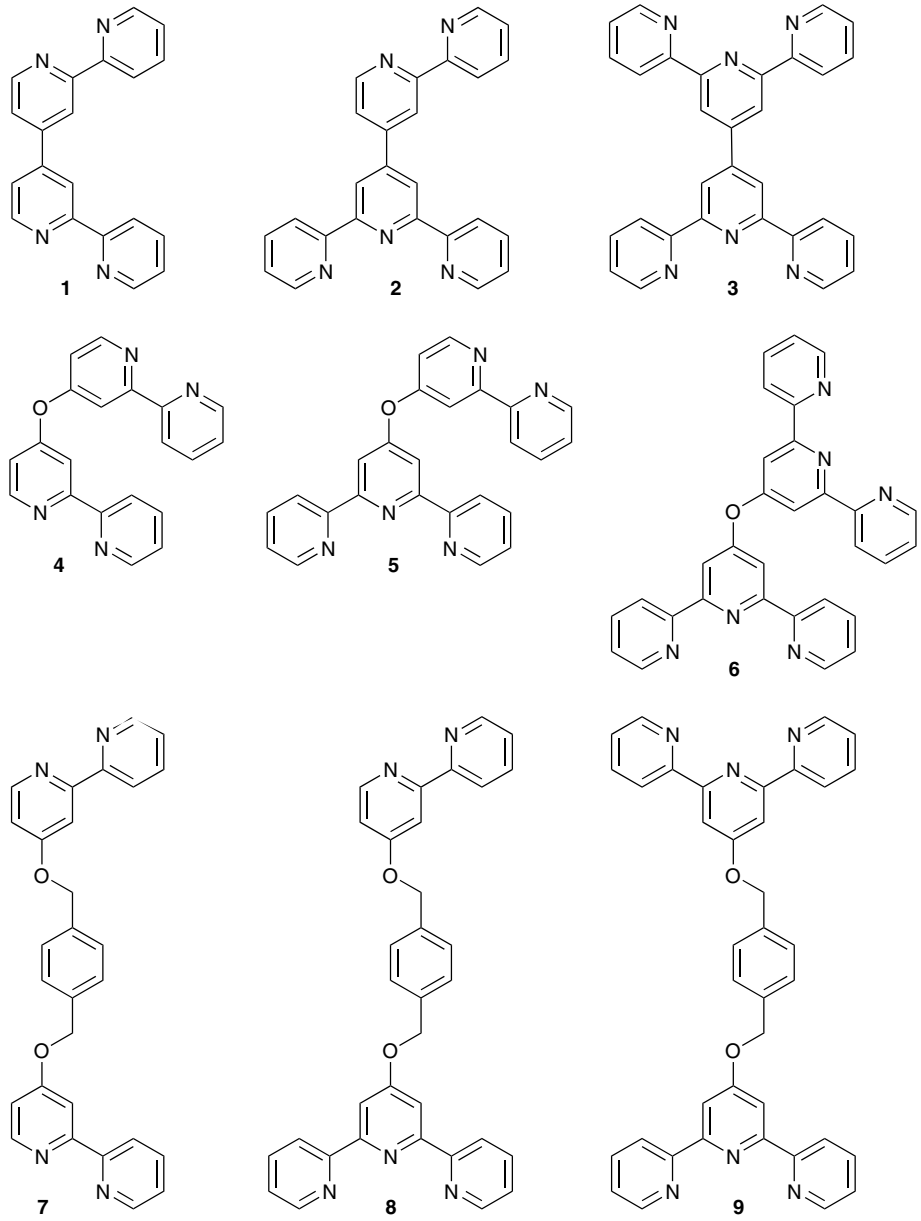

Scheme 1. Homo- and heteroditopic bpy and tpy ligands discussed in this paper.

3 [58] has been followed up by studies of coordination oligomers and polymers incorporating this species [22,65–83]. We have made brief reports concerning the bpy-tpy compound **2** [84,85] and will discuss further aspects of its coordination behaviour in this manuscript. In general, complexes containing ligands **1**–**3** will be prepared by conventional methods involving initial synthesis of the free ligand. The second class is typified by the linkage of the two metal-binding domains by a single ether oxygen atom, giving a greater degree of conformational freedom at the expense of conjugation of the subunits; of this ligand series, we have described the tpy–tpy compound **6** [30,86,87] and the bpy–bpy analogue **4** has been reported [20,88,89] but the heteroditopic species **5** has not hitherto been described. Synthetic strategies for ligands of this type are of four main types: (i) synthesis and subsequent coordination of the appropriate free ligand, (ii) reactions of coordinated electrophilic Xbpy or Xtpy ligands (Xbpy = 4-chloro-2,2′-bipyridine or 4-bromo-2,2′-bipyridine, Xtpy = 4′-chloro-2,2′:6′,2″-terpyridine or 4′-bromo-2,2′:6′,2″-terpyridine) with nucleophilic HObpy or HOtpy (HObpy = 2,2′-bipyridin-4(1*H*)-one, HOtpy = 4′-hydroxy-2,2′:6′,2″-terpyridine), (iii) reactions of coordinated HObpy or HOtpy with Xbpy or Xtpy or (iv) reactions of coordinated HObpy or HOtpy with Xbpy or Xtpy complexes. The final ligand type that we discuss incorporates a 1,4-$OCH_2C_6H_4CH_2O$ spacer between the metal-binding domains; we have reported a few complexes containing the tpy–tpy compound **9** [87] but compounds **7** and **8** have not yet been described. Synthetic approaches resemble those for ligands **4**–**6**, although the commonest strategies involve reaction of 1,4-bis(bromomethyl)benzene with HObpy or HOtpy or their complexes.

3.2. Ligand synthesis

This section briefly presents the synthesis of the key electrophilic and nucleophilic tpy derivatives that are used for the preparation of the multitopic ligands. The overview represents many years investigating synthetic routes to these compounds and presents the strategies which we consider to be the best.

3.2.1. Simple 2,2′-bipyridine derivatives

The synthesis of 4-heteroatom-substituted bpy ligands almost always commences with bpy itself which is activated by conversion to the *N*-oxide **10** by reaction with 3-chloroperbenzoic acid in chlorinated solvent or H_2O_2 in acetic acid [38–51]. In our hands, the latter procedure is more reliable and gives higher yields (>70%). The *N*-oxide **10** is readily nitrated in classical conditions to give 4-nitro-2,2′-bipyridine *N*-oxide **11** in yields ≈65% [40,45,47,50,51]. In our hands, the reaction of **11** with acetyl bromide in acetic acid gives a mixture of 4-bromo-2,2′-bipyridine *N*-oxide **12** and 4-bromo-2,2′-bipyridine, Brbpy, **13**. Subsequent reduction of **12** with PBr_3 in $CHCl_3$ gives **13** in quantitative yield and the overall conversion of **11**–**13** is usually greater than 90% [40,51–53]. We find the most convenient route to 4-chloro-2,2′-bipyridine, Clbpy, **14** is directly from **10** rather than the more classical route from **11** [44,49,51,54,55]. We have investigated routes to HObpy **15** starting from the halo-compounds Brbpy or Clbpy, but have found no reliable hydrolysis method for the preparation of the free ligands, and the method of choice for the preparation is reduction of **11** to 4-amino-2,2′-bipyridine **16** [47,54,57] followed by diazotization and hydrolysis [56]. These transformations are summarized in Scheme 2.

3.2.2. Simple 2,2′:6′,2″-teripyridine derivatives

The key intermediates in the tpy series are Cltpy and HOtpy; HOtpy **17** is readily prepared in good yield in a two step process from ethyl picolinate. The reaction of ethyl picolinate with the enolate of acetone gives the triketone **18** [58], which is cyclized by reaction with ammonium acetate to give HOtpy. The conversion of HOtpy to Cltpy **19** by reaction with PCl_5 in $POCl_3$ is quantitative [58]. These transformations are presented in Scheme 3.

3.2.3. Synthesis of free ditopic ligands

Of the directly-linked ditopic ligands, **1**–**3**, we only present new results for ligand **2** in this paper. The heteroditopic ligand **2** was prepared as a white crystalline solid in 23% yield by the literature method [84,85].

The free ligand **6** is prepared by the reaction of HOtpy with Cltpy in the presence of base for prolonged periods [86]. Although it would be possible to prepare the ditopic ligands **4** and **5** by analogous reactions (HObpy with Clbpy for **4**, HObpy with Cltpy or Clbpy with HOtpy for **5**) it is more convenient to make use of reactions of coordinated Clbpy or Cltpy to give complexes of unambiguous constitution in a single step.

The homoditopic tpy–tpy free ligand **9** was prepared in 82% yield by the reaction of HOtpy with 1,4-$BrCH_2C_6H_4CH_2Br$ in DMF in the presence of K_2CO_3 as a white crystalline solid. The bpy–bpy analogue **7** was prepared in a similar manner from HObpy as a white solid in 91% yield Scheme 4. The two new ligands were fully characterized by conventional methods. The EI mass spectrum of **9** exhibited a parent ion at *m*/*z* 601 whilst the FAB MS of **7** showed a parent ion at *m*/*z* 447. The high symmetry of the new ligands is seen in both the ^{13}C and ^{1}H NMR spectra; in the ^{1}H NMR spectra in $CDCl_3$ the phenylene and methylene protons appear as equal intensity singlets at δ 7.54 and 5.35 ppm in **7** and at δ 7.56 and 5.36 ppm in **9**. We have not attempted to prepare the heteroditopic free ligand **8** for two reasons. Firstly, selective reaction of one side of the 1,4-$BrCH_2C_6H_4CH_2Br$ with HOtpy or HObpy

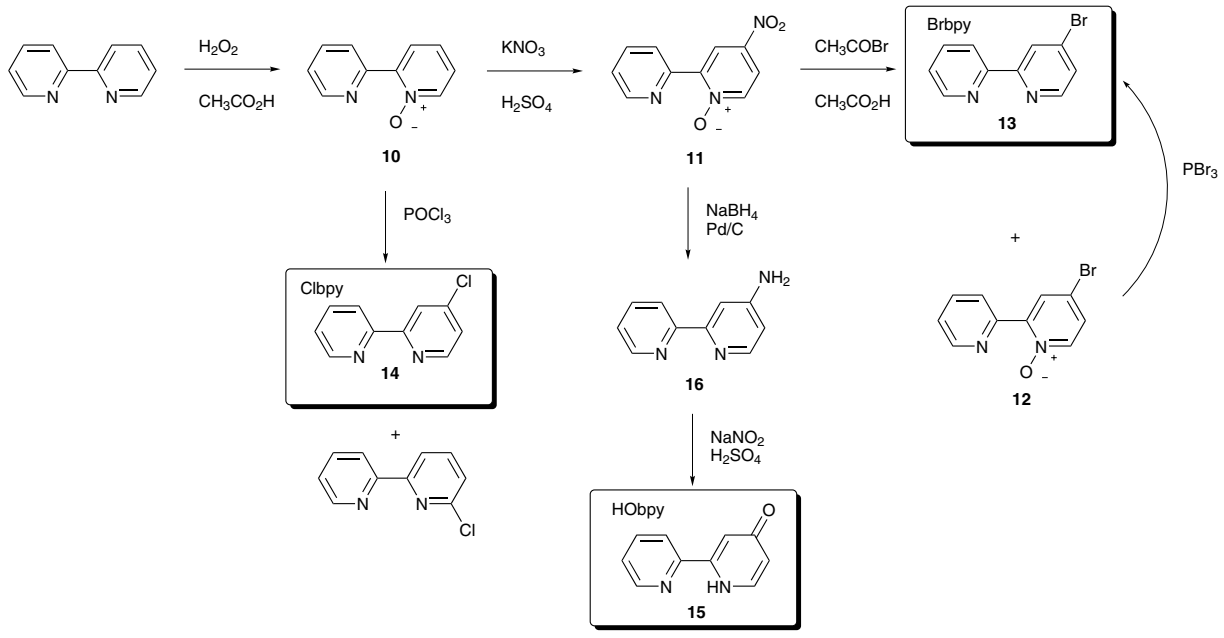

Scheme 2. Key transformations within the 2,2′-bipyridine ligand series.

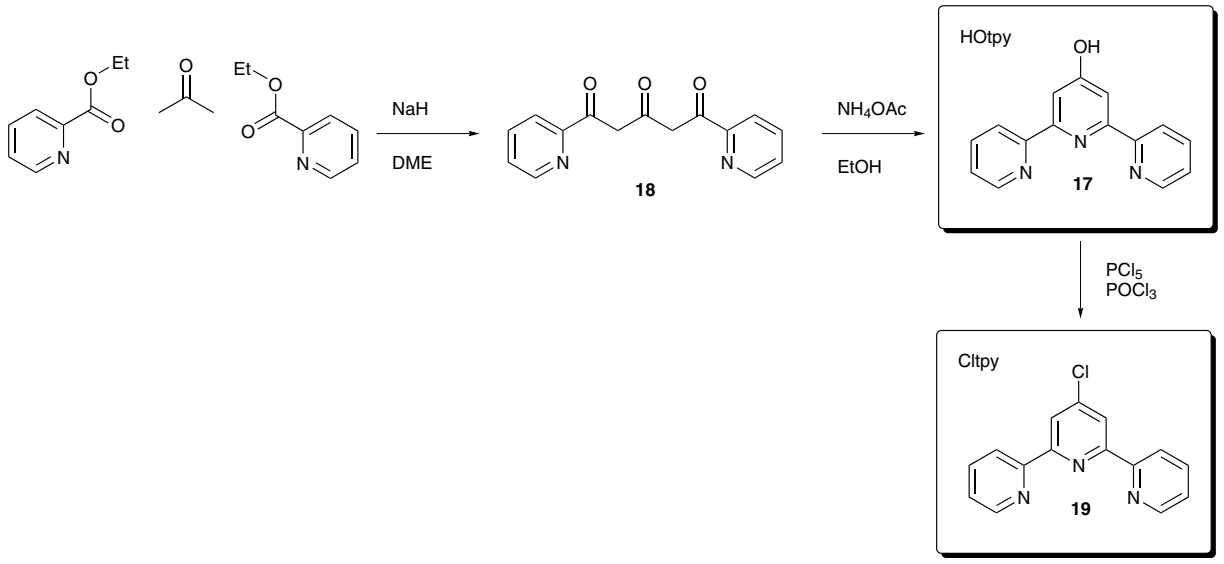

Scheme 3. Key transformations within the 2,2′:6′,2″-terpyridine ligand series.

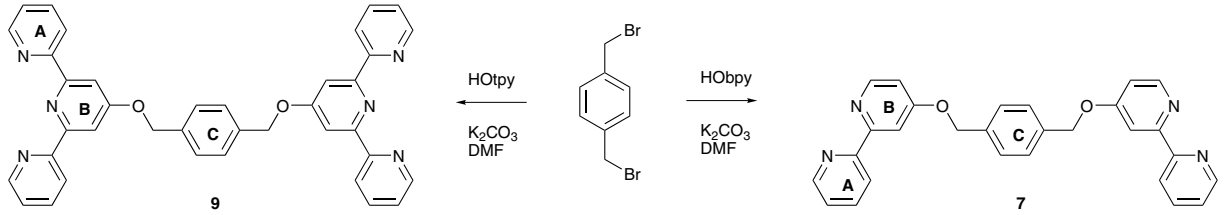

Scheme 4. Synthesis of heterotopic bridging ligands **7** and **9** showing the nomenclature system adopted to distinguish the aromatic rings.

followed by subsequent reaction with HObpy or Hotpy, respectively, seemed likely to give mixtures of mono- and bis-functionalized compounds. Secondly, even if we did obtain **8**, it would be necessary to selectively address the bpy or tpy metal-binding domains. Accordingly, for all compounds containing **8**, we adopted alternative approaches based upon reactions of coordinated ligands.

3.3. Synthesis of mononuclear ruthenium(II) complexes and simple ligand reactions

In the majority of the chemistry reported in this paper we utilize kinetically inert ruthenium(II) complexes, both as reaction scaffolds for reactions at coordinated ligands and as synthetic targets in their own right. We are primarily interested in tuning the redox and photophysical properties of multinuclear species containing metal-centred chromophores and lumophores, and $\{Ru(bpy)_3\}$ and $\{Ru(tpy)_2\}$ motifs are at the core of these studies.

The complexes $[Ru(bpy)_2(Clbpy)][PF_6]_2$ [90–92] and $[Ru(bpy)_2(Brbpy)][PF_6]_2$ [20,64,89] were prepared by the reaction of *cis*-$[Ru(bpy)_2Cl_2]$ with Clbpy or Brbpy, respectively, in refluxing $HOCH_2CH_2OH$ in a modified domestic microwave oven. This technique allows for very fast reaction times of the order of minutes in contrast to conventional thermal reactions which require many hours at reflux. The crude products were precipitated as hexafluorophosphate salts and purified by chromatography over silica using a highly polar mobile phase (acetonitrile, water, aqueous KNO_3). The complexes $[Ru(bpy)_2(Clbpy)][PF_6]_2$ and $[Ru(bpy)_2(Brbpy)][PF_6]_2$ were obtained as bright red solids in yields of 75% and 87% respectively. These two compounds will be used as electrophilic bpy complexes for the unambiguous introduction of $\{Ru(bpy)_3\}$ motifs. The two complexes are luminescent with absorption and emission spectra essentially identical to $[Ru(bpy)_3]^{2+}$. The ligands are slightly more electron withdrawing than bpy, and the ruthenium(II)–(III) redox process is shifted to slightly more positive potentials (+0.92 and +0.90 V for the Brbpy and Clbpy complexes, respectively, all potentials quoted vs. internal Fc/Fc^+, MeCN solution) than $[Ru(bpy)_3]^{2+}$ (+0.85 V). We note at this point that all $\{Ru(bpy)_2(Xbpy)\}$ centres described in this paper are racemates comprising equal amounts of the Δ and Λ enantiomers, as is the starting *cis*-$[Ru(bpy)_2Cl_2]$.

An analogous reaction of *cis*-$[Ru(bpy)_2Cl_2]$ with the amino compound **16** under microwave conditions gave an uncharacterized mixture of compounds possessing various colours, but prolonged (5 h) reaction in aqueous methanol under normal thermal conditions, followed by chromatographic purification gave $[Ru(bpy)_2(\mathbf{16})][PF_6]_2$ [90–92] as a red solid in 42% yield. All attempts to use $[Ru(bpy)_2(\mathbf{16})][PF_6]_2$ as a nitrogen nucleophile in reactions with electrophiles were unsuccessful. The amino group is highly conjugated with the bpy and this is observed in the properties of the complex; the MLCT absorption is red shifted to 458 nm and the ruthenium(II)–(III) redox process is now observed at +0.70 V, shifted 150 mV to less positive potential than $[Ru(bpy)_3]^{2+}$. The luminescence is also significantly red-shifted to 645 nm with respect to $[Ru(bpy)_3]^{2+}$ (620 nm).

The phenolic hydroxy group in complexes of HObpy and HOtpy is readily deprotonated to give complexes of enhanced (but still very low) nucleophilicity. Regardless of the tautomeric state of the free ligands (pyridone or hydroxypyridine), the complexes are forced to adopt the hydroxypyridine structure. Attempts to prepare salts of either $[Ru(bpy)_2(HObpy)]^{2+}$ or $[Ru(bpy)_2(Obpy)]^{+}$ from HObpy and $[Ru(bpy)_2Cl_2]$ under microwave or thermal conditions only resulted in mixtures of numerous products in our hands. However, although we could not obtain good yields of HObpy by alkaline hydrolysis of Clbpy or Brbpy, we considered that the enhanced electrophilicity of coordinated Clbpy might allow us to perform the hydrolysis in the coordination sphere and prepare $[Ru(bpy)_2(HObpy)]^{2+}$ or $[Ru(bpy)_2(Obpy)]^{+}$ directly from $[Ru(bpy)_2(Clbpy)][PF_6]_2$. Upon heating $[Ru(bpy)_2(Clbpy)][PF_6]_2$ to reflux overnight with 2 M aqueous sodium hydroxide solution, a red solution was obtained from which the orange complex $[Ru(bpy)_2(Obpy)][PF_6]$ was isolated. Protonation yielded the parent complex $[Ru(bpy)_2(HObpy)][PF_6]_2$ as a red solid. In contrast to the complex with the amino compound **16**, the HOtpy complex shows no great difference in its electrochemical or spectroscopic behaviour from $[Ru(bpy)_3]^{2+}$. These compounds will act as nucleophilic complexes for the introduction of $\{Ru(bpy)_3\}$ moieties upon reaction with electrophiles. These reactions are summarized in Scheme 5.

In the series of complexes based upon $\{Ru(tpy)_2\}$ motifs, the complexes $[Ru(tpy)(Cltpy)][PF_6]_2$ and $[Ru(tpy)(HOtpy)][PF_6]_2$ act as electrophilic and nucleophilic species, respectively. The standard method for the preparation of $[Ru(tpy)(Xtpy)][PF_6]_2$ complexes involves the reaction of $[Ru(tpy)Cl_3]$ with Xtpy or $[Ru(Xtpy)Cl_3]$ with tpy under reducing conditions (Scheme 6) [24]. It is most convenient to use an alcohol solvent containing an amine such as *N*-ethylmorpholine as the reductant. The desired ruthenium(III) complexes $[Ru(Xtpy)Cl_3]$ are prepared by the reaction of Xtpy with ethanolic solutions of commercial hydrated ruthenium trichloride and obtained as very dark brown or black insoluble solids. The electrophilic complex $[Ru(tpy)(Cltpy)][PF_6]_2$ is prepared in 45% yield as a red solid from the reaction of $[Ru(tpy)Cl_3]$ with Cltpy.

We were somewhat surprised to find that the two complementary routes for the preparation of $[Ru(tpy)(HOtpy)][PF_6]_2$, $[Ru(tpy)Cl_3]$ with HOtpy or $[Ru(HOtpy)Cl_3]$ with tpy, proceeded in significantly different

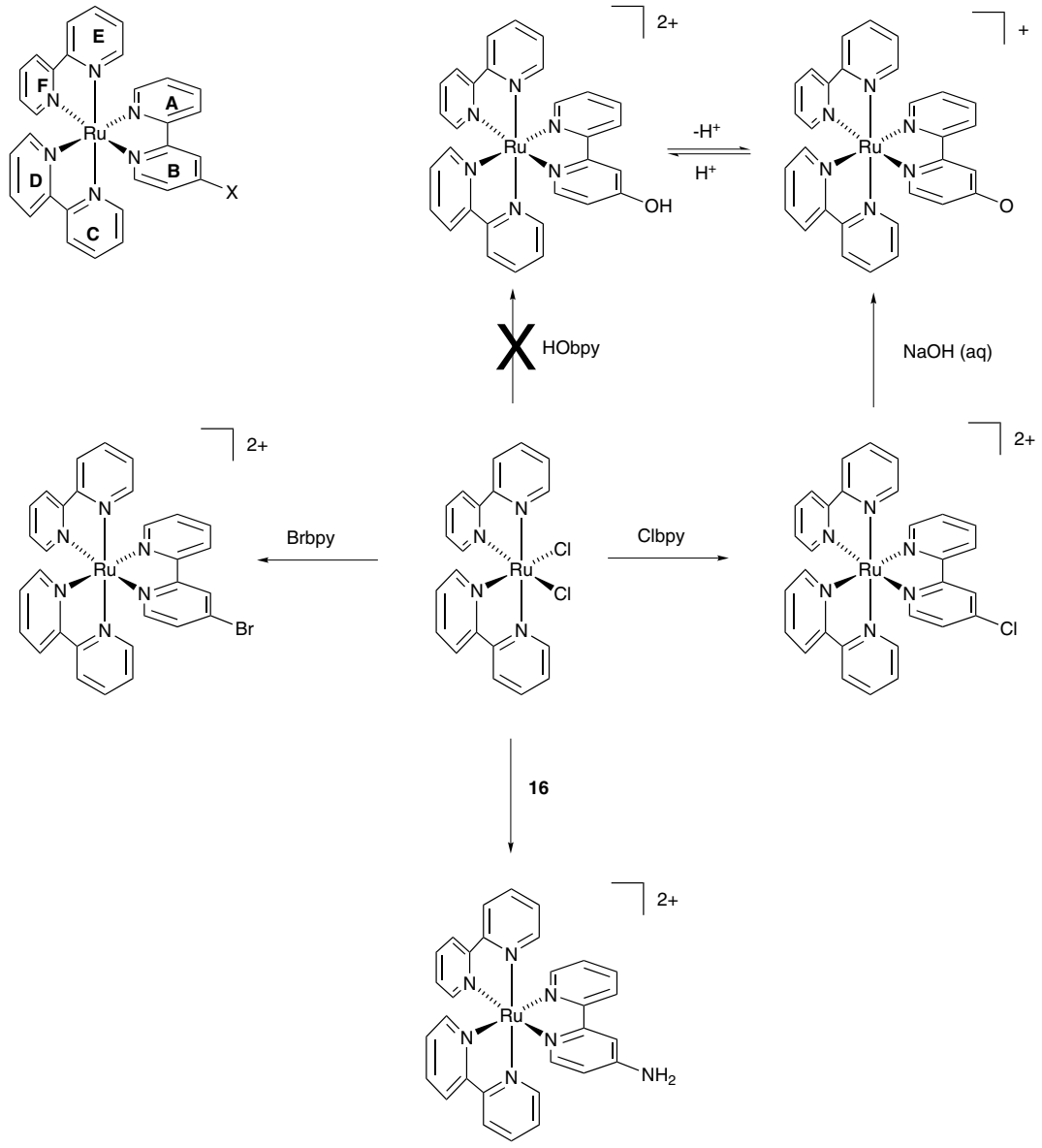

Scheme 5. The preparation and reactivity of mononuclear $[Ru(bpy)_2(Xbpy)]^{n+}$ complexes. The numbering scheme used to describe the various aromatic rings is also given.

manners. The compound $[Ru(HOtpy)Cl_3]$ is obtained as a brown solid in 75% yield from the reaction of HOtpy with "$RuCl_3 \cdot 3H_2O$" and subsequent reaction with tpy in ethanol containing *N*-ethylmorpholine gave $[Ru(tpy)(HOtpy)][PF_6]_2$ [24] as a red solid in 40% yield after chromatographic purification. In contrast, the reaction of $[Ru(tpy)Cl_3]$ with HOtpy in methanol containing *N*-ethylmorpholine gave a dark coloured solution. Chromatographic workup gave $[Ru(tpy)(HOtpy)][PF_6]_2$ as a red solid in 50% yield and a purple compound $\{Ru(tpy)(HOtpy)Cl(PF_6)\}$ in 21% yield. This latter complex has a number of characteristic features in its ^1H NMR spectrum; the tpy ligand remains symmetrical with the two terminal rings magnetically equivalent, but in the HOtpy ligand the two terminal rings are non-equivalent. Furthermore, the H_6 resonance of one of the terminal rings of the HOtpy ligand has a very characteristic chemical shift of δ 10.31 ppm which is typical of an oligopyridine *cis* to chlorine in which the C–Cl bond is approximately parallel to the Ru–Cl bond. In the other terminal ring of the HOtpy, H_6 (δ 8.63 ppm) is to higher frequency (down-field) than H_3 (δ 8.32 ppm) with the assignments being made by COSY methods, and H_6 and H_3 being distinguished on the basis of the coupling constants ($J_{5,6} < 6$ Hz, $J_{3,4} > 7$ Hz) [93]; this pattern is typical of a non-coordinated pyridine. The purple compound is the hypodentate [94–104] complex $[Ru(tpy)(HOtpy)Cl][PF_6]$ which contains a bidentate tpy ligand. On the NMR time-scale, rings C and F appear equivalent. It is unclear why the

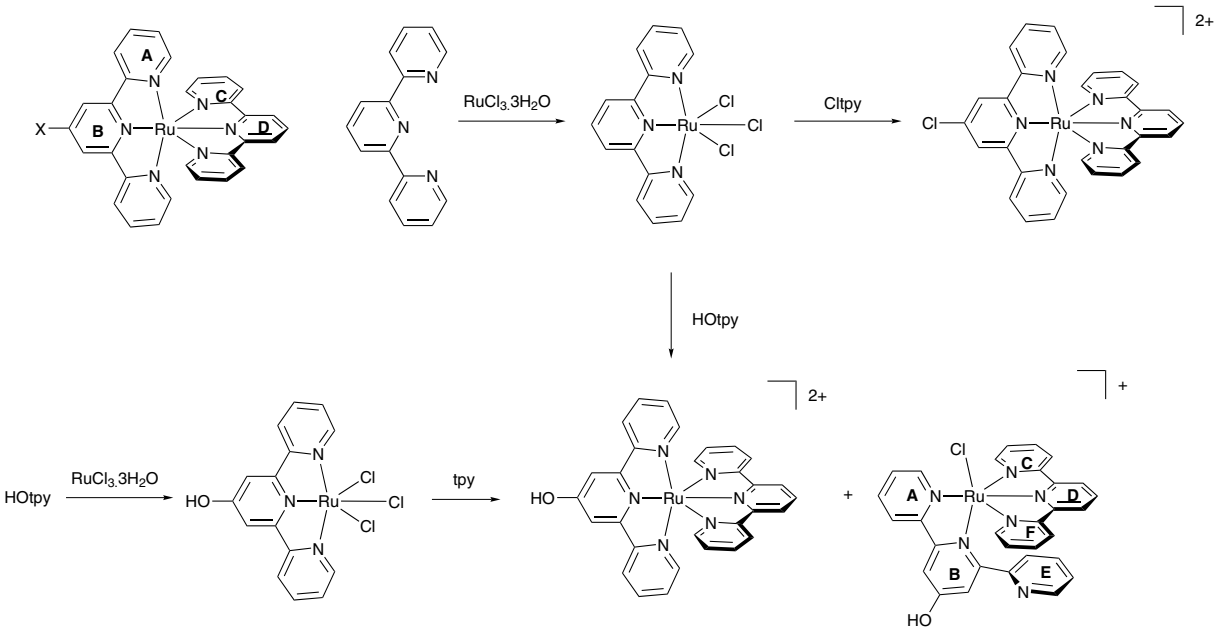

Scheme 6. Preparation of electrophilic and nucleophilic {Ru(tpy)$_2$} complexes and the hypodentate complex [Ru(tpy)(HOtpy)Cl][PF$_6$]. The labelling scheme for the normal and the hypodentate complexes is indicated.

hypodentate complex should be particularly favoured in this reaction.

3.4. Structural development of mononuclear ruthenium(II) complexes and complexes with pendant metal-binding domains

For the specific preparation of heterodinuclear and higher nuclearity complexes it is necessary to have metal-containing building blocks with pendant metal-binding domains. These species are often conveniently prepared from reactions of functionalized metal complexes with appropriate ligand species. We attempted to extend this methodology to the new spaced ligands **7**–**10**.

The reaction of the nucleophilic metal complex [Ru(tpy)(HOtpy)][PF$_6$]$_2$ with one equivalent of 1,4-BrCH$_2$C$_6$H$_4$CH$_2$Br in MeCN containing K$_2$CO$_3$ gave a red solution from which a new complex, [Ru(tpy)(**20**)]-[PF$_6$]$_2$ may be isolated in good yield (Scheme 7). This complex contains the new ligand (4′-bromomethylphenylmethyloxy)-2,2′:6′,2″-terpyridine which has been generated in situ by nucleophilic attack of the oxygen of the HOtpy ligand on the electrophilic 1,4-BrCH$_2$C$_6$H$_4$CH$_2$Br; indeed, the free ligand **20** has never been prepared. The new complex has been fully characterized and pertinent spectroscopic features include the observations of peak envelopes in the mass spectrum possessing the calculated isotopomer distributions for RuBr$_2$ species, together with the observation of two methylene singlets in the ^{1}H NMR spectrum typical of BrCH$_2$ (δ 4.66 ppm) and ArOCH$_2$ (δ 5.60 ppm) species. This complex with a pendant bromomethyl group is not particularly activated by coordination and may be recrystallized from aqueous acetonitrile without hydrolysis. Accordingly, we planned to use [Ru-(tpy)(**20**)][PF$_6$]$_2$ for the preparation of the homoditopic and heteroditopic pendant ligand complexes [Ru-(tpy)(**9**)][PF$_6$]$_2$ and [Ru(tpy)(**8**)][PF$_6$]$_2$ by reaction with HOtpy and HObpy, respectively. However, although the complex [Ru(tpy)(**20**)][PF$_6$]$_2$ is reasonably water stable, all attempts to react it with HOtpy or HObpy in MeCN containing potassium carbonate resulted in the formation of the [Ru(tpy)(**21**)][PF$_6$]$_2$ in which the bromine has been displaced by an acetoxy group in a mechanistically obscure reaction, but which presumably involves hydrolysis of the acetonitrile. Confirmation of this comes from the observation of a C=O stretch in the IR spectrum (1736 cm^{-1}), the observation of the parent ion in the mass spectrum and an acetate methyl resonance at δ 2.09 ppm in the ^{1}H NMR spectrum.

Attempts to prepare [Ru(bpy)$_2$(**7**)][PF$_6$]$_2$ by a similar route were also unsuccessful. The reaction of [Ru-(bpy)$_2$(Obpy)][PF$_6$] with 1,4-BrCH$_2$C$_6$H$_4$CH$_2$Br proceeded smoothly and the complex [Ru(bpy)$_2$(**22**)][PF$_6$]$_2$ was obtained as an orange solid in 25% yield after chromatographic purification. Once again, two methylene singlets are observed in the ^{1}H NMR spectrum typical of BrCH$_2$ (δ 4.58 ppm) and ArOCH$_2$ (δ 5.28 ppm) species and comparing well with [Ru(tpy)(**20**)][PF$_6$]$_2$. Attempts to prepare [Ru(bpy)$_2$(**7**)][PF$_6$]$_2$ or [Ru(bpy)$_2$(**8**)][PF$_6$]$_2$ by the reaction of [Ru(bpy)$_2$(**22**)][PF$_6$]$_2$ with HObpy or HOtpy in acetonitrile only gave the acetoxy derivative [Ru(bpy)$_2$(**23**)][PF$_6$]$_2$.

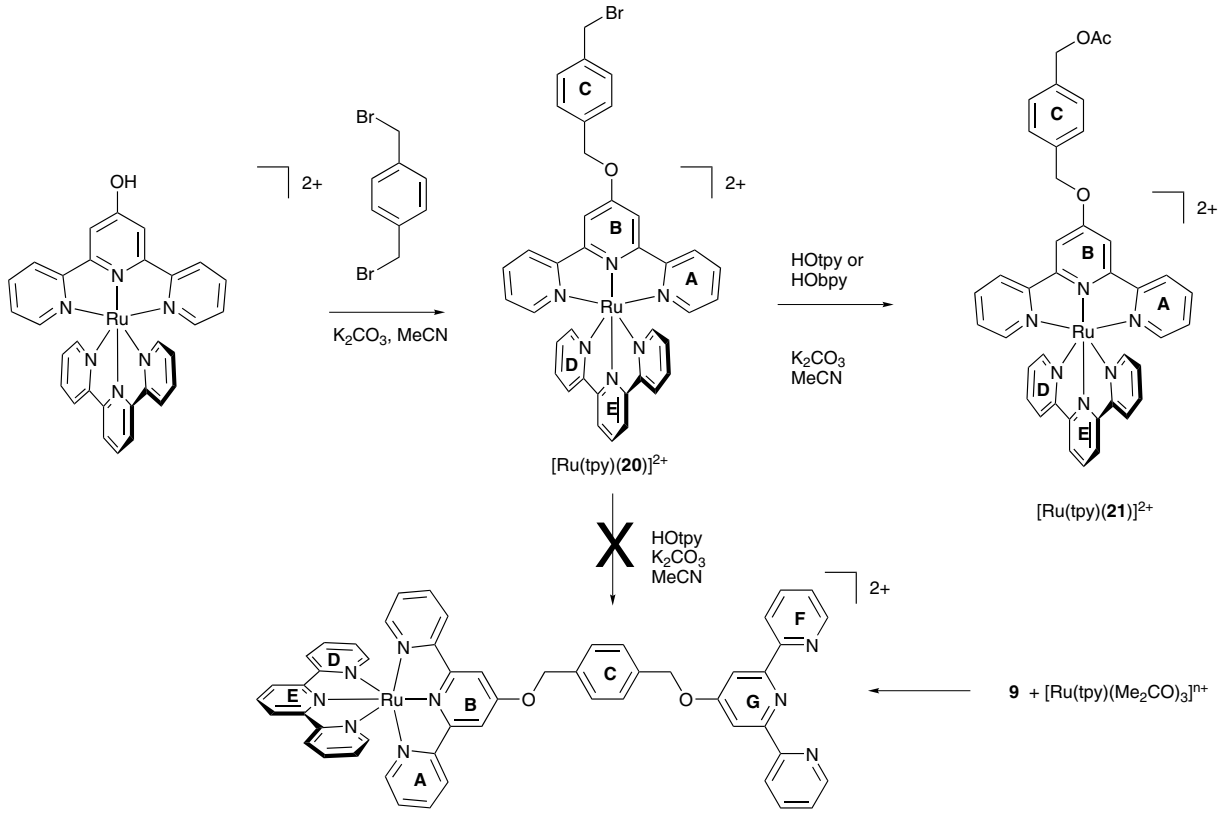

Scheme 7. Synthesis of mononuclear complex [Ru(tpy)(**9**)][PF_6]$_2$ with a pendant tpy metal-binding domain.

The complex [Ru(tpy)(**9**)][PF_6]$_2$, which has a free tpy metal-binding domain can, however, be prepared by the reaction of **9** with the solvento complex [Ru(tpy)(Me_2CO)$_3$]$^{n+}$. The new complex has the expected ^{1}H NMR spectroscopic characteristics for a species which has an uncoordinated tpy residue, with H_6 appearing at the typical free ligand position of δ 8.94 ppm. The bpy analogue [Ru(bpy)$_2$(**7**)][PF_6]$_2$, which has a free bpy metal-binding domain is prepared in a similar manner by the reaction of **7** with the solvento complex [Ru(bpy)$_2$(Me_2CO)$_2$]$^{n+}$ (prepared in situ by the reaction of silver tetrafluoroborate with [Ru(bpy)$_2$Cl$_2$] in acetone). The new complex has the expected ^{1}H NMR spectroscopic characteristics for a species which has an uncoordinated bpy residue. The {Ru(bpy)$_3$} luminophore is unperturbed and the complex shows an emission from the ^{3}MLCT level at 623 nm. The introduction of the ether-functionality at the 4-position of the bpy results in slightly greater ligand field and the ruthenium(II)–(III) process is shifted to slightly lower potential (+0.83 V) (see Scheme 8).

Metal-directed approaches to complexes containing the heteroditopic ligand **5** would involve the reaction of [Ru(tpy)(Cltpy)][PF_6]$_2$ with HObpy or [Ru(bpy)$_2$(Clbpy)][PF_6]$_2$ with HOtpy under the conditions used for the preparation of complexes of **1** or **3**. We elected to utilize the latter approach on the basis that the future use of enantiomerically pure [Ru(bpy)$_2$(Clbpy)][PF_6]$_2$ would allow the preparation of homochiral metallopolymers and metallodendrimers. The complex [Ru(bpy)$_2$(**5**)][PF_6]$_2$ was obtained in 41% yield from the reaction of either [Ru(bpy)$_2$(Clbpy)][PF_6]$_2$ or [Ru(bpy)$_2$(Brbpy)][PF_6]$_2$ with HOtpy in acetonitrile containing K_2CO_3 (Scheme 9). Again, the complex has characteristic properties associated with the non-coordinated tpy metal-binding domain (H_6 of the tpy domain at δ 8.77 ppm), behaves as a typical {Ru(bpy)$_3$} luminophore with an emission at 620 nm and exhibits a ruthenium(II)–(III) redox process at +0.88 V.

The principle of selectively addressing bpy or tpy domains in heteroditopic ligands is illustrated by the preparation of [Ru(bpy)$_2$(**2**)][PF_6]$_2$ from [Ru(bpy)$_2$Cl$_2$] and **2**. The complex [Ru(bpy)$_2$Cl$_2$] has two labile monodentate ligands and will react with bidentate oligopyridine metal-binding domains. In the case of ligand **2**, bidentate bpy and tpy domains are available, but the steric effects associated with the non-coordinated terminal pyridine ring of the didentate tpy destabilize this complex with respect to that with a coordinated bipyridine. The reaction of [Ru(bpy)$_2$Cl$_2$] with **2** in ethanol containing *N*-ethylmorpholine gives the complex [Ru(bpy)$_2$(**2**)][PF_6]$_2$ in 55% yield as an orange solid. The ^{1}H NMR spectrum clearly indicates that it is the tpy domain that is not-coordinated. The complex behaves as

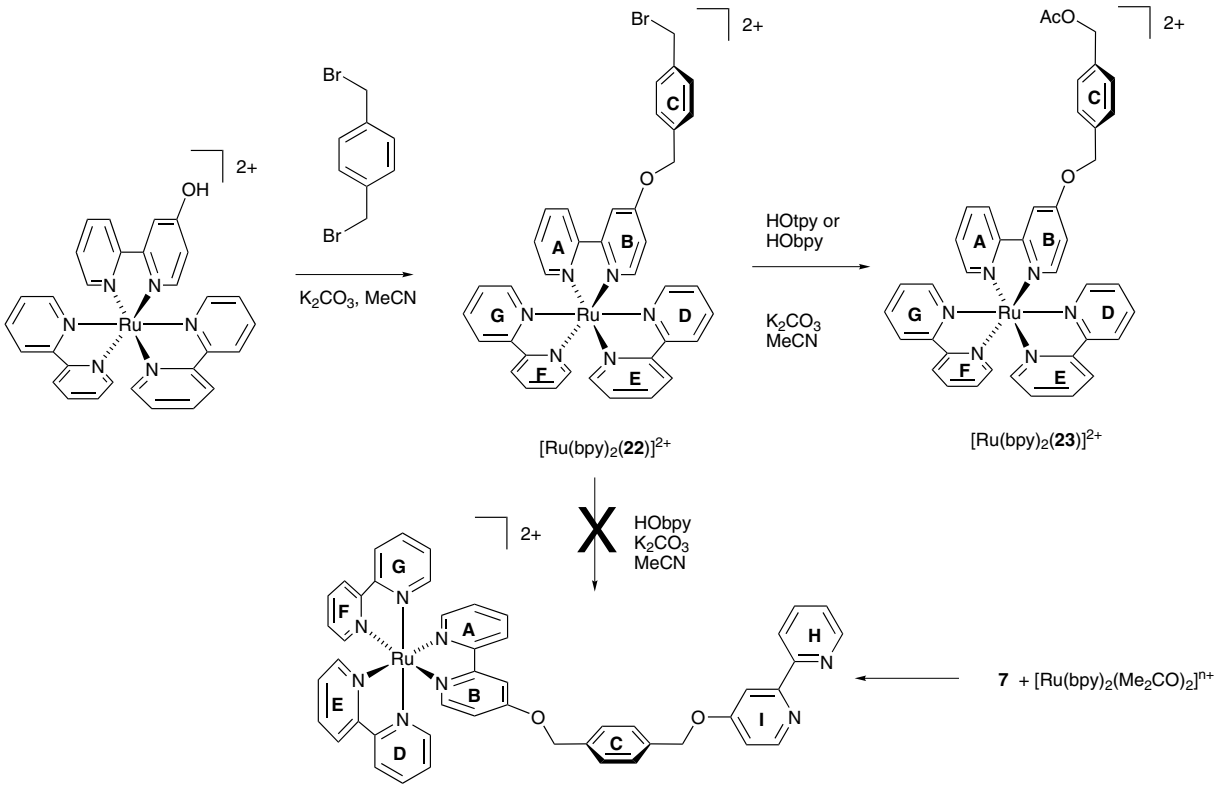

Scheme 8. Synthesis of mononuclear complex [Ru(tpy)(**7**)][PF_6]$_2$ with a pendant bpy metal-binding domain.

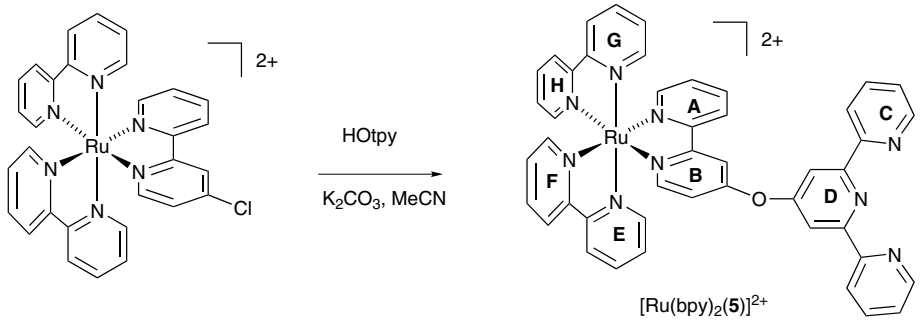

Scheme 9. Reaction of coordinated Cltpy with HObpy to form the new heteroditopic ligand **5**, coordinated to Ru(II).

a typical {Ru(bpy)$_3$} derivative, with essentially no perturbation of the ruthenium(II)–(III) redox process (+0.93 V) or the MLCT absorption (461 nm) and also retains the typical luminescent properties of this luminophore and shows an emission at 628 nm.

3.5. Preparation of diruthenium complexes of homoditopic and heteroditopic ligands

In this section, the various ways of preparing diruthenium complexes will be exemplified. The simplest method is the reaction of a ditopic ligand with two equivalents of a commensurate ruthenium complex. For every tpy metal-binding domain, use of complex [Ru(tpy)Cl$_3$] will give a new {Ru(tpy)$_2$} motif whilst for every bpy metal-binding domain reaction with [Ru(bpy)$_2$Cl$_2$] will give a new {Ru(bpy)$_3$} motif. In the case of the homoditopic ligands this procedure is trivial, although the complexes containing two {Ru(bpy)$_3$} groups will exist as a mixture of ΔΔ, ΔΛ and ΛΛ diastereoisomers. It is unlikely that the heteroditopic ligands can be selectively addressed.

A typical example is the preparation of [(bpy)$_2$-Ru(**7**)Ru(bpy)$_2$][PF_6]$_4$ from **7** and [Ru(bpy)$_2$Cl$_2$] (Scheme 10). The complex is obtained (as an uncharacterized mixture of diastereoisomers) as a red solid. We cannot state anything about the presence or ratio of diastereoisomers on the basis of the ^{1}H NMR spectra. There is no strong electronic interaction between the ruthenium centres and a single ruthenium(II)–(III)

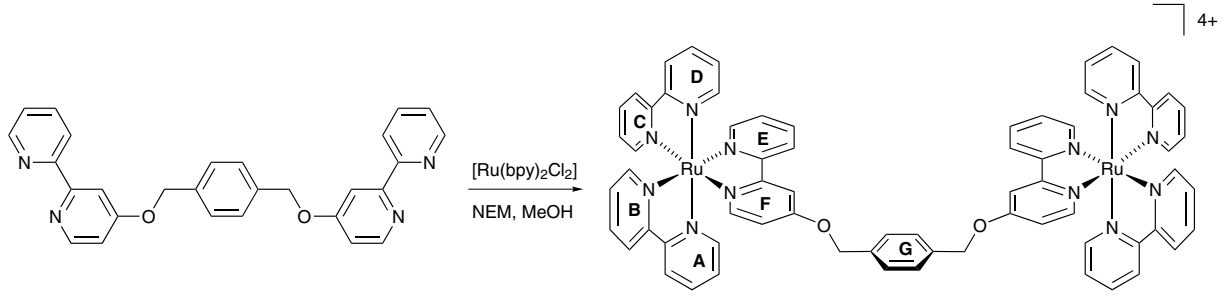

Scheme 10. Preparation of $[(bpy)_2Ru(\mathbf{7})Ru(bpy)_2][PF_6]_4$ from **7** and $[Ru(bpy)_2Cl_2]$ (only the ΛΔ diastereoisomer is shown).

redox process is observed at +0.81 V. The molar absorption coefficients are roughly twice that of model mononuclear complexes (or rather, the molar absorptivity per ruthenium centre is roughly constant) (see Schemes 11 and 12).

For heteroditopic ligands, the best strategy is to prepare a complex with a pendant metal-binding domain and to cap with a commensurate complex. The reaction of ruthenium complexes with pendant tpy metal-binding domains is exemplified by the use of the complexes $[Ru(bpy)_2(\mathbf{2})][PF_6]_2$ and $[Ru(bpy)_2(\mathbf{5})][PF_6]_2$ with $[Ru(tpy)Cl_3]$ to give the dinuclear complexes $[(bpy)_2Ru(\mathbf{2})Ru(tpy)][PF_6]_4$ and $[(bpy)_2Ru(\mathbf{5})Ru(tpy)][PF_6]_4$. These complexes, which contain only a single $\{Ru(bpy)_3\}$ motif are obtained as a racemate of the Δ and Λ enantiomers. The complexes exhibit a single observable ruthenium(II)–(III) process in their cyclic voltammogram or differential pulse voltammogram, although these are very broad and can be deconvoluted to two Gaussians for the $\{Ru(bpy)_3\}$ and $\{Ru(tpy)_2\}$ motifs. Both complexes are red-brown, but the absorption for $[(bpy)_2Ru(\mathbf{2})Ru(tpy)][PF_6]_4$ is red shifted to 500 nm with respect to $[(bpy)_2Ru(\mathbf{5})Ru(tpy)][PF_6]_4$ (467 nm). Both complexes are luminescent with $[(bpy)_2Ru(\mathbf{5})Ru(tpy)][PF_6]_4$ showing a typical $\{Ru(bpy)_3\}$ emission at 626 nm, but the emission from $[(bpy)_2Ru(\mathbf{2})Ru(tpy)][PF_6]_4$ is observed at 689 nm.

3.6. Preparation of trinuclear complexes of homoditopic and heteroditopic ligands

In the final section, we demonstrate the utility of complexes containing pendant tpy metal-binding domains as building blocks and illustrate their use for

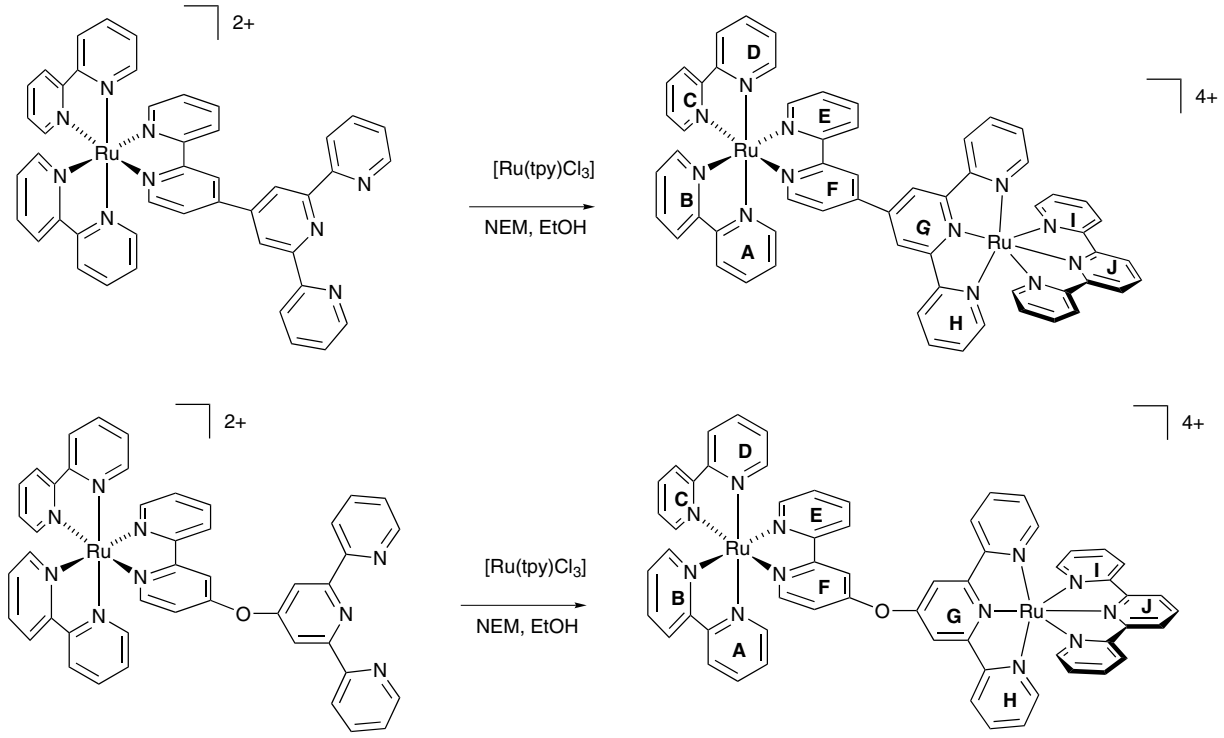

Scheme 11. The preparation of $[(bpy)_2Ru(\mathbf{2})Ru(tpy)][PF_6]_4$ and $[(bpy)_2Ru(\mathbf{5})Ru(tpy)][PF_6]_4$ by selectively capping the pendant tpy metal-binding domain with a (tpy)Ru unit.

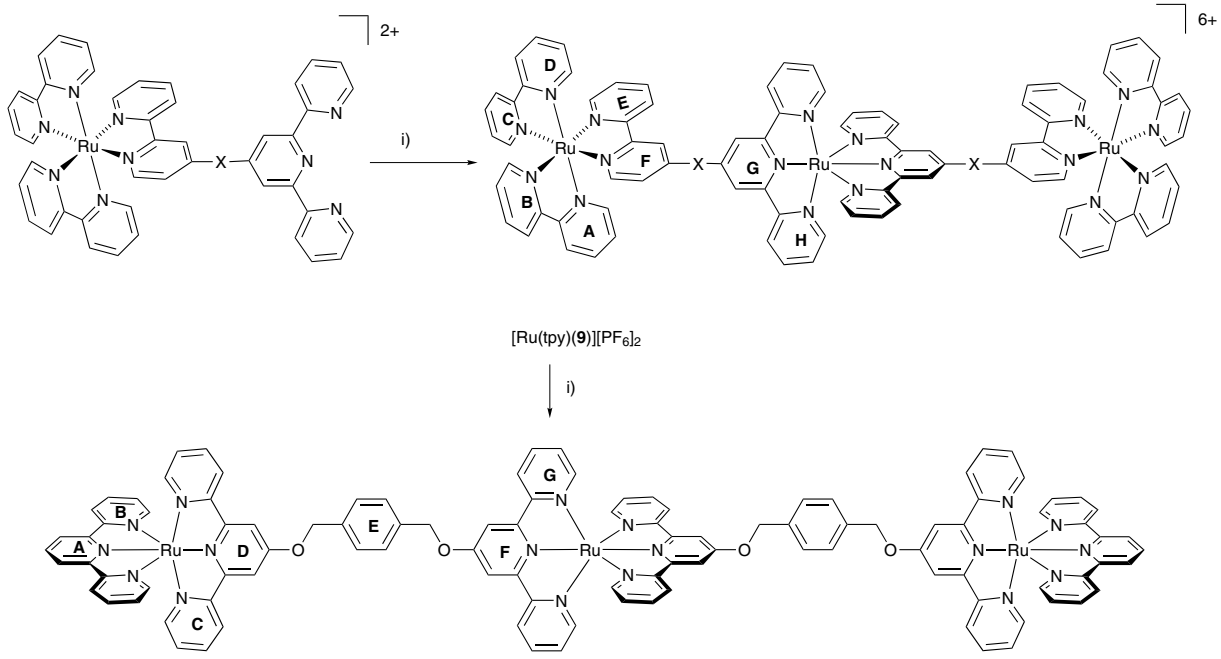

Scheme 12. Preparation of homo- and heterotrinuclear complexes with $\{Ru(bpy)_3\}$ and $\{M(tpy)_2\}$ domains: X = nothing or O, M = Ru (only for X = nothing) (i) $RuCl_3 \cdot 3H_2O$, $HOCH_2CH_2OH$, microwave; M = Co (i) $Co(OAc)_2 \cdot 4H_2O$; M = Fe (i) $Fe(BF_4)_2 \cdot 4H_2O$, MeOH; M = Mn (i) $Mn(OAc)_2 \cdot 4H_2O$.

the formation of a range of homo and heterotrinuclear complexes. The complex $[Ru(bpy)_2(\mathbf{2})][PF_6]_2$ contains a non-coordinated metal binding domain and is expected to react rapidly with labile first row divalent transition metal salts to give heterotrinuclear $[(bpy)_2Ru(\mathbf{2})M(\mathbf{2})Ru(bpy)_2]^{6+}$ species and under forcing conditions with less-labile ruthenium sources to give the homotrinuclear compound $[(bpy)_2Ru(\mathbf{2})Ru(\mathbf{2})Ru(bpy)_2]^{6+}$ with two $\{Ru(bpy)_3\}$ and one $\{Ru(tpy)_2\}$ motif.

The reaction of $[Ru(bpy)_2(\mathbf{2})][PF_6]_2$ with commercial $RuCl_3 \cdot 3H_2O$ under microwave conditions in $HOCH_2CH_2OH$ gave an orange solution from which the trinuclear compound $[(bpy)_2Ru(\mathbf{2})Ru(\mathbf{2})Ru(bpy)_2][PF_6]_6$ was isolated in 51% yield. The ^1H NMR spectrum reveals the high symmetry and the presence of the $\{Ru(bpy)_3\}$ and $\{Ru(tpy)_2\}$ motifs. The complex is presumably a statistical mixture of ΔΔ, ΔΛ and ΛΛ diastereoisomers. The nuclearity of these trinuclear complexes is very conveniently determined by the high resolution mass spectrometry, where the envelope of isotopomer peaks arising from the various ruthenium isotopes is very characteristic. This is illustrated in Fig. 1, where calculated isotopomer distributions are compared with the experimental electrospray mass spectrum for the dipositive ion $\{[(bpy)_2Ru(\mathbf{2})Ru(\mathbf{2})Ru(bpy)_2][PF_6]_4\}^{2+}$.

The presence of the $\{Ru(bpy)_3\}$ and $\{Ru(tpy)_2\}$ motifs domains is also seen in the spectroscopic and electrochemical properties of the complex. The differential pulse voltammogram of $[(bpy)_2Ru(\mathbf{2})Ru(\mathbf{2})Ru(bpy)_2][PF_6]_6$ (MeCN vs. Fc/Fc^+, $[^nBu_4N][PF_6]$ supporting electrolyte) is presented in Fig. 2, showing the asymmetric process associated with the two different ruthenium centres. The peak fitting to two Gaussians in a ratio of 2:1 is shown and allows us to extract E^0 values of +0.91 and +0.98 V for the $\{Ru(bpy)_3\}$ and $\{Ru(tpy)_2\}$ domains, respectively. The complex also shows two overlapping but distinct MLCT absorptions at 460 and 512 nm, assigned to the $\{Ru(bpy)_3\}$ and $\{Ru(tpy)_2\}$ domains, respectively. As expected, the complex is luminescent and shows a red-shifted $\{Ru(bpy)_3\}$-type emission at 670 nm.

The complexes $[(bpy)_2Ru(\mathbf{2})M(\mathbf{2})Ru(bpy)_2][PF_6]_6$ (M = Co, Fe, Mn) are even simpler to prepare and are isolated by the addition of NH_4PF_6 to methanol solutions containing $[Ru(bpy)_2(\mathbf{2})][PF_6]_2$ and appropriate salts in a 2:1 ratio. All of the complexes are luminescent with MLCT absorption maxima 460–470 nm and a typical $\{Ru(bpy)_3\}$-type emission at 628–636 nm. In the case of the purple iron(II) complex $[(bpy)_2Ru(\mathbf{2})Fe(\mathbf{2})Ru(bpy)_2][PF_6]_6$, there is a second MLCT absorption due to the $\{Fe(tpy)_2\}$ chromophore at 591 nm. The complexes all show a ruthenium(II)–(III) process in their cyclic voltammograms at +0.92–0.95 V. In the cases of the iron(II) and cobalt(II) complexes, an additional metal-centred process due to the central first row metal is observed at +0.79 and −0.07 V, respectively. Taken collectively, these data argue strongly for uncoupled metal centres in the heterotrinuclear species. The ^1H NMR spectra of the complexes are of varying degrees of utility, the diamagnetic iron complex is assigned by usual

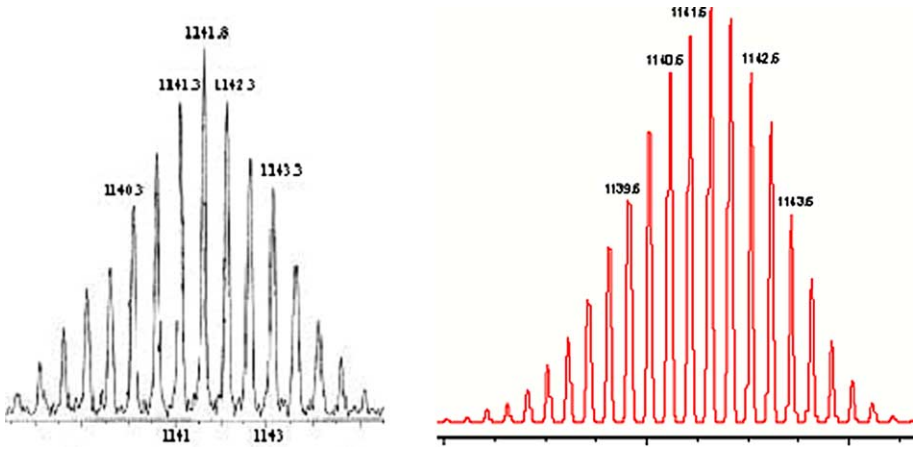

Fig. 1. Experimental (left) and calculated (right) isotopomer distribution for the species $\{[(bpy)_2Ru(\mathbf{2})Ru(\mathbf{2})Ru(bpy)_2][PF_6]_4\}^{2+}$.

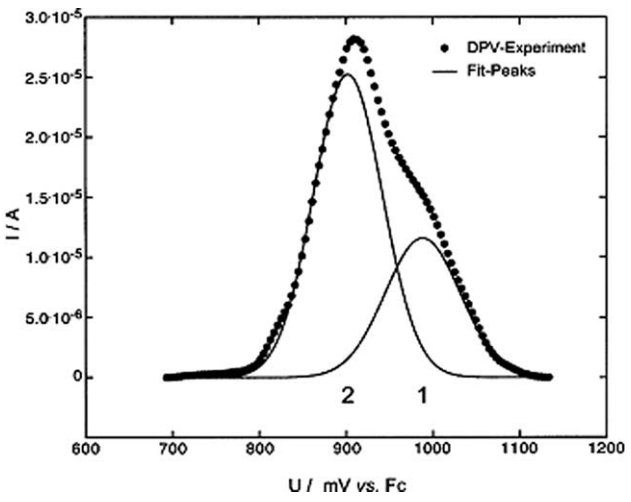

Fig. 2. Differential pulse voltammogram of $[(bpy)_2Ru(\mathbf{2})Ru(\mathbf{2})Ru(bpy)_2][PF_6]_6$ (MeCN vs. Fc/Fc^+, $[^nBu_4N][PF_6]$ supporting electrolyte) and fitting of two Gaussian curves for the $\{Ru(bpy)_3\}$ and $\{Ru(tpy)_2\}$ processes at +0.91 and +0.98 V, respectively.

methods. Both the cobalt(II) and manganese(II) complexes are paramagnetic; in the case of $[(bpy)_2Ru(\mathbf{2})Mn(\mathbf{2})Ru(bpy)_2][PF_6]_6$ all signals are exceptionally broad and no assignments can be made, but for $[(bpy)_2Ru(\mathbf{2})Co(\mathbf{2})Ru(bpy)_2][PF_6]_6$ the peaks of the $\{Co(tpy)_2\}$ domain are shifted but not excessively broadened, allowing a full assignment [93].

The analogous heterotrinuclear compounds $[(bpy)_2Ru(\mathbf{5})M(\mathbf{5})Ru(bpy)_2][PF_6]_6$ and $[(bpy)_2Ru(\mathbf{9})M(\mathbf{9})Ru(bpy)_2][PF_6]_6$ (M = Co, Fe, Mn) were prepared using $[Ru(bpy)_2(\mathbf{5})][PF_6]_2$ or $[Ru(bpy)_2(\mathbf{9})][PF_6]_2$, respectively. No significant differences from the compounds discussed above were observed: all compounds with **5** exhibited $\{Ru(bpy)_3\}$ MLCT absorption maxima at 450–458 nm and a typical $\{Ru(bpy)_3\}$-type emission at 620–625 nm, whilst those with **9** were non-luminescent in fluid solution having only a $\{Ru(tpy)_2\}$ luminophore, and show typical $\{Ru(tpy)_3\}$ MLCT absorption maxima at 478–482 nm. The iron(II) complexes with both **5** and **9** show an additional iron-centred MLCT absorption at 550–560 nm. The complexes are redox active showing essentially unperturbed $\{Ru(bpy)_3\}$ ruthenium(II)–(III) processes at +0.86 to +0.90 V, $\{Ru(tpy)_2\}$ ruthenium(II)–(III) processes at +0.80 to +0.90 V, {Co(tpy)} cobalt(II)–(III) processes at +0 V, and $\{Fe(tpy)_2\}$ iron(II)–(III) processes at ≈+0.70 V.

4. Conclusions

We have demonstrated that combinations of conventional ligand and complex synthesis with metal-directed reactions of coordinated ligands may be used to prepare a suite of building blocks containing hetero- and homoditopic ligands. Representative homo- and heterotrinuclear complexes with these building blocks have been prepared.

Acknowledgements

We thank the Universities of Basel and Birmingham, the Swiss National Science Foundation and COST action D31 for financial support.

References

[1] J.A. McCleverty, T.J. Meyer (Eds.), Comprehensive Coordination Chemistry II, Vol. 7, Elsevier Pergamon, Oxford, 2004.
[2] J.A. McCleverty, T.J. Meyer (Eds.), Comprehensive Coordination Chemistry II, Vol. 9, Elsevier Pergamon, Oxford, 2004.
[3] E.C. Constable, in: J.A. McCleverty, T.J. Meyer (Eds.), Comprehensive Coordination Chemistry II, vol. 7, Oxford, 2004, p. 263.
[4] Z.S. Hou, Q.Z. Zhang, G.Y. Li, M.G. Zhu, Progr. Chem. 14 (2002) 469.
[5] K. Onitsuka, S. Takahashi, Top. Curr. Chem. 228 (2003) 39.

[6] H.J. van Manen, F.C.J.M. van Veggel, D.N. Reinhoudt, Top. Curr. Chem. 217 (2001) 121.
[7] D. Astruc, Pure Appl. Chem. 75 (2003) 461.
[8] D. Astruc, J.C. Blais, E. Cloutet, L. Djakovitch, S. Rigaut, J. Ruiz, V. Sartor, C. Valerio, 2000; vol. 210; p. 229.
[9] I. Cuadrado, M. Moran, C.M. Casado, B. Alonso, J. Losada, Coord. Chem. Rev. 195 (1999) 395.
[10] M. Dasgupta, M.B. Peori, A.K. Kakkar, Coord. Chem. Rev. 233 (2002) 223.
[11] G.R. Newkome, E.F. He, C.N. Moorefield, Chem. Rev. 99 (1999) 1689.
[12] J.F. Nierengarten, Chem.-Eur. J. 6 (2000) 3667.
[13] S. Serroni, S. Campagna, F. Puntoriero, C. Di Pietro, N.D. McClenaghan, F. Loiseau, Chem. Soc. Rev. 30 (2001) 367.
[14] S.C. Zimmerman, L.J. Lawless, Top. Curr. Chem. 217 (2001) 95.
[15] E.C. Constable, Metals and ligand reactivity, An Introduction to the Organic Chemistry of Metal Complexes, VCH, Weinheim, 1995.
[16] E.C. Constable, P. Harverson, M. Oberholzer, J. Chem. Soc., Chem. Commun. (1996) 1821.
[17] L.E. Hansen, E.R. Glowacki, D.L. Arnold, G.J. Bernt, B. Chi, R.J. Fites, R.A. Freeburg, R.F.N. Rothschild, M.C. Krieg, W.A. Howard, J.M. Tanski, Inorg. Chim. Acta 348 (2003) 91.
[18] C.J. Aspley, J.A.G. Williams, New J. Chem. 25 (2001) 1136.
[19] E.C. Constable, R.W. Handel, C.E. Housecroft, A.F. Morales, L. Flamigni, F. Barigelletti, Dalton Trans. (2003) 1220.
[20] A. Boerje, O. Koethe, A. Juris, New J. Chem. 25 (2001) 191.
[21] E.C. Constable, C.E. Housecroft, M.. Neuburger, I. Poleschak, M. Zehnder, Polyhedron 22 (2003) 93.
[22] E.C. Constable, A.M.W.C. Thompson, J. Chem. Soc., Dalton Trans. (1995) 1615.
[23] M. Maestri, N. Armaroli, V. Balzani, E.C. Constable, A.M.W.C. Thompson, Inorg. Chem. 34 (1995) 2759.
[24] E.C. Constable, A.M.W.C. Thompson, D.A. Tocher, M.A.M. Daniels, New J. Chem. 16 (1992) 855.
[25] E.C. Constable, Inorg. Chim. Acta 82 (1984) 53.
[26] A.G. Blackman, Adv. Heterocycl. Chem. 58 (1993) 123.
[27] E.C. Constable, C.E. Housecroft, L.A. Johnston, D. Armspach, M. Neuburger, M. Zehnder, Polyhedron 20 (2001) 483.
[28] E.C. Constable, P. Harverson, Inorg. Chim. Acta 252 (1996) 9.
[29] D. Armspach, E.C. Constable, C.E. Housecroft, M. Neuburger, M. Zehnder, J. Organomet. Chem. 550 (1998) 193.
[30] E.C. Constable, P. Harverson, J. Chem. Soc., Chem. Commun. (1996) 33.
[31] E.C. Constable, Adv. Inorg. Chem. 34 (1989) 1.
[32] C. Kaes, A. Katz, M.W. Hosseini, Chem. Rev. 100 (2000) 3553.
[33] V. Balzani, A. Juris, Coord. Chem. Rev. 211 (2001) 97.
[34] K. Kalyanasundaram, Coord. Chem. Rev. 46 (1982) 159.
[35] A. Juris, V. Balzani, F. Barigelletti, S. Campagna, P. Belser, A. Von Zelewsky, Coord. Chem. Rev. 84 (1988) 85.
[36] E.C. Constable, A.M.W. Cargill Thompson, D.A. Tocher, in: V. Balzani, L. De Cola (Eds.), Supramolecular Chemistry, Kluwer Academic Press, Dordrecht, 1992, p. 219.
[37] E.C. Constable, in: A.M. Trzeciak, P. Sobota, J.J. Ziolkowski (Eds.), Education in Advanced Chemistry, Perspectives in Coordination Chemistry, vol. 7, University Publishing House (Wydawnictwa Uniwersytetu Wroclawskiego), Poznan-Wroclaw, 2000, p. 159.
[38] T. Norrby, A. Boerje, L. Zhang, B. Akermark, Acta Chem. Scand. 52 (1998) 77.
[39] F.W.J. Demnitz, M.B. d'Heni, Maria Betania; Org. Prep. Proced. Int. 30 (1998) 467.
[40] J. Polin, E. Schmohel, V. Balzani, Synthesis (1998) 321.
[41] R. Bernardi, B. Novo, G. Resnati, J. Chem. Soc. Perkin Trans. 1 (1996) 2517.
[42] I. Antonini, F. Claudi, G. Cristalli, P. Franchetti, M. Grifantini, S. Martelli, J. Med. Chem. 24 (1981) 1181.
[43] J.C. Plaquevent, I. Chichaoui, Bull. Soc. Chim. Fr. 133 (1996) 369.
[44] D.B. Moran, G.O. Morton, J.D. Albright, J. Heterocycl. Chem. 23 (1986) 1071.
[45] D. Wenkert, R.B. Woodward, J. Org. Chem. 48 (1983) 283.
[46] J.C. Plaquevent, I. Chichaoui, Tetrahedron Lett. 34 (1993) 5287.
[47] T.Q. Nguyen, F.Q. Qu, X.L. Huang, A.F. Janzen, Can. J. Chem.-Rev. Can. Chim. 70 (1992) 2089.
[48] S. Dayan, M. Kol, S. Rozen, Synthesis (1999) 1427.
[49] F. Wang, A.W. Schwabacher, Tetrahedron Lett. 40 (1999) 4779.
[50] F. Trecourt, B. Gervais, O. Mongin, C. Le Gal, F. Mongin, G. Queguiner, J. Org. Chem. 63 (1998) 2892.
[51] R.A. Jones, B.D. Roney, W.H.F. Sasse, K.O. Wade, J. Chem. Soc. B (1967) 106.
[52] M.J. Cook, A.P. Lewis, G.S.G. McAuliffe, V. Skarda, A.J. Thomson, J.L. Glasper, D.J. Robbins, J. Chem. Soc.-Perkin Trans. 2 (1984) 1293.
[53] T. Mizuno, M. Takeuchi, I. Hamachi, K. Nakashima, S. Shinkai, J. Chem. Soc.-Perkin Trans. 2 (1998) 2281.
[54] K. Araki, T. Mutai, Y. Shigemitsu, M. Yamada, T. Nakajima, S. Kuroda, I. Shimao, J. Chem. Soc.-Perkin Trans. 2 (1996) 613.
[55] A.J. Downard, G.E. Honey, L.F. Phillips, P.J. Steel, Inorg. Chem. 30 (1991) 2259.
[56] M. Sprecher, R. Breslow, O. Uziel, T.M. Link, Org. Prep. Proced. Int. 26 (1994) 696.
[57] J. Otsuki, H. Ogawa, N. Okuda, K. Araki, M. Seno, Bull. Chem. Soc. Jpn. 70 (1997) 2077.
[58] E.C. Constable, M.D. Ward, J. Chem. Soc., Dalton Trans. (1990) 1405.
[59] K.O. Johansson, J.A. Lotoski, C.C. Tong, G.S. Hanan, Chem. Commun. (2000) 819.
[60] Y.G. Fang, M.I.J. Polson, G.S. Hanan, Inorg. Chem. 42 (2003) 5.
[61] K. Bierig, R.J. Morgan, S. Tysoe, H.D. Gafney, T.C. Strekas, A.D. Baker, Inorg. Chem. 30 (1991) 4898.
[62] P.A. Anderson, G.B. Deacon, K.H. Haarmann, F.R. Keene, T.J. Meyer, D.A. Reitsma, B.W. Skelton, G.F. Strouse, N.C. Thomas, J.A. Treadway, A.H. White, Inorg. Chem. 34 (1995) 6145.
[63] L. Ding, K.B. Ma, G. Durner, M. Bolte, F.F. de Biani, P. Zanello, M. Wagner, J. Chem. Soc.-Dalton Trans. (2002) 1566.
[64] G.R. Pabst, O.C. Pfueller, J. Sauer, Tetrahedron 55 (1999) 8045.
[65] W. Goodall, K. Wild, K.J. Arm, J.A.G. Williams, J. Chem. Soc. Perkin Trans. 2 (2002) 1669.
[66] E.C. Constable, A.M.W.C. Thompson, J. Chem. Soc., Dalton Trans. (1992) 3467.
[67] A. Gelling, M.D. Olsen, K.G. Orrell, A.G. Osborne, V. Sik, Vladimir, J. Chem. Soc., Dalton Trans. (1998) 3479.
[68] E.C. Constable, A.M.W.C. Thompson, New J. Chem. 20 (1996) 65.
[69] E.C. Constable, A.M.W.C. Thompson, S. Greulich, J. Chem. Soc., Chem. Commun. (1993) 1444.
[70] F. Barigelletti, L. Flamigni, V. Balzani, J.P. Collin, J.P. Sauvage, A. Sour, E.C. Constable, A. Thompson, J. Am. Chem. Soc. 116 (1994) 7692.
[71] H. Torieda, A. Yoshimura, K. Nozaki, S. Sakai, T. Ohno, J. Phys. Chem. A 106 (2002) 11034.
[72] J.P. Collin, P. Laine, J.P. Launay, J.P. Sauvage, A. Sour, J. Chem. Soc., Chem. Commun. (1993) 434.
[73] M.T. Indelli, F. Scandola, J.P. Collin, J.P. Sauvage, A. Sour, Inorg. Chem. 35 (1996) 303.
[74] C. Patoux, J.P. Launay, M. Beley, S. ChodorowskiKimmes, J.P. Collin, S. James, J.P. Sauvage, J. Am. Chem. Soc. 120 (1998) 3717.

[75] L. Hammarstrom, F. Barigelletti, L. Flamigni, M.T. Indelli, N. Armaroli, G. Calogero, M. Guardigli, A. Sour, J.P. Collin, J.P. Sauvage, J. Phys. Chem. A 101 (1997) 9061.
[76] F. Barigelletti, L. Flamigni, V. Balzani, J.P. Collin, J.P. Sauvage, A. Sour, E.C. Constable, A.M.W.C. Thompson, J. Chem. Soc., Chem. Commun. (1993) 942.
[77] F. Barigelletti, L. Flamigni, G. Calogero, L. Hammarstrom, J.P. Sauvage, J.P. Collin, Chem. Commun. (1998) 2333.
[78] F. Barigelletti, L. Flamigni, M. Guardigli, J.P. Sauvage, J. Collin, A. Sour, Chem. Commun. (1996) 1329.
[79] B.K. Koo, L. Bewley, V. Golub, R.S. Rarig, E. Burkholder, C.J. O'Connor, J. Zubieta, Inorg. Chim. Acta 351 (2003) 167.
[80] B.K. Koo, W. Ouellette, E.M. Burkholder, V. Golub, C.J. O'Connor, J. Zubieta, Solid State Sci. 6 (2004) 461.
[81] W. Ouellette, B.K. Koo, E. Burkholder, V. Golub, C.J. O'Connor, J. Zubieta, Dalton Trans. (2004) 1527.
[82] H. Torieda, K. Nozaki, A. Yoshimura, T. Ohno, J. Phys. Chem. A 108 (2004) 4819.
[83] A. Yoshimura, H. Torieda, T. Ohno, J. Phys. Chem. A 108 (2004) 2149.
[84] E.C. Constable, E. Figgemeier, C.E. Housecroft, J. Olsson, Y.C. Zimmermann, Dalton Trans. (2004) 1918.
[85] E. Figgemeier, L. Merz, B. Hermann, Y.C. Zimmermann, C.E. Housecroft, H.-J. Güntherodt, E.C. Constable, J. Phys. Chem. B 107 (2003) 1157.
[86] E.C. Constable, A. Thompson, P. Harveson, L. Macko, M. Zehnder, Chem.-Eur. J. 1 (1995) 360.
[87] E.C. Constable, P. Harverson, C.E. Housecroft, J. Chem. Soc., Dalton Trans. (1999) 3693.
[88] A. Juris, L. Prodi, New J. Chem. 25 (2001) 1132.
[89] A. Boerje, O. Koethe, A. Juris, J. Chem. Soc., Dalton Trans. (2002) 843.
[90] W. Nussbaumer, H. Gruber, G.F. Greber, Monatsh. Chem. 119 (1988) 1.
[91] K.O. Johansson, J.A. Lotoski, C.C. Tong, G. Hanan, Chem. Commun. (2000) 819.
[92] V. Marvaud, D. Astruc, Chem. Commun. (1997) 773.
[93] H.S. Chow, E.C. Constable, C.E. Housecroft, K. Kulicke, Y. Tao, Dalton Trans. (2005) 236.
[94] B. Akermark, J. Bjernemose, A. Borje, P.J. Chmielewski, H. Paulsen, O. Simonsen, P.C. Stein, H. Toftlund, J.A. Wolny, Dalton Trans. (2004) 1215.
[95] R. Chotalia, E.C. Constable, M.J. Hannon, D.A. Tocher, J. Chem. Soc., Dalton Trans. (1995) 3571.
[96] E.C. Constable, C.J. Cathey, M.J. Hannon, D.A. Tocher, J.V. Walker, M.D. Ward, Polyhedron 18 (1999) 159.
[97] K.M. Rao, C.R.K. Rao, P.S. Zacharias, Polyhedron 16 (1997) 2369.
[98] E.K. Rymmai, K.M. Rao, Indian J. Chem., Sect. A: Inorg., Bioinorg., Phys., Theor. Anal. Chem. 42 (2003) 1892.
[99] E.C. Constable, A.M.W. Cargill Thompson, Inorg. Chim. Acta 223 (1994) 177.
[100] A.G. Blackman, C.R. Acad. Sci., Ser. IIc: Chim. 8 (2005) 107.
[101] R.L. Fanshawe, A. Mobini-Khaledi, C.R. Clark, A.G. Blackman, Inorg. Chim. Acta 307 (2000) 26.
[102] N.J. Lundin, I.G. Hamilton, A.G. Blackman, Polyhedron 23 (2004) 97.
[103] D.A. McMorran, S. Pfadenhauer, P.J. Steel, Inorg. Chem. Commun. 5 (2002) 449.
[104] M. Sokolov, K. Umakoshi, Y. Sasaki, Inorg. Chem. 41 (2002) 6237.

Available online at www.sciencedirect.com
SCIENCE DIRECT®
Polyhedron 25 (2006) 459–468
POLYHEDRON
www.elsevier.com/locate/poly

Cleavage of F–C(sp^2) bonds by MHR(CO)(P^tBu_2Me)$_2$ (M = Os and Ru; R = H, CH_3 or Aryl): Product dependence on M and R

Dejian Huang, Kenton B. Renkema, Kenneth G. Caulton *

Department of Chemistry, Indiana University, 800 E. Kirkwood, CHEM A250B, Bloomington, IN 47405-4001, USA

Received 12 May 2005; accepted 9 August 2005
Available online 4 October 2005

In celebration of the coming of age of Malcolm Harold Chisholm.

Abstract

Both MH(Ph)(CO)L_2 (L = P^tBu_2Me; M = Ru and Os) react with vinyl fluoride to form M–F bonds; however, Ru eliminates benzene, while Os eliminates ethylene. In contrast, Ru(H)$_2$(CO)L_2 and Os(H)$_2$(CO)(1-butene)L_2 both react with vinyl fluoride to give ethylene and MHF(CO)L_2. Ethylene production from *both* dihydrides is attributed to β-F migration to M from an MCH_2CH_2F transient, while the unique behavior of RuH(Ph)(CO)L_2 (giving the C–F oxidative addition product Ru(η^1-vinyl)F(CO)L_2) is attributed to the difficulty of achieving Ru^{IV}, and the ability of the strongly π-acidic vinyl fluoride to rapidly trigger reductive elimination of benzene. The products of reaction of RuH(Ar)(CO)L_2 with vinyl fluoride are redirected more towards ethylene formation when Ar carries fluorine substituents. The reaction products of OsH(R)(CO)L_2 with vinyl fluoride revert to R-H elimination when R is methyl. Finally, the more π-acidic $H_2C{=}CF_2$ triggers very rapid CH_4 elimination from OsH(CH_3)(CO)L_2; cleavage of the second C–F bond yields the vinylidene $OsF_2(CCH_2)(CO)L_2$. All selectivity is rationalized via the fate of the adduct MH(R)($C_2H_{4-n}F_n$)(CO)L_2.
© 2005 Elsevier Ltd. All rights reserved.

Keywords: Fluorocarbons; Ruthenium; Osmium; Organometallic; Mechanisms

1. Introduction

C–F bond cleavage is a goal for accomplishing catalytic transformation of perfluoroalkanes (and arenes) and Freons to valuable or environmentally benign materials [1–5]. This is also a topic of interest in organic synthesis [6–19]. The early transition elements have a strong tendency to cleave F–C(sp^2) bonds [20–25]. A fundamental problem in C–F activation by soluble transition metal complexes is selective cleavage of the C–F in preference to the C–H bond in partially fluorinated alkanes and arenes since the C–F bond is normally stronger than the C–H bond [26]. That is, kinetic selectivity is required [27–32]. In at least one case, C–F bond cleavage is thermodynamically favored, but kinetically disfavored [33]. However, rarely has there been a report of different selectivity for reaction of a metal complex with vinyl fluoride versus aryl fluoride. Such an example is documented here.

2. Results

2.1. MH(Ph) Reactivity with $H_2C{=}CHF$

(a) M = Os. The molecule OsH(Ph)(CO)L_2 (L = P^tBu_2Me) (**1**), is reported to be "triggered" by reaction with fluoroarenes ($C_6H_{6-n}F_n$, with $n = 1, 2, 5$) at 25 °C to eliminate C_6H_6 and oxidatively add an arene C–H

* Corresponding author. Tel.: +1 812 855 4798; fax: +1 812 855 8300.
E-mail address: caulton@indiana.edu (K.G. Caulton).

0277-5387/$ - see front matter © 2005 Elsevier Ltd. All rights reserved.
doi:10.1016/j.poly.2005.08.012

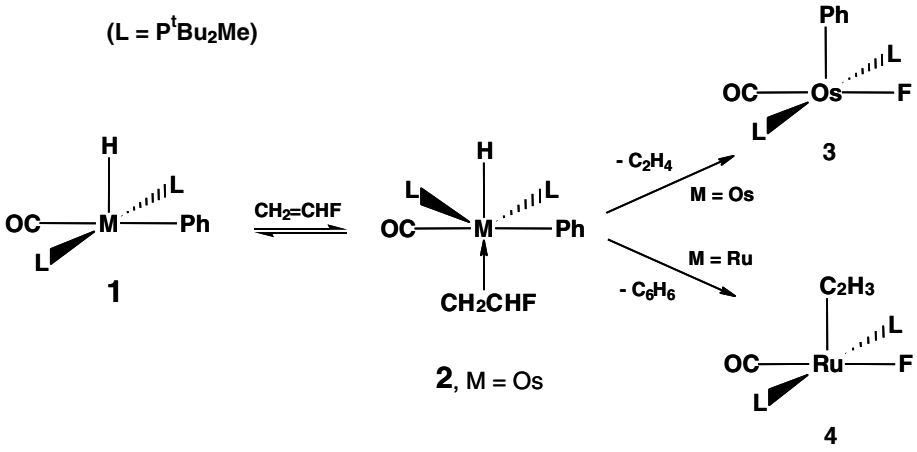

Scheme 1.

bond, to yield $OsH(Ar^F)(CO)L_2$ [34]. The reactions are thus selective *against* C–F bond scission; indeed, C_6F_6 does not react. In contrast, **1** is now reported to react with vinyl fluoride to ultimately produce a C–F bond-cleaved product. Reaction of $OsH(Ph)(CO)L_2$ with excess vinyl fluoride at −90 °C in toluene (Scheme 1) gives a π-adduct (**2**), $OsH(Ph)(CO)L_2(C_2H_3F)$. The ^1H NMR spectrum of **2** shows a hydride peak at −3.7 ppm as an apparent triplet. The coordinated vinyl protons appear at 2.7, 2.9 and 7.6 ppm and the ^{19}F NMR signal of the bound vinyl fluoride (−171 ppm) is shifted significantly upfield, compared to that of free vinyl fluoride (−113 ppm) [35]. The $^{31}P\{^1H\}$ NMR spectrum of this adduct at −50 °C is an AB quartet and the relatively small $J'_{PP} = 162$ Hz is indicative of two phosphines bent significantly away from a ~180° P–Os–P angle, consistent with strong back donation to this olefin [35]. At 25 °C, **2** reacts further (complete in 4 h) to release ethylene and form **3**, $OsPh(F)(CO)L_2$. The ^{19}F NMR spectrum shows a triplet ($^2J_{PF} = 28$ Hz) at a chemical shift (−202.1 ppm) consistent with F bonded to osmium (not carbon), and $^{31}P\{^1H\}$ NMR shows a doublet with the same splitting. The ^{t}Bu groups are diastereotopically inequivalent and they, as well as the PCH_3 groups, are virtual triplets consistent with structure **3**. The ν_{CO} value (1874 cm^{-1}) is low enough to be consistent with a push/pull F → COπ* donation when these ligands are mutually *trans*. There are four (one of intensity 2) distinct phenyl proton NMR signals, suggesting slow rotation of the Ph around the Os–C(*ipso*) bond [36].

(b) M = Ru. $RuH(Ph)(CO)L_2$ also cleaves the C–F bond of vinyl fluoride but it gives a different product. Combination of $RuH(Ph)(CO)L_2$ with 1 atm $CH_2=CHF$ in benzene[1] gives quantitative formation of $Ru(CH{=}CH_2)F(CO)L_2$ (**4**), after 12 h at room temperature (Scheme 1). The ^{19}F NMR spectrum of **4** shows a broad triplet ($^3J_{PF} = 22$ Hz) and the $^{31}P\{^1H\}$ NMR spectrum shows a doublet with the same J_{PF} value. The ^1H NMR spectrum of **4** features an α-vinyl proton at 8.3 ppm (ddd, $J_{HH} = 14.7$ Hz, $J_{HH} = 7.5$, $J_{FH} = 6.9$ Hz) with the β-protons at higher field (5.4 and 5.1 ppm). The low ν(CO) value (1894 cm^{-1}) is consistent with CO *trans* to F. For comparison, **4** can also be synthesized from $RuHF(CO)L_2$ and C_2H_2. Combination of $RuHF(CO)L_2$ and 1 atm C_2H_2 in benzene gives $Ru(C_2H_3)F(CO)L_2$ quantitatively in 30 min at room temperature.

(c) Mechanism. We interpret these results without invoking a wholly different mechanism for the reaction of the Ru and Os species $MH(Ph)(CO)L_2$ with vinyl fluoride. The idea that an oxidant, including even an electron deficient olefin like $(NC)_2C{=}C(CN)_2$, can trigger reductive elimination is termed oxidatively induced reductive elimination [37–41]. We suggest that the absence of *detectable* vinyl fluoride adduct for M = Ru is of quantitative (i.e., a few kcal/mol) rather than qualitative significance. Indeed, it serves as a reminder that Os is a more potent π base than Ru, since back-bonding is an important component of binding of the fluorinated olefin. This difference in π-basicity can also be used to interpret the distinct selectivities shown by Ru and Os. In brief (Scheme 2), osmium is more tolerant to high oxidation states, so the C–F oxidation product, containing Os^{IV}, can be achieved. This seven-coordinate species will be sufficiently persistent and nonrigid, to permit isomerization of H to a site *cis* to the vinyl group; reductive elimination of ethylene follows. For M = Ru, η^2 binding of π-acidic $H_2C{=}CHF$ triggers rapid reductive elimination of H with C_6H_5 as the lowest energy process, in order to avoid the high (versus Os) energy of Ru^{IV}; the prompt character of these two events prohibits establishing any inherent (i.e., thermodynamic) preference for phenyl versus vinyl remaining on ruthenium. That is, selectivity is truly kinetically controlled for Ru

[1] No detectable amount of adduct is formed from $RuH(Ph)(CO)L_2$ under 1 atm vinyl fluoride in d_{14}-methylcyclohexane at −70° by ^1H and ^{31}P NMR spectroscopy.

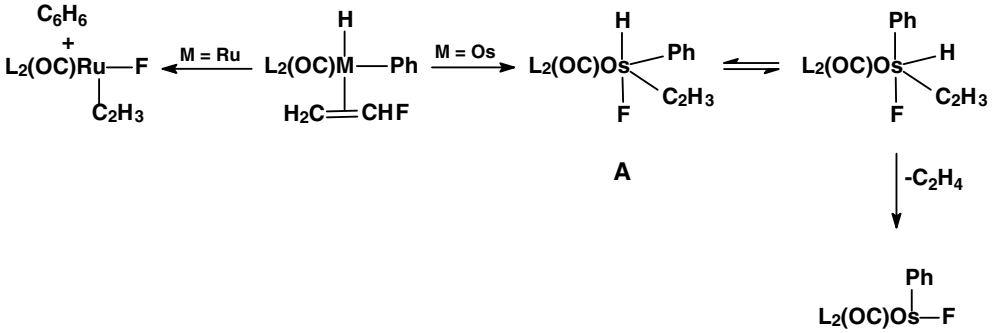

Scheme 2.

but probably not so for Os. Based on our earlier evidence that M–F bond formation is thermodynamically favored for the reactions of the various five-coordinate species studied here [33], the metal dependent products in Scheme 1 probably involve very small differences in reaction enthalpy (i.e., they differ by vinyl versus phenyl on the metal (Eq. (1)) but share the production of a M–F bond). The different products are thus best explained by being under kinetic control via the distinct accessibility of redox changes at a 4d versus a 5d metal.

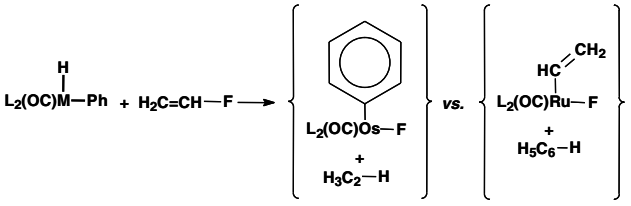

(1)

In order to test for possible phosphine dissociation at or prior to the rate determining step in the reaction of $MH(Ph)(CO)L_2$ with vinyl fluoride, a rate comparison was made in the absence and presence of 2–5 equivalents of free phosphine (P^tBu_2Me). For either M = Ru or Os, the half-lives for product appearance were observed to be comparable with and without added L, eliminating phosphine dissociation as a mechanistic component.

Based on the mechanism previously deduced for reaction of $OsHCl(CO)(P^iPr_3)_2$ with RCCH [42], a direct attack of the M–H bond on the olefin must also be considered here (Eq. (2)). Here, no prior η^2-olefin adduct is on the reaction path and the first M/C interaction is concurrent with C/H bond formation.

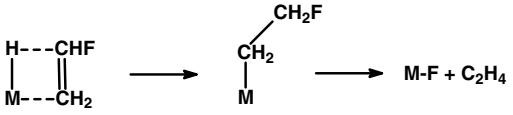

(2)

Since this is a path to M–F and ethylene, it might explain the results when M = Os, but not for Ru. Because it is not clear *why* this mechanism would have higher $\Delta G^{\ddagger}$ for Ru, we discount it. In contrast, the known redox differences of Ru and Os naturally account for the observed selectivity difference via Scheme 2.

$M(H)_2$ reactivity with H_2C=CHF. A mechanism which incorporates the adduct $MHR(H_2C{=}CHF)(CO)L_2$ also naturally explains the high rate and *similar* products, for M = Ru and Os, when R = H, as will now be described. The feature common to the reactions in Scheme 1 is that the hydride ligand cannot react immediately with a vinyl fluoride ligand *trans* to itself, and thus metal-dependent selectivity develops from within the adduct. To create the contrasting situation of hydride *cis* to the olefin, excess vinyl fluoride was reacted with $Ru(H)_2(CO)L_2$ [36]: immediately at −80 °C ethylene and $RuHF(CO)L_2$ are formed. We propose the reaction proceeds by insertion of vinyl fluoride into the *cis* Ru–H bond, followed by β-F migration (Scheme 3).

To compare this dihydride reactivity of Ru to that for Os, $Os(H)_2$(1-butene)$(CO)L_2$ [43,44] (as a source of the currently unknown $Os(H)_2(CO)L_2$) was prepared from $Os(H)_2(H_2)(CO)L_2$ and 1-butene. This molecule reacts with excess (19 equivalents) vinyl fluoride within 30 min at 25 °C in C_6D_6 to give ethylene and $OsHF(CO)L_2$; since this product molecule shows dynamic NMR effects from binding olefin, identification is simplified by first removing all volatiles, then redissolving in benzene.

Thus, and in contrast to $MH(Ph)(CO)L_2$, unsaturated Ru and Os show analogous reactivity when a hydride is *adjacent* to the empty coordination site.

2.2. Influence of R group identity in $MH(R)(CO)L_2$

The essential feature of species **A** is that C_2H_3 and H are *not* mutually *cis* because H, Ph, C_2H_3, and F are coplanar. Therefore, the different results seen for Ru and Os were argued to occur because the unstable Ru(IV) intermediate analogous to **A** would not allow time for rearrangement, followed by elimination of the most thermodynamically favorable products, $MF(Ar)(CO)L_2$ and olefin. The furthest extension of this mechanism, where a Ru(IV) intermediate never exists, is represented in Scheme 4.

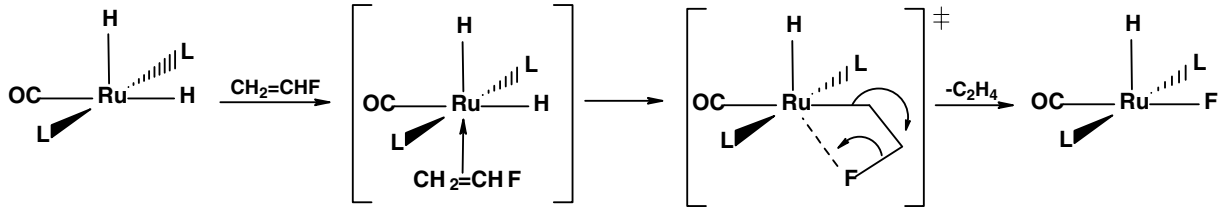

Scheme 3.

In order to understand what role M–R bond strength plays in these reactions, we synthesized $RuH(2\text{-}C_6H_4F)(CO)L_2$ and $RuH(C_6F_5)(CO)L_2$ by reacting $RuH(Ph)(CO)L_2$ with monofluorobenzene and pentafluorobenzene, respectively. We expect that these species will have greater thermal stability against arene elimination with increasing number of fluorines on the aryl ring since $OsH(2,6\text{-}C_6F_2H_3)(CO)L_2$ persists unchanged after 30 h at 70 °C in d_{12}-cyclohexane, but $OsH(C_6H_5)(CO)L_2$ decomposes to free benzene, phosphine and unidentified osmium products under the same conditions. Previous DFT-calculations on $OsH(C_6H_5)(CO)(PH_3)_2$ showed that π donation was partially responsible for restricted rotation about the M–C(*ipso*) bond. The calculated and observed thermodynamic preference for metal–aryl complexes with fluorine *ortho* to the metal suggest that fluorines on the aryl ring increase the amount of π donation from a fluoroaryl ring to a metal.

(a) Ru–Ar^F. When $RuH(2\text{-}C_6H_4F)(CO)L_2$ was reacted with one equivalent of vinyl fluoride for 20 h at 50 °C, the products, $Ru(C_2H_3)F(CO)L_2$ and C_6H_5F, are analogous to those in Eq. (2), i.e., aryl/H reductive elimination. Reaction of the less oxidizable $RuH(C_6F_5)(CO)L_2$ with less than one equivalent C_2H_3F for 7 days at 85 °C yields $Ru(C_2H_3)F(CO)L_2$, C_6F_5H, $Ru(C_6F_5)F(CO)L_2$, and C_2H_4. These last two products therefore indeed indicate that reactions of *both* types in Scheme 2 compete for this more stable ruthenium hydrido-fluoroaryl reagent, consistent with Ru–C bond strength influencing the decay mode of the intermediate.

(b) Os–CH$_3$. Continuing this hypothesis, an osmium species with a *weaker* Os–C bond than Os–C_6H_5 should change reaction selectivity. To that end, $OsH(CH_3)(CO)L_2$ (**5**), was synthesized by reaction of $OsHCl(CO)L_2$ with one equivalent of MeLi. Centrifugation of the solution most efficiently removed the LiCl co-product. The NMR signatures of **5** are consistent with other five-coordinate osmium complexes where hydride is in the apical position. The hydride chemical shift is far upfield (−33.2 ppm). The methyl ^{1}H NMR signal (integrated to intensity 3) is a triplet at 0.46 ppm. The *t*-butyl signals are diastereotopic virtual triplets and the ^{31}P NMR spectrum shows one sharp singlet. In benzene at 22 °C, **5** undergoes slow conversion to $OsH(Ph)(CO)L_2$. Species **5** thus has a weaker Os–C bond than $OsH(Ph)(CO)L_2$.

Compound **5** is completely consumed by excess vinyl fluoride at −75 °C in d_8-toluene; *two* new species were observed by ^{19}F NMR. The ^{31}P NMR spectrum of *one* of these showed an AB pattern ($J_{PP} = 161$ Hz). ^{1}H NMR gave two defining signals, a hydride signal at −6.3 ppm (d of d) and signal intensity 3 at −1.1 ppm (assigned to Os–CH_3). These spectroscopic features are consistent with assignment of (Eq. (3)) the most abundant primary product as the simple adduct $OsH(CH_3)(CO)L_2(C_2H_3F)$.

$$\begin{aligned} &OsH(CH_3)(CO)L_2 + H_2C{=}CHF \\ &\quad \rightleftharpoons OsH(CH_3)(CO)L_2(C_2H_3F) \\ &\quad \xrightarrow{RT} OsF(CH_3)(CO)L_2 + H_2C{=}CH_2 \end{aligned} \tag{3}$$

Warming the mixture to −15 °C increased the rate of olefin exchange sufficiently to cause the ^{19}F NMR signals at −169 ppm for bound olefin to broaden nearly into the baseline. Significant conversion of this olefin adduct to the final product did not occur until room temperature, but this is faster than the corresponding reaction of $OsH(Ph)(CO)L_2$. A ^{19}F NMR triplet (−198 ppm, $J_{FP} = 27$ Hz), a $^{31}P\{^1H\}$ NMR doublet (26.0 ppm, $J_{PF} = 27$ Hz), the loss of the hydride signal, and the production of ethylene are all consistent with assignment of the new compound as $OsF(CH_3)(CO)L_2$. This represents reactivity analogous to that of $OsH(Ph)(CO)L_2$ with vinyl fluoride.

The amount and spectral features of the *second* low temperature product change very little upon warming the sample from −45 to 20 °C. Over those temperatures,

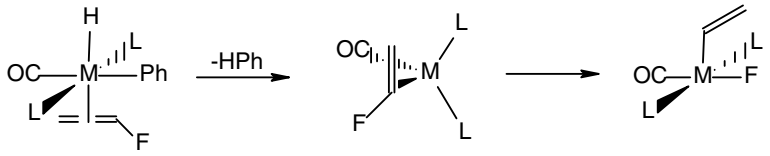

Scheme 4.

the $^{31}P\{^{1}H\}$ NMR spectrum showed an AM pattern ($\Delta\delta = 32$ ppm) with a J_{PP} of 148 Hz. One of the phosphorus nuclei showed coupling to fluorine ($J_{PF} = 15$ Hz) whose magnitude is consistent with F on Os. This fluorine is detected at −195 ppm as a doublet of multiplets. AM patterns with large $\Delta\delta$ are typical for metallated alkyl ligands on phosphines; we propose structure **6**. The presence of this second product where the osmium complex has lost methane, HR, shows the competitive occurrence of a second mechanism, that used by Ru in Scheme 2, prior to activation of a C–F bond. This species declines in intensity as the temperature is raised and ultimately disappears from both ^{31}P and ^{19}F NMR spectra.

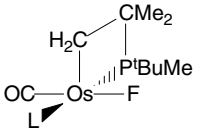

6

Detection of this species is especially important because it has the stoichiometry of $Os(CO)L_2$ *minus* one H and *plus* one F. It is thus a plausible product of a second fate for $OsH(Me)(CO)L_2$, following olefin-induced reductive elimination of methane. The primary product would then be zerovalent, unsaturated **7** (Scheme 5), in which oxidative addition of a *t*-Bu C–H bond would permit hydrogen migration to vinyl fluoride, then fluorine migration to Os, with liberation of ethylene.

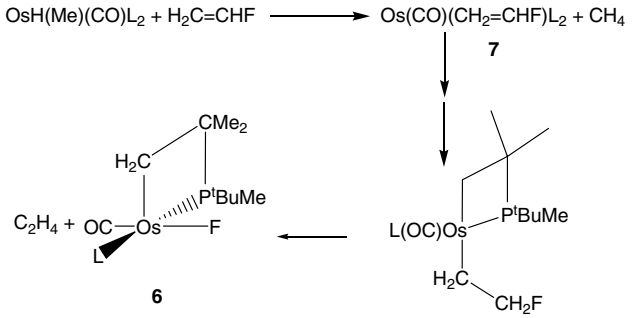

Scheme 5.

The detection of a second competitive reaction channel for $OsHMe(CO)L_2$ in reacting with vinyl fluoride thus links the ruthenium chemistry ($RuH(Ph)(CO)L_2$) to that of osmium; the more facile elimination of H with an sp^3 carbon (versus sp^2 in $OsH(Ph)(CO)L_2$) makes this oxidatively induced reductive elimination now detectable (but not dominant) for $OsHMe(CO)L_2$.

2.3. A more oxidizing olefin

(a) Os–CH₃. The *gem*-difluoro olefin $H_2C{=}CF_2$ provides an additional test of mechanism. An insertion mechanism for reaction of $H_2C{=}CF_2$ with **5** would yield vinyl fluoride (Scheme 6). If, on the other hand, this more π-acidic difluoro olefin promptly triggers methane elimination, then the first C–F oxidative addition to Os(0) could be followed by a second F migration (Scheme 7). Reaction of $OsH(CH_3)(CO)L_2$ with gem-difluoroethylene at 0 °C with subsequent slow warming to room temperature, then removal of excess olefin, gave 75% yield of product **8** with 100% conversion of **5**. The $^{31}P\{^{1}H\}$ NMR spectrum of **8** is a doublet of doublets ($J_{PF} = 41$, 25 Hz). ^{19}F NMR revealed an AB pattern due to inequivalent F on Os. The lower field doublet ($J_{FF} = 143$ Hz) also showed triplet coupling to phosphorus ($J_{FP} = 25$ Hz), while the lines of the higher field doublet were each triplets of triplets, due to two phosphorus ($J_{PF} = 41$ Hz) and two protons ($J_{FH} = 7$ Hz). ^{1}H NMR showed the absence of a hydride chemical shift as well as the appearance of a new signal at 2.0 ppm (vinylidene CH_2), which was a doublet of triplets ($J_{HF} = 7$ Hz,

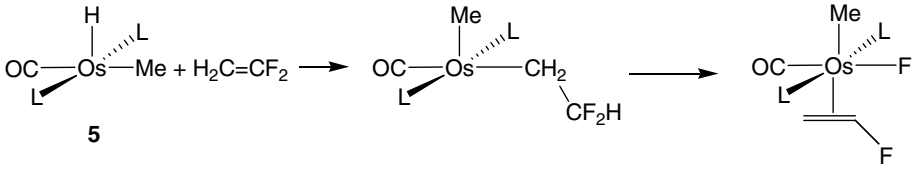

Scheme 6.

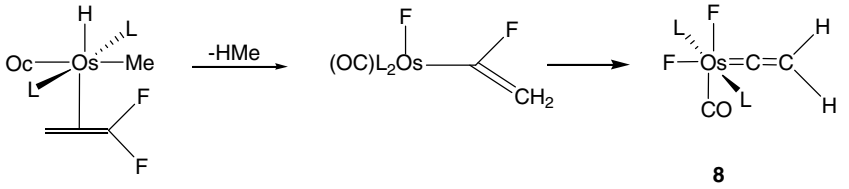

Scheme 7.

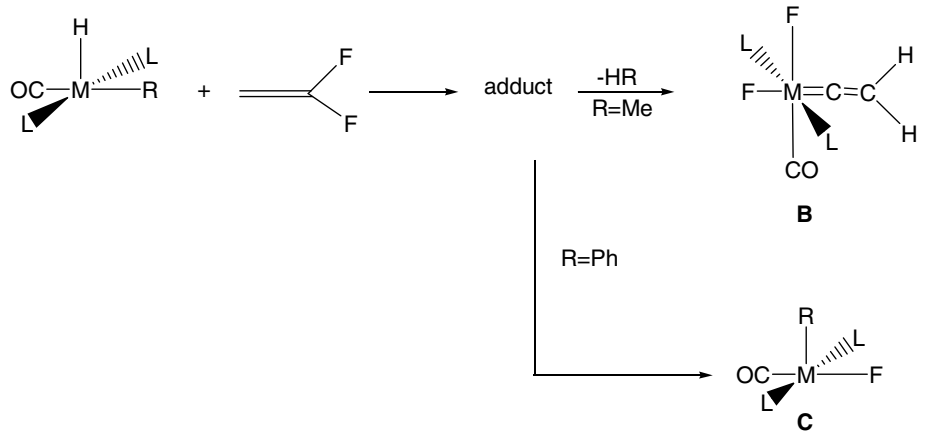

Scheme 8.

$J_{HP} = 3$ Hz). $^{13}C\{^1H\}$ NMR showed the β-carbon signal at 94 ppm as a doublet ($J_{CF} = 16$ Hz).

An osmium difluoride product is consistent with an intermediate with fluorine located α to the metal because such species exhibit α-fluoro migration. The "prompt" elimination of H–CH_3 in Scheme 7 contrasts to the reaction of $OsH(Ph)(CO)L_2$ with vinyl fluoride, and may be attributed to the more oxidizing (cf. π-acid) character of $H_2C{=}CF_2$ (versus $H_2C{=}CHF$).

(b) Os–Ph. To test the influence of Os–C(sp^3) versus C(sp^2) on reactivity, the reaction of $OsH(Ph)(CO)L_2$ with excess $H_2C{=}CF_2$ was studied. This yielded primarily $Os(Ph)F(CO)L_2$ on the same time scale as vinyl fluoride; only a trace amount of $OsF_2(CO)(CCH_2)L_2$ forms. This result further illustrates how the energetics of HR elimination from the proposed M(IV) intermediate affects the outcome of the reaction (Scheme 8). When HR elimination is the fastest process from the adduct, then metal difluoride **B** would result. However, if rearrangement (to hydride *cis* to olefin) and elimination of the vinyl species are faster, five-coordinate $OsRF(CO)L_2$ (**C**), forms. Clearly, the latter is favored for osmium: the Os–Ph bond persists through reaction with both $H_2C{=}CHF$ and $H_2C{=}CF_2$.

3. Conclusion

We have demonstrated here several C–F bond cleavage reactions of vinyl fluoride by five-coordinate hydrides $MHR(CO)L_2$ (R = Ph, CH_3, H; M = Os, Ru). The reaction products are highly dependent on the identity of the metal when R = Ph. For Os, Os–H/C–F "exchange" is the dominant pathway, while for Ru and R = Ph, the reaction features reductive elimination of C_6H_6, followed by C–F bond cleavage of vinyl fluoride. The facility for H-Ph formation and the relative stability of (II versus IV) oxidation states are the two factors influencing the metal-dependence. It is also remarkable that benzene loss from $RuH(Ph)(CO)L_2$ is followed by oxidative addition of the C–H bond of partially fluorinated arene [33], but of the C–F bond of vinyl fluoride. It is noteworthy that both metals show kinetic selectivity (C–H cleavage) when reacting with fluorinated arenes to give $MH(Ar^F)(CO)L_2$ but thermodynamic selectivity (M–F bond formation) when reacting with fluorinated olefins.

In a sense, this reaction of $RuH(Ph)(CO)L_2$ as a "$Ru^0(CO)L_2$ equivalent" is analogous to that of elemental magnesium, to generate a Grignard reagent by C–F oxidative addition [45]. In contrast, in *both* dihydride cases reported here, the net reaction is M–H/ C–F exchange, but apparently by a β-F migration mechanism.

This work began by raising the question of the curious selectivity for C–H over C–F scission in reaction of $OsH(Ph)(CO)L_2$ with partially fluorinated arenes. However, vinyl fluoride substrate shows quite the opposite selectivity, and what was discovered here is contrasting *metal* selectivity: Ru versus Os. The question of reversion to "normal" selectivity for C–F scission with fluoro olefins (cf. fluoroarenes) probably relates to the greater ease of binding olefins (versus arenes) to metals, together with the very different ability of metal to attack F–C(H)CH_2 versus F–$C(CH)_2$ (i.e., arene) moieties.

4. Experimental

4.1. General procedures

All manipulations were performed using standard Schlenk techniques or in an argon filled glovebox unless otherwise noted. Solvents were distilled from Na, Na/benzophenone, CaH_2, or 4 Å molecular sieves, degassed

prior to use, and stored in air-tight vessels. OsHCl(CO)(P^tBu_2Me)$_2$ [46], OsH(Ph)(CO)(P^tBu_2Me)$_2$ [34], RuHF(CO)(P^tBu_2Me)$_2$ [47], Ru(H)$_2$(CO)(P^tBu_2Me)$_2$ [36] and RuH(Ph)(CO)(P^tBu_2Me)$_2$ [36] were prepared according to published procedures. All other reagents were purchased from commercial vendors and used as received after drying/degassing when necessary. ^{1}H NMR chemical shifts are reported in ppm relative to protio impurities in the deuterated solvents; ^{31}P (always proton-decoupled) and ^{19}F spectra are referenced to external standards of 85% H_3PO_4 and $CFCl_3$, respectively (both at 0 ppm). NMR spectra were recorded with a Varian Gemini 2000 (300 MHz ^{1}H; 121 MHz ^{31}P; 75 MHz ^{13}C, 282 MHz ^{19}F), a Varian Unity Inova instrument (400 MHz ^{1}H; 162 MHz ^{31}P; 101 MHz ^{13}C, 376 MHz ^{19}F), or a Varian Unity Inova instrument (500 MHz ^{1}H, 126 MHz ^{13}C). Infrared spectra were recorded on a Nicolet 510P FT-IR spectrometer.

4.2. *Os(Ph)F(CO)(P^tBu_2Me)$_2$*

An NMR tube containing OsH(Ph)(CO)(P^tBu_2Me)$_2$ (16.5 mg, 2.68×10^{-5} mol) in 500 μL d_8-toluene had 200 Torr (7.7×10^{-4} mol) of vinyl fluoride condensed into it. At low temperature the η^2-adduct formed: diagnostic ^{1}H NMR (C_7D_8, −90 °C) −3.7, (t, 1H, Os*H*, $J_{PH}=29$ Hz); 2.7, (d, 1H, CCH, $J_{HF}=20.4$ Hz); 2.9 (d, 1H, CCH, $J_{HF}=22$ Hz); 7.54, (d, 1H, CCH, $J_{FH}=72.0$ Hz). ^{31}P NMR (C_7D_8, −90 °C) −2.5, (AB, $J_{PP}=162$ Hz). ^{19}F(C_7D_8, −90 °C) −171.3 (dt, 1F, CCF, $J_{FH}=73$ Hz, $J_{FH}=20$ Hz). Conversion to the final product did not occur until 10 °C and was complete within 4 h at room temperature. The ^{1}H NMR detection of ethylene confirmed product identity. ^{1}H NMR (C_7D_8, 20 °C) 1.00, (vt, 18H, OsPCC*H*$_3$, $J_{PH}=5.8$ Hz); 1.04, (vt, 18H, PCC*H*$_3$, $J_{PH}=5.8$ Hz); 1.29, (broad s, 6H, PC*H*$_3$); 6.39, (t, 1H, Ar-*H*, $J_{PH}=6.0$ Hz); 6.5, (t, 2H, Ar-*H*, $J_{HH}=6$ Hz); 7.32, (d, Ar-*H*, $J_{HH}=6$ Hz); 7.64, (d, Ar-*H*, $J_{HH}=6.0$ Hz). ^{31}P NMR (C_7D_8, 20 °C) 26.5, (d, 2P, $J_{PF}=28$ Hz). ^{19}F(C_7D_8, 20 °C) −202.1 (t, 1F, CCF, $J_{FP}=28$ Hz) ν(CO) = 1874 cm^{-1}.

4.3. *Reaction of OsH(Ph)(CO)(P^tBu_2Me)$_2$ + C_2H_3F in the presence of P^tBu_2Me*

When OsH(Ph)(CO)(P^tBu_2Me)$_2$ (10.5 mg, 1.70×10^{-5} mol) was dissolved in 500 μL C_6D_6 and reacted with two equivalents P^tBu_2Me and C_2H_3F (600 Torr, 5.2 equivalents) the reaction reached completion in 4 h. A similar time scale was observed in the absence of free phosphine.

4.4. *Ru(C_2H_3)F(CO)(P^tBu_2Me)$_2$*

RuHF(CO)L$_2$ (150 mg, 0.32 mmol) was dissolved in diethyl ether (3 mL). The solution was degassed and the headspace was charged with acetylene gas (1 atm). The mixture was stirred at room temperature for 30 min before the volatiles were removed under vacuum. The residue was dissolved in pentane, filtered through a Celite pad and concentrated to ca. 2 mL. After cooling the solution at −40 °C for one day, dark orange crystals were obtained. Yield: 120 mg (76%). ^{1}H NMR (C_6D_6, 20 °C, 300 MHz): 1.20 (vt, N = 12.5, 18H, PC(CH$_3$)$_3$), 1.25 (vt, 18H, N = 12 Hz, PC(CH$_3$)$_3$), 1.21 (vt, 6H, N = 5.9, PCH$_3$), 5.10 (dt, $J_{HH}=14.5$, $J_{PH}=2.0$ Hz, 1H β-H(vinyl)), 5.45 (dt, $J_{HH}=6.4$ Hz, $J_{PH}=2.4$ Hz, 1H, β-vinyl), 8.30 (doublet of apparent triplets, 1H, $J_{HH}=14.5$ Hz, $J_{HH}=7.5$ Hz, $J_{HF}=6.9$ Hz, α-H of vinyl). ^{13}C{^{1}H} NMR (toluene-d_8, 75 MHz, 20 °C): 3.16 (vt, N = 15 Hz, PCH$_3$), 29.7, 29.8 (s, PC(*C*H$_3$)$_3$), 35.4, 35.5 (s, P*C*(CH$_3$)$_3$), 117.5 (s, =CH$_2$), 156.3 (t, J = 20.3 Hz, Ru–CH). ^{31}P{^{1}H} NMR: 41.2 (d, $J_{PF}=22$ Hz). ^{19}F NMR: −214 (t, $J_{PF}=22$ Hz). IR (C_6D_6): 1894 (ν(CO)).

4.5. *Reaction of RuH(Ph)(CO)L$_2$ with vinyl fluoride*

RuH(Ph)(CO)(P^tBu_2Me)$_2$ (10 mg, 0.019 mmol) was dissolved in C_6D_6 (0.5 mL) and degassed by three freeze–pump–thaw cycles. To the tube, C_2H_3F (1 atm) was charged. The mixture was agitated for 12 h. NMR spectroscopies reveal clean formation of Ru(C_2H_3)(F)(CO)L$_2$ by comparison to data in the preceding experiment.

4.6. *Reaction of RuH(Ph)(CO)(P^tBu_2Me)$_2$ with vinyl fluoride in the presence of added phosphine ligand*

In an NMR tube, RuH(Ph)(CO)L$_2$ (10 mg, 0.019 mmol) and P^tBu_2Me (15 mg, 5 eq.) were dissolved in cyclohexane-d_{12}. The solution was degassed and the headspace of the tube was charged with 1 atm vinyl fluoride. After 12 h at room temperature, RuH(Ph)(CO)L$_2$ was completely consumed and Ru(C_2H_3)F(CO)L$_2$ was formed as revealed by its ^{31}P{^{1}H} NMR spectrum.

4.7. *Os(H)$_2$(η^2-1-butene)(CO)(P^tBu_2Me)$_2$*

Reaction of OsH$_2$(H$_2$)(CO)(P^tBu_2Me)$_2$ (5.6 mg, 1.04×10^{-5} mol) with 1-butene (100 Torr, 6.95×10^{-5} mol) in C_6D_6 at room temperature gives the title compound within 5 min. The room temperature NMR signals are broadened by dynamic equilibrium. ^{1}H NMR (C_6D_6, 293 K) −11.2 (t, OsH, 1H, $J_{PH}=23$ Hz); −8.66 (t, OsH, 1H, $J_{PH}=33.5$ Hz); 0.86 (t, CH$_2$C*H*$_3$, 3H, $J_{HH}=4$ Hz); 1.26 (vt, PCCH$_3$, 18H, $J_{PH}=6.3$ Hz); 1.28 (vt, PCCH$_3$, 18H, $J_{PH}=6.3$ Hz); 1.62 (m, C*H*$_2$CH$_3$); 2.2 (br s, vinyl CH, 1H); 2.6 (br s, vinyl CH, 1H); 3.2 (br s, vinyl CH, 1H). ^{31}P NMR (C_6D_6, 293 K) 29.6, 29.9 (AB, $J_{PP}=148$ Hz).

4.8. Reaction of $OsH_2(\eta^2\text{-1-butene})(CO)(P^tBu_2Me)_2$ with C_2H_3F

To $OsH_2(\eta^2$-1-butene)(CO)$(P^tBu_2Me)_2$ (1.83×10^{-5} mol) was added C_2H_3F (150 Torr, 19 equivalents); $OsHF(\eta^2\text{-}C_2H_3F)(CO)(P^tBu_2Me)_2$ was formed within 30 min. The signals for this species were broad due to exchange of olefin. The species was identified by ^{1}H NMR (C_6D_6, 293 K); 2.8, (br s, C_2H_3F); −3.1 (br s, Os*H*) and ^{31}P NMR (C_6D_6, 293 K): 24.5 (br s). Evacuation of the excess olefin left $OsHF(CO)(P^tBu_2Me)_2$. ^{1}H NMR (C_6D_6, 293 K) −32.2 (td, OsH, 1H, $J_{PH}=13$ Hz, $J_{HF}=8.7$ Hz); 1.20 (vt, $PCCH_3$, 18H, $J_{PH}=6.9$ Hz); 1.22 (vt, $PCCH_3$, 18H, $J_{PH}=6.9$ Hz). ^{31}P NMR (C_6D_6, 293 K) 44.78 (d, $J_{PF}=26$ Hz). ^{19}F NMR (C_6D_6, 293 K): −184.6 (t, $J_{FP}=26$ Hz).

4.9. Reaction of $Ru(H)_2(CO)(P^tBu_2Me)_2$ with vinyl fluoride

$Ru(H)_2(CO)(P^tBu_2Me)_2$ (10 mg) in toluene-d_8 (0.5 mL) in an NMR tube was freeze–pump–thaw degassed, and the headspace of the NMR tube was charged with vinyl fluoride (1 atm) at −80 °C. The tube was transferred to a precooled NMR probe for observation. At −80 °C, no $Ru(H)_2(CO)L_2$ but only $RuHF(CO)L_2$ was detected by its $^{31}P\{^1H\}$ NMR spectrum (52.5 ppm, doublet $J_{PF}=20$ Hz). The volatiles of the reaction mixture were vacuum transferred to another NMR tube where the ^{1}H NMR spectrum revealed ethylene (5.34, singlet).

4.10. Reaction of $RuH(2\text{-}C_6FH_4)(CO)(P^tBu_2Me)_2$

$RuH(Ph)(CO)(P^tBu_2Me)_2$ (200 mg, 0.38 mmol), cyclohexane (10 mL), and fluorobenzene (1 mL) were stirred together for 18 h. After removal of the volatiles, the residue was extracted with pentane. The pentane solution was filtered through a Celite pad, concentrated to ca. 3 mL, and cooled to −78 °C for 2 h to give yellow crystals after 12 h. The crystals were filtered, washed with pentane and dried in vacuo to yield 125 mg (70%) of the title compound. Newly prepared product contains two rotamers about the Ru–Aryl bond, with 10:6 ratio based on NMR integration of the PCH_3 peaks. Spectroscopic data for the major isomer: ^{1}H NMR (C_6D_6, 20 °C) −28.7 (td, $J_{PH}=19.2$, $J_{FH}=7.6$ Hz, 1H, RuH); 0.70 (vt, 5.5 Hz, 6H, PCH_3); 1.13 (vt, 13 Hz, 18H, $PCCH_3$); 1.20 (vt, 12.7 Hz, 18H, $PCCH_3$); 6.9, 7.1, 7.6 (m, 4H, ArH). ^{31}P NMR (C_6D_6, 20 °C) 57.0 (s). ^{19}F (C_6D_6, 20 °C) −96.7(s). Minor isomer: ^{1}H NMR: −27.2 (td, $J_{PH}=20$ Hz, $J_{HF}=5.2$ Hz, 1H, Ru–H), 0.66 (vt, 5.5 Hz, PCH_3), 1.09 (vt, 12 Hz, 18H, $PC(CH_3)_3$), 1.19 (vt, 13 Hz, 18H, $PC(CH_3)_3$), 6.87, 7.03, 7.55 (4H, Ar). $^{31}P\{^1H\}$ NMR: 57.1 (s). ^{19}F NMR: −84.5 (s).

4.11. Reaction of $RuH(2\text{-}C_6FH_4)(CO)(P^tBu_2Me)_2$ with vinyl fluoride

$RuH(2\text{-}C_6FH_4)(CO)(P^tBu_2Me)_2$ (10 mg, 1.8×10^{-5} mol) was dissolved in C_6D_6 (0.5 mL) and degassed by three freeze–pump–thaw cycles. To the NMR tube, 400 Torr vinyl fluoride was charged. The resulting mixture was heated at 50 °C for 20 h to give $Ru(C_2H_3)F(CO)(P^tBu_2Me)_2$ and fluorobenzene.

4.12. Reaction of $RuH(C_6F_5)(CO)(P^tBu_2Me)_2$

The same procedure as $RuH(2\text{-}C_6FH_4)(CO)(P^tBu_2Me)_2$ was followed except C_6F_5H was used instead of C_6H_5F. Alternatively, it can be prepared from reaction of $RuHF(CO)(P^tBu_2Me)_2$ with $Me_3SiC_6F_5$ in the presence of a catalytic amount of CsF.

4.13. Reaction of $RuH(C_6F_5)(CO)(P^tBu_2Me)_2$ with vinyl fluoride

In an NMR tube, $RuH(C_6F_5)(CO)(P^tBu_2Me)_2$ (10 mg, 0.016 mmol) was dissolved in C_6D_6 (0.5 mL) and degassed by three freeze–pump–thaw cycles. To the tube, vinyl fluoride (400 mm Hg) was added. The mixture was heated at 85 °C for three days to give (based on $^{31}P\{^1H\}$ NMR integration) conversion to $RuF(C_6F_5)(CO)(P^tBu_2Me)_2$ (85%) and $Ru(C_2H_3)(F)(CO)(P^tBu_2Me)_2$ (15%). Addition of CsF to the NMR tube was necessary to resolve all couplings. Spectroscopic data for $RuF(C_6F_5)(CO)(P^tBu_2Me)_2$: ^{1}H NMR (400 MHz, C_6D_6, 20 °C) 0.92 (vt, 13 Hz, 18H, PCH_3,); 0.99 (vt, 6.5 Hz,18H, $PCCH_3$,); 1.22 (broad, 6H, $PCCH_3$). $^{31}P\{^1H\}$ NMR (C_6D_6, 20 °C): 42.7 (d, 2P, $J_{PF}=24.6$Hz). ^{19}F NMR (376.3 MHz): −111.5 (dd, $J_{FRuF}=53.3$ Hz, $J_{FF}=28.8$ Hz, 1F, *o*-ArF); −113.7 (d, $J_{FF}=26.5$ Hz, 1F, *o*-ArF,); −162.3 (dt, $J_{FF}=53$ Hz, $J_{PF}=25$ Hz, Ru–F), −164.4 (dd, $J_{FF}=J_{FF}=21$ Hz, *para*-F), −164.9 (dddd, $J_{FF}=26.2$, 21, 5, 5 Hz, *meta*-F); −167.4 (dddd, $J_{FF}=28$, 23, 5, 5 Hz, *meta*-F). The volatiles of the reaction mixture were vacuum transferred to another NMR tube and ^{1}H and ^{19}F NMR spectra showed C_2H_4 and C_6F_5H.

4.14. Reaction of $OsH(CH_3)(CO)(P^tBu_2Me)_2$

A solution containing 40.5 mg (7.04×10^{-5} mol) $OsHCl(CO)(P^tBu_2Me)_2$ in 3 mL of pentane was prepared in a centrifuge tube. Dropwise addition of 49.0 μL (7.11×10^{-5} mol) MeLi solution caused a gradual darkening of the solution concurrent with the appearance of a white suspension. The solution was centrifuged and the supernate was pipetted to a Schlenk flask. The solvent was then removed to leave an orange-red solid. ^{1}H NMR (C_6D_{12}, 20 °C) −33.3, (t, 1H, Os*H*, $J_{PH}=15.1$ Hz); 0.46 (t, 3H, $OsCH_3$, $J_{PH}=7.2$ Hz); 1.18 (vt, 18H, $PCCH_3$,

$J_{PH} = 6.0$ Hz); 1.21 (vt, 18H, PCCH_3, $J_{PH} = 6.0$ Hz); 1.49 (t, 6H, PCH_3, $J_{PH} = 2.8$ Hz). ^{31}P NMR (C_6D_{12}, 20 °C) 36.5, IR(C_6D_6): 1864(ν_{CO}).

4.15. $Os(CH_3)F(CO)(P^tBu_2Me)_2$

The reaction was run in a sealed NMR tube containing 9.2 mg $OsH(CH_3)(CO)(P^tBu_2Me)_2$ (1.658×10^{-5} mol) with 100 Torr vinyl fluoride (6.786×10^{-5} mol) in d_8-toluene. At −75 °C, the adduct $OsH(Me)(\eta^2\text{-}C_2H_3F)(CO)(P^tBu_2Me)_2$ was formed. Its diagnostic spectral features were: ^{1}H NMR (C_7D_8, −75 °C) −6.3 (1H, OsH); −1.1 (3H, OsCH_3); 2.9 (d, 1H, C=CH, $J_{PH} = 22.0$ Hz); 3.2 (m, 1H, C=CH); 6.3 (1H, C=CH). ^{31}P NMR (C_7D_8, −75 °C): 15.2, 12.7 (AB, 2P, $J_{PP} = 161$Hz). ^{19}F(C_7D_8, −75 °C) −170.0 (dt, 1F, CCF, $J_{FH} = 73$Hz, $J_{FH} =$ 20 Hz). Conversion to the final product (the title compound) occurred at 20 °C; its spectroscopic features were: ^{1}H NMR (C_7D_8, 20 °C) −1.1 (3H, OsCH_3); 1.28 (vt, 18H, OsPCCH_3, $J_{PH} = 6$Hz); 1.30 (vt, 18H, PCCH_3, $J_{PH} = 6$Hz); 1.86 (6H, PCH_3). ^{31}P NMR (C_7D_8, 20 °C) 26.0, (d, 2P, $J_{PF} = 27$ Hz). ^{19}F (C_7D_8, 20 °C) −198.0 (t, 1F, OsF, $J_{FP} = 27$Hz).

4.16. $OsF_2(CCH_2)(CO)(P^tBu_2Me)_2$

When 8.5 mg (1.53×10^{-5} mol) of $OsHMe(CO)(P^tBu_2Me)_2$ was warmed slowly with 25 equivalents (3.83×10^{-4}) of *gem*-difluoroethylene, $OsF_2(CCH_2)(CO)(P^tBu_2Me)_2$ formed in 60% yield. Following vacuum removal of excess $C_2H_2F_2$, and other volatiles, the diagnostic spectroscopic signals of the major product were: ^{1}H NMR (C_6D_6, 20 °C) 1.31 (vt, 36H, PCCH_3, $J_{PH} = 7.0$ Hz); 1.44 (vt, 6H, OsPCH_3, $J_{PH} = 4.1$ Hz); 2.01 (dt, 2H, CCH_2, $J_{FH} = 7$ Hz, $J_{PH} = 3$ Hz). ^{13}C NMR (C_6D_6, 20 °C) 3.6 (t, 2C, PCH_3, $J_{CP} = 5$ Hz); 29.7 (s, 6C, PCCH$_3$): 29.5 (s, 6C, PCCH$_3$); 36.2 (t, 2C, PCCH$_3$, $J_{PC} = 10.4$); 36.4 (t, 2C, PCCH$_3$, $J_{PC} = 10.4$); 94.8 (d, 1C, OsCC, $J_{CF} = 16$). ^{31}P NMR (C_6D_6, 20 °C) 34.65 (dd, 2P, $J_{PF} = 41.9$ Hz, $J_{PF'} = 25.1$ Hz). ^{19}F (C_6D_6, 20 °C) −277.45 (dt, 1F, OsF, $J_{FF} = 143$, $J_{FP} = 25$ Hz); −278.6 (dtt, 1F, OsF, $J_{FF} = 143$, $J_{FP} = 41$, $J_{HF} = 7$ Hz).

Acknowledgment

This work was supported by the US National Science Foundation.

References

[1] J.L. Kiplinger, T.G. Richmond, C.E. Osterberg, Chem. Soc. Rev. 94 (1994) 373.
[2] M. Aizenberg, D. Milstein, Science 265 (1994) 359.
[3] M. Aizenberg, D. Milstein, J. Am. Chem. Soc. 117 (1995) 8674.
[4] J. Burdeniuc, R.H. Crabtree, Science 271 (1996) 340.
[5] P.L. Timms, J. Chem. Soc., Dalton Trans. (1999) 815.
[6] B.L. Pagenkopf, E.M. Carreira, Chemistry A 5 (1999) 3437.
[7] K. Fagnou, M. Lautens, Ange. Chem. Int. Ed. 41 (2002) 26.
[8] P. Barthazy, R.M. Stoop, M. Woerle, A. Togni, A. Mezzetti, Organometallics 19 (2000) 2844.
[9] P. Barthazy, A. Togni, A. Mezzetti, Organometallics 20 (2001) 3472.
[10] P. Barthazy, D. Broggini, A. Mezzetti, Can. J. Chem. 79 (2001) 904.
[11] C. Becker, I. Kieltsch, D. Broggini, A. Mezzetti, Inorg. Chem. 42 (2003) 8417.
[12] A. Mezzetti, C. Becker, Helv. Chim. Acta 85 (2002) 2686.
[13] V.V. Grushin, Organometallics 19 (2000) 1888.
[14] V.V. Grushin, W.J. Marshall, Angew. Chem. Int. Ed. 41 (2002) 4476.
[15] V.V. Grushin, Chemistry A 8 (2002) 1006.
[16] V.V. Grushin, W.J. Marshall, J. Am. Chem. Soc. 126 (2004) 3068.
[17] R.J. Young Jr., V.V. Grushin, Organometallics 18 (1999) 294.
[18] T.G. Richmond, Angew. Chem. Int. Ed. 39 (2000) 3241.
[19] C.E. Osterberg, T.G. Richmond, ACS Symp. Ser. 555 (1994) 392.
[20] S.A. Strazisar, P.T. Wolczanski, J. Am. Chem. Soc. 123 (2001) 4728.
[21] E. Clot, C. Megret, B.M. Kraft, O. Eisenstein, W.D. Jones, J. Am. Chem. Soc. 126 (2004) 5647.
[22] W.D. Jones, Dalton Trans. (2003) 3991.
[23] B.M. Kraft, W.D. Jones, J. Am. Chem. Soc. 124 (2002) 8681.
[24] B.M. Kraft, R.J. Lachicotte, J. Rene, W.D. Jones, Organometallics 21 (2002) 727.
[25] T.G. Richmond, Top. Organomet. Chem. 3 (1999) 243.
[26] B.E. Smart, in: M. Audlicky, A.Z. Pavlath (Eds.), Chemistry of Organic Fluorine Compounds. A Critical Review, ACS Monograph 187, American Chemical Society, Washington, DC, 1995.
[27] N.A. Jasim, R.N. Perutz, A.C. Whitwood, T. Braun, J. Izundu, B. Neumann, S. Rothfeld, H.-G. Stammler, Organometallics 23 (2004) 6140.
[28] M. Reinhold, J.E. McGrady, R.N. Perutz, J. Am. Chem. Soc. 126 (2004) 5268.
[29] E. Clot, B. Oelckers, A.H. Klahn, O. Eisenstein, R.N. Perutz, Dalton Trans. 21 (2003) 4065.
[30] E. Clot, M. Besora, F. Maseras, C. Megret, O. Eisenstein, B. Oelckers, R.N. Perutz, Chem. Commun. (Cambridge) 4 (2003) 490.
[31] T. Braun, S. Rothfeld, V. Schorlemer, H.-G. Stammler, Inorg. Chem. Commun. 6 (2003) 752.
[32] D. Noveski, T. Braun, M. Schulte, B. Neumann, H.-G. Stammler, Dalton Trans. (2003) 4075.
[33] R. Bosque, E. Clot, S. Fantacci, F. Maseras, O. Eisenstein, R.N. Perutz, K.R. Renkema, K.G. Caulton, J. Am. Chem. Soc. 120 (1998) 12634.
[34] K.B. Renkema, R. Bosque, W.E. Streib, F. Maseras, O. Eisenstein, K.G. Caulton, J. Am. Chem. Soc. 121 (1999) 10895.
[35] A.J. Edwards, S. Elipe, M.A. Esteruelas, F.J. Lahoz, L.A. Oro, C. Valero, Organometallics 16 (1997) 3828.
[36] R.H. Heyn, S.A. Macgregor, T.T. Nadasdi, M. Ogasawara, O. Eisenstein, K.G. Caulton, Inorg. Chim. Acta 259 (1997) 5.
[37] J.K. Kochi, Organometallic Mechanisms and Catalysis, Academic Press, New York, 1978.
[38] T. Yamamoto, A. Yamamoto, S. Ikeda, J. Am. Chem. Soc. 93 (1971) 3350.
[39] D.G. Morrell, J.K. Kochi, J. Am. Chem. Soc. 97 (1975) 7262.
[40] A. Pedersen, M. Tilset, K. Folting, K.G. Caulton, Organometallics 14 (1995) 875.
[41] A. Ceccanti, P. Diversi, G. Ingrosso, F. Laschi, A. Lucherini, S. Magagna, P. Zanello, J. Organomet. Chem. 526 (1996) 251.
[42] A.V. Marchenko, H. Gerard, O. Eisenstein, K.G. Caulton, New J. Chem. 25 (2001) 1244.

[43] J.N. Coalter III, K.G. Caulton, New J. Chem. 24 (2000) 9.
[44] M.J. Albèniz, M.L. Buil, M.A. Esteruelas, A.M. Lopez, L.A. Oro, B. Zeier, Organometallics 13 (1994) 3746.
[45] R.E. Banks, Fluorocarbons and Their Derivatives, American Elsevier, New York, 1970.
[46] A. Andriollo, M.A. Esteruelas, U. Meyer, L.A. Oro, R.A. Sanchez-Delgado, E. Sola, C. Valero, H. Werner, J. Am. Chem. Soc. 111 (1989) 7431.
[47] J.T. Poulton, M.P. Sigalas, K. Folting, W.E. Streib, O. Eisenstein, K.G. Caulton, Inorg. Chem. 33 (1994) 1476.

Available online at www.sciencedirect.com
SCIENCE DIRECT
Polyhedron 25 (2006) 469–476
POLYHEDRON
www.elsevier.com/locate/poly

Potential Group IV olefin polymerization catalysts that contain a diamido ligand substituted with hexaisopropylterphenyl groups

Zachary J. Tonzetich, Richard R. Schrock *

Department of Chemistry, MIT, 77 Massachusetts Avenue, Cambridge, MA 02139, United States

Received 26 August 2005; accepted 12 September 2005
Available online 27 October 2005

This paper is dedicated to Malcolm H. Chisholm on the occasion of his 60th birthday.

Abstract

The diamine *rac*-H_2[HIPTN$_2$] (HIPTN$_2$ = (*N-hexa-iso*-propyl-3,5-terphenyl)diaminobinaphthalene) has been prepared through palladium-catalyzed *N*-aryl coupling of diaminobinaphthalene and 3,5-bis(2,4,6-triisopropylphenyl)bromobenzene. The reaction between H_2[HIPTN$_2$] and M(NMe$_2$)$_4$ (M = Ti, Zr, and Hf) yields [HIPTN$_2$] M(NMe$_2$)$_2$ complexes. Other complexes of [HIPTN$_2$]$^{2-}$ that have been prepared include [HIPTN$_2$]ZrCl$_2$, [HIPTN$_2$]ZrMe$_2$, [HIPTN$_2$]Zr(CH$_2$CMe$_3$)$_2$, [HIPTN$_2$]HfCl$_2$, [HIPTN$_2$]HfMe$_2$, and [HIPTN$_2$]Hf(CH$_2$CHMe$_2$)$_2$. Activation of [HIPTN$_2$]ZrMe$_2$ with a variety of Lewis acids gives rise to different species depending on the nature of the activator employed. For example, [HIPTN$_2$]ZrMe$_2$ reacts with [Ph$_3$C][B(C$_6$F$_5$)$_4$] to give a cationic complex that is active toward oligomerization of 1-hexene, while activation with B(C$_6$F$_5$)$_3$ leads to formation of [HIPTN$_2$]Zr(C$_6$F$_5$)$_2$. No polymerization of 1-hexene by activated complexes was observed.
© 2005 Elsevier Ltd. All rights reserved.

Keywords: Olefin; Polymerization; Zirconium; Hafnium

1. Introduction

The number of non-metallocene-based catalysts for the polymerization of ordinary olefins has increased markedly in the last decade [1]. Some of these catalysts offer activity that is comparable to metallocene catalysts, and also in some cases display characteristics of a living polymerization [2]. Many of the most successful catalysts contain nitrogen-based ligands, and examples of both early and late metal catalysts are abundant. Amido ligands have been found to be especially useful for preparing early transition metal polymerization catalysts [3].

We have been interested in the synthesis of complexes that contain new amido-based supporting ligands, particularly those that when activated display characteristics of a living olefin polymerization [4–12]. However, we have yet to prepare catalysts that effect both living and stereospecific olefin polymerizations [13]. A binaphthyl-based ligand system in which pyridine donors are incorporated has demonstrated that six-coordinate dialkyl complexes of zirconium and hafnium could be prepared and activated cleanly [14]. However, activated versions of these compounds do not polymerize 1-hexene, presumably because the pyridine donors prevent coordination of the olefin to the cationic metal center. We felt that a potential remedy for this situation might involve C_2-symmetric amido complexes that lacked a pendant donor moiety. Cationic complexes that contain diamido ligands were among the first that were found to exhibit living characteristics, as long as large aryl groups (e.g., mesityl or 2,4,6-triisopropylphenyl) were present on nitrogen [15,16].

In this paper, we report the preparation and Group IV chemistry of complexes that contain a diamido ligand derived from diaminobinaphthalene, one that is N-substituted with the bulky *hexa-iso*-propyl-3,5-terphenyl, or HIPT, group. The HIPT group recently has been useful

* Corresponding author. Tel.: +1 617 253 1596; fax: +1 617 253 7670.
E-mail address: rrs@mit.edu (R.R. Schrock).

0277-5387/$ - see front matter © 2005 Elsevier Ltd. All rights reserved.
doi:10.1016/j.poly.2005.09.005

as a substituent in triamidoamine ligands bound to molybdenum. Such species are catalysts for the catalytic reduction of dinitrogen to ammonia with protons and electrons at a single Mo center [17–21]. The HIPT group is believed to provide a significant degree of steric hindrance "at a distance" that leads to the success of catalytic dinitrogen reduction.

2. Results and discussion

2.1. Synthesis of the ligand and Group IV complexes that contain it

The parent diamine, *rac*-H_2[HIPTN$_2$], was prepared through a palladium-catalyzed *N*-aryl coupling between *rac*-diaminobinaphthalene and 3,5-bis(2,4,6-triisopropylphenyl)bromobenzene (HIPTBr). Using the XPHOS [22] ligand, the reaction is complete in less than 4 h, and can be scaled up to 15 g with yields of >80% after purification by flash chromatography (Eq. (1)).

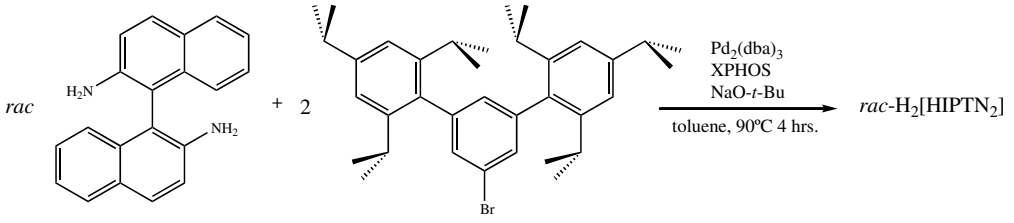

(1)

White, crystalline H_2[HIPTN$_2$] is readily soluble in all organic solvents including pentane and diethyl ether. The NMR spectrum contains three septets of area 4 for each of the methine protons of the triisopropylphenyl ring, indicating that rotation about the aryl–aryl bond of the terphenyl groups is not possible, but rotation about the *N*-aryl bond is facile. Other features of the ^{1}H NMR spectrum are consistent with C_2-symmetry and no rotation about the aryl–aryl bond.

The ligand can be attached to Ti, Zr, or Hf readily upon addition of it to M(NMe$_2$)$_4$ (Scheme 1). In the case of hafnium and zirconium, the parent diamine reacts with M(NMe$_2$)$_4$ in pentane at room temperature to yield [HIPTN$_2$]M(NMe$_2$)$_2$ as yellow microcrystals after 24 h. The titanium complex is somewhat more difficult to prepare, requiring elevated temperatures and significantly longer reaction time to go to completion. Heating H_2[HIPTN$_2$] and Ti(NMe$_2$)$_4$ in toluene at 110 °C for 6 days affords [HIPTN$_2$]Ti(NMe$_2$)$_2$ as an orange solid. The ^{1}H NMR spectra of the dimethylamido complexes are similar, and all show the expected C_2-symmetry. A large singlet of area 12 near 2.7 ppm is assigned to the NMe$_2$ protons. The sharp resonances suggest that rotation about the metal–nitrogen bond is fast on the NMR time scale at room temperature, as is typically observed for early transition metal dimethylamido complexes.

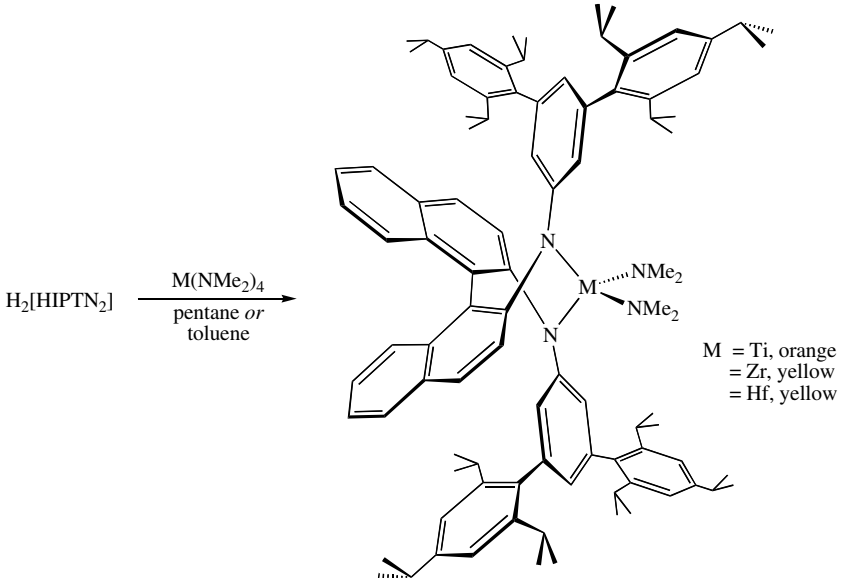

Scheme 1.

Treatment of $[HIPTN_2]M(NMe_2)_2$ (M = Zr, Hf) with two equivalents of Me_3SiCl in benzene at 60 °C affords $[HIPTN_2]MCl_2$. Proton NMR spectra of the yellow hafnium species show the expected sharp features of the ligand in a C_2-symmetric environment. However, proton spectra of the zirconium species reveal relatively broad resonances. The zirconium dichloride complex is deep red, but its solutions in diethyl ether are orange-yellow. Proton NMR spectra of samples recrystallized from diethyl ether show a broad peak for two equivalents of diethyl ether near 3.70 ppm. Combustion analyses of the Zr compound were also consistent with the presence of two molecules of diethyl ether. We suggest that a dynamic mixture of monomer and dimer exists in the zirconium case at room temperature, which gives rise to a broadened spectrum. Dimers of this type have been structurally characterized in the zirconium chemistry of diamidodonor ligands [9].

Attempts to prepare $[HIPTN_2]TiCl_2$ were unsuccessful. Heating solutions of $[HIPTN_2]Ti(NMe_2)_2$ with excess Me_3SiCl for several days resulted only in formation of $[HIPTN_2]Ti(NMe_2)Cl$, according to ^1H NMR spectra. A reaction between $[HIPTN_2]Ti(NMe_2)_2$ and $TMSOSO_2CF_3$ also resulted in formation of only $[HIPTN_2]Ti(NMe_2)(OTf)$, according to NMR spectra. These results are similar to those found in the titanium chemistry of a related diamidodonor ligand [23].

Alkylation of "$[HIPTN_2]MCl_2$" (M = Zr, Hf) yielded $[HIPTN_2]MR_2$ complexes (R = Me, CH_2CMe_3, CH_2CHMe_2; Scheme 2). The dialkyl species are all yellow solids which are readily soluble in common organic solvents, including pentane. Proton NMR spectra are consistent with monomeric C_2-symmetric species with resonances for the alkyl ligands appearing in a range typically encountered for d^0 alkyl complexes of hafnium and zirconium (Table 1). Attempts to grow X-ray quality crystals of dialkyl complexes were unsuccessful, leading in each case to small needle-like crystals or amorphous solids.

2.2. Activation of dialkyl species

Activation of $[HIPTN_2]ZrMe_2$ was attempted with $B(C_6F_5)_3$, $[Ph_3C][B(C_6F_5)_4]$, and $[HNMe_2Ph][B(C_6F_5)_4]$ with the aim of preparing a cationic monomethyl species. Reaction of $[HIPTN_2]ZrMe_2$ with $B(C_6F_5)_3$ in C_6D_6 yielded a deep red solution, a proton NMR spectrum of which showed it to contain a C_2-symmetric species,

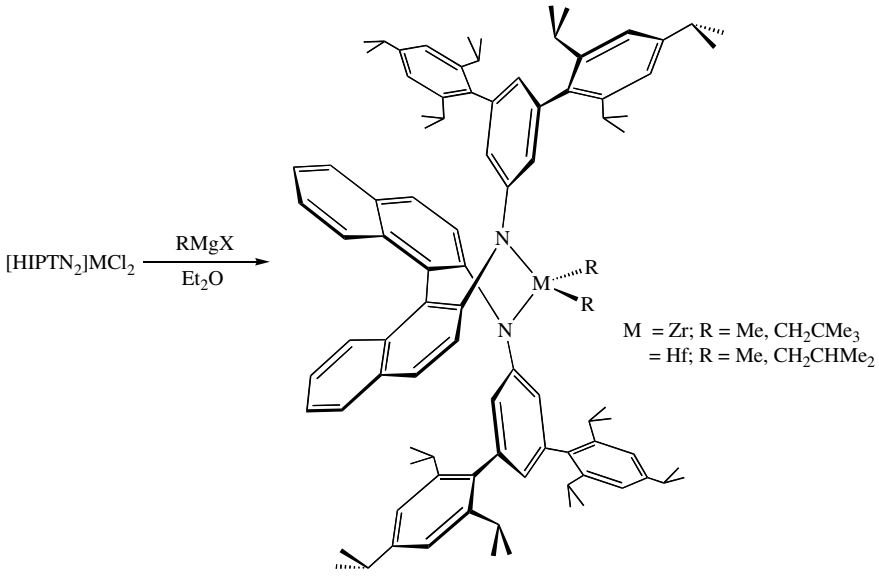

Scheme 2.

Table 1
Selected NMR data for the alkyl ligands of complexes of $[HIPTN_2]^{2-}$

Compound	^1H NMR	^{13}C NMR
$[HIPTN_2]ZrMe_2$	0.60[a]	53.17[c]
$\{[HIPTN_2]Zr(Me)(NMe_2Ph)\}^+$	0.73[b]	51.95[b]
$\{[HIPTN_2]Zr(Me)\}^+$	0.42[b] (major); 0.64 (minor)	47.51[b] (major); 49.76 (minor)
$[HIPTN_2]Zr(C_6F_5)_2$	N/A	148.52[c] (*o*); 146.11 (*ipso*); 142.71 (*p*); 136.48 (*m*)
$[HIPTN_2]Zr(CH_2CMe_3)_2$	1.60[a], 1.11 (CH_2); 0.91 (*Me*)	99.91[c] (CH_2); 37.24 (CMe_3); 34.76 (*Me*)
$[HIPTN_2]HfMe_2$	0.46[a]	63.16[c]
$\{[HIPTN_2]Hf(Me)(NMe_2Ph)\}^+$	0.49[b]	
$\{[HIPTN_2]Hf(Me)\}^+$	0.66[b]	
$[HIPTN_2]Hf(CH_2CHMe_2)_2$	2.25[a] (*CH*); 0.97, 0.85 (CH_2); 0.81, 0.63 (*Me*)	98.11[c] (CH_2)

Measured in [a]C_6D_6, [b]C_6D_5Br, [c]CD_2Cl_2.

although no resonance could be found that could be assigned to a methyl group. Examination of the ^{19}F NMR spectrum of the product showed that the expected $[MeB(C_6F_5)_3]^-$ anion was not present, although one major species appeared to be present. Activation of the ^{13}C labeled derivative gave identical ^1H and ^{19}F NMR spectra to those obtained upon activation of the unlabeled compound. The ^{13}C NMR spectrum was more enlightening, showing only a very broad resonance at 17 ppm in bromobenzene-d_5 assignable to the $^{13}CH_3$ groups. The appearance and chemical shift of these methyl resonances points to a species with both methyl groups bound to boron. Decomposition of the $[MeB(C_6F_5)_3]^-$ anion by C_6F_5 transfer to the metal is a documented reaction pathway for Group IV methyl cations [24–26]. Such a decomposition would explain the presence of a C_2-symmetric species, which we believe to be $[HIPTN_2]Zr(C_6F_5)_2$, and one equivalent of $Me_2B(C_6F_5)$ (Eq. (2)). A double exchange of methyl for pentafluorophenyl is more rare than a single exchange and may be due to the highly electron deficient nature of the metal center and its relatively open

$$[HIPTN_2]ZrMe_2 + B(C_6F_5)_3 \longrightarrow [HIPTN_2]Zr(C_6F_5)_2 + Me_2B(C_6F_5) \quad (2)$$

architecture. This reaction can be used on larger scales to prepare $[HIPTN_2]Zr(C_6F_5)_2$ in good yield. Proton, carbon, and fluorine NMR spectra, as well as combustion analysis of the recrystallized material are all consistent with the product being $[HIPTN_2]Zr(C_6F_5)_2$; NMR spectra are also all identical to those obtained in NMR scale activation experiments. Attempts to polymerize 1-hexene by a cationic species that may be formed transiently upon activation of $[HIPTN_2]$ $ZrMe_2$ with $B(C_6F_5)_3$ were unsuccessful, even when the reaction was conducted in neat 1-hexene at −30 °C. This result contrasts with that obtained by McConville for a titanium diamido catalyst where decomposition of the $[MeB(C_6F_5)_3]^-$ anion could be avoided by conducting polymerization experiments in neat 1-hexene [25].

The reaction between $[HIPTN_2]ZrMe_2$ and $[HNMe_2Ph][B(C_6F_5)_4]$ in bromobenzene-d_5 proceeded as anticipated with elimination of methane and formation of a dimethylaniline adduct of the monomethyl cation, as shown in Eq. (3). The activation required several hours at

$$[HIPTN_2]ZrMe_2 + [HNMe_2Ph][B(C_6F_5)_4] \xrightarrow{-CH_4} \{[HIPTN_2]Zr(Me)(NMe_2Ph)\}\{B(C_6F_5)_4\} \quad (3)$$

room temperature to go to completion, perhaps as a consequence of the limited solubility of $[HNMe_2Ph][B(C_6F_5)_4]$ in bromobenzene. Proton and carbon NMR spectra are both consistent with the product being asymmetric and containing one methyl group. Two singlet resonances are found for the Me groups of dimethylaniline in the ^1H NMR spectrum, consistent with it being tightly bound. The low coordination number of (formally) a three-coordinate and sterically accessible metal in the cation apparently allows tight binding of dimethylaniline. Only one diastereomer is observed. Not surprisingly, addition of 1-hexene to $\{[HIPTN_2]Zr(Me)(NMe_2Ph)\}[B(C_6F_5)_4]$ yielded no polymer, even at 60 °C, presumably as a consequence of tight binding of dimethylaniline.

Reaction of $[HIPTN_2]ZrMe_2$ with $[Ph_3C][B(C_6F_5)_4]$ in bromobenzene-d_5 at −10 °C over a period of 20–30 min yielded a dark red solution whose ^1H and ^{13}C NMR spectra were consistent with formation of an asymmetric monomethyl cation. When a full equivalent of trityl was employed, two similar species were formed in a roughly 1:1 ratio. The two compounds have nearly identical NMR spectra, which suggests that they may be diastereomers (Table 1). The two species do not grow in at the same rate; one is formed before all $[HIPTN_2]ZrMe_2$ is consumed, while the other grows in as $[HIPTN_2]ZrMe_2$ reacts with the remaining trityl. The dimethyl species therefore may play a role in conversion of one diastereomer to the other.

Activation of dimethyl species with trityl has been shown to produce monocationic dimers through capture of the monomethyl cation by unreacted dimethyl species [27,28]. In order to test the likelihood of dimer formation upon activation of $[HIPTN_2]ZrMe_2$, activation was carried out with 0.5 equivalents of trityl. Proton NMR spectra from this reaction show a 1:1 ratio of starting material to one of the diastereomers observed above, indicating that monocationic dimeric species probably are not present. The $^1J_{C-H}$ coupling constants of 120 Hz for the methyl groups in each diastereomer also argue in favor of monomeric species. At this stage, we can only suggest that relatively strong ion pairing is the origin of two different species being observable in NMR spectra.

Solutions of $[HIPTN_2]ZrMe_2$ activated with trityl react instantly and exothermically with several equivalents of 1-hexene at −30 °C. Examination of these reactions by ^{13}C and ^1H NMR revealed that the 1-hexene had been oligomerized, not polymerized. The NMR spectrum, which is similar to that found with the $[(MesN\text{-}o\text{-}C_6H_4)_2O]^{2-}$ ligand system, suggests that chain termination by β-H elimination (from either the 1,2 or especially a 2,1 insertion product) is facile [29–31]. The relatively open environment at the metal may not allow effective discrimination between 1,2 and 2,1 olefin insertion, thereby leading to an enhanced proclivity towards β-H elimination [29–31].

Activation of the $[HIPTN_2]HfMe_2$ species with the three activators discussed above yielded results that are essentially identical to those observed with zirconium (see Section 4). Interestingly, the $[HIPTN_2]Hf(C_6F_5)_2$ formed by reaction with $B(C_6F_5)_3$ we believe to be the first such compound of hafnium to be formed by aryl transfer from boron. The $[HIPTN_2]Hf(CH_2CHMe_2)_2$ species showed similar behavior to the dimethyl species when activated with $[Ph_3C][B(C_6F_5)_4]$ and $[HNMe_2Ph][B(C_6F_5)_4]$. Unlike the methyl species, however, the isobutyl complex did not undergo exchange with $B(C_6F_5)_3$, but rather reacted slowly to give an asymmetric Hf species and isobutene as judged by ^1H NMR. This asymmetric species could not be identified positively as the isobutyl cation, but the fact that it did

not react with 1-hexene at room temperature to yield polymer or oligomer argues against it being the isobutyl cation.

The dineopentyl zirconium species was also examined as an initiator. The complex did not react readily with $B(C_6F_5)_3$, and it reacted only very slowly with the other two activators to give products which could not be identified by NMR spectroscopy.

3. Conclusions

Complexes that contain the $[HIPTN_2]^{2-}$ ligand appear to be similar in some ways to other early transition metal polymerization catalysts that contain diamido supporting ligands. Unfortunately, the "steric hindrance at a distance" that is provided by the HIPT substituents is not sufficient to stabilize pseudo three-coordinate cations against various decomposition reactions, and only oligomerization of 1-hexene was observed as a consequence of insufficient steric protection close to the metal. We conclude that although three HIPT substituents on amido nitrogens provides a significant amount of steric protection in five-coordinate complexes that contain a triamidoamine ligand [17–21], only two HIPT substituents cannot counteract the consequences of an inherently open architecture in a diamido alkyl metal cation.

4. Experimental

General comments. All manipulations of air- and moisture-sensitive materials were performed in oven-dried (200 °C) glassware under an atmosphere of nitrogen on a dual-manifold Schlenk line or in a Vacuum Atmospheres glovebox. NMR experiments were carried out in Teflon-valve sealed J. Young-type NMR tubes. HPLC grade organic solvents were sparged with nitrogen and dried by passage through activated alumina (for diethyl ether, toluene, pentane, THF, and methylene chloride) followed by passage through Q-5 supported copper catalyst (for benzene) prior to use then stored over 4 Å Linde-type molecular sieves. Benzene-d_6, toluene-d_8, and THF-d_8 were dried over sodium/benzophenone ketyl and vacuum-distilled. Methylene chloride-d_2 and bromobenzene-d_5 were dried over CaH_2, vacuum distilled and stored over 4 Å Linde-type molecular sieves. NMR spectra were recorded on a Varian 500 or Varian 300 spectrometer. Chemical shifts for ^1H and ^{13}C spectra were referenced to the residual $^1H/^{13}C$ resonances of the deuterated solvent (^1H: C_6D_6, δ 7.16; $C_6D_5CD_3$, δ 2.15; CD_2Cl_2, δ 5.32; C_6D_5Br, δ 7.29. ^{13}C: C_6D_6, δ 128.32; C_6D_5Br, δ 121.19) and are reported as parts per million relative to tetramethylsilane. ^{19}F NMR spectra were referenced externally to fluorobenzene (δ −113.15 ppm relative to $CFCl_3$). In the following discussion of NMR shifts, BINAP refers to protons on the binaphthyl rings, whereas *o*, *m*, and *p* refer to the aryl positions of the terphenyl substituent. High-resolution mass spectrometry measurements were performed at the MIT Department of Chemistry Instrument Facility, and elemental analyses were performed by H. Kolbe Microanalytics Laboratory, Mülheim de Ruhr, Germany.

2,2′-Diamino-1,1′-binaphthalene, 3,5-bis(2,4,6-triisopropylphenyl)bromobenzene, $Ti(NMe_2)_4$, $Zr(NMe_2)_4$, and $Hf(NMe_2)_4$ [32] were prepared according to published procedures, or slightly modified versions thereof. Me_3SiCl, *iso*-BuMgBr, and MeMgBr were purchased from Aldrich Chemical Co. and used as received. Tris(pentafluorophenyl)borane, trimethylsilyl trifluoromethanesulfonate (TMSOTf), $Pd_2(dba)_3$, and XPHOS were purchased from Strem Chemical Co. and used as received. Trityl tetrakis(pentafluorophenyl)borate, $\{Ph_3C\}[\{B(C_6F_5)_4\}]$, was obtained as a gift from the Exxon Mobile Corp. and used as received.

$H_2[HIPTN_2]$. A 500 mL Schlenk flask was charged with 3.97 g (14.0 mmol) of 2,2′-diamino-1,1′-binaphthalene, 17.15 g (30.5 mmol) of 3,5-bis(2,4,6-triisopropylphenyl)bromobenzene, 4.30 g (44.7 mmol) of NaO-*t*-Bu, and 300 mL of toluene. To the mixture was added a solution of 0.130 g (1 mol%) of $Pd_2(dba)_3$ and 0.138 g (2 mol%) of XPHOS dissolved in 5 mL of toluene. The resulting mixture was stirred at 90 °C for 5 h during which time the mixture became brown and a large amount of precipitate had formed. The mixture was filtered through celite and the volatiles were removed from the filtrate in vacuo. The brown residue was dissolved in a minimal amount of pentane and left to stand overnight. The compound precipitated as a white crystalline solid over a period of 18 h. The remaining mother liquor was purified by flash chromatography on silica gel eluting with 20% toluene in pentane. The pooled column fractions were evaporated to dryness in vacuo leaving a white solid; total yield 13.04 g (75%): ^1H NMR (CD_2Cl_2) δ 7.87 (d, 2 BINAP*H*), 7.82 (d, 2 BINAP*H*), 7.77 (d, 2 BINAP*H*), 7.26 (t, 2 BINAP*H*), 7.15 (t, 2 BINAP*H*), 7.09 (d, 2 BINAP*H*), 7.00 (app d, 8 *m*-*H*), 6.80 (s, 4 *o*-*H*), 6.56 (s, 2 *p*-*H*), 5.73 (s, 2 N*H*), 2.89 (sep, 4 *p*-C*H*Me$_2$), 2.73 (m, 8 *o*-C*H*Me$_2$), 1.26 (d, 24 *p*-CH*Me*$_2$), 1.09 (d, 12 *o*-CH*Me*$_2$), 1.03 (app q, 36 *o*-CH*Me*$_2$); $^{13}C\{^1H\}$ NMR (CD_2Cl_2) δ 148.59, 147.06, 142.45, 142.25, 141.54, 137.26, 134.41, 130.18, 129.98, 128.78, 127.47, 126.31, 124.63, 123.99, 120.98, 120.43, 118.45, 116.85, 34.93, 30.96, 24.84, 24.50, 24.48, 24.41; HRMS Calc. $[M+H]^+$ 1245.8898. Found $[M+H]^+$ 1245.8889. *Anal*. Calc. for $C_{92}H_{112}N_2$: C, 88.69; H, 9.06; N, 2.25. Found: C, 88.62; H, 8.94; N, 2.17%.

$[HIPTN_2]Ti(NMe_2)_2$. A sealable Schlenk vessel was charged with 1.145 g (0.919 mmol) of $H_2[HIPTN_2]$, 0.21 g (0.94 mmol) of $Ti(NMe_2)_4$, and 30 mL of toluene. The sealed vessel was heated at 110 °C for 6 days during which time the solution became bright red-orange. The toluene was removed in vacuo and the residue was crystallized from a minimal amount of pentane at −25 °C. Yield: 0.733 g (58%). ^1H NMR (C_6D_6) δ 7.73 (app s, 4 BINAP*H*), 7.47 (d, 2 BINAP*H*), 7.20 (s, 4 *m*-*H*), 7.19 (s, 4 *m*-*H*), 7.03 (d, 2 BINAP*H*), 7.02 (s, 4 *o*-*H*), 6.98 (t, 2 BINAP*H*), 6.56 (s, 2 *p*-*H*), 6.54 (t, 2 BINAP*H*),

3.15 (sep, 4 *o*-C*H*Me$_2$), 3.07 (sep, 4 *o*-C*H*Me$_2$), 2.87 (sep, 4 *p*-C*H*Me$_2$), 2.85 (s, 6 N *Me*$_2$), 1.30 (m, 48 CH*Me*$_2$), 1.21 (d, 12 CH*Me*$_2$), 1.08 (d, 12 CH*Me*$_2$). *Anal*. Calc. for $C_{96}H_{122}N_4Ti$: C, 83.56; H, 8.91; N, 4.06. Found: C, 83.37; H, 9.06; N, 3.94%.

[HIPTN$_2$]Zr(NMe$_2$)$_2$. A round bottom flask was charged with 6.269 g (5.03 mmol) of H$_2$[HIPTN$_2$], 1.278 g (4.78 mmol) of Zr(NMe$_2$)$_4$, and 60 mL of pentane. The reaction was allowed to stir for 2 days at room temperature during which time it became bright yellow. The solution was set aside at −25 °C from which the compound crystallized as yellow microcrystals. Yield: 5.538 g (82%). ^{1}H NMR (C$_6$D$_6$) δ 7.92 (d, 2 BINAP*H*), 7.75 (d, 2 BINAP*H*), 7.41 (d, 2 BINAP*H*), 7.22 (s, 4 *m*-*H*), 7.21 (s, 4 *m*-*H*), 7.16 (s, 4 *o*-*H*), 7.08 (d, 2 BINAP*H*), 6.94 (t, 2 BINAP*H*), 6.60 (t, 2 BINAP*H*), 6.57 (s, 2 *p*-*H*), 3.15 (m, 8 *o*-C*H*Me$_2$), 2.65 (s, 12 N *Me*$_2$), 2.87 (sep, 4 *p*-C*H*Me$_2$), 2.64 (s, 12 N *Me*$_2$), 1.27 (m, 60 CH*Me*$_2$), 1.18 (d, 12 *o*-CH*Me*$_2$). *Anal*. Calc. for $C_{96}H_{122}N_4Zr$: C, 78.16; H, 8.40; N, 1.82. Found: C, 77.96; H, 8.31; N, 1.75%.

[HIPTN$_2$]ZrCl$_2$(Et$_2$O)$_2$. A sealable Schlenk vessel was charged with 5.532 g (3.89 mmol) of [HIPTN$_2$]Zr(NMe$_2$)$_2$, 1.0 mL (8.1 mmol) of Me$_3$SiCl, and 70 mL of benzene. The reaction was stirred at 70 °C for 18 h during which time it became deep red. The benzene was removed in vacuo and the residue crystallized from diethyl ether at −25 °C. Attempts at crystallizing the compound from pentane were unsuccessful. The ^{1}H NMR spectrum of the orange-yellow compound was very broad and difficult to interpret with a peak assignable to ~2 equivalents of coordinated diethyl ether (see text). Yield: 3.640 g (67%). ^{1}H NMR (C$_6$D$_6$) *all peaks very broad* δ 7.62, 7.37, 7.27, 7.16, 6.98, 6.85, 6.60, 6.38, 3.70 (*Et*$_2$O), 2.97 (C*H*Me$_2$), 2.87 (C*H*Me$_2$), 1.36–1.10 (CH*Me*$_2$), 1.01, 0.72. *Anal*. Calc. for $C_{100}H_{130}N_2Cl_2O_2Zr$: C, 77.28; H, 8.43; N, 1.80; Cl, 4.56. Found: C, 76.94; H, 8.12; N, 1.90; Cl, 4.75%.

[HIPTN$_2$]ZrMe$_2$. A flask was charged with 2.005 g (1.43 mmol) of [HIPTN$_2$]ZrCl$_2$ (Et$_2$O)$_2$ and dissolved in 40 mL of diethyl ether. The solution was chilled to −25 °C at which point 0.91 mL (2.9 mmol) of MeMgBr (3.15 M in Et$_2$O) was added dropwise. The reaction mixture was allowed to stir at room temperature for 60 min during which time the solution changed from orange to yellow, and a precipitate formed. The ether was removed in vacuo and the residue extracted with pentane and filtered through celite. The pentane solution was concentrated to ~5 mL and set aside at −25 °C for several days. The complex crystallized as a yellow solid in several crops. Yield: 1.514 g (78%). ^{1}H NMR (C$_6$D$_6$) δ 7.84 (d, 2 BINAP*H*), 7.59 (d, 2 BINAP*H*), 7.47 (s, 4 *o*-*H*), 7.26 (d, 2 BINAP*H*), 7.24 (s, 4 *m*-*H*), 7.22 (s, 4 *m*-*H*), 6.96 (d, 2 BINAP*H*), 6.90 (t, 2 BINAP*H*), 6.71 (s, 2 *p*-*H*), 6.57 (t, 2 BINAP*H*), 3.13 (m, 8 *o*-C*H*Me$_2$), 2.88 (sep, 4 *p*-C*H*Me$_2$), 1.28 (m, 60 CH*Me*$_2$), 1.17 (d, 12 *o*-CH*Me*$_2$), 0.60 (s, 6 C*H*$_3$); ^{13}C{^{1}H} NMR (CD$_2$Cl$_2$) δ 150.58, 148.53, 147.17, 147.16, 142.57, 138.31, 137.55, 135.05, 133.09, 131.63, 128.61, 128.00, 126.72, 125.98, 125.27, 124.92, 123.90, 121.05, 121.01, 119.29, 53.17 (*Me*), 34.90 (*p*-*C*HMe$_2$), 31.07 (*o*-*C*HMe$_2$), 31.01 (*o*-*C*HMe$_2$), 24.87, 24.76, 24.69, 24.61, 24.49, 24.47. *Anal*. Calc. for $C_{94}H_{116}N_2Zr$: C, 82.70; H, 8.56; N, 2.05. Found: C, 82.59; H, 8.50; N, 1.96%.

[HIPTN$_2$]Zr(^{13}*CH$_3$)$_2$* was prepared similarly from ^{13}CH$_3$MgI: ^{13}C NMR (C$_6$D$_6$) δ 54.50 (q, *C*H$_3$, $^1J_{C-H}$ = 115 Hz).

[HIPTN$_2$]Zr(CH$_2$CMe$_3$)$_2$. This complex was prepared in a fashion analogous to that used to prepare [HIPTN$_2$]ZrMe$_2$ starting from 0.584 g (0.376 mmol) of [HIPTN$_2$]ZrCl$_2$(Et$_2$O)$_2$ and 0.54 mL (0.86 mmol) of Me$_3$CCH$_2$MgCl (1.6 M in Et$_2$O). The pentane extract was evaporated to dryness to give the complex as a yellow solid. Yield: 0.538 g (88%). ^{1}H NMR (C$_6$D$_6$) δ 7.86 (d, 2 BINAP*H*), 7.80 (s, 2 BINAP*H*), 7.44 (s, 4 *o*-*H*), 7.36 (d, 2 BINAP*H*), 7.21 (s, 4 *m*-*H*), 7.20 (s, 4 *m*-*H*), 6.89 (m, 4 BINAP*H*), 6.64 (s, 2 *p*-*H*), 6.39 (t, 2 BINAP*H*), 3.16 (sep, 4 *o*-C*H*Me$_2$), 3.08 (sep, 4 *o*-C*H*Me$_2$), 2.86 (sep, 4 *p*-C*H*Me$_2$), 1.60 (d, 2 C*H*$_2$CMe$_3$, $^2J_{H-H}$ = 12.5 Hz), 1.34 (d, 12 CH*Me*$_2$), 1.27 (m, 36 CH*Me*$_2$), 1.22 (d, 12 CH*Me*$_2$), 1.17 (d, 12 CH*Me*$_2$), 1.11 (d, 2 C*H*$_2$CMe$_3$), 0.91 (s, 18 CH$_2$C*Me*$_3$); ^{13}C{^{1}H} (CD$_2$Cl$_2$) δ 151.69, 148.35, 147.19, 147.15, 142.13, 139.29, 137.69, 135.19, 132.36, 131.59, 128.38, 127.68, 127.20, 126.55, 125.78, 125.55, 124.69, 120.90, 120.85, 120.50, 99.91 (*C*H$_2$CMe$_3$), 37.24 (*C*Me$_3$), 34.88 (*p*-*C*HMe$_2$), 34.76 (C *Me*$_3$), 30.94 (*o*-*C*HMe$_2$), 30.82 (*o*-*C*HMe$_2$), 25.02, 24.91, 24.85, 24.64, 24.47, 24.46 (CH*Me*$_2$). *Anal*. Calc. for $C_{102}H_{132}N_2Zr$: C, 82.92; H, 9.01; N, 1.90. Found: C, 82.84; H, 8.96; N, 1.86%.

[HIPTN$_2$]Zr(C$_6$F$_5$)$_2$. A flask was charged with 0.343 g (0.251 mmol) of [HIPTN$_2$]ZrMe$_2$ and dissolved in 30 mL of pentane. The yellow solution was chilled to −25 °C at which point 0.135 g (0.264 mmol) of B(C$_6$F$_5$)$_3$ was added as a solid. The solution immediately became bright orange upon addition of borane. The orange solution was stirred at room temperature for 60 min and then evaporated to dryness. The orange residue was crystallized from hot hexane. Yield: 0.318 g (76%). ^{1}H NMR (C$_6$D$_6$) δ 7.65 (d, 2 BINAP*H*), 7.41 (d, 2 BINAP*H*), 7.26 (d, 2 BINAP*H*), 7.16 (s, 4 *o*-*H*), 7.12 (s, 4 *m*-*H*), 7.11 (s, 4 *m*-*H*), 7.00 (t, 2 BINAP*H*), 6.84 (d, 2 BINAP*H*), 6.69 (s, 2 *p*-*H*), 6.51 (t, 2 BINAP*H*), 2.92 (m, 8 *o*-C*H*Me$_2$), 2.79 (sep, 4 *p*-C*H*Me$_2$), 1.22 (d, 24 *p*-CH*Me*$_2$), 1.15 (m, 36 *o*-CH*Me*$_2$), 1.07 (d, 12 *o*-CH*Me*$_2$); ^{13}C{^{1}H} NMR (CD$_2$Cl$_2$) δ 148.72, 148.71, 148.52 (dd, *o*-*C*F, $^1J_{C-F}$ = 228 Hz), 147.07, 146.83, 146.11 (t, *C*$_{ipso}$, $^2J_{C-F}$ = 65 Hz), 142.99, 142.71 (d, *p*-*C*F, $^1J_{C-F}$ = 257 Hz), 137.52, 136.90, 136.48 (d, *m*-*C*F, $^1J_{C-F}$ = 261 Hz), 135.03, 133.16, 132.58, 128.53, 128.47, 127.78, 127.70, 127.17, 126.71, 125.55, 120.95, 120.84, 119.71, 34.92 (*p*-*C*HMe$_2$), 30.97 (*o*-*C*HMe$_2$), 30.86 (*o*-*C*HMe$_2$), 24.65, 24.47, 24.43, 24.39, 24.28, 24.10; ^{19}F NMR (C$_6$D$_6$) δ −124.12 (d, 4 *o*-*F*), −148.80 (t, 2 *p*-*F*), −159.10 (t, 4 *m*-*F*). *Anal*. Calc. for $C_{104}H_{110}N_2F_{10}$ Zr: C, 74.83; H, 6.64; N, 1.68. Found: C, 74.91; H, 6.73; N, 1.66%.

[HIPTN$_2$]Hf(NMe$_2$)$_2$. This complex was prepared in a manner strictly analogous to that used to prepare [HIPTN$_2$]Zr(NMe$_2$)$_2$ starting from 4.092 g (3.28 mmol) of H$_2$[HIPTN$_2$] and 1.189 g (3.35 mmol) of Hf(NMe$_2$)$_4$. Yield: 3.635 g (71%). ^{1}H NMR (C$_6$D$_6$) δ 7.90 (d, 2 BINAP*H*), 7.75 (d, 2 BINAP*H*), 7.41 (d, 2 BINAP*H*), 7.21 (s, 4 *m*-*H*), 7.20 (s, 4 *m*-*H*), 7.18 (s, 4 *o*-*H*), 7.04 (d, 2 BINAP*H*), 6.95 (t, 2 BINAP*H*), 6.56 (m, 2 *p*-*H*/2 BINAP*H*), 3.13 (m 8 *o*-C*H*Me$_2$), 2.87 (sep, 4 *p*-C*H*Me$_2$), 2.70 (s, 12 N *Me*$_2$), 1.27 (m, 60 CH*Me*$_2$), 1.15 (d, 12 CH*Me*$_2$). *Anal*. Calc. for C$_{96}$H$_{122}$N$_4$Hf: C, 76.33; H, 8.14; N, 3.71. Found: C, 76.25; H, 8.05; N, 3.57%.

[HIPTN$_2$]HfCl$_2$. This complex was prepared in a manner similar to that used to prepare [HIPTN$_2$]ZrCl$_2$ starting from 3.02 g (2.00 mmol) of [HIPTN$_2$] Hf(NMe$_2$)$_2$ and 0.53 mL (4.2 mmol) of Me$_3$SiCl. The reaction solution remained yellow after heating in contrast to the Zr complex. All volatiles were removed in vacuo giving a yellow solid. Yield: 2.90 g (97%). ^{1}H NMR (C$_6$D$_6$) δ 7.64 (d, 2 BINAP*H*), 7.49 (d, 2 BINAP*H*), 7.34 (s, 4 *o*-*H*), 7.16 (m, 2 BINAP*H*/8 *m*-*H*), 6.87 (m, 4 BINAP*H*), 6.63 (s, 2 *p*-*H*), 6.50 (t, 2 BINAP*H*), 2.98 (m, 8 *o*-C*H*Me$_2$), 2.82 (sep, 4 *p*-C*H*Me$_2$), 1.20 (m, 60 CH*Me*$_2$), 1.11 (d, 12 *o*-CH*Me*$_2$). *Anal*. Calc. for C$_{92}$H$_{110}$N$_2$Cl$_2$Hf: C, 74.00; H, 7.42; N, 1.88; Cl, 4.75. Found: C, 73.85; H, 7.51; N, 1.83; Cl, 4.77%.

[HIPTN$_2$]HfMe$_2$. A flask was charged with 1.138 g (0.762 mmol) of [HIPTN$_2$]HfCl$_2$ and dissolved in 20 mL of diethyl ether. The solution was chilled to −25 °C at which point 0.47 mL (1.6 mmol) of MeMgBr (3.3 M in Et$_2$O) was added dropwise. The reaction mixture was allowed to stir at room temperature for 60 min during which time a precipitate formed. The ether was removed in vacuo and the residue extracted with pentane and filtered through celite. The pentane solution was evaporated to dryness yielding a yellow solid. Yield: 0.978 g (88%). ^{1}H NMR (C$_6$D$_6$) δ 7.83 (d, 2 BINAP*H*), 7.60 (d, 2 BINAP*H*), 7.42 (s, 4 *o*-*H*), 7.28 (d, 2 BINAP*H*), 7.23 (s, 4 *m*-*H*), 7.21 (s, 4 *m*-*H*), 6.96 (d, 2 BINAP*H*), 6.92 (t, 2 BINAP*H*), 6.68 (s, 2 *p*-*H*), 6.55 (t, 2 BINAP*H*), 3.12 (m, 8 *o*-C*H*Me$_2$), 2.88 (sep, 4 *p*-C*H*Me$_2$), 1.30–1.20 (m, 72 CH*Me*$_2$), 0.46 (s, 6 C*H*$_3$). ^{13}C{^{1}H} NMR (CD$_2$Cl$_2$) δ 150.74, 148.52, 147.19, 147.16, 142.53, 137.82, 137.61, 135.05, 133.10, 131.65, 128.61, 127.98, 126.81, 126.00, 125.40, 125.21, 124.64, 121.05, 121.01, 119.58, 63.16 (*Me*), 34.92 (*p*-*C*HMe$_2$), 31.05 (*o*-*C*HMe$_2$), 31.00 (*o*-*C*HMe$_2$), 24.88, 24.77, 24.69, 24.63, 24.51, 24.48. *Anal*. Calc. for C$_{94}$H$_{116}$N$_2$Hf: C, 77.73; H, 8.05; N, 1.93. Found: C, 77.62; H, 8.15; N, 1.87%.

[HIPTN$_2$]Hf(CH$_2$CHMe$_2$)$_2$. This compound was prepared in a manner analogous to that used to prepare [HIPTN$_2$]HfMe$_2$ starting from 1.076 g (0.721 mmol) of [HIPTN$_2$]HfCl$_2$ and 0.62 mL (1.5 mmol) of Me$_2$CHCH$_2$-MgBr (2.4 M in Et$_2$O). Yield: 1.008 g (91%). ^{1}H NMR (C$_6$D$_6$) δ 7.87 (d, 2 BINAP*H*), 7.76 (d, 2 BINAP*H*), 7.39 (s, 4 *o*-*H*), 7.37 (d, 2 BINAP*H*), 7.21 (s, 4 *m*-*H*), 7.20 (s, 4 *m*-*H*), 6.93 (m, 4 BINAP*H*), 6.64 (s, 2 *p*-*H*), 6.43 (t, 2 BINAP*H*), 3.15 (sep, 4 *o*-C*H*Me$_2$), 3.07 (sep, 4 *o*-C*H*Me$_2$), 2.87 (sep, 4 *p*-C*H*Me$_2$), 2.25 (sep, 2 CH$_2$C*H*Me$_2$), 1.33 (d, 6 CH*Me*$_2$), 0.97 (dd, 2 C*H*$_2$CHMe$_2$), 0.85 (dd, 2 C*H*$_2$CHMe$_2$), 0.81 (d, 6 CH$_2$CH*Me*$_2$), 0.63 (d, 6 CH$_2$CH*Me*$_2$). ^{13}C{^{1}H} NMR (CD$_2$Cl$_2$) δ 151.19, 148.42, 147.19, 147.14, 142.31, 138.47, 137.72, 135.22, 132.69, 131.62, 128.45, 127.79, 127.04, 126.06, 125.81, 125.25, 125.12, 120.95, 120.91, 120.27, 98.11 (*C*H$_2$CHMe$_2$), 34.91 (*p*-*C*HMe$_2$), 30.98 (*o*-*C*HMe$_2$), 30.90 (*o*-*C*HMe$_2$), 29.87, 28.98, 28.20, 24.91, 24.81, 24.74, 24.72, 24.51, 24.48. *Anal*. Calc. for C$_{100}$H$_{128}$N$_2$Hf: C, 78.16; H, 8.40; N, 1.82. Found: C, 77.96; H, 8.31; N, 1.75%.

Activation experiments. Activation of [HIPTN$_2$]ZrMe$_2$ and [HIPTN$_2$]Zr(^{13}CH$_3$)$_2$ were conducted as follows. Equimolar amounts of the complex and activator were dissolved in ~0.4 mL of bromobenzene-*d*$_5$. The solutions were cooled to −30 °C, at which point they were mixed and quickly transferred to the J-Young tube. The NMR data of the activated zirconium species are listed below.

{[HIPTN$_2$]Zr(Me)(NMe$_2$Ph)}{B(C$_6$F$_5$)$_4$}. ^{1}H NMR (C$_6$D$_5$Br) δ 8.17 (d, 1 Ar*H*), 7.87 (d, 1 Ar*H*), 7.80 (d, 1 Ar*H*), 7.77 (d, 2 Ar*H*), 7.75 (t, 1 Ar*H*), 7.69 (d, 1 Ar*H*), 7.34 (t, 1 Ar*H*), 7.23 (s, 2 Ar*H*), 7.21 (s, 2 Ar*H*), 7.19 (s, 2 Ar*H*), 7.15 (s, 2 Ar*H*), 7.05–6.85 (m, 7 Ar*H*), 6.77 (s, 2 Ar*H*), 6.68 (t, 1 Ar*H*), 6.62 (m, 4 Ar*H*), 6.43 (t, 1 Ar*H*), 3.01–2.79 (m, 12 C*H*Me$_2$), 2.21 (br s, 3 *Me*$_2$NPh), 1.47 (br s, 3 *Me*$_2$NPh), 1.35–1.12 (m, 72 CH*Me*$_2$), 0.53 (s, 3 *Me*).

{[HIPTN$_2$]Zr(Me)}{B(C$_6$F$_5$)$_4$} (*minor isomer only*). ^{1}H NMR (C$_6$D$_5$Br) d 8.15 (d, 1 Ar*H*), 7.78 (t, 2 Ar*H*), 7.66 (d, 1 Ar*H*), 7.21–6.98 (m, 32 Ar*H*), 6.81 (m, 3 Ar*H*), 6.73 (m, 2 Ar*H*), 2.91 (m, 6 C*H*Me$_2$), 2.81 (m, C*H*Me$_2$), 2.03 (s, 3 Ph$_3$CC*H*$_3$), 1.32–1.12 (m, 72 CH*Me*$_2$), 0.43 (s, 3 *Me*); ^{13}C NMR (C$_6$D$_5$Br) d 49.76 (*Me*, minor isomer, $^1J_{C-H} = 120$ Hz), 47.51 (*Me*, major isomer, $^1J_{C-H} =$ 120 Hz).

[HIPTN$_2$]Hf(C$_6$F$_5$)$_2$. ^{1}H NMR (C$_6$D$_6$) δ 7.68 (d, 2 BINAP*H*), 7.45 (d, 2 BINAP*H*), 7.31 (d, 2 BINAP*H*), 7.16 (s, 4 *o*-*H*), 7.13 (s, 4 *m*-*H*), 7.12 (s, 4*m*-*H*), 7.01 (t, 2 BINAP*H*), 6.85 (d, 2 BINAP*H*), 6.69 (s, 2 *p*-*H*), 6.51 (t, 2 BINAP*H*), 2.94 (m, 8 *o*-C*H*Me$_2$), 2.82 (sep, 4 *p*-C*H*Me$_2$), 1.25 (d, 24 *p*-CH*Me*$_2$), 1.18 (m, 36 *o*-CH*Me*$_2$), 1.06 (d, 12 *o*-CH*Me*$_2$). ^{19}F NMR (C$_6$D$_6$) δ −122.85 (br s, 4 *o*-*F*), −148.33 (br s, 2 *p*-*F*), −159.03 (br s, 4 *m*-*F*).

{[HIPTN$_2$]Hf(Me)(NMe$_2$Ph)}{B(C$_6$F$_5$)$_4$}. ^{1}H NMR (C$_6$D$_5$Br) δ 8.18 (d, 1 Ar*H*), 7.82 (d, 1 Ar*H*), 7.77 (d, 1 Ar*H*), 7.72 (d, 1 Ar*H*), 7.36 (d, 1 Ar*H*), 7.22–7.14 (m, 10 Ar*H*), 7.01 (m, 3 Ar*H*), 6.93 (d, 1 Ar*H*), 6.91 (s, 2 Ar*H*), 6.85 (t, 1 Ar*H*), 6.83 (s, 2 Ar*H*), 6.71 (s, 2 Ar*H*), 6.66 (t, 1 Ar*H*), 6.60 (s, 1 Ar*H*), 6.53 (m, 2 Ar*H*), 6.36 (t, 1 Ar*H*), 2.93 (m, 6 C*H*Me$_2$), 2.79 (m, 6 C*H*Me$_2$), 2.21 (br s, 3 *Me*$_2$NPh), 1.46 (br s, 3 *Me*$_2$NPh), 1.34–1.10 (m, 72 CH*Me*$_2$), 0.49 (s, 3 *Me*).

{[HIPTN$_2$]Hf(Me)}{B(C$_6$F$_5$)$_4$} (*major isomer only*). ^{1}H NMR (C$_6$D$_5$Br) δ 7.97 (br s, 1 Ar*H*), 7.67 (t, 1 Ar*H*), 7.56 (br d, 1 Ar*H*), 7.31 (t, 2 Ar*H*), 7.18–7.05 (m, 30 Ar*H*), 7.01 (s, 1 Ar*H*) 6.80 (br d, 1 Ar*H*), 6.74 (s, 2 Ar*H*), 6.62 (m, 2 Ar*H*), 2.92 (m, 6 C*H*Me$_2$), 2.78 (m, 6 C*H*Me$_2$), 2.03 (s, 3 Ph$_3$CC*H*$_3$), 1.31–1.11 (m, 72 CH*Me*$_2$), 0.66 (s, 3 *Me*).

Acknowledgments

R.R.S. thanks the Department of Energy (DE-FG02-86ER13564) for research support and Z.J.T. thanks the National Science Foundation for a predoctoral fellowship. We thank W.W. Weare for assistance with synthetic details.

References

[1] V.C. Gibson, S.K. Spitzmesser, Chem. Rev. 103 (2003) 283.
[2] G.W. Coates, P.D. Hustad, S. Reinartz, Angew. Chem., Int. Ed. 41 (2002) 2236.
[3] R. Kempe, Angew. Chem., Int. Ed. 39 (2000) 468.
[4] M. Aizenberg, L. Turculet, W.M. Davis, F. Schattenmann, R.R. Schrock, Organometallics 17 (1998) 4795.
[5] R. Baumann, W.M. Davis, R.R. Schrock, J. Am. Chem. Soc. 119 (1997) 3830.
[6] M.A. Flores, M. Manzoni, R. Baumann, W.M. Davis, R.R. Schrock, Organometallics 18 (1999) 3220.
[7] L.-C. Liang, R.R. Schrock, W.M. Davis, J. Am. Chem. Soc. 120 (1999) 5797.
[8] P. Mehrkhodavandi, R.R. Schrock, P.J.J. Bonitatebus, Organometallics 21 (2002) 5785.
[9] R.R. Schrock, R. Baumann, S.M. Reid, J.T. Goodman, R. Stumpf, W.M. Davis, Organometallics 18 (1999) 3649.
[10] P. Mehrkhodavandi, L.L. Pryor, R.R. Schrock, Organometallics 22 (2003) 4569.
[11] R.R. Schrock, P.J. Bonitatebus Jr., Y. Schrodi, Organometallics 20 (2001) 1056.
[12] R. Baumann, R.R. Schrock, J. Organomet. Chem. 557 (1998) 69.
[13] G.W. Coates, J. Chem. Soc., Dalton Trans. (2002) 467.
[14] Z.J. Tonzetich, R.R. Schrock, A.S. Hock, P. Müller, Organometallics 24 (2005) 3335.
[15] J.D. Scollard, D.H. McConville, J.J. Vittal, Organometallics 14 (1995) 5478.
[16] J.D. Scollard, D.H. McConville, J. Am. Chem. Soc. 118 (1996) 10008.
[17] D. Yandulov, R.R. Schrock, J. Am. Chem. Soc. 124 (2002) 6252.
[18] D.V. Yandulov, R.R. Schrock, A.L. Rheingold, C. Ceccarelli, W.M. Davis, Inorg. Chem. 125 (2003) 796.
[19] D.V. Yandulov, R.R. Schrock, Science 301 (2003) 76.
[20] V. Ritleng, D.V. Yandulov, W.W. Weare, R.R. Schrock, A.R. Hock, W.M. Davis, J. Am. Chem. Soc. 126 (2004) 6150.
[21] D.V. Yandulov, R.R. Schrock, Inorg. Chem. 44 (2005) 1103.
[22] X. Huang, K.W. Anderson, D. Zim, L. Jiang, A. Klapars, S.L. Buchwald, J. Am. Chem. Soc. 125 (2003) 6653.
[23] L.-C. Liang, R.R. Schrock, W.M. Davis, Organometallics 19 (2000) 2526.
[24] T. Wondimagegn, Z. Xu, K. Vanka, T. Ziegler, Organometallics 23 (2004) 3847.
[25] J.D. Scollard, D.H. McConville, S.J. Rettig, Organometallics 16 (1997) 1810.
[26] F. Guerin, J.C. Stewart, C. Beddie, D.W. Stephan, Organometallics 19 (2000) 2994.
[27] P. Mehrkhodavandi, P.J. Bonitatebus Jr., R.R. Schrock, J. Am. Chem. Soc. 122 (2000) 7841.
[28] R.R. Schrock, A.L. Casado, J.T. Goodman, L.-C. Liang, P.J. Bonitatebus Jr., W.M. Davis, Organometallics 19 (2000) 5325.
[29] C.R. Landis, K.A. Rosaaen, J. Uddin, J. Am. Chem. Soc. 124 (2002) 12062.
[30] C.R. Landis, K.A. Rosaaen, D.R. Sillars, J. Am. Chem. Soc. 125 (2003) 1710.
[31] Z. Liu, E. Somsook, C.B. White, K.A. Rosaaen, C.R. Landis, J. Am. Chem. Soc. 123 (2001) 11193.
[32] G.M. Diamond, R.F. Jordan, J.L. Petersen, Organometallics 15 (1996) 4030.

Available online at www.sciencedirect.com
SCIENCE DIRECT®
Polyhedron 25 (2006) 477–483
POLYHEDRON
www.elsevier.com/locate/poly

New terphenylphenoxides of group 13 and 14 elements

Corneliu Stanciu, Anne F. Richards, Matthias Stender, Marilyn M. Olmstead, Philip P. Power *

Department of Chemistry, University of California, Davis, One Shields Avenue, Davis, CA 95616, USA

Received 26 May 2005; accepted 7 July 2005
Available online 26 September 2005

Dedicated to Professor Malcolm Chisholm on the occasion of his 60th birthday.

Abstract

The reaction of the sterically hindered terphenol Ar*OH (Ar* = C_6H_3-2,6(C_6H_2-2,4,6-Pr^i_3)$_2$) with trimethylaluminum or trimethylgallium in ether led to the isolation of the corresponding ether-coordinated monophenoxide species Ar*OM(CH_3)$_2$(Et_2O) (M = Al (**1**) or Ga (**2**)). The reaction of the lithium salt of the related bulky terphenol Ar′OH (Ar′ = C_6H_3-2,6(C_6H_3-2,6-Pr^i_3)$_2$) with the divalent species MCl_2 (M = Ge, Sn) afforded the novel germanium (II) and tin (II) mono- and bisphenoxides [{Ar′OGeCl}(dioxane)] · toluene (3 · toluene), Ge(OAr′)$_2$ (**4**) and Sn(OAr′)$_2$ (**5**). The compounds were characterized by ^{1}H, ^{13}C and ^{119}Sn NMR (**5**) spectroscopy, and by IR spectroscopy and X-ray crystallography.
© 2005 Elsevier Ltd. All rights reserved.

Keywords: Terphenyl; Aryloxide; Steric effects

1. Introduction

Previous work by us has shown that the very bulky phenols Ar*OH (Ar* = C_6H_3-2,6(C_6H_2-2,4,6-Pr^i_3)$_2$) and Ar′OH (Ar′ = C_6H_3-2,6(C_6H_3-2,6-Pr^i_2)$_2$) and some of their alkali metal salts could be synthesized and characterized by simple routes [1]. Although their oxygen atoms carry only one substituent, aryloxide ligands can be good protecting groups if the aryl substituent is very large. Thus, bulky aryloxides have been used as substituents on a wide variety of metallic centers [2,3], for the stabilization of low coordinate compounds [4], persistent odd-electron species [5] or heavier main group compounds with multiple bonds [6]. Very bulky aryloxide complexes of aluminum or gallium are an attractive target for synthesis in view of their potential applications in catalysis [7] or for isolation of new low valent, low coordinate species. In addition, despite the fact that aryloxide derivatives are well known for the majority of main group and transition metals [2], for germanium (II) and tin (II) they are rather uncommon. The first examples (M(OAr)$_2$, Ar = 2,6-Bu^t_2-4-MeC_6H_2, M = Ge or Sn) were reported by Lappert et al. [4] and some recent germanium derivatives have been reported by Rothwell et al. [8,9]; for example (*R*,*R*)-[Ge{$OC_{20}H_{10}$($OSiMe_3$)-2′-($SiMe_3$)$_2$-3,3′}$_2$], (*R*)-[Ge{$O_2C_{20}H_{10}$($SiMe_2Ph$)$_2$-3,3′}{NH_3}], or [Ge(OAr)$_2$]$_n$, where (n = 2, ArO = $OC_6H_2Me_3$-2,4,6; $OC_6H_3Pr^i_2$-2,6; n = 1, ArO = $OC_6H_3Ph_2$-2,6; OC_6HPh_4-2,3,5,6), and by Barrau et al. [10,11] (M(OAr)$_2$, Ar = 2,4,6-[$(CH_3)_2NCH_2$]$_3C_6H_2$, M = Ge, Sn and M($OCH_2CH_2NMe_2$)$_2$). However, structural data remain scarce and no ^{119}Sn spectroscopic data for a tin (II) aryloxide or alkoxide complex, in which the tin is unambiguously two coordinate, have been reported. We now describe the synthesis and characterization of some new group 13 and 14 mono and

* Corresponding author. Tel.: +1 520 752 6913/530 752 6435; fax: +1 530 752 8995/530 752 9463.
E-mail address: pppower@ucdavis.edu (P.P. Power).

0277-5387/$ - see front matter © 2005 Elsevier Ltd. All rights reserved.
doi:10.1016/j.poly.2005.07.025

bisterphenoxides as potentially important species for further low valent chemistry involving both homo and hetero main group or transition metal derivatives.

2. Results and discussion

2.1. Synthesis and spectroscopy

The aluminum and gallium derivatives **1** and **2** were synthesized by direct reaction of the bulky phenol Ar*OH [1] with 1.0 M ethereal solutions of trimethylaluminum and trimethylgallium, at room temperature, according to the reaction

$$Ar^*OH + M(CH_3)_3 \xrightarrow[RT]{Et_2O} Ar^*OM(CH_3)_2(Et_2O) + CH_4$$

$$M = Al(\mathbf{1}) \text{ and } Ga(\mathbf{2})$$

This method was chosen because of the commercial availability of the metal alkyls, the high solubility of the terphenylphenol in ether solvents and because X-ray quality crystals of **1** and **2** could be grown from ether solvents. Numerous attempts were made to grow crystals of unsolvated complexes from reaction mixtures in non-coordinating solvents, such as hexane, benzene or toluene. Changing the solvent or the temperature at which crystal growth was attempted (−78, −30, 5 °C, and RT) did not produce the desired result. In the absence of a coordinating solvent (i.e., Et_2O) only microcrystalline material was formed.

The reaction route employed the for synthesis of group 14 derivatives consisted of the treatment of lithium terphenoxide Ar′OLi and the divalent tin or germanium chlorides, as described below

$$2Ar'OLi + MCl_2 \xrightarrow[RT]{Et_2O} M(OAr')_2 + 2LiCl$$

$$M = Ge(\mathbf{4}) \text{ and } Sn(\mathbf{5})$$

In the case of germanium, the monoterphenoxide could also be isolated, in the form of the 1,4-dioxane solvate **3**, if a 1:1 ratio of reagents was used. Despite numerous efforts to prepare an analogous tin monoterphenoxide, we were unable to isolate a pure sample of such a compound. Likewise, efforts to synthesize the mono and bisphenoxide derivatives of lead (II) were unsuccessful. The synthesis of the latter species was attempted in many ways: by reaction of lithium phenoxide with lead (II) chloride, bromide or iodide, or by direct reaction of lead (II) bis(*N*,*N*-diisopropyl)amide with phenols. One possible explanation for the failure of these reactions could be the pronounced difference in hard/soft character between the phenoxide moiety and lead (II). In all cases the starting material used (i.e., Ar*OH or Ar′OLi) was recovered unchanged, which suggested a difference in chemical behavior of the reacting species rather than occurrence of side-reactions.

Table 1
^{1}H and ^{13}C NMR chemical shifts for the $M(CH_3)_2$ group in compounds **1** and **2**

–$M(CH_3)_2$	^{1}H NMR (ppm)	^{13}C NMR (ppm)
1, M = Al	−1.07	−9.28
2, M = Ga	−0.61	−4.65

Crystals of **3**–**5** were obtained readily from toluene solutions. The products **1**–**5** were investigated by ^{1}H and ^{13}C NMR spectroscopy, as well as by ^{119}Sn NMR spectroscopy in the case of **5**. The ^{1}H and ^{13}C NMR chemical shifts followed the expected patterns in terphenyl derivatives. For **1** and **2**, the shift values for the $M(CH_3)_2$ moiety (M = Al, Ga) are listed in Table 1.

These shifts are in agreement with the different electronegativities of the two metals, Al (EN = 1.613) being less electronegative than Ga (EN = 1.756) [12].

For **5**, the ^{119}Sn NMR spectroscopy afforded a signal that had a chemical shift of −289.7 ppm (in C_6D_6). The only other comparative literature value was reported by Barrau and coworkers [10,11] for the tin bisphenoxide $Sn[OC_6H_2\text{-}2,4,6(CH_2NMe_2)_3]_2$ which displayed a ^{119}Sn NMR signal well upfield at −529.8 ppm. The shift value for **5** is much further upfield than those found in other two coordinate tin (II) compounds. For example: 2272 ppm in $Sn[CH(SiMe_3)_2]_2$ [13], 2208 ppm in $Sn(C_6H_2\text{-}2,4,6\text{-}Pr^i_3)\{C_6H_2\text{-}2,4,6\text{-}[CH(SiMe_3)_2]_3\}$ [14], 1197 ppm in $Sn(Ar^*)[N(SiMe_3)_2]$ [15], 980 ppm in $SnMes^*_2$ [16], 776 ppm in $Sn[N(SiMe_3)_2]_2$ [17] or 723 ppm in $Sn[C_6H_2\text{-}2,4,6\text{-}(CF_3)_3]_2$ [18]. In fact, the trend found in these divalent species is opposite to that expected on the basis of σ-inductive effects. The unexpected trend in these shifts have been explained on the basis of the mixing of a low lying paramagnetic excited state which causes deshielding of the ^{119}Sn nucleus [19]. This mixing occurs to the greatest extent when electron releasing substituents are used which afford a small singlet–triplet gap and strongly deshield the tin environment. With electronegative amide or aryloxide substituents this gap becomes much larger and upfield shifts are observed as a result. The particularly large upfield shift of Barrau's compound may be a result of an increase in the effective coordination number at tin due to complexation of the tin by pendant CH_2NMe_2 groups. The upfield shift of **5** in which tin is two coordinate is surprising since the value is in the range of a tetracoordinated [20,21] rather than a dicoordinated tin compound.

3. Structures

The main feature of compounds **1**–**5** is that they all are monomers in solid state. Selected structural data for **1**–**5** are provided in Table 2 (see Fig. 1).

The structures of **1** and **2** display distorted tetrahedral metal coordination in which the metal is bound to two

Table 2
Selected bond distances (Å) and angles (°) for compounds **1**–**5**

Compound **1**		Compound **2**		Compound **3**	
Al(1)–O(1)	1.7547(17)	Ga(1)–O(1)	1.8618(12)	Ge(1)–O(1)	1.830(2)
Al(1)–O(2)	1.9208(19)	Ga(1)–C(38)	1.966(2)	Ge(1)–O(2)	2.214(2)
Al(1)–C(37)	1.951(3)	Ga(1)–C(37)	1.965(2)	Ge(1)–Cl(1)	2.2752(10)
Al(1)–C(38)	1.959(3)	Ga(1)–O(2)	2.082(14)	O(1)–C(1)	1.367(3)
O(1)–C(1)	1.351(3)	O(1)–C(1)	1.353(2)	O(1)–Ge(1)–O(2)	84.75(9)
O(2)–C(41)	1.456(3)	O(1)–Ga(1)–C(38)	110.27(7)	O(1)–Ge(1)–Cl(1)	93.80(8)
O(2)–C(39)	1.459(3)	O(1)–Ga(1)–C(38)	113.81(7)	O(2)–Ge(1)–Cl(1)	88.34(7)
O(1)–Al(1)–O(2)	95.83(8)	C(38)–Ga(1)–C(38)	128.97(8)	C(1)–O(1)–Ge(1)	134.06(18)
O(1)–Al(1)–C(37)	118.48(11)	O(1)–Ga(1)–O(2)	92.56(10)	O(1)–C(1)–C(6)	122.0(2)
O(2)–Al(1)–C(37)	102.62(10)	C(38)–Ga(1)–O(2)	104.08(14)	O(1)–C(1)–C(2)	116.8(2)
O(1)–Al(1)–C(38)	111.28(11)	C(37)–Ga(1)–O(2)	98.41(13)		
O(2)–Al(1)–C(38)	105.17(11)	C(1)–O(1)–Ga(1)	122.12(17)		
C(37)–Al(1)–C(38)	119.00(13)	O(1)–C(1)–C(2)	119.4(1)		
C(1)–O(1)–Al(1)	134.46(15)	O(1)–C(1)–C(6)	120.5(1)		
C(41)–O(2)–C(39)	114.94(19)				
Compound 4		**Compound 5**			
Ge(1)–O(2)	1.8245(13)	Sn(1)–O(1)	2.0450(16)		
Ge(1)–O(1)	1.8296(14)	Sn(1)–O(2)	2.0493(16)		
O(1)–C(1)	1.376(2)	O(1)–C(1)	1.359(3)		
O(2)–C(31)	1.380(2)	O(2)–C(31)	1.361(3)		
O(2)–Ge(1)–O(1)	92.54(6)	O(1)–Sn(1)–O(2)	92.18(6)		
C(1)–O(1)–Ge(1)	131.25(12)	C(1)–O(1)–Sn(1)	127.93(14)		
C(31)–O(2)–Ge(1)	124.81(12)	C(31)–O(2)–Sn(1)	130.57(14)		
O(1)–C(1)–C(2)	117.77(17)	O(1)–C(1)–C(2)	122.2(2)		
O(1)–C(1)–C(6)	122.16(18)	O(1)–C(1)–C(6)	118.4(2)		

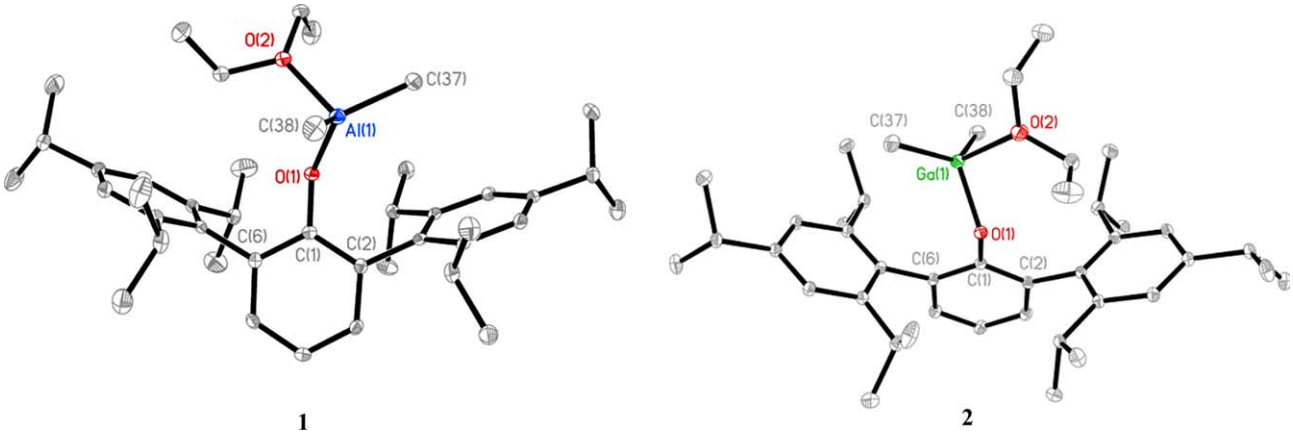

Fig. 1. Thermal ellipsoid (30%) drawings for compounds **1** and **2**. H atoms are not shown.

oxygens and two carbons. There are significant differences between the aluminum and gallium environments and between the alkoxide ligand parameters in each complex. For example: the C(1)–O(1)–Al(1) and C(1)–O(1)–Ga(1) angles are 134.46(15)° and 122.12(17)°, respectively, and the Al–O(1) bond (1.755(2) Å) involving terphenoxide is ca 0.1 Å shorter than the Ga–O(1) bond (1.861(2) Å). This is due to the greater electropositive character of aluminum in comparison to gallium, which causes a larger ionic component in the Al–O bond which shortens it and increases steric congestion [22]. Consequently, the C(1)–O(1)–Al(1) angle widens to decrease steric strain. The M–OAr distances in **1** and **2** are ca. 0.05 Å longer than those in the compounds $Me_2MOC_6H_2$-2, 6-Bu^t_2-4-Me owing to the higher coordination number of the metals as a result of ether coordination. Also, the Ga–O(2) bond involving diethyl ether is ca. 0.16 Å longer than the corresponding Al–O(2) bond, which is consistent with the higher electronegativity and lower Lewis acidity of Ga in comparison to Al. The differences between the M–C bond lengths are much less (Al–C = 1.955(4) Å, Ga–C = 1.971(3) Å), probably because the ionic character of these bonds is lower.

Molecule **3** is, to the best of our knowledge, the first example of a fully characterized aryloxygermanium (II) chloride species. The structure involves the complexation

of two Ar′OGeCl units to each oxygen of a 1,4-dioxane molecule (see Fig. 2).

The Ge(1)–O(1) distance is 1.830(2) Å, which is shorter than the sum of the covalent radii, but it is in the range for other germanium (II) phenoxides reported in the literature [4,23]. The Ge(1)–Cl(1) distance of 2.2752(10) Å is also consistent with distances found in other Ge(II)–Cl structures and are in the normal range and approximately equal to the sum of their respective covalent radii [24–26], with correction for ionic effects [27,28]. Other distances in molecule fall within the expected range for the terphenyl derivatives. The germanium has a pyramidal geometry, with bond angles of O(1)–Ge(1)–O(2), O(1)–Ge(1)–Cl(1) and O(2)–Ge(1)–Cl(1) of 84.75(9)°, 93.80(8)°, and 88.34(7)°, respectively. Attempts to synthesize a tin analogue of **3** were unsuccessful.

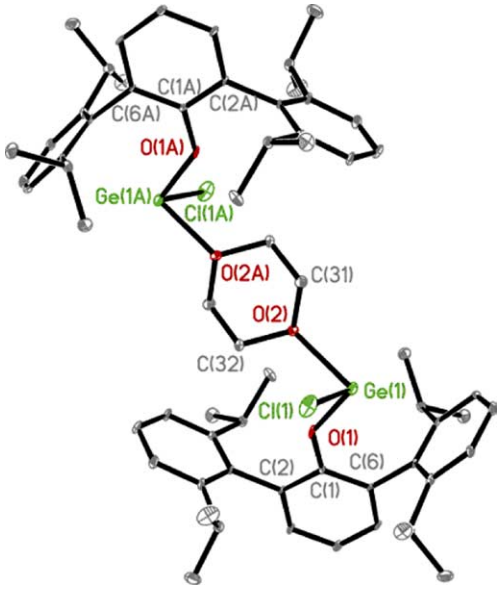

Fig. 2. Thermal ellipsoid (30%) diagram of Ar′OGeCl complex with 1,4-dioxane, **3**. H atoms and toluene solvate are not shown.

The homoleptic bis aryloxide carbene-like species **4** and **5** were readily obtained by reaction of two equivalents of terphenylphenoxide Ar′OLi and MCl_2 (M = Ge, Sn) in ether (see Fig. 3).

After extraction in toluene (in later experiments hexane also proved to be a good solvent) and storage in a ca. 5 °C refrigerator for 2 days, large, colorless blocks of **4** or **5** were obtained. The crystallographic studies revealed that the two molecules are isostructural, and that they display a V-shaped geometry with angles of O(2)–Ge(1)–O(1) and O(1)–Sn(1)–O(2) of 92.54(6)° and 92.18(6)°, respectively. This feature is somewhat different from similar examples reported in the literature [4], where O–Ge–O angle was larger than the O–Sn–O angle (i.e., 92.0(4)° and 88.8(2)° in $M(OC_6H_2Me\text{-}4\text{-}Bu^t_2\text{-}2,6)_2$ for M = Ge or M = Sn, respectively). However, this difference can be attributable to a larger steric bulk of the ligands employed in our case, which can result in an increase of the angle at tin, making it very similar to the germanium analog. The Ge–O (1.8296(14) Å) and Sn–O (2.0450(16) Å) distances are slightly shorter than expected from the sum of the radii of Ge or Sn and O because of the ionic character of the Ge–O and Sn–O bonds, but fall in the range of other similar carbene-like species reported previously [4] i.e., 1.802(8) and 1.812(7) Å for M = Ge and 1.995(4) and 2.022(4) Å for M = Sn in $M(OC_6H_2Me\text{-}4\text{-}Bu^t_2\text{-}2,6)_2$. The colorless nature of **4** and **5** is noteworthy and shows that the n → p chromophore has been shifted into the UV region of the spectrum in comparison to more highly colored alkyl, aryl, and amide analogues. In other

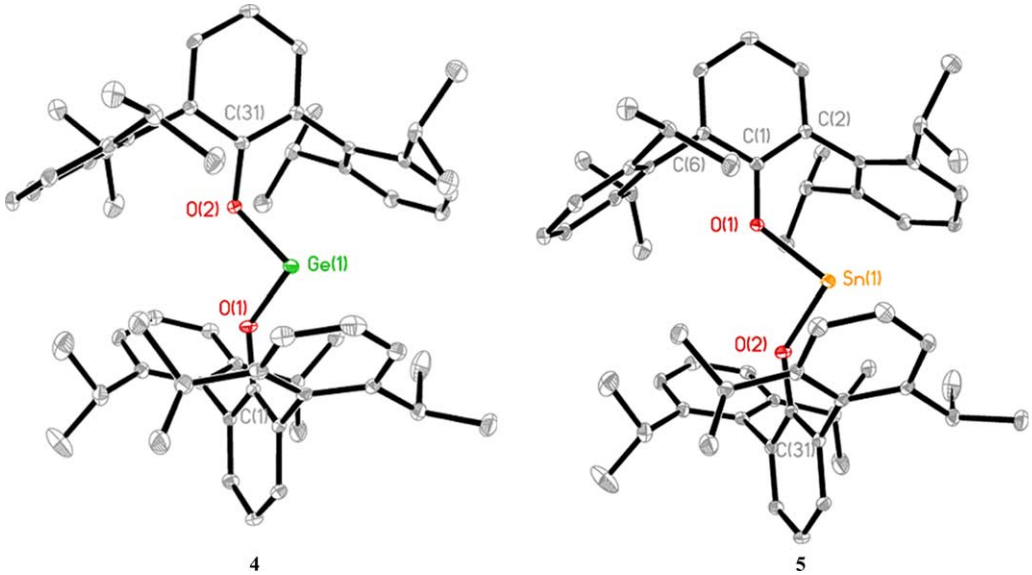

Fig. 3. Thermal ellipsoid (30%) drawings of molecules **4** and **5**. H atoms are not shown.

words the energy difference between n and p levels has been increased by the more electronegative oxygen substituents which lowers the energy of the metal lone pair. The increase in the n → p energy difference is consistent with the arguments made earlier for the ^{119}Sn NMR shifts.

4. Conclusion

The present study resulted in the synthesis and full structural characterization of new aluminum and gallium bulky monophenoxides as well as new bis-terphenylphenoxides of Sn(II) and Ge(II). A new aryloxygermanium (II) chloride was synthesized and its structure determined to be an unusual 2:1 complex with 1,4-dioxane. The yields were good in all cases, ranging from 78% to 93%, making these syntheses a very efficient and useful synthetic pathway for the title compounds.

5. Experimental

5.1. General procedures

All manipulations were carried out by using modified Schlenk techniques under an atmosphere of N_2 or Ar or in Vacuum Atmospheres HE-43 or NEXUS dryboxes. All solvents were distilled from molten Na/K alloy and degassed twice prior to use. $AlMe_3$ and $GaMe_3$ were used as 1.0 M solutions in diethyl ether, accurately prepared from pure $AlMe_3$ and $GaMe_3$. Ar*OH and Ar′OLi were prepared as described previously [1]. The ^{1}H and ^{13}C NMR spectra were recorded on a Varian 300 or 400 MHz spectrometer and referenced to known standards. Melting points were recorded in glass capillaries under N_2 and are uncorrected. Infrared spectra were recorded as Nujol mulls between CsI plates on a Perkin–Elmer 1430 spectrometer.

5.2. Ar*OAl(CH$_3$)$_2$(Et$_2$O) (1)

Ar*OH (0.5 g, 1 mmol) was dissolved in diethyl ether (30 mL) and 1 mL of a 1.0 M ethereal solution of $AlMe_3$ was added dropwise, at room temperature, via syringe, with rapid stirring. Immediate gas evolution was observed. The resulting mixture was stirred for an additional hour whereupon the solvent was pumped off and toluene (ca. 10 mL) was added to the remaining pale yellow residue. The clear solution obtained was concentrated to about 5 mL and placed in a −20 °C freezer. No crystals were formed after 3 days so about 0.1 mL ether was added to the solution and the flask was left in the freezer overnight, to afford **1** as large colorless crystals. These proved suitable for X-ray crystallographic studies. Yield: 0.585 g, 93%, m.p. 133–134 °C. ^{1}H NMR (300 MHz, C_6D_6, 25 °C): $\delta = -1.07$ [s, 6H, $AlMe_2$], 0.54 [t, $^3J_{H-H} = 6.9$ Hz, 6H, ether CH_3], 1.17 [d, $^3J_{H-H} = 6.6$ Hz, 12H, *o*-CH(CH$_3$)$_2$], 1.27 [d, $^3J_{H-H} = 6.9$ Hz, 12H, *o*-CH(CH$_3$)$_2$], 1.38 [d, $^3J_{H-H} = 6.3$ Hz, 12H, *p*-CH(CH$_3$)$_2$], 2.84 [sept, $^3J_{H-H} = 6.9$ Hz, 2H, *p*-C*H*(CH$_3$)$_2$], 2.94 [q, $^3J_{H-H} = 7.2$ Hz, 4H, ether CH_2], 3.15 [sept, $^3J_{H-H} = 6.8$ Hz, 4H, *o*-C*H*(CH$_3$)$_2$], 6.88 [t, $^3J_{H-H} = 7.4$ Hz, 1H, *p*-C_6H_3], 7.16 [s, 4H, *m*-Trip], 7.18 [d, $^3J_{H-H} = 7.4$ Hz, 2H, *m*-C_6H_3] ppm. ^{13}C NMR (300 MHz, C_6D_6, 25 °C): $\delta = -9.28$ [$AlMe_2$], 13.25 [ether CH_3], 23.68 [*o*-$CHMe_2$], 24.39 [*o*′-$CHMe_2$], 25.85 [*p*-$CHMe_2$], 30.72 [*o*-*C*HMe_2], 34.74 [*p*-$CHMe_2$], 64.96 [ether CH_2], 117.30 [*o*-C_6H_3], 120.70 [*m*-C_6H_3], 130.82 [*p*-C_6H_3], 131.52 [*p*-Trip], 136.83 [*i*-Trip], 147.59 [*o*-Trip], 147.76 [*m*-Trip], 155.60 [*i*-C_6H_3] ppm. IR (Nujol): $\nu = 680$–720 cm^{-1} (Al–O, broad).

5.3. Ar*OGa(CH$_3$)$_2$(Et$_2$O) (2)

The same procedure as that described for **1** was employed in the reaction of Ar*OH (0.5 g, 1 mmol) with 1 mL of a 1.0 M ethereal solution of $GaMe_3$ at room temperature. Gas evolution was also observed during the reaction. After a similar work up procedure as that described for **1**, the resulting ethereal reaction mixture was left in the freezer for 3 days to afford large colorless crystals of **2** that were suitable for crystallographic studies. Yield: 0.613 g, 91%, m.p. 92–94 °C. ^{1}H NMR (300 MHz, C_6D_6, 25 °C): $\delta = -0.61$ [s, 6H, $GaMe_2$], 0.66 [t, $^3J_{H-H} = 6.9$ Hz, 6H, ether CH_3], 1.17 [d, $^3J_{H-H} = 7.2$ Hz, 12H, *o*-CH(CH$_3$)$_2$], 1.25 [d, $^3J_{H-H} = 6.3$ Hz, 12H, *o*-CH(CH$_3$)$_2$], 1.37 [d, $^3J_{H-H} = 6.9$ Hz, 12H, *p*-CH(CH$_3$)$_2$], 2.82 [sept, $^3J_{H-H} = 6.9$ Hz, 2H, *p*-C*H*(CH$_3$)$_2$], 2.93 [q, $^3J_{H-H} = 6.7$ Hz, 4H, ether CH_2], 3.19 [sept, $^3J_{H-H} = 6.7$ Hz, 4H, *o*-C*H*(CH$_3$)$_2$], 6.87 [t, $^3J_{H-H} = 7.2$ Hz, 1H, *p*-C_6H_3], 7.16 [s, 4H, *m*-Trip], 7.21 [d, $^3J_{H-H} = 7.5$ Hz, 2H, *m*-C_6H_3] ppm. ^{13}C NMR (300 MHz, C_6D_6, 25 °C): $\delta = -4.65$ [$GaMe_2$], 14.53 [ether CH_3], 24.12 [*o*-$CHMe_2$], 24.75 [*o*′-$CHMe_2$], 26.49 [*p*-$CHMe_2$], 31.14 [*o*-*C*HMe_2], 35.12 [*p*-$CHMe_2$], 64.54 [ether CH_2], 117.08 [*o*-C_6H_3], 121.09 [*m*-C_6H_3], 131.31 [*p*-C_6H_3], 131.55 [*p*-Trip], 136.70 [*i*-Trip], 147.92 [*o*-Trip], 148.31 [*m*-Trip], 159.21 [*i*-C_6H_3] ppm. IR (Nujol): $\nu = 530$–580 cm^{-1} (Ga–O, broad).

5.4. Ar′OGeCl(0.5dioxane) (3)

A solution of 0.21 g (0.5 mmol) LiOAr′ in 20 mL diethyl ether was added via cannula, with rapid stirring, to a suspension of 0.115 g (0.5 mmol) $GeCl_2 \cdot$ dioxane in ca. 20 mL diethyl ether. The reaction mixture was stirred at room temperature overnight. The solvent was pumped off and the pale yellow solid residue was extracted in ca. 30 mL toluene. The solution was filtered through a Celite pad and concentrated to about 5 mL. After being stored in a −20 °C freezer overnight, large,

colorless crystals of **3** were formed, which were analyzed by X-ray crystallographic methods. Yield: 0.235 g, 83%, m.p. 175–180 °C. ^{1}H NMR (300 MHz, C_6D_6, 25 °C): $\delta = 1.03$ [d, $^3J_{H-H} = 6$ Hz, 12H, *o*-CH(CH$_3$)$_2$], 1.08 [d, $^3J_{H-H} = 6$ Hz, 12H, *o′*-CH(CH$_3$)$_2$], 2.82 [sept, $^3J_{H-H} = 6.7$ Hz, 4H, *o*-C*H*(CH$_3$)$_2$], 4.31 [s, 8H, dioxane CH$_2$], 6.78 [t, $^3J_{H-H} = 7.3$ Hz, 1H, *p*-C$_6$H$_3$], 6.91 [d, $^3J_{H-H} = 7.5$ Hz, 2H, *m*-C$_6$H$_3$], 7.06 [d, $^3J_{H-H} = 6.8$ Hz, 4H, *m*-Dipp], 7.18 [t, $^3J_{H-H} = 6.8$ Hz, 2H, *p*-Dipp] ppm. ^{13}C NMR (300 MHz, C_6D_6, 25 °C): $\delta = 23.89$ [*o*-CHMe$_2$], 24.03 [*o*-CHMe$_2$], 30.72 [*o*-*C*HMe$_2$], 66.70 (dioxane), 120.07 [*p*-C$_6$H$_3$], 123.04 [*m*-Dipp], 126.73 [*p*-Dipp], 128.81 [*m*-C$_6$H$_3$], 129.99 [*i*-Dipp], 133.64 [*o*-Dipp], 147.84 [*o*-C$_6$H$_3$], 150.91 [*i*-C$_6$H$_3$] ppm.

5.5. Ge(OAr′)$_2$ (4)

LiOAr′ 0.84 g (2 mmol) was dissolved in ca. 50 mL diethyl ether and this solution was added via cannula, with rapid stirring at room temperature, to a suspension of 0.23 g (1 mmol) of $GeCl_2 \cdot$ dioxane in 30 mL ether. The resulting reaction mixture was stirred overnight. The solvent was pumped off and toluene (ca. 30 mL) was added to the pale yellow solid residue. After filtration through a Celite pad, the volume of the solution was reduced by half and the flask was stored in a −5 °C fridge for 2 days. Large, colorless crystals of **4** were obtained which were suitable for X-ray analysis. Yield: 0.7 g, 78%, m.p. 190–195 °C (becomes red). ^{1}H NMR (400 MHz, C_6D_6, 25 °C): $\delta = 0.95$ [d, $^3J_{H-H} = 6.8$ Hz, 12H, *o*-CH(CH$_3$)$_2$], 0.99 [d, $^3J_{H-H} = 6.8$ Hz, 12H, *o′*-CH(CH$_3$)$_2$], 2.73 [sept, $^3J_{H-H} = 6.8$ Hz, 4H, *o*-C*H*(CH$_3$)$_2$], 6.73 [t, $^3J_{H-H} = 6.9$ Hz, 1H, *p*-C$_6$H$_3$], 6.90 [d, $^3J_{H-H} = 7.6$ Hz, 2H, *m*-C$_6$H$_3$], 7.04 [d, $^3J_{H-H} = 7.6$ Hz, 4H, *m*-Dipp], 7.19 [t, $^3J_{H-H} = 7.2$ Hz, 2H, *p*-Dipp] ppm. ^{13}C NMR (400 MHz, C_6D_6, 25 °C): $\delta = 24.70$ [*o*-CHMe$_2$], 24.79 [*o*-CHMe$_2$], 30.99 [*o*-*C*HMe$_2$], 119.99 [*p*-C$_6$H$_3$], 123.77 [*m*-Dipp], 128.65 [*i*-Dipp], 128.76 [*p*-Dipp], 131.10 [*m*-C$_6$H$_3$], 140.92 [*o*-C$_6$H$_3$], 146.70 [*o*-Dipp], 153.89 [*i*-C$_6$H$_3$] ppm.

5.6. Sn(OAr′)$_2$ (5)

In a similar manner to that described for **4**, an ethereal solution of 0.84 g (2 mmol) LiOAr′ was added to a suspension of 0.19 g (1 mmol) $SnCl_2$ via cannula, at room temperature. The reaction mixture was stirred overnight and the solvent was then removed under reduced pressure. The remaining dark yellow viscous residue was extracted with 30 mL toluene, filtered through Celite, concentrated to about 5 mL and stored in freezer for 3d to yield colorless crystals suitable for X-ray analysis. Yield: 0.8 g, 85%, m.p. 234–236 °C. ^{1}H NMR (400 MHz, C_6D_6, 25 °C): $\delta = 0.99$ [d, $^3J_{H-H} = 7.2$ Hz, 12H, *o*-CH(CH$_3$)$_2$], 1.01 [d, $^3J_{H-H} = 6.8$ Hz, 12H, *o*-CH(CH$_3$)$_2$], 2.82 [sept, $^3J_{H-H} = 6.8$ Hz, 4H, *o*-C*H*(CH$_3$)$_2$], 6.71 [t, $^3J_{H-H} = 7.6$ Hz, 1H, *p*-C$_6$H$_3$], 6.81 [t, $^3J_{H-H} = 7.6$ Hz, 2H, *p*-Dipp], 6.96 [d, $^3J_{H-H} = 7.2$ Hz, 4H, *m*-Dipp], 7.08 [d, $^3J_{H-H} = 7.6$ Hz, 2H, *m*-C$_6$H$_3$] ppm. ^{13}C NMR (400 MHz, C_6D_6, 25 °C): $\delta = 23.79$ [*o*-CHMe$_2$], 24.95 [*o*-CHMe$_2$], 30.92 [*o*-*C*HMe$_2$], 122.89 [*p*-C$_6$H$_3$], 124.39 [*m*-Dipp], 128.98 [*p*-Dipp], 130.31 [*m*-C$_6$H$_3$], 130.83 [*i*-Dipp], 139.02 [*o*-C$_6$H$_3$], 146.89 [*o*-Dipp], 158.57 [*i*-C$_6$H$_3$] ppm. ^{119}Sn NMR: −289.68 ppm.

Table 3
Selected crystallographic and refinement data for compounds **1**–**5**

	1	**2**	**3**	**4**	**5**
Formula	$C_{42}H_{65}AlO_2$	$C_{42}H_{65}GaO_2$	$C_{71}H_{90}C_{12}Ge_2O_4$	$C_{60}H_{74}GeO_2$	$C_{60}H_{74}O_2Sn$
Formula weight	628.92	671.66	1223.51	899.78	945.88
Color, habit	colorless, needle	colorless, block	colorless, plate	colorless, chunk	colorless, block
Crystal system	monoclinic	monoclinic	triclinic	monoclinic	monoclinic
Space group	$P2_1/a$	$P2_1/n$	$P\bar{1}$	$P2_1$	$P2_1$
a (Å)	8.9644(12)	12.4470(8)	8.6021(8)	11.5193(12)	11.6179(8)
b (Å)	24.484(3)	15.3429(10)	11.5267(11)	17.0623(18)	17.1068(12)
c (Å)	18.474(3)	21.2631(14)	16.4582(16)	12.8898(13)	12.8192(9)
α (°)	90	90	79.680(2)	90	90
β (°)	91.866(3)	105.3278(1)	86.345(2)	90.890(2)	90.803(2)
γ (°)	90	90	80.032(2)	90	90
V (Å^3)	4052.6(10)	3917.2(4)	1580.3(3)	2533.1(5)	2547.5(3)
Z	4	4	1	2	2
Crystal dimensions (mm)	$0.51 \times 0.17 \times 0.14$	$0.37 \times 0.35 \times 0.24$	$0.14 \times 0.09 \times 0.07$	$0.31 \times 0.22 \times 0.18$	$0.23 \times 0.19 \times 0.10$
d_{calc} (g cm^{-3})	1.031	1.139	1.286	1.180	1.233
μ (mm^{-1})	0.081	0.734	1.083	0.646	0.543
Number of reflections	9294	12289	7184	11596	11691
Number of observed reflections	4936	8500	5810	10045	10631
R_1 observed reflections[a]	0.0615	0.0432	0.0483	0.0336	0.0281
wR_2[b], all	0.1672	0.1163	0.1583	0.0766	0.0662

[a] $R_1 = \sum(|F_o| - |F_c|)/\sum|F_o|$.
[b] $wR_2 = |\sum[w(F_o^2 - F_c^2)^2/\sum[w(Fo^2)^2]]^{1/2}$.

6. X-ray crystallographic studies

Crystals of **1**–**5**, after removal from the Schlenk tube, were covered with a hydrocarbon oil under a rapid flow of argon, mounted on a glass fiber attached to a copper pin and placed in the cold stream of N_2 of the diffractometer. X-ray data were collected on a Bruker SMART 1000 diffractometer at 90(2) K with use of Mo Kα ($\lambda = 0.71073$ Å) radiation. Absorption corrections were applied using SADABS [29]. The structures were solved with use of direct methods or the Patterson option in SHELXS and refined by the full-matrix least-squares procedure in SHELXL [30]. All non-hydrogen atoms were refined anisotropically, while hydrogen atoms were placed at calculated positions and included in refinement using a riding model. Some details of the data collection and refinement are given in Table 3. Further details can be found in the supporting information.

7. Supplementary material

Crystallographic data have been deposited with the Cambridge Crystallographic Data Centre, CCDC 273256-273260. Copies of this information may be obtained free of charge from the Director, CCDC, 12, Union Road, Cambridge CD2 1EZ, UK (fax: +44 1223 336033; e-mail: deposit@ccdc.cam.ac.uk or http://www.ccdc.cam.ac.uk).

Acknowledgments

We are grateful to the National Science Foundation and the Donors of the Petroleum Research Fund administered by the American Chemical Society for its generous support.

References

[1] C. Stanciu, M.M. Olmstead, A.D. Phillips, M. Stender, P.P. Power, Eur. J. Inorg. Chem. (2003) 3495.
[2] D.C. Bradley, R.C. Mehrotra, I.P. Rothwell, A. Singh, Alkoxo and Aryloxo Derivatives of Metals, Academic Press, San Diego, 2001.
[3] P.P. Power, J. Organomet. Chem. 690 (2004) 1638.
[4] B. Cetinkaya, I. Gumrukcu, M.F. Lappert, J.L. Atwood, R.D. Rogers, M.J. Zawarotko, J. Am. Chem. Soc. 102 (1980) 2088.
[5] B. Cetinkaya, A. Hudson, M.F. Lappert, P.P. Power, H. Goldwhite, J. Chem. Soc., Chem. Commun. (1982) 609.
[6] P.P. Power, Chem. Rev. 99 (1999) 3463.
[7] T. Ooi, Y. Kondo, K. Maruoka, Angew. Chem., Int. Ed. Engl. 37 (1998) 3039.
[8] C.S. Weinert, P.E. Fanwick, I.P. Rothwell, J. Chem. Soc., Dalton Trans. (2002) 2948.
[9] C.S. Weinert, A.E. Fenwick, P.E. Fanwick, I.P. Rothwell, J. Chem. Soc., Dalton Trans. (2003) 532.
[10] J. Barrau, G. Rima, T. El Amraoui, Organometallics 17 (1998) 607.
[11] N.N. Zemlyanski, I.V. Boresova, M.G. Kuznetsova, V.N. Khristalev, Y.A. Ustynynk, M.S. Nechaev, V.V. Lunin, J. Barrau, G. Rima, Organometallics 22 (2003) 1875.
[12] J.B. Mann, T.L. Meek, L.C. Allen, J. Am. Chem. Soc. 122 (2000) 2780.
[13] K.W. Zilm, G.A. Lawless, R.M. Merrill, M.M. Millar, G.G. Webb, J. Am. Chem. Soc. 109 (1987) 7236.
[14] N. Tokitoh, N. Kano, K. Shibata, R. Okazaki, Organometallics 14 (1995) 3121.
[15] L. Pu, M.M. Olmstead, B. Schiemenz, P.P. Power, Organometallics 17 (1998) 5602.
[16] M. Weidenbruch, J. Schlaefke, A. Shäfer, K. Peters, H.G. von Schnering, H. Marsmann, Angew. Chem., Int. Ed. Engl. 33 (1994) 1846.
[17] B. Wrackmeyer, J. Magn. Reson. 61 (1985) 536.
[18] H. Grützmacher, H. Pritzkow, F.T. Edelmann, Organometallics 10 (1991) 23.
[19] B. Wrackmeyer, Ann. Rep. NMR Spectrosc. 38 (1999) 203.
[20] M. Nadvornik, J. Holecek, K. Handlir, A. Lycka, J. Organomet. Chem. 275 (1984) 43.
[21] J. Holecek, M. Nadvornik, K. Handlir, A. Lycka, J. Organomet. Chem. 315 (1986) 299.
[22] M.A. Petrie, M.M. Olmstead, P.P. Power, J. Am. Chem. Soc. 113 (1991) 8704.
[23] C. Glidewell, D.C. Liles, J. Chem. Commun. (1979) 93.
[24] P. Jutzi, C. Leue, Organometallics 13 (1994) 2898.
[25] R.S. Simons, L. Pu, M.M. Olmstead, P.P. Power, Organometallics 16 (1997) 1920.
[26] J.E. Huheey, E.A. Keiter, R.L. Keiter, Inorganic Chemistry, fourth ed., Harper and Row, New York, 1993, p. 187.
[27] V. Schomaker, D.P. Stevenson, J. Am. Chem. Soc. 63 (1941) 37.
[28] R. Blom, A. Haaland, J. Mol. Struct. 129 (1985) 1.
[29] SADABS: Area Detector Absorption Connections, Bruker AXS Inc., Madison, WI, 2003.
[30] SHELXTL, Version 5.1, Bruker AXS Inc., Madison, WI, 1997.

Available online at www.sciencedirect.com
SCIENCE DIRECT®
Polyhedron 25 (2006) 484–492
POLYHEDRON
www.elsevier.com/locate/poly

Synthesis of heteroleptic uranium compounds including an asymmetric, sterically unsaturated, bimetallic, organouranium(IV) halide: $(C_5Me_5)(C_8H_8)ClU(\mu\text{-}Cl)U(C_8H_8)(C_5Me_5)$

William J. Evans *, Stosh A. Kozimor, Joseph W. Ziller

Department of Chemistry, University of California, Irvine, CA 92697-2025, USA

Received 1 June 2005; accepted 11 July 2005
Available online 24 August 2005

Dedicated to Professor Malcolm Chisholm whose accomplishments in inorganic chemistry and enthusiasm for advancing the field have inspired us all.

Abstract

$K_2C_8H_8$ reacts with $(C_5Me_5)_2UCl_2$ not by substitution of both chlorides, but by Cl^{1-} and $(C_5Me_5)^{1-}$ ligand displacement to form an asymmetric, sterically unsaturated, mixed ligand metallocene chloride complex, $(C_5Me_5)(C_8H_8)ClU(\mu\text{-}Cl)U(C_8H_8)(C_5Me_5)$ (**1**). Complex **1** is a tetravalent uranium analogue of the asymmetric trivalent yttrium bimetallic complex, $(C_5Me_5)_2ClY(\mu\text{-}Cl)Y(C_5Me_5)_2$ (**2**), that has been used to evaluate coordination of bases with electropositive trivalent metallocenes. Tetravalent **1** similarly coordinates Lewis bases as demonstrated by its reaction with ε-caprolactam that generates a complex with four different ligands, $(C_5Me_5)(C_8H_8)UCl[OCNH(CH_2)_5]$ (**3**). Complex **1** also participates in ionic salt metathesis reactions with $KN(SiMe_3)_2$ to form $(C_5Me_5)(C_8H_8)U[N(SiMe_3)_2]$ (**4**).
© 2005 Elsevier Ltd. All rights reserved.

Keywords: Cyclopentadienyl; Cyclooctatetraenyl; Uranium; Heteroleptic; Chiral metal complex; Bimetallic

1. Introduction

The synthesis of sterically unsaturated f element complexes is challenging because the presence of an open coordination site on an electropositive metal with a +3 or +4 formal charge generally results in high reactivity. Sterically unsaturated f element species tend to either react to form more stable sterically saturated products or to increase their electrostatic stabilization by interacting with any nearby available electron density [1–3]. The common occurrence of agostic interactions in f element complexes is indicative of the latter tendency [4–6]. As a consequence, sterically unsaturated complexes are difficult to isolate and crystallographically characterize.

Previously, using the lanthanide mimic, yttrium, a trivalent complex of formula $(C_5Me_5)_2ClY(\mu\text{-}Cl)Y(C_5Me_5)_2$ was isolated that had one sterically unsaturated seven-coordinate metal center as well as one metal site with the more common eight-coordinate environment [7]. The isolation of this unsaturated species was attributed to the steric bulk of the four pentamethylcyclopentadienyl ligands that prevented formation of a symmetric dimer involving two eight coordinate metal centers. This compound subsequently proved to be

* Corresponding author. Tel.: +1 949 824 5174; fax: +1 949 824 2210.
E-mail address: wevans@uci.edu (W.J. Evans).

0277-5387/$ - see front matter © 2005 Elsevier Ltd. All rights reserved.
doi:10.1016/j.poly.2005.07.015

useful in evaluating the relative binding ability of Lewis bases to a metallocene complex of an electropositive trivalent metal since it was soluble in arenes and formed base adducts cleanly according to Eq. (1) [8]:

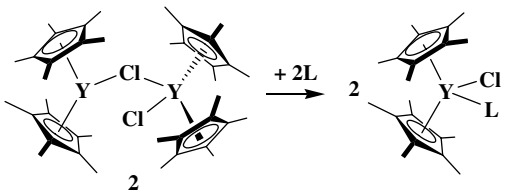

(1)

We report here the synthesis, structural characterization, and coordination chemistry of a tetravalent uranium analog of the yttrium complex, namely $(C_5Me_5)(C_8H_8)ClU(\mu\text{-}Cl)U(C_8H_8)(C_5Me_5)$ (**1**). Due to the higher valence of U(IV) compared to Y(III), a cyclooctatetraenyl dianion is used in place of a pentamethylcyclopentadienyl monoanion to make the metallocene component in this complex. As a result, it is a mixed ligand metallocene. A Th(IV) complex analogous in composition to **1** was synthesized years ago from $(C_8H_8)ThCl_2(THF)_2$ and $(C_5Me_5)MgCl(THF)$ followed by desolvation at 100 °C, but no structural information was reported on this species [9]. In contrast to the thorium synthesis, the mixed ligand uranium metallocene chloride **1** was obtained from the common precursor $(C_5Me_5)_2UCl_2$ [10] in a room temperature reaction that uses both normal substitution of a chloride ligand as well as an unusual $(C_5Me_5)^{1-}$ substitution.

Complex **1** appears to be suitable to evaluate U(IV) Lewis acid/base reactions like those examined with trivalent $(C_5Me_5)_2ClY(\mu\text{-}Cl)Y(C_5Me_5)_2$ (**2**), in Eq. (1). Structural data on a $(C_5Me_5)(C_8H_8)UCl(L)$ reaction product of this type is presented for L = ε-caprolactam, a substrate that gave unusual results with $(C_5Me_5)_2ClY(\mu\text{-}Cl)Y(C_5Me_5)_2$ [8]. In addition, we report that **1** undergoes subsequent chloride substitution to generate a uranium analog of the thorium complex, $(C_5Me_5)(C_8H_8)Th[N(SiMe_3)_2]$, reported earlier [9] that contains U(IV) ligated by three of the most common ancillary ligands in f element chemistry.

2. Experimental section

2.1. General experimental

The syntheses and manipulations of the extremely air and moisture sensitive compounds described below were conducted under nitrogen or argon with rigorous exclusion of air and water by Schlenk, vacuum line, and glovebox techniques. Unless specified otherwise, all glovebox manipulations were carried out in an argon filled glovebox that was free of coordinating solvents. THF, toluene, benzene, diethyl ether and *n*-hexane were saturated with Ar and passed through a GlassContour® column.[1] Benzene-d_6 and toluene-d_8 were distilled over NaK alloy and benzophenone and degassed by three freeze–pump–thaw cycles. $KN(SiMe_3)_2$ (Aldrich) was recrystallized from toluene before use. C_8H_8 (Aldrich) was distilled onto Type 4 activated molecular sieves, and degassed by three freeze–pump–thaw cycles. ε-Caprolactam (Aldrich) was sublimed before use. $K_2C_8H_8$ [11] and $(C_5Me_5)_2UCl_2$ [10] were prepared as previously described. NMR experiments were conducted with Bruker 400 and 500 MHz spectrometers. IR samples were analyzed as thin films using an ASI ReactIR1000 [12]. GC–MS data were obtained on a Waters (Micromass) Autospec with fused silica 30 m × 0.32 mm i.d. DB-5 GC columns. Elemental analyses were provided by Analytische Laboratorien, Lindlar Germany.

2.2. $(C_5Me_5)(C_8H_8)ClU(\mu\text{-}Cl)U(C_8H_8)(C_5Me_5)$ (1)

A dark red solution of $(C_5Me_5)_2UCl_2$ (480 mg, 0.825 mmol) in toluene (10 mL) was slowly added to a stirred suspension of $K_2C_8H_8$ (150 mg, 0.828 mmol) in toluene (5 mL). The mixture was stirred for 3 h and a white insoluble powder was removed from the red solution by centrifugation. The solvent was removed by rotary evaporation and $(C_5Me_5)(C_8H_8)ClU(\mu\text{-}Cl)U(C_8H_8)(C_5Me_5)$ was isolated as a red solid (400 mg, 95%). ^1H NMR (C_6D_6, 21 °C) $\delta = 7.6$ (s, C_5Me_5, 30 H) −29.3 (s, C_8H_8, 16H) ppm. The ^1H NMR spectrum of **1** showed no sign of monomer/ dimer equilibrium between −75 and 75 °C. ^{13}C NMR (C_6D_6, 21 °C) $\delta = 274$ (s, C_8H_8), 273 (s, C_8H_8), 10.3 (s, C_5Me_5), −23.4 (s, C_5Me_5) ppm. IR 2964s, 2907s, 2856s, 2725w, 1640w, 1602m, 1482m, 1436s, 1378s, 1262s, 1092s, 1061s, 1019s, 903m, 861w, 803s, 722s, 676s cm^{-1}. **1** readily crystallizes from saturated solutions of hot toluene cooled to −35 °C with one molecule of toluene per formula unit. *Anal.* Calc. for $C_{36}H_{46}Cl_2U_2 \cdot C_7H_8$: C, 46.22; H, 4.83; Cl, 6.35; U, 42.61. Found: C, 46.27; H, 4.88; Cl, 6.21; U, 43.40%.

2.3. $(C_5Me_5)(C_8H_8)UCl[OCNH(CH_2)_5]$ (3)

A red solution of **1** (58 mg, 0.568 mmol) in C_6D_6 was added to an a flask charged with ε-caprolactam (13 mg, 0.112 mmol). After 2 h, the solvent was removed by rotary evaporation leaving a red oil. The oil was washed with hexane (3×), the washings were discarded, and the remaining insoluble red solids were dried under vacuum. ^1H NMR spectroscopy (C_6D_6) indicated 8.0 (s, 15H) and −32.7 (s, 8H) ppm as the major resonances, but small peaks at 0.18 (s, 3.6H) and −32.8 (s, 2H) as well

[1] THF and diethyl ether were dried over activated alumina and sieves. Toluene and *n*-hexanes were dried over Q-5 and molecular sieves. For more information on the drying system see www.glasscontour.com.

as resonances for C_5Me_5H were also present. The resonances of the ε-caprolactam were not located. **3** crystallized from toluene at −35 °C overnight.

2.4. $(C_5Me_5)(C_8H_8)U[N(SiMe_3)_2]$ (4)

A solution of **1** (280 mg, 0.272 mmol) in toluene (10 mL) was added to a solution of $KN(SiMe_3)_2$ (110 mg, 0.547 mmol) in toluene (5 mL) and the red solution was stirred for 12 h. White solids were removed by centrifugation and the solvent was removed by rotary evaporation leaving $(C_5Me_5)(C_8H_8)U[N(SiMe_3)_2]$ (310 mg, 92%) as a red solid. ^{1}H NMR (C_6D_6, 298 K) $\delta = 2.8$ (s, 15H, C_5Me_5), −11 [s br, $\Delta\upsilon_{1/2} = 3000$ Hz, $N(SiMe_3)_2$], −35.5 (s, 8H, C_8H_8) ppm. ^{1}H NMR (Toluene-d_8, 298 K) $\delta = 2.8$ (s, 15H, C_5Me_5), −12 [s br, $\Delta\upsilon_{1/2} =$ 3000 Hz, $N(SiMe_3)_2$], −35.0 (s, 8H, C_8H_8) ppm. ^{1}H NMR (Toluene-d_8, 208 K) $\delta = 29.1$ [s, 6H, $N(SiMe_3)_2$], 12.5 [s, 6H, $N(SiMe_3)_2$], 0.9 (s, 15H, C_5Me_5), −56.2 (s, 8H, C_8H_8), −93.2 [s, 6H, $N(SiMe_3)_2$] ppm. ^{1}H NMR (Toluene-d_8, 336 K) $\delta = 3.2$ (s, 15H, C_5Me_5), −9.8, [s, 18H, $N(SiMe_3)_2$], −27.7, (s, 8H, C_8H_8). IR: 2957s, 2907s, 2856s, 2725w, 1640m, 1598w, 1567w, 1482w, 1436m, 1378m, 1258s, 1092m, 1065m, 1019s, 930s, 903m, 857s, 803s, 779s, 722s, 676s cm^{-1}.

2.5. X-ray data collection, structure solution and refinement for $(C_5Me_5)(C_8H_8)ClU(\mu\text{-}Cl)U(C_8H_8)(C_5Me_5)\cdot C_6H_5Me$

A red crystal of approximate dimensions $0.07 \times 0.26 \times 0.28$ mm was mounted on a glass fiber and transferred to a Bruker CCD platform diffractometer. The SMART [13] program package was used to determine the unit-cell parameters and for data collection (25 s/frame scan time for a sphere of diffraction data). The raw frame data was processed using SAINT [14] and SADABS [15] to yield the reflection data file. Subsequent calculations were carried out using the SHELXTL [16] program. The diffraction symmetry was 2/*m* and the systematic absences were consistent with the centrosymmetric monoclinic space group $P2_1/n$ which was later determined to be correct. Details are in Table 1.

The structure was solved by direct methods and refined on F^2 by full-matrix least-squares techniques. The analytical scattering factors [17] for neutral atoms were used throughout the analysis. There was one molecule of toluene solvent present per formula unit. Hydrogen atoms were included using a riding model. Carbon atoms C(25) and C(37) were refined using isotropic temperature parameters. At convergence, $wR_2 = 0.1427$ and GOF = 1.151 for 414 variables refined against 7879 data (0.80 Å). As a comparison for refinement on *F*, $R_1 = 0.0599$ for those 6591 data with $I > 2.0\sigma(I)$.

2.6. $(C_5Me_5)(C_8H_8)UCl[OCNH(CH_2)_5]$ (3)

A red plate of approximate dimensions $0.02 \times 0.16 \times 0.17$ mm was handled as described above, with the exception that a 30 s/frame scan time for a sphere of diffraction data was used. There were no systematic absences nor any diffraction symmetry other than the Friedel condition. The centrosymmetric triclinic space group $P\bar{1}$ was assigned and later determined to be correct. The structure was solved by direct methods and refined on F^2 by full-matrix least-squares techniques. The analytical scattering factors [17] for neutral atoms were used throughout the analysis. Hydrogen atoms were included using

Table 1
X-ray data collection parameters for $(C_5Me_5)(C_8H_8)ClU(\mu\text{-}Cl)U(C_8H_8)(C_5Me_5)$ (**1**), $(C_5Me_5)(C_8H_8)UCl[OCNH(CH_2)_5]$ (**3**), and $(C_5Me_5)(C_8H_8)U[N(SiMe_3)_2]$ (**4**)

	1	3	4
Empirical formula	$C_{36}H_{46}Cl_2U_2\cdot C_7H_8$	$C_{24}H_{34}ClNO\cdot 1/2(C_6H_{14})U$	$C_{24}H_{41}NSi_2U$
Formula weight	1117.82	669.09	637.79
Crystal system	monoclinic	triclinic	monoclinic
Space group	$P2_1/n$	$P\bar{1}$	$P2_1/c$
a (Å)	8.7702(6)	8.856(7)	15.5878(13)
b (Å)	30.238(2)	12.104(10)	11.8752(10)
c (Å)	14.5724(10)	13.566(11)	13.7049(11)
α (°)	90	68.305(13)	90
β (°)	92.9340(10)	73.604(14)	96.7560(10)
γ (°)	90	75.722(13)	90
Volume (Å^3)	3859.5(5)	1279.7(18)	2519.3(4)
Z	4	2	4
λ (Å)	0.71073	0.71073	0.71073
ρ_{calc} (Mg/m^3)	1.924	1.736	1.682
Absorption coefficient (mm^{-1})	8.549	6.465	6.548
Goodness-of-fit on F^2	1.151	1.241	1.084
R^a [$I > 2\sigma(I)$]: R_1	0.0599	0.1186	0.0296
R^b (all data): wR_2	0.1427	0.3030	0.0840

[a] $R_1 = \sum||F_o| - |F_c||/\sum|F_o|$.
[b] $wR_2 = \sum[w(F_o^2 - F_c^2)^2]/\sum[w(F_o^2)^2]^{1/2}$.

a riding model. There was a solvent molecule present that was presumed to be hexane. It was included as a half-molecule of hexane (located about an inversion center). The poor quality of the crystal prevented anisotropic refinement. All atoms were assigned isotropic temperature parameters. The final least-squares analysis yielded $wR_2 = 0.3030$ and GOF = 1.241 for 128 variables refined against 3926 data (0.85 Å resolution). As a comparison for refinement on F, $R_1 = 0.1186$ for those 3144 data with $I > 2.0\sigma(I)$. The structure has been established but the metric data are not reliable.

2.7. $(C_5Me_5)(C_8H_8)U[N(SiMe_3)_2]$ (4)

A red crystal of approximate dimensions $0.07 \times 0.12 \times 0.13$ mm was handled as described above. The diffraction symmetry was $2/m$ and the systematic absences were consistent with the centrosymmetric monoclinic space group $P2_1/c$ which was later determined to be correct. The structure was solved by direct methods and refined on F^2 by full-matrix least-squares techniques. The analytical scattering factors [17] for neutral atoms were used throughout the analysis. Hydrogen atoms were included using a riding model. At convergence, $wR_2 = 0.0840$ and GOF = 1.084 for 253 variables refined against 5120 data (0.80 Å). As a comparison for refinement on F, $R_1 = 0.0296$ for those 4398 data with $I > 2.0\sigma(I)$.

3. Results

3.1. Synthesis of $(C_5Me_5)(C_8H_8)ClU(\mu\text{-}Cl)U(C_8H_8)(C_5Me_5)$ (1)

The reaction of $(C_5Me_5)_2UCl_2$ with $K_2C_8H_8$ does not result in the formation of two equivalents of KCl as is typical of reactions of $(C_5Me_5)_2UCl_2$ with potassium reagents [4–6,10,18–21]. ^{1}H NMR spectroscopy of the benzene-soluble, uranium-containing, product suggested that one $(C_5Me_5)^{1-}$ ligand had been lost since the spectrum contained resonances attributable to $(C_5Me_5)^{1-}$ and $(C_8H_8)^{2-}$ ligands with peak area ratios of 15 to 8. This observation was surprising since $(C_5Me_5)^{1-}$ is typically an unreactive ancillary ligand. Indeed, one of the important features of $(C_5Me_5)_2UCl_2$ as a reagent in organouranium chemistry is that the $[(C_5Me_5)_2U]^{2+}$ unit remains intact during reaction sequences [4–6].

Confirmation that $(C_5Me_5)^{1-}$ was lost as KC_5Me_5 via an ionic salt metathesis reaction was obtained by both hydrolysis and deuterolysis of the insoluble white solids that precipitate during the reaction. GC–MS analysis showed these to be C_5Me_5H and C_5Me_5D, respectively.

Since the NMR data on the paramagnetic uranium product were not definitive, an X-ray crystallographic study was conducted. This confirmed that substitution

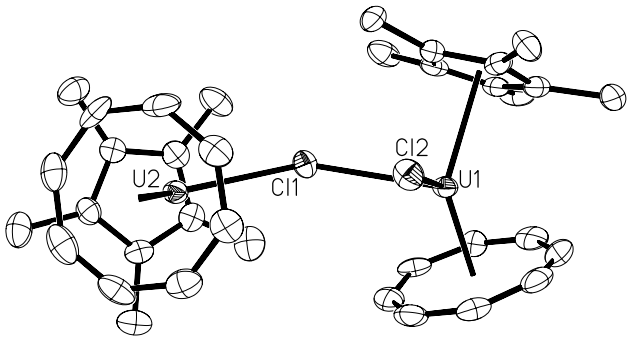

Fig. 1. Thermal ellipsoid plot of $(C_5Me_5)(C_8H_8)ClU(\mu\text{-}Cl)U(C_8H_8)(C_5Me_5)$ (**1**), drawn at the 50% probability level. The molecule of toluene that co-crystallized with **1** has been omitted.

of both Cl^{1-} and $(C_5Me_5)^{1-}$ had occurred: $(C_5Me_5)(C_8H_8)ClU(\mu\text{-}Cl)U(C_8H_8)(C_5Me_5)$ (**1**), Fig. 1, was identified as the product, Eq. (2). Unlike the symmetrical trimeric trivalent

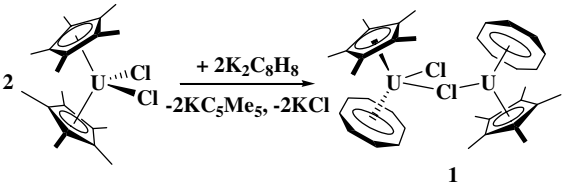

(2)

uranium metallocene chloride, $[(C_5Me_5)_2U(\mu\text{-}Cl)]_3$, which is insoluble in alkanes and arene solvents, complex **1** readily dissolves in arenes.

An analogous reaction of $(C_5Me_5)_2ThCl_2$ with $K_2C_8H_8$ forms a product with NMR spectra consistent with those reported for $[(C_5Me_5)(C_8H_8)ThCl]_2$ [9]. Crystallographic characterization of this product has been elusive.

3.2. Structure of $(C_5Me_5)(C_8H_8)ClU(\mu\text{-}Cl)U(C_8H_8)(C_5Me_5)$ (1)

Complex **1** is structurally similar to $(C_5Me_5)_2ClY(\mu\text{-}Cl)Y(C_5Me_5)_2$ (**2**), in that both compounds contain two metal centers that differ in coordination number by one, both have a single bridging chloride and a single terminal chloride, and both have the four ring centroids arranged in a roughly tetrahedral geometry. The "end on" view in Fig. 2 clearly shows the tetrahedral nature of the four ring centroids in **1**. The 138.0° and 140.7° (C_5Me_5 ring centroid)–U–(C_8H_8 ring centroid) angles are typical of $(C_5Me_5)/(C_8H_8)$ mixed metallocene complexes and are also similar to bis(pentamethylcyclopentadienyl) metallocenes of the f elements. For example, analogous angles in $(C_5Me_5)(C_8H_8)U(bipy)$ [22] and $(C_5Me_5)_2UCl_2$ [23] are 131° and 138.2°, respectively. U(1) is a chiral center and the complex crystallizes as a racemic mixture of enantiomers.

The U(1)–C(C_5Me_5) distances, which range from 2.67(1) to 2.80(1) Å and average 2.74(4) Å, are similar

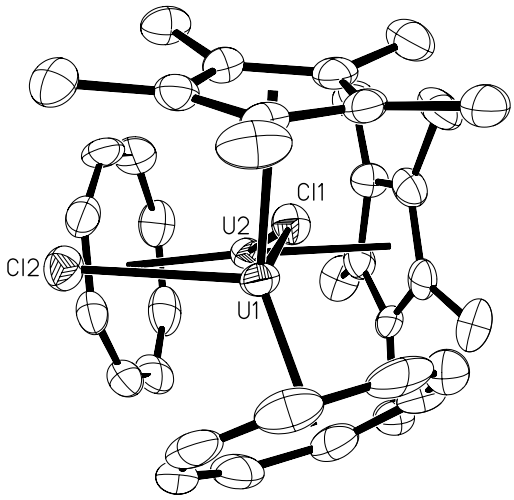

Fig. 2. Thermal ellipsoid plot $(C_5Me_5)(C_8H_8)ClU(\mu\text{-}Cl)U(C_8H_8)(C_5Me_5)$ (**1**), drawn at the 50% probability level.

to the 2.73(1)–2.75(2) Å distances in the mixed ligand metallocene $[(C_5Me_5)(C_8H_8)U(THF)_2](BPh_4)$ [24] and overlap with the 2.78(2)–2.81(2) Å distances in the bimetallic $[(C_5Me_5)(C_8H_8)U]_2(C_8H_8)$ complex [25]. The 2.74(4) Å mean U–(C_5Me_5) distance in **1** is also similar to the analogous distances in eight coordinate bis(pentamethylcyclopentadienyl) complexes, e.g. $(C_5Me_5)_2UMe_2$, 2.732(7) and 2.739(6) Å [26,27]. This shows that the U–$C(C_5Me_5)$ unit in the mixed metallocene **1** does not deviate substantially from those in metallocenes containing two $(C_5Me_5)^{1-}$ ligands.

In **1**, the $(C_8H_8)^{2-}$ ligands bind with η^8-hapticity and have U(1)–$C(C_8H_8)$ bond distances in the range 2.61(1)–2.71(1) Å that average 2.66(3) Å. These lengths are similar to analogous distances in $(C_8H_8)_2U$, 2.635(10)–2.675(11) Å [28,29], $(C_8H_8)(PC_4Me_4)U(BH_4)THF$, 2.688(9)–2.740(9) Å [30], $[(C_5Me_5)(C_8H_8)U(THF)_2](BPh_4)$, 2.62(2)–2.68(2) Å [24], and $\{[(^tBu)(C_6H_4Me_2)C{=}N]_3U(C_8H_8)\}[Na(OEt_2)]$, 2.717(7)–2.757(7) Å [31]. In complex **1**, the 2.42 and 2.49 Å U–(C_5Me_5 ring centroid) distances are substantially longer than the 1.89 and 1.98 Å U–(C_8H_8 ring centroid) distances which is typical for dianionic $(C_8H_8)^{2-}$ vs. monoanionic $(C_5Me_5)^{1-}$ ligands in uranium complexes.

The U(1) ion in **1** attaches to the terminal chloride ligand, Cl(2), with a 2.673(3) Å U(1)–Cl(2) bond distance that is longer than analogous bonds in monometallic U(IV) metallocene bis-chloride complexes such as $(C_5Me_5)_2UCl_2$ [23], $[1,3\text{-}(Me_3Si)_2C_5H_3]_2UCl_2$ [32,33], $[1,3\text{-}(^tBu)_2C_5H_3]_2UCl_2$ [33], and $[1,2\text{-}(^tBu)_2C_5H_3]_2UCl_2$ [34] which have U(IV)–Cl lengths of 2.583(6) Å [23], 2.579(2) Å [32,33], 2.577(4) Å [33], and 2.591(4) and 2.576(4) Å [34], respectively. Since these latter complexes are formally eight coordinate and U(1) is formally ten coordinate [counting the three electron pairs of $(C_5Me_5)^{1-}$ and five electron pairs of $(C_8H_8)^{2-}$], the longer distance in **1** is consistent with the higher coordination number [35]. The U(1)–Cl(2) bond distance is more similar to the 2.638(1) Å terminal U–Cl distance in $\{[Me_3SiN(CH_2CH_2NSiMe_3)_2]ClU(\mu\text{-}Cl)\}_2$ [36] which contains a sterically demanding ligand.

Both U–(μ-Cl) distances in **1** are longer than the terminal U(1)–Cl(2) length as is typical of bridging ligands. The U–(μ-Cl)–U bridge is asymmetric since the 2.738(3) Å U(2)–Cl(1) distance to the nine coordinate U(2) ion is shorter than the 2.921(3) Å U(1)–Cl(1) distance to the ten coordinate U(1) ion. Since the radii of uranium ions typically increase by only 0.05 Å with an increase of one in coordination number, the large difference between U(1)–Cl(1) and U(2)–Cl(1) cannot be explained by ionic radius alone. The long U(1)–Cl(1) distance in **1** is substantially longer than the 2.79(2) and 2.82(2) Å distances in the more symmetrically bridged trivalent complex $[(THF)_2(18\text{-crown-}6)Na]\{[(C_5H_5)_3U]_2(\mu\text{-}Cl)\}$ [37] and more similar in length to the 2.901(5) distance in the trivalent uranium complex $[(C_5Me_5)_2U(\mu\text{-}Cl)]_3$ [38]. Since the short U–Cl distance in **1** is associated with U(2), the complex appears to be more of a combination of two $(C_5Me_5)(C_8H_8)UCl$ units rather than a $[(C_5Me_5)(C_8H_8)UCl_2]^{1-}[(C_5Me_5)(C_8H_8)U]^{1+}$ cation/anion pair.

The 148.11(11)° U(1)–Cl(1)–U(2) angle, Fig. 2, is considerably more bent than the 162.8(2)° Y–Cl–Y angle in $(C_5Me_5)_2ClY(\mu\text{-}Cl)Y(C_5Me_5)_2$ [7]. The U–Cl–U angle in **1** is also more bent than the analogous 180° angle in mixed valent $\{N[CH_2N(Si^tBuMe_2)]_3U\}_2(\mu\text{-}Cl)$ [39] and the 157.5(7)° angle in trivalent $[(THF)_2(18\text{-crown-}6)Na]\{[(C_5H_5)_3U]_2(\mu\text{-}Cl)\}$ [37]. The U–Cl–U angle in trivalent $[(C_5Me_5)_2U(\mu\text{-}Cl)]_3$ is 84.5(3)°, however [38].

Recent structural studies of $(C_5Me_5)_2MeLu(\mu\text{-}Me)Lu(C_5Me_5)_2$ [40] and $(C_5Me_5)_2MeSm(\mu\text{-}Me)Sm(C_5\text{-}Me_5)_2(\mu\text{-}Me)Sm(C_5Me_5)_2$ [40], which have asymmetric bridged oligomeric structures like those of **1** and $(C_5Me_5)_2ClY(\mu\text{-}Cl)Y(C_5Me_5)$ (**2**), have revealed that in the solid state the molecules are located with the terminal Me ligand of one unit, i.e. $(C_5Me_5)_2LnMe$, oriented at long distances toward the sterically unsaturated metal center of another unit. In light of these structures, intermolecular geometries in **1** and **2** were examined.

Fig. 3 shows a portion of the extended structure of **2** that is similar to the $(C_5Me_5)_2MeLu(\mu\text{-}Me)Lu(C_5Me_5)_2$ complex and exists as a one-dimensional chain of repeating $(C_5Me_5)_2ClY(\mu\text{-}Cl)Y(C_5Me_5)_2$ units with intermolecular Y···Cl distances, such as Y(2A)···Cl(2B), of approximately 5.1 Å. The intermolecular Y(1B)–Cl(2B)–Y(1A) angle of 168° is similar to the 162.8(2)° intramolecular Y(1A)–Cl(1A)–Y(2A) angle.

The solid state structure of **1** also has the terminal ligand oriented toward the metal center of another molecule. However, as shown in Fig. 4, the terminal Cl(2)

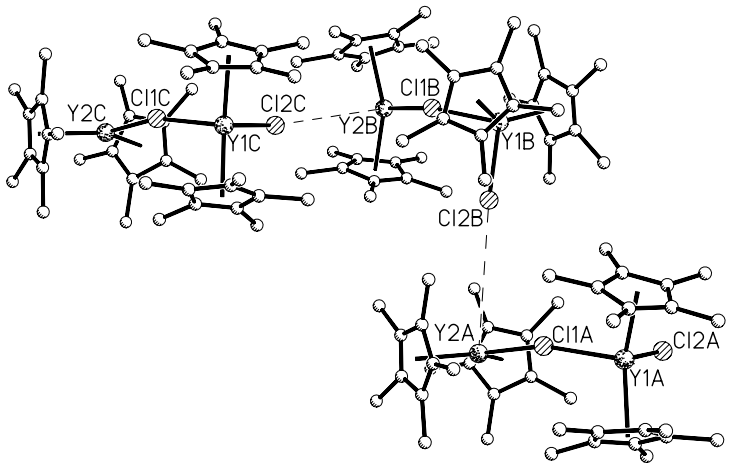

Fig. 3. A ball and stick representation of $(C_5Me_5)_2ClY(\mu\text{-}Cl)Y(C_5Me_5)_2$ (**2**), showing the 1-dimensional extended network. The dashed lines show the orientation of the chloride ligands toward the yttrium ions in adjacent molecules.

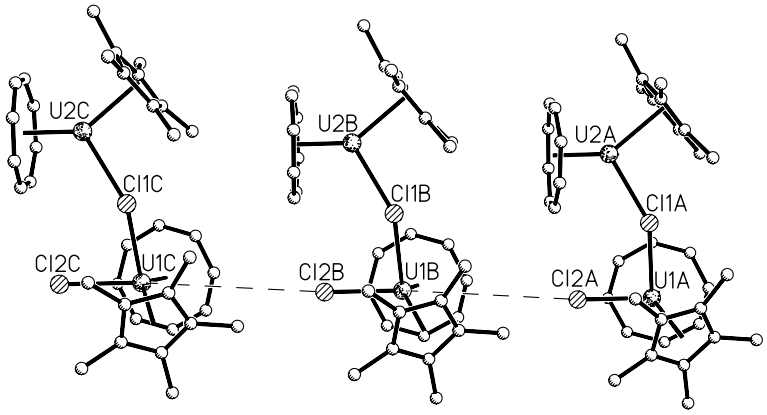

Fig. 4. Ball and stick diagram of $(C_5Me_5)(C_8H_8)ClU(\mu\text{-}Cl)U(C_8H_8)(C_5Me_5)$ (**1**), showing the 1-dimensional extended network. The dashed lines show the orientation of the chloride ligands toward the uranium ions in adjacent molecules.

ligands in **1** are oriented to the higher coordinate U(1) positions instead of sterically less saturated U(2). The intermolecular Cl···U–Cl angles are 175° and the intermolecular distances, such as Cl(2A)···U(1C), are approximately 6.1 Å.

3.3. Coordination chemistry of *1*

To determine if **1** might be useful as a U(IV) metallocene platform for evaluating Lewis acid/base interactions analogous to $(C_5Me_5)_2ClY(\mu\text{-}Cl)Y(C_5Me_5)_2$ (**2**), in Eq. (1), complex **1** was treated with ε-caprolactam. This base generated one of the more unusual results with **2**: a bis-adduct formed that had hydrogen bonding between the amide protons and the chloride ligand [8]. Complex **1** reacts with two equiv of ε-caprolactam to form a mixture of products from which the simple mono-base adduct $(C_5Me_5)(C_8H_8)UCl[OCNH(CH_2)_5]$ (**3**), crystallizes, Eq. (3):

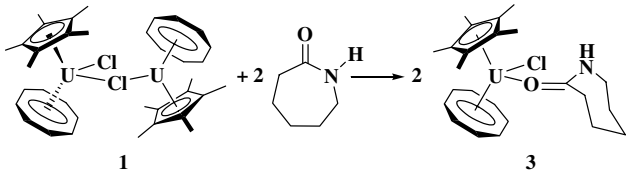

(3)

Complex **3** was identified by X-ray crystallography, Fig. 5. Analysis of the reaction by ^1H NMR spectroscopy in C_6D_6 reveals that other products are formed as well. Broad resonances at 0.18 and −32.8 ppm increased in size with addition of more ε-caprolactam, but these could not be definitively identified. C_5Me_5H was also observed, suggesting that the lactam can cleave a $(C_5Me_5)^{1-}$ ring from **1** by protonation. Deprotonation of ε-caprolactam would form caprolactamate, a ligand that is known to complex Ti, Y, Yb, and Er [41,42].

The crystallographic data on **3** were sufficient only to determine connectivity. Complex **3** contains four

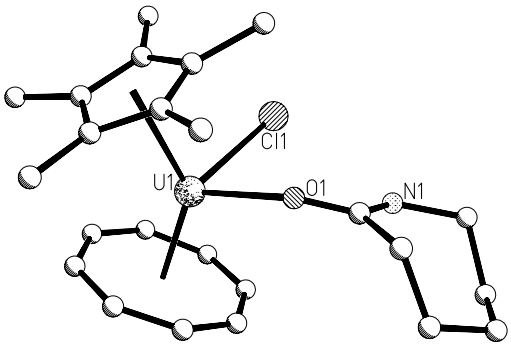

Fig. 5. A ball and stick representation of one enantiomer of $(C_5Me_5)(C_8H_8)U(Cl)[OCNH(CH_2)_5]$ (**3**). The molecules of hexane that co-crystallize with **3** have been omitted.

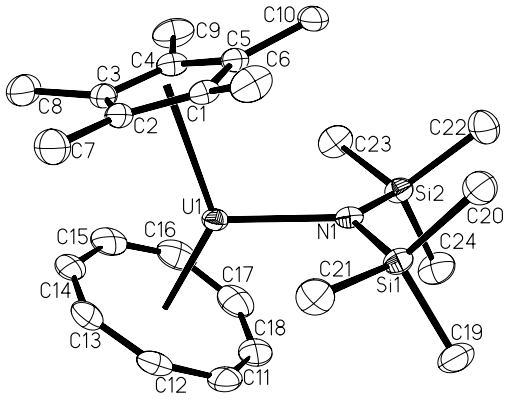

Fig. 6. Thermal ellipsoid plot of $(C_5Me_5)(C_8H_8)U[N(SiMe_3)_2]$ (**4**), drawn at the 50% probability level.

different ligands with the $(C_5Me_5)^{1-}$ and $(C_8H_8)^{2-}$ ring centroids occupying two corners of a distorted tetrahedron. The chloride and ε-caprolactam ligands occupy the other two sites and the caprolactam ring is oriented to allow the amide proton to hydrogen bond to the chloride. Enantiomers of **3** co-crystallize as a racemic mixture in the solid state, Fig. 5.

3.4. Substitution chemistry of *1*

Although addition of $K_2C_8H_8$ did not result in substitution of both chloride ligands in $(C_5Me_5)_2UCl_2$, the second chloride can eventually be removed when **1** is treated with $KN(SiMe_3)_2$. The reaction of **1** with $KN(SiMe_3)_2$ to form $(C_5Me_5)(C_8H_8)U[N(SiMe_3)_2]$ (**4**), Eq. (4), is analogous to a $[(C_5Me_5)(C_8H_8)ThCl]_2$/$KN(SiMe_3)_2$ reaction reported earlier [9]:

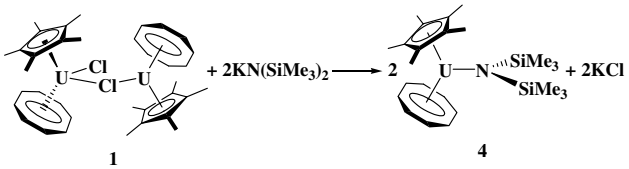

(4)

Complex **4** was characterized by ^1H NMR spectroscopy and its structure was confirmed by X-ray crystallographic analysis, Fig. 6. The resonances attributable to the $(C_5Me_5)^{1-}$ and $(C_8H_8)^{2-}$ ligands in the ^1H NMR spectra of **4** in benzene-d_6 and toluene-d_8 at 298 K are well resolved while the resonance for the $[N(SiMe_3)_2]^{1-}$ ligand is broadened almost completely into the baseline. At 336 K, the $[N(SiMe_3)_2]^{1-}$ resonance sharpens and the peak areas for the three ligands are as expected, 15:8:18, respectively. At 208 K, three resonances are observed for the $[N(SiMe_3)_2]^{1-}$ ligand with equal peak areas of 6. This suggests that the rotation of the trimethylsilyl substituents of the amide ligand is frozen at lower temperatures rendering each pair of methyl groups inequivalent as found in the solid state structure, Fig. 6. Complex **4** undergoes hydrolysis to form C_5Me_5H, $HN(SiMe_3)_2$, and C_8H_8 as the major products. Deuterolysis of **4** similarly gives C_5Me_5D, $DN(SiMe_3)_2$, and C_8H_8. Only small amounts of the reduced 1,3,5-cyclooctatriene and 1,5,7-cyclooctatriene were observed by GC–MS (<10% of the C_8H_8 peak).

3.5. Structure of $(C_5Me_5)(C_8H_8)U[N(SiMe_3)_2]$ (*4*)

The U–C(C_5Me_5) bond distances in **4**, which range from 2.763(5) to 2.823 Å and average 2.79(3) Å, are similar to those observed in **1**. As in other uranium mixed $(C_5Me_5)^{1-}/(C_8H_8)^{2-}$ metallocenes [43], the U–C(C_5Me_5) distances in **4** are longer than the U–C(C_8H_8) distances which range from 2.659(6) to 2.737(5) Å and average 2.70(3) Å. The 2.515 Å U–(C_5Me_5 ring centroid) and 1.990 Å U–(C_8H_8 ring centroid) distances are shorter than analogous distances in $(C_5Me_5)(C_8H_8)Th[CH(SiMe_3)_2]$, 2.54 and 2.03 Å [9], respectively, which is consistent with difference in ionic radii [35]. The 134.7° (C_5Me_5 ring centroid)–U–(C_8H_8 ring centroid) angle is similar to the analogous angles in **1**, Table 2, and the 138.1° angle in $(C_5Me_5)(C_8H_8)Th[CH(SiMe_3)_2]$ [9].

As was observed for the trivalent analogue of **4**, namely $(C_5Me_5)_2U[N(SiMe_3)_2]$ [21], the amide is bound symmetrically to the uranium ion as evidenced by the U(1)–N(1)–Si angles of 119.5(2)° and 117.7(2)° and the similar U(1)–Si distances. The 2.284(4) Å U(1)–N(1) distance is similar to those in other U(IV) amides [44] such as $[(Me_3Si)_2N]_2UCl_2$, 2.231(8) and 2.238(7) Å [45], $[(Me_3Si)_2N]_3U[O(C_6H_3{}^tBu_2)]$, 2.29(1), 2.29(1) and 2.28(1) Å [46], and $[Me_2Si(C_5Me_4)(^tBuN)]U(NMe_2)$, 2.278(4) and 2.207(4) Å [47]. The U(1)–N(1) distance in **1** is shorter than the 2.352(2) Å U–N distance in trivalent $(C_5Me_5)_2U[N(SiMe_3)_2]$ which is consistent with the differences in ionic radii and coordination number [35]. The U(1)–N(1) distance is substantially shorter than the 2.54(1) Å Th–C[$CH(SiMe_3)_2$] distance in $(C_5Me_5)(C_8H_8)Th[CH(SiMe_3)_2]$ [9].

Table 2
Selected bond distances (Å) and angles (deg) for $(C_5Me_5)(C_8H_8)ClU(\mu\text{-}Cl)U(C_8H_8)(C_5Me_5)$ (**1**) and $(C_5Me_5)(C_8H_8)U[N(SiMe_3)_2]$ (**4**)

Complex **1**				Complex **4**	
U–C(C_5Me_5)				U–C(C_5Me_5)	
U(1)–Cnt(C_5Me_5)	2.491	U(2)–Cnt(C_5Me_5)	2.423	U(1)–Cnt(C_5Me_5) 2.515	
U(1)–C(1)	2.749(11)	U(2)–C(11)	2.673(12)	U(1)–C(1)	2.769(4)
U(1)–C(2)	2.769(11)	U(2)–C(12)	2.678(11)	U(1)–C(2)	2.806(5)
U(1)–C(3)	2.795(11)	U(2)–C(13)	2.708(11)	U(1)–C(3)	2.823(5)
U(1)–C(4)	2.764(11)	U(2)–C(14)	2.759(12)	U(1)–C(4)	2.783(5)
U(1)–C(5)	2.754(11)	U(2)–C(15)	2.696(13)	U(1)–C(5)	2.763(5)
U–(C_8H_8)				U–(C_8H_8)	
U(1)–Cnt(C_8H_8)	1.980	U(2)–Cnt(C_8H_8)	1.894	U(1)–Cnt(C_8H_8)	1.990
U(1)–C(21)	2.692(11)	U(2)–C(29)	2.617(12)	U(1)–C(11)	2.715(5)
U(1)–C(22)	2.691(12)	U(2)–C(30)	2.614(12)	U(1)–C(12)	2.682(5)
U(1)–C(23)	2.712(12)	U(2)–C(31)	2.647(13)	U(1)–C(13)	2.704(5)
U(1)–C(24)	2.684(13)	U(2)–C(32)	2.634(13)	U(1)–C(14)	2.735(5)
U(1)–C(25)	2.656(12)	U(2)–C(33)	2.618(12)	U(1)–C(15)	2.689(6)
U(1)–C(26)	2.713(12)	U(2)–C(34)	2.630(13)	U(1)–C(16)	2.659(6)
U(1)–C(27)	2.690(13)	U(2)–C(35)	2.663(12)	U(1)–C(17)	2.701(6)
U(1)–C(28)	2.665(12)	U(2)–C(36)	2.667(12)	U(1)–C(18)	2.737(5)
Cnt(C_5Me_5)–U(2)–Cnt(C_8H_8)	138.0	Cnt(C_5Me_5)–U(2)–Cnt(C_8H_8)	140.7	Cnt(C_5Me_5)–U(2)–Cnt(C_8H_8)	134.7
U(1)–Cl(1)	2.921(3)	U(2)–Cl(1)	2.738(3)	U(1)–N(1)	2.284(4)
Cnt(C_5Me_5)–U(1)–Cl(1)	96.1	Cnt(C_8H_8)–U(1)–Cl(1)	113.7	Cnt(C_5Me_5)–U(1)–N(1)	104.9
Cnt(C_5Me_5)–U(1)–Cl(2)	97.3	Cnt(C_8H_8)–U(1)–Cl(2)	115.6	Cnt(C_8H_8)–U(1)–N(1)	120.3
Cnt(C_5Me_5)–U(2)–Cl(1)	100.0	Cnt(C_8H_8)–U(2)–Cl(1)	119.2		
U(1)–Cl(2)	2.673(3)	U(2)–Cl(1)–U(1)	148.11(11)		
Cl(2)–U(1)–Cl(1)	80.68(9)				

4. Discussion

The formation of **1** from $(C_5Me_5)_2UCl_2$ and $K_2C_8H_8$ represents a rare example of $(C_5Me_5)^{1-}$ ligand displacement for $(C_5Me_5)_2UCl_2$, a complex which has been such an important source of the $[(C_5Me_5)_2U]^{2+}$ unit in tetravalent uranium metallocene chemistry. $(C_5Me_5)^{1-}$ displacement via ionic salt metathesis has been recently observed with the sterically crowded complexes $(C_5Me_5)_3U$ and $[(C_5Me_5)_2U]_2(C_6H_6)$, Eqs. (5) and (6) [48],

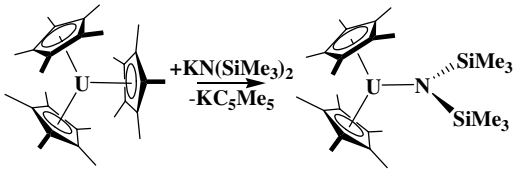

(5)

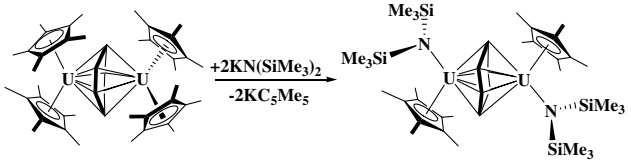

(6)

but this is more reasonable since it relieves steric strain. Steric factors could also explain the unexpected loss of $(C_5Me_5)^{1-}$ in the synthesis of **1** if the reaction proceeded through some highly crowded intermediates, such as "$(C_5Me_5)_2UCl(C_8H_8)K$." In addition, the product that would form if two chlorides were displaced, "$(C_5Me_5)_2U(C_8H_8)$", has never been isolated, but is expected to be sterically crowded [25].

In any case, the $(C_5Me_5)_2UCl_2/K_2C_8H_8$ reaction provides a convenient route using mild conditions to an unsolvated U(IV) metallocene that contains an open coordination site. As demonstrated by the ε-caprolactam reaction, Eq. (3), complex **1** is an arene soluble option for the evaluation of the coordination chemistry of U(IV) in a metallocene environment when a mixed ligand metallocene coordination geometry is acceptable. An advantage of the mixed ligand nature of **1** is that addition of any ligand immediately generates a chiral metal center ligated with four different groups.

Replacement of the chloride in **1** with another anion generates heteroleptic complexes like **4** that have three different ligands. Such completely heteroleptic complexes are generally difficult to synthesize because ligand redistribution reactions lead to the more common and favored bis(pentamethylcyclopentadienyl) complexes or tris(cyclopentadienyl) complexes in the case of the smaller $(C_5H_5)^{1-}$ ligands.

5. Conclusion

The synthesis of $(C_5Me_5)(C_8H_8)ClU(\mu\text{-}Cl)U(C_8H_8)$-$(C_5Me_5)$ (**1**), provides a soluble, sterically unsaturated U(IV) complex that can be conveniently prepared and used to evaluate U(IV) coordination chemistry in a

neutral metallocene environment. The fact that this complex can be prepared by $(C_5Me_5)^{1-}$ displacement demonstrates that the pentamethylcyclopentadienyl ligands of $(C_5Me_5)_2UCl_2$ can be separately cleaved using the appropriate reagents. Complex **1** should be a good precursor to completely heteroleptic tri- and tetrasubstituted U(IV) metallocenes [4–6].

6. Supporting material

Details on data collection and refinement, fractional atomic coordinates, anisotropic displacement parameters and full list of bond lengths and angles in CIF format has been deposited at the Cambridge Crystallographic Data Centre, CCDC No. 269609–269611 for compounds **1–3**, respectively. Copies of this information may be obtained free of charge from The Director, CCDC, 12 Union Road, Cambridge, CB2 1EZ, UK (fax: +44 1223 336033; e-mail: deposit@ccdc.cam.ac.uk or http://www.ccdc.cam.ac.uk).

Acknowledgments

We thank the Chemical Sciences, Geosciences, and Biosciences Division of the Office of Basic Energy Sciences of the Department of Energy for support.

References

[1] C.J. Schaverian, Adv. Organomet. Chem. 36 (1994) 283.
[2] R. Anwander, W.A. Herrmann, Top. Curr. Chem. 179 (1996) 1.
[3] W.J. Evans, Polyhedron 6 (1987) 803.
[4] T.J. Marks, R.D. Ernst, in: G. Wilkinson, F.G.A. Stone, E.W. Abel (Eds.), Comprehensive Organometallic Chemistry, Pergamon, Oxford, 1982, p. 211 (Chapter 21).
[5] F.T. Edelmann, Comprehensive Organometallic Chemistry II, in: G. Wilkinson, F.G.A. Stone, E.W. Abel (Eds.), Pergamon, Oxford, 1995, p. 131 (Chapter 2).
[6] T.J. Marks, Prog. Inorg. Chem. 25 (1979) 223.
[7] W.J. Evans, T.T. Perterson, M.D. Rausch, W.E. Hunter, H. Zhang, J.L. Atwood, Organometallics 4 (1985) 554.
[8] W.J. Evans, C.H. Fujimoto, M.A. Johnston, J.W. Ziller, Organometallics 21 (2002) 1825.
[9] T.M. Gilbert, R.R. Ryan, A.P. Sattelberger, Organometallics 8 (1989) 857.
[10] P.F. Fagan, J.M. Manriquez, E.A. Maatta, A.M. Seyam, T.J. Marks, J. Am. Chem. Soc. 103 (1981) 6650.
[11] A.L. Wayda, Inorg. Synth., vol. 27, p. 150.
[12] W.J. Evans, M.A. Johnston, R.D. Clark, J.W. Ziller, Inorg. Chem. 39 (2000) 3421.
[13] SMART Software Users Guide, version 5.1, Bruker Analytical X-Ray Systems, Inc.; Madison, WI, 1999.
[14] SAINT Software Users Guide, version 6.0, Bruker Analytical X-Ray Systems, Inc.; Madison, WI, 1999.
[15] G.M. Sheldrick, SADABS, version 2.10, Bruker Analytical X-Ray Systems, Inc., Madison, WI, 2001.
[16] G.M. Sheldrick, SHELXTL version 6.12, Bruker Analytical X-Ray Systems, Inc., Madison, WI, 2001.
[17] International Tables for X-Ray Crystallography, vol. C., Kluwer Academic Publishers, Dordrecht, 1992.
[18] T. Arliguie, M. Fourmigue, M. Ephritikhine, Organometallics 19 (2000) 109.
[19] K.A.N.S. Ariyaratne, R.E. Cramer, J.W. Gilje, Organometallics 21 (2002) 5799.
[20] J.L. Kiplinger, D.E. Morris, B.L. Scott, C.J. Burns, Organometallics 21 (2002) 3073.
[21] W.J. Evans, G.W. Nyce, K.J. Forrestal, J.W. Ziller, Organometallics 21 (2002) 1050.
[22] A.R. Schake, L.R. Avens, C.J. Burns, D.L. Clark, A.P. Sattelberger, W.H. Smith, Organometallics 12 (1993) 1497.
[23] M.R. Spirlet, J. Rebizant, C. Apostolidis, B. Kanellakopulos, Acta Cryst. C48 (1992) 2135.
[24] J.-C. Berthey, C. Boisson, M. Lance, J. Vigner, M. Nierlich, M. Ephritikhine, J. Chem. Soc. Dalton Trans. (1995) 3027.
[25] W.J. Evans, G.W. Nyce, J.W. Ziller, Angew. Chem. Int. Ed. 39 (2000) 240.
[26] K.C. Jantunen, C.J. Burns, I. Castro-Rodriguez, R.E. Da Re, J.T. Golden, D.E. Morris, B.L. Scott, F.L. Taw, J.L. Kiplinger, Organometallics 23 (2004) 4682.
[27] E. Barnea, T. Andrea, M. Kapon, J.-C. Berthey, M. Ephritikhine, M.S. Eisen, J. Am. Chem. Soc. 126 (2004) 10860.
[28] A. Zalkin, K.E. Raymond, J. Am. Chem. Soc. 91 (1969) 5667.
[29] A. Avdeef, K.N. Raymond, K.O. Hodgson, A. Zalkin, Inorg. Chem. 11 (1972) 1083.
[30] S.M. Cendrowski-Guillaume, M. Nierlich, M. Ephritikhine, J. Organomet. Chem. 643–644 (2002) 209.
[31] P.L. Diaconescu, C.C. Cummins, J. Am. Chem. Soc. 124 (2002) 7660.
[32] P.C. Blake, M.F. Lappert, R.G. Taylor, J.L. Atwood, W.E. Hunter, H. Zhang, J. Chem. Soc. Dalton Trans. (1995) 3335.
[33] W.W. Lukens Jr., S.M. Beshouri, L.L. Blosch, A.L. Stuart, R.A. Andersen, Organometallics 18 (1999) 1235.
[34] R.P. Hughes, J.R. Lomprey, A.L. Rheingold, B.S. Haggerty, G.P.A. Yap, J. Organomet. Chem. 517 (1996) 89.
[35] R.D. Shannon, Acta. Crystallogr. A32 (1976) 751.
[36] D.J. Wilson, A. Sebastian, F.G.N. Cloke, A.G. Avent, P.B. Hitchcock, Inorg. Chim. Acta 345 (2003) 89.
[37] J.F. LeMaréchal, C. Villiers, P. Charpin, M. Nierlich, M. Lance, J. Vigner, M. Ephritikhine, J. Organomet. Chem. 379 (1989) 259.
[38] J.M. Manriquez, P.J. Fagan, T.J. Marks, S.H. Vollmer, C.D. Day, V.W. Day, J. Am. Chem. Soc. 101 (1979) 5075.
[39] P. Roussel, P.B. Hitchcock, N. Tinker, P. Scott, J. Chem. Comm. (1996) 2053.
[40] W.J. Evans, J.M. Perotti, J.W. Ziller, J. Am. Chem. Soc. 127 (2005) 3894.
[41] W.J. Evans, C.H. Fujimoto, M.A. Greci, J.W. Ziller, Eur. J. Inorg. Chem. (2001) 745, and references therein.
[42] W.J. Evans, C.H. Fujimoto, J.W. Ziller, Organometallics 20 (2001) 4529, and references therein.
[43] D. Seyferth, Organometallics 23 (2004) 3562.
[44] J.C. Berthet, M. Ephritikhine, Coord. Chem. Rev. 178–180 (1998) 83.
[45] L.G. McCullough, H.W. Turner, R.A. Andersen, A. Zalkin, D.H. Templeton, Inorg. Chem. 20 (1981) 2869.
[46] J.M. Berg, D.L. Clark, J.C. Huffman, D.E. Morris, A.P. Sattelberger, W.E. Streib, W.G. Van der Sluys, J.G. Watkin, J. Am. Chem. Soc. 114 (1992) 10811.
[47] B.D. Stubbert, C.L. Stern, T.J. Marks, Organometallics 22 (2003) 4836.
[48] W.J. Evans, S.A. Kozimor, J.W. Ziller, N. Kaltsoyannis, J. Am. Chem. Soc. 126 (2004) 14533.

Available online at www.sciencedirect.com
SCIENCE DIRECT®
Polyhedron 25 (2006) 493–498
POLYHEDRON
www.elsevier.com/locate/poly

Solid state aggregation of lithium and thallium(I) bis(alkylamido)phenylboranes

David R. Manke, Daniel G. Nocera *

Department of Chemistry, 6-335, Massachusetts Institute of Technology, 77 Massachusetts Avenue Cambridge, MA 02139-4307, United States

Received 31 May 2005; accepted 9 August 2005
Available online 23 September 2005

Abstract

The conversion of *N*,*N*′-dilithiobis(alkylamido)phenylboranes [RN–B^{Ph}–NR]Li_2 (R = ^{t}Bu (**1**), ^{i}Pr (**2**)) to the equivalent dithallium(I) bisamides proceeds readily through the reaction with two molar equivalents of thallous chloride. The thallium amides [RN–B^{Ph}–NR]Tl_2 (R = ^{t}Bu (**3**), ^{i}Pr (**4**)) have been prepared and characterized by ^{1}H and ^{11}B{^{1}H} NMR. Single crystal X-ray structures of **2**–**4** reveal the formation of aggregates in the solid state.
© 2005 Elsevier Ltd. All rights reserved.

Keywords: Thallium amides; Lithium amides; Borylamides; Aggregation; Infinite chains

1. Introduction

Many metal amides form aggregates in the solid state [1,2]. Aggregate formation is governed by steric constraints of the solid state structure, the presence of bridging ligands, and electrostatic interactions between the metal ion and amide [3]. Most extended amide structures involve lithium as the metal ion with a paucity of structurally characterized amide aggregates of other non-alkali metal cations such as thallium(I). The latter cation is of interest because extended structures may involve metallophillic interactions between the two $6s^2$ filled shell thallium(I) atoms due to dispersion forces [4]. Recent work by Gade [5] has begun to shed light on the aggregation properties of such systems. In these instances, closed-shell metal–metal interaction, as well as metal–arene interactions and the relatively low coordination numbers common to thallium(I) play a significant role in supporting extended structures of unusual patterns of aggregation.

We have recently developed a transition metal chemistry for bis(alkylamido)phenylboranes, [RN–B^{Ph}–NR]$^{2-}$, by reacting dilithio salts of bisamides with metal dihalides [6–8]. Since the dilithiobis(amido) species are so important to our synthetic schemes, they warranted characterization. Similarly, we wished to develop analogous dithallium(I) diamides as a metathetical alternative owing to the less reducing properties of thallium transmetallation agents. We now report the synthesis, spectroscopic characterization, and solid state structures of lithium and thallium aggregates of bis(alkylamido)phenylborane ligands. We find that the thallium amido complexes produce brightly colored species possessing interesting extended solid state structures.

2. Experimental

2.1. General procedures

All manipulations were carried out using modified Schlenk techniques under an atmosphere of N_2 or in a Vacuum Atmosphere HE-553-2 glove box. Solvents for synthesis were of reagent grade or better and were dried according to standard methods [9]. *N*,*N*′-dilithiobis(isopropylamido)phenylborane and *N*,*N*′-dilithiobis(*tert*-butylamido)phenylborane were prepared by literature methods [10]. All other materials were used as received.

* Corresponding author. Tel.: +1 617 253 5537; fax: +1 617 253 7670.
E-mail address: nocera@mit.edu (D.G. Nocera).

0277-5387/$ - see front matter © 2005 Elsevier Ltd. All rights reserved.
doi:10.1016/j.poly.2005.08.021

2.2. Preparation of [RN–B^{Ph}–NR]Tl_2, R = ^{t}Bu (3) and R = ^{i}Pr (4)

Pentane solutions (7 ml) containing 400 mg of [RN–B^{Ph}–NR]Li_2 (R = ^{t}Bu (**1**) (1.64 mmol); R = ^{i}Pr (**2**) (1.85 mmol)) were frozen. Upon partial thawing, solid thallous chloride was added in three parts (800 mg (3.34 mmol) to **1**; 900 mg (3.75 mmol) to **2**) to the dilithiodiamide solutions. Some black precipitate formed immediately (thallium metal). The solution slowly turned yellow over the course of 3 h, with significant black precipitate forming. The mixture was allowed to stir for 24 h. Solvent was removed in vacuo, and 15 ml of toluene was added. The solution was then filtered through Celite to remove thallium metal and LiCl. Solvent was removed in vacuo from the resulting clear red-orange solution, yielding 539 mg (51.4% yield) of red crystalline solid **3** and 620 mg (54.5% yield) of orange powder **4**. Yields are based upon dilithium starting material. The resulting complexes readily decompose at room temperature in solution or in the solid state, but are stable for months when stored at −35 °C. *Anal.* data for **3**. ^{1}H NMR (300 MHz, C_6D_6, 25 °C) δ 1.330 (s, 18H), 7.0-7.4 (m, 5H) $^{11}B\{^1H\}$ NMR (160.490 MHz, C_6D_6, 25 °C) δ 25.454. *Anal.* data for **4**. ^{1}H NMR (300 MHz, C_6D_6, 25 °C) δ 1.280 (d, 12H, $J = 6.000$ Hz), 5.578 (br s, 2H), 7.2–7.5 (m, 5H) $^{11}B\{^1H\}$ NMR (160.490 MHz, C_6D_6, 25 °C) δ 26.843.

Table 1
Crystallographic data for [^{i}PrN–B^{Ph}–N^{i}Pr]Li_2 **(2)**, [^{t}BuN–B^{Ph}–N^{t}Bu]Tl_2 **(3)** and [^{i}PrN–B^{Ph}–N^{i}Pr]Tl_2 **(4)**

	2	**3**	**4**
Empirical formula	$C_{12}H_{19}BLi_2N_2$	$C_{17.50}H_{27}BN_2Tl_2$	$C_{12}H_{23}BN_2Tl_2$
Formula weight	215.99	684.99	614.90
Temperature (K)	100(2)	183(2)	100(2)
λ (Å)	0.71073	0.71073	0.71073
Space group	$I4_1/acd$	$P\bar{1}$	$Pna2_1$
a (Å)	15.1389(8)	6.5486(14)	10.611(3)
b (Å)	15.1389(8)	13.055(3)	11.936(3)
c (Å)	72.654(5)	13.408(3)	48.733(12)
α (°)	90	62.398(3)	90
β (°)	90	80.039(4)	90
γ (°)	90	83.695(4)	90
V (Å^3)	16651.3(17)	1000.0(4)	6172(3)
Z	54	2	16
d_{calcd} (Mg/m^3)	1.034	2.261	2.629
Absorption coefficient (mm^{-1})	0.058	16.093	20.840
R_1[a]	0.0385	0.0763	0.0466
wR_2[b]	0.0955	0.2027	0.1095

[a] $R_1 = \sum \||F_o| - |F_c|\| / \sum |F_o|$.
[b] $wR_2 = \left[\sum w(F_o^2 - F_c^2)^2 / \sum w(F_o^2)^2\right]^{1/2}$.

2.3. Physical methods

^{1}H NMR spectra were recorded on solutions at 25 °C within the magnetic fields of a Varian Mercury 300 spectrometer, which was located in the Department of Chemistry Instrumentation Facility (DCIF). Chemical shifts are reported using the standard δ notation in ppm. ^{1}H NMR spectra were referenced to residual solvent peak. $^{11}B\{^1H\}$ NMR spectra were collected at the DCIF on a Varian Inova 501 spectrometer and referenced to an external $BF_3 \cdot OEt_2$ standard at 0 ppm.

X-ray diffraction experiments were performed on single crystals grown from concentrated pentane (**2**), toluene (**3**) or pentane/ether (**4**) solutions at −35 °C. Crystals were removed from the supernatant liquid and transferred onto a microscope slide coated with Paratone N oil. Selected crystals were affixed to a glass fiber in Paratone N oil and cooled to −90 (**3**) or −173 (**2**, **4**) °C. Data collection was performed by shining Mo Kα ($\lambda = 0.71073$ Å) radiation onto crystals mounted onto a Bruker CCD diffractometer. The data were processed and refined by using the program SAINT supplied by Siemens Industrial Automation, Inc. The structures were solved by direct methods (SHELXTL v6.10,

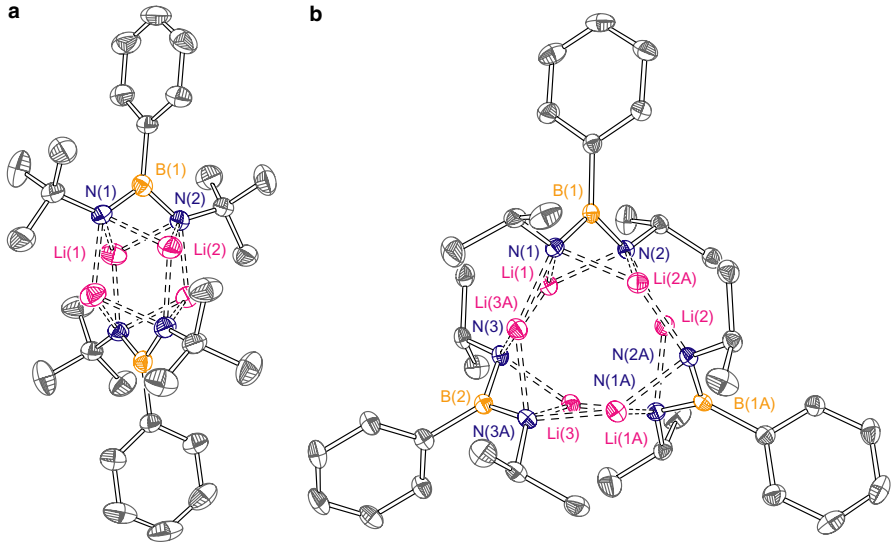

Fig. 1. Solid state structure of (a) [^{t}BuN–B^{Ph}–N^{t}Bu]Li_2 (**1**) and (b) [^{i}PrN–B^{Ph}–N^{i}Pr]Li_2 (**2**) with thermal ellipsoids shown at the 40% probability level.

Sheldrick, G.M., and Siemens Industrial Automation, Inc., 2000) in conjunction with standard difference Fourier techniques. All non-hydrogen atoms were refined anisotropically unless otherwise noted. Hydrogen atoms were placed in calculated positions. An AFIX 66 instruction was used to restrain a disordered solvent toluene molecule in **3**. Complex **4** was refined as a racemic twin, with a BASF refining to 0.47042. Some details regarding the refined data and cell parameters are provided in Table 1.

Table 2
Selected bond lengths (Å) and bond angles (°) of [^{i}PrN–B^{Ph}–N^{i}Pr]Li$_2$ (**2**)

Bond lengths (Å)	
B(1)–N(1)	1.437(2)
B(1)–N(2)	1.438(2)
B(2)–N(3)	1.439(2)
Li(1)–N(3)	2.004(7)
Li(1)–N(2)	2.012(7)
Li(1)–N(1)	2.104(7)
Li(2)–N(2)	1.997(7)
Li(2)–N(1A)	2.012(7)
Li(2)–N(2A)	2.101(7)
Li(3)–N(1A)	1.995(7)
Li(3)–N(3)	2.026(7)
Li(3)–N(3A)	2.117(7)
Li(3)–C(3A)	2.419(8)
Bond angles (°)	
N(2)–B(1)–N(1)	112.03(15)
N(3)–B(2)–N(3A)	112.9(2)
N(3)–Li(1)–N(2)	147.7(4)
N(2)–Li(2)–N(1A)	147.3(3)
N(1A)–Li(3)–N(3)	148.5(4)
B(1)–N(1)–Li(1)	73.4(3)
B(1)–N(1)–Li(2A)	76.3(3)
B(1)–N(2)–Li(1)	76.4(3)
B(1)–N(2)–Li(2A)	73.3(3)
B(2)–N(3)–Li(3)	76.5(3)
B(2)–N(3)–Li(3A)	73.4(3)
N(2)–Li(1)–N(1)	70.9(2)
N(1A)–Li(2)–N(2A)	70.9(2)
N(3)–Li(3)–N(3A)	70.8(3)

3. Results and discussion

The dilithio salts of bis(alkylamido)phenylboranes are readily prepared from the reaction of the parent amine with 2 equiv. of *n*-BuLi. The *tert*-butyl analogue [^{t}BuN–B^{Ph}–N^{t}Bu]Li$_2$ (**1**) has previously been prepared [11] and structurally characterized [12]. The structure exhibits a heterocubane Li and N core that is familiar to other difunctional lithium amides [13–15]. The isopropyl derivative has also been reported previously, but is presented structurally here for the first time. The structure of [^{i}PrN–B^{Ph}–N^{i}Pr]Li$_2$ possesses a trimeric configuration, demonstrating a distorted Li_6N_6 hexagonal prismatic core (Fig. 1). Such configurations have been observed in iminolithium hexamers [16]. Table 2 lists selected bond lengths and angles for **2**. The monomeric Li_2N_2 core possesses metric parameters similar to that observed for the *tert*-butyl analogue, with N–B distances ranging from 1.437(2) to 1.439(2) Å and Li–N distances of 2.012(7) to 2.117(7) Å. The N–B–N angle (112.03(15)–112.9(2)°) and bite angle (N–Li–N = 70.9(2)–76.5(3)°) are also consistent with the monomeric core of [^{t}BuN–B^{Ph}–N^{t}Bu]Li$_2$. One methyl unit on each isopropyl group appears to have an agostic C(–H)···Li contact (d(C–Li) = 2.419(8) Å). This is consistent with the ^{1}H NMR, which exhibits two methyl resonances [8], indicating that the trimeric structure is maintained in solution. It is interesting to note the change in aggregation from a dimeric to a trimeric unit, with this

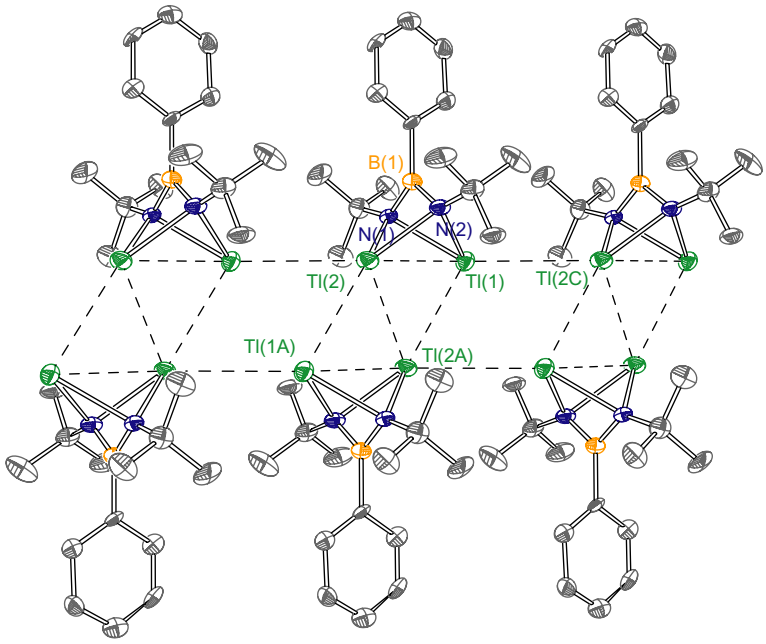

Fig. 2. Solid state structure of [^{t}BuN–B^{Ph}–N^{t}Bu]Tl$_2$ (**3**) showcasing three dimeric units and weak intermolecular thallium–thallium contacts. Thermal ellipsoids are shown at the 50% probability level.

small variance in steric bulk. This has also been observed by Brask et al. [17] for [^{t}BuN–B$^{n\text{Bu}}$–N^{t}Bu]Li$_2$ and [^{t}BuN–B$^{\text{Et}}$–N^{t}Bu]Li$_2$ with analogous dimeric and trimeric structures, respectively. In this instance, however, the difference in the steric bulk originates from the substituents on the boron bridgehead, rather than on the amido nitrogens.

Table 3
Selected bond lengths (Å) and bond angles (°) of [^{t}BuN–B$^{\text{Ph}}$–N^{t}Bu]Tl$_2$ (**3**)

Bond lengths (Å)	
Tl(1)–N(1)	2.47(2)
Tl(1)–N(2)	2.53(3)
Tl(1)–Tl(2)	3.3877(18)
Tl(1)–Tl(2A)	3.5394(19)
N(1)–B(1)	1.44(4)
Tl(2)–N(2)	2.40(3)
Tl(2)–N(1)	2.41(2)
Tl(2)–Tl(2A)	3.228(3)
Tl(1)–Tl(2C)	3.772(2)
N(2)–B(1)	1.43(4)
Bond angles (°)	
N(1)–Tl(1)–N(2)	55.7(8)
N(2)–Tl(2)–N(1)	58.0(8)
B(1)–N(2)–Tl(1)	85.4(19)
B(1)–N(1)–Tl(2)	85.1(18)
B(1)–N(1)–Tl(1)	87.4(19)
B(1)–N(2)–Tl(2)	85.9(19)
Tl(1)–Tl(2)–Tl(1A)	124.50(4)
Tl(1)–Tl(2)–Tl(1B)	132.24(6)
Tl(2A)–Tl(2)–Tl(1)	64.63(5)
Tl(2)–Tl(1)–Tl(2A)	55.50(4)
N(2)–B(1)–N(1)	109(3)

Taking these dilithio salts and stirring them in a pentane solution with thallous chloride for 24 h led to the formation of the thallium(I) amides **3** and **4**.

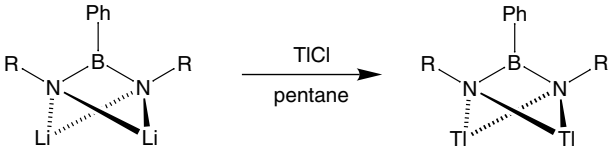

(1)

R = ^{t}Bu (**1**), ^{i}Pr (**2**) R = ^{t}Bu (**3**), ^{i}Pr (**4**)

Both complexes are soluble in aromatic and ethereal solvents, and are stable in solution or the solid state in a nitrogen atmosphere at −35 °C for months. Warming to room temperature or exposure to air results in the facile decomposition of these thallium(I) diamides to generate thallium metal. ^{1}H NMR exhibits only a single *tert*-butyl resonance for **3** and a single set of isopropyl resonances for **4**. A single peak is observed in the ^{11}B{^{1}H} NMR spectra of both species. Single crystal X-ray analysis of these thallium(I) bisamides demonstrate an interesting pattern of molecular packing in the solid state.

Recrystallization of **3** from a concentrated toluene solution afforded deep red single crystals. The asymmetric unit of the complex possesses a single dithallium unit that has a molecular structure in which two nitrogen and two thallium(I) atoms form a puckered spirocycle. This structure is

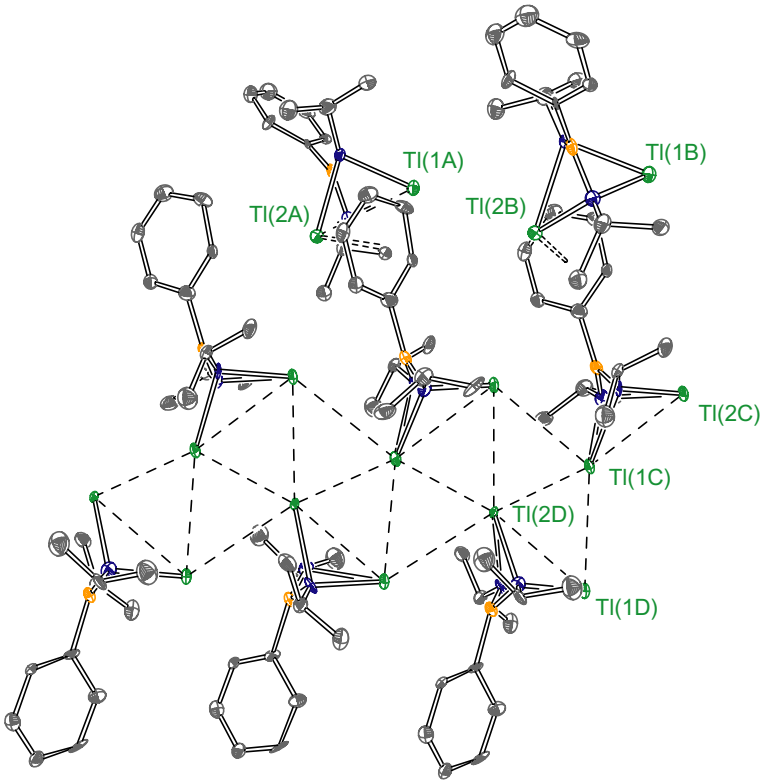

Fig. 3. Solid state structure of [^{i}PrN–B$^{\text{Ph}}$–N^{i}Pr]Tl$_2$ (**4**) demonstrating both thallium–thallium and thallium–arene interactions. Thermal ellipsoids are shown at the 50% probability level.

consistent with the observed motif in the monomeric units of the dilithium structures, with ligand metrics almost identical to those observed in **1** and **2**. This monomeric unit has been observed previously by Hellmann et al. [18] for other difunctional thallium(I) amides. Table 3 lists selected bond lengths and bond angles for **3**. The fairly short Tl···Tl distance in **3** is likely due to the nature of the bridging ligand, though it is of an appropriate length for a Tl···Tl metallophilic interaction (d(Tl···Tl) = 3.3877(18) Å). In the solid, molecular units of **3** aggregate into dimeric sets, where each thallium ion has a close contact with two intermolecular thallium atoms. The result is a pair of edge sharing triangles, with Tl···Tl distances of 3.228(3) along the shared edge and 3.5394(19) Å along the outer edge (Fig. 2). Hellmann et al. [19] have observed this type of edge sharing triangular dimerization previously in a trithallium system. Unlike the trithallium system, however, this system has additional intermolecular Tl···Tl contacts of 3.772(2) Å, resulting in a rare example [18,20,21] of an infinite chain thallium(I) amide compound.

Recrystallization of **4** from a pentane/ether solution at −35 °C, yields dark orange single crystals that demonstrate a truly unique solid state structure. Selected bond lengths and angles for **4** are listed in Table 4. The asymmetric unit possesses four dithallium units, all of which possess similar Tl_2N_2 cores and ligand metrics as **3** with slightly shorter Tl···Tl contacts (d(Tl···Tl) = 3.2653(16)–3.2667(14) Å). Two of these monomeric units aggregate to form an infinite chain of edge sharing triangles (Fig. 3). Each dithallium set of a monomeric unit forms a triangle with one thallium of another dithallium set through very close contacts of 2.950(2) and 3.004(2) Å. The remaining Tl···Tl contacts are significantly longer, ranging from 3.3727(8) to 3.5330(18) Å. The other two monomeric units are not involved in aggregation, but instead demonstrate a metal–arene interaction. One thallium from each of these units has a contact of 3.496(18) Å from the plane of the phenyl rings of the ligands in the aggregation polymer. This distance is consistent with other arene interactions in thallium(I) amide species (d(Tl···C) = 3.34–3.74 Å) [22]. The effects of thallium–arene interactions in the aggregation of thallium(I) amides has been examined by Gade and co-workers [22,23], who have shown the Tl–arene interaction to be close to the Tl···Tl interaction in influence on aggregate formation.

The marked change in the mode of aggregation between **3** and **4** results from the modest size difference between *tert*-butyl to isopropyl amido substituents, respectively. The *tert*-butyl derivative has two symmetrically inequivalent thallium atoms that possess three and four Tl···Tl close contacts, respectively. The reduced steric encumbrance of isopropyl groups permits greater access to thallium atoms. The result is an increased number of Tl···Tl contacts to a maximum of five for thallium atoms in the infinite chain of **4**. The *tert*-butyl derivative possesses thallium triangles that share a single edge, while the isopropyl derivative possesses thallium triangles sharing two edges, as well as exhibiting closer Tl···Tl contacts. Interestingly, though **4**

Table 4
Selected bond lengths (Å) and bond angles (°) of [^{i}PrN–B^{Ph}–N^{i}Pr]Tl$_2$ (**4**)

Bond lengths (Å)	
Tl(1)–Tl(2)	3.2667(14)
Tl(5)–Tl(6)	3.2653(16)
Tl(7)–Tl(8)	3.2056(16)
Tl(5A)–Tl(8)	3.004(2)
Tl(5)–Tl(8)	2.950(2)
Tl(5)–Tl(7)	3.3727(18)
Tl(6A)–Tl(8)	3.3995(18)
Tl(5)–Tl(6A)	3.5330(18)
Tl(7A)–Tl(8)	3.4892(17)
B(1)–N(1)	1.43(2)
B(1)–N(2)	1.62(2)
Tl(4)···Ph	3.496(18)
Tl(1)–N(1)	2.383(14)
Tl(1)–N(2)	2.314(12)
Tl(2)–N(1)	2.703(14)
Tl(2)–N(2)	2.452(13)
Tl(5)–N(5)	2.448(17)
Tl(5)–N(6)	2.459(17)
Tl(6)–N(5)	2.427(16)
Tl(6)–N(6)	2.386(17)
B(3)–N(5)	1.54(3)
B(3)–N(6)	1.52(4)
Tl(2)···Ph	3.496(18)
Bond angles (°)	
Tl(5)–Tl(8)–Tl(7)	66.29(5)
Tl(5)–Tl(8)–Tl(5A)	126.94(4)
Tl(5)–Tl(8)–Tl(7A)	160.31(4)
Tl(5)–Tl(8)–Tl(6A)	67.18(3)
Tl(7)–Tl(5)–Tl(6A)	120.95(4)
Tl(7)–Tl(8)–Tl(7A)	106.48(5)
Tl(7)–Tl(8)–Tl(6A)	130.95(4)
Tl(5A)–Tl(7A)–Tl(8)	51.88(4)
Tl(5A)–Tl(8)–Tl(7)	166.48(5)
Tl(5A)–Tl(8)–Tl(7A)	62.06(4)
Tl(5A)–Tl(8)–Tl(6A)	60.95(2)
Tl(5A)–Tl(6A)–Tl(5)	103.11(5)
Tl(5A)–Tl(6A)–Tl(8)	53.53(4)
N(1)–B(1)–N(2)	109.1(13)
N(2)–Tl(1)–N(1)	63.9(5)
N(2)–Tl(2)–N(1)	57.4(4)
B(1)–N(1)–Tl(1)	80.8(9)
B(1)–N(1)–Tl(2)	86.5(10)
B(1)–N(2)–Tl(1)	79.6(8)
B(1)–N(2)–Tl(2)	91.7(9)
Tl(6)–Tl(5)–Tl(7)	131.05(5)
Tl(6)–Tl(5)–Tl(6A)	104.37(5)
Tl(8)–Tl(5)–Tl(7)	60.49(3)
Tl(8)–Tl(5)–Tl(6)	166.56(5)
Tl(8)–Tl(5)–Tl(6A)	62.49(4)
Tl(8)–Tl(7)–Tl(5)	53.22(4)
Tl(8)–Tl(5A)–Tl(7A)	66.06(3)
Tl(8)–Tl(5A)–Tl(6A)	65.52(4)
Tl(8)–Tl(5A)–Tl(8A)	126.54(4)
Tl(8)–Tl(5A)–Tl(6B)	164.10(6)
Tl(8)–Tl(6A)–Tl(5A)	50.33(4)
Tl(6A)–Tl(8)–Tl(7A)	122.57(4)
Tl(8A)–Tl(7A)–Tl(8)	105.10(5)
N(5)–B(3)–N(6)	118.6(12)
N(5)–Tl(5)–N(6)	65.0(5)
N(5)–Tl(6)–N(6)	66.4(5)
B(3)–N(5)–Tl(6)	73.2(10)
B(3)–N(5)–Tl(5)	81.4(11)
B(3)–N(6)–Tl(6)	74.8(11)
B(3)–N(6)–Tl(5)	81.4(11)

possesses an increase in number and a shortening of Tl···Tl contacts in the infinite chain, half of the thallium units are instead occupied with aryl interactions.

We began our foray into the synthesis and structural investigation of the dilithium and dithallium complexes **1**–**4** to develop viable transmetallation agents for the delivery of bis(alkylamido)phenylborane ligands. The dilithio species have proven to be effective in this transmetallation. We have found, in the case of the dithallium species, that the thermal instability of the complexes appears to limit the effectiveness of **3** and **4** as metathesis reagents. Regardless of the effectiveness of these complexes for transmetallation reactions, the investigation into their solid state structures showed interesting new aggregation patterns. The effects of the metallophilic Tl···Tl interactions play a significant role in the formation of an unprecedented structure-type.

Acknowledgment

This work was supported by a Grant from the National Science Foundation (CHE-0132680).

Appendix A. Supplementary data

Table of X-ray crystallographic data for complex **2**–**4** including a fully labeled thermal ellipsoid plot, final atomic coordinates, equivalent isotropic displacement parameters, anisotropic displacement parameters, and bond distances and bond angles. Crystallographic data for the structural analyses have been deposited with the Cambridge Crystallographic Data Center, CCDC Nos. 273690, 273691, and 273689 for compounds **2**–**4**, respectively. Copies of this information may be obtained free of charge from the Director, CCDC, 12 Union Road, Cambridge, CB2 1EZ, UK (fax: +44 1223 336033; e-mail: deposit@ccdc.cam.ac.uk or on the web http://www.ccdc.cam.ac.uk). Supplementary data associated with this article can be found, in the online version, at doi:10.1016/j.poly.2005.08.021.

References

[1] R.D. Rogers, J.L. Atwood, R. Grüning, J. Organomet. Chem. 157 (1978) 229.
[2] D. Mootz, A. Zinnius, B. Böttcher, Angew. Chem., Int. Ed. Engl. 8 (1969) 378.
[3] K. Gregory, P.v.R. Schleyer, R. Snaith, Adv. Inorg. Chem. 37 (1991) 47.
[4] P. Pyykkö, Chem. Rev. 97 (1997) 597.
[5] L.H. Gade, Dalton 3 (2003) 267.
[6] D.R. Manke, D.G. Nocera, Inorg. Chim. Acta 345 (2003) 235.
[7] D.R. Manke, D.G. Nocera, Inorg. Chem. 42 (2003) 4431.
[8] D.R. Manke, Z.-H. Loh, D.G. Nocera, Inorg. Chem. 43 (2004) 3618.
[9] W.L.F. Armarego, D.D. Perrin, Purification of Laboratory Chemicals, 4th ed., Butterworth–Heinmann, Oxford, 1996.
[10] C.D. Habben, A. Heine, G.M. Sheldrick, D. Stalke, Z. Naturforsch. B 47 (1992) 1367.
[11] D. Fest, C.D. Habben, A. Meller, G.M. Sheldrick, D. Stalke, F. Pauer, Chem. Ber. 123 (1990) 703.
[12] T. Chivers, C. Fedorchuk, G. Schatte, J.K. Brask, Can. J. Chem. 80 (2002) 821.
[13] K.W. Hellmann, A. Bergner, L.H. Gade, I.J. Scowen, M.J. McPartlin, J. Organomet. Chem. 573 (1999) 156.
[14] D.J. Brauer, H. Bürger, G.R. Liewald, J. Organomet. Chem. 30 (1986) 119.
[15] M.G. Gardiner, C.L. Raston, Inorg. Chem. 34 (1995) 4206.
[16] D. Barr, W. Clegg, R.E. Mulvey, R. Snaith, K.J. Wade, Chem. Commun. (1986) 295.
[17] J.K. Brask, T. Chivers, G. Schatte, Chem. Commun. (2000) 1805.
[18] K.W. Hellmann, L.H. Gade, R. Fleischer, D. Stalke, Chem. Commun. (1997) 527.
[19] K.W. Hellmann, L.H. Gade, R. Fleischer, T. Kottke, Chem. Eur. J. 3 (1997) 1801.
[20] J.C. Peters, S.B. Harkins, S.D. Brown, M.W. Day, Inorg. Chem. 40 (2001) 5083.
[21] K.W. Hellmann, L.H. Gade, I.J. Scowen, M. McPartlin, Chem. Commun. (1996) 2515.
[22] C.H. Galka, L.H. Gade, Inorg. Chem. 38 (1999) 1038.
[23] K.W. Hellmann, C. Galka, L.H. Gade, A. Steiner, D.S. Wright, T. Kottke, D. Stalke, Chem. Commun. (1998) 549.

Available online at www.sciencedirect.com
SCIENCE DIRECT®
Polyhedron 25 (2006) 499–512
POLYHEDRON
www.elsevier.com/locate/poly

Carbon–hydrogen versus carbon–chalcogen bond cleavage of furan, thiophene and selenophene by *ansa* molybdenocene complexes

David G. Churchill, Brian M. Bridgewater, Guang Zhu, Keliang Pang, Gerard Parkin *

Department of Chemistry, Columbia University, New York, NY 10027, USA

Received 1 June 2005; accepted 9 August 2005
Available online 7 October 2005

Dedicated with respect to Professor Malcolm H. Chisholm on the occasion of his 60th birthday. Happy birthday Malcolm!

Abstract

$[Me_2Si(C_5Me_4)_2]MoH_2$ reacts with furan and benzofuran to yield products resulting from C–H bond cleavage, namely $[Me_2Si(C_5Me_4)_2]Mo(\eta^1\text{-}C\text{-}C_4H_3O)H$ and $[Me_2Si(C_5Me_4)_2]Mo(\eta^1\text{-}C\text{-}C_8H_5O)H$, whereas the corresponding reactions of selenophene and benzoselenophene yield products resulting from C–Se bond cleavage, namely $[Me_2Si(C_5Me_4)_2]Mo(\eta^2\text{-}C,Se\text{-}SeC_4H_4)$ and $[Me_2Si(C_5Me_4)_2]Mo(\eta^2\text{-}C,Se\text{-}SeC_8H_6)$. On this basis, the reactivity of the selenophene derivatives is analogous to that of previously reported thiophene derivatives, while the reactivity of the furan derivatives is unique. DFT calculations indicate that C–E (E = O, S, Se) bond cleavage is thermodynamically more favored than C–H bond cleavage for each of the chalcogen derivatives. As such, the calculations provide evidence that C–O bond cleavage of the furan derivatives is not observed because of kinetic factors. DFT calculations also demonstrate that the observation of C–S bond cleavage of thiophene by the *ansa* metallocene $[Me_2Si(C_5Me_4)_2]MoH_2$ and C–H bond cleavage by Cp_2MoH_2 is dictated by thermodynamic factors. Specifically, the Me_2Si *ansa* bridge thermodynamically favors $[Me_2Si(C_5Me_4)_2]Mo(\eta^2\text{-}C,S\text{-}SC_4H_4)$ over $[Me_2Si(C_5Me_4)_2]Mo(\eta^1\text{-}C\text{-}SC_4H_3)H$ because the bridge promotes a shift in the coordination of the cyclopentadienyl rings from η^5-coordination towards η^3-coordination and this thermodynamically unfavorable modification is stabilized by sulfur-to-metal π-donation within $[Me_2Si(C_5Me_4)_2]Mo(\eta^2\text{-}C,S\text{-}SC_4H_4)$.
© 2005 Elsevier Ltd. All rights reserved.

Keywords: Molybdenum; Hydrodesulfurization; Hydrodenitrogenation; Ansa metallocene; Furan; Thiophene; Seleneophen

1. Introduction

Hydrodesulfurization (HDS) is the largest volume and most important industrial catalytic application of transition metals and is the process by which sulfur containing impurities are removed from crude petroleum feedstocks and fuels [1,2]. Thiophenes, in particular, are a class of molecules that are most resistant towards hydrodesulfurization and have consequently featured prominently as substrates for model studies [2,3]. However, despite the fact that molybdenum is the most essential transition metal component of a typical HDS catalyst [4], the majority of model studies pertaining to HDS of thiophene has focused on metals other than molybdenum [5–9]. For this reason, we have initiated a series of studies directed towards activating thiophene by molybdenum compounds and have reported the first examples of thiophene C–S bond cleavage by molybdenum. Specifically, we have demonstrated that: (i) the *ansa* molybdenocene dihydride complex $[Me_2Si(C_5Me_4)_2]MoH_2$ photochemically achieves cleavage of the C–S bond of thiophene to give $[Me_2Si(C_5Me_4)_2]Mo(\eta^2\text{-}C,S\text{-}SC_4H_4)$ (Scheme 1) [10]; (ii) $Mo(PMe_3)_6$ reacts with thiophene to yield the η^5-thiophene adduct $(\eta^5\text{-}C_4H_4S)Mo(PMe_3)_3$ and the butadiene–thiolate complex $(\eta^5\text{-}C_4H_5S)Mo(PMe_3)_2(\eta^2\text{-}CH_2PMe_2)$ (Scheme 2) [11–13]. In this paper, we describe the reactivity of $[Me_2Si(C_5Me_4)_2]MoH_2$ towards the oxygen and selenium counterparts of thiophene, namely furan and selenophene. These studies demonstrate that the course of the reaction between

* Corresponding author.
E-mail address: parkin@chem.columbia.edu (G. Parkin).

0277-5387/$ - see front matter © 2005 Elsevier Ltd. All rights reserved.
doi:10.1016/j.poly.2005.08.016

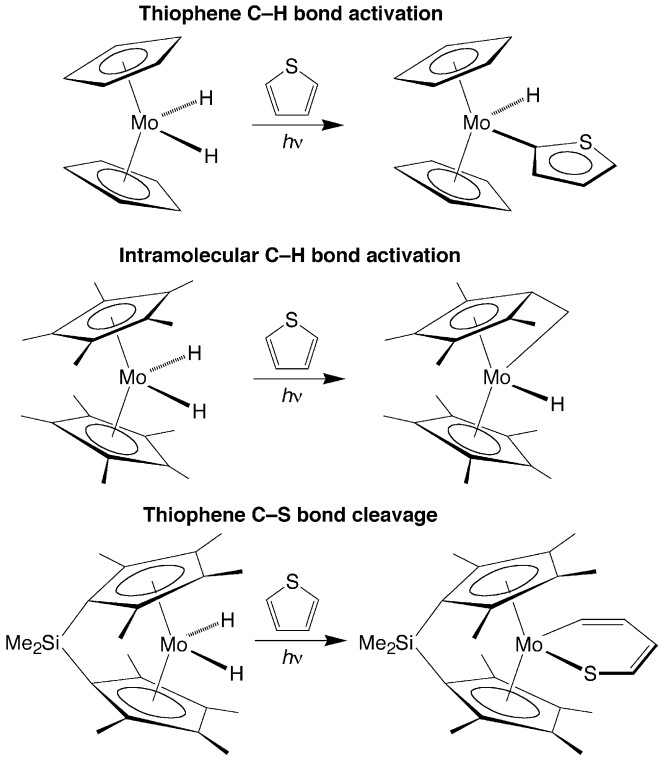

Scheme 1.

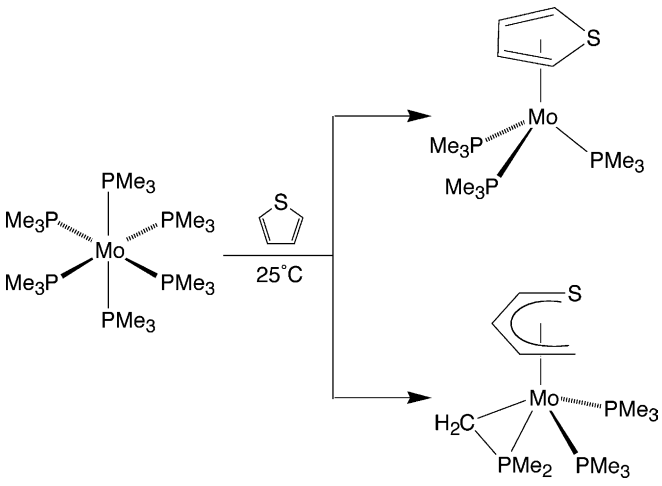

Scheme 2.

$[Me_2Si(C_5Me_4)_2]MoH_2$ and EC_4H_4 is strongly influenced by the nature of the chalcogen (E = O, S, Se).

2. Results and discussion

2.1. Computational analysis of the thermodynamics of thiophene C–H versus C–S bond cleavage

The ability of $[Me_2Si(C_5Me_4)_2]MoH_2$ to cleave the C–S bond of thiophene and give the metallacycle $[Me_2Si(C_5Me_4)_2]Mo(\eta^2\text{-}C,S\text{-}SC_4H_4)$ is not only significant because it represents the first example of thiophene C–S bond cleavage by a molybdenum compound, but it is also noteworthy because related molybdenocene complexes such as $Cp^*_2MoH_2$ and Cp_2MoH_2 do not exhibit analogous reactivity [10]. For example, the non-*ansa* counterpart $Cp^*_2MoH_2$ is inert to thiophene under comparable conditions and yields only a product of *intramolecular* C–H bond activation, namely $Cp^*(\eta^5,\eta^1\text{-}C_5Me_4CH_2)MoH$ (Scheme 1), thereby providing an interesting example of an *ansa* effect [14]. In contrast to the inertness of $Cp^*_2MoH_2$ towards thiophene, Cp_2MoH_2 is reactive. However, the reaction of Cp_2MoH_2 with thiophene gives a thienyl–hydride complex $Cp_2Mo(\eta^1\text{-}C\text{-}SC_4H_3)H$ via cleavage of the α C–H bond (Scheme 1) [5a,15], rather than a metallathiacycle $Cp_2Mo(\eta^2\text{-}C,S\text{-}SC_4H_4)$ via cleavage of the C–S bond; the corresponding tungsten complex, Cp_2WH_2, however, reacts with thiophene to give products derived from both C–H and C–S bond cleavage [5a,16].

While the difference in reactivity between $[Me_2Si(C_5Me_4)_2]MoH_2$ and $Cp^*_2MoH_2$ may be readily interpreted in terms of $Cp^*(\eta^5,\eta^1\text{-}C_5Me_4CH_2)MoH$ being exceptionally stable with respect to $[Cp^*_2Mo]$ compared to that of the *ansa* counterpart [17,18], the C–S versus C–H bond cleavage reactivity of $[Me_2Si(C_5Me_4)_2]MoH_2$ and Cp_2MoH_2, respectively, is not so easily rationalized. Therefore, to help explain this difference in reactivity, we have performed DFT calculations to establish the relative energies of the various C–H and C–S bond cleavage products. Furthermore, since the reaction of $[Me_2Si(C_5Me_4)_2]MoH_2$ with dibenzothiophene resulted in the formation of an η^1-*S*-dibenzothiophene adduct [10,19], we have also calculated the energies of the corresponding η^1-*S*-thiophene isomers that result from coordination of thiophene to the molybdenum center without either C–H or C–S bond cleavage.

With respect to the $\{[Me_2Si(C_5Me_4)_2]Mo\}$ system, the geometry optimized structures of $[Me_2Si(C_5Me_4)_2]Mo(\eta^2\text{-}C,S\text{-}SC_4H_4)$, *endo*-$[Me_2Si(C_5Me_4)_2]Mo(\eta^1\text{-}C\text{-}SC_4H_3)H$, *exo*-$[Me_2Si(C_5Me_4)_2]Mo(\eta^1\text{-}C\text{-}SC_4H_3)H$, and $[Me_2Si(C_5Me_4)_2]Mo(\eta^1\text{-}SC_4H_4)$ are illustrated in Fig. 1. The thiophene-derived fragment in each of these complexes lies in the equatorial metallocene plane, with the exception of the thiophene adduct $[Me_2Si(C_5Me_4)_2]Mo(\eta^1\text{-}SC_4H_4)$, for which the angle between the molybdenum and the thiophene plane is 170°. The displacement of the metal out of the thiophene plane in η^1-thiophene complexes has been attributed to minimizing filled–filled repulsions between the sulfur π-lone pair and the metal center [20].

The relative energies of the geometry optimized structures are listed in Table 1. Significantly, the calculations indicate that the experimentally observed metallathiacycle $[Me_2Si(C_5Me_4)_2]Mo(\eta^2\text{-}C,S\text{-}SC_4H_4)$ obtained by C–S bond cleavage is more stable than both (i) the thienyl–hydride resulting from C–H bond cleavage $[Me_2Si(C_5Me_4)_2]Mo(\eta^1\text{-}C\text{-}SC_4H_3)H$ and (ii) the η^1-thiophene adduct $[Me_2Si(C_5Me_4)_2]Mo(\eta^1\text{-}SC_4H_4)$ resulting from coordination without bond cleavage, as illustrated in Fig. 2. However, while the calculations indicate that the C–S bond cleavage product is the most stable, the calculations do not provide any indication as to whether the formation of $[Me_2Si(C_5\text{-}$

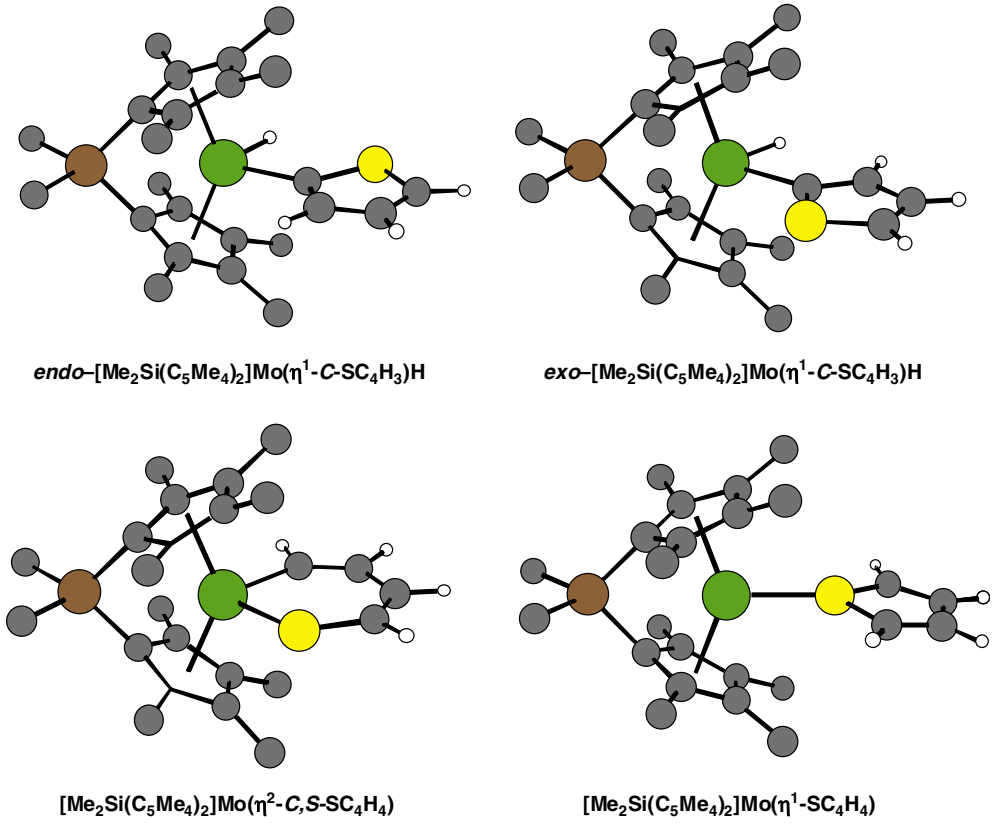

Fig. 1. Geometry optimized structures of $[Me_2Si(C_5Me_4)_2]Mo(\eta^2\text{-}C,S\text{-}SC_4H_4)$, $[Me_2Si(C_5Me_4)_2]Mo(\eta^1\text{-}C\text{-}SC_4H_3)H$, and $[Me_2Si(C_5Me_4)_2]Mo(\eta^1\text{-}SC_4H_4)$ (hydrogen atoms on methyl groups omitted for clarity).

Table 1
DFT calculated relative energies (kcal mol^{-1}) of $(Cp^R)_2Mo(\eta^2\text{-}C,E\text{-}EC_4H_4)$, $(Cp^R)_2Mo(\eta^1\text{-}C\text{-}EC_4H_3)H$, and $(Cp^R)_2Mo(\eta^1\text{-}EC_4H_4)$ isomers (cc-pVTZ(-f)/LACV3P basis sets)

	O	S	Se
$[Me_2Si(C_5Me_4)_2]Mo(\eta^2\text{-}C,E\text{-}EC_4H_4)$	0	0	0
$[Me_2Si(C_5Me_4)_2]Mo(\eta^1\text{-}C\text{-}EC_4H_3)H$ (*endo*)	11.4	5.3	7.8
$[Me_2Si(C_5Me_4)_2]Mo(\eta^1\text{-}C\text{-}EC_4H_3)H$ (*exo*)	8.9	6.1	9.3
$[Me_2Si(C_5Me_4)_2]Mo(\eta^1\text{-}EC_4H_4)$	31.9	16.1	20.5
$Cp_2Mo(\eta^2\text{-}C,E\text{-}EC_4H_4)$		0	
$Cp_2Mo(\eta^1\text{-}C\text{-}EC_4H_3)H$ (*endo*)		0.2	
$Cp_2Mo(\eta^1\text{-}C\text{-}EC_4H_3)H$ (*exo*)		0.1	
$Cp_2Mo(\eta^1\text{-}EC_4H_4)$		9.6	
$Cp^*_2Mo(\eta^2\text{-}C,E\text{-}EC_4H_4)$		0	
$Cp^*_2Mo(\eta^1\text{-}C\text{-}EC_4H_3)H$ (*endo*)		1.1	
$Cp^*_2Mo(\eta^1\text{-}C\text{-}EC_4H_3)H$ (*exo*)		1.2	
$Cp^*_2Mo(\eta^1\text{-}EC_4H_4)$		12.6	

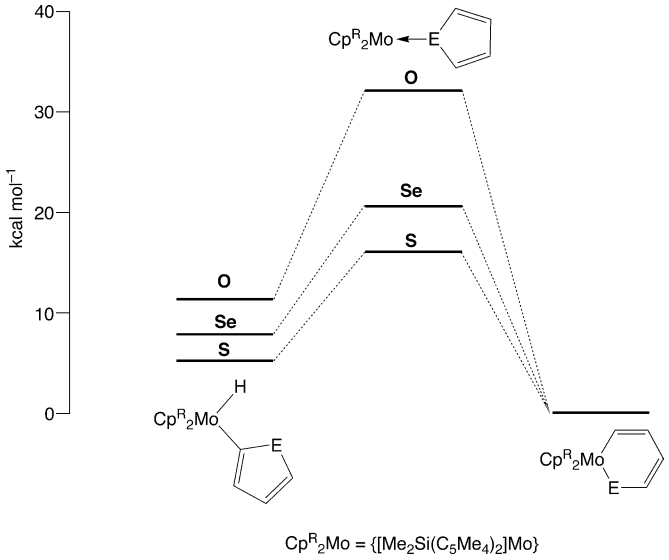

Fig. 2. Relative energies of geometry optimized structures of $[Me_2Si(C_5Me_4)_2]Mo(\eta^2\text{-}C,E\text{-}EC_4H_4)$, $[Me_2Si(C_5Me_4)_2]Mo(\eta^1\text{-}C\text{-}EC_4H_3)H$, and $[Me_2Si(C_5Me_4)_2]Mo(\eta^1\text{-}EC_4H_4)$ (E = O, S, Se).

$Me_4)_2]Mo(\eta^2\text{-}C,S\text{-}SC_4H_4)$ is actually dictated by kinetic factors, i.e., is $[Me_2Si(C_5Me_4)_2]Mo(\eta^2\text{-}C,S\text{-}SC_4H_4)$ obtained because the molybdenum center is kinetically incapable of cleaving the C–H bond of thiophene? Evidence against the latter is provided by the fact that $\{[Me_2Si(C_5Me_4)_2]Mo\}$ reacts with the C–H bond of benzene to give $[Me_2Si(C_5Me_4)_2]Mo(Ph)H$ [14,17], thereby indicating that there should not be an inherent kinetic problem with the ability of the $\{[Me_2Si(C_5Me_4)_2]Mo\}$ molybdenocene fragment to react with the C–H bond of thiophene. Thus, assuming that both molybdenocene fragments $\{[Me_2Si(C_5Me_4)_2]Mo\}$ and $[Cp_2Mo]$ have the ability to react with C–H and C–S bonds, the different reactivities towards thiophene may be attributed to thermodynamic factors. In this

regard, products of thiophene C–S bond cleavage are often considered to be more thermally stable than those of C–H bond activation [21], but examples are known in which the order is reversed [22]. For example, Jones has reported that the thienyl–hydride $Cp^*Rh(PMe_3)(\eta^1\text{-}C\text{-}C_4H_3S)H$ converts to the more stable metallathiacycle $Cp^*Rh(PMe_3)(\eta^2\text{-}C,S\text{-}SC_4H_4)$ at 25 °C [21b,23], whereas Carmona has reported that the closely related metallathiacycle $[Tp^{Me_2}]Rh(PMe_3)(\eta^2\text{-}C,S\text{-}C_4H_4)$ converts to the thienyl–hydride $[Tp^{Me_2}]Rh(PMe_3)(\eta^1\text{-}C\text{-}SC_4H_3)H$ upon heating at 90 °C [22].

To ascertain the influence of the molybdenocene fragment on the relative stabilities of the three isomers, i.e., thienyl–hydride, metallathiacycle, and thiophene adduct, analogous DFT calculations were performed on the $[Cp_2Mo]$ and $[Cp^*_2Mo]$ systems (Table 1). Most interestingly, whereas the C–S bond cleavage product $(Cp^R)_2Mo(\eta^2\text{-}C,S\text{-}C_4H_4)$ is 5.1 kcal mol^{-1} more stable than the C–H bond cleavage product $(Cp^R)_2Mo(\eta^1\text{-}C\text{-}C_4H_3S)H$ for the *ansa*-molybdenocene $\{[Me_2Si(C_5Me_4)_2]Mo\}$ system, the calculations indicate that the isomers are of comparable energy for the $[Cp_2Mo]$ ($\Delta E =$ 0.1 kcal mol^{-1}) and $[Cp^*_2Mo]$ ($\Delta E = 1.0$ kcal mol^{-1}) systems, as illustrated in Fig. 3 [24]. The calculations, therefore, demonstrate that the *ansa* bridge confers stability to the metallathiacycle relative to the thienyl–hydride and thereby provide a thermodynamic explanation for the different reactivities of Cp_2MoH_2 and $[Me_2Si(C_5Me_4)_2]MoH_2$ towards thiophene.

The origin of the stabilizing effect for the metallathiacycle isomer in the *ansa* metallocene system is the geometrical perturbation that results from the presence of a Me_2Si bridge. In general, upon incorporating a Me_2Si bridge, the cyclopentadienyl groups are displaced from their natural positions such that (i) the Cp_{cent}–M–Cp_{cent} (γ) angle decreases and (ii) the angle between the M–Cp_{cent} vector and the ring normal (τ) increases, thereby resulting in a

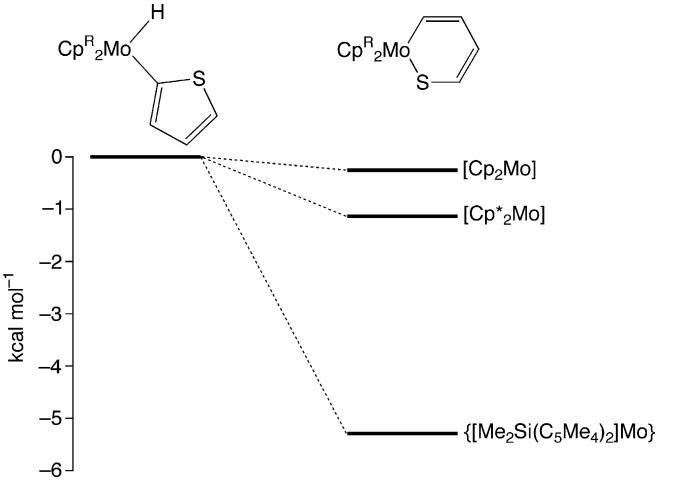

Fig. 3. Relative energies of geometry optimized structures of $(Cp^R)_2Mo(\eta^2\text{-}C,S\text{-}SC_4H_4)$ and $(Cp^R)_2Mo(\eta^1\text{-}C\text{-}SC_4H_3)H$. The Me_2Si *ansa* bridge thermodynamically favors the $(Cp^R)_2Mo(\eta^2\text{-}C,S\text{-}SC_4H_4)$ derivative.

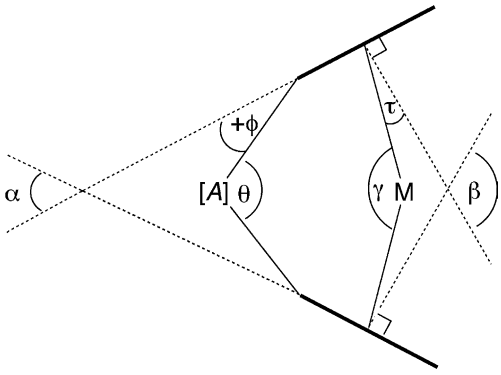

$\alpha = 180 - \beta$; $\alpha = 2\tau - \gamma + 180$; $\tau = 0.5(\gamma - \beta)$

Fig. 4. Parameters that define metallocene geometries and their relationships.

shift in coordination of the cyclopentadienyl rings from η^5-coordination towards η^3-coordination (Fig. 4) [25,26]. While this shift in coordination mode results in destabilization of a molybdenocene complex, the extent of the destabilization would be less for the metallathiacycle than for the thienyl–hydride derivative because sulfur-to-metal lone pair donation in the former isomer provides an ameliorating effect, as conceptually illustrated in Fig. 5. Thus, relative to the thienyl–hydride compound, the metallathiacycle derivative becomes more stable for the *ansa* molybdenocene system (Fig. 5). The effect is synergistic, with sulfur-to-metal lone pair donation providing a mechanism to facilitate displacement of the cyclopentadienyl rings. An indication of the displacement of the cyclopentadienyl ligands in the metallathiacycle is provided by consideration of the geometry optimized structures of $[Me_2Si(C_5Me_4)_2]Mo(\eta^2\text{-}C,S\text{-}SC_4H_4)$, $[Me_2Si(C_5Me_4)_2]Mo(\eta^1\text{-}C\text{-}SC_4H_3)H$ and $[Me_2Si(C_5Me_4)_2]Mo(SC_4H_4)$. For example, the calculated Mo–C bond lengths for the cyclopentadienyl groups in $[Me_2Si(C_5Me_4)_2]Mo(\eta^2\text{-}C,S\text{-}SC_4H_4)$ (2.32–2.53 Å), *endo*-$[Me_2Si(C_5Me_4)_2]Mo(\eta^1\text{-}C\text{-}SC_4H_3)H$ (2.28–2.48 Å) and $[Me_2Si(C_5Me_4)_2]Mo(\eta^1\text{-}SC_4H_4)$ (2.28–2.39 Å) clearly indicate that the cyclopentadienyl ligands in the metallathiacycle are displaced from the molybdenum center to a greater degree than for the other two derivatives.

While a simplified description of the effect of the Me_2Si *ansa* bridge is that it causes the electron count of the molybdenum center in $[Me_2Si(C_5Me_4)_2]Mo(\eta^2\text{-}C,S\text{-}SC_4H_4)$ to be reduced from 18 such that sulfur lone pair donation provides an important component to the bonding, a more complete understanding is provided by a molecular orbital analysis. In this regard, the electronic structure of a bent metallocene fragment is well established and the most important feature is that the three frontier orbitals that are available for interacting with additional ligands lie in the equatorial *xz* plane of the metallocene fragment [27,28]. None of these frontier orbitals, however, is of appropriate symmetry for interacting in a π-manner with a lone pair on sulfur. Rather, the only d orbitals that are of appropriate symmetry are the d_{xy} and d_{yz} orbitals, but

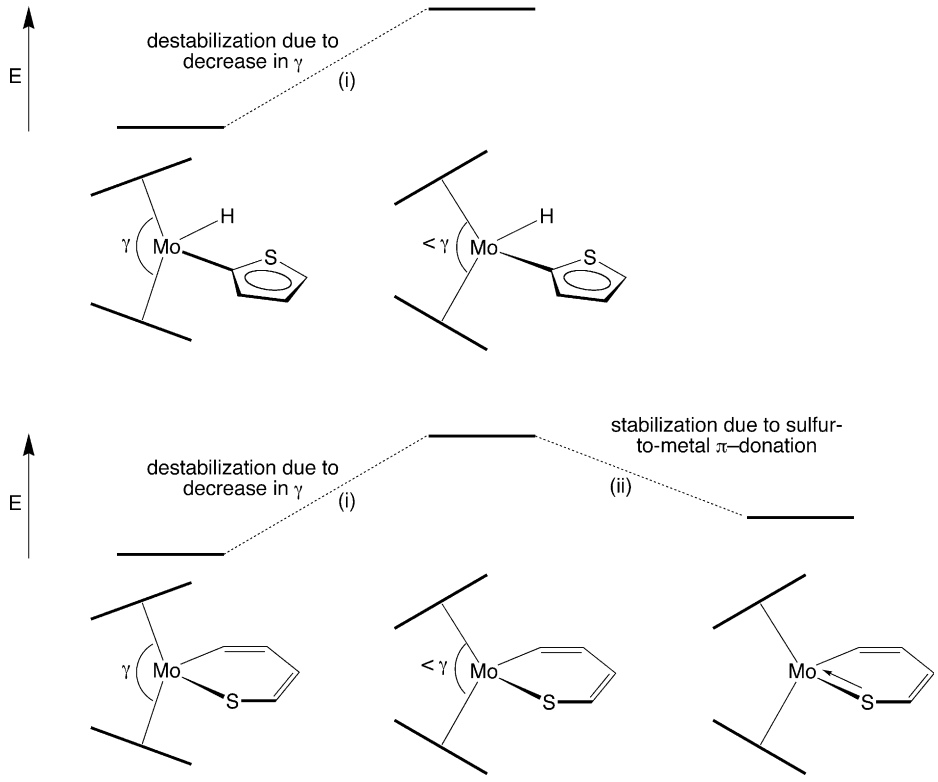

Fig. 5. Schematic illustration of (i) the destabilization of a molybdenocene fragment by bending a Cp–Mo–Cp fragment and (ii) the stabilization resulting from sulfur-to-metal π-donation. The latter interaction is not possible for the product of C–H bond cleavage and so is destabilized relative to that of C–S bond cleavage upon reducing γ.

these orbitals are involved in metal–cyclopentadienyl bonding. As such, π-donation from sulfur necessarily competes with metal–cyclopentadienyl bonding in a manner that is closely analogous to the perpendicular π-interaction in Cp_2MoO [29], $Cp_2Mo(NBu^t)$ [30] and $(\eta^3\text{-}Cp^*)_2Mo(N)(N_3)$ [31]. Specifically, π-donation from sulfur is a component of a 3-center 4-electron interaction involving the molybdenum, cyclopentadienyl, and $\eta^2\text{-}C,S\text{-}SC_4H_4$ fragments, as illustrated schematically in Fig. 6. Thus, the molybdenum d_{xy} orbital interacts with (i) an orbital combination of the cyclopentadienyl ligands and (ii) an orbital of the $\eta^2\text{-}C,S\text{-}SC_4H_4$ ligand, resulting in a bonding orbital, a "nonbonding" ligand based orbital [32], and an antibonding orbital, of which the lattermost is unoccupied (Fig. 6) [33]. Previous studies have shown that the interaction between the cyclopentadienyl orbital and d_{xy} orbital decreases as the Cp_{cent}–M–Cp_{cent} angle decreases [27], and, as a consequence, increased bending of the metallocene fragment provides a mechanism to increase π-donation from the sulfur atom. The two occupied molecular orbitals of the 3-center 4-electron interaction for both $[Me_2Si(C_5Me_4)_2]Mo(\eta^2\text{-}C,S\text{-}SC_4H_4)$ and $Cp_2Mo(\eta^2\text{-}C,S\text{-}SC_4H_4)$ are illustrated in Fig. 7, indicating that the Mo–S π-bonding interaction is greater for the *ansa* derivative $[Me_2Si(C_5Me_4)_2]Mo(\eta^2\text{-}C,S\text{-}SC_4H_4)$. Thus, for $Cp_2Mo(\eta^2\text{-}C,S\text{-}SC_4H_4)$, MO ⟨62⟩ is primarily a metal-$(\eta^2\text{-}C,S\text{-}SC_4H_4)$ nonbonding orbital that is localized on the ligand, whereas MO ⟨56⟩ is primarily a metal–cyclopentadienyl bonding orbital with little contribution from the $\eta^2\text{-}C,S\text{-}SC_4H_4$ ligand. In contrast, the corresponding orbital for $[Me_2Si(C_5Me_4)_2]Mo(\eta^2\text{-}C,S\text{-}SC_4H_4)$, i.e., MO ⟨104⟩, has a noticeably greater bonding component between the d_{xy} orbital and the p_π-orbitals on sulfur and carbon of the metallathiacycle. In accord with the enhanced π-bonding interaction, MO ⟨108⟩, which is the counterpart to the nonbonding orbital in $Cp_2Mo(\eta^2\text{-}C,S\text{-}SC_4H_4)$ (⟨62⟩), possesses metal-$(\eta^2\text{-}C,S\text{-}SC_4H_4)$ antibonding character.

2.2. Experimental evidence for sulfur-to-metal π-donation within $[Me_2Si(C_5Me_4)_2]Mo(\eta^2\text{-}C,S\text{-}SC_4H_4)$: metallathiacyclohexa-1,3-diene versus metallathiabenzene character

In view of the possibility of sulfur-to-metal π-donation within metallathiacycles, two general classes of compounds have been identified according to whether or not the interaction is significant. These classes are distinguished according to whether or not the metal center is electronically saturated or unsaturated in the absence of lone pair donation [34]. The former class of metallathiacycle is identified by a single principal resonance structure corresponding to that of a metallathiacyclohexa-1,3-diene, whereas the latter class possesses additional resonance structures (Fig. 8). In view of the additional resonance structures, molecules in the latter class have been termed metallathiabenzenes [35]. Representative examples of these two classes of

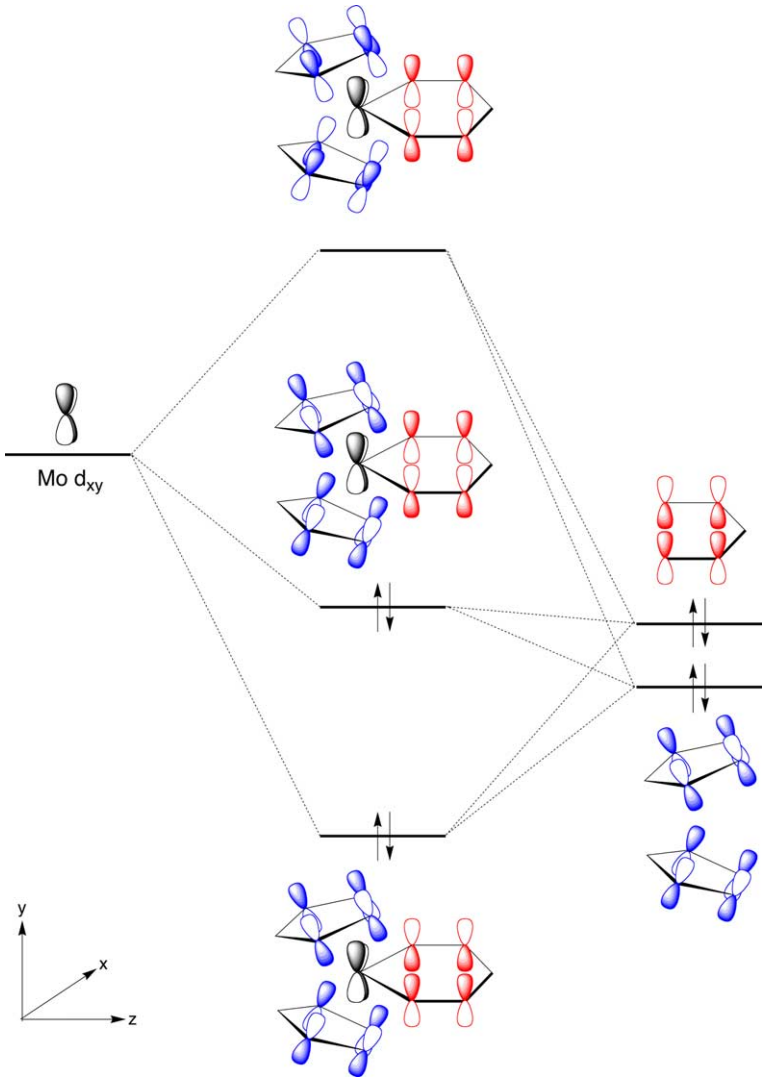

Fig. 6. 3-Center–4-electron interaction between a (Cp_2^R) fragment, a molybdenum d_{xy} orbital, and a η^2-*C*,*S*-SC_4H_4 ligand.

compounds are provided by the 2,5-dimethylthiophene derivatives, Cp*Ir(η^2-*C*,*S*-$SC_4H_2Me_2$)(PMe_2Ph) and Cp*Ir(η^2-*C*,*S*-$SC_4H_2Me_2$) (Fig. 9). Thus, the former complex is electronically saturated with an 18-electron configuration in the absence of lone pair donation from sulfur and is classified as a metallathiacyclohexa-1,3-diene derivative. In contrast, Cp*Ir(η^2-*C*,*S*-$SC_4H_2Me_2$) is electronically unsaturated with a 16-electron configuration in the absence of lone pair donation from sulfur and is classified as a metallathiabenzene derivative. It is important to note, however, that the concept of electronic saturation with respect to the feasibility of sulfur lone pair donation does not necessarily imply an 18-electron configuration. For example, square planar Ni and Pt favors 16-electron configurations and so complexes such as (PEt_3)$_2$Pt(η^2-*C*,*S*-SC_4H_4) [9f] and (dippe)Ni(η^2-*C*,*S*-SC_4H_4) [9b] are better described as metallathiacyclohexa-1,3-diene derivatives rather than metallathiabenzene complexes.

Calculations indicate that there is little electronic preference for favoring planar over bent metallathiacycles and that bent geometries are a consequence of steric interactions [36,37]. The planarity of a metallathiacycle cannot, therefore, be used as a definitive indication of metallathiabenzene character. Furthermore, in view of the twofold disorder that is prevalent in many metallathiacycles [38,39], the variation in bond lengths within the six membered ring can likewise not be used as a reliable indicator of metallathiabenzene character. It is, therefore, significant that Angelici has proposed that the ^{13}C NMR shift of the carbon attached to the metal center in a metallathiacycle may be used to provide a criterion to distinguish between localized and delocalized π-bonding [34]. Specifically, a large downfield shift of the ^{13}C signals for the carbon attached to the metal center is proposed to be indicative of a delocalized structure because the metal–carbon bond possesses more alkylidene character. The ^{13}C NMR spectroscopic data for a series of six-membered metallathiacycles are summarized in Table 2, from which it is evident that metallathiacyclohexa-1,3-diene complexes are characterized by ^{13}C NMR signals in the range 106–142 ppm, whereas bona fide

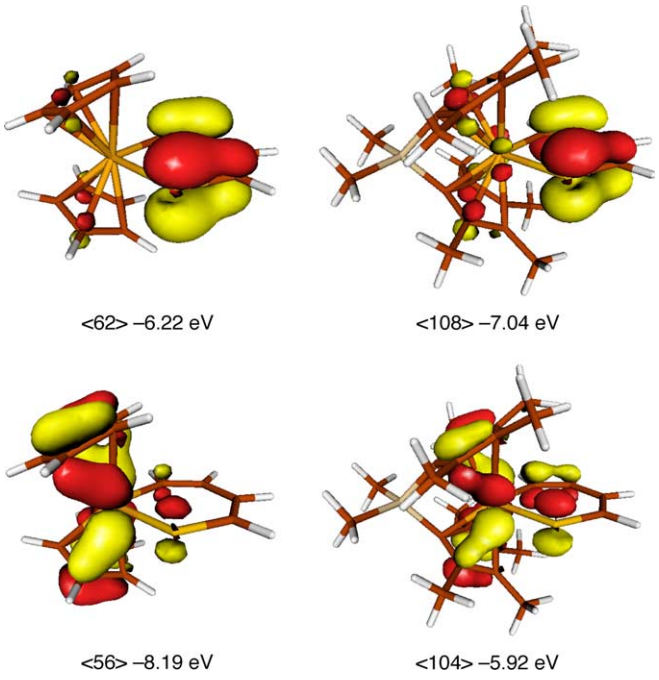

Fig. 7. The two occupied molecular orbitals of the 3-center–4-electron interaction for $Cp_2Mo(\eta^2\text{-}C,S\text{-}SC_4H_4)$ (left) and $[Me_2Si(C_5Me_4)_2]Mo(\eta^2\text{-}C,S\text{-}SC_4H_4)$ (right). MO ⟨62⟩ of $Cp_2Mo(\eta^2\text{-}C,S\text{-}SC_4H_4)$ is primarily a metal-$(\eta^2\text{-}C,S\text{-}SC_4H_4)$ nonbonding orbital that is localized on the ligand, while MO ⟨56⟩ is primarily a metal–cyclopentadienyl bonding orbital with little contribution from the $\eta^2\text{-}C,S\text{-}SC_4H_4$ ligand. In contrast, ⟨104⟩, the corresponding bonding orbital for $[Me_2Si(C_5Me_4)_2]Mo(\eta^2\text{-}C,S\text{-}SC_4H_4)$, has a noticeably greater bonding component between the d_{xy} orbital and the p_π-orbitals on sulfur and carbon of the metallathiacycle.

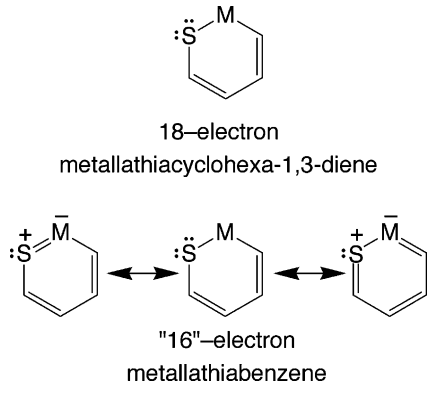

Fig. 8. Bonding descriptions of metallathiacyclohexa-1,3-diene and metallathiabenzene derivatives.

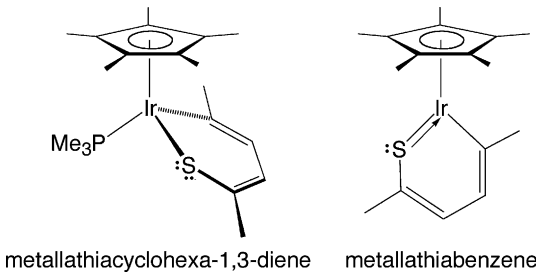

Fig. 9. Examples of metallathiacyclohexa-1,3-diene and metallathiabenzene derivatives.

Table 2
^{13}C NMR spectroscopic data for the carbon attached to the metal in six membered metallathiacycles

	δ (ppm)	Reference
Metallathiacyclohexa-1,3-dienes		
$(\eta^2\text{-}C,S\text{-}SC_4H_4)Ir(PMe_3)_3Cl$	113.1	[8j]
$(\eta^2\text{-}C,S\text{ -}SC_4H_2Me_2)Ir(PEt_3)_3Cl$	106.4 and 131.2[a]	[35g]
$[(\eta^2\text{-}C,S\text{-}SC_4H_2Me_2)Ir(PEt_3)_4]^+$	115.8	[35g]
$(\eta^2\text{-}C,S\text{-}SC_4H_2Me_2)Ir(PEt_3)_3H$	118.8	[35g]
$(\eta^2\text{-}C,S\text{-}SC_4H_4)Ir(PEt_3)_3H$	121.1	[35e]
$(PEt_3)_2Pt(\eta^2\text{-}C,S\text{-}SC_4H_4)$	131.1	[9e]
$Cp^*Ir(\eta^2\text{-}C,S\text{-}SC_4H_2Me_2)(PMe_2Ph)$	$\leqslant$136[b]	[8i]
$Cp_2W(\eta^2\text{-}C,S\text{-}SC_4H_4)$	$\leqslant$136.1[b]	[5a]
$Cp^*Rh(\eta^2\text{-}C,S\text{-}SC_4H_4)(PMe_3)$	137.4	[8c]
$(dippe)Ni(\eta^2\text{-}C,S\text{-}SC_4H_4)$	142.0	[9b]
Metallathiabenzenes		
$[Me_2Si(C_5Me_4)_2]Mo(\eta^2\text{-}C,S\text{-}SC_4H_4)$	162.6	[10]
$[(\eta^2\text{-}C,S\text{-}SC_4H_2Me_2)Ir(PEt_3)_3]^+$	165.1	[35g]
$[\eta^3\text{-}MeC(CH_2PPh_2)_3]Ir(\eta^2\text{-}C,S\text{ -}SC_4H_4)$	178.9	[8k]
$Cp^*Ir(\eta^2\text{-}C,S\text{-}SC_4H_2Me_2)$	181.0	[8h]
$Cp^*Ir(\eta^2\text{-}C,S\text{-}SC_4H_3Me)$	182.8	[8h]

[a] Values for 2 isomers.
[b] Assignment of the carbon of the metallathiacycle attached to the metal not determined and so only an upper limit to the chemical shift is known.

metallathiabenzene complexes are characterized by ^{13}C NMR signals in the range 165–183 ppm. On this basis, the ^{13}C NMR chemical shift of 162.6 ppm for $[Me_2Si(C_5Me_4)_2]Mo(\eta^2\text{-}C,S\text{-}SC_4H_4)$ is consistent with significant metallathiabenzene character and hence sulfur-to-metal π-donation.

2.3. Reactivity of $[Me_2Si(C_5Me_4)_2]MoH_2$ towards furan and selenophene

In order to obtain a more detailed appreciation of the factors that influence the energy surface relating the three isomeric thiophene complexes, we have investigated the reactivity of $[Me_2Si(C_5Me_4)_2]MoH_2$ towards furan and selenophene derivatives. Interestingly, furan exhibits reactivity which is distinct from that of thiophene (Scheme 3). Thus, rather than cleave the C–O bond, $[Me_2Si(C_5Me_4)_2]MoH_2$ reacts with the C–H bond of furan to give the furyl–hydride compound $[Me_2Si(C_5Me_4)_2]Mo(\eta^1\text{-}C\text{-}C_4H_3O)H$ (Fig. 10) [40]. ^1H NMR spectroscopic analysis indicates that there is an approximately 2:1 selectivity for cleaving the two different types of C–H bonds, although it is not definitive whether this corresponds to α/β or β/α selectivity [41], preferential cleavage of the α-C–H bond has, however, been noted for other reactions of furan with transition metal compounds [42]. Benzofuran also reacts with $[Me_2Si(C_5Me_4)_2]MoH_2$ to give the β-isomer $[Me_2Si(C_5Me_4)_2]Mo(\eta^1\text{-}C\text{-}C_8H_5O)H$ (Scheme 3 and Fig. 11). The observation of C–H bond cleavage in the reactions of furan and benzofuran with $[Me_2Si(C_5Me_4)_2]MoH_2$ provides further support for the notion that C–H bond cleavage of thiophene would not be kinetically prohibitive. Also of note, the oxidative addition of the C–H bond of furan is

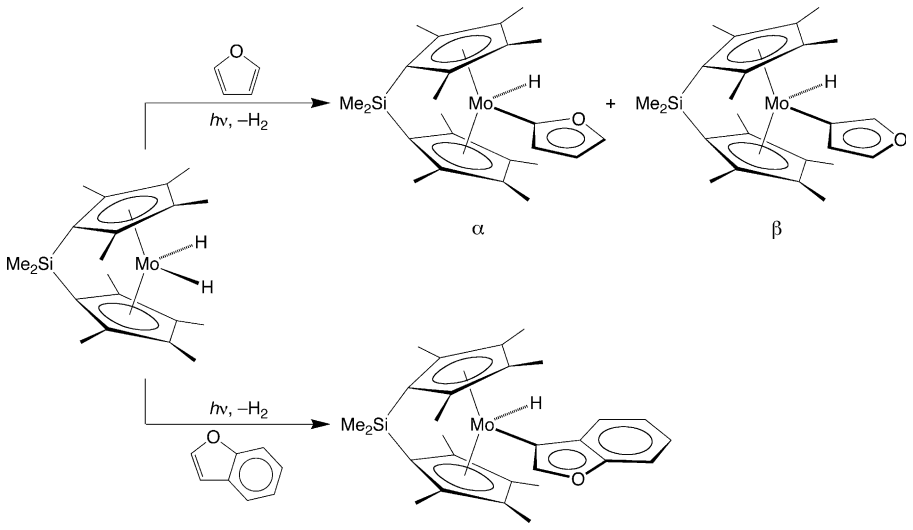

Scheme 3.

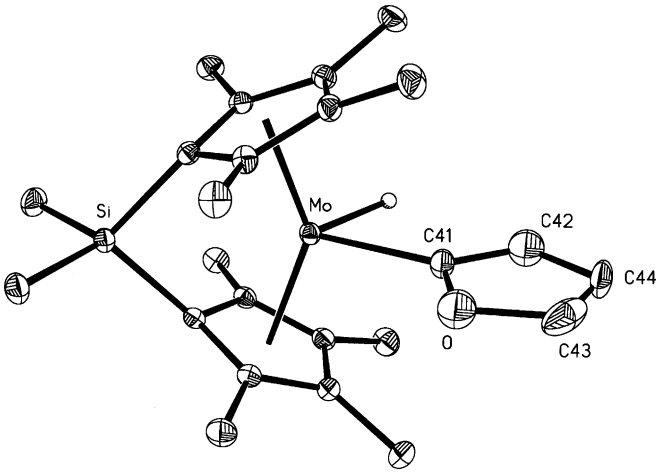

Fig. 10. Molecular structure of $[Me_2Si(C_5Me_4)_2]Mo(\eta^1\text{-}C\text{-}C_4H_3O)H$. The $\eta^1\text{-}C\text{-}C_4H_3O$ ligand is disordered and only one of the disordered configurations is illustrated for clarity.

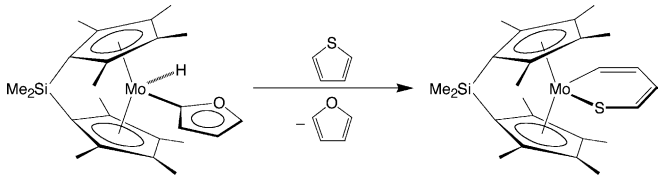

Scheme 4.

In contrast to the C–H bond cleavage reactions of $[Me_2Si(C_5Me_4)_2]MoH_2$ with furan and benzofuran, $[Me_2Si(C_5Me_4)_2]MoH_2$ reacts with selenophene and benzoselenophene to give the product of C–Se bond cleavage, namely $[Me_2Si(C_5Me_4)_2]Mo(\eta^2\text{-}C,Se\text{-}SeC_4H_4)$ and $[Me_2Si(C_5Me_4)_2]Mo(\eta^2\text{-}C,Se\text{-}SeC_8H_6)$, as illustrated in Scheme 5. The molecular structures of $[Me_2Si(C_5Me_4)_2]Mo(\eta^2\text{-}C,Se\text{-}SeC_4H_4)$ and $[Me_2Si(C_5Me_4)_2]Mo(\eta^2\text{-}C,Se\text{-}SeC_8H_6)$ have been determined by X-ray diffraction, as

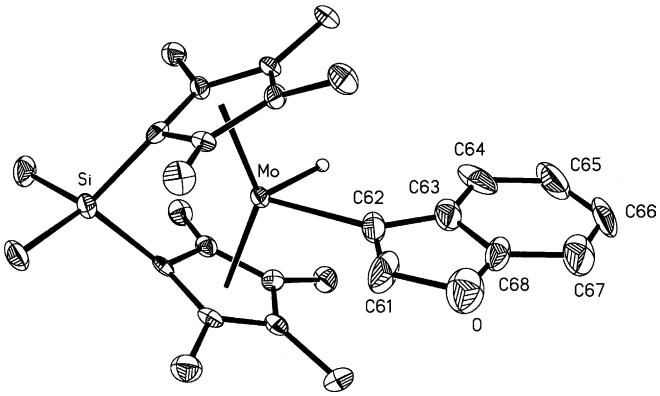

Fig. 11. Molecular structure of $[Me_2Si(C_5Me_4)_2]Mo(\eta^1\text{-}C\text{-}C_8H_5O)H$.

reversible and treatment of $[Me_2Si(C_5Me_4)_2]Mo(\eta^1\text{-}C\text{-}C_4H_3O)H$ with thiophene yields $[Me_2Si(C_5Me_4)_2]Mo(\eta^2\text{-}C,S\text{-}SC_4H_4)$ (Scheme 4).

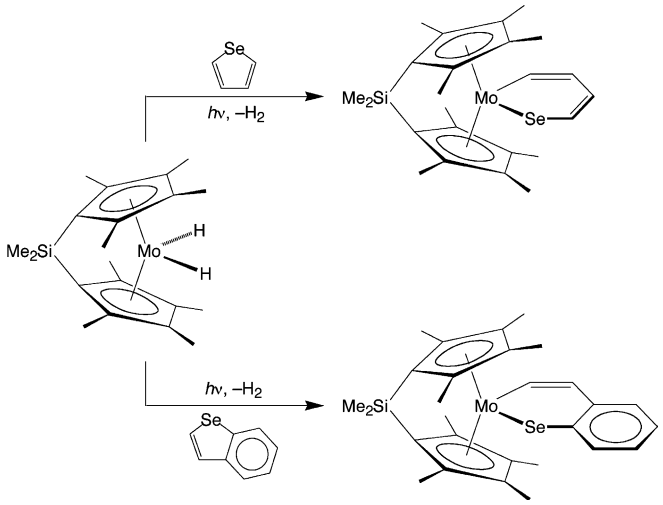

Scheme 5.

illustrated in Figs. 12 and 13, and are analogous to the sulfur counterparts [10]. The reactivity of selenophene and benzoselenophene, therefore, corresponds closely to that of thiophene and benzothiophene [10]. By comparison to the C–S bond cleavage reactivity of thiophene, however, complexes derived from C–Se bond cleavage of selenophene are not common, although two notable examples are provided by Jones' $Cp^*Rh(PMe_3)(\eta^2\text{-}C,Se\text{-}SeC_4H_4)$ [43] and Angelici's $Cp^*Ir(\eta^2\text{-}C,Se\text{-}SeC_4H_2Me_2)$ [44,45]. The ^{13}C NMR chemical shift of the metallaselenacycle carbon atom attached to molybdenum in $[Me_2Si(C_5Me_4)_2]Mo(\eta^2\text{-}C,Se\text{-}SeC_4H_4)$ is 163.1 ppm, comparable to the value of 162.6 ppm for the corresponding carbon atom in $[Me_2Si(C_5Me_4)_2]Mo(\eta^2\text{-}C,S\text{-}SC_4H_4)$. On the basis of the above discussion pertaining to the bonding within $[Me_2Si(C_5Me_4)_2]Mo(\eta^2\text{-}C,S\text{-}SC_4H_4)$, it is evident that $[Me_2Si(C_5Me_4)_2]Mo(\eta^2\text{-}C,Se\text{-}SeC_4H_4)$ possesses a significant amount of metallaselenobenzene character. In this regard,

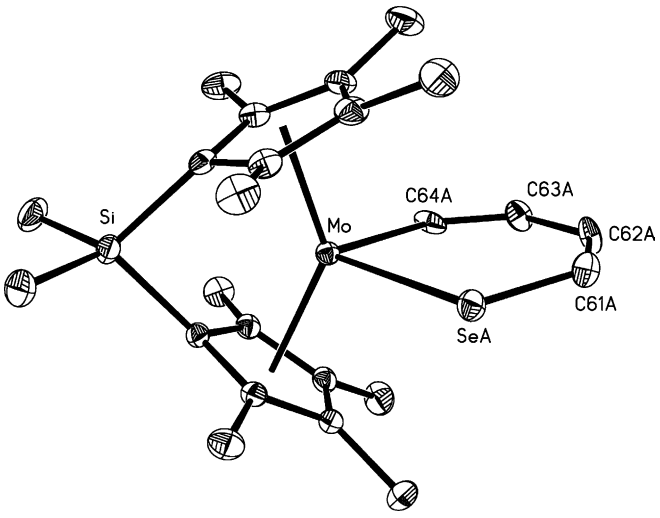

Fig. 12. Molecular structure of $[Me_2Si(C_5Me_4)_2]Mo(\eta^2\text{-}C,Se\text{-}SeC_4H_4)$. The $\eta^2\text{-}C,Se\text{-}SeC_4H_4$ ligand exhibits a twofold disorder and only one of the disordered configurations is illustrated for clarity.

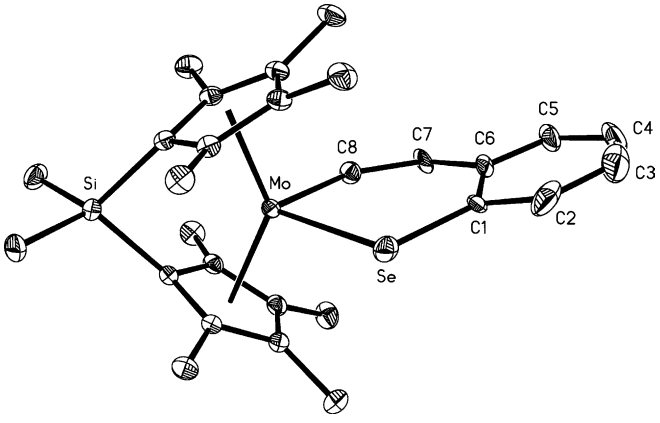

Fig. 13. Molecular structure of $[Me_2Si(C_5Me_4)_2]Mo(\eta^2\text{-}C,Se\text{-}SeC_8H_6)$. The $\eta^2\text{-}C,Se\text{-}SeC_8H_6$ ligand exhibits a twofold disorder and only one of the disordered configurations is illustrated for clarity.

the ^{77}Se NMR spectroscopic signal for $[Me_2Si(C_5Me_4)_2]Mo(\eta^2\text{-}C,Se\text{-}SeC_4H_4)$ is observed at 209 ppm, a value which is intermediate between those for $Cp^*Rh(PMe_3)(\eta^2\text{-}C,Se\text{-}SeC_4H_4)$ (31.9 ppm) [43], a metallaselenacyclohexa-1,3-diene derivative, and $Cp^*Ir(\eta^2\text{-}C,Se\text{-}SeC_4H_2Me_2)$ (905.4 ppm) [44], a bona fide metallaselenabenzene derivative.

The different reactivity of furan, vis-à-vis thiophene and selenophene, towards $[Me_2Si(C_5Me_4)_2]MoH_2$ poses an interesting question: specifically, why is the molybdenocene center incapable of cleaving the C–O bond? In this regard, DFT calculations indicate that C–E (E = O, S, Se) bond cleavage is thermodynamically more favored than C–H bond cleavage for all of the chalcogen derivatives (Table 1 and Fig. 2). As such, the calculations indicate that the inability to cleave the C–O bond in furan is a kinetic problem. In support of this notion, it is pertinent to note that six-membered metallaoxacycles, the products of formal furan C–O bond cleavage, e.g., $(\eta^2\text{-}C,O\text{-}OC_4H_2Me_2)Ir(PEt_3)_3X$ (X = H, Me, Cl) and $[(\eta^2\text{-}C,O\text{-}OC_4H_2Me_2)Ir(PEt_3)_3]^+$, have been reported [46], but these complexes are synthesized by metathesis with a potassium oxapentadienide derivative and not via reactions that involve cleavage of a C–O bond. Cleavage of the C–O bond in furan has, nevertheless, been observed in the reaction of $(Ph_3P)_2ReH_7$ with furan in the presence of $Bu^tCH{=}CH_2$, but the product obtained is a hydrogenated 1-oxapentadienyl derivative, $(Ph_3P)_2Re(\eta^5\text{-}C_4H_5O)(CO)$ [47].

Preferential C–H bond cleavage of furan and C–S cleavage of thiophene has been previously noted, as illustrated by the observation that $[Ir(PMe_3)_3(COD)][Cl]$ reacts with thiophene to give a metallathiacycle $Ir(PMe_3)_3(\eta^2\text{-}C,S\text{-}SC_4H_4)(H)Cl$, whereas furan gives the furyl–hydride complex $Ir(PMe_3)_3(\eta^1\text{-}C\text{-}OC_4H_3)Cl$ [8i]. However, in contrast to these reactions where the discontinuity in reactivity occurs between furan and thiophene, the reactions of $Os_3(CO)_{10}(MeCN)_2$ with furan, thiophene, selenophene and tellurophene exhibit a discontinuity between thiophene and selenophene. Thus, $Os_3(CO)_{10}(MeCN)_2$ reacts with furan and thiophene via C–H bond cleavage to give $Os_3(\mu\text{-}H)(\mu\text{-}2\text{-}C_4H_3E)(CO)_{10}$ (E = O, S), whereas the reactions with selenophene and tellurophene occur via C–E bond cleavage to give $Os_3(CO)_{10}(EC_4H_4)$ (E = Se, Te) [45b,45c].

3. Conclusions

In summary, DFT calculations provide evidence that the observation of C–S bond cleavage of thiophene by the *ansa* metallocene $[Me_2Si(C_5Me_4)_2]MoH_2$ but C–H bond cleavage by Cp_2MoH_2 is dictated by thermodynamic considerations. Specifically, the Me_2Si *ansa* bridge favors $[Me_2Si(C_5Me_4)_2]Mo(\eta^2\text{-}C,S\text{-}SC_4H_4)$ over $[Me_2Si(C_5Me_4)_2]Mo(\eta^1\text{-}C\text{-}SC_4H_3)H$ because the bridge promotes a shift in the coordination of the cyclopentadienyl rings from η^5-coordination towards η^3-coordination and this thermodynamically unfavorable modification is stabilized by

sulfur-to-metal π-donation within $[Me_2Si(C_5Me_4)_2]Mo(\eta^2$-*C*,*S*-$SC_4H_4)$. Selenophene reacts with $[Me_2Si(C_5Me_4)_2]$-MoH_2 in a manner analogous to that of thiophene, but furan reacts via C–H bond cleavage to give a furyl–hydride complex $[Me_2Si(C_5Me_4)_2]Mo(\eta^1$-*C*-$C_4H_3O)H$. DFT calculations indicate that C–E (E = O, S, Se) bond cleavage is thermodynamically favored for all of the chalcogens and thus the inability to cleave the C–O of furan derivatives is due to kinetic factors.

4. Experimental

4.1. General considerations

All manipulations were performed using a combination of glovebox, high-vacuum and Schlenk techniques under a nitrogen or argon atmosphere. Solvents were purified and degassed by standard procedures. ^1H and ^{13}C NMR spectra were measured on Bruker 300 DRX, Bruker 400 DRX, and Bruker Avance 500 DMX spectrometers. Chemical shifts are reported in ppm relative to $SiMe_4$ ($\delta = 0$) and were referenced internally with respect to the protio solvent impurity (δ 7.15 for C_6D_5H) and ^{13}C resonances (δ 128.0 for C_6D_6). ^{77}Se chemical shifts are reported in ppm relative to neat Me_2Se ($\delta = 0$) and were referenced using a solution of Ph_2Se_2 in C_6D_6 ($\delta = 460$) as external standard [48]. Coupling constants are given in hertz. Infrared spectra were recorded on Perkin–Elmer 1430 and 1600 spectrometers and are reported in cm^{-1}. $[Me_2Si(C_5Me_4)_2]MoH_2$ was prepared by the method previously reported [26].

4.2. Synthesis of $[Me_2Si(C_5Me_4)_2]Mo(\eta^1$-*C*-$C_4H_3O)H$

A solution of $[Me_2Si(C_5Me_4)_2]MoH_2$ (15 mg, 0.04 mmol) and furan (0.05 mL, 0.69 mmol) in cyclohexane (ca. 1 mL) was photolyzed with UV light for 2 days, resulting in the deposition of yellow crystals. The crystals were isolated, washed with pentane (2 × 0.3 mL) and dried in vacuo giving $[Me_2Si(C_5Me_4)_2]Mo(\eta^1$-*C*-$C_4H_3O)H$ (8 mg, 46%). Anal. Calc. for $C_{24}H_{34}OSiMo$: C, 62.3; H, 7.4. Found: C, 62.0; H, 7.1%. IR data (KBr pellet, cm^{-1}): 2901 (vs), 1817 (s), 1776 (s), 1644 (m), 1345 (s), 1296 (s), 1253 (vs), 1124 (s), 1020 (vs), 892 (m), 864 (m), 836 (s), 763 (s), 712 (m), 672 (m). ^1H NMR data (C_6D_6): Isomer A (minor): −6.18 [br m, 1H of $Mo(OC_4H_3)H$], 0.28 [s, 1Me of $(CH_3)_2Si\{C_5(CH_3)_4\}_2$], 0.40 [s, 1Me of $(CH_3)_2Si\{C_5(CH_3)_4\}_2$], 1.13 [s, 2Me of $(CH_3)_2Si\{C_5(CH_3)_4\}_2$], 1.87 [s, 2Me of $(CH_3)_2Si\{C_5(CH_3)_4\}_2$], 1.95 [d, $^4J_{H-H} = 3$, 2Me of $(CH_3)_2Si\{C_5(CH_3)_4\}_2$], 1.99 [s, 2Me of $(CH_3)_2Si\{C_5(CH_3)_4\}_2$], 6.41 [t, $^3J_{H-H} = 2$, 1H of $Mo(OC_4H_3)$], 6.54 [br, 1H of $Mo(OC_4H_3)$], 7.66 [br, 1H $Mo(OC_4H_3)$]. Isomer B (major): −6.22 [septet, $J_{H-H} = 3$, 1H of $Mo(OC_4H_3)H$], 0.29 [s, 1Me of $(CH_3)_2Si\{C_5(CH_3)_4\}_2$], 0.37 [s, 1Me of $(CH_3)_2Si\{C_5(CH_3)_4\}_2$], 1.12 [s, 2Me of $(CH_3)_2Si\{C_5(CH_3)_4\}_2$], 1.76 [s, 2Me of $(CH_3)_2Si\{C_5(CH_3)_4\}_2$], 1.83 [d, $^4J_{H-H} = 3$, 2Me of $(CH_3)_2Si\{C_5(CH_3)_4\}_2$], 1.87 [s, 2Me of $(CH_3)_2Si\{C_5(CH_3)_4\}_2$], 5.71 [br, 1H of $Mo(OC_4H_3)$], 7.34 [br, 1H of $Mo(OC_4H_3)$], 7.45 [br, 1H $Mo(OC_4H_3)$]. ^{13}C NMR data for the major isomer (B) (C_6D_6): 2.7 [q, $^1J_{C-H} = 115$, 1Me of $(CH_3)_2Si\{C_5(CH_3)_4\}_2$], 2.9 [q, $^1J_{C-H} = 125$, 1C of $(CH_3)_2Si\{C_5(CH_3)_4\}_2$], 11.5 [q, $^1J_{C-H} = 127$, 4Me of $(CH_3)_2Si\{C_5(CH_3)_4\}_2$], 12.4 [q, $^1J_{C-H} = 131$, 2Me of $(CH_3)_2Si\{C_5(CH_3)_4\}_2$], 13.4 [q, $^1J_{C-H} = 126$, 2Me of $(CH_3)_2Si\{C_5(CH_3)_4\}_2$], 48.6 [s, 2C, $(CH_3)_2Si\{C_5(CH_3)_4\}_2$], 90.3 [s, 2C of $(CH_3)_2Si\{C_5(CH_3)_4\}_2$], 93.1 [s, 2C of $(CH_3)_2Si\{C_5(CH_3)_4\}_2$], 106.1 [s, 2C of $(CH_3)_2Si\{C_5(CH_3)_4\}_2$], 123.2 [s, 2C of $(CH_3)_2Si\{C_5(CH_3)_4\}_2$], 121.0 [d, $^1J_{C-H} = 158$, 1C of $Mo(OC_4H_3)$], 140.1 [d, $^1J_{C-H} = 194$, 1C of $Mo(OC_4H_3)$], 150.8 [d, $^1J_{C-H} = 199$, 1C of $Mo(OC_4H_3)$], 187.3 [s, $1C_{ipso}$ of $Mo(OC_4H_3)$].

4.3. Synthesis of $[Me_2Si(C_5Me_4)_2]Mo(\eta^2$-*C*,*Se*-$SeC_4H_4)$

A solution of $[Me_2Si(C_5Me_4)_2]MoH_2$ (30 mg, 0.08 mmol) and selenophene (75 μL, 0.81 mmol) in cyclohexane (ca. 1 mL) was photolyzed with UV light for 1 day, resulting in the deposition of red crystals of $[Me_2Si(C_5Me_4)_2]Mo(\eta^2$-*C*,*Se*-$SeC_4H_4)$ which were isolated and dried in vacuo (20 mg, 50%). Anal. Calc. for $C_{24}H_{34}SiSeMo$: C, 54.9; H, 6.5. Found: C, 54.8; H, 6.6%. IR data (KBr pellet, cm^{-1}): 2988 (s), 2900 (s), 1569 (w), 1449 (w), 1376 (m), 1349 (vs), 1305 (s), 1253 (m), 1127 (m), 1018 (s), 946 (vs), 813 (s), 796 (s), 769 (s), 675 (vs), 660 (vs), 642 (vs), 605 (m). ^1H NMR data (C_6D_6): 0.16 [s, 1Me of $(CH_3)_2Si\{C_5(CH_3)_4\}_2$], 0.18 [s, 1Me of $(CH_3)_2Si\{C_5(CH_3)_4\}_2$], 1.45 [s, 2Me of $(CH_3)_2Si\{C_5(CH_3)_4\}_2$], 1.49 [s, 2Me of $(CH_3)_2Si\{C_5(CH_3)_4\}_2$], 1.59 [s, 2Me of $(CH_3)_2Si\{C_5(CH_3)_4\}_2$], 2.00 [s, 2Me of $(CH_3)_2Si\{C_5(CH_3)_4\}_2$], 6.83 [m, 1H of Mo-$(SeC_4H_4)$], 6.94 [m, 1H of $Mo(SeC_4H_4)$], 7.18 [m, 1H of $Mo(SeC_4H_4)$], 7.19 [m, 1H of $Mo(SeC_4H_4)$] (the signals due to SeC_4H_4 are a complex ABCD multiplet that may be simulated with the following coupling constants: $J_{AB} = 10$, $J_{AC} = 5$, $J_{AD} = 3$, $J_{CD} = 10$.) ^{13}C NMR data (C_6D_6): 2.2 [q, $^1J_{C-H} = 120$, 1C of $(CH_3)_2Si\{C_5(CH_3)_4\}_2$], 2.4 [q, $^1J_{C-H} = 121$, 1C of $(CH_3)_2Si\{C_5(CH_3)_4\}_2$], 10.0 [q, $^1J_{C-H} = 126$, 2C of $(CH_3)_2Si\{C_5(CH_3)_4\}_2$], 11.7 [q, $^1J_{C-H} = 126$, 2C of $(CH_3)_2Si\{C_5(CH_3)_4\}_2$], 12.4 [q, $^1J_{C-H} = 128$, 2C of $(CH_3)_2Si\{C_5(CH_3)_4\}_2$], 14.5 [q, $^1J_{C-H} = 128$, 2C of $(CH_3)_2Si\{C_5(CH_3)_4\}_2$], 57.8 [s, 2C of $(CH_3)_2Si\{C_5(CH_3)_4\}_2$], 92.8 [s, 2C of $(CH_3)_2Si$-$\{C_5(CH_3)_4\}_2$], 94.2 [s, 2C of $(CH_3)_2Si\{C_5(CH_3)_4\}_2$], 119.1 [s, 2C of $(CH_3)_2Si\{C_5(CH_3)_4\}_2$], 124.5 [s, 2C of $(CH_3)_2Si\{C_5(CH_3)_4\}_2$], 113.4 [d, $^1J_{C-H} = 166$, 1C of Mo-(SeC_4H_4)], 130.7 [d, $^1J_{C-H}$ = obscured by solvent peak, 1C of $Mo(SeC_4H_4)$], 133.3 [d, $^1J_{C-H} = 188$, 1C of Mo-(SeC_4H_4)], 161.6 [d, $^1J_{C-H} = 140$, 1C of Mo-(SeC_4H_4)]. ^{77}Se NMR data (C_6D_6): 209 [s, $Mo(SeC_4H_4)$].

4.4. Synthesis of $[Me_2Si(C_5Me_4)_2]Mo(\eta^2$-*C*,*Se*-$SeC_8H_6)$

A solution of $[Me_2Si(C_5Me_4)_2]MoH_2$ (30 mg, 0.08 mmol) and benzoselenophene (14 mg, 0.083 mmol) in cyclohexane (ca. 1 mL) was photolyzed with UV light for

1 day, resulting in the deposition of dark red crystals. The crystals were isolated, washed with pentane and dried in vacuo giving $[Me_2Si(C_5Me_4)_2]Mo(\eta^2\text{-}C,Se\text{-}SeC_8H_6)$ (15 mg, 34%). Anal. Calc. for $C_{28}H_{36}SeSiMo$: C, 58.4; H, 6.3. Found: C, 58.5; H, 6.5%. IR data (KBr pellet, cm^{-1}): 2836 (vs), 1464 (s), 1444 (m), 1412 (s), 1376 (m), 1361 (m), 1343 (m), 1307 (m), 1253 (s), 1178 (w), 1129 (m), 1076 (w), 1052 (m), 1036 (m), 1014 (s), 839 (s), 812 (s), 770 (m), 745 (vs), 726 (s), 674 (s), 654 (m). ^1H NMR data (C_6D_6): 0.17 [s, 1Me of $(CH_3)_2Si\{C_5(CH_3)_4\}_2$] 0.18 [s, 1Me of $(CH_3)_2Si\{C_5(CH_3)_4\}_2$], 1.35 [s, 2Me of $(CH_3)_2Si\{C_5(CH_3)_4\}_2$], 1.47 [s, 2Me of $(CH_3)_2Si\{C_5(CH_3)_4\}_2$], 1.56 [s, 2Me of $(CH_3)_2Si\{C_5(CH_3)_4\}_2$], 1.89 [s, 2Me of $(CH_3)_2Si\{C_5(CH_3)_4\}_2$], 6.87 [t, $^3J_{H-H} = 7$; d, $^4J_{H-H} = 2$, 1H of $Mo(SeC_8H_6)$], 6.99 [t, $^3J_{H-H} = 7$; d, $^4J_{H-H} = 1$, 1H of $Mo(SeC_8H_6)$], 7.03 [d, $^3J_{H-H} = 8$; d, $^4J_{H-H} = 2$, 1H of $Mo(SeC_8H_6)$], 7.23 [d, $^3J_{H-H} = 12$, 1H of $Mo(SeC_8H_6)$], 7.73 [d, $^3J_{H-H} = 12$, 1H of $Mo(SeC_8H_6)$], 8.13 [d, $^3J_{H-H} = 7$, 1H of $Mo(SeC_8H_6)$]. ^{13}C NMR data (C_6D_6): 2.2 [q, $^1J_{C-H} = 120$, 1Me of $(CH_3)_2Si\{C_5(CH_3)_4\}_2$], 2.4 [q, $^1J_{C-H} = 119$, 1Me of $(CH_3)_2Si\{C_5(CH_3)_4\}_2$], 9.9 [q, $^1J_{C-H} = 127$, 2Me of $(CH_3)_2Si\{C_5(CH_3)_4\}_2$], 11.7 [q, $^1J_{C-H} = 127$, 2Me of $(CH_3)_2Si\{C_5(CH_3)_4\}_2$], 12.5 [q, $^1J_{C-H} = 128$, 2Me of $(CH_3)_2Si\{C_5(CH_3)_4\}_2$], 14.5 [q, $^1J_{C-H} = 127$, 2Me of $(CH_3)_2Si\{C_5(CH_3)_4\}_2$], 57.6 [s, 2C of $(CH_3)_2Si\{C_5(CH_3)_4\}_2$], 92.3 [s, 2C of $(CH_3)_2Si\{C_5(CH_3)_4\}_2$], 94.7 [s, 2C of $(CH_3)_2Si\{C_5(CH_3)_4\}_2$], 118.4 [s, 2C of $(CH_3)_2Si\{C_5(CH_3)_4\}_2$], 123.1 [d, $^1J_{C-H} = 160$, 1C of $Mo(SeC_8H_6)$], 125.0 [s, 1C of $Mo(SeC_8H_6)$], 125.7 [d, $^1J_{C-H}$ = ca. 140, 1C of $Mo(SeC_8H_6)$], 131.7 [d, $^1J_{C-H} = 153$, 1C of $Mo(SeC_8H_6)$], 134.2 [d, $^1J_{C-H} = 151$, 1C of $Mo(SeC_8H_6)$], 140.5 [d, $^1J_{C-H} = 147$, 1C of $Mo(SeC_8H_6)$], 144.3 [s, 1C of $Mo(SeC_8H_6)$], 163.1 [d, $^1J_{C-H}$ = ca. 140, 1C of $Mo(SeC_8H_6)$], 2C of $(CH_3)_2Si\{C_5(CH_3)_4\}_2$ are obscured by solvent.

4.5. X-ray structure determinations

X-ray diffraction data were collected on a Bruker P4 diffractometer equipped with a SMART CCD detector and crystal data, data collection and refinement parameters are summarized in Table 3. The structures were solved using direct methods and standard difference map techniques, and were refined by full-matrix least-squares procedures on F^2 with SHELXTL (Version 5.10) [49]. The crystallographic data for $[Me_2Si(C_5Me_4)_2]Mo(\eta^1\text{-}C\text{-}C_4H_3O)H$ (CCDC # 272896), $[Me_2Si(C_5Me_4)_2]Mo(\eta^1\text{-}C\text{-}C_8H_5O)H$ (CCDC # 272894), $[Me_2Si(C_5Me_4)_2]Mo(\eta^2\text{-}C,Se\text{-}SeC_4H_4)$ (CCDC # 272895) and $[Me_2Si(C_5Me_4)_2]Mo(\eta^2\text{-}C,Se\text{-}SeC_8H_6)$ (CCDC # 272893) have been deposited with the Cambridge Crystallographic Data Center. $[Me_2Si(C_5Me_4)_2]Mo(\eta^2\text{-}C,Se\text{-}SeC_4H_4)$ and $[Me_2Si(C_5\text{- }Me_4)_2]Mo(\eta^2\text{-}C,Se\text{-}SeC_8H_6)$ exhibit a two-fold disorder of the metallaselenacycle which is common to this type of complex [10,39,43]. $[Me_2Si(C_5Me_4)_2]Mo(\eta^1\text{-}C\text{-}C_4H_3O)H$ also exhibits disorder and was refined with occupancies as suggested by ^1H NMR spectroscopic analysis.

4.6. Computational details

All calculations were carried out using DFT as implemented in the Jaguar 6.0 suite of ab initio quantum

Table 3
Crystal, intensity collection and refinement data

	$[Me_2Si(C_5Me_4)_2]Mo(\eta^1\text{-}C\text{-}C_4H_3O)H$	$[Me_2Si(C_5Me_4)_2]Mo(\eta^1\text{-}C\text{-}C_8H_5O)H$	$[Me_2Si(C_5Me_4)_2]Mo(\eta^2\text{-}C,Se\text{-}SeC_4H_4)$	$[Me_2Si(C_5Me_4)_2]Mo(\eta^2\text{-}C,Se\text{-}SeC_8H_6)$
Lattice	orthorhombic	triclinic	monoclinic	monoclinic
Formula	$C_{24}H_{34}MoOSi$	$C_{28}H_{36}MoOSi$	$C_{24}H_{34}MoSeSi$	$C_{28}H_{36}MoSeSi$
Formula weight	462.54	512.60	525.50	575.56
Space group	*Pnma*	$P\bar{1}$	$P2_1/c$	$P2_1/c$
a (Å)	22.564(11)	8.689(3)	9.809(1)	10.0081(8)
b (Å)	11.316(5)	9.598(3)	24.957(2)	27.639(2)
c (Å)	8.629(4)	16.373(6)	9.883(1)	9.9429(8)
α (°)	90	75.160(7)	90	90
β (°)	90	81.562(8)	112.642(2)	114.205(1)
γ (°)	90	68.323(60	90	90
V (Å^3)	2203(2)	1224.5(7)	2232.8(4)	2508.6(3)
Z	4	2	4	4
Temperature (K)	238	238	238	243
Radiation (λ, Å)	0.71073	0.71073	0.71073	0.71073
ρ_{calc} (g cm^{-3})	1.394	1.390	1.563	1.524
μ (Mo Kα) (mm^{-1})	0.661	0.602	2.278	2.035
θ_{max} (°)	28.3	28.3	28.3	28.1
Number of data	2665	5505	5050	5637
Number of parameters	132	282	281	373
R_1	0.0390	0.0806	0.0349	0.0263
wR_2[a]	0.1042 (0.1126)	0.1629 (0.2064)	0.0841 (0.0865)	0.0644 (0.0664)
Goodness-of-fit	1.055	1.010	1.155	1.063

[a] $I > 2\sigma(I)$; value in parentheses for all data.

chemistry programs [50]. Geometry optimizations were performed with the B3LYP functional and the 6-31G** (C, H, S, Si), LAV3P (Se) and LACVP (Mo) basis sets. The energies of the optimized structures were reevaluated by additional single point calculations on each optimized geometry using the cc-pVTZ(-f) (C, H, S, Si, Se) and LACV3P (Mo) basis sets.

Acknowledgments

We thank the U.S. Department of Energy, Office of Basic Energy Sciences (DE-FG02-93ER14339) for support of this research.

References

[1] For recent review articles, see: (a) Stirling, D. The Sulfur Problem: Cleaning up Industrial Feedstocks, RSC Clean Technology Monographs, 2000;
(b) H. Topsøe, B.S. Clausen, F.E. Massoth, in: J.R. Anderson, M. Boudart (Eds.), Hydrotreating Catalysis in Catalysis: Science and Technology, vol. 11, Springer-Verlag, New York, 1996;
(c) S. Brunet, D. Mey, G. Pérot, C. Bouchy, F. Diehl, Appl. Catal. A: General 278 (2005) 143;
(d) I. Mochida, K.-H. Choi, J. Jpn. Pet. Inst. 47 (2004) 145;
(e) D.D. Whitehurst, T. Isoda, I. Mochida, Adv. Catal. 42 (1998) 345.

[2] For review articles concerned with modeling HDS, see: (a) R.A. Sánchez-Delgado, Organometallic Modelling of the Hydrodesulfurization and Hydrodenitrogenation Reactions, Kluwer Academic Publishers, Boston, 2002;
(b) R.A. Sánchez-Delgado, J. Mol. Catal. 86 (1994) 287;
(c) R.J. Angelici, Organometallics 20 (2001) 1259;
(d) R.J. Angelici, Polyhedron 16 (1997) 3073;
(e) C. Bianchini, A. Meli, Trans. Met. Sulph., NATO ASI Ser. 3 60 (1998) 129;
(f) C. Bianchini, A. Meli, Acc. Chem. Res. 31 (1998) 109;
(g) C. Bianchini, A. Meli, F. Vizza, J. Organomet. Chem. 689 (2004) 4277;
(h) W.D. Jones, D.A. Vicic, R.M. Chin, J.H. Roache, A.W. Myers, Polyhedron 16 (1997) 3115;
(i) W.D. Jones, Inorg. Chem. 44 (2005) 4475.

[3] For review articles featuring metal-thiophene chemistry, see Ref. [2] and: (a) R.J. Angelici, Trans. Met. Sulph., NATO ASI Ser. 3 60 (1998) 89;
(b) R.J. Angelici, Bull. Soc. Chim. Belg. 104 (1995) 265;
(c) T.B. Rauchfuss, Prog. Inorg. Chem. 39 (1991) 259;
(d) R.J. Angelici, Coord. Chem. Rev. 105 (1990) 61;
(e) S. Harris, Polyhedron 16 (1997) 3219;
(f) A.P. Sadimenko, Adv. Heterocycl. Chem. 78 (2001) 1.

[4] Typical HDS catalysts are comprised of a mixture of MoS_2 and Co_9S_8 supported on Al_2O_3. See Ref. [1] and J.V. Lauritsen, S. Helveg, E. Laegsgaard, I. Stensgaard, B.S. Clausen, H. Topsoe, F. Besenbacher, J. Catal. 197 (2001) 1.

[5] For examples of C–S bond cleavage of thiophene and related derivatives by tungsten, see: (a) W.D. Jones, R.M. Chin, T.W. Crane, D.M. Baruch, Organometallics 13 (1994) 4448;
(b) R.C. Mills, K.A. Abboud, J.M. Boncella, Chem. Commun. (2001) 1506.

[6] For examples of C–S bond cleavage of thiophene and related derivatives by manganese and rhenium, see: (a) C.A. Dullaghan, S. Sun, G.B. Carpenter, B. Weldon, D.A. Sweigart, Angew. Chem., Int. Ed. Engl. 35 (1996) 212 (Mn);
(b) C.A. Dullaghan, G.B. Carpenter, D.A. Sweigart, D.S. Choi, S.S. Lee, Y.K. Chung, Organometallics 16 (1997) 5688 (Mn);
(c) D.S. Choi, I.S. Lee, S.U. Son, Y.K. Chung, Organometallics 20 (2001) 3617 (Mn);
(d) M.A. Reynolds, I.A. Guzei, R.J. Angelici, Organometallics 20 (2001) 1071 (Re);
(e) M.A. Reynolds, I.A. Guzei, R.J. Angelici, J. Am. Chem. Soc. 124 (2002) 1689 (Re).

[7] For examples of C–S bond cleavage of thiophene and related derivatives by iron and ruthenium, see: (a) I.E. Buys, L.D. Field, T.W. Hambly, A.E.D. McQueen, J. Chem. Soc., Chem. Commun. (1994) 557 (Fe);
(b) H.D. Kaesz, R.B. King, T.A. Manuel, L.D. Nichols, F.G.A. Stone, J. Am. Chem. Soc. 82 (1960) 4749 (Fe);
(c) P. Hübener, E. Weiss, J. Organomet. Chem. 129 (1977) 105 (Fe);
(d) A.E. Ogilvy, M. Draganjac, T.B. Rauchfuss, S.R. Wilson, Organometallics 7 (1988) 1171 (Fe);
(e) T. Morikita, M. Hirano, A. Sasaki, S. Komiya, Inorg. Chim. Acta 291 (1999) 341 (Fe);
(f) K.M.K. Dailey, T.B. Rauchfuss, A.L. Rheingold, G.P.A. Yap, J. Am. Chem. Soc. 117 (1995) 6396 (Ru);
(g) C. Bianchini, D. Masi, A. Meli, M. Peruzzini, F. Vizza, F. Zanobini, Organometallics 17 (1998) 2495 (Ru).

[8] For examples of C–S bond cleavage of thiophene and related derivatives by cobalt, rhodium, and iridium, see: (a) W.D. Jones, R.M. Chin, Organometallics 11 (1992) 2698 (Co);
(b) W.D. Jones, R.M. Chin, J. Organomet. Chem. 472 (1994) 311 (Co);
(c) W.D. Jones, L. Dong, J. Am. Chem. Soc. 113 (1991) 559 (Rh);
(d) L. Dong, S.B. Duckett, K.F. Ohman, W.D. Jones, J. Am. Chem. Soc. 114 (1992) 151 (Rh);
(e) C. Blonski, A.W. Myers, M. Palmer, S. Harris, W.D. Jones, Organometallics 16 (1997) 3819;
(f) M. Paneque, S. Taboada, E. Carmona, Organometallics 15 (1996) 2678 (Rh);
(g) M. Paneque, P.J. Pérez, A. Pizzano, M.L. Poveda, S. Taboada, M. Trujillo, E. Carmona, Organometallics 18 (1999) 4304 (Rh);
(h) J. Chen, L.M. Daniels, R.J. Angelici, J. Am. Chem. Soc. 112 (1990) 199 (Ir);
(i) J. Chen, L.M. Daniels, R.J. Angelici, Polyhedron 9 (1990) 1883 (Ir);
(j) H.E. Selnau, J.S. Merola, Organometallics 12 (1993) 1583 (Ir);
(k) C. Bianchini, A. Meli, M. Peruzzini, F. Vizza, P. Frediani, V. Herrera, R.A. Sanchez-Delgado, J. Am. Chem. Soc. 115 (1993) 2731 (Ir);
(l) J. Chen, R.J. Angelici, Coord. Chem. Rev. (2000) 206, 63 (Ir);
(m) J. Chen, V.G. Young Jr., R. Angelici, J. Organomet. 21 (2002) 5951;
(n) J. Chen, R.J. Angelici, J. Organomet. Chem. 621 (2001) 55;
(o) J. Chen, R.J. Angelici, Inorg. Chim. Acta 334 (2002) 204.

[9] For examples of C–S bond cleavage of thiophene and related derivatives by nickel, palladium and platinum, see: (a) D.A. Vicic, W.D. Jones, J. Am. Chem. Soc. 121 (1999) 7606 (Ni);
(b) D.A. Vicic, W.D. Jones, J. Am. Chem. Soc. 119 (1997) 10855 (Ni);
(c) M. Hernández, G. Miralrio, A. Arévalo, S. Bernès, J.J. García, C. López, P.M. Maitlis, F. del Rio, Organometallics 20 (2001) 4061 (Ni, Pd, Pt);
(d) D.A. Vicic, W.D. Jones, Organometallics 17 (1998) 3411 (Ni, Pt);
(e) J.J. Garcia, B.E. Mann, H. Adams, N.A. Bailey, P.M. Maitlis, J. Am. Chem. Soc. 117 (1995) 2179 (Pt);
(f) A. Arevalo, S. Bernes, J.J. Garcia, P.M. Maitlis, Organometallics 18 (1999) 1680 (Pt);
(g) K. Yu, H. Li, E.J. Watson, K.L. Virkaitis, G.B. Carpenter, D.A. Sweigart, Organometallics 20 (2001) 3550 (Pt);
(h) A. Iretskii, J.J. García, G. Picazo, P.M. Maitlis, Catal. Lett. 51 (1998) 129 (Pt);
(i) C.A. Dullaghan, X. Zhang, D.L. Greene, G.B. Carpenter, D.A. Sweigart, C. Camiletti, E. Rajaseelan, Organometallics 17 (1998) 3316 (Pt);

(j) J. Chantson, H. Görls, S. Lotz, J. Organomet. Chem. 687 (2003) 39 (Pt).
[10] D.G. Churchill, B.M. Bridgewater, G. Parkin, J. Am. Chem. Soc. 122 (2000) 178.
[11] K.E. Janak, J.M. Tanski, D.G. Churchill, G. Parkin, J. Am. Chem. Soc. 124 (2002) 4182.
[12] For another example of C–S bond cleavage of thiophene accompanied by hydrogenation, see: G.P. Rosini, W.D. Jones, J. Am. Chem. Soc. 114 (1992) 10767.
[13] Hydrogenation of thiophene without cleavage of the C–S bond has also been reported. For example, $[RuH_2(\eta^2\text{-}H_2)_2(PCy_3)_2]$ reacts with thiophene to give an η^4-thioallyl complex $(\eta^4\text{-}S,C\text{-}SC_4H_5)Ru(PCy_3)_2H$ and is an effective catalyst precursor for the homogeneous hydrogenation of thiophene to 2,3,4,5-tetrahydrothiophene. See: A.F. Borowski, S. Sabo-Etienne, B. Donnadieu, B. Chaudret, Organometallics 22 (2003) 4803.
[14] For other examples of the "*ansa* effect" in this system, see: (a) D. Churchill, J.H. Shin, T. Hascall, J.M. Hahn, B.M. Bridgewater, G. Parkin, Organometallics 18 (1999) 2403;
(b) K.E. Janak, J.H. Shin, G. Parkin, J. Am. Chem. Soc. 126 (2004) 13054.
[15] A. Samat, J. Sala-Pala, R. Guglielmetti, J. Guerchais, Nouv. J. Chem. 2 (1978) 13.
[16] For another example of C–H bond cleavage of thiophene by tungsten, see: H. Sakaba, T. Yumoto, S. Watanabe, C. Kabuto, K. Kabuto, Chem. Lett. 32 (2003) 14.
[17] D.G. Churchill, K.E. Janak, J.S. Wittenberg, G. Parkin, J. Am. Chem. Soc. 125 (2003) 1403.
[18] In essence, geometric constraints imposed by the *ansa* bridge destabilize the product of intramolecular C–H bond cleavage, $[Me_2Si(\eta^5\text{-}C_5Me_4)(\eta^6\text{-}C_5Me_3CH_2)]MoH$, such that it is not a thermodynamic sink for the system.
[19] For other examples of thiophene adducts, see Refs. [2,3] and: (a) R.H. Schultz, Organometallics 23 (2004) 4349;
(b) M.A. Reynolds, I.A. Guzei, B.C. Logsdon, L.M. Thomas, R.A. Jacobson, R.J. Angelici, Organometallics 18 (1999) 4075;
(c) X. Fang, J.G. Watkin, B.L. Scott, K.D. John, G.J. Kubas, Organometallics 21 (2002) 2336;
(d) P.A. Vecchi, A. Ellern, R.J. Angelici, J. Am. Chem. Soc. 125 (2003) 2064;
(e) C. Slugovc, I. Padilla-Marti'nez, S. Sirol, E. Carmona, Coord. Chem. Rev. 213 (2001) 129;
(f) M. Paneque, M.L. Poveda, E. Carmona, V. Salazar, Dalton Trans. (2005) 1422;
(g) D.A. Delafuente, W.H. Myers, M. Sabat, W.D. Harman, Organometallics 24 (2005) 1876.
[20] For calculations on η^1-thiophene complexes, see: (a) L. Rincón, J. Terra, D. Guenzburger, R.A. Sánchez-Delgado, Organometallics 14 (1995) 1292;
(b) A.L. Sargent, E.P. Titus, C.G. Riordan, A.L. Rheingold, P. Ge, Inorg. Chem. 35 (1996) 7095;
(c) A.L. Sargent, E.P. Titus, Organometallics 17 (1998) 65;
(d) O. Maresca, F. Maseras, A. Lledos, New J. Chem. 28 (2004) 625.
[21] See, for example: (a) C. Bianchini, J.A. Casares, R. Osman, D.I. Pattison, M. Peruzzini, R.N. Perutz, F. Zanobini, Organometallics 16 (1997) 4611, and references therein;
(b) Ref. [8c];
(c) Ref. [8d];
(d) M. Paneque, M.L. Poveda, V. Salazar, S. Taboada, E. Carmona, E. Gutiérrez-Puebla, A. Monge, C. Ruiz, Organometallics 18 (1999) 139;
(e) M. Paneque, M.L. Poveda, L. Rey, S. Taboada, E. Carmona, C. Ruiz, J. Organomet. Chem. 504 (1995) 147.
[22] (a) M. Paneque, S. Taboada, E. Carmona, Organometallics 15 (1996) 2678;
(b) Ref. [8g].
[23] Although the conversion of $Cp^*Rh(PMe_3)(\eta^1\text{-}C\text{-}C_4H_3S)H$ to $Cp^*Rh(PMe_3)(\eta^2\text{-}C,S\text{-}SC_4H_4)$ occurs via initial C–H bond formation,[a] it is important to note that σ-thienyl compounds which do not have a hydride co-ligand may also undergo C–S bond cleavage. For example, it has been demonstrated that a dinuclear tungsten σ-thienyl compound undergoes a reaction that results in C–S cleavage and formation of a bridging vinylidene thiolate ligand (μ-C=CH=CH=CHS).[b]
(a) Refs. [8d,20c];
(b) M.H. Chisholm, S.T. Haubrich, J.C. Huffman, W.E. Streib, J. Am. Chem. Soc. 119 (1997) 1634.
[24] These calculations are for isomers of $(Cp^R)_2Mo(\eta^1\text{-}C\text{-}C_4H_3S)H$ that have sulfur *endo* to the hydride ligand. The *exo* isomers are slightly less stable: $[Me_2Si(C_5Me_4)_2]Mo(\eta^1\text{-}C\text{-}C_4H_3S)H$ ($\Delta E = 1.0$ kcal mol^{-1}), $Cp_2Mo(\eta^1\text{-}C\text{-}C_4H_3S)H$ ($\Delta E = 0.3$ kcal mol^{-1}), and $Cp^*_2Mo(\eta^1\text{-}C\text{-}C_4H_3S)H$ ($\Delta E = 0.2$ kcal mol^{-1}).
[25] C.E. Zachmanoglou, A. Docrat, B.M. Bridgewater, G. Parkin, C.G. Brandow, J.E. Bercaw, C.N. Jardine, M. Lyall, J.C. Green, J.B. Keister, J. Am. Chem. Soc. 124 (2002) 9525.
[26] For a specific comparison of $\{[Me_2Si(C_5Me_4)_2]Mo\}$ and $[Cp^*_2Mo]$ derivatives, see Ref. [14].
[27] (a) J.W. Lauher, R. Hoffmann, J. Am. Chem. Soc. 98 (1976) 1729;
(b) J.C. Green, Chem. Soc. Rev. 27 (1998) 263.
[28] Note that different conventions are used to define the equatorial metallocene plane and these results in different symmetry labels for the frontier orbitals. With z defining the C_2 axis and xz defining the metallocene plane, the frontier oribitals of the metallocene fragment have a_1, b_1 and a_1 symmetry (Ref. [27b]); with yz defining the metallocene plane, the frontier oribitals of the metallocene fragment have a_1, b_2 and a_1 symmetry (Ref. [27a]).
[29] A.J. Bridgeman, L. Davis, S.J. Dixon, J.C. Green, I.N. Wright, J. Chem. Soc., Dalton Trans. (1995) 1023.
[30] M.L.H. Green, P.C. Konidaris, D.M. Michaelidou, P. Mountford, J. Chem. Soc., Dalton Trans. (1995) 155.
[31] J.H. Shin, B.M. Bridgewater, D.G. Churchill, M.-H. Baik, R.A. Friesner, G. Parkin, J. Am. Chem. Soc. 123 (2001) 10111.
[32] For a symmetric AX_2 molecule in which the bonding utilizes, for simplicity, a single s orbital on each atom, it is well known that the molecular orbital pattern consists of three orbitals which have the following character: (i) A–X bonding with no nodes, (ii) A–X nonbonding with a single node, and (iii) A–X antibonding with two nodes. However, although the A–X nonbonding orbital for an AX_2 molecule is localized on the X ligands with no contribution from the central atom, the corresponding "nonbonding" orbital for an asymmetric X–A–Y species may have varying degrees of X–A and A–Y bonding or antibonding character. As such, it is not completely appropriate to describe the orbital as "nonbonding"; it is, nevertheless, still characterized by a single node.
[33] The d_{yz} orbital is also of appropriate symmetry to interact with the $\eta^2\text{-}C,S\text{-}SC_4H_4$ ligand, but the overlap is not significant.
[34] (a) Ref. [8h];
(b) Ref. [8i].
[35] For examples of metallathiabenzenes, see: (a) Ref. [34];
(b) R.M. Chin, W.D. Jones, Angew. Chem., Int. Ed. Engl. 31 (1992) 357;
(c) Ref. [9j];
(d) J.R. Bleeke, P.V. Hinkle, J. Am. Chem. Soc. 121 (1999) 595;
(e) J.R. Bleeke, M.F. Ortwerth, M.Y. Chiang, Organometallics 11 (1992) 2740;
(f) M.A. Iron, J.M.L. Martin, M.E. van der Boom, Chem. Commun. (2003) 132;
(g) J.R. Bleeke, P.V. Hinkle, N.P. Rath, Organometallics 20 (2001) 1939;
(h) C. Bianchini, A. Meli, M. Peruzzini, F. Vizza, S. Moneti, V. Herrera, R.A. Sánchez-Delgado, J. Am. Chem. Soc. 116 (1994) 4370.
[36] (a) Ref. [8e];
(b) M. Palmer, K. Carter, S. Harris, Organometallics 16 (1997) 2448.
[37] For other calculations pertaining to metallathiacycles, see: (a) S. Harris, Organometallics 13 (1994) 2628;
(b) A.L. Sargent, E.P. Titus, Organometallics 17 (1998) 65;
(c) M.S. Palmer, S. Rowe, S. Harris, Organometallics 17 (1998) 3798.

[38] For specific examples of twofold disorder of metallathiacycle ligands, see: (a) Ref. [8e];
(b) Ref. [9a].
[39] For general examples in which disorder influences the observed bond lengths, see: (a) G. Parkin, Acc. Chem. Res. 25 (1992) 455;
(b) G. Parkin, Chem. Rev. 93 (1993) 887;
(c) K. Yoon, G. Parkin, A.L. Rheingold, J. Am. Chem. Soc. 113 (1991) 1437;
(d) K. Yoon, G. Parkin, A.L. Rheingold, J. Am. Chem. Soc. 114 (1992) 2210;
(e) K. Yoon, G. Parkin, J. Am. Chem. Soc. 113 (1991) 8414;
(f) K. Yoon, G. Parkin, Inorg. Chem. 31 (1992) 1656.
[40] Structurally characterized molybdenum–furyl compounds are not common, but an example is provided by $CpMo(CO)_2(PPh_3)(\eta^1\text{-}C\text{-}C_4H_3O)$. See: K.H. Pannell, R. Cea-Olivares, R.A. Toscano, R.N. Kapoor, Organometallics 6 (1987) 1821.
[41] Although it is possible that the two isomers could correspond to rotamers, the ^{1}H NMR spectra do not show any evidence of interconversion at 70 °C, thereby suggesting that the isomers are not rotamers.
[42] For other examples of α-C–H bond cleavage of furan, see: (a) Ref. [7e];
(b) Ref. [15];
(c) Ref. [8j];
(d) S.N. Ringelberg, A. Meetsma, S.I. Troyanov, B. Hessen, J.H. Teuben, Organometallics 21 (2002) 1759;
(e) W.D. Jones, L. Dong, A.W. Myers, Organometallics 14 (1995) 855;
(f) K.A. Pittard, J.P. Lee, T.R. Cundari, T.B. Gunnoe, J.L. Petersen, Organometallics 23 (2004) 5514.
[43] D.A. Vicic, A.W. Myers, W.D. Jones, Organometallics 16 (1997) 2751.
[44] C.J. White, R.J. Angelici, M.-G. Choi, Organometallics 14 (1995) 332.
[45] For other examples of C–Se cleavage in selenophenes, see: (a) M.L. Spera, W.D. Harman, Organometallics 18 (1999) 1559;
(b) A.J. Arce, R. Machado, C. Rivas, Y. De Sanctis, A.J. Deeming, J. Organomet. Chem. 419 (1991) 63;
(c) A.J. Arce, A.J. Deeming, Y. De Sanctis, R. Machado, J. Manzur, C. Rivas, J. Chem. Soc., Chem. Commun. (1990) 1568;
(d) D.S. Choi, I.S. Lee, S.U. Son, Y.K. Chung, Organometallics 20 (2001) 3617.
[46] (a) J.R. Bleeke, J.M.B. Blanchard, E. Donnay, Organometallics 20 (2001) 324;
(b) J.R. Bleeke, J.M.B. Blanchard, J. Am. Chem. Soc. 119 (1997) 5443;
(c) J.R. Bleeke, T. Haile, P.R. New, M.Y. Chiang, Organometallics 12 (1993) 517.
[47] D. Baudry, J.-C. Daran, Y. Dromzee, M. Ephritikhine, H. Felkin, Y. Jeannin, J. Zakrzewski, J. Chem. Soc., Chem. Commun. (1983) 813.
[48] M. Lardon, J. Am. Chem. Soc. 92 (1970) 5063.
[49] G.M. Sheldrick, SHELXTL, An Integrated System for Solving, Refining and Displaying Crystal Structures from Diffraction Data, University of Göttingen, Göttingen, Federal Republic of Germany, 1981.
[50] Jaguar 6.0 Schrödinger, Inc., Portland, OR, 2005.

Available online at www.sciencedirect.com
SCIENCE DIRECT®
Polyhedron 25 (2006) 513–520
POLYHEDRON
www.elsevier.com/locate/poly

Metal complexes of *N*,*N*,*N*′,*N*′-tetrakis(2-pyridylmethyl)ethylenediamine (TPEN): Variable coordination numbers and geometries

Claudia A. Blindauer [a,b], M. Tahir Razi [a,c], Simon Parsons [a], Peter J. Sadler [a,*]

[a] *School of Chemistry, University of Edinburgh, West Mains Road, Edinburgh, EH9 3JJ, UK*
[b] *Department of Chemistry, University of Warwick, Gibbet Hill Road, Coventry CV4 7AL, UK*
[c] *Department of Pharmacy, Bahauddin Zakariya University, Multan, Pakistan*

Received 2 June 2005; accepted 11 August 2005
Available online 5 October 2005

Abstract

We report X-ray crystal structures of complexes of the membrane-permeable metal chelator *N*,*N*,*N*′,*N*′-tetrakis(2-pyridylmethyl)ethylenediamine (TPEN) with Cu(II) and Zn(II), and solution studies of the Zn(II) and Cd(II) complexes. $[Zn(II)(TPEN)](PF_6)_2$ exhibits a distorted octahedral geometry with hexadentate TPEN, whilst $[Cu(II)(TPEN)](PF_6)_2$ contains penta-coordinated Cu(II), with one pendant picolyl arm of TPEN. A survey of structures of metal–TPEN complexes reveals the versatility of the TPEN ligand. Complexes of V(V), Cr(III), Rh(III), Re(VII), Fe(II), as well as Cu(II) are known which contain hypodentate TPEN with 3–5 of its nitrogens coordinated to the metal. Solution NMR spectroscopic studies also suggest that there is dynamic conformational flexibility in the structures of the $[Zn(TPEN)]^{2+}$ and $[Cd(TPEN)]^{2+}$ complexes in aqueous solution.
© 2005 Elsevier Ltd. All rights reserved.

Keywords: Denticity; Zinc; Copper; Cadmium; X-ray; NMR spectroscopy

1. Introduction

N,*N*,*N*′,*N*′-Tetrakis(2-pyridyl-methyl)ethylenediamine (TPEN, Fig. 1) is a potentially hexadentate ligand. The ability of TPEN to cross-natural and artificial membranes and to chelate d-block metals preferentially makes it a useful tool for investigating the role of these metals inside cells. It has thus been used extensively in the past 15 years to study metal ion, in particular zinc, homeostasis [1,2]. Studies using TPEN have demonstrated that intracellular zinc depletion causes oxidative stress and DNA damage [3], upregulates hundreds of genes [4], and leads to (programmed) cell death [5]. TPEN has also been shown to be active against botulinum neurotoxins A and B in vivo [6], by a mechanism which presumably involves abstraction of the active site Zn(II) from the metalloprotease component of the toxins. However, since this chelating action is not limited to the toxin, TPEN is also considerably cytotoxic.

Despite its ubiquitous use as zinc chelator in biological systems, no X-ray structure of the TPEN complex of Zn(II) had been reported until very recently [7] (and after preparation of this script had begun), and little is known about the solution properties of this complex. We report here NMR spectroscopic studies of the Zn(II) and Cd(II) complexes of TPEN in solution and a comparison of the X-ray structures of Zn(II) and Cu(II) complexes. We show that TPEN is highly versatile in terms of the denticity and geometry that it adopts in metal complexes.

Abbreviations: TPEN, *N*,*N*,*N*′,*N*′-tetrakis(2-pyridylmethyl)ethylenediamine; EDTA, ethylenediamine-tetraacetate.

* Corresponding author. Tel.: +44 131 650 4729; fax: +44 131 650 6453.
E-mail address: p.j.sadler@ed.ac.uk (P.J. Sadler).

0277-5387/$ - see front matter © 2005 Elsevier Ltd. All rights reserved.
doi:10.1016/j.poly.2005.08.019

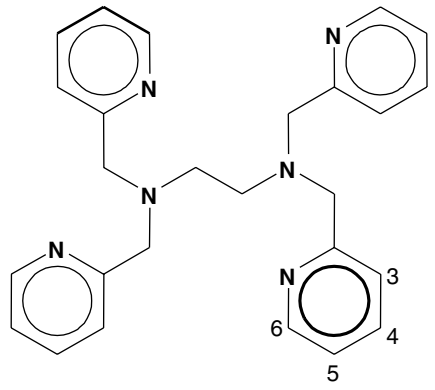

Fig. 1. Chemical structure of *N*,*N*,*N*′,*N*′-tetrakis(2-pyridylmethyl)ethylenediamine (TPEN).

2. Experimental

2.1. X-ray crystallography

Diffraction data for compounds were collected on a Bruker Smart APEX diffractometer equipped with an Oxford Cryosystems low-temperature device operating at 150 K. Absorption corrections were based on the multiscan procedure SADABS. Structures were solved by Patterson methods using DIRDIF [8]. A summary of X-ray crystallographic data for [Zn(TPEN)]$(PF_6)_2$ and [Cu(TPEN)]$(PF_6)_2$ is given in Table 1.

2.1.1. [Zn(II)(TPEN)]$(PF_6)_2$

TPEN (8.5 mg, 20 μmol) was dissolved in 2 ml H_2O at 353 K. $ZnCl_2$ (20 μmol) was added from a 0.2 M aqueous stock solution. NH_4PF_6 (40 μmol) was added from a 0.1 M aqueous stock solution, and the pH was readjusted to 8.0 using NaOH. Subsequently, MeOH was added dropwise at 353 K, until the appearance of a precipitate. Water was added to re-dissolve this precipitate, and the solution was left to cool, first at room temperature, then at 277 K. Colourless blocks suitable for crystallography formed within days.

Refinement of 425 parameters by full-matrix least-squares on F^2 using SHELX-97 [9] gave $wR_2 = 0.1142$ based on all data and $R_1 = 0.0448$, based on 6598 data with $F > 4\sigma(F)$, $S = 1.055$, maximum Δ/σ on last cycle 0.006, maximum/minimum residual electron density = +0.73/−0.50 Å^{-3}. All non-hydrogen atoms refined anisotropically; hydrogen atoms of the complex were placed in calculated positions and allowed to ride on their parent atoms.

2.1.2. [Cu(II)(TPEN)]$(PF_6)_2$

TPEN (8.5 mg, 20 μmol) was dissolved in 5 ml of H_2O by adding 1 M HCl and the pH of the solution was adjusted to 7.0. To this solution 1 ml of an aqueous solution of $CuCl_2 \cdot 2H_2O$ (3.4 mg, 20 μmol) was added slowly with constant stirring. After 30 min stirring at room temperature, an aqueous solution (1 ml) of NH_4PF_6 (6.5 mg, 40 μmol) was added slowly to the reaction mixture. A blue microcrystalline product was obtained by concentrating the resultant solution on a rotary evaporator. The product was filtered off, washed with cold water and methanol, dried in air, and recrystallised from water. Blue crystals for X-ray structure determination formed after 1 week at 277 K.

Refinement of 424 parameters by full-matrix least-squares on F^2 using SHELX-97 [9] gave $wR_2 = 0.1069$ based on all data and $R_1 = 0.0439$, based on 6203 data with $F > 4\sigma(F)$, $S = 1.027$, maximum Δ/σ on last cycle 0.002, maximum/minimum residual electron density = +0.64/−0.45 Å^{-3}. All non-hydrogen atoms refined anisotropically; hydrogen atoms of the complex were placed in calculated positions and allowed to ride on their parent atoms.

Table 1
Crystallographic data collection and refinement details

Complex	[Cu(II)(TPEN)]$(PF_6)_2$	[Zn(II)(TPEN)]$(PF_6)_2$
Formula	$C_{26}H_{28}CuF_{12}N_6P_2$	$C_{26}H_{28}F_{12}N_6P_2Zn$
Formula weight	778.02	779.85
Crystal system	triclinic	monoclinic
Colour	blue	colourless
Size (mm)	0.56 × 0.40 × 0.18	0.30 × 0.15 × 0.12
Space group	$P\bar{1}$	$P2_1/c$
a (Å)	10.1461 (4)	10.5880 (6)
b (Å)	12.4869 (4)	19.0543 (11)
c (Å)	14.0604 (6)	15.3555 (9)
α (°)	70.064 (3)	90
β (°)	68.947 (2)	98.6340 (10)
γ (°)	70.881 (2)	90
V (Å^3)	1519.54 (10)	3062.8 (3)
Z	2	4
λ (Å)	0.71073	0.71073
ρ_{calc} (g/cm^3)	1.700	1.691
T (K)	150 (2)	150 (2)
R_1	0.0439	0.0448
wR_2	0.1069	0.1142
Goodness-of-fit	1.027	1.055

2.2. ^1H NMR spectroscopy

^{1}H NMR experiments were carried out on 5 mM [Zn(TPEN)]Cl_2 solutions in either 10% D_2O at pH 7.1, or 100% D_2O at pH* 7.1, and on 2.5 mM [^{111}Cd(TPEN)]Cl_2 (^{111}Cd isotopic purity 95.29%, Oak Ridge National Laboratory, TN) in 10% D_2O at pH 7.4. No buffers were added to the solutions. In each case, the solutions were prepared by mixing the appropriate amounts of TPEN and the respective metal chloride.

^{1}H spectra were acquired at 298 K on a Bruker DMX 500 spectrometer (500.13 MHz for ^{1}H) using an inverse multinuclear probehead (TBI) with 16 k time domain data points over a frequency width of 10000 Hz (20 ppm), giving an acquisition time of 0.625 s, and a relaxation delay of 2 s. The water signal was suppressed by presaturation during the relaxation delay, or using excitation sculpting [10]. Data were zero-filled to 64 k, apodised by exponential multiplication, applying a line-broadening factor of 0.3 Hz prior to Fourier transformation.

2.3. ^{111}Cd NMR spectroscopy

For ^{111}Cd NMR experiments, the reference was external 0.1 M $Cd(ClO_4)_2$ (natural abundance). Spectra were acquired on a 2.5 mM enriched sample (95.29% ^{111}Cd; Oak Ridge National Laboratory, TN) of the TPEN complex in 10% D_2O, pH 7.4, on a Bruker DMX 500 spectrometer operating at 106.046 MHz for ^{111}Cd, using a multinuclear broad-band observe (BBO) probehead with a pulsewidth of 17.5 μs (90°), acquisition time of 387 ms, recycle-delay of 1.5 s, 1024 transients, and frequency widths of 100, 200, and 400 ppm with varying offset frequencies. Spectra were zero-filled, and apodised by exponential multiplication with a line-broadening factor of 3, 15 or 30 Hz. Spectra were acquired without and with ^{1}H decoupling using GARP; no $^3J(^1H–^{111}Cd)$ coupling could be resolved.

2.4. Electrospray mass spectrometry

A Micromass Platform II ESI-MS instrument operating in positive ion mode was used for recording mass spectra (source temperature 373 K, capillary 3.52, HV lens 6.5). For MS samples, $[Cu(TPEN)](PF_6)_2$ was dissolved in water to a concentration of 100 μM. The cone voltage was varied over the range 10–35 V. MASS-LYNX (version 2.3) software was used for data processing.

2.5. UV–Vis spectroscopy

A CARY 300 Scan UV–Vis spectrophotometer was used for recording UV–Vis spectra (200–800 nm) in 1 cm pathlength cells. Samples were prepared by dissolving $[Cu(TPEN)](PF_6)_2$ in water at a concentration of 1.3 mM.

3. Results and discussion

3.1. Structure of $[Zn(TPEN)](PF_6)_2$

$[Zn(TPEN)](PF_6)_2$ crystallises in the monoclinic space group $P2_1/c$. The complex is chiral, and the crystals are racemic, with one crystallographically independent molecule in the unit cell. Fig. 2(a) shows the structure of one of the two stereoisomers. The recently characterized perchlorate salt $[Zn(TPEN)](ClO_4)_2$ crystallises in the monoclinic space group $C2/c$ [7] and contains two crystallographically independent molecules, with slightly different structures, and different stereochemistry. In both the perchlorate and hexafluorophosphate salts, Zn(II) has distorted octahedral coordination, with two picolyl rings *trans* to each other (labelled 2 and 4 in Fig. 2(a)), and the other two *cis* to each other (labelled 1 and 3). Table 2 gives selected distances and angles. The Zn–N distances in $[Zn(TPEN)](PF_6)_2$ vary between 2.117(2) and 2.2185(19) Å, with the shortest distances being observed for the two nitrogens in the *cis* picolyl rings, and the longest for the two ethylenediamine nitrogens. The largest deviation from ideal octahedral geometry is observed for the angles in the equatorial plane defined by the "en" nitrogens and the two *cis* picolyl nitrogens (N31–Zn–N33 = 124.64(7)°, and N1–Zn–N4 = 80.67(7)°). The planes defined by the two *cis* picolyl rings are at an angle of 22.5°. In the perchlorate salt, twist angles of 8° and 16.4° are observed. The planes of the *trans* picolyl rings are almost perpendicular to one another, at an angle of 79.9° in the PF_6 salt.

3.2. Structure of $[Cu(II)(TPEN)](PF_6)_2$

$[Cu(TPEN)](PF_6)_2$ is blue in colour and soluble in water and methanol. The UV–Vis spectrum of an aqueous solution

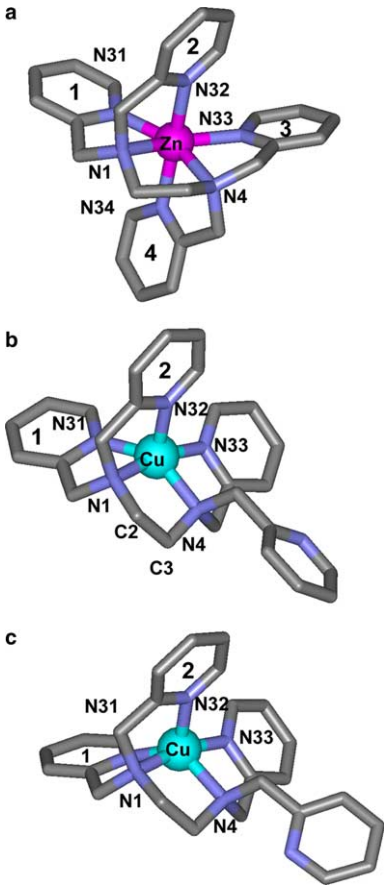

Fig. 2. View towards the "en" backbone of equivalent stereoisomers of the complex cations in (a) $[Zn(TPEN)](PF_6)_2$, (b) $[Cu(II)(TPEN)](PF_6)_2$, and (c) $[Cu(II)(TPEN)](ClO_4)_2$ [11]. The molecules have been positioned in such a way that ring 2, N1 and N4 are in similar orientations. Hydrogen atoms have been omitted for clarity. The comparison of (a) with (b) illustrates how differences in the conformation of the backbone allow for changes in the coordination number. The conformations of the five-membered chelate rings involving the "en" backbone can be described as "twist" (with C2 and C3 deviating from the plane defined by N1, Zn, and N4) for the Zn(II) complex, and as "envelope" for the Cu(II) complex, with C3 being the "flap" (the torsional angle between N4–Cu–N1–C2 is only 7°). As a consequence, the stereochemistry at N4 in $[Cu(TPEN)]^{2+}$ is inverted. The angle between the two "equatorial" picolyl rings (1 and 3) is 22.5° for the Zn(II) complex, and 51.0° for the Cu(II) complex. This larger angle in the Cu(II) complex is also a direct consequence of the stereochemistry at N4. A comparison of (b) and (c) demonstrates that the geometry of complex in the PF_6 salt is closer to tetragonal-pyramidal than trigonal-bipyramidal, as observed in the ClO_4 salt. This difference is mainly due to the altered position of ring 1 in relation to the rest of the molecule (see text).

Table 2
Selected bond lengths (Å) and angles (°)

[Cu(II)(TPEN)](PF$_6$)$_2$		[Zn(II)(TPEN)](PF$_6$)$_2$[a]	
Cu–N(1)	2.0252 (18)	Zn–N(4)	2.2185 (19)
Cu–N(4)	2.0475 (18)	Zn–N(1)	2.2062 (19)
Cu–N(31)	2.0240 (19)	Zn–N(34)	2.204 (2)
Cu–N(32)	2.109 (2)	Zn–N(33)	2.1195 (19)
Cu–N(33)	1.9872 (19)	Zn–N(31)	2.117 (2)
		Zn–N (32)	2.1665 (19)
N(33)–Cu–N (1)	168.01 (8)	N(31)–Zn–N(4)	153.83 (7)
N(33)–Cu–N (4)	82.53 (8)	N(31)–Zn–N(1)	77.62 (7)
N(33)–Cu–N (31)	104.09 (8)	N(31)–Zn–N(34)	88.67 (7)
N(33)–Cu–N(32)	105.06 (8)	N(31)–Zn–N(33)	124.64 (7)
N(31)–Cu–N(1)	82.02 (8)	N(34)–Zn–N(4)	78.42 (7)
N(31)–Cu–N(4)	143.35 (8)	N(34)–Zn–N(1)	93.89 (7)
N(31)–Cu–N(32)	104.63 (7)	N(34)–Zn–N(33)	92.64 (7)
N(1)–Cu–N(4)	86.48 (7)	N(4)–Zn–N(1)	80.67 (7)
N(1)–Cu–N(32)	82.92 (7)	N(4)–Zn–N(33)	79.03 (7)
N(4)–Cu–N(32)	108.31 (7)	N(4)–Zn–N(33)	156.95 (8)
		N(32)–Zn–N(31)	95.43 (7)
		N(32)–Zn–N(33)	91.20 (7)
		N(32)–Zn–N(31)	171.45 (7)
		N(32)–Zn–N(1)	79.72 (7)
		N(32)–Zn–N(4)	94.84 (7)

For atom labelling schemes see Fig. 2.
[a] The labelling of atoms in this table has been adjusted for [Zn(II)(TPEN)](PF$_6$)$_2$ to facilitate comparisons between the zinc and copper complexes, and is not identical with the numbering in the deposited cif file (see Section 5).

of this complex at pH 7.0 shows a single absorption band with λ_{max} at 691 nm ($\varepsilon = 165\ M^{-1}\ cm^{-1}$) which is in agreement with the reported value [16]. The X-ray crystal structure of this complex is shown in Fig. 2(b). A summary of selected data are given in Table 1, and selected bond lengths and angles are given in Table 2. [Cu(TPEN)](PF$_6$)$_2$ forms triclinic crystals (space group $P\bar{1}$), and there are two molecules in the unit cell. The copper in this complex is five-coordinate, with one dangling, non-coordinating picolyl arm. The geometry is distorted, and can be described (see below) either as trigonal-bipyramidal, with N1 and N33 as axial ligands (N1–Cu–N33 = 168.01(8)°), or as tetragonal-pyramidal, with N32 as axial ligand, displaying a markedly longer bond distance (Cu–N32 = 2.109(2) Å) than the other four nitrogen ligands (1.9872(19)–2.0475(19) Å). The angles N33–Cu–N4, N31–Cu–N1, N1–Cu–N32 between picolyl and aliphatic nitrogen atoms are in the range of 82.0–82.9°, whereas the angle between the aliphatic nitrogens (N1–Cu–N4) is slightly larger, 86.5°. [Cu(TPEN)]$^{2+}$ is chiral, and the two molecules in the unit cell are enantiomers.

There are some interesting differences between the structures of the PF$_6$ salt of [Cu(TPEN)]$^{2+}$ reported here and that of the perchlorate salt reported recently [11]. The perchlorate salt is described as green in powder and crystalline forms, whereas the PF$_6$ salt is strongly blue in colour, as expected for all-nitrogen coordination. They crystallise in different space groups (monoclinic, $C2/c$ versus triclinic, $P\bar{1}$) with different packing.

In the perchlorate salt, the complex cation has a similar, but not identical, structure as that in [Cu(TPEN)](PF$_6$)$_2$ reported here. [Cu(TPEN)](ClO$_4$)$_2$ (Fig. 2(c)) has distorted trigonal-bipyramidal geometry with N1 and N33 (labelling according to Fig. 2) as the axial ligands, giving a N1–Cu–N33 angle of 167.3(2)°, very close to the corresponding angle in [Cu(TPEN)](PF$_6$), 168.01(8)°. A remarkable difference between the structures of the perchlorate and the hexafluorophosphate salts is the position of N31 in relation to N32 and N4 (the aliphatic nitrogen with the non-coordinating picolyl arm): In the perchlorate structure, the angles N31–Cu–N32, and N31–Cu–N4 are similar, 125.9(2)° and 127.2(2)°, respectively, whilst in the hexafluorophosphate structure, they differ considerably, with the N31–Cu–N4 angle being much larger (143.35(8)°) than the N31–Cu–N32 angle (104.63(7)°). Another striking difference is the bond length between Cu and N4: 2.148 Å in the perchlorate salt, the longest bond length in the complex, but only 2.0475(18) Å in the hexafluorophosphate salt, with the longest Cu–N bond length being that to the aromatic N32 (2.109(2) Å; the corresponding distance in the perchlorate salt is only 2.028(4) Å). In summary, the coordination geometry of the hexafluorophosphate structure is closer to tetragonal-pyramidal (with N32 as the apical ligand) than that of the perchlorate salt complex. The finding that the [Cu(TPEN)]$^{2+}$ complex can adopt various geometries in the solid state has implications for its solution behaviour.

Electrospray ionization mass spectra (ESI-MS) of [Cu(TPEN)]$^{2+}$ in water were recorded at different cone voltages (CV). At 10 or 15 V, a peak at 243.3 amu (m/z) clearly showed the presence of the [Cu(TPEN)]$^{2+}$ ion (calc. m/z 488/2 = 244). A peak at 486.9 amu corresponds to a species bearing one positive charge (calc. 487 Da). Upon using higher cone voltages (35 V), in-source fragmentation was observed, giving peaks at 92.5 amu, corresponding to a picolyl residue (calc. 92 amu) and at 393.6 amu, corresponding to the singly charged parent ion with one picolyl group less (calc. 395 amu). In contrast, there was no indication of Cu loss from the complex (no peaks detected for free TPEN). It is notable that the coordinative Cu(II)–N bonds remain intact whilst a C–N bond (305 kJ mol^{-1}) is cleaved. This demonstrates the high stability of these chelate complexes, and confirms that the pentadentate coordination mode is not only adopted in the solid state and solution, but also in the gas phase.

The variable denticity of TPEN has been noted previously, e.g., in the case of Fe(II), Cr(III), or Rh(III) complexes [12–15]. The pentadentate coordination of Cu(II) was predicted by Anderegg et al. [16] as early as 1977, who noticed that the Cu(II) complex was less stable than expected based on the Irving-Williams series. This is illustrated in Fig. 3. The maximum stability for octahedral [M(II)(TPEN)]$^{2+}$ complexes [16] would be expected for Cu(II), but the series observed for TPEN complexes peaks at Ni(II).

The versatility of TPEN was further highlighted by a survey of X-ray crystal structures of its complexes currently deposited in the Cambridge Crystallographic Database (version 5.26; November 2004), summarised in Table 3.

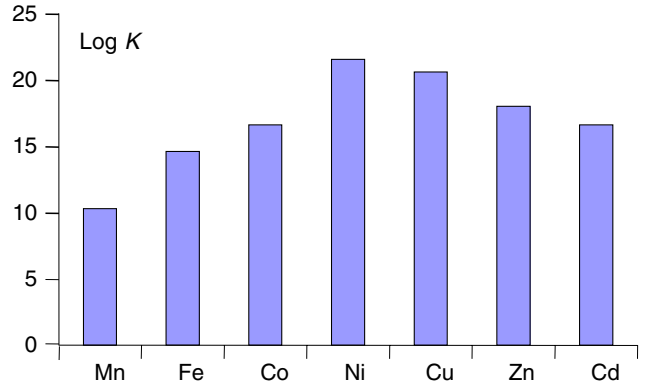

Fig. 3. Summary of stabilities of M(II) complexes of TPEN [16]. The stabilities do not strictly follow the Irving-Williams series. In particular, the Cu(II) complex is less stable than expected for octahedral coordination with Jahn–Teller distortion. This is attributable to its five-coordinate structure compared to the octahedral structure expected for the other metal ions.

The structures of mononuclear complexes $[M(TPEN)]^{n+}$ of M = Cr(III), Fe(II), Fe(III), Co(III), Ni(II), Zn(II), and Ru(II) have been reported [7,12–15,17–22]. All of these complexes have distorted octahedral geometry. Higher coordination numbers (7–10) for hexadentate TPEN complexes with additional ligands have been observed in mononuclear complexes of Mn(II), Cd(II), Sm(III), Tl(III), La(III) and Tb(III) [23–26]. Several examples for mononuclear complexes in which TPEN acts as a hypodentate ligand, coordinating metals via only 3 to 5 of its nitrogens, have been reported for V(V), Cr(III), Rh(III), Re(VII), Fe(II), and Cu(II) [11,12,14,15,18,27–29]. In every case, the "en" nitrogens are coordinated, and the hypodenticity is due to un-coordinated picolyl rings. In the complexes of V(V), Cr(III), Rh(III), Re(VII) and Fe(II), the hypodenticity is due to the presence of other competing ligands (Cl^-, oxo-O, sulfato-O, acetato-O), whereas the penta-coordinate Cu(II) complex is the only one with no additional ligands present. In this case, it is apparently the preference of Cu(II) for penta-coordination that governs the coordination geometry.

In addition, TPEN can form dinuclear complexes with the two symmetrical halves (comprising two pyridyl nitrogens and one aliphatic nitrogen) coordinating to one metal ion each. Depending on the nature of the metal and the additional ligands present, the two metals can be in close proximity, forming a metal–metal bond, as observed for complexes with Cu(I and II), Cr(III), Mn(III and IV), V(V), Mo(V) and W(V) [30–35]. The dinuclear complexes with metal–metal bonds have bridging oxo, hydroxo, and/or acetate ligands, with the exception of $[Cu(I)_2(TPEN)](BF_4)_2$ [30], (Cu–Cu 2.779 Å). Alternatively, the TPEN ligand can adopt an extended conformation, as in $[Cu(II)_2Cl_2(TPEN)](ClO_4)_2 \cdot H_2O$ (Cu–Cu 7.196 Å) [11], or $[Cu(II)_2Cl_4(TPEN)]$ (Cu–Cu 7.316 Å) [36]. A recent report has shown that Cu(II) interactions with TPEN in the presence of Cl^- can lead to the formation of $[Cu(II)_2Cl_2(TPEN)]^{2+}$ in solution [37].

In summary, depending on stoichiometry and conditions of the reaction, including the presence of competing ligands, TPEN shows a wide versatility in its interactions with metal ions, with Cu(I) and Cu(II) complexes displaying various features that are unparalleled in complexes with any other metal ions.

3.3. ^1H NMR spectroscopy of $[Zn(TPEN)]^{2+}$

Fig. 4 shows the 1-D ^1H NMR spectra of free TPEN, and mixtures of Zn(II) and TPEN, all at pH 7.1. The free ligand gives two resonances in the aliphatic, and four in the aromatic region. The peak assignments are also shown. In contrast to the other resonances, the line-width of the resonance for the ethylene "backbone" protons is temperature- and pH-dependent (at 298 K, 10% D_2O, pH 7.1: 7.8 Hz, pH 0: 4.2 Hz).

The reported pK_a values for TPEN are 7.19, 4.86, 3.35, and 2.95 [38]. Protonation occurs exclusively at the picolyl rings [16], as these exert a pronounced inductive effect on the tertiary amine nitrogens, making them much less basic than, e.g., triethylamine ($pK_a = 11$). This conclusion from solution data has been confirmed for the solid state; the X-ray structure of $H_4TPEN(ClO_4)_4$ shows four protonated picolyl residues [39]. No intramolecular H-bonds are observed, but the acidic protons show H-bonds to the counter-anions. From the protonation constants it can be concluded that at pH 7.1, about 50% of the TPEN molecules are protonated at one nitrogen (i.e., in total, ca. 13% of all picolyl nitrogens are protonated). The shift differences between the predominant species at pH 7.1 and the fully protonated form (observed at pH 0) are between 0.147 ppm for H6 and 0.583 ppm for H4. The methylene protons shift by 0.180 ppm and the ethylene protons by −0.227 ppm. All proton resonances shift downfield upon protonation, except for the ethylene protons, which shift upfield. Generally, downfield shifts are expected upon protonation, and the largest change in shift would be expected for the proton next to the protonation site (i.e., H6, which shifts only by 0.147 ppm); thus it is likely that the shift changes are influenced by changes in the preferred conformations of the protonated and deprotonated forms. Although caution must be applied when interpreting solution data based on solid-state structures, the X-ray crystal structures of protonated and deprotonated [40] TPEN are compatible with the upfield shift observed for the ethylene protons: in the structure of $H_4TPEN(ClO_4)_4$, all four ethylene protons are in a position to experience shielding from the electron cloud of the picolyl rings, whereas this is the case for only two protons in the deprotonated structure.

Complex formation between TPEN and Zn(II) in solution is rapid, as expected since the ligand is flexible. With substoichiometric amounts of zinc, two separate sets of ^1H NMR signals are observed for the free ligand and the complex. This indicates that exchange between these two species is slow on the NMR time scale, consistent with the reported high stability of the complex [16]; an upper

Table 3
TPEN metal complexes

Compound	Nucleus	Z	Geometry	TPEN dentate	Description	Other ligands	Reference
Mononuclear complexes							
$[Re(VII)O_3(TPEN)](ClO_4)_2 \cdot 2CH_3CN$	mono	6	octahedral	3	2 N free, 1 Npy proton	3 O	[29]
$[V(V)O_2(TPEN)]Cl \cdot H_2O$	mono	6	octahedral	4	2 Npy free	2 O	[27]
$[Cr(III)(OH)_2(TPEN)](ClO_4) \cdot 3H_2O$	mono	6	octahedral	4	2 Npy free	2 O	[14]
$[Rh(III)Cl_2(TPEN)]PF_6 \cdot 2CH_3CN$	mono	6	octahedral	4	2 Npy free	2 Cl	[15]
$[Cu(II)(TPEN)](ClO_4)_2$	mono	5	tetragonal pyramidal	5			[11]
$[Cr(III)(OOCCH_3)(TPEN)](ClO_4)_2 \cdot H_2O$	mono	6	octahedral	5	1 Npy free	OAc	[13]
$[Cr(III)(OH)(TPEN)](ClO_4)_2$	mono	6	octahedral	5	1 Npy free	OH	[13]
$[Fe(II)(TPEN)(SO_4)] \cdot 4H_2O$	mono	6	octahedral	5	1 Npy free	SO_4	[12]
$[Fe(II)(TPEN)(SO_4)] \cdot 2.5H_2O \cdot 0.5CH_3CN$	mono	6	octahedral	5	1 Npy free	SO_4	[18]
$[Rh(III)Cl(TPEN)](PF_6)_2 \cdot CH_3CN$	mono	6	octahedral	5	1 Npy free	Cl	[15]
$[V(V)(SO_4)(TPEN)]$ $(0.75HSO_4/0.25SO_4) \cdot 1.25H_2O$	mono	7	pentagonal bipyramidal	5	1 Npy free	SO_4	[28]
$[Zn(II)(TPEN)](ClO_4)_2$	mono	6	octahedral	6			[7]
$[Cr(III)(TPEN)](ClO_4)_3$	mono	6	octahedral	6			[12]
$[Fe(II)(TPEN)](ClO_4)_2$	mono	6	octahedral	6			[13]
$[Fe(II)(TPEN)](ClO_4)_2 \cdot 0.66H_2O$	mono	6	octahedral	6			[13,17]
$[Fe(II)(TPEN)](ClO_4)_2 \cdot 0.5H_2O$	mono	6	octahedral	6			
$[Fe(II)(TPEN)](PF_6)_2$	mono	6	octahedral	6			[17]
$[Fe(III)(TPEN)](ClO_4)_3$	mono	6	octahedral	6			[20]
$[Co(III)(TPEN)](ClO_4)_3$	mono	6	octahedral	6			[21]
$[Ni(II)(TPEN)](ClO_4)_2 \cdot 0.67H_2O$	mono	6	octahedral	6			[22]
$[Ru(II)(TPEN)](ClO_4)_2 \cdot 0.5H_2O$	mono	6	octahedral	6			[15]
$[Mn(II)(H_2O)(TPEN)](ClO_4)_2$	mono	7	pentagonal bipyramidal	6		H_2O	[23]
$[Cd(II)(NO_3)(TPEN)](NO_3) \cdot (CH_3)_2CO$	mono	7	pentagonal bipyramidal	6		NO_3	see footnote 1
$[Sm(III)Cl_2(TPEN)](ClO_4)$	mono	8	dodecahedral	6		2 Cl	[24]
$[Tl(III)(NO_3)(TPEN)](ClO_4)_2$	mono	8	dodecahedral	6		2 O	[25]
$[La(III)(NO_3)_2(TPEN)](NO_3) \cdot 3H_2O$	mono	10	bicapped square antiprism	6	4 O from 2 bidentate NO_3	2 NO_3	[26]
$[Tb(III)(NO_3)_2(TPEN)](NO_3) \cdot 3H_2O$	mono	10	bicapped square antiprism	6	4 O from 2 bidentate NO_3	2 NO_3	[26]
Dinuclear complexes							
$[Cu(I)_2(TPEN)](BF_4)_2$	di	4	tetrahedral	2*3	3 N to each Cu; Cu–Cu 2.779 Å		[30]
$[Cu(I)_2(TPEN)(CO)_2](BF_4)_2$	di	4	tetrahedral	2*3	3 N to each Cu; Cu–Cu: 4.764 Å	2 CO	[30]
$[Cu(II)_2Cl_4(TPEN)]$	di	5	square pyramidal	2*3	3 N to each Cu; Cu–Cu: 7.316 Å	Cl	[36]
$[Cr(III)_2(OH)_2(TPEN)(OOCCH_3)](ClO_4)_3$	di	6		2*3	3 N to each Cr, 2 μ-OH, μ-acetato; Cr–Cr: 2.818 Å	2 OH, OAc	[30]
$[Mn(IV)_2O_2(TPEN)(OOCCH_3)]$ $(ClO_4)_3 \cdot CH_3CN$	di	6		2*3	3 N to each Mn, 2 μ-O, μ-acetato; Mn–Mn: 2.591 Å	2 O, OAc	[32]
$[Mn(III)Mn(IV)O_2(TPEN)(OOCCH_3)]$ $(ClO_4)_2 \cdot 2CH_3CN$	di	6		2*3	3 N to each Mn, 2 μ-O, μ-acetato; Mn–Mn: 2.591 Å	2 O, 2OAc	[33]
$[Mo(V)_2O_4(TPEN)](ClO_4)_2 \cdot 2H_2O$	di	7	basket type	2*3	3 N, oxo-O, 2 μ-O for each Mo. Mo–Mo: 2.546 Å	4 O	[34]
$[Mo(V)_2O_4(TPEN)][MoCl_4O(H_2O)]Cl \cdot 2H_2O$	di	7	basket type	2*3	3 N, oxo-O, 2 μ-O for each Mo. Mo–Mo: 2.546 Å	4 O	[34]
$[W(V)_2O_4(TPEN)](ClO_4)_2 \cdot 2CH_3CN$	di	7	basket type	2*3	3 N, O, 2 μ-O for each W. W–W: 2.561 Å	4 O	[34]
$[V(IV)_2(OH)_2(O)_2(TPEN)]I_2 \cdot 4H_2O$	di	8	octahedral	2*3	3 N to each V, μ-OH, 1 oxo-O, V–V: 2.965 Å	O,OH	[35]

limit for the exchange rate can be estimated from the shift difference between the two closest peaks (for H3: 60.9 Hz). As the peaks are well resolved, the exchange rate must be well below 135 s^{-1}, corresponding to lifetimes for the two species of >7.4 ms. The protons of the side-arm methylene groups are magnetically inequivalent (diastereotopic) in the complex, as they are part of a chelate ring system. Interestingly, the singlet for the "en" CH_2 protons is much sharper (half-height width in 10% D_2O, 298 K, pH 7.1: 3.1 Hz) for the complex than for the free ligand (7.8 Hz under the same

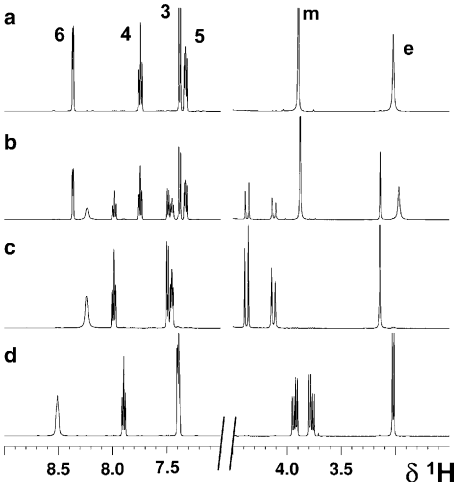

Fig. 4. 1-D ^{1}H NMR spectra of TPEN (pH* 7.1, 10% D_2O) (a) in the absence of metal ions, (b) with ca. 0.5 mol equiv. of $ZnCl_2$, (c) with 1 mol equiv. of $ZnCl_2$, (d) with 1 mol equiv. of $^{111}CdCl_2$ (prepared from ^{111}CdO by dissolution in 1 M HCl).

conditions); this suggests that the relative broadness of the signal in the free ligand is due to an exchange process that is no longer possible in the complex, e.g., rotation around the C–C bond.

In contrast, the H6 resonance is broader for the complex. For the free ligand, the width at half-height is ca. 6 Hz, and a small coupling to H5 (5.3 Hz) can be observed; this coupling is no longer resolved for the Zn(II) complex, for which the width at half-height is ca. 15 Hz. Exchange of the picolyl rings between equatorial (rings 1 and 3, Fig. 2(a)) and axial (rings 2 and 4) environments may account for some of the broadening. This exchange might occur through a trigonal prismatic ''twist'' mechanism, as has been reported for the Fe(II) complex [13]. The complex is stable at pH values as low as 2.0 (data not shown; spectra taken at this pH have essentially the same appearance as that shown in Fig. 4(c), and no peaks for free TPEN are observed). Addition of 10 M HCl is required to displace Zn(II) from the complex. Titrations with NaCl (data not shown) gave no indication of either additional binding of a seventh ligand in $[Zn(TPEN)]^{2+}$, or of the displacement of one picolyl ligand.

3.4. ^{1}H and ^{111}Cd NMR spectroscopy of $[Cd(II)(TPEN)]^{2+}$

The crystal structure of the Cd(II) complex of TPEN (as the nitrate salt) has been determined previously.[1] We have studied $[Cd(TPEN)]^{2+}$ in solution by ^{1}H and ^{111}Cd NMR spectroscopy. The ^{111}Cd NMR chemical shift of 151 ppm is within the expected range for Cd(II) coordinated to nitrogen ligands [41]. The half-height width of the ^{111}Cd peak in non-^{1}H decoupled spectra is ca. 80 Hz, precluding the resolution of coupling to ^{1}H, but heteronuclear coupling can be observed in the ^{1}H spectrum (Fig. 5). For both methylene and ethylene protons, ^{3}J coupling between ^{1}H and ^{111}Cd is easily observed. All heteronuclear $^{3}J(^{1}H–^{111}Cd)$ coupling constants for these protons are between 5 and 9 Hz. ^{3}J couplings are dependent on the torsional angle; thus, in principle two different coupling constants would be expected for coupling of ^{111}Cd to a pair of geminal protons, if the conformation in solution is rigid. However, only one coupling constant is observed for the two methylene protons, thus it appears that conformational changes occur rapidly on the NMR time-scale. The same is true for the ethylene protons. The coupling pattern for the methylene protons in $[Cd(TPEN)]^{2+}$ can be compared with that observed for $[Cd(EDTA)]^{2-}$ (Fig. 5). Two average $^{3}J(^{1}H–^{111}Cd)$ coupling constants can be determined for the methylene protons in $[Cd(EDTA)]^{2-}$ (11.3 and 13.3 Hz), whereas the corresponding coupling constant for $[Cd(TPEN)]^{2+}$ is only 8.7 Hz. The major difference between the EDTA and TPEN complexes is that there are two possible pathways for coupling between ^{111}Cd(II) and the methylene protons in $[Cd(TPEN)]^{2+}$, namely through the aliphatic nitrogens and/or the aromatic nitrogens, whereas for EDTA, the 3-bond coupling can occur only through the aliphatic nitrogens, as there are four bonds via the carboxylates. Four-bond couplings are expected to be too small to contribute to the observed coupling pattern. A comparison of the crystal structures of the two hepta-coordinate complexes $[Cd(H_2O)(EDTA)]^{2-}$ and $[Cd(NO_3)(TPEN)]^{2+}$ reveals that overall, the Cd–N–C–H torsional angles are similar in both complexes (70–90° and 150–170° for the two diastereotopic protons, respectively). Assuming that the ''sum'' of torsional angles is the same at any given time, the differences between the coupling constants observed in $[Cd(EDTA)]^{2-}$ and $[Cd(TPEN)]^{2+}$ might be attributable to contributions to the coupling via the aromatic nitrogens. Resolution enhancement allowed the peak at 8.44 ppm (H6), see Fig. 4(d) to be resolved into a pseudo-triplet, indicating that this proton is also coupled to ^{111}Cd, with a ^{3}J coupling

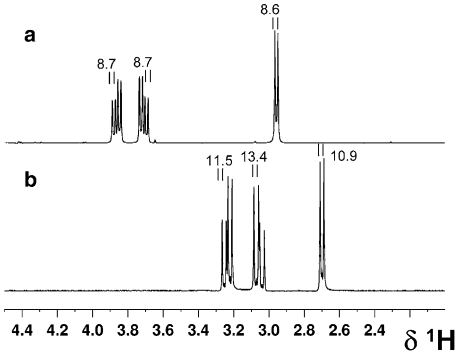

Fig. 5. Comparison of the $^{3}J(^{1}H–^{111}Cd)$ coupling in $[Cd(TPEN)]^{2+}$ (a) and $[Cd(EDTA)]^{2-}$ (b) (numbers given are in Hz). The homonuclear coupling between the geminal methylene protons is 15.8 Hz in $[Cd(TPEN)]^{2+}$, 16.4 Hz in $[Cd(EDTA)]^{2-}$, and 17.2 Hz in $[Zn(TPEN)]^{2+}$ (shown in Fig. 4(c)).

[1] The structure of $[Cd(II)(NO_3)(TPEN)](NO_3) \cdot$ acetone has been deposited in the CSD by M. Nieger, J. Ratilainen, K. Rissanen in 2002, but no literature reference is available.

constant of ca. 5 Hz. No coupling to other protons was detectable in the ^{1}H NMR spectrum.

4. Conclusions

TPEN forms very strong complexes with d-block metal ions and is often used to control the concentration of "free" metal ions, especially Zn(II), in biochemical experiments. The stability constant for $[Cu(TPEN)]^{2+}$ is anomalous in that it does not obey the Irving-Williams series for first row M(II) transition metal ions, with the Cu(II) complex being unexpectedly less stable than the Ni(II) complex (Fig. 3). We have crystallised $[Zn(TPEN)](PF_6)_2$ and $[Cu(TPEN)](PF_6)_2$. The Zn(II) complex is octahedral whereas the Cu(II) complex is five-coordinate with a dangling arm picolyl ring. The anomalous position of $[Cu(TPEN)]^{2+}$ in the Irving-Williams series can therefore be attributed to its five-coordinate structure compared to six-coordination for the other M(II) first-transition-series complexes. Moreover, it is apparent that these complexes possess considerable conformational flexibility. The perchlorate salt of $[Cu(TPEN)]^{2+}$ for example has a trigonal bipyramidal structure [11] which contrasts with the more closely tetragonal pyramidal structure of the hexafluorophosphate complex. Solution NMR studies also suggest that there is dynamic conformational flexibility in the structures of the $[Zn(TPEN)]^{2+}$ and $[Cd(TPEN)]^{2+}$ complexes in aqueous solution.

5. Supplementary data

The structures of $[Zn(II)(TPEN)](PF_6)_2$ and $[Cu(II)(TPEN)](PF_6)_2$ have been deposited in the Cambridge Crystallographic Data Centre under the accession numbers 273732 and 273733, respectively. Copies of this information may be obtained free of charge from The Director, CCDC, 12 Union Road, Cambridge CB2 1EZ, UK (fax: +44 1223 336 033; e-mail: deposit@ccdc.cam.ac.uk or www: http://www.ccdc.cam.ac.uk).

Acknowledgements

We thank the EC (Marie Curie Fellowship to CAB), The Wellcome Trust (Edinburgh Protein Interaction Centre and Fellowship to CAB), HEC of Pakistan (Postdoctoral Fellowship to MTR), and the Royal Society (Olga Kennard University Research Fellowship for CAB) for their support of this work.

References

[1] S. Devergnas, F. Chimienti, N. Naud, A. Pennequin, Y. Coquerel, J. Chantegrel, A. Favier, M. Seve, Biochem. Pharmacol. 68 (2004) 699.
[2] C.E. Outten, T.V. O'Halloran, Science 292 (2001) 2488.
[3] E. Ho, C. Courtemanche, B.N. Ames, J. Nutr. 133 (2003) 2543.
[4] B. Kindermann, F. Doring, M. Pfaffl, H. Daniel, J. Nutr. 134 (2004) 57.
[5] G.R. Sauer, D.M. Smith, M. Cahalane, L.N.Y. Wu, R.E. Wuthier, J. Cell. Biochem. 88 (2003) 954.
[6] M. Adler, R.E. Dinterman, R.W. Wannemacher, Toxicon 35 (1997) 1089.
[7] Y. Mikata, M. Wakamatsu, S. Yano, Dalton Trans. (2005) 545.
[8] P.T. Beurskens, G. Beurskens, W.P. Bosman, R. de Gelder, S. Garcia-Granda, R.O. Gould, R. Israel, J.M.M. Smits, DIRDIF-96: Program System, Crystallography Laboratory, University of Nijmegen, The Netherlands, 1996.
[9] G.M. Sheldrick, SHELX-97: Programs for Crystal Structure Analysis (Release 97-2), Institut für Anorganische Chemie der Universität, Tammannstrasse 4, D-3400 Göttingen, Germany, 1998.
[10] T.-L. Hwang, A.J. Shaka, J. Magn. Reson. A 112 (1995) 275.
[11] D.C. Yoon, U. Lee, C.E. Oh, Bull. Korean Chem. Soc. 25 (6) (2004) 796.
[12] T. Hirano, M. Hirobe, K. Kobayashi, A. Odani, O. Yamauchi, M. Ohsawa, Y. Satow, T. Nagano, Chem. Pharm. Bull. 48 (2000) 223.
[13] H.R. Chang, J.K. McCusker, H. Toftlund, S.R. Wilson, A.X. Trautwein, H. Winkler, D.N. Hendrickson, J. Am. Chem. Soc. 112 (1990) 6814.
[14] J. Eriksen, P. Goodson, A. Hazell, D.J. Hodgson, K. Michelsen, O. Monsted, J.C. Rasmussen, H. Toftlund, Acta Chem. Scand. 53 (1999) 1083.
[15] M. Sokolov, K. Umakoshi, Y. Sasaki, Inorg. Chem. 41 (2002) 6237.
[16] G. Anderegg, E. Hubmann, N.G. Podder, F. Wenk, Helv. Chim. Acta 60 (1977) 123.
[17] X. Solans, L. Ruiz-Ramirez, R. Moreno-Esparza, M. Labrador, A. Escuer, J. Solid State Chem. 109 (1994) 315.
[18] M. Osawa, Y. Satow, SR Kagaku Gijutsu Joho 4 (1994) 2.
[19] G. Chen, G. Espinosa-Perez, A. Zentella-Dehesa, I. Silaghi-Dumitrescu, F. Lara-Ochoa, Inorg. Chem. 39 (2000) 3440.
[20] L. Duelund, R. Hazell, C.J. McKenzie, L. Preuss Nielsen, H. Toftlund, J. Chem. Soc., Dalton Trans. (2001) 152.
[21] J.B. Mandel, C. Maricondi, B.E. Douglas, Inorg. Chem. 27 (1988) 2990.
[22] D. Da Luz, C.V. Franco, I. Vencato, A. Neves, Y.P. Mascarenhas, J. Coord. Chem. 26 (1992) 269.
[23] J.-D. Lee, M.-H. Lee, J. Ind. Eng. Chem. 7 (2001) 137.
[24] H.Y. Jin, M. Akiba, K. Umakoshi, Y. Sasaki, K. Kabuto, Acta Crystallogr., Sect. C 53 (1997) 338.
[25] S. Musso, G. Anderegg, H. Ruegger, C.W. Schlaepfer, V. Gramlich, Inorg. Chem. 34 (1995) 3329.
[26] L.R. Morss, R.D. Rogers, Inorg. Chim. Acta 255 (1997) 193.
[27] A. Neves, M. Horner, H. Fenner, J. Straehle, Acta Crystallogr., Sect. C 49 (1993) 1737.
[28] K. Kanamori, E. Kameda, K.-i. Okamoto, Bull. Chem. Soc. Jpn. 69 (1996) 2901.
[29] A. Mitani, M. Abe, K. Tsuge, Y. Sasaki, Chem. Lett. 32 (2003) 502.
[30] R.R. Gagne, R.P. Kreh, J.A. Dodge, R.E. Marsh, M. McCool, Inorg. Chem. 21 (1982) 254.
[31] H. Toftlund, O. Simonsen, E. Pedersen, Acta Chem. Scand. 44 (1990) 676.
[32] S. Pal, J.W. Gohdes, W.C.A. Wilisch, W.H. Armstrong, Inorg. Chem. 31 (1992) 713.
[33] S. Pal, W.H. Armstrong, Inorg. Chem. 31 (1992) 5417.
[34] R. Hazama, K. Umakoshi, A. Ichimura, S. Ikari, Y. Sasaki, T. Ito, Bull. Chem. Soc. Jpn. 68 (1995) 456.
[35] A. Neves, K. Wieghardt, B. Nuber, J. Weiss, Inorg. Chim. Acta 150 (1988) 183.
[36] D.-C. Yoon, C.E. Oh, U. Lee, Acta Crystallogr., Sect. E 58 (2002) m113.
[37] N. Hirayama, S. Iimuro, K. Kubono, H. Kokusen, T. Honjo, Talanta 43 (1996) 621.
[38] G. Anderegg, F. Wenk, Helv. Chim. Acta 50 (1967) 2330.
[39] S.S. Gunatilleke, R.E. Norman, Acta Crystallogr., Sect. E 59 (2003) o269.
[40] T. Fujihara, M. Saito, A. Nagasawa, Acta Crystallogr., Sect. E 60 (2004) o262.
[41] G.L. Öz, D.L. Pountney, I.M. Armitage, Biochem. Cell Biol. 76 (1998) 223.

Available online at www.sciencedirect.com
SCIENCE DIRECT®
Polyhedron 25 (2006) 521–529
POLYHEDRON
www.elsevier.com/locate/poly

Synthesis and characterization of the $[Ni_6Ge_{13}(CO)_5]^{4-}$ and $[Ge_9Ni_2(PPh_3)]^{2-}$ Zintl ion clusters

Emren N. Esenturk, James Fettinger, Bryan Eichhorn *

Department of Chemistry and Biochemistry, University of Maryland, College Park, MD 20742, United States

Received 3 June 2005; accepted 21 July 2005
Available online 31 August 2005

Abstract

Reactions between K_4Ge_9, $Ni(CO)_2(PPh_3)_2$, and 2,2,2-crypt in ethylenediamine solutions give two different products depending on reaction conditions. The $[Ni_6Ge_{13}(CO)_5]^{4-}$ ion (**1**) is formed at low temperatures (~40 °C) and short reaction times whereas the $[Ge_9Ni_2(PPh_3)]^{2-}$ ion (**2**) forms at higher temperatures (~118 °C). Both complexes were isolated as $[K(2,2,2\text{-crypt})]^+$ salts and characterized by single-crystal X-ray diffraction, electrospray mass spectrometry (ESI-MS) and NMR studies (^{13}C and ^{31}P). **1** has a hypo-*closo* cluster electron count (Wades Rules) and adopts an interpenetrating biicosahedral structure with 17 vertices and 2 interstitials, which is unique in transition metal Zintl ion clusters. **2** also has a hypo-*closo* cluster electron count but displays an open, *nido*-like 10-vertex structure with a Ni interstitial. The composition of **2** was established through ESI-MS studies and corrects an earlier report that characterized the cluster as $[Ge_{10}Ni(PPh_3)]^{2-}$ with an interstitial Ge.
© 2005 Elsevier Ltd. All rights reserved.

Keywords: Polygermanide; Zintl; Icosahedron

1. Introduction

Interest in "ligand-free" transition metal derivatives of Zintl ions has received much attention of late due to their close relationship to nanoparticles and fullercages [1–4], their remarkable molecular and electronic structures [5,6] and their utility in preparing low temperature alloys and intermetallics [7,8]. In particular, group 14 Zintl ions (i.e., Ge_9^{4-}, Sn_9^{4-}, Pb_9^{4-}) react with labile transition metal precursors to give high symmetry clusters that often contain centered transition metals. These include the $[M@Pb_{12}]^{2-}$ and $[M@Pb_{10}]^{2-}$ ions where M = Ni, Pd, Pt [9–11], and the recently reported $[Pd_2@Ge_{18}]^{4-}$ and $[Ni_3@Ge_{18}]^{4-}$ clusters [12,13]. The structures of these clusters depend on both the steric demands of the constituent elements and the cluster electron count. Many have structures similar to the boranes and are predicted by Wades rules [14] whereas others, such as $[Sn_9Pt_2(PPh_3)]^{2-}$, seem to violate Wade's structure prediction principles [15]. The latter complex has 20 cluster electrons with 10 surface vertices, which corresponds to a hypo-*closo* system in a Wade type analysis. The observed structure is not the anticipated closed, deltahedral type but a more open, *nido*-like framework [16] with fewer Sn–Sn contacts that predicted. This structural variance presumably results from the steric demands of the centered Pt atom and the weak nature of the Sn–Sn bonds. For comparison, the closely related $[Sn_9Ni_2(CO)]^{3-}$, which has a smaller Ni interstitial, adopts the expected closo structure in accord with its 21 electron, $2n + 1$ configuration [15].

Our initial studies with group 14 Zintl ions involved the use of ML_n subunits that did not contribute electrons to cluster bonding and were not expected to alter the cluster electron count or Zintl ion precursor framework structure. For example, the 9-vertex, 22-electron *nido*-Sn_9^{4-} complex forms the expected 10-vertex,

* Corresponding author.
E-mail address: eichhorn@umd.edu (B. Eichhorn).

0277-5387/$ - see front matter © 2005 Elsevier Ltd. All rights reserved.
doi:10.1016/j.poly.2005.07.031

22-electron *closo*-$[Sn_9M(CO_3)]^{4-}$ series of complexes (M = Cr, Mo, W) [17]. The first transition metal polygermanide was prepared from the reaction between Ge_9^{4-} and $Ni(CO)_2(PPh_3)_2$ in ethylenediamine solvent. The product was characterized as $[K(2,2,2\text{-crypt})]_2[Ge_9(\mu_{10}\text{-Ge})Ni(PPh_3)]$ on the basis of X-ray analysis and Wade's electron counting principles [18]. By inserting an interstitial Ge instead of an interstitial Ni atom, one achieves a nido electron count that is consistent with the observed *nido*-like structure. With the discovery [15] of the isostructural $[Sn_9Pt_2(PPh_3)]^{2-}$ ion that violates Wades rules, we were prompted to reinvestigate the identity of the $[Ge_9(\mu_{10}\text{-Ge})Ni(PPh_3)]^{2-}$ ion by way of electrospray mass spectrometry (ESI-MS) and a new single-crystal X-ray analysis. During the course of our investigation, we discovered a new type of transition metal Zintl cluster, $[Ge_{13}Ni_6(CO)_5]^{4-}$, that possesses an interpenetrating biicosahedral structure [19,20]. Herein we report the synthesis and characterization of this cluster in addition to the correct structure and composition of the $[Ge_9Ni_2(PPh_3)]^{2-}$ ion that was previously described [18] as the $[Ge_9(\mu_{10}\text{-Ge})Ni(PPh_3)]^{2-}$ ion. The interconversion of these complexes and their relationships to other transition metal group 14 Zintl complexes are described.

2. Experimental

2.1. General data

All reactions were performed in a nitrogen atmosphere drybox (Vacuum Atmosphere Co.). The $^{31}P\{^1H\}$ NMR spectrum was recorded on a Bruker DRX400 spectrometer at 162 MHz. Electrospray Mass Spectra (ESI-MS) were obtained by direct injection of DMF solutions into a Finnigan mass spectrometer. Samples were detected in the negative ion mode. An AMRAY 1820K scanning electron microscope with a potential of 20 kV was used for energy dispersive X-ray (EDX) studies.

2.2. Chemicals

Melts of nominal composition K_4Ge_9 was made by fusion (at high temperature) of stoichiometric ratios of the elements. The chemicals were sealed in evacuated, silica tubes and heated carefully with a natural gas/oxygen flame. *CAUTION:* the synthesis of polygermanides can result in explosive mixtures and all fusion reactions should be conducted behind a blast shield inside of a well functioning hood. 4,7,13,16,21,24-Hexaoxa-1,10-diazobicyclo[8,8,8]-hexacosane (2,2,2-crypt) and $Ni(CO)_2(PPh_3)_2$ were purchased from Aldrich. Anhydrous ethylenediamine (en) and dimethylformamide (DMF) were purchased from Fisher, vacuum distilled from K_4Sn_9, and stored under dinitrogen.

2.3. Synthesis

2.3.1. Preparation of $[K(2,2,2\text{-crypt})]_4[Ni_6Ge_{13}(CO)_5]\cdot 1.5en$ (1)

In a vial K_4Ge_9 (54 mg, 0.07 mmol), 2,2,2-crypt (100 mg, 0.27 mmol), and $[Ni(CO)_2(PPh_3)_2]$ (84 mg, 0.14 mmol) were dissolved in 4 ml of en yielding a red/brown mixture. This mixture was heated ($35\ ^\circ C < T < 45\ ^\circ C$) and stirred for about 15 min. and filtered through a hot filter. After a week small thin black crystals of $[K(2,2,2\text{-crypt})]_4[Ni_6Ge_{13}(CO)_5]\cdot 1.5en$ precipitated. Yield: ~20 mg (~30%). EDX Ge:Ni:K = 3.8:1.7:1. ESI-MS data: (*m*/*z*, ion) 1850 $[K(2,2,2\text{-crypt})Ni_6Ge_{13}(CO)_5]^{1-}$; 1821 $[K(2,2,2\text{-crypt})Ni_6Ge_{13}(CO)_4]^{1-}$; 1296 $[Ni_6Ge_{13}]^{1-}$; 1214 $[K(2,2,2\text{-crypt})Ge_9Ni_2(CO)]^{1-}$; 838 $K[Ge_9Ni_2(CO)]^{1-}$; 810 $K[Ge_9Ni_2]^{1-}$; 770 $[Ge_9Ni_2]^{1-}$; 677 $K[Ge_4Ni_4(CO)_4]^{1-}$.

2.3.2. Preparation of $[K(2,2,2\text{-crypt})]_2[Ni_2Ge_9(PPh_3)]\cdot en$ (2)

In a vial K_4Ge_9 (54 mg, 0.007 mmol), 2,2,2-crypt (100 mg, 0.27 mmol), and $[Ni(CO)_2(PPh_3)_2]$ (84 mg, 0.14 mmol) were dissolved in 4 ml of en yielding a red/brown mixture. This mixture was boiled and stirred for about 15 min, and filtered through a hot filter. After 3–4 days block-shaped black crystals of $[K(2,2,2\text{-crypt})]_2[Ni_2Ge_9(PPh_3)]\cdot en$ started to precipitate. Yield: ~20 mg (~30%). EDX analysis on crystals showed presence of K, P, Ge, and Ni. ESI-MS data: (*m*/*z*, ion) 1447 $[K(2,2,2\text{-crypt})Ni_2Ge_9(PPh_3)]^{-1}$, 1072 $K[Ni_2Ge_9(PPh_3)]^{-1}$, 838 $K[Ni_2Ge_9(CO)]^{-1}$, 810 $K[Ni_2Ge_9]^{-1}$.

2.3.3. Interconversion studies

Conversion of ***1*** *to* ***2***. In a dry box, 36 mg of $[K(2,2,2\text{-crypt})]_4[Ni_6Ge_{13}(CO)_5]$ crystals were dissolved in 4 ml DMF. ESI-MS data were recorded to confirm the presence of $[Ni_6Ge_{13}(CO)_5]^-$ and $[K(2,2,2\text{-crypt})][Ni_6Ge_{13}(CO)_5]^-$, $[Ni_2Ge_9(CO)]^-$ and $[Ni_2Ge_9]^-$ ions before the interconversion experiments. 3 mg of PPh_3 was added to the starting solution and the reaction mixture was stirred for 30 min at ~118 °C. The resulting ESI-MS spectra showed signals of $K[Ni_2Ge_9(PPh_3)]^-$ and $[Ni_2Ge_9(PPh_3)]^-$ ions.

Attempted conversion of ***2*** *to* ***1***. In dry box, 20 mg of $[K(2,2,2\text{-crypt})]_2[Ni_2Ge_9(PPh_3)]\cdot en$ crystals were dissolved in 4 ml DMF. ESI-MS data were recorded to confirm the presence of $[Ni_2Ge_9(PPh_3)]^-$ and $[K(2,2,2\text{-crypt})][Ni_2Ge_9(PPh_3)]^-$ ions before the interconversion experiment. The solution was placed in a Schlenk flask, the head gases evacuated and the flask back filled with CO gas. The reaction mixture was stirred for 3 h under the CO atmosphere. The resulting ESI-MS spectra showed decomposition of the starting material but did not show the formation of **1** or the $[Ni_2Ge_9(CO)]^-$ ion.

2.4. Crystallographic studies

2.4.1. $[K(2,2,2\text{-crypt})]_4[Ni_6Ge_{13}(CO)_5]\cdot 1.5en$ (1)

A black plate with approximate orthogonal dimensions $0.260\times0.196\times0.101\ mm^3$ was placed and optically centered on the Bruker SMART CCD system at −80 °C. The initial unit cell was indexed using a least-squares analysis of a random set of reflections collected from three series of 0.3° wide ω-scans. Data frames were collected [Mo Kα] with 0.2° wide ω-scans, 40 s per frame and 909 frames per series. Five data series were collected at varying ϕ angles ($\phi = 0°$, 72°, 144°, 216°, 288°), and finally, a partial repeat of the first series, 300 frames, for decay purposes. The crystal to detector distance was 4.903 cm, thus, providing a complete sphere of data to $2\theta_{max} = 55.0°$. A total of 96 582 reflections were collected and corrected for Lorentz and polarization effects and absorption using Blessing's method as incorporated into the program SADABS [21] with 27 463 unique ($R_{int} = 0.0330$).

System symmetry, lack of systematic absences and intensity statistics indicated the centrosymmetric triclinic space group $P\bar{1}$ (no. 2). The structure was determined by direct methods with the successful location of the heavy atom cluster and a few potassium atoms using the program XS [22]. The structure was refined with XL [22]. A multitude of least-squares difference-Fourier cycles were required to locate the remaining non-hydrogen atoms. All non-hydrogen, full occupancy, atoms were refined anisotropically. All of the hydrogen atoms were placed in calculated positions. Various disorders were found for the potassium crypt-and cations and each was optimized independently. A full and half occupancy ethylenediamine molecules were located and also optimized. The final difference-Fourier map possessed several large peaks that were all near heavy atoms while the remainder of the map was featureless indicating that the structure is both correct and complete. An empirical correction for extinction was also attempted but found to be negative and therefore not applied.

2.4.2. $[K(2,2,2\text{-crypt})]_2[Ni_2Ge_9(PPh_3)]\cdot en$ (2)

A black block with approximate orthogonal dimensions $0.152\times0.139\times0.068\ mm^3$ was mounted as above and cooled −100 °C. The data collection was performed as described above. A total of 75 805 reflections were collected and corrected for Lorentz and polarization effects and absorption using Blessing's method as incorporated into the program SADABS with 17 295 unique ($R_{int} = 0.0615$).

The structure was solved and refined using the SHELXTL program package [22] as described above. An empirical correction for extinction was also attempted but found to be negative and therefore not applied. The final difference-Fourier map possessed several large peaks that were all near heavy atoms while the remainder of the map was featureless indicating that the structure is both correct and complete.

3. Results and discussion

K_4Ge_9 and $Ni(CO)_2(PPh_3)_2$ react in ethylenediamine (en) in the presence of 2,2,2-crypt to give two different products that depend on reaction conditions. At moderate temperatures (30 °C < T < 40 °C), the $[Ni_6Ge_{13}(CO)_5]^{4-}$ ion (**1**) formed as the $[K(2,2,2\text{-crypt})]^+$ salt in moderate yield. The $[K(2,2,2\text{- crypt})]^+$ salt of **1** forms small, thin dark brown crystals is air and moisture sensitive in solution and the solid state. The salt is highly soluble in DMF and CH_3CN and forms dark brown solutions. The 19-atom cluster has a fused biicosahedral capsule-like structure with 17 Ge/Ni vertices and 2 centered Ni atoms. The structure and properties of this cluster will be discussed in subsequent sections.

At higher temperatures ($T \sim 118$ °C), the same reaction yields the $[Ge_9Ni_2(PPh_3)]^{2-}$ ion (**2**) in moderate yields, which crystallizes as large, block-like dark brown crystals of the $[K(2,2,2\text{-crypt})]^+$ salt. The structure of the anion has 1 Ni and 9 Ge vertices with a centered Ni atom and will also be discussed in subsequent sections. Both complexes have been characterized by single-crystal X-ray diffraction, NMR spectroscopy (^{13}C and ^{31}P where appropriate), Energy dispersive X-ray analysis (EDX), electrospray ionization mass spectrometry (ESI-MS) and infrared spectroscopy. Both salts are highly soluble in DMF and CH_3CN and decompose upon exposure to air in the solid state or in solution.

A proposed scheme for the interconversion of anions **1** and **2** is illustrated in Scheme 1. The transformation involves the initial formation of the cluster anion $[Ni_6Ge_{13}(CO)_5]^{4-}$ (**1**) followed by an irreversible conversion to $[Ge_9Ni_2(PPh_3)]^{2-}$ (**2**). This conclusion is based on the following results and observations:

(i) The same Ni precursor, $Ni(CO)_2(PPh_3)_2$, is used in the synthesis of **1** and **2**. However, anion **1** is isolated from reactions conducted at relatively lower temperatures (35–40 °C) and short reaction times whereas the formation of **1** is favored at high temperatures and long reaction times.

(ii) Electrospray mass spectra of DMF solutions of **1** (see following section) show anion **1** as well as, $[Ge_9Ni_2(CO)]^-$ and $[Ge_9Ni_2]^-$, that result from fragmentation of the parent. These ions have the same Ge_9Ni_2 core composition of **2**.

(iii) Addition of PPh_3 to en solutions of pure $[K(2,2,2\text{-crypt})]_4[Ni_6Ge_{13}(CO)_5]$ results in the formation of **2** after ~30 min of reaction at 118 °C. The ESI-MS spectra of these solutions show signals

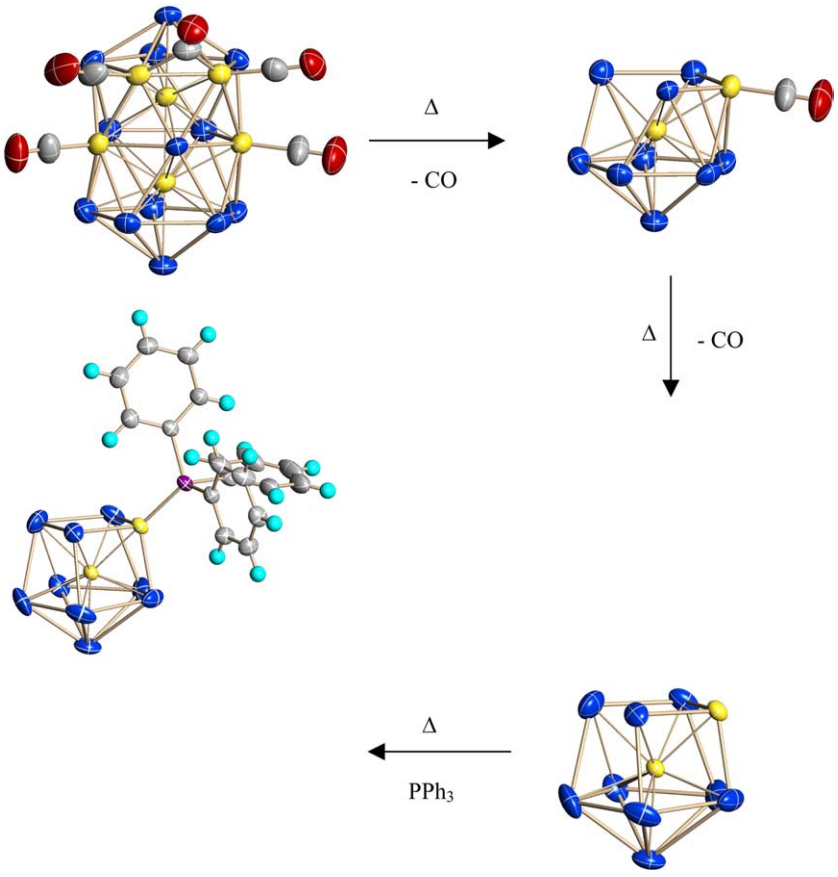

Scheme 1.

corresponding to $K[Ge_9Ni_2(PPh_3)]^{1-}$ and $[Ge_9Ni_2(PPh_3)]^{1-}$ ions, that coincide with those of the authentic sample.

(iv) Reactions between **2** and carbon monoxide result in cluster decomposition but do not regenerate **1** or result in the formation of $[Ge_9Ni_2(CO)]^-$ according to ESI-MS analysis.

While these experiments show that **2** can be generated from **1** under appropriate conditions, they do not preclude the direct formation of **2** from Ge_9^{4-} and $Ni(CO)_2(PPh_3)_2$.

Indeed, the synthesis of closely related clusters such as $[Sn_9Pt_2(PPh_3)]^{2-}$ appear to form directly from Sn_9^{4-} with sequential addition of Pt fragments (NMR analysis) [15] and do not seem to involve intermediates akin to **1**. Moreover, the proposed mechanism for the formation of the closely related $[Ni_3@Ge_{18}]^{4-}$ involves direct insertion of Ni into a Ge_9 cluster and a subsequent coupling [13].

3.1. Mass spectrometry

The electrospray mass spectrum for each sample was recorded in the negative ion mode from DMF solutions of crystalline $[K(2,2,2\text{-crypt})]^+$ salts. The distinctive mass envelopes arising from the multiple isotopes of Ge and Ni have been simulated to facilitate assignments and verify nuclearities. The spectrum for $K[Ge_9Ni_2(PPh_3)]^{1-}$ is shown in Fig. 1 as an example and the remaining spectra and simulations are given in the Supporting Information. The spectrum of **1** (Fig. S1) shows weak signals of the [K(2,2,2-crypt)]-coordinated molecular ion of $[Ni_6Ge_{13}(CO)_5]^-$ along with the decarbonyl loss products $Ni_6Ge_{13}(CO)_4^-$, $Ni_6Ge_{13}(CO)_2^-$ and ligand-free binary ion $Ni_6Ge_{13}^-$. Patterns of new compounds, $Ge_9Ni_2(CO)^-$ and $Ge_9Ni_2^-$ are also observed as well as peaks for the $Ge_4Ni_4(CO)_4^-$ cluster ion paired to K^+ and $[K(2,2,2\text{-crypt})]^+$.

The negative ion electrospray mass spectrum of DMF solution constituted from crystalline $[K(2,2,2\text{-crypt})]_2[Ge_9Ni_2(PPh_3)]$ shows an intense signal for the $K[Ge_9Ni_2(PPh_3)]^{1-}$ molecular ion with the expected mass envelope (Fig. 1). As is common for these types of Zintl ions, the potassium-coordinated ion pair, $K[Ge_9Ni_2(PPh_3)]^{1-}$, appears as the parent ion, (m/z 1072.1) and the fully charged anion is not observed. The ligand-free Ge–Ni cluster anion $K[Ge_9Ni_2]^{1-}$ was also observed as well as the CO substituted cluster, $K[Ge_9Ni_2(CO)]^{1-}$, which presumably results from a trace contamination in the sample.

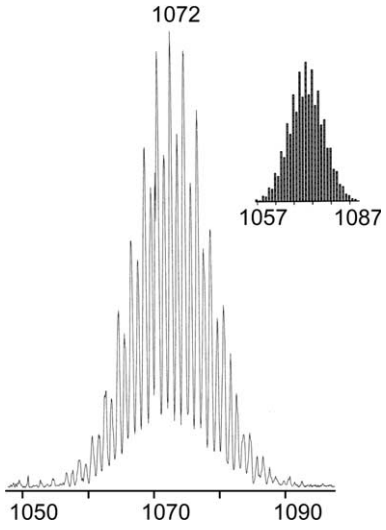

Fig. 1. ESI-mass spectrum of the $K[Ge_9Ni_2(PPh_3)]^{1-}$ molecular ion. The inset shows the simulated mass envelope.

3.2. Solid-state structures

The $[Ni_6Ge_{13}(CO)_5]^{4-}$ (**1**) and $[Ge_9Ni_2(PPh_3)]^{2-}$ (**2**) anions crystallize as the $[K(2,2,2\text{-crypt})]^{+}$ salts with triclinic crystal symmetry, space group $P\bar{1}$. The former has 1.5en solvate molecules per formula unit. A summary of the crystal data is given in Table 1, and selected bond distances are given in Tables 2 and 3, respectively. A previous report of the $[K(2,2,2\text{-crypt})]_2[Ge_9Ni_2(PPh_3)]$ structure was incorrectly characterized as having an anion formula $[Ge_{10}Ni(PPh_3)]^{2-}$. We correct this interpretation here and present a new refinement of the crystal structure from new X-ray data.

The $[Ni_6Ge_{13}(CO)_5]^{4-}$ anion possesses C_s point symmetry with a symmetry plane defined by Ge1, Ge8, Ge19 and the bridging carbonyl (Fig. 2). The anion is a 17-vertex deltahedral cluster defined by 13 Ge atoms and 4 Ni atoms. The cluster is centered by two additional interstitial Ni atoms. Each of the 4 vertex Ni atoms has a terminal CO ligand bound in a radial fashion with an additional bridging CO spanning the Ni2–Ni3 edge. The 17-atom deltahedron possesses 126 total valence electrons and has 32 cluster electrons according to Wades rules of electron counting [14]. According to Wades Rules, each of the Ge atoms contributes 2 electrons whereas each Ni(CO) vertex unit and interstitial Ni contributes zero electrons. The bridging CO ligand and the cluster charge contribute 2 and 4 electrons, respectively, to give 32 cluster electrons

$$13 \times 2(\text{Ge}) + 2(\text{CO}) + 4(\text{charge}) = 32\text{e}.$$

The 17-vertex, 32 electron cluster corresponds to a hypo-*closo* electron count and is consistent with the closed, deltahedral structure type.

The $[Ni_6Ge_{13}(CO)_5]^{4-}$ structure can be viewed as two interpenetrating icosahedral units (**Ih1** and **Ih2**) that share the central $Ge_3Ni_2(CO)_2$ penagonal ring and the 2 interstitial Ni atoms of the biicosahedral cluster (see Fig. 2(b)). **Ih1** has a composition $Ge_7Ni_6(CO)_5$ where Ni7 is interstitial and Ni13 occupies a vertex. **Ih2** has a $Ge_9Ni_4(CO)_2$ composition where Ni7 occupies a vertex and Ni13 occupies the interstitial site. This type of interpenetrating biicosahedral structure is new for transition metal Zintl clusters but is known in some of Teo's bimetallic Au–Ag and trimetallic Au–Ag–M; M = Pt, Pd, Ni supraclusters. In particular, the structure of **1** is highly

Table 1
Summary of crystallographic data for the $[Ni_6Ge_{13}(CO)_5]^{4-}$ and $[Ge_9Ni_2(PPh_3)]^{2-}$ ions

Empirical formula	$[K(2,2,2\text{-crypt})]_2[\mathbf{2}]\cdot$ en	$[K(2,2,2\text{-crypt})]_4[\mathbf{1}]\cdot 1.5$en
Compound formula	$C_{78.5}H_{150}Ge_{13}K_4N_{9.5}Ni_6O_{29}$	$C_{56}H_{95}Ge_9K_2N_6Ni_2O_{12}P$
Formula weight	3143.41	1924.28
Temperature (K)	193(2)	173(2)
Wavelength (Å)	0.71073	0.71073
Crystal system	triclinic	triclinic
Space group	$P\bar{1}$	$P\bar{1}$
a (Å)	15.2287(4)	12.9083(11)
b (Å)	16.1988(4)	13.0373(11)
c (Å)	26.1824(7)	23.569(2)
α (°)	92.7560(10)	96.546(2)
β (°)	91.3490(10)	104.757(2)
γ (°)	11.2730(10)	96.868(2)
Volume (Å^3)	6006.0(3)	3764.7(6)
Z	2	2
D_{calc} (g/cm^3)	1.738	1.698
Absolute coefficient (mm^{-1})	4.319	4.212
Data/restraints/parameters	27463/2340/1437	17295/5/790
Goodness-of-fit on F^2	1.118	1.029
Final R indices $[I > 2\sigma(I)]$[a]	$R_1 = 0.0549$; $wR_2 = 0.1794$	$R_1 = 0.0428$; $wR_2 = 0.1007$
R indices (all data)[a]	$R_1 = 0.0839$; $wR_2 = 0.1936$	$R_1 = 0.0834$; $wR_2 = 0.1111$

[a] The function minimized during the full-matrix least-squares refinement was $\sum w(F_o^2 - F_c^2)$ where $w = 1/[\sigma^2(F_o^2) + (0.050 * P)^2 + 1.3423 * P]$ and $P = \max(F_o^2, 0) + 2 * F_c^2)/3$.

Table 2
Selected bond distances (Å) and angles (°) for the $[Ge_{13}Ni_6(CO)_5]^{4-}$ ion

Ge(1)–Ni(2)	2.668(1)
Ge(1)–Ni(7)	2.474(1)
Ge(4)–Ni(3)	2.610(1)
Ge(4)–Ni(7)	2.438(1)
Ge(4)–Ni(9)	2.557(1)
Ge(5)–Ni(7)	2.431(1)
Ge(8)–Ni(2)	2.508(1)
Ge(8)–Ni(7)	2.381(1)
Ge(1)–Ge(4)	2.658(1)
Ge(1)–Ge(5)	2.906(1)
Ge(4)–Ge(5)	2.892(1)
Ge(4)–Ge(10)	2.735(1)
Ge(5)–Ge(10)	2.659(1)
Ge(5)–Ge(11)	2.706(1)
Ge(8)–Ge(15)	2.703(1)
Ge(10)–Ge(11)	2.862(1)
Ni(2)–Ni(7)	2.606(1)
Ni(2)–Ni(12)	2.742(1)
Ni(3)–Ni(9)	2.771(1)
Ni(7)–Ni(13)	2.564(1)
Ni(7)–Ni(9)	2.637(1)
Ni(9)–Ni(13)	2.610(1)
Ge(8)–Ni(9)	2.497(1)
Ge(10)–Ni(7)	2.522(1)
Ge(10)–Ni(9)	2.574(1)
Ge(10)–Ni(13)	2.595(1)
Ge(14)–Ni(12)	2.666(1)
Ge(14)–Ni(13)	2.575(1)
Ge(15)–Ni(9)	2.605(1)
Ge(16)–Ni(13)	2.499(1)
Ge(10)–Ge(16)	2.638(1)
Ge(10)–Ge(17)	2.820(1)
Ge(14)–Ge(15)	2.749(1)
Ge(14)–Ge(19)	2.741(1)
Ge(15)–Ge(16)	2.675(1)
Ge(16)–Ge(17)	2.777(1)
Ge(16)–Ge(19)	2.808(1)
Ge(17)–Ge(19)	2.772(1)
Ni(2)–C(2)	1.694(8)
Ni(2)–C(23′)	1.859(8)
Ni(3)–C(3)	1.712(8)
Ni(3)–C(23′)	1.898(8)
Ni(9)–C(9)	1.715(8)
Ni(12)–C(12)	1.750(8)
Ni(2)–Ge(1)–Ni(3)	54.80(3)
Ge(4)–Ge(1)–Ge(5)	62.44(3)
Ge(4)–Ge(5)–Ge(6)	97.67(3)
Ge(1)–Ni(7)–Ni(13)	173.03(4)
Ge(5)–Ni(7)–Ge(8)	173.04(4)
Ge(6)–Ni(7)–Ni(9)	169.49(4)
Ge(4)–Ni(9)–Ge(16)	122.46(4)
Ge(6)–Ge(11)–Ge(17)	157.25(4)
Ge(8)–Ni(13)–Ge(15)	65.11(3)
Ge(16)–Ni(13)–Ni(12)	171.06(4)
Ge(19)–Ni(13)–Ni(7)	176.55(4)
Ge(16)–Ni(17)–Ge(18)	106.81(3)
C(23′)–Ni(2)–Ge(6)	140.70(2)
C(3)–Ni3–C(23)	106.10(4)
C(9)–Ni(9)–Ge(8)	127.50(3)
Ni(3)–C(23′)–Ni(2)	81.40(2)

Table 3
Selected bond distances (Å) and angles (°) for the $[Ge_9Ni_2(PPh_3)]^{2-}$ ion

Ni(1)–P(1)	2.121(1)
Ge(1)–Ni(1)	2.381(1)
Ge(3)–Ni(1)	2.371(1)
Ge(9)–Ni(1)	2.370(1)
Ni(1)–Ni(2)	2.359(1)
Ge(1)–Ni(2)	2.350(1)
Ge(2)–Ni(2)	2.433(1)
Ge(3)–Ni(2)	2.368(1)
P(1)–C(1)	1.847(4)
P(1)–C(2)	1.843(4)
P(1)–C(3)	1.840(4)
Ge(1)–Ge(2)	2.640(1)
Ge(1)–Ge(8)	2.608(1)
Ge(2)–Ge(3)	2.634(1)
Ge(2)–Ge(5)	2.722(1)
Ge(2)–Ge(6)	2.733(1)
Ge(3)–Ge(4)	2.594(1)
Ge(4)–Ge(9)	2.633(1)
Ge(4)–Ge(7)	2.692(1)
Ge(4)–Ge(5)	2.788(1)
Ge(5)–Ge(7)	2.642(1)
Ge(5)–Ge(6)	2.656(1)
Ge(6)–Ge(7)	2.657(1)
Ge(6)–Ge(8)	2.808(1)
Ge(7)–Ge(8)	2.692(1)
Ge(8)–Ge(9)	2.635(1)
Ni(2)–Ge(1)–Ni(1)	59.82(2)
Ni(1)–Ge(1)–Ge(8)	92.35(3)
Ni(1)–Ge(1)–Ge(2)	82.29(2)
Ge(8)–Ge(1)–Ge(2)	108.20(2)
Ni(2)–Ge(2)–Ge(3)	55.56(2)
Ge(3)–Ge(2)–Ge(1)	89.45(2)
Ge(3)–Ge(2)–Ge(5)	68.03(2)
Ge(1)–Ge(2)–Ge(5)	107.92(2)
Ni(2)–Ge(4)–Ge(3)	56.16(2)
Ge(3)–Ge(4)–Ge(9)	82.94(2)
Ge(9)–Ge(4)–Ge(7)	76.38(2)
Ge(9)–Ge(4)–Ge(5)	109.40(2)
Ge(7)–Ge(4)–Ge(5)	57.60(2)
Ge(9)–Ni(2)–Ge(1)	94.80(3)
Ge(1)–Ni(2)–Ni(1)	60.75(2)
Ge(1)–Ni(2)–Ge(3)	103.73(3)
Ge(1)–Ni(2)–Ge(7)	128.30(3)
Ni(1)–Ni(2)–Ge(7)	148.06(3)
Ge(3)–Ni(2)–Ge(8)	157.16(3)
Ni(2)–Ni(1)–Ge(3)	60.08(2)
P(1)–Ni(1)–Ni(2)	177.23(4)
P(1)–Ni(1)–Ge(9)	122.79(4)
P(1)–Ni(1)–Ge(3)	117.45(4)
C(1)–P(1)–Ni(1)	119.34(1)
C(2)–P(1)–Ni(1)	112.37(1)
C(2)–P(1)–C(1)	100.69(2)
C(3)–P(1)–C(2)	102.21(2)
C(3)–P(1)–C(1)	117.79(1)

reminiscent of the *sss* rotamer of the $[(PPh_3)_{10}Au_{13}Ag_{12}Br_8]^+$ triicosahedral cluster [20].

The Ge–Ge, Ni–Ni, and Ni–Ge bond distances are in the range of 2.658(1)–2.894(1) Å (avg. 2.746(4) Å), 2.450(1)–2.771(1) Å (avg. 2.624(4) Å), and 2.381(1)–2.668(1) Å (avg. 2.522(5) Å), respectively (see Table 2). As expected, $Ni–CO_{(terminal)}$ contacts (avg. 1.718(8) Å) are shorter than the $Ni–CO_{(bridge)}$ contacts (avg. 1.879(8) Å). The structure is slightly flattened along the Ge8–Ge14 and Ge8–Ge5 vectors. This distortion is best illustrated by the differences between the 6 diagonal distances in each icosahedral subunit. In both of the icosahedral cages, diagonal distances involving Ge8, (Ge8–

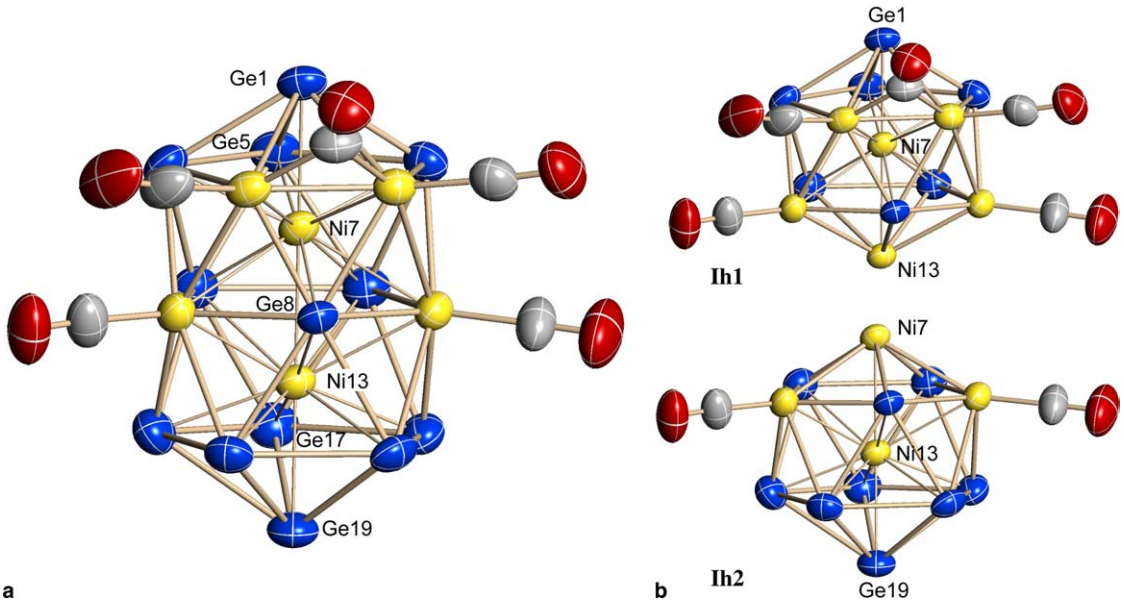

Fig. 2. (a) ORTEP drawing of the $[Ni_6Ge_{13}(CO)_5]^{4-}$ anion. Ni is yellow, Ge is blue, C is gray and oxygen is red. A fully labeled drawing is given in the Supporting material. (b) The two interpenetrating icosahedral subunits, Ih1 and Ih2.

Ge5 = 4.812(1) Å for **Ih1**, and Ge8–Ge17 = 4.878(2) Å for **Ih2**) are shorter than the other 5 diagonals in the respective subunits (5.087(5) Å, avg. for **Ih1**, and 5.115(4) Å avg. for **Ih2**).

The Ge–Ge bond distances for the anion **1** (2.6335(9)–2.9064(11); 2.750(6) Å avg.) are similar to those in other polygermenide clusters such as $[K(2,2,2\text{-crypt})]_3[P(C_6H_5)_3Ge_9]$, where Ge–Ge distances vary from 2.53 to 3.27 Å [23–25]. The Ni–Ge (2.3808(9)–2.6681(11) Å; 2.523(5) Å av.) and Ni–Ni (2.450(1)–2.771(1) Å, 2.624(4) Å av.) contacts are similar to the reported compounds (2.470–2.691 and 2.553–2.721 Å, respectively) [26].

As mentioned previously, the structure of the $[Ge_9Ni_2(PPh_3)]^{2-}$ ion, (**2**), was incorrectly reported to have the formula $[Ge_{10}Ni(PPh_3)]^{2-}$ in which the interstitial atom was refined as Ge. The formula has been unequivocally established by ESI-MS studies and the structure re-determined. The structure (Fig. 3) is identical to that previously reported except for the identity of the centered atom. The anion has virtual C_{3v} point symmetry and is isoelectronic and isostructural to $[Sn_9Pt_2(PPh_3)]^{2-}$ [15]. It is defined by nine surface Ge atoms, one interstitial Ni atom and a capping $[Ni(PPh_3)]$ fragment. The cluster is a 10-vertex 20-electron hypo-*closo* system that has an open, *nido*-like structure. For comparison, it is isostructural to the 24-electron 10-vertex $[Sb_7Ni_3(CO)_3]^{3-}$ ion that adopts a *nido*-type architecture [27]. Note that replacing the centered Ni atom with a Ge atom would add 4 electrons to cluster bonding and would be consistent with the observed structure. Although this does not occur, this

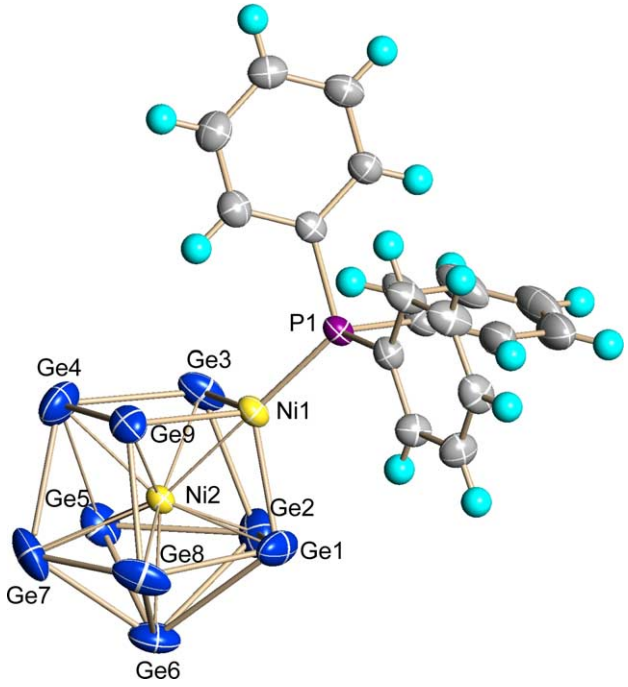

Fig. 3. ORTEP drawing of the $[Ge_9Ni_2(PPh_3)]^{2-}$ ion, (**2**). Ni is yellow, Ge is blue, C is gray, P is purple and H is turquoise.

electron counting rationale gave rise to the erroneous assignment in the original publication [18].

The centered Ni atom has nine Ni–Ge contacts in the range of 2.342(6)–2.447(6) Å. The 3 Ni–Ge bonds to Ni1 average 2.37(2) Å. The Ge–Ge contacts are in the range 2.594(1)–2.808(1) Å and are typical of polygerminide cages.

3.3. NMR spectroscopic studies

The ^{13}C NMR spectrum of $[Ni_6Ge_{13}(CO)_5]^{4-}$ (DMSO-d_6, 25 °C) shows carbonyl resonances at 194.6, 217.9, 224.9 ppm, which is consistent with the solid state structure.

The room temperature ^{31}P NMR spectrum of $[Ge_9Ni_2(PPh_3)]^{2-}$ crystals shows only free triphenylphosphine in DMF solution ($\delta = -5.1$ ppm), suggesting that PPh_3 ligand dissociation is fast on the NMR time scale. This observation is somewhat surprising in view of the static nature of the PPh_3 ligand in the isoelectronic, isostructural $[Sn_9Pt_2(PPh_3)]^{2-}$ ion and the electron deficient nature of the cluster.

4. Conclusions

In our original report, the centered atom of **2** was modeled as both Ni and Ge with ultimate selection of the latter. Due to the similarities in the scattering factors of Ni and Ge, the refinement of the X-ray data did not allow for the discrimination between the two models. The assignment of a centered Ge atom was primarily based on electron counting principles (Wades rules) and striking structural similarities to other clusters of the same nuclearity (e.g., $[Sb_7Ni_3(CO)_3]^{3-}$). With the discovery of $[Sn_9Pt_2(PPh_3)]^{2-}$, we were prompted to reinvestigate the Ni–Ge system and the identity of **2**. The higher precision CCD data reported here and, more importantly, the ESI-MS data unequivocally identify the ion as $[Ge_9Ni_2(PPh_3)]^{2-}$ with a centered Ni atom. The non-deltahedral *nido*-like structures of these hypo-*closo* clusters are presumably due to steric demands of the centered metal atom.

During our re-investigation of the synthesis of **2**, we found that the $[Ni_6Ge_{13}(CO)_5]^{4-}$ ion, **1**, was formed at lower temperatures and shorter reaction times. While we have shown that **2** can be formed from **1** (Scheme 1), it seems quite possible that it also forms directly from Ge_9^{4-} and the $Ni(CO)_2(PPh_3)_2$. The biicosahedral structure of **1** is unique to Zintl ion chemistry but is a known feature in bimetallic clusters of the coinage metals [20]. The recently reported $[Pd_2@Ge_{18}]^{4-}$ and $[Ni_3@(Ge_9)_2]^{4-}$ cluster anions also in this general class of compounds. The former is an 18 vertex, 2 focus, 40 electron cluster with the expected *closo* architecture ($2n + 2$ cluster electrons per focus) whereas the latter does not easily fit into a Wadian description. Interestingly, neither forms icosahedral structures and are structurally distinct from **1**.

Recently, we have shown that ligand-free deltahedral clusters of Pb and Sn that are compositionally similar to the ligand-free ions identified here. For example, $[Ni@Pb_{10}]^{2-}$ and the gas phase $[Ni@Pb_{10}]^{1-}$ ions are centered 10-vertex clusters [10] similar to $Ge_9Ni_2^{-1}$ (or $[Ni@Ge_9Ni]^{-1}$). The later presumably adopts the *nido*-like C_{3v} structure of **2** despite having *5 fewer electrons* than the 22-electron *closo*-$[Ni@Pb_{10}]^{2-}$ cluster. While many of Zintl clusters of the group 14 elements and their transition metal derivatives adopt Wadian like structures, there are now several examples that do not. It is certain that more exceptions will be discovered as research continues.

Acknowledgments

We dedicate this manuscript to Professor Malcolm Chisholm on the occasion of his 60th birthday. This material is based upon work supported by the National Science Foundation under Grant No. 0401850.

Appendix A. Supplementary data

Crystallographic data for the compounds have been deposited with the Cambridge Crystallographic Data Centre, CCDC Nos. 273776 (**1**) and 273777 (**2**). Copies of this information may be obtained free of charge from The Director, CCDC, 12 Union Road, Cambridge, CB2 1EZ, UK (fax: +44 1223 3360333 or e-mail: deposit@ccdc.cam.ac.uk or http://www.ccdc.cam.ac.uk). Supplementary data associated with this article can be found, in the online version, at doi:10.1016/j.poly.2005.07.031.

References

[1] T.F. Fassler, S.D. Hoffmann, Angew. Chem. Int. Ed. 43 (2004) 6242.
[2] L. Yong, S.D. Hoffmann, T.F. Fassler, Z. Anorg. Allg. Chem. 630 (2004) 1977.
[3] T.F. Fassler, Angew. Chem. Int. Ed. 40 (2001) 4161.
[4] J.M. Goicoechea, S.C. Sevov, Inorg. Chem. 44 (2005) 2654.
[5] S. Neukermans, E. Janssens, Z.F. Chen, R.E. Silverans, P.V. Schleyer, P. Lievens, Phys. Rev. Lett. 92 (2004).
[6] R.B. King, T. Heine, C. Corminboeuf, P.V. Schleyer, J. Am. Chem. Soc. 126 (2004) 430.
[7] M.J. Moses, J.C. Fettinger, B.W. Eichhorn, Science 300 (2003) 778.
[8] R.C. Haushalter, C.M. O'Connor, J.P. Haushalter, A.M. Umarji, G.K. Shenoy, Angew. Chem. Int. Ed. 23 (1984) 169.
[9] E.N. Esenturk, B. Eichhorn, J. Fettinger (to be published).
[10] E.N. Esenturk, J. Fettinger, B. Eichhorn, Chem. Commun. (2005) 247.
[11] E.N. Esenturk, J. Fettinger, Y.F. Lam, B. Eichhorn, Angew. Chem. Int. Ed. 43 (2004) 2132.
[12] J.M. Goicoechea, S.C. Sevov, J. Am. Chem. Soc. 127 (2005) 7676.
[13] J.M. Goicoechea, S.C. Sevov, Angew. Chem. Int. Ed. 44 (2005) 4026.
[14] K.J. Wade, Adv. Inorg. Chem. Radiochem. 18 (1976) 1.
[15] B. Kesanli, J. Fettinger, D.R. Gardner, B. Eichhorn, J. Am. Chem. Soc. 124 (2002) 4779.
[16] S. Lee, Inorg. Chem. 31 (1992) 3063.

[17] B. Kesanli, J.C. Fettinger, D.R. Gardner, B.W. Eichhorn, Chem. Eur. J. (2001) 5277.
[18] D.R. Gardner, B.W. Eichhorn, J. Fettinger, Angew. Chem. Int., Ed. Engl. 35 (1996) 2852.
[19] B.K. Teo, H. Zhang, Y. Kean, H. Dang, X.B. Shi, J. Chem. Phys. 99 (1993) 2929.
[20] B.K. Teo, H. Zhang, Coord. Chem. Rev. 143 (1995) 611.
[21] G.M. Sheldrick, Universitat Gottingen, Gottingen, Germany, 1996.
[22] G.M. Sheldrick, Siemens Analytical X-ray Instruments, Inc., Madison, WI, 1994.
[23] C. Belin, H. Mercier, V. Angilella, New J. Chem. 15 (1991) 931.
[24] L. Yong, S.D. Hoffmann, T.F. Fassler, Z. Anorg. Allg. Chem. 631 (2005) 1149.
[25] C. Downie, Z.J. Tang, A.M. Guloy, Angew. Chem. Int. Ed. 39 (2000) 338.
[26] A. Ceriotti, F. Demartin, B.T. Heaton, P. Ingallina, G. Longoni, M. Manassero, M. Marchionna, N. Masciocchi, J. Chem. Soc., Chem. Commum. (1989) 786.
[27] S. Charles, B.W. Eichhorn, S.G. Bott, J. Am. Chem. Soc. 115 (1993) 5837.

Available online at www.sciencedirect.com
SCIENCE DIRECT®
Polyhedron 25 (2006) 530–538
POLYHEDRON
www.elsevier.com/locate/poly

Structures and magnetic behaviour of hydroxo-bridged Cr^{III} aggregates: $[Cr_4(\mu\text{-}OH)_4(hpdta)_2]^{2-}$ and $[Cr_6(\mu\text{-}OH)_8(hpdta)_2(en)_2]$

Saratchandra B. Mukkamala [a,1], Rodolphe Clérac [b], Christopher E. Anson [a], Annie K. Powell [a,*]

[a] Institut für Anorganische Chemie der Universität Karlsruhe, Engesserstrasse Geb. 30.45, D-76128 Karlsruhe, Germany
[b] Centre de Recherche Paul Pascal, CRPP-CNRS UPR 8641, 115 Avenue du Dr A. Schweitzer, 33600 Pessac, France

Received 9 June 2005; accepted 18 July 2005
Available online 29 September 2005

Dedicated to Prof. Malcolm H. Chisholm on the occasion of his 60th birthday.

Abstract

The syntheses and crystal structures of the tetra- and hexanuclear Cr^{III} aggregates $(enH_2)[Cr_4(\mu\text{-}OH)_4(hpdta)_2]\cdot 5\frac{1}{2}H_2O$ (**1a**), $[Ba(OH_2)_5\{Cr_4(\mu\text{-}OH)_4(hpdta)_2\}]\cdot 13H_2O$ (**1b**) $[Cr_6(\mu\text{-}OH)_8(hpdta)_2(en)_2]\cdot 10H_2O$ (**2a**) and $[Cr_6(\mu\text{-}OH)_8(hpdta)_2(en)_2]\cdot 14H_2O$ (**2b**) (H_5hpdta = 2-hydroxypropane-1,3-diaminetetraacetic acid) are reported and discussed. The antiferromagnetic interactions mediated by the bridging hydroxo ligands have been quantified. The fact that there are only a few such examples in the literature with similar bridges leads to the conclusion that a meaningful magnetostructural correlation, such as that recently proposed for oxo- and hydroxo-bridged Fe^{III} aggregates, is not yet possible in the case of Cr^{III}.
© 2005 Elsevier Ltd. All rights reserved.

Keywords: Chromium; Hydroxo-bridged aggregates; Magnetic properties; Structures; Coordination compounds

1. Introduction

We have previously described how hydrolysis reactions controlled by the use of chelating organic ligands containing amino, carboxylato and often alkoxo functionalities can be used to obtain polymetal aggregates of iron(III) and aluminium(III) held together by oxygen bridges deriving from the solvent water with further oxygen bridges often provided by groups on the ligand [1,2]. The structures of the resulting compounds are often analogous, although not always strictly isostructural [1]. This is probably a reflection of the relative lability and Lewis acidity of the two metal ions. For example, we find that whilst oxide bridges are common in the iron(III) complexes, hydroxide bridges tend to predominate in the aluminium(III) systems. We also found that the proligand hydroxypropanediaminotetraacetic acid, H_5hpdta (Scheme 1) is useful for providing dinuclear metal units as the central alcohol function provides an alkoxide bridge between the two metal ions [3–5].

With this in mind, we thought it would be interesting to see if this type of chemistry can be extended to the chromium(III) ion. Although several bis-(hydroxo)dichromium complexes have been reported [6] there are currently very few examples of larger hydroxo-bridged chromium(III) aggregates in the literature, although

* Corresponding author.
E-mail address: powell@chemie.uni-karlsruhe.de (A.K. Powell).
[1] Present address: Department of Chemistry, Gandhi Institute of Technology and Management, Visakhapatnam 530 045, India.

0277-5387/$ - see front matter © 2005 Elsevier Ltd. All rights reserved.
doi:10.1016/j.poly.2005.08.001

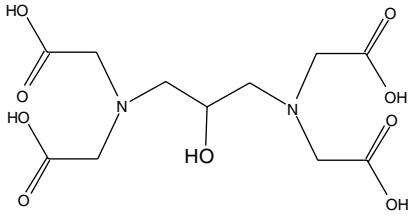

Scheme 1. The proligand H_5hpdta.

speciation studies suggest that hydrolytic clusters similar to those found for iron(III) and aluminium(III) should exist [7]. It is possible that the dual effects of the inertness of the chromium(III) ion and its tendency to form stable mononuclear octahedral complexes make the crystallisation of such aggregated species difficult. Thus, whilst mononuclear complexes of chromium(III) with chelating aminocarboxylate ligands have been extensively studied [8] only a few dinuclear hydroxo-bridged complexes with such ligands have been reported [9]. Apart from some tri- and tetranuclear complexes with ammine or cyclic polyamine ligands [10] the known higher nuclearity complexes are predominantly cyclic or cubane-based species in which the hydroxo bridges are supported by carboxylate co-ligands [11].

The magnetic interactions in the dinuclear hydroxo-bridged complexes have been extensively studied and it has been concluded that the magnitude of the antiferromagnetic interaction depends on the Cr–O(H) bond lengths, the Cr–O(H)–Cr angle and the extent to which the O–H bond is bent out of the Cr_2O plane [12]. The latter structural parameter, which reflects the nature of the hybridisation at the bridging oxygen, is at least as important as the other two which is in contrast to the situation for iron(III) complexes where a useful magnetostructural correlation was obtained using only the Fe–O–Fe bond lengths and angles [13]. More recently, ab initio DDCI2 methods have been used to calculate the magnitude of the magnetic interactions in such bis-(hydroxo)dichromium systems and these largely support the earlier correlations between the three geometrical parameters described above and the magnitude of the antiferromagnetic interaction [14].

In this paper, we report on the successful synthesis and isolation of tetranuclear and hexanuclear hydroxo-bridged chromium(III) aggregates using $hpdta^{5-}$ as the organic ligand. These have been structurally characterised using single crystal X-ray diffraction studies and their magnetic behaviour is described.

2. Experimental

H_5hpdta, $CrCl_3 \cdot 6H_2O$, $Cs(OH) \cdot H_2O$ and $BaCl_2 \cdot 2H_2O$ were purchased from Aldrich Chemical Co., 1,2-diaminoethane (en) (99%) from Lancaster Synthesis and all were used as received. $[Cr_3O(O_2CCH_3)_6(OH_2)_3]Cl \cdot 6H_2O$ was prepared by the method of Brauer [15]. All compounds gave satisfactory microanalyses.

2.1. Synthesis and characterisation

2.1.1. $(enH_2)[Cr_4(\mu\text{-}OH)_4(hpdta)_2] \cdot 5\frac{1}{2}H_2O$ (**1a**)

H_5hpdta (97 mg, 0.3 mmol) and 1,2-diaminoethane (72 mg, 80 μl, 1.2 mmol) in 10 ml water were stirred for 10 min. $CrCl_3 \cdot 6H_2O$ (160 mg, 0.6 mmol) was added with further stirring for 5 min. The solution was then heated to 85 °C under reflux with stirring for 24 h. After cooling, slow evaporation over 3–4 weeks gave purple crystals of **1a** in 15% yield.

2.1.2. $[Ba(OH_2)_5\{Cr_4(\mu\text{-}OH)_4(hpdta)_2\}] \cdot 13H_2O$ (**1b**)

H_5hpdta (97 mg, 0.3 mmol), $CrCl_3 \cdot 6H_2O$ (160 mg, 0.6 mmol), $BaCl_2 \cdot 2H_2O$ (37 mg, 0.15 mmol) and 1,2-diaminoethane (60 mg, 67 μl, 1.0 mmol) in 10 ml water were stirred for 10 min. The solution was heated to 85 °C under reflux with stirring for 20 h. The pH of the solution was then raised to 8.1 by dropwise addition of aqueous 1,2-diaminoethane followed by heating for a further 4 h. After cooling, slow evaporation over 2 weeks gave purple rod-shaped crystals of **1b** in 11% yield.

2.1.3. $[Cr_6(\mu\text{-}OH)_8(hpdta)_2(en)_2] \cdot 10H_2O$ (**2a**)

H_5hpdta (81 mg, 0.25 mmol) and 1,2-diaminoethane (66 mg, 74 μl, 1.1 mmol) in 10 ml water were stirred for 10 min. $[Cr_3O(O_2CCH_3)_6(OH_2)_3]Cl \cdot 6H_2O$ (362 mg, 0.5 mmol) was added, with further stirring until the trinuclear complex had dissolved. The solution was then heated to 85 °C under reflux with stirring for 4 h. The pH of the solution was then raised to 7.3 by dropwise addition of aqueous 1,2-diaminoethane followed by heating for a further 20 h. After cooling, slow evaporation over 2 weeks gave purple needle-shaped crystals of **2a** in 8% yield.

2.1.4. $[Cr_6(\mu\text{-}OH)_8(hpdta)_2(en)_2] \cdot 14H_2O$ (**2b**)

H_5hpdta (97 mg, 0.30 mmol), $CsOH \cdot H_2O$ (84 mg, 0.5 mmol) and 1,2-diaminoethane (30 mg, 34 μl, 0.5 mmol) in 10 ml water were stirred for 10 minutes. $CrCl_3 \cdot 6H_2O$ (160 mg, 0.6 mmol) was added with further stirring for 5 min. The solution was then heated to 85 °C under reflux with stirring for 24 h. The pH of the solution was then raised to 7.6 by dropwise addition of aqueous 1,2-diaminoethane, followed by heating for a further 1 h. After cooling, slow evaporation over 5 days gave purple block-shaped crystals of **2b** in 7% yield.

Table 1
Crystal data

Compound	1a	1b	2a	2b
Formula	$C_{24}H_{51}Cr_4N_6O_{27.5}$	$C_{22}H_{66}BaCr_4N_4O_{40}$	$C_{26}H_{70}Cr_6N_8O_{36}$	$C_{26}H_{78}Cr_6N_8O_{40}$
Formula weight	1071.71	1372.13	1382.90	1454.96
Crystal system	monoclinic	triclinic	triclinic	triclinic
Space group	$C2/c$	$P\bar{1}$	$P\bar{1}$	$P\bar{1}$
a (Å)	24.8071(17)	12.2856(13)	8.8031(12)	8.9756(10)
b (Å)	15.7492(8)	13.4172(13)	12.7952(17)	13.1054(15)
c (Å)	23.1461(16)	16.1851(16)	13.5853(19)	13.3370(15)
α (°)		80.337(12)	61.926(3)	62.842(2)
β (°)	120.654(8)	74.543(12)	72.261(2)	76.443(2)
γ (°)		88.075(12)	70.690(3)	75.694(2)
U (Å^3)	7779.2(9)	2534.8(4)	1253.6(3)	1339.0(3)
Z	8	2	1	1
T (K)	200	200	200	100
$F(000)$	4424	1396	714	754
D_{calc} (Mg m^{-3})	1.830	1.798	1.832	1.804
μ (Mo Kα) (mm^{-1})	1.197	1.708	1.368	1.291
Data measured	18545	16726	7833	6605
Unique data	6895	9299	5418	5608
R_{int}	0.0657	0.0323	0.0387	0.0175
Data with $I \geqslant 2\sigma(I)$	4197	7222	2938	4366
$2\theta_{max}$ (°)	50.3	52.2	56.4	56.0
Completeness to $2\theta = 50°$ (%)	98.9	93.7	98.6	98.0
wR_2 (all data)	0.0669	0.1324	0.0733	0.1076
S (all data)	0.982	0.972	0.838	0.971
R_1 [$I \geqslant 2\sigma(I)$]	0.0391	0.0475	0.0465	0.0399
Parameters	619	732	397	436
Biggest difference peak/hole (e Å^{-3})	+0.78/−0.30	+1.17/−0.57	+0.55/−0.48	+0.89/−0.71

2.2. Crystal structure determinations

Data were measured on Stoe IPDS (**1a** and **1b**) and Bruker SMART Apex (**2a** and **2b**) area detector diffractomers, respectively, using graphite-monochromated Mo-Kα radiation ($\lambda = 0.71073$ Å). The structures were solved by direct methods and refined by full-matrix least-squares against F^2 for all data, using the SHELXTL software package [16]. In **1b** many water molecules (those coordinated to Ba and lattice waters) were two- or threefold disordered. All non-H atoms were refined anisotropically except for some disordered lattice water molecules; H-atoms bonded to O or N were refined isotropically; those bonded to C were placed in calculated positions. Crystal data and details of the data collection and structural refinement are summarised in Table 1.

2.3. Magnetic measurements

Magnetic susceptibility measurements on **1a** (5.6 mg), **1b** (10.6 mg), **2a** (1.67 mg) and **2b** (9.93 mg) were obtained on a finely ground polycrystalline sample with the use of a Quantum Design SQUID magnetometer MPMS-XL. The dc measurements were collected from 1.8 to 300 K and from −70 to 70 kOe. Experimental data were also corrected for the sample holder and for the diamagnetic contribution calculated from Pascal constants [17].

3. Results and discussion

3.1. Description of the structures

The structure of the tetranuclear complex in **1a** is shown in Fig. 1; a similar numbering scheme is used for that in **1b**. Each hpdta^{5-} ligand coordinates two Cr(III) centres with the alkoxo oxygen bridging between the two as expected. Each Cr(III) is ligated in a tetradentate fashion through the alkoxo and two carboxylato oxygens and the amino nitrogen. Two such $\{Cr_2(hpdta)\}^-$ moieties are linked by the four bridging hydroxo ligands, two of which coordinate to each Cr(III) in a *cis* relationship. The Cr–O(H) bond lengths for **1a** and **1b** all lie in the range 1.938–1.996 Å with the Cr–O(H)–Cr angles of 130.7–135.9°. The corresponding values for the alkoxo bridges are 1.947–1.992 Å and 131.3–132.0° reflecting the fact that the geometry of the alkoxo bridge is constrained by the overall coordination of the hpdta^{5-} ligand. The geometries of the hydroxo-bridges compare well with those previously reported for unsupported single hydroxo-bridges, which are all in the range 132–137° [10]. The $\{Cr_4(\mu\text{-}OH)_4(\mu\text{-}OR)_2\}$ core thus has approximate tetrahedral symmetry, although this is reduced if the organic ligand as a whole is considered. Bond lengths and angles for the aggregates in **1a** and **1b** are summarised in Table 2.

The tetranuclear aggregate is thus isostructural with the aluminium analogue in $(enH_2)[Al_4(\mu\text{-}OH)_4$-

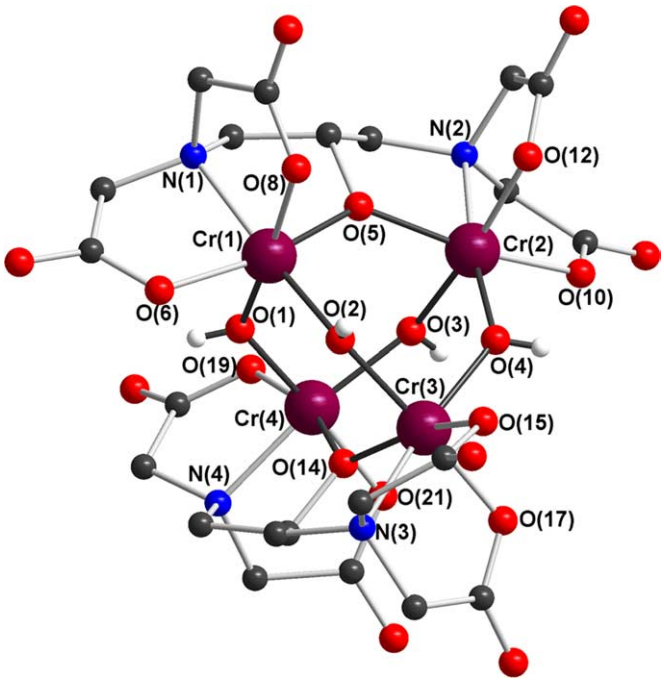

Fig. 1. Structure of the $[Cr_4(\mu\text{-}OH)_4(hpdta)_2]^{2-}$ aggregate in **1a**. The same numbering scheme is used in **1b**.

$(hpdta)_2] \cdot 7\frac{1}{2}H_2O$ [1]. In the corresponding tetrahedral iron(III) aggregates $X[Fe_4(\mu\text{-}O)(\mu\text{-}OH)_3(hpdta)_2] \cdot 5H_2O$ ($X = enH_2$, $pipH_2$) [2,18], one of these bridging hydroxo ligands is found to be deprotonated to an oxo bridge, which is probably a consequence of the higher Lewis-acidity of Fe(III) compared to Cr(III) or Al(III), noting that the relative acidities of metal ions can be judged from what is often termed the hydrolysis constant, which corresponds to the first pK_a for deprotonation of a coordinated water ligand with values of 2.1 for Fe(III), 4.0 for Cr(III) and 5.0 for Al(III).

In the crystal lattice of **1a**, the aggregates are linked via a three-dimensional network of hydrogen bonds. Three of the bridging hydroxo ligands (O(2), O(3) and O(4)) make hydrogen bonds to non-coordinated carboxylate oxygens of adjacent aggregates. In addition, one of the two NH_3^+ groups of the organic cation, N(31), forms hydrogen bonds to carboxylate oxygens from three different aggregates and three of the lattice waters also act as hydrogen-bonding linkages between different aggregates. In the lattice of **1b**, however, the aggregates are linked into chains via the Ba^{2+} countercations (Fig. 2). In each aggregate one carboxylate ligand, that involving O(6) and O(7), chelates to Ba(1), while O(7) also coordinates to the inversion-related Ba(1′) (at $-x$, $1-y$, $1-z$) such that two aggregates are linked through a dimeric $\{Ba_2(OH_2)_{10}\}^{4+}$ unit. Further coordination of the carboxylate oxygen O(16) to Ba(1″) (at $1-x$, $1-y$, $1-z$) leads to the one-dimensional motif in which two parallel rows of Cr_4 aggregates are joined through the dibarium units.

The structure of the hexanuclear Cr_6 aggregate in **2a** and **2b** is shown in Fig. 3. Unlike that in **1a** and **1b**, this aggregate has no direct analogue from our work with $hpdta^{5-}$ complexes of Fe(III) or Al(III). Selected bond lengths and angles are listed in Table 3; the same atom numbering system is used for the two isostructural aggregates. As before, a $hpdta^{5-}$ ligand chelates two chromium centres, Cr(1) and Cr(2), with the alkoxo oxygen bridging between them. Cr(1) is then linked to Cr(3) by two hydroxo ligands, O(1) and O(2), while Cr(2) is linked to Cr(3) by a further hydroxo bridge, O(3). Two such trichromium moieties form the centrosymmetric hexanuclear aggregate being joined by two further hydroxo bridges with O(4) bridging between Cr(2) and Cr(3′) and a corresponding bridge formed by its symmetry equivalent O(4′). The coordination sphere of Cr(3) is completed by the nitrogen atoms N(3) and N(4) of an ethylenediamine ligand. The geometries of the double bridges between Cr(1) and Cr(2), involving O(1) and O(2) are again comparable with previously reported systems [4,10]. However, unlike in **1a** and **1b**, the angles at the single hydroxo-bridges are now smaller than for such bridges in the literature [7,10], although still more obtuse than the angles reported for carboxylate-supported bridges [11]. To the best of our knowledge, the alkoxo-bridges at O(5) in **2a** and **2b** represent the first examples of single unsupported alkoxo-bridges between two chromium(III) centres. The unit cell parameters for **2a** and **2b** are closely related, and the packing of the Cr_6 aggregates in the lattice similar for both with extensive hydrogen bonding interactions in evidence through the lattice waters.

Table 2
Selected bond lengths (Å) and angles (°) for the Cr_4 aggregates in **1a** and **1b**

	1a	1b
Cr(1)–O(1)	1.989(3)	1.938(3)
Cr(1)–O(2)	1.961(3)	1.968(4)
Cr(1)–O(5)	1.967(3)	1.947(3)
Cr(1)–O(6)	1.965(3)	1.984(3)
Cr(1)–O(8)	1.991(3)	1.983(3)
Cr(1)–N(1)	2.090(3)	2.081(4)
Cr(2)–O(3)	1.956(3)	1.967(3)
Cr(2)–O(4)	1.957(3)	1.985(3)
Cr(2)–O(5)	1.981(2)	1.971(2)
Cr(2)–O(10)	1.986(3)	1.994(3)
Cr(2)–O(12)	1.999(3)	1.972(4)
Cr(2)–N(2)	2.067(3)	2.092(4)
Cr(3)–O(2)	1.957(3)	1.968(3)
Cr(3)–O(4)	1.966(3)	1.996(3)
Cr(3)–O(14)	1.992(3)	1.961(3)
Cr(3)–O(15)	1.998(3)	1.982(3)
Cr(3)–O(17)	1.977(2)	1.977(4)
Cr(3)–N(3)	2.091(3)	2.080(4)
Cr(4)–O(1)	1.988(3)	1.945(3)
Cr(4)–O(3)	1.949(3)	1.965(3)
Cr(4)–O(14)	1.970(2)	1.968(4)
Cr(4)–O(19)	1.971(3)	1.997(3)
Cr(4)–O(21)	1.985(2)	1.974(4)
Cr(4)–N(4)	2.082(3)	2.094(4)
Cr(1)···Cr(2)	3.6070(9)	3.6070(9)
Cr(3)···Cr(4)	3.6098(9)	3.6098(9)
Cr(1)···Cr(3)	3.6190(8)	3.6190(8)
Cr(1)···Cr(4)	3.6239(9)	3.6239(9)
Cr(2)···Cr(3)	3.6082(8)	3.6082(8)
Cr(2)···Cr(4)	3.6066(8)	3.6066(8)
Cr(1)–O(5)–Cr(2)	132.00(11)	131.94(15)
Cr(3)–O(14)–Cr(4)	131.30(12)	132.01(16)
Cr(1)–O(1)–Cr(4)	131.34(16)	135.88(18)
Cr(1)–O(2)–Cr(2)	134.98(16)	135.72(18)
Cr(2)–O(3)–Cr(4)	134.89(16)	135.11(17)
Cr(2)–O(4)–Cr(3)	133.78(15)	130.76(18)

3.2. Magnetic behaviour

The magnetic susceptibilities of polycrystalline samples of **1a** and **1b** were measured over the temperature range 1.8–300 K at 1 kOe, and the results are shown in Fig. 4.

For each compound, the high temperature data above 100 K can be fitted to a Curie–Weiss law, with $C = 8.6$ and 9.5 cm^3 K/mol and $\theta = -98$ and -106 K for **1a** and **1b**, respectively. The estimation of the Curie constant is in good agreement with the presence of four $S = 3/2$ Cr(III) metal ions (expected value for $g = 2.0$ is $C = 7.5$ cm^3 K/mol). Moreover, the Weiss constant indicates dominating antiferromagnetic interactions between the magnetic centres. According to the molecular structure of these Cr_4 units (vide supra), four different hydroxo and two alkoxo groups link the magnetic centres, potentially resulting in six different magnetic interactions. Although it is known that the magnitudes of these interactions depend critically on (inter alia) the degree of out-of-plane bending of the O–H and O–R bonds we used a simplified model with only two different interactions, one for the hydroxo and one for the alkoxo bridges. A similar simplification has previously been used to interpret the magnetism of a tetranuclear complex with a $\{Cr_4(\mu\text{-}OH)_6\}$ core [10e]. Therefore, the susceptibility was calculated using the following Heisenberg spin Hamiltonian (see inset Fig. 4):

$$H = -2J\{S_1S_3 + S_1S_4 + S_2S_3 + S_2S_4\} - 2J_1\{S_1S_2 + S_3S_4\}.$$

Here J corresponds to the average magnetic interaction through the four hydroxo bridges, and J_1 to that through the two alkoxo bridges. Using this model, the simulation shown in Fig. 4 was obtained using the MAGPACK program [19]. The final values obtained were $J/k_B = -8.5(2)$ K ($-5.9(1)$ cm^{-1}), $J_1/k_B = -8.0(2)$ K ($-5.6(1)$ cm^{-1}), $g = 1.98$ for **1a**, and $J/k_B = -10.6(2)$ K ($-7.4(1)$ cm^{-1}), $J_1/k_B = -1.8(2)$ K ($-1.3(1)$ cm^{-1}), $g = 1.98$ for **1b**. It is worth noting that these values are robust in that they could be obtained from a range of different starting values.

For **1a**, the values of J and J_1 are very similar. It would seem that the larger out-of-plane bending of the O–H bonds (18–29°) compared to that for the O–C bonds (13.9° and 11.3°) is largely compensated by the replacement of the H substituent on the oxygen bridge by an alkoxo group. In the case of **1b**, however, it appears not to be so straightforward with J similar to that found for **1a**, but J_1 much smaller (-1.8 K compared to -8.0 K). Paine et al. reported the magnetic analysis of two related bis-(methoxy)-bridged dinuclear chromium complexes, in which the two $\{Cr_2(\mu\text{-}OMe)_2\}$ cores had very similar geometries but very different J values; however they attributed the difference to the presence of an additional hydrogen-bonded {Cr–MeOH···OMe–Cr} bridge [20]. For **1b**, a further possibility is that J_1 might not be assignable to the alkoxo bridges, but to two opposite hydroxo-bridges. Inspection of the structure of **1b** shows that the O–H bonds on O(1) and O(4) are substantially more bent out-of-plane (by 39° and 28°) than those on O(2) and O(3) (16° and 8°) and the small value for J_1 might reflect the possibly weaker coupling through O(1) and O(4) with J then assigned to the O(2) and O(3) and alkoxo bridges. Such arguments must, however, remain speculative, particularly as the out-of-plane O–H angles cannot be obtained with any degree of accuracy from even a low-temperature X-ray crystal structure. We merely note here that the observed susceptibilities can be simulated with just two J values. Ab initio calculations [20] using a structure obtained from neutron diffraction would probably be the only way to define precisely the magnetic interactions, but this is outside the scope of the present work.

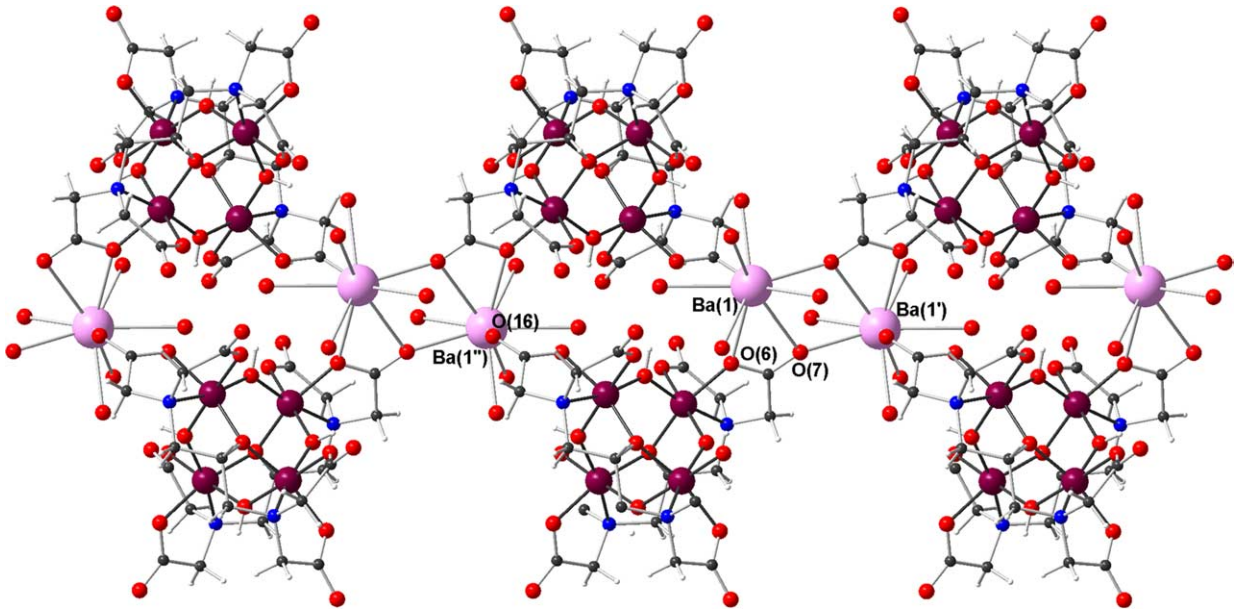

Fig. 2. Linkage of the Cr_4 aggregates by coordination of O(6), O(7) and O(16) to Ba^{2+} cations forming double-chains in the structure of **1b**.

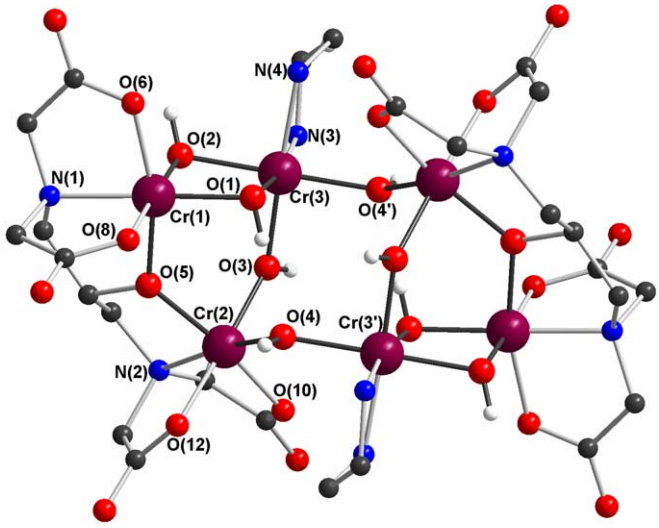

Fig. 3. Structure of the $[Cr_6(\mu\text{-}OH)_8(hpdta)_2(en)_2]$ aggregate in **2a**. The same numbering scheme is used in **2b**.

The magnetic susceptibilities of polycrystalline samples of **2a** and **2b** were similarly measured over the temperature range 1.8–300 K at 1 kOe, and the results are shown in Fig. 5. The high temperature data above 100 K can be fitted to a Curie–Weiss law for both compounds with $C = 12.0$ and 12.3 cm^3 K/mol and $\theta = -74$ and -105 K for **2a** and **2b**, respectively. The estimation of the Curie constants is in agreement with the presence of six $S = 3/2$ Cr(III) metal ions (expected value for $g = 2$ is $C = 11.25$ cm^3 K/mol). As before, the Weiss constants indicate dominating antiferromagnetic interactions. In the molecular structure of these Cr_6 units (vide supra), four chemically distinct types of bridges between the chromium(III) centres are present: the double hydroxo bridge between Cr(1) and Cr(3), the alkoxo bridge between Cr(1) and Cr(2), and the two single hydroxo bridges O(3) and O(4). However, the latter two bridges have very similar geometries and we have therefore considered only three different interactions in a simplified model. The susceptibility was thus calculated using the following Heisenberg spin Hamiltonian (see inset Fig. 5):

$$H = -2J_1\{S_1S_3 + S_5S_6\} - 2J_2\{S_1S_2 + S_4S_6\} - 2J_3\{S_2S_3 + S_3S_4 + S_4S_5 + S_2S_5\}.$$

Table 3
Selected bond lengths (Å) and angles (°) for the Cr_6 aggregates in **2a** and **2b**

	2a	2b
Cr(1)–O(1)	1.944(3)	1.954(2)
Cr(1)–O(2)	1.956(4)	1.963(2)
Cr(1)–O(5)	1.933(3)	1.962(2)
Cr(1)–O(6)	1.974(3)	2.009(2)
Cr(1)–O(8)	1.971(3)	1.991(2)
Cr(1)–N(1)	2.044(3)	2.070(2)
Cr(2)–O(3)	1.926(3)	1.985(2)
Cr(2)–O(4)	1.974(3)	1.984(2)
Cr(2)–O(5)	1.953(3)	1.988(2)
Cr(2)–O(10)	1.976(3)	1.987(2)
Cr(2)–O(12)	1.950(3)	1.990(2)
Cr(2)–N(2)	2.058(4)	2.082(2)
Cr(3)–O(1)	1.953(3)	1.980(2)
Cr(3)–O(2)	1.979(3)	1.978(2)
Cr(3)–O(3)	1.969(3)	1.979(2)
Cr(3)–O(4′)	1.989(3)	1.999(2)
Cr(3)–N(3)	2.062(4)	2.078(3)
Cr(3)–N(4)	2.067(4)	2.073(3)
Cr(1)···Cr(2)	3.4900(10)	3.5585(7)
Cr(1)···Cr(3)	2.9447(10)	2.9728(7)
Cr(2)···Cr(3)	3.5462(10)	3.5728(7)
Cr(2)···Cr(3′)	3.5839(11)	3.6199(7)
Cr(1)–O(5)–Cr(2)	127.79(14)	128.57(10)
Cr(1)–O(1)–Cr(3)	98.13(13)	98.15(9)
Cr(1)–O(2)–Cr(3)	96.90(14)	97.91(9)
Cr(2)–O(3)–Cr(3)	131.16(16)	130.71(11)
Cr(2)–O(4)–Cr(3′)	129.46(16)	130.71(10)

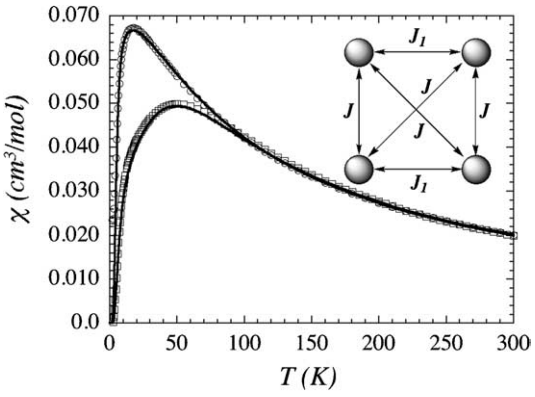

Fig. 4. Plots of magnetic susceptibility χ against temperature for compounds **1a** (○) and **1b** (□), the solid lines are the best fits using the models described in the text. Inset: Schematic view of the magnetic interaction topology.

Here J_1, J_2 and J_3 correspond to the magnetic interactions through the double-hydroxo, mono-hydroxo and alkoxo bridges, respectively. This Hamiltonian was fully diagonalized using MAGPACK [19] and the susceptibility calculated. The simulation agrees very well with the experimental data with $J_1/k_B = -15.0(2)$ K ($-10.4(1)$ cm^{-1}), $J_2/k_B = -6.6(2)$ K ($-4.6(1)$ cm^{-1}), $J_3/k_B = -4.5(2)$ K ($-3.1(1)$ cm^{-1}), $g = 1.98$ for **2a**, and $J_1/k_B = -12.0(2)$ K ($-8.3(1)$ cm^{-1}), $J_2/k_B = -9.6(2)$ K

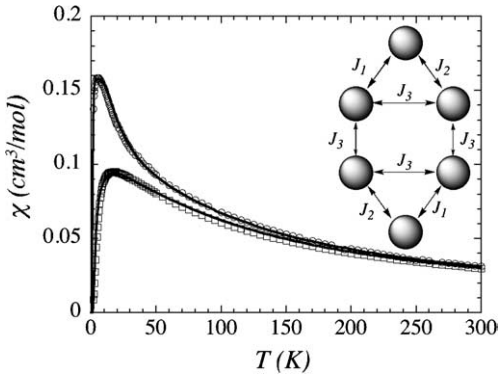

Fig. 5. Plots of magnetic susceptibility χ against T for compounds **2a** (○) and **2b** (□), the solid lines are the best fits using the models described in the text. Inset: Schematic view of the magnetic interaction topology.

($-6.7(1)$ cm^{-1}), $J_3/k_B = -7.6(2)$ K ($-5.3(1)$ cm^{-1}), $g = 1.98$ for **2b**. Although individual J values differ between the two compounds in both cases the interaction through the double-hydroxo bridges is the most strongly antiferromagnetic, followed by the mono-hydroxo and alkoxo bridges. In spite of the fact that the geometries of the aggregates in **2a** and **2b** are very similar, it is likely that even relatively small changes in the hydrogen-bonding environments of the (μ-OH) ligands, resulting from changes in the crystal packing, with concomitant effects on the extent to which the O–H bonds are bent out-of-plane, are responsible for the small differences in corresponding J values for the two compounds.

For iron(III) aggregates linked by (μ_3-O), (μ-OR) and (μ-OH) bridges a rather successful correlation between bridge geometry and magnetic interaction has been proposed, based on the Fe–O distances and Fe–O–Fe angles [13]. For the d^5 metal cation it was not found necessary to include the out-of-plane O–H bending to obtain a useful correlation. For chromium(III), by contrast, such a correlation is not practical for two main reasons. Firstly, the magnitudes of the J values are much less than for iron(III) and are indeed comparable to the degree of experimental scatter found for the iron system [13]. Secondly, while the M–O bond lengths and M–O–M angles can be determined to a good degree of precision in an X-ray structural analysis, this is not the case for the out-of-plane bend of the O–H bonds and the precise location of the hydrogen atom has been shown to have a dominant influence on the magnetic interaction in hydroxo-bridged chromium(III) complexes [21]. Furthermore, Glerup et al. [10e] have commented that it may be unwise to compare J values from chromium(III) complexes of differing nuclearity. We also note that, in contrast to iron(III) complexes, in the chromium complexes so far reported, the hydroxo-bridges have Cr–O–Cr angles that fall into three well-defined groups: double-hydroxo bridges with Cr–O–Cr ca. 96-99°, carboxylate-supported hydroxo-bridges with Cr–O–Cr ca.

120°, and unsupported hydroxo-bridges with Cr–O–Cr ca. 131–137°. In order to develop any sort of magneto-structural correlation a much wider spread of geometries is clearly required.

4. Conclusion

Overall these results indicate that the Cr(III) ion can be used to produce aggregates via hydrolytic routes similar to some of the Fe(III) and Al(III) compounds already known. The inert nature of the Cr(III) centre requires fairly harsh reaction conditions with compounds forming only when solutions are left refluxing and then in rather small yields compared with the other two metal ions. This inertness together with the fact that the compounds formed only have hydroxo bridges and no oxo bridges makes them more comparable to the Al(III) than the Fe(III) compounds previously observed. The magnetic behaviour of these new Cr(III) hydroxo-bridged systems can be modelled and the dominant interactions are antiferromagnetic. However, until further examples of aggregates containing three or more Cr(III) centres linked by hydroxo bridges are available it is not possible to propose any definitive rules for a magnetostructural correlation.

5. Supplementary material

Crystallographic data (excluding structure factors) for the structures in this paper have been deposited with the Cambridge Crystallographic Data Centre as supplementary publication nos. CCDC 273330–273333. Copies of the data can be obtained, free of charge, on application to CCDC, 12 Union Road, Cambridge CB2 1EZ, UK: http://www.ccdc.cam.ac.uk/perl/catreq/catreq.cgi, e-mail: data_request@ccdc.cam.ac.uk, or fax: +44 1223 336 033.

Acknowledgements

This work was supported by the DFG (via the Schwerpunkt Programm SPP 1137 "Molecular Magnetism" and the Center for Functional Nanostructures), the Conseil Régional d'Aquitaine, Bordeaux I University and the CNRS. The authors are also grateful to J. Modesto Clemente-Juan for providing the MAGPACK package.

References

[1] W. Schmitt, P.A. Jordan, R.K. Henderson, G.R. Moore, C.E. Anson, A.K. Powell, Coord. Chem. Rev. 228 (2002) 115.
[2] W. Schmitt, M. Murugesu, J.C. Goodwin, J.P. Hill, A. Mandel, R. Bhalla, C.E. Anson, S.L. Heath, A.K. Powell, Polyhedron 20 (2001) 1687.
[3] W. Schmitt, E. Baissa, A. Mandel, C.E. Anson, A.K. Powell, Angew. Chem. Int. Ed. 40 (2001) 3578.
[4] W. Schmitt, C.E. Anson, B. Pilawa, A.K. Powell, Z. Anorg. Allg. Chem. 628 (2002) 2443.
[5] W. Schmitt, W. Wernsdorfer, C.E. Anson, A.K. Powell, Chem. Commun. (2005) 2098.
[6] (a) J. Springborg, Adv. Inorg. Chem. 32 (1988) 55;
(b) P. Andersen, Coord. Chem. Rev. 94 (1989) 47;
(c) P.A. Lay, A. Levina, in: J.A. McCleverty, T.J. Meyer (Eds.), Comprehensive Coordination Chemistry II, vol. 4, Elsevier, Amsterdam, 2004, pp. 367–368.
[7] P.A. Lay, A. Levina, in: J.A. McCleverty, T.J. Meyer (Eds.), Comprehensive Coordination Chemistry II, vol. 4, Elsevier, Amsterdam, 2004, p. 369.
[8] P.A. Lay, A. Levina, in: J.A. McCleverty, T.J. Meyer (Eds.), Comprehensive Coordination Chemistry II, vol. 4, Elsevier, Amsterdam, 2004, pp. 361–362.
[9] (a) e.g. for the nitrilotriacetate ligand: H.G. Visser, W. Purcell, S.S. Basson, Polyhedron 18 (1999) 2795;
(b) J.-H. Choi, T. Suzuki, S. Kaizaki, Acta Crystallogr., Sect. E 59 (2003) m812;
(c) G. Novitchi, J.-P. Costes, V. Ciornea, S. Shova, I. Filippova, Y.A. Simonov, A. Gulea, Eur. J. Inorg. Chem. (2005) 929.
[10] (a) E. Bang, Acta Chem. Scand. 22 (1968) 2671;
(b) E. Bang, Acta Chem. Scand. A 38 (1984) 417;
(c) P. Andersen, T. Damhus, E. Pedersen, A. Petersen, Acta Chem. Scand. A 38 (1984) 359;
(d) P. Andersen, E. Bang, Acta Chem. Scand. A 40 (1986) 476;
(e) J. Glerup, H. Weihe, P.A. Goodson, D.J. Hodgson, Inorg. Chim. Acta 212 (1993) 281.
[11] (a) A. Harton, K. Terell, J.C. Huffman, C. MacDonald, A. Beatty, S. Li, C.J. O'Connor, J.B. Vincent, Inorg. Chem. 36 (1997) 4875;
(b) F.E. Mabbs, E.J.L. McInnes, M. Murrie, S. Parsons, G.M. Smith, C.C. Wilson, R.E.P. Winpenny, Chem. Commun. (1999) 643;
(c) I.M. Atkinson, C. Benelli, M. Murrie, S. Parsons, R.E.P. Winpenny, Chem. Commun. (1999) 285;
(d) M. Eshel, A. Bino, I. Felner, D.C. Johnston, M. Luban, L.L. Miller, Inorg. Chem. 39 (2000) 1376;
(e) S. Parsons, A.A. Smith, R.E.P. Winpenny, Chem. Commun. (2000) 579;
(f) E.J.L. McInnes, C. Anson, A.K. Powell, A.J. Thomson, S. Poussereau, R. Sessoli, Chem. Commun. (2001) 89;
(g) M. Eshel, A. Bino, Inorg. Chim. Acta 320 (2001) 127;
(h) M. Eshel, A. Bino, Inorg. Chim. Acta 329 (2002) 45;
(i) A.C. Royer, R.D. Rogers, D.L. Arrington, S.C. Street, J.B. Vincent, Polyhedron 21 (2002) 155;
(j) P. Christian, G. Rajaraman, A. Harrison, J.J.W. McDouall, J.T. Raftery, R.E.P. Winpenny, Dalton Trans. (2004) 1511.
[12] (a) R.P. Scaringe, D.J. Hodgson, W.E. Hatfield, Transition Met. Chem. 6 (1981) 340;
(b) J. Glerup, D.J. Hodgson, E. Pedersen, Acta Chem. Scand. A 37 (1983) 161;
(c) D.J. Hodgson, in: R.D. Willet, D. Gatteschi, O. Kahn (Eds.), Magnetostructural Correlations in Exchange Coupled Systems, NATO Advanced Study Series C, vol. 140, Riedel, Dordrecht, 1985, p. 497ff.
[13] C. Cañada-Vilalta, T.A. O'Brien, E.K. Brechin, M. Pink, E.R. Davidson, G. Christou, Inorg. Chem. 43 (2004) 5505.
[14] O. Castell, R. Caballol, Inorg. Chem. 38 (1999) 668.
[15] G. Brauer, Handbook of Preparative Inorganic Chemistry, vol. 2, Academic Press, New York, 1965, pp.1371-1372.
[16] G.M. Sheldrick, SHELXTL 5.1, Bruker AXS Inc., 630, Enterprise Lane, Madison, WI 53719-1173, USA, 1997.
[17] E.A. Boudreaux, L.N. Mulay (Eds.), Theory and Applications of Molecular Paramagnetism, Wiley, New York, 1976.

[18] W. Schmitt, Ph.D. Thesis, Universität Karlsruhe, 2002.
[19] J.J. Borrás-Almenar, J.M. Clemente-Juan, E. Coronado, B.S. Tsukerblat, J. Comput. Chem. 22 (2001) 985.
[20] T.K. Paine, T. Weyhermüller, K. Wieghardt, P. Chaudhuri, Inorg. Chem. 41 (2002) 6358.
[21] T. Schönherr, Theochem 93 (1992) 203.

Available online at www.sciencedirect.com
SCIENCE DIRECT®
Polyhedron 25 (2006) 539–549
POLYHEDRON
www.elsevier.com/locate/poly

Di-2-pyridyl ketone in lanthanide(III) chemistry: Mononuclear and dinuclear erbium(III) complexes

Katerina A. Thiakou [a], Vassilios Nastopoulos [a], Aris Terzis [b], Catherine P. Raptopoulou [b,*], Spyros P. Perlepes [a,*]

[a] Department of Chemistry, University of Patras, 265 04 Patras, Greece
[b] Institute of Materials Science, NCSR "Demokritos", 153 10 Aghia Paraskevi Attikis, Athens, Greece

Received 15 June 2005; accepted 19 July 2005
Available online 29 August 2005

Dedicated to Malcolm Chisholm, one of the giants in inorganic chemistry, on the occasion of his 60th birthday.

Abstract

The use of di-2-pyridyl ketone ($(py)_2CO$)/SCN^- "blend" in erbium(III) chemistry has yielded mononuclear and dinuclear complexes. The Er^{III}/SCN^-/$(py)_2CO$ reaction mixture in alcohols (MeOH, EtOH) gives complexes $[Er(NCS)_3\{(py)_2C(OR)(OH)\}_3]$ (R = Me (**1**), Et (**2**)), where $(py)_2C(OR)(OH)$ is the neutral hemiacetal derivative of $(py)_2CO$. Incorporation of hydroxides in the methanolic reaction system leads to the isolation of $[Er_2(NCS)_3\{(py)_2C(OMe)O\}_3(MeOH)]$ (**3**). Complex **3** can also be isolated by the reaction of **1** with three equivalents of NMe_4OH in MeOH. The crystal structures of $\mathbf{2}\cdot 0.3EtOH\cdot 0.4H_2O$ and $\mathbf{3}\cdot MeOH$ have been solved by single-crystal X-ray crystallography. The Er^{III} atom in the former is in a nine-coordinate, tricapped trigonal prismatic ligand environment. The $(py)_2C(OEt)(OH)$ molecules adopt the novel N(2-pyridyl), O(hydroxyl)-bidentate chelating mode, while three isothiocyanate ligands complete the coordination sphere of Er^{III}. In complex $\mathbf{3}\cdot MeOH$ the two Er^{III} atoms are triply bridged by the deprotonated hydroxyl oxygen atoms of the $\eta^1{:}\eta^2{:}\eta^1{:}\mu_2(py)_2C(OMe)O^-$ ligands; three 2-pyridyl nitrogen atoms belonging to three different ligands and two isothiocyanate anions complete eight-coordination at one Er^{III} atom, while eight-coordination at the other Er^{III} atom is completed by three 2-pyridyl nitrogen atoms, one isothiocyanate ligand and one MeOH molecule. The coordination polyhedra of the eight donor atoms about both Er^{III} atoms are best described as distorted dodecahedra. The complexes were studied by room-temperature effective magnetic moments and spectroscopic (IR, solid-state f–f) methods. All data are discussed in terms of the nature of bonding and known (**2**, **3**) or assigned (**1**) structures.
© 2005 Elsevier Ltd. All rights reserved.

Keywords: Di-2-pyridyl ketone-based ligands; Dodecahedral coordination geometry; Er(III) isothiocyanate complexes; f–f spectra; Tricapped trigonal prismatic geometry

1. Introduction

Lanthanide elements (Ln), bearing special electronic and spectroscopic properties mainly associated with their 4f electronic configuration, represent a unique series of metals in the periodic table [1]. The paramagnetic and optical properties of trivalent lanthanides, their hard acid character and their high coordination numbers make lanthanide(III) complexes attractive for applications such as magnetic resonance imaging (MRI) contrast agents [2], mild reagents and catalysts in organic synthesis [3], molecular magnetic materials [4], in luminescence studies [1] and in solvent extraction of actinides(III) [5]. For example, due to the impressive luminescence characteristics of several Ln^{3+} ions, they

* Corresponding authors. Tel.: +30 2610 997146; fax: +30 2610 997118.
E-mail addresses: craptop@ims.demokritos.gr (C.P. Raptopoulou), perlepes@patreas.upatras.gr (S.P. Perlepes).

0277-5387/$ - see front matter © 2005 Elsevier Ltd. All rights reserved.
doi:10.1016/j.poly.2005.07.029

are increasingly used as highly efficient electroluminescent components for light emitting diodes [6], luminescence probes for analytes [7], labels for proteins and amino acids [8], and for molecular recognition and chirality sensing of biological substrates [9]. Moreover, by incorporating Ln^{3+} ions into liquid crystals, it is possible to obtain mesogenic complexes that are useful for the design of emissive liquid crystal displays and magnetically addressable liquid crystals [10]. Consequently, lanthanide coordination chemistry has been thoroughly investigated over the last twenty years [11–20], and the position of Ln(III) complexes, primarily mononuclear ones, in various technologically and medically important areas, has now been firmly established.

Despite the great progress in the synthesis and physical (mainly magnetic) properties of polynuclear complexes (clusters) of the d-block metals at intermediate oxidation states [21–25], the number of Ln(III) clusters is still rather limited [26–34]. Dinuclear and polynuclear Ln(III) complexes exhibit a fascinating variety of unusual symmetries and structural patterns, and are expected to find such important applications as precursors for metalloorganic chemical vapour deposition (MOCVD) [35] and sol–gel technology [36], synthetic nucleases [37], new biomedical imaging contrast agents [38] and single-molecule magnets [39], the last potential application being currently confined to 3d-4f mixed-metal clusters.

Almost all clusters are made from complex reaction mixtures, which provide metal ions, ligand or ligands, solvent molecules, counter-ions and, perhaps, traces of absorbed oxygen. Each component may influence the final product. Other variables include the pH and ionic strength of the solution, and the temperature of the reaction. One route to polynuclear complexes – a route perhaps best termed "designed assembly" – controls the reaction pathway by making a specific metal–ligand interaction the most significant in the system [40]. This approach finds limited application in Ln(III) chemistry. A complementary approach is "serendipitous assembly" [41], where the variables in the complex system are modified following certain rationales to influence the product found, rather than to control or design the target molecule [42].

The future of the field of 4f-metal clusters and the chances of identifying new complexes with interesting properties will both benefit from the development of new reaction systems with suitable organic ligands. Our group [43–49] and others [50–52] have been exploring reaction systems involving (i) the monoanion $(py)_2C(OH)O^-$, or the dianion, $(py)_2CO_2^{2-}$, of the *gem*-diol form (derivative), $(py)_2C(OH)_2$, of di-2-pyridyl ketone, $(py)_2CO$, or (ii) the monoanion, $(py)_2C(OR)O^-$ (R = Me, Et, etc.), of the hemiacetal form (derivative), $(py)_2C(OR)(OH)$, of di-2-pyridyl ketone in Mn, Fe, Co, Ni, Cu, Zn, and Cd chemistries. The formulae of these ligands and their abbreviations are shown in Fig. 1. The reactions of $(py)_2CO$ with 3d-metal ions have been well-studied over the last ten years or so [43]. There

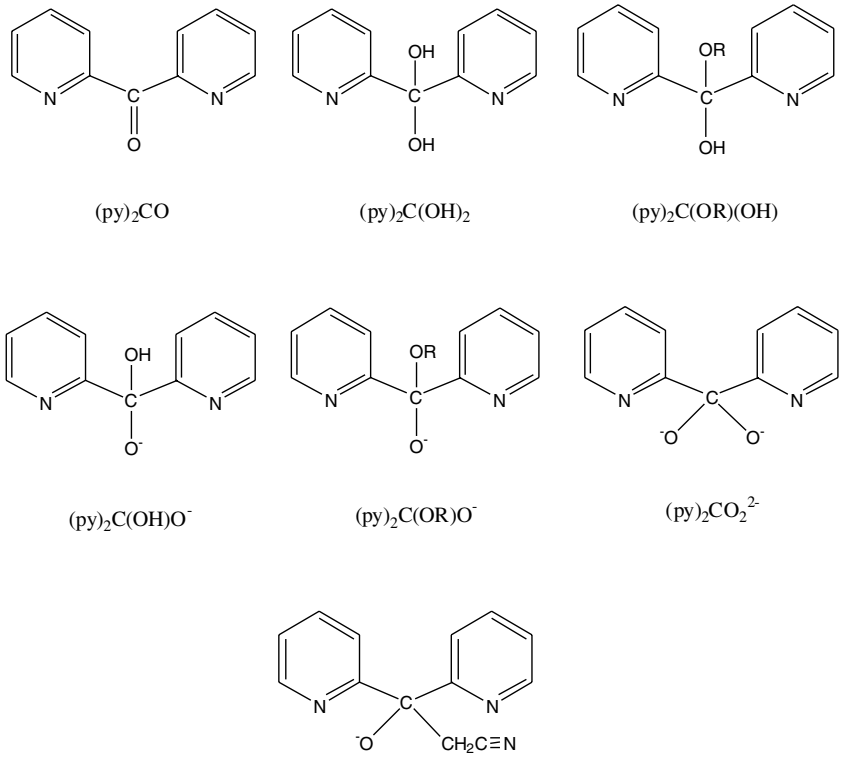

Fig. 1. The derivatives of di-2-pyridyl ketone, $(py)_2CO$, discussed in the text; note that $(py)_2C(OH)_2$, $(py)_2C(OR)(OH)$ and all four anions do not exist as free species – they exist only as ligands in their metal complexes.

is a chemical characteristic of $(py)_2CO$ that makes this molecule special as ligand; this is its carbonyl group. Water and alcohols (ROH) have been shown to add to the carbonyl group *upon coordination of the 2-pyridyl rings* forming the ligands $(py)_2C(OH)_2$ (the *gem*-diol form of $(py)_2CO$) and $(py)_2C(OR)(OH)$ (the hemiacetal form of $(py)_2CO$), respectively (Fig. 1). Recently [53] it has also been reported that the ligand $(py)_2C(OH)(CH_2CN)^-$, see Fig. 1, can be generated in situ during the preparation of a heterometallic $Ni_{12}K_4$ cluster by the reaction of CH_3CN and $(py)_2CO$ at room temperature under aerobic conditions. The neutral ligands coordinate to the metal ion as tridentate *N,N,O* chelates, with the M–O bond often being weak; therefore, both neutral ligands do not present interest from the cluster formation viewpoint [43]. Completely different and much more interesting (for cluster chemistry) coordination modes are seen when the ligands $(py)_2C(OH)_2$ and $(py)_2C(OR)(OH)$ are deprotonated. Upon deprotonation, the latter becomes monoanionic, whereas the former can function either as mono- or dianionic. The presence of deprotonated hydroxyl group(s) leads to a great coordinative flexibility, due to the well known ability of the negatively charged oxygen to bridge two or three 3d-metal ions. The immense structural diversity displayed by the complexes reported stems in part from the ability of $(py)_2C(OH)O^-$, $(py)_2CO_2^{2-}$ and $(py)_2C(OR)O^-$ to exhibit no less than nine distinct bridging coordination modes ranging from μ_2 to μ_5 [43]. Employment of carboxylates, β-diketonates or organic oxo anions (NO_3^-, SO_4^{2-}, etc.) as ancillary ligands in the reaction mixtures gives an extraordinary structural flexibility in the mixed-ligand systems, allowing the isolation of a variety of 3d-metal clusters with nuclearities ranging from 3 to 14 [43] and with interesting physical properties including single-molecule magnetism [46].

Surprisingly, however, $(py)_2CO$-based ligands have been completely ignored in Ln(III) chemistry. Here, we report some experiments that lead to the first members of the new and diverse family of Ln(III) complexes with $(py)_2CO$-based ligands.

2. Experimental

2.1. General and physical measurements

All manipulations were performed under aerobic conditions using materials (reagent grade) and solvents as received. For the preparation of the complexes, a methanolic solution of "$Er(NCS)_3$" (solution A) was prepared as follows: A solution (10 ml) of KSCN (6.0 mmol) in MeOH was treated with $ErCl_3 \cdot 6H_2O$ (2.0 mmol). The solid erbium(III) chloride soon dissolved, the mixture was stirred for 30 min and the white crystals of KCl were removed by filtration. The resulting filtrate (~11 ml) has a known concentration of "$Er(NCS)_3$". An ethanolic solution (~25 ml) of "$Er(NCS)_3$" (solution B) was prepared by an analogous manner using a solution (23 ml) of KSCN (6.0 mmol) in warm EtOH and $ErCl_3 \cdot 6H_2O$ (2.0 mmol). Solutions A and B contain less than 10% of the original Cl^- ions (in the form of KCl) as deduced by the potentiometric determination of chlorides. It seems that the chloride concentration in solutions A and B does not affect the reactions.

Microanalyses (C, H, N) were performed by the University of Ioannina (Greece) Microanalytical Laboratory using an EA 1108 Carlo Erba analyser. The metal content was determined volumetrically with ethylenediaminetetra-acetate using xylenol orange as indicator. IR spectra (4000–450 cm^{-1}) were recorded on a Perkin–Elmer 16 PC FT spectrometer with samples prepared as KBr pellets. Magnetic susceptibilities were measured at room temperature using the Faraday method with a Cahn-Ventron RM-2 balance standardized with $HgCo(NCS)_4$; diamagnetic corrections were estimated from Pascal's constants. Solid-state (diffuse reflectance) spectra in the 200–800 nm range were recorded on a Varian Cary 3 spectrometer equipped with an integration sphere.

2.2. Compound preparation

2.2.1. $[Er(NCS)_3\{(py)_2C(OMe)(OH)_3\}]$ (**1**)

To a pale pink solution A (1.1 ml, 0.2 mmol "$Er(NCS)_3$") was slowly added a solution of $(py)_2CO$ (0.074 g, 0.40 mmol) in MeOH (8 ml). The resulting almost colourless solution was kept under stirring at room temperature for about 5 min, and then layered with Et_2O (15 ml). Slow mixing gave a pink polycrystalline solid, which was collected by filtration, washed with ice-cold MeOH (1 ml) and Et_2O (2 × 5 ml), and dried in vacuo over silica gel. Yield: 62% (based on the ligand). *Anal.* Calc. for $C_{39}H_{36}ErN_9O_6S_3$: C, 47.30; H, 3.67; N, 12.73; Er, 16.89. Found: C, 47.45; H, 3.50; N, 12.81; Er, 17.44%. IR (KBr, cm^{-1}): 3420 (mb), 3057 (w), 3044 (w), 2966 (w), 2902 (w), 2062 (s), 1598 (s), 1570 (m), 1472 (m), 1434 (s), 1294 (w), 1258 (m), 1234 (m), 1152 (sh), 1124 (m), 1104 (sh), 1050 (s), 1016 (m), 984 (m), 778 (s), 756 (sh), 684 (s), 636 (s), 530 (w), 501 (w), 454 (m). Effective magnetic moment (μ_{eff}): 9.56 BM (23 °C). Diffuse reflectance spectrum (DRS, nm): 261, 368, 378, 406, 447, 450, 488, 523, 530 (sh), 542, 552 (sh), 652, 657.

2.2.2. $[Er(NCS)_3\{(py)_2C(OEt)(OH)\}_3] \cdot 0.3EtOH \cdot 0.4H_2O$ (**2** $\cdot 0.3EtOH \cdot 0.4H_2O$)

To a pale pink solution B (2.5 ml, 0.2 mmol "$Er(NCS)_3$") was slowly added a solution of $(py)_2CO$ (0.074 g, 0.40 mmol) in EtOH (7 ml). The resulting

homogeneous, almost colourless solution was allowed to stand undisturbed for one day at 5 °C, during which time X-ray quality pink crystals of the product were precipitated. The crystals were collected by filtration, washed with ice-cold EtOH (2 × 1 ml) and Et_2O (2 × 5 ml), and dried in vacuo over silica gel. Yield: 49% (based on the ligand). A sample for crystallography was covered with epoxy glou to prevent collapse. The vacuum-dried sample analysed as unsolvated. *Anal.* Calc. for $C_{42}H_{42}ErN_9O_6S_3$: C, 48.86; H, 4.11; N, 12.21; Er, 16.20. Found: C, 48.67; H, 4.20; N, 12.07; Er, 16.99%. IR (KBr, cm^{-1}): 3446 (mb), 3058 (w), 3045 (w), 2976 (w), 2930 (w), 2894 (w), 2062 (s), 1598 (s), 1572 (sh), 1468 (w), 1438 (m), 1336 (w), 1268 (w), 1236 (s), 1156 (w), 1118 (m), 1065 (sh), 1050 (s), 1018(m), 962 (w), 886 (w), 806 (w), 762 (s), 670 (sh), 642 (m), 628 (m), 572 (m), 532 (w), 486 (w), 464 (w). μ_{eff} (BM): 9.51 (20 °C). DRS (nm): 262, 365, 374 (sh), 380, 405, 448, 451, 489, 523, 529 (sh), 543, 553 (sh), 653, 659.

2.2.3. $[Er_2(NCS)_3\{(py)_2C(OMe)O\}_3(MeOH)] \cdot MeOH$ (**3** · MeOH)

2.2.3.1. Method A. Solids $(py)_2CO$ (0.037 g, 0.20 mmol), $LiOH \cdot H_2O$ (0.0084 g, 0.20 mmol) and $LiClO_4 \cdot 3H_2O$ (0.064 g, 0.40 mmol) were dissolved in MeOH (15 ml), resulting in a colourless solution. This was added to a pale pink solution A (1.1 ml, 0.2 mmol). The resulting new pinkish solution was stirred for about 1 h and filtered to remove a very small quantity of insoluble material. The filtrate was allowed to stand undisturbed for 4 days during which time the product slowly crystallized. The pink crystals were collected by filtration, washed with cold MeOH (1 ml) and Et_2O (2 × 5 ml), and dried in vacuo. Yield: 79% (based on the ligand). A sample for crystallography was kept in contact with the mother liquor to prevent interstitial MeOH loss. The air-dried sample analysed as unsolvated. *Anal.* Calc. for $C_{40}H_{37}Er_2N_9O_7S_3$: C, 40.49; H, 3.15; N, 10.63; Er, 28.19. Found: C, 40.61; H, 3.20; N, 10.99; Er, 27.71%. IR (KBr, cm^{-1}): 3430 (mb), 3072 (w), 2962 (w), 2930 (w), 2066 (s), 1600 (s), 1570 (m), 1472 (m), 1436 (s), 1340 (w), 1294 (m), 1258 (s), 1230 (s), 1124 (s), 1108 (sh), 1054 (s), 1038 (sh), 1010 (m), 984 (m), 968 (sh), 952 (sh), 778 (s), 752 (sh), 686 (s), 634 (s), 576 (w), 534 (w), 492 (w), 456 (m). μ_{eff} (BM): 9.54 (21 °C). DRS (nm): 269, 366, 379, 408, 442, 451, 488, 522, 525 (sh), 533 (sh), 543, 655, 670 (sh).

2.2.3.2. Method B. Treatment of a slurry of complex **1** (0.099 g, 0.10 mmol) in MeOH (20 ml) with NMe_4OH (0.054 g, 0.30 mmol) resulted in a pink solution. The solution was heated at 40 °C for 5 min, during which time no noticeable colour change was observed. The solution was filtered through celite and allowed to slowly evaporate at room temperature. The resulting microcrystalline solid was collected by filtration, washed with Et_2O (2 × 3 ml), and dried in vacuo over silica gel. Yield 30% (based on **1**). The dried solid analysed satisfactorily as **3**. The identity of the product was further confirmed by IR spectroscopic comparison with the authentic sample prepared by Method A.

2.3. Single-crystal X-ray crystallography

Crystals of **2** · 0.3EtOH · $0.4H_2O$ and **3** · MeOH were mounted in air and covered with epoxy glou, and in capillary, respectively. Diffraction measurements were made on a Crystal Logic Dual Goniometer diffractometer using graphite-monochromated Mo radiation. Complete crystal data and parameters for data collection and processing are reported in Table 1. Unit cell dimensions were determined and refined by using the angular settings of 25 automatically centered reflections in the range $11 < 2\vartheta < 23°$. Three standard reflections monitored every 97 reflections showed less than 3% variation and no decay. Lorentz, polarization and Ψ-scan absorption corrections were applied using Crystal Logic software.

Table 1
Crystallographic data for complexes **2** · 0.3EtOH · $0.4H_2O$ and **3** · MeOH

Parameter	**2** · 0.3EtOH · $0.4H_2O$	**3** · MeOH
Formula	$C_{42.6}H_{44.6}ErN_9O_{6.7}S_3$	$C_{41}H_{41}Er_2N_9O_8S_3$
Formula weight	1053.31	1218.53
Crystal colour, habit	pale pink, prism	pale pink, prism
Crystal dimensions (mm)	0.50 × 0.50 × 0.60	0.08 × 0.18 × 0.40
Crystal system	hexagonal	triclinic
Space group	$P3_1$	$P\bar{1}$
Unit cell dimensions		
α (Å)	12.218(6)	10.458(6)
b (Å)	12.218(6)	14.128(8)
c (Å)	30.30(2)	16.747(9)
α (°)	90	84.14(2)
β (°)	90	75.52(2)
γ (°)	120	85.68(2)
V (Å^3)	3917(4)	2380(2)
Z	3	2
ρ_{calc} (g cm^{-3})	1.339	1.700
Radiation, λ (Å)	Mo Kα, 0.71073	Mo Kα, 0.71073
Temperature (K)	298	298
Scan mode/speed (° min^{-1})	ϑ–2ϑ/4.0	ϑ–2ϑ/5.0
$2\theta_{max}$ (°)	50.0	50.04
μ (mm^{-1})	1.777	3.691
Reflections collected/ unique (R_{int})	8201/7672(0.1096)	8504/8035(0.0221)
Data with $I > 2\sigma(I)$	7299	6340
Parameters refined	563	580
$(\Delta\rho)_{max}$, $(\Delta\rho)_{min}$ (e Å^{-3})	0.915, −0.963	0.675, −0.535
Goodness-of-fit (on F^2)	0.0690, 0.01797	1.137
R_1,[a] wR_2[b] (all data)	0.0729, 0.1880	0.0481, 0.0953
R_1,[a] wR_2[b] ($I > 2\sigma(I)$)	0.0690, 0.1797	0.0312, 0.0868

[a] $R_1 = \sum(|F_o| - |F_c|)/\sum(|F_o|)$.
[b] $wR_2 = \{\sum[w(F_o^2 - F_c^2)^2]/\sum[w(F_o^2)^2]\}^{1/2}$.

The structures were solved by direct methods using SHELXS-86 [54] and refined by full-matrix least squares techniques on F^2 with SHELXL-97 [55]. For both structures, all hydrogen atoms were introduced at calculated positions as riding on bonded atoms. For **3** · MeOH, all non-hydrogen atoms were refined using anisotropic thermal parameters. For **2** · 0.3EtOH · 0.4H_2O, all non-hydrogen atoms – except those of the solvate molecules – were refined anisotropically.

3. Results and discussion

3.1. Synthetic comments

The chemical and structural identities of the products from the "Er(NCS)$_3$"/(py)$_2$CO reaction system in alcohols depend on the OH^- concentration. The mononuclear complexes **1** and **2** were isolated from the direct reaction between "Er(NCS)$_3$" and (py)$_2$CO, whereas employment of hydroxides leads to the dinuclear complex **3**. The formation of these Er(III) complexes can be summarized in balanced Eqs. (1) and (2).

$$\text{“Er(NCS)}_3\text{”} + 3(\text{py})_2\text{CO} + 3\text{ROH} \xrightarrow[\text{R=Me,Et}]{\text{ROH}} [\text{Er(NCS)}_3\{(\text{py})_2\underset{\mathbf{1,2}}{\text{C(OR)(OH)}}\}_3] \quad (1)$$

$$2\text{“Er(NCS)}_3\text{”} + 3(\text{py})_2\text{CO} + 3\text{LiOH} \cdot \text{H}_2\text{O} + 4\text{MeOH} \xrightarrow{\text{MeOH}} [\text{Er}_2(\text{NCS})_3\{(\text{py})_2\underset{\mathbf{3}}{\text{C(OMe)O}}\}_3(\text{MeOH})] + 3\text{LiNCS} + 6\text{H}_2\text{O} \quad (2)$$

The Er(III)-mediated addition of solvent (MeOH, EtOH) to (py)$_2$CO to give the neutral hemiacetal derivative of di-2-pyridyl ketone, (py)$_2$C(OR)(OH) (Fig. 1), in **1** and **2**, and the monoanion of this derivative, (py)$_2$C(OR)O^- (Fig. 1), in **3** involves a nucleophilic attack of the ROH molecule on the carbonyl group [43]. The electrophilic character of the carbonyl group of (py)$_2$CO is increased by coordination of the carbonyl oxygen to the metal ion (direct polarization) and/or coordination of the more remote 2-pyridyl sites (induced polarization) [43].

Two features of the reactions represented by Eqs. (1) and (2) deserve comments. First, the "wrong" stoichiometries employed for the preparation of **1**–**3** (see Section 2.2), compared to those required by Eqs. (1) and (2), obviously did not prove detrimental to the formation of the complexes. With the identities of **1**–**3** established, the "correct" stoichiometries, i.e., Er(III): (py)$_2$CO = 1:3, were employed and led to pure compounds in high yields. Second, the presence of $LiClO_4 \cdot 3H_2O$ in the reaction mixture that leads to **3** might imply that cationic complexes are capable of existing; we did *not* have such an evidence during our synthetic efforts. $LiClO_4 \cdot 3H_2O$ is beneficial only for the isolation of single crystals of **3**; in other words, its presence does not affect the identity of the product, but only its crystallization, most probably through the alteration of the ionic strength of the reaction solution. We have not performed experiments to see how different ratios of $LiClO_4$ affect the yield of **3**. If no $LiClO_4$ is added, the same product is isolated (elemental analyses and IR confirmation) in ~70% yield, but in the form of microcrystalline powder.

The fact that complexes **1** and **3** contain basically the same ligand set (the only difference being in the protonation state of the ligand), led us to suspect that **1** would be transformed to **3**; this has, indeed, turned out to be the case. This Brönsted acidity of **1** is summarized in Eq. (3).

$$2[\text{Er(NCS)}_3\{\underset{\mathbf{1}}{(\text{py})_2\text{C(OMe)(OH)}}\}_3] + 6\text{NMe}_4\text{OH} + \text{MeOH} \xrightarrow{\text{MeOH}} [\text{Er}_2(\text{NCS})_3\{\underset{\mathbf{3}}{(\text{py})_2\text{C(OMe)O}}\}_3(\text{MeOH})] + 3\text{NMe}_4\text{SCN} + 3\text{NMe}_4\{(\text{py})_2\text{C(OMe)O}\} + 6\text{H}_2\text{O} \quad (3)$$

3.2. Description of structures

Partially labelled plots of the mononuclear and dinuclear molecules present in complexes **2** · 0.3EtOH · 0.4H_2O and **3** · MeOH are shown in Figs. 2 and 4, respectively. The coordination polyhedra of the Er^{III} atoms are shown in Figs. 3 and 5. Selected interatomic distances and angles are listed in Tables 2 and 3.

The crystal structure of **2** · 0.3EtOH · 0.4H_2O consists of discrete [Er(NCS)$_3${(py)$_2$C(OEt)(OH)}$_3$] molecules and solvate molecules; the latter will not be further discussed.

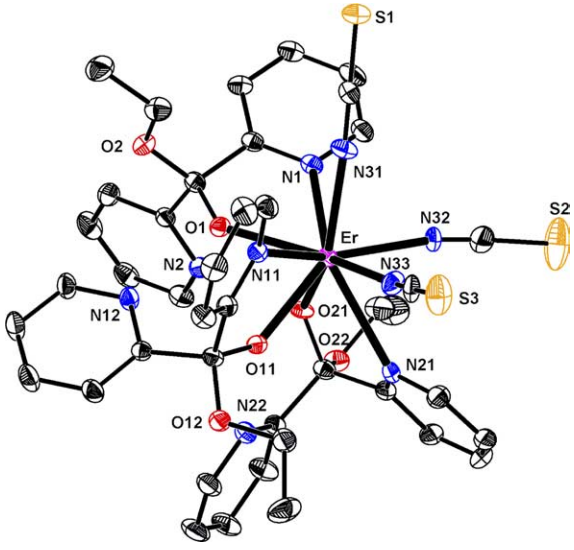

Fig. 2. The structure of the mononuclear complex molecule present in complex **2** · 0.3EtOH · 0.4H_2O.

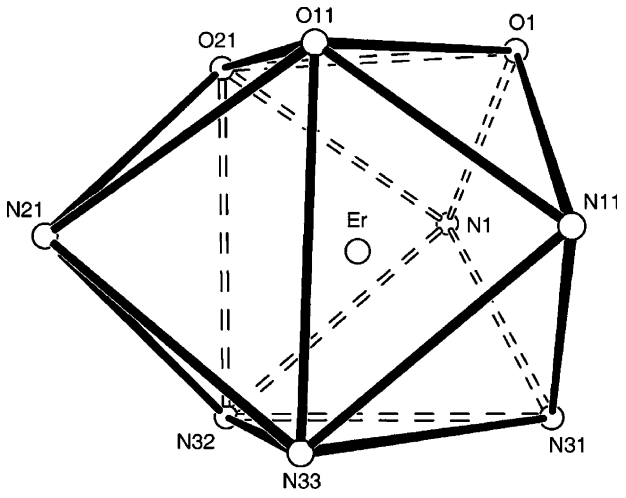

Fig. 3. A view of the inner coordination polyhedron of **2** · 0.3EtOH · $0.4H_2O$ showing the tricapped trigonal prismatic coordination of the Er^{III} atom.

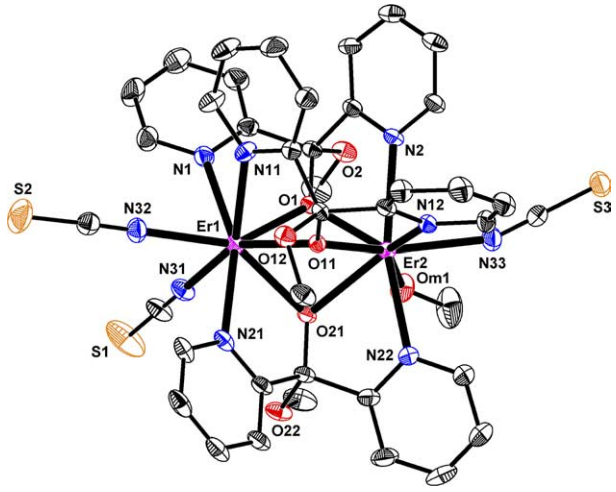

Fig. 4. The structure of the dinuclear molecule present in complex **3** · MeOH.

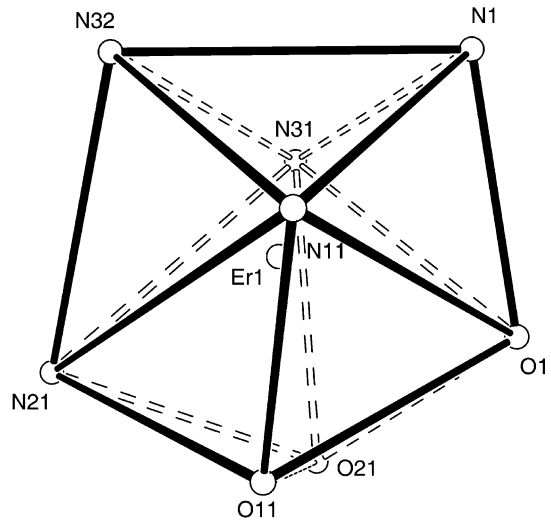

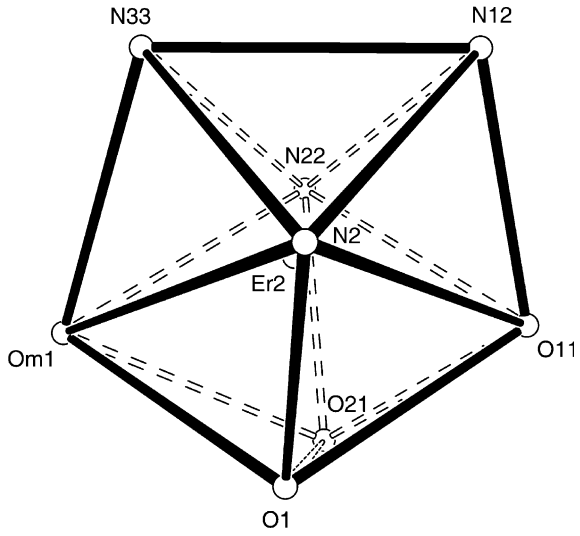

Fig. 5. The dodecahedral stereochemistry about the Er^{III} atoms in complex **3** · MeOH.

The Er^{III} atom is in a nine-coordinate ligand environment comprising three hydroxyl oxygen atoms and three 2-pyridyl nitrogen atoms from the three $(py)_2C(OEt)(OH)$ ligands, and the three nitrogen atoms from the isothiocyanate anions. The Er–N bond lengths fall into two distinct categories; those involving the organic ligands (2.707(10)–2.755(11) Å) and those involving the isothiocyanate ligands (2.356(11)–2.376(11) Å). The Er–N(isothiocyanate) distances have an average value of 2.364(11) Å which is slightly longer, as expected, than that of an eight-coordinated Er(III) complex containing terminal isothiocyanate ligands (2.327(6) Å) [56]. The SCN^- ions are not perfectly linear, the N–C–S bond angles being in the range 175.9(18)–179.0(12)°. The terminal isothiocyanate anions involving N(31) and N(33) as donor atoms are coordinated in a slightly bent fashion, as indicated by the Er–NC angles (160.7(11)°, 161.5(11)°); the third SCN^-ion is coordinated in a more linear fashion (Er–N(32)–C(62) = 170.5(14)°). No hydrogen bonds are involved in the crystal lattice.

The coordination polyhedron of the Er^{III} atom is best described as a distorted tricapped trigonal prism with the three 2-pyridyl nitrogen donor atoms, N(1), N(11) and N(21), forming the three rectangular face caps. The angle sum subtended by the three capping atoms at Er is 358.3°.

The $(py)_2C(OEt)(OH)$ molecules behave as $\eta^1{:}\eta^1$ ligands in **2**, see Fig. 6. The ethoxy oxygen atom remains unbound to the Er^{III} atom. The ligand forms one five-membered ErNCCO chelating ring. Ligands based on the *gem*-diol or the hemiacetal forms of di-2-pyridyl ketone have been observed in numerous ligation modes over the years [43], but the particular bidentate chelating coordination mode (Fig. 6) observed for $(py)_2C(OEt)$-

Table 2
Selected bond distances (Å) and angles (°) for the mononuclear erbium(III) complex $2 \cdot 0.3EtOH \cdot 0.4H_2O$

Bond distances	
Er–O(1)	2.378(7)
Er–O(11)	2.358(7)
Er–O(21)	2.388(8)
Er–N(1)	2.717(10)
Er–N(11)	2.707(10)
Er–N(21)	2.755(11)
Er–N(31)	2.376(11)
Er–N(32)	2.361(10)
Er–N(33)	2.356(11)
C(61)[a]–N(31)	1.156(17)
C(61)[a]–S(1)	1.615(13)
C(62)[a]–N(32)	1.10(2)
C(62)[a]–S(2)	1.657(19)
C(63)[a]–N(33)	1.193(19)
C(63)[a]–S(3)	1.613(15)
Bond angles	
O(1)–Er–O(11)	71.9(3)
O(1)–Er–N(11)	74.6(3)
O(1)–Er–N(32)	134.7(4)
O(11)–Er–O(21)	73.5(2)
O(11)–Er–N(1)	127.8(3)
O(11)–Er–N(33)	90.0(4)
O(21)–Er–N(11)	129.4(3)
O(21)–Er–N(21)	62.0(3)
O(21)–Er–N(32)	86.9(4)
N(1)–Er–N(11)	120.8(3)
N(1)–Er–N(31)	67.3(4)
N(1)–Er–N(32)	74.6(4)
N(11)–Er–O(11)	61.0(3)
N(11)–Er–N(21)	117.8(3)
N(11)–Er–N(32)	142.7(4)
N(21)–Er–O(11)	72.1(3)
N(21)–Er–N(31)	143.1(4)
N(21)–Er–N(33)	73.1(4)
N(31)–Er–O(11)	135.6(4)
N(31)–Er–N(11)	75.5(4)
N(31)–Er–N(32)	81.6(4)
N(32)–Er–O(11)	139.6(4)
N(32)–Er–N(21)	86.9(4)
N(32)–Er–N(33)	79.1(5)
N(33)–Er–O(21)	134.9(3)
N(33)–Er–N(11)	68.8(4)
N(33)–Er–N(31)	81.9(4)
N(31)–C(61)[a]–S(1)	179.0(12)
N(32)–C(62)[a]–S(2)	175.9(18)
N(33)–C(63)[a]–S(3)	178.3(12)

[a] These carbon atoms, which have not been labelled in Fig. 2, belong to the isothiocyanate ligands.

Table 3
Selected interatomic distances (Å) and bond angles (°) for the dinuclear erbium(III) complex $3 \cdot MeOH$

Interatomic distances	
Er(1)···Er(2)	3.380(2)
Er(1)–O(1)	2.253(4)
Er(1)–O(11)	2.331(4)
Er(1)–O(21)	2.317(4)
Er(1)–N(1)	2.528(5)
Er(1)–N(11)	2.589(6)
Er(1)–N(21)	2.483(5)
Er(1)–N(31)	2.346(6)
Er(1)–N(32)	2.364(6)
Er(2)–O(1)	2.269(4)
Er(2)–O(11)	2.231(4)
Er(2)–O(21)	2.327(4)
Er(2)–N(2)	2.529(5)
Er(2)–N(12)	2.549(5)
Er(2)–N(22)	2.472(5)
Er(2)–Om(1)	2.380(5)
Er(2)–N(33)	2.367(6)
Bond angles	
O(1)–Er(1)–O(21)	67.3(1)
O(1)–Er(1)–N(31)	96.5(2)
O(11)–Er(1)–N(21)	76.8(2)
O(11)–Er(1)–N(31)	149.4(2)
O(21)–Er(1)–N(21)	67.3(2)
O(21)–Er(1)–N(31)	81.6(2)
N(1)–Er(1)–O(11)	123.9(2)
N(1)–Er(1)–N(21)	158.0(2)
N(11)–Er(1)–O(21)	129.0(1)
N(11)–Er(1)–N(32)	76.2(2)
N(21)–Er(1)–O(1)	133.1(2)
N(21)–Er(1)–N(31)	87.9(2)
N(31)–Er(1)–N(1)	76.6(2)
N(31)–Er(1)–N(11)	147.0(2)
N(32)–Er(1)–O(21)	145.1(2)
N(32)–Er(1)–N(21)	81.0(2)
O(1)–Er(2)–O(11)	77.9(1)
O(1)–Er(2)–Om(1)	79.6(2)
O(11)–Er(2)–N(22)	91.2(2)
O(11)–Er(2)–N(33)	142.0(2)
O(21)–Er(2)–N(22)	67.1(2)
O(21)–Er(2)–N(33)	141.8(2)
N(2)–Er(2)–O(11)	89.9(2)
N(2)–Er(2)–Om(1)	107.7(2)
N(12)–Er(2)–O(21)	126.0(2)
N(12)–Er(2)–N(33)	76.8(2)
N(22)–Er(2)–N(12)	85.7(2)
N(22)–Er(2)–Om(1)	82.7(2)
Om(1)–Er(2)–N(12)	150.3(2)
Om(1)–Er(2)–N(33)	75.4(2)
N(33)–Er(2)–N(2)	80.0(2)
N(33)–Er(2)–N(22)	87.4(2)

(OH) in **2** is unprecedented. In all the up-to-now structurally characterized d-metal complexes containing O-bound $(py)_2C(OR)(OH)$ ligands (R = Me, Et), the alkylated oxygen is the ligated atom [43,57,58].

Complex $3 \cdot MeOH$ crystallizes in monoclinic space group $P\bar{1}$. Its structure consists of dinuclear $[Er_2(NCS)_3\{(py)_2C(OMe)O\}_3(MeOH)]$ molecules and solvate MeOH molecules; the latter will not be further discussed. In the dinuclear molecule, the monoanionic hemiacetal form of the organic ligand bridges the metal centers through the deprotonated hydroxyl group and the –OMe group points away from the metals. The two Er^{III} atoms are triply bridged by the deprotonated hydroxyl oxygen atoms (O(1), O(11), O(21)) of the $(py)_2C(OMe)O^-$ ligands. Three 2-pyridyl nitrogen atoms (N(1), N(11), N(21)) and two isothiocyanate ligands complete eight-coordination at Er(1), while eight-coordination at Er(2)

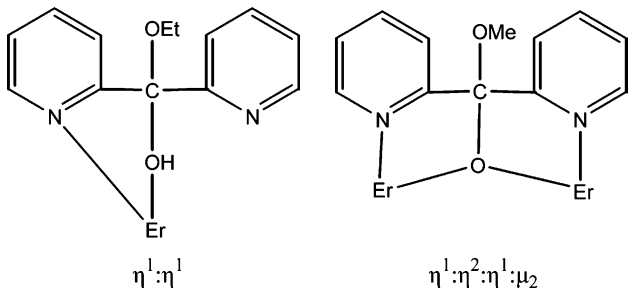

Fig. 6. The crystallographically established coordination modes of $(py)_2C(OEt)(OH)$ and $(py)_2C(OMe)O^-$ in complexes $\mathbf{2}\cdot 0.3EtOH\cdot 0.4H_2O$ and $\mathbf{3}\cdot MeOH$, respectively.

is completed by three 2-pyridyl nitrogen atoms (N(2), N(12), N(22)), one isothiocyanate ligand and one methanol molecule.

The Er–O distances are in the relatively narrow range 2.231(4)–2.380(5) Å; this range is typical for eight-coordinate Er(III) complexes [59–61]. The Er–N bond lengths again fall into two distinct categories; those involving the organic ligands (2.472(5)–2.589(6) Å) and those involving the isothiocyanate ligands (2.346(6)–2.367(6) Å). The Er–N(2-pyridyl) distances in $\mathbf{3}\cdot MeOH$ have an average value of 2.525(6) Å, which is shorter than the corresponding value in $\mathbf{2}\cdot 0.3EtOH\cdot 0.4H_2O$ (2.726(11) Å); the decreased Er–N(2-pyridyl) distances in the former are a consequence of the lower coordination number of the Er^{III} atoms compared to that in the latter (eight versus nine). However, an analogous trend does not hold true for the Er–N(isothiocyanate) distances. These bond distances have similar average values in $\mathbf{2}\cdot 0.3EtOH\cdot 0.4H_2O$ (2.364(11) Å) and $\mathbf{3}\cdot MeOH$ (2.359(6) Å). This discrepancy emphasizes the fact that in lanthanide complexes, where the bonding is regarded as being substantially ionic, the coordination number is determined by packing considerations, this in turn determining the bond lengths between the central metal ion and the atoms surrounding it [62]. The bridging Er–O distances involving O(11) are asymmetric (Er(1)–O(11) = 2.331(4) Å, Er(2)–O(11) = 2.231(4) Å). The terminal isothiocyanate ligands bind to Er(1) in an almost linear fashion, as indicated by the Er–N≡C angles (175.6(6)°, 177.5(6)°); the third isothiocyanate ligand binds to Er(2) in a slightly bent fashion (Er(2)–N(33)–C(63) = 159.5(6)°). The Er(1)···Er(2) distance is 3.380(2) Å.

The coordination polyhedra of the eight donor atoms about the Er^{III} atoms are best described as distorted dodecahedra [63], see Fig. 5. For example, if we consider the polyhedron of Er(2), atoms N(33), N(12), O(1), O(21) constitute a distorted tetrahedron that has been elongated along the fourfold inversion axis of the idealized polyhedron, whereas the set of atoms N(2), N(22), O(11), Om(1) form a distorted tetrahedron that has been squashed along the same axis. An alternative way of viewing the dodecahedron about Er(2) is to consider it [63] as two interpenetrating planar trapezoids N(12)N(33)O(11)Om(1) and N(2)N(22)O(1)O(21).

The $(py)_2C(OMe)O^-$ anions behave as $\eta^1{:}\eta^2{:}\eta^1{:}\mu_2$ ligands in **3**, see Fig. 6. The methoxy oxygen atom remains unbound to the metals. The monoanionic ligand forms two five-membered ErNCCO chelating rings with two different Er^{III} atoms; these rings share a common C–O edge. This ligation mode is common in the coordination chemistry of the hemiacetal forms of di-2-pyridyl ketone [43,44].

No hydrogen bonds are involved in the crystal structure of $\mathbf{3}\cdot MeOH$. The crystal structure is stabilized by two intermolecular π–π stacking interactions. The first involves the two 2-pyridyl rings that involve N(21) and is shown in Fig. 7; the centroid···centroid distance is 3.505 Å (the symmetry code is $-x$, $-y$, $-z+1$). The two rings are strictly parallel due to the presence of a crystallographically imposed inversion center at $c/2$. The second type of the π–π stacking interactions involves the two 2-pyridyl rings that involve N(2) and are in the symmetry relationship x, y, z and $-x+1$, $-y+1$, $-z$; the centroid···centroid distance is 3.653 Å. There also appears to be a weak intramolecular stacking interaction between the two 2-pyridyl rings involving N(2) and N(11), the centroid···centroid distance being 3.934 Å.

3.3. Magnetic moments, electronic and IR spectra

The experimental, room-temperature μ_{eff} values per Er^{III} for complexes **1**–**3** (see Section 2.2) show very little deviation from the theoretical value of 9.6 BM predicted by Eq. (4), suggesting that the 4f electrons in the com-

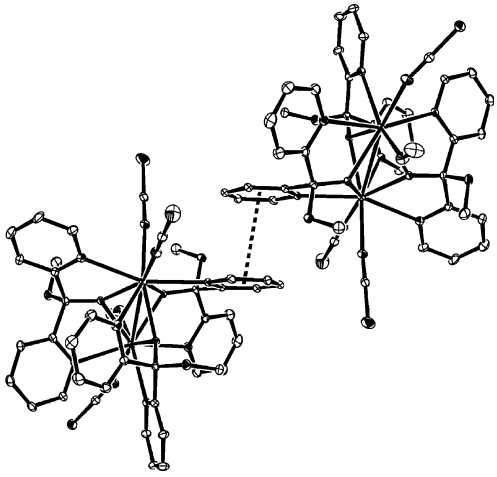

Fig. 7. A view of the intermolecular π–π stacking interaction between the parallel 2-pyridyl rings that involve N(21) in complex $\mathbf{3}\cdot MeOH$. The symmetry codes of the two rings are x, y, z and $-x$, $-y$, $-z+1$. Only two neighbouring dinuclear molecules have been drawn; the centroid···centroid distance is 3.505 Å.

plexed Er^{III} atoms are well-shielded by the outermost 5s and 5p electrons [64]

$$\mu_{eff} = g[J(J+1)]^{1/2}. \quad (4)$$

The solid-state (diffuse reflectance) electronic spectra of the prepared complexes involve mainly intraligand and f–f transitions. Detailed assignments of the main f–f-bands for complex **2** (considered as a representative example) are given in Table 4. The values of the bonding parameters $\bar{\beta}$ (nephelauxetic ratio), δ (Sinha's parameter) and $b^{1/2}$ (covalent factor), calculated [65–67] from the solid-state f–f spectra by Eqs. (5)–(7), are listed in Table 5. The values indicate that the interaction between Er^{III} and the ligands is essentially electrostatic and that there is a minor participation of the 4f orbitals in bonding [65–67]

$$\bar{\beta} = \frac{1}{2}\sum_{n=1}^{n}\frac{\bar{V}_{complex}}{\bar{V}_{aquo}}, \quad (5)$$

$$\delta\ (\%) = \frac{1-\bar{\beta}}{\bar{\beta}} \times 100, \quad (6)$$

$$b^{1/2} = \left[\frac{1}{2}(1-\bar{\beta})\right]^{1/2}. \quad (7)$$

The shape and fine structure of the f–f band assigned to the "hypersensitive" transition $^4I_{15/2} \rightarrow {}^2H_{11/2}$ (Er–I) are sensitive to coordination number [68]. By comparing the spectra of **1**–**3** with the spectra of Er(III) complexes of known structures [59,68,69] in the region of the above-mentioned transition, it is confirmed (complex **2**) or concluded (complex **1**) that the metal ion is nine-coordinate; similarly, this comparison confirms that the Er^{III} atoms in **3** are eight-coordinate (the bands/shoulders due to this transition appear at 522, 525 and 533 in the spectrum of **3**).

The IR spectra of **1** and vacuum-dried (solvent free) **2** exhibit a medium intensity band at 3420 (**1**) and 3446 (**2**) cm^{-1}, assignable to ν(OH) vibration of the $(py)_2C(OR)(OH)$ ligands [57]. The presence of coordinated MeOH in vacuum-dried **3** is manifested by the medium intensity band at 3430 cm^{-1} assigned to ν(OH) [70]. The spectra of the three complexes do not exhibit bands in the region expected for ν(C=O) vibration (1684 cm^{-1} for free $(py)_2CO$) with the nearest IR absorptions at 1598 (**1**, **2**) and 1600 (**3**) cm^{-1} assigned as a 2-pyridyl stretching mode raised from 1582 cm^{-1} on coordination, as observed earlier on complex formation involving alcoholysis or hydration of $(py)_2CO$ [44,71]. The bands at ~1050, ~770 and ~640 cm^{-1} can be assigned [58] to pyridyl ring breathing, pyridyl C–H out-of-plane bending and in-plane pyridyl ring deformation vibrations, respectively. The IR spectra of **1**–**3** exhibit the ν(CN) mode of the SCN^- ligands at ~2065 cm^{-1}; this wavenumber is typical of terminal isothiocyanate groups [72,73]. The expected ν(CS) and δ(NCS) bands could not be located and unambiguously assigned because they are obscured by $(py)_2C(OR)(OH)/(py)_2C(OMe)O^-$ absorptions.

Table 4
Main, solid-state f–f bands of the representative complex **2**

λ (nm)	Assignment
659, 653	$^4I_{15/2} \rightarrow {}^4F_{9/2}$
543	$^4I_{15/2} \rightarrow {}^4S_{3/2}$
529 (sh), 523	$^4I_{15/2} \rightarrow {}^2H_{11/2}$ (Er–I)[a]
489	$^4I_{15/2} \rightarrow {}^4F_{7/2}$
380, 374 (sh)	$^4I_{15/2} \rightarrow {}^4G_{11/2}$ (Er–II)[a]

[a] These transitions are "hypersensitive".

Table 5
Bonding parameters[a,b] for the Er(III) complexes **1**–**3**

Complex	$\bar{\beta}$	δ (%)	$b^{1/2}$
1	0.996	+0.40	0.045
2	0.995	+0.50	0.050
3	0.994	+0.60	0.055

[a] Calculated from solid-state f–f spectra taking into account the wavenumbers of the $^4I_{15/2} \rightarrow {}^4F_{9/2}$, $^4S_{3/2}$, $^2H_{11/2}$, $^4F_{7/2}$, $^4F_{5/2}$, $^4F_{3/2}$, (^2G, ^4F, $^2H)_{9/2}$ and $^4G_{11/2}$ transitions.

[b] For the definition of the bonding parameters $\bar{\beta}$, δ (%) and $b^{1/2}$, see text.

4. Conclusions and perspectives

Complexes $[Er(NCS)_3\{(py)_2C(OEt)(OH)\}_3]$ (**2**) and $[Er_2(NCS)_3\{(py)_2C(OMe)O\}_3(MeOH)]$ (**3**) cover a gap in the literature, because these are the first structurally characterized lanthanide(III) complexes with $(py)_2CO$-based ligands. Thus, the principal objective of our studies has been realized. Based on analytical and spectroscopic data, it seems that complex **1** has a similar molecular structure with that of **2**. It is also of interest that complex **2** (and presumably **1**) exhibits a novel coordination mode for the ligand $(py)_2C(OEt)(OH)$.

Although only mononuclear and dinuclear complexes have been discovered from our work, clearly the $Ln^{III}/(py)_2CO$ chemistry warrants further study and expansion to other solvents (e.g., H_2O, MeCN, DMF, etc.) that favour the formation of the *gem*-diol form of di-2-pyridyl ketone, $(py)_2C(OH)_2$ (Fig. 1). For example, the ability of this form to act as a dianionic ligand and to bridge 3, 4 or 5 metal ions [43] gives hopes for the isolation of high-nuclearity Ln(III) clusters. A ligand "blend" that might prove highly successful for this synthetic purpose is $(py)_2CO_2^{2-}/RCO_2^-$ [43]. The isothiocyanate terminal ligands present in **1**–**3** could have future utility as sites for facile incorporation of other monodentate ligands by metathesis, or as a means to access higher-nuclearity neutral or cationic clusters using bis(monodentate) and/or bis(bidentate) bridging

ligands, including aromatic heterocycles and dicarboxylates.

5. Supplementary data

Full crystallographic details have been deposited with the Cambridge Crystallographic Data Centre. Copies of the data can be obtained free of charge on request from the CCDC, 12 Union Road, Cambridge CB2 1EZ, UK (fax: +44 1233 336033; e-mail: deposit@ccdc.cam.ac.uk or http://www.ccdc.cam.ac.uk) quoting the deposition numbers 274911 ($\mathbf{2}\cdot 0.3\mathrm{EtOH}\cdot 0.4\mathrm{H_2O}$) and 274912 ($\mathbf{3}\cdot \mathrm{MeOH}$).

Acknowledgements

K.A.T. and S.P.P. thank the Research Committee of the University of Patras (K. CARATHEODORY Program No. 3016) for financial support of this work. We also thank Prof. Kordoulis (Catalysis Laboratory, Department of Chemistry, University of Patras) for helpful discussions concerning the solid-state f–f spectra of the three Er(III) complexes.

References

[1] See the various chapters in G.R. Choppin, J.-C.G. Bünzli (Eds.), Lanthanide Probes in Life, Chemical and Earth Science, Elsevier, Amsterdam, 1989.
[2] S. Aime, M. Botta, M. Fasano, E. Terreno, Chem. Soc. Rev. 27 (1998) 19.
[3] T. Imamoto, Lanthanides in Organic Synthesis, Academic Press, New York, 1994.
[4] N. Ishikawa, M. Sugita, T. Ishikawa, S. Koshihara, Y. Kaizu, J. Am. Chem. Soc. 125 (2003) 8694.
[5] M.G.B. Drew, P.B. Iveson, M.J. Hudson, J.O. Liljenzin, L. Spjuth, P.-Y. Cordier, A. Enarsson, C. Hill, C. Madic, J. Chem. Soc., Dalton Trans. (2000) 821.
[6] J. Kido, Y. Okamoto, Chem. Rev. 102 (2002) 2357.
[7] D. Parker, Coord. Chem. Rev. 205 (2000) 109.
[8] V.W.W. Yam, K.K.W. Lo, Coord. Chem. Rev. 184 (1999) 157.
[9] H. Tsukube, S. Shinoda, H. Tamiaki, Coord. Chem. Rev. 226 (2002) 227.
[10] K. Binnemans, C. Görller-Walrand, Chem. Rev. 102 (2002) 2303.
[11] R. Wietzke, M. Mazzanti, J.-M. Latour, J. Pécaut, P.-V. Cordier, C. Madic, Inorg. Chem. 37 (1998) 6690.
[12] A. Bellusci, G. Barberio, A. Crispini, M. Ghedini, M. La Deda, D. Pucci, Inorg. Chem. 44 (2005) 1818.
[13] G. Mancino, A.J. Ferguson, A. Beeby, N.J. Long, T.S. Jones, J. Am. Chem. Soc. 127 (2005) 524.
[14] C. Piguet, J.-C.G. Bünzli, Chem. Soc. Rev. 28 (1999) 347.
[15] D.R. van Staveren, G.A. van Albada, S. Gorter, J.G. Haasnoot, J. Reedijk, Inorg. Chim. Acta 300–302 (2004) 1104.
[16] M.K. Thompson, A.J. Lough, A.J. White, D.J. Williams, I.A. Kahwa, Inorg. Chem. 42 (2003) 4828.
[17] G. Champion, N. Lalioti, V. Tangoulis, M.-A. Arrio, P. Sainctavit, F. Villain, A. Caneschi, D. Gatteschi, C. Giorgetti, Baudelet, M. Verdaguer, C.C. dit Moulin, J. Am. Chem. Soc. 125 (2003) 8371.
[18] V. Monga, B.O. Patrick, C. Orvig, Inorg. Chem. 44 (2005) 2666.
[19] S.W. Magennis, S. Parsons, Z. Pikramenou, Chem. Eur. J. 8 (2002) 5761.
[20] C. Benelli, A. Caneschi, D. Gatteschi, L. Pardi, P. Rey, D.P. Shum, R.L. Carlin, Inorg. Chem. 28 (1989) 272.
[21] R.E.P. Winpenny, Adv. Inorg. Chem. 52 (2001) 1.
[22] G. Christou, D. Gatteschi, D.N. Hendrickson, R. Sessoli, MRS Bull. 25 (2000) 66.
[23] D. Gatteschi, R. Sessoli, Angew. Chem., Int. Ed. 42 (2003) 268.
[24] A.J. Tasiopoulos, A. Vinslava, W. Wernsdorfer, K.A. Abboud, G. Christou, Angew. Chem., Int. Ed. 43 (2004) 2117.
[25] S. Mukhopadhyay, S.K. Mandal, S. Bhaduri, W.H. Armstrong, Chem. Rev. 104 (2004) 3981.
[26] Z. Zheng, R. Wang, Comments Inorg. Chem. 22 (2000) 1.
[27] Z. Zheng, Chem. Commun. (Feature Article) (2001) 2521.
[28] J.-C.G. Bunzli, C. Piguet, Chem. Rev. 102 (2002) 1897.
[29] L.G. Westin, M. Kritikos, A. Caneschi, Chem. Commun. (2003) 1012.
[30] I.A. Setyawati, S. Liu, S.J. Rettig, C. Orvig, Inorg. Chem. 39 (2000) 496.
[31] A.J. Blake, D.M.J. Doble, W.-S. Li, M. Schröder, J. Chem. Soc., Dalton Trans. (1997) 3655.
[32] G.B. Deacon, T. Feng, D.C.R. Hockless, P.C. Junk, B.W. Skelton, A.H. White, Chem. Commun. (1997) 341.
[33] X.-M. Chen, Y.-L. Wu, Y.-X. Tong, Z. Sun, D.N. Hendrickson, Polyhedron 16 (1997) 4265.
[34] T. Kujiwara, H. Wu, T. Ito, N. Iki, S. Miyano, Angew. Chem., Int. Ed. 43 (2004) 1832.
[35] L.G. Hubert-Pfalzgraf, New J. Chem. 19 (1995) 727.
[36] P. Chanaud, A. Julbe, P. Vaija, M. Persin, L. Cot, J. Mater. Sci. 29 (1994) 4244.
[37] N.H. Williams, B. Takasaki, M. Wall, J. Chin. Acc. Chem. Res. 32 (1999) 485.
[38] S. Yu, A. Watson, Chem. Rev. 99 (1999) 2353.
[39] A. Mishra, W. Wernsdorfer, S. Parsons, G. Christou, E.K. Brechin, Chem. Commun. (2005) 2086, and references therein.
[40] M. Ruben, J. Rojo, F.J. Romero-Salguero, L.H. Uppadine, J.-M. Lehn, Angew. Chem., Int. Ed. 43 (2004) 3644.
[41] R.E.P. Winpenny, J. Chem. Soc., Dalton Trans. (Dalton Perspective) (2002) 1.
[42] G. Aromi, A.R. Bell, M. Helliwell, J. Raftery, S.J. Teat, G.A. Timco, O. Roubeau, R.E.P. Winpenny, Chem. Eur. J. 9 (2003) 3024.
[43] G.S. Papaefstathiou, S.P. Perlepes, Comments Inorg. Chem. 23 (2002) 249, and references therein.
[44] E. Katsoulakou, V. Bekiari, C.P. Raptopoulou, A. Terzis, P. Lianos, E. Manessi-Zoupa, S.P. Perlepes, Spectrochim. Acta Part A 61 (2005) 1627.
[45] G.S. Papaefstathiou, A. Escuer, F.A. Mautner, C. Raptopoulou, A. Terzis, S.P. Perlepes, R. Vicente, Eur. J. Inorg. Chem. (2005) 879.
[46] A.K. Boudalis, B. Donnadieu, V. Nastopoulos, J. Modesto Clemente-Juan, A. Mari, Y. Sanakis, J.-P. Tuchagues, S.P. Perlepes, Angew. Chem. 116 (2004) 2316.
[47] A.K. Boudalis, F. Dahan, A. Bousseksou, J.-P. Tuchagues, S.P. Perlepes, Dalton Trans. (2003) 3411.
[48] C.J. Milios, E. Kefalloniti, C.P. Raptopoulou, A. Terzis, R. Vicente, N. Lalioti, A. Escuer, S.P. Perlepes, Chem. Commun. (2003) 819.
[49] G.S. Papaefstathiou, A. Escuer, M. Font-Bardia, S.P. Perlepes, X. Solans, R. Vicente, Polyhedron 21 (2002) 2027.
[50] K.N. Crowder, S.J. Garcia, R.L. Burr, J.M. North, M.H. Wilson, B.L. Conley, P.E. Fanwick, P.S. White, K.D. Sienerth, R.M. Granger II, Inorg. Chem. 43 (2004) 72.

[51] M.-L. Tong, S.-L. Zheng, J.-X. Shi, Y.-X. Tong, H.K. Leey, X.-M. Chen, J. Chem. Soc., Dalton Trans. (2002) 1727.
[52] Z.E. Serna, M.K. Urtiaga, M.G. Barandika, R. Cortes, S. Martin, L. Lezama, M.I. Arriortua, T. Rojo, Inorg. Chem. 40 (2001) 4550.
[53] M.-L. Tong, M. Monfort, J.M. Clemente Juan, X.-M. Chen, X.-H. Bu, M. Ohba, S. Kitagawa, Chem. Commun. (2005) 233.
[54] G.M. Sheldrick, SHELXS-86, Structure Solving Program, University of Göttingen, Germany, 1986.
[55] G.M. Sheldrick, SHELXL-97, Program for the Refinement of Crystal Structures from Diffraction Data, University of Göttingen, Germany, 1997.
[56] R.A. Coxall, S.G. Harris, D.K. Henderson, S. Parsons, P.A. Tasker, R.E.P. Winpenny, J. Chem. Soc., Dalton Trans. (2000) 2349.
[57] A representative reference: V. Tangoulis, C.P. Raptopoulou, S. Paschalidou, A.E. Tsohos, E.G. Bakalbassis, A. Terzis, S.P. Perlepes, Inorg. Chem. 36 (1997) 5270.
[58] A representative reference: Z.E. Serna, R. Cortés, M.K. Urtiaga, M.G. Barandika, L. Lezama, M.I. Arriortua, T. Rojo, Eur. J. Inorg. Chem. (2001) 865.
[59] A. Messimeri, V. Nastopoulos, A. Terzis, C.P. Raptopoulou, C. Papadimitriou, S.P. Perlepes, Inorg. Chem. Commun. (2005) 578.
[60] R.E. Morris, A.P. Wilkinson, A.K. Cheetham, Inorg. Chem. 31 (1992) 4774.
[61] J.A. Darr, D.M.P. Mingos, D.E. Hibbs, M.B. Hursthouse, K.M.A. Malik, Polyhedron 15 (1996) 3225.
[62] J.F. Bower, S.A. Cotton, J. Fawcett, R.S. Hughes, D.R. Russell, Polyhedron 22 (2003) 347.
[63] D.L. Kepert, Inorganic Stereochemistry, Springer-Verlag, Berlin, 1982, p. 152.
[64] S. Liu, L. Gelmini, S.J. Rettig, R.C. Thompson, C. Orvig, J. Am. Chem. Soc. 114 (1992) 6081.
[65] C.K. Jorgensen, Modern Aspects of Ligand Field Theory, North-Holland, Amsterdam, 1971.
[66] S.P. Sinha, Spectrochim. Acta 22 (1966) 57.
[67] D.E. Henrie, G.R. Choppin, J. Chem. Phys. 49 (1968) 477.
[68] (a) D.G. Karraker, Inorg. Chem. 6 (1967) 1863;
(b) D.G. Karraker, Inorg. Chem. 7 (1968) 473.
[69] A. Messimeri, C.P. Raptopoulou, V. Nastopoulos, A. Terzis, S.P. Perlepes, C. Papadimitriou, Inorg. Chim. Acta 336 (2002) 8.
[70] V. Tangoulis, C.P. Raptopoulou, V. Psycharis, A. Terzis, K. Skorda, S.P. Perlepes, O. Cador, O. Kahn, E.G. Bakalbassis, Inorg. Chem. 39 (2000) 2522.
[71] P.K. Byers, A.J. Canty, L.M. Engelhardt, J.M. Patrick, A.H. White, J. Chem. Soc., Dalton Trans. (1985) 981.
[72] J.L. Burmeister, S.D. Patterson, E.A. Diardorff, Inorg. Chim. Acta 3 (1969) 105.
[73] K. Nakamoto, Infrared and Raman Spectra of Inorganic and Coordination Compounds, 4th ed., Wiley, New York, 1986, p. 283.

Available online at www.sciencedirect.com
SCIENCE DIRECT®
Polyhedron 25 (2006) 550–558
POLYHEDRON
www.elsevier.com/locate/poly

Thioether coordinated metalloenediynes: Syntheses, structures and thermal reactivity comparison ☆

Sibaprasad Bhattacharyya, Maren Pink, John C. Huffman, Jeffrey M. Zaleski *

Department of Chemistry and Molecular Structure Center, Indiana University, Bloomington, IN 47405, USA

Received 17 June 2005; accepted 15 July 2005
Available online 9 September 2005

Abstract

Two novel, thioether containing benzannulated enediyne ligands, 1,2-bis(3-(quinolin-8-ylsulfanyl)prop-1-ynyl)benzene (**1**), and 1,2-bis(3-(pyridin-2-ylmethylsulfanyl)prop-1-ynyl)benzene (**2**) have been synthesized and characterized along with their corresponding Cu(I), Ag(I), Cu(II), and Pd(II) metalloenediyne complexes (**3**–**10**). Single crystal X-ray structures of the d^{10} and d^8 N_2S_2 complexes show thioether coordination leading to distorted tetrahedral and *trans* square planar geometries about the metal centers, respectively. Based on their X-ray structures, all complexes are expected to exhibit high Bergman cyclization temperatures (>200 °C), and indeed this is the case for the Cu(I) and Ag(I) complexes (211–218 °C). In contrast, the corresponding divalent, tetragonal and *trans* square planar complexes of Cu(II) and Pd(II) exhibit more facile reactivity and lower solid state Bergman cyclization temperatures (186–190 °C) which more closely resemble values expected for *cis*-complexes. The unusual order in the thermal reactivities of these constructs can be attributed to a previously evaluated mechanism by which weak thioether coordination permits an elevated temperature *trans*-to-*cis* geometric rearrangement prior to Bergman cyclization.
© 2005 Elsevier Ltd. All rights reserved.

Keywords: Metalloenediynes; Diradical; Bergman cyclization; Copper; Palladium; Thioether

1. Introduction

For over 30 years [1,2] the (*Z*)-hexa-3-ene-1,5-diyne unit has intrigued chemists due to the ability of this functionality to cyclize to form a highly reactive 1,4-benzenoid diradical intermediate [3]. The discovery of this reactive species within natural products isolated from microbial fermentation broths [4–8] reignited interest in systematically evaluating the geometric (e.g., alkyne termini separation, acyclic versus cyclic structures, H-bonding at the alkyne termini) and electronic contributions (e.g., benzannulation, electron donating/withdrawing groups at both *–ene–* and *–yne–* positions, through space electron lone-pair electron repulsion) to Bergman cyclization [3]. One fundamental and common goal of much of this work was to understand and gain control over the reactivity of the enediyne unit. To this end, photochemical cyclization strategies [9–12] have also been evaluated as a means to initiate cyclization in compounds with pronounced thermal stability such as benzannulated and aromatic acyclic enediyne constructs.

The principles derived from these geometric and electronic studies paved the way for the use of metal ions as reagents to activated enediynes toward Bergman cyclization [3,13]. The first key examples demonstrated that Bergman cyclization could be strongly influenced by metal ion coordination to a ligating enediyne framework. For example, binding of Hg^{2+} to a bipyridyl-enediyne conjugate forced the ligand into a planar conformation which labilized the enediyne toward cyclization [14,15].

☆ In celebration of the 60th birthday of Professor Malcolm H. Chisholm, and his more than 35 years of outstanding chemical achievement.

* Corresponding author.
E-mail address: zaleski@indiana.edu (J.M. Zaleski).

0277-5387/$ - see front matter © 2005 Elsevier Ltd. All rights reserved.
doi:10.1016/j.poly.2005.07.032

In parallel, 1,2-bis(diphenylphosphinoethynyl)benzene was shown to cyclization spontaneously upon binding to divalent platinum or palladium [16]. In this case, later work on the same ligand showed that this effect was dependent upon the geometry of the metal center [17,18]; for chelating enediyne motifs, tetrahedral structures result in high cyclization temperatures relative to the much more facile reactivity of *cis* tetragonal or planar analogues [17,19,20]. The same guidelines also apply to a set of tetradentate enediyne ligands, but the effects of geometry on the cyclization temperature are not as pronounced [20–22]. Electronic effects, such as ancillary halogen lone pair donation [23,24], π-complexation at the alkyne carbons [25,26], as well as coordination of electron withdrawing, high valent metals near the alkyne termini (e.g., Mo^{IV}–S^{-} coordination), have also been shown to be capable of driving enediyne reactivity at ambient temperature [27]. The emerging theme from this body of work is that ligand design, and correspondingly, choice of metal ion activator, are critically important to the resulting Bergman cyclization kinetics and thermodynamics.

The conceptual developments highlighted above have fueled the syntheses of more diverse tetradentate chelating ligands containing mixed N,S coordination [28]. Structures containing coordinatively fluxional thiother ligands have not been previously examined and may yield unusual reactivity due to the weak thioether ligand. This work reports the syntheses of two benzannulated tetradentate thioether–imine (quinoline, pyridine) enediyne ligands and their corresponding Cu(I), Ag(I), Cu(II), and Pd(II) complexes. The thermal reactivities of these complexes are unusual and suggest an atypical reaction mechanism based on fluxional thioether coordination.

2. Experimental

2.1. General considerations

Compounds 1,2-bis-(3-bromopropynyl)benzene and pyridin-2-yl-methanethiol were prepared according to literature methods [29,30] All the metal salts (e.g., $Cu(MeCN)_4PF_6$, $Cu(BF_4)_2 \cdot XH_2O$, $AgPF_6$ and $Pd(MeCN)_4(BF_4)_2$) were purchased from Strem. Reactions were carried out under nitrogen using Schlenk line and drybox techniques. Hydrocarbon solvents such as diethyl ether and benzene were dried by distillation over sodium/benzophenone prior to use. Methylene chloride and *n*-butylamine were dried by distillation over calcium hydride. Organic enediynes were purified by flash chromatography using silica gel (200–440 mesh). All other chemicals and solvents were used as received from Aldrich, Strem, and Fluka.

^{1}H NMR and ^{13}C NMR spectra were recorded on a VXR 400 NMR spectrometer using the residual proton resonance of the solvent as an internal reference. Elemental analyses on all samples were obtained from Robertson Microlit Laboratories Inc., and mass spectra were measured at the Indiana University Mass Spectrometer Facility. Differential scanning calorimetry (DSC) traces were recorded on a V4.1 Dupont 910 calorimeter coupled to a Dupont thermal analyst 2100, or on a TA Instruments Q10 series calorimeter at a heating rate of 10 °C min^{-1}.

2.2. Ligand syntheses

2.2.1. 1,2-Bis(3-(quinolin-8-ylsulfanyl)prop-1-ynyl)-benzene (L, **1**)

A flask was charged with thioxine hydrochloride (1.6 g, 8.12 mmol) and dry dimethylformamide (30 mL). Anhydrous potassium carbonate (4.0 g, 28.9 mmol) was then added and the mixture was allowed to stir for 5 h at 20 °C. A solution of 1,2-bis-(3-bromopropynyl)benzene (1.2 g, 3.87 mmol) in dry dimethylformamide (20 mL) was then added dropwise over 1 h. The reaction mixture was stirred for 3 h at ambient temperature. After completion of the reaction, the solid was filtered and washed with dimethylformamide (2 × 10 mL). The combined organic layers were then poured into water (300 mL) and then extracted with methylene chloride (50 mL). The organic layer was washed with water (3 × 200 mL) and dried over anhydrous sodium sulfate. Finally, the solvent was removed under reduced pressure. The crude product was purified on a silica gel column with 1% methanol in methylene chloride. Yield: 0.70 g (35%); yellow solid. ^{1}H NMR (400 MHz, $CDCl_3$) δ (ppm) 8.87 (s, 2H), 8.09 (d, 2H), 7.67 (d, 2H), 7.56 (d, 2H), 7.48 (d, 2H), 7.36 (m, 2H), 7.25 (m, 2H), 7.17 (m, 2H), 3.88 (s, 4H); ^{13}C NMR (400 MHz, CD_3CN) δ (ppm) 149.45, 145.74, 137.32, 136.58, 132.12, 128.39, 127.98, 127.02, 125.82, 125.69, 124.81, 121.87, 89.18, 82.03, 20.95. MS (EI, HRMS) 472.1066, Calc. 472.1067 (M^{+}).

2.2.2. 1,2-Bis(3-(pyridin-2-ylmethylsulfanyl)prop-1-ynyl)benzene (L′, **2**)

A flask was charged with pyridin-2-yl-methanethiol (1 g, 8.12 mmol) and dry dimethylformamide (30 mL). Sodium hydroxide (0.36 g, 9.00 mmol) was then added and the mixture was allowed to stir for 1 h at 0 °C. A solution of 1,2-bis-(3-bromopropynyl)benzene (1.2 g, 3.87 mmol) in dry dimethylformamide (20 mL) was then added dropwise over 1 h. The reaction mixture was stirred for 3 h at 0 °C. The combined reaction mixture was poured into water (300 mL) and then extracted with methylene chloride (50 mL). The methylene chloride layer was washed with water (3 × 200 mL) and dried over anhydrous sodium sulfate. Finally, the solvent was removed under reduced pressure. The crude product was purified on a silica gel column with 1% methanol in methylene chloride. Yield: 0.60 g (50%); yellow viscous oil. ^{1}H NMR (400 MHz, $CDCl_3$) δ (ppm) 8.53 (s, 2H),

7.61 (t, 2H), 7.40 (m, 2H), 7.35 (d, 2H), 7.22 (m, 2H), 7.12 (m, 2H), 4.03 (s, 2H), 4.04 (s, 4H); ^{13}C NMR (400 MHz, CD_3CN) δ (ppm) 158.17, 149.97, 136.78, 132.38, 128.07, 125.84, 123.35, 122.20, 89.39, 82.43, 37.69, 20.51. MS (EI, HRMS) 400.5667, Calc. 400.5682 (M^+).

2.3. Metalloenediyne syntheses

Metalloenediyne complexes (**3**–**10**) are all prepared by reaction of ligands **1** and **2** with appropriate metal salts following the same general method. The case of [Cu(L1)]PF_6 (**3**) is described in detail below.

Ligand **1** (0.25 mmol) was dissolved in 6 mL chloroform and an equimolar amount of the $(MeCN)_4CuPF_6$ was separately dissolved in 6 mL of MeCN. To a 100 mL Schlenk flask containing 25 mL MeCN, these ligand and metal salt solutions were slowly and simultaneously added dropwise (to avoid polymer formation) under nitrogen at ambient temperature. After the complete addition, the mixture was stirred for 30 min at ambient temperature. The volume of the solution was reduced to 15 mL and filtered to remove the insoluble components. To the filtrate, 50 mL of dry ether was added and the resulting solution kept in freezer for 3 h. The yellow precipitate was subsequently collected by filtration. Yield: 80% ^{1}H NMR (400 MHz, CD_3CN) δ (ppm) 8.81 (d, 2H), 8.37 (m, 4H), 8.11 (d, 2H), 7.81 (t, 2H), 7.51 (m, 2H), 7.10 (m, 2H), 6.99 (m, 2H), 4.23 (s, 4H). MS (ESI, HRMS): m/z 535.0360, Calc. 535.0364 ($M - PF_6$).

[Ag(L1)]PF_6 (**4**): Yield: 70% ^{1}H NMR (400 MHz, CD_3CN) δ (ppm) 8.83 (d, 2H), 8.33 (d, 2H), 8.09 (d, 2H), 7.95 (d, 2H), 7.68 (t, 2H), 7.44 (m, 2H), 7.12 (m, 4H), 4.01 (s, 4H); ^{13}C NMR (400 MHz, CD_2Cl_2) δ (ppm) 154.47, 146.55, 140.47, 138.62, 132.91, 132.53, 130.97, 130.89, 129.89, 128.77, 125.38, 123.69, 89.25, 85.42, 30.32. MS (EI): m/z 579 (^{107}Ag), 581(^{109}Ag) ($M - PF_6$). *Anal*. Calc. for $C_{30}H_{20}N_2S_2AgPF_6$: C, 49.67; H, 2.78; N, 3.86. Found: C, 49.81; H, 3.03; N, 3.64%.

[Cu(L1)]$(BF_4)_2$ (**5**): Yield: 65%, MS (EI): m/z 535(^{63}Cu), 537(^{65}Cu) ($M - 2BF_4$). *Anal*. Calc. for $C_{30}H_{20}N_2S_2Cu(BF_4)_2$: C, 50.76; H, 2.84; N, 3.94. Found: C, 50.25; H, 2.84; N, 3.94%.

[Pd(L1)]$(BF_4)_2$ (**6**): Yield: 90% ^{1}H NMR (400 MHz, $CDCl_3$) δ (ppm) 9.21 (d, 2H), 8.87 (d, 2H), 8.66 (d, 2H), 8.44 (d, 2H), 8.08 (t, 2H), 7.87 (m, 2H), 7.29 (m, 2H), 7.13 (m, 2H), 4.82 (d, 2H), 4.56 (d, 2H); ^{13}C NMR (400 MHz, $CDCl_3$) δ (ppm) 159.68, 153.76, 144.40, 139.03, 134.73, 132.57, 132.13,130.97, 127.22, 125.70, 123.63, 122.25, 89.88, 87.78, 39.32. *Anal*. Calc. for $C_{30}H_{20}N_2S_2Pd(BF_4)_2$: C, 47.87; H, 2.67; N, 3.78. Found: C, 47.11; H, 2.67; N, 3.65%.

[Cu(L2)]PF_6 (**7**): Yield: 80%, ^{1}H NMR (400 MHz, $CDCl_3$) δ (ppm) 8.43 (d, 2H), 7.67 (d, 2H), 7.45 (d, 2H), 7.21 (d, 2H), 7.17 (m, 4H), 4.34 (s, 4H), 3.81 (s, 4H). *Anal*. Calc. for $C_{24}H_{20}N_2S_2CuPF_6$: C, 47.33; H, 3.31; N, 4.60. Found: C, 47.11; H, 3.67; N, 4.35%.

[Ag(L2)]PF_6 (**8**): Yield: 75%, ^{1}H NMR (400 MHz, $CDCl_3$) δ (ppm) 8.50 (d, 2H), 7.73 (t, 2H), 7.48 (d, 2H), 7.25 (d, 2H), 7.15 (m, 4H), 4.27 (s, 4H), 3.74 (s, 4H); MS (ESI, HRMS): m/z 507.0105 (^{107}Ag), Calc. 507.0113 ($M - PF_6$).

[Cu(L2)]$(BF_4)_2$ (**9**): Yield: 70%, MS (ESI, HRMS): m/z 463.0360(^{63}Cu), Calc. 463.0358 ($M - 2BF_4$).

[Pd(L2)]$(BF_4)_2$ (**10**): Yield: 90%, ^{1}H NMR (400 MHz, $CDCl_3$) δ (ppm) 8.58 (d, 2H), 8.05 (t, 2H), 7.76 (d, 2H), 7.36 (d, 2H), 7.32 (m, 4H), 4.98 (d, 2H), 4.61 (d, 2H), 4.43 (d, 2H), 4.10 (d, 2H). *Anal*. Calc. for $C_{24}H_{20}N_2S_2Pd(BF_4)_2$: C, 42.35; H, 2.96; N, 4.11. Found: C, 42.11; H, 3.07; N, 4.31%.

2.4. X-ray crystallography

X-ray quality crystals of **1** were grown by slow evaporation from a methanol:dichloromethane mixture (1:1). For complexes **3**, **6**, **7**, **8a**, single crystals were obtained by slow vapor diffusion of diethyl ether into an acetonitrile solution of the complex at 0 °C. Suitable crystals were placed onto the tip of a 0.1 mm diameter glass capillary and mounted on a SMART6000 (Bruker) at 120 K. The data collection was carried out using Mo Kα radiation (graphite monochromator) and a detector distance of 5.0 cm. A randomly oriented region of reciprocal space was surveyed to at least the extent of a hemisphere, collection several major sections of frames with 0.30° steps in ω at 3 different ϕ settings and a detector position of −43° in 2θ. Final cell constants were calculated from the xyz centroids of strong reflections from the actual data collection after data reduction. The intensity data were corrected for absorption [31].

Space groups were determined based on intensity statistics and systematic absences. The structures were solved using SIR-92 [32] and refined with SHELXL-97 [33]. Direct-methods solutions were calculated which provided most non-hydrogen atoms from the E-map. Full-matrix least squares/difference Fourier cycles were performed, which located the remaining non-hydrogen atoms. All non-hydrogen atoms were refined with anisotropic displacement parameters. The hydrogen atoms were placed in ideal positions and refined as riding atoms with individual or relative isotropic displacement parameters.

3. Results

3.1. Synthesis and characterization

Acyclic enediyne ligands **1** and **2** were prepared by mixing 1,2-bis-(3-bromopropynyl)benzene [29] in DMF with the pre-formed Na^+ or K^+ salt of the desired thiol in a nucleophilic substitution reaction (Scheme 1). Strong base (NaOH) was employed for the preparation

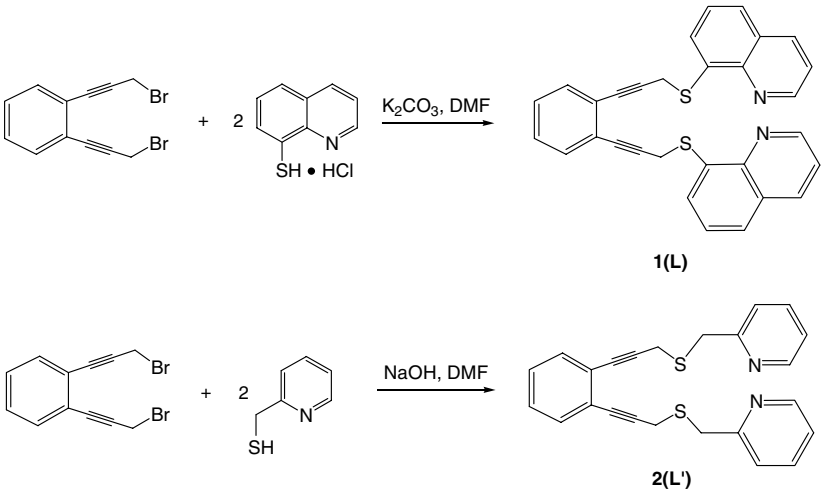

Scheme 1. Syntheses of tetradentate enediyne ligands **1** (L) and **2** (L′).

of **2** due to the sluggish reactivity of pyridin-2-yl-methanethiol with K_2CO_3. Both ligands can be isolated in moderate yields (35–50%).

Weakly coordinating, thioether metalloenediynes of soft metals (e.g., Pd(II), Cu(I), Ag(I)) can be readily prepared by complexation with the appropriate PF_6^- (e.g., Cu^+, Ag^+) or BF_4^- (Cu^{2+}, Pd^{2+}) salts (Scheme 2). These ions form the tetrahedral or tetragonal/square planar geometries that modulate the enediyne conformation. All the metal complexes were prepared following same general method. In order to avoid possible polymer formation ligand and appropriate metal salt were dissolved separately and simultaneously added at room temperature maintaining sufficient dilution. The reaction mixture was subsequently filtered to eliminate insoluble materials. The desired metalloenediyne complexes were isolated by recrystallization from diethylether in very good yields (70–90%).

Both ligands display well-resolved ^1H and ^{13}C NMR spectra in solution. In ^1H NMR spectra, all aromatic

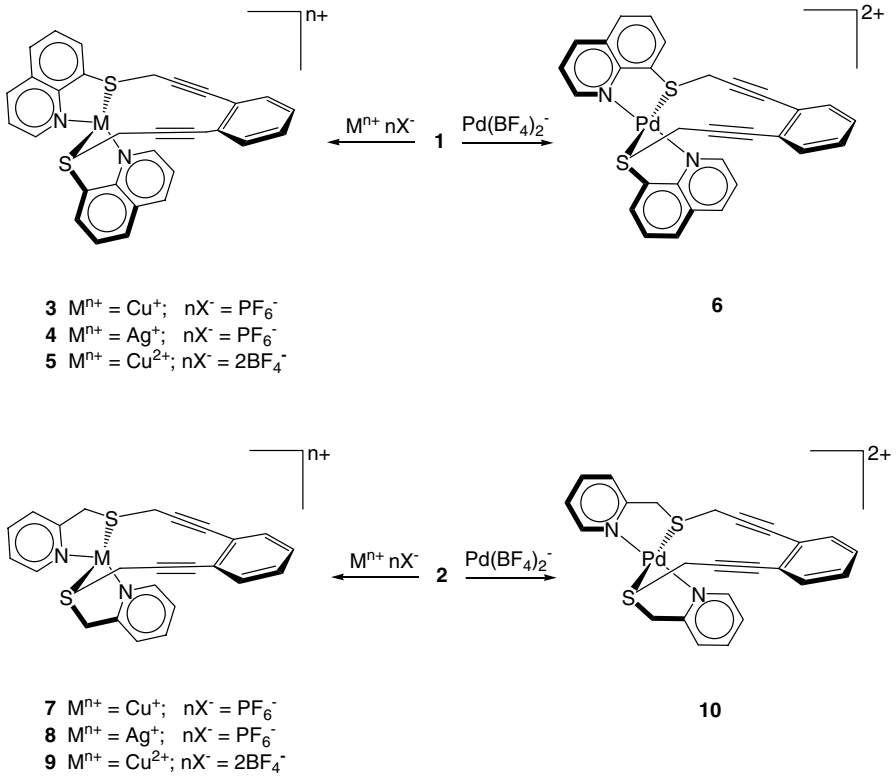

Scheme 2. Preparation of metalloenediynes complexes **3**–**10**.

resonances appear between 7 and 9 ppm while the methylene protons adjacent to the enediyne linkage are detected below 3.8 ppm. Upon diamagnetic metal ion complexation, downfield shifts of all proton signals are observed. Due to thioether coordination and metal ion proximity, the methylene protons show dramatic shifts upon complexation. For Cu(I) and Ag(I), the downfield shift of the methylene protons signal is ~0.4 ppm, while for the Pd(II) complex, the shift is slightly larger (~0.7 ppm). In both cases, the shift serves as a useful diagnostic of metal coordination by the thioether linkage. Similarly, in the ^{13}C NMR spectra of these metalloenediyne complexes, the methylene carbon resonance is also markedly shifted from the free ligand value (~20 ppm) to ~30 ppm for the Ag(I) complex and ~39 ppm for the Pd(II) analogue, thereby revealing the Lewis acidity/electron withdrawing capability of the metal ion as a function of oxidation state. All other resonances are observed as expected.

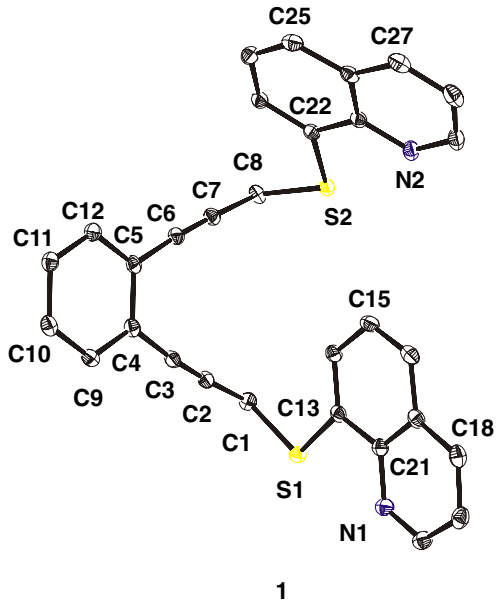

1

Fig. 1. X-ray structure and atom labeling scheme for **1**. Thermal ellipsoids are illustrated at 40% probability. The alkyne termini separation (C2···C7) is 3.76 Å.

3.2. Molecular structure

Ligand **1** was crystallized by slow evaporation of methanol-chloroform solution (Fig. 1, Table 1). X-ray quality crystals of metalloenediyne complexes of ligands **1** (**3**, **6**), and **2** (**7**, **8a**) were obtained by vapor diffusion of ether into an acetonitrile solution of the complexes (Figs. 2 and 3, Table 1). The Ag(I) complex **8** did not readily yield X-ray quality crystals; however counter ion exchange of PF_6 for SbF_6 afforded the desired single crystals (**8a**). Selected bond parameters are listed in Tables 2 and 3.

In the X-ray structure of ligand **1** (Fig. 1) the two thioxine (8-mercaptoquinoline) groups lie in a *syn* con-

Table 1
Crystallographic data for **1**,**3** · CH_2Cl_2,**6** · CH_3CN, **7**, and **8a**

	1	**3** · CH_2Cl_2	**6** · CH_3CN	**7**	**8a**
Empirical formula	$C_{30}H_{20}N_2S_2$	$C_{31}H_{22}Cl_2N_2S_2CuPF_6$	$C_{32}H_{23}B_2F_8N_3PdS_2$	$C_{24}H_{20}CuF_6N_2PS_2$	$C_{24}H_{20}N_2S_2AgSbF_6$
Formula weight	472.60	766.04	793.67	609.05	744.16
Color of crystal	colorless	yellow	yellow	yellow	colorless
Crystal system	monoclinic	monoclinic	monoclinic	monoclinic	monoclinic
Space group	$P2_1/n$	$P2_1/n$	$P2_1/c$	$P2_1/c$	$P2_1/c$
a (Å)	21.9054(19)	12.8102(11)	14.912(2)	13.1335(5)	13.1428(7)
b (Å)	4.9336(4)	12.0201(11)	11.8170(16)	12.6210(5)	12.8945(7)
c (Å)	23.425(2)	21.365(2)	17.597(2)	14.7333(6)	15.2240(8)
α (°)					
β (°)	115.647(2)	105.565(3)	91.245(4)	94.699(1)	94.344(1)
γ (°)					
V (Å^3)	2282.1(3)	3169.2(5)	3100.0(7)	2433.95(17)	2572.62(2)
Z	4	4	4	4	4
ρ_{calc} (g cm^{-3})	1.375	1.605	1.701	1.662	1.921
Linear absorption coefficient (mm^{-1})	0.256	1.102	0.812	1.198	2.034
Goodness-of-fit[a] on F^2	1.022	1.034	1.067	1.053	1.068
Final R indices[b] [$I > 2\sigma(I)$]	$R_1 = 0.0337$, $wR_2 = 0.0804$	$R_1 = 0.0397$, $wR_2 = 0.0915$	$R_1 = 0.0286$, $wR_2 = 0.0699$	$R_1 = 0.0331$, $wR_2 = 0.838$	$R_1 = 0.0414$, $wR_2 = 0.1317$
R indices[c] (all data)	$R_1 = 0.0474$, $wR_2 = 0.0875$	$R_1 = 0.0580$, $wR_2 = 0.1035$	$R_1 = 0.0349$, $wR_2 = 0.0753$	$R_1 = 0.0424$, $wR_2 = 0.0903$	$R_1 = 0.0519$, $wR_2 = 0.1385$
Largest difference peak and hole (e Å^{-3})	0.300 and −0.276	0.954 and −0.610	0.885 and −0.539	0.533 and −0.314	2.188 and −1.939

[a] Goodness-of-fit = $[\sum[w(F_o^2 - F_c^2)^2]/N_{observns} - N_{params})]^{1/2}$, all data.
[b] $R_1 = \sum(|F_o| - |F_c|)/\sum|F_o|$.
[c] $wR_2 = [\sum[w(F_o^2 - F_c^2)^2]/\sum[w(F_o^2)^2]]^{1/2}$.

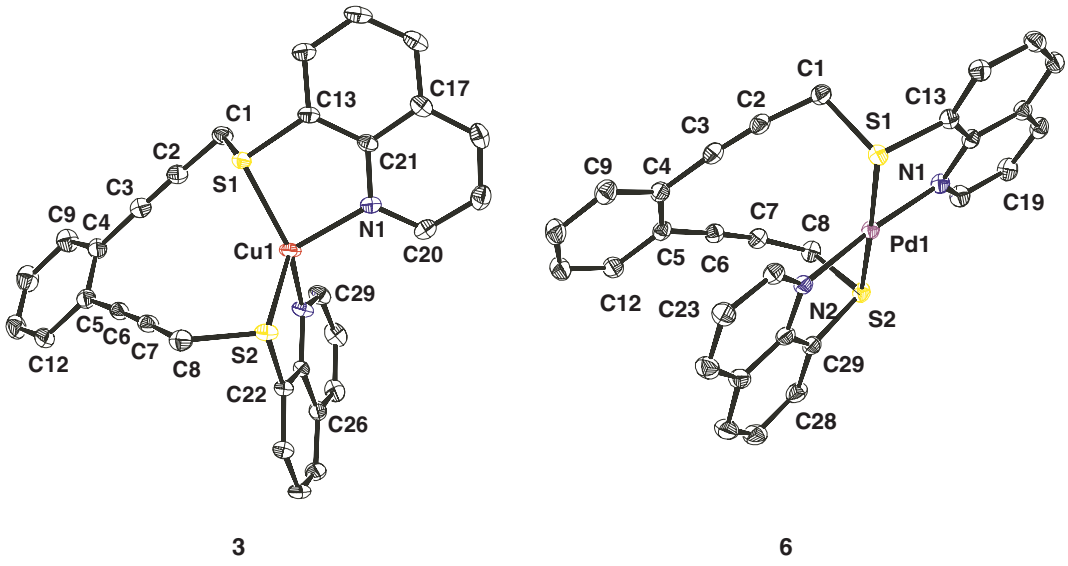

Fig. 2. X-ray structures and atom labeling scheme for **3** and **6**. Thermal ellipsoids are illustrated at 40% probability. Counter ions are omitted for clarity. The alkyne termini separation (C2···C7) **3**: 4.05 Å; **6**: 3.98 Å.

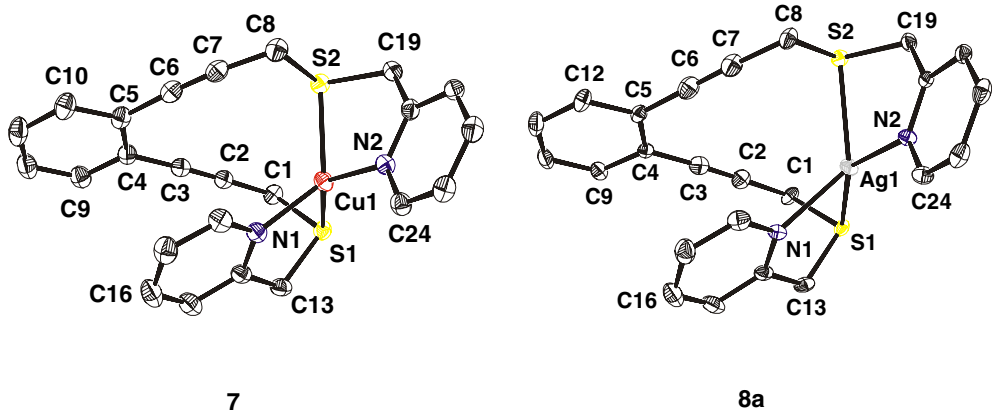

Fig. 3. X-ray structures and atom labeling scheme for **7** and **8a**. Thermal ellipsoids are illustrated at 40% probability. Counter ions are omitted for clarity. Alkyne termini separation (C2···C7) **7**: 3.95 Å; **8a**: 4.09 Å.

figuration with respect to the enediyne plane with their rings oriented at ~45° to each other. The alkyne termini (C2···C7) separation is relaxed (3.76 Å) and shows no evidence of steric crowding as occurs in more rigid enediyne constructs with large metal binding functionalities near the alkyne termini, due in part to the flexibility engendered by the additional methylene linkage [20]. For d^{10} metalloenediynes **3**, **7** (Cu(I)), and **8a** (Ag(I)), the N_2S_2 ligand donor atoms coordinate in a distorted tetrahedral fashion. The N1–M–N2 and S1–M–S2 bond angles range from ~106° to 113° and ~113° to 123°, respectively, reflective of the structural flexibility of the ligand and the elongated M–S bond lengths (~0.15–0.3 Å) over their M–N counterparts (Tables 2 and 3). In contrast, the Pd(II) complex **6** is square planar with the two weakly coordinating thioether linkages in a *trans* relationship leading to S1–Pd–S2 and N1–Pd–N2 bond angles of ~175°. Although the *cis* conformation is also a plausible structure, it is energetically uphill by ~6–9 kcal/mol from the *trans* geometry [28]. Despite the coordination geometry differences between the complexes, the alkyne termini separation (C2···C7) is almost same for all complexes (~4 Å). This arises from the large S1–M–S2 bite angles that range from 113° to 175° across all complexes.

3.3. Thermal Bergman cyclization

The thermal Bergman cyclization temperatures of these enediyne compounds have been measured by differential scanning calorimetry (DSC) and are given in Table 4. DSC is a convenient technique for comparing and correlating the thermal reactivities of enediynes, and is especially useful for complexes that react with solvent and decompose under thermal conditions in solution.

Table 2
Selected bond lengths (Å) and angles (°) of **1**, **3**, and **6**

Distances	
1	
S1–C1	1.8186(18)
C1–C2	1.457(2)
C2–C3	1.192(2)
C3–C4	1.438(2)
C4–C5	1.419(2)
S1–C13	1.7608(17)
3	
Cu1–N2	2.024(2)
Cu1–S1	2.2575(8)
Cu1–N1	2.043(2)
Cu1–S2	2.2851(8)
S1–C1	1.844(3)
C1–C2	1.452(4)
C2–C3	1.196(4)
6	
Pd1–N2	2.0468(18)
Pd1–N1	2.0440(18)
Pd1–S1	2.3171(6)
Pd1–S2	2.2871(6)
S1–C1	1.860(2)
C1–C2	1.450(3)
C2–C3	1.189(5)
Angles	
1	
C1–S1–C13	102.41(8)
S1–C1–C2	113.61(13)
C1–C2–C3	176.85(18)
C2–C3–C4	174.16(18)
C3–C4–C5	118.80(15)
S1–C13–C21	114.89(12)
3	
N1–Cu1–N2	105.92(10)
N1–Cu1–S1	88.08(7)
N1–Cu1–S2	120.60(7)
S1–Cu1–S1	118.83(3)
S1–C1–C2	107.1(2)
Cu1–S1–C1	107.47(10)
6	
N1–Pd1–N2	174.91(7)
N1–Pd1–S1	84.88(5)
N1–Pd1–S2	93.79(5)
S1–Pd1–S2	175.91(2)
S1–C1–C2	108.65(16)
Pd1–S1–C1	102.12(7)

Table 3
Selected bond lengths (Å) and angles (°) of **7** and **8a**

Distances	
7	
Cu1–N1	2.039(2)
Cu1–N2	2.014(2)
Cu1–S1	2.2832(6)
Cu1–S2	2.3348(7)
S1–C1	1.829(2)
C1–C2	1.457(3)
C2–C3	1.199(3)
8a	
Ag1–N1	2.288(4)
Ag1–N2	2.341(4)
Ag1–S2	2.4905(12)
Ag1–S1	2.5635(13)
S1–C1	1.821(5)
C1–C2	1.465(7)
C2–C3	1.193(7)
Angles	
7	
N1–Cu1–N2	112.88(8)
N1–Cu1–S1	88.19(6)
N2–Cu1–S1	135.06(6)
S1–Cu1–S2	112.61(2)
S1–C1–C2	114.79(16)
Cu1–S1–C1	103.35(8)
8a	
N1–Ag1–N2	108.51(14)
N1–Ag1–S1	146.23(11)
N2–Ag1–S1	80.32(10)
S1–Ag1–S2	123.04(4)
S1–C1–C2	108.8(3)
Ag1–S1–C1	101.6(2)

Table 4
Bergman cyclization temperatures of **1**–**10** (DSC)

Compound	Cyclization temperature (°C)
L (**1**)	230
[CuL]PF_6 (**3**)	218
[AgL]PF_6 (**4**)	214
[CuL]$(BF_4)_2$ (**5**)	186
[PdL]$(BF_4)_2$ (**6**)	190
L′ (**2**)	228
[CuL′]PF_6 (**7**)	215
[AgL′]PF_6 (**8**)	211
[CuL′]$(BF_4)_2$ (**9**)	188
[PdL′]$(BF_4)_2$ (**10**)	189

Upon heating, ligand **1** exhibits a sharp, endothermic peak at 105 °C characteristic of a melting transition. At higher temperature, a broad exothermic peak is also observed at 230 °C, which is characteristic of and at the expected temperature for the Bergman cyclization reaction of the neat liquid (Fig. 4). Ligand **2**, which is a liquid at ambient temperature, displays a similar exotherm at 226 °C, indicative of diradical formation by a similar construct.

Unlike **1**–**2**, the metalloenediyne complexes are all solids and do not show melting endotherms at temperatures below the cyclization reaction. For these complexes, cyclization occurs in the solid state, whereas the ligands react as neat liquids. Thus, direct comparison of the specific cyclization temperatures between the ligands and complexes cannot be readily made. However, it should be noted that the ligand cyclization temperatures would likely be considerably higher if encapsulated within an inert matrix, thereby illustrating the ability of the metal to reduce the cyclization temperatures relative to the free ligands [17,19,20].

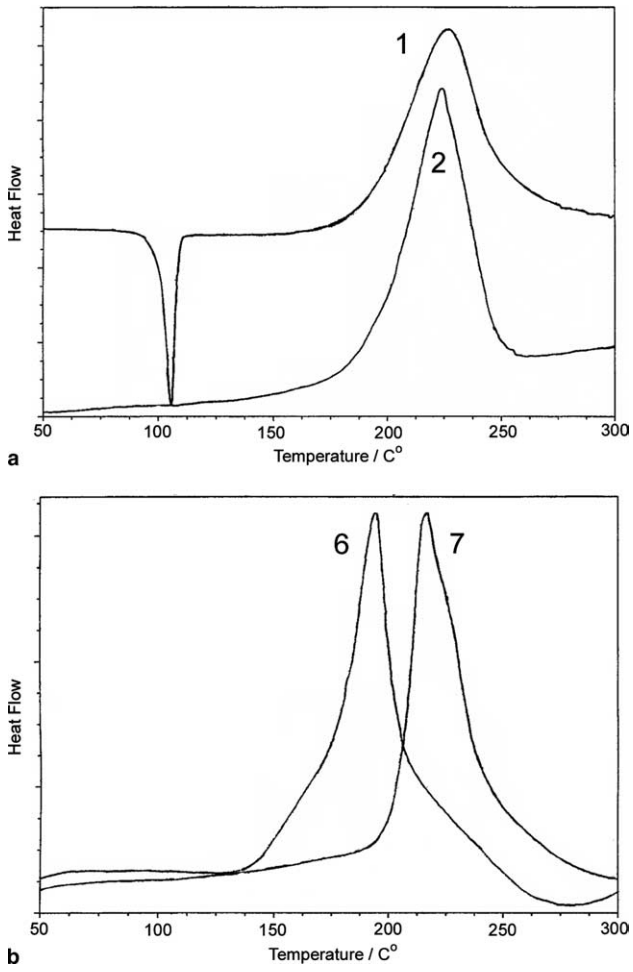

Fig. 4. Differential scanning calorimetry traces for the thermal cyclization of (a) **1**, **2** and (b) **6**, **7** in the solid state.

To this end, the cyclization temperatures of monovalent metalloenediyne complexes such as those of Cu(I) and Ag(I) displaying tetrahedral geometries (211–218 °C) are ~20–25 °C higher than their corresponding divalent, tetragonal and *trans* square planar complexes of Cu(II) and Pd(II) (186–190 °C). This trend is invariant to ligand and virtually identical for both sets of complexes derived from ligands **1** and **2**, despite the change of pyridine for quinoline coordination. It is also noteworthy that the alkyne termini separation in the X-ray structures *increases* upon metal coordination, while the cyclization temperatures actually *decrease*. This behavior is in stark contrast to the typical relationship between cyclization temperature and alkyne termini separation that has been well-established for analogous chelating metalloenediyne constructs [18–22].

4. Discussion

Ligands **1** and **2**, and their corresponding metalloenediyne complexes **3**–**10** represent a new class of thioether-coordinated enediyne framework. These constructs are very intriguing because they generate possibilities for using the thioether to geometrically, electronically, or substitutionally modulate the bound enediyne conformation and hence the Bergman cyclization temperature.

Earlier studies have shown that tetradentate amine/imine enediyne ligands [21,22,34] could give rise to, in some cases, extremely facile Bergman cyclization at ambient temperature [34]. In this sense, use of the thioether linkage as a mechanism to draw the alkyne termini into close proximity has attractive potential. Yet similar studies also revealed the importance of metal geometry in controlling coordinated enediyne conformation [16–22,35]. It is now well-established that *cis*-planar structures often have markedly lower cyclization temperatures than their tetrahedral or more rarely, their *trans*-planar [35] counterparts. As shown in Table 4, these thioether coordinated complexes do not adhere to this clearly defined paradigm, but rather exhibit cyclization temperatures for the *trans*-planar complexes that are ~25 °C *lower* than their tetrahedral counterparts. Since these complexes exhibit the same trend as their non-benzannulated structures, albeit ~50–60 °C lower in temperature [28], the variational thermal reactivities of these constructs is clearly not disrupted by benzannulation. With the wealth of data of metalloenediyne complexes and the established relationships with geometric structure, why then do the *trans* planar complexes react more readily than the tetrahedral structures?

Bergman cyclization temperatures also exhibit electronic contributions to reduction or enhancement of the thermal barrier to cyclization [36–40]. More specifically, electron withdrawing functionalities at the alkyne termini have been shown both theoretically [38] and experimentally [40] to decrease the onset temperature for the cyclization reaction. Although these effects are relevant in metalloenediyne constructs, their observation typically requires careful synthetic isolation of geometric and electronic components by locking the ligand conformation in order to systematically evaluate such contributions [24]. Within this theme, such enhancements in reactivity have recently been shown to be accessible by high valent metal ion coordination (e.g., Mo^{IV}–S^{-}) near the alkyne termini [27]. Ligands such as **1** and **2** displa- ying thioether coordination in the vicinity of the alkyne termini have potential for just this mode of electronic enediyne activation. However, in these cases, the neutral charge of the thioether leads to long metal–ligand bond lengths and poor orbital overlap, which is the basis for electronic activation. Additionally, the tetrahedral or *trans* planar geometry (e.g., Pd(II)) negates significant electronic enhancement via less than favorable geometric considerations. Thus, these fundamental guidelines for metalloenediyne reactivity do not explain the thermal chemistry of thioether-coordinated constructs such as **3**–**10**.

In very recent work on the non-benzannulated derivatives of **3**–**6**, detailed NMR and DFT studies implicated elevated temperature formation of a *cis* isomer with reduced alkyne termini separation by dissociation of the thioether ligand and rotation about the M–N bond [28]. This species then serves as the active precursor to Bergman cyclization. In fact, ambient temperature cyclization can be initiated via competitive ligand exchange by addition of 1 eq of pyridine. Under these conditions, the methylene protons from the dissociated thioether ligand appear in the ^{1}H NMR (δ 3.9 ppm) and new resonances from the cyclized product between δ 6 and 7 ppm emerge [28]. In light of the increased cyclization temperatures and the parallel thermal reactivity trends between related metalloenediyne complexes, these benzannulated derivatives likely follow the same reaction pathway.

5. Conclusion

We have prepared two novel thioether-coordinated enediyne ligands and a set of metalloenediyne complexes of Cu(I), Ag(I), Cu(II), and Pd(II). The d^{10} species exhibit distorted but near tetrahedral geometries with weak thioether coordination, while the d^9 and d^8 species are likely *trans* tetragonal and square planar, respectively. Remarkably, the latter structures exhibit Bergman cyclization temperatures ~25 °C lower than their tetrahedral counterparts. These values are much lower than those expected for complexes with *trans* geometries. The rationale for this chemical behavior can be traced to the fluxional nature of the thioether linkage and a *trans* to pseudo *cis* conformational change about the metal center via M–N bond rotation. This reactivity reveals the complex and untapped potential for using metal coordination to activate enediyne ligands toward Bergman cyclization.

6. Supplementary material

Crystallographic data for the X-ray structure analyses have been deposited with the Cambridge Crystallographic Data Center, CCDC Nos. 268 255 (**6**), 275 063 (**7**), 275 064 (**3**), 275 065 (**1**), and 275 066 (**8a**).

Acknowledgement

The support of the National Institutes of Health (R01 GM62541) is gratefully acknowledged.

References

[1] N. Darby, C.U. Kim, J.A. Salaun, K.W. Shelton, S. Takada, S. Masamune, Chem. Commun. (1971).
[2] R.G. Bergman, Acc. Chem. Res. 6 (1973) 25.
[3] D.S. Rawat, J.M. Zaleski, Synlett (2004) 393.
[4] M.D. Lee, T.S. Dunne, C.C. Chang, G.A. Ellestad, M.M. Siegal, G.O. Morton, W.J. McGahren, D.B. Borders, J. Am. Chem. Soc. 109 (1987) 3466.
[5] M.D. Lee, J.K. Manning, D.R. Williams, N.A. Kuck, R.T. Testa, D.B. Borders, J. Antibiot. 42 (1989) 1070.
[6] M. Konishi, H. Ohkuma, T. Tsuno, T. Oki, G.D. VanDuyne, J. Clardy, J. Am. Chem. Soc. 112 (1990) 3715.
[7] J. Golik, J. Clardy, G. Dubay, G. Groenewold, H. Kawaguchi, M. Konishi, B. Krishnan, H. Ohkuma, K. Saitoh, T.W. Doyle, J. Am. Chem. Soc. 109 (1987) 3461.
[8] J. Golik, G. Dubay, G. Groenewold, H. Kawaguchi, M. Konishi, B. Krishnan, H. Ohkuma, K. Saitoh, T.W. Doyle, J. Am. Chem. Soc. 109 (1987) 3462.
[9] R.L. Funk, E.R.R. Young, R.M. Williams, M.F. Flanagan, T.L. Cecil, J. Am. Chem. Soc. 118 (1996) 3291.
[10] A. Evenzahav, N.J. Turro, J. Am. Chem. Soc. 120 (1998) 1835.
[11] T. Kaneko, M. Takahashi, M. Hirama, Angew. Chem., Int. Ed. Engl. 38 (1999) 1267.
[12] M. Nath, M. Pink, J.M. Zaleski, J. Am. Chem. Soc. 127 (2005) 478.
[13] A. Basak, S. Mandal, S.S. Bag, Chem. Rev. 103 (2003) 4077.
[14] B. König, H. Hollnagel, B. Ahrens, P.G. Jones, Angew. Chem., Int. Ed. Engl. 34 (1995) 2538.
[15] B. König, W. Pitsch, I. Thondorf, J. Org. Chem. 61 (1996) 4258.
[16] B.P. Warner, S.P. Millar, R.D. Broene, S.L. Buchwald, Science 269 (1995) 814.
[17] N.L. Coalter, T.E. Concolino, W.E. Streib, C.G. Hughes, A.L. Rheingold, J.M. Zaleski, J. Am. Chem. Soc. 122 (2000) 3112.
[18] E.W. Schmitt, J.C. Huffman, J.M. Zaleski, Chem. Commun. (2001) 167.
[19] P.J. Benites, D.S. Rawat, J.M. Zaleski, J. Am. Chem. Soc. 122 (2000) 7208.
[20] D.S. Rawat, P.J. Benites, C.D. Incarvito, A.L. Rheingold, J.M. Zaleski, Inorg. Chem. 40 (2001) 1846.
[21] T. Chandra, M. Pink, J.M. Zaleski, Inorg. Chem. 40 (2001) 5878.
[22] T. Chandra, R.A. Allred, B.J. Kraft, L.M. Berreau, J.M. Zaleski, Inorg. Chem. 43 (2004) 411.
[23] S. Bhattacharyya, A.E. Clark, M. Pink, J.M. Zaleski, Chem. Commun. (2003) 1156.
[24] S. Bhattacharyya, J.M. Zaleski, Curr. Top. Med. Chem. 4 (2004) 1637.
[25] J.M. O'Connor, L.I. Lee, P. Gantzel, A.L. Rheingold, K.-C. Lam, J. Am. Chem. Soc. 122 (2000) 12057.
[26] J.M. O'Connor, S.J. Friese, M. Tichenor, J. Am. Chem. Soc. 124 (2002) 3506.
[27] S. Bhattacharyya, M. Pink, M.-H. Baik, J.M. Zaleski, Angew. Chem., Int. Ed. Engl. 44 (2005) 592.
[28] S. Bhattacharyya, D.F. Dye, M. Pink, J.M. Zaleski, Chem. Commun. (submitted).
[29] H. Hopf, P.G. Jones, P. Bubenitschek, C. Werner, Angew. Chem., Int. Ed. Engl. 34 (1995) 2367.
[30] R. Deziel, E. Malenfant, Bioorg. Med. Chem. Lett. 8 (1998) 1437.
[31] R. Blessing, Acta Crystallogr. A51 (1995) 33.
[32] A. Altomare, G. Cascarno, C. Giacovazzo, A. Gualardi, J. Appl. Crystallogr. 26 (1993) 343.
[33] SHELXTL-PLUS V6.14, Bruker Analytical X-ray Systems, Madison, WI.
[34] D.S. Rawat, J.M. Zaleski, J. Am. Chem. Soc. 123 (2001) 9675.
[35] Y.-Z. Hu, C. Chamchoumis, J.S. Grebowicz, R. Thummel, Inorg. Chem. 41 (2002) 2296.
[36] G.B. Jones, G.W. Plourde II, Org. Lett. 2 (2000) 1757.
[37] G.B. Jones, P.M. Warner, J. Am. Chem. Soc. 123 (2001) 2134.
[38] M. Prall, A. Wittkopp, A.A. Fokin, P.R. Schreiner, J. Comp. Chem. 22 (2001) 1605.
[39] I.V. Alabugin, M. Manoharan, S.V. Kovalenko, Org. Lett. 4 (2002) 1119.
[40] M. Nath, J.C. Huffman, J.M. Zaleski, J. Am. Chem. Soc. 125 (2003) 11484.

Available online at www.sciencedirect.com
SCIENCE DIRECT®
Polyhedron 25 (2006) 559–567
POLYHEDRON
www.elsevier.com/locate/poly

Dinuclear coordination of a novel four-electron reduced μ-η^1,η^3-allene ligand with β-agostic C–H···Ta interaction: Direct addition of allene to $(C_5Me_5)_2Ta_2(\mu\text{-}X)_4$ (X = Cl, Br), and molecular structure of $(C_5Me_5)_2Ta_2(\mu\text{-}\eta^1,\eta^3\text{-}C_3H_4)(\mu\text{-}Cl)Cl_3$

Jui-Hsien Huang, Ting-Yu Lee, Dale C. Swenson, Louis Messerle *

Department of Chemistry, The University of Iowa, Madison & Market Streets, Iowa City, IA 52242, USA

Received 17 June 2005; accepted 4 August 2005
Available online 5 October 2005

Dedicated to Professor Malcolm Chisholm for his numerous creative contributions to and leadership in transition metal–metal multiple bond and dinuclear allene chemistries, and for advancing the metal–metal multiple bond paradigm from synthesis and structure to reactivity.

Abstract

The organoditantalum complexes $(\eta\text{-}C_5Me_5)_2Ta_2(\mu\text{-}X)_4$ (X = Cl, Br) react with 1–5 equiv. of allene under mild conditions to afford the fluxional allene adducts $(C_5Me_5)_2Ta_2(\mu\text{-}\eta^1,\eta^3\text{-}C_3H_4)(\mu\text{-}X)X_3$ as shown by spectroscopic and spectrometric data. Low-temperature-limit proton NMR data at −95 °C for $(C_5Me_5)_2Ta_2(\mu\text{-}\eta^1,\eta^3\text{-}C_3H_4)(\mu\text{-}Cl)Cl_3$ show a large chemical shift range for the inequivalent allene hydrogens, with a high-field value for one hydrogen at δ −0.36, and inequivalent Cp* groups. The low-temperature-limit ^{13}C NMR resonances for the allene ligand are found at δ 204.4 (central C), δ 70.3 (CH_2, $^1J_{CH} = 154$ Hz), and the substantially upfield value of δ 42.9. The latter resonance has remarkably different coupling constants ($^1J_{CH} = 173$, 154 Hz). The allene coordinates in a novel alkylidene-diyl fashion in the solid-state, as shown by X-ray diffractometry on $(C_5Me_5)_2Ta_2(\mu\text{-}\eta^1,\eta^3\text{-}C_3H_4)(\mu\text{-}Cl)Cl_3$ at 200 K. One tantalum is doubly-bonded to the central allenic carbon (Ta1=C22 distance, 2.011(7) Å) and interacts with an allene hydrogen in a probable β-agostic manner (Ta1–H21A distance of 2.25(10) Å). The second tantalum is coordinated to the allene in a hybrid of η^3-allylic and sigma bonding, with Ta2–C distances to the allene methylenes of 2.206(8) and 2.276(9) Å and a Ta2–C22 bond distance to the central allenic carbon of 2.253(7) Å. The allene hydrogens are oriented above and below the C–C–C plane, consistent with appreciable σ-bonding between the Ta(2) and the allene methylenes. The bent allene ligand has a C–C–C angle of 106.0(6)° and can be viewed as reduced by four electrons, with concomitant oxidation of the two d^2 tantalum centers of the organoditantalum(III) reactant. The long Ta···Ta nonbonded distance of 3.3052(8) Å is consistent with two d^0 tantalum centers in an organoditantalum(V) product.
© 2005 Elsevier Ltd. All rights reserved.

Keywords: Tantalum; Organoditantalum; Allene complex; C–H agostic interaction; Dinuclear

1. Introduction

There is considerable structural diversity in the products from reactions of the simplest cumulene, allene, and its derivatives with organotransition metal compounds. A variety of allene coordination modes (Scheme 1) and metal-mediated rearrangements have been observed in mononuclear [1] and dinuclear chemistries. The course of these reactions depends in part on the functional groups of the organotransition metal reactant. For example, migratory insertion of allene into metal hydride [2–5], μ-vinyl [6], and η^3-allyl [6] groups has

* Corresponding author. Tel.: +1 319 335 1372; fax: +1 319 335 1270.
E-mail address: lou-messerle@uiowa.edu (L. Messerle).

0277-5387/$ - see front matter © 2005 Elsevier Ltd. All rights reserved.
doi:10.1016/j.poly.2005.08.008

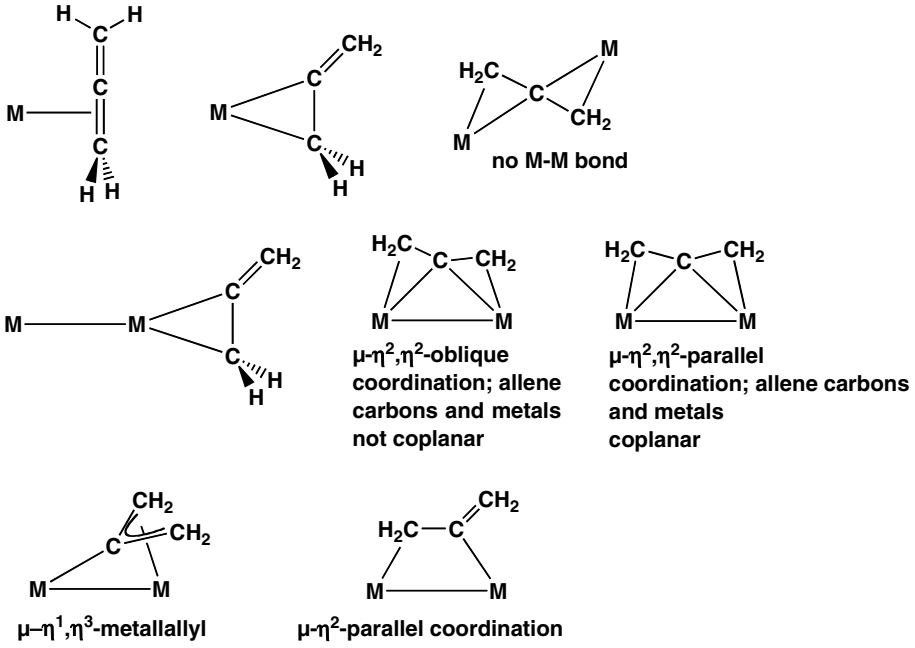

Scheme 1.

been shown to yield η^3-allyl complexes and other hydrocarbon-coupled products. Allene coupling with CO, phosphido [7], μ-methylene [8], and allene [9–11] ligands has also been reported.

There are only a small number of reported homo- and heterodinuclear allene adducts. Solid-state structures, as well as solution structures proposed on the basis of spectroscopic data, fall into several classes. These include η^2-coordination to one of the metal centers [12–17], μ-η^2,η^2-coordination oblique or parallel to the metal–metal vector (with or without metal–metal bonding) [12,18–28], μ-η^2-coordination (i.e., 1,2-dimetallacyclobutane with an exocyclic methylene group) [29,30], and μ-η^1,η^3-coordination [7,10,12,23,27,29,31–37]. The latter mode, which contains a formal doubly-reduced allene ligand, can be described as a 2-metallaallyl that is η^3-bonded to the second metal. In one case, a μ-η^1,η^3-coordinated allene has been described formally as quadruply-reduced (i.e., tetraanionic) [27]. Dinuclear allene adducts have been observed in matrix isolation experiments [38].

Dinuclear complexes with allene ligands have been prepared by a variety of methods, including: (1) direct addition of allene to dinuclear complexes, (2) sequential nucleophilic/electrophilic attack [39] or diazoalkane addition [9,40–42] to μ-vinylidene complexes, (3) rearrangements of μ-cyclopropylidene ligands [43,44], and (4) photochemical decarbonylation of a μ-η^1,η^3-β-carbonylallylic ligand [19]. Of the reports of direct allene addition to dinuclear reactants, only a few involve compounds possessing metal–metal multiple bonds.

The formally metal–metal doubly-bonded, mid-valent organoditantalum(III) complexes (η-$C_5Me_4R)_2$-$Ta_2(\mu\text{-}X)_4$ (**1**; R = Me, Cp*; R = Et; X = Cl, Br) react with a variety of substrates, including dihydrogen [45], borohydride [46], 3,3-disubstituted cyclopropenes [47], and 1-alkenes [48]. This reactivity may be associated with the fact that **1** possesses a d^2–d^2 electron poor double bond of $\sigma^2\delta^2$ electronic configuration (or the alternate [49] non-bonded $\sigma^2\delta^{*2}$, depending on the degree of interaction of the μ-halide lone pairs with the δ-symmetry d_{xy} orbitals and the concomitant destabilization of δ relative to δ*). $(C_5Me_4R)_2Ta_2(\mu\text{-}X)_4$ reacts under mild conditions (25 °C, 15 psi) with simple 1-alkenes ($H_2C{=}CHR'$) to give the organoditantalum complexes $(C_5Me_4R)_2Ta_2(\mu\text{-}CHCHR')(\mu\text{-}H)(\mu\text{-}X)X_3$, the formal products from vinylic C–H bond activation [48]. Olefins such as styrene or butadiene react at kinetically-convenient rates only at higher temperatures (80 °C) to yield mononuclear Ta(V) organometallics such as $Cp^*Ta(\eta^2\text{-}H_2CCHPh)X_2$ or the metallacyclopentene $Cp^*Ta(CH_2CH{=}CHCH_2)X_2$, respectively [45]. We investigated whether allene would react with **1** via a C–H activation pathway or via complexation in mononuclear or dinuclear products, and report here our results that represent an unusual coordination mode for allene in organodimetallic chemistry.

2. Results and discussion

2.1. Reaction of allene with $Cp^*_2Ta_2(\mu\text{-}X)_4$

The injection of 1–5 equiv. of allene via gas-tight syringe to a cooled (−78 °C) toluene solution of

$Cp^*_2Ta_2(\mu\text{-}X)_4$, **1**, followed by warming to room temperature and stirring overnight, converts the solution from the forest-green reactant color to deep red solutions from which the brownish-red allene adducts $Cp^*_2Ta_2(\mu\text{-}X)_4(H_2CCCH_2)$ (X = Cl, **2a**; X = Br, **2b**) can be isolated in 55% (X = Cl) or 53% (X = Br) yield via concentration and low-temperature fractional crystallization. The best yields are obtained from use of 2 equiv. of allene per equivalent of **1**. The reaction of excess allene, at greater than one atmosphere pressure in a pressure reaction vessel [50], with a toluene solution of $Cp^*_2Ta_2(\mu\text{-}X)_4$ yields a mixture of presently uncharacterized products. Elemental analysis and mass spectrometric data confirm that allene has added to **1**, and NMR spectroscopic data are consistent with formulation of **2** as dinuclear allene adducts rather than as products derived from vinylic C–H bond activation or mononuclear coordination via one C=C double bond.

2.2. Spectroscopic studies

The ^{1}H NMR spectra of the allene adducts **2** at 25 °C are simple, with resonances consistent with a single Cp* group and two types of allene protons. At 25 °C the allene hydrogen atoms in the chloride complex **2a** appear as broad singlets at δ 1.66 and δ 2.60 in C_6D_6, and as multiplets at δ 1.41 and δ 1.70 in CD_2Cl_2. For the bromide **2b**, the allene hydrogen atoms appear as broad singlets at δ 1.88 and δ 2.26 in C_6D_6. At lower temperatures the two Cp* groups and the four allene hydrogen atoms of **2a** are nonequivalent, with resonances over a surprisingly large chemical shift range (Fig. 1). At −95 °C (CD_2Cl_2) the four allene proton resonances are found at δ −0.36 (double doublet), δ 0.09 (doublet), and δ 2.60 (overlapped doublet and broad singlet). Homonuclear decoupling experiments at −95 °C establish that the two high-field resonances at δ −0.36 and δ 0.09 are geminal protons, and we postulate that they are H21A and H21B because of the unusual chemical shifts and structural features associated with the two hydrogen atoms on C21 in the solid-state structure (vide infra). Since the Cp* resonances become equivalent at room temperature, the fluxional process must involve a substantial reorganization of the C_3H_4 ligand to a symmetric intermediate followed by rearrangement to bond the central allene carbon atom to the other tantalum atom. Such fluxional behavior has been noted often in dinuclear allene coordination chemistry.

The ^{13}C NMR spectra of **2a** also change appreciably with temperature. Resonances for a single Cp* group and equivalent allene methylene groups are observed at 25 °C, with allene ligand chemical shifts of δ 62.9 (CH_2, $^1J_{CH}$ = 160 Hz) and δ 206.9 (central C). At −95 °C, the Cp* groups and allene methylenes become nonequivalent, with the inequivalent methylene carbon atoms appearing at δ 70.3 and the substantially upfield value of δ 42.9. The resonance at δ 42.9 has remarkably different C–H coupling constants ($^1J_{CH}$ = 173 and 154 Hz) to the geminal protons in the gated {^{1}H} spectrum, whereas the δ 70.3 resonance is a deceptively simple triplet with $^1J_{CH}$ = 154 Hz. The 19 Hz difference in the $^1J_{CH}$ coupling constants for the methylene carbon atom at δ 42.9 and the unusual spread of the proton NMR resonances for the four allene protons are suggestive of an agostic [51] interaction of one or more of the allene hydrogen atoms with a tantalum atom. The spread in $^1J_{CH}$ values for **2a** may be related to the fact that C21 is β to Ta1 and α to Ta2. $^1J_{CH}$ values for α-agostic interactions should be used with caution since the $^1J_{CH}$ for σ-bonded carbons depends on the electron density at the metal center [52].

Infrared spectroscopy has been used to characterize, with partial success, agostic interactions [51b]. Infrared spectra of **2a** and **2b** (recorded as KBr pellets and concentrated Nujol mulls) show no evidence of unusual C–H stretching absorptions in the 2750–2200 cm^{-1} range.

Allene ^{1}H NMR resonances in dinuclear complexes are related to the metal as well as coordination mode and allene carbon rehybridization, so chemical shifts are not a reliable indicator of the coordination mode in complexes with other metals. However, no other reported dinuclear allene complex has a slow-exchange-limit ^{1}H NMR spectral range with such high field values nor such a range of chemical shifts as those seen for **2a**. The ^{1}H chemical shifts of the allene ligand in **2a** are quite different from that of allene itself (δ 4.49 in C_6D_6, 25 °C). Among early transition metal complexes, an organodimolybdenum complex [18] with a $\mu\text{-}\eta^2,\eta^2$-oblique allene coordination had allene resonances in C_6D_6 at δ 3.67 and δ 2.52, versus δ 4.46 and δ 2.82 for the tungsten analog. A μ-parallel allene ligand in an organoditungsten complex had an allenic ^{1}H NMR chemical shift at δ 6.59 [12]. The proton chemical shifts for two ditungsten $\mu\text{-}\eta^1,\eta^3$-metallallyls ranged from δ 5.88 to δ 2.40 [12].

Carbon-13 NMR shifts for allene ligands in dinuclear complexes are also related to the metal and coordination mode. Of early transition metal examples, $Cp_2Mo_2(CO)_4(\mu\text{-}\eta^2,\eta^2\text{-}C_3H_4)$ had a central allene ^{13}C chemical shift of δ 197.0 and methylene carbon value of δ 36.7, with $^1J_{CH}$ values of 160 and 170 Hz; the tungsten analog had a central allene carbon resonance at δ 31.6 [18]. In one ditungsten $\mu\text{-}\eta^2,\eta^2$-parallel allene complex, the central allene carbon resonance was found at δ 249.7 and the methylene at δ 89.1, with $^1J_{CH}$ = 156 Hz [12]. Another ditungsten allene complex, $W_2(OCMe_3)_4(\mu\text{-}OCMe_3)_2$ ($\mu\text{-}\eta^1,\eta^3\text{-}C_3H_4$) ($\eta^2\text{-}C_3H_4$) with a metallallyl allene coordination mode, had resonances for $C_{central}$ at δ 177.1 and CH_2 at δ 67.9 (interestingly, with two $^1J_{CH}$ values differing by 10 Hz) [12].

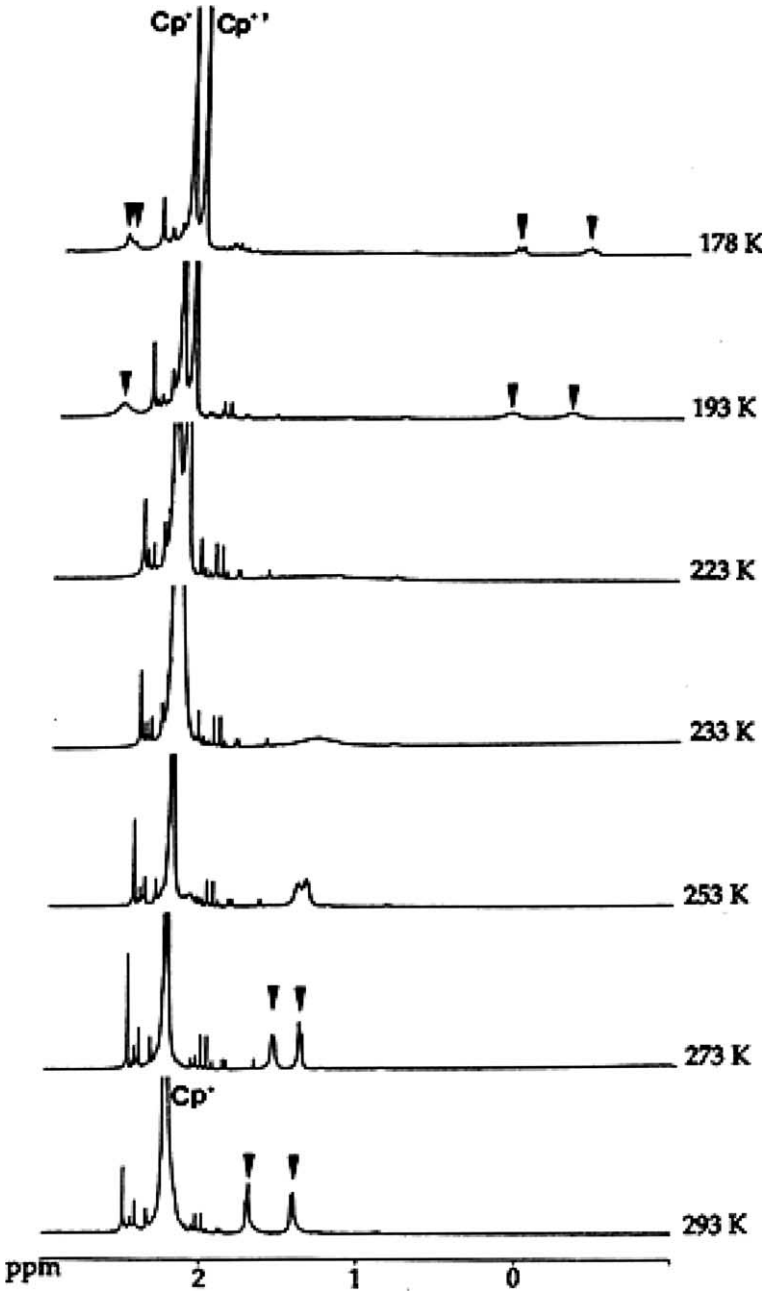

Fig. 1. Variable temperature ^{1}H NMR spectra of $(C_5Me_5)_2Ta_2(\mu\text{-}\eta^1,\eta^3\text{-}C_3H_4)(\mu\text{-}Cl)Cl_3$ (**2a**) in CD_2Cl_2. The arrows denote resonances for the allene hydrogen atoms, Cp* denotes the methyl resonances of the C_5Me_5 groups. Remaining resonances are solvent impurities.

*2.3. Solid-state structure determination of **2a** by X-ray diffractometry*

The thermal ellipsoid plot in Fig. 2 depicts the molecular structure of **2a** as determined from single-crystal X-ray diffraction data collected at 200 K. Fig. 3 is the thermal ellipsoid plot obtained by rotating the structure in Fig. 2 by ~90° about the Ta1···Ta2 vector. Key bond distances and bond angles are listed in Tables 1 and 2, respectively, while crystallographic and data collection parameters are summarized in Section 4.

Important structural parameters include: (1) a nonbonded Ta1···Ta2 distance of 3.3052(8) Å, bridged by the allene ligand and one chlorine atom directly opposite the allene ligand, (2) an unsymmetric $\mu\text{-}\eta^1,\eta^3$-allene coordination mode with twisting of the C21–C22–C23 moiety with respect to the Ta1···Ta2 vector, (3) a small allene ligand C21–C22–C23 angle of 106.0(6)°, (4) a long allene C21–C22 distance of 1.537(10) Å and C22–C23 distance of 1.435(11) Å, respectively, (5) rotation of the allene hydrogen atoms on C21 and C23 out of the C21–C22–C23 plane, with

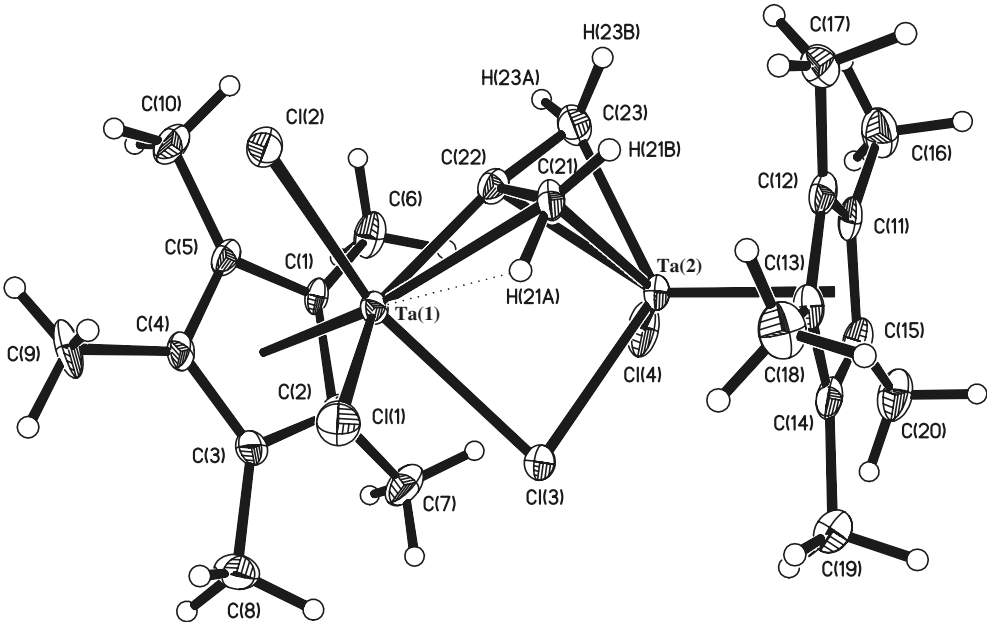

Fig. 2. Thermal ellipsoid plot of the molecular structure of $(C_5Me_5)_2Ta_2(\mu\text{-}\eta^1,\eta^3\text{-}C_3H_4)(\mu\text{-}Cl)Cl_3$ (**2a**) viewed approximately perpendicular to the Ta1···Ta2 vector and Ta1–C22 bond. Ellipsoids are drawn at 35% probability level.

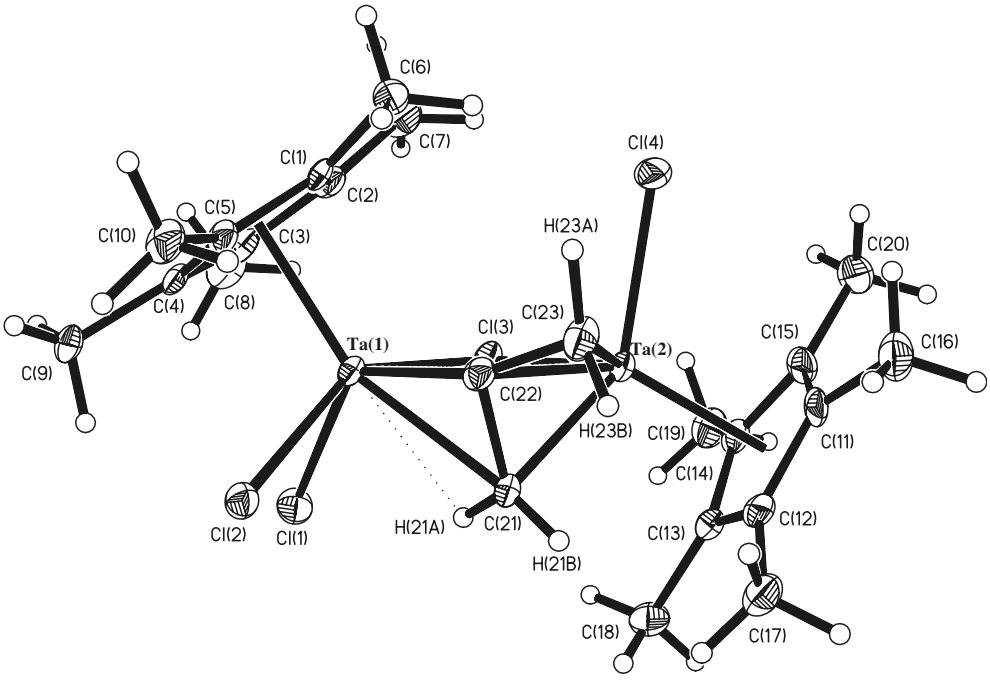

Fig. 3. Thermal ellipsoid plot of the molecular structure of $(C_5Me_5)_2Ta_2(\mu\text{-}\eta^1,\eta^3\text{-}C_3H_4)(\mu\text{-}Cl)Cl_3$ (**2a**), rotated 90° about the Ta1···Ta2 vector from that in Fig. 2 and viewed perpendicular to the Ta1···Ta2 vector and parallel to a vector passing through C22 and the bridge chlorine CL3. Ellipsoids are drawn at 35% probability level.

dihedral angles between the H21A–C21–H21B plane and the C21–C22–C23 plane of 22.7° and between the H23A–C23–H23B plane and the C21–C22–C23 plane of 53.3°, (6) a short Ta1–C22 distance of 2.011(7) Å, (7) a nearly planar C22, with summation of angles (Ta1–C22–C21, Ta–C22–C23, and C21–C22–C23) of 354.5° and deviation of Ta1 from the C21–C22–C23 plane of 0.4606(1) Å, (8) Ta2 interaction with the three allene carbons, with Ta2–C21, Ta2–C22, and Ta2–C23 distances of 2.206(8), 2.253(7), and 2.276(9) Å, respectively, and (9) a short Ta1···H21A distance of 2.25(10) Å.

Table 1
Selected bond distances (Å) in $(C_5Me_5)_2Ta_2(\mu\text{-}\eta^1,\eta^3\text{-}C_3H_4)(\mu\text{-}Cl)Cl_3$ (**2a**)

Ta(1)–Ta(2)	3.3052(8)
Ta(1)–H(21A)	2.25(10)
Ta(2)–C(23)	2.276(9)
Ta(1)–Cl(1)	2.4731(18)
Ta(2)–Cl(3)	2.4363(19)
Ta(1)–C(2)	2.475(7)
Ta(1)–C(5)	2.409(7)
Ta(2)–C(13)	2.403(7)
Ta(1)–C(21)	2.461(7)
Ta(2)–C(21)	2.206(8)
C(21)–C(22)	1.537(10)
Ta(1)–Cl(2)	2.459(2)
Ta(2)–Cl(4)	2.381(2)
Ta(1)–C(3)	2.422(7)
Ta(2)–C(11)	2.406(7)
Ta(2)–C(14)	2.403(7)
Ta(1)–C(22)	2.011(7)
Ta(2)–C(22)	2.253(7)
C(22)–C(23)	1.435(11)
Ta(1)–Cl(3)	2.568(2)
Ta(1)–C(1)	2.464(7)
Ta(1)–C(4)	2.411(7)
Ta(2)–C(12)	2.422(7)
Ta(2)–C(15)	2.444(8)

Standard deviations given in parentheses.

Table 2
Selected bond angles (°) in $(C_5Me_5)_2Ta_2(\mu\text{-}\eta^1,\eta^3\text{-}C_3H_4)(\mu\text{-}Cl)Cl_3$ (**2a**)

C(21)–C(22)–C(23)	106.0(6)
Cl(1)–Ta(1)–C(100)	114.5
C(100)–Ta(1)–H(21A)	173.5
Cl(1)–Ta(1)–Cl(2)	80.04(7)
Cl(3)–Ta(2)–Cl(4)	94.94(8)
C(23)–Ta(2)–Cl(4)	83.2(3)
C(22)–Ta(2)–C(200)	140.0
C(21)–Ta(2)–Cl(3)	83.0(2)
Ta(2)–C(21)–Ta(1)	90.0(3)
Ta(2)–Cl(3)–Ta(1)	82.63(6)
Cl(2)–Ta(1)–C(100)	105.1
C(22)–Ta(1)–Cl(1)	130.0(2)
Cl(1)–Ta(1)–Cl(3)	76.51(7)
C(21)–Ta(2)–Cl(4)	138.6(2)
Cl(4)–Ta(2)–C(200)	110.6
C(23)–Ta(2)–C(200)	118.6
C(22)–Ta(2)–Cl(3)	87.00(19)
Ta(1)–C(22)–Ta(2)	101.5(3)
C(22)–Ta(1)–C(100)	115.5
Cl(3)–Ta(1)–C(100)	107.0
C(22)–Ta(1)–Cl(3)	88.9(2)
Cl(2)–Ta(1)–Cl(3)	145.89(6)
C(22)–Ta(2)–Cl(4)	98.31(19)
C(21)–Ta(2)–C(200)	107.2
Cl(3)–Ta(2)–C(200)	116.3
C(23)–Ta(2)–Cl(3)	121.8(2)

C(100) and C(200) are the centroids of the C_5Me_5 rings. Standard deviations given in parentheses.

The structural data is consistent with an unusual coordination mode for an allene ligand in a dinuclear complex, which is depicted below in idealized fashion.

The actual structure has some twisting of the allene ligand which results in inequality of the C22–C23 (1.43(1) Å) and long C21–C22 (1.54(1) Å) distances. The four allene hydrogens are above and below the C21–C22–C23 plane, rather than in the C21–C22–C23 plane as would be expected for a $\mu\text{-}\eta^1,\eta^3$-metallaallyl ligand. This suggests a significant rehybridization of the allene methylene carbon atoms towards sp^3. The short Ta1=C22 distance of 2.011(7) Å is in the Ta=C double bond range, showing that tantalum–carbon multiple bonding competes with C=C double bonding. The near planarity of the central allene carbon C22 is consistent with this alkylidene formulation.

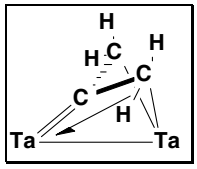

A number of $\mu\text{-}\eta^1,\eta^3$-metallallyl complexes have been studied by X-ray diffractometry. In the first reported structure, on $Fe_2(CO)_6(PPh_3)(C_3H_4)$, the two C–C distances were 1.45(2) and 1.41(2) Å and the C–C–C angle was 116(1)° [31,32]. Among earlier transition metal examples, the ditungsten complex $W_2(OCMe_3)_4(\mu\text{-}OCMe_3)_2(\mu\text{-}\eta^1,\eta^3\text{-}C_3H_4)(\eta^2\text{-}C_3H_4)$ had allene C–C distances of 1.434(16) and 1.458(16) Å (average 1.45(2) Å), and an allene C–C–C angle of 109.8(10)° [12]. Interestingly, the allene ligand protons lie in the allene C–C–C plane, as would be expected for a normal metallallyl coordination. In both this structure and the related [12] carbonyl derivative $W_2(OCMe_3)_4(\mu\text{-}OCMe_3)_2(\mu\text{-}\eta^1,\eta^3\text{-}C_3H_4)(CO)_2$ the W–C σ-bonding distances to the central allene carbon were consistent with single bonds, and the allene C–C distances were 1.32(7) and 1.49(6) Å.

All four allene hydrogen atoms in **2a** were located and refined in the structure determination. The C–H distances were not constrained during refinement, and thus range from an unreasonably short though statistically acceptable 0.64(9) Å for C21–H21A (the postulated agostic hydrogen) to 0.8(1) Å for C23–H23A to 1.0(1) Å for both C21–H21B and C23–H23B. Because of the short C21–H21A distance, it is not possible to state with complete certainty that H21A is interacting with Ta1 in a β-agostic manner despite the short Ta1···H21A distance. However, an important criterion for the existence of an agostic interaction is the presence of a suitable acceptor orbital on the metal [51b]. Fig. 4 shows a partial molecular view through the top of the Cp* group (carbon atoms removed) along the Ta1–C100 ring centroid vector. The C21–H21A bond is located along one of the legs of the four-legged piano stool geometry about

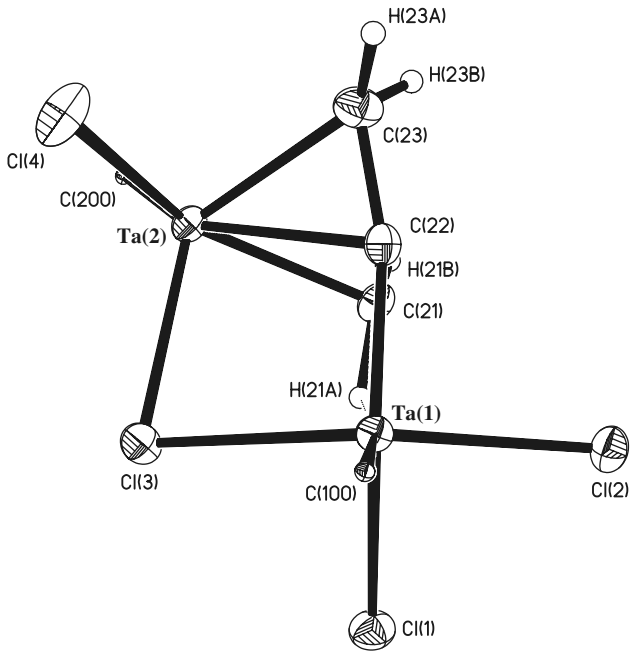

Fig. 4. Thermal ellipsoid plot emphasizing the Ta1 coordination sphere of $(C_5Me_5)_2Ta_2(\mu\text{-}\eta^1,\eta^3\text{-}C_3H_4)(\mu\text{-}Cl)Cl_3$ (**2a**) as viewed down the centroid C100···Ta1 vector from above the Cp* group (with carbons removed for clarity). Ellipsoids are drawn at 35% probability level.

Ta1, with H21A pointing toward the location of the empty Ta1 orbital projecting from the base of the piano stool. Therefore, we conclude that the location of the C21–H21A bond in a coordination position on Ta1 and the short Ta1···H21A distance, combined with the unusual NMR spectroscopic data, are consistent with a β-agostic interaction of H21A with Ta1. A partially deuterated allene version of **2** is needed in order to confirm this conclusion.

β-Agostic interactions in Group 5 chemistry are rare, with the vast majority of agostic interactions being α-agostic interactions in alkylidene and alkyl complexes [51b]. Tantalum– and niobium–hydrogen distances in cases of α-agostic interactions are typically 2.13 [51b] to 2.36 Å [53]. There is one report [54] of a β-agostic interaction in tantalum chemistry, as postulated on the basis of an unusual upfield ^{1}H chemical shift (δ −0.09) and ^{13}C NMR spectroscopic data for the ethyl group in the alkylidene(ethyl) complex $Ta(CHCMe_3)(CH_2CH_3)Cl_2(PMe_3)_2$. β-Agostic interactions in dinuclear complexes are, to our knowledge, unknown, in contrast to the numerous reports of α-agostic interactions in dinuclear and particularly trinuclear cluster chemistry [51b,55]. While in most cases of agostic interactions the C–H bond is lengthened 5–10%, it is not always true that such bond lengthening is observed [51b]. The lack of possible back donation in **2a** from the d^0 Ta1 to the C21–H21A bond means that the postulated β-agostic interaction in **2a** would involve σ-activation without σ*-activation [56,57].

3. Conclusions

We have shown that allene reacts with **1** to give a new type of dinuclear allene coordination mode rather than mononuclear adducts or products derived from vinylic C–H bond activation. The allene ligand in **2a** is coordinated in a rarely observed bonding mode that can be described as a four-electron reduced metallallyl or, more properly, an alkylidene-diyl ligand. The remarkably short Ta1=C22 distance, planarity at C22, and twisting of the allene hydrogen atoms out of the C21–C22–C23 plane are consistent with this formulation. The probable existence of a β-agostic Ta1···H21A–C21 interaction is supported by the short Ta1···H21A distance, the location of the C21–H21A bond in a favorable position for interaction with an empty orbital on Ta1, the unusual high field ^{1}H NMR resonance for one allene hydrogen atom, and the disparate $^1J_{CH}$ values for the associated allene carbon atom.

We have shown recently that **2a** can be reduced by alkali metal amalgams in solution to the first propynylidene complex $(C_5Me_5)_2Ta_2Cl_2(\mu\text{-}H)_2(\mu\text{-}HCCCH)$ [58]. The proposed agostic C–H interaction in **2a** may assist the initial stages of this formal double C–H activation reaction.

The mechanism of reaction of allene with **1** is not known at present. The remote possiblility that **1** dissociates in solution to give solvated Cp^*TaX_2 which then reacts with allene to give a mononuclear allene adduct, followed by addition of a second equivalent of Cp^*TaX_2, has not yet been excluded. Addition of allene to the metal–metal triply-bonded $Cp_2Mo_2(CO)_4$ probably occurs by direct addition to the organodimolybdenum reactant, since no crossover product was noted [18] in the reaction of a mixture of $Cp_2Mo_2(CO)_4$ and $Cp_2W_2(CO)_4$ with allene.

4. Experimental

4.1. General

General procedures for glove box and Schlenk line manipulations, solvent purification, ligand preparation, mass spectrometry, infrared spectroscopy, and X-ray diffractometry have been published [59]. NMR spectroscopy was performed on a Bruker AMX-360 spectrometer operated in the internal deuterium lock mode with all chemical shifts reported in ppm (positive chemical shifts representing resonances at lower field strength than that of the standard). Proton spectra and selectively homodecoupled proton spectra at 360.17 MHz were referenced to the residual protio solvent impurity (C_6D_5H, δ 7.15; $CDHCl_2$, δ 5.32) in the respective perdeuterated solvent. Carbon-13 NMR spectra at 90.58 MHz were recorded in either the fully {^{1}H} or gated {^{1}H} mode and were

referenced to the solvent carbon-13 resonance (C_6D_6, δ 128.0; CD_2Cl_2, δ 53.8). Infrared spectra were recorded as either KBr pellets or concentrated Nujol mulls.

$Cp^*_2Ta_2(\mu\text{-}X)_4$ (X = Cl, Br) was prepared by sodium amalgam reduction [45] of Cp*TaX_4 [59] in toluene using mechanical stirring and filtration through oven-dried Celite prior to fractional crystallization. Allene (Matheson, Aldrich) was used as received.

4.2. Synthesis of $Cp^*_2Ta_2(\mu\text{-}Cl)Cl_3(\mu\text{-}C_3H_4)$

$Cp^*_2Ta_2Cl_4$ (0.50 g., 0.65 mmol) was dissolved in toluene (80 cm^3) in a 150 cm^3 2-neck flask equipped with magnetic stir bar, gas inlet adapter and septum. The flask was cooled to −78 °C and then allene (36 cm^3 at 20 °C, 1.5 mmol, 2.3 equiv.) was introduced into the green reactant solution via gas-tight syringe. The cooling bath was removed after one hour and the solution allowed to warm to room temperature with stirring. After 12 hours, the dark red solution was filtered to remove a very small quantity of insoluble impurity and the filtrate concentrated in vacuo to low volume. After cooling the solution to −35 °C, two crops of brown red crystals were collected by fractional crystallization and filtrate concentration, washed with hexane, and dried in vacuo. Total weight: 0.29 g (55% yield based on $Cp^*_2Ta_2Cl_4$). *Anal.* Calc. for $C_{23}H_{34}Cl_4Ta_2$: C, 33.93; H, 4.22; Cl, 17.41. Found: C, 34.13; H, 4.22; Cl, 15.74%. ^{1}H NMR (δ, C_6D_6, 25 °C): 1.66 (broad s, 2H, CH_2), 1.97 (s, 30H, C_5Me_5), 2.60 (broad s, 2H, CH_2). ^{1}H NMR (δ, CD_2Cl_2, 25 °C): 1.41 (m, 2H, CH_2), 1.70 (m, 2H, CH_2), 2.33 (s, 30H, C_5Me_5). ^{1}H NMR (δ, CD_2Cl_2, −95 °C, J_{HH} values based on selective decoupling of each allene ligand resonance): −0.36 (dd, 1H, CH, $^2J_{HH} = 14$ Hz, $^4J_{HH} = 10$ Hz), 0.09 (d, 1H, CH, $^2J_{HH} = 14$ Hz), 2.12 (s, 15H, C_5Me_5), 2.19 (s, 15H, C_5Me_5), 2.6 (overlapped d and broad singlet, *J* not resolvable, 2H, CHH). ^{13}C NMR (δ, gated {^{1}H}, CD_2Cl_2, 25 °C): 12.4 (q, $C_5\mathit{Me}_5$, $^1J_{CH} = 129$ Hz), 62.9 (t, CH_2, $^1J_{CH} = 160$ Hz), 122.5 (s, C_5Me_5), 206.9 (s, $CH_2=\mathit{C}=CH_2$). ^{13}C NMR (δ, gated {^{1}H}, CD_2Cl_2, −95 °C): 11.8 (q, C_5Me_5, $^1J_{CH} = 129$ Hz), 12.6 (q, $C_5\mathit{Me}_5$, $^1J_{CH} = 129$ Hz), 42.9 (dd, $\mathit{C}H_2=C=CH_2$, $^1J_{CH} = 173$, 154 Hz), 70.3 (t, $CH_2=C=\mathit{C}H_2$, $^1J_{CH} = 154$ Hz), 118.3 (s, C_5Me_5), 124.0 (s, C_5Me_5), 204.4 (s, $CH_2=\mathit{C}=CH_2$). MS (*m*/*e*): no parent ion observed; the highest ion, at *m*/*e* 776, was assigned to $Cp^*_2Ta_2Cl_3(C_3H_4)^+$ based on chlorine isotope pattern. IR (KBr pellet, concentrated Nujol mull): no discernible absorption between 2750 and 2200 cm^{-1}.

4.3. Synthesis and spectroscopic characterization of $Cp^*_2Ta_2Br_4(C_3H_4)$

The brown red bromide analog was prepared by the same procedure used for the chloride compound, by reaction of $Cp^*_2Ta_2$ (μ-Br)$_4$ (0.52 g, 0.55 mmol) with allene (26 cm^3 at 20 °C, 1.08 mmol, 2 equiv). Yield from two crops, 0.29 g (53%). ^{1}H NMR (δ, C_6D_6, 25 °C): 1.88 (s, broad, 2H, CH_2); 2.01 (s, 30H, C_5Me_5); 2.26 (s, broad, 2H, CH_2). ^{1}H NMR (δ, CD_2Cl_2, 25 °C): 1.30 (s, broad, 2H, CH_2); 1.49 (s, broad, 2H, CH_2); 2.32 (s, 30H, C_5Me_5). IR (KBr pellet, concentrated Nujol mull): no discernible absorption between 2750 and 2200 cm^{-1}.

4.4. X-ray data collection and structure determination

Crystals of **2a** were grown from toluene/hexane solution as dark red plates. A single crystal was mounted under nitrogen in a thin-walled glass capillary. Data was collected at 200 K on an Enraf-Nonius CAD-4 diffractometer and processed with the Enraf-Nonius MOLEN software package. Of 10090 total reflections collected in the range of $4° < 2\theta < 55°$, 5037 reflections with $F^2 > 2.0\sigma(I)$ were used in the structure solution and refinement.

4.4.1. Crystal data

$Ta_2Cl_4C_{23}H_{34}$, $M = 814.2$, triclinic, $a = 11.121(2)$ Å, $b = 16.979(4)$ Å, $c = 8.298(2)$ Å, $\alpha = 114.42(2)°$, $\beta = 105.49(2)°$, $\gamma = 105.01(2)°$; (35 reflections, $25° < 2\theta < 36°$, used in cell dimension determination), $D_c = 2.15$, $Z = 2$, space group $P\bar{1}$ (No. 2), $V = 1247(5)$, crystal dimensions = 0.17 × 0.28 × 0.34 mm, intensity standards decay = <2%, absorption coefficient = 9.20 mm^{-1}, analytical absorption correction method used, agreement between equivalent reflections = 0.035.

The structure was solved by direct methods. All the non-H atoms were refined with anisotropic thermal parameters, and the H atoms on C21 and C23 were located in a difference map and refined with $U_{iso} = 1.2 * U_{iso}$(carbon). The remaining H atoms on Cp* groups were included at calculated positions with calculated thermal parameters. $R = 0.054$ and $R_{w2} = 0.151$ with standard SHELXL97 weighting scheme $w = [\sigma^2(F_o^2) + (0.1105p)^2 + (4.9728p)]^{-1}$ (with $p = (F_o^2 + 2F_c^2)/3$) were obtained at final refinement. Standard deviation of unit weight was 1.071.

5. Supplemental material

Crystallographic data for structural analysis has been deposited with the Cambridge Crystallographic Data Center, CCDC 275641 for compound $(C_5Me_5)_2Ta_2(\mu\text{-}\eta^1,\eta^3\text{-}C_3H_4)(\mu\text{-}Cl)Cl_3$ (**2a**). Copies of this information may be obtained free of charge from The Director, CCDC, 12 Union Road, Cambridge, CB2 IEZ, UK (fax: +44-1223-336-033; e-mail: deposit@ccdc.cam.ac.uk or http://www.ccdc.cam.ac.uk).

Acknowledgements

The authors gratefully acknowledge support from the National Science Foundation for the purchase of the CAD-4 diffractometer system (CHE85-07623) and the Department of Energy for the purchase of the Bruker AMX-360 NMR spectrometer (DE-FG05-89ER75503).

References

[1] F.L. Bowden, R. Giles, Coord. Chem. Rev. 20 (1976) 81.
[2] A.D. Horton, M.J. Mays, J. Chem. Soc., Dalton Trans. (1990) 155.
[3] L.-S. Wang, M. Cowie, Can. J. Chem. 73 (1995) 1058.
[4] V.C. Gibson, G. Parkin, J.E. Bercaw, Organometallics 10 (1991) 220.
[5] B.T. Sterenberg, R. McDonald, M. Cowie, Organometallics 16 (1997) 2297.
[6] G. Conole, K. Henrick, M. McPartlin, A.D. Horton, M.J. Mays, E. Sappa, J. Chem. Soc., Dalton Trans. (1990) 2367.
[7] S.A.R. Knox, D.A.V. Morton, A.G. Orpen, M.L. Turner, Inorg. Chim. Acta 220 (1994) 201.
[8] M.J. Fildes, S.A.R. Knox, A.G. Orpen, M.L. Turner, M.I. Yates, J. Chem. Soc., Chem. Commun. (1989) 1680.
[9] G.S. Lewandos, N.M. Doherty, S.A.R. Knox, K.A. MacPherson, A.G. Orpen, Polyhedron 7 (1988) 837.
[10] M.J. Chetcuti, P.E. Fanwick, S.R. McDonald, N.N. Rath, Organometallics 10 (1991) 1551.
[11] W. Lin, S.R. Wilson, G.S. Girolami, Organometallics 16 (1997) 2356.
[12] S.T. Chacon, M.H. Chisholm, K. Folting, J.C. Huffman, M.J. Hampden-Smith, Organometallics 10 (1991) 3722.
[13] S.W. Carr, B.L. Shaw, M. Thornton-Pett, J. Chem. Soc., Dalton Trans. (1987) 1763.
[14] A. Borrini, G. Ingrosso, J. Organomet. Chem. 132 (1977) 275.
[15] P. Racanelli, G. Pantini, A. Immirzi, G. Allegra, L. Porri, Chem. Commun. (1969) 361.
[16] L.-S. Wang, M. Cowie, Organometallics 14 (1995) 3040.
[17] D.S.A. George, R. McDonald, M. Cowie, Organometallics 17 (1998) 2553.
[18] W.I. Bailey, M.H. Chisholm, F.A. Cotton, C.A. Murillo, L.A. Rankel, J. Am. Chem. Soc. 100 (1978) 802.
[19] I.-Y. Wu, T.-W. Tseng, C.-T. Chen, M.-C. Cheng, Y.-C. Lin, Y. Wang, Inorg. Chem. 32 (1993) 1539.
[20] Y.N. Al-Obaidi, P.K. Baker, M. Green, N.D. White, G.E. Taylor, J. Chem. Soc., Dalton Trans. (1981) 2321.
[21] C.G. Kreiter, M. Leyendecker, W.S. Sheldrick, J. Organomet. Chem. 302 (1986) 35.
[22] J.R. Briggs, C. Crocker, W.S. McDonald, B.L. Shaw, J. Chem. Soc., Dalton Trans. (1981) 121.
[23] W.A. Herrmann, J. Weichmann, M.L. Ziegler, H. Pfisterer, Angew. Chem., Int. Ed. Engl. 21 (1982) 551.
[24] C.G. Kreiter, W. Michels, G. Heeb, J. Organomet. Chem. 502 (1995) 9.
[25] T.A. Budzikiewicz, M.H. Chisholm, K. Folting, J.C. Huffman, W.E. Streib, D.B. Tiedtke, Polyhedron 17 (1998) 857.
[26] D. Lentz, N. Nickelt, S. Willemsen, Chem. - Eur. J. 8 (2002) 1205.
[27] M.H. Chisholm, W.E. Streib, D.B. Tiedtke, D.-D. Wu, Chem. - Eur. J. 4 (1998) 1470.
[28] J.N.L. Dennett, S.A.R. Knox, J.P.H. Charmant, A.L. Gillon, A.G. Orpen, Inorg. Chim. Acta 354 (2003) 29.
[29] X.L.R. Fontaine, G.B. Jacobsen, B.L. Shaw, M. Thornton-Pett, J. Chem. Soc., Dalton Trans. (1988) 1185.
[30] N. Spetseris, J.R. Norton, C.D. Rithner, Organometallics 14 (1995) 603.
[31] R.E. Davis, Chem. Commun. (1968) 248.
[32] R. Ben-Shoshan, R. Pettit, Chem. Commun. (1968) 247.
[33] R.E. Colborn, A.F. Dyke, S.A.R. Knox, K.A. Mead, P. Woodward, J. Chem. Soc., Dalton Trans. (1983) 2099.
[34] A. Wojcicki, C.E. Shuchart, Coord. Chem. Rev. 105 (1990) 35.
[35] A.J. Arce, Y. De Sanctis, A.J. Deeming, K.I. Hardcastle, R. Lee, J. Organomet. Chem. 406 (1991) 209.
[36] D. Seyferth, L.L. Anderson, W.B. Davis, M. Cowie, Organometallics 11 (1992) 3736.
[37] T.A. Hanna, A.M. Baranger, R.G. Bergman, J. Am. Chem. Soc. 117 (1995) 11363.
[38] D.W. Ball, R.G.S. Pong, Z.H. Kafafi, J. Am. Chem. Soc. 115 (1993) 2864.
[39] L.N. Lewis, J.C. Huffman, K.G. Caulton, Inorg. Chem. 19 (1980) 1246.
[40] N.M. Doherty, C. Elschenbroich, H.-J. Kneuper, S.A.R. Knox, J. Chem. Soc., Chem. Commun. (1985) 170.
[41] M. Bamber, G.C. Console, R.J. Deeth, S.F.T. Froom, M. Green, J. Chem. Soc., Dalton Trans. (1994) 3569.
[42] C.P. Casey, E.A. Austin, J. Am. Chem. Soc. 110 (1988) 7106.
[43] C.P. Casey, E.A. Austin, Organometallics 5 (1986) 584.
[44] E.L. Hoel, G.B. Ansell, S. Leta, Organometallics 5 (1986) 585.
[45] C. Ting, N.C. Baenziger, L. Messerle, J. Chem. Soc., Chem. Commun. (1988) 1133.
[46] C. Ting, L. Messerle, J. Am. Chem. Soc. 111 (1989) 3449.
[47] J.-H. Huang, T.-Y. Lee, D.C. Swenson, L. Messerle, Inorg. Chim. Acta 345 (2003) 209.
[48] C. Ting, L. Messerle, J. Am. Chem. Soc. 109 (1987) 6506.
[49] J.C. Green, M.L.H. Green, P. Mountford, M.J. Parkington, J. Chem. Soc., Dalton Trans. (1990) 3407.
[50] L. Messerle, ACS Symp. Ser. 357 (1987) 198.
[51] (a) M. Brookhart, M.L.H. Green, J. Organomet. Chem. 250 (1983) 395;
(b) M. Brookhart, M.L.H. Green, L.L. Wong, Prog. Inorg. Chem. 36 (1988) 1, and references therein;
(c) R.H. Crabtree, D.G. Hamilton, Adv. Organomet. Chem. 28 (1988) 299.
[52] W.C. Finch, E.V. Anslyn, R.H. Grubbs, J. Am. Chem. Soc. 110 (1988) 2406.
[53] A.D. Poole, D.N. Williams, A.M. Kenwright, V.C. Gibson, W. Clegg, D.C.R. Hockless, P.A. O'Neill, Organometallics 12 (1993) 2549.
[54] J.D. Fellmann, R.R. Schrock, D.D. Traficante, Organometallics 1 (1982) 481.
[55] D.L. Davies, B.P. Gracey, V. Guerchais, S.A.R. Knox, A.G. Orpen, J. Chem. Soc., Chem. Commun. (1984) 841.
[56] O. Eisenstein, Y. Jean, J. Am. Chem. Soc. 107 (1985) 1177.
[57] D.L. Lichtenberger, G.E. Kellogg, J. Am. Chem. Soc. 108 (1986) 2560.
[58] J.-H. Huang, J.J. Luci, T.-Y. Lee, D.C. Swenson, J.H. Jensen, L. Messerle, J. Am. Chem. Soc. 125 (2003) 1688.
[59] T.Y. Meyer, L.R. Garner, N.C. Baenziger, L. Messerle, Inorg. Chem. 29 (1990) 4045.

Available online at www.sciencedirect.com
SCIENCE DIRECT
Polyhedron 25 (2006) 568–574
POLYHEDRON
www.elsevier.com/locate/poly

Synthesis of micro-crystals of transparent cobalt aluminate, shrouded in siliceous material, from Co(II)-exchanged zeolite X

Matthew Thomas Jamie Lodge [a], Peter P. Edwards [a,*], Paul A. Anderson [b], Martin O. Jones [a], Ian Gameson [b]

[a] *Inorganic Chemistry Laboratory, University of Oxford, South Parks Road, Oxford, OX1 3QR, UK*
[b] *School of Chemistry, The University of Birmingham, Haworth Building, Edgbaston, Birmingham, B15 2TT, UK*

Received 5 July 2005; accepted 12 August 2005
Available online 11 October 2005

Abstract

We report an investigation of the synthesis of a cobalt aluminate spinel composite from the heat-induced collapse of cobalt ion-exchanged sodium zeolite X. The work presented here adds to earlier studies by illustrating that by careful control of synthesis and reaction conditions, both the phase composition and crystallite size of the spinel can be controlled. The spinel crystallites grow within siliceous materials formed by the collapse of the zeolite framework, with the crystalline particles being completly shrouded by the siliceous matrix.
© 2005 Elsevier Ltd. All rights reserved.

Keywords: Cobalt Aluminate; Synthesis; Zeolite; Transparent; Pigment; Ion-exchange

1. Introduction

Cobalt aluminate spinel, $CoAl_2O_4$, which imparts an intense royal blue colour arising from tetrahedral coordinated Co(II) ions, has been used extensively as an inorganic pigment [1–3]. This pigment is usually prepared by the calcination of the constituent oxides [4,5] or via a sol–gel reaction using mixed alkoxides or other metal organic compounds as starting materials [6–9].

Here we explore the potential of a process [10–14] which involves the heat-induced collapse of ion-exchanged zeolite X precursors for the synthesis of aluminate ceramics. Following the collapse of the framework structure, an amorphous phase is formed from the zeolite precursors, followed by the crystallisation of dense aluminate spinel particles. Interestingly, this synthesis route results in optically transparent aluminate micro-crystals which are completely shrouded by an amorphous siliceous phase from which the spinel particles have crystallised.

Zeolites [15–19] are microporous aluminosilicates which carry a counter cation to balance the negative framework charge that results from the substitution of silicon by aluminium. The materials reported in this paper were all prepared using sodium zeolite X – a Faujasite type zeolite having an approximate Si/Al ratio of 1.2 (Fig. 1). The extra-framework ions can be replaced by the process of ion-exchange and the balance of charge between this cation and the framework maintains charge neutrality. Therefore, assuming a complete ion-exchange of sodium zeolite X with cobalt(II) to synthesise cobalt zeolite X, the cobalt will be in a ratio of 1:2 with respect to the framework aluminium.

A Co(II)/Al(III) ratio of 1/2 for a fully ion-exchanged zeolite is therefore precisely the composition ratio of the cations in the target spinel phase. The ion-exchange procedure thus ensures that the elemental components of the aluminate are present in the correct stoichiometric ratio (see Scheme 1).

The elemental distribution of both constituent framework ions and guest (ion-exchange) cations is highly uniform since all of these elements are fixed at crystallographically defined sites. This perfect elemental distribution – on the atomic scale – ensures the uniform nucleation of phases from the zeolite 'precursor' [10,12]. Following the heat-induced

* Corresponding author.
E-mail address: peter.edwards@chem.ox.ac.uk (P.P. Edwards).

0277-5387/$ - see front matter © 2005 Elsevier Ltd. All rights reserved.
doi:10.1016/j.poly.2005.08.041

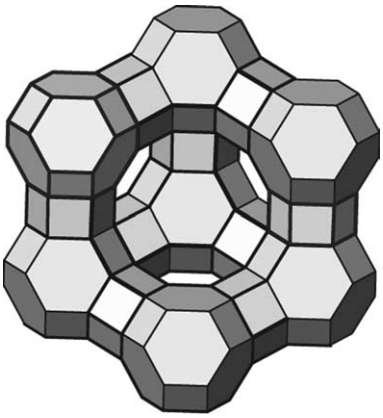

Fig. 1. A representation of zeolite X showing only the aluminosilicate framework. Extra-framework cations, for example Na^+, can be replaced by Co^{2+} (see Scheme 1) and this assembly forms the basis for the "precursor" for the cobalt aluminate spinel.

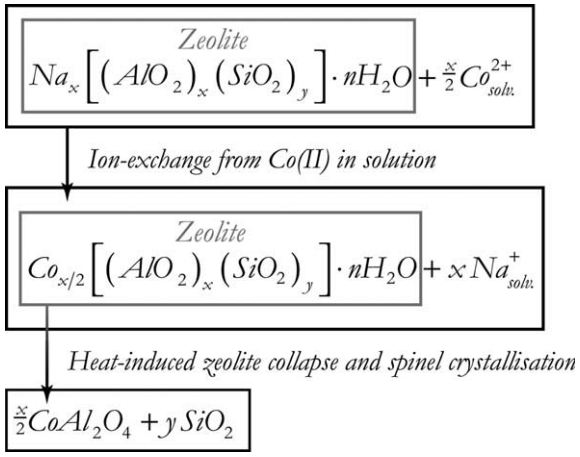

Scheme 1. A representation of the preparation of cobalt aluminate from a zeolite involving the process of (solution-based) ion-exchange and the heat-induced collapse of the ion-exchanged zeolite precursor to synthesise $CoAl_2O_4$ and siliceous materials.

collapse of the zeolite X framework, the elemental dispersion is maintained and the nucleation of the dense cobalt aluminate spinel phase precipitates homogeneously from within the amorphous matrix. By carefully adjusting the reaction and processing conditions, a high degree of control can therefore be exerted on the resulting cobalt aluminate micro-crystals.

The remaining framework silicon and oxygen form a siliceous shroud upon collapse that encases the micro crystals of cobalt aluminate. Thus, this synthesis route has the benefit of potentially limiting the escape of the harmful cobalt ion into the environment.

2. Experimental

Sodium zeolite X was prepared by a traditional hydrothermal synthesis route [19] using solutions of sodium metasilicate and sodium aluminate. The concentration of aqueous sodium metasilicate was increased slightly above the normal stoichiometric level to discourage the formation of zeolite A.

Cobalt zeolite X was prepared by ion-exchange, at 80 °C, of sodium zeolite X with an aqueous solution of cobalt chloride of concentration 0.1 M.

The cobalt-exchanged zeolite was then heated at various temperatures and samples interrogated using powder X-ray diffraction. Individual samples were synthesised at specific temperatures ranging from 200 to 1200 °C, for 12 h with a heating rate of 300 °C per hour.

X-ray diffraction measurements were carried out using a Bruker Axs D5005 diffractometer operating in reflection mode. The diffractometer was fitted with a Gobel Mirror, which produced a parallel Cu Kα beam of wavelength 1.5418 Å. Normally the D5005 is fitted with a position sensitive detector, PSD. For variable temperature work the PSD was replaced with a scintillation detector and an Anton-Parr HTK 1200 °C furnace was fitted. Phase identification was undertaken using the Diffrac-AT software and JCPDS database card system.

Electron microscopy images were obtained using a Philips CM20 transmission electron microscope (TEM), operating at a voltage of 100 kV, and a JEOL JSM-5410 Scanning Electron Microscope (SEM), using an operating voltage of 40 kV. UV–Vis measurements were obtained using a Unicam UV500 UV/Vis spectrometer operating in diffuse reflectance mode.

3. Results and discussion

Sodium zeolite X (Na–X) and corresponding cobalt zeolite X (Co–X) were examined by X-ray diffraction in order to assess their phase purity and crystallinity. The results are presented in Fig. 2.

These diffraction data reveal that the Na–X was highly crystalline, particularly evident in the sharp diffraction peaks at high angle. Conversely, the lack of high angle reflections in the Co–X zeolite suggests that the acidic cobalt ion-exchange solution has initiated some damage to the zeolite framework with a corresponding reduction in sample crystallinity. The diffraction data also demonstrate that no zeolite A is present.

As cobalt aluminate is a highly coloured material, it was apparent from visual examination that for samples fired at temperatures below 800 °C there was little or no evidence of cobalt aluminate formation (Fig. 3). This was evident in the marked colour difference between the sample synthesised at 700 °C, where the sample appears beige, and 800 °C where a blue colour can clearly be seen.

The conclusions drawn from the visual examination were confirmed using variable temperature X-ray diffraction; data were collected over a 20–70 ° 2θ range from 25 to 1100 °C in incremental steps of 25 °C (Fig. 4).

The variable temperature diffraction data reveal that diffraction peaks corresponding to the zeolite X completely disappeared before those corresponding to cobalt aluminate began to appear. Thus it appears that the cobalt aluminate

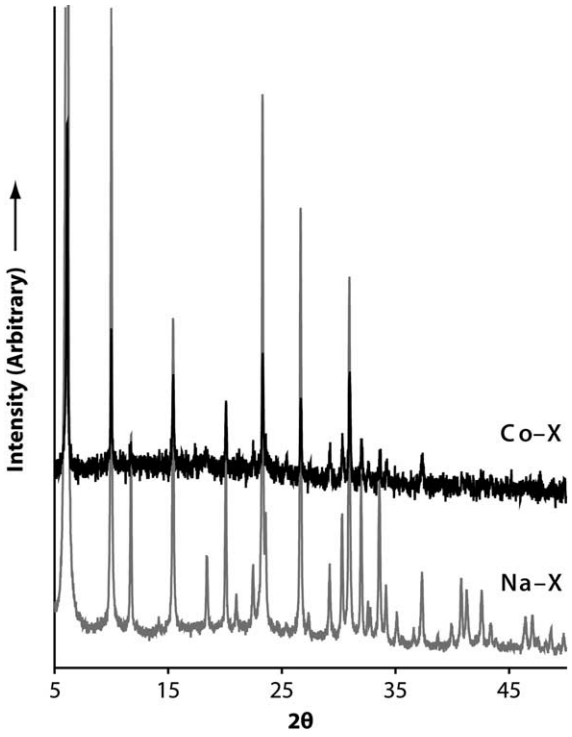

Fig. 2. X-ray diffraction patterns for synthesised Na–X and ion-exchanged Co–X.

Fig. 3. Co–X materials thermally collapsed at various temperatures. The onset of a blue colouration, characteristic of cobalt aluminate formation, can clearly be seen for the sample fired at 800 °C.

and other phases crystallise from the initial amorphous phase which is synthesised as a result of the heat-induced zeolite collapse. We can further ascertain the temperature for the initiation of aluminate formation. The horizontal

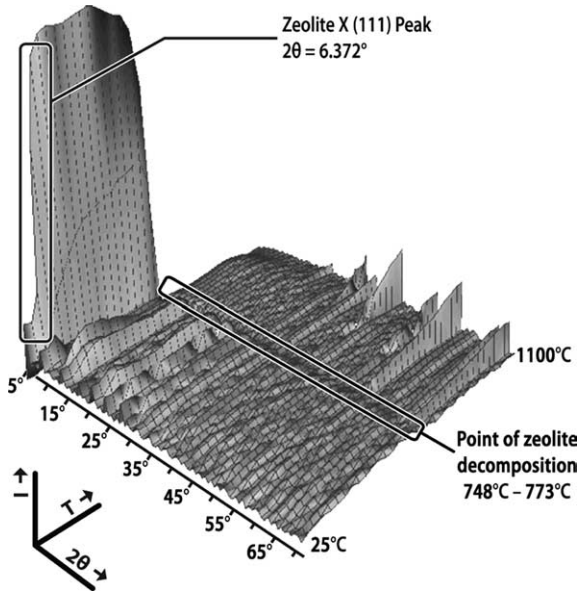

Fig. 4. X-ray diffraction data collected from a sample of cobalt zeolite X at various temperatures from 25 to 1100 °C.

box which runs parallel along the 2θ axis in Fig. 4 shows the position of this transition as being between 748 and 773 °C, which confirmed our visual observation that the sample synthesised at 700 °C contained no cobalt aluminate. The increase in relative intensity of the zeolite (111) peak at $2\theta = 6.372°$ is also noteworthy (highlighted by a vertical box in Fig. 4) and is due to the gradual dehydration of the zeolite. Because of the speed at which the X-ray diffraction scans were obtained, the data were of insufficient quality to provide further detailed information. Furthermore, due to the nature of the change in phase from Co–X zeolite, an open framework solid, to cobalt aluminate – a condensed solid – a decrease in sample volume occurred. As a result the surface of the alumina sample holder became exposed to the incident X-ray beam and a partial diffraction pattern of the alumina was recorded with that of the sample, further complicating any detailed interpretation.

X-ray data were therefore collected on a range of samples, each fired at a given temperature, from 800 to 1200 °C, to further probe the growth mechanism of the cobalt aluminate and associated phases (Fig. 5).

From Fig. 5 one can see that at synthesis temperatures below 1100 °C mullite [20] – general formula $Al_6Si_2O_{13}$ – was synthesised along with cobalt aluminate [21]. The reflections of cobalt aluminate have been identified by arrows in Fig. 5 bearing the *hkl* indices to which they relate. A reflection of mullite is highlighted in dark grey. At higher synthesis temperatures the mullite reflection disappears and is replaced by a diffuse diffraction peak running between 2θ values of 15° and 25°, highlighted in pale grey in Fig. 5. This is indicative of a poorly crystalline material and is attributed to siliceous material, since this is the most likely co-product given the composition of the amorphous phase formed by the zeolite collapse (Scheme 1). Finally, for samples prepared at 1200 °C there is evidence of the silica coe-

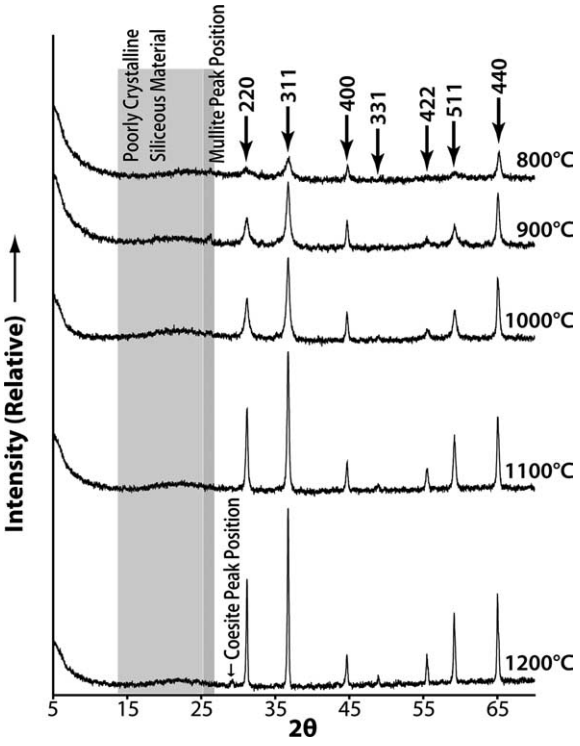

Fig. 5. X-ray diffraction data for separate materials synthesised from 800 to 1200 °C in 100 °C steps.

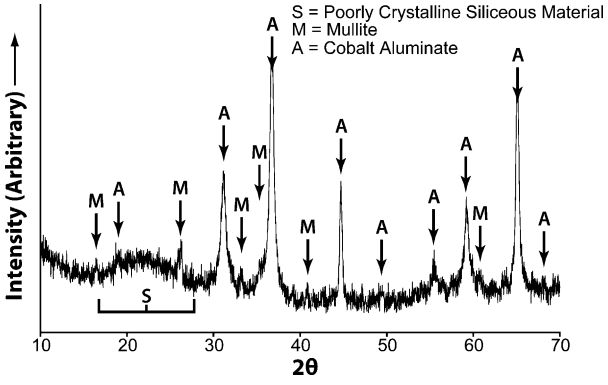

Fig. 6. X-ray diffraction data for cobalt aluminate synthesised at 900 °C.

site [22] of general formula SiO_2. The evidence for these phases can be more readily be seen by examining the individual patterns where the reflections are strongest (Figs. 6 and 7).

In Fig. 6 we can clearly identify mullite [20] and cobalt aluminate [21] as well as a diffuse diffraction peak that most likely represents some residual poorly crystalline siliceous material.

The formation of mullite, $Al_6Si_2O_{13}$ suggests that there was insufficient cobalt to allow all of the framework aluminium to be utilised in cobalt aluminate formation. This could possibly arise because of incomplete ion-exchange. If this is the case then sodium should also be present in the amorphous phase formed after zeolite collapse, represented by the diffuse diffraction peak, labelled 'S' in

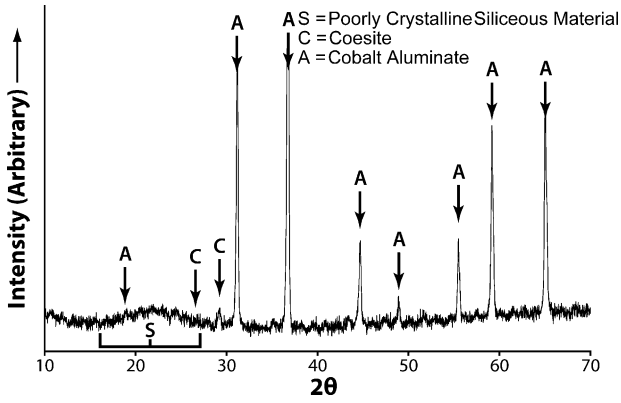

Fig. 7. X-ray diffraction data for cobalt aluminate synthesised at 1200 °C.

Fig. 6. Further elaboration of the composition of this amorphous phase is ongoing. Evidence of the presence of mullite was visible in the diffraction patterns of the samples synthesised in the range 800–1100 °C. Weidenthaler et al. [12] found only the reflections of cobalt aluminate in their collapsed Co–X materials at temperatures below 1100 °C and no evidence of mullite was reported.

As the synthesis temperature increases, the high temperature silica, coesite [22], gradually becomes visible (Fig. 7) together with a clear sharpening of the powder X-ray diffraction peaks for cobalt aluminate. The reflections from coesite are weak, however, and it is likely that the majority of the silica from the zeolite's framework is still poorly crystalline. This phase could also contain elements other than silicon and oxygen: aluminium and sodium, for example. At temperatures above 1100 °C Weidenthaler et al. [12] report finding the silica cristobalite, where we find coesite.

The growth of various phases and their subsequent disappearance can be partially explained in terms of Si/Al ratio, the ion-exchange level and the initial composition of the amorphous phase formed from the collapsed zeolite precursor. Once the zeolite has collapsed, there will exist a complex system of reactions, which result in the growth of many phases in competition each other. For example, the aluminium-containing mullite phase disappears at high temperature. It is possible that at high temperature the formation of cobalt aluminate becomes more favourable than that of mullite, thus the mullite phase is dissolved into the low crystallinity siliceous phase as the aluminium is scavenged by the formation of cobalt aluminate. At higher temperatures (above 1100 °C), a crystalline silicate, coesite, appeared. The growth of the coesite phase seems to coincide with the disappearance of the mullite phase. It could also be possible that the coesite is a product of the reconfiguration of the mullite, after sacrifice of the aluminium in the formation of cobalt aluminate.

The cobalt aluminate crystallite size was determined from the X-ray powder diffraction data (Fig. 5) using the Scherrer equation, below [23]

$$L_{hkl} = \frac{K\lambda}{\beta_{hkl}\cos\theta}$$

Table 1
A table of cobalt aluminate crystallite dimensions as calculated by the Scherrer equation

Synthesis temperature (°C)	Particle size in nm	
	$2\theta = 31.294$ (220) Peak	$2\theta = 36.743$ (311) Peak
800	14.6	12.5
900	14.3	19.6
1000	17.7	21.7
1100	28.8	32.1
1200	43.1	44.8

where K is a constant, normally equal to 1, λ is the wavelength of the incident X-ray radiation, 1.5418 Å in this case. The value θ is half of 2θ the position of the reflection, in radians, from which the value β_{hkl} is taken. β_{hkl} is the full width at half maximum height of the analysed reflection, given in angstroms and L_{hkl} is the particle diameter in angstroms. Table 1 shows the calculated particle diameters, in nm, for materials produced at various temperatures.

The Scherrer equation provides a volume-weighted statistical average of particle diameters. Thus it is best to treat the derived particle sizes obtained in this way as no more than a guide. However, one can readily discern that the spinel particle size increases with increasing synthesis temperature, as observed in earlier studies [12–14].

In Fig. 8 we show the trends in spinel crystallite size with increasing temperature of the synthesis process. Obviously, heating the material at higher temperatures leads to the formation of larger spinel micro-crystals, as indicated by the sharper powder X-ray diffraction reflections. We note that the rate of increase is approximately the same for each reflection. We have also used TEM (Fig. 9) to provide further direct information on crystallite size and morphology.

From these TEM data one can readily discern the cobalt aluminate micro-crystals suspended in, and covered by, a substrate which is more permeable to electrons; we believe that the particles consist of spinel micro-crystals covered by a siliceous matrix. This matrix shrouds the micro-crystals and blocks their surfaces. The micro-crystals, also noted by earlier workers [10–14], appear to be in the size regime

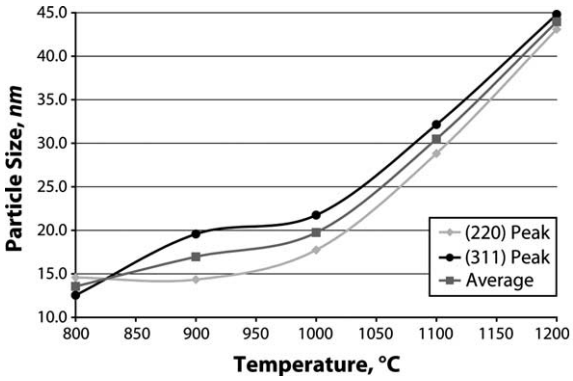

Fig. 8. A graph showing the trend in cobalt aluminate crystallite diameter against synthesis temperature.

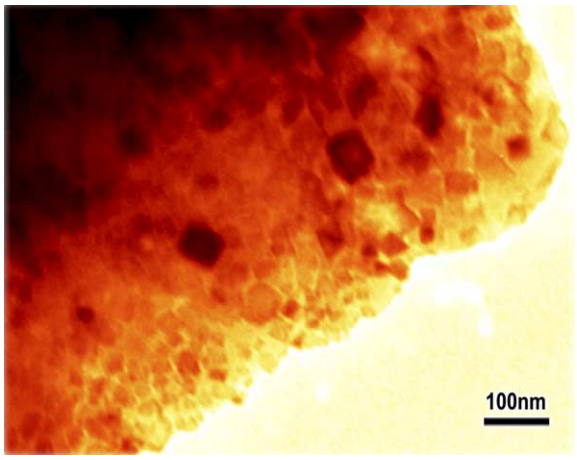

Fig. 9. A TEM micrograph of cobalt-exchanged zeolite X collapsed at 1000 °C. The cobalt aluminate spinel micro-crystals can clearly be seen in contrast to the encapsulating siliceous host.

between 15 and 60 nm, as suggested by the Scherrer equation.

SEM images were also obtained from samples produced at 800 °C (image 'a'), 900 °C (image 'b') and 1000 °C (images 'c' and 'd'). At lower temperatures the particles were irregular in shape and had uneven surfaces. As the synthesis temperature is increased the siliceous compounds start to become mobile and some of the particles exhibit a spherical shape. One such particle is shown enlarged in Fig. 10 image 'd'. The small white areas on the surface may be exposed areas of cobalt aluminate.

As our primary interest in these compounds was as potential pigment materials, UV/Vis spectroscopic measurements were also obtained for samples produced at 800 °C and above (Fig. 11).

The UV/Vis spectra reveal that the intensity of the cobalt aluminate colour centre increased with increasing synthesis temperature. This can be seen in the increase in absorbance in the 200–400 nm and 500–675 nm regions.

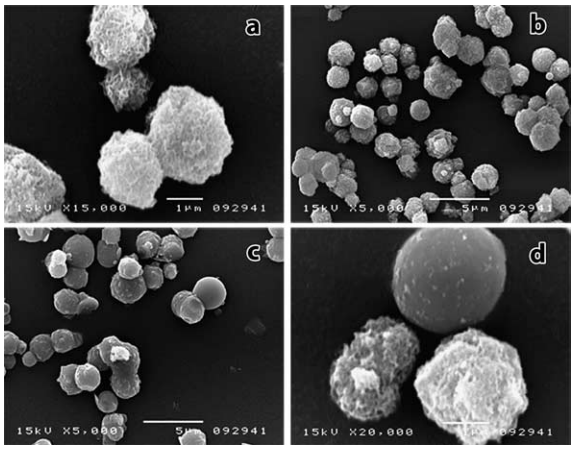

Fig. 10. Four SEM images from samples produced at 800 °C, image 'a', 900 °C, image 'b', and 1000 °C, images 'c' and 'd'. The scale bars represent 1 μm (a,d) and 5 μm (b,c).

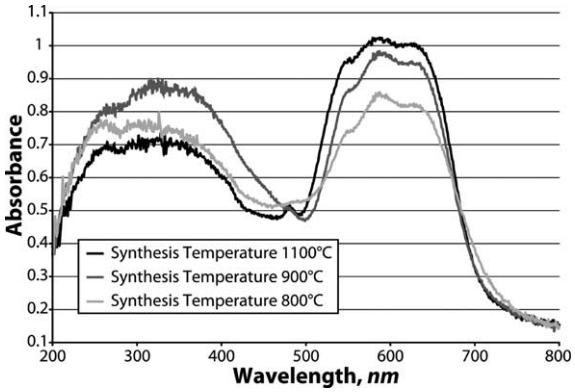

Fig. 11. Diffuse reflectance UV/Vis spectra of samples produced at various temperatures.

These data support our visual observation of the samples (Fig. 3) and also explain the paleness of the blue colour seen in samples produced at low temperature. This difference in colour intensity could be due to a particle size effect, the more divided the material, the more diffuse and less intense the colour [1], or simply due to the fact that less cobalt aluminate is present in the sample. If the particle size is small enough, however, there exists the possibility that the particles will be optically transparent [1].

In order to test this proposition, samples were suspended in silicone oil. The particular oil was chosen as it has a refractive index close to that of glass and is colourless and transparent. By observing the suspensions in front of cards of various colours and under various lighting conditions, it was possible to determine that the colour of the samples was due largely to transmitted light. For cobalt aluminate samples prepared at lower synthesis temperatures almost all the colour was the result of transmitted light. Further experimentation demonstrated the transparency of our samples within a polymer host (Fig. 12).

Fig. 12 shows our sample dispersed in a polymer and spread on a glass slide, part of which is black and part of which is white. The observation that the blue colouration was only evident on the white part demonstrated that the colour was due to transmission and not reflection.

Fig. 12. A film of micro crystals of cobalt aluminate dispersed in a polymer and deposited on a glass support.

4. Conclusions

We have shown that the controlled heat-induced collapse of cobalt zeolite X provides a highly effective route to producing micro crystals of cobalt aluminate shrouded in a coating of siliceous materials, which should help prevent leaching of cobalt into the environment. Schmidt et al. [13,14] found that the cobalt aluminate micro-crystals could be freed from their siliceous shroud for use as high surface area catalysts.

Our results suggest that the collapse of cobalt-exchanged zeolite X produced an amorphous phase in which a complex series of competing reactions take place to produce a dense spinel micro-crystals covered by a siliceous matrix. The fact that the work of Weidenthaler et al. [12] showed different crystalline phases is thus perhaps not surprising as there are many factors which could alter the components of the final crystalline phase after the collapse of the zeolite. These include; the Si/Al ratio of the original zeolite, the extent of ion-exchange, the temperature at which the zeolite was collapsed and, most probably, the duration of the heating of the amorphous phase after zeolite collapse. There exists here a system of great interest worthy of further study and experimentation.

This work, therefore, adds to the earlier pioneering work of Colyer et al. [10,11] in demonstrating the significant potential of materials prepared from the heat-induced collapse of ion-exchange zeolites for the synthesis of aluminosilicate-based ceramics.

Acknowledgements

We thank the EPSRC for their financial support. It is a great pleasure – and a great honour – to be part of these celebrations for our colleague Professor Chisholm on this very happy occasion.

References

[1] R.J.D. Tilley, Colour and Optical Properties of Materials, John Wiley and Sons, New York, 2000.
[2] R.J.H. Clark, Chem. Soc. Rev. (1995) 187.
[3] A.M. Ferrari, C. Leonelli, T. Manfredini, P. Miselli, G. Monari, G.C. Pellacani, Ind. Ceram. 18 (1998) 7.
[4] T. He, K.D. Becker, Solid State Ionics 101 (1) (1997) 337.
[5] P.H. Bolt, F.H.P.M. Habraken, J.W. Geus, J. Solid State Chem. 135 (1998) 59.
[6] G. Busca, V. Lorenzelli, V. Bolis, Mater. Chem. Phys. 31 (1992) 221.
[7] M. Sales, C. Valentín, J. Alarcón, J. Eur. Ceram. Soc. 17 (1997) 41.
[8] M. Zayat, D. Levy, Chem. Mater. 12 (2000) 2763.
[9] J. Merikhi, H. Jungk, C. Feldmann, J. Mater. Chem. 10 (2000) 1311.
[10] L.M. Colyer, G.N. Greaves, A.J. Dent, S.W. Carr, K.K. Fox, R.H. Jones, in: J. Weitkamp, H.G. Karge, H. Pfeifer, W. Hölderich (Eds.), Studies in Surface Science and Catalysis, vol. 84, Elseiver, Amsterdam, 1994, p. 387.
[11] L.M. Colyer, G.N. Greaves, A.J. Dent, K.K. Fox, S.W. Carr, R.H. Jones, Nucl. Instr. Meth. Phys. Res. Sect. B 97 (1995) 107.
[12] C. Weidenthaler, W. Schmidt, Chem. Mater. 12 (2000) 3811.
[13] W. Schmidt, C. Weidenthaler, Chem. Mater. 13 (2001) 607.
[14] W. Schmidt, C. Weidenthaler, Micropor. Mesopor. Mater. 48 (2001) 89.

[15] A. Dyer, An Introduction to Zeolite Molecular Sieves, John Wiley and Sons, New York, 1988.
[16] D.W. Breck, Zeolite Molecular Sieves, Wiley, New York, 1974.
[17] R.M. Barrer, Zeolites and Clay Minerals as Sorbents and Molecular Sieves, Academic Press, London, 1982.
[18] J.V. Smith, Chem. Rev. 88 (1988) 149.
[19] D.W. Breck, Synthesis and Properties of Union Carbide Zeolites L, X and Y, Union Carbide Corporation, USA, 1982.
[20] JCPDS card number 15-776. Primary reference, NBSMA6, 3, 1964, 3.
[21] JCPDS card number 44-160. R. Sailer and G. McCarthy, ICDD Grant-in-Aid, 1992, North Dakota State University, Fargo, North Dakota.
[22] JCPDS card number 83-1833. Primary reference, L. Levien and C.T. Prewitt, AMMIAY, 66, 324, 1981.
[23] H.P. Klug, L.E. Alexander, X-ray Diffraction Procedures for Polycrystalline and Amorphous Materials, 2nd ed., John Wiley and Sons, New York, 1977.

Available online at www.sciencedirect.com
SCIENCE DIRECT®
Polyhedron 25 (2006) 575–584
POLYHEDRON
www.elsevier.com/locate/poly

Theoretical studies of π-loading and structural diversity in Cp_3MX (M = Zr, Hf; X = H, CH_3, OR, NR_2) compounds

Erick J. Palmer, Bruce E. Bursten *

Department of Chemistry, The Ohio State University, 100 W. 18th Avenue, Columbus, OH 43210, USA

Received 20 June 2005; accepted 19 July 2005
Available online 30 August 2005

In celebration of Professor Malcolm H. Chisholm, our inspirational friend, colleague and mentor, on the occasion of his 60th birthday.

Abstract

Density functional theory has been used to explore the bonding and geometric preferences of tris-Cp zirconium and hafnium compounds of the type Cp_3MX. In most cases, two primary isomers were found: a "**3-5**" isomer, which contains three η^5-Cp ligands, and a "**2-5,1-1**" isomer, which contains two η^5-Cp and one η^1-Cp ligands. The relative energies of these isomers are dependent upon the π-donor ability of the X ligand. For the tris-Cp methyl compounds, the "**3-5**" isomers are more stable by 1–4 kcal/mol. The "**2-5,1-1**" isomers of the tris-Cp alkoxide and amido compounds are more stable by 3–6 and 6–11 kcal/mol, respectively. Bonding analyses show these binding preferences can be understood in terms of π-competition between the tris-Cp ligand set and the lone pair of the X ligand. π-loading on the X ligand decreases the π-donor ability of the "**3-5**" tris-Cp ligand set, which increases the preference for the "**2-5,1-1**" ground state geometry in the complexes with strong π-donors. In addition, molecular orbital theory provides evidence for destabilization effects arising from filled–filled interactions between the "**3-5**" Cp_3M fragment and the X lone pair.
© 2005 Elsevier Ltd. All rights reserved.

Keywords: Organometallics; Density functional theory; tris-Cyclopentadienyl; π-donation; Alkoxide and amido complexes; Molecular orbital theory

1. Introduction

The bonding of three cyclopentadienyl (Cp) ligands to a metal center in Cp_3MX (M = Zr, Hf; X = H, CH_3, OR, NR_2) compounds leads to a variety of different bonding modes. The three Cp ligands can all bind in an η^5 fashion, which we refer to as a "**3-5**" geometry. Another bonding mode involves two η^5-Cp ligands and one η^1-Cp ligand, which we refer to as a "**2-5,1-1**" geometry. Alternatively, two Cp ligands can bind in an η^5 fashion with the other Cp ligand binding in an η^2 fashion, which we refer to as a "**2-5,1-2**" geometry. These bonding modes are shown in Fig. 1.

Our current interest in tris-cyclopentadienyl (tris-Cp) compounds of the Group IV transition metals stems from our earlier theoretical work on tris-Cp f-element compounds [1]. tris-Cp lanthanide complexes have been structurally characterized and shown to exhibit interesting structural chemistry across the lanthanide series [2]. Although these complexes exhibit very little notable reactivity, Evans has recently shown that reductive chemistry can be induced in tris-Cp lanthanide complexes when the Cp ligands are replaced with larger pentamethylcyclopentadienyl (Cp*) ligands [3]. The availability of a variety of oxidation states in the actinide series leads to a much richer reaction chemistry involving tris-Cp actinide compounds relative to their lanthanide counterparts [4]. For example, tris-Cp actinide compounds have been used as precursors to compounds containing actinide-transition metal single

* Corresponding author. Tel.: + 1 614 292 1866; fax: + 1 614 688 3306.
E-mail address: bursten.1@osu.edu (B.E. Bursten).

0277-5387/$ - see front matter © 2005 Elsevier Ltd. All rights reserved.
doi:10.1016/j.poly.2005.07.033

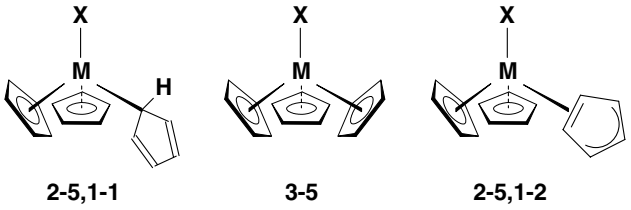

Fig. 1. Known bonding modes of three cyclopentadienyl (Cp) ligands around a transition metal center. Compounds containing two η^5-Cp and one η^1-Cp ligands (left) are referred to as having a "**2-5,1-1**" geometry. Compounds containing three η^5-Cp ligands (middle) are referred to as having a "**3-5**" geometry. Compounds containing two η^5-Cp and one η^2-Cp ligands (right) are referred to as having a "**2-5,1-2**" geometry.

bonds [5], and substituted tris-Cp actinide compounds were seminal in isolating the first terminal end-on actinide metal dinitrogen compound [6].

Despite the large number of tris-Cp lanthanide and actinide compounds that have been synthesized and structurally charaterized, only a few examples of tris-Cp compounds involving transition metals have been reported in the literature. Although tris-Cp compounds of Group III [7] and Group VI [8] transition metals are known, the Group IV transition metals provide the most examples and greatest diversity within the tris-Cp class of compounds. The crystal structure of Cp_3Ti exhibits a "**2-5,1-2**" structure [9], while the crystal structure of Cp_3Zr exhibits a "**3-5**" structure [10]; this structural difference is attributed to the larger size of zirconium, which is better suited to accommodate the sterically cumbersome "**3-5**" ligand set.

Oxidation of the M(III) Cp_3M compounds to M(IV) Cp_3MX compounds allows for a diverse set of Cp_3MX complexes, where X can be a hydride, alkyl, or halide. The tetrakis-Cp compounds, which can be viewed as a special case of tris-Cp compounds where X is a cyclopentadienyl ligand, are the most familiar examples within the organometallic community. The crystal structures of Cp_4Ti, which contains two η^5-Cp and two η^2-Cp ligands [11], and Cp_4Zr, which contains three η^5-Cp and one η^1-Cp ligands [12], are consistent with those observed for the Cp_3M(III) compounds. The crystal structure of Cp_4Hf shows that Cp_4Hf is isostructural with Cp_4Ti rather than Cp_4Zr [13]. Interestingly, this was the first example of analogous zirconium and hafnium compounds that exhibited significantly different structural chemistry. We have shown that the chloride complexes Cp_3ZrCl and Cp_3HfCl (Cp = cyclopentadienyl or substituted cyclopentadienyl) exhibit similar structural duality; the Zr complexes invariably adopt "**3-5**" structures whereas the Hf complexes exhibit "**2-5,1-1**" structures [14].

There have been relatively few studies of the structures of other Cp_3MX complexes. The synthesis of Cp_3MH (M = Zr, Hf) was reported by Brainina and co-workers [15]. Although no crystal structure data were obtained, IR spectroscopy indicated that both compounds exhibit a "**3-5**" structure. This "**3-5**" structure for Cp_3ZrH was supported by the X-ray structure of the triethyl aluminum adduct of Cp_3ZrH [16]. The efforts of Erker and co-workers [17] have led to the characterization of a large number of Group IV tris-Cp compounds. They have shown that the crystal structure of Cp_3ZrCH_3 exhibits a "**3-5**" tris-Cp geometry. In addition, Erker et al. [18] also reported a variety of Cp_3M^+ (M = Zr, Hf) cations stabilized by weak σ-donor ligands, all of which were shown to exhibit a "**3-5**" structure in the solid state. The addition of bulky substituents onto one of the Cp ligands in tris-Cp zirconium compounds can influence the overall binding preference of the tris-Cp ligand set. Lawless and co-workers [19] reported a crystal structure for $(C_5H_5)_2(C_5H_3t\text{-}Bu_2)ZrBr$, which possesses two η^5-Cp ligands and an asymmetrically bound η^2-C_5H_3t-Bu_2 ligand. This complex is the only reported tris-Cp zirconium compound that has been structurally characterized and does not have a "**3-5**" geometry.

The structural diversity exhibited by these Cp_3MCl complexes has caused us to ask what factors about the axial ligand X can affect the ultimate structure. Theoretical investigations have been used previously to explain the apparent exception to the 18-electron rule found for "**3-5**" Cp_3MX compounds [20], but few investigations have focused on the structural preferences for the bonding mode of the three Cp ligands around a transition metal center. Erker and Berke have shown that density functional theory (DFT) calculations of their Cp_3M^+ cations stabilized by weak σ-donor ligands correctly predict the "**3-5**" isomer to be more stable than the "**2-5,1-1**" isomer for all of these compounds [18], an observation that leads one to ask what factors of ligand X can cause the structure of the Cp_3M moiety to change. In their seminal studies of metal–alkoxide and metal–amido complexes, Chisholm and co-workers [21], and others, have demonstrated the influence of ligand π-donation on overall structure. In this contribution, we will use DFT to examine the importance of the π-donor ability of the X ligand in Cp_3MX compounds on the binding preferences of the tris-Cp ligand set. The relative bonding energies of the "**3-5**" and "**2-5,1-1**" isomers of tris-Cp metal hydride and alkyl compounds will be compared with those of the analogous tris-Cp metal alkoxide and amido compounds. Population analyses and molecular orbital theory will be used to explain the different ground state geometries calculated for these two groups of compounds.

2. Computational details

DFT calculations were performed using the Amsterdam density functional (ADF) package, Version

2003.01, developed by Baerends et al. [22–24]. All geometry optimizations were carried out with no symmetry constraints under the C_1 point group using the local exchange-correlation potential of Vosko et al. [25] and the non-local exchange and correlation corrections of Perdew and Wang (PW91) [26]. The frozen core approximation was applied to all atoms except H. 1s was frozen for C, N and O, 1s–3d was frozen for Zr, and 1s–4f was frozen for Hf. For H, C, N, and O, the ADF Basis TZ2P was used, which is a core double-ζ, valence triple-ζ Slater-type orbital (STO) doubly-polarized basis set. For Zr and Hf, the ADF Basis TZP was used, which is a core double-ζ, valence double-ζ STO doubly-polarized basis set. Relativistic effects were included in all calculations using the zero-order regular approximation (ZORA) formalism and ZORA basis sets [27–31]. All geometry optimizations were performed using an integration parameter of 6.0 and were optimized to a maximum gradient of no more than 0.0001 hartree/Å. Frequencies were calculated by numerical differentiation of the first derivatives of the energy gradients in slightly displaced geometries using double-sided displacements [32,33].

3. Results and discussion

3.1. MO description of the Cp bonding in 3-5 Cp_3MX compounds

First presented by Reynolds and Wilkinson [34] in relation to organoactinide compounds and Pappalardo and Jørgensen [35] in connection with tris-Cp lanthanide complexes, the bonding of "**3-5**" tris-Cp transition metal compounds has been discussed previously by Hoffmann [20] and our group [1e], but a brief review is warranted here. In "**3-5**" tris-Cp compounds, the major orbital interactions involve the doubly-degenerate π_2 orbitals of the Cp ligands and the valence metal d-orbitals. When three Cp ligands are bonded to a metal under C_{3v} symmetry, the set of six π_2 Cp orbitals transforms as $a_1 + a_2 + 2e$ with the a_2 orbital being the ligand–ligand anti-bonding HOMO. Under C_{3v} symmetry, the metal d-orbitals transform as $a_1 + 2e$. As a result, the Cp_3-based a_1 combination is allowed by symmetry to interact with the p_z and d_{z^2} metal valence orbitals, although these contributions are small; the d_{z^2} orbital interacts primarily in a σ-fashion with the X ligand. The lower energy Cp_3-based e orbital interacts with the $d_{x^2-y^2}$ and d_{xy} metal orbitals to form the 14e molecular orbital, while the higher energy Cp_3-based e orbital interacts with the d_{xz} and d_{yz} metal orbitals to form the 15e molecular orbital. The principal M–Cp_3 interactions that result are illustrated in Fig. 2.

Interestingly, the Cp_3-based $5a_2$ HOMO does not have the appropriate symmetry for interaction with a transition metal due to the threefold symmetry of the molecule. As a result, the π_2 $5a_2$ orbital is rigorously ligand–metal non-bonding for a transition metal (although the $5a_2$ is allowed to interact with an f orbital in Cp_3-actinide complexes). The tris-Cp ligand set is thus formally a 16-electron donor to a transition metal [20]. Therefore, with the donation of two electrons from the X ligand, "**3-5**" Cp_3MX complexes obey the 18-electron rule. Similar symmetry arguments have been used to explain the bonding in several $(acetylene)_3WCO$ compounds [36] and $Zr(BH_4)_4$ [37].

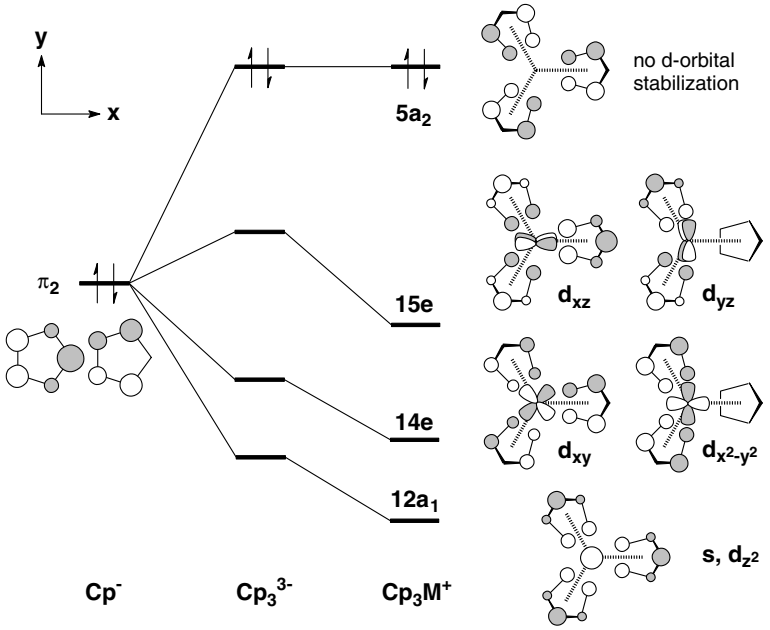

Fig. 2. Bonding interactions between the metal d-orbitals and the π_2 orbitals of the Cp_3 ligand set.

3.2. Calculated structures and relative energies

Full geometry optimizations of Cp_3ZrH (**1**) and Cp_3HfH (**2**) located the "**3-5**" structures along the potential energy surface. However, all attempts to locate either a "**2-5,1-1**" or "**2-5,1-2**" local-minimum geometry failed as these calculations always optimized to the "**3-5**" structure when no symmetry constraints were placed on the system.[1] Selected calculated bond distances and angles for **1** and **2** are compiled in Table 1. These results are consistent with IR data provided by Brainina and co-workers [15], which suggested that both **1** and **2** exhibit a "**3-5**" structure. A double-sided frequency calculation of **1** calculated a Zr–H stretching frequency of 1600 cm^{-1}, which is in excellent agreement with the experimental value of 1603 cm^{-1}. A similar frequency calculation of **2** determined a Hf–H stretching frequency of 1656 cm^{-1}, which agrees well with the experimental value of 1670 cm^{-1}. The good agreement between the calculated and experimental M–H stretching frequencies suggests that DFT is a viable tool for correctly predicting experimental observables of tris-Cp compounds.

In addition to the "**3-5**" isomers, full geometry optimizations located a "**2-5,1-2**" isomer for Cp_3ZrCH_3 (**3**), which has an asymmetrically bound η^2-Cp ligand,[2] and a "**2-5,1-1**" isomer for Cp_3HfCH_3 (**4**). **3** and **4** were found to be more stable in the "**3-5**" geometry by 4.3 and 1.3 kcal/mol, respectively, which is consistent with the crystal structure of **3** as reported by Erker [17]. The calculated Cent-Zr–Cent and Cent-Zr–CH_3 bond angles of 98° and 118°, respectively, are in agreement with the crystal structure data. Not surprisingly, the calculated average Zr–C(π) distances are 0.06 Å longer than those determined from the crystal structure (2.65 Å calculated versus 2.59 Å from the crystal data). Computational problems associated with correctly predicting M–C(π) bond distances involving Cp ligands have been well documented in the literature [38]. Surprisingly, the DFT calculations grossly overestimate the Zr–CH_3 length by 0.059 Å (2.354Å calculated versus 2.295 Å from the crystal data). All attempts to search for a geometry with a shorter Zr–CH_3 bond length while maintaining a "**3-5**" geometry failed. One may conclude that DFT does a poor job at reproducing the crystal structure of **3**, but the crystal structure determination of **3** was not without problems.[3] It is important to note that despite these shortcomings in predicting the Zr–CH_3 bond length, the relative bonding energies are consistent with the experimentally observed ground state structure of **3**.

Not unexpectedly, the calculated M–C(π) bond distances in the "**3-5**" structures are considerably longer than those calculated for the "**2-5,1-2**" and "**2-5,1-1**" structures due to the increased steric bulk of the "**3-5**" tris-Cp ligand set. This elongation of the M–C(π) bond distances in the "**3-5**" structures is consistent with X-ray crystal data, which shows considerably longer M–C(π) bond distances in Cp_4Zr [12], Cp_3ZrCl [14], and Cp_3ZrCH_3 [17] than in other bent bis-metallocene zirconium compounds [39]. The relief of steric congestion around the metal center is also responsible for shortening the Zr–Me bond length in the "**2-5,1-2**" structure.

A comparison of the total bonding energies of the "**3-5**" and "**2-5,1-1**" geometries of Cp_3ZrOH (**5**) and Cp_3HfOH (**6**) indicates that the "**2-5,1-1**" structures are more stable for **5** and **6** by 2.8 and 6.3 kcal/mol, respectively. Similar results are obtained for Cp_3ZrOCH_3 (**7**) and Cp_3HfOCH_3 (**8**), which are more stable as "**2-5,1-1**" isomers by 3.0 and 6.1 kcal/mol, respectively. One primary structural difference between the "**3-5**" and "**2-5,1-1**" geometries of complexes **5** through **8** is the M–O bond distance, which is much shorter in the "**2-5,1-1**" structures than in the "**3-5**" structures. Although this observation is consistent with the relief of steric congestion on going from a "**3-5**" geometry to a "**2-5,1-1**" geometry as was observed for **3** and **4**, a major contribution to the bond contraction in complexes **5** through **8** is the increase in π-donation from the hydroxide and alkoxide ligands to the electron-deficient metal center in the "**2-5,1-1**" geometry. The importance of π-donation is demonstrated by comparing the magnitude of the decrease in the M–X bond

[1] A "**2-5,1-1**" geometry for both Cp_3ZrH and Cp_3HfH was located when the molecules were forced to have C_s symmetry containing a mirror plane bisecting the Cent–M–Cent plane and lying in the C(σ)–M–H plane. In this conformation, the geometry optimization led to an unusual α-agostic interaction between the C(σ)–H bond of the η^1-Cp ligand with a M–C(σ)–H bond angle of less than 90°. A frequency calculation produced one imaginary frequency and is indicative of a transition state for the rotation about the M–C(σ) bond vector.

[2] The two Zr–C bond lengths involving the η^2-Cp ligand were calculated to be 2.488 and 2.673 Å. Although these distances indicate a much more asymmetrically bound η^2-Cp ligand than that found in the crystal structure of $Cp_2(\eta^2\text{-}C_5H_3tBu_2)ZrBr$, Erker and Berke reported a similar structure for Cp_3TiMe (see footnote 3 in [18]).

[3] The wR_2 for the final R indices was 0.1696 and the goodness-of-fit of F^2 was 1.121, both of which are unusually large values. The crystal structure indicates essentially five equivalent Zr–C(π) lengths, which vary by only 0.007 Å, and three symmetry-equivalent η^5-Cp ligands. This disagrees with our optimized geometry, which shows a variation of about 0.05 Å in the Zr–C(π) distances and three η^5-Cp ligands that are considerably distorted from an idealized C_3 symmetry. This calculated variation in the Zr–C(π) distances is consistent with other structurally characterized tris-Cp zirconium compounds, all of which show significant variations in their Zr–C(π) bond lengths. In addition, the fact that the Zr–C(σ) distance determined from the crystal structure of **3** is comparable to those found in bis-zirconocene compounds is bothersome. The increased steric demands of the "**3-5**" geometry would be expected to increase the Zr–C(σ) bond length in **3**. This trend is observed in all of our calculations, for the Zr–Cl distance in the crystal structure of Cp_2ZrCl_2 versus Cp_3ZrCl (see [14]), and for the M–C(σ) distances in the crystal structure of Cp_4Zr versus Cp_4Hf.

Table 1
Selected calculated bond distances and angles for **1** through **12**

	Cp_3ZrH		Cp_3HfH		Cp_3ZrCH3		Cp_3HfCH_3	
	3-5		**3-5**		**3-5**	**2-5,1-2**	**3-5**	**2-5,1-1**
M–X (Å)	1.842		1.834		2.354	2.331	2.332	2.306
M–C(π) (Å)	2.628		2.628		2.648	2.573	2.649	2.567
Cp–M–Cp (°)	119		119		118	127	118	127
X–M–Cent (°)	95		96		98	101	99	102
	Cp_3ZrOH		Cp_3HfOH		Cp_3ZrOCH_3		Cp_3HfOCH_3	
	3-5	**2-5,1-1**	**3-5**	**2-5,1-1**	**3-5**	**2-5,1-1**	**3-5**	**2-5,1-1**
M–X (Å)	2.054	2.015	2.068	2.029	2.019	1.960	2.044	1.992
M–C(π) (Å)	2.671	2.57	2.667	2.566	2.680	2.582	1.674	2.574
Cp–M–Cp (°)	117	130	117	130	117	128	117	128
X–M–Cent (°)	100	106	100	106	101	108	101	107
M–O–R (°)	115	120	114	118	139	158	136	149
	Cp_3ZrNH_2		Cp_3HfNH_2		$Cp_3ZrN(CH_3)_2$		$Cp_3HfN(CH_3)_2$	
	3-5	**2-5,1-1**	**3-5**	**2-5,1-1**	**3-5**	**2-5,1-1**	**3-5**	**2-5,1-1**
M–X (Å)	2.143	2.085	2.142	2.085	2.157	2.119	2.160	2.119
M–C(π) (Å)	2.673	2.563	2.670	2.561	2.694	2.579	2.687	2.577
Cp–M–Cp (°)	117	132	117	131	116	127	116	126
X–M–Cent (°)	100	105	100	106	102	109	102	109
M–N–Mid (°)	144	180	144	180	162	180	162	180

length, which is 0.02 Å in methyl complex **3** and 0.04 Å in hydroxide complex **5**. In addition, this increased π-donation is supported structurally by the observation that the dihedral angle between the C(σ)–M–O and M–O–H planes is 90° in **5** and **6**, a conformation that maximizes π-donation, and by an increase in the M–O–R bond angle of 18° and 13° in the "**2-5,1-1**" geometries of **7** and **8**, respectively. These calculated structural data are summarized in Table 1, and the calculated structures of **5** and **7** are shown in Fig. 3.

Similar binding preferences were observed for tris-Cp zirconium and hafnium amido complexes. Both "**3-5**" and "**2-5,1-1**" geometries were located on the potential energy surfaces for Cp_3ZrNH_2 (**9**) and Cp_3HfNH_2 (**10**), each preferring the "**2-5,1-1**" geometry by 6.3 and 9.9 kcal/mol, respectively. The geometry of the amido ligand nicely illustrates the change in π-donation in going from the electronically saturated metal center in the "**3-5**" geometry to the electron-deficient metal center in the "**2-5,1-1**" geometry. In the "**3-5**" structure of **9**, the amido ligand is pyramidalized as the Zr–N–Mid angle is 144°, where Mid is the midpoint between the two hydrogen atoms of the amido ligand. Although highly unusual, transition metal compounds containing pyramidal amido ligands are not unprecedented but are limited to electron-rich late-transition metal complexes [40]. In the "**2-5,1-1**" structure of **9**, the geometry of the amido ligand is trigonal planar as evidenced by a Zr–N–Mid angle of 180°, and the dihedral angle between the C(σ)–Zr–N and H-N–H planes is 90°, which is consistent with optimum π-donation into the metal center.

Comparable relative binding energies were obtained for $Cp_3ZrN(CH_3)_2$ (**11**) and $Cp_3HfN(CH_3)_2$ (**12**), which were more stable in the "**2-5,1-1**" geometry by 7.3 and 10.8 kcal/mol, respectively. However, the amido ligand is less pyramidalized in the "**3-5**" structure of **11** than in **9** as is shown by the increased Zr–N–Mid angle to 162° in **11**, where Mid is the midpoint between the two carbon atoms of the amido ligand. In addition, in the "**2-5,1-1**" structure of **11**, the dihedral angle between the C(σ)–Zr–N and Me–N–Me planes was calculated to be 73°, which is smaller than the 90° value calculated for **9**. This gearing of the amido ligand in **11** is caused by increased steric interactions between the larger methyl groups and the two η^5-Cp ligands and is consistent with X-ray crystal data of other bis-metallocene zirconium amido compounds reported by Bercaw and co-workers [41]. These structural data are summarized in Table 1, and the calculated structures of **9** and **11** are shown in Fig. 4.

3.3. Effect of π-loading on bonding energies and orbital interactions

Table 2 summarizes the relative bonding energies for the "**3-5**" and "**2-5,1-1**" isomers of complexes **1** through **12**. The binding preferences calculated for Cp_3MX (M = Zr, Hf; X = H, OR, NR_2) compounds in conjunction with the differences observed for the alkoxide and amido geometries in the "**3-5**" and "**2-5,1-1**" structures indicate that the π-donor ability of the X ligand is important in determining which isomer is more stable.

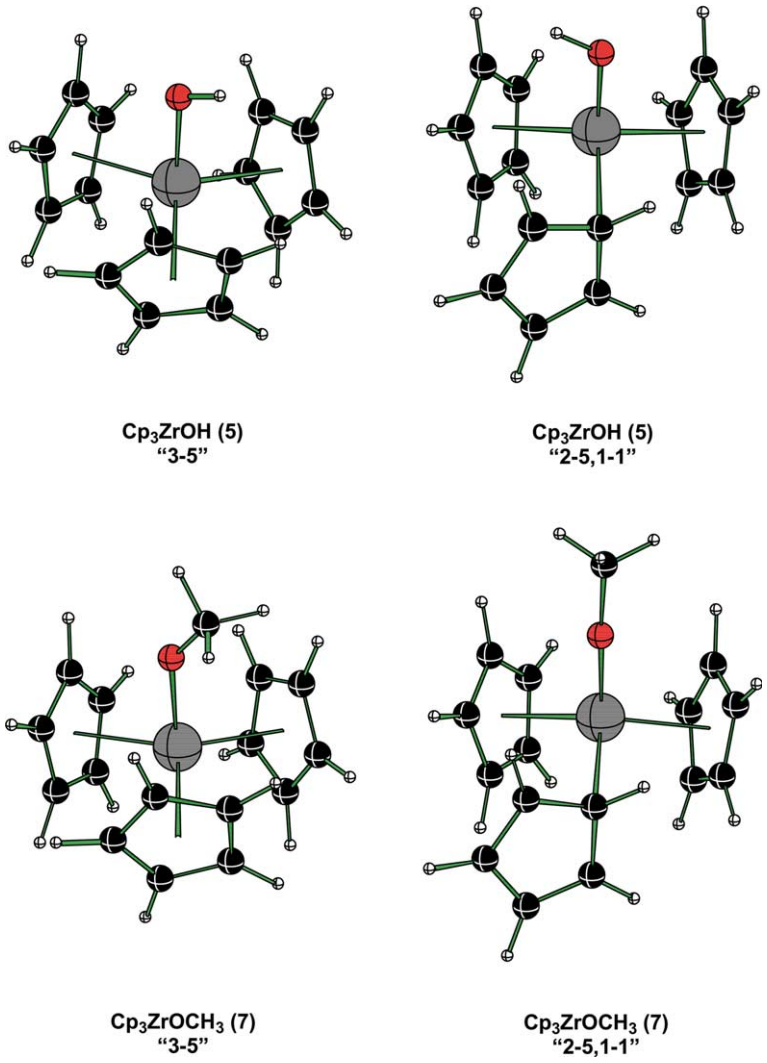

Fig. 3. Optimized geometries of the "**3-5**" and "**2-5,1-1**" structures of Cp_3ZrOH (**5**) and Cp_3ZrOCH_3 (**7**).

When X is not a π-donor, as is the case for **3** and **4**, the "**3-5**" isomer is calculated to be more stable than the "**2-5,1-1**" isomer. In contrast, when X is a strong π-donor, as in the alkoxide and amido compounds, the "**2-5,1-1**" isomers are found to be more stable than the "**3-5**" isomers. Interestingly, the amido compounds have a higher preference for the "**2-5,1-1**" geometry than the corresponding hydroxide and alkoxide complexes, which is consistent with an $–NR_2$ ligand being a stronger π-donor than an –OR ligand [42]. Notice also that in all cases, the Hf complex shows a greater preference for the "**2-5,1-1**" structure than does the corresponding Zr complex. This observation, which is consistent with the differing structures of the Zr and Hf complexes when X = Cp or Cl, will be the focus of a separate contribution.

Because "**3-5**" Cp_3MX compounds are electronically saturated, π-donation from the X ligand is minimized in comparison to the π-donation in the "**2-5,1-1**" isomers. This should be evident from inspection of the charges on the metal atom, the tris-Cp ligand set, and the X ligand in **3** through **6**, **9** and **10**, which are compiled in Table 3. Analysis of the Mulliken charges is not consistent with this expected increase in π-donation in the "**2-5,1-1**" geometries as there is no significant difference in the Mulliken charges of the X ligands in the "**3-5**" and "**2-5,1-1**" isomers. In fact, the Mulliken charges of the X ligands in all of these compounds are more negative in the "**2-5,1-1**" structures than in the "**3-5**" structures, indicating less electron donation from the X ligand in the "**2-5,1-1**" isomers. In light of these results, which are contrary to those expected from chemical intuition, and the well-documented problems associated with Mulliken population analyses involving diffuse basis sets [43], the Mulliken charges are not considered further in this study.

Hirshfeld [44] and Voronoi deformation density (VDD) [45] charges have been shown to be more useful than Mulliken charges in the interpretation of calculations involving other organometallic systems [46].

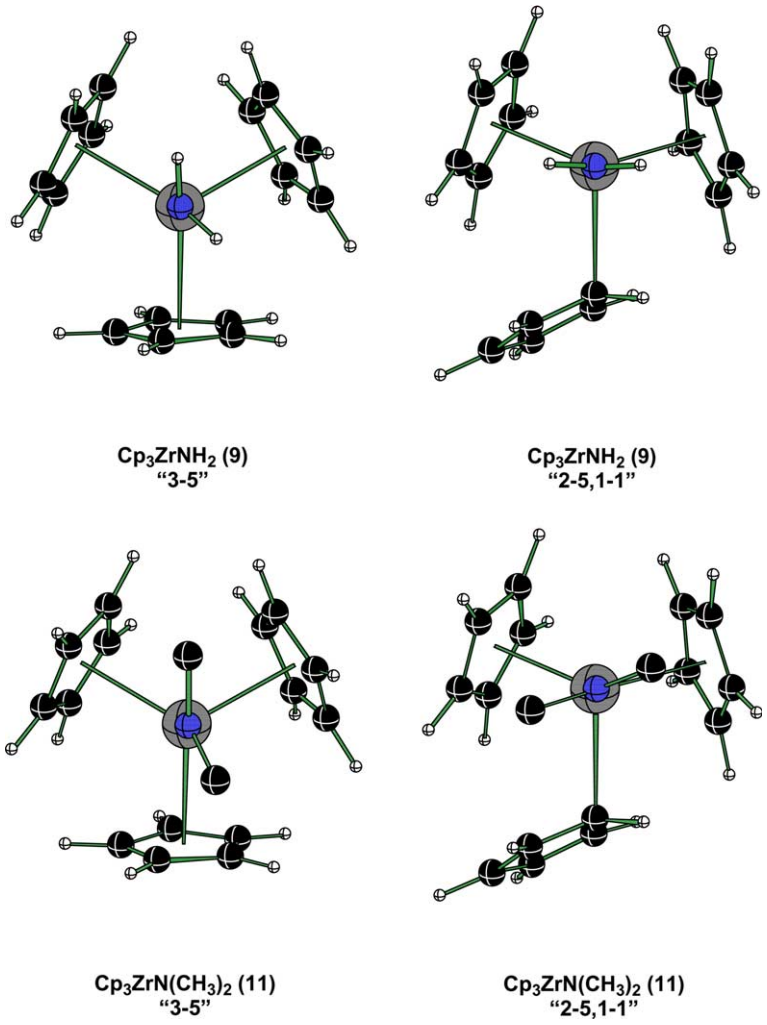

Fig. 4. Optimized geometries of the "**3-5**" and "**2-5,1-1**" structures of Cp_3ZrNH_2 (**9**) and $Cp_3ZrN(CH_3)_2$ (**11**). The view is shown along the Zr–N bond vector. In **11**, the hydrogen atoms of the amido methyl groups are omitted for clarity.

A comparison of the Hirshfeld and VDD charges of the "**3-5**" isomers of **3**, **5** and **9** indicates electron donation from the tris-Cp ligand set to the metal center is greatest for **3** and follows the order **3** > **5** > **9**. A similar trend is observed for the corresponding "**3-5**" hafnium compounds **4**, **6** and **10**. Inspection of the charges of the X ligands indicates that the electron donation from the X ligand to the metal center follows the order $NH_2 > OH \approx CH_3$. This is not unexpected as CH_3 is a stronger σ-donor than OH but OH is a stronger π-donor than CH_3 and NH_2 is a stronger π-donor than OH. In addition, both charge analyses show a smaller charge on the metal atom in the "**2-5,1-1**" structure than in the "**3-5**" structure for compounds **5**, **6**, **9**, and **10**. Because there are only slight variations in the tris-Cp donation in the "**3-5**" and "**2-5,1-1**" geometries, the decrease in the metal charge in the "**2-5,1-1**" isomer is primarily caused by greater donation from the –OH and $–NH_2$ ligands to the metal center.

Interestingly, the Hirshfeld and VDD charge analyses show that the charge of the metal center in the hafnium compounds is more positive than the charge of the metal center in the analogous zirconium complexes, which indicates more electron donation from the ligands in

Table 2
Relative bonding energies (kcal/mol) for complexes **1** through **10**

Compound	**3-5**	**2-5,1-1**
1	0.0	(–)
2	0.0	(–)
3	0.0	4.3[a]
4	0.0	1.3
5	2.8	0.0
6	6.3	0.0
7	3.0	0.0
8	6.1	0.0
9	6.3	0.0
10	9.9	0.0
11	7.3	0.0
12	10.8	0.0

(–) indicates the "**2-5,1-1**" structures for **1** and **2** were not located on the potential energy surface.

[a] The geometry optimization of **3** located a "**2-5,1-2**" isomer rather than a "**2-5,1-1**" isomer.

Table 3
Mulliken, Hirshfeld, and Voronoi deformation density (VDD) charges for the metal atom, tris-Cp ligand set, and X ligand in compounds **3**–**6**, **9**, and **10**

Compound	Geometry	Mulliken			Hirshfeld			Voronoi deformation density (VDD)		
		M	Cp_3	X	M	Cp_3	X	M	Cp_3	X
Cp_3ZrCH_3	**3-5**	1.318	−0.972	−0.346	0.528	−0.296	−0.232	0.407	−0.183	−0.224
	2-5,1-2	1.426	−1.058	−0.368	0.536	−0.307	−0.229	0.401	−0.182	−0.219
Cp_3HfCH_3	**3-5**	1.388	−1.099	−0.289	0.595	−0.352	−0.243	0.505	−0.263	−0.242
	2-5,1-1	1.396	−1.072	−0.324	0.594	−0.357	−0.237	0.487	−0.252	−0.235
Cp_3ZrOH	**3-5**	1.547	−1.033	−0.514	0.595	−0.357	−0.238	0.470	−0.243	−0.227
	2-5,1-1	1.699	−1.179	−0.520	0.584	−0.378	−0.206	0.429	−0.240	−0.188
Cp_3HfOH	**3-5**	1.578	−1.096	−0.482	0.656	−0.410	−0.246	0.560	−0.317	−0.241
	2-5,1-1	1.530	−1.038	−0.493	0.632	−0.416	−0.215	0.509	−0.305	−0.202
Cp_3ZrNH_2	**3-5**	1.476	−1.015	−0.461	0.573	−0.370	−0.203	0.457	−0.258	−0.198
	2-5,1-1	1.690	−1.209	−0.481	0.549	−0.407	−0.143	0.410	−0.275	−0.136
Cp_3HfNH_2	**3-5**	1.494	−1.099	−0.395	0.636	−0.426	−0.210	0.550	−0.338	−0.211
	2-5,1-1	1.510	−1.080	−0.431	0.598	−0.446	−0.151	0.491	−0.341	−0.150

the zirconium compounds. This effect appears to be relativistic in nature [47]. Non-relativistic Hirshfeld and VDD charges indicate no difference in the metal charges of the analogous zirconium and hafnium compounds. These results are consistent with the relativistic destabilization of the 5d orbitals of hafnium relative to the 4d orbitals of zirconium, leading to a poorer energy match between the metal 5d orbitals and the ligand orbitals in the hafnium complexes.

The above population analyses indicate that the geometry preferences of tris-Cp Group IV transition metal compounds can be viewed as a competition between the π-donation of the X ligand and the third Cp ligand. This π-competition model is illustrated in Fig. 5. The calculations indicate that the alkoxide and amido groups are stronger π-donors than the third Cp ligand in Cp_3MX compounds. As the metal accepts more electron density from the π orbital of the X ligand, π-donation from the third η^5-Cp ligand is decreased to such an extent that it becomes a better electron donor as an η^1-Cp ligand. This model is consistent with the 90° orientation of the alkoxide and amide ligands relative to the η^1-Cp ligand in the "**2-5,1-1**" geometry as discussed in the previous section.

The stability of the "**2-5,1-1**" geometry in the alkoxide and amido compounds can also be explained using molecular orbital theory. Inspection of the molecular orbitals of the tris-Cp metal fragment in Fig. 2 shows that the 15e molecular orbital involving the metal d_{xz} orbital has the appropriate symmetry and orientation for interaction with the π-donor orbital of the X ligand. Because both the 15e orbital and the π orbital of the X ligand are filled, this leads to a filled–filled destabilizing interaction, which increases the energy of this molecular orbital. As a result, the degenerate 15e orbital in Cp_3ZrCH_3 is split into two non-degenerate orbitals in Cp_3ZrOH, with the one involving the metal d_{xz} orbital substantially increased in energy. In Cp_3ZrNH_2, the π-donation is strong enough that the energy of this

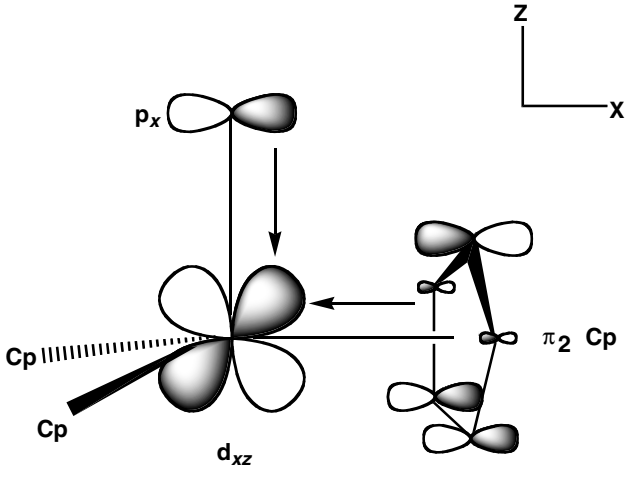

Fig. 5. Orbital interactions between the metal d_{xz} orbital, the π-donor orbital of X, and one of the π_2 orbitals of the third η^5-Cp ligand in Cp_3MX compounds. Increased π-donation from the X ligand decreases the π-contribution of the third Cp ligand, which becomes a pure σ-donor when X is an alkoxide or amido ligand. The other two η^5-Cp ligands are labeled as "Cp" for clarity.

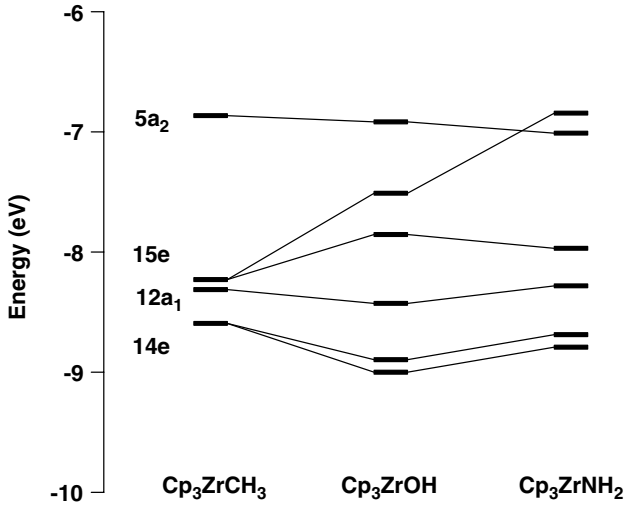

Fig. 6. Molecular orbital energies of **3**, **5** and **9**.

orbital rises above the $5a_2$ orbital. This destabilization is responsible for the relative stability of the "**2-5,1-1**" isomers of the tris-Cp alkoxide and amido compounds. The molecular orbital energies of Cp_3ZrX ($X = CH_3$, OH, NH_2) are shown in Fig. 6.

4. Conclusion

The DFT calculations presented here indicate that the bonding of the tris-Cp ligand set in transition metal compounds of the type Cp_3MX ($M = Zr$, Hf) is dependent upon the nature of the X ligand. When X is a pure σ-donor (e.g., H, CH_3), the complexes are more stable in a "**3-5**" geometry. However, the preference for a "**2-5,1-1**" geometry increases as the π-donor ability of the X ligand increases. Thus, when X is an alkoxide or amido ligand, the tris-Cp ligand set prefers a "**2-5,1-1**" geometry. This preference for the "**2-5,1-1**" geometry can be understood in terms of a π-competition model, which indicates that the π-donor ability of the alkoxide and amido ligands is greater than that of the third η^5-Cp ligand. Molecular orbital theory also suggests that the presence of strong π-donor X ligands in Cp_3MX complexes leads to filled–filled interactions between the π orbital of the X ligand and one of the 15e orbitals of the Cp_3M fragment. This unfavorable interaction destabilizes the "**3-5**" geometry and contributes to the relative stability of the "**2-5,1-1**" isomers of Cp_3MOH and Cp_3MNH_2.

Acknowledgements

Acknowledgment is made to the Donors of The Petroleum Research Fund, administered by the American Chemical Society, for support of this research (Grant 38438-AC3). We are also grateful to the Ohio Supercomputing Center for a generous grant of computer time.

References

[1] (a) B.E. Bursten, R.J. Strittmatter, J. Am. Chem. Soc. 109 (1987) 6606;
(b) B.E. Bursten, L.F. Rhodes, R.J. Strittmatter, J. Am. Chem. Soc. 111 (1989) 2756;
(c) B.E. Bursten, L.F. Rhodes, R.J. Strittmatter, J. Am. Chem. Soc. 111 (1989) 2758;
(d) B.E. Bursten, L.F. Rhodes, R.J. Strittmatter, J. Less-Common Met. 149 (1989) 207;
(e) R.J. Strittmatter, B.E. Bursten, J. Am. Chem. Soc. 113 (1991) 552;
(f) M. Pepper, B.E. Bursten, Chem. Rev. 91 (1991) 719;
(g) B.E. Bursten, R.J. Strittmatter, Angew. Chem., Int. Ed. Engl. 30 (1991) 1069;
(h) N. Kaltsoyannis, B.E. Bursten, J. Organomet. Chem. 528 (1997) 19.

[2] (a) J.M. Birmingham, G. Wilkinson, J. Am. Chem. Soc. 78 (1956) 42;
(b) E.O. Fischer, H. Fischer, J. Organomet. Chem. 3 (1965) 181;
(c) S.G. Krasnova, G.K. Borisov, G.G. Devyatykh, Russ. J. Inorg. Chem. 16 (1971) 918;
(d) V.T. Aleksanyan, G.K. Borisov, I.A. Garbuzova, G.G. Devyatykh, J. Organomet. Chem. 131 (1977) 251;
(e) S.H. Eggers, M. Adam, E.T.K. Haupt, R.D. Fischer, Inorg. Chim. Acta 139 (1987) 315;
(f) W.J. Evans, B.L. Davis, Chem. Rev. 102 (2002) 2119, and references therein.

[3] (a) W.J. Evans, J. Organomet. Chem. 652 (2002) 61;
(b) W.J. Evans, S.A. Kozimor, G.W. Nyce, J.W. Ziller, J. Am. Chem. Soc. 125 (2003) 13831.

[4] (a) For recent examples, see: P.C. Blake, M.A. Edelman, P.B. Hitchcock, J. Hu, M.F. Lappert, S. Tian, G. Müller, J.L. Atwood, H. Zhing, J. Organomet. Chem. 551 (1998) 261;
(b) M.d.M. Conejo, J.S. Parry, E. Carmona, M. Schultz, J.G. Brennann, S.M. Beshouri, R.A. Andersen, R.D. Rogers, S. Coles, M. Hursthouse, Chem. Eur. J. 5 (1999) 3000.

[5] (a) R.S. Sternal, T.J. Marks, Organometallics 6 (1987) 2621;
(b) S.P. Nolan, M. Porchia, T.J. Marks, Organometallics 10 (1991) 1450.

[6] W.J. Evans, S.A. Kozimor, J.W. Ziller, J. Am. Chem. Soc. 125 (2003) 14264.

[7] (a) M. Adam, U. Behrens, R.D. Fischer, Acta Crystallogr., Sect. C 47 (1991) 968;
(b) S.H. Eggars, J. Kopf, R.D. Fischer, Organometallics 5 (1986) 383;
(c) J.L. Atwood, K.D. Smith, J. Am. Chem. Soc. 95 (1973) 1488;
(d) J. Rebizant, C. Apostolidis, M.R. Spirlet, B. Kanellakopulos, Acta Crystallogr., Sect. C 44 (1988) 614.

[8] (a) F.A. Cotton, P. Legzdins, J. Am. Chem. Soc. 90 (1968) 6232;
(b) J.L. Calderon, F.A. Cotton, P. Legzdins, J. Am. Chem. Soc. 91 (1969) 2528.

[9] (a) C.R. Lucas, M.L.H. Green, R.A. Forder, K. Prout, J. Chem. Soc., Chem Commun. (1973) 97;
(b) R.A. Forder, K. Prout, Acta Crystallogr., Sect. B 30 (1974) 491.

[10] W.W. Lukens, R.A. Andersen, Organometallics 14 (1995) 3435.

[11] J.L. Calderon, F.A. Cotton, B.G. DeBoer, J. Takats, J. Am. Chem. Soc. 93 (1971) 3592.

[12] R.D. Rogers, R. Vann Bynum, J.L. Atwood, J. Am. Chem. Soc. 100 (1978) 5238.

[13] R.D. Rogers, R. Vann Bynum, J.L. Atwood, J. Am. Chem. Soc. 103 (1981) 692.

[14] (a) R.J. Strittmatter, Ph.D. Dissertation, The Ohio State University, 1990;
(b) E.J. Palmer, Ph.D. Dissertation, The Ohio State University, 2005.

[15] B.V. Lokshin, Z.S. Klemenkova, M.G. Ezernitskaya, L.I. Strunkina, E.M. Brainina, J. Organomet. Chem. 235 (1982) 69.

[16] J. Kopf, H.J. Vollmer, W. Kaminsky, Cryst. Struct. Commun. 9 (1980) 985.

[17] T. Brackemeyer, G. Erker, R. Fröhlich, Organometallics 16 (1997) 531.

[18] H. Jacobsen, H. Berke, T. Brackemeyer, T. Eisenblatter, G. Erker, R. Frölich, O. Meyer, K. Bergander, Helv. Chim. Acta 81 (1998) 1692.

[19] M.M. Corradi, D.J. Duncalf, G.A. Lawless, M.P. Waugh, Chem Commun. (1997) 203.

[20] J.W. Lauher, R. Hoffmann, J. Am. Chem. Soc. 98 (1976) 1729.

[21] (a) See, for example: M.H. Chisholm, L.S. Tan, J.C. Huffman, J. Am. Chem. Soc. 104 (1982) 4879;
(b) M.H. Chisholm, M.J. Hampden-Smith, J.C. Huffman, K.G. Moodley, J. Am. Chem. Soc. 110 (1988) 4070;

(c) M.H. Chisholm, I.P. Parkin, W.E. Streib, O. Eisenstein, Inorg. Chem. 33 (1994) 812.
[22] G. te Velde, S.J.A. Bickelhaupt, C.F. Guerra, E.J. Baerends, J.G. Snijders, T. Ziegler, J. Comput. Chem. 22 (2001) 931.
[23] C.F. Guerra, J.G. Snijders, G. te Velde, E.J. Baerends, Theoret. Chem. Acc. 99 (1998) 391.
[24] ADF2003.01, SCM, Theoretical Chemistry, Vrije Universiteit, Amsterdam, The Netherlands. Available from: <http://www.scm.com>.
[25] S.H. Vosko, L. Wilk, M. Nusair, Can. J. Phys. 58 (1980) 1200.
[26] J.P. Perdew, Phys. Rev. B 46 (1992) 6671.
[27] E. van Lenthe, E.J. Baerends, J.G. Snijders, J. Chem. Phys. 99 (1993) 4597.
[28] E. van Lenthe, E.J. Baerends, J.G. Snijders, J. Chem. Phys. 101 (1994) 9783.
[29] E. van Lenthe, A.E. Ehlers, E.J. Baerends, J. Chem. Phys. 110 (1999) 8943.
[30] E. van Lenthe, J.G. Snijders, E.J. Baerends, J. Chem. Phys. 105 (1996) 6505.
[31] E. van Lenthe, R. van Leeuwen, E.J. Baerends, J.G. Snijders, Int. J. Quantum Chem. 57 (1996) 281.
[32] L. Fan, T. Ziegler, J. Chem. Phys. 96 (1992) 9005.
[33] L. Fan, T. Ziegler, J. Phys. Chem. 96 (1992) 6937.
[34] L.T. Reynolds, G. Wilkinson, J. Inorg. Nucl. Chem. 2 (1956) 246.
[35] R. Pappalardo, C.K. Jørgensen, J. Chem. Phys. 46 (1967) 632.
[36] (a) D.P. Tate, J.M. Augl, W.M. Ritchey, B.L. Ross, J.G. Grasselli, J. Am. Chem. Soc. 86 (1964) 3261;
(b) R.B. King, Inorg. Chem. 7 (1968) 1044;
(c) R.M. Laine, R.E. Moriarty, R. Bau, J. Am. Chem. Soc. 94 (1972) 1402.
[37] A. Davison, S.S. Wreford, Inorg. Chem. 14 (1975) 703.
[38] (a) H. Koch, P. Jorgensen, T. Helgaker, J. Chem. Phys. 104 (1996) 9528;
(b) K. Pierloot, B.J. Persson, B.O. Roos, J. Phys. Chem. 99 (1995) 3465;
(c) C. Park, J. Almlof, J. Chem. Phys. 95 (1991) 1829;
(d) H.P. Lüthi, P.E.M. Siegbahn, J. Almlof, K. Faegri Jr., A. Heiberg, Chem. Phys. Lett. 111 (1984) 1;
(e) T.E. Taylor, M.B. Hall, Chem. Phys. Lett. 114 (1985) 338.
[39] D.J. Cardin, M.F. Lappert, C.L. Raston, Chemistry of Organo-zirconium and Hafnium Compounds, Wiley, New York, 1986.
[40] (a) M.A. Dewey, A.M. Arif, J.A. Gladysz, Chem. Commun. (1991) 712;
(b) M.A. Dewey, D.A. Knight, A. Arif, J.A. Gladysz, Chem. Ber. 125 (1992) 815.
[41] (a) G.L. Hillhouse, J.L. Bercaw, Organometallics 1 (1982) 1025;
(b) G.L. Hillhouse, A.R. Bulls, B.D. Santarsiero, J.E. Bercaw, Organometallics 7 (1988) 1309.
[42] (a) W.W. Lukens, M.R. Smith, R.A. Andersen, J. Am. Chem. Soc. 118 (1996) 1719;
(b) M. Horacek, R. Gyepes, J. Kubista, K. Mach, Inorg. Chem.Commun. 7 (2004) 155.
[43] (a) F. Jensen, Introduction to Computational Chemistry, Wiley, New York, 1999, pp. 217–219;
(b) C.J. Cramer, Essentials of Computational Chemistry: Theories and Models, Wiley, New York, 2002, pp. 278–283;
(c) A.E. Reed, R.B. Weinstock, F. Weinhold, J. Chem. Phys. 83 (1985) 735.
[44] (a) F.L. Hirshfeld, Theoret. Chim. Acta 44 (1977) 129;
(b) K.B. Wiberg, P.R. Rablen, J. Comput. Chem. 14 (1993) 1504.
[45] (a) G. te Velde, E.J. Baerends, J. Comput. Chem. 99 (1992) 84;
(b) F.M. Bickelhaupt, N.J.R. van Eikema Hommes, C.F. Guerra, E.J. Baerends, Organometallics 15 (1996) 2923.
[46] C.F. Guerra, J.-W. Handgraaf, E.J. Baerends, M. Bickelhaupt, J. Comput. Chem. 25 (2004) 189.
[47] (a) K.S. Pitzer, Acc. Chem. Res. 12 (1979) 271;
(b) P. Pyykkö, J.P. Desclaux, Acc. Chem. Res. 12 (1979) 276;
(c) P. Pyykkö, J.G. Snijders, E.J. Baerends, Chem. Phys. Lett. 83 (1981) 432;
(d) N. Kaltsoyannis, J. Chem. Soc., Dalton Trans. (1997) 1.

Available online at www.sciencedirect.com
SCIENCE DIRECT®
Polyhedron 25 (2006) 585–590
POLYHEDRON
www.elsevier.com/locate/poly

A dendrimer-based Co_{32} nanocluster: Synthesis and application in diameter-controlled growth of single-walled carbon nanotubes

Junfeng Geng [a,1], Hongwei Li [b], Dejian Zhou [a], Wilhelm T.S. Huck [b], Brian F.G. Johnson [a,*]

[a] Department of Chemistry, University of Cambridge, Lensfield Road, Cambridge, CB2 1EW, UK
[b] Melville Laboratory for Polymer Synthesis, Department of Chemistry, University of Cambridge, Cambridge, CB2 1EW, UK

Received 27 June 2005; accepted 19 August 2005
Available online 5 October 2005

Abstract

We report the synthesis and characterization of a dendrimer-based Co_{32} nanocluster molecule and its use as uniform-size catalytic seed for diameter-controlled growth of single-walled carbon nanotubes.
© 2005 Elsevier Ltd. All rights reserved.

Keywords: Cluster molecule; Cobalt; Nanoparticles; Chemical vapour deposition; Single-walled carbon nanotubes

1. Introduction

Cobalt (Co) nanoparticles have been under intense investigation because of their importance in the development of nanoscale ferromagnets [1,2], high-density magnetic memory storage materials [3,4], and as catalytic seeds in the growth of single-walled carbon nanotubes (CNTs) [5]. As far as the single-walled CNTs are concerned, the control of the tube diameter has been a challenge to the scientific community for a decade since their discovery in 1993 [6]. Although the exact mechanism involved in their growth remains incompletely understood, it has been demonstrated that the diameter of single-walled CNTs often matches the size of the catalytic metal nanoparticles employed [7–10]. Thus, in the control of the nanotube diameter, the first and most critical step is the control of the size of the catalytic metal nanoparticles.

To date, metal nanoparticles (Co, Fe or Ni) are produced either from colloids [7,11,12], or by thermal decomposition of metal-containing precursors of inorganic or organometallic salts [13–18,23]. Despite great efforts by several research groups, no uniform-size metal nanoparticles down to a scale of ~1.0 nm have been prepared from either a colloidal system or a salt precursor. For applications that require monodispersed Co small particles, and in particular, for seeking diameter-controlled growth of single-walled CNTs, it is clearly desirable to develop new synthetic approaches to control the particle size and molecular structure. Here we report the synthesis and characterization of a dendrimer-based Co_{32} nanocluster molecule. The ability of precisely controlling the cluster size, the number of metal atoms and surface functionality distinguishes such molecules from Co colloidal nanoparticles and other cobalt nanoparticles formed from decomposition of salt precursors. As an initial and preliminary application study, we also demonstrate the employment of such nanoclusters as uniform-size catalytic particles for diameter-controlled growth of single-walled CNTs.

2. Experimental

2.1. General technique in synthesis and characterization

All reactions were carried out with the exclusion of air under an argon atmosphere using standard vacuum-line techniques. Solvents were freshly distilled prior to use. Except tetracobalt carbonyl that was purchased from

* Corresponding author. Tel.: +44 1223 336337; fax: +44 1223 336017.
E-mail addresses: jg201@cam.ac.uk (J. Geng), bfgj1@cam.ac.uk (B.F.G. Johnson).
[1] Tel.: +44 1223 763881; fax: +44 1223 336362.

0277-5387/$ - see front matter © 2005 Elsevier Ltd. All rights reserved.
doi:10.1016/j.poly.2005.08.036

Strem Chemicals Ltd., other chemicals were obtained from the Aldrich. IR spectra were recorded on a FT-IR spectrometer (Perkin Elmer, RX I system) using a CaF_2 sample cell. ^{31}P NMR spectra were recorded on a 400-MHz Bruker spectrometer. The employed SiO_2/Si substrates (commercial chips) were first cleaned by a mixture of ethanol and acetone, then by water. All substrates were polished by O_2 plasma for 10 min before use. Atomic force microscopy (AFM) images were acquired on a digital dimensional 3100 AFM mechine equiped with the nanoscope IV controller.

2.2. Synthesis of compound *1*

The synthesis was based on a literature method but with some modification [19]. Briefly, 0.34 g of paraformaldehyde and 2.0 ml diphenylphosphine was heated in methanol (20 ml) at 60–65 °C for 30 min. The reaction mixture was cooled to room temperature and treated with a solution of DAB-dendr-$[NH_2]_8$ (0.50 ml dendrimer in 5 ml methanol). After half an hour of stirring at room temperature, toluene (40 ml) was added. Temperature was raised to 60 °C, and the solution was kept at that temperature for an hour. The volume of the reaction mixture was then reduced to 3 ml under a reduced pressure. Cold methanol was added to yield a glassy colorless solid, DAB-dendr-$[N(CH_2PPh_2)_2]_8$ (**1**). The product was washed by methanol and dried under high vacuum at 40 °C for at least 17 h. ^{31}P NMR (CD_2Cl_2, δ): −27.9 ppm (sharp, closely-nested doublet).

2.3. Synthesis of compound *2*

0.146 g of tetracobalt carbonyl was dissolved in 30 ml of dichloromethane. The resulting solution was stirred at room temperature for 30 min. A dichloromethane solution of compound **1** (0.105 g) was then added in drop wise. After about 24 h of stirring at room temperature, the volume of the reaction mixture was reduced to 3 ml under a reduced pressure. Separation of the product, DAB-dendr-$[N(CH_2PPh_2)_2Co_4(CO)_9]_8$ (**2**), was achieved by precipitation using hexane. The un-purified product contains Co_4 metal clusters (already in excess as the starting reactant). They were removed by washing using hexane. The remaining solution containing unreacted cluster was discarded and the entire process was repeated 3–5 times. The solid product has a dark brown color. It was dried under high vacuum for 3 h. IR (cm^{-1}): 2060(s), 2017(vs), 1979(m), 1956(m), 1887(m), 1825(w) and 1804(w). ^{31}P NMR (CD_2Cl_2, δ in ppm): 37.4 (main), 25.0 (weak). Elemental *Anal.* Calc. (wt%): C, 48.9; H, 3.5; N, 2.5; P, 6.3. Found: C, 45.6; H, 3.7; N, 2.5; P, 5.7%.

2.4. Growth of the carbon nanotubes

The SiO_2/Si wafers employed were first cleaned by ethanol. The dendrimer-based Co_{32} nanocluster molecules were deposited onto the substrate from their CH_2Cl_2 solution, with an approximate concentration of 8×10^{-5} M or less. After dipped into the solution for 10 min, the substrate was rinsed by dichloromethane and dried by nitrogen. The sample was then transferred into a quartz boat, which was placed in a tube-shape reactor under a flow of argon. The sample was first heated at 300–400 °C. Such heating treatment of the cluster molecules made their organic dendritic-core and all the carbonyl ligands burned off and subsequently, the formed gaseous species were taken out of the reactor by the flow of argon. This process was immediately followed by the introduction of methane (CH_4) into the reactor to initiate the growth of the carbon nanotubes. The temperature of the reactor was kept at 850 °C during the carbon deposition. The flow rate of the methane was 1.1 L min^{-1}. The carbon deposition lasted for 30 min.

3. Results and discussion

The Co_{32} nanocluster was constructed on a host dendrimer molecule, DAB-dendr-$[N(CH_2PPh_2)_2]_8$ (**1**), which was prepared in situ by double phosphinomethylation of each of the eight peripheral amino groups of a commercially available dendrimer, DAB-dendr-$[NH_2]_8$, through the use of Ph_2PCH_2OH prepared from HCHO and $HPPh_2$. This synthesis was based on a literature method with some modification [19], and its successful double phosphinomethylation is evident by the observation of the ^{31}P NMR spectrum which shows a sharp peak at $\delta = -27.9$ ppm. Binding eight $Co_4(CO)_{12}$ cluster units onto the 8[P–N–P] tridentate terminals of compound **1** leads to formation of a nanoscale dendrimer-based supercluster, with each produced molecule containing 32 Co atoms (see Scheme 1).

The coordination reaction of the dendrimer and cluster was monitored by infrared spectroscopy (IR) in the (CO) region. On comparison with the starting cluster, a new set of absorption bands at 1956, 1979 and 2017 cm^{-1} gradually emerged, indicating formation of the product. The band at 2060 cm^{-1} is a strong carbonyl absorption which arises from the parent cluster. The band at 1887 cm^{-1} is medium in intensity for the product, but weak for the parent cluster. Bands of 1824 and 1804 cm^{-1} are weak for the product and not obvious for the starting cluster. To ensure a full coordination of all the tridentate terminals by the $Co_4(CO)_{12}$ clusters, it was found necessary to keep the clusters in excess and the reaction under mild conditions. A normally encountered problem may be a partial coordination, which was also found in our previous studies using other metal clusters [20,21].

Successful completion of the coordination herein is evident from the ^{31}P NMR spectrum. The original resonant peak at $\delta = -27.9$ ppm, corresponding to non-coordinated phosphorous atoms in the parent dendrimer, has disappeared completely (Fig. 1). Donation of the electron density from the P atoms to the Co centers leads to a significant downfield shift in the coordinated product. Elemental analysis is in agreement with that expected for each

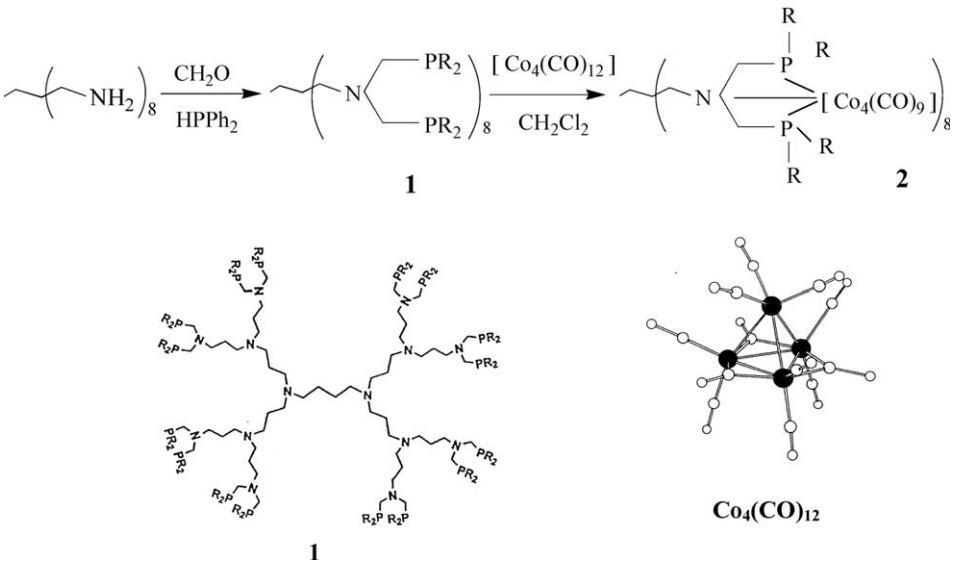

Scheme 1. Synthetic route to compound **2**. In this scheme are also shown the molecular structures of **1** and the starting tetracobalt cluster R = Ph.

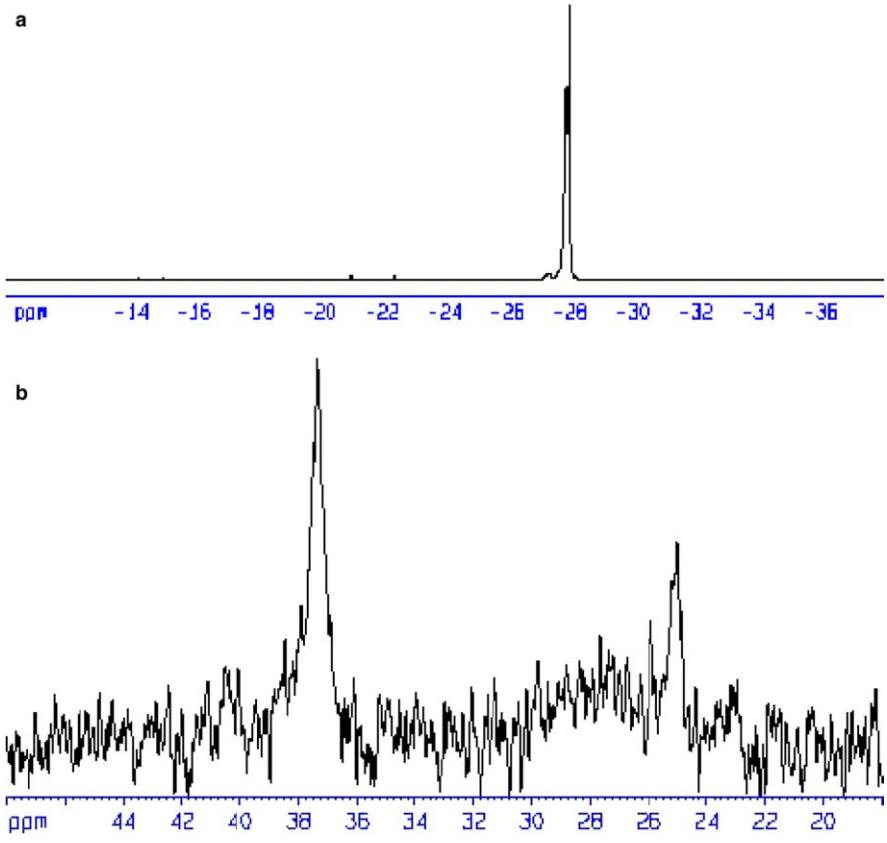

Fig. 1. NMR spectrum of the compound **1**: (a) at $\delta = -27.9$ ppm; and of the compound **2**; (b) at $\delta = 25.0$ and 37.4 ppm. The spectra were taken by dissolving the compounds into CD_2Cl_2 solvent. The relatively low ratio of signal to noise in the spectrum (b) arises from the low weight percentage (6.3%) of the phosphorous within the supermolecular structure of compound **2**.

dendrimer molecule containing eight tetracobalt cluster units. Whilst the analysis results for H, N and P are close to their calculated values, the C value is over 3% lower. This may possibly result from the Co–C reaction at high temperatures in the burning process of the analysis, which made some part of C to be transformed into metal carbide, bearing in mind that a large percentage of Co metal (~24 wt%) exists in the molecular structure. In this case, not all the carbon would form CO_2 gas for counting in the analysis. A lower C value from the measurement is thus expected. A second minor peak in the ^{31}P NMR spectrum of the product was frequently observed in our studies using

the same type of dendrimer to react with metal clusters (Co, Fe, Ru and Au). The two peaks reported in this work are believed to arise from two different coordination modes between the chelating dendritic ligands and the Co4 cluster units [20–22], but with the one corresponding to the peak at 37.4 ppm in dominance. Integration of the major and minor peak gives relative sizes in a ratio of about 4:1.

To acquire the molecular size and morphology information, atomic force microscopy (AFM) was carried out for the molecules deposited onto a SiO_2/Si substrate. The deposition was performed by dipping the substrate into a CH_2Cl_2 solution of the complex for 2 min, followed by washing with CH_2Cl_2 and evaporation. The topographic image indicated that upon evaporation of solvent, the Co_{32} nanocluster molecules did not crystallize into grains. Instead, the molecules existed as isolated single entities on the substrate (Fig. 2). Topographical height measurements revealed a dominant height of ~1.5 nm for such single molecules. Considering these dendrimer-based molecules are soft and may be flattened when adsorbed onto the substrate, we believe that the molecular diameter may be slightly larger than the measured height. The isolated cluster molecules arose from their electronically neutral nature, coupled with the large molecular size. In addition, the hydrogen bonding between the OH groups on the SiO_2/Si substrate and the CO ligands of the clusters might have played an important role because these bonds were able to enhance the surface adsorption, which helped to anchor the clusters on the substrate.

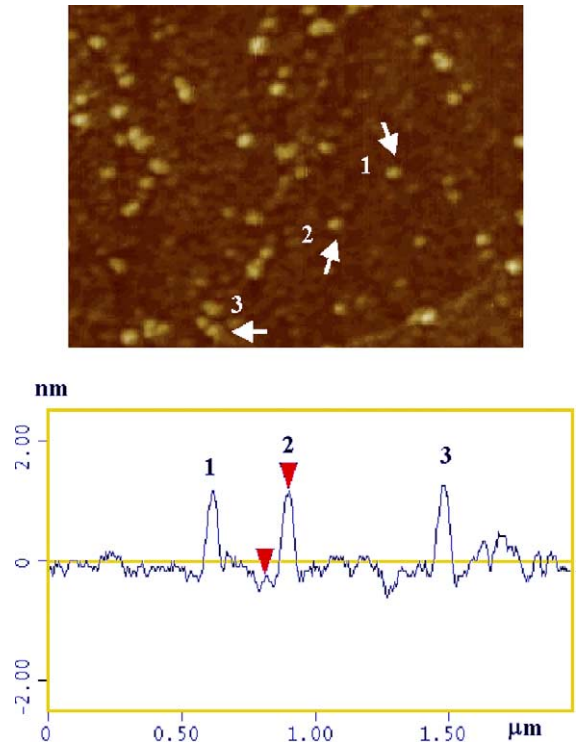

Fig. 2. Top: the AFM topographic image of the dendrimer-based Co_{32} nanoclusters on a SiO_2/Si surface. Bottom: topographical height measurements showing the size of the clusters. In this case, the measured heights correspond to the three single molecules indicated by arrows on the top image.

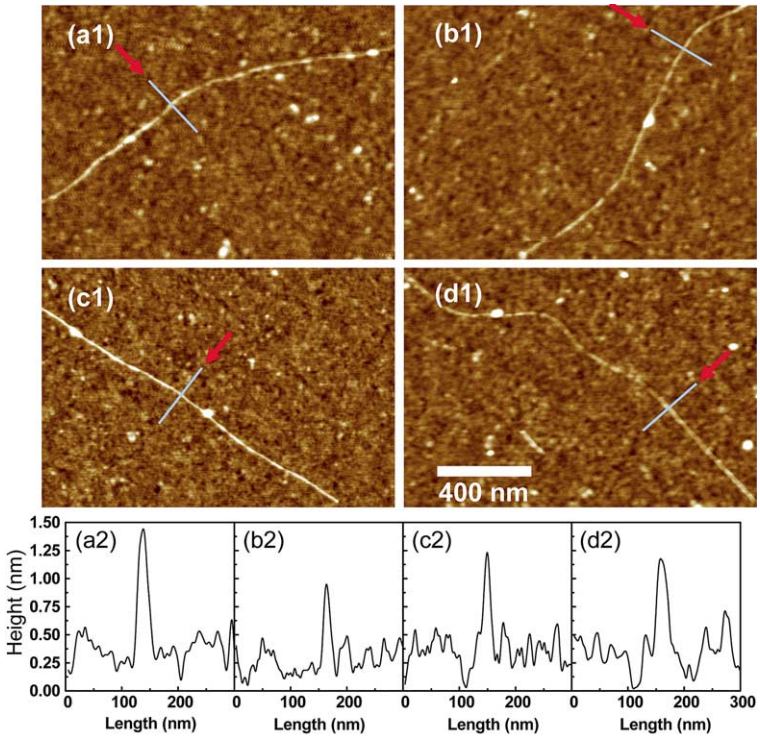

Fig. 3. Top (a1–d1): images of the single-walled carbon nanotubes under AFM (tapping mode); Bottom (a2–d2): the corresponding topographical height measurements for the diameters of the nanotubes.

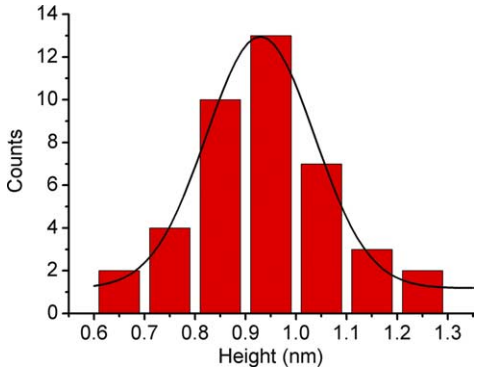

Fig. 4. The measured topographical heights of more than 40 single-walled CNTs on the substrate, showing the tube diameters and distribution. The nanotubes were grown in a CVD process at 850 °C using CH_4 as the carbon feedstock.

We would stress that the existence as isolated single molecules on the SiO_2/Si substrate may be regarded as a bonus in view of a potentially diameter-controlled growth of single-walled CNTs. Metallic Co_{32} nanoparticles may be obtained from the corresponding single parent molecules after burning off the organic dendritic core and carbonyl ligands at elevated temperatures. By such means, each produced Co nanoparticle may be identical in size due to the fixed number of metal atoms in the molecules. This nanocluster molecule may be also compared with colloidal nanoparticles or other nanoparticles produced from an inorganic or organometallic salt. For a given colloidal system, a size distribution is almost certainly unavoidable due to the complex kinetic factors involved in the formation of the colloids, particularly at the atomic nucleation and aggregation stages. When an inorganic or organometallic salt is used, the two electronically opposite ions within a salt tend to attract each other and thus force the molecules to crystallize into grains when the solvent is dried up. As the consequence of crystallization, solid-state grains with varied sizes are formed. This size difference in the grains finally leads to the size variation of the metal nanoparticles formed from thermal decomposition of the crystal grains.

For a preliminary application study, we have employed these synthesized Co_{32} nanoclusters as catalytic seeds in the growth of single-walled CNTs. Examination of the growth product by tapping mode AFM indicated that individually distributed CNTs were formed on the substrate (Fig. 3). Along with the topography, phase mode images of the CNTs were simultaneously recorded. The result displayed similar nanotube morphologies. Topographical height measurements for more than 40 such nanotubes showed a narrow diameter distribution (Fig. 4), and none of the tubes was thicker than 1.3 nm. Such small diameters indicate that the produced tubes are single-walled because no measured height reaches the threshold diameter of a double-walled CNT ($d = 1.4$ nm). Fig. 4 also shows that the average height is ~0.95 nm, the best representation of the nanotube diameter, taken all the possible errors in the measurements into account. This measured diameter clearly matches the size of a single Co_{32} metallic nanoparticle, ~0.9 nm, calculated by assuming that the particle takes a sphere shape and all the 32 Co atoms are closely packed. This result suggests that at least, the majority of the individually distributed single-walled CNTs seeded from their corresponding Co_{32} single clusters.

4. Conclusion

To summarize, we have successfully synthesized a dendrimer-based Co_{32} nanocluster molecule. Since the molecules possess uniform size and well-defined molecular structure, they are fundamentally different from Co colloids or other nanoparticles formed from decomposition of a salt precursor. The existence as isolated single molecules on the SiO_2/Si wafer is an interesting feature of such nanoclusters, which is of significant appeal in a potential application where monodispersed Co nanoentities are important. We have also demonstrated that individual single-walled CNTs can be obtained utilizing these molecules as uniform-size catalytic precursor, and the measured average tube diameter matches the size of a single Co_{32} cluster seed. In addition, the success of this synthetic route also offers feasibility of making similar metal nanoclusters with precisely controlled cluster sizes, for example, using the same cobalt starting cluster but changing the generation number of the dendrimer host molecules to prepare metal clusters with different sizes. Given all these, we believe that such development paves a new way for the exploration of utilizing uniform-size cobalt nanoclusters for applications, and in particular, for future studies of seeking an entirely diameter-controlled growth of single-walled carbon nanotubes.

Acknowledgements

J.G. thanks Thomas Swan Ltd. & Co. UK for financial support during the tenure of which this work was carried out. We also thank helpful discussions given by Dr. Ian Kinlock, Professor Alan Windle (Department of Materials Science) and Dr. Vladimir Golovko (Department of Chemistry) at University of Cambridge.

References

[1] M.L. Billas, J.A. Becker, A. Chatelain, W.A. de Heer, Phys. Rev. Lett. 71 (1993) 4067.
[2] C.B. Murry, S. Sun, J. Appl. Phys. 85 (1999) 4325.
[3] S. Sun, C.B. Murray, D. Weller, L. Folks, A. Moser, Science 287 (2000) 1989.
[4] T. Hayashi, S. Hirono, M. Tomita, S. Umemura, Nature 381 (1996) 772.
[5] M.S. Dresselhaus, G. Dresselhaus, P.C. Eklund, Science of Fullerenes and Carbon Nanotubes, Academic Press, New York, 1996.
[6] S. Iijima, T. Ichihashi, Nature 363 (1993) 603.
[7] C.L. Cheung, A. Kurtz, H. Park, C.M. Lieber, J. Phys. Chem. B 106 (2002) 2429.
[8] Y. Li, W. Kim, Y. Zhang, M. Rolandi, D. Wang, H. Dai, J. Phys. Chem. B 105 (2001) 11424.

[9] H.C. Choi, W. Kim, D. Wang, H. Dai, J. Phys. Chem. B 106 (2002) 12361.
[10] L. An, J.M. Owens, L.E. McNeil, J. Liu, J. Am. Chem. Soc. 124 (2002) 13688.
[11] B. Kleinsorge, V.B. Golovko, S. Hofmann, J. Geng, D. Jefferson, J. Robertson, B.F.G. Johnson, Chem. Commun. (2004) 1416.
[12] H. Ago, T. Komatsu, S. Ohshima, Y. Kuriki, M. Yumura, Appl. Phys. Lett. 77 (2000) 79.
[13] J. Geng, C. Singh, D.S. Shephard, M.S.P. Shaffer, B.F.G. Johnson, A.H. Windle, Chem. Commun. (2002) 2666.
[14] J. Geng, H. Li, V.B. Golovko, D.S. Shephard, D.A. Jefferson, B.F.G. Johnson, S. Hofmann, B. Kleinsorge, J. Robertson, C. Ducati, J. Phys. Chem. B. 108 (2004) 18446.
[15] Y.Q. Xu, H.Q. Peng, R.H. Hauge, R.E. Smalley, Nano Lett. 5 (2005) 163.
[16] Y. Li, I.A. Kinloch, M.S.P. Shaffer, J. Geng, B.F.G. Johnson, A.H. Windle, Chem. Phys. Lett. 384 (2004) 98.
[17] R.H. Baughman, A.A. Zakhidov, W.A. de Heer, Science 297 (2002) 787.
[18] H.W. Zhu, C.L. Xu, D.H. Wu, B.Q. Wei, R. Vajtai, P.M. Ajayan, Science 296 (2002) 884.
[19] M.T. Reetz, G. Lohmer, R. Schwickardi, Angew. Chem., Int. Ed. Engl. 36 (1997) 1526.
[20] N. Feeder, J. Geng, P.G. Goh, B.F.G. Johnson, C.M. Martin, D.S. Shephard, W. Zhou, Angew. Chem., Int. Ed. Engl. 39 (2000) 1661.
[21] J. Geng, H. Li, W.T.S. Huck, B.F.G. Johnson, Chem. Commun. (2004) 2122.
[22] D. Salter, V. Sik, S.A. Williams, T.J. Adatia, Chem. Soc., Dalton Trans. (1996) 643.
[23] M. Green, Chem. Commun. (2005) 3002.

Available online at www.sciencedirect.com
SCIENCE DIRECT
Polyhedron 25 (2006) 591–598
POLYHEDRON
www.elsevier.com/locate/poly

Synthesis and structure of gold(III) complexes of asymmetric dithiolene ligands

Josephine M. Tunney, Alexander J. Blake, E. Stephen Davies, Jonathan McMaster, Claire Wilson, C. David Garner *

School of Chemistry, The University of Nottingham, University Park, Nottingham NG7 2RD, UK

Received 4 July 2005; accepted 1 September 2005
Available online 19 October 2005

We are pleased to mark Professor Malcolm Chisholm's many significant contributions to Inorganic Chemistry, using the occasion of his 60th birthday to congratulate him on his achievements, wishing him health, happiness, and continued scientific success.

Abstract

Four new $[Au(dithiolene)_2]^-$ complexes, each involving two asymmetrically substituted dithiolene ligands (SC(H)C(R)S; R = phenyl, pyridin-2-yl, pyridin-3-yl, or pyridin-4-yl), have been synthesized by reacting $K[AuCl_4]$ with the corresponding dithiolene, generated by base hydrolysis of the thione-protected 1,3-dithiolate. Each complex has been isolated as its $[PPh_4]^+$ salt and the structures of these $[PPh_4][Au(dithiolene)_2]$ compounds have been determined by X-ray crystallography; each anion possesses a square planar $\{AuS_4\}$ core with a *cis*-arrangement of the R groups for R = phenyl and pyridin-2-yl complexes, but a *trans*-arrangement for R = pyridin-3-yl and pyridin-4-yl. In each compound, the lengths of the C–C (1.34 ± 0.01 Å) and C–S (1.75 0.03 Å) bonds of the metallocycle are consistent with the ene-1,2-dithiolate form of the dithiolene, i.e., these are [Au(III)bis(ene-1,2-dithiolate)]$^-$ complexes. Each compound is diamagnetic and ^{1}H NMR studies indicate that, in solution in d^6-acetone, both the *cis* and *trans* isomers of the $[Au(SC(H)C(R)S)_2]^-$ anion are present and do not interconvert at room temperature. Each $[Au(dithiolene)_2]^-$ complex undergoes an oxidation ($80 < E_p^a < 230$ mV) and a reduction ($-1880 < E_p^c(red) < -2020$ mV; versus $[Fc]^+/[Fc]$); the particular potentials observed correlate with the electron withdrawing ability of the dithiolene substituent (R), as expressed by the Hammett σ_p-parameter. Comparison of the information obtained in these studies with that determined for related systems leads to the conclusion that the oxidation is a ligand-based process and that reduction involves addition of an electron to an orbital that possesses both metal and ligand character.
© 2005 Elsevier Ltd. All rights reserved.

Keywords: Gold; Dithiolene; Structure; Redox properties

1. Introduction

An extensive range of bis-dithiolene complexes of Au and their properties have been reported [1–31]; the majority are $[Au(dithiolene)_2]^-$ complexes with a square planar $\{AuS_4\}$ core, diamagnetic, and generally considered to involve a Au(III) (d^8) centre. The redox properties of $[Au(dithiolene)_2]^-$ complexes have been investigated and related $[Au(dithiolene)_2]^z$ ($z = 0$ or $2-$) complexes identified [2–4,7,8,12,15–18,23,25,26,30,31]; the electronic structure of these systems, notably the role of the dithiolene ligands in the redox processes, has been probed by ab initio and density functional calculations [21,32].

There are a range of strategies available to synthesize dithiolene complexes [33]. We have adapted the procedure developed by Davies et al. [34,35] to synthesize four new $[Au(dithiolene)_2]^-$ complexes, each of which involves the metal coordinated by two asymmetrically substituted dithiolenes.

* Corresponding author. Tel.: +44 115 951 4188; fax: +44 115 951 3563.
E-mail address: Dave.Garner@nottingham.ac.uk (C.D. Garner).

0277-5387/$ - see front matter © 2005 Elsevier Ltd. All rights reserved.
doi:10.1016/j.poly.2005.09.002

2. Experimental

Anhydrous *N*,*N*-dimethylformamide (DMF), over molecular sieves, was purchased from Fluka and used as received. Potassium *O*-isopropyl xanthate [36], 4-(phenyl)-1,3-dithiol-2-one [37], 2-bromoacetylpyridine hydrobromide, 3-bromoacetylpyridine hydrobromide and 4-bromoacetylpyridine hydrobromide [38,39] were prepared by the literature methods or modifications thereof.

2.1. Synthesis of 4-(pyridin-2-yl)-1,3-dithiol-2-one

2–Bromoacetylpyridine hydrobromide (8.41 g, 29.9 mmol) was suspended in CH_2Cl_2 (60 cm^3) and triethylamine (3.64 g, 36.0 mmol) added to give a pink solution. Potassium *O*-isopropyl xanthate (6.26 g, 36.0 mmol) was added and the orange suspension stirred for 2 h. The reaction was quenched by the addition of water (100 cm^3) and the CH_2Cl_2 layer separated. The aqueous phase was washed with CH_2Cl_2 (2×10 cm^3), the CH_2Cl_2 phases were combined, dried ($MgSO_4$), filtered, and the filtrate evaporated in vacuo to give a brown solid. The solid was treated with H_2SO_4 (10 cm^3, 98%) resulting in an exothermic reaction. After 5 min, ice was added to the reaction until no further heat was generated. The solution was diluted with water and then neutralised with $NaHCO_3$. The pale precipitate was extracted into CH_2Cl_2, the organic phase dried ($MgSO_4$), and the filtrate evaporated to dryness to yield a pale brown solid. Recrystallization from hot EtOH afforded a cream colored solid (0.80 g, 14%). Elemental *Anal*. Calc. for $C_8H_5NOS_2$: C, 49.27; H, 2.58; N, 7.18. Found: C, 49.18; H, 2.57; N, 6.98%. EI-MS *m*/*z*: 195 ($C_8H_5NOS_2^+$), 167 ($C_7H_5NS_2^+$), 123 ($C_6NSH_5^+$), 78 ($C_5H_4N^+$). ^{1}H NMR (300 MHz, $CDCl_3$, 298 K): δ_H 8.60–8.58 (m, 1H, H^6), 7.79–7.73 (m, 1H, H^3), 7.53–7.50 (m, 1H, H^4), 7.36 (s, 1H, H^{dithio}), 7.28–7.24 (m, 1H, H^5).

2.2. Synthesis of 4-(pyridin-3-yl)-1,3-dithiol-2-one

This compound was prepared as for 4-(pyridin-2-yl)-1,3-dithiol-2-one from 3-bromoacetylpyridine hydrobromide (8.11 g, 28.9 mmol), triethylamine (3.51 g, 34.8 mmol), potassium *O*-isopropyl xanthate (6.06 g, 34.8 mmol) and H_2SO_4 (10 cm^3, 98%), and obtained as a cream colored solid 0.90 g (16%). Elemental *Anal*. Calc. for $C_8H_5NOS_2$: C, 49.27; H, 2.58; N, 7.18. Found: C, 49.26; H, 2.52; N, 7.18%. EI-MS *m*/*z*: 195 ($C_8H_5NOS_2^+$), 167 ($C_7H_5NS_2^+$), 122 ($C_6NSH_4^+$), 78 ($C_5H_4N^+$). ^{1}H NMR (300 MHz, $CDCl_3$, 298 K): δ_H 8.73–8.72 (m, 1H, H^2), 8.63–8.60 (m, 1H, H^6), 7.73–7.69 (m, 1H, H^4), 7.38–7.33 (m, 1H, H^5), 6.94 (s, 1H, H^{dithio}).

2.3. Synthesis of 4-(pyridin-4-yl)-1,3-dithiol-2-one

This compound was prepared as for 4-(pyridin-2-yl)-1,3-dithiol-2-one from 4-bromoacetylpyridine hydrobromide (7.63 g, 27.2 mmol), triethylamine (3.30 g, 32.7 mmol), potassium *O*-isopropyl xanthate (5.57 g, 32.0 mmol) and H_2SO_4 (10 cm^3, 98%), and obtained as a cream colored solid (1.14 g, 22%). Elemental *Anal*. Calc. for $C_8H_5NOS_2$: C, 49.27; H, 2.58; N, 7.18. Found: C, 48.88; H, 2.52; N, 6.97%. EI-MS *m*/*z*: 195 ($C_8H_5NOS_2^+$), 167 ($C_7H_5NS_2^+$), 122 ($C_6NSH_4^+$), 78 ($C_5H_4N^+$). ^{1}H NMR (300 MHz, $CDCl_3$, 298 K): δ_H 8.67 (dd, 2H, H^2, H^6, J_{H-H} 4.5, 1.7 Hz), 7.30 (dd, 2H, H^3, H^5, J_{H-H} 4.4, 1.6 Hz), 7.15 (s, 1H, H^{dithio}).

2.4. Synthesis of [PPh_4][Au(sdt)$_2$] (**1**)

4-Phenyl-1,3-dithiol-2-one (0.10 g, 0.5 mmol) and NaOH (0.10 g, 2.5 mmol) were suspended in EtOH (10 cm^3). A solution of K[$AuCl_4$] (0.10 g, 0.3 mmol) in water (10 cm^3) was added and a dark yellow colored solution was obtained. This solution was heated at reflux for 3 h and then allowed to cool to room temperature. A solution of [PPh_4]Br (0.20 g, 0.5 mmol) in water (10 cm^3) was then added and a pale brown solid precipitated. The volume of the solvent was reduced in vacuo and the precipitate collected by filtration. This solid was recrystallized from a CH_2Cl_2 solution layered with *n*-hexane; the product was isolated by decantation of the mother liquor and then dried in vacuo to yield a golden crystalline solid (0.11 g, 51%). Elemental *Anal*. Calc. for $AuS_4PC_{40}H_{32}$: C, 55.29; H, 3.71. Found: C, 54.35; H, 3.69%. FAB-MS *m*/*z*: 530 $[Au(sdt)_2]^-$. ^{1}H NMR (300 MHz, $(CD_3)_2CO$, 298 K): δ_H 8.03–7.94 (m, 4H, PPh_4), 7.88–7.82 (m, 16H, PPh_4), 7.57 (m, 4H, H^2, H^6), 7.19 (m, 4H, H^3, H^5), 7.08 (m, 2H, H^4), 6.63, 6.62 (2s, 2H, H^{dithio}).

2.5. Synthesis of [PPh_4][Au(2-pedt)$_2$] (**2**)

This compound was prepared as described for **1** from 4-(pyridin-2-yl)-1,3-dithiol-2-one (0.10 g, 0.5 mmol), NaOH (0.10 g, 2.5 mmol) and K[$AuCl_4$] (0.10 g, 0.3 mmol). Addition of a solution of [PPh_4]Br (0.20 g, 0.5 mmol) in water (10 cm^3) to the dark yellow solution resulted in the precipitation of a pale brown solid. The volume of the solvent was reduced in vacuo, the precipitate was collected by filtration and then recrystallized from a solution in CH_2Cl_2 layered with *n*-hexane. The product was isolated by decantation of the mother liquor and then dried in vacuo to yield a golden crystalline solid (0.04 g, 18%). Elemental *Anal*. Calc. for $AuS_4N_2PC_{38}H_{30}$: C, 52.41; H, 3.47; N, 3.22. Found: C, 52.21; H, 3.34; N, 3.04%. FAB-MS *m*/*z*: 532 $[Au(2\text{-}pedt)_2]^-$. ^{1}H NMR (300 MHz, $(CD_3)_2CO$, 298 K): δ_H 8.32 (m, 2H, H^6), 8.03–7.96 (m, 4H, PPh_4), 7.89–7.81 (m, 16H, PPh_4), 7.62, 7.61 (2s, 2H, H^{dithio}), 7.60–7.58 (m, 4H, H^3, H^4), 6.99 (m, 2H, H^5).

2.6. Synthesis of [PPh_4][Au(3-pedt)$_2$] (**3**)

This compound was prepared as described for **1** from 4-(pyridin-3-yl)-1,3-dithiol-2-one (0.10 g, 0.5 mmol), NaOH (0.10 g, 2.5 mmol) and K[$AuCl_4$] (0.10 g, 0.3 mmol).

Addition of a solution of $[PPh_4]Br$ (0.20 g, 0.5 mmol) in water (10 cm^3) to the dark yellow solution resulted in the precipitation of a pale brown solid. The volume of the solvent was reduced in vacuo, the precipitate was collected by filtration and then recrystallized from a solution in CH_2Cl_2 layered with *n*-hexane. The product was isolated by decantation of the mother liquor and then dried in vacuo to yield a golden crystalline solid (0.08 g, 37%). Elemental *Anal*. Calc. for $AuS_4N_2PC_{38}H_{30}$: C, 52.41; H, 3.47; N, 3.22. Found: C, 52.26; H, 3.49; N, 3.10%. FAB-MS *m*/*z*: 532 $[Au(3\text{-pedt})_2]^-$. ^1H NMR (300 MHz, $(CD_3)_2CO$, 298 K): δ_H 8.80 (d, 2H, H^2, J_{H-H} 2.1 Hz), 8.30 (dd, 2H, H^6, J_{H-H} 4.9, 1.6 Hz), 8.03–7.97 (m, 4H, PPh_4), 7.89–7.83 (m, 18H, PPh_4, H^4), 7.19 (m, 2H, H^5) 6.79, 6.78 (2s, 2H, H^{dithio}).

2.7. Synthesis of $[PPh_4][Au(4\text{-pedt})_2]$ (4)

This compound was prepared as described for **1** from 4-(pyridin-4-yl)-1,3-dithiol-2-one (0.10 g, 0.5 mmol), NaOH (0.10 g, 2.5 mmol) and $K[AuCl_4]$ (0.10 g, 0.3 mmol). Addition of a solution of $[PPh_4]Br$ (0.20 g, 0.5 mmol) to the dark yellow solution resulted in the precipitation of a pale brown solid. The volume of the solvent was reduced in vacuo, the solid was separated by filtration and then recrystallized from a solution in CH_2Cl_2 layered with *n*-hexane. The product was isolated by decantation of the mother liquor and then dried in vacuo to yield a golden crystalline solid (0.04 g, 18%). Elemental *Anal*. Calc. for $AuS_4N_2PC_{38}H_{30}$: C, 52.41; H, 3.47; N, 3.22. Found: C, 51.99; H, 3.48; N, 3.15%. FAB-MS *m*/*z*: 532 $[Au(4\text{-pedt})_2]^-$. ^1H NMR (300 MHz, $(CD_3)_2CO$, 298 K): δ_H 8.36 (dd, 4H, H^2, H^6, J_{H-H} 4.7, 1.6 Hz), 8.03–7.94 (m, 4H, PPh_4), 7.89–7.83 (m, 16H, PPh_4), 7.49 (dd, 4H, H^3, H^5, J_{H-H} 4.9, 1.6 Hz), 7.15, 7.14 (2s, 2H, H^{dithio}).

3. Physical characterization

Elemental analyses of the compounds isolated in these studies were accomplished by the Microanalytical Laboratory of the School of Chemistry, the University of Nottingham, and by the Elemental Analysis Service at London Metropolitan University. FAB and EI mass spectra were recorded on a Fisons VG Trio 200 or a Fisons VG Autospec spectrometer. ^1H NMR spectra were recorded on a Bruker DPX300 NMR spectrometer and UV/Vis spectra were recorded on a Perkin–Elmer Lambda 16 spectrophotometer.

The cyclic voltammogram of each compound (1 mM) in DMF, containing $[N^nBu_4][BF_4]$ (0.2 M) as the background electrolyte, was recorded at room temperature using a glassy carbon working electrode, a Pt wire secondary electrode, and a saturated calomel reference electrode. To avoid overlapping redox couples, the $[(Me_5C_5)_2Fe]^+$/$[(Me_5C_5)_2Fe]$ ($[Fc^*]^+$/Fc^*]) couple was used as the internal reference and the potentials of the redox processes observed were referenced to that of the $[Fc]^+$/[Fc] couple by an independent calibration ($\Delta E_{1/2}$, $[Fc]^+$/[Fc] versus $[Fc_2^*]^+$/$[Fc_2^*]$, = 0.475 V). Measurements were performed using an Autolab PGSTAT20 potentiostat and compensation for internal resistance was not applied.

Golden, single crystals of **1**, **2**, **3** and **4** were grown by dissolution of the corresponding compound in CH_2Cl_2 followed by the slow diffusion of *n*-hexane into the solution. Details of the unit cell dimensions, data collection, and refinement are given in Table 1. Data for the structures of **1**, **2** and **3** were collected on a Bruker SMART 1000 CCD area detector diffractometer, whilst data for **4** were collected on a Bruker SMART APEX detector diffractometer. Both systems were equipped with an Oxford Cryosystems open flow cryostat. Structures **1** and **2** were solved by direct methods and structures **3** and **4** by Patterson heavy-atom

Table 1
Unit cell dimensions, data collected and refined for the crystal structures of $[PPh_4][Au(sdt)_2]$ (**1**), $[PPh_4][Au(2\text{-pedt})_2]$ (**2**), $[PPh_4][Au(3\text{-pedt})_2]$ (**3**), and $[PPh_4][Au(4\text{-pedt})_2]$ (**4**)

Compound	1	2	3	4
Empirical formula	$C_{40}H_{32}$ Au P S_4	$C_{38}H_{30}$ Au N_2 P S_4	$C_{38}H_{30}$ Au N_2 P S_4	$C_{38}H_{30}$ Au N_2 P S_4
M	868.83	870.82	870.82	870.82
Crystal system	monoclinic	monoclinic	monoclinic	monoclinic
Space group	$P2_1/n$	$P2_1/n$	$I2/a$	$I2/a$
a (Å)	14.7438(11)	14.3534(8)	18.187(4)	18.169(2)
b (Å)	13.7638(10)	13.8681(7)	17.332(4)	17.452(2)
c (Å)	17.0507(13)	17.0646(9)	21.346(5)	21.532(2)
α (°)	90	90	90	90
β (°)	92.199(2)	91.873(1)	90.960(4)	94.417(2)
γ (°)	90	90	90	90
V (Å^3)	3457.6(4)	3395.0(5)	6728(3)	6807(2)
Z	4	4	8	8
μ (mm^{-1})	4.572	4.658	4.701	4.646
Reflections collected	30951	19494	20743	19270
Independent reflections	8584	8226	8115	7918
R_{int}	0.032	0.038	0.062	0.033
Final R_1 [$I > 2\sigma(I)$], wR_2	0.0264, 0.0571	0.0344, 0.0803	0.0540, 0.135	0.0473, 0.115

methods, using SHELXS-97 [40]. In each case, a full-matrix least-squares refinement was carried out using SHELXL-97 [41]. All hydrogen atoms were placed in geometrically calculated positions and thereafter refined using a riding model with $U_{iso}(H) = 1.2U_{eq}(C)$, unless otherwise stated. All non-hydrogen atoms were refined with anisotropic atomic displacement parameters (adps), except partially occupied atoms of **2** and **4**. Compound **2** had a disorder in the pyridine ring containing the atoms C13–C18. The initial refined values of the isotropic adp (U_{iso}) suggested a misassignment of the carbon and nitrogen atoms C18 and N2. However, further investigation suggested an electron density intermediate between C and N at both sites. Therefore, the ring was modeled with two coincident half-occupied sites, with attendant half-occupied hydrogen atom positions corresponding to those of the C atoms. Compound **4** had a disorder in the anion containing Au2. All atoms of this anion, except the gold and sulfur, were positioned in two sites with occupancies of 0.70 and 0.30. Geometric restraints were applied to the distances in all the partial occupancy disorder models, such that the bond lengths were restrained to be the same in each component. Hydrogen atoms were geometrically placed.

4. Results and discussion

4.1. Syntheses

Each of the $[Au(SC(H)C(R)S)_2]^-$ (R = phenyl, pyridin-2-yl, pyridin-3-yl, or pyridin-4-yl: dithiolene abbreviations = sdt, 2-pedt, 3-pedt, and 4-pedt, respectively) complexes have been prepared (Scheme 1) by reacting $K[AuCl_4]$ with the appropriate dithiolene, generated by base hydrolysis of the corresponding thione-protected 1,3-dithiolate. Each $[Au(SC(H)C(R)S)_2]^-$ complex has been isolated as its $[PPh_4]^+$ salt (compounds **1**, **2**, **3**, and **4**, respectively) in a reasonable (18–51%) yield.

4.2. Structural information

The asymmetric unit of compounds **1** and **2** each comprises a $[PPh_4]^+$ cation and a $[Au(dithiolene)_2]^-$ (dithiolene = sdt or 2-pedt) anion, each of which has a *cis*-configuration (Fig. 1(a) and (b)). The asymmetric unit of compounds **3** and **4** each comprises a $[PPh_4]^+$ cation and two independent half $[Au(dithiolene)_2]^-$ (dithiolene = 3-pedt or 4-pedt) anions, the Au atoms of which are situated on an inversion center, i.e., each anion has a *trans*-configuration (Fig. 1(c) and (d)). The dimensions of each $[Au(dithiolene)_2]^-$ complex are presented in Table 2. In each anion, the AuS_4 center is essentially square planar: the length of the four Au-S bonds is essentially the same (2.30 ± 0.02 Å); the S–Au–S angles are all close to 90°; and the AuS_4 array is precisely planar in compounds **3**

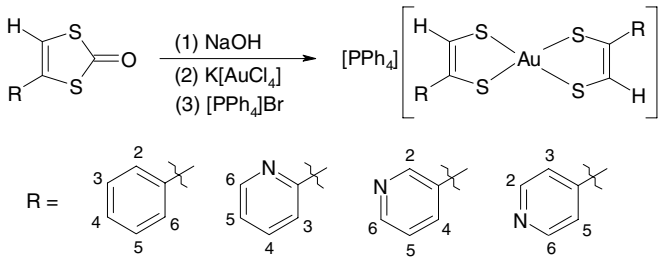

Scheme 1. Route used for the synthesis of $[PPh_4][Au(dithiolene)_2]$ (dithiolene = SC(H)C(R)S, R = phenyl (sdt), pyridin-2-yl (2-pedt), pyridin-3-yl (3-pedt) and pyridin-4-yl (4-pedt)) compounds. The numbering scheme for the various ligand substituents has been used in the assignment of the ^1H NMR spectra of these compounds.

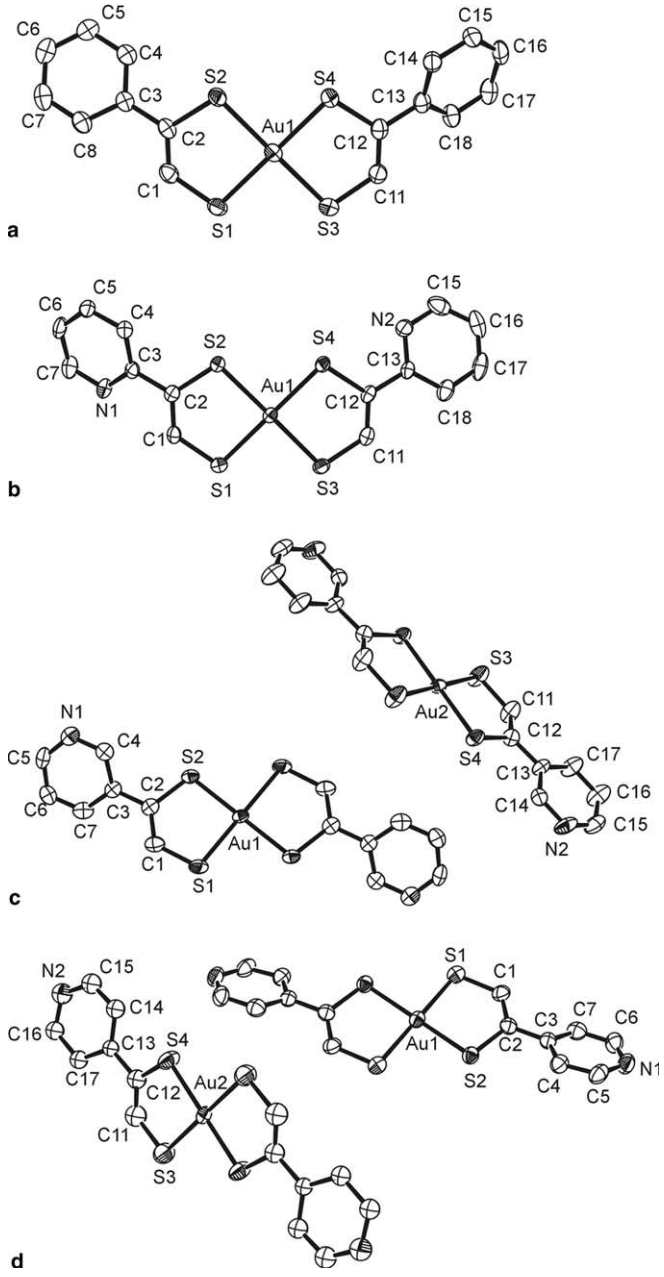

Fig. 1. Structure of: (a) $[Au(sdt)_2]^-$; (b) $[Au(2\text{-pedt})_2]^-$; (c) $[Au(3\text{-pedt})_2]^-$; and (d) $[Au(4\text{-pedt})_2]^-$ in the corresponding $[PPh_4][Au(dithiolene)_2]$ compound (**1**, **2**, **3** and **4**, respectively).

Table 2
Dimensions (bond length/Å; interbond angle/°) of the $[Au(dithiolene)_2]^-$ anions of $[PPh_4][Au(sdt)_2]$ (**1**), $[PPh_4][Au(2\text{-}pedt)_2]$ (**2**), $[PPh_4][Au(3\text{-}pedt)_2]$ (**3**) and $[PPh_4][Au(4\text{-}pedt)_2]$ (**4**)

Structure	1	2	3	4
Au1–S1	2.3126(9)	2.3124(12)	2.297(2)	2.308(2)
Au1–S2	2.3141(9)	2.3173(12)	2.298(2)	2.3054(18)
Au(A)–S3	2.3199(9)	2.3083(12)	2.301(2)	2.311(2)
Au(A)–S4	2.3149(9)	2.3116(12)	2.299(2)	2.2817(19)
S1–C1	1.737(4)	1.732(4)	1.732(9)	1.741(8)
S2–C2	1.777(3)	1.768(5)	1.770(8)	1.777(8)
S3–C11	1.744(3)	1.732(5)	1.730(9)	1.766(8)
S4–C12	1.770(3)	1.769(4)	1.759(9)	1.749(8)
C1–C2	1.336(5)	1.335(6)	1.349(10)	1.335(10)
C11–C12	1.337(4)	1.343(7)	1.337(12)	1.343(16)
S1–Au1–S2	89.66(3)	89.80(4)	89.95(8)	89.97(7)
S3–Au(A)–S4	89.95(3)	89.90(4)	89.62(8)	90.00(8)
Au1–S1–C1	101.15(12)	101.25(17)	101.7(3)	101.6(3)
Au1–S2–C2	102.32(11)	101.59(15)	102.6(3)	102.1(2)
Au(A)–S3–C11	100.82(12)	101.39(15)	101.4(3)	98.4(5)
Au(A)–S4–C12	101.82(10)	101.71(17)	102.8(3)	105.2(5)
S1–C1–C2	126.2(3)	125.4(4)	125.4(6)	125.1(6)
S2–C2-C1	120.3(3)	121.7(4)	120.3(7)	121.3(6)
S3–C11–C12	125.6(3)	125.2(4)	125.7(7)	129.1(10)
S4–C12–C11	121.3(2)	121.3(4)	120.4(7)	116.2(10)

The labelling of the atoms is shown in Figure 1 and Au(A) corresponds to Au(1) for **1** and **2** (the asymmetric unit of which involve one $[Au(dithiolene)_2]^-$ anion) and Au(2) for **3** and **4** (the asymmetric unit of which involve two independent half $[M(dithiolene)_2]^-$ anions).

and **4** and very close to planar in compounds **1** and **2** (the maximum deviation of an atom from the AuS_4 plane is 0.044 Å in **1** and 0.043 Å in **2**). Also, each {AuSCCS} metallodithiolene ring is essentially planar with the maximum displacement from the mean plane being $\leqslant 0.05$ Å. These structural details are in good agreement with those reported for other $[Au(dithiolene)_2]^-$ anions [6,9,13,16,19,20,22,29–31], as are the C–S (1.75 ± 0.03 Å) and dithiolene C–C (1.34 ± 0.01 Å) bond lengths (provided that the C–C bond is not part of an aromatic ring).

The four crystal structures described herein are the first such examples of gold bound to two asymmetrically substituted dithiolenes; also, $[Au(sdt)_2]^-$ and $[Au(2\text{-}pedt)_2]^-$ represent the first *cis*-isomers of a bis-dithiolene complex to be structurally characterized. The essential equivalence of the four M–S and four C–S bonds of each $[Au(dithiolene)_2]^-$ (dithiolene = sdt, 2-pedt, 3-pedt, or 4-pedt) complex indicates that the asymmetric nature of the dithiolene does not significantly affect the nature of the metal–sulfur interactions. However, the asymmetric nature of the dithiolene ligands *is* reflected in the S–C–C interbond angles; the S–C(H)–C(R) angles (125.1(6)–126.2(3)°) are significantly larger than the S–C(R)–C(H) angles (116.2(10)–121.7(4)°).

An important aspect to the nature of a dithiolene complex is the "non-innocence" of this ligand, the two extreme forms being the ene-1,2-dithiolate ($^-S–C{=}C–S^-$) and the dithioketone (S=C–C=S) [42]. Thus, the lengths of the C–C and C–S bonds can be used to comment on the nature of a dithiolene ligand in a complex, especially when – as in the present cases – the dithiolene ring is not fused to an aromatic ring. For sp^2 hybridized carbon atoms, typical bond lengths are: C–C, 1.43–1.48 Å; C=C, 1.30–1.36 Å; C–S, 1.71–1.75 Å; and C=S 1.67–1.68 Å [43]. Thus, the length of both the C–C (1.34 ± 0.01 Å) and the C–S (1.75 ± 0.03 Å) bonds of the ligands in each of the compounds **1**–**4** are consistent with the ene-1,2-dithiolate form of the dithiolene. Therefore, these $[Au(dithiolene)_2]^-$ anions can, to a first approximation, be formulated as Au(III) bis(ene-1,2-dithiolate) complexes, as proposed for $[Au(1,2\text{-}C_6H_4S_2)_2]^-$ by Ray et al. on the basis of the C–S bond lengths of this complex (average 1.762 Å) [31]. Consistent with this proposal, the electronic spectrum of compound **1** contains two weak absorptions at ca. 720 nm ($\varepsilon \sim 100\ M^{-1}\ cm^{-1}$) and ca. 465 nm ($\varepsilon \sim 260\ M^{-1}\ cm^{-1}$), similar to those of $[Au(1,2\text{-}C_6H_4S_2)_2]^-$ and related $[Au(dithiolene)_2]^-$ complexes [21,31].

4.3. ^1H NMR spectroscopy

The dithiolene proton of these $[Au(SC(H)C(R)S)_2]^-$ complexes provides a valuable probe of the nature of these complexes in solution. In the ^1H NMR spectrum of each $[PPh_4][Au(dithiolene)_2]$ (dithiolene = sdt, 2-pedt, 3-pedt, or 4-pedt) compound in $(CD_3)_2CO$ at 298 K the dithiolene (H^{dithio}) resonances were observed as two singlets, consistent with the presence of both *cis* and *trans* isomers of the square-planar anion in solution. The resonances observed and the ratio of the integrals were: $[PPh_4][Au(sdt)_2]$, 6.63 and 6.62 ppm, ca. 1:1; $[PPh_4][Au(2\text{-}pedt)_2]$, 7.62 and 7.61 ppm, ca. 1:1; $[PPh_4][Au(3\text{-}pedt)_2]$, 6.79 and 6.78 ppm, ca. 9:1; and $[PPh_4][Au(4\text{-}pedt)_2]$, 7.16 and 7.15, ca. 1:1. These H^{dithio} resonances vary with the nature of the dithiolene as 2-pedt > 4-pedt > 3-pedt > sdt, as observed for the $[MO(dithiolene)_2]^{2-}$ (M = Mo or W) complexes of these ligands. This order is consistent with nature of the ligands, in respect of: (i) inductive effects and (ii) the relative ability of the aromatic substituent to stabilize a resonance form in which a positive charge is localized at the C atom carrying the dithiolene proton [34,35].

The resolution of two environments for the dithiolene protons of compounds **1**–**4** contrasts with the ^1H NMR spectra observed for $[Ni(sdt)_2]$, in CD_2Cl_2; at >198 K a single dithiolene resonance is manifest but, at 198 K two resonances, of relative intensity ca. 1:1 and separated by 9.8 Hz are resolved. This latter information is consistent with a rapid interconversion of the *cis* and *trans* isomers of $[Ni(sdt)_2]$ at >198 K and has been attributed to a facile rotation of the ligand(s) around the metal [44]. Noting these results, the ^1H NMR spectrum of $[PPh_4][Au(sdt)_2]$ in $(CD_3)_2SO$ was recorded at ca. 298, 320, 330, 340, 355 and 365 K. At each temperature, the dithiolene proton resonances appeared as two singlets with a relative intensity of ca. 1:1. The splitting between these two singlets decreased slightly as the temperature was increased, from 3.28 Hz at 298 K to 2.96 Hz at 365 K, suggesting that coalescence may occur at >365 K. However, it is clear that the

activation energy for the interconversion of the *cis* and *trans* isomers of $[Au(sdt)_2]^-$ is significantly greater than that for the corresponding process of $[Ni(sdt)_2]$ [44]; this could be due to stronger metal–ligand bonds for Au (a 5d-metal) than Ni (a 3d-metal).

The presence of essentially equal amounts of the *cis* and *trans* isomers of $[Au(sdt)_2]^-$, $[Au(2\text{-pedt})_2]^-$, and $[Au(4\text{-pedt})_2]^-$ in solution and the lack of any significant interconversion of these isomers at room temperature suggests that solid samples of their $[PPh_4]^+$ salts contain an essentially equal amounts of the two isomers. However, from the structural studies, it appears that one isomer of the anion may preferentially crystallize and/or been present in the crystal selected for X-ray analysis. In respect of $[PPh_4][Au(3\text{-pedt})_2]$, we presume that the *trans* isomer identified by X-ray crystallography predominates in the sample for which the ^1H NMR spectrum was recorded.

4.4. Redox behavior

The cyclic voltammogram of each $[PPh_4][Au(\text{dithiolene})_2]$ (dithiolene = sdt, 2-pedt, 3-pedt, or 4-pedt) compound has been recorded in dmf solution containing $[N^nBu_4][BF_4]$ (0.2 M) as the background electrolyte. Each compound (Table 3) exhibits both an oxidation and a reduction process.

The oxidation of the compounds **1**–**4** occurs in the range $80\text{ mV} < E_p^a(\text{ox}) < 230\text{ mV}$ (versus $[Fc]^+/[Fc]$). The relative values of these potentials (Table 3) correlates with the electron withdrawing nature of the substituent (R), as measured by the Hammett parameter, σ_p [45]; thus, **1** (R = Ph; $\sigma_p = -0.01$) is the easiest to oxidize ($E_p^a(\text{ox}) = 80\text{ mV}$) and **4** (R = pyridin-4-yl; $\sigma_p = 0.44$) is the most difficult to oxidize ($E_p^a(\text{ox}) = 230\text{ mV}$). For each compound **1**–**4**, a variation in the scan rate (from 20 to 300 mV s^{-1}), monitoring the wave profile, the separation of the peak potentials (ΔE generally >70 mV), and the ratio of the cathodic and anodic currents ($-I_p^c : I_p^a \neq 1.0$) indicated that the oxidation is not electrochemically reversible. The most promising results were obtained for compound **1** (Fig. 2). At a scan rate >50 mV s^{-1}, ΔE is ca. 70 mV and comparable with that of the $[Fc^*]^+/[Fc^*]$ couple used as an internal standard. Also, the oxidation was monitored by UV/Vis spectroscopy and the profile seen to change through a series of isosbestic points. However, application of a potential sufficient to reverse the oxidation did not reproduce the original UV/Vis spectrum (even at 243 K). Therefore, the product of the oxidation of **1** is not stable within the timescale of the bulk electrolysis experiment. Also, oxidation of **1** with I_2 did not produce a stable product.

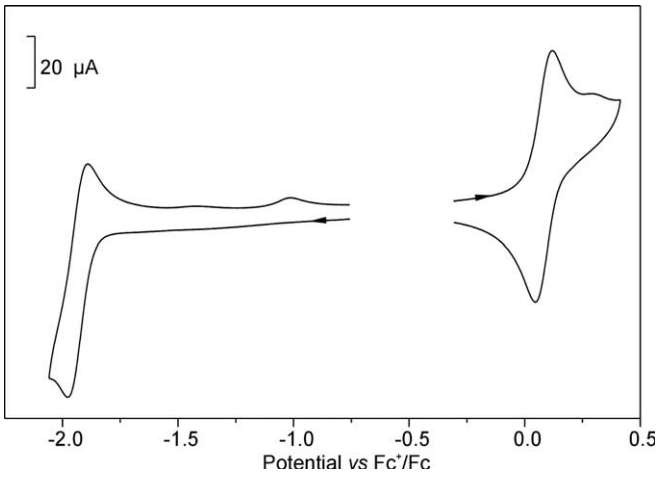

Fig. 2. Cyclic voltammogram of $[PPh_4][Au(sdt)_2]$ (**1**) (1 mM), at room temperature in DMF containing $[N^nBu_4][BF_4]$ (0.2 M), recorded using a glassy carbon working electrode, a Pt wire secondary electrode, and a saturated calomel reference electrode; potentials are vs. the $[Fc]^+/[Fc]$ couple.

The reduction of the compounds **1**–**4** occurs in the range $-1880\text{ mV} < E_p^c(\text{red}) < -2020\text{ mV}$ (versus $[Fc]^+/[Fc]$). As for oxidation of these compounds, the relative values of these reduction potentials (Table 3) correlate with the electron withdrawing nature of the dithiolene substituent (R), as measured by the Hammett parameter, σ_p [45]; thus, **1** is the most difficult to reduce ($E_p^c(\text{red}) = -2020\text{ mV}$) and **4** is the easiest to reduce ($E_p^c(\text{red}) = -1880\text{ mV}$). For each compound the reduction wave is accompanied by a corresponding oxidation wave upon reversal of the potential (Fig. 2). The electrochemical characteristics of the process were examined for a range of scan rates (20–300 mV s^{-1}) and, in each case, the reduction was not reversible. Also, following the reduction of each compound, scans at a more positive potential revealed other, relatively minor, oxidation processes, suggesting that each reduced species is reactive and/or unstable.

The cyclic voltammogram (CV) of **1** (Fig. 2) is remarkably similar, in respect of both the overall profile and the potentials of the redox processes, to the CV of $[Au(3,5\text{-di-}tert\text{-butyl-}1,2\text{-benzenedithiolate})_2]^-$ ($[Au(3,5\text{-}(^tBu)_2bdt)_2]^-$) [31]. This latter complex, in CH_2Cl_2 solution, undergoes two, reversible, one-electron processes; an oxidation at 74 mV and a reduction at −2280 mV (versus $[Fc]^+/[Fc]$). The correspondence in redox behavior and the one-electron nature of both redox couples of $[Au(3,5\text{-}(^tBu)_2bdt)_2]^-$ implies that oxidation of **1** involves the

Table 3
Potentials (vs. $[Fc]^+/[Fc]$) observed for the oxidation and reduction of $[PPh_4][Au(sdt)_2]$ (**1**), $[PPh_4][Au(2\text{-pedt})_2]$ (**2**), $[PPh_4][Au(3\text{-pedt})_2]$ (**3**), and $[PPh_4][Au(4\text{-pedt})_2]$ (**4**) (1 mM) at room temperature in DMF containing $[N^nBu_4][BF_4]$ (0.2 M)

Compound	$E_p^a(\text{ox})$	$E_{1/2}(\text{ox})$	$E_p^c(\text{red})$	$E_{1/2}(\text{red})$	$\Delta E([Fc^*]^+/[Fc^*])$
1	80	50(70)	−2020	−1970(90)	70
2	120		−1970	−1920(90)	80
3	180		−1920	−1880(90)	70
4	230	200(70)	−1880	−1840(90)	70

The shape of the voltammogram observed for the oxidation of **2** and **3** does not allow an accurate determination of $E_{1/2}$. For each compound, other redox processes were observed outside the potential range 1000 to −2100 mV.

$[Au(dithiolene)_2]/[Au(dithiolene)_2]^-$ couple and reduction involves the $[Au(dithiolene)_2]^-/[Au(dithiolene)_2]^{2-}$ couple.

The nature of the frontier orbitals of $[Au(dithiolene)_2]^-$ complexes has been investigated by performing ab initio calculations for $[Au(bdt)_2]^-$ [21] and the results of density functional calculations for $[Au(bdt)_2]^z$ ($z = 0$ or 1) and related complexes of Ni, Pd, Pt, and Cu [32]. Schiødt et al. [21] showed that, as observed by Schultz et al. [12], the two highest occupied molecular orbitals (HOMOs) of $[Au(bdt)_2]^-$ have π-character and comprise the antisymmetric and symmetric combination of the ligand HOMOs with 4 and 0% contribution from Au orbitals, respectively; each of these orbitals is C–S antibonding and C–C bonding in character. The LUMO of $[Au(bdt)_2]^-$ has σ-character, is the antibonding combination of the metal d_{xy} and ligand $1b_{1g}$ orbitals with significant contributions from both the metal (Au d_{xy} ca. 48%) and the ligand orbitals [21]. Similar results were obtained by density functional calculations accomplished for $[Au(bdt)_2]^z$ ($z = 0$ or 1) [32].

As described in 4.2, the length of the C–C and C–S bonds of the dithiolene ligands of compounds **1**–**4** are consistent with formulation as $[Au(III)(ene\text{-}1,2\text{-}dithiolate)_2]^-$, as indicated by structural [31] and theoretical [32] studies of $[Au(bdt)_2]^-$. One-electron oxidation of a $[Au(dithiolene)_2]^-$ complex, electrochemically or chemically (e.g., I_2), yields the corresponding, paramagnetic, $[Au(dithiolene)_2]$ complex, examples of which have been structurally characterized [12,16,30]. Dautel et al. [30] and Ray et al. [31] have compared the dimensions of a $[Au(dithiolene)_2]^-$ complex with those of its a $[Au(dithiolene)_2]$ counterpart and shown that conversion of the former to the latter leaves the Au–S bond length essentially unchanged, but the C–S bond shortens and the C–C bond lengthens. These structural changes are consistent with the loss of an electron from the HOMO of a $[Au(dithiolene)_2]^-$ complex, i.e., this ligand-based orbital[1] is Au–S non-bonding, C–S antibonding, and C–C bonding [21,32].

One-electron reduction of a $[Au(dithiolene)_2]^-$ complex yields the corresponding $[Au(dithiolene)_2]^{2-}$ complex that possesses one unpaired electron and EPR spectra of several of these systems have been reported [2,7,8,25,26]. A single-crystal EPR-ENDOR study of ^{13}C enriched $[^nBu_4N]_2[Au(mnt)_2]$ diluted in $[^nBu_4N]_2[Ni(mnt)_2]$ found that the majority (ca. 64%) of the unpaired spin density is located on the *S*-atoms [25,26]. This information is in qualitative agreement with the significant involvement of ligand orbitals in the LUMO of $[Au(dithiolene)_2]^-$ complexes [21,32].

A comparison of redox potentials for $[Au(L)_2]^-$ (L = sdt, 2-pedt, 3-pedt or 4-pedt) with those of their $[M(L)_2]^-$ (M = Ni, Pd or Pt) analogs [43] indicates that oxidation is less sensitive to a change in the metal than that of the corresponding reduction process. This is consistent with an oxidation being predominantly ligand-based and reduction involving an orbital with both ligand and metal character (vide infra). The trends within this series of $[Au(L)_2]^-$ complexes indicate a tuning of the ligand energy levels by the appended aromatic substituents.

5. Conclusions

Four new $[Au(dithiolene)_2]^-$ complexes, each involving two asymmetrically substituted dithiolene ligands (SC(H)-C(R)S; R = phenyl, pyridin-2-yl, pyridin-3-yl, or pyridin-4-yl) have been synthesised, isolated as the $[PPh_4]^+$ salt and structurally characterized. The lengths of the C–C and C–S bonds of the ligands in each $[Au(dithiolene)_2]^-$ complex is consistent with the dithiolene being present as an ene-1,2-dithiolate and, hence these are [Au(III)bis(ene-1,2-dithiolate)]$^-$ complexes. Each compound is diamagnetic and ^1H NMR studies indicate that, in solution in d^6-acetone, both the *cis* and *trans* isomers of the $[Au(SC(H)C(R)S)_2]^-$ anion are present and do not interconvert at room temperature. Each $[Au(dithiolene)_2]^-$ complex undergoes a ligand-based oxidation process and a reduction that involves the addition of an electron to an orbital that possesses considerable ligand character. These $[PPh_4][Au(dithiolene)_2]$ compounds are suitable diamagnetic hosts that facilitate EPR studies of corresponding $[M(dithiolene)_2]^-$ (M = Ni, Pd, or Pt) complexes [46].

Acknowledgements

We thank the EPSRC for the provision of a studentship to J.M.T.

Appendix A. Supplementary data

Crystallographic data for the structure of compounds **1**–**4** have been deposited with the Cambridge Crystallographic Data Centre, CCDC Nos. 275968, 275969, 275970 and 275971, respectively. Copies of the information may be obtained from The Director, CCDC, 12 Union Road, Cambridge CB2 1EZ, UK (Tel.: +44 1223 336408; fax: +44 1223 336033). Supplementary data associated with this article can be found, in the online version, at doi:10.1016/j.poly.2005.09.002.

References

[1] A. Davison, N. Edelstein, R.H. Holm, A.H. Maki, Inorg. Chem. 2 (1963) 1227.
[2] J.H. Waters, H.B. Gray, J. Am. Chem. Soc. 87 (1965) 3534.
[3] R. Williams, E. Billig, J.H. Waters, H.B. Gray, J. Am. Chem. Soc. 88 (1966) 43.

[1] Ray et al. [31,32] favor a description of the oxidized species as $[Au^{III}(L)(L^{\cdot})]$ (L = dithiolene). This implies that oxidation of a $[Au(dithiolene)_2]^-$ complex removes an electron from *one* ligand, *whereas* the theoretical results [12,21,32] indicate that the electron is lost from an orbital that involves an equal contribution from each ligand and the dimensions observed for $[Au(dithiolene)_2]$ complexes provide no such distinction between the ligands [12,16,30].

[4] M.J. Baker-Hawkes, E. Billig, H.B. Gray, J. Am. Chem. Soc. 88 (1966) 4870.
[5] A. Davison, D.V. Howe, E.T. Shawl, Inorg. Chem. 6 (1967) 458.
[6] J.H. Enemark, J.A. Ibers, Inorg. Chem. 7 (1968) 2636.
[7] R.L. Schlupp, A.H. Maki, Inorg. Chem. 13 (1974) 44.
[8] A. Domingos, R.T. Henriques, V. Gama, M. Almeida, A. Lopes, L. Alcacer, Syn. Met. 27 (1988) B411.
[9] M.A. Mazid, M.T. Razi, P.J. Sadler, Inorg. Chem. 20 (1981) 2872.
[10] P. Kuppusamy, N. Venkatalakshmi, P.T. Manoharan, J. Cryst. Spectros. Res. 15 (1985) 629.
[11] J.C. Fitzmaurice, A.M.Z. Slawin, D.J. Williams, J.D. Woollins, A.J. Lindsay, Polyhedron 9 (1990) 1561.
[12] A.J. Schultz, H.H. Wang, L.C. Soderholm, T.L. Sifter, J.M. Williams, K. Bechgaard, M.-H. Whangbo, Inorg. Chem. 26 (1987) 3757.
[13] T.W. Hijmans, W.P. Beyermann, Phys. Rev. Lett. 58 (1987) 2351.
[14] U. Geiser, A.J. Schultz, H.H. Wang, M.A. Beno, J.M. Williams, Acta Crystallogr., Sect. C 44 (1988) 259.
[15] G. Matsubayashi, A. Yokozawa, J. Chem. Soc., Dalton Trans. (1990) 3535.
[16] G. Rindorf, N. Thorup, T. Bjørnholm, K. Bechgaard, Acta Crystallogr., Sect. C 46 (1990) 1437.
[17] S.P. Best, S.A. Ciniawsky, R.J.H. Clark, R.C.S. McQueen, J. Chem. Soc., Dalton Trans. (1993) 2267.
[18] N.C. Schiødt, T. Bjørnholm, C.S. Jacobsen, K. Bechgaard, Synth. Met. 56 (1993) 2164.
[19] M.C. Gimeno, P.G. Jones, A. Laguna, M. Laguna, R. Terroba, Inorg. Chem. 33 (1994) 3932.
[20] R.M. Dávila, R.J. Staples, J.P. Fackler Jr., Acta Crystallogr., Sect. C 50 (1994) 1898.
[21] N.C. Schiødt, P. Sommer-Larsen, T. Bjørnholm, M. Folmer Nielsen, J. Larsen, K. Bechgaard, Inorg. Chem. 34 (1995) 3688.
[22] A. Charlton, A.E. Underhill, A. Kobayashi, H. Kobayashi, J. Chem. Soc., Dalton Trans. (1995) 1285.
[23] N.C. Schiødt, T. Bjørnholm, K. Bechgaard, J.J. Neumeier, C. Allgeier, C.S. Jacobsen, N. Thorup, Phys. Rev. B 53 (1996) 1773.
[24] M. Nakano, A. Kuroda, G. Matsubayashi, Inorg. Chim. Acta 254 (1997) 189.
[25] L. Ihlo, R. Böttcher, R.-M. Olk, R. Kirmse, Inorg. Chim. Acta 281 (1998) 160.
[26] L. Ihlo, R. Stosser, W. Hofbauer, R. Böttcher, R. Kirmse, Z. Naturforsch. 54 (1999) 597.
[27] M. Takahashi, N. Robertson, A. Kobayashi, H. Becker, R.H. Friend, A.E. Underhill, J. Mater. Chem. 8 (1998) 319.
[28] E. Cerrada, J. Garrido, M. Laguna, N. Lardiés, I. Romeo, Synth. Met. 102 (1999) 1709.
[29] S. Lo Schiavo, F. Nicolò, R. Scopelliti, G. Tresoldi, P. Piraino, Inorg. Chim. Acta 304 (2000) 108.
[30] O.J. Dautel, M. Fourmigué, E. Canadell, P. Auban-Senzier, Adv. Funct. Mater. 12 (2002) 693.
[31] K. Ray, T. Weyhermüller, A. Goossens, M.W.J. Crajé, K. Wieghardt, Inorg. Chem. 42 (2003) 4082.
[32] K. Ray, T. Weyermüller, F. Neese, K. Wieghardt, Inorg Chem. 44 (2005) 5345.
[33] T.B. Rauchfuss, Prog. Inorg. Chem. 52 (2003) 1.
[34] E.S. Davies, R.L. Beddoes, D. Collison, A. Dinsmore, A. Docrat, J.A. Joule, C.R. Wilson, C.D. Garner, J. Chem. Soc., Dalton Trans. (1997) 3985.
[35] E.S. Davies, G.M. Aston, R.L. Beddoes, D. Collison, A. Dinsmore, A. Docrat, J.A. Joule, C.R. Wilson, C.D. Garner, J. Chem. Soc., Dalton Trans. (1998) 3647.
[36] J. Berger, I. Uldall, Acta Chem. Scan. 18 (1964) 1353.
[37] A.K. Bhattacharya, A.G. Hortmann, J. Org. Chem. 39 (1974) 95.
[38] K. Schank, Chem. Ber. 102 (1969) 383.
[39] W. Wunderlich, J. Prackt. Chem. 2 (1955) 302.
[40] G.M. Sheldrick, SHELXS-97, University of Göttingen, Göttingen, Germany, 1997.
[41] G.M. Sheldrick, SHELXL-97, University of Göttingen, Göttingen, Germany, 1997.
[42] J.A. McCleverty, Prog. Inorg. Chem. 10 (1968) 49.
[43] F.H. Allen, O. Kennard, D.G. Watson, L. Brammer, A.G. Orpen, R. Taylor, J. Chem. Soc., Perkin Trans. II (1987) S1.
[44] A. Sugimori, N. Tachiya, M. Kajitani, T. Akiyama, Organometallics 15 (1996) 5664.
[45] C. Hansch, A. Leo, R.W. Taft, Chem. Rev. 91 (1991) 165.
[46] J. Tunney, Ph.D. Thesis, The University of Nottingham, 2003.

Available online at www.sciencedirect.com
SCIENCE DIRECT
Polyhedron 25 (2006) 599–612
POLYHEDRON
www.elsevier.com/locate/poly

Improved synthetic methods to mixed-donor thiacrown ethers

Mark W. Glenny [a], Leon G.A. van de Water [b], Joanna M. Vere [a], Alexander J. Blake [a], Claire Wilson [a], Willem L. Driessen [b,*], Jan Reedijk [b], Martin Schröder [a,*]

[a] School of Chemistry, University of Nottingham, University Park, Nottingham, NG7 2RD, United Kingdom
[b] Leiden Institute of Chemistry, Leiden University, P.O Box 9502, 2300 RA Leiden, The Netherlands

Received 30 August 2005; accepted 7 November 2005
Available online 15 December 2005

Abstract

A series of azathia- and azaoxathiacrown ether macrocycles have been prepared in good yields via the use of *N*-boc-bis(2-chloroethyl)amine as a precursor, which minimises undesirable side reactions and facilitates subsequent deprotection to the free cyclic amine. The mono-aza macrocycles, [12]aneNS$_3$, [12]aneNOS$_2$, [15]aneNS$_4$, [15]aneNO$_2$S$_2$ and [16]aneNS$_4$ have been prepared via this route. The single-crystal X-ray structure of [12]aneNS$_3$ · HBr · 2H$_2$O confirms the macrocycle to be distorted quadrangular with the S-centres lying along the edges and six out of 12 torsion angles less than 90°. The synthesis of di-aza macrocycles utilising the diamide precursors, *N*,*N*′-bis(chloroacetyl)-1,2-diaminoethane and *N*,*N*′-bis(chloroacetyl)-1,3-diaminopropane, affords the free macrocycles [12]aneN$_2$S$_2$, [15]aneN$_2$S$_3$, [15]aneN$_2$OS$_2$, [16]aneN$_2$S$_3$ and [19]aneN$_2$S$_4$ after reduction of the intermediate cyclic amides. Reaction of 3,6-dioxa-1,8-octanediamine with the dimethyl ester of thiadiglycolic acid followed by reduction affords [15]aneN$_2$O$_2$S, while the hydroxy-substituted macrocycles [20]aneS$_6$(OH)$_2$, [13]aneS$_4$(OH), and [26]aneS$_8$(OH)$_2$ have been prepared by reaction of 1,3-dichloro-2-hydroxypropane with the appropriate dithiol. The crystal structure of [20]aneS$_6$(OH)$_2$ shows two endo- and four exo-dentate S-centres as observed in the parent [18]aneS$_6$. The *N*-aryl substituted macrocycles *N*-4-NO$_2$Ph-[12]aneNS$_3$ (*N*-4-nitrophenyl-7-aza-1,4,10-trithiacyclododecane) and *N*-4-NH$_2$COPh-[12]aneNS$_3$ (*N*-4-benzamido-7-aza-1,4,10-trithiacyclododecane) have been prepared by reaction of 4-substituted bis-tosylated *N*,*N*-bis(2-hydroxyethyl)aniline with 3-thia-1,5-pentanedithiol.
© 2005 Elsevier Ltd. All rights reserved.

Keywords: Macrocycles; Thioether; Aza; Synthetic methods; Crown

1. Introduction

The ability of oxygen donor crown ethers to co-ordinate specifically to cations has been used extensively to bind and isolate alkali and alkaline earth metal ions from solution [1,2]. Macrocycles containing nitrogen and/or sulfur donor atoms are of interest as they exhibit high affinities towards heavy transition metal ions, and their selectivity is readily tunable by altering the composition of the donor-atom set and ring size. Mixed *N*,*O*,*S*-donor crowns, therefore, form an interesting class of compounds, which have found use as selective extractants for soft metal cations [3,4], and as models for the active sites of some enzymes [5]. The availability of mixed-donor crowns, however, is often limited by synthetic difficulties and many different approaches have been developed. We describe herein new synthetic routes to the formation of mixed *N*,*O*,*S*-donor crowns in reasonable yields. Such ligands have proven to be valuable in the selective extraction of transition-metal ions after immobilisation of these ligands onto organic polymeric resins, where the selectivity can be tuned by variation of the macrocyclic ligand [6,7]. Furthermore, *N*-substituted mixed-donor crown ethers may find application as redox chemosensors [8,9] or as hosts for the simultaneous binding of anions and cations [10,11].

Crown ethers containing only oxygen donors are generally accessible by reaction of the appropriate diol with a dihalide or ditosylate species in the presence of a base,

* Corresponding authors. Fax: +31 71 527 4451 (W.L. Driessen), +44 115 9513563 (M. Schröder).
E-mail address: M.Schroder@nottingham.ac.uk (M. Schröder).

0277-5387/$ - see front matter © 2005 Elsevier Ltd. All rights reserved.
doi:10.1016/j.poly.2005.11.006

for example NaOH [1]. This type of ring closure is relatively successful due to a strong template effect of the alkali metal ions with the polyether units. The synthesis of sulfur analogues, however, is less straightforward due to the absence of such a template effect, which can be attributed to the much lower affinity of sulfur for alkali metal ions compared to oxygen. Thus, the reaction of 3-thia-1,5-pentanedithiol with 1,2-dichloroethane in the presence of NaOH in EtOH affords low yields (0.04%) of the cyclic product [9]aneS$_3$ [12].

More recently, an improved method for the synthesis of thiacrown ethers has been developed by Buter and Kellogg [13] (Scheme 1). This method involves the Cs_2CO_3-mediated cyclisation of a dithiol and a dihalide in DMF under high-dilution conditions coupled with prolonged reaction times. It is believed that the Cs^+ ions form relatively weak ion pairs with the thiolate moieties, thereby making the sulfur atom highly nucleophilic and hence more reactive. Using this method [9]aneS$_3$ can be synthesised in multigram quantities in 50% yield [14]. Similarly, by variation of the dithiol or the dihalide species, oxathiacrown ethers and macrocycles bearing substituents have become available [15–17].

N-Tosylated amines are generally used for cyclisation reactions involving C–N bond formation [3] as dialkylation and quaternisation can result when unprotected amines are used. Thus, the cyclisation reaction is generally undertaken either in the presence of Cs_2CO_3 or by employing the disodium salts of the tosylated diamine. Ditosylates rather than dihalides are often used as the co-cyclisation reagents in these reactions [18] and an example is shown in Scheme 2. The major disadvantage of this method of cyclisation is the deprotection step that is necessary to obtain the tosylate-free macrocycle. Vigorous conditions such as concentrated H_2SO_4 at 90 °C [19], prolonged refluxing in HBr/acetic acid [20] or lithium in liquid ammonia [21] are required to remove the protecting group, but these can result, depending upon the ligand system, in degradation of the macrocyclic product. A variation on this method is provided by the reaction between a ditosylate and a dithiol (instead of a ditosylated diamine) in which [9]aneNS$_2$ can be synthesised from tritosylated diethanolamine and ethane dithiol, using Cs_2CO_3 in DMF [22].

Alternative synthetic procedures for azathiacrown ethers, which avoid tosylated intermediates, have also been reported. [15]aneNS$_4$ has been prepared directly from 3,6-dithia-1,8-octanedithiol and 1,5-dichloro-3-azapentane under high dilution conditions in DMF in the presence of Cs_2CO_3 [23] (Scheme 3(i)), although the yield of the macrocycle was rather low. [12]aneNS$_3$, [15]aneNS$_4$ and [18]aneNS$_5$ have been prepared from the 1,5-dichloro-3-azapentane and the appropriate dithiols (Scheme 3(ii)) with yields in the range from 26% to 39% [24]. Similarly, [12]aneNOS$_2$ can be prepared from 3-oxa-1,5-pentanedithiol and 1,5-dibromo-3-azapentane in MeOH in the presence of NaOMe (Scheme 3(iii)) [25]. The occurrence of *N*-alkylation and competing polymerisation reactions appear to be the major disadvantages of using a dithiol and an unprotected bis(2-haloethyl)amine.

An entirely different approach to unsubstituted oxaazathiacrown ethers involves the reaction of a diamine with a diacid chloride. Thus, Pelissard and Louis [26] have described the synthesis of a wide range of potentially pentadentate macrocycles using the same general procedure (Scheme 4). The reduction of the diamide is accomplished by either $LiAlH_4$ or BH_3 in THF. An alternative to this method is provided by the reaction of diamines with dimethyl esters instead of diacid chlorides [27], where only medium dilution conditions are required with reagent concentrations of the order of 0.1 mol/L, and the reaction proceeds under ambient conditions using MeOH as the solvent, typically over 7 days at 25 °C. Unlike the reactions involving diacid chlorides, non-protected polyamines can also be utilised in this type of cyclisation reaction due to the higher reactivity of the terminal primary amines compared to the internal secondary amines. Again, the resulting diamide may be reduced either by $LiAlH_4$ or by BH_3 in THF to afford the macrocyclic amine [27]. The fact that neither nitrogen protection nor high dilution conditions are required makes this method very attractive.

A series of 16–19-membered mixed-donor dibenzocrown ethers has been synthesised via the Schiff-base condensation of a linear diamine with dialdehyde [28]. The resulting

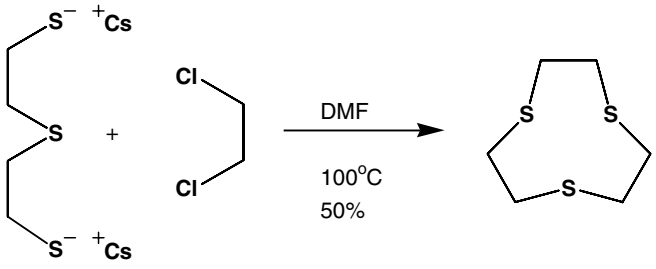

Scheme 1. Cs_2CO_3-mediated cyclisation of [9]aneS$_3$.

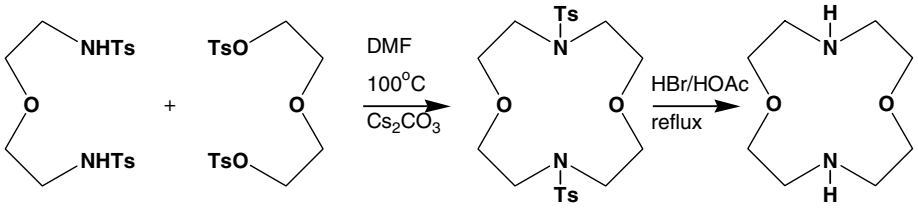

Scheme 2. Scheme for the synthesis of an oxa-azacrown ether.

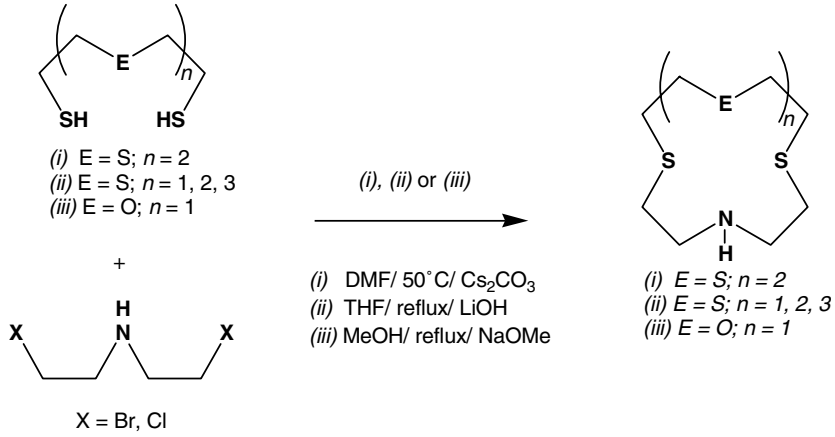

Scheme 3. Synthesis of mixed-donor crown ethers without the use of protecting groups.

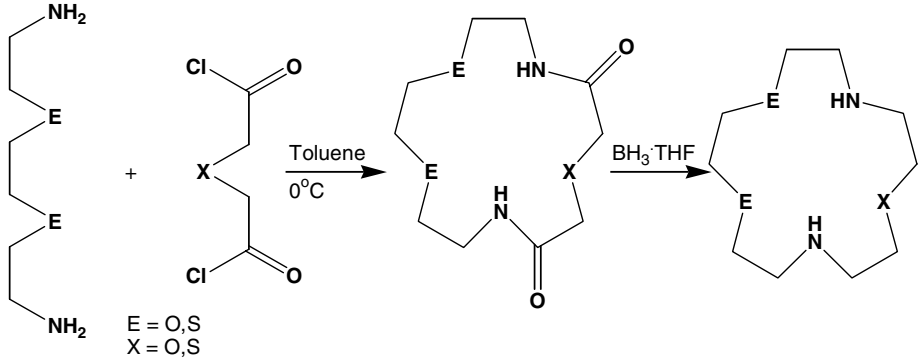

Scheme 4. Synthesis of 15-membered macrocycles from diamines and diacid chloride precursors.

diimines can be subsequently reduced with $NaBH_4$ to give the saturated macrocycles. Protection of the nitrogen atoms is not necessary as the initial formation of the imine species prevents undesired dialkylation reactions. Izatt and co-workers have used a different strategy to avoid side-reactions involving *N*-centres [29]. In this method a bis(α-chloroamide), prepared from the appropriate diamine by acylation using chloroacetic anhydride, undergoes ring-closure in a reaction with bis-secondary amines. The final reduction to yield the tetraamine can be achieved by reaction with $LiAlH_4$ (Scheme 5).

Metal templates have also been used to facilitate ring closing reactions; for example [9]aneS_3 has been prepared using the $Mo(CO)_3$ fragment with reaction between 1,2-dibromoethane and a 3-thia-1,5-pentanedithiol molybdenum adduct giving the cyclic product in good yield. This reaction can be made catalytic in terms of molybdenum [30].

Thus, the synthetic challenges in macrocycle synthesis are the result of: (i) elaborate protection and deprotection steps prior to and after ring closure, (ii) side reactions resulting in branched and polymeric products, and (iii) high-dilution conditions or simultaneous addition of two reagents. The tosyl group is the most widely used protective group in macrocyclic synthesis and has the advantages of high stablity towards harsh reaction conditions and ease of purification [19]. The main disadvantage is the often troublesome removal of the tosyl groups from mixed-donor crown ethers [21], particularly in the presence of oxidisable *S*-centres.

In order to overcome difficulties in deprotection, we have chosen to use a *t*-butyloxycarbonyl (boc) group to protect secondary amines in cyclisation reactions. The advantages of boc groups are that: (i) they can be readily introduced into secondary amines, (ii) they are not removed during cyclisation reactions, (iii) boc-protected crown ethers can be easily purified by column chromatography, and (iv) boc groups are generally removed under mild acidic conditions without affecting the macrocycle. We report herein the use of *N*-boc-bis(2-chloroethyl)amine (**1**) as the key intermediate for the synthesis of a series of unsubstituted oxamonoazathiacrown ethers. Secondly, a series of diazathiacrown ethers is presented, prepared by reaction of *N*,*N*′-bis(chloroacetyl)-diaminoalkanes with dithiols. In this way, no branched side products are formed during the cyclisation reaction as the nitrogen atoms are protected by the amide bond, and subsequent mild reduction in borane–THF affords the unsubstituted diazathiacrown ethers. Finally, we also report the synthesis of hydroxy-substituted thiacrown ethers and of *N*-aryl-substituted monoazathiacrown ethers.

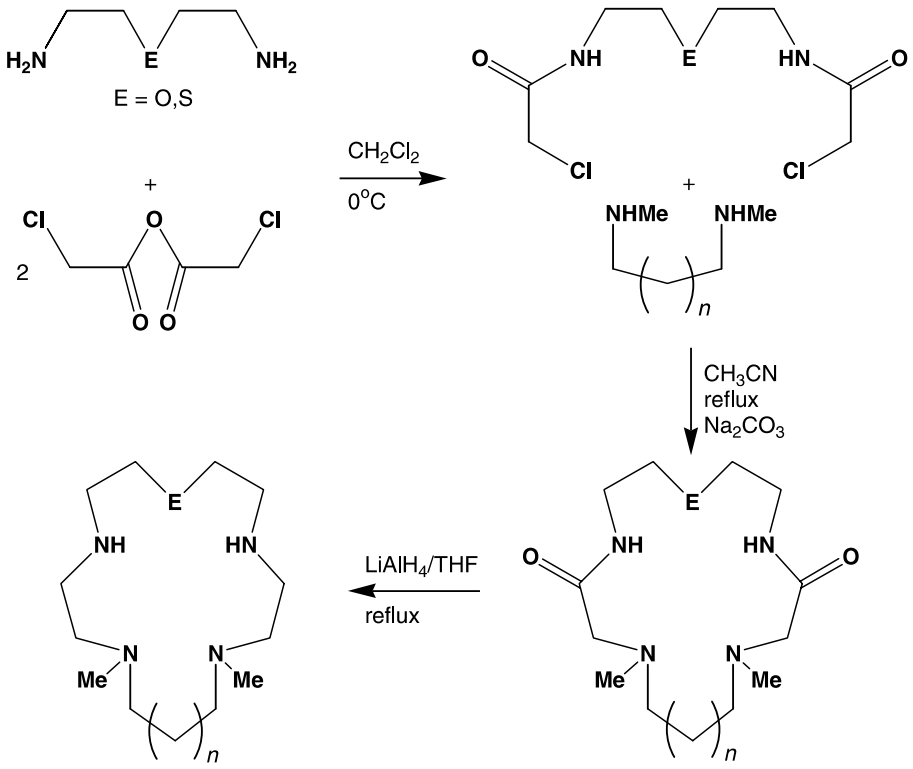

Scheme 5. Synthesis of polyaza-crown ethers via a diamide intermediate.

2. Results and discussion

2.1. Macrocycle synthesis

Reaction of **1** with the corresponding dithiol was carried out in a rapidly stirred suspension of Cs_2CO_3 in DMF, usually at concentrations in the range from 50 to 100 mmol/L at temperatures ranging from 65 to 100 °C, following the procedure of Buter and Kellogg [13]. The synthesis of the macrocyles [12]aneNS$_3$ (**2**), [12]aneNOS$_2$ (**3**), [15]aneNS$_4$ (**4**) and [15]aneNO$_2$S$_2$ (**5**) is illustrated in Scheme 6. Similarly, [16]aneNS$_4$ (**6**) was prepared from **1** and 3,7-dithia-1,9-nonanedithiol. The crude boc-protected products were purified by column chromatography yielding 35–40% of the pure boc-protected macrocycle, or by crystallisation (boc-**2**, 55% yield). In each case boc deprotection was carried out by stirring the boc-protected crown ethers with a TFA/CH_2Cl_2 mixture to give the deprotected macrocycle in 90% isolated yield.

A series of mixed-donor macrocycles containing two adjacent N-centres, [12]aneN$_2$S$_2$ (**7**), [15]aneN$_2$S$_3$ (**8**), [15]aneN$_2$OS$_2$ (**9**), [16]aneN$_2$S$_3$ (**10**) and [19]aneN$_2$S$_4$ (**11**) has been prepared utilising the precursors *N*,*N*′-bis(chloroacetyl)-1,2-diaminoethane and *N*,*N*′-bis(chloroacetyl)-1,3-diaminopropane (Scheme 7). The cyclisation is mediated by Cs_2CO_3 in DMF under medium dilution conditions using a dithiol as the co-cyclisation reagent. The intermediate macrocyclic diamide is readily separated from the polymeric material formed in competition with the macrocycle by extraction with CH_2Cl_2, with the exception of [12]aneN$_2$S$_2$ (**7**). Yields of the 15-membered diamide macrocycles were high (60–70%) while the yield of 1,4-dithia-7,10-diazacyclododecane-6,11-dione was lower and was difficult to estimate due to the presence of polymeric material.

The saturated macrocycles were obtained in good yield by reduction of the diamide precursors with borane–THF and, in the case of [12]aneN$_2$S$_2$ (**7**), no difficulty was experienced in the separation from the polymeric material. The reaction time is important in the reduction step with shorter times (8–12 h) giving optimum yields and longer times (20–40 h) resulting in lower yields (5–10%). The crude material was suitable, in most cases, for further use without purification, although column chromatography can be used to obtain analytically pure samples. We also report here the reduction of 7,13-diaza-1,4-dioxa-10-thiacyclopentadecane-8,12-dione, prepared from 3,6-dioxa-1,8-octanediamine and the dimethylester of thiadiglycolic acid in dry MeOH [31] using the same procedure. The reduction step is effective and affords the macrocycle [15]aneN$_2$O$_2$S (**12**) in 60% yield.

Employing the same methodology as used to prepare the other aza-thioether macrocyles with the intermediate **1**, the macrocycles [20]aneS$_6$(OH)$_2$ (**13**, Scheme 8), [13]aneS$_4$(OH) (**14**) [32] and [26]aneS$_8$(OH)$_2$ (**15**) (Scheme 9) were prepared via reaction of 1,3-dichloro-2-hydroxypropane with the appropriate dithiol. The preparation of the 20-membered macrocycle, **13**, also afforded small amounts of the [1+1] 10-membered macrocycle which proved difficult to purify, while the 13- and 26-membered macrocycles were obtained

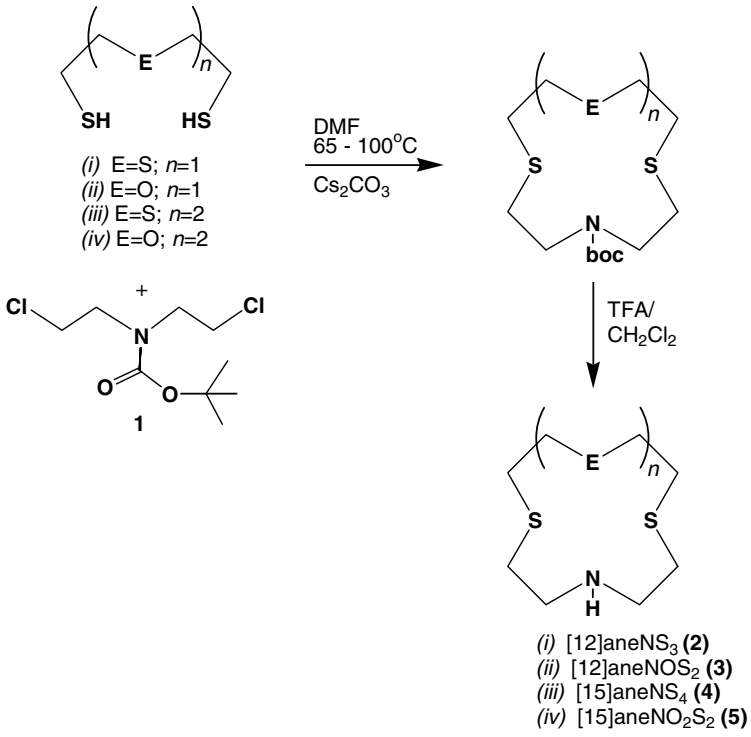

Scheme 6. Synthesis of (oxa)monoazathia crown ethers **2**, **3**, **4** and **5** from boc-protected bis(2-chloroethyl)amine **1**.

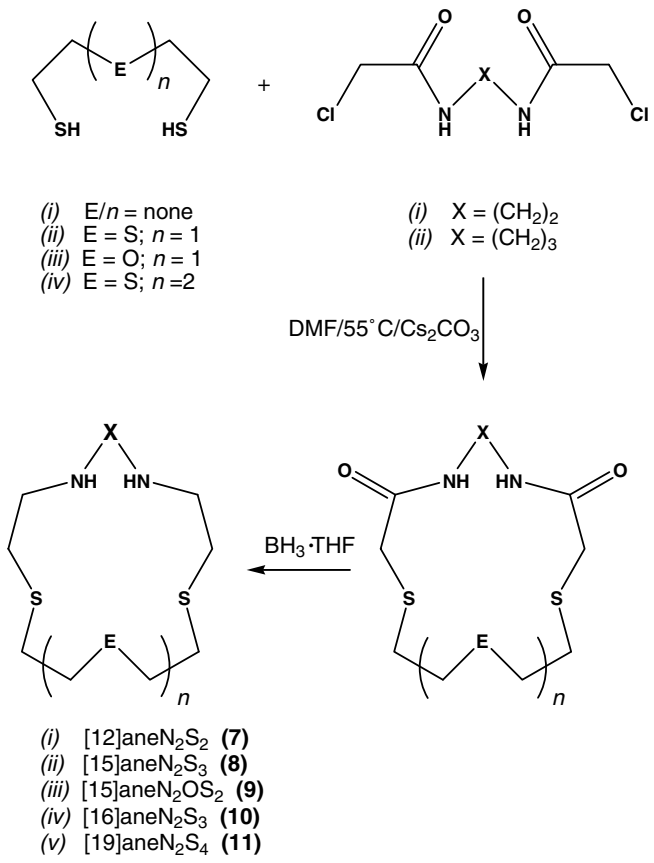

Scheme 7. Synthesis of *syn*-nitrogen containing macrocycles.

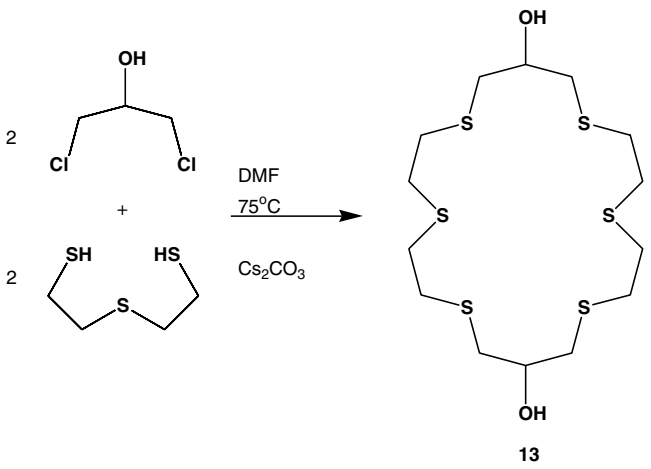

Scheme 8. Synthesis of hydroxyl-substituted [20]aneS$_6$(OH)$_2$ (**13**).

from the same reaction mixture and were separated by column chromatography on silica gel. These macrocycles are obtained as a mixture of *syn*/*anti* isomers which we were unable to resolve; however, due to the crystalline nature of [20]aneS$_6$(OH)$_2$ (**13**) crystals suitable for X-ray analysis could be grown.

While modifications to the aza moiety in macrocycles is often facile and accompanied in some cases with high yields [15–17], attempts to introduce aryl groups directly onto the

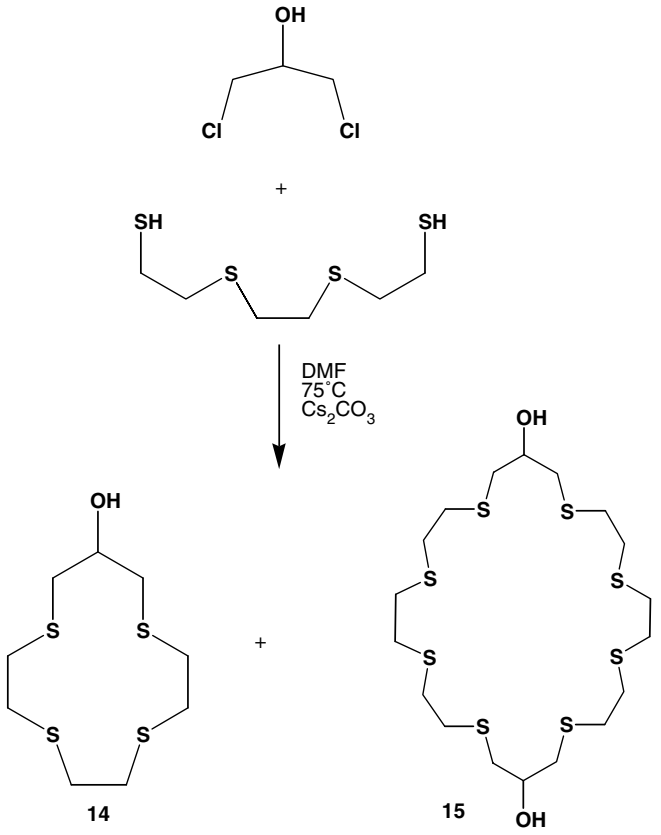

Scheme 9. Synthesis of hydroxy-substituted [13]aneS$_4$(OH) (**14**) and [26]aneS$_8$(OH)$_2$ (**15**).

macrocylic N-centre of the parent macrocycle is often problematic, even via Pd-catalysed coupling reactions which give good yields in analogous oxacrown ethers [33]. The main setback to Pd-catalysed routes to *N*-aryl-substituted azathiacrowns appears to be the high affinity and binding of these macrocycles to the palladium centre, thus rendering the catalyst ineffective. There are, however, some reports of aryl-subsitituted aza-thioether macrocycles in the literature: although their preparative routes and yields vary [17,34] they tend to utilise *N*-aryl substituted precursors.

Our interest in these types of macrocycles lies in their many potential uses, for example selective metal sensors, enhanced metal extraction and molecular switches. We, therefore, developed another route to aryl-substituted aza-thioether macrocycles in reasonable yields using tosylate leaving-groups, which is based upon the general cyclisation procedure already discussed above. This methodology also uses *N*-aryl substituted precursors and tosylates under Kellogg conditions [13]. Although it has been noted that tosylates are not as reactive toward thiolates as iodide leaving groups under the conditions used [34d], in our hands the macrocycles were obtained in satisfactory yields after a straightforward workup.

Thus, when a mixture of the ditosylated derivative of *N*,*N*-bis(2-hydroxyethyl)-4-nitroaniline, prepared in good yield from the reaction of the parent diol with tosyl chloride in a THF/water mixture, and 3-thia-1,5-pentanedithiol in DMF were added slowly to a rapidly stirred sus-

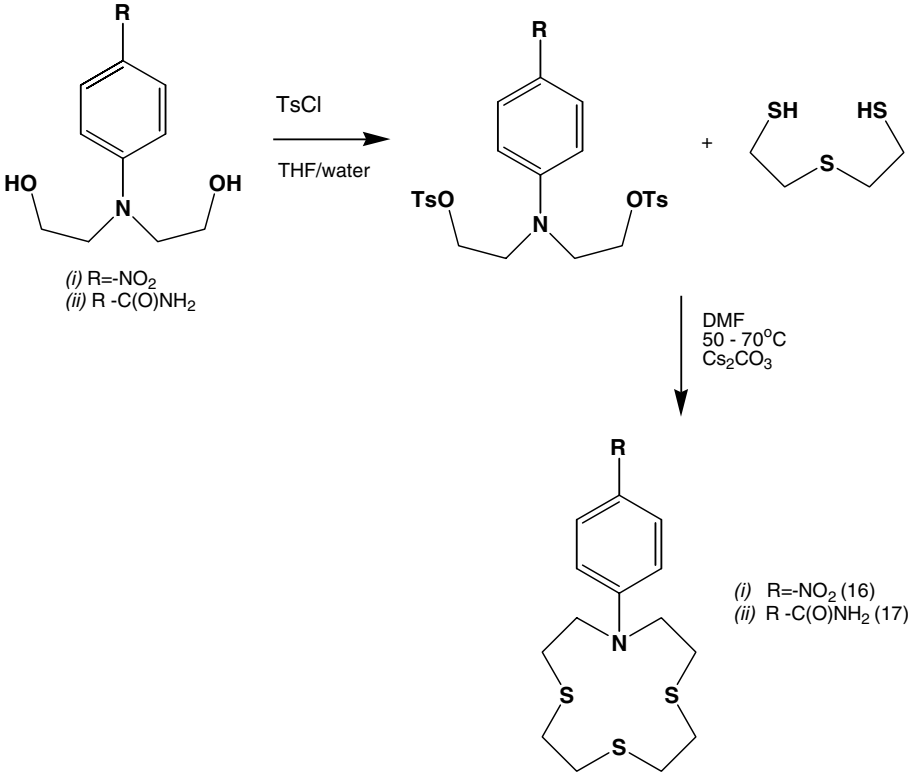

Scheme 10. Synthesis of *N*-4-NO$_2$Ph-[12]aneNS$_3$ (**16**) and *N*-4-NH$_2$COPh-[12]aneNS$_3$ (**17**).

pension of Cs_2CO_3 in DMF at 70 °C (Scheme 10), the resulting macrocyclic product *N*-4-NO_2Ph-[12]aneNS$_3$ (*N*-4-nitrophenyl-7-aza-1,4,10-trithiacyclododecane) (**16**) was obtained in 47% yield after purification by recrystallisation. The addition of Cs_2CO_3 is necessary for the reaction to take place smoothly, and heating to 50–70 °C was necessary to avoid the recovery of starting materials and/or polymeric material. In a similar fashion, *N*-4-NH_2COPh-[12]aneNS$_3$ (*N*-4-benzamido-7-aza-1,4,10-trithiacyclododecane) (**17**) was also prepared, the presence of the amide functionality allowing facile subsequent derivatisation via reduction to an amino group.

2.2. Single crystal structures of [12]aneNS$_3$ · HBr · 2H$_2$O (**2** · HBr · 2H$_2$O) and [20]aneS$_6$(OH)$_2$ (**13**)

A single-crystal X-ray structure of the HBr salt of [12]aneNS$_3$, **2** · HBr · 2H$_2$O (Fig. 1) was determined with the unit cell containing four molecules of **2** · HBr and eight molecules of water. The geometry of the molecule is rather unusual and may be described as a distorted quadrangular crown. The tendency of sulfur atoms in macrocyclic ligands to occupy the corners of quadrangular type structures is well documented [35], and in the majority of cases the sulfur atoms are oriented with their lone pairs pointing out of the ring (exodentate). This has been attributed to the preference of C–S bonds to adopt *gauche* conformations [35–37] while the C–C bonds take up the more energetically favourable *anti* conformations. In the structure of **2** · HBr · 2H$_2$O, the sulfur atoms do not occupy the corners of a quadrangle as found in [12]aneS$_4$ [35] and many other structures [38,39]; rather, they lie along the edges of a distorted crown. Significantly, there are only two *gauche* C–S conformations and three unfavorable eclipsed C–S conformations, while the remaining C–S torsion angle approaches a more favourable *anti* conformation (−158.9°). It has been noted [35] that an asymmetric distribution of donor atoms can make conformational preferences of ring segments act in opposition to each other which, in conjunction with amine protonation and hydrogen-bonding to the water molecules in the unit cell, may explain the abnormal conformation observed. Thus, six out of 12 torsion angles in the macrocyclic ring are less than 90°. Interestingly, the S atom (S7) lies out of the plane defined by N1, S4 and S10; however, all donor atoms are endodentate, an unusual orientation in thioether macrocycles although endodentate S centres have been observed in the structures of [9]aneS$_3$ [37] and [18]aneS$_6$ [35]. The transannular S···S distances in **2** · HBr · 2H$_2$O (3.476 and 3.600 Å for S4···S7 and S7···S10, respectively) are also shorter than the sum of the van der Waals radius of two sulfur atoms (3.7 Å) [40], and all C–C distances are slightly shorter than that expected for a C–C single bond (1.54 Å) as is commonly observed in other macrocyclic thioethers [35–37]. Selected bond distances, angles and torsion angles are given in Table 1. The extended structure of **2** · HBr · 2H$_2$O is a three-dimensional network of macrocycles, water molecules and bromide ions linked by N–H···O, O–H···O and O–H···Br interactions. Part of this network is shown in Fig. 2.

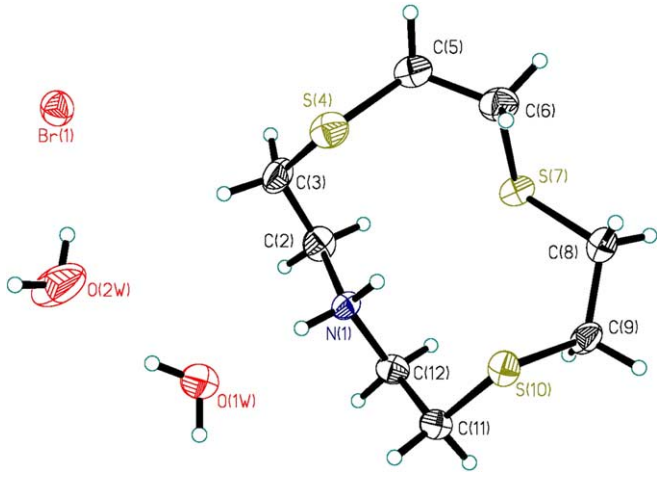

Fig. 1. Structure of **2** · HBr · 2H$_2$O (thermal ellipsoids shown at 50% probability level).

Table 1
Bond lengths (Å), bond angles (°) and torsion angles (°) for **2** · HBr · 2H$_2$O

N1–C12	1.485(8)
N1–C2	1.495(8)
C2–C3	1.524(10)
C3–S4	1.803(8)
S4–C5	1.817(7)
C5–C6	1.512(10)
C6–S7	1.812(7)
S7–C8	1.806(7)
C8–C9	1.531(10)
C9–S10	1.820(7)
S10–C11	1.815(7)
C11–C12	1.528(9)
C12–N1–C2	114.5(5)
N1–C2–C3	109.6(5)
C2–C3–S4	115.8(5)
C3–S4–C5	106.3(4)
C6–C5–S4	113.6(5)
C5–C6–S7	111.2(5)
C8–S7–C6	103.6(3)
C9–C8–S7	112.9(5)
C8–C9–S10	112.4(5)
C11–S10–C9	101.5(3)
C12–C11–S10	114.0(5)
N1–C12–C11	109.9(5)
C12–N1–C2–C3	−174.7(6)
N1–C2–C3–S4	48.1(7)
C2–C3–S4–C5	75.0(6)
C3–S4–C5–C6	−113.8(6)
S4–C5–C6–S7	79.4(6)
C5–C6–S7–C8	−158.9(5)
C6–S7–C8–C9	130.6(5)
S7–C8–C9–S10	−68.1(6)
C8–C9–S10–C11	126.5(5)
C9–S10–C11–C12	−72.6(5)
C2–N1–C12–C11	7.5(5)
S10–C11–C12–N1	−54.0(7)

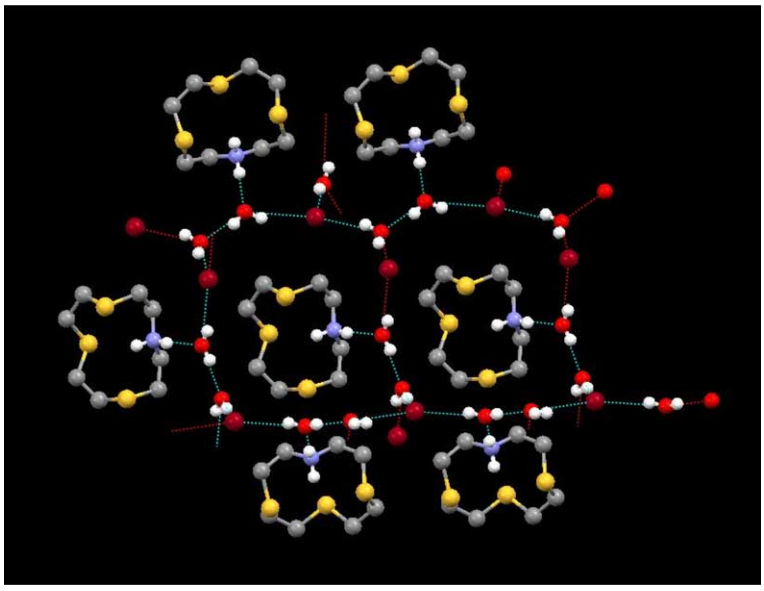

Fig. 2. Packing diagram of **2** · HBr · $2H_2O$. O: red, S: yellow, C: grey, H: white, N: blue. Hydrogens on carbon have been omitted for clarity.

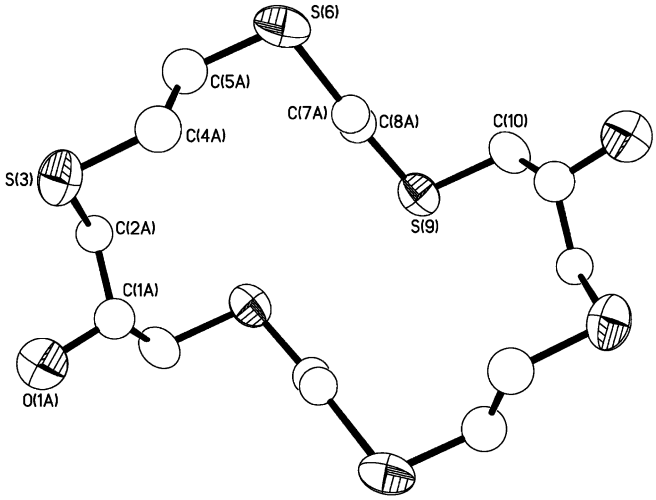

Fig. 3. Structure of **13** showing one disordered component. Carbon and oxygen atoms, except C(10) are isotropic, sulfur atoms are anisotropic (thermal ellipsoids shown at 50% probability level). Hydrogen atoms have been omitted for clarity.

The structure of [20]ane$S_6(OH)_2$ (**13**) is rather disordered, as may be expected from a mixture of isomers. Although the weakness of the diffraction resulted in a structure of limited precision, the main features of the compound are easily discernable. For clarity only the major (85%) disorder component is shown in Fig. 3. With two S atoms endodentate and four exodentate, the structure of [20]ane$S_6(OH)_2$ is reminiscent of that of [18]aneS_6 [35]. The molecule lies across a crystallographic twofold axis. Molecules are linked into a two-dimensional array by O–H···O hydrogen bonding interactions, as shown in Fig. 4.

3. Conclusions

We have demonstrated that mixed azathiacrown ether and oxaazathiacrown ether macrocycles can be obtained in good yields by utilising simple precursors under Kellogg conditions [13]. The methods described here are gen-

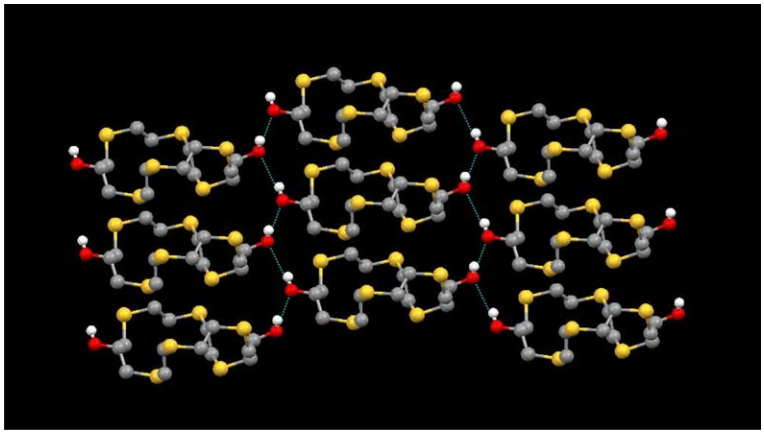

Fig. 4. Packing diagram of **13**. O: red, S: yellow, C: grey, H: white. Hydrogens on carbon have been omitted for clarity.

erally applicable to a wide range of mixed donor macrocyles and we are currently further exploring their derivatisation, co-ordination chemistry and applicability to metal ion extraction. The structure of [12]aneNS$_3$ · HBr · 2H$_2$O is found to be unusual compared to its homoleptic thioether analogues in that the macrocycle is rather distorted and contains endodentate donor atoms and few *gauche* C–S conformations which we attribute to protonation of the nitrogen donor. The structure of [20]aneS$_6$(OH)$_2$, although of limited precision, shows features similar to those in [18]aneS$_6$. Two *N*-aryl substituted aza-thioether macrocycles, *N*-4-NO$_2$Ph-[12]aneNS$_3$ and *N*-4-NH$_2$COPh-[12]aneNS$_3$, have also been prepared and are, due to their ease of purification, amenable to large scale synthesis.

4. Experimental

4.1. General remarks

All reagents and solvents were purchased from commercial sources and were used as received, unless stated otherwise. DMF was stored under an atmosphere of N_2 over molecular sieves. Elemental analyses (C, H, N, S) were carried out using the analytical facilities at the School of Chemistry, University of Nottingham, at Leiden University and University College Dublin. ^{1}H NMR and ^{13}C NMR spectra were recorded on either 200 MHz JEOL JNM FT NMR or Bruker AX 300 FT NMR spectrometers. Chemical shifts are quoted with respect to TMS as an internal reference. Mass spectra were recorded on either a Finnigan MAT TSQ-700 or a Finnigan MAT 900 XLT equipped with a custom-made electrospray interface (ESI), and by the EPSRC National Mass Spectrometry Facility at the University of Wales, Swansea. Single crystal *X*-ray data collections were performed on a Bruker SMART APEX CCD area detector diffractometer.

4.2. Single-crystal X-ray structural analyses of [12]aneNS$_3$ · HBr · 2H$_2$O [2 · HBr · 2H$_2$O] and [20]aneS$_6$(OH)$_2$ (**13**)

Single crystals of [12]aneNS$_3$ · HBr · 2H$_2$O suitable for analysis by X-ray diffraction were grown from a solution containing HBr/acetic acid and *N*-boc-[12]aneNS$_3$, which had been stirred at room temperature for 1 h. The solvent was reduced in vacuo and the colourless columnar crystals formed immediately at room temperature.

4.2.1. Crystal data

$C_8H_{22}BrNO_2S_3$, $M = 340.36$, tetragonal, $a = 8.609(3)$ Å, $c = 19.591(8)$ Å, $V = 1882.2(13)$ Å^3, $T = 220$ K, space group $P4_1$ (No. 76), $Z = 4$, μ(Mo Kα) = 3.247 mm^{-1}, $D_{calc} = 1.557$ g cm^{-3}, 1622 reflections measured, 1317 unique ($R_{int} = 0.037$) which were used in all calculations. The H atoms of the water molecules were found from the difference map and were given distance and angle restraints. The final *wR* (all F^2) was 0.0717, R_1 [1232 $F \geqslant 4\sigma(F)$] was 0.0327, and the Flack parameter refined to 0.00(3).

Lath-like single crystals of [20]aneS$_6$(OH)$_2$ were grown by slow evaporation of an ethyl acetate/hexane solution.

4.2.2. Crystal data

$C_{14}H_{28}O_2S_6$, $M = 420.72$, monoclinic, $a = 17.370(2)$ Å, $b = 5.4019(6)$ Å, $c = 22.146(3)$ Å, $\beta = 106.617(2)°$, $V = 1991.2(4)$ Å^3, $T = 150$ K, space group *I*/2*a* (alt. *C*2/*c*, No. 15), $Z = 4$, μ(Mo Kα) = 0.690 mm^{-1}, $D_{calc} = 1.403$ g cm^{-3}, 6961 reflections measured, 2558 unique ($R_{int} = 0.021$) which were used in all calculations. The crystal gave only weak diffraction and extensive disorder of the methylene and hydroxy groups was observed. All carbon atoms except C10 adopt extreme displacement parameters unless they remain isotropic, and C–C, C–O and C–S distances were refined subject to distance restraints of 1.52, 1.42 and 1.82 Å, respectively. The final *wR* (all F^2) was 0.333, R_1 [1575 $F \geqslant 4\sigma(F)$] was 0.103. Crystallographic Information Files (CIFs) for both structures have been deposited with the Cambridge Crystallographic Data Centre, UK.

4.2.3. *N*-Boc-bis(2-chloroethyl)amine (**1**)

Bis(2-chloroethyl)amine hydrochloride (36.0 g, 202 mmol) was added to a solution of NaOH (32.3 g, 807 mmol) in water (500 mL) at 0 °C. Di-*tert*-butyl dicarbonate [(Boc)$_2$O] (48.4 g, 222 mmol) was carefully added over a period of 30 min and the reaction mixture was stirred overnight at room temperature. The product was extracted with EtOAc (3 × 300 mL), dried over MgSO$_4$ and concentrated in vacuo to obtain the protected amine *N*-boc-bis(2-chloroethyl)amine as a pale yellow oil (45.2 g, 187 mmol, 93%); ^{1}H NMR ($CDCl_3$): δ (ppm) = 1.46 (s, 9H, C(CH$_3$)$_3$), 3.59 (m, 8H, CH$_2$); FAB-MS *m*/*z* ($C_9H_{18}Cl_2NO_2$, 242): 242 (M^+), IR (KBr disc) ν/cm^{-1} 2977, 1697. The product can also be obtained by heating the reagents under reflux in MeOH with the addition of a slight excess of triethylamine.

4.2.4. [12]aneNS$_3$(7-aza-1,4,10-trithiacyclododecane) (**2**)

N-Boc-[12]aneNS$_3$ was prepared by slowly adding a solution of 3-thia-1,5-pentanedithiol (16.4 g, 106 mmol) and *N*-boc-bis(2-chloroethyl)amine (25.6 g, 106 mmol) in dry DMF (1 L) to a suspension of Cs_2CO_3 (53.3 g, 164 mmol) in DMF (1.5 L) at 65 °C over a period of 96 h. Solvent was then removed in vacuo and the crude product dissolved in CH_2Cl_2 (300 mL) and washed with water to remove cesium salts. After drying over MgSO$_4$, filtering, and evaporation of the solvent, the crude product was purified by recrystallisation from warm toluene, yielding *N*-boc-[12]aneNS$_3$ (18.8 g, 58.1 mmol, 55%) as white crystals.

N-Boc-[12]aneNS$_3$ was deprotected with a mixture of TFA (60 mL) and CH_2Cl_2 (60 mL) for 15 min at room temperature. After evaporation of excess TFA and CH_2Cl_2, water was added (50 mL) and the reaction mixture was adjusted to pH 14 with Na_2CO_3 and NaOH. After

extraction with CH_2Cl_2 (5×50 mL), drying over $MgSO_4$, filtering, and removal of the solvent in vacuo, [12]aneNS$_3$ was obtained as a white solid in a 76% yield. *Anal*. Calc. for $C_8H_{17}NS_3$: C, 43.01; H, 7.67; N, 6.27; S, 43.05. Found: C, 43.11; H, 7.62; N, 5.98; S, 43.61%. ^{1}H NMR ($CDCl_3$): δ (ppm) = 1.98 (br s, 1H, NH), 2.69–2.90 (m, 16H, CH_2); ^{13}C NMR ($CDCl_3$): δ (ppm) = 31.15, 32.23 (CH_2–S), 49.81 (CH_2–N); ESI-MS *m*/*z* ($C_8H_{17}NS_3$, 223): 223 ($M^{+\cdot}$).

4.2.5. [12]aneNOS$_2$ (7-aza-1-oxa-4,10-dithiacyclododecane) (**3**)

3-Oxa-1,5-pentanedithiol (12.9 g, 93.3 mmol) was reacted with *N*-boc-bis(2-chloroethyl)amine (22.6 g, 93.3 mmol), using the same procedure as for *N*-boc-[12]aneNS$_3$, yielding *N*-boc-[12]aneNOS$_2$ (15.0 g, 48.9 mmol, 52%) as a colourless oil. After deprotection with TFA/CH_2Cl_2, the crude product was purified by column chromatography on SiO_2 eluting with CH_2Cl_2:methanol (20:1) to afford [12]aneNOS$_2$ in 39% yield. NMR analysis of the column fractions revealed that partial decomposition of the product on the column had occurred. No attempts were made to optimise the purification of the deprotected product. Analytical data for [12]aneNOS$_2$ have been reported previously [25a].

4.2.6. [15]aneNS$_4$ (7-aza-1,4,10,13-tetrathiacyclopentadecane) (**4**)

3,6-Dithia-1,8-octanedithiol was prepared by converting 3,6-dithia-1,8-octanediol to the dithiol according to the literature procedure [41]. *N*-Boc-[15]aneNS$_4$ was prepared by reacting *N*-boc-bis(2-chloroethyl)amine (4.23 g, 17.5 mmol) with the 3,6-dithia-1,8-octanedithiol (3.75 g, 17.5 mmol) in the same manner as for the syntheses of *N*-boc-[12]aneNS$_3$ and *N*-boc-[12]aneNOS$_2$. The product was purified by column chromatography on SiO_2 eluting with CH_2Cl_2. Yield: 2.32 g (6.05 mmol, 35%). The boc-protected product was deprotected with a 50% TFA-solution in CH_2Cl_2 for 15 min at room temperature (90% yield). *Anal*. Calc. for $C_{10}H_{21}NS_4$: C, 42.36; H, 7.47; N, 4.94; S, 45.23. Found: C, 42.39; H, 7.27; N, 4.27; S, 45.26%. ^{1}H NMR ($CDCl_3$): δ (ppm) = 1.86 (br s, 1H, NH), 2.60–2.90 (m, 20H, CH_2); ^{13}C NMR ($CDCl_3$): δ (ppm) = 32.26, 32.58, 32.73 (CH_2–S), 48.64 (CH_2–N); ESI-MS *m*/*z* ($C_{10}H_{21}NS_4$, 283): 284 $(M+H)^+$.

4.2.7. [15]aneNO$_2$S$_2$ (10-aza-1,4-dioxa-7,13-dithiacyclopentadecane) (**5**)

3,6-Dioxa-1,8-octanedithiol (2.80 g, 15.4 mmol) was reacted with *N*-boc-bis(2-chloroethyl)amine (3.72 g, 15.4 mmol), via the same procedure described above for *N*-boc-[15]aneNO$_2$S$_2$, resulting in a 35% yield after column chromatography on SiO_2. Deprotection was carried out using a TFA/CH_2Cl_2 mixture to give the product in 87% yield. *Anal*. Calc. for $C_{10}H_{21}NO_2S_2$: C, 47.76; H, 8.43; N, 5.57. Found: C, 47.55; H, 8.45; N, 5.18%. ^{1}H NMR ($CDCl_3$): δ (ppm) = 2.19 (br s, 1H, NH), 2.71–2.89 (m, 12H, CH_2–S and CH_2–N), 3.63 (s, 4H, CH_2–O), 3.70 (t, 4H, CH_2–O); ^{13}C NMR ($CDCl_3$): δ (ppm) = 32.11, 33.22 (CH_2–S), 48.35 (CH_2–N), 70.75, 72.01 (CH_2–O); ESI-MS *m*/*z* ($C_{10}H_{21}O_2NS_2$, 251): 251 ($M^{+\cdot}$).

4.2.8. [16]aneNS$_4$(7-aza-1,4,10,13-tetrathiacyclohexadecane) (**6**)

A mixture of 3,7-dithia-1,9-nonanedithiol [41] (3.74 g, 16.4 mmol) and *N*-boc-bis(2-chloroethyl)amine (3.97 g, 16.4 mmol) in dry DMF (50 mL) was slowly added to a well-stirred suspension of Cs_2CO_3 (5.99 g, 18.4 mmol) in DMF (70 mL) at 100 °C over 10 h under N_2. Stirring and heating was continued for a further 10 h, and the reaction mixture was filtered, and the DMF removed in vacuo. The crude product was extracted with CH_2Cl_2 (50 mL) and dried over $MgSO_4$. The volume of the yellow solution was then reduced to 25 mL and the product purified by column chromatography on SiO_2 eluting with CH_2Cl_2, affording *N*-boc-[16]aneNS$_4$ in 36% yield as a colourless oil which crystallised upon standing. ^{1}H NMR ($CDCl_3$): δ (ppm) = 1.45 (s, 9H, $C(CH_3)_3$), 1.94 (p, 2H, CH_2–C*H*$_2$–CH_2), 2.65–2.84 (m, 16H, CH_2–S), 3.44 (t, 4H, CH_2–N).

Deprotection was carried out using a TFA/CH_2Cl_2 mixture to give the product in 90% yield. *Anal*. Calc. for $C_{13}H_{24}F_3NO_2S_4$ ([16]aneNS$_4$ · TFA): C, 37.94; H, 5.88; N, 3.40; S, 31.16. Found: C, 37.91; H, 5.77; N, 3.40; S, 30.25%. ^{1}H NMR ($CDCl_3$): δ (ppm) = 1.91 (p, 2H, CH_2–C*H*$_2$–CH_2), 2.44 (br s, 1H, NH, absent on adding D_2O), 2.65–2.83 (m, 16H, CH_2–S), 2.83–2.93 (m, 4H, CH_2–N), ^{13}C NMR ($CDCl_3$): δ (ppm) = 30.01 (CH_2–*C*H$_2$–CH_2), 30.62, 32.41 (CH_2–S), 48.15 (CH_2–N); ESI-MS *m*/*z* ($C_{11}H_{23}NS_4$, 297): 298 $(M+H)^+$.

4.2.9. [12]aneN$_2$S$_2$ (7,10-diaza-1,4-dithiacyclododecane) (**7**)

The preparation of 7,10-diaza-1,4-dithiacyclododecane followed the analogous procedure as for the preparation of 10,13-diaza-1,4,7-trithiacyclopentadecane, with the exception that the diamide precursor, 7,10-diaza-1,4-dithiacyclododecane-6,11-dione, was not purified before use. The yield of the product, which was obtained as a pale yellow solid, was 30%. Analytical data for [12]aneN$_2$S$_2$ have been reported previously [42].

4.2.10. [15]aneN$_2$S$_3$ (10,13-diaza-1,4,7-trithiacyclopentadecane) (**8**)

The procedure for preparation of 10,13-diaza-1,4,7-trithiacyclopentadecane (using 3-thia-1,5-pentane dithiol) followed the procedure for preparation of 1-oxa-7,10-diaza-4,13-dithiacyclopentadecane with the exception that the crude product from the cyclisation was first isolated by filtration after addition of water. The cyclic diamide, 10,13-diaza-1,4,7-trithiacyclopentadecane-9,14-dione, was purified by Soxhlet extraction into CH_2Cl_2 in 60% yield, and the reduced product was extracted with ethyl acetate. The yield of the reduction step to give 1,4,7-trithia-10,13-diazacyclopentadecane as a pale yellow oil was 77%. The product was pure enough for further reactions, but an analytically

pure sample was obtained by column chromatography on SiO_2, eluting with CH_2Cl_2:MeOH (20:1), followed by crystallisation as the dihydrochloride salt from a methanol–water mixture.

10,13-diaza-1,4,7-trithiacyclopentadecane-9,14-dione. *Anal*. Calc. for $C_{10}H_{18}N_2O_2S_3$: C, 40.79; H, 6.16; N, 9.51. Found: C, 40.67; H, 5.74; N, 9.53%. ^{1}H NMR ($CDCl_3$): δ (ppm) = 2.82 (s, 8H, CH_2), 3.31 (s, 4H, CH_2CO), 3.56 (s, 4H, CH_2N), 7.28 (s, 2H, NH); ^{13}C NMR (75 MHz, 25 °C, $CDCl_3$): 29.53, 31.42, 33.29, 36.11, 170.03; EI MS *m/z* ($C_{10}H_{18}N_2O_2S_3$, 294) 294 ($M^{+\cdot}$).

10,13-diaza-1,4,7-trithiacyclopentadecane. *Anal*. Calc. for $C_{10}H_{24}Cl_2N_2S_3 \cdot 0.5H_2O$: C, 43.60; H, 8.41; N, 10.17. Found: C, 44.31; H, 8.14; N, 9.91%. ^{1}H NMR (300 MHz, 25°C, $CDCl_3$): δ (ppm) = 2.28 (s, 2H, NH), 2.65–2.81 (m, 20H, CH_2); ^{13}C NMR (75 MHz, 25°C, $CDCl_3$): δ (ppm) = 32.47 (s, S*C*H$_2$), 32.97 (s, S*C*H$_2$), 33.22 (s, S*C*H$_2$), 48.25 (s, N*C*H$_2$), 48.85 (s, N*C*H$_2$); FAB$^+$-MS *m/z* ($C_{10}H_{22}N_2S_3$, 266) 267 $(M+H)^+$.

4.2.11. [15]aneN_2OS_2 (1-oxa-7,10-diaza-4,13-dithiacyclopentadecane) (**9**)

To a rapidly stirred suspension of Cs_2CO_3 (43 g, 132 mmol) in DMF (800 mL) at 55 °C was added dropwise over 6 h a solution of 3-oxa-1,5-pentanedithiol (10.9 mL, 88 mmol) and *N*,*N*′-bis(chloroacetyl)-1,2-diaminoethane [43] (18.7 g, 88 mmol) in DMF (450 mL). After the addition was completed the mixture was stirred for 15 h at 55 °C and the solvent was then evaporated. Addition of water (300 mL) and extraction with CH_2Cl_2 afforded 1-oxa-7,10-diaza-4,13-dithiacyclopentadecane-6,11-dione in 67% yield as a white solid after evaporation of the solvent.

1-oxa-7,10-diaza-4,13-dithiacyclopentadecane-6,11-dione (6.8 g, 24.4 mmol) in 1 M borane–THF (80 mL) was heated under reflux for 15 h followed by careful addition of MeOH to quench excess borane. The volatile components were removed in vacuo which was repeated 4 times with the addition of MeOH (40 mL) before each evaporation cycle. To the resulting white solid was added 3 M HCl (150 mL) and the mixture heated under reflux for 5 h after which time the resulting solution was filtered through celite and basified to pH 13 with 5 M NaOH solution. The aqueous mixture was extracted with CH_2Cl_2 and dried over $MgSO_4$ to obtain 1-oxa-7,10-diaza-4,13-dithiacyclopentadecane in 84% yield as a colourless oil after evaporation of the solvent and drying under reduced pressure. The product was pure enough for further reactions. Analytical data for [15]aneN_2OS_2 have been reported previously [26].

4.2.12. [16]aneN_2S_3 (10,14-diaza-1,4,7-trithiacyclohexadecane) (**10**)

The preparation of 10,14-diaza-1,4,7-trithiacyclohexadecane (using 3-thia-1,5-pentanedithiol and *N*,*N*′-bis(chloroacetyl)-1,3-diaminopropane[1]) followed the same procedure as for the preparation of 10,13-diaza-1,4,7-trithiacyclopentadecane. The unsaturated macrocyclic precursor, 10,14-diaza-1,4,7-trithiacyclohexadecane-9,15-dione, was formed in 67% yield after purification by extraction into CH_2Cl_2, while the reduced product was extracted with $CHCl_3$. The yield at the reduction step to give 10,14-diaza-1,4,7-trithiacyclohexadecane as a pale yellow oil was 59%. Although this product was pure enough for most further applications, an analytically pure sample was obtained by column chromatography on SiO_2, eluting with CH_2Cl_2:MeOH (20:1).

10,14-diaza-1,4,7-trithiacyclohexadecane-9,15-dione. ^{1}H NMR ($CDCl_3$): δ (ppm) = 1.78 (tt, 2H, CH_2–CH_2–CH_2), 2.83 (m, 8H, CH_2–S), 3.25 (s, 4H, CH_2–CO), 3.44 (q, 4H, CH_2–N); ^{13}C NMR ($CDCl_3$): δ (ppm) = 109.67 (C=O), 49.06, 48.36, 32.92, 32.76, 32.25, 29.08 (CH_2–CH_2–CH_2); EI-MS *m/z* ($C_{11}H_{20}N_2O_2S_3$, 308) 308 ($M^{+\cdot}$).

10,14-diaza-1,4,7-trithiacyclohexadecane. ^{1}H NMR ($CDCl_3$): δ (ppm) = 1.70 (quin, 2H, CH_2–CH_2–CH_2), 1.98 (br s, 2H, NH), 2.74 (m, 8H, CH_2N), 2.80 (s, 12H, CH_2S); ^{13}C NMR ($CDCl_3$): δ (ppm) = 48.95, 48.28, 33.10, 32.84, 32.27, 28.93; FAB$^+$-MS *m/z* ($C_{11}H_{24}N_2S_3$, 280) 281 $(M+H)^+$.

4.2.13. [19]aneN_2S_4 (14,17-diaza-1,4,8,11-trithiacyclononadecane) (**11**)

The procedure for preparation of 14,17-diaza-1,4,8,11-trithiacyclononadecane (using 3,7-dithia-1,9-nonanedithiol and *N*,*N*′-bis(chloroacetyl)-1,2-diaminoethane) followed same procedure as for the preparation of 10,13-diaza-1,4,7-trithiacyclopentadecane. The unsaturated macrocyclic precursor, 14,17-diaza-1,4,8,11-trithiacyclononadecane-13,18-dione, was purified by extraction into CH_2Cl_2 and isolated in 37% yield. The crude reduced product was extracted into $CHCl_3$ and after evaporation of the solvent, a yellow oil was obtained which was purified by repeated extraction into Et_2O. Subsequent reduction gave 14,17-diaza-1,4,8,11-trithiacyclononadecane as a pale yellow oil in 47% yield.

14,17-diaza-1,4,8,11-trithiacyclononadecane-13,18-dione. ^{1}H NMR ($CDCl_3$): δ (ppm) = 7.38 (br s. 2H, NHCO), 2.9–2.65 (m, 12H, CH_2–S), 2.69 (t, 4H, CH_2–N); ^{13}C NMR ($CDCl_3$): δ (ppm) = 170.0, 53.5, 40.6, 38.7, 33.5, 31.6, 31.0, 30.4; EI-MS *m/z* ($C_{13}H_{24}N_2O_2S_4$, 366) 366 ($M^{+\cdot}$).

14,17-diaza-1,4,8,11-trithiacyclononadecane. ^{1}H NMR ($CDCl_3$): δ (ppm) = 2.80–2.55 (m, 24H, CH_2), 1.93 (br s, 2H, NH), 1.82 (quin, 2H, CH_2–CH_2–CH_2); ^{13}C NMR ($CDCl_3$): δ (ppm) = 48.7, 48.5, 33.0, 32.7, 32.6, 30.7 ppm; FAB$^+$-MS *m/z* ($C_{13}H_{28}N_2S_4$, 340) 341 $(M+H)^+$.

4.2.14. [15]aneN_2O_2S (7,13-diaza-1,4-dioxa-10-thiacyclopentadecane) (**12**)

This procedure is similar to the one used by Gryko et al. [31] for the preparation of the corresponding dione but to the best of our knowledge the reduction to the saturated macrocycle has not been reported.

3,6-Dioxa-1,8-octanediamine (16.0 g, 108 mmol) and the dimethylester of thiadiglycolic acid (19.2 g, 108 mmol,

[1] Prepared using the same procedure as *N*,*N*′-bis(chloroacetyl)-1,2-diaminoethane.

1 eq.) were dissolved in dry MeOH (1 L) and the mixture was heated at reflux under N_2 for 7 days. The solvent was removed in vacuo and the product, 7,13-diaza-1,4-dioxa-10-thiacyclopentadecane-8,12-dione, was recrystallised from a mixture of CH_2Cl_2 and hexane yielding the cyclic diamide as white crystals in 21% yield. *Anal.* Calc. for $C_{10}H_{18}N_2O_4S$: C, 45.78; H, 6.92; N, 10.67. Found: C, 45.72; H, 6.81; N, 10.51%. ^{1}H NMR ($CDCl_3$): δ (ppm) = 3.32 (s, 4H, CH_2–S), 3.51 (m, 4H, CH_2–N), 3.61 (t, 4H, CH_2–O), 3.65 (s, 4H, CH_2–O); ^{13}C NMR ($CDCl_3$): δ (ppm) = 37.00 (CH_2–S), 39.42 (CH_2–N), 68.98 (CH_2–O), 69.59 (CH_2–O), 167.70 (C=O); FAB$^+$-MS *m/z* ($C_{10}H_{18}N_2O_4S$, 262): 263 $(M+H)^+$.

7,13-Daza-1,4-dioxa-10-thiacyclopentadecane-8,12-dione (5.90 g, 22.5 mmol) was reduced with a 1.0 M solution of borane in THF (125 mL) by heating the mixture at reflux for 24 h under a N_2. The excess borane was quenched with MeOH and the solvent was removed in vacuo. The crude product was treated with MeOH (25 mL) and evaporated again in order to remove low-boiling borates. The product was then heated at reflux for 4 h in a mixture of 2 M HCl and MeOH (1:1). The reaction mixture was cooled and basified (pH 13) with a KOH solution. The product was extracted with CH_2Cl_2 (5 × 30 mL), the solution dried over $MgSO_4$, filtered, and the solvent removed in vacuo. The product was purified by column chromatography on SiO_2, eluting with CH_2Cl_2:MeOH (4:1) to give [15]aneN_2O_2S as a light yellow oil in 61% yield. *Anal.* Calc. for $C_{10}H_{22}O_2N_2S$: C, 51.25; H, 9.46; N, 11.95; S, 13.68. Found: C, 49.29; H, 8.87; N, 10.28; S, 12.26%. ^{1}H NMR ($CDCl_3$): δ (ppm) = 2.70 (s, 4H, CH_2–S), 2.73 (m, 8H, CH_2–N), 2.86 (br s, 2H, NH), 3.55 (m, 8H, CH_2–O); ^{13}C NMR ($CDCl_3$): δ (ppm) = 33.61 (CH_2–S), 47.85 (CH_2–N), 48.98 (CH_2–N), 69.75 (CH_2–O), 69.92 (CH_2–O); FAB$^+$-MS *m/z* ($C_{10}H_{22}N_2O_2S$, 234): 235 $(M+H)^+$.

4.2.15. [20]ane$S_6(OH)_2$ (1,11-Dihydroxy-3,6,9,13,16,19-hexathiacycloeicosane) (**13**)

To a rapidly stirred suspension of Cs_2CO_3 in DMF (550 mL) at 75 °C was added a solution of 3-thia-1,5-pentanedithiol (5.45 mL, 42 mmol) and 1,3-dichloro-2-hydroxypropane (5.42 g, 42 mmol) in DMF (42 mL) at a rate of 1.2 mL/hr. After the addition was complete the reaction mixture was heated at 75 °C for a further 12 h. The solution was allowed to cool, was filtered and the resulting yellow solution evaporated to yield a yellow oil which solidified on standing. Addition of CH_2Cl_2 afforded a white solid which was filtered off and washed with CH_2Cl_2. Slow evaporation of the filtrate afforded white crystals which were washed with hexane and recrystallised from EtOH–hexane (50:50). Further product was obtained by recrystallisation of the evaporated mother liquor from EtOH–hexane (50:50) to remove small quantities of the 1+1 macrocycle. Total isolated yield was 1.97 g (22%). Resolution of the two isomers was not achieved. *Anal.* Calc. for $C_{14}H_{28}O_2S_6$: C, 39.96; H, 6.71. Found: C, 39.99; H, 6.64%. ^{1}H NMR ($CDCl_3$): δ (ppm) = 2.65–2.70 (m, 4H, CH_2), 2.80–2.89 (m, 20H, CH_2), 3.90 (m, 2H, CH); ^{13}C NMR ($CDCl_3$): δ (ppm) = 32.27, 32.97, 38.26 (CH_2–S), 70.25 and 70.30 (CH–OH); FAB$^+$-MS *m/z* ($C_{14}H_{28}O_2S_6$, 420): 421 $(M+H^+)$, CI$^+$-MS *m/z* ($C_{14}H_{28}O_2S_6$+NH_4, 438): 438 $(M+NH_4)^+$.

4.2.16. [13]aneS_4(OH) (1-Hydroxy-3,6,9,12-tetrathiacyclotridecane) (**14**) and [26]ane$S_8(OH)_2$ (1,14-dihydroxy-3,6,9,12,16,19,22,25-octathiacyclohexacosane) (**15**)

The preparations of 1-hydroxy-3,6,9,12-tetrathiacyclotridecane and 1,14-dihydroxy-3,6,9,12,16,19,22,25-octathiacyclohexacosane (using 3,6-dithiaoctane-1,8-dithiol) followed the same cyclisation procedure and used reagents on the same millimolar scale as for the preparation of 1,11-dihydroxy-3,6,9,13,16,19-hexathiacycloeicosane. Purification of the product was achieved through column chromatography on SiO_2 with an EtOAc:hexane (50:50) eluent. The first band to be eluted was [13]aneS_4(OH) (1.85 g), [26]ane$S_8(OH)_2$ (0.32 g) being obtained from the second band after evaporation. Total yield of combined products was 2.17 g (17%). Resolution of the isomers was not achieved.

1-Hydroxy-3,6,9,12-tetrathiacyclotridecane. *Anal.* Calc. for $C_9H_{18}OS_4$: C, 39.96; H, 6.71. Found: C, 39.75; H, 6.52%. ^{1}H NMR ($CDCl_3$): δ (ppm) = 2.60 (d, 1H, CH_2), 2.64 (d, 1H, CH_2), 2.77–2.95 (m, 14H, CH_2), 3.87 (m, 1H, CH–O); ^{13}C NMR ($CDCl_3$): δ (ppm) = 31.52, 31.70, 32.23, 37.71 (CH_2–S), 67.55 (CH–OH); FAB$^+$-MS *m/z* ($C_{18}H_{36}O_2S_8$, 270): 270 (M^+).

1,14-dihydroxy-3,6,9,12,16,19,22,25-octathiacyclohexacosane. *Anal.* Calc. for $C_{18}H_{36}O_2S_8$: C, 39.96; H, 6.71. Found: C, 39.73; H, 6.79%. ^{1}H NMR ($CDCl_3$): δ (ppm) = 2.65–2.82 (m, 32H, CH_2), 3.88 (m, 2H, CH_2); ^{13}C NMR ($CDCl_3$): δ (ppm) = 32.40, 32.92, 32.97, 38.26 (CH_2–S), 69.93 (CH–OH); FAB$^+$-MS *m/z* ($C_{18}H_{36}O_2S_8$, 540): 541 $(M+H)^+$.

4.2.17. N,N-Bis(hydroxyethyl)-4-nitroaniline

To a solution of 4-nitroaniline (12.88 g, 93.2 mmol) in glacial acetic acid (80 mL) was added ethylene oxide (30 g, 680 mmol) and the bright yellow mixture stirred for 2 days at room temperature. The solvent was removed at 40 °C and a mixture of water (50 mL) and CH_2Cl_2 (50 mL) added to the resulting oil from which a yellow solid precipitated. The precipitate was filtered and washed with water then CH_2Cl_2 and dried in vacuo (7.2 g). Further product (6 g) was obtained by concentration and cooling of the CH_2Cl_2 filtrate. The total yield of the yellow product was 13.2 g (63%). *Anal.* Calc. for $C_{10}H_{14}N_2O_4$: C, 53.09; H, 6.24; N, 12.38. Found: C, 52.39; H, 6.10; N, 12.26%. ^{1}H NMR ($CDCl_3$): δ (ppm) = 3.71 (t, 4H, CH_2), 3.81 (t, 4H, CH_2), 4.19 (m, 2H, OH), 6.84 (m, 2H, Ar), 8.01 (m, 2H, Ar); ^{13}C NMR ($CDCl_3$): δ (ppm) = 54.86 (CH_2), 59.85 (CH_2), 111.69 (CH), 126.46 (CH), 137.34 (C_{quat}), 154.40 (C_{quat}); FAB$^+$-MS *m/z* ($C_{10}H_{14}N_2O_4$, 226): 227 $(M+H)^+$.

4.2.18. N,N-Bis(tosylethyl)-4-nitroaniline

To an aqueous NaOH solution (1.1 M, 100 mL) was added *N*,*N*-bis(hydroxyethyl)-4-nitroaniline (5.9 g, 26.1 mmol) in THF (80 mL) and the mixture cooled to 0 °C in an ice-salt bath. Tosyl chloride (9.94 g, 52.2 mmol) in THF (50 mL) was added dropwise to the cooled solution ensuring that the temperature remained below 3 °C. The resulting suspension was stirred for 1 h at 5 °C and then for 15 h at room temperature. The bright yellow precipitate was filtered, washed with water and dried (7.8 g, 56%). Further product was obtained by recrystallisation of the residue derived from the filtrate from a dichloromethane–hexane mixture. *Anal*. Calc. for $C_{24}H_{26}N_2O_8S_2$: C, 53.92; H, 4.90; N, 5.24. Found: C, 53.73; H, 4.71; N, 5.28%. ^{1}H NMR ($CDCl_3$): δ (ppm) = 2.40 (s, 6H, CH_3), 3.69 (t, 4H, CH_2), 4.15 (t, 4H, CH_2), 6.42 (d, 2H, Ar), 7.25 (d, 4H, Ar), 7.68 (d, 4H, Ar), 8.00 (d, 2H, Ar); ^{13}C NMR ($CDCl_3$): δ (ppm) = 21.57 (CH_3), 50.25 (CH_2), 65.87 (CH_2), 110.67 (CH_{phenyl}), 126.01 (CH_{phenyl}), 127.78 (CH_{tosyl}), 129.93 (CH_{tosyl}), 132.25 (C_{quat}), 138.24 (C_{quat}), 145.37 (C_{quat}), 150.93 (C_{quat}); FAB$^+$-MS *m*/*z* ($C_{24}H_{26}N_2O_8S_2$, 534): 535 $(M+H)^+$.

4.2.19. N-4-NO_2Ph-[12]aneNS$_3$(N-4-Nitrophenyl-7-aza-1,4,10-trithiacyclododecane) (**16**)

The preparation of *N*-4-nitrophenyl-7-aza-1,4,10-trithiacyclododecane (using *N*,*N*-bis(tosylethyl)-4-nitroaniline) followed the same procedure as for the preparation of 7-aza-1,4,10-trithiacyclododecane using reagents on the same millimolar scale. Purification of the product was achieved by recrystallisation from CH_2Cl_2–hexane. The isolated yield of the yellow solid was 0.63 g (47%). *Anal*. Calc. for $C_{14}H_{20}N_2O_2S_3$: C, 48.81; H, 5.85; N, 8.13. Found: C, 47.55; H, 5.59; N, 7.94%. ^{1}H NMR ($CDCl_3$): δ (ppm) = 2.82–2.92 (m, 12H, CH_2), 3.71 (m, 4H, CH_2), 6.68 (d, 2H, Ar), 8.13 (d, 4H, Ar); ^{13}C NMR ($CDCl_3$): δ (ppm) = 28.48 (CH_2), 31.49 (CH_2), 31.50 (CH_2), 51.14 (CH_2), 110.48 (CH_{phenyl}), 126.40 (CH_{phenyl}), 145.47 (C_{quat}), 152.14 (C_{quat}); FAB$^+$-MS *m*/*z* ($C_{14}H_{20}N_2O_2S_3$, 344): 345 $(M+H)^+$.

4.2.20. N,N-Bis(hydroxyethyl)-4-benzamide

Using the procedure outlined for the preparation of *N*,*N*-bis(hydroxyethyl)-4-nitroaniline and reagents on the same millimolar scale, the product was obtained as a white powder (60%). *Anal*. Calc. for $C_{11}H_{16}N_2O_3$: C, 58.91; H, 7.19; N, 12.49. Found: C, 58.22; H, 7.13; N, 11.62%. ^{1}H NMR (CD_3OD): δ (ppm) = 3.59 (t, 4H, CH_2), 3.73 (t, 4H, CH_2), 6.75 (d, 2H, Ar), 7.72 (d, 2H, Ar); ^{13}C NMR (CD_3OD): δ (ppm) = 54.73 (CH_2), 60.17 (CH_2), 112.01 (CH), 120.97 (C_{quat}), 130.46 (CH), 152.38 (C_{quat}), 172.63 (CO); EI-MS *m*/*z* ($C_{11}H_{16}N_2O_3$, 224): 224 ($M^{+\cdot}$).

4.2.21. N,N-Bis(tosylethyl)-4-benzamide

Using the procedure outlined for the preparation of *N*,*N*-bis(tosylethyl)-4-nitrobenzamide and reagents on the same millimolar scale, recrystallisation from methanol to remove mono-tosylated product yielded the product as a white solid (3.3 g, 48%). *Anal*. Calc. for $C_{25}H_{28}N_2O_7S_2$: C, 56.37; H, 5.30; N, 5.26. Found: C, 56.14; H, 5.24; N, 5.21%. ^{1}H NMR (CD_3OD): δ (ppm) = 2.35 (s, 6H, CH_3), 3.56 (t, 4H, CH_2), 4.11 (t, 4H, CH_2), 6.39 (d, 2H, Ar), 7.24 (d, 4H, Ar), 7.60 (m, 6H, Ar); FAB$^+$-MS *m*/*z* ($C_{25}H_{28}N_2O_7S_2$, 532): 533 $(M+H)^+$.

4.2.22. N-4-NH_2COPh-[12]aneNS$_3$(N-4-Benzamido-7-aza-1,4,10-trithiacyclododecane) (**17**)

The preparation of *N*-4-benzamido-7-aza-1,4,10-trithiacyclododecane (using *N*,*N*-bis(tosylethyl)-4-benzamide) followed the cyclisation procedure and used reagents on the same millimolar scale as for the preparation of 7-aza-1,4,10-trithiacyclododecane. Purification was achieved by extraction into hot toluene followed by slow cooling to obtain the product as a white microcrystalline solid (0.40 g, 23%). *Anal*. Calc. for $C_{15}H_{22}N_2OS_3$: C, 52.60; H, 6.47; N, 8.18. Found: C, 53.66; H, 6.45; N, 7.73%. ^{1}H NMR ($CDCl_3$): δ (ppm) = 2.84 (m, 12H, CH_2), 3.64 (m, 4H, CH_2), 5.66 (br s, NH_2), 6.72 (d, 2H, Ar), 7.70 (d, 2H, Ar); ^{13}C NMR ($CDCl_3$): δ (ppm) = 28.36 (CH_2), 31.19 (CH_2), 32.27 (CH_2), 50.80 (CH_2), 111.08 (CH), 128.21 (C_{quat}), 129.48 (CH), 150.26 (C_{quat}), 168.85 (CO); FAB$^+$-MS *m*/*z* ($C_{15}H_{22}N_2OS_3$, 342): 343 $(M+H)^+$.

Acknowledgments

L. vd W. is indebted to the Council for Chemical Sciences of the Netherlands Organisation for Scientific Research (CW-NWO) for financial support. We thank the EPSRC for support to MWG and for the provision of diffractometers. We also thank the Universities of Leiden and Nottingham for support and the EPSRC National Mass Spectrometry Service at the University of Wales, Swansea for mass spectra. M.S. gratefully acknowledges receipt of a Royal Society Wolfson Merit Award and of a Royal Society Leverhulme Trust Senior Research Fellowship.

Appendix A. Supplementary data

Crystallographic data have been deposited and are available from the CCDC, 12 Union Road, Cambridge CB2 1EZ, UK on request, quoting the deposition numbers CCDC 288182 and 288183. Supplementary data associated with this article can be found, in the online version, at doi:10.1016/j.poly.2005.11.006.

References

[1] C.J. Pedersen, J. Am. Chem. Soc. 89 (1967) 7017.
[2] R.M. Izatt, K. Pawlak, J.S. Bradshaw, R.L. Bruening, Chem. Rev. 91 (1991) 1721.
[3] A.S. Craig, R. Kataky, R.C. Matthews, D. Parker, G. Ferguson, A. Lough, H. Adams, N. Bailey, H. Schneider, J. Chem. Soc., Perkin Trans. 2 (1990) 1523.
[4] J.S. Bradshaw, R.M. Izatt, Acc. Chem. Res. 30 (1997) 338.
[5] K. Krylova, C.P. Kulatilleke, M.J. Heeg, C.A. Salhi, L.A. Ochrymowycz, D.B. Rorabacher, Inorg. Chem. 38 (1999) 4322.

[6] L.G.A. van de Water, W.L. Driessen, M.W. Glenny, J. Reedijk, M. Schröder, React. Funct. Polym. 51 (2002) 33.
[7] L.G.A. van de Water, F. ten Hoonte, W.L. Driessen, J. Reedijk, D.C. Sherrington, Inorg. Chim. Acta 303 (2000) 77.
[8] C. Caltagirone, A. Bencini, F. Demartin, F.A. Devillanova, A. Garau, F. Isaia, V. Lippolis, P. Mariani, U. Papke, L. Tei, G. Verani, Dalton Trans. (2003) 901.
[9] A.J. Blake, A. Bencini, C. Caltagirone, G. De Filippo, L.S. Dolci, A. Garau, F. Isaia, V. Lippolis, P. Mariani, L. Prodi, M. Montalti, N. Zaccheroni, C. Wilson, Dalton Trans. (2004) 2771.
[10] J.B. Love, J.M. Vere, M.W. Glenny, A.J. Blake, M. Schröder, Chem. Commun. (2001) 2678.
[11] M.W. Glenny, A.J. Blake, C. Wilson, M. Schröder, Dalton Trans. (2003) 1941.
[12] D. Gerber, P. Chongsawangvirod, A.K. Leung, L.A. Ochrymowycz, J. Org. Chem. 42 (1977) 2644.
[13] J. Buter, R.M. Kellogg, J. Chem. Soc., Chem. Commun. (1980) 466.
[14] P.J. Blower, S.R. Cooper, Inorg. Chem. 26 (1987) 2009.
[15] J. Buter, R.M. Kellogg, F. van Bolhuis, J. Chem. Soc., Chem. Commun. (1991) 910.
[16] N.R. Champness, D.W. Bruce, M. Schröder, New J. Chem. 23 (1999) 671.
[17] R.C.W. Liu, P.-S. Fung, F. Xue, T.C.W. Mak, D.K.P. Ng, J. Chem. Res. (S) (1998) 414.
[18] D. Parker (Ed.), Macrocycle Synthesis, vol. 28, Oxford University Press, Oxford, 1996.
[19] M. Lachkar, R. Guilard, A. Atmani, A. de Cian, J. Fischer, R. Weiss, Inorg. Chem. 37 (1998) 1575.
[20] H. Koyama, T. Yoshino, Bull. Chem. Soc. Jpn. 45 (1972) 481.
[21] A.J. Blake, J.P. Danks, A. Harrison, S. Parsons, P. Schooler, G. Whittaker, M. Schröder, J. Chem. Soc., Dalton Trans. (1998) 2335.
[22] A.J. Blake, J.P. Danks, I.A. Fallis, A. Harrison, W.-S. Li, S. Parsons, S.A. Ross, G. Whittaker, M. Schröder, J. Chem. Soc., Dalton Trans. (1998) 3969.
[23] V.V. Pavlishchuk, P.E. Strizhak, Chem. Heterocycl. Compd. 25 (1989) 553.
[24] M. Tanaka, M. Nakamura, T. Ikeda, K. Ikeda, H. Ando, Y. Shibutani, S. Yajima, K. Kimura, J. Org. Chem. 66 (2001) 7008.
[25] (a) D.St.C. Black, I.A. McLean, Aust. J. Chem. 24 (1971) 1401;
(b) D.St.C. Black, I.A. McLean, Tetrahedron Lett. 45 (1969) 3961;
(c) S. Shinkai, K. Shigematsu, Y. Honda, O. Manabe, Bull. Chem. Soc. Jpn. 57 (1984) 2879.
[26] D. Pelissard, R. Louis, Tetrahedron Lett. 45 (1972) 4589.
[27] J. Jurczak, S. Kasprzyk, P. Salański, T. Stankiewicz, J. Chem. Soc., Chem. Commun. (1991) 956.
[28] D. Baldwin, P.A. Duckworth, G.R. Erickson, L.F. Lindoy, M. McPartlin, G.M. Mockler, W.E. Moody, P.A. Tasker, Aust. J. Chem. 40 (1987) 1861.
[29] Z. Yang, J.S. Bradshaw, X.X. Zhang, P.B. Savage, K.E. Krakowiak, N.K. Dalley, N. Su, R.T. Bronson, R.M. Izatt, J. Org. Chem. 64 (1999) 3162.
[30] D. Sellmann, L. Zapf, Angew. Chem., Int. Ed. Engl. 23 (1984) 807.
[31] D.T. Gryko, D. Gryko, J. Jurczak, Synlett 8 (1999) 1310.
[32] K. Krylova, K.D. Jackson, J.A. Vroman, A.J. Grall, M.R. Snow, L.A. Ochrymowycz, D.B. Rorabacher, Inorg. Chem. 36 (1997) 6216.
[33] B. Witulski, Synlett 8 (1999) 1223.
[34] (a) L.R. Hoover, T. Pryor, J.A. Wetgenant, P.E. Williams, B.N. Storhoff, J.C. Huffman, Phosphorous Sulfur Silicon Relat. Elem. 122 (1997) 155;
(b) J. Ishikawa, H. Sakamoto, M. Nakamura, K. Doi, H. Wada, J. Chem. Soc., Dalton Trans. 191 (1999);
(c) R.C. Liu, P.-S. Fung, F. Xue, T.C.W. Mak, D.K.P. Ng, J. Chem. Res. Synop. 8 (1998) 1744;
(d) H. Sakamoto, J. Ishikawa, M. Otomo, Bull. Chem. Soc. Jpn. 68 (1995) 2631.
[35] R.E. Wolf Jr., J.-A.R. Hartman, J.M.E. Storey, B.M. Foxman, S.R. Cooper, J. Am. Chem. Soc. 109 (1987) 4328.
[36] R.E. DeSimone, M.D. Glick, J. Am. Chem. Soc. 98 (1976) 762.
[37] R.S. Glass, G.S. Wilson, W.N. Setzer, J. Am. Chem. Soc. 102 (1980) 5068.
[38] N.K. Dalley, J.S. Smith, S.B. Larson, K.L. Matheson, J.J. Christensen, R.M. Izatt, J. Chem. Soc., Chem. Commun. 84 (1975).
[39] N.K. Dalley, S.B. Larson, J.S. Smith, K.L. Matheson, R.M. Izatt, J.J. Christensen, J. Heterocycl. Chem. 18 (1981) 463.
[40] L. Pauling, The Nature of the Chemical Bond, 3rd ed., Cornell University Press, Ithaca, NY, 1960, p. 260.
[41] W. Rosen, D.H. Busch, J. Am. Chem. Soc. 91 (1969) 4694.
[42] L. Siegfried, T.A. Kaden, Helv. Chim. Acta 67 (1) (1984) 29.
[43] W.O Lin, J.A.de.A. Figueira, H.G. Alt, Monatsh. Chem. 116 (2) (1985) 217.

Available online at www.sciencedirect.com
SCIENCE DIRECT®
Polyhedron 25 (2006) 613–625
POLYHEDRON
www.elsevier.com/locate/poly

Mixed 3d/4d and 3d/4f metal clusters: Tetranuclear $Fe^{III}_2M^{III}_2$ (M^{III} = Ln, Y) and $Mn^{IV}_2M^{III}_2$ (M = Yb, Y) complexes, and the first Fe/4f single-molecule magnets

Muralee Murugesu [a], Abhudaya Mishra [a], Wolfgang Wernsdorfer [b], Khalil A. Abboud [a], George Christou [a,*]

[a] Department of Chemistry, University of Florida, Gainesville, FL 32611-7200, USA
[b] Laboratoire Louis Néel-CNRS, BP 166, 25 Avenue des Martyrs, 38042 Grenoble, Cedex 9, France

Received 6 July 2005; accepted 18 August 2005
Available online 21 November 2005

Dedicated to Malcolm H. Chisholm on the occasion of his 60th birthday; an outstanding scientist, colleague, and friend.

Abstract

The synthesis, structure and magnetic properties are reported of Fe_2Ln_2, Fe_2Y_2, Mn_2Yb_2 and Mn_2Y_2 complexes. The compound $[Fe_2Ho_2(OH)_2(teaH)_2(O_2CPh)_4(NO_3)_2]$ (**1**), where $teaH_3$ is triethanolamine, was obtained from the reaction of eight equivalents of $teaH_3$ with one equivalent each of $Ho(NO_3)_3$ and $[Fe_3O(O_2CPh)_6(H_2O)_3](O_2CPh)$ in MeCN/MeOH. The use instead of $Dy(NO_3)_3$ or $Tb(NO_3)_3$ leads to the structurally similar products $[Fe_2Dy_2(OH)_2(teaH)_2(O_2CPh)_6]$ (**2**) and $[Fe_2Tb_2(OH)_2(teaH)_2(O_2CPh)_6]$ (**3**). The compounds $[Fe_2Y_2(pdmH)_6Cl_4]Cl_2$ (**4**) and isostructural $[Fe_2Ho_2(pdmH)_6Cl_4]Cl_2$ (**5**), where $pdmH_2$ is pyridine-2,6-dimethanol, were prepared from the reaction of four equivalents of $pdmH_2$ with two equivalents of YCl_3 or $HoCl_3$, respectively, and $FeCl_2$ in MeOH. The compounds $[Mn_2Y_2O_2(O_2CPh)_6(OMe)_4(MeOH)_4]$ (**6**) and $[Mn_2Yb_2O_2(O_2CPh)_6(OMe)_4(MeOH)_4]$ (**7**) were prepared by methanolysis of (NBu^n_4)-$[Mn_4O_2(O_2CPh)_9(H_2O)]$ in the presence of $Yb(NO_3)_3$ or $Y(NO_3)_3$, respectively. Complexes **1**–**3**, **6** and **7** contain a 'defect dicubane' M_4 core (including the first mixed 3d/4f examples of this type to contain Fe^{III} or Mn^{IV}), whereas **4** and **5** have a U-shaped core. Variable-temperature solid-state magnetic susceptibility studies of **1**–**6** in the temperature range 5.00–300 K were carried out, and for all the complexes predominantly antiferromagnetic exchange interactions between the metal centers was observed. Magnetization versus applied field sweeps on single crystals of **1** and **2** at low temperature reveal hysteresis loops, confirming these species to be new examples of single-molecule magnets (SMMs). Thus, complexes **1** and **2** are the first examples of Fe/4f SMMs.
© 2005 Elsevier Ltd. All rights reserved.

Keywords: Iron; Manganese; Lanthanide; Single-molecule magnet; Crystal structures; Hysteresis

1. Introduction

A major reason for the current intense interest by many groups around the world in polynuclear 3d transition metal clusters is the often unusual and even novel magnetic properties such species possess. In particular, some of these clusters have been found to be single-molecule magnets (SMMs), which are individual molecules capable of functioning as nanoscale magnetic particles and which thus represent a molecular approach to nanomagnetism [1–3]. In addition, there continues to be a great bioinorganic chemistry interest in 3d metal clusters, which are of relevance to objectives such as understanding the assembly of the multinuclear Fe/O core of the iron-storage protein ferritin, and elucidating the nature and mechanism of action of the Mn_4Ca core of the water oxidizing complex of

* Corresponding author.
E-mail addresses: christou@chem.ufl.edu, polyhedron@chem.ufl.edu (G. Christou).

0277-5387/$ - see front matter © 2005 Elsevier Ltd. All rights reserved.
doi:10.1016/j.poly.2005.08.029

photosystem II [4–8]. For these and other areas, there continues to be a great need for synthetic methods to new examples of homometallic and heterometallic metal clusters, to increase our knowledge of the structural, magnetic, and other properties of high nuclearity paramagnetic species.

The present paper reports results of relevance to the nanomagnetism field. SMMs, which are molecular superparamagnets, derive their properties from the combination of a large ground state spin (S) value and a large and negative magnetoanisotropy (negative zero-field splitting parameter, *D*). This combination results in a significant energy barrier to magnetization reversal, and hence slow relaxation of the magnetization is observed at low temperatures. The latter can be detected as: (i) frequency-dependent signals in AC susceptibility measurements; (ii) hysteresis in magnetization versus applied DC field sweeps [1–3,9–12]. There are now many homometallic SMMs, most of them Mn species [13], and new approaches into heterometallic species have been more recently explored as a route to distinctly different properties. As a result of such work, we and others have recently reported some mixed transition metal/lanthanide SMMs [14–16]. In this paper, we report the extension of our studies along these lines and describe new Fe/Ln and Mn/Ln clusters. Not all of these are new SMMs, but they are all nevertheless valuable new additions to the growing family of mixed 3d/4f clusters possessing a variety of structural and other properties. We also have extended this work to Y instead of Ln, which has proven useful for understanding the magnetic properties of the isostructural Ln-containing species.

To facilitate the formation of polynuclear products, this work has employed the polydentate chelate-forming molecules triethanolamine ($teaH_3$) and pyridine-2,6-dimethanol ($pdmH_2$). Both molecules contain alcohol arms, which are good metal-bridging groups on deprotonation and thus foster formation of polynuclear products [17–20]. In addition, since lanthanides show strong affinity towards oxygen donors [23], both chelates were thought likely to lead to mixed 3d/4f products, and this has proven to be the case. We herein report the synthesis, crystallographic characterization and magnetic properties of a family of mixed 3d/4f M/Ln (M = Mn, Fe) and mixed M/Y (M = Mn, Fe) complexes. These are also the first crystallographically characterized tetranuclear Fe^{III}/Ho^{III}, Fe^{III}/Y^{III}, Mn^{IV}/Yb^{III} and Mn^{IV}/Y^{III} complexes in general.

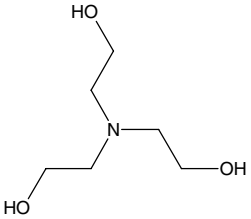

$teaH_3$

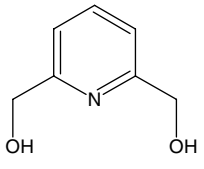

$pdmH_2$

2. Experimental

2.1. Compound preparations

All manipulations were performed under aerobic conditions using materials and solvents as received. $[Fe_3O(O_2CR)_6(H_2O)_3](O_2CR)$ and $(NBu^n_4)[Mn_4O_2(O_2CPh)_9(H_2O)]$ complexes were prepared using the procedures reported previously [24,25].

2.1.1. $[Fe_2Ho_2(OH)_2(teaH)_2(O_2CPh)_4(NO_3)_2]\cdot 6MeCN$ (**1**·6MeCN)

Solutions of $[Fe_3O(O_2CPh)_6(H_2O)_3](O_2CPh)$ (0.26 g, 0.25 mmol) in MeCN (30 mL), and $Ho(NO_3)_3\cdot 5H_2O$ (0.11 g, 0.25 mmol) and $teaH_3$ (0.298 g, 2 mmol) in MeCN/MeOH (50/5 mL) were mixed to give a yellow/orange solution. This was layered with Et_2O and left undisturbed at room temperature. After 7 days, small yellow rectangular crystals of **1**·6MeCN were collected in 40% yield and dried in vacuum. *Anal.* Calc. for **1**: C, 34.85; H, 3.51; N, 4.06. Found: C, 34.99; H, 3.54; N, 4.38%. Selected IR data (cm^{-1}): 3510 (br), 2860 (s), 1595 (s), 1541 (m), 1381 (m), 1095 (s), 909 (s), 723 (m), 674 (m), 595 (s), 460 (s).

2.1.2. $[Fe_2Dy_2(OH)_2(teaH)_2(O_2CPh)_6]\cdot 4MeCN\cdot 3H_2O$ (**2**·4MeCN·3H$_2$O)

This was prepared in a similar way as **1**, but using $Dy(NO_3)_3\cdot 6H_2O$ instead of $Ho(NO_3)_3\cdot 5H_2O$. After 2 days, pale yellow rectangular crystals of $\mathbf{2}\cdot 4MeCN\cdot 3H_2O$ were collected in 52% yield and dried in air. *Anal.* Calc. for $\mathbf{2}\cdot 4MeCN\cdot 3H_2O$: C, 43.55; H, 4.47; N, 4.91. Found: C, 43.48; H, 4.20; N, 4.90%. Selected IR data (cm^{-1}): 3420 (br), 2860 (m), 1595 (s), 1544 (m), 1448 (m), 1095 (m), 1025 (s), 907 (s), 721 (m), 674 (s), 594 (s), 460 (s).

2.1.3. $[Fe_2Tb_2(OH)_2(teaH)_2(O_2CPh)_6]\cdot 4MeCN\cdot 3H_2O$ (**3**·4MeCN·3H$_2$O)

This was prepared in a similar way as **1**, but using $Tb(NO_3)_3\cdot 6H_2O$ instead of $Ho(NO_3)_3\cdot 5H_2O$. After 2 days, pale yellow rectangular crystals of $\mathbf{3}\cdot 4MeCN\cdot 3H_2O$ were collected in 49% yield and dried in air. *Anal.* Calc. for $\mathbf{3}\cdot 4MeCN\cdot 3H_2O$: C, 43.73; H, 4.49; N, 4.93. Found: C, 43.66; H, 4.15; N, 4.86%. Selected IR data (cm^{-1}): 3380 (br), 2860 (m), 1595 (s), 1545 (m), 1448 (m), 1094 (m), 1025 (s), 905 (s), 718 (m), 674 (s), 593 (s), 459 (s).

2.1.4. $[Fe_2Y_2(pdmH)_6Cl_4]Cl_2\cdot 2MeOH$ (**4**·2MeOH)

Solutions of $FeCl_2\cdot 4H_2O$ (0.10 g, 0.50 mmol) in MeOH (20 mL), and $YCl_3\cdot 6H_2O$ (0.15 g, 0.50 mmol) and $pdmH_2$ (0.14 g, 1.0 mmol) in MeOH (20 mL) were mixed to give a yellow solution. This was layered with Et_2O and left undisturbed at room temperature. After 7 days, small yellow rectangular crystals of **4**·2MeOH were collected in 42% yield and dried in vacuum. *Anal.* Calc. for **4**: C, 37.87; H,

4.05; N, 6.02. Found: C, 37.51; H, 3.93; N, 5.87%. Selected IR data (cm^{-1}): 3376 (br), 3075 (br), 1607 (m), 1579 (s), 1447 (m), 1368 (s), 1360 (s), 1163 (s), 1072 (m), 1046 (m), 783 (m), 654 (s), 554 (s), 497 (s).

2.1.5. $[Fe_2Ho_2(pdmH)_6Cl_4]Cl_2 \cdot 2MeOH$ (**5** · 2MeOH)

Solutions of $FeCl_2 \cdot 4H_2O$ (0.10 g, 0.50 mmol) in MeOH (20 mL), and $HoCl_3 \cdot 6H_2O$ (0.19 g, 0.50 mmol) and $pdmH_2$ (0.14 g, 1.0 mmol) in MeOH (20 mL) were mixed to give a yellow/green solution. This was layered with Et_2O and left undisturbed at room temperature. After 7 days, small yellow/green rectangular crystals of **5** were collected in 37% yield and dried in vacuum. *Anal.* Calc. for **5**: C, 34.15; H, 3.65; N, 5.43. Found: C, 34.23; H, 3.54; N, 5.26%. Selected IR data (cm^{-1}): 3437 (br), 3317 (br), 3007 (br), 2834 (br), 2713 (br), 2621 (br), 1609 (m), 1582 (s), 1448 (m), 1310 (m), 1042 (m), 797 (s), 725 (s), 667(s), 576(s), 475(s).

2.1.6. $[Mn_2Y_2O_2(O_2CPh)_6(OMe)_4(MeOH)_4] \cdot 2MeOH$ (**6** · 2MeOH)

$(NBu^n_4)[Mn_4O_2(O_2CPh)_9(H_2O)]$ (0.50 g, 1.0 mmol) was dissolved in a solution of $Y(NO_3)_3 \cdot 6H_2O$ (0.24 g, 2.0 mmol) in MeCN/MeOH (20/5 mL) and stirred for 25 min to give a brown solution. This was filtered and more MeOH (10 mL) added to the filtrate. The resulting solution was left undisturbed at room temperature for a week to slowly produce orange crystals of **6** · 2MeOH, which were collected in 25% yield and dried in vacuum. The same product was obtained using $YCl_3 \cdot 6H_2O$ instead of $Y(NO_3)_3 \cdot 6H_2O$. *Anal.* Calc. for **6**: C, 46.24; H, 4.50. Found: C, 46.15; H, 4.46%. Selected IR data (cm^{-1}): 3412 (br), 1594 (m), 1545 (s), 1448 (w), 1391 (s), 1025 (w), 718 (s), 681 (m), 623 (s), 540 (m), 474 (w).

2.1.7. $[Mn_2Yb_2O_2(O_2CPh)_6(OMe)_4(MeOH)_4] \cdot 2MeOH$ (**7** · 2MeOH)

$(NBu^n_4)[Mn_4O_2(O_2CPh)_9(H_2O)]$ (0.50 g, 1.0 mmol) was dissolved in a solution of $Yb(NO_3)_3 \cdot 5H_2O$ (0.31 g, 2.0 mmol) in MeCN/MeOH (20/5 mL) and stirred for 25 min to give a brown solution. This was filtered and more MeOH (10 mL) added to the filtrate. The resulting solution was slowly concentrated by evaporation at room temperature for 5 days, during which time brown crystals of **7** · 2MeOH slowly grew. These were collected in 10% yield and dried in vacuum. *Anal.* Calc. for **7**: C, 40.94; H, 3.99. Found: C, 40.87; H, 3.96%. Selected IR data (cm^{-1}): 3426 (br), 1600 (m), 1540 (m), 1384 (s), 1026 (w), 718 (s), 682 (m), 624 (s), 545 (m), 476 (w).

2.2. General and physical measurements

Elemental analyses (C, H and N) were performed in the in-house facilities of the University of Florida Chemistry Department. Infrared spectra in the 400–4000 cm^{-1} range were recorded in the solid state (KBr pellets) on a Nicolet Nexus 670 FTIR spectrometer. Variable temperature DC magnetic susceptibility data down to 5.0 K were collected using a Quantum Design MPMS-XL SQUID susceptometer equipped with a 7 T DC magnet. Pascal's constants were used to estimate the diamagnetic corrections, which were subtracted from the experimental susceptibilities to give the molar magnetic susceptibilities (χ_M). Microcrystalline samples were restrained in eicosane by suspending the solid for 15 min in eicosane maintained at a temperature above its melting point (35–37 °C), and then the temperature was gradually decreased below the melting point to solidify the eicosane. Low-temperature (<1.8 K) hysteresis loop and DC relaxation measurements were performed at Grenoble using an array of micro-SQUIDs [26].

Table 1
Crystallographic data for complexes **1**, **4**, **5**, **6** and **7**

Compound	**1**	**4**	**5**	**6**	**7**
Formula	$C_{52}H_{66}Fe_2Ho_2N_{10}O_{22}$	$C_{46}H_{64}Cl_6Fe_2N_6O_{16}Y_2$	$C_{46}H_{64}Cl_6Fe_2N_6O_{16}Ho_2$	$C_{52}H_{66}Mn_2O_{24}Y_2$	$C_{52}H_{66}Mn_2O_{24}Yb_2$
Formula weight	1624.17	1459.25	1611.29	1362.75	1531.01
Space group	$P\bar{1}$	$I2/a$	$I2/a$	$P2_1/c$	$P2_1/c$
a (Å)	12.0151(8)	20.9871(15)	20.9871(15)	15.6620(12)	15.5610(11)
b (Å)	12.1189(8)	19.1467(14)	19.1467(14)	24.9417(19)	24.9105(18)
c (Å)	12.8580(8)	14.6204(11)	14.6204(11)	7.8231(6)	7.8259(6)
α (°)	116.348(2)	90	90	90	90
β (°)	94.752(2)	92.745(2)	92.7450(10)	95.819(2)	96.120(2)
γ (°)	103.419(2)	90	90	90	90
V (Å^3)	1594.42(18)	5868.2(7)	5868.2(7)	3040.2(4)	3016.3(4)
Z	1	4	4	2	2
T (°C)	173(2)	173(2)	173(2)	173(2)	173(2)
Radiation	Mo Kα	Mo Kα	Mo Kα	Mo Kα	Mo Kα
ρ_{calc} (g/cm^{-3})	1.692	1.652	1.824	1.489	1.686
μ (mm^{-1})	2.981	2.785	3.494	2.372	3.558
R_1[a,b]	3.55	4.02	3.59	3.48	3.11
wR_2[a,c]	8.62	9.94	9.62	7.27	7.67

[a] $I > 2\sigma(I)$.
[b] $R_1 = 100 \sum(||F_0| - |F_c||)/\sum|F_0|$.
[c] $wR_2 = 100[\sum[w(F_o^2 - F_c^2)^2]/\sum[w(F_o^2)^2]]^{1/2}$, $w = 1/[\sigma^2(F_o^2) + [(ap)^2 + bp]$, where $p = [\max(F_o^2, 0) + 2F_c^2]/3$.

2.2.1. X-ray crystallography and solution of structures

Data were collected at 173 K on a Siemens SMART PLATFORM equipped with a CCD area detector and a graphite monochromator utilizing Mo Kα radiation ($\lambda = 0.71073$ Å). Cell parameters were refined using up to 8192 reflections. A full sphere of data (1850 frames) was collected using the ω-scan method (0.3° frame width). The first 50 frames were re-measured at the end of data collection to monitor instrument and crystal stability (maximum correction on I was <1%). Absorption corrections by integration were applied based on measured indexed crystal faces.

The structures were solved by the direct methods in SHELXL6 [27], and refined using full-matrix least squares. The non-hydrogen atoms were refined anisotropically, whereas the hydrogen atoms were placed in ideal, calculated positions and refined isotropically as riding on their respective carbon atoms. For complex **1** · 6MeCN, a total of 405 parameters were refined in the final cycle of refinement using 5899 reflections with $I > 2\sigma(I)$. For complex **4** · 2MeOH, a total of 365 parameters were refined in the final cycle of refinement using 4504 reflections with $I > 2\sigma(I)$. For complex **5** · 2MeOH, a total of 365 parameters were refined in the final cycle of refinement using 4670 reflections with $I > 2\sigma(I)$. For complex **6** · 2MeOH, a total of 378 parameters were refined in the final cycle of refinement using 2803 reflections with $I > 2\sigma(I)$. For complex **7** · 2MeOH , a total of 378 parameters were refined in the final cycle of refinement on F^2 using 4821 reflections with $I > 2\sigma(I)$. Unit cell data and the final refinement indices R_1 and wR_2 are listed in Table 1.

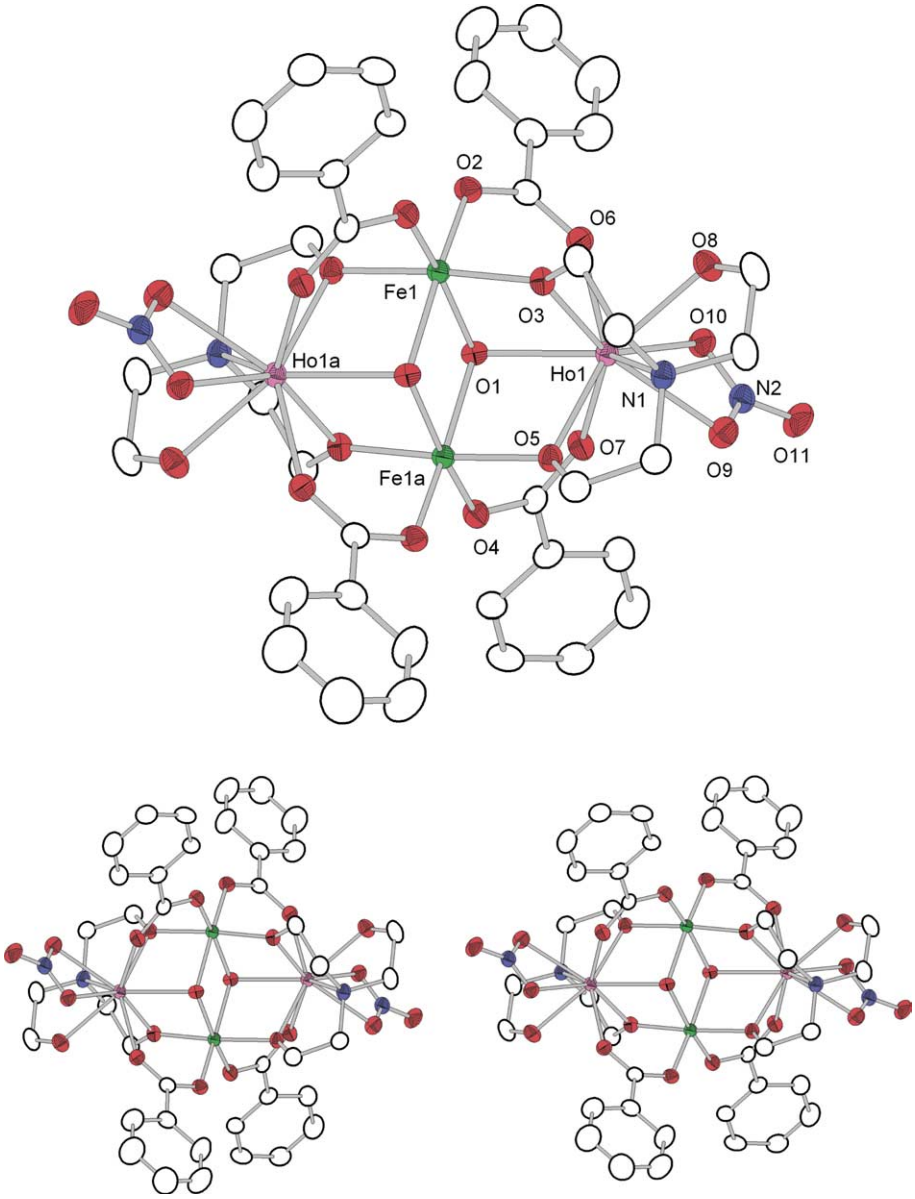

Fig. 1. ORTEP representation and stereopair at the 50% probability level of complex **1**. All H atoms have been removed for clarity.

3. Results and discussion

3.1. Syntheses

The reaction of a $[M_3O(O_2CR)_6L_3]^{0,+}$ (M = Mn, Fe; L = py, H_2O, etc.) complex with a chelating ligand represents a commonly employed and successful route to a wide range of higher nuclearity clusters of Fe and Mn. For example, the use of triethanolamine ($teaH_3$) or 2-(hydroxymethyl)pyridine (hmpH) has led to a large variety of products, depending on the precise reaction conditions and ratios, including Mn_4 [28], Mn_6 [21], Fe_8 [22], Mn_7 [29], Mn_{10} [30], Mn_{12} [31], and Fe_6 [32] clusters. As stated earlier, the alkoxide arms of the tea^{3-} and hmp^- ligands normally adopt bridging modes, fostering formation of higher nuclearity products. Thus, we have employed $[Fe_3O(O_2CPh)_6(H_2O)_3]^+$ or $FeCl_2$ and a lanthanide Ln^{3+} (or Y^{3+}) source in reactions with $teaH_3$ or $pdmH_2$ in MeOH or a mixed MeOH/MeCN solvent system (to ensure adequate solubility of all reagents).

The reaction of $[Fe_3O(O_2CPh)_6(H_2O)_3](O_2CR)$, $Ln(NO_3)_3$ (Ln = Ho, Dy, Tb) and $teaH_3$in a 1:1:8 molar ratio in MeCN/MeOH gave yellow solutions from which yellow rectangular crystals of $[Fe_2Ho_2(OH)_2(teaH)_2(O_2CPh)_4(NO_3)_2]$ (**1**), $[Fe_2Dy_2(OH)_2(teaH)_2(O_2CPh)_6]$ (**2**) and $[Fe_2Tb_2(OH)_2(teaH)_2(O_2CPh)_6]$ (**3**) slowly formed in ~40–50% yields. If the reaction solutions were left undisturbed for longer periods (~2 weeks), orange crystals of the known homometallic complex $[Fe_8O_3(O_2CPh)_9(tea)(teaH)_3]$ were also obtained [22]. The reactions are likely complicated equilibria involving several species of various nuclearities, both homo- and heterometallic, and the crystallization of the main product directly from the reaction solution is probably beneficial in providing pure material. In all cases, the filtrates are still colored, but we have not pursued isolation of other species (other than $[Fe_8O_3(O_2CPh)_9(tea)(teaH)_3]$).

Treatment of an equimolar mixture of $FeCl_2$ and YCl_3 in MeOH with two equivalents of $pdmH_2$ gave a yellow solution, and layering this with Et_2O gave small rectangular yellow crystals of $[Fe_2Y_2(pdmH)_6Cl_4]Cl_2$ (**4**) in 42% yield. The same reaction but with $HoCl_3$ gave the analogous $[Fe_2Ho_2(pdmH)_6Cl_4]Cl_2$ (**5**) complex in 37% yield. Small changes to the Fe:Ln:$pdmH_2$ ratio still gave the same products.

A different strategy was used for the Mn reactions. In this case, neither $teaH_3$ or $pdmH_2$ were employed, the reaction instead comprising the methanolysis of a Mn^{III} species in the presence of a Yb^{3+} or Y^{3+} source. The chosen Mn starting material was the readily prepared, tetranuclear $(NBu^n_4)[Mn_4O_2(O_2CPh)_9(H_2O)]$ ($4Mn^{III}$) complex [25], and treatment of this with $Yb(NO_3)_3 \cdot 5H_2O$ in a 1:2 molar ratio in MeCN/MeOH led to brown crystals of $[Mn_2Y_2O_2(O_2CPh)_6(OMe)_4(MeOH)_4]$ (**6**) or $[Mn_2Yb_2O_2(O_2CPh)_6(OMe)_4(MeOH)_4]$ (**7**) in 10–25% yields. Note that in both these Mn-containing complexes that there are also MeO^- groups from the MeOH solvent, whereas none of the Fe-containing complexes **1**–**5** contain MeO^- groups. Again, there are likely other products from these complicated reactions in the colored filtrates, but we have not pursued any further separations.

3.2. Structural description of $[Fe_2Ho_2(OH)_2(teaH)_2(O_2CPh)_4(NO_3)_2]$ (1)

A labeled ORTEP plot and stereoview of the $[Fe_2Ho_2(OH)_2(teaH)_2(O_2CPh)_4(NO_3)_2]$ (**1**) are provided in Fig. 1. Selected bond distances and angles are listed in Table 2. Complex **1** · 6MeCN crystallizes in triclinic space group $P\bar{1}$, the cluster lying on an inversion center and consisting of a planar Fe_2Ho_2 rhombus. Each Fe_2Ho trinuclear sub-unit is bridged by a μ_3-OH^- ion (oxygen atoms O1 and O1a). Each of the two $teaH^{2-}$ ligands binds in a tetradentate chelate fashion to Ho1 or Ho1a, with their protonated alcohol arms (O8 and O8a) binding terminally to the Ho, and their two deprotonated alkoxide arms each bridging to an adjacent Fe atom (O3 bridging Fe1/Ho1, and O5 bridging Fe1a/Ho1). There is also a chelating NO_3^- group on each Ho atom, and ligation is completed by a *syn*, *syn*, bridging benzoate group across each of the four HoFe edges of the rhombus. The Fe and Ho atoms are six- and nine-coordinate, respectively.

The overall structure of the core of complex **1** can be described as two face-sharing $[M_4O_4]$ cubanes with a metal atom missing from one vertex in each cubane. Such a 'defect double-cubane' unit with a resulting planar M_4 rhombus is relatively common in both homo- and heterometallic cluster chemistry, and is often on a crystallographic center of symmetry. Such examples are known

Table 2
Selected bond distances (Å) and angles (°) for complex **1**

Fe1···Fe1a	3.243(6)
Fe1···Ho1	3.3935(6)
Fe1···Ho1a	3.4027(6)
Fe1–O1	2.067(3)
Fe1–O2	2.031(3)
Fe1–O3	1.943(3)
Fe1–O4a	2.002(3)
Fe1–O5a	1.972(3)
Fe1–O1a	2.044(3)
Ho1–O1a	2.356(3)
Ho1–O3	2.293(3)
Ho1–O5	2.313(3)
Ho1–O6	2.329(3)
Ho1–O7	2.408(3)
Ho1–O8	2.414(3)
Ho1–O9	2.494(3)
Ho1–O10	2.514(3)
Ho1–N1	2.572(3)
Ho1–N2	2.911(4)
Fe1a–O1–Fe1	104.13(12)
Fe1a–O1–Ho1a	100.68(12)
Fe1–O1–Ho1a	100.35(12)
Fe1–O3–Ho1	106.18(12)
Fe1a–O5–Ho1	104.87(12)

with different transition metals [28,33], and there are also a very few examples of mixed 3d/4f examples [14b,34], but no mixed iron–lanthanide complexes have previously been obtained. We also carried out preliminary X-ray crystallographic studies on complexes **2** and **3** and found that they are isostructural with **1** except that the two chelating NO_3^- groups have been replaced by two chelating $PhCO_2^-$ groups, as we had suspected from the similar formulas and IR spectra of **1**–**3**. For this reason, the structures of **2** and **3** will not be discussed further here.

3.3. Structural descriptions of $[Fe_2Y_2(pdmH)_6Cl_4]Cl_2$ (**4**) and $[Fe_2Ho_2(pdmH)_6Cl_4]Cl_2$ (**5**)

Labeled ORTEP plots and stereoviews of the cations of complexes **4** · 2MeOH and **5** · 2MeOH are shown in Figs. 2 and 3, respectively. Selected bond lengths and angles are listed in Tables 3 and 4, respectively. The complexes both crystallize in monoclinic space group $I2/a$, with the cations on a crystallographic C_2 rotation axis; the two complexes are isostructural. The cores of the cations (Fig. 4) can best

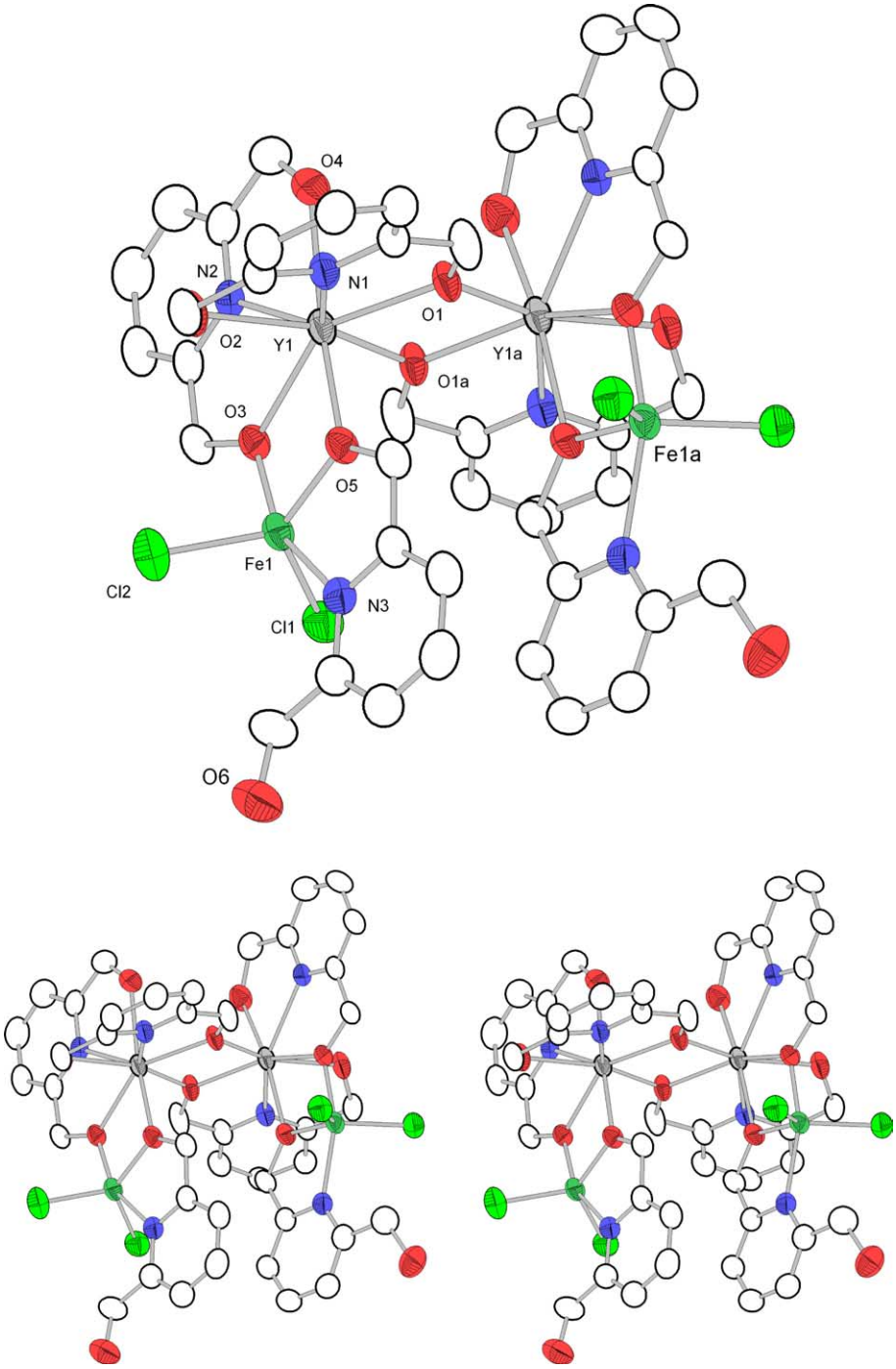

Fig. 2. ORTEP representation and stereopair of the cation of complex **4** at the 50% probability level. All H atoms have been removed for clarity.

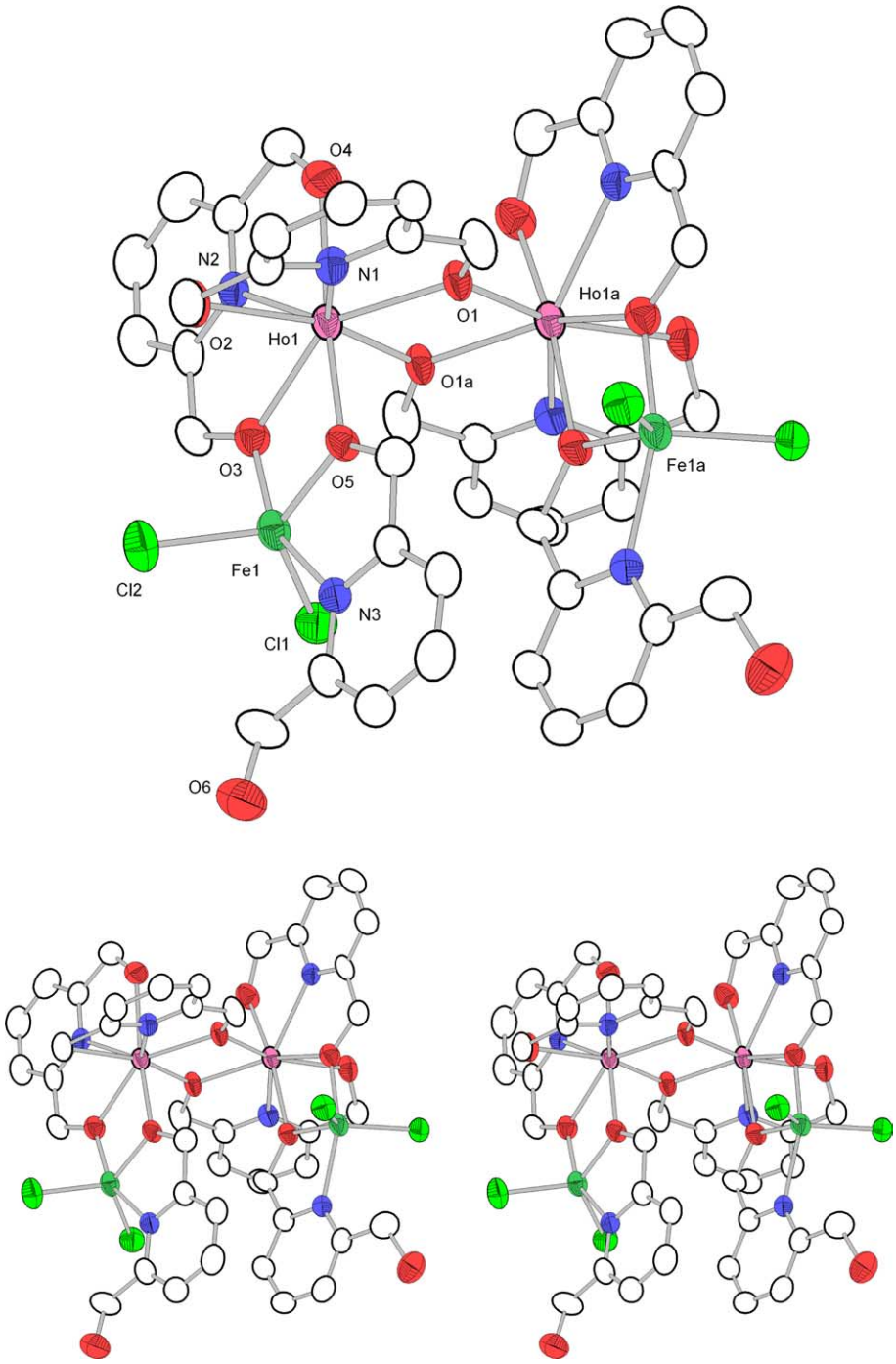

Fig. 3. ORTEP representation and stereopair of the cation of complex **5** at the 50% probability level. All H atoms have been removed for clarity.

be described as twisted U-shaped, with the Fe^{III} atoms at the two ends, and either two Y^{III} (complex **4**) or two Ho^{III} (complex **5**) atoms on the inside. Each pair of adjacent metal atoms is bridged by two alkoxide O atoms from monodeprotonated $pdmH^-$ groups. There are two of the latter as tridentate chelates on each of the inner Y^{III} (**4**) or Ho^{III} (**5**) atoms, with their alkoxide arm bridging to an adjacent atom (O1, O3), as mentioned, and their protonated (alcohol) arm (O2, O4) and N atom binding terminally. There are two additional $pdmH^-$ groups, attached in a bidentate chelate fashion to the Fe^{III} atoms, their alkoxide arm (O5) bridging to an inner metal and their protonated arm unligated (O6). Ligation is completed by two terminal Cl^- ions on each of the Fe^{III} atoms. The two Fe atoms are five-coordinate and the two inner Y^{III} or Ho^{III} atoms are eight-coordinate. There are intramolecular π–π stacking interactions, and many intermolecular hydrogen-bonds involving the $pdmH^-$, MeOH and Cl^- groups, the latter serving to bridge separate $Fe_2Y_2(Ho)_2$ clusters. For example for **4**, the unbound $pdmH^-$ alcohol group (O6) hydrogen-bonds to interstitial MeOH atom O7 ($O6\cdots O7 = 2.695$ Å), with the latter also hydrogen-bonding to free

Table 3
Selected bond distances (Å) and angles (°) for complex **4**

Y1···Fe1	3.4487(6)
Y1···Y1a	3.7121(7)
Y1–O1	2.283(2)
Y1–O1a	2.252(2)
Y1–O2	2.416(3)
Y1–O3	2.316(2)
Y1–O4	2.374(3)
Y1–O5	2.329(2)
Y1–N1	2.466(3)
Y1–N2	2.480(3)
Fe1–O3	1.943(2)
Fe1–O5	1.926(2)
Fe1–N3	2.218(3)
Fe1–Cl1	2.2541(10)
Fe1–Cl2	2.2209(11)
Y1–O1–Y1a	109.87(9)
Fe1–O3–Y1	107.80(9)
Fe1–O5–Y1	107.94(10)

Table 4
Selected bond distances (Å) and angles (°) for complex **5**

Ho1···Ho1a	3.7153(5)
Ho1···Fe1	3.4702(9)
Ho1–O1	2.286(3)
Ho1–O1a	2.248(3)
Ho1–O2	2.419(4)
Ho1–O3	2.325(3)
Ho1–O4	2.375(4)
Ho1–O5	2.316(4)
Ho1–N1	2.462(4)
Ho1–N2	2.482(4)
Fe1–O3	1.983(4)
Fe1–O5	1.928(3)
Fe1–N3	2.211(4)
Fe1–Cl1	2.2532(15)
Fe1–Cl2	2.2331(16)
Ho1–O1–Ho1a	110.04(13)
Fe1–O3–Ho1	107.04(14)
Fe1–O5–Ho1	109.35(15)

Cl^- ion Cl3 (O7···Cl3 = 3.072 Å). In addition, this Cl^- ion hydrogen-bonds to bound pdm^{2-} O atom O2 (Cl3···O2 = 2.976 Å) of a neighboring cluster.

The U-shaped core seen in these complexes is not common, although it is with precedent, for example in the complex $[Mn_4(6Me\text{-}hmp)Cl_4]\cdot 4H_2O$ (6Me-hmp = 6-methyl-2-(hydroxymethyl)pyridine) [35].

3.4. Structural descriptions of $[Mn_2Y_2O_2(O_2CPh)_6(OMe)_4(MeOH)_4]$ (6) and $[Mn_2Yb_2O_2(O_2CPh)_6(OMe)_4(MeOH)_4]$ (7)

Labeled ORTEP representations of the centrosymmetric structures of **6** · 2MeOH and **7** · 2MeOH are presented in Fig. 5, and selected bond distances and angles are listed in Table 5. The two complexes both crystallize in the monoclinic space group $P2_1/c$ with the molecules lying on an inversion center; the two complexes are isostructural. The cores of the complexes possess the defect-dicubane

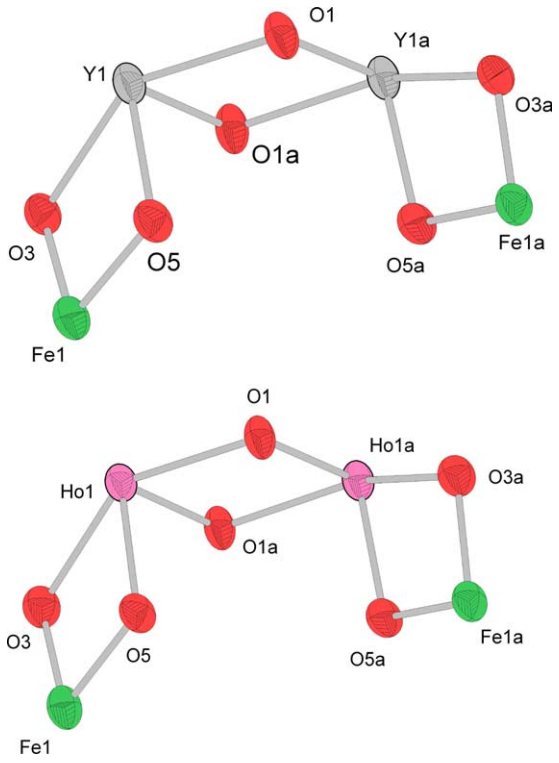

Fig. 4. Comparison of the cores of the cations of complexes **4** (top) and **5** (bottom).

structure of complex **1**, with two Mn^{IV} atoms at the central positions and either two $2Y^{III}$ (complex **6**) or two Yb^{III} (complex **7**) atoms at the end positions. However, there are two major differences between the cores of **6**/**7** and that of **1**: First, the two μ_3-O atoms (O8, O8a) capping each triangular sub-unit are O^{2-} ions rather than OH^- ones; and secondly, each of the four edges of the M_4 rhombus in **6**/**7** is bridged by a MeO^- ion (O7, O7a, O11, O11a) rather than an alkoxide arm of a chelate. The fully labeled cores of **6** and **7** are provided in Fig. 6, which emphasize the near superimposibility of the mixed 3d/4d complex **6** with the mixed 3d/4f complex **7**. Peripheral ligation about the cores is provided by four *syn*, *syn* bridging benzoate groups bridging each Y/Mn or Yb/Mn edge of the rhombus, two monodentate benzoate groups, one on each of the Y/Yb atoms, and four terminal MeOH molecules, two on each of the Y/Yb ions. As a result, the Y^{III} and Yb^{III} atoms of **6** and **7**, respectively, are eight-coordinate, and the Mn^{IV} atoms are six-coordinate. There are intramolecular OH···H hydrogen bonds between the unbound O atom (O1) and the terminal MeOH ligand (O1···O10 = 2.577 Å). In addition, there are intermolecular OH···H hydrogen bonds between the bound MeOH (O9) and interstitial MeOH (O12) molecules (O9···O12 = 2.656 Å), and between this interstitial MeOH and the unbound O atom (O1) of a neighboring cluster (O12···O1 = 2.687 Å). Thus, the hydrogen-bonding through the interstitial MeOH molecules links adjacent metal clusters in the crystal, which also likely provides a pathway for superexchange interactions between molecules (vide infra).

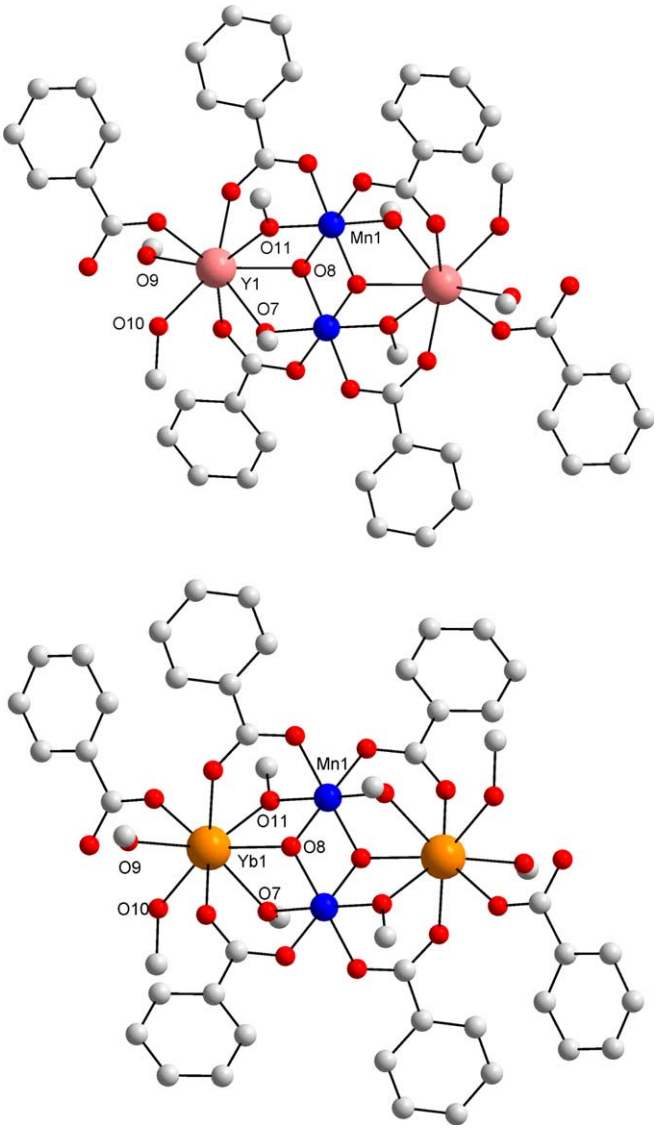

Fig. 5. PovRay representations of complexes **6** (top) and **7** (bottom).

Table 5
Selected bond distances (Å) and angles (°) for complexes **6** and **7**

Complex ***6***	
Y1···Mn1	3.3168(7)
Mn1···Mn1a	2.7819(9)
Y1–O7	2.365(2)
Y1–O8	2.356(2)
Y1–O9	2.416(2)
Y1–O10	2.351(2)
Y1–O11	2.299(2)
Mn1–O8	1.859(2)
Mn1–O11	1.913(2)
Y1–O11–Mn1	102.08(9)
Mn1–O8–Mn1a	97.52(9)
Y1–O8–Mn1	103.18(9)
Complex 7	
Yb1···Mn1	3.2886(6)
Mn1···Mn1a	2.7769(11)
Yb1–O7	2.336(2)
Yb1–O8	2.331(2)
Yb1–O9	2.383(3)
Yb1–O10	2.323(3)
Yb1–O11	2.269(2)
Mn1–O8	1.866(2)
Mn1–O11	1.912(3)
Yb1–O11–Mn1	101.79(11)
Mn1–O8–Mn1a	97.05(11)
Yb1–O8–Mn1	102.61(10)

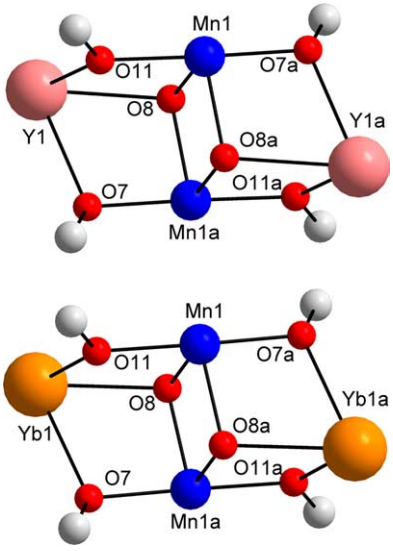

Fig. 6. Comparison of the cores of complexes **6** (top) and **7** (bottom), emphasizing their near superimposibility.

It should be noted that mixed Mn_2Ln_2 complexes with the same kind of defect-dicubane core have previously been reported for Ln = Dy, Gd and Tb [14b,34]. However, in all of these previous cases, the Mn atoms were in the Mn^{III} oxidation state, so **6** and **7** are the first to instead contain Mn^{IV}. The Mn^{IV} oxidation level is suggested by overall charge considerations and inspection of metric parameters; in particular, Mn–O bond distances all lie in the range 1.84–1.97 Å, as expected for Mn^{IV}, and thus do not show the Jahn-Teller axial distortion expected for Mn^{III} in near octahedral geometry. The Y–O and Yb–O bond distances are very similar, lying in the 2.30–2.42 and 2.27–2.38 Å ranges, respectively, consistent with eight-coordinate Y^{III}/Yb^{III} centers. The Mn^{IV} oxidation states and the protonation levels of the O^{2-}, MeO^- and MeOH were confirmed by bond valence sum (BVS) calculations, shown in Tables 6 and 7. The BVS values for the Mn atoms are clearly ~4, confirming the Mn^{IV} oxidation level. Values of ~2 are expected for O atoms in the O^{II-} oxidation level and that have no attached atoms that cannot be seen in X-ray crystallography (i.e., H atoms). This confirms that O7, O8 and O11 are MeO^-, O^{2-}, and MeO^-, respectively. In contrast, if there is a H atom which is not visible and its contribution to the BVS of that O atom is therefore not included, a lower BVS value is expected, typically 1–1.5 (depending on the degree of its participation in hydrogen-bonding); this is clearly the case for O9 and O10, which are therefore confirmed as MeOH groups.

Table 6
Bond valence sums (BVS)[a] for the Mn atoms of complexes **6** (Y) and **7** (Yb)

Atom	Mn^{II}	Mn^{III}	Mn^{IV}	Assignment
Mn1 (**6**)	4.132	3.779	3.967	Mn^{IV}
Mn1 (**7**)	4.124	3.772	3.959	Mn^{IV}

[a] The underlined value is the one closest to the charge for which it was calculated. The oxidation state of a particular metal is the nearest whole number to that value.

Table 7
Bond valence sums (BVS) for the O atoms of complexes **6** (Y) and **7** (Yb)

Atom	BVS (**6**)	BVS (**7**)	Assignment
O7	1.972	1.972	MeO^-
O8	1.898	1.859	O^{2-}
O9	1.210	1.198	MeOH
O10	1.339	1.342	MeOH
O11	2.038	2.016	MeO^-

The occurrence of Mn^{IV} in **6** and **7** is noteworthy given that the reaction employed a Mn_4^{III} starting material and either Y^{III} or Yb^{III}, neither of which are good oxidizing agents. This points to either the participation of atmospheric O_2 gas as the oxidizing agent or the disproportionation of Mn^{III} to Mn^{IV} and Mn^{II}. We favor the latter possibility given the low yields of these complexes, but we have not sought Mn^{II} species in the filtrates to confirm this.

4. Magnetochemistry

4.1. DC magnetic susceptibility

The magnetic properties of **1**–**6** were investigated by solid state magnetic susceptibility (χ_M) measurements in the 5.0–300 K range in a 0.1 tesla (T) DC field. The resulting data for complexes **1**–**3**, **4**–**5** and **6** are shown as $\chi_M T$ versus T plot in Figs. 7–9, respectively. For complex **1**, the $\chi_M T$ value of 33.1 cm^3 K mol^{-1} at 300 K is slightly less than the value expected for $2Fe^{III}$ ($S = 5/2$, $g = 2$) and $2Ho^{III}$ ($S = 2$, $L = 6$, $^5I_8$) non-interacting ions of 36.9 cm^3 K mol^{-1}, consistent with antiferromagnetic exchange interactions, and decreases steadily to 24.2 cm^3 $kmol^{-1}$ at 50 K and then 13.7 cm^3 $kmol^{-1}$ at 5.0 K. Complexes **2** and **3** behave in a similar fashion to complex **1**. For complex **2**, the $\chi_M T$ value of 37.1 cm^3 $kmol^{-1}$ at 300 K is essentially that expected for $2Fe^{III}$ ($S = 5/2$, $g = 2$) and $2Dy^{III}$ ($S = 5/2$, $L = 5$, $^6H_{15/2}$) non-interacting ions of 36.94 cm^3 $kmol^{-1}$, and it decreases with decreasing temperature to 30.3 cm^3 $kmol^{-1}$ at 50 K, and then to 23.8 cm^3 $kmol^{-1}$ at 5.0 K. For complex **3**, the $\chi_M T$ value of 35.5 cm^3 $kmol^{-1}$ at 300 K is slightly greater than that expected for $2Fe^{III}$ ($S = 5/2$, $g = 2$) and $2Tb^{III}$: $S = 3$, $L = 3$, $^7F_6$ non-interacting ions of 32.4 cm^3 $kmol^{-1}$, and it decreases with decreasing temperature to 29.1 cm^3 $kmol^{-1}$ at 50 K, and then to 22.4 cm^3 $kmol^{-1}$ at 5.0 K. The data suggest predominantly antiferromagnetic exchange interactions within all three

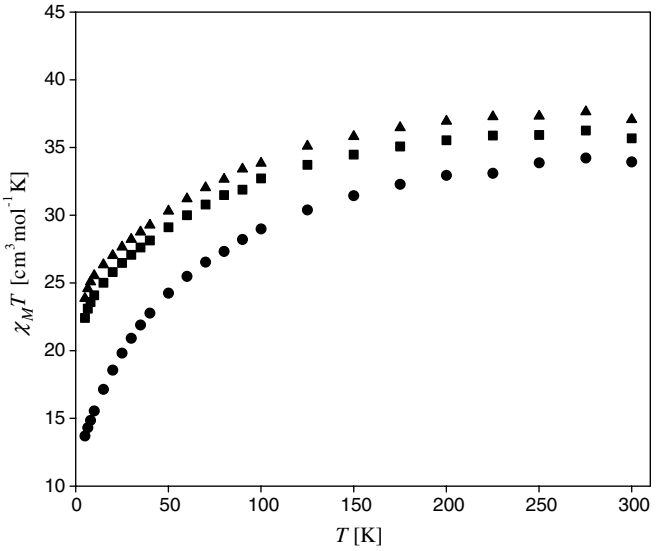

Fig. 7. Plot of $\chi_M T$ vs. T for complexes **1** (●), **2** (▲) and **3** (■).

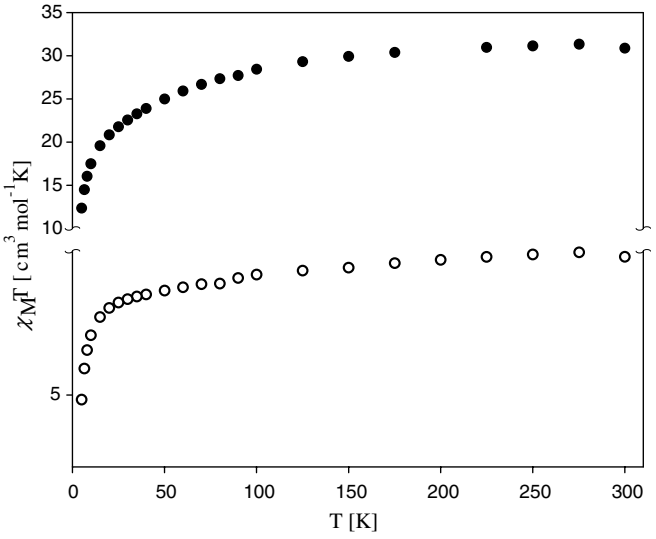

Fig. 8. Plot of $\chi_M T$ vs. T for complexes **4** (○) and **5** (●).

complexes, but with perhaps some ferromagnetic contributions. The presence of strong spin–orbit coupling effects in these three lanthanide derivatives makes the fitting of the data to obtain $Fe^{III}Fe^{III}$ and $Fe^{III}Ln^{III}$ exchange parameters far from straightforward. Such an analysis would in fact greatly benefit from the availability and parallel study of the corresponding Gd^{3+} ($S = 7/2$, $L = 0$) and Y^{3+} ($S = 0$) derivatives, but unfortunately neither of these are available at the present time. A more complete magnetic analysis of complexes **1**–**3** and other derivatives is thus the objective of future work.

Complex **4** has a $\chi_M T$ value at 300 K of 6.9 cm^3 $kmol^{-1}$ which is less than that expected for two non-interacting Fe^{III} centers of 8.8 cm^3 $kmol^{-1}$ with $g = 2$, and it decreases only slightly with decreasing temperature to 6.3 cm^3 $kmol^{-1}$ at 35 K, but then much more rapidly to 4.9 cm^3 $kmol^{-1}$ at 5.0 K (Fig. 8). This behavior is probably due to a very weak

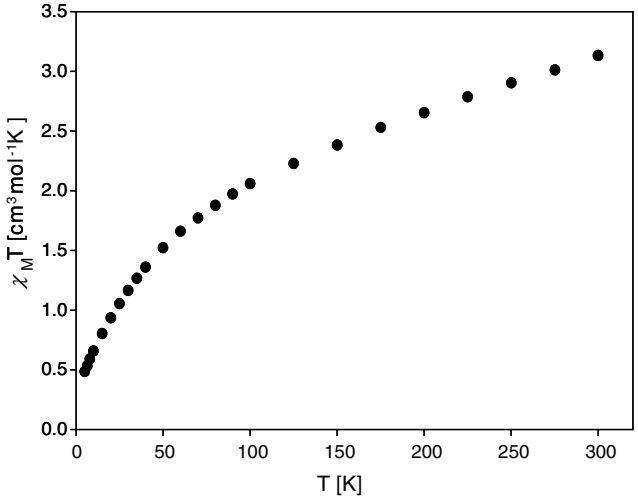

Fig. 9. Plot of $\chi_M T$ vs. T for complex **6**.

antiferromagnetic exchange interaction between the Fe^{III} ions via the intervening, diamagnetic Y^{III} ions, but we cannot get a good fit of the data over the entire temperature range to the Van Vleck equation for a $S_1 = S_2 = 5/2$ dimer. We suspect this is due to the exchange interaction being so weak as a result of the large separation between Fe^{III} atoms that it is thus comparable in magnitude to intermolecular interactions mediated by the multiple intermolecular hydrogen-bonds between adjacent clusters, as described above. Complex **5** has a $\chi_M T$ value of 30.8 $cm^3\,kmol^{-1}$ at 300 K, which, as for **1**, is again less than the 36.9 $cm^3\,kmol^{-1}$ expected for two Fe^{III} ($S = 5/2$) and two Ho^{III} ($S = 2$, $L = 6$, $^5I_8$) non-interacting ions; it then decreases to 28.4 $cm^3\,kmol^{-1}$ at 100 K, and then more rapidly to 20.8 $cm^3\,kmol^{-1}$ at 20 K then finally to 12.3 $cm^3\,kmol^{-1}$ at 5.0 K (Fig. 8). The overall behavior is consistent with antiferromagnetic exchange interactions between the constituent metal atoms.

Complex **6** has a $\chi_M T$ value that steadily decreases almost linearly from 3.13 $cm^3\,kmol^{-1}$ at 300 K to 1.52 $cm^3\,kmol^{-1}$ at 50 K, and then more rapidly decreases to 0.49 $cm^3\,kmol^{-1}$ at 5.0 K (Fig. 9). The value at 300 K is less than the expected spin-only ($g = 2$) value for a complex consisting of two non-interacting Mn^{IV} ions ($S = 3/2$; the $2Y^{III}$ ions are diamagnetic) of 3.75 $cm^3\,kmol^{-1}$, indicating an antiferromagnetic exchange interaction between the Mn^{IV} ions and a resultant $S = 0$ spin ground state. Attempts to fit the $\chi_M T$ versus T data using the isotropic Heisenberg–Dirac–van Vleck Hamiltonian described by $\mathscr{H} = -2J\hat{S}_1\hat{S}_2$, where $S_1 = S_2 = 3/2$ and J is the magnetic exchange interaction gave poor fits that did not reproduce the data over the whole temperature range, particularly the higher T data. However, it did suggest the J value is relatively weak, in the $J = -10$ to $-15\ cm^{-1}$ range, which in fact is consistent with the relatively acute Mn^{4+}–O^{2-}–Mn^{4+} (Mn1–O8–Mn1a) angles of 97.52°. As for **4**, we believe the problem is intermolecular exchange interactions, via the hydrogen-bonding network described above, which are not incorporated in the model. These points are being considered further as we seek to reach a more detailed magnetic understanding of this whole family of mixed-metal species, as well as others being prepared.

4.2. AC magnetic susceptibility

AC magnetic susceptibility measurements are a very convenient method to assess whether a molecule exhibits a slow magnetization relaxation rate, which is a necessary (but not sufficient) property of a species that might be a single-molecule magnet (SMM). Thus, such measurements were carried out in the 1.8–10 K range using a 3.5 G AC field oscillating at 50–1000 Hz, seeking the detection of a non-zero out-of-phase AC susceptibility signal (χ''_M). The latter indicates that the sample's magnetization vector cannot relax (reorient) fast enough to keep up with the oscillating field. None of the complexes in this work gave a clear χ''_M signal above 1.8 K, the operating minimum of our SQUID magnetometer, but complex **2** showed a weak, frequency-dependent tail of what might be a peak lying at <1.8 K. We thus chose **1** and **2** for more detailed studies involving single-crystal magnetization versus applied DC field sweeps on a micro-SQUID apparatus down to millikelvin temperatures [26]. The observation of hysteresis loops in such studies is the classical diagnostic property of a magnet.

The magnetization versus applied DC field sweeps for a single crystal of complex **1** · 6MeCN are shown in Fig. 10. At very low temperatures (0.3 K and below) and at a 0.14 T/s applied field sweep rate, hysteresis loops are observed with a very small coercivity and only a slight temperature dependence. The small coercive field and the overall shape of the loops suggest the presence of intermolecular interactions and some degree of ordering as the main source of the hysteresis. Indeed, a closer examination

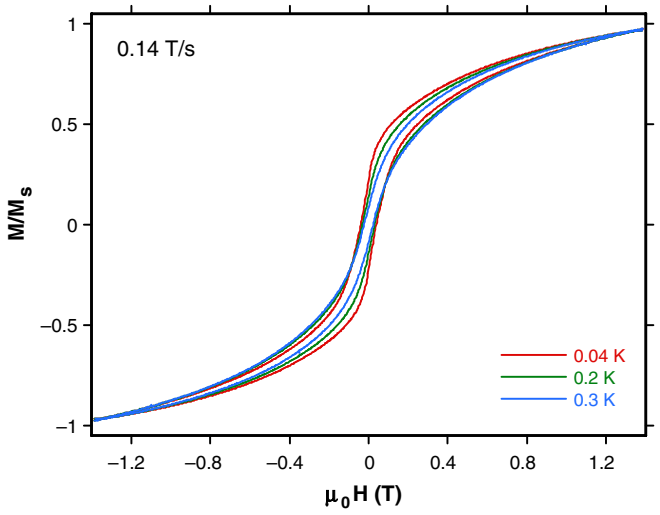

Fig. 10. Magnetization (M) vs. applied DC field hysteresis loops for a single crystal of **1** · 6MeCN at the indicated temperatures and a 0.14 T/s sweep rate. The magnetization is normalized to its saturation value, M_S.

of the crystal structure of **1** · 6MeCN reveals intermolecular π–π stacking overlaps (~3.7 Å) between the aromatic rings of benzoate groups, and this is likely the pathway for intermolecular exchange interactions. At best, therefore, complex **1** could be regarded as an exchange-biased SMM [36], although it is clearly difficult to separate the intermolecular interactions and the SMM behavior.

Clearer evidence for a SMM was observed when the same studies were performed on **2** · 4MeCN · $3H_2O$. Hysteresis loops were again obtained, and now they were much more characteristic of a SMM. The hysteresis loops obtained with a field sweep rate of 0.14 T/s and at various temperatures below 1.1 K are shown in Fig. 11 (top), and those obtained from a sweep rate dependence at a constant temperature of 0.04 K are shown in Fig. 11 (bottom). The coercivities increase with decreasing temperature and with increasing sweep rate, as expected for the superparamagnet-like behavior of a SMM. The dominating feature in these loops is the large relaxation step at zero-field, which can be assigned to fast quantum tunneling of the magnetization (QTM) through the barrier to relaxation. This is commonly seen in previous SMMs containing lanthanide ions [14b]. In fact, this very fast QTM step at zero field makes the magnetization decay very rapidly in zero field and prevents magnetization versus time decay data being collected and used to construct an Arrhenius plot; the latter kinetic analysis is commonly used to determine the effective barrier to relaxation. Again, this is as found for previous mixed 3d/4f SMMs, which show fast QTM at zero field. Steps at other field positions are also expected, but they are poorly resolved, almost unobservable, and this is assigned to broadening effects from a distribution of molecular environments, which would give a distribution of relaxation barriers and thus a distribution in step positions. Additional broadening is also expected from intermolecular interactions from both dipolar and superexchange pathways.

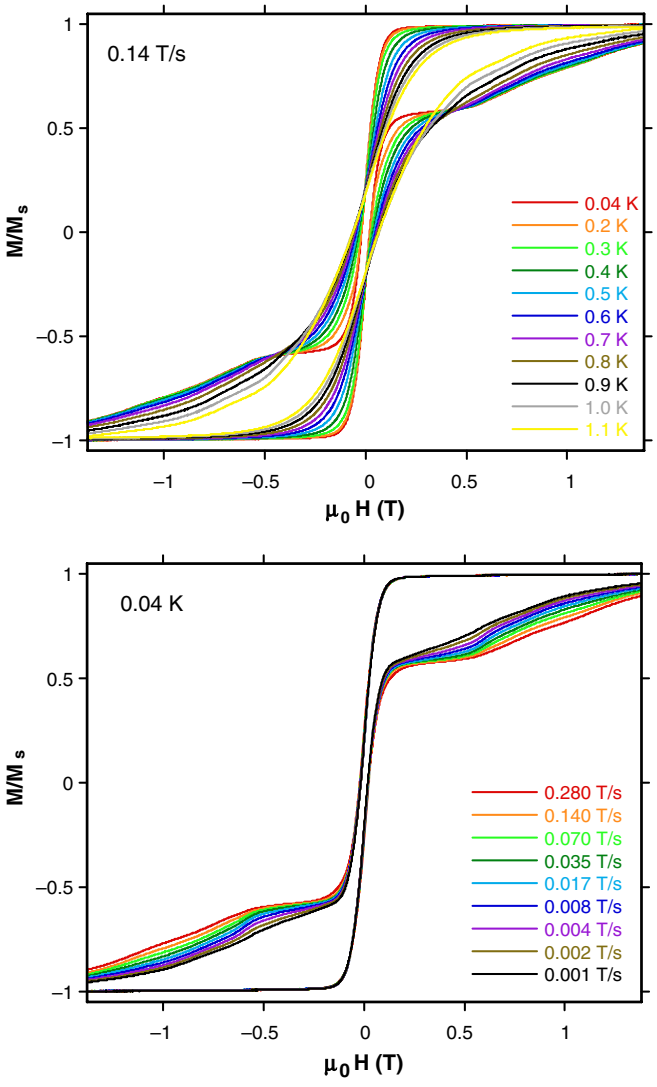

Fig. 11. Magnetization (M) vs. applied DC field hysteresis loops for a single crystal of **2** · 4MeCN · $3H_2O$ at (top) the indicated temperatures and a 0.14 T/s sweep rate, and (bottom) at the indicated field sweep rates and a temperature of 0.04 K. The magnetization is normalized to its saturation value, M_S.

5. Conclusions

A new group of mixed 3d/4f and 3d/4d tetranuclear clusters have been synthesized from the reactions of Fe^{III} or Mn^{III} sources with $teaH_3$ or $pdmH_2$, or simply by methanolysis. These products represent new additions to what is still a very small family of such mixed-metal species. While the magnetic properties are complicated by the large spin–orbit coupling effects of most Ln^{III} ions, making difficult the quantitative elucidation of the magnitude of the exchange parameters within these molecules and their resulting ground state description, hysteresis loop determinations have established that additional examples of SMMs have been provided from this area. However, lanthanide-containing SMMs still suffer from the disadvantage of fast QTM rates. This represents a diminution of the effective barrier for magnetization relaxation, and thus the temperature below which the relaxation is blocked and the complex will function as a SMM. Nevertheless, the use of lanthanides to modulate the magnetic properties of transition metal SMMs is still an interesting area that promises much new science as it matures.

6. Supplementary material

Crystallographic data have been deposited with Cambridge Crystallographic Data centre, CCDC Nos. 276642–276646. Copies of this information may be obtained from The Director, CCDC, 12 Union Road, Cambridge, CB2 1EZ, UK (fax: +44 1233 336033; email: deposit@ccdc.cam.ac.uk or www.ccdc.cam.ac.uk).

Acknowledgment

This work was supported by the National Science Foundation.

References

[1] G. Christou, D. Gatteschi, D.N. Hendrickson, R. Sessoli, MRS Bull. 25 (2000) 66.
[2] R. Sessoli, H. Tsai, A.R. Schake, S. Wang, J.B. Vincent, K. Folting, D. Gatteschi, G. Christou, D.N. Hendrickson, J. Am. Chem. Soc. 115 (1993) 1804.
[3] M. Soler, W. Wernsdorfer, K.A. Abboud, D.N. Hendrickson, G. Christou, Polyhedron 22 (2003) 1777.
[4] E.C. Theil, Annu. Rev. Biochem. 57 (1987) 289, and references therein.
[5] B. Xu, N.D. Chasteen, J. Biol. Chem. 266 (1991) 19965.
[6] R.A. Grant, D.J. Filman, S.E. Finkel, R. Kolter, J. Hogle, Nat. Struct. Biol. 5 (1998) 294.
[7] (a) V.K. Yachandra, K. Sauer, Biochim. Biophys. Acta 1655 (2004) 140;
(b) K.N. Ferreira, T.M. Iverson, K. Maghlaoui, J. Barber, S. Iwata, Science 303 (2004) 1831.
[8] A. Mishra, W. Wernsdorfer, K.A. Abboud, G. Christou, Chem. Commun. (2005) 54.
[9] R. Sessoli, D. Gatteschi, A. Caneschi, M.A. Novak, Nature 365 (1993) 141.
[10] S.M. Aubin, N.R. Gilley, L. Pardi, J. Krzystek, M.W. Wemple, L.C. Brunel, M.B. Marple, G. Christou, D.N. Hendrickson, J. Am. Chem. Soc. 120 (1998) 4991.
[11] S.M. Aubin, M.W. Wemple, D.M. Adams, H.-L. Tsai, G. Christou, D.N. Hendrickson, J. Am. Chem. Soc. 118 (1996) 7746.
[12] E.K. Brechin, J. Yoo, J.C. Huffman, D.N. Hendrickson, G. Christou, Chem. Commun. (1999) 783.
[13] (a) G. Aromi, S.M.J. Aubin, M.A. Bolcar, G. Christou, H.J. Eppley, K. Folting, D.N. Hendrickson, J.C. Huffman, R.C. Squire, H.-L. Tsai, S. Wang, M.W. Wemple, Polyhedron 17 (1998) 3005;
(b) G. Christou, Polyhedron (in press), and references therein.
[14] (a) A. Mishra, W. Wernsdorfer, K.A. Abboud, G. Christou, J. Am. Chem. Soc. 126 (2004) 15648;
(b) A. Mishra, W. Wernsdorfer, S. Parsons, G. Christou, E.K. Brechin, Chem. Commun. (2005) 2086;
(c) A.J. Tasiopoulos, W. Wernsdorfer, B. Moulton, M.J. Zaworotko, G. Christou, J. Am. Chem. Soc. 125 (2003) 15274.
[15] C.M. Zaleski, E.C. Depperman, J.W. Kampf, M.L. Kirk, V.L. Pecoraro, Angew. Chem., Int. Ed. 43 (2004) 3912.
[16] S. Osa, T. Kido, N. Matsumoto, N. Re, A. Pochaba, J. Mrozinski, J. Am. Chem. Soc. 126 (2004) 420.
[17] M. Murugesu, M. Habrych, W. Wernsdorfer, K.A. Abboud, G. Christou, J. Am. Chem. Soc. 126 (2004) 4766.
[18] M. Murugesu, W. Wernsdorfer, K.A. Abboud, G. Christou, Polyhedron (in press).
[19] E.K. Brechin, J. Yoo, M. Nakano, J.C. Huffman, D.N. Hendrickson, G. Christou, Chem. Commun. (1999) 783.
[20] C. Boskovic, W. Wernsdorfer, K. Folting, J.C. Huffman, D.N. Hendrickson, G. Christou, Inorg. Chem. 41 (2002) 5107.
[21] M. Murugesu, W. Wernsdorfer, K.A. Abboud, G. Christou, Angew. Chem. 44 (2005) 792.
[22] M. Murugesu, K.A. Abboud, G. Christou, Dalton. Trans. (2003) 4552.
[23] F.A. Hart, in: G. Wilkinson (Ed.), Comprehensive Coordination Chemistry, vol. 3, Pergamon, Oxford, 1987, p. 1073.
[24] R.F. Weinland, A. Herz, Ber. Deutsch. Chem. Ges. 45 (1912) 2662.
[25] M.W. Wemple, H.-L. Tsai, S. Wang, J.-P. Claude, W.E. Streib, J.C. Huffman, D.N. Hendrickson, G. Christou, Inorg. Chem. 35 (1996) 6450.
[26] W. Wernsdorfer, Adv. Chem. Phys. 118 (2001) 99.
[27] G.M. Sheldrick, SHELXL-97, Program for Refinement of Crystal Structures, University of Gottingen, Germany, 1997.
[28] L. Wittick, K. Murray, B. Moubaraki, S. Batten, L. Spiccia, K. Berry, Dalton Trans. (2004) 1003.
[29] M.A. Bolcar, S.M.J. Aubin, K. Folting, D.N. Hendrickson, G. Christou, Chem. Commun. (1997) 1485.
[30] N.C. Harden, M.A. Bolcar, W. Wernsdorfer, K.A. Abboud, W.E. Streib, G. Christou, Inorg. Chem. 42 (2003) 7067.
[31] C. Boskovic, E.K. Brechin, W.E. Streib, K. Folting, J.C. Bollinger, D.N. Hendrickson, G. Christou, J. Am. Chem. Soc. 124 (2002) 3725.
[32] E.K. Brechin, M.J. Knapp, J.C. Huffmann, D.N. Hendrickson, G. Christou, Inorg. Chim. Acta 297 (2000) 389.
[33] P. King, R. Clérac, W. Wernsdorfer, C.E. Anson, A.K. Powell, Dalton Trans. (2004) 2670.
[34] C. Benelli, M. Murrie, S. Parsons, R.E.P. Winpenny, Dalton Trans. (1999) 4125.
[35] J. Yoo, A. Yamaguchi, M. Nakano, J. Krzystek, W.E. Streib, L.-C. Brunel, H. Ishimoto, G. Christou, D. Hendrickson, Inorg. Chem. 40 (2001) 4604.
[36] W. Wernsdorfer, N. Aliaga-Alcalde, D.N. Hendrickson, G. Christou, Nature 416 (2002) 406.

Available online at www.sciencedirect.com
SCIENCE DIRECT®
Polyhedron 25 (2006) 627–634
POLYHEDRON
www.elsevier.com/locate/poly

Unique copper ion catalyzed hydrolytic cleavage of C–N(2) bond of thiosemicarbazide

S.K. Chawla [a,*], M. Arora [a], K. Nättinen [b], K. Rissanen [b]

[a] Department of Chemistry, Guru Nanak Dev University, Amritsar 143005, India
[b] Department of Chemistry, University of Jyvaskyla, Jyvaskyla, Finland

Received 24 September 2004; accepted 25 May 2005
Available online 5 December 2005

Abstract

For the first time, stable but coordinatively unsaturated Cu(II) complexes $[Cu(2,2'\text{-bpy})X_2]\cdot xH_2O$ (X = ClO_4, NO_3, CH_3COO and 2,2′-bpy = 2,2′-bipyridyl) have been found to promote the hydrolysis of C–N(2) bond of thiosemicarbazide (tsc) at 25 °C and at neutral pH yielding monomeric $[Cu(2,2'\text{-bpy})(NCS)_2]$. Direct reaction between $[Cu(2,2'\text{-bpy})_2]Cl_2\cdot 6H_2O$, KSCN and $CuCl_2$ results in polymeric $[Cu(2,2'\text{-bpy})(NCS)_2]_n$ [1] [Inorg. Chim. Acta. 286 (1999) 108]. Similarly tsc is cleaved by Cu(I) complex $[Cu(\phi_3P)_2(CH_3CN)_2]ClO_4$ [ϕ_3P = triphenylphosphine] which itself is converted into dimeric $[Cu(\phi_3P)_2(NCS)]_2$.
© 2005 Published by Elsevier Ltd.

Keywords: 2,2′-Bipyridyl; Thiosemicarbazide; Triphenylphosphine; Copper; Thiocyanate

1. Introduction

In the past considerable attention has been paid to study the complexation behavior of various thiosemicarbazides and thiosemicarbazones(tscz) because of their broad pharmacological activity [2–12]. Such ligands generally act as bidentate chelating through hydrazinic N(1) and S [13–17] [$H_2N(1)$–N(2)H–C(3)S–N(4)H_2].

Only a few complexes are known with tsc acting as monodentate ligand binding through S [18–22]. The strength of S-donor atom has been found to be the most important single factor affecting the biological activity of such ligands [23]. The donor properties of S are modulated by nature of metal ion and stereochemistry of the complex which in turn are monitored by the substitution on N [4] of tsc and tscz [23]. Because of good σ donor properties and π-bonding abilities supplemented by the chelate and steric effects; 2,2′-bpy is expected to substantially affect the stability of M–S bond. With a view to study the effect of 2,2′-bpy on the stability of M–S bond and hence its biological activity, we employed tsc in combination with 2,2′-bpy in the syntheses of Cu(II) complexes.

2. Experimental

Thiosemicarbazide, 2,2′-bipyridyl, hydrazine hydrate and triphenyl phosphine were purchased from CDH Lab., Bombay and copper(II) perchlorate was purchased from Aldrich Chemical Co. Copper(I) perchlorate [24] and phenylisothiocyanate [25] were prepared by known methods and their purity was checked through IR spectra. All other chemicals were of reagent grade and were used as such without further purification.

IR spectra were recorded on FTIR-NICOLET 320, Fourier-Transform spectrometer using KBr pellets. Elemental analyses were performed by Regional Sophisticated Instrumentation Centre, Punjab University, Chandigarh on Carlo Erba model 1106. HPLC was

* Corresponding author. Tel.: +91 183 258845; fax: +91 183 258820.
E-mail address: dcsegndu@yahoo.com (S.K. Chawla).

0277-5387/$ - see front matter © 2005 Published by Elsevier Ltd.
doi:10.1016/j.poly.2005.05.021

performed on 501 Waters pump with C-18 bonda packed column using Waters 484 UV detector.

2.1. X-ray crystallography

The single-crystal X-ray diffraction was done with Nonius Kappa CCD diffractometer with graphite monochromatized Mo Kα($\lambda = 0.71073$ Å) radiation. Collect–software was used in the measurement and DENZO-SMN in the processing of the data. The structures were solved and refined by full-matrix least-squares on F^2 with WinGX-software package [26] utilizing SHELXS-97 [27] and SHELXL-97 [28] modules. Hydrogen atoms were refined by a riding model. Empirical absorption correction was performed for the compound **2**. The graphic presentations of the structures were created with the software Diamond [29].

2.2. Preparative method

2.2.1. Preparation of 4-phenylthiosemicarbazide

It was prepared by reacting hydrazine with phenylisothiocyanate in chloroform. Its purity was checked by melting point 135 °C (136 – 138 °C) and IR spectrum 3395m, 3100s(ν_{N-H}), 1650s(δ_{N-H}) and 820w(ν_{C-S}) cm^{-1}.

2.2.2. Preparation of [Cu(2,2′-bpy)(NCS)$_2$] (*1*)

To the acetonitrile solution of $[Cu(2,2'\text{-bpy})(ClO_4)_2]\cdot 4H_2O$ (0.0489 g, 0.1 mmol) was added tsc (0.018 g, 0.2 mmol) in methanol. The reaction contents were refluxed for half an hour and filtered. The resulting solution was left undisturbed. After two days green needles of 1 separated out which were filtered and dried over calcium chloride. Yield 30% based upon $[Cu(2,2'\text{-bpy})(ClO_4)_2]\cdot 4H_2O$. *Anal.* Calc. for $C_{12}H_8CuN_4S_2$: C, 42.9; H, 2.3; N, 16.7. Found: C, 42.5; H, 2.0; N, 16.0%. IR spectrum 2080s ($\nu_{C\equiv N}$), 1620s ($\nu_{C=N}$) and 828w (ν_{C-S}) cm^{-1}.

In analogous reactions all other Cu(II) salts (X = NO_3, Cl and CH_3COO) resulted in the formation of $[Cu(2,2'\text{-bpy})(NCS)_2]$, which were analyzed through CHN, IR spectral and X-ray crystal (in case of ClO_4, NO_3, and Cl complexes) studies.

2.2.3. Preparation of [Cu(ϕ_3P)$_2$(NCS)]$_2$ (*2*)

Solution of $[Cu(CH_3CN)_4]ClO_4$ (0.032 g, 0.1 mmol) and ϕ_3P (0.026 g, 0.1 mmol) in methanol–acetonitrile mixture was refluxed for half an hour. It was followed by addition of tsc (0.018 g, 0.2 mmol) in methanol and further refluxed, cooled and filtered. The filtrate was left undisturbed. Colorless crystals suitable for X-ray studies were obtained after 2 days which were filtered, washed with methanol and dried over calcium chloride. Yield 40% based upon $[Cu(CH_3CN)_4]ClO_4$. *Anal.* Calc. for $C_{37}H_{30}CuNP_2S$: C, 68.7; H, 4.6; N, 2.1. Found: C, 68.4; H, 4.8; N, 2.4%. IR spectrum 2120s ($\nu_{C\equiv N}$), 1090m (ν_{P-C}), 820w, 745s and 700 cm^{-1} (due to bridging ν_{C-S}).

2.2.4. Preparation of [Cu(2,2′-bpy)(4-tscph)][ClO$_4$]$_2$ (*3*)

Addition of methanolic solution of 4-tscph (0.016 g, 0.1 mmol) to the refluxing solution of $[Cu(2,2'\text{-bpy})(ClO_4)_2]\cdot 4H_2O$ (0.0489 g, 0.1 mmol) resulted in the formation of immediate precipitates of complex which were separated by filtration, washed with methanol and dried in vacuo. Yield 55% based upon $[Cu(2,2'\text{-bpy})(ClO_4)_2]\cdot 4H_2O$. *Anal.* Calc. for $C_{17}H_{16}CuN_5SCl_2O_8$: C, 40.7; H, 3.2; N, 13.9. Found: C, 39.9; H, 4.0; N, 13.6%. IR spectrum 3365b, 3090s(ν_{N-H}), 1632s(δ_{N-H}), 835w(ν_{C-S}), 1100s($\nu_{3\ ClO_4}$) and 600w ($\nu_{4\ ClO_4}$) cm^{-1}.

2.2.5. Preparation of [Cu(ϕ_3P)$_2$ (4-tscph)][ClO$_4$] (*4*)

The corresponding reaction of 4-tscph with $[Cu(\phi_3P)_2(CH_3CN)_2]ClO_4$ under analogous conditions yielded white precipitates of **4**. Yield 60% based upon $[Cu(\phi_3P)_2(CH_3CN)_2]ClO_4$. Anal. Calc. for $C_{43}H_{39}CuN_3P_2SClO_4$: C, 60.3; H, 4.6; N, 4.9. Found: C, 59.7; H, 3.9; N, 4.6%. IR spectrum 3370b(ν_{N-H}), 1625s(δ_{N-H}), 840w(ν_{C-S}), 1100s($\nu_{3\ ClO_4}$) and 600w($\nu_{4\ ClO_4}$)cm^{-1}.

2.2.6. Preparation of precursor complexes

The precursor complexes $[M(N\text{–}N)X_2]\cdot xH_2O$ [N–N = 2,2′-bpy, M = Ni(II), Co(II), Cu(II) and Zn(II), X = NO_3, ClO_4, Cl and CH_3COO and N–N = 1, 10-phenanthroline (1, 10-phen), ethylenediammine (en) and $2NH_3$, M = Cu and X = NO_3, ClO_4] and Cu(2,2′-bpy). $(ClO_4)_2(L')$ [4-tscph, 2thiourea(tu) and semicarbazide(sc)] were prepared by known methods.

3. Results

For the preparation of mixed donor ligand complex of the type $[Cu(2,2'\text{-bpy})(tsc)][ClO_4]_2$, we reacted $[Cu(2,2'\text{-bpy})(ClO_4)_2]\cdot 4H_2O$ with stoichiometric amount of tsc in methanol–acetonitrile. But to our unexpected surprise the reaction yielded green complex of composition $[Cu(2,2'\text{-bpy})(NCS)_2]$. The IR spectrum of 1 reports $\nu_{C\equiv N}$ at 2080 cm^{-1} and ν_{C-S} at 828 cm^{-1} diagnostic of N bonded thiocyanate. Further, various absorption bands in the region 3400–3100 cm^{-1} (ν_{N-H}), characteristic of tsc and 1100 cm^{-1} (ν_3) and 600 cm^{-1} (ν_4) consistent with presence of ClO_4 anion are entirely absent [30]. Peaks for $\nu_{C=N}$ (2,2′-bpy) appears at ca. 1620 cm^{-1}. The structure of complex has been confirmed X-ray crystallography.

3.1. The crystal structure of [Cu(2,2′-bpy)(NCS)$_2$]

The crystal data and structure refinement are given in Table I and important bond lengths and angles are

Table I
Crystal data structural refinement for **1** and **2**

Compound	**1**	**2**
Empirical formula	$C_{12}H_8CuN_4S_2$	$C_{36}H_{30}CuN_2P_2S$
Formula weight	335.88	648.16
Crystal color, shape	green, prisms	colorless, prisms
Crystal dimensions (mm)	$0.15 \times 0.20 \times 0.4$	$0.40 \times 0.20 \times 0.15$
Crystal system	monoclinic	triclinic
Space group	$C2/c$ No. 15	$P\bar{1}$ No. 2
a (Å)	8.7345(2)	10.2110(2)
b (Å)	12.6745(3)	13.0204(3)
c (Å)	13.6299(4)	13.3572(3)
α (°)	105.144(1)	114.840(1)
β (°)	107.182(1)	92.888(1)
γ (°)	105.112(1)	100.714(1)
V (Å^3)	1294.74(6)	1566.94(6)
Calculated density (mg/m^3)	1.998	1.374
Temperature of collection (K)	173	173
Z	4	2
R_{obs}	$R_1 = 0.0293$, $wR_2 = 0.0570$	$R_1 = 0.0385$, $wR_2 = 0.0840$
R_{all}	$R_1 = 0.0386$, $wR_2 = 0.0597$	$R_1 = 0.0550$, $wR_2 = 0.0910$
Goodness-of-fit	1.077	1.019
θ Range for data collection (°)	3.27–25.03	2.94–24.99
Scan type	Φ/Ω, 2°	Φ, 1°
Reflections collected/unique	3828/1149	15,035/5491
Refined parameters	87	379
Residual electron density (e/Å^3)	0.490/−0.403	0.340/−0.575

represented in Table II. The coordination geometry around Cu(II) center can be described as a distorted square planar. It coordinates to 2 N from 2,2′-bpy and 2 N from thiocyanate (Fig. 1). The inter pyridyl planar dihedral angle is 80.96°. The Cu7–N8 bond is in 71.3° angle to the normal of the plane formed by bipyridyl, while the angle of the thiocyanate group from normal of above mention plane is 60.1°. The angle between these two lines is 11.2°. The two thiocyanate groups are 119.9° degree in respect to each other. The individual molecules are arranged in zigzag chains in herringbone design with 2,2′-bpy and thiocyanate alternating on either side of the stack making a head to tail arrangement (Fig. 2). The bipyridyl double rings are coplanar, except for 0.7° twist inside the molecule. The pairs of symmetry related chains are packed in 2D sheets. The most intriguing feature is that a chain within a particular layer and molecules within a chain are unsupported by any interaction. The molecules are linked together in chains or sheets through π–π interactions between aromatic units of the immediate layers (Fig. 3(a) and (b)). The layers are arranged

Table II
Selected bond lengths (Å) and bond angles (°) in **1**

N(1)–Cu(7)	2.003(2)
N(8)–Cu(7)	1.952(2)
Cu(7)–N(1)#1	2.003(2)
Cu(7)–N(8)#1	1.952(2)
N(8)–Cu(7)–N(8) #1	96.70(13)
N(8)–Cu(7)–N(1)	161.60(9)
N(8)#1–Cu(7)–N(1)	93.56(9)
N(8)–Cu(7)–N(1)#1	93.56(9)
N(8)#1–Cu(7)–N(1)#	161.60(9)
N(1)–Cu(7)–N(1)	80.96(12)

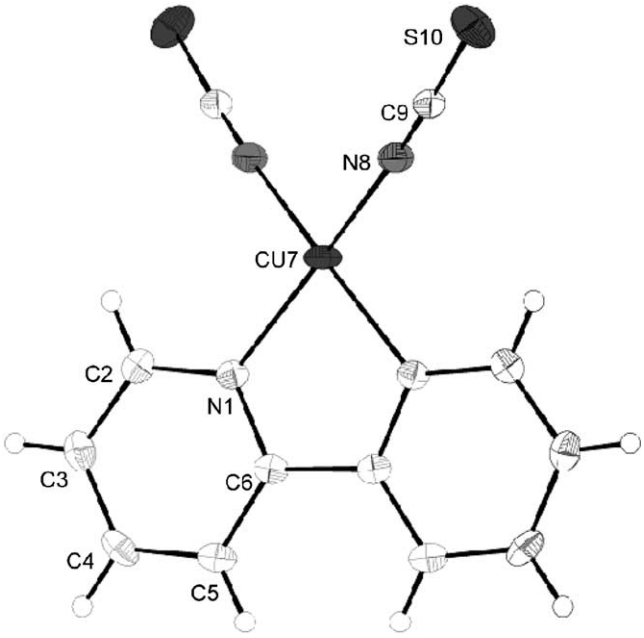

Fig. 1. ORTEP diagram of asymmetric unit of 1 with labeling scheme.

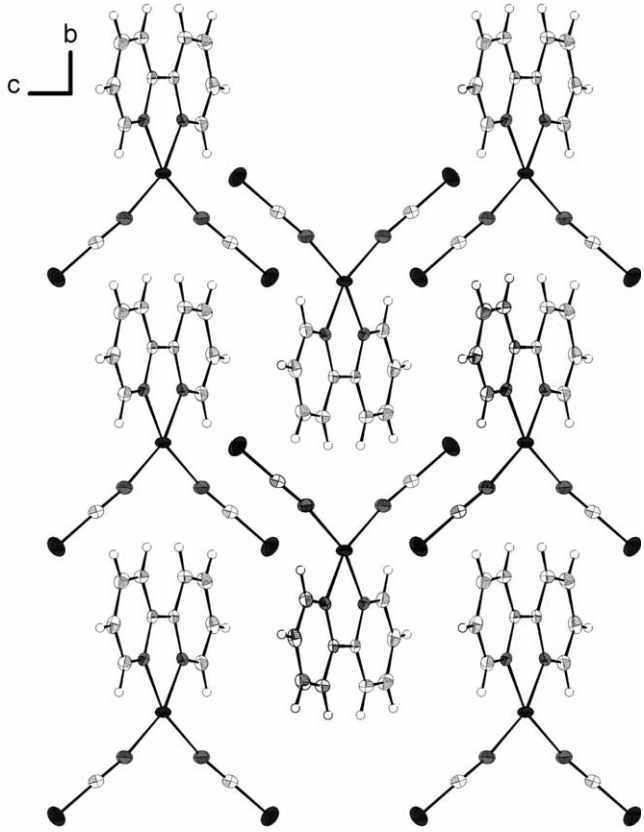

Fig. 2. A view of layer (bc plane) depicting the packing of molecules in zigzag chains in herringbone fashion in 1.

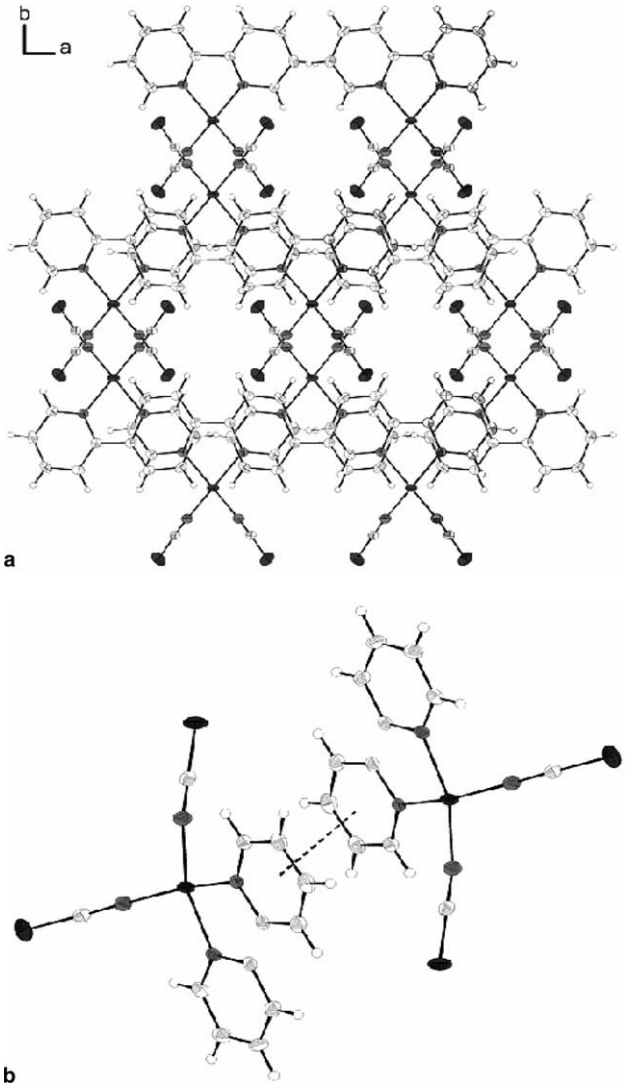

Fig. 3. (a) Two layers of network of 1, (b) a view along *c*-axis showing the stacking of layers.

in rare face to face (OFF) motif [31]. The superimposed bipyridyl rings are half the width of bipyridyl unit so that each 2,2′-bpy molecule interacts with the two 2,2′-bpy molecules of the adjacent layer covering one half of each molecule (Fig. 3(a)). The distance from one bipyridyl ring to the other calculated between C2 and C4 of the neighboring molecules is 3.29 Å. This mode of packing not only links two layers together but also keeps the molecules of the adjacent layer in position.

There is also a weak hydrogen bond between S10 and H3 of the adjacent molecule. The D–H···A and D···H distances are 3.042 and 3.699 Å, respectively. The D–H···A angle is 128.98°.

To investigate the probable mechanism of this unusual cleavage, series of experiments as tabulated below were carried out and were followed through IR spectroscopy for the presence or absence of thiocyanate peak.

3.1.1. Role of metal ion

The role of metal ion in hydrolysis of tsc was investigated by reacting $[M(2,2'\text{-bpy})X_2]\cdot xH_2O$, [M = Co, Ni, Cu and Zn and X = Cl, NO_3, ClO_4, CH_3COO] with tsc in methanol–acetonitrile mixture.

3.1.2. Effect of anion

A range of $[Cu(2,2'\text{-bpy})X_2]\cdot xH_2O$ precursors were reacted with tsc where X ranges from very weak to strong coordinating anion. The reaction completion is indicated by change of initial brown color to green color characteristic of $[Cu(2,2'\text{-bpy})(NCS_2]$.

3.1.3. Participation of co-ligand(N–N)

The participation of co-ligand to assist the cleavage of tsc in $Cu(N\text{–}N)(ClO_4)_2\cdot xH_2O$ was studied by employing π-bonding bulky ligands and non-π-bonding non-bulky ligands. The following sets of experiments were carried out.

3.1.4. Role of O/S and N/S ligand

Finally the reaction of $Cu(2,2'\text{-bpy})(ClO_4)_2\cdot 4H_2O$ with other similar ligands containing O/N or S/N donor atoms were employed. As indicated by IR studies only tsc is cleaved.

The above observations suggest that

(a) The hydrolysis is promoted only by copper complexes (Table 1).
(b) The stronger the coordinating ability of the anion, longer is the time taken to yield thiocyanate complex (Table 2).
(c) The hydrolysis is catalysed only with strong π-bonding and sterically hindered co-ligand (Table 3).

Table 1
Role of metal ion

S. no.	Precursor complex	ν, $\delta_{NH(tsc)}$ (cm^{-1})	$\nu_{CN\ (NCS)}$ (cm^{-1})	$\nu_{CS\ (NCS)}$ (cm^{-1})	$\nu_{CS\ (tsc)}$ (cm^{-1})
1	$Cu(2,2'\text{-bpy})\cdot X_2\cdot xH_2O$		ca. 2080	ca. 830	
2	$Co(2,2'\text{-bpy})\cdot X_2\cdot xH_2O$	3290, 3250, 1650, 1625			700
3	$Ni(2,2'\text{-bpy})\cdot X_2\cdot xH_2O$	3350, 3260, 1630, 1600			710
4	$Zn(2,2'\text{-bpy})\cdot X_2\cdot xH_2O$	3280, 3130, 1630, 1600			690

X = ClO_4, All other metal anions also show similar results.

Table 2
Effect of anion

S. no.	Precursor complex	Final complex	Time required for the completion of the reaction
1	$Cu(2,2'bpy)(ClO_4)_2 \cdot xH_2O$	$[Cu(2,2'bpy)(NCS)_2]$	Instant
2	$Cu(2,2'bpy)(NO_3)_2 \cdot xH_2O$	$[Cu(2,2'bpy)(NCS)_2]$	5 min
3	$Cu(2,2'bpy)(Cl)_2 \cdot xH_2O$	$[Cu(2,2'bpy)(NCS)_2]$	3–4 h
4	$Cu(2,2'\text{-}bpy)(CH_3COO)_2 \cdot xH_2O$	$[Cu(2,2'bpy)(NCS)_2]$	5–6 h

Table 3
Participation of co-ligand (N–N)

S. no.	(N–N)	ν, $\delta_{NH(tsc)}$ (cm^{-1})	$\nu_{CN\ (NCS)}$ (cm^{-1})	$\nu_{CS(NCS)}$ (cm^{-1})	$\nu_{CS(tsc)}$ (cm^{-1})
1	2,2′-bpy		ca. 2080	ca. 830	
2	1,10-phen		2030	810	
3	$2NH_3$	3295, 3210, 1620, 1580			740
4	en	3340, 3200, 1610, 1590			765

Table 4
Role of O/S and N/S ligand

S. no.	Ligand	ν_{NH} (cm^{-1})	δ_{NH} and ν_{CN} (cm^{-1})	$\nu_{CN\ (NCS)}$ (cm^{-1})	ν_{CS} (cm^{-1})
1	tsc			2100	ca. 835
2	4-tscph	3355, 3250	1635, 1600		745
3	tu	3265	1655, 1610		695
4	sc	3280	1635, 1600		

(d) The thiosemicarbazide species are hydrolysed only under special conditions. 4-Phenyl thiosemicarbazide and other similar ligands fail to undergo cleavage (Table 4).

4. Discussion

The common mode of bidentate coordination in tsc is through hydrazinic N(1) and S. However, based upon the above results it is possible that in the presence of 2,2′-bpy or other bulky π-bonding ligands both nitrogen atoms N(1) and N(4) instead of N(1) and S coordinate to Cu(II) due to the following reasons:

(1) In the presence of bulky amine ligands like 2,2′-bpy and 1,10-phen, Cu ion may react preferentially through amidic N(4) instead of S due to steric clashes. With non-bulky co-ligands like en, NH_3 the conventional S, N chelation may be dominating. Such effects

Table III
Selected bond lengths (Å) and bond angles (°) in **2**

Cu(1)–N(4)	2.034(2)
Cu(1)–P(24)	2.2819(7)
Cu(1)–P(5)	2.3095(7)
Cu(1)–S(2)	2.3968(7)
N(4)–Cu(1)–P(24)	112.83(6)
N(4)–Cu(1)–P(5)	105.09(6)
P(24)–Cu(1)–P(5)	121.76(2)
N(4)–Cu(1)–S(2)	98.22(6)
P(24)–Cu(1)–S(2)	111.23(3)
P(5)–Cu(1)–S(2)	104.89(3)

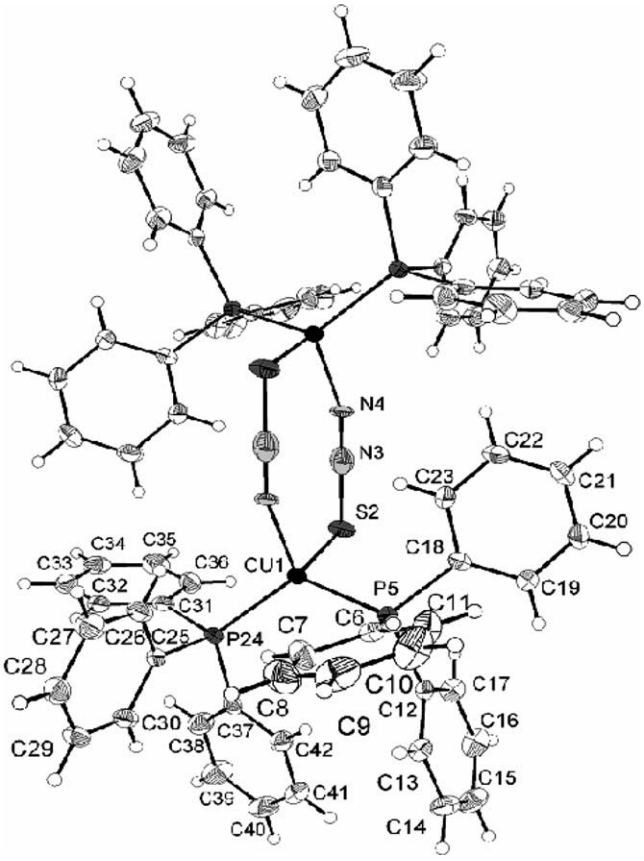

Fig. 4. The local coordination environment around Cu(I) ion in **2**.

have already been observed by Williams et al. in Pt(II) diammine complexes with methionine and *N*-acetyl methionine [32]. In the presence of bulky diammine ligands Pt(II) bind through S, N or S, O instead of S, S atoms due to interligand clashes. Their studies are also supported by molecular mechanics calculations.

(2) Copper being a borderline metal ion should preferentially coordinate through S of thiosemicarbazide. But this mode of bonding may be reversed in presence of strong π-acceptor ligands like 2,2′-bpy or 1,10-phen. Their strong π-acceptor nature makes the d-orbitals of Cu ion in $Cu(2,2'\text{-bpy}) \cdot X_2 \cdot xH_2O$ less available for bonding with π orbitals of sulphur. Therefore, metal orbitals of Cu(II) in $Cu(2,2'\text{-bpy}) \cdot X_2 \cdot xH_2O$ are not quite as basic as that of Cu(II) tsc, making the N(4) amidic nitrogen to coordinate to Cu(II) instead of S. Similar effects have also been observed earlier in [Pd(2,2′-bpy)(NCS)(SCN)] complex [33,34]. Although the soft nature of Pd(II) calls for bonding of SCN through its S end but for the second thiocyanate the bonding through N is preferred, because the less availability of electron density on Pd(II) due to back bonding with 2,2′-bpy makes Pd(II)–S bond interaction very weak.

(3) Bonding through N instead of S may also be preferred due to symbiotic effects.

The participation of π bonding in catalyzing the cleavage of tsc is further proved by substituting 2,2′-bpy with ϕ_3P- another π bonding ligand. The $[Cu(\phi_3P)_2(CH_3CN)_2]ClO_4$ was reacted with tsc under similar conditions and here again tsc is cleaved to generate $[Cu(\phi_3P)_2(NCS)]_2$. Another support to the proposed mechanism comes from the failure of both $[Cu(2,2'\text{-bpy})(ClO_4)_2] \cdot 4H_2O$ and $[Cu(\phi_3P)_2(CH_3CN)_2]ClO_4$ to hydrolyse 4-tscph and yield $[Cu(2,2'\text{-bpy})(4\text{-tscph})][ClO_4]_2$ and $[Cu(\phi_3P)_2(4\text{-tscph})]$-

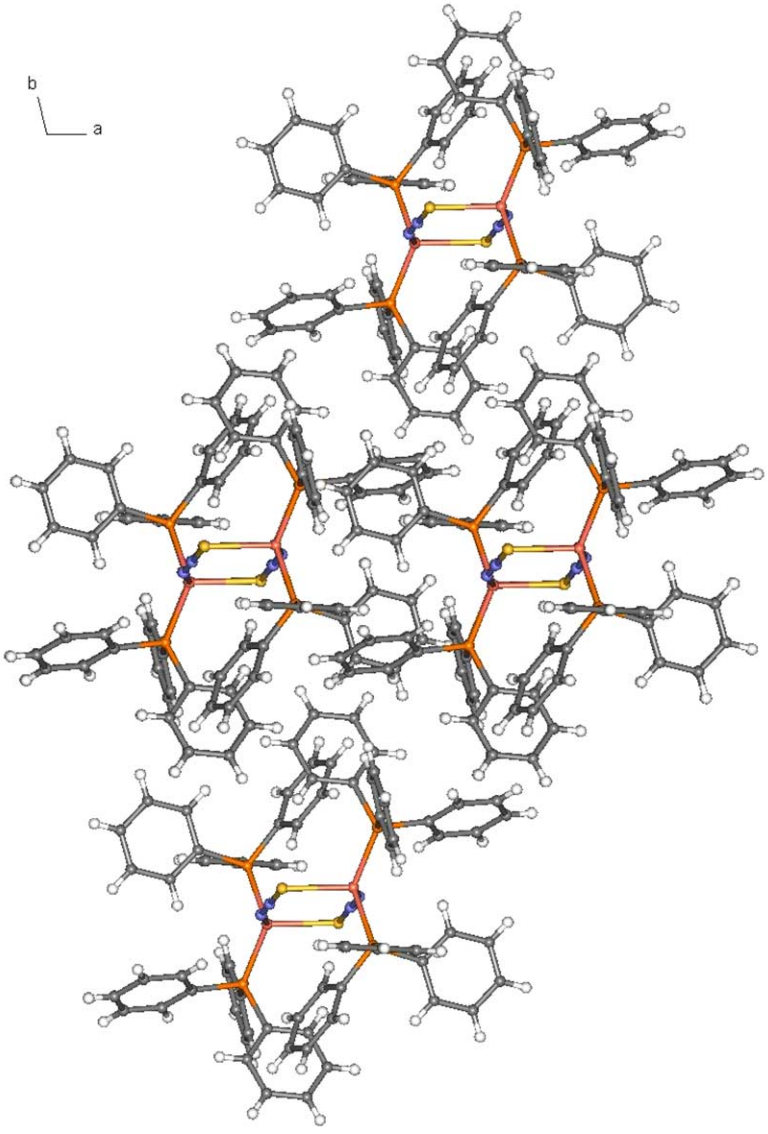

Fig. 5. Packing view along *c*-axis of complex **2**.

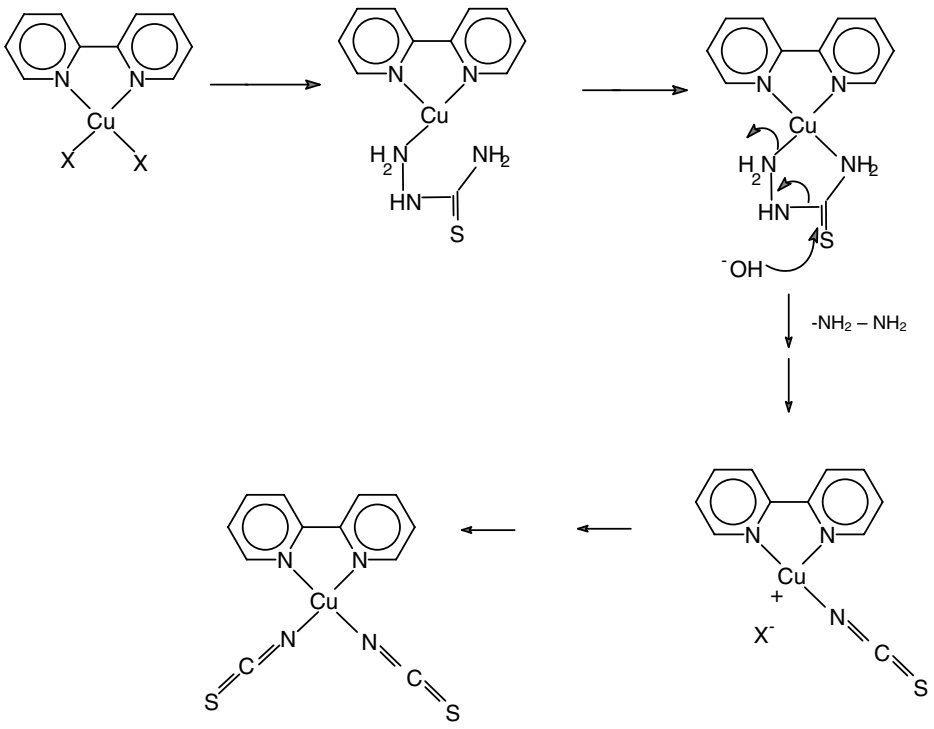

Evolution of hydrazine was confirmed through HPLC.

Scheme 1. Proposed mechanism of hydrolysis of tsc.

(ClO_4) respectively. Due to the presence of bulky phenyl group N(4) is both sterically hindered and electron deficient. Here 4-tscph probably binds through S and hydrazinic N which is supported by shifting of C=S peak from 820w cm^{-1} in 4-tscph to ca. 840 cm^{-1} in the complexes. As the coordinated sulphur is difficult to cleave, the hydrolysis of 4-tscph fails. Similarly other similar ligands tu (binding through S) sc binding through (O or O and N) are not hydrolyzed.

*4.1. Crystal structure of [Cu(ϕ_3P)$_2$ (NCS)]$_2$ (**2**)*

The crystal data and structure refinement and important bond length and angles are reported in Tables I and III, respectively. The molecule exists as a dimer in which each of the Cu(I) is significantly deviated from idealised tetrahedral geometry towards square planar (Fig. 4). Two Cu(I) ions are bridged by two NCS groups through S and N atoms. The tetrahedral geometry is completed by coordination of each Cu atom to two triphenyl phosphines. The $Cu_2(NCS)_2$ forms 8 membered ring and has inversion center between two copper atoms. Packing of various layers is shown in Fig. 5.

5. Proposed mechanism

Based upon above observations that in case of $[Cu(2,2'\text{-bpy})X_2]\cdot xH_2O$, Cu perhaps bind through N(1), N(4) instead of N, S and binding through N(4) withdraws most of the electron density from S making it electropositive and susceptible to hydrolysis. The following mechanism is proposed (Scheme 1).

6. Conclusion

The ability of copper ion to promote the hydrolytic cleavage of tsc when coordinated to π acceptor ligands has been noticed for the first time. Both electronic and steric effects may be playing a significant role.

7. Supplementary data

Supplementary data are available from the Cambridge Crystallographic Data Center, 12 Union Road, Cambridge CB2 1EZ, UK (fax: (+44)1223-336-033; e-mail: deposit@ccdc.cam.ac.uk) quoting the deposition numbers 208696 and 208697.

Acknowledgements

M. Arora is indebted to Guru Nanak Dev University for providing financial assistance, K.R. thanks the Finnish Academy for the financial support and K.N. thanks graduate School of Bio-organic Chemistry.

References

[1] S. Ferlay, G. Francese, H.W. Schmalle, S. Decurtins, Inorg. Chim. Acta 286 (1999) 108.
[2] M.A. Ali, A.H. Mirza, A. Monsur, S. Hossain, M. Nazimuddin, Polyhedron 20 (2001) 1045.
[3] M.B. Ferrari, S. Capacchi, G. Pelosi, G. Reffo, P. Tarasconi, R. Albertini, S. Pinelli, P. Lunghi, Inorg. Chim. Acta 286 (1999) 134.
[4] M.C. Miller, C.N. Stineman, J.R. Vance, D.X. West, I.H. Hall, Anticancer Res. 18 (1998) 4131.
[5] M.C. Miller, C.N. Stineman, J.R. Vance, D.X. West, I.H. Hall, Appl. Organomet. Chem. 13 (1999) 9.
[6] W.E. Antholine, J.M. Knight, D.H. Petering, J. Med. Chem. 19 (1976) 339.
[7] L.A. Saryan, E. Ankel, C. Krishnamurti, D.H. Petering, J. Med. Chem. 22 (1979) 1218.
[8] M.R. Taylor, J.P. Glusker, E.J. Gabe, J.A. Minkin, Bioinorg. Chem. 3 (1974) 189.
[9] F.B. Colin, C.R. Theocharis, Acta Crystallogr. Sect. C. 43 (1987) 26.
[10] M. Mohan, M.P. Gupta, L. Chandra, N.K. Jha, Inorg. Chim. Acta 151 (1988) 61.
[11] S. Padhye, G.B. Kauffman, Coord. Chem. Rev. 63 (1985) 127.
[12] D. K-Demertzi, J.R. Miller, N. Kourkoumelis, S.K. Hadjikakou, M.A. Demertzis, Polyhedron 18 (1999) 1005.
[13] L.M. Fostiak, I. Garcia, J.K. Swearingen, E. Bermejo, A. Castineiras, D.X. West, Polyhedron 22 (2003) 83.
[14] C. Bellitto, A.A.G. Tomlinson, C. Furlani, G. Demunno, Inorg. Chim. Acta 27 (1978) 269.
[15] G. Dessy, V. Fares, L. Scaramuzza, A.A.G. Tomlinson, G. DeMunnu, J. Chem. Soc., Dalton Trans. (1978) 1549.
[16] M.E. Rusanovskii, I.D. Samus, N.M. Samus, O.A. Bologa, N.V. Belov, Dolk. Akad. Nauk SSSR. 260 (1981) 98.
[17] I.D. Samus, M.E. Rusanovskii, O.A. Bologa, N.M. Samus, Koord. Khim. 7 (1981) 120.
[18] A.K. Barik, S. Paul, S.K. Kar, R.J. Butcher, J.C. Bryan, Polyhedron 18 (1998) 571.
[19] M. Nardelli, G.F. Gasparri, G.G. Battistini, A. Musatti, Chem. Commun. (1965) 187.
[20] G.F. Gasparri, A. Mangia, A. Musatti, M. Nardelli, Acta. Crystallogr. Sect B. 24 (1968) 367.
[21] L.C. Capacchi, G.F. Gasparri, M. Ferrari, M. Nardelli, Chem. Commun. (1968) 910.
[22] L.C. Capacchi, G.F. Gasparri, M. Ferrari, M. Nardelli, Ric. Sci. 38 (1968) 974.
[23] M.J.M. Campbell, Coord. Chem. Rev. 15 (1975) 279.
[24] I. Csoregh, P. Kieregaard, R. Nerrestom, Acta Crystallogr. Sect. B. 31 (1975) 314.
[25] A.I. Vogel, A Text Book of Practical Organic Chemistry, fourth ed., 1978.
[26] L.J. Farrugia, J. Appl. Cryst. 32 (1999) 837.
[27] G.M. Sheldrick, Acta Cryst. A 46 (1990) 467.
[28] G.M. Sheldrick, SHELXL-97 – A Program for Crystal Structure Refinement, University of Göttingen, Germany, 1997.
[29] DIAMOND – Visual Crystal Structure Information System, Prof. Dr. G. Bergerhoff, Gerhard-Domagk-Strasse 1, 53121 Bonn, Germany, 2001.
[30] K. Nakamoto, Infrared Spectra of Inorganic and Coordination Compounds, fifth ed., Wiley, New York, 1997.
[31] V. Russell, M. Scudder, I. Dance, J. Chem. Soc., Dalton Trans. (2001) 789.
[32] K.M. Williams, C. Rowan, J. Mitchell, Inorg. Chem. 43 (2004) 1190.
[33] J. Burmeister, F. Basolo, Inorg. Chem. 3 (1964) 1587.
[34] A. Sabatini, I. Bertini, Inorg. Chem. 4 (1965) 1665.

Available online at www.sciencedirect.com
SCIENCE DIRECT®
Polyhedron 25 (2006) 635–644
POLYHEDRON
www.elsevier.com/locate/poly

Design and syntheses of blue luminescent zinc(II) and cadmium(II) complexes with bidentate or tridentate pyridyl-imidazole ligands

Shu-Mei Yue, Hong-Bin Xu, Jian-Fang Ma, Zhong-Min Su *, Yu-He Kan, Heng-Jun Zhang

Institute of Functional Material Chemistry, Faculty of Chemistry, Northeast Normal University, Changchun, Jilin 130024, PR China

Received 4 April 2005; accepted 3 July 2005
Available online 25 August 2005

Abstract

A series of luminescent Zn(II) and Cd(II) complexes have been prepared based on three different π-conjugated ligands, 2-(2-pyridyl)-imidazole (HL1), 2-(2-pyridyl)-benzimidazole (HL2) and 2,6-bis(benzimidazol-2yl)-pyridine (H_2L3). The PL spectra of the ligands exhibit a bathochromic shift in agreement with the extended π-conjugation of the ligand. The spectra of the complexes with the ligands follow the same rule. The structures of $Zn(L2)_2H_2O$ (**5**), $[Cd(L2)_2(H_2O)_2]\cdot 2DMSO$ (**6**), $Zn(HL3)_2$ (**9**) and $Cd(HL3)_2$ (**10**) have been established by X-ray crystallography. The structure of **5** can be best described as a square pyramid. The coordination geometries of **6**, **9** and **10** can be described as distorted octahedrons. In the solid state and in DMSO, these complexes show emission maxima in the blue region. The complexes have a bathochromic shift of the emission energy in sharp contrast to the free ligands. They display blue luminescence and have high luminescence quantum efficiency. A theoretical study reveals that the emissions are assigned to intraligand transitions of the deprotonated L2 and HL3 ligands, and the metal ions in the complexes play a key role in stabilizing the ligand and promoting the luminescence, which is consistent with the experimental results.
© 2005 Elsevier Ltd. All rights reserved.

Keywords: 2-(2-Pyridyl)-imidazole; 2-(2-Pyridyl)-benzimidazole; 2,6-Bis(benzimidazol-2yl)-pyridine; Complex; Luminescence

1. Introduction

Since Tang and Van Slyke [1] reported the first double-layer green organic electroluminescent devices (OELDs) using Alq_3 (q = 8-hydroxyquinolinyl) in 1987, there has been intense research activity in organic EL devices [2,3]. Studies on OELDs have proliferated because of their application in the next generation of full-color flat panel displays, and extensive studies have been performed on the use of small molecular complexes to make organic EL devices with high brightness, multi-color emission, improved durability and desirable efficiency [4,5]. Research into ligand design for EL materials has been dominated by the 8-hydroxyquinoline, dipyridine and azaindole moiety. Despite recent advances in red and green light OLEDs, useful blue electroluminescent materials are still sparse and sought-after in the literature, with notable examples being Zn(II) metal–organic compounds [6]. Che and Wang groups [7] have reported a series of Zn(II) compounds containing 7-azaindole or 2,2′-dipyridylamine ligands, which display blue light photoluminescence. However, practical applications of these compounds in OELDs would require a new generation of organic ligands that are inexpensive and robust.

In organic polymers, such as poly(*p*-phenylene vinylene) (PPV) and polythiophenes, etc., the length,

* Corresponding author. Tel.: +86 431 5099747; fax: +86 431 5684009.
E-mail address: zmsu@nenu.edu.cn (Z.-M. Su).

0277-5387/$ - see front matter © 2005 Elsevier Ltd. All rights reserved.
doi:10.1016/j.poly.2005.07.021

substitution, regioregularity and degree of conjugation can be modulated to tune color. A common approach to control the emitted color of organic materials is to append fluorescent chromophores to a polymeric backbone or to blend dyes into inert polymeric matrices [8]. Similarly, the emission wavelength of most metal–organic complexes can be tuned or changed by adjusting the length of conjugation of the ligand since fluorescent emission is mostly dominated by the coordinated ligand transition [9–11].

Imidazole and its derivatives were found to have a broad scope of biological activity. For example, they were found to be essential in the biosynthesis of purine nucleotides and DNA binding studies of their complexes [12,13]. On the other, transition metal complexes with imidazole and its derivatives have attracted much attention due to not only their interesting structural and chemical properties but also their applications in materials science [14,15]. Recently, homoleptic rare earth 2-(2-pyridyl)-benzimidazole [16], *cis*-dichloro (2-pyridyl)-benzothiazole platinum (II) [17] and [Cu(pmda)(2-(2-pyridyl)-benzimidazole)] were obtained [18]. Only a few transition metal complexes of 2-(2-pyridyl)-imidazole (HL1), 2-(2-pyridyl)-benzimidazole (HL2) and 2,6-bis(benzimidazol-2yl)-pyridine (H_2L3) are known [16–19]. By integrating the design features described above, we have prepared three different conjugated length ligands including imidazole, HL1, HL2 and H_2L3, which are inexpensive and commercially available. As far as we know, there are no reports about the crystal structures of the neutral Cd(II), Zn(II) complexes in the literature until now.

According to these considerations, We designed and synthesized theses ligands, which can coordinate to Cd(II) and Zn(II) ions via the nitrogen atoms in a bidentate or tridentate mode. At the same time molecular orbital calculations are performed to study the structures and spectra of the complexes.

2. Experimental

2.1. Syntheses

2.1.1. Preparation of ligand HL1

HL1 was prepared according to the literature procedures [20]. A solution of 20 g (190 mmol) of pyridine-2-carboxaldehyde and 20 ml of 95% ethanol was cooled to 0 °C and added to a solution of 27 ml of 40% aqueous glyoxal in 20 ml of 95% ethanol, also at 0 °C. The mixture was stirred in an ice bath, and 64 ml of cold aqueous NH_3 (30%) was added as quickly as possible while maintaining the temperature of the entire mixture below about 5 °C. The stirring solution gradually turned brown and was allowed to warm to room temperature after 1 h. The volume was reduced by gentle warming under vacuum, and the remaining solution was extracted several times with ether, and the ether was then removed under vacuum to yield a brown oil which was distilled under vacuum. A clear yellow oil was obtained and then recrystallized from ethyl acetate yielding 9 g (33%) of light yellow needles.

2.1.2. Preparation of ligand HL2

A mixture of 2-picoline (0.1 mol), *o*-phenylenediamine (0.1 mol) and sulfur (0.3 mol) was heated at 170 °C for 10 h. After the reaction was over, the reaction mixture was concentrated in vacuo, becoming gummy. The residue was extracted with hot ethanol. The extract was evaporated in vacuo and recrystallized after purification with active charcoal [21].

2.1.3. Preparation of ligand H_2L3

According to the literature procedures [26], pyridine-2,6-dicarboxylic acid (3.35 g) was stirred with *o*-phenylenediamine (4.7 g) in syrupy phosphoric acid (40 ml) at ca. 230 °C for 4 h. The colored molten mixture was poured into and vigorously stirred in cold water. When cooled the bulky blue-green precipitate was collected by filtration and then stirred in hot, 10% aqueous sodium carbonate solution (300 ml). The resulting solid was filtered off and recrystallized from methanol to give long, white prisms (3.3 g, 53%).

2.1.4. $Zn(L1)_2 \cdot H_2O$ (**1**)

A solution of 2-(2-pyridyl)imidazole (1.5 mmol) in methanol (20 ml) was heated to boiling, mixed with a solution of zinc (II) acetate dihydrate (1 mmol in 30 ml methanol), and triethylamine (1 ml) was added. A white precipitate was obtained after filtration. Yield: 36%. *Anal*. Calc. for $C_{16}H_{14}N_6OZn$: C, 51.70; H, 3.80; N, 22.61. Found: C, 51.64; H, 3.79; N, 23.70%. IR (cm^{-1}) 1539, 1529, 1308, 744, 640.

2.1.5. $Cd(L1)_2 \cdot 2H_2O$ (**2**)

Complex **2** was synthesized using the same method as for complex **1**. Yield: 39%. *Anal*. Calc. for $C_{16}H_{16}N_6O_2Cd$: C, 40.00; H, 3.69; N, 18.33. Found: C, 39.96; H, 3.64; N, 18.33%. IR (cm^{-1}) 1599, 1500, 1218, 784, 633.

2.1.6. $[Zn(HL1)_2]Cl_2$ (**3**)

A solution of 2-(2-pyridyl)imidazole (1.5 mmol) in methanol (20 ml) was heated to boiling and then mixed with a solution of $NaClO_4$ and $ZnCl_2 \cdot 2H_2O$ (1 mmol in 30 ml methanol). A white precipitate was obtained after filtration. Yield: 36%. *Anal*. Calc. for $C_{16}H_{14}N_6ZnCl_2$: C, 45.47; H, 3.31; N, 18.76. Found: C, 45.45; H, 3.29; N, 18.76%. IR (cm^{-1}) 1540, 1510, 1218, 765, 609.

2.1.7. $[Cd(HL1)_2]Cl_2$ (**4**)

Complex **4** was synthesized using the same method as for complex **3**. A white precipitate was obtained after

filtration. Yield: 38%. *Anal*. Calc. for $C_{16}H_{14}N_6$- $CdCl_2$: C, 40.58; H, 2.98; N, 17.74. Found: C, 40.54; H, 2.96; N, 17.73%. IR (cm^{-1}) 1560, 1489, 1268, 801, 703.

2.1.8. $Zn(L2)_2 \cdot H_2O$ (**5**)

A solution of 2-(2-pyridyl)benzimidazole (1.5 mmol) in methanol (20 ml) was heated to boiling, mixed with a solution of zinc (II) acetate dihydrate (1 mmol in 30 ml methanol) and then triethylamine (1 ml) was added. A white precipitate (yield 40%) was obtained after filtration, crystals of $Zn(L2)_2 \cdot H_2O$ were obtained by slow evaporation of a DMSO solution of the precipitate. Yield: 43%. *Anal*. Calc. for $C_{24}H_{18}N_6OZn$: C, 61.10; H, 3.84; N, 17.81. Found: C, 61.02; H, 3.69; N, 17.95%. IR (cm^{-1}) 1604, 1445, 1424, 796, 746.

2.1.9. $[Cd(L2)_2(H_2O)_2] \cdot 2DMSO$ (**6**)

The complex **6** was prepared in exactly the same way as for complex **5**. The crystals of $[Cd(L2)_2 \cdot (H_2O)_2] \cdot 2DMSO$ were obtained by slow evaporation of a DMSO solution. Yield: 39%. *Anal*. Calc. for $C_{28}H_{32}N_6O_4S_2Cd$: C, 48.55; H, 4.62; N, 12.13. Found: C, 48.13; H, 4.38; N, 12.02%. IR (cm^{-1}) 1599, 1500, 1418, 744, 643.

2.1.10. $[Zn(HL2)_2](ClO_4)_2$ (**7**)

A solution of 2-(2-pyridyl) benzimidazole (1.5 mmol) in methanol (20 ml) was heated to boiling and then mixed with a solution of $NaClO_4$ and $ZnCl_2 \cdot 2H_2O$ (1 mmol in 30 ml methanol). A white precipitate (yield 40%) was obtained after filtration. Yield: 33%. *Anal*. Calc. for $C_{24}H_{18}N_6O_8Cl_2Zn$, C, 44.03, H, 2.77, N, 12.84. Found: C, 44.15, H, 2.62, N, 12.65%.

2.1.11. $[Cd(HL2)_2](ClO_4)_2$ (**8**)

The complex **8** was prepared in exactly the same way as for complex **7**. Yield: 33%. *Anal*. Calc. for $C_{24}H_{18}N_6O_8Cl_2Cd$: C, 41.08, H, 2.56, N, 11.98. Found: C, 41.15, H, 2.63, N, 11.60%.

2.1.12. $Zn(HL3)_2$ (**9**)

Zinc(II) chloride dihydrate (5.5 mmol) was heated in glycerol (50 ml) under nitrogen for 1 h at 150 °C. To the resulting solution was added solid 2,6-bis(benzimidazol-2yl)pyridine (10 mmol) and triethylamine (3 ml), and then the mixture was heated for 5 h at 200 °C. After dilution of the resulting solution with water (100 ml), $NaClO_4$ (5.6 mmol) was added to give a precipitate, which was collected and recrystallized from methanol. Yield: 35%. *Anal*. Calc. for $C_{38}H_{24}N_{10}Zn$: C, 66.53; H, 3.53; N, 20.41. Found: C, 66.51; H, 3.52; N, 20.41%. IR (cm^{-1}) 1601, 1502, 1437, 744, 669.

2.1.13. $Cd(HL3)_2$ (**10**)

The complex **10** was prepared in exactly the same way as for complex **9**. Yield: 43%. *Anal*. Calc. for $C_{38}H_{24}N_{10}Cd$: C, 62.26; H, 3.30; N, 19.11. Found: C, 62.14; H, 3.49; N, 18.91%. IR (cm^{-1}) 1574, 1500, 1437, 744, 670.

2.2. Materials and physical measurements

All solvents and reagents were of commercially analytical grade and used without further purification. The starting materials were purchased from Aldrich and used without further purification. Infrared spectra were recorded from KBr plates in a MAGNA-560 spectrometer. Excitation and emission spectra were recorded on a Cary Eclipse fluorescence spectrophotometer. Elemental analyses were performed on a Perkin–Elmer 240c analyzer. Absorption spectra were recorded at 293 K using a Cary-Varian 500 Spectrophotometer in the 220–700 nm range.

2.3. X-ray crystallographic analyses

Crystals, which were obtained directly from solution, were suitable for X-ray diffraction study. Diffraction intensities for these complexes were collected on a Rigaku RAXIS–RAPID image plate diffractometer using the ω scan technique with Mo Kα radiation ($\lambda = 0.71073$ Å). Absorption corrections were applied using the multi-scan technique [22]. The structures were solved with the direct method of SHELXS-97 [23] and refined with full-matrix least-squares techniques using the SHELXL-97 program [24]. Non-hydrogen atoms were refined anisotropically. The hydrogen atoms on carbon atoms were generated geometrically, while the aqua hydrogen atoms were not located. An analytical expression of neutral-atom scattering factors was employed and anomalous dispersion correction incorporated [25]. The crystallographic data for complexes **5**, **6**, **9** and **10** are given in Table 1. Selected bond lengths and angles are given in Tables 2–5.

3. Results and discussion

3.1. Syntheses

3.1.1. Ligands

Our previous work has established that the deprotonated benzimidazole ligand is an efficient blue emitter when bonded to a central atom in a bridging mode [26]. Based on the inherent character of the benzimidazole group which allows easy derivation and potentially strong π–π stacking interactions to form supramolecular structures, we have now synthesized three derivatives of the imidazole ligand, the bidentate or tridentate ligands HL1, HL2 and H_2L3 (Scheme 1), with increasing extended conjugation.

Table 1
Experimental details for the single crystal structure determination in this study

	Complex **5**	Complex **6**	Complex **9**	Complex **10**
Empirical formula	$C_{24}H_{18}N_6OZn$	$C_{28}H_{32}CdN_6O_4S_2$	$C_{36}H_{27}ZnN_{10}$	$C_{38}H_{24}CdN_{10}$
Formula weight	471.81	693.12	665.04	733.07
Temperature (K)	193(2)	193(2)	293(2)	293(2)
Crystal system	monoclinic	monoclinic	monoclinic	monoclinic
Space group	$P2_1/c$	$P2_1/c$	Cc	Cc
a (Å)	12.569(6)	10.653(3)	14.146(3)	14.082(3)
b (Å)	12.954(4)	14.6551(3)	15.231(3)	15.231(3)
c (Å)	13.293(4)	18.856(4)	18.704(4)	18.726(4)
β (°)	102.919(1)	97.675(7)	112.1(3)	112.1(3)
V (Å^3)	2109.8(1)	2917.1(1)	3733.8(1)	3722.0(1)
Z	4	4	4	4
D_c (Mg m^{-3})	1.485	1.578	1.181	1.308
$F(000)$	968	1416	1368	1480
Reflections collected/unique	9148/4800	12922/6669	4292/3937	4279/3994
Goodness-of-fit on F^2	1.012	0.951	1.158	1.187
R_{int}	0.0433	0.0432	0.0350	0.0304
Final $R(I > 2(I))$ R_1[a], wR_2[b]	0.0951, 0.0516	0.0382, 0.0824	0.0564, 0.1882	0.0369, 0.1175

[a] $\sum\|F_o| - |F_c\|/\sum|F_o|$.
[b] $wR_2 = \sum[w(F_o^2 - F_c^2)^2]/\sum[w(F_o^2)^2]$.

Table 2
Selected bond lengths (Å) and angles (°) for complex **5**

Bond lengths (Å)	
Zn(1)–N(2)	1.993(2)
Zn(1)–N(5)	1.996(2)
Zn(1)–O(1)	2.025(2)
Zn(1)–N(1)	2.232(2)
Zn(1)–N(4)	2.242(2)
N(1)–C(1)	1.340(3)
Bond angles (°)	
N(2)–Zn(1)–N(5)	127.2(9)
N(2)–Zn(1)–O(1)	117.5(8)
N(5)–Zn(1)–O(1)	115.2(8)
O(1)–Zn(1)–N(1)	89.5(9)
N(1)–Zn(1)–N(4)	172.3(8)
N(5)–Zn(1)–N(4)	77.8(9)

Table 3
Selected bond lengths (Å) and angles (°) for complex **6**

Bond lengths (Å)	
Cd(1)–N(5)	2.256(4)
Cd(1)–N(2)	2.256(4)
Cd(1)–O(2)	2.311(3)
Cd(1)–O(1)	2.348(4)
Cd(1)–N(1)	2.388(4)
Cd(1)–N(4)	2.402(4)
Bond angles (°)	
N(5)–Cd(1)–N(2)	157.8(2)
O(2)–Cd(1)–N(1)	167.4(1)
O(2)–Cd(1)–O(1)	90.2(1)
O(1)–Cd(1)–N(1)	87.1(1)
O(1)–Cd(1)–N(4)	175.0(1)
N(2)–Cd(1)–O(1)	92.7(1)

Table 4
Selected bond lengths (Å) and angles (°) for complex **9**

Bond lengths (Å)	
Zn(1)–N(8)	2.294(8)
Zn(1)–N(3)	2.321(8)
Zn(1)–N(2)	2.329(9)
Zn(1)–N(6)	2.336(8)
Zn(1)–N(1)	2.343(8)
Zn(1)–N(7)	2.411(8)
Bond angles (°)	
N(1)–Zn(1)–N(7)	93.7(3)
N(2)–Zn(1)–N(7)	91.3(3)
N(3)–Zn(1)–N(7)	95.1(3)
N(6)–Zn(1)–N(1)	160.0(3)
N(8)–Zn(1)–N(2)	100.3(3)
N(3)–Zn(1)–N(6)	120.2(3)

Table 5
Selected bond lengths (Å) and angles (°) for complex **10**

Bond lengths (Å)	
Cd–N(9)	2.421(6)
Cd–N(5)	2.304(5)
Cd–N(8)	2.337(5)
Cd–N(3)	2.336(5)
Cd–N(1)	2.337(5)
Cd–N(6)	2.278(5)
Bond angles (°)	
N(1)–Cd–N(6)	99.6(2)
N(3)–Cd–N(6)	126.8(2)
N(9)–Cd–N(5)	92.1(2)
N(5)–Cd–N(8)	99.4(2)
N(9)–Cd–N(3)	93.9(2)
N(9)–Cd–N(1)	93.6(2)

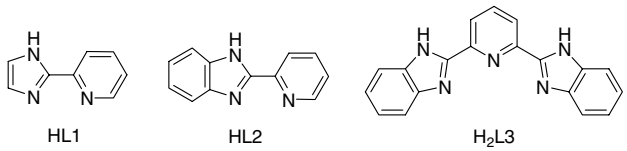

Scheme 1. Illustration of the three ligands.

3.1.2. Complexes

These complexes were synthesized by the reaction of the corresponding ligands (HL1, HL2, H_2L3) with the metal ion M^{2+} ($M^{2+} = Cd^{2+}$, Zn^{2+}). They are either neutral complexes or ionic ones due to deprotonation of HL1, HL2, H_2L3 (with additional triethylamine). We compared the properties of these complexes and found that the neutral complexes are more stable than the ionic complexes, especially as they have melting points greater than 240 °C, which is a highly desired property for the practical application in electroluminescent devices [27]. The crystal structures of **5**, **6**, **9** and **10** have been determined by X-ray diffraction.

3.2. Crystal structures of the complexes

3.2.1. $Zn(L2)_2 \cdot H_2O$ (**5**)

The structure of **5** can be best described as a square pyramid surrounded by O(1), N(1), N(2), N(4) and N(5). Two L1 ligands are chelated to the Zn(II) center (Fig. 1). The shortest bond is between Zn(II) and the negatively charged imidazole atom N(2), 1.993(2) Å, while the longest bond is 2.242(2) Å, between Zn(II) and the pyridine N atom. Zinc complexes with the bipyridine ligand commonly have Zn–N bond lengths ranging from 2.1 to 2.2 Å [28]. Five-coordinated Zn(II) complexes are quite common and many examples have been reported previously [27,28].

3.2.2. $[Cd(L2)_2(H_2O)_2] \cdot 2DMSO$ (**6**)

Each Cd(II) ion is six-coordinated by four nitrogen atoms from the two bidentate L2 anions and two water molecules. The coordination geometry of the Cd(II) ion can be described as a distorted octahedral (Fig. 2). The average Cd–O (water) distance of 2.329 Å is near to the values found in other Cd(II) complexes [29,30]. Cd–N (pyridine)distance of 2.395 Å is longer than the Cd–N (imidazole) distance (2.256 Å). Each deprotonated ligand L2 coordinates to one Cd(II) ion through its pyridine N atom and imidazole N atom. The $[Cd(L1)_2(H_2O)_2]$ molecules are linked through hydrogen bonds between water molecules and nitrogen atoms. All of the other bond distances and angles are similar to those found for the related rhenium (I) polypyridyl complexes [31].

3.2.3. $Zn(HL3)_2$ (**9**)

The molecular structure of **9** with the atom numbering is shown in Fig. 3. The structure contains one zinc atom and two $HL3^-$ anionic ligands. N(3) and N(8) are deprotonated with Zn(1)–N(3) 2.321(8) and Zn(1)–N(8) 2.294(8) Å, respectively. The corresponding protonated nitrogens, as expected, form marginally longer bonds with Zn(1)–N(2) 2.329(9) and Zn(1)–N(7) 2.411(8) Å. The coordination geometry shows considerable distortion from a regular octahedron as is evident from the bond

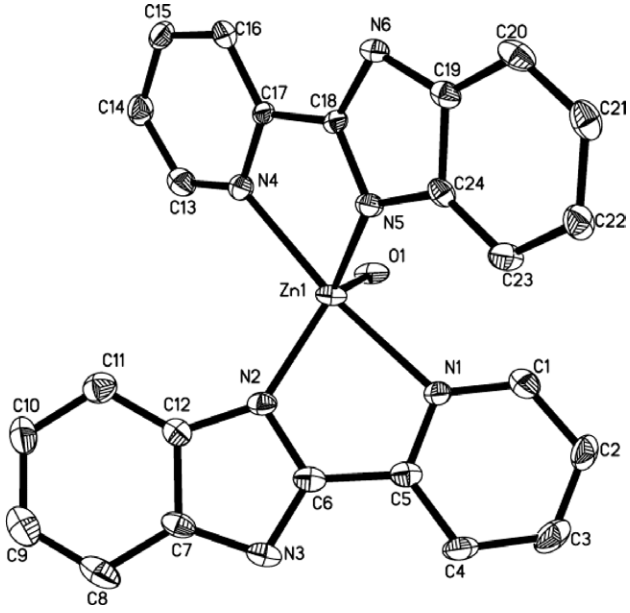

Fig. 1. The molecular structure of complex **5**. Thermal ellipsoids are plotted at the 30% probability level and the hydrogen atoms are omitted for simplicity.

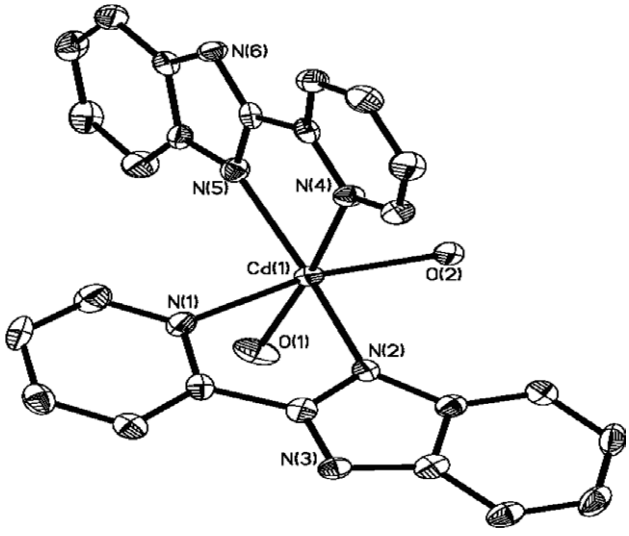

Fig. 2. The molecular structure of complex **6**. Thermal ellipsoids are plotted at the 30% probability level and the hydrogen atoms are omitted for simplicity.

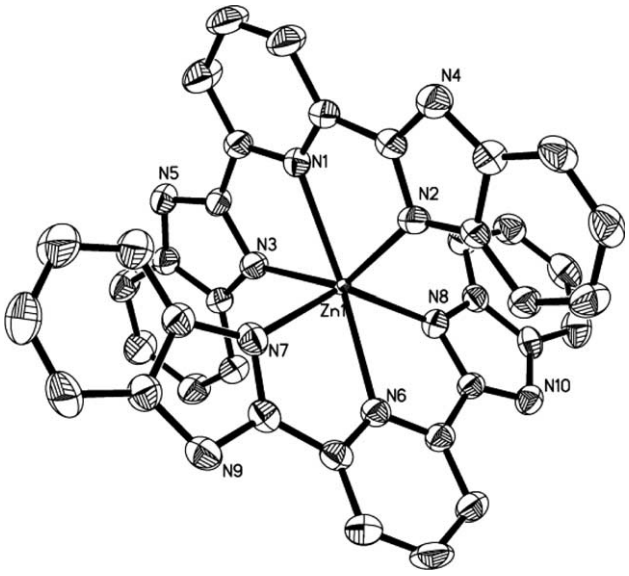

Fig. 3. The molecular structure of complex **9**. Thermal ellipsoids are plotted at the 30% probability level and the hydrogen atoms are omitted for simplicity.

angles around zinc: N(3)–Zn(1)–N(1) 70.30(3)° is considerably smaller than the ideal 90°. The molecular structure of **9** is similar to the Mn(II) complex [32].

3.2.4. $Cd(HL3)_2$ (*10*)

The molecular structure of **10** with the atom numbering is shown in Fig. 4. The structure of $Cd(HL3)_2$ is similar to that of $Zn(HL3)_2$ (**9**). N(4) and N(9) are deprotonated with Cd–N(4) 2.303(4) and Cd–N(9) 2.277(4) Å, respectively. The corresponding protonated nitrogens, as expected, form marginally longer bonds with Cd–N(1) 2.337(4) Å and Cd–N(6) 2.425(4) Å. The coordination geometry shows considerable distortion from a regular octahedron as is evident from the bond angles around cadmium: N(3)–Cd–N(1) 70.49(13)° is considerably smaller than the ideal 90°. The previously reported structure of $Cd(H_2L3)Cl_2$ can be best described as a distorted trigonal bipyramidal geometry. The ligand affords three N atoms to coordinate to Cd(II) and two chloride ions lie each side of the planar pyridine ring [33].

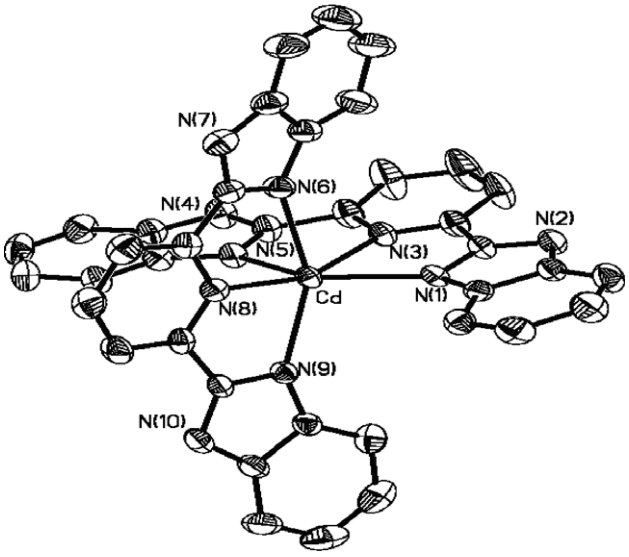

Fig. 4. The molecular structure of complex **10**. Thermal ellipsoids are plotted at the 30% probability level and the hydrogen atoms are omitted for simplicity.

3.3. Luminescent properties

Compounds HL1, HL2 and H_2L3 have a similar structures, however the bathochromic shifts of the emission energy of compound HL2 ($\lambda_{max} = 369$ nm), compared to that of HL1 ($\lambda_{max} = 363$ nm), is due to the extended conjugation through the phenyl units. In the same way the emission energy of compound H_2L3 ($\lambda_{max} = 407$ nm) exhibits more obvious bathochromic shifts. The emission energy of H_2L3 has 38 and 44 nm bathochromic shifts relative to that of HL1 and HL2, respectively. H_2L3 is much more π-conjugated than HL1 and HL2, which apparently decreases the π–π* energy gap, thus resulting in a bathochromic shift in emission wavelength.

Complexes with L1 emit a purple or blue color in the solid state and in solution. The dramatic bathochromic shift of the emission energy of complexes with HL1 in comparison to that of free HL1 can be attributed to the coordination of the central metal and the ligand HL1. The excitation and emission spectra for all the complexes **1**–**10** are showed in Fig. 5, and the excitation and emission data of the complexes in the solid state and DMSO are shown in Table S1 in ESI.

While each of the complexes gives a blue emission in the solid state and in solution. The emission energy for

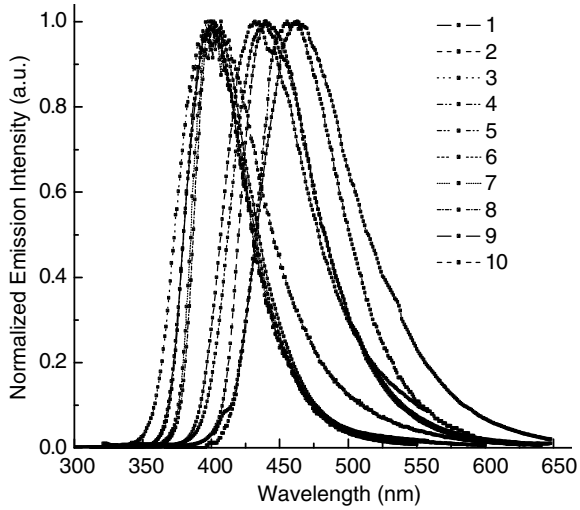

Fig. 5. Normalized solid PL spectra of the complexes **1**–**10**.

these complexes is similar despite the differences of the geometry and ligand environment of the complexes. This is not surprising because the blue luminescence of the complexes is believed to originate from a π*–π transition of the ligands. The luminescent curves of these complexes are in sharp contrast to that of the free ligands which have either no emission at all in the visible region or a weak emission. For complexes with HL1, **1** ($\lambda_{max} = 402$ nm) and **2** ($\lambda_{max} = 432$ nm) have a larger red shift in emission energy than the corresponding values for **3** ($\lambda_{max} = 398$ nm) and **4** ($\lambda_{max} = 400$ nm), because the deprotonation of the ligand decreases the π*–π gap. The same phenomena has been found for the complexes (**5**–**8**) with HL2. In comparison to the free HL2 ligand, a bathochromic shift for the complexes was observed. This bathochromic shift is undoubtedly due to the deprotonation of the ligand when forming the neutral complexes, which is consistent with the results of Wang's work in luminescent 7-azaindole complexes [34].

Complexes **9** and **10** exhibit blue-fluorescent emission in the solid state and in solution. As a result of the same reason, there are dramatic bathochromic shifts of the emission energies of the complexes in comparison to that of free H_2L3, which is consistent with the results of complexes **1**–**8**. The role of the central ion in complexes **1**, **2**, **5**, **6**, **9** and **10** is simply to stabililize the negatively charged ligand via the formation of coordination bonds. Their bidentate and tridentate complexes have the same luminescent properties. The emission properties of these complexes are attributed to the L–L (ligand–ligand) charge transfer, and the metal ions in the complexes play a key role in increasing the ligands' conformational rigidity, thereby reducing the non-radiative decay of the intraligand (π–π* transition) excited state. Similar to other complexes containing the benzimidazole group, the luminescence for the ligand is predominantly π–π* transition fluorescence [33,35].

In order to obtain blue luminescence, we have to make adjustments by chemical means to obtain the emission maximum (π-conjugation) according to the fact that the greater the conjugation is, the less the emission energy is, and the maximum emission shows a bathochromic shift. To understand the effect on the emission energy on going from the free ligand to the complex, we performed DFT calculations for the free ligand HL2 (2-(2-pyridyl)benzimidazole) and complex **6** at the DFT/B3LYP level using the SDD [36] basis set employing the GAUSSIAN 98 suite of programs [37]. The geometric parameters were taken from the X-ray diffraction crystal structural data for complex **6** and optimized employing B3LYP/6-31g(d) for HL2. The energies of the frontier molecular orbitals (FMOs) of the free ligand and complex **6** are ploted in Fig. 6. As one may see, the FMOs of complex **6** are significantly different from those of HL2; the highest occupied molecular orbital (HOMO) of HL2 is a π orbital with contributions from 2p orbitals of the carbon atoms in benzimidazole and pyridine rings, with the latter contributing less than the former. Analogously, the HOMO of complex **6** is also a π orbital, localized on the lone pair of non-coordinating nitrogen atoms (N(3), N(6)) and the carbon atom in the benzimidazole ring, owing to the low symmetry (C_1). Compared with the free ligand, the electronic density is more concentrated at the benzimidazole ring again. The nodal structure of the HOMO of the ligand, however, is not compatible with that of the complex. The energy of the HOMO level of the complex is much lower

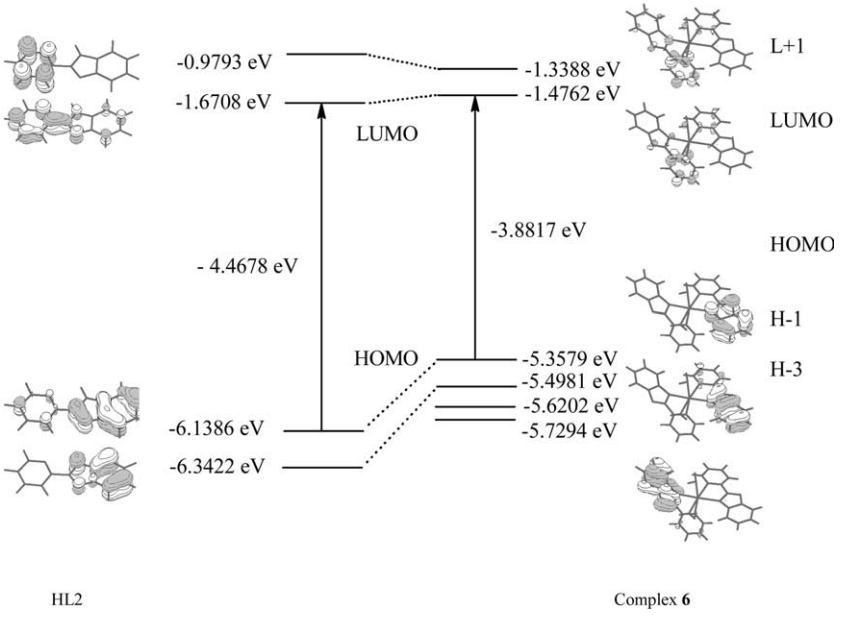

Fig. 6. Frontier molecular orbitals of HL2 and complex **6**.

than that of the free ligand. The lowest unoccupied molecular orbital (LUMO) of the free ligand is a π* orbital with contributions from both benzimidazole and pyridyl rings, while the LUMO of the complex is a π* orbital consisting of mostly atomic orbitals from one of the non-coordinated pyridyl rings. There are essentially few contributions from the benzimidazole ring in the LUMOs of the complex. The role of the Cd(II) ion is to stabilize the negatively charged ligand and decrease the π–π* energy gap, leading to a bathochromic shift in the transition energy from HL2 to $Cd(L2)_2$. The excitation energies were obtained at the density functional level by using the time-dependent perturbation theory approach (TDDFT) [38] with the adiabatic local density approximation, which have high reliability in obtaining accurate predictions for excitation energies and oscillator strengths. It was found that the absorption spectrum of the complex $Cd(L2)_2$ predicts an absorption maximum at 320.62 nm and therefore is in good agreement with the experimental values of 323 nm. The dominant contribution to this peak were assigned as ligand-to-ligand charge transfer (LLCT) which is associated with excitations from HOMO − 3 to LUMO + 1.

The quantum yields of **1**–**10** in solution were determined to be 0.17, 0.09, 0.06, 0.04, 0.59, 0.34, 0.28, 0.11, 0.25 and 0.26, respectively, relative to that of quinine sulfate (0.55) [39]. The quantum yields of complexes **1**, **2**, **5**, **6** are higher than those of the corresponding complexes **3**, **4**, **7**, **8** containing chloride anions, respectively. The quantum yields of complexes **6**, **7**, **9** and **10** are similar to those of the related compounds $(Me_2PyrPy)_2Zn$ (0.32) and $(^iPr_2PyrPy)_2Zn$ (0.31) [28]. Complex **5** shows the highest quantum field (0.59) among these complexes.

In compounds **5** and **6**, a water molecule is involved in the metal complex. In order to know the effect of the water molecule on luminescence, we measure their luminescence intensities. The results show that the intensity of the complexes with coordinated water is three times greater than that of complexes without water. Although there is a water molecule in the direct environment of the luminescent complex, the efficiency of the emission is relatively high [40]. In our paper, complex **5** and **6** have relatively high photoluminescent efficiencies. It has been reported that the coordination of a water molecule makes luminescence lifetimes fall and result in luminescence decay [41], but we think that the existence of water molecules may increase coplane and conformational rigidity in the molecule structure.

4. Conclusion

Three different ligands including imidazole, 2-(2′-pyridyl)imidazole (HL1), 2-(2′-pyridyl)benzimidazole (HL2) and 2,6-bis(benzimidazol-2yl)pyridine (H_2L3) have been designed and synthesized so as to increase the π-conjugation, based on the fact that a large π-conjugation of the ligand decreases the π–π* energy gap, and thus leads to a bathochromic shift in emissive spectra. At the same time complexes with these ligands, including Cd^{2+} and Zn^{2+}, have been obtained in the neutral or ionic state, and their absorption and fluorescent spectra have been studied. Also the photoluminescent efficiencies of the complexes have been determined. Among them, complex **5**, with HL2, has the most efficient PL property. We are applying the new complexes in an electroluminescent device and are further improving electroluminescent performances in our future work.

Acknowledgments

Authors acknowledge financial support from the National Natural Science Foundation of China (Project Nos. 20162005 and 20373009).

Appendix A. Supplementary data

Crystallographic data for the structural analyses have been deposited with the Cambridge Crystallographic Data Centre, CCDC Nos. 268938, 198727, 237768 and 237767 for **5**, **6**, **9** and **10**, respectively. These data can be obtained free of charge at www.ccdc.cam.ac.uk/conts/retrieving.html (or from the Cambridge Crystallographic Data Centre, 12 Union Road, Cambridge CB2 1EZ, UK; fax: (internat.) +44 1223/336 033; e-mail: deposit@ccdc.cam.ac.uk). Supplementary data associated with this article can be found, in the online version, at doi:10.1016/j.poly.2005.07.021.

References

[1] (a) C.W. Tang, S.A. VanSlyke, Appl. Phys. Lett. 51 (1987) 913;
(b) C.W. Tang, S.A. VanSlyk, C.H. Chen, J. Appl. Phys. 65 (1989) 361.
[2] (a) C. Adachi, T. Tsutsui, S. Saito, Appl. Phys. Lett. 56 (1990) 799;
(b) C. Adachi, T. Tsutsui, S. Saito, Appl. Phys. Lett. 57 (1990) 531;
(c) Y. Hamada, IEEE Trans. Electron. Dev. 44 (1997) 1208;
(d) S.A. VanSlyke, C.H. Chen, C.W. Tang, Appl. Phys. Lett. 69 (1996) 2160.
[3] (a) C.H. Chen, J. Shi, Coord. Chem. Rev. 171 (1998) 161;
(b) N.X. Hu, M. Esteghamatian, S. Xie, Z. Popovic, A.M. Hor, B. Ong, S. Wang, Adv. Mater. 11 (1999) 17;
(c) J.F. Wang, G.E. Jabbour, E.A. Mash, J. Anderson, Y. Zhang, P.A. Lee, N.R. Armstrong, N. Peryhambarian, B. Kippelen, Adv. Mater. 11 (1999) 1266.
[4] (a) C.H. Chen, J. Shi, C.W. Tang, Macromol. Symp. 125 (1997) 1;

(b) C. Hoskawa, H. Higashi, H. Nakamura, T. Kusumoto, Appl. Phys. Lett. 67 (1995) 3853;
(c) C.H. Chen, C.W. Tang, J. Shi, K.P. Klubek, Macromol. Symp. 125 (1997) 49;
(d) J. Kido, Y. Lizumi, Appl. Phys. Lett. 73 (1998) 2721;
(e) S.A. VanSlyke, C.H. Chen, C.W. Tang, Appl. Phys. Lett. 69 (1996) 2160;
(f) J. Shi, C.W. Tang, Appl. Phys. Lett. 70 (1997) 1665.

[5] (a) M.A. Baldo, D.F.O. Brien, Y. You, A. Shoustikov, S. Sibley, M.E. Thompson, S.R. Forrest, Nature 395 (1998) 151;
(b) P.E. Burrows, S.R. Forrest, T.X. Zhou, L. Michalski, Appl. Phys. Lett. 76 (2000) 2493;
(c) M.A. Baldo, M.E. Thompson, S.R. Forrest, Nature 403 (2000) 750;
(d) Q. Wu, Q. Esteghamatian, N.X. Hu, Z. Popovic, G. Enright, S.R. Breeze, S. Wang, Angew. Chem. 121 (1999) 9447;
(e) N.X. Hu, M. Esteghamatian, S. Xie, Z. Popovic, A.M. Hor, B. Ong, S. Wang, Adv. Mater. 11 (1999) 1460;
(f) T. Virgili, D.G. Lidzey, D.D.C. Bradley, Adv. Mater. 12 (2000) 58;
(g) V. Cleave, G. Yahioglu, P.L. Barny, R.H. Friend, N. Tessler, Adv. Mater. 11 (1999) 285;
(h) S. Capecchi, O. Renault, D.G. Moon, M. Halim, M. Etchells, P.J. Dobson, O.V. Salata, V. Christou, Adv. Mater. 12 (2000) 1591.

[6] (a) C.F. Lee, K.F. Chin, S.M. Peng, C.M. Che, J. Chem. Soc., Dalton Trans. (1993) 467;
(b) T.A. Hopkins, K. Meerholz, S. Shaheen, M.L. Anderson, A. Schmidt, B. Kippelen, A.B. Padias, H.K. Hall Jr., N. Peyghambarian, N.R. Armstrong, Chem. Mater. 8 (1996) 3;
(c) Q. Wu, J.A. Lavigne, Y. Tao, M. D'Iorio, S. Wang, Inorg. Chem. 39 (2000) 5248;
(d) H. Zhu, M. Ströbele, Z. Yu, Z. Wang, H.J. Meyer, X. You, Inorg. Chem. Commun. 4 (2001) 577;
(e) L.S. Sapochak, F.E. Benincasa, R.S. Schofield, J.L. Baker, K.K.C. Riccio, D. Fogarty, H. Kohlmann, K.F. Ferris, P.E. Burrows, J. Am. Chem. Soc. 124 (2002) 6119.

[7] (a) Y. Ma, H.Y. Chao, Y. Wu, S.T. Lee, W.Y. Yu, C.M. Che, Chem. Commun. (1998) 2491;
(b) K.Y. Ho, W.Y. Yu, K.K. Cheung, C.M. Che, Chem. Commun. (1998) 2101;
(c) W. Yang, H. Schmider, Q. Wu, Y.S. Zhang, S. Wang, Inorg. Chem. 39 (2000) 2397;
(d) S.F. Liu, Q. Wu, H.L. Schmider, H. Aziz, N.X. Hu, Z. Popović, S. Wang, J. Am. Chem. Soc. 122 (2000) 3671;
(e) C. Seward, J. Pang, S. Wang, Eur. J. Inorg. Chem. (2002) 1390.

[8] (a) M. Berggren, O. Inganas, G. Gustafsson, J. Rasmusson, M.R. Andersson, T. Hjertberg, O. Wennerstrom, Nature 372 (1994) 444;
(b) M. Aguiar, F.E. Karasz, L. Akcelrud, Macromolecules 28 (1995) 4598;
(c) S.J. Chung, J.I. Jin, K.K. Kim, Adv. Mater. 9 (1997) 551;
(d) T. Christ, A. Greiner, R.V. Sander, J. Stumpflen, H. Wendorff, Adv. Mater. 9 (1997) 219;
(e) S.E. Dottinger, M. Hohloch, J.L. Segura, E. Steinhuber, M. Hanack, A. Tompert, D. Oelkrug, Adv. Mater. 9 (1997) 233;
(f) E.M. Girotto, M.A. De Paoli, Adv. Mater. 10 (1998) 790;
(g) D.E. Biller, H. Baumgartel, Angew. Chem., Int. Ed. 37 (1998) 646.

[9] (a) R.G. Xiong, J.L. Zuo, X.Z. You, B.F. Abrahams, Z.P. Bai, C.M. Che, H.K. Fun, Chem. Commun. (2000) 2061;
(b) R.G. Xiong, J.L. Zuo, X.Z. You, H.K. Fun, S.S.S. Raj, Organometallics 19 (2000) 4183;
(c) H.K. Fun, S.S.S. Raj, R.G. Xiong, J.L. Zuo, Z. Yu, X.Z. You, J. Chem. Soc., Dalton Trans. (1998) 1915;
(d) J. Zhang, W. Lin, Z.F. Chen, R.G. Xiong, B.F. Abrahams, H.K. Fun, J. Chem. Soc., Dalton Trans. (2001) 1804;
(e) Z.F. Chen, R.G. Xiong, J. Zhang, X.T. Chen, Z.L. Xue, X.Z. You, Inorg. Chem. 40 (2001) 4075;
(f) R.X. Yuan, R.G. Xiong, Z.F. Chen, X.Z. You, S.M. Peng, G.H. Lee, Inorg. Chem. Commun. 4 (2001) 430.

[10] (a) D.M. Ciurtin, N.G. Pschirer, M.D. Smith, U.H.F. Bunzand, H.C. Zur Loye, Chem. Mater. 13 (2001) 2743;
(b) E. Fiscus, S. Shotwell, R.C. Layland, M.D. Smith, H.C. Zur Loye, U.H.F. Bunz, Chem. Commun. (2001) 2674;
(c) O. Teichert, W.S. Sheldrick, Z. Anorg. Allg. Chem. 625 (1999) 1860.

[11] J. Zhang, Y.R. Xie, Q. Ye, R.G. Xiong, Z.L. Xue, X.Z. You, Eur. J. Inorg. Chem. (2003) 2572.

[12] (a) R.B. Martin, H. Sigel (Eds.), Metal Ions in Biological Systems, vol. 9, Markker, New York, 1979, p. 1 (Chapter 1);
(b) L.D. Pettit, J.E. Gregor, H.R. Kozlowski, W. Hay, J.R. Dilworth, K.B. Nolan (Eds.), Perspectives in Bioinorganic Chemistry, vol. 1, JAI Press, London, 1991, p. 1.

[13] (a) V.G. Vaidyanathan, B.U. Nair, J. Inorg. Biochem. 91 (2002) 405;
(b) V.G. Vaidyanathan, B.U. Nair, J. Inorg. Biochem. 94 (2003) 121;
(c) V.G. Vaidyanathan, B.U. Nair, Eur. J. Inorg. Chem. (2003) 3633.

[14] (a) M. Leirer, G. Knör, A. Vogler, Inorg. Chim. Acta 288 (1999) 150;
(b) S.X. Wang, Y. Zhu, Y.X. Cui, L.F. Wang, Q.H. Luo, J. Chem. Soc., Dalton Trans. (1994) 2523;
(c) L. Huang, K.Z. Wang, C.H. Huang, F.Y. Li, Y.Y. Huang, J. Mater. Chem. 11 (2001) 790;
(d) M. Hasegawa, F. Renz, T. Hara, Y. Kikuchi, Y. Fukuda, J. Okubo, T. Hoshi, W. Linert, Chem. Phys. 277 (2002) 21.

[15] (a) M. Boca, R. Boca, G. Kickelbick, W. Linert, I. Svoboda, H. Fuess, Inorg. Chem. Acta 338 (2002) 36;
(b) M. Haga, H.G. Hong, Y. Shiozawa, Y. Kawata, H. Monjushiro, T. Fukuo, R. Arakawa, Inorg. Chem. 39 (2000) 4566;
(c) A.E. Ceniceros-Gómez, N. Barba-Behrens, M.E. Quiroz-Castro, S. Bernès, H. Nöth, S.E. Castillo-Blum, Polyhedron 19 (2000) 1821;
(d) H. Yi, J.A. Crayston, J.T.S. Irvine, J. Chem. Soc., Dalton Trans. (2003) 685.

[16] M.B. Klaus, C.Q. Catharina, Inorg. Chem. 42 (2003) 2742.

[17] X.F. He, C.M. Vogels, A. Decken, S.A. Westcott, Polyhedron 23 (2004) 155.

[18] D. Choquesillo-Lazarte, B. Covelo, J.M. González-Pérez, A. Castiñeiras, J. Niclós-Gutiérrez, Polyhedron 21 (2002) 1485.

[19] R. Bocaňa, M. Boca, L. Dlháň, K. Falk, H. Fuess, W. Haase, R. Jarošciak, B. Papánková, F. Renz, M. Vrbová, R. Werner, Inorg. Chem. 40 (2001) 3025.

[20] H.J. Wagner, R.O. Loutfy, C.K. Hsiao, J. Mater. Sci. 17 (1982) 2781.

[21] (a) A.W. Addison, P.J. Burke, J. Heterocycl. Chem. 18 (1981) 803;
(b) A. Tavman, B. Ülküseven, Synth. React. Inorg. Met.Org. Chem. 29 (1999) 1805.

[22] T. Higashi, Program for Absorption Correction, Rigaku Corporation, Tokyo, Japan, 1995.

[23] G.M. Sheldrick, SHELXS-97, Program for Automatic Solution of Crystal Structures, University of Goettingen, Germany, 1997.

[24] G.M. Sheldrick, SHELXL-97, Program for Crystal Structure Refinement, University of Goettingen, Germany, 1997.

[25] International Tables for X-ray Crystallography, vol. C, Kluwer Academic Publisher, Dordrecht, 1992.

[26] (a) S.M. Yue, Z.M. Su, J.F. Ma, H.J. Zhang, Z.H. Huang, R.S. Wang, in: International Conference on Science and Technology

of Synthetic Metals (ICSM'2002), vol. 216, Shanghai, China, 200;
(b) S.M. Yue, Z.M. Su, J.F. Ma, Y. Liao, Y.H. Kan, H.J. Zhang, Chin. J. Struct. Chem. (English) 22 (2003) 174.
[27] S.F. Liu, Q. Wu, H.L. Schmider, H. Aziz, N.X. Hu, Z. Popović, S. Wang, J. Am. Chem. Soc. 122 (2000) 3671.
[28] J.J. Klappa, S.A. Geers, S.J. Schmidtke, L.A. MacManus-Spencer, K. McNeill, J. Chem. Soc., Dalton Trans. (2004) 883.
[29] A. Wojciechowska, Z. Staszak, W. Bronowska, A. Pietraszko, M. Cieslak-Golonka, Polyhedron 20 (2001) 2063.
[30] (a) T.C. Ramalho, J.D. Figueroa-Villar, J. Mol. Struct. (Theochem.) 580 (2002) 217;
(b) A.S.G. Mohamed, A.M. Franz, K.H. Afaf, A.M.A. Morsy, G. Christian, M.A.B. Ahmed, Polyhedron 22 (2003) 975.
[31] T. Rajendran, B. Manimaran, F.Y. Lee, G.H. Lee, S.M. Peng, C.M. Wang, K.L. Lu, Inorg. Chem. 39 (2000) 2016.
[32] R. Rajan, R. Rajaram, B.U. Nair, T. Ramasami, S.K. Mandal, J. Chem. Soc., Dalton Trans. (1996) 2019.
[33] S.G. Liu, J.L. Zuo, Y.Z. Li, X.Z. You, J. Mol. Struct. 705 (2004) 153.
[34] (a) W. Liu, A. Hassan, S. Wang, Organometallics 16 (1997) 4257;
(b) J. Ashenhurst, G. Wu, S. Wang, J. Am. Chem. Soc. 122 (2000) 2541.
[35] S.F. Liu, C. Seward, H. Aziz, N.X. Hu, Z. Popovic, S. Wang, Organometallics 19 (2000) 5709.
[36] (a) T. Leininger, A. Nicklass, H. Stoll, M. Dolg, P. Schwerdtfeger, J. Chem. Phys. 105 (1996) 1052;
(b) M. Nicklass, H. Dolg, H. Stoll, H. Preuss, J. Chem. Phys. 102 (1995) 8942;
(c) W. Kuechle, M. Dolg, H. Stoll, H. Preuss, J. Chem. Phys. 100 (1994) 7535.
[37] M.J. Frisch, G.W. Trucks, H.B. Schlegel, GAUSSIAN 98 Revision A.9, Gaussian, Inc., Pittsburgh PA, 1998.
[38] (a) R. Bauernschmitt, R. Ahlrichs, Chem. Phys. Lett. 256 (1996) 454;
(b) R. Bauernschmitt, R. Ahlrichs, J. Chem. Phys. 104 (1996) 9047;
(c) R. Bauernschmitt, M. Häser, O. Treutler, R. Ahlrichs, Chem. Phys. Lett. 264 (1997) 573.
[39] S.R. Meech, D. Phillips, J. Photochem. 23 (1983) 193.
[40] L. Thompson, J. Lwgendziewicz, J. Cybinska, P. Li, W. Bremmessel, J. Alloys Compos. 341 (2002) 312.
[41] X.P. Yang, C.Y. Su, B.S. Kang, X.L. Feng, W.L. Xiao, H.Q. Liu, J. Chem. Soc., Dalton Trans. (2000) 3253.

Available online at www.sciencedirect.com
SCIENCE DIRECT®
Polyhedron 25 (2006) 645–653
POLYHEDRON
www.elsevier.com/locate/poly

Architectures in two crystalline homo and hetero two-dimensional polymers of the type $[Cd_3(tren)_2(NCS)_6]_n$ and $[Ni_2Cd(tren)_2(NCS)_6]_n$ [tren = Tris(2-aminoethyl)amine] through molecular ion bridges

Doyel Bose [a], Sk Hafijur Rahaman [a], Rajarshi Ghosh [a], Golam Mostafa [b], Joan Ribas [c], Chen-Hsiung Hung [d], Barindra K. Ghosh [a,*]

[a] *Department of Chemistry, The University of Burdwan, Golapbag, Burdwan 713104, India*
[b] *Department of Physics, Jadavpur University, Kolkata 700 032, India*
[c] *Departament de Quimica Inorginica, Universitat de Barcelona, Diagonal 647 08028 Barcelona, Spain*
[d] *Department of Chemistry, National Changhua University of Education, Changhua, Taiwan, ROC*

Received 15 March 2005; accepted 5 July 2005
Available online 6 September 2005

Abstract

Cadmium(II) nitrate tetrahydrate – a metal ion template, tris(2-aminoethyl)amine (tren) – a tripodal amine and thiocyanate – a versatile intermediatary in a 3:2:6 mole ratio in water afford a homopolymer, $[Cd_3(tren)_2(NCS)_6]_n$ (**1**). Replacement of two equivalents of cadmium(II) salt by two equivalents of nickel(II) nitrate hexahydrate results in the heteropolymer, $[Ni_2Cd(tren)_2(NCS)_6]_n$ (**2**). Compound **1** crystallizes in the monoclinic $C2/c$ space group with $a = 20.3480(17)$ Å, $b = 10.8796(9)$ Å, $c = 16.3495(10)$ Å, $\beta = 110.009(7)°$ and $Z = 4$; **2** crystallizes in the same space group as in **1** with $a = 19.584(5)$ Å, $b = 11.034(3)$ Å, $c = 15.760(4)$ Å, $\beta = 100.712(4)°$ and $Z = 4$. **1** and **2** are new examples of homo- and hetero-polymers with the multiconnecting molecular ion bridge $[Cd(NCS)_6]^{4-}$ in different geometric configurations. The single crystal X-ray structures of both neutral polymers consist of infinite two-dimensional sheets with two alternating environmentally different octahedral metal ion [M(II) = Ni(II)/Cd(II)] coordination spheres connected by four 1,3-thiocyanato bridging *cis*-/*trans*-$[Cd(NCS)_2(SCN)_4]^{4-}$. The Cd(1) centres in **1** and **2** with the CdN_2S_4 chromophore are surrounded by four S atoms of the bridging thiocyanate and two terminal N atoms of the pseudohalide, while the CdN_6 chromophore of Cd(2) in **1** and NiN_6 chromophore of Ni(1) in **2** are completed by four tren N atoms and two N atoms of the bridging NCS^- in *cis* alignment. In **1**, the three tripodal amine N atoms and two bridging S atoms are engaged in strong intermolecular hydrogen bondings, which is responsible for the conformation and stability of the supramolecular network. The absence of such hydrogen bonding in **2** is due to a difference in the orientation of the tripodal amine from that in **1** in the polymeric net. The magnetic property of **2** has been investigated over the 2–300 K temperature range. The feature is characteristic of a Curie law for a typical magnetically isolated nickel(II) ion with very weak antiferromagnetic interactions ($J < 0.01$ cm^{-1}). The presence of a diamagnetic molecular ion with two 1,3-thiocyanate bridges may be one of the major reasons to hinder effective coupling of the paramagnetic centres.
© 2005 Elsevier Ltd. All rights reserved.

Keywords: Cadmium(II); Nickel(II); Tripodal amine; Polymers; Supramolecules

* Corresponding author. Tel.: +913422558545; fax: +913422530452.
E-mail address: barin_1@yahoo.co.uk (B.K. Ghosh).

0277-5387/$ - see front matter © 2005 Elsevier Ltd. All rights reserved.
doi:10.1016/j.poly.2005.07.041

1. Introduction

A vast majority of current work centres around the use of molecular components to prepare inorganic-organic hybrid [1,2] functional materials [3–9] of different shapes and sizes [10] through control and manipulation of covalent bonds [11,12] with malleable coordination spheres and multiple lateral non-covalent forces [13–19] like hydrogen bonding, C–H...π and π...π interactions. One of the popular approaches in the synthetic strategy to the construction of these materials has been the use of two complementary building blocks like cyanometallates $[M(CN)_n]^{z-}$ ($M = V^{II}$, Cr^{III}, Mn^{III} and Fe^{III}, $n = 6$, $z = 4$ or 3; $M = Ni^{II}$, $n = 4$, $z = 2$; $M = Mo^{V}$, $n = 8$, $z = 3$) as bridging units in combination with other metal templates containing potential coordination site(s) [20–33]. Hexacyanometallates [20–29] with potential donor sites are used extensively as multiple bridging units and polyamine or Schiff base transition metal complexes, as complementary units with potential acceptor site(s). A sizeable number of one-dimensional (1D), two-dimensional (2D) and three-dimensional (3D) extended arrays of homo- and hetero-polymers have been characterized with novel structures and physicochemical [34,35] properties. To the best of our knowledge no such report is found with other hexapseudohalogenometallates like $[M(X)_6]^{n-}$ ($X^- = N_3^-$, NCS^-, NCO^- and $NCSe^-$). We are interested in extending this view to a molecular ion, $[Cd(NCS)_6]^{4-}$, as a bridging unit with other transition/non-transition metal templates containing controlled vacant coordination site(s) to prepare multidimensional homo- and heterometallic coordination polymers and polymer-based superstructures [36,37]. Diamagnetic cadmium(II) is chosen for its d^{10} configuration, permitting a wide variety of geometries and coordination numbers [38–40]. The ambidenticism of the thiocyanate ligand [41,42], with a hard nitrogen and a soft sulfur donor centre, tends to form homo- and hetero-polymeric chains with both hard and soft transition and non-transition metal ions. The tripodal amine [28,43] tris(2-aminoethyl)amine (tren), with its four nitrogen centres may be used as a blocker to control the dimensionalities and architectures of polymers and superstructures. The in situ preparation of the $[Cd(NCS)_6]^{4-}$ unit may have dynamic Cd(II) and NCS^- linkages of the type $[Cd(NCS)_{6-n}(SCN)_n]^{4-}$ ($n = 0$–6) in solution which in the presence of varied complementary units may result in different coordination matrices like $[Cd(NCS)_6]^{4-}$, $[Cd(NCS)_5(SCN)]^{4-}$, *cis*-/*trans*-$[Cd(NCS)_4(SCN)_2]^{4-}$, *fac*-/*mer*-$[Cd(NCS)_3(SCN)_3]^{4-}$, *cis*-/*trans*-$[Cd(NCS)_2(SCN)_4]^{4-}$, $[Cd(NCS)(SCN)_5]^{4-}$ and $[Cd(SCN)_6]^{4-}$. The present work stems from our interest to isolate polymeric complexes with the use of this molecular ion in combination with different complementary units having variable potential vacant site(s). Successfully we have synthesized and X-ray structurally characterized a homonuclear polymer of the type $[Cd_3(tren)_2(NCS)_6]_n$ (**1**) and a heteronuclear analogue of the type $[Ni_2Cd(tren)_2(NCS)_6]_n$ (**2**), where respectively *cis*-$[Cd(NCS)_2(SCN)_4]^{4-}$ and *trans*-$[Cd(NCS)_2(SCN)_4]^{4-}$ geometries are engaged in propagating the 1,3-thiocyanato bridges among the environmentally different metal ions. The presence of strong interchain N–H...S hydrogen bondings in **1** leads to the formation of a polymer based superstructure whereas such non-covalent forces are absent in **2** arising from the difference in the orientation of the tripodal amine in the lattice. The details of the synthesis, spectroscopic, magnetic and some physicochemical properties of these complexes are described below.

2. Experimental

2.1. Materials

Cadmium nitrate tetrahydrate (E. Merck, India), nickel nitrate hexahydrate (E. Merck, India), tris(2-aminoethyl)amine (tren) (Lancaster, UK) and ammonium thiocyanate (E. Merck, India) were purchased from the respective concerns and used as received. All other chemicals and solvents for preparative and spectroscopic work were of reagent grade and were used as received.

2.2. Physical measurements

IR spectra (KBr discs, 4000–200 cm^{-1}) were recorded on a Jasco FTIR model 420 spectrophotometer. Microanalyses (C, H and N) were done with a Perkin–Elmer 2400 CHNS/O elemental analyzer. The diffuse reflectance spectrum was run at room temperature on a Jasco UV–Vis–NIR V-570 spectrophotometer in the 200–1000 nm range. Magnetic measurements on powdered samples were performed in the temperature range 2–300 K using a Quantum Design MPMS-7 SQUID magnetometer in a magnetic field of 0.1 T. The experimental susceptibilities were corrected for the diamagnetism of the constituent atoms (Pascal tables).

2.3. Preparation of the complexes

2.3.1. $[Cd_3(tren)_2(NCS)_6]_n$ (1)

An aqueous solution (5 cm^3) of NH_4NCS (0.456 g, 6 mmol) was added dropwise to $Cd(NO_3)_2\cdot 4H_2O$ (0.308 g, 1 mmol) in the same solvent (5 cm^3) in a container. A solution (5 cm^3) of $Cd(NO_3)_2\cdot 4H_2O$ (0.616 g, 2 mmol) in water was added to an aqueous (5 cm^3) solution of tren (0.252 g, 2 mmol). These two solutions were mixed slowly to result in a colourless solution which was filtered through a fine glass frit. Well-formed faint yellow single crystals of **1** appeared on allowing the

resulting solution to evaporate slowly at room temperature. Yield: 0.024 g (75%) based on cadmium. *Anal.* Calc. for $C_{18}H_{36}N_{14}S_6Cd_3$ (978.26) (**1**): C, 27.92; H, 3.04; N 30.21. Found: C, 27.77; H, 3.07; N, 30.43%. IR (KBr)/cm^{-1}: ν(CN) 2108, 2089, 2068; ν(N–H) 3327, 3275. Λ_M (DMF, ohm^{-1} cm^2 mol^{-1}): 5. UV–Vis (λ, nm): 275.

2.3.2. $[Ni_2Cd(tren)_2(NCS)_6]_n$ (2)

This is prepared similarly as in **1**. To a solution (10 cm^3) of NH_4NCS (0.456 g, 6 mmol) and $Cd(NO_3)_2\cdot 4H_2O$ (0.308 g, 1 mmol), a mixture of $Ni(NO_3)_2\cdot 6H_2O$ (0.594 g, 2 mmol) and tren (0.252 g, 2 mmol) in water (10 cm^3) was added dropwise. The final blue violet solution was filtered through a fine glass frit. Violet single crystals of **2** were isolated on evaporation of this solution at room temperature. Yield: 0.027 g (75%) based on cadmium. *Anal.* Calc. for $C_{18}H_{36}N_{14}S_6Ni_2Cd$ (870.79) (**2**): C, 24.92; H, 3.01; N, 32.21. Found: C, 24.77; H, 3.00; N, 32.49%. IR (KBr)/cm^{-1}: ν(CN) 2138, 2121, 2066; ν(N–H), 3329, 3278. Λ_M (DMF, ohm^{-1} cm^2 mol^{-1}): 8. UV–Vis (λ, nm): 359, 563, 890.

2.4. X-ray crystallographic study

Suitable single crystals of the title complexes **1** and **2** for X-ray analyses were mounted on diffractometers equipped with a graphite monochromated Mo Kα(λ = 0.71073 Å) radiation source. The intensity data were corrected for Lorentz and polarization effects and an empirical absorption correction was also employed using the SAINT program [44]. A summary of the crystallographic data and structure refinement parameters is given in Table 1. The structure was solved by the Patterson method using SHELXS-97 [45] followed by Fourier and difference Fourier synthesis. Full-matrix least-squares refinements on F^2 were carried out using SHELXL-97 [46] with anisotropic displacement parameters for all non-hydrogen atoms. The hydrogen atoms were fixed geometrically and refined using a riding model. In the final difference Fourier map the residual maxima and minima were 0.516 and −1.197 (**1**) and −0.425 and 5.096 (**2**) e Å^{-3}. The maximum residual density 5.096 e Å^{-3} of **2** is 1.114 Å away from Ni1 and so it is not possible for any other type of heavy atom or molecule to be present there and this does not create any problem in structure solution. All calculations were carried out using SHELXL-97, ORTEP-3 [47] and PLATON-99 [48] programs.

3. Results and discussion

3.1. Synthesis and formulation

Homonuclear $[Cd_3(tren)_2(NCS)_6]_n$ (**1**) and heteronuclear $[Ni_2Cd(tren)_2(NCS)_6]_n$ (**2**) polymers were synthesized by the reaction of $[M(tren)(S)_2]^{2+}$ (M = Cd in **1**, Ni in **2**; S = H_2O) with $[Cd(NCS)_{6-n}(SCN)_n]^{4-}$ (n = 0–6) at room temperature (298 K). The molecular ion, $[Cd(NCS)_{6-n}(SCN)_n]^{4-}$, was generated in solution by the addition of six moles of ammonium thiocyanate to

Table 1
Summary of the crystal data and details of the structure determination for **1** and **2**

Compounds	**1**	**2**
Chemical formula	$C_{18}H_{36}N_{14}S_6Cd_3$	$C_{18}H_{36}N_{14}S_6CdNi_2$
Formula weight	978.16	870.9
T (K)	293(2)	293(2)
Radiation (Å)	0.71073	0.71073
Crystal system	monoclinic	monoclinic
Space group	$C2/c$	$C2/c$
a (Å)	20.3480(17)	19.584(5)
b (Å)	10.8796(9)	11.034(3)
c (Å)	16.3495(12)	15.760(4)
α (°)	90	90
β (°)	110.009(7)	100.712(4)
γ (°)	90	90
V (Å^3)	3400.9(5)	3346.5(13)
Z	4	4
D_c (g cm^{-3})	1.910	1.728
μ (mm^{-1})	2.262	2.153
F(000)	1928	1768
Crystal size (mm)	0.19 × 0.22 × 0.25	0.46 × 0.25 × 0.22
Reflections collected	3688	9890
Independent reflections	3447	3791
Final R indices [$I > 2\sigma(I)$]	$R_1 = 0.0251$, $wR_2 = 0.0668$	$R_1 = 0.0604$, $wR_2 = 0.1417$
R indices (all data)	$R_1 = 0.033$, $wR_2 = 0.0684$	$R_1 = 0.0841$, $wR_2 = 0.1495$
Largest peak and hole (e Å^{-3})	0.516 and −1.197	−0.425 and 5.096

one mole of cadmium(II) nitrate tetrahydrate in water. The complementary units $[Cd(tren)(S)_2]^{2+}$ and $[Ni(tren)(S)_2]^{2+}$ were prepared by dropwise addition of two moles of tren to a two molar cadmium(II) nitrate tetrahydrate solution in water and another two moles of tren to a two molar nickel(II) nitrate hexahydrate in separate containers. **1/2** resulted through union of *cis*-$[Cd(NCS)_2(SCN)_4]^{4-}$/*trans*-$[Cd(NCS)_2(SCN)_4]^{4-}$ and *cis*-$[Cd(tren)(S)_2]^{2+}$/*cis*-$[Ni(tren)(S)_2]^{2+}$ in a 1:2 ratio of these building blocks. The details of the sequential reactions are summarized in Scheme 1.

The principle involved is the union of two complementary units viz. $[Cd(NCS)_{6-n}(SCN)_n]^{4-}$, a molecular ion with multiconnectors behaving as potential donors and the $[M(tren)(OH_2)_2]^{2+}$, disolvento species with two labile reaction sites acting as potential acceptors. Use of the tetradentate tripodal amine, tren in $[M(tren)(OH_2)_2]^{2+}$ in conjunction with cadmium(II) or nickel(II) generates hexacoordinated metal cores facilitating polymers. The displacement of the weakly bound solvent molecules from the solvento complexes in $[M(tren)(OH_2)_2]^{2+}$ by the putative pseudohalide bridging unit in $[Cd(NCS)_{6-n}(SCN)_n]^{4-}$ triggers such multinuclear homomer and heteromer formation. The mole ratios are adjusted so as to have neutral homo- and heteropolymers, avoiding counter ions which might inter alia disrupt the solid state packing due to additional cation–anion interactions that would be difficult to control [49].

The preparation of homonuclear **1** and heteronuclear **2** were also achieved in good yield by single-pot [50,51] reactions using stoichiometric amounts [3:2:6 molar ratio of $Cd(NO_3)_2\cdot 4H_2O$, tren and NH_4NCS for **1** and 1:2:2:6 molar ratio of $Cd(NO_3)_2\cdot 4H_2O$, $Ni(NO_3)_2\cdot 6H_2O$, tren and NH_4NCS for **2**] of the individual metal ion template, organic blocker and the pseudohalide bridge/terminal. It is worth noting that an aqueous solution of a 1:2:2:6 molar ratio of $Ni(NO_3)_2\cdot 6H_2O$, $Cd(NO_3)_2\cdot 4H_2O$, tren and NH_4NCS to generate complementary units, $[Ni(NCS)_6]^{4-}$ and $[Cd(tren)(OH_2)_2]^{2+}$ and thereby to isolate a heteropolymer of the type $[Ni_2Cd(tren)_2(NCS)_6]_n$ also resulted in **2** in low yield, reflecting its special stability. This shows that molecular scrambling occurs and the result is the formation of $[Ni(tren)(OH_2)_2]^{2+}$ and $[Cd(NCS)_6]^{4-}$, which accounts for the low yield of **2**.

The complexes were characterized using microanalytical, spectroscopic, magnetic and some physicochemical properties. They are stable over long periods of time in powdery or crystalline states and are insoluble in water and other common organic solvents. However they are soluble in warm dimethylformamide and dimethylsulfoxide. In dimethylformamide they behave as non-electrolytes as evident from their low conductivity values [52]. In IR spectra three well resolved ν_{CN} bands (at 2108, 2089, 2068 cm^{-1} in **1** and at 2138, 2121, 2066 cm^{-1} in **2**) are observed indicating the existence of different force constants of the thiocyanato groups [53] in the crystal lattice. The band corresponding to the ν_{CS} stretching frequency appears at 765 cm^{-1} in **1** and 759 cm^{-1} in **2**. Bands belonging to the deformation frequency δ_{NCS} are found as doublets (at 468, 472 cm^{-1} for **1** and 450, 465 cm^{-1} for **2**). The ν_{NH} stretching frequency of the NH_2 group is observable at 3327 and 3275 cm^{-1} in **1** and at 3329 and 3278 cm^{-1} in **2**. Several weak bands in the range 2980–2807 cm^{-1} assignable to the aliphatic C–H stretching vibration are routinely observed.

The electronic spectrum of **2** in the solid state (Nujol mull) as well as in DMF solution show bands at λ_{max} values of 563 and 359 nm, assignable to spin allowed transitions $^3T_{1g} \leftarrow {}^3A_{2g}$ and $^3T_{1g}(P) \leftarrow {}^3A_{2g}$ respectively, typical of octahedral nickel(II). The close similarity in d–d maxima reflects similar gross structure and electronic structure in the solid state and in solution. The shoulder at around 890 nm originates from the spin-forbidden $^1E_g \leftarrow {}^3A_{2g}$ transition, frequently observed in Ni(II) octahedral complexes [54]. **1** exhibits a strong band at 275 nm presumably [55] belonging to a ligand based charge transfer.

$$n\,Cd(NO_3)_2.4H_2O + 6n\,NH_4NCS \longrightarrow n\,(NH_4)_4[Cd(NCS)_6] + 2n\,NH_4NO_3 + 4n\,H_2O \quad \ldots (1)$$

$$2n\,Cd(NO_3)_2.4H_2O + 2n\,tren \longrightarrow 2n\,[Cd(tren)(OH_2)_2](NO_3)_2 + 4n\,H_2O \quad \ldots (2)$$

$$2n\,Ni(NO_3)_2.6H_2O + 2n\,tren \longrightarrow 2n\,[Ni(tren)(OH_2)_2](NO_3)_2 + 8n\,H_2O \quad \ldots (3)$$

$$n\,(NH_4)_4[Cd(NCS)_6] + 2n\,[Cd(tren)(OH_2)_2](NO_3)_2 \longrightarrow [Cd_3(tren)_2(NCS)_6]_n + 4n\,NH_4NO_3 + 4n\,H_2O \quad \ldots (4)$$

$$n\,(NH_4)_4[Cd(NCS)_6] + 2n\,[Ni(tren)(OH_2)_2](NO_3)_2 \longrightarrow [Ni_2Cd(tren)_2(NCS)_6]_n + 4n\,NH_4NO_3 + 4n\,H_2O \quad \ldots (5)$$

Scheme 1.

3.2. Structure description

3.2.1. $[Cd_3(tren)_2(NCS)_6]_n$ (1)

X-ray crystallography was performed for the exact definition of the coordination sphere as well as the long range structure. A perspective view of the asymmetric unit with the atom numbering scheme of **1** is shown in Fig. 1. The polymeric network of the complex with alternating CdN_6 and CdN_2S_4 chromophores are shown in Fig. 2 and its projection onto the *b*-axis with hydrogen bonding is shown in Fig. 3. Selected bond lengths and angles with their estimated standard deviations are listed in Table 2.

In the structure, each *cis*-$[Cd(NCS)_2(SCN)_4]^{4-}$ is connected to four $[Cd(tren)]^{2+}$ units through 1,3-thiocyanate bridges in the *ab*-plane, leading to a two-dimensional (2D) sheet with two alternating environmentally different octahedral cadmium(II) coordination spheres. The geometry around the 4d ion, Cd(1), is a distorted octahedron with a relatively soft *cis*-CdN_2S_4 matrix produced from four S atoms of four different bridging NCS^- ligands and two N atoms of the two terminal pseudohalides. Cd(2) of $[Cd(tren)]^{2+}$ is also in a distorted octahedral environment with a hard CdN_6 chromophore produced through attachment of four N atoms of the tripodal amine and two N atoms of two bridging NCS ligands in a *cis* alignment (Fig. 1). The sequence in one branch is represented as –Cd(1)–S(1)–C(1)–N(1)–Cd(2)–N(2*)–C(2*)–S(2*)–Cd(1*)– (Fig. 2).

The equatorial plane of Cd(1) consists of three of the four sulfur atoms [S(1*), S(2), S(2*); * indicates a symmetry operation $-x$, y, $1/2 - z$] of the bridging thiocyanates and one (N3*) of the two terminal pseudohalide nitrogens. Axial positions are occupied by S(1) and N(3). Cd(1)–S bond lengths lie within the range 2.6666(7)–2.8819(8) Å whereas Cd(1)–N bond lengths

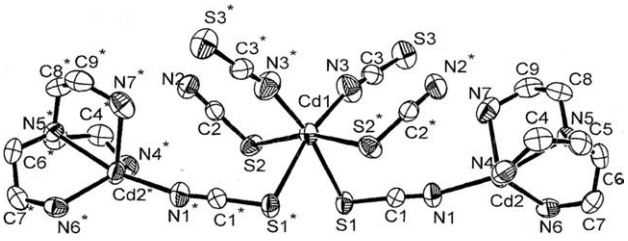

Fig. 1. ORTEP diagram of **1** with the atom numbering scheme. Symmetry code: * $-x$, y, $1/2 - z$.

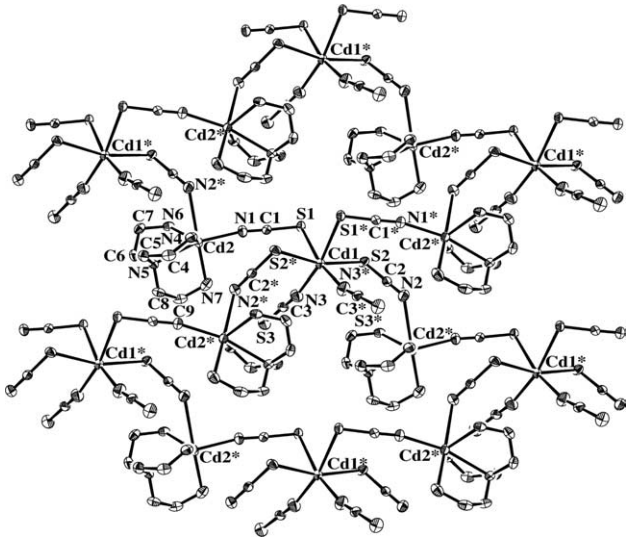

Fig. 2. Perspective view of the 2D sheet in **1**. Symmetry code: * $-x$, y, $1/2 - z$.

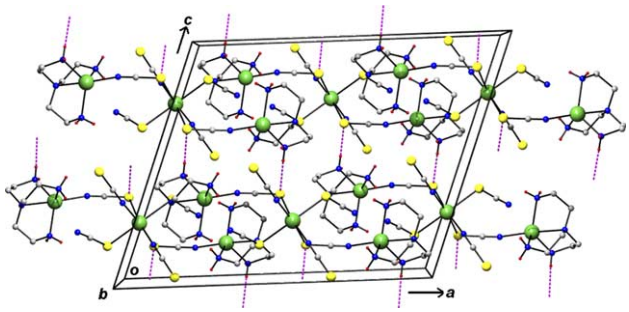

Fig. 3. Projection onto the *b*-axis of **1** showing stacking of sheets approximately perpendicular to the *c*-axis. Intermolecular N–H...S interactions are indicated by dotted lines.

Table 2
Selected bond distances (Å) and angles (°) for **1**

Bond distances	
Cd(1)–S(1)	2.8819(8)
Cd(1)–S(2)	2.6666(7)
Cd(1)–N(3)	2.242(3)
Cd(1)–N(1)	2.226(3)
Cd(2)–N(4)	2.291(3)
Cd(2)–N(5)	2.441(2)
Cd(2)–N(6)	2.267(2)
Cd(2)–N(7)	2.321(3)
Bond angles	
S(1)–Cd(1)–S(2)	78.40(2)
S(1)–Cd(1)–N(3)	92.09(10)
S(1)–Cd(1)–S(1*)	78.55(3)
S(1)–Cd(1)–S(2*)	88.57(2)
S(1)–Cd(1)–N(3*)	168.35(9)
S(2)–Cd(1)–N(3)	96.39(8)
S(2)–Cd(1)–S(2*)	163.21(3)
S(2*)–Cd(1)–N(3)	94.60(8)
N(1)–Cd(2)–N(5)	165.44(10)
N(6)–Cd(2)–N(7)	107.60(10)
N(5)–Cd(2)–N(6)	76.25(8)
N(3)–Cd(1)–N(3*)	98.00(2)
N(1)–Cd(2)–N(6)	111.02(10)
N(1)–Cd(2)–N(7)	91.66(11)
N(1)–Cd(2)–N(4)	108.08(11)
N(4)–Cd(2)–N(6)	124.23(9)
N(4)–Cd(2)–N(7)	109.37(10)
N(4)–Cd(2)–N(5)	75.67(9)
N(5)–Cd(2)–N(7)	73.94(10)

Symmetry code: * $-x$, y, $1/2 - z$.

lie within the range 2.226(3)–2.242(3) Å. The range of *cisoid* angles [78.40(2)–98.00(2)°] and that of the *transoid* angles [163.21(3)–168.35(9)°] reflect the deviation of the chromophore from an ideal octahedron. Two pendant pseudohalide arms around Cd(1) are mutually in a *cis* orientation [N(3)–Cd(1)–N(3*), 98.00(2)°]. Four bridging thiocyanate nitrogens [N(1), N(1*), N(2), N(2*)] of $[Cd(NCS)_6]^{4-}$ coordinate to the adjacent $[Cd(tren)]^{2+}$ forming a 2D sheet. Three amine nitrogens [N(4), N(6), N(7)] of the tripodal amine and a bridging thiocyanate nitrogen [N(2)] constitute the equatorial plane of Cd(2) in each $[Cd(tren)]^{2+}$. The tertiary nitrogen [N(5)] of the blocker and another bridging nitrogen [N(1)] occupy the axial sites. Cd(2)–N bond lengths of this unit lie within a close range [2.227(3)–2.441(2) Å] and are similar to those of Cd(1)–N. Bond angles around Cd(2) are indicative of large deviation from ideality [*cisoid* angles: 73.94(10)–111.02(10)°; *transoid* angles: 124.23(9)–165.44(10)°]. The intrachain Cd...Cd separation is 6.006(6) Å for Cd(1)...Cd(2) and 11.7359(10) Å for Cd(2)...Cd(2*) whereas the Cd...Cd separation between two sheets is 9.767 Å.

Three distinct hydrogen bonds (Table 3) involving three tripodal amine N atoms [N(4), N(6) and N(7)] and bridging S(1) atoms are present in this polymer leading to a superstructure; of the three, two are intrachain N–H...N–H-bonds [H(7B)···N(2) 2.360 Å, ∠N(7)–H(7B)···N(2) 147.6°; H(4B)···N(2) 2.493 Å, ∠N(4)–H(4B)···N(2) 120.8°] and the other is a N–H...S [40] interchain bonding [H(6B)···S(1) 2.713 Å, ∠N(6)–H(6B)···S(1) 164.7°]. The latter arises due to the specific orientation of the tripodal ligand of one sheet towards the bound thiocyanate sulfur in the molecular ion of the adjacent sheet. This type of non-covalent interaction throughout the lattice is responsible for the conformation and stability of supramolecular framework. The 2D sheets are stacked along the *c*-axis by such multiple interactions, forming a 3D network (Fig. 3).

3.2.2. $[Ni_2Cd(tren)_2(NCS)_6]_n$ (2)

The polymer **2** bears a fair resemblance to **1** in the asymmetric unit. An ORTEP diagram of this unit, the two-dimensional (2D) sheet found in the covalently bonded polymer and the arrangement of these sheets perpendicular to the *a*-axis are respectively shown in Figs. 4–6. Selected bond distances and bond angles are set in Table 4. The two different metal centres [diamagnetic 4d ion, cadmium(II) and paramagnetic 3d ion, nickel(II)] with varied coordination environments are propagated in an alternate fashion bridged by thiocyanates in an end-to-end motif. Each *trans*-$[Cd(NCS)_2(SCN)_4]^{4-}$ is connected to four $[Ni(tren)]^{2+}$ units to yield the heteropolymeric network in contrast to **1** where a homopolymer is the result. The geometry around Cd(1) is a distorted octahedron with a *trans*-CdN_2S_4 chromophore instead of a *cis*-CdN_2S_4 chromophore, and it lies on an inversion centre. Ni(1) has a hard NiN_6 chromophore in a distorted octahedral environment. Cd(1) is attached to four sulfur atoms [S(2), S(2^c), S(3), S(3^c); ^{c} indicates a symmetry operation $-x+1/2, -y+1/2, -z$] of the bridging thiocyanates in

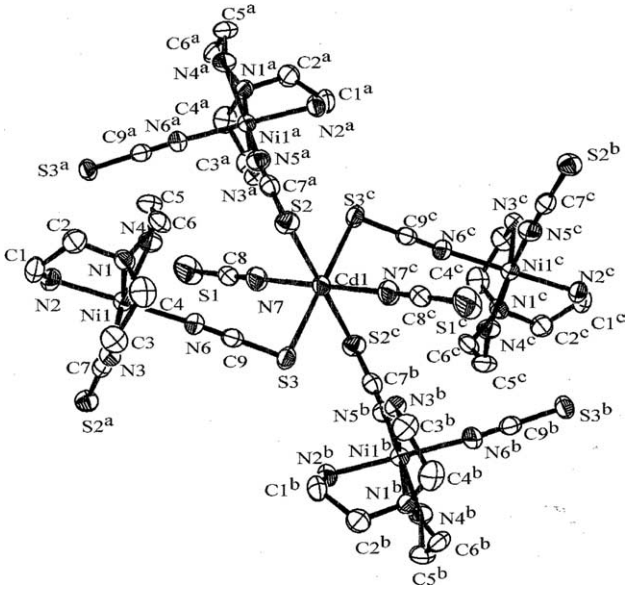

Fig. 4. ORTEP diagram of **2** with the atom numbering scheme. Symmetry code: $^a -x+1/2,\ y+1/2,\ -z+1/2$; $^b x,\ -y,\ z+1/2$; $^c -x+1/2,\ -y+1/2,\ -z$.

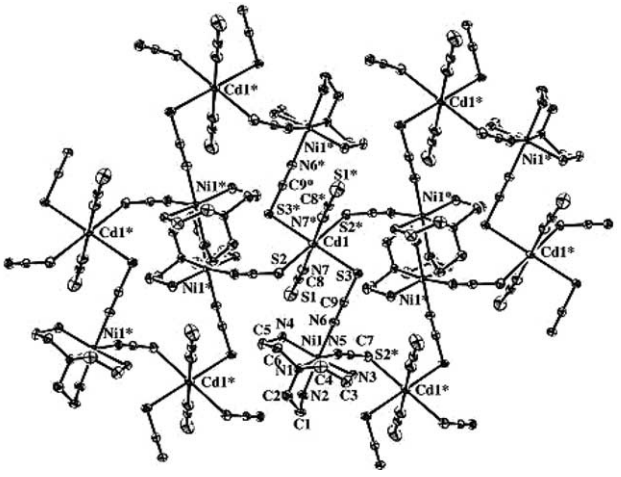

Fig. 5. Perspective view of the 2D sheet in **2**. Symmetry code: $^a -x+1/2, y+1/2, -z+1/2$; $^b x, -y, z+1/2$; $^c -x+1/2, -y+1/2, -z$.

Table 3
Hydrogen bond distances (Å) and angles (°) for **1**

Compound	D–H...A	D–H	H...A	D...A	∠D–H...A
1	N4–H4B...N2^{i}	0.89	2.49	3.05(4)	120
	N6–H6B...S1^{ii}	0.89	2.71	3.58(2)	164
	N7–H7B...N2^{iii}	0.90	2.35	3.15(4)	147

Symmetry code: $^{i}\ -1/2+x,\ +1/2+y,\ z$; $^{ii}\ -1/2-x,\ 3/2-y,\ -z$; $^{iii}\ -x,\ y,\ 1/2-z$.

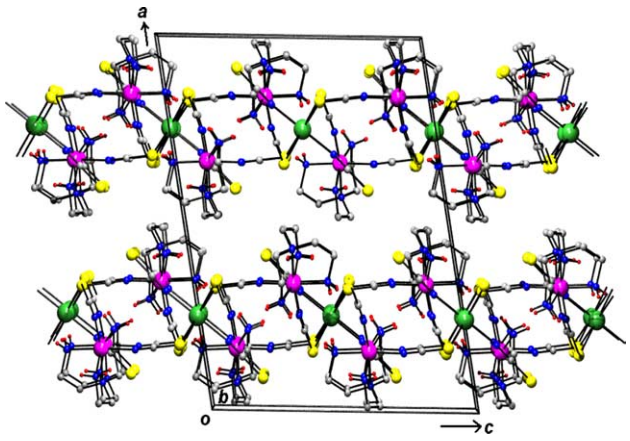

Fig. 6. Projection onto the *b*-axis of **2** showing stacking of sheets approximately perpendicular to the *a*-axis.

the equatorial plane and two nitrogen atoms [N(7), N(7^c)] of the terminal pseudohalides in axial positions (Fig. 4). The sequence of the arrangement of the atoms in polymeric **2** is –Cd(1)–S(3)–C(9)–N(6)–Ni(1)–N(5)–C(7)–S(2^c)–Cd(1^c)– (Fig. 5). Ranges of Cd(1)–S [2.7587(16)–2.7621(14) Å] and Cd(1)–N [2.254(5) Å] bond lengths are similar to those of **1**. *Transoid* angles around Cd(1) are exactly 180.00° but *cisoid* angles are of variable magnitude [87.21(14)–92.79(14)°], but are close to 90.00°. The two pendant pseudohalide arms around Cd(1) are mutually in a *trans* orientation with a N(7)–Cd(1)–N(7^c) angle of 180.0(3)°. The environment around Ni(1) is comparable to Cd(2) of **1** with three amine nitrogens [N(2), N(4), N(6)] of the tripodal amine and a bridging thiocyanate nitrogen [N(3)] constituting the equatorial plane. The remaining bridging nitrogen, N(1) and tertiary nitrogen [N(5)] of the blocker occupy axial positions of the paramagnetic 3d metal ion. Ni(1)–N bond lengths lie within a close range [2.046(5)–2.122(4) Å]. Bond angles around Ni(1) are indicative of deviation from ideality [*cisoid* angles: 81.68(17)–96.02(18)°; *transoid* angles: 161.53(18)–176.9(2)°]. The Cd...Ni separation is 5.6837(17) Å whereas the shortest Cd...Cd and Ni...Ni distances are 9.619(3) and 5.7705(18) Å respectively within the discrete sheet. The N atoms of the tripodal amine in one sheet are housed into the spaces (holes) below cadmium centres of another adjacent sheet and N–H...S type of hydrogen bonding as is present in **1** is inhibited due to such an orientation (Fig. 6).

Table 4
Selected bond distances (Å) and angles (°) for **2**

Bond distances	
Cd(1)–N(7)	2.254(5)
Cd(1)–S(3)	2.7621(14)
Cd(1)–S(2)	2.7587(16)
Ni(1)–N(1)	2.122(4)
Ni(1)–N(2)	2.119(4)
Ni(1)–N(5)	2.046(5)
Ni(1)–N(3)	2.109(4)
Ni(1)–N(6)	2.109(5)
Ni(1)–N(4)	2.119(4)
Bond angles	
N(7)–Cd(1)–N(7^c)	180.0(3)
N(7)–Cd(1)–S(2^c)	90.17(15)
S(3^c)–Cd(1)–S(3)	180.00
N(7)–Cd(1)–S(2)	89.83(15)
S(2)–Cd(1)–S(3)	91.88(5)
S(2^c)–Cd(1)–S(2)	180.00(6)
N(7)–Cd(1)–S(3^c)	87.21(14)
S(2)–Cd(1)–S(3^c)	88.12(5)
N(7)–Cd(1)–S(3)	92.79(14)
N(5)–Ni(1)–N(3)	94.16(18)
N(2)–Ni(1)–N(1)	81.89(18)
N(6)–Ni(1)–N(1)	95.85(18)
N(4)–Ni(1)–N(1)	83.93(18)
N(5)–Ni(1)–N(6)	90.40(19)
N(3)–Ni(1)–N(6)	84.13(17)
N(5)–Ni(1)–N(2)	91.68(18)
N(3)–Ni(1)–N(2)	93.36(18)
N(6)–Ni(1)–N(2)	176.9(2)
N(5)–Ni(1)–N(4)	101.42(19)
N(3)–Ni(1)–N(4)	161.53(18)
N(6)–Ni(1)–N(4)	85.88(18)
N(2)–Ni(1)–N(4)	96.02(18)
N(5)–Ni(1)–N(1)	172.08(18)
N(3)–Ni(1)–N(1)	81.68(17)

Symmetry code: ^{c} $-x+1/2, -y+1/2, -z$.

3.3. Magnetic behaviour of $[Ni_2Cd(tren)_2(NCS)_6]_n$ (2)

The magnetic behaviour in the form of $\chi_m T$ versus T and χ_m versus T (inset) plots indicates (Fig. 7) that the $\chi_m T$ value (1.188 $cm^3\,mol^{-1}\,K$ at 300 K) remains constant down to 10 K and then decreases to 0.181 $cm^3\,mol^{-1}\,K$ at 2 K. The global feature is characteristic of a Curie-law typical for a magnetically isolated nickel(II) ion ($S=1$ with $g=2.16$–2.18) with a very

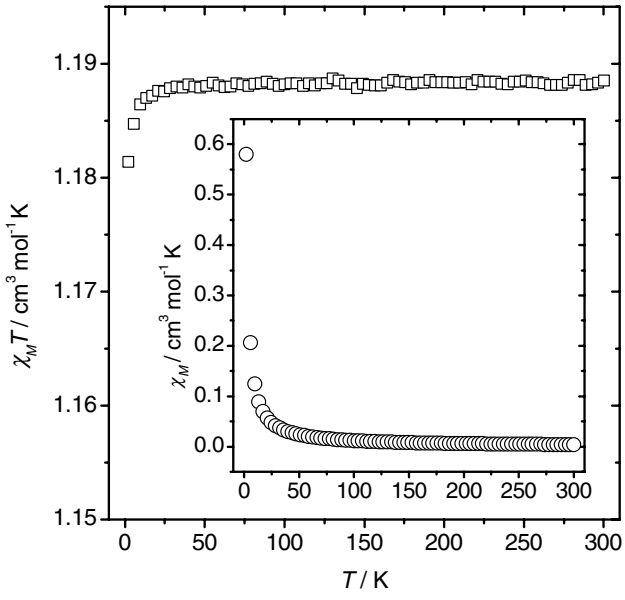

Fig. 7. Plots of (a) $\chi_m T$ vs. T and (b) χ_m vs. T.

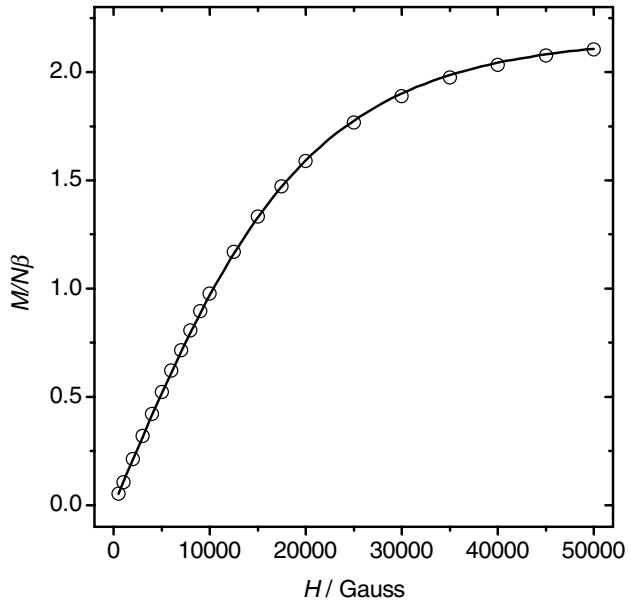

Fig. 8. Field dependence magnetization plot for **2**.

small zero-field splitting (D parameter typical for an $S = 1$ system) or a very weak antiferromagnetic interaction ($J < 0.01\ cm^{-1}$). The χ_M curve starts at $0.004\ cm^3\ mol^{-1}$ at room temperature and increases in a uniform way to $0.58\ cm^3\ mol^{-1}$ at 2 K. The reduced molar magnetization ($M/N\beta$) per nickel(II) entity tends to two electrons (Fig. 8). Assuming an isolated nickel(II) system, the fit to the Brillouin formula gives $g = 2.17$ with $R = 2.04 \times 10^{-5}$ (agreement factor, R, being defined as $\chi_i[(\chi_m T)_{obs} - (\chi_m T)_{calc}]^2/\chi_i[(\chi_m T)_{obs}]^2$). The lack of coupling among paramagnetic centres linked by complex species of diamagnetic ions is known for $[M(CN)_n]^{z-}$ systems [M = Ni(II), Co(III), etc.] with either weak ferro- or antiferromagnetic coupling [25,28].

4. Conclusion

1 and **2** are good examples of inorganic organic hybrid polymers where the ambidentate intermediary thiocyanate is the dynamic molecular ion $[Cd(NCS)_6]^{4-}$ bridges in different geometries (*cis*/*trans*) of the formulation $[Cd(NCS)_2(SCN)_4]^{4-}$. The versatility of the pseudohalide connectors in the cadmium(II) bound state is revealed through coordination as terminal and end-to-end bridging motifs. The polymers show significant differences in molecular and crystalline architectures. The fundamental difference between **1** and **2** is the orientations of the tripodal amine in the crystals that result in hydrogen bonded superstructures in **1** and inhibits such non-covalent forces between adjacent sheets in **2**. The latter represents the first report of a molecular ion bridged species involving 3d and 4d transition metal ions. The variable temperature magnetic study of **2** show weak antiferromagnetic interactions hindered by the diamagnetic molecular ion. We are currently investigating how to extend such work on paramagnetic molecular ions $[M(X)_6]^{z-}$ ($M = Fe^{III}$, Mn^{II}, Co^{II}, etc.) containing pseudohalides (X^-) like N_3^-, NCO^- and $NCSe^-$ with other paramagnetic complementary units to create extended paramagnetic homo-/heteropolymeric networks resulting in new supramolecular magnetic materials, particularly nanomagnets.

5. Supplementary data

Crystallographic data for the structural analyses have been deposited with the Cambridge Crystallographic Data Center, CCDC Nos. 200290 (**1**) and 200289 (**2**). Copies of this information can be obtained free of charge from the Director, CCDC, 12 Union Road, Cambridge, CB2 IEZ, UK (fax: +44 1223 336033; e-mail: deposit@ccdc.cam.ac.uk or www.ccdc.cam.ac.uk).

Acknowledgements

B.K.G. thanks the Department of Science and Technology (DST) and Council of Scientific and Industrial Research, (CSIR) New Delhi, India for the financial support.

References

[1] D.B. Mitzi, Progr. Inorg. Chem. (1999) 48.
[2] B. Moulton, M.J. Zaworotko, Chem. Rev. 101 (2001) 1629.
[3] J.S. Miller, in: M. Drillon (Ed.), Magnetism: Molecules to Materials IV, Wiley-VCH, Weinheim, 2003.
[4] S.R. Marder, in: D.W. Bruce, D. O'Hare (Eds.), Metal Containing Materials for Nonlinear Optics in Inorganic Materials, 2nd ed., Wiley, Chichester, 1996, p. 121.
[5] O.R. Evans, W. Lin, Acc. Chem. Res. 35 (2002) 511.
[6] Chemical Sensors, Chem. Rev. 100 (2000) 7 (special issue).
[7] B. Cornils, W.A. Herrmann, R. Schlogl (Eds.), Catalysis from A to Z: A Concise Encyclopedia, John Wiley & Sons, New York, 2000.
[8] D. Demus, J.W. Goodby, G.W. Gray, H.-W. Spiess, V. Vill (Eds.), Handbbook of Liquid Crystals, Wiley-VCH, Weinheim, 1998.
[9] J.R. Farraro, J.M. Williams, Introduction to Synthetic Electrical Conductors, Academic Press, New York, 1987.
[10] S.T. Hyde, B. Ninham, S. Anderson, Z. Blum, T. Landh, K. Larsson, S. Liddin, The Language of Shape, Elsevier, Amsterdam, 1997.
[11] S. Leininger, B. Olenyuk, P.J. Stang, Chem. Rev. 100 (2000) 853.
[12] P. Comba, T.W. Hambley, Molecular Modelling of Inorganic and Coordination Compounds, 2nd ed., VCH, Weinheim, 2001.
[13] T. Steiner, Angew. Chem. Int. Ed. 41 (2002) 48.
[14] G.R. Desiraju (Ed.), Crystal Design: Structure and Function, Perspectives in Supramolecular Chemistry, vol. 7, John Wiley & Sons, Ltd., Chichester, 2003.

[15] C. Janiak, J. Chem. Soc., Dalton Trans. (2003) 2781.
[16] S.L. James, Chem. Soc. Rev. 32 (2003) 276.
[17] O. Almarsson, M.J. Zawarotko, Chem. Commun. (2004) 1889.
[18] C.D. Abernethy, C.L.B. Macdonald, J.A.C. Clyburne, A.H. Cowley, Chem. Commun. (2001) 61.
[19] L. Rong-Guang, T. Zhu, X. Sai-Feng, Z. Quin-Jiang, W.G. Jackson, W. Zhan-Bing, L. La-Sheng, Polyhedron 22 (2003) 3467.
[20] M.S. El Falah, E. Rentchler, A. Caneschi, R. Sessoli, D. Gatteschi, Angew. Chem. Int. Ed. 35 (1996) 1947.
[21] K.V. Langenberg, S.R. Batten, K.J. Berry, D.C.R. Hockless, B. Moubaraki, K.S. Murray, Inorg. Chem. 36 (1997) 5006.
[22] H. Miyasaka, H. Ieda, N. Matsumoto, N. Re, R. Crescenzi, C. Floriani, Inorg. Chem. 37 (1998) 255.
[23] M. Ohba, N. Usuki, N. Fukita, H. Okawa, Inorg. Chem. 37 (1998) 3349.
[24] S. Ferlay, T. Mallah, R. Ouahes, P. Veillet, M. Verdaguer, Inorg. Chem. 38 (1999) 229.
[25] T. Lu, H. Xiang, C. Su, P. Cheng, Z. Mao, L. Ji, New J. Chem. 25 (2001) 216.
[26] R.J. Parker, L. Spiccia, K.J. Berry, G.D. Fallon, B. Moubaraki, K.S. Murray, Chem. Commun. (2001) 333.
[27] M. Clemente-Leon, E. Coronado, J.R. Galan-Mascaros, C.J. Gomez-Garcia, T. Woike, J.M. Clemente-Juan, Inorg. Chem. 40 (2001) 87.
[28] R.J. Parker, L. Spiccia, S.R. Batten, J.D. Cashion, G.D. Fallon, Inorg. Chem. 40 (2001) 4696.
[29] J. Larinova, R. Clerac, J. Sanchiz, O. Kahn, S. Golhen, L. Ouahab, J. Am. Chem. Soc. 120 (1998) 13088.
[30] G. Rombaut, S. Golhen, L. Ouahab, C. Mathoniere, O. Kahn, J. Chem. Soc., Dalton Trans. (2000) 3609.
[31] W.-F. Yeung, W.-L. Man, W.-T. Wong, T.-C. Lau, S. Gao, Angew. Chem. Int. Ed. 40 (2001) 3031.
[32] R. Pradhan, C. Desplanches, P. Guionneau, J.-P. Sutter, Inorg. Chem. 42 (2003) 6607.
[33] V. Marvaud, C. Decroix, A. Scuiller, C.G. Duhayon, J. Vaissermann, F. Gonnet, M. Verdaguer, Chem. Eur. J. 9 (2003) 1677.
[34] V. Balzani, M.G. -Lopez, J.F. Stoddart, Acc. Chem. Res. 31 (1998) 405.
[35] Molecular Materials in Electronic and Optoelectronic Devices, Acc. Chem. Res. 32 (1999) 3 (special issue).
[36] J.-M. Lehn, Supramolecular Chemistry: Concepts and Perspectives, VCH, Weinheim, 1995.
[37] J.W. Steed, J.L. Atwood, Supramolecular Chemistry, John Wiley & Sons, New York, 2000.
[38] F.A. Cotton, G. Wilkinson, C.A. Murillo, M. Bochmann, Advanced Inorganic Chemistry, 6th ed., John Wiley & Sons, Inc., 1999.
[39] A. Mondal, G. Mostafa, A. Ghosh, I.R. Laskar, N.R. Chaudhuri, J. Chem. Soc., Dalton Trans. (1999) 9.
[40] D. Bose, J. Banerjee, Sk H. Rahaman, G. Mostafa, H.-K. Fun, R.D.B. Walsh, M.J. Zaworotko, B.K. Ghosh, Polyhedron 23 (2004) 2045.
[41] H. Zhang, X. Wang, K. Zhang, B.K. Teo, Coord. Chem. Rev. 183 (1993) 157.
[42] J.M. Clemente-Juan, B. Chansou, B. Donnadieu, J.-P. Tuchagues, Inorg. Chem. 39 (2000) 5515.
[43] Z.-L. Lu, C.-Y. Duan, Y.-P. Tian, Z.-W. Wu, J.-J. You, Z.-Y. Zhou, T.C.W. Mak, Polyhedron 16 (1997) 909.
[44] G.M. Sheldrick, SAINT V4, Software Reference Manual, Siemens Analytical X-ray Systems, Madison, WI, USA, 1996.
[45] G.M. Sheldrick, SHELXL-PLUS, Siemens Analytical X-ray Systems, Madison, WI, USA, 1990.
[46] G.M. Sheldrick, SHELXL 97, Program for Refinement of Crystal Structures, University of Gottingen, Gottingen, Germany, 1997.
[47] L.J. Farrugia, ORTEP-3, J. Appl. Crystallogr. 30 (1997) 565.
[48] A.L. Spek, PLATON 99, Molecular Geometry Program, University of Utrecht, The Netherlands, 1999.
[49] G. Guilera, J.W. Steed, Chem. Commun. (1999) 1563.
[50] Focus on Self-Assembly, Acc. Chem. Res. 32 (1999) 4 (special issue).
[51] B.J. Holliday, C.A. Mirkin, Angew. Chem. Int. Ed. 40 (2001) 2022.
[52] W.J. Geary, Coord. Chem. Rev. 7 (1971) 81.
[53] K. Nakamoto, Infrared and Raman Spectra of Inorganic and Coordination Compounds, Part B, 5th ed., John Wiley & Sons, New York, 1997, p. 116.
[54] B. Zurowska, J. Mrozinski, M. Julve, F. Lloret, A. Maslejova, W.S. Dobrowolska, Inorg. Chem. 41 (2002) 1771.
[55] A.B.P. Lever, Inorganic Electronic Spectroscopy, 2nd ed., Elsevier Science, New York, 1984.

Available online at www.sciencedirect.com
SCIENCE DIRECT®
Polyhedron 25 (2006) 654–662
POLYHEDRON
www.elsevier.com/locate/poly

Synthesis and structural elucidation of some novel aluminium(III) complexes with Schiff bases: Crystal and molecular structure of $[Al\{O(C_6H_4)CH{=}NC_6H_5\}_2\{HO(C_6H_4)CH{=}NC_6H_5\}_2]Br$

Amit K. Jain [a], Anjali Gupta [a], Rakesh Bohra [a,*], Ingo-Peter Lorenz [b], Peter Mayer [b]

[a] Department of Chemistry, University of Rajasthan, Jaipur-302004, India
[b] Department of Chemistry and Biochemistry, Ludwig Maximilian University, Munich, Germany

Received 18 December 2004; accepted 5 July 2005
Available online 26 September 2005

Dedicated in the memory of (Late) Prof. R.C. Mehrotra (11.07.2004), a giant in Inorganic Chemistry, who was known all over the world for his pioneering work on "Metal Alkoxide Chemistry".

Abstract

Reactions of $Et_3Al \cdot Et_2O$ with bidentate Schiff base ligands in 1:1 and 1:2 molar ratios in diethyl ether yield $Et_2Al\{O(C_6H_4)CH{=}NC_6H_5\}$, $EtAl\{O(C_6H_4)CH{=}NC_6H_5\}_2$, $Et_2Al\{OC(R){=}CHC(R^1){=}NC_6H_5\}$ and $EtAl\{OC(R){=}CHC(R^1){=}NC_6H_5\}_2$ (where $R = R^1{=}CH_3$, C_6H_5; $R = CH_3$, $R^1 = C_6H_5$). The reaction of Et_2AlBr with $HO(C_6H_4)CH{=}NC_6H_5$ in a 1:4 molar ratio in diethyl ether yields $[Al\{O(C_6H_4)CH{=}NC_6H_5\}_2\{HO(C_6H_4)CH{=}NC_6H_5\}_2]Br$. All the above complexes are soluble in common organic solvents and have been characterized by elemental analysis, as well as IR and multinuclear NMR (^1H, ^{13}C and ^{27}Al) spectroscopy. Molecular weight measurements in refluxing benzene show the monomeric nature of the monoethyl complexes and dimeric nature of the diethyl complexes, which is further supported from the FAB mass spectra of three representative compounds, $Et_2Al\{O(C_6H_4)CH{=}NC_6H_5\}$, $Et_2Al\{OC(CH_3){=}CHC(CH_3){=}NC_6H_5\}$ and $EtAl\{O(C_6H_4)CH{=}NC_6H_5\}_2$. ^{27}Al NMR spectra show that in both types of complex, the aluminium is pentacoordinated. The crystal structure of $[Al\{O(C_6H_4)CH{=}NC_6H_5\}_2\{HO(C_6H_4)CH{=}NC_6H_5\}_2]Br$ displays a unique octahedral symmetry with the ligand bonded in two different patterns to the aluminium(III) center.
© 2005 Elsevier Ltd. All rights reserved.

Keywords: Aluminium complexes; Schiff base ligands; Salicylaldiminato-N,O chelates; Salicylaldimine complexes

1. Introduction

Aluminium alkyls as well as their heteroleptic derivatives are important industrial chemicals. Triethylaluminium, for example, is an activator in the Z–N polymerization of olefins [1], while methylaluminoxanes (MAO) are used as co-catalysts for the homogeneous polymerization of olefins [2,3].

In Schiff base complexes of aluminium, the coordination environment at the metal center can be modified by attaching different substituents to the ligand, providing useful steric and electronic properties [4] essential for the fine tuning of structures and reactivity. Therefore, it is not surprising that p-block metal derivatives of Schiff bases have been shown to catalyze a wide variety of reactions [5,6]. For example, aluminium based complexes which are closely related to the compounds reported in this paper have been used as catalysts in the polymerization of ethylene [7] and methacrylate [8,9], as well as the ring opening polymerization of heterocyclic monomers [10].

Furthermore, our choice of target complexes was also based on the fact that the organometallic chemistry of

* Corresponding author. Tel./fax: +911412700364.
E-mail address: rkbohra@satyam.net.in (R. Bohra).

0277-5387/$ - see front matter © 2005 Elsevier Ltd. All rights reserved.
doi:10.1016/j.poly.2005.07.028

group 13 elements with bidentate salicylideneminate ligands remains relatively poorly investigated. The structurally characterized four coordinated aluminium complexes of this type are only reported with sterically encumbered ligands [11,12]. Recently, structural investigations of complexes of aluminium and indium with Schiff bases have been investigated [13].

In our recent publications [14–18], it has been shown that binuclear metallo-organic complexes with bidentate ligands usually adopt unsymmetrical structures containing aluminium atoms with the coordination numbers four and six, rather than a symmetric five coordinated structure. More recently, we have also reported the five coordinate heteroleptic metallo-organic complex $Al[\{O(C_6H_4)CH{=}NC_6H_5\}_2Al\{ON{=}C(CH_3)C_4H_3S\text{-}2\}]$ [19].

In a continuation of our systematic studies, we report here the synthesis and structure elucidation of organoaluminium(III) complexes with Schiff bases and the crystal structure of a unique hexacoordinated aluminium(III) complex $[Al\{O(C_6H_4)CH{=}NC_6H_5\}_2\{HO(C_6H_4)CH{=}NC_6H_5\}_2]Br$.

2. Experimental

All the complexes described in the present investigation were manipulated in a vacuum line or in a purified argon atmosphere. The solvents and reagents were purified by conventional techniques. The $Et_3Al \cdot Et_2O$ and Et_2AlBr were synthesized and purified according to the literature methods [20]. The Schiff base ligands were prepared by condensing salicylaldehyde, acetylacetone, benzylacetone and dibenzoylmethane with the appropriate aniline and distilled prior to use. Aluminium was estimated gravimetrically as the oxinate [21] and bromide was estimated by Volhard's method [21]. Microanalyses were carried out on a Perkin–Elmer C, H, N & S II series 2400 analyzer. The IR spectra were recorded as Nujol mulls on a Nicolet Magna-550 spectrometer in the range 4000–400 cm^{-1}. ^1H, ^{13}C and ^{27}Al NMR spectra were recorded in 5 mm NMR tubes as freshly prepared $CDCl_3$ solutions on a Bruker DPX-300 spectrometer operating at 300, 75.5 and 111.9 MHz, respectively. Spectra were referenced with the internal chloroform peak (*7.26 for ^1H and 77.0 for ^{13}C). Molecular weight measurements in anhydrous benzene were carried out by the elevation in boiling point method using Beckmanns Thermometer fitted in a glass assembly. The instrument was calibrated using samples of known molecular weight such as naphthalene/benzophenone/benzil in anhydrous benzene ($M = 1000\ K_b w/\Delta T_b W$, where M is the molecular weight, w is the weight of solute in g, K_b is the molar elevation constant, W is the weight of solvents in g, ΔT_b is the elevation in boiling point).

2.1. Preparation of $Et_2Al\{O(C_6H_4)CH{=}NC_6H_5\}$ (1)

A solution of $Et_3Al \cdot Et_2O$ (1.49 g, 7.91 mmol) in 20 ml of anhydrous diethyl ether was slowly added to an etheral solution of $HO(C_6H_4)CH{=}NC_6H_5$ (1.57 g, 7.95 mmol) under an argon atmosphere and the reaction mixture was stirred at room temperature for 4h. The solvents were evaporated under vaccum and the product was washed (2×10 ml) with *n*-hexane. The compound was dried under vaccum to give a yellow solid (Yield 97%), which was recrystallized from a mixture of dichloromethane and *n*-hexane (7:1).

The diethylaluminium(III) complexes **3**, **5** and **7** were prepared using a similar route. Their synthetic details and analytical data are summarized in Table 1.

2.2. Preparation of $EtAl\{O(C_6H_4)CH{=}NC_6H_5\}_2$ (2)

An ethereal solution of $Et_3Al \cdot Et_2O$ (1.29 g, 6.85 mmol) was gradually added to an ethereal solution of $HO(C_6H_4)CH{=}NC_6H_5$ (2.72 g, 13.78 mmol) under an argon atmosphere. The reaction mixture was stirred at room temperature for 4 h. After removal of the solvent under reduced pressure the product obtained was washed (2×10 ml) with *n*-hexane and dried in vacuum to afford a yellow solid (Yield 96%), which was recrystallized from a mixture of dichloromethane and *n*-hexane (7:1).

The monoethylaluminium(III) complexes **4**, **6** and **8** were prepared using a similar route. Their synthetic details and analytical data are also summarized in Table 1.

2.3. Preparation of $[Al\{O(C_6H_4)CH{=}NC_6H_5\}_2\{HO(C_6H_4)\text{-}CH{=}NC_6H_5\}_2]Br$ (9)

A solution of Et_2AlBr (0.74 g, 4.48 mmol) in 20 ml of anhydrous diethyl ether was slowly added to an ethereal solution of $HO(C_6H_4)CH{=}NC_6H_5$ (3.55 g, 17.96 mmol) under an argon atmosphere and the reaction mixture was stirred at room temperature for 4 h. The solvents were evaporated under vacuum and dried to give a yellow coloured paste, which was washed (2×10 ml) with petroleum ether to give a yellow solid (89%). The solid product obtained was recrystallized from a mixture of dichloromethane and *n*-hexane (7:1). After several hours, shiny yellow crystals were obtained. *Anal.* Calc.: Al, 3.02; N, 6.27; Br, 8.94. Found: Al, 3.00; N, 6.24; Br, 8.90% (see Table 2).

2.4. X-ray diffraction analysis

Single crystals of **9** suitable for X-ray diffraction analysis were obtained by covering a solution of **9** in CH_2Cl_2 with a layer of *n*-hexane. A pale yellow, needle shape crystal of $[Al\{O(C_6H_4)CH{=}NC_6H_5\}_2\{HO(C_6H_4)\text{-}$

Table 1
Synthetic and analytical data of ethylaluminium(III) complexes **1**–**8**

S.No.	Complexes	Yield (%)	Colour and state	Elemental analysis (%) Found (Calc.)				Molecular weight Found (Calc.)	MP (°C)
				C	H	N	Al		
1	$Et_2Al\{O(C_6H_4)CH{=}NC_6H_5\}$	97	Yellow solid	72.3 (72.6)	7.05 (7.17)	4.96 (4.98)	9.52 (9.59)	586 (281)	146
2	$EtAl\{O(C_6H_4)CH{=}NC_6H_5\}_2$	96	Yellow solid	74.8 (75.0)	5.60 (5.62)	6.21 (6.25)	5.88 (6.02)	464 (448)	120
3	$Et_2Al\{OC(CH_3){=}CHC(CH_3){=}NC_6H_5\}$	99	Yellow orange viscous liquid	69.2 (69.5)	8.52 (8.55)	5.38 (5.40)	10.4 (10.4)	526 (259)	–
4	$EtAl\{OC(CH_3){=}CHC(CH_3){=}NC_6H_5\}_2$	96	Yellow solid	71.0 (71.3)	7.15 (7.23)	6.90 (6.93)	6.65 (6.67)	(404)	145
5	$Et_2Al\{OC(CH_3){=}CHC(C_6H_5){=}NC_6H_5\}$	98	Yellow solid	74.4 (74.7)	7.48 (7.53)	4.33 (4.36)	8.37 (8.40)	(321)	87
6	$EtAl\{OC(CH_3){=}CHC(C_6H_5){=}NC_6H_5\}_2$	98	Yellow solid	77.0 (77.3)	6.20 (6.29)	5.27 (5.30)	5.00 (5.10)	(528)	93
7	$Et_2Al\{OC(C_6H_5){=}CHC(C_6H_5){=}NC_6H_5\}$	96	Yellow solid	78.0 (78.3)	7.00 (6.83)	3.62 (3.65)	7.00 (7.04)	(383)	dec.
8	$EtAl\{OC(C_6H_5){=}CHC(C_6H_5){=}NC_6H_5\}_2$	96	Yellow solid	80.5 (80.9)	5.58 (5.71)	4.28 (4.29)	4.02 (4.13)	(652)	

Table 2
IR and NMR (^{1}H and ^{13}C) spectra of free Schiff bases

S.No.	Schiff bases	IR	^{1}H NMR in δ ppm	^{13}C NMR in δ ppm
1	$HO(C_6H_4)CH{=}NC_6H_5$	2926 s ν(OH) 1457 s ν(C=N)	6.97–7.61 m (Phenyl), 8.75 s (C*H*=N), 13.4 s (–O*H*)	117.5–133.3 (aromatic carbons), 162.8 (*C*H=N)
2	$HOC(CH_3){=}CHC(CH_3){=}NC_6H_5$	2924 s ν(OH) 1378 s ν(C=N)	1.96, 2.09 s (CH_3), 5.26 s (C*H*), 7.03–7.41 m (Phenyl), 12.61 br (–O*H*)	19.7, 29.1 (*C*H_3), 97.8 (*C*H), 124.7–139.0 (aromatic carbons), 159.9 (*C*=N), 196.0 (–O*C*)
3	$HOC(CH_3){=}CHC(C_6H_5){=}NC_6H_5$	2915 s ν(OH) 1465 s ν(C=N)	2.21 s (CH_3), 6.02 s (C*H*), 6.27–8.05 m (Phenyl), 13.25 br (–O*H*)	20.3 (CH_3), 94.5 (*C*H), 124.9–140.4 (aromatic carbons), 162.1 (*C*=N), 188.8 (–O*C*)
4	$HOC(C_6H_5){=}CHC(C_6H_5){=}NC_6H_5$	2928 s ν(OH) 1460 s ν(C=N)	5.90 s (C*H*), 6.81–8.71 m (C_6H_5), 13.26 br (–O*H*)	122.4–140.5 (aromatic carbons), 172.6 (*C*=N), 196.0 (–O*C*)

Table 3
FAB mass spectral data for complexes **1**, **2** and **3**

m/e	$Et_2Al\{O(C_6H_4)CH{=}NC_6H_5\}$ (**1**)
562	$[Et_2Al\{O(C_6H_4)CH{=}NC_6H_5\}]_2$
549	$[Et_2Al\{O(C_6H_4)CH{=}NC_6H_5\}][Et_2Al\{O(C_6H_4)NC_6H_5\}]$
548	$[Et_2Al\{O(C_6H_4)C{=}NC_6H_5\}][Et_2Al\{O(C_6H_4)NC_6H_5\}]$
514	$[Et_2Al\{O(C_6H_4)C{=}NC_6H_5\}][Et_2Al\{O(C_6H_4)NC_3H_5\}]\cdot H_2$
513	$[Et_2Al\{O(C_6H_4)C{=}NC_6H_5\}][Et_2Al\{O(C_6H_4)NC_3H_5\}]\cdot H$
504	$[Et_2Al\{O(C_6H_4)C{=}NC_6H_5\}][Et_2Al\{O(C_6H_4)CNH_3\}]\cdot H_2O$
480	$[Et_2Al\{O(C_6H_4)C{=}NC_4H_5\}][Et_2Al\{O(C_6H_4)CNH_3\}]\cdot H_2O$
461	$[Et_2Al\{O(C_6H_4)C{=}NC_4H_5\}][Et_2Al\{O(C_6H_4)CNH_2\}]$
419	$[Et_2Al\{O(C_6H_4)C{=}C_2H\}][Et_2Al\{O(C_6H_4)CNH_2\}]$
407	$[Et_2Al\{O(C_6H_4)C{=}CH\}][Et_2Al\{O(C_6H_4)CNH_2\}]$
395	$[Et_2Al\{O(C_6H_4)CH\}][Et_2Al\{O(C_6H_4)CNH_2\}]$
363	$[Et_2Al\{O(C_6H_4)CH\}][Et_2Al(C_6H_4)C]$
349	$[Et_2Al\{O(C_6H_4)CH\}][EtCH_3Al(C_6H_4)C]$
333	$[Et_2Al\{O(C_6H_4)CH\}][(C_2H_4)Al(C_6H_4)C]$
307	$[C_2H_8Al\{O(C_6H_4)CH\}][(C_2H_4)Al(C_6H_4)C]$
257	$[C_2H_8Al\{O(C_6H_4)CH\}][(C_2H_4)Al(C_3H_2)]$
227	$[C_2H_8Al\{O(C_6H_4)CH\}][Al(C_3)]$
214	$[C_2H_8Al\{O(C_6H_4)\}][Al(C_3)]$
198	$[C_2H_8Al(C_6H_4)][Al(C_3)]$
197	$[C_2H_7Al(C_6H_4)][Al(C_3)]$
m/e	$EtAl\{O(C_6H_4)CH{=}NC_6H_5\}_2$ (**2**)
460	$EtAl\{O(C_6H_4)CH{=}NC_6H_5\}_2\cdot C$
429	$Al\{O(C_6H_4)C{=}NC_6H_5\}_2\cdot C$
345	$\{O(C_6H_4)CH{=}NC_6H_5\}Al\{O(C_6H_4)CH_2NH_2\}$
333	$\{O(C_6H_4)CH{=}NC_6H_5\}Al\{O(C_6H_4)\}\cdot H_2O$
258	$\{O(C_6H_4)CH{=}NC_6H_5\}Al(OH)\cdot H_2O$
240	$\{O(C_6H_4)CH{=}NC_6H_5\}Al(OH)$
223	$\{O(C_6H_4)CH{=}NC_6H_5\}Al$
196	$\{O(C_6H_4)CH{=}NC_6H_5\}$
154	$\{O(C_6H_4)CN\}\cdot(H_2O)_2$
136	$\{O(C_6H_4)CN\}\cdot(H_2O)$
120	$\{O(C_6H_4)CHNH\}$
104	$\{O(C_6H_4)C\}$
m/e	$Et_2Al\{OC(CH_3){=}CHC(CH_3){=}NC_6H_5\}$ (**3**)
518	$[Et_2Al\{OC(CH_3){=}CHC(CH_3){=}NC_6H_5\}]_2$
504	$[Et_2Al\{OC(CH_3){=}CHC(CH_3){=}NC_6H_5\}][Et_2Al\{OC(CH_3){=}CHC(CH_3){=}NC_5H_3\}]$
488	$[Et_2Al\{OC(CH_3){=}CHC(CH_3){=}NC_6H_5\}][Et_2Al\{OC(CH_3){=}CHC(CH_3){=}C_5H\}]$
476	$[Et_2Al\{OC(CH_3){=}CHC(CH_3){=}NC_6H_5\}][Et_2Al\{OC(CH_3){=}CHC(CH_3){=}C_4H\}]$
464	$[Et_2Al\{OC(CH_3){=}CHC(CH_3){=}NC_6H_5\}][Et_2Al\{OC(CH_3){=}CHC(CH_3){=}C_3H\}]$
433	$[Et_2Al\{OC(CH_3){=}CHC(CH_3){=}C_5\}][Et_2Al\{OC(CH_3){=}CHC(CH_3){=}C_3H\}]$
418	$[Et_2Al\{OC(CH_3){=}CHC(CH_3){=}C_5\}][Et_2Al\{OC{=}CHC(CH_3){=}C_3H\}]$
393	$[Et_2Al\{OC(CH_3){=}CHC(CH_3){=}C_5\}][Et_2Al\{OC{=}CHC(CH_3){=}C\}]$
367	$[Et_2Al\{OC(CH_3){=}CH_2C_5\}][Et_2Al\{OC{=}CHC(CH_3){=}C\}]$
351	$[Et_2Al\{OC(CH_3){=}CH_2C_5\}][Et_2Al\{C{=}CHC(CH_3){=}C\}]$
327	$[Et_2Al\{OC(CH_3){=}CH_2C_3\}][Et_2Al\{C{=}CHC(CH_3){=}C\}]$
311	$[Et_2Al\{C(CH_3){=}CH_2C_3\}][Et_2Al\{C{=}CHC(CH_3){=}C\}]$
295	$[Et_2Al\{C(CH_3){=}CH_2C_3\}][Et_2Al\cdot C_4]$
282	$[Et_2Al\{C(CH_3){=}C_3H\}][Et_2Al\cdot C_4]$
281	$[Et_2Al\{C(CH_3){=}C_3\}][Et_2Al\cdot C_4]$
267	$[Et_2Al\{CH.C_3\}][Et_2Al\cdot C_4]$
175	$[Et_2Al][CH_3Al\cdot C_4]$
160	$[Et_2Al][Al\cdot C_4]$
134	$[C_2H_8Al][Al\cdot C_4]$
132	$[C_2H_6Al][Al\cdot C_4]$
118	$[CH_4Al][Al\cdot C_4]$
91	$[CH_4Al]\cdot C_4$
89	$[CH_2Al]\cdot C_4$
76	$[HAl]\cdot C_4$

$CH{=}NC_6H_5\}_2$]Br was mounted on a glass fiber. The data collection and cell refinement gave cell constants corresponding to a monoclinic cell whose dimensions are given in Table 6 along with other experimental and refinement parameters. The structure was solved by direct methods using SIR97 [22], and refined with SHELX-97 [23]. The graphical representation of the molecular structure of **9** was generated with ORTEP [24].

3. Results and discussion

3.1. Syntheses

All the above reactions were carried out under a strictly anhydrous and inert atmosphere. Reactions of $Et_3Al{\cdot}Et_2O$ with the corresponding Schiff base ligands in 1:1 and 1:2 molar ratios in diethyl ether afforded products of the types $Et_2Al\{O(C_6H_4)CH{=}NC_6H_5\}$ (**1**), $EtAl\{O(C_6H_4)CH{=}NC_6H_5\}_2$ (**2**), $Et_2Al\{OC(R){=}CHC(R^1){=}NC_6H_5\}$(**3**, **5**, **7**) and $EtAl\{OC(R){=}CHC(R^1){=}NC_6H_5\}_2$ (**4**, **6**, **8**) ($R = R^1 = CH_3$, C_6H_5; $R = CH_3$, $R^1 = C_6H_5$), whereas the reaction of Et_2AlBr with $HO(C_6H_4)CH{=}NC_6H_5$ in a 1:4 molar ratio in diethyl ether afforded the product $[Al\{O(C_6H_4)CH{=}NC_6H_5\}_2\{HO(C_6H_4)CH{=}NC_6H_5\}_2]Br$ (**9**). The general reactions may be illustrated schematically as:

$$Et_3Al\cdot Et_2O + nLH \xrightarrow[\text{stirring}]{Et_2O} \underset{\mathbf{1\text{–}8}}{Et_{3-n}AlL_n} + nEtH$$

$$LH{=}HO(C_6H_4)CH{=}NC_6H_5; HOC(R){=}CHC(R^1){=}NC_6H_5$$
$$(R = R^1 = CH_3, C_6H_5; R = CH_3, R^1 = C_6H_5; n = 1, 2)$$

$$Et_2AlBr + 4HO(C_6H_4)CH{=}NC_6H_5 \xrightarrow[\text{stirring}]{Et_2O} \underset{\mathbf{9}}{[Al\{O(C_6H_4)CH{=}NC_6H_5\}_2\{HO(C_6H_4)CH{=}NC_6H_5\}_2]Br} + 2EtH$$

All the above complexes are yellow or orange solids or pastes (Table 1) and are soluble in common organic solvents. These compounds were purified by recrystallization from a mixture of dichloromethane and *n*-hexane. Molecular weight measurements indicate the monomeric nature of the monoethyl complexes (**2**, **4**, **6** and **8**) and the dimeric nature of the diethylaluminium(III) complexes (**1**, **3**, **5** and **7**) in refluxing benzene.

3.2. FAB mass spectra

The FAB mass spectra of three representative compounds, $Et_2Al\{O(C_6H_4)CH{=}NC_6H_5\}$ (**1**), $EtAl\{O(C_6H_4)CH{=}NC_6H_5\}_2$ (**2**) and $Et_2Al\{OC(CH_3){=}CHC(CH_3){=}NC_6H_5\}$ (**3**) have been recorded and the characteristic signals for the fragmentation of these compounds are summarized in Table 3.

The FAB mass spectral studies of the representative compounds suggest the monomeric nature of the monoethyl complexes and the dimeric nature of the diethyl complexes. The molecular ion peaks for the dimeric complexes (**1**) and (**3**) appear at the expected positions. However, the FAB mass spectrum of complex (**2**) exhibits signals with higher *m*/*e* than the molecular ion peak, suggesting that the complex is associated in the solid state.

3.3. IR spectra

Tentative assignments of the important IR bands have been made and are summarized in Table 4. Broad stretching vibrations at $\sim$2900 cm^{-1} due to the –OH group of the free Schiff bases (Table 2) disappeared in the IR spectra of the above derivatives, suggesting the deprotonation of the –OH group and formation of Al–O bonds. Formation of Al–O [25,26] bonds is further supported by the appearance of a band of medium to strong intensity in the 684–725 cm^{-1} region.

Table 4
Some relevant IR spectral data of aluminium(III) complexes **1**–**8** (in cm^{-1})

S.No.	Complexes	Schiff base moiety ν(C=N)	ν(Al–C)	ν(Al–O)	ν(Al–N)	ν(Al–O–Al)
1	$Et_2Al\{O(C_6H_4)CH{=}NC_6H_5\}$	1580 s	550 w	725 s	683 s	750 vs
2	$EtAl\{O(C_6H_4)CH{=}NC_6H_5\}_2$	1550 s	550 m	708 m	683 m	
3	$Et_2Al\{OC(CH_3){=}CHC(CH_3){=}NC_6H_5\}$	1583 s	600 m	684 s	634 m	750 vs
4	$EtAl\{OC(CH_3){=}CHC(CH_3){=}NC_6H_5\}_2$	1583 s	550 m	700 s	616 m	
5	$Et_2Al\{OC(CH_3){=}CHC(C_6H_5){=}NC_6H_5\}$	1550 s	600 w	684 m	634 w	750 vs
6	$EtAl\{OC(CH_3){=}CHC(C_6H_5){=}NC_6H_5\}_2$	1540 s	600 w	700 m	649 w	
7	$Et_2Al\{OC(C_6H_5){=}CHC(C_6H_5){=}NC_6H_5\}$	1550 s	550 m	708 m	616 m	750 vs
8	$EtAl\{OC(C_6H_5){=}CHC(C_6H_5){=}NC_6H_5\}_2$	1566 s	583 m	718 s	633 s	

The shifting of ν(C=N) stretching frequencies to lower wave numbers as compared to the free ligand moieties (Table 2), indicates the coordination of the nitrogen atom of the ligand to aluminium. This was further confirmed by the appearance of a new medium-sized band in the 616–683 cm^{-1} region, which may be assigned to the ν(Al–N) mode [14,16]. The weak to medium absorptions in the 550–600 cm^{-1} region were assigned to ν(Al–C). In the 1:1 complexes, an additional medium-sized band at 750 cm^{-1} was also observed and assigned as ν(Al–O–Al) [15,16].

3.4. ^1H NMR spectra

The important signals in ^1H NMR spectra of these derivatives are summarized in Table 4. A comparison of the spectra of the free Schiff bases (Table 2) with the spectra of the corresponding derivatives (Table 5) shows the absence of –OH signals, indicating deprotonation of the hydroxy group of the Schiff bases and formation of Al–O bonds occurred. This is supported by the significant shift of the methyl, phenyl and CH signals of the ligand moiety. The ^1H NMR spectra of these derivatives exhibit characteristic peaks and peak multiplicities for the Et–Al and ligand protons [27,28], whereby the CH_2 and CH_3 protons of the Et–Al group appear in the δ 0.06–0.19 ppm and δ 1.07–1.58 ppm range, respectively. Other resonances appeared at their expected positions (Table 4).

3.5. ^{13}C NMR spectra

The mode of bonding suggested above has also been confirmed by the ^{13}C NMR spectral data (Table 5). In the ^{13}C NMR spectra of the complexes, the CH_2 and CH_3 carbon signals of the EtAl group appear in the ranges δ 0.92–1.09 ppm and δ 9.30–20.30 ppm, respectively. The azomethine (C=N) carbon is deshielded on complexation and a signal appears in the δ 160.0–176.5 ppm range. This deshielding provides further support for the coordination of the ligand through the azomethine nitrogen to the aluminium atom (see Fig. 1).

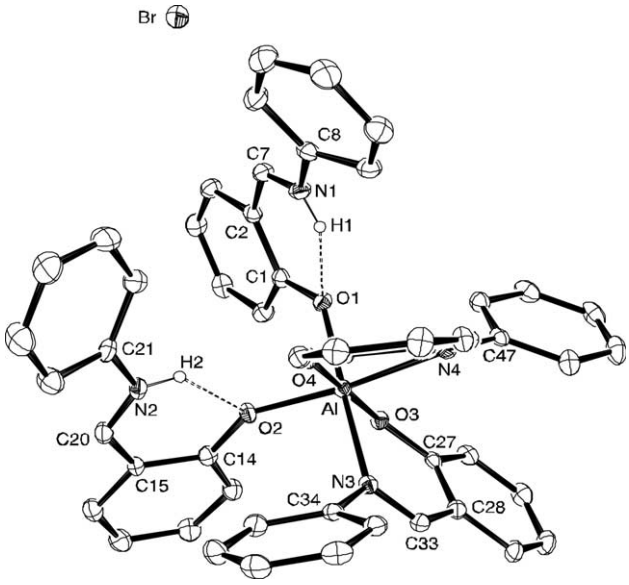

Fig. 1. Molecular structure of $[Al\{O(C_6H_4)CH{=}NC_6H_5\}_2\{HO(C_6H_4)CH{=}NC_6H_5\}_2]Br$ (**9**).

3.6. ^{27}Al NMR spectra

^{27}Al NMR spectra of the complexes **1**–**8** exhibit a broad signal in the region δ 68.0–71.2 ppm, indicating that the central aluminium atom is pentacoordinated [28–32]. It is interesting to mention here that in contrast

Table 5
NMR (^1H, ^{13}C, and ^{27}Al) spectral data of aluminium(III) complexes **1**–**8**

Complex No.	^1H NMR		^{13}C NMR		^{27}Al NMR
	Ethyl moiety	Schiff base moiety	Ethyl moiety	Schiff base moiety	
1	0.12 m (CH_2); 1.07 t (CH_3)	6.59–7.67 m (Phenyl); 8.37 s (*CH*=N)	1.07 (CH_2); 9.30 (CH_3)	116.3–135.3 (aromatic carbons); 167.5 (*C*H=N)	68.7
2	0.12 m (CH_2); 1.26 m (CH_3)	6.65–7.48 m (Phenyl); 8.05 s (*CH*=N)	1.07 (CH_2); 18.8 (CH_3)	115.3–135.0 (aromatic carbons); 168.7 (*C*H=N)	71.2
3	0.09 m (CH_2); 1.30 m (CH_3)	1.80 s, 2.06 s (CH_3); 5.23 s (*CH*); 7–7.48 m (NC_6H_5)	1.09 (CH_2); 19.7 (CH_3)	29.0, 29.1 (CH_3); 97.7 (*C*H); 115.1–139.0 (aromatic carbons); 160.0 (*C*=N); 196.1 (–O*C*)	70.5
4	0.06 br (CH_2); 1.26 m (CH_3)	1.65 s, 1.74 s (CH_3); 4.91 s (*CH*); 6.97–7.35 m (NC_6H_5)	0.95 (CH_2); 19.6 (CH_3)	25.0, 29.0 (CH_3); 97.6 (*C*H); 123.9–132.2 (aromatic carbons); 169.7, 171.6 (*C*=N); 196.0 (–O*C*)	68.9
5	0.06 m (CH_2); 1.35 t (CH_3)	2.18 s (CH_3); 5.80 s (*CH*); 6.78–8.05 m (C_6H_5)	1.04 (CH_2); 19.0 (CH_3)	24.0 (CH_3); 94.4 (*C*H); 122.9–140.1 (aromatic carbons); 172.7 (*C*=N); 188.9 (–O*C*)	68.0
6	0.15 m (CH_2); 1.58 m (CH_3)	2.21 s (CH_3); 5.95 s (*CH*); 6.78–8.05 m (C_6H_5)	1.04 (CH_2); 20.3 (CH_3)	24.6 (CH_3); 94.4 (*C*H); 123.0–140.7 (aromatic carbons); 162.0 (*C*=N); 188.9 (–O*C*)	70.2
7	0.12 m (CH_2); 1.07 t (CH_3)	5.95 s (*CH*); 6.97–7.35 m (C_6H_5)	1.07 (CH_2); 9.30 (CH_3)	95.0 (*C*H); 123.0–140.1 (aromatic carbons); 173.2 (*C*=N); 196.0 (–O*C*)	70.5
8	0.19 m (CH_2); 1.26 t (CH_3)	6.21 s (*CH*); 6.72–8.05 m (C_6H_5)	0.92 (CH_2); 10.2 (CH_3)	95.5 (*C*H); 123.9–140.3 (aromatic carbons); 176.5 (*C*=N); 196.1 (–O*C*)	71.2

to the above, the crystal structure analysis of the dimethyl corresponding derivative, Me_2AlL, suggests a monomeric nature and tetracoordination around the central aluminium(III) atom in the solid state [13,32]. This difference in behavior appears to be quite unusual and difficult to explain without single crystal X-ray analysis. As mentioned earlier, the molecular weight measurement in boiling benzene suggest a monomeric nature for the complexes of the type $EtAlL_2$ (**2**, **4**, **6** and **8**) but a dimeric nature for Et_2AlL (**1**, **3**, **5** and **7**), this observation gets further support from the FAB mass spectral studies of the three representative compounds (Table 3).

Therefore, on the basis of the above studies the following tentative structures may be proposed (Figs. 2 and 3) see Table 6.

3.7. Molecular structure of $[Al\{O(C_6H_4)CH{=}NC_6H_5\}_2\{HO(C_6H_4)\text{-}CH{=}NC_6H_5\}_2]Br$ (9)

The most important bond lengths and angles of **9** are given in Table 7, and its molecular structure is shown in Fig. 1. Octahedrally coordinated by 4 oxygen and 2 nitrogen atoms, the Al(III) center is surrounded by two anionic salicylaldiminato ligands, acting as bidentate N,O-chelates and two O-bound salicylaldimine ligands in *cis*-positions (O1–Al1–O2 = 89.2(1)°). The latter ones coordinate in a *trans*-position to the N atom of the chelate system (O1–Al1–N3 = 175.18(11)° and O2–Al1–N4 = 172.99(11)°). The four Al–O bond lengths vary between 1.81 and 1.89 Å, whereas both Al–N bonds are almost constant (Al1–N3 = 2.107(3) and Al1–N4 = 2.102(3) Å). The distortion of the octahedron at Al1 mainly results from the different angles, e.g., those from the monodentate O1 or O2 to the O or N atoms of the chelates vary between 86.43(11)° (O–Al1–N4) and 96.58(10)° (O2–Al1–O3). It is noteworthy that only three angles are almost 90° (O1–Al1–O2 = 89.20(10)°, O3–Al1–N4 = 89.33(10)° and N3–Al1–N4 = 90.69(10)°), whereas the two angles resulting from the chelating function are somewhat smaller than 90° (O3–Al1–N3 = 88.19(10°) and O4–Al1–N4 = 87.76 (10)°).

Two facts must be emphasized: first, within both monodentate salicylaldiminato-O ligands strong hydrogen bridges exist between the atoms O1 and N1 or O2 and N2. Their lengths are about 2.61 Å, whereby in both

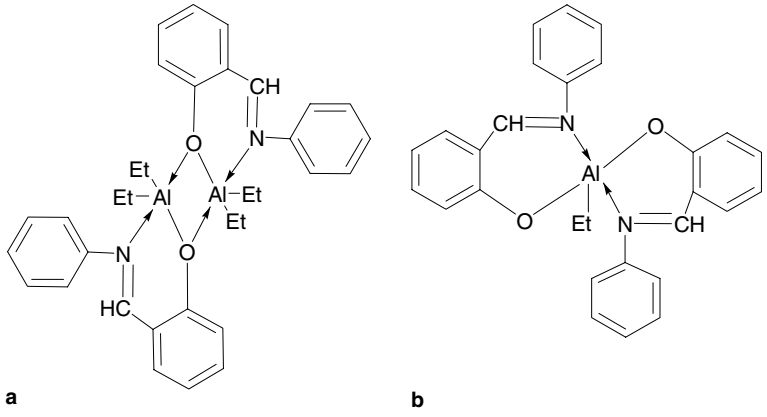

Fig. 2. Proposed structures of $Et_2Al\{O(C_6H_4)CH{=}NC_6H_5\}$ (a) and $EtAl\{O(C_6H_4)CH{=}NC_6H_5\}_2$ (b).

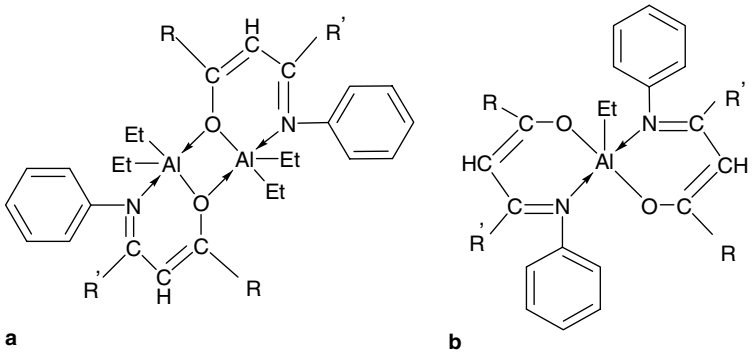

Fig. 3. Proposed structures of $Et_2Al\{OC(R){=}CHC(R^1){=}NC_6H_5\}$ (a) and $EtAl\{OC(R){=}CHC(R^1){=}NC_6H_5\}_2$ (b) (where $R = R^1 = CH_3$, C_6H_5; $R = CH_3$, $R^1 = C_6H_5$).

Table 6
Crystal data and structure refinement for $[Al\{O(C_6H_4)CH{=}NC_6H_5\}_2\{HO(C_6H_4)CH{=}NC_6H_5\}_2]Br$ (**9**)

	1
Empirical formula	$C_{52}H_{42}AlBrN_4O_4$
M_r (g mol^{-1})	893.800
Crystal system	monoclinic
Space group	$P2_1/n$
a (Å)	12.1230(2)
b (Å)	14. 4654(2)
c (Å)	25.7494(4)
α (°)	90
β (°)	101.1286(5)
γ (°)	90
V (Å^3)	4430.61(12)
Z	4
ρ (g cm^{-3})	1.33996(4)
μ (mm^{-1})	0.999
Crystal size (mm)	$0.20 \times 0.11 \times 0.06$
Temperature (K)	200(2)
Diffractometer	'KappaCCD'
Radiation	Mo Kα (0.71073)
Anode	'rotating anode'
Absorption capacity (kW)	4.125
θ-Range (°)	3.47–25.00
Reflections	80 007
Absorption correction	numerical
Transmission factors	0.8698–0.9427
F(000)	1848
Observed reflections	43 323
Independent reflections	7783
R_{int}	0.0702
Average value $\sigma(I)/I$	0.0487
Reflections with $I \geqslant 2\sigma(I)$	5790
x, y (weighting factor)	0.0775, 5.5128
Parameters refined	727
Restraints	2
R (F_{obs})	0.0522
R_w (F^2)	0.1516
S	1.028
Shift/error$_{max}$	0.001
Residuals (e Å^{-3})	0.326, −0.975

cases the hydrogen atoms come significantly closer to nitrogen (N–H ≈ 0.8 Å) than to oxygen (O···H ≈ 2.0 Å). Again this hydrogen bonding interaction gets weakened on complexation with the central aluminium(III) atom in comparison to the free ligand (O–N: 2.598(8) Å) [33]. Furthermore, in the free state the salicylaldimine molecule is nearly planar. In **9**, however, the two planes of each of the four ligands are distorted to each other as indicated in Table 7 [C_{Ph2}–C_{Ph8} = 23.6(2), C_{Ph18}–C_{Ph21} = 33.4(2), C_{Ph27}–C_{Ph34} = 50.47(18) and C_{Ph40}–C_{Ph47} = 37.95(18)]. The dihedral angles between both planes in the monocoordinated ligands are significantly smaller (C1–C13: 23.6(2)° and C14–C26: 33.4(2)°) than those in the bidentate ligands (C27–C39: 50.47(18)° and C40–C52. 37.95(18)°). The reason may be due to steric hindrance of the two chelating ligands in the *cis*-position.

Table 7
Selected bond lengths (Å) and angles (°) for $[Al\{O(C_6H_4)CH{=}NC_6H_5\}_2\{HO(C_6H_4)CH{=}NC_6H_5\}_2]Br$ (**9**)

Bond lengths	
Al(1)–O(1)	1.893(2)
Al(1)–O(2)	1.855(2)
Al(1)–O(3)	1.816(2)
Al(1)–O(4)	1.850(2)
Al(1)–N(3)	2.107(3)
Al(1)–N(4)	2.102(3)
O(1)–C(1)	1.309(4)
O(2)–C(14)	1.315(4)
O(3)–C(27)	1.324(4)
O(4)–C(40)	1.322(4)
N(1)–C(8)	1.423(5)
N(2)–C(21)	1.425(5)
N(3)–C(34)	1.451(4)
N(4)–C(47)	1.450(4)
N (1)–C(7)	1.300(4)
N (2)–C(20)	1.286(5)
N (3)–C(33)	1.288(4)
N (4)–C(46)	1.298(4)
N(1)–H(1)	0.79(3)
N (2)–H(2)	0.79(2)
O(1)···H(1)	1.98(3)
O(2)···H(2)	2.03(3)
O(1)···N(1)	2.625(4)
O(2)···N(2)	2.605(4)
Bond angles	
O(1)–Al(1)–O(2)	89.20(10)
O(1)–Al(1)–O(3)	96.15(10)
O(1)–Al(1)–O(4)	87.84(10)
O(1)–Al(1)–N(3)	175.18(11)
O(1)–Al(1)–N(4)	86.43(11)
O(2)–Al(1)–O(3)	96.58(10)
O(2)–Al(1)–O(4)	86.60(10)
O(2)–Al(1)–N(3)	93.29(10)
O(2)–Al(1)–N(4)	172.99(11)
O(3)–Al(1)–O(4)	174.91(11)
O(3)–Al(1)–N(3)	87.67(10)
O(3)–Al(1)–N(4)	89.33(10)
O(4)–Al(1)–N(3)	88.19(10)
O(4)–Al(1)–N(4)	87.76(10)
O(3)–Al(1)–N(4)	90.69(10)
C_{Ph2}–C_{Ph8}	23.6(2)
C_{Ph18}–C_{Ph21}	33.4(2)
C_{Ph27}–C_{Ph34}	50.47(18)
C_{Ph40}–C_{Ph47}	37.95(18)

4. Conclusion

Above studies indicates that in all ethylaluminium(III) (both Et_2AlL and $EtAlL_2$) complexes the central aluminium atom is pentacoordinated, either by inter or intramolecular coordinating interactions. However, the existence of pentacoordination in dimeric Et_2AlL type complexes is in contrast to what was reported for their corresponding dimethyl derivatives (monomeric and tetracoordinated). The crystal structure analysis of compound **9** revealed the presence of two types of ligand moieties in the complex. The dihedral angles between the two rings of all four ligand moieties are

increased on complexation with the aluminium atom. The hydrogen atom of the monodentate ligands are much closer to the nitrogen atom in comparison to the oxygen atom.

5. Supplementary material

The crystal code for $[Al\{O(C_6H_4)CH{=}NC_6H_5\}_2\{HO(C_6H_4)CH{=}NC_6H_5\}_2]Br$ is CCDC No. (gn 147) 258319. Supplementary data are available from the Director, 12 Union Road, Cambridge, CB2 1EZ, UK, fax: +44 1223 336033, e-mail: deposit@ccdc.cam.ac.uk or www: http://www.ccdc.cam.ac.uk on request, quoting the deposition number (gn 147) 258319 Additional material available from the Cambridge Crystallographic Data Centre comprises the final atomic coordinates for all atoms, parameters and a complete listing of bond distances and angles.

Acknowledgements

One of the authors (A.K. Jain) is grateful to DST, New Delhi for the award of JRF and another (A.G.) is thankful to CSIR, New Delhi for the award of RA. We are thankful to DST and UGC, New Delhi for financial support.

References

[1] B. Gates, Catalytic Chemistry, Wiley, New York, 1992.
[2] M.R. Mason, J.M. Smith, S.G. Bott, A.R. Barron, J. Am. Chem. Soc. 115 (1993) 4791.
[3] R.L. Graham, J.C. Christopher, S. Lothar, Organometallics 20 (2001) 1629.
[4] D.A. Atwood, M.J. Harvey, Chem. Rev. 101 (2001) 37.
[5] L. Canali, D.C. Sherrington, Chem. Soc. Rev. 28 (1999) 85.
[6] V.C. Gibson, S.K. Spitzmesser, Chem. Rev. 103 (2003) 283.
[7] P.A. Camerson, V.C. Gibson, C. Redshaw, J.A. Segal, M.D. Bruce, A.J.P. White, D.J. Williams, Chem. Commun. (1999) 1883.
[8] P.A. Cameron, V.C. Gibson, D.J. Jrvine, Angew. Chem. 112 (2000) 2225.
[9] P.A. Cameron, V.C. Gibson, D.J. Jrvine, Angew. Chem., Int. Ed. 39 (2000) 2141.
[10] (a) T.M. Ovitt, G.W.J. Coates, J. Am. Chem. Soc. 124 (2002) 1316;
(b) N. Nomura, R. Ishii, M. Akakura, K. Aol, J. Am. Chem. Soc. 124 (2002) 5938.
[11] P.A. Cameron, V.C. Gibson, C. Redshaw, J.A. Segal, G.A. Solan, A.J.P. White, D.J. Williams, J. Chem. Soc., Dalton Trans. (2001) 1472.
[12] M.S. Hills, A.R. Hutchison, T.S. Keizer, S. Perkin, M.A. Van-Aelstyn, D.A. Atwood, J. Organomet. Chem. 628 (2001) 71.
[13] J. Lewinski, J. Zachara, K.B. Starowiegski, Z. Ochal, I. Justyniak, T. Kopec, P. Stolarzewicz, M. Dranka, Organometallics 22 (2003) 3773.
[14] A. Dhammani, R. Bohra, R.C. Mehrotra, Polyhedron 15 (1996) 733.
[15] N. Sharma, R.K. Sharma, R. Bohra, Main Group Met. Chem. 24 (2001) 781.
[16] N. Sharma, R.K. Sharma, R. Bohra, J.E. Drake, M.B. Hursthouse, M.E. Light, J. Chem. Soc., Dalton Trans. (2002) 1631.
[17] N. Sharma, R.K. Sharma, R. Bohra, J. Chem. Res. (2003) 622.
[18] A.K. Jain, R. Bohra, R.C. Mehrotra, S. Nagar, S. Sharma, Heteroatom Chem. 14 (2003) 518.
[19] N. Sharma, A.K. Jain, R.K. Sharma, R. Bohra, J.E. Drake, M.B. Hursthouse, M.E. Light, Polyhedron 22 (2003) 2943.
[20] N. Auner, U. Klingebiel, Synthetic Methods of Organometallic and Inorganic Chemistry, vol. 2, Georg Thieme Verlag Stuttgart, New York, 1996.
[21] A.I. Vogel, Text Book of Quantitative Chemical Analysis, fifth ed., Longmans, London, 1998.
[22] A. Altomare, M.C. Burla, M. Camalli, G.L. Cascarano, C. Giacovazzo, A. Guagliardi, A.G.G. Moliterni, G. Polidori, R. Spagna, J. Appl. Crystallogr. 32 (1999) 115.
[23] SHELXL-97 (G.M. Sheldrick, University of Gottingen, 97-2 version).
[24] ORTEP (M.N. Burnett, C.K. Johnson, ORTEP-III: Oak Ridge Thermal Ellipsoid Plot Program for Crystal Structure Illustrations, Oak Ridge National Laboratory Report ORNL-6895, 1996). Windows version (L.J. Farrugia, University of Glasgow)
[25] A. Singh, A.K. Rai, R.C. Mehrotra, Indian J. Chem. 11 (1973) 478.
[26] R. Bohra, A. Dhammani, R.K. Sharma, R.C. Mehrotra, Synth. React. Inorg. Met. Org. Chem. 36 (2001) 681.
[27] J. Lewinski, I. Justyniak, J. Zachara, E. Tratkiewicz, Organometallics 22 (2003) 4151.
[28] C.J. Carmalt, J.D. Mileham, A.J.P. White, D.J. Williams, Organometallics 22 (2003) 1554.
[29] S.J. Dzugan, V.L. Goedken, Inorg. Chem. 25 (1986) 2858.
[30] Z. Jiang, L.V. Interrante, D. Kwon, F.S. Tham, R. Kulling, Inorg. Chem. 30 (1991) 995.
[31] W. Ziemkowska, S. Pasynkiewicz, T. Skrok, Main Group Met. Chem. 21 (1998) 105.
[32] R.-C. Yu, C.-H. Hung, J.-H. Huang, H.-Y. Lee, J.-T. Chen, Inorg. Chem. 41 (2002) 6450.
[33] R. Destro, A. Gavezzotti, M. Simonetta, Acta Crystallogr. B 34 (1978) 2867.

Available online at www.sciencedirect.com
SCIENCE DIRECT®
Polyhedron 25 (2006) 663–670
POLYHEDRON
www.elsevier.com/locate/poly

Bimetallic complex of the type $[Cu(tren)(NCS)]_4[Mn(NCS)_6]$: A hydrogen bonded network structure

Doyel Bose [a], Golam Mostafa [b], Rosa D. Bailey Walsh [c], Michael J. Zaworotko [c], Barindra K. Ghosh [a,*]

[a] Department of Chemistry, The University of Burdwan, Golapbag, Burdwan 713 104, India
[b] Department of Physics, Jadavpur University, Kolkata 700 032, India
[c] Department of Chemistry, The University of South Florida, SCA 400, 4202 East Fowler Avenue, Tampa, FL 33620-5250, USA

Received 1 July 2005; accepted 7 August 2005
Available online 5 October 2005

Abstract

$MnCl_2 \cdot 4H_2O$, $Cu(NO_3)_2 \cdot 3H_2O$, tris(2-aminoethyl)amine (tren) and NH_4NCS in a 1:4:4:10 molar ratio in aqueous solution results a bimetallic compound of the type $[Cu(tren)(NCS)]_4[Mn(NCS)_6]$ (**1**) which has been characterized by microanalytical, physicochemical, spectroscopic and magnetic results. The structure of the complex is determined by X-ray diffraction study. Some pertinent crystal data are: monoclinic, space group $P21/c$, $a = 11.0442(9)$ Å, $b = 14.4923(12)$ Å, $c = 19.2505(16)$ Å, $\beta = 91.95(10)°$, and $Z = 4$. The crystal structure consists of a hydrogen bonded 3D network of $[Cu(tren)(NCS)]^+$ and $[Mn(NCS)_6]^{4-}$ ions. Manganese(II) has an MnN_6 chromophore bound by six N atoms of the terminal thiocyanates. Each copper(II) centre is five coordinated by one N atom of terminal thiocyanate and four N atoms of the tripod ligand. Four copper(II) units are hydrogen bonded to form a hydrogen bonded tetramer. Each manganese(II) in turn is further engaged in hydrogen bonding to four such tetramers leading to the 3D network. Variable-temperature magnetic study shows no significant magnetic interactions among the metal ions connected by hydrogen bonding.
© 2005 Elsevier Ltd. All rights reserved.

Keywords: Copper(II)/manganese(II); Bimetallic; Tris(2-aminoethylamine); Molecular ion; Supramolecular chemistry

1. Introduction

In recent times great effort has been devoted to the self-assembly of organic and inorganic molecules in the solid state because it extends the range of new solids with desirable physical and chemical properties [1]. The range and variety of self-assembled inorganic structures that can be constructed relies on suitable metal–ligand interactions and hydrogen bondings [2,3] and the various types of polymeric structures include 1D, 2D and 3D networks [4]. Cyanometallates with multiple connectors have been used to prepare such multidimensional polymers and supramers in combination with suitable complementary units containing potential acceptor site(s) [5–7]. We are interested in extending this view with other hexapseudohalogenometallates specially thiocyanate and have reported on the use of the molecular ion $[Cd(NCS)_6]^{4-}$ as multiple connector in combination with suitable complementary unit containing 3d/4d metal ion centres ligated by tris(2-aminoethylamine) (tren) and with potential acceptor sites [8]. Cadmium(II) [9] being a d^{10} ion does not permit any magnetic interaction between the paramagnetic centres. The present work stems from our interest to synthesize coordination compounds with a molecular ion containing paramagnetic metal centre, for example $[Mn(NCS)_6]^{4-}$ to observe its role on

* Corresponding author. Tel.: +91 342 2558545; fax: +91 342 2530452.
E-mail address: barin_1@yahoo.co.uk (B.K. Ghosh).

0277-5387/$ - see front matter © 2005 Elsevier Ltd. All rights reserved.
doi:10.1016/j.poly.2005.08.009

magnetic exchange between the paramagnetic [Cu(tren)-$(OH_2)]^{2+}$ complementary units. Copper was specifically chosen [10,11] as it offers a variety of geometries, like tetrahedral, square pyramidal or trigonal-bipyramidal coordination environment of comparable stability and this often leads to significant differences in the metal–ligand geometry and molecular overall shape. This metal ion as well as manganese(II) also finds significant use in bioinorganic chemistry [12] and magnetism [13]. Using $[Mn(NCS)_6]^{4-}$ as building block in conjunction with $[Cu(tren)(OH_2)]^{2+}$, results a bimetallic complex of the type $[Cu(tren)(NCS)]_4[Mn(NCS)_6]$ (**1**) instead of covalently bonded trinuclear entity $[Cu_2Mn(tren)_2(NCS)_6]$ or polymeric $[Cu_2Mn(tren)_2(NCS)_6]_n$. X-ray crystallography study shows the presence of discrete $[Cu(tren)(NCS)]^+$ and $[Mn(NCS)_6]^{4-}$ ions hydrogen bonded to form a 3D supramolecular continuum. Although the magnetic behaviour of this complex is less important yet its structure establishes the fact that non-covalent forces play a vital role in structure determination. The details of synthesis, structure and properties are described below.

2. Experimental

2.1. Materials

High purity tris(2-aminoethyl)amine (Fluka, Germany), copper nitrate trihydrate (E. Merck, India), manganese chloride tetrahydrate (E. Merck, India), and ammonium thiocyanate (E. Merck, India) were purchased from respective concerns and used as received. All other chemicals and solvents were AR grade and were used as received.

2.2. Physical measurements

Elemental analyses (carbon, hydrogen and nitrogen) were performed on a Perkin–Elmer 2400 CHNS/O elemental analyzer. IR spectra (KBr discs, 4000–300 cm^{-1}) were recorded using a Perkin–Elmer model RX 1 spectrometer. Molar conductance was measured using a Systronics conductivity meter where the cell constant was calibrated with 0.01 M KCl solution and dry MeOH was used as solvent. Ground state absorption measurements were made with a Jasco model V-530 UV–Vis spectrophotometer. Magnetic susceptibilities at room temperature were measured with a PAR 155 vibrating sample magnetometer with $Hg[Co(SCN)_4]$ as the reference. Measurements on powdered samples were performed in the temperature range 2–300 K using a Quantum Design MPMS-7 SQUID magnetometer in a magnetic field of 0.1 T. The experimental susceptibilities were corrected for the diamagnetism of the constituent atoms (Pascal Tables).

2.3. Preparation of $[Cu(tren)(NCS)]_4[Mn(NCS)_6]$

The bimetallic complex was synthesised by the reaction of $MnCl_2 \cdot 4H_2O$, $Cu(NO_3)_2 \cdot 3H_2O$, tren and NH_4NCS in aqueous solution at room temperature using four different procedures with varied yields. These are described below. Powder X-ray diffraction of the compounds obtained from the different methods have been performed and all the four powder X-ray diffraction (PXRD) data are identical. It indicates that all four compounds are same and are in same phase. X-ray crystallography was performed with the compound obtained from Method D.

2.3.1. Method A

An aqueous solution (5 cm^3) of NH_4NCS (0.457 g, 6 mmol) was added to a solution of $MnCl_2 \cdot 4H_2O$ (0.197 g, 1 mmol) in the same solvent (10 cm^3) with the formation of a colourless solution. In an another container $Cu(NO_3)_2 \cdot 3H_2O$ (0.483 g, 2 mmol) and tren (0.293 g, 2 mmol) were mixed together in water (10 cm^3) producing a bluish green solution. This coloured solution was added dropwise to the above colourless solution. The final bluish green mixture was filtered and left for slow evaporation in air. Bluish green rectangular crystals of **1** suitable for X-ray diffraction were formed after a week. Yield: 0.221 g (30%). *Anal.* Calc. for $C_{17}H_{36}N_{13}S_5Mn_{0.5}Cu_2$ (**1**): C, 27.63; H, 4.90; N, 24.67. Found: C, 27.56; H, 4.81; N, 24.47%. IR (KBr, cm^{-1}): ν(NCS) 2124, 2075, 2048. Λ_M (DMF, $ohm^{-1}\,cm^2\,mol^{-1}$): 139. UV–Vis (λ, nm): 260, 675, 885.

2.3.2. Method B

$MnCl_2 \cdot 4H_2O$ (0.197 g, 1 mmol), $Cu(NO_3)_2 \cdot 3H_2O$ (0.483 g, 2 mmol), tren (0.293 g, 2 mmol) and NH_4NCS (0.457 g, 6 mmol) were mixed in a single container containing 20 cm^3 water, which resulted a bluish green solution. The mixture was filtered and left for slow evaporation in air. Bluish green rectangular crystals were formed after a week. Yield: 0.235 g (32%). *Anal.* Calc. for $C_{17}H_{36}N_{13}S_5Mn_{0.5}Cu_2$ (**1**): C, 27.63; H, 4.90; N, 24.67. Found: C, 27.49; H, 4.79; N, 24.46%. IR (KBr, cm^{-1}): ν(NCS) 2125, 2074, 2048. Λ_M (DMF, $ohm^{-1}\,cm^2\,mol^{-1}$): 141. UV–Vis (λ, nm): 265, 675, 885.

2.3.3. Method C

$Cu(NO_3)_2 \cdot 3H_2O$ (0.242 g, 1 mmol), $MnCl_2 \cdot 4H_2O$ (0.394 g, 2 mmol), tren (0.293 g, 2 mmol) and NH_4NCS (0.457 g, 6 mmol) were mixed in a single container containing 20 cm^3 water, which resulted a bluish green solution. The mixture was filtered and left for slow evaporation. Bluish green crystals were formed after a few days. Yield: 0.294 g (40%). *Anal.* Calc. for $C_{17}H_{36}N_{13}S_5Mn_{0.5}Cu_2$ (**1**): C, 27.63; H, 4.90; N, 24.67. Found: C, 27.49; H, 4.85; N, 24.50%. IR (KBr, cm^{-1}):

ν(NCS) 2124, 2075, 2048. Λ_M (DMF, ohm^{-1} cm^2 mol^{-1}): 140. UV–Vis (λ, nm): 262, 670, 887.

2.3.4. Method D

To an aqueous solution (10 cm^3) of tren (0.966 g, 4 mmol) a solution of $Cu(NO_3)_2 \cdot 3H_2O$ (0.586 g, 4 mmol) in same solvent (5 cm^3) was added slowly in a glass beaker. In an another container, solution (10 cm^3) of NH_4NCS (0.761 g, 10 mmol) was added to $MnCl_2 \cdot 4H_2O$ (0.197 g, 1 mmol) in water (10 cm^3). The former blue solution was added dropwise to the latter colourless solution yielding a bluish green mixture. This was filtered and left for slow evaporation in air. Bluish green rectangular crystals of **1** suitable for X-ray diffraction were formed after two weeks. Yield: 0.626 g (85%). *Anal.* Calc. for $C_{17}H_{36}N_{13}S_5Mn_{0.5}Cu_2$ (**1**): C, 27.63; H, 4.90; N, 24.67. Found: C, 27.52; H, 4.82; N, 24.48%. IR (KBr, cm^{-1}): ν(NCS) 2124, 2075, 2048. Λ_M (DMF, ohm^{-1} cm^2 mol^{-1}): 140. UV–Vis (λ, nm): 262, 675, 883.

2.4. X-ray crystallography

Single crystals were obtained by slow evaporation of an aqueous solution of the reaction mixture. The crystal data and data collection parameters are listed in Table 1. Bluish green crystals suitable for X-ray crystallographic analyses were selected following examination under a microscope. Diffraction data were collected on a Bruker-AXS SMART APEX/CCD diffractometer using Mo Kα radiation, which were corrected for Lorentz and polarization effects and for absorption using the SADABS program [14]. The structure was solved by direct methods and the structure solution and refinement were based on $|F|^2$. All non-hydrogen atoms were refined with anisotropic displacement parameters whereas hydrogen atoms were placed in calculated positions and given isotropic U values 1.2 times that of the atom to which they are bonded. The crystallographic calculations were conducted with the SHELXTL v.6.1 program package [15].

Table 1
Crystal data and structure refinement parameters for **1**

Chemical formula	$C_{17}H_{36}N_{13}S_5Mn_{0.5}Cu_2$
Formula weight	737.44
Colour	blue green
Temperature (K)	200(2)
Wavelength (Å)	0.71073
Diffractometer	Bruker-AXS SMART
Crystal system, space group	monoclinic, $P2(1)/c$
a (Å)	11.0442(9)
b (Å)	14.4923(12)
c (Å)	19.2505(16)
β (°)	91.9510(10)
V (Å^3)	3079.4(4)
Z	4
ρ (Mg m^{-3})	1.591
μ (mm^{-1})	1.949
$F(000)$	1518
Crystal size (mm)	$0.35 \times 0.30 \times 0.20$
θ Range for data collection (°)	1.76–28.32
Limiting indices	$-14 \leqslant h \leqslant 14$, $-19 \leqslant k \leqslant 13$, $-18 \leqslant l \leqslant 25$
Reflections collected	18 800
Independent reflections [$R_{(int)}$]	7237 [0.0323]
Completeness to $\theta = 28.32°$ (%)	94.3
Data/restraints/parameters	7237/0/340
Goodness-of-fit on F^2	1.036
Final R indices [$I > 2\sigma(I)$]	$R_1 = 0.0343$, $wR_2 = 0.0835$
R indices (all data)	$R_1 = 0.0451$, $wR_2 = 0.0878$
Largest difference peak and hole (e Å^{-3})	0.434 and −0.279

3. Results and discussion

3.1. Synthesis and formulation

The bimetallic complex (**1**) was initially synthesised by reaction of $[Cu(tren)(OH_2)]^{2+}$ with $[Mn(NCS)_6]^{4-}$ at room temperature (298 K) with the aim to obtain heteropolymer $[Cu_2Mn(tren)_2(NCS)_6]_n$ or heterotrinuclear $[Cu_2Mn(tren)_2(NCS)_6]$. However, to our surprise a bimetallic compound of the type $[Cu(tren)(NCS)]_4[Mn(NCS)_6]$ (**1**) was obtained in low yield. The molecular ion, $[Mn(NCS)_6]^{4-}$, was generated in solution by addition of six moles of ammonium thiocyanate to one mole of manganese(II) chloride tetrahydrate in water. The complementary unit $[Cu(tren)(OH_2)]^{2+}$ was prepared by dropwise addition of two moles of tren to a two molar copper(II) nitrate trihydrate solution in water in separate containers. **1** resulted in low yield through union of $[Mn(NCS)_6]^{4-}$ and $[Cu(tren)(OH_2)]^{2+}$ building blocks (Method A; see Section 2.3.1). The details of the sequential reactions are summarised in Eqs. (1)–(3).

$$MnCl_2 \cdot 4H_2O + 6NH_4NCS \rightarrow (NH_4)_4[Mn(NCS)_6] + 2NH_4Cl + 4H_2O \quad (1)$$

$$2Cu(NO_3)_2 \cdot 3H_2O + 2tren \rightarrow 2[Cu(tren)(OH_2)](NO_3)_2 + 2H_2O \quad (2)$$

$$(NH_4)_4[Mn(NCS)_6] + 2[Cu(tren)(OH_2)](NO_3)_2 \rightarrow [Cu(tren)(NCS)]_4[Mn(NCS)_6] \quad (3)$$

The principle involved is the union of two complementary units viz. $[Mn(NCS)_6]^{4-}$, a molecular ion with multiconnectors behaving as potential donor and $[Cu(tren)(OH_2)]^{2+}$, monosolvento species with one labile reaction site acting as potential acceptor. The displacement of the weakly bound solvent molecule from the solvento complex in $[Cu(tren)(OH_2)]^{2+}$ by putative pseudohalide unit in $[Mn(NCS)_6]^{4-}$ triggers such complex. The mole ratios are so adjusted as to have neutral complex avoiding counter ions which might inter alia disrupt the solid state packing due to additional cation–anion interactions that would be difficult to control [16]. The preparation of **1** was also achieved by single-pot

[17] reaction using 1:2:2:6 molar ratio of $MnCl_2 \cdot 4H_2O$, $Cu(NO_3)_2 \cdot 3H_2O$, tren and NH_4NCS, respectively (Method B; see Section 2.3.2). It is to note that an aqueous solution of 1:2:2:6 molar ratio of $Cu(NO_3)_2 \cdot 3H_2O$, $MnCl_2 \cdot 4H_2O$, tren and NH_4NCS to generate complementary units, $[Cu(NCS)_6]^{4-}$ and $[Mn(tren)(OH_2)_2]^{2+}$ and thereby to isolate a heterocomplex also resulted **1** in low yield reflecting its special stability (Method C; see Section 2.3.3). However reactant ratio (1:4:4:10) of $MnCl_2 \cdot 4H_2O$, $Cu(NO_3)_2 \cdot 3H_2O$, tren and NH_4NCS corresponding to the product stoichiometry affords (Eq. (4)) **1** in good yield (Method D; see Section 2.3.4).

$$MnCl_2 \cdot 4H_2O + 4Cu(NO_3)_2 \cdot 3H_2O + 4tren + 10NH_4NCS \rightarrow [Cu(tren)(NCS)]_4[Mn(NCS)_6] + 2NH_4Cl + 8NH_4NO_3 + 16H_2O \quad (4)$$

The air-stable moisture-insensitive complex is moderately soluble in methanol, ethanol, acetonitrile, dimethylformamide and dimethylsulfoxide and the solubility increases on warming. However it is insoluble in water but soluble in polar organic solvents which indicates strong hydrogen bonding between the cations and anions. In methanol it shows conductivity value of 140 $ohm^{-1}\,cm^2\,mol^{-1}$ which reflects molecular association of the complex ions [18]. In IR three well resolved peaks are observed at 2124, 2075, 2048 cm^{-1} attributed to the ν(NCS) stretching mode [19]. Although all the pseudohalides are present as terminals but both N- and S- of the thiocyanates are engaged in different types of hydrogen bondings with the amine nitrogens. Presence of multiple bands is in line with different force constants of the thiocyanates. A band corresponding to ν(CS) stretching frequency appears at 769 cm^{-1}. The bands belonging to deformation frequency δ(NCS) are found as doublets at 468 and 472 cm^{-1}. The bimetallic assembly shows bands around 3325–3265 cm^{-1} due to N–H stretching of the NH_2 groups and weak bands in the range 2980–2900 cm^{-1} are assignable to the aliphatic C–H stretching vibration [20]. The complex displays multiple absorption bands and shoulders in the 200–1000 nm range in MeOH solution. A band at 883 nm is assignable to a d–d transition ($d_{x^2-y^2}, d_{xy} \rightarrow d_{z^2}$) of copper(II) moieties in trigonal bipyramidal (tbp) geometry. A higher energy shoulder is observed at 675 nm which is typical of copper(II) complexes with tbp geometry [21]. Absorption at 262 nm may be assigned due to ligand origin. The solid state reflectance spectrum shows a good correspondence to the solution spectrum indicating similar gross geometric and electronic structure in solid state and in solution.

3.2. Structure

$[Cu(tren)(NCS)]_4[Mn(NCS)_6]$ (**1**) exhibits a hydrogen bonded network of the asymmetric unit containing $[Cu(tren)(NCS)]^+$ and $[Mn(NCS)_6]^{4-}$ ions. An ORTEP plot of the asymmetric unit, a view of the supramolecular tetramer formed by four $[Cu(tren)(NCS)]^+$ units and a 3D network formed by N–H···N and N–H···S hydrogen bondings are shown in Figs. 1–3, respectively. Selected interatomic distances and angles are given in Table 2.

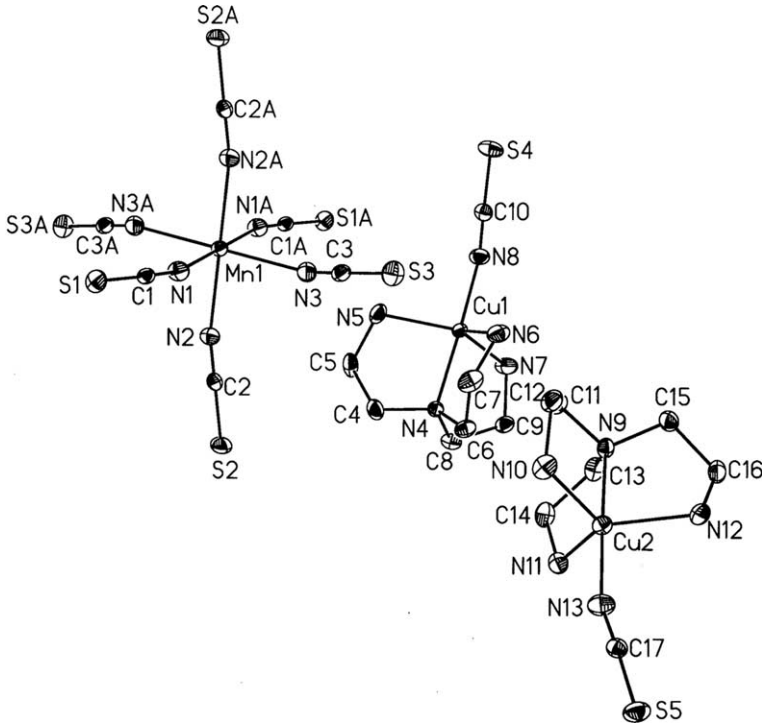

Fig. 1. ORTEP representation of the asymmetric unit in $[Cu(tren)(NCS)]_4[Mn(NCS)_6]$ (**1**).

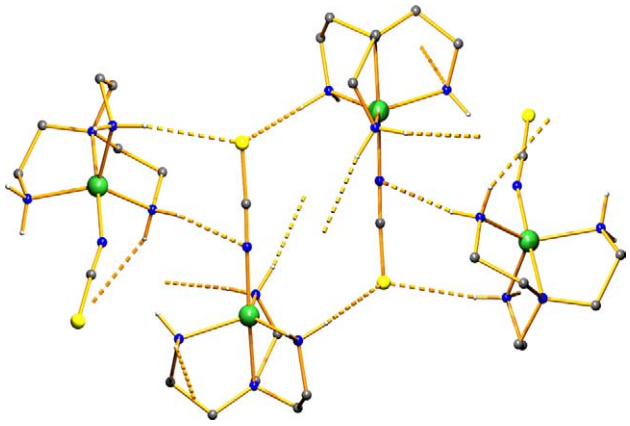

Fig. 2. Intermolecular N–H···S and N–H···N hydrogen bonded supramolecular tetramer formed by four $[Cu(tren)(NCS)]^{+}$ units. The dotted lines indicate N–H···X (X = N/S) hydrogen bonding.

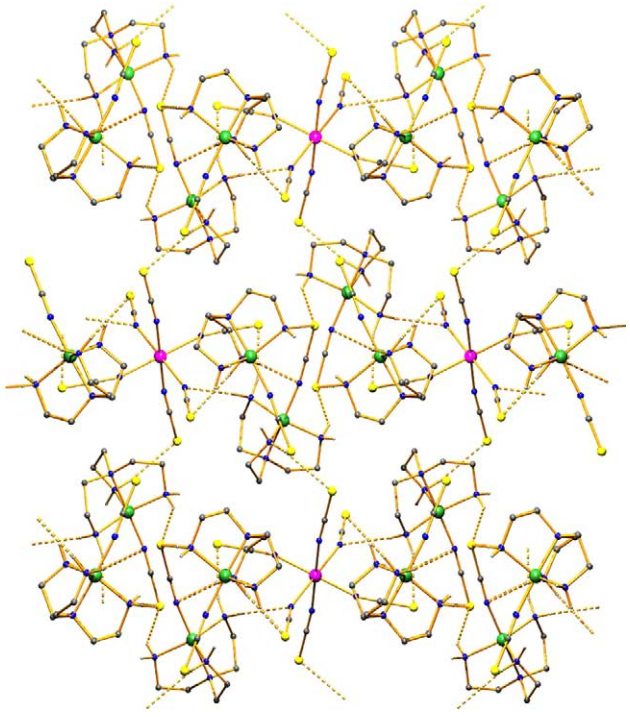

Fig. 3. 3D network formed by intermolecular N–H···S and N–H···N hydrogen bondings between the supramolecular tetramers and $[Mn(NCS)_6]^{4-}$ units. The dotted lines indicate N–H···X (X = N/S) hydrogen bonding.

The geometry around the manganese(II) atom in tetraanionic $[Mn(NCS)_6]^{4-}$ is best described as distorted octahedron with an MnN_6 chromophore. Manganese(II) is coordinated by N atoms of six terminal thiocyanate ligands (Fig. 1). The Mn-N bond lengths lie within a close range [2.208(2)–2.264(2) Å]. *Transoid* angles around Mn are exactly 180.00° whereas the *cisoid* angles [89.10(8)–90.90(8)°] are also close to ideal value (90°). The N–C–S angles [178.1(2)–179.8(2)°] of the six thiocyanates show their linear coordination.

Table 2
Selected bond distances (Å) and angles (°) for **1**

Bond distances	
Cu(1)–N(8)	1.952(2)
Cu(1)–N(7)	2.042(2)
Cu(1)–N(4)	2.0464(18)
Cu(1)–N(5)	2.054(2)
Cu(1)–N(6)	2.156(2)
Cu(2)–N(13)	1.941(2)
Cu(2)–N(9)	2.0333(19)
Cu(2)–N(11)	2.078(2)
Cu(2)–N(12)	2.078(2)
Cu(2)–N(10)	2.108(2)
Mn(1)–N(1*)	2.208(2)
Mn(1)–N(1)	2.208(2)
Mn(1)–N(2*)	2.217(2)
Mn(1)–N(2)	2.217(2)
Mn(1)–N(3*)	2.264(2)
Mn(1)–N(3)	2.264(2)
Bond angles	
N(8)–Cu(1)–N(7)	95.53(9)
N(8)–Cu(1)–N(4)	176.94(9)
N(7)–Cu(1)–N(4)	84.25(8)
N(8)–Cu(1)–N(5)	93.54(9)
N(7)–Cu(1)–N(5)	131.25(11)
N(4)–Cu(1)–N(5)	84.36(8)
N(8)–Cu(1)–N(6)	98.98(9)
N(7)–Cu(1)–N(6)	111.54(11)
N(4)–Cu(1)–N(6)	83.92(8)
N(5)–Cu(1)–N(6)	114.10(10)
N(13)–Cu(2)–N(9)	177.35(9)
N(13)–Cu(2)–N(11)	94.72(9)
N(9)–Cu(2)–N(11)	84.15(8)
N(13)–Cu(2)–N(12)	94.18(9)
N(9)–Cu(2)–N(12)	84.51(8)
N(11)–Cu(2)–N(12)	124.42(9)
N(13)–Cu(2)–N(10)	98.32(9)
N(9)–Cu(2)–N(10)	84.33(8)
N(12)–Cu(2)–N(10)	116.92(9)
N(11)–Cu(2)–N(10)	115.75(9)
N(1*)–Mn(1)–N(1)	180.00(10)
N(1*)–Mn(1)–N(2*)	90.19(7)
N(1)–Mn(1)–N(2*)	89.81(7)
N(1*)–Mn(1)–N(2)	89.81(9)
N(1)–Mn(1)–N(2)	90.19(7)
N(1*)–Mn(1)–N(3*)	89.84(8)
N(2*)–Mn(1)–N(3*)	89.10(8)
N(2)–Mn(1)–N(3*)	90.90(8)
N(1)–Mn(1)–N(3)	89.84(8)
N(1*)–Mn(1)–N(3)	90.16(8)
N(2*)–Mn(1)–N(2)	180.00(8)
N(1)–Mn(1)–N(3*)	90.16(8)
N(2)–Mn(1)–N(3)	89.10(8)
N(2*)–Mn(1)–N(3)	90.90(8)
N(3*)–Mn(1)–N(3)	180.00

The coordination geometry of the two types of copper(II) centres [Cu(1) and Cu(2)] in the asymmetric unit is best described as distorted trigonal bipyramid (tbp) with a CuN_5 chromophore (Fig. 1). Primary amine nitrogen atoms [N(5), N(6), N(7) for Cu(1), and N(10), N(11), N(12) for Cu(2)] of each tren occupy the equatorial positions around the metal ion. The tertiary amine nitrogen [N(4) for Cu(1) and N(9) for Cu(2)] is

located in the axial position *trans* to the pseudohalide nitrogen [N(8) for Cu(1) and N(13) for Cu(2)]. The bivalent metal centres are displaced [0.210 Å for Cu(1) and 0.206 Å for Cu(2)] from the equatorial plane towards the thiocyanate ligand. There is significant variation of the Cu–N distances [2.033(19)–2.156(2) Å] in the equatorial plane and these are longer compared to the Cu–N distances [1.941(2)–1.952(2) Å] of the pseudohalide. For Cu(2), the N–Cu–N bond angles in the equatorial plane [116.92(9)–124.42(9)°] span tight around 120°; whereas around Cu(1) these angles show greater deviation [111.54(11)–131.25(11)°]. The N(amine)–Cu–N(NCS) angles in the Cu(II) moieties are close [176.94(9)–177.35(9)°] to ideal value as found in regular tbp geometry [21b]. Distances between Cu(1)···Cu(1), Cu(2)···Cu(2) and Cu(1)···Cu(2) within the tetramer are 6.620, 6.078 and 5.550 Å, respectively. Shortest Mn(1)···Cu(1) and Mn(1)···Cu(2) distances are 6.999 and 7.018 Å, respectively.

The hydrogen bonding network that connects the thiocyanates and tren primary amines is an important feature of **1** (Table 3). Establishment of the network seems to be aiding the crystallization. Two sets of hydrogen bondings among different Cu(1) and Cu(2) centres form a supramolecular tetramer (Fig. 2). Within the tetramer, Cu(1) and its symmetry related counterpart participates in N–H···S hydrogen bonding [22] to form a cyclic motif, with $R_2^2(12)$ in Etter's graph notation [23]. This is further linked to Cu(2) and to its symmetry counterpart through two N–H···N hydrogen bonds [24] to complete the tetrameric form (Fig. 2). Each tetramer is alternately placed with the $[Mn(NCS)_6]^{4-}$ molecular ion and the pendant S atoms and bound N atoms of the manganese(II)-bound NCS groups are engaged in hydrogen bonding as detailed below.

In Cu(1) all the three primary amine nitrogen atoms [N(5), N(6) and N(7)] are engaged in hydrogen bonding of which one N–H···N and three N–H···S hydrogen bondings are present. N(5) involves in hydrogen bonding to a bound nitrogen [N(3)] of a terminal thiocyanate of the adjacent $[Mn(NCS)_6]^{4-}$ unit. Another N–H···S bond is formed between N(5) and pendant S(1) of the same $[Mn(NCS)_6]^{4-}$ unit. N(6) participates in N–H···S bonding with S(2), a terminal sulphur atom of a different $[Mn(NCS)_6]^{4-}$ unit. [N(7)] is engaged in hydrogen bonding with a terminal thiocyanate sulphur [S(4)] of its symmetry related counterpart which is one of the two N–H···S bonds forming the cyclic loop in the tetramer (Fig. 2). In contrast to Cu(1), in Cu(2) only two primary amine nitrogen atoms [N(10) and N(11)] are involved in hydrogen bonding. An N–H···S type of bonding is noticed between N(10) of Cu(2) and S(4) of Cu(1), completing the loop in the tetramer and the other between N(11) and S(3) of $[Mn(NCS)_6]^{4-}$ unit of the same layer. Bound nitrogen N(8) of the terminal thiocyanate of Cu(1) forms hydrogen bond to N(11) of Cu(2) within the tetramer. In summary, each of the supramolecular tetramers formed by $[Cu(tren)(NCS)]^{+}$ units, are hydrogen bonded to four $[Mn(NCS)_6]^{4-}$ units, and these each in turn hydrogen bonded to four such tetramers leading to an infinite 3D network (Fig. 3).

Table 3
Hydrogen bond distances (Å) and angles (°) for**1**

D–H···A	D–H	H···A	D···A	∠D–H···A
N(5)–H(5C)···N(3)	0.9200	2.5800	3.471(3)	164.00
N(5)–H(5D)···S(1)[a]	0.9200	2.5300	3.420(2)	162.00
N(6)–H(6C)···S(2)[b]	0.9200	2.8500	3.724(3)	159.00
N(7)–H(7C)···S(4)[c]	0.9200	2.7800	3.577(3)	145.00
N(10)–H(10A)···S(4)[d]	0.9200	2.8200	3.677(2)	155.00
N(11)–H(11C)···S(3)[d]	0.9200	2.6600	3.517(2)	156.00
N(11)–H(11D)···N(8)[d]	0.9200	2.4700	3.376(3)	170.00
C(12)–H(12A)···S(1)[e]	0.9900	2.8300	3.735(2)	152.00

Symmetry code: [a] $1-x, 1-y, 1-z$; [b] $1-x, 1/2+y, 1/2-z$; [c] $1-x, 2-y, -z$; [d] $x, 3/2-y, 1/2+z$; [e] $-x, 1/2+y, 1/2-z$.

3.3. Magnetism

Variable-temperature magnetic susceptibility measurements were performed in the range of 2–300 K. The thermal variation of molar susceptibility χ_M together with a plot of $\chi_M T$ versus T of the complex is shown in Fig. 4. The magnetic moment (μ_{eff}) per copper(II) and manganese(II) centre is same as that expected for an isolated paramagnetic system [$S = 1/2$ ($\mu_{eff} = 1.732$ BM) for copper(II) and $S = 5/2$ ($\mu_{eff} = 5.916$ BM) for manganese(II)]. **1** consists of four copper(II) and one manganese(II) ion as its basic unit. For each copper(II), $\chi_M T$ is, as indicated, close to 0.4 $cm^3\ mol^{-1}$ K and for manganese(II) is close to 4.4 $cm^3\ mol^{-1}$ K. Thus the total value should be 6.0 $cm^3\ mol^{-1}$ K. The experimental value is 5.9 $cm^3\ mol^{-1}$ K at room temperature. At 4 K the value is 5.5 $cm^3\ mol^{-1}$ K. This shows coupling between the paramagnetic centres is negligible. Each magnetic centre

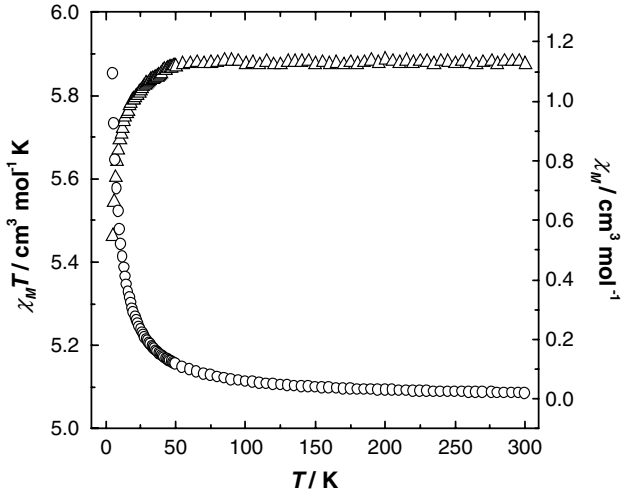

Fig. 4. Plots of $\chi_M T$ vs. T and χ_M vs. T in **1**.

behaves as discrete unit which implies that hydrogen bonded bridges have no effect on magnetic exchange.

4. Conclusion

The formation of such bimetallic compound [Cu(tren)(NCS)]$_4$[Mn(NCS)$_6$] (**1**) with hydrogen bonded network structure instead of covalently bonded polymers shows that hydrogen bond is a masterkey interaction in superstructure formation with a novel architecture. Presence of acidic hydrogen in the organic ligand and pendant arm with basic centre in pseudohalide lead to different varieties of architectures with different metal ions. The variable temperature magnetic study of **1** show negligible magnetic interactions due the formation of discrete units bridged by non-covalent hydrogen bonds.

5. Supplementary data

Crystallographic data for the structural analysis have been deposited with the Cambridge Crystallographic Data Centre, CCDC No. 212268 (**1**). Copies of this information can be obtained free of charge from the Director, CCDC, 12 Union Road, Cambridge, CB2 1EZ, UK, fax: +44 1223 336 033; e-mail: deposit@ccdc.cam.ac.uk or on the web www.ccdc.cam.ac.uk).

Acknowledgements

Financial support from the Department of Science and Technology (DST) and Council of Scientific and Industrial Research (CSIR), New Delhi, India is gratefully acknowledged.

References

[1] (a) G.R. Desiraju, Angew. Chem., Int. Ed. Engl. 34 (1995) 2311;
(b) J.M. Lehn, Supramolecular Chemistry, VCH, Weinheim, 1995;
(c) G.R. Desiraju, Chem. Commun. (1997) 1475.

[2] (a) G.A. Jeffrey, An Introduction to Hydrogen Bonding, Oxford University Press, Oxford, 1997;
(b) G.R. Desiraju, Nature 412 (2001) 397;
(c) G.R. Desiraju, Acc. Chem. Res. 35 (2002) 565;
(d) T. Steiner, Angew. Chem. Int. Ed. 41 (2002) 48.

[3] (a) G.R. Desiraju, T. Steiner, The Weak Hydrogen Bond in Structural Chemistry and Biology, Oxford University Press, Oxford, 1999;
(b) G.R. Desiraju (Ed.), Crystal Design: Structure and Function. Perspectives in Supramolecular Chemistry, vol. 7, John Wiley & Sons, Chichester, 2003.

[4] (a) A.J. Blake, N.R. Champness, P. Hubberstey, W.-S. Li, M.A. Withersby, M. Schroder, Coord. Chem. Rev. 183 (1999) 117;
(b) S. Muthu, J.H.K. Yip, J.J. Vittal, J. Chem. Soc., Dalton Trans. (2002) 4561, and references therein.

[5] (a) S. Ferlay, T. Mallah, R. Ouahes, P. Veillet, M. Verdaguer, Inorg. Chem. 38 (1999) 229;
(b) R.J. Parker, L. Spiccia, K.J. Berry, G.D. Fallon, B. Moubaraki, K.S. Murray, Chem. Commun. (2001) 333;
(c) M. Clemente-Leon, E. Coronado, J.R. Galan-Mascaros, C.J. Gomez-Garcia, T. Woike, J.M. Clemente-Juan, Inorg. Chem. 40 (2001) 87;
(d) R.J. Parker, L. Spiccia, S.R. Batten, J.D. Cashion, G.D. Fallon, Inorg. Chem. 40 (2001) 4696.

[6] (a) F.H. Liu, W.Z. Chen, X.Z. You, J. Solid State Chem. 169 (2002) 199;
(b) R. Podganjy, C. Desplanches, B. Sieklucka, R. Sessoli, V. Villar, C. Paulsen, W. Wernsdorfer, Y. Dromzee, M. Verdauger, Inorg. Chem. 41 (2002) 1323;
(c) J.H. Zhou, Y.F. Peng, Y.P. Zhang, B.L. Li, Y. Zhang, Inorg. Chem. Commun. 7 (2004) 1181;
(d) F. Bonadio, M.-C. Senna, J. Ensling, A. Sieber, A. Neels, H.S. Evans, S. Decurtins, Inorg. Chem. 44 (2005) 969.

[7] (a) R. Pradhan, C. Desplanches, P. Guionneau, J.-P. Sutter, Inorg. Chem. 42 (2003) 6607;
(b) V. Marvaud, C. Decroix, A. Scuiller, C.G. Duhayon, J. Vaissermann, F. Gonnet, M. Verdaguer, Chem. Eur. J. 9 (2003) 1677;
(c) J.R. Withers, C. Ruschmann, P. Bojang, S. Parkin, S.M. Holmes, Inorg. Chem. 44 (2005) 969.

[8] D. Bose, Sk H. Rahaman, R. Ghosh, G. Mostafa, J. Ribas, C.-H. Hung, B.K. Ghosh, Polyhedron (in press).

[9] (a) F.A. Cotton, G. Wilkinson, C.A. Murillo, M. Bochmann, Advanced Inorganic Chemistry, 6th ed., John Wiley & Sons, Inc., 1999, p. 598;
(b) C. Caltagirone, A. Bencini, F. Dermatin, F.A. Devillanova, A. Garan, F. Isaia, V. Lippolis, P. Mariani, U. Papke, L. Tei, G. Verani, Dalton Trans. (2003) 901;
(c) R. Wang, M. Hong, D. Yuan, Y. Sun, L. Xu, J. Luo, R. Cao, A.S.C. Chan, Eur. J. Inorg. Chem. (2004) 37;
(d) C.-D. Wu, W. Lin, Inorg. Chem. 44 (2005) 1178.

[10] (a) Y.-H. Li, X.-S. Wang, H. Zhao, R.-X. Yuan, J. Zhang, R.-G. Xiong, X.-Z. You, H.-X. Ju, Z.-L. Xue, Inorg. Chem. 43 (2004) 712;
(b) M. Kawahara, M.K. Kabir, K. Yamada, A. Adachi, H. Kumagai, Y. Narumi, K. Kindo, S. Kitagawa, S. Kawata, Inorg. Chem. 43 (2004) 92;
(c) Y.Z. Zhang, S. Gao, H.L. Sun, G. Su, Z.M. Wang, S.W. Zhang, Chem. Commun. (2004) 1906.

[11] (a) Y.S. You, C.S. Hong, K.M. Kim, Polyhedron 24 (2005) 249;
(b) J.K. Clegg, L.F. Lindoy, J.C. McMurtie, D. Schilter, Dalton Trans. (2005) 857;
(c) Z.-K. Chan, Y.-Y. Wu, J.-D. Chen, C.-Y. Yeh, C.-C. Wang, Y.-F. Tsai, J.-C. Wang, Dalton Trans. (2005) 985.

[12] (a) A.K. Patra, S. Dhar, M. Nethaji, A.R. Chakravarty, Dalton Trans. (2005) 896;
(b) J.W. Whittmaker, Mn and Its Role in Biological Processes, vol. 37, Marcel Dekker, New York, 2000, p. 587.

[13] (a) G.-Y. Hsu, C.-W. Chen, S.-C. Cheng, S.-H. Lin, H.-H. Wei, C.-J. Lee, Polyhedron 24 (2005) 487;
(b) M.A.M. Abu-Youssef, A. Escuer, R. Vicente, F.A. Mautner, L. Öhrstrom, M.A.S. Goher, Polyhedron 24 (2005) 557.

[14] SADABS v2.02: Area-Detector Absorption Correction, Siemens Industrial Automation, Inc., Madison, WI, 1996.

[15] SHELXTL 6.1, Bruker AXS Inc., Madison, WI, 2001.

[16] G. Guilera, J.W. Steed, J. Chem. Soc., Chem. Commun. (1999) 1563.

[17] (a) Special issue on Focus on Self-Assembly, Acc. Chem. Res. 32 (1999) 4;
(b) B.J. Holliday, C.A. Mirkin, Angew. Chem. Int. Ed. 40 (2001) 2022.

[18] W.J. Geary, Coord. Chem. Rev. 7 (1971) 81.
[19] K. Nakamoto, Infrared and Raman Spectra of Inorganic and Coordination Compounds, Part B, 5th ed., John Wiley & Sons, New York, 1997, p. 116.
[20] Z.-L. Lu, C.-Y. Duan, Y.-P. Tian, Z.-W. Wu, J.-J. You, Z.-Y. Zhou, T.C.W. Mak, Polyhedron 16 (1997) 909.
[21] (a) A.B.P. Lever, Inorganic Electronic Spectroscopy, 2nd ed., Elsevier Science, New York, 1984;
(b) H.-Y. Mao, X.-Q. Shen, G. Li, H.-Y. Zhang, C. Xu, H.-L. Liu, E.-B. Wang, Q.-A. Wu, H.-W. Hou, Y. Zhu, Polyhedron 23 (2004) 1961.
[22] D. Bose, J. Banerjee, Sk H. Rahaman, G. Mostafa, H.-K. Fun, R.D.B. Walsh, M.J. Zaworotko, B.K. Ghosh, Polyhedron 23 (2004) 2045.
[23] M.C. Etter, J. Phys. Chem. (1991) 4601.
[24] J. Luo, X.-G. Zhou, S. Gao, L.-H. Weng, Z.-H. Shao, C.-M. Zhang, Y.-R. Li, J. Zhang, R.-F. Cai, Polyhedron 23 (2004) 1243.

Available online at www.sciencedirect.com
SCIENCE DIRECT®
Polyhedron 25 (2006) 671–677
POLYHEDRON
www.elsevier.com/locate/poly

Synthesis, characterization and X-ray crystal structures of [Ni(Me-sal)$_2$dpt] and [Ni(Me-sal)dpt]Cl

Mehdi Amirnasr [a,*], Kurt J. Schenk [b], Soraia Meghdadi [a], Mahbod Morshedi [a]

[a] Department of Chemistry, Isfahan University of Technology, Isfahan 84156-83111, Iran
[b] Institut de cristallograohie EPFL, Lausanne, Switzerland

Received 4 June 2005; accepted 7 July 2005
Available online 8 September 2005

Abstract

Two Ni(II) complexes, [Ni(Me-sal)$_2$dpt] (**1**) and [Ni(Me-sal)dpt]Cl (**2**), with penta- and tetradentate ligands ((H_2L^1)=H_2(Me-sal)$_2$dpt=*N*,*N*-bis(α-methylsalicylidene)dipropylenetriamine and (HL^2)=H(Me-sal)dpt=*N*-(α-methylesalicylidene)dipropylenetriamine) containing N_3O_2 and N_3O donor sets, respectively, have been synthesized and characterized by elemental analyses, FT-IR and UV–Vis spectroscopy. The green five coordinate complex [Ni(Me-sal)$_2$dpt] (**1**) forms on reaction of H_2(Me-sal)$_2$dpt with $Ni^{II}(OAc)_2 \cdot 4H_2O$ in boiling methanol, whereas at reflux temperature in ethanol the red diamagnetic [Ni(Me-sal)dpt]Cl (**2**) is formed on reaction of H_2(Me-sal)$_2$dpt with $NiCl_2 \cdot 6H_2O$. In the ligand (Me-sal)dpt one of the imine groups is hydrolysed resulting in a new tetradentate N_3O ligand. Complex (**2**) is also prepared in a higher yield by the direct reaction of H(Me-sal)dpt with $NiCl_2 \cdot 6H_2O$. The crystal and molecular structures of (**1**) and (**2**) were determined by X-ray crystallography. Complex (**1**) crystallizes in the monoclinic space group $P2_1/c$ and complex (**2**) crystallizes in the triclinic space group $P\bar{1}$. The coordination polyhedron about the Ni(II) center in complex (**1**) is best described as distorted trigonal bipyramidal and that of complex (**2**) as distorted square planar. The FT-IR and UV–Vis spectra of the complexes are also discussed.
© 2005 Elsevier Ltd. All rights reserved.

Keywords: Schiff base complexes; Nickel(II); Half unit ligand; Crystal structures

1. Introduction

The chemistry of multidentate Schiff base ligands has been studied extensively [1–8] owing to their potential for binding to one, two or more metal centers and their use in the synthesis of homo and heteronuclear metal complexes with interesting stereochemistry [9–12]. Among others, the synthesis of Schiff base ligands through the 1:1 condensation of diamines to form "half-unit" ligands has attracted much attention in recent years [13–16]. These ligands, apart from being used in the synthesis of metal complexes, afford the possibility of synthetic routes to additional unsymmetrical tetradentate and pentadentate [14] Schiff base ligands.

Nickel can exhibit several oxidation states and Schiff base ligands have been employed in the development of new Schiff base complexes containing nickel with different oxidation states [17]. Such complexes play an important role in bioinorganic chemistry and redox enzyme systems [18] and may provide the basis of models for active sites of biological systems [19] or act as catalysts [20–23]. In the present paper, we describe the synthesis of pentadentate H_2L^1 and tetradentate HL^2 ligands (Fig. 1) and their Ni(II) complexes. An interesting feature observed during this work was the hydrolysis of the coordinated pentadentate Schiff base ligand L^1 in the presence of KOH under reflux conditions in an ethanolic solution, leading to the formation of the [Ni(L^2)]Cl complex.

* Corresponding author. Tel.: +98 311 391 2351; fax: +98 311 391 2350.
E-mail address: amirnasr@cc.iut.ac.ir (M. Amirnasr).

0277-5387/$ - see front matter © 2005 Elsevier Ltd. All rights reserved.
doi:10.1016/j.poly.2005.07.040

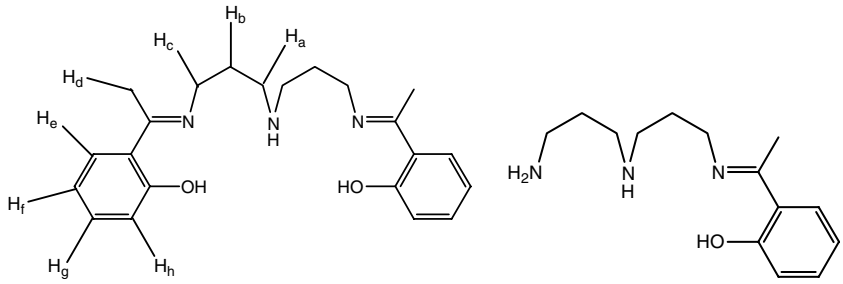

H_2L^1 HL^2

Fig. 1. Schematic presentation of the ligands H_2L^1 and HL^2.

2. Experimental

All chemicals were used as supplied by Merck and Fluka without further purification. Solvents were either of reagent or spectroscopic grade and were dried by conventional procedures prior to use.

2.1. Physical measurements

Elemental analyses were performed by using a Heraeus CHN-O-RAPID elemental analyzer. UV–Vis spectra were recorded on a JASCO V-570 spectrophotometer, λ_{max} (ε) in nm. Infrared spectra (KBr pellet) were obtained on a FT-IR JASCO 680 plus spectrophotometer. The ^{1}H NMR spectrum of the ligand was obtained on a BRUKER AVANCE DR X500 (500 MHz) spectrometer. Proton chemical shifts are reported in parts per million (ppm) relative to an internal standard of Me_4Si.

2.2. Synthesis

2.2.1. H_2(Me-sal)$_2$dpt (H_2L^1) ligand

N,*N*-bis(α-methylsalicylidene)dipropylenetriamine (H_2(Me-sal)$_2$dpt) was prepared by following the syntheses outlined for related Schiff base ligands [6], via the condensation of (394 mg, 3.00 mmol) dipropylenetriamine (dpt) with (817 mg, 6.00 mmol) 2-hydroxyacetophenone in methanol (or ethanol) at room temperature, and was purified by recrystallization from hot ethanol [24–26]. Yield: 1.05 g (95%). IR (KBr, cm^{-1}): ν_{max} 3300–3400 (m, br, OH), 3295 (s N–H), 1613 (s, C=N). UV–Vis: λ_{max} (nm) (ε, M^{-1} cm^{-1}) (methanol): 362 (12 100), 337 (14 500). ^{1}H NMR (CD_3COCD_3, 500 MHz):δ = 7.58 (2H, d, J_{HH} = 8 Hz, H_e), 7.26 (2H, t, J_{HH} = 8 Hz, H_g), 6.78 (2H, d, J_{HH} = 8 Hz, H_h), 6.75 (2H, t, J_{HH} = 8 Hz, H_f), 3.63 (4H, t, J_{HH} = 6.8 Hz, H_c), 2.71 (4H, t,J_{HH} = 6.8 Hz, H_a), 2.34 (6 H, s, H_d), 2.15 (1H, br, N–H), 1.88 (4H, m, J_{HH} = 6.8 Hz, H_b).

2.2.2. H(Me-sal)dpt (HL^2) ligand

N-(α-methylesalicylidene)dipropylenetriamine (H(Me-sal)dpt) was prepared according to a procedure for similar "half-unit" ligands, by the condensation of dipropylenetriamine with 2-hydroxyacetophenone (1:1 molar ratio) at room temperature [15]. To a solution of dipropylenetriamine (dpt) (131 mg, 1.00 mmol) in 10 ml chloroform was added dropwise a solution of 2-hydroxyacetophenone (136 mg, 1.00 mmol) in 10 ml chloroform over a 30 min period and the mixture was stirred for 1 h. The solvent was then evaporated under vacuum leaving a yellow oil (HL^2). The resulting yellow oil was used for the synthesis of complex (**2**) by method 2.

2.2.3. [Ni(Me-sal)$_2$dpt] (**1**)

To a boiling solution of H_2(Me-sal)$_2$dpt (367 mg, 1.00 mmol) in 10 ml dichloromethane was added slowly a solution of $Ni^{II}(OAc)_2 \cdot 4H_2O$ (249 mg, 1.00 mmol) in 10.0 ml methanol, and the resulting solution was stirred until the dichloromethane evaporated. Solid KOH (112 mg, 2.00 mmol) was then added to the remaining solution and the mixture was stirred for an additional 5 min. A green precipitate was finally obtained. The reaction mixture was cooled to room temperature and the green precipitate was filtered off and washed with methanol. The product was then recrystallized from hot toluene. Yield: 280 mg (66%). *Anal*. Calc. for $C_{22}H_{27}N_3NiO_2$: C, 62.3; H, 6.42; N, 9.91. Found: C, 62.2; H, 6.40; N, 9.40%. IR (KBr, cm^{-1}): ν_{max} 3176 (m, NH), 1608 (s, C=N). UV–Vis: λ_{max} (nm) (ε, M^{-1} cm^{-1}) (chloroform): 1218 (18.04), 974(5.88), 877(2.94), 600(59.03).

2.2.4. [Ni(Me-sal)dpt]Cl (**2**) method 1

Solid KOH (112 mg, 2.00 mmol) was added to a solution of H_2(Me-sal)$_2$dpt (367 mg, 1.00 mmol) in 25 ml ethanol and the mixture was refluxed for 5 min. A solution of $Ni^{II}Cl_2 \cdot 6H_2O$ (238 mg, 1.00 mmol) in 10 ml methanol was then added and a green precipitate appeared which instantly dissolved to form a deep red solution. The solution was refluxed for 1 h and then cooled to room temperature and filtered off. The solvent of the resulting filtrate was evaporated under vacuum to give a red precipitate. Crystals of (**2**) suitable for X-ray crystallography were obtained by the diffusion of diethyl ether into a saturated solution of the red product in

ethanol at room temperature. Yield: 65.1 mg (19%). *Anal*. Calc. for $C_{14}H_{22}ClN_3NiO$: C, 47.5; H, 6.14; N, 12.8. Found: C, 48.6; H, 6.5; N, 12.0%. IR (KBr, cm^{-1}): ν_{max} 3229, 3197 (m, NH), 1597 (s, C=N). UV–Vis: λ_{max} (nm) (ε, $M^{-1}\,cm^{-1}$) (chloroform): 510 (127), 450 (160), 393 (2968).

2.2.5. [Ni(Me-sal)dpt]Cl (2) method 2

To a solution of 1.00 mmol (249 mg) of the freshly prepared H(Me-sal)dpt (as described in Section 2.2.2.) in 25 mmol ethanol was added a solution of triethylamine (101 mg, 1.00 mmol) in ethanol and the mixture was refluxed for 5 min. A solution of $Ni^{II}Cl_2 \cdot 6H_2O$ (238 mg, 1.00 mmol) in 10 ml methanol was then added upon which the color of the solution turned deep red. The reflux was continued for an additional 1 h. The final reaction mixture was cooled to room temperature and filtered off. The solvent of the resulting filtrate was evaporated under vacuum to give a red precipitate. Crystals of (**2**) suitable for X-ray crystallography were obtained by the diffusion of diethyl ether into a saturated solution of the red product in ethanol at room temperature. Yield: 151 mg (40%). *Anal*. Calc. for $C_{14}H_{22}ClN_3NiO$: C, 47.5; H, 6.14; N, 12.8. Found: C, 48.3; H, 6.5; N, 12.2%. IR (KBr, cm^{-1}): ν_{max} 3229, 3197 (m, NH), 1597 (s, C=N). UV–Vis: λ_{max} (nm) (ε, $M^{-1}\,cm^{-1}$) (chloroform): 510 (127), 450 (160), 393 (2968).

2.3. X-ray crystallography

Green crystals of [Ni(Me-sal)$_2$dpt] (**1**) suitable for X-ray crystallography were grown by slow evaporation of a hot toluene solution of the complex at 78 °C and red crystals of [Ni(Me-sal)dpt]Cl (**2**) suitable for X-ray crystallography were grown by slow diffusion of diethylether vapour into a saturated solution of the complex in ethanol at room temperature. The crystals were mounted on glass fibers. Data collections were carried out on a Stoe IP diffraction system at 293 K using graphite monochromatized Mo Kα radiation (λ = 0.71073 Å). A crystal-to-detector distance of 100 cm was chosen and 180 one-degree-wide images were exposed for 5 min for (**1**) and 10 min for (**2**). Crystal data and details of the structure determination are given in Table 1. The data were corrected for Lorentz and polarization effects and a numerical absorption correction (Stoe X-Red 1.24) was applied [27]. The structures were solved with the help of DirDif-96 for (**1**) [28] and SHELXL-97 for (**2**) [29a]. The structure refinement was performed using the full-matrix against F^2 method (SHELXL-97) [29b]. Anisotropic displacement parameters were refined for non-hydrogen atoms, all hydrogen atoms were made to ride on their carrier atoms.

3. Results and discussion

3.1. Synthesis

The ligand H_2L^1 was synthesized and reacted with nickel salts in an attempt to prepare five or four coordinate species as have been reported for related ligands [19,30]. Our first attempt on the synthesis of [Ni(Me-sal)$_2$dpt] (**1**) was based on the procedure reported by

Table 1
Crystallographic and refinement data of (**1**) and (**2**)

Empirical formula	$C_{22}H_{27}N_3NiO_2$ (**1**)	$C_{14}H_{22}ClN_3NiO$ (**2**)
Habitus	{0 1 1} prism, {1 0 0} pinacoid ($\bar{1}$01) pedion (bevel face)	{1 1 1}, {0 1 0} pinacoids, (00$\bar{1}$), (1$\bar{1}\bar{1}$), (3 1 7) pedions
Formula weight	424.18	342.51
Temperature (K)	293(1)	293(1)
Crystal system	monoclinic	triclinic
Space group	$P2_1/c$	$P\bar{1}$
a (Å)	10.458(2)	7.6070(8)
b (Å)	14.580(3)	10.3755(11)
c (Å)	13.679(3)	10.6948(11)
α (°)	90	70.921(8)
β (°)	104.20(3)	73.948(8)
γ (°)	90	71.718(8)
V (Å^3)	2022.1(7)	743.09(13)
Z, $D_{calc.}$ (Mg/m^3)	4, 1.393	2, 1.531
μ (mm^{-1})	0.982	1.484
Crystal size (mm)	0.4 × 0.4 × 0.12	0.55 × 0.29 × 0.18
Reflections collected	9242	7419
Independent reflections (R_{int})	4987 (0.0215)	3786 (0.0385)
Maximum and minimum transmission	0.8779, 0.6867	0.7705, 0.5221
Data/restraints/parameters	4986/0/256	3786/0/210
Goodness-of-fit on F^2	2.963	3.043
Final R indices [$I > 2\sigma(I)$]	$R_1 = 0.0339$, $wR_2 = 0.0440$	$R_1 = 0.0318$, $wR_2 = 0.0513$
R indices (all data)	$R_1 = 0.0442$, $wR_2 = 0.0448$	$R_1 = 0.0344$, $wR_2 = 0.0514$

Kawamoto and co-workers [30], and H_2(Me-sal)dpt was reacted with $NiCl_2 \cdot 6H_2O$. Instead, a diamagnetic red product with a low yield (19%) was obtained that was assumed to be a four coordinate nickel complex similar to [Ni(2,6Bis[2-acetylphenyl)carbamoyl]pyridine)] [30]. The presence of only one Me-sal coupled with dipropylenetriamine is evident from the elemental analysis data and the IR spectrum of this complex. In addition, the structural analysis of the red crystals of the product by X-ray crystallography (vide infra) proved that one of the imine fragments of the ligand H_2L^1 had been removed, presumably by undergoing hydrolysis in the presence of KOH while the reaction mixture was refluxed. The product was identified as the four coordinate [Ni(Me-sal)dpt]Cl (**2**). In an alternative method for the synthesis of [Ni(Me-sal)$_2$dpt] (**1**), described in Section 2, a green product was obtained. The X-ray crystal structure analysis showed that this compound was a five coordinate nickel complex, (**1**), with a distorted trigonal bipyramidal geometry.

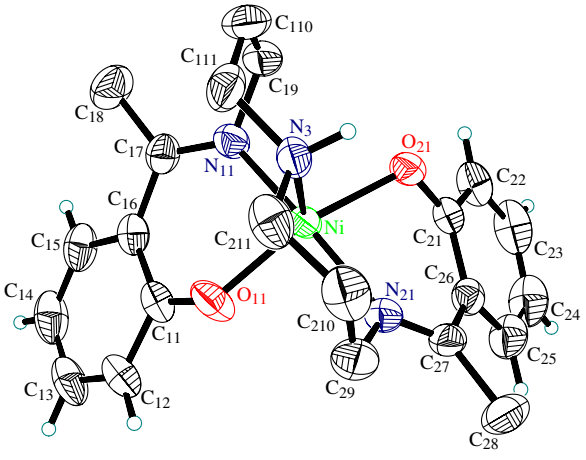

Fig. 2. Representation of molecular structure of **1** with the atom labelling scheme. Ring labels B and C are used in the text.

In order to have a more consistent procedure and to get a higher yield of the red complex an alternative method was developed for the synthesis of H(Me-sal)dpt and the complex [Ni(Me-sal)dpt]Cl (**2**), as described in Section 2. In this method, 2-hydroxyacetophenone and dipropylenetriamine were reacted in a 1:1 molar ratio and the resulting yellow oily product was used directly for the synthesis of the complex. The yield was improved from 19% in method 1 to 40% in method 2.

3.2. Description of structures

The structure of [Ni(Me-sal)$_2$dpt] (**1**) consists of isolated NiL^1 units in which the nickel is coordinated by three nitrogen and two oxygen atoms of the quinquedentate (Me-sal)$_2$dpt ligand (Fig. 2). The geometry of the $\{NiO_2N_2N'\}$ coordination core is that of a distorted trigonal bipyramid with two imine nitrogen atoms N(11) and N(21) being located in the axial positions, subtending an angle N(11)–Ni–N(21) of 173.82(5)°. The secondary amine nitrogen atom N(3) lies in the position just perpendicular to the near linear N(11)–Ni–N(21) arrangement with angles N(11)–Ni–N(3), 91.98(5)° and N(21)–Ni–N(3), 94.16(5)°. The donor oxygen atoms are bound equatorially and form the angle O(11)–Ni–O(21), 158.38(5)°. The whole molecule is butterfly shaped but offers enough space for the coordination of a sixth ligand.

In the conformation adopted by the (Me-sal)$_2$dpt ligand, the phenyl rings are unsymmetrically bent away from the axial position occupied by N(3) due to the difference in the conformations of the six membered rings linking the salycilidene rings to the secondary amine nitrogen N(3). A boat conformation for the chain to ring B and a chair conformation for the chain to ring C is observed (Fig. 2). The set of torsion angles for both the boat and chair ring conformations are presented in Table 2. The angles between the normal to the equatorial plane [Ni, O(11), O(21), N(11), N(21)] and the normals to the benzene rings C(11) → C(16) (ring B)

Table 2
Torsion angles for the propylene chains [deg]

Chair		Boat	
*[Ni(Me-sal)$_2$dpt] (**1**)*			
Ni–N(21)–C(29)–C(210)	−59.07(17)	Ni–N(11)–C(19)–C(110)	−71.35(15)
N(21)–C(29)–C(210)–C(211)	67.2(2)	N(11)–C(19)–C(110)–C(111)	17.6(2)
C(29)–C(210)–C(211)–N(3)	−71.1(2)	C(19)–C(110)–C(111)–N(3)	56.0(2)
C(210)–C(211)–N(3)–Ni	63.59(16)	C(110)–C(111)–N(3)–Ni	−61.41(18)
C(211)–N(3)-Ni–N(21)	−48.53(10)	C(111)–N(3)–Ni–N(11)	9.16(12)
N(3)–Ni–N(21)–C(29)	47.85(12)	N(3)–Ni–N(11)–C(19)	53.39(12)
*[Ni(Me-sal)dpt]Cl (**2**)*			
Ni–N(21)–C(29)–C(210)	42.9(3)	Ni–N(11)–C(19)–C(110)	−20.9(2)
N(21)–C(29)–C(210)–C(211)	−61.6(2)	N(11)–C(19)–C(110)–C(111)	74.2(2)
C(29)–C(210)–C(211)–N(3)	70.4(2)	C(19)–C(110)–C(111)–N(3)	−42.7(2)
C(210)–C(211)–N(3)–Ni	−53.9(2)	C(110)–C(111)–N(3)–Ni	−30.93(19)
C(211)–N(3)–Ni–N(21)	26.94(15)	C(111)–N(3)–Ni N(11)	65.70(14)
N(3)–Ni–N(21)–C(29)	−23.32(19)	N(3)–Ni–N(11)–C(19)	−36.23(14)

and C(21) → C(26) (ring C) are 38.64(6)° and 61.17(6)°, respectively.

Selected bond lengths and angles for (**1**) are presented in Table 3. The Ni–O_{av} (1.93 Å), Ni–N_{av} (2.03 Å) and Ni–N(3) (2.049 Å) bond lengths are comparable with the corresponding bond lengths reported for analogous structures [31]. By comparing the structural parameters of (**1**) with those of Ni(salMedpt) [31] (Table 4), and most notably the O–Ni–O angle, one can conclude that [Ni(Me-sal)$_2$dpt] (**1**) shows a greater tendency to form a square pyramidal arrangement than Ni(salMedpt). The square pyramidal structure with the metal atom above the basal plane cannot be attained presumably because the N(11)–Ni–N(3) angles are bound to be close to 90°. Some evidence in support of this interpretation is given by the strain present in the trimethylene chains, where the angles of the carbon atoms are larger than the expected tetrahedral value. For example, C(19)–C(110)–C(111) = 116.6 (2)°. The same steric factors would prevent the O–Ni–O angle from attaining higher values through a rotation of the sal ring around the Ni–N bonds.

The X-ray structure of [Ni(Me-sal)dpt]Cl (**2**) shows that the nickel ion is in a distorted square planar environment, formed by a primary and a secondary amine, an imino nitrogen and a phenolic oxygen group (Fig. 3). The average displacement of the O(11), N(11), N(3), and N(21) atoms from the least-squares plane through these atoms is 0.124 Å, consistent with this geometry. In the conformation adopted by the (Me-sal)dpt ligand in (**2**), the N(11)–C(19)–C(110)–C(111)–N(3)–Ni and the N(21)–C(29)–C(210)–C(211)–N(3)–Ni chelate rings of dpt, adopt a boat and a chair conformation, respectively (Fig. 3). The set of torsion angles for both the boat and chair ring conformations are presented in Table 2.

Selected bond distances and angles for (**2**) are given in Table 3. The bond distances and angles are in agreement with the values for tetracoordinate low-spin divalent nickel complexes. The Ni–O(11) (1.8269(14) Å), Ni–N(11) (1.8966(16) Å), Ni–N(3) (1.9285(17) Å) and Ni–N(21) (1.9207(16) Å) distances are comparable with the corresponding Ni–O (1.79 Å) and Ni–N(imine) (1.88 Å) distances in [Ni($Me_2NCH_2CH_2N$(Me)-C_6H_4O)N_3] [32], and Ni–N (*sec*-amine) (1.94 Å) [19] and Ni–N(amine) (1.91 Å) in [Ni(*N*-(thiobenzenylidene)-diethylenetriamine)]Cl, respectively.

Table 3
Selected bond lengths [Å] and angles [°]

Complex	[Ni(Me-sal)$_2$dpt]Cl (**1**)	[Ni(Me-sal)dpt] (**2**)
Bond lengths		
Ni–O(11)	1.9514(16)	1.8269(14)
Ni–O(21)	2.0034(15)	
Ni–N(11)	2.0310(18)	1.8966(16)
Ni–N(21)	2.0432(17)	1.9207(16)
Ni–N(3)	2.0490(18)	1.9288(17)
Bond angles		
O(11)–Ni–N(11)	88.93(8)	82.17(8)
O(21)–Ni–N(11)	94.38(7)	
O(11)–Ni–N(21)	89.24(8)	83.38(7)
O(21)–Ni–N(21)	85.27(7)	
N(11)–Ni–N(21)	173.95(8)	169.61(7)
O(11)–Ni–O(21)	158.38(5)	
O(11)–Ni–N(3)	103.07(8)	173.40(7)
O(21)–Ni–N(3)	97.95(7)	
N(11)–Ni–N(3)	92.05(8)	91.22(7)
N(21)–Ni–N(3)	93.98(7)	94.17(8)

Table 4
Selected bond lengths [Å] and angles [°] for [Ni(Me-sal)$_2$dpt] (**1**) and Ni(salMedpt) complex

Complex	Ni–O	Ni–N	Ni–N′	O–Ni–O	N–Ni–N
[Ni(Me-sal)$_2$dpt]	1.95 2.003	2.03 2.04	2.05	158.38(5)	173.95(8)
Ni(salMedpt)[a]	1.956 1.954	2.017 2.001	2.086	140.6	177.0

[a] Data from reference [31].

3.3. Spectral studies

The splitting of the terms of the Ni(II) ion in crystal fields of D_{3h} and C_{4v} symmetry has been calculated and the spectra of several complexes have been measured experimentally [6,33,34]. It has been shown that for a similar set of donor atoms in a regular trigonal bipyramidal configuration only one band is expected in the near infrared region at ca. 7000 cm^{-1} (1428 nm) while two bands are expected for a regular square pyramidal configuration at ca. 7200 cm^{-1} (1388 nm) and ca. 10 800 cm^{-1} (925 nm). The reported experimental data are in good agreement with the theoretical predictions [6,33,34]. The spectrum of [Ni(Me-sal)$_2$dpt] (**1**) complex in dichloromethane shows a band at 1218 nm and a shoulder at 974 nm in the near infrared region which

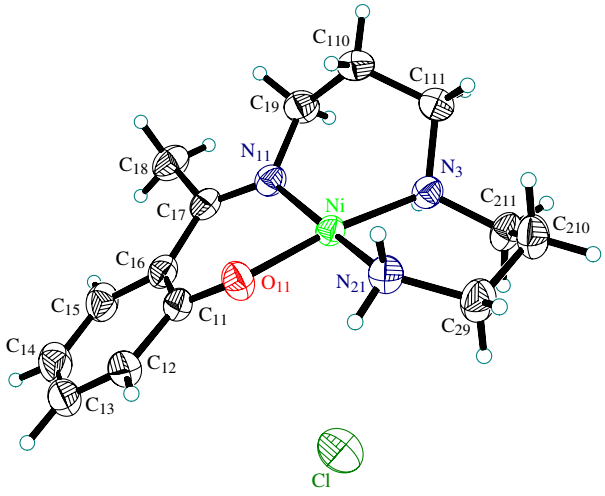

Fig. 3. Representation of the molecular structure of **2** with the atom labelling scheme.

is in accord with a distorted square pyramidal configuration [6] and confirmed by the X-ray crystal analysis.

The red [Ni(Me-sal)dpt]Cl (**2**) complex shows two shoulders at 510 and 450 nm, which are characteristic of square planar diamagnetic Ni(II) complexes [34], and resemble the absorption bands observed in the spectrum of an analogous Ni(II) complex, [Ni(*N*-(thiobenzyline)-ethylenetriamine)]Cl, reported by Bouwman [19]. A third band which is expected to appear at a higher energy is apparently hidden under the CT band.

In the IR spectrum of the H_2(Me-sal)$_2$dpt ligand, a broad band characteristic of the OH group at 3300–3400 cm^{-1} is observed. The disappearance of this band in the IR spectra of the complexes is indicative of the fact that the equatorial ligand is coordinated in its deprotonated form. The ν(C=N) band of H_2(Me-sal)$_2$dpt at 1615 cm^{-1} also shifts to 1608 cm^{-1} in [Ni(Me-sal)$_2$dpt] (**1**) correspondingly due to the loss of the intramolecular hydrogen bonding and the formation of a new chelate ring between the imine nitrogens and Ni(II). The ν(C=N) stretching of [Ni(Me-sal)dpt]Cl (**2**) appears at 1597 cm^{-1}. The bands corresponding to the amine ν(N–H) stretching vibrations of the free (Me-sal)$_2$dpt (H_2L^1) appears at 3295 cm^{-1}. This band, as expected, is shifted by about 119 cm^{-1} in the complex [Ni(Me-sal)$_2$dpt] (**1**) relative to the uncoordinated amine. The complex [Ni(Me-sal)dpt]Cl (**2**) shows two medium bands at 3229 and 3197 cm^{-1} that correspond to ν(N–H) stretching vibrations of the primary and secondary amines of the coordinated ligand.

4. Conclusion

We have prepared two nickel complexes of different geometries by reacting the Schiff base ligand H_2(Me-sal)$_2$dpt with nickel acetate and nickel chloride. Interestingly, the reaction with nickel acetate under milder conditions led to a green five coordinate ($N_2N'O_2$) complex with a distorted trigonal bipyramidal geometry. However, nickel chloride under more severe conditions, gave an orange four coordinate ($NN'N''O$) complex with a distorted square planar structure containing a ''half unit'' ligand (Me-sal)dpt, resulting from the hydrolysis of one imine fragment of (Me-sal)$_2$dpt. The ''half unit'' ligand H(Me-sal)dpt was also prepared and used freshly for the direct synthesis of [Ni(Me-sal)dpt]Cl in which the yield improved significantly relative to the indirect method.

Acknowledgements

Partial support of this work by the Isfahan University of Technology Research Council through Grant 1CHJ832 is gratefully acknowledged.

Appendix A. Supplementary data

Full tables of bond lengths and angles, listings of atom coordinates and thermal parameters, and details of least-squares planes have been deposited with the Cambridge Crystallographic Data Center, CCDC Nos. 268596 for (**1**) and 268597 for (**2**). Copies of this information may be obtained free of charge from The Director, CCDC, 12 Union Road, Cambridge, CB2 1EZ, UK (Fax: +44 1223 336033; e-mail: deposit@ccdc.cam.ac.uk or www: http://www.ccdc.cam.ac.uk). Supplementary data associated with this article can be found, in the online version at doi:10.1016/j.poly.2005.07.040.

References

[1] D.H. Lee, N.N. Murthy, K.D. Karlin, Inorg. Chem. 35 (1996) 804.
[2] B.C. Whitmore, R. Eisenberg, Inorg. Chem. 22 (1983) 1.
[3] H. Adam, S. Clunas, D.E. Fenton, Inorg. Chem. Commun. 4 (2001) 667.
[4] D.E. Fenton, Inorg. Chem. Commun. 5 (2002) 537.
[5] J.L. Sessler, J.W. Sibert, V. Lynch, Inorg. Chem. 29 (1990) 4143.
[6] L. Sacconi, I. Bertini, J. Am. Chem. Soc. 88 (1966) 5180.
[7] H.A. Goodwin, J.C. Bailar Jr., J. Am. Chem. Soc. 83 (1961) 2467.
[8] S. Yamada, Coord. Chem. Rev. 190–192 (1999) 537.
[9] M.D. Timken, W.A. Marritt, D.N. Henderickson, R.A. Gagne, E. Sinn, Inorg. Chem. 24 (1985) 4202.
[10] R. Karmakar, C.R. Choudhury, G. Bravic, J.P. Sutter, S. Mitra, Polyhedron 23 (2004) 949.
[11] C. Piguet, G. Bernardinelli, G. Hopfgartner, Chem. Rev. 97 (1997) 2005.
[12] H. Adams, S. Clunas, D.E. Fenton, Inorg. Chem. Commun. 5 (2002) 1063.
[13] E. Kwiatkowski, G. Romanowski, K. Suwin'ska, Polyhedron 21 (2001) 2071.
[14] E. Kwaitkowski, M. Klein, G. Romanowski, Inorg. Chim. Acta 293 (1999) 115.
[15] J. Pierre, F. Dahan, J.M. Dominguez-vera, J.P. Laurent, J. Ruiz, J. Sotiropouos, Inorg. Chem. 33 (1994) 3908.
[16] J.P. Costes, F. Dahan, J.P. Laurent, Inorg. Chem. 30 (1991) 1887.
[17] G. Foulds, Coord. Chem. Rev. 169 (1998) 3.
[18] A.F. KolodZiej, Prog. Inorg. Chem. 41 (1994) 493.
[19] E. Bouwman, R.K. Henderson, J. Reedijk, N. Veldman, A.L. Spek, Inorg. Chim. Acta 278 (1999) 105.
[20] M. Meseguer, M. Moreno-Mañas, A. Vallribera, Tetrahedron Lett. 41 (2000) 4093.
[21] A. Gennaro, A.A. Isse, F. Maran, J. Electroanal. Chem. 507 (2001) 124.
[22] S. Bunce, R.J. Cross, L.J. Farrugia, S. Kunchandy, L.L. Meason, K.W. Muir, M.O. Donnell, R.D. Peacock, D. Stirling, S.J. Teat, Polyhedron 17 (1998) 4179.
[23] M. Salavati-Niasari, S.H. Banitaba, J. Mol. Catal. A: Chem. 201 (2003) 43.
[24] H. Chen, J.A. Cronin, R.D. Archer, Inorg. Chem. 34 (1995) 2306.
[25] S.D. Bella, I. Fragala, I. Ledoux, M.A. Diaz-Garcia, T.J. Marks, J. Am. Chem. Soc. 119 (1997) 9550.
[26] R.D. Archer, H. Chen, L.C. Thompson, Inorg. Chem. 37 (1998) 2089.
[27] X-Red 1.24. Program for Data Reduction, Stoe & Cie GmbH, Hilpertstraße 10, D-64295 Darmstadt, Germany.
[28] P.T. Beurskens, G. Beurskens, W.P. Bosman, R. de Gelder, S. Garcia-Granda, R.O. Gould, R. Israël, M.M. Smits, The

DirDif-96 System of Programs, Laboratorium voor Kristallografie, Katholieke Universiteit Nijmegen, 1996.
[29] (a) G.M. Sheldrick, SHELXS-97., Release 97-2, Program for the Solution of Crystal Structures, Universität Göttingen, Germany, 1997;
(b) G.M. Sheldrick, SHELXL-97, Release 97-2, Program for the Refinement of Crystal Structures, Universität Göttingen, Germany, 1997.
[30] T. Kavamato, B.S. Hammes, R. Ostrander, A.L. Rheingold, A.S. Borovik, Inorg. Chem. 37 (1998) 3424.
[31] M. DiVaira, P.L. Orioli, L. Sacconi, Inorg. Chem. 10 (1971) 553.
[32] N. Mondal, S. Mitra, V. Gramilich, S.O. Ghodsi, K.M.A. Malik, Polyhedron 20 (2001) 135.
[33] M. Ciapolini, Inorg. Chem. 5 (1966) 35.
[34] A.B.P. Lever, Inorganic Electronic Spectroscopy, second ed., Elsevier, Amsterdam, 1984.

Available online at www.sciencedirect.com
SCIENCE DIRECT®
Polyhedron 25 (2006) 678–686
POLYHEDRON
www.elsevier.com/locate/poly

The role of the carboxylic group in the copper(II) mixed-ligand complexes of DL-aspartic acid-β-hydroxamic acid and polyamines

Danuta Kroczewska [a,*], Barbara Kurzak [a], Julia Jezierska [b]

[a] Department of Chemistry, University of Podlasie, 3 Maja 54, 08-110 Siedlce, Poland
[b] Faculty of Chemistry, University of Wrocław, F.Joliot-Curie 14, 50-383 Wrocław, Poland

Received 28 February 2005; accepted 8 July 2005
Available online 23 September 2005

Abstract

Equilibrium studies of the mixed-ligand complexes of the Cu^{2+} ion with polyamines {ethylenediamine (1,2-diaminoethane, en), diethylenetriamine (bis(2-aminoethyl)amine, dien) or pentamethyldiethylenetriamine (*N*,*N*,*N*′,*N*″,*N*″-pentamethyl-[bis(2-aminoethyl)amine], Me_5dien)} as a primary ligand A, and DL-aspartic acid-β-hydroxamic acid (*N*-hydroxyasparagine, Asp-β-ha) as a secondary ligand L were performed by potentiometric titration and UV–Vis and EPR spectroscopy. The results show that the parent and two mixed-ligand complexes, [CuA(HL)] and [CuA(L)], are formed. In the first [CuA(HL)] species the amino nitrogen and carboxylate oxygen of Asp-β-ha are the coordinating donor atoms (glycine-like coordination) and in the second [CuA(L)] species the amino and hydroxamate nitrogens are the coordinating donor atoms of this ligand. The first manner of coordination predominates in acidic and neutral solutions while the second one in basic solution.

Absorption (UV–Vis) and EPR spectra at various pH values indicate a five-coordinate structure of the formed complexes with a geometry close to a square-pyramid in the case of dien and trigonal bipyramid in the case of Me_5dien. In the binary copper(II)–aspartic acid-β-hydroxamic acid system the occurrence of a pentanuclear complex was confirmed.
© 2005 Elsevier Ltd. All rights reserved.

Keywords: Aminohydroxamic acids; Five-coordinate complexes; Mixed-ligand complexes; Equilibria; Polyamines; Spectroscopic studies

1. Introduction

Mixed-ligand copper(II) complexes in which polyamines play a role as a primary ligand and aminohydroxamic acid as a secondary one have been studied by us since 1998 [1–4]. The studies allowed us to ascertain that in these mixed-ligand complexes the geometry around the copper(II) is controlled first of all by the polyamines, i.e., by the number of nitrogen atoms of the polyamines which may occupy coordination sites [3].

Now we are interested in ternary systems with polyamines in which the secondary ligand possesses two donor groups: amino-acid and hydroxamate. These two groups are bidentate and have their own different geometries – hydroxamate is planar [5,6] and amino acid is less planar, e.g., in the glycine molecule the N_α (amino) atom is deviated from the plane defined by the O–C=O atoms [7]. The acidities of these groups are: $pK_{NHOH} = 9.27$ [8] and $pK_{NH_3^+} + pK_{COOH} = 11.91$ [9] for acetohydroxamic acid ($CH_3CONHOH$) and glycine, respectively.

Aspartic acid β-hydroxamic acid – $HO_2CCH(NH_2)$-$CH_2CONHOH$ – (Asp-β-ha) may be considered as a derivative of aspartic acid in which the hydroxamate group is in a β-position to the amino group. Then, the mutual influence between the amino and the hydroxamate

* Corresponding author. Tel.: +48 25 643 10 77; fax: +48 25 643 10 25.
E-mail address: danutak@ap.siedlce.pl (D. Kroczewska).

0277-5387/$ - see front matter © 2005 Elsevier Ltd. All rights reserved.
doi:10.1016/j.poly.2005.07.043

group is negligible [10,11]. The binary copper(II)–aspartic acid β-hydroxamic acid system has been studied by several authors [12–14] who obtained different equilibrium models. To render the situation relating to this system more comprehensive, and to acquire more reliable data, we have performed new studies on binary and ternary systems containing aspartic acid β-hydroxamic acid. Our aim is to answer the following question: what coordination mode, glycine-like or aminohydroxamate-like, will be preferred for Asp-β-ha in the ternary system with polyamines. In order to resolve this problem we undertook studies on the complexes equilibria in the systems: Cu^{2+}–(Asp-β-ha), Cu^{2+}–en–(Asp-β-ha), Cu^{2+}–dien–(Asp-β-ha), Cu^{2+}–Me_5dien–(Asp-β-ha) using pH-metric, spectrophotometric and EPR methods. The obtained results are compared with those for β-alaninehydroxamic acid (β-Alaha) [1,3].

2. Experimental

2.1. Materials

Aspartic acid β-hydroxamic acid monohydrate (Asp-β-ha · H_2O) and ethylenediamine dihydrochloride (en · 2 HCl) were purchased from Sigma (USA). Diethylenetriamine (dien) was used from Aldrich (Germany), *N*,*N*′,*N*″,*N*″-pentamethyldiethylenetriamine (Me_5dien) was from Fluka (Switzerland). All ligands were used without further purification and their purity was greater than 99%.

The exact concentrations of the ligand solutions were determined by the Gran method [15]. Copper(II) chloride solution was purchased from Merck as a Titrisol ampoule. Carbonate-free potassium hydroxide (the titrant) was prepared and standardized against a standard potassium hydrogenphthalate solution.

All solutions were prepared with deionized water. The study of aspartic acid β-hydroxamic acid was difficult because of the relative instability of its aqueous solution. Given the relative instability of stock solutions of Asp-β-ha, its solutions as well as amines were prepared immediately prior to use for each experiment.

2.2. Methods

2.2.1. Potentiometric measurements

The potentiometric measurements were carried out at 25.0 ± 0.1 °C using a constant-temperature water-bath. A summary of the experimental details is given in Table 1. The data for the Cu^{2+}-amines binary systems can be found in our early papers [1–3,16]. The metal ions:ligand molar ratios were 1.2:1, 1.14:1, 1:1, 1:2 and 1:4 for the Cu^{2+}–(Asp-β-ha) binary system. Within the whole studied pH range (i.e., from ca. 2 to 11), no precipitate was observed even if the copper(II) to Asp-β-ha molar ratio was 1.2:1. Titration emf data, together with E^0 and pK_w, were used to calculate the hydrogen ion concentration, [H^+].

For clarity, the charges of the complexes are omitted in the text and tables. It has to be mentioned, however, the fully deprotonated form of aspartic acid β-hydroxamic acid (Asp-β-ha) is L^{2-} while the amines are neutral.

2.2.2. Spectroscopic studies

The electronic absorption spectra were recorded on a SPECORD M-40 (Vis) spectrophotometer using 2 or 1-cm quartz cells at room temperature. The individual spectra of the copper(II) complexes were calculated according to the law of additivity of absorption. To extract the net ligand-field absorption band of each mixed-ligand species, the spectrum measured at a pH value where each of these species exhibits maximal contribution was resolved into the components corresponding to the individual

Table 1
Summary of experimental parameters for the potentiometric measurements

Systems	Binary: Asp-β-ha with H^+ or Cu^{2+} in water solution Ternary: dien/Me_5dien/en and Asp-β-ha with Cu^{2+} in water solution
Solution composition	[dien], [Me_5dien], [en] and [Asp-β-ha] range – 0.002–0.008 M, [Cu^{2+}] range – 0.001–0.004 M; ionic strength – 0.200 M; electrolyte KCl
Experimental method	pH-metric titration of 5 cm^3 samples in the range of pH 2–12; pK_w = 13.72
Instruments	MOLSPIN automatic titrator and autoburette ABU 80 with SINGLE PORE combination pH electrode (Hamilton)
Calibration	By periodic titrations of an HCl solution (0.01 M) against standard KOH solution; I = 0.2 M (KCl)
T (°C)	25.0 ± 0.1
n_{tot}[a]	100–150
n_{tit}[b]	6–8
Method of calculation	SUPERQUAD[c]

[a] Number of titration points per titration.
[b] Number of titrations per copper(II)–ligand (or copper(II)–amine–Asp-β-ha) system.
[c] P. Gans, A. Sabatini, A. Vacca, J. Chem. Soc., Dalton Trans. (1985) 1195.

species existing at that pH (as described in [1]). The molar absorptivity for the individual species was then calculated taking into account their distribution.

EPR measurements were performed on a Bruker 300E X-band spectrophotometer equipped with a Bruker NMR gaussmeter ER 035M and a Hewlett–Packard frequency counter HP 5350B at 77 K in water/ethyleneglycol (4:1 v/v) solution. The EPR parameters were calculated by computer simulation of the experimental spectra using Bruker's WIN-EPR SimFonia Software Version 1.25. The metal ion concentrations for both spectroscopic measurements were 4×10^{-3} M and metal-to-ligand molar ratios were the same as for the potentiometric measurement.

3. Results and discussion

The acid dissociation constants of the studied ligands are given in Table 2. The totally protonated aspartic acid-β-hydroxamic acid (Asp-β-ha, H_3L^+) can release three protons in the measurable pH region.

The first value, $pK_1 = 2.12$, is assigned to the dissociation of the –COOH group, but the other two processes overlap each other which means that the pK_2 and pK_3 macroconstants are not characteristic of the real acidity of the $-NH_3^+$ and –NHOH groups. It is well known that dissociation microconstants for β-alaninehydroxamic acid show that the $-NH_3^+$ group is less acidic than –NHOH in contrast to α-alaninehydroxamic acid [11]. For Asp-β-ha the dissociation constants are: $pK_{COOH} = 2.12$, $pK_{NHOH} = 8.24$, $pK_{NH_3^+} = 9.45$.

Additionally, from the data in Table 2, it is seen that the presence of the carboxylate group in Asp-β-ha causes the increase of acidity of both $-NH_3^+$ and –NHOH groups when compared to those of β-Alaha.

The general four-component equilibria can be written as

$$pCu + qA + rL + sH \leftrightarrows Cu_pA_qL_rH_s$$

where p, q, r and s are the stoichiometric coefficients corresponding to the copper(II) metal ion, A = dien or Me_5dien, L = Asp-β-ha, and H, respectively; charges are omitted for simplicity.

The cumulative formation constants are defined as

$$\beta_{pqrs} = [Cu_pA_qL_rH_s]/[Cu]^p[A]^q[L]^r[H]^s.$$

The β_{1111} and β_{1110} constants express the stability of the [CuAHL] and [CuAL] mixed-ligand species, respectively.

3.1. Copper(II)–DL-aspartic acid-β-hydroxamic acid system

The evaluation of the experimental pH-metric data for the Cu^{2+}–(Asp-β-ha) system demonstrates that two different equilibrium models yield acceptable fittings (Table 3). Model I is the same as the model presented by Careri et al. [14]. In this model, only two species exist in the whole pH range. The first species, $[Cu(H\text{-}Asp\text{-}\beta\text{-}ha)]^+$, is seen above pH 2 whereas above pH 4.5 only one species, $[Cu_5(Asp\text{-}\beta\text{-}ha)_4H_{-4}]^{2-}$, exists. This equilibrium model is identical with that for the copper(II)–β-alaninehydroxamic acid system [17].

Table 2
Cumulative protonation constants ($\log\beta^H$) and dissociation constants (pK) of the ligands at 25 °C and $I = 0.2$ M (KCl) in water solutions

	en	dien	Me_5dien	Asp-β-ha	β-Alaha
$\log\beta_1^H$	9.89(0)	9.85(2) 9.86(2)[a]	9.33(0) 9.42(1)[b]	9.45(0)	9.74(1)[b]
$\log\beta_2^H$	17.07(0)	18.85(2) 18.92(2)[a]	17.86(0) 17.95(1)[b]	17.69(0)	18.21(1)[b]
$\log\beta_3^H$		23.28(2) 23.30(3)[a]	20.08(2) 20.03(1)[b]	19.81(1)	
pK_1		4.43 4.38[a]	2.22 2.09[b]	2.12 2.12[c]	
pK_2	7.18	9.00 9.06[a]	8.53 8.41[b]	8.24 8.29[c]	8.47[b]
pK_3	9.89	9.85 9.86[a]	9.33 9.22[b]	9.45 9.42[c]	9.74[b]
$pK^{micro}_{NH_3^+}$					8.85[d]
pK^{micro}_{NHOH}					8.47[d]

[a] Ref. [16].
[b] Ref. [3].
[c] Ref. [13].
[d] Ref. [11].

Table 3
Cumulative formation constants ($\log\beta$) for Cu^{2+} complexes formed with Asp-β-ha in binary systems at 25 °C and $I = 0.2$ M (KCl) in water solutions

Assignments	Literature data			This work	
	Ref. [12]	Ref. [13]	Ref. [14]	Model I	Model II
$\log\beta[Cu(H\text{-}Asp\text{-}\beta\text{-}ha)]^{+}$		16.41(16)	17.07(1)	17.02(4)	16.74(3)
$\log\beta[Cu(Asp\text{-}\beta\text{-}ha)]$	12.60(1)	13.24(5)			13.06(3)
$\log\beta[Cu_5(Asp\text{-}\beta\text{-}ha)_4H_{-4}]^{2-}$			50.70(3)	50.31(16)	49.90(6)
$\log\beta[Cu_4(Asp\text{-}\beta\text{-}ha)_4H_{-2}]^{2-}$		52.82(16)			53.41(6)
$\log\beta[Cu_4(Asp\text{-}\beta\text{-}ha)_4H_{-3}]^{3-}$		42.30(20)			44.36(8)
$\log\beta[Cu_2(Asp\text{-}\beta\text{-}ha)_3]^{2-}$	37.45(5)				
$\log\beta[Cu_3(Asp\text{-}\beta\text{-}ha)_4]^{2-}$	53.43(9)				
$\log\beta[Cu(Asp\text{-}\beta\text{-}ha)_2]^{2-}$	19.07(4)				
$\log\beta[Cu(Asp\text{-}\beta\text{-}ha)_2]^{3-}$	9.08(4)				

The major difference between model II and the model presented by Farkas and Buglyo [13] concerns the formation of the pentanuclear species; according to our model II, this species is formed and reaches a maximum concentration (ca. 50%) at pH 4.5. Additionally, the stability constants for the $[Cu_4(Asp\text{-}\beta\text{-}ha)_4H_{-2}]^{2-}$ and $[Cu_4(Asp\text{-}\beta\text{-}ha)_4H_{-3}]^{3-}$ species obtained in [13] and in this work are different.

Plots of $\bar{n}_H$ versus pH ($\bar{n}_H$ = means number of bound protons per mole of ligand) are given in Fig. 1. From this, we can see that in the system with metal ions 'extra' deprotonation of the hydroxamate group of Asp-β-ha occurs, already in acidic solution. With an excess of Cu^{2+}, the values of $\bar{n}_H$ are close to −1 (above pH 4). Hence, such 'extra' deprotonation leads to the formation of the LH_{-1} form of the ligand as it has been observed during the formation of polynuclear complexes with other aminohydroxamic acids [17,18].

The absorption spectra in the d–d region exhibit a distinctive band at 617 nm in the 4.5–11 pH region, the energy of which is independent on the metal-to-ligand molar ratios (Fig. 2). This indicates that in the whole pH range only one species exists. A plot of absorbance at 617 nm versus $c_{Cu^{2+}}/c_{Asp\text{-}\beta\text{-}ha}$ (Fig. 3) indicates a copper(II)-to-Asp-β-ha ratio of 1.25:1. Hence, we can describe this species as $[Cu_5L_4]$. Due to the fact that $L = LH_{-1}$, the real formula of this species is

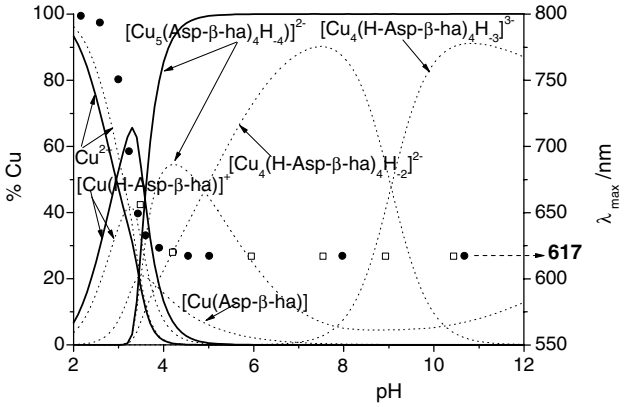

Fig. 2. Concentration distribution curves as a function of pH and variations of visible absorption maximum wavelength for the Cu^{2+}–(Asp-β-ha) system at 1:2 molar ratio; model I – solid line and circles; model II – dotted line and squares; $c_{Cu} = 4 \times 10^{-3}$ M.

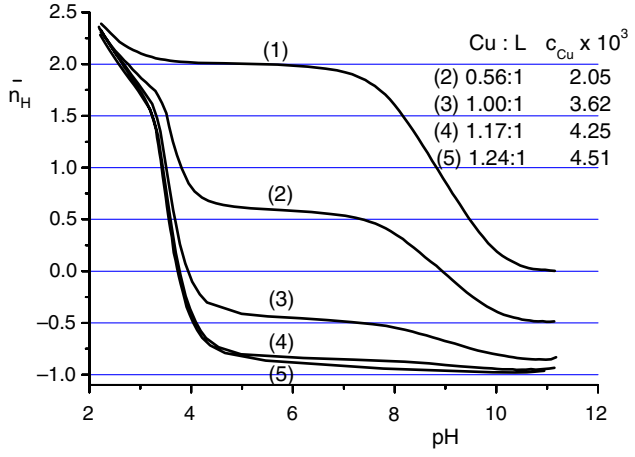

Fig. 1. Mean number of bound protons per mole of ligand, $\bar{n}_H$, for Asp-β-ha (L) alone (1) and in the presence of Cu^{2+} (2-5); $c_{Asp\text{-}\beta\text{-}ha} = 3.64 \times 10^{-3}$ M.

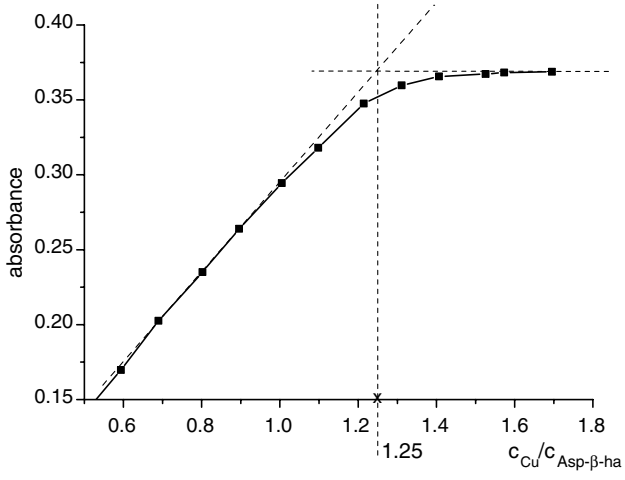

Fig. 3. Dependence of the absorbance of the d–d transition at 617 nm on the copper(II)-to-(Asp-β-ha) molar ratio; $c_{Asp\text{-}\beta\text{-}ha} = 5 \times 10^{-3}$ M; 1 cm cells.

$[Cu_5(LH_{-1})_4]$. From the above considerations, the most probable species in the pH range 4.5–11 is the pentanuclear species $[Cu_5(Asp\text{-}\beta\text{-}ha)_4H_{-4}]^{2-}$ in which the carboxylato groups are not coordinated [14]. Thus, we can see that model I in Table 2 is preferred.

The molar absorption coefficient (ε) for the $[Cu_5(Asp\text{-}\beta\text{-}ha)_4H_{-4}]^{2-}$ species may be calculated from a plot of absorbance versus Cu^{2+}-concentration for a series of samples with Asp-β-ha. This relation exhibits a linear behaviour from 0.5 to 5.5 mM with the slope of the line giving $\varepsilon = 61\ dm^3\ mol^{-1}\ cm^{-1}$, calculated per Cu^{2+} ion.

3.2. Copper(II)-amine-DL-aspartic acid-β-hydroxamic acid systems

In the Cu^{2+}–en–(Asp-β-ha) system, the mixed-ligand complexes are not formed. The results of potentiometric studies on the ternary systems with triamines are collected in Table 4, together with our previous stability constants values concerning ternary systems with β-alaninehydroxamic acid [1,3]. Concentration distribution curves for these systems are presented in Figs. 4(a) and (b) together with their variations of visible absorption maximum wavelengths with pH.

The calculated concentrations of the copper(II) complex species for the Cu^{2+}–dien–(Asp-β-ha) 1:1:2 molar ratio system as a function of pH (shown in Fig. 4(a)) indicate that under these conditions, the $[Cu(dien)]^{2+}$ species is present in concentration ca. 95% in the 4–6 pH range. The $[Cu(dien)_2]^{2+}$ complex is formed in significant concentration at copper(II):dien:Asp-β-ha molar ratios of 1:2:2 and 1:2:1, but at the discussed 1:1:2 molar ratio it is a minor product (ca 1%), so it can be regarded as negligible.

From comparative analysis of potentiometric data and EPR spectra for the Cu^{2+}–dien–(Asp-β-ha) system, it may be established that in the 7–11 pH range two mixed-ligand complexes, $[Cu(dien)(H\text{-}Asp\text{-}\beta\text{-}ha)]^{+}$ and $[Cu(dien)(Asp\text{-}\beta\text{-}ha)]$ exist (Fig. 4(a)). The EPR spectra of the species formed in the Cu^{2+}–dien–(Asp-β-ha) system depending on pH are demonstrated in Fig. 5. The spectra observed within pH range 2.5 and 4.5, with parameters $g_{\|} = 2.334$, $A_{\|} = 158 \times 10^{-4}\ cm^{-1}$ (Table 5), are ascribed to the first complex $[Cu(H\text{-}Asp\text{-}\beta\text{-}ha)]^{+}$ being in equilibrium with Cu^{2+}_{aqua} (Fig. 4(a)). The parameters are close to those found for Cu^{2+} with β-Alaha at pH 3 [1]. Between pH 3.56 and 5.51, the spectrum with parameters $g_{\|} = 2.234$, $A_{\|} = 190 \times 10^{-4}\ cm^{-1}$ is characteristic for $[Cu(dien)]^{2+}$. It is still observed to a small extent at pH 7.58. At this pH a new spectrum with $g_{\|} = 2.218$, $A_{\|} = 190 \times 10^{-4}\ cm^{-1}$ is dominant. These parameters are close to those for $[Cu(dien)_2]^{2+}$ ($g_{\|} = 2.214$, $A_{\|} = 186 \times 10^{-4}\ cm^{-1}$, Table 5) and are different from those observed for the Cu^{2+}–dien-β-Alaha system ($g_{\|} = 2.244$, $A_{\|} = 183 \times 10^{-4}\ cm^{-1}$) at pH 7 [1]. It suggests that the coordination sphere in the Cu^{2+} plane in $[Cu(dien)(H\text{-}Asp\text{-}\beta\text{-}ha)]^{+}$ consists of four nitrogen atoms whereas the oxygen of Asp-β-ha may

Table 4
Cumulative formation constants ($\log\beta$) and derived equilibrium constants ($\log K$) for complexes formed in the Cu^{2+}–dien and Cu^{2+}–Me_5dien systems with aspartic acid-β-hydroxamic acid or β-alaninehydroxamic acid (L) at 25 °C and $I = 0.2$ M (KCl) in water solutions (the ion charges are omitted)

No.	Assignment	A = dien		A = Me_5dien	
		L = Asp-β-ha	L = β-Alaha	L = Asp-β-ha	L = β-Alaha
		This work	Ref. [1]	This work	Ref. [3]
1.	$\log\beta_{CuALH_2}$			33.51(7)	34.01(2)
2.	$\log\beta_{CuALH}$	29.32(2)	28.77(3)	27.66(4)	27.76(2)
3.	$\log\beta_{CuAL}$	20.54(3)	19.99(2)	18.74(4)	18.91(2)
4.	$pK_{Cu(HA)HL}$			5.85	6.25
5.	pK_{CuAHL}	8.78	8.78	8.92	8.85
6.	$[CuA] + H_2L \rightleftharpoons [CuAHL] + H^+$ $\log K_{[CuAHL]} = \log\beta^{Cu^{2+}}_{[CuAHL]} - \log\beta^{Cu^{2+}}_{[CuA]} - pK_{NHOH} - \log K_{NH_2} - \log K_{COO^-}$	−6.50		−4.49	
7.	$[CuA] + HL \rightleftharpoons [CuAHL]$ $\log K_{[CuAHL]} = \log\beta^{Cu^{2+}}_{[CuAHL]} - \log\beta^{Cu^{2+}}_{[CuA]} - pK_{NH_3^+} - \log K_{NHO^-}$		−5.45		−2.92
8.	$[CuA] + L \rightleftharpoons [CuAL]$ $\log K_{[CuAL]} = \log\beta^{Cu^{2+}}_{[CuAL]} - \log\beta^{Cu^{2+}}_{[CuA]}$	4.53	3.98	6.40	6.44
9.	$\log K_{[CuAL]} - \log K_{NHO^-} - \log K_{NH_2}$	−13.16	−14.40	−11.29	−11.77

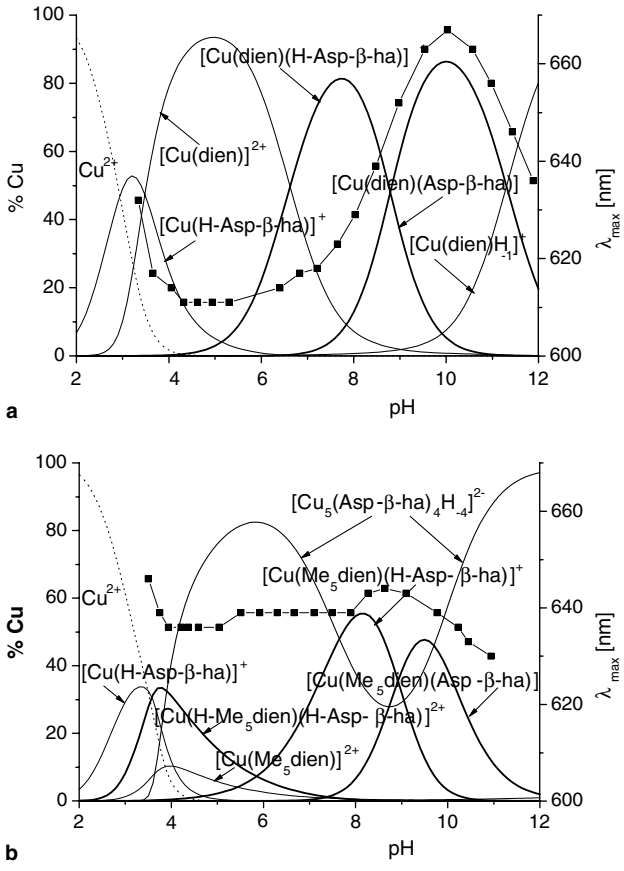

Fig. 4. Variations of visible absorption (■) maximum wavelengths in the Cu^{2+}–dien–(Asp-β-ha) system at 1:1:2 molar ratio, 2 cm cells (a) and Cu^{2+}–Me_5dien–(Asp-β-ha) system at 1:2:1 molar ratio, 1 cm cells (b), as a function of the distribution of copper(II) into its free and complexed forms; $c_{Cu} = 4 \times 10^{-3}$ M.

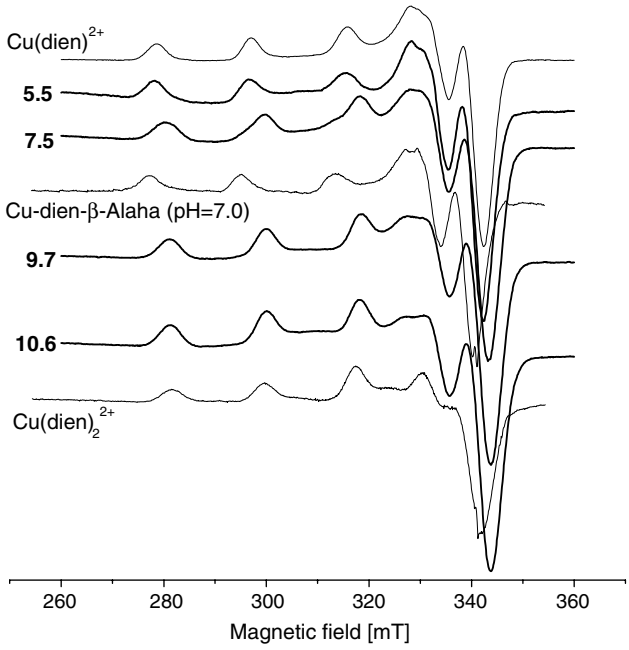

Fig. 5. EPR spectra of Cu^{2+} complexes formed in the Cu^{2+}–dien–(Asp-β-ha) system as a function of pH. For a comparison, the spectrum for the $[Cu(dien)(H\text{-}\beta\text{-}Alaha)]^{2+}$ species is added.

occupy an axial position leading to a geometry close to square-pyramid. So, the most probable explanation is that Asp-β-ha in $[Cu(dien)(H\text{-}Asp\text{-}\beta\text{-}ha)]^{+}$ coordinates in a bidentate manner through N_{amino} and $O_{carboxylate}$ donor atoms (Scheme 1), whereas three nitrogens of dien complete the coordination in the Cu^{2+} plane. The formation of this complex is reflected by a slight change in visible spectra in comparison with those manifested by $[Cu(dien)]^{2+}$ and $[Cu_5(Asp\text{-}\beta\text{-}ha)_4H_{-4}]^{2-}$ species separately (Fig. 6). The spectrum of this mixed-ligand species exhibits one band with a maximum at 618 nm with $\varepsilon = 75\ dm^3\ mol^{-1}\ cm^{-1}$, which is more asymmetric in the wavelength region 700–900 nm than that for $[Cu(dien)]^{2+}$. Such asymmetry is characteristic of the five-coordinate complexes. The coordination of the

Table 5
EPR parameters of the binary and ternary systems

System	Identified species	pH	g_z	g_x	g_y	A_z	A_x	A_y
Cu^{2+}–dien–Asp-β-ha	$[Cu(H\text{-}Asp\text{-}\beta\text{-}ha)]^{+}$	3.25	2.334	2.067	2.067	158	10	10
	$[Cu(dien)]^{2+}$	4.52–5.51	2.234	2.050	2.050	190	20	20
	$[Cu(dien)(H\text{-}Asp\text{-}\beta\text{-}ha)]^{+}$	7.58	2.218	2.050	2.050	190	20	25
	$[Cu(dien)(Asp\text{-}\beta\text{-}ha)]$	9.72	2.215	2.055	2.045	186	35	15
Cu^{2+}–Me_5dien–Asp-β-ha	$[Cu(H\text{-}Asp\text{-}\beta\text{-}ha)]^{+}$	3.19	2.332	2.067	2.067	160	10	10
	$[Cu(H\text{-}Me_5dien)(H\text{-}Asp\text{-}\beta\text{-}ha)]^{2+}$	3.92	2.240	2.055	2.055	175	15	15
	$[Cu(Me_5dien)(H\text{-}Asp\text{-}\beta\text{-}ha)]^{+}$	7.58	2.235	2.055	2.030	174	30	15
	$[Cu(Me_5dien)(Asp\text{-}\beta\text{-}ha)]$	9.67	2.233	2.065	2.035	174	50	20
	$[Cu_5(Asp\text{-}\beta\text{-}ha)_4H_{-4}]^{2-}$	4–9	a very broad and weak line					
Cu^{2+}–dien (1:1)	$[Cu(dien)]^{2+}$	5.3	2.234	2.055	2.055	190	20	20
Cu^{2+}–dien (1:2)	$[Cu(dien)]_2{}^{2+}$	7.90–9.40	2.214	2.054	2.044	186	25	15
Cu^{2+}–Me_5dien (1:1)	$[Cu(Me_5dien)]^{2+}$	5.65	2.240	2.060	2.045	175	30	15
Cu^{2+}–Asp-β-ha	$[Cu(H\text{-}Asp\text{-}\beta\text{-}ha)]^{+}$	3.16	2.334	2.067	2.067	160	10	10
	polynuclear species	4.5–11	a very broad and weak line					

The anisotropic parameters are estimated on the basis of computer simulation of the experimental spectra measured at 77 K. Parameters A are given in $[10^{-4}\ cm^{-1}]$.

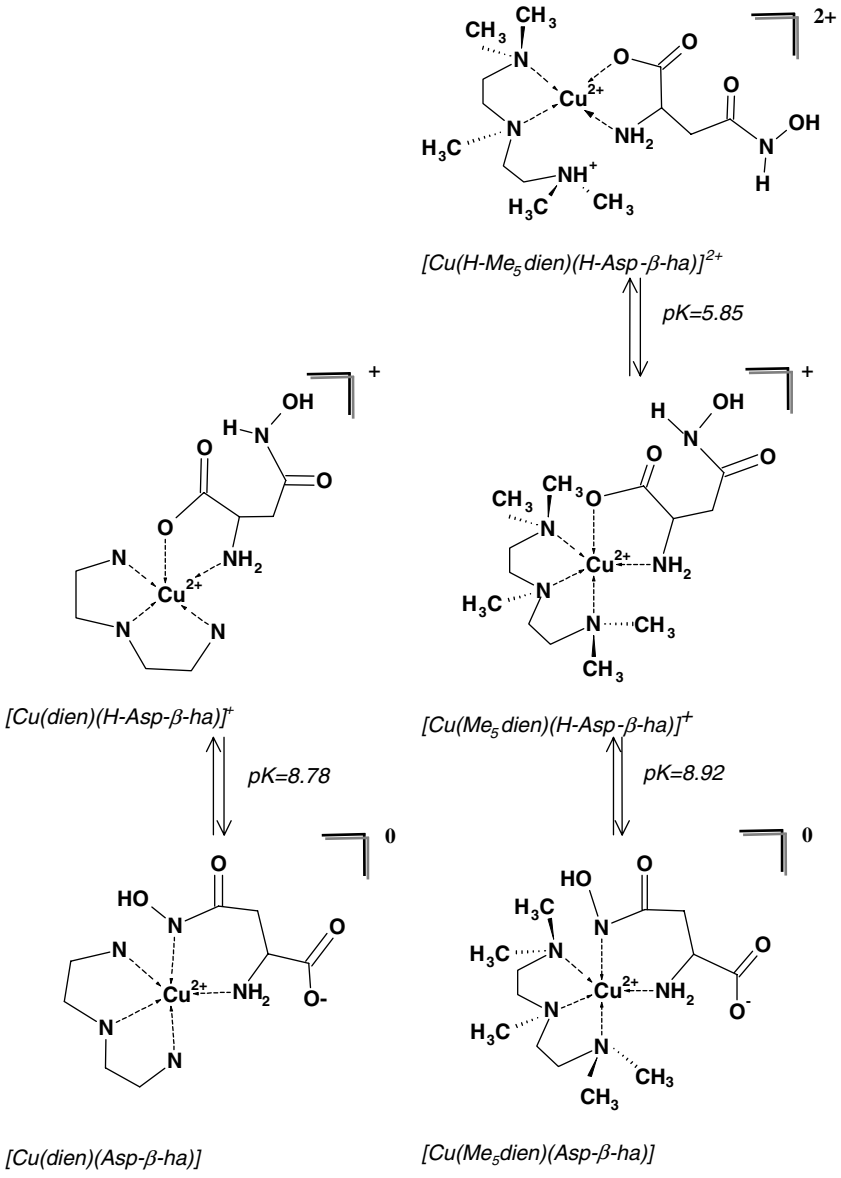

Scheme 1.

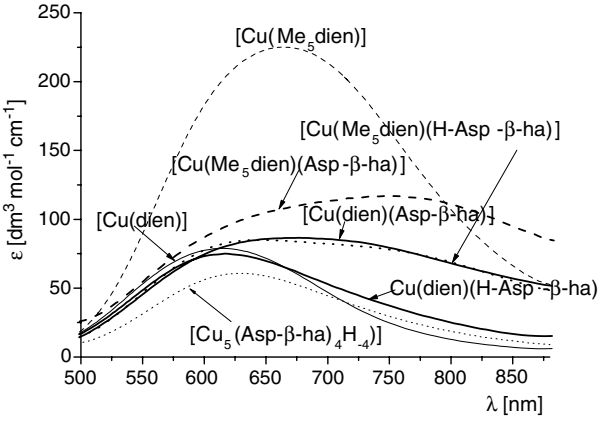

Fig. 6. Calculated electronic spectra of individual mixed-ligand species.

nitrogen donor atom in an equatorial position generally causes a blue-shift (ca. 40 nm) of the d–d absorption band relative to λ_{max} for $[Cu(dien)]^{2+}$, while in an axial position – a red-shift, more widely than for an oxygen donor atom. As a result of the two opposite effects (blue and red-shift), a 7 nm shift to lower energies occurs in λ_{max} of the spectrum for $[Cu(dien)(H\text{-}Asp\text{-}\beta\text{-}ha)]^{+}$ as compared to that for $[Cu(dien)]^{2+}$.

Thus H-Asp-β-ha in $[Cu(dien)(H\text{-}Asp\text{-}\beta\text{-}ha)]^{+}$ is coordinated via $O_{carboxylate}$ and N_{amino} donor atoms in a glycine-like mode (the neutral hydroxamate group is not coordinated), whereas in $[Cu(dien)(H\text{-}\beta\text{-}Alaha)]^{2+}$ it is bound via oxygen donor atoms from the hydroxamate group, and the amino group is protonated [1]. In both cases five-membered chelate rings are formed. A comparison of the basicity-adjusted stability constants

of [Cu(dien)(H-Asp-β-ha)]$^{+}$ and [Cu(dien)(H-β-Ala-ha)]$^{2+}$ shows that the stability of the former complex is lower than that of the latter (Eqs. (6) and (7) in Table 4). This relation is similar to those observed for [Cu(dien)(acetohydroxamic acid)]$^{+}$ and [Cu(dien)(glycine)]$^{+}$, their basicity-adjusted stability constants are −5.67 (obtained from data published in [19]) and −7.42 (obtained from data published in [20]), respectively. From the above considerations it is possible to ascertain that in the ternary Cu^{2+}–dien–Asp-β-ha system at pH ca. 7.5, the glycine-like coordination is chosen for Asp-β-ha, although this group forms less stable complexes.

The deprotonation of [Cu(dien)(H-Asp-β-ha)]$^{+}$ results to the formation of [Cu(dien)(Asp-β-ha)] above pH 8. This process is reflected by a distinct change in visible spectra starting from pH 8 (circles in Fig. 4(a)). Additionally, the isolated electronic absorption spectrum for the [Cu(dien)(Asp-β-ha)] species demonstrates a broad band in the wavelength range 600–800 nm. The EPR spectra at pH 9.7 and 10.6, where [Cu(dien)(Asp-β-ha)] is dominant, (Fig. 5) differ from that at pH about 8 (ascribed to the previous mixed-ligand species) by the presence of a weak rhombic distortion ($A_x \neq A_y$ and $g_x \neq g_y$) together with smaller A_z and g_z parameters. These spectral changes are indicative of some lowering of the geometry from square-pyramid towards trigonal bipyramid. The structural transformation around the copper(II) centre is consistent with participation of the hydroxamate nitrogen instead of the carboxylate oxygen donor atom. The modification of bonding mode from five-membered (N_{amino}, $O_{carboxylate}$) to six-membered (N_{amino}, $N_{hydroxamate}$) chelate-ring leads also to the geometry distortion. The tentative structures for the discussed mixed-ligand species are presented in Scheme 1.

The stability constants obtained for the complexes formed in the Cu^{2+}–Me_5dien–(Asp-β-ha) system are given in Table 4. The concentration distribution curves for this system are presented in Fig. 4(b). From Table 4, it can be seen that the equilibrium model contains parent and mixed-ligand species: [Cu(Me_5dien)(H-Asp-β-ha)]$^{+}$, [Cu(Me_5dien)(Asp-β-ha)], similar to those observed in the Cu^{2+}–dien–Asp-β-ha system, and an additional [Cu(H-Me_5dien)(H-Asp-β-ha)]$^{2+}$ species at lower pH.

The EPR spectra for the Cu^{2+}–Me_5dien–Asp-β-ha system are presented in Fig. 7. At pH 3.19 two sets of signals of parallel and perpendicular orientations should be assigned to the equilibrium between Cu^{2+}-aqua ions ($g_{\parallel} = 2.413$ and $A_{\parallel} = 125 \times 10^{-4}$ cm^{-1}) and the first Cu(II) complex whose parameters ($g_{\parallel} = 2.332$ and $A_{\parallel} = 160 \times 10^{-4}$ cm^{-1}) are consistent with coordination of one chelating H-Asp-β-ha molecule to Cu^{2+}. The spectrum due to the first complex is also seen at pH 3.92 in equilibrium with new spectra. One of them, almost similar to that observed for [Cu(Me_5dien)]$^{2+}$,

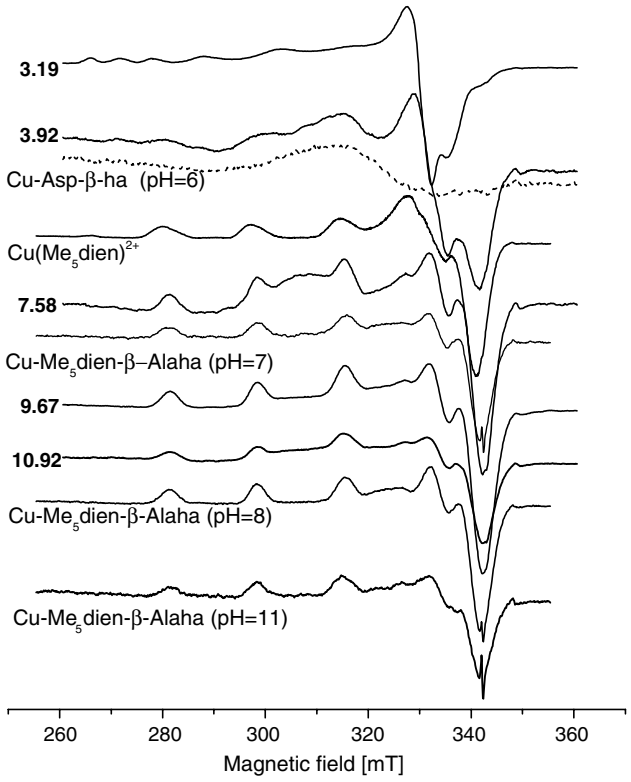

Fig. 7. EPR spectra of Cu^{2+} complexes formed in the Cu^{2+}–Me_5dien–(Asp-β-ha) system as a function of pH. For comparison, spectra for the [Cu(Me_5dien)(H-β-Alaha)]$^{2+}$ and [Cu(Me_5dien)(β-Alaha)]$^{+}$ species are added.

should be assigned to the first mixed-ligand species, [Cu(H-Me_5dien)(H-Asp-β-ha)]$^{2+}$, predicted at this pH. Its spectrum was fitted using axial symmetry parameters ($g_{\parallel} = 2.240$, $g_{\perp} = 2.055$ and $A_{\parallel} = 175 \times 10^{-4}$ cm^{-1}, $A_{\perp} = 15 \times 10^{-4}$ cm^{-1}), whereas for [Cu(Me_5dien)]$^{2+}$ the presence of rhombic distortion is evident ($g_z = 2.240$, $g_x = 2.060$, $g_y = 2.045$ and $A_z = 175$, $A_x = 30$, $A_y = 15 \times 10^{-4}$ cm^{-1} [3]). The EPR parameters suggest that the coordination in the Cu^{2+} plane in this mixed-ligand complex may be realized by two nitrogens of triamine as well as nitrogen and oxygen donors of H-Asp-β-ha. In the pH range 3.9–7 the signals corresponding to the monomeric species are overlapped by the broad line associated with formation of the polynuclear [Cu_5(Asp-β-ha)$_4H_{-4}$]$^{2-}$ complex. The broadening and small intensity of the spectrum results from the strong spin–spin interaction between Cu^{2+} centers. The same weak and broad spectrum is observed at pH 6 in the binary Cu^{2+}–(Asp-β-ha) system (Fig. 7). The change of the EPR spectrum observed at pH 7.58 supports that a new complex, predicted as [Cu(Me_5dien)(H-Asp-β-ha)]$^{+}$, is formed with parameters $g_z = 2.235$, $g_x = 2.055$, $g_y = 2.030$ and $A_z = 174$, $A_x = 30$, $A_y = 15 \times 10^{-4}$ cm^{-1}. A rhombic character of the parameters indicate that the geometry distortion for [Cu(Me_5dien)(H-Asp-β-ha)]$^{+}$ species is higher than for the mixed-ligand complex

containing dien. The visible spectrum, calculated for this complex, shows a broad band in the 600–800 nm range with two shoulders: at 610 nm ($\varepsilon = 85$) and 750 ($\varepsilon = 78$) (Fig. 6) indicating again a rhombic distortion of the geometry towards trigonal bipyramid.

At pH about 11 the intensity of the EPR signals observed for the monomeric species decreases more than two times as compared to that at pH 9.5. This explains the increase of concentration of polynuclear $[Cu_5(Asp\text{-}\beta\text{-}ha)_4H_{-4}]^{2-}$ species in basic solution. Thus, the distribution curve of the pentanuclear species has two maxima and one minimum in which two mixed-ligand species are formed (as observed in our previous work [3]). Such a situation is often observed in various systems in which polynuclear and mixed-ligand species are formed [21].

A comparison of the basicity-adjusted stability constants shows that the stability of $[Cu(Me_5dien)(H\text{-}Asp\text{-}\beta\text{-}ha)]^{+}$ is lower than that for $[Cu(Me_5dien)(H\text{-}\beta\text{-}Alaha)]^{2+}$ (Eqs. (6) and (7) in Table 4). This relation is similar to those observed for $[Cu(Me_5dien)(acetohydroxamic\ acid)]^{+}$ and $[Cu(Me_5dien)(glycine)]^{+}$. Their basicity-adjusted stability constants are −3.18 [22] and −6.61 (calculated from data published in [20]), respectively. Hence, it is possible to ascertain that in the ternary Cu^{2+}–Me_5dien–Asp-β-ha system, at pH ca. 7.5, for Asp-β-ha the glycine-like coordination is chosen which results in formation of less stable complexes as was observed in the ternary systems with dien (see above). An increasing distortion of the $[Cu(Me_5dien)H_2O]^{2+}$ complex geometry in comparison with $[Cu(dien)H_2O]^{2+}$ is the reason for the higher stability of the mixed-ligand complexes with Me_5dien than those with dien (Table 4).

The absorption curve for the next mixed-ligand species, $[Cu(Me_5dien)(Asp\text{-}\beta\text{-}ha)]$, which exhibits a broad band with a maximum at 750 nm, is different from that for the previous species. The molar absorption coefficient, ε, equal to 117 $dm^3\ mol^{-1}\ cm^{-1}$, is higher than for $[Cu(Me_5dien)(H\text{-}Asp\text{-}\beta\text{-}ha)]$. The EPR spectrum (at pH 9.67), corresponding to formation of $[Cu(Me_5dien)(Asp\text{-}\beta\text{-}ha)]$, displays a higher degree of rhombic distortion (Table 5) as compared to that observed for the previous mixed-ligand complex. A similar trend is found for the complexes present in the Cu^{2+}–Me_5dien–β-Alaha system [3]. This spectral behavior reveals a structural transformation around the copper(II) ion, suggesting the participation of all nitrogen-donor atoms in the coordination sphere in the $[Cu(Me_5dien)(Asp\text{-}\beta\text{-}ha)]$ species.

4. Conclusion

In the ternary Cu^{2+}–dien–(Asp-β-ha) and Cu^{2+}–Me_5-dien–(Asp-β-ha) systems at pH ca. 7.5, H-Asp-β-ha coordinates to $[Cu(dien)]^{2+}$ as well as to $[Cu(Me_5dien)]^{2+}$ by the carboxylate group, in addition to the amino nitrogen (glycine-like coordination), whereas the hydroxamate group remains in the form CONHOH. At higher pH the hydroxamate ligand is coordinated by N_{amino} and $N_{hydrox.}$ donor atoms.

The presence of the carboxylate group in Asp-β-ha causes the changes in the bonding mode of Asp-β-ha in the mixed-ligand species in relation to β-Alaha (in the binary systems both aminohydroxamic acids form stable pentanuclear species over a wide pH range). The basicity-adjusted stability constants for the complexes with Asp-β-ha are higher than those with β-Alaha (Eq. (9) in Table 4) because of the neutral charge of $[Cu(amine)(Asp\text{-}\beta\text{-}ha)]$, while the charge of $[Cu(amine)\beta\text{-}Alaha]^{+}$ is positive. An increasing distortion of the $[Cu(Me_5dien)H_2O]^{2+}$ complex geometry in comparison with $[Cu(dien)H_2O]^{2+}$ results in a higher stability of the mixed-ligand complexes with Me_5dien compared to that with dien.

References

[1] B. Kurzak, D. Kroczewska, J. Jezierska, Polyhedron 17 (1998) 1831.
[2] B. Kurzak, K. Bogusz, D. Kroczewska, J. Jezierska, Polyhedron 20 (2001) 2627.
[3] D. Kroczewska, K. Bogusz, B. Kurzak, J. Jezierska, Polyhedron 21 (2002) 295.
[4] D. Kroczewska, B. Kurzak, E. Matczak-Jon, Polyhedron 21 (2002) 2183.
[5] B.H. Bracher, R.W.H. Small, Acta Cystallogr. B26 (1970) 1705.
[6] T. Głowiak, M. Koralewicz, Cryst. Spectrosc. Res. 15 (1985) 621.
[7] A. Kvick, W.M. Canning, T.F. Koetzle, G.J.B. Williams, Acta Cystallogr. B36 (1980) 115.
[8] E. Farkas, E.A. Enyedy, H. Csoka, J. Inorg. Biochem. 79 (2000) 205.
[9] A. Gergely, I. Sovago, J. Inorg. Nucl. Chem. 35 (1973) 4355.
[10] T. Głowiak, B. Kurzak, J. Crystallogr. Spectr. Res. 22 (1992) 95.
[11] T. Kiss, E. Farkas, B. Kurzak, J. Chem. Soc., Perkin Trans. (1990) 1255.
[12] E. Leporati, J. Chem. Soc., Dalton Trans. (1988) 953.
[13] E. Farkas, P. Buglyo, J. Chem. Soc., Dalton Trans. (1990) 1549.
[14] M. Careri, F. Dallavalle, M. Tegoni, I. Zagnoni, J. Inorg. Biochem 93 (2003) 174.
[15] G. Gran, Acta Chem. Scand. 4 (1959) 599.
[16] B. Kurzak, D. Kroczewska, J. Coord. Chem. 34 (1995) 67.
[17] B. Kurzak, E. Farkas, T. Głowiak, H. Kozłowski, J. Chem. Soc., Dalton Trans. (1991) 163.
[18] E. Farkas, J. Szoke, T. Kiss, H. Kozłowski, W. Bal, J. Chem. Soc., Dalton Trans. (1989) 2247.
[19] E. Farkas, E.A. Enyedy, G. Micera, E. Garribba, Polyhedron 19 (2000) 1727.
[20] T. Murakami, K. Murata, Y. Ishikawa, Inorg. Chim. Acta 244 (1996) 51.
[21] (a) M. Dyba, M. Jeżowska-Bojczuk, E. Kiss, H. Kozłowski, Y. Leroux, D. El Manouni, J. Chem. Soc., Dalton Trans. (1996) 1119; (b) T. Kiss, T. Jakusch, M. Kilyen, E. Kiss, A. Lakatos, Polyhedron 19 (2000) 2389.
[22] B. Kurzak, D.Kroczewska, unpublished data.

Available online at www.sciencedirect.com
SCIENCE DIRECT®
Polyhedron 25 (2006) 687–694
POLYHEDRON
www.elsevier.com/locate/poly

Synthesis and characterization of Co(II), Cu(II) and Zn(II) complexes with 1,1-cyclobutanedicarboxylic acid

Zofia Rzączyńska [a], Agata Bartyzel [a,*], Elżbieta Olszewska [a], Wanda Sawka-Dobrowolska [b]

[a] *Department of General and Coordination Chemistry, Faculty of Chemistry, Maria Curie-Skłodowska University, 20-031 Lublin, Poland*
[b] *Faculty of Chemistry, University of Wrocław, 50-383 Wrocław, Poland*

Received 4 April 2005; accepted 14 July 2005
Available online 5 October 2005

Abstract

The compounds of 1,1-cyclobutanedicarboxylic acid with cobalt(II), copper(II) and zinc(II) ions have been prepared in aqueous solutions. The complexes were characterized by elemental analysis, IR spectroscopy, thermal analysis (TG, DSC/DTA and TG-FTIR) and X-ray analysis. The polycrystalline cobalt(II) and zinc(II) complexes were obtained as the hydrated compounds $Co(C_6H_6O_4)\cdot 2H_2O$ and $Zn_2(C_6H_6O_4)_2\cdot 3H_2O$, whereas the polycrystalline copper compound is anhydrous $Cu(C_6H_6O_4)$. During slow recrystallization we obtained single crystals of cobalt(II) and copper(II) compounds where the number of water molecules is different from that of the polycrystalline compounds and the formula are $[Co_2(C_6H_6O_4)_2(H_2O)_3]$ (**1**) and $[Cu(C_6H_6O_4)H_2O]$ (**2**). The polycrystalline cobalt(II) and copper(II) complexes crystallize in the monoclinic system, the zinc(II) compound crystallizes in the triclinic system. During heating the hydrated complexes lose water molecules and become anhydrous. Next the anhydrous compounds decompose to the corresponding oxides. The thermal decomposition is connected with the release of water molecules (328 K), carbon dioxide (502 K) and cyclobutanecarboxylic acid (546 K). The IR spectra of the salt are discussed.
© 2005 Elsevier Ltd. All rights reserved.

Keywords: Cobalt 1,1-cyclobutanedicarboxylate; Copper 1,1-cyclobutanedicarboxylate; Zinc 1,1-cyclobutanedicarboxylate; X-ray analysis; Crystal structure; IR spectra; Thermal analysis; TG-FTIR analysis

1. Introduction

There has been major interest in metal carboxylates in the last few years [1–7]. Metal carboxylates exhibit interesting biological properties, antibacterial and antifungal activities. Moreover, the carboxylate ion often participates as an important ligand in many metalloenzymes [4,8–10]. Carboxylate metal complexes are also interesting from a structural point of view. The carboxylate group can adopt a wide range of coordination modes. These are very attractive for the study and design of metal-organic framework solids. Polycarboxylates compounds are of particular significance [9,11].

Metal compounds with 1,1-cyclobutanedicarboxylic are the subjects of our research. The 1,1-cyclobutanedicarboxylate ligand has been often used as a component of platinum complexes, studied as potential antitumor drugs. The most common compound is platinum(II) *cis*-diamin(1,1-cyclobutanedicarboxylate), carboplatin, widely used as a drug in cancer chemotherapy [12–17]. Lanthanide complexes were first studied by us [18,19]. We also studied transition metal compounds. In a previous paper [20], we presented a manganese(II) complex with 1,1-cyclobutanedicarboxylic acid which is isostructural with the cobalt(II) complex ($[Co_2(C_6H_6O_4)_2(H_2O)_3]$) presented in this paper. The manganese(II)

* Corresponding author. Tel.: +48 81 5375754; fax: +48 81 5333348.
E-mail address: abartyze@hermes.umcs.lublin.pl (A. Bartyzel).

0277-5387/$ - see front matter © 2005 Elsevier Ltd. All rights reserved.
doi:10.1016/j.poly.2005.07.044

complex crystallizes in the monoclinic system and in the space group $C2/c$. The polymeric structure comprises dimeric units bridged by carboxylate groups. The metal ions in dimeric units are bonded with one water molecule and carboxylate groups [20].

The present work reports the properties of cobalt(II), copper(II) and zinc(II) complexes with 1,1-cyclobutanedicarboxylic acid. We have synthesized and characterized the compounds by X-ray crystallography, IR spectra and thermal analysis. Polycrystalline cobalt(II) and copper(II) compounds with 1,1-cyclobutanedicarboxylic acid were also investigated by Allan and Dalrymple [3]. They obtained complexes with a different number of water molecules from that presented in this paper. Polycrystalline cobalt(II) and copper(II) 1,1-cyclobutanedicarboxylates were obtained as monohydrate compounds whereas the complexes synthesized by us are dihydrate and anhydrous, $Co(C_6H_6O_4)\cdot 2H_2O$ and $Cu(C_6H_6O_4)$.

2. Experimental

2.1. Synthesis

1,1-Cyclobutanedicarboxylic acid was dissolved in boiling water and neutralized by the addition of the corresponding metal(II) carbonate. The solution was filtered to remove any excess of metal carbonates and the filtrate was then reduced in volume to yield the polycrystalline metal complexes. The contents of carbon and hydrogen were determined on the basis of elemental analysis using a CHN 2400 Perkin–Elmer analyzer. Chemical analysis confirms the composition (Table 1). Single crystals were obtained by recrystallization from an aqueous solution of the compounds after a few weeks. Crystals were isolated, washed with ethanol and dried at room temperature.

2.2. Magnetism

Magnetic susceptibility measurement was conducted at 294 K using a magnetic susceptibility balance MSB-MKI, Sherwood Scientific Ltd., Cambridge. The data were corrected for diamagnetic susceptibilities. The effective magnetic moment was calculated from the equation $\mu_{eff} = 2.828(\chi_{cor}T)^{1/2}$.

2.3. IR

The IR spectra of complexes were recorded over the range 4000–400 cm^{-1} using a FTIR 1725X Perking–Elmer spectrometer. The samples were prepared as KBr discs.

2.4. X-ray powder diffraction

The powder diffraction data were collected on a PHILIPS XPERT PRO (Holland) automated X-ray diffractometer. The experimental conditions were: Cu target X-ray tube operated at 45 kV and 30 mA, 6° take-off angle, 1° divergence slit, 0.15 mm receiving slit, curved graphite diffracted beam monochromator and scintillation counter with pulse height analyzer. The powder diffraction pattern was collected by step scanning between 4° and 70° in 2θ with a step equal to 0.02° and a count time of 10 s/step. The diffractometer was calibrated by using a SRM 1976 standard. Throughout the measurement, the ambient temperature was maintained at 20 ± 1 °C. The XRAYAN program was used for determining peak intensities and positions. Pattern indexing was carried out with the PC-version of the TREOR program [21]. For this sample, all the 2θ peak positions were used. The unit cell data are presented in Table 2.

2.5. X-ray structure determination

Both crystals, $Co_2(C_6H_6O_4)_2(H_2O)_3]$ (**1**) and $[Cu(C_6H_6O_4)H_2O]$ (**2**), were mounted on a glass fiber and then flash-frozen to 100 K (Oxford Cryosystem-Cryostream Cooler). Preliminary examination and intensity data collections were carried out on a Kuma KM4CCD κ-axis diffractometer with graphite-monochromated Mo Kα radiation. The crystallographic data and the refinement procedure details are given in Table 3. All data were corrected for Lorentz, polarization and absorption effects [22]. The structures were solved by direct methods (program SHELXS97 [23,24]) and refined by the full-matrix least-squares method on all F^2 data using the SHELXL97 [25] programs. Hydrogen atoms were found by Fourier syntheses (all in **1** and OH in **2**) or included in calculated positions (in **2**) with the isotropic thermal parameters

Table 1
Characterization data of polycrystalline cobalt(II), copper(II) and zinc(II) 1,1-cyclobutanedicarboxylates

Complex	Elemental analysis (%)						Color	Magnetic moment, μ_{eff} (μ_B)
	M		C		H			
	Calc.	Found	Calc.	Found	Calc.	Found		
$CoL\cdot 2H_2O$	24.88	24.73	30.39	30.55	4.22	4.21	pink–violet	5.12
CuL	30.92	30.46	35.02	34.54	2.92	2.99	deep blue	1.94
$Zn_2L_2\cdot 3H_2O$	27.87	27.48	30.72	30.88	3.84	3.83	white	diamagnetic

$L = C_6H_6O_4$.

Table 2
The unit cell parameters for polycrystalline 1,1-cyclobutanedicarboxylates

	$CoL \cdot 2H_2O$	CuL	$Zn_2L_2 \cdot 3H_2O$
Crystal system	monoclinic	monoclinic	triclinic
a (Å)	21.06	18.31	14.36
b (Å)	7.91	11.23	14.31
c (Å)	9.75	9.76	15.64
α (°)			102.38
β (°)	108.74	109.35	128.93
γ (°)			52.28
Volume (Å^3)	1538	1894	1900

Table 3
Crystal data and structure refinement

Compound	**1**	**2**
Formula	$C_{12}H_{18}Co_2O_{11}$	$C_6H_8CuO_5$
M_r	456.12	223.66
Crystal system	monoclinic	orthorhombic
Space group	$C2/c$	$Pnma$
T (K)	100(1)	100(1)
Wavelength (Å)	0.71073	0.71073
a (Å)	20.262(4)	18.252(4)
b (Å)	7.827(2)	7.063(1)
c (Å)	9.711(2)	5.488(1)
β (°)	98.11(3)	
Volume (Å^3)	1524.7(6)	707.5(2)
Z	4	4
$F(000)$	928	452
Absorption coefficient (mm^{-1})	2.237	3.062
Absorption correction	analytical	analytical
Maximum and minimum transmission	0.817 and 0.681	0.901 and 0.544
D_{calc} (Mg/m^3)	1.987	2.100
Crystal size (mm)	$0.20 \times 0.15 \times 0.12$	$0.3 \times 0.2 \times 0.15$
θ Range for data collection (°)	3.42–28.34	3.65–28.48
Reflections measured	5005	6806
Reflections unique	1775	927
R_{int}	0.042	0.056
Data [$I > 2\sigma(I)$]/parameters	1482/161	846/62
Goodness-of-fit on F^2	1.069	1.252
Final R indices [$I > 2\sigma(I)$]	$R_1 = 0.0331$, $wR_2 = 0.0650$	$R_1 = 0.0474$, $wR_2 = 0.0746$
R indices (all data)	$R_1 = 0.0487$, $wR_2 = 0.0699$	$R_1 = 0.0573$, $wR_2 = 0.0769$
Largest difference peak and hole (e Å^{-3})	0.482 and −0.373	0.531 and −0.486

$R_1 = \sum(F_o - F_c)/\sum F_o$; $wR_2 = \{\sum[w(F_o^2 - F_c^2)^2]/\sum[w(F_o^2)^2]\}^{1/2}$.

proportional to those of the connected carbon atoms. Unfortunately, we could not obtain untwinned single crystals with a good quality for compound **2**, and the data of the X-ray analysis were poorer than the other crystals. In the case of the structure of the cobalt complex, the water molecule O21 is disordered occupying two statistical positions represented by O21 and O21′ with site occupancy factors of 0.55 and 0.45. Crystal structures of complexes **1** and **2** are shown in Figs. 1–4.

2.6. Thermal analysis

The thermal stability and decomposition of the prepared complexes in air were determined with the aid of Setsys 16/18, recording TG, DTA and DTG curves. Samples (8.24–9.90 mg) were heated in Al_2O_3 crucibles at 293–1273 K in flowing air atmosphere with a heating rate of 10 K min^{-1}. The products of decomposition were calculated from TG curves (Figs. 5 and 6).

Using a Netzsch TG apparatus coupled with a Bruker FTIR IFS66 spectrophotometer, the gas-phase products of decomposition were identified (Fig. 7). The samples (7.40–19.38 mg) were heated to 1250 K, using Al_2O_3 crucibles, in an argon atmosphere, at a heating rate of 10 K min^{-1}.

3. Results and discussion

The polycrystalline 1,1-cyclobutanedicarboxylates of cobalt(II) and zinc(II) were obtained as hydrated

compounds whereas the polycrystalline copper complex is anhydrous. The characterization data of polycrystalline cobalt(II), copper(II) and zinc(II) 1,1-cyclobutanedicarboxylates are listed in Table 1. For cobalt(II) and copper(II) 1,1-cyclobutanedicarboxylates we obtained single crystals. Both single crystals contain a different number of water molecules from that of the polycrystalline complexes. In the case of polycrystalline cobalt(II) 1,1-cyclobutanedicarboxylate $Co(C_6H_6O_4)\cdot 2H_2O$, the molar ratio of metal to water is 1:2 but in the single crystal it is 1:1.5 and general formula is $[Co_2(C_6H_6O_4)_2(H_2O)_3]$ (**1**). Polycrystalline copper(II) is anhydrous whereas the single crystal was obtained as the monohydrate $[Cu(C_6H_6O_4)H_2O]$ (**2**).

The magnetic moment of $Co(C_6H_6O_4)\cdot 2H_2O$ (5.12 μ_B) is in the range of values expected for a high-spin complex. This value indicates the influence of orbital moment on the effective magnetic moment that it is characteristic of cobalt ions with octahedral geometry. The magnetic moment of $Cu(C_6H_6O_4)$ equals 1.94 μ_B. This value is characteristic of an antiferromagnetic compounds of copper.

The IR spectrum of 1,1-cyclobutanedicarboxylic acid shows a strong band, observed at 1698 cm^{-1}, due to COOH-groups. This band is absent in the complexes due to the formation of COO^- groups. Values of the frequency separation ($\Delta\nu$) between COO^- asymmetric and symmetric stretching vibrations $\nu(COO^-)$ can be used for predicting the coordination mode of the carboxyl group. In $Co(C_6H_6O_4)\cdot 2H_2O$, the $\Delta\nu$ value is lower than that of the sodium salt, which suggests that the carboxylate groups are bidentate chelating. In the structure of cobalt(II) 1,1-cyclobutanedicarboxylate, the carboxyl groups occur as monodentate and tridentate-bridging. This disagreement results from the fact that the coupling mode of symmetric $\nu_{as}(COO)$ and $\delta(CH_2)$ makes it difficult to estimate the coordination mode based on the IR spectrum. In $Cu(C_6H_6O_4)$, the asymmetric stretching vibration $\nu(COO^-)$ splits, giving both greater and lower $\Delta\nu$ values than those of the sodium salt. According to Nakamoto [26], they indicate monodentate and chelating carboxyl groups, respectively. In $Zn_2(C_6H_6O_4)_2\cdot 3H_2O$, the asymmetric stretching vibration $\nu(COO^-)$ is also split and the calculated $\Delta\nu$ values are similar and as well as lower than those of the sodium salt. Thus, the COO^- groups can coordinate to the metal atom in a bridging and chelating fashion [26]. The polycrystalline cobalt(II) and zinc(II) compounds spectra show strong bands characteristic for water molecules; the bands at 3404 cm^{-1} for the Co(II) and 3516 cm^{-1} for the Zn(II) complexes are assigned to OH stretching vibrations. This band does not occur the polycrystalline copper(II) compound spectrum.

The X-ray diffraction patterns show excellent quality. The unit cell data are presented in Table 2. The crystal structures of Co(II) and Cu(II) 1,1-cyclobutanedicarboxylates depends on the method of crystallization. During precipitation of the Co(II) compound from aqueous solution there forms a dihydrated complex which crystallizes in the monoclinic system. After dissolution of $Co(C_6H_6O_4)\cdot 2H_2O$ in water and recrystallization we obtained single crystal $[Co_2(C_6H_6O_4)_2(H_2O)_3]$ (**1**) which also crystallize in the monoclinic system. The values of elemental cell parameters of both compounds are similar; they change by about 1%. Engaging one water molecule to bind cobalt ions in dimeric units may cause the decrease of the water molecule number in the monocrystal structure. The polycrystalline $Cu(C_6H_6O_4)$ complex crystallizes in the monoclinic system. Slow recrystallization from the water solution gives a different form of complex. The monocrystal is hydrated $[Cu(C_6H_6O_4)H_2O]$ (**2**) and crystallizes in the orthorhombic system. Polycrystalline zinc(II) 1,1-cyclobutanedicarboxylate crystallizes in the triclinic system.

The crystal structure of compound **1** consists of infinite chains that run parallel to the *a*-axis (Fig. 1), where neighboring chains are connected via hydrogen bonds. A fragment of crystal structure is shown in Fig. 2. The chains comprise dimeric $[Co_2(C_6H_6O_4)_2(H_2O)_3]$ repeating units, which are linked by two carboxylate groups from two different ligands. The cobalt ions in dimeric units are bonded by bridging carboxylate groups and a water molecule, and the distance between them is 3.4995(9) Å. The distance between neighboring Co(II)

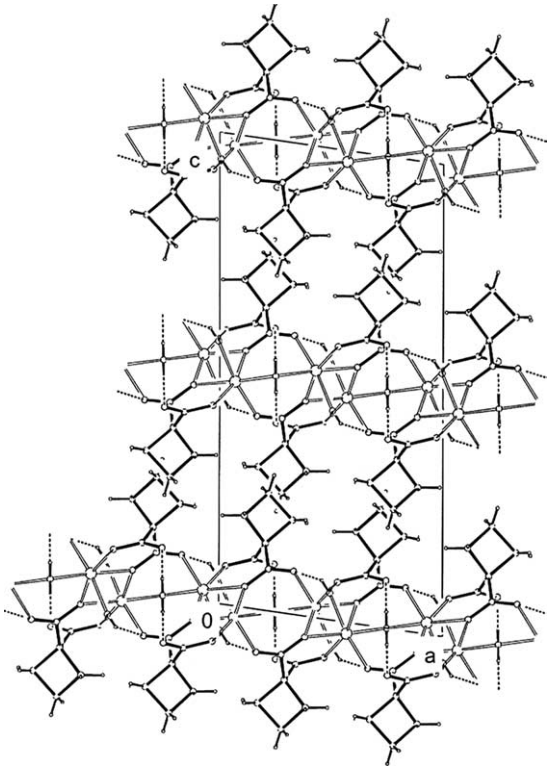

Fig. 1. Projection along the *b*-axis of $[Co_2(C_6H_6O_4)_2(H_2O)_3]$. Dotted lines symbolize hydrogen bonds.

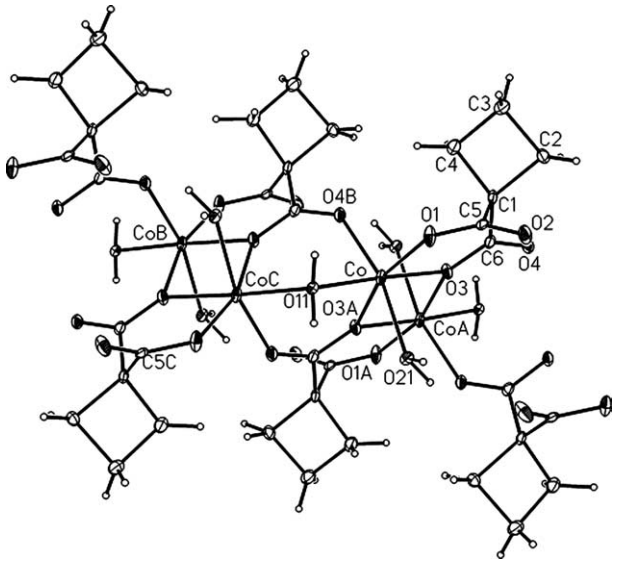

Fig. 2. ORTEP drawing (50% probability) of $[Co_2(C_6H_6O_4)_2(H_2O)_3]$. Symmetry transformations used to generate equivalent atoms: (A) $1-x, -y, -z$; (B) $x, -y, 0.5+z$; (C) $1-x, y, 0.5-z$.

atoms in chains is 3.2700(6) Å, the shortest interchain Co···Co separation is 5.3791(12) Å. Each cobalt(II) cation is surrounded by two water oxygen atoms and four carboxylate oxygen atoms from three different 1,1-cyclobutanedicarboxylic anions, exhibiting a significantly distorted octahedron. The Co–$O_{carboxyl}$ distances vary in the range 2.048(2)–2.145(2) Å while the Co–O_{water} bond lengths are 2.140(10) Å for O(21), 2.043(12) Å for O(21)′ and 2.125(1) Å (Table 4). The *cis* angles around the metal center change between 78.58(7)° and 104.10(7)°, whereas the *trans* angles vary from 163.70(7)° to 177.32(5)°. The carboxylate groups in this complex have the tridentate-bridging (O(3)–C(6)–O(4)) and monodentate (O(1)–C(5)–O(2)) character. The carboxylate groups O(3)–C(6)–O(4) and O(1)–C(5)–O(2) are rotated by 60.7(3)° and 57.5(3)° from the C1–C2–C4 plane of the cyclobutane ring. The length of C–O bonds are in the range 1.232(3)–1.291(3) Å and the O–C–O angles are 123.9(2)° and 124.3(2)°. The water molecule, which bridges two metal ions, is located in a particular position on a twofold axis of symmetry. Additionally, this water molecule acts as a proton donor in a strong hydrogen bond; the O(11)–H(1)···O(2) length is 2.610(2) Å. The water molecule O(21) is also engaged in three weak hydrogen bonds as a proton donor; the hydrogen bond length distances are in the range 2.691(10)–3.164(10) Å (Table 5).

The crystal structure of compound **2** comprises a chain in which bridging carboxylate groups bind copper ions. The structure is shown in Figs. 3 and 4. The shorter distance between two neighboring Cu(II) atoms in the chain is 4.8390(5) Å. Each copper ion is surrounded by four oxygen atoms of carboxylate groups from three different 1,1-cyclobutanedicarboxylate ligands and one water oxygen achieves the coordination number 5. The

Table 4
Selected bond lengths (Å) and angles (°)

$[Co_2(C_6H_6O_4)_2(H_2O)_3]$ (**1**)	
Co–O(1)	2.048(2)
Co–O(3)^{i}	2.080(2)
Co–O(21)	2.140(10)
Co–O(21)′	2.043(12)
Co–O(3)	2.145(2)
Co–O(4)^{ii}	2.089(2)
Co–O(11)	2.125(1)
O(1)–C(5)	1.281(3)
O(2)–C(5)	1.232(3)
O(3)–C(6)	1.291(3)
O(4)–C(6)	1.247(3)
O(2)–C(5)–O(1)	123.9(2)
O(1)–Co–O(3)^{i}	163.70(7)
O(1)–Co–O(21)	90.1(3)
O(3)^{i}–Co–O(21)	80.3(3)
O(1)–Co–O(4)^{ii}	104.07(7)
O(3)^{i}–Co–O(4)^{ii}	87.04(7)
O(21)–Co–O(4)^{ii}	164.7(2)
O(1)–Co–O(11)	91.21(7)
O(3)^{i}–Co–O(11)	100.52(6)
O(21)–Co–O(11)	82.5(2)
O(4)^{ii}–Co–O(11)	91.49(6)
O(1)–Co–O(3)	89.18(7)
O(4)–C(6)–O(3)	124.3(2)
O(3)^{i}–Co–O(3)	78.58(7)
O(21)–Co–O(3)	94.9(2)
O(4)^{ii}–Co–O(3)	90.99(7)
O(11)–Co–O(3)	177.32(5)
Co^{i}–O(3)–Co	101.42(7)
Co–O(11)–Co^{iv}	110.89(10)
C(5)–O(1)–Co	119.68(16)
C(6)–O(3)–Co^{i}	130.58(15)
C(6)–O(3)–Co	127.93(15)
C(6)–O(4)–Co^{iii}	135.24(16)
$[Cu(C_6H_6O_4)H_2O]$ (**2**)	
Cu–O(2)	1.940(2)
Cu–O(1)^{iii}	1.958(2)
Cu–O(11)	2.377(4)
O(1)–C(5)	1.270(3)
O(2)–C(5)	1.253(4)
O(2)–C(5)–O(1)	122.6(3)
O(2)–Cu–O(2)^{i}	89.50(13)
O(2)–Cu–O(1)^{ii}	90.21(9)
O(2)^{i}–Cu–O(1)^{ii}	179.63(9)
O(2)–Cu–O(1)^{iii}	179.63(9)
O(2)^{i}–Cu–O(1)^{iii}	90.21(9)
O(1)^{ii}–Cu–O(1)^{iii}	90.08(12)
O(2)–Cu–O(11)	89.81(9)
O(2)^{i}–Cu–O(11)	89.81(9)
O(1)^{ii}–Cu–O(11)	90.42(9)
O(1)^{iii}–Cu–O(11)	90.42(9)
C(5)–O(1)–Cu^{iv}	117.63(2)
C(5)–O(2)–Cu	124.5(2)

Symmetry codes for **1**: (i) $-x+1, -y, -z$; (ii) $x, -y, z+1/2$; (iii) $x, -y, z-1/2$; (iv) $-x+1, y, -z+1/2$. Symmetry codes for **2**: (i) $x, -y+1/2, z$; (ii) $-x+1/2, -y, z+1/2$; (iii) $-x+1/2, y+1/2, z+1/2$; (iv) $-x+1/2, -y, z-1/2$.
O21 and O21′ occupancy factors are 0.55 and 0.45, respectively.

Table 5
Hydrogen-bonds lengths (Å) and angles (°)

D–H···A	D–H	H···A	D···A	∠DH···A
$[Co_2(C_6H_6O_4)_2(H_2O)_3]$ (**1**)				
O(11)–H(1)···O(2)^{v}	0.97(1)	1.64(3)	2.610(2)	176(2)
O(21)–H(2)···O(1)^{vi}	0.97(1)	1.83(3)	2.691(10)	146(4)
O(21)–H(2)···O(2)^{vii}	0.97(1)	2.55(5)	3.083(10)	114(3)
O(21)–H(3)···O(4)^{vii}	0.97(1)	2.39(4)	3.164(10)	136(3)
$[Cu(C_6H_6O_4)H_2O]$ (**2**)				
O(11)–H(1)···O(1)^{iv}	1.12	2.20	3.138(4)	140
O(11)–H(1)···O(1)^{v}	1.12	2.20	3.138(4)	140
C(4)–H(41)···O(1)^{vi}	0.97	2.42	2.834(4)	105
C(4)–H(42)···O(1)	0.97	2.42	2.834(4)	105

Symmetry codes for **1**: (v) $x, -y+1, z+1/2$; (vi) $-x+1, -y+1, -z$; (vii) $-x+1, y, -z-1/2$. Symmetry codes for **2**: (iv) $-x+1/2, -y, z-1/2$; (v) $x, -y-1/2, z-1$; (vi) $-x-1/2, y-1/2, z-1/2$.

coordination polyhedron around the Cu(II) ion takes the form of a tetragonal pyramid. The Cu–$O_{carboxyl}$ distances are 1.940(2) and 1.958(2) Å while the Cu–O_{water} bond length is longer, 2.377(4) Å (Table 4). Copper ions, the cyclobutane ring and the water molecule are situated in a particular position on the symmetry plane. The carboxylate groups are located over and under plane. The carboxylate groups in this complex have bidentate bridging character with a *syn-anti* conformation. The lengths of the C–O bond are equal to 1.270(3) and 1.253(4) Å; the O–C–O angles are 122.6(3)°.

The carboxylate groups of 1,1-cyclobutanedicarboxylic ligands take part in hydrogen bond formation as proton acceptors in O–H···O bonds, where a water molecule is the proton donor, but only hydrogen atom H1 is engaged in hydrogen bonds. In the structure of the copper(II) complex, a weak C–H ··· O hydrogen bond is also observed (Table 5).

1,1-Cyclobutanedicarboxylates of cobalt(II), copper(II) and zinc(II) are stable at room temperature (Table 6, Figs. 5 and 6). On heating to about 324–393 K, the hydrated compounds lose the molecules of

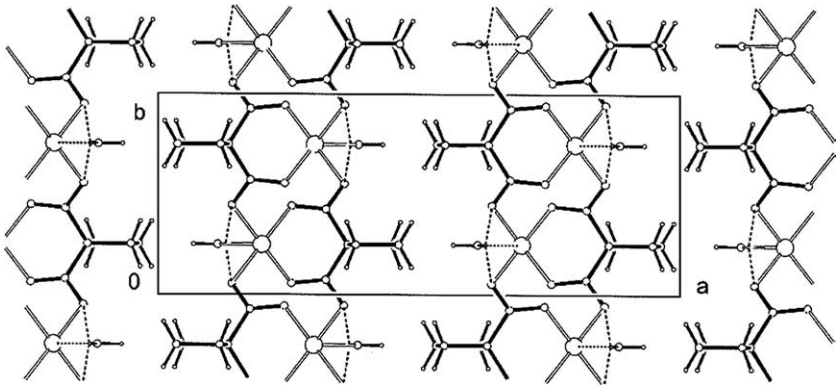

Fig. 3. Projection along the *c*-axis of $[Cu(C_6H_6O_4)_2(H_2O)]$. Dotted lines symbolize hydrogen bonds.

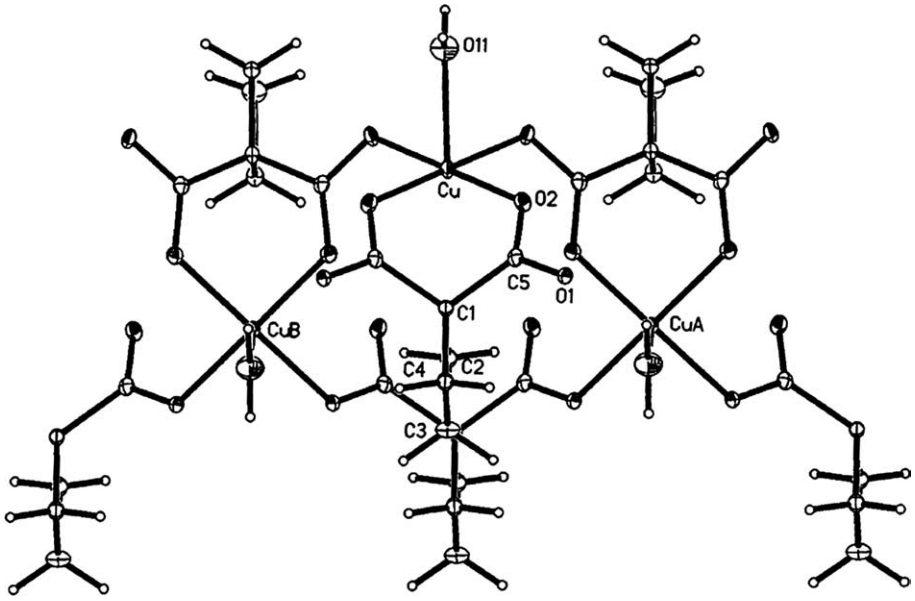

Fig. 4. ORTEP drawing (50% probability) of $[Cu(C_6H_6O_4)H_2O]$. Symmetry transformations used to generate equivalent atoms: (A) $0.5-x, -y, 0.5+z$; (B) $0.5-x, 1-y, 0.5+z$.

Table 6
Temperature of dehydration and decomposition of 1,1-cyclobutanedicarboxylates

Compound L = $C_6H_6O_4$	ΔT_1 (K)	Mass loss (%)		n	ΔT_2 (K)	Mass loss (%)		ΔT_3 (K)	Mass loss (%)	
		Calc.	Found	H_2O		Calc.	Found		Calc.	Found
$CoL \cdot 2H_2O$	324–403	3.81	3.50	0.5	518–608[b]	50.20	50.70	1136–1203	68.37	68.78
	433–506	15.06	15.29	1.5	608–715	66.13	66.79			
$Co_2L_2 \cdot 3H_2O$[a]	393–516	11.85	12.20	3	525–675	64.90	65.50	1182–1216	67.13	67.50
CuL					495–652	61.29	61.60			
$CuL \cdot H_2O$[a]	391–487	8.05	8.15	1	541–664	63.41	63.85			
$Zn_2L_2 \cdot 3H_2O$	340–458	11.52	11.62	3	485–717	65.28	65.67			

ΔT_1, temperature of dehydration; ΔT_2, temperature of decomposition of anhydrous compounds to oxides; ΔT_3, temperature of transformation of Co_3O_4 to CoO.
[a] Single crystal.
[b] Decomposition to $CoCO_3$.

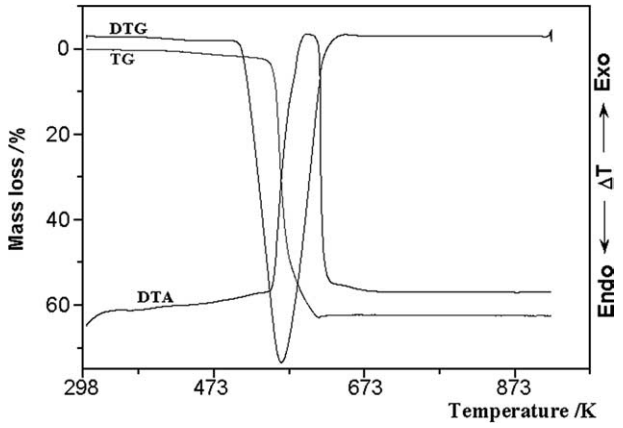

Fig. 5. TG, DSC and DTG curves of $Cu(C_6H_6O_4)$ in air atmosphere.

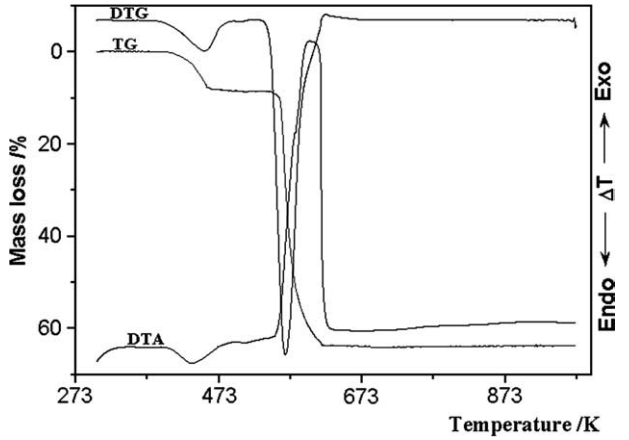

Fig. 6. TG, DSC and DTG curves of $[Cu(C_6H_6O_4)H_2O]$ in air atmosphere.

water. For the zinc(II) complex and for single crystals of the cobalt(II) and copper(II) compounds the dehydration process proceeds in one stage and the compounds become anhydrous. In the case of polycrystalline cobalt(II) 1,1-cyclobutanedicarboxylate, the dehydration proceeds in two stages; first it loses part of one half the water molecules and then the remaining part of the water molecules. In the first stage, the dehydration process is reflected by the FTIR spectra of the gaseous product decomposition. The characteristic valence and deformation vibration bands of water molecules appear at 328–365 K in the wavenumber ranges 3950–3500 and 2000–1350 cm^{-1}, respectively. These bands do not occur in the FTIR spectra of the gaseous decomposition of $Cu(C_6H_6O_4)$, confirming the anhydrous character of the polycrystalline copper(II) compound (Fig. 7). The anhydrous compounds are stable at 485–541 K, but upon heating above these temperatures they decompose to the corresponding oxides. The polycrystalline cobalt(II) complex decomposes to Co_3O_4 with the intermediate formation of unstable $CoCO_3$. Decomposition is connected with the release of carbon dioxide and cyclobutanecarboxylic acid, and for cobalt(II) also water molecules. The bands characteristic of carbon dioxide molecules appear at 490–530 K in the wavenumber ranges 2350–2250 and 750–600 cm^{-1}, due to valence and deformation vibrations, respectively. At 545–581 K bands characteristic for cyclobutanecarboxylic acid appear in the FTIR spectra of the gaseous products. Bands characteristic for water molecules occurred at 597–722 K in the FTIR spectra of gaseous products of $Co(C_6H_6O_4) \cdot 2H_2O$ decomposition. Above 1100 K Co_3O_4 transforms into CoO. The decomposition scheme for complexes can be presented as follows:

$$Co(C_6H_6O_4) \cdot 2H_2O \xrightarrow{Endo} Co(C_6H_6O_4) \cdot 1.5H_2O \xrightarrow{Endo} CoC_6H_6O_4 \xrightarrow{Exo} CoCO_3 \xrightarrow{Exo} Co_3O_4 \xrightarrow{Endo} CoO$$

$$[Co_2(C_6H_6O_4)_2(H_2O)_3] \xrightarrow{Endo} Co_2(C_6H_6O_4)_2 \xrightarrow{Exo} Co_3O_4 \xrightarrow{Endo} CoO$$

$$Cu(C_6H_6O_4) \xrightarrow{Exo} CuO$$

$$Cu(C_6H_6O_4) \cdot H_2O \xrightarrow{Endo} Cu(C_6H_6O_4) \xrightarrow{Exo} CuO$$

$$Zn_2(C_6H_6O_4)_2 \cdot 3H_2O \xrightarrow{Endo} Zn_2(C_6H_6O_4)_2 \xrightarrow{Exo} ZnO$$

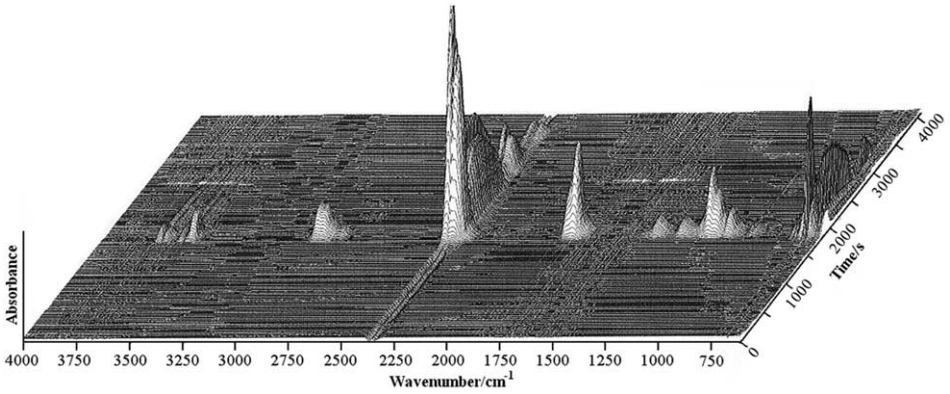

Fig. 7. FTIR spectra of gaseous products from the thermal decomposition of $Cu(C_6H_6O_4)$.

4. Supplementary data

Supplementary data are available from the CCDC, 12 Union Road, Cambridge CB2 1EZ, UK, on request, quoting the deposition numbers 243102 and 249929 (fax: +44 1223 336033; e-mail: deposit@ccdc.cam.ac.uk; http://www.ccdc.cam.ac.uk).

Acknowledgment

This work was supported by the Polish State Committee Scientific Research, Grant 4T09A 131 24.

References

[1] A. Petri, Th. Schwarz, A. Lentz, Thermochim. Acta 317 (1998) 85.
[2] A. Petri, Th. Schwarz, A. Lentz, Thermochim. Acta 323 (1998) 131.
[3] J.R. Allan, J. Dalrymple, Thermochim. Acta 221 (1993) 205.
[4] J. Kim, J.M. Lim, M.Ch. Suh, H. Yun, Polyhedron 20 (2001) 1947.
[5] J.D. Zubkowski, D. Washington, N. Njoroge, E.J. Valente, T. Cannon, C.D. Parks, P. Berdahl, D.L. Perry, Polyhedron 16 (1997) 2341.
[6] M. Petric, F. Pohleven, I. Turel, P. Šegedin, A.J.P. White, D.J. Williams, Polyhedron 17 (1998) 255.
[7] Y.M. Liu, L.F. Wang, Z.P. Wang, Z.H. Zhang, Y.R. Chen, Trans. Met. Chem. 24 (1999) 1.
[8] M. Geraghty, J.F. Cronim, M. Devereux, M. McCann, BioMetals 13 (2000) 1.
[9] F.D. Rochon, G. Massarweh, Inorg. Chim. Acta 304 (2000) 190.
[10] G.M. McCann, M.T. Casey, M. Devereux, M. Curran, G. Ferguson, Polyhedron 16 (1997) 2547.
[11] A. Dimos, A. Michaelides, S. Skoulika, Chem. Mater. 12 (2000) 3256.
[12] J. Kuduk-Jaworska, Poszukiwania cytostatycznych związków koordynacyjnych platyny, Wydawnictwo Uniwersytetu Wrocławskiego, Wrocław, 1993.
[13] R. Gust, B. Schnurr, R. Krauser, G. Bernhardt, M. Koch, B. Schmid, E. Hummel, H. Schönenberger, J. Cancer, Res. Clin. Oncol. 124 (1998) 585.
[14] J. Yoo, Y.S. Sohn, Y. Do, J. Inorg. Biochem. 73 (1999) 187.
[15] E. Wong, Ch.M. Giandomenico, Chem. Rev. 99 (1999) 2451.
[16] J. Burgess, D.N. Drasdo, M.S. Patel, BioMetals 8 (1995) 137.
[17] D. Lebwohl, R. Canetta, Eur. J. Cancer 34 (1998) 1522.
[18] Z. Rzączyńska, A. Bartyzel, J. Therm. Anal. Cal. 68 (2002) 937.
[19] Z. Rzączyńska, A. Bartyzel, T. Głowiak, J. Coord. Chem. 56 (2003) 1525.
[20] Z. Rzączyńska, A. Bartyzel, T. Głowiak, Polyhedron 22 (2003) 2595.
[21] P.E. Werner, TREOR, Trial and Error Program for Indexing of Unknown Powder Patterns, University of Stockholm, S 106 91, Stockholm, Sweden, 1984.
[22] Kuma Diffraction. KM-4 CCD Software: version 1.171. KUMA Diffraction Instruments GmbH, Poland, 1995–1999.
[23] G.M. Sheldrick, Acta Crystallogr. A46 (1990) 467.
[24] G.M. Sheldrick, SHELXS-97, Program for Crystal Structure Solution, University of Göttingen, Germany, 1997.
[25] G.M. Sheldrick, SHELXL-97, Program for Refinement of Crystal Structures, University of Göttingen, Germany, 1997.
[26] K. Nakamoto, Infrared and Raman Spectra of Inorganic Coordination Compounds, Wiley, New York, 1986.

Available online at www.sciencedirect.com
SCIENCE DIRECT®
Polyhedron 25 (2006) 695–701
POLYHEDRON
www.elsevier.com/locate/poly

Structural relationships in the homologous series of alkyltriphenylstannane compounds of formula $Ph_3Sn(CH_2)_{n-1}CH_3$, with *n* even and in the range 4–14 and 18

Gillian M. Allan [a], R. Alan Howie [a,*], John N. Low [a], Janet M.S. Skakle [a], James L. Wardell [b], Solange M.S.V. Wardell [c]

[a] *Department of Chemistry, University of Aberdeen, Meston Walk, Old Aberdeen AB24 3UE, Scotland, UK*
[b] *Departamento de Química Inorgânica, Instituto de Química, Universidade Federal do Rio de Janeiro, CP 68563, 21945-970 Rio de Janeiro, RJ, Brazil*
[c] *Fundação Oswaldo Cruz, Far-Manguinhos, Rua Sizenando Nabuco 100, Manguinhos, 21041-250 Rio de Janeiro, RJ, Brazil*

Received 14 June 2005; accepted 14 July 2005
Available online 29 August 2005

Abstract

The solid state structures of several compounds in the homologous series of alkyltriphenylstannanes of general formula $Ph_3Sn(CH_2)_{n-1}CH_3$ have been determined. For *n* in the range 4–10 the structures are monoclinic with space group $P2_1/c$. For *n* greater than 10 they are, instead, triclinic with space group $P\bar{1}$. The structural difference between the two classes is attributable to a change in the degree of control over the packing of the molecules exerted by the triphenylstannyl entity on the one hand and the alkyl chain on the other.
© 2005 Elsevier Ltd. All rights reserved.

Keywords: Alkyltriphenylstannane; Homologous series; X-ray structures

1. Introduction

Tetraorganotin compounds, with few recognized exceptions, have near tetrahedral geometries and four coordinate tin centres, even for compounds having quite distinct organic groups, an example being $Ph_3SnCH_2CMe_2Ph$ [1]. The exceptions arise when suitably positioned donor centres are located in the molecules, which allow tin–donor intramolecular interactions. Examples include (*Z*)-3,4,4-trimethylstannyl)-1-pentene-3-ol [2], bis[3-pyridine-2-yl-thien-2-yl]bis(*p*-tolyl)stannane [3] and 1,2:5,6-di-*O*-isopropylidene-3-C-triphenylstannylmethyl-α-D-allofuranose [4].

As part of a study concerned with the properties and structures of organotin compounds having long-chain alkyl groups, we have prepared a number of compounds of general formula $Ph_3Sn(CH_2)_{n-1}CH_3$ (**1**: $n = 4$, 6, 8, 10, 12, 14, 18 and 22). While we understood that the geometries about tin will be distorted tetrahedral in all cases, we wished to investigate such matters as how the alkyl chains, in particular the longer alkyl chains, will pack, the influence throughout the series of π-intermolecular interactions involving the phenyl groups and whether disorder would, in some cases, be an intractable problem. Comparatively few of the solid state structures of **1** have been reported. Indeed, recourse to the Cambridge Structural Database (version 5.26) [5], accessed by means of the Chemical Database Service of the EPSRC [6] reveals only

* Corresponding author. Tel.: +44 1224 272907; fax: +44 1224 272921.
E-mail address: r.a.howie@abdn.ac.uk (R.A. Howie).

0277-5387/$ - see front matter © 2005 Elsevier Ltd. All rights reserved.
doi:10.1016/j.poly.2005.07.024

two relevant entries. These are the structures of ethyltriphenyltin, (**1**: $n = 2$), [7] and triphenyltetradecylstannane, (**1**: $n = 14$), [8]. We now report the solid state structures of (**1**: $n = 4$–12 and $n = 18$). In addition infrared and NMR spectra are reported.

2. Experimental

Infrared spectra were recorded in KBr or CsI disks on a Nicolet-Magna IR 760 instrument. NMR spectra were recorded on Bruker 250 MHz and Varian 400 MHz instruments. Melting points were measured using a Kofler hot-stage microscope.

2.1. Preparation of compounds

To the Grignard reagent from alkyl bromide (4.3 mmol) and Mg (4.5 mmol) in Et_2O (30 ml) was added a solution of Ph_3SnCl (1.54 g, 4.0 mmol) in Et_2O (20 ml). The reaction mixture was refluxed for 30 min and water carefully added. The organic layer was collected, dried over magnesium sulfate and evaporated. The residues were purified by a combination of column chromatography (on silica gel with petroleum ether as eluent) and recystallizations from EtOH.

M.p. (**1**: $n = 4$) 61–62 °C, lit. 61–62 °C [9]; (**1**: $n = 6$) 55–56 °C, lit. 54 °C [9]; (**1**: $n = 8$) 53–54 °C, lit. 54–55 °C [9]; (**1**: $n = 10$) 49–50 °C; (**1**: $n = 12$) 52–53 °C; (**1**: $n = 14$) 58–59 °C; (**1**: $n = 16$) 63–64 °C; (**1**: $n = 18$) 68–70 °C; (**1**: $n = 22$) 75–77 °C.

Selected spectral data.

^{1}H NMR (400 MHz, $CDCl_3$) for (**1**: $n > 4$): δ 1.2–1.8 [$(2n + 1)$H, ms], 7.3–7.4 [9H, *p*- + *m*-aryl-H], 7.5–7.6 [6H, *o*-aryl-H].

^{13}C NMR (100 MHz, $CDCl_3$) for (**1**: $n > 4$): δ: 11.1 [$J(^{13}C–^{119,117}Sn) = 398/381$ Hz, C_α], 14.0–32.0 [alkyl C, $(n - 2)$ carbon atoms], 34.2 [$J(^{13}C–^{119,117}Sn) = 50$ Hz], 128.4 [$J(^{13}C–^{119,117}Sn) = 48$ Hz, C_{meta}], 128.7 [$J(^{13}C–^{119,117}Sn) = 10.7$ Hz, C_{para}], 137.0 [$J(^{13}C–^{119,117}Sn) = 45.8$ Hz, C_{ortho}], 139.2 [$J(^{13}C–^{119,117}Sn) = 478/458$ Hz, C_{ipso}].

^{119}Sn NMR (93 MHz, $CDCl_3$) for (**1**: $n > 4$): δ -100 ± 0.5.

IR: (KBr or CsI).

All compounds from $n = 4$ to $n = 22$ had common IR bands at: 3060–2852, 1577, 1479, 1470, 1427, 1375, 1330, 1300, 1259, 1188, 1153, 1074, 1022, 996, 861, 729, 698, 658, 445, 447–444, 264–262, ca. 240 cm^{-1}. The relative

Table 1
Crystal data and structure refinement for monoclinic **1**

Compound	$n = 4$	$n = 6$	$n = 8$	$n = 10$
Empirical formula	$C_{22}H_{24}Sn$	$C_{24}H_{28}Sn$	$C_{26}H_{32}Sn$	$C_{28}H_{36}Sn$
Formula weight	407.10	435.15	463.21	491.26
Temperature (K)	120(2)	150(2)	150(2)	150(2)
Crystal system	monoclinic	monoclinic	monoclinic	monoclinic
Space group	$P2_1/c$	$P2_1/c$	$P2_1/c$	$P2_1/c$
Unit cell dimensions				
a (Å)	17.2815(10)	18.8103(6)	20.5732(7)	21.9317(13)
b (Å)	15.0892(7)	15.1779(4)	15.1268(4)	14.8018(7)
c (Å)	7.3345(4)	7.5151	7.5183(2)	7.6859(3)
β (°)	92.996(2)	99.1096(12)	97.7961(11)	92.936(2)
Volume (Å^3)	1910.0(3)	2118.51(10)	2318.12(12)	2491.8(2)
Z	4	4	4	4
D_{calc} (Mg m^{-3})	1.416	1.364	1.327	1.310
Absorption coefficient (mm^{-1})	1.336	1.209	1.109	1.036
$F(000)$	824	888	952	1016
Crystal size (mm)	$0.20 \times 0.20 \times 0.15$	$0.44 \times 0.15 \times 0.03$	$0.28 \times 0.10 \times 0.03$	$0.15 \times 0.10 \times 0.05$
θ Range for data collection (°)	2.95–27.58	3.06–27.48	3.00–26.37	2.99–27.50
Index ranges	$-15 \leqslant h \leqslant 22$; $-19 \leqslant k \leqslant 17$; $-9 \leqslant l \leqslant 9$	$-21 \leqslant h \leqslant 24$; $-19 \leqslant k \leqslant 19$; $-9 \leqslant l \leqslant 9$	$-25 \leqslant h \leqslant 25$; $-17 \leqslant k \leqslant 18$; $-9 \leqslant l \leqslant 9$	$-23 \leqslant h \leqslant 26$; $-17 \leqslant k \leqslant 19$; $-9 \leqslant l \leqslant 9$
Maximum and minimum transmission	0.9750 and 0.5860	0.9660 and 0.5780	0.9670 and 0.8890	0.9700 and 0.9010
Reflections collected/unique/observation[a]	13912/4340/2735	16457/4815/3540	16182/4696/3443	18801/5461/2371
R_{int}	0.1140	0.0886	0.0543	0.1550
Data/restraints/parameters	4340/0/209	4815/0/227	4696/0/245	5461/26/299
Goodness-of-fit on F^2	1.213	0.976	0.996	0.906
Final R indices [$I > 2\sigma(I)$]	$R_1 = 0.0796$; $wR_2 = 0.1965$	$R_1 = 0.0428$; $wR_2 = 0.0972$	$R_1 = 0.0373$; $wR_2 = 0.0886$	$R_1 = 0.0519$; $wR_2 = 0.0738$
Final R indices (all data)	$R_1 = 0.1356$; $wR_2 = 0.2114$	$R_1 = 0.0656$; $wR_2 = 0.1075$	$R_1 = 0.0613$; $wR_2 = 0.0996$	$R_1 = 0.1874$; $wR_2 = 0.0989$
Largest difference peak and hole (e Å^{-3})	2.887 and −1.971	0.957 and −2.196	0.815 and −0.976	0.796 and −0.637

[a] Condition for observed status $I > 2\sigma(I)$.

intensities of the medium-strong bands at 1479 and 1470 cm^{-1} decreased as n increased, such that the 1470 cm^{-1} band was by far the weaker for $n = 4$ but became the more intense for $n = 14$. The weak band at 863–850 cm^{-1} becomes progressively weaker as n increases from $n = 4$.

2.2. X-ray structure determinations

2.2.1. Data collection

Intensity data for all of the structures presented here were obtained with Mo Kα radiation ($\lambda = 0.71073$ Å) from colourless crystals, at 120 K for (**1**: $n = 4$), 100 K for (**1**: $n = 18$) and 150 K for the remainder, by means of the Enraf Nonius Kappa CCD area detector diffractometer of the National Crystallography Centre of the EPSRC at Southampton. Data collection, cell refinement and data reduction were all achieved by means of the programs DENZO [10] and COLLECT [11]. Correction for absorption by comparison of the intensities of equivalent reflections was carried out by means of the program SORTAV [12,13].

2.2.2. Structure solution and refinement

All of the structures were solved by application of the direct methods routine of SHELXS97 [14] and the initial solutions completed and the structures fully refined on F^2 with SHELXL97 [15]. In all cases, in the final stages of refinement, hydrogen atoms were introduced in calculated positions with C–H bond lengths set to 0.95, 0.98 and 0.99 Å for phenyl, methyl and methylene hydrogen atoms, respectively, and refined with a riding model with the isotropic displacement parameter of hydrogen set to 1.5 times for methyl, or 1.2 times otherwise, the equivalent isotropic displacement parameter of the carbon atom to which the hydrogen is attached. The rotational orientation of the methyl groups was also refined. The refinement of the structure of (**1**: $n = 10$) was slightly complicated by disorder over pairs of sites of equal occupancy of carbon atoms C(4), C(6), C(8) and C(10). The disordered atoms in each pair are distinguished by suffix D and E as C(4D)/C(4E) and the disorder taken into account in the placement of the hydrogen atoms. The program ORTEP-3 for Windows [16] was used in the preparation of Figs. 2–5 and PLATON [17] was used to generate the data for

Table 2
Crystal data and structure refinement for triclinic **1**

Compound	$n = 12$	$n = 14$[a]	$n = 18$
Empirical formula	$C_{30}H_{40}Sn$	$C_{32}H_{44}Sn$	$C_{36}H_{52}Sn$
Formula weight	519.31	547.36	603.47
Temperature (K)	150(2)	150(2)	100(2)
Crystal system	triclinic	triclinic	triclinic
Space group	$P\bar{1}$	$P\bar{1}$	$P\bar{1}$
Unit cell dimensions			
a (Å)	7.5658(2)	7.5417(2)	7.5141(2)
b (Å)	9.8632(2)	9.8665(2)	9.9055(3)
c (Å)	19.1427(4)	20.3571(6)	23.0264(8)
α (°)	83.1364(7)	95.2205(10)	80.6766(12)
β (°)	85.0506(7)	91.5327(9)	83.6935(12)
γ (°)	69.6585(7)	110.1477(18)	70.127(2)
Volume (Å^3)	1328.27(5)	1413.45(6)	1587.75(8)
Z	2	2	2
D_{calc} (Mg m^{-3})	1.298	1.286	1.262
Absorption coefficient (mm^{-1})	0.976	0.921	0.826
$F(000)$	540	572	636
Crystal size (mm)	0.20 × 0.10 × 0.10	0.20 × 0.07 × 0.002	0.20 × 0.06 × 0.01
θ Range for data collection (°)	1.07–27.48	1.01–27.52	2.97–27.50
Index ranges	$-9 \leqslant h \leqslant 9$; $-11 \leqslant k \leqslant 12$; $-24 \leqslant l \leqslant 24$	$-7 \leqslant h \leqslant 9$; $-12 \leqslant k \leqslant 12$; $-26 \leqslant l \leqslant 26$	$-9 \leqslant h \leqslant 9$; $-12 \leqslant k \leqslant 12$; $-29 \leqslant l \leqslant 29$
Maximum and minimum transmission	0.9760 and 0.6830	0.8750 and 0.7820	0.3690 and 0.3690
Reflections collected/unique/observation[b]	17645/5914/5305	14968/6317/4900	24524/6933/5233
R_{int}	0.0585	0.0903	0.1505
Data/restraints/parameters	5914/0/281	6317/0/299	6933/0/335
Goodness-of-fit on F^2	1.115	1.034	1.024
Final R indices [$I > 2\sigma(I)$]	$R_1 = 0.0355$; $wR_2 = 0.0874$	$R_1 = 0.0400$; $wR_2 = 0.0827$	$R_1 = 0.0532$; $wR_2 = 0.1097$
Final R indices (all data)	$R_1 = 0.0439$; $wR_2 = 0.1005$	$R_1 = 0.0646$; $wR_2 = 0.1069$	$R_1 = 0.0836$; $wR_2 = 0.1214$
Largest difference peak and hole (e Å^{-3})	0.723 and −1.839	0.793 and −0.711	1.062 and −1.499

[a] Replicates structure reported in [8].
[b] Condition for observed status $I > 2\sigma(I)$.

Tables 4 and 5 and Supplementary Tables S2–S7. Further details of data collection and structure refinement are given in Tables 1 and 2.

3. Results and discussion

3.1. Synthesis

The Grignard synthesis of compounds, **1**, proceeded readily. However, for the longer chain compounds, i.e. (**1**: $n > 12$), separation from other long chain material, such as any unreacted alkyl bromide or the alkane formed on hydrolysis of the Grignard reagent, was more troublesome and purification required repeated crystallizations. As expected for members of a homologous series, compounds **1** exhibited similar spectral properties, see Section 2. Particularly noteworthy, in this respect, were the IR spectra, in general, and specifically in the NMR spectra, the δ ^{119}Sn values (all ~100 ppm), the $J(^{119,117}\mathrm{Sn}–^{13}\mathrm{C})$ values for the *ipso*-aromatic and α-aliphatic carbons, 478/458 and 398/381 Hz, respectively. It is apparent from these data that the tin environment is similar throughout the studied series.

The melting points of $Ph_3Sn(CH_2)_{n-1}CH_3$ cover a relatively short range, from 49–50 to 75–77 °C. Interestingly, the melting points of **1** show a slight U-shaped dependence on n (Fig. 1), with the lowest melting point obtained for (**1**: $n = 10$). In contrast, the similar shaped graphs for compounds of the series $X(CH_2)_{n-1}CH_3$ (X = H, Br or OH) show overall larger ranges of m.p. and a general increase in m.p. with, however, reducing increments as n is increased (see Fig. 1). For each of the four series, $X(CH_2)_{n-1}CH_3$ (X = H, Br, OH and $SnPh_3$), there appears to be a convergence of melting point values. Of interest, the m.p.s show little differences for $n = 22$ between the values for each series. It is clear that as n increases, the specific effects of the Ph_3Sn group have diminishing influences on the m.p.s.

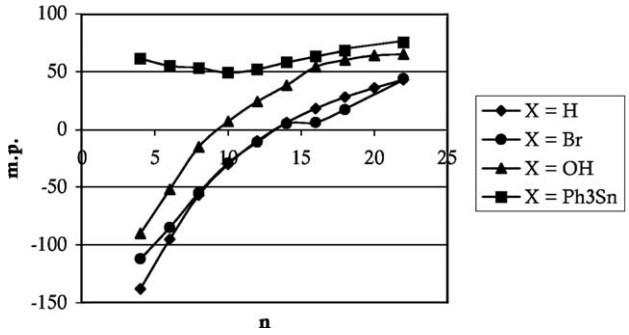

Fig. 1. Melting points (°C) for $X(CH_2)_{n-1}CH_3$ for n even and X = Ph_3Sn, OH, Br and H. See Supplementary Table S1 for numerical values.

The slight U-shaped melting point dependence for the organotin derivatives suggests opposing factors are at play, e.g., as n increases, the significance of the Ph_3Sn moiety is initially reduced and later overtaken by an increasing influence of the long chain alkyl groups. As we now report below, the structure determinations reveal two distinct packing arrangements, with the space group change occurring as n changes from 10 to 12.

3.2. Crystallography

3.2.1. Atom labelling scheme

Fig. 2 shows, as an example of the molecular conformation and atom labelling scheme of the molecules of all of the compounds whose structures are described in this paper, the molecule of (**1**: $n = 8$). In all cases, the carbon atoms of the alkyl group are numbered from 1 to n with C(1) bonded to tin. The sole exception to this is the use of suffices D and E to distinguish between individual atoms in the disordered pairs which, as noted above, occur in the structure of (**1**: $n = 10$). In all cases, the carbon atoms of the phenyl groups are numbered cyclically with C(1) bonded to tin. The phenyl groups are then distinguished by suffix a, b and c. No attempt has been made,

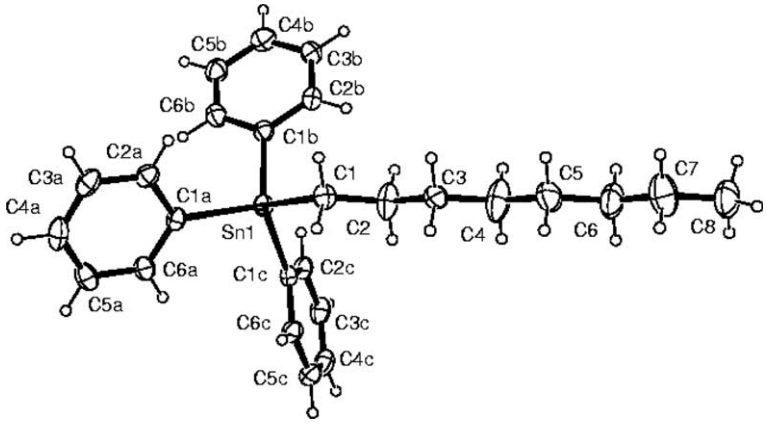

Fig. 2. The labelling scheme exemplified by the molecule of (**1**: $n = 8$). Ellipsoids are drawn at the 30% probability level and hydrogen atoms are shown as small spheres of arbitrary radii.

however, to ensure the use of completely consistent clockwise or anticlockwise cyclical order nor have the suffices been applied with strict regard to subtle variations in the functionality of the phenyl groups.

3.2.2. Molecular geometry

Selected bond lengths and bond angles for the compounds are given in Table 3. In all cases tin is in a slightly distorted tetrahedral environment with, in all but two cases, the Sn–C_{alkyl} bond the longest bond to tin. The C–Sn–C angles are in the range 106.6(2)–113.9(3)°, where these limiting values are found in the data for (**1**: $n = 2$) [7]. The bond lengths and bond angles in the phenyl groups and the alkyl chains are generally within the normal ranges and do not merit detailed discussion although the Sn(1)–C(1)–C(2) angles in the range 113.7(2)–115.6(7)° are of some interest.

3.2.3. Molecular packing and intermolecular contacts

For convenience, in what follows the structures of (**1**: $n = 4$–10) are designated type M (for monoclinic, with space group $P2_1/c$) and those of (**1**: $n = 12$, 14 and 18) type T (for triclinic, with space group $P\bar{1}$).

In the type M structures, as shown for (**1**: $n = 6$) in Fig. 3 in which two adjacent layers are seen edge on, the molecules form layers parallel to (1 0 0) with the alkyl groups directed towards the centre of the layer and the phenyl groups on the layer surfaces. Similar layers

Table 3
Selected bond lengths and bond angles (Å, °) for various **1**

	$n = 2$[a]	$n = 4$	$n = 6$	$n = 8$	$n = 10$	$n = 12$	$n = 14$[b]	$n = 18$
Sn(1)–C(alkyl)	2.172(9)	2.145(11)	2.150(3)	2.154(3)	2.137(5)	2.153(3)	2.151(3)	2.149(4)
Sn(1)–C(aryl)	2.131(6)9	2.124(11)c	2.138(3)b	2.137(3)a	2.123(5)a	2.140(3)c	2.134(3)b	2.143(4)b
	2.133(5)15	2.137(10)b	2.142(3)a	2.138(3)c	2.133(5)b	2.142(3)b	2.140(4)a	2.148(3)c
	2.137(6)3	2.148(11)a	2.144(3)c	2.141(4)b	2.133(5)c	2.145(3)a	2.144(3)c	2.149(4)a
C(aryl)-Sn(1)–C(alkyl)	109.8(3)9	111.9(4)c	110.05(13)b	111.28(13)a	107.0(2)a	112.98(10)c	108.57(13)b	108.49(15)b
	110.3(3)15	107.7(4)b	108.64(12)a	108.75(12)c	112.8(2)b	108.60(10)b	112.85(14)a	107.35(14)c
	113.9(3)3	109.1(4)a	111.48(13)c	110.98(14)b	111.5(2)c	107.20(10)a	107.14(13)c	113.02(15)a
C(aryl)-Sn(1)–C(aryl)	108.99(17)9,15	108.1(4)bc	110.22(12)ab	109.56(12)ac	109.4(2)ab	108.20(10)bc	108.59(13)ab	108.78(15)bc
	107.1(2)3,9	110.3(4)ac	107.74(12)bc	107.83(12)ab	108.7(2)ac	110.56(10)ac	109.33(13)bc	108.57(14)ab
	106.6(2)3,15	109.7(4)ab	108.70(14)ac	108.39(14)bc	107.4(2)bc	109.23(10)ab	110.30(13)ac	110.53(13)ac
C(alkyl)–C(alkyl)-Sn(1)	115.6(7)	115.0(7)	113.7(2)	113.9(3)	114.1(4)	113.96(17)	114.1(2)	114.1(3)

The bond and angle designations are those of (**1**: $n = 8$) as in Fig. 1. The Sn–C_{phenyl} bonds are arranged in increasing order of length and the suffices, as used in the refinements of the structures, are appended to the table entries, where appropriate, in order to identify which C_{phenyl} atoms, and therefore phenyl groups, are involved in each case.

[a] Calculated from previously published [7] data.

[b] From a replicate of a previously reported [8] structure.

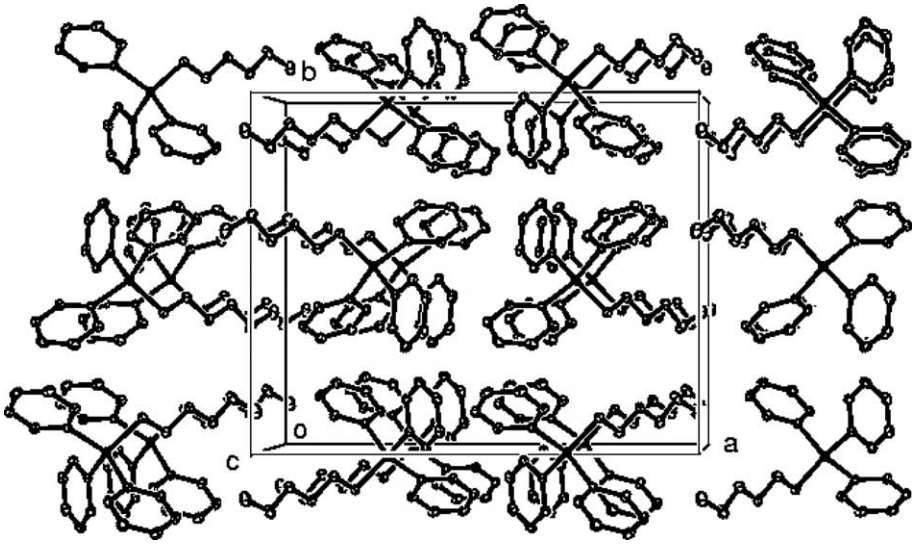

Fig. 3. The packing of the molecules in a type M structure. The example shown is (**1**: $n = 6$). Ellipsoids are shown at the 20% probability level and hydrogen atoms have been omitted for clarity.

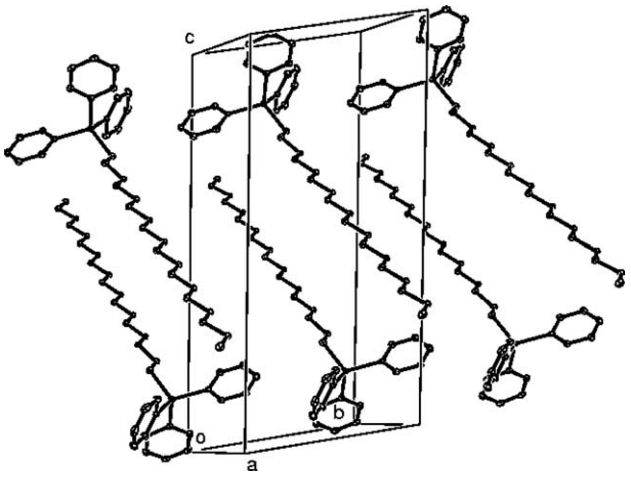

Fig. 4. A section, one unit cell thick in the direction of *a*, through a layer of molecules in a type T structure. The example shown is (**1**: $n = 18$). Ellipsoids are shown at the 20% probability level and hydrogen atoms have been omitted for clarity.

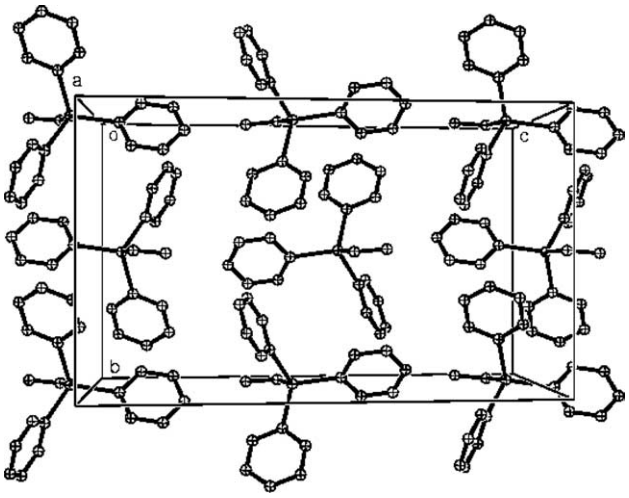

Fig. 5. Molecules in (**1**: $n = 2$) in columns propagated in the direction of *b*. Ellipsoids are shown at the 20% probability level and hydrogen atoms have been omitted for clarity.

(Fig. 4) are found in the type T structures but the layers are much thicker and the alkyl chains oriented in a different manner with respect to the thickness of the layer.

The molecules in the type T structures are packed in layers parallel to (0 0 1). In this case crystallographic centres of symmetry are the only factor, other than unit cell translations, relating the molecules throughout the structure. In the layers of the type M structures, the centrosymmetric relationship between the molecules within the layers is augmented by the operations of a crystallographic *c*-glide plane (extending the layers in the direction of *c*) and a crystallographic twofold screw axis extending the layers in the direction of *b*. The compound (**1**: $n = 2$) [7] is a very different case from the type M and type T structures. Here, although the unit cell is monoclinic the space group is $C2/c$ and the molecules, related to one another by the operation of a crystallographic twofold screw axis, are found in columns (Fig. 5).

Another difference between the type M and type T structures is to be found in the lists of intermolecular C–H···π interactions exemplified in Tables 4 and 5 for (**1**: $n = 8$) and (**1**: $n = 18$), respectively, and available in Supplementary Tables S3–S7 for the other **1** noted in Tables 1 and 2. In the type M structures (Table 4), there are six intermolecular contacts which satisfy the PLATON [17] criteria but only four are found for the type T structures (Table 5). The implication of this is that the presence of the longer alkyl chains in the type T structures creates greater separation between the triphenyl groups at the surface of the layers of molecules. Supplementary Table S2 shows the presence of five C–H···π contacts in the case of (**1**: $n = 2$). Casas et al. [7] have discounted the significance of the C–H···π contacts in the structure of (**1**: $n = 2$) on the grounds of the length of the H···Cg distances but this does not preclude their use as an estimate, allbeit crude, of the degree of association of the phenyl groups.

It is of interest to consider the increment in the volume occupied by a single molecule as the alkyl chain increases in length. In the transition from (**1**: $n = 2$) to (**1**: $n = 4$) it is of the order of only 25 Å^3 which is very small for the addition of two methylene groups when the volume commonly associated with one carbon atom is 20 Å^3. In this case the lengthening of the alkyl chain

Table 4
Geometry (Å, °) of intermolecular C–H···π interactions in (**1**: $n = 8$) (type M structure)

C–H···Cg	H···Cg	H_{perp}	γ	C–H···Cg	C···Cg
C(3A)–H(3D)···Cg(1^{i})	3.038	2.868	19	138	3.802
C(4)–H(4A)···Cg(2^{ii})	2.973	2.847	17	140	3.781
C(5A)–H(5D)···Cg(3^{iii})	3.279	3.209	12	122	3.873
C(5C)–H(5F)···Cg(1^{ii})	3.256	3.000	23	116	3.774
C(6B)–H(6E)···Cg(3^{iv})	3.056	2.955	15	138	3.810
C(6C)–H(6F)···Cg(1^{ii})	3.356	2.994	27	113	3.825

Notes. Ring (1) C(1A)–C(6A), ring (2) C(1B)–C(6B), ring (3) C(1C)–C(6C). H_{perp} is the perpendicular distance of the hydrogen atom from the plane of phenyl group *n* with centroid Cg(*n*) and γ is the angle at hydrogen between H_{perp} and H···Cg. Symmetry codes: (i) x, $3/2 - y$, $1/2 + z$; (ii) x, y, $-1 + z$; (iii) $1 - x$, $1 - y$, $1 - z$; (iv) x, y, $1 + z$.

Table 5
Geometry (Å, °) of intermolecular C–H···π interactions in (**1**: $n = 18$) (type T structure)

C–H···Cg	H···Cg	H_{perp}	γ	C–H···Cg	C···Cg
C(4)–H(4B)···Cg(1^{i})	3.012	2.926	14	158	3.950
C(4A)–H(4D)···Cg(2^{ii})	3.235	3.211	7	141	4.020
C(5C)–H(5F)···Cg(2^{i})	3.085	2.964	16	117	3.615
C(6A)–H(6D)···Cg(3^{iii})	2.960	2.897	12	139	3.733

Notes. As Table 4 but symmetry codes now (i) $-1 + x$, y, z; (ii) x, $1 + y$, z; (iii) $1 + x$, y, z.

is, however, accompanied by a dramatic change of structure and of the way in which the molecules pack together. As n increases from 4 to 10 the volume changes start at 52 $Å^3$ and reduce progressively to 49 $Å^3$. On further increase of chain length from 10 to 18 the volume changes remain comparatively constant in the range 41–44 $Å^3$, now much as would be expected for a two carbon increment in chain length. These changes in the volume of individual molecules suggest that in (**1**: $n = 12$–18) increase in alkyl chain length has no more effect than to increase the thickness of the layers of molecules. The small volume increase as n changes from 2 to 4 is accounted for, in general terms, by the change in molecular packing which occurs at this point. The comparatively large, but decreasing, volume changes accompanying the change of n from 4 to 10 is taken to imply optimum packing of the phenyl groups accompanied by comparatively inefficient packing of the alkyl chains, culminating in the disorder in the alkyl chain for (**1**: $n = 10$) noted above.

4. Conclusions

The occurrence of the minimum m.p. at (**1**: $n = 10$) and the abrupt change in symmetry from monoclinic to triclinic as n changes from 10 to 12 are clearly indicative of a significant change in molecular packing at the break-point. The decrease in m.p. accompanied by rather large, but decreasing, values of incremental changes in volume per molecule as n changes from 4 to 10 suggests that in this region the increase in chain length is accommodated in a comparatively inefficient manner which increases the internal energy of the structure without affecting the packing of the Ph_3Sn groups. For $n = 12$ and upwards, however, the comparatively regular increase in m.p. with increasing molecular weight is characteristic of a homologous series in which van der Waals interactions are becoming increasingly important as the number of atoms increases as shown, for example, by the alkane series (X = H) in Fig. 1. This taken together with the more or less constant incremental molecular volume suggests that efficient packing of the alkyl chains is now in operation.

Acknowledgements

The authors are grateful to the EPSRC, UK for access to both the National Crystallography Centre at Southampton and the Chemical Database Service at Daresbury and to Norma Thomson for her skill and endeavour in preparing some of the compounds.

Appendix A. Supplementary data

Supplementary cif format structural data is available from the Cambridge Crystallographic Data Centre, 12 Union Road, Cambridge CB2 IEZ, UK (fax: +44 1223 336033; e-mail: deposit@ccdc.cam.ac.uk or http://www.ccdc.cam.ac.uk), quoting the deposition numbers CCDC 274515–274521. Supplementary Tables S1–S7 are available electronically along with the Web version of this paper. Supplementary data associated with this article can be found, in the online version, at doi:10.1016/j.poly.2005.07.024.

References

[1] R.A. Howie, J.L. Wardell, Acta Crystallogr. Sect. E E60 (2004) m1536.
[2] F. Kayser, M. Biesemans, A. Delmonte, I. Verbruggen, I. deBorger, M. Gielen, R. Willem, E.R.T. Tiekink, Organometallics 13 (1994) 4026.
[3] K.M. Lo, S.W. Ng, V.G.K. Das, J. Crystallogr. Spectrosc. Res. 23 (1993) 933.
[4] L.A. Burnett, S.M.S.V. Doidge-Harrison, S.J. Garden, R.A. Howie, O.J. Taylor, J.L. Wardell, J. Chem. Soc., Perkin Trans. 1 (1993) 1621.
[5] F.H. Allen, Acta Crystallogr. Sect. B B58 (2002) 380.
[6] D.A. Fletcher, R.F. McMeeking, D. Parkin, J. Chem. Inf. Comput. Sci. 36 (1996) 746.
[7] J.S. Casas, E.F. Castellano, J. Ellena, M.S. García-Tasende, J.P. Goméz-Torres, A. Sánchez, J. Sordo, Appl. Organometal. Chem. 18 (2004) 99.
[8] G. Allan, J.N. Low, J.M.S. Skakle, J.L. Wardell, S.M.S.V. Wardell, Acta Crystallogr. Sect. E E57 (2001) m95.
[9] R.K. Ingham, S.D. Rosenberg, H. Gilman, Chem. Rev. 60 (1960) 459.
[10] Z. Otwinowski, W. Minor, Methods in enzymology, in: C.W. CarterJr., R.M. Sweet (Eds.), Macromolecular Crystallography, Part A, vol. 276, Academic Press, New York, 1997, p. 307.
[11] R.W.W. Hooft, COLLECT, Nonius BV, Delft, The Netherlands, 1998.
[12] R.H. Blessing, Acta Crystallogr. Sect. A A51 (1995) 33.
[13] R.H. Blessing, J. Appl. Crystallogr. 30 (1997) 421.
[14] G.M. Sheldrick, SHELXS97, Program for the Solution of Crystal Structures, University of Göttingen, Germany, 1997.
[15] G.M. Sheldrick, SHELXL97, Program for Crystal Structure Refinement, University of Göttingen, Germany, 1997.
[16] L.J. Farrugia, J. Appl. Crystallogr. 30 (1997) 565.
[17] A.L. Spek, J. Appl. Crystallogr. 36 (2003) 7.

Available online at www.sciencedirect.com
SCIENCE DIRECT®
Polyhedron 25 (2006) 702–710
POLYHEDRON
www.elsevier.com/locate/poly

Coordination induced 2-(2′-hydroxyphenyl) imidazolidine ring hydrolysis of dinucleating amine–imine–phenol ligands: X-ray structures of hardness-matched mononuclear cobalt(III) complexes as end products having isomeric N_4O_2 coordination spheres

Prasant Kumar Nanda, Debashree Mandal, Debashis Ray *

Department of Chemistry, Indian Institute of Technology, Kharagpur, West Bengal 721 302, India

Received 8 June 2005; accepted 19 July 2005
Available online 29 August 2005

Abstract

Two dinucleating ligands $H_3L_I^x$ (subscript I for imidazolidine; $x = 1, 2$) having pendant imidazolidine rings have been reacted with cobalt salts in aqueous methanol at room temperature to obtain the mononuclear complexes $[Co^{III}L^1]Cl \cdot 2H_2O$ ($\mathbf{1} \cdot 2H_2O$) and $[Co^{III}L^2]ClO_4 \cdot H_2O$ ($\mathbf{2} \cdot H_2O$) of hydrolyzed ligands H_2L^x. Expected dicobalt complexes were not obtained due to the coordination induced hydrolytic cleavage of the central substituted imidazolidine rings. The complexes $\mathbf{1} \cdot 2H_2O$ and $\mathbf{2} \cdot H_2O$ were structurally characterized by X-ray crystallography. Both *mer*- and *fac*-ON_2 binding modes of the two halves of the hexadentate ligands have been identified in these complexes. The mononuclear complexes have CoN_4O_2 coordination spheres with a N_4O_2 donor atom set of the two hexadentate ligands, forming isomeric distorted octahedral coordination geometries around the metal atoms. As a result, the imine nitrogen pairs coordinated trans to each other in $[CoL^1]^+$, whereas the phenolic oxygens are trans in $[CoL^2]^+$. In complex $\mathbf{1} \cdot 2H_2O$ the average Co–N(imine), Co–N(amine), and Co–O(phenolate) distances are 1.910, 1.959, 1.894 Å, respectively, and in $\mathbf{2} \cdot H_2O$ the corresponding average distances are 1.944, 1.991 and1.887 Å, respectively. Both the cobalt(III) complexes are diamagnetic. The UV–Vis spectra of the end products, after the imidazolidine ring hydrolysis, is different from the spectrum of the initial reaction mixture containing the μ-bis(tetradentate) ligands, $H_3L_I^x$ ($x = 1, 2$) and metal salts.
© 2005 Elsevier Ltd. All rights reserved.

Keywords: Bis(tetradentate); Imidazolidine ring hydrolysis; Schiff-base; Hexadentate; Crystal structure

1. Introduction

Among various products from the condensation of aromatic aldehydes with α,ω-tetramine containing both primary and secondary amino groups is a binucleating Schiff base ligand with a in-built spacer imidazolidine ring, which can take up two same or different metal ions [1,2]. Chiral imidazolidine ring grafted ligands are important for the development of various enantioselective catalysts [3]. Intermolecular nucleophilic attack on incoming aldehyde carbon atom by imine nitrogens of the parent hexadentate ligand lead to the formation of saturated heterocyclic ring in place of the ethylenediamine part of the parent hexadentate ligands. Terminal imidazolidine rings are not formed in the first step of reaction with 2-hydroxy benzaldehyde/acetophenone as observed previously with 2-pyridinecarboxaldehyde-*N*-oxide [4]. The use of such binucleating ligands for

* Corresponding author. Tel.: +91 3222283324; fax: +91 3222755303.
E-mail address: dray@chem.iitkgp.ernet.in (D. Ray).

0277-5387/$ - see front matter © 2005 Elsevier Ltd. All rights reserved.
doi:10.1016/j.poly.2005.07.030

the synthesis of new family of di-3d-metal complexes has been receiving considerable attention in recent years. In view of the importance of the imidazolidine ring formation and its cleavage in various fields, [3] we examined the complexation behavior of two 2′-hydroxy-2-phenyl imidazolidine ring containing ligands toward cobalt salts to identify the stabilization of the ligand heterocyclic backbone to bridge hard cobalt(III) ions.

In the present work a pair of functionally dinucleating bis(tetradentate) type ligands incorporating amine, imine, and phenol functions have been used for mononuclear binding of cobalt(III) ions establishing the selective role of metal ions for ligand hydrolysis. As a result the corresponding Co_2^{II} or Co_2^{III} complexes are not obtained in this study (Scheme 1). Both the mononuclear complexes, as the end products of the complexation reactions, have been structurally characterized revealing the $Co^{III}N_4O_2$ coordination spheres in two different geometrical forms. The meridional or facial coordination of the ONN halves of the ligands, before hydrolysis, does not contribute much to the imidazolidine ring stabilization. In dinuclear $Cu^{II}Zn^{II}$ and $Cu^{II}Cu^{II}$ complexes this coordination was meridional due to the presence of semi-rigid imidazolidine ring. We report the synthesis and structural characterizations of two isomeric mononuclear cobalt complexes as the end product of the reactions of known H_2L^1 and hitherto unknown H_2L^2 ligands with two different cobalt salts.

2. Experimental

2.1. Physical measurements

Triethylenetetramine (trien) was obtained from S.D.Fine Chem, India. Salicylaldehyde and Cobaltous

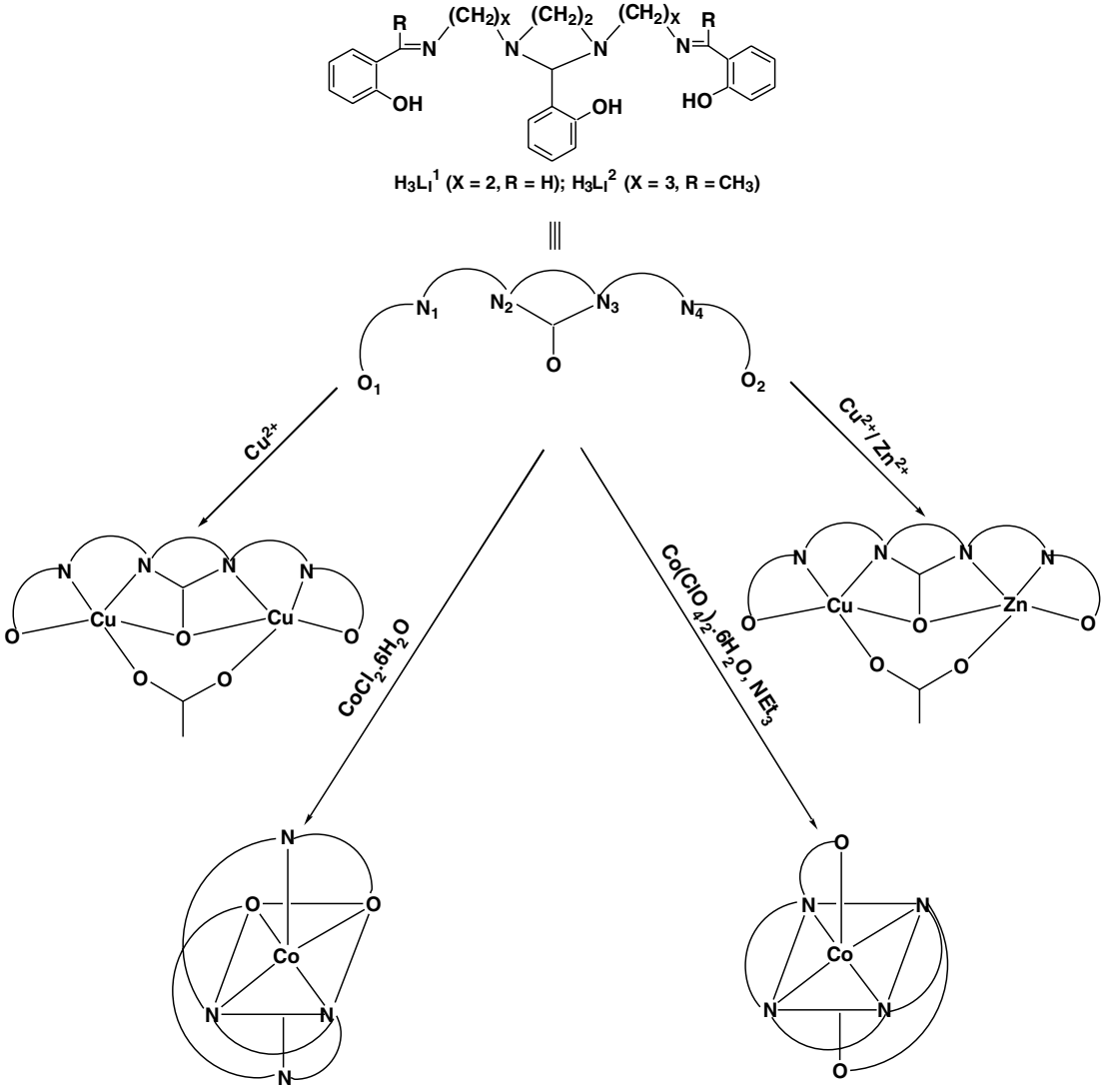

Scheme 1.

chloride were purchased from SRL, India. All other chemicals and solvents were reagent grade materials and were used as received without further purification. Purification of acetonitrile and preparation of tetraethylammonium perchlorate (TEAP) for electrochemical work was performed as reported in the literature [5]. Microanalyses (C, H, N) were performed using a Perkin–Elmer 240C elemental analyzer. IR spectra were obtained on a Perkin–Elmer 883 spectrometer (200–4000 cm^{-1}) prepared as KBr pellets. The commercial grade KBr was used after being dried in air oven at 110 °C followed by cooling to room temperature in a desiccator before use. Electronic spectra were recorded on a Shimadzu UV/Vis/NIR 3100 (190–3200 nm) (1 cm quartz cell) spectrophotometer. Diamagnetic corrections for ligand susceptibilities were made using Pascal's constants. ^1H and ^{13}C NMR spectra were obtained on a Bruker AC 200 NMR spectrometer using TMS as the internal standard. 2D CH-COSY spectrum is recorded on Brucker DRX-400 spectrometer. Electrochemical measurements were made using a PAR model 173 potentiostat/galvanostat, 175 universal programmer, 178 electrometer, and 377-cell system. A planar Beckman 39273 platinum disk working-electrode, a platinum-wire auxiliary-electrode, and an aqueous saturated calomel reference electrode (SCE) were used in a three-electrode configuration. A digital series 2000 Omni Graphic recorder was used to trace the voltammograms. Electrochemical measurements were made under a dinitrogen atmosphere. All chemical data were collected at 298 K and are uncorrected for junction potentials. Solution electrical conductivity was measured using a Unitech type UI31C digital conductivity meter with a solute concentration of about 10^{-3} M.

2.2. Preparation of $H_3L_I^1$

The ligand has been prepared following a modified literature procedure [6]. The product was collected by filtration, washed with hexane, diethyl ether and dried in air. Comparing the analytical and spectroscopic data with the literature values has checked identity and purity of the ligand.

2.3. Preparation of $H_3L_I^2$

A solution of *N*,*N*′-bis-(3-aminopropyl)ethylenediamine (2.0 g, 11.47 mmol) in methanol (50 ml) was added to a solution of 2-hydroxyacetaphenone (3.1 g, 22.95 mmol) in methanol (20 ml). The resulting pale-yellow solution was refluxed for ca. 5 h to give a yellow solid (H_2L^2) on evaporation. The product was isolated by filtration, washed with Et_2O, and finally dried in vacuo over fused $CaCl_2$ for a total yield of 4.0 g (86%), m.p. 89–90 °C. $C_{24}H_{34}N_4O_2$ (410.27): Calc. C, 70.21; H, 8.35; N, 13.65. Found: C, 70.06; H, 8.26; N, 13.57%. Mass spectrum (EI): *m*/*z* 410 ($M^+ = L^+$); Relative intensity of $M^+ = 40\%$. Infrared spectrum (cm^{-1}, KBr disk): *ν*(phenolic OH) 3439(b); *ν*(C=N) 1604(s); *ν*(phenolic CO) 1445(s); *ν*(CH_2) 850(m); *ν*(aromatic CH) 753(s). ^1H NMR ($CDCl_3$, ppm): *δ*(phenolic OH) 16.35(s, 2H); (H_8) 3.63 (t, 4H); (H_{25}) 6.69–7.51 (m, 8H); (H_9) 1.68 (m, 4H); (H_{10}) 2.73 (t, 4H); (H_{11}) 1.98 (t, 4H); (H_{12}) 2.33 (s, 6H); (amine NH) 2.63 (s, 1H). ^{13}C NMR ($CDCl_3$, ppm): *δ* (C_1) 157.16; (C_2) 116.80; (C_3) 131.92; (C_4) 121.77; (C_5) 128.06; (C_6) 123.40 (C_7) 161.07; (C_8) 43.52; (C_9) 30.62; (C_{10}) 46.38; (C_{11}) 49.96; (C_{12}) 14.21.

In the next step, a solution of salicylaldehyde (0.3 g, 2.43 mmol) in methanol (25 ml) was added to the solution of H_2L^2 (1 g, 2.43 mmol) in methanol (25 ml). The yellow solution was then stirred at room temperature for 30 min to give a yellow solid ($H_3L_I^2$). The product was isolated by filtration, washed with water and hexane, and finally dried in vacuo over fused $CaCl_2$ for a total yield of 1 g (78%), m.p. 160 °C. $C_{31}H_{38}N_4O_3$ (514.66): Calc. C, 72.35; H, 7.44; N,10.89; found C, 72.51; H, 7.32; N, 10.51%. Mass spectrum (EI): *m*/*z* 514 ($M^+ = L^+$); Relative intensity of $M^+ = 40\%$. Infrared spectrum (cm^{-1}, KBr disk): *ν*(phenolic OH) 3418(b); *ν*(C=N) 1625(s); *ν* (phenolic CO) 1438(s); *ν*(CH_2) 877(m); *ν*(aromatic CH) 753(s). ^1H NMR ($CDCl_3$, ppm): *δ*(terminal phenolic OH) 16.62(s, 2H); *δ*(pendent phenolic OH) 10.95(s, 1H); (H_8) 3.53 (m, 4H); (H_{16-19}) 7.22–7.46 (m, 8H); (H_9) 1.72 (m, 4H); (H_{10}) 3.32 (t, 4H); (H_{11}) 2.37 (m, 4H); (H_{12}) 2.22 (s, 6H); (H_{13}) 3.67 (s, 1H); (H_{2-5}) 6.58–6.94 (m, 4H); ^{13}C NMR ($CDCl_3$, ppm): *δ* (C_1) 157.96; (C_{15}) 165.68 (C_2) 118.43; ($C_{3,5}$) 121.09; (C_4) 117.51; (C_6) 132.40; (C_7) 171.28; (C_8) 44.52; (C_9) 28.70; (C_{10}) 46.38; (C_{11}) 49.96; (C_{12}) 14.21; (C_{13}) 89.55; (C_{14}) 129.91; (C_{16}) 132.37 (C_{17}) 134.87; (C_{18}) 127.43; (C_{19}) 129.76.. UV–Vis spectra (MeOH), [λ_{max}, nm (*ε*, 1 mol^{-1} cm^{-1})]: 389 (9980), 273 (18 880), 254 (18 645).

2.4. Preparation of $[Co^{III}L^1]Cl \cdot 2H_2O$

To a solution of $H_3L_I^1$ (0.5 g, 1.09 mmol) in methanol (30 ml), aqueous solution of $CoCl_2 \cdot 6H_2O$ (0.5 g, 2.18 mmol) was added dropwise with stirring. The reaction mixture was then stirred at ambient temperature for 2 h. Resulting deep brown color solution was then evaporated in air. The brown color solid separated was collected by filtration through glass frit and washed thoroughly with hexane.The compound was finally dried in vacuo over P_4O_{10}. Yield: 0.6 g (95%). *Anal*. Calc. for $C_{20}H_{26}ClCoN_4O_4$ (480.89): C, 49.95; H, 5.45; N, 11.65; Co, 12.26. Found: C, 49.96; H, 5.69; N, 11.45; Co, 11.80%. IR (KBr, cm^{-1}): $\nu = 3376$(s), 1632(vs), 1597(vs), 1535(s), 1452(s), 1306(s), 1203(s), 1057(s), 760(vs). Molar conductance, Λ_M: (MeOH solution) 95 Ω^{-1} cm^2 mol^{-1}. UV–Vis spectra [λ_{max}, nm (*ε*, 1 mol^{-1} cm^{-1})]: (MeOH solution) 605 (180), 490 (500), 392 (1706), 251 (17 515), 219 (17 071).

2.5. Preparation of $[Co^{III}L^2]ClO_4 \cdot H_2O$

To a solution of $H_3L_I^2$ (0.5 g, 0.97 mmol) in methanol (30 ml), aqueous solution of $(Co(ClO_4)_2 \cdot 6H_2O)$ (0.6 g, 2.18 mmol) was added dropwise with magnetic stirring during 15 min. After half-an-hour, a methanolic solution of NEt_3 (0.2 g, 1.16 mmol) was slowly added to the previous solution during 10 min. The reaction mixture was then stirred for another 30 min. The deep green color solid was separated on solvent evaporation in air. The product was collected by filtration through glass frit and washed thoroughly with hexane. The compound was finally dried in vacuo over P_4O_{10}. Yield: 0.5 g (82%). *Anal.* Calc. for $C_{24}H_{32}ClCoN_4O_7$ (582.98): C, 49.44; H, 5.53; N, 9.61; Co, 10.11. Found: C, 49.56; H, 5.69; N, 9.56; Co, 10.20%. IR (KBr, cm^{-1}): $\nu = 3480$(s), 1597(vs), 1547(s), 1438(s), 1327(s), 1106(vs), 760(s), 607(s). Molar conductance, Λ_M: (MeOH solution) 92 Ω^{-1} cm^2 mol^{-1}. UV–Vis spectra [λ_{max}, nm (ε, 1 mol^{-1} cm^{-1})]: (MeOH solution) 630 (212), 555 (259), 386 (5182), 438 (2327).

2.6. X-ray data collection and structural determination

Diffraction data for complexes $\mathbf{1} \cdot 2H_2O$ and $\mathbf{2} \cdot H_2O$ were collected at 293(2) K on Bruker-Nonius Mach3 CAD4 X-ray diffractometer using graphite-monochromated Mo Kα radiation ($\lambda = 0.71073$ Å). The intensities of three reference reflections of each complex were monitored every one-hour though out the data collection shows no sign of crystal deterioration. The structures was solved by direct method SHELXS-97 [7], followed by successive Fourier synthesis and least-square refinement using SHELXS-97 program [8]. Direct phase determination yielded Co, and most of the C, N, O atoms. Anisotropic thermal parameters are used for the nonhydrogen atoms and isotropic parameters for the hydrogen atoms. For the complex $\mathbf{2} \cdot H_2O$ the two hydrogen atom of the uncoordinated water molecule were detected in the process of successive refinement stages during structure determination. The crystallographic data and other pertinent information are summarized in Table 1. Due to the crystal instability absorption correction was not applied on the collected reflections, as a result the minute hole seems to be big.

Table 1
Crystallographic data for complexes $\mathbf{1} \cdot 2H_2O$ and $\mathbf{2} \cdot H_2O$

Molecular formula	$C_{20}H_{26}N_4O_4CoCl$	$C_{24}H_{32}N_4O_7CoCl$
Molecular weight	480.89	582.98
Crystal system	monoclinic	monoclinic
Space group	*P21/c*	*P21/c*
a (Å)	18.356(4)	9.166(2)
b (Å)	10.099(2)	24.148(4)
c (Å)	12.054(2)	12.517(2)
α (°)	90	90
β (°)	103.25(3)	96.99(2)
γ (°)	90	90
U (Å^3)	2176.1(8)	2749.9(10)
D_{calc} (g cm^{-3})	1.455	1.408
Z	4	4
F(000)	984	1216
Crystal size (mm)	0.30 × 0.30 × 0.20	0.40 × 0.25 × 0.30
μ (mm^{-1})	0.945	0.769
θ Range (°)	1.14–25.16	1.69–24.98
R_1, wR_2 [$I > 2\sigma(I)$]	0.0803, 0.2468	0.0879, 0.2264
Goodness-of-fit on F^2	1.584	1.019
Final difference map maximum, minimum (e Å^{-3})	0.965, −2.829	0.980, −0.504

$R_1 = \sum(||F_o| - |F_c||)/\sum|F_o|$. $wR_2 = [\sum w(|F_o| - |F_c|)^2/\sum w(F_o)^2]^{1/2}$, $w = 0.75/(\sigma^2(F_o) + 0.0010F_o^2)$.

3. Results and discussion

3.1. Synthesis

The ligands used in this work belong to a family of μ-bis(tetradentate) type with a semi-rigid 2-hydroxyphenyl substituted five-membered imidazolidine spacer and has easy synthetic accessibility. The five-membered imidazolidine ring is introduced inside the hexadentate precursor to act as a spacer-cum-bridging-cum-heterocyclic backbone unit. The ligand $H_3L_I^2$ is new. Earlier we reported a similar symmetrical binucleating ligand having unsymmetrical compartments containing 1-methyl-3-oxobut-1-enyl end groups [9]. Synthesis of $H_3L_I^2$ has been achieved by the introduction of 2-hydroxy phenyl substituted imidazolidine ring in the second step of the reaction with 2-hydroxy benzaldehyde as shown in Scheme 2. Terminal imidazolidine rings are not formed at the two ends of the tetramine during ligand synthesis, which is also another possibility.

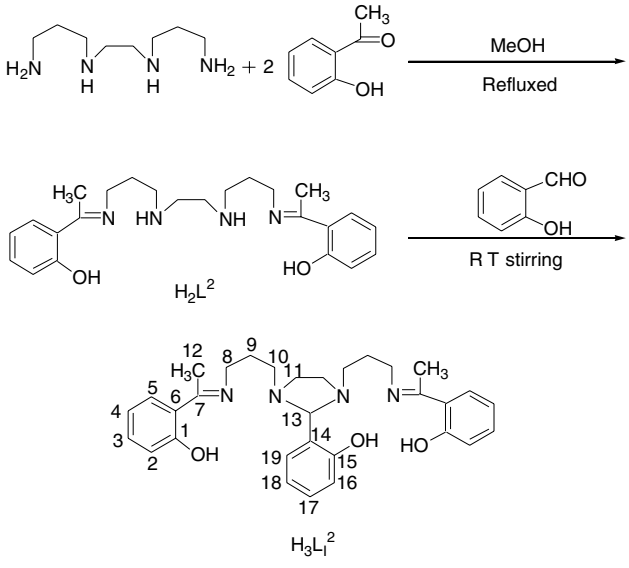

Scheme 2.

The ligand $H_3L_I^2$ is characterized by elemental analysis, IR, ^1H, ^{13}C and CH-COSY NMR and mass spectral analyses. In IR spectrum, a strong band at 1625 cm^{-1} indicates the $\nu_{C=N}$ stretching frequency. The ^1H NMR spectrum of $H_3L_I^2$ in $CDCl_3$ shows a characteristic signal of the imidazolidine ring proton (H_{13}) at 3.67 ppm. The 2D CH-COSY NMR spectrum confirms the atom connectivity of $H_3L_I^2$ as assigned from the ^1H and ^{13}C spectra. In COSY the signal at δ 171.28 is due to the imine carbon C_7 and at 165.68 and 157.96 are for C_{15} and C_1 which are not connected to any proton (Fig. 1). The signals at δ 134.87, 132.37, 129.91 and 127.43 is due to the pendent phenolic carbons (C_{16-19}) attached to the protons (H_{16-19}) at δ 7.22–7.46 and the next four signals at 121.09 (two peaks), 118.43 and 117.51 are due to the terminal phenolic carbons (C_{2-5}) attached to the protons (H_{2-5}) at δ 6.58–6.94. The peak at δ 89.55 is assigned to the C_{13} attached to H_{13} at δ 3.67 ppm. The δ 49.96 peak corresponds to C_{11} bonded to H_{11} (δ 2.37 ppm). The peaks at δ 46.38 and 44.52 are due to C_{10} and C_8 connected to the respective protons at δ 3.32 and 3.53, respectively. Among the up field signals the peak at δ 28.70 can be assigned to the carbon C_9 connected to the corresponding proton at δ 1.72 ppm and the most up field peak at δ 14.21 is for the methyl carbon C_{12} connected the protons at δ 2.22 ppm.

In mass spectrum the molecular ion peak (*m*/*z*) is observed at 514, which indicates the formation of the desired imidazolidino Schiff base ligand.

The mononuclear complexes have been obtained by reacting the ligands with cobalt(II) chloride hexahydrate and cobalt(II) perchlorate hexahydrate, respectively, in aqueous methanol in air. All the solution measurements reported in this work were made in methanol and DMF. Two $Co^{III}N_4O_2$ complexes of the parent hexadentate ligands (H_2L^1 and H_2L^2) have been obtained from two binucleating ligands $H_3L_I^1$ and $H_3L_I^2$. The phenyl substituted imidazolidine rings are removed completely instead of reductive-cleavages to any 2-hydroxy-*N*-benzyl derivative of the parent hexadentate ligand [10]. Recently, similar trisphenolate ligand was reported from borohydride reduction of imidazolidino reduced Salen ligand [11]. The mononuclear complexes having $Co^{III}N_4O_2$ coordination sphere have been structurally characterized to establish the coordination driven imidazolidine ring hydrolysis.

3.2. Crystal and molecular structures of the complex

Atom labeling scheme and molecular views of the mononuclear complexes is shown in Fig. 2. Selected bond lengths and angles around the metal center are listed in Table 2. Both the monomeric complexes are composed of an approximate octahedral $[Co^{III}L^{1-2}]^+$ cation with Cl^- and ClO_4^- anions. The metal center in

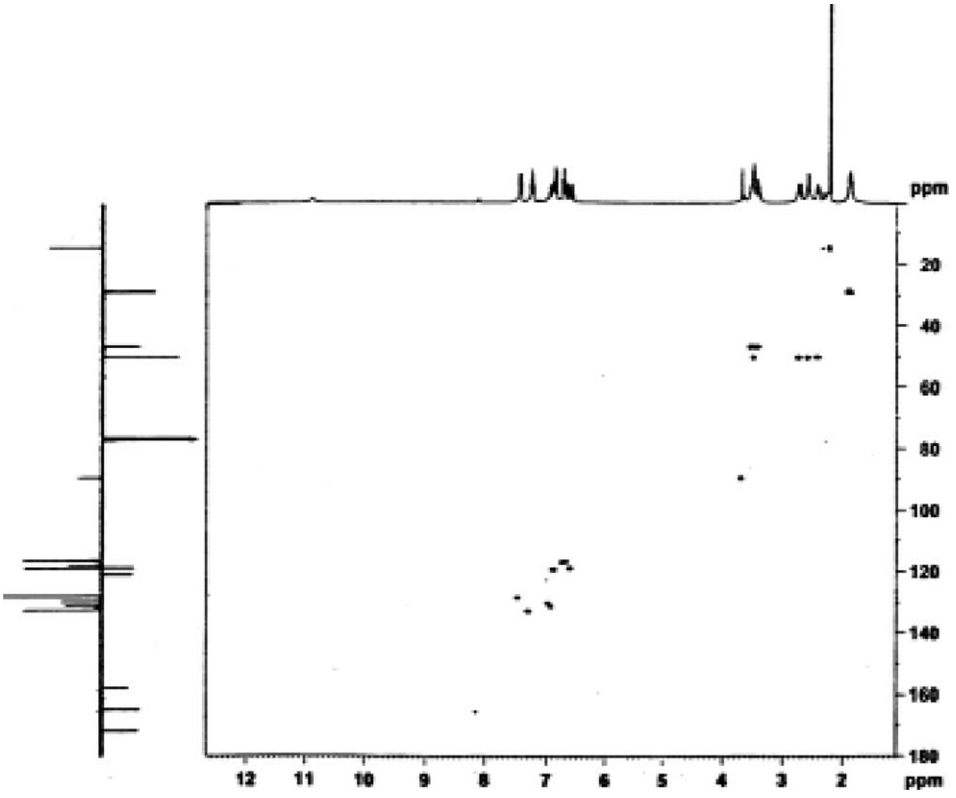

Fig. 1. 2D CH-COSY spectrum of $H_3L_I^2$ recorded on Bruker DRX-400 specrtometer in $CDCl_3$.

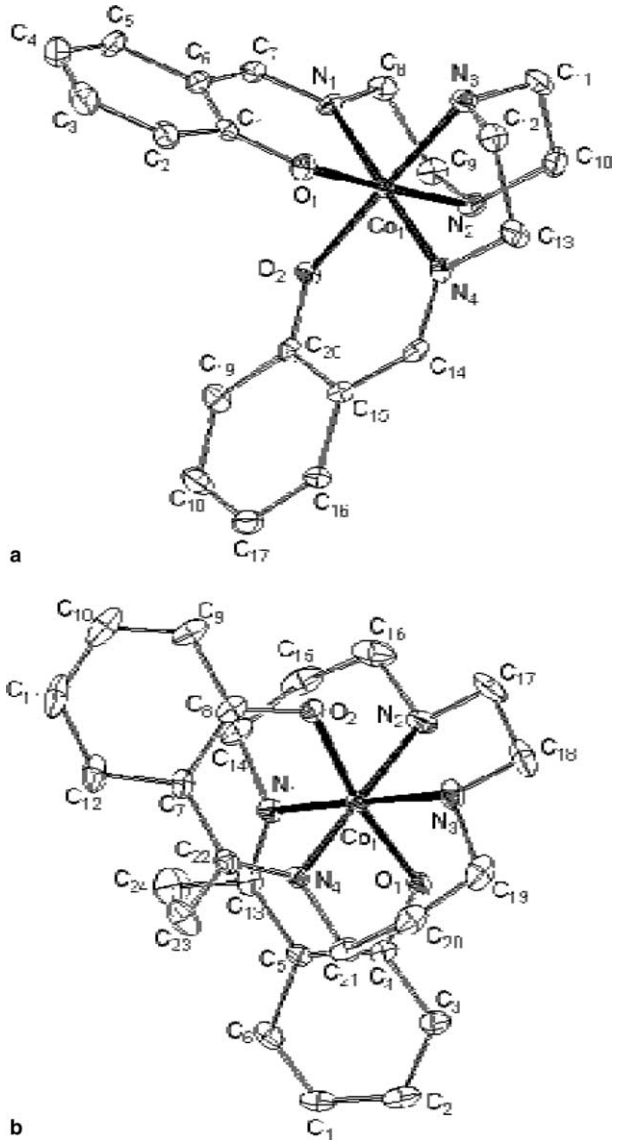

Fig. 2. ORTEP views of (a) $[Co^{III}L^1]^+$ and (b) $[Co^{III}L^2]^+$ cations with atom numbering scheme and thermal ellipsoids drawn at 30% probability level. Hydrogen atoms are omitted for clarity.

both the structures are in distorted octahedral CoN_4O_2 environment from two different types of ligand chelation. There are, however, four ways in which the linear tetramine based hexadentate ligand can span octahedral position through meridional (A) and facial (B–D) (Chart 1) binding of two tridentate N_2O halves of

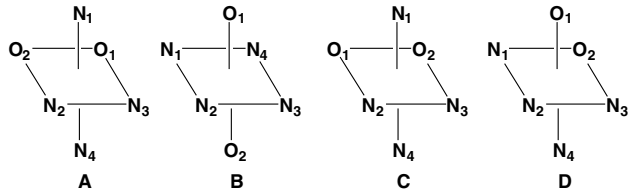

Chart 1.

Table 2
Selected bond lengths (Å) and angles (°) in $\mathbf{1} \cdot 2H_2O$ (a) and $\mathbf{2} \cdot H_2O$ (b)

Bond lengths (a)	
Co(1)–O(1)	1.883(4)
Co(1)–O(2)	1.905(3)
Co(1)–N(4)	1.910(4)
Co(1)–N(3)	1.958(4)
Co(1)–N(2)	1.960(4)
Co(1)–N(1)	1.910(4)
Bond lengths (b)	
Co(1)–O(1)	1.882(6)
Co(1)–O(2)	1.893(6)
Co(1)–N(1)	1.940(7)
Co(1)–N(4)	1.949(8)
Co(1)–N(3)	1.970(8)
Co(1)–N(2)	2.012(9)
Bond angles (a)	
O(2)–Co(1)–N(4)	94.69(15)
N(4)–Co(1)–N(3)	85.04(17)
N(3)–Co(1)–N(2)	87.60(18)
N(2)–Co(1)–N(1)	86.00(17)
N(1)–Co(1)–O(1)	94.22(16)
O(1)–Co(1)–O(2)	91.47(15)
O(1)–Co(1)–N(4)	86.93(16)
O(2)–Co(1)–N(1)	86.27(15)
N(4)–Co(1)–N(1)	178.48(17)
O(1)–Co(1)–N(3)	89.51(17)
O(2)–Co(1)–N(3)	178.96(16)
N(1)–Co(1)–N(3)	93.98(17)
O(1)–Co(1)–N(2)	177.11(16)
O(2)–Co(1)–N(2)	91.41(16)
N(4)–Co(1)–N(2)	92.80(16)
Bond angles (b)	
O(1)–Co(1)–O(2)	170.2(3)
O(1)–Co(1)–N(1)	96.4(3)
O(2)–Co(1)–N(1)	88.8(3)
O(1)–Co(1)–N(4)	89.4(3)
O(2)–Co(1)–N(4)	98.7(3)
N(1)–Co(1)–N(4)	92.2(3)
O(1)–Co(1)–N(3)	85.2(3)
O(2)–Co(1)–N(3)	89.0(3)
N(1)–Co(1)–N(3)	175.6(4)
N(4)–Co(1)–N(3)	91.9(4)
O(1)–Co(1)–N(2)	87.2(3)
O(2)–Co(1)–N(2)	84.6(3)
N(1)–Co(1)–N(2)	90.2(4)
N(4)–Co(1)–N(2)	176.0(3)
N(3)–Co(1)–N(2)	85.8(4)

hexadentate ligands. Out of three possible structures B–D in facial binding mode only B is obtained exclusively. The fundamental geometric difference between the two structures lies in the isomeric nature of coordination spheres. The imine nitrogen pairs are coordinated trans to each other in $\mathbf{1} \cdot 2H_2O$, and the remaining four atoms (two cis amine and two cis phenolic oxygen) complete the coordination sphere where as the phenolic oxygens are trans in $\mathbf{2} \cdot H_2O$ and the remaining four nitrogen atoms (two cis amine and two cis imine) complete the coordination sphere. The two coordinating ONN ligand halves are meridional in complex

$\mathbf{1} \cdot 2H_2O$ but are facial in complex $\mathbf{2} \cdot H_2O$ The difference is sustained by the greater flexibility of the trimethylene chains compared to dimethylene chains. Of the five chelate rings two are six-membered and three are five-membered in complex $\mathbf{1} \cdot 2H_2O$, and the corresponding numbers in complex $\mathbf{2} \cdot H_2O$ are four and one, respectively. The dimethylene bridges in complex $\mathbf{1} \cdot 2H_2O$ have the gauche configuration, and the six-membered trimethylene containing rings in complex $\mathbf{2} \cdot H_2O$ have chair like configurations.

The coordinated $\geq$C=N– pairs from the terminal imine groups with the two adjacent carbon atoms, in both the complexes, are planar within experimental error. The Co–N(imine) bond distances are equal 1.910 (4) Å in complex $\mathbf{1} \cdot 2H_2O$ and 1.940 (7), 1.949 (8) in complex $\mathbf{2} \cdot H_2O$ which are significantly shorter than Co–N(amine) distances 1.958 (4), 1.960 (4) Å in $\mathbf{1} \cdot 2H_2O$ and 2.012 (9), 1.970 (8) Å in $\mathbf{2} \cdot H_2O$. The Co–O(phenolic) distances lie in the range 1.882(6)–1.905(3) Å which are consistent with those reported for other similar structurally characterized mononuclear Schiff base Co^{III} complexes [12]. The facial chelation of ONN halves in $\mathbf{2} \cdot H_2O$ is responsible for greater N–C–C–N torsion angle (57.82°) of the central ethylenediamine part of H_2L^2 compared to meridional spanning of H_2L^1 in $\mathbf{1} \cdot 2H_2O$ (37.74°).

Intramolecular hydrogen bonding is observed between the Cl^- anions with the amine nitrogen and uncoordinated water molecule in complex $\mathbf{1} \cdot 2H_2O$. The same uncoordinated water molecule forms intermolecular hydrogen bonding with the amine nitrogen atom of the neighboring molecule to form hydrogen bonded chain like structure as shown in the Fig. 3. No hydrogen bonding is observed between ClO_4^- anion and the uncoordinated water molecules in complexes $\mathbf{2} \cdot H_2O$, in which the perchlorate anion is at a distance of 3.835 Å from the uncoordinated water molecule.

There are significant difference in bond lengths between the equatorial Co–O(phenolic), Co–N(amine) pairs and the axial Co–N(imine) pairs in complex $\mathbf{1} \cdot 2H_2O$ as well as in the equatorial Co–N(imine), Co–N(amine) pairs and the axial Co–O(phenolic) pairs in complex $\mathbf{2} \cdot H_2O$. The chloride and perchlorate anions are at 4.495 and 4.692 Å distance from the cobalt centers in $\mathbf{1} \cdot 2H_2O$ and $\mathbf{2} \cdot H_2O$, respectively. The perchlorate ion in the complex $\mathbf{2} \cdot H_2O$ have the expected regular tetrahedral geometry, with the average Cl–O bond lengths and the average O–Cl–O bond angles of 1.326 Å and 108.40°, respectively. Oxygen disorders are not observed, which is very common otherwise.

3.3. Stability of the imidazolidine ring towards cobalt(III) coordination

In solution, the expulsion of one mole of 2-hydroxy benzaldehyde molecule takes place when cobalt(III) ions react with the ligands $H_3L_I^1$ and $H_3L_I^2$, which are different from the selective imidazolidine ring opening reaction as observed earlier in a different ligand system with no loss of aldehyde molecule [4]. This type of imidazolidine ring-cleavage reaction with removal of one aldehyde molecule was not observed earlier for reactions of similar binucleating imidazolidine based ligands with vanadium, iron, copper and zinc [1,13–15]. Air oxidation of the starting +2 state of cobalt is responsible for the imidazolidine ring hydrolysis for hardness matching and the transformation is dependent on the metal ion and coordinated acidic water molecules (pK_1 for $Co(H_2O)_6^{3+}$ is 1.75) [16] (Scheme 3). The coordinated water has a pK_a sizably lower than free water and can release a proton easily. Protonation of first imidazolidine nitrogen atom followed by nucleophilic attack of $[Co–OH]^{2+}$ to the 2-imidazolidinyl carbon leads to the resulting ring hydrolysis. Cobalt(III) coordination driven imidazolidine ring hydrolysis transforms

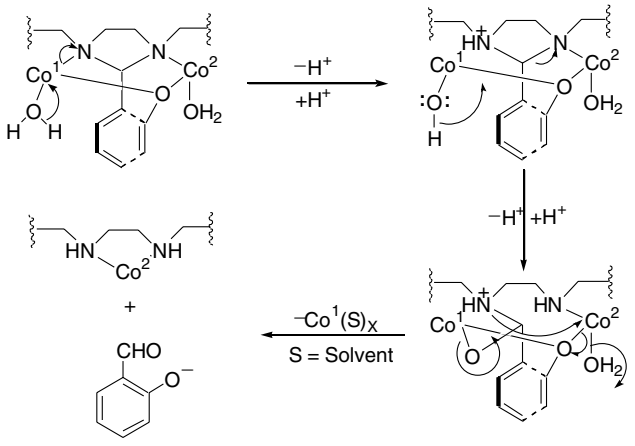

Scheme 3.

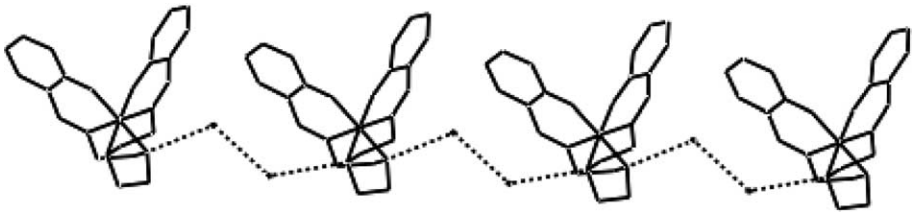

Fig. 3. 1-D hydrogen bonding chain in complex $\mathbf{1} \cdot 2H_2O$.

ethylenediamine (part of the imidazolidine ring) bridging coordination to a favored chelating coordination. Recently, we have identified polynuclear bridging coordination against chelating coordination of the central ethylenediamine part of any polydentate ligand. Ligands $H_3L_I^1$ and $H_3L_I^2$ are stable in methanol, acetonitrile and DMF against any hydrolytic cleavage for weeks. Greater hardness (η; Pearson) [17], of the central cobalt (III) ion (which also serves as a measure of the Lewis acidity) is responsible for the hardness-matched monocobalt complex formation with parent hexadentate ligands following hydrolytic cleavage of the ligands $H_3L_I^1$ and $H_3L_I^2$.

3.4. Physical characterizations

The molar conductivity (Λ_M) values of complexes $\mathbf{1}\cdot 2H_2O$ and $\mathbf{2}\cdot H_2O$ in MeOH are 95 and 92 $\Omega^{-1}\,cm^2\,mol^{-1}$ indicating a behavior attributable to 1:1 electrolytes. In IR spectra of the complexes a strong C=N stretching frequency due to the coordinated imine functions are observed at 1632 and 1597 cm^{-1} in $\mathbf{1}\cdot 2H_2O$ and $\mathbf{2}\cdot H_2O$, respectively, which are shifted from the free ligand values at 1642 and 1625 cm^{-1}. Broad bands at around 3376 and 1535 cm^{-1} in $\mathbf{1}\cdot 2H_2O$ are assigned to the stretching and bending vibrations of the uncoordinated water molecule and the corresponding values for $\mathbf{2}\cdot H_2O$ are 3480 and 1547 cm^{-1}, respectively. The strong unsplit band (ν_{ClO4^-}) at around 1106 cm^{-1} in $\mathbf{2}\cdot H_2O$ suggests no coordination of perchlorate ions [9], but presence of the same outside the coordination sphere.

The electronic spectra of $H_3L_I^1$ and $H_3L_I^2$ show characteristic $n\rightarrow\pi^*$ and $\pi\rightarrow\pi^*$ transitions at 285 and 321 nm ($\varepsilon\sim 5520$ and 4555 $l\,mol^{-1}\,cm^{-1}$) and 254 and 273 nm ($\varepsilon\sim 18\,880$ and 18 645 $l\,mol^{-1}\,cm^{-1}$), respectively. The spectrum observed immediately after addition of the metal salt to the methanolic solution of ligand $H_3L_I^1$ in air shows bands at 630 nm ($\varepsilon\sim 65\,l\,mol^{-1}\,cm^{-1}$), 512 nm ($\varepsilon\sim 230\,l\,mol^{-1}\,cm^{-1}$), 327 nm ($\varepsilon\sim 6780\,l\,mol^{-1}\,cm^{-1}$), 254 nm ($\varepsilon\sim 28\,590\,l\,mol^{-1}\,cm^{-1}$) and 222 nm ($\varepsilon\sim 29\,205\,l\,mol^{-1}\,cm^{-1}$). After 24 h of mixing the initial spectrum changes to one which exactly matches with the solution spectrum of the crystals of the corresponding mononuclear complex $\mathbf{1}\cdot 2H_2O$. It shows several shifted absorption bands at 605 nm ($\varepsilon\sim 180\,l\,mol^{-1}\,cm^{-1}$), 490 nm ($\varepsilon\sim 500\,l\,mol^{-1}\,cm^{-1}$), 392 nm ($\varepsilon\sim 1705\,l\,mol^{-1}\,cm^{-1}$), 251 nm ($\varepsilon\sim 17\,515\,l\,mol^{-1}\,cm^{-1}$) and 219 nm ($\varepsilon\sim 17\,070\,l\,mol^{-1}\,cm^{-1}$). Similarly the spectrum after 24 h from time of metal salt addition to the methanolic solution of ligand $H_3L_I^2$ shows transitions at 630 nm ($\varepsilon\sim 170\,l\,mol^{-1}\,cm^{-1}$), 560 nm ($\varepsilon\sim 202\,l\,mol^{-1}\,cm^{-1}$), 386 nm ($\varepsilon\sim 4155\,l\,mol^{-1}\,cm^{-1}$), which are shifted from 645 nm ($\varepsilon\sim 76\,l\,mol^{-1}\,cm^{-1}$), 391 nm ($\varepsilon\sim 2685\,l\,mol^{-1}\,cm^{-1}$), 362 nm ($\varepsilon\sim 10\,800\,l\,mol^{-1}\,cm^{-1}$) obtained after immediate addition. It also matches with the solution spectrum of the isolated single crystals of $\mathbf{2}\cdot H_2O$.

The redox behavior of both the mononuclear complexes in solution was examined electrochemically in DMF solution at a glassy carbon working electrode. The complexes are electroactive with respect to the metal center and exhibit one redox processes each. in the potential range ±1.5 V versus a saturated calomel electrode (SCE) (tetraethylammonium perchlorate as supporting electrolyte, at 298 K). A quasi-reversible one-electron response is observed at $E_{1/2}=1.33$ V versus SCE (ΔE_p, 150 mV) and $E_{1/2}=1.38$ V versus SCE (ΔE_p, 160 mV) for complexes $\mathbf{1}\cdot 2H_2O$ and $\mathbf{2}\cdot H_2O$, respectively.

4. Conclusion

Cobalt(III) coordination driven imidazolidine ring hydrolysis following air oxidation of the metal centre transforms *N*,*N*-imidazolidine bridging coordination to a favored *N*,*N*-chelating coordination with a change in hardness of the nitrogen donors. The greater the hardness of the cobalt center (which also serves as a measure of the Lewis acidity), the greater the preference to form $[Co^{III}L^x]^+$ complex with the hexadentate ligand. Thus expected dicobalt(II/II) complexes can be obtained when weak Lewis acids such as Co^{2+} are incapable of splitting of imidazolidine rings and favor imidazolidine nitrogen coordination. Both the ligands presumably bind two Co^{2+} centers initially in solution. Metal ion coordination driven imidazolidine ring hydrolysis is responsible for an increase in nitrogen donor basicity. Imidazolidine nitrogen donors present in binucleating ligands are soft bases compared to the secondary amine nitrogens in hexadentate ligands. Both *mer*- and *fac*-ON_2 binding modes of the two halves of the parent ligands have been identified in two structure determinations establishing no conformational preference for ligand hydrolysis.

5. Supplementary material

Further details of the structure determinations, including atomic coordinates, bond lengths and angles and thermal parameters of all non-hydrogen atoms for the structure are available on request as supplementary material from The Director, Cambridge Crystallographic Data Center, 12, Union Road, Cambridge CB2 1EZ, UK (fax: +44 1223 336 033; e-mail: deposit @ccdc.cam.ac.uk) (CCDC Deposition Nos. 268225 and 268226).

Acknowledgments

We thank DST, New Delhi, for the Single Crystal X-ray Diffractometer facility in the Department of

Chemistry, IIT Kharagpur under its FIST program. We thank Dr. S. Mukherjee, Delaware, USA for the CH-COSY spectra. We also acknowledge the comments of the referees at the revision stage.

References

[1] U. Mukhopadhyay, L. Govindasamy, K. Ravikumar, D. Velmurugan, D. Ray, Inorg. Chem. Commun. 1 (1998) 152.
[2] M. Bera, W.T. Wong, G. Aromi, D. Ray, Eur. J. Inorg. Chem. (2005) 2526.
[3] E.K. Lee, S.H. Kim, B.H. Jung, W.S. Ahn, G.J. Kim, Tetrahedron Lett. 44 (2003) 1971.
[4] M. Boca, P. Baran, R. Boca, H. Fuess, G. Kickelbick, W. Linert, F. Renz, I. Svoboda, Inorg. Chem. 39 (2000) 3205.
[5] (a) D.T. Sawyer, J.L. Roberts Jr., Experimental Electrochemistry for chemists, Wiley, New York, 1974, p. 167;
(b) M. Walter, L. Ramaley, Anal. Chem. 45 (1973) 165;
(c) D.D. Perrin, W.L.F. Armango, D.R. Perrin, Purification of Laboratory Chemicals, Pergamon, Oxford, 1980.
[6] B.D. Sarma, J.C. Bailar Jr., J. Am. Chem. Soc. 77 (1955) 5476.
[7] G.M. Sheldrick, SHELXS-97, Program for the Solution of Crystal Structures, University of Göttinegen, Germany, 1997.
[8] G.M. Sheldrick, SHELXS-97, Program for the Refinement of Crystal Structures, University of Göttinegen, Germany, 1997.
[9] U. Mukhopadhyay, L.R. Falvallo, D. Ray, Eur. J. Inorg. Chem. (2001) 2823.
[10] L.-W. Yang, S. Liu, E. Wong, S.J. Retting, C. Orvig, Inorg. Chem. 34 (1995) 2164.
[11] H. Schmitt, R. Lomoth, A. Magnuson, J. Park, J. Fryxelius, M. Kritikos, J. Martensson, L. Hammarstorm, L. Sun, B. Akemark, Chem. Eur. J. (2002) 3757.
[12] Y.S. Xie, X.T. Liu, M. Zhang, K.J. Wei, Q.L. Liu, Polyhedron 24 (2005) 165.
[13] B. Chiari, O. Piovesana, T. Tarantelli, P.F. Zanazzi, Inorg. Chem. 21 (1982) 2444.
[14] M. Fondo, A.M. Garcia-Deibe, M.R. Bermejo, J. Sanmar-tin, A.L. Liamas-Saiz, J. Chem. Soc., Dalton Trans. (2002) 4746.
[15] E.P. Copeland, I.A. Kahwa, J.T. Mague, G.L. Mcpherson, J. Chem. Soc., Dalton Trans. (1997) 2849.
[16] J.A. Dean, Lange's Handbook of Chemistry, 13th ed., McGraw-Hill, New York, 1987, p. 15 (Section 5).
[17] (a) R.G. Pearson, J. Am. Chem. Soc. 85 (1963) 3533;
(b) R.G. Pearson, J. Am. Chem. Soc. 105 (1983) 7512.

Available online at www.sciencedirect.com
SCIENCE DIRECT®
Polyhedron 25 (2006) 711–721
POLYHEDRON
www.elsevier.com/locate/poly

Syntheses, spectroscopic characterization and crystal structures of some new phosphoramidates and an organotin(IV) complex of *N*-(4-fluorobenzoyl)-*N*′,*N*″-bis(piperidinyl)phosphoric triamide

Khodayar Gholivand *, Zahra Shariatinia, Mehrdad Pourayoubi

Department of Chemistry, Tarbiat Modarres University, Gisha Bridge, P.O. Box 14115-175, Tehran, Iran

Received 18 June 2005; accepted 25 July 2005
Available online 30 August 2005

Abstract

Some new phosphoramidates with formula 4-F-$C_6H_4C(O)N(H)P(O)X_2$, $X = NC_4H_8$ (**1**), NC_5H_{10} (**2**), 4-CH_3-NC_5H_9 (**3**), NC_4H_8O (**4**), NC_6H_{12} (**5**), $N(CH_2CH_3)_2$ (**6**), $N(CH_2CH_2CH_3)_2$ (**7**) were synthesized. The reaction of compound **2** with dimethyltin(IV) dichloride leads to an octahedral organotin(IV) complex, $SnCl_2(CH_3)_2$[4-F-$C_6H_4C(O)N(H)P(O)(NC_5H_{10})_2]_2$ (**8**) with equal ligands in *trans* positions. These compounds were characterized by IR, ^1H, ^{13}C, ^{31}P, ^{119}Sn NMR, mass spectroscopy and elemental analysis. The structures have been determined for compounds **1**, **2**, **4**, **5** and **8**. Compound **2** exists as four symmetrically independent molecules in the crystalline lattice. Compounds **1**, **4** and **5** form dimmers via intermolecular –P=O···H–N– hydrogen bonds that in **1** is centrosymmetric. In compound **2**, two dimmers were formed; each of them was produced between two adjacent independent molecules. In compounds **1**, **2**, **3**, **4** and **8**, containing five- and six-membered ring amine groups, $^3J(P,C_{aliphatic}) > {}^2J(P,C_{aliphatic})$. Compound **5** with seven-membered ring amine, similar to compounds **6** and **7** with acyclic aliphatic amines, shows that $^2J(P,C_{aliphatic}) > {}^3J(P,C_{aliphatic})$. Mass spectra of these compounds indicate the 4-F-$C_6H_4CO^+$ and 4-F-$C_6H_4CN^+$ fragments.
© 2005 Elsevier Ltd. All rights reserved.

Keywords: X-ray crystallography; NMR spectroscopy; Phosphoramidate; Organotin(IV) complex

1. Introduction

The chemistry of phosphoramidates is recently developed due to the biological activity [1–3] and also the coordination chemistry [4–6] of these compounds. Some of them with $RC(O)N(H)P(O)R^1_2$ formula were used as *O*,*O*′-donor ligands for metal ions, particularly for rare earth metal cations [7,8]. Although the crystal structures of several phosphoramidates and their complexes are already known [4–6,9–12], there are little discussions about the substituent effects on the structural and NMR parameters. Among coordination compounds, the organometallic compounds of tin(IV) are very important antitumor agents [13,14]. Organotin(IV) compounds have been extensively used as wood preservatives, agrochemical fungicides and biocides [15,16]. The coordination compounds of organotin(IV) are a matter of interest in recent researches [17–20]. In our previous studies, we obtained some structures with two conformers in the lattice [21–23]. Cain et al. reported the crystal structure of compound {(5*R*,4*S*)-*N*-Pr-ephedrine}P(S)[NH(Si)$(CH_3)_3$] that has three independent molecules in the unit cell [24]. The first phosphoramidate with four crystallographically independent molecules in the crystalline network was $C_6H_5C(O)N(H)P(O)(NC_5H_{10})_2$ [25] and in this work we report its analogous compound 4-F-$C_6H_4C(O)N(H)P(O)(NC_5H_{10})_2$ (**2**). There are several articles that have been discussed

* Corresponding author. Tel. +98 21 8011001x3443; fax: +98 21 8006544.
E-mail address: gholi_kh@modares.ac.ir (K. Gholivand).

0277-5387/$ - see front matter © 2005 Elsevier Ltd. All rights reserved.
doi:10.1016/j.poly.2005.07.035

on noticeable information on the coupling constants between ^{31}P and ^{13}C (or ^{1}H) nuclei [26,27]. Herein, we represent the synthesis of some new phosphoramidates with general formula 4-F-$C_6H_4C(O)N(H)P(O)X_2$, X = NC_4H_8 (**1**), NC_5H_{10} (**2**), 4-NC_5H_9-CH_3 (**3**), NC_4H_8O (**4**), NC_6H_{12} (**5**), $N(CH_2CH_3)_2$ (**6**), $N(CH_2CH_2CH_3)_2$ (**7**). Also, we studied the behavior of **2** as *O*-donor ligand to interaction with $SnCl_2(CH_3)_2$ and an octahedral organotin(IV) complex, $SnCl_2(CH_3)_2$[4-F-$C_6H_4C(O)$-$N(H)P(O)(NC_5H_{10})_2]_2$ (**8**) was prepared. The structures of compounds **1**, **2**, **4**, **5** and **8** were determined by X-ray crystallography. Furthermore, we discussed on structural, NMR and Mass spectral parameters in these compounds and their analogous derivatives.

2. Experimental

2.1. Materials

Dipropylamine (⩾99%), morpholine (>98%) (Merck) and 4-fluorobenzamide (98%), formic acid (98%), phosphorus pentachloride (⩾98%), pyrrolidine (>98%), piperidine (⩾99.5%), hexemethyleneimine (⩾97%), diethylamine (⩾99.7%), dimethyltin dichloride (~95%) (Fluka) were used as supplied. In all reactions, the low temperature condition was used.

2.2. X-ray measurements

X-ray data of compounds **1**, **2**, **5** and **8** were collected on a Bruker SMART 1000 CCD [28] and for compound **4** on a Siemens P3/PC [29] single crystal diffractometer with graphite monochromated Mo Kα radiation ($\lambda = 0.71073$ Å). The structures were refined with SHELXL-97 [30] by full-matrix least-squares on F^2. The positions of hydrogen atoms were obtained from the difference Fourier map. Routine Lorentz and polarization corrections were applied and an absorption correction was performed using the SADABS program [31].

2.3. Spectroscopic measurements

All reactions were performed under argon atmosphere and in dry solvents. ^{1}H, ^{13}C, ^{31}P and ^{119}Sn NMR spectra were recorded on a Bruker Avance DRS 500 spectrometer. ^{1}H and ^{13}C chemical shifts were determined relative to internal TMS, ^{31}P chemical shifts relative to 85% H_3PO_4 as external standard and ^{119}Sn chemical shift relative to $Sn(CH_3)_4$ solution. Infrared (IR) spectra were recorded on a shimadzu model IR-60 spectrometer. Elemental analysis was performed using a Heraeus CHN-O-RAPID apparatus. High resolution mass spectra were obtained with a Shimadzu model QP-1100EX spectrometer (EI, 70 eV). 4-F-$C_6H_4C(O)NHP(O)Cl_2$ was prepared according to the literature method [32].

2.4. Syntheses

2.4.1. General procedure for synthesis of compounds 1–8

Compounds **1**–**7** were prepared by the reaction of 10 mmol *N*-(4-fluorobenzoyl) phosphoramidic dichloride with 40 mmol of corresponding amines in dry chloroform and stirred at −5 °C. After about 5 h, the solvent was removed and product was washed with H_2O and recrystallized from methanol/chloroform. Compound **8** was synthesized by the reaction of 20 mmol of **2** with 10 mmol dimethyltin(IV) dichloride in methanol at room temperature.

3. Results and discussion

3.1. NMR and IR study

Synthesis of compounds **1**–**7** were performed by the reaction of *N*-(4-fluorobenzoyl) phosphoramidic dichloride [32] with corresponding amines, Scheme 1. Compound **8** was obtained from the reaction of compound **2** with dimethyltin(IV) dichloride. ^{13}C NMR spectra of compounds **1**, **2**, **3**, **4** and **8**, containing five- and six-membered ring amine groups, show that $^{3}J(P,C_{aliphatic})$ is greater than $^{2}J(P,C_{aliphatic})$. For compound **5** with seven-membered ring amine, similar to compounds **6** and **7** with acyclic aliphatic amines, $^{2}J(P,C_{aliphatic}) > {}^{3}J(P,C_{aliphatic})$. Compound **6** shows an opposite result for $^{2,3}J(P,C_{aliphatic})$ relative to compound **1** (with diethylamine group), Scheme 2. Also, it is observed from Table 1 that with increasing the ring size of amine groups in compounds **1**–**5**, the $^{3}J(P,C_{aliphatic})$ becomes smaller and it varies from 8.0 Hz in **1** to 3.8 Hz in **5**. These results are in good agreement with our previous studies on the similar compounds **9**–**12**, Table 1. The carbon atoms of C=O groups in compounds **6**, **7**, **8** and **10** couple with their related phosphorus atoms with $^{2}J(P,C(O))$ coupling constant values in the range from 1.9 Hz in **6** and **8** to 3.9 Hz in **10**. The *ipso* carbon atoms of phenyl rings in compounds **1**–**12** show $^{3}J(P,C_{aromatic})$ coupling constants in the range from 7.6 Hz in **3** to 8.9 Hz in **6** and **7**.

^{13}C NMR spectrum of compound **3** indicates eight peaks for the two unequivalent aliphatic rings of 4-methylpiperidinyl groups. The four doublet signals with two various $^{2}J(P,C_{aliphatic})$ [and also $^{3}J(P,C_{aliphatic})$] coupling constant values are related to the carbon atoms with two and three bond distances from phosphorus atom, Table 1 and Fig. 1.

The δ (^{31}P) of compounds **1**, **2** and **5** indicates that with increasing the ring size of amine groups, it shifts to down fields (Table 1). The phosphorus-31 chemical

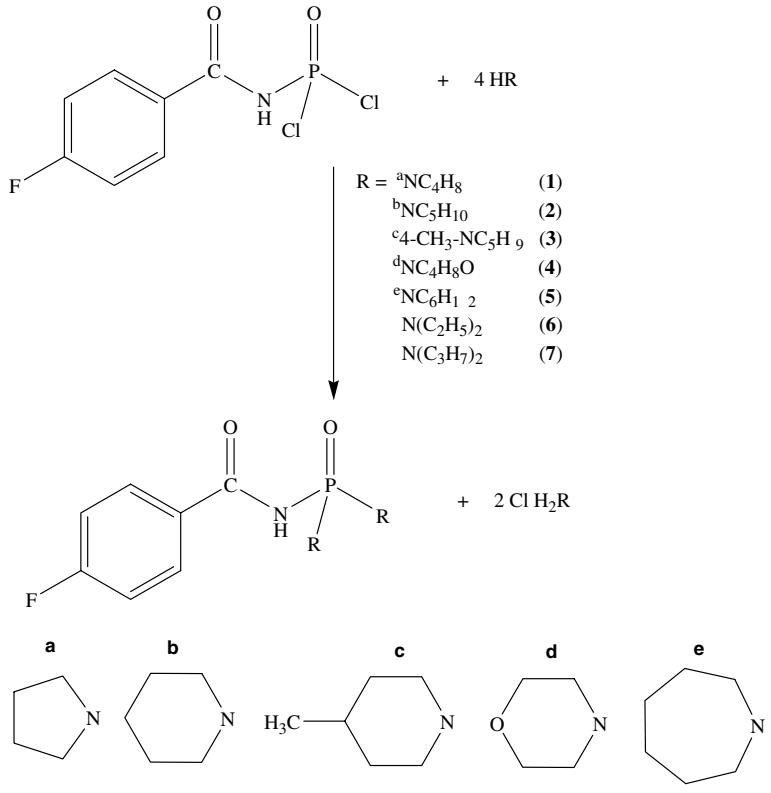

Scheme 1. Preparation of compounds **1**–**7**.

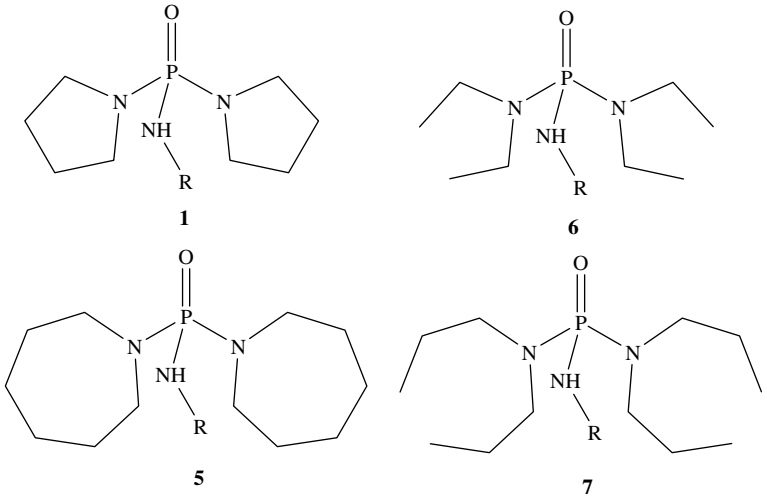

Scheme 2. The formula of compounds **1**, **5**–**7**.

shifts of compounds **1**, **2** and **5** with 4-fluorobenzoyl moiety are in upfields relative to their analogous compounds **10**–**12** with formula $C_6H_5C(O)N(H)P(O)R_2$ ($R = NC_4H_8$, NC_5H_{10}, NC_6H_{12}). The δ (^{31}P) of compounds **2** and its organotin(IV) complex, **8**, are close to each other, 10.34 ppm in **2** and 10.15 ppm in **8**. ^{119}Sn NMR of compound **8** shows a signal at −210.75 ppm for the Sn atom. ^1H NMR spectrum of this molecule indicates two separate signals for the NH protons of two ligands. The fluorine substituent couple with aromatic carbon and proton atoms of phenyl ring and we observed $^{1-4}J(F,C_{aromatic})$ and $^4J(F,H_{aromatic})$ in compounds **1**–**8**.

IR spectra of compounds **1**–**8** show that the $\nu_{P=O}$; $\nu_{P-N(amine)}$; $\nu_{P-N(amide)}$ and $\nu_{C=O}$ frequencies are in the range from 1162 in **8** to 1215 in **1**; 870 in **1** to 964 in **4**; 752 (**1**) to 757 (**5** & **8**) and 1661 (**5**) to 1680 (**8**), respectively. The C=O frequency in structurally similar com-

Table 1
$^{2}J(P,C_{aliphatic})$, $^{3}J(P,C_{aliphatic})$ and $^{3}J(P,C_{aromatic})$ (Hz), $\delta(^{31}P)$ (ppm) for compounds **1**–**12** and m.p. (°C), yield (%) of **1**–**8**

No.	Compound	$^{2}J(P,C_{aliphatic})$	$^{3}J(P,C_{aliphatic})$	$^{3}J(P,C_{aromatic})$	$\delta(^{31}P)$	M.p. (°C)	Yield (%)
1	4-F-$C_6H_4C(O)N(H)P(O)R^1_2$	5.0 (CH_2)	8.0 (CH_2)	8.5	7.05	181	88
2	4-F-$C_6H_4C(O)N(H)P(O)R^2_2$	0.0 (CH_2)	4.8 (CH_2)	8.7	10.34	194	83
3	4-F-$C_6H_4C(O)N(H)P(O)R^3_2$	3.4 (CH_2), 1.9 (CH_2)	5.8 (CH_2), 4.8 (CH_2)	7.6	10.39	189	79
4	4-F-$C_6H_4C(O)N(H)P(O)R^4_2$	0.0 (CH_2)	5.4 (CH_2)	8.6	9.44	193	70
5	4-F-$C_6H_4C(O)N(H)P(O)R^5_2$	4.5 (CH_2)	3.8 (CH_2)	8.7	12.72	144	68
6	4-F-$C_6H_4C(O)N(H)P(O)[N(C_2H_5)_2]_2$	1.9 (C=O), 5.0 (CH_2)	0.0 (CH_3)	8.9	12.92	126	73
7	4-F-$C_6H_4C(O)N(H)P(O)[N(C_3H_7)_2]_2$	2.4 (C=O), 4.5 (CH_2)	2.3 (CH_2)	8.9	13.44	81	82
8	$Sn(CH_3)_2Cl_2[4\text{-F-}C_6H_4C(O)N(H)P(O)R^2_2]_2$	1.9 (C=O), 2.6 (CH_2)	4.9 (CH_2)	8.1	10.15	176	31
9[a]	$C_6H_5C(O)N(H)P(O)R^1_2$	5.5 (CH_2)	8.6 (CH_2)	8.7	8.84		
10[b]	$C_6H_5C(O)N(H)P(O)R^2_2$	3.9 (C=O), 2.7 (CH_2)	4.7 (CH_2)	8.5	12.02		
11[b]	$C_6H_5C(O)N(H)P(O)R^3_2$	2.9 (CH_2), 0.0 (CH_2)	4.9 (CH_2), 5.1 (CH_2)	8.6	12.04		
12[c]	$C_6H_5C(O)N(H)P(O)R^5_2$	4.7 (CH_2)	4.2 (CH_2)	8.7	14.70		

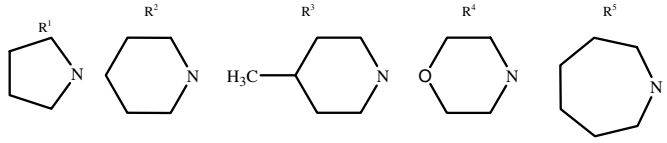

[a] The data of this compound are given in [23].
[b] The data of these compounds are given in [25].
[c] The data of this compound are given in [42].

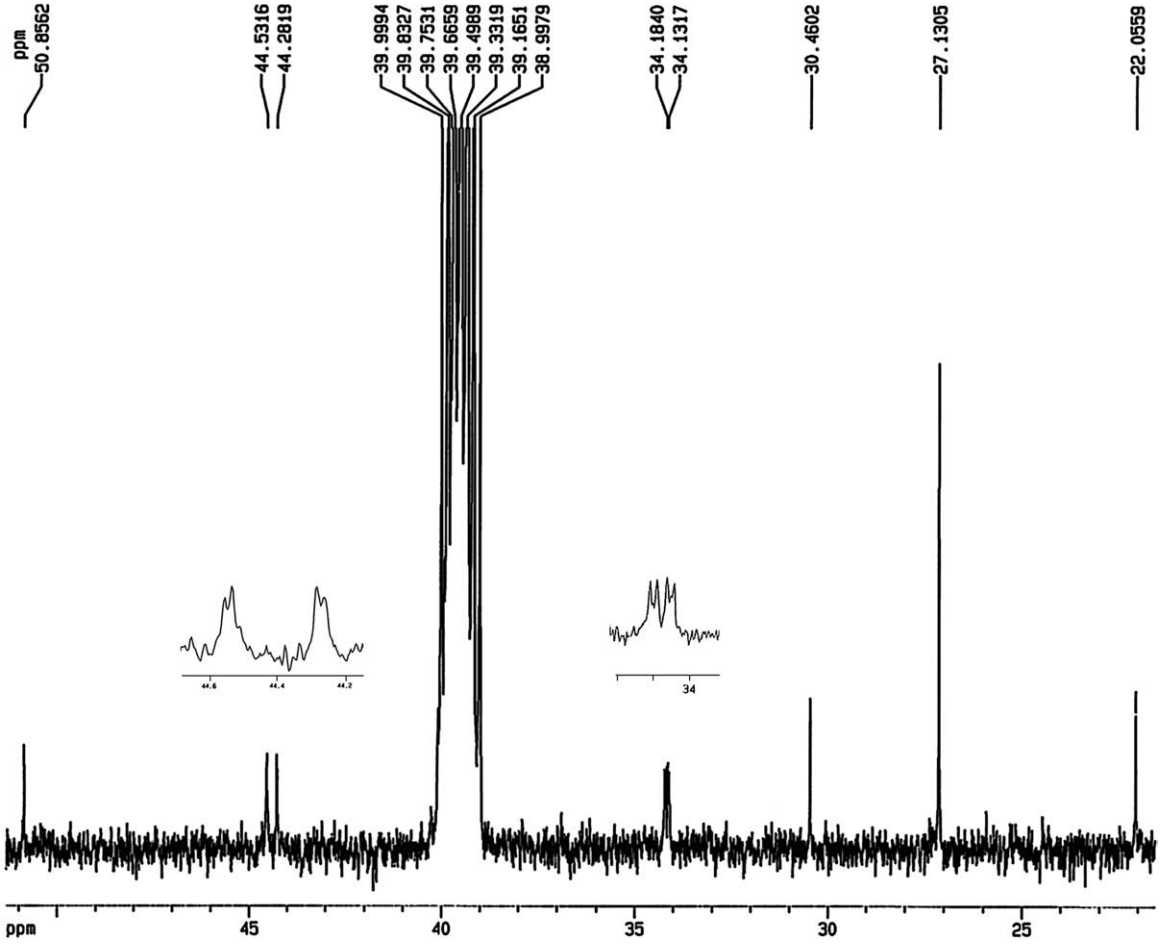

Fig. 1. Selected region of ^{13}C NMR spectrum of compound **3**.

Table 2
Crystallographic data for **1**, **2** and **4**

	1	**2**	**4**
Empirical formula	$C_{15}H_{21}FN_3O_2P$	$C_{17}H_{25}FN_3O_2P$	$C_{15}H_{21}FN_3O_4P$
Formula weight	325.32	353.37	357.32
T (K)	120(2)	120(2)	293(2)
λ (Å)	0.71073	0.71073	0.71073
Crystal system	monoclinic	triclinic	monoclinic
Space group	$P2_1/n$	$P\bar{1}$	$C2/c$
Unit cell dimensions			
a (Å)	9.4043(19)	9.4800(11)	15.732(3)
b (Å)	9.4365(19)	17.5062(19)	10.740(2)
c (Å)	17.744(4)	22.439(2)	21.553(4)
α (°)	90	76.168(2)	90
β (°)	90.044(4)	84.962(3)	106.93(3)
γ (°)	90	84.366(3)	90
V (Å^3)	1574.6(6)	3590.4(7)	3483.9(12)
Z	4	8	8
D_{calc} (Mg m^{-3})	1.372	1.307	1.362
Absorption coefficient (mm^{-1})	0.196	0.177	0.192
F(000)	688	1504	1504
Crystal size (mm^3)	$0.4 \times 0.5 \times 0.6$	$0.3 \times 0.2 \times 0.2$	$0.4 \times 0.36 \times 0.32$
θ Range for data collection (°)	2.30–28.99	0.94–26.00	3.30–28.06
Limiting indices	$-12 \leqslant h \leqslant 12$, $-12 \leqslant k \leqslant 12$, $-20 \leqslant l \leqslant 24$	$-11 \leqslant h \leqslant 11$, $-21 \leqslant k \leqslant 21$, $-27 \leqslant l \leqslant 27$	$0 \leqslant h \leqslant 20$, $0 \leqslant k \leqslant 14$, $-28 \leqslant l \leqslant 27$
Reflections collected/unique (R_{int})	13097/4107 (0.0307)	25752/13810 (0.0412)	4311/4165 (0.0092)
Completeness to θ (%)	($\theta = 28.99°$) 98.0	($\theta = 26.00°$) 97.7	($\theta = 28.06°$) 98.2
Absorption correction	none	semi-empirical from equivalents	none
Maximum and minimum transmission	0.928 and 0.197	0.9654 and 0.9487	
Refinement method	full-matrix least-squares on F^2	full-matrix least-squares on F^2	full-matrix least-squares on F^2
Data/restraints/parameters	4107/0/199	13810/12/857	4165/0/253
Goodness-of-fit on F^2	1.000	1.020	1.025
Final R indices	$R_1 = 0.0410$, $wR_2 = 0.1093$	$R_1 = 0.0698$, $wR_2 = 0.1490$	$R_1 = 0.0488$, $wR_2 = 0.1178$
R indices (all data)	$R_1 = 0.0451$, $wR_2 = 0.1143$	$R_1 = 0.1258$, $wR_2 = 0.1705$	$R_1 = 0.0765$, $wR_2 = 0.1346$
Largest difference in peak and hole (e Å^{-3})	0.957 and −0.329	0.654 and −0.516	0.251 and −0.228

pounds **1**, **6** and also in **5**, **7** (see Scheme 2) are very close to each other. The P=O stretching frequency in complex **8** (1162 cm^{-1}) is weaker than in its ligand **2** (1178 cm^{-1}), but for C=O frequency an opposite result was obtained (1680 cm^{-1} in **8** and 1668 cm^{-1} in **2**). The two bands at 542 and 511 cm^{-1} are related to the asymmetric and symmetric stretching frequencies of Sn–C bonds, respectively [33] and the band at 467 cm^{-1} corresponds to the vibration of Sn–O bond [34].

3.2. X-ray crystallography investigation

Single crystals of compounds **1**, **2**, **4**, **5** and **8** were obtained from a solution of methanol and chloroform after slow evaporation at room temperature. The crystal data and the details of the X-ray analysis are given in Tables 2 and 3, selected bond lengths and angles in Tables 4 and 5. Molecular structures of these compounds are shown in Figs. 2–6.

The two aliphatic rings of pyrrolidine groups in compound **1** have puckered shape and they are not planar. Compound **2** with six-membered ring amine group exists as four symmetrically independent molecules in the crystal lattice. This is due to the differences in similar torsion angles of these four independent molecules. This phenomenon was also observed for compound $C_6H_5C(O)N(H)P(O)(NC_5H_{10})_2$ [25]. The complexation of compound **2** with dimethyltin dichloride (compound **8**) produced a coordination compound with two symmetrically equal phosphoramidate ligands, Fig. 6.

Compounds **1**, **4** and **5** each contain one amidic hydrogen atom and form dimmers via intermolecular –P=O···H–N– hydrogen bonds that in **1** is a centrosymmetric dimmer (Table 6). In compound **2** (with four independent molecules in the unit cell), the two conformers labeled with P(1), P(1A) [and also the two others labeled with P(1B), P(1C)] are connected to each other via two different –P=O···H–N– hydrogen bonds and form a noncentrosymmetric dimmer. The earlier studied *N*-benzoyl, phosphoric triamides exist either in the form of dimmeric aggregates [35] or as polymeric chains [36].

In molecules **1**, **2**, **4**, **5** and **8** the phosphoryl and the carbonyl groups are anti, Figs. 2–6. The phosphorus atoms in these structures have slightly distorted tetrahedral configuration. The bond angles around P(1) atoms

Table 3
Crystallographic data for **5** and **8**

	5	**8**
Empirical formula	$C_{19}H_{29}FN_3O_2P$	$C_{36}H_{56}Cl_2F_2N_6O_4P_2Sn$
Formula weight	381.42	926.40
T (K)	120(2)	120(2)
λ	0.71073 Å	0.71073 Å
Crystal system	monoclinic	monoclinic
Space group	$C2/c$	$P2_1/c$
Unit cell dimensions		
a (Å)	23.030(4)	14.906(3)
b (Å)	9.2745(13)	8.6132(17)
c (Å)	20.585(3)	16.538(3)
α (°)	90	90
β (°)	116.684(4)	101.483(4)
γ (°)	90	90
V (Å^3)	3928.6(11)	2080.8(7)
Z	8	2
D_{calc} (Mg m^{-3})	1.290	1.479
Absorption coefficient (mm^{-1})	0.167	0.873
$F(000)$	1632	956
Crystal size (mm^3)	$0.23 \times 0.21 \times 0.18$	$0.45 \times 0.3 \times 0.15$
θ Range for data collection (°)	1.98–29.00	1.39–28.00
Limiting indices	$-29 \leqslant h \leqslant 31$, $-12 \leqslant k \leqslant 12$, $-26 \leqslant l \leqslant 27$	$-19 \leqslant h \leqslant 18$, $-11 \leqslant k \leqslant 9$, $-21 \leqslant l \leqslant 19$
Reflections collected/unique (R_{int})	13691/5065 (0.0281)	15430/4900 (0.0178)
Completeness to θ (%)	($\theta = 29.00°$) 97.0	($\theta = 28.00°$) 97.5
Absorption correction	semi-empirical from equivalents	semi-empirical from equivalents
Maximum and minimum transmission	0.970 and 0.962	0.877 and 0.696
Refinement method	full-matrix least-squares on F^2	full-matrix least-squares on F^2
Data/restraints/parameters	5065/130/362	4900/0/243
Goodness-of-fit on F^2	1.018	1.001
Final R indices	$R_1 = 0.0948$, $wR_2 = 0.1608$	$R_1 = 0.0276$, $wR_2 = 0.0549$
R indices (all data)	$R_1 = 0.1676$, $wR_2 = 0.1782$	$R_1 = 0.0357$, $wR_2 = 0.0566$
Largest difference in peak and hole (e Å^{-3})	0.842 and −0.688	1.274 and −0.509

Table 4
Selected bond lengths (Å) and angles (°) for compounds **1**, **2**, **4** and **5**

	1	2	4	5
P(1)–O(1)	1.4863(10)	1.480(2)	1.4801(17)	1.472(2)
P(1)–N(1)	1.6899(11)	1.683(3)	1.6839(16)	1.675(3)
P(1)–N(2)	1.6239(12)	1.636(3)	1.6246(18)	1.634(3)
P(1)–N(3)	1.6390(12)	1.625(3)	1.6318(18)	1.626(4)
O(2)–C(1)	1.2207(16)	1.223(4)	1.212(2)	1.328(4)
N(1)–C(1)	1.3763(15)	1.378(4)	1.375(3)	1.365(4)
N(2)–C(8)	1.4841(16)	1.460(5)	1.468(3)	1.445(4)
F(1)–C(5)	1.3615(16)	1.366(4)	1.358(2)	1.321(4)
O(1)–P(1)–N(1)	104.66(5)	104.60(15)	104.63(9)	106.88(14)
O(1)–P(1)–N(2)	110.37(6)	118.86(16)	111.11(9)	109.89(19)
O(1)–P(1)–N(3)	119.59(6)	110.78(15)	118.30(11)	106.41(18)
N(2)–P(1)–N(1)	115.73(6)	105.13(16)	112.22(9)	116.41(19)
N(3)–P(1)–N(1)	102.89(6)	112.94(17)	106.52(9)	116.1(2)
N(2)–P(1)–N(3)	103.93(6)	104.64(16)	104.16(10)	100.7(3)
C(1)–N(1)–P(1)	125.81(9)	127.4(3)	127.28(14)	129.2(3)

Table 5
Selected bond lengths (Å) and angles (°) for compound **8**

P(1)–O(1)	1.5012(14)
P(1)–N(1)	1.6921(17)
P(1)–N(2)	1.6260(17)
P(1)–N(3)	1.6201(17)
O(2)–C(1)	1.222(2)
N(1)–C(1)	1.384(3)
F(1)–C(5)	1.355(2)
Sn(1)–C(18)	2.1238(19)
Sn(1)–O(1)	2.2176(13)
Sn(1)–Cl(1)	2.5617(6)
C(18)–Sn(1)–C(18)#1	180.000(1)
C(18)–Sn(1)–O(1)	87.51(7)
C(18)–Sn(1)–O(1)#1	92.49(7)
O(1)#1–Sn(1)–O(1)	180.0
C(18)–Sn(1)–Cl(1)	90.25(6)
C(18)#1–Sn(1)–Cl(1)	89.75(6)
O(1)–Sn(1)–Cl(1)	91.91(4)
O(1)#1–Sn(1)–Cl(1)	88.09(4)
Cl(1)#1–Sn(1)–Cl(1)	180.0
P(1)–O(1)–Sn(1)	145.42(9)

Symmetry code: #1: $-x, -y+2, -z+2$.

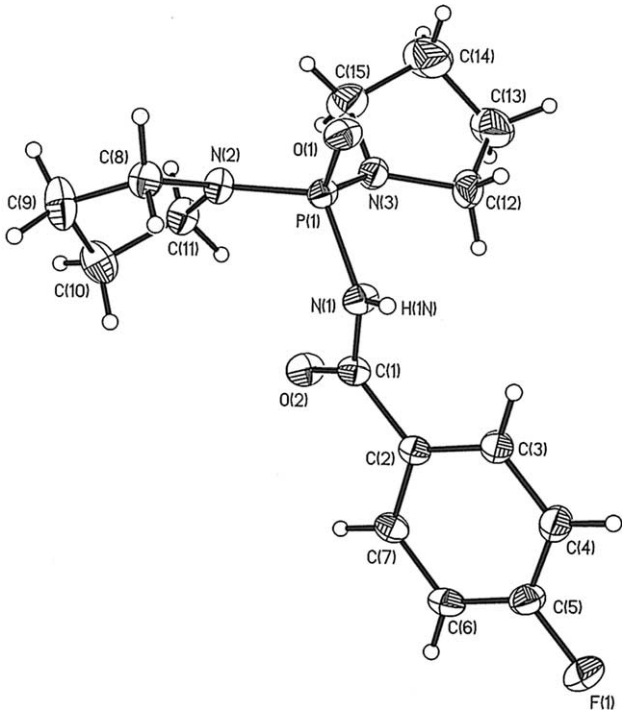

Fig. 2. Molecular structure and atom-labeling scheme for P(O)(4-F-$C_6H_4C(O)NH)(NC_4H_8)_2$, compound **1** (50% probability ellipsoids).

in these compounds are in the range from 119.59(6)° in **1** to 100.7(3)° in **5**, for the angles O(1)–P(1)–N(3) and N(2)–P(1)–N(3), respectively, Tables 4 and 5. In these compounds, the angles OPN_{amide} (N_{amide} is the nitrogen atom of P(O)N(H)C(O) moiety) are lower than the angles OPN_{amine} (N_{amine} is the nitrogen atom of P(O)NR moiety). The P=O bond lengths in molecules **1**, **2**, **4**, **5** and **8** are 1.4863(10), [1.480(2), 1.479(2), 1.471(2), 1.475(3)], 1.4801(17), 1.472(2) and 1.5012(14) Å that are larger than the normal P=O bond length (1.45 Å) [37]. The P=O bond lengths in our previously reported structures are in the range from 1.4875(14) Å in **12** to 1.459(12) Å in **10** (Table 7). The P=O and $P–N_{amide}$ bond lengths in complex **8** is longer than those of ligand **2**, but the C=O bond length in **8** is shorter than in **2**, Table 7. The C=O bond length in compound **5** with seven-membered ring amine group has the longest, 1.328(4) Å, and in compound **4**, 1.212(2) Å, has the lowest value.

The $P–N_{amide}$ bond lengths are longer than the $P–N_{amine}$ bond lengths, because of the resonance interaction of the N_{amide} with the C=O π system that cause a partial multiple bond character in $C–N_{amide}$ (the $C–N_{amide}$

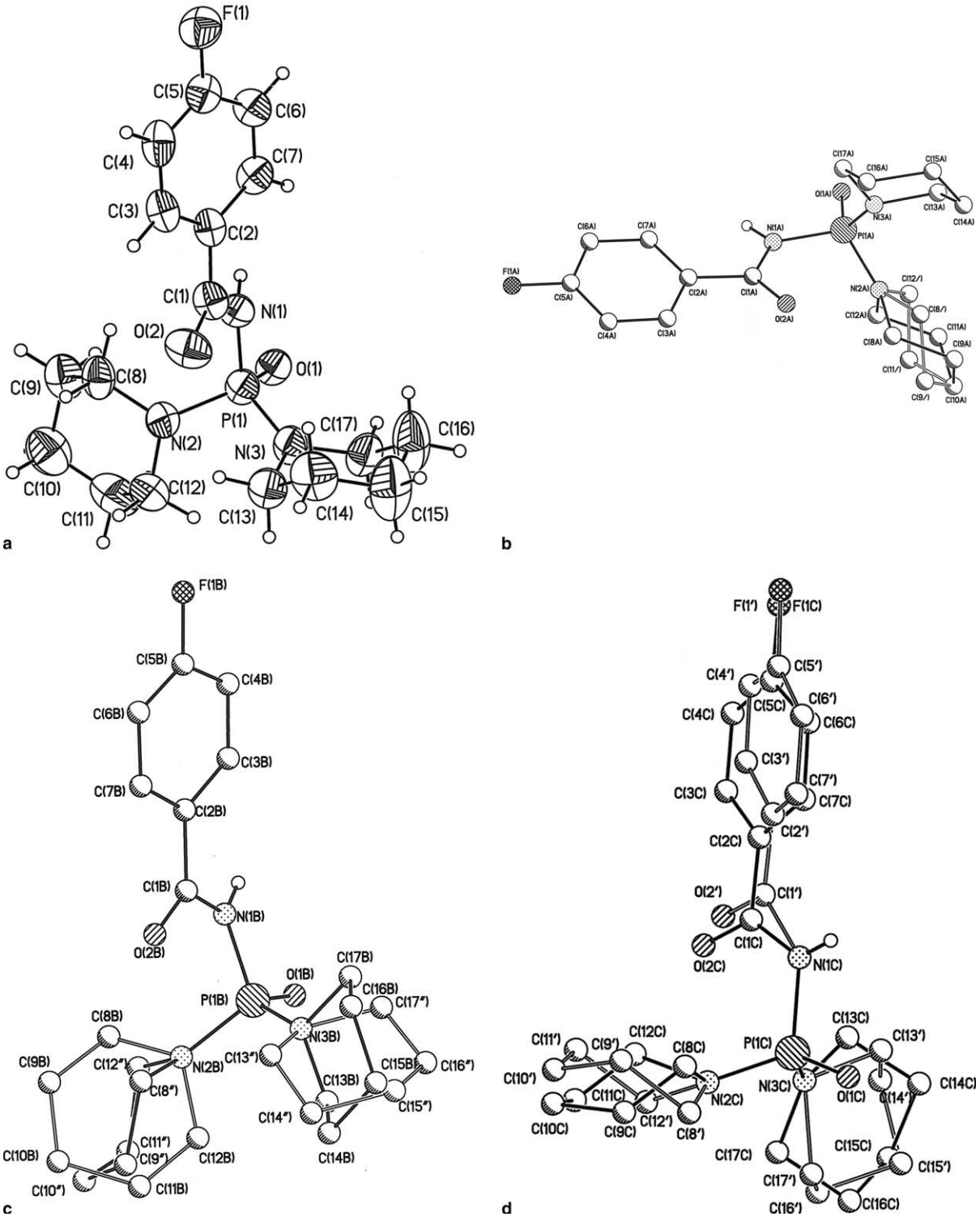

Fig. 3. Molecular structure and atom-labeling scheme for $P(O)(4\text{-}F\text{-}C_6H_4C(O)NH)(NC_5H_{10})_2$, compound **2** showing four crystallographically independent molecules in the lattice three of them have disordered forms (50% probability ellipsoids).

bond lengths are shorter than the $C–N_{amine}$ bond lengths). All of these P–N bonds are shorter than the typical P–N single bond length (1.77 Å [37]). This is likely due to the electrostatic effects (polar bonds) which overlap with P–N σ bond [38]. The P–N bond lengths in the previously reported structures were in the range from 1.6916(16) Å ($P–N_{amide}$ in **12**) to 1.590(15) Å ($P–N_{amine}$ in **10**), respectively (Table 7).

The environment of the nitrogen atoms is practically planar. In compound **1** the angles C(11)–N(2)–C(8),

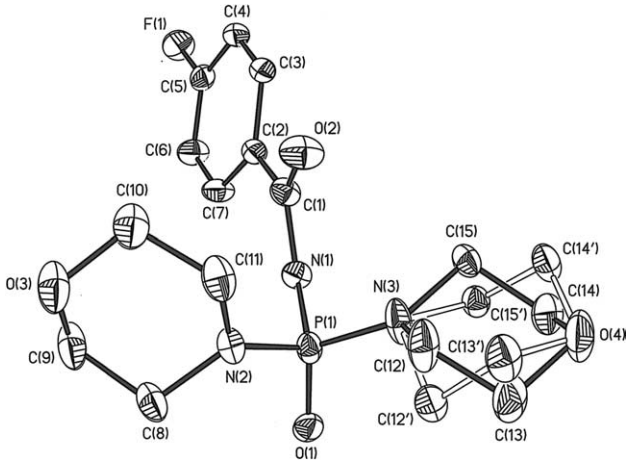

Fig. 4. Molecular structure and atom-labeling scheme for P(O)(4-F-$C_6H_4C(O)NH)(NC_4H_8O)_2$, compound **4** (50% probability ellipsoids).

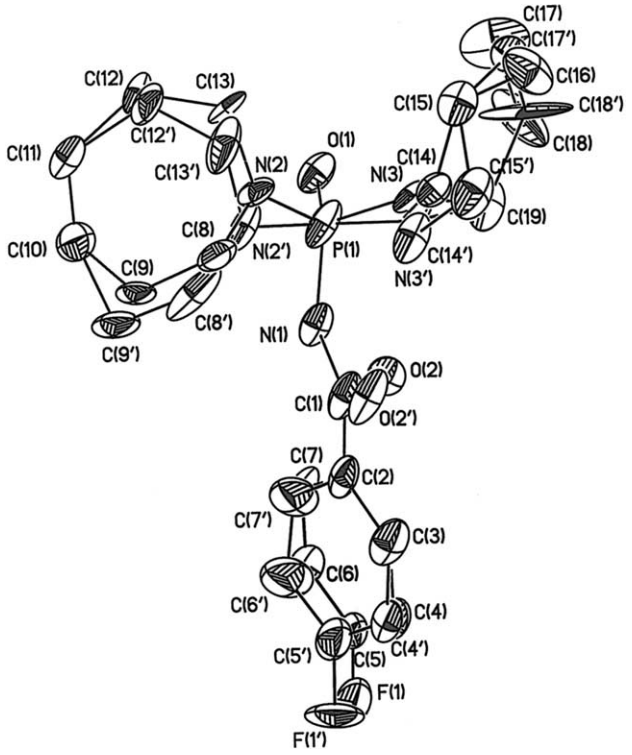

Fig. 5. Molecular structure and atom-labeling scheme for P(O)(4-F-$C_6H_4C(O)NH)(NC_6H_{12})_2$, compound **5** (50% probability ellipsoids).

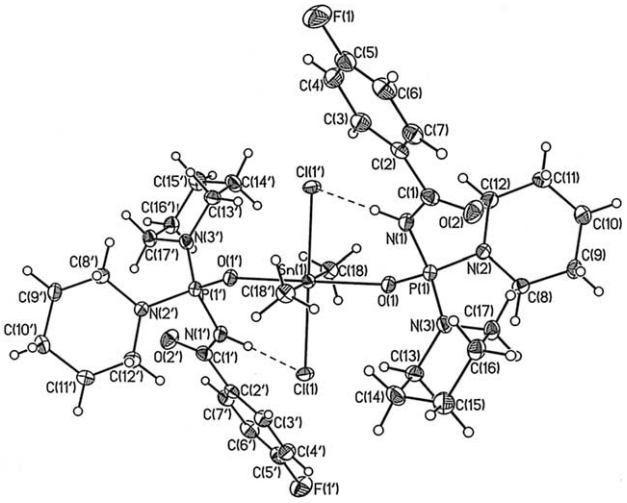

Fig. 6. Molecular structure and atom-labeling scheme for $Sn(CH_3)_2Cl_2[P(O)(4\text{-}F\text{-}C_6H_4C(O)NH)(NC_5H_{10})_2]_2$, compound **8** (50% probability ellipsoids).

C(11)–N(2)–P(1) and C(8)–N(2)–P(1) are 110.39(10)°, 126.80(9)° and 118.78(8)°, respectively, with average 118.7°. The sum of surrounding angles around N(1) and N(3) atoms are 359.99° and 351.69°, respectively. Similar results were obtained for the nitrogen atoms of other structures that confirm the sp^2 hybridization for the N atoms, although due to the repulsion and steric interactions, some angles are greater, and the others are smaller than 120°.

In compound **8**, the structure is symmetric and the central Sn atom has octahedron coordination. The two methyl groups (and also the two phosphoramidates and the two chlorine atoms) are in *trans* positions and the C(18)–Sn(1)–C(18)#1, O(1)–Sn(1)–O(1)#1 and Cl(1)–Sn(1)–Cl(1)#1 bond angles are 180.0° and the C–Sn–O, C–Sn–Cl and O–Sn–Cl bond angles are about 90°, Table 5. The Sn–C bond lengths (both are 2.1238(19) Å) are quite close to those reported in the literature [39]. The Sn–Cl bond lengths are 2.5617(6) Å lying in the normal covalent radii 2.37–2.60 Å [40]. The Sn–O bond lengths are 2.2176(13) Å that are shorter than sum of the van der Waals radii of Sn and O atoms (3.70 Å) [41].

Table 6
Hydrogen bonds D–H···A for compounds **1**, **2**, **4**, **5**, and **8** (Å and °)

Compound	D–H···A	*d*(D–H)	*d*(H···A)	*d*(D···A)	∠DHA
1	N1–H1N···O1 [$-x+1, -y+1, -z$]	0.845	2.001	2.842(2)	173.85
2	N1–H1N···O1A	0.86	1.96	2.818(4)	172
	N1A–H1NA···O1	0.91	1.99	2.886(4)	170
	N1C–H1C···O1B	0.75	2.17	2.912(4)	170
	N1B–H1B···O1C	0.85	2.07	2.916(4)	171
4	N1–H1A···O1 [$-x, y, -z+1/2$]	0.86	2.06	2.904(3)	166
5	N1–H1N···O1 [$-x, -y+1, -z+1$]	0.82	2.02	2.820(4)	165
8	N1–H1N···Cl1 [$-x, -y+2, -z+2$]	0.90	2.50	3.320(2)	152

Table 7
P=O, P–N_{amide}, P–N_{amine} and C=O bond lengths (Å) in compounds with five-, six- and seven-membered ring amine groups

No.	Compound	P=O	P–N_{amide}	P–N_{amine}	C=O
1	4-F-$C_6H_4C(O)N(H)P(O)R^1{}_2$	1.4863(10)	1.6899(11)	1.6239(12), 1.6390(12)	1.2207(16)
2	4-F-$C_6H_4C(O)N(H)P(O)R^2{}_2$	1.480(2), 1.479(2), 1.471(2), 1.475(3)	1.683(3), 1.681(3), 1.670(3), 1. 678(4)	1.625(3), 1.618(3) [conformer 1] 1.625(3), 1.633(3) [conformer 2] 1.636(3), 1.632(3) [conformer 3] 1.633(3), 1.626(3) [conformer 4]	1.223(4), 1.222(4), 1.222(4), 1.229(9), 1.238(10)
4	4-F-$C_6H_4C(O)N(H)P(O)R^3{}_2$	1.4801(17)	1.6839(16)	1.6246(18), 1.6318(18)	1.212(2)
5	4-F-$C_6H_4C(O)N(H)P(O)R^4{}_2$	1.472(2)	1.675(3)	1.626(4), 1.634(3), 1.635(4), 1.641(4) [disordered form]	1.328(4), 1.312(4)
8	$Sn(CH_3)_2Cl_2$[4-F-$C_6H_4C(O)N(H)P(O)R^2{}_2$]$_2$	1.5012(14)	1.6921(17)	1.6260(17), 1.6201(17)	1.222(2)
9[a]	$C_6H_5C(O)N(H)P(O)R^1{}_2$	1.487(3), 1.485(3)	1.679(4), 1.687(4)	1.618(4), 1.625(4) [conformer 1] 1.615(4), 1.618(3) [conformer 2]	1.217(5), 1.207(4)
10[b]	$C_6H_5C(O)N(H)P(O)R^2{}_2$	1.465(12), 1.459(12), 1.461(13), 1.464(13)	1.672(13), 1.690(13), 1.691(14), 1.656(13)	1.614(13), 1.605(15) [conformer 1] 1.615(17), 1.590(15) [conformer 2] 1.644(14), 1.631(14) [conformer 3] 1.623(13), 1.647(14) [conformer 4]	1.235(17), 1.229(17), 1.230(17), 1.236(18)
12[c]	$C_6H_5C(O)N(H)P(O)R^4{}_2$	1.4875(14)	1.6916(16)	1.6369(16), 1.6345(15)	1.227(2)

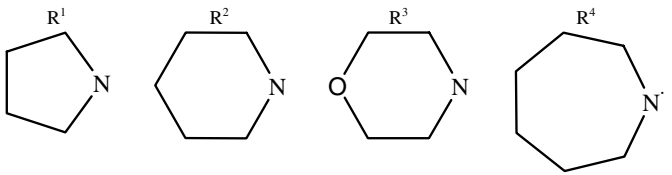

[a] The data of this compound are given in [23].
[b] The data of these compounds are given in [25].
[c] The data of this compound are given in [42].

Appendix A. Supplementary data

Spectroscopic data of compounds **1**–**8** can be obtained as supplementary materials. Crystallographic data for the structures in this paper have been deposited with Cambridge Crystallographic Data Center as supplementary publication nos. CCDC 259182 ($C_{15}H_{21}F_1N_3O_2P_1$), CCDC 259186 ($C_{17}H_{25}F_1N_3O_2P_1$), CCDC 259185 ($C_{15}H_{21}F_1N_3O_4P_1$), CCDC 259184 ($C_{19}H_{29}F_1N_3O_2P_1$) and CCDC 259187 ($C_{36}H_{56}Cl_2F_2N_6O_4P_2Sn_1$). Copies of the data may be obtained on application to CCDC, 12 Union Road, Cambridge CB2 1EZ, UK (fax: +44 1223 336033; e-mail: deposit @ccdc.cam.ac.uk or www: http://www.ccdc.cam.ac.uk). Supplementary data associated with this article can be found, in the online version, at doi:10.1016/j.poly.2005.07.035.

References

[1] W.D. Mallender, T. Szegletes, T.L. Rosenberry, Biochemistry 39 (2000) 7753.
[2] A. Baldwin, Z. Huang, Y. Jounaidi, D.J. Waxman, Arch. Biochem. Biophys. 409 (2003) 197.
[3] Y. Pang, T.M. Kollmeyer, F. Hong, J. Lee, P.I. Hammond, S.P. Haugabouk, S. Brimijoin, Biochem. Biol. 10 (2003) 491.
[4] K.E. Gubina, V.A. Ovchynnikov, V.M. Amirkhanov, H. Fischer, R. Stumpf, V.V. Skopenko, Z. Naturforsch. B 55 (2000) 576.
[5] V.M. Amirkhanov, V.A. Ovchinnikov, A.V. Turov, V.V. Skopenko, Russ. J. Coord. Chem. 23 (2) (1997) 126.
[6] V.A. Trush, K.V. Domasevitch, V.M. Amirkhanov, J. Sieler, Z. Naturforsch. B 54 (1999) 451.
[7] K.E. Gubina, J.A. Shatrava, V.A. Amirkhanov, V.A. Ovchynnikov, V.M. Amirkhanov, Polyhedron 19 (2000) 2203.
[8] V.M. Amirkhanov, V.A. Trush, A.A. Kapshuk, V.V. Skopenko, Russ. J. Inorg. Chem. 41 (1996) 1947.
[9] K. Gholivand, M. Pourayoubi, Z. Shariatinia, H. Mostaanzadeh, Polyhedron 24 (2005) 655.
[10] K. Gholivand, Z. Shariatinia, M. Pourayoubi, Z. Anorg. Allg. Chem. 631 (2005) 961.
[11] K.E. Gubina, V.M. Amirkhanov, Z. Naturforsch. B 55 (2000) 1015.
[12] K.E. Gubina, V.A. Ovchynnikov, V.M. Amirkhanov, T. Yu, Silva, V.V. Skopenko, T. Glowiak, H. Kozlowski, Z. Naturforsch. B 54 (1999) 1357.
[13] E. Wong, C.M. Iandomenico, Chem. Rev. 99 (1999) 2541.
[14] M.J. Clarke, F. Zhu, D.R. Frasca, Chem. Rev. 99 (1999) 2511.
[15] L. Pellerito, L. Nagy, Coord. Chem. Rev. 626 (2001) 161.
[16] A. Matsuno-Yagi, Y. Hatefi, J. Biol. Chem. 268 (1993) 1539.
[17] S.E. Denmark, J. Fu, J. Am. Chem. Soc. 125 (2003) 2208.
[18] M.C. Cassani, M.J. Davis, P.B. Hitchcock, M.F. Lappert, Inorg. Chim. Acta 358 (2005) 1595.
[19] A. Deák, S. Kárpáti, G. Vankó, A. Kálmán, I. Haiduc, Inorg. Chim. Acta 358 (2005) 1012.
[20] R. Zhang, J. Sun, C. Ma, Inorg. Chim. Acta 357 (2004) 4322.
[21] K. Gholivand, M. Pourayoubi, Z. Anorg. Allg. Chem. 630 (2004) 1330.
[22] K. Gholivand, Z. Shariatinia, M. Pourayoubi, Z. Naturforsch. B 52 (2005) 67.
[23] K. Gholivand, M. Pourayoubi, H. Mostaanzadeh, Anal. Sci. 20 (2004) x51.
[24] M.J. Cain, A. Cawley, V. Sum, D. Brown, M. Thornton-Pett, T.P. Kee, Inorg. Chim. Acta 345 (2003) 154.
[25] K. Gholivand, C.O. Vedova, A. Anaraki Firooz, A. Madani Alizadegan, M.C. Michelini, R. Pis Diez, J. Mol. Struct. 750 (2005) 64.
[26] K. Gholivand, S. Ghadimi, H. Naderimanesh, A. Forouzanfar, Magn. Reson. Chem. 39 (2001) 684.
[27] L.B. Krivdin, E.W. Della, Prog. Nucl. Magn. Reson. Spectrosc. 23 (1991) 301.
[28] Bruker, SMART. Bruker Molecular Analysis Research Tool, v. 5.059. Bruker AXS, Madison, WI, USA, 1998.
[29] Siemens (1989). P3 and XDISK. Release 4.1. Siemens AXS, Madison, WI, USA, 1998.
[30] G.M. Sheldrick, SHELXTL v. 5.10, Structure Determination Software Suit, Bruker AXS, Madison, WI, USA, 1998.
[31] G.M. Sheldrick, SADABS v. 2.01, Bruker/Siemens Area Detector Absorption Correction Program, Bruker AXS, Madison, WI, USA, 1998.
[32] L.D. Protsanko, I.A. Avrutskaya, T.N. Dneprova, E. Yu Kodintseva, S.M. Andrianova, P. Ya Sologub, Khim.-Farm. Zh. (Kiev. NII Farmakol. Toksikol., Kiev, USSR) 22 (7) (1998) 803.
[33] C. Ma, J. Sun, Polyhedron 23 (2004) 1547.
[34] C. Ma, Y. Han, R. Zhang, J. Organomet. Chem. 689 (2004) 1675.
[35] V. Mizrahi, T.A. Modro, Crystallogr. Struct. Commun. 11 (1982) 627.
[36] O.N. Rebrova, V.N. Biyushkin, T.I. Malinovski, V.M. Ovrutskii, L.D. Protsenko, T.N. Dneprova, M.D. Mazus, Dokl. AN. SSSR (Russia) 324 (1992) 103.
[37] D.E.C. Corbridge, Phosphorus an Outline of its Chemistry Biochemistry and Technology, 5th ed., Elsevier, Amsterdam, 1995.
[38] D.G. Gilheany, Chem. Rev. 94 (1994) 1339.
[39] C.L. Ma, F. Li, Q. Jiang, R.F. Zhang, J. Organomet. Chem. 689 (2004) 96.
[40] F.H. Allen, S.A. Bellard, M.D. Brice, B.A. Cartwright, A. Doubleday, H. Higgs, T. Hummelink, B.G. Hummelink-Peters, O. Kennard, W.D.S. Motherwell, J.R. Rogers, D.G. Watson, Acta Crystallogr., Sect. B 35 (1979) 2331.
[41] J. Beckmann, M. Henn, K. Jurkschat, M. Schürmann, D. Dakterniek, A. Duthie, Organometallics 21 (2002) 192.
[42] K. Gholivand, Z. Hosseini, M. Pourayoubi, Z. Shariatinia, Z. Anorg. Allg. Chem. 2005, in press.

Available online at www.sciencedirect.com
SCIENCE DIRECT®
Polyhedron 25 (2006) 722–736
POLYHEDRON
www.elsevier.com/locate/poly

Potentiometric, spectrophotometric, theoretical studies and binding properties of a novel tripodal polycatechol-amine ligand with lanthanide(III) ions

Suban K. Sahoo, Minati Baral *, B.K. Kanungo

Department of Chemistry, Sant Longowal Institute of Engineering and Technology, Longowal, Sangrur, Punjab 148106, India

Received 15 June 2005; accepted 26 July 2005

Abstract

A new tripodal ligand *cis*,*cis*-1,3,5-tris[(2,3-dihydroxybenzylamino)aminomethyl] cyclohexane (TMACHCAT), bearing three catechol units attached to a tris-methylaminocyclohexane (TMACH) ring has been synthesized and characterized by elemental analyses, UV–VIS, IR and ^{1}H NMR spectral data. The lowest energy molecular geometry of TMACHCAT was obtained through empirical followed by quantum mechanical treatment. Theoretical UV–VIS, IR and ^{1}H NMR spectral data were calculated from the energy-minimized structure by applying semi-empirical ZINDO, PM3 and TNDO/2 method, respectively and compared with the experimental data. The complexation behaviour of the ligand with H^+, La(III), Gd(III) and Lu(III) in an aqueous medium of 0.1 M KCl at 25 ± 1 °C was studied by potentiometric and spectrophotometric methods. Six protonation constants were determined for the ligand and used as input data to evaluate the formation constants of the metal complexes. The formation of complexes between the partially protonated ligand and lanthanide ions of the types MLH_3, MLH_2, MLH, ML_2H_6 have been observed. The solution structures of the metal complexes were proposed through experimental evidences along with the calculated minimum strain energy through molecular mechanics calculation using CAChe's augmented MM3 force field.
© 2005 Elsevier Ltd. All rights reserved.

Keywords: Tripodal polycatechol-amine ligand; Lanthanum; Gadolinium; Lutetium; Protonation constants; Formation constants; Molecular mechanics and semi-empirical method

1. Introduction

Lanthanide (III) coordination chemistry has recently received growing interest because of the numerous applications of lanthanide (III) complexes, such as relaxation agents in nuclear magnetic resonance imaging [1], luminescent probes in biology and medicine [2] or catalysts for the cleavage of RNA and DNA [3,4]. While dealing with such applications, the greatest interest is focused on the use of these complexes, gadolinium compounds in particular, as contrast agents in magnetic resonance imaging (MRI) [5], due to its effective magnetic moment and electronic relaxation time associated with the f^7 configuration. For this purpose, the most stringent requirement is high thermodynamic stability and possibly kinetic inertness, which can be achieved by complexation of suitable designed ligands. Much of this work has been based on the application of gadolinium complexes of poly(aminocarboxylate) ligands such as Gd-DTPA (DTPA = diethylenetriaminepentaacetic acid) [6] and Gd-DOTA (DOTA = 1,4,7,10-*N*,*N*′,*N*″,*N*‴-tetraacetic acid) [7] and their derivatives [8]. Recently, efforts have been taken to synthesize multidentate tripodal ligands because of their intermediate chelation between open chain ligands and those based on macrocycles, where metal can be encapsulated by three arms of the suitably designed ligand [9–12]. Among such ligands,

* Corresponding author. Tel./fax: +91 1672284840.
E-mail address: minatik@vsnl.net (M. Baral).

0277-5387/$ - see front matter © 2005 Elsevier Ltd. All rights reserved.
doi:10.1016/j.poly.2005.07.039

the natural occurring siderophore, enterobactin has a tripodal architecture with one catechol binding unit in each arm [13,14] shows the highest binding constants [15]. This led not only to model it through simple artificially synthetic molecules for the ultimate development of iron removal drugs for therapeutic use [16] and to mimic the various biological functions such as redox, spectroscopic, binding or assimilation [17] but also the study of the coordination chemistry of catechol-based ligands with 3d transition elements [18], trivalent group 13 metal ions [19], actinides [20] and trivalent lanthanides [21,22].

Again, the complexation of lanthanide ions in aqueous medium has been studied mostly with carboxylato- and phosphonato-oxygen donors because of their oxoplilicity [23]. Very less attention has been given to the phenolato-group as anionic oxygen donor for these metal ions [24,25]. The main reason why the coordination of lone phenol is hindered is the weak acidity of the hydroxy group (pK_a of phenol ~10) [24] and since the lanthanide aqueous ions are themselves weak Lewis acids, they generally cannot compete with the hydrogen ion for complexation of phenol in water and precipitate as hydroxides above pH 8. Thus, a ligand containing only amines and phenols could not be expected to be a particularly good ligand for aqueous lanthanide chelation as it should simply be too basic. Nevertheless, it has been reported that introduction of phenol groups into a well-preorganized structure allows the ligand to form strong lanthanide (III) complexes [25,26]. Coordination chemistry of different sulfonated water soluble tripodal amino-phenolate ligands tris-((2-hydroxy-5-sulfobenzylamino)ethyl)amine (TRNS), 1,1,1-tris-(((2-hydroxy-5-sulfobenzyl)amino)-methyl)ethane (TAMS), 1,2,3-tris-((2-hydroxy-5-sulfobenzyl)amino)propane (TAPS) have been investigated by Orvig et al. in solution where it was found that Ln(III) was encapsulated by podands possessing short and rigid tripods to give $[Ln(TAPS)]^{3-}$ and $[Ln(TAMS)]^{3-}$, while the more flexible TREN spacer in TRNS prevented regular wrapping of the chelating side arms around Ln(III), thus leading to monocapped $[Ln(H_3TRNS)(H_2O)_x]$ and bicapped $[Ln(H_3TRNS)_2]^{3-}$ podates (Fig. 1) [25,26]. Recently, Di Bernardo and others suggested that introduction of catechol group in tris((2,3-dihydroxybenzyl-amino)ethyl) amine (TRENCAT) as binding units instead of phenolate donor showed high complexing ability towards lanthanide metal ions at nearly physiological pH [27,28].

Based on these above facts we were interested to study the coordination behaviour of a new polycatechol-amine ligand by changing the spacer unit TREN into a cyclohexane based tripod tris-aminomethylcyclohexane (TMACH), which is expected (i) to increase the degree of freedom and flexibility of podants and (ii) to reduce the steric constraints within the tripod thus favouring regular wrapping of the binding side arms. Thus, in this communication, we present the synthesis and structural characterization of a multidentate tripodal ligand *cis*,*cis*-1,3,5-tris[(2,3-dihydroxybenzyl-

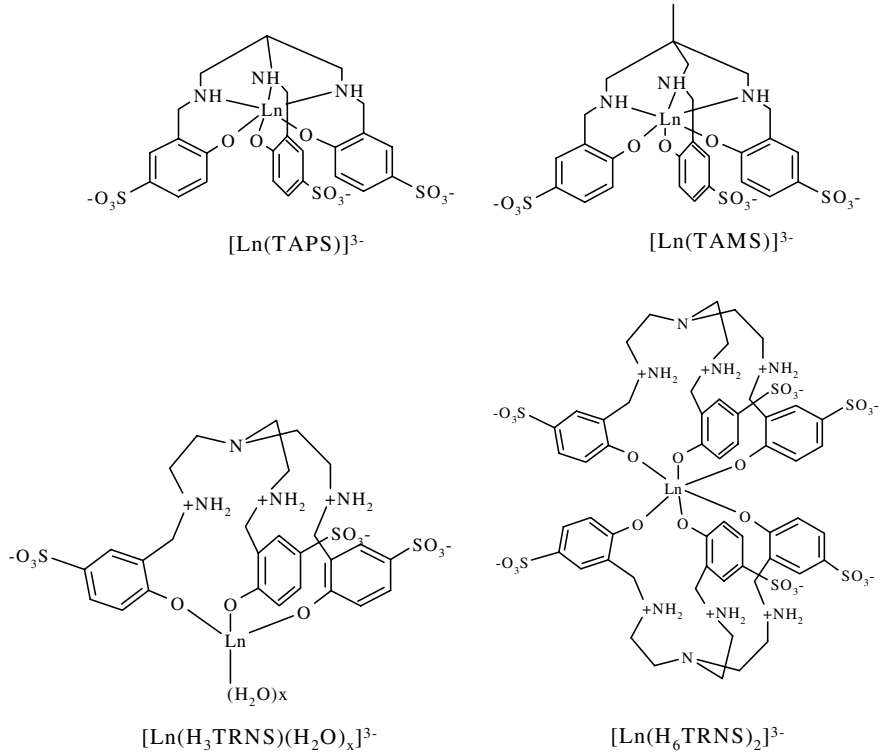

Fig. 1. Coordination modes of lanthanide metal ions with different tripodal aminophenolate ligands in solution.

amino)aminomethyl]cyclohexane (TMACHCAT) having three catechol units linked through methylene moieties to the backbone of TMACH. We were also interested to study the coordination behaviour of the ligand with some lanthanide ions in aqueous solution to see if coordination geometries are function of pH and whether phenolato coordination could provide an anchoring effect, which would enable the amine nitrogen atoms to coordinate in water. The complexation behaviour of the newly synthesized ligand towards La(III), Gd(III) and Lu(III) in water and the solution structures of the metal complexes were proposed through the molecular modeling calculations.

2. Experimental

2.1. Materials and measurements

The compound *cis*,*cis*-1,3,5-tris(methylamino)cyclohexane (TMACH) was synthesized as in Scheme 1 [29]. All chemicals: 1,3,5-benzenetricarboxylic acid, platinum dioxide, lithiumaluminiumhydride, *p*-toluenesulphonyl chloride, sodium azide, 2,3-dihydroxybenzaldehyde and sodiumborohydride were obtained from Sigma–Aldrich and used directly. Nitrate salts of lanthanides (purity > 99.9%) were obtained from Indian Rare Earths Ltd., India. The absolute ethanol (99.9%) was obtained from Les Alcools Commerce Inc., Canada. Dry solvents (methanol and THF), KOH, HCl, KCl were obtained from Ranbaxy Chemicals Ltd., India.

Proton and ^{13}C NMR spectra were recorded on a Brucker DPX-300 spectrometer in $CDCl_3$ or D_2O and chemical shifts were reported relative to Me_4Si. IR (KBr pellets, 450–4000 cm^{-1}) spectra were recorded on Perkin–Elmer RX I FT-IR spectrometer. The electronic spectra were recorded on an Agilent-8453 diode array spectrometer. Elemental analyses were determined for C, H and N using the Exeter Analytical CE-440. FAB mass spectra were recorded on a Jeol-SX-102 spectrometer.

2.2. Synthesis of cis,cis-1,3,5-tris(methylamino)-cyclohexane

cis,*cis*-1,3,5-Tris(methylamino)cyclohexane was synthesized as per Scheme 1 [29]. Mass spectra (CI+): $m/z = 172$ (calc. 171.3); ^1H NMR (D_2O, δ ppm): 0.53 (3H, q, CH_2 axial), 1.41 (3H, m, CH_2 equatorial), 1.75 (3H, d, CH axial), 2.44 (6H, d, CH_2 of $–NH_2$); ^{13}C NMR (D_2O, δ ppm): 34.38 (ring CH_2), 39.38 (ring CH), 47.57 (CH_2 of NH_2).

2.3. Synthesis of cis,cis-1,3,5-tris[(2,3-dihydroxy-benzylidene)aminomethyl]cyclohexane (L′)

To a magnetically stirred solution of TMACH (0.3 g, 1.75 mmol) in 10 ml absolute ethanol, 2,3-dihydroxybenzaldehyde (0.75 g, 5.43 mmol) in 5 ml absolute ethanol was added drop wise. A bright yellow precipitate obtained, which was filtered off and washed with cold ethanol followed by ether and then dried in vacuum.

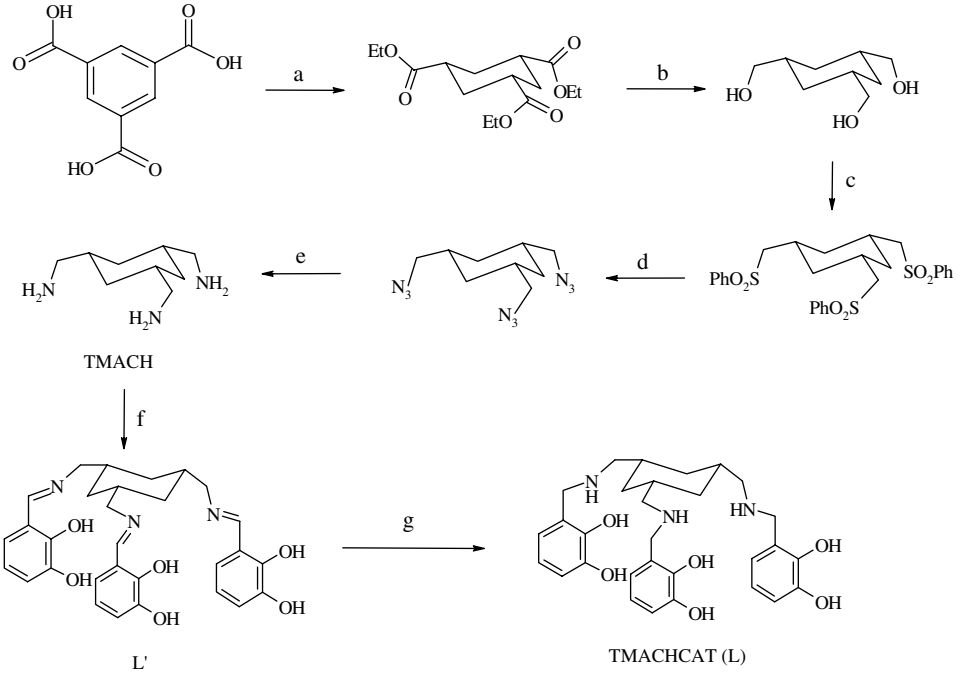

Scheme 1. Reagents and conditions: (a) (i) EtOH, dry HCl and (ii) PtO_2/H_2, room temp, 24 h; (b) (i) $LiAlH_4$, dry THF; (c) $PhSO_2Cl$; (d) NaN_3; (e) $LiAlH_4$, dry THF; (f) 2,3-dihydroxybenzaldehyde/EtOH; (g) $NaBH_4$/MeOH, conc. HCl/MeOH.

Yield = 92%; IR (KBr pellet, cm^{-1}): 3401, 2918, 2833, 2717, 1632, 1596, 1508, 1458, 1384, 1363, 1276, 1227, 1163, 853, 777, 739; ^1H NMR ($CDCl_3$, δ ppm): 0.84 (3H, q), 1.81 (3H, b), 1.93 (3H, d), 3.49 (6H, d), 8.24 (3H, s), 6.60 (3H, t), 6.77 (3H, d), 6.88 (3H, d); ^{13}C NMR ($CDCl_3$, δ ppm): 34.21, 37.52, 62.98, 116.47, 116.63, 121.37, 145.74, 153.05, 164.86; Mass spectrum (FAB): $m/z = 532$.

2.4. Synthesis of cis,cis-1,3,5-tris[(2,3-dihydroxybenzylamine)aminomethyl]cyclohexane (L)

To a suspension of L′ (0.699 g, 1.31 mmol) in 50 ml dry methanol, sodium borohydride (0.155 g, 4.09 mmol) was added with stirring over a period of 2 h under N_2 atmosphere. When the solid phase disappeared and the solution became colourless, an excess of conc. HCl in methanol was added and kept overnight at −40 °C. A white residue was removed by filtration. The solvent was evaporated under reduced pressure. The crude product obtained was dissolved in dry methanol and evaporated. This process was repeated thrice. Then, the residue was dissolved again in dry methanol and to it decolourizing charcoal was added which was filtered after vigorous shaking. When the solvent was evaporated under reduced pressure, a white product was obtained, which was dried under vacuum. Yield = 77%; IR (KBr pellet, cm^{-1}): 3401, 3230, 2923, 2831, 2715, 1597, 1508, 1479, 1384, 1361, 1285, 1208, 836, 776, 738; ^1H NMR (D_2O, δ ppm): 0.79 (3H, q), 1.77 (3H, d), 1.86 (3H, b), 2.90 (6H, d), 4.17 (6H, s), 6.78 (3H, t), 6.84 (3H, d) and 6.94 (3H, d); Elemental analysis: *Anal.* Calc. for $C_{30}H_{39}N_3O_6 \cdot 3HCl \cdot 2H_2O$: C, 52.85; H, 6.81; N, 6.17. Found: C, 52.67; H, 6.82; N, 6.14%.

2.5. Titration procedure

The protonation constants of the ligand and the formation constants of the metal complexes were determined by potentiometric and spectrophotometric titrations at 25 ± 1 °C maintained from a double wall glass jacketed titration cell connected to a constant temperature circulatory bath. For all titrations, the observed pH was measured as $-\log[H^+]$ using a ThermoOrion $720A^+$ pH meter equipped with a combined glass electrode. The electrode was calibrated to read pH according to the classical method [30]. A standard hydrochloric acid solution was titrated with a standard KOH solution and the calculated hydrogen ion concentrations ($pK_w = 13.77 \pm 0.05$) was used to convert the pH-meter reading to hydrogen ion concentration.

All solutions were prepared prior to the experiments in double distilled deoxygenated water. KOH solution of 0.1 M was prepared and standardized against potassium hydrogen phthalate. HCl solution (0.1 M) was prepared and standardized against standard KOH. The ionic strength was maintained at 0.1 M by adding appropriate amount of 1 M KCl. Solutions of 0.01 M ligand and 0.01 M metal ions were also prepared in deoxygenated water. Final concentration of ligand (1×10^{-3}M) and metal (1×10^{-3}M and 5×10^{-4}M) were maintained for the different titrations. Following titrations with metal-to-ligand molar ratios: $C_M/C_L = 0{:}1$; $C_M/C_L = 1{:}1$, 1:2 (M = La^{+3}, Gd^{+3} and Lu^{+3}) were carried out. The protonation constants of the ligand and the formation constants of the metal complexes were determined using computer program Hyperquad 2000 [31].

The apparatus and method used for the potentiometric and spectrophotometric titrations are very similar except dilute solutions of ligand (4.02×10^{-5}M) and metal ions (4.02×10^{-5}M or 2.02×10^{-5}M) were used. After each adjustment of pH, an aliquot was removed and spectra were recorded. The protonation constants and formation constants were calculated by global fitting of the whole spectral data using a non-linear least-square fitting program, pHAb [32].

2.6. Molecular modeling calculation

All calculations were carried out on a Pentium IV 3.0 GHz machine on windows 2000 environment using the computer program CAChe version 6.01 [33] and/or GAUSSIAN-03 [34]. The initial geometry of TMACHCAT leading to minimum strain energy was achieved through molecular mechanics calculation using MM3 force field and then reoptimized by semi-empirical PM3 self-consistent fields (SCF) method, at the Restricted Hartree–Fock (RHF) level. The geometry optimizations were obtained by the application of the Polak–Ribiere method with convergence limit of 0.0001 kcal/mol and RMS gradient of 0.001 kcal/mol. The full vibrational analysis was carried out for the various acid–base species of TMACHCAT to obtain the free energy in vacuo by applying semi-empirical PM3 Hamiltonian. The ^1H NMR of TMACHCAT was calculated through TNDO/2 (Typed Neglect of Differential Overlap) semi-empirical method (with convergence limit 0.001 and maximum iterations 50) using the program HyperNMR Version 7.0 [35].

The structures of the lanthanide complexes were optimized through the molecular mechanics calculation using CAChe augmented MM3 force field. CAChe's augmented force field automatically estimates any missing parameters for any element in the molecule. These estimated parameters will be less accurate than either MM2 or MM3, however it allows calculations on structures containing any element up to 103. A coordination scan [36] was tried for the species MLH_3 but no suitable curve was obtained to ascertain the coordination number. Hence, based on the available literature [37], a nine-coordinated structure was drawn for the metal

complexes for optimization. Both equatorial and axial conformer for the ligand was taken for optimization for each metal complex.

3. Results and discussion

3.1. Ligand synthesis

The synthetic procedure of TMACHCAT is given in Scheme 1. The reduced TMACHCAT was tried to isolate in its organic-form by precipitating the crude reduced product in aqueous NH_4OAc/NH_4Cl, but it was found that the catechol groups got oxidized in basic conditions giving light pink colour. So the ligand was isolated as hydrochloride salt and care was taken to avoid contact with atmosphere throughout the procedure. The compound is highly hygroscopic, soluble in water, methanol and ethanol but insoluble in chloroform, ether and acetonitrile. The ligand was characterized on the basis of elemental analyses, electronic, IR, ^{1}H NMR spectral data (Fig. 2(a)).

The infrared spectra of L′ showed strong band at 1632 cm^{-1}, characteristic of imine Schiff base. Upon reduction, infrared spectrum of L (Fig. 3(a)) showed the disappearance of the characteristic imine C=N band at 1632 cm^{-1} and appearance of a new band at 3230 and 1497 cm^{-1} were observed from N–H stretching and bending vibrations, respectively. These observations confirm that the C=N bonds were reduced to the –NH–CH_2– linkage. The ligand (L) showed a broad ν_{O-H} stretching vibration at 3401 cm^{-1}. This is an indication for intramolecular hydrogen bonding, because the normal position for stretching vibration of non-hydrogen bonded or free hydroxyl group absorbs strongly in the range of 3700-3584 cm^{-1} [38]. The deformation δ_{O-H} peaks were observed at 1384 and 1361 cm^{-1}. The bands observed at 1208 cm^{-1} was attributed to ν_{C-O}. Aromatic carbon–carbon stretching vibrations were observed at 1597 and 1508 cm^{-1}, whereas two bands at 836 and 776 cm^{-1} were assigned for ring substituted bending vibration and one band at 738 cm^{-1} obtained for ring bending vibration. Theoretical infrared spectrum of L calculated using semi-empirical PM3 Hamiltonian is shown in Fig. 3(b) and assignment was made through the structural animation at every peak. The PM3 force field is the most widely used functional for predicting infrared spectrum compared to other semi-empirical methods [39]. The computed vibrational frequencies in comparison to the experimental values showed the closest correspondence for bending vibrations but slightly higher values were noted for stretching vibrations. However, the trends are consistent with the experiment and helpful for interpreting the different modes of vibrations.

Experimental ^{1}H NMR spectra of L′ displayed a resonance signal at 8.25 ppm due to imine hydrogens. Upon reduction, the characteristic imine band disappeared and the ^{1}H NMR spectra of TMACHCAT (Fig. 4(a)) showed the presence of benzylic signals at 4.17 ppm. The spectrum showed three distinct peaks for the three different kinds of protons found in cyclohexane ring. A quartet and doublet was obtained at 0.73 and 1.77 ppm for the axial and equatorial protons attached with the three methylene groups, respectively, whereas a broad peak at 1.86 ppm was observed for the three axial protons attached with the appended groups in the cyclohexane ring, which confirm the *cis,cis*-configuration for TMACHCAT. Theoretical ^{1}H NMR spectrum of TMACHCAT obtained from the PM3 optimized structure through semi-empirical TNDO/2 method is shown in Fig. 4(b). Due to virtual memory problem, after calculating shielding constant and chemical shift, only the noted 14 protons were considered for calculation of the spectrum. The methylene protons in cyclohexane ring shows two peaks in the spectrum at 2.97 and 3.26 ppm for the axial and equatorial protons,

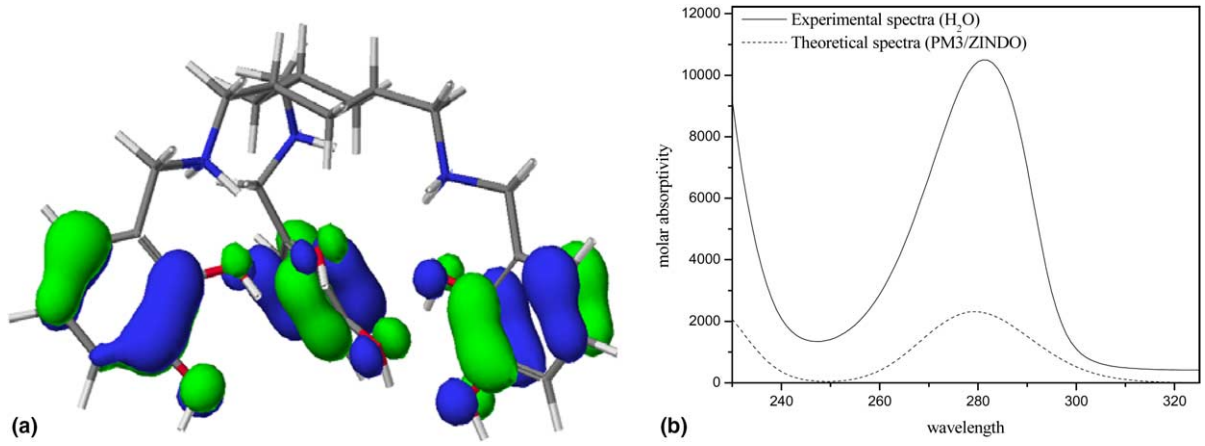

Fig. 2. (a) The HOMO molecular orbital diagrams at λ_{max} 279 nm (calculated applying semiempirical ZINDO method and (b) experimental and theoretical spectra for TMACHCAT.

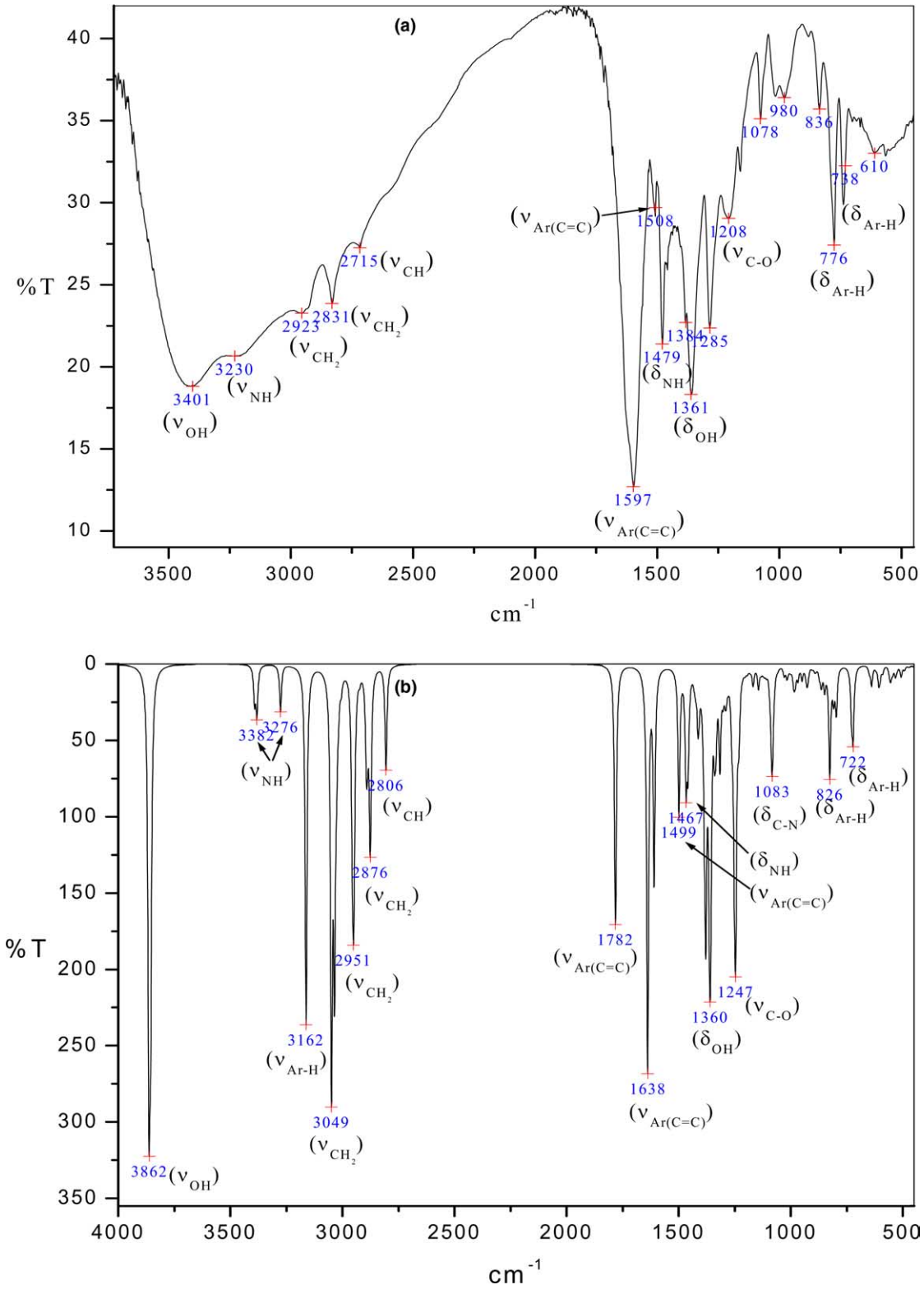

Fig. 3. Infrared spectrum of TMACHCAT: (a) experimental (KBr pellet) and (b) calculated (applying semi-empirical PM3 method).

respectively, whereas peak at 3.48 ppm was observed for the methine protons. The two peaks for the methylene groups one attached to cyclohexane ring and another to benzene ring were observed at 4.36 and 4.77 ppm, respectively. Three peaks for aromatic protons were observed at 6.62, 7.13 and 7.38 ppm. The calculated peaks for hydroxyl (H_{13}, H_{14}) and amine protons (H_1, H_5) were not observed experimentally.

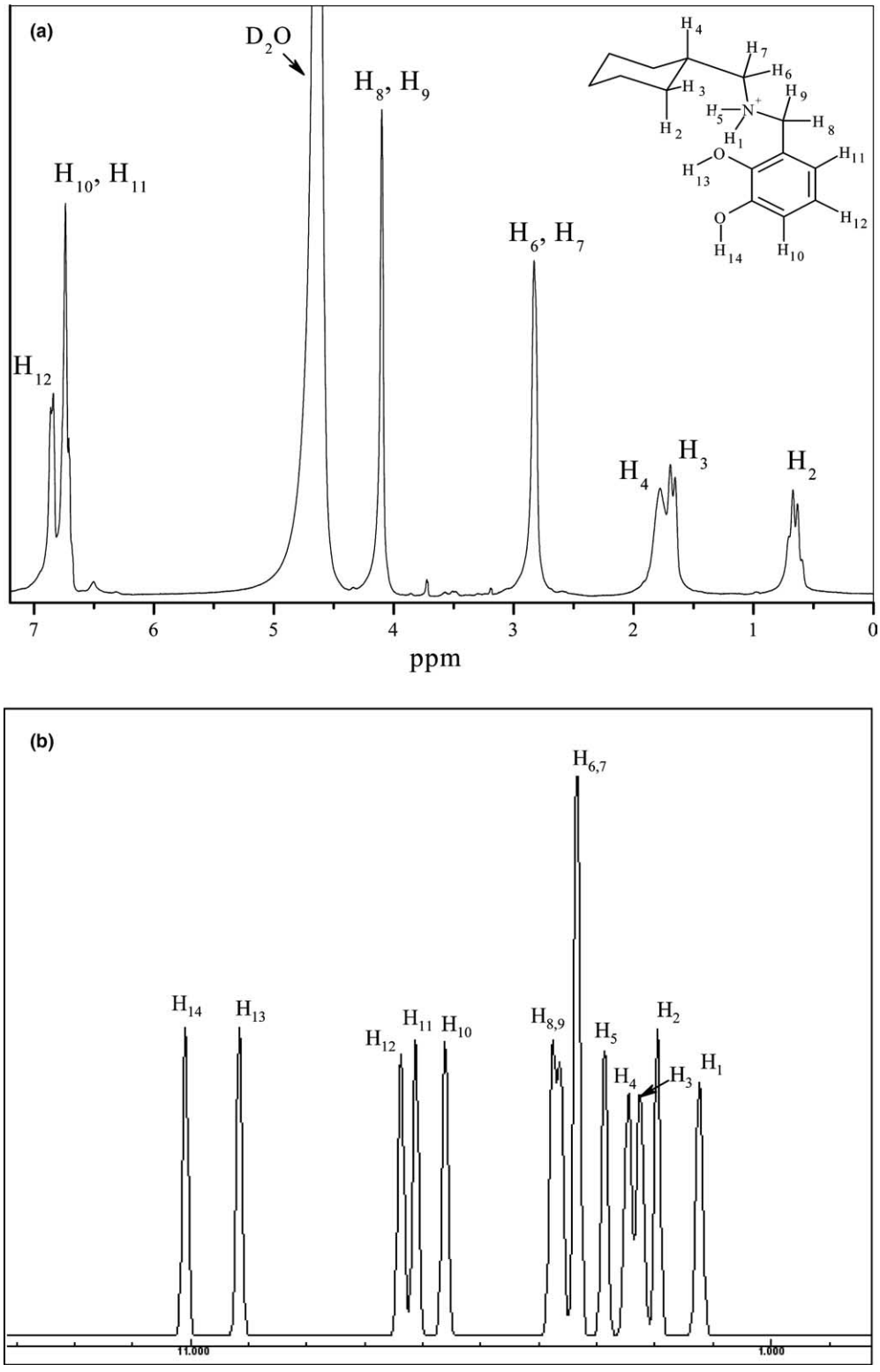

Fig. 4. ^{1}H NMR spectrum of TMACHCAT: (a) experimetral (D_2O, 300 MHz) and (b) calculated (applying semi-empirical TNDO/2 method).

Theoretical ^{1}H NMR chemical shifts gave qualitative trends although the values are not in quantitative agreement with the experiment measurements.

The trihydrochloride salt of the ligand in aqueous medium exhibits only one peaks at 281 nm attributed to $\pi \rightarrow \pi^*$ transitions associated with the chromophoric phenyl ring. Calculated electronic spectrum of TMACHCAT from PM3 (RHF) optimized structure by employing semi-empirical ZINDO method showed peaks with λ_{max} at 279 nm. The optimize structure along

with the HOMO at 279 nm is shown in Fig. 2(a) and the experimental and theoretical spectra are shown in Fig. 2(b).

3.2. Ligand protonation constants

The potentiometric titration of the ligand was carried out by adding excess measured amount of standard HCl to the ligand and titrating against standard KOH at $\mu = 0.1$ M KCl and 25 ± 1 °C in aqueous medium. The titration curve of the ligand is given in Fig. 5. Though upon addition of KOH deprotonation occurs, representation of the acid dissociation constants (K_a) in stability study usually expressed in terms of proton-ligand formation constant or protonation constant (Eq. (1)), and also used in the present communication. Analysis of the potentiometric titration curve using the program Hyperquad 2000 gave best fit for six protonation constants (Table 1) for the ligand as proposed by the Eq. (1) (charges are omitted for clarity):

$$LH_{n-1} + H \rightleftharpoons LH_n, \quad K_{1n} = \frac{[LH_n]}{[LH_{n-1}][H]} \tag{1}$$

The ligand TMACHCAT is a potentially hexa-protic acid. However, due to very low acidity of catechol ($pK_{a1} = 9.13$, $pK_{a2} = 13.00$) [24] subunits it is to be considered as a triprotic acid. In fact, in the present experimental conditions adopted here (pH < 11) only one of the two acidic functions of catechol can be deprotonated, while a very high basic condition is required to deprotonate the second one. It was possible to determine only the protonation constants of the secondary amino groups and three of the phenolic oxygens of the ligand.

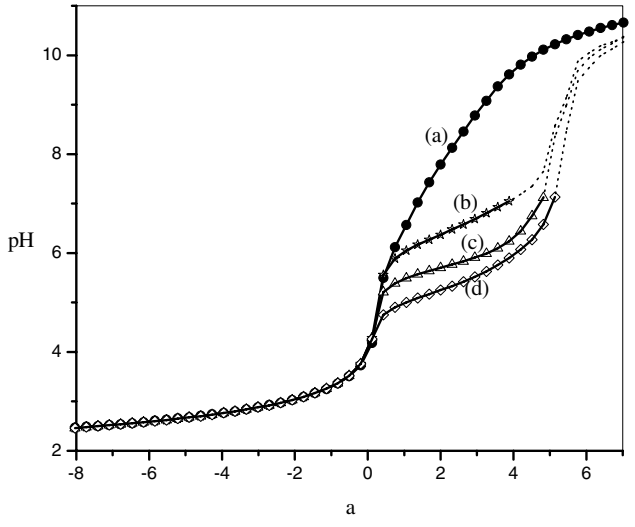

Fig. 5. Potentiometric titration curves of TMACHCAT in absence (a) and presence of metal ions (b) La(III), (c) Gd(III) and (d) Lu(III) in 1:1 ligand–metal molar ratio, where '*a*' is moles of base added per mole of ligand present (symbols and solid lines indicate the experimental values and simulated results, respectively).

Table 1
Protonation constants (log *K*) of TMACHCAT at 25 °C and $\mu = 0.1$ mol dm^{-3} (A = potentiometry and B = spectrophotometry)

TMACHCAT	TRENCAT	TRNS	TMACH	TREN	TACH	TAME	TAP	Proton type	TACS	TAMS	TAPS	Proton type
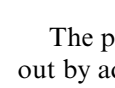	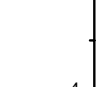			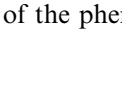	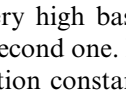	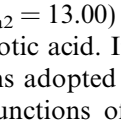	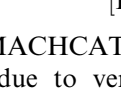		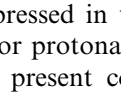	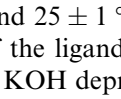	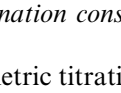	
A	A	A	A	A	A	A	A		A	A	A	
11.26 ± 0.04	11.21 ± 0.05	11.23	11.2	10.53	10.13	10.16	10.16	9.64	N–H	11.24	11.19	11.24	N–H
10.65 ± 0.02	10.65 ± 0.02	10.61	10.6	9.84	9.43	8.66	8.25	7.98	N–H	9.84	9.81	9.77	N–H
9.80 ± 0.03	9.79 ± 0.05	9.75	9.59	8.88	8.41	7.17	5.85	3.72[i]	N–H	8.95	8.91	8.73[i]	O–H
8.48 ± 0.03	8.47 ± 0.03	8.51	8.07						O–H	7.85	7.95	7.78	O–H
7.61 ± 0.06	7.60 ± 0.04	7.58	7.29						O–H	7.08	6.56	6.54	O–H
6.23 ± 0.03	6.22 ± 0.02	6.32	6.17						O–H	6.01	2.92	1.7[i]	N–H

The superscript i refer to the shorter arms.

Accordingly, the neutral TMACHCAT is addressed as LH_3 and the fully protonated form is considered as LH_6^{+3}. The simulated titration curve obtained using the results (Table 1) for the ligand titration is given as solid line whereas experimental titration data are marked as • in Fig. 5. There is a close agreement of the above two. The titration curve for ligand showed a sharp inflection at $a = 0$, where 'a' is moles of base added per mole of ligand present, which is due to the neutralization of excess hydrogen ions whereas other sharp inflection was observed for deprotonation from –OH or $-NH_2^+$ groups. The species distribution diagram of TMACHCAT as a function of pH (Fig. 6) indicates that in acidic solution TMACHCAT initially exists 100% in the fully protonated form as LH_6 below pH < 4.5. As the pH is increases, deprotonation starts with formation of LH_5 which exists between pH 5–8 with maximum concentration (75%) at pH ~ 7. The other species LH_4, LH_3, LH_2 and LH are formed and successively with increase in pH and show maximum concentration of 55%, 75%, 55% and 40% at pH ~ 8, ~9, ~10 and ~11, respectively.

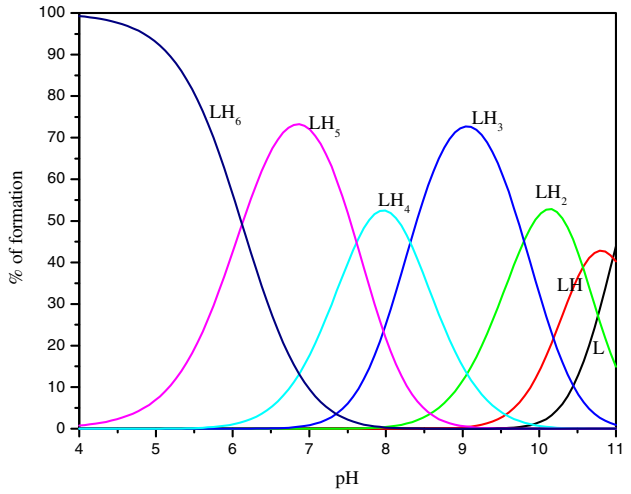

Fig. 6. pH-dependent species distribution curves for TMACHCAT.

The protonation constants of the ligand were also determined by spectrophotometric method. The electronic spectra (220–400 nm) of the ligand were recorded in the pH range 4.29–10.32 and given in Fig. 7(a). Inclusion of whole range of data resulted six protonation constants (Table 1). The predicted electronic spectra of the ligand at various experimental pH ranges are given in Fig. 7(b) and agreeable with the experimental one (Fig. 7(a)) while that of all the species whose protonation constants have been determined and the protonated ligands are given in Fig. 8. The state of equilibrium between deprotonated ligand and protonated ligand was examined from the shifting of peaks towards longer wavelength and formation of isosbestic points. No appreciable change in the electronic spectra was observed below the experimental pH < 4.29 and the spectra overlapped with each other. As the pH increases, the spectra showed a bathochromic shift in the absorption band from 281 nm (assigned for $\pi \rightarrow \pi^*$ transitions) to 292 nm and a concomitant increase in absorbance. The shifting was continued till pH 8.27 and between this, the spectra showed two isosbestic points at 270 and 283 nm. Calculation by exclusion of spectra above pH 8.27 gave only three protonation constants, which may be due to the basic $-O^-$ groups of catechol. Since the catechol group is the only significant

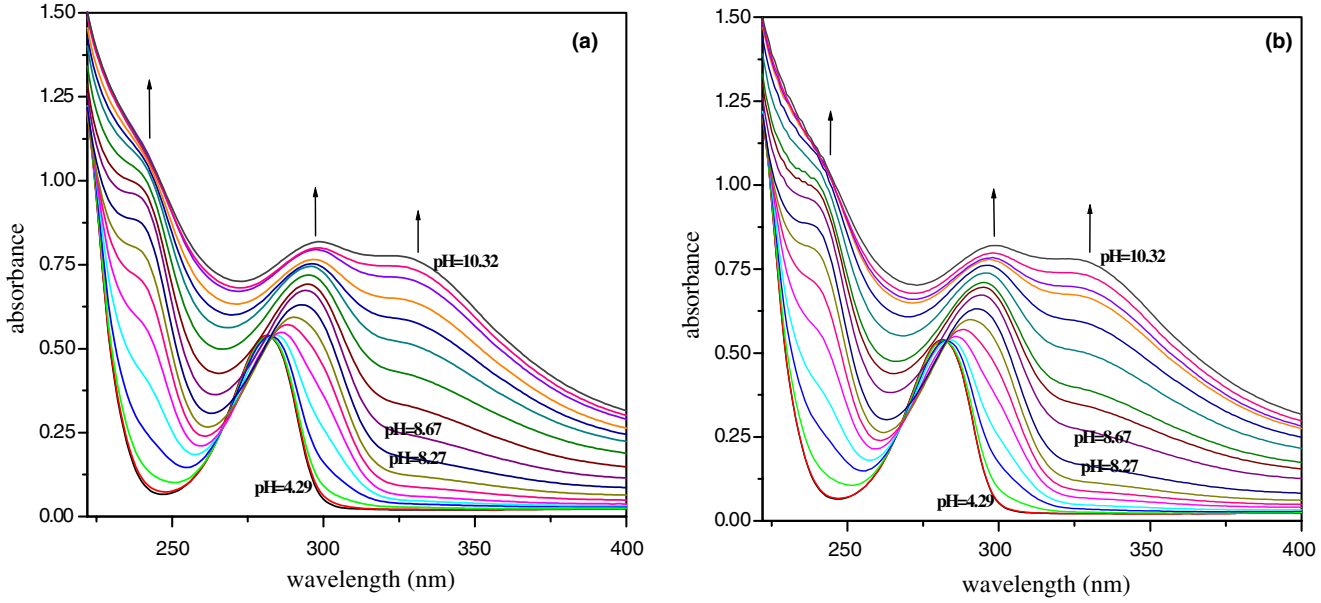

Fig. 7. (a) Experimental electronic spectra and (b) predicted electronic spectral data of TMACHCAT as a function of pH (4.29–10.32) during a spectrophotometric titration: [TMACHCAT] = 0.041 mM; [KCl] = 0.1 M and $T = 25 \pm 1$ °C.

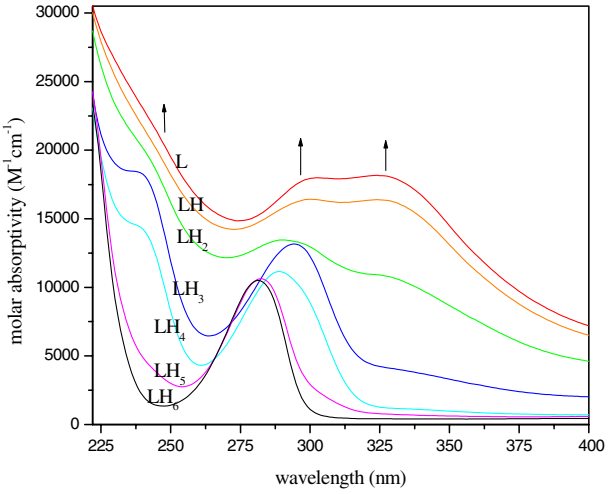

Fig. 8. Electronic spectra of the seven species as a function of molar absorptivity and wavelength predicted from pHAb using experimental data for TMACHCAT.

chromophore in TMACHCAT, any major change in the electronic spectra is attributable to deprotonation from any one of the hydroxy groups, which can able to provide additional opportunity for charge delocalization and thus providing smaller energy increments for transition to excited state. Further, as the deprotonation started from $-NH_2^+$ groups above pH 8.27, no more isosbestic points were observed for the spectra and shifted hyperchromically.

Table 1 summarizes the protonation constants of TMACHCAT along with the related compounds TRENCAT [27], TRNS [40], TAMS [40], TAPS [40] and TACS [40] and their parent tripodal amine TMACH [41], TREN [24], TACH [42], TAME [43] and TAP [44] for comparison. The first three values for TMACHCAT are similar with TRENCAT and TRNS (assigned for deprotonation from –NH– group), while differences are observed for pK_{a3} with TAPS, TACS and TAMS (assigned for deprotonation from OH group). It has been suggested by Orvig et al. that [40], if the parent amine has a $pK_a < 8$, the first deprotonation takes place from amine group followed by phenolic –OH, whereas when $pK_a > 8$ in the parent amine becomes elevated in the corresponding amine phenol. This hypothesis also indicates that in TMACHCAT, the deprotonation reactions started from catecholic –OH groups. Thus, the first three protonation constants viz., 11.26, 10.65 and 9.80 correspond to the secondary amino groups (–NH–) and the next three values viz., 8.48, 7.61 and 6.23 for the protonation of phenolate ($-O^-$) groups of the three catechol units; the later is clearly shown by variable pH UV spectroscopy where, between pH 4.24 and 8.27 there is a bathochromic shift in absorption maxima typical of phenols. Although the protonation constants for the amino groups of TMACHCAT, TRENCAT and TRNS are very similar, these values are higher than their parent amine TMACH and TREN and also the protonation constants for the phenolic groups of TMACHCAT (also for TRENCAT and TRNS) are lower than the 4-sulfophenol ($pK_{1a} = 8.60$) and catechol ($pK_{1a} = 9.13$). This significant difference in the values of protonation constants may be due to the formation of strong ion-hydrogen bonds between the protonated amine and the closest deprotonated phenolate ions. Further, the difference in basicity of the hydroxyl groups for TMACHCAT with respect to catechol ($\Delta \log K = 9.13 - 8.48 = 0.65$) is similar to TRENCAT ($\Delta \log K = 9.13 - 8.51 = 0.62$) but larger than TRNS as compared to with 4-sulfophenol ($\Delta \log K = 8.60 - 8.07 = 0.53$) can be attributed for the formation of secondary hydrogen bonding between the phenolate and the phenolic groups in each catechol units. These observations indicate that the farthest hydroxyl groups are unaffected by change of pH.

In order to verify the validity and assignment made for the experimental protonation constants, gas-phase free energy for the entire representative species was calculated through semi-empiric PM3 quantum mechanical approach. For an acid species AH, the pK_a defined as the negative logarithm of the dissociation constant of the reaction $AH = A^- + H^+$, is given by the thermodynamics relation $pK_a = \Delta G_{gas,AH}/2.303RT$. The change in free energy in gas phase is obtained according to the following equation:

$$\Delta G_{gas,AH} = (G_{gas,A^-} + G_{gas,H^+}) - G_{gas,AH}. \quad (2)$$

For which the proton free energy [45] at 298 K and 1 atm is:

$$G_{gas,H^+} = 2.5RT - T\Delta S^\circ = 1.48 - 7.76 = -6.28 \text{ kcal/mol}$$

The greater acidity belongs to the group in which its hydrogen release is easier and there must be a decrease in ΔG values in the deprotonation process. A clear decrease in ΔG was observed in case TMACHCAT (Fig. 9) as the deprotonation take place from catecholic oxygens followed by protonated amines from fully protonated free ligand, LH_6. The validity of this calculated ΔG_{gas} for the different species of TMACHCAT was compared with the calculated experimental pK_a, which resulted an acceptable correlation with $R^2 = 0.9987$.

3.3. Metal complex formation

Potentiometric titrations of TMACHCAT (L) with La(III), Gd(III) and Lu(III) ions were carried out in 1:1 and 1:2 metal–ligand molar ratios at $\mu = 0.1$ M KCl and 25 ± 1 °C in aqueous medium. The experimental titration curves for the 1:1 metal–ligand molar ratio are given in Fig. 5. The deviation in the metal–ligand titration curves from the free ligand titration curve implies the formation of metal complexes. Complexes

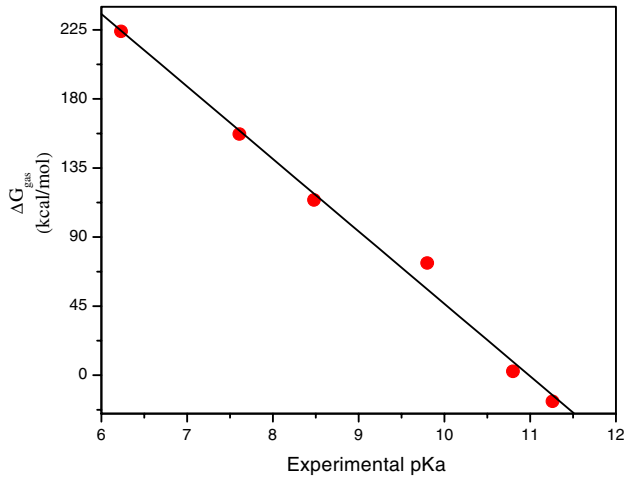

Fig. 9. Correlation between experimental pK_a and the calculated free energy $\Delta G_{gas,AH}$.

due to La(III) formed at higher pH (~5.5), while Lu(III) at the lowest (~4.0) and Gd(III) in between La(III) and Lu(III) (i.e., at ~5), which indicate that the stability of the complexes depends significantly on the charge density of the metal ions. Formation of turbidity and precipitate appeared only after $a > 5$ (a = moles of OH^-/moles of ligand), which implies that five protons have been displaced before hydrolysis of lanthanide ions, and complexation occurred prior to this. Data beyond this (after pH ~ 7) were excluded from calculation. Keeping in view these preliminary observations many sets of possible complexes were tested in the minimization programme and the best-fit model was obtained when formation of protonated species of the types MLH_3, MLH_2 and MLH were considered. From the data of 1:2 metal–ligand molar ratio an additional species ML_2H_6 was also observed. The overall formation constants ($\log\beta$) of the species were calculated using Hyperquad 2000 program and the derived stepwise formation constants ($\log K$) of complexes are summarized in Table 2. The equilibrium reactions for the overall formations of the complexes are given below by Eqs. (3)–(6) (charges are omitted for clarity):

$$M + L + H \rightleftharpoons MLH, \quad \log\beta_{111} = \frac{[MLH]}{[M][L][H]} \tag{3}$$

$$M + L + 2H \rightleftharpoons MLH_2, \quad \log\beta_{112} = \frac{[MLH_2]}{[M][L][H]^2} \tag{4}$$

$$M + L + 3H \rightleftharpoons MLH_3, \quad \log\beta_{113} = \frac{[MLH_3]}{[M][L][H]^3} \tag{5}$$

$$M + 2L + 6H \rightleftharpoons ML_2H_6, \quad \log\beta_{126} = \frac{[ML_2H_6]}{[M][L]^2[H]^6} \tag{6}$$

In order to predict the reaction path sometime it is advantageous to represent the equilibrium reactions in terms of successive formation of complexes. MLH_3 may be regarded to be formed by the reaction of M and LH_3, whereas MLH_2 and MLH may be formed due to dissociation of protons in steps from MLH_3. Also, the species ML_2H_6 is treated as the product of reaction between MLH_3 and LH_3. Accordingly, the derived successive formation constants may be represented as Eqs. (7)–(9).

$$M + LH_3 \rightleftharpoons MLH_3, \quad \log K^{LH_3}_{MLH_3} = \frac{[MLH_3]}{[M][LH_3]} \tag{7}$$

$$MLH_3 \rightleftharpoons MLH_2 + H, \quad \log K^{MLH_3}_{MLH_2} = \frac{[MLH_2][H]}{[MLH_3]} \tag{8}$$

$$MLH_2 \rightleftharpoons MLH + H, \quad \log K^{MLH_2}_{MLH} = \frac{[MLH][H]}{[MLH_2]} \tag{9}$$

$$MLH_3 + LH_3 \rightleftharpoons ML_2H_6, \quad \log K^{MLH_3}_{ML_2H_3} = \frac{[ML_2H_3]}{[MLH_3][LH_3]} \tag{10}$$

The interaction of lanthanide ions with TMACHCAT (L) was also studied by spectrophotometric method to explain the different possible coordination modes of the species in solution. Spectrometric titrations of TMACHCAT was carried out in 1:1 and 1:2 metal-to-ligand ratios with the ligand concentration $[L] = 4.02 \times 10^{-5}$M and

Table 2
Overall ($\log\beta$) and stepwise formation constants ($\log K$ or pK) of the metal complexes at 25 ± 1 °C and μ = 0.1 M KCl, (A = potentiometry and B = spectrophotometry)

	La(III)			Gd(III)			Lu(III)	
	TMACHCAT		TRENCAT	TMACHCAT		TRENCAT	TMACHCAT	
	A	B	A	A	B	A	A	B
$[MLH_3]/[M][L][H]^3$	39.01 ± 0.03	38.80 ± 0.02	38.53	40.52 ± 0.01	40.81 ± 0.02	40.08	42.27 ± 0.06	42.8 ± 10.03
$[MLH_2]/[M][L][H]^2$	31.75 ± 0.02	32.01 ± 0.01	31.25	34.84 ± 0.03	34.54 ± 0.01	34.17	36.23 ± 0.02	36.48 ± 0.03
[MLH]/[M][L][H]	24.86 ± 0.03	25.09 ± 0.03	24.28	28.01 ± 0.05	27.73 ± 0.03	27.51	30.27 ± 0.01	30.53 ± 0.03
$[ML_2H_6]/[M][L]^2[H]^6$	77.17 ± 0.09	77.23 ± 0.06	76.41	80.11 ± 0.08	79.97 ± 0.07	79.10	82.01 ± 0.09	82.29 ± 0.03
$[MLH_3]/[M][LH_3]$	7.30	7.15	6.94	8.81	9.16	8.49	10.56	11.16
$[MLH_2][H]/[MLH_3]$[a]	7.26	6.79	7.28	5.68	6.27	5.91	6.04	6.33
[MLH][H]/$[MLH_2]$[a]	6.89	6.92	6.97	6.83	6.81	6.66	5.96	5.95
$[ML_2H_6]/[MLH_3][LH_3]$	6.45	6.78	6.29	7.88	7.51	7.43	8.03	7.83

[a] Represents pK values (p$K = -\log K$).

the metal ion concentrations $[M(III)] = 4.02 \times 10^{-5}$M (M:L::1:1) and 2.01×10^{-5}M (M:L::1:2) with increasing pH between 2.5 and 8.0. No spectral changes were observed at low pH (between pH ~ 2.5–4.0) and graphs in this region are excluded. The experimental electronic spectra of TMACHCAT-M(III) systems are given in Fig. 10. Major spectral changes were observed between pH ~ 4.5–8.0, which may be due to the formation of metal complexes. After pH ~ 8, the solution became turbid. The variations in electronic spectra for all metal ions at different pH are almost similar with respect to TMACHCAT indicate similar mode of complexation. The ligand peak at 281 nm (pH ~ 4) was shifted towards higher wavelength with formation of two isosbestic points. No additional band specific to the chelate(s) appeared at long wavelengths. The best-fit model was obtained when formation of the species MLH_3, MLH_2, MLH and ML_2H_6 were considered. The formation constants were calculated from the spectral data using computer program pHAb and the values are given in Table 2.

The pH dependent species distribution curves (Fig. 11) indicate that in acidic condition MLH_3 and MLH_2 predominate whereas in neutral condition MLH and ML_2H_6 predominate. Also, Fig. 11 shows that interaction of ligand with the metal ion takes place in the form of LH_3 to give MLH_3 at pH 4.5, where the free ligand started releasing protons from the more acidic hydroxyl group of catechol (Fig. 6). Comparison of the electronic spectra of LH_3 and MLH_3 also support the above fact. The species LH_3 shows maximum absorbance at 294 nm in the free ligand, whereas in 1:1 M/L solution the said peak appeared at 280 nm assignable

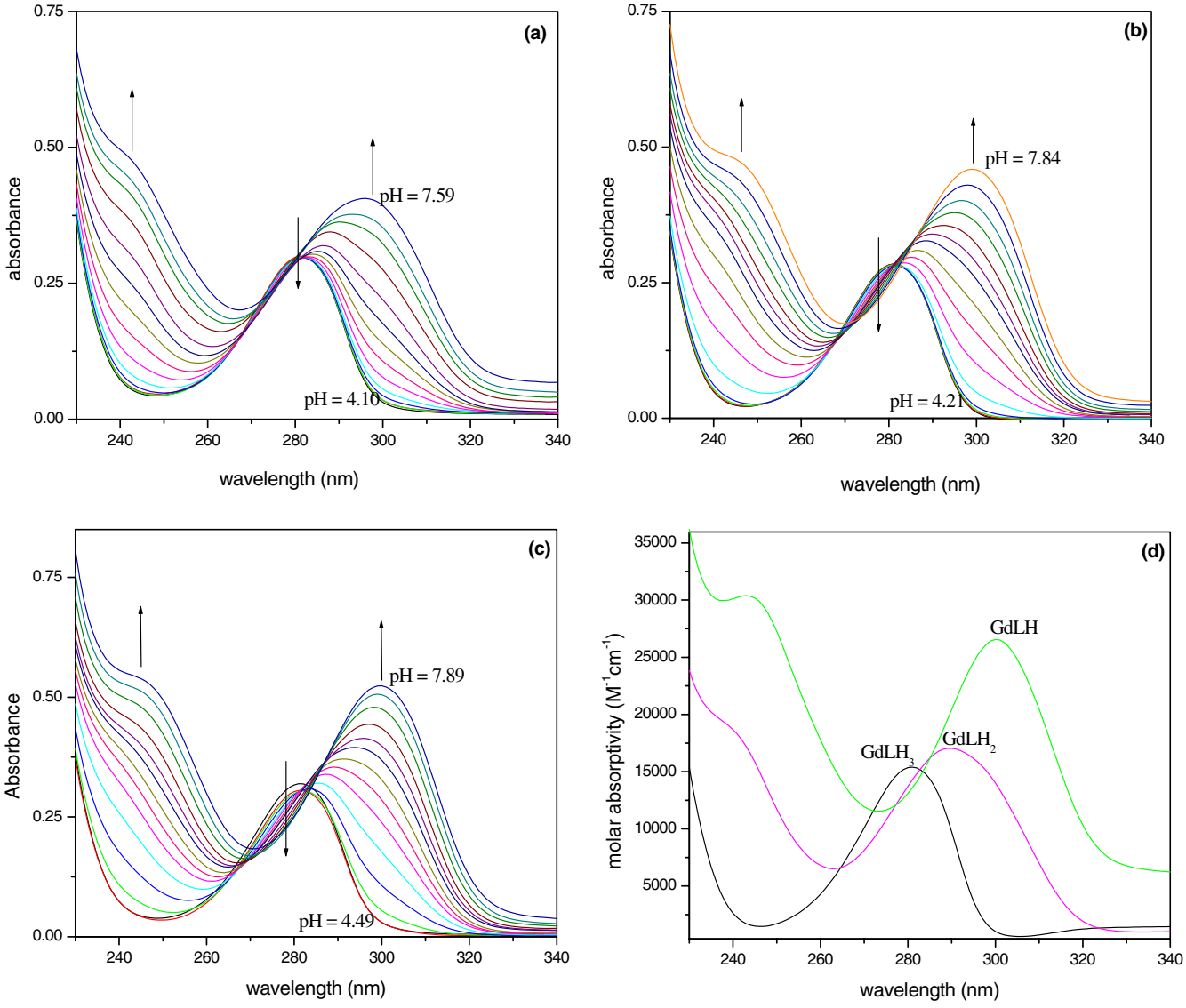

Fig. 10. Experimental electronic spectra of 1:1 metal to ligand ratio: (a) La(III), (b) Gd(III), (c) Lu(III) with increasing pH and (d) predicated electronic spectra of the three species for 1:1 Gd(III)-TMACHCAT system.

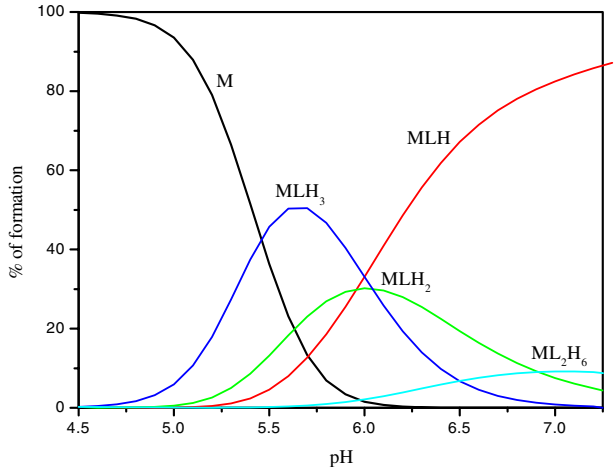

Fig. 11. Speciation diagram (% of formation vs. pH) calculated for 1:2 Gd(III)-TMACHCAT system.

to the coordination of the three catecholic groups to the metal ion. Thus, MLH_3 may be presented as a capped configuration with the coordination of three more acidic catecholic oxygen at *ortho* (Fig. 12a). Raymond et al. have reported the formation constant for the protonated mononuclear catecholate complex $\log K_{Eu(Hcat)}$ to be 7.3 [21]. To the best of our knowledge $\log K_2$, $\log K_3$ or $\log \beta_3$ for catechol with lanthanides have not been reported so far. Considering only the statistical factor, the theoretical $\log \beta_3$ for the formation of $[Eu(Hcat)_3]$ should be 20.9. Since the ligand under study contains three catechol units, the expected formation constant is about 20.9. The stability of MLH_3 ($\log \beta_1 = 39$–42, Table 2) compared with that of $[Eu(Hcat)_3]$ reveals that there is definitely a chelate effect and preorganization in the ligand favouring coordination to lanthanide ions. Molecular modeling calculation of free ligand species LH_3 and $GdLH_3$ (Fig. 13) also indicates that the geometry is stabilized due to the preorganization of ligand architecture by intramolecular hydrogen bonding between protonated nitrogens and phenolic oxygens.

As the pH increases, successive deprotonation from MLH_3 leads to the formation of partially protonated MLH_2 and MLH. Release of these protons from MLH_3 can either take place from the NH_2^+ groups for which the protonation constant values have been evaluated or from catechol ones, for three of which the protonation constant values are unknown. These two probabilities lead to two distinct geometries either nitrogen–oxygen encapsulated or oxygen–oxygen encapsulated. In the first case, for nitrogen–oxygen encapsulated, if the metal ion enters into the nitrogen–oxygen cavity with release of one/two protons from NH_2^+ upon coordination may get repulsive force due to its larger size in the presence of two or one protonated NH_2^+ groups, which on coordination results a six membered chelate ring. However, in second case oxygen–oxygen encapsulated, the ligand coordinates through its more basic catecholic oxygens as anionic donor to form five membered chelate rings. Since the five membered chelate rings is more stable than six membered chelate rings [46] and the latter is more preferable. Also, the bathochromic spectral shifting with concomitant rise in absorbance upon deprotonation from MLH_3 assignable to the coordination of chromophoric catecholic oxygens. This type of coordination is expected for the large size lanthanide (III) metal ions because the binding between lanthanide metals and donor atoms is predominantly ionic in character, and the cations display a strong preference for negatively charged O donor ligands [47]. Moreover, reported results show that tripodal ligands derived from TREN possessing six oxygen functions yielded cationic or neutral complexes in which the nitrogen atoms (imine or amide functions) were not involved

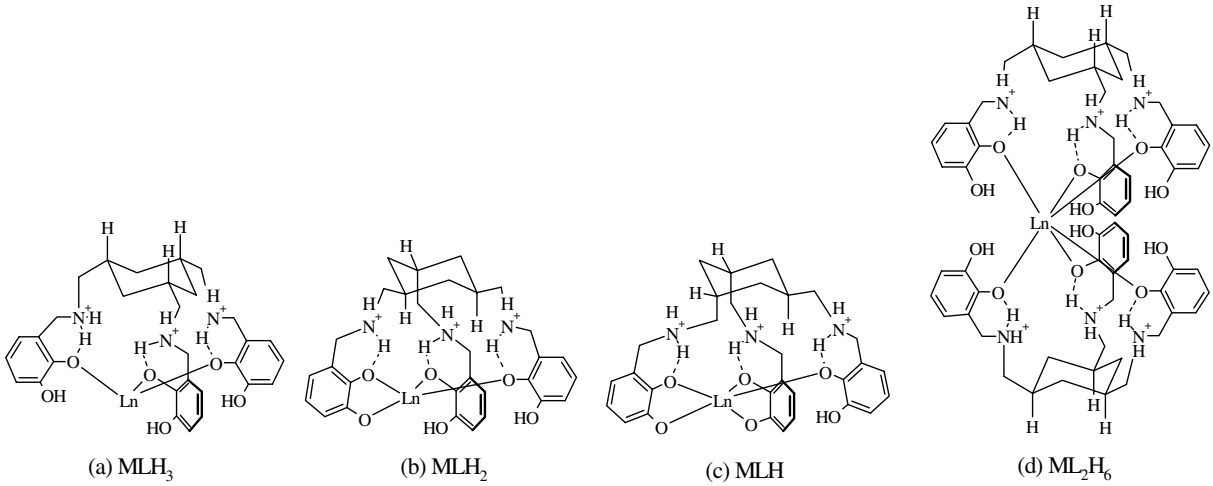

Fig. 12. Proposed modes of complexation of TMACHCAT with Ln(III): Capped (a) MLH_3; encapsulated (b) MLH_2, (c) MLH; and bicapped (d) ML_2H_6 structure.

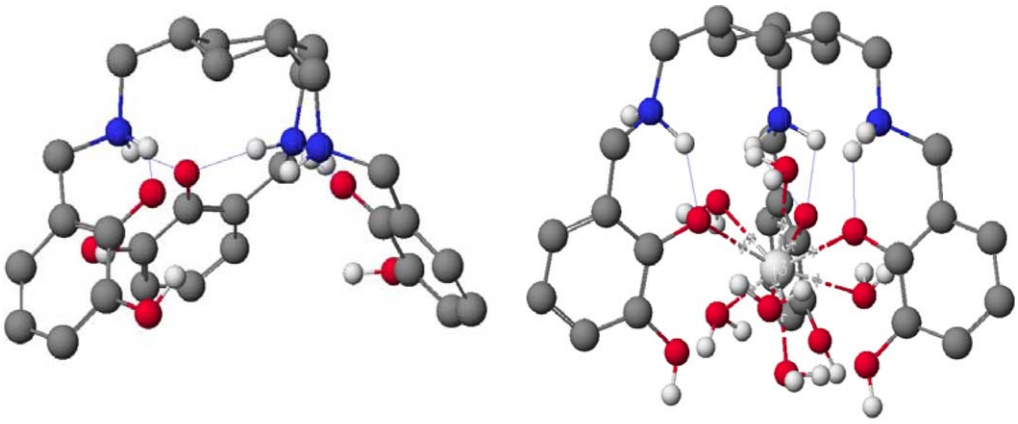

Fig. 13. Energetically optimized structure of free ligand species LH_3 (applying semi-empirical PM3 method) and $GdLH_3$ (applying MM3 force field).

Table 3
Calculated least strain energy (E_T in kcal/mol) structures of [M(TMACHCAT)][a]

M(III)	MLH_3		MLH_2			MLH		
	3-axial	3-equitorial	3-axial	3-equitorial	1-axial + 2-equitorial	3-axial	3-equitorial	2-axial + 1-equitorial
La(III)	246.32	192.95	287.98	280.03	241.66	387.90	371.82	366.56
Gd(III)	275.52	214.14	293.42	258.09	244.26	413.64	411.52	410.88
Lu(III)	279.70	231.97	313.91	318.66	279.83	431.61	421.67	405.91

[a] Axial and equatorial denoted for the conformational position of the three arms of TMACHCAT on complexation.

in coordination [48], which was also confirmed by X-ray crystal structure study. This observation strongly suggests that M(III) in the capped MLH_3 is not efficiently protected by the wrapped podand and remain accessible for further complexation to give encapsulated partially protonated complex as shown in Fig. 12(b) and (c). Again, the negative logarithms of stepwise formation constants indicate the instability of the partially protonated complexes. Molecular modeling calculations were carried out to calculate the strain energy for the proposed metal complexes formed in solution. Based on the strain energy (Table 3), it can be suggested that in capped MLH_3 complex, the ligand retain its equatorial conformation but in the encapsulated complex the ligand prefers axial conformation. This change involves a ring-flip into energetically disfavour axial conformer, which is compensated due to coordination to form the encapsulated metal complex. Such ring-flip upon complexation was observed with many TACH derived tripodal ligands [49], but no evidence was reported for conformational interconversion in the uncomplexed ligand. This interconversion in TMACHCAT on forming encapsulated complexes may leads to the negative logarithms of stepwise formation constants.

Formation of ML_2H_6 species was also observed at higher pH for which a bicapped configuration may be proposed (Fig. 12(d)). Comparison of results with other phenol–amines and catechol–amine complexes of lanthanides (Table 2) reveals that, the stability of MLH_3 complexes of TMACHCAT are higher than TRNS lanthanides complexes [$\Delta \log K = 1.65$ for La(III) and 2.14 for Gd(III)]. These increases in stabilizing effect may be due to preorganization of the ligand and easy deprotonation of three highly basic catechol hydrogens of the ligand on complexation profit the coordination of lanthanides to TMACHCAT. Moreover, the stability of TMACHCAT complexes are slightly higher than TRENCAT lanthanide complexes, reflects that increase in cavity size on introducing cyclohexane ring as spacer group, favours more towards the encapsulation chelation of hard cations.

4. Conclusion

Experimental and theoretical studies of the newly synthesized ligand TMACHCAT indicate the presence of intramolecular H-bond, which provide a rigid tripodal framework for complexation. The ligand shows effective binding properties towards trivalent lanthanides due to the increase in cavity size by introducing cyclohexane as spacer unit. The stability increases with decrease in metal ions size. The pH dependent metal–ligand species shows formation of three different structures: (i) capped, (ii) bicapped and (iii) encapsulated, in which only catecholic oxygens take part in complexation whereas protonated amines formed intramolecular hydrogen bonding. It is important to mention here from the ligand

TMACHCAT shows a potential to form mononuclear encapsulated complex at nearly physiological condition, which is important for use as contrast agents in magnetic resonance imaging.

References

[1] S. Aime, M. Botta, M. Fasano, E. Terreno, Chem. Soc. Rev. 27 (1998) 19.
[2] J.C.G Bunzli, in: J.C.G. Bunzli, G.R. Choppin (Eds.), Lanthanide Probes in Life, Chemical and Earth Sciences, Elsevier, Amsterdam, 1989.
[3] T.C. Bruice, A. Tsubouchi, R.O. Dempcy, L.P. Olson, J. Am. Chem. Soc. 118 (1996) 9867.
[4] S.J. Oh, Y.S. Choi, S. Hwangbo, S.C. Bae, J.K. Ku, J.W. Park, Chem. Commun. (1998) 2189.
[5] G.R. Choppin, K.M. Schaab, Inorg. Chim. Acta 252 (1996) 299.
[6] A.D. Watson, J. Alloys Compd. 207/208 (1994) 14.
[7] K. Kumar, T. Jin, X. Wang, J.F. Desreux, M.F. Tweedle, Inorg. Chem. 33 (1994) 3823.
[8] R.B. Lauffer, Chem. Rev. 87 (1987) 901.
[9] C. Orvig, D.J. Berg, S.J. Rettig, J. Am. Chem. Soc. 113 (1991) 2528.
[10] R.M. Kirchner, C. Mealli, M. Bailey, M. Howe, L.P. Torre, L.J. Wilson, L.C. Andrews, N.J. Rose, E.C. Lingafelter, Coord. Chem. Rev. 77 (1987) 89.
[11] K.G. Ragunathan, P.K. Bharadwaj, J. Chem. Soc. Dalton Trans. (1992) 2417.
[12] P. Ghosh, R. Shukla, D.K. Chand, P.K. Bharadwaj, Tetrahedron 51 (1995) 3265.
[13] I.G. O'Brien, F. Gibson, Biochim. Biophys. Acta 215 (1970) 393.
[14] J.R. Pollack, J.B. Neilands, Biochim. Biophys. Res. Commun. 38 (1978) 989.
[15] (a) W.R. Harris, C.J. Carrano, S.R. Cooper, A.E. Avdeef, J.V. McArdle, K.N. Raymond, J. Am. Chem. Soc. 101 (1979) 6097;
(b) W.R. Harris, C.J. Carrano, K.N. Raymond, J. Am. Chem. Soc. 101 (1979) 2213.
[16] A.E. Martell, W.F. Anderson, D.E. Badman, Development of Iron Chelators for Clinical Use, Elsevier, The Netherlands, 1981.
[17] K.N. Raymond, Coord. Chem. Rev. 105 (1990) 135.
[18] M.J. Sever, J.J. Wilker, J. Chem. Soc. Dalton Trans. (2004) 1061.
[19] (a) S.M. Cohen, K.N. Raymond, Inorg. Chem. 39 (2000) 3624;
(b) A.R. Bulls, C.G. Pippin, F.E. Hahn, K.N. Raymond, J. Am. Chem. Soc. 112 (1990) 1617.
[20] (a) K.N. Raymond, G.E. Freeman, M.J. Kappel, Inorg. Chim. Acta 94 (1984) 193;
(b) P.W. Durbin, N. Jeung, E.S. Jones, F.L. Weitl, K.N. Raymond, Radiat. Res. 99 (1984) 85.
[21] D. Zhu, M.J. Kappel, K.N. Raymond, Inorg. Chim. Acta 147 (1988) 115.
[22] G.E. Freeman, K.N. Raymond, Inorg. Chem. 24 (1985) 1410.
[23] G.R. Choppin, Pure Appl. Chem. 27 (1971) 23.
[24] A.E. Martell, R.M. Smith, Critical Stability Constants, vols. 1–6, Plenum, New York, 1974–1989.
[25] M.P. Lowe, P. Caravan, S.J. Rettig, C. Orvig, Inorg. Chem. 37 (1998) 1637.
[26] P. Caravan, T. Hedlund, S. Liu, S. Sjoberg, C. Orvig, J. Am. Chem. Soc. 117 (1995) 11230.
[27] A. Bismondo, C. Comuzzi, P. Di Bernardo, P.L. Zanonato, Inorg. Chim. Acta 286 (1999) 103.
[28] A. Bismondo, P. Di Bernardo, R. Portanova, M. Tolazzi, P.L. Zanonato, Polyhedron 21 (2002) 1393.
[29] M. Baral, B.K. Kanungo, P. Moore, unpublished work.
[30] A.E. Martell, R.J. Motekaitis, The Determination and Use of Stability Constants, VCH Publishers, New York.
[31] P. Gans, A. Sabatini, A. Vacca, Talanta 43 (1996) 1739.
[32] P. Gans, A. Sabatini, A. Vacca, Annali di Chim. 89 (1999) 45.
[33] User guide manual for CAChe version 6.01, Fujitsu limited, 2003.
[34] Gaussian-03, Revision B.5, Gaussian, Inc., Pittsburgh, PA, 2003.
[35] Computational Chemistry manual for HyperNMR version 7.0, Hypercube Inc., 419 Philip Street, Waterloo, Ont., Canada N2L 3X2.
[36] (a) E.L. Muetterties, C.M. Wright, Quart. Rev. Lond. 21 (1967) 109;
(b) J.H. Forsberg, T. Moeller, Inorg. Chem. 8 (1969) 883.
[37] D.E. Reichert, M.J. Welch, Coord. Chem. Rev. 212 (2001) 111.
[38] R.M. Silverstein, F.X. Webster, Spectrometric Identification of Organic Compounds, sixth ed., Wiley, New York, 1996.
[39] D.M. Seeger, C. Korzeniewski, W. Kowalchyk, J. Phys. Chem. 95 (1991) 68.
[40] P. Caravan, C. Orvig, Inorg. Chem. 36 (1997) 236.
[41] S.E. Muthu, Ph.D. thesis, Punjab Technical University, India, 2004.
[42] R.F. Childers, R.A.D. Wentworth, L.J. Zompa, Inorg. Chem. 10 (1971) 302.
[43] M. Micheloni, A. Sabatini, A. Vacca, Inorg. Chim. Acta 25 (1977) 41.
[44] R. Cini, G. Giorgi, D. Masi, A. Sabatini, A. Vacca, J. Chem. Soc. Perkin Trans. (1991) 765.
[45] I.A. Topol, G.J. Tawa, S.K. Burt, A.A. Rashin, J. Chem. Phys. 111 (1999) 10998.
[46] R.D. Hancock, A.E. Martell, Chem. Rev. 89 (1989) 1875.
[47] N.N. Greenwood, A. Earnshaw, Chemistry of the Elements, Pergamon, Toronto, 1987.
[48] (a) S.J. Archibald, A.J. Blake, M. Schroder, R.E.P. Winpenny, J. Chem. Soc. Chem. Commun. (1994) 1669;
(b) S.J. Archibald, A.J. Blake, M. Schroder, S. Parsons, R.E.P. Winpenny, J. Chem. Soc. Chem. Commun. (1997) 173;
(c) J. Xu, S.J. Franflin, D.W. Whisenhunt Jr., K.N. Raymond, J. Am. Chem. Soc. 117 (1995) 7245.
[49] J.E. Bollinger, J.T. Mague, W.A. Banks, A.J. Kastin, D.M. Roundhill, Inorg. Chem. 34 (1995) 2134.

Available online at www.sciencedirect.com
SCIENCE DIRECT®
Polyhedron 25 (2006) 737–746
POLYHEDRON
www.elsevier.com/locate/poly

Synthesis, characterization, conduction and gas sensing properties of novel multinuclear metallo phthalocyanines (Zn, Co) with alkylthio substituents

Tanju Ceyhan [a,1], Ahmet Altındal [b,2], Mehmet K. Erbil [a,1], Özer Bekaroğlu [c,*]

[a] Department of Biochemistry, Division of Organic Chemistry, Gülhane Medical Academy, (GATA), Ankara, Turkey
[b] Department of Physics, Marmara University, 34722 Göztepe-Istanbul, Turkey
[c] Department of Chemistry, Marmara University, 34722 Göztepe-Istanbul, Turkey

Received 14 April 2005; accepted 20 July 2005
Available online 3 October 2005

Abstract

Compound **1** has been prepared by the reaction of 4-nitrophthalonitrile and 2-nitro-2-methyl-1,3-propanediol by the common method of nucleophilic substitution of an activated nitro group in an aromatic ring. Interesting binuclear metallophthalocyanines (M = Zn and Co), compounds **2** and **3**, respectively, of a new type have been synthesized from compound **1**, 4,5-bis(hexylthio)phthalonitrile, and the corresponding metal salts [$Zn(OAc)_2$ and $CoCl_2$] by the method of statistically mixed condensation. Compound **2** was converted to the tetranuclear zinc (II) phthalocyanine **4** by the reaction with NaOH solution and activated zinc powder in a mixture of MeOH and THF as the solvent. Impedance spectroscopy (IS) and d.c conductivity ($\sigma_{d.c}$) measurements were performed on spin coated films of these compounds as a function of temperature (290–400 K) and frequency (40–10^5 Hz.) The sensing properties for volatile organic compounds (VOCs) were also investigated. Although the d.c conductivity shows typical Arrehenius behaviour for compound **2**, a discontinous point was observed in the slope of $\ln \sigma_{d.c}$ versus $1/T$ plot for compound **4**. Unlike the films of **2** and **4,** the d.c behaviour of compound **3** obeys the variable range hopping (VRH) model. At room temperature, a curved line was observed from the complex plane plots of impedance for all compounds. These curved lines transformed into a full semicircle with increasing temperature. The a.c conductivity of the films is represented by the form ω^s. The dependency of the frequency exponent s on temperature suggests a correlated barrier hopping. A sensor using compound **4** as the sensing layer had the highest sensitivity for all volatile organic compounds investigated and showed complete reversibility even at room temperature. The results indicated that the film of compound **4** has potential as a sensitive coating for the monitoring of VOC vapours.
© 2005 Elsevier Ltd. All rights reserved.

Keywords: Phthalocyanine; VOC sensing; Variable range hopping; CBH

1. Introduction

Metal phthalocyanines (MPcs) have been well studied as liquid crystals [1,2], photosensitizers [3], catalysts [4–9], molecular thermometers [10], magnets [11], electrochromic displays [12,13], photovoltaic cells [14], optical limiting devices [15] and gas sensors [16–18] over the last few years. Especially, cobalt phthalocyanine (CoPc) and its derivatives are shown to catalyze reactions like the reduction of oxygen, CO_2, formic acid, formaldehyde, trichloro acetic acid and cysteine-containing proteins. The catalytic behaviour of CoPc complexes is associated with the redox activity of the central metal which undergoes oxidation and reduction related with the Co(3+)/Co(2+) and Co(2+)/Co(I) electrochemical reactions [4–9]. The values of the oxidation or reduction potentials of the central metal in

* Corresponding author. Tel.: +90 216 359 0130; fax: +90 216 386 0824.
E-mail addresses: aaltindal@marmara.edu.tr (A. Altındal), obekaroglu@marmara.edu.tr (Ö. Bekaroğlu).
[1] Fax: +90 312 3043300.
[2] Fax: +90 216 3478783.

0277-5387/$ - see front matter © 2005 Elsevier Ltd. All rights reserved.
doi:10.1016/j.poly.2005.07.046

CoPc thus strongly influence the catalytic behaviour of the complexes which is essential for the design of more efficient catalysts. Spectroelectrochemical studies of the phthalocyanines facilitate the understanding of the nature of the redox processes which may occur at either the central metal atom or the phthalocyanine ring, but this cannot usually be distinguished by using electrochemistry alone. Spectroelectrochemical studies of the phthalocyanines are also important with regard to their possible use as electrochromic materials which display several colours depend on the applied potential on the electrode surface [19]. In these respects, the synthesis [20–23], electrochemical [23–25], spectroelectrochemical [23,25–27] and electrocatalytic behaviour [4–9] of cobalt phthalocyanine derivatives have been extensively investigated under different experimental conditions. In particular, multinuclear cobalt phthalocyanines having various kinds of linkage have been the subject of interest in electrocatalysis for the reduction of oxygen at a fuel cell cathode, because the electrocatalyst can participitate in a concerted fashion with a multi-electron reduction which makes it an effective oxygen reduction catalyst to hydrogen peroxide [25].

It is well known that the adsorption of the oxidizing or reducing gases on the surface of MPc films affects their electronic properties. Although many recent reports have been published on the response of MPc films to electron donor and electron acceptor gases such as NH_3 [28], NO_x [29] and halogens [16], very little work has appeared on volatile organic compound (VOC) sensing properties of MPc films. The use of MPcs for the detection of VOC vapours is limited due to the low reactivities of organic gases compared with inorganic gases. In spite of the inadequacy of MPcs for VOC sensing, there has been increasing effort towards the design and synthesis of new molecules to detect and identify VOCs at low concentration that are important in many fields. The determination of the electrical properties of the MPc films is crucial in order to realize the sensing mechanism and their future applications.

We have previously synthesized a triazine carrying three phthalocyaninato zinc (II) macrocycles through amino groups [30] and a new type of sandwich dilutetium tetraphthalocyanine, which exhibits variable range hopping conductivity, as inorganic semiconductors and also observed electrochromic effects from cyclic voltammetric (CV) measurements [31]. In the present work, novel binuclear zinc (II) and cobalt (II) phthalocyanines with alkyl thio substituents have been synthesized from compound **1** and 4,5-bis-(hexylthio)phthalonitrile as two different dinitriles and the corresponding metal salts [$Zn(OAc)_2$ and $CoCl_2$] in a mixed condensation [32]. Binuclear zinc (II) phthalocyanine (**2**) has been converted to a new type of tetranuclear zinc (II) phthalocyanine (**4**). Both d.c and a.c behaviour of the spin coated films of these compounds were studied by using complex impedance spectroscopy. In addition, the response characteristics of the films to organic solvent molecules has been investigated as a function of temperature.

2. Experimental

Routine IR were recorded on a Shimadzu IR-470 Infrared spectrometer as KBr pellets, electronic spectra on a UNICAM UV 500 UV–Vis spectrometer. Elemental analysis was performed by the LECO CHNS 932 in the Instrumental Analysis Laboratory of TUBITAK Ankara Research Center. ^1H NMR spectra were recorded on a Bruker Avance DPX-400 spectrometer. Ten-finger interdigital gold electrodes with 100 μm gap were deposited photolithographically on a pre-cleaned corning glass substrate (substrates were first cleaned thoroughly with soap solution and distilled water). Prior to vacuum evaporation, the glass substrates were cleaned ultrasonically in 2-propanol for 5 min. Thin films of the compounds were obtained by spin-coating chloroform solutions (5×10^{-6} M) of the product over the electrode arrays to obtain devices suitable for electrical and gas sensing measurements. A close-cycle liquid helium cryostat was used to allow electrical characteristics to be measured over a wide temperature range. D.c conductivity measurements were performed between 290 and 400 K by using a Keithley 617 electrometer. A.c conductivity measurements were carried out with a Keithley 3330 LCZ meter in the frequency range 40 Hz to 100 kHz, in the temperature range from 290 to 400 K. During the measurement the temperature of the sample was controlled with a Leybold LTC 60 temperature controller. All the measurements were performed under 10^{-3} mbar in the dark, but the values did not change under illumination with indoor lighting. The conductivity data were recorded using an IEEE 488 data acqusition system incorporating a personal computer. For the gas sensing measurements, the sensors were placed in a teflon chamber and when the sensors were stable, they were exposed to five VOC gases: chloroform, carbon tetrachloride, acetone, methanol and ethanol. The test gases were mixed with dry nitrogen (N_2) using computer derived mass flow controllers (Heastings 200/202 series). The concentration of the target gas was adjusted to 200 ppm. A typical experiment consisted of repeated exposure to an organic solvent vapour and subsequent purging with dry N_2 to reset the baseline. The results obtained under these conditions were reproducible with an uncertainity of less than 3%.

All reagents and solvents were of reagent grade quality, obtained from commercial suppliers. The solvents were stored over molecular sieves (4 Å). 4-Nitrophthalonitrile [33] and 4,5-bis(hexylthio)phthalonitrile [34] were prepared by the literature methods.

3. Syntheses

*3.1. 2-Nitro-2-methyl-1,3-bis(3,4 dicyanophenoxymethyl) propane (**1**)*

A mixture of 2-nitro-2-methyl-1,3-propanediol (2.56 g, 0.019 mol), 4-nitrophthalonitrile (7.96 g, 0.046 mol) and K_2CO_3 (2 g) in 100 ml of DMSO was intensively stirred

for 22 h at 70 °C. After that, 2 g of K_2CO_3 was added and reaction was continued for 11 h at the same temperature. The reaction was monitored by thin layer chromotography (TLC). Then, the reaction mixture was poured into 500 ml of water, and acetic acid (140 ml) was added to the mixture. The residue was filtered off, flushed several times with water until the filtrate was neutral. After that it was washed with diethyl ether (40 ml) and dried in vacuo. After the product had been refluxed in EtOH (400 ml), it was filtered while hot. The yellow precipitate was washed successively with water, ethanol and diethyl ether prior to drying in vacuum at room temperature. The pure product was soluble in DMF, DMSO, ethyl acetate and THF but insoluble in hexane, chloroform and diethyl ether. Yield: 3.49 g, 47%. Melting point 121–123 °C. IR (KBr), $\nu(cm^{-1})$: 3065 (H–Ar), 2215 (C≡N), 1580 (Ar C=C), 1552 (NO_2), 1477, 1406, 1332 (NO_2), 1276, 1249 (Ar–O–C), 1161, 1090, 965, 918, 849, 521. ^{1}H NMR (d_6-DMSO): $\delta = 8.38$–7.28 (m, 6H, ArH), 5.37 (s, 4H, $ArOCH_2$), 1.79 (s, 3H, O_2NCCH_3).

3.2. [(RS)$_6$ZnPc]$_2$NO$_2$ (2)

A mixture of compound **1** (0.100 g, 0.258 mmol), 4,5-bis (hexylthio) phthalonitrile (0.558 g, 1.55 mmol), $Zn(OAc)_2 \cdot 2H_2O$ (0.119 g, 0.542 mmol) and dry quinoline (2 ml) was heated and stirred at 180–190 °C under argon for 24 h. After cooling to room temperature, the dark green mixture was diluted with ethanol (10 ml) and the crude product precipitated. This was filtered off. After having been washed with hot water and hot ethanol to remove the unreacted organic materials, the precipitate was dissolved in chloroform (90 ml), the solution was filtered and the filtrate evaporated to a smaller volume (ca. 20 ml) from which a dark green precipitate was obtained by addition of acetone (180 ml). It was filtered, washed successively with DMSO (3×20 ml), ethyl acetate (3×20 ml), ethanol (3×20 ml) and acetone (3×20 ml) prior to drying in vacuo. Finally, pure **2** was obtained by chromatography with silica gel using $CHCl_3$ as the first eluent and then CCl_4:THF = 10:1. The dark green product was soluble in $CHCl_3$, benzene and THF but only moderately soluble in diethyl ether. Yield: 0.252g, 36%. Melting point >300 °C IR (KBr, cm^{-1}): 3010 (CH aromatic), 2890–2830 (CH_2, CH_3), 2340, 1580 (Ar C=C), 1540 (NO_2), 1447, 1393, 1367 (NO_2), 1232 (Ar–O–C), 1177, 1075, 1054, 935, 443, 426. ^{1}H NMR (*d*-chloroform) δ: 7.94–6.96 (m, 18H, ArH), 5.34 (s, 4H, $ArOCH_2$), 2.11 (br s, 24H, SCH_2), 1.72 (s, 3H, O_2NCCH_3), 1.50–1.09 (m, 96H, CH_2), 0.82 (s, 36H, CH_3).

3.3. [(RS)$_6$CoPc]$_2$NO$_2$ (3)

A mixture of compound **1** (0.100 g, 0.258 mmol), 4,5-bis(hexylthio) phthalonitrile (0.558 g, 1.55 mmol), $CoCl_2 \cdot 6H_2O$ (0.128 g, 0.535 mmol) and ethylene glycol (4 ml) was heated and stirred at 170–180 °C under argon for 22 h. After cooling to room temperature, water (5ml) was added to the mixture. The precipitate was filtered and washed with hot water several times followed by hot ethanol and acetone, and then dried. The crude product was dissolved in $CHCl_3$ (150 ml) and filtered. After the filtrate had been evaporated to a smaller volume (ca. 20 ml), it was reprecipitated with ethyl acetate (170 ml) and the precipitate was washed with hexane (3×20 ml), CCl_4 (3×20 ml), hot DMSO (3×20 ml), ethyl acetate (3×20 ml), ethanol (3×20 ml), acetone (3×20 ml) nad diethyl ether (3×20 ml). It was then dried in a vacuum at room temperature. Compound **3** was isolated on a silica gel column first with $CHCl_3$ and then with CCl_4:THF = 10:1 as eluents. The dark green product was soluble in $CHCl_3$ and THF. Yield: 0.168g, 24%. Melting point >300 °C IR (KBr, cm^{-1}): 3010 (CH aromatic), 2895–2830 (CH_2, CH_3), 2340, 1584 (Ar C=C), 1540 (NO_2), 1401, 1370 (NO_2), 1232, (Ar–O–C), 1061, 948.

3.4. [(RS)$_6$ZnPc]$_4$N$_2$ (4)

A mixture of compound **2** (90 mg, 0.0336 mmol), NaOH solution (1 ml, 0.268 M), MeOH (4 ml) and THF (20 ml) was stirred at room temperature for 15 min. Then, activated zinc powder (8.71 mg, 0.134 mmol) was added to the reaction mixture and refluxed for 8 h. After completion of the reaction, the reaction mixture was filtered while hot and the residue on the filter was washed with 15 ml of MeOH. After that, concentrated HCl (12 ml, 37%) was added to the filtrate until it was neutral and the precipitate was filtered, washed successively with water, MeOH (2×20 ml), EtOH (2×20 ml), ethyl acetate (2×20 ml), benzene (2×20 ml),acetone (2×20 ml), chloroform (2×20 ml) and diethyl ether (2×20 ml) prior to drying in vacuo. The dark green product was soluble in hot DMF, hot DMSO and hot THF. Yield: 60 mg, 68%. Melting point >300 °C IR (KBr, cm^{-1}): 3010 (CH aromatic), 2915–2840 (CH_2, CH_3), 2340, 1580 (Ar C=C), 1401, 1232 (Ar–O–C), 1075, 1054, 935, 443, 426. ^{1}H NMR (*d*-DMSO) δ: 8.62–6.92 (m, 36 H, ArH), 4.17 (s, 8H, $ArOCH_2$), 3.31–2.63 (m, 48H, SCH_2), 1.73 (s, 192H, CH_2), 1.47 (s, 6H, –N=NCCH$_3$), 0.95 (s, 72H, CH_3).

4. Results and discussion

Our key starting material is compound **1** which can be obtained via a single step reaction of 2-nitro-2-methyl-1,3-propanediol with 4-nitrophthalonitrile in dry DMSO as the solvent in the presence of K_2CO_3 as the base in a yield of 47% (Scheme 1). A new type of binuclear metallo phthalocyanine (M = Zn, Co) was synthesized from compound **1** and 4,5-bis(hexylthio)phthalonitrile and the corresponding metal salts [$Zn(OAc)_2$, $CoCl_2$] by the method of statistically mixed condensation. The high boiling solvents of choice for these reactions were quinoline for binuclear zinc (II) phthalocyanine (**2**) and ethylene glycol for binuclear cobalt (II) phthalocyanine (**3**). After work-up, the product mixtures were purified by chromatography over silica. The first fraction proved to be the corresponding

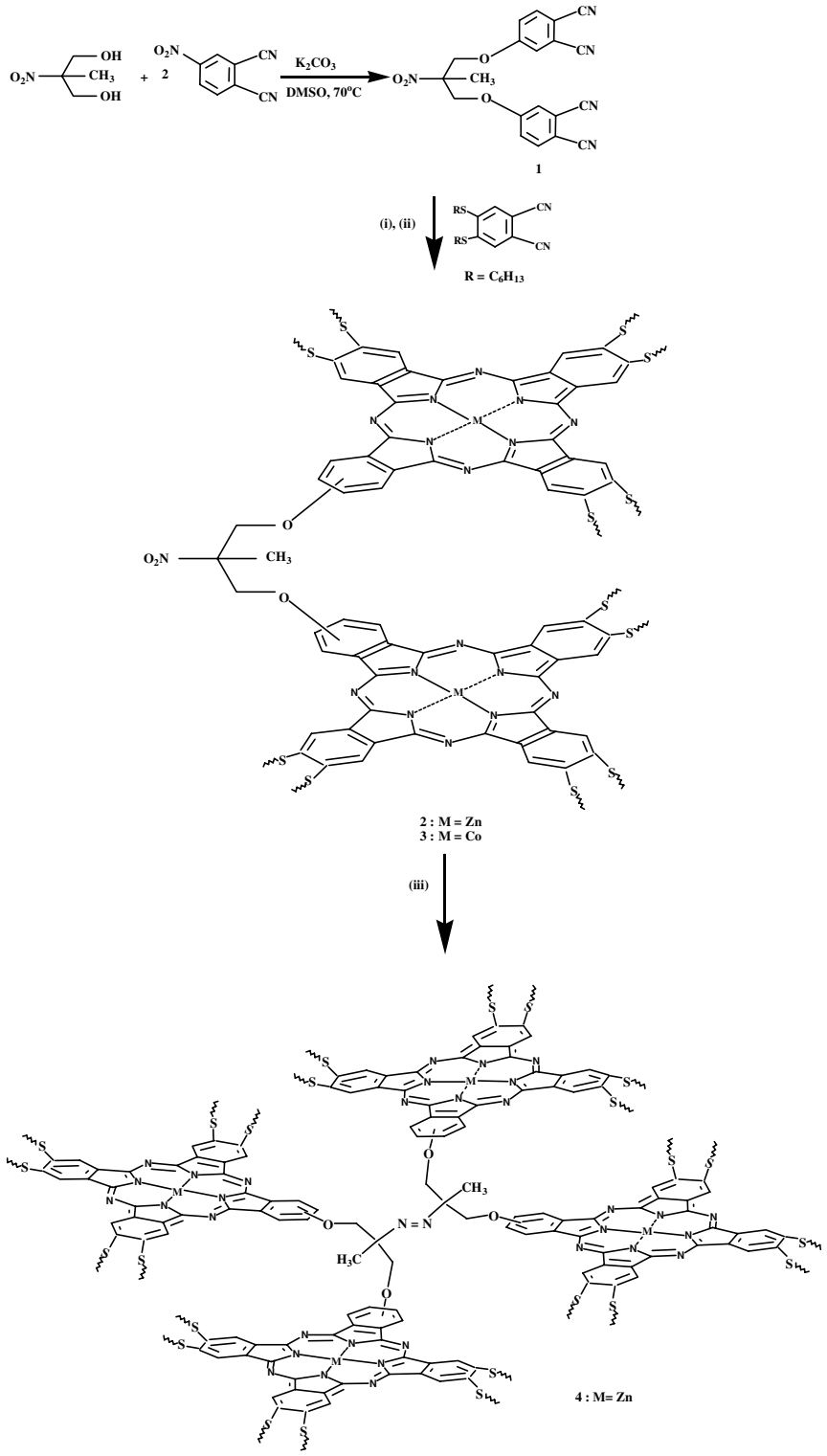

Scheme 1. Summary of the synthesis of the compounds **1**–**4**; (i) $CoCl_2 \cdot 6H_2O$, ethylene glycol, 170–180 °C; (ii) $Zn(OAc)_2 \cdot 2H_2O$, quinoline, 180–190 °C; (iii) NaOH solution, powdered Zn, MeOH/THF, reflux.

octa(hexylthio)phthalocyanine, identified by TLC comparison with an authentic sample [34]. The second fraction, which still contained traces of the octa(hexylthio)phthalocyanine together with the slower moving compound, gave after additional chromatography the products **2** and **3**. Binuclear zinc (II) phthalocyanine (**2**) was converted to the novel tetranuclear zinc (II) phthalocyanine (**4**) by the reaction with NaOH solution and activated zinc powder in a mixture of MeOH and THF. All of the new compounds were characterized by elemental analysis (Table 1), IR, UV–Vis (Table 2) and ^{1}H NMR spectroscopic techniques.

Table 1
Analytical[a] data for compounds **1**–**4**

Compounds	Yield (%)	Molecular formula (M)	Analysis (%)			
			C	H	N	S
1	47	$C_{20}H_{13}N_5O_4$ (387)	(62.01) 61.44	(3.36) 2.93	(18.08) 18.96	–
2	36	$C_{140}H_{181}N_{17}S_{12}O_4Zn_2$ (2677)	(62.75) 61.67	(6.76) 5.75	(8.89) 9.51	(14.34) 14.92
3	24	$C_{140}H_{181}N_{17}S_{12}O_4Co_2$ (2665)	(63.03) 65.63	(6.79) 6.56	(8.93) 9.51	(14.40) 13.70
4	68	$C_{280}H_{362}N_{34}S_{24}O_4Zn_4$ (5290)	(63.51) 62.60	(6.84) 6.33	(8.99) 9.36	(14.51) 13.14

[a] Required values are given in parentheses.

Table 2
UV–Vis data for the phthalocyanines **2**–**4**

Compounds	Solvent	λ/nm (log ε/dm^3 mol^{-1} cm^{-1})
2	$CHCl_3$	712 (4.59), 322 (4.57)
3	$CHCl_3$	715 (4.42), 639 sh (4.27), 315 (4.61)
4	DMF	697 (4.63), 634 sh (4.03), 367 (4.30)

sh, shoulder.

The spectroscopic data of the new compounds were in accordance with the structures. The IR spectra taken with KBr pellets showed a $-NO_2$ peak at 1552 and 1332 cm^{-1} and an intense absorption attributable to Ar–O–C at 1249 cm^{-1}, an Ar C=C peak at 1580 cm^{-1} and an aromatic CH peak at 3065 cm^{-1} for compound **1**. After conversion of compound **1** to pc **2** and **3**, the sharp C≡N vibration at 2215 cm^{-1} disappeared. The IR spectra of the metal phthalocyanines, which are very similar to each other, showed Ar–O–C peaks at 1232 cm^{-1} for all of the phthalocyanines. In addition, the stretching peaks at 2890–2830, 2895–2830 and 2915–2840 cm^{-1} indicate the presence of $-CH_2$ and $-CH_3$ in the substituents for the phthalocyanines **2**–**4**, respectively.

The ^{1}H NMR spectra were also in good correlation with the structures of the synthesized compounds. In the ^{1}H NMR spectrum of compound **1**, which was taken in DMSO, the aromatic protons appeared at 8.38–7.28 ppm as a multiplet. The peaks at 5.37 and 1.79 ppm indicated the presence of a $ArOCH_2$ group and a O_2NCCH_3 group in the structure, respectively. In the ^{1}H NMR spectrum of zinc (II) phthalocyanine **2**, which was taken in *d*-chloroform, the aromatic protons appeared at 7.94–6.96 ppm, $ArOCH_2$ protons at 5.34 ppm, O_2NCCH_3 protons at 1.72 ppm, the $-CH_2-$ protons in the long aliphatic chain at 1.50–1.09 ppm and the $-CH_3$ at the end of the chain at 0.82 ppm. The peak at 2.11 ppm indicated the presence of a $-SCH_2-$ group neighboring an aromatic ring in the structure. The ^{1}H NMR spectrum of compound **4** was similar to that of compound **2**. The aromatic protons were found at 8.62–6.92 ppm, the $ArOCH_2$ protons at 4.17 ppm and the $N{=}NCCH_3$ protons at 1.47 ppm. The $-CH_2-$ protons in the long aliphatic chain were observed at 1.73 ppm, $-SCH_2$ protons neighboring an aromatic ring at 3.31–2.63 ppm and the $-CH_3$ protons at the end of the chain at 0.95 ppm. ^{1}H NMR measurements were precluded for the cobalt (II) phthalocyanine (**3**) owing to its paramagnetic nature [35–38].

The phthalocyanines show typical electronic spectra with two strong absorption regions, one of them in the UV region at about 300–400 nm (B band) and the other in the visible portion at 600–700 nm (Q band). While the monomeric species with D_{2h} symmetry, i.e metal-free derivatives, show two intense absorptions of comparable intensity around 600–700 nm, those having D_{4h} symmetry give only a single band in this region.

The typical UV–Vis spectra of phthalocyanine **2** exhibited characteristic Q and B bands, one in the visible region at 712 nm (Q-band) attributed to the the $\pi \rightarrow \pi^*$ transition from the highest occupied molecular orbital (HOMO) to the lowest unoccupied molecular orbital (LUMO) of the pc^{2-} ring, and the other in the UV region at 322 nm (B-band) arising from the deeper π levels $\rightarrow$ LUMO transition. The electronic spectra are especially fruitful in establishing the structure of phthalocyanines **3** and **4**. The electronic spectra of the metal phthalocyanines show the characteristic Q-band absorptions as a single peak at 715 nm in the binuclear cobalt phthalocyanine **3** (Fig. 1) and at 697 nm in the tetranuclear zinc phthalocyanine **4** (Fig. 2). B bands of the phthalocyanines **3** and **4**, arising from the deeper π levels $\rightarrow$ LUMO transitions, are observed in the UV region at about 315 and 367 nm, respectively. The phthalocyanine **3** shows an additional band centered at ca. 70 nm to the blue of the normal Q-band as a result of aggregation through exciton coupling of the phthalocyanine units [25] (Table 2). In compound **4**, this band is attributed as a Q-band satellite. The intensity of

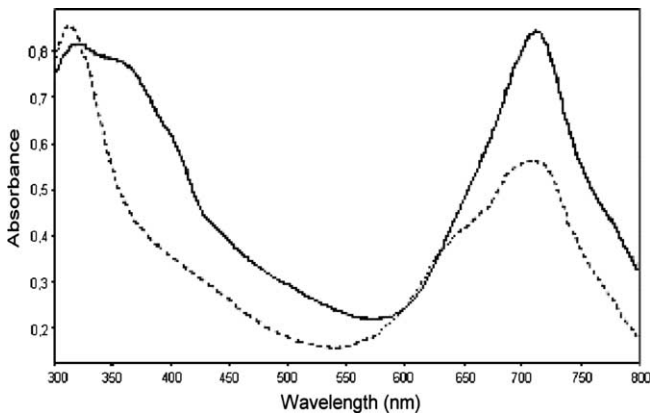

Fig. 1. UV–Vis spectra for the phthalocyanines **2**(—-) and **3** (·····).

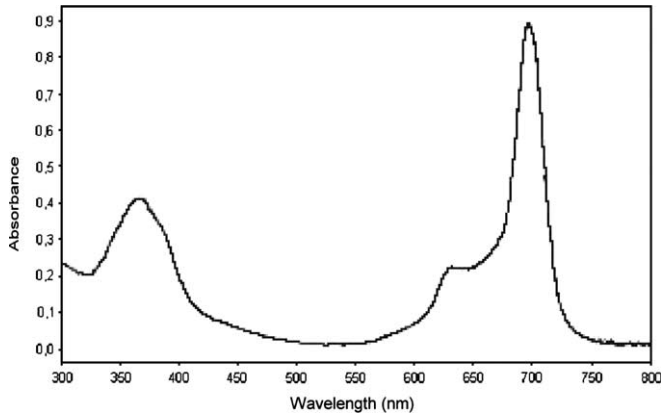

Fig. 2. UV–Vis spectra for the phthalocyanine **4.**

the Q-band relative to B is also low for binuclear cobalt phthalocyanine **3** (Fig. 1). This result is similar to those previously observed for binuclear cobalt phthalocyanines [24].

The temperature dependence of the dark d.c conductivity was obtained by the rapid cooling method which allows the avoidance of the influence of the sorption-desorption process. Fig. 3 shows the variation of d.c conductivity of compounds **2**–**4** as a function of reciprocal temperature in the temperature range 290–400 K. The well defined straight line obtained from the Arrehenius plot suggests the presence of only one conduction mechanism in the temperature range of 290–400 K for the film **2**. Thus, it is reasonable to represent the temperature dependence of conductivity for the film **2** by the well known expression,

$$\sigma_{d.c} = \sigma_0 \exp\left(-\frac{E_A}{kT}\right), \quad (1)$$

where E_A is the activation energy and k is the Boltzmann's constant. The value of the activation energy, derived from the slope of the $\log\sigma_{d.c}$ versus $1/T$ graph, is 0.91 eV for compound **2**. A deviation from linearity of the $\log\sigma_{d.c}$ versus $1/T$ plot at ~353 K was observed for compound **4**. As seen from Fig. 3, the graph splits into two different linear regions, and each region can be ascribed a different activation energy corresponding to a different dominant excitation. The activation energies obtained for region I and II were found to be 0.46 and 1.24 eV, respectively. Two different linear regions in the Arrehenius plot and hence two activation energy values, as in our case, is interpreted as a transition from extrinsic to intrinsic conduction by Nakada et al. [39]. Robinet and Clarisse [40] reported that adsorbed O_2 molecules introduce an acceptor level within the band gap and demonstrates itself as a break in the $\ln\sigma_{d.c}$ versus $1/T$ graph indicating the change from an extrinsic to an intrinsic region. A discussion of the O_2 kinetics is not the aim of this paper, but indicating that the anamoly in conductivity is not an intrinsic phenomenon. A completely different conduction mechanism was observed for compound **3**. It is clear from Fig. 3 that the temperature dependence of d.c conductivity cannot be explained by the band conduction model. This type of conduction is described by variable range hopping (VRH) of barriers in 3-dimensions, as proposed by Mott [41]. The VRH model has been extensively applied to various amorphous semiconductors over the last few decades, and recently has also been applied with a varying degree of success to conducting polymers [42]. Recently Altındal et al. [43] have shown the applicability of Mott's VRH model in spin coated phthalocyanine films. According to the VRH model, the temperature dependence of conductivity is given by

$$\sigma_{d.c} = \sigma_0 \exp\left[-\left(\frac{T_0}{T}\right)^{\gamma}\right], \quad (2)$$

where σ_0 is the high temperature limit of conductivity and T_0 is associated with the degree of localization of the electronic wave function. The exponent γ determines the dimensionality of the medium. We have plotted the d.c conductivity data as a function of $T^{-1/4}$ in Fig. 4. It is evident from the plot of $\ln\sigma_{d.c}$ versus $T^{-1/4}$ that the three-dimensional VRH model gives an excellent fit

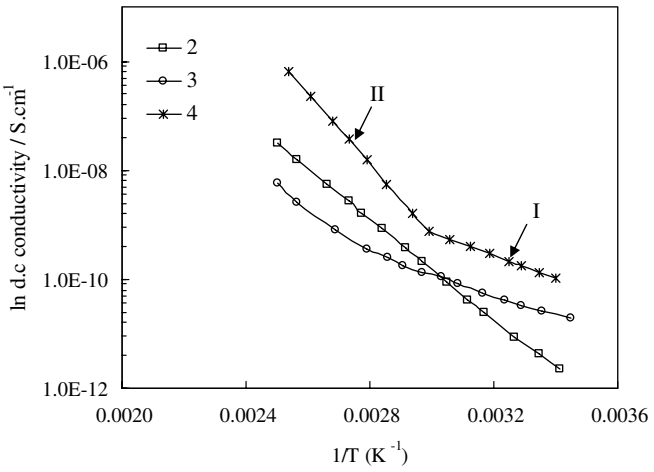

Fig. 3. Dependence of d.c conductivity on the inverse of temperature for spin coated films of compounds **2** –**4**.

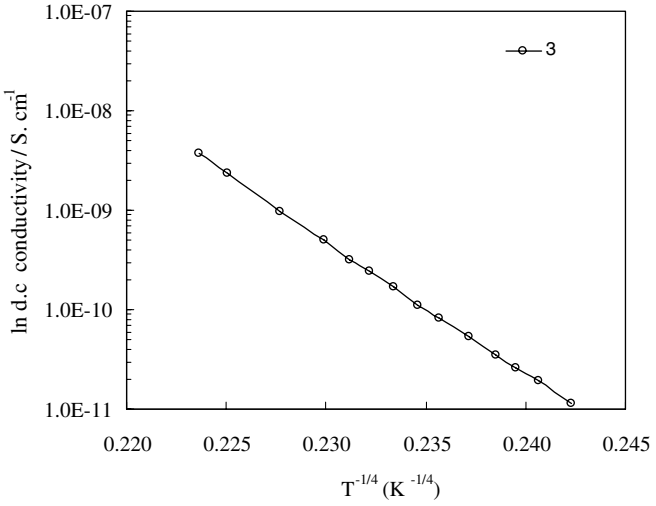

Fig. 4. D.c conductivity of film **3** as plotted against $T^{-1/4}$.

to the experimental results. Fig. 4 predicts that three-dimensional charge transport occurs in film **3**.

Cole–cole spectra of the complex impedance, $Z = Z' + jZ''$, of the pc films were recorded in the frequency range from 40 Hz to 100 kHz. The impedance spectra of compounds **2**–**4** measured at room temperature (Fig. 5(a)) and 400 K (Fig. 5(b)) are shown in Fig. 5. A quasi-vertical line was observed in the Nyquist plot for all the samples at room temperature. This results means that the impedance becomes capacitive even at a relatively high frequency. In this case, the measured impedance data can be modelled as a capacitor in parallel with a resistor in series with another resistor as shown in Fig. 5(a). The resistance R_0 in the equivalent circuit is defined as $R_0 = R_{d.c} - R_\infty$. R_∞ and $R_{d.c}$ represent the resistance at $\omega \to \infty$ and $\omega \to 0$, respectively. The impedance response of the compounds significantly changes with temperature. On the complex plane plot, only depressed semicircles with different radius were observed for compounds **2**–**4** at 400 K, indicating deviation from the Debye dispersion relation. In the case of a depressed semicircle in the impedance spectra, the relaxation time is considered as a distribution of values, rather than a single relaxation time.

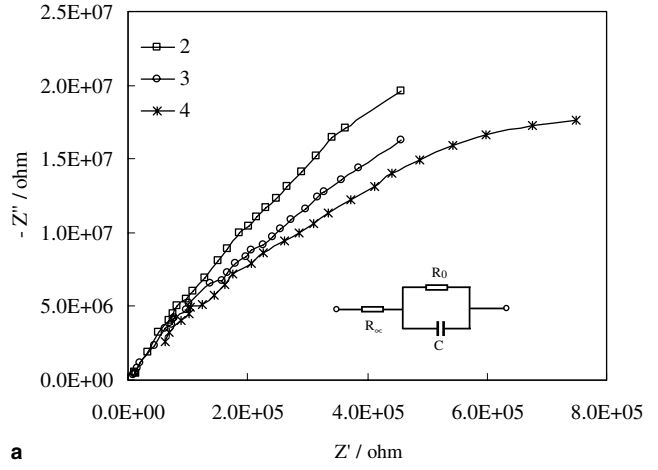

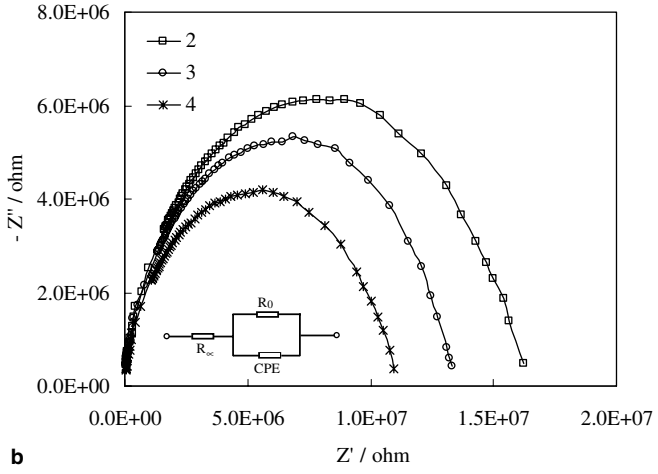

Fig. 5. Nyquist plot (Z'' vs. Z') of the samples: at room temperature (a) and 400 K (b).

Therefore, the equivalent circuit is modified to include a constant phase element (CPE) as shown in Fig. 5(b). The series resistance in the equivalent circuit represents the ohmic losses in the test fixture and electrode sheet resistance. The parallel resistance is of the coating material in parallel with that of the substrate. The presence of the constant phase element represents a slight distribution of relaxation times instead of a discrete relaxation time. This conclusion was supported by another type of Bode plot (log $|Z|$ versus log $|f|$). The Bode plot for compound **4** is shown in Fig. 6. The dependence of log $|Z|$ versus log $|f|$ shows a slope of -0.987, corresponding to capacitive behaviour at room temperature. At 400 K, the slope for log $|Z|$ versus log |f| is -0.505 which indicates the presence of a CPE . Similar results of the Bode plot were found for compounds **2** and **3**.

The total conductivity, $\sigma_{tot.}$, over a range of frequencies, may often be expressed according to the following expression:

$$\sigma_{tot.} = \sigma_0 + \sigma(\omega), \tag{3}$$

where σ_0 is the d.c conductivity. The frequency dependent part of the total conductivity, $\sigma(\omega)$, is given by the power law of the form [44],

$$\sigma(\omega) = A\omega^s \tag{4}$$

where A and s are temperature dependent parameters. As a representative result, the temperature dependence of the measured a.c conductivity as a function of frequency at the indicated temperature are shown in Fig. 7 for film **4.** Low frequency conductivity measurements could not be performed below 337 K due to its high resistivity. As seen from Fig. 7 for a temperature above 337 K, there is a nearly constant conductivity at low frequency and after a certain characteristic frequency it increases with the power law. Similar results were obtained for films **2** and **3**. Various models such as quantum mechanical tunelling (QMT) and correlated barrier hopping (CBH) has been proposed to explain this type of behaviour, but it is not easy to decide which of those mechanism is responsible for the observed

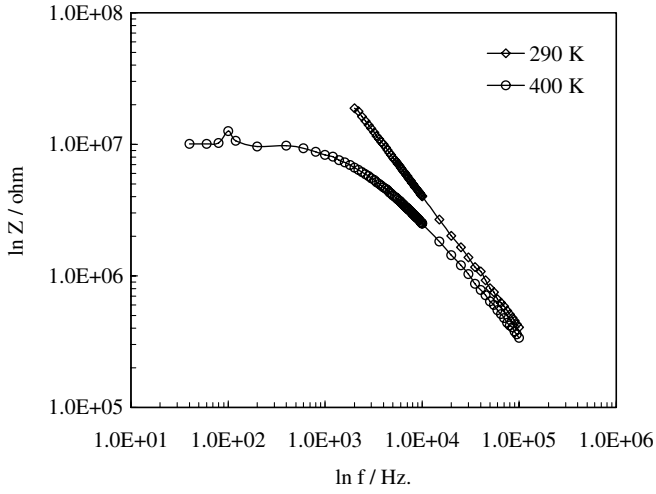

Fig. 6. Bode plot for compound **4** at room temperature and 400 K.

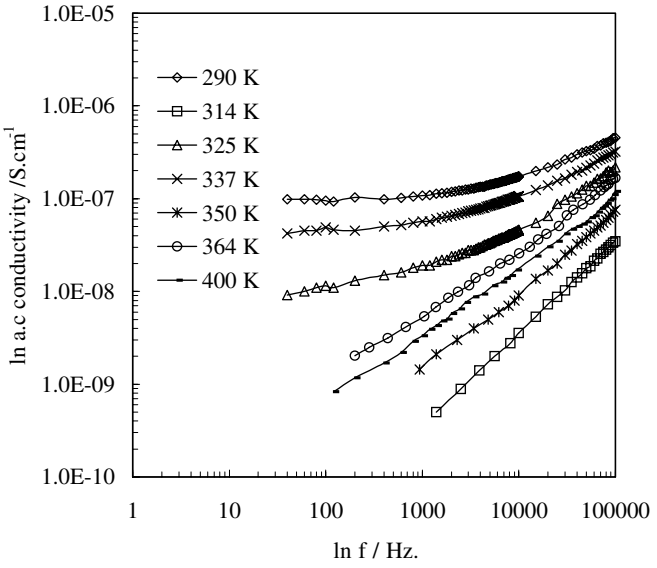

Fig. 7. Frequency dependent conductivity of film **4** at selected temperatures.

conduction mechanism. However, the behaviour of the exponent s with temperature can help in determining the possible conduction mechanism. Fig. 8 shows the thermal variation of the frequency exponent s for all compounds The values of s are calculated from the slope of $\ln\sigma(\omega, T)$ versus ln f graphs and were generally found to decrease with increasing temperature. The behaviour of s with temperature cannot be explained by the QMT model. This model, which is based on phonon asissted tunnelling of electrons predicts a temperature independent frequency exponent s with a constant value around 0.8. According to the CBH model, which was developed by Eliot [45], the a.c conductivity which can be expressed to a first-order approximation as

$$\sigma(\omega) = \frac{\pi^2 N^2 \varepsilon}{24}\left[\frac{8e^2}{eW_m}\right]^6 \frac{\omega^s}{\tau_0^\beta}, \tag{5}$$

where N is the density of localized states, ε the permittivity, τ_0 the effective relaxation time, e the electronic charge and s is predicted to be temperature dependent following an equation of the form,

$$s = 1 - \frac{6kT}{W_m} \tag{6}$$

where W_m is the optical band gap. Unlike the QMT model, the CBH model predicts a temperature dependent s parameter which decreases with increasing temperature.

It is clear from the temperature dependence of the frequency exponent s (Fig. 8) that our data are quantitatively consistent with the prediction of the CBH model.

It is known that when a test gas molecule is adsorbed on the surface of a phthalocyanine film it causes a variation in physical or chemical properties, such as conductivity. The effect of the same concentration (200 ppm) of five different VOC vapours on the conductivity of the film of **4** is shown in Fig. 9 at room temperature. As usual, a d.c voltage of 0.6 volt was applied to the sensor during the measurements. At a sensing temperature of 290 K, the current level in nitrogen environment was 1.05×10^{-10} A. After exposure to 200 ppm VOC vapours, the current increased sharply in the initial doping stage for a few minutes and then the rate of increase slowed down to reach a current of 5.6×10^{-10} and 2.42×10^{-10} A after 10 min for chloroform (maximum current change) and ethanol (minimum current change), respectively. Although a complete steady-state current, which quantifies the VOC concentration, cannot be approached during a period of 10 min even at an operating temperature of 400 K, the incease in current is adequate to indicate the presence of VOC vapours in the atmosphere. Fig. 9 also shows that the response characteristics of compound **4** to VOC vapours are different. It is noticed that there are two stages of current changes, an initial fast decrease followed by a slow drift, in the recovery processes. The kinetics of adsorption can be described, bearing in

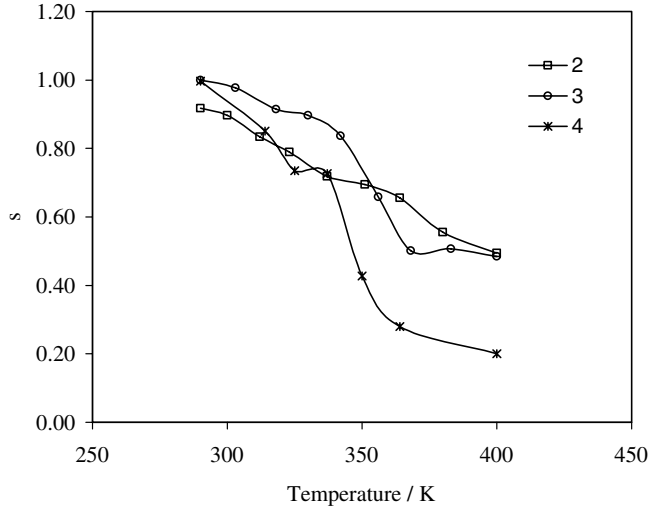

Fig. 8. The variation of the frequency exponent s with temperature for compounds **2**–**4**.

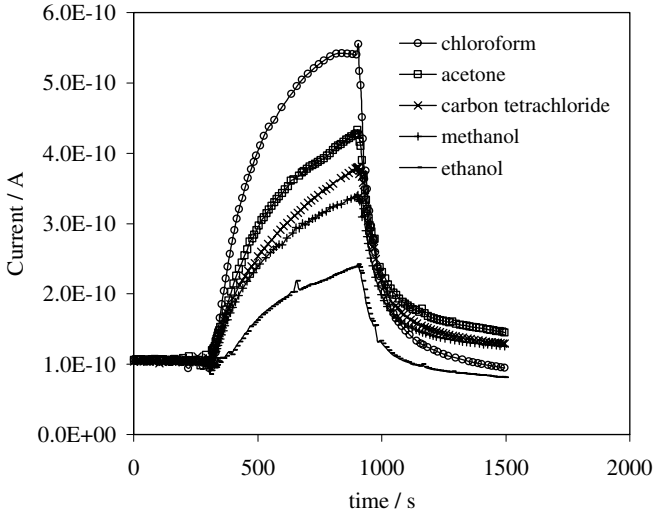

Fig. 9. Current vs. time of a spin coated film of **4** exposed to 200 ppm of five different VOC vapours.

mind that phthalocyanines are p-type semiconductors, in terms of a charge transfer interaction between the phthalocyanine and VOC vapours.

In our case the VOCs would play an electron acceptor role. When the VOC molecules interact with the π-elecron network of the phthalocyanines, it causes the transfer of an electron from the phthalocyanine ring to the VOC molecule. Thus, the induced positive holes on the film surface give rise to an increase in the p-type conductivity of the film. The failure to return to baseline after the VOC vapours are removed originates from the strong bonding of the VOC molecules on the surface. Similar response characteristics were obtained for other sensors based on phthalocyanine films [46]. In order to determine the optimal working temperature, the sensing measurements were carried out in the temperature range of 290–400 K. Fig. 10 shows the sensitivity of the film **4** to 200 ppm concentrations of VOC vapours as a function of sensing temperature, where the sensitivity (S) is defined as

$$S = \frac{1}{C}\left[\frac{\Delta I}{I_0}\right], \tag{7}$$

where ΔI is the change in current at a concentration of organic solvent vapor (C), I_0 is the reference value of the coated devices expoed to dry nitrogen (without the doping VOC vapours). Maximum sensitivity was obtained at room temperature and the sensitivity of the film decreases rapidly with increasing temperature (Fig. 10). This type of behaviour has previously been reported [47] and was explained on the basis of the negative heat of adsorption. In general, the sensitivity of the sensor has been related to the number of the active adsorption sites on the sensing layer.

The present result shows that the increase in temperature gives a significant effect in reducing the sensitivity. Electron microscopy studies of thin phthalocyanine films show that heat treatment induces crystallization of the amorphous region [48]. The decrease of sensitivity with increasing temperature is consistent with the thermally induced structural changes. Like the device coated with **4**, the sensors coated with **2** and **3** also exhibited a reduction of sensitivity with increasing temperature. Consequently, the sensitivity of the compound **4** film is the highest for all the VOC vapours investigated. The maximum sensitivity with all the sensors are obtained at room temperature for all organic solvents. In light of the above result, it seems that the surface processes occuring on the sensing layer during the exposure to VOC vapours still need to be given detailed research.

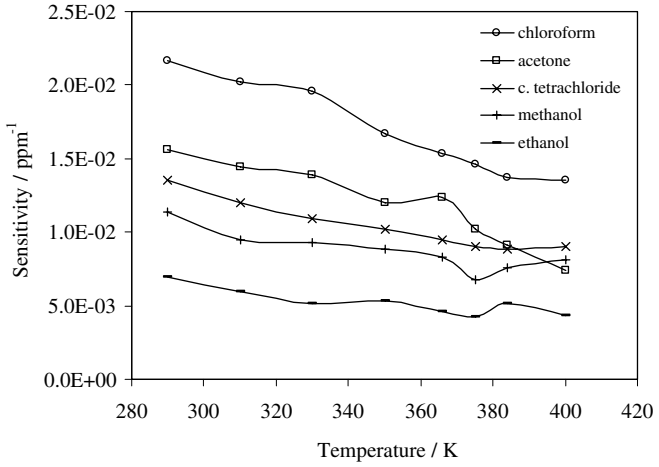

Fig. 10. The variation of the sensitivity with temperature for film **4** for the indicated VOC vapours.

5. Conclusion

2-Nitro-2methyl-1,3-bis(3,4-dicyanophenoxymethyl)propane was synthesized and used as a key compound for the preparation and characterization of novel multinuclear metallophthalocyanines (Zn, Co) with alkylthio substituents. The d.c and detailed a.c impedance spectroscopy techniques have been used to investigate the charge transport mechanism and the response characteristics of novel multinuclear metallophthalocyanines with alkylthio substituents to VOC vapors. While the d.c conductivity of film **2** shows an Arrhenius dependence in the temperature range of 290–400 K, a transition from extrinsic to intrinsic conductivity at ~353 K was observed for film **4.** The temperature dependence of the d.c conductivity of compound **3** was well represented by the variable range hopping model, $T^{-1/4}$ law, in the whole temperature range. The a.c. conductivity $\sigma(\omega)$ varied as ω^s , where the exponent s was found to be a temperature dependent variable and always less than unity. An analysis of the measured a.c conductivity data and the dependency of frequency exponent s on temperature indicated that the conduction mechanism can be explained by the correlated barrier hopping (CBH) model for all compounds. It was found from the gas sensing measurements that the increase in temperature reduces the sensitivity of the films to VOC vapors. The impedance spectra of the films can be represented by an electrical equivalent circuit.

Acknowledgements

Financial assistance from the Research Fund of Gülhane Medical Academy of Ankara and in part from the Turkish Academy of Sciences (TUBA) are gratefully acknowledged. We also gratefully acknowledge Mr. Mesut Akyol, computer expert, Gülhane Medical Academy of Ankara for valuable help.

References

[1] H. Eichhorn, D. Wöhrle, D. Pressner, Liq. Cryst. 22 (1997) 643.
[2] D. Lelievre, M.A. Petit, J. Simon, Liq. Cryst. 4 (1989) 707.
[3] I. Rosenthal, in: C.C. Leznoff, A.B.P. Lever (Eds.), The Phthalocyanines Properties and Applications, 4, VCH, New York, 1996, p. 485.
[4] J.H. Zagal, Coordin. Chem. Rev. 119 (1992) 89.
[5] P. Janda, N. Kobayashi, P.R. Auburn, H. Lam, C.C. Leznoff, A.B.P. Lever, Can. J. Chem. 67 (1989) 1109.

[6] N. Kobayashi, W.A. Nevin, Appl. Organomet. Chem. 10 (1996) 579.
[7] W.J. Todd, F. Bailly, J. Pavez, P.W. Faguy, R.P. Baldwin, R.M. Buchanan, J. Am. Chem. Soc. 120 (1998) 4887.
[8] M.K. Halbert, R.P. Baldwin, Anal. Chem. 57 (1985) 591.
[9] E. Karmann, D. Schlettwein, N.I. Jaeger, J. Electroanal. Chem. 405 (1996) 149.
[10] J.M. Lupton, Appl. Phys. Lett. 81 (2002) 2478.
[11] D.K. Rittenberg, K.I. Sugiyra, Y. Sakata, S. Mikami, A.J. Epstein, J.S. Miller, Adv. Mater. 12 (2000) 126.
[12] N. Toshima, T. Tominaga, S. Kawamura, Bull. Chem. Soc. Jpn. 69 (1996) 245.
[13] B. Lukas, J. Silver, M.J. Lovett, M.J. Cook, Chem. Phys. Lett. 241 (1995) 351.
[14] D. Wöhrle, L. Kreienhoop, G. Schnurpfeil, J. Elbe, B. Tennigkeit, S. Hiller, D. Schlettwein, J. Mater. Chem. 5 (1995) 1819.
[15] M.O. Liu, C.H. Tai, W.Y. Wang, J.R. Chen, A.T. Hu, T.H. Wei, J. Organomet. Chem. 689 (2004) 1078.
[16] A. Altındal, Z.Z. Öztürk, S. Dabak, Ö. Bekaroğlu, Sens. Actuat. B 77 (2001) 389.
[17] M.I. Newton, T.K.H. Starke, M.R. Willis, G. Mchale, Sens. Actuat. B 67 (2003) 307.
[18] R. Rella, J. Spadavecchia, G. Ciccarella, P. Siciliano, G. Vasapollo, L. Valli, Sens. Actuat. B 89 (2003) 86.
[19] Ş. Abdurrahmanoğlu, A.R. Özkaya, M. Bulut, Ö. Bekaroğlu, J. Chem. Soc., Dalton Trans. (2004) 4022.
[20] M. Kandaz, I. Yılmaz, Ö. Bekaroğlu, Polyhedron 19 (2000) 19115.
[21] I. Yılmaz, Ö. Bekaroğlu, Chem. Ber. 129 (1996) 967.
[22] M. Koçak, A.G. Gürek, A. Gül, Ö. Bekaroğlu, Chem. Ber. 127 (1994) 355.
[23] Ö. Bekaroğlu, Appl. Organomet. Chem. 10 (1996) 605.
[24] W.A. Nevin, M.R. Hempstead, W. Liu, C.C. Leznoff, A.B.P. Lever, Inorg. Chem. 26 (1987) 570.
[25] W.A. Nevin, W. Liu, M.R. Hempstead, S.M. Marcuccio, M. Melnik, C.C. Leznoff, A.B.P. Lever, Inorg. Chem. 26 (1987) 891.
[26] K.J. Balkus, A.G. Gabrielov, S.I. Bell, F. Bedioui, L. Roue, J. Devynck, Inorg. Chem. 33 (1994) 67.
[27] A.B.P. Lever, Inorg. Chim. Acta. 203 (1993) 171.
[28] K. Morishige, S. Tomayasu, G. Iwano, Langmuir 13 (1997) 5284.
[29] Y.-L. Lee, C.-Y. Sheu, R. Hsio, Sens. Actuat. B 99 (2004) 281.
[30] N. Ozan, Ö. Bekaroğlu, Polyhedron 22 (2003) 819.
[31] Ş. Abdurrahmanoğlu, A. Altındal, A.R. Özkaya, M. Bulut, Ö. Bekaroğlu, Chem. Commun. (2004) 2096.
[32] T. Ceyhan, M. Korkmaz, T. Kutluay, Ö. Bekaroğlu, J. Porphyr. Phthalocyanine. 8 (2004) 1383.
[33] J.G. Young, W. Onyebuagu, J. Org. Chem. 55 (1990) 2155.
[34] A.G. Gürek, Ö. Bekaroğlu, J. Chem. Soc., Dalton Trans. (1994) 1419.
[35] C.C. Leznoff, A.B.P. Lever (Eds.), Phthalocyanines Properties and Applications, VCH, Weinheim, 1989.
[36] A.R. Koray, V. Ahsen, Ö. Bekaroğlu, J. Chem. Soc., Chem. Commun. (1986) 932.
[37] V. Ahsen, E. Yılmazer, M. Ertaş, Ö. Bekaroğlu, J. Chem. Soc., Dalton Trans. (1988) 401.
[38] G. Gümüş, Z.Z. Öztürk, V. Ahsen, A. Gül, Ö. Bekaroğlu, J. Chem. Soc., Dalton Trans. (1992) 2485.
[39] I. Nakada, K. Ariga, A. Ichimaya, J. Appl. Phys. Soc. Jpn. 19 (1964) 1587.
[40] S. Robinet, C. Clarisse, Thin Solid Films 170 (1989) L51.
[41] N.F. Mott, E.A. Davis, Electronic Processes in Non-crystalline Materials, Calerendon, Oxford, 1979.
[42] P. Dutta, S.K. De, Synthetic Met. 139 (2003) 201.
[43] A. Altındal, Ş. Abdurrahmanoğlu, M. Bulut, Ö. Bekaroğlu, Synthetic Met. 150 (2005) 181.
[44] W.K. Lee, J.F. Lin, S. Walker, Phys. Rev. Lett. 67 (1991) 1559.
[45] S.R. Eliot, Philos. Mag. 36 (1977) 1291.
[46] P. Roisin, J.D. Wright, R.J.M. Nolte, O.E. Sielcken, S.C. Thorpe, J. Mater. Chem. 2 (1992) 131.
[47] C. Choi, S. Lee, W.-J. Lee, Sens. Actuat. B 32 (1996) 77.
[48] J.R. Fryer, in: 37th Ann. Proc. Electron Microscopy Soc. Amer. San Antonio, TX, 1979, p. 616.

Available online at www.sciencedirect.com
SCIENCE DIRECT®
Polyhedron 25 (2006) 747–752
POLYHEDRON
www.elsevier.com/locate/poly

Role of electronic factors in the formation of anionic complexes of tellurium(IV): Crystal structure of bis(4-methylbenzoylmethyltriphenylphosphonium) hexabromotellurate(IV)

Ashok K.S. Chauhan [a,*], Arun Kumar [a], Shobhit Charan [a,1], Ramesh C. Srivastava [a], Ray J. Butcher [b]

[a] *Department of Chemistry, University of Lucknow, Lucknow 226007, India*
[b] *Department of Chemistry, Howard University, Washington, DC 20059, USA*

Received 21 July 2005; accepted 21 July 2005
Available online 8 September 2005

Abstract

Reactions of $[(4\text{-}MeOC_6H_4COCH_2)Ph_3P]Br$ (**1c**) with $(4\text{-}XC_6H_4COCH_2)_2TeBr_2$ (X = H, **2a**; Me, **2b**; OMe, **2c**) lead to Te–C bond cleavage to afford $[(4\text{-}MeOC_6H_4COCH_2)Ph_3P]_2[TeBr_6]$ (**3c**). The analogous complexes $[(4\text{-}MeC_6H_4COCH_2)Ph_3P]_2[TeBr_6]$ (**3b**) and $[(C_6H_5COCH_2)Ph_3P]_2[TeBr_6]$ (**3a**) are obtained from the reaction of the corresponding phosphonium bromide with **2c**. The 1:1 adducts $[(4\text{-}XC_6H_4COCH_2)Ph_3P]^+[(4\text{-}XC_6H_4COCH_2)_2TeBr_3]^-$, formed as intermediates, could be isolated only in case of X = H or Me. The crystal structure of **3b**, which crystallizes with one molecule of dichloromethane, shows the presence of close C–H···Br/Cl contacts among the ions and solvated molecules. These weak interactions distort, though marginally, the otherwise ideal octahedral shape of the $[TeBr_6]^-$ anion adopted as a consequence of stereochemical inertness of the lone pair on the central tellurium atom. The supramolecular extended arrays of ionic molecular units formed by means of solvated head-to-tail linkers are identified.
© 2005 Elsevier Ltd. All rights reserved.

Keywords: Te–C bond cleavage; Intramolecular coordination; Secondary interaction; Anionic complexes; Supramolecular association

1. Introduction

Hexahalotellurates(IV) and their oligomeric anionic species are interesting examples of stereochemical inertness of a lone pair on the central atom. Similar anionic species containing one or two Te–C bonds have been comparatively less studied [1,2] though the first of such five-coordinate anions, $[MeTeCl_4]^-$, was prepared as early as 1929 [3]. Anions with two Te–C bonds are comparatively rare and appear to be particularly stable when the two Te–C bonds are part of a cycle, e.g., $[-(CH_2)_4-TeX_4]^{2-}$ [2]. We have recently reported the preparation and structural characterization of bis(4-substitutedbenzoylmethyl)tellurium dihalides (**2**) [4]. The crystal structure of **2a**, its iodide anologue and **2c** showed the presence of rare intramolecular 1,4-Te···O(C) secondary interactions which tend to saturate the Te atom coordinatively and discourage ubiquitous intermolecular Te···X (halide) bonding in the solid state. It appeared, therefore, of interest to examine the acceptor property of **2** towards a few phosphonium bromides with varying electronic environments at the phosphorus center.

* Corresponding author.
E-mail address: akschauhan@hotmail.com (A.K.S. Chauhan).
[1] Present address: Centre for Material for Electronic Technology (C-MET), Pune 411 008, India.

0277-5387/$ - see front matter © 2005 Elsevier Ltd. All rights reserved.
doi:10.1016/j.poly.2005.07.038

2. Results and discussion

Reactions of (4-substitutedbenzoylmethyl)triphenylphosphonium bromides, $[(4\text{-}XC_6H_4COCH_2)Ph_3P]Br$, (X = H, **1a**; Me, **1b**; OMe, **1c**) with bis(4-substitutedbenzoylmethyl)tellurium dibromides, $(4\text{-}XC_6H_4COCH_2)TeBr_2$ (X = H, **2a**; Me, **2b**; OMe, **2c**) have been carried out in dichloromethane or chloroform. The isolable product in the reaction of **1c** with **2a**, **2b** or **2c** is the phosphonium salt of hexabromotellurate(IV), $[(4\text{-}MeOC_6H_4COCH_2)Ph_3P]_2[TeBr_6]$ (**3c**). Similarly, reaction of **1a** or **1b** with **2c** affords the corresponding $[(4\text{-}XC_6H_4COCH_2)Ph_3P]_2[TeBr_6]$, [X = H, **3a**; Me, **3b**]. All these reactions must involve cleavage of both the Te–C bonds of **2** while the P–C bonds remain intact. The ^{1}H NMR spectra of **3** show a multiplet for aryl protons and a doublet for P–CH_2 protons with $^2J(^{31}P\text{–}^1H)$ ~12 Hz. The molar conductivity of **3** in nitrobenzene (40–42 Ω^{-1} cm^{-1} mol^{-1}) is consistent with the 2:1 electrolytic nature.

The reaction between **1a** and **2a** or **1b** and **2b** in 1:1 or 2:1 ratios initially affords the expected 1:1 adduct, $[(4\text{-}C_6H_4COCH_2)Ph_3P]^+[(4\text{-}XC_6H_4COCH_2)_2TeBr_3]^-$ (X = H, **4a**; Me, **4b**) along with the separation of traces of elemental tellurium. Both **4a** and **4b** give reasonably good elemental analyses and are 1:1 electrolytes as shown by their conductivity measurements. It is their ^{1}H NMR spectra which are intriguing. The ^{1}H NMR spectra of **4a** and **4b** show, in addition to a multiplet for aryl protons, a doublet for P–CH_2[$^1J(^{31}P\text{–}^1H)$ = 12.01–12.30 Hz] and a singlet for Te–CH_2 protons in a 1:1 ratio rather than the expected 1:2 ratio. The spectrum of **4b** (X = Me) also consists of an additional two singlets in a 1:1 ratio for the methyl protons. These observations suggest disproportionation of the 1:1 adducts (**4a** or **4b**) in $CDCl_3$ (Eq. (1)). While the formation of **A** is less likely as the reaction of **1a** with **2a** or **1b** with **2b** even in a 2:1 molar ratio affords only **4a** or **4b**, the complex **B** receives support from

$$[RPh_3P]_2[TeBr_6.TeR_2]_{\mathbf{B}} \xleftarrow[\text{or}-2RH]{-R-R} 2[RPh_3P][R_2TeBr_3] \xrightarrow[-R_2TeBr_2]{} \underset{\mathbf{A}}{[RPh_3P]_2[R_2TeBr_4]}$$
$$R = 4 - XC_6H_4COCH_2; (X = H, Me) \quad (1)$$

the recent isolation of $[TeBr_6\cdot(SeBr_2)_2]^-$ and $[TeBr_6\cdot(Se_2Br_2)_2]^-$ anions with unsymmetrical phosphonium cations [5]. However, repeated attempts to crystallize **4b**, in dichloromethane, eventually afford X-ray grade crystals of **3b**. It is thus interesting to note that the MeO substituent in the phenyl ring of the phenacyl ligand promotes the cleavage of Te–C bonds and leads to the instantaneous formation of **3** while the Me substituent initially gives the 1:1 adduct.

2.1. Crystal structure of *3b*

The crystal structure of $[(4\text{-}MeC_6H_4COCH_2)Ph_3P]_2[TeBr_6]\cdot CH_2Cl_2$ together with the atom numbering scheme is shown in Fig. 1, and the bond parameters are presented in Table 1. The lattice is composed of discrete $[TeBr_6]^-$ anions and $[(4\text{-}MeC_6H_4COCH_2)Ph_3P]^+$ cations together with dichloromethane molecules. The asymmetric unit consists of one cation and only halves of the anion and the solvated molecule. The geometry of the hexabromotellurate anion is nearly octahedral,

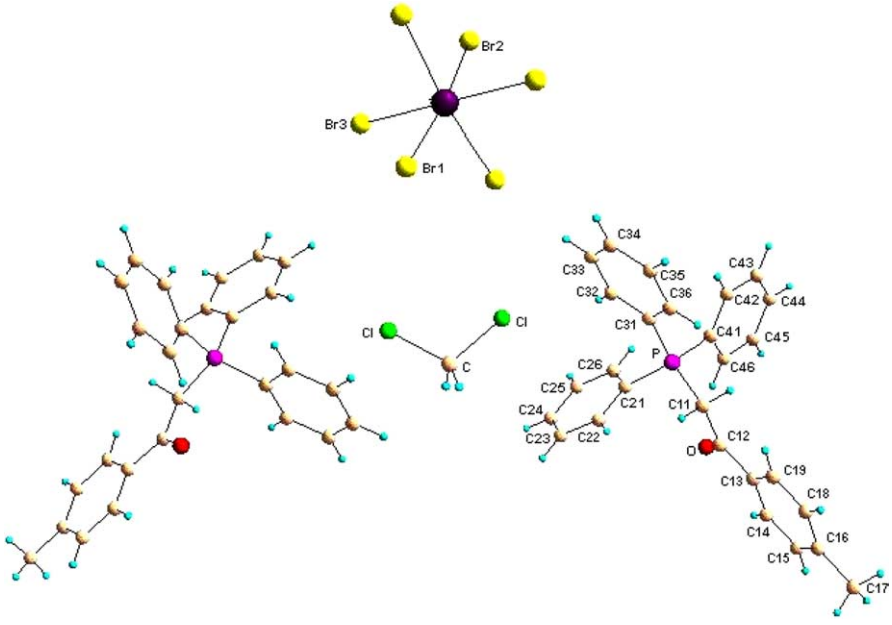

Fig. 1. Molecular structure of compound **3b**.

Table 1
Selected bond parameters for **3b**

Bond lengths (Å)	
Te–Br(2)	2.6638(3)
Te–Br(2)#1	2.6638(3)
Te–Br(3)#1	2.7052(3)
Te–Br(3)	2.7052(3)
Te–Br(1)	2.7434(3)
Te–Br(1)#1	2.7434(3)
P–C(21)	1.791(2)
P–C(41)	1.800(2)
P–C(31)	1.806(2)
P–C(11)	1.818(2)
O–C(12)	1.221(3)
C–Cl	1.744(3)
C–Cl#1	1.744(3)
Bond angles (°)	
Br(2)–Te–Br(2)#1	85.724(13)
Br(2)–Te–Br(3)#1	93.749(9)
Br(2)#1–Te–Br(3)#1	86.354(8)
Br(2)–Te–Br(3)	86.354(9)
Br(2)#1–Te–Br(3)	93.749(9)
Br(3)#1–Te–Br(3)	179.860(14)
Br(2)–Te–Br(1)	173.801(9)
Br(2)#1–Te–Br(1)	89.580(9)
Br(3)#1–Te–Br(1)	89.981(8)
Br(3)–Te–Br(1)	89.924(8)
Br(2)–Te–Br(1)#1	89.580(9)
Br(2)#1–Te–Br(1)#1	173.801(9)
Br(3)#1–Te–Br(1)#1	89.924(8)
Br(3)–Te–Br(1)#1	89.981(8)
Br(1)–Te–Br(1)#1	95.380(13)
C(21)–P–C(41)	111.86(11)
C(21)–P–C(31)	106.96(11)
C(41)–P–C(31)	108.39(11)
C(21)–P–C(11)	111.30(11)
C(41)–P–C(11)	110.11(11)
C(31)–P–C(11)	108.05(11)
Cl#1–C–Cl	112.9(3)
C(12)–C(11)–P	112.90(16)
P–C(11)–H(11A)	109.0
P–C(11)–H(11B)	109.0
O–C(12)–C(13)	121.7(2)
O–C(12)–C(11)	119.5(2)
C(26)–C(21)–P	120.91(18)
C(22)–C(21)–P	118.70(18)
C(32)–C(31)–P	118.41(18)
C(36)–C(31)–P	122.00(18)
C(42)–C(41)–P	119.24(17)
C(46)–C(41)–P	120.90(18)

Symmetry transformations used to generate equivalent atoms: #1x, $-y-1/2$, $-z+2$.

typical of TeX_6^{2-} (X = Cl [6], Br [7], I [8]) anions, which are reported to be unaffected by the size of the counter cations [9]. This geometry is reminiscent of stereochemical inactivity of the lone pair on the central atom in 14-electron AX_6E species, which is believed to be a manifestation of interligand repulsion that predominates when the separation among the large monoatomic electronegative X ligands becomes less than the van der Waals' separation. It is thus assumed that the lone pair on Te atom resides in the stereochemically inert 6s orbital. In the compound **3b**, although the three independent Te–Br bond lengths vary over a wider range (2.6638(3)–2.7434(3) Å) in comparison to those in K_2TeBr_6 [7a], $[H_9O_4][TeBr_6]$ [7b] or $[Me_3PhN][TeBr_6]$ [7d], the mean value, 2.7036 Å, remains almost the same. However, the angular distortion (with the largest deviation of 6.202° and 3.655° in the *trans* and *cis* Br–Te–Br angles, respectively) is greatest of the observed values so far. Besides other crystal forces, the interionic C–H···Br contacts, closer than the van der Waals' separation (3.05 Å) and listed in Table 2, may also be held responsible for the observed distortion of the octahedral anion. Each of the bromine ligands with a partial negative charge interacts with the benzene ring or methylene C–H proton donors of neighboring cations (Fig. 2). Similar, though smaller, distortion of the $TeBr_6$ octahedron in the anions $[TeBr_6(Se_2Br_2)]^{2-}$ [5a] and $[TeBr_6(SeBr_2)]^{2-}$ [5b] due to non-covalent Se···Br interactions (involving only four of the six bromine ligands) has been observed earlier. The significant importance of the relatively weak C–H···X interactions (X = P, O, N, Cl, Br, I) to the organization of the solid state has been widely recognized [10].

The benzoylmethyl group in the phosphonium cation $[(4\text{-}MeC_6H_4COCH_2)Ph_3P]^+$ adopts a cisoidal conformation and the intramolecular distance between the phosphorus and the carbonyl oxygen atom [2.9161(18) Å], is shorter than the sum of their van der Waals radii (3.32 Å).This suggests a significant direct electron-donative interaction from the carbonyl oxygen atom to the positively charged P atom. A comparable intramolecular P···O separation 2.878(12) Å observed in the crystal structure of the benzyl(2-methoxyphenyl)phosphonium bromide was also supported by energy minimization calculations [11]. The short P···O distance in the present case is not a result of geometrical constrain as could be in the case of the 2-methoxyphenylphosphonium cation. However, there is no appreciable lengthening of the P–C31 bond compared to the other three P–C bonds, in spite of an almost linear O···P–C31 alignment {∠O···P–C31 = 160.990(76)°}. The P···O interaction may, therefore, be electrostatic in nature instead of a σ^*(P–C) ← n(O) covalent interaction. The observed cisoidal orientation of the benzoylmethyl group also facilitates the C17–H···Cl(CH_2Cl_2) close contact. The methylene fragment of the dichloromethane solvate simultaneously acts as a multiple proton donor to the Br2 atoms of a $TeBr_6^{2-}$ anion. Extended supramolecular chains of molecular units (consisting of a $TeBr_6^{2-}$ anion encompassed by a pair of phosphonium cations) linked by means of solvated CH_2Cl_2 molecules thus become apparent (Fig. 3). In addition, there are other C–H···Br van der Waals' contacts that govern the packing of such chains in the solid state.

Table 2
Hydrogen bond parameters for **3b**

D–H···A	d(D–H)	d(H···A)	d(D···A)	∠(DHA)
C(14)–H(14A)···O#5	0.9511(25)	2.5045(18)	2.8003(31)	98.016(160)
C(46)–H(46A)···O#1	0.9496(28)	2.3698(17)	3.0225(32)	125.565(170)
C(19)–H(19A)···Br(1)#2	0.9499(25)	2.9346(3)	3.8421(24)	160.255(147)
C(11)–H(11B)···Br(3)#2	0.9894(24)	2.6814(3)	3.6419(25)	163.780(142)
C(35)–H(35A)···Br(2)#4	0.9498(25)	2.8303(3)	3.5807(27)	136.633(159)
C(44)–H(44A)···Br(2)#5	0.9513(21)	2.9429(1)	3.6457(25)	131.714(139)
C–H(0A)···Br(2)#3	0.9601(35)	2.9469(2)	3.6832(51)	134.414(5)
C(17)–H(17C)···Cl#5	0.9798(28)	2.8443(9)	3.7162(29)	148.651(164)

Symmetry transformations used to generate equivalent atoms: #1x, $-y-1/2$, $-z+2$; #2$x+1/2$, $-y-1/2$, $z-1/2$; #3$x+1$, $-y-1/2$, $-z+2$; #4$x+1/2$, y, $-z+3/2$; #5 $-x+3/2$, $y+1/2$, $-z+3/2$.

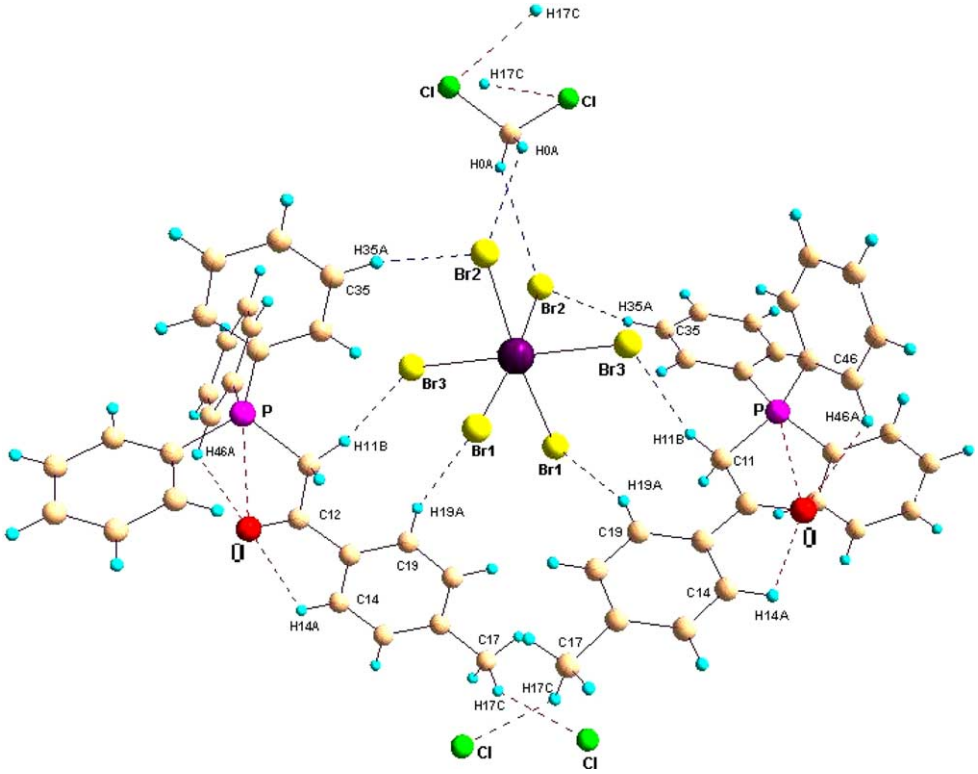

Fig. 2. A selected segment of the crystal lattice depicting interlinking of $TeBr_6^-$ anions through C–H···Br interactions.

3. Experimental

3.1. General

Commercial tellurium powder (Fluka) was dried at 120 °C and ground for 15 min just before use. 4-Substitutedbenzoylmethyl bromides were prepared by bromination of the parent acetophenones in glacial acetic acid. The phosphonium salts, $[(4\text{-}XC_6H_4COCH_2)Ph_3P]Br$, (X = H, **1a**; Me, **1b**; OMe, **1c**) were prepared and characterized following the literature method [12]. Bis(4-substitutedbenzoylmethyl)tellurium dibromides, $(4\text{-}XC_6H_4COCH_2)_2TeBr_2$ (X = H, **2a**; Me, **2b**; OMe, **2c**) were prepared as reported earlier [4]. Melting points were recorded in capillary tubes and are uncorrected. ^1H NMR spectra were recorded at 300.13 MHz in $CDCl_3$on Varian 300 spectrometers, using Me_4Si as internal standard. Microanalyses (carbon and hydrogen) were carried out using a Carlo Erba 1108 make analyzer. Conductance measurements were made using Toshniwal conductivity bridge and dip type cell (cell constant 0.80) in 10^{-3} M nitrobenzene solutions. Tellurium was estimated volumetrically and the halogen content gravimetrically as silver halide.

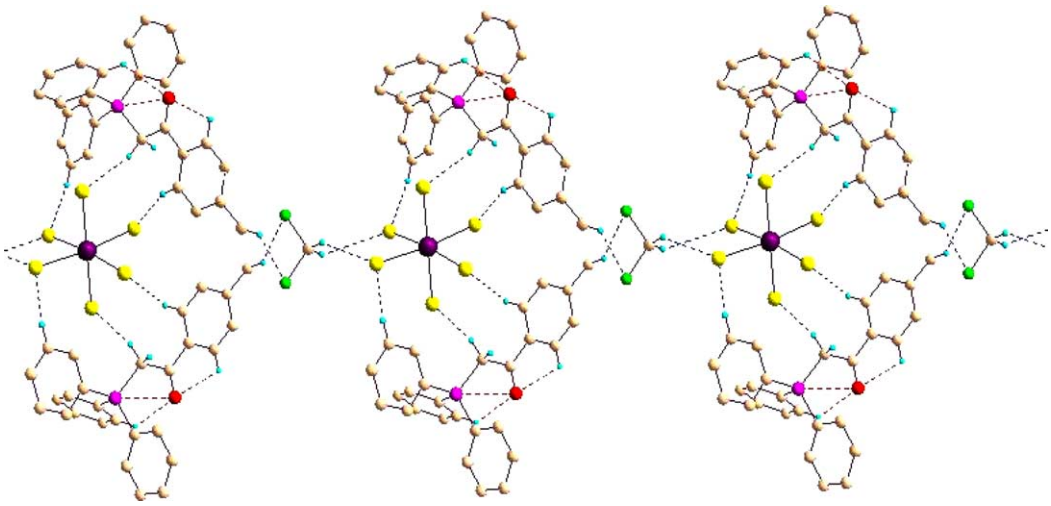

Fig. 3. Projection of a segment of the crystal lattice of **3b** showing an extended array.

*3.1.1. (I) Reaction of [(4-MeOC$_6$H$_4$COCH$_2$)Ph$_3$P]Br (**1c**) with (4-XC$_6$H$_4$COCH$_2$)$_2$TeBr$_2$ (X = H, **2a**; Me, **2b**; OMe, **2c**)*

To a solution of **1c** (0.5 g, 1 mmol) in dichloromethane (15 ml) was added **2c** (0.58 g, 1 mmol) in the same solvent (15 ml) and stirred for 5 h. A dark greyish residue (~0.06 g) was filtered off. After concentrating the filtrate to ~10 ml, pet-ether (~15 ml) was added. The yellow solid was filtered, washed with pet-ether and crystallized from dichloromethane to give orange needles of [(4-MeOC$_6$H$_4$COCH$_2$)Ph$_3$P]$_2$[TeBr$_6$] (**3c**). Yield: 0.3 g (40%; based on **2c**); m.p. 92 °C (shrank), 211 °C (dec.); *Anal.* Calc. for C$_{54}$H$_{48}$O$_4$Br$_6$P$_2$Te: C, 45.36; H, 3.38; Br, 33.53; Te, 8.92. Found: C, 45.21; H, 3.40; Br, 33.50; Te, 8.58%. ^{1}H NMR (CDCl$_3$), δ(ppm), 6.97–8.43 (m, arom.), 6.20 (d, CH$_2$–P) [^2J(^{31}P–^{1}H), 12.01 Hz], 3.96 (s, OCH$_3$); Cond. (nitrobenzene), 41.82 Ω^{-1} cm^{-1} mol^{-1}.

The same product was obtained in ~45% yield when **1c** was reacted with **2a** or **2b** under similar conditions.

*3.1.2. (II) Reaction of [(4-MeC$_6$H$_4$COCH$_2$)Ph$_3$P]Br (**1b**) with (4-XC$_6$H$_4$COCH$_2$)$_2$TeBr$_2$ (X = H, **2a**; Me, **2b**; OMe, **2c**)*

(a) A solution of **1b** (0.48 g, 1 mmol) (15 ml) and **2b** (0.55 g, 1 mmol) in dichloromethane or chloroform (40 ml) was stirred vigorously for 6 h at room temperature. A very small amount of elemental tellurium separated. It was filtered off and the filtrate concentrated to ~10 ml before adding pet-ether (~10 ml). A yellow solid precipitated which was filtered and washed with pet-ether (2 × 5 ml), until it showed a single spot on TLC. It was found to be the 1:1 adduct [(4-MeC$_6$H$_4$COCH$_2$)Ph$_3$P]$^+$[(4-MeC$_6$H$_4$COCH$_2$)$_2$TeBr$_3$]$^-$. Yield: 0.44 g (43%); m.p. 183 °C; *Anal.* Calc. for C$_{45}$H$_{42}$O$_3$Br$_3$PTe: C, 52.52; H, 4.11; Br, 23.29; Te, 12.40. Found: C, 51.90; H, 4.00; Br, 23.63; Te, 12.03%. ^{1}H NMR (CDCl$_3$), δ (ppm), 7.30–8.26 (m, arom.), 6.22 (d, CH$_2$–P) [^2J(^{31}P–^{1}H), 12.03 Hz], 5.44 (s, CH$_2$–Te), 2.46 (s, CH$_{3(cation)}$), 2.30 (s, CH$_{3(anion)}$); Cond. (nitrobenzene), 20.12 Ω^{-1} cm^{-1} mol^{-1}.

The same product was obtained when the reaction was carried out in 2:1 molar ratio.

Attempted crystallization for diffraction quality crystals by dissolving the adduct in dichloromethane and adding pet-ether initially gave a semi-solid which was triturated with pet-ether to give an orange solid. On repeated attempts it eventually afforded orange crystals of [(4-MeC$_6$H$_4$COCH$_2$)Ph$_3$P]$_2$[TeBr$_6$]. CH$_2$Cl$_2$, **3b**. m.p. 192 °C; *Anal.* Calc. for C$_{55}$H$_{50}$O$_2$Br$_6$Cl$_2$P$_2$Te: C, 44.55; H, 3.40; Br, 32.23; Te, 8.60. Found: C, 43.91; H, 3.40; Br, 31.80; Te, 8.86%. ^{1}H NMR (CDCl$_3$), δ (ppm), 7.32–8.03 (m, arom.), 5.88 –5.92 (d, CH$_2$–P) [^2J(^{31}P–^{1}H), 12.30 Hz], 2.60 (s, CH$_3$); Cond. (nitrobenzene), 40.02 Ω^{-1} cm^{-1} mol^{-1}.

(b) The same product was obtained directly in ~45% yield when **1b** and **2c** were stirred together in dichloromethane. After filtering off the traces of elemental tellurium, the solvent was distilled off. The residue on crystallization afforded **3b**, m.p. 192 °C.

*3.1.3. (III) Reaction of [(C$_6$H$_5$COCH$_2$)Ph$_3$P]Br (**1a**) with (4-XC$_6$H$_4$COCH$_2$)$_2$TeBr$_2$ (X = H, **2a**; Me, **2b**; OMe, **2c**)*

(a) The reaction between **1a** and **2a**, as in (IIa), afforded the 1:1 adduct, [(C$_6$H$_5$COCH$_2$)Ph$_3$P]$^+$[(C$_6$H$_5$COCH$_2$)$_2$TeBr$_3$]$^-$. Yield: 49%; m.p. 225 °C; *Anal.* Calc. for C$_{42}$H$_{36}$O$_3$Br$_3$PTe: C, 51.11; H,

3.68; Br, 24.29; Te, 12.93. Found: C, 50.65; H, 3.61; Br, 24.01; Te, 12.63%. ^{1}H NMR ($CDCl_3$), δ (ppm), 7.34–8.36 (m, arom.), 6.23–6.23 (d, CH_2–P) [$^2J(^{31}P–^1H)$, 12.02 Hz], 5.50 (s, CH_2–Te); Cond. (nitrobenzene), 20.65 Ω^{-1} cm^{-1} mol^{-1}.

(b) Reaction of **1a** with **2b** or **2c**, as in (I), afforded $[(C_6H_5COCH_2)Ph_3P]_2[TeBr_6]$, **3a**, Yield: ~42%; m.p. 216 °C; *Anal*. Calc. for $C_{52}H_{44}O_2Br_6P_2Te$: C, 45.59; H, 3.24; Br, 35.00; Te, 9.31. Found: C, 45.21; H, 3.30; Br, 35.21; Te, 8.90%. ^{1}H NMR ($CDCl_3$), δ (ppm), 7.32–8.40 (m, arom.), 6.34–6.38 (d, CH_2–P) [$^2J(^{31}P–^1H)$, 12.06 Hz]; Cond. (nitrobenzene), 42.00 Ω^{-1} cm^{-1} mol^{-1}.

3.2. Crystallography

The X-ray diffraction measurements were performed at 103(2) K on a Bruker PS4 diffractometer employing graphite monochromated Mo Kα radiation (λ = 0.71073 Å) to a θ_{max} value of 28.47° via ω scans (completeness 97.0% to θ_{max}). A total of 40 887 reflections were collected and the data were reduced and corrected for absorption using the programs SAINT and SADABS [13]. The structure was solved by direct methods and difference Fourier synthesis using SHELXS-97, implemented in WIN GX 2002 [14]. The non-hydrogen atoms were refined anisotropically while the hydrogen atoms, introduced at calculated positions, were refined isotropically. An acceptance criterion of $I > 2\sigma(I)$ was used and the final cycle of full-matrix least squares refinement based on 6806 independent reflections and 309 parameters converged with unweighted (R_1) and weighted (wR_2) agreement factors of 0.0245 and 0.0537, respectively. Lattice parameters and structure solution of the title compound are: $C_{55}H_{49}Br_6Cl_2O_2P_2Te$, M = 1481.84, orthorhombic, *Pbna*, a = 14.6483(10) Å, b = 17.0962(10) Å, c = 22.1458(10) Å, V = 5546.0(6) Å^3, Z = 4, D_x = 1.775 Mg/m^3, $F(000)$ = 2884, μ = 5.053 mm^{-1}. The max. and min. residual electron densities were 0.667 and −1.023 e Å^{-3}. Figures were created using the DIAMOND package.

4. Supplementary material

Crystallographic data for the structure analysis have been deposited with the Cambridge Crystallographic Data Center, CCDC No. 269986 for $[(4\text{-}MeC_6H_4COCH_2)Ph_3P]_2[TeBr_6]$. CH_2Cl_2 (**3b**). Copies of this information may be obtained free of charge from the Director, CCDC, 12 Union Road, Cambridge CB2 1EZ, UK, fax: +44 1223 336 033, or e-mail: deposite @ccdc.cam.ac.uk or www: http://www.ccdc.cam. ac.uk.

Acknowledgment

Financial assistance by the University Grants Commission, New Delhi, India is gratefully acknowledged.

References

[1] N. Petragnani, L.T. Castellanos, K.J. Wynne, W. Maxwell, J. Organomet. Chem. 55 (1973) 295.
[2] (a) T.N. Srivastava, R.C. Srivastava, M. Singh, J. Organomet. Chem. 157 (1978) 405;
(b) T.N. Srivastava, R.C. Srivastava, M. Srivastava, J. Indian, Chem. Soc. LIX (1982) 1028, and references therein.
[3] H.D.K. Drew, J. Chem. Soc. (1929) 560.
[4] (a) A.K.S. Chauhan, A. Kumar, R.C. Srivastava, R.J. Butcher, J. Organomet. Chem. 658 (2002) 169;
(b) A.K.S. Chauhan, A. Kumar, R.C. Srivastava, J. Beckmann, A. Duthie, R.J. Butcher, J. Organomet. Chem. 689 (2004) 345.
[5] (a) V. Janickis, M. Necas, J. Novosad, M. Dusek, V. Petricek, Acta Crystallogr. B 58 (2002) 977;
(b) V. Janickis, M. Herberhold, W. Milius, A. Anorg. Allg. Chem. 629 (2003) 29.
[6] (a) E.E. Aynsley, A.C. Hazell, Chem Ind. (London) (1963) 611;
(b) A.C. Hazell, Acta Chem. Scand. 20 (1966) 165;
(c) S.M. Narhi, R. Oilunkaniemi, R.S. Laitinen, M. Ahlgren, Acta Crystallogr. E 60 (2004) o798.
[7] (a) I.D. Brown, Can. J. Chem. 42 (1964) 2758;
(b) B. Krebs, S. Bonmann, K. Erpenstein, Z. Natureforsch 46b (1991) 919;
(c) S. Hauge, V. Jainickis, K. Marey, Acta Chem. Scand. 52 (1998) 441;
(d) S. Hauge, K. Maroy, Acta Chem. Scand. 52 (1998) 445.
[8] (a) D. Katryniok, R. Kniep, D. Mootz, Z. Anorg. Allg. Chem. 461 (1980) 96;
(b) P.C. Srivastava, H.G. Schmidt, H.W. Roesky, Z. Natureforsch 50 (1995) 695.
[9] B. Krebs, F.P. Ahlers, Adv. Inorg. Chem. 35 (1990) 235.
[10] C.B. Aakeroy, K.R. Seddon, Chem. Soc. Rev. (1993) 397.
[11] J.S. Wood, R.J. Wikholm, W.E. McEven, Phosphorus Sulfur 3 (1977) 163.
[12] (a) G. Aksnes, J. Songstad, Acta Chem. Scand. 18 (1964) 655;
(b) F. Ramirez, S. Dershowitz, J. Org. Chem. 22 (1957) 41.
[13] SMART, SAINT and SADABS, Siemens Analytical X-ray Instruments Inc., Madison, WI, USA, 1999.
[14] L.J. Farrugia, J. Appl. Cryst. 32 (1999) 837.

Available online at www.sciencedirect.com
SCIENCE DIRECT®
Polyhedron 25 (2006) 753–758
POLYHEDRON
www.elsevier.com/locate/poly

Coordination modes of 3-aminosalicylic and 3-hydroxyanthranilic acids in palladium(II), platinum(II) and rhenium(V) complexes. The crystal structure of *cis*-$[Pt(HsalNH)(PPh_3)_2]\cdot 0.25C_2H_5OH$

Susana M.O. Quintal [a], Vitor Félix [a], Michael G.B. Drew [b], Helena I.S. Nogueira [a,*]

[a] *Department of Chemistry, CICECO, University of Aveiro, Campus de Santiago, 3810-193 Aveiro, Portugal*
[b] *School of Chemistry, University of Whiteknights, Reading RG6 6AD, UK*

Received 19 April 2005; accepted 25 July 2005
Available online 5 October 2005

Abstract

New Pd(II), Pt(II) and Re(V) complexes of 3-aminosalicylic acid (H_2salNH_2) and 3-hydroxyantranilic acid (HantOH) have been prepared, *cis*-[Pt (HsalNH)$(PPh_3)_2$]· $0.25C_2H_5OH$ (**1**), *trans*-[PdCl$(salNH_2)(PPh_3)_2$] (**2**), *trans*-[$ReOI_2(HsalNH_2)(PPh_3)$]$\cdot(CH_3)_2CO$ (**3**), *cis*-[Pt(HantO)$(PPh_3)_2$] (**4**), *trans*-[PdCl(antOH)$(PPh_3)_2$]$\cdot 4H_2O$ (**5**), [PdCl(antOH)(bipy)]$\cdot C_2H_5OH$ (**6**), [$PdCl_2$(HantOH)$_2$] (**7**) and *trans*-[ReOI(HantO)$(PPh_3)_2$]$\cdot(CH_3)_2CO$ (**8**). The crystal structure of complex **1** was determined showing chelation of $HsalNH^{2-}$ through the adjacent nitrogen and oxygen atoms of the amino and phenolate groups. Infrared and ^1H NMR spectroscopic data for the complexes are presented.
© 2005 Elsevier Ltd. All rights reserved.

Keywords: 3-Aminosalicylic acid; 3-Hydroxyanthranilic acid; Crystal structure; Palladium; Platinum; Rhenium

1. Introduction

We have been studying the coordination modes of aromatic ambidentade ligands, such as 3-hydroxypicolinic acid [1,2], 2-hydroxynicotinic acid [3] and 2,3-, 3,4- and 2,6-dihydroxybenzoic acids, with 2nd and 3rd row transition metals and the lanthanides [4–6]. In the present work a comparative study was done on Pd(II), Pt(II) and Re(V) complexes with 3-aminosalicylic (H_2salNH_2) and 3-hydroxyantranilic acids (HantOH), respectively. The two ligands are constitutional isomers: 3-aminosalicylic acid is 3-amino-2-hydroxybenzoic acid (Fig. 1(a)), and 3-hydroxyanthranilic acid is 2-amino-3-hydroxybenzoic acid (Fig. 1(b)).

3-Aminosalicylic acid can bind to metals by several coordination modes: monodentate O or N donor, bridging, or by two different chelates either the O,O-chelate, involving the carboxylate group and the oxygen in position-2, resulting in a six-membered chelate-ring, or the N,O-chelate, involving the amino group nitrogen and the oxygen in position-2, with the formation of a five-membered chelate-ring. A similar O,O-chelate is found in complexes of salicylic acid and derivatives, such as $[MoO_2L_2]^{2-}$ (H_2L = salicylic acid, 4- or 5-methylsalicylic acids), $[PdL_2]$ (H_2L = salicylic acid) [7], $[MoO_2L_2]^{2-}$, $[OsO_2(py)_2L]$, [ReOIL(PPh_3)] (H_2L = 2,6-dihydroxybenzoic acid; py = pyridine) [8].

When deprotonated, 3-hydroxyanthranilic acid can also bind to metals by several coordination modes: monodentate O or N donor, bridging, or by two possible N,O-chelating modes, involving the nitrogen atom and the oxygen atom of either the hydroxyl group (forming a five-membered chelate-ring) or the carboxyl group (forming a six-membered chelate-ring). The former is found in complexes with 2-aminophenolate and

* Corresponding author. Tel.: +351234370727; fax: +351234370084.
E-mail address: helena@dq.ua.pt (H.I.S. Nogueira).

0277-5387/$ - see front matter © 2005 Elsevier Ltd. All rights reserved.
doi:10.1016/j.poly.2005.07.034

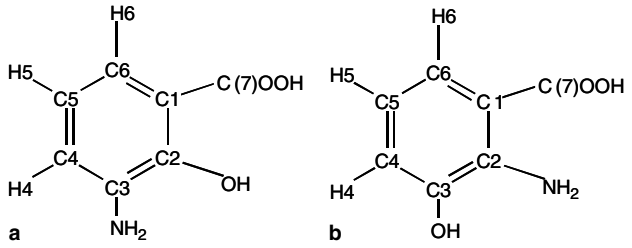

Fig. 1. 3-Aminosalicylic (a) and 3-hydroxyanthranilic (b) acids and numbering scheme adopted.

derivatives such as $[MoO_2(HL)_2]$ (H_2L = 2-amino-4-clorophenol, 2-amino-4-methylphenol) and $[OsL_3]$ (H_2L = 2-amino-4-methylphenol, 2-amino-4-^{t}butylphenol), $[MoO_2(HL)_2]$ [9] and $[PtL(PPh_3)_2]$ [10] (H_2L = 2-aminophenol), $[V(=NPh)(OC_6H_2(CH_2NMe_2)\text{-}2\text{-}Me_2\text{-}4,6)_2]$ [11], $[V(OC_6H_2(CH_2NMe_2)\text{-}2,6\text{-}Me\text{-}4)_3]$ and $[VCl(OC_6H_2(CH_2NMe_2)\text{-}2\text{-}Me\text{-}4)_2]$ [12]. The latter chelating mode is found in complexes of anthranilic acid like $[MoCl_3\{2\text{-}(HN)C_6H_4CO_2\}\{2\text{-}Me_3SiO_2CC_6H_4N\}]^-$, $[MoCl_3\{2\text{-}(HN)C_6H_4CO_2\}(NC_6H_3Pr^i_2\text{-}2,6)]^-$ [13] and $[Ba(2\text{-}NH_2C_6H_4CO_2)_2(OH_2)]_n$ [14].

The N,O-chelating mode in H_2salNH_2 is similar to the N,O-chelating mode with HantOH, forming five-membered chelate-rings. The formation of six-membered chelate-rings is in the case of H_2salNH_2 achieved through bonding to a carboxylate O atom and a hydroxyl O atom, and in the case of HantOH to a carboxylate O atom and an amino N atom. The coordination modes described were investigated in Pd(II), Pt(II) and Re(V) complexes using spectroscopic data and in one case X-ray diffraction data. The crystal structure of the Pt(II) compound **1** was determined and in this complex the 3-aminosalicylato ligand shows coordination through the nitrogen and oxygen atoms of the amino and phenolate groups (N,O-chelating mode). Spectroscopic characterisation of the remaining compounds suggests that other coordination modes may occur.

2. Results and discussion

2.1. Preparations

Suspensions of *cis*-$[PtCl_2(PPh_3)_2]$ or *trans*-$[PdCl_2(PPh_3)_2]$ and H_2salNH_2 or HantOH in an ethanol/methanol mixture in the presence of triethylamine gave complexes *cis*-$[Pt(HsalNH)(PPh_3)_2]\cdot 0.25C_2H_5OH$ (**1**), *trans*-$[PdCl(HsalNH_2)(PPh_3)_2]$ (**2**), *cis*-$[Pt(HantO)(PPh_3)_2]$ (**4**) and *trans*-$[PdCl(antOH)(PPh_3)_2]\cdot 4H_2O$ (**5**). When $K_2[PdCl_4]$ was used as starting material, the compound obtained was $[PdCl_2(HantOH)_2]$ (**7**). Reaction of the 2,2′-bipyridine (bipy) complex $[PdCl_2(bipy)]$ with HantOH gave compound **6**, $[PdCl(antOH)(bipy)]\cdot C_2H_5OH$. The complexes *trans*-$[ReOI_2(HsalNH_2)(PPh_3)]\cdot(CH_3)_2CO$ (**3**) and *trans*-$[ReOI(HantO)(PPh_3)_2]\cdot(CH_3)_2CO$ (**8**) were synthesised by refluxing *trans*-$[ReOI_2(OEt)(PPh_3)_2]$ with H_2salNH_2 or HantOH in acetone.

2.2. Crystal structure of *1*

The X-ray diffraction study of **1** shows that its crystal structure is built up from an asymmetric unit composed of one molecule of *cis*-$[Pt(HsalNH)(PPh_3)_2]$ and several solvent molecules of ethanol all with reduced occupancy. An ORTEP view showing the overall geometry of the complex and the atomic notation scheme is presented in Fig. 2. Bond lengths and angles are listed in Table 1 for complex **1**. The platinum(II) centre is surrounded by the nitrogen and oxygen atoms from the amino and phenol groups of the $HsalNH^{2-}$ ligand and the phosphorus atoms of the two PPh_3 ligands in a distorted square planar coordination environment. The angle N–Pt–O of 79.32(3)° is dictated by the O–N bite angle of the $HsalNH^{2-}$ ligand while the remaining angles in the metal coordination sphere are the result of

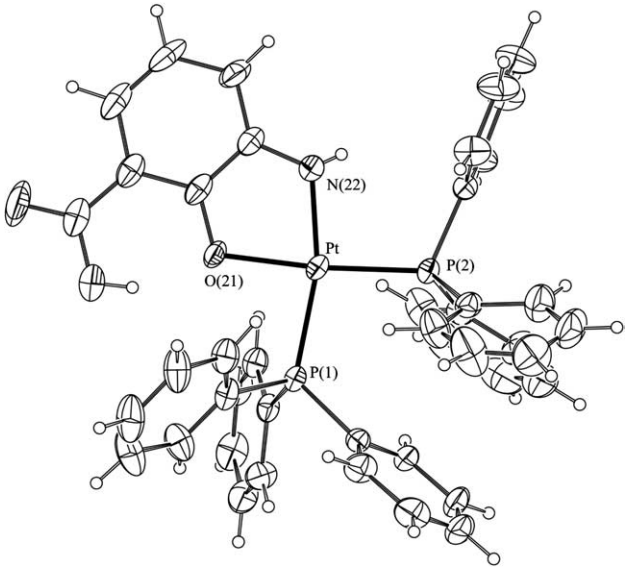

Fig. 2. An ORTEP view of *cis*-$[Pt(HsalNH)(PPh_3)_2]$ (**1**) showing the overall molecular geometry. Ellipsoids are drawn at 30% probability level.

Table 1
Selected distances (Å) and angles (°) for complex **1**

Pt–N(22)	2.014(6)
Pt–P(1)	2.289(2)
Pt–O(21)	2.069(5)
Pt–P(2)	2.226(2)
N(22)–Pt–P(1)	166.5(2)
P(2)–Pt–O(21)	174.2(2)
N(22)–Pt–P(2)	95.0(2)
P(1)–Pt–P(2)	99.4(1)
N(22)–Pt–O(21)	80.4(2)
P(1)–Pt–O(21)	86.1(2)

the minimisation of the steric interactions between the $HsalNH^{2-}$ ligand and the two bulky PPh_3 ligands. The bond lengths to the metal centre are within the values found for related complexes such as *cis*-[PtCl(picOH)$(PPh_3)_2$] [1] and *cis*-[PtCl(HnicO)$(PPh_3)_2$] [3].

2.3. Infrared spectra

Infrared data for H_2salNH_2, HantOH and complexes **1**–**8** are given in Table 2. Tentative assignments are based on those found in the literature for 3-aminosalicylic acid [15], salicylic acid [7], anthranilic acid and derivatives [16,17], 2-aminophenol [9], 3-hydroxypicolinic acid [1,2], and respective complexes. The most sensitive bands to metal coordination were selected, namely the C=O and C–O stretches of the carboxyl group, ν(C=O) and $\nu(C–O)_c$, the bending mode of the amino group, $\delta(NH_2)$, the C–O stretch of the phenolic group, $\nu(C–O)_{OH}$, and the C–NH_2 stretch, $\nu(C–NH_2)$.

The bending frequency of the NH_2 group, $\delta(NH_2)$, of 3-aminosalicylic acid is assigned at 1537 cm^{-1} and of 3-hydroxyanthranilic acid at 1548 cm^{-1}. In all complexes, this frequency shifts to higher wavenumbers. For complexes **5** and **6** it shifts only 3 cm^{-1}. For complexes **1**, **3**, **4**, **7** and **8** this shift is higher than 42 cm^{-1} showing that the amino group may be involved in the coordination to metals. It suggests that in complexes **5** and **6** the coordination may involve only the carboxylate or phenolate groups.

Two strong bands at 1651 and 1394 cm^{-1} in the spectrum of 3-aminosalicylic acid are assigned to the C=O and C–O stretches, ν(C=O) and $\nu(C–O)_c$, of the carboxyl group, respectively. In the spectrum of 3-hydroxyanthranilic acid these bands are seen at 1651 cm^{-1} and 1344 cm^{-1}, respectively. The ν(C=O) frequency decreases in complexes **5** and **6**, and the $\nu(C–O)_c$ frequency increases. The calculated $\Delta\nu(CO_2)$ values, defined by Deacon and Phillips as $\nu_{as}(CO_2) - \nu_s(CO_2)$, of 267 and 233 cm^{-1} for **5** and **6**, respectively, indicate a typical COO^- coordination fashion, possibly unidentate [18,19]. In **1**–**4**, **7** and **8**, the carboxyl group is possibly not involved in the coordination because of the increase of the ν(C=O) frequency. In complex **1**, the charge balance constrains a 2− charge in the deprotonated form of the 3-aminosalicylic acid. Assuming the 1721 cm^{-1} frequency as the C=O stretch, characteristic of the carboxyl group, the deprotonation possibly occurs in the phenolic and amino groups (according to crystal structure data). Similar deprotonation was described for $[MoCl_3\{2\text{-}(HN)C_6H_4CO_2\}\{2\text{-}Me_3SiO_2CC_6H_4N\}]^-$, $[MoCl_3\{2\text{-}(HN)C_6H_4CO_2\}(NC_6H_3Pr^i{}_2\text{-}2,6)]^-$ [13] and $[Pt\{2\text{-}(HN)C_6H_4O\}(PPh_3)_2]$ [10]. The stretching C–O frequency of the phenolic group, $\nu(C–O)_{OH}$, (1319 cm^{-1} in H_2salNH_2 spectra and 1299 cm^{-1} in HantOH) shifts to lower wavenumbers in the spectra of all complexes. It is particularly significant for complexes **1**–**4** and **8**, suggesting that in these complexes the oxygen atom of the phenolic group may be involved in coordination to the metals. The decrease in the C–NH_2 stretch frequency, $\nu(C–NH_2)$, in the spectra of the complexes **1**, **3**, **4**, **7** and **8** indicates that the amino group may be coordinated to the metals.

The results described suggest the following coordination modes of 3-aminosalicylic or 3-hydroxyanthranilic acids: in complexes **1**, **3**, **4** and **8** via chelation-NO through the nitrogen atom of the amino group and the oxygen atom of the phenolate group; in complexes **5** and **6** through one of the oxygen atoms of the carboxylate group; in complex **2** via monodentate-O of the phenolate group; and in complex **7** via monodentate-N.

The spectra of compounds **1**–**5** and **8** show three characteristic bands of the PPh_3 ligands, around 1480, 1435 and 1095 cm^{-1}, assigned to the symmetric and asymmetric stretching and bending of P–Ph bonds, respectively [17,19]. The strong bands at 974 and 979 cm^{-1} in the spectra of the rhenium complexes **3** and **8**, respectively, are assigned to Re=O stretch [1].

Table 2
Infrared data (cm^{-1}) for 3-aminosalicylic and 3-hydroxyanthranilic acids and complexes **1**–**8**

Compound	ν(C=O)	$\delta(NH_2)$[a]	$\nu(C–O)_c$	$\nu(C–O)_{OH}$	$\nu(C–NH_2)$[b]	ν(M–N)	ν(M–Cl)
3-Aminosalicylic acid	1651 vs	1537 vs	1394 vs	1319 vs	1262 vs		
cis-[Pt(HsalNH)$(PPh_3)_2]\cdot 0.25C_2H_5OH$ (**1**)	1721 vs	1587 m	1373 m	1302 vs	1227 s	399 w	
trans-[PdCl$(HsalNH_2)(PPh_3)_2$] (**2**)	1700 m	1571 m	1390 m	1308 m	1283 m		389 m
trans-[$ReOI_2(HsalNH_2)(PPh_3)]\cdot(CH_3)_2CO$ (**3**)	1671 m	1581 s	1370 s	1303 m	1240 m	457 m	
3-Hydroxyanthranilic acid	1651 vs	1548 vs	1344 s	1299 vs	1221 vs		
cis-[Pt(HantO)$(PPh_3)_2$] (**4**)	1679 sh	1615 s	1323 s	1251 vs	1213 vs	350 w	
trans-[PdCl(antOH)$(PPh_3)_2]\cdot 4H_2O$ (**5**)	1635 m	1551 m	1368 s	1275 vs	1249 m		350 w
[PdCl(antOH)(bipy)]$\cdot C_2H_5OH$ (**6**)	1603 vs	1551 s	1370 vs	1276 vs	1250 sh		336 m
$[PdCl_2(HantOH)_2]$ (**7**)	1666 vs	1590 s	1337 s	1293 vs	1215 vs		328 s, 307 s
trans-[ReOI(HantO)$(PPh_3)_2]\cdot(CH_3)_2CO$ (**8**)	1680 m	1602 m	1296 s	1242 vs	1215 s	458 m	

vs, very strong; s, strong; m, medium; w, weak; sh, shoulder.
[a] δ(NH) in complexes **1**, **4** and **8**.
[b] ν(C–NH) in complexes **1**, **4** and **8**.

Table 3
^{1}H NMR data for for 3-aminosalicylic and 3-hydroxyanthranilic acids and its complexes

Compound	Chemical shift (ppm)[A]		
	H4	H5	H6
3-Aminosalicylic acid[a]	7.02 dd (5, 26)	6.72 t (26)	7.37 dd (5, 26)
cis-[Pt(HsalNH)(PPh_3)$_2$] · 0.25C_2H_5OH (**1**)[b]	6.31 d (25)	6.44 t (26)	6.96 d (25)
trans-[$ReOI_2$(HsalNH_2)(PPh_3)] · (CH_3)$_2$CO (**3**)[c]	7.49 dd (5, 26)	6.99 t (26)	7.73 dd (5, 26)
3-Hydroxyanthranilic acid[a]	6.80 dd (5, 26)	6.45 t (26)	7.35 dd (5, 27)
cis-[Pt(HantO)(PPh_3)$_2$] (**4**)[b]	6.47 d (25)	6.25 t (25)	7.05 d (27)
[PdCl(antOH)(bipy)] (**6**)[d]	7.21 d (26)	6.74 t (26)	8.02 d (25)
[$PdCl_2$(HantOH)$_2$] (**7**)[c]	6.79 d (25)	6.36 t (26)	7.20 d (27)
trans-[ReOI(HantO)(PPh_3)$_2$] · (CH_3)$_2$CO (**8**)[c]	6.98 dd (5, 26)	6.74 t (26)	7.33 dd (5, 27)

[A] *J* values in parentheses (Hz); dd, doublet-doublet; t, triplet; d, doublet.
[a] In CD_3OD.
[b] In $CDCl_3$.
[c] In dmso-d_6.
[d] D_2O.

2.4. ^{1}H NMR spectra

^{1}H NMR data and tentative assignments for 3-aminosalicylic and 3-hydroxyanthranilic acids and its complexes are shown in Table 3. Assignments are based on those find in the literature for salicylic acid [20] and derivates [16] and 2-aminophenol [9,21], anthranilic acid [13,18] and derivates [17] and salicylic acid complexes [7].

The ^{1}H NMR spectrum of 3-aminosalicylic acid in CD_3OD shows a triplet at 6.72 ppm assigned to the H5 proton and two doublet-doublets at 7.02 and 7.37 ppm assigned to the H4 and H6 protons, respectively. Similarly the ^{1}H NMR spectrum of 3-hydroxyanthranilic acid in CD_3OD shows a triplet at 6.45 ppm assigned to the H5 proton, a doublet-doublet at 6.80 ppm assigned to the H4 proton and another doublet-doublet at 7.35 ppm assigned to the H6 proton.

The proton signals of $HsalNH_2^-$ in complex **2** and of $antOH^-$ in complex **5** are overlapped with the PPh_3 signals. In the spectra of complex **6**, the major shifts downfield are observed for H4 and H6 protons. These are higher than the shifts observed in complexes **4** and **8** with suggested NO-chelation. Relative to the free ligand, the protons of $HsalNH^{2-}$ ligand in the Pt complex **1** shift upfield and in the Re complex **3** shift downfield; the same trend is observed for the protons of $HantO^-$ ligand in complexes **4** (Pt) and **8** (Re), having all the suggested NO-chelation .

3. Experimental

3.1. Preparation of complexes

All chemicals were of at least reagent grade and used as supplied by Aldrich. The starting complexes, *trans*-[$PdCl_2$(PPh_3)$_2$] [22], *cis*-[$PtCl_2$(PPh_3)$_2$] [23], [$PdCl_2$(bipy)] [24] and *trans*-[$ReOI_2$(OEt)(PPh_3)$_2$] [25] were prepared by the respective literature procedures.

3.1.1. *cis*-[Pt(HsalNH)(PPh_3)$_2$] · 0.25C_2H_5OH (**1**)

To a stirred suspension of *cis*-[$PtCl_2$(PPh_3)$_2$] (0.12 g, 0.15 mmol) in ethanol (5 cm^3) was added a methanolic suspension (5 cm^3) of 3-aminosalicylic acid (0.05 g, 0.3 mmol) and triethylamine (0.08 cm^3, 0.6 mmol). The resulting yellow suspension was stirred for one day. It was centrifuged and a yellow solid isolated. Orange crystals were formed by recrystallisation in ethanol, washed whith water and dried over silica gel. Yield: 0.05 g, 0.06 mmol, 40%.

Elemental analysis. Calc.: C, 58.3; H, 4.3; N, 1.6. Exp.: C, 59.9; H, 4.1; N, 1.6%. MS = 871; MW = 870.768 calculated for [Pt(HsalNH)(PPh_3)$_2$].

3.1.2. *trans*-[PdCl(HsalNH_2)(PPh_3)$_2$] (**2**)

To a stirred suspension of *trans*-[$PdCl_2$(PPh_3)$_2$] (0.15 g, 0.15 mmol) in ethanol (5 cm^3) was added a methanolic suspension (5 cm^3) of 3-aminosalicylic acid (0.05 g, 0.3 mmol) and triethylamine (0.08 cm^3, 0.6 mmol). The resulting suspension was refluxed for 1 h and filtered. To the orange filtrate was added 10 cm^3 of water and a orange solid was formed. It was centrifuged, washed with water and dried over silica gel. Yield: 0.05 g, 0.06 mmol, 40%.

Elemental analysis. Calc.: C, 63.1; H, 4.4; N, 1.7. Exp.: C 61.4, H 4.6, N 1.7%.

3.1.3. *trans*-[$ReOI_2$(HsalNH_2)(PPh_3)] · (CH_3)$_2$CO (**3**)

A suspension of *trans*-[ReOI(OEt)$_2$(PPh_3)$_2$] (0.31 g, 0.3 mmol) and 3-aminosalicylic acid (0.05 g, 0.3 mmol) in acetone (20 cm^3) was refluxed for 1 h. It was centrifuged and a green solid obtained. It was washed with acetone and dried over silica gel. Yield: 0.20 g, 0.21 mmol, 68%.

Elemental analysis. Calc.: C, 36.2; H, 2.9; N, 1.5. Exp.: C, 36.3; H, 3.1; N, 1.6%.

3.1.4. *cis*-[Pt(HantO)(PPh$_3$)$_2$] (**4**)

To a stirred suspension of *cis*-[PtCl$_2$(PPh$_3$)$_2$] (0.12 g, 0.15 mmol) in ethanol (5 cm^3) was added a methanolic suspension (5 cm^3) of 3-hydroxyanthranilic acid (0.05 g, 0.3 mmol) and triethylamine (0.08 cm^3, 0.6 mmol). The resulting yellow suspension was stirred for one day. It was centrifuged and a yellow solid isolated, washed with ethanol and dried over silica gel. Yield: 0.11 g, 0.13 mmol, 87%.

Elemental analysis. Calc.: C, 59.3; H, 4.1; N, 1.6. Exp.: C, 59.9; H, 4.1; N, 1.6%. MS = 871; MW = 870.768 calculated for [Pt(HantO)(PPh$_3$)$_2$].

3.1.5. *trans*-[PdCl(antOH)(PPh$_3$)$_2$] · 4H$_2$O (**5**)

To a stirred suspension of *trans*-[PdCl$_2$(PPh$_3$)$_2$] (0.35 g, 0.5 mmol) in ethanol (5 cm^3) was added a methanolic suspension (4 cm^3) of 3-hydroxyanthranilic acid (0.15 g, 1 mmol) and triethylamine (0.28 cm^3, 2 mmol). The resulting suspension was stirred for 1 h. It was centrifuged and a orange solution was obtained. Part of the solvent was evaporated and a red solid was obtained by addition of an equal amount of water. This solid was washed with water and dried over silica gel. Yield: 0.13 g, 0.27 mmol, 54%.

Elemental analysis. Calc.: C, 58.0; H, 5.0; N, 1.6. Exp.: C, 58.0; H, 5.3; N, 2.1%.

3.1.6. [PdCl(antOH)(bipy)] · C$_2$H$_5$OH (**6**)

To a stirred suspension of [PdCl$_2$(bipy)] (0.05 g, 0.15 mmol) in ethanol (5 cm^3) was added a methanolic suspension (5 cm^3) of 3-hydroxyanthanilic acid (0.05 g, 0.3 mmol) and triethylamine (0.08 cm^3, 0.6 mmol). The resulting yellow suspension was stirred for three days. It was centrifuged and a brownish solid isolated, washed with ethanol and dried over silica gel. Yield: 0.07 g, 0.14 mmol, 93%.

Elemental analysis. Calc.: C, 46.0; H, 4.1; N, 8.5. Exp.: C, 45.9; H, 4.1; N, 9.9%. MS = 413; MW = 414.731 calculated for [Pd(antOH)(bipy)]$^+$.

3.1.7. [PdCl$_2$(HantOH)$_2$] (**7**)

A methanolic suspension (4 cm^3) of 3-hydroxyanthranilic acid (0.15 g, 1 mmol) was added to an aqueous solution (5 cm^3) of K$_2$[PdCl$_4$] (0.16 g, 0.5 mmol). The resulting orange suspension was stirred for one day. It was centrifuged and a yellow solid isolated, washed with ethanol and dried over silica gel. Yield: 0.22 g, 0.45 mmol, 90%.

Elemental analysis. Calc.: C, 34.8; H, 2.9; N, 5.8. Exp.: C, 34.6; H, 3.4; N, 6.2%. MS = 485; MW = 483.596 calculated for [PdCl$_2$(antOH)$_2$]. MS = 411; MW = 412.690 calculated for [Pd(antOH)$_2$]$^{2+}$.

3.1.8. *trans*-[ReOI(HantO)(PPh$_3$)$_2$] · (CH$_3$)$_2$CO (**8**)

A suspension of *trans*-[ReOI$_2$(OEt)(PPh$_3$)$_2$] (0.31 g, 0.3 mmol) and 3-hydroxyantharanilic acid (0.05 g, 0.3 mmol) in acetone (10 cm^3) was refluxed for 30 min. After cooling to room temperature, 10 cm^3 of water were added and a brownish solid was formed, isolated, washed with water and dried over silica gel. Yield: 0.20 g, 0.19 mmol, 63%.

Elemental analysis. Calc.: C, 51.9; H, 4.0; N, 1.3. Exp.: C, 54.9; H, 4.1; N, 1.5%.

3.2. X-ray diffraction

$C_{44.50}H_{40}NO_{3.75}P_2Pt$ (**1**), $M_r = 905.80$, triclinic, space group $P\bar{1}$, $a = 9.749(12)$ Å; $b = 13.954(15)$ Å; $c = 16.333(17)$ Å; $\alpha = 74.23(1)°$; $\beta = 84.14(1)°$, $\gamma = 74.15(1)°$, $U = 2056.0$ Å^3, $Z = 2$, $\rho_{calc} = 1.463$ Mg m^{-3}, μ(Mo Kα) = 3.531 mm^{-1}.

X-ray data were collected at room temperature on a MAR research plate system using graphite monochromatised Mo Kα radiation ($\lambda = 0.71073$ Å) at Reading University. The crystal was positioned at 70 mm from the image plate. 95 frames were taken at 2° intervals with an adequate counting time. Data analysis was performed with the XDS program [26]. Intensities were corrected empirically for absorption effects, using a DIFABS version modified for image plate geometry [27].

The structure was solved by a combination of direct methods and difference Fourier syntheses. The hydrogen atoms on the parent carbon atoms and aliphatic nitrogen atoms were included in calculated positions and giving thermal parameters equivalent 1.2 times those of the atom to which were attached. The non-hydrogen atoms were refined with anisotropic thermal parameters

The final refinement of 464 parameters by full-matrix least-squares method against F^2 until convergence to be achieved leading to final indices $R_1 = 0.0412$ and $wR_2 = 0.1126$ for 5710 reflections with $I > 2\sigma(I)$ and $R_1 = 0.0521$ and $wR_2 = 0.1205$, for all intensity data comprising 6578 reflections. The residual electronic density was in the range −1.189 to 2.347 e Å^{-3}, with positive hole 0.96 Å within platinum coordination sphere while the negative one is only 1.44 Å way from the calculated position for an hydrogen atom. All calculations required to solve and to refine the structure were carried out using the SHELX-97 system programs [28]. Molecular diagrams were drawn with PLATON [29].

3.3. Instrumentation

Infrared spectra were measured as KBr pellets on a Mattson 7000 FT instrument. ^{1}H NMR spectra were recorded on a Brüker AMX300 spectrometer at 300 MHz and referenced to SiMe$_4$ or the solvent. Microanalyses

(C, H and N) were measured by the Department of Chemistry, University of Aveiro.

Acknowledgements

The authors acknowledge Fundação para a Ciência e a Tecnologia (FCT, Portugal) for financial support. S.M.O. Quintal thanks FCT for a postgraduate grant. We also thank EPSRC (UK) and the University of Reading (UK) for funds for the Image Plate System.

Appendix A. Supplementary data

Crystallographic data for the structure reported in this paper have been deposited with the Cambridge Crystallographic Data Centre as supplementary publication no. CCDC 269712. Copies of the data can be obtained free of charge on application to CCDC, 12 Union Road, Cambridge CB2 2EZ, UK (fax: (+44) 1223 336033; e-mail: deposit@ccdc.cam.ac.uk, and http://www.ccdc.cam.ac.uk). Supplementary data associated with this article can be found, in the online version at doi:10.1016/j.poly.2005.07.034.

References

[1] S.M.O. Quintal, H.I.S. Nogueira, V. Félix, M.G.B. Drew, New J. Chem. 24 (2000) 511.
[2] S.M.O. Quintal, H.I.S. Nogueira, H. Carapuça, V. Félix, M.G.B. Drew, J. Chem. Soc., Dalton Trans. (2001) 3196.
[3] S.M.O. Quintal, H.I.S. Nogueira, V. Félix, M.G.B. Drew, Polyhedron 21 (2002) 2783.
[4] P.C.R. Soares-Santos, H.I.S. Nogueira, V. Félix, M.G.B. Drew, R.A. Sá Ferreira, L.D. Carlos, T. Trindade, Chem. Mater. 15 (2003) 100.
[5] P.C.R. Soares-Santos, H.I.S. Nogueira, J. Rocha, V. Félix, M.G.B. Drew, R.A. Sá Ferreira, L.D. Carlos, T. Trindade, Polyhedron 22 (2003) 3529.
[6] P.C.R. Soares-Santos, H.I.S. Nogueira, F.A. Almeida Paz, R.A. Sá Ferreira, L.D. Carlos, J. Klinowski, T. Trindade, Eur. J. Inorg. Chem. (2003) 3609.
[7] C.F. Edwards, W.P. Griffith, A.J.P. White, D.J. Williams, J. Chem. Soc., Dalton Trans. (1993) 3813.
[8] W.P. Griffith, H.I.S. Nogueira, B.C. Parkin, R.N. Sheppard, A.J.P. White, D.J. Williams, J. Chem. Soc., Dalton Trans. (1995) 1775.
[9] W.P. Griffith, T.Y. Hoh, D.J. Williams, J. Chem. Soc., Dalton Trans. (1993) 3459.
[10] J.M. Clemente, C.Y. Wong, P. Bhattacharyya, A.M.Z. Slawin, D. Williams, J.D. Woollins, Polyhedron 13 (1994) 261.
[11] H. Hagen, C. Bezemer, J. Boersma, H. Kooijman, M. Lutz, A.L. Spek, G. Koten, Inorg. Chem. 39 (2000) 3970.
[12] H. Hagen, J. Boersma, M. Lutz, A.L. Spek, G. Koten, Eur. J. Inorg. Chem. 117 (2001) 123.
[13] V.C. Gibson, C. Redshaw, W. Clegg, M.R.J. Elsegood, J. Chem. Soc., Dalton Trans. (1997) 3207.
[14] R. Murugavel, V.V. Karambelkar, G. Anantharaman, M.G. Walawalkar, Inorg. Chem. 39 (2000) 1381.
[15] H.I.S. Nogueira, Spectrochim. Acta, Part A 54 (1998) 1461.
[16] G.S. Denisov, L.A. Kusina, J. Mol. Struct. 322 (1994) 205.
[17] A.F. Borowski, D.J. Cole-Hamilton, Polyhedron 12 (1993) 1757.
[18] G.B. Deacon, R.J. Phillips, Coord. Chem. Rev. 33 (1980) 227.
[19] D.H. Gibson, Y. Ding, R.L. Miller, B.A. Sleadd, M.S. Mashuta, J.F. Richardson, Polyhedron 18 (1999) 1189.
[20] H. Esaki, H. Onozaki, S. Kawakishi, T. Osawa, J. Agric. Food Chem. (1996) 696.
[21] R. Murugavel, V.V. Karambelkar, G. Anantharaman, M.G. Walawalkar, Inorg. Chem. 39 (2000) 1381.
[22] C. Cookson, D.W. Jones, J. Chem. Soc. (1965) 1881.
[23] J.C. Bailar Jr., H. Itatani, Inorg. Chem. 4 (1965) 1618.
[24] W.P. Griffith, S.I. Mostafa, Polyhedron 11 (1992) 871.
[25] G.F. Ciani, G. D'Alfonso, P.F. Romiti, A. Sironi, M. Freni, Inorg. Chim. Acta 72 (1983) 29.
[26] W. Kabsch, J. Appl. Crystallogr. 21 (1988) 916.
[27] N. Walker, D. Stuart, DIFABS, Acta Crystallogr. Sect. A 39 (1983) 158.
[28] G.M. Sheldrick, SHELX-97, University of Göttingen, 1997.
[29] A.L. Spek, PLATON, a Multipurpose Crystallographic Tool, Utrecht University, Utrecht, The Netherlands, 1999.

Available online at www.sciencedirect.com
SCIENCE DIRECT®
Polyhedron 25 (2006) 759–766
POLYHEDRON
www.elsevier.com/locate/poly

Density functional study of the properties of isomeric aminophenylhydroxamic acids and their copper (II) complexes

Rita Kakkar *, Rajni Grover, Pragya Gahlot

Department of Chemistry, University of Delhi, Delhi 110 007, India

Received 20 June 2005; accepted 26 July 2005
Available online 1 September 2005

Abstract

The three isomeric aminophenylhydroxamic acids and their copper (II) complexes have been investigated by the density functional theory using different potentials. The GGA-PBE approach is found to be best suited for such studies. A comparison is made of the electronic structures of the acids to understand why they form different types of complexes. 2-Aminophenylhydroxamic acid is found to be the most stable of the three isomers due to extensive hydrogen bonding, but the complex formation energy for square planar complexes is highest for the 4-aminophenyl isomer. The different properties of the three acids and their Cu(II) complexes are satisfactorily explained from these studies. The nature of bonding in these complexes is also investigated.
© 2005 Elsevier Ltd. All rights reserved.

Keywords: DFT; GGA-PBE; Hydroxamic acids; Copper complexes; Bonding; Electronic structures

1. Introduction

The accurate calculation of properties of transition metal complexes by refined theories is very difficult for several reasons. The first is the vast number of electrons that needs to be considered, and the significant relativistic effects, which implies the use of relativistic pseudopotentials or relativistic calculations. The second is the existence of unpaired electrons in the d shells of most transition metals (except d^{10} systems), which makes an unambiguous assignment of the ground state difficult. Jahn–Teller distortions and other such effects imply that even the symmetry of the complex is often unknown; thus, open-shell calculations that take approximately twice the computational time required for restricted closed shell calculations, need to be performed on these systems. The SCF convergence is also slow for these systems because of the mixing of d orbitals and the s orbitals.

The significance of transition metals in chemistry, however, is immense [1], e.g. in organometallic and bioinorganic chemistry, organic catalysis, etc., and hence the need of having reliable and precise theoretical methods for their calculation. Significant progress in this direction has been made in recent years, and today we have several theoretical papers describing accurate calculations on these systems. The first and foremost conclusion that emerges from these studies is the remarkable accuracy that even surpasses and challenges experimental results. In particular, density functional (DFT) methods (especially gradient-corrected and hybrid functionals) achieve good results for relatively low computational cost. Gradient corrected functionals are much faster and can be efficiently used with plane wave basis sets in solid state calculations. However, for the dissociation of transition metal–oxygen bonds, these functionals produce large errors for the dissociation energy [2], but they do reproduce trends correctly. Hybrid

* Corresponding author. Tel.: +91 011 27666313.
E-mail address: rita_kakkar@vsnl.com (R. Kakkar).

0277-5387/$ - see front matter © 2005 Elsevier Ltd. All rights reserved.
doi:10.1016/j.poly.2005.07.036

functionals, such as B3LYP, though more accurate for metal-oxide dissociation energies, cannot efficiently be used with plane waves, and are hence not useful for calculations on solid materials.

The model complexes used in the present study contain the hydroxamic acid moiety. Metal–hydroxamate complexes exhibit structural diversity [3–10]. Hydroxamate ions have two oxygen atoms and may bond to the metal ion in two different ways: monodentate and bidentate configurations. Besides, they may also coordinate through the nitrogen atom and one oxygen atom. However, the bulk of experimental data favor the bidentate mode using two oxygen atoms. Investigations on the complex formation with simple primary hydroxamic acid ligands in aqueous solution demonstrated clearly that, depending on the pH, two (*O*,*O*) binding modes of the ligands are accessible to metal ions like Cu(II) and V(IV) [3,4]. The more common hydroxamato (1-) type mode arises from the first deprotonation step and involves the coordination of the NHO^- moiety. The hydroximato (2-) form of the ligand is produced by further metal-induced deprotonation of the NHO^- at high pH.

The coordination of the nitrogen atom of the hydroxamic moiety was never found in metal complexes formed by simple hydroxamic acids even if this nitrogen atom can be converted into a very effective binding site in aminohydroxamates, as demonstrated by studies on aminohydroxamates, both in solution and in the solid state [5].

Hydroxamic acids have been found to bind in other coordination modes as well [10]. It was therefore also considered worthwhile to investigate the Cu(II) complexes of three isomeric aminophenylhydroxamic acids, whose crystal data have become available [9], and seek an explanation for their different structures.

2. Computational details

DFT methods are best suited for electronic structure calculations on inorganic complexes. We have performed these calculations using the DMol^3 program [11,12] available from Accelrys Inc. in the Materials Studio package Ver. 3.1. DMol^3 supports two local gradient-corrected exchange-correlation functionals (LDA) and eight nonlocal gradient-corrected exchange-correlation functionals (GGA). VWN [13] and PWC [14] are the two local functionals available in DMol^3. The LDA description tends to overbind atoms, so that the bond lengths are usually underestimated by a few percent. GGA corrects this error, but can underbind instead, leading to slightly long bond lengths. We, therefore, carried out calculations with the ten methods for a model compound whose structure has recently been elucidated by X-ray crystallography [9], and compared the optimized geometry with the experimental one to gauge the relative accuracy of the methods. The eight GGA functionals explored are PW91 [14], BP [14,15], PBE [16], BLYP [15,17], BOP [18], VWN-BP [13–15], RPBE [19] and HCTH [20].

Our calculations employed numerical basis sets of double-ζ quality plus polarization functions (DNP) to describe the valence orbitals. This is the numerical equivalent of the Gaussian 6-31G** basis set. The use of numerical basis sets minimizes the basis set superposition error (BSSE) [21]. The core electrons were treated using DFT semi-local pseudopotentials (DSPP) [22], which replace the effects of core electrons with a simple potential. These core potentials include some degree of relativistic effects and are thus very useful approximations for heavier elements, and the calculation is less computationally expensive since the core electrons are dropped. Complete geometry optimizations were carried out, and the energies corrected for the zero-point vibrational contribution.

The charge distributions were estimated using the molecular electrostatic potential fitting approach [23], since the Mulliken method has well-known shortcomings because of the uncertainty in uniquely defining a charge-partitioning scheme [24], particularly for unbalanced basis sets. For the sake of comparison, however, we also report the Mulliken populations. Since our model complexes contain a Cu(II) ion, which is an open-shell system (d^9), we have performed unrestricted calculations. Mayer bond orders [25] were calculated to describe the bonding in the complexes.

3. Results and discussion

3.1. Choice of an appropriate methodology

As our test ligands, we have chosen the three isomeric aminophenylhydroxamic acids. As mentioned in the introduction, although hydroxamate ions usually bind to metal ions through the two oxygen atoms (i.e. as (*O*,*O*)-bidentate chelating agents), other binding modes are also possible, and this range can be greatly increased if the hydroxamate ligand contains secondary binding groups, resulting in many diverse and intriguing structures [10]. This was found in the complexes formed between the isomeric aminophenylhydroxamic acids ($AphaH_2$) and $CuSO_4 \cdot 5H_2O$ [9]. Whilst 4-aminophenylhydroxamic acid (4-$AphaH_2$) gives the simple square planar complex Cu(4-$AphaH)_2 \cdot 2H_2O$, 2-aminophenylhydroxamic acid (2-$AphaH_2$) gives a fused 'dimeric' metallocrown of the formula $[Cu_5(2\text{-}Apha)_4(\mu\text{-}SO_4) \cdot (H_2O)_2]_2$, in which the metal ions display extensive magnetic coupling (with potential applications in the field of magnetoelectronics). The complex has a 'clam-like' structure, in which (2-$Apha^{2-}$) is doubly deprotonated 2-aminophenylhydroxamic acid. The

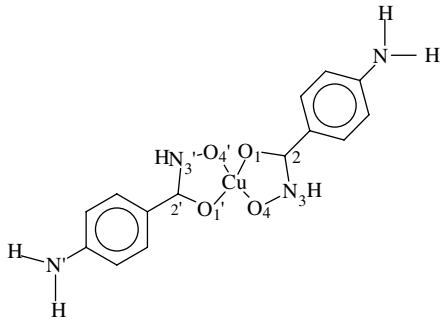

Fig. 1. Structure of the Cu(II) complex of 4-aminophenylhydroxamic acid.

coordination is through deprotonated nitrogen and it contains bridging hydroximate (2-) functions, combined with the $\{O, \mu_2\text{-}O'\}$ chelating/bridging mode. 3-Aminophenylhydroxamic acid (3-AphaH$_2$) gives a trinuclear helical polymer of formula $[Cu_3(3\text{-AphaH})_4SO_4\cdot(H_2O)]_n\cdot 8H_2O$, which has a supramolecular structure with large open cavities, which can be useful in trapping guest molecules.

We optimized the geometries of the 4-aminophenylhydroxamic acid copper complex (see Fig. 1) with the different potentials available in DMol^3, and calculated the relative errors in comparison with experimental determinations (Table A1, Supplementary information). The following conclusions can be drawn: Both the LDA geometries, particularly VWN, are in good agreement with experiment, but the gradient-corrected DFT methods tend to exaggerate the Cu–O$_1$ bond length when compared with the experimental [9] value. This agrees with similar observations made earlier [26,27] for inorganic complexes. On the other hand, LDA-VWN overbinds the Cu–O$_4$ bond, yielding a bond length that is too short by 0.034 Å. Some of the GGA functionals, namely BOP, RPBE and HCTH, are particularly bad when it comes to predicting Cu–O bond lengths. The only GGA functional that gives good agreement with experiment is PBE, for which the error is only 1.6% in relation to experiment, in spite of the fact that the latter refer to the solid state, which is subject to deformation because of solid state effects. In particular, this is the only method that predicts equal Cu–O$_1$ and Cu–O$_4$ bond lengths (see Fig. 1) for the two rings, in agreement with experiment. All other methods predict asymmetry in the two rings. We have, therefore, performed further calculations with the GGA-PBE functional. Table A1 also reveals that, in most cases, the overall errors are smaller for bond angles than for bond distances.

3.2. Structures of the three isomeric aminophenylhydroxamic acids

Table 1 gives the zero-point corrected binding energies of the various structures investigated here. As for other similar systems, the keto tautomer of pyruvic acid is found to be more stable [28]. Moreover, this tautomer may exist in two conformations, namely *Z* and *E*.

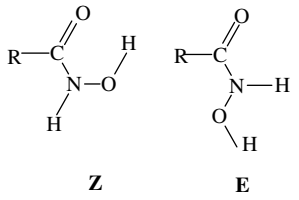

Z **E**

It may be noted that the *Z* conformers of 2- and 4-aminophenylhydroxamic acid isomers have the same energy before zero-point corrections, but 4-aminophenylhydroxamic acid turns out to be lowest in energy after application of the correction (see Table 1). Contrary to expectations, the 2-aminophenyl isomer is lower in energy than the 3-aminophenyl isomer despite the two hydrogens in close proximity in the former. The structures of the *Z* forms of the isomeric aminophenylhydroxamic acids in the free-state are shown in Fig. 2 and Table 2 gives the optimized bond lengths, along with the calculated bond orders.

All three acids are stabilized by intramolecular hydrogen bonding. The existence of the hydrogen bond is indicated from the following:

(i) the distances (∼1.8 Å, see Table 2) between the protons of OH and the carbonyl oxygens are smaller than the sum of the van der Waals radii (ca. 2.7 Å) of the hydrogen and oxygen atoms,
(ii) the high positive charge densities (∼0.4) on the protons of the OH groups, as well as the negative charge densities (∼−0.5) on the carbonyl oxygens,
(iii) the OH···O bond angles of ∼124° are higher than the cut-off angle (90° of arc) [29], and
(iv) the Mayer bond orders (Table 2) of the carbonyl oxygen to hydroxyl hydrogen (0.13), and total valences, 2.03 and 1.02, respectively, on the carbonyl oxygen and hydroxyl hydrogen, which are slightly higher than the ideal values of 2 and 1.

For the simple hydroxamic acids investigated earlier [28], the *trans E* conformers were also found to be stable. For the aminophenylhydroxamic acids, in each case, the *Z* form is found to be more stable by several

Table 1
Zero-point energy corrected GGA-PBE binding energies (kcal/mol) for various structures

	2-	3-	4-
Aminophenylhydroxamic acid (*Z*)	−2064.4	−2063.3	−2065.0
Aminophenylhydroxamic acid (*E*)	−2057.1	−2056.1	−2059.8
Anion *a*	−2029.1	−2028.0	−2027.2
Anion *b*	−2048.6	−2041.9	−2040.8
Cu^{2+} complex	−4091.1	−4090.6	−4090.3

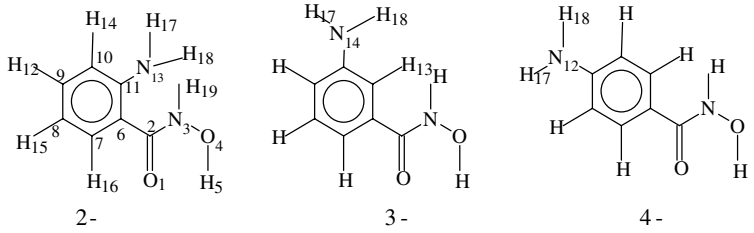

Fig. 2. Structures of the *Z* forms of the three isomeric, 2-, 3- and 4-aminohydroxamic acids.

Table 2
Optimized bond lengths (Å), along with the calculated Mayer bond orders for the three isomeric acids

Bond[a]	2- (X = N, Y = Z = H)		3- (X = H, Y = N, Z = H)		4- (X = Y = H, Z = N)	
	Length	Order	Length	Order	Length	Order
O_1C_2	1.234	1.679	1.234	1.675	1.234	1.673
O_1N_3	2.229	0.095	2.223	0.108	2.232	0.097
C_2N_3	1.372	1.131	1.359	1.165	1.369	1.145
N_3O_4	1.390	1.025	1.388	1.019	1.394	1.018
O_1H_5	1.826	0.131	1.848	0.130	1.826	0.133
O_4H_5	0.981	0.871	0.979	0.873	0.981	0.871
C_2C_6	1.465	1.031	1.470	0.999	1.461	1.023
C_6C_7	1.397	1.326	1.390	1.328	1.394	1.310
C_7C_8	1.377	1.416	1.384	1.386	1.376	1.446
C_8C_9	1.390	1.351	1.383	1.409	1.399	1.284
C_9C_{10}	1.379	1.422	1.397	1.293	1.399	1.282
C_6C_{11}	1.410	1.247	1.391	1.343	1.395	1.300
$C_{10}C_{11}$	1.396	1.315	1.395	1.318	1.377	1.450
C_9Z_{12}	1.072	0.991	1.073	0.990	1.369	1.120
$C_{11}X_{13}$	1.383	1.100	1.074	0.983	1.073	0.982
$C_{10}Y_{14}$	1.074	0.989	1.377	1.106	1.074	0.992
C_8H_{15}	1.071	0.993	1.073	0.991	1.074	0.990
C_7H_{16}	1.072	0.981	1.071	0.986	1.072	0.983
NH_{17}[b]	1.062	0.981	0.998	0.980	0.998	0.981
NH_{18}[b]	1.004	0.941	0.998	0.982	0.998	0.981
N_3H_{19}	1.005	0.924	1.000	0.947	1.002	0.946

[a] See Fig. 2 for numbering. The complete set of optimized geometrical parameters can be found in the Supplementary information.

[b] N is the amino nitrogen, which is N_{13} for 2-, N_{14} for 3-, and N_{12} for 4-aminophenylhydroxamic acid.

kcal/mol (see Table 1) as a result of intramolecular hydrogen bonding. Besides, we found that the *E* forms are nonplanar and do not represent energy minima in the case of 2-aminophenylhydroxamic acid, which possesses a small imaginary frequency (155 cm^{-1}) and the 4-aminophenyl isomer, for which the imaginary frequency is 45 cm^{-1}.

The aminophenylhydroxamic acids could also be *N*-acids (*a*) or *O*-acids (*b*).

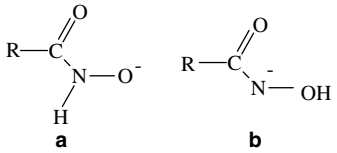

Our earlier calculations for simple hydroxamic acids [28] had shown that only the *cis* form of the *a* anion (shown above) is important, and this is the one formed by deprotonation from the hydroxyl hydrogen of the more stable *Z* conformer, while the *trans* isomer would be the result of deprotonation from the *E* conformer. Moreover, this has the correct conformation for chelation with metal ions. We, therefore, restricted our calculations to the *a* (*cis*) and *b* anions formed by ionization of an OH proton or NH proton, respectively, from the *Z* conformers of the acids. For the hydroxamic acids investigated earlier, the *b* anions were found to be more stable, making them *N*-acids. In this case, too, the acids are *N*-acids, as the *b* anion is more stable than *a* in all cases. The difference in energies between the two anions is highest for the anion of 2-aminophenylhydroxamic acid (see Table 1), as there is extensive hydrogen bonding in the *b* anion in this case (see Fig. 3). This partly explains why this isomer has a tendency to form complexes by deprotonation from both nitrogen and oxygen, while the other acids undergo deprotonation at oxygen only on complex formation.

Since the *a* anion is the one involved in chelation with metal ions, we have collected the bond lengths and bond orders of these anions in Table 3. It is found that anion formation increases the O_1C_2 bond length and decreases the C_2N_3 bond length.

3.3. Structures of the three isomeric aminophenylhydroxamic acid complexes

The binding energies for the 2-, 3- and 4- isomeric complexes are given in Table 1. Again, the 2-amino isomer complex appears to be more stable despite the two hydrogens in close proximity. However, the relative stabilities of the complexes may be determined more accurately from the complexation energies, $\Delta E = E_{\text{product}} - E_{\text{reactant}}$, i.e.

$$\Delta E = E_{\text{complex}} - E_{Cu^{2+}} - 2E_{\text{anion}},$$

where $E_{Cu^{2+}}$, the binding energy of the Cu^{2+} ion, is 669.6 kcal/mol, and E_{anion} is the energy of the *a* anion.

The complexation energies for the three complexes are −702.5, −704.2 and −705.5 kcal/mol. These calculations prove the slightly greater stability of the 4-aminophenyl isomer. In these calculations, the effects of hydrogen bonding get cancelled as it is present in both the reactant and the product. Moreover, for the 2-amino-

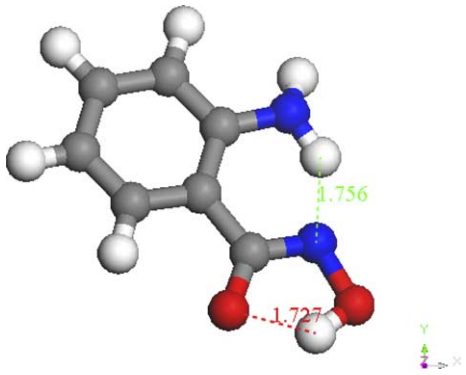

Fig. 3. Structure of the *b* anion of 2-aminophenylhydroxamic acid, showing the extensive hydrogen bonding. Distances are in Å.

Table 3
Optimized bond lengths (Å), along with the calculated Mayer bond orders for the *a* anions of the three isomeric acids

Bond[a]	2- (X = N, Y = Z = H)		3- (X = H, Y = N, Z = H)		4- (X = Y = H, Z = N)	
	Length	Order	Length	Order	Length	Order
O_1C_2	1.246	1.634	1.249	1.621	1.250	1.612
O_1N_3	2.304	0.107	2.305	0.115	2.308	0.113
C_2N_3	1.359	1.173	1.351	1.199	1.350	1.207
C_2O_4	2.382	0.108	2.384	0.106	2.387	0.109
N_3O_4	1.304	1.260	1.300	1.255	1.303	1.250
C_2C_6	1.488	1.009	1.481	1.014	1.482	1.010
C_6C_7	1.401	1.321	1.404	1.288	1.401	1.294
C_7C_8	1.382	1.399	1.380	1.417	1.382	1.408
C_8C_9	1.390	1.361	1.390	1.367	1.391	1.321
C_9C_{10}	1.389	1.376	1.397	1.296	1.394	1.302
C_6C_{11}	1.414	1.238	1.405	1.296	1.400	1.297
$C_{10}C_{11}$	1.393	1.349	1.389	1.362	1.383	1.423
C_9Z_{12}	1.074	0.992	1.075	0.991	1.410	1.027
$C_{11}X_{13}$	1.399	1.062	1.075	0.977	1.074	0.978
$C_{10}Y_{14}$	1.017	0.988	1.405	1.041	1.076	0.990
C_8H_{15}	1.074	0.993	1.076	0.992	1.077	0.990
C_7H_{16}	1.073	0.977	1.072	0.977	1.073	0.974
NH_{17}[b]	1.002	0.984	1.001	0.985	1.004	0.987
NH_{18}[b]	1.007	0.984	1.002	0.987	1.002	0.987
N_3H_{19}	1.011	0.931	1.010	0.947	1.010	0.949

[a] See Fig. 2 for numbering. The proton removed is H_5. The complete set of optimized geometrical parameters can be found in the Supplementary information.

[b] N is the amino nitrogen, which is N_{13} for 2-, N_{14} for 3-, and N_{12} for 4-aminophenylhydroxamic acid.

phenylhydroxamate complex, there are three small imaginary frequencies, 32, 37 and 50 cm^{-1}.

Selected optimized bond lengths and bond orders for the three complexes are given in Table 4. It can be observed that complexation leads to a further increase in the O_1C_2 bond length (and consequent decrease in bond order) and further strengthening of the C_2N_3 bond, particularly for the Cu(II) complex of 4-aminophenylhydroxamic acid. In each complex, both five-membered Cu–hydroxamate rings are planar, causing delocalization of electrons in the $O_1C_2N_3$ moiety. The C_2C_6 bond is essentially single, permitting the phenyl ring to rotate about this bond. The phenyl rings are twisted with respect to the hydroxamate grouping by ~20° in each case. Similar results were obtained in single-crystal studies of three bis(*N*-methylbenzohydroxamato-*O*,*O*′) copper (II) complexes, except the observation [30] of significant angular strain on the sp^2 carbonyl carbon, which was not found to be the case in the present studies.

3.4. Charge population analysis

Table 5 presents the ESP fitted and Mulliken atomic charges and group charges of the three complexes. The group charge was calculated by the summation over the atomic charges of all of the atoms that comprise the group. As shown in Table 5, the group charge of the hydroxamate ligand in the free state is −1.0, while the ESP charges of the ligands in the three complexes, 2-, 3- and 4-aminophenylhydroxamic acid, are −0.308, −0.314 and −0.301, respectively. It is seen that the group charges of the ligand decrease in magnitude in the complexes coordinating with Cu(II), which indicates that electron transfer from the ligands to Cu(II) has occurred and the coordination bonds have formed. This is also evident from the calculated Cu–O_4 bond distance

Table 4
Selected optimized bond lengths (Å), along with the calculated Mayer bond orders for the three isomeric Cu(II) complexes

Bond[a]	2-(X = N, Y = Z = H)		3-(X = H, Y = N, Z = H)		4-(X = Y = H, Z = N)	
	Length	Order	Length	Order	Length	Order
O_1Cu_5	1.947	0.472	1.917	0.502	1.964	0.455
O_1C_2	1.275	1.340	1.276	1.324	1.276	1.351
O_1N_3	2.224	0.093	2.222	0.098	2.223	0.095
C_2N_3	1.323	1.263	1.318	1.275	1.320	1.377
O_4Cu_5	1.932	0.513	1.892	0.542	1.928	0.515
N_3O_4	1.344	1.094	1.334	1.096	1.345	1.097
C_2C_6	1.461	1.069	1.456	1.056	1.456	1.050
C_6C_7	1.395	1.298	1.392	1.314	1.397	1.317
C_7C_8	1.378	1.432	1.385	1.424	1.325	1.429
C_8C_9	1.387	1.356	1.383	1.354	1.398	1.282
C_9C_{10}	1.381	1.364	1.400	1.298	1.399	1.310
C_6C_{11}	1.407	1.240	1.392	1.281	1.394	1.284
$C_{10}C_{11}$	1.391	1.371	1.396	1.345	1.377	1.422
C_9Z_{12}	1.072	0.989	1.095	0.985	1.372	1.092
$C_{11}X_{13}$	1.393	1.074	1.096	0.975	1.074	0.980
$C_{10}Y_{14}$	1.075	0.985	1.367	1.106	1.074	0.986
C_8H_{15}	1.072	0.989	1.093	0.986	1.075	0.987
C_7H_{16}	1.071	0.971	1.092	0.972	1.072	0.973
NH_{17}[b]	1.001	0.983	1.016	0.972	0.998	0.983
NH_{18}[b]	1.004	0.952	1.016	0.974	0.998	0.980
N_3H_{19}	1.005	0.930	1.022	0.944	1.001	0.959

[a] See Figs. 1 and 2 for numbering. Geometrical parameters of only one ligand are given. The complete set of optimized geometrical parameters can be found in the Supplementary information.

[b] N is the amino nitrogen, which is N_{13} for 2-, N_{14} for 3-, and N_{12} for 4-aminophenylhydroxamic acid.

(1.93 Å), which is slightly smaller than the sum of the ionic radii of Cu^{2+} and O^{2-}, which is 1.97 Å.

The atomic charge calculations can give a feature for the relocation of the electron density of the ligands. As shown in Table 5, the atomic charges of the coordinated atoms, O_4, remain unchanged (∼−0.438) for the 2-aminophenyl isomer. In contrast, the atomic charges of O_1 (from −0.483 to −0.409) decrease for the 2-aminophenyl isomer. This indicates that there is no general rule to predict the atomic charges for the coordinated atoms. There is a large variation in the charge densities on nitrogen and carbon, too. Instead of gaining electron density in the anion, the nitrogen becomes almost neutral in the anion and complex. The carbon remains almost constantly positively charged throughout. However, the charges on Cu^{2+} (Table 5) demonstrate that 1.384 e transfers from the ligands to Cu(II) in the complex, suggesting that an electron moves from the coordinated atoms to Cu(II) and the electron transfers synchronously from other parts of the ligands to the coordinated atoms. For the other two complexes, the situation is similar. For the 4-aminophenyl isomer, there is a slightly larger transfer of charge from the ligands to the Cu^{2+} ion, as the positive charge on Cu^{2+} is the least in this case.

A comparison with the Mulliken charges indicates that the Mulliken partial charge on Cu in the three complexes is smaller, ∼0.4 e, compared to ∼0.6 e for the ESP charges. This indicates that Mulliken charges ascribe higher covalency to the complex. This is a failing of Mulliken charges. Another drawback of the Mulliken charges is their tendency to be basis-size dependent. To confirm this, we calculated the partial charge on copper as a function of the size of the basis set for the 4-aminophenylhydroxamate copper (II) complex. The calculated Mulliken charges for the minimal (MIN), double zeta (DN), 6-31G* (DND) and 6-31G** (DNP) basis sets are 0.928, 0.380, 0.434 and 0.392, respectively, while the corresponding ESP charges are 0.893, 0.725, 0.607 and 0.602, respectively. It can be seen that the latter converge to 0.6 as the basis set is increased in size, while the former do not follow any particular order. Therefore, the ESP charges may be considered reliable.

The calculated Mayer bond orders for the *Z* forms of the acids, their corresponding anions and the Cu(II) complexes are given in Tables 2–4, where we have given all bond orders $\geqslant 0.1$, even when the two atoms are not connected. Both in the *Z* conformers of the three acids (Table 2) and their anions formed by deprotonation of the hydroxyl proton (Table 3), it may be noted that the carbonyl bond of the hydroxamate grouping is weak, with an average bond order of 1.67 in the former and 1.62 for the latter, compared to the expected value of 2. For the acids, this can be traced to hyperconjugative interactions with N_3 and hydrogen bonding with H_5. The interaction with the N_3 lone pair puts electron density into the carbonyl π* orbital, reducing its bond

Table 5
The calculated partial charges of the optimized complexes and free ligands (*Z*), anions and complexes for the isomeric aminophenylhydroxamic acids[a]

	ESP			Mulliken		
	Free	Anion	Complexed	Free	Anion	Complexed
2-Aminophenylhydroxamic acid						
O_1	−0.483	−0.620	−0.409	−0.495	−0.549	−0.507
C_2	0.388	0.434	0.286	0.389	0.288	0.467
N_3	−0.225	−0.017	−0.050	−0.133	−0.24	0.013
O_4	−0.438	−0.595	−0.439	−0.349	−0.558	−0.443
Cu^{2+}			0.616			0.401
Hydroxamate		−1.0	−0.308		−1.0	−0.201
3-Aminophenylhydroxamic acid						
O_1	−0.466	−0.622	−0.386	−0.493	−0.563	−0.504
C_2	0.381	0.421	0.266	0.386	0.289	0.480
N_3	−0.265	−0.053	−0.134	−0.083	0.018	0.036
O_4	−0.400	−0.563	−0.396	−0.351	−0.549	−0.445
Cu^{2+}			0.628			0.409
Hydroxamate		−1.0	−0.314		−1.0	−0.205
4-Aminophenylhydroxamic acid						
O_1	−0.473	−0.620	−0.403	−0.498	−0.567	−0.499
C_2	0.382	0.408	0.299	0.383	0.288	0.470
N_3	−0.275	−0.066	−0.173	−0.097	0.015	0.035
O_4	−0.410	−0.572	−0.386	−0.361	−0.562	−0.453
Cu^{2+}			0.602			0.392
Hydroxamate		−1.0	−0.301		−1.0	−0.196

[a] See Figs. 1 and 2 for numbering. The complete set of partial atomic charges and Mayer free valences is available as Supplementary information.

order. In the anion, removal of H_5 removes hydrogen bonding interaction, but increases hyperconjugative interaction with N_3, as reflected in the further decrease in the carbonyl bond order and decreased electron density at nitrogen in the anion. The Mayer total valence on the nitrogen also increases from an average value of 3.27 in the acids to 3.60 in the anions.

The calculated Cu–O Mayer bond orders for the 4-aminophenylhydroxamate complex show that the Cu–O_4 bonds are stronger than the Cu–O_1 bonds (Table 4). This is also evident from the shorter bond length of the former. The complexes have sizeable covalent character, the total valence of copper being 2.24. For the 2-aminophenylhydroxamate Cu(II) complex, however, all four Cu–O bonds have similar bond orders, 0.58, and the total valence on copper is 2.36. The case of the 3-aminophenylhydroxamate Cu(II) complex is similar (Table 4).

However, the electron distribution is not apparent from the partial atomic charges. In Fig. 4 is given the plot of the electrostatic potential for the *a* forms of the anions. It can be seen that the negative charge (yellow areas) is distributed throughout. In the case of the 4-aminophenylhydroxamic acid complex, there is greater accumulation of charge density away from the two coordinating oxygens. Thus the difference in the three complexes is a result of the different electronic distributions in the anions themselves.

We have also plotted the electrostatic potential maps for the three complexes in Fig. 5. These maps give an idea about the range of electron density around the complex. For 2- and 3-aminophenylhydroxamate complexes, the isoelectronic contour plotted is at 0.016 au (10 kcal/mol). However, this was not possible for the 4-aminophenylhydroxamate complex, as the potential extends only between -5.1×10^{-4} and 2.9×10^{-7} au, and hence the contour is for 1×10^{-10} au.

The three maps demonstrate the differences in the electronic behavior of the three complexes. The 2- and 3-aminophenylhydroxamate complexes have similar maps, but that of the 3-aminophenyl isomer is smaller and hence more compact, showing that the charge is concentrated in the latter. However, the map for the 4-aminophenylhydroxamate complex bears no resemblance to that of the other two. While in the former cases, the potential near the Cu(II) ion is positive (yellow), in this case it is negative at the center, but positive elsewhere. The smaller extent of the potential in the case of the 4-aminophenylhydroxamate complex may explain its reluctance to polymerize.

One can also note that in the 2- and 3-aminophenylhydroxamic acid complexes, the potential is

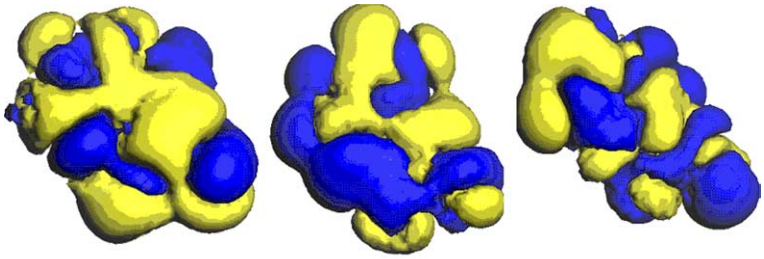

Fig. 4. Isopotential maps for the *a* anions of 2-, 3- and 4-aminophenylhydroxamic acid (isovalue $= 1\times10^{-17}$ au).

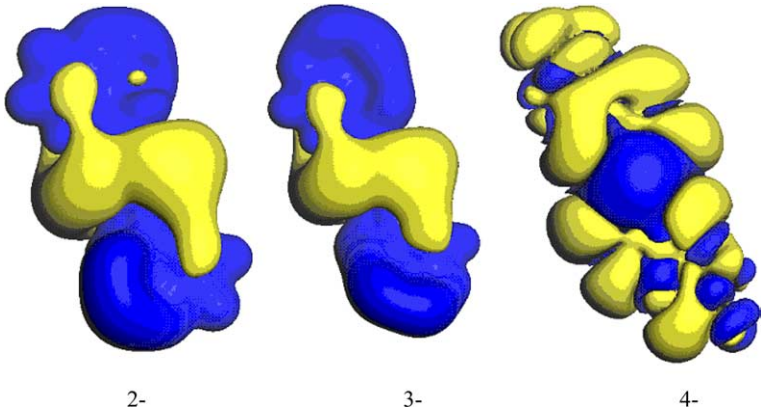

Fig. 5. Isopotential maps for the Cu(II) complex of 2- and 3-aminophenylhydroxamic acid (isovalue = 0.016 au), and 4-aminophenylhydroxamic acid (isovalue $= 1\times10^{-10}$ au).

positive throughout (blue areas) unlike the case of the hydroxamate ions.

4. Conclusions

Density functional calculations have been performed on a copper hydroxamate complex of experimentally determined structure to determine the applicability of this approach to study the properties of inorganic complexes. It has been found that:

- Most of the potentials yield very good geometries when compared with experiment.
- The GGA-PBE and LDA-VWN pseudopotentials, in particular, are best suited for these studies, but because of a tendency to overbind atoms in the latter, the former is preferred.
- The results demonstrate that 2-aminophenylhydroxamic acid is the most stable of the three isomers in spite of two hydrogens in close proximity, but the complex formation reaction is most exothermic for the 4-aminophenylhydroxamic acid complex, although the differences are small.
- All the acids are *N*-acids, but bind in the (*O*,*O*)-coordination mode. The 2-aminophenyl isomer, however, has a more acidic proton at the nitrogen and therefore undergoes further deprotonation.
- Hyperconjugative interactions with the nitrogen lone pair weaken the carbonyl bond.
- Electrostatic potential fitted charges give a better description of the charge distribution than the Mulliken charges.
- The complexes have considerable covalent character, the Cu–O bond orders being slightly higher than 0.5 in each case.
- There is greater delocalization of charge away from the coordinating oxygens, both in the anion and in the complex, for the 4-aminophenyl isomer.
- The differences in the coordination geometries of the three complexes can be satisfactorily explained using DFT calculations.

Acknowledgements

Two of the authors (R.G. and P.G.) thank the Council of Scientific and Industrial Research (CSIR), New Delhi, for Research Fellowships.

Appendix A. Supplementary data

Supplementary data associated with this article can be found, in the online version, at doi:10.1016/j.poly.2005.07.036.

References

[1] G. Berthon (Ed.), Handbook of Metal–Ligand Interactions in Biological Fluids, Marcel Dekker, New York, 1995.
[2] J. Sauer, J. Döbler, Dalton Trans. (2004) 3116.
[3] E. Farkas, E. Kozma, M. Pethö, K.M. Herlihy, G. Micera, Polyhedron 17 (1998) 3331.
[4] A. Dessi, G. Micera, D. Sanna, L.S. Erre, J. Inorg. Biochem. 48 (1992) 279.
[5] B. Kurzak, H. Kozlowski, E. Farkas, Coord. Chem. Rev. 114 (1992) 169.
[6] E. Farkas, E.A. Enyedy, H. Csoka, J. Inorg. Biochem. 79 (2000) 205.
[7] E. Farkas, K. Megyeri, L. Somsák, L. Kováks, J. Inorg. Biochem. 70 (1998) 41.
[8] C.J. Marmion, D. Griffith, K.B. Nolan, Eur. J. Inorg. Chem. 15 (2004) 3003.
[9] D. Gaynor, Z.A. Starikova, W. Haase, K.B. Nolan, J. Chem. Soc., Dalton Trans. (2001) 1578.
[10] C.J. Milios, E. Manessi-Zoupa, S.P. Perlepes, Transit. Metal Chem. 27 (2002) 864.
[11] B. Delley, J. Chem. Phys. 92 (1990) 508.
[12] B. Delley, J. Chem. Phys. 113 (2000) 7756.
[13] S.H. Vosko, L. Wilk, M. Nusair, Can. J. Phys. 58 (1980) 1200.
[14] J.P. Perdew, Y. Wang, Phys. Rev. B45 (1992) 13244.
[15] A.D. Becke, J. Chem. Phys. 88 (1988) 2547.
[16] J.P. Perdew, K. Burke, M. Ernzerhof, Phys. Rev. Lett. 77 (1996) 3865.
[17] C. Lee, W. Yang, R.G. Parr, Phys. Rev. B 37 (1988) 785.
[18] T. Tsuneda, T. Suzumura, K. Hirao, J. Chem. Phys. 110 (1999) 10664.
[19] B. Hammer, L.B. Hansen, J.K. Norskov, Phys. Rev. B 59 (1999) 7413.
[20] A.D. Boese, N.C. Handy, J. Chem. Phys. 114 (2001) 5497.
[21] N. Matsuzawa, J. Seto, D.A. Dixon, J. Phys. Chem. A 101 (1997) 9391.
[22] B. Delley, Phys. Rev. B 66 (2002) 155125/1.
[23] U.C. Singh, P.A. Kollman, J. Comput. Chem. 5 (1984) 129.
[24] K.B. Wiberg, P.R. Rablen, J. Comput. Chem. 14 (1993) 1504.
[25] I. Mayer, Int. J. Quantum Chem. 29 (1986) 477.
[26] Y. Zhang, Z. Guo, X.–Z. You, J. Am. Chem. Soc. 123 (2001) 9378.
[27] P.N. Kapoor, R. Kakkar, J. Mol. Struct.-Theochem 679 (2004) 149.
[28] R. Kakkar, R. Grover, P. Chadha, Org. Biomol. Chem. 1 (2003) 2200.
[29] G.A. Jeffrey, W. Saenger, Hydrogen Bonding in Biological Structures, Springer-Verlag, Berlin, Germany, 1991.
[30] R.G. Baughman, D.J. Brink, J.M. Butler, P.R. New, Acta Crystallogr. C56 (2000) 528.

Available online at www.sciencedirect.com
SCIENCE DIRECT®
Polyhedron 25 (2006) 767–775
POLYHEDRON
www.elsevier.com/locate/poly

Dioxomolybdenum(VI) and -tungsten(VI) complexes with tetradentate aminobis(phenol)s

Ari Lehtonen [a,*], Mikael Wasberg [a], Reijo Sillanpää [b]

[a] Materials Chemistry and Chemical Analysis, Department of Chemistry, University of Turku, Vatselantie, FIN-20014, Turku, Finland
[b] Laboratory of Inorganic Chemistry, Department of Chemistry, University of Jyväskylä, FIN-40351 Jyväskylä, Finland

Received 1 July 2005; accepted 26 July 2005
Available online 31 August 2005

Abstract

Aminobis(phenol) ligands (H_2L^n) carrying either a dimethylamino, a pyridyl or a methoxy sidearm donor were used in the preparation of new tungsten and molybdenum complexes. Treatment of $[W(eg)_3]$ (eg = 1,2-ethanediolate dianion) with H_2L^n under hydrolytic conditions in a $CHCl_3$–MeOH mixture gave the *cis*-dioxotungsten(VI) complexes $[WO_2(L^n)]$ in good yields. The corresponding molybdenum complexes $[MoO_2(L^n)]$ were prepared from $[MoO_2(acac)_2]$ and respective ligands. The solid-state structures of two molybdenum and one tungsten compounds were determined by single crystal X-ray diffraction, which revealed that the dianionic aminobis(phenolate) backbones of the ligands have coordinated to the metal centre as [O,N,O] donors, whereas the last coordination sphere has been occupied by a N or O donor atom of the ligand sidearm. All synthesized new complexes can catalyse the oxotransfer reaction between benzoin and dmso at 120 °C.
© 2005 Elsevier Ltd. All rights reserved.

Keywords: Alkoxide complexes; Phenolate ligands; Molybdenum; Tungsten; Crystal structure

1. Introduction

High-valent molybdenum and tungsten complexes which bear *cis*-MO_2 units have attracted considerable interest due to their applications in catalytic oxotransfer reactions [1,2]. In particular, these complexes are known to catalyse various industrially valuable processes, e.g. asymmetric olefin epoxidation and alcohol oxidation [3]. Molybdenum and tungsten are also necessary elements in diverse biological systems, since nature has made use of these metal centres in numerous redox enzymes [4]. Catalytic activities of artificial and biological catalysts are commonly associated with the coordinative unsaturation of the metal centre, which allows the substrate molecules to coordinate to the reactive metal species. There are few reports on tetrahedral 4-coordinate [5–7] and trigonal bipyramidal 5-coordinate [3d,7,8] dioxomolybdenum(VI) complexes, but generally *cis*-dioxo complexes of molybdenum(VI) and tungsten(VI) have saturated octahedral coordination. The coordination sphere around the metal centre is frequently completed by solvent molecules or through dimerization.

In respect to occurrence, metallurgy, and properties of the metals, molybdenum and tungsten are remarkably similar elements [9]. They have also rather similar chemical properties, as they are able to form structurally identical compounds. However, there are some differences between these metals in various categories of compounds, thus compounds of the same structural type may differ noticeably in their formation and reactivities. For example, numerous *cis*-dioxomolybdenum(VI) complexes with a variety of supporting ligands have been prepared and studied as catalyst model compounds [10], whereas chemistry of analogous tungsten complexes is still inadequately

* Corresponding author. Tel.: +358 2 333 6733; fax: +358 2 333 6700.
E-mail address: Ari.Lehtonen@utu.fi (A. Lehtonen).

0277-5387/$ - see front matter © 2005 Elsevier Ltd. All rights reserved.
doi:10.1016/j.poly.2005.07.037

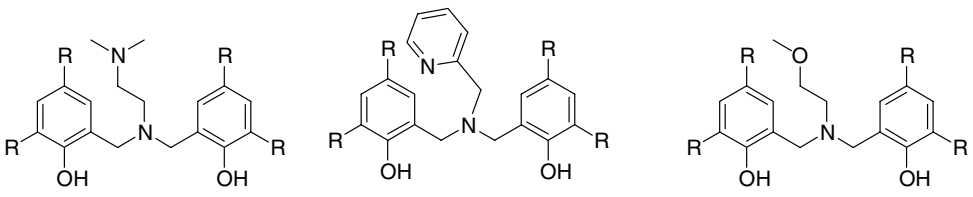

Chart 1. Aminobis(phenolato) ligands used in this study.

studied [2,3,11]. One reason for the relatively low number of known *cis*-dioxotungsten(VI) complexes is apparently the poor availability of suitable starting materials, whereas appropriate precursor for corresponding molybdenum complexes are easily accessible. In some cases, tungstate ion [WO_4^{2-}] can be used in acidic, aqueous solution to prepare new *cis*-dioxotungsten(VI) complexes [11,12]. Other procedures employ moisture-sensitive, poorly soluble [WO_2Cl_2] or its more convenient derivatives, i.e., [WO_2Cl_2(dme)] and [WO_2(acac)$_2$] (dme = 1,2-dimethoxyethane) [2,11,13,14]. Monomeric trisdiolatotungsten(VI) complex [W(eg)$_3$] (eg = ethylene glycolate) [15] is a straightforwardly available, air-stable and moderately soluble compound, which can be easily converted to a variety of new tungsten(VI) alkoxide and phenoxide complexes [16]. Therefore, we have previously used it as a precursor for various oxotungsten(VI) complexes with aminobis(phenol)s [16c,16d,16e]. During these studies we have found that [W(eg)$_3$] can react with linear, tetradentate diaminobis(phenol)s (H_2ONNO^R) under hydrolytic conditions to produce air-stable *cis*-dioxocomplexes [$WO_2(ONNO^R)$] [16e]. In this article, we shall describe the synthesis and characterization of a series of new 6-coordinate *cis*-dioxomolybdenum(VI) complexes [$MoO_2(L^n)$] as well as structurally analogous tungsten complexes [$WO_2(L^n)$] with potentially tetradentate symmetric aminobis(phenolate) ligands (Chart 1).

We have earlier observed that dioxomolybdenum(VI) complexes with tridentate aminobis(phenolate)s tend to dimerize in the absence of strongly coordinating solvent, which causes poor solubility and may also inhibit catalytic activity [17]. In the present study, the ligand design is used to prevent unwanted dimerization. Consequently, the aminobis(phenolate) backbones of the ligands coordinate to the *cis*-MO_2 moieties as dianionic tridentate [O,N,O] donors, while the sixth coordination sites are occupied by N or O sidearm donor atoms.

2. Results and discussion

2.1. Syntheses and spectroscopic characterization of complexes

Some dioxomolybdenum(VI) complexes with tripodal tetradentate aminobis(phenolate)s have been previously prepared from [MoO_2(acac)$_2$] and relevant ligand precursors in high yields using a simple ligand displacement reactions [18], whereas other examples employ the use of an acidic solution of [NH_4]$_6$[Mo_7O_{24}]·4H_2O [2a,2b,2c]. In our experiments, the syntheses involved the treatment of [MoO_2(acac)$_2$] with ligand precursors H_2L^n (see Chart 1) in chloroform solutions (Scheme 1). When starting materials dissolved and the ligand substitution reactions were initiated, the reaction mixtures turned yellow. These yellow solutions were treated with methanol to enhance crystallization and the reaction mixtures were then kept overnight at room temperature. Filtration followed by washing with methanol led to the isolation of pure complexes [$MoO_2(L^n)$] as yellow prismatic crystals or crystalline solids in high yields. All solid complexes are stable in air under ambient conditions. Complex **6** with bulky ligand tends to crystallize as a methanol triadduct, which decomposes slowly due to the partial loss of solvent molecules. All complexes [$MoO_2(L^n)$] were also prepared by the reaction of ligand precursors with [MoO_2Cl_2(dmf)$_2$], but the yields were generally lower and obtained materials had to be purified by recrystallization, as the initial depositions were disturbed by the co-precipitation of additional base or unreacted ligand as a hydrochloride adduct.

Although useful precursors for new dioxomolybdenum(VI) complexes are easily available, there are just a few appropriate starting materials for corresponding dioxotungsten(VI) chemistry. The rare examples of aminobis(phenolate) complexes of dioxotungsten(VI) have been prepared using [WO_2Cl_2(dme)] as a tungsten precursor [2a,2b,2c]. In this study, tungsten trisdiolate [W(eg)$_3$] was allowed to react with tripodal, tetradentate aminobis(phenol)s H_2L^n in a mixture of $CHCl_3$ and MeOH. The pale yellow reaction mixtures were then stirred at 70 °C for an hour and subsequently kept at room temperature for 12 h. Slow crystallization provided analytically pure complexes [$WO_2(L^n)$] in moderate to good yields (Scheme 1). Sterically most hindered ligand precursor H_2L^4 appears to react slower than other studied aminobis(phenols), therefore the formation of the complex **8** in a synthetically useful yield required 8 h reaction in EtOH at reflux temperature. Presumably the mechanism for the formation of these dioxocomplexes includes alkoxide ligand displacement

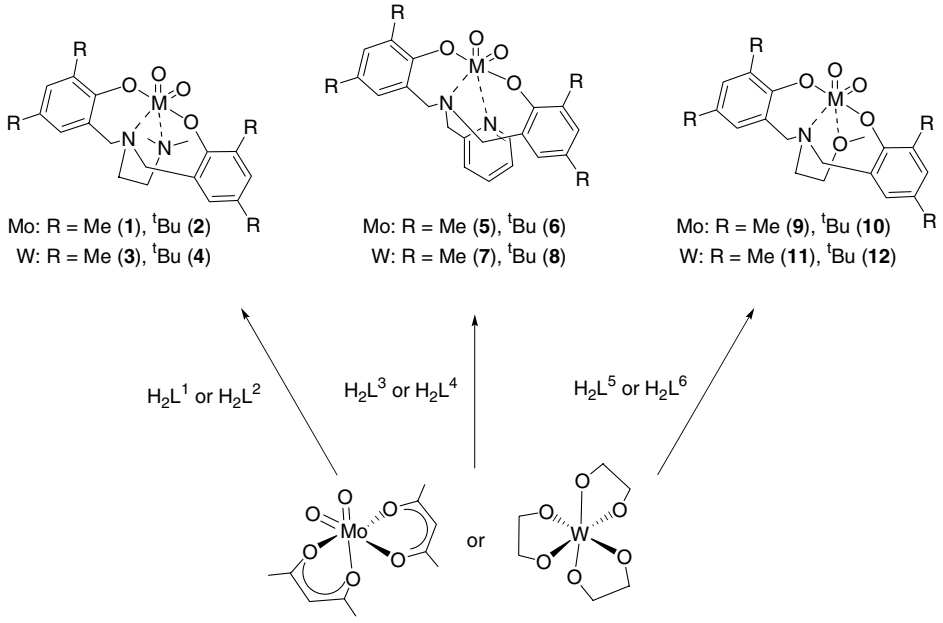

Scheme 1. Formation of complexes $[MO_2(L^n)]$.

reaction in association with hydrolytic cleavage of two diolato groups, so the role of the alcohol solvents is most likely to carry a necessary amount of water to the reaction.

All complexes $[MoO_2(L^n)]$ and $[WO_2(L^n)]$ are moderately soluble in chloroform, dmf and dmso. In general, *tert*-butyl-substituted complexes are more soluble in organic solvents than their methyl-substituted counterparts. Unsurprisingly, structurally analogous Mo and W complexes have considerably similar IR and NMR spectra. The most significant differences between particular molybdenum complex and its tungsten counterpart can been seen in their M=O stretching frequencies. The IR spectra of compounds $[MoO_2(L^n)]$ present two distinctive absorption maxima for MoO_2^{2+} moiety in the expected IR region [2]. The symmetric and asymmetric stretches are observed at 915–935 and 890–905 cm^{-1}, respectively. Similarly, $[WO_2(L^n)]$ show two characteristic *cis*-WO_2 vibrational bands at 935–950 and 900–910 cm^{-1} in their IR spectra [2]. The former bands occur generally at 10–25 cm^{-1} higher frequencies than those for their molybdenum congeners. ^1H and ^{13}C NMR spectra of these molybdenum and tungsten complexes in $CDCl_3$ are consistent with supposed distorted octahedral structures, and they present typical resonances for C_s-symmetric aminobis(phenolate) complexes [2a,19,20].

2.2. Solid-state structures

Complexes **1**, **3**, and **9** crystallized from reaction mixtures as single crystals suitable for X-ray crystallographic analyses (see Table 1). All three complexes form mononuclear molecules, in which the aminobis(phenolate) moiety is coordinated to the dioxometal(VI) unit as a tripodal tetradentate ligand (see Figs. 1–3, Table 2). In all cases, the coordination sphere around the central metal presents distorted octahedral geometry with the terminal oxo ligands *cis* to each other. Two anionic phenolate oxygens and two neutral donor atoms of the ligands are *trans* and *cis*, respectively, as expected for octahedral dioxo complexes. The O=M=O angles and M=O distances are typical for six-coordinated dioxomolybdenum(VI) and -tungsten(VI) complexes [2,6,11]. In complex **1**, the rather long Mo–$O_{aryloxide}$ distances are associated with small Mo–O–C_{aryl} angels. In principal, these two parameters may correlate with the electron donation from aryloxide oxygen lone pair to the metal centre [21]. However, it has been shown that the M–O–C distances and angles in early d-block transition metal aryloxides are exceedingly flexible parameters, which give little insight into M–OAr bonding [22], whereas bonding parameters in these solid-state structures may be mostly controlled by steric effects and packing forces.

2.3. Oxotransfer studies and electrochemistry

Dioxomolybdenum(VI) and tungsten(VI) complexes are known to catalyze oxotransfer reaction from dmso to organic substrates or phosphines [1,2,10a,10b]. Generally, molybdenum-based catalysts are more active in these reactions than their tungsten counterparts. In the present study, the utility of new dioxomolybdenum(VI) and -tungsten(VI) complexes to catalyze oxotransfer reactions was investigated in dmso solutions using benzoin as the substrate, while the conversion of benzoin to benzil was detected by ^1H NMR spectroscopy. As expected, all studied complexes catalyzed oxotransfer from

Table 1
Summary of crystallographic data for **1**, **3**, and **9** at 173 K

	1	**3**	**9**
Formula	$C_{22}H_{30}MoN_2O_4$	$C_{22}H_{30}N_2O_4W$	$C_{21}H_{27}MoNO_5$
M_r	482.42	570.33	469.38
Crystal system	monoclinic	orthorhombic	orthorhombic
Space group (no.)	$P2_1/n$ (14)	*Pbnm* (62)	*Pbnm* (62)
a (Å)	10.5432(4)	7.7966(2)	7.7210(2)
b (Å)	15.8698(9)	15.9781(7)	16.0454(4)
c (Å)	12.5285(6)	17.1642(8)	16.4600(5)
β (°)	90.001(3)	90	90
V (Å^3)	2096.25(17)	2138.23(15)	2039.17(10)
Z	4	4	4
μ(Mo Kα) (cm^{-1})	6.57	54.33	6.75
Observed reflections	4496	2179	2220
R_{int}	0.0314	0.0615	0.0461
Parameters	268	158	145
R_1	0.053 (0.035)[a]	0.041 (0.027)	0.039 (0.029)
wR_2	0.080 (0.075)	0.051 (0.054)	0.065 (0.069)
Peak, hole (e Å^{-3})	0.408, −0.564	0.530, −1.059	0.455, −0.433

$R_1 = \sum||F_o| - |F_c||/\sum|F_o|$.
$wR_2 = \{\sum[w(F_o^2 - F_c^2)_2]/\sum[w(F_o^2)_2]\}^{1/2}$ and $w = 1/[^2(F_o^2) + (aP)^2 + bP)]$, where $P = (2F_c^2 + F_o^2)/3$.
[a] Values in parentheses for reflections with $I > 2.0\sigma(I)$.

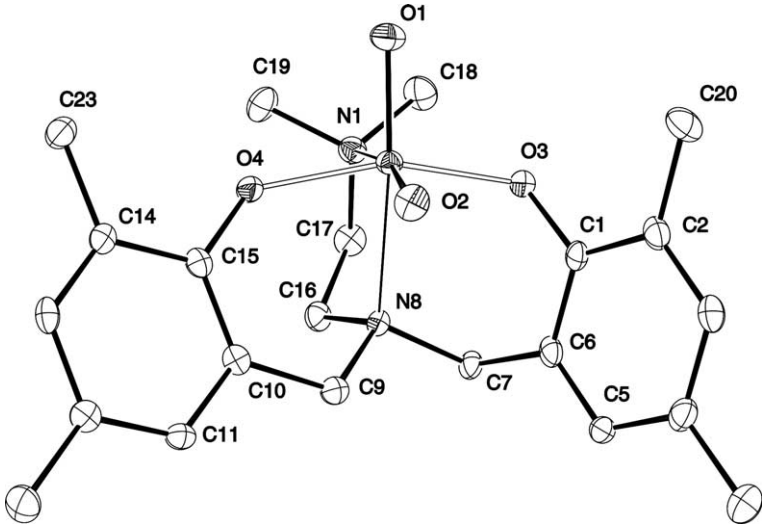

Fig. 1. Molecular structure of $[MoO_2(L^1)]$ (**1**). Thermal ellipsoids have been drawn at 50% probability level. The hydrogen atoms are omitted for clarity in all ORTEP figures.

dmso to benzoin. In individual experiments, the detected yields of oxidized products were 40–60% after 24 h heating at 120 °C. These oxotransfer reactions turned out to be very slow at lower temperatures, and no reactions were noticed at room temperature. Although molybdenum-based oxotransfer catalysts are usually reported to be more active than their tungsten counterparts [2], we did not observe any noteworthy differences between these metals. On the grounds of structurally comparable molybdenum and tungsten-based catalyst systems, we can suppose, that the dioxometal(VI) complexes react with benzoin to yield oxometal(IV) complexes and benzil. The central metal ions are then rapidly oxidized back to the initial dioxocompounds with dmso to complete the catalytic cycle [2a,2b]. Although reduced molybdenum and tungsten species are expected to be strongly coloured, no colour changes were observed during these catalytic reactions, which indicates that the re-oxidation process of metal is very rapid and/or only small amount of complex units are actually reactive. We also attempted to gather possible reduced species by running stoichiometric reactions of benzoin and dioxometal(VI) complexes in various solvents (dmf, $CHCl_3$, MeCN). However, even though the reactions in dmf at high temperatures yielded slight coloration of solutions, we could not isolate any reduced metal complexes.

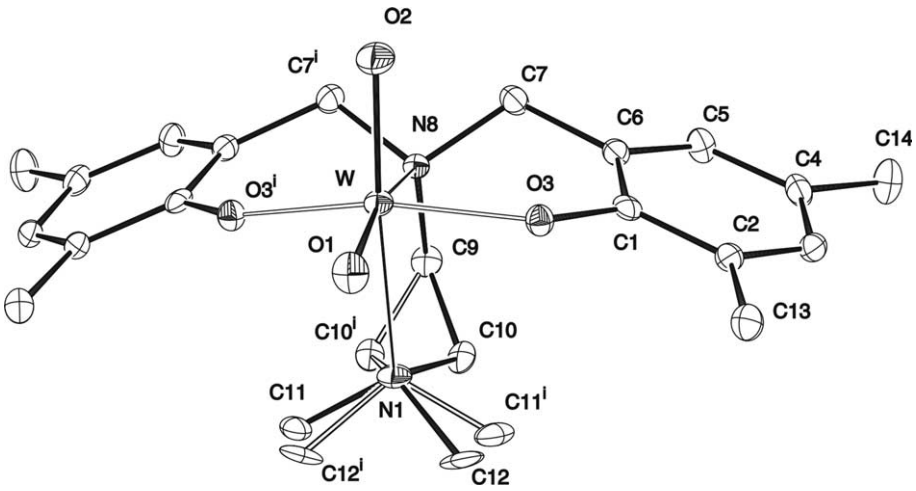

Fig. 2. Molecular structure of $[WO_2(L^1)]$ (**3**). Thermal ellipsoids have been drawn at 30% probability level. Symmetry operation i = x, y, $-z + 1/2$.

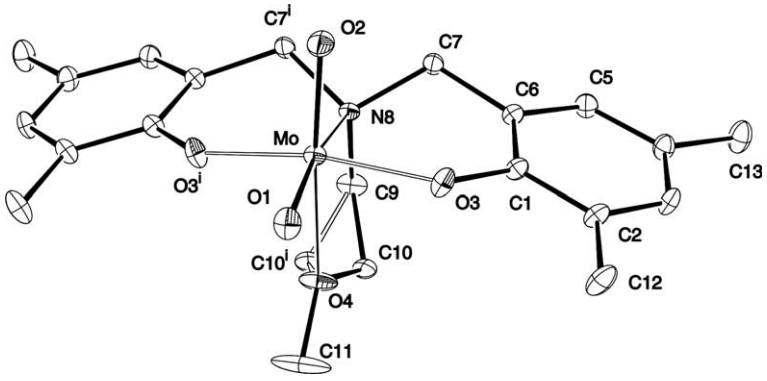

Fig. 3. Molecular structure of $[MoO_2(L^5)]$ (**9**). Thermal ellipsoids have been drawn at 30% probability level. Symmetry operation i = x, y, $-z + 1/2$.

Table 2
Selected bond lengths (Å) and angles (°) for **1**, **3** and **9**

	1	**3**	**9**
M–O1	1.7099(19)	1.731(4)	1.703(2)
M–O2	1.7046(19)	1.727(4)	1.700(2)
M–O3	1.9704(17)	1.925(3)	1.9163(17)
M–O4	1.9449(17)		
M–N1/O4	2.429(2)	2.409(4)	2.349(2)
M–N8	2.409(2)	2.412(5)	2.390(3)
O1–M–O2	108.31(9)	106.94(19)	107.15(12)
O3–M–O4/O3^i	154.80(8)	157.72 (15)	156.12(10)
O1–M–N8	159.09(8)	163.98(16)	162.12(11)
O2–M–N1/O4	166.12(9)	162.21(19)	162.17(10)
C1–O3–M	116.87(15)	141.8(3)	141.87(15)
C15 –O4 –M	128.31(16)		

Symmetry operation i = x, y, $-z + 1/2$.

Table 3
Electrochemical data for selected complexes

Compound	Reduction peak potential (V)
$[MoO_2(L^1)]$ (**1**)	−1.52
$[MoO_2(L^2)]$ (**2**)	−1.77
$[MoO_2(L^{13})]$ (**5**)	−1.38
$[MoO_2(L^4)]$ (**6**)	−1.47
$[MoO_2(L^5)]$ (**9**)	−1.55
$[MoO_2(L^6)]$ (**10**)	−1.52
$[WO_2(L^4)]$ (**8**)	−1.94
$[WO_2(L^6)]$ (**12**)	−1.85

The electrochemical properties of the complexes $[MoO_2(L^n)]$ ($n = 1$–6) and $[WO_2(L^n)]$ ($n = 4$, 6) were studied by cyclic voltammetry (Table 3). All these complexes present an irreversible one-electron reduction process characteristic for the conversion of M^{VI} to M^{V}. For molybdenum complexes this reduction peak shows reversible character as the scan rate is increased, which indicates that the formed molybdenum(V) species decompose rapidly via some homogeneous reactions. The metal-based reduction potentials for the tungsten complexes are more negative by 0.4–0.5 V and reductions are more irreversible than those of the analogous molybdenum compounds, which is in accordance with earlier studies of dioxomolybdenum(VI) and tungsten(VI) compounds [2,3c]. The substituents on the phenolic ring of the ligand seem to have a minor effect on the reduction potential, which is also consistent with

the electron donating characters of methyl and *tert*-butyl groups.

3. Conclusion

Potentially tetradentate aminobis(phenol) ligands (H_2L^n), which carry either a dimethylamino, a pyridyl or a methoxy sidearm donor were used in the preparation of new tungsten and molybdenum complexes. Tris-diolatotungsten(VI) $[W(eg)_3]$ (eg = 1,2-ethanediolate dianion) reacts with H_2 L^n in a $CHCl_3$–MeOH mixture under hydrolytic conditions to yield the *cis*-dioxotungsten(VI) complexes $[WO_2(L^n)]$. The corresponding molybdenum complexes $[MoO_2(L^n)]$ were prepared by the reaction of $[MoO_2(acac)_2]$ with respective ligands. The spectral analyses and crystal structure investigations revealed that the dianionic aminobis(phenolate) backbones of the ligands have coordinated as [O,N,O] donors, whereas the last coordination sphere has been occupied by a N or O donor atom of the ligand sidearm. All synthesized new complexes can catalyse the oxo-transfer reaction between benzoin and dmso at 120 °C, while little difference is observed between activities of Mo and W complexes.

4. Experimental

Starting materials $[MoO_2(acac)_2]$ [23], $[W(eg)_3]$ [15] and H_2L^n [19,24,25] were prepared according literature procedures. Solvents were of HPLC grade and were used as purchased. All syntheses were performed under ambient laboratory atmosphere. ^1H and ^{13}C NMR spectra (400 MHz) were recorded in $CDCl_3$ solutions and were referenced internally to $SiMe_4$. IR spectra were recorded as Nujol mulls. Crystalline samples were dried in vacuum at 40 °C for 4 h prior to elemental analyses. Cyclic voltammograms of studied complexes were recorded at ambient temperature with a Princeton Applied Research model 283 potentiostat using a platinum working electrode, a 1 mm diameter platinum counter electrode and a Ag/AgCl reference electrode (3.4 M KCl). Samples were dissolved in MeCN containing 0.1 M of $(Bu_4N)ClO_4$ as the supporting electrolyte. Typically, a 1.0 mM solution of sample was purged with argon and then the voltammograms were recorded at scan rate of 50 mV s^{-1} over the potential range of 0.0 to −2.0 at ambient temperature.

4.1. Preparation of $[MoO_2(L_n)]$

General procedure. 1.0 mmol of $[MoO_2(acac)_2]$ and 1.0 mmol of a ligand precursor H_2L^n were dissolved in 10 ml of $CHCl_3$ by gentle heating during 15 min. Orange-yellow solution that formed was cooled to room temperature, then 15 ml of MeOH was added to enhance the precipitation of solid product $[MoO_2(L^n)]$. The reaction mixture was then allowed to stand for 12 h at room temperature to complete the crystallization. Bright yellow crystals or crystalline solids were then collected by filtration and washed with cold MeOH.

*$[MoO_2(L^1)]$ (**1**)*. Yellow crystals, yield 90% (434 mg). IR: 1456vs, 1327w, 1312w, 1238vs, 1213s, 1175s, 1101m, 1040w, 1015m, 959w, 947w, 924vs, 901vs, 881m, 860m, 833m, 820m, 801s, 775m, 752m, 727w, 694w, 590m, 554s. ^1H NMR: δ 6.96 (2H, aryl), 6.72 (2H, aryl), 4.51 (d, $J = 14$ Hz, 2H, CH_2), 3.71 (d, $J = 14$ Hz, 2H, CH_2), 2.66 (overlapping s + t, 8H, $N(CH_3)_2 + CH_2$), 2.46 (t, $J = 6$ Hz, 2H, CH_2), 2.25 (6H, CH_3), 2.23 (6H, CH_3). ^{13}C NMR: δ 158.17, 131.60, 129.51, 127.16, 126.03, 122.12, 63.06, 57.38, 52.03, 49.55, 20.53, 16.30. *Anal*. Calc. for $C_{22}H_{30}MoN_2O_4$: C, 54.8; H, 6.3; N, 5.8. Found: C, 54.6; H, 6.1; N, 5.5%.

*$[MoO_2(L^2)]$ (**2**)*. Yellow crystalline solid, yield 69% (448 mg). IR: 1458vs, 1412m, 1364s, 1310m, 1244vs, 1202s, 1169s, 1126m, 1094m, 1028s, 974w, 916s, 894vs, 874s, 871s, 843m, 828s, 806m, 779m, 773m, 752s, 650 w, 602m, 594w, 556m, 496m. ^1H NMR: δ 7.30 (2H, aryl), 7.00 (2H, aryl), 4.14 (d, $J = 14$ Hz, 2H, CH_2), 4.01 (d, $J = 14$ Hz, 2H, CH_2), 3.50 (2H, CH_2) 2.88 (overlapping s + d, 8H, $N(CH_3)_2 + CH_2$), 1.40 (18H, $C(CH_3)_3$), 1.30 (18H, $C(CH_3)_3$). ^{13}C NMR: δ 161.15, 142.62, 136.28, 123.63, 123.39, 122.76, 61.26, 56.63, 53.76, 50.87, 50.59, 35.01, 34.28, 31.66, 30.43. *Anal*. Calc. for $C_{34}H_{54}MoN_2O_4$: C, 62.8; H, 8.4; N, 4.3. Found: C, 62.4; H, 8.1; N, 4.1%.

*$[MoO_2(L^3)]$ (**5**)*. Yellow microcrystals, yield 93% (467 mg). IR: 1611s, 1574w, 1454vs, 1379s, 1319m, 1304m, 1256s, 1221m, 1159m, 1098m, 1059m, 1024m, 961w, 916vs, br, 878s, 851vs, 829vs, 787m, 783m, 731m, 727m, 691w, 648m, 594m, 558m, 519w, 488w. *Anal*. Calc. for $C_{24}H_{26}MoN_2O_4$: C, 57.4; H, 5.2; N, 5.6. Found: C, 57.1; H, 5.4; N, 5.3%.

*$[MoO_2(L^4)] \cdot 3MeOH$ (**6**)*. Yellow crystals, yield 65% (499 mg). IR: 1611s, 1576w, 1456vs,br, 1410w, 1364s, 1304m, 1238s, 1202m, 1157s, 1128m, 1099m, 1057m, 1028m, 972w, 951w, 930s, 905vs, 872s, 833s, 808m, 788m, 746m, 732m, 652w, 602m, 592m, 557m, 498w.^1H NMR: δ 9.11 (d, $J = 5$ Hz, 1H, Py), 7.50 (t, $J = 8$ Hz, 1H, Py), 7.12 (t, $J = 8$ Hz, 1H, Py), 7.10 (2H, aryl), 6.96 (2H, aryl), 6.74 (d, $J = 8$ Hz, 1H, Py), 4.98 (d, $J = 14$ Hz, 2H, CH_2), 3.97 (2H, CH_2Py), 3.75 (d, $J = 14$ Hz, 2H, CH_2), 3.71 (q, J = 23 Hz, 9H, CH_3OH) 1.27 (18H, $C(CH_3)_3$), 1.23 (18H, $C(CH_3)_3$). ^{13}C NMR: δ 159.38, 155.31, 151.41, 142.23, 139.05, 137.64, 123.90, 123.75, 122.68, 121.56, 121.17, 69.17, 63.80, 59.24, 58.35, 50.66 (CH_3OH), 34.93, 34.20, 31.60, 29.89, 18.33. *Anal*. Calc. for $C_{36}H_{50}MoN_2O_4$: C, 64.5; H, 7.5; N, 4.2. Found: C, 64.1; H, 7.4; N, 4.3%.

*[$MoO_2(L^5)$] (**9**)*. Yellow crystals, yield 63% (296 mg): 1456vs,br, 1322w, 1316 m, 1268s, 1254s, 1219s, 1161s, 1101m, 1069m, 1032m, 976w, 953w, 920vs, 897vs, 864vs, 849s, 831m, 789m, 746w, 735m, 693w, 686w, 592m, 557m, 514w. ^{1}H NMR: δ 6.97 (2H, aryl), 6.76 (2H, aryl), 4.46 (d, $J = 14$ Hz, 2H, CH_2), 3.87 (3H, OCH_3), 3.77 (d, $J = 14$ Hz, 2H, CH_2), 3.41 (t, $J = 6$ Hz, 2H, CH_2), 2.83 (t, $J = 6$ Hz, 2H, CH_2), 2.26 (6H, CH_3), 2.25 (6H, CH_3). ^{13}C NMR: δ 158.02, 131.60, 129.73, 126.72, 126.42, 121.78, 69.09, 62.70, 62.34, 52.87, 20.54, 16.24. *Anal*. Calc. for $C_{21}H_{27}MoNO_5$: C, 53.7; H, 5.8; N, 3.0. Found: C, 53.8; H, 5.6; N, 2.8%.

*[$MoO_2(L^6)$] (**10**)*. Yellow microcrystals, yield 64% (296 mg): IR: 1456vs, 1412m, 1364m, 1316m, 1244s, 1202m, 1167m, 1123m, 1096m, 1067vs, 1013m, 972w, 934s, 909vs, 878s, 858s, 833m, 812w, 746w, 735w, 669w, 606w, 592w, 557m, 510w. ^{1}H NMR: δ 7.32 (2H, aryl), 6.96 (2H, aryl), 4.65 (d, $J = 14$ Hz, 2H, CH_2), 3.81 (3H, OCH_3), 3.77 (d, $J = 14$ Hz, 2H, CH_2), 3.34 (t, $J = 6$ Hz, 2H, CH_2), 2.88 (t, $J = 6$ Hz, 2H, CH_2), 1.43 (18H, $C(CH_3)_3$), 1.29 (18H, $C(CH_3)_3$). ^{13}C NMR: δ 158.00, 142.66, 137.53, 124.15, 123.65, 121.90, 69.17, 63.68, 63.04, 58.31, 56.18, 52.94, 35.02, 34.03, 31.62, 29.92, 18.32. *Anal*. Calc. for $C_{33}H_{51}MoNO_5$: C, 62.2; H, 8.1; N, 2.2. Found: C, 62.6; H, 8.1; N, 2.3%.

4.2. Preparation of *[$WO_2(L^n)$]*

General procedure. 1.0 mmol of [W(eg)$_3$] and 1.0 mmol of aminobis(phenol) H_2L^n were dissolved in a combination of $CHCl_3$ (10 ml) and MeOH (10 ml) by heating the reaction mixture to ca. 70 °C for an hour. The pale yellow solution that formed was cooled to room temperature and subsequently allowed to stand for 12 h to precipitate [$WO_2(L^n)$]. White or pale yellow (**7**) crystalline solids were then collected by filtration and washed with cold MeOH. Complex **8** was prepared by refluxing 1.0 mmol of [W(eg)$_3$] and 1.0 mmol of H_2L^4 in 20 ml of EtOH for 8 h, whereas pale yellow solid material crystallized upon cooling to the room temperature.

*[$WO_2(L^1)$] (**3**)*. White crystals, yield 67% (382 mg). IR: 1456vs, 1327w, 1312m, 1254vs, 1219s, 1161s, 1094m, 1040w, 1015m, 962w, 947w, 932vs, 906m, 891vs, 864vs, 849s, 801m, 788m, 735w, 694w, 591m, 556m. ^{1}H NMR: δ 7.00 (2H, aryl), 6.78 (2H, aryl), 4.57 (d, $J = 14$ Hz, 2H, CH_2), 3.60 (d, $J = 14$ Hz, 2H, CH_2), 2.69 (overlapping s + t, 8H, $N(CH_3)_2 + CH_2$), 2.57 (t, $J = 6$ Hz, 2H, CH_2), 2.29 (6H, CH_3), 2.22 (6H, CH_3). ^{13}C NMR: δ 158.27, 131.00, 129.22, 126.96, 126.11, 121.72, 63.00, 57.03, 51.99, 49.51, 20.91, 16.33. *Anal*. Calc. for $C_{22}H_{30}N_2O_4W$: C, 46.3; H, 5.3; N, 4.9. Found: C, 46.0; H, 5.3; N, 4.7%.

*[$WO_2(L^2)$] (**4**)*. White crystalline solid, yield 57% (421 mg). IR: 1454vs, 1364s, 1312m, 1238s, 1202m, 1169m, 1094m, 1028m, 974w, 945s, 904vs, 874s, 849m, 829s, 806m, 779m, 754m, 650 w, 602m, 594w, 556m. ^{1}H NMR: δ 7.36 (d, $J = 2.5$ Hz, 2H, aryl), 6.99 (d, $J = 2.5$ Hz, 2H, aryl), 4.21 (d, $J = 14$ Hz, 2H, CH_2), 4.11 (d, $J = 14$ Hz, 2H, CH_2), 3.50 (2H, CH_2) 2.99 (overlapping s + d, 8H, $N(CH_3)_2 + CH_2$), 1.50 (18H, $C(CH_3)_3$), 1.30 (18H, $C(CH_3)_3$). ^{13}C NMR: δ 159.00, 143.02, 137.51, 124.03, 123.22, 122.58, 61.74, 57.26, 54.31, 51.03, 50.88, 35.00, 34.25, 31.68, 30.55. *Anal*. Calc. for $C_{34}H_{54}N_2O_4W$: C, 55.3; H, 7.4; N, 3.8. Found: C, 55.6; H, 7.3; N, 4.0%.

*[$WO_2(L^3)$] (**7**)*. Pale yellow crystalline solid, yield 46% (271 mg). IR: 1611s, 1574w, 1454vs, 1393m, 1377s, 1321m, 1304m, 1246s, br, 1223m, 1159s, 1098s, 1059m, 1032m, 961w, 934vs, 901vs, 878s, 853vs, 829s, 770m, 763m, 727m, 721m, 689w, 648m, 590m, 556s, 519w, 488w. *Anal*. Calc. for $C_{24}H_{26}N_2O_4W$: C, 48.8; H, 4.4; N, 4.8. Found: C, 48.9; H, 4.6; N, 4.9%.

*[$WO_2(L^4)$] (**8**)*. Pale yellow crystalline solid, yield 41% (310 mg). IR: 1611s, 1574w, 1456vs,br, 1412w, 1388s, 1364s, 1304m, 1238s, 1202m, 1167s, 1128m, 1096m, 1057m, 1028m, 972w, 948vs, 906vs, 874s, 835s, 808m, 770m, 760m, 748m, 732m, 650w, 602m, 588m, 556m, 498m. ^{1}H NMR: δ 9.18 (d, $J = 5$ Hz, 1H, Py), 7.54 (t, $J = 8$ Hz, 1H, Py), 7.17 (2H, aryl), 7.15 (t, $J = 8$ Hz, 1H, Py), 6.95 (2H, aryl), 6.77 (d, $J = 11$ Hz, 1H, Py), 5.09 (d, $J = 13$ Hz, 2H, CH_2), 4.10 (2H, CH_2Py), 3.80 (d, $J = 14$ Hz, 2H, CH_2), 1307 (18H, $C(CH_3)_3$), 1.27 (18H, $C(CH_3)_3$). ^{13}C NMR: δ 157.27, 156.02, 152.06, 142.65, 139.45, 138.60, 124.15, 123.81, 122.82, 121.46, 120.93, 64.05, 59.49, 53.45, 50.89, 34.91, 34.20, 31.63, 30.30, 29.89, 18.30. *Anal*. Calc. for $C_{36}H_{50}N_2O_4W$: C, 57.0; H, 6.6; N, 3.7. Found: C, 56.7; H, 6.6; N, 3.8%.

*[$WO_2(L^5)$] (**11**)*. White crystalline solid, yield 86% (479 mg). IR: 1456vs, 1323m, 1302m, 1269m, 1254s, 1219s, 1163s, 1094m, 1063s, 1032s, 972w, 939s, 899vs, 864vs, 858s, 831m, 789m, 739w, 733m, 693w, 688m, 592m, 556m, 514w. ^{1}H NMR: δ 7.04 (2H, aryl), 6.80 (2H, aryl), 4.79 (d, $J = 14$ Hz, 2H, CH_2), 3.86 (3H, OCH_3), 3.77 (d, $J = 14$ Hz, 2H, CH_2), 3.27 (t, $J = 6$ Hz, 2H, CH_2), 2.95 (t, $J = 6$ Hz, 2H, CH_2), 2.31 (6H, CH_3), 2.29 (6H, CH_3). ^{13}C NMR: δ 155.56, 132.06, 130.08, 127.74, 126.68, 121.46, 70.72, 63.59, 52.87, 20.52, 16.16. *Anal*. Calc. for $C_{21}H_{27}NO_5W$: C, 45.3; H, 4.9; N, 2.5. Found: C, 45.6; H, 4.7; N, 2.6%.

*[$WO_2(L^6)$] (**12**)*. White crystalline solid, yield 63% (455 mg). IR: 1456vs, 1412m, 1366m, 1318m, 1244s, 1204m, 1169m, 1123m, 1092m, 1069vs, 1026m, 1010m, 970w, 957s, 941m, 909vs, 880s, 851s, 835m, 820w, 812w, 744w, 735w, 669w, 608w, 592w, 557m, 510w. ^{1}H NMR: δ 7.34 (2H, aryl), 6.86 (2H, aryl), 4.59 (d, $J = 14$ Hz, 2H, CH_2), 3.83 (3H, OCH_3), 3.76 (d, $J = 14$ Hz, 2H, CH_2), 3.29 (t, $J = 6$ Hz, 2H, CH_2), 2.90 (t, $J = 6$ Hz, 2H, CH_2), 1.30 (18H, $C(CH_3)_3$), 1.26 (18H, $C(CH_3)_3$). ^{13}C NMR: δ 157.26, 142.65, 138.59,

124.14, 123.63, 121.71, 69.17, 64.65, 64.04, 59.47, 53.45, 53.08, 35.03, 34.33, 31.63, 29.90, 18.28. *Anal*. Calc. for $C_{33}H_{51}NO_5W$: C, 54.6; H, 7.1; N, 1.9. Found: C, 54.9; H, 7.5; N, 2.2%.

4.3. Oxotransfer catalysis

In a typical test reaction, 0.10 mmol (21 mg) of benzoin was dissolved in 0.7 ml of deoxygenated dmso in a NMR tube and then treated with 0.01 mmol of catalyst. The reaction mixture was kept at 120 °C for 24 h and subsequently cooled to the room temperature. The conversion of benzoin to benzil was detected by ^{1}H NMR. Detected yield of benzil was 40–60% in all experiments.

4.4. X-ray crystallography

Crystals suitable for X-ray measurements were grown from reaction mixtures. Crystallographic data for **1**, **3** and **9** along with other experimental details are summarized in Table 1. The crystal data were collected at 173 K on a Nonius Kappa CCD area-detector diffractometer using graphite monochromatised Mo Kα radiation ($\lambda = 0.71073$ Å). The data collection was performed using φ and ω scans. The data were processed using DENZO-SMN v0.93.0 [26]. SHELXA [27] absorption correction was applied for the data of all compounds. The structures were solved by direct methods using the SHELXS-97 program and full-matrix least-squares refinements on F^2 were performed using the SHELXL-97 program [28]. For all compounds the heavy atoms were refined anisotropically. The CH hydrogen atoms were included at the fixed distances with fixed displacement parameters from their host atoms. Figures were drawn with ORTEP-3 for Windows [29].

Appendix A. Supplementary data

Crystallographic data (excluding structure factors) for the structures reported in this paper have been deposited with the Cambridge Crystallographic Data Centre as deposition numbers CCDC 276480–276482 for **1**, **3**, and **9**, respectively. Copies of the data can be obtained free of charge on application to CCDC, 12 Union Road, Cambridge CB2 1EZ, UK [fax: +44 1223/336 033; e-mail: deposit@ccdc.cam.ac.uk]. Supplementary data associated with this article can be found, in the online version at doi:10.1016/j.poly.2005.07.037.

References

[1] H. Arzoumanian, Coord. Chem. Rev. 178–180 (1998) 191.
[2] (a) Y.-L. Wong, Y. Yan, E.S.H. Chan, Q. Yang, T.C.W. Mak, D.K.P. Ng, J. Chem. Soc., Dalton Trans. (1998) 3057;
(b) R. Dinda, P. Sengupta, S. Ghosh, W.S. Sheldrick, Eur. J. Inorg. Chem. (2003) 363;
(c) Y.-L. Wong, J.-F. Ma, W.-F. Law, Y. Yan, W.T. Wong, Z.-Y. Zhang, T.C.W. Mak, D.K.P. Ng, Eur. J. Inorg. Chem. (1999) 313.
[3] (a) F.E. Kühn, W.-M. Xue, A. Al-Ajlouni, A.M. Santos, S. Zang, C.C. Romão, G. Eickerling, E. Herdtweck, Inorg. Chem. 41 (2002) 4468;
(b) F.E. Kühn, M. Groarke, É. Bencze, E. Herdtweck, A. Prazeres, A.M. Santos, M.J. Calhorda, C.C. Romão, I.S. Gonçalves, A.D. Lopes, M. Pillinger, Chem. Eur. J. 8 (2002) 2370;
(c) W.A. Herrmann, J. Fridgen, G.M. Lobmaier, M. Spiegler, New J. Chem. (1999) 5;
(d) Y.-L. Wong, A.R. Cowley, J.R. Dilworth, Inorg. Chim. Acta 357 (2004) 4358.
[4] (a) J.H. Enemark, J.J.A. Cooney, J.-J. Wang, R.H. Holm, Chem. Rev. 104 (2004) 1175;
(b) M.K. Johnson, D.C. Rees, M.W.W. Adams, Chem. Rev. 96 (1996) 2817.
[5] T.A. Hanna, C.D. Incarvito, A.L. Rheingold, Inorg. Chem. 39 (2000) 630.
[6] M. Huang, C.W. DeKock, Inorg. Chem. 32 (1993) 2287.
[7] T.A. Hanna, A.K. Ghosh, C. Ibarra, M.A. Mendez-Rojas, A.L. Rheingold, W.H. Watson, Inorg. Chem. 43 (2004) 1511.
[8] K. Most, S. Köpke, F. Dall'Antonia, N.C. Mösch-Zanetti, Chem. Commun. (2002) 1676.
[9] F.A. Cotton, G. Wilkinson, Advanced Inorganic Chemistry, 5th ed., John Wiley & Sons, New York, 1988, p. 804.
[10] (a) J.T. Hoffman, S. Einwaechter, B.S. Chohan, P. Basu, C.J. Carrano, Inorg. Chem. 43 (2004) 7573;
(b) A.J. Millar, C.J. Doonan, P.D. Smith, V.N. Nemykin, P. Basu, C.G. Young, Chem. Eur. J. 11 (2005) 3255;
(c) J. Jarupatracorn, M.P. Coles, T.D. Tilley, Chem. Mater. 17 (2005) 1818.
[11] W.A. Herrmann, J.J. Haider, J. Fridgen, G.M. Lobmaier, M. Spiegler, J. Organomet. Chem. 603 (2000) 69.
[12] A. Cervilla, E. Llopis, A. Ribera, A. Doménech, E. Sinn, J. Chem. Soc., Dalton Trans. (1994) 3511.
[13] K. Dreisch, C. Andersson, C. Stålhandske, Polyhedron 10 (1991) 2417.
[14] S. Yu, R.H. Holm, Inorg. Chem. 28 (1989) 4385.
[15] F.A. Schröder, J. Scherle, Z. Naturforsch. 28b (1973) 46.
[16] (a) A. Lehtonen, R. Sillanpää, J. Chem. Soc., Dalton Trans. (1994) 2119;
(b) A. Lehtonen, R. Sillanpää, Inorg. Chem. 40 (2001) 6047;
(c) A. Lehtonen, R. Sillanpää, Inorg. Chem. 43 (2004) 6501;
(d) A. Lehtonen, R. Sillanpää, Organometallics 24 (2005) 2795;
(e) A. Lehtonen, Inorg. Chem. Commun. 8 (2005) 122.
[17] A. Lehtonen, R. Sillanpää, Polyhedron 24 (2005) 257.
[18] C.J. Hinshaw, G. Peng, R. Singh, J.T. Spence, J.H. Enemark, M. Bruck, J. Kristofski, S.L. Merbs, R.B. Ortega, P.A. Wexler, Inorg. Chem. 28 (1989) 4483.
[19] T. Toupance, S.R. Dubberley, N.H. Rees, B.R. Tyrrell, P. Mountford, Organometallics 21 (2002) 1367.
[20] F. Wolff, C. Lorber, R. Choukroun, B. Donnadieu, Inorg. Chem. 42 (2003) 7839.
[21] N. Kanehisa, Y. Kai, N. Kasai, H. Yasuda, Y. Nakayama, A. Nakamura, Bull. Chem. Soc. Jpn. 65 (1992) 1197.
[22] B.D. Steffey, P.E. Fanwick, I.P. Rothwell, Polyhedron 9 (1990) 963.
[23] G.J.-J. Chen, J.W. McDonald, W.E. Newton, Inorg. Chem. 15 (1976) 2612.
[24] E.Y. Tsuva, I. Goldberg, M. Kol, Organometallics 21 (2002) 3017.
[25] E.Y. Tsuva, I. Goldberg, M. Kol, Z. Goldschmidt, Organometallics 20 (2001) 3017.

[26] Z. Otwinowski, W. Minor, Methods in Enzymology, in: C.W. Carter Jr., R.M. Sweet (Eds.), Macromolecular Crystallography, Part A, vol. 276, Academic Press, New York, 1997, p. 307.
[27] G.M. Sheldrick, (anon) SHELX-97 Release 97-2, 1998.
[28] G.M. Sheldrick, SHELXL-97. Program for Crystal Structure Refinement, University of Göttingen, Germany, 1997.
[29] L.J. Farrugia, J. Appl. Crystallogr. 32 (1999) 837.

Available online at www.sciencedirect.com
SCIENCE DIRECT®
Polyhedron 25 (2006) 776–782
POLYHEDRON
www.elsevier.com/locate/poly

Copper (I) and (II) complexes of melamine

Austin B. Wiles [a], Daniel Bozzuto [b], Christopher L. Cahill [b], Robert D. Pike [a,*]

[a] Department of Chemistry, College of William and Mary, P.O. Box 8795, Williamsburg, VA 23187-8795, United States
[b] Department of Chemistry, The George Washington University, Washington, DC 20052, United States

Received 18 May 2005; accepted 15 August 2005
Available online 23 September 2005

Abstract

Coordination of copper (I) and (II) salts to melamine (Mel) produces [CuX(Mel)] [X = Cl (**5a**), Br (**5b**), I (**5c**), NO_3 (**5d**)], [CuX_2-$(Mel)_2$] · S [X = Cl, S = H_2O (**6a**); X = Cl, S = 2 MeOH (**6b**); X = Br, S = 1/2H_2O (**6c**); X = OAc, S = none (**6d**)], and [$Cu(OAc)_2$(Mel)] (**7**). The chemical identity of the complexes has been confirmed by elemental analysis, X-ray powder diffraction, thermogravimetry, and infrared analysis.
© 2005 Elsevier Ltd. All rights reserved.

Keywords: Copper; Complex; Infrared; Melamine; Thermogravimetry; X-ray

1. Introduction

Melamine (2,4,6-triamino-*s*-triazine, **1**) has long been known as a monomer for melamine formaldehyde resins, but it is also an important fire retardant additive for polymers [1]. As part of our ongoing studies of copper complexes as fire retardant/smoke suppression additives for chlorinated polymers [2], we decided to undertake an investigation of the coordination chemistry of copper salts with melamine (Mel). Despite its apparent promise as a ligand, investigations into the coordination chemistry of melamine in the literature are remarkably few (see below). This fact probably owes much to the insolubility of melamine in all common solvents, except hot water. Nevertheless, our studies have also shown that melamine is a surprisingly poor ligand, especially in aqueous medium. The likely reason for the foregoing observations is the extensive hydrogen bonding that causes melamine to form a robust network structure [3].

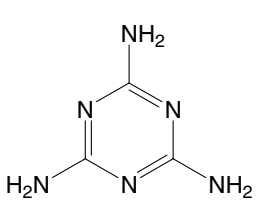

1

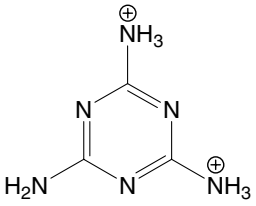

2

The metal compounds of melamine that have been reported to date are almost exclusively limited to group 11 metals and largely fall into one of three categories: melaminium dication (**2**) salts associated with coordination anions [4], inorganic salts cocrystallized with melamine (showing hydrogen bonding but not coordination between the two networks) [5], and a few serendipitously formed coordination complexes [6]. Two of the latter complexes have been structurally characterized. Reaction of diacetylmelamine with $Cu(NO_3)_2$ in methanol provided melamine complex **3**, and $AgClO_4$ reacted with melamine in water/methanol produced **4**. The dimer units that comprise the Cu(II) complex **3** contain internal hydrogen bonds between methanol or methoxide oxygen atoms and melamine

* Corresponding author. Tel.: +1757 2212555; fax: +1757 2212715.
E-mail address: rdpike@wm.edu (R.D. Pike).

0277-5387/$ - see front matter © 2005 Elsevier Ltd. All rights reserved.
doi:10.1016/j.poly.2005.08.022

hydrogen atoms. In addition, the intermolecular hydrogen bonds knit the dimer units into sheets, similar to those found for melamine itself [3]. The structure of the Ag(I) cation **4** is simpler, consisting of $[Ag(Mel)_2]^+$ units linked into chains through weakly bridging perchlorate–silver interactions and additionally by hydrogen bonds between the perchlorate oxygen atoms and melamine hydrogen atoms. The coordination of melamine in both of these complexes occurs through one aromatic nitrogen atom, with no evidence of chelation to the amine nitrogen atoms.

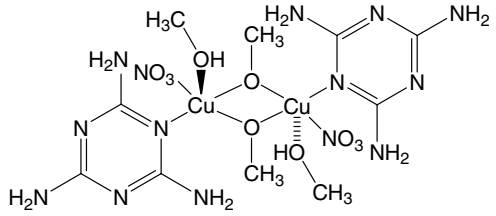

3

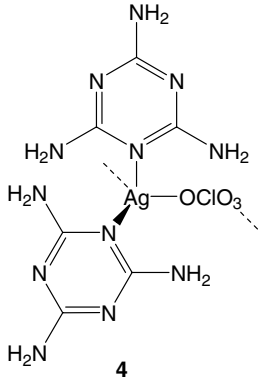

4

There has been a report of Cu(II) salt reactions with melamine [7]. The reported complexes $[CuCl_2(Mel)_2]$ and $[CuX_2(Mel)]$ (X = Cl, Br, OAc) were formed by heating butanol or methanol solutions of Cu(II) salt with melamine. No crystal structures were reported in this study. Herein we report the synthesis and characterization of a series of Cu(I) and Cu(II) melamine complexes.

2. Experimental

2.1. General

All compounds were reagent grade and were used as received, except for CuCl and CuBr, which were freshly recrystallized from HCl and HBr, respectively. $[Cu(NCMe)_4]BF_4$ was prepared according to a literature method [8]. All copper-containing products were analyzed for copper content by atomic absorption as previously described [9]. Analyses for C, H, and N were carried out by Atlantic Microlabs, Norcross, GA. Thermogravimetric analyses (TGA) were run using a TA Instruments Q500 instrument in high resolution mode (heating rate dependent upon mass loss activity) under 60 mL/min N_2 flow. X-ray powder diffraction analyses were carried out on a Scintag XDS 2000 diffractometer (Cu Kα, 3–60°, 0.05° step, 1.0 s/step) and manipulated using the JADE software package [10]. Infrared (IR) spectra were collected from KBr pellets on a Digilab FTS 7000 FTIR spectrophotometer.

2.2. Preparation of *[CuBr(Mel)]* (*5b*)

Copper (I) bromide (217 mg, 1.51 mmol) was dissolved in 30 mL Ar-degassed MeCN. The solution was filtered through Celite. Melamine (126 mg, 1.00 mmol) was added. The suspension was sealed in a thick-walled glass tube and heated to 100 °C with stirring in an oil bath. After 20 h, the MeCN had lost the pale green color associated with the solution of CuBr. The suspended solid was collected by means of filtration, washed with fresh MeCN and diethyl ether, and then dried under vacuum (white solid, 235 mg, 0.872 mmol, 87.4%). *Anal.* Calc. for **5b**: Cu, 26.73; C, 16.67; H, 2.80; N, 38.35. Found: Cu, 26.67; C, 16.63; H, 2.79; N, 38.84%. Selected IR data (cm^{-1}): 3459, 3425, 3352, 3195, 3140, 1659, 1600, 1575, 1541, 1477, 1448, 1028, 798.

2.3. Preparation of *[CuCl(Mel)$_{1.1}$]* (*5a*)

Synthesized as for **5b** but CuCl was added. Mint solid, yield 87.5%. *Anal.* Calc. for **5a**: Cu, 26.73; C, 16.67; H, 2.80; N, 38.35. Found: Cu, 26.67; C, 16.63; H, 2.79; N, 38.84%. Selected IR data (cm^{-1}): 3454, 3426, 3348, 3199, 3137, 1664, 1601, 1577, 1540, 1467, 1447, 1031, 797.

2.4. Preparation of *[CuI(Mel)]* (*5c*)

Synthesized as for **5b** but CuI was added. White solid, yield 91.6%. *Anal.* Calc. for **5c**: Cu, 20.07; C, 11.38; H, 1.91; N, 26.55. Found: Cu, 20.03; C, 11.54; H, 1.84; N, 26.31%. Selected IR data (cm^{-1}): 3469, 3408, 3326, 3145, 1703, 1688, 1653, 1623, 1566, 1530, 1498, 1020, 816.

2.5. Preparation of *[CuNO$_3$(Mel)]* (*5d*)

Synthesized as for **5b** except "$CuNO_3$" was first prepared in MeCN solution through conproportionation of $Cu(NO_3)_2 \cdot 2.5H_2O$ with Cu wool until the solution was colorless. Excess copper wool was then removed, melamine was added, and the procedure for **5b** was followed. White solid, yield 93.5%. *Anal.* Calc. for **5d**: Cu, 25.25; C, 14.32; H, 2.40; N, 38.96. Found: Cu, 24.57; C, 14.53; H, 2.37; N, 38.68%. Selected IR data (cm^{-1}): 3459, 3426, 3337, 3195, 3143, 1672, 1660, 1618, 1571, 1541, 1466, 1450, 1026, 790.

2.6. Preparation of *[CuCl$_2$(Mel)$_2$] · 2MeOH* (*6b*)

Copper (II) chloride dihydrate (171 mg, 1.00 mmol) was dissolved in 30 mL Ar-degassed MeOH. Melamine (252 mg, 2.00 mmol) was added. The mixture was sealed

in a thick-walled glass tube and heated to 100 °C with stirring in an oil bath. After 14 h, the lime green MeOH had bleached to a very pale green color and the white solid had become yellow-green. The solid was collected by means of filtration, washed with fresh MeOH and diethyl ether and then dried under vacuum. (white solid, 347 mg, 0.770 mmol, 77.0%). *Anal*. Calc. for **6b**: Cu, 14.10; C, 21.32; H, 4.47; N, 37.29. Found: Cu, 14.64; C, 20.60; H, 4.37; N, 37.95%. Selected IR data (cm^{-1}): 3331, 3157, 1651, 1540, 1474, 1017, 801, 783.

2.7. Preparation of $[CuCl_2(Mel)_2] \cdot H_2O$ (6a)

Synthesized as for **6b** except the solvent used was BuOH. Yellow solid, yield 92.5%. *Anal*. Calc. for **6a**: Cu, 15.70; C, 17.81; H, 3.49; N, 41.53. Found: Cu, 15.77; C, 17.67; H, 3.44; N, 40.65%. Selected IR data (cm^{-1}): 3425, 3410, 3373, 3312, 3177, 1702, 1680, 1652, 1622, 1561, 1535, 1475, 1023, 804, 782.

2.8. Preparation of $[CuBr_2(Mel)_2] \cdot 1/2H_2O$ (6c)

Synthesized as for **6b** except $CuBr_2$ was added and the solvent used was MeCN. Pea green solid, yield 99.6%. *Anal*. Calc. for **6c**: Cu, 13.11; C, 14.87; H, 2.70; N, 34.68. Found: Cu, 13.19; C, 15.06; H, 2.94; N, 34.50%. Selected IR data (cm^{-1}): 3425, 3410, 3373, 3312, 3214, 3171, 1702, 1680, 1652, 1622, 1535, 1475, 1020, 804, 781.

2.9. Preparation of $[Cu(OAc)_2(Mel)_2] \cdot H_2O$ (6d)

Synthesized as for **6b** except $Cu(OAc)_2 \cdot H_2O$ was added and the solvent used was MeCN. Aqua solid, yield 85.5%. *Anal*. Calc. for **6d**: Cu, 14.00; C, 27.68; H, 4.18 ; N, 38.74. Found: Cu, 14.06; C, 27.61; H, 4.09; N, 38.63%. Selected IR data (cm^{-1}): 3470, 3410, 3337, 3249, 3191, 3133, 1653, 1627, 1553, 1468, 1437, 1028, 814.

2.10. Preparation of $[Cu(OAc)_2(Mel)]$ (7)

Synthesized as for **6b** except $Cu(OAc)_2 \cdot H_2O$ and melamine were reacted in equimolar proportions in MeCN. Aqua solid, yield 91.5%. *Anal*. Calc. for **7**: Cu, 20.65; C, 27.32; H, 3.93; N, 27.31. Found: Cu, 20.43; C, 27.00; H, 3.96; N, 28.18%. Selected IR data (cm^{-1}): 3470, 3420, 3353, 3244, 3137, 1651, 1626, 1553, 1467, 1437, 1031, 813.

3. Results and discussion

3.1. Synthesis

Initial attempts to form Cu(I)–melamine complexes in our lab focused on the use of aqueous ammoniacal solutions of copper (I) ion, which are produced via hydroxylamine reduction of $CuSO_4 \cdot 5H_2O$ [11]. Melamine (Mel) was dissolved in warm degassed water and was added via syringe to a nitrogen-purged colorless solution of "Cu_2SO_4" prepared as previously described [11]. Encouragingly, the solution remained colorless, showing no sign of copper oxidation. Slow cooling of the solution to 5 °C, resulted in the formation of colorless crystals. However, these crystals contained no copper and were shown by melting point analysis to be merely recrystallized melamine. Thus, under these experimental conditions (0.20 M Cu_2SO_4, 0.60 M melamine 3.0 M NH_3), ammonia coordination proved to be favored over that of melamine.

A non-aqueous approach was pursued next. The use of organic solvents necessitated working with melamine as a suspended solid in copper-containing solutions. Acetonitrile was the solvent of choice for most of the reactions, however, methanol and *n*-butanol were also effective for several of the copper (II) salt reactions. The reaction mixtures containing the dissolved copper salt and solid melamine were heated overnight in sealed, thick-wall reaction tubes. Typically, the solution color lessened during the reaction, indicating the transfer of copper to the suspended melamine. The products were filtered and subjected to chemical analysis.

The favored products of CuX (X = Cl, Br, I, NO_3) with melamine conformed to the formula [CuX(Mel)] (**5**). The only problematic results came from the CuCl reaction, which reproducibly formed **5a** as $[CuCl(Mel)_{1.1–1.3}]$. A replicate CuCl reaction was carried out in the presence of copper wool to help prevent possible formation of Cu(II). Although the product of this reaction was whiter in color, chemical analysis still revealed excess melamine. The use of large excesses (about 10-fold) of copper salt resulted in the materials roughly conforming to $[(CuX)_2(Mel)]$ for X = Cl, Br. However, elemental analyses for these products were not of high quality. Although X-ray powder diffraction and thermogravimetry results suggested that $[(CuX)_2(Mel)]$ might be an independent phase (see below), a mixture of **5** and CuX could not be ruled out. Nevertheless, no evidence was found for the formation of $[(CuX)_2(Mel)]$ products for X = I, NO_3; instead the isolated solids invariably analyzed as **5c** and **5d**. Attempts to dissolve away any adsorbed (rather than bonded) copper salt were carried out by heating the various Cu(I)–melamine complexes in fresh acetonitrile at 100 °C over several days. These experiments produced no changes in sample composition. Products of reactions involving the use of excess melamine yielded irreproducible chemical analyses. Subsequent X-ray analysis of these powders clearly revealed the presence of both **5** and free melamine. Hence, copper-poor phases with melamine do not appear to exist.

When $[Cu(NCMe)_4]BF_4$ was dissolved in MeCN and heated with melamine, the solid recovered proved to be unreacted melamine. What makes this result particularly surprising is the demonstrated reaction of the nitrate salt with melamine. Conproportionation of $Cu(NO_3)_2 \cdot 2.5H_2O$ with Cu in acetonitrile produces "$CuNO_3$", which almost certainly exists in solution as $[Cu(NCMe)_4]NO_3$. The formation of $[CuNO_3(Mel)]$ (**5d**) but not of $[CuBF_4(Mel)]$ under essentially identical conditions points to the possible

necessity of anion coordination since NO_3^- is a superior ligand to BF_4^-.

All of the Cu(I)–melamine products were white or nearly white in color. This absence of color suggests that copper coordination is occurring through the amine nitrogen atoms, rather than those of triazine. The known Cu(I) complexes of diazine and triazine ligands invariably show significant color due to metal to ligand charge transfer absorptions in the visible spectrum [9,12].

In contrast to the results obtained with Cu(I), the Cu(II) salts generally formed products analyzing as $[CuX_2(Mel)_2]$ (**6**). Water or alcohol solvent was retained in several cases, presumably as an additional ligand for copper. The only 1:1 Cu(II):Mel product realized was $[Cu(OAc)_2(Mel)]$ (**7**). The lack of isolated 1:1 complexes for $CuCl_2$ and $CuBr_2$ with melamine in the current study stands in contrast to the results reported previously [7].

3.2. X-ray powder diffraction

X-ray powder diffraction analysis was used to help characterize the new products. Sharp line diffractograms were obtained in all cases, indicating good sample crystallinity. Comparison of diffraction patterns was used to help confirm that the products were single-phase materials. Thus for example, the powder diffraction pattern of **5a** was compared to those of CuCl and melamine, see Fig. 1. The diffraction pattern of **5a** revealed no evidence of CuCl or melamine peaks. The diffractogram from the material provisionally identified as $[(CuCl)_2(Mel)]$ also appeared to be distinct from those of CuCl, melamine and **5a** (Fig. 1). Within the sensitivity constraints of X-ray powder diffraction, neither melamine nor copper salts were observed as contaminant phases in any of the copper–melamine products. Although the X-ray data were not of sufficient quality to allow for cell indexing, the occurrence of similar powder

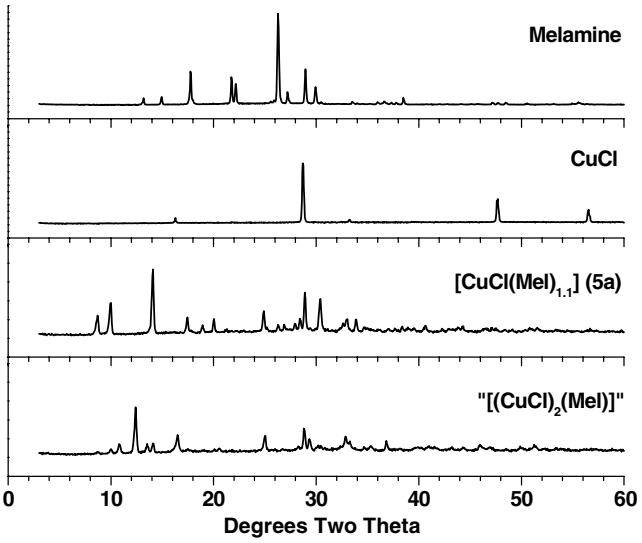

Fig. 1. X-ray powder diffraction traces for CuCl–melamine compounds.

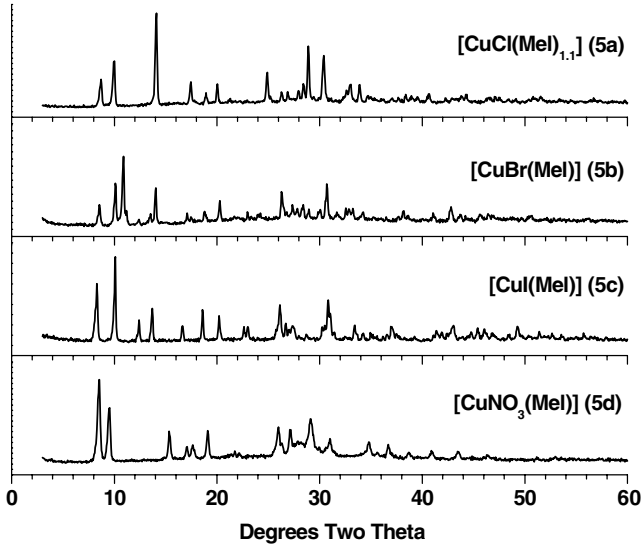

Fig. 2. X-ray powder diffraction traces for the Cu(I)–melamine compounds (**5**).

patterns for the **5** products shown in Fig. 2 suggests possible crystallographic isomorphism between these apparently low symmetry phases.

3.3. Thermogravimetric analysis

All of the melamine complexes were examined using TGA. The results and interpretations are collected in Table 1. Melamine itself sublimes between about 210 and 260 °C under the TGA conditions used. The TGA results for compounds **5** are shown in Fig. 3. Thermal analysis results for **5a** show four closely spaced mass losses occurring above 300 °C and separated from one another by shallow plateaus. The first three steps appear to represent the stepwise loss of melamine illustrated in the following equations:

$$2[CuX(Mel)]\ (\mathbf{5}) \rightarrow [(CuX)_2(Mel)] + Mel\uparrow \quad (1)$$

$$2[(CuX)_2(Mel)] \rightarrow [(CuX)_4(Mel)] + Mel\uparrow \quad (2)$$

$$[(CuX)_4(Mel)] \rightarrow 4CuX + Mel\uparrow \quad (3)$$

The mass percent represented in the first plateau corresponds well to $[(CuCl)_2(Mel)]$. Also suggestive is the fact that, after the initial mass loss from **5a**, the subsequent mass loss profiles for the **5a** residue and that of the material provisionally identified as $[(CuCl)_2(Mel)]$ were identical. The plateau at about 380–390 °C may represent $[(CuCl)_4(Mel)]$, a phase that has not been synthesized. Volatilization of the remainder of the melamine leaves CuCl. The decomposition temperature of the residual CuCl from the melamine complexes corresponds to that of free CuCl. However, while authentic CuCl largely sublimes, leaving only a few percent residual mass, the decomposition of CuCl from the melamine complexes leaves significant residual mass, nearing that of the initial copper content. Hence, in addition to CuCl sublimation, reductive elimination, reaction (4) is also occurring, as has previously been observed [12].

Table 1
Thermogravimetric analysis results

Complex	Temp. (°C)	Possible product	wt% (theory)	wt% (expt)
5a	205–340	$(CuCl)_2(Mel)$	68	66
	340–390	$(CuCl)_4(Mel)$	55	51
	390–425	CuCl	42	37
	425–510	Cu	27	24
5b	235–335	$(CuBr)_2(Mel)$	77	75
	335–380	CuBr	53	60
	380–620	Cu/sublimation		9
5c	215–330	CuI	60	58
	500–580	Cu	24	21
5d	220–410	$CuNO_3$	50	57
	410–435	Cu	25	29
6a	190–350	$CuCl_2$	33	33
	350–590	Cu	16	14
6b	45–240	$CuCl_2(Mel)_2$	86	91
	240–335	$CuCl_2$	30	35
	335–590	Cu	14	15
6c	200–350	$(CuBr_2)_2(Mel)$	59	58
	350–480	$CuBr_2$	46	47
	350–675	Cu	13	14
6d	195–215	$Cu(OAc)_2(Mel)$	71	76
	215–290	CuOAc	28	30
	300–630	Cu	15	16
7	185–210	$Cu(OAc)_2$	59	64
	210–270	CuOAc	40	45
	315–470	Cu	21	26

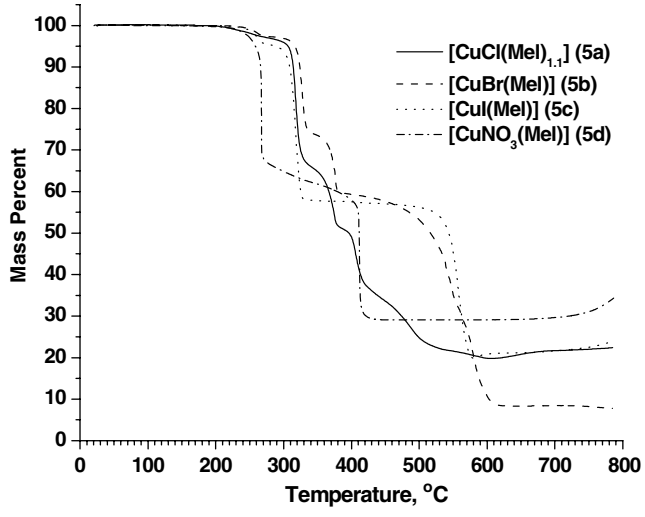

Fig. 3. TGA traces for the Cu(I)–melamine compounds (**5**).

$$2\ CuX \rightarrow Cu + X_2\uparrow \quad (4)$$

The behavior of the copper (I) bromide sample **5b** was similar to that of the **5a**, with the notable exception that there is no evidence of a $[(CuBr)_4(Mel)]$ phase. In addition, the residual CuBr undergoes sublimation to a greater extent, leaving little final residue at high temperature. Nevertheless, the onset of decomposition for the analogous CuCl- and CuBr-derived materials is similar. In contrast to the behavior of the chloride and bromide complexes, **5c** and **5d** fail to show evidence of any more copper-rich phases, see Fig. 3. Consistent with this observation is the fact that no copper-rich CuI or $CuNO_3$ materials could be synthesized. Reductive elimination (Eq. (4)) is favored for the iodide and nitrate, the residual mass corresponding closely to the original copper content of the samples.

The copper (II) complexes exhibited somewhat more complicated decomposition behavior (see Fig. 4). The $[CuCl_2(Mel)_2]$ complexes (**6a** and **6b**) underwent the loss of solvent and melamine to give $CuCl_2$, which then reduced to copper in a complicated series of steps. The TGA traces showed only slight inflections during the loss of melamine. In contrast to this behavior, the bromide **6c** trace presented several possible intermediates during the loss of melamine. The most significant plateau corresponded to a possible formula $[(CuBr_2)_2(Mel)]$. Following this possible intermediate, an inflection corresponding to $CuBr_2$ was noted, followed by a series of steps ending with copper metal. The two $Cu(OAc)_2$–melamine complexes appear to undergo a series of decomposition steps that are summed up in the following equation:

$$[Cu(OAc)_2(Mel)_2]\ (\mathbf{6d}) \rightarrow [Cu(OAc)_2(Mel)]\ (\mathbf{7}) \rightarrow Cu(OAc) \rightarrow Cu \quad (5)$$

3.4. Infrared analysis

The IR spectrum of melamine has long been known and has been reinterpreted fairly recently [13,14]. The IR spectrum of melamine consists of three principal absorption regions. The 2800–3500 cm^{-1} region encompasses the N–H stretching modes, the sharp higher frequency bands corresponding to non-hydrogen bonded N–H and the broad lower frequency bands representing hydrogen bonded N–H. The 1440–1650 cm^{-1} region contains ring distortion, N–H bending, and two complex

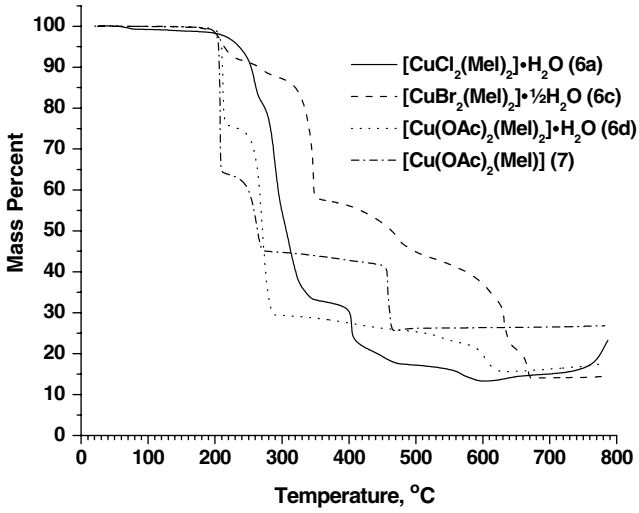

Fig. 4. TGA traces for the Cu(II)–melamine compounds (**6** and **7**).

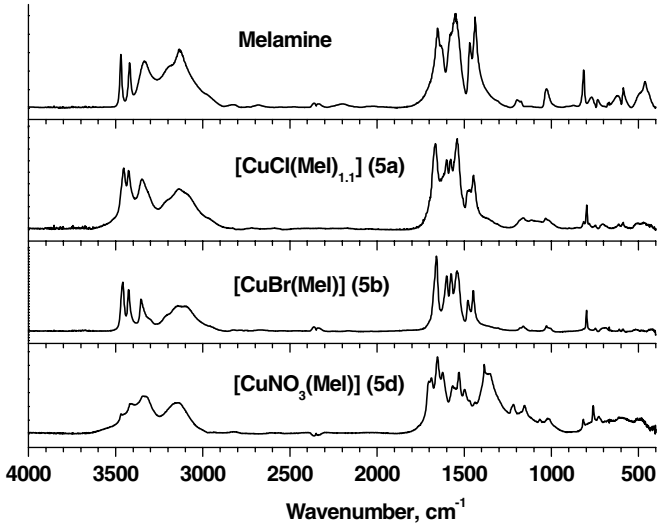

Fig. 5. IR spectra for Cu(I)–melamine compounds (**5**).

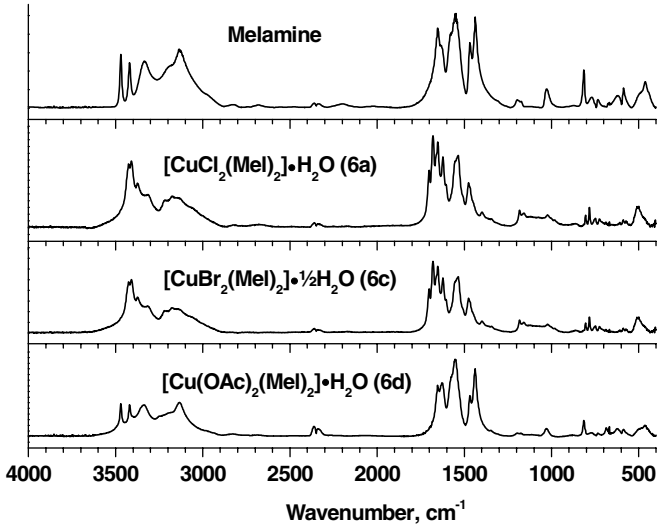

Fig. 6. IR spectra for Cu(II)–melamine compounds (**6** and **7**).

molecular modes. The 800–1050 cm^{-1} region contains two additional complex molecular modes. The spectrum of melamine is compared with those of the copper–melamine complexes in Figs. 5 and 6 and in Table 2. The band identities are adapted from the literature [14] and are interpreted under D_{3h} symmetry.

Several trends can be noted from examination of the data. All of the copper complexes retain both free and hydrogen bonded N–H stretching bands. Relative to melamine, the Cu(I)–melamine complexes' two free amine bands tend to move closer to one another in frequency, while the hydrogen bonded amine bands shift to higher frequencies. The Cu(II) complexes show a primarily downward shift in N–H stretching frequency. The fact that all of the copper–melamine products, with the exception of the acetate complexes (see below), show changes in the N–H stretching region is consistent with the lack of color in these complexes in suggesting amine, rather than triazine, coordination.

In the N–H stretching region, and throughout the IR spectrum, the $Cu(OAc)_2$–melamine complexes **6d** and **7** show almost no differences from melamine itself. This result possibly indicates little or no melamine coordination with copper, possibly due to the presence of the chelating acetate anion. Two hydrogen bonded hybrid networks between melamine and $Cu(PyHy)_2$ and $Cu(H_2NTA)Cl$ [PyHy = 5-(2-pyridylmethylene)hydantoin and H_2NTA = dihydrogen nitrilotriacetate] have been characterized previously [5], representing precedent for non-coordinating metal–melamine network formation.

The E′ ring distortion IR band is blue shifted for all of the Cu complexes except **5c**, **6b** and the aforementioned acetate complexes. This shift suggests an increase in ring rigidity, perhaps due to increased network interaction. Removal of E′ band degeneracy is evident in many of the Cu compound spectra. This removal of degeneracy is even more evident in the N–H bending bands. Once again, it is noteworthy that the acetate complexes show neither splitting nor shifting of these bending bands. Upon coordination there is a consistent red shift of the A_1' symmetrical bending mode (1626 cm^{-1} for melamine). The four low frequency bands (1468, 1436, 1027, and 814 cm^{-1} for melamine) show fairly consistent trends in their coordination shifts: the 1468 cm^{-1} band shows blue shifts, 1436 cm^{-1}

Table 2
IR data for melamine and copper–melamine complexes[a,b]

Compound	Free N–H	Hydrogen bonded N–H	E′ ring distortion	A_1' and E′ N–H bending		E′ and A_1' modes		E′ mode	A_2'' mode
Melamine	3470, 3420	3334, 3187, 3137	1651	1626	1553	1468	1436	1027	814
5a	3454, 3426	3348, 3199, 3137	1664	1601	1577, 1540	1467	1447	1031	797
5b	3459, 3425	3352, 3195, 3140	1659	1600	1575, 1541	1477	1448	1028	798
5c	3462, 3424	3355, 3195, 3134	1651	1604	1570, 1540	1472	1449	1018	799
5d	3469, 3408	3326, 3145	1703, 1688, 1653	1623	1566, 1530	1498	Obscured	1020	816
6a	3425, 3410, 3373	3312, 3177	1702, 1680, 1652	1622	1561, 1535	1475		1023	804, 782
6b	Obscured	3331, 3157	1651		1540	1474		1017	801, 783
6c	3425, 3410, 3373	3312, 3214, 3171	1702, 1680, 1652	1622	1535	1475		1020	804, 781
6d	3470, 3410	3337, 3249, 3191, 3133	1653	1627	1553	1468	1437	1028	814
7	3470, 3420	3353, 3244, 3137	1651	1626	1553	1467	1437	1031	813

[a] All data in cm^{-1}.
[b] See [13] for more detailed melamine band assignments.

shows blue shifts for Cu(I) products, and 1027 and 814 cm^{-1} bands show red shifts. No splitting of these bands is evident. Given the vibrational complexity of the underlying modes, the trends for these low frequency bands are difficult to interpret.

4. Conclusion

Melamine has been shown to act as a ligand for both Cu(I) and Cu(II) salts. The resulting insoluble networks reveal 1:1 metal salt:melamine stoichiometry for Cu(I), with the exception of CuCl, which forms $[CuCl(Mel)_{1.1–1.3}]$. In addition 2:1 complexes were realized for CuCl and CuBr. For Cu(II) salts 1:2 stoichiometry was favored. Only $Cu(OAc)_2$ produced a 1:1 compound. Thermogravimetric analysis results suggested step-wise removal of melamine for the CuCl and CuBr complexes. Infrared analysis reveals modest shifts and symmetry removal in the complexes, with the possible exception of the $Cu(OAc)_2$ products. It is possible that the latter materials are composed of separate $Cu(OAc)_2$ and melamine networks, probably associated through hydrogen bonds. Lack of Cu(I) charge transfer color and analysis of IR data suggest melamine coordination occurs through amine groups.

Acknowledgments

Grateful acknowledgement is made to Prof. Steven Aubuchon (Virginia Commonwealth University) for the use of thermogravimetric equipment. This research was supported in part by the National Science Foundation (Grant No. CHE-9983374), the Camille and Henry Dreyfus Foundation (Grant No. TH-99-010), the Thomas F. and Kate Miller Jeffress Memorial Trust (J-678), and also a Howard Hughes Medical Institute grant through the Undergraduate Biological Sciences Education Program to the College of William and Mary.

References

[1] (a) E.D. Weil, V. Choudhary, J. Fire Sci. 13 (1995) 104, and references cited therein;
(b) E.D. Weil, M. Lewin, H.S. Lin, J. Fire Sci. 16 (1998) 383;
(c) C.M. Dick, C. Denecker, J.J. Liggat, M.H. Mohammed, C.E. Snape, G. Seeley, C. Lindsay, B. Eling, P. Chaffanjon, Polym. Int. 49 (2000) 1177;
(d) A.I. Balabanovich, C.F. Levchik, S.V. Levchik, J. Engelmann, J . Fire Sci. 20 (2002) 71.

[2] (a) R.D. Pike, W.H. Starnes Jr., J.P. Jeng, W.S. Bryant, P. Kourtesis, C.W. Adams, S.D. Bunge, Y.M. Kang, A.S. Kim, J.H. Kim, J.A. Macko, C.P. O'Brien, Macromolecules 30 (1997) 6957;
(b) R.D. Pike, W.H. Starnes Jr., J.R. Cole, A.S. Doyal, P.M. Graham, T.J. Johnson, E.J. Kimlin, E.R. Levy, ACS Symp. Ser. 797 (2001) 267;
(c) R.D. Pike, W.H. Starnes Jr., P.M. Graham, Copper(I) networks: potential smoke suppression agents in poly(vinyl chloride), in: S. Al-Malaika, A. Golovoy, C.A. Wilkie (Eds.), Specialty Polymer Additives: Principles and Applications, Blackwell Science, Oxford, UK, 2001, pp. 343–357;
(d) W.H. Starnes Jr., R.D. Pike, J.R. Cole, A.S. Doyal, E.J. Kimlin, J.T. Lee, P.J. Murray, R.A. Quinlan, J. Zhang, Polym. Degrad. Stab. 82 (2003) 15.

[3] H.A. Ma, X. Jia, Z.L. Cui, Y.W. Pan, P.W. Zhu, B.B. Liu, H.J. Liu, X.C. Wang, J. Liu, G.T. Zou, Chem. Phys. Lett. 368 (2003) 668, and references cited therein.

[4] (a) A. Colombo, L. Menabue, A. Motori, G.C. Pellacani, W. Porzio, F. Sandrolini, R.D. Willett, Inorg. Chem. 24 (1985) 2900;
(b) B. Scott, U. Geiser, R.D. Willett, B. Patyal, C.P. Landee, R.E. Greeney, T. Manfredini, G.C. Pellancani, A.B. Corradi, L.P. Battaglia, Inorg. Chem. 27 (1988) 2454.

[5] (a) M. Chowdhry, D.M.P. Mingos, A.J.P. White, D.J. Williams, Chem. Commun. (1996) 899;
(b) Y. Zheng, L. Jianmin, M. Nishiura, T. Imamoto, Chem. Lett. (1999) 543.

[6] (a) H. Zhu, Z. Yu, X. You, H. Hu, X. Huang, J. Chem. Cryst. 29 (1999) 239;
(b) D.M.L. Goodgame, I. Hussain, A.J.P. White, D.J. Williams, J. Chem. Soc., Dalton Trans. (1999) 2899.

[7] M. Bicher, C. Guran, J. Jitaru, Rev. Roum. Chim. 39 (1994) 1203.

[8] G.J. Kubas, Inorg. Synth. 28 (1990) 68.

[9] P.M. Graham, R.D. Pike, M. Sabat, R.D. Bailey, W.T. Pennington, Inorg. Chem. 39 (2000) 5121.

[10] JADE, V6.1, Materials Data Inc., Livermore, CA, 2002.

[11] L.M. Nguyen, M.E. Dellinger, J.T. Lee, R.A. Quinlan, A.L. Rheingold, R.D. Pike, Inorg. Chim. Acta 358 (2005) 1331.

[12] J.T. Maeyer, T.J. Johnson, A.K. Smith, B.D. Borne, R.D. Pike, W.T. Pennington, M. Krawiec, A.L. Rheingold, Polyhedron 22 (2003) 419.

[13] (a) W.J. Jones, W.J. Orville-Thomas, Trans. Faraday Soc. 55 (1959) 203;
(b) W. Sawodny, K. Niedenzu, J.W. Davidson, J. Chem. Phys. 45 (1966) 3155;
(c) J.R. Schneider, B. Schrader, J. Mol. Struct. 29 (1975) 1.

[14] R.J. Meier, J.R. Maple, M.-J. Hwang, A.T. Hagler, J. Phys. Chem. 99 (1995) 5445.

Available online at www.sciencedirect.com
SCIENCE DIRECT®
Polyhedron 25 (2006) 783–792
POLYHEDRON
www.elsevier.com/locate/poly

Different nuclearities of M(II) nitrate complexes (M = Co, Ni, Cu and Cd) with a tetrapyridyl pendant-armed hexaazamacrocyclic ligand

M[a] del Carmen Fernández-Fernández [a], Rufina Bastida [a,*], Alejandro Macías [a], Laura Valencia [a,*], Paulo Pérez-Lourido [b]

[a] *Departamento de Química Inorgánica, Facultad de Química, Universidad de Santiago de Compostela, Avenida de las Ciencias s/n 15782, Santiago de Compostela, Spain*
[b] *Departamento de Química Inorgánica, Facultad de Ciencias, Universidade de Vigo, 36310 Vigo, Pontevedra, Spain*

Received 14 July 2005; accepted 29 July 2005
Available online 3 October 2005

Abstract

A new series of nitrate M(II) (M = Co, Ni, Cu and Cd) complexes with a tetrapyridyl pendant-armed hexaazamacrocyclic ligand (L) has been synthesized. The complexes have been characterized by microanalysis, FAB-MS, conductivity measurements, IR, UV–Vis, ^{1}H NMR spectroscopy and magnetic measurements at room temperature. In all cases, complexes with 1:1 and 2:1 metal:ligand molar ratios were obtained depending on the stoichiometry. Crystal structures of $[Co_2L(NO_3)_4]\cdot 2H_2O$, $[Cu_2L(H_2O)_2](NO_3)_4$, $[Cd_2L(NO_3)_2](NO_3)_2\cdot 5H_2O\cdot CH_3CN$ and $[CdL](NO_3)_2\cdot 6H_2O$ have been determined. The X-ray studies show that in $[Co_2L(NO_3)_4]\cdot 2H_2O$ and $[Cu_2L(H_2O)_4](NO_3)_4$, the metal atoms are exocyclically coordinated to the pyridine pendant arms and the tertiary amine nitrogen atoms in a distorted square pyramid [N4O] and distorted octahedral geometry [N4O2], respectively. In both cases, the pyridine rings of the macrocyclic backbone (bridgehead) are not coordinated. In contrast, in $[Cd_2L(NO_3)_2](NO_3)_2\cdot 5H_2O\cdot CH_3CN$ the metal atoms are coordinated by both types of pyridine group (bridgehead and pendant arm) and the tertiary amine with an [N5O2] core in a distorted capped octahedral geometry. Finally, the structure of the 1:1 cadmium complex $[CdL](NO_3)_2\cdot 6H_2O$ was also resolved and this showed the metal centre in a distorted octahedral geometry [N6] with the metal coordinated by both types of pyridine group and the tertiary amine.
© 2005 Elsevier Ltd. All rights reserved.

Keywords: Pyridyl macrocyclic ligand; *N*-alkylation; Metal complex; X-ray structure

1. Introduction

Over the last three decades, the chemistry of polyazamacrocycles has become a fruitful research area due to the ability of these systems to interact with different substrates such as metal ions or anionic species [1]. The presence of pyridine groups in the macrocyclic framework offers the possibility of obtaining complexes with high levels of metal and this has attracted considerable interest in recent years [2].

A great deal of effort has since been focused on pendant-armed ligands and their metal complexes due to the fact that the ligating groups attached to the macrocyclic backbone can offer additional donor groups and enhance complex stability [3]. The flexibility of the pyridyl pendant arms together with the steric requirements of the metal ion employed and the coordinative behaviour of the counterions, make it possible for intramolecular coordination to the parent metal ion to occur as well as intermolecular coordination to other metal ions.

* Corresponding authors. Tel.: +34 981 591076; fax: +34 981597525.
E-mail addresses: qibastid@usc.es (R. Bastida), qilaura@usc.es (L. Valencia).

0277-5387/$ - see front matter © 2005 Elsevier Ltd. All rights reserved.
doi:10.1016/j.poly.2005.07.045

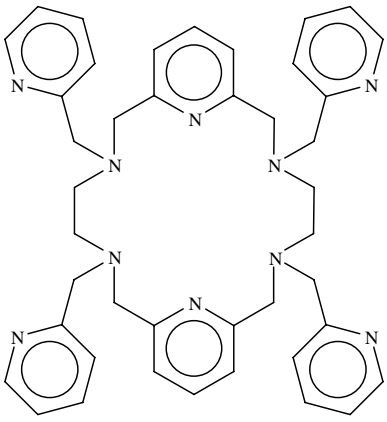

L

Fig. 1. Tetrapyridyl pendant-armed hexaazamacrocyclic ligand, L.

Such an arrangement could give rise to higher nuclearity or polymeric structures [4].

We have previously reported the synthesis of metal complexes of different nuclearity starting from silver nitrate [5] and perchlorate metal salts [6] and the hexaazamacrocyclic pendant-armed ligand L (Fig. 1), which bears tetrapyridyl pendant groups. In order to investigate possible modifications of the coordination behaviour of the macrocyclic ligand and, consequently, changes in the crystal structure due to the well-known different coordinative properties between perchlorate and nitrate anions, we report here our results obtained in the synthesis of a series of nitrate metal complexes.

Metal complexes of L with Co(II), Ni(II), Cu(II) and Cd(II) nitrate salts were prepared and characterized by microanalysis, FAB-MS, conductivity measurements, IR, UV–Vis, ^{1}H NMR spectroscopy and magnetic studies. The X-ray crystal structures of $[Co_2L(NO_3)_4]\cdot 2H_2O$, $[Cu_2L(H_2O)_2](NO_3)_4$, $[Cd_2L(NO_3)_2](NO_3)_2\cdot 5H_2O\cdot CH_3CN$ and $[CdL](NO_3)_2\cdot 6H_2O$ were also determined.

2. Experimental

2.1. Chemicals and starting materials

2,6-Pyridinedimethanol, ethylenediamine, 2-picolyl chloride hydrochloride and hydrated nitrate salts were commercial products (from Alfa and Aldrich) and were used without further purification. Solvents were of reagent grade and were purified by standard methods.

2.2. Synthesis of the macrocycle L

The ligand L was prepared from the hexaazamacrocycle precursor [7] by alkylation with picolyl chloride using a previously reported method [8].

2.3. Synthesis of the metal complexes

2.3.1. General procedure

The appropriate metal salt (0.25 mmol in a 1:1 synthesis or 0.5 mmol in a 2:1 synthesis) was dissolved in acetonitrile (10 mL) and the solution added to a stirred solution of the ligand L (0.25 mmol) in acetonitrile (30 mL) under reflux. The reaction mixture was heated under reflux for 2 h and concentrated using a rotary evaporator to give a volume of ca. 5–6 mL. The resulting product was filtered off and dried. In all cases, the complexes were obtained in a 1:1 or 2:1 metal:ligand molar ratio.

2.3.2. $[CoL](NO_3)_2\cdot 5H_2O$

Anal. Calc. for $C_{42}H_{56}N_{12}O_{11}Co$ (MW: 963): C, 52.3; H, 5.8; N, 17.4. Found: C, 51.4; H, 5.5; N, 17.7%. Yield: 49%. IR (KBr, cm^{-1}): 1609, 1591, 1475, 1437 [ν(C=N)$_{py}$ and ν(C=C)], 1384, [$\nu(NO_3^-)$]. MS (FAB, m/z): 812 $[CoL(NO_3)]^+$, 750 $[CoL]^{2+}$. $\Lambda_M/\Omega^{-1}\,cm^2\,mol^{-1}$ (in CH_3CN): 260 (2:1). Colour: brown.

2.3.3. $[Co_2L(NO_3)_4]\cdot 2H_2O$

Anal. Calc. for $C_{42}H_{50}N_{14}O_{14}Co_2$ (MW: 1092): C, 46.1; H, 4.6; N, 18.0. Found: C, 46.5; H, 4.5; N, 18.3%. Yield: 47%. IR (KBr, cm^{-1}): 1606, 1590, 1475, 1436 [ν(C=N)$_{py}$ and ν(C=C)], 1443, 1383, 1314, 810 [$\nu(NO_3^-)$]. MS (FAB, m/z): 994 $[Co_2L(NO_3)_3]^+$, 812 $[CoL(NO_3)]^+$. $\Lambda_M/\Omega^{-1}\,cm^2\,mol^{-1}$ (in CH_3CN): 365 (3:1). Colour: pink.

2.3.4. $[NiL](NO_3)_2\cdot 4H_2O$

Anal. Calc. for $C_{42}H_{54}N_{12}O_{10}Ni$ (MW: 946): C, 53.3; H, 5.7; N, 17.9. Found: C, 53.3; H, 5.7; N, 17.9%. Yield: 58%. IR (KBr, cm^{-1}): 1609, 1591, 1475, 1437 [ν(C=N)$_{py}$ and ν(C=C)], 1384 [$\nu(NO_3^-)$]. MS (FAB, m/z): 812 [NiL(NO$_3$)]+, 750 $[NiL]^{2+}$. $\Lambda_M/\Omega^{-1}\,cm^2\,mol^{-1}$ (in CH_3CN): 290 (2:1). Colour: brown.

2.3.5. $[Ni_2L(NO_3)_4]\cdot 2H_2O$

Anal. Calc. for $C_{42}H_{50}N_{14}O_{14}Ni_2$ (MW: 1092): C, 46.2; H, 4.6; N, 17.9. Found: C, 46.1; H, 4.7; N, 18.0%. Yield: 53%. IR (KBr, cm^{-1}): 1607, 1589, 1472, 1432 [ν(C=N)$_{py}$ and ν(C=C)], 1445, 1384, 1312, 811 [$\nu(NO_3^-)$]. MS (FAB, m/z): 994 $[Ni_2L(NO_3)_3]^+$, 932 $[Ni_2L(NO_3)_2]^{2+}$, 811 $[NiL(NO_3)]^+$, 750 $[NiL]^{2+}$. $\Lambda_M/\Omega^{-1}\,cm^2\,mol^{-1}$ (in CH_3CN): 402 (3:1). Colour: blue.

2.3.6. $[CuL](NO_3)_2\cdot 2H_2O$

Anal. Calc. for $C_{42}H_{50}N_{12}O_8Cu$ (MW: 913): C, 55.2; H, 5.5; N, 18.4. Found: C, 53.7; H, 5.5; N, 18.1%. Yield: 48%. IR (KBr, cm^{-1}): 1612, 1591, 1476, 1436 [ν(C=N)$_{py}$ and ν(C=C)], 1384 [$\nu(NO_3^-)$]. MS (FAB, m/z): 815 $[CuL(NO_3)]^+$, 753 $[CuL]^{2+}$. $\Lambda_M/\Omega^{-1}\,cm^2\,mol^{-1}$ (in CH_3CN): 275 (2:1). Colour: green.

2.3.7. $[Cu_2L(H_2O)_2](NO_3)_4$

Anal. Calc. for $C_{42}H_{50}N_{14}O_{14}Cu_2$ (MW: 1102): C, 37.8; H, 4.0; N, 16.4. Found: C, 37.7; H, 3.9; N, 16.4%. Yield: 52%. IR (KBr, cm^{-1}): 1609, 1588, 1481, 1434 [ν(C=N)$_{py}$ and ν(C=C)], 1384 [$\nu(NO_3^-)$]. MS (FAB, *m/z*): 1002 $[Cu_2L(NO_3)_3]^+$, 942 $[Cu_2L(NO_3)_2]^{2+}$, 880 $[Cu_2L(NO_3)]^{3+}$, 753 $[CuL]^{2+}$. $\Lambda_M/\Omega^{-1}\,cm^2\,mol^{-1}$ (in CH_3CN): 460 (4:1). Colour: blue.

2.3.8. $[CdL](NO_3)_2 \cdot 6H_2O$

Anal. Calc. for $C_{42}H_{58}N_{12}O_{12}Cd$ (MW: 1036): C, 48.6; H, 5.6; N, 16.2. Found: C, 48.9; H, 5.4; N, 16.0%. Yield: 48%. IR (KBr, cm^{-1}): 1602, 1588, 1436 [ν(C=N)$_{py}$ and ν(C=C)], 1383 [$\nu(NO_3^-)$]. MS (FAB, *m/z*): 866 $[CdL(NO_3)]^+$, 803 $[CdL]^{2+}$. $\Lambda_M/\Omega^{-1}\,cm^2\,mol^{-1}$ (in CH_3CN): 258 (2:1). Colour: white.

2.3.9. $[Cd_2L(NO_3)_2](NO_3)_2 \cdot 5H_2O \cdot CH_3CN$

Anal. Calc. for $C_{44}H_{59}N_{15}O_{17}Cd_2$ (MW: 1297): C, 40.7; H, 4.6, N, 16.2. Found: C, 40.6, H, 4.7, N, 15.9%. Yield: 71%. IR (KBr, cm^{-1}): 1602, 1588, 1436 [ν(C=C) and ν(C=N)$_{py}$], 1436, 1383, 1316, 817 [$\nu(NO_3^-)$]. MS (FAB, *m/z*): 1040 $[Cd_2L(NO_3)_2]^{2+}$, 866 $[CdL(NO_3)]^+$, 803 $[CdL]^{2+}$. $\Lambda_M/\Omega^{-1}\,cm^2\,mol^{-1}$ (in CH_3CN): 392 (3:1). Colour: white.

2.4. Physical measurements

Elemental analyses were performed in a Carlo-Erba EA microanalyser. Infrared spectra were recorded as KBr discs on a Bruker IFS-66V spectrophotometer. FAB mass spectra were recorded using a Kratos-MS-50T spectrometer connected to a DS90 data system using 3-nitrobenzyl alcohol as the matrix. Conductivity measurements were carried out in 10^{-3} mol dm^{-3} acetonitrile solutions at 20 °C using a WTW LF3 conductivimeter. ^1H NMR spectra were recorded on a Bruker 500 MHz spectrometer and CD_3CN was used as the solvent in all cases. Solid-state electronic spectra were recorded on a Hitachi 4-3200 spectrophotometer using $MgCO_3$ as reference. Magnetic studies were determined at room temperature on a vibration sample magnetometer (VSM) (Digital Measurement System 1660) with a magnetic field of 5000 G.

2.5. Crystal structure determination

The X-ray crystal measurements were made on a Bruker SMART CCD 1000 area diffractometer. All data were corrected for Lorentz and polarization effects. Empirical absorption corrections were also applied for all the crystal structures obtained [9]. Complex scattering factors were taken from the program package SHELXTL [10]. The structures were solved by direct methods, which revealed the position of all non-hydrogen atoms. All the structures were refined on F^2 by a full-matrix least-squares procedure using anisotropic displacement parameters for all non-hydrogen atoms. The hydrogen atoms were located in their calculated positions and refined using a riding model. Molecular graphics were generated using ORTEP-3 [11].

3. Results and discussion

Metal complexes of Co(II), Ni(II), Cu(II) and Cd(II) with 1:1 and 2:1 stoichiometries were prepared by reaction of a tetrapyridyl pendant-armed hexaazamacrocyclic ligand (L) with hydrated metal nitrate salts, in acetonitrile, in 1:1 and 2:1 metal:ligand molar ratios. The complexes were synthesized by a one-step procedure as described in Section 2 and the reactions gave good yields of analytically pure products.

The complexes appear to be air stable; they are soluble in acetonitrile, dimethylformamide and dimethylsulfoxide, some of them are soluble in water, methanol and ethanol, but are insoluble in dichloromethane and chloroform.

3.1. Crystal structures

The details of the X-ray crystal structure solutions and refinement are given in Table 1.

3.1.1. Crystal structure of $[Co_2L(NO_3)_4] \cdot 2H_2O$

Pink crystals of $[Co_2L(NO_3)_4] \cdot 2H_2O$ were obtained by slow recrystallization of the complex from acetonitrile. The molecular structure of the complex and selected bond lengths (Å) and angles (°) relating to the coordination environment of the metal are given in Fig. 2. The unit cell contains a dinuclear complex with the two cobalt atoms separated by 9.33 Å. Both metal centres present a similar six-coordinate N4O2 core in a distorted octahedral geometry. Each cobalt is bound to four nitrogen atoms – two contiguous tertiary amines from the macrocyclic backbone and their corresponding two pyridyl pendant groups – and two oxygen atoms from two monodentate nitrate anions. All the donor atoms are disposed in a *cis* arrangement. Neither of the bridgehead pyridyl groups are coordinated. Examination of the coordination spheres in more detail shows that there are few differences between the two metal ions. The equatorial plane of Co(1) can be considered to be formed by two pyridyl pendant nitrogen atoms [N(7), N(8)], one amine nitrogen, N(3), and an oxygen from a nitrate molecule, O(4n), [N(7) N(8) N(3) O(4n), rms 0.3619] and the axial axis consists of the other amine nitrogen N(2) and O(1n) [N(2)–Co(1)–O(1n), 164.2(4)°]. In contrast, the equatorial plane for Co(2) is better described by the other two amine nitrogen atoms [N(6), N(5)], one pyridyl pendant nitrogen atom, N(9), and an oxygen atom from a nitrate molecule, O(10n), [N(6)

Table 1
Crystal data and structure refinement for $[Co_2L(NO_3)_4]\cdot 2H_2O$, $[Cu_2L(H_2O)_2](NO_3)_4$, $[Cd_2L(NO_3)_2](NO_3)_2\cdot 5H_2O\cdot CH_3CN$ and $[CdL](NO_3)_2\cdot 6H_2O$

	$[Co_2L(NO_3)_4]\cdot 2H_2O$	$[Cu_2L(H_2O)_2](NO_3)_4$	$[Cd_2L(NO_3)_2](NO_3)_2\cdot 5H_2O\cdot CH_3CN$	$[CdL](NO_3)_2\cdot 6H_2O$
Empirical formula	$C_{42}H_{46}Co_2N_{14}O_{14}$	$C_{21}H_{25}CuN_7O_7$	$C_{44}H_{49}Cd_2N_{15}O_{17}$	$C_{42}H_{58}CdN_{12}O_{12}$
Formula weight	1088.79	551.02	1284.78	1035.40
Temperature (K)	293(2)	293(2)	120(2)	293(2)
Wavelength (Å)	0.71073	0.71073	0.71073	0.71073
Crystal system	orthorrombic	monoclinic	triclinic	monoclinic
Space group	*Cc*	*P*2(1)/*n*	$P\bar{1}$	*C*2/*c*
Unit cell dimensions				
a (Å)	30.274(3)	9.281(2)	10.337(2)	15.765(3)
b (Å)	8.7941(7)	15.844(4)	11.680(2)	18.350(3)
c (Å)	18.1442(15)	16.112(4)	12.027(2)	16.967(3)
α (°)			109.657(3)	
β (°)	100.506(2)	91.443(4)	98.007(3)	104.454(3)
γ (°)			101.949(3)	
Volume (Å^3)	4749.6(7)	2368.5(10)	1303.0(4)	4752.9(14)
Z	4	4	1	4
Density (calculated) (Mg/m^3)	1.523	1.545	1.637	1.447
Absorption coefficient (mm^{-1})	0.780	0.980	0.901	0.532
F(000)	2248	1140	650	2152
Crystal size (mm)	$0.36\times0.24\times0.07$	$0.50\times0.48\times0.43$	$0.27\times0.25\times0.19$	$0.27\times0.18\times0.15$
Theta range for data collection (°)	2.28–27.98	1.80–26.43	1.85–26.52	1.74–24.71
Index ranges	$-39\leqslant h\leqslant 35$, $-11\leqslant k\leqslant 10$, $-18\leqslant l\leqslant 23$	$-11\leqslant h\leqslant 11$, $-19\leqslant k\leqslant 19$, $-20\leqslant l\leqslant 19$	$-12\leqslant h\leqslant 12$, $-14\leqslant k\leqslant 13$, $0\leqslant l\leqslant 15$	$-18\leqslant h\leqslant 17$, $0\leqslant k\leqslant 21$, $0\leqslant l\leqslant 19$
Reflections collected	13432	19804	14837	15065
Independent reflections [R_{int}]	7817 [0.0420]	4854 [0.0287]	5369 [0.0226]	4047 [0.0493]
Completeness to theta =	93.8% (27.98°)	99.8% (26.43°)	99.2% (26.52°)	99.7% (24.71°)
Absorption correction	empirical	empirical	empirical	empirical
Maximum and minimum transmission	0.9474 and 0.7666	0.6780 and 0.6401	0.8474 and 0.7929	0.9244 and 0.8696
Refinement method	full-matrix least-squares on F^2	full-matrix least-squares on F^2	full-matrix least-squares on F^2	full-matrix least-squares on F^2
Data/restraints/parameters	7817/2/650	4854/0/333	5369/0/403	4047/36/320
Goodness-of-fit on F^2	0.854	1.029	1.089	1.005
Final *R* indices [$I>2\sigma(I)$]	$R_1=0.0481$, $wR_2=0.1064$	$R_1=0.0446$, $wR_2=0.1298$	$R_1=0.0326$, $wR_2=0.0855$	$R_1=0.0720$, $wR_2=0.2125$
R indices (all data)	$R_1=0.0931$, $wR_2=0.1211$	$R_1=0.0567$, $wR_2=0.1410$	$R_1=0.0375$, $wR_2=0.0897$	$R_1=0.1301$, $wR_2=0.2561$
Largest difference peak and hole (e Å^{-3})	0.533 and −0.416	0.647 and −0.415	1.223 and −0.747	1.154 and −0.732

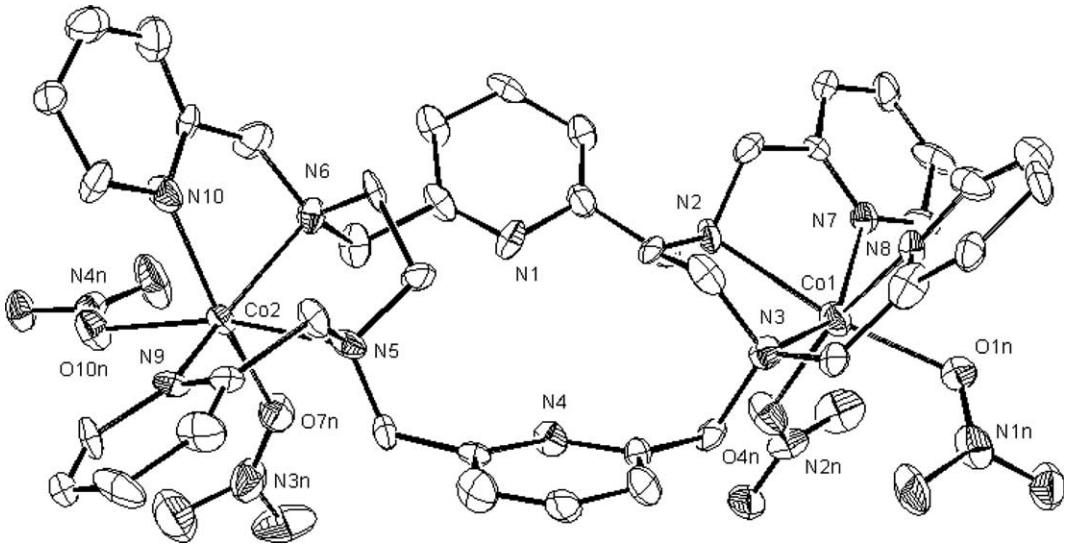

Fig. 2. Crystal structure of $[Co_2L(NO_3)_4] \cdot 2H_2O$ and selected bond lengths (Å) and angles (°). Co(1)–N(2) 2.356(9), Co(1)–N(3) 2.277(9), Co(1)–N(7) 2.166(10), Co(1)–N(8) 2.187(10), Co(1)–O(1n) 2.066(9), Co(1)–O(4n) 2.092(9), Co(2)–N(5) 2.279(10), Co(2)–N(6) 2.188(10), Co(2)–N(9) 2.125(10), Co(2)–N(10) 2.149(11), Co(2)–O(7n) 2.027(9), Co(2)–O(10n) 2.130(8), O(4n)–Co(1)–O(1n) 94.7(4), O(1n)–Co(1)–N(7) 91.3(4), O(4n)–Co(1)–N(8) 161.0(4), O(1n)–Co(1)–N(8) 81.4(4), N(7)–Co(1)–N(8) 91.1(4), O(4n)–Co(1)–N(3) 92.0(3), N(7)–Co(1)–N(3) 143.6(3), O(4n)–Co(1)–N(2) 86.0(3), O(1n)–Co(1)–N(2) 164.2(4), O(7n)–Co(2)–O(10n) 95.6(3), O(10n)–Co(2)–N(9) 87.7(4), O(7n)–Co(2)–N(10) 163.3(4), N(9)–Co(2)–N(10) 87.9(4), O(7n)–Co(2)–N(6) 92.6(4), O(10n)–Co(2)–N(6) 118.9(4), N(9)–Co(2)–N(6) 144.5(4), O(7n)–Co(2)–N(5) 84.4(3), O(10n)–Co(2)–N(5) 161.2(3).

N(5) N(9) O(10n), rms 0.2459]. The axial axis is now determined by the other pyridyl pendant nitrogen atom N(10) and O(7n) [N(10)–Co(2)–O(7n), 163.3(4)°]. The main distortions from a regular octahedral geometry can be attributed to the five-membered chelate rings formed on the macrocyclic ligand.

The average values of the bond lengths between the metal ions and the N atoms of the macrocycle are 2.275 and 2.156 Å for $Co–N_{am}$ and $Co–N_{py}$, respectively, with the longer distance corresponding to Co(1)–N(2), 2.356(9) Å. The average value of the Co–O bond length is 2.078 Å, which is similar to that found in other monodentate nitrate complexes of octahedral Co(II) [12].

The macrocyclic backbone is slightly folded with a dihedral angle between the pyridyl groups of 46.14°. Finally, the crystal structure is completed by two water solvent molecules that are not coordinated to the metal centre.

3.1.2. Crystal structure of $[Cu_2L(H_2O)_2](NO_3)_4$

The molecular structure of $[Cu_2L(H_2O)_2](NO_3)_4$ is shown in Fig. 3 together with selected bond lengths (Å) and angles (°). The complex structure is similar to that found for the corresponding perchlorate complex [6]. The dinuclear complex is disposed around a crystallographic inversion centre. The symmetry-related metal ions are separated by 8.76 Å. The crystal structure shows that the copper atoms are also exocyclically coordinated by two contiguous amine nitrogen atoms from the macrocyclic backbone and their corresponding two pyridyl pendant groups. The fifth coordination position is, in this case, completed by one water molecule. Therefore, the copper atoms are five-coordinate with an N_4O donor set. The τ factor is 0.27 and this show that the coordination geometry around the metal ion is best described as a fairly distorted square pyramid than a distorted trigonal bipyramid [13], with the basal plane formed by the amine nitrogen atoms N(2) and N(3)#1 and their corresponding pyridyl pendant groups N(4) and N(5) also in a *cis* disposition. The apical position of the pyramid is occupied by oxygen atom O(1w) of a water molecule. The largest deviation from the mean N(2) N(3)#1 N(4) N(5) basal plane (rms = 0.1876) is 0.2044 Å for N(2). The copper atom is displaced by 0.2792 Å toward the apical site. The angles at the metal atom in the three five-membered chelate rings deviate significantly from 90° [83.00(10)°, 85.59(10)° and 81.96(10)° for N(5)–Cu(1)–N(3)#1, N(2)–Cu(1)–N(3)#1 and N(2)–Cu(1)–N(4), respectively] due to the geometrical constrains of the macrocyclic ligand. All of the Cu–N distances are similar, with the pyridyl pendant-arm distances [Cu(1)–N(4) 2.017(2) Å, Cu(1)–N(5) 2.018(3) Å] shorter than the amine nitrogen atom distances [Cu(1)–N(2) 2.030(2) Å, Cu(1)–N(3)#1 2.072(2) Å]. The average Cu–N bond length is 2.034 Å. The longer coordination bond corresponds to the Cu(1)–O(1w) distance, 2.216(2) Å, and this is in the range found for axially coordinated water molecules in other similar pentacoordinated Cu(II) complexes [14].

The macrocyclic backbone is almost in a plane. The bridgehead pyridine groups are parallel to one another and the planes containing each of them are 0.59 Å away. The nitrate ions are not coordinated to the metal centres but interact with the water molecules through hydrogen

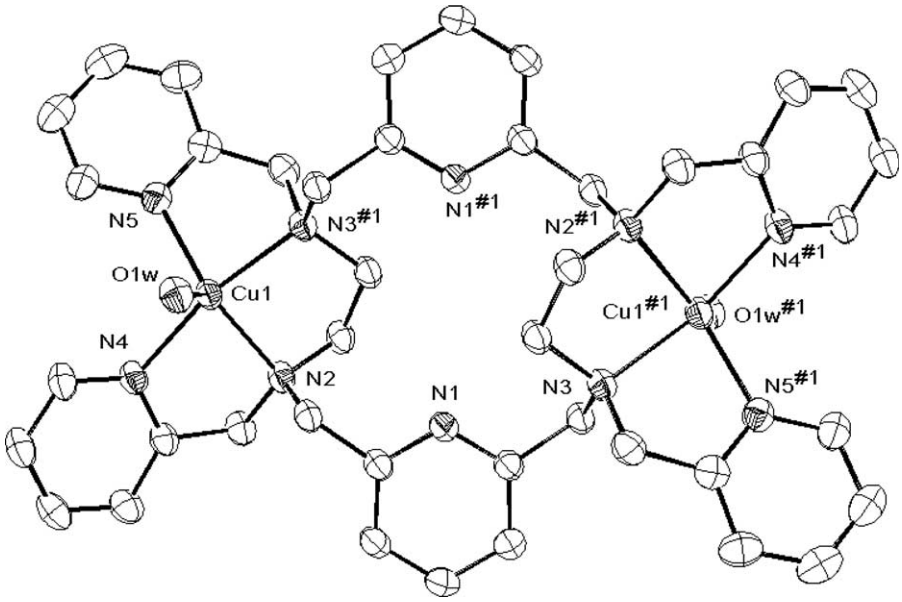

Fig. 3. Crystal structure of $[Cu_2L(H_2O)_2](NO_3)_4$ and selected bond lengths (Å) and angles (°). Cu(1)–N(3)#1 2.072(2), Cu(1)–N(5) 2.018(3); Cu(1)–N(4) 2.017(2), Cu(1)–N(2) 2.030(2), Cu(1)–O(1w), 2.216(2), N(4)–Cu(1)–N(5) 107.04(11), N(4)–Cu(1)–N(2) 81.96(10), N(5)–Cu(1)–N(2) 151.34(10), N(4)–Cu(1)–N(3)#1 167.34(10), N(5)–Cu(1)–N(3)#1 83.00(10), N(2)–Cu(1)–N(3)#1 85.59(10), N(4)–Cu(1)–O(1w) 87.02(10), N(5)–Cu(1)–O(1w) 96.14(10), N(2)–Cu(1)–O(1w) 111.70(11), N(3)#1–Cu(1)–O(1W) 99.77(9). Symmetry transformations used to generate equivalent atoms: #1 $-x, -y, -z$.

bonds [2.716(0) Å, 169.14(0.02)° for O(2n)—O(1w) and O(1w)–H(1s)–O(2n), respectively, and 2.729(0) Å, 175.46(0.02)° for O(5n)–O(1w) and O(1w)–H(2s)–O(5n), respectively].

3.1.3. Crystal structure of $[Cd_2L(NO_3)_2](NO_3)_2 \cdot 5H_2O \cdot CH_3CN$

The dinuclear complex $[Cd_2L(NO_3)_2](NO_3)_2 \cdot 5H_2O \cdot CH_3CN$ was obtained by recrystallization (acetonitrile) of the complex obtained from the reaction between Cd(II) nitrate and the macrocyclic ligand in a 2:1 molar ratio. The crystal structure was studied by X-ray diffraction and the molecular structure of the complex is shown in Fig. 4 together with the atomic numbering scheme adopted and selected bond length distances (Å) and angles (°).

The complex presents a crystallographically imposed symmetry in the unit cell. The intramolecular Cd–Cd distance is 5.784 Å. The metal atoms are seven-coordinate with an N5O2 core. In this case, all the nitrogen atoms of the ligand are coordinated. Each cadmium ion is coordinated to one pyridyl bridgehead unit, two tertiary amine nitrogens contiguous to that pyridyl bridgehead, and to their corresponding pyridyl pendant arms. The coordination environment is completed by a bidentate nitrate anion. The geometry around the metal ions can be described as distorted capped octahedral, or distorted octahedral if both oxygen atoms of the nitrate anion are considered to occupy one coordination position.

In this case, the pyridyl bridgehead of the macrocyclic backbone provides the strongest bond to the metal atoms [Cd–N1, 2.304(2) Å]. This distance is slightly shorter than that corresponding to pyridyl pendant arms [Cd–N3, 2.319(3) Å and Cd–N4, 2.346(2) Å]. The longer Cd–N distance corresponds to the amine groups [Cd–N2, 2.536(3) Å and Cd–N5, 2.502(3) Å] and these distances are in the range expected for this type of bond [15]. Two of the nitrate ions act in anisobidentate mode [Cd–O4n, 2.397(2) Å and Cd–O5n, 2.579(3) Å] and the average value of 2.488 Å is in accordance with other similar seven-coordinate nitrate Cd(II) complexes [12,16].

The macrocyclic ligand is in a step conformation. The dihedral angle between the pyridyl bridgeheads is 0° due to crystallographic symmetry requirements and the angle between these rings and the plane described for the tertiary amine nitrogen atoms (rms 0) is 76.31°.

3.1.4. Crystal structure of $[CdL](NO_3)_2 \cdot 6H_2O$

Crystals of $[CdL](NO_3)_2 \cdot 6H_2O$ were obtained by the reaction between Cd(II) nitrate and the macrocyclic ligand in a 1:1 molar ratio. The molecular structure of the complex together with selected bond lengths (Å) and angles (°) relating to the coordination environment of the metal are given in Fig. 5. The structure is similar to that found for the metal complex obtained from the perchlorate cadmium salt and the same ligand [6]. The X-ray crystal structure confirms the presence of a mononuclear endomacrocyclic complex constituted by the cation $[CdL]^{2+}$, two well-separated nitrate anions and three water molecules of hydration. The crystal structure is centrosymmetric and the metal atom is six-coordinate with a distorted octahedral geometry [N6] arising from coordination of the two pyridyl bridgehead rings of the macrocyclic backbone, two opposite tertiary amine

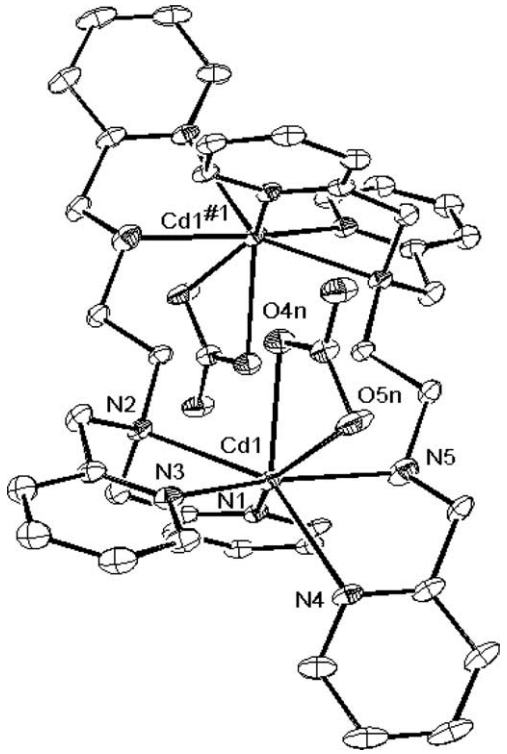

Fig. 4. Crystal structure of $[Cd_2L(NO_3)_2](NO_3)_2 \cdot 5H_2O \cdot CH_3CN$ and selected bond lengths (Å) and angles (°). Cd–N(1) 2.304(2), Cd–N(3) 2.319(3), Cd–N(4) 2.346(2), Cd–O(4n) 2.397(2), Cd–N(5) 2.502(3), Cd–N(2) 2.536(3), Cd–O(5n) 2.579(3), N(1)–Cd–N(3) 124.12(9), N(1)–Cd–N(4) 95.82(9), N(3)–Cd–N(4) 95.93(9), N(1)–Cd–O(4n) 124.23(8), N(3)–Cd–O(4n) 85.85(8), N(4)–Cd–O(4n) 129.81(8), N(1)–Cd–N(5) 71.51(9), N(3)–Cd–N(5) 161.41(9), N(4)–Cd–N(5) 70.79(9), O(4N)–Cd–N(5) 92.79(8), N(1)–Cd–N(2) 68.93(8), N(3)–Cd–N(2) 71.22(8), N(4)–Cd–N(2) 145.94(9), O(4n)–Cd–N(2) 81.82(8), N(5)–Cd–N(2) 126.98(8), N(1)–Cd–O(5n) 153.68(9), N(3)–Cd–O(5n) 82.20(9), N(4)–Cd–O(5n) 79.06(8), O(4n)–Cd–O(5n) 51.39(7), N(5)–Cd–O(5n) 82.50(9), N(2)–Cd–O(5n) 127.71(8).

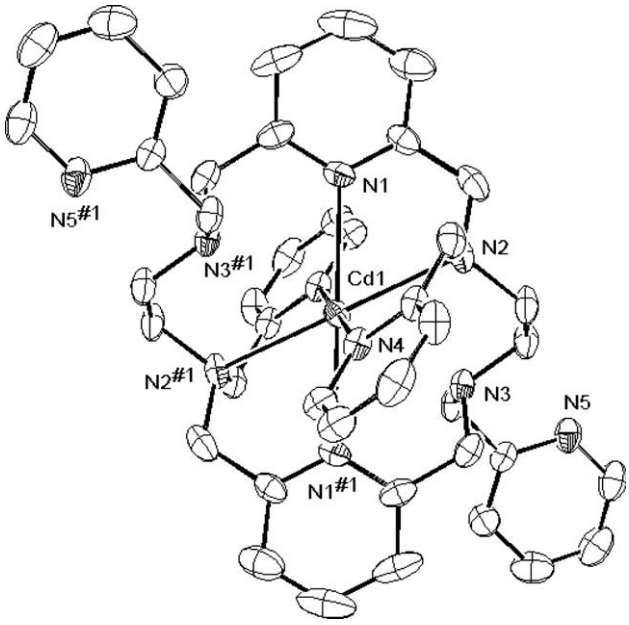

Fig. 5. Crystal structure of $[CdL](NO_3)_2 \cdot 6H_2O$ and selected bond lengths (Å) and angles (°). Cd(1)–N(4) 2.352(6), Cd(1)–N(4)#1 2.352(6), Cd(1)–N(1)#1 2.546(7), Cd(1)–N(1) 2.546(7), Cd(1)–N(2)#1 2.610(7), Cd(1)–N(2) 2.610(7), N(4)–Cd(1)–N(4)#1 180.000(1), N(4)–Cd(1)–N(1)#1 80.0(2), N(4)#1–Cd(1)–N(1)#1 100.0(2), N(4)–Cd(1)–N(1) 100.0(2), N(4)#1–Cd(1)–N(1) 80.0(2), N(1)#1–Cd(1)–N(1) 180.0, N(4)–Cd(1)–N(2)#1 110.9(3), N(4)#1–Cd(1)–N(2)#1 69.1(3), N(1)#1–Cd(1)–N(2)#1 64.2(3), N(1)–Cd(1)–N(2)#1 115.8(3), N(4)–Cd(1)–N(2) 69.1(3), N(4)#1–Cd(1)–N(2) 110.9(3), N(1)#1–Cd(1)–N(2) 115.8(3), N(1)–Cd(1)–N(2) 64.2(3), N(2)#1–Cd(1)–N(2) 180.000(1). Symmetry transformations used to generate equivalent atoms: #1 $-x+1/2$, $-y+1/2$, $-z+1$.

nitrogen atoms and their corresponding pyridyl pendant arms – all of which are in a *trans* disposition. The other two aliphatic amine nitrogen atoms and their corresponding pyridyl pendant arms are not coordinated. The main distortion from a regular octahedral geometry can also be attributed to the three five-membered chelate rings of the macrocyclic ligand.

The Cd–N bond distances are different and are slightly shorter than that observed for the perchlorate complex mentioned above. The pyridyl pendant-arm nitrogen atoms provide the strongest bond to the ion [Cd–N4, 2.352(6) Å]. This is shorter than pyridyl bridgehead [Cd–N1, 2.546(7)] and tertiary amine [Cd–N2, 2.610(7)] bond lengths. The macrocycle is not folded and the pyridyl bridgehead units are parallel with one another.

3.2. Spectroscopic and magnetic studies

The IR spectra of the complexes were recorded as KBr discs and all show similar features. The ν(C=N) and ν(C=C) of the pyridine rings are generally shifted to higher wave numbers than in the free ligand, suggesting coordination of the pyridyl groups to the metal ions [17]. In the all of the mononuclear as well as the dinuclear Cu(II) complexes, the band at 1383 cm^{-1} associated with the presence of ionic nitrate is observed. This shows that uncoordinated nitrate groups are present, as it has been found in the crystal structures of $[CdL](NO_3)_2 \cdot 6H_2O$ and $[Cu_2L(H_2O)_2](NO_3)_4$. On the other hand, in Co(II), Ni(II) and Cd(II) dinuclear complexes, the band at 1383 cm^{-1} (probably due to the interchange between nitrate and bromide groups of the KBr disc) is accompanied by several bands in the region associated with nitrate vibrations and these clearly identify the coordinated nitrate groups [18] – as found in the crystal structures of $[Co_2L(NO_3)_4] \cdot 2H_2O$ and $[Cd_2L(NO_3)_2](NO_3)_2 \cdot 5H_2O \cdot CH_3CN$.

The reflectance spectra of $[CoL](NO_3)_2 \cdot 5H_2O$ and $[Co_2L(NO_3)_4] \cdot 2H_2O$ show two d–d transition bands at ca. 10000 and 20000 cm^{-1}, which are due to the $^4T_{2g} \leftarrow {}^4T_{1g}$ and $^4T_{1g}(P) \leftarrow {}^4T_{1g}(F)$ transitions, respectively, and are of the type expected for distorted octahedral high spin Co(II) complexes [19].

The reflectance spectra of the nickel complexes $[NiL](NO_3)_2 \cdot 4H_2O$ and $[Ni_2L(NO_3)_4] \cdot 2H_2O$ show three bands at ca. 10 300, 16 400 and 26 000 cm^{-1}. These bands are attributable to the $^3T_{2g} \leftarrow {}^3A_{2g}$, $^3T_{1g}(F) \leftarrow {}^3A_{2g}$ and $^3T_{1g}(P) \leftarrow {}^3A_{2g}$ transitions, respectively, and are indicative of octahedral Ni(II) compounds. One absorption band at ca. 14 780 cm^{-1} is also present in $[Ni_2L(NO_3)_4] \cdot 2H_2O$, probably due to the spin forbidden transition $^1E_g \leftarrow {}^3A_{2g}$ usually observed in Ni(II) complexes [20].

The electronic reflectance spectrum of the pentacoordinated complex $[Cu_2L(H_2O)_2](NO_3)_4$ shows one broadband, probably a multicomponent band, between 17 200 and 12 500 cm^{-1}. This band is consistent with a five-coordinate $[CuN_4O]$ square pyramidal geometry around the metal [21]. Nevertheless, the UV–Vis spectrum of the 1:1 complex $[CuL](NO_3)_2 \cdot 2H_2O$ exhibits a broadband at ca. 17 000 cm^{-1} and an octahedral geometry is proposed for this system by analogy with the corresponding mononuclear perchlorate complex [6].

The room temperature magnetic moments obtained for $[CoL](NO_3)_2 \cdot 5H_2O$ and $[Co_2L(NO_3)_4] \cdot 2H_2O$ are 4.7 BM (per Co atom), which is consistent with the presence of high-spin octahedral Co(II) ions [22]. The magnetic moments at room temperature for the Ni(II) and Cu(II) complexes were 2.9 and 1.8 BM (per metal atom), respectively, and these values are within the range usually observed for octahedral Ni(II) and d^9 systems, respectively [22].

The molar conductance values for the complexes of L measured in acetonitrile at 25 °C lie in the range reported for 2:1 electrolytes for the complexes $[CoL](NO_3)_2 \cdot 5H_2O$, $[NiL](NO_3)_2 \cdot 4H_2O$, $[CuL](NO_3)_2 \cdot 2H_2O$ and $[CdL](NO_3)_2 \cdot 6H_2O$, 3:1 electrolytes for $[Co_2L(NO_3)_4] \cdot 2H_2O$, $[Ni_2L(NO_3)_4] \cdot 2H_2O$ and $[Cd_2L(NO_3)_2](NO_3)_2 \cdot 5H_2O \cdot CH_3CN$, while the complex $[Cu_2L(H_2O)_2](NO_3)_4$ acts as 4:1 electrolytes in this solvent [23].

The FAB mass spectra for all the complexes indicate the presence of the macrocyclic ligand and the metal ion and, as is common with complexes of this type, a characteristic fragmentation pattern resulting from stepwise loss of counterions from the neutral parent ion is observed.

The ^1H NMR spectra of $[CdL](NO_3)_2 \cdot 6H_2O$ and $[Cd_2L(NO_3)_2](NO_3)_2 \cdot 5H_2O \cdot CH_3CN$ were recorded in CD_3CN and D_2O, respectively.

The ^1H NMR spectrum for $[CdL^1](NO_3)_2 \cdot 6H_2O$ is complicated and contains a large number of signals, indicating that the complex adopts an asymmetric structure in solution where the ligand has lost its fourfold symmetry. Nevertheless, the ^1H NMR spectrum of $[Cd_2L(NO_3)_2](NO_3)_2 \cdot 5H_2O \cdot CH_3CN$ is very clear (Table 2). The assignments of the proton signals were based upon standard 2D homonuclear (COSY) and $^1H/^{13}C$ heteronuclear spectra (HMQC). The pyridine hydrogens H_a and H_b appear as the expected triplet and doublet, respectively. The geminal protons H_{4a} and H_{4b}, H_{5a} and H_{5b} and H_{6a} and H_{6b} appear as separate doublets, showing that they are chemically and magnetically inequivalent. In general, all the proton signals are shifted downfield in comparison to those in the free ligand.

Table 2
^1H NMR spectrum for $[Cd_2L(NO_3)_2](NO_3)_2 \cdot 5H_2O \cdot CH_3CN$ in D_2O

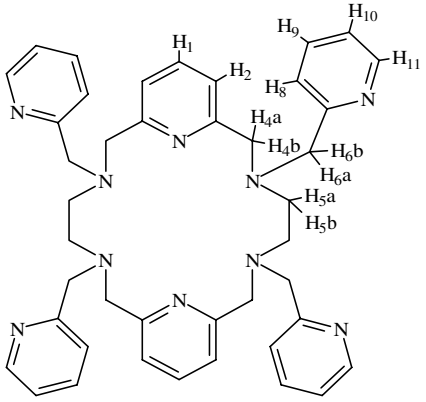

Assignment	δ (ppm)
H_1	7.65 (t, 2H)
H_2	7.15 (d, 4H)
H_{4a} and H_{4b}	4.16 (d, 4H) and 4.41 (d, 4H)
H_{5a} and H_{5b}	2.45 (m, 4H) and 2.99 (m, 4H)
H_{6a} and H_{6b}	3.86 (d, 4H) and 4.05 (d, 4H)
H_8, H_9, H_{10} and H_{11}	8.17 (d, 4H), 7.43 (t, 4H), 8.03 (t, 4H) and 7.58 (d, 4H)

4. Conclusion

The position and number of donor atoms together with the flexibility of the tetrapyridyl pendant-armed macrocyclic ligand, L, make this a versatile molecule that can bind the metal through different nitrogen donor atoms and can adopt different conformations depending on the steric requirements of the metal ion employed.

Reaction of this ligand with Co(II), Ni(II), Cu(II) and Cd(II) nitrate salts gives metal complexes with 1:1 or 2:1 stoichiometries depending on the metal:ligand molar ratio employed in the synthesis.

Different features were found for the dinuclear complexes $[Co_2L(NO_3)_4] \cdot 2H_2O$, $[Cu_2L(H_2O)_2](NO_3)_4$ and $[Cd_2L(NO_3)_2](NO_3)_2 \cdot 5H_2O \cdot CH_3CN$. For example, the Co(II) and Cu(II) complexes are exocyclically bonded to all the pyridyl pendant arms and tertiary amine nitrogen atoms but the pyridyl bridgehead of the macrocyclic ligand is not coordinated. In the case of Cd(II), all the pyridyl groups (pendant arms and bridgehead) and also the tertiary amine nitrogen atoms are coordinated.

In the mononuclear complex $[CdL](NO_3)_2 \cdot 6H_2O$ the metal ion is coordinated to six nitrogen donor atoms: the two pyridyl bridgehead groups and to half of the tertiary amine nitrogen atoms and their pyridyl pendant arms.

Crystal data for other mononuclear metal complexes were not obtained, but the microanalysis, spectroscopic and magnetic results suggest in all cases the formation of mononuclear complexes in which the metal atom is in an octahedral environment – similar to that found for the Cd(II) nitrate described above or to the equivalent perchlorate complexes. Finally, a dinuclear structure similar to $[Co_2L(NO_3)_4] \cdot 2H_2O$ is suggested for the 2:1 Ni(II) complex.

Acknowledgements

We thank the Xunta de Galicia (PGIDT01PXI20901PR) for financial support. Intensity measurements were performed at the Unidade de Raios X, RIAIDT, University of Santiago de Compostela, SPAIN.

Appendix A. Supplementary data

Crystallographic data for the structural analyses have been deposited with the Cambridge Crystallographic Data Centre, CCDC Nos. 277410 for $[Co_2L(NO_3)_4] \cdot 2H_2O$, 277411 for $[Cu_2\ L(H_2O)_2\ ](NO_3)_4$, 277412 for $[Cd_2L(NO_3)_2]\ (NO_3)_2 \cdot 5H_2O \cdot CH_3CN$ and 277413 for $[CdL](NO_3)_2 \cdot 6H_2O$. Copies of this information may be obtained free of charge from The Director, CCDC, 12 Union Road, Cambridge, CB2 1EZ, UK (fax: +44 1233 336033; e-mail: deposit@ccdc.cam.ac.uk or http://www.ccdc.ac.uk). Supplementary data associated with this article can be found, in the online version, at doi:10.1016/j.poly.2005.07.045.

References

[1] (a) R.M. Izatt, J.S. Bradshaw, S.A. Nielsen, J.D. Lamb, J.J. Christensen, D. Sen, Chem. Rev. 85 (1985) 271;
(b) K.B. Mertes, J.M. Lehn, in: G. Wilkinson (Ed.), Comprehensive Coordination Chemistry, Pergamon Press, Oxford, 1987, p. 915;
(c) J.M. Lehn, Angew. Chem., Int. Ed. Engl. 27 (1988) 89;
(d) K.E. Krakowiak, J.S. Bradshaw, D.J. Zamecka-Krakowiak, Chem. Rev. 89 (1989) 929;
(e) J.S. Bradshaw, Aza-Crown Macrocycles, Wiley, New York, 1993.

[2] (a) E.C. Constable, M.G.B. Drew, G. Forsyth, M.D. Ward, J. Chem. Soc., Chem. Commun. (1988) 1450;
(b) D.E. Fenton, R.W. Matthews, M. McPartlin, B.P. Murphy, I.J. Scowen, P.A. Tasker, J. Chem. Soc., Chem. Commun. (1994) 1391;
(c) L.H. Bryant Jr., A. Lachgar, K.S. Coates, S.C. Jackels, Inorg. Chem. 33 (1994) 2219.

[3] (a) G.A. Mclachlan, S.J. Brudenell, G.D. Fallon, R.L. Martin, L. Spiccia, E.R.T. Tiekink, J. Chem. Soc., Dalton Trans. (1995) 439;
(b) H. Adams, H.A. Bailey, D.E. Fenton, M.B. Hursthouse, W. Kanda, M. Kanesato, K.M.A. Malik, E.J. Sadler, J. Chem. Soc., Chem. Commun. (1997) 921.

[4] (a) I.M. Atkinson, J.D. Chartres, G.W. Everett, X.-K. Ji, L.F. Lindoy, F. Leonard, O.A. Matthews, G.V. Meehan, B.W. Skelton, W. Brian, G. Wei, A.H. White, J. Chem. Soc., Dalton Trans. (2000) 1191;
(b) P. Xue, Q. Yuan, E. Fu, C. Wu, J. Organomet. Chem. 327 (2001) 637;
(c) W.S. Szulbinski, R.S. Czernuszewicz, Inorg. Chim. Acta 247 (1996) 11;
(d) S.J. Brudenell, L. Spiccia, A.M. Bond, P. Comba, D.C.R. Hockless, Inorg. Chem. 37 (1998) 3705.

[5] L. Valencia, R. Bastida, A. Macías, M. Vicente, P. Pérez-Lourido, New J. Chem. 29 (2005) 424.

[6] R. Bastida, D.E. Fenton, M. López-Deber, A. Macías, L. Valencia, M. Vicente, Inorg. Chim. Acta 355 (2003) 292.

[7] G.L. Rothermel Jr., L. Miao, A.L. Hill, S.C. Jackels, Inorg. Chem. 31 (1992) 4854.

[8] (a) I.M. Atkinson, A.R. Carroll, R.J.A. Janssen, L.F. Lindoy, O.A. Matthews, G.V. Meehan, J. Chem. Soc., Perkin Trans. 1 (1997) 295;
(b) S.J. Brudenell, L. Spiccia, E.R.T. Tiekink, Inorg. Chem. 35 (1996) 1974.

[9] G.M. Sheldrick, SADABS, Program for Empirical Absorption Correction of Area Detector Data, University of Göttingen, Germany, 1996.

[10] SHELXTL version, An Integrated System for Solving and Refining Crystal Structures from Diffraction Data (Revision 5.1), Bruker AXS LTD.

[11] L.J. Farrugia, J. Appl. Cryst. 30 (1997) 565.

[12] (a) M. Ciurtin, Y.-B. Dong, M.D. Smith, T. Barclay, H.-C. zur Loye, Inorg. Chem. 40 (2001) 2825;
(b) J.M. Grevy, F. Tellez, S. Bernes, H. Noth, R. Contreras, N. Barba-Behrens, Inorg. Chim. Acta 339 (2002) 532;
(c) J. Ratilainen, K. Airola, R. Frohlich, M. Nieger, K. Rissanen, Polyhedron 18 (1999) 2265.

[13] J.A.W. Addison, T.N. Rao, J. Reedijk, J. van Rinj, G.C. Verschoor, J. Chem. Soc., Dalton Trans. (1984) 1349.

[14] (a) H. Matsushima, H. Hamada, K. Watanabe, M. Koikawa, T. Tokii, J. Chem. Soc., Dalton Trans. (1999) 971;
(b) L.R. Falvello, M. Tomas, Chem. Commun. (1999) 273;
(c) S.L. Jain, P. Bhattacharyya, H.L. Milton, A.M.Z. Slawin, J.A. Crayston, J.D. Woollins, J. Chem. Soc., Dalton Trans. (2004) 862.

[15] (a) G.J. Kleywegt, W.G.R. Wiesmeijer, G.J. Van Driel, W.L. Driessen, J. Reedijk, J.H. Noordik, J. Chem. Soc., Dalton Trans. (1985) 2177;
(b) S. Loukiala, J. Ratilainen, K. Airola, J. Valkonen, K. Rissanen, Acta Chem. Scand. 52 (1998) 593.

[16] K.R. Adam, S.P.H. Arshad, D.S. Baldwin, P.A. Duckworth, A.J. Leong, L.F. Lindoy, B.J. McCool, M. McPartlin, B.A. Tailor, P.A. Tasker, Inorg. Chem. 33 (1994) 1194.

[17] (a) N.S. Gill, R.H. Nuttall, D.E. Scaife, D.W.J. Sharp, Inorg. Nucl. Chem. 18 (1961) 79;
(b) S. Aime, M. Botta, U. Casellato, S. Tamburini, P.A. Vigato, Inorg. Chem. 34 (1995) 5825.

[18] W.T. Carnall, S. Siegel, J.R. Ferraro, B. Tani, E. Gebert, Inorg. Chem. 12 (1973) 560.

[19] B.P. Lever, Inorganic Electronic Spectroscopy, 2nd ed., Elsevier, Amsterdam, 1984.

[20] (a) W.J. Eilbeck, F. Holmes, A.E. Underhill, J. Chem. Soc. (A) 5 (1967) 757;
(b) J. Reedijk, T.M. Mulder, J.A. Smit, Inorg. Chim. Acta 13 (1975) 219.
[21] (a) Z. Xu, L.K. Thompson, C.J. Matthews, D.O. Miller, A.E. Goeta, C. Wilson, J.A.K. Howard, M. Ohba, H. Okawa, J. Chem. Soc., Dalton Trans. (2000) 69;
(b) I. Beloso, J. Borrás, J. Castro, J.A. García-Vázquez, P. Pérez-Lourido, J. Romero, A. Sousa, Eur. J. Inorg. Chem. (2004) 635 (and references therein).
[22] B.N. Figgis, Introduction to Ligand Fields, Interscience, New York, 1967.
[23] W.J. Geary, Coord. Chem. Rev. 7 (1971) 81.

Available online at www.sciencedirect.com
SCIENCE DIRECT®
Polyhedron 25 (2006) 793–800
POLYHEDRON
www.elsevier.com/locate/poly

Monoinsertion of but-2-ynedioic acid dimethyl ester into palladium–carbon σ bonds of cyclopalladated compounds derived from biphenyl-2-ylamine: X-ray molecular structure of biphenyl-2-yl-(2,4,6-trimethoxy-benzylidene)-amine

Joan Albert [a,*], Jaume Granell [a], Ana Luque [a], Mercè Font-Bardia [b], Xavier Solans [b]

[a] Departament de Química Inorgànica, Universitat de Barcelona, Martí i Franquès, 1-11, E-08028 Barcelona, Spain
[b] Departament de Cristal.lografia, Mineralogia i Dipòsits Minerals, Universitat de Barcelona. Martí i Franquès s/n, E-08028 Barcelona, Spain

Received 6 July 2005; accepted 2 August 2005
Available online 8 September 2005

Abstract

Dinuclear cyclopalladated compounds (μ-Br)$_2$[κ^2-***N2′***,***C1***-1-Pd-2-{(2′-RCH=NC$_6$H$_4$)C$_6$H$_4$}]$_2$ [**1a** (R = 2,4,6-trimethoxyphenyl), **1b** (R = 2,6-dichlorophenyl) and **1c** (R = 2,6-difluorophenyl)] and (μ-Br)$_2$[κ^2-***N2′***,***C1***-1-Pd-2-{(2′-NH$_2$C$_6$H$_4$)C$_6$H$_4$}]$_2$ (**1d**) reacted with but-2-ynedioic acid dimethyl ester (molar ratio 1–2) to afford the dinuclear cyclopalladated compounds (μ-Br)$_2$[κ^2-***N2′***,***C1***-1-Pd-2-{(2′-RCH=NC$_6$H$_4$)C$_6$H$_4$}-*cis*-1,2-(CO$_2$Me)$_2$–C=C]$_2$ [**2a** (R = 2,4,6-trimethoxyphenyl), **2b** (R = 2,6-dichlorophenyl) and **2c** (R = 2,6-difluorophenyl)] and (μ-Br)$_2$[κ^2-***N2′***,***C1***-1-Pd-2-{(2′-NH$_2$C$_6$H$_4$)C$_6$H$_4$}-*cis*-1,2-(CO$_2$Me)$_2$–C=C]$_2$ (**2d**), which derived from the monoinsertion of the alkyne into the palladium–carbon σ bonds of the cyclopalladated dimers **1**. Compounds **2a** and **2b** reacted with PPh$_3$ (molar ratio 1–4) to give a mixture of the mononuclear compound *trans*-***N***,***P***-{[κ^2-***N2′***,***C1***-1-Pd-2-{(*Z*-2′-RCH=NC$_6$H$_4$)C$_6$H$_4$}-*cis*-1,2-(CO$_2$Me)$_2$–C=C]Br(PPh$_3$)} and *trans*-***P***,***P***-{[κ^1-***C1***-1-Pd-2-{(*E*-2′-RCH=NC$_6$H$_4$)C$_6$H$_4$}-*cis*-1,2-(CO$_2$Me)$_2$–C=C]Br(PPh$_3$)$_2$} in a molar ratio of 1–2 and ca. 1–12, respectively. Compound **2c** reacted with PPh$_3$ in a molar ratio 1–4 giving *trans*-***P***,***P***-{[κ^1-***C1***-1-Pd-2-{(*E*-2′-RCH=NC$_6$H$_4$)C$_6$H$_4$}-*cis*-1,2-(CO$_2$Me)$_2$–C=C]Br(PPh$_3$)$_2$} (R = 2,6-difluorophenyl)-(compound **4c**) and compound **2d** reacted with PPh$_3$ in a molar ratio of 1–2, affording the mononuclear cyclopalladated compound *trans*-***N***,***P***-{[*cis*-κ^2-***N2′***,***C1***-1-Pd-2-{(2′-NH$_2$C$_6$H$_4$)C$_6$H$_4$}-1,2-(CO$_2$Me)$_2$–C=C]Br(PPh$_3$)} (compound **3d**). Notably, the ^{31}P{^{1}H} NMR of compounds **4** produced an AB spin system, showing that compounds **4** were chiral. In addition, we report the X-ray molecular structure of the *E* isomer of the free Schiff base **a** [biphenyl-2-yl-(2,4,6-trimethoxy-benzylidene)-amine].
© 2005 Elsevier Ltd. All rights reserved.

Keywords: Palladacycle; Schiff base; Insertion; Alkyne

1. Introduction

Cyclopalladated compounds containing a biphenyl cyclopalladated unit have been used as starting materials in organic and organometallic synthesis [1–8] and as precursors of catalytic species in C–C and C–N coupling reactions [9,10]. Furthermore, an intramolecular C–H bond activation of a biphenyl group in a palladium(II) centre has been proposed in catalytic cycles that transform a C–H bond into a C–C bond [11,12].

In earlier papers [13–15], we have described the synthesis of the dinuclear cyclopalladated compounds **1a**–**d** containing a biphenyl cyclopalladated unit (see Scheme 1 for their structural formula). The *exo*-cyclopalladated imine **1a** consisted, in relation to the *E* or *Z* configuration adopted by their azomethine functional groups, almost exclusively of the (*E*,*E*) isomer, while compounds **1b**

* Corresponding author. Tel.: +34 93 4039131; fax: +34 93 4907725.
E-mail address: joan.albert@qi.ub.es (J. Albert).

0277-5387/$ - see front matter © 2005 Elsevier Ltd. All rights reserved.
doi:10.1016/j.poly.2005.08.002

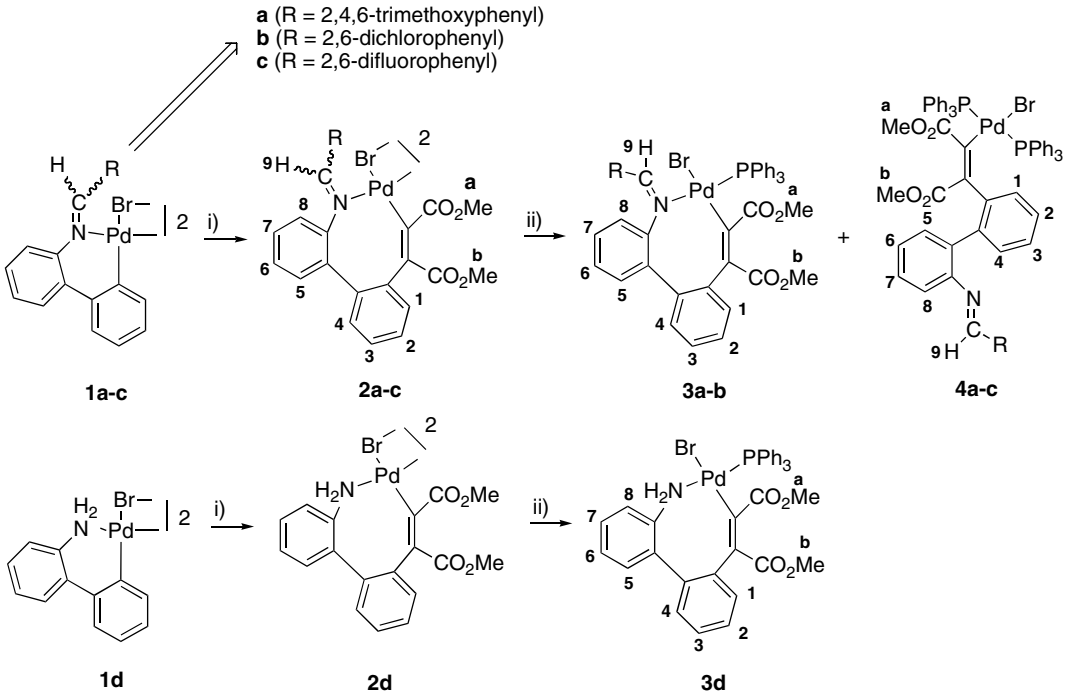

Scheme 1. (i) but-2-ynedioic acid dimethyl ester, chloroform (**a**: reflux, 24 h; **b**: 0 °C, 72 h; **c**: 0 °C, 48 h; **d**: 0 °C, 24 h), molar ratio **1**/but-2-ynedioic acid dimethyl ester = 1/2; (ii) PPh_3 (**a**: THF, 0 °C, 24 h, molar ratio **2a**/PPh_3 = 1/4; **b** (or **c**): THF, 0 °C, 6 h, molar ratio **2b** (or **2c**)/PPh_3 = 1/4; **d**: $CHCl_3$, −10 °C, 4 h, molar ratio **2d**/PPh_3 = 1/2).

and **1c** were a mixture of the (*E*,*E*), (*E*,*Z*) and (*Z*,*Z*) isomers. ^{1}H NMR spectra of compounds **1b** and **1c** suggested that the ratio of their azomethine functional groups in *E* and *Z* form was about one to one. Note that the metal atom is not accounted for the *E* or *Z* assignment of the configuration of the azomethine functional group in *exo*-cyclometallated imines and that the *endo*- and *exo*-descriptors are used to differentiate between the regioisomers of cyclometallated imines; the *exo*-descriptor indicates that the double bond of the azomethine functional group is not included in the metallacycle [13,16]. These conventions have been also applied throughout the present paper. Fig. 1 shows the structure of the (*E*,*E*), (*E*,*Z*) and (*Z*,*Z*) isomers of compound **1b**.

It is well known that the reaction between internal alkynes and cyclometallated compounds may produce mono-, di- or tri-inserted compounds, which depending on their electronic or steric properties may evolve to the formation of organic compounds. Internal alkynes with electron-withdrawing substituents favour the monoinsertion reaction, while internal alkynes with electron-donating substituents favour the diinsertion reaction. In some cases the chemoselectivity of the reaction cannot be controlled and the product of double insertion is formed, regardless the stoichiometry between the cyclometallated compound and the alkyne [17–23].

In this context, we were interested in expanding a six-membered palladacycle to an eight-membered palladacycle by monoinsertion of an alkyne into its palladium–carbon σ bond. Few examples of this transformation have been described in the literature for six-membered palladacyles, starting from cyclopalladated

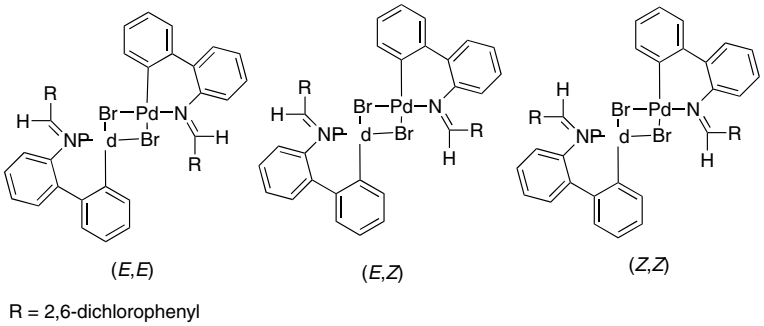

Fig. 1. Structure of the (*E*,*E*), (*E*,*Z*) and (*Z*,*Z*) isomers of compound **1b**.

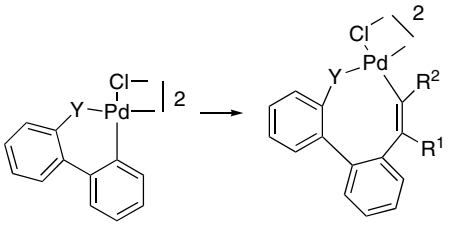

Y	R^1	R^2	Reference
N=CHFc	Ph	Ph	1
SMe	Me	^{t}Bu	3
SMe	Ph	Ph	5
NMe_2	CF_3	CF_3	7
NMe_2	CO_2Me	CO_2Me	7

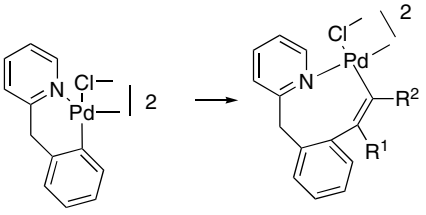

R^1	R^2	Reference
Me	^{t}Bu	3
Ph	Ph	23
CO_2Me	CO_2Me	23

Fig. 2. Examples of expansion of a six-membered palladacycle to an eight-membered palladacycle by monoinsertion of an alkyne into the σ palladium–carbon bond of the precursor six-membered palladacycle.

compounds containing a biphenyl cyclopalladated unit or an *ortho*-palladated 2-benzylpyridine (Fig. 2) [1,3,5,7,23]. Thus, we chose to study the reactivity of compounds **1a**–**d** towards but-2-ynedioic acid dimethyl ester in a molar ratio of 1–2. The results of this study are described here. In addition, we report the X-ray crystal structure of the *E* isomer of the free Schiff base **a** [biphenyl-2-yl-(2,4,6-trimethoxy-benzylidene)-amine].

2. Results and discussion

Scheme 1 shows the new compounds described in this paper and the numbering of their protons.

In a first attempt to prepare the monoinserted compounds **2**, we treated compounds **1** with but-2-ynedioic acid dimethyl ester in a molar ratio 1–2 in refluxing chloroform for 24 h. These reaction conditions afforded only positive results for the reaction between compound **1a** and but-2-ynedioic acid dimethyl ester, allowing the isolation of the dinuclear cyclopalladated compound **2a** in high yield (70–90%). In spite of this result, this reaction using as starting materials compounds **1b**–**d** was complicated by the formation of palladium(0). Thus, in order to optimize the reaction between compounds **1b**–**d** and but-2-ynedioic acid dimethyl ester in chloroform in a molar ratio of 1–2, this reaction was studied at different temperatures and reaction times. The best results were obtained at 0 °C and reaction times of three days, two days and one day for the reactions with **1b**, **1c** and **1d**, respectively. In the latter reaction conditions the formation of palladium(0) was not observed, and from the red solutions that formed, after concentration of the solvent and elution of the crude of the reactions through a flash column chromatography, the monoinserted compounds **2c**–**d** were isolated in high yield (70–90%).

Compounds **2** were stable yellow (**2a**) or orange (**2c**–**d**) solids. Their IR spectra presented a strong band at 1710–1720 cm^{-1}, corresponding to the C=O stretching of the ester groups of the inserted alkynes. Furthermore, the IR spectra of the azomethine compounds **2a**–**c** presented a band of medium intensity in the interval 1621–1609 cm^{-1}, which was assigned to the C=N stretching of their azomethine functional groups, and the IR spectrum of the amino compound **2d** showed two bands of low intensity at 3286 and 3218 cm^{-1}, which were assigned to the N–H stretchings of its amino groups. The FAB^+ spectra of compounds **2** produced intense signals corresponding to $M + H^+ - MeOH$ and $M + H^+ - HBr$, which were consistent with a dinuclear bromo-bridged structure [24].

$CDCl_3$ solutions of compounds **2** were stable at room temperature. Thus, we registered their ^1H NMR spectra at 200 MHz. The ^1H NMR spectrum of compound **2a** presented a single set of signals. The proton of its azomethine functionality appeared as a singlet at 8.41 ppm, high field shifted relative to the free imine, which indicated that its azomethine functional groups presented an *E* configuration [13,25]. The aromatic protons of the 2,4,6-trimethoxyphenyl group appeared as a singlet at 6.14 ppm. This result indicated that, in compound **2a**, there was free rotation through the carbon–carbon σ bond between the azomethine carbon and the 2,4,6-trimethoxyphenyl group. The aliphatic protons of the 2,4,6-trimethoxyphenyl group appeared as a singlet at 3.84 ppm with an integral corresponding to nine protons. Note that the 4-methoxy group resonated at the same frequency of the 2,6-dimethoxy groups by accident. In addition, the methyls of the inserted alkyne gave place to two singlets at 3.69 and 3.49 ppm. The precedent data indicated that compound **2a** consisted of only a single geometrical isomer, which we assigned, according to the literature [25], to the *trans*-(*E*,*E*) geometrical isomer.

In contrast, compounds **2b** and **2c** gave place to complex ^{1}H NMR spectra, but three groups of well-separated signals were observed in the intervals 9.04–8.40, 8.07–6.55 and 4.00–3.20 ppm, which were assigned to azomethinic, aromatic and aliphatic protons, respectively. The azomethinic region presented eight singlets and their chemical shift suggested that compounds **2b** and **2c** were a mixture of the (*E*,*E*), (*E*,*Z*) and (*Z*,*Z*) geometrical isomers, some of them consisting of a mixture of *trans* and *cis* geometrical isomers or of a mixture of conformational isomers [13]. In addition, the ^{1}H NMR spectrum of compound **2d** produced broad signals for the aromatic and some of the aliphatic protons, suggesting the presence in solution of a dynamic equilibrium between different isomers of this compound [13,25].

Compounds **2** were treated with PPh_3 in a molar ratio of 1/2 in acetone at room temperature. Usually, this treatment converts cyclopalladated dimers of general formula $(\mu\text{-}X)_2[Pd(C,N)]_2$ into mononuclear cyclopalladated compounds of formula *trans*-***N***,***P***-[Pd(C,N)X(PPh_3)] (X = OAc, Cl or Br) [13–15,25–27]. But this reaction in the latter conditions and using as starting material the imino compounds **2a**–**c** was complicated by the hydrolysis of the azomethine functionality, as indicated by the ^{1}H NMR spectra of the reaction crudes. In addition; in all cases, including the reaction which used as starting material the amino compound **2d**, the initial yellow solution slowly changed to a red solution. This change of color could be related to a reorganization of the eight-membered palladacycle of compound **3d** to a spirocyclic compound, such as that described in reference [23]. Attempts to obtain mononuclear derivatives of general formula *trans*-***N***,***N***-[Pd(C,N)Br(py-d_5)] by reacting solutions of compounds **2** in $CDCl_3$ with py-d_5 at room temperature were not successful.

In view of the precedent results, the imino compounds **2a**–**c** were treated with PPh_3 in a molar ratio of 1/4 in anhydrous tetrahydrofuran at 0 °C and the amino compound **2d** was treated with PPh_3 in a molar ratio of 1/2 in chloroform at −10 °C. In these conditions, stable yellow solutions were formed which after concentration of the solvent and addition of a minimum volume of diethyl ether to the residues yielded stable yellow solids. Analysis of freshly prepared solutions of these solids in C_6D_6 by ^{1}H and ^{31}P{^{1}H} NMR showed that they were a mixture of compounds **3a** and **4a** in a molar ratio of 1/2, a mixture of compounds **3b** and **4b** in a molar ratio of ca. 1/12, compound **4c** and compound **3d**.

Compounds **3d** and **4c** produced satisfactory elemental analyses, FAB$^+$, IR, ^{1}H and ^{31}P{^{1}H} NMR spectra, and the mixtures of compounds **3a** and **4a** and **3b** and **4b** gave rise to satisfactory IR, FAB$^+$, ^{1}H and ^{31}P{^{1}H} NMR spectra. The molar fraction between compound **3a** and **4a** and **3b** and **4b** in these latter mixtures was determined by the ratio between the integrals of the azomethine protons.

In the ^{1}H NMR spectra of the imino compounds **3a** and **3b**, the azomethine protons appeared downfield shifted relative to the free imines, indicating that the azomethine functionality in these compounds presented the *Z* configuration. Furthermore, consistent with their *Z* configuration and the *cis* arrangement between the phosphorus nuclei and the proton of the azomethine functionality, the coupling constant between these two nuclei was ca. 4 Hz. In contrast, the azomethinic proton of compounds **4a**–**c** gave a singlet, whose chemical shift was consistent with an *E* configuration for their azomethine functional group [25]. Furthermore, the protons of the amino group of compound **3d** appeared at 4.60 ppm as a broad signal. This latter result showed that the interconversion between the enantiomeric conformations of the palladacycle of compound **3d** was in the fast exchange region at room temperature [15]. The ^{31}P{^{1}H} NMR spectra of compounds **3** and **4** produced a singlet and a second order spectrum derived from an AB spin system, respectively. It should be noted that according to the different *trans* influence of the atom *trans* to the phosphorus in compounds **3** and **4**, a nitrogen atom for compounds **3** and a phosphorus atom for compounds **4**, the ^{31}P signal of compounds **3** was downfield shifted in relation to the ^{31}P signal of compounds **4** [28]. In addition, the ^{31}P signals of compounds **3** and **4** appeared between 30 and 15 ppm, which is the expected interval for compounds of general formula *trans*-***N***,***P***-[Pd(C,N)X(PPh_3)] and *trans*-***P***,***P***-[PdRX(PPh_3)$_2$] [13–15,25,29].

Notably, the fact that compounds **4** in the ^{31}P{^{1}H} NMR produced a second order spectrum, indicated that these compounds were chiral. In order to study the origin of the chirality in compounds **4**, 2D ^{1}H–^{1}H COSY and ROESY experiments at 500 MHz were undertaken for compound **4c**. These experiments allowed the assignment of all of its protons (see Section 3). The data from the 1D ^{1}H and the 2D ^{1}H–^{1}H ROESY experiments suggested that compound **4c** adopted in solution the conformation shown in Fig. 3. In the 1D experiment, two doublets corresponding to aromatic protons appeared at the unusual chemical shifts of 9.95 and 5.44 ppm.

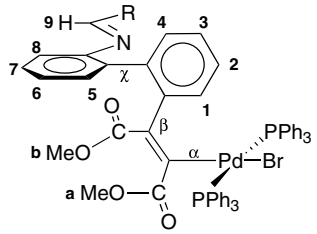

R = 2,6-difluorophenyl

Fig. 3. Proposed conformation in solution for compound **4c**.

The signal at 9.95 was assigned to proton **1**. This assignment was consistent with the presence in the ROESY experiment of negative off-diagonal peaks between proton **1** and the protons of the PPh_3 ligands. These NMR data were consistent with proton **1** residing in a pseudo fifth coordination position above the square planar palladium(II) centre and therefore with a restricted rotation through the σ bonds labeled as α and β in Fig. 3 [30]. In addition a negative off-diagonal peak between **9** and **8** protons was consistent with and *E* configuration for the azomethine functionality and the ^1H–^1H COSY experiment allowed the assignment of the **5**–**8** protons. These assignments showed that the second aromatic proton with the unusual chemical shift of 5.44 ppm was proton **5**. The chemical shift of proton **5** should be a consequence of its proximity to the carbonyl group of the inserted alkyne, and this suggested that rotation through the σ bond labeled as χ in Fig. 3 was restricted and that the biphenyl group adopted an orthogonal conformation. Note that in this particular conformation the molecule is asymmetric and the phosphorus atoms are not equivalent. Therefore, they could produce a spectrum derived from an AB spin system. In support of this, we should note that 2,2′-disubstitued biphenyls with bulky substituents are usually chiral [31].

During the progress of this work we obtained monocrystals of the *E* isomer of the free imine **a** [biphenyl-2-yl-(2,4,6-trimethoxy-benzylidene)-amine]. Thus, its X-ray molecular structure is reported here. It should be noted that the benzaldimine **a** in solution consisted of only one isomer [13]; which was assumed to be, according to the literature [32], the *E* isomer. Fig. 4 shows the X-ray molecular structure of **a** and Table 1 gives selected bond distances angles for **a**.

Compound **a** crystallized in the $P\bar{1}$ triclinic space group with $Z = 2$. The structure consisted of discrete molecules separated by van der Waals distances and presented interactions between C–H bonds and aromatic π systems which produced dimers and chains in the crystal [33]. As expected, the imines adopted the *E* configuration around the azomethine functional group [dihedral angle C14–C13–N–C12 = 177.41(18)°], and differences in distances and angles with the molecules of the *E* isomer of phenyl–benzilidene–amine of formula Ph–CH=N–Ph, were a consequence of the electronic and steric requirements introduced by the substituents on going from the phenyl–benzilidene–amine to the Schiff base **a** [34]. The most noticeable feature of the σ coordination through the N and the deprotonated C1 atoms of the Schiff base **a** to the $PdBr(PPh_3)$ fragment turned out to be an increase of the C14–C13–N angle from 126.1(2)° to 130.5(6)°, due to the steric repulsion between the 2,4,6-trimethoxyphenyl group bonded to the C13 atom and the $PdBr(PPh_3)$ fragment [13]. Note that the driving force for the $E \rightarrow Z$ isomerization of *exo*-cyclic cyclopalladated Schiff bases has been related to the steric repulsion between the PdX fragment (X represents the co-ligands of the palladium atom) and the aryl group bonded to the carbon of the azomethine functionality [13,25].

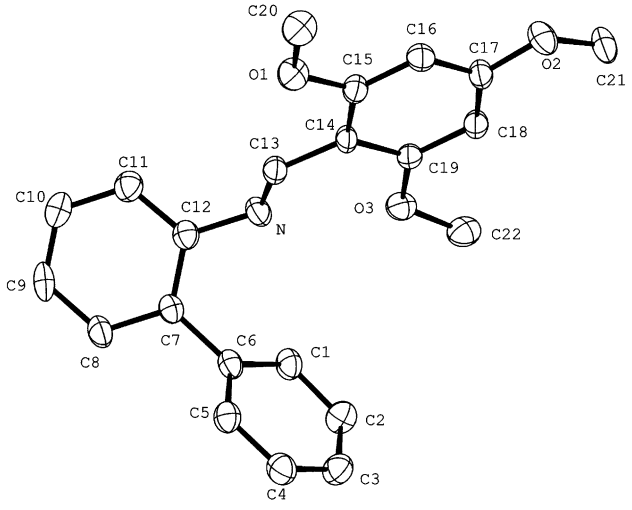

Fig. 4. X-ray molecular structure of **a**.

Table 1
Selected bond distances (Å), bond angles (°) and dihedral angles (°) for **a**

C22–O3	1.425(2)
O3–C19	1.359(2)
C19–C14	1.418(2)
C14–C13	1.458(2)
C13–N	1.251(2)
N–C12	1.413(2)
C12–C7	1.393(3)
C7–C6	1.506(2)
C6–C1	1.403(2)
C22–O3–C19	119.33(16)
O3–C19–C14	115.50(13)
C19–C14–C13	124.4(2)
C14–C13–N	126.1(2)
C13–N–C12	119.20(19)
N–C12–C7	119.26(14)
C12–C7–C6	121.74(19)
C7–C6–C1	120.5(2)
C22–O3–C19–C14	174.11(19)
O3–C19–C14–C13	0.9(3)
C19–C14–C13–N	5.7(3)
C14–C13–N–C12	177.41(18)
C13–N–C12–C7	127.0(2)
N–C12–C7–C6	−3.2(2)
C12–C7–C6–C1	58.2(2)

3. Experimental

3.1. General remarks

Compounds **1a**–**d** were prepared as previously reported [13–15]. Elemental analyses of C, H and N were

performed with Eager 1108 or Carlo Erba 1106 microanalyzers. Infrared spectra were recorded on a Nicolet 520 FT-IR spectrophotometer using pressed discs of diluted samples of the compounds in KBr. ^{1}H NMR at 200 and 500 MHz were recorded on Varian Gemini 200 and VRX-500 instruments, respectively. ^{31}P{^{1}H} NMR at 101.2 MHz were recorded on a Varian Bruker 250 instrument. Chemical shifts are reported in δ values (ppm) relative to $SiMe_4$ for ^{1}H and relative to $P(OMe)_3$ ($\delta = 140.18$ ppm) for ^{31}P. FAB$^+$ mass spectra were obtained with a VG-Quatro Fisions instrument, using 3-(nitro-phenyl)-methanol as matrix. All chemicals were of commercial grade and used as received. Solvents were distilled before use as follows: chloroform over CaO; methanol over $CaCl_2$; and tetrahydrofuran and diethyl ether over sodium and benzophenone.

3.2. Preparation of compounds 2

Compound ***2a***. A suspension formed by 300 mg of **1a** (0.28 mmol) and 80 mg of but-2-ynedioic acid dimethyl ester (0.56 mmol) was treated at reflux of chloroform (20 mL) for 24 h. The red solution formed was concentrated under vacuum and the residue was eluted through a SiO_2 flash column chromatography with a solution of methanol in chloroform in a 2-to-100 volume ratio. The first coloured band was concentrated under vacuum. Addition of diethyl ether (5 cm^3) to the residue produced the precipitation of **2a** as a yellow powder, which was filtered and dried under vacuum. Compound **2b**: A suspension formed by 300 mg of **1b** (0.29 mmol) and 83 mg of but-2-ynedioic acid dimethyl ester (0.58 mmol) was treated in chloroform (20 mL) at 0 °C for 72 h. The red solution formed was concentrated under vacuum at 0 °C and the residue was eluted through a SiO_2 flash column chromatography with a solution of methanol in chloroform in a 2-to-100 volume ratio. The intense coloured bands were concentrated under vacuum. Addition of diethyl ether (5 cm^3) to the residue produced the precipitation of **2b** as an orange powder, which was filtered and dried under vacuum. Compound **2c**: A suspension formed by 300 mg of **1c** (0.31 mmol) and 89 mg of but-2-ynedioic acid dimethyl ester (0.63 mmol) was treated in chloroform (20 mL) at 0 °C for 48 h. The red solution formed was concentrated under vacuum at 0 °C and the residue was eluted through a SiO_2 flash column chromatography with a solution of methanol in chloroform in a 2-to-100 volume ratio. The intense coloured bands were concentrated under vacuum. Addition of diethyl ether (5 cm^3) to the residue produced the precipitation of **2c** as an orange powder, which was filtered and dried under vacuum. Compound **2d**: A suspension formed by 300 mg of **1d** (0.42 mmol) and 117 mg of but-2-ynedioic acid dimethyl ester (0.83 mmol) was treated in chloroform (20 mL) at 0 °C for 24 h. The red solution formed was concentrated under vacuum at 0 °C and the residue was eluted through a SiO_2 flash column chromatography with a solution of methanol in chloroform in a 4-to-100 volume ratio. The intense coloured bands were concentrated under vacuum. Addition of diethyl ether (5 cm^3) to the residue produced the precipitation of **2d** as an orange powder, which was filtered and dried under vacuum. The yield of isolation of compounds **2** ranged between 70% and 90%. Compound **2a** consisted almost exclusively of the (*E*,*E*) isomer and **2b** and **2c** consisted of a mixture of the (*E*,*E*), (*E*,*Z*) and (*Z*,*Z*) isomers. *Characterization data*: **2a**: *Anal*. Calc. for $C_{56}H_{52}Br_2N_2O_{14}Pd_2$: C, 49.8; H, 3.9; N, 2.1. Found C, 49.2; H, 3.9; N, 2.0%. FAB$^+$ (most intense peaks): 1269 ($M + H^+ - HBr$); 644 ($M/2 + H^+ - MeOH$); 594 ($M/2 + H^+ - HBr$). IR (cm^{-1}): 1712 (C=O st); 1621 (C=N st); 1206 (C–O st). ^{1}H NMR (200 MHz, $CDCl_3$): 8.41 s (1H, H^9); 7.70–7.05 (8H, H^1–H^8); 6.14 s (2H, aromatic protons of 2,4,6-trimethoxyphenyl); 3,84 s (9H, Me groups of 2,4,6-trimethoxyphenyl); 3.69 s (3H, Me, inserted alkyne); 3.49 s (3H, Me, inserted alkyne). Compound **2b**: *Anal*. Calc. for $C_{50}H_{36}Br_2Cl_4N_2O_8Pd_2$: C, 45.9; H, 2.8; N, 2.1. Found C, 45.4; H, 2.8; N, 2.0%. FAB$^+$ (most intense peaks): 1227 ($M + H^+ - HBr$); 622 ($M/2 + H^+ - MeOH$); 574 ($M/2 + H^+ - HBr$). IR (cm^{-1}): 1711 (C=O st); 1609 (C=N st); 1208 (C–O st). ^{1}H NMR (200 MHz, $CDCl_3$): 9.04–8.40, 8 singlets, H^9; 8.07–6.55 aromatic protons; 3.90–3.35, 10 singlets, Me, inserted alkyne. Compound **2c**: *Anal*. Calc. for $C_{50}H_{36}Br_2F_4N_2O_8Pd_2$: C, 48.4; H, 2.9; N, 2.3. Found C, 47.3; H, 3.0; N, 2.2%. FAB$^+$ (most intense peaks): 1211 ($M + H^+ - MeOH$); 1161 ($M + H^+ - HBr$); 540 ($M/2 + H^+ - HBr$). IR (cm^{-1}): 1711 (C=O st); 1609 (C=N st); 1208 (C–O st). ^{1}H NMR (200 MHz, $CDCl_3$): 9.00–8.40, 8 singlets, H^9; 7.95–6.55 aromatic protons; 4.00–3.20, singlets, Me inserted alkyne. Compound **2d**: *Anal*. Calc. for $C_{36}H_{32}Br_2N_2O_8Pd_2$: C, 43.5; H, 3.2; N, 2.9. Found C, 42.5; H, 3.4; N, 2.8%. FAB$^+$ (most intense peaks): 963 ($M + H^+ - MeOH$); 913 ($M + H^+ - HBr$). IR (cm^{-1}): 3286 and 3218 (N–H st), 1715 (C=O st); 1251 and 1216 (C–O st). ^{1}H NMR (200 MHz, $CDCl_3$): 7.80–6.80, broad signals, aromatic protons; 4.00–3.20, NH_2 and Me inserted alkyne.

3.3. Preparation of the mixture of compounds 3a and 4a

A suspension formed by 100 mg (0.074 mmol) of compound **2a**, 78 mg (0.296 mmol) of PPh_3 and anhydrous THF (30 mL) was stirred at 0 °C for 24 h. The yellow solution formed was concentrated at 0 °C under vacuum, the residue was treated with diethyl ether (5 mL) and the solid was filtered and dried under vacuum. A sample of ca. 100 mg was obtained which was a mixture of compounds **3a** (*Z* isomer) and **4a** (*E* isomer) in a ca. 1–2 molar ratio. *Characterization data*: ^{1}H NMR (500 MHz, C_6D_6) (selected data): 10.69 d $^4J_{HP} = 4.1$ Hz (H^9, **3a**); 10.05 d $^3J_{HH} = 7.5$ Hz (H^1,

4a); 9.06 s (H^9, **4a**), 5.97 s (aromatic protons of the 2,4,6-trimethoxy group of **4a**); 5.66 s (aromatic protons of the 2,4,6-trimethoxy group of **3a**); 5.54 d $^3J_{HH} = 8.1$ Hz (H^5, **4a**). $^{31}P\{^1H\}$ NMR (101.2 MHz, C_6D_6): 22.02 s (**3a**); 15.59 AB spin system (**4a**). FAB^+ (most intense peaks): 1199 ($M_{4a} + H^+$); 938 ($M_{3a} + H^+$ or $M_{4a} + H^+ - PPh_3$); 856 ($M_{3a} + H^+ - HBr$ or $M_{4a} + H^+ - HBr - PPh_3$). IR ($cm^{-1}$): 1721, 1700 (C=O st) (**3a** and **4a**).

3.4. Preparation of the mixture of compounds *3b* and *4b*

A suspension formed by 100 mg (0.076 mmol) of compound **2b**, 80 mg (0.306 mmol) of PPh_3 and anhydrous THF (30 mL) was stirred at 0 °C for 6 h. The yellow solution formed was concentrated at 0 °C under vacuum, the residue was treated with diethyl ether (5 mL) and the solid was filtered and dried under vacuum. A sample of ca. 100 mg was obtained which was a mixture of compounds **3b** (*Z* isomer) and **4b** (*E* isomer) in a ca. 1–12 molar ratio. *Characterization data*: ^1H NMR (500 MHz, C_6D_6) (selected data): 9.96 d $^3J_{HH} = 7.5$ Hz (H^1, **4b**); 9.92 d $^4J_{PH} = 4.1$ Hz (H^9, **3b**); 8.76 s (H^9, **4b**); 5.54 d $^3J_{HH} = 8.1$ Hz (H^6, **4b**); 3.30 s and 3.07 s (Me inserted alkyne **3b)**, 2.99 s and 2.78 s (Me inserted alkyne **4b)**. $^{31}P\{^1H\}$ NMR (101.2 MHz, C_6D_6): 28.43 s (**3b**); 21.44 AB spin system (**4b**). FAB^+ (most intense peaks): 916 ($M_{3b} + H^+$ or $M_{4b} + H^+ - PPh_3$); 836 ($M_{3b} + H^+ - HBr$ or $M_{4b} + H^+ - HBr - PPh_3$). IR ($cm^{-1}$): 1717, 1703 (C=O st) (**3b** and **4b**).

3.5. Preparation of compound *4c*

A suspension formed by 100 mg (0.081 mmol) of compound **2c** and 87 mg (0.322 mmol) of PPh_3 and anhydrous THF (30 mL) was stirred at 0 °C for 6 h. The yellow solution formed was concentrated at 0 °C under vacuum and the residue was treated with diethyl ether (5 mL). This treatment produced the precipitation of compound **4c** (*E* isomer), which was filtered and dried under vacuum. Yield: 65%. *Characterization data*: *Anal.* Calc. for $C_{61}H_{48}BrF_2NO_4P_2Pd$: C, 64.0; H, 4.2; N, 1.2. Found C, 62.6; H, 4.1; N, 1.2%. FAB^+ (most intense peaks): 884 ($M + H^+ - PPh_3$); 802 ($M + H^+ - HBr - PPh_3$). IR (cm^{-1}): 1718 and 1681 (C=O st); 1621 (C=N st); 1238 (C–O st), 1095 (*q* X-sensitive mode of the coordinated PPh_3). ^1H NMR (500 MHz, C_6D_6): 9.95 d $^3J_{HH} = 8.1$ Hz (1H, H^1); 8.76 s (1H, H^9); 7.85–7.73 m (12H, *ortho* protons of PPh_3), 7.56 d $^3J_{HH} = 8.1$ Hz (1H, H^4), 7.28 t $^3J_{HH} = 8.1$ Hz (1H, H^2); 7.21 t $^3J_{HH} = 8.1$ Hz (1H, H^3); 6.98 m (19 h, H^7 and *para* and *meta* protons of PPh_3); 6.92 d $^3J_{HH} = 8.1$ Hz (1H, H^8); 6.60 t $^3J_{HH} = 8.1$ Hz (1H, H^6); 6.38 m (1H, proton in position 4 of 2,6-difluorophenyl); 6.25 t $^3J_{HH} = {}^3J_{FH} = 8.1$ Hz (2H, protons in position 3 and 5 of 2,6-difluorophenyl), 5.44 d $^3J_{HH} = 8.1$ Hz (1H, H^5); 2.98 s (3H, Me^a inserted alkyne); 2.77 s (3H, Me^b inserted alkyne). $^{31}P\{^1H\}$ NMR (101.2 MHz, C_6D_6): 21.44 AB spin system.

3.6. Preparation of compound *3d*

A suspension formed by 100 mg (0.101 mmol) of compound **2d** and 53 mg (0.202 mmol) of PPh_3 and anhydrous THF (30 mL) was stirred at −10 °C for 4 h. The yellow solution formed was concentrated at −10 °C under vacuum and the residue was eluted through a SiO_2 column chromatography with a solution of methanol in chloroform in a 2-to-100 volume ratio. The second yellow band was collected and concentrated under vacuum. Addition of diethyl ether (5 cm^3) to the residue produced the precipitation of **2d** as pale yellow powder, which was filtered and dried in vacuum. Yield: 63%. *Characterization data*: *Anal.* Calc. for $C_{36}H_{31}BrNO_4PPd$: C, 57.0; H, 4.1; N, 1.8. Found C, 57.1; H, 4.3; N, 1.9%. FAB^+ (most intense peaks): 728 ($M + H^+ - MeOH$); 678 ($M + H^+ - HBr$); 416 ($M + H^+ - HBr - PPh_3$). IR (cm^{-1}): 3297 and 3184

Table 2
Crystal data and structure refinement for biphenyl-2-yl-(2,4,6-trimethoxy-benzylidene)-amine

Empirical formula	$C_{22}H_{21}NO_3$
Formula weight	347.40
T (K)	293(2)
λ (Å)	0.71069
Crystal system	triclinic
Space group	$P\bar{1}$
Unit cell dimensions	
a (Å)	9.247(3)
b (Å)	9.843(2)
c (Å)	10.856(3)
α (°)	95.13(2)
β (°)	102.54(2)
γ (°)	108.43(2)
V (Å^3)	901.6(4)
Z	2
D_{calc} (Mg/m^3)	1.280
Absorption coefficient (mm^{-1})	0.085
$F(000)$	368
Crystal size (mm)	$0.1 \times 0.1 \times 0.2$
θ Range for data collection (°)	2.21–29.95
Index ranges	$-12 \leqslant h \leqslant 12$, $-13 \leqslant k \leqslant 13$, $0 \leqslant l \leqslant 15$
Reflections collected/unique (R_{int})	2703/2703 (0.0121)
Completeness to $\theta = 29.95°$ (%)	51.6
Refinement method	full-matrix least-squares on F^2
Data/restraints/parameters	2703/0/238
Goodness-of-fit on F^2	1.009
Final R indices [$I > 2\sigma(I)$]	$R_1 = 0.0363$, $wR_2 = 0.0494$
R indices (all data)	$R_1 = 0.0777$, $wR_2 = 0.0534$
Largest difference in peak and hole (e Å^{-3})	0.113 and −0.140

(N–H st), 1704 (C=O st); 1206 (C–O st), 1097 (*q* X-sensitive mode of the coordinated PPh_3). ^1H NMR (200 MHz, $CDCl_3$): 7.63–7.20 (15 h, H^{4-8} and protons of PPh_3), 7.14 t $^3J_{HH} = 7.7$ Hz (1H, H^3); 6.98 t $^3J_{HH} = 7.7$ Hz (1H, H^2); 6.22 d $^3J_{HH} = 7.7$ Hz (1H, H^1); 4.60 broad signal (2H, NH_2), 3.37 s (3H, Me inserted alkyne); 3.25 s (3H, Me inserted alkyne). $^{31}P\{^1H\}$ NMR (101.2 MHz, C_6D_6): 29.82 s.

3.7. Crystallographic studies

Crystals for the X-ray molecular structure determination of biphenyl-2-yl-(2,4,6-trimethoxy-benzylidene)-amine were obtained by slow evaporation of a solution of this imine in ethanol/chloroform. A prismatic crystal was selected and mounted on an Enraf-Nonius CAD4 four-circle diffractometer. The structure was solved by direct methods using the SHELXS computer program [35] and refined by the full-matrix least-squares method, with the SHELXL computer program [36]. A summary of crystallographic data and some details of the refinement are given in Table 2.

4. Supplementary material

Crystallographic data for the structural analyses of biphenyl-2-yl-(2,4,6-trimethoxy-benzylidene)-amine has been deposited at the Cambridge Crystallographic Data Centre, CCDC No. 274705. Copies of this information can be obtained from The Director, CCDC, 12 Union Road, Cambridge CB2 1EZ, UK (fax: +44 1233 336 033; e-mail: deposit@ccdc.ac.uk or www: http://www.ccdc.cam.ac.uk).

Acknowledgements

We are grateful to the Ministerio de Ciencia y Tecnología and to the Generalitat de Catalunya for financial support (Grants BQU2003-0096 and 2001SGR 00054).

References

[1] M. Benito, C. López, X. Morvan, X. Solans, M. Font-Bardia, J. Chem. Soc., Dalton Trans. (2000) 4470.
[2] M.S. Driver, J.F. Hartwig, J. Am. Chem. Soc. 117 (1995) 4708.
[3] J. Spencer, M. Pfeffer, N. Kyritsakas, J. Fischer, Organometallics 14 (1995) 2214.
[4] A. Macchioni, P.S. Pregosin, P.F. Engel, S. Mecking, M. Pfeffer, J.-C. Daran, J. Vaisserman, Organometallics 14 (1995) 1637.
[5] J. Spencer, M. Pfeffer, A. DeCian, J. Fischer, J. Org. Chem. 60 (1995) 1005.
[6] P.E. Engel, M. Pfeffer, J. Fischer, Organometallics 13 (1994) 4751.
[7] J. Dupont, M. Pfeffer, L. Theurel, M.A. Rotteveel, A. de Cian, J. Fischer, New J. Chem. 15 (1991) 551.
[8] J. Dupont, M. Pfeffer, M.C. Rottevell, A. de Cian, J. Fischer, Organometallics 8 (1989) 1116.
[9] A. Schnyder, A.F. Indolese, M. Studer, H.-U. Blaser, Angew. Chem. Int. Ed. 41 (2002) 3668.
[10] O. Navarro, R.A. Kelly, S.P. Nolan, J. Am. Chem. Soc. 125 (2003) 16194.
[11] G. Dyker, Angew. Chem. Int. Ed. 38 (1999) 1698, and references therein.
[12] M. Miura, T. Tsuda, T. Satoh, S. Pivsa-Art, M. Nomura, J. Org. Chem. 63 (1998) 5211.
[13] J. Albert, J. Granell, A. Luque, M. Font-Bardia, X. Solans, J. Organomet. Chem. 545–546 (1997) 131.
[14] J. Albert, J. Granell, A. Luque, J. Mínguez, R. Moragas, M. Font-Bardía, X. Solans, J. Organomet. Chem. 522 (1996) 87.
[15] J. Albert, J. Granell, J. Zafrilla, M. Font-Bardia, X. Solans, J. Organomet. Chem. 690 (2005) 422.
[16] J. Albert, J.M. Cadena, J. Granell, X. Solans, M. Font-Bardia, J. Organomet. Chem. 689 (2004) 4889.
[17] J. Spencer, M. Pfeffer, Adv. Metal-Org. Chem. 6 (1998) 103.
[18] M. Pfeffer, Recl. Trav. Chim. Pays-Bas 109 (1990) 567.
[19] W. Ferstl, I.K. Sakodinskaya, N. Beydoun-Sutter, G. Le Borgne, M. Pfeffer, A.D. Ryabov, Organometallics 16 (1997) 411.
[20] J. Vicente, I. Saura-Llamas, M.G. Palin, Peter G. Jones, J. Chem. Soc., Dalton Trans. (1995) 2535.
[21] J. Vicente, I. Saura-Llamas, M.C. Ramírez de Arellano, J. Chem. Soc., Dalton Trans. (1995) 2529.
[22] A.D. Ryabov, R. van Eldik, G. Le Borgne, M. Pfeffer, Organometallics 12 (1993) 1386.
[23] F. Maassarani, M. Pfeffer, G. Le Borgne, J. Chem. Soc., Chem. Commun. (1986) 488.
[24] M.A. Cinellu, G. Minghetti, G. Banditelli, A.L. Bandini, B. Peli, P. Traldi, Inorg. Chim. Acta 161 (1989) 57.
[25] J. Albert, J. Granell, J. Sales, M. Font-Bardia, X. Solans, Organometallics 14 (1995) 1393.
[26] J. Vicente, A. Arcas, D. Bautista, P.G. Jones, Organometallics 16 (16) (1997) 2127.
[27] A. Amoedo, M. Graña, J. Martínez, T. Pereira, M. López-Torres, A. Fernández, J.J. Fernández, J.M. Vila, Eur. J. Inorg. Chem. (2002) 613.
[28] A. Fernández, D. Vázquez García, J.J. Fernández, M. López-Torres, A. Súarez, S. Castro-Juiz, J.M. Ortigueira, J.M. Vila, New J. Chem. 26 (2002) 105.
[29] J. Albert, M. Gómez, J. Granell, J. Sales, Organometallics 9 (1990) 1405.
[30] P.S. Pregosin, F. Wombacher, Magn. Reson. Chem. 29 (1991) S106.
[31] E.L. Eliel, S.H. Wilen, L.N. Mander, in: Stereochemistry of Organic Compounds, Wiley–Interscience, New York, 1994, p. 1143.
[32] J. Bjørgo, D.R. Boyd, C.G. Watson, W.B. Jennings, D.M. Jerina, J. Chem. Soc., Perkin. Trans. II (1974) 1081.
[33] A.L. Spek, Acta Crystallogr., Sect. A 46 (1990) C-34.
[34] H.B. Bürgi, J.D. Dunitz, Helv. Chim. Acta 53 (1970) 1747.
[35] G.M. Sheldrick, SHELXL: A Computer Program for Determination of Crystal Structures, University of Göttingen, Göttingen, Germany, 1997.
[36] G.M. Sheldrick, SHELXS: A Computer Program for Determination of Crystal Structures, University of Göttingen, Göttingen, Germany, 1997.

Available online at www.sciencedirect.com
SCIENCE DIRECT®
Polyhedron 25 (2006) 801–808
POLYHEDRON
www.elsevier.com/locate/poly

New phosphathiamacrocycles containing polypypiridine units

Lluis Escriche [a,*], Jaume Casabó [a], Vicens Muns [a], Raikko Kivekäs [b], Reijo Sillanpää [c]

[a] Departmento de Química, Universitat Autónoma de Barcelona, Campus de Bellaterra, 08193 Cerdanyola del Vallés, Barcelona, Spain
[b] Department of Chemistry, P.O. Box 55, University of Helsinki, FIN 00014, Finland
[c] Department of Chemistry, University of Jyväskylä, 40351 Jyväskylä, Finland

Received 8 June 2005; accepted 3 August 2005
Available online 30 September 2005

Abstract

A new 2,2′-bipyridine-based phosphadithiamacrocycle: 3,3′-5-phenyl-2,8-dithia-5-phospha[9]-2,2′-bipyridinophane (L) has been synthesized by reacting 6,6′-bis(bromomethyl)-2,2′-bipyridine and dilithium 3-phenyl-3-phosphapenta-1,5-dithiolate. The phosphoryl derivative: 3,3′-5-oxo-5-phenyl-2,8-dithia-5-phospha[9]-2,2′-bipyridinophane (Lox) synthesized by direct oxidation of L at open atmosphere. Both compounds have been isolated as white solids containing different amounts of LiBr.

The reaction of acetonitrile solutions of these solids with Fe(II) perchlorate gave the complexes $[FeBr(L)](ClO_4)\cdot 2H_2O$ and $[FeBr(Lox)](ClO_4)\cdot 3H_2O$, which were crystallized as $[FeBr(L)]Br\cdot H_2O$ and $[FeBr(Lox)](ClO_4)\cdot 1\frac{1}{6}MeOH$ salts from nitromethane or methanol, respectively. Both compounds were characterized by X-ray diffraction analysis. In both cases, a distorted octahedral environment is achieved at the Fe(II), with five sites occupied by the macrocycles L and Lox and the sixth by a monodentate bromine ligand. The bond distances found in the complex cation $[FeBr(Lox)]^+$ are compatible with a high-spin configuration. However, the same parameters for $[FeBr(L)]^+$ and their magnetic character are only compatible with a low-spin configuration.
© 2005 Elsevier Ltd. All rights reserved.

Keywords: Phosphathiamacrocycles; Polypyridine; Iron(II) complexes

1. Introduction

The chemistry of macrocyclic ligands containing phosphane groups as donor atoms has been less developed than those of their oxygen or nitrogen equivalents [1]. This fact has been mainly attributed to the air-sensitivity behavior of these compounds and the poor yields obtained in their preparations by high-dilution or template methods, although several high yield synthesis of homoleptic triphosphamacrocycles have recently been reported [2]. However, phosphathiamacrocycles seem to be more accessible as free ligands, and several examples can be found in the literature [3–6]. As a general trend, the interest in the chemistry of asymmetric phosphorus–sulfur donor ligands is mainly focused on the phenomenon of their hemilability and their potential use in catalytic processes [7,8]. Other possibilities are found when these P–S donor systems are integrated in macrocyclic systems, such as the documented ability of their phosphoryl [9,10], and thiophosphoryl [11] derivatives to interact selectively with ionic species that act as chemical sensors for anions.

On the other hand, the introduction of heteroaromatic subunits, such as bipyridine or 1,10-phenantroline into the macrocyclic structures generates different families of compounds which combine the special complexation features of these macrocycles [12] with the well-known photophysical, photochemical or electrochemical properties exhibited by the metal complexes of these heterocycles [13]. In this context, several 1,10-phenantroline containing polyaza and polythiamacrocycles have recently

* Corresponding author. Tel.: +34935811369; fax: +34935812947.
E-mail address: lluis.escriche@uab.es (L. Escriche), jaume.casabo@uab.es (J. Casabó).

0277-5387/$ - see front matter © 2005 Elsevier Ltd. All rights reserved.
doi:10.1016/j.poly.2005.08.006

been reported and their complexing [14], luminescent [15] and sensing [16] properties studied.

Examples may be found of similar studies on polyaza and polyamidamacrocycles containing 2,2′-bipyridene units [14a,17], but less information is available on mono or polybipyridine-containing macrocycles [18], including the softer donor atoms.

As a part of our work in this field, we report herein on the synthesis of the new bipyridine-based phosphadithiamacrocycle: 3,3′-5-phenyl-2,8-dithia-5-phospha[9]-2,2′-bipyridinophane (L) and their phosphoryl derivative: 3,3′-5-oxo-5-phenyl-2,8-dithia-5-phospha[9]-2,2′-bipyridinophane (Lox). The reactivity of these systems in the presence of Fe(II) salts is also investigated. At present, this is the first example of a phosphathmacrocycles containing polypyridine units.

2. Results and discussion

The synthetic pathway leading to the ligand L (Scheme 1) starts with the bromination of the 2-amino-6-picoline, followed by the reaction of the 2-bromo-6-picoline with Raney-Ni to afford the 6,6′-dimethyl-2,2′-bipyridine, which was finally halogenated with NBS to produce the 6,6′-bis(bromomethyl)-2,2′-bipyridine in an overall 10% yield [19,20]. Subsequent cyclisation of equimolar amounts of this dibromo derivative under high dilution conditions with the dilithium 3-phenyl-3-phosphapenta-1,5-dithiolate (obtained by previously reported methods [21]) produced low yields of the required macrocycle.

The $^{31}P\{^{1}H\}$ NMR spectrum of L shows a single signal at −21.29 ppm, which is in the range observed for similar dialkylarylphosphane-containing macrocyclic molecules [2d,5b,5d,22]. No additional downfield signals were observed, indicating that no phosphoryl or phosphonium derivatives are present in the final product obtained via this procedure.

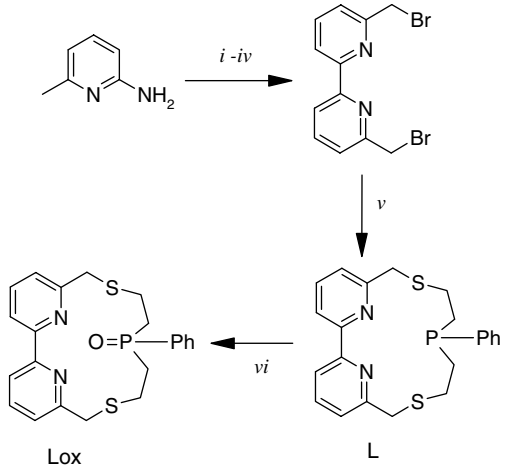

Scheme 1. Reagents and conditions: (i) $NaNO_2$ 1 M, Br_2 and HBr 98%; (ii) Ni-Raney, toluene; (iii) H_2O, 40 °C, 2 h; (iv) NBS, CCl_4, 3 h; (v) $Ph–P(–CH_2–CH_2–S^-Li^+)_2$, thf; (vi) stirring at open atmosphere, 24 h.

The ^{1}H NMR spectrum displays a complex pattern due to the high inversion barrier of the phosphane group [23], which makes non-equivalent the geminal methylene protons. The S–CH_2-bipy protons appear as a pair of doublets centered at 4.0 ppm (AB system), and three groups of signals attributed to the —S–CH_2–CH_2–P– methylene protons coupled with the phosphorus atom are observed in the interval 2.4–3.1 ppm. The COSY spectrum shows coupling between three multiplets, which evidences that all four methylene protons and the phosphorus atom define an ABMNX system similar to those found in related macrocyclic molecules [24,6].

The $^{13}C\{^{1}H\}$ NMR spectrum shows a singlet for each different carbon atom in the molecule, split in some cases by the P–C coupling, thus indicating the conformational flexibility of the ligand L. The assignation of this spectrum was made on the basis of the literature data for the P–C coupling constants [25] and the observed chemical shifts of related phosphane macrocycles [5b,6]. Alkyl phosphanes are easily oxidized to their phosphoryl derivatives [26] and ligand L is no exception to this behavior. Exposing stirred chloroformic solutions of L to air yields almost quantitatively the phosphorylic macrocycle Lox. The patterns of the ^{1}H and $^{13}C\{^{1}H\}$ NMR spectra of Lox are very similar to that described for L, whereas the $^{31}P\{^{1}H\}$ NMR spectrum again shows a single signal at 37.21 ppm, which is in the expected position for a dialkyl aryl phosphine oxide [25,27].

The spectroscopic properties of the ligands L and Lox, including mass spectra, were consistent with the proposed structure; however, the elemental analyses of the two compounds were not coincident with those calculated from their empirical formulas. Taking into account that there was no spectroscopic evidence for the presence of additional organic compounds and no insoluble residues remained when L and Lox were dissolved in organic solvents, we proceeded with the study of their complexing abilities.

The reaction of the ligands L and Lox with equimolar amounts of hydrated $Fe(ClO_4)_2$ in a CH_2Cl_2–CH_3CN mixture affords red–purple microcrystalline materials corresponding to the respective iron (II) complexes. As in the case of the free ligands, elemental analysis of both complexes did not fit any empirical formula derived from simple metal to ligand to perchlorate counteranion relations. Hopefully, these complexes may easily crystallize, producing suitable materials for X-ray diffraction analysis, which could reveal (Figs. 1 and 2) the presence of the monocationic complex units $[\mathbf{1}]^+$ and $[\mathbf{2}]^+$, which contain one ligand (L and Lox, respectively), and one bromine atom bound to a Fe(II) atom in an octahedral environment. The presence of bromine in both compounds could only be explained if some of the LiBr generated in the synthesis of L is not completely removed by the purifica-

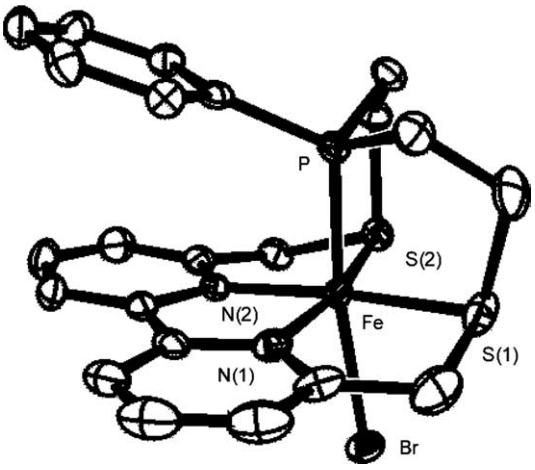

Fig. 1. Perspective view of the complex cation $[\mathbf{1}]^+$ showing 30% displacement ellipsoids. Hydrogen atoms are omitted for clarity.

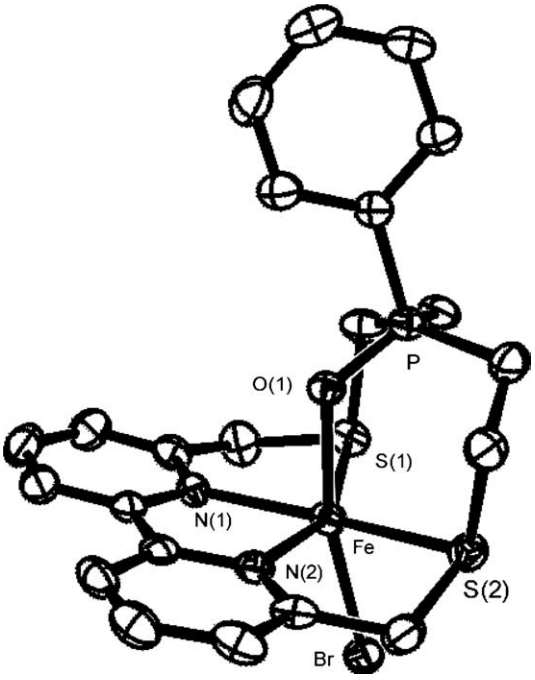

Fig. 2. Perspective view of complex cation $[\mathbf{2}]^+$ showing 30% displacement ellipsoids. Hydrogen atoms are omitted for clarity.

tion procedures used in the isolation of L and Lox. This assumption was confirmed by the Li analysis of both ligands using atomic emission spectrometry. The LiBr present in the Lox ligand can be easily removed by treating its chloroformic solutions with water. However, all the attempts made to purify L by the same or other procedures gave rise to its partial oxidation, and the separation of these L and Lox mixtures was unsuccessful. Furthermore, all attempts to synthesize Fe(II) complexes with the purified Lox ligand were also unsuccessful.

The complex cations $[\mathbf{1}]^+$ and $[\mathbf{2}]^+$ were initially obtained as purple microcrystalline perchlorate salts showing a different degree of solubility in organic solvents. The $[\mathbf{1}]^+$ perchlorate salt was sufficiently soluble in acetonitrile to be fully studied by NMR spectroscopy, a fact which reflects diamagnetic character, whereas the low solubility of $[\mathbf{2}]^+$ perchlorate salt prevented further solution studies. The $^{31}P\{^1H\}$ NMR spectrum of $[\mathbf{1}](ClO_4)$ shows a single signal at 132.52 ppm which suggests the presence of only one species in solution. These low-field shifts are characteristic of co-ordinated phosphanes in fused five-membered chelate rings [28] and several Fe(II)–triphosphamacrocyclic complexes showing similar shifts in the ^{31}P NMR spectra have recently been reported [2a,2c]. Between 4.8 and 2.4 ppm, the ^1H NMR spectrum presents the same groups of multiplets, corresponding to the methylene protons found in the free ligand, but low-field shifted. However, the number of signals of the bipyridine rings increases with respect to the ligand L, which reflects the loss of the local symmetry by the effect of the co-ordination to the metal centre.

The $^{13}C\{^1H\}$ NMR spectrum also shows the same number of signals as the free ligand, but in this latter case the most important differences are found in the region corresponding to the methylene groups, where the pair of doublets corresponding to the $–S–CH_2–CH_2–P–$ carbon atoms (22.4 and 33.5 ppm) appears high and low field displaced with respect to the L ligand (27.7 and 28.7 ppm). These data suggest that in solution the complex cation $[\mathbf{1}]^+$ maintains its monomeric character, which is in agreement with the well-known kinetic stability of the low-spin octahedral Fe(II) complexes [29].

The crystal structures of the L and Lox Fe(II) complexes, which crystallize as $[\mathbf{1}]Br \cdot H_2O$ and $[\mathbf{2}](ClO_4) \cdot 1\frac{1}{6}MeOH$ salts, showed the presence of the aforementioned $[\mathbf{1}]^+$ and $[\mathbf{2}]^+$ complex cations without significant interactions with the counter-anions and the solvate molecules. The diagrams for these complex cations are shown in Figs. 1 and 2, respectively. Crystallographic data for the structures are listed in Table 1; selected bond distances and angles for $[\mathbf{1}]^+$ and $[\mathbf{2}]^+$ are summarized in Tables 2 and 3, respectively.

As was mentioned above, the co-ordination geometry at the Fe(II) atoms in both complex cations is a distorted octahedron defined by the five donor atoms of the ligands and an additional bromine atom which is placed in a *trans* position with respect to the phosphorus-phophane atom for $[\mathbf{1}]^+$ or to the oxygen-phosphoryl atom for $[\mathbf{2}]^+$. The major distortion in both octahedral environments is observed in the value of the S–Fe–S bond angles (105.30(6)° and 120.99(9)° for $[\mathbf{1}]^+$ and $[\mathbf{2}]^+$, respectively), and this can be attributed to the geometric constraint imposed by the simultaneous co-ordination of the two bipyridine nitrogen atoms and the two thioether sulfur atoms, thus defining three contiguous five-membered chelate rings. These four donor atoms and the metal ion are almost coplanar in

Table 1
Crystallographic data for [**1**]Br · H_2O and [**2**](ClO_4) · $1\frac{1}{6}$MeOH

	[**1**]Br · H_2O	[**2**](ClO_4) · $1\frac{1}{6}$MeOH
Formula	$C_{22}H_{25}Br_2FeN_2OPS_2$	$C_{23.17}H_{27.67}BrClFeN_2O_{6.17}PS_2$
M	644.20	699.11
Crystal system	triclinic	trigonal
Space group	$P\bar{1}$ (no. 2)	$R\bar{3}$ (no. 148)
a (Å)	10.1594(15)	30.855(4)
b (Å)	14.376(2)	30.855(4)
c (Å)	9.2397(15)	16.083(4)
α (°)	92.537(15)	90
β (°)	110.820(12)	90
γ (°)	76.067(13)	120
V (Å^3)	1223.0(3)	13260(4)
Z	2	18
T (K)	294(2)	294(2)
D_c (g cm^{-3})	1.749	1.576
μ (mm^{-1})	4.138	2.194
R_1[a] ($I > 2\sigma(I)$)	0.0397	0.0643
wR_2[b] ($I > 2\sigma(I)$)	0.0962	0.1590

[a] $R_1 = \sum\|F_o| - |F_c\|/\sum|F_o|$.
[b] $wR_2 = [\sum w(|F_o^2| - |F_c^2|)^2/\sum w|F_o^2|^2]^{1/2}$.

Table 2
Selected bond distances (Å) and angles (°) for compound [**1**]Br · H_2O

Br(1)–Fe	2.5108(9)
Fe–N(1)	1.918(4)
Fe–N(2)	1.921(4)
Fe–P	2.1780(13)
Fe–S(1)	2.2604(15)
Fe–S(2)	2.2667(14)
N(1)–Fe–N(2)	81.42(16)
N(1)–Fe–P	91.35(11)
N(2)–Fe–P	93.46(11)
N(1)–Fe–S(1)	86.71(13)
N(2)–Fe–S(1)	168.12(12)
P–Fe–S(1)	86.73(5)
N(1)–Fe–S(2)	167.92(13)
N(2)–Fe–S(2)	86.57(12)
P–Fe–S(2)	88.10(5)
S(1)–Fe–S(2)	105.30(6)
N(1)–Fe–Br(1)	93.52(11)
N(2)–Fe–Br(1)	93.28(10)
P–Fe–Br(1)	172.21(4)
S(1)–Fe–Br(1)	87.49(4)
S(2)–Fe–Br(1)	88.40(4)

the complex cation $[\mathbf{1}]^+$ whereas in $[\mathbf{2}]^+$ the iron atom deviates 0.191(2) Å from the N_2S_2 plane.

The Fe–Br bond distances observed for both complexes are similar (2.5108(9) and 2.4887(15) Å for $[\mathbf{1}]^+$ and $[\mathbf{2}]^+$, respectively), and lie in the same range as those reported for related octahedral Fe(II) complexes containing non-bridging bromine ligands [30]. This situation is similar for the Fe–O(phosphoryl) bond distance in $[\mathbf{2}]^+$, which shows a value (2.107(5) Å) comparable to that observed in the few reported structures containing octahedral Fe(II) complexes with coordinated phosphoryl ligands [31]. However, the Fe–P(phosphine) bond distance for $[\mathbf{1}]^+$ (2.1780(13) Å) is somewhat less when compared with those observed in other low-spin Fe(II) complexes with aryl-dialkyl phosphines [32,33].

Table 3
Selected bond distances (Å) and angles (°) for compound [**2**](ClO_4) · $1\frac{1}{6}$MeOH

Br–Fe	2.4887(15)
Fe–O(1)	2.107(5)
Fe–N(2)	2.113(7)
Fe–N(1)	2.134(7)
Fe–S(1)	2.558(3)
Fe–S(2)	2.579(3)
P–O(1)	1.502(5)
O(1)–Fe–N(2)	86.3(2)
O(1)–Fe–N(1)	84.9(2)
N(2)–Fe–N(1)	77.5(3)
O(1)–Fe–Br	167.55(15)
N(2)–Fe–Br	102.41(8)
N(1)–Fe–Br	105.56(18)
O(1)–Fe–S(1)	86.00(15)
N(2)–Fe–S(1)	156.9(2)
N(1)–Fe–S(1)	80.1(2)
Br–Fe–S(1)	89.07(7)
O(1)–Fe–S(2)	84.55(16)
N(2)–Fe–S(2)	79.9(2)
N(1)–Fe–S(2)	155.5(2)
Br–Fe–S(2)	88.23(7)
S(1)–Fe–S(2)	120.99(9)
P–O(1)–Fe	124.3(3)

The Fe–N(bipyridine) distances for $[\mathbf{1}]^+$ (1.918(4) and 1.921(4) Å) are also slightly less than the average Fe–N bond length (ca. 2.00 Å) obtained through a Cambridge Crystallographic Data Base (CCDB) search [34] on octahedral Fe(II) complexes containing bipyridine as ligand and covering 47 structures. However, the same distances for $[\mathbf{2}]^+$ (2.134(7) and 2.113(7) Å) are ca. 0.20 Å longer than those found in $[\mathbf{1}]^+$ and similar to those reported for related octahedral high-spin Fe(II)–bipyridine complexes [35]. The same trends are also observed for the Fe–S(thioether) distances, which in the case of $[\mathbf{1}]^+$ (2.2604(15) and 2.2667(14) Å) are very close to the Fe–S bond lengths observed in low-spin Fe(II) complexes of homoleptic polythiamacrocycles [36] and azathiamacrocycles [37] whereas in the complex cation $[\mathbf{2}]^+$ these distances are noticeably longer (2.558(3) and 2.579(3) Å) and similar to those reported for high-spin Fe(II) complexes with different thioether containing ligands [32,38]. These structural data confirm the low-spin nature of the Fe(II) metal ion in the complex $[\mathbf{1}]^+$. However the bond distances and angles in the complex cation $[\mathbf{2}]^+$ are only compatible with a high-spin electronic configuration for the Fe(II) metal ion, a fact that can be attributed to the increase in the macrocyclic ligand hardness when the phosphane group in L is replaced by their phosphoryl derivative. Only the Br–Fe distance is slightly short in $[\mathbf{2}]^+$ than in $[\mathbf{1}]^+$, which may be due to the *trans*-effect of the P(phosphane) atom in $[\mathbf{1}]^+$ in comparison with the O(phosphoryl) atom in [**2**] [2].

3. Experimental

The syntheses were carried out using standard Schlenk techniques under dry dinitrogen atmosphere. The solvents were dried by conventional methods and distilled under dinitrogen before use. Dilithium 3-phenyl-3-phosphapenta-1,5-dithiolate and 6,6′-bis(bromomethyl)-2,2′-bipyridine [20,21] were prepared according to published procedures. Chemical analyses were performed in the Chemical Analysis Service of the Universitat Autònoma de Barcelona. Elemental analyses were carried out using a Carlo Erba EA-1108 instrument. Li determinations were made by atomic emission spectrometry (AES) using a Perkin–Elmer 2100 instrument; the samples were previously prepared treating them with HNO_3/H_2O (1:1) at 180 psi during 40 min in a microwaves digestor (CEM2000). The NMR spectra were run in the NMR Service of the Universitat Autònoma de Barcelona. ^1H and $^{13}C\{^1H\}$ NMR spectra were recorded using a Bruker 400 MHz AM instrument and the $^{31}P\{^1H\}$ NMR spectra were recorded using a Bruker 250 MHz AC instrument with chemical shifts given as ppm relative to 85% H_3PO_4. COSY and HNQC experiments were made in order to assign the ^1H and ^{13}C spectra by using general standard parameters. Mass spectra were recorded using a HP298S GC/MS system.

4. Syntheses

4.1. 3,3′-5-phenyl-2,8-dithia-5-phospha[9]-2,2′-bipyridinophane (L)

Under a dinitrogen atmosphere, a solution of dilithium 3-phenyl-3-phosphapenta-1,5-dithiolate in thf (100 cm^3, 0.09 M) and a solution of 6,6′-bis(bromomethyl)-2,2′-bipyridine (3.10 g, 9 mmol) in thf (100 cm^3) were added simultaneously to thf (500 cm^3) over a period of 5 h at room temperature. After the addition, the mixture was stirred for a further 48 h. The thf was removed under vacuum and the resulting oily yellow residue was extracted with diethyl ether (3×60 cm^3). The ethereal layer was separated, evaporated under vacuum, and the residue was dissolved in the minimum amount of CH_2Cl_2. After slow addition of petroleum ether (40–60°) to this solution a white precipitate appeared which was filtered off and vacuum dried. Yield (calculated for L · 2LiBr) 0.54 g, 10%. *Anal.* Calc. for $C_{22}H_{23}N_2PS_2Li_2Br_2$: C, 45.23; H, 3.97; N, 4.79; S, 10.98; Li, 2.38. Found: C, 44.4; H, 3.8; N, 4.1; S, 10.2%; Li (determined by AES), 21.7 mg Li/1 g sample, 2.2%. ^1H NMR (400 MHz, $CDCl_3$): δ 2.07 (m, 2, –S–CH_2–CH_2–P–), 2.45 (m, 2, –S–CH_2–CH_2–P–), 2.84 (m, 4, –S–CH_2–CH_2–), 3.90 (d, 2, –S–CH_2–Ph, $J = 13.9$ Hz), 4.02 (d, 2, –S–CH_2–Ph, $J = 13.9$ Hz), 7.42–7.77 (m, 11, Ar). $^{13}C\{^1H\}$ NMR (100 MHz, $CDCl_3$): δ 27.71 (d, S–CH_2–CH_2–P–, $J = 10.5$ Hz), 28.72 (d, –S–CH_2–CH_2–P–, $J = 20.9$ Hz), 37.92 (–S–CH_2–Ph), 119.32, 124.62, 139.31 (Bipy), 128.08 (d, P–Ph, $J = 7.0$ Hz), 128.54 (d, P–Ph, $J = 15.7$ Hz), 131.45 (d, P–Ph, $J = 19.2$ Hz), 131.86 (d, P–Ph, $J = 19.4$ Hz), 152.45, 158.58 (Bipy). $^{31}P\{^1H\}$ NMR (101 MHz, $CDCl_3$): δ − 21.29. Mass spectrum (EI); *m/z* 410 (M^+).

4.2. 3,3′-5-oxo-5-phenyl-2,8-dithia-5-phospha[9]-2,2′-bipyridinophane (Lox)

A solution of L · 2LiBr (0.200 g, 0.34 mmol) in $CHCl_3$ (30 cm^3) was stirred at open atmosphere and room temperature for 24 h. The resulting solution was evaporated to dryness and the resulting solid collected. Yield (calculated for Lox · 2LiBr) 0.198 g, 97%. *Anal.* Calc. for $C_{22}H_{23}N_2OPS_2Li_2Br_2$: C, 44.02; H, 3.86; N, 4.67; S, 10.68; Li, 2.31. Found: C, 43.8; H, 3.4; N, 4.6; S, 10.3%; Li (determined by AES), 24.8 mg Li/1 g sample, 2.5%. ^1H NMR (400 MHz, $CDCl_3$): δ 2.35 (m, 2, –S–CH_2–CH_2–P–), 2.80 (m, 6, –S–CH_2–CH_2–P–), 3.81 (d, 2, –S–CH_2–Ph, $J = 13.9$ Hz), 3.92 (d, 2, –S–CH_2–Ph, $J = 13.9$ Hz), 7.38–7.89 (m, 11, Ar). $^{13}C\{^1H\}$ NMR (100 MHz, $CDCl_3$): δ 30.98 (d, –S–CH_2–CH_2–P–, $J = 14.8$ Hz), 31.95 (d, S–CH_2–CH_2–P–, $J = 18.5$ Hz), 36.27 (–S–CH_2–Ph), 120.60, 123.66 (Bipy), 128.81 (d, P–Ph, $J = 11.09$ Hz), 130.09 (d, P–Ph, $J = 9.2$ Hz), 130.50 (d, P–Ph, $J = 9.4$ Hz), 132.04 (s, P–Ph), 138.78, 138.93, 160.46 (Bipy). $^{31}P\{^1H\}$ NMR (101 MHz, $CDCl_3$): δ 37.21. Mass spectrum (EI); *m/z* 426 (M^+).

4.3. [FeBr(L)](ClO4) · 2H2O · [1](ClO4) · 2H2O

A solution of $Fe(ClO_4)_2 \cdot 6H_2O$ (44 mg, 0.122 mmol) in acetonitrile (5 cm^3) was slowly added to a solution of L · 2LiBr (50 mg, 0.086 mmol) in dichloromethane (2 cm^3). The solution changed immediately to red–purple and a solid of the same colour appeared which was filtered off, washed with dichloromethane and vacuum dried. Yield: 17 mg, 29%. *Anal.* Calc. for $C_{22}H_{27}BrClFeN_2O_6PS_2$: C, 38.76; H, 3.99; N, 4.11; S, 9.45. Found: C, 38.9; H, 3.6; N, 4.2; S, 9.3%. ^1H NMR (400 MHz, CD_3NO_2): δ 2.37 (m, 4, –S–CH_2–CH_2–P–), 3.13 (m, 4, –S–CH_2–CH_2–P–), 4.67 (d, 2, –S–CH_2–Ph, $J = 18.0$ Hz), 4.81 (d, 2, –S–CH_2–Ph, $J = 18.0$ Hz), 6.24–7.00 (m, 6, Bipy), 7.78 (m, 5, P–Ph). $^{13}C\{^1H\}$ NMR (100 MHz, CD_3NO_2): δ 22.51 (d, –S–CH_2–CH_2–P–, $J = 29.7$ Hz), 33.41 (d, S–CH_2–CH_2–P–, $J = 31.5$ Hz), 44.36 (–S–CH_2–Ph), 117.18, 117.56 (Bipy), 128.81 (d, P–Ph, $J = 11.09$ Hz), 124.42 (d, P–Ph, $J = 8.9$ Hz), 124.89 (d, P–Ph, $J = 9.1$ Hz), 126.53 (s, P–Ph), 130.41, 153.59, 159.14 (Bipy). $^{31}P\{^1H\}$ NMR (101 MHz, $CDCl_3$): δ 132.52.

4.4. [FeBr(Lox)](ClO$_4$) · 3H$_2$O · [2](ClO$_4$) · 3H$_2$O

The compound was prepared as for [**1**](ClO$_4$) · 2H$_2$O using Lox as ligand. Yield: 19 mg, 29%. *Anal.* Calc. for $C_{22}H_{29}BrClFeN_2O_8PS_2$: C, 36.92; H, 4.08; N, 3.91; S, 8.96. Found: C, 36.4; H, 3.9; N, 3.8; S, 8.2%.

5. Crystallography

The slow evaporation of a nitromethane solution of [**1**](ClO$_4$) · 2H$_2$O and a methanol solution of [**2**](ClO$_4$) · 3H$_2$O produced crystalline materials corresponding to [**1**]Br · H$_2$O and [**2**](ClO$_4$) · $1\frac{1}{6}$MeOH, respectively. Single-crystal data were performed at ambient temperature on a Rigaku AFC5S diffractometer using graphite monochromatized Mo Kα radiation. The unit cell parameters for both compounds were determined by least-squares refinement of 25 carefully centered reflections. All data obtained were corrected for empirical absorption (P scan). A total of 4563 and 5557 reflections giving 4296 and 5198 unique reflections ($R_{int} = 0.0179$ and 0.0562) were collected by T/2 scan mode ($2\theta_{max} = 50°$) for [**1**]Br · H$_2$O and [**2**](ClO$_4$) · $1\frac{1}{6}$MeOH, respectively.

Both structures were solved by direct methods and least-squares refinements were performed using the SHELX-97 program system [39]. For [**1**]Br · H$_2$O non-hydrogen atoms were refined with anisotropic displacement parameters. Hydrogen atoms were included in the calculations at the fixed distances from their host atoms and treated as riding atoms using the SHELX-97 default parameters.

The asymmetric unit of [**2**](ClO$_4$) · $1\frac{1}{6}$MeOH consists of the complex unit [**2**]$^+$, disordered perchlorate ion, one methanol molecule at common position and 1/6 of disordered methanol molecule at threefold axis. The perchlorate ion shows rotational disorder, the Cl–O(2) bond being common shared by both rotamers. The disordered oxygen atoms of the perchlorate ion and the methanol molecules were refined with isotropic displacement parameters; the rest of the non-hydrogen atoms were refined with anisotropic displacement parameters. Hydrogen atoms of the methanol molecules could not be reliably positioned but the remainder of the hydrogen atoms were included in the calculations at fixed distances from their host atoms and treated as riding atoms by using the SHELX-97 default parameters.

6. Supplementary data

Supplementary data are available from the CCDC, 12 Union Road, Cambridge CB2 1EZ, UK on request. CCDC Nos.: 274557 and 274558 for [**1**]Br · H$_2$O and [**2**](ClO$_4$) · $1\frac{1}{6}$MeOH, respectively. Copies of this information may be obtained free of charge from The Director, CCDC, 12 Union Road, Cambridge, CB2 1EZ, UK (fax: +44 1223 336 033; e-mail: deposit@ccdc.cam.ac.uk or www: http://www.ccdc.cam.ac.uk)

Acknowledgements

The authors acknowledge to "Ministerio de Educación y Ciencia (Spain)" and "Generalitat de Catalunya (Spain)" for Grants CTQ20004-04134 and 2001SGR 00177, respectively.

References

[1] A.M. Caminade, J.P. Majoral, Chem. Rev. 94 (1994) 1183.
[2] (a) P.G. Edwards, P.D. Newman, A.K.M. Malik, Angew. Chem., Int. Ed. 39 (2000) 2922;
(b) P.G. Edwards, P.D. Newman, D.E. Hibbs, Angew. Chem., Int. Ed. 39 (2000) 2722;
(c) P.G. Edwards, M.L. Whatton, R. Haigh, Organometallics 19 (2000) 2652;
(d) A.J. Price, P.G. Edwards, Chem. Commun. (2000) 899.
[3] M. Ciampolini, Pure Appl. Chem. 58 (1986) 1429, and references therein.
[4] E.P. Kyba, R.E. Davis, M.A. Fox, C.N. Clubb, S.T. Liu, G.A. Reitz, V.J. Scheuler, R.P. Kashyap, Inorg. Chem. 26 (1987) 1647, and references therein.
[5] (a) P.J. Blower, A.V. Chadwick, J.C. Jeffery, G.E.D. Mullen, A.K. Powell, S.N. Salek, R.J. Smith, M.J. Went, Inorg. Chim. Acta 294 (1999) 170;
(b) J.A. Muñoz, L. Escriche, J. Casabó, C. Pérez-Jiménez, R. Kivekäs, R. Sillanpää, Inorg. Chem. 36 (1997) 947;
(c) P.J. Blower, J.C. Jeffery, J.R. Miller, S.N. Salek, D. Schmaljohann, R.J. Smith, M.J. Went, Inorg. Chem. 36 (1997) 1578;
(d) N.R. Champness, C.S. Frampton, G. Reid, D.A. Tocher, J. Chem. Soc., Dalton Trans. (1994) 3031;
(e) R.J. Smith, A.K. Powell, N. Barnard, J.R. Dilworth, P.J. Blower, J. Chem. Soc., Chem. Commun. (1993) 54;
(f) P.B. Savage, S.K. Holmgren, J.M. Desper, S.H. Gellman, Pure Appl. Chem. 65 (1993) 461;
(g) T.L. Jones, A.C. Willis, S.B. Wild, Inorg. Chem. 31 (1992) 1411.
[6] L. Escriche, J.A. Muñoz, R. Kivekäs, R. Sillanpää, J. Casabó, Eur. J. Inorg. Chem. 12 (2002) 3258.
[7] J.R. Dilworth, N. Wheatley, Coord. Chem. Rev. 199 (2000) 89.
[8] C.S. Slone, D.A. Weinberger, C.A. Mirkin, Prog. Inorg. Chem. 48 (1999) 233.
[9] P.B. Savage, S.K. Holmgren, S.H. Gellman, J. Am. Chem. Soc. 116 (1994) 4069.
[10] J. Casabó, L. Escriche, C. Pérez- Jiménez, J.A. Muñoz, F. Teixidor, J. Baucells, A. Errachid, Anal. Chim. Acta 320 (1996) 63.
[11] (a) E.I. Sinyavskaya, Koord. Khim. 12 (1986) 1155;
(b) E.N. Tsvetkov, A.N. Bovin, V.K. Syundyukova, Russ. Chem. Rev. (1988) 776;
(c) R.M. Izatt, K. Pawlak, J.S. Bradshaw, R.L. Bruening, Chem. Rev. 91 (1991) 1721.
[12] B.G. Cox, H. Schneider, Studies in physical and theoretical chemistry. Coodination and Transport properties of Macrocyclic Compounds in Solution, vol. 74, Elsevier, Amsterdam, 1992.

[13] (a) S. Campagna, C. Di Pietro, F. Loiseau, B. Maubet, N. McClenaghan, R. Passalacqua, F. Pantoriero, V. Ricevuto, S. Serroni, Coord. Chem. Rev. 229 (2002) 67;
(b) H. Yersin, C. Kratzer, Coord. Chem. Rev. 229 (2002) 75;
(c) L. Fabbrizzi, M. Licchelli, P. Pallavichini, D. Sacchi, Supramol. Chem. 13 (2001) 569;
(d) M. Venturi, A. Credi, V. Balzani, Coord. Chem. Rev. 186 (1999) 233;
(e) K. Kalyanasundaram, M. Grätzel, Coord. Chem. Rev. 177 (1998) 347;
(f) M.D. Ward, C.M. White, F. Barigelletti, N. Armaroli, G. Calogero, L. Flamini, Coord. Chem. Rev. 171 (1998) 481;
(g) V. Balzani, A. Juris, M. Venturi, S. Campagna, S. Serroni, Chem. Rev. 96 (1996) 759.

[14] (a) A. Bencini, A. Bianchi, P. Fornasari, C. Giorgi, P. Paoleti, C. Giorgi, B. Valtancoli, Polyhedron 21 (2002) 1329;
(b) A.J. Blake, M.H.M. Caçote, F.A. Devillanova, A. Garau, F. Isaia, V. Lippolis, C.M. Pereira, F. Silva, L. Tei, Eur. J. Inorg. Chem. 7 (2002) 1816;
(c) A.J. Blake, F.A. Devillanova, A. Garau, A. Harrison, F. Isaia, V. Lippolis, S.K. Tiwary, M. Schröder, G. Verani, G. Whittaker, J. Chem. Soc., Dalton Trans. (2002) 4389;
(d) M. Arca, A.J. Blake, J. Casabó, F. Demartino, F.A. Devillanova, A. Garau, F. Isaia, V. Lippolis, R. Kivekäs, V. Muns, M. Schröder, R. Sillanpää, G. Verani, J. Chem. Soc., Dalton Trans. (2001) 1180;
(e) A.J. Blake, J. Casabó, F.A. Devillanova, L. Escriche, A. Garau, F. Isaia, V. Lippolis, R. Kivekäs, V. Muns, M. Schröder, R. Sillanpää, G. Verani, J. Chem. Soc., Dalton Trans. (1999) 1085.

[15] M.C. Aragoni, M. Arca, F. Demartino, F.A. Devillanova, F. Isaia, A. Garau, V. Lippolis, F. Jalali, U. Papke, M. Shamsipur, L. Tei, A. Yari, G. Verani, Inorg. Chem. 41 (2002) 6623.

[16] M. Shamsipur, M. Javanbakht, V. Lippolis, A. Garau, G.D. Filippo, M.R. Ganjali, A. Yari, Anal. Chim. Acta 462 (2002) 225.

[17] (a) C. Bazzicalupi, A. Bellusci, A. Bencini, E. Berni, A. Bianchi, S. Ciattini, C. Giorgi, B. Valtancoli, J. Chem. Soc., Dalton Trans. (2002) 2151, and references therein;
(b) C. Calaup, M.-C. Carrié, P. Tisnès, C. Picard, Eur. J. Org. Chem. (2001) 2165, and references there in;
(c) R.B. Hopkins, J.S. Albert, D. Van Engen, A.D. Hamilton, Bioorg. Med. Chem. 4 (1996) 1121;
(d) Z. Wang, J. Reibenspies, A.E. Martell, Inorg. Chem. 36 (1997) 629.

[18] C. Kaes, A. Katz, M.W. Hosseini, Chem. Rev. 100 (2000) 3553.

[19] G.R. Newkome, D.C. Pantalio, W.E. Puckett, P.L. Zieple, W.A. Deutsch, J. Inorg. Nucl. Chem. 43 (1981) 1529.

[20] Z. Wang, J. Reibenspies, R.J. Motekaitis, A.E. Martell, J. Chem. Soc., Dalton Trans. (1995) 1511.

[21] J.A. Muñoz, L. Escriche, J. Casabó, C. Pérez-Jiménez, R. Kivekäs, R. Sillanpää, Inorg. Chim. Acta 257 (1997) 99.

[22] (a) E.P. Kiva, A.M. John, S.B. Brown, C.W. Hudson, M.J. McPhaul, A. Harding, K. Larsen, S. Niedzwiecki, R.E. Davis, J. Am. Chem. Soc. 102 (1980) 139;
(b) E.P. Kiva, S.S.P. Chou, J. Am. Chem. Soc. 102 (1980) 7012;
(c) J.S. Edwards, J.S. Fleming, S.S. Liyanage, Inorg. Chem. 35 (1996) 4563;
(d) D.J. Jones, P.G. Edwards, R.P. Tooze, T. Albers, J. Chem. Soc., Dalton Trans. (1999) 1045;
(e) T. Lebbe, P. Machnitzki, O. Stelzer, W. Sheldrick, Tetrahedron 56 (2000) 157;
(f) P.-H. Leung, A. Liu, K.F. Mok, A.J.P. White, D.J. Williams, J. Chem. Soc., Dalton Trans. (1999) 1277.

[23] R.D. Baechler, K. Mislow, J. Am. Chem. Soc. 92 (1970) 3090.

[24] R. Boese, R. Boetzel, G. Hägele, Magn. Reson. Chem. 32 (1994) 409.

[25] (a) L.M. Green, D.W. Meek, Polyhedron 9 (1990) 35;
(b) J.G. Verkade, L.D. Quin (Eds.), Phosphorus-31 NMR Spectral Properties in Compounds. Characterization and Structural Analysis, VCH, New York, 1994.

[26] L.H. Pignolet (Ed.), Homogeneus Catalysis with Metal Phosphine Complexes, in: J.P. Fackler Jr. (Ed.), Modern Inorganic Series, Plenum Press, New York, 1983.

[27] S.K. Homgren, P.B. Savage, J.M. Desper, K.D. Schladetzky, D.R. Powell, S.H. Gellman, Tetrahedron 53 (1997) 12249.

[28] (a) P.S. Pregosin, R.W. Kunz, ^{31}P and ^{13}C NMR of Transition Metal Complexes, Springer, Berlin, 1979;
(b) P.E. Garrou, Chem. Rev. 81 (1981) 229.

[29] G. Wilkinson, R.D. Gillard, J.A. McCleverty (Eds.), Comprehensive Coordination Chemistry. vol. 4, in: P.N. Hawker, M.V. Twigg (Series Eds.), Pergamon Press, UK, 1987, Chapter 44.1.

[30] (a) Wu Chi-Cheng, J. Jung, P.K. Gantzel, P. Gutlich, D.N. Hendrickson, Inorg. Chem. 36 (1997) 5339;
(b) L.D. Field, T.W. Hambley, B.C.K. Yau, Acta Crystallogr. C49 (1993) 224;
(c) D.J. Evans, R.A. Henderson, A. Hills, D.L. Hughes, K.E. Oglieve, J. Chem. Soc., Dalton Trans. (1992) 1259;
(d) R. Albrecht, E. Weiss, J. Organomet. Chem. 399 (1990) 163.

[31] (a) Kuang Shan-Ming, Zhang Zheng-Zhi, Xue Fen, T.C.W. Mak, Polyhedron 18 (1999) 3465;
(b) Li Song-Lin, Zhang Zheng-Zhi, Wu Bo-Mu, T.C.W. Mak, Inorg. Chim. Acta 255 (1997) 239;
(c) Dong Yanhong, Yan Shiping, V.G. Young Jr., L. Que Jr., Angew. Chem., Int. Ed. Engl. 35 (1996) 618;
(d) I. Ondrejkovicova, M. Melnik, K. Smolander, M. Ahlgren, Acta Chem. Scand. 49 (1995) 475;
(e) J.E. Barclay, D.J. Evans, D.L. Hughes, G.J. Leigh, J. Chem. Soc., Dalton Trans. (1993) 69.

[32] D. Sellmann, T. Hofmann, F. Knoch, Inorg. Chim. Acta 224 (1994) 61.

[33] (a) F.E. Sowrey, P.J. Blower, J.C. Jeffery, E.J. MacLean, M.J. Went, Inorg. Chem. Commun. 5 (2002) 832;
(b) M. Mealli, F. Sabat, M. Zanobini, C. Ciampolini, C. Nardi, J. Chem. Soc., Dalton Trans. (1985) 479;
(c) M. Di Vaira, S. Midollini, L. Sacconi, Inorg. Chem. 18 (1979) 3466.

[34] 3D search and research using the Cambridge structural database F.H. Allen, O. Kennard, Chem. Design Automat. News 8 (1) (1993) 1&31.

[35] (a) A. Ion, J.-C. Moutet, E. Saint-Aman, G. Royal, S. Tingry, J. Pecaut, S. Menage, R. Ziessel, Inorg. Chem. 40 (2001) 3632;
(b) Zhong Zhuang Jin, Tao Jian-Qing, Yu Zhi, Dun Chun-Ying, Liu Yong-Jian, You Xiao-Zeng, J. Chem. Soc., Dalton Trans. (1998) 327;
(c) J.A. Real, M.C. Munoz, J. Faus, X. Solans, Inorg. Chem. 36 (1977) 3008;
(d) M. Konno, M. Mikami-Kido, Bull. Chem. Soc. Jpn. 64 (1991) 339;
(e) E. König, Prog. Inorg. Chem. 35 (1987) 527.

[36] (a) A.J. Blake, M. Schroeder, Adv. Inorg. Chem. 35 (1990) 1;
(b) V.A. Grillo, L.R. Gahan, G.R. Hanson, R. Stranger, T.W. Hambley, K.S. Murray, B. Moubaraki, J.D. Cashion, J. Chem. Soc., Dalton Trans. (1998) 2341;
(c) V.A. Grillo, L.R. Gahan, G.R. Hanson, T.W. Hambley, Polyhedron 15 (1996) 559;
(d) G.J. Grant, S.M. Isaac, W.N. Setzer, D.G. Van Derveer, Inorg. Chem. 32 (1993) 4284;
(e) W.N. Setzer, E.L. Cacioppo, Guo Qin, G.J. Grant, D.D. Kim, J.L. Hubbard, D.G. Van Derveer, Inorg. Chem. 29 (1990) 2672.

[37] (a) U. Heinzel, A. Henke, R. Mattes, J. Chem. Soc., Dalton Trans. (1997) 501;
(b) N. Atkinson, A.J. Lavery, A.J. Blake, G. Reid, M. Schroder, Polyhedron 9 (1990) 2641.
[38] (a) D. Sellmann, J. Utz, F.W. Heinemann, Inorg. Chem. 38 (1999) 459;
(b) C. Zhou, R.H. Holm, Inorg. Chem. 36 (1997) 4066;
(c) D. Sellmann, G. Mahr, F. Knoch, F. Moll, Inorg. Chim. Acta 224 (1994) 45;
(d) D. Sellmann, W. Soglowek, F. Knoch, G. Ritter, J. Dengler, Inorg. Chem. 31 (1992) 3711.
[39] G.M. Sheldrick, SHELX-97, Program for Crystal Structure Refinement, University of Göttingen, Germany, 1997.

Available online at www.sciencedirect.com
SCIENCE DIRECT®
Polyhedron 25 (2006) 809–814
POLYHEDRON
www.elsevier.com/locate/poly

Binuclear complexes of lanthanides with 1,4-bis(diphenylphosphino)butane dioxide

Zdenek Spichal [a], Marek Necas [a,*], Jiri Pinkas [a], Zbynek Zdrahal [b]

[a] Department of Inorganic Chemistry, Faculty of Science, Masaryk University, Kotlarska 2, CZ-61137 Brno, Czech Republic
[b] LMFR, Faculty of Science, Masaryk University, Kotlarska 2, CZ-61137 Brno, Czech Republic

Received 16 June 2005; accepted 3 August 2005
Available online 9 September 2005

Abstract

A series of binuclear complexes of a general formula $[(dppbO_2)Ln(NO_3)_3(\mu\text{-}dppbO_2)Ln(NO_3)_3(dppbO_2)]$ (Ln = Pr (**1**), Nd (**2**), Sm (**3**), Dy (**4**), Lu (**5**)) were prepared by reacting bis(diphenylphosphino)butane dioxide ($dppbO_2$) with lanthanide nitrates under solvothermal conditions. All compounds were characterized by analytical and spectroscopic techniques, such as infrared spectroscopy and mass spectrometry with electrospray ionization, and their molecular structures were determined by single crystal X-ray diffraction analysis in four cases. In contrast to the majority of lanthanide complexes with bis(diphenylphosphino)ethane dioxide which were previously reported as 2D polymeric networks, the present compounds are strictly molecular. This is evidently manifestation of the longer and flexible ligand backbone that allows a chelating binding mode.
© 2005 Elsevier Ltd. All rights reserved.

Keywords: Bis(diphenylphosphino)butane dioxide; Lanthanides; Binuclear complexes; X-ray crystallography; Electrospray mass spectrometry

1. Introduction

Recently we have studied the reactivity of bis(diphenylphosphino)ethane dioxide $Ph_2P(O)–CH_2CH_2–P(O)Ph_2$ ($dppeO_2$) with lanthanide salts [1]. While bis(diphenylphosphino)methane dioxide ($dppmO_2$) had already been known to form a range of various chelates with lanthanide cations [2], we have prepared a series of coordination polymers with its one-carbon longer homologue. We have observed different coordination geometries and polymeric architectures, depending on the ancillary non-bridging ligands and the reaction conditions involved.

Our current investigation was targeted on the reactivity of diphosphine dioxide ligands with longer central chains. There have been several publications studying the steric properties of the bidentate diphosphine ligands in connection with the structural and catalytic features of resulting complexes [3–5]. The $Ph_2P–(CH_2)_n–PPh_2$ series in particular, provided the opportunity to study the steric effects by the simple variations in *n*, without significantly affecting the electronic properties of ligands [6]. The oxidized series, $Ph_2P(O)–(CH_2)_n–P(O)Ph_2$, seemed suitable for similar investigations on lanthanides, which are generally coordinated by phosphorus to a lesser extent.

We will show in the following, that in contrast to the observed polymeric nature of $dppeO_2$ complexes, the reversal to the molecular character was featured in lanthanide complexes of bis(diphenylphosphino)butane dioxide ($dppbO_2$). These were prepared by the solvothermal reactions of $dppbO_2$ with lanthanide nitrates and characterized structurally and spectroscopically. Electrospray ionization technique has been used successfully to ionize both non-volatile and thermally labile inorganic compounds for mass spectrometric detection [7] and it proved a valuable tool in the characterization of the prepared lanthanide complexes **1**–**6**.

* Corresponding author.
E-mail address: man@chemi.muni.cz (M. Necas).

0277-5387/$ - see front matter © 2005 Elsevier Ltd. All rights reserved.
doi:10.1016/j.poly.2005.08.007

2. Results and discussion

The solvothermal synthesis is a variation to the well-known hydrothermal process, in which water is substituted by a general solvent. The hydrothermal and solvothermal methods are widely used in material design and crystal engineering, with the view to obtain the products of desired structure, texture and crystallinity [8–11]. Using solvothermal synthesis, we have successfully prepared good quality crystals of coordination polymers of $dppeO_2$ with lanthanides [1]. We have therefore used the reaction in an autoclave for the preparation of coordination compounds of $dppbO_2$. One-day heating of the ligand with a respective lanthanide nitrate in methanol yielded block-shaped crystals of excellent quality. In all cases, the single crystal X-ray diffraction analysis revealed the binuclear complexes of a general formula [($dppbO_2$)-$Ln(NO_3)_3$-(μ-$dppbO_2$)-$Ln(NO_3)_3$($dppbO_2$)] (Ln = Pr (**1**), Nd (**2**), Sm (**3**), Dy (**4**)) (see Fig. 1). The reaction with $Lu(NO_3)_3 \cdot 2H_2O$ led to a microcrystalline solid, which decomposed to powder on exposure to air, most probably because of a loss of the solvent of crystallization. Even though the lutetium complex was not studied by the X-ray diffraction, its binuclear nature is apparent from the electrospray mass spectra (see Table 3).

The molecular structures of **1**–**4** are similar to the binuclear complex [($dppeO_2$)$Lu(NO_3)_3$-(μ-$dppeO_2$)-$Lu(NO_3)_3$($dppeO_2$)] (**6**), which was isolated as the only molecular compound from the solvothermal reaction of $dppeO_2$ with lanthanide nitrates [1]. The fact that all other $dppeO_2$ complexes with lighter lanthanides were polymeric, we ascribed to the effect of the lanthanide contraction. The formation of binuclear compounds with $dppbO_2$ is obvious throughout the whole rare earth metal series, thus the longer ligand backbone is clearly responsible for the transition from polymeric to molecular complexes.

All compounds combine chelating as well as bridging bonding modes for the bidentate $dppbO_2$. While the bridging ligands have their P=O groups in an *anti* conformation as they do in their uncoordinated form [12], in chelate rings they naturally adopt the *syn* conformation. Mean deviations from P1–O1–P2–O2 planes are 0.049, 0.049, 0.047, and 0.043 Å for **1**–**4**, respectively. Considering the coordination sphere of the lanthanide cation as being pseudooctahedral, the ligands are meridionally disposed. The selected bond lengths and angles are listed in Table 2. With decreasing ionic radius of Ln^{3+}, the oxygen atoms get progressively closer to the cation, with consistent difference of about 0.2 Å in Ln–O(N) and Ln–O(P) distances.

The IR spectra are very similar to those obtained for the $dppeO_2$ coordination polymers [1]. Again we observe the grouping of bands at 1467–1487, 1291–1323, 1029–1031, and 816–820 cm^{-1}, which we assign to the bidentate nitrate groups, in agreement with previous data [13,14]. The band at 1384–1385 cm^{-1} is also apparent and belongs to the ionic nitrate. According to Lees et al. [14], the NO_3^- anion is displaced from the complex by Br^- from the KBr pellet. The most prominent bands are at 1139–1159 cm^{-1} which correspond to the P=O stretching frequency. In the present compounds, they usually appear in pairs, suggesting the chelating and bridging nature of the P=O moieties.

We studied the binuclear complexes of the $dppbO_2$ ligand **1**–**5** and the complex **6** with the shorter $dppeO_2$

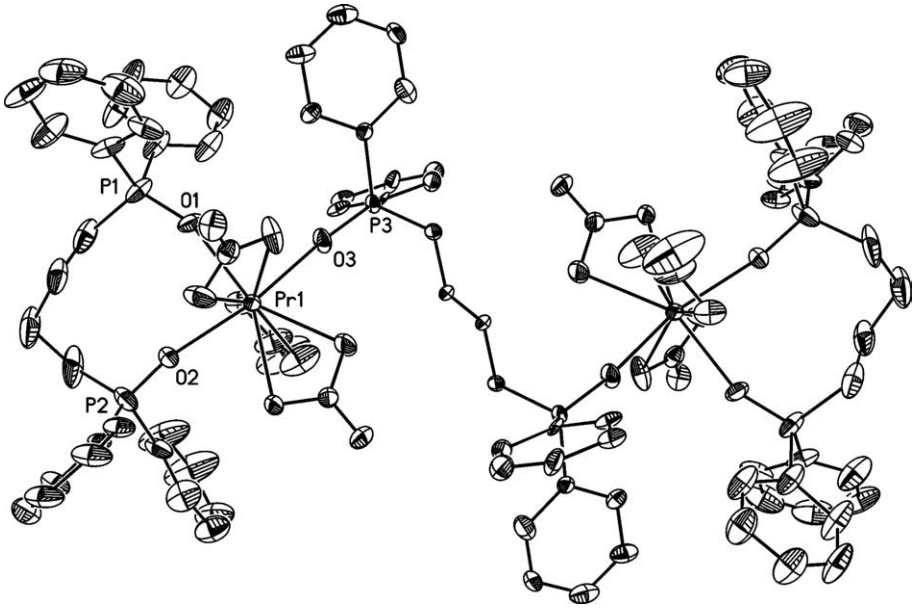

Fig. 1. The molecular structure of [($dppbO_2$)$Pr(NO_3)_3$-(μ-$dppbO_2$)-$Pr(NO_3)_3$($dppbO_2$)] (**1**). The thermal ellipsoids were drawn at the 50% probability level and hydrogen atoms were omitted for clarity. The compounds **2**–**4** are isostructural with **1**.

Table 1
Crystal data and structure refinement parameters

	1	2	3	4
Empirical formula	$C_{42}H_{42}N_3O_{12}P_3Pr \cdot C_{0.75}O_{0.75}$	$C_{42}H_{42}N_3O_{12}P_3Nd \cdot C_{0.75}O_{0.75}$	$C_{42}H_{42}N_3O_{12}P_3Sm \cdot C_{0.75}O_{0.75}$	$C_{42}H_{42}N_3O_{12}P_3Dy \cdot C_{0.75}O_{0.75}$
Formula weight	1035.61	1038.94	1045.05	1057.20
Crystal system	monoclinic	monoclinic	monoclinic	monoclinic
Space group	$P2_1/n$	$P2_1/n$	$P2_1/n$	$P2_1/n$
a (Å)	12.577(3)	12.422(1)	12.432(1)	12.338(1)
b (Å)	17.035(3)	16.931(1)	16.931(1)	16.894(1)
c (Å)	21.789(4)	21.731(2)	21.778(1)	21.787(1)
α (°)	90	90	90	90
β (°)	90.96(3)	90.70(1)	90.89(1)	91.19(1)
γ (°)	90	90	90	90
Volume (Å^3)	4667.6(16)	4570.2(5)	4583.5(3)	4540.1(4)
Z	4	4	4	4
ρ (Mg/m^3)	1.474	1.510	1.514	1.547
μ (mm^{-1})	1.210	1.306	1.451	1.817
Reflections collected/ unique	24000/8196	27059/8017	41977/8039	39406/7986
Data/ parameters	8196/766	8017/771	8039/761	7986/751
Final R indices [$I > 2\sigma(I)$]	0.0458/0.1018	0.0341/0.0798	0.0373/0.0784	0.0466/0.0884
R indices (all data)	0.0513/0.1038	0.0459/0.0832	0.0442/0.0807	0.0606/0.0927
$\Delta\rho_{max}/\Delta\rho_{min}$ (e Å^{-3})	1.901/−1.390	0.941/−0.780	0.996/−1.111	1.025/−0.598

Table 2
Selected average bond lengths (Å) and angles (°) for prepared compounds and the parent $dppbO_2$ ligand

	$dppbO_2$[b]	**1** (Pr)	**2** (Nd)	**3** (Sm)	**4** (Dy)
Ln–O (to N)		2.579	2.543	2.523	2.472
Ln–O (to P)		2.385	2.354	2.334	2.281
P–O	1.482(2)	1.521	1.510	1.511	1.509
P–C[a]	1.812(2)	1.795	1.787	1.790	1.789
Ln–O–P		162.3	162.3	162.1	161.8
O–P–C[a]	114.9(1)	112.5	112.8	112.8	113.0

[a] C is the carbon atom in $(CH_2)_4$ central moiety; the average value was calculated for both chelating and bridging ligands.
[b] The values taken from [12].

ligand by ESI–MS in acetonitrile/water (1:1) solutions to ascertain their stability and ionization and fragmentation pathways (see Fig. 2). Molecular ions of all compounds were not visible in the positive mode most probably because of an easy loss of a nitrate group and a ligand to form the positively charged fragments of the highest observed mass (see Table 3). The signal for $[M - NO_3]^+$ cation was registered as a weak peak in the spectrum of **6**. In the spectra of **1**–**5**, the signal for $[M - NO_3]^+$ is very weak or absent but the binuclear $[(dppbO_2)_2Ln_2(NO_3)_5]^+$ fragments, formed by further loss of a neutral $dppbO_2$ ligand, are quite prominent in all compounds and substantiate the existence of the intact binuclear species in solution. The presence of two lanthanide atoms in these ions was clearly demonstrated by the correspondence of measured and theoretical isotope pattern for the Nd, Sm, and Dy (see Fig. 3) complexes. A subsequent loss of a neutral $Ln(NO_3)_3$

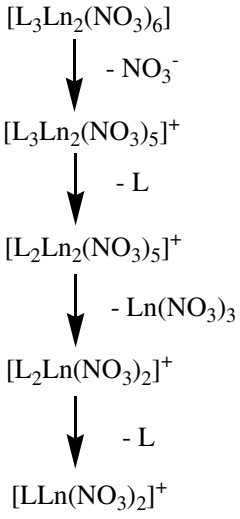

Fig. 2. The fragmentation pathway for the complexes **1**–**6** in ESI–MS.

Table 3
Electrospray mass spectral data for prepared compounds, m/z (rel. intensity)

Complex	**1** (Pr)	**2** (Nd)	**3** (Sm)	**4** (Dy)	**5** (Lu)	**6** (Lu)
Fragment						
M^+	2028[a]	2030[a]	2050[a]	2074[a]	2096[a]	2012[a]
$[M - NO_3]^+$	1966[a]	1968[a]	1988[a]	2012[a]	2034[a]	1950 (1)
$[M - L - NO_3]^+$	1508 (20)	1515 (20)	1530 (10)	1551 (10)	1576 (15)	1520 (20)
$[L_2Ln(NO_3)_2]^+$	1181 (100)	1184 (100)	1194 (100)	1204 (100)	1215 (100)	1159 (100)
$[LLn(NO_3)_2]^{+b}$	723	724	736	744	757	729
$[LLn(NO_3)_2–HNO_2]^{+c}$	676	677	689	699	710	682

[a] Not observed.
[b] MS^2 experiments.
[c] MS^3 experiments.

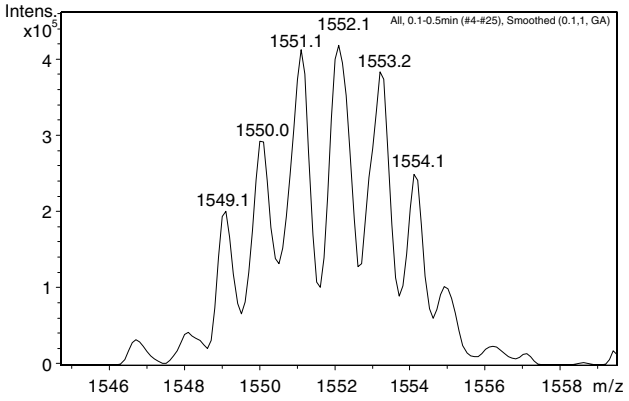

Fig. 3. The experimental isotope pattern of the binuclear $[M - L - NO_3]^+$ fragment with the composition of $C_{56}H_{56}N_5O_{19}Dy_2P_4$.

moiety provides the most intense signals $[(dppbO_2)_2Ln(NO_3)_2]^+$ in all spectra (see Table 3). Two most abundant ions $[(dppbO_2)_2Ln_2(NO_3)_5]^+$ and $[(dppbO_2)_2Ln(NO_3)_2]^+$ were mass selected and fragmented in MS^2 experiments. The loss of neutral $Ln(NO_3)_3$ and the sequential detachment of $dppbO_2$ was corroborated in every complex. In the next MSMS step (MS^3) all fragments $[(dppbO_2)Ln(NO_3)_2]^+$ were found to lose 47 amu. This loss could correspond to HNO_2. The general fragmentation pathway is summarized in Fig. 2. Addition of 0.1% of HCOOH to enhance ionization or changing the solvent to methanol/water (1:1) had no effect on the signal intensities or the appearance of the spectra. Experiments acquired in the negative ion mode displayed fragmentation patterns similar to the positive mode but with much weaker signal intensities and the spectra were dominated by the $[Ln(NO_3)_4]^-$ ions.

To conclude, we have prepared and characterized five binuclear lanthanide complexes as a continuation of our thorough study on the interaction of lanthanide cations with the ligands of diphosphine dioxide type. In the series of $Ph_2P(O)–(CH_2)_n–P(O)Ph_2$ ($n = 1, 2, 4$) ligands, the shortest one was previously found to form chelates with lanthanides [2]; we have prepared 2D coordination polymers with the medium length ligand [1]; and finally, in the present work, we observed the restoration of the molecularity in the complexes with $dppbO_2$. It is obvious, that the lack of rigid backbone allows the aliphatic ligands to take upon chelate arrangements. Thus, for the preparation of polymeric complexes the appropriate combination of length and rigidity will be of crucial importance.

3. Experimental

The preparation of $Ph_2P(O)–(CH_2)_4–P(O)Ph_2$-($dppbO_2$) was based on the previously described method [15]. IR spectra (KBr pellets, 4000–400 cm^{-1}) were collected on an EQUINOX 55/S/NIR FTIR spectrometer. Microanalyses were performed using a ThermoFinnigen Co. CHN Analyzer Flash EA 1112. Melting points were measured on a Boetius melting-point apparatus.

A mixture of $dppbO_2$ (250 mg, 0.545 mmol) and the lanthanide nitrate (0.273 mmol) in methanol (30 ml) was sealed in a 250-ml stainless-steel reactor Berghof HR-200 with a Teflon liner, heated for 24 h to 140 °C with a RHS-295 heater controlled by a BAR-945 unit, and then slowly cooled to room temperature. After next 24 h the autoclave was opened and a crystalline solid was collected and washed with methanol.

*3.1. $(dppbO_2)Pr(NO_3)_3(\mu\text{-}dppbO_2)Pr(NO_3)_3(dppbO_2)$ (**1**)*

Yield: 258 mg (93.1%). M.p. >300 °C. *Anal.* Calc.: C, 49.72; H, 4.17; N, 4.14. Found: C, 48.70, H, 4.23, N, 4.91%. IR: 481 vw, 505 w, 542 m, 553 s, 671 vw, 694 m, 712 w, 723 m, 733 m, 744 m, 780 vw, 794 vw, 820 vw, 881 vw, 895 vw, 998 vw, 1029 w, 1072 w, 1098 s, 1124 s, 1146 vs, 1152 vs, 1171 m, 1217 vw, 1240 vw, 1291 s, 1311 s, 1355 vw, 1384 s, 1438 vs, 1468 vs, 1591 vw, 2939 vw, 3059 vw, 3419 vw.

*3.2. $(dppbO_2)Nd(NO_3)_3(\mu\text{-}dppbO_2)Nd(NO_3)_3(dppbO_2)$ (**2**)*

Yield: 125 mg (45.0%). M.p. >300 °C. *Anal.* Calc.: C, 49.56; H, 4.16; N, 4.13. Found: C, 48.20; H, 4.06; N,

4.90%. IR: 480 w, 504 m, 537 m, 542 m, 552 vs, 671 w, 694 s, 711 m, 723 s, 734 m, 743 m, 780 vw, 794 vw, 820 vw, 880 vw, 895 vw, 997 w, 1029 m, 1072 w, 1099 s, 1124 s, 1138 s, 1147 vs, 1154 vs, 1173 m, 1217 vw, 1239 vw, 1291 s, 1313 vs, 1355 vw, 1385 m, 1438 vs, 1467 vs, 1591 vw, 2940 vw, 3059 vw.

3.3. $(dppbO_2)Sm(NO_3)_3(\mu\text{-}dppbO_2)Sm(NO_3)_3(dppbO_2)$ (**3**)

Yield: 220 mg (78.6%). M.p. >300 °C. *Anal*. Calc.: C, 49.26; H, 4.13; N, 4.10. Found: C, 47.30, H, 4.00, N, 4.82%. IR: 481 vw, 504 w, 513 w, 537 m, 542 m, 553 s, 672 vw, 695 m, 711 w, 723 m, 737 m, 744 m, 756 w, 781 vw, 795 vw, 819 vw, 882 vw, 897 vw, 998 vw, 1030 w, 1072 w, 1100 s, 1124 s, 1139 s, 1156 vs, 1176 m, 1225 vw, 1240 vw, 1291 m, 1318 s, 1354 vw, 1384 s, 1438 vs, 1467 vs, 1591 vw, 2944 vw, 3059 vw, 3649 vw.

3.4. $(dppbO_2)Dy(NO_3)_3(\mu\text{-}dppbO_2)Dy(NO_3)_3(dppbO_2)$ (**4**)

Yield: 198 mg (70.0%). M.p. >300 °C. *Anal*. Calc.: C, 48.68; H, 4.09; N, 4.06. Found: C, 46.10, H, 3.93, N, 4.73%. IR: 478 vw, 505 w, 513 w, 537 m, 542 m, 553 s, 672 vw, 695 m, 711 w, 723 m, 742 m, 756 w, 781 vw, 795 vw, 819 vw, 882 vw, 899 vw, 998 vw, 1031 w, 1073 vw, 1102 s, 1124 s, 1141 s, 1159 vs, 1180 m, 1221 vw, 1293 s, 1323 vs, 1353 vw, 1384 m, 1438 vs, 1472 vs, 1591 vw, 2941 vw, 3059 vw, 3649 vw.

3.5. $(dppbO_2)Lu(NO_3)_3(\mu\text{-}dppbO_2)Lu(NO_3)_3(dppbO_2)$ (**5**)

Yield: 223 mg (75.5%). M.p. 241–242 °C. *Anal*. Calc.: C, 48.10; H, 4.04; N, 4.01. Found: C, 50.30, H, 4.29, N, 4.07%. IR: 484 vw, 508 w, 538 m, 553 s, 694 m, 710 w, 723 m, 746 m, 807 vw, 998 vw, 1030 vw, 1072 vw, 1100 m, 1124 m, 1148 vs, 1183 w, 1236 vw, 1299 m, 1384 s, 1438 m, 1480 m, 1591 vw, 2937 vw, 3058 vw, 3654 vw.

4. Mass spectrometry

The ion trap mass spectrometer Esquire 2000 (Bruker, Germany) with electrospray ionization was used for ESI–MS analyses. Solid samples were dissolved in water and diluted in acetonitrile/water (1:1). The samples were injected directly into the electrospray ion source at a flow rate of 4 μl min^{-1}. The spectra were recorded both in positive and negative mode. The capillary voltage was 4500 V. Smart Parameter Settings mode was used to optimize other parameters for MS and MSMS operation. The temperature of sampling capillary was set to 200 °C (or 250 °C).

5. Crystallography

Diffraction data were collected on a KUMA KM-4 κ-axis diffractometer equipped with a CCD detector, with Mo Kα radiation ($\lambda = 0.71073$ Å). The temperature during data collection was 120(2) K. The intensity data were corrected for Lorentz and polarization effects; absorption correction was applied for all data. The structures were solved by direct methods and refined by full-matrix least-squares methods. The structures are isomorphous, the contraction in lattice parameters reflects the decreasing ionic radius in the lanthanide series. The asymmetric part is built of the $(dppbO_2)Ln(NO_3)_3(Ph_2P(O)CH_2CH_2)$ mononuclear unit, which yields the whole binuclear molecule upon inversion operation. There is a significant disorder in all structures, mainly in the bridging $dppbO_2$ ligand. Its Ph_2P moieties were refined over two sites with almost equal occupancies; the central chain was modelled over three paths in an approximately 0.5:0.25:0.25 ratio. To ensure the reasonable description of a thermal motion in disordered phenyl groups, the rigid-bond restraint was applied for the ring carbon atoms. Nevertheless, in sporadic cases some of the anisotropic displacement parameters became 'non-positive definite' (mainly the *ipso* carbons in phenyl groups), therefore the attempts to describe them anisotropically were abandoned. For all other non-hydrogen atoms the anisotropic thermal parameters were used. The amount of the solvent was initially refined, and later fixed to 0.75 molecules of methanol per asymmetric unit.

The software packages used were: XCALIBUR CCD system for the data collection/reduction [16], and SHELXTL for the structure solution, refinement, and drawing preparation [17]. Details of the data collection and structure refinement are listed in Table 1. Crystallographic data for structures reported in this paper are available from the CCDC, 12 Union Road, Cambridge CB2 1EZ, UK (fax: +44 1223 336 033; e-mail: deposit@ccdc.cam.ac.uk; www: http://www.ccdc.cam.ac.uk) on request, quoting the Deposition Nos. CCDC 275118–275121.

Acknowledgements

This work was supported by the Ministry of Education of the Czech Republic (MSM0021622410 and MSM0021622415). We thank Professor Zdenek Travnicek, Palacky University, Olomouc, for elemental analyses.

References

[1] Z. Spichal, M. Necas, J. Pinkas, Inorg. Chem. 44 (2005) 2074.
[2] A.M.J. Lees, A.W.G. Platt, Inorg. Chem. 42 (2003) 4673.
[3] C.A. Tolman, Chem. Rev. 77 (1977) 313.

[4] H.A. Mayer, W.C. Kaska, Chem. Rev. 94 (1994) 1239.
[5] P. Dierkes, P.W.N.M. van Leeuwen, J. Chem. Soc., Dalton Trans. (1999) 1519.
[6] G.J. Palenik, M. Mathew, W.L. Steffen, G. Beran, J. Am. Chem. Soc. 97 (1975) 1059.
[7] W. Henderson, B.K. Nicholson, L.J. McCaffrey, Polyhedron 17 (1998) 4291.
[8] C. Burda, X. Chen, R. Narayanan, M.A. El-Sayed, Chem. Rev. 105 (2005) 1025.
[9] G. Bonavia, R.C. Haushalter, C.J. O'Connor, J. Zubieta, Inorg. Chem. 35 (1996) 5603.
[10] P.M. Forster, P.M. Thomas, A.K. Cheetham, Chem. Mater. 14 (2002) 17.
[11] S. Feng, R. Xu, Acc. Chem. Res. 34 (2001) 239.
[12] M.R.M. Fontes, G. Oliva, J. Zukerman-Schpector, Acta Cryst. C47 (1991) 2699.
[13] W. Levason, E.H. Newman, M. Webster, Polyhedron 19 (2000) 2697.
[14] A.M.J. Lees, J.M. Charnock, R.A. Kresinski, A.W.G. Platt, Inorg. Chim. Acta 312 (2001) 170.
[15] P. Calcagno, B.M. Kariuki, S.J. Kitchin, J.M.A. Robinson, D. Philp, K.D.M. Harris, Chem. Eur. J. 6 (2000) 2338.
[16] Oxford Diffraction Ltd., XCALIBUR CCD System, CrysAlis Software System, Version 1.170. Oxford, UK, 2003.
[17] SHELXTL, Version 5.10, Bruker AXS, Inc., Madison, WI, 1997.

Available online at www.sciencedirect.com
SCIENCE DIRECT®
Polyhedron 25 (2006) 815–820
POLYHEDRON
www.elsevier.com/locate/poly

Synthesis and reaction kinetics of Pd(1,5-cyclooctadiene)Cl_2 with *N*,*N*′-methylene-bis(2-aminopyridyl): An efficient catalyst for Suzuki-cross-coupling reactions

Sasmita Mohanty, Benudhar Punji, Maravanji S. Balakrishna *

Department of Chemistry, Indian Institute of Technology Bombay, Powai, Mumbai 400 076, India

Received 24 July 2005; accepted 10 August 2005
Available online 5 October 2005

Abstract

An inexpensive bidentate ligand *N*,*N*′-methylene-bis(2-aminopyridyl) (**1**) has been synthesized. Reaction of **1** with [Pd(COD)Cl_2] affords a stable chelate complex, [{$NC_5H_4N(H)(\mu\text{-}CH_2)(H)NC_5H_4N\text{-}\kappa N,\kappa N$}$PdCl_2$] (**2**). The kinetics of the pseudo-unimolecular reaction of *N*,*N*′-methylene-bis(2-aminopyridyl) with Pd(1,5-cyclooctadiene)Cl_2 has been studied over the range $3.0 \leqslant 10^3$ [**1**] $\leqslant 7.0$ mol dm^{-3}, 30 °C $\leqslant t \leqslant$ 40 °C. The rate constants and equilibrium constants were calculated. Entropy and enthalpy of the reaction are found to be -42 ± 1 J K^{-1} mol^{-1} and 75 ± 1 kJ mol^{-1}, respectively, which clearly indicates that the substitution reaction follows associative mechanism. The complex **2** was tested for the Suzuki-cross-coupling reaction of a variety of aryl halides with aryl boronic acids in methanol at room temperature or at 60 °C, giving generally high yields for both activated and inactivated aryl bromides. The effect of solvents as well as the effect of base on the Suzuki-coupling reaction is also investigated.
© 2005 Elsevier Ltd. All rights reserved.

Keywords: Reaction kinetics; Nitrogen donor ligands; Palladium complex; Catalysis; Suzuki-cross-coupling reactions

1. Introduction

In general, substitution reactions of square-planar complexes and particularly that of Pd(II) and Pt(II) have received much attention from various investigations over the past two decades [1]. Palladium or platinum complexes containing nitrogen donor ligands are widely employed in kinetics and mechanistic investigations. Most of the palladium(II) complexes exhibit 10^4–10^5 times higher reactivity than platinum(II) complexes, although their structural and equilibrium behavior is similar [2]. This interest of studying the Pd(II) and Pt(II) complexes mainly focuses on the ability to use steric and electronic effects to tune the solubility, acidity and reactivity of such complexes for their probable utility as antitumor drugs [3] and as homogeneous catalysts [4].

Palladium complexes containing phosphines [5], phosphates [6], and phosphine oxides [7] are widely used as catalyst in Suzuki-Miyaura cross-coupling reactions. However, these catalysts are sensitive to moisture and air, therefore require air free handling to minimize ligand oxidation or stable oxidative addition products. Recently, nitrogen donor ligands have emerged as efficient partners for the Suzuki reaction in order to circumvent the problems associated with tertiary phosphine derivatives [8]. The nitrogen donor ligands such as *N*-heterocyclic carbenes [9] imine and amine palladacycles [10], oxime palladacycles [11] and diazobutadiene derivatives [12] have shown excellent activity for Suzuki-reactions. Current technologies demand new catalysts that are inexpensive, accessible, moisture and air stable,

* Corresponding author. Tel.: +91 22 2576 7181; fax: +91 22 2576 7152/2572 3480.
E-mail address: krishna@iitb.ac.in (M.S. Balakrishna).

0277-5387/$ - see front matter © 2005 Elsevier Ltd. All rights reserved.
doi:10.1016/j.poly.2005.08.013

non-toxic, and most importantly effective under mild experimental conditions towards aryl halides. In view of this and as a continuation of our work in designing new ligand systems for exploring their organometallic chemistry and catalytic utility in organic synthesis [13], here in we report the synthesis of a cheap, air and moisture stable, phosphine free ligand *N*,*N*′-methylene-bis(2-aminopyridyl) (**1**) and the kinetic study of **1** with $Pd(COD)Cl_2$. The catalytic utility of $[\{NC_5H_4N(H)\text{-}(\mu\text{-}CH_2)(H)NC_5H_4N\text{-}\kappa N,\kappa N\}PdCl_2]$ (**2**) in Suzuki-cross-coupling reactions is also described.

2. Results and discussion

Reaction of two equivalent of 2-amino pyridine with 37% aqueous solution of formaldehyde at 0 °C gives the *N*,*N*′-methylene-bis(2-aminopyridyl) (**1**) in 72% yields (Scheme 1). The IR spectrum of **1** shows two major bands at 3394 and 3023 cm^{-1} for ν(N–H) and ν(C–H), respectively. The ^1H NMR spectrum shows a broad singlet at 6.35 ppm for N–H protons and a triplet at 5.03 ppm for methylene protons. Treatment of **1** with $[Pd(COD)Cl_2]$ in toluene gives the metal complex **2** in good yield, which is insoluble in most of the organic solvents so it cannot be characterized fully. The IR spectrum of complex **2** shows ν(N–H) at 3343 cm^{-1}. The elemental analysis is in good agreement with the proposed molecular compositions.

2.1. Spectra and kinetics

Spectral changes resulting from mixing metal precursor $[Pd(COD)Cl_2]$ and ligand **1** solution were recorded over the range 250–600 nm to establish a suitable wavelength at which kinetic measurements could be performed. Addition of $Pd(COD)Cl_2$ solution to a solution of *N*,*N*′-methylene-bis(2-aminopyridyl) resulted in an increase in absorbance in the visible range. The absorbance spectra of the mixture of $Pd(COD)Cl_2$ and *N*,*N*′-methylene-bis(2-aminopyridyl) and shifting of λ_{max} from ~330 to ~350 nm indicates the formation of complex **2** (Fig. 1).

Pd(II) complexes are usually considered as soft acids [14]. In $Pd(COD)Cl_2$ complex, palladium(II) is in square planner geometry. Rate is very sensitive to the nature of entering group. In the ligand *N*,*N*′-methylene-bis (2-aminopyridyl), the nucleophilicity of the pyridyl nitrogens is more as compared to the nitrogen of the secondary amine groups. Hence the ligand binds the metal through the pyridine nitrogen rather than the amine nitrogen (Scheme 1).

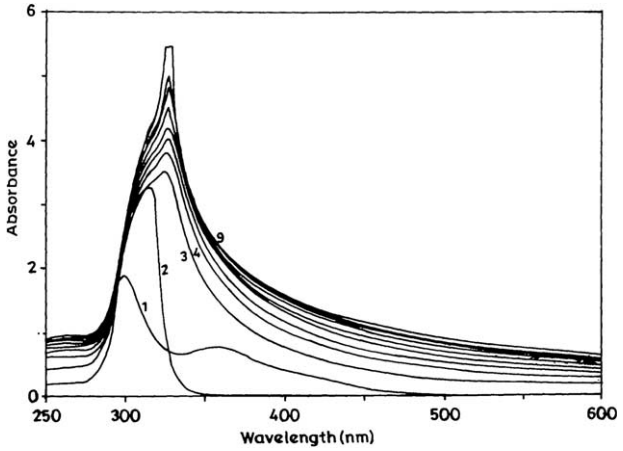

Fig. 1. Spectral difference among $[Pd(COD)Cl_2]$, *N*,*N*′-methylene-bis(2-aminopyridyl) and the product complex. 1. $[Pd(COD)Cl_2] = 3.0 \times 10^{-4}$ mol dm^{-3} at 30 °C; 2. *N*,*N*′-methylene-bis(2-aminopyridyl) = 9.0×10^{-3} at 30 °C; 3. product complex after 4 min at 30 °C; 4. after 5 min; 5. after 6 min; 6. after 7 min; 7. after 9 min; 8. after 11 min and 9. after 14 min.

2.2. Effect of $[Pd(COD)Cl_2]$ on the reaction rate

In the first set of kinetic experiments, the $[Pd^{2+}]_T$ was varied at constant concentration of ligand 5.0×10^{-3} mol dm^{-3} at 40 °C temperature and toluene medium. The pseudo-first-order plots are linear, giving $10^3 k_{obs} = 4.5$ s^{-1} when $[Pd^{2+}]_T$ was changed from 3.0×10^{-4} to 1.0×10^{-3} mol dm^{-3}. The independence of k_{obs} at 40 °C under the condition $[\mathbf{1}] = 5.0 \times 10^{-3}$ and over the $[Pd^{2+}]_T$ range from 3.0×10^{-4} to 1.0×10^{-3} mol dm^{-3} is in agreement with first-order dependence on $[Pd^{2+}]_T$. To verify this we have also carried out the reaction of two equivalent of $[Pd(COD)Cl_2]$ with *N*,*N*′-methylene-bis(2-aminopyridyl)} and the product was characterized through FT IR and elemental analysis. The product showing a strong N–H peak at 3342 cm^{-1}, which

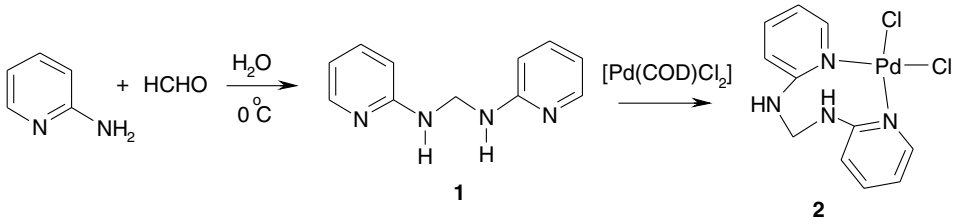

Scheme 1.

indicates only pyridine nitrogen atoms are coordinating to the palladium center. The rate law therefore is given by the following equation:

$$\text{Rate} = -\mathrm{d}[\mathrm{Pd}^{2+}]_T/\mathrm{d}t = k_{obs}[\mathrm{Pd}^{2+}]_T. \quad (1)$$

2.3. Effect of N,N′-methylene-bis(2-aminopyridyl) on reaction rate

The effect of ligand concentration on the reaction rate was studied at fixed metal concentration 3.0×10^{-4} mol dm^{-3} at various temperatures. The concentration of ligand was varied from 3.0×10^{-3} to 7.0×10^{-4} mol dm^{-3}. The rate constants are presented in Table 1, which are comparable with previous literature data [1a]. It is observed that as ligand concentration increases, the rate constant increases in a linear fashion (Fig. 2), which is characteristic of the ligand substitution reactions of square planar complexes. It proceeds according to the associative mechanism [15].

The probable mechanism for the substitution reaction may be delineated as in Scheme 2.

The rate law can be derived for the substitution reaction in the following manner:

$$\mathrm{d}[C]/\mathrm{d}t = k_{ip}[\mathrm{B}]_e = k_{ip}K_{ip}[\mathrm{A}]_e[\mathrm{LH}_2], \quad (2)$$

$$\begin{aligned}[\mathrm{A}]_T &= [\mathrm{A}]_e + [\mathrm{B}]_e \\ &= [\mathrm{A}]_e + K_{ip}[\mathrm{A}]_e[\mathrm{LH}_2] \\ &= [\mathrm{A}]_e\{1 + K_{ip}[\mathrm{LH}_2]\} \\ &= [\mathrm{A}]_e = [\mathrm{A}]_T/\{1 + K_{ip}[\mathrm{LH}_2]\},\end{aligned}$$

$$\mathrm{d}[C]/\mathrm{d}t = k_{ip}K_{ip}[\mathrm{A}]_T[\mathrm{LH}_2]/\{1 + K_{ip}[\mathrm{LH}_2]\},$$

$$\text{Rate} = k_{obs}[\mathrm{A}]_T, \quad (3)$$

Table 1
Effect of reaction rate on *N*,*N*′-methylene-bis(2-aminopyridyl)[a]

10^3[**1**] (mol dm^{-3})	T (°C)	$10^3 k_{obs}$ (s^{-1})	$10^2 k_{ip}$ (s^{-1})	K_{ip}
3.0	30	1.7	0.4	207.5
4.0	30	1.8		
5.0	30	2.0		
6.0	30	2.4		
7.0	30			
3.0	35	2.0	0.69	158.0
4.0	35	2.7		
5.0	35	2.8		
6.0	35	3.2		
7.0	35	4.1		
3.0	40	3.3	1.03	145.6
4.0	40	4.2		
5.0	40	4.4		
6.0	40	4.8		
7.0	40	5.0		

[a] Values of $10^3 k_{obs}$ (s^{-1}) at different ligand concentrations and different temperatures keeping the metal concentration constant $[\mathrm{Pd}^{+2}] = 3.0 \times 10^{-4}$ mol dm^{-3}.

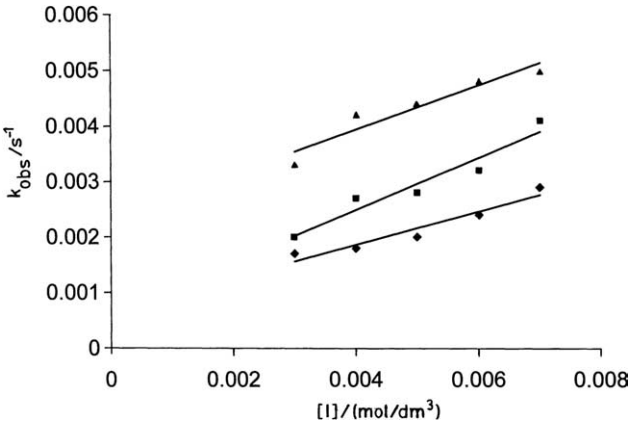

Fig. 2. Rate constants vs. ligand concentration at various temperatures. ▲, at 40 °C, ■, at 35 °C, ◆, at 30 °C.

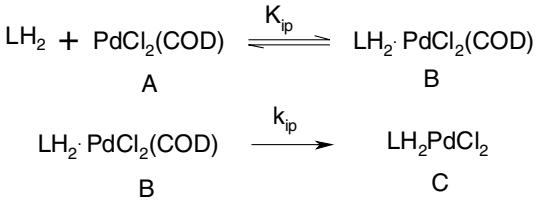

Where LH_2 = N, N'-methylene-bis(2-aminopyridyl)
K_{ip} = equilibrium constant
k_{ip} = ion-pair rate constant

Scheme 2.

$$k_{obs} = k_{ip}K_{ip}[\mathrm{LH}_2]/\{1 + K_{ip}[\mathrm{LH}_2]\},$$

$$1/k_{obs} = 1/k_{ip} + 1/k_{ip}K_{ip}[\mathrm{LH}_2]. \quad (4)$$

The plot of $1/k_{ip}$ versus $1/[\mathrm{LH}_2]$ should be linear with an intercept $1/k_{ip}K_{ip}$. This plot is linear at all temperatures studied. k_{ip} is determined from the reciprocal of the intercept and K_{ip} is calculated from intercept/slope ratio. The values of k_{ip}, K_{ip} are given in Table 1.

2.4. Effect of temperature on the rate

The reaction is studied at three different temperatures with different ligand concentrations. Activation parameters were calculated using Eyring equation and compared with literature data of the analogous systems. The low $\Delta H^{\#}$ value with negative $\Delta S^{\#}$ value, suggest an associative mechanism [1a,16]. The values of $\Delta H^{\#}$ and $\Delta S^{\#}$ are 75 kJ mol^{-1} and -42 J K^{-1} mol^{-1}, respectively, which are comparable with the analogous systems (Table 2). ΔH^0 and ΔS^0 values were calculated from the $\ln K$ versus $10^3/T$ plot. ΔH^0 is calculated from the slope and ΔS^0 is calculated from the intercept. ΔH^0 and ΔS^0 values were found to be 32.68 kJ mol^{-1} and 148.5 J K^{-1} mol^{-1}, respectively.

Table 2
Effect of temperature on the rate

System	$\Delta H^{\#}$ (kJ mol^{-1})	$\Delta S^{\#}$ (J K^{-1} mol^{-1})	Ref.
Diethylamine	23 ± 1	−9 ± 5	[1a]
L-Cysteine	38 ± 1	−68 ± 2	[1e]
L-Glutathione	33 ± 1	−73 ± 2	[1e]
DL-Penicillamine	47 ± 1	−43 ± 1	[16]
N,*N*′-methylene-bis(2-aminopyridyl)	75 ± 1	−42 ± 1	this work

Comparison of activation parameters with analogous systems.

2.5. Catalytic studies

The complex **2** effectively catalyses the Suzuki-cross-coupling reaction of a variety of aryl halides with phenyl boronic acid, affording the desired biaryls in high yields (Table 3). All the reactions were carried out at room temperature using 1 mol% of catalyst in methanol. It is notable that the deactivated, electron-rich aryl halides (entries 3 and 4) as well as activated, electron poor ones (entry 1) also resulted in high yields. In general, this coupling can be satisfactorily carried out at room temperature. When there is a need to improve the yield, it is carried out at elevated temperature (60 °C). We have also studied the coupling of some heterocycles and sterically bulky or highly substituted aryl bromides with phenyl boronic acid. The coupling of 2-bromo pyridine and 2-bromo thiophene with phenyl boronic acid give the moderate yield (54% and 66%, respectively), at room temperature. Surprisingly, when these reactions were carried out at 60 °C, both 2-bromo pyridine and 2-bromo thiophene give excellent conversions (entries 6 and 7). The highly substituted 2,4-dimethoxy-1-bromo benzene gives low coupling product at room temperature as well as at elevated temperature (entry 8). The high efficiency of the catalyst at room temperature and 60 °C makes it a valuable for thermally sensitive substrates. In the literature, few catalysts are known for Suzuki-cross-coupling reactions, which are effective at room temperature [5c,10a,17].

The activity of complex **2** is found to be superior to that in $Pd(OAc)_2$/Dabco, where reaction were carried out with 3 mol% and at 110 °C [18]. In comparison with other N-coordinated palladium catalysts, the catalytic activity of **2** is similar to those found in the $Pd_2(dba)_3$/pyrazole-tethered system whose reaction were carried out in dioxane at 55 °C [19], and a palladium ferrocenylamine complex at room temperature in methanol [4c].

To examine the solvent effect, the coupling between 4-bromoacetophenone and phenyl boronic acid catalyzed by the catalyst **2** with a number of solvents (Table 4). It is found that polar solvent such as MeOH is more productive. This may be due to higher complex solubility. Although, non-polar solvents like toluene also give good conversions, it takes more time for the reaction.

The influence of base on the coupling reaction of 4-bromoacetophenone and phenyl boronic acid is also carried out. The inorganic bases (Cs_2CO_3, KOH, Na_2CO_3, KF and K_2CO_3) and organic base (Et_3N) are

Table 3
Suzuki-cross-coupling of aryl halides with phenyl boronic acid[a]

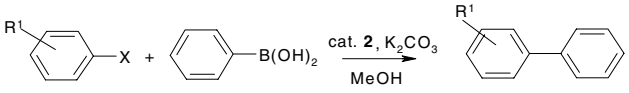

Entry	Aryl halides	Product	Time (h)	Yield (%)[b]
1	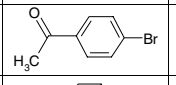	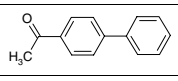	1	100
2	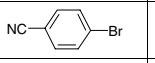	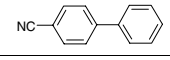	1	99
3	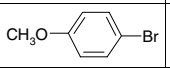	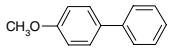	3	92
4	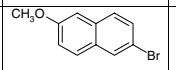	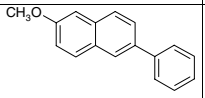	1	92
5	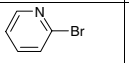	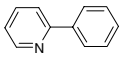	5	54 (98)[c]
6	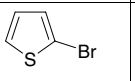	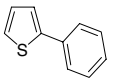	12	66 (98)[c]
7	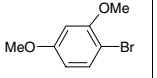	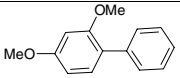	12	36 (47)[c]
8	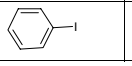	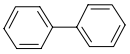	3	96

[a] Reaction conditions: aryl bromide (0.5 mmol), phenyl boronic acid (0.75 mmol), K_2CO_3 (1 mmol), MeOH (5 mL).
[b] Conversion to the coupled product determined by GC, based on aryl bromide or dodecane; average of two runs.
[c] At 60 °C for 2 h.

Table 4
Effect of solvent on the coupling reaction[a]

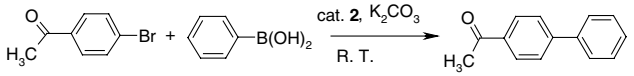

Entry	Solvent	Yield(%)[b]
1	Methanol	100
2	Toluene	91
3	Acetone	79
4	THF	75
5	Dioxane	73

[a] Reaction conditions: 4-bromo acetophenone (0.5 mmol), phenyl boronic acid (0.75 mmol), K_2CO_3 (1 mmol). Catalyst **2** (1 mol%), solvent (5 mL), reaction time was not optimized.
[b] Conversion to the coupled product determined by GC, based on aryl bromide or dodecane; average of two runs.

Table 5
Effect of base on the coupling reaction[a]

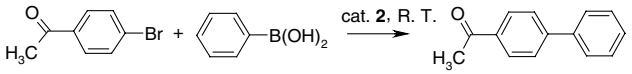

Entry	Base	Yield(%)[b]
1	K_2CO_3	>99
2	Na_2CO_3	>99
3	KOH	99
4	Et_3N	98
5	Cs_2CO_3	98
6	KF	97

[a] Reaction conditions: catalyst 1 mol%, 4-bromo acetophenone (0.5 mmol), phenyl boronic acid (0.75 mmol), base (1 mmol), MeOH (5 mL), 1 h.
[b] Conversion to the coupled product determined by GC, based on aryl bromide or dodecane; average of two runs.

taken into consideration for the coupling reaction. It is observed that all most all the bases are giving excellent conversions with in 1 h (Table 5).

3. Summary

In conclusion, we have synthesized an inexpensive ligand *N*,*N*′-methylene-bis(2-aminopyridyl) and its palladium complex **2**. We also studied the substitution reaction kinetics of **1** with [Pd(COD)Cl_2], which follows the associative mechanism. The complex **2** was found to be excellent catalyst for the Suzuki-coupling reaction for a variety of aryl halides with phenyl boronic acid under mild conditions. The Suzuki-coupling reactions of other highly substituted and bulky aryl halides as well as other reactions such as Heck reaction, amination, hydrogenation using this catalyst system are underway.

4. Experimental

The metal precusor $PdCl_2$ (1,5-cyclooctadiene) is prepared according to the published procedure. Others chemicals were obtained locally and used without further purifications. Solvents were dried and distilled prior to use by conventional methods. The kinetic studies were done using JASCO V-570 UV/VIS/NIR spectrophotometer. The ^{1}H NMR (δ in ppm) spectra were obtained on a VRX 400 spectrometer operating at frequency of 400 MHz. The spectra were recorded in $CDCl_3$ (or DMSO-d_6) solutions with $CDCl_3$ as an internal lock; TMS was used as external standards for ^{1}H NMR. Positive shifts lie downfield of the standard in all of the cases. Infrared spectra were recorded on a Nicolet Impact 400 FT IR instrument in KBr disk or nujol mull. Microanalyses were carried out on a Carlo Erba Model 1106 elemental analyzer. Melting points of all compounds were determined on Veego melting point apparatus and were uncorrected. GC analyses were performed on a Perkin–Elmer Clarus 500 GC fitted with packed column.

4.1. Synthesis of *N*,*N*′-methylene-bis(2-aminopyridyl) (**1**)

To the solution of 2-aminopyridine (2 g, 0.02 mol) in water (20 mL), 37% formaldehyde solution (0.86 mL, 0.01 mol) was added dropwise at 0 °C and the reaction mixture was stirred at room temperature for 8 h. The white precipitate formed was filtered, washed several times with water and then with diethyl ether and dried. It was dissolved in acetone, dried over Na_2SO_4 and concentrated, which on cooling to −25 °C, gives analytically pure product of **1**. Yield: 72% (1.53 g). m.p.: 122–124 °C. *Anal*. Calc. for $C_{11}H_{12}N_4$: C, 65.97; H, 6.06; N, 27.97. Found: C, 65.76; H, 5.98; N, 27.89%. FT IR (KBr disk) cm^{-1}: ν_{NH} 3394 s, 3258 s; ν_{CH}, 3023 s. ^{1}H NMR (400 MHz, $CDCl_3$): δ 8.11 (d, 2H, Py), 7.36 (t, 2H, Py), 6.59 (t, 2H, Py), 6.41 (d, 2H, Py), 6.35 (br, 2H, NH), 5.03 (t, 2H, CH_2).

4.2. Synthesis of $(NC_5H_4NH)CH_2PdCl_2$ (**2**)

To the solution of Pd(COD)Cl_2 (0.05 g, 0.175 mmol) in toluene (6 mL) was added a solution of ligand **1** (0.035 g, 0.175 mmol) also in toluene (8 mL) and stirred at room temperature for 3 h. The yellow precipitate formed was filtered and washed with Et_2O and dried. This product **2** was insoluble in almost all the organic solvent. Yield: 88% (0.058 g). m.p.:196 °C (dec). *Anal*. Calc. for $C_{11}H_{12}Cl_2N_4Pd$: C, 34.99; H, 3.20; N, 14.84. Found: C, 34.75; H, 3.09; N, 14.78%. FT IR (KBr disk) cm^{-1}: ν_{NH} 3343 s, ν_{CH} 3023 s.

4.3. Procedure for kinetic study

A small measured volume (0.1 mL) of 0.01 M metal solutions was taken in an UV–visible cell. The calculated amount of 0.01 M ligand solution was added to it. The total solution taken was 3 mL. So the required amount of toluene is added to the cell to maintain the fixed volume. The contents of the cell were thoroughly mixed by rapid shaking and variations of the absorbance were monitored at 480 nm as a function of time. All the reactions were carried out under pseudo-first-order conditions with ligand in at least 10-fold excess. The temperature dependence of k_{obs} was studied over the range 30-40 °C. The rate constants k_{obs} were obtained from the slopes of $\ln(A_\infty - A_t)$ versus 't' plots

$$\ln(A_\infty - A_t) = k_{obs}t + C, \quad (5)$$

where A_t and A_∞ are absorbance of the reaction at time 't' and at equilibrium, respectively.

4.4. General procedure for the coupling reaction

In a two-necked round bottom flask under dry nitrogen were placed metal complex **2** (1.9 mg, 0.005 mmol) and 5 mL of methanol. After stirring for 5 min, aryl bromide (0.5 mmol), phenyl boronic acid (0.091 g, 0.75 mmol) and K_2CO_3 (0.138 g, 1 mmol) were introduced into the reaction flask. The mixture was stirred at room temperature or 60 °C for the required time under atmosphere of nitrogen (the course of reaction was monitored by GC analysis). Then the solvent was removed under reduced pressure. The resultant residual mixture was diluted with H_2O (10 mL) and Et_2O (10 mL), followed by extraction twice (2×6 mL) with Et_2O. The combined organic fraction was dried ($MgSO_4$), stripped of the solvent under vacuum and the residue was redissolved in 5 mL of dichloromethane. An aliquot was taken with a syringe and subjected to GC analysis. Yields were calculated versus aryl bromide or dodecane as an internal standard.

Acknowledgements

We are grateful to the Department of Science and Technology (DST), New Delhi for funding through Grant SR/S1/IC-05/2003. S.M. thanks IIT Bombay for Research Fellowship (RA) and B.P. thanks CSIR, New Delhi for Fellowship (JRF and SRF).

References

[1] (a) S. Matsumoto, S. Kawaguchi, Bull. Chem. Soc. Jpn. 53 (1980) 1577;
(b) Z.D. Bugarcic, G. Liehr, R. van Eldik, J. Chem. Soc., Dalton Trans. 14 (2002) 2825;
(c) Z.D. Bugarcic, G. Liehr, R. van Eldik, J. Chem. Soc., Dalton Trans. (2002) 951;
(d) S. Aizawa, Y. Sone, T. Kawamoto, S. Yamada, M. Nakamura, Inorg. Chem. Acta 338 (2002) 235;
(e) Z.D. Bugarcic, D.M. Jancic, A.A. Shoukry, M.M. Shoukry, Monatsh Chem. 135 (2004) 151.

[2] T. Rau, R. van Eldik, in: A. Sigel, H. Sigel (Eds.), Metal Ions in Biological Systems, vol. 32, Marcel Dekker, New York, 1996, p. 339.

[3] (a) B. Lippert (Ed.), Cisplatin Chemistry and Biochemistry of Leading Anticancer Drugs, CHIPS, Weimer, TX, 1999;
(b) J. Reedijk, Chem. Rev. 99 (1999) 2499;
(c) E.R. Jamieson, S.J. Lippard, Chem. Rev. 99 (1999) 2467.

[4] (a) J.P. Wolfe, R.A. Singer, B.H. Yang, S.L. Buchwald, J. Am. Chem. Soc. 121 (1999) 9550;
(b) T.E. Pickett, C.J. Richards, Tetrahedron. Lett. 42 (2001) 3767;
(c) Z. Weng, S. Teo, L.L. Koh, T.S. Andy Hor, Organometallics 23 (2004) 3603.

[5] (a) X. Bei, H.W. Turner, W.H. Weinberg, A.S. Guram, J. Org. Chem. 64 (1999) 6797;
(b) A. Zapf, A. Ehrentraut, M. Beller, Angew. Chem., Int. Ed. Engl. 22 (2000) 4153;
(c) A.F. Littke, C. Dai, G.C. Fu, J. Am. Chem. Soc. 122 (2000) 4020;
(d) M. Feuerstein, D. Laurenti, C. Bougeant, H. Doucet, M. Santelli, Chem. Commun. 4 (2001) 325;
(e) S.Y. Liu, M.J. Choi, G.C. Fu, Chem. Commun. 23 (2001) 2408.

[6] A. Zapf, M. Beller, Chem. Eur. 6 (2000) 1830.

[7] G.Y. Li, Angew. Chem., Int. Ed. Engl. 40 (2001) 1513.

[8] O. Navarro, R.A. Kelly, S.P. Nolan, J. Am. Chem. Soc. 125 (2003) 16194.

[9] (a) T. Weskamp, V.P.W. Bohm, W.A. Herrmann, J. Organomet. Chem. 585 (1999) 348;
(b) C. Zhang, J. Huang, M.L. Trudell, S.P. Nolan, J. Org. Chem. 64 (1999) 3804;
(c) C. Zhang, M.L. Trudell, Tetrahedron Lett. 41 (2000) 595;
(d) V.P.W. Bohm, C.W.K. Gstottmayr, T. Weskamp, W.A. Herrmann, J. Organomet. Chem. 595 (2000) 186.

[10] (a) H. Weissman, D. Milstein, Chem. Commun. 18 (1999) 1901;
(b) R.B. Bedford, C.S.J. Cazin, Chem. Commun. 17 (2001) 1540.

[11] (a) D.A. Alonso, C. Nájera, M.C. Pacheco, Org. Lett. 2 (2000) 1823;
(b) L. Botella, C. Nájera, Angew. Chem., Int. Ed. Engl. 41 (2002) 179.

[12] G.A. Grasa, A.C. Hillier, S.P. Nolan, Org. Lett. 3 (2001) 1077.

[13] (a) M.S. Balakrishna, R.M. Abhyankar, J.T. Mague, J. Chem. Soc., Dalton Trans. (1999) 1407;
(b) M.S. Balakrishna, R. Panda, J.T. Mague, Inorg. Chem. 40 (2001) 5620;
(c) M.S. Balakrishna, R. Panda, J.T. Mague, J. Chem. Soc., Dalton Trans. (2002) 4617;
(d) S. Priya, M.S. Balakrishna, J.T. Mague, S.M. Mobin, Inorg. Chem. 42 (2003) 1272;
(e) S. Priya, M.S. Balakrishna, J.T. Mague, J. Organomet. Chem. 689 (2003) 3335;
(f) M.S. Balakrishna, P.P. George, J.T. Mague, J. Organomet. Chem. 689 (2003) 3388;
(g) M.S. Balakrishna, P.P. George, S.M. Mobin, Polyhedron 24 (2005) 475.

[14] (a) C.G. Swain, C.B. Scott, J. Am. Chem. Soc. 75 (1953) 141;
(b) R.G. Pearson, J. Am. Chem. Soc. 85 (1963) 3533.

[15] (a) E.F. Basolo, R.G. Pearson, Mechanism of Inorganic Reactions, 2nd ed., Wiley, New York, 1967 (Chapter 5).

[16] Z.D. Bugarcic, D. Ilic, M.I. Djuran, Aust. J. Chem. 54 (2001) 237.

[17] J.P. Wolfe, S.L. Buchwald, Angew. Chem., Int. Ed. Engl. 38 (1999) 2413.

[18] J. Li, W. Liu, Org. Lett. 6 (2004) 2809.

[19] A. Mukherjee, A. Sarkar, Tetrahedron Lett. 46 (2005) 15.

Available online at www.sciencedirect.com
SCIENCE DIRECT®
Polyhedron 25 (2006) 821–822
POLYHEDRON
www.elsevier.com/locate/poly

Preface

In Honour of Professor Mike Hursthouse

Professor Michael B. Hursthouse

When we were recruiting a Lecturer in Inorganic Chemistry at QMC in 1966 I insisted that we should appoint someone who had experience in X-ray crystallography and fortunately we were able to appoint Mike to that post.

Although he had only a second-hand manual diffractometer at his disposal, Mike swiftly settled in and, with his characteristic drive and energy, established a productive X-ray structural group. He was a charismatic teacher who introduced his subject into the undergraduate curriculum. Soon he was attracting substantial research funds and in 1978 obtained a computer-controlled automated diffractometer which transformed the output of structures and enabled him to broaden his collaborations both within and outside the Department. A particularly fruitful collaboration was with Sir Geoffrey Wilkinson at Imperial College. Mike was appointed Reader in Structural Chemistry in 1979 and to a Personal Chair in 1987. Meanwhile he had established a National Crystallographic Service with funding from the Science Research Council, a resounding success, and was becoming recognised worldwide. He also played a leading role with the RSC Chemical Crystallography Group being Chairman from 1983 to 1986.

When I became Executive Editor of *Polyhedron* in 1981, I was fortunate in persuading Mike to deal with the X-ray structural content of all papers submitted to the journal thus establishing the high standards associated with that publication.

Sadly for QMC, Mike was appointed to the Established Chair of Structural Chemistry in the University of Wales, Cardiff, in 1991, then moving to his present Chair at Southampton in 1998.

Mike Hursthouse was an inspiring teacher of undergraduate and postgraduate students and a congenial colleague who enlivened Staff meetings with his forthright contributions.

It was a privilege and a great pleasure having him as a colleague and a friend for life.

Donald C. Bradley
Queen Mary College, University of London, London, UK

0277-5387X/$ - see front matter © 2005 Elsevier Ltd. All rights reserved.
doi:10.1016/j.poly.2005.10.017

Note from the Editors

As past PhD students of Mike Hursthouse we were pleased to be asked to serve as guest editors for this special issue of *Polyhedron*. It is testimony to the respect and affection that colleagues have for Mike that all the authors we approached were immediately enthusiastic about contributing to the issue. We thank them for their submissions, the referees for their hard work and constructive comments, and the editorial and production staff at Elsevier for bringing this issue to fruition to coincide with Mike's 65th birthday.

Alan J. Welch
Department of Chemistry, Heriot-Watt University, Edinburgh, UK
E-mail address: a.j.welch@hw.ac.uk

Paul R. Raithby
Department of Chemistry, University of Bath, Bath, UK

Available online 2 December 2005

Available online at www.sciencedirect.com
SCIENCE DIRECT®
Polyhedron 25 (2006) 823–826
POLYHEDRON
www.elsevier.com/locate/poly

The preparation and characterisation of a series of group IV metallocene dithiolato complexes containing a naphthalene backbone

Stuart D. Robertson, Alexandra M.Z. Slawin, J. Derek Woollins *

School of Chemistry, University of St. Andrews, St. Andrews, Fife KY16 9ST, Scotland, UK

Received 24 June 2005; accepted 4 July 2005
Available online 19 August 2005

Dedicated to Prof. M.B. Hursthouse on the occasion of his 65th birthday, in recognition of the enormous contibution he has made to chemical crystallography.

Abstract

Reduction of the sulfur–sulfur bond of naphtho[1,8-*cd*]-1,2-dithiole with 2 equivalents of $Li(BEt)_3H$ to give the dilithium salt followed by the addition of an equivalent of bis(pentamethyl)metallocene dichloride $[(Cp)^*_2MCl_2, M = Ti, Zr, Hf, Cp^* = C_5Me_5]$ gives the sulfur bonded complexes $(Cp)^*_2TiS_2C_{10}H_6$ (**1**), $(Cp)^*_2ZrS_2C_{10}H_6$ (**2**) and $(Cp)^*_2HfS_2C_{10}H_6$ (**3**) containing six-membered MS_2C_3 rings. The products were obtained in moderate yield as crystals and have been fully characterised and had their X-ray crystal structures determined.
© 2005 Elsevier Ltd. All rights reserved.

Keywords: Complex; Thiolates; X-ray structure; Titanium; Sulfur

1. Introduction

The chemistry of the group IV metallocenes has been extensively studied with the majority of the work on complexes of titanocene. Complexes containing a bidentate ligand bound to titanium are quite common, with many examples via a pair of chalcogen atoms. These chalcogens can be bridged by groups such as other chalcogen atoms to give a polychalcogen ring [1,2], phosphorus [3], alkyl groups [4] or nitrogen [5]. Titanocene can also give complexes bound to two monodentate ligands which are essentially similar complexes where the two chalcogen atoms are not connected to each other [6]. These have practical uses in that they can be used in ligand transfer to give platinum thiolato complexes [7]. More recently, we have synthesised a series of titanocene complexes containing a mixture of thiolato, sulfinato and sulfenato ligands [8] linked by an organic aromatic backbone. Dimeric titanocene complexes with two bridging thiolato ligands have been reported [9] and shown to exhibit crown ether like properties, with a silver or copper cation contained in the centre of the structure.

Complexes of zirconocene with a bidentate phosphorus ring [10] or sulfur ring [1], or with two monodentate nitrogen bound ligands have been described [11]. The majority of other chalcogen containing zirconocene complexes contain either two monodentate ligands [12–15] or exist as dimers with two bridging chalcogen atoms [16–18].

Hafnocene is known to exist in a similar complex to zirconocene with two phosphorus atoms bound to the hafnium atom and another phosphorus atom bridging the two to give a four-membered ring [10] and $Cp^*_2HfH_2$ has also been shown to react with RN_3 to give

* Corresponding author. Fax: +44 1334 463384.
E-mail address: jdw3@st-and.ac.uk (J.D. Woollins).

0277-5387/$ - see front matter © 2005 Elsevier Ltd. All rights reserved.
doi:10.1016/j.poly.2005.07.009

an interesting complex with a bidentate N_3 ligand which will lose N_2 at 80 °C [19]. Hafnocene complexes with two monodentate ligands bound through carbon [20] which will thermally decompose to give a complex containing one bidentate ligand are known. Similarly to titanocene and zirconocene complexes, hafnocene complexes with two monodentate sulfur bound ligands have also been described [21] while a dimeric structure with two bridging chalcogen atoms has been reported [18].

However, there are very few examples of a homologous series of complexes being produced to allow comparison of all three members of the group. Here, we report the synthesis and X-ray crystal structures of a series of three group IV metallocene complexes containing a bidentate aromatic ligand bound to the metal centre through two sulfur atoms.

2. Results and discussion

The salt elimination reactions of the dilithium salt of naphtho[1,8-*cd*]-1,2-dithiole with the group IV bis(pentamethyl)metallocene dichlorides $Cp^*_2MCl_2$ (M = Ti, Zr, Hf) proceed smoothly in tetrahydrofuran at room temperature to give $Cp^*_2TiS_2C_{10}H_6$ (**1**), $Cp^*_2ZrS_2C_{10}H_6$ (**2**) and $Cp^*_2HfS_2C_{10}H_6$ (**3**) in moderate yield (34–64%)

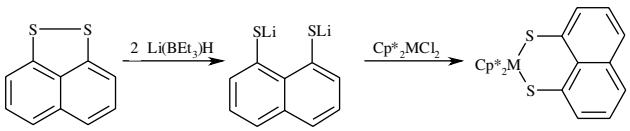

(1)

The purification and isolation of these compounds is straightforward; removal of insoluble salts by re-dissolving in toluene and filtering through celite followed by recrystallisation from toluene/hexane gives crystals which are of extremely high purity. The ^{1}H NMR data (CD_2Cl_2) for complexes **1**–**3** all show the expected peaks, with three separate multiplets in the aromatic region (7.05–7.52 ppm) representing the three pairs of different protons on the naphthalene backbone and a singlet at 1.81, 1.84 and 1.87 ppm, respectively, representing the 10 methyl groups on the cyclopentadienyl rings. No fluxionality was noticed in the ^{1}H NMR spectra of these complexes down to 183 K. The ^{13}C NMR (CD_2Cl_2) are also excellent, each displaying the three quaternary and three non quaternary peaks of the naphthalene backbone plus a peak representing the quaternary carbon atoms of the cyclopentadienyl rings and a single peak at 12.7, 11.6 and 10.5 ppm, respectively, representing the carbon of the ten methyl groups bound to the cyclopentadienyl rings.

Excellent elemental analyses were obtained for all complexes and electrospray mass spectral data were consistent with the proposed structures showing in each case $[M]^+$ and $[M + Na]^+$.

3. Molecular structures

The crystal structures of **1**–**3** (Fig. 1, Tables 1 and 2) are very similar, indeed they are isomorphous which allows for a comparison of bond lengths and angles which are not influenced by packing effects. All three complexes exist in an envelope conformation folded along the sulfur–sulfur axis. The S–M–S bond angles are in the range 82.40(2)–83.82(4)°; close to previously studied complexes containing a six-membered TiS_2C_3 ring [8]. The other angles in these six-membered rings are also in accord with the literature values. The angle which varies most markedly between the three complexes is the splay angle (the deviation from the two S–C bonds being parallel). The splay angles of complexes **1**–**3** are 21.0°, 22.8° and 22.9°, respectively. This can be explained by the size of the metal atom which is between the two sulfur atoms, resulting in longer M–S distances and causing the S–C bonds to stray from being parallel. Zirconium has a greater atomic radius than titanium, therefore it forces the sulfur atoms further apart and gives a larger splay angle. Hafnium has a very similar atomic radius to zirconium so has a similar effect on the splay angle. The bond lengths in **1**–**3** are also very similar and are close to the values in related complexes. The only bond lengths which differ slightly are the M–S and M–Cp bond lengths. The M–S(1) bond lengths of complexes **1**–**3** are 2.406(2), 2.5033(7) and 2.4832(13) Å, respectively, while the M–S(9) bond lengths are 2.428(2), 2.5107(7) and 2.4901(10) Å. These results are to be expected when the atomic radii of the three metal atoms are considered. The M–S bond lengths are very close to similar complexes [12–14,17,21–25]. This pattern where the Zr–S and Hf–S bond lengths are both very similar and noticeably longer than the Ti–S bond length has been seen before in a series of group IV metallocene complexes [26]. The M–Cp bond lengths show an identical pattern to that previously mentioned for the M–S bond lengths.

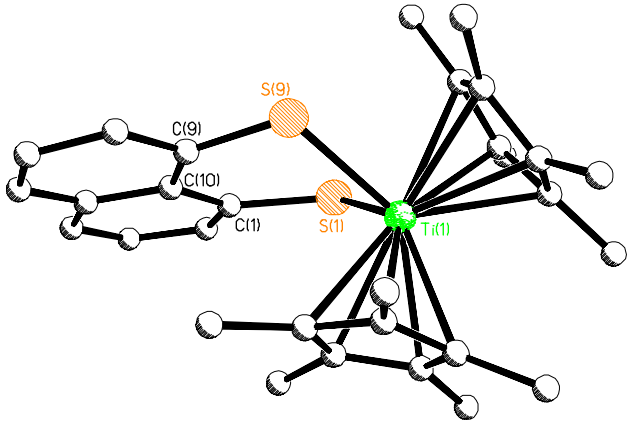

Fig. 1. Molecular structure of $Cp^*_2Ti(S_2C_{10}H_6)$ **1** in the crystal. The structures of **2** and **3** are isomorphous and have been numbered analogously.

Table 1
Crystallographic data for complexes **1**–**3**

	1	**2**	**3**
Empirical formula	$C_{30}H_{36}S_2Ti$	$C_{30}H_{36}S_2Zr$	$C_{30}H_{36}S_2Hf$
M	508.61	551.93	639.20
Crystal system	orthorhombic	orthorhombic	orthorhombic
Space group	*Pna*2(1)	*Pna*2(1)	*Pna*2(1)
a (Å)	17.873(10)	18.1276(19)	18.074(2)
b (Å)	8.468(5)	8.4311(13)	8.4295(11)
c (Å)	16.735(9)	16.722(3)	16.721(2)
α (°)	90	90	90
β (°)	90	90	90
γ (°)	90	90	90
U (Å)^3	2533(2)	2555.7(6)	2547.5(6)
ρ_{calc} (g/cm^3)	1.334	1.434	1.667
μ (mm^{-1})	0.520	0.611	4.276
Reflections measured	13438	14822	14755
Independent reflections	3640	4132	4039
Final $R1$, $wR2$ [$I > 2\sigma(I)$]	0.0678, 0.1456	0.0215, 0.0513	0.0195, 0.0438
Flack parameter	−0.03(5)	0.03(5)	−0.008(8)

Table 2
Bond lengths (Å) and angles (°) for complexes **1**–**3**

	1	**2**	**3**
M(1)–S(1)	2.406(2)	2.5033(7)	2.4832(13)
M(1)–S(9)	2.428(2)	2.5107(7)	2.4901(10)
S(1)–C(1)	1.788(6)	1.779(2)	1.781(4)
S(9)–C(9)	1.772(6)	1.779(2)	1.788(4)
C(1)–C(10)	1.440(8)	1.448(3)	1.464(5)
C(9)–C(10)	1.440(9)	1.445(3)	1.437(6)
M(1)–Cp*(1)	2.432(6)–2.490(6)	2.537(2)–2.579(2)	2.508(4)–2.564(4)
M(1)–Cp*(2)	2.418(6)–2.494(6)	2.520(3)–2.578(3)	2.509(6)–2.561(6)
S(1)–M(1)–S(9)	83.70(7)	82.40(2)	83.82(4)
M(1)–S(1)–C(1)	114.3(2)	112.32(8)	112.45(14)
M(1)–S(9)–C(9)	112.6(2)	110.73(8)	110.42(14)
S(1)–C(9)–C(10)	127.7(4)	128.25(18)	128.4(3)
S(9)–C(9)–C(10)	126.9(5)	127.11(18)	128.1(3)
C(1)–C(10)–C(9)	126.4(5)	127.4(2)	126.4(4)
Splay angle	21.0	22.8	22.9

4. Conclusion

We have prepared and fully characterised a series of new group IV complexes (M = Ti, Zr, Hf) by reduction of the sulfur–sulfur bond of naphtho[1,8-*cd*]-1,2-dithiole with two equivalents of super hydride ($LiBEt_3H$) followed by the addition of one equivalent of $Cp^*_2MCl_2$. We have also made a good comparison of the bond lengths and angles around the central metal atom.

5. Experimental

5.1. General

Manipulations were performed under an oxygen free nitrogen atmosphere using standard Schlenk techniques and glassware. Solvents were dried, purified and stored according to common procedures [27]. The compound, naphtho[1,8-*cd*]-1,2-dithiole, was prepared according to the literature procedures [28,29].

^{1}H (270 MHz) and ^{13}C (67.9 MHz) NMR spectra were recorded on a Jeol DELTA GSX270 spectrometer with δ(H) and δ(C) referenced to external Me_4Si. Elemental analyses were performed by the University of St. Andrews Microanalysis Service and ES$^+$ mass spectra were carried out by the University of St. Andrews Mass Spectrometry Service.

5.2. Bis(pentamethyl)titanocene 1,8-dithiolato-naphthalene (*1*)

Naphtho[1,8-*cd*]-1,2-dithiole (0.072 g, 0.38 mmol) was dissolved in tetrahydrofuran (10 cm^3) and a 1.0 M solution of $LiBEt_3H$ (0.75 cm^3, 0.75 mmol) was added via syringe. Upon addition, an immediate colour change

from red to pale yellow was observed along with the evolution of gas. Bis(pentamethyl) titanocene dichloride (0.147 g, 0.38 mmol) was added and this solution was allowed to stir for 24 h. The solvent was removed under reduced pressure and the residue extracted into hot toluene. This was filtered through celite, dried and recrystallised from toluene/hexane to give green crystals. Yield: 0.125 g, 64%. Microanalysis: *Anal.* Calc. for $C_5Me_{52}TiS_2C_{10}H_6$: C, 70.84; H, 7.13; S, 12.58. Found: C, 70.79; H, 7.55; S, 12.36%. ^{1}H NMR (CD_2Cl_2): $\delta =$ 7.41 (dd, 2H, aromatics), 7.33 (dd, 2H, aromatics), 7.05 (td, 2H, aromatics), 1.81 (s, 30H, $10 \times$ Me). ^{13}C NMR (CD_2Cl_2): $\delta = 147.8$, 137.0, 120.6 (all quaternary aromatic), 134.4, 124.6, 123.6 (all aromatic), 125.1 (aromatic Cp groups), 12.7 (methyl). ES$^+$ MS: *m*/*z*, 531 $[M + Na]^+$, 508 $[M]^+$.

5.3. Bis(pentamethyl)zirconocene 1,8-dithiolatonaphthalene (2)

This was prepared as per compound **1** using naphtho[1,8-*cd*]-1,2-dithiole (0.072 g, 0.38 mmol) and Bis(pentamethyl) zirconocene dichloride (0.164 g, 0.38 mmol) to give **2** as dark red crystals. Yield: 0.071 g, 34%. Microanalysis: *Anal.* Calcd. for $C_5Me_{52}ZrS_2C_{10}H_6$: C, 65.43; H, 6.59; S, 11.62. Found: C, 65.26; H, 6.58; S, 11.83%. ^{1}H NMR (CD_2Cl_2): $\delta = 7.52$ (dd, 2H, aromatics), 7.38 (dd, 2H, aromatics), 7.07 (td, 2H, aromatics), 1.84 (s, 30H, $10 \times$ Me). ^{13}C NMR (CD_2Cl_2): $\delta = 144.8$, 139.9, 121.8 (all quaternary aromatic), 136.4, 123.8, 122.1 (all aromatic), 125.8 (aromatic Cp groups), 11.6 (methyl). ES$^+$ MS: *m*/*z*, 573 $[M + Na]^+$, 550 $[M]^+$.

5.4. Bis(pentamethyl)hafnocene 1,8-dithiolatonaphthalene (3)

This was prepared as per compound **1** using naphtho[1,8-*cd*]-1,2-dithiole (0.072 g, 0.38 mmol) and Bis(pentamethyl) hafnocene dichloride (0.197 g, 0.38 mmol) to give **3** as dark red crystals. Yield. 0.087 g, 36%. Microanalysis: *Anal.* Calc. for $(C_5Me_5)_2HfS_2C_{10}H_6$: C, 56.23; H, 5.66; S, 9.52. Found: C, 56.70; H, 5.91; S, 9.99%. ^{1}H NMR (CD_2Cl_2): $\delta = 7.51$ (dd, 2H, aromatics), 7.34 (dd, 2H, aromatics), 7.08 (td, 2H, aromatics), 1.87 (s, 30H, $10 \times$ Me). ^{13}C NMR (CD_2Cl_2): $\delta = 137.4$, 126.2, 123.7 (all quaternary aromatic), 128.0, 121.7, 116.0 (all aromatic), 117.3 (aromatic Cp groups), 10.5 (methyl). ES$^+$ MS: *m*/*z*, 663 $[M + Na]^+$, 640 $[M]^+$.

5.5. Crystal structure analysis

Single crystals suitable for X-ray diffraction studies of compounds $Cp^*_2TiS_2C_{10}H_6$ (**1**), $Cp^*_2ZrS_2C_{10}H_6$ (**2**) and $Cp^*_2HfS_2C_{10}H_6$ (**3**) were obtained by recrystallisation from toluene/hexane.

Data for **1**, **2** and **3** were collected at 93 K using a Rigaku MM007/Mercury CCD diffractometer (Mo Kα radiation, confocal optic $\lambda = 0.71073$ Å). All refinements were performed using SHELXTL (Version 6.10, Bruker AXS, 2002). In **3**, the large residual peak in the final map is located close to the Hf atom.

6. Supplementary material

CCDC reference Nos. 268066–268068. See http://www.rsc.org/suppdata/dt/b4/b409700a/ for crystallographic data in CIF or other electronic format.

References

[1] A. Shaver, J.M. McCall, Organometallics 3 (1984) 1823.
[2] P. Petkonen, Y. Hiltunen, R.S. Laitenen, J. Valkonen, Inorg. Chem. 30 (1991) 1874.
[3] L. Gelmini, D.W. Stephan, Organometallics 6 (1987) 1515.
[4] D.M. Giolando, T.B. Rauchfuss, Organometallics 3 (1984) 487.
[5] R. Steudel, O. Schumann, J. Buschmann, P. Luger, Angew. Chem., Int. Ed. 37 (4) (1998) 492.
[6] H. Kopf, M. Schmidt, J. Organomet. Chem. 4 (1965) 426.
[7] K. Osakada, Y. Kawaguchi, T. Yakamoto, Organometallics 14 (1995) 4542.
[8] S.M. Aucott, P. Kilian, H.L. Milton, S.D. Robertson, A.M.Z. Slawin and J.D. Woollins, Inorg. Chem. 44 (2005) 2710.
[9] T.T. Nadasdi, D.W. Stephan, Organometallics 11 (1992) 116.
[10] J. Ho, T.L. Breen, A. Ozarowski, D.W. Stephan, Inorg. Chem. 33 (1994) 865.
[11] G. Chandra, M.F. Lappert, J. Chem. Soc. A (1968) 1940.
[12] W.A. Howard, T.M. Trnka, G. Parkin, Inorg. Chem. 34 (1995) 5900.
[13] V.W.-W. Yam, G.-Z. Qi, K.-K. Cheung, J. Chem. Soc., Dalton Trans. (1998) 1819.
[14] V.W.-W. Yam, G.-Z. Qi, K.-K. Cheung, J. Organomet. Chem. 548 (1997) 289.
[15] S. Pouly, G. Tainturier, B. Gatheron, J. Organomet. Chem. 232 (1982) C65.
[16] D.W. Stephan, Organometallics 10 (1991) 2037.
[17] F. Bottomley, D.F. Drummond, G.O. Egharevba, P.S. White, Organometallics 5 (1986) 1620.
[18] G. Tainturier, M. Fahim, B. Gatheron, J. Organomet. Chem. 362 (1989) 311.
[19] G.L. Hillhouse, J.E. Bercaw, Organometallics 1 (1982) 1025.
[20] A.R. Bulls, W.P. Schaefer, M. Serfas, J.E. Bercaw, Organometallics 6 (1987) 1219.
[21] V.W.-W. Yam, G.-Z. Qi, K.-K. Cheung, Organometallics 17 (1998) 5448.
[22] T.A. Wark, D.W. Stephan, Organometallics 8 (1989) 2836.
[23] R. Steudel, M. Kustos, A. Prenzel, Z. Nat. 52b (1997) 79.
[24] S. Ogawa, S. Yoshimura, N. Nagahora, Y. Kawai, Y. Mikata, R. Sato, Chem. Commun. (2002) 1918.
[25] W.A. Howard, G. Parkin, Organometallics 12 (1993) 2363.
[26] O.M. Kekia, A.L. Rheingold, Organometallics 16 (1997) 5142.
[27] D.D. Perrin, W.L.F. Armarego, Purification of Laboratory Chemicals, third ed., Pergammon Press, Oxford, 1988.
[28] W.B. Price, S. Smiles, J. Chem. Soc. (1928) 2372.
[29] A. Zweig, A.K. Hoffman, J. Org. Chem. (1965) 3997.

Available online at www.sciencedirect.com
SCIENCE DIRECT®
Polyhedron 25 (2006) 827–833
POLYHEDRON
www.elsevier.com/locate/poly

Crystal and molecular structure of $W_2(OBu^t)_6$ and electronic structure calculations on various conformers of $W_2(OMe)_6$

Malcolm H. Chisholm *, Judith C. Gallucci, Carl B. Hollandsworth [1]

Department of Chemistry, The Ohio State University, 100 W. 18th Avenue, Columbus, OH 43210-1185, USA

Received 25 June 2005; accepted 4 July 2005
Available online 18 August 2005

Dedicated to Professor M.B. Hursthouse on the occasion of his 65 birthday.

Abstract

The structure of $W_2(OBu^t)_6$ was determined via a single crystal X-ray diffraction study. In the space group *C2/c*, there are 1.5 $W_2(OBu^t)_6$ molecules in the asymmetric unit, with one half molecule located on a crystallographic inversion center and one full molecule in a general position. The W≡W bond distances are 2.328(1) and 2.335(1) Å and the average W–O distances are 1.89(1) Å. The alkoxide alkyl groups are found oriented in the "one distal, two proximal" arrangement with respect to the W–W vector, giving on average, W–W–O angles of 99(1)° for the distal alkoxide and 110(1)° for the proximal. This arrangement is common to other $W_2(OR)_6$ compounds. Computational studies employing density functional theory on several conformers of the model compound $W_2(OMe)_6$ were undertaken. The results for the total bonding energies for each conformer indicate that this "one distal, two proximal" arrangement is only slightly more stable than the all-distal, D_{3d} and the alkoxide-eclipsed D_{3h} structures in the gas phase. This small difference in conformer energy suggests that the proximality preference is likely due to steric effects that are important in the solid state.
© 2005 Published by Elsevier Ltd.

Keywords: Tungsten; Alkoxide; Metal–metal bonds; Density functional theory

1. Introduction

$W_2(OBu^t)_6$ was among the first of the reported ethane-like $(M{\equiv}M)^{6+}$ triply-bonded dimers of formula $X_3M{\equiv}MX_3$, where M = Mo, W [1]. It is prepared by the alcoholysis of $W_2(NMe_2)_6$ with 6 or more equivalents of Bu^tOH in hydrocarbon solvents [2]. The preferred method of purification is crystallization by the cooling of concentrated solutions of $W_2(OBu^t)_6$ in aliphatic hydrocarbon solvents. Crystallization in this manner yields ruby-red, plate-like crystals [2].

$W_2(OBu^t)_6$ exhibits a varied and rich chemistry. It undergoes reversible association with Lewis bases such as pyridine [3]. It also undergoes metathesis with various alkynes and organic nitriles to give alkylidynes $(Bu^tO)_3W{\equiv}CR$ and the nitride $(Bu^tO)_3W{\equiv}N$ [4]. It reacts with NO to give oxidative cleavage of the WW triple bond [5]. and with ethyne [6] and allene [7] to give π-adducts. The ethyne adduct exists in equilibrium with the methylidyne complex and undergoes coupling with additional ethyne to give $W_2(\mu\text{-}C_4H_4)(OBu^t)_6$ [6a]. The addition of CO to $W_2(OBu^t)_6$ yields a carbonyl adduct $[W_2(\mu\text{-}CO)(OBu^t)_6]_2$ with a remarkably low CO stretching frequency, $\upsilon(CO) = 1575\ cm^{-1}$ [8]. The W–O bonds are labile toward insertion reactions with CO_2 [9] and arylcyanates, ArNCO [10]. In reactions with less sterically-demanding alcohols, tetranuclear clusters such as $W_4(OPr^i)_{12}$ [11] and $W_4(OR)_{12}(HOR)$ [12] are obtained where R = CH_2-c-Bu and CH_2-c-Pen.

Despite this extensive coordination chemistry, the molecular structure of $W_2(OBu^t)_6$ was not previously

* Corresponding author. Tel.: +1 614 292 7216; fax: +1 614 292 0368.
E-mail addresses: chisholm@chemistry.ohio-state.edu (M.H. Chisholm), hollandsworth@mail.chem.sc.edu (C.B. Hollandsworth).
[1] Tel.: +1 614 519 8751.

0277-5387/$ - see front matter © 2005 Published by Elsevier Ltd.
doi:10.1016/j.poly.2005.07.010

determined. Several attempts (by various research groups) have been made to study the compound by single-crystal X-ray crystallography. In all cases, the ruby-red crystals either failed to yield good diffraction data or the data proved insufficient for a structure determination. Other $W_2(OR)_6$ compounds have been crystallographically characterized, e.g., for $R = Pr^i$, C_6H_{11}, and $SiMe_2Bu^t$ [13]. The latter compound contained a disordered W_2 unit within the cage of a pseudo octahedral $OSiMe_2Bu$ ligands. There was little doubt that $W_2(OBu^t)_6$ was structurally related to these compounds; however, interest has remained in its structure as it sometimes shows different reactivity from other members of this family. Furthermore, spectroscopic studies have been conducted on $W_2(OBu^t)_6$, in which knowing the experimental bonding parameters, especially the W–W–O and W–O–C angles, would prove useful.

One interesting characteristic of the $X_3W{\equiv}WX_3$ compounds, where $X = CH_2R$ or OR was pointed out by Gilbert et al. in a recent study [13a]. This characteristic is the varied arrangements of the R-alkyl substituents with respect to the WW vector. The $M_2(NMe_2)_6$ compounds, where M = Mo and W, exhibit well-defined proximal and distal methyl substituents due to a strong N(p) to unfilled WW δ and δ^* donation [14]. This donation relieves some of the electronic deficiency on the formally 12 e^- W atoms. However, within the $W_2(OR)_6$ compounds, the O(p) WW δ and δ^* donation may occur when the alkyl substituents align in either of the proximal/distal combinations. This preference has been further examined in this work by employing DFT computations on several conformers of the model compound $W_2(OMe)_6$.

2. Experimental

2.1. Synthesis and X-ray structure determination of $W_2(OBu^t)_6$

$W_2(OBu^t)_6$ was synthesized via the alcoholysis of $W_2(NMe_2)_6$ with a fourfold excess (24 equiv.) of Bu^tOH in thf. The reaction is slow in this solvent and the reaction solution must be stirred for several days for the reaction to proceed to completion at room temperature. Crystals of the product were grown by a slow evaporation of the thf/Bu^tOH solution. The identity of the product was confirmed by ^1H NMR spectroscopy (δ 1.62 in benzene-d_6 solution).

The data collection crystal was a red-orange plate. Examination of the diffraction pattern on a Nonius Kappa CCD diffractometer indicated a monoclinic crystal system. All work was done at 200 K using an Oxford Cryosystems Cryostream Cooler. The data collection strategy was set up to measure a quadrant of reciprocal space with a redundancy factor of 4.2, which means that 90% of the reflections were measured at least 4.2 times. A combination of φ and ω scans with a frame width of 1.0° was used.

The initial unit cell obtained at 200 K for the data collection crystal was a C-centered monoclinic cell with $a = 28.614$ Å, $b = 17.339$ Å, $c = 9.845$ Å and $\beta = 95.27°$. But data integration did not proceed well with this cell and it was discovered that the unit cell had changed during data collection. A new unit cell was obtained at the end of data collection by using only the latter half of the frames. This new unit cell is also C-centered monoclinic, but it has twice the volume of the original unit cell with the c axis almost doubled and the β angle slightly smaller by 3°: $a = 29.196(2)$ Å, $b = 17.349(2)$ Å, $c = 19.227(2)$ Å and $\beta = 92.222(3)°$. The crystal quality at the end of data collection was not as good as it was at the beginning of data collection. It appeared that the crystal had undergone a phase transition during data collection. [A DSC scan of $W_2(OBu^t)_6$ revealed that there is a phase transition for the crystalline solid near −10 °C.] With the data crystal still on the diffractometer, the temperature of the Cryostream was increased from 200 to 260 K and the unit cell was redetermined. The original small unit cell was found at this temperature.

In order to salvage this data set, only the latter half of the data set was used and it was integrated with the larger unit cell. This latter half of the data set consists of 253 frames out of a total of 531 frames, or 48% of the data. Because the data set was collected with a redundancy factor of 4, we were able to salvage enough of the data set to obtain a reasonable structure. Data integration was done with Denzo [15], and scaling and merging of the data were done with Scalepack [15]. Merging the data and averaging the symmetry equivalent reflections resulted in an R_{int} value of 0.085.

The structure was solved by the Patterson method in *C2/c* using SHELXS-97 [16a]. There are 1.5 molecules in the asymmetric unit: one molecule (labeled as A) contains a crystallographic inversion center and the second one (labeled as B) is located on a general position. During the final stages of refinement, the difference electron density map shows large peaks at about 4–5 e $Å^{-3}$ located near the W–W portions of both molecule A and molecule B. These peaks could be construed to be alternate positions of the W–W atoms, with the assumption that the dimer is disordered over several orientations.

Some of these large residual peaks associated with molecule B were labeled as W atoms, with pairs of peaks chosen which are approximately 2.3 Å apart. Among these, there are three W–W pairs, which may represent alternative orientations of the W–W vector. All of the occupancy factors for these W atoms were tied together with the SUMP command. One of the Bu^t groups of molecule A is disordered and is treated with a second orientation (C6AA, C7AA and C8AA). Both sets of carbon atoms for this group are kept isotropic. Full-matrix

least-squares refinements based on F^2 were performed in SHELXL-97 [16b], as incorporated in the WINGX package [17].

The hydrogen atoms were included in the model at calculated positions using a riding model with U(H) = 1.5* Ueq(attached C atom). The final refinement cycle was based on 7785 intensities, 459 variables and 22 restraints and resulted in agreement factors of $R_1(F) = 0.135$ and $wR_2(F^2) = 0.208$. For the subset of data with $I > 2^*\sigma(I)$, the $R_1(F)$ value is 0.072 for 4562 reflections. The final difference electron density map contains maximum and minimum peak heights of 5.00 and −1.94 e Å^{-3}. The largest peaks are still near the W atoms. Neutral atom scattering factors were used and include terms for anomalous dispersion [18]. The experimental details for the X-ray structure determination of $W_2(OBu^t)_6$ are summarized in Table 1. Two separate attempts to conduct X-ray studies at other temperatures, 260 and 120 K, resulted in data sets from which no solution could be obtained.

Table 1
Crystallographic, experimental details for $W_2(OBu^t)_6$

Empirical formula	$C_{24}H_{54}O_6W_2$
Formula weight	806.37
Temperature	200(2) K
Wavelength	0.71073 Å
Crystal system	monoclinic
Space group	*C2/c*
Unit cell dimensions	
a (Å)	29.196(2)
b (Å)	17.349(2)
c (Å)	19.227(2)
β (°)	92.222(3)
Volume (Å)	9732(2)
Z	12
D_{calc} (Mg m^{-3})	1.651
Absorption coefficient (mm^{-1})	7.116
F(000)	4728
Crystal size (mm^3)	0.08 × 0.19 × 0.23
θ Range for data collection (°)	2.12–25.03
Index ranges	$-34 \leqslant h \leqslant 34$, $-20 \leqslant k \leqslant 20$, $-22 \leqslant 1 \leqslant 22$
Reflections collected	25016
Independent reflections [R_{int}]	7785 [0.085]
Completeness to $\theta = 25.03°$	90.5%
Refinement method	full-matrix least-squares on F^2
Data/restraints/parameters	7785/22/459
Goodness of fit on F^2	1.069
Final *R* indices [$I > 2\sigma(I)$]	$R_1 = 0.0719$, $wR_2 = 0.1710$
R indices (all data)	$R_1 = 0.1348$, $wR_2 = 0.2078$
Largest difference in peak and hole	5.00 and −1.94 e Å^{-3}

2.2. DFT computational study of several isomers of $W_2(OMe)_6$

Density functional theory calculations were performed using the Amsterdam Density Functional (ADF) program, version 2002.03, developed by Baerends et al. [19] and vectorized by Ravenck [20]. The numerical integration scheme used was developed by te Velde et al. [21], and the geometry optimizations were carried out under full symmetry using the local exchange-correlation potential of Vosko et al. [22] and the non-local exchange and correlation corrections of Perdew and Wang (PW91) [23]. For tungsten, the electronic configuration was described using a double-ζ STO basis for 5s and a triple-ζ for 6s, 5p, 5d and 4f, augmented by a 6p and a 5f polarization function. The core was frozen and was defined to be 4d and below. For oxygen and carbon, a triple-ζ STO basis was used for the valence 2s and 2p orbitals, augmented by a 3d and a 4f polarization function, with the core 1s frozen. Hydrogen was also treated using a triple-ζ STO basis for its 1s, and was augmented with a 2p and a 3d polarization function. All atoms were also corrected for relativistic effects using the zeroth order regular approximation (ZORA) [24] method. All accuracy and convergence parameters were left at the default level, with the exception of the general integration accuracy, which was set to 7.0. Total bonding energies in ADF are calculated with respect to dissociation into spin-restricted fragment atomic in the gas phase.

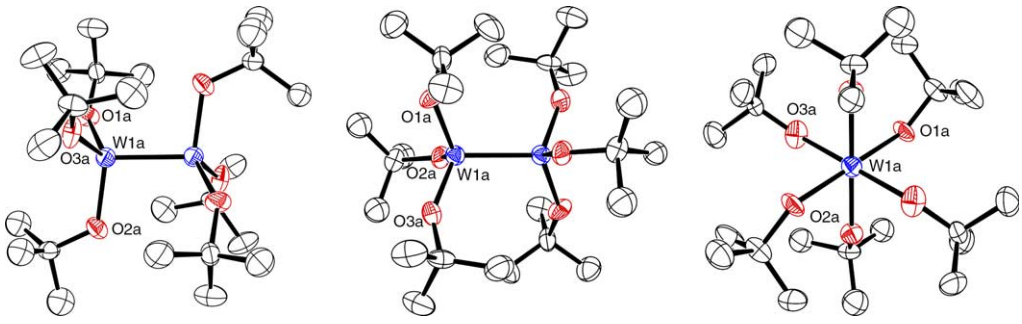

Fig. 1. Three orientations of $W_2(OBu^t)_6$; molecule **A**. Only one Bu^t orientation is shown for the disordered Bu^t group. Only one set of symmetry equivalent atoms is labeled. The symmetry transformation to generate equivalent atoms is: $-x+2,-y+1,-z+1$. Thermal ellipsoids are drawn at the 30% probability level.

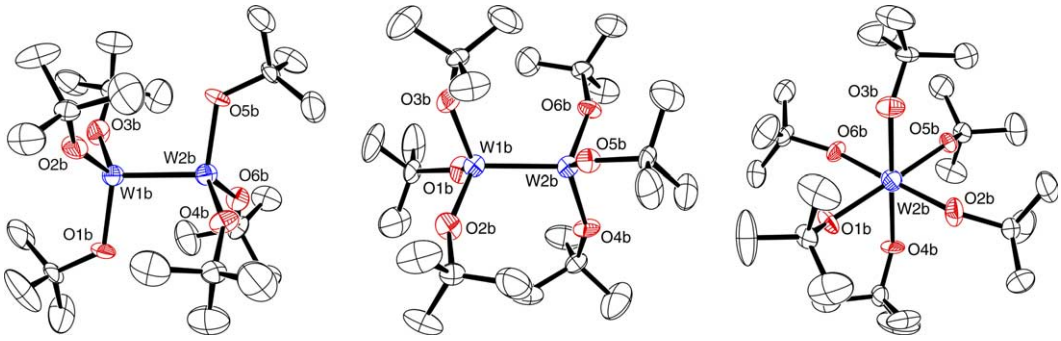

Fig. 2. Three orientations of $W_2(OBu^t)_6$; molecule **B**. Thermal ellipsoids are drawn at the 30% probability level.

3. Results and discussion

3.1. X-ray crystal structure of $W_2(OBu^t)_6$

The structure solution reveals 1.5 molecules in the asymmetric unit, which give two dinuclear species upon expansion of the unit cell. The molecule located on a crystallographic inversion center is labeled **A**, and the molecule located on a general position is labeled molecule **B**. Several views of the refined geometries for these molecules **A** and **B** are shown in Figs. 1 and 2.

For both independent molecules **A** and **B**, there were extra peaks located in the difference map corresponding to what may be construed as different orientations of W atoms within the six alkoxide ligand framework. The W atoms depicted for molecule **A** were the only W atoms refined for molecule **A**. Although there was one other "W" atom of less than 4% occupancy that gives a WW bond of ca. 2.5 Å, this tungsten atom was not included in the model for molecule **A**. The W–W orientation depicted for molecule **B** in Fig. 1 is the major W–W contributor found at 86% occupancy. There are three other W–W atom pairs of less occupancy located for molecule **B** and these can be construed as alternate representations of the W–W species within the ligand environment of six alkoxides (see Figs. 3 and 4). The problem of multiple W–W orientations was also reported to occur in the X-ray structure refinement for the related compounds: $W_2(OAdamantyl\text{-}C_5H_{11})_6$ [13a] and $W_2(OSiMe_2Bu^t)_6$ [13c].

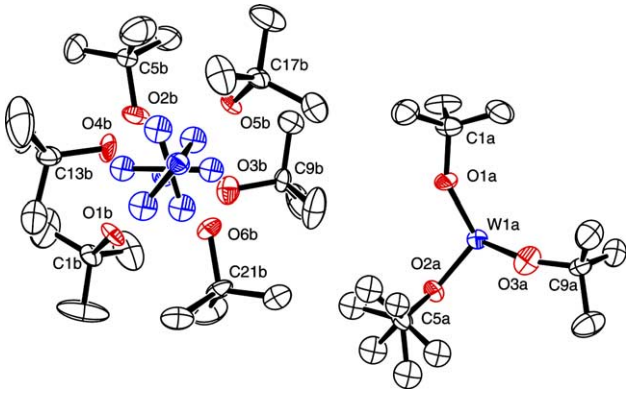

Fig. 3. The asymmetric unit of $W_2(OBu^t)_6$. All three major W–W orientations for molecule **B** are shown. The alternate Bu^t orientation for C(5) on molecule **A** is also shown. Only the quaternary carbon atoms for each Bu^t group are labeled.

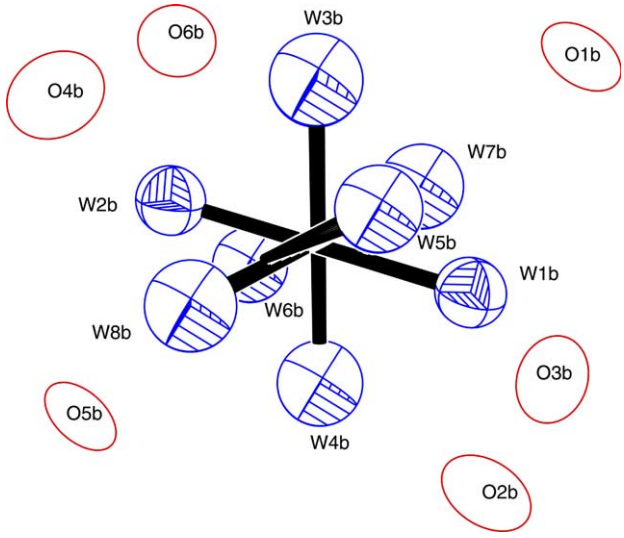

Fig. 4. Diagram indicating the refined W–W moieties for molecule **B** of $W_2(OBu^t)_6$. W(1b)–W(2b) is the unit that refined with the largest occupancy (>86%).

Table 2
Selected W–W and W–O bond distances and e.s.d.'s for $W_2(OBu^t)_6$; molecules **A** and **B**

Bond type	Molecule **A**		Molecule **B**	
	Bond descriptor	Distance (Å)	Bond descriptor	Distance (Å)
W–W	W(1A)–W(1A)*	2.328(1)	W(1B)–W(2B)	2.335(1)
W–O	W(1A)–O(1A)	1.88(1)	W(1B)–O(1B)	1.92(1)
	W(1A)–O(2A)	1.92(1)	W(1B)–O(2B)	1.84(1)
	W(1A)–O(3A)	1.89(1)	W(1B)–O(3B)	1.91(1)
			W(2B)–O(4B)	1.87(1)
			W(2B)–O(5B)	1.91(1)
			W(2B)–O(6B)	1.84(1)

Table 3
Refined W–W bond distances and occupancy factors for molecules **A** and **B**

Bond descriptor	Distance (Å)	Occupancy factor
W(1A)–W(1A)*	2.328(1)	1.000
W(1B)–W(2B)	2.335(1)	0.864(3)
W(3B)–W(4B)	2.27(2)	0.063(3)
W(5B)–W(6B)	2.30(2)	0.046(3)
W(7B)–W(8B)	2.24(3)	0.049(3)

Selected bond distances and angles for molecules **A** and **B** are shown in Tables 2–4. Table 3 contains the W–W bond lengths and occupancy factors for all of the refined W–W units in the structure of $W_2(OBu^t)_6$. The W–O bond distances for the lesser W–W contributors for molecule **B** are not reported here. They have been calculated for each W–W orientation and fall within the range of 1.74 to 2.53 Å. It is likely that the refined orientation of oxygen atoms does not represent the true environment of alkoxide oxygen atoms for the smaller W–W contributors and that the true oxygen peaks are lost within the background of this problematic structure.

4. Electronic structure calculations

$W_2(OR)_6$ compounds are only isolable when R is bulky. Bulky alkoxide ligands lead to a staggered W_2O_6 skeleton as a result of the minimization of alkyl–alkyl repulsions across the WW bond. However, for $W_2(O\text{-}c\text{-}C_6H_{11})_6$, a near eclipsed W_2O_6 skeleton is present. One other interesting feature is seen in the geometries of $W_2(OR)_6$ compounds and that is the orientation of alkyl groups with respect to the W–W bond. These can be either directed over the WW bond and termed "proximal" or directed away or "distal". An all proximal arrangement leads to steric congestion over the MM bond although this arrangement is seen for the secondary alkoxide $W_2(O\text{-}c\text{-}C_6H_{11})_6$. An all-distal arrangement maximizes steric repulsion along the axes of the WW bond and has not been observed in the known structures of $W_2(OR)_6$ compounds. A more common geometry is that wherein one distal and two proximal alkoxide arrangement is present at each tungsten center with an overall approximation to C_{2h} symmetry. Intuitively, this would seem to represent a best structure based on a compromise or minimization of steric repulsive interactions. This structure is seen here for

Table 4
Selected WWO, OWO, and WOC bond angles for molecules **A** and **B**

Angle type	Molecule **A**		Molecule **B**	
	Angle descriptor	Angle (°)	Angle descriptor	Angle (°)
W–W–O	W(1A)*–W(1A)–O(1A)	110.3(4)	W(2B)–W(1B)–O(1B)	99.4(4)
	W(1A)*–W(1A)–O(2A)	98.6(3)	W(2B)–W(1B)–O(2B)	109.7(4)
	W(1A)*–W(1A)–O(3A)	111.0(4)	W(2B)–W(1B)–O(3B)	109.8(4)
			W(1B)–W(2B)–O(4B)	107.7(4)
			W(1B)–W(2B)–O(5B)	99.6(4)
			W(1B)–W(2B)–O(6B)	109.8(4)
O–W–O	O(1A)–W(1A)–O(2A)	116.3(5)	O(1B)–W(1B)–O(2B)	113.9(6)
	O(1A)–W(1A)–O(3A)	106.8(5)	O(1B)–W(1B)–O(3B)	116.0(6)
	O(2A)–W(1A)–O(3A)	113.7(5)	O(2B)–W(1B)–O(3B)	107.7(6)
			O(4B)–W(2B)–O(5B)	117.3(6)
			O(4B)–W(2B)–O(6B)	110.1(6)
			O(5B)–W(2B)–O(6B)	111.6(6)
W–O–C	W(1A)–O(1A)–C(1A)	145.7(9)	W(1B)–O(1B)–C(1B)	123(1)
	W(1A)–O(2A)–C(5A)	122.8(9)	W(1B)–O(2B)–C(5B)	154(1)
	W(1A)–O(3A)–C(9A)	150(1)	W(1B)–O(3B)–C(9B)	146(1)
			W(2B)–O(4B)–C(13B)	150(1)
			W(2B)–O(5B)–C(17B)	123(1)
			W(2B)–O(6B)–C(21B)	154(1)

The symmetry transformation (*) for molecule A is: $-x+2$, $-y+1$, $-z+1$.

Table 5
Summary of $W_2(OR)_6$ compounds bearing bulky alkoxide ligands

Compound	Distribution of alkoxides	Conformation	Ref.	Only example?
$W_2(OBu^t)_6$	all tertiary	distal, proximal, proximal	this work	no
$W_2(OAd\text{-}C_5H_{11})_6$	all tertiary	distal, proximal, proximal	[13a]	no
$W_2(OCMe_2CF_3)_6$	all tertiary	distal, distal, proximal	[13d]	yes
$W_2(OCy)_6$	all secondary	all proximal	[13b]	yes

Table 6
Figures showing several orientations for the converged geometries of the **ddd** (bottom), **dpp** (top), and **ecl** (middle) conformers and the relative calculated total bonding energy (TBE) for each conformer

	View down x-axis	View down y-axis	View down z-axis	relative TBE (kcal mol^{-1})
dpp	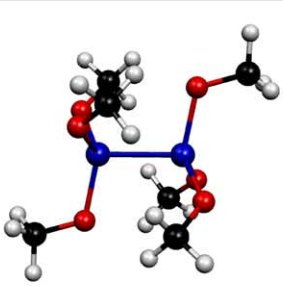	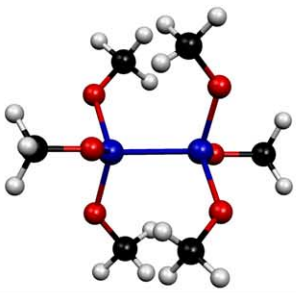	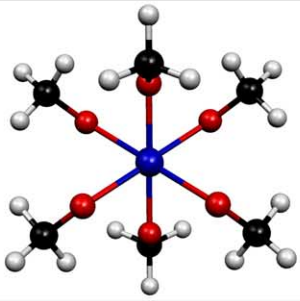	0
ecl	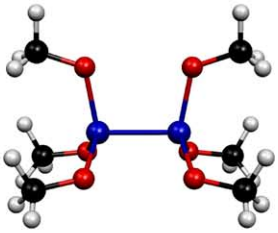	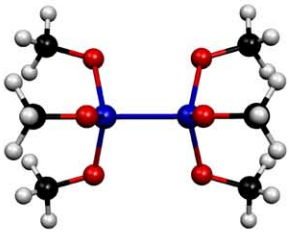	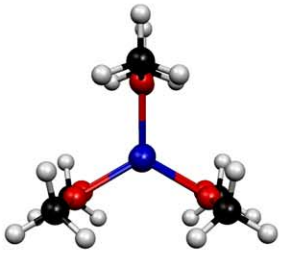	+ 20.89
ddd	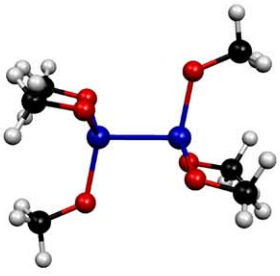	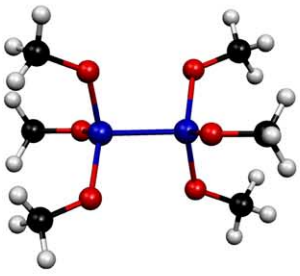	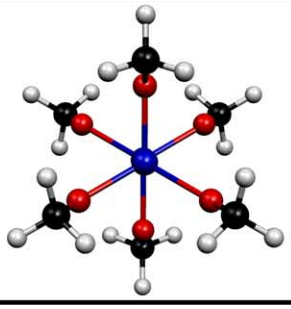	+ 21.17

$W_2(OBu^t)_6$ and was also found for W_2(OAdamantyl-$C_5H_{11})_6$ [13a] (see Table 5).

In order to interrogate the role of steric and electronic factors influencing the structures of the $W_2(OR)_6$ molecule, we carried out electronic structure calculations on the model compound $W_2(OMe)_6$ in various conformations. The specific conformers investigated were D_{3d} and D_{3h} isomers having all distal methyl groups and the C_{2h} molecule having two distal and one proximal alkoxide alkyl substituents. Each structure was allowed to optimize within the overall symmetry constraint: D_{3h}, D_{3d} or C_{2h}. The calculated metric parameters are listed in Table 6. The calculated energies of these three structures varied by less than 22 kcal mol^{-1} with the C_{2h} structure being the calculated minimum energy structure. This small difference in energy certainly supports the view that geometries seen in the solid-state are almost entirely a consequence of steric factors. Inversion at oxygen (through W–O–C = 180°) will readily allow the interconversion of a proximal/distal arrangement of alkyl groups about the WW axis (see Table 7).

Table 7
Calculated bonding parameters for the converged geometries of the three $W_2(OMe)_6$ isomers

Distance (Å) or angle (°)	ddd	dpp	ecl
W–W	2.319	2.326	2.330
W–O	1.935	1.899 (p) 1.930 (d)	1.927
O–C	1.444	1.436 (p) 1.426 (d)	1.432
W–W–O	100.9	101.0 (p) 104.8 (d)	100.8
O–W–O	116.5	110.2 (p. to d.) 117.0 (d. to d.)	116.6
W–O–C	124.2	116.7 (p) 132.7 (d)	119.0

5. Concluding remarks

The crystal and molecular structure of $W_2(OBu^t)_6$ has finally been solved and the problems observed in determining its structure reveal insight into why earlier attempts were unsuccessful. The arrangement of the Bu^t groups in a two-proximal plus one distal manner at each W center, together with the disorder of the WW axis and one Bu^t alkyl group is as seen for other $W_2(OR)_6$ compounds (R = adamantly and $SiMe_2Bu^t$) [13] and, together with the electronic structure calculations on the model compound $W_2(OMe)_6$, testify to the dominant role of steric factors in the packing of the R groups at the dimetal center.

6. Crystallographic data

Crystallographic data for the title compound is available from the Cambridge Crystallographic Center, CCDC #263305. Copies of this information may be obtained free of charge from The Director, CCDC, 12 Union Road, Cambridge, CB2 1EZ, UK (fax: + 44 1223 336 033; e-mail: deposit@ccdc.cam.ac.uk or www: http://www.ccdc.cam.ac.uk).

Acknowledgements

We thank the National Science Foundation, CHE – 0131832 for financial support of this work and the Ohio Supercomputing Center for computational resource units.

References

[1] M.H. Chisholm, C.B. Hollandsworth, in: F.A. Cotton, R.A. Walton, C.A. Murillo (Eds.), Multiple Bonds between Metal Atoms, 3rd ed., Springer-Verlag, New York, 2005 (Chapter 6).
[2] M. Akiyama, M.H. Chisholm, F.A. Cotton, M.W. Extine, D.A. Haitko, D. Little, P.E. Fanwick, Inorg. Chem. 18 (1979) 2266.
[3] T.A. Budzichowski, M.H. Chisholm, K. Folting, J.C. Huffman, W.E. Streib, D.B. Tiedtke, Polyhedron 17 (1998) 857.
[4] (a) R.R. Schrock, M.L. Listemann, L.G. Sturgeoff, J. Am. Chem. Soc. 104 (1982) 4291;
(b) M.H. Chisholm, J.C. Huffman, N.L. Marchant, J. Am. Chem. Soc. 105 (1983) 6162;
(c) M.H. Chisholm, D.M. Hoffmann, J.C. Huffman, J. Am. Chem. Soc. 106 (1984) 6794;
(d) M.L. Listemann, R.R. Schrock, Organometallics 4 (1985) 74.
[5] M.H. Chisholm, F.A. Cotton, M.W. Extine, R.L. Kelly, Inorg. Chem. 18 (1979) 116.
[6] (a) M.H. Chisholm, K. Folting, D.M. Hoffman, J.C. Huffman, J. Am. Chem. Soc. 106 (1984) 6794;
(b) S.T. Chacon, M.H. Chisholm, K. Folting, J.C. Huffman, M.J. Hampden-Smith, Polyhedron 16 (1996) 839.
[7] (a) R.H. Cayton, M.H. Chisholm, M.J. Hampden-Smith, J. Am. Chem. Soc. 110 (1988) 4438;
(b) S.T. Chacon, M.H. Chisholm, K. Folting, J.C. Huffman, M.J. Hampden-Smith, Organometallics 10 (1991) 3722.
[8] M.H. Chisholm, D.M. Hoffman, J.C. Huffman, Organometallics 4 (1985) 986.
[9] M.H. Chisholm, F.A. Cotton, M.W. Extine, W.W. Reichert, J. Am. Chem. Soc. 100 (1978) 1727.
[10] F.A. Cotton, E.S. Shamshoum, J. Am. Chem. Soc. 107 (1985) 4662.
[11] M.H. Chisholm, D.L. Clark, J.C. Huffman, M.J. Hampden-Smith, J. Am. Chem. Soc 109 (1987) 7750.
[12] M.H. Chisholm, K. Folting, C.E. Hammond, M.J. Hamden-Smith, K.G. Moodley, J. Am. Chem. Soc. 111 (1989) 5300.
[13] (a) R = 1-adamantyl: T.M. Gilbert, J.C. Littrell, C.E. Talley, M.A. Vance, R.F. Dallinger, R.D. Rodgers, Inorg. Chem. 43 (2004) 1762;
(b) R = cyclohexyl:M.H. Chisholm, K. Folting, M.J. Hampden-Smith, C.A. Smith, Polyhedron 6 (1987) 1747;
(c) R = $SiMe_2Bu^t$:M.H. Chisholm, C.M. Cook, J.C. Huffman, W.E. Streib, J. Chem. Soc. Dalton Trans. (1991) 929;
(d) R = $CMe(CF_3)_2$:T.M. Gilbert, C.B. Bauer, A.H. Bond, R.D. Rodgers, Polyhedron 18 (1999) 1293;
(e) R = (+) menthyl:I.P. Patkin, K. Folting, J. Chem. Soc. Dalton Trans. (1992) 2343;
(f) R = Pr^i: Ref. [11].
[14] B.E. Bursten, F.A. Cotton, J.C. Green, E.A. Seddon, G.G. Stanley, J. Am. Chem. Soc. 102 (1980) 4579.
[15] DENZO: Z. Otwinowski, W. Minor, Methods in enzymology, in: C.W. CarterJr., R.M. Sweet (Eds.), Macromolecular Crystallography, part A, vol. 276, Academic Press, New York, 1997, pp. 307–326.
[16] (a) G.M. Sheldrick, SHELXS-97, Universität Göttingen, Germany, 1997;
(b) G.M. Sheldrick, SHELXL-97, Universität Göttingen, Germany, 1997.
[17] WINGX-Version 1.64.05: L.J. Farrugia, J. Appl. Cryst. 32 (1999) 837.
[18] International Tables for Crystallography. Volume C. Kluwer Academic Publishers, Dordrecht, 1992.
[19] (a) E.J. Baerends, D.E. Ellis, P. Ros, Chem. Phys. 2 (1973) 41;
(b) E.J. Baerends, P. Ros, Chem. Phys. 2 (1973) 52;
(c) G. te Velde, E.J. Baerends, J. Comput. Phys. 92 (1992) 84;
(d) C.G. Fonseca, O. Visser, J.G. Snijders, G. te Velde, E.J. Baerends, in: E. Clementi, G. Corongiu (Eds.), Methods and techniques in computational chemistry, METECC-95, STEF: Cagliara, Italy, 1995, p. 305.
[20] W. Ravenek, in: H.J.J. te Riele, T.J. Dekker, H.A. van de Horst (Eds.), Algorithms and Applications on Vector and Parallel Computers, Elsevier, Amsterdam, The Netherlands, 1987.
[21] (a) G. te Velde, E.J. Baerends, J. Comput Chem. 99 (1992) 84;
(b) P.M. Boerrigter, G. te Velde, E.J. Baerends, Int. J. Quantum Chem. 33 (1998) 87.
[22] S.H. Vosko, L. Wilk, M. Nusair, Can. J. Phys. 58 (1980) 1200.
[23] J.P. Perdew, Phys. Rev. B. 46 (1992) 6671.
[24] E. van Lenthe, A.E. Ehlers, E.J. Baerends, J. Chem. Phys. 110 (1999) 8943.

Available online at www.sciencedirect.com
SCIENCE DIRECT®
Polyhedron 25 (2006) 834–842
POLYHEDRON
www.elsevier.com/locate/poly

Unusual hetero-atomic RhSCNSb(Rh) co-ordination ring: Synthesis and X-ray structure of [Rh($\underline{N}^1$,$\underline{S}^2$-2-thiopyrimidinato)$_2$($\underline{N}^1$(Sb),$\underline{S}^2$(Rh)-2-thiopyrimidinato){Sb(C_6H_5)$_3$}] and long time sought structure of *mer*-[$RhCl_3${Sb(C_6H_5)$_3$}$_3$]

Renzo Cini [a,*], Gabriella Tamasi [a], Sandra Defazio [a], Maddalena Corsini [a,1], Francesco Berrettini [b], Alessandro Cavaglioni [a,2]

[a] *Department of Chemical and Biosystem Sciences and Technologies, University of Siena, Via A. Moro 2, I-53100 Siena, Italy*
[b] *Centro Interdipartimentale di Analisi e Determinazioni Strutturali (CIADS), University of Siena, Via A. Moro 2, I-53100 Siena, Italy*

Received 29 July 2005; accepted 13 September 2005
Available online 7 November 2005

This study is dedicated to Prof. Mike Hursthouse, University of Southampton, on the occasion of his 65th birthday.

Abstract

The reaction of $RhCl_3 \cdot 3H_2O$ with $SbPh_3$ (Ph, C_6H_5) in ethanol produced *mer*-[$RhCl_3(SbPh_3)_3$] (**1**), as the main product, together with *trans*-[$RhCl_2(Ph)(SbPh_3)_3$] (**2**) (R. Cini, G. Giorgi, L. Pasquini, Inorg. Chim. Acta 196 (1992) 7; A. Cavaglioni, R. Cini, J. Chem. Soc., Dalton Trans. (1997) 1149). Ways to improve the yield for **1** and **2** were a subject of further works by this laboratory during the past decade and the reactivity of the organometallic compound **2** was investigated towards a variety of bases. Long sought single crystals of **1** suitable for X-ray diffraction have been obtained from hot acetone solution. The metal centre has a pseudo-octahedral coordination environment with the three chloride anions and the three $SbPh_3$ molecules in *mer* positions. The Rh–Cl bond *trans* to Sb is significantly weakened by the high *trans* influence by antimony itself. This gives the rationale for the formation of **2** from $RhCl_3$ and $SbPh_3$ via the preliminary formation of **1**, followed by dissociation of the activated chloride anion, and the subsequent formation of the Rh–C(Ph) linkage. The reaction of **1** with 2-thio-1,3-pyrimidine (Htpym) in ethanol produces crystalline [Rh($\underline{N}^1$,$\underline{S}^2$-tpym)$_2$($\underline{N}^1$(Sb),$\underline{S}^2$(Rh)-tpym)($SbPh_3$)] (**3**). Single crystals suitable for X-ray diffraction studies as obtained from ethanol/diethyl-ether contain a complex molecule and a quarter of an ethanol molecule in the asymmetric unit. Two out of three $tpym^-$ anions chelate the metal centre via the N^1 and S^2 atoms, whereas the third $tpym^-$ anion behaves as mono-dentate through the S^2 atom only. The sixth co-ordination position is occupied by the Sb atom. Interestingly, one of the N atoms of the monodentate $tpym^-$ anion behaves as electron donor to Sb and a Sb–N linkage forms ($d_{(Sb-N)}$, 2.846 Å). As a consequence, an unusual totally hetero-atomic five-membered co-ordination ring of the type RhSCNSb(Rh) forms. A molecular modelling analysis at the hybrid density functional level DFT-B3LYP was performed on selected co-ordination molecules.
© 2005 Elsevier Ltd. All rights reserved.

Keywords: Rhodium; Thiopyrimidine; X-ray crystallography; Coordination chemistry; Density Functional

1. Introduction

The synthesis of platinum group metal complexes with pyrimidine and purine derivatives as ligands has acquired new impetus in the past decade. This happened because several reasons, some of which are the following. First, on the basis of pure co-ordination chemistry pyrimidines

* Corresponding author. Tel.: +39 0577 234368; fax: +39 0577 234177.
E-mail address: cini@unisi.it (R. Cini).
[1] Present address: Department of Chemistry, University of Siena, Via A. Moro 2, I-53100 Siena, Italy.
[2] Present address: ISVEA srl, Laboratorio di Analisi, Via Basilicata 1/3, Località Fosci, I-53036 Poggibonsi, Italy.

0277-5387/$ - see front matter © 2005 Elsevier Ltd. All rights reserved.
doi:10.1016/j.poly.2005.09.010

and purines are very versatile ligands and show a huge variety of ligating modes as a function of the metal and the environmental conditions. Much has to be learnt on this matter even though a large amount of experimental and theoretical work has already been done [1–11]. The information collected from the preparative, structural and reactivity studies have high significance for several fields which span from the bio-sciences to the material sciences. Second, pyrimidines and purines, often called nucleobase derivatives (to stress their importance in the life of the cell), have in some cases pharmaceutical activity, for instance as anti-tumoral or anti-viral agents. Third, for this type of drugs the complex formation with specific metals may improve the activity towards certain diseases and hopefully may increase the activity spectrum [12]. The combination of two or more different molecules into the same compound may bring to a multi-therapeutic agent which can be expanded by the synergic action of the metal residue (especially for platinum group metals) once the co-ordination compound dissociate inside the target tissue. Fourth, it has recently been suggested that photo-activation of DNA thiobases, may offer a novel approach for the treatment of non-malignant diseases like psoriasis or of superficial tumours that are accessible via photo-therapy [13]. Rhodium–thiopyrimidine and –thiopurine systems are not much investigated by the community of inorganic and co-ordination chemists, at least as it is revealed by the small number of structures deposited at the Cambridge Structural Database (CSD) (Release November 2004, ca. 10 structures) [14].

We reasoned that the synthesis of platinum group metal–thiopyrimidine complexes would be worth of efforts. On continuing our project on co-ordination chemistry of rhodium, we found that this metal has a renewed interest in oncology [15]. These ideas and the search for comparative analyses with ruthenium complexes from here [11f] suggested to prepare rhodium–thiopyrimidine complexes. We wish to report in this paper on the synthesis and the structural characterisation of $[Rh(\underline{N}^1,\underline{S}^2\text{-tpym})_2(\underline{N}^1(Sb),\underline{S}^2(Rh)\text{-tpym})(SbPh_3)]$ (**3**) (see Scheme 1 for the structural formulas of Htpym and $tpym^-$). The structure of the parent compound $[RhCl_3(SbPh_3)_3]$ (**1**), has also been studied and is here reported. The complex eluded many crystal growth attempts carried out for many years. The finding of the activation of a Rh–Cl bond helps in understanding the process of formation of $[RhCl_2(Ph)(SbPh_3)_3]$ from the reaction of $RhCl_3$ with $SbPh_3$ [11a,11b].

2. Experimental

2.1. Materials

$RhCl_3 \cdot 3H_2O$ (reagent grade, r.g., Acros), Htpym (r.g., Sigma), $SbPh_3$ (r.g., Fluka), Ethanol (EtOH, analytical grade, a.g., Baker), Acetone (a.g., Baker), Diethylether (Et_2O, a.g., Baker), DMSO-d_6 (99.5 at.% D, Fluka) were used as purchased.

2.2. Syntheses

2.2.1. *mer-*$[RhCl_3(SbPh_3)_3] \cdot CH_3COCH_3$ (**1** $\cdot CH_3COCH_3$)

The compound was prepared according to the procedures previously reported from this laboratory [11a]. Single crystals suitable for X-ray diffraction studies were prepared by slowly evaporating a saturated solution of the crude compound in acetone, at 22 °C. The solution was stored in dust-free, dark, thermostated room, carefully devoid of vibrations. The crystals that formed within three weeks as thin orange plates were filtered, washed with acetone and then stored at 5 °C. *Anal.* Calc. for $C_{57}H_{51}Cl_3ORhSb_3$ (MW = 1326.6): C, 51.61; H, 3.88; Cl, 8.02. Found: C, 51.30; H, 3.70; Cl, 8.22%.

2.2.2. $[Rh(\underline{N}^1,\underline{S}^2\text{-tpym})_2(\underline{N}^1(Sb),\underline{S}^2(Rh)\text{-tpym})(SbPh_3)] \cdot 0.25C_2H_5OH$ (**3** $\cdot 0.25C_2H_5OH$)

A suspension consisting of **1** $\cdot CH_3COCH_3$ (260 mg, ca. 0.2 mmol), Htpym (70 mg, ca. 0.6 mmol) and EtOH (12 mL) was refluxed in air. After some 15 mins of reflux the solid material dissolved and the resulting orange clear solution was refluxed for two more hours. The solution was cooled down to 22 °C, then concentrated to 3 mL and added by 30 mL of Et_2O. Finally, the mixture was covered and stored at room temperature (22 °C). Orange-red crystals suitable for X-ray diffraction studies formed within 24 h, which were filtered off and then stored in the air atmosphere at 5 °C. Yield: 50%. *Anal.* Calc. For

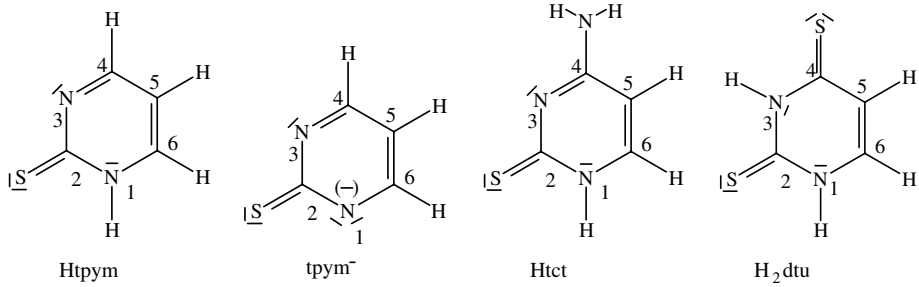

Scheme 1. Structural formulas for 2-thio-1,3-pyrimidine (Htpym) and 2-thio-1,3-pyrimidinate ($tpym^-$), and the atom numbering. The formulas of thiocytosine (Htct) and dithiouracil (H_2dtu) are also represented.

$C_{30.25}H_{26.5}N_6O_{0.25}RhS_3Sb$ (MW = 800.9): C, 45.74; H, 3.31; N, 10.49; S, 12.01. Found: C, 45.97; H, 3.38; N, 10.60; S, 11.80%.

IR. Selected absorption bands: Htpym, 1605 cm^{-1} (strong, s; ring motion), 1211 (medium, m; NCS vibrations), 1053 (m; CS vibration); **3**, 1562 cm^{-1} (s), no band detectable in the regions around 1200 and 1050 cm^{-1}.

^{1}H NMR. Selected signals: Htpym, 8.21 ppm (doublet, 2H, H^4 and H^6), 6.77 (triplet, 1H, H^5); **2**, 7.20–7.55 ppm (multiplet, ca. 17H, $SbPh_3$ protons and H^4 and H^6 protons of tpym(3)), 7.05, 6.71 and 6.52 (three triplets, 1H each, H^5 of tpyms), 8.55–8.05 (four multiplets, 1H each, tpym(1) and tpym(2)).

2.3. Spectroscopy

IR spectra were recorded by using the KBr pellet technique through a Perkin–Elmer FT1600 spectrometer.

^{1}H NMR spectra were recorded in DMSO-d_6 solutions (0.01 mol L^{-1}) through a Varian XL 200 Machine at 200 MHz and 25 °C.

2.4. X-ray crystallography

2.4.1. *mer*-$[RhCl_3(SbPh_3)_3]\cdot CH_3COCH_3$ (**1**$\cdot CH_3COCH_3$)

2.4.1.1. Data collection. An orange thin crystal fragment was selected under the polarising microscope and mounted on a glass capillary. Preliminary X-ray diffraction experiments, performed through the Weissenberg technique allowed the evaluation of the approximate cell constants, the crystal setting (monoclinic) and the space group ($P2_1/c$). The accurate cell parameters (Table 1) and data set were measured through a Siemens P4 automatic four circle diffractometer at 292 ± 2 K. Graphite mono-chromatised Mo Kα radiation ($\lambda = 0.71073$ Å) was used. The data were corrected for Lorentz-polarisation and absorption effects (ψ-scan technique). The collected reflections totalled 7286, 4519 of which were independent with $I > 2\sigma(I)$. No appreciable decay was observed on monitoring periodically three standard reflections. The intensities of diffraction were very weak at angles beyond $2\theta = 46°$, probably because of the shape and quality of the crystal (thin fragment) and the presence of some cracks, probably due to some efflorescence of co-crystallised acetone. For this reason the data collection was not performed beyond $2\theta = 46°$.

2.4.1.2. Structure solution and refinement. The structure was solved via the Patterson and Fourier techniques. The difference-Fourier map computed after a 12-cycle refinement at the isotropic level on the non-hydrogen atoms of the complex molecule showed four new peaks attributable to the atoms of a co-crystallised molecule of acetone, in agreement with the analytical data. The hydrogen atoms for the two molecules of the asymmetric unit were included in calculated positions through the HFIX and AFIX options of SHELX-97 [16] and were allowed to ride on the atoms to which they are linked (with the thermal parameter equal to 1.2 times the value for the corresponding heavy atom). All the non-hydrogen atoms were treated as anisotropic whereas all the hydrogen atoms were treated as isotropic during the last cycles of refinement. The final agreement factors converged to $R_1 = 0.0491$ and $wR_2 = 0.0938$ over the observed reflections. All the calculations

Table 1
Selected crystal data (at 292 ± 2 K) and structure refinement for *mer*-$[RhCl_3(SbPh_3)_3]\cdot CH_3COCH_3$ (**1**$\cdot CH_3COCH_3$) and for $[Rh(\underline{N}^1,\underline{S}^2\text{-tpym})_2(\underline{N}^1(Sb),\underline{S}^2(Rh)\text{-tpym})(SbPh_3)]\cdot 0.25C_2H_5OH$ (**3**$\cdot 0.25C_2H_5OH$)

Parameter	Value	
	1$\cdot CH_3COCH_3$	**3**$\cdot 0.25C_2H_5OH$
Empirical formula	$C_{57}H_{51}Cl_3ORhSb_3$	$C_{30.50}H_{26.50}N_6O_{0.25}RhS_3Sb$
Formula weight	1326.49	801.92
Wavelength/Å	0.71073	0.71073
Crystal system	monoclinic	triclinic
Space group	$P2_1/c$	$P\bar{1}$
Unit cell dimensions		
a (Å)	19.892(2)	10.254(1)
b (Å)	13.232(4)	11.006(5)
c (Å)	20.672(3)	17.231(2)
α (°)	90	85.96(1)
β (°)	98.23(1)	85.62(1)
γ (°)	90	62.62(1)
V (Å^3)	5385.1(19)	1720.4(8)
Z	4	2
D_{calc} (Mg m^{-3})	1.636	1.548
Absorption coefficient (mm^{-1})	1.976	1.476
Crystal size (mm)	0.3 × 0.2 × 0.03	0.4 × 0.3 × 0.2
Reflections collected/unique (R_{int})	7286/7045 (0.0338)	7111/6006 (0.0094)
Data/restraints/parameters	7045/0/586	6006/2/395
Final R indices [$I > 2\sigma(I)$]	$R_1 = 0.0491$, $wR_2 = 0.0938$	$R_1 = 0.0373$, $wR_2 = 0.1040$
R indices (all data)	$R_1 = 0.0986$, $wR_2 = 0.1135$	$R_1 = 0.0464$, $wR_2 = 0.1091$

were carried out with the SHELX-97, PARST-97 [17] and ORTEP3 [18] computer programs implemented on Pentium machines.

2.4.2. [Rh($\underline{N}^1$,$\underline{S}^2$-tpym)$_2$($\underline{N}^1$(Sb),$\underline{S}^2$(Rh)-tpym)-($SbPh_3$)] · 0.25C_2H_5OH (**3** · 0.25C_2H_5OH)

2.4.2.1. Data collection. An orange-red crystal was selected under the polarising microscope, mounted on a glass capillary. The accurate cell parameters (Table 1) and data set were measured with device and method above reported for **1** · CH_3COCH_3. The collected reflections were 7111, 6006 of which were independent with $I > 2\sigma(I)$. No appreciable decay was observed on monitoring periodically three standard reflections.

2.4.2.2. Structure solution and refinement. The structure was solved via the procedure as reported above for **1** · CH_3COCH_3. The difference-Fourier map computed after a 12-cycle refinement at the isotropic level on the non-hydrogen atoms of the complex molecule showed three new peaks attributable to the atoms of a co-crystallised molecule of ethanol. The peak assigned to the oxygen atom was sitting on an inversion centre, so that the ethanol molecule is affected by a statistical disorder. The occupancy of the three non-hydrogen atoms of the co-crystallised ethanol molecule was refined via a trial and error method based on the thermal parameters and on the analytical data (C, H, N, S). An acceptable fitting of the experimental data and the thermal parameter was obtained by fixing the occupancy of the oxygen atom (namely O1E) at 0.125 and that of the carbon atoms at 0.25. The hydrogen atoms were included in calculated positions through the HFIX and AFIX options of SHELX-97 and were allowed to ride on the atoms to which they are linked (with the thermal parameter equal to 1.2 times the value for the corresponding heavy atom). The non-hydrogen atoms were treated as anisotropic whereas all the hydrogen atoms were treated as isotropic during the last cycles of refinement. The final agreement factors converged to $R_1 = 0.0373$ and $wR_2 = 0.1040$ over the observed reflections. All the calculations were carried out as above reported for **1** · CH_3COCH_3.

2.5. Molecular modelling: density functional methods

All the density functional calculations were carried out through the GAUSSIAN-98/RevA.7 package [19] implemented on an Origin 3800 SG machine at CINECA (Inter-University Computing Centre, Casalecchio di Reno, Bologna, Italy). Geometry optimisations, population analysis and vibration frequency calculations have been obtained by using the B3LYP method [20] and different basis sets [20] depending on the atom type and on the molecule (see Section 3). The models optimised were: $SbH_2CH{=}CH_2$; $M(SbH_2CH{=}CH_2)^+$ for M = Cu, Ag, Au; $M(SbH_2CH{=}CH_2)^{2+}$ for M = Zn, Cd, Hg; Htpym; $tpym^-$; M(tpym) for M = Cu, Ag, Au; $M(tpym)^+$ for M = Zn, Cd, Hg; Rh($\underline{N}^1$,$\underline{S}^2$-tpym)$^{2+}$ for quintet, triplet, singlet. Molecular drawings were obtained through the ORTEP3 package [18].

3. Results and discussion

3.1. X-ray crystallography

3.1.1. mer-[$RhCl_3(SbPh_3)_3$] · CH_3COCH_3 (**1** · CH_3COCH_3)

The complex molecule **1** is depicted in Fig. 1 whereas the selected bond lengths and bond angles are listed in Table 2. The rhodium(III) centre has a pseudo-octahedral co-ordination environment, the donors being the three chloride anions (*mer* position) and the three antimony atoms from triphenylstibine.

The three Rh–Cl bond distances differ significantly, the two vectors *trans* to each other being significantly shorter (2.350(3) and 2.362(3) Å) than the one *trans* to Sb (2.399(3) Å). This effect is related to the higher *trans* influence exerted by Sb when compared to Cl. The Rh–Sb bond distances are 2.558(1) Å (*trans* to Cl), and 2.577(1) and 2.626(1) Å. Interestingly, all the three chloride anions are involved in several C–H···Cl interactions. Cl(1) is the H-acceptor for the intramolecular interactions: C(126)–H···Cl(1) (CH···Cl, 2.946 Å; 146°); C(326)–H···Cl(1) (CH···Cl, 3.115 Å; 106°); C(236)–H···Cl(1) (CH···Cl, 2.768 Å; 147°); and the intermolecular interaction: C(124)–H($-x+2$, $y-0.5$, $-z+0.5$)···Cl(1) (CH···Cl, 2.927 Å; 138°). Cl(2) is the H-acceptor for the intramolecular interactions: C(116)–H···Cl(2) (CH···Cl, 2.939 Å; 111°); C(236)–H···Cl(2) (CH···Cl, 3.038 Å; 104°); and the intermolecular interactions: C(223)–H(x, $-y-0.5$, $z+0.5$)···Cl(2) (CH···Cl, 3.100 Å; 134°); C(4s)–H($-x+1$, $y-0.5$, $-z+0.5$)···Cl(2) (2.726 Å; 176°). Cl(3) is the H-acceptor for the intramolecular interactions:

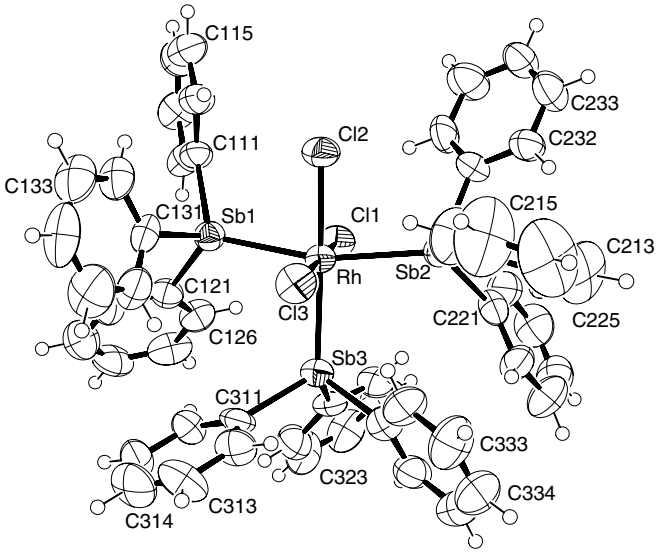

Fig. 1. Drawing of the complex molecule for *mer*-[$RhCl_3(SbPh_3)_3$] · CH_3COCH_3 (**1** · CH_3COCH_3). The ellipsoids enclose 50% probability. The labelling of selected atoms only is included for the sake of clarity.

Table 2
Selected bond lengths (Å) and angles (°) for *mer*-$[RhCl_3(SbPh_3)_3]\cdot CH_3COCH_3$ ($\mathbf{1}\cdot CH_3COCH_3$)

Vectors	Lengths (Å)/Angles (°)
Rh–Cl(1)	2.362(3)
Rh–Cl(2)	2.399(3)
Rh–Cl(3)	2.350(3)
Rh–Sb(1)	2.577(1)
Rh–Sb(2)	2.626(1)
Rh–Sb(3)	2.558(1)
Sb(1)–C(111)	2.14(1)
Sb(1)–C(121)	2.14(1)
Sb(1)–C(131)	2.14(1)
Sb(2)–C(211)	2.14(1)
Sb(2)–C(221)	2.14(1)
Sb(2)–C(231)	2.14(1)
Sb(3)–C(311)	2.14(1)
Sb(3)–C(321)	2.14(1)
Sb(3)–C(331)	2.12(1)
Cl(3)–Rh–Cl(1)	175.24(11)
Cl(3)–Rh–Cl(2)	89.74(11)
Cl(1)–Rh–Cl(2)	93.58(11)
Cl(3)–Rh–Sb(3)	82.54(8)
Cl(1)–Rh–Sb(3)	94.15(7)
Cl(2)–Rh–Sb(3)	172.27(9)
Cl(3)–Rh–Sb(1)	91.13(8)
Cl(1)–Rh–Sb(1)	85.96(8)
Cl(2)–Rh–Sb(1)	81.93(8)
Sb(3)–Rh–Sb(1)	98.46(4)
Cl(3)–Rh–Sb(2)	97.12(9)
Cl(1)–Rh–Sb(2)	86.58(8)
Cl(2)–Rh–Sb(2)	84.85(8)
Sb(3)–Rh–Sb(2)	95.76(4)
Sb(1)–Rh–Sb(2)	164.38(4)

C(332)–H···Cl(3) (2.676 Å; 145°); C(216)–H···Cl(3) (2.853 Å; 134°); and intermolecular interactions: C(214)–H($-x+1$, $y-0.5$, $-z+0.5$) (2.801 Å; 161°); C(3s)–H($-x$, $y+0.5$, $-z+0.5$)···Cl(3) (3.112 Å; 132°). The analysis of the bond distances reveals the activation of the Rh–Cl (*trans* to Sb) bond towards dissociation and formation of chloride anion and of a penta-co-ordinate intermediate state. It is reasonable to assume that the activation of a $SbPh_3$ ligand towards dissociation of a Sb–C linkage occurs at the level of the intermediate state. Some activation on $Sb(2)Ph_3$ towards the formation of $SbClPh_2$ [11a] and the Rh–Ph linkage [11a,11b] occurs. In favour of this hypothesis is the fact that the C(111)–Sb(2)–C(131) bond angle (105.1(4)°) is the largest of all the C–Sb–C angles for **1** and $[RhCl_2(Ph)(SbPh_3)_3]$ and that the Cl(2)···Sb(2) contact distance (3.265 Å) is short. However, it has to be noted that no lengthening of any Sb–C bond is observed in the structure of **1**. Although, the intra-molecular activation of a Sb–C bond for a Rh(III)–$SbPh_3$ molecule is evident from the structure of **3** (see below).

3.1.2. $[Rh(\underline{N}^1,\underline{S}^2\text{-tpym})_2(\underline{N}^1(Sb),\underline{S}^2(Rh)\text{-tpym})\text{-}(SbPh_3)]\cdot 0.25C_2H_5OH$ ($\mathbf{3}\cdot 0.25C_2H_5OH$)

The complex molecule **3** is shown in Fig. 2 and the selected geometrical parameters are reported in Table 3. The rhodium centre has the usual octahedral co-ordination arrangement and it is chelated by two $tpym^-$ anions. Two *cis* positions are occupied by the sulfur atom from the third $tpym^-$ anion and by the Sb atom from triphenylstibine. Interestingly, the antimony donor is five-co-ordinate, being linked to one of the nitrogen atoms from the mono-dentate $tpym^-$ anion, to the three phenyl groups and the metal centre. A completely hetero-atomic five-membered co-ordination ring of the type Rh–S–C–N-Sb(Rh) is unusually operating in the complex molecule. The sulfur atoms (S(1) and S(2)) from the chelating $tpym^-$ molecules are *trans* to each other and at longer distances (2.365(2), 2.378(1) Å) from Rh than the sulfur donor of the third ligand (S(3), 2.322(1) Å). The two Rh–N bond distances are equal within one time the standard deviations and average 2.082(4) Å in agreement with corresponding values found previously for Rh(III) complexes [11,21]. The Rh–Sb bond distance, 2.5344(8) Å is slightly short when compared to other octahedral Rh(III) complexes which contain only one $SbPh_3$ ligand [11b]. The Rh···N(13) contact distance 3.469 Å is rather long and excludes a significant linking interaction between the two atoms. Bond angles around the Rh(III) centre deviate significantly from the idealised values of 90° and 180°, mostly because the strains related to the presence of two four-membered chelate rings. For instance, the S(1)–Rh–N(11) and S(2)–Rh–N(12) bond angles are 69.2(1)° and 68.9(1)°, respectively; the S(1)–Rh–S(2) angle is 162.58(6)° whereas the S(3)–Rh–N(12) angle is 166.2(1)°. The linking interaction between the $tpym^-$ and the $SbPh_3$ ligand is evidenced by a short Sb–N(13) distance: 2.846(3) Å and by the geometrical parameters for the sphere around the antimony atom. In fact, the N(13) atom is roughly *trans* with respect to the C(111) atom, the N(13)–Sb–C(111) angle being 168.7(1)°. The *trans* influence exerted by the nitrogen atom is evidenced by the lengthening of the Sb–C(111) vector (bond distance, 2.164(5) Å) with respect to the Sb–C(121) and Sb–C(131) vectors (bond distances, 2.129(4) and 2.114(5) Å, respectively). Moreover, the enlarging of the C(121)–Sb–C(131) bond angle (110.1(2)°) upon the formation of the N-Sb linkage is evident from the inspection of the C(111)–Sb–C(121) (95.8(2)°) and C(111)–C(131) (95.9(2)°) bond angles. A sort of activation of the $SbPh_3$ ligand can therefore be hypothesised via the formation of the complex molecule **3**, which could evolve towards the release of a phenyl group. This type of mechanism, has been proposed for the formation of *trans*-$[RhCl_2(Ph)(SbPh_3)_3]$ and $ClSbPh_2$ from a mixture of $RhCl_3$ and $SbPh_3$ in ethanol via the complex molecule of *mer*-$[RhCl_3(SbPh_3)_3]$ [11a,11b].

3.2. Molecular modelling

3.2.1. $SbH_2CH{=}CH_2$ (structures **I** and **II**), $M(SbH_2CH{=}CH_2)^+$, and $M(SbH_2CH{=}CH_2)^{2+}$ for M = Cu, Ag, Au, and Zn, Cd, Hg (structures **III**–**VIII**, respectively)

The goal of the analysis was that to investigate the reliability of the computational method for metal-stibine co-ordination molecules and to study the influence of the

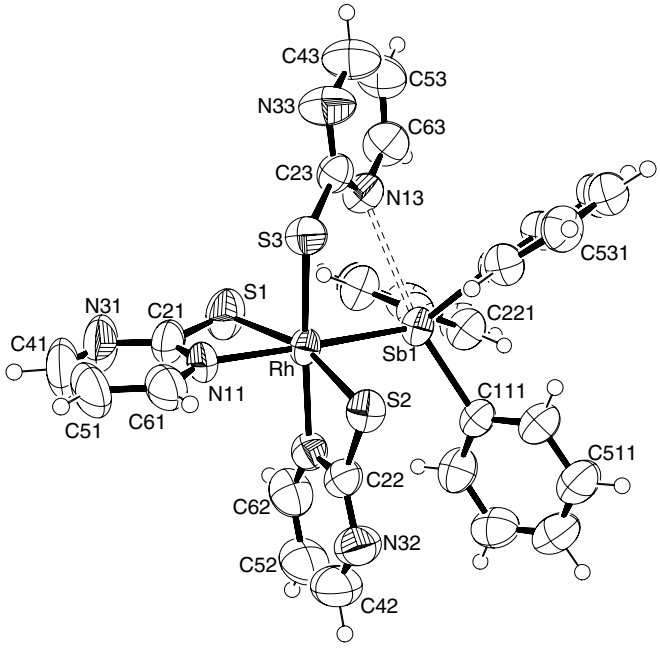

Fig. 2. Drawing of the complex molecule for $[Rh(\underline{N}^1,\underline{S}^2\text{-tpym})_2(\underline{N}^1(Sb),\underline{S}^2(Rh)\text{-tpym})(SbPh_3)]\cdot 0.25C_2H_5OH$ ($\mathbf{3}\cdot 0.25C_2H_5OH$). The ellipsoids enclose 50% probability. The labelling of selected atoms only is included for the sake of clarity.

metal ligation to antimony on the Sb–C and (Sb)C–C bond distances. The computation have been performed at the B3LYP/Lanl2dz level. The $SbH_2CH{=}CH_2$ molecule was used as a model for triphenylstibine with the aim to reduce the computational costs. Several attempts to optimise $Rh(SbH_2CH{=}CH_2)^{3+}$, singlet, triplet and quintet states did not succeed. The $CH{=}CH_2$ system was restrained to be planar; no other restraint was applied. Two computed minimum energy structures were obtained for $SbH_2CH{=}CH_2$, namely **I** and **II** (Fig. 3), for which the H–Sb–C–C torsion angle is 134.6° and −10.5°, respectively, and the difference between the electronic energy ΔE_{el} is small (0.596 kcal), **I** being the most stable. The computed Sb–C bond distance is 2.158 Å in nice agreement with the experimental value found for tris(2-thienyl)stibine [22] and for triphenylstibine [23]. Even the H–Sb–C and H–Sb–H bond angles (**I**, 94.0° and 90.5°) compare well with the C–Sb–C angles for $SbPh_3$ and for several of its metal-complexes (solid state) [11a,11b,24]. The computed C–C bond distance is 1.352 Å (**I**), slightly larger than the corresponding computed value for ethene, 1.348 Å.

The computed structures of closed shell complexes $M(SbH_2CH{=}CH_2)^+$ for M = Cu(I) (structure **III**), Ag(I) (**IV**), Au(I) (**V**) (Fig. 4), have the metal almost coplanar with the $CH{=}CH_2$ group (M–Sb–C–C torsion angle, 0.0°, 0.0° and 1.5°, respectively). The computed M–Sb bond distances are 2.515, 2.718 and 2.584 Å, respectively, in agreement with the X-ray data at the solid state for related structures [25,26]. The computed Sb–C bond distances for **III**, **IV** and **V** are 2.115, 2.117 and 2.107 Å, respectively, significantly shorter than for free $SbH_2CH{=}$

Table 3
Selected bond lengths (Å) and angles (°) $[Rh(\underline{N}^1,\underline{S}^2\text{-tpym})_2(\underline{N}^1(Sb),\underline{S}^2(Rh)\text{-tpym})(SbPh_3)]\cdot 0.25C_2H_5OH$ ($\mathbf{3}\cdot 0.25C_2H_5OH$)

Vectors	Lengths (Å)/Angles (°)
Rh–N(12)	2.078(4)
Rh–N(11)	2.086(4)
Rh–S(3)	2.3222(14)
Rh–S(1)	2.3650(16)
Rh–S(2)	2.3779(14)
Rh–Sb(1)	2.5344(8)
Sb(1)–N(13)	2.846(3)
Sb(1)–C(131)	2.114(5)
Sb(1)–C(121)	2.129(4)
Sb(1)–C(111)	2.164(5)
S(1)–C(21)	1.723(7)
S(2)–C(22)	1.720(6)
S(3)–C(23)	1.737(5)
N(11)–C(61)	1.304(8)
N(11)–C(21)	1.357(8)
N(12)–C(62)	1.314(7)
N(12)–C(22)	1.358(7)
N(13)–C(23)	1.332(6)
N(13)–C(63)	1.350(7)
N(31)–C(21)	1.314(8)
N(31)–C(41)	1.332(13)
N(32)–C(22)	1.318(7)
N(32)–C(42)	1.337(10)
N(33)–C(43)	1.330(8)
N(33)–C(23)	1.351(7)
N(12)–Rh–N(11)	88.30(17)
N(12)–Rh–S(3)	166.17(12)
N(11)–Rh–S(3)	89.48(13)
N(12)–Rh–S(1)	98.58(13)
N(11)–Rh–S(1)	69.21(14)
S(3)–Rh–S(1)	93.38(6)
N(12)–Rh–S(2)	68.86(12)
N(11)–Rh–S(2)	97.59(14)
S(3)–Rh–S(2)	97.94(5)
S(1)–Rh–S(2)	162.58(6)
N(12)–Rh–Sb(1)	91.30(11)
N(11)–Rh–Sb(1)	171.79(13)
S(3)–Rh–Sb(1)	92.82(4)
S(1)–Rh–Sb(1)	102.77(5)
S(2)–Rh–Sb(1)	89.90(4)
C(131)–Sb(1)–C(121)	110.13(19)
C(131)–Sb(1)–C(111)	95.89(19)
C(121)–Sb(1)–C(111)	95.84(18)
N(13)–Sb(1)–C(111)	168.70(10)

CH_2. The same trend happens in the solid state for selected structures [23,25,26]. The computed M–Sb–C bond angles are 116.9°, 118.1° and 113.7° in perfect agreement with

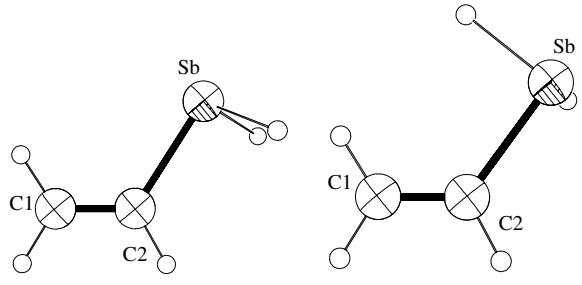

Fig. 3. Drawings of the optimised structures for $SbH_2CH{=}CH_2$.

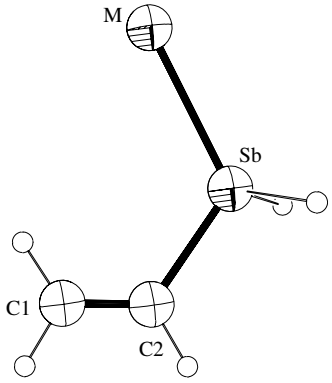

Fig. 4. Drawing of the general structures for $M(SbH_2CH{=}CH_2)^+$ (M = Cu, Ag, Au).

the experimental values found for Rh–$SbPh_3$ groupings from this work.

The computed M′–Sb bond distances are 2.835, 2.970 and 2.983 Å, for $M(SbH_2CH{=}CH_2)^{2+}$, M = Zn(II) (structure **VI**), Cd(II) (**VII**) and Hg(II) (**VIII**), larger than those for the copper triad. The only structure of stibine ligands with zinc triad bivalent cations, deposited in the CSD [14] is that of $I_2CdSb(CH_2CH_3)_2Sb(CH_2CH_3)_2CdI_2$ [27] whose Cd–Sb bond distance is 2.822 Å.

From this analysis, one can say that first the method and level of theory used in this analysis reproduces fairly well the main structural features of the SbR_3 ligands both free and in metal complexes. Second, no any activating effect on the Sb–C linkage upon metal co-ordination could be revealed.

3.2.2. Htpym (structure *IX*) and tpym$^-$ (structure *X*)

The structure **IX** (Fig. 5), as optimised at the B3LYP/(6-31G**) level, has the C^2-S^2 and N^1–C^2 bond lengths of 1.667 and 1.374 Å in agreement with the X-ray structure of thiocytosine [28]. The corresponding bond lengths for structure **X** (same computation level) are 1.719 and 1.382 Å, somewhat larger than those for **IX** (in agreement with deprotonation). In the case the B3LYP/(Lanl2dz(C,H,N);6-31G**(S)) [20] level was used the computed C^2-S^2 and N^1–C^2 bond distances are 1.666 and 1.393 Å for **IX** and 1.713 and 1.408 Å for **X**, respectively. Therefore, the two basis sets compute very close distances for corresponding bonds both for Htpym and tpym$^-$ molecules.

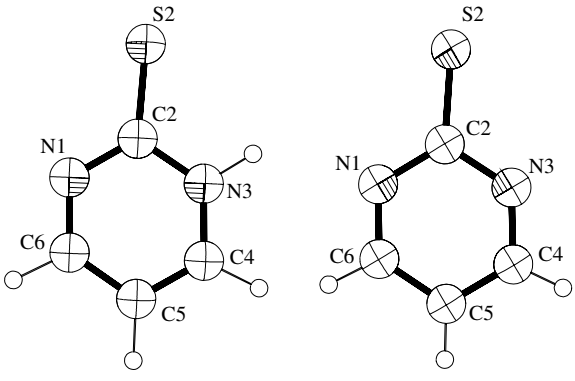

Fig. 5. Drawings of the optimised structures for Htpym and tpym$^-$.

3.2.3. M($\underline{N}^1$,$\underline{S}^2$-tpym) for M = Cu, Ag, Au (structures *XI*, *XII*, *XIII*), and M($\underline{N}^1$,$\underline{S}^2$-tpym)$^+$ for M = Zn, Cd, Hg (structures *XIV*, *XV*, *XVI*)

The structures **XI**–**XIII** (Fig. 6) have the tpym$^-$ anion as chelator via S and N and were optimised at the B3LYP/(Lanl2dz(C,H,N);6-31G**(S)) level. The computed M–S bond distances are 2.315, 2.503, 2.328 Å, whereas the M–N bond distances are 2.085, 2.473 and 3.054 Å. The CSD [14] reports only a complicate structure of a Cu(I)-complex (polycentric) with a tpym$^-$ derivative (*N*,*S*-chelate) as ligand [29]. The Cu–S and Cu–N bond distances are around 2.25 and 2.03 Å, respectively. The only Ag(I)-($\underline{N}^1$,$\underline{S}^2$-tpym) complex found through CSD (it also has a complicate polycentric structure) has Ag-S and Ag-N bond distances of 2.48-2.99 and 2.40 Å [30]. The search on CSD for Au(I)-($\underline{N}^1$,$\underline{S}^2$-tpym) species shows the absence of any effective chelation of the tpym$^-$ anion to a single gold centre. A dimeric structure for bis(μ_2-4,6-dimethylpyrimidine-2-thiolato)digold(I) has Au(1)–S, Au(2)–N, Au(1)–N and Au(2)–S bond distances of 2.26, 2.09, 3.50 and 3.51 Å, respectively [31]. The C–S bond distances are 1.742, 1.745 and 1.768 Å in agreement with the computed values for the free tpym$^-$ anion (see above).

The computed M–S and M–N bond distances are 2.302 and 2.039, 2.494 Å and 2.273, 2.546 and 2.461 Å for **XIV**, **XV**, **XVI**, respectively. A variety of Zn–S and Zn–N bond distances were found for the four structures that contain the Zn(II)-($\underline{N}^1$,$\underline{S}^2$-tpym) group from the CSD. The structure of bis(6-amino-2-thiouracilato)aquazinc(II) has Zn–S and Zn–N lengths of 2.35 and 2.23 Å [32]. The structure of (1,10-phenanthroline)-bis(pyrimidine-2-thionato-*N*,*S*)-cadmium(II) has Cd–S and Cd–N lengths of 2.55–2.59 and 2.42–2.52 Å [33]. The structure of (4-amino-5-methylthiopyrimidine)methylmercury(II) has Hg–S and Hg–N bond distances of 2.39 and 2.81 Å, respectively [34]. The

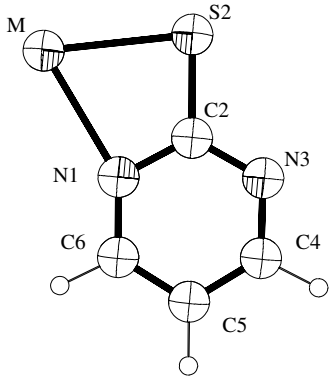

Fig. 6. Drawing of the general structures for M($\underline{N}^1$,$\underline{S}^2$-tpym) (M = Cu, Ag, Au) and M($\underline{N}^1$,$\underline{S}^2$-tpym)$^+$ (M = Zn, Cd, Hg) and Rh($\underline{N}^1$,$\underline{S}^2$-tpym)$^{2+}$.

computed C–S bond distances are 1.773, 1.771 and 1.772 Å, i.e., longer than those for the copper triad.

3.2.4. $Rh(\underline{N}^1,\underline{S}^2\text{-tpym})^{2+}$ (structure *XVII*)

The computed Rh–S bond distances at the B3LYP/(Lanl2dz(C,H,N,Rh);6-31G**(S)) level are 2.177, 2.320, 2.296 Å for the singlet, triplet and quintet states. The experimental data found for **3** (diamagnetic, singlet) are in the range 2.322(1)–2.378(1) Å. The singlet state reproduces well the co-ordination to N found at the solid state, the computed Rh–N distance being 2.016 Å (found for **3**, 2.082 Å, average for tpym(1) and tpym(2)).

3.2.5. $Rh(\underline{N}^1(Sb),\underline{S}^2(Rh)\text{-tpym})(SbH_3)^{2+}$

Several attempts to optimise reasonable structures for $Rh(\underline{N}^1(Sb),\underline{S}^2(Rh)\text{-tpym})(SbH_3)^{2+}$ (in different multeplicity states) to simulate the possible formation of a Rh–S–C–N-Sb(Rh) co-ordination ring, starting from Sb···N contact distance of 2.86 Å, did not converge. The calculations were interrupted when the Sb···N distance reached 4.5 Å.

4. Conclusion

In conclusion, this work produced an efficient method for the synthesis of the new crystalline complex $[Rh(\underline{N}^1,\underline{S}^2\text{-tpym})_2(\underline{N}^1(Sb),\underline{S}^2(Rh)\text{-tpym})(SbPh_3)]$ (**3**). The novelty of this compound consists in having two different types of co-ordinated thiopyrimidine moieties, and a Rh–S–C–N-Sb(Rh) co-ordination ring for which the antimony atom acts both as electron donor to Rh and acceptor from nitrogen. The work shows that the co-ordination of the third $tpym^-$ anion via S only causes an activation of a Sb–C(Ph) bond through the N···Sb intramolecular interaction. The density functional analysis shows that the DFT-B3LYP methods is able to reproduce fairly well the main co-ordination behaviour of $tpym^-$ but it does not model the RhSCNSb(Rh) ring. This suggests to perform further investigation by using more sophisticate molecular models and more accurate computational tools to theoretically investigate the unusual co-ordination mode.

The X-ray diffraction analysis for **1** has confirmed an activation of a Rh–Cl bond through the *trans* influence from an antimony atom assisted by (Ph)C–H···Cl(Rh) hydrogen bond type interactions. The short Cl(2)···Sb(2) contact distance and the lengthening of the Rh–Sb(2) bond suggests that Cl(2) could behave like the $tpym(3)^-$ ligand of **3** and it can activate a Sb–C bond toward dissociation. The X-ray diffraction data and the DFT analysis did not unveil any direct lengthening of Sb–C bonds via metal ligation to antimony that can give a rationale for the formation of *trans*-$[RhCl_2(Ph)(SbPh_3)_3]$ (**2**), from **1**. Instead, the solid state data from this work and from the literature, and theory show a shortening of Sb–C bonds upon metal ligation. From the experimental data at the solid state both for **3** and **1**, it appears that the intervention of a nucleophilic particle on the Sb atom of a $SbPh_3$ ligand is requested to activate the triphenylstibine molecule towards a Sb–C bond breakage and a Rh–Sb dissociation. The effect of an approaching chloride anion to antimony has not been investigated through theoretical and experimental tools, yet. It has to be noted that even the solvent molecules may play a role in the formation of **2**. Further experimental and theoretical efforts must therefore be performed to understand the reaction mechanism.

Acknowledgements

CIADS (Centro Interdipartimentale di Analisi e Determinazioni Strutturali), University of Siena, is acknowledged for the X-ray data collections. University of Siena and MIUR (Ministero della Istruzione, dell'Università e della Ricerca, Rome) are acknowledged for funding through Project PRIN 2004–2005.

Appendix A. Supplementary data

Crystallographic data for the structural analyses have been deposited with the Cambridge Crystallographic Data Centre CCDC Nos. 265735 and 265737 for compounds **1** and **3**. Copies of this information may be obtained free of charge from the Director, CCDC, 12 Union Road, Cambridge CB2 1EZ, UK (fax: +44 1223 336033; e-mail: deposit@ccdc.cam.ac.uk or www: http://www.ccdc.cam.ac.uk). The atomic coordinates for the molecular structures optimised via DFT methods, Tables XIS–XXIXS, 19 pages, have been deposited with the journal. Supplementary data associated with this article can be found, in the online version, at doi:10.1016/j.poly.2005.09.010.

References

[1] (a) E. Freisinger, S. Meier, B. Lippert, J. Chem. Soc., Dalton Trans. (2000) 3274;
(b) M. Roitzsch, B. Lippert, Inorg. Chem. 43 (2004) 5483.
[2] C.X. Zhang, P.V. Chang, S.J. Lippard, J. Am. Chem. Soc. 126 (2004) 6536.
[3] A. Egger, V.B. Arion, E. Reisner, B. Cebrián-Losantos, S. Shova, G. Trettenhahn, B.K. Keppler, Inorg. Chem. 44 (2005) 122.
[4] (a) M. Carlone, L.G. Marzilli, G. Natile, Inorg. Chem. 43 (2004) 584;
(b) G. Colonna, N.G. Di Masi, L.G. Marzilli, G. Natile, Inorg. Chem. 42 (2003) 997.
[5] A.C.G. Hotze, E.P.L. van der Geer, S.E. Caspers, H. Kooijman, A.L. Spek, J.G. Haasnoot, J. Reedijk, Inorg. Chem. 43 (2004) 4935.
[6] P. Mura, M. Camalli, L. Messori, F. Piccioli, P. Zanello, M. Corsini, Inorg. Chem. 43 (2004) 3863.
[7] (a) U. Bierbach, M. Sabat, N. Farrell, Inorg. Chem. 39 (2000) 1882;
(b) U. Bierbach, M. Sabat, N. Farrell, Inorg. Chem. 39 (2000) 3734;
(c) U. Bierbach, M. Sabat, N. Farrell, Inorg. Chem. 39 (2000) 2960.
[8] (a) C.A. Blindauer, T.I. Sjåstad, A. Holý, E. Sletten, H. Sigel, J. Chem. Soc., Dalton Trans. (1999) 3661;
(b) A.H. Velders, A. Bergamo, E. Alessio, E. Zangrando, J.G. Haasnoot, C. Casarsa, M. Cocchietto, S. Zorzet, G. Sava, J. Med. Chem. 47 (2004) 1110;
(c) E. Iengo, G. Mestroni, S. Geremia, M. Calligaris, E. Alessio, J. Chem. Soc., Dalton Trans. (1999) 3361;
(d) S. Rojas, J.L. Garcia Fierro, R. Fandos, A. Rodriguez, P. Terreros, J. Chem. Soc., Dalton Trans. (2001) 2316.

[9] J. Kasparkova, O. Delalande, M. Stros, M.-A. Elizondo-Riojas, M. Vojtiskova, J. Kozelka, V. Brabec, Biochemistry 42 (2003) 1234.
[10] K.S. Schmidt, J. Reedijk, K. Weisz, E.M. Basilio Janke, J.E. Sponer, J. Sponer, B. Lippert, Inorg. Chem. 41 (2002) 2855.
[11] (a) R. Cini, G. Giorgi, L. Pasquini, Inorg. Chim. Acta 196 (1992) 7;
(b) A. Cavaglioni, R. Cini, J. Chem. Soc., Dalton Trans. (1997) 1149;
(c) C. Pifferi, R. Cini, J. Chem. Soc., Dalton Trans. (1998) 2679;
(d) R. Cini, A. Cavaglioni, Inorg. Chem. 38 (1999) 3751;
(e) R. Cini, M. Corsini, A. Cavaglioni, Inorg. Chem. 39 (2000) 5874;
(f) R. Cini, G. Tamasi, S. Defazio, M. Corsini, P. Zanello, L. Messori, G. Marcon, F. Piccioli, P. Orioli, Inorg. Chem. 42 (2003) 8038.
[12] S. Ramadan, T.V. Hambley, B.J. Kennedy, P.A. Lay, Inorg. Chem. 43 (2004) 2943.
[13] (a) A. Massey, Y.Z. Xu, P. Karran, Curr. Biol. 11 (2001) 1142;
(b) Y.Z. Xu, X. Zhang, H.C. Wu, A. Massey, P. Karran, Bioorg. Med. Chem. Lett. 14 (2004) 995.
[14] The Cambridge Crystallographic Data Base, version 5.25, The Cambridge Crystallographic Data Center, Cambridge, UK, November, 2004.
[15] (a) B. Desoize, Anticancer Res. 24 (2004) 1529;
(b) B. Weber, A. Serafin, J. Michie, C. Van Rensburg, J.C. Swarts, L. Bohm, Anticancer Res. 24 (2004) 763;
(c) N. Katsaros, A. Anagnostopoulou, Crit. Rev. Onc. Hematol. 42 (2002) 297.
[16] G.M. Sheldrick, SHELX-97: Program for the Solution and Refinement of Crystal Structures, University of Göttingen, Göttingen, Germany, 1997.
[17] M. Nardelli, PARST-97: A System of Computer Routines for Calculating Molecular Parameters from Results, University of Parma, Parma, Italy, 1997.
[18] C.K. Johnson, M.N. Burnett, ORTEP3 for Windows; Oak Ridge National Laboratory: Oak Ridge, TN. 32-bit Implementation by L.J. Farrugia, University of Glasgow, Glasgow, Scotland, 1998.
[19] M.J. Frisch, G.W. Trucks, H.B. Schlegel, G.E. Scuseria, M.A. Robb, J.R. Cheeseman, V.G. Zakrzewski, J.A. Montgomery Jr., R.E. Stratmann, J.C. Burant, S. Dapprich, J.M. Millam, A.D. Daniels, K.N. Kudin, M.C. Strain, O. Farkas, J. Tomasi, V. Barone, M. Cossi, R. Cammi, B. Mennucci, C. Pomelli, C. Adamo, S. Clifford, J. Ochterski, G.A. Petersson, P.Y. Ayala, Q. Cui, K. Morokuma, J.V. Malick, A.D. Rabuck, K. Raghavachari, J.B. Foresman, J. Cioslowski, J.V. Ortiz, A.G. Baboul, B.B. Stefanov, G. Liu, A. Liashenko, P. Piskorz, I. Komaromi, R. Gomperts, R.L. Martin, D.J. Fox, T. Keith, M.A. Al-Laham, C.Y. Peng, A. Nanayakkara, C. Gonzalez, M. Challacombe, P.M.W. Gill, B. Johnson, W. Chen, M.W. Wong, J.L. Andres, C. Gonzalez, M. Head-Gordon, E.S. Replogle, J.A. Pople, GAUSSIAN-98, Revision A.7, Gaussian, Inc., Pittsburgh, PA, 1998.
[20] A. Frish, M.J. Frisch, GAUSSIAN-98, User's Reference, second ed., Gaussian, Inc., Pittsburgh, PA, 1998.
[21] R. Cini, Trends Inorg. Chem. 7 (2001) 57.
[22] J. Vela, P. Sharma, A. Cabrera, C. Álvarez, N. Rosas, S. Hernández, A. Toscano, J. Organomet. Chem. 634 (2001) 5.
[23] E.A. Adams, J.W. Kolis, W.T. Pennington, Acta Crystallogr., Sect. C 46 (1990) 917.
[24] R. Cini, A. Cavaglioni, E. Tiezzi, Polyhedron 18 (1999) 669.
[25] G.A. Bowmaker, R.D. Hart, E.N. De Silva, B.W. Skelton, A.H. White, Aust. J. Chem. 50 (1997) 621.
[26] P.G. Jones, Acta Crystallogr., Sect. C 48 (1992) 1487.
[27] R.S. Dickson, K.D. Heazle, G.N. Pain, G.B. Deacon, B.O. West, G.D. Fallon, R.S. Rowe, P.W. Leech, M. Faith, J. Organomet. Chem. 449 (1993) 131.
[28] S. Furberg, L.H. Jensen, Acta Crystallogr., Sect. B 26 (1970) 1260.
[29] R. Castro, M.L. Duran, J.A. Garcia-Vazquez, J. Romero, A. Sousa, E.E. Castellano, J. Zukerman-Schpector, J. Chem. Soc., Dalton Trans. (1992) 2559.
[30] W. Su, R. Cao, M. Hong, W.-T. Wong, J. Lu, Inorg. Chem. Commun. 2 (1999) 241.
[31] L. Hao, R.J. Lachicotte, H.J. Gysling, R. Eisenberg, Inorg. Chem. 38 (1999) 4616.
[32] M.A. Romero, M.P. Sanchez, M. Quiros, F. Sanchez, J.M. Salas, M.N. Moreno, Can. J. Chem. 71 (1993) 29.
[33] R. Castro, M.L. Duran, J.A. Garcia-Vazquez, J. Romero, A. Sousa, A. Castineiras, W. Hiller, J. Strahle, Z. Naturforsch. B 47 (1992) 1067.
[34] D.A. Stuart, L.R. Nassimbeni, A.T. Hutton, K.R. Koch, Acta Crystallogr., Sect. B 36 (1980) 2227.

Available online at www.sciencedirect.com
SCIENCE DIRECT
Polyhedron 25 (2006) 843–852
POLYHEDRON
www.elsevier.com/locate/poly

Synthesis and structures of diphosphinoamide complexes of nickel, palladium and platinum

Musa Said, David L. Hughes, Manfred Bochmann *

Wolfson Materials and Catalysis Centre, School of Chemical Sciences and Pharmacy, University of East Anglia, Norwich NR4 7TJ, UK

Received 21 June 2005; accepted 15 July 2005
Available online 29 August 2005

Dedicated to Professor Mike Hursthouse, in gratitude for his friendship over the last three decades. Happy Birthday Mike!

Abstract

Lithium bis(diphenylphosphino)amide, $(THF)_3LiN(PPh_2)_2$ reacts with $Ni(COD)_2$ or $PtMe_2(COD)$ to give the corresponding bimetallic complexes $(THF)_3LiN(PPh_2)_2Ni(COD)$ and $(THF)_3LiN(PPh_2)_2PtMe_2$. Reaction of $(THF)_3LiN(PPh_2)_2Ni(COD)$ with Me_3SnCl gave the Ni–Sn derivative, also accessible from $Me_3SnN(PPh_2)_2$. The silyl derivatives $Me_3SiN(PPh_2)_2M$ [M = Ni(COD), $PtMe_2$] were obtained similarly as red and colourless crystals, respectively. By contrast, the reaction with $PdCl_2(COD)$ afforded an insoluble yellow adduct which, on attempted recrystallisation afforded a small amount of a Pd(I) product, $[PdCl\{HN(PPh_2)_2\}]_2$. The crystal structures of the Ni and Pt complexes are based on MP_2N four-membered rings. The geometric parameters proved rather insensitive to changes in the N-main group element bond. In all cases the amido-nitrogen atom deviated slightly from trigonal-planar geometry, most probably as the consequence of packing forces.
© 2005 Elsevier Ltd. All rights reserved.

Keywords: Nickel; Platinum; Bimetallic complexes; Phosphine complexes; Lithium phosphinoamide

1. Introduction

The control of steric and electronic properties of catalytically active metal centres is a fundamental problem in catalyst design [1]. As part of a general study of new ligands directed towards olefin polymerisation catalysts, we became interested in the possibility of influencing the electronic characteristics of one, potentially active metal centre by connecting it to a second metal complex via a ligand capable of allowing electronic interactions, as shown schematically in structures **I** and **II**.

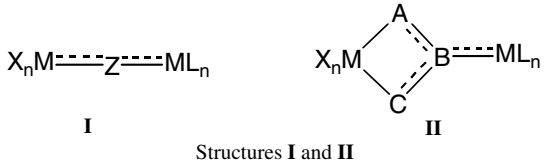

I **II**

Structures **I** and **II**

As a preliminary to such studies we became interested in complexes of bis(diphenylphosphino)amine, since on the one hand derivatives of this ligand have been shown to produce active catalysts [2], while on the other the amine can be deprotonated and metallated [3]. We report here the synthesis and structures of bis(diphenylphosphino) amide complexes of group 10 metals of type **II**, where $ML_n = Li(THF)_3$, $SiMe_3$ and $SnMe_3$. Neutral complexes of the type $(Ph_2PNPPh_2)MX(L)$

* Corresponding author.
E-mail address: m.bochmann@uea.ac.uk (M. Bochmann).

0277-5387/$ - see front matter © 2005 Elsevier Ltd. All rights reserved.
doi:10.1016/j.poly.2005.07.027

(M = Ni, Pd; X = Cl or Br; L = phosphine) as well as bis(diphenylphosphino)amine complexes [PtCl(L)-(dppa)]Cl are well known [4,5] [dppa = $HN(PPh_2)_2$].

2. Results and discussion

2.1. Syntheses

Lithium bis(diphenylphosphino)amide, $(THF)_3LiN(PPh_2)_2$ (**1**) is readily accessible from butyllithium and $HN(PPh_2)_2$ in THF [3] and was isolated as a crystalline solid. Treatment of **1** in THF with $Ni(COD)_2$ or $PtMe_2$-(COD) afforded the corresponding phosphine complexes of Ni(0) and Pt(II), dark-red **NiLi** and colourless **PtLi**, respectively (Scheme 1).

As a test for the coordination of metals other than lithium to the nitrogen in the $dppa^-$ anion, **1** was reacted with trimethyltin chloride to give $Me_3SnN(PPh_2)_2$ (**2**) which on treatment with $Ni(COD)_2$ gave the expected complex $Me_3SnN(PPh_2)_2Ni(COD)$ (**NiSn**). The same product was obtained by reacting **NiLi** with Me_3SnCl. The compound was isolated as red crystals in good yield (Scheme 2).

In a similar manner, the reaction of $Me_3SiN(PPh_2)_2$ with $Ni(COD)_2$ and $PtMe_2(COD)$ gave the complexes $Me_3SiN(PPh_2)_2Ni(COD)$ (**NiSi**) and $Me_3SiN(PPh_2)_2$-$PtMe_2 \cdot$ toluene (**PtSi**) as crystalline products in good yields.

^{31}P NMR spectroscopy was found to be a convenient way of following these reactions (Table 1). There is remarkably little difference in chemical shift on substituting lithium in **1** for the rather more covalently bonded $SnMe_3$ group. Similarly, complexation of **1** to a Ni(COD) residue results in only a relatively small low-field shift of ca. 13 ppm. By contrast, coordination of **1** to Pt(II) produces a shift of ca. 20 ppm to higher field, with platinum–phosphorus coupling constants of 740–770 Hz.

While these reactions of nickel and platinum compounds readily gave crystalline products, the analogous

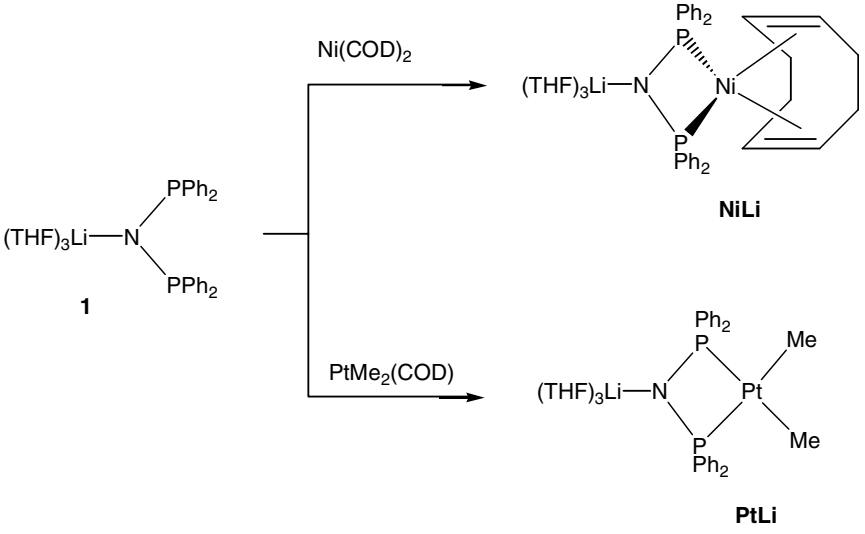

Scheme 1.

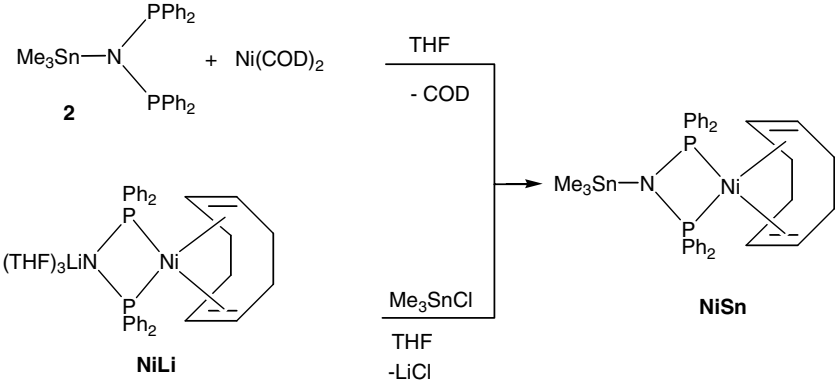

Scheme 2.

Table 1
^{31}P NMR data of dppa derivatives

Compound	δ ^{31}P	Conditions
$(THF)_3LiN(PPh_2)_2$	53.56[a]	THF-d_8, 30 °C
$Me_3SnN(PPh_2)_2$	61.24	C_6D_6, 25 °C
NiLi	66.22	THF-d_8, 25 °C
NiSn	83.67	C_6D_6, 25 °C
NiSi	82.84	C_6D_6, 25 °C
PtLi	29.77 ($J_{Pt-P} = 740$ Hz)	THF-d_8, 25 °C
PtSi	35.00 ($J_{Pt-P} = 769.9$ Hz)	C_6D_6, 25 °C

[a] Ref. [3].

reaction of $Me_3SiN(PPh_2)_2$ with $PdCl_2(COD)$ generated a poorly soluble yellow powder which analysed for $Me_3SiN(PPh_2)_2PdCl_2$. During attempted recrystallisations from a large volume of THF/CH_2Cl_2 a few crystals were isolated which turned out to be a decomposition product and were identified by X-ray diffraction as a Pd(I)–dppa complex, $[PdCl\{HN(PPh_2)_2\}]_2 \cdot 3CH_2Cl_2$ (Scheme 3). This compound has previously been made as the acetone solvate by a more rational route, the comproportionation of $PdCl_2(NCPh)_2$ and $Pd_2(dba)_3 \cdot CHCl_3$ in the presence of dppa (dba = dibenzylideneacetone) [6].

The reactivity of these complexes in polymerisation reactions and as synthons for bimetallic species will be reported elsewhere.

2.2. Molecular structures

The crystal structures of **NiLi**, **NiSn**, **PtLi** and **PtSi** were determined. In all cases the structures of the complexes are based on MP_2N four-membered rings. Although the polarities of the N–Li, N-Si and N–Sn bonds are expected to differ widely in reflection of the differences in electronegativity, these changes turned out to have remarkably little effect on the geometric parameters of the resulting complexes.

The nickel–lithium compound $(THF)_3LiN(PPh_2)_2$-Ni(COD) (**NiLi**) has a core of a planar, four-membered NiP_2N ring, with the lithium atom bound to the nitrogen atom N(2) (Fig. 1). Selected bond distances and angles are collected in Table 2. The lithium ion is displaced 0.415(3) Å from the NiP_2N plane. The nitrogen atom is almost trigonal-planar, with an angle sum of 357.75°, and is moved 0.151(2) Å out of the LiP_2 plane. As

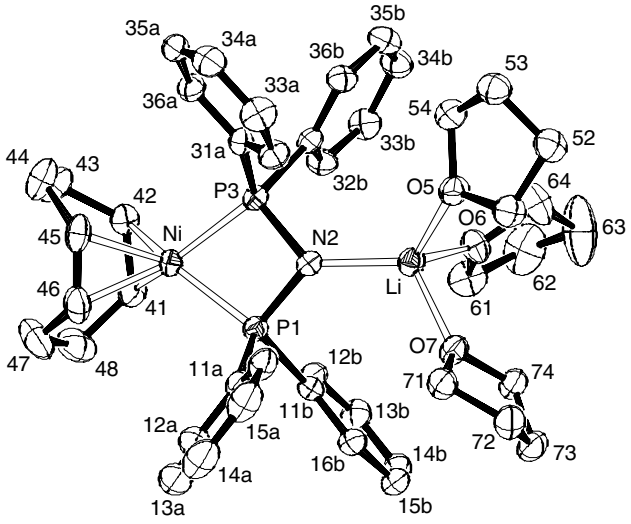

Fig. 1. Molecular structure of $(THF)_3LiN(PPh_2)_2Ni(COD)$ (**NiLi**), indicating the atom numbering scheme; the atoms labelled '*n*' denote the carbon atoms C(*n*). Thermal ellipsoids are shown at the 50% probability level.

expected for a bidentate chelate, the P–N–P angle in **NiLi** is 95.46(9)°, very much smaller than the PNP angle of 124.7(3)° in uncoordinated $(THF)_3LiN(PPh_2)_2$ [3]. The mean Ni–P–N angle is 97.59(14)°.

The nickel atom is four-coordinate (taking the two Ni–π interactions to the centres of the C=C bonds as occupying two coordination sites) in a roughly tetrahedral pattern. The chelating P–Ni–P angle is acute, at 69.36(2)°. The COD ligand is saddle-shaped, with a twist (so that there is no eclipsing of bonds). The lithium atom is four-coordinate. In spite of the angular changes around N the Li–N(2) distance in **NiLi** of 2.012(4) Å is very close to that in free $(THF)_3LiN(PPh_2)_2$ [2.030(1) Å]. The coordination geometry of Li is completed by three THF ligands, in a more obviously tetrahedral pattern. The THF ligands of O(6) and O(7) have envelope-like conformations, with C(63) and C(72) forming the out-of-plane flap atoms. The O(5) THF ring has a minimum torsion angle of 10.8(2)°, and the overall ring shape is more 'half-chair' than 'envelope'.

Overall the shape of $Me_3SnN(PPh_2)_2Ni(COD)$ (**NiSn**) is rather similar to **NiLi** (Fig. 2 and Table 3). There are two independent molecules in the asymmetric unit. They

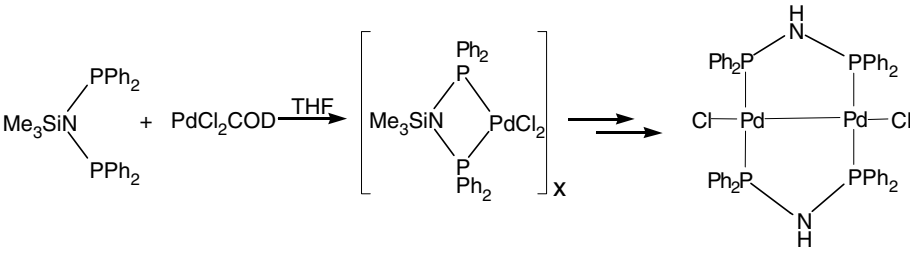

Scheme 3.

Table 2
Selected bond lengths (Å) and angles (°) of $Me_3SnN(PPh_2)_2Ni(COD)$ (**NiLi**)

Ni–P(1)	2.2007(6)
Ni–P(3)	2.1922(6)
Ni–C(41)	2.071(2)
P(1)–N(2)	1.6882(17)
P(1)–C(11a)	1.844(2)
P(1)–C(11b)	1.854(2)
N(2)–Li	2.012(4)
Li–O(5)	2.071(4)
C(41)–C(42)	1.388(3)
C(41)–C(48)	1.508(3)
Ni–C(42)	2.074(2)
Ni–C(45)	2.099(2)
Ni–C(46)	2.099(2)
N(2)–P(3)	1.6897(17)
P(3)–C(31a)	1.841(2)
P(3)–C(31b)	1.846(2)
Li–O(6)	1.964(4)
Li–O(7)	2.037(4)
C(44)–C(45)	1.508(3)
C(45)–C(46)	1.379(3)
P(3)–Ni–P(1)	69.36(2)
C(41)–Ni–P(1)	115.39(6)
P(1)–N(2)–P(3)	95.46(9)
P(1)–N(2)–Li	132.00(13)
N(2)–Li–O(5)	122.91(17)
O(6)–Li–N(2)	115.43(18)
N(2)–Li–O(7)	117.91(18)
C(42)–Ni–P(1)	145.85(6)
C(46)–Ni–P(3)	135.62(7)
P(3)–N(2)–Li	130.29(14)
O(6)–Li–O(5)	98.45(16)
O(7)–Li–O(5)	97.81(16)
O(6)–Li–O(7)	100.12(16)

look very similar but show some subtle conformational differences.

The nickel atom is four-coordinate, with a much distorted tetrahedral pattern. The mean P–Ni–P angle is 73.21(7)°. The four atoms of the NiP_2N core in molecule A (containing Ni(1)) are coplanar, but in molecule B (of Ni(2)) there is a mean deviation of 0.024(2) Å of these atoms from their mean-plane. As in **NiLi**, the nitrogen atoms are not quite trigonal-planar, with angle sums of 356.8° and 358.4° for molecules 1 and 2, respectively. The N–Sn bonds are tilted slightly out of the core planes, so that Sn(2) lies 0.653(2) Å and Sn(6) 0.394(2) Å from those planes. Correspondingly, the nitrogen atoms N(2) and N(6) are displaced 0.188(5) and 0.133(6) Å from their SnP_2 planes.

The tin atoms show little distortion from regular tetrahedra in their bonds to the nitrogen atoms and three methyl carbon atoms. The COD ligands have the same twisted saddle-shapes as in **NiLi**. However, when the molecules are viewed down the Ni–N vectors and the orientations of the $SnMe_3$ groups are aligned, we note that the COD ligands are twisted in opposite directions. In molecule A, the projection of Sn(2)–C(21) bisects the

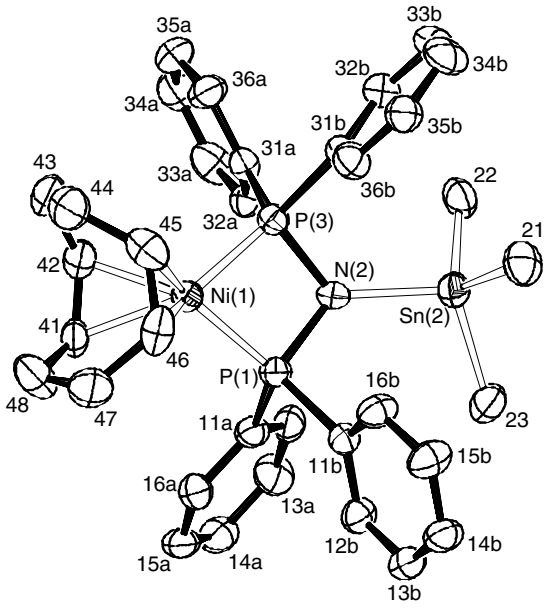

Fig. 2. Views of one of the two independent molecules of $Me_3SnN(PPh_2)_2Ni(COD)$ (**NiSn**), indicating the atom numbering schemes. Hydrogen atoms have been omitted for clarity. Thermal ellipsoids are drawn at the 50% probability level.

Table 3
Selected bond lengths (Å) and angles (°) of $Me_3SnN(PPh_2)_2Ni(COD)$ (**NiSn**)

Molecule 1		Molecule 2	
Ni(1)–P(1)	2.177(2)	Ni(2)–P(5)	2.1585(19)
Ni(1)–P(3)	2.1624(19)	Ni(2)–P(7)	2.1532(18)
Ni(1)–C(41)	2.116(7)	Ni(2)–C(81)	2.090(8)
Ni(1)–C(42)	2.077(9)	Ni(2)–C(82)	2.120(8)
Ni(1)–C(45)	2.101(7)	Ni(2)–C(85)	2.080(6)
Ni(1)–C(46)	2.087(7)	Ni(2)–C(86)	2.083(7)
N(2)–Sn(2)	2.101(6)	N(6)–Sn(6)	2.132(5)
Sn(2)–C(21)	2.143(7)	Sn(6)–C(61)	2.120(9)
Sn(2)–C(22)	2.150(7)	Sn(6)–C(62)	2.127(9)
Sn(2)–C(23)	2.145(7)	Sn(6)–C(63)	2.139(7)
P(1)–C(11a)	1.835(6)	P(5)–C(51a)	1.842(7)
P(1)–C(11b)	1.840(7)	P(5)–C(51b)	1.816(8)
P(1)–N(2)	1.715(5)	P(5)–N(6)	1.691(5)
N(2)–P(3)	1.724(6)	N(6)–P(7)	1.722(6)
P(3)–C(31a)	1.831(7)	P(7)–C(71a)	1.828(8)
P(3)–C(31b)	1.849(6)	P(7)–C(71b)	1.841(7)
C(41)–C(42)	1.352(10)	C(81)–C(82)	1.378(9)
C(41)–C(48)	1.530(11)	C(81)–C(88)	1.495(9)
P(3)–Ni(1)–P(1)	73.22(7)	P(7)–Ni(2)–P(5)	73.20(7)
C(11a)–P(1)–Ni(1)	121.0(3)	C(51b)–P(5)–Ni(2)	121.1(2)
C(11b)–P(1)–Ni(1)	127.2(2)	C(51a)–P(5)–Ni(2)	120.2(2)
N(2)–P(1)–Ni(1)	94.4(2)	N(6)–P(5)–Ni(2)	94.9(2)
P(1)–N(2)–Sn(2)	131.3(3)	P(5)–N(6)–Sn(6)	127.7(3)
P(1)–N(2)–P(3)	97.6(3)	P(5)–N(6)–P(7)	97.7(3)
P(3)–N(2)–Sn(2)	127.9(3)	P(7)–N(6)–Sn(6)	133.0(3)
N(2)–P(3)–Ni(1)	94.64(18)	N(6)–P(7)–Ni(2)	94.19(19)
C(31a)–P(3)–Ni(1)	118.1(2)	C(71a)–P(7)–Ni(2)	115.5(2)
C(31b)–P(3)–Ni(1)	127.0(2)	C(71b)–P(7)–Ni(2)	128.2(2)

C(45)–C(46) bond (similar to the arrangement in **NiLi**), whereas Sn(6)–C(61) lies parallel to the projection of the Ni–C(85) bond.

The structures of the platinum(II) complexes **PtLi** and **PtSi** are shown in Figs. 3 and 4, respectively. Bond lengths and angles are given in Tables 4 and 5. In both cases the platinum centres are square planar with two methyl groups in a *cis* arrangement, and a chelating PPh_2NPPh_2 ligand. In **PtLi** the Pt atom is displaced

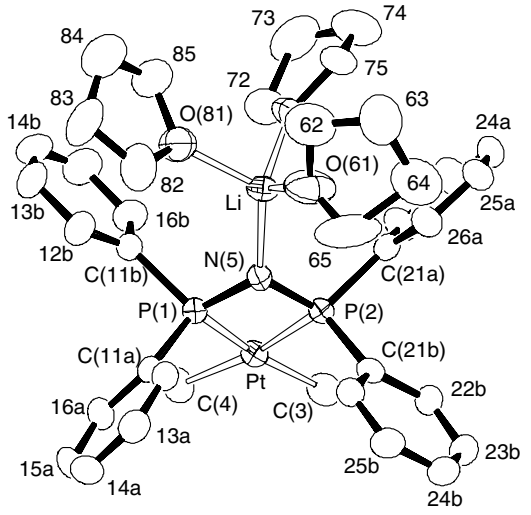

Fig. 3. View a molecule of $(THF)_3LiN(PPh_2)_2PtMe_2$ (**PtLi**). Atoms labelled as "*n*" represent the carbon atoms C(*n*). Hydrogen atoms are omitted for clarity. Thermal ellipsoids are drawn at the 50% probability level.

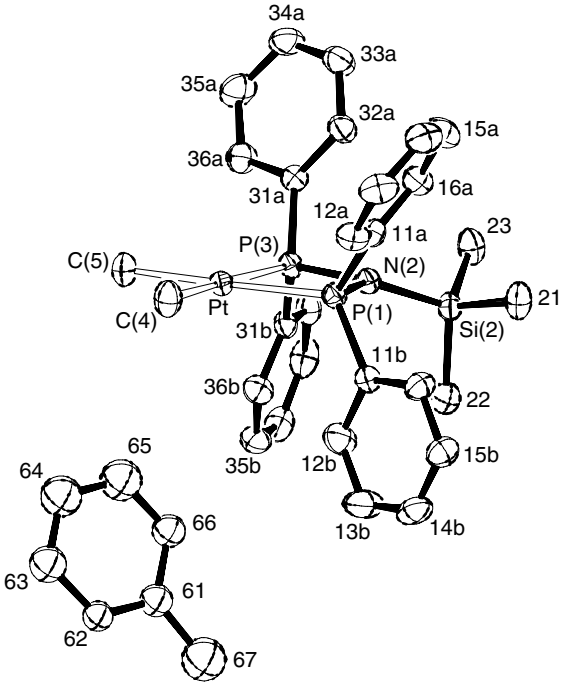

Fig. 4. Molecular structure of $Me_3SiN(PPh_2)_2PtMe_2 \cdot 0.5$ toluene (**PtSi**). Hydrogen atoms are omitted for clarity. Thermal ellipsoids are drawn at the 50% probability level.

0.016(3) Å to one side of the P_2C_2 mean-plane; N(5) and Li are on the opposite side, at −0.194(5) and −1.314(11) Å from the plane. The nitrogen atom of the PNP ligand is bonded to the Li atom, and the three angles about N(5) add up to 351.5°, the most highly pyramidalised N atom of all the structures considered here. The central core of the molecule is thus seen to curve gently from the methyl carbon atoms through the Pt, P and N atoms to the Li atom.

The three THF ligands give Li a distorted tetrahedral coordination pattern. The three N–Li–O angles are all rather larger than the regular tetrahedral value, and two of the three O–Li–O angles are much smaller than 109.5°. There is disorder (which has been clearly resolved) of a methylene group in one THF ligand; several other carbon atoms in these ligands have large thermal parameters but no further disorder has been identified.

Table 4
Selected bond lengths (Å) and angles (°) of $(THF)_3LiN(PPh_2)_2PtMe_2$ (**PtLi**)

Pt–P(1)	2.2827(15)
Pt–P(2)	2.2941(15)
P(1)–N(5)	1.690(5)
P(1)–C(11a)	1.833(6)
P(1)–C(11b)	1.836(6)
N(5)–Li	2.031(11)
Li–O(61)	1.970(12)
Pt–C(3)	2.101(6)
Pt–C(4)	2.131(6)
P(2)–N(5)	1.688(5)
P(2)–C(21b)	1.827(6)
P(2)–C(21a)	1.838(6)
Li–O(71)	1.950(11)
Li–O(81)	2.035(11)
P(1)–Pt–P(2)	66.43(5)
C(3)–Pt–P(1)	169.9(2)
C(4)–Pt–P(1)	103.4(2)
N(5)–P(1)–Pt	98.60(17)
C(11a)–P(1)–Pt	118.47(19)
C(11b)–P(1)–Pt	119.0(2)
N(5)–P(1)–C(11a)	108.2(3)
N(5)–P(1)–C(11b)	110.9(3)
C(11a)–P(1)–C(11b)	101.4(3)
P(1)–N(5)–Li	128.3(4)
P(2)–N(5)–Li	127.4(4)
O(61)–Li–N(5)	118.2(5)
O(71)–Li–N(5)	112.6(5)
N(5)–Li–O(81)	122.3(5)
C(3)–Pt–P(2)	103.5(2)
C(4)–Pt–P(2)	169.6(2)
C(3)–Pt–C(4)	86.6(3)
N(5)–P(2)–Pt	98.26(17)
C(21b)–P(2)–Pt	117.37(19)
C(21a)–P(2)–Pt	122.56(19)
N(5)–P(2)–C(21b)	109.6(3)
N(5)–P(2)–C(21a)	109.9(2)
C(21b)–P(2)–C(21a)	99.0(3)
P(2)–N(5)–P(1)	95.8(2)
O(71)–Li–O(61)	110.8(5)
O(61)–Li–O(81)	93.7(5)
O(71)–Li–O(81)	96.2(5)

Table 5
Selected bond lengths (Å) and angles (°) of $Me_3SiN(PPh_2)_2PtMe_2$ (**PtSi**)

Pt–P(1)	2.2790(10)
Pt–P(3)	2.2675(10)
N(2)–Si(2)	1.789(3)
P(1)–N(2)	1.735(3)
P(1)–C(11b)	1.825(4)
P(1)–C(11a)	1.827(4)
Pt–C(4)	2.093(4)
Pt–C(5)	2.087(4)
N(2)–P(3)	1.732(3)
Si(2)–C(21)	1.861(5)
Si(2)–C(22)	1.865(5)
Si(2)–C(23)	1.871(5)
P(3)–Pt–P(1)	70.37(4)
C(4)–Pt–P(1)	103.02(13)
C(5)–Pt–P(1)	170.08(13)
N(2)–P(1)–Pt	95.45(11)
N(2)–P(1)–C(11a)	108.53(18)
N(2)–P(1)–C(11b)	107.27(17)
C(11a)–P(1)–Pt	119.76(13)
C(11b)–P(1)–Pt	120.74(13)
C(11b)–P(1)–C(11a)	103.76(19)
P(3)–N(2)–P(1)	98.17(16)
P(1)–N(2)–Si(2)	130.0(2)
N(2)–Si(2)–C(21)	109.55(19)
N(2)–Si(2)–C(22)	110.79(19)
C(4)–Pt–P(3)	173.15(13)
C(5)–Pt–P(3)	99.71(13)
C(5)–Pt–C(4)	86.90(18)
N(2)–P(3)–Pt	95.94(12)
N(2)–P(3)–C(31a)	108.41(17)
N(2)–P(3)–C(31b)	107.86(17)
C(31a)–P(3)–Pt	118.78(12)
C(31b)–P(3)–Pt	119.24(14)
C(31a)–P(3)–P(31b)	105.40(19)
P(3)–N(2)–Si(2)	128.0(2)
N(2)–Si(2)–C(23)	108.75(19)

The platinum atom in $Me_3SiN(PPh_2)_2PtMe_2 \cdot 0.5$ toluene (**PtSi**) lies close to the mean-plane through the C_2P_2 coordinating atoms. Atom N(2) lies only 0.044(4) Å from that plane and Si(2) dips away rather more, to lie 0.601(3) Å out-of-plane. The arrangement about N(2) is close to trigonal planar (angle sum 356.2°), and the N-atom is 0.193(3) Å from the P_2Si plane, a distortion presumably resulting from the close packing of the $SiMe_3$ methyl groups against the phenyl groups on the P atoms.

Pairs of toluene molecules lie disordered about centres of symmetry; one or other of the pair is present at any centre, and the atoms of this molecule are well resolved.

The main geometric parameters of these four complexes are compared in Table 6. In all cases the P–N bonds are elongated compared to uncomplexed $(THF)_3LiN(PPh_2)_2$ [3]. The P–N–P angles are reduced from 124.7° to ca. 95–98°, irrespective of the metal. Whereas in free $(THF)_3LiN(PPh_2)_2$ there are two P–N–Li angles due to the interaction of one of the PPh_2 groups with the Li atom, in the complexes all these angles substantially exceed 120°. In all cases the N atom deviates slightly from ideal trigonal-planar geometry, although there is no correlation between the size of this deviation and the nature of the N-bound main group element.

The molecular structure and selected geometric parameters of the Pd(I) product $[PdCl\{HN(PPh_2)_2\}]_2 \cdot 3CH_2Cl_2$ are given in Fig. 5 and Table 7, respectively.

The Pd complex molecule is dimeric, the two halves related by a twofold symmetry axis which passes through the two nitrogen atoms. The N–H bonds lie along the symmetry axis and are directed towards the solvent chlorine atoms, Cl(41′) and Cl(41″) which also lie on the symmetry axis at H···Cl distances of 2.88 and 2.82 Å. Viewed down the symmetry axis, the angle between the normals to the two PNP planes is 67.1°. There are three principal arrangements of the CH_2Cl_2 solvent molecules: that of Cl(41), C(42), Cl(43) lies to one side of the symmetry axis or to the other side; on the opposite side of the axis to that molecule, the molecule of Cl(51) and Cl(53) lies in one of several orientations; the third molecule, of Cl(61), etc., lies disordered about a centre of symmetry in one of several possible orientations.

Since the remaining structural features are essential identical to those reported by Uson for the acetone solvated compound the bonding parameters will not be discussed here further.

Table 6
Comparison of main geometric parameters in bis(diphenylphosphino) amide complexes

	$(THF)_3LiN(PPh_2)_2$[a]	**NiLi**	**NiSn**	**PtLi**	**PtSi**
M–P	–	2.1964(4)[b]	2.163(5)[b]	2.288(6)[b]	2.273(6)[b]
P–N	1.672(15)	1.6889(8)[b]	1.713(8)[b]	1.689(1)[b]	1.734(2)[b]
N–E	2.030(1) (E = Li)	2.012(4) (E = Li)	2.117(16)[b] (E = Sn)	2.031(11) (E = Li)	1.789(3) (E = Si)
P–M–P	–	69.36(2)	73.21(1)[b]	66.43(5)	70.37(4)
P–N–P	124.7(3)	95.46(9)	97.65(5)[b]	95.8(2)	98.17(16)
P–N–E	106.5(3), 128.7(4)	131.1(9) [b]	130.0(13)[b]	127.9(5)[b]	129.0(10)[b]
N angle sum	359.9	357.75	358.4, 356.8	351.5	356.2

[a] From [3].
[b] Mean value.

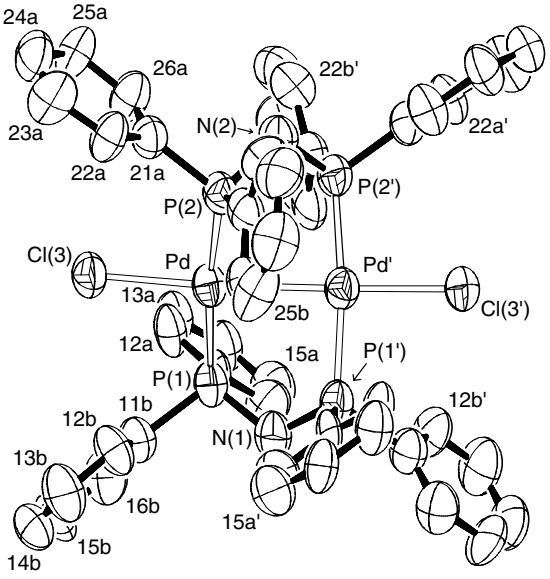

Fig. 5. View of the Pd dimeric complex, $[PdCl(Ph_2PNHPPh_2)]_2$, indicating the atom numbering scheme. Hydrogen atoms have been omitted for clarity. Thermal ellipsoids are drawn at the 50% probability level.

Table 7
Selected bond lengths (Å) and angles (°) of $[PdCl\{HN(PPh_2)_2\}]_2 \cdot 3CH_2Cl_2$

Pd–Pd′	2.637(2)
Pd–P(1)	2.281(4)
P(1)–N(1)	1.677(11)
P(1)–C(11a)	1.813(14)
P(1)–C(11b)	1.843(15)
Pd–P(2)	2.276(4)
Pd–Cl(3)	2.406(4)
P(2)–N(2)	1.716(12)
P(2)–C(21a)	1.806(14)
P(2)–C(21b)	1.777(14)
P(1)–Pd–Pd′	88.68(8)
P(2)–Pd–Pd′	84.98(8)
Cl(3)–Pd–Pd′	173.63(11)
N(1)–P(1)–Pd	111.7(6)
P(1)–N(1)–P(1′)	119.2(12)
P(2)–Pd–P(1)	171.99(13)
P(1)–Pd–Cl(3)	91.86(12)
P(2)–Pd–Cl(3)	94.98(12)
N(2)–P(2)–Pd	111.9(5)
P(2)–N(2)–P(2′)	112.0(11)

3. Conclusion

The reaction of $(THF)_3LiN(PPh_2)_2$ with $Ni(COD)_2$ or $PtMe_2(COD)$ readily affords Ni(0) and Pt(II) bimetallic complexes of type II containing the $LiN(PPh_2)_2$ ligand framework, in which lithium is covalently rather than ionically bonded. In an effort to test the suitability of these compounds as synthons for the preparation of other bimetallic derivatives, the substitution of Li by Me_3Sn or Me_3Si was investigated. A comparison of the solid-state structures of these complexes showed the geometric parameters of the NP_2 bridge to be remarkably insensitive to changes of either the transition or the main group metal.

4. Experimental

4.1. Methods and materials

Syntheses were performed under nitrogen using standard Schlenk techniques. Solvents were distilled over sodium–benzophenone (diethyl ether, THF), sodium (toluene), sodium–potassium alloy (light petroleum, bp. 40–60 °C), or CaH_2 (dichloromethane). NMR solvents (C_6D_6, THF-d_8, CD_2Cl_2) were dried over activated 4 Å molecular sieves and degassed by several freeze–thaw cycles. NMR spectra were recorded using a Bruker Avance DPX-300 spectrometer. Chemical shifts are reported in ppm and referenced to residual solvent resonances. Nitrogen and argon were purified by passing through columns of supported P_2O_5 with moisture indicator, and activated 4 Å molecular sieves. Elemental analyses were performed by the Microanalysis Services of the School of Chemical Sciences and Pharmacy. $HN(PPh_2)_2$ [1], $LiN(PPh_2)_2 \cdot 3THF$ [3] and $Ni(COD)_2$ [7] were prepared according to the literature procedures.

4.2. Preparation of $(THF)_3LiN(PPh_2)_2Ni(COD)$, *NiLi*

To a mixture of solid $(THF)_3LiN(PPh_2)_2$ (1.0 g, 1.65 mmol) and $Ni(COD)_2$ (0.45 g, 1.65 mmol) in a round bottom flask was added THF (30 mL) at −78 °C. The solution was allowed to warm to room temperature and stirred for 5 h. Reduction of the solvent volume to one third induced the formation of microcrystals which were dissolved by warming. Crystallisation at −26 °C gave dark-red crystals of the title compound (1.1 g, 86%). *Anal.* Calc. for $C_{44}H_{56}LiNNiO_3P_2$: C, 64.89; H, 6.66; N, 2.10. Found: C, 63.55; H, 6.62; N, 1.82%. ^1H NMR (300.13 MHz): δ 1.74 (br, THF), 1.89 (s, CH_2), 2.04 (s, CH_2), 3.58 (br, THF), 3.97 (s, CH), 7.09–7.57 (Ph). $^{13}C\{^1H\}$ NMR (75.46 MHz): δ 36.18 (s, CH_2), 83.04 (s, CH), 130.03–151.93 (Ph). ^{31}P NMR (121.49 MHz): δ 66.22.

4.3. Preparation of $(THF)_3LiN(PPh_2)_2PtMe_2$, *PtLi*

To a mixture of $(THF)_3LiN(PPh_2)_2$ (0.39 g, 0.65 mmol) and $PtMe_2(COD)$ (0.22 g, 0.65 mmol) was added THF (20 mL) at −78 °C. The solution was allowed to warm to RT and stirred for 3 h. The solvent was then reduced to 5 mL and the solution cooled to −26 °C to give colourless crystals of the product, yield 0.39 g (72%). *Anal.* Calc. for $C_{38}H_{50}LiNO_3P_2Pt$: C, 54.81; H, 6.05; N, 1.68. Found: C, 54.50; H, 6.20; N, 1.76%. ^1H

NMR (300.13 MHz): δ 0.31 (t, $J_{P-H} = 37$ Hz, $PtMe_2$), 1.74 (m, THF), 3.58 (m, THF), 7.20–7.73 (Ph). ^{31}P NMR (121.49 MHz): δ 29.77 (t, $J_{Pt-P} = 740$ Hz).

4.4. Preparation of $Me_3SnN(PPh_2)_2$ (2)

To a solution of $(THF)_3LiN(PPh_2)_2$ (2.9 g, 4.77 mmol) in THF (30 mL) was added Me_3SnCl (0.95 g, 4.77 mmol) in small portions using a bent finger. The reaction was complete within 1 h. The solvent was removed and the product extracted with light petroleum (50 mL) to give white microcrystals, yield 2.2 g (84%). ^1H NMR (300.13 MHz, C_6D_6): δ 0.26 (s, $SnMe_3$), 7.01–7.67 (Ph). $^{13}C\{^1H\}$ NMR (75.46 MHz): δ −1.31 (s, Me), 129.00–143.39 (Ph). ^{31}P NMR (121.49 MHz): δ 61.24.

4.5. Preparation of $Me_3SnN(PPh_2)_2Ni(COD)$, NiSn

Method 1: A mixture of **2** (1.0 g, 1.82 mmol) and Ni(COD)$_2$ (0.50 g, 1.82 mmol) in THF (30 mL) was stirred for 3 h at 25 °C. The solvent volume was reduced to 10 mL, and crystallisation was initiated by adding light petroleum (ca. 30 mL). On cooling to −26 °C the product was obtained as red crystals, yield 0.95 g (73%). *Anal.* Calc. for $C_{35}H_{41}NNiP_2Sn$: C, 58.79; H, 5.78; N, 1.96. Found: C, 58.57; H, 5.91; N, 1.86%. ^1H NMR (300.13 MHz): δ −0.27 (s, Me_3Sn), 2.38 (br, CH_2), 4.77 (br, CH), 7.12–7.93 (Ph). $^{13}C\{^1H\}$ NMR (75.46 MHz): δ −2.70 (s, Me_3Sn), 28.50 (s, CH_2), 85.07 (s, CH), 128.94–142.20 (Ph). ^{31}P NMR (121.49 MHz): δ 83.67.

Method 2: To a suspension of **NiLi** (0.32 g, 0.41 mmol) in toluene (20 mL) was added Me_3SnCl (0.08 g, 0.41 mmol) in small portions using a bent finger. The mixture was stirred overnight at room temperature and filtered. The solvent volume was reduced to ca. 5 mL and light petroleum was added (3 mL) to give a product identical to that from method 1 (0.15 g, 51%).

4.6. Preparation of $Me_3SiN(PPh_2)_2PtMe_2 \cdot 0.5$ toluene, PtSi

A mixture of $Me_3SiN(PPh_2)_2$ (0.34 g, 0.74 mmol) and $PtMe_2(COD)_2$ (0.25 g, 0.74 mmol) in THF (20 mL) was stirred for 3 h at room temperature. The solvent volume was reduced to 2 mL, and light petroleum (30 mL) and toluene (2 mL) were added to induce crystallisation. Red microcrystals formed on cooling to −26 °C, yield 0.35 g (61%). *Anal.* Calc. for $C_{29}H_{35}NP_2PtSi \cdot 0.5C_7H_8$: C, 55.80; H, 5.59; N, 1.90. Found: C, 54.98; H, 5.49; N, 1.81%. ^1H NMR (300.13 MHz): δ −0.39 (s, $SiMe_3$), 1.47 (t, $J_{P-H} = 36.7$ Hz $PtMe_2$), 7.03–8.05 (Ph). ^{31}P NMR (121.49 MHz): δ 35.00 (t, $J_{Pt-P} = 769.9$ Hz).

4.7. Preparation of $Me_3SiN(PPh_2)_2Ni(COD)$, NiSi

To a mixture of $Me_3SiN(PPh_2)_2$ (0.50 g, 1.09 mmol) and Ni(COD)$_2$ (0.30 g, 1.09 mmol) in a round bottomed flask was added THF (30 mL). The solution was stirred at room temperature for 5 h. The solution was concentrated to 5 mL and light petroleum was added (10 mL). Cooling to −26 °C gave red crystals, yield 0.45 g (66%). *Anal.* Calc. for $C_{35}H_{41}NNiP_2Si$: C, 67.32; H, 6.62; N, 2.42. Found: C, 66.94; H, 6.69; N, 2.12%. ^1H NMR (300.13 MHz, C_6D_6): δ −0.30 (s, $SiMe_3$), 2.32 (s, CH_2), 4.64 (s, CH), 7.14–8.01 (Ph). $^{13}C\{^1H\}$ NMR (75.46 MHz): δ 36.18 (s, CH_2), 83.04 (s, CH), 127.89–140.08 (Ph). ^{31}P NMR (121.49 MHz): δ 82.84.

4.8. Preparation of $Me_3SiN(PPh_2)_2PdCl_2$ and formation of $[PdCl(dppa)]_2 \cdot 3CH_2Cl_2$

A mixture of $Me_3SiN(PPh_2)_2$ (0.21 g, 0.46 mmol) and $PdCl_2(COD)_2$ (0.13 g, 0.46 mmol) in THF (15 mL) was stirred overnight at 20 °C. The product was poorly soluble in THF and was isolated by filtration as a yellow powder, yield 0.22 g (76%). *Anal.* Calc. for $C_{27}H_{29}Cl_2NP_2PdSi$: C, 51.08; H, 4.60; N, 2.21; Cl, 11.17. Found: C, 51.35; H, 4.47; N, 2.18; Cl, 11.22%. ^1H NMR (300.13 MHz, THF-d_8): δ 0.41 (s, $SiMe_3$), 7.30–8.14 (Ph). ^{31}P NMR (121.49 MHz, THF-d_8): δ −35.85.

Attempts to recrystallise the complex from a large amount of THF in the presence of dichloromethane over a period of two weeks led to the isolation of a few crystals of the Pd(I)–dppa complex $[PdCl(dppa)]_2 \cdot 3CH_2Cl_2$ which was identified by X-tray diffraction.

4.9. X-ray crystallography

Crystals were mounted on glass fibres and fixed in the cold nitrogen stream on a Rigaku R-Axis IIc image plate diffractometer equipped with a rotating anode X-ray source (Mo Kα radiation) and graphite monochromator. Data were collected at 140(1) K and processed using the DENZO/SCALEPACK [8] programs. The structures were determined by the direct methods routines in the SHELXS program [9] and refined by full-matrix least-squares methods, on F^2's, in SHELXL [9]. Non-hydrogen atoms were refined with anisotropic thermal parameters, and hydrogen atoms were included in idealised positions with their U_{iso} values set to ride on the U_{eq} values of the parent carbon and nitrogen atoms. Scattering factors for neutral atoms were taken from reference [10]. Computer programs used in this analysis have been noted above or in Table 4 of [11], and were run on a Silicon Graphics Indy at the University of East Anglia, or a DEC-AlphaStation 200 4/100 in the Biological Chemistry Department, John Innes Centre.

Crystal data are collected in Table 8.

Table 8
Crystal data and summary of data collection and refinement details

Complex	**NiLi**	**NiSn**	**PtLi**	**PtSi**	$[PdCl(dppa)]_2 \cdot 3CH_2Cl_2$
Empirical formula	$C_{44}H_{56}LiNNiO_3P_2$	$C_{35}H_{41}NNiP_2Sn$	$C_{38}H_{50}LiNO_3P_2Pt$	$C_{29}H_{35}NP_2PtSi \cdot 0.5C_7H_8$	$C_{48}H_{42}Cl_2N_2P_4Pd_2 \cdot 3CH_2Cl_2$
Formula weight	774.5	715.0	832.8	728.8	1309.2
Crystal size (mm)	$0.53 \times 0.40 \times 0.20$	$0.25 \times 0.13 \times 0.10$	$0.15 \times 0.20 \times 0.42$	$0.33 \times 0.35 \times 0.45$	$0.69 \times 0.42 \times 0.38$
Crystal system	monoclinic	monoclinic	monoclinic	monoclinic	monoclinic
Space group	$P2_1/n$	$P2_1/n$	$P2_1/c$	$P2_1/n$	$C2/c$
a (Å)	10.726(1)	9.852(1)	20.949(2)	10.766(1)	23.302(5)
b (Å)	20.658(2)	20.358(6)	9.868(1)	22.219(1)	13.485(3)
c (Å)	18.692(1)	32.548(8)	19.777(6)	13.232(1)	20.301(4)
β (°)	96.19(1)	96.15(1)	114.11(1)	92.22(1)	114.30(3)
V (Å^3)	4117.6(6)	6490(3)	3731.7(12)	3162.8(4)	5814(2)
Z	4	8	4	4	4
D_{calc} (g cm^{-3})	1.249	1.463	1.482	1.530	1.496
μ (mm^{-1})	0.588	1.473	3.881	4.597	1.131
$F(000)$	1648	2928	1680	1452	2624
θ Range (°)	$2.1 \leqslant \theta \leqslant 25.4$	$2.0 \leqslant \theta \leqslant 25.4$	$2.1 \leqslant \theta \leqslant 25.4$	$2.6 \leqslant \theta \leqslant 25.4$	$2.2 \leqslant \theta \leqslant 20.0$
Number of reflections collected	22170	23302	15934	17266	7624
Number of unique reflections (R_{int})	6920 (0.054)	9744 (0.083)	6116 (0.056)	5434 (0.117)	2513 (0.481)
Number of 'observed' reflections	5903	6908	5109	5191	1761
Data/restraints/parameters	6920/0/469	9744/0/721	6116/0/426	5434/0/338	2513/0/350
Goodness-of-fit on F^2, S	1.055	1.032	1.029	1.081	1.185
$R_1[I > 2\sigma(I)]$	0.035	0.057	0.043	0.031	0.110
wR_2 (all data)	0.097	0.167	0.119	0.083	0.311
Weighting parameters A, B[a]	0.0471, 1.30	0.0910, 6.17	0.0728, 5.37	0, 3.68	0.20, 0
largest difference in peak and hole (e Å^{-3})	0.35 and −0.43	0.58 and −1.43	1.55 and −1.74	1.17 and −1.37	1.08 and −0.88
Location of largest difference peak	close to COD ligand	close to Sn atom	close to Pt atom	close to Pt atom	around Pd atom

[a] Reflection weighting scheme: $w = [\sigma^2(F_o^2) + (AP)^2 + BP]^{-1}$ where $P = (F_o^2 + 2F_c^2)/3$.

The crystal of $[PdCl\{HN(PPh_2)_2\}]_2 \cdot 3CH_2Cl_2$, the best of several examined, diffracted strongly but reflection profiles were large and poorly defined, with patterns from small crystals in addition to that from the major crystal. Using 4° oscillations, 48 exposures of 27 min. each were made. Total no. of reflections accepted, to $\theta_{max} = 20°$, was 7624 of which 2513 were unique ($R_{int} = 0.48$); 1761 were 'observed' with $[I > 2\sigma(I)]$. In addition to the Pd complex, there are regions of solvent, CH_2Cl_2, molecules which are disordered and not fully resolved.

5. Supplementary material

Full tables of bond lengths and angles, tables of non-hydrogen and hydrogen atomic coordinates and anisotropic thermal parameters for non-hydrogen atoms are available from the Cambridge Crystallographic Data Centre, quoting CCDC deposition numbers 275633 (**NiLi**), 275634 (**NiSn**), 275635 (**PtLi**), 275636 (**PtSi**) and 275636 ($[PdCl\{HN(PPh_2)_2\}]_2$). Copies of the information may be obtained free of charge from The Director, CCDC, 12 Union Road, Cambridge CB2 1EZ, UK (fax: +44 1223 336 033; e-mail: deposit@ccdc.cam.ac.uk or www: http://www.ccdc.cam.ac.uk).

Acknowledgement

This work was supported by the Engineering and Physical Sciences Research Council.

References

[1] (a) S.D. Ittel, L.K. Johnson, Chem. Rev. 100 (2000) 1169;
(b) G.W. Coates, Chem. Rev. 100 (2000) 1223;
(c) G.W. Coates, P.D. Hustad, S. Reinartz, Angew. Chem. Int. Ed. 41 (2002) 2237;
(d) V.C. Gibson, S.K. Spitzmesser, Chem. Rev. 103 (2003) 283.
[2] (a) A. Carter, S.A. Cohen, N.A. Cooley, A. Murphy, J. Scutt, D.F. Wass, Chem. Commun. (2002) 858;
(b) D.S. McGuinness, P. Wasserscheid, W. Keim, C. Hu, U. Englert, J.T. Dixon, C. Grove, Chem. Commun. (2003) 334.
[3] T. Kremer, F. Hampel, F.A. Knoch, W. Bauer, A. Schmidt, P. Gabold, M. Schütz, J. Ellermann, P.v. Ragué Schleyer, Organometallics 15 (1996) 4776.
[4] M. Gomez, G. Muller, J. Sales, X. Solans, J. Chem. Soc., Dalton Trans. (1993) 221.
[5] P. Bhattacharyya, R.N. Sheppard, A.M.Z. Slawin, D.J. Williams, J.D. Woollins, J. Chem. Soc., Dalton Trans. (1993) 2393.
[6] R. Uson, J. Fornies, R. Navarro, M. Tomas, C. Fortuño, J.I. Cebollada, A.J. Welch, Polyhedron 8 (1989) 1045.
[7] M.J. Tenorio, M.C. Puertra, I. Salcedo, P. Valerga, J. Chem. Soc., Dalton Trans. (2001) 653.
[8] Z. Otwinowski, W. Minor, in: Methods in Enzymology, in: C.W. Carter, Jr., R.M. Sweet (Eds.), Macromolecular Crystallography: Part A, vol. 276, Academic Press, New York, 1997, pp. 307–326.
[9] G.M. Sheldrick, SHELX-97: Programs for Crystal Structure Determination (SHELXS) and Refinement (SHELXL), University of Göttingen, Göttingen, Germany, 1997.
[10] 'International Tables for X-ray Crystallography', vol. C, Kluwer Academic Publishers, Dordrecht, 1992, pp. 500, 219 and 193.
[11] S.N. Anderson, R.L. Richards, D.L. Hughes, J. Chem. Soc., Dalton Trans. (1986) 245.

Available online at www.sciencedirect.com
SCIENCE DIRECT
Polyhedron 25 (2006) 853–858
POLYHEDRON
www.elsevier.com/locate/poly

Synthesis and crystal structures of bromo- and ester-functionalised polyhedral silsesquioxanes

Ewan A. Drylie, Christopher D. Andrews, Meredith A. Hearshaw, Cristina Jimenez-Rodriguez, Alexandra Slawin, David J. Cole-Hamilton, Russell E. Morris *

EaStChem School of Chemistry, University of St. Andrews, Purdie Building, St. Andrews, Scotland KY16 9ST, United Kingdom

Received 29 July 2005; accepted 12 September 2005
Available online 20 October 2005

Dedicated to Professor Mike Hursthouse on the occasion of his 65th birthday.

Abstract

Radical initiated hydrobromination and methoxycarbonylation using a Pd(0) complex have been used to convert octavinylsilsesquioxane to species functionalised with alkyl bromide and linear methyl propanoate groups on all eight reactive sites, respectively. The two new molecules, 1,3,5,7,9,11,13,15-octakis[ethylbromide]octasiloxane and 1,3,5,7,9,11,13,15-octakis[methylpropanoate]octasiloxane, have been characterised using NMR (^{1}H, ^{13}C and ^{29}Si) and IR spectroscopy, elemental analysis and single crystal X-ray diffraction.
© 2005 Elsevier Ltd. All rights reserved.

Keywords: Silsesquioxanes; Methoxycarbonylation; Hydrobromination; X-ray diffraction

1. Introduction

Polyhedral oligomeric silsesquioxanes (POSS) are a class of molecules commonly derived from the hydrolytic condensation of organotrihalosilanes. These molecules have the general formula $(RSiO_{3/2})_n$ (where R is an organic group and n is an even number >6) and provide excellent platforms for the synthesis of new inorganic-organic hybrid materials [1,2]. The most common members of the family have an almost cubic silica-like core surrounded by eight organic groups ($n = 8$), which makes them topologically ideal for the preparation of intimate nanocomposite materials [3] with the size of the inorganic region precisely defined by the size of the core. This has led to proposed uses of these molecules as hard blocks or reinforcing particles in high performance polymer materials [4].

The cubic topology of these molecules offers opportunities to prepare interesting micro- or mesoporous materials as it is geometrically difficult to link cubes through their corners and fill all available space [5–7]. The shape of the silsesquioxane core also lends itself well to the preparation of dendrimers, where the large number of external branching sites on the core leads to a high concentration of branch ends after relatively few generations [8,9]. Dendrimers of this type have been studied as potential catalysts, where phosphine functionalised molecules have been found to have positive effects on the selectivity of hydroformylation reactions [10].

Key to all these potential uses of silsesquioxanes is the ease with which their external organic functionality can be altered in controlled and high yielding ways to produce new molecules suitable for further reaction. A relatively wide range of derivatisation reactions is possible, although care must be taken to avoid acidic, basic or overly oxidising environments as the silsesquioxane core is vulnerable under such conditions. Even with these restrictions there are now many examples in the literature of functional silsesquioxanes. Many of these preparations are based on addition to multiple bonds. In this paper, we report two methods of functionalising the vinyl functionalised POSS species

* Corresponding author. Tel.: +44 1334 463818; fax: +44 1334 463808.
E-mail addresses: rem1@st-andrews.ac.uk, rem1@st-and.ac.uk (R.E. Morris).

0277-5387/$ - see front matter © 2005 Elsevier Ltd. All rights reserved.
doi:10.1016/j.poly.2005.09.007

(**1**). Firstly, regiospecific radical addition of hydrogen bromide across the double bond leads to a high yield of the terminally bromide functionalised material **2** (Fig. 1). Clearly, alkyl halide functionality of this type is a useful potential starting point for further derivatisation of the molecule.

A potentially very interesting target for functional silsesquioxanes is those functionalised with carboxylic acid or ester groups because they can be further functionalised to provide novel molecules. In a previous paper, we reported the use of platinum-catalysed hydrosilation using protected aldehyde reactants as a route to aldehyde- and carboxylic acid-functionalised silsesquioxanes [11]. However, the oxidation reactions in this route are difficult to control. Another approach involves the formation of carboxylic ester functionalised silsesquioxanes. Feher et al. [12] have reported previously the hydrosilation of methyl-3,3-dimethyl-4-pentenoate onto the octahydrido silsesquioxane core to form the methyl ester functionalised silsesquioxane. Here, we report an alternative route to the preparation of ester functionalised molecules using direct methoxycarbonylation of the octavinyl silsesquioxane **1**.

Methoxycarbonylation of terminal and internal alkenes under mild conditions in the presence of a palladium bis-(di-*tert*-butylphosphinomethyl)benzene complex, $L_2Pd(dba)_3$ (where L_2 = 1,2-bis(di-*tert*-butylphosphinomethyl)benzene and dba = *trans*,*trans*-dibenzylideneacetone) has been reported recently as a highly selective route to industrially important methyl esters [13]. In this paper, we describe how this methodology can also be applied to form the terminal methyl ester **3** with high selectivity (Fig. 1).

One of the reasons that silsesquioxanes of this type are of interest is their rather unusual architectures, and so structural studies are important in assessing and predicting the properties of the materials. For example, some phosphine-terminated silsesquioxane-based dendrimers are highly selective catalytic ligands in hydroformylation reactions, [10,14] and this can be traced back, at least to some extent, to the structure of the silsesquioxane core based on molecular modelling [15]. Unfortunately, however these types of silsesquioxanes are notoriously difficult to crystallise and single crystal X-ray diffraction is often problematical because of the disorder in the organic groups [9,16]. In this paper we do, however, report single crystal X-ray diffraction structures of both compounds **2** and **3**. Both structures illustrate some of the problems associated with structure determinations on such highly functional molecules. They are weakly scattering crystals with relatively poor data:parameter ratios in the refinement. However, while **2** has a relatively well-behaved structural characterisation **3** is more troublesome; problems that are probably caused by unresolved disorder leading to poor crystallinity.

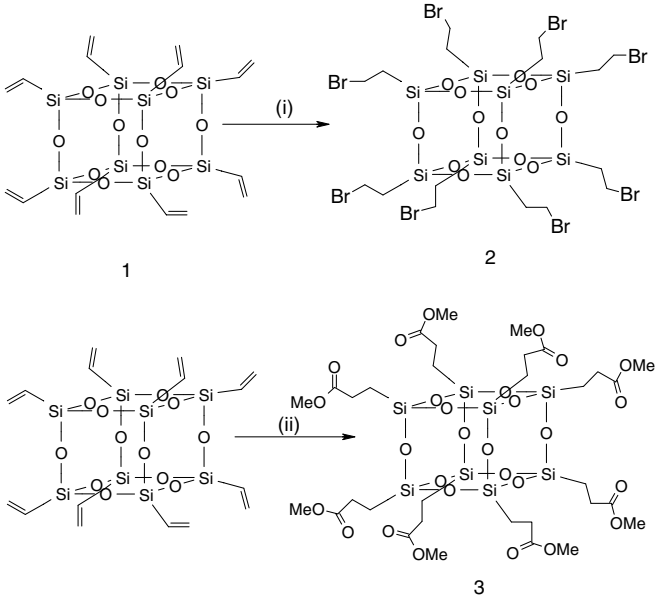

Fig. 1. The synthesis of compounds **2** and **3**. Reaction conditions (i) and (ii) are given in Section 2.

2. Experimental

All manipulations were carried out under an atmosphere of argon. Solvents were dried according to established procedures. NMR spectra were recorded on a Varian 300 or a Bruker 300 spectrometer. FTIR spectra were recorded on a Perkin–Elmer 1710 spectrometer. Chemical analysis was carried out by the University of St. Andrews Microanalysis service on a Carlo Erba model 1106 elemental analyser.

2.1. Synthesis

The starting materials for these preparations, octavinyl-octa-silsesquioxane (**1**), was prepared according to the literature methods [17].

2.1.1. 1,3,5,7,9,11,13,15-Octakis[ethylbromide]octasiloxane (**2**)

Hydrogen bromide gas was bubbled through octavinylsilsesquioxane (0.90 g, 1.42 mmol) and benzoyl peroxide (0.30 g, 1.24 mmol) in toluene (50 ml) at 50 °C for 2 h. After 1 h more benzoyl peroxide (0.30 g, 1.24 mmol) in toluene (10 ml) was added. The reaction mixture was stirred at RT overnight. Argon was then bubbled through the reaction mixture to quench any remaining radicals. The solvent was removed in vacuo and the residue dissolved in dichloromethane (150 ml) and washed with sodium carbonate solution (2×50 ml, 0.05 mol dm^{-3}) and water (50 ml). The resulting colourless liquid was dried over Na_2SO_4, filtered and the solvent removed. The residue was recrystallised using acetone and methanol to yield white crystals (0.87 g, 48%). ^1H NMR ($CDCl_3$, 300 MHz): δ_H 1.45 (16H, t, J_H 8.3, CH_2CH_2Br) and 3.45 (16H, t, J_H 8.3, CH_2CH_2Br). ^{16}C NMR ($CDCl_3$): δ_C 17.90 (16H, CH_2CH_2Br) and 27.10 (16H, CH_2CH_2Br). ^{29}Si NMR ($CDCl_3$): δ_{Si} −70.45 (8Si, s, O_3SiCH_2). IR (nujol mull): ν/cm^{-1} 790 (C–Br str), *Anal*. Calc. for CHN: C, 15.01; H, 2.52. Found: C, 14.35; H, 2.15%.

2.1.2. 1,3,5,7,9,11,13,15-Octakis[methylpropanoate] octasiloxane (**3**)

$Pd_2(dba)_3$ (45.7 mg, 7.283×10^{-5} mol) [dba = dibenzylidene-acetone], 1,2-bis(di-*tert*-butylphosphinomethyl)benzene (198 mg, 5.018×10^{-4} mol) and **1** (500 mg, 7.90×10^{-4} mol) were dissolved in toluene (30 ml) under argon. Methanol (5 ml) and methanesulfonic acid (65 μl, 1×10^{-3} mol) were added and the reaction mixture was transferred into a Hastelloy autoclave, which had been evacuated and fitted with a paddle stirrer. The autoclave was pressurised to 30 bar CO and heated to 80 °C for 41 h. The autoclave was then cooled, vented, the contents removed and the product purified on a fluorosil column (ethyl acetate/petroleum ether). The product was recrystallised from ethyl acetate/petroleum ether to yield small, white needle like crystals (0.38 g, 43%). ^{1}H NMR ($CDCl_3$, 300 MHz): δ_H 0.9 (16H, m, SiCH_2CH$_2$), 2.3 (16H, m, SiCH$_2$$CH_2$) and 3.6 (24H, s, OMe). ^{13}C NMR ($CDCl_3$, 75 MHz) δ_C 7.17 (8C, SiCH_2CH$_2$), 27.64 (8C, SiCH$_2$$CH_2$), 52.10 (8C, OMe) and 174.65 (8C, COO). ^{29}Si NMR ($CDCl_3$, 59.6 MHz): δ_{Si} −67 (8Si, CH_2SiO_3). IR (nujol mull): ν/cm^{-1} 1738 (–O–C=O str.), 1236 (CO str.) and 1095 (CO str.). *Anal.* Calc. for CHN: C, 34.52; H, 5.07. Found: C, 34.90; H, 4.71%.

2.2. X-ray crystallography

The single crystal X-ray diffraction studies on crystals of **2** and **3** were performed at 293 K using a Bruker SMART diffractometer with graphite-monochromated Mo Kα radiation ($\lambda = 0.71074$). The crystal structures were solved using the direct methods program SHELXS-97 and refined with a full-matrix least-squares technique using the program SHELXL-97.

3. Results and discussion

3.1. Synthesis and structure of **2**

Radical addition of HBr across olefinic double bonds is a well known synthetic reaction in organic chemistry, leading to Markovnikov addition. Here we have shown that such an approach leads to quantitative addition of the bromide on all eight corners of the vinyl functionalised POSS species. The reaction is regioselective; there is no evidence for addition of the bromine atom to anything other than the terminal carbon of the vinyl group. ^{1}H NMR spectroscopy indicated that complete conversion of **1** to the linear ethyl bromide product (δ_H 1.45 and 3.45) could be achieved after 2 h of bubbling HBr gas through the reaction mixture and then allowing the reaction to stir overnight. NMR (^{1}H and ^{13}C), IR and single crystal X-ray crystallography all reveal the expected structure. Despite the crystals used in this structure determination exhibiting relatively poor scattering of X-rays the refinement against the X-ray diffraction data is reasonable given the fact that the data:parameter ratio is only just acceptable at ~10. The details of the refinement are shown in Table 1 and the final refined crystal structure is shown in Figs. 2 and 3. All non-hydrogen atoms in

Table 1
Crystal data and structure refinement details for compounds **2** and **3**

Identification code	Compound **2**	Compound **3**
Empirical formula	$(Si_8O_{12})(CH_2CH_2Br)_8$	$(Si_8O_{12})(CH_2CH_2CO_2CH_3)_8$
Formula weight	1280.34	1273.45
Temperature (K)	293(2)	293(2)
Wavelength (Å)	0.71074	0.71074
Crystal system	monoclinic	tetragonal
Space group	$P12_1/n1$	$P4/ncc$
Unit cell dimensions		
a (Å)	9.326(6)	17.813(2)
b (Å)	20.288(10)	17.813(2)
c (Å)	11.229(6)	15.704(3)
α (°)	90	90
β (°)	102.85(4)	90
γ (°)	90	90
V (Å^3)	2071(1)	4982.9(12)
Z,	2	4
Calculated density (Mg/m^3)	2.053	1.654
$F(000)$	1232	2592
Crystal size (mm)	$0.09 \times 0.09 \times 0.09$	$0.07 \times 0.07 \times 0.07$
Reflections collected/unique [R_{int}]	7943/1963 [0.045]	20040/1797 [0.131]
Refinement method	full-matrix least-squares on F^2	full-matrix least-squares on F^2
Data/restraints/parameters	1963/0/199	1797/70/170
Goodness-of-fit on F^2	1.006	2.544
Final R indices [$I > 2\sigma(I)$]	$R_1 = 0.0559$, $wR_2 = 0.1367$	$R_1 = 0.1989$, $wR_2 = 0.5647$
R indices (all data)	$R_1 = 0.1266$, $wR_2 = 0.1615$	$R_1 = 0.2221$, $wR_2 = 0.5745$
Largest difference in peak and hole (e Å^{-3})	1.002 and −0.749	1.156 and −1.027

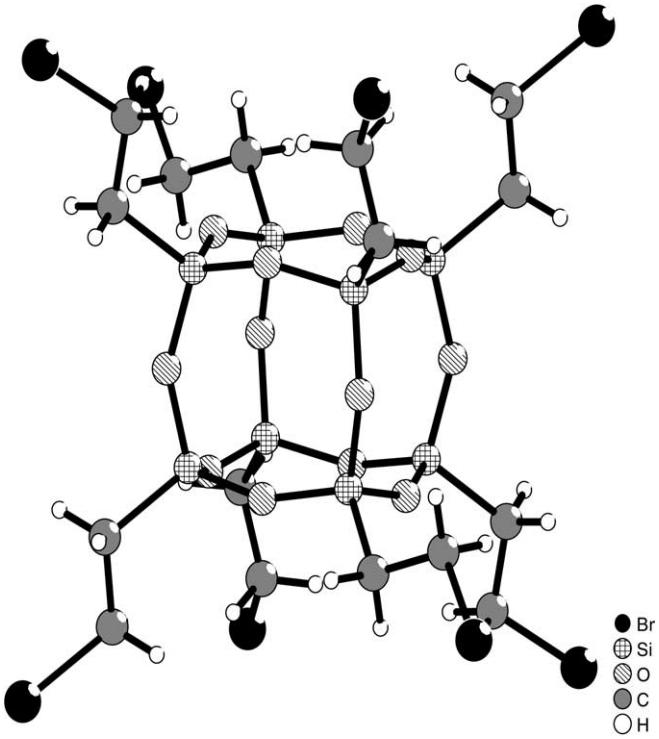

Fig. 2. The structure of compound **2**.

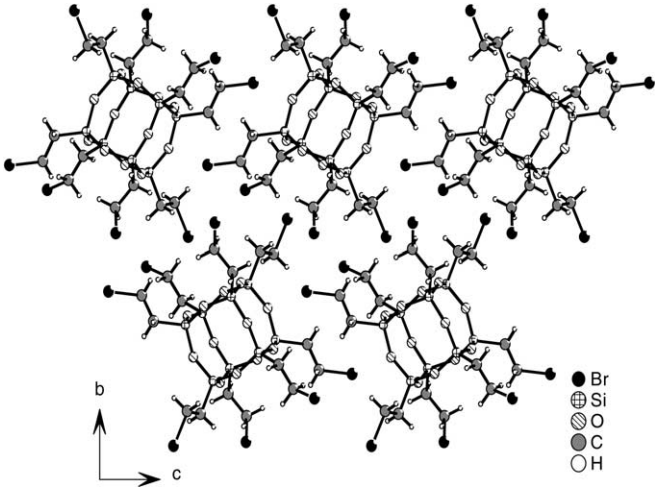

Fig. 3. Packing diagram for compound **2**.

the structure were refined using anisotropic displacement parameters and the hydrogen atoms were geometrically placed and restrained to refine as riding atoms together with the carbon atoms to which they are bonded.

The structure of **2** comprises half of the molecule in the asymmetric unit, 4 independent silicon atoms and four ethylbromide units. The geometry of the core is as would be expected from crystal structures of other silsesquioxane molecules. The Si–O interatomic distances range from 1.603 (10) to 1.629 (10) Å, the O–Si–O angles indicate almost regular tetrahedral coordination about silicon, ranging from 108.1 (7)° to 111.5 (7)° and the Si–O–Si angles from 145.9 (7)° to 152.8 (7)°. The ethyl bromide arms on the structure also show reasonably good geometry with Si–C, C–C and C–Br interatomic distances ranging from 1.827 (14) to 1.854 (14) Å, 1.45 (2) to 1.50 (2) Å and 1.893 (17) to 1.967 (15) Å, respectively. The atomic displacement parameters for the individual atoms in the core have relatively normal values; the equivalent isotropic displacement parameters for the silicon atoms 0.044 $Å^2$ and the oxygen atoms 0.050 $Å^2$. However, the atoms on the periphery of the molecule the displacement parameter values have larger values of around 0.090 $Å^2$ for the bromine atoms. The packing diagram for **2** is shown in Fig. 3 and shows that there are two orientations of the silsesquioxane cores. The arms of the molecules interlink in such a way as to produce the closest intermolecular contact between the bromine on the periphery of one molecule and one of the faces of the cubic core of another. The bromine points almost at the centre of one of these faces with Br–O interatomic distances ranging from 3.715 to 3.909 Å.

The crystal structure of a related molecule where the starting molecule was an allyl terminated POSS has been reported before [18] but we believe this is the first time that reaction of a vinyl-POSS species has been reported in this reaction. Clearly, the presence of alkyl-bromide functionality in the exterior of these silsesquioxane molecules opens up the possibility of many further reactions.

3.2. Synthesis and structure of *3*

Alkoxycarbonylation of alkenes is an important process in which vinyl groups are converted to alkyl esters. A wide range of products is accessible using this approach; from high molecular weight 'polyketones' [19] to methyl propanoate [20,21]. Here, we report the methoxycarbonylation of octavinylsilsesquioxane to form a silsesquioxane species functionalised with eight methyl propanoate groups, **3**, accomplished using the zero valent $L_2Pd(dba)_3$ complex [where L_2 = 1,2-bis(di-*tert*-butylphosphinomethyl)benzene and dba = *trans*,*trans*-dibenzylideneacetone] as the catalyst. The reaction was performed under 30 bar CO at 80 °C in a Hastelloy autoclave. The reaction could also be performed at room temperature on a smaller scale by bubbling CO through the solution, however the scale up of this procedure proved problematic.

Nuclear magnetic resonance (^1H and ^{13}C) spectroscopy indicated that all the vinyl resonances (δ_H 5.7–6.1) of **1** had disappeared after 41 h. The ^1H NMR showed the emergence of two multiplet resonances (δ_H 0.9 and 2.3), which were assigned to the CH_2 groups of the alkyl chains in the molecule and a singlet peak (δ_H 3.6) assigned to the methoxy group. In line with steric requirements of the system, there was no evidence of formation of the branched ester product. Therefore, as a far as could be deduced from NMR 100% conversion to the linear ester product had been achieved. Chemical analysis and ^{29}Si NMR further proved that addition to all corners of the silsesquioxane cube had been achieved. The IR spectrum showed the expected ester carbonyl stretch at 1738 cm^{-1}. Purification of

the product by chromatography followed by recrystallisation resulted in the formation of white needle-like crystals. Diffraction data were collected at room temperature on a laboratory diffractometer equipped with a CCD detector. It was clear that the low angle scattering was relatively strong but that the intensity of the diffraction decreased markedly at high 2θ angles. Structure solution was accomplished using direct methods techniques, and revealed the location of the central silsesquioxane core of the molecule (Fig. 2). Difference Fourier syntheses were used to complete the molecule. The final cycle of least-squares refinement included anisotropic displacement parameters for all the non-hydrogen atoms except those of the minor disordered ester group, which were refined isotropically. Hydrogen atoms on the methylene groups were placed geometrically and were refined as riding atoms on the carbon atoms to which they were attached. Hydrogen atoms on the ester methyl groups were not modelled. To ensure that the external ester groups retained chemically sensible geometry some restraints on bond distances and angles were required. Details of the refinement are listed in Table 1 and Figs. 4 and 5 show the final refined structure.

The structure of **3** comprises one quarter of the molecule in the asymmetric unit; two independent silicon atoms together with two of the organic arms of the molecule. The silsesquioxane core of the structure is crystallographically well-behaved with good inferred geometry and anisotropic displacement parameters of the expected magnitude. Comparison with the structure of compound **2** indicate very similar geometry for the silsesquioxane core, with Si–O interatomic distance ranges (1.601 (10)–1.650 (10) Å) and O–Si–O angle ranges (107.6 (6)–111.4 (7)°) show no statistically significant difference between compounds **2** and **3**. The Si–O–Si angle ranges (143.7 (8)–148.7 (8)°) are slightly smaller than those for compound **2** but fall well in the range seen in other molecules of this type. However, the least-squares refinement of the atoms on the organic arms of the molecule is less satisfactory. The further away from the silsesquioxane core the atom is the larger the anisotropic displacement parameters become, as would be expected, but the magnitudes of the displacement parameters are such that they must be due to some unresolved disorder and/or severe molecular motion of the terminal units. Disorder of the terminal carbon and oxygen atoms was resolvable on half of the ester groups (i.e., one of the two crystallographically independent units), with occupancy factors for the two disordered units of 0.66 (4) and 0.31 (4). However, there remains some significant disorder of the remaining ester group that we were not able to model satisfactorily. Collecting data at lower temperature (150 K) using the synchrotron source at Daresbury did not improve the quality of the diffraction experiment to any great degree. This type of problem is by no means unusual in the structural chemistry of silsesquioxane materials of this kind. In fact there are examples where the crystallinity of the materials is such that only the cubic silsesquioxane core can be located using these techniques, the organic groups being so disordered as to render them unlocatable using X-ray diffraction [17]. However, for **3** all the non-hydrogen atoms were found from the difference Fourier syntheses, but the subtle details of the structure cannot be elucidated unambiguously. The packing diagram for **3** is shown in Fig. 5. It shows a number of similarities to that of **2**. Again there are two different orientations of

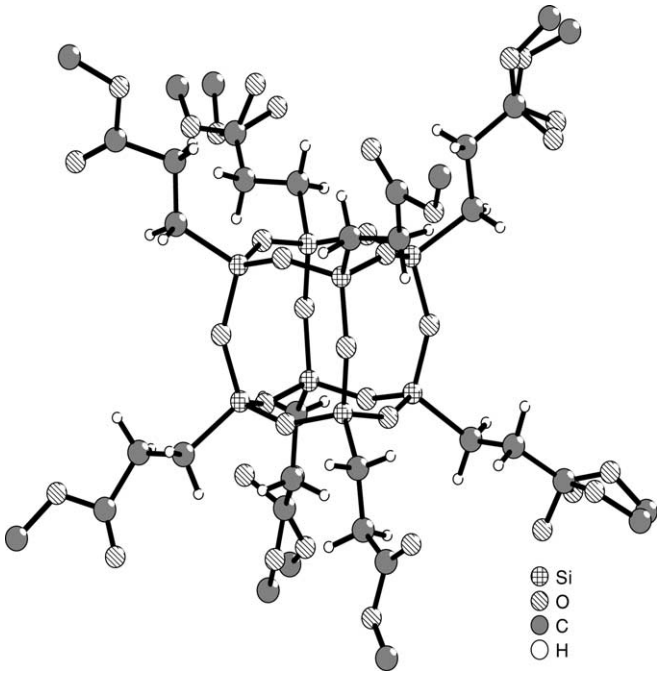

Fig. 4. The structure of compound **3**. The disorder the external ester groups can be seen on half the arms of the molecule.

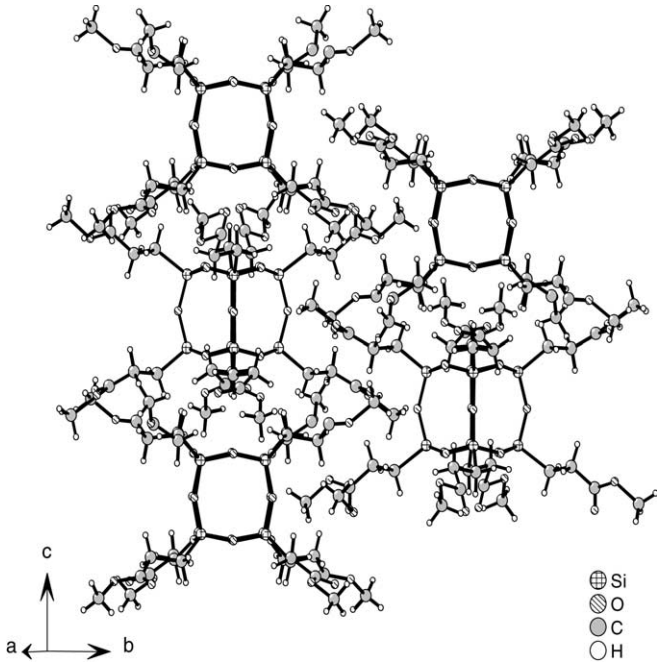

Fig. 5. Packing diagram for compound **3**. For clarity, only the major component of the disordered ester groups are shown.

the polyhedral silsesquioxane core and the organic arms of the molecules interlock so that the methyl carbon of one molecules points approximately towards the centre of the face of the silsesquioxane core on the next molecule. The distance from the methyl carbon to the oxygen atoms of the nearest face range from 3.817 to 4.019 Å.

We have the reported the synthesis and characterisation of two new octafunctionalised silsesquioxane molecules. The new molecules present potentially useful starting materials for the further preparation of further functionalised molecules. The direct methoxycarbonylation reaction to produce ester groups on the exterior of the molecules is a particularly interesting reaction. We are currently exploring further synthetic uses of this molecule using hydrolysis of the ester and also transesterification reactions.

4. Supplementary material

CCDC 279579, corresponding to **2**, and CCDC 263076, to **3** contain the supplementary crystallographic data for this paper. These data can be obtained free of charge via www.ccdc.cam.ac.uk/conts/retrieving.html (or from the CCDC, 12 Union Road, Cambridge CB2 1EZ, UK; fax: +44 1223 336033; e-mail: deposit@ccdc.cam.ac.uk).

Acknowledgements

We thank the EPSRC and SHEFC for funding. R.E.M. thanks the Royal Society for the provision of a University Research Fellowship.

References

[1] P.G. Harrison, J. Organomet. Chem. 542 (1997) 141.
[2] F. Ribot, C. Sanchez, Comments Inorg. Chem. 20 (1999) 327.
[3] C.X. Zhang, R.M. Laine, J. Am. Chem. Soc. 122 (2000) 6979.
[4] J.D. Lichtenhan, Comments Inorg. Chem. 17 (1995) 115.
[5] P.G. Harrison, P. Kannengisser, Chem. Commun. (1996) 415.
[6] C. Zhang, F. Babonneau, C. Bonhomme, R.M. Laine, C.L. Soles, H.A. Hristov, A.F. Yee, J. Am. Chem. Soc. 120 (1998) 8380.
[7] J.J. Morrison, C.J. Love, B.W. Manson, I.J. Shannon, R.E. Morris, J. Mater. Chem. 12 (2002) 3208.
[8] P.I. Coupar, P.-A. Jaffrès, R.E. Morris, J. Chem. Soc., Dalton Trans. (1999) 2183.
[9] P.-A. Jaffrès, R.E. Morris, J. Chem. Soc., Dalton Trans. (1998) 2767.
[10] L. Ropartz, R.E. Morris, D.F. Foster, D.J. Cole-Hamilton, Chem. Commun. (2001) 361.
[11] B.W. Manson, J.J. Morrison, P.I. Coupar, P.-A. Jaffres, R.E. Morris, J. Chem. Soc. Dalton Trans. (2001) 1123.
[12] F.J. Feher, K.D. Wyndham, Chem. Commun. (1998) 323.
[13] C. Jimenez Rodriguez, D.F. Foster, G.R. Eastham, D.J. Cole-Hamilton, Chem. Commun. (2004) 1720.
[14] L. Ropartz, R.E. Morris, D.F. Foster, D.J. Cole-Hamilton, J. Mol. Catal. A 182 (2002) 99.
[15] K.J. Haxton, D.J. Cole-Hamilton, R.E. Morris, Dalton Trans. (2004) 1665.
[16] R.E. Morris, J. Mater. Chem. 9 (2005) 931.
[17] M. Voronkov, T.N. Marinova, R.G. Mirskov, V.I. Bely, J. Gen. Chem. USSR (Eng. Transl.) 49 (1979) 1328.
[18] A. Provatas, M. Luft, J.C. Mu, A.H. White, J.G. Matisons, B.W. Skelton, J. Organometal. Chem. 565 (1998) 159.
[19] J.K. Liu, B.T. Heaton, J.A. Iggo, R. Whyman, Chem. Commun. (2004) 1326.
[20] W. Clegg, G.R. Eastham, M.R.J. Elsegood, R.P. Tooze, X.L. Wang, K. Whiston, Chem. Commun. (1999) 1877.
[21] G.R. Eastham, R.P. Tooze, M. Kilner, D.F. Foster, D.J. Cole-Hamilton, J. Chem. Soc., Dalton Trans. (2002) 1613.

Available online at www.sciencedirect.com
SCIENCE DIRECT
Polyhedron 25 (2006) 859–863
POLYHEDRON
www.elsevier.com/locate/poly

Dimethylxanthene- and dibenzofuran-diamido complexes of titanium

Robin M. Porter, Andreas A. Danopoulos *

School of Chemistry, University of Southampton, Highfield Campus, Southampton, Hants SO17 1BJ, UK

Received 4 July 2005; accepted 21 September 2005
Available online 27 October 2005

Honouring the outstanding chemist and special friend Professor Michael B. Hursthouse on the occasion of his retirement.

Abstract

The new ligands 4,5-dialkyl-and-diaryl-amido-9,9-dimethylxanthene and 4,6-dialkyl-and-diaryl-amido dibenzofuran serve as rigid, pre-organised and tunable 'spectators' for group 4 metals. The structure of a titanium complex with 4,5-di-cyclohexylamido-9,9-dimethylxanthene is reported.
© 2005 Elsevier Ltd. All rights reserved.

Keywords: Amido titanium; Crystal structure; Xanthene dibenzofuran; Catalytic amination

1. Introduction

The development of new rigid, pre-organised ligands is an active area of research. Of particular interest is their use in homogeneous catalysis, where a geometric perturbation introduced by such ligands could improve the activity or selectivity of the catalyst. Demonstrations of this concept in the catalytic aziridination, cyclopropanation, C–H/C–C activation and hydroformylation reactions appeared recently [1]. The use of rigid preorganised ligands with early transition metals is less common. In addition to certain *ansa*-cyclopentadienyls [2], recent work has focussed on amido ligands, which could offer wide scope for electronic and steric tuning and ligand design [3]. The generation of low coordination number, electronically/sterically unsaturated metal species, the suppression of β-hydrogen elimination and the modulation of the rate of insertion reactions are attractive goals, where ligand preorganisation may prove useful. Rigid xanthene and dibenzofuran bridged chelating diphosphines have successfully been used in Rh catalysed hydroformylation. In this case, the *n*-/*i*-aldehyde ratio is influenced by the bite angle of the chelating diphosphine [1d].

As part of our ongoing research aiming at the development of novel ligands for the early transition metals, we report here a facile method for the synthesis of chelating dialkyl- and diaryl-amido ligands with xanthene and dibenzofuran backbones and initial results on the synthesis of their titanium complexes. The tunable rigidity, bite-angle, N-attached bulk and donor characteristics make these ligands useful building blocks for the design of the metal coordination environment. They are complementary to the family of the tridentate diamido ligands developed by Schrock et al. [4]. Hagadorn et al. [5] has recently prepared bimetallic xanthene bis-amidinate complexes of Zr and Ti. A review on the catalytic activity of Ti complexes in C–C and C–N bond formation reactions has recently appeared [6].

2. Experimental

2.1. General methods

Elemental analyses were carried out by the University College, London, microanalytical laboratory. All manipulations were performed under nitrogen in a Braun

* Corresponding author. Tel.: +02380594116; fax: +02380596805.
E-mail address: ad1@soton.ac.uk (A.A. Danopoulos).

0277-5387/$ - see front matter © 2005 Elsevier Ltd. All rights reserved.
doi:10.1016/j.poly.2005.09.011

glove-box or using standard Schlenk techniques, unless stated otherwise. Solvents were dried using standard methods and distilled under nitrogen prior use.

The starting materials 4,5-dibromo-2,7-di-*tert*-butyl-9,9-dimethylxanthene [7], 4,5-dibromo-dibenzofuran [8], Ti$(NMe_2)_2Cl_2$ [9] and Ti(benzyl)$_4$ [10] were prepared by literature methods.

NMR data were recorded on Bruker AMX-300 and DPX-400 spectrometers, operating at 300 and 400 MHz (^{1}H), respectively. The spectra were referenced internally using the signal from the residual protio-solvent (^{1}H) or the signals of the solvent (^{13}C). Mass spectra (ES^+) were run from acetonitrile solutions on a VG Biotec platform.

2.2. 4,5-(N,N′-bis-cyclohexylamino)-2,7-di-tert-butyl-9,9-dimethyl-xanthene ($L_a{}^{cy}H_2$)

An ampoule was charged with 4,5-dibromo-2,7-di-*tert*-butyl-9,9-dimethyl-xanthene (2.80 g, 5.83 mmol), sodium *tert*-butoxide (1.70 g, 17.5 mmol), Pd(dba)$_2$ (0.10 g, 0.175 mmol), 1,3-bis-(2,6-diisopropylphenyl)imidazolinium chloride (0.15 g, 0.35 mmol) and 1,4-dioxane (40 cm^3). To the mixture was added cyclohexylamine (1.27 g, 12.83 mmol) and the ampoule was closed under reduced pressure and heated at 100 °C for 60 h. The reaction was allowed to cool and water (40 cm^3) was added. The mixture was extracted with diethyl ether (2×100 cm^3 then 50 cm^3). The combined organic extracts were filtered and dried with $MgSO_4$. Evaporation of the volatiles under reduced pressure yielded a pale yellow solid that was recrystallised from boiling petroleum (60/80) to give $L_a{}^{cy}H_2$ as a pale yellow solid. Yield: 2.29 g, 76%. Mass spectrometry (EI): *m*/*z*, 517 $(M+1)^+$ δ_H ($CDCl_3$): 1.20–2.15 (20H, m, cyclohexyl CH_2), 1.35 (18H, s, Bu^t), 1.62 (6H, s, CH_3), 3.40–3.50 (2H, m, cyclohexyl CH α to amino N), 4.03 (2H, d, NH), 6.62 (2H, s, aromatics), 6.77 (2H, s, aromatics). ^{13}C{^{1}H} ($CDCl_3$): 25.30, 26.75 (cyclohexyl CH_2s), 32.25 (methyls), 32.32 (Bu^t), 34.07 (cyclohexyl CH_2), 35.30, 35.58 (tertiary carbons), 52.04 (cyclohexyl CH α to amino N), 107.61, 110.58 (aromatic CHs), 130.12, 135.59, 137.36, 146.13 (quaternary aromatics).

2.3. 4,5-(N,N′-bis-mesitylamino)-2,7-di-tert-butyl-9,9-dimethyl-xanthene ($L_a{}^{mes}H_2$)

An ampoule was charged with 4,5-dibromo-2,7-di-*tert*-butyl-9,9-dimethyl-xanthene (3.00 g, 6.25 mmol), sodium *tert*-butoxide (1.80 g, 18.75 mmol), Pd(dba)$_2$ (0.18 g, 0.3 mmol), 1,3-bis-(2,6-diisopropylphenyl)imidazolinium chloride (0.26 g, 0.6 mmol) and 1,4-dioxane (60 cm^3). To this was added 2,4,6-trimethylaniline (1.86 g, 13.74 mmol), the ampoule was closed under reduced pressure and heated at 105 °C for 4 days. The reaction was allowed to cool and water (40 cm^3) was added. The mixture was extracted with diethyl ether (3×100 cm^3). The combined organic extracts were filtered and dried with $MgSO_4$. Volatiles were removed in vacuo and the residue was recrystallised from boiling ethanol to yield the product as a cream coloured solid. Yield: 2.53 g, 69%. Mass spectrometry (EI): *m*/*z*, 590 $(M+1)^+$. δ_H ($CDCl_3$): 1.39 (18H, s, Bu^t), 1.89 (6H, s, xanthene CH_3), 2.38 (12H, s, mesityl CH_3), 2.44 (6H, s, mesityl CH_3), 5.73 (2H, s, NH), 6.37 (2H, s, aromatics), 7.03 (2H, s, aromatics), 7.09 (4H, s, mesityl aromatics). ^{13}C{^{1}H} ($CDCl_3$): 18.98, 21.55 (mesityl CH_3), 32.15 (xanthene CH_3), 32.20 (But), 35.18, 35.67 (tertiary carbons), 108.34, 111.49 (aromatic CHs), 129.86 (mesityl aromatic CHs), 130.35, 134.60, 135.43, 135.77, 136.45, 137.55, 146.11 (quaternary aromatics).

2.4. 4,6-(N,N′-bis-mesitylamino)-dibenzofuran ($L_b{}^{mes}H_2$)

An ampoule was charged with 4,6-dibromo-dibenzofuran (1.00 g, 3.1 mmol), sodium *tert*-butoxide (0.88 g, 9.2 mmol), Pd(dba)$_2$ (0.18 g, 0.3 mmol), 1,3-bis-(2,6-diisopropylphenyl)imidazolinium chloride (0.26 g, 0.6 mmol) and 1,4-dioxane (20 cm^3). To this was added 2,4,6-trimethylaniline (0.99 g, 7.3 mmol) and the ampoule was closed under reduced pressure and heated at 105 °C for 18 h. The reaction was allowed to cool and water (100 cm^3) was added before extracting the reaction into diethyl ether (3×100 cm^3). The organic extracts were combined, filtered and dried with $MgSO_4$. Volatiles were removed in vacuo and the residue was recrystallised from boiling ethanol to yield the product as a white solid. Yield: 0.82 g, 61%. Mass spectrometry (EI): *m*/*z*, 435 $(M+1)^+$ δ_H ($CDCl_3$): 2.28 (12H, s, mesityl methyls), 2.36 (6H, s, mesityl methyls), 5.69 (2H, s, NH), 6.28 (2H, d, aromatics), 7.01 (4H, s, mesityl aromatics), 7.09 (2H, t, aromatics), 7.33 (2H, d, aromatics). ^{13}C{^{1}H} ($CDCl_3$): 18.94, 21.64 (mesityl methyls), 109.86, 110.46, 124.27 (aromatic CHs), 125.85 (quaternary aromatic), 129.98 (mesityl aromatic CHs), 133.23, 135.55, 136.43, 136.79, 145.01 (quaternary aromatics).

2.5. Bis-(N,N′-mesitylamido-dibenzofuran) dilithium salt ($L_b{}^{mes}Li_2$)

To a stirred, cooled (−78 °C) solution of ($L_b{}^{mes}H_2$) (0.22 g, 0.5 mmol) in petroleum (20 cm^3), was added slowly via cannula Bu^{n}Li (0.4 cm^3 of 2.45 M solution in hexanes, 1.0 mmol). The mixture was stirred at −78 °C for 1 h, allowed to reach room temperature and stirred for 15 h. This gave a colourless precipitate, which was isolated by filtration and dried in vacuo. Yield: 0.190 g, 85%. δ_H (C_6D_6): 1.65 (12H, s, mesityl methyls), 2.09 (6H, s, mesityl methyls), 6.32 (2H, d, aromatics), 6.63 (4H, s, mesityl aromatics), 6.90–7.05 (4H, m, aromatics). ^{13}C{^{1}H} (C_6D_6): 19.70, 21.33 (mesityl methyls), 107.27, 112.15 (aromatic CHs), 126.94 (quaternary aromatics), 127.84 (aromatic CHs), 131.27 (mesityl aromatic CHs), 131.94, 132.12, 142.25, 145.49, 146.40 (quaternary aromatics). The dilithium salts of ($L_a{}^{cy}H_2$), and ($L_a{}^{mes}H_2$) were prepared in an analogous way.

2.6. $(L_b^{mes})Ti(NMe_2)_2$

To a stirred, cooled (−78 °C) solution of ($L_b^{mes}H_2$) (0.24 g, 0.41 mmol) in diethyl ether (10 cm^3), was added slowly via cannula Bu^nLi (0.34 cm^3 of 2.45 M solution in hexanes, 0.81 mmol). The mixture was stirred at −78 °C for 1 h, allowed to reach room temperature and stirred for a further hour to give an orange solution with a colourless precipitate. The mixture was cooled to −25 °C and a cooled (−25 °C) solution of $Ti(NMe_2)_2Cl_2$ in diethyl ether (7 cm^3) was added slowly via cannula. The reaction was slowly allowed to reach room temperature and stirred for ca. 15 h to give a red solution and grey precipitate. The volatiles were removed in vacuo and the residue extracted into petroleum (20 cm^3) and filtered through Celite. Removal of the volatiles in vacuo gave (L_b^{mes})$Ti(NMe_2)_2$ as an orange/red oil. Yield: 0.157 g, 53%. δ_H (C_6D_6): 1.23 (18H, s, Bu^t), 1.74 (6H, s, xanthene methyls), 2.17 (6H, s, mesityl methyls), 2.22 (12H, s, mesityl methyls), 2.83 (12H, s, dimethylamides), 6.26 (2H, s, aromatics), 6.80–7.00 (6H, m, aromatics). $^{13}C\{^1H\}$ (C_6D_6): 19.92, 21.64 (mesityl methyls), 29.20 (xanthene methyls), 32.64 (Bu^t), 35.76, 37.38 (tertiary carbons), 45.99 (dimethylamides), 108.18, 109.01 (aromatic CHs), 129.79 (mesityl aromatic CHs), 132.04, 133.66, 134.23, 142.57, 147.73, 148.01, 149.39 (quaternary aromatics).

2.7. $(L_a^{cy})Ti(NMe_2)_2$

This was prepared as the complex described above from $L_a^{cy}H_2$ (0.18 g, 0.35 mmol) and $Ti(NMe_2)_2Cl_2$ (0.072 g, 0.35 mmol). It was isolated as orange solid from petroleum. X-ray quality crystals were obtained from concentrated diethyl ether solutions by cooling at 0 °C for one week. Yield: 0.14 g, 65%.

δ_H (C_6D_6) 1.10–2.10 (20H, m, cyclohexyl), 1.44 (18H, s, Bu^t), 1.64 (6H, s, methyls), 3.10 (12H, s, dimethylamides), 4.04 (2H, br m, cyclohexyl CH α to amido N), 6.77 (2H, s, aromatic), 7.12 (2H, s, aromatic).

2.8. $(L_a^{cy})Ti(Bz)_2$

In the absence of light an NMR tube equipped with Young's tap was charged with a C_6D_6 solution of ($L_a^{cy}H_2$) (0.020 g, 0.039 mmol) and $Ti(benzyl)_4$ (0.016 g, 0.039 mmol) and the base of the NMR tube was covered in foil. A ^1H NMR spectrum was run after the mixing and showed only the presence of the two starting materials. The sample was left at RT for ca. 15 h before the ^1H NMR spectrum was recorded again. The spectrum now contained a small set of peaks assignable to the (L_a^{cy})$Ti(benzyl)_2$ complex and free toluene as well as the more pronounced peaks due to the two starting materials. The NMR tube was then heated at 80 °C for 3 h and appeared to show complete conversion of the starting materials to the product. The volatiles were removed in vacuo and the dark red residue redissolved in C_6D_6 to obtain the spectra of the pure product.

δH (C_6D_6): 1.10–2.65 (20H, m, cyclohexyl CH2s), 1.35 (18H, s, Bu^t), 1.57 (6H, s, methyls), 2.92 (4H, s, benzyl CH_2s), 5.78 (2H, br m, cyclohexyl CH α to amido N), 6.70–6.85 (4H, m, aromatics), 6.95–7.05 (6H, m, aromatics), 7.10–7.20 (4H, m, aromatics). $^{13}C\{^1H\}$: 27.57, 28.24, 29.86 (cyclohexyl CH_2s), 32.57 (Bu^t), 33.05 (methyls), 35.02, 35.74 (cyclohexyl CH2s), 38.56, 38.86 (tertiary carbons), 60.57 (cyclohexyl CH α to amido N), 84.53 (benzyl CH_2s), 107.85, 111.75, 123.50 (aromatic CHs), 127.94 (quaternary aromatic), 128.02, 129.16 (aromatic CHs), 142.32, 143.74, 148.52, 149.01 (quaternary aromatics).

2.9. Structure determination of $(L_a^{cy})Ti(NMe_2)_2$

The data set was collected on a Bruker Nonius Kappa CCD area detector diffractometer with rotating anode FR591 and an Oxford Cryosystems low-temperature device operating in omega scanning mode with phi and omega scans to fill the Ewald sphere. The programs used for control and integration were COLLECT, SCALEPACK and DENZO [11,12]. An orange air sensitive crystal was mounted on a glass fibre with silicon grease, from Fomblin vacuum oil. Chemical formula $C_{39}H_{62}N_4OTi$. $C_4H_{10}O$; crystal system triclinic; space group $P\bar{1}$; cell dimensions $a = 10.2581(4)$ Å, $b = 12.2629(6)$ Å, $c = 18.6460(11)$ Å, $\alpha = 94.693(2)°$, $\beta = 95.234(3)°$, $\gamma = 107.671(2)°$; $Z = 2$, μ/mm^{-1} 0.230; $F(000)$ 708.0; number of data collected 23,300; number of unique data 7739; R_{int} 0.0981; final $R(|F|)$ for $I > 2\sigma(I)$ 0.0955; final $R(F^2)$ for all data 0.1547. All solutions and refinements were performed using the WINGX package [13] and all software packages within. All non-hydrogen atoms were refined using anisotropic thermal parameters and hydrogens were added using a riding model. The quality of the data was affected by the small size of the crystal and the rapid deterioration of the crystal quality during crystal selection possibly due to solvent loss. The structure contains a highly disordered molecule of diethylether and attempts to satisfactorily model this failed. As a result it was removed using the squeeze algorithm (P.v.d. Sluis, A.L. Spek, Acta Crystallogr., Sect. A 46 (1990) 194).

3. Results and discussion

The ligands $L_a^{mes}H_2$, $L_a^{cy}H_2$ and $L_b^{mes}H_2$ can be easily synthesised in multigram quantities from commercially available or easily accessible dibromo-xanthene or -dibenzofurans by Buchwald–Hartwig amination (Scheme 1).

The best conversions and selectivities are obtained with primary alkyl and aryl amines with a catalytic system comprising [1, 3-bis(2, 6-$Pr^i_2C_6H_3$)imidazolinium]chloride/$Pd_2(dba)_3$/Bu^tONa in dioxane [14]. Low catalyst loadings result in monoamination and dehalogenation giving rise to monoamines. The only alternative methods that have been used for the introduction of the amino (NH_2) group to xanthene ring were based on Curtius rearrangement with diphenylphosphorylazide and benzyl alcohol followed by

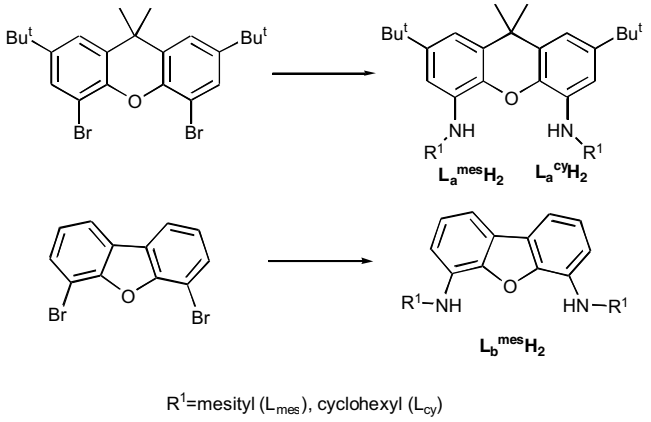

Scheme 1. Reagents and conditions: 2.2 equiv. R^1NH_2, 6 equiv. Bu^{t}ONa, 0.2 equiv. [1,3-bis(2,6-$Pr^i_2C_6H_3$)imidazolinium] chloride, 0.2 equiv. $Pd(dba)_2$, dioxane 100 °C, 12 h.

hydrogenolysis of the resulting carbamate [15]. Introduction of one dimethylamino (NMe_2) group has been accomplished by Ullman amination of the iodides under forcing conditions [16] and is of limited scope.

The new diamines were converted in almost quantitative yields to extremely air/moisture sensitive dilithium salts by reaction with Bu^{n}Li in petroleum.

The introduction of the L_a and L_b to group 4 transition metals has been successfully carried out by salt elimination from dilithium amides and metal halides or by alkane elimination from Ti tetralkyls and $L_a^{cy}H_2$ as shown in Scheme 2.

Even though the conversions are quantitative (by ^{1}H NMR spectroscopy) the yields of the isolated products are lower due to their high solubility in non-polar solvents. The new complexes were characterised by ^{1}H and $^{13}C\{^1H\}$ NMR spectroscopy. Elemental analysis data were not reproducible, possibly due to the formation of solvates (see below). The spectroscopic data support the presence of a C_s symmetric structure in solution with the plane of symmetry being perpendicular to the aromatic plane of the ligand and passing through the metal centre and the oxygen donor. The structure of $\mathbf{L_a^{cy}Ti(NMe_2)_2}$ in the solid state was determined by single crystal X-ray diffraction. A diagram of the molecule is shown in Fig. 1.

The coordination geometry around the metal can be best described as distorted square pyramidal ($\tau = 0.0186$), [17] with one dimethylamide nitrogen occupying the axial position. The diamidoxanthene ligand coordinates in the

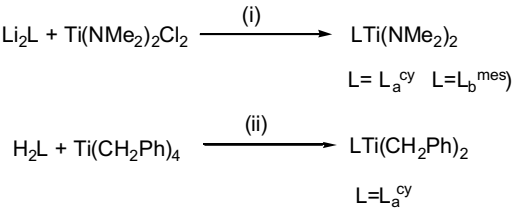

Scheme 2. Reagents and conditions: (i) ether, −78 °C to room temperature; (ii) Me_3SiCl, toluene; (iii) toluene, 80 °C, 3 h.

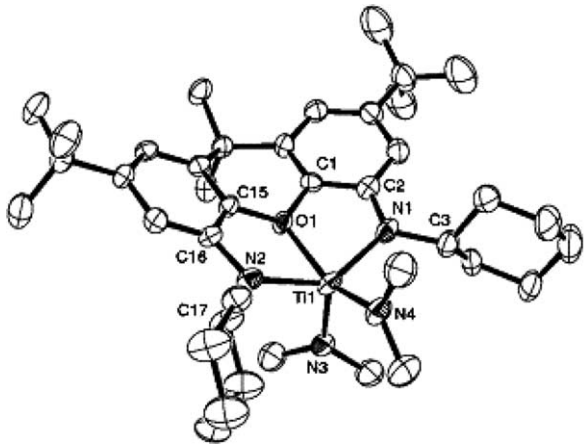

Fig. 1. ORTEP representation of the structure of $\mathbf{L_a^{cy}Ti(NMe_2)_2}$. One disordered ether molecule present in the unit cell as well as hydrogen atoms are omitted for clarity. Selected bond lengths (Å) and angles (°): N(1)–Ti(1) = 2.057(4); N(2)–Ti(1) = 2.040(4); N(3)–Ti(1) = 1.887(4); N(4)–Ti(1) = 1.893(4): O(1)–Ti(1) = 2.132(3) and N(3)–Ti(1)–N(4) = 105.15(18); N(3)–Ti(1)–N(2) = 103.92(17); N(4)–Ti(1)–N(2) = 101.64(17); N(3)–Ti(1)–N(1) = 105.55(17); N(4)–Ti(1)–N(1) = 97.36(17); N(2)–Ti(1)–N(1) = 139.08(15); N(3)–Ti(1)–O(1) = 99.97(16); N(4)–Ti(1)–O(1) = 154.80(16); N(2)–Ti(1)–O(1) = 73.73(13); N(1)–Ti(1)–O(1) = 73.72(13).

'*mer* fashion' as anticipated. The two Ti–dimethylamido bond lengths [Ti(1)–N(3) 1.888(4) Å; Ti(1)–N(2) 1.892(4) Å] are equal within the observed e.s.d.'s and shorter than the cyclohexylarylamido bonds [Ti(1)–N(1) 2.056(4) Å; Ti(1)–N(2) 2.039(4) Å]. The latter are in the range reported for less rigid 'pincer' or NON^{2-} diamido ligands [18]. All the amido groups are virtually planar. Of particular interest is the deviation of the ligand backbone from planarity due to structural constraint imposed by the linking groups (O and CMe_2). The angle defined by the two aromatic rings is ca. 15^0. In solution the structure is possibly non-rigid (idealised C_{2v}) with equivalent dimethylamido groups and methyl substituents on the 9-position.

In solution, complexes $\mathbf{L_b^{mes}Ti(NMe_2)_2}$ and $\mathbf{L_a^{cy}Ti(Bz)_2}$ exhibit spectra with features similar to $\mathbf{L_a^{cy}Ti(NMe_2)_2}$ and, therefore, are expected to adopt analogous structures. We have been unable to grow crystals of $\mathbf{L_b^{mes}Ti(NMe_2)_2}$ and $\mathbf{L_a^{cy}Ti(Bz)_2}$ suitable for X-ray diffraction. The electron deficient $\mathbf{L_a^{cy}Ti(Bz)_2}$ is stable at room temperature in solution. This behaviour contrasts with the more flexible and less bulky (NON)Ti(alkyl)$_2$ which show limited stability in solution and the solid state [18b].

In summary, we have developed a general method based on Pd catalysed aromatic amination for the preparation of preorganised xanthene and dibenzofuran diamines. The diamido ligands that originate from them provide a useful tunable environment for the stabilisation of early transition metals. Extension of the scope of the catalytic amination to the synthesis of preorganised carbazole and dibenzothiophenes as well as studies of the chemistry of the new early transition metal amides as a function of ligand structural parameters is currently in progress.

4. Supplementary material

The crystallographic data for this paper have been pre-deposited at the Cambridge Crystallographic Database (CCDC 276930). These data can be obtained free of charge via www.ccdc.cam.ac.uk/data_request/cif, or by emailing data_request@ccdc.cam.ac.uk, or by contacting The Cambridge Crystallographic Data Centre, 12, Union Road, Cambridge CB2 1EZ, UK (fax: +44 1223 336033).

Acknowledgement

We thank Professor M.B. Hursthouse for helpful discussions and the EPSRC for support and provision of X-ray facilities.

References

[1] (a) For leading references see: A.N. Vedernikov, K.G. Caulton, Org. Lett. 5 (2003) 2591;
(b) A.N. Vedernikov, K.G. Caulton, Angew. Chem. Int. Ed. 41 (2002) 4102;
(c) B. Rybtchinski, D. Milstein, Angew. Chem. Int. Ed. 38 (1999) 870;
(d) P.W.N.M. van Leeuwen, C. Claver (Eds.), Rhodium Catalysed Hydroformylation, Kluwer Academic Publishers, Dortrecht, 2000.

[2] A.H. Hoveyda, J.P. Morken, in: A. Togni, R.L. Halterman (Eds.), Metallocenes – Synthesis, Reactivity – Applications, Wiley-VCH, Weinheim, 1998.

[3] (a) L.H. Gade, Chem. Commun. (2000) 173;
(b) J.A.R. Schmidt, G.R. Giesbrecht, C. Cui, J. Arnold, Chem. Commun. (2003) 1025;
(c) V.C. Gibson, S.K. Spitzmesser, Chem. Rev. 103 (2003) 183.

[4] (a) R. Baumann, W.M. Davis, R.R. Schrock, J. Am. Chem. Soc. 119 (1997) 3830;
(b) D.D. Graf, W.M. Davis, R.R. Schrock, Organometallics 17 (1998) 5820;
(c) R. Baumann, R.R. Schrock, J. Organomet. Chem. 557 (1998) 69;
(d) R. Baumann, R. Stumpf, W.M. Davis, L.C. Liang, R.R. Schrock, J. Am. Chem. Soc. 121 (1999) 7822;
(e) R.R. Schrock, R. Baumann, S.M. Reid, T.J. Goodman, R. Stumpf, W.M. Davis, Organometallics 18 (1999) 3649;
(f) J.T. Goodman, R.R. Schrock, Organometallics 20 (2001) 5205.

[5] (a) M.J. McNevin, J.R. Hagadorn, Inorg. Chem. 43 (2004) 8547;
(b) J.R. Hagadorn, M.J. McNevin, G. Wiedenfeld, R. Shoemaker, Organometallics 22 (2003) 4818, and references cited therein.

[6] A.L. Odom, Dalton Trans. (2005) 225.

[7] J.S. Novick, P. Ballester, F. Ebmeyer, J. Rebek, J. Am. Chem. Soc. 112 (1990) 8902.

[8] E.B. Schwartz, C.B. Knobler, D.J. Cram, J. Am. Chem. Soc. 114 (1992) 10775.

[9] E. Benzing, W. Kornicker, Chem. Ber. 94 (1961) 2263.

[10] A. van der Linden, C.J. Schaverien, N. Meijboom, C. Canter, A.G. Orpen, J. Am. Chem. Soc. 117 (1995) 3008.

[11] R. Hooft, COLLECT, Nonius BV, 1997–2000.

[12] Z. Otwinowski, W. Minor, SCALEPACK, DENZO, Methods Enzymol. 276 (1997) 307.

[13] L.J.J. Farrugia, Appl. Crystallogr. 32 (1999) 83.

[14] (a) S. Caddick, F.G.N. Cloke, P.B. Hitchcock, J. Leonard, A.K. de K. Lewis, D. McKerrecher, L.R. Titcomb, Organometallics 21 (2002) 4318;
(b) S.R. Stauffer, S.W. Lee, J.P. Stambuli, S.I. Hauck, J.F. Hartwig, Org. Lett. 2 (2000) 1423;
(c) R.M. Porter, A.A. Danopoulos, Dalton Trans. (2004) 2556.

[15] B. Hamann, N. Branda, J. Rebek, Tetrahedron Lett. 34 (1993) 6837.

[16] L.A. van der Veen, P.K. Keeven, P.C.J. Kamer, P.W.N.M. van Leeuwen, J. Chem. Soc., Dalton Trans. (2000) 2105.

[17] A.W. Addison, T.N. Rao, J. Reedijk, J. van Rijn, G.C. Verschoor, J. Chem. Soc., Dalton Trans. (1984) 1349.

[18] (a) F. Guérin, D.H. McConville, N.C. Payne, Organometallics 15 (1996) 5085;
(b) R. Baumann, R. Stumpf, W.M. Davis, L.-C. Liang, R.R. Schrock, J. Am. Chem. Soc. 121 (1999) 7822.

Available online at www.sciencedirect.com
SCIENCE DIRECT
Polyhedron 25 (2006) 864–868
POLYHEDRON
www.elsevier.com/locate/poly

Synthesis of novel mixed indium(III) chalcogenolato complexes: Potential precursors for indium chalcogenides

Mohammad A. Malik [a], Mohammad Afzaal [a], Paul O'Brien [a,*], Madeleine Halliwell [b]

[a] The School of Materials and School of Chemistry, The University of Manchester, Oxford Road, Manchester M13 9PL, UK
[b] The School of Chemistry, The University of Manchester, Oxford Road, Manchester M13 9PL, UK

Received 22 June 2005; accepted 21 September 2005
Available online 27 October 2005

Dedicated to Professor Mike Hursthouse for his 65th birthday.

Abstract

Novel organometallic and metal–organic indium complexes, $[Et_2In(OS_2CNMe^nBu)]_2$ (**1**), $[In\{(SeP^iPr_2)_2N\}(S_2CNEt_2)_2]$ (**2**) and $[In\{(SeP^iPr_2)_2N\}(S_2P^iBu_2)_2]$ (**3**), have been synthesised and characterised. Compound (**1**) was formed by the insertion of oxygen atoms into the M–S bonds of thiocarbamate ligands, whereas the mixed-chalcogenide complexes (**2**) and (**3**) were prepared by the reaction of $Na(S_2CNEt_2)_2$ or $Na(S_2P^iBu_2)_2$ with $In[(SeP^iPr_2)_2N]_2Cl$. The structures of all three compounds were determined by X-ray single crystallographic methods. The dimeric structure of (**1**) consists of two five membered and one four membered rings formed by chelating and bridging of both dithioperoxycarbamato ligands. The structures of both (**2**) and (**3**) are based on monomers in each case the coordination around indium is distorted octahedral.
© 2005 Elsevier Ltd. All rights reserved.

Keywords: Synthesis; Indium; Chalcogenolato; Oxygen insertion; Thiocarbamate

1. Introduction

A significant amount of work has been carried out on tetraorganodichalcogeno-diphosphinato $[R_2P(E)–N–P(E)R_2]$-(E = O, S, Se) ligands because of their versatility in forming inorganic chelate rings that are the analogs of β-diketonates [1]. Metal complexes of such ligands show a variety of structural and coordination modes. For example, indium complexes of the bidentate ligand tetraphenylimidodiphosphinate and its derivatives form six coordinate complexes, i.e., $[In\{(EPPh_2)_2N]_3$ (E = O, S, Se) [2,3]. While five coordinate indium(III) bis-chelate complexes with general formula $In[(EP^iPr_2)_2N]_2Cl$ (E = S, Se) have also been reported [4]. Metal complexes of such ligands have been shown to be effective single source molecular precursors for the synthesis of thin films by chemical vapour deposition (CVD) [5] and the preparation of quantum dots [6].

A number of mixed-alkyl indium dithiocarbamate complexes, $(R_2InS_2CNR'_2)$ (R = Me, Et, Np; R′ = Et, Me^nBu), have been synthesised and used as single-source precursors for indium sulfide thin films [7]. One closely related complex $[Et_2In(S_2CNMe^nBu)]$, a clear liquid, has been successfully utilised to prepare nanorods of tetragonal β-In_2S_3 [8].

The oxidation of 1,1 dithiolate ligands by elemental sulfur in nickel(II) complex, was first reported by Coucouvanias and Fackler [9]. Insertion of sulfur expanded the ring from four to five membered ring and gave rise to a new chelate perthiodithiolate ligand. This sulfur insertion was further established in the X-ray structure of $[Fe(p\text{-}MeC_6H_4SC_2)_2$ $(p\text{-}MeC_6H_4CS_3)]$ in which sulfur has been inserted into a Fe–S bond [10]. Similar ring expansion by the insertion of

* Corresponding author. Tel.: +44 161 275 4652; fax: +44 161 275 4616.
E-mail address: paul.obrien@machester.ac.uk (P. O'Brien).

0277-5387/$ - see front matter © 2005 Elsevier Ltd. All rights reserved.
doi:10.1016/j.poly.2005.09.012

oxygen instead of sulfur has been reported by Martin et al. [11] in a chromium complex prepared by the reaction of $Na(S_2CNR_2)$ (R = Et or Me) with $K_2Cr_2O_7$ in aqueous solution. The X-ray single crystal structure of this complex is based on a monomer in which chromium is pseudo-octahedral with two normal dithiocarbamato (dtc) ligands and one dithioperoxycarbamato (odtc) ligand resulting from the insertion of oxygen into a Cr–S bond $[Cr(S_2CNR_2)_2(OS_2CNR_2)]$ [12]. This chromium complex has been further studied electrochemically along with the dithiocarbamato complex.

In this work, we report a unique complex with a double ring expansion where oxygen is inserted in both dithiocarbamato ligands of $[Et_2In(S_2CNMe^nBu)]$ to form $[Et_2In(OS_2CNMe^nBu)]_2$ (**1**). Initially, the compound was prepared serendipitously when the toluene solution of $[In(S_2CNMe^nBu)_3]$ and triethylindium was exposed to air through a leak in the system. The reaction gave reproducible results when repeated with stirring in an open flask for 2 min. The same reaction in dry toluene under strict air sensitive conditions produced the complex $[Et_2In(S_2CNMe^nBu)]$ as a clear viscous liquid. Furthermore, we report the synthesis and structural characterisation of indium complexes containing both imidodiphosphinates and dithiocarbamate or dithiophosphinate ligands.

2. Experimental

The synthesis of $[NH(SeP^iPr_2)_2]$, [1d] $In[(SeP^iPr_2)_2N]_2Cl$ [4] and $[In(S_2CNMe^nBu)_3]$ [13] was carried out according to the reported methods. Carbon disulfide, sodium hydroxide, sodium diisobutyldithiophosphinate and diethylamine were bought from Aldrich Chemical Company Limited and used as received. All manipulations and reactions were carried out in an inert atmosphere using Schlenk techniques and a vacuum line. The solvents were distilled and degassed prior to use. ^1H, ^{13}C and ^{31}P NMR studies were carried out using a Bruker AC300 FTNMR instrument. Elemental analysis was performed by the University of Manchester micro-analytical laboratory.

2.1. Synthesis of $[Et_2In(OS_2CNMe^nBu)]_2$ (1)

Tris(methyl(*n*-butyl)dithiocarbamato)indium(III) and triethylindium were reacted in 1:2 stoichiometric ratio at room temperature under nitrogen for 10 min and then allowed to stir in open air for 2 min. Yield: 85%. ^1H NMR (C_6D_6, 300 MHz) δ/ppm: 0.90 (q, 4H, In–CH_2), 1.41 (t, 6H, In–CH_2–CH_3), 3.41 (s, 6H, N–CH_3), 3.85 (t, 4H, N–CH_2–CH_2–), 1.79 (q, 4H, N–CH_2–CH_2), 1.40 (m, N–CH_2–CH_2–CH_2), 1.0 (t, 6H, N–CH_2–CH_2–CH_2–CH_3); $^{13}C\{H\}$ NMR (C_6D_6, 125 MHz) δ/ppm: 203.19 (CS), 55.32 (N–CH_2), 40.67 (N–CH_3), 28.75 (N–CH_2–CH_2), 19.90 (In–CH_2–CH_3), 13.71 (N–CH_2–CH_2–CH_2–CH_3), 12.22 (N–CH_2-CH_2–CH_2–CH_3), 9.92 (In–CH_2). *Anal.* Calc. for $C_{20}H_{44}O_2N_2S_4In_2$: C, 34.2; H, 6.3; N, 4.0, S, 18.3. Found: C, 33.8; H, 6.2; N, 3.8; S, 18.4%.

2.2. Synthesis of $[In\{(SeP^iPr_2)_2N\}(S_2CNEt_2)_2]$ (2)

CS_2 (0.4 ml, 6.25 mmol) was added to a cold, stirring solution of $NH(C_2H_5)_2$(0.65 ml, 6.25 mmol) in NaOH (0.25 g, 6.25 mmol). After stirring for 30 min, while on ice bath, $In[(SeP^iPr_2)_2N]_2Cl$ [4] (5.8 g, 6.02 mmol) dissolved in 40 ml THF was added dropwise to the solution and stirred overnight. The colour of the solution changed from orange to light yellow. Removal of solvent in vacuo led to a viscous liquid, which was crystallised by adding hexane. The product was recrystallised from THF. Yield: 72%. ^1H NMR ($CDCl_3$, 300 MHz) δ/ppm: 1.10–1.30 (m, 24H, P–CH(CH_3)$_2$) 1.10–1.30 (m, 12H, N–CH_2–CH_3), 3.85 (qs, 8H, N–CH_2–CH_3), 2.10–2.75 (ms, 4H, P–CH(CH_3)$_2$) $^{31}P\{H\}$ NMR ($CDCl_3$, 400, 162 MHz) δ/ppm: 59.90, 60.93 (m, 2P, *P*–CH–) *Anal.* Calc. for $C_{20}H_{48}InN_3P_2S_4Se_2$: C, 32.3; H, 5.9; N, 5.1, S, 15.8. Found: C, 31.5; H, 5.9; N, 5.1; S, 15.7%.

2.3. Synthesis of $[In\{(SeP^iPr_2)_2N\}(S_2P^iBu_2)_2]$ (3)

$Na(S_2P^iBu_2)_2$ (0.39 g, 1.34 mmol) was added to a stirred solution of $In[(SeP^iPr_2)_2N]_2Cl$ (1.28 g, 6.01 mmol) in 20 ml THF and the colour immediately turned into intense yellow. The reaction was refluxed for 1 h after which a orange colour solution was obtained. After removal of the solvent

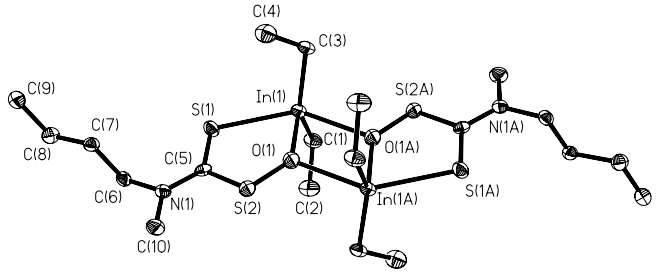

Fig. 1. Molecular structure of $[Et_2In(OS_2CNMe^nBu)]_2$. Hydrogen atoms have been omitted for clarity.

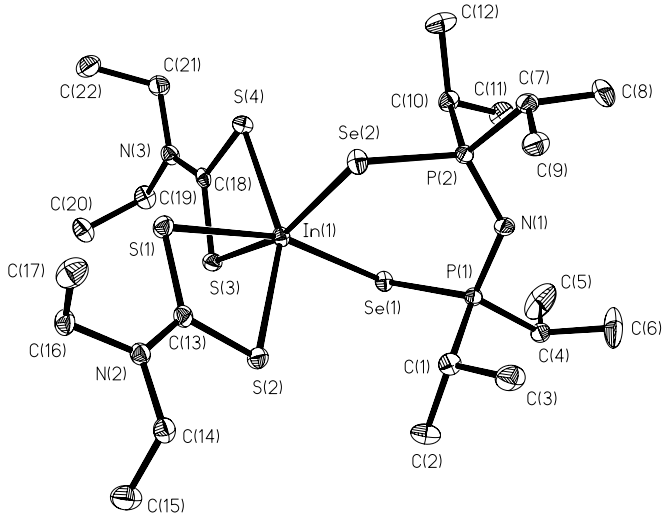

Fig. 2. Molecular structure of $[In\{(SeP^iPr_2)_2N\}(S_2CNEt_2)_2]$. Hydrogen atoms have been omitted for clarity.

in vacuo, an orange colour powder was obtained which was recrystallised from DCM. Yield: 78%. ^{1}H NMR ($CDCl_3$, 300 MHz) δ/ppm: 1.15–1.30 (m, 24H, P–CH_2–CH(CH_3)$_2$), 1.30–1.39 (m, 24H, P–CH(CH_3)$_2$), 2.18 (m, 4H, P–CH(CH_3)$_2$), 2.32–2.58 (m, 12H, P–CH_2–CH(CH_3)$_2$) ^{31}P{H} NMR ($CDCl_3$, 400, 162 MHz) δ/ppm: 59.95 (d/d, 2P, *P*–CH–), 66.07 (d/d, 2P, *P*–CH_2–). *Anal*. Calc. for $C_{28}H_{64}InNP_4S_4Se_2$: C, 35.2; H, 6.9; N, 1.5, P, 13.2. Found: C, 33.9; H, 6.4; N, 2.0; P, 12. 8%.

2.4. X-ray single crystallography

Measurements were made using graphite monochromated Mo Kα radiation on a Bruker APEX diffractometer.

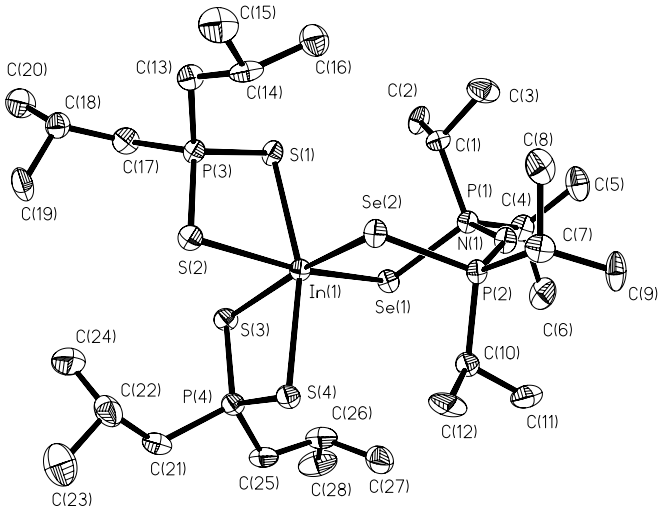

Fig. 3. Molecular structure of [In{(SeP^{i}Pr$_2$)$_2$N}(S$_2$P^{i}Bu$_2$)$_2$].

The structures were solved by direct methods and refined by full-matrix least-squares on F^2 [14]. All calculations were carried out using the SHELXTL package [15]. All non-hydrogen atoms were refined with anisotropic atomic displacement parameters. Hydrogen atoms were placed in calculated positions and assigned isotropic atoms. Figs. 2 and 3 have 50% thermal ellipsoids. Crystallographic details and selected interatomic distances and angles are summarised in Tables 1 and 2.

3. Results and discussion

Compound (**1**) was initially prepared serendipitously by exposure of [In(S$_2$CNMe^{n}Bu)$_3$] and triethylindium solution to air. The reaction gave reproducible results when repeated by stirring the reaction mixture in an open flask for 2 min. The same reaction in dry toluene under strictly air sensitive conditions produced a viscous liquid [Et$_2$In(S$_2$CNMe^{n}Bu)] which has successfully been used for the deposition of In_2S_3 nanorods by AACVD [8]. Compound (**1**) is soluble in most organic solvents and was crystallised from a toluene solution to give transparent cubic crystals. It gave satisfactory microelemental analysis. ^{1}H NMR spectrum gave an overlapping quartet and a triplet at 0.90–1.00 ppm for methylene protons of ethyl group attached with indium and for methyl protons of *n*-butyl group. A clear singlet for N–CH_3 at 3.41 ppm and a triplet at the lowest field (3.85 ppm) for the *N*-methylene protons of the *n*-butyl group are seen. A quintet is shown for β-methylene protons N–CH_2–CH_2 at 1.79 ppm and a triplet for methyl protons of ethyl group at indium and a multiplet appears for γ-proton of *n*-butyl group at 1.40 ppm. ^{13}C NMR gives an eight line spectrum as expected. CS

Table 1
Crystal data and structure refinement for compounds (**1**), (**2**) and (**3**)

Compound	$C_{20}H_{44}In_2N_2O_2S_4$ (**1**)	$C_{22}H_{48}InN_3P_2S_4Se_2$ (**2**)	$C_{28}H_{64}InNP_4S_4Se_2$ (**3**)
F_w	702.45	817.55	939.66
Temperature (K)	100(2)	100(2)	100(2)
Crystal system	triclinic	triclinic	triclinic
Space group	$P\bar{1}$	$P\bar{1}$	$P\bar{1}$
a (Å)	9.005(4)	10.018(8)	10.176(5)
b (Å)	9.561(4)	11.037(9)	10.179(5)
c (Å)	10.042(5)	15.484(13)	20.948(5)
α (°)	62.493(6)	74.186(10)	81.315(5)
β (°)	68.731(7)	87.822(10)	81.052(5)
γ (°)	74.726(7)	85.719(10)	86.451(5)
Volume (Å^3)	709.8(6)	1642.4(2)	2117.2(16)
Z	1	2	2
D_{calc} (Mg/m^3)	1.643	1.653	1.474
Absorption coefficient (mm^{-1})	1.937	3.305	2.645
F(000)	356	824	960
Index ranges	$-11 \leqslant h \leqslant 11$, $11 \leqslant k \leqslant 12$, $-12 \leqslant i \leqslant 12$	$-12 \leqslant h \leqslant 12$, $-13 \leqslant k \leqslant 13$, $-19 \leqslant i \leqslant 19$	$-12 \leqslant h \leqslant 11$, $-9 \leqslant k \leqslant 12$, $-25 \leqslant i \leqslant 26$
Collected/unique	5514/2860	13244/6647	11898/8301
Data/restraints/parameters	2860/0/141	16647/0/319	8310/0/378
Goodness-of-fit on F^2	1.022	1.066	1.102
R_1, wR_2 [$I>2\sigma(I)$]	0.0341, 0.0826	0.0229, 0.0513	0.0559, 0.1375
R_1, wR_2 (all data)	0.0413, 0.0850	0.0266, 0.0566	0.0626, 0.1414
Difference in peak, hole (e Å^{-3})	1.377, −0.662	0.585, −0.317	1.699, −1.835

Table 2
Selected bond lengths (Å) and angles (°) for compounds (**1**)–(**3**)

*Compound (**1**)*			
In(1)–C(1)	2.144(4)	S(1)–In(1)–O(1a)	143.40(7)
In(1)–C(3)	2.149(3)	C(1)–In(1)–C(3)	141.77(16)
In(1)–O(1)	2.186(3)	O(1)–In(1)–O(1A)	67.12(12)
In(1)–O(1a)	2.489(3)	C(1)–In(1)–O(1a)	89.68(14)
In(1)–S(1)	2.692(3)	C(3)–In(1)–O(1a)	90.30(13)
S(2)–O(1)	1.571(3)	S(1)–In(1)–C(1)	95.94(12)
		S(1)–In(1)–C(3)	106.37(12)
		S(1)–In(1)–O(1)	77.48(8)
*Compound (**2**)*			
In(1)–S(1)	2.638(6)	S(4)–In(1)–S(3)	68.30(19)
In(1)–S(2)	2.592(7)	S(1)–In(1)–S(3)	94.03(2)
In(1)–S(3)	2.648(6)	S(2)–In(1)–Se(2)	100.1(16)
In(1)–S(4)	2.620(6)	S(4)–In(1)–Se(4)	92.65(15)
In(1)–Se(1)	2.689(4)	S(1)–In(1)–Se(2)	88.43(16)
In(1)–Se(2)	2.697(3)	S(3)–In(1)–Se(2)	160.68(16)
Se(1)–P(1)	2.202(7)	S(2)–In(1)–Se(1)	96.792(16)
Se(2)–P(2)	2.20(7)	S(4)–In(1)–Se(1)	103.75(17)
		S(1)–In(1)–Se(1)	164.72(16)
S(2)–In(1)–S(4)	153.63(2)	S(3)–In(1)–Se(3)	82.48(15)
S(2)–In(1)–S(1)	68.93(2)	Se(2)–In(1)–Se(1)	99.79(19)
S(4)–In(1)–S(1)	88.59(2)	P(1)–Se(1)–In(1)	103.08(19)
S(2)–In(1)–S(3)	98.70(2)	P(2)–Se(2)–In(1)	103.59(19)
*Compound (**3**)*			
In(1)–S(1)	2.649(2)	S(1)–In(1)–S(2)	76.27(7)
In(1)–Se(1)	2.655(16)	Se1(4)–In(1)–S(2)	166.61(5)
In(1)–S(4)	2.66(2)	S(4)–In(1)–S(2)	90.51(7)
In(1)–S(2)	2.665(2)	S(1)–In(1)–Se(2)	96.70(16)
In(1)–Se(2)	2.672(15)	S(4)–In(1)–Se(4)	92.65(15)
In(1)–S(3)	2.68(2)	Se(1)–In(1)–Se(2)	100.68(3)
Se(1)–P(1)	2.213(2)	S(4)–In(1)–Se(2)	94.80(5)
Se(2)–P(2)	2.19(2)	S(2)–In(1)–Se(2)	87.19(5)
		S(1)–In(1)–S(3)	91.64(7)
		Se(1)–In(1)–Se(3)	85.20(5)
S(1)–In(1)–Se(1)	91.95(5)	S(4)–In(1)–S(3)	75.64(7)
S(1)–In(1)–S(4)	161.97(6)	S(2)–In(1)–S(3)	88.76(7)
Se(1)–In(1)–S(4)	99.52(6)	Se(2)–Se(1)–S(3)	169.58(5)

carbon gives a signal at the lowest field (203.19 ppm) and the In–CH_2 carbon at the highest field (9.92 ppm).

Our repeated attempts to prepare a *tris* indium complex $In[(SeP^iPr_2)_2N]_3$ even on addition of excess ligand were unsuccessful. This behaviour of the indium complex $In[(SeP^iPr_2)_2N]_2Cl$ has also been reported previously [4]. However, the reaction between $In[(SeP^iPr_2)_2N]_2Cl$ and NaS_2CNEt_2 at room temperature readily produced a mixed ligand (imidodiphosphinate and dithiocarbamate)indium (III) complex $[In\{(SeP^iPr_2)_2N\}(S_2CNEt_2)_2]$ (**2**). Using similar method, another mixed ligand complex (imidodiphosphinate and dithiophosphinate) $[In\{(SeP^iPr_2)_2N\}(S_2P^iBu_2)_2]$ (**3**) was prepared by the reaction of $In[(SeP^iPr_2)_2N]_2Cl$ and $NaS_2P^iBu_2$. Both compounds are soluble in common organic solvents and were crystallised from THF and DCM, respectively, and are air and moisture stable for months.

^1H NMR and ^{31}P NMR data for compounds (**2**) and (**3**) are given in Section 2. In ^1H NMR spectrum of compound (**2**), methyl protons of isopropyl group are shown as overlapping multiplets at δ 1.10–1.1.30 ppm. Similarly, the methyl protons of ethyl group also appear in the same range as overlapping multiplets. The methylene protons of ethyl group appear as overlapping quartets at δ 3.85 ppm and the methyne protons of isopropyl group give four sets of multiplets in the range δ 2.10–2.75 ppm. ^1H NMR spectrum of compound (**3**) gives multiplets for methyl protons of isobutyl groups at δ 1.15–1.30 ppm and the methyl protons of isopropyl groups appear at δ 1.30–1.39 ppm as multiplets as well. Methylene protons and methyne protons of both isobutyl and isopropyl groups give multiplets in the range δ 2.18–2.58 ppm. Only two phosphorus signals are observed at δ 59.95 and δ 66.07 ppm as expected.

3.1. X-ray structures

The structure of complex (**1**) is based on a dimer in which each indium is five co-ordinated with bonding to two ethyl groups, two oxygen and one sulfur atom (Fig. 1). Both dithioperoxycarbamato ligands (odtc) act as both chelating and bridging through oxygen atoms, hence forming two five membered rings (S(1), C(5), S(2), O(1), In (1)) and (S(2A), C(5A), S(1A), In(1A), O(1A)) and a four membered ring (In, O, O, In). The geometry around indium is highly distorted which is reflected in its bond angles; C(1)–In–C(3) being 141.8°, O(1)–In–O(1A) is 67.12° and C(1)–In–O(1) is 113.0°. The bond length In(1)–O(1A) 2.489(3) Å is considerably longer than In(1)–O(1) (2.186(3) Å) as the first one is bridging and the latter is chelating. A similar effect on the bond lengths of In–O was observed in $[Et_2In(\mu,\lambda O_2C)–C_6H_4–2\text{-}NH_2]_n$ where indium to bridging oxygen bond length was In(1)–O(1a) 2.554(4) Å and indium to non-bridging oxygen was In(1)–O(2a) 2.264(3) Å [16]. In–C bond lengths are normal, 2.144(4) Å. In–S bond distances are longer In(1)–S(1) (2.691(13) Å) than those observed in $[In(SOCN^iPr_2)_3]$ In–S(3) 2.481(2) Å [17] but are comparable to those reported for ($Me_2InS_2CNEt_2$) where In–S distances are 2.56(10) and 2.68(10) Å [18].

X-ray structures of compounds (**2**) and (**3**) are shown in Figs. (2) and (3). The reaction of sodium salts of dithiocarbamate or dithiophosphinate with parent compound $In[(SeP^iPr_2)_2N]_2Cl$ replaces axial chlorine and one of the iminobis(diisopropylphosphine selenide) in the trigonal bipyramidal geometry to give a distorted octahedron. In compound (**2**), two distinct sets of In–S bond lengths are seen with the distances of one set longer (In(1)–S(3) 2.648(6) Å) than the other (In(1)–S(2) 2.592(7) Å). Similar pattern has been noted before in other indium dithiocarbamates, e.g. $[Me_2InS_2CNEt_2]$ [18], $In(S_2CNEt)_3$ [19] and $In[S_2P(OEt)_2]_3$ [20]. The In–S bond lengths [2.649(2)–2.68(2) Å] in compound (**3**) are also noticeably different but lie with in the range observed for other indium dithiophosphinate species [21]. No significant difference between In and Se bond lengths is observed in both compounds. Nevertheless, these are comparatively shorter than the In–Se bond lengths found in $In[(SePPh_2)_3N]_3$ (2.75(3) Å) [3] and $In[(SeP^iPr_2)_2N]_2Cl$ (2.720(3) Å) [4].

These In–Se bond lengths are closer to those measured for the less crowded $[In\{Se(2,4,6\text{-}^tBu_3C_6H_2)\}_3]$ compound [22].

In compound (**2**), the S–In–S bite angles (av. 68.62 (10) Å) are smaller than the corresponding Se–In–Se bite angles (99.79 (19) Å) due to the constraint imposed by the dithiocarbamato groups. Similar S–In–S bite angles are observed in $[Et_2InS_2CNEt_2]$ (68.77(3) Å) [18]. The Se–In–Se angle in compound (**2**) readily compares with other octahedral compounds having symmetrical ligands [3]. Similar bonding mode is observed in compound (**3**). In both compounds, P–S bond lengths are enlarged and the N–P bond lengths are shortened as compared to those in their free acids, reflecting the increased delocalisation as a consequence of deprotonation.

4. Conclusion

Three novel indium complexes have been synthesised and completely characterised including their X-ray structures. The insertion of oxygen atoms into the M–S bonds of indium complex, $[Et_2In(S_2CNMe^nBu)]$, produced a unique compound with a dimeric structure. The structure consists of two five membered and one four membered rings formed by chelating and bridging of both dithioperoxycarbamato ligands. Both compounds (**2**) and (**3**) which contain more than one type of ligand are monomers, and in each case indium is six coordinate as compared to the parent indium compound which is five coordinate.

5. Supplementary material

Crystallographic data for the structural analysis have been deposited with the Cambridge Crystallographic Data Center. CCDC reference numbers for the compounds are 234614, 267172 and 267173. Supplementary data are available from the CCDC, 12 Union Road, Cambridge CB2 1EZ, UK (fax: +44 1223 336 033; e-mail: deposit@ccdc.cam.ac.uk or www: http://www.ccdc.cam.ac.uk).

Acknowledgements

The authors are grateful to the EPSRC for funding.

References

[1] (a) F.T. Wang, J. Najdzionek, K.L. Leneker, H. Wasserman, D.M. Braitsch, Synth. React. Inorg. Met.-Org. Chem. 8 (1978) 119;
(b) R.O. Day, R.R. Holmes, A. Schmidpeter, K. Stoll, L. Howe, Chem. Ber. 124 (1991) 2443;
(c) P. Bhattacharyya, A.M.Z. Slawin, M.B. Smith, J. Chem. Soc. Dalton Trans. (1998) 2467;
(d) D. Cupertino, D.J. Birdsall, A.M.Z. Slawin, J.D. Woollins, Inorg. Chim. Acta 290 (1999) 1;
(e) J.D. Woollins, J. Chem. Soc., Dalton Trans. (1996) 2893, and references within;
(f) P. Bhattacharyya, J.D. Woollins, Polyhedron 14 (1995) 3367;
(g) D. Cupertino, R. Keyte, A.M.Z. Slawin, D.J. Williams, J.D. Woollins, Inorg. Chem. 35 (1996) 2695.

[2] R. Cea-Olivares, R.A. Toscano, G. Carreon, J. Valdes-Martínez, Monatsh. Chem. 123 (1992) 391.

[3] R. Cea-Olivares, V. García-Montalvo, J. Novosad, J.D. Woollins, R.A. Toscano, G. Espinosa-Perez, Chem. Ber. 129 (1996) 919.

[4] K. Darwin, L.M. Gilby, P.R. Hodge, B. Piggott, Polyhedron 18 (1999) 3729.

[5] (a) M. Afzaal, S.M. Ascott, D. Crouch, P. O'Brien, J.D. Woollins, J.-H. Park, Chem. Vapor Depos. 8 (2002) 187;
(b) M. Afzaal, D. Crouch, M.A. Malik, M. Motevalli, P. O'Brien, J.-H. Park, J. Mater. Chem. 13 (2003) 1;
(c) M. Afzaal, D. Crouch, M.A. Malik, M. Motevalli, P. O'Brien, J.-Ho Park, J.D. Woollins, Eur. J. Inorg. Chem. (2004) 171.

[6] D.J. Crouch, P. O'Brien, M.A. Malik, P.J. Skabara, S.P. Wright, Chem. Commun. (2003) 1454.

[7] S.W. Haggata, M.A. Malik, M. Motevalli, P. O'Brien, J.C. Knowles, Chem. Mater. 7 (1995) 716.

[8] M. Afzaal, M.A. Malik, P. O'Brien, J. Chem. Soc., Chem. Commun. (2004) 334.

[9] D. Coucouvanias, J.P. Fackler Jr., J. Am. Chem. Soc. 89 (1967) 1346.

[10] D. Coucouvanias, S.J. Lippard, J. Am. Chem. Soc. 90 (1968) 3281, 91 (1969) 307;
J. Am. Chem. Soc. 91 (1969) 307.

[11] J.M. Hope, R.L. Martin, D. Taylor, A.H. White, J. Chem. Soc., Chem. Commun. (1977) 99.

[12] A.M. Bond, G.J. Wallace, Inorg. Chem. 23 (1984) 1858.

[13] P. O'Brien, D.J. Otway, J.R. Walsh, Thin Solid Films 315 (1998) 57.

[14] G.M. Sheldrick, SHELXL 97 and SHELXS 97, University of Göttingen, Germany, 1997.

[15] Bruker, SHELXTL. Version 6.10, Bruker AXS Inc., Madison, WI, USA, 2000.

[16] J. Lewinski, I. Justyniak, J. Lipkowski, J. Zachara, Inorg. Chem. Commun. 3 (2000) 700.

[17] G.A. Horley, P. O'Brien, J. Ho-Park, A.J.P. White, D.J. Williams, J. Mater. Chem. 9 (1999) 1289.

[18] S.W. Haggata, M.A. Malik, M. Motevalli, P. O'Brien, J.C. Knowles, Chem. Mater. 7 (1995) 716.

[19] K. Dymock, G.J. Palenik, J. Slezak, C.L. Raston, A.H. White, J. Chem. Soc., Dalton Trans. (1976) 28.

[20] P. Coggan, J.D. Lebbeda, A.T. McPhail, R.A. Palmer, J. Chem. Soc., Chem. Commun. (1970) 78.

[21] (a) J. Zukerman-Schpector, I. Haiduc, C. Silvestru, R. Cea-Olivares, Polyhedron 14 (1995) 3087;
(b) G. Svensson, J. Albertsson, Acta Chem. Scand. 43 (1989) 511;
(c) P. Coggon, J.D. Lebedda, A.T. McPhail, R.A. Palmer, J. Chem. Soc. D (1970) 78.

[22] K. Ruhlandt-Senge, P.P. Power, Inorg. Chem. 32 (1993) 3478, and reference cited therein.

Available online at www.sciencedirect.com
SCIENCE DIRECT®
Polyhedron 25 (2006) 869–875
POLYHEDRON
www.elsevier.com/locate/poly

Syntheses and structures of two- and three-dimensional cyanide-bridged coordination networks derived from crystallization of diimine-tetracyanoruthenate anions with gadolinium(III) cations

Juan-Manuel Herrera, Svetlana G. Baca [1], Harry Adams, Michael D. Ward *

Department of Chemistry, University of Sheffield, Sheffield S3 7HF, UK

Received 7 June 2005; accepted 21 September 2005
Available online 27 October 2005

This paper is dedicated to Prof. Mike Hursthouse on the occasion of his 65th birthday.

Abstract

This paper describes the syntheses and structures of two coordination networks based on reaction of diimine-tetracyanoruthenate(II) complexes with lanthanide(III) cations, in the presence of additional bidentate ligands to occupy some of the coordination sites on the lanthanide(III) centres. Reaction of the known complex $K_2[Ru(phen)(CN)_4]$ (phen = 1,10-phenanthroline) with $Gd(NO_3)_3 \cdot 6H_2O$ in the presence of additional phen afforded crystals of $[Ru(phen)(CN)_4]_3[Gd(phen)(H_2O)_3]_2 \cdot 6H_2O$, in which each $[Ru(phen)(CN)_4]^{2-}$ unit is connected to two Gd(III) centres via Ru–CN–Gd bridges using the equatorial pair of cyanide ligands *trans* to the phen ligand. Each Gd(III) centre is the recipient of three bridging cyanide interactions (all from different Ru units) and is additionally coordinated by one phen and three water ligands, making it 8-coordinate. The structure consists of two-dimensional sheets in which the Ru–CN–Gd bridges result in formation of $Ru_6Gd_6(\mu\text{-}CN)_{12}$ rings with a Gd(III) ion at each corner and a Ru(II) ion in the centre of each edge; this sheet is capped above and below by the phen ligands. The new dinuclear cyanometallate $[\{Ru(CN)_4\}_2(\mu\text{-bpym})]^{4-}$ (bpym = 2,2′-bipyrimidine) was prepared by reaction of bpym with >2 equivalents of hexacyanoruthenate, and contains eight cyanide ligands which can potentially bridge. Reaction with $Gd(hfac)_3(H_2O)_2$ in MeCN/water afforded $[\{Ru(CN)_4\}_2(\mu\text{-bpym})][Gd(hfac)(H_2O)_4]_2 \cdot 10H_2O$, (hfac = 1,1,1,5,5,5,-hexafluoro-pentane-2,4-dionate) which has a three-dimensional network structure based on Ru–CN–Gd bridges. Six of the cyanide ligands of each $[\{Ru(CN)_4\}_2(\mu\text{-bpym})]^{4-}$ unit connect to Gd(III) ions, and each Gd(III) centre has in additional bidentate hfac ligand and four waters, making it nine-coordinate. The three-dimensional cyanide-bridged lattice contains square cross-section channels which are occupied by water molecules.
© 2005 Elsevier Ltd. All rights reserved.

Keywords: Coordination network; Gadolinium; Ruthenium; Cyanide; Crystal structures

1. Introduction

As part of our ongoing study into the use of d-block chromophores to act as antennae for generating sensitized near-infrared luminescence from lanthanide(III) ions [1,2], we have recently prepared a series of coordination oligomers and polymers in which the cyanometallate luminophore $[Ru(bipy)(CN)_4]^{2-}$ [3] was crystallized with lanthanide(III) cations, affording networks based on Ru–CN–Ln bridges [2]. These short bridges were effective at facilitating energy-transfer from the ^{3}MLCT state of $[Ru(bipy)(CN)_4]^{2-}$ to the lanthanide centre, as long as the lanthanide had low energy f–f excited states which were available to act as energy-acceptors, i.e., using the series of near-IR emitting lanthanide(III) ions Yb(III), Er(III), Nd(III) and Pr(III). In these cases the Ru-based emission was largely quenched, and sensitized lanthanide

* Corresponding author. Fax: +44 114 2229484.
E-mail address: m.d.ward@sheffield.ac.uk (M.D. Ward).
[1] Present address: Moldova Academy of Sciences, Academeistrasse 3, Chisinau, Republic of Moldova.

0277-5387/$ - see front matter © 2005 Elsevier Ltd. All rights reserved.
doi:10.1016/j.poly.2005.09.013

luminescence was observed, following excitation of the $[Ru(bipy)(CN)_4]^{2-}$ unit and energy-transfer to a low-lying f–f excited state of the lanthanide(III) centre.

Accordingly, we are interested in the further study of hybrid coordination networks based on combination of other cyanometallate luminophores with lanthanide(III) ions. Such cyanometallate/lanthanide networks have attracted interest from other workers [4–6], largely for their beautiful structures (e.g. Shore and co-workers) [4], although there has been interest in the photophysical properties of networks based on $[M(CN)_2]^-$ (M = Ag, Au) and lanthanide(III) cations from Patterson and co-workers [5] as the high energy of these cyanometallate excited states makes them effective sensitizers for visible-emitting lanthanides. The magnetic properties of mixed-metal cyanometallate networks has also attracted attention [6]. In this paper, we describe prototypes of two new series of cyanide-bridged d–f coordination networks, viz. the structures derived from (i) crystallisation of $[Ru(phen)(CN)_4]^{2-}$ with Gd(III) in the presence of extra phen to block some of the Gd(III) coordination sites, and (ii) crystallization of the new cyanometallate $[\{Ru(CN)_4\}_2(\mu\text{-bpym})]^{4-}$ with $Gd(hfac)_3 \cdot 2H_2O$.

2. Results and discussion

Our aims were twofold: firstly, to use cyanometallate chromophores other than the relatively well-known $[Ru(bipy)(CN)_4]^{2-}$ as components of the networks; secondly, to use additional ligands (such as phenanthroline or a β-diketonate) to block coordination sites on the lanthanide(III) centre which would otherwise be occupied by solvent molecules and possibly have an inhibiting effect on the luminescence [7]. We chose $[Ru(phen)(CN)_4]^{2-}$ as it has superior photophysical properties to $[Ru(bipy)(CN)_4]^{2-}$, with a higher luminescence quantum yield and longer lifetime [8], and so it is likely to be a more effective energy donor. In contrast, the dinuclear complex $[\{Ru(CN)_4\}_2(\mu\text{-bpym})]^{4-}$ was chosen for structural reasons, because it has eight externally directed cyanide groups to act as potentially bridging ligands, and may therefore result in more structurally elaborate coordination networks than species such as $[Ru(bipy)(CN)_4]^{2-}$ which can form, at most, four bridging interactions to lanthanide(III) ions [2]. $[Ru(phen)(CN)_4]^{2-}$ is available from the literature [8]; $[\{Ru(CN)_4\}_2(\mu\text{-bpym})]^{4-}$ was prepared by reaction of 2,2′-bipyrimidine with >2 equivalents of potassium hexacyanoruthenate under forcing conditions, followed by ion-exchange chromatography to separate it from mononuclear $[Ru(CN)_4(bpym)]^{2-}$.

Slow evaporation of an aqueous solution containing a 3:2 mixture of $K_2[Ru(phen)(CN)_4]$ and $Gd(NO_3)_3$ did not initially yield any crystalline products, However, in the presence of excess phenanthroline [1 equivalent per Gd(III) centre] a good crop of orange block-like crystals grew, whose structure is shown in Figs. 1 and 2. The compound so formed is $[Ru(phen)(CN)_4]_3[Gd(phen)(H_2O)_3]_2 \cdot 6H_2O$, and consists of two-dimensional sheets based on Ru–CN–Gd bridges. Fig. 1 shows the asymmetric unit, plus a few additional atoms to complete the coordination sphere around each of the metal centres. The structure contains two independent $[Ru(phen)(CN)_4]^{2-}$ units, of which one [containing Ru(1)] is in a general position, and the second [containing Ru(2)] lies on a twofold axis such that half of it is in the asymmetric unit. The Gd(III) centre, connected to both of these via cyanide bridges, is also in a general position; the asymmetric unit therefore contains 1.5 cyanoruthenate anions (charge 2- each) to balance the Gd^{3+} cation. The Gd(III) centre is 8-coordinate, from a chelating phenanthroline ligand, three water molecules, and the N-termini of three cyanide bridges from Ru(II) centres.

Fig. 2 illustrates the sheet-like structure of the extended network, viewed from two perspectives. The top view shows the Ru–CN–Gd sheet 'edge-on' and shows how it is capped above and below by the phenanthroline ligands. Successive sheets like this fit together by intermeshing of the 'downward' pointing phenanthroline units from one sheet with the 'upward' pointing phenanthrolines of the layer below. The lower view shows the latter structure face-on, with everything except the Ru, Gd, and cyanide

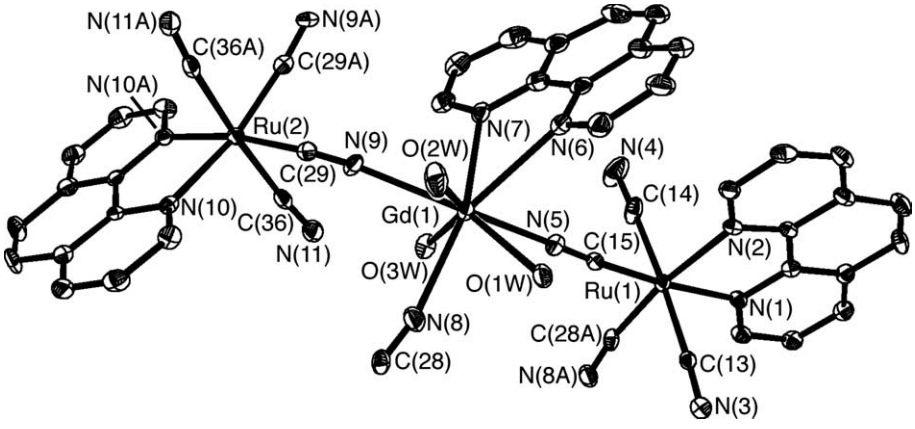

Fig. 1. ORTEP diagram (thermal ellipsoids at 40% level) of the asymmetric unit of $[Ru(phen)(CN)_4]_3[Gd(phen)(H_2O)_3]_2 \cdot 6H_2O$ (solvent molecules omitted).

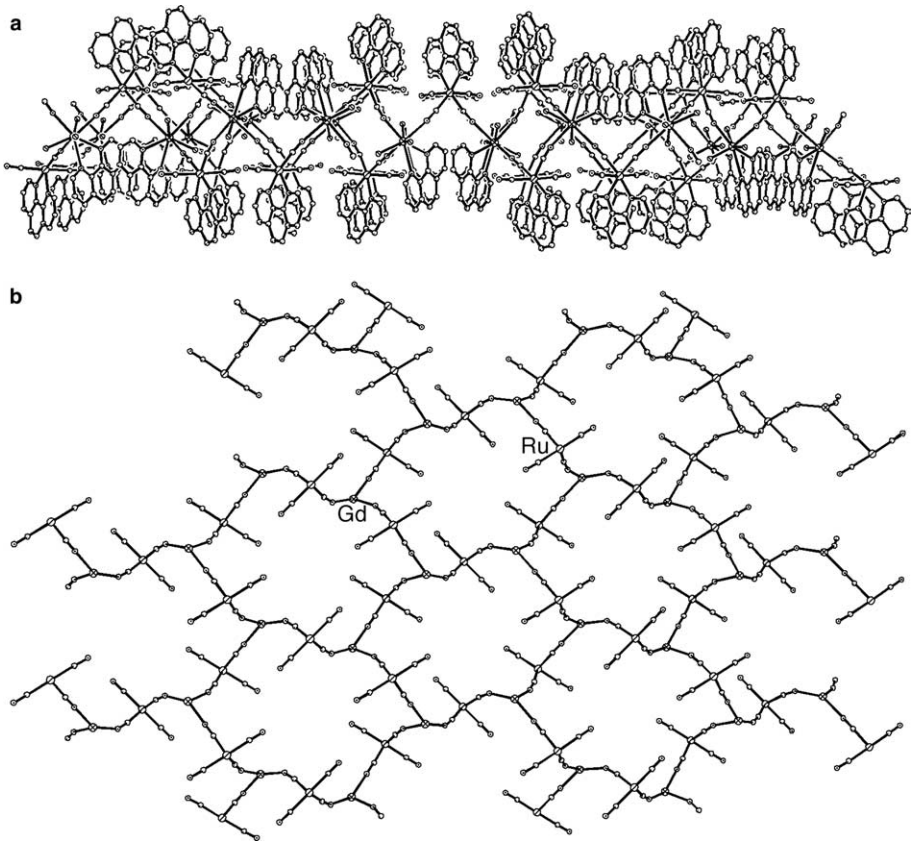

Fig. 2. (a) Edge-on view of a two-dimensional layer in $[Ru(phen)(CN)_4]_3[Gd(phen)(H_2O)_3]_2 \cdot 6H_2O$, with lattice solvent molecules omitted for clarity and (b) face-on view of the two-dimensional layer with only Ru, Gd and cyanide atoms showing.

atoms shown for clarity. It is clear that the sheet structure consists of 36-membered rings consisting of 6 Ru centres, 6 Gd centres and 12 bridging cyanide ligands. Each Ru(II) unit is connected to two adjacent Gd(III) centres via the 'equatorial' pair of cyanide ligands that are *trans* to the phenanthroline group; the 'axial' pair of cyanide ligands is not involved in bridging. In contrast each of the Gd(III) centres is connected to three Ru(II) centres via bridging cyanides, and this provides a mechanism for the rings to fuse together, with each Gd(III) centre being at the point where three $Ru_6Gd_6(CN)_{12}$ rings meet. The topology of this network is accordingly similar to that of a layer of fused hexagons in graphite, with the Ru atoms in the centre of each edge (connected to two vertices) and the Gd atoms at the vertices, connected to three different edges. The Ru···Gd separations are 5.45 Å [Ru(2)···Gd(1)], 5.55 Å [Ru(1A)···Gd(1A)] and 5.34 Å [Ru(2)···Gd(1)].

Reaction of $K_4[\{Ru(CN)_4\}_2(\mu\text{-bpym})]$ with $Gd(hfac)_3(H_2O)_2$ would, it was hoped, generate a network in which the two labile water ligands of $Gd(hfac)_3(H_2O)_2$ would be replaced by cyanide ligands, such that the lanthanide(III) centre would be solvent-free and coordinated only by three diketonate and two cyanide ligands. However, slow evaporation of a mixture of these components from aqueous MeCN solution afforded a good crop of crystals of $[\{Ru(CN)_4\}_2(\mu\text{-bpym})][Gd(hfac)(H_2O)_4]_2 \cdot 10H_2O$ (Figs. 3 and 4) in which each Gd centre has lost two of its hfac ligands; thus, two $\{Gd(hfac)\}^{2+}$ units balance the charge of each $[\{Ru(CN)_4\}_2(\mu\text{-bpym})]^{4-}$ unit. Fig. 3 shows the asymmetric unit of the structure, with a few extra symmetry-equivalent atoms included to complete the coordination sphere about each metal ion. Gd(1) is 9-coordinate, from the remaining bidentate diketonate ligand, four water ligands, and three N atoms from bridging cyanides; one of the water ligands [O(3)] is disordered over two sites, so there is little point in analyzing the coordination geometry. The F atoms of the hfac ligands were likewise disordered over two sites corresponding to different orientations of the CF_3 substituents. The $[\{Ru(CN)_4\}_2(\mu\text{-bpym})]^{4-}$ unit is involved in six Ru–CN–Gd bridging interactions, with all four cyanide ligands on Ru(1) interacting with Gd(III) centres, wheras only two cyanides on Ru(2) – the equatorial 'cis'-related pair in the same plane as the bpym ligand – are bridging to Gd(III) centres.

The bridging cyanide interactions in this case result in a three-dimensional network, as shown in Figs. 4 and 5. The view down the *a* or *b* axis (Fig. 4, with the water and hfac ligands removed for clarity) shows how the interaction of each $[\{Ru(CN)_4\}_2(\mu\text{-bpym})]^{4-}$ unit with six Gd(III) centres generates the three-dimensional network. The view down the *c* axis (Fig. 5, with hfac and water ligands included) shows how the Ru–CN–Gd network contains

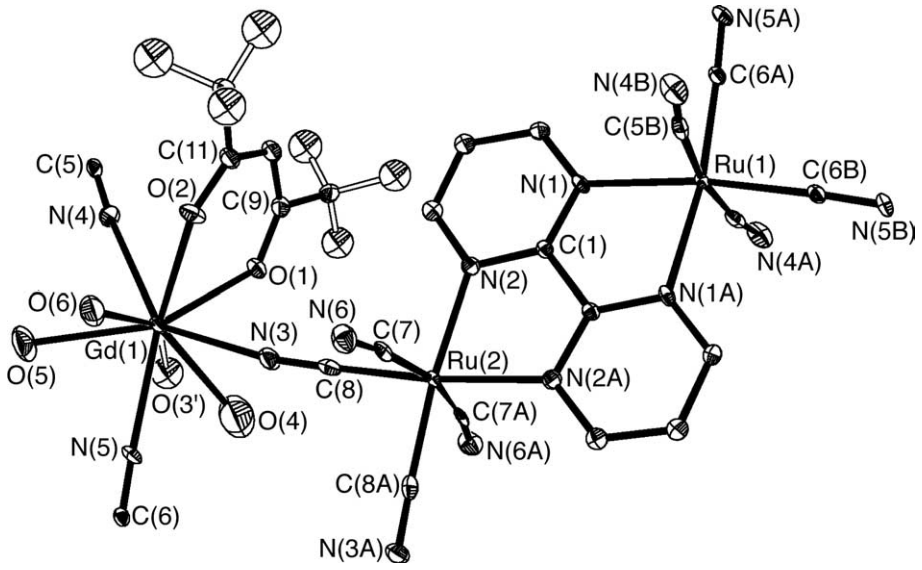

Fig. 3. ORTEP diagram (thermal ellipsoids at 40% level) of the asymmetric unit of $[\{Ru(CN)_4\}_2(\mu\text{-bpym})][Gd(hfac)(H_2O)_4]_2 \cdot 10H_2O$ (solvent molecules omitted). The F atoms and O(3) are disordered over two sites; only the major component is shown, with the bonds to these atoms being hollow.

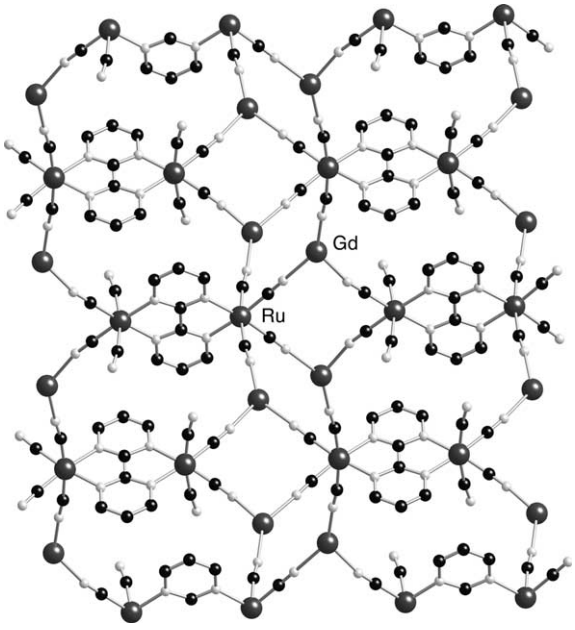

Fig. 4. A view of the three-dimensional lattice in $[\{Ru(CN)_4\}_2(\mu\text{-bpym})][Gd(hfac)(H_2O)_4]_2 \cdot 10H_2O$, showing only the Ru, Gd, bipyrimidine and cyanide atoms.

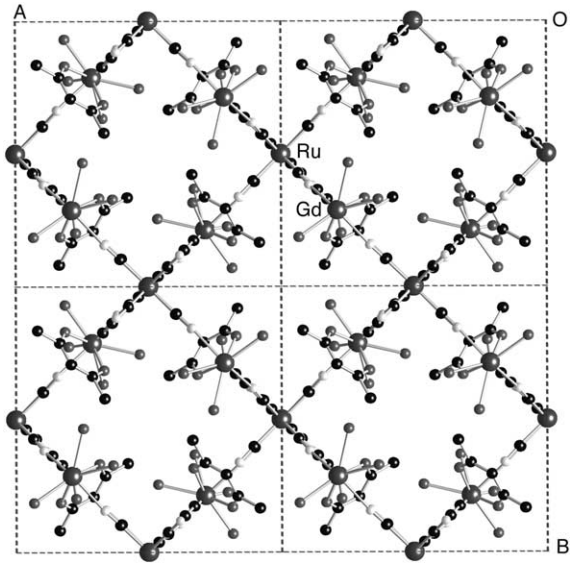

Fig. 5. Alternative view (down the *c* axis) of the three-dimensional lattice in $[\{Ru(CN)_4\}_2(\mu\text{-bpym})][Gd(hfac)(H_2O)_4]_2 \cdot 10H_2O$, emphasizing the square cross-section array of channels which contain water molecules (omitted for clarity).

square channels; these are filled with water molecules which are involved in hydrogen-bonding interactions with each other and with the water ligands coordinated to Gd(III), as shown by numerous O···O separations of 2.7–3 Å. The Ru···Gd separations are 5.53 Å [Ru(2)···Gd(1)], 5.68 Å [Ru(1)···Gd(1)] and 5.61 Å [Ru(1A)··· Gd(1)].

In conclusion, the cyanoruthenate chromophores that we have been interested in for their photophysical properties also form attractive coordination networks with lanthanide ions, in which we expect that, with an appropriate choice of lanthanide(III) ion, photoinduced d → f energy will transfer will occur following the examples we described recently [2]. Photophysical studies are in progress and will be described separately.

3. Experimental

3.1. General details

The compounds $K_2[Ru(phen)(CN)_4]$ [8] and $Gd(hfac)_3 \cdot (H_2O)_2$ [9] were prepared according to the literature procedures. 2,2′-Bipyrimidine and potassium hexacyanoruthenate

were purchased from Aldrich and Alfa respectively, and used as received.

3.2. Preparation of $K_4[\{Ru(CN)_4\}_2(\mu\text{-bpym})]$

A solution of 2,2′-bipyrimidine (0.079 g, 0.5 mmol) and $[K_4Ru(CN)_6]\cdot 3H_2O$ (0.513 g, 1.1 mmol) in aqueous HCl at pH 1.3 was heated to reflux with stirring for 24 h and then cooled down to room temperature. The resulting dark red–brown solution was neutralised with KOH and the solution was evaporated to dryness. The solid residue was dissolved in the minimum quantity of water, and MeOH was added to precipitate unreacted $K_4[Ru(CN)_6]\cdot 3H_2O$ which was filtered off. The residue was again evaporated to dryness, dissolved in the minimum quantity of water; addition of acetone precipitated the crude product which was filtered off and washed with acetone. The product was purified by column chromatography on SEPHADEX QAE-25, eluting with aqueous KI. Use of 0.15 M KI resulted in elution of the mononuclear by-product $K_2[Ru(bpym)(CN)_4]$ (which is the major product); increasing the KI concentration to 0.25 M then resulted in elution of dark red $K_4[\{Ru(CN)_4\}_2(\mu\text{-bpym})]$, which was collected and reduced in volume to 5 cm^3. The complex was precipitated by the addition of acetone and further recrystallized from H_2O/acetone, and dried in vacuo to give the pure product as a red solid. Yield: 34%. *Anal.* Calc. for $K_4[\{Ru(CN)_4\}_2\text{-}(\mu\text{-bpym})]$: C, 26.5; H, 0.8; N, 23.2. Found: 27.5; H, 1.0; N, 23.9%. ^{1}H NMR (D_2O): δ 7.80 (1H, t; $J = 5.5$ Hz), 9.35 (2H, d; $J = 5.5$ Hz).

3.3. Preparation of $[Ru(phen)(CN)_4]_3[Gd(phen)(H_2O)_3]_2\cdot 6H_2O$

An aqueous solution containing $K_2[Ru(phen)(CN)_4]$, $Gd(NO_3)_3\cdot 6H_2O$ and 1,10-phenanthroline in a 3:2:2 ratio afforded crystals of the product as orange blocks following slow evaporation over several weeks. *Anal.* Calc. for $[Ru(phen)(CN)_4]_3[Gd(phen)(H_2O)_3]_2\cdot 6H_2O$: C, 42.2; H, 3.2; N, 15.0. Found: C, 42.5; H, 3.0; N, 14.6%.

3.4. Preparation of $[\{Ru(CN)_4\}_2(\mu\text{-bpym})][Gd(hfac)(H_2O)_4]_2\cdot 10H_2O$

A solution of $K_4[\{Ru(CN)_4\}_2(\mu\text{-bpym})]$ (0.015 g, 20 μmol) in MeCN/water (1:1, 1.5 cm^3) was added to a solution of $Gd(hfac)_3(H_2O)_2$ (0.080 g, 200 μmol) in MeCN/water (1:1, 2.5 cm^3) with stirring. Slow evaporation of the resulting solution afford red plate-like crystals in 75% yield. *Anal.* Calc. for $[\{Ru(CN)_4\}_2(\mu\text{-bpym})][Gd(hfac)(H_2O)_4]_2\cdot 10H_2O$: C, 19.3; H, 2.7; N, 10.4. Found: C, 19.5; H, 2.3; N, 10.7%.

3.5. X-ray crystallography

X-ray crystallographic data are summarised in Tables 1–3. For each compound a suitable crystal was coated with hydrocarbon oil and attached to the tip of a glass fibre and transferred to Bruker-SMART diffractometer under a stream of cold N_2. Data were collected using a Siemens SMART CCD area diffractometer (graphite monochromated Mo Kα radiation, $\lambda = 0.71073$ Å) with an Oxford Cryosystems low temperature system. The data were corrected for Lorentz and polarisation effects and for absorption by semi-empirical methods (SADABS) based on symmetry-equivalent and repeated reflections. The structures were solved by direct methods or heavy atom Patterson methods and refined by full-matrix least-squares methods on F^2. Hydrogen atoms were placed geometrically and refined with a riding model and with U_{iso} constrained to be 1.2 (1.5 for methyl groups) times U_{eq} of the carrier atom. All non-hydrogen atoms were refined anisotropically unless otherwise stated. The programs used in the determination and refinement of the structures were Siemens

Table 1
Crystallographic data for the two complexes[a]

Complex	$[Ru(phen)(CN)_4]_3[Gd(phen)(H_2O)_3]_2\cdot 6H_2O$	$[\{Ru(CN)_4\}_2(\mu\text{-bpym})][Gd(hfac)(H_2O)_4]_2\cdot 10H_2O$
Empirical formula	$C_{72}H_{64}Gd_2N_{22}O_{12}Ru_3$	$C_{13}H_{22}F_6GdN_6O_{11}Ru$
Formula weight	2047.16	810.69
T (K)	150(2)	100 (2)
Crystal size (mm^3)	$0.26\times 0.25\times 0.18$	$0.35\times 0.30\times 0.11$
Crystal system, space group	orthorhombic, *Pbcn*	tetragonal, $P\bar{4}$
a (Å)	25.571(2)	13.9009(16)
b (Å)	26.472(2)	13.9009(16)
c (Å)	11.7944(9)	13.049(3)
V ($Å^3$)	7983.7	2521.5(7)
Z	4	4
ρ (calc) ($g\,cm^{-3}$)	1.703	2.136
μ (mm^{-1})	2.265	3.313
Data/restraints/parameters	9180, 0, 502	5741, 60, 339
R_1, wR_2[b]	0.0486, 0.1163	0.0386, 0.0970

[a] Data in common. Diffractometer, Siemens SMART; $\lambda = 0.71073$ Å.
[b] R_1 is based on data with $I > 2\sigma(I)$; wR_2 is based on all data.

Table 2
Selected bond distances (Å) and angles (°) for $[Ru(phen)(CN)_4]_3$-$[Gd(phen)(H_2O)_3]_2 \cdot 6H_2O$

Ru(1)–C(28A)	1.965(5)		
Ru(1)–C(15)	1.972(5)	Ru(2)–C(29)	1.976(5)
Ru(1)–C(13)	2.035(5)	Ru(2)–C(36)	2.049(6)
Ru(1)–C(14)	2.050(6)		
Ru(1)–N(2)	2.118(4)	Ru(2)–N(10)	2.113(4)
Ru(1)–N(1)	2.118(4)		
Gd(1)–O(2W)	2.404(4)	Gd(1)–N(9)	2.440(4)
Gd(1)–O(1W)	2.422(3)	Gd(1)–O(3W)	2.457(4)
Gd(1)–N(5)	2.422(4)	Gd(1)–N(7)	2.592(4)
Gd(1)–N(8)	2.431(5)	Gd(1)–N(6)	2.613(4)
O(2W)–Gd(1)–O(1W)	73.60(14)	N(8)–Gd(1)–O(3W)	75.21(15)
O(2W)–Gd(1)–N(5)	142.17(14)	N(9)–Gd(1)–O(3W)	77.28(14)
O(1W)–Gd(1)–N(5)	73.24(14)	O(2W)–Gd(1)–N(7)	113.96(15)
O(2W)–Gd(1)–N(8)	86.92(16)	O(1W)–Gd(1)–N(7)	133.94(13)
O(1W)–Gd(1)–N(8)	71.74(14)	N(5)–Gd(1)–N(7)	78.05(15)
N(5)–Gd(1)–N(8)	99.47(16)	N(8)–Gd(1)–N(7)	149.36(15)
O(2W)–Gd(1)–N(9)	72.99(15)	N(9)–Gd(1)–N(7)	78.85(14)
O(1W)–Gd(1)–N(9)	141.00(14)	O(3W)–Gd(1)–N(7)	75.25(14)
N(5)–Gd(1)–N(9)	144.09(15)	O(2W)–Gd(1)–N(6)	77.76(14)
N(8)–Gd(1)–N(9)	86.92(16)	O(1W)–Gd(1)–N(6)	75.95(13)
O(2W)–Gd(1)–O(3W)	145.98(13)	N(5)–Gd(1)–N(6)	77.01(14)
O(1W)–Gd(1)–O(3W)	125.08(13)	N(8)–Gd(1)–N(6)	147.03(15)
N(5)–Gd(1)–O(3W)	70.47(14)	N(9)–Gd(1)–N(6)	115.38(14)
N(7)–Gd(1)–N(6)	62.85(14)	O(3W)–Gd(1)–N(6)	131.13(14)

Table 3
Selected bond distances (Å) and angles (°) for $[\{Ru(CN)_4\}_2(\mu\text{-bpym})]$-$[Gd(hfac)(H_2O)_4]_2 \cdot 10H_2O$

Gd(1)–O(1)	2.423(5)	Gd(1)–O(3)	2.456(9)
Gd(1)–O(2)	2.428(5)	Gd(1)–O(6)	2.475(6)
Gd(1)–O(3′)	2.435(11)	Gd(1)–N(5)	2.479(6)
Gd(1)–N(3)	2.447(6)	Gd(1)–N(4)	2.516(5)
Gd(1)–O(5)	2.453(6)	Gd(1)–O(4)	2.552(9)
Ru(1)–C(6)	1.986(7)	Ru(2)–C(8)	1.950(7)
Ru(1)–C(5)	2.038(7)	Ru(2)–C(7)	2.035(6)
Ru(1)–N(1)	2.139(5)	Ru(2)–N(2)	2.126(6)
O(1)–Gd(1)–O(2)	72.53(17)	O(3)–Gd(1)–O(6)	152.4(6)
O(1)–Gd(1)–O(3′)	71.0(6)	N(3)–Gd(1)–O(6)	84.0(2)
O(2)–Gd(1)–O(3′)	140.7(6)	O(5)–Gd(1)–O(6)	70.4(2)
O(1)–Gd(1)–N(3)	77.1(2)	O(3)–Gd(1)–O(6)	141.3(3)
O(2)–Gd(1)–N(3)	73.7(2)	O(1)–Gd(1)–N(5)	133.62(19)
O(3′)–Gd(1)–N(3)	111.2(7)	O(2)–Gd(1)–N(5)	133.1(2)
O(1)–Gd(1)–O(5)	138.8(2)	O(3')–Gd(1)–N(5)	84.0(6)
O(2)–Gd(1)–O(5)	114.3(2)	N(3)–Gd(1)–N(5)	76.65(19)
O(3′)–Gd(1)–O(5)	85.1(7)	O(5)–Gd(1)–N(5)	73.4(2)
N(3)–Gd(1)–O(5)	144.0(2)	O(3)–Gd(1)–N(5)	93.5(3)
O(1)–Gd(1)–O(3)	76.1(3)	O(6)–Gd(1)–N(5)	77.1(2)
O(2)–Gd(1)–O(3)	133.3(3)	O(1)–Gd(1)–N(4)	72.13(19)
N(3)–Gd(1)–O(3)	130.8(4)	O(2)–Gd(1)–N(4)	69.50(19)
O(5)–Gd(1)–O(3)	71.0(3)	O(3)–Gd(1)–N(4)	85.8(7)
O(1)–Gd(1)–O(6)	136.33(19)	N(3)–Gd(1)–N(4)	137.4(2)
O(2)–Gd(1)–O(6)	64.44(19)	O(5)–Gd(1)–N(4)	73.1(2)
N(5)–Gd(1)–N(4)	145.6(2)	O(3)–Gd(1)–N(4)	68.4(3)
O(1)–Gd(1)–O(4)	69.6(3)	O(6)–Gd(1)–N(4)	98.5(2)
O(2)–Gd(1)–O(4)	130.9(3)	O(3)–Gd(1)–O(4)	63.9(4)
O(3′)–Gd(1)–O(4)	43.9(7)	O(6)–Gd(1)–O(4)	137.1(3)
N(3)–Gd(1)–O(4)	68.3(3)	N(5)–Gd(1)–O(4)	65.4(3)
O(5)–Gd(1)–O(4)	114.8(3)	N(4)–Gd(1)–O(4)	124.1(3)

SMART [10] and SAINT [11] for control and integration software, and the SHELXTL package [12] comprising SHELXS-97 [13] and SHELXL-97 [14] for structure solution and refinement.

In the structure of $[\{Ru(CN)_4\}_2(\mu\text{-bpym})][Gd(hfac)$-$(H_2O)_4]_2 \cdot 10H_2O$, atom O(3) [coordinated to Gd(1)] is disordered over two closely spaced sites with site occupancies of 0.69 and 0.31; these disordered atoms were refined with isotropic thermal parameters. The minor component O(3′) ends up quite close to O(4) [1.87 Å] but atom O(4) shows no sign of also being disordered, with unit site occupancy and unremarkable thermal parameters. The six F atoms of the CF_3 groups on the hfac ligand were also all disordered over two sites which refined with site occupancies of 0.57 and 0.43; these F atoms were also refined with isotropic thermal parameters.

4. Supplementary material

Supplementary data (cif files for the two structures) are available on request from the Cambridge Crystallographic Data Centre, 12 Union Road, Cambridge, CB2 1EZ, UK, quoting deposition Nos. 274160 and 274161 (see www: http://www.ccdc.cam.ac.uk).

Acknowledgements

We thank the Spanish Ministry of Science for a post-doctoral grant to J.-M. H. and the Royal Society for a fellowship to S.B.

References

[1] (a) N.M. Shavaleev, L.P. Moorcraft, S.J.A. Pope, Z.R. Bell, S. Faulkner, M.D. Ward, Chem. Eur. J. 9 (2003) 5283;
(b) N.M. Shavaleev, G. Accorsi, D. Virgili, Z.R. Bell, T. Lazarides, G. Calogero, N. Armaroli, M.D. Ward, Inorg. Chem. 44 (2005) 61.
[2] (a) T.A. Miller, J.C. Jeffery, M.D. Ward, H. Adams, S.J.A. Pope, S. Faulkner, J. Chem. Soc., Dalton Trans. (2004) 1524;
(b) G.M. Davies, S.J.A Pope, H. Adams, S. Faulkner, M.D. Ward, Inorg. Chem. 44 (2005) 4656.
[3] C.J. Timpson, C.A. Bignozzi, B.P. Sullivan, E.M. Kober, T.J. Meyer, J. Phys. Chem. 100 (1996) 2915.
[4] C.E. Plecnik, S. Liu, S.G. Shore, Acc. Chem. Res. 36 (2003) 499.
[5] M.A. Rawashdeh-Omary, C.L. Larochelle, H.H. Patterson, Inorg. Chem. 39 (2000) 4527.
[6] (a) M. Ohba, H. Okawa, Coord. Chem. Rev. 198 (2000) 313;
(b) M. Verdaguer, A. Bleuzen, V. Marvaud, J. Vaissermann, M. Seuleiman, C. Desplanches, A. Scuiller, C. Train, R. Garde, G. Gelly, C. Lomenech, I. Rosenman, P. Veillet, C. Cartier, F. Villain, Coord. Chem. Rev. 190–192 (1999) 1023;
(c) T. Korzeniak, K. Stadnicka, M. Rams, B. Sieklucka, Inorg. Chem. 43 (2004) 4811;
(d) J.-M. Herrera, A. Bleuzen, Y. Dromzee, M. Julve, F. Lloret, M. Verdaguer, Inorg. Chem. 42 (2003) 7052;
(e) L.M. Toma, F.S. Delgado, C. Ruiz-Pérez, R. Carrasco, J. Cano, F. Lloret, M. Julve, Dalton Trans. (2004) 2836.
[7] A. Beeby, I.M. Clarkson, R.S. Dickins, S. Faulkner, D. Parker, L. Royle, A.S. de Sousa, J.A.G. Williams, M. Woods, J. Chem. Soc., Perkin Trans. 2 (1999) 493.

[8] M. Kovács, A. Horváth, Inorg. Chim. Acta 335 (2002) 69.
[9] Y. Hasegawa, Y. Kimura, K. Murakoshi, Y. Wada, J. Kim, N. Nakashima, T. Yamanaka, S. Yanagida, J. Phys. Chem. 100 (1996) 10201.
[10] Siemens SMART Data Collection Software, version 4.050; Siemens Analytical X-ray Instruments Ltd, Madison, WI, 1996.
[11] Siemens SAINT Data Reduction Software, version 4.050; Siemens Analytical X-ray Instruments Ltd, Madison, WI, 1996.
[12] Siemens SHELXTL version, An integrated system for solving and refining crystal structures from diffraction data, revision 5.1; Siemens Analytical X-ray Instruments Ltd, Madison, WI, 1996.
[13] G.M. Sheldrick, SHELXS-97, a Program for Automatic Solution of Crystal Structures, University of Gottingen, Gottingen, Germany, 1997.
[14] G.M. Sheldrick, SHELXL-97, a Program for Crystal Structure Refinement, University of Gottingen, Gottingen, Germany, 1997.

Available online at www.sciencedirect.com
SCIENCE DIRECT
Polyhedron 25 (2006) 876–880
POLYHEDRON
www.elsevier.com/locate/poly

Syntheses and characterization of mono(6,6-dimethylcyclohexadienyl) complexes of titanium and zirconium

Atta M. Arif, Rehan Basta, Richard D. Ernst *

Department of Chemistry, University of Utah, 315 S. 1400 E., Salt Lake City, UT 84112-0850, USA

Received 8 June 2005; accepted 27 September 2005
Available online 9 November 2005

Dedicated to Professor Michael B. Hursthouse on the occasion of his 65th birthday.

Abstract

Reactions of appropriate bis(6,6-dmch) (dmch = dimethylcyclohexadienyl) complexes of titanium(II) or zirconium(IV) with dichloroethane or phosphines, respectively, have led to loss of one dienyl ligand, and the formation of mono(6,6-dmch) complexes of Ti(III) or Zr(IV). The polymeric $[Ti(6,6\text{-dmch})Cl_2]_n$ and $Zr(6,6\text{-dmch})Br_3(dmpe)$ (dmpe = 1,2-bis(dimethylphosphino)ethane) have thus been isolated, and fully characterized.
© 2005 Elsevier Ltd. All rights reserved.

Keywords: Dimethylcyclohexadienyl complex; Pentadienyl titanium(III) structure; Pentadienyl zirconium(IV) structure

1. Introduction

A substantial body of chemistry has developed based on open and half-open metallocenes [1]. In these compounds, two dienyl ligands are present, both being the electronically open pentadienyl ligand or a substituted variant in the former class of compounds, while in the second class, one electronically open pentadienyl ligand is joined by an aromatic cyclopentadienyl ligand. Particularly for the early transition metal systems, whose pentadienyl chemistry has been found to be quite rich [2], it would be advantageous to have available mono(pentadienyl) metal halide complexes as starting materials for further exploration. Herein, we report reactions of $Ti(6,6\text{-dmch})_2$ and of $Zr(6,6\text{-dmch})_2Br_2$ that lead readily to such species.

2. Experimental

All reactions were conducted under a nitrogen atmosphere in Schlenk apparatus. Solvents were dried and deoxygenated by passing them through columns of activated alumina under a nitrogen atmosphere, while benzene-d_6 was dried and deoxygenated by vacuum transfer from sodium benzophenone ketyl. Spectroscopic studies were carried out as previously described [3]. ^{13}C NMR spectra were not precisely integrated, but numbers of carbon atoms are given in accord with their assignments. $Ti(6,6\text{-dmch})_2$ [4] and $Zr(6,6\text{-dmch})_2(PMe_3)_2$ [5] were prepared as previously described. Due to the high solubility of the former in hydrocarbons, its crude solutions were used directly for further reactions. Elemental analyses were obtained from Desert Analytics.

2.1. Dichloro(6,6-dimethylcyclohexadienyl)titanium(III), $[Ti(6,6\text{-dmch})Cl_2]_n$

To a brown-green solution of $Ti(6,6\text{-dmch})_2$ (nominally 0.58 g, 2.2 mmol) in 20 mL of hexane, 1,2-dichloroethane (0.18 mL, 2.2 mmol) was added. The color of the solution slowly changed to dark brown. The reaction mixture was left overnight unstirred. The next day, brown crystals suitable for X-ray analysis had grown on the bottom of the

* Corresponding author.
E-mail address: ernst@chem.utah.edu (R.D. Ernst).

0277-5387/$ - see front matter © 2005 Elsevier Ltd. All rights reserved.
doi:10.1016/j.poly.2005.09.026

reaction flask (0.12 g, 24%). The compound was insoluble in common organic solvents.

Anal. Calc. for $C_8H_{11}Cl_2Ti$: C, 42.52; H, 4.91. Found: C, 42.00; H, 5.11%.

2.2. Tribromo[1,2-bis(dimethylphosphino)ethane](6,6-dimethylcyclohexadienyl)zirconium(IV), Zr(6,6-dmch)(dmpe)(Br)$_3$

To a dark black-red solution of Zr(6,6-dmch)$_2$(PMe$_3$)$_2$ (0.61 g, 1.3 mmol) in 30 mL of hexanes was added 1,2-dibromoethane (0.23 mL, 2.4 mmol). A bright red-orange precipitate immediately formed. The reaction mixture was allowed to stir for 30 min. The solvent was removed in vacuo, leaving a red-orange residue which was dissolved in 20 mL of THF. Next, 1,2-bis(dimethylphosphino)ethane (dmpe, 0.45 mL, 2.4 mmol) was added and the solution color immediately changed to dark purple. After ~1 h of stirring at room temperature the color of the solution changed again to bright orange-red. After the reaction mixture was stirred for an additional 2 h, the solvent was removed, leaving an orange residue. The solid was extracted with ca. 40 mL of toluene and filtered through a Celite pad on a coarse frit. The product was crystallized by concentrating the solution to 5 mL and placement in a −60 °C freezer, yielding 0.42 g (54% yield) of red-orange solid.

^{1}H NMR (benzene-d_6, ambient): δ 0.62 (s, 3H, *exo* CH$_3$(dmch)), 0.96 (d, 6H, $J = 7.5$ Hz, *exo* CH$_3$ (dmpe)), 1.36 (s, 3H, *endo* CH$_3$ (dmch)), 1.49 (m, 4H, (dmpe)), 1.59 (d, 6H, $J = 8.4$ Hz, *endo* CH$_3$ (dmpe)), 4.85 (m, 2H, H$_{1,5}$), 5.87 (t, 1H, $J = 5.7$ Hz, H$_3$), 6.49 (t, 2H, $J = 6.6$ Hz, H$_{2,4}$).

^{13}C NMR (benzene-d_6, ambient): δ 14.2 (q, 2C, $J = 130.8$ Hz, CH$_3$ (dmpe)), 14.5 (q, 2C, $J = 129.9$ Hz, CH$_3$ (dmpe)), 23.9 (m, 1C, dmpe), 27.4 (m, 1C, dmpe), 28.5 (q, 1C, $J = 128.2$ Hz, *exo* CH$_3$ (dmch)), 32.4 (s, 1C, C$_6$), 35.1 (q, 1C, $J = 127.7$ Hz, *endo* CH$_3$ (dmch)), 96.3 (d, 1C, $J = 173.8$ Hz, C$_3$), 112.0 (d, 2C, $J = 160.4$ Hz, C$_{1,5}$), 126.0 (s, 2C, C$_{2,4}$).

Anal. Calc. for $C_{14}H_{27}Br_3P_2Zr$: C, 28.59; H, 4.63. Found: C, 28.57; H, 4.76.

2.3. Crystallographic studies

Single crystals of each compound were protected from the air by a coating of Paratone oil, and then fixed to a glass fiber and transferred to a Nonius Kappa CCD diffractometer. Structure solutions and refinements were carried out using the SIR-97 and SHELXL-97 program packages. The Ti(6,6-dmch)Cl$_2$ structure suffered a disorder involving a 75:25 ratio of overlapping images. The C4, C6, C7, and chlorine atom positions overlapped their analogues in the second image, and hence appeared as single atoms. As such, their bonding parameters must be considered less reliable than indicated. Most nonhydrogen atoms could be refined anisotropically. The exceptions were the resolved carbon atoms of the minor image, C1′, C2′, C3′, C5′, and C8′, which were refined isotropically. Hydrogen atoms were allowed to ride on their respective carbon atoms. An alternative solution in the centrosymmetric space group $P2_1/m$ was judged incorrect due to the 3:1 ratio of the images that would be averaged, and the fact that refinements of the structure in this space group were poorly behaved and led to *R* factors of ca. 20%. For Zr(6,6-dmch)Br$_3$(dmpe), all nonhydrogen atoms were refined anisotropically, while the hydrogen atoms were refined isotropically (see Table 1).

Table 1
Crystallographic parameters for [Ti(6,6-dmch)Cl$_2$]$_n$ and Zr(6,6-dmch)Br$_3$(dmpe)

Empirical formula	$C_8H_{11}Cl_2Ti$	$C_{14}H_{27}Br_3P_2Zr$
Formula weight	225.97	588.25
Temperature (K)	150(1)	150(1)
Wavelength (Å)	0.71073	0.71073
Crystal system	monoclinic	triclinic
Space group	$P2_1$	$P\bar{1}$
Unit cell dimensions		
a (Å)	6.7075(11)	9.0164(1)
b (Å)	6.3995(12)	9.9650(2)
c (Å)	10.988(2)	12.3247(3)
α (°)	90	95.3452(7)
β (°)	103.296(6)	107.3134(7)
γ (°)	90	101.3236(10)
Volume (Å^3)	459.0(1)	1022.92(3)
Z	2	2
D_{calc}	1.635	1.910
Absorption coefficient (cm^{-1})	1.44	6.54
θ Range (°)	3.8–27.5	4.1–27.5
Limiting indices	$-8 \leqslant h \leqslant 8$, $-7 \leqslant k \leqslant 8$, $-14 \leqslant l \leqslant 14$	$-11 \leqslant h \leqslant 11$, $-12 \leqslant k \leqslant 12$, $-15 \leqslant l \leqslant 15$
Reflections collected	1848	7498
Independent reflections, n; $I > n\sigma(I)$	1848; 2	4632; 2
$R(F)$	0.0405	0.0287
$R_w(F^2)$	0.1041	0.0695
Max/min difference in Fourier peak (e Å^{-3})	0.50/−0.40	0.98/−1.13

3. Results and discussion

Earlier studies have demonstrated that Zr(6,6-dmch)$_2$(PMe$_3$)$_2$ and Zr(C$_5$H$_5$)(6,6-dmch)(PMe$_3$)$_2$ react with 1,2-C$_2$H$_4$X$_2$ to yield the first general series of higher valent metal pentadienyl complexes, Zr(6,6-dmch)$_2$X$_2$ and Zr(C$_5$H$_5$)(6,6-dmch)X$_2$ (X = Cl, Br, I) [6,7]. Prior to these reports, few such higher valent species were known [8], nearly all of which incorporated strong π-donor ligands [9], whose function may have been to reduce the buildup of positive charge on the metal center, thereby allowing for better overlap between the metal valence orbitals and those of the wide pentadienyl ligands. Conceivably, the added electron density might also have allowed for some δ backbonding, which can be an especially strongly bonding interaction for metal pentadienyl compounds [1]. It has therefore become of interest to investigate the possibility of preparing a general series of high valent titanium

pentadienyl complexes. As in the case of zirconium, it appeared that the 6,6-dmch ligand (**1**) would be ideal for such attempts. Early work with this ligand by the Wolczanski group has shown that this ligand displays electronic properties which are intermediate between those of cyclopentadienyl and typically strongly δ acidic pentadienyl ligands [4,10]. Indeed, a reaction readily occurred between Ti(6,6-dmch)$_2$ and 1,2-$C_2H_4Cl_2$, leading to the loss of one 6,6-dmch ligand and the formation of a brown, crystalline product having the stoichiometry Ti(6,6-dmch)Cl_2, analogous to the known $[Ti(C_5H_5)Cl_2]_n$ [11]. A single crystal X-ray diffraction study (Table 2, Fig. 1) revealed that the titanium centers achieved a four-legged piano stool structure through the formation of a one-dimensional polymeric network involving chloride bridges. A similar structure is thus conceivable for the C_5H_5 analogue. Although the +3 oxidation state is not generally considered to be that high, it is not all that common for metal pentadienyl complexes, presumably for the same reasons that tetravalent and higher oxidation states are rare. Indeed, one observes a similar though somewhat less exaggerated pattern in the M–C bond distances as observed for the tetravalent zirconium analogues. In particular, the Ti–C(3) distance (2.333(4) Å) is shorter than the Ti–C(2,4) distances (2.337(6), 2.416(4) Å), and still shorter than the Ti–C(1,5) distances (2.457(5), 2.526(6) Å). As for the Zr(IV) complexes, it appears that the contracted Ti(III) orbitals do not overlap effectively with those of a wide pentadienyl ligand, leading to a strong interaction with the central dienyl carbon atom, and progressively longer interactions with the subsequent carbon atoms. Thus, one observes what may be regarded as the initiation of the expulsion of a pentadienyl ligand from a higher valent metal center. The C–C bond distances follow a short-long-long-short pattern, consistent with the above formulation, and with **2**. Given that the chlorine atom positions are really composites of two images, the Ti–Cl distances for the major one, ranging from 2.458(1) to 2.519(1) Å, are fairly regular. Those for the second image appear to be less regular, with two long interactions being compensated by two short ones. If real, this could reflect packing requirements for the attached Ti(6,6-dmch) residue.

Table 2
Pertinent bonding parameters for $[Ti(6,6\text{-dmch})Cl_2]_n$

Bond distances (Å)			
Ti1–Cl	2.457(5)	Ti1′–C1′	2.46(2)
Ti1–C2	2.337(6)	Ti1′–C2′	2.26(2)
Ti1–C3	2.333(4)	Ti1′–C3′	2.33(3)
Ti1–C4	2.416(4)	Ti1′–C4	2.460(5)
Ti1–C5	2.526(6)	Ti1′–C5′	2.51(3)
Ti1–Cl1	2.5092(12)	Ti1′–Cl1	2.610(3)
Ti1–Cl2	2.5187(12)	Ti1′–Cl2	2.584(3)
Ti1–Cl1′	2.4581(13)	Ti1′–Cl1′	2.335(3)
Ti1–Cl2′	2.4725(12)	Ti1′–Cl2′	2.394(3)
C1–C2	1.381(10)	C3–C4	1.426(9)
C2–C3	1.417(10)	C4–C5	1.358(7)
Bond angles (°)			
Cl1–Ti1–Cl2	76.90(4)	Cl2–Ti1–Cl1′	83.67(4)
Cl1–Ti1–Cl1′	131.51(4)	Cl2–Ti1–Cl2′	131.99(4)
Cl1–Ti1–Cl2′	82.24(4)	Cl1′–Ti1–Cl2′	78.71(4)

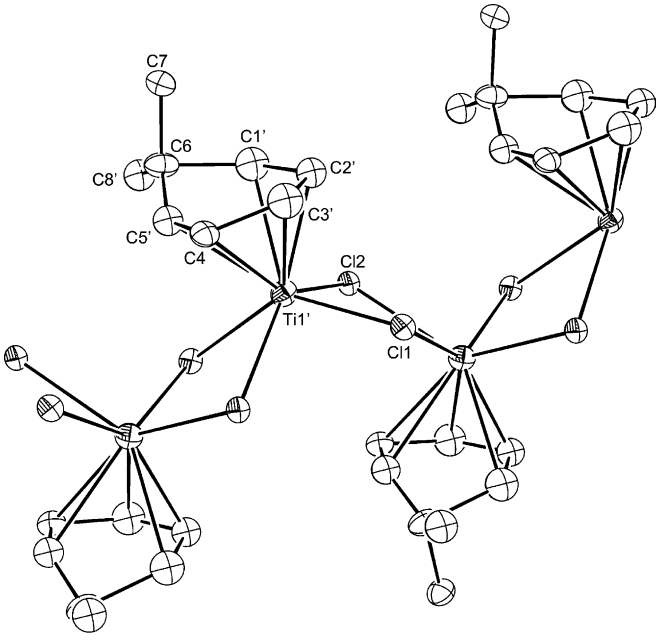

Fig. 1. Perspective view of the one-dimensional chain structure of [Ti(6,6-dmch)Cl_2]$_n$.

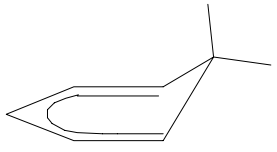

1

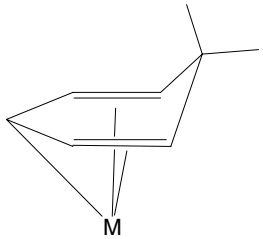

2

Access to a mono(6,6-dmch) complex of zirconium(IV) was obtained from the reaction of Zr(6,6-dmch)$_2Br_2$ with dmpe [1,2-bis(dimethylphosphinoethane)]. Interestingly, a dark purple intermediate was immediately formed, of unknown formulation, and this slowly was converted to the orange-red color of the subsequently isolated product. The rapid incorporation of the dmpe into a sterically crowded Zr(6,6-dmch)$_2Br_2$ complex seems unusual, but could be promoted by the slipped nature of the 6,6-dmch ligand in the high valent complex. Spectroscopic, analyti-

cal, and structural characterization revealed the product to be Zr(6,6-dmch)Br_3(dmpe), **3**.

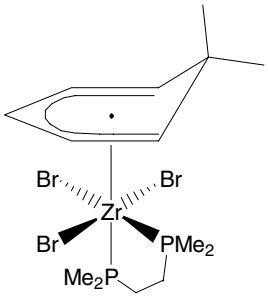

3

As the product contains more bromine than the starting complex, the addition of dmpe to Zr(6,6-dmch)$_2Br_2$ led to some sort of disproportionation. Whether this simply involves a redistribution of 6,6-dmch ligands, or perhaps loss of 6,6-dmch ligand to yield a Zr(III) intermediate which then undergoes redox and bromide redistribution processes is unclear, but further investigation of the purple intermediate would be of interest. Notably, the reaction of Zr(6,6-dmch)$_2$(PMe_3)$_2$ with 1,2-$C_2H_4I_2$ has been found to lead to an analogous species, Zr(6,6-dmch)I_3(PMe_3)$_2$, as well as Zr(6,6-dmch)$_2I_2$ [6].

The structure of **3** (Fig. 2, Table 3) may be regarded as a *mer*,*cis*-pseudooctahedral coordination geometry. Such an arrangement has been established earlier for U($C_5H_4CH_3$)Cl_3(THF)$_2$ [12]. Subsequently, this geometry has been established for numerous transition metal complexes,

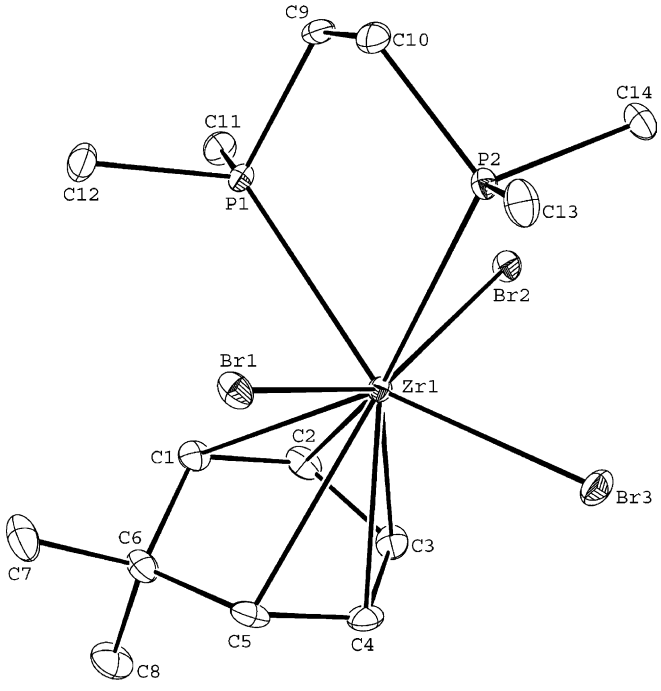

Fig. 2. Perspective view of Zr(6,6-dmch)Br_3(dmpe).

Table 3
Pertinent bonding parameters for Zr(6,6-dmch)Br_3(dmpe)

Bond distances (Å)			
Zr–C1	2.712(3)	Zr–Br1	2.6652(4)
Zr–C2	2.539(3)	Zr–Br2	2.6751(3)
Zr–C3	2.482(3)	Zr–Br3	2.6652(3)
Zr–C4	2.556(3)	C1–C2	1.382(4)
Zr–C5	2.757(3)	C2–C3	1.409(4)
Zr–P1	2.7725(7)	C3–C4	1.422(4)
Zr–P2	2.7836(7)	C4–C5	1.370(5)
Bond angles (°)			
P1–Zr–P2	71.75(2)	Br1–Zr–Br2	148.387(12)
P1–Zr–Br1	81.74(2)	Br1–Zr–Br3	94.859(12)
P1–Zr–Br2	75.67(2)	Br2–Zr–Br3	91.669(11)
P1–Zr–Br3	145.78(2)	C1–C2–C3	121.1(3)
P2–Zr–Br1	74.35(2)	C2–C3–C4	116.4(3)
P2–Zr–Br2	77.71(2)	C3–C4–C5	121.3(3)
P2–Zr–Br3	74.55(2)		

including a number of Zr(C_5H_5)Cl_3(L)$_2$ species (L$_2$ = dme [13], L = H_2O [14], and L = THF or dmf [15]), as well as for Ti(C_5H_5)Cl_3(dmpe) [16]. Interestingly, appropriate tethering of the Lewis bases (L) to the dienyl ligand has led to the alternative *mer*,*trans* [17,18] and *fac* [19] isomers (**4**, **5**). A pseudo-octahedral arrangement has also been found for Zr(*c*-C_8H_{11})(H)(dmpe)$_2$ (C_8H_{11} = octadienyl), and presumably also exists for Zr(*c*-C_6H_7)(H)(dmpe)$_2$ (C_6H_7 = hexadienyl) [20]. Given the large size of the 6,6-dmch ligand, it is not surprising that the four adjacent ligands tilt substantially down toward the P(2) donor site, with P2–Zr–Br angles ranging from 74.35(2)° to 77.71(2)°. The P2–Zr–P1 angle is still smaller, at 71.75(2)°, as a result of the chelating nature of the dmpe ligand. The Zr-dmch bonding follows the expected trend for a higher valent metal pentadienyl complex, having the shortest interaction involving the central dienyl carbon atom, with the subsequent carbon atoms being located progressively further from the metal center. The short–long–long–short pattern in dienyl C–C bond distances is consistent with this (cf., **2**). As in the case of [Ti(6,6-dmch)Cl_2]$_n$ and the other high valent metal pentadienyl complexes, the structural data reflect an inability of the contracted metal orbitals to interact effectively with the entire dienyl fragment, leading to the initiation of ligand slippage. The observed structure may be viewed as an intermediate between η^5 and η^1 coordination modes, which can play a major role in facilitating the loss of pentadienyl ligands from their high valent complexes, and thus helps explain the extreme preference

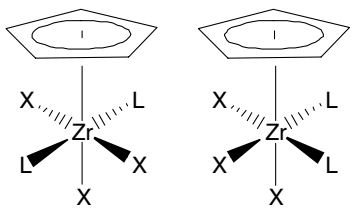

4 **5**

exhi-bited by pentadienyl ligands to bond to metals in lower oxidation states.

Some additional indications of the $\eta^5-\eta^1$ slippage can be seen in the dienyl fragment. As noted above for $[Ti(6,6\text{-dmch})Cl_2]_n$ and the other high valent complexes, one observes a short–long–long–short pattern of C–C bond distances, consistent with **2**. Furthermore, resonance form **2** implicates a partial contribution of sp^3 hybridization on the central carbon atom, and this is reflected by the C2–C3–C4 bond angle being smaller than those for C1–C2–C3 and C3–C4–C5 (116.4(3) vs. 121.1(3)° and 121.3(3)°). Finally, tilts of the hydrogen atom substituents out of the plane are telling. Typically in metal-pentadienyl compounds, the dienyl substituents tilt significantly down toward the metal center, in an attempt to improve metal–ligand overlap, as in **6**. That is indeed observed here for H1, H2, H4, and H5. The tilts for H2 and H4 (0.13, 0.21 Å) seem to be greater than those for H1 and H5 (0.11, 0.14 Å). This may indicate that the Zr–C(1,5) distances have become so long that little can be gained from the substituent tilting. In contrast, the central hydrogen atom experiences essentially no tilt, 0.02(3) Å, and in fact, in other high valent complexes the tilting actually occurs in a direction *away from* the metal center, in accord with the partial contribution of sp^3 hybridization on C3.

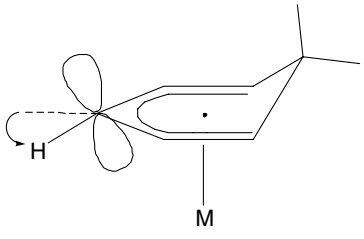

6

The availability of these mono(dmch) complexes of Ti(III) and Zr(IV), along with the previously reported $Zr(C_5H_5)(6,6\text{-dmch})X_2$ and $Zr(6,6\text{-dmch})_2X_2$ complexes, should now allow for the first extensive investigations of higher valent metal pentadienyl chemistry. Already it is clear that this chemistry differs dramatically from the lower valent species, and many worthwhile possibilities await exploration.

4. Supplementary material

Crystallographic data for the structural analysis has been deposited with the Cambridge Crystallographic Data Centre, CCDC, Nos. 273154-273155 for compounds $[Ti(6,6\text{-dmch})Cl_2]_n$ and $Zr(6,6\text{-dmch})Br_3(dmpe)$, respectively. Copies of this information may be obtained free of charge from The Director, CCDC, 12 Union Road, Cambridge, CB2 1EZ, UK, fax: +44 1223 366 033, e-mail: deposit@ccdc.ac.uk or on the web www: http://www.ccdc.cam.ac.uk.

Acknowledgements

Acknowledgement is made to the Donors of the American Chemical Society Petroleum Research Fund and the University of Utah for partial support of this work.

References

[1] (a) R.D. Ernst, Chem. Rev. 88 (1988) 1255;
(b) R.D. Ernst, Comments Inorg. Chem. 21 (1999) 285.
[2] (a) V. Kulsomphob, B. Harvey, A.M. Arif, R.D. Ernst, Inorg. Chim. Acta 334 (2002) 17, and references therein;
(b) R.D. Ernst, R. Basta, A.M. Arif, Z. Kristallogr. NCS 219 (2004) 403.
[3] T.D. Newbound, L. Stahl, M.L. Ziegler, R.D. Ernst, Oganometallics 9 (1990) 2962.
[4] P.T. DiMauro, P.T. Wolczanski, Organometallics 6 (1987) 1947.
[5] R. Basta, R.D. Ernst, A.M. Arif, J. Organomet. Chem. 64 (2003) 683.
[6] R. Basta, Ph.D. dissertation, University of Utah, 2004.
[7] A. Rajapakshe, N.E. Gruhn, D.L. Lichtenberger, R. Basta, A.M. Arif, R.D. Ernst, J. Am. Chem. Soc. 126 (2004) 14105.
[8] (a) A. Gutierrez, G. Wilkinson, B. Hussain-Bates, M.B. Hursthouse, Polyhedron 9 (1990) 2081;
(b) S. Feng, J. Klosin, W.J. Kruper Jr., M.H. McAdon, D.R. Neithamer, P.N. Nickias, J.T. Patton, D.R. Wilson, K.A. Abboud, C.L. Stern, Organometallics 18 (1999) 1159;
(c) M.R. Lentz, P.E. Fanwick, I.P. Rothwell, Organometallics 22 (2003) 2259;
(d) J. Gavenonis, T.D. Tilley, J. Am. Chem. Soc. 124 (2002) 8536;
(e) J. Gavenonis, T.D. Tilley, Organometallics 21 (2002) 5549;
(f) S. Pillet, G. Wu, V. Kulsomphob, B.G. Harvey, R.D. Ernst, P. Coppens, J. Am. Chem. Soc. 125 (2003) 1937.
[9] V. Kulsomphob, A.M. Arif, R.D. Ernst, Organometallics 21 (2002) 3182.
[10] (a) P.T. DiMauro, P.T. Wolczanski, L. Parkanyi, H.H. Petach, Organometallics 9 (1990) 1097;
(b) P.T. DiMauro, P.T. Wolczanski, Polyhedron 14 (1995) 149.
[11] P.D. Bartlett, B. Seidel, J. Am. Chem. Soc. 83 (1961) 581.
[12] R.D. Ernst, W.J. Kennelly, C.S. Day, V.W. Day, T.J. Marks, J. Am. Chem. Soc. 101 (1979) 2656.
[13] N.J. Wells, J.C. Huffman, K.G. Caulton, J. Organomet. Chem. 213 (1981) C17.
[14] G. Erker, C. Sarter, S. Werner, C. Krüger, J. Organomet. Chem. 377 (1989) C55.
[15] G. Erker, C. Sarter, M. Albrecht, S. Dehnicke, C. Krüger, E. Raabe, R. Schlund, R. Benn, A. Rufinska, R. Mynott, J. Organomet. Chem. 382 (1990) 89.
[16] D.L. Hughes, G.J. Leigh, D.G. Walker, J. Organomet. Chem. 355 (1988) 113.
[17] M.D. Fryzuk, S.S.H. Mao, P.B. Duval, S.J. Rettig, Polyhedron 14 (1995) 11.
[18] M.D. Fryzuk, P.B. Duval, B.O. Patrick, S.J. Rettig, Organometallics 20 (2001) 1608.
[19] A.A.H.v.d. Zeuden, C. Mattheis, R. Fröhlich, Acta Cryst. C54 (1998) 458.
[20] M.B. Fisher, E.J. James, T.J. McNeese, S.C. Nyburg, B. Posin, W. Wong-Ng, S.S. Wreford, J. Am. Chem. Soc. 102 (1980) 4941.

Available online at www.sciencedirect.com
SCIENCE DIRECT
Polyhedron 25 (2006) 881–887
POLYHEDRON
www.elsevier.com/locate/poly

Supramolecular assembly of nanometer-sized heterobimetallic 3d–4f complexes formed with benzimidazole based N,O-donor ligands

Xiaoping Yang [a], Richard A. Jones [a,*], Rachel J. Lai [a], Abdul Waheed [a], Michael M. Oye [b], Archie L. Holmes [b]

[a] Department of Chemistry and Biochemistry, The University of Texas at Austin, 1 University Station A 5300, Austin, TX 78712-0165, USA
[b] Microelectronics Research Center and Texas Materials Institute, The University of Texas at Austin, 1 University Station Stop R9900, Austin, TX 78712-0165, USA

Received 12 August 2005; accepted 27 September 2005
Available online 3 November 2005

Dedicated with admiration to Professor Michael B. Hursthouse on the occasion of his 65th birthday.

Abstract

Five heterobimetallic Cu–Ln complexes of general formula $[CuLn(HL)_2(NO_3)_3(MeCN)_2]\cdot 2Et_2O$ (Ln = Eu **1**, Tb **2**, Er **3**, Yb **4** and Nd **5**) were prepared with a new multidentate benzimidazole ligand based on 4-bromo-2-[2-(5-bromo-2-hydroxy-3-methoxy-phenyl)-benzoimidazol-1-ylmethyl]-6-methoxy-phenol ($\mathbf{H_2L^1}$) or its bis-methoxy substituted analog ($\mathbf{H_2L^3}$). In the solid state the structures of **1**–**4** exhibit supramolecular 3D-networks which are formed by the linking of C–H···O and C–H···π interactions. Compound **5** does not exhibit an extended supramolecular network.
© 2005 Elsevier Ltd. All rights reserved.

Keywords: 3d–4f Complex; X-ray crystallography; Supramolecular assemblies; C–H···O/π interactions

1. Introduction

Mononuclear transition metal complexes are now well established as versatile building blocks in supramolecular chemistry [1]. In many cases successful strategies for engineering the assemblies of materials take advantage of non-bonded interactions such as hydrogen-bonding and π–π stacking between building blocks. More recently molecular assemblies incorporating dinuclear metal species as rigid or semi-rigid corner units have become the focus of active research [2]. Although heterobimetallic 3d–4f metal complexes are of interest for their catalytic, electronic, magnetic or optical properties there are relatively few reports of supramolecular assemblies which comprise these units as building blocks [3]. As part of our ongoing interest in 3d–4f complexes we have investigated the use of modified "salen" type Schiff base complexes such as $\mathbf{H_2L^2}$ [4]. This ligand may be conveniently prepared at room temperature. However, in refluxing ethanol it is converted into the benzimidazole ligand $\mathbf{H_2L^1}$ (Scheme 1). This type of transformation is well known and in the case of $\mathbf{H_2L^1}$ produces a substituted benzimidazole with two 5-bromo-3-methoxy-phenolic substituents. One is linked directly to the center carbon of the benzimidazole group and the other via a CH_2 group to a nitrogen atom [5]. Despite the asymmetric nature of $\mathbf{H_2L^1}$ we have found that two deprotonated units of it can stabilize 3d–4f heterobimetallic complexes via benzimidazole nitrogen, phenolic oxygen and methoxy oxygen atoms. Interestingly, in the solid state the structures of these compounds exhibit supramolecular 3D-networks formed by C–H···O hydrogen bonding and C–H···π interactions.

We have also isolated and characterized an analogous Cu–Nd complex which has a similar benzimidazole ligand but with two OMe substituents on the phenylene backbone.

* Corresponding author. Tel.: +1 512 471 1706.
E-mail address: rajones@mail.utexas.edu (R.A. Jones).

0277-5387/$ - see front matter © 2005 Elsevier Ltd. All rights reserved.
doi:10.1016/j.poly.2005.09.029

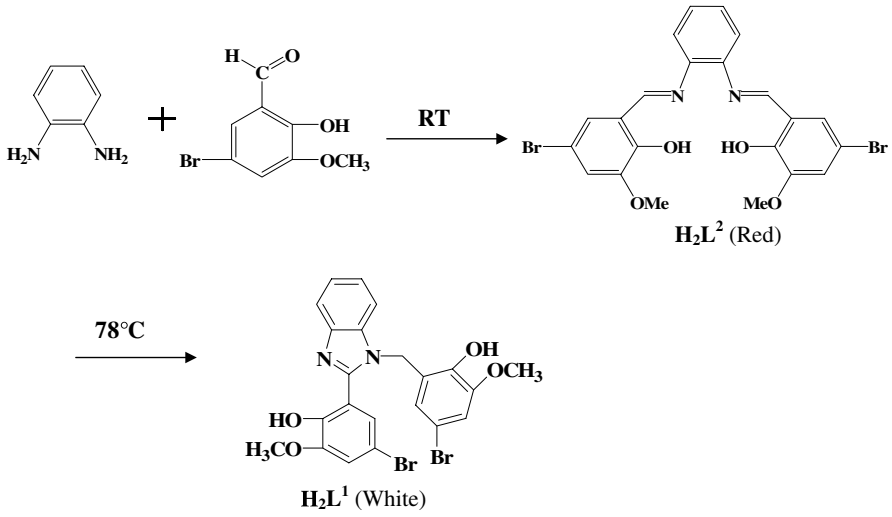

Scheme 1.

In this case, no supramolecular 3D-network was found in the solid state.

2. Results and discussion

2.1. Free Schiff base ligand H_2L^1

The reaction of *o*-phenylenediamine with 5-bromo-2-hydroxy-3-methoxybenzaldehyde in ethanol of room temperature gives the bright-red Schiff base $\mathbf{H_2L^2}$ in high yield (Scheme 1) [4]. However if this reaction is carried out under refluxing conditions (10 h) the colorless benzimidazole derivative $\mathbf{H_2L^1}$ is produced in good yield. In order to confirm the identity of this product the solid state structure of $\mathbf{H_2L^1}$ was determined via an X-ray crystallographic study (Table 1). Two views of the molecule are shown in Fig. 1. The two substituted aryl groups are both twisted with respect to the planar benzimidazole unit, no doubt in order to reduce steric interactions. The dihedral angles are 53.6° and 78.1°. Hydrogen bonding interactions (O–H···N) link adjacent molecules of the free ligand into one-dimensional strands ($N_{1A}\cdots O_{4B} = 2.691$ Å), as shown in Fig. 1. Key bond lengths and angles for $\mathbf{H_2L^1}$ are given in Table 2.

Table 1
Crystal data and structure refinement for the free $\mathbf{H_2L^1}$, **1**–**5**

	$\mathbf{H_2L^1}$	**1**	**2**	**3**	**4**	**5**
Formula	$C_{22}H_{18}Br_2N_2O_4$	$C_{56}H_{60}Br_4CuN_9O_{19}Eu$	$C_{56}H_{60}Br_4CuN_9O_{19}Tb$	$C_{56}H_{60}Br_4CuN_9O_{19}Er$	$C_{56}H_{60}Br_4CuN_9O_{19}Yb$	$C_{60}H_{66}Br_4CuN_9O_{23}Nd$
Formula weight	534.20	1698.25	1705.21	1713.57	1719.35	1808.64
Crystal system	monoclinic	monoclinic	monoclinic	monoclinic	monoclinic	monoclinic
Space group	*P*2(1)/*c*	*C*2/*c*	*C*2/*c*	*I*2/*a*	*I*2/*a*	*C*2/*c*
a (Å)	17.041(3)	26.4002(3)	26.484(5)	16.137(3)	16.173(5)	27.571(6)
b (Å)	8.8444(18)	21.5673(4)	21.307(4)	21.649(4)	21.559(5)	19.821(4)
c (Å)	14.963(3)	16.2285(3)	16.239(3)	21.399(4)	21.437(5)	16.218(3)
β (°)	107.57(3)	125.736(1)	125.42(3)	92.11(3)	91.917(5)	124.51(3)
V (Å^3)	2150.1(7)	7500.4(2)	7468(3)	7471(3)	7473(3)	7303(3)
Z	4	4	4	4	4	4
D_{calc} (g cm^{-3})	1.650	1.495	1.510	1.522	1.529	1.645
Temperature (K)	153(1)	153(1)	153(1)	153(1)	153(1)	153(1)
F(000)	1064	3332	3348	3392	3400	3608
μ (mm^{-1})	3.801	3.309	3.431	3.606	3.735	3.261
θ range (°)	3.16–27.48	2.99–27.50	2.99–27.49	3.01–27.50	3.00–27.50	3.05–25.00
Reflections measured	7382	16468	15834	16333	16603	11799
Reflections used	4875	8589	8479	8476	8527	6426
Parameters	272	398	408	411	411	444
R^a ($I > 2\sigma(I)$)	$R_1 = 0.0520$	$R_1 = 0.0756$	$R_1 = 0.0669$	$R_1 = 0.0515$	$R_1 = 0.0641$	$R_1 = 0.0864$
	$wR_2 = 0.1210$	$wR_2 = 0.1750$	$wR_2 = 0.1714$	$wR_2 = 0.1267$	$wR_2 = 0.1588$	$wR_2 = 0.2335$
R^a (all data)	$R_1 = 0.0713$	$R_1 = 0.1043$	$R_1 = 0.1526$	$R_1 = 0.0626$	$R_1 = 0.0845$	$R_1 = 0.1515$
	$wR_2 = 0.1283$	$wR_2 = 0.1878$	$wR_2 = 0.2030$	$wR_2 = 0.1328$	$wR_2 = 0.1694$	$wR_2 = 0.2771$
S	1.139	1.101	1.038	1.090	1.066	1.087

[a] $R_1 = \sum|F_o| - |F_c|\sum|F_o|$. $wR_2 = [\sum w[(F_o^2 - F_c^2)^2]/\sum|[w(F_o^2)^2]]^{1/2}$. $w = 1/[\sigma^2(F_o^2) + (0.075P)^2]$, where $P = [\max(F_o^2, 0) + 2F_c^2]/3$.

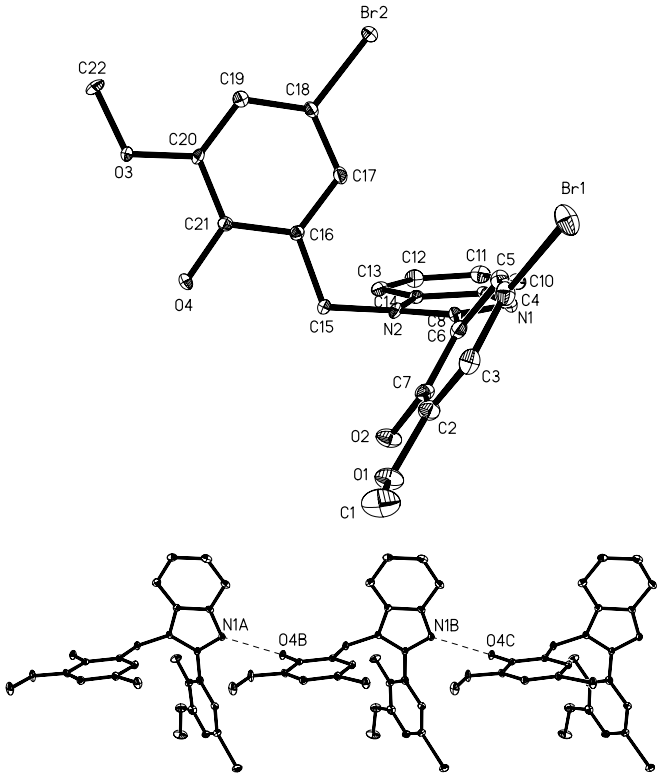

Fig. 1. Views of the crystal structure of the free ligand $\mathbf{H_2L^1}$. Thermal ellipsoids are drawn at the 25% probability level. Hydrogen atoms are omitted for clarity.

Table 2
Selected bond lengths (Å) and angles (°) for $\mathbf{H_2L^1}$

N(2)–C(8)	1.364(6)	C(8)–N(1)–C(9)	106.1(4)
N(2)–C(14)	1.390(6)	N(1)–C(8)–N(2)	112.5(4)
N(2)–C(15)	1.457(6)	N(1)–C(8)–C(6)	123.1(4)
N(1)–C(8)	1.317(6)	N(2)–C(8)–C(6)	124.4(4)
N(1)–C(9)	1.392(6)	C(13)–C(14)–N(2)	131.8(4)
C(6)–C(8)	1.469(7)	C(13)–C(14)–C(9)	122.8(5)
C(14)–C(9)	1.407(7)	N(2)–C(14)–C(9)	105.4(4)
C(8)–N(2)–C(14)	107.1(4)	N(1)–C(9)–C(10)	131.1(5)
C(8)–N(2)–C(15)	127.8(4)	N(1)–C(9)–C(14)	108.9(4)
C(14)–N(2)–C(15)	123.9(4)	C(10)–C(9)–C(14)	120.0(5)

2.2. Metal complexes

Reactions of $\mathbf{H_2L^1}$ with $Cu(OAc)_2$ and $Ln(NO_3)_3 \cdot 6H_2O$ in MeCN/EtOH produce blue solutions from which the dinuclear complexes $[CuLn(HL^1)_2(NO_3)_3(MeCN)_2] \cdot 2Et_2O$ (Ln = Eu **1**, Tb **2**, Er **3** and Yb **4**) may be isolated in 30–60% yields as blue crystalline solids. X-ray crystallographic studies have shown that **1**–**4** are isomorphous with central dinuclear units comprising neutral $[CuLn(HL^1)_2(NO_3)_3(MeCN)_2]$ moieties. The minor differences in the metric parameters for these molecules reflect the effects of the lanthanide contraction. A view of **1** is shown in Fig. 2 and important bond lengths and angles are presented in Table 3. The molecular structure of **1** features Cu(II) and Eu(III) ions complexed by two deprotonated $\mathbf{HL^1}$ ligands.

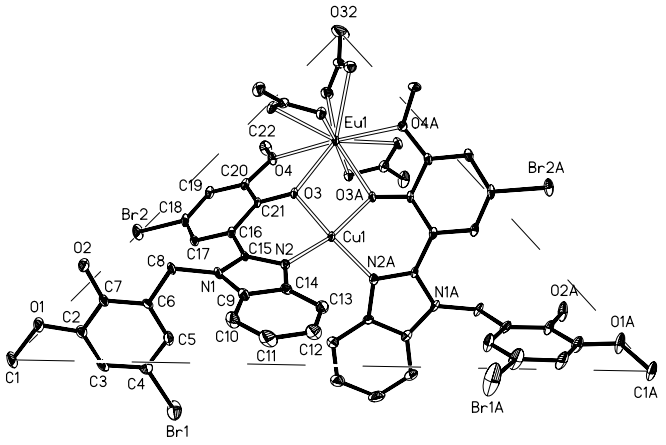

Fig. 2. View of the crystal structure of **1** (C(1)···C(1A): 20.005 Å, C(1)···O(32): 15.650 Å). Thermal ellipsoids are drawn at the 25% probability level. Two weakly coordinated MeCN molecules bond to Cu(1) and all hydrogen atoms are omitted for clarity.

Table 3
Selected bond lengths (Å) and angles (°) for **1**

Eu(1)–O(3)	2.369(4)	O(3)#1–Eu(1)–O(31)	133.32(16)
Eu(1)–O(42)	2.479(5)	O(3)–Eu(1)–O(31)	146.73(17)
Eu(1)–O(41)	2.497(5)	O(42)–Eu(1)–O(31)	115.48(18)
Eu(1)–O(31)	2.528(5)	O(41)–Eu(1)–O(31)	82.31(17)
Eu(1)–O(4)	2.607(5)	O(31)#1–Eu(1)–O(31)	50.5(3)
Cu(1)–N(2)	1.960(6)	O(3)#1–Eu(1)–O(4)	114.13(15)
Cu(1)–O(3)	1.964(4)	O(3)–Eu(1)–O(4)	62.40(15)
O(3)#1–Eu(1)–O(3)	65.4(2)	O(42)#1–Eu(1)–O(4)	113.38(15)
O(3)–Eu(1)–O(42)#1	79.62(15)	O(42)–Eu(1)–O(4)	66.31(15)
O(3)–Eu(1)–O(42)	93.10(15)	O(41)#1–Eu(1)–O(4)	65.82(16)
O(42)#1–Eu(1)–O(42)	171.4(2)	O(41)–Eu(1)–O(4)	115.09(15)
O(3)–Eu(1)–O(41)#1	74.07(16)	O(31)#1–Eu(1)–O(4)	71.31(16)
O(42)–Eu(1)–O(41)#1	130.92(16)	O(31)–Eu(1)–O(4)	112.27(17)
O(42)–Eu(1)–O(41)	51.58(16)	O(4)–Eu(1)–O(4)#1	176.3(2)
O(41)#1–Eu(1)–O(41)	154.1(2)	N(2)#1–Cu(1)–N(2)	101.9(3)
O(3)–Eu(1)–O(31)#1	133.32(16)	N(2)#1–Cu(1)–O(3)	162.8(2)
O(42)–Eu(1)–O(31)#1	72.87(18)	N(2)–Cu(1)–O(3)	90.0(2)
O(41)#1–Eu(1)–O(31)#1	82.31(18)	O(3)–Cu(1)–O(3)#1	81.4(3)

In each case the molecule sits on a crystallographic 2-fold axis which runs through the lanthanide and Cu atoms. The unsubstituted nitrogen atoms of the benzimidazole group are bound to the Cu(II) center while the deprotonated phenolic groups bridge both metals. The Cu^{2+} ion has a pseudo-octahedral coordination environment which is completed by two weakly bond molecules of MeCN in axial positions (N(3)–Cu(1) = 2.564 Å). The Cu(1)–Eu(1) distance is 3.482 Å. The overall structure has a distinctly triangular structure of nanoscale proportions (20.0 × 15.7 × 15.7 Å) and has a C_2-axis which runs through O(32)–Cu(1)–Eu(1). The Eu^{3+} ion is 10 coordinate with an inner coordination environment provided by oxygen atoms; four from two $\mathbf{HL^1}$ ligands and six from the three bidentate nitrates. The pseudo-octahedral coordination geometry of Cu(1) (pseudo-square planar if the two weakly bound MeCN groups are ignored) causes the deprotonated $\mathbf{HL^1}$ ligand to adopt a more planar configuration. Thus, the dihedral angle between the benzimidazole group and the aryl ring which bears the deprotonated

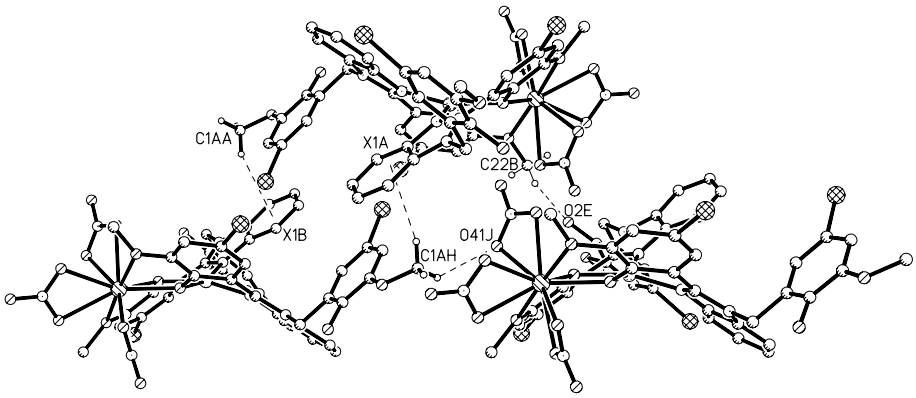

Fig. 3. View of the intermolecular interactions in **1**: C–H···π interactions (H(1AH)···X1A: 2.854 Å, C–H–π: 153.3°; H(1AA)···X1B: 2.860 Å, C–H–π: 147.3°) and hydrogen bonds (O(2E)···H–C(22B): 2.473 Å, O–H–C: 102.7°; O(41J)···H–C(1AH): 2.619 Å, O–H–C: 99.5°).

phenolic group is now considerably smaller than that in the free ligand (31.2° versus 53.6°).

The crystal packing behavior for **1**–**4** is of particular interest. Both intermolecular C–H···O hydrogen bonding and C–H···π_{aryl} interactions combine to give these compounds 3D supramolecular frameworks. Fig. 3 shows details of the C–H···π_{aryl} interactions between methoxy hydrogens and the phenylene rings of the benzimidazole groups as well as C–H···O interactions between methoxy hydrogens and either phenolic or nitrate oxygen atoms. The C–H···O(phenolic) interactions create a one-dimensional strand along the *b*-axis. The C–H···π_{aryl} interactions and C–H··· O(nitrate) interactions then create a 3D open network structure with extended channels running along the *b*-axis (Fig. 4). These channels measure approximately 8×9 Å and accommodate guest molecules of diethylether. There are short hydrogen bonded interactions between the entrapped diethylether molecules and the surrounding supramolecular framework (aryl-OH···O(ether) O···O = 2.722 Å). Fig. 5 provides a view of the supramolecular formwork of **1** showing the diethylether located in the channels of the open framework.

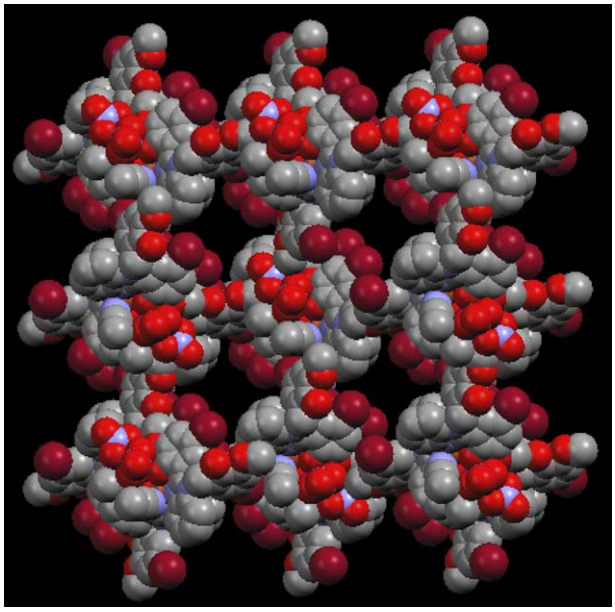

Fig. 4. View of **1** along the *b*-axis showing the 3D-network.

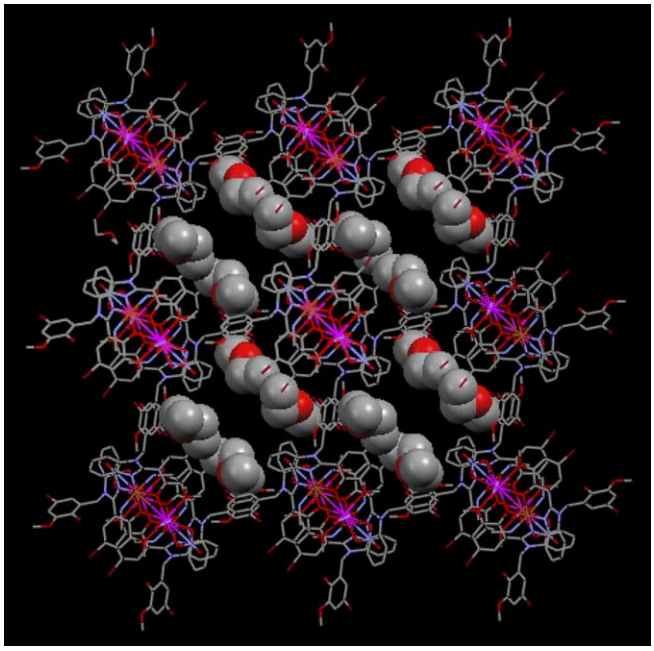

Fig. 5. View of **1** showing the entrapped diethylether molecules.

As part of our studies of Schiff base ligands capable of stabilizing 3d–4f combinations we have also investigated the use of $\mathbf{H_2L^4}$, the methoxy substituted analog of $\mathbf{H_2L^2}$. In refluxing ethanol in the presence of Cu(II) and Nd(III) $\mathbf{H_2L^4}$ is converted into the benzimidazole derivative ($\mathbf{H_2L^3}$) (Scheme 2) and, in deprotonated form, this serves as a ligand to stabilize a heterobimetallic Cu–Nd species. Thus the reaction of $\mathbf{H_2L^4}$ with a mixture of $Cu(ClO_4)_2 \cdot 6H_2O$ and $Nd(NO_3)_3 \cdot 6H_2O$ in MeCN/EtOH under reflux gave a red-brown solution from which crystals of $[CuNd(HL^3)_2(NO_3)_3(MeCN)_2] \cdot 2Et_2O$ (**5**) were isolated in 42% yield. The molecular structure of **5** is shown in Fig. 6, crystallographic details are in Table 1 and selected bond lengths and angles are in Table 4. We were interested in the effects that the two methoxy groups had on both the

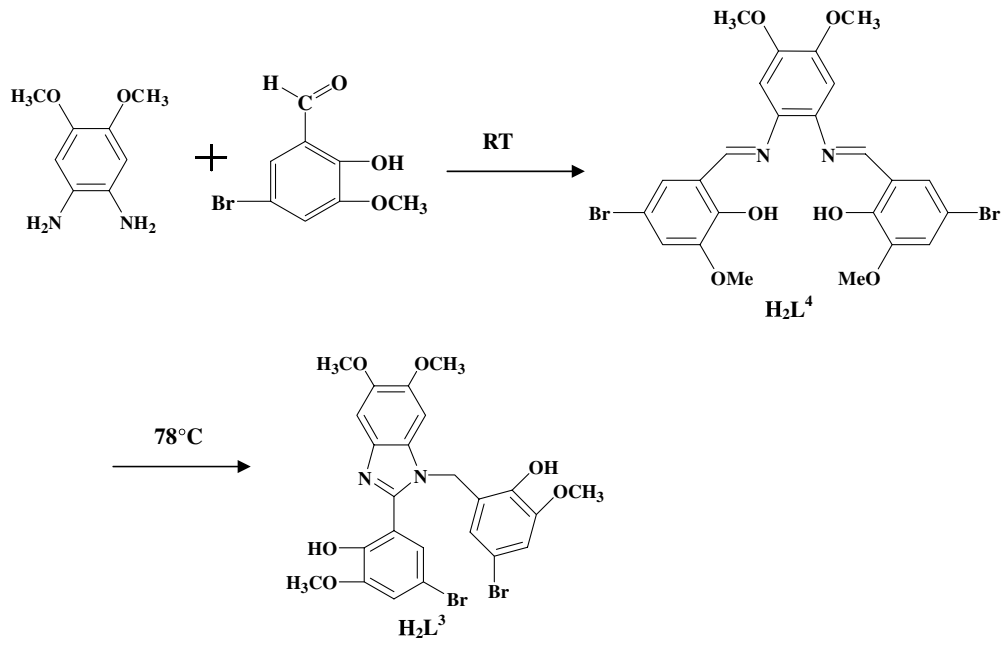

Scheme 2.

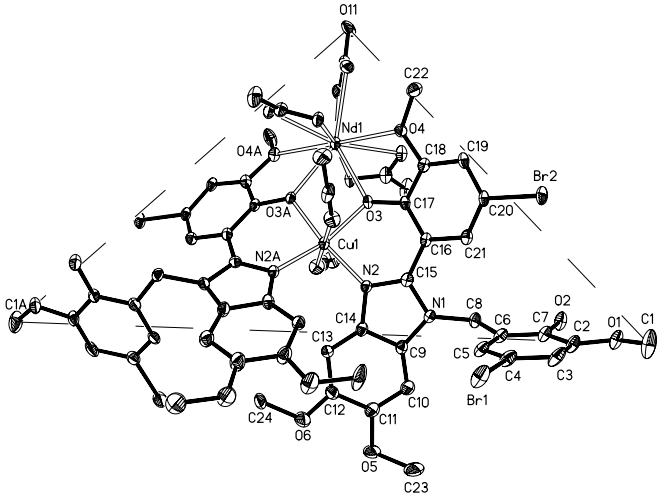

Fig. 6. View of the crystal structure of **5** (C(1)···C(1A): 20.749 Å, C(1)···O(32): 14.976 Å).

Table 4
Selected bond lengths (Å) and angles (°) for **5**

Nd(1)–O(3)	2.389(8)
Nd(1)–O(8)	2.502(9)
Nd(1)–O(10)	2.556(11)
Nd(1)–O(7)	2.563(9)
Nd(1)–O(4)	2.605(9)
Cu(1)–N(2)	1.959(10)
Cu(1)–O(3)	1.977(8)
O(3)–Nd(1)–O(3)#1	64.8(3)
O(3)–Nd(1)–O(8)	87.6(3)
O(3)–Nd(1)–O(8)#1	82.3(3)
O(8)–Nd(1)–O(8)#1	168.1(5)
O(3)–Nd(1)–O(10)	145.8(3)
O(3)#1–Nd(1)–O(10)	135.9(3)
O(8)–Nd(1)–O(10)	118.2(4)
O(8)#1–Nd(1)–O(10)	73.6(4)
O(10)–Nd(1)–O(10)#1	47.6(6)
O(3)–Nd(1)–O(7)	123.3(3)
O(3)#1–Nd(1)–O(7)	72.9(3)

molecular structure and the overall crystal packing. The core structure of **5** is similar to those of **1**–**4** and so a detailed discussion of it is unnecessary. However, the methoxy groups appear to disrupt the molecular packing of dinuclear units so that there are no significant intermolecular contacts which would result in an extended supramolecular framework.

3. Experimental

All operations were performed under a dry oxygen-free dinitrogen atmosphere using standard Schlenk techniques. Metal salts, methylenechloride, acetonitrile and absolute ethanol were purchased from Aldrich Chemicals. The solvents were distilled under nitrogen prior to use. Physical measurements: mass spec: ESI and FAB; Finnigan MAT TSQ 700; NMR: Varian 300 Unity Plus spectrometer (^{1}H, 300 MHz) at 298 K (chemical shifts referenced to the deuterated solvent). IR: Nicolet IR 200 FTIR spectrometer. UV–Vis Beckman DU 640 spectrophotometer. Melting points were obtained in sealed glass capillaries under dinitrogen and are uncorrected. Microanalytical data for the metal complexes were not reproduceable, probably due to eratic loss of solvent molecules.

3.1. Synthesis

3.1.1. Preparation of ligand H_2L^1

A solution of *o*-phenylenediamine (1.08 g, 0.01 mol) in ethanol (20 ml) was added to a solution of 5-bromo-2-hydroxy-3-methoxybenzaldehyde (4.62 g, 0.02 mol) in

ethanol (60 ml). The mixture was refluxed for 10 h and the colorless solid product filtered and washed with ethanol (20 ml). The material was recrystallized from hot ethanol. Yield 2.90 g, 60%. m.p. 195 °C. ESI-MS (CH_3CN) *m/z* (%): 534 (100) $[M + H^+]^+$. ^1H NMR (DMSO-d_6, δ, ppm): 3.806 (s, 3H), 3.828 (s, 3H), 5.378 (s, 2H), 6.635 (s, 1H), 6.857 (s, 1H), 7.013 (s, 1H), 7.212 (s, 1H), 7.428 (m, 2H), 7.480 (d, 1H), 8.052 (d, 1H). IR (CH_3CN, cm^{-1}): 3748, 1655, 1635, 1619, 1560, 1521, 1505, 1458, 1416, 1254, 745, 671. Single crystals for X-ray crystallographic analysis were obtained by vapor diffusion of diethyl ether into solutions of $\mathbf{H_2L^1}$ in EtOH.

3.1.2. Preparation of ligand H_2L^4

1,2-Dimethoxy-4,5-diaminobenzene was prepared using the published procedure [6]. A solution of 1,2-dimethoxy-4,5-diaminobenzene (0.74 ml, 5.0 mmol) in ethanol (5 ml) was added dropwise with stirring to a solution of 5-bromo-3-methoxysalicylaldehyde (2.31 g, 10 mmol) in ethanol (30 ml). The reaction mixture was stirred at room temperature (2 h), after which the solvent was removed under vacuum using a rotary evaporator. The product *N*,*N*′-bis(5-bromo-3-methoxysalicylidene)-4,5-dimethoxy phenylene-1,2-diamine was obtained as a reddish-brown solid. Yield: 91%. m.p. 179–186 °C; IR, (Nujol, cm^{-1}): 3410 b, 2934 s, 2851 b, 1627 s, 1572 b, 1473 b, 1396 s, 1343 s, 1250 b, 1101 s, 1048 b, 975 s; FAB-MS *m/z*: 596 $[M^+ - CO]$; ^1H NMR (DMSO-d_6, δ, ppm): –OCH_3, 3.74–3.92 (m, 12H); aromatic *H*, 6.9–8.9 (m, 6H); N=C*H* 8.57 (m, 2H).

3.1.3. Preparation of complexes 1–4

All complexes were prepared by the same procedure. A typical procedure is given for **1**.

3.1.4. $[CuEu(HL^1)_2(NO_3)_3(MeCN)_2]\cdot 2Et_2O$ (1)

A mixture of $\mathbf{H_2L^1}$ (0.106 g, 0.20 mmol) and $Cu(OAc)_2\cdot 2H_2O$ (0.022 g, 0.10 mmol) in 1:1 MeCN/EtOH (20 ml) was stirred and heated under reflux (20 min). A solution of $Eu(NO_3)_3\cdot 6H_2O$ (0.045 g, 0.10 mmol) in EtOH (10 ml) was added and the mixture was stirred and refluxed for (2 h). The mixture was allowed to cool to room temperature and filtered. Diethylether was allowed to diffuse slowly into the solution in a closed vessel at room temperature. Blue single crystals of **1** were formed after 1 month. Yield 0.093 g, 55%. ESI-MS (CH_3CN) *m/z* (%): 1129 (85) $[M + H^+ - 2Et_2O - 2MeCN - 3(NO_3^-) - Eu^{3+}]^+$, 1506 (10) $[M + H^+ - 2Et_2O - MeCN]^+$. m.p. > 330 °C (dec). IR (CH_3CN, cm^{-1}): 3514, 1653, 1635, 1613, 1589, 1558, 1489, 1473, 1349, 1233, 745, 669.

3.1.5. $[CuTb(HL^1)_2(NO_3)_3(MeCN)_2]\cdot 2Et_2O$ (2)

$Tb(NO_3)_3\cdot 5H_2O$ (0.044 g, 0.10 mmol) was used. Yield: 0.068 g, 40%, blue crystals. ESI-MS (CH_3CN) *m/z* (%): 1129 (80) $[M + H^+ - 2Et_2O - 2MeCN - 3(NO_3^-) - Tb^{3+}]^+$. m.p. > 315 °C (dec). IR (CH_3CN, cm^{-1}): 3642, 1656, 1632, 1611, 1591, 1540, 1492, 1470, 1353, 1230, 746, 668.

3.1.6. $[CuEr(HL^1)_2(NO_3)_3(MeCN)_2]\cdot 2Et_2O$ (3)

$Er(NO_3)_3\cdot 5H_2O$ (0.044 g, 0.10 mmol) was used. Yield: 0.089 g, 52%, blue crystals. ESI-MS (CH_3CN) *m/z* (%): 685 (30) $[M - 2Et_2O - 2MeCN - 2(NO_3^-)]^{2+}$, 1129 (85) $[M + H^+ - 2Et_2O - 2MeCN - 3(NO_3^-) - Er^{3+}]^+$, 1517 (15) $[M + H^+ - 2Et_2O - MeCN]^+$. m.p. > 320 °C (dec). IR (CH_3CN, cm^{-1}): 3533, 1652, 1630, 1615, 1590, 1555, 1483, 1475, 1348, 1232, 745, 670.

3.1.7. $[CuYb(HL^1)_2(NO_3)_3(MeCN)_2]\cdot 2Et_2O$ (4)

$Yb(NO_3)_3\cdot 5H_2O$ (0.045 g, 0.10 mmol) was used. Yield: 0.060 g, 35%, blue crystals. ESI-MS (CH_3CN) *m/z* (%): 1129 (90) $[M + H^+ - 2Et_2O - 2MeCN - 3(NO_3^-) - Yb^{3+}]^+$. m.p. > 310 °C (dec). IR (CH_3CN, cm^{-1}): 3520, 1650, 1636, 1613, 1586, 1553, 1487, 1472, 1357, 1230, 745, 669.

3.1.8. Preparation of complex 5

A solution of $Cu(ClO_4)_2\cdot 6H_2O$ (0.1 g, 0.32 mmol) in ethanol (5 ml) was added to a solution of *N*,*N*′-bis(5-bromo-3-methoxysalicylidene)-4,5-dimethoxyphenylene-1,2-diamine ($\mathbf{H_2L^4}$), 0.014 g, 0.024 mmol) in acetonitrile (3 ml) giving a reddish-brown solution. The mixture was heated under reflux (40 min) and the resulting solution was allowed to cool to room temperature after which a solution of $Nd(NO_3)_3\cdot 6H_2O$ (0.01 g, 0.027 mmol) in ethanol (3 ml) was added. The mixture was heated under reflux (40 min) and then filtered and the filtrate transferred into a test tube. Diethylether was allowed to diffuse slowly into the filtrate at room temperature in an enclosed vessel. After six weeks, crystals suitable for X-ray diffraction studies were obtained. They were collected and dried under vacuum. Yield: 42%. $[CuNd(HL^3)_2(NO_3)_3(MeCN)_2]\cdot 2Et_2O$ m.p. > 310 °C; IR (Nujol, cm^{-1}): 2923 s, 2853 b, 1626 s, 1558 b, 1467 s, 1295 s, 1231 s, 1106 b, 789 s; FAB-MS *m/z*: 612 $[M - 2Et_2O - 2MeCN]^+$; ^1H NMR (DMSO-d_6, δ, ppm): –OCH_3, 3.7–3.9 (m, 12H); –N=C*H*, 8.6 (m, 2H); aromatic *H*, 6.9–8.9 (m, 6H); UV–Vis (DMSO, 1.7 μM): very broad absorption at λ_{max} 325 nm.

3.2. X-ray crystallographic studies

Details of crystallographic parameters, data collection and refinements are listed in Table 1. Selected bond lengths (Å) and angles (°) for $\mathbf{H_2L^1}$, **1** and **5** are listed in Tables 2–4, respectively. Crystallographic data files for **2**–**4** are supplied as supplementary material. Intensities were collected on a Nonius Kappa CCD diffractometer with graphite monochromated Mo Kα radiation ($\lambda = 0.71073$ Å) at 153 K. Absorption corrections were applied using GAUSSIAN. The structures were solved by direct methods and refined anisotropically using full-matrix least-squares methods with the SHELX 97 program package [7]. The coordinates of the non-hydrogen atoms were refined anisotropically, while hydrogen atoms were included in the calculation isotropically but not refined. Neutral atom scattering factors were taken from Cromer and Waber [8].

4. Supplementary material

Crystallographic data for the complexes have been deposited with the Cambridge Crystallographic Data Centre, CCD 278165–278170 for $\mathbf{H_2L^1}$, **1**–**5**. Copies of this information may be obtained free of charge from The Director, CCDC, 12 Union Road, Cambridge, CB2 1EZ, UK (fax: +44 1223 336033; e-mail: deposit@ccdc.cam.ac.uk or web: http://www.ccdc.cam.ac.uk).

Acknowledgment

We thank the Robert A. Welch Foundation (Grant F-816) for financial support.

References

[1] (a) S. Leninger, B. Olenyuk, P.J. Stang, Chem. Rev. 100 (2000) 853;
(b) C.J. Jones, Chem. Soc. Rev. 27 (1998) 289;
(c) B.J. Holliday, C.A. Mirkin, Angew. Chem. Int. Ed. 40 (2001) 2022;
(d) M. Fujita, K. Umemoto, M. Yoshizawa, N. Fujita, T. Kusukawa, K. Biradha, Chem. Commun. (2001) 509;
(e) M. Munakata, L.P. Wu, T. Kuroda-Sowa, Adv. Inorg. Chem. 46 (1999) 173.

[2] (a) F.A. Cotton, C. Lin, C.A. Murillo, Acc. Chem. Res. 34 (2001) 759;
(b) R.P. Bonar-Law, T.D. McGrath, N. Singh, J.F. Bickley, C. Femoni, A. Steiner, J. Chem. Soc., Dalton Trans. (2000) 4343.

[3] (a) M.P. Hogerheide, J. Boersma, G.V. Konten, Coord. Chem. Rev. 155 (1996) 87;
(b) D. Imbert, M. Cantuel, J.-C.G. Bünzli, G. Bemardinelli, C. Piguet, J. Am. Chem. Soc. 125 (2003) 15698;
(c) N.M. Shavaleev, L.P. Moorcraft, S.J.A. Pope, Z.R. Bell, S. Faulkner, M.D. Ward, Chem. Commun. (2003) 1134;
(d) S.I. Klink, H. Keizer, F.C.J.M. van Veggel, Angew. Chem., Int. Ed. 39 (2000) 4319.

[4] (a) X.-P. Yang, R.A. Jones, V. Lynch, M.M. Oye, A.L. Holmes, J. Chem. Soc., Dalton Trans. 5 (2005) 849;
(b) X.-P. Yang, R.A. Jones, Q.-Y. Wu, M.M. Oye, A.L. Holmes, Polyhedron (2005) in press.

[5] T. Kitazume, N. Ishikawa, Bull. Chem. Soc. Jpn. 47 (1974) 785.

[6] S.M. Malinak, O.T. Rosa, D. Coucouvanis, Inorg. Chem. 37 (1998) 1175.

[7] G.M. Sheldrick, SHELX 97A Software Package for the Solution and Refinement of X-ray Data, University of Göttingen, Göttingen, Germany, 1997.

[8] D.T. Cromer, J.T. WaberInternational Tables for X-ray Crystallography, vol. 4, Kynoch Press, Birmingham, 1974 (Table 2.2A).

Available online at www.sciencedirect.com
SCIENCE DIRECT
Polyhedron 25 (2006) 888–900
POLYHEDRON
www.elsevier.com/locate/poly

Synthesis, structure, and redox states of homoleptic d-block metal complexes with bis-1,2,4-triazin-3-yl-pyridine and 1,2,4-triazin-3-yl-bipyridine extractants

Michael G.B. Drew [a], Mark R.St.J. Foreman [a,*], Andreas Geist [b], Michael J. Hudson [a], Frank Marken [c], Virginia Norman [a], Michael Weigl [b]

[a] *School of Chemistry, The University of Reading, P.O. Box 224, Whiteknights, Reading, Berks RG6 6AD, UK*
[b] *Forschungszentrum Karlsruhe, Institut fur Nukleare Entsorgung, P.O. Box 3640, D-76021, Karlsruhe, Germany*
[c] *Department of Chemistry, University of Bath, Bath BA2 7AY, UK*

Received 1 July 2005; accepted 30 September 2005
Available online 28 November 2005

Dedicated to Professor Mike Hursthouse on the happy occasion of his 65th birthday.

Abstract

It has been established that triazinyl bipyridines (*hemi*-BTPs) and bis-triazinyl pyridines (BTPs), ligands which are currently being investigated as possible ligands for the separation of actinides from lanthanides in nuclear waste, are able to form homoleptic complexes with first row transition metals such as cobalt(II), copper(II), iron(II), manganese(II), nickel(II) and zinc(II). The metal complexes exhibit six-co-ordinate octahedral structures and redox states largely analogous to those of the related terpyridine complexes. The reactivity of the different redox states of cobalt bis-*hemi*-BTP complex in aqueous environments has been studied with two-phase electrochemistry by immobilisation of the essentially water-insoluble metal complexes on graphite electrodes and the immersion of this modified electrode in an aqueous electrolyte.

It was found that redox potentials for the metal-centred reactions were pH-independent whereas the potentials for the ligand-centred reactions were strongly pH-dependent. The reductive degradation of these complexes has been investigated by computational methods. Solvent extraction experiments have been carried out for a range of metals and these show that cobalt(II) and nickel(II) as well as palladium(II), cadmium(II) and lead(II) were all extracted with the ligands **1e** and **2c** with higher distribution ratios that was observed for americium(III) under the same conditions. The implications of this result for the use of these ligands to separate actinides from nuclear waste are discussed.
© 2005 Elsevier Ltd. All rights reserved.

Keywords: Redox potentials; Crystal structures; Transition metals; Bis-1,2,4-triazine-3-yl-pyridines

1. Introduction

The aqueous solution (PUREX first cycle raffinate) remaining after the extraction of uranium and plutonium from dissolved used nuclear fuel by the PUREX process is a complex mixture of fission products and corrosion products [1] that also contains the transplutonium actinides, americium and curium. These actinides, together with the residual plutonium, are responsible for the majority of the radiotoxicity that will be present between 300 and 20 000 years in the future [2]. If these metals were removed from the PUREX raffinate then the majority of the radiotoxicity will decay during the likely lifetime of a stainless steel drum [3]. After removal from the PUREX raffinate, the actinides could be disposed of separately, or transmutated by nuclear means or employed in medical [4] or industrial applications. The lanthanides have similar properties to the trivalent

* Corresponding author. Tel.: +44 118 378 8789; fax: +44 118 378 6331.
E-mail address: m.r.s.foreman@reading.ac.uk (M.R.St.J. Foreman).

0277-5387/$ - see front matter © 2005 Elsevier Ltd. All rights reserved.
doi:10.1016/j.poly.2005.09.030

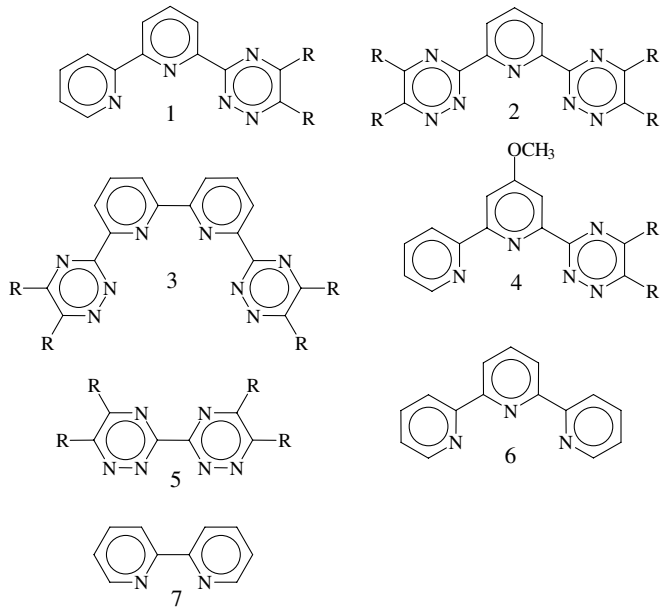

Fig. 1. Key to parent structures. *Hemi*-BTP (**1**), BTP (**2**), BTBP (**3**), methoxy-*hemi*-BTP (**4**), 3,3′-bi-1,2,4-triazinyl (**5**), terpyridine (**6**), 2,2′-bipyridine (**7**). Key to ancillary groups, hydrogen (**a**), methyl (**b**), ethyl (**c**), *n*-propyl (**d**) and *n*-pentyl (**e**).

actinides since they have high neutron cross-sections and they are abundant among the fission products of ^{235}U (the atom yield for the lanthanides is ca. 28%). Recently, we have investigated the lanthanide coordination chemistry of triazinyl pyridines such as the triazinyl bipyridines (*hemi*-BTPs, **1**) [5], the bis-triazinyl pyridines (BTPs, **2**) [6] and the bis-triazinyl bipyridines (BTBPs, **3**) [7]. However, when compared with the oligopyridines, little is known about the coordination chemistry of the 1,2,4-triazines with the first row transition metals [8–10]. It has been shown during an actinide extraction test using tetrapropyl-BTP (**2d**) that much of the iron, ruthenium and palladium present in the acid aqueous feed solution enters the organic phase [11] so that a transition metal could inhibit the extraction of the desired metals by sequestering the extractant. Also the transition metal could enter a product or waste stream where it could cause undesirable reactions such an exothermic reactions during the bituminisation of waste [12]. It is therefore appropriate to carry out a systematic investigation of the first row transition metal coordination chemistry of tridentate triazinyl-pyridines. In this paper, we report the synthesis and the spectroscopic, crystallographic and electrochemical characterisation of a series of transition metal complexes with a variety of 1,2,4-triazinyl pyridine ligands shown in Fig. 1.

2. Experimental

2.1. Synthesis

All organic reagents were purchased from Acros or Aldrich, while inorganic reagents were obtained from either BDH or Aldrich. 6-(5,6-diethyl-[1,2,4]triazin-3-yl)-[2,2′]bipyridinyl (diethyl-*hemi*-BTP, **1c**) and 6-(5,6-dimethyl-[1,2,4]triazin-3-yl)-[2,2′]bipyridinyl (dimethyl-*hemi*-BTP, **1b**) were prepared as previously described [5] while 6-(5,6-diethyl-[1,2,4]triazin-3-yl)-[2,2′]bipyridinyl (dipentyl-*hemi*-BTP, **1e**) was prepared by an analogous procedure. 4-Methoxy-2,2′-bipyridine-*N*-oxide was obtained by the nitration and subsequent methanolysis of 2,2′-bipyridine-*N*-oxide [13]. Oxalodihydrazonic acid diamide was formed by the reaction of dithiooxamide (rubeanic acid) and hydrazine in ethanol (*WARNING*: The reaction forms a large volume of toxic gas [hydrogen sulfide]) [14]. ^{1}H, ^{13}C-{^{1}H} and ^{13}C NMR spectra were recorded using either a Bruker AMX400 or an Avance DPX250 instrument. Chemical shifts are reported in ppm downfield from tetramethylsilane. Magnetic moments were determined in dichloromethane also using the Avance DPX250 by the Evans' NMR method. Carbon, hydrogen and nitrogen microanalysis was performed by Medac Limited.

2.1.1. 2,6-Bis-(5,6-diethyl-[1,2,4]triazin-3-yl)-pyridine (tetramethyl BTP, **2b**) [15]

Pyridine-2,6-dihydrazonic acid diamide (3.19 g) was combined with THF (100 mL), triethyl amine (3 mL) and butane-2,3-dione (6 mL) and heated under reflux (3 h). After cooling toluene was added to the reaction flask, and the mixture heated briefly under reflux. After allowing the mixture to cool, the orange solid was isolated by filtration. After washing with ethanol and diethyl ether the solid (2.66 g; 55%) was allowed to dry in air. δ_H 8.81 (2H, d, 7.9 Hz), 8.14 (1H, t, 7.9 Hz), 2.80 (3H, s) and 2.74 (3H, s) ppm.

2.1.2. 2,6-Bis-(5,6-diethyl-[1,2,4]triazin-3-yl)-pyridine (tetraethyl BTP, **2c**)

Pyridine-2,6-dihydrazonic acid diamide (5.47 g) was combined with THF (175 mL), triethyl amine (10 mL) and hexane-3,4-dione (10 mL). The resulting mixture was heated under reflux (2 h). After allowing the mixture to cool, the first crop (4.61 g; 47%) was obtained by filtration and washing with a small volume of ethanol. By concentration of the mother liquor a second crop (2.18 g; 22%) was obtained giving an overall yield of 69%. *Anal.* Calc. for $C_{19}H_{23}N_7 \cdot 0.5EtOH$: C, 62.0; H, 6.7; N, 25.3. Found: C, 62.0; H, 6.9; N, 26.7%. δ_H 8.77 (2H, d, 7.9 Hz), 8.12 (1H, t, 7.9Hz), 3.06 (8H, m) and 1.47 (12 H, m). δ_C 163.36 (quat), 161.41 (quat), 161.00 (quat), 154.00 (quat), 138.62, 125.70, 27.67 (CH_2), 26.15 (CH_2), 12.82 and 12.13. MS (CI) 350 $(MH)^+$ and 240 amu. Molecular ion found at 350.2104 amu, $^{12}C_{19}{}^{1}H_{24}{}^{14}N_7$ requires 350.2093 amu (error of 3.2 ppm).

2.1.3. 6-(5,6-Dimethyl-[1,2,4]triazin-3-yl)-4-methoxy-[2,2′]bipyridinyl (dimethyl methoxy hemi BTP, **4b**)

To a solution of 4-methoxy-2,2′-bipyridine-*N*-oxide (6.67 g) in dichloromethane (100 mL) was added trimethylsilyl cyanide (5 mL) and dimethyl carbomyl chloride (3.5 mL). After allowing the mixture to stand for 3 days,

the solvent was evaporated. The solid was redissolved in dichloromethane, and the resulting solution was filtered through a silica pad before being evaporated again to give the nitrile as a white solid (5.70 g; 82%). δ_H ($CDCl_3$) 8.59 (1H, m), 8.37 (1H, m), 8.11 (1H, d, 2.4 Hz), 7.77 (1H, ddd 7.8, 7.8 and 1.8 Hz), 7.29 (1H, m), 7.15 (1H, d, 2.4 Hz). δ_C 167.36, 159.84, 154.38, 149.52, 137.58, 134.46, 125.20, 122.12, 117.78, 116.62, 108.96 and 56.38. The nitrile (2.03 g) was suspended in a mixture of ethanol (25 mL) and hydrazine monohydrate (8 mL), and the resulting slurry was heated to 50 °C (4 h). After allowing the mixture to cool, the volatile solvents were removed in vacuum to furnish a damp solid. Water (30 mL) was added and the mixture stirred to form a slurry and the solid was collected by filtration. The solid was washed with water (2 × 10 mL). In all 4.92 g of the damp solid was obtained. δ_H (CD_3OD) 8.66 (1H, m), 8.53 (1H, m), 7.97 (1H, ddd, 7.8, 7.8 and 1.8 Hz), 7.92 (1H, d, 2.4 Hz), 7.56 (1H, d, 2.4 Hz), 7.47 (1H, m) and 3.99 (3H, s). Part of the damp solid (2.32 g) was stirred in THF (60 mL), butane-2,3-dione (7 mL) was added and the resulting mixture boiled under reflux (2 h). After cooling, all volatile solvents were removed in vacuum before the resulting solid was recrystallised from hot ethanol to form a bright yellow crystalline solid (944 mg; 71% from nitrile, 58% overall). *Anal.* Calc. for $C_{16}H_{15}N_5O$ C, 65.5; H, 5.2; N, 23.9. Found: C, 65.3; H, 5.2; N, 23.7%. δ_H ($CDCl_3$) 8.60 (2H, m), 8.08 (1H, d, 2.5 Hz), 8.06 (1H, d, 2.5 Hz), 7.77 (1H, ddd, 7.7, 7.7 and 1.9 Hz), 7.26 (1H, m), 3.98 (3H, s), 2.71 (3H, s) and 2.63 (3H, s). δ_C ($CDCl_3$) 168.10 (quat), 162.00 (quat), 159.76 (quat), 158.85 (quat), 157.35 (quat), 156.05 (quat), 154.54 (quat), 149.37, 137.32, 124.49, 122.39, 111.00, 108.33, 56.12, 22.52 and 20.06.

2.1.4. 6-(5,6-Diethyl-[1,2,4]triazin-3-yl)-4-methoxy-[2,2′]bipyridinyl (diethyl methoxy hemi BTP, **4c**)

A sample of the dihydrazonic acid diamide formed from the nitrile (0.52 g) was dissolved in THF (10 mL), hexane-3,4-dione (2 mL) was added and the resulting mixture heated under reflux (2 h). After cooling, the product (502 mg; 63%) was isolated by removal of the solvent in vacuum. δ_H ($CDCl_3$) 8.60 (2H, m), 8.07 (2H, m), 7.77 (1H, ddd, 7.7, 7.7 and 1.8 Hz), 7.25 (1H, m), 3.97 (3H, s), 3.02 (2H, q, 7.5 Hz), 2.90 (2H, q, 7.4 Hz) and 1.38 (6H, m). δ_C ($CDCl_3$) 168.05 (quat), 162.78 (quat), 161.68 (quat), 160.63 (quat), 158.72 (quat), 156.10 (quat), 154.74 (quat), 149.30, 137.33, 124.46, 122.34, 111.08, 107.93, 56.06, 27.49 (CH_2), 26.08 (CH_2), 12.65 and 11.58. MS (CI) 322 $(MH)^+$ and 212 amu. Molecular ion found at 322.1669 amu, $^{12}C_{18}{}^{1}H_{20}{}^{14}N_5{}^{16}O$ requires 322.1668 amu (error of 0.4 ppm).

2.1.5. 5,6,5′,6′-Tetraethyl-[3,3′]bi[[1,2,4]triazinyl] (**5c**)

Oxalodihydrazonic acid diamide (26.7 g) was dissolved in a mixture of ethanol (300 mL) and THF (300 mL). To this solution was added triethyl amine (75 mL) and hexane-3,4-dione (75 mL). The mixture was heated under reflux (3 h), before being allowed to cool. The mixture was treated with decolourising charcoal, and filtered. The filtrate was concentrated in vacuum. The residue was triturated with petrol (100 mL, 40–60 °C fraction) before the solid was collected by filtration. After washing with diethyl ether (4 × 50 mL), the solid was dried in air (44.54 g; 71%). *Anal.* Calc. for $C_{14}H_{20}N_6$ C, 61.7; H, 7.4; N, 30.8. Found: C, 60.9; H, 7.4; N, 29.9%. δ_H 3.12 (4H, q, 7.5 Hz), 2.99 (4H, q, 7.5 Hz), 1.44 (12 H, m). δ_C 163.32 (quat), 161.78 (quat), 160.58 (quat), 27.63 (CH_2), 26.26 (CH_2), 12.76 and 11.96. MS (CI) 273 $(MH)^+$ and 163 amu. Molecular ion found at 273.1823 amu, $^{12}C_{14}{}^{1}H_{21}{}^{14}N_6$ requires 273.1827 amu (error of 1.6 ppm).

2.1.6. Typical procedure for the synthesis of the complexes of manganese, iron, copper and zinc

In method A, a solution of **1b** (201 mg) in hot ethanol (10 mL) was treated with iron(II) chloride tetrahydrate (76 mg) dissolved in water (3 mL). After cooling this red solution was treated with the sodium perchlorate solution, before concentrating in vacuum. The resulting solid was collected on a paper filter before being washed twice with water, ethanol and diethyl ether to give a deep red solid (280 mg; 94%). Method B is similar to method A except that the reaction mixture was evaporated to remove all the organic solvent before the addition of water.

2.1.7. Typical procedure for the synthesis of a complex of cobalt

Method C: To a deoxygenated suspension of **4b** (141.6 mg) in a mixture of ethanol (10 mL) and THF (5 mL) was added cobalt(II) chloride hexahydrate (57.6 mg). After stirring (4.5 h) this mixture was concentrated by evaporation. After dissolution in water (10 mL), a sodium perchlorate solution was added. The resulting red solid was collected by filtration before being washed with water, ethanol and ether.

2.1.8. Typical procedure for the synthesis of a complex of nickel

Method D: To a deoxygenated suspension of **4b** (145.7 mg) in a mixture of ethanol (10 mL) and THF (5 mL) was added nickel(II) chloride hexahydrate (59.0 mg). After being heated under reflux (4 h), the mixture was allowed to cool to room temperature before being concentrated by evaporation. After dissolution in water (10 mL), a sodium perchlorate solution was added. The resulting tan solid was collected by filtration before being washed with water, ethanol and ether.

CAUTION: Treat all materials containing both organic matter and perchlorate anions as potential explosives [16].

2.2. Crystallography

Crystallographic data are given in Table 1. All data were measured with Mo Kα radiation using the MARresearch Image Plate System. The crystals were positioned at

Table 1
Cell data for the structures

Complex	$[Mn(\mathbf{1c})_2]_2ClO_4 \cdot 3H_2O$	$[Fe(\mathbf{1c})_2]_2ClO_4$	$[Fe(\mathbf{4c})_2]_2ClO_4$	$[Co(\mathbf{1c})_2]_2ClO_4 \cdot CH_2Cl_2 \cdot H_2O$	$[Zn(\mathbf{1c})_2]_2ClO_4 \cdot 0.5CH_2Cl_2 \cdot 0.5H_2O$
Formula	$C_{34}H_{40}C_{12}MnN_{10}O_{11}$	$C_{34}H_{34}Cl_2FeN_{10}O_8$	$C_{36}H_{38}Cl_2FeN_{10}O_{10}$	$C_{35}H_{38}Cl_4CoN_{10}O_9$	$C_{34.5}H_{36}Cl_3ZnN_{10}O_{8.5}$
Molecular weight	890.60	837.5	897.51	943.49	898.45
Crystal system	triclinic	triclinic	monoclinic	triclinic	triclinic
Spacegroup	$P\bar{1}$	$P\bar{1}$	$P2_1/n$	$P\bar{1}$	$P\bar{1}$
Unit cell dimensions					
a (Å)	10.025(14)	9.207(11)	10.162(14)	11.199(14)	10.096(12)
b (Å)	11.780(14)	10.831(12)	37.40(4)	12.144(14)	11.454(14)
c (Å)	19.50(2)	17.570(19)	11.015(14)	20.02(2)	19.78(2)
α (°)	102.47(1)	96.61(1)	(90)	87.88(1)	101.25(1)
β (°)	95.35(1)	91.73(1)	96.63(1)	86.89(1)	94.21(1)
γ (°)	104.77(1)	92.27(1)	(90)	67.36(1)	105.34(1)
V (Å^3)	2148	1738	4159	2509	2145
Z	2	2	4	2	2
D_{calc} (g cm^{-3})	1.377	1.597	1.433	1.248	1.391
Number of reflections/R_{int}	8094/0.064	10476/0.0386	16672/0.0900	13216/0.0732	13146/0.0491
Reflections/constraints/parameters	6099/0/511	6167/0/501	6540/0/538	8790/0/552	7137/0/535
R_1, wR_2 [$I > 2\sigma(I)$]	0.1177, 0.2119	0.1175, 0.2579	0.1071, 0.2195	0.1098, 0.2682	0.1055, 0.2600
R_1, wR_2 (all data)	0.2544, 0.2660	0.1342, 0.2651	0.1590, 0.2483	0.2176, 0.3105	0.1415, 0.2852
Largest difference in peak and hole (e Å^{-3})	0.344 and −0.260	1.338 and −0.736	0.730 and −0.559	0.503 and −0.324	0.875 and −0.467

70 mm from the Image Plate and 100 frames were measured at 2° intervals with a counting time of 5 min. Data analyses were carried out with the XDS program [17]. The structures were solved using direct methods with the SHELX-86 program [18]. Non-hydrogen atoms were refined with anisotropic thermal parameters. The hydrogen atoms bound to carbon were included in geometric positions and given thermal parameters equivalent to 1.2 times those of the atom to which they were attached. The majority of structures contained some disordered solvent. All crystals were of poor quality and gave misshapen spots and as a result the crystal structures were solved with high R values. Empirical absorption corrections were applied using DIFABS [19]. The structures were refined on F^2 using SHELXL [20]. Crystal data have been deposited at the Cambridge Crystallographic Data Centre (reference numbers CCDC 277000–277004 inclusive).

2.3. Electrochemistry

All electrochemical experiments were conducted using a computer-controlled Autolab potentiostat (PGSTAT 30, Eco-chemie, Netherlands). Solution state electrochemical experiments were performed in deoxygenated acetonitrile in the presence of tetraethyl ammonium perchlorate (0.25 M). The tetraethyl ammonium perchlorate was obtained by the addition of perchloric acid to aqueous tetraethyl ammonium bromide, and was recrystallised twice from water before being dried in vacuum to a constant mass. *CAUTION: Treat all organic perchlorates as potential explosives; tetraethylammonium perchlorate is a known explosive* [16]. The working electrode was a 3 mm glassy carbon disk purchased from Bioanalytical Systems, a silver wire was used as a quasi-reference electrode and the counter-electrode was a platinum wire. Solution state potentials were measured using the ferrocene/ferrocenium couple (ferrocene added as an internal standard). Cyclic voltammetry was performed using a staircase waveform with a step size typically of 0.1 mV, while differential square wave experiments were performed at 25 Hz using an amplitude of 10 mV and a step size of 1 mV. For reversible electrochemical events, the formal potentials were calculated as the midpoint of potentials of the anodic and cathodic current peaks. For both reversible and irreversible redox processes formal potentials were also measured by using the peak potential obtained with differential square wave voltammetry. Two-phase voltammetry was performed using a 4.9 mm diameter basal plane pyrolytic graphite working electrode with microparticles adhering to the surface, a saturated calomel reference electrode, and a platinum gauze counter-electrode all immersed in an aqueous electrolyte solution. All experiments were conducted in argon (BOC) atmosphere and at a temperature of 22 ± 2 °C.

2.4. Computational chemistry

Density functional calculations were performed by using the ADF program [21]. Slater-type orbital basis sets of triple zeta quality for the valence orbitals were employed with polarisation functions on the ligand atoms (2p for H, and 3d for C and N) and additional valence p-orbitals on metal atom. Scalar relativistic effects were included via the Zora protocol. The Generalised Gradient Approximation was used with Becke88 exchange and Perdew86 correlation gradient corrections.

2.5. Metal extraction

All solvent extraction experiments were performed as previously described [22]. Organic phases were either solutions of **2c** (different concentrations) in kerosene/*n*-octan-1-ol (7:3 vol.) or solutions of **1e** (different concentrations) with 0.5 M 2-bromohexanoic acid in *tert*-butylbenzene. Aqueous solutions were Cr(III), Mn(II), Fe(III), Co(II), Ni(II), Cu(II), Zn(II), Sr(II), Y(III), Zr(IV), Ru(II) (added as $RuNO(NO_3)_3$), Rh(III), Pd(II), Cd(II), Ba(II), La(III)–Lu(III) (without Pm and Tm), Pb(II) (1 mg/L each) + ^{241}Am(III) (900 Bq/mL) in nitric acid of different concentrations. Equal volumes (1 mL each) of organic and aqueous phases were contacted for 4.5 h by vigorous shaking using an orbital shaker (IKA KS 250), the diameter of the circular path was ca. 15 mm, and the rotation rate was 9.2 Hz. During mixing the temperature was 20 °C. Samples were centrifuged, and phases were separated. Aliquots of each phase were taken for analysis. ^{241}Am activity was determined in 0.2 mL of each sample by gamma counting. 0.2 mL of each aqueous sample was diluted with 4.8 mL HNO_3 2% (suprapur) and analysed by ICP-MS. 50 μL (kerosene/octanol samples) or 25 μL (*tert*-butylbenzene samples) of each organic sample was dissolved in 4.95 or 4.975 mL of a solution of (10 g/L Triton X-100 in HNO_3 2% (suprapur)) and analysed by ICP-MS. In each case, standards were prepared accordingly.

3. Results and discussion

3.1. Metal extraction

Extraction experiments were carried out with Mn(II), Ni(II), Sr(II), Zr(IV), Ru(II) nitrosyl, Rh(III), Cd(II), Ba(II), Pb(II) and Am(III). Am(III), Pb(II), Cd(II) and Zr(IV) were extracted by an ion exchange process (Eq. (1) and Fig. 2), which was favoured by a low nitric acid concentration. The lanthanides were only weakly extracted; when the concentrations of **1e** and nitric acid were 0.020 and 0.1 M, respectively, the lanthanide distribution ratios were 2×10^{-3} or lower

$$M_{(aq)}^{n+} + n\mathrm{RCOOH}_{(org)} + x\mathbf{1e}_{(org)} \leftrightarrow [M(\mathrm{RCOO})_n(\mathbf{1e})_x]_{(org)} + n\mathrm{H}_{(aq)}^{+} \quad (1)$$

Similar behaviour was observed for americium with a solution of diethyl-*hemi*-BTP + bromodecanoic in an aliphatic diluent (Hydrogenated propylene trimer, also known as TPH) [5]. the ruthenium nitrosyl distribution ratio was independent of the nitric acid concentration indicating that a solvation mechanism (such as that in Eq. (2)) was also in operation

$$M_{(aq)}^{n+} + n\mathrm{NO}_3^- + x\mathbf{1e}_{(org)} \leftrightarrow [M(\mathbf{1e})_x] \cdot n\mathrm{NO}_{3(org)} \quad (2)$$

No extraction of either strontium or barium observed, and rhodium and manganese were only very weakly extracted (D_M was always less than 10^{-3}, NB: $D_M = [M_{organic}]/[M_{aqueous}]$). Nickel was totally extracted from all samples of the aqueous phase and hence it was not possible to elucidate the mechanism of the nickel extraction. The solutions of **3e** in *tert*-butylbenzene/bromohexanoic acid mixtures were only able to weakly extract nickel and it was deduced that nickel(II) has a high affinity for *hemi*-BTP [22] (see Fig. 3).

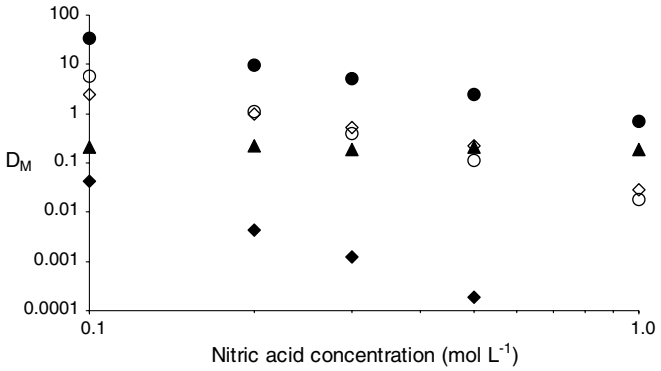

Fig. 2. Distribution ratios for metals with **1e** (0.02 M) in bromohexanoic acid (0.5 M) in *tert*-butylbenzene from nitric acid solutions. The *x*-axis has a logarithmic scale. *Key*: ◆, Am; ◇, Zr; ▲, Ru; ●, Cd; and ○, Pb.

In a similar way, solutions of **2c** in a 3:7 (v/v) mixture of octanol and keroscene were tested for their ability to extract metals. In common with the solution of **1e** the solution of **2c** did not extract strontium or barium, and the rhodium was only weakly extracted. cobalt(II), nickel(II), palladium(II), cadmium(II) and lead(II) were all extracted with higher distribution ratios than was observed for americium(III) under the same conditions. Zirconium(IV) and ruthenium nitrosyl were both extracted but the distribution ratios are lower than those observed for americium(III). Many of the metals are extracted by a solvation mechanism similar to that in Eq. (2), further work will be required in order to clearly identify the extraction mechanims. It is clear that metals such as nickel and palladium would, if present at high concentrations, be able to disrupt an americium extraction process by sequestering the extraction agent. Since it had been shown that nickel(II) has an exceptional ability to bind to **1e** and **2c**, a detailed investigation of the coordination chemistry of the triazinyl pyridines with the first row transition metals was initiated (see Fig. 3).

3.2. Synthesis and some properties of the metal complexes

An immediate colour change occurred on combining **1c**, **2c**, **4b**, **4c** or terpyridine (**6**) with manganese(II) chloride, iron(II) chloride, cobalt(II) chloride or copper(II) nitrate, and it can be assumed that aqueous zinc acetate reacts rapidly with the tridentate ligands although no colour change is discernable. While nickel(II) chloride started to react within seconds, owing to the lower water exchange rate of this metal, all reactions using nickel salts were heated under reflux for at least 3 h [23,24]. Iron(II) chloride was reacted with a bis-triazinyl (**5c**), bis-(5,6-dimethyltriazinyl)

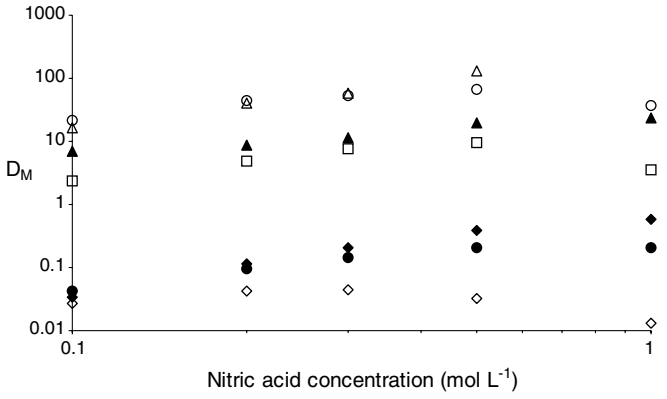

Fig. 3. Distribution ratios for selected metals with **2c** (0.01 M) in 3:7 (v/v) octanol/kerosene mixture from nitric acid solutions. The *x*-axis has a logarithmic scale. *Key*: ◆, Am; ◇, Zr; ▲, Pd; ●, Mn; △, Ni; □, Co; and ○, Pb.

pyridine (dimethyl-BTP, **2b**) and dimethyl-*hemi*-BTP (**1b**). All the complexes were collected as solids after anion metathesis with sodium perchlorate or ammonium perrhenate: Acceptable microanalytical data were obtained for all the solids (Table 2).

In common with iron(II) bis-terpyridine salts, the perchlorate salts of the iron(II) homoleptic complexes of **1c**, **2c**, **4b**, **4c** and **5c** were examined by NMR experiments and found to be diamagnetic indicating that the two triazinyl pyridine ligands provide the metal with an octahedral coordination environment that has a strong ligand field. The iron complexes of **1b** and **2b** were too insoluble for NMR experiments to be carried out but it can be assumed that they would also be diamagnetic. It is interesting that the metal complexes of **4b** were soluble in both dichloromethane and acetonitrile, suggesting that the methoxy group significantly enhances the solubility. Owing to the paramagnetism of the manganese, cobalt, nickel and copper complexes only the iron and zinc complexes were characterised by ^{1}H and ^{13}C NMR, the NMR spectra are in agreement with the proposed homoleptic distorted octahedral structure of the complexes. The Evans' NMR method was used to examine the nickel complexes in dichloromethane solution and it was found that each nickel atom in **1c** has 2.3 unpaired electrons and in **4b** had 2.2 unpaired electrons suggesting that, in these octahedral complexes, the axial perturbation of the ligand field is too weak to permit a singlet ground state.

Table 2
Data for the metal complexes formed using compounds **2c**, **1c**, **4b**, **4c**, **5c**, **1b**, **2b** and **6**

Complex	Yield (%)	Colour	Method of synthesis	Redox potentials (V)				CHN microanalyses					
				Ligand-centred		Metal-centred		Found (%)			Required (%)		
						I/II	II/III	C	H	N	C	H	N
$[Mn(\mathbf{4b})_2]\cdot 2ClO_4$	73	yellow	A	−1.53*	−1.42*	–	0.807	45.0	3.6	16.2	45.7	3.7	16.7
$[Fe(\mathbf{4b})_2]\cdot 2ClO_4\cdot 0.5H_2O$	91	black	B	−1.68*	−1.46*		0.651	45.1	3.5	16.1	45.2	3.6	16.5
$[Co(\mathbf{4b})_2]\cdot 2ClO_4$	59	red	C	−2.08*	−1.79*	−1.158	−0.212	45.2	3.6	16.3	45.5	3.6	16.6
$[Ni(\mathbf{4b})_2]\cdot 2ClO_4$	76	tan	D	−2.14*$	−1.62*$	−1.50*$	1.10	45.9	3.6	16.4	45.5	3.6	16.6
$[Cu(\mathbf{4b})_2]\cdot 2ClO_4\cdot H_2O$	84	green	A	–	–	−0.582	–	44.8	3.6	16.1	44.3	3.7	16.1
$[Zn(\mathbf{4b})_2]\cdot 2ClO_4$	86	pale green	A	–	–	–	–	44.6	3.6	16.1	44.2	3.7	16.1
$[Mn(\mathbf{1c})_2]\cdot 2ClO_4\cdot 0.5H_2O$	84	yellow	A	−1.72*	−1.50*	–	0.875	48.3	4.1	16.5	48.3	4.1	16.6
$[Fe(\mathbf{1c})_2]\cdot 2ClO_4$	80	deep red	A	−1.76*	−1.48*	–	0.753	47.9	3.8	16.1	47.7	4.2	16.4
$[Co(\mathbf{1c})_2]\cdot 2ClO_4\cdot H_2O$	85	red	C	−2.07*	−1.82*	−1.065	−0.195	47.9	4.0	16.4	47.6	4.2	16.3
$[Ni(\mathbf{1c})_2]\cdot 2ClO_4$	90	tan	D	−2.17*$	−1.73*	−1.450	1.196	48.7	4.1	16.6	48.6	4.0	16.7
$[Cu(\mathbf{1c})_2]\cdot 2ClO_4\cdot H_2O$	89	green	A	–	−1.14*	−0.536	–	47.1	4.0	16.0	47.3	4.2	16.2
$[Zn(\mathbf{1c})_2]\cdot 2ClO_4$	85	white	A	–	–	–	–	47.4	4.0	16.1	47.2	4.2	16.2
$[Mn(\mathbf{2c})_2]\cdot 2ClO_4$	97	yellow	A	–	–	–	–	47.1	4.9	20.2	47.9	4.9	20.6
$[Fe(\mathbf{2c})_2]\cdot 2ClO_4\cdot H_2O$	59	brick red	B	−1.60*	−1.40*	–	0.837	47.1	4.5	20.0	47.0	4.9	20.2
$[Co(\mathbf{2c})_2]\cdot 2ClO_4\cdot 2H_2O$	76	red	C	−1.92*	−1.73*	−0.925	−0.194	45.7	4.6	19.6	46.0	5.0	19.7
$[Ni(\mathbf{2c})_2]\cdot 2ClO_4\cdot H_2O$	61	tan	D	−2.12*$	−1.546£	−1.270	1.186	46.8	4.9	20.0	46.8	4.9	20.1
$[Cu(\mathbf{2c})_2]\cdot 2ClO_4\cdot H_2O$	83	green	A	–	1.20*	−0.344	–	46.7	4.7	20.2	46.6	4.9	20.0
$[Zn(\mathbf{2c})_2]\cdot 2ClO_4$	81	white	A	–	–	–	–	47.0	4.9	20.4	47.4	4.8	20.4
$[Y(\mathbf{1c})_2]\cdot 3ClO_4$	75	white	A	–	–	–	–	50.1	4.6	17.1	42.1	3.5	14.4
$[Zn(\mathbf{1c})_2]\cdot 2ReO_4\cdot H_2O$	76	white	A	–	–	–	–	35.0	3.0	12.0	35.0	3.1	12.0
$[Fe(\mathbf{4c})_2]\cdot 2ClO_4\cdot 0.5H_2O$	91	black	A	−1.78*	−1.50*	–	0.629	47.6	3.8	14.5	47.7	4.3	15.4
$[Fe(\mathbf{1b})_2]\cdot 2ClO_4\cdot 2H_2O$	94	deep red	A	–	–	–	–	44.1	3.2	16.7	44.1	3.7	17.1
$[Fe(\mathbf{2b})_2]\cdot 2ClO_4$	95	brick red	B	–	–	–	–	41.8	3.4	22.6	41.9	3.7	22.8
$[Fe(\mathbf{6})_2]\cdot 2ClO_4$	n/a	purple	A	−1.790	−1.652	–	0.702	–	–	–	–	–	–
$[Co(\mathbf{6})_2]\cdot 2ClO_4$	n/a	red	C	–	−2.056	−1.183	−0.139	–	–	–	–	–	–
$[Ni(\mathbf{6})_2]\cdot 2ClO_4$	n/a	tan	D	–	−1.827	−1.622	1.257	–	–	–	–	–	–
$[Cu(\mathbf{6})_2]\cdot 2ClO_4$	n/a	green	A	–	–	−0.660	–	–	–	–	–	–	–
$[Fe(\mathbf{5c})_3]\cdot 2ClO_4\cdot H_2O$	90	red	A	−1.561 −1.825	−1.368	–	0.946	45.8	5.6	22.1	45.6	5.8	22.7

All redox potentials are expressed relative to the ferrocene/ferrocenium couple (Fc/Fc^{+}). For reversible couples the redox potentials are the mean of the anodic and cathodic peaks observed during cyclic voltammetry experiments (200 mV s^{-1}). For irreversible reductions the redox potential expressed is the potential of the cathodic peak relative to the cathodic peak for the reduction of ferrocenium ions.
Key: *, irreversable reduction; £, partly reversible reduction; $, measured using differential square wave voltammetry; and –, not observed.

3.3. Crystallography

Crystals of the complexes formed between Mn, Fe, Co and Zn with diethyl-*hemi*-BTP (**1c**) were obtained by the liquid diffusion of diethyl ether and petrol (60–80 °C fraction) into dichloromethane solutions of the metal complexes and crystal structures were obtained (Fig. 4). The structure of the iron compound with **4c** was also determined (Fig. 5). A search was made of the crystallographic database [25,26] for related structures. The triazine nitrogens in $[Fe(\mathbf{4c})_2]\cdot 2ClO_4$ are at similar distances from the iron at 1.955(6) and 1.946(6) Å to the triazine nitrogens in $[Fe(\mathbf{5b})_3]^{2+}$ [10] which are at 1.940 and 1.932 Å. The M–N bond lengths listed in Table 3 for the five structures suggest that of all the metals, iron has the highest affinity and manganese the lowest affinity for the *hemi*-BTPs. The Fe(II) and Co(II) complexes have coordination environments which are closest to ideal octahedral and for these metals the triazine nitrogens form shorter bonds to the metal than the outer pyridine nitrogens which contrasts with the fact that the pyridine and triazine nitrogens in the dichlorocopper complex of 2-(5,6-diphenyl-[1,2,4]triazin-3-yl)-[1,10]phenanthroline are approximately equidistant from the metal atom at lengths of 2.100 and 2.116 Å [27]. In common with the iron and cobalt complexes of **1c** in the ruthenium(II) complexes of 2-(5,6-diphenyl-[1,2,4]triazin-3-yl)-[1,10]phenanthroline, 9-[1,10]phenanthrolin-2-yl-7,8,10-triaza-fluoranthene and 3-[1,10]phenanthrolin-2-yl-phenanthro[9,10-*e*][1,2,4]triazine, the triazine nitrogen to metal bond is shorter than the pyridine nitrogen to metal bond, e.g., 2.072 versus 2.106 Å in the case of the diphenyl-triazinyl ligand [28]. This difference, which was observed for the ruthenium, iron and cobalt complexes can be readily rationalised by the difference in the steric demands of the two different heterocylic rings. The two rings differ in steric demands because in the case of the 2-pyridyl group adjacent to the nitrogen atom is a carbon bearing a hydrogen, in the triazinyl group this CH unit has been replaced by a nitrogen atom which has a smaller steric effect. The structures of the zinc and manganese complexes are more distorted from ideal octahedral geometry. In the Mn(II) complex the bonds to triazine are shorter than those to pyridine, while in the Zn(II) complex in one ligand these bonds are equivalent while in the other ligand the bond to the triazine nitrogen is significantly longer than that to pyridine nitrogen. For these d^{10} and high-spin d^5 complexes the N(21)–M–N(51) angle is distorted by more than 15° away from the expected angle (180°) for a perfect octahedral complex compared to a value of ca. 5° in the iron (d^6) and cobalt (d^7) complexes. The steric crystal packing effects are more likely to be able to distort the coordination environment of a d^{10} or a high spin d^5 metal centre, where ligand field energy effects are absent, than d^6 and d^7 octahedral metal centres.

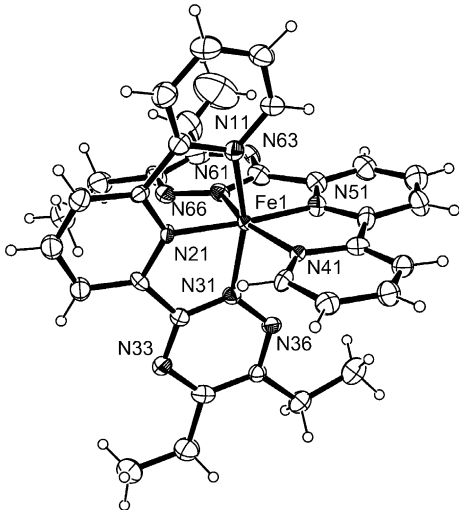

Fig. 4. The $[Fe(\mathbf{1c})_2]^{2+}$ cation present in the perchlorate salt, with ellipsoids at 25% probability.

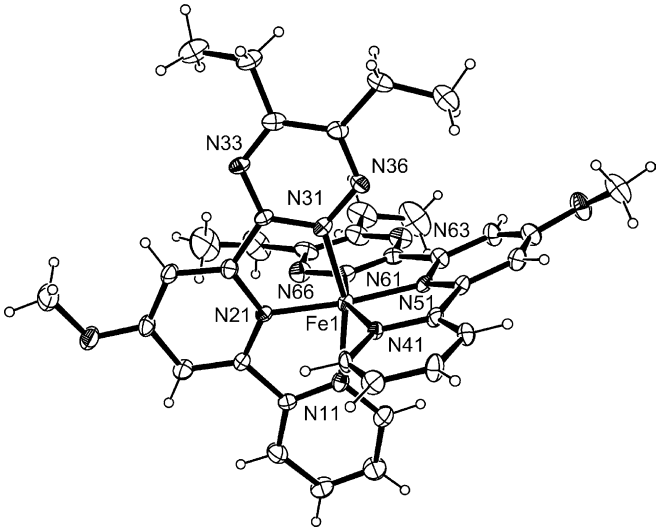

Fig. 5. The $[Fe(\mathbf{4c})_2]^{2+}$ cation present in the perchlorate salt, with ellipsoids at 25% probability.

3.4. Electrochemical characterisation

Next, the electrochemical characteristics of the homoleptic metal complexes of Mn, Fe, Co, Ni, and Zn with 1,2,4-triazin-3-yl-pyridine ligands were explored. A change in redox state during the extraction process is likely to have a significant impact on the rate of formation or on the degradation of these metal complexes and, therefore, voltammetric measurements were undertaken in both organic and aqueous environments. In order to study the metal complexes in organic solution, acetonitrile was employed as the solvent. The very low solubility of the metal complexes in aqueous media, required for the successful two-phase extraction process, prevented the study of electrochemical properties in aqueous solution. However, two-phase (solid metal complex|aqueous electrolyte solution) electrochemical data were readily obtained by immobilisation of the solid metal complexes at basal plane pyrolytic graphite electrodes and immersion into aqueous media [35].

Table 3
Experimental and theoretical M–N bond lengths (Å) in the metal coordination spheres

Metal nitrogen distance (Å)	Nitrogen type	Metal complex					
		$[Mn(\mathbf{1c})_2]^{2+}$	$[Fe(\mathbf{1c})_2]^{2+}$	$[Fe(\mathbf{4c})_2]^{2+}$	$[Co(\mathbf{1c})_2]^{2+}$	$[Zn(\mathbf{1c})_2]^{2+}$	
Experimental							
M–N(11)	outer py	2.274(8)	1.917(7)	1.979(7)	2.032(7)	2.198(6)	
M–N(21)	inner py	2.217(7)	1.886(6)	1.918(6)	1.897(7)	2.074(6)	
M–N(31)	outer tz	2.252(7)	1.869(7)	1.955(6)	2.029(7)	2.205(7)	
M–N(41)	outer py	2.240(10)	1.961(6)	2.011(6)	2.094(7)	2.123(7)	
M–N(51)	inner py	2.217(12)	1.875(7)	1.896(6)	1.934(7)	2.097(6)	
M–N(61)	outer tz	2.303(8)	1.868(7)	1.946(6)	2.043(7)	2.256(7)	
		$[Mn(\mathbf{1a})_2]^{2+}$	$[Fe(\mathbf{1a})_2]^{2+}$	$[Co(\mathbf{1a})_2]^{2+}$	$[Ni(\mathbf{1a})_2]^{2+}$	$[Cu(\mathbf{1a})_2]^{2+}$	$[Zn(\mathbf{1a})_2]^{2+}$
Theoretical							
M–N(11)	outer py	2.216	1.927	1.934	2.181	2.112	2.052
M–N(21)	inner py	2.121	1.839	1.843	1.898	2.013	1.933
M–N(31)	outer tz	2.095	1.876	1.875	2.112	2.169	2.033

In acetonitrile solution, several metal and ligand-centred redox processes were observed (see Table 2) for all metal complexes. The metal-centred redox reactions were reversible, and were analogous to the reported metal-centred redox chemistry of the homoleptic bis-terpyridine complexes of Mn, Fe, Co and Ni [29,30]. The Cu(II)/Cu(I) redox chemistry of the copper complexes was very similar to that of the bis-4′-methylsulfanyl-[2,2′;6′,2″]terpyridine complex [31]. In contrast, many of the ligand-centred reductions appeared to be chemically irreversible at a scan rates of 0.1 V s^{-1}. In some cases the reduction of the ligand led to the formation of a coating on the glassy carbon working electrode (vide infra), which could be partly removed during the subsequent oxidation (for Co and Fe) or only by polishing with alumina (for Cu). In contrast to the formation of copper metal during reduction of the bis-4′-methylsulfanyl-[2,2′;6′,2″]terpyridine copper(I) complex [31], unreactive non-conductive coatings were formed during the reduction of copper(I) complexes.

When scanning over a wide potential window (from +1.2 to −2.4 V) three reduction processes (ligand-centred) and one oxidation process (metal-centred) for $[Fe(\mathbf{1c})_2]^{2+}$ were observed (see Fig. 6). The oxidation process is highly reversible and well defined. The reduction processes appear to be one electron in nature (by comparison with the oxidation) and diffusion-controlled. However, the smaller re-oxidation signals and spurious product signals at −0.7 V versus $Fc^{+/0}$ indicate a follow-up reaction and limited chemical inertness of the reduction products.[1] Sharp peaks are observed for the reduction at −2.3 V versus $Fc^{+/0}$ and the re-oxidation at −1.7 V versus $Fc^{+/0}$ which are consistent with the precipitation of a neutral intermediate $[Fe(\mathbf{1c})_2]^0$ onto the electrode, followed by either a solid state phase transformation or a stripping reaction during either the reduction or oxidation. An analogous process has been reported for the formation of the neutral complexes $[M(bipy)_3]^0$ (M = Fe, Ru and Os) [32].

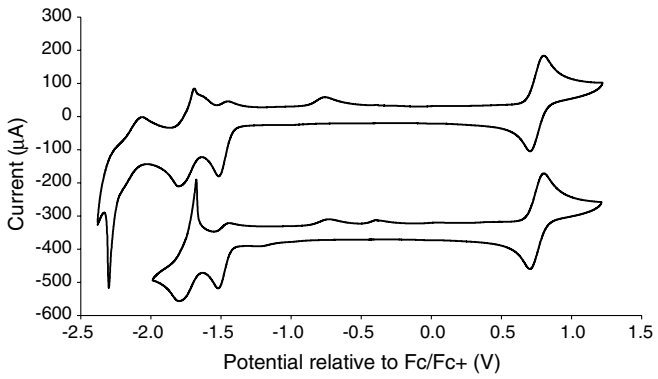

Fig. 6. Cyclic voltammograms of $[Fe(\mathbf{1c})_2]^{2+}$ scanned at 200 mV s^{-1} over two different potential ranges.

Since no adsorption of electroactive materials was observed during experiments using solutions of $[Fe(\mathbf{5c})_3]^{2+}$, it was considered possible that the formation of an anionic complex through a reversible reaction might prevent electrocrystallisation on the electrode. To test this hypothesis cobalt complexes of *hemi*-BTP and BTP ligands were prepared and examined with cyclic voltammetry, as it is known that for the bis-terpyridine cobalt complex the Co(I)/(II) couple has a potential intermediate between the Co(II)/(III) and ligand-centred redox couples. It was found for the cobalt complexes of BTP and *hemi*-BTP ligands that the ligand-centred reduction events were irreversible and resulted in the formation of an electroactive coating on the electrode, indicating that after reduction the triazinyl pyridine ligands were converted to other species. The electroactive coating was readily removed by polishing the electrode. Such degradations have not been observed

[1] The exact provenance of the small anodic peaks is unclear. When the potential range for the iron, cobalt and nickel complexes is restricted to the range in which only the reversible metal centred redox events occur, these anodic peaks are absent, upon the irreversible ligand centred reductions these anodic peaks appeared suggesting a redox active coating was formed upon the working electrode. For example, when $[Ni(\mathbf{1c})_2]^{2+}$ and $[Ni(\mathbf{4b})_2]^{2+}$ was reduced (respectively) to −2.5 and −1.5 V on subsequent scans, new oxidation peaks at 0.26 and −0.04 V were observed. By polishing the working electrode the material responsible for these new peaks were removed.

for the bis-vinylterpyridine complex of iron in either acetonitrile or dimethylformamide in the range from −0.4 to −2.1 V versus Fc/Fc^+ [29,33].

For the metal-centred redox events, the methoxy groups in ligand (**4b**) caused a cathodic shift in redox potential for the complexes by an average of 61 mV. This cathodic shift due to the resonance effect of the methoxy group can be contrasted with the anodic shift caused by the introduction of a pyridyl group at the 4′ positions of the terpyridines attached to an iron-centre [34]. On the other hand, the replacement of the two *hemi*-BTP ligands by BTP ligands resulted in a higher anodic shift of 98 mV. One rationalisation for this higher value is that the triazine ligands are stronger π-acids and weaker σ donors.

In order to obtain an understanding of the redox chemistry of the metal complexes of the 1,2,4-triazin-3-yl-pyridines in the presence of aqueous media, an investigation of the solid metal complexes adhered to graphite electrodes and immersed in aqueous electrolyte media was undertaken [35,36]. The resulting two-phase system (solid metal complex|aqueous electrolyte) allows well-defined voltammograms to be recorded and the aqueous redox chemistry related to the solution phase redox chemistry in acetonitrile. While microparticles of $[Co(\mathbf{2c})_2]\cdot 2ClO_4$, $[Co(\mathbf{1c})_2]\cdot 2ClO_4$ and $[Co(\mathbf{4b})_2]\cdot 2ClO_4$ on a graphite surface immersed in aqueous sodium perchlorate solution gave reversible and reproducible electrochemical responses, microparticles of the analogous Mn(II), Fe(II), Ni(II) and Cu(II) solids gave weaker and often less well-defined responses. This difference can be rationalised by the fact that the Co(II) complexes are the only metal complexes, which can be both reduced and oxidised reversibly (metal-centred) hence facilitating electrical conduction through the passage of electrons and holes through the crystal lattice (a requirement for the solid state electrochemical process to occur). All further microparticle voltammetry was performed using $[Co(\mathbf{1c})_2]\cdot 2ClO_4$.

It was found that microparticles of $[Co(\mathbf{1c})_2]\cdot 2ClO_4$ exhibit a chemically reversible Co(II)/Co(III) redox couple at 35 mV versus SCE (Fig. 7) when the solid is in contact with neutral sodium perchlorate solution. The anodic and cathodic current peaks are at 0 and 70 mV versus SCE, respectively. This process is consistent with the metal-centred Co(II)/Co(III) process observed in acetonitrile solution (see Table 2).

For the solid-state process, it is likely that perchlorate anions can be reversibly inserted into the solid in order to allow charge neutrality to be maintained during the redox process. In contrast to the solution state cyclic voltammetry, the anodic and cathodic current peaks were proportional not to the square root of the scan rate suggesting that an immobilised redox system reacts and that diffusion was not rate limiting. On increasing the scan-rate the anodic current peak occurred at a more cathodic (reducing) potential. This is the opposite of the relationship between the potential of the anodic peak and the scan-rate that was observed for a quasi-reversible couple with slow

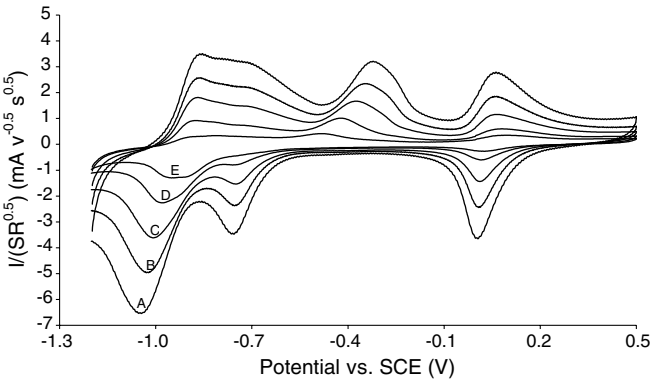

Fig. 7. Two-phase cyclic voltammetry of solid $[Co(\mathbf{1c})_2]\cdot 2ClO_4$ immobilised at a 4.9 mm diameter basal plane pyrolytic graphite electrode. Voltammograms were recorded at 100 (A), 50 (B), 25 (C), 10 (D) and 5 (E) mV s^{-1}. For clarity the current has been divided by the square root of the scan-rate (SR).

electron transfer. Over the range of scan-rates used the cathodic peak appears to be normal for a redox event with fast electron transfer.

A clear reduction peak can be observed also for the second metal-centred Co(I)/Co(II) reduction process at −742 mV versus SCE, while the peak due to the corresponding anodic process is at −706 mV versus SCE. This potential is in good agreement with that predicted based on the solution phase study (see Table 2). At even more negative potentials (−1045 mV versus SCE) the ligand-centred reductions can be observed and these seem to be chemically reversible based on the detection of the Co(II)/Co(III) system at more positive potentials. The ligand-centred reduction processes are multi-electron in nature and may involve protonation of the ligand. In contrast with the solution phase electrochemical observations this ligand-centred reduction appears to be chemically reversible probably owing to the stabilising nature of counterions and the solid matrix. It is possible that by constraining the shape of the ligand by coordination to a metal, and embedding the resulting complex in a crystal lattice that the reduced form of the ligand was stabilised.

It is interesting to explore the mechanism for the metal and ligand-based reductions in more detail. The magnitude of the currents suggests that the ligand-centred reduction was a multielectron process associated with corresponding anodic reactions at −848 mV versus SCE. For the metal-centred Co(II)/Co(I) reduction process a corresponding oxidation process was observed only at −250 mV versus SCE which was much more positive than expected. By varying the cathodic limit of the cyclic voltammetry scan (see Fig. 8) it was shown that the Co(II)/Co(I) metal centred redox system was fully reversible, resulting in a symmetric reduction–oxidation couple. However, scanning the potential into the ligand centred potential results in the formation of a new product detected at −300 mV versus SCE. The ligand reduction appears to stabilise the Co(I) centre that is possible by protonation of the triazine ligand. When this experiment was repeated using aqueous

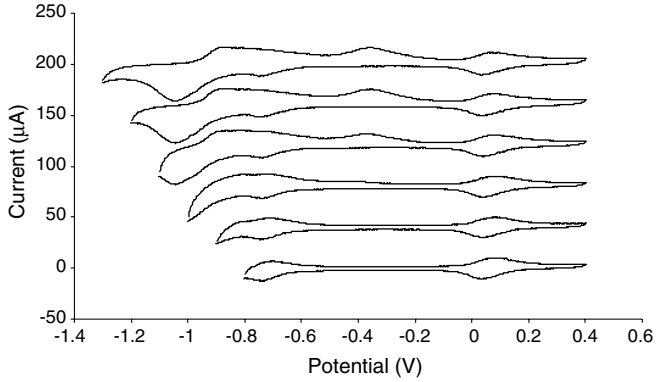

Fig. 8. Two-phase voltammetry of solid $[Co(\mathbf{1c})_2]\cdot 2ClO_4$ immobilised at a 4.9 mm diameter basal plane pyrolytic graphite electrode recorded at 100 mV s^{-1} with variation of the negative potential limit.

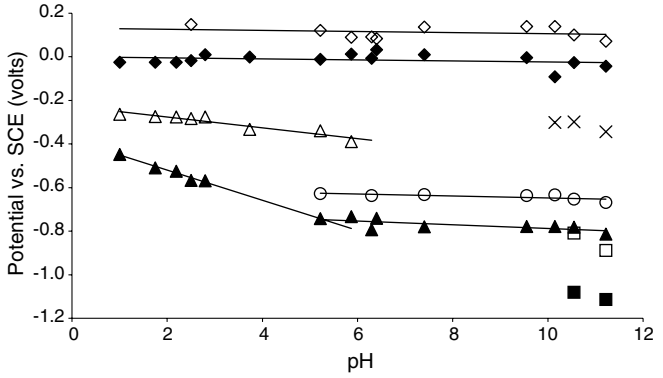

Fig. 9. Redox potentials of $[Co(\mathbf{1c})_2]\cdot 2ClO_4$ plotted against pH. *Key*: ◇, Co(II) → Co(III) oxidation; ◆, Co(III) → Co(II) reduction; ×, ligand-centred oxidation; □, either a ligand or metal-centred oxidation; ■, either a ligand or metal-centred reduction; △, ligand-centred oxidation; ▲, ligand-centred or Co(II) → Co(I) reduction; and ○, ligand-centred oxidation.

potassium perchlorate (0.1 M) in place of the sodium perchlorate solution the redox chemistry was unchanged indicating that the reversible intercalation of alkali metal ions does not facilitate the solid state redox chemistry.

In order to test the protonation hypothesis, the pH of the aqueous solution was varied. On replacement of the sodium perchlorate solution with perchloric acid (0.1 M), it was found that while the Co(II)/Co(III) couple remained as before (confirming the charge compensation mechanism via perchlorate exchange), the ligand-centred reduction was subject to a clear anodic shift and it was no longer possible to observe the Co(I)/Co(II) redox event independently. This anodic shift confirmed that the ligand-centred reduction involves protonation. In order to investigate this further a series of experiments employing aqueous electrolytes with different pH values were performed. In order to ensure that the majority of the anions present in the aqueous phase were perchlorates, a large amount of sodium perchlorate (0.2 M) and a small amount of sodium phosphate (0.02 M) were dissolved in water. This aqueous solution was then titrated with aqueous perchloric acid (0.1 M) in order to provide aqueous solutions with pH values between 11.0 and 1.8. When the pH was high, an additional reduction was observed with (cathodic and anodic peaks at −1.114 and −0.888 V, respectively), which could be due to a reversible Co(I) → Co(O) or a ligand-centred reduction. It is likely that this reduction can only be observed at low proton concentrations because protons interfere with this chemistry either by reacting with the Co(O) species or by obscuring this new peak with the peak arising from the formation of dihydrogen from protons. When the pH was below 4 it was found that the potential at which the ligand reduction occurred was subject to an anodic shift of −69 mV per pH unit, which suggests that 1.2 protons were required for the transfer of every electron. This compares well with the proton facilitated reduction of 1,2,4-triazines which has been reported in *N*,*N*-dimethylformamide [37]. The ligand-centred reduction observed between pH 1 and 6, was subject also to an anodic shift of −25 mV per pH unit suggesting that the loss of 0.43 protons could be required for the loss of each electron (see Fig. 9).

It is interesting to compare these results with those for $[Fe(\mathbf{1c})_2]^{2+}$ shown in Fig. 6. The formation of the product peak in acetonitrile was very similar to that observed in aqueous media and protonation due to traces of water present in acetonitrile cannot be ruled out.

3.5. Computational chemistry

Within an industrial plant separating the transplutonium metals from spent fuel the extractant will be exposed to high doses of radiation. It is vital that the radiolysis of the extraction agent should be addressed. It is known that when dissolved in hexanol, gamma irradiation (1 kGy) is able to degrade **2c** and that electrochemical reduction of the triazinyl ligands can result in degradation it was thought that the reduction of the iron complexes should be modelled. It has been demonstrated by trapping experiments that radiolytically generated solvated electrons are responsible for the dechlorination of polychlorobiphenyls (PCBs) [38] and for the degradation of **2a** [39]. Calculations was performed upon the homoleptic transition metal complexes $[ML_2]^{n+}$ with tridentate ligands and $[ML_3]^{n+}$ with bidentate ligands using density functional theory (DFT) via the ADF program [21]. Since the alkyl side groups attached to the triazinyl have little influence on the metal coordination chemistry, the complexes of the parent unsubstituted BTP (**2a**), *hemi*-BTP (**1a**) and the related ligands (**6**, **5a**, **7**, **8a**, and **4a**) were studied in the gas phase. Geometry optimisations were carried out for these species with alternative charges 2, 1, and 0 and possible spin states. Starting models were taken from the crystal structures, but C_2 or D_{2d} symmetry was imposed on all models. The geometry of all structures converged successfully and in all cases one specific spin state was easily identifiable as the lowest energy. For complexes with **1a**, for Mn(II) the lowest energy was obtained with 1 unpaired electron compared to 3 with relative energy at 1.06 eV and to 5 at 0.86 eV, for Fe(II) the lowest energy structure contained no

unpaired electrons rather than 2 and 4 at 1.14, 1.44 eV higher in energy and for Co(II), the complex with one unpaired electron was lower in energy by 2.03 eV than the complex with three unpaired electrons. All these results confirm that the low spin complex is the most stable, consistent with the magnetic measurements detailed above. For Ni(II), 2 unpaired electrons were preferred to 0 by 1.02 eV against consistent with the experimental results.

Thus, the triazinyl pyridine ligands provided the metals with a strong ligand field M–N bond lengths somewhat shorter by between 0.05 and 0.10 Å than those obtained in the crystal structures. The one anomaly, however, was found for calculations with Mn. Here, the three energies for 1,3 and 5 unpaired electrons were −13.57632, −13.52898, and −13.53661 a.u suggesting that the cation was likely to have only 1 unpaired electron. However, the bond lengths in the crystal structure are typical of Mn–N bond lengths in octahedral structures [25,26] in which the metal has 5 unpaired electrons rather than 1. Indeed, the DFT calculations also bear this out with Mn–N distances of 1.978 Å to the outer pyridine nitrogen), 1.882 Å to the inner pyridine nitrogen, 1.902 Å to the triazine nitrogen for 1 unpaired electron, compared to 1.997, 1.898, 1.923 Å, respectively, for three unpaired electrons and 2.216, 2.121, 2.095 Å, respectively, for five unpaired electrons. It seems most likely therefore that in the crystal the Mn has 5 unpaired electrons rather than the 1 predicted for the isolated cation due no doubt to the effect of the anion and the crystal packing. A recent experimental paper [40] describing Fe(II) terpy complexes has shown that different anions give rise to different spin states for the metal even in identical cations.

As shown in Table 3, the trends in distances between the three M–N bonds, calculated with the ADF program and found in the crystal structures are the same in that the bond to the inner pyridine N(21) is the shortest bond while for Mn, Fe, Co and Cu the distance to the outer pyridine N(11) is longer than the distance to the triazine N(31), while the reverse is the case for Zn. We were unable to obtain crystals of the Ni(II) complex, but the DFT calculations provide distances between the metal and N(11) and N(31) of 2.052 and 2.033 Å, respectively. There is very little difference in dimensions between those found in $[Fe(\mathbf{1a})_2]^{2+}$ and in $[Fe(\mathbf{4a})_2]^{2+}$ and it is clear that the presence of the methoxy group makes little difference to the bonding of the ligand to the iron atom. In $[Fe(\mathbf{1a})_2]^{2+}$ and $[Fe(\mathbf{4a})_2]^{2+}$, the bonds to the outer pyridine rings via N(11) and N(41) are ca. 0.051 and 0.059 Å, respectively, shorter than those to the outer triazine rings via N(31) and N(61). It is noteworthy that the outer pyridine nitrogen to iron distance in $[Fe(\mathbf{6})_2]^{2+}$ is at 1.915 Å slightly shorter than the analogous bond (1.927 Å) in $[Fe(\mathbf{1a})_2]^{2+}$ and the triazine nitrogen iron bond lengths in $[Fe(\mathbf{2a})_2]^{2+}$ (1.894 Å) are longer than the equivalent bond to the triazine ring in $[Fe(\mathbf{1a})_2]^{2+}$ (1.876 Å). It appears that the M–N(triazine) bond in $[Fe(\mathbf{1a})_2]^{2+}$ is strengthened at the expense of the M–N(pyridine) bond. Within the crystallographic literature a large number of metal complexes of 1,2,4-triazines exist in which N(31) is bonded to the metal [33,34], but none with N(33) bonded have been reported (see Figs. 4 and 5 for numbering scheme). To investigate this the complex of iron with **1a** (designated as **1a′**) binding through N(33) of the triazine ring rather than N(31) was calculated to be 0.76 eV less stable. This is due primarily to electronic effects in unsubstituted ligands, though the steric effects of any alkyl groups bonded to C(34) of the triazine ring will reinforce the preference of binding through N(31) rather than N(33). Hence, coordination via N(33) is so unlikely that it does not need to be considered further.

The LUMO/HOMO energy gap for the complexes show some variations. The latest value is found for $[Fe(\mathbf{1a})_2]^{2+}$ 1.986 eV while complexes with ligands **2a**, **1a**, and **1a′** are similar at 1.919, 1.852 and 1.877 eV, while **4a** is significantly lower at 1.614 eV. In the iron complexes of **6**, **1a**, **2a**, **4a**, the three highest occupied orbitals are all concentrated within d-orbitals of the iron, while the next two have no iron component. On the other hand, the LUMOs are primarily concentrated on the ligands rather than the metal and distributed out over many atoms. From the HOMO–LUMO gaps, assuming that the energy required to spin-pair an electron is the same for all three complexes, the ligand-field stabilisation energy of the complexes of the triazinyl pyridines are slightly smaller (BTP complex 1.9%, and *hemi*-BTP complex 4.2%) than that which is predicted for the terpyridine complex. The HOMO/LUMO energy gap of the tris-bipyridine complex $\{[Fe(\mathbf{7})_3]^{2+}\}$ is 0.036 eV larger than that of the tris-[3,3′-bi-(1,2,4-triazinyl)] complex $\{[Fe(\mathbf{5a})_3]^{2+}\}$, while the HOMO/LUMO energy gap for *fac*-$[Fe(\mathbf{8a})_3]^{2+}$ is 0.029 eV greater than that of the tris-bipyridine complex. The iron complexes with ligands **6, 2a, 1a** and **1a′** were also considered with charges of +1 and 0 and were geometry optimised with the ADF program at various spin states and the results together with those from the complexes with charge +2 are shown in Table 4. For complexes with **2a, 1a, 1a′** and **4a**, in all cases the outer pyridine nitrogens are less electron rich than the inner pyridine nitrogens. The charges on the metal atom are significantly less for the **2a** complex at 0.87e compared to ca. 1.0 for the other ligands which allied to the large HOMO–LUMO gap again demonstrates the uniqueness of the BTP ligand. The Mulliken atomic charges on the iron and pyridine nitrogen atoms varied little as the charge on the complex is reduced from 2 to 1 to 0. Indeed, the extra electron(s) is distributed primarily over the ligand. The most marked increase in electron density was observed for the triazine nitrogen N(33) which is not bonded to the metal but even in this case the increase is less than 0.1e. The lone pair associated with N(33) points outwards from the molecule and is an obvious point at which an electrophile could attack a metal complex for example following an electrochemical or radiochemical reduction process (vide infra).

Of the triazinyl-pyridine complexes of iron studied by cyclic voltammetry $[Fe(\mathbf{5c})_3]^{2+}$ was unique by virtue of

Table 4
The energies, Fe–N bond lengths and selected atomic charges for the iron complexes of tridentate ligands following DFT geometry optimisation

Complex	Unpaired electrons	Relative energy (eV)	Metal nitrogen distance (Å)			Mulliken atomic charges					
						Nitrogen atoms					Iron atom
			Triazine	Pyridine		Pyridine		Triazine			
				Outer	Inner	Outer	Inner	N36	N31	N33	
$[Fe(\mathbf{6})_2]^{2+}$	0	0		1.915	1.836	−0.361	−0.484				0.993
$[Fe(\mathbf{6})_2]^{+}$	1	−7.17		1.912	1.837	−0.368	−0.506				1.017
$[Fe(\mathbf{6})_2]^{0}$	0	−11.10		1.910	1.839	−0.365	−0.484				1.008
$[Fe(\mathbf{6})_2]^{0}$	2	−11.27		1.909	1.839	−0.370	−0.503				1.016
$[Fe(\mathbf{2a})_2]^{2+}$	0	0	1.895		1.843		−0.384	−0.127	−0.204	−0.225	0.874
$[Fe(\mathbf{2a})_2]^{+}$	1	−7.97	1.891		1.843		−0.378	−0.150	−0.201	−0.268	0.875
$[Fe(\mathbf{2a})_2]^{0}$	0	−12.73	1.888		1.839		−0.374	−0.171	−0.198	−0.309	0.875
$[Fe(\mathbf{2a})_2]^{0}$	2	−12.77	1.888		1.840		−0.388	−0.168	−0.223	−0.294	0.892
$[Fe(\mathbf{1a})_2]^{2+}$	0	0	1.873	1.920	1.836	−0.357	−0.429	−0.128	−0.206	−0.224	0.923
$[Fe(\mathbf{1a})_2]^{+}$	1	−7.66	1.875	1.920	1.834	−0.360	−0.424	−0.169	−0.201	−0.280	0.925
$[Fe(\mathbf{1a})_2]^{0}$	0	−11.30	1.873	1.911	1.832	−0.337	−0.511	−0.200	−0.293	−0.201	1.048
$[Fe(\mathbf{1a})_2]^{0}$	2	−12.26	1.870	1.913	1.832	−0.364	−0.447	−0.156	−0.222	−0.289	0.943
$[Fe(\mathbf{1a}')_2]^{2+}$	0	0.76[a]	1.902	1.924	1.842	−0.362	−0.468	−0.116	−0.135	−0.306	0.989
$[Fe(\mathbf{1a}')_2]^{+}$	1	−7.17[a]	1.893	1.921	1.842	−0.367	−0.488	−0.160	−0.156	−0.326	1.010
$[Fe(\mathbf{1a}')_2]^{0}$	0	−11.98[a]	1.891	1.910	1.841	−0.360	−0.470	−0.200	−0.172	−0.307	1.003
$[Fe(\mathbf{1a}')_2]^{0}$	2	−11.90[a]	1.889	1.909	1.839	−0.373	−0.507	−0.190	−0.176	−0.332	1.031
$[Fe(\mathbf{4a})_2]^{2+}$	0	0	1.875	1.934	1.843	−0.359	−0.442	−0.131	−0.215	−0.236	0.926
$[Fe(\mathbf{4a})_2]^{+}$	1	−7.24	1.877	1.925	1.837	−0.360	−0.435	−0.157	−0.204	−0.285	0.920
$[Fe(\mathbf{4a})_2]^{0}$	0	−11.47	1.876	1.916	1.836	−0.360	−0.427	−0.178	−0.200	−0.328	0.921
$[Fe(\mathbf{4a})_2]^{0}$	2	−11.40	1.885	1.921	1.849	−0.361	−0.441	−0.145	−0.208	−0.297	0.908

[a] Energies for complexes containing **1a**′ are relative to that of $[Fe(\mathbf{1a})_2]^{2+}$.

the fact that after the ligand-centred reduction no degradation occurred, one explanation is that the additional electron density is spread over a larger number of triazine rings. According to the DFT calculations the N(4) triazine nitrogen has an unusually low electron density (−0.175 in the complex $[Fe(\mathbf{5a})_3]^{2+}$) hence making the attack of electrophiles much less likely.

Metal complexes of tetraethyl-BTP (**2c**) with iron, cobalt and nickel in a range of oxidation states were studied with the ADF program in the gas phase and also in solution via the COSMO method. From these results it was possible to calculate the potential at which a series of redox event would occur using the general method of Peover [41] as later adapted by Shalev and Evans [42]. For the three metals, the energies of the metal complexes of **2a** with different charges and all possible spin states were calculated in the gas phase. Subsequently, the spin states with the lowest energy were used in calculations with **2c** complexes with the same range of metals and charges were calculated both with and without solvation in acetonitrile ($\varepsilon_r = 38$). It was found that solvation had little influence upon the structure of the complex; the atoms whose positions changed most were on the periphery of the complex. In common with the iron complexes, the atomic charge on either the cobalt or nickel atom did not vary with the overall charge of the complex. It was noted that on going from Fe to Co to Ni that the metal atom became more positively charged.

Hence, the nickel complex is more reducible than the cobalt or iron complexes. As the complexes become more positively charged, the atoms within the ethyl groups become more positively charged, due to inductive effects but this is less noticeable for the atoms in the terminal methyl groups.

A graph of calculated redox potentials against experimental values suggested that, while the absolute difference between the redox potentials of the nickel BTP complexes were overestimated, the order and relative magnitude of these redox potentials were correctly predicted. The calculations confirmed that of the three metal complexes (Fe, Co, Ni), the nickel can be most readily reduced to the uncharged zero-valent metal complex. The DFT calculations predicted that the difference between the $E^{2/3}$ and $E^{1/2}$ would be less for cobalt than it would be for nickel, but this potential gap for cobalt was significantly overestimated (see Table 5).

$$E^{2/3} = \text{Energy } (+2 \text{ form}) - \text{Energy } (+3 \text{ form}).$$
$$E^{1/2} = \text{Energy } (+1 \text{ form}) - \text{Energy } (+2 \text{ form}).$$
$$E^{0/1} = \text{Energy } (+0 \text{ form}) - \text{Energy } (+1 \text{ form}).$$

Table 5
Absolute redox potentials of $[M(\mathbf{2c})_2]^{2+}$ predicted by DFT calculations (M = Fe, Co and Ni)

Redox potential (V)	Metal		
	Fe	Co	Ni
$E^{2/3}$	5.34	3.77	4.83
$E^{1/2}$	−3.19	−3.45	−3.07
$E^{0/1}$	−6.22	−6.38	−3.91

4. Conclusions

It has been established that the triazinyl pyridines were able to bind strongly to the transition metals, in a manner analogous to that of terpyridine. The 1,2,4-triazine rings are more electron withdrawing than pyridine rings. Upon solution state reduction of the triazinyl pyridine ligands degradation was often observed, an accumulation of negative charge at N(33) of the triazine ring has been predicted computationally and is a possible step in a reductive degradation. It is hoped that it will be possible to design metal extraction agents lacking N(33) like nitrogens which will have a better resistance to radiolytic degradation. A solid-state electrochemical study of a cobalt complex indicates that the ligand reduction is a reversible event that is promoted and modified by the presence of a Brönsted acid.

Acknowledgements

We are grateful for the financial support by the European Union Nuclear Fission Safety Programme (EUROPART (FI6W-CT-2003-508854) and PARTNEW (FIKW-CT-2000-0087) contracts). We also thank the EPSRC and the University of Reading for funding of the image-plate system.

Appendix A. Supplementary material

Crystallographic data are available from the CCDC, 12 Union Road, Cambridge CB2 1EZ, UK (fax +44 1223 336 033; e-mail: deposit@ccdc.cam.ac.uk or www: http://www.ccdc.cam.ac.uk) quoting deposition numbers CCDC 277000–277004. NMR and extraction data are deposited. Supplementary data associated with this article can be found, in the online version, at doi:10.1016/j.poly.2005.09.030.

References

[1] I. Svantesson, I. Hagström, G. Persson, J.O. Liljenzin, J. Inorg. Nucl. Chem. 41 (1979) 383.
[2] H. Takahashi, H. Rief, in: Proceedings of the Specialist Meeting on Accelerator Based Transmutation, Villigen, 1992.
[3] I.G. Crossland, Interdiscipl. Sci. Rev. 23 (1998) 269.
[4] M.J. Rivard, B.L. Kirk, L.J. Stapleford, D.E. Wazer, Appl. Radiat. Isot. 61 (2004) 1211.
[5] M.J. Hudson, M.G.B. Drew, M.R.S. Foreman, C. Hill, N. Huet, C. Madic, T.G.A. Youngs, Dalton Trans. (2003) 1675.
[6] M.G.B. Drew, D. Guillaneux, M.J. Hudson, P.B. Iveson, C. Madic, Inorg. Chem. Commun. 4 (2001) 462.
[7] M.G.B. Drew, M.R.S. Foreman, C. Hill, M.J. Hudson, C. Madic, Inorg. Chem. Commun. 8 (2005) 239.
[8] Z. Kolarik, Solvent Extr. Ion Exc. 21 (2003) 381.
[9] R. Uma, M. Palaniandavar, R.J. Butcher, J. Chem. Soc., Dalton Trans. (1996) 2061.
[10] J. Breu, K.-J. Range, E. Herdtweck, Monatsh. Chem. 125 (1994) 119.
[11] C. Hill, D. Guillaneux, X. Hérès, N. Boubals, L. Ramain, Atalante2000, Avignon, October 2000.
[12] K. Okada, M. Nomura, Y. Fujii, Nucl. Technol. 129 (2000) 131.
[13] D. Wenkert, R.B. Woodward, J. Org. Chem. (1983) 283.
[14] F.H. Case, J. Org. Chem. 30 (1965) 931.
[15] F.H. Case, J. Heterocycl. Chem. 8 (1971) 1043.
[16] W.R. Robinson, J. Chem. Educ. 62 (1985) 1001.
[17] W. Kabsch, J. Appl. Crystallogr. 21 (1988) 916.
[18] G.M. Sheldrick, SHELX-86, Acta Crystallogr., Sect. A 46 (1990) 467.
[19] N. Walker, D. Stuart, DIFABS program, Acta Crystallogr., Sect. A 39 (1983) 158.
[20] G.M. Sheldrick, SHELXL: Program For Crystal Structure Refinement, University of Göttingen, Göttingen, Germany, 1993.
[21] ADF-2000 program: E.J. Baerends, A. Berces, C. Bo, P.M. Boerrigter, L. Cavallo, L. Deng, R.M. Dickson, D.E. Ellis, L. Fan, T.H. Fisher, C. Fonseca-Guerra, S.J.A. van Gisbergen, J.A. Groeneveld, O.V. Gritsenko, F.E. Harris, D. van Hoek, P.H. Jacobson, G. van Kessel, F. Kootstra, E. van Lenthe, V.E. Osinga, P.H.T. Philipson, D. Post, C.C. Pye, W. Ravenek, P. Ros, P.R.T. Schipper, G. Schreckenback, J.G. Snijders, M. Sola, D. Swerhone, G. te Velde, P. Vernooijs, L. Versluis, O. Visser, E. van Wezenbeek, G. Wiesenekker, S.K. Wolff, T. Woo, T. ZieglerSCM Inc., Theoretical Chemistry, Vrije Universiteit, Amsterdam, The Netherlands, 2000.
[22] M.R.S.J. Foreman, M.J. Hudson, A. Geist, C. Madic, M. Weigl, Solvent Extr. Ion Exc. 23 (2005) 645.
[23] S.F. Lincoln, A.E. Merbach, Adv. Inorg. Chem. 42 (1995) 1.
[24] F.A. Dunand, L. Helm, A.E. Merbach, Adv. Inorg. Chem. 54 (2003) 1.
[25] F.H. Allen, O. Kennard, Chem. Des. Autom. News 8 (1993) 31.
[26] D.A. Fletcher, R.F. MeMeeking, D. Parkin, J. Chem. Inf. Comput. Sci. 36 (1996) 746.
[27] S.W. Ng, Acta Crystallogr., Sect. E 60 (2004) m937.
[28] Hui Chao, Guang Yang, Gen-Qiang Xue, Hong Li, Hao Zang, I.D. Williams, Liang-Nian Ji, Xiao-Ming Chen, Xiao-Yuan Li, J. Chem. Soc., Dalton Trans. (2001) 1326.
[29] J.A.R. Sende, C.R. Arana, L. Hernández, K.T. Potts, M. Keshevarz-K, H.D. Abruña, Inorg. Chem. 34 (1995) 3339.
[30] J.M. Rao, M.C. Hughes, D.J. Macero, Inorg. Chim. Acta 18 (1976) 127.
[31] K.T. Potts, M. Keshavarz-K, F.S. Tham, H.D Abruña, C. Arana, Inorg. Chem. 32 (1993) 4450.
[32] E. Perezcordero, R. Buigas, N. Brady, L. Echegoyen, C. Arana, J.M. Lehn, Helv. Chim. Acta 77 (1994) 1222.
[33] C. Arana, M. Keshavarz, K.T. Potts, H.D. Abruña, Inorg. Chim. Acta 225 (1994) 285.
[34] E.C. Constable, A.M.W. Cargill Thompson, J. Chem. Soc., Dalton Trans. (1992) 2947.
[35] T. Grygar, F. Marken, U. Schroder, F. Scholz, Collect. Czech. Chem. Commun. 67 (2002) 163.
[36] F. Marken, S. Cromie, V. McKee, J. Solid State Electrochem. 7 (2003) 141.
[37] A. Nurhadi, E. Graf, M. Gross, Electrochim. Acta 36 (1991) 1997.
[38] B.J. Mincher, R.E. Arbon, W.B. Knighton, D.H. Meikrantz, Appl. Radiat. Isot. 45 (1994) 879.
[39] S. Andersson, C. Ekberg, M.R.S. Foreman, M.J. Hudson, M. Nilsson, G. Skarnemark, Chalmers University, 2005, unpublished work.
[40] E.C. Constable, G. Baum, E. Bill, R. Dyson, R. van Eldik, D. Fenske, S. Kaderli, D. Morris, A. Neubrand, M. Neuburger, D.R. Smith, K. Wieghardt, M. Zehnder, A.D. Zuberbuhler, Chem. Eur. J. 5 (1999) 498.
[41] M.E. Peover, Nature 193 (1962) 475.
[42] H. Shalev, D.H. Evans, J. Am. Chem. Soc. 111 (1989) 2667.

Available online at www.sciencedirect.com
SCIENCE DIRECT®
Polyhedron 25 (2006) 901–909
POLYHEDRON
www.elsevier.com/locate/poly

Formation and X-ray crystal structures of neutral 3D networks by charge-assisted hydrogen bonds between tetrakis(thiourea)platinum(II) complexes and dicarboxylates

Philip A. Gale *, Mark E. Light, Roberto Quesada

School of Chemistry, University of Southampton, Southampton UK SO17 1BJ, United Kingdom

Received 17 August 2005; accepted 15 October 2005
Available online 28 November 2005

This paper is dedicated to Professor Mike Hursthouse.

Abstract

Five new complex salts $[Pt(SC(NH_2)_2)_4][dc]$ (dc = adipate (**1**), isophthalate (**2**), terephthalate (**3**), 4,4′-biphenyldicarboxylate (**4**), 1,4-naphthalenedicarboxylate (**5**)) have been characterized by single-crystal X-ray diffraction. Thiourea–carboxylate interactions have proven to be a reliable supramolecular synthon, yielding in all the examples charge-assisted hydrogen-bonded 3D networks via N–H···O interactions.
© 2005 Elsevier Ltd. All rights reserved.

Keywords: Platinum complexes; Crystal engineering; Hydrogen bonds; Crystal structures; Dicarboxylates; Supramolecular networks

1. Introduction

Recently, developments in inorganic crystal engineering have made significant progress towards the goal of the rational synthesis of crystalline materials [1–5]. Employing metal-containing building blocks allows the use of co-ordinate bonds in addition to non-covalent bonds to design molecular networks. Metal-organic frameworks (MOFs) represent a fast growing class of materials which have a variety of applications [6,7]. On the other hand, hydrogen-bonded frameworks derived from metal complexes have also attracted a great deal of interest [8–11]. One frequently employed strategy in the production of networks is the use of pyridine ligands bearing carboxylic acid or amide groups, as the hydrogen-bonded dimers of these groups are well known supramolecular synthons in organic crystal engineering [12–14]. Although this approach has proven very successful, there are very few examples of 3D structures assembled through ligand–ligand hydrogen bonds (which may be classed as 'second sphere' coordination complexes) [8–10]. The use of metal cations and neutral ligands means that the resultant cationic network must be balanced by the presence of counterions. A possible solution to avoid this is the inclusion of the anions in the network design [15,16]. Similar approaches involving crystallization of organic cations with hydrogen bond donor groups and metallate anions has been used by Orpen, Hosseini and others [17–20], resulting in the characterization of one, two and 3D networks stabilized by charge-assisted hydrogen bonds.

Urea and thiourea derivatives have been widely used in organic crystal engineering, being the bidentate urea–carboxylate interactions a well known and exploited motif in carboxylate recognition chemistry, forming complexes which show appreciable stability in polar solvents [21]. Despite these examples, the supramolecular aggregation of metal complexes containing these ligands is largely unexplored [22–24]. This prompted us to test the suitability of

* Corresponding author. Tel: +44(0)23 8059 3332; fax: +44(0)23 8059 6805.
E-mail address: philip.gale@soton.ac.uk (P.A. Gale).

0277-5387/$ - see front matter © 2005 Elsevier Ltd. All rights reserved.
doi:10.1016/j.poly.2005.10.007

the tetrakis(thiourea)platinum(II) complex with dicarboxylates as molecular building blocks in the synthesis of hydrogen-bonded networks. The stability of the complex toward ligand substitution allow the use of carboxylate anions, which might otherwise displace some of the neutral ligands or co-ordinate to the metal centre, as demonstrated by Burrows et al. [25–27] in the case of Zn(II) thiourea complexes. The set of four coordinated thiourea groups in a semiflexible square planar arrangement is capable of propagating hydrogen bonding interactions in three dimensions through the interactions with the dicarboxylate dianions (see Chart 1).

2. Experimental

2.1. Materials

Tetrakis(thiourea)platinum(II)dichloride was prepared according to published procedures [28]. Dipotassium tetrachloroplatinate, adipic acid, terephthalic acid, isophthalic acid, 1,4-naphthalene dicarboxylic acid and 4,4′-biphenyl dicarboxylic acid were obtained commercially and used without further purification. Methanolic solutions of dicarboxylic acids were treated with two equivalents of potassium hydroxide and the resulting dipotassium dicarboxylate salts obtained as white microcrystalline powder by removing the solvents.

2.2. Synthesis of the complex salts *[Pt(SC(NH$_2$)$_2$)$_4$][dicarboxylate]*

2.2.1. *[Pt(SC(NH$_2$)$_2$)$_4$][adip] (**1**)*

Tetrakis(thiourea)platinum(II)dichloride (0.05 g, 0.088 mmol) was dissolved in 1.5 mL of DMSO. To this solution, an aqueous solution (1 mL) of adipic acid dipotassium salt (0.02 g, 0.089 mmol) was added and acetone allowed to diffuse slowly into the mixture. Colourless crystals suitable for X-ray diffraction appeared within five days. Yield 0.028 g (49%).

Elemental analysis calc. for **1** · 2DMSO: C, 21.02; H, 4.54; N, 14.01. Found: C, 20.51; H, 4.50; N, 13.67%.

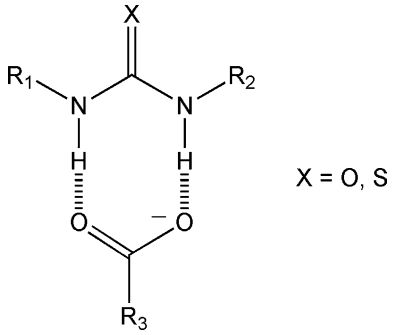

Chart 1. Schematic representation of the urea/thiourea–carboxylate interaction.

2.2.2. *[Pt(SC(NH$_2$)$_2$)$_4$][ipht] (**2**)*

A DMSO solution (1.5 mL) of tetrakis(thiourea)platinum(II)dichloride (0.05 g, 0.088 mmol) was mixed with an aqueous solution of isophthalic acid dipotassium salt (0.022 g, 0.088 mmol). Acetone vapour was allowed to diffuse slowly into the mixture, and yellow blocks appeared within five days. Yield 0.024 g (36%).

Elemental analysis calc. for **2**: C, 21.72; H, 3.04; N, 16.88. Found: C, 21.50; H, 3.08; N, 16.66%.

2.2.3. *[Pt(SC(NH$_2$)$_2$)$_4$][tpht] (**3**)*

Tetrakis(thiourea)platinum(II)dichloride (0.04 g, 0.07 mmol) was dissolved in 1.5 mL of DMSO. To this solution, an aqueous solution of terephthalic acid dipotassium salt (0.017 g, 0.07 mmol) was added and acetone allowed diffusing slowly into the mixture. Yellow crystals suitable for X-ray diffraction appeared within three days. Yield 0.024 g (36%).

Elemental analysis calc. for **3** · 2DMSO · 2H$_2$O: C, 22.45; H, 4.24; N, 13.09. Found: C, 22.08; H, 4.14 H; N, 13.08%.

2.2.4. *[Pt(SC(NH$_2$)$_2$)$_4$][bphdc] (**4**)*

A DMSO solution (1.5 mL) of tetrakis(thiourea)platinum(II)dichloride (0.05 g, 0.088 mmol) was mixed with an aqueous solution of 4,4′-biphenyldicarboxylic acid dipotassium salt (0.028 g, 0.088 mmol). Acetone vapour was allowed to diffuse slowly into the mixture, and colourless blocks appeared within five days. Yield 0.036 g (55%).

Elemental analysis calc. for **4** · 3OC(CH$_3$)$_2$: C, 35.48; H, 4.63; N, 12.26. Found: C, 35.68; H, 4.73; N, 12.36%.

2.2.5. *[Pt(SC(NH$_2$)$_2$)$_4$][naphdc] (**5**)*

Two solutions containing tetrakis(thiourea)platinum(II)dichloride (0.05 g, 0.088 mmol) and 1,4-naphthalene dicarboxylic acid dipotassium salt (0.027 g, 0.088 mmol) in DMSO and water, respectively, were mixed and acetone allowed to slow diffuse into it. Pale yellow crystals suitable for X-ray diffraction appeared within two days. Yield 0.031 g (47%).

Elemental analysis calc. for **5** · 2DMSO: C, 27.61; H, 3.94; N, 12.88. Found: C, 27.97; H, 4.05; N, 12.69%.

2.3. Crystal structure determination

Data for all structures were collected using Phi and omega scans on a Bruker Nonius Kappa CCD area detector diffractometer with a rotating Mo (0.71073 Å) anode following standard procedures. Data were corrected for absorption using SADABS [29]. Structure solution was performed using SHELXS 97 [30] and refinement carried out on F^2 using SHELXL 97 [31]. Hydrogen atoms were placed in idealized positions and refined using a riding model. The non-merohedrally twinned data for **1** were processed using evalCCD [32] and the data were not merged; the

Table 1
Crystal data and structure refinement details for compounds **1**–**5**

Compound	**1**	**2**	**3**	**4**	**5**
Formula	$C_4H_{16}S_4N_8Pt \cdot C_6H_8O_4 \cdot 2C_2H_6SO$	$C_4H_{16}N_8PtS_4 \cdot C_8H_4O_4$	$C_4H_{16}S_4N_8Pt \cdot C_8H_4O_4 \cdot 2C_2H_6SO \cdot 2H_2O$	$C_4H_{16}N_8PtS_4 \cdot C_{14}H_8O_4 \cdot 3C_3H_6O$	$C_4H_{16}N_8PtS_4 \cdot C_{12}H_6O_4 \cdot 2C_2H_6SO$
Colour	colourless	yellow	yellow	colourless	pale yellow
Habit	block	block	block	block	blade
Size (mm^3)	$0.4 \times 0.3 \times 0.1$	$0.2 \times 0.15 \times 0.1$	$0.2 \times 0.15 \times 0.1$	$0.12 \times 0.1 \times 0.06$	$0.2 \times 0.04 \times 0.03$
Crystal system	triclinic	monoclinic	monoclinic	triclinic	triclinic
Space group	$P\bar{1}$	$C2/c$	$C2/c$	$P\bar{1}$	$P\bar{1}$
a (Å)	9.203(5)	11.849(2)	11.3740(10)	12.041(5)	9.9576(6)
b (Å)	12.471(5)	12.957(3)	20.610(4)	12.569(5)	10.9835(6)
c (Å)	14.381(5)	13.200(3)	13.7650(11)	14.040(5)	15.0119(10)
α (°)	75.296(5)			104.238(5)	78.355(5)°
β (°)	82.555(5)	91.60(3)	91.491(8)	91.001(5)	85.736(5)°
γ (°)	73.001(5)			118.461(5)	88.838(4)°
Z	2	4	4	2	2
Reflections	13430	22379	14399	33089	27233
Independent	13430 (not merged)	2326 [$R_{int} = 0.0304$]	3695 [$R_{int} = 0.0467$]	8196 [$R_{int} = 0.0402$]	7311 [$R_{int} = 0.0619$]
Completeness to $\theta = 27.48°$	70.3	99.7	99.6	99.8	99.4
Transmission maximum and minimum	0.6318 and 0.2369	0.5258 and 0.3200	0.6460 and 0.4476	0.7862 and 0.6319	0.8690 and 0.4161
Parameters	320	135	193	430	378
Final R indices [$F^2 > 2\sigma(F^2)$]	$R_1 = 0.0749$	$R_1 = 0.0149$	$R_1 = 0.0291$	$R_1 = 0.0255$	$R_1 = 0.0417$
	$wR_2 = 0.1383$	$wR_2 = 0.0321$	$wR_2 = 0.0671$	$wR_2 = 0.0590$	$wR_2 = 0.0836$
R indices (all data)	$R_1 = 0.1158$	$R_1 = 0.0187$	$R_1 = 0.0315$	$R_1 = 0.0287$	$R_1 = 0.0694$
	$wR_2 = 0.1605$	$wR_2 = 0.0337$	$wR_2 = 0.0682$	$wR_2 = 0.0605$	$wR2 = 0.0927$
CCDC code	281330	281333	281331	281332	281329

twin relationship was a 180° rotation about 0 0 1. The carbon chains of the two half adipate molecules in **1** were modelled as disordered 50:50 over two conformations. The DMSO in **3** was disordered 60:40 over two positions. CCDC Nos. 281329–281333 contain the supplementary crystallographic data for this paper. These data can be obtained free of charge from The Cambridge Crystallographic Data Centre via www.ccdc.cam.ac.uk/data_request/cif. Crystal data and structure refinement details are summarized in Table 1. Selected hydrogen bond parameters are given in Table 2.

3. Results and discussion

Reaction of $[Pt(SC(NH_2)_2)_4]Cl_2$ in DMSO with potassium salts of the dicarboxylates shown in Chart 2 led to the corresponding complex salts in which the chloride anions have been substituted by the dicarboxylates. These salts were crystallized and characterized by single-crystal X-ray diffraction.

The crystal structure determination of complex **1** revealed that the salt crystallizes in the presence of two DMSO molecules. The coordinated thiourea groups

Table 2
Hydrogen bond parameters for compounds **1**–**5**

Compound	D–H···A	*d*(D–H) (Å)	*d*(H···A) (Å)	*d*(D···A) (Å)	∠(DHA) (°)	Symmetry codes
1	N1–H1A···O5A	0.88	1.92	2.772(9)	162.3	(v) $-x, -y+1, -z$
	N1–H1A···O5B	0.88	1.92	2.772(9)	162.3	(vi) $-x+1, -y, -z+1$
	N2–H2A···O6A	0.88	2.02	2.891(9)	171.8	
	N2–H2A···O6B	0.88	2.02	2.891(9)	171.8	
	N1–H1B···O5A^{v}	0.88	1.98	2.810(9)	156.0	
	N1–H1A···O5B	0.88	1.92	2.772(9)	162.3	
	N2–H2B···O2^{vi}	0.88	2.51	3.323(9)	153.3	
	N4–H4B···O2^{vi}	0.88	2.08	2.883(9)	151.7	
2	N1–H1A···O1^{iii}	0.88	1.93	2.805(3)	171.1	(i) $-x+3/2, -y+1/2, -z+1$
	N2–H2A···O2^{iii}	0.88	1.99	2.864(3)	170.4	(ii) $-x+2, y, -z+3/2$
	N3–H3A···O1^{i}	0.88	2.06	2.843(3)	148.2	(iii) $x+1/2, y-1/2, z$
	N4–H4A···O1^{i}	0.88	2.23	2.970(3)	141.8	(iv) $-x+3/2, y-1/2, -z+3/2$
	N2–H2B···O2^{iv}	0.88	2.35	3.130(3)	147.9	(v) $x, -y+1, z-1/2$
	N3–H3B···O2^{v}	0.88	2.12	2.920(3)	151.2	(vi) $x, y-1, z$
	N4–H4B···O2^{vi}	0.88	2.40	3.134(3)	140.7	
3	N2–H2B···O1	0.88	2.13	2.989(5)	166.5	(iii) $-x+1, y, -z+1/2$
	O4–H98···O1	0.837(10)	1.971(14)	2.800(4)	171(5)	(iv) $x-1/2, -y+1/2, z+1/2$
	O4-H98···O2	0.837(10)	2.66(4)	3.296(4)	134(4)	(v) $-x+1/2, y+1/2, -z+1/2$
	N2–H2A···O4^{iii}	0.88	2.03	2.826(5)	149.5	(vi) $-x+1/2, -y+1/2, -z$
	O4–H99···N2^{iii}	0.831(10)	2.15(4)	2.826(5)	139(5)	
	N3–H3A···O4^{iv}	0.88	2.31	3.026(4)	138.3	
	N4–H4A···O1^{v}	0.88	1.95	2.819(5)	171.4	
	N4–H4B···O2^{vi}	0.88	1.96	2.777(4)	153.5	
4	N1–H1A···O2	0.88	2.19	2.855(3)	132.2	(i) $-x+2, -y, -z+1$
	N2–H2B···S2	0.88	2.84	3.532(3)	136.4	(ii) $-x+1, -y, -z+1$
	N3–H3B···S1	0.88	2.74	3.405(3)	133.1	(iii) $x-1, y, z+1$
	N1–H1B···O4^{i}	0.88	1.93	2.805(3)	172.2	(iv) $x, y, z+1$
	N2–H2A···O1^{ii}	0.88	1.94	2.781(3)	160.4	(v) $-x+1, -y-1, -z+1$
	N3–H3A···O4^{iii}	0.88	2.08	2.934(3)	162.4	(vi) $x, y-1, z$
	N4–H4A···O3^{iii}	0.88	1.89	2.767(3)	171.9	
	N8–H8A···O3^{iv}	0.88	2.01	2.883(4)	170.4	
	N4–H4B···O3^{v}	0.88	2.11	2.832(4)	138.8	
	N5–H5A···O1^{vi}	0.88	2.03	2.894(4)	168.3	
	N6–H6A···O2^{vi}	0.88	1.89	2.754(4)	167.7	
5	N5–H5A···O2	0.88	2.02	2.883(6)	167.3	
	N6–H6A···O3	0.88	2.08	2.948(6)	169.2	
	N3–H3A···O4^{iii}	0.88	2.03	2.885(6)	163.7	
	N4–H4A···O5^{iii}	0.88	1.95	2.816(7)	168.2	
	N7–H7A···O3^{iv}	0.88	2.08	2.906(6)	157.0	
	N8–H8A···O3^{iv}	0.88	2.36	3.121(7)	144.4	
	N1–H1B···O3^{iv}	0.88	2.14	3.010(6)	172.1	
	N1–H1A···O5^{v}	0.88	2.04	2.847(6)	152.0	
	N2–H2B···O1^{i}	0.88	2.15	2.997(6)	161.5	
	N1–H1A···O5^{v}	0.88	2.04	2.847(6)	152.0	
	N2–H2A···O4^{vi}	0.88	1.91	2.772(6)	165.9	
	N4–H4B···O2^{vii}	0.88	2.08	2.844(6)	145.0	
	N1–H1A···O5^{v}	0.88	2.04	2.847(6)	152.0	

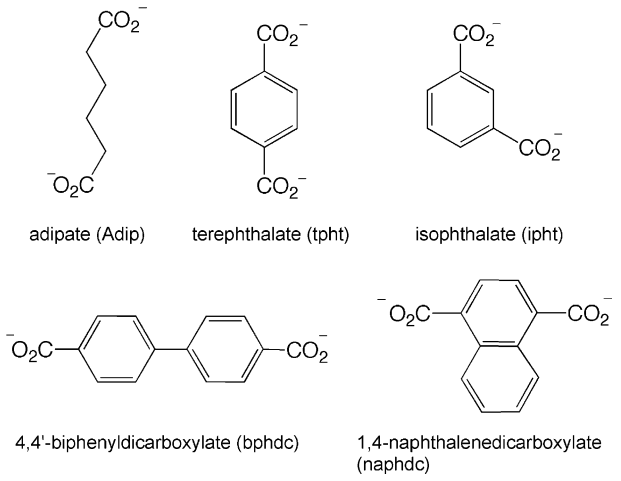

Chart 2. Dicarboxylates used as counter anions within this work.

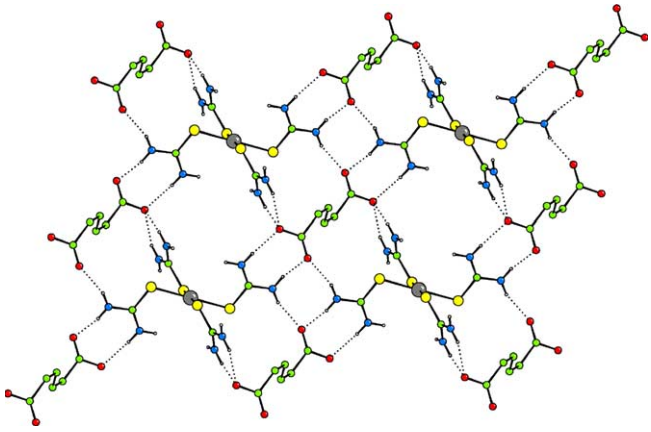

Fig. 1. Hydrogen bonding interactions within sheets in compound **1**.

adopted a 1,2-alternate[1] conformation with respect to the plane containing the platinum and sulfur atoms. Adipate dianions form strong double hydrogen bond interactions with thiourea groups forming infinite 1D chains. These chains are inter-linked via N–H···O interactions involving four thiourea groups (graph set $R_2^1(6)$ and *D*) to form two crystallographically independent sheets cross-linked via one DMSO and one adipate molecule (Fig. 1). The two crystallographically independent DMSO molecules are bound in slightly different ways. The first DMSO is bound by two hydrogen bonds from adjacent thiourea groups in the same platinum complex. The second DMSO is also bound by two hydrogen bonds but bridges two thiourea groups in different platinum complexes. When viewed down the *a*-axis these DMSO molecules sit in pseudo-channels (Fig. 2).

X-ray analysis of complex **2** reveals that the structure does not contain additional solvent molecules. The hydrogen bonding pattern is very similar to that found in the case of compound **1**, with three types of hydrogen bond interactions between the coordinated thiourea groups and the isophthalate dianions. Two thiourea groups in a *trans* disposition form DD:AA hydrogen bonding interactions with the isophthalate (graph set $R_2^2(8)$) with N···O distances 2.864 (3) and 2.805 (3) Å and bond angles 171.1°

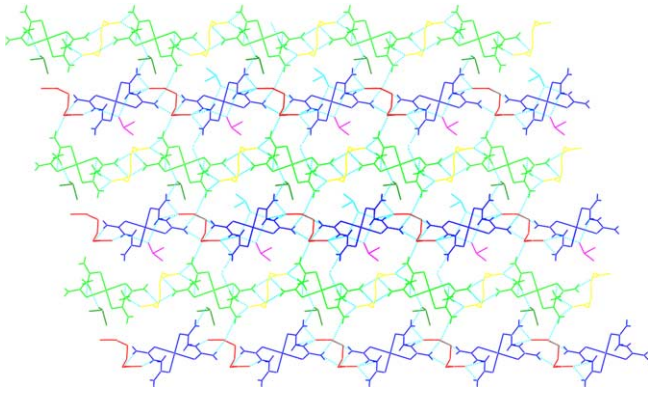

Fig. 2. View down crystallographic axis *a* of compound **1** network (solvents shown in magenta).

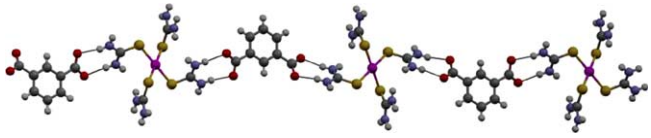

Fig. 3. View of the neutral chain defined by thiourea–carboxylate interactions in compound **2**.

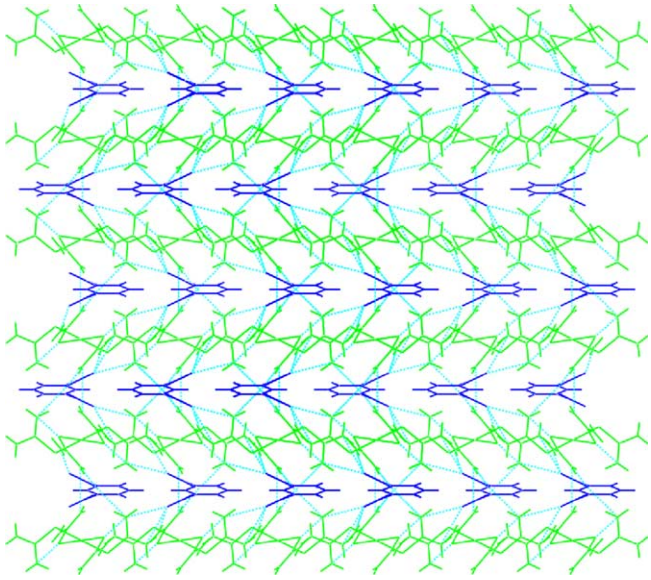

Fig. 4. Hydrogen-bonded 3D network of compound **2** viewed down crystallographic axis *a*.

[1] The nomenclature used to describe the conformation of the platinum complexes has been 'borrowed' from calix[4]arene chemistry. 1,3-Alternate means each thiourea group is oriented away from the PtS_4 plane in an alternating fashion whilst 1,2-alternate describes an arrangement where two adjacent thiourea molecules are oriented in one direction away from the PtS_4 plane whilst the other two thiourea molecules are oriented in the opposite direction.

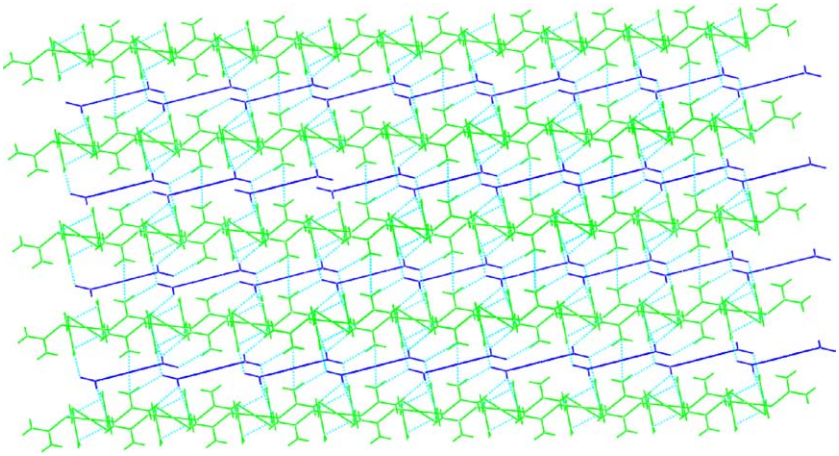

Fig. 5. Hydrogen-bonded 3D network of compound **2** viewed down crystallographic axis *b*.

and 170.4°, forming a neutral chain (Fig. 3), which is cross-linked to form a 3D network by two hydrogen bond interactions (graph set *D* and $R_2^1(6)$) between the other two urea groups and four additional isophthalate groups (Figs. 3–6).

In the case of compound **3** the complex salt crystallized together with two molecules of water and two molecules of DMSO. Again, the coordinated thiourea groups are found in a 1,2-alternate conformation but in this case only discrete hydrogen bond interactions (graph set *D*) are found between them and the terephthalate dianions (N2–H2B···O1 bond distance 2.989(5) Å, bond angle 166.5°). The hydrogen bonding environment of each complex cation included four molecules of water and four molecules of DMSO (Fig. 7). Water molecules were found bridging

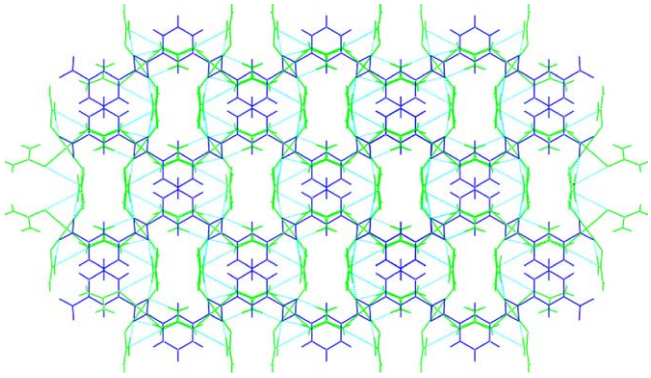

Fig. 6. Hydrogen-bonded 3D network of compound **2** viewed down crystallographic axis *c*.

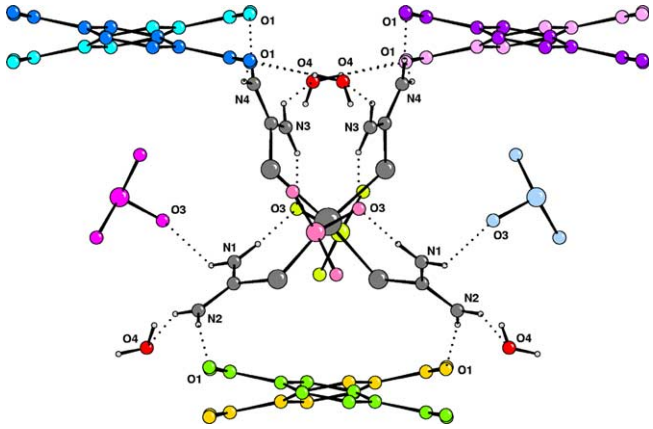

Fig. 7. Hydrogen bonding environment of a $[Pt(SC(NH_2)_2)_4]^{2+}$ cation in compound **3**.

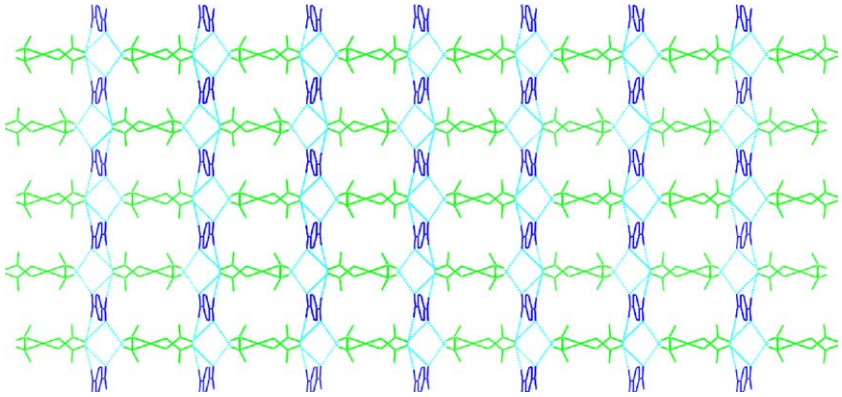

Fig. 8. View down crystallographic axis *a* of compound **3** network (solvents omitted for clarity).

the terephthalate and platinum complexes meanwhile the DMSO molecules are contained in channels running along the crystallographic *a*-axis, with two of these molecules displaying discrete contacts and the other two bridging two coordinated thiourea ligands (graph set $R_2^1(10)$) (Fig. 8).

The crystal structure of **4** revealed that the lattice contains three acetone molecules. In this case, the co-ordinated thiourea ligands adopt a 1,3-alternate conformation and this arrangement is stabilized by two intramolecular hydrogen bonds between adjacent thiourea groups S(6) with N2–H2B···S2 3.532(3) Å and N3–H3B···S1 3.405(3) Å. The hydrogen bond network might be explained in terms of a neutral chain composed by strong DD:AA interactions between two thiourea groups in *cis* arrangement and two dicarboxylate anions (Fig. 9) which is inter-linked by discrete contacts with thiourea groups belonging to other five platinum complexes (Figs. 10 and 11). The acetone molecules form N–H···O interactions with coordinated thiourea groups with one of them bridging two thiourea groups belonging to two different platinum complexes. The platinum complexes form centro-symmetric dimers via N–H···S hydrogen bonds with the N···S distance being 3.263(7) Å.

The complex salt **5** was found to contain two molecules of DMSO as solvent included in the crystal structure. There are two half platinum complexes in the asymmetric unit as the central atoms sit on special positions. The coordinate thiourea ligands again adopt a 1,2-alternate conformation around the platinum(II) centre. A neutral 1D chain along the crystallographic *b*-axis is formed by means of strong DD:AA interactions between two of the thiourea ligands in *trans* disposition and the dicarboxylate dianion, with N···O distances 2.883(3) and 2.948 (3) Å and bond angles from 167.3° and 169.2° (graph set $R_2^2(8)$) (Fig. 12). This motif is expanded into a 3D network through additional interactions with other coordinated ligands (Fig. 13). The crystal structure included two DMSO molecules which are found displaying N–H···O hydrogen bonds with two thiourea groups in a *cis* position within a platinum complex (graph set $R_2^1(10)$) (Fig. 14).

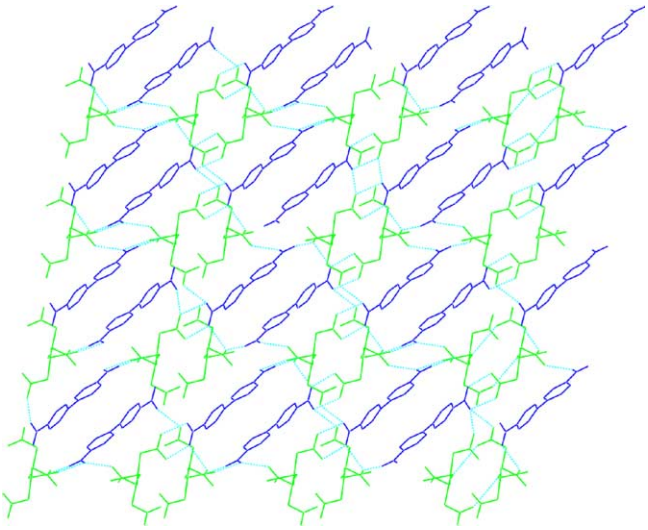

Fig. 11. 3D network viewed down crystallographic axis *b* of compound **4** (solvents omitted for clarity).

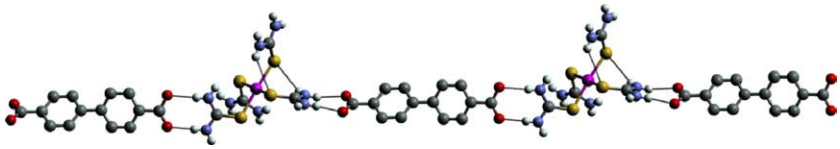

Fig. 9. Infinite 1D neutral chain in compound **4**.

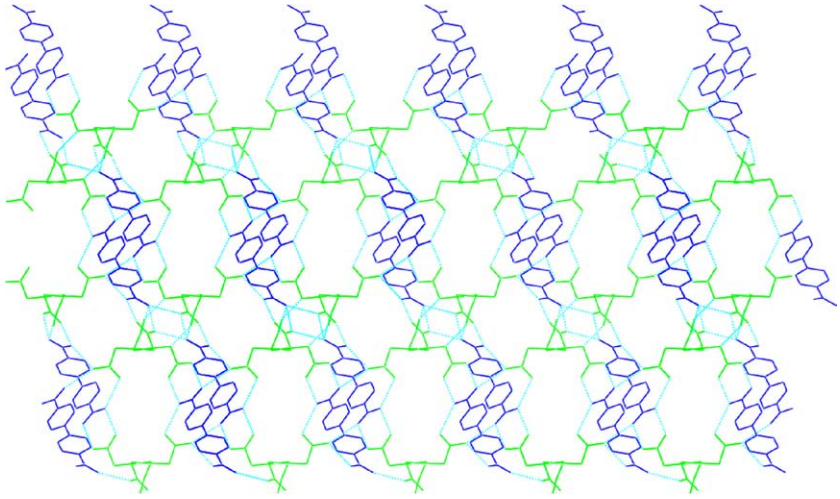

Fig. 10. 3D network viewed down crystallographic axis *a* of compound **4** (solvents omitted for clarity).

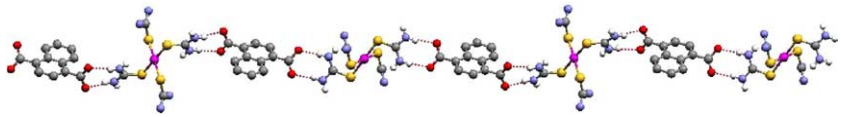

Fig. 12. Infinite 1D neutral chain defined by thiourea–carboxylate interactions in compound **5**.

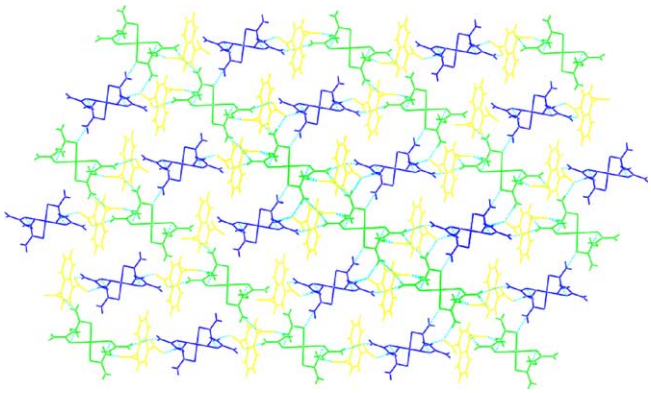

Fig. 13. Crystal structure of compound **5** viewed down crystallographic axis *a* (solvents omitted for clarity).

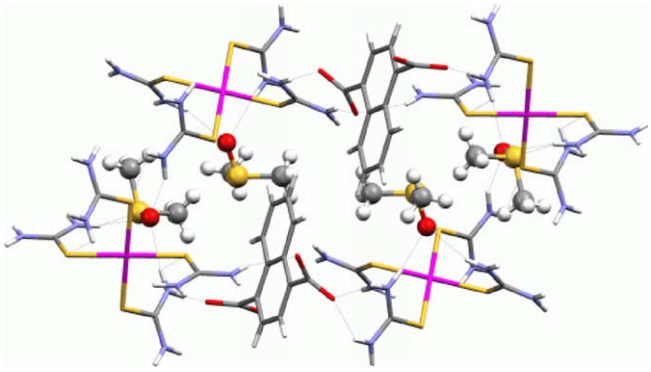

Fig. 14. Detail of the hydrogen bonding environment of the DMSO molecules included in the crystal structure of compound **5**.

Compounds **1**, **2**, **4** and **5** contain in their structures neutral 1D chains resulting from bidentate N–H···O interactions ($R_2^2(8)$) between coordinated thiourea ligands and carboxylate groups. These chains are formed by thiourea groups in *trans* disposition but in the case of compound **4**, in which the 1,3-alternate disposition of thiourea groups means that the chains are propagated through mutually *cis*-ligands. These chains are inter-linked by secondary thiourea–carboxylate interactions to yield in all the examples 3D networks.

Formally, only two carboxylate groups are needed to balance the positive charge carried by the platinum complex, which include four thiourea ligands. This result in an "excess" of hydrogen bond donors relative to hydrogen bond acceptors, making the nets prone to include guest molecules with hydrogen bond acceptor properties. In fact, all compounds except compound **2** were crystallized including solvent molecules in their structure, e.g., DMSO or acetone, acting as hydrogen bond acceptors fulfilling the donor properties of the thiourea groups. Compound **3** includes in its crystal structure not only DMSO but water. This event has a profound effect in the resultant structure and no bidentate thiourea–carboxylate interactions are present but only discrete N–H···O interactions. Water molecules participate in the hydrogen-bonded network bridging the terephthalate dianions and the coordinated thiourea molecules creating a series of channels where the DMSO molecules are included. Overall, this structure can be seen as a failure in the ligand-anion recognition process, induced by the inclusion of the water molecules.

4. Conclusions

Tetrakis(thiourea)platinum(II) is an adequate molecular tecton for the construction of hydrogen-bonded networks. Its inertness towards ligand substitution makes it ideal for studies employing anions with high coordinative potential, like the carboxylates employed in this work, whereas the spatial disposition of the thiourea groups allowed the translation of the interactions into the three dimensions of the crystal. Double thiourea–carboxylate hydrogen bond interactions appeared in four of the five structures presented, a supramolecular yield of 80%, despite the presence of competitive anions and solvent in the reaction media, making of this motif a reliable supramolecular synthon. We are continuing to study the use of the tetrakis(thiourea)platinum(II) unit in crystal engineered network formation. The results of these studies will be published shortly.

Acknowledgements

P.A.G. thanks the Royal Society for a University Research Fellowship, R.Q. thanks the Spanish Ministerio de Educación y Ciencia for a Postdoctoral Grant. The authors thank the EPSRC and Prof. Mike Hursthouse for access to the crystallographic facilities at the University of Southampton.

References

[1] D. Braga, L. Brammer, N.R. Champness, Cryst. Eng. Commun. 7 (2005) 1.
[2] L. Brammer, Chem. Soc. Rev. 33 (2004) 476.
[3] Entire issue devoted to Inorganic Crystal Engineering J. Chem. Soc., Dalton Trans. (2000) 3705.
[4] A.J. Blake, N.R. Champness, P. Hubberstey, W.-S. Li, M.A. Withersby, M. Schroder, Coord. Chem. Rev. 183 (1999) 117.
[5] D. Braga, F. Grepioni, G.R. Desiraju, Chem. Rev. 98 (1998) 1375.
[6] S.L. James, Chem. Soc. Rev. 32 (2003) 276.
[7] B. Moulton, M.J. Zaworotko, Chem. Rev. 101 (2001) 1629.

[8] S.J. Loeb, in: J.L. Atwood, J.E.D. Davis, D.D. MacNicol, F. Vögtle (Eds.), Comprehensive Supramolecular Chemistry, vol. 1, Elsevier Science, New York, 1996, p. 733.
[9] D.A. Beauchamp, S.J. Loeb, in: J.L. Atwood, J.W. Steed (Eds.), Encyclopedia of Supramolecular Chemistry, Marcel Dekker, New York, 2004, p. 1209.
[10] A.M. Beatty, Coord. Chem. Rev. 246 (2003) 131.
[11] A.M. Beatty, Cryst. Eng. Commun. 3 (2001) 1.
[12] J. Lu, K. Zhao, Q.-R. Fang, J.-Q. Xu, J.-H. Yu, X. Zhang, H.-Y. Bie, T.-G. Wang, Cryst. Growth Des. 5 (2005) 1091.
[13] T.J. Wadas, Q.-M. Wang, Y.-J. Kim, C. Flaschenreim, T.N. Blanton, R. Eisenberg, J. Am. Chem. Soc. 126 (2004) 16841.
[14] K. Uemura, S. Kitagawa, K. Fukui, K. Saito, J. Am. Chem. Soc. 126 (2004) 3817.
[15] M.T. Allen, A.D. Burrows, M.F. Mahon, J. Chem. Soc., Dalton Trans. (1999) 215.
[16] A.J. Blake, P. Hubberstey, U. Suksangpanya, C.L. Wilson, J. Chem. Soc., Dalton Trans. (2000) 3873.
[17] C.J. Adams, P.C. Crawford, A.G. Orpen, T.J. Podesta, B. Salt, Chem. Commun. (2005) 2457.
[18] A. Angeloni, P.C. Crawford, A.G. Orpen, T.J. Podesta, B.J. Shore, Chem. Eur. J. 10 (2004) 3783.
[19] B. Dolling, A.L. Gillon, A.G. Orpen, J. Starbuck, X.-M. Wang, Chem. Commun. (2001) 567.
[20] M.W. Hosseini, Coord. Chem. Rev. 240 (2003) 157, and references therein.
[21] Z.-Y. Wu, S.A. Van Arman, S. Kincaid, A.D. Hamilton, J. Am. Chem. Soc. 115 (1993) 369.
[22] E. Fan, D.-J. Xua, C.-H. Hung, J. Coord. Chem. 57 (2004) 791.
[23] E. Diamantopoulou, G.S. Papaefstathiou, A. Terzis, C.P. Raptopoulou, H.O. Desseyn, S.P. Perlepes, Polyhedron 22 (2003) 825.
[24] R. Keuleers, H.O. Desseyn, G.S. Papaefstathiou, L. Drakopoulou, S.P. Perlepes, C.P. Raptopoulou, A. Terzis, Transition Met. Chem. 28 (2003) 548.
[25] A.D. Burrows, R.W. Harrington, M.F. Mahon, C.E. Price, J. Chem. Soc., Dalton Trans. (2000) 3845.
[26] N.J. Burke, A.D. Burrows, A.S. Donovan, A.W. Harrington, M.F. Mahon, C.E. Price, Dalton Trans. (2003) 3840.
[27] A.D. Burrows, A.S. Donovan, A.W. Harrington, M.F. Mahon, Eur. J. Inorg. Chem. 23 (2004) 4686.
[28] J.M. Bret, P. Castan, J.P. Laurent, Inorg. Chim. Acta 51 (1981) 103.
[29] G.M. Sheldrick, Bruker Nonius area detector scaling and absorption correction – V2.10.
[30] G.M. Sheldrick, SHELXS 97, Acta Crystallogr. A 46 (1990) 467.
[31] G.M. Sheldrick, SHELXL 97, University of Göttingen, Germany, 1997.
[32] A.J.M. Duisenberg, L.M.J. Kroon-Batenburg, A.M.M. Schreurs, J. Appl. Crystallogr. 36 (2003) 220.

Available online at www.sciencedirect.com
SCIENCE DIRECT
Polyhedron 25 (2006) 910–914
POLYHEDRON
www.elsevier.com/locate/poly

Lanthanide(III) ion coordination by a concave reagent

Jan P.W. Eggert [a], Jack M. Harrowfield [b,c], Ulrich Lüning [a], Brian W. Skelton [c], Allan H. White [c,*]

[a] *Otto-Diels-Institut für Organische Chemie, Universität Kiel, Olshausenstrasse 40, D-24098, Kiel, Germany*
[b] *Institut de Science et de Ingénierie Supramoléculaires, Universite Louis Pasteur, 8, allée Gaspard Monge, 67083 Strasbourg Cedex, Bas-Rhin, France*
[c] *Chemistry M313, University of Western Australia, 35 Stirling Highway, Crawley, WA 6009, Australia*

Received 26 September 2005; accepted 25 October 2005
Available online 2 December 2005

Dedicated to Professor Mike Hursthouse on the occasion of his 65th birthday.

Abstract

A macrobicylic ligand **1** formed by the A,D-bridging of a calix[6]arene with a 2,9-disubstituted 1,10-phenanthroline unit reacts with Yb(III) under basic conditions in dimethylformamide (dmf) to give a neutral, mononuclear complex characterised by X-ray crystallography as [Yb(**1**-3H)(dmf)] · 3dmf. The structure shows that although the metal can be considered to lie within a cavity formed by the "concave reagent" ligand, this does not entirely prevent its coordination to a dmf molecule between arms of the macrobicycle. Stability constant measurements indicate that **1** forms complexes of similar strength across the lanthanide(III) series.
© 2005 Elsevier Ltd. All rights reserved.

Keywords: Concave reagent; Calixarenes; Lanthanide complexes; Crystal structure; Stability constants

1. Introduction

In analogy with many enzyme active sites where a metal ion is held within a cavity of restricted dimensions [1], the complexation of metal ions by donor atoms attached to or within a hollow synthetic receptor raises prospects for many forms of catalysis [2,3]. The synthesis of ligands for such purposes is not straightforward, though one simplification is to use as reactants molecules which already have the capacity to adopt conformations of a cavity form. This property is well known for the calixarenes, including in particular calix[6]arenes [4], and we have previously described [3,5] the synthesis and structure of a calix[6]arene, bridged between the A,D rings by a 1,10-phenanthroline moiety (**1**, Fig. 1), which does indeed appear to behave as a "concave reagent" for binding metal ions [3]. An analogous derivative of calix[8]arene has also been recently described [6].

One of the unanticipated properties of **1** was its conformational lability, theoretical calculations indicating the probable presence of numerous forms of similar energy [5]. This implies that an interaction such as metal ion coordination might well enforce conformations quite different from those of the free ligand [5], an extreme case being that where ligands completing the coordination sphere of the metal, potentially those involved in catalysis, do not lie within the cavity of **1**. The formation of 2:1 M:L complexes of **1** with transition metals [7] provides evidence in support of this possibility. Thus, it was of interest to establish the structure of a metal complex of **1**, a lanthanide (Ln) ion complex, given the typically high coordination numbers and irregular geometry of simple Ln(III) ions [8], being seen as offering a stringent test of the capacity of **1** to restrict the full coordination environment of a bound metal. It is well known, in the case of cryptand complexes, for example [9], that simple unidentate ligands can bind to

* Corresponding author.
E-mail addresses: harrowfield@isis.u-strasbg.fr (J.M. Harrowfield), ahw@chem.uwa.edu.au (A.H. White).

0277-5387/$ - see front matter © 2005 Elsevier Ltd. All rights reserved.
doi:10.1016/j.poly.2005.10.018

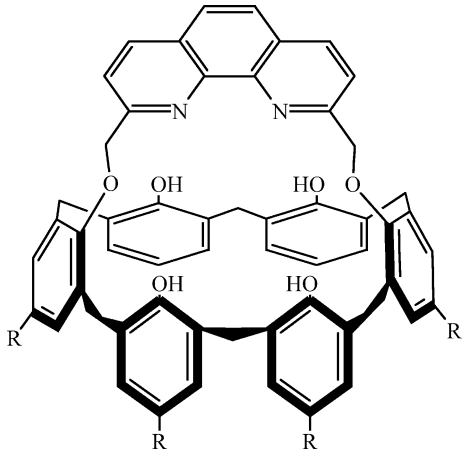

Fig. 1. The A,D-bridged calix[6]arene **1** (R = *t*-butyl, for clarity omitted from the two remote phenyl rings), shown in its idealised form as a "concave reagent".

Ln(III) centres between the arms of macrobicyclic ligands (of which **1** is an example). We report here the crystal structure of the complex [Yb(**1**-3H)(dmf)] · 3dmf (dmf = *N*,*N*-dimethylformamide) along with preliminary stability constant measurements indicating that **1** binds with similar strength to all members of the lanthanide(III) series.

2. Experimental

2.1. Synthesis

*[Yb(**1**-3H)(dmf)] · 3dmf*. Addition of a solution of $[Yb(dmso)_8](ClO_4)_3$ [10] (45 mg) in dry dmf (1 mL) to a solution of **1** (50 mg) in dmf (1 mL) containing a fourfold molar amount of triethylamine led to a yellow solution from which small yellow crystals slowly (over days) deposited. After one week, the crystals, one of which proved suitable for a structure determination, were collected and washed with acetonitrile followed by diethyl ether. Yield: 28 mg (50%). FAB-MS: *m*/*z* 1349 (parent peak) = $[Yb(\mathbf{1}\text{-}2H)]^+$.

2.2. Stability constant determinations

A solution of **1** (10^{-3} mol L^{-1}) in dimethylsulfoxide (dmso) containing a fourfold molar amount of triethylamine was titrated with an equimolar solution prepared from either $[Ln(dmso)_4(NO_3)_3]$ [11] (Ln = La) or $[Ln(dmso)_8](ClO_4)_3$ (Ln = Eu, Tb, Yb) in dmso, spectral changes being monitored in the visible region (350–700 nm). Measurements were made at 298 K, with data being analysed using Specfit 32 [12].

2.3. Crystallography

2.3.1. Structure determination

A full sphere of CCD area-detector diffractometer data were measured (Bruker AXS instrument, ω-scans, $2\theta_{max} = 50°$; monochromatic Mo Kα radiation, $\lambda = 0.71073$ Å; *T* ca. 153 K) yielding 150 882 total reflections, these merging to 14 424 independent after 'empirical'/multiscan 'absorption correction' (proprietary software; $R_{int} = 0.095$. $\mu = 1.14$ mm^{-1}; specimen: $0.30 \times 0.06 \times 0.05$ mm; '*T*'$_{min/max} = 0.87$), 7434 with $F > 4\sigma(F)$ being used in the large block least squares refinement (anisotropic displacement parameters for the non-hydrogen atoms, $(x, y, z, U_{iso})_H$ included at estimated values). Conventional residuals on |*F*| at convergence were $R = 0.055$, $R_w = 0.057$ (reflection weights: $(\sigma^2(F) + 0.0006F^2)^{-1}$). Neutral atom complex scattering factors were employed within the Xtal 3.7 program system [13]. *t*-Butyl groups 14, 44, 54 were modelled as disordered (about their pendent bonds), as also were the coordinated and solvent dmf molecules. The disorder is apparently concerted, site occupancies refining to 0.613(9) and complement for major and minor components (exception: *t*-butyl 54 where the occupancies were set at 0.5); for the minor components, the isotropic displacement parameter form was used, solvent dmf 4 being modelled with a rigid body constraint. The geometries of dmf(30) and *t*-Bu(54) were constrained at idealised values. The phenolic O(51) was assigned as protonated on the basis of difference map evidence, coupled with geometrical considerations. Pertinent results are presented below, and in Table 1, and Fig. 1, the latter showing the non-hydrogen atoms with 50% probability amplitude displacement envelopes, hydrogen atoms having arbitrary radii of 0.1 Å.

2.3.2. Crystal data

$[Yb(\mathbf{1}\text{-}3H)(dmf)] \cdot 3dmf \equiv C_{92}H_{117}N_6O_{10}Yb$, $M = 1640.0$. Orthorhombic, space group *Pbca* (D_{2h}^{15}, No. 61), $a =$

Table 1
The metal environment in the molecule of [Yb(**1**-3H)(dmf)]

Atom	*r*	O(21)	O(31)	O(61)	O(10)	N(01)	N(01′)
O(11)	2.532(6)	69.0(2)	158.3(2)	82.3(2)	92.3(2)	118.4(2)	60.0(2)
O(21)	2.103(6)		89.3(2)	97.8(2)	83.7(3)	167.1(2)	120.3(2)
O(31)	2.183(6)			101.8(2)	84.6(2)	82.8(2)	137.0(2)
O(61)	2.110(6)				173.4(2)	93.8(2)	103.8(2)
O(10)	2.296(7)					85.5(2)	70.1(2)
N(01)	2.712(8)						61.7(2)
N(01′)	2.622(7)						

r (Å) is the Yb–ligand atom distance; other entries in the matrix are the angles subtended by the relevant atoms at the head of the row and column. Yb–O(n1)–C(n1) ($n = 1,2,3,6$) are 120.8(5), 147.1(6), 138.2(5), 165.5(6); Yb–O(10)–C(10,10′) 153(1), 133(2)°.

30.707(6) Å, $b = 17.440(4)$ Å, $c = 32.377(8)$ Å, $V = 17339$ Å^3. D_{calc} ($Z = 8$) = 1.25$_6$ g cm^{-3}.

3. Results and discussion

The molecular entity [Yb(**1**-3H)(dmf)] found within the lattice of [Yb(**1**-3H)(dmf)] · 3dmf in the present low-temperature, single-crystal X-ray diffraction study is shown, with atom numbering, in Fig. 2(a). It is an addition to the relatively short list of mononuclear Ln(III) complexes of phenoxide-form calixarenes known [14] and presumably the essential inclusion of the metal within the ligand cavity retards association through such means as phenoxide-*O* bridging (otherwise commonly observed [14]). The Yb centre shows O_5N_2 seven-coordination (Fig. 2(b); Table 1), again not unusual for a lanthanide/calixarene species, with the longest Yb–O interaction involving one of the ether-*O* donor centres formed as a result of alkylation of the calixarene by the phenanthroline unit. This interaction may explain the unsymmetrical binding of the metal to the

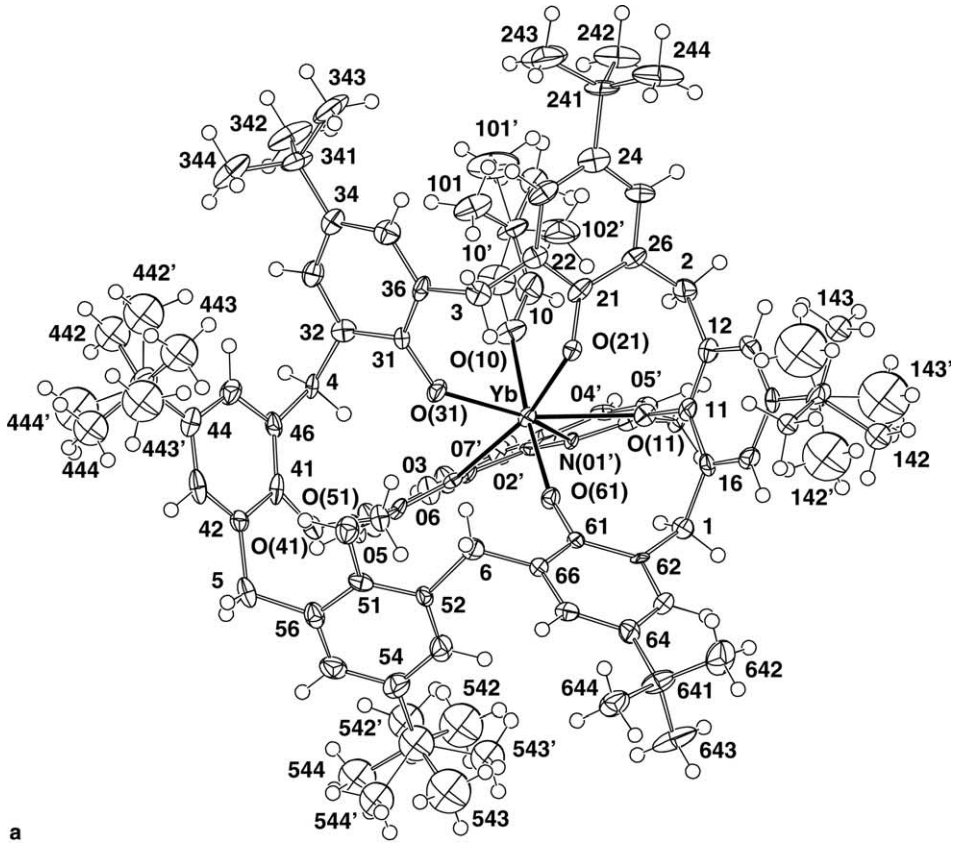

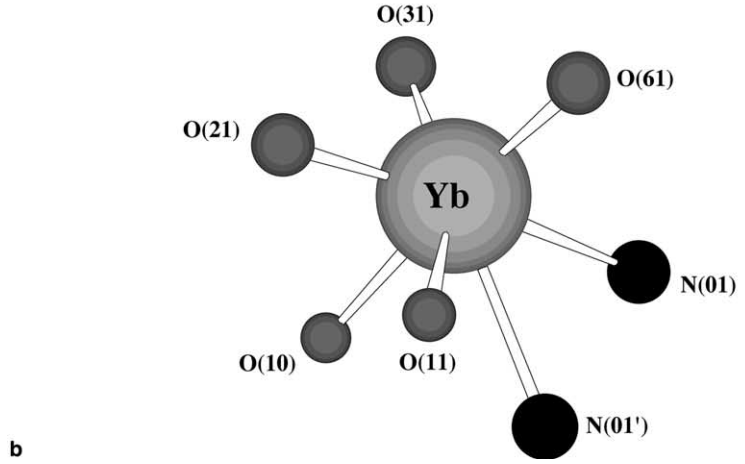

Fig. 2. (a) Projection of a molecule of [Yb(**1**-3H)(dmf)] through the macrocycle. (b) The coordination environment of Yb(III) in [Yb(**1**-3H)(dmf)].

phenanthroline-*N* donors, though this also is not unusual in very heavy metal complexes of 1,10-phenanthroline itself [15]. That the Yb–O bond distances, including those involving uncharged oxygen, are shorter than Yb–N is typical of Ln(III) ions [8]. The metal ion thus does not appear to be under particular geometric constraints in its interaction with **1**. O(41), which is directed away from the Yb centre, is assigned as carrying the residual ligand proton required for charge balance.

A significant feature of the metal ion environment in [Yb(**1**-3H)(dmf)] is that the *O*-bound dmf ligand approaches the metal between the ligand arms defined by the phenanthroline bridge and half the calixarene macrocycle, so that it cannot be considered to have been drawn into what it was hoped would be a cone-like cavity formed by the calix[6]arene entity. In fact, the coordination of three phenoxide-*O* atoms to Yb, although it may be regarded as assisting the formation of a cavity by orienting three *p*-*t*-butylphenyl rings in the same sense as the two attached to the phenanthroline unit, actually orients these "blocking" entities away from the sides of the phenanthroline plane so that they must do little to inhibit approach of a

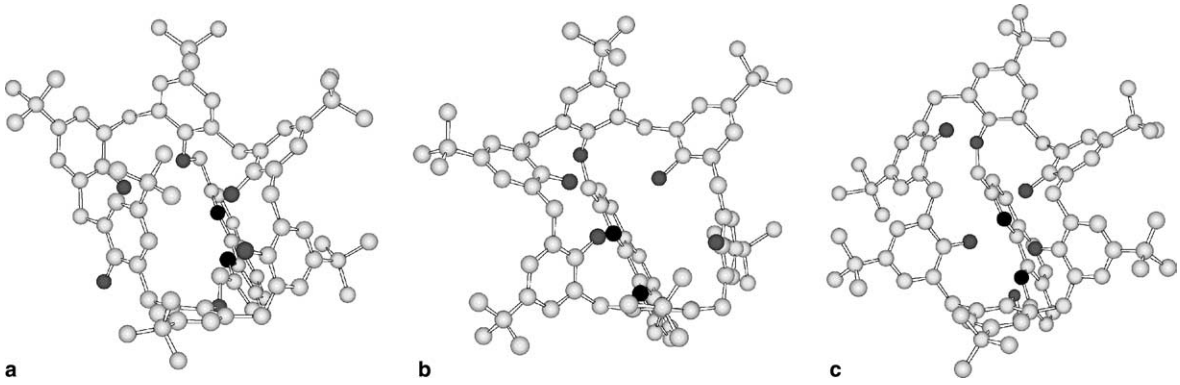

Fig. 3. Conformations of the molecule **1**, viewed with similar projections of the phenanthroline unit and with only one component of disordered sections of the molecule shown, as found in: (a) the water/acetonitrile/chloroform solvate of the ligand; (b) the water/pyridine solvate of the ligand; and (c) the formally trianionic form of the ligand found in its Yb(III) complex. (Atom colour coding: C, white; N, black; O, pale grey.)

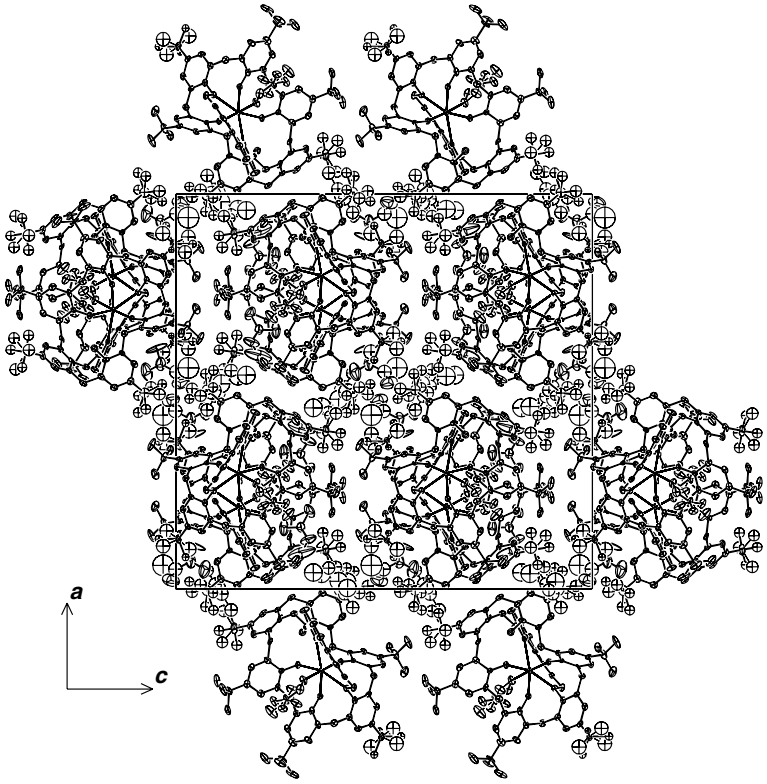

Fig. 4. The unit cell contents projected down *b*, i.e., down the columns of complex molecules parallel to that axis within which the Yb sites undulate. The complex columns are partitioned by columns of disordered solvent molecules.

small molecule such as dmf. Nonetheless, it may be noted that the (disordered) *N*-methyl groups of the bound dmf do come within ~3.5 Å of the centroids of two phenyl rings, indicating that inclusion effects of the ''side pockets'' might still be possible.

The conformation of **1** as its trianion bound to Yb(III) differs markedly from those of the neutral ligand as its water/acetonitrile/chloroform and water/pyridine solvates (Fig. 3), though the latter two conformations also differ markedly, apparently in response to different H-bonding interactions, as has been discussed previously [5]. In all three cases, nonetheless, the ligand can be regarded as forming a cavity offering a site for inclusion of other molecules. In the case of the Yb(III) complex, it is not the lattice dmf which occupies these cavities but adjacent, similarly oriented complex units, possibly largely due to edge-to-face phenanthroline–phenyl interactions, so that the complexes can be viewed as forming zig-zag chains down *b* through the lattice, with Yb···Yb 9.117(2) Å (Fig. 4). Such inclusion of a neighbouring molecule is seen in many metal complexes of calixarenes, sometimes resulting in hermaphrodite pair formation [16] rather than polymer formation as in the present case. Since the nature of the cavity is influenced, even if indirectly, by the metal ion, a prospect for catalysis by inclusion but without direct coordination still exists.

While the binding of the trianion of **1** to Yb(III) does not seem to restrict further binding of at least one small ligand, it does appear to eliminate interaction with a second molecule of **1**, since analysis of the spectral changes on addition of Ln(III), Ln = La, Eu, Tb, Yb, to **1** in dmso solution were consistent with the formation of just a 1:1 species in all instances. Given the apparent flexibility of **1** and the unexceptional nature of the coordination sphere of Yb in [Yb(**1**-3H)(dmf)]·3dmf, marked selectivity in the solution complexation of Ln(III) by **1** would be surprising, and indeed the values ($\log K_{stab}$) obtained of 4.0 ± 0.3 (La), 4.7 ± 0.3 (Eu), 4.5 ± 0.3 (Tb) and 4.2 ± 0.3 (Yb) indicate, assuming linear interpolations are justified, that **1** shows little discrimination across the lanthanide series. (Note that these values correspond to effective stability constants, since the K_a values for **1** in dmso are unknown.)

4. Conclusions

Ligand design for a specific objective is difficult [17] and it is somewhat ironic that the carefully planned synthesis of the ligand **1** appears not to have resulted in a desired objective, the placing of reactive substrates within a protected environment through coordination drawing them into a molecular cavity, when this has been achieved unintentionally in a much simpler calixarene system [18]. However, the fact that La(III), for example, frequently shows higher coordination numbers than Yb(III) [8], this being true in particular in complexes of a simple podand polyaryloxide [19], may justify further examination of lanthanide complexes of **1** to see whether lighter lanthanides may attract not only a ligand sited between the macrocyclic arms but also one drawn through the calixarene cavity. The similar affinity of **1** for all the lanthanides means, of course, that the full gamut of magnetic and spectroscopic properties of the lanthanides would be available for exploitation in such complexes.

5. Supplementary information

Full crystallographic data have been deposited with the CCDC under deposition number 284795. These data may be obtained free of charge via www.ccdc.cam.ac.uk/conts/retrieving.html or from the Cambridge Crystallographic Data Centre, 12 Union Road, Cambridge CB2 1EZ, UK (fax: +44 1223 336 033 or e-mail: deposit@ccdc.cam.ac.uk).

Acknowledgement

J.E. thanks the Deutscher Akademische Austauschdienst (DAAD) for a scholarship to carry out experiments at the University of Western Australia.

References

[1] R.H. Holm, E.I. Solomon, Chem. Rev. 104 (2004) 347.
[2] E. Engeldinger, D. Armspach, D. Matt, Chem. Rev. 103 (2003) 4147.
[3] (a) R. Cacciapaglia, S. Di Stefano, F. Fahrenkrug, U. Lüning, L. Mandolini, J. Phys. Org. Chem. 17 (2004) 350, and references therein; (b) M. Bühl, F. Terstegen, F. Löffler, B. Meynhardt, S. Kierse, M. Müller, C. Näther, U. Lüning, Eur. J. Org. Chem. (2001) 2151.
[4] U. Lüning, F. Löffler, J.P.W. Eggert, in: Z. Asfari, V. Böhmer, J.M. Harrowfield, J. Vicens (Eds.), Calixarenes 2001, Kluwer Academic Publishers, Dordrecht, 2001, pp. 71–88 (Chapter 4).
[5] J.P.W. Eggert, J. Harrowfield, U. Lüning, B.W. Skelton, A.H. White, F. Löffler, S. Konrad, Eur. J. Org. Chem. (2005) 1348.
[6] S. Konrad, C. Näther, U. Lüning, Eur. J. Org. Chem. (2005) 2330.
[7] F. Löffler, U. Lüning, G. Gomar, New J. Chem. 24 (2000) 935.
[8] J.M. Harrowfield, in: A. Sigel, H. Sigel (Eds.), The Lanthanides and their Interrelationships with Biosystems, Metal Ions in Biological Systems, vol. 40, Marcel Dekker, New York, 2003 (Chapter 4).
[9] I. Bkouche-Waksman, J. Guilhem, C. Pascard, B. Alpha, R. Deschenaux, J.-M. Lehn, Helv. Chim. Acta 74 (1991) 1163.
[10] J.-C.G. Bünzli, A. Militic-Tang, in: K.A. GschneidnerJr., L. Eyring (Eds.), Handbook of the Chemistry and Physics of the Rare Earths, vol. 21, Elsevier, Amsterdam, 1995, p. 305.
[11] P.C. Junk, D.L. Kepert, B.W. Skelton, A.H. White, Aust. J. Chem. 52 (1999) 497, and references therein.
[12] Specfit 32 from Spectrum Software Associates, PMB 361, Marlborough MA, USA..
[13] S.R. Hall, D.J. du Boulay, R. Olthof-Hazekamp (Eds.), The Xtal 3.7 System, University of Western Australia, 2001.
[14] P. Thuéry, M. Nierlich, J.M. Harrowfield, M.I. Ogden, in: Z. Asfari, V. Böhmer, J.M. Harrowfield, J. Vicens (Eds.), Calixarenes 2001, Kluwer Academic Publishers, Dordrecht, 2001, pp. 561–582 (Chapter 30).
[15] A.A. Soudi, F. Marandi, A. Ramasami, E. Elmadi, A. Morsali, C.R. Chimie 8 (2005) 157.
[16] A. Bilyk, A.K. Hall, J.M. Harrowfield, M.W. Hosseini, B.W. Skelton, A.H. White, Inorg. Chem. 40 (2001) 672.
[17] P.J. Steel, Acc. Chem. Res. 38 (2005) 243.
[18] Z. Asfari, J.M. Harrowfield, M.I. Ogden, A.H. White, Angew. Chem. Int. Ed. 30 (1991) 854.
[19] Z. Xu, P.W. Read, D.E. Hibbs, M.B. Hursthouse, K.M.A. Malik, B.O. Patrick, S.J. Rettig, M. Seid, D.A. Summers, M. Pink, R.C. Thompson, C. Orvig, Inorg. Chem. 39 (2000) 508.

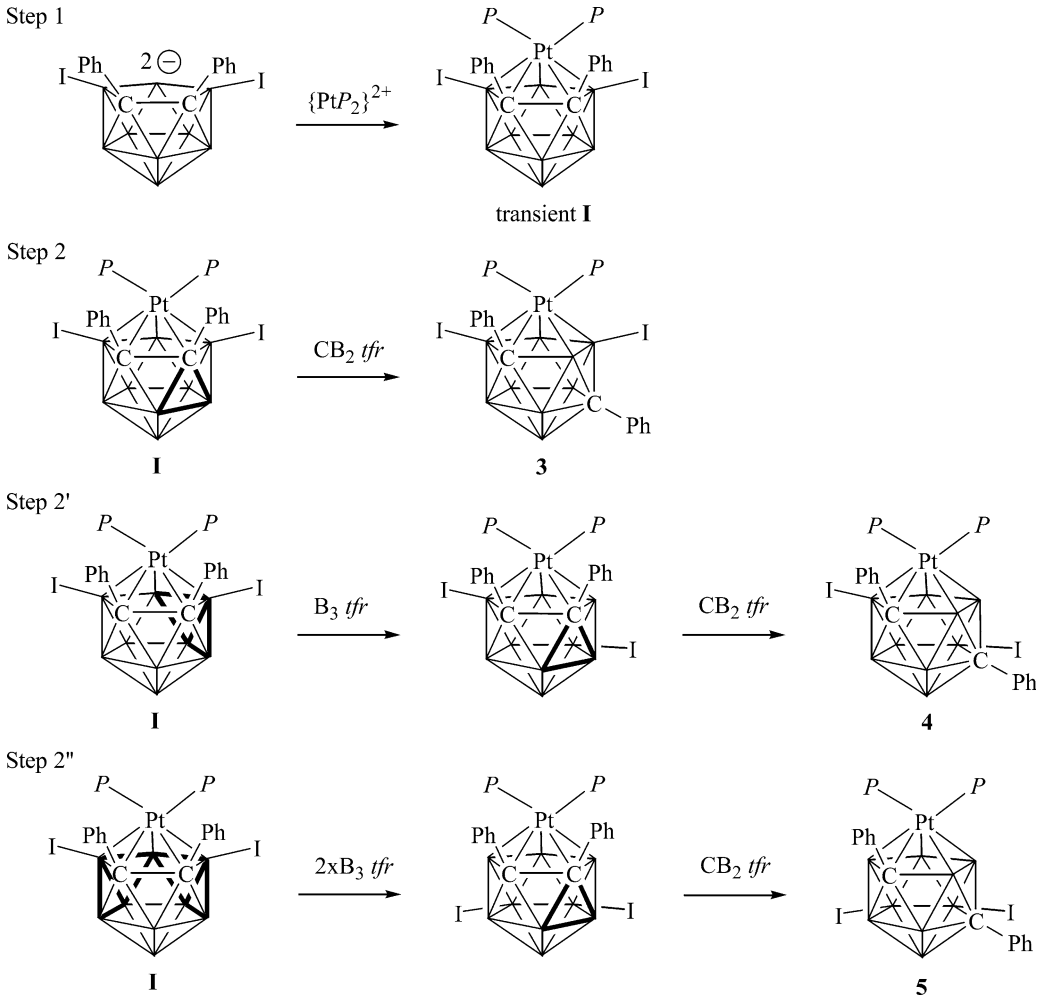

Scheme 1. Possible formation of platinacarboranes **3**–**5** by triangle face rotations (tfrs) starting from an implied transient species **I**. In each tfr the face highlighted in bold is assumed to rotate by 120°. In Steps 2′ and 2″ the B_3 and CB_2 tfrs could be sequential or synchronous. $P = PMe_2Ph$.

are also formed [7c,7d], whereas addition of bulky $\{PtL_2\}^{2+}$ always gives 2,1,8-PtC_2B_9 products [4,7b,7d], although in one case [7b] we were also able to isolate a 3,1,2-PtC_2B_9 species and show that it represented an intermediate by its isomerisation to 2,1,8-PtC_2B_9 on gentle warming.

In this paper, we extend these studies by describing the synthesis of new mono- and disubstituted nido-diphenylcarboranes and the results of subsequent metallation of the latter with a $\{PtL_2\}^{2+}$ fragment.

2. Experimental

2.1. Synthetic and spectroscopic studies

Experiments were performed under dry, oxygen-free N_2 using standard Schlenk techniques, with some subsequent manipulation in the open laboratory. Solvents were freshly distilled over CaH_2 (CH_2Cl_2) or Na wire (THF, Et_2O, 40–60 petroleum ether), or were stored over 4 Å molecular sieves [$CDCl_3$, $(CD_3)_2CO$]. Preparative thin layer chromatography (TLC) employed 20 × 20 cm Kieselgel 60 F_{254} glass plates. NMR spectra at 200.13 (^{1}H), 400.13 MHz (^{1}H), 128.38 (^{11}B) or 161.98 MHz (^{31}P) were recorded on Bruker AC 200 or DPX 400 spectrometers from $CDCl_3$ or $(CD_3)_2CO$ solutions at ambient temperature, chemical shifts being recorded relative to $SiMe_4$ (^{1}H), $BF_3 \cdot OEt_2$ (^{11}B) or H_3PO_4 (^{31}P). IR spectra were recorded from KBr disks on a Perkin–Elmer Spectrum RX FT-IR spectrophotometer. Elemental analyses were determined by the EPS School service. The starting materials 1,2-Ph_2-1,2-*closo*-$C_2B_{10}H_{10}$ [9] and *cis*-$PtCl_2(PMe_2Ph)_2$ [10] were prepared by literature methods or slight variants thereof. All other reagents and solvents were supplied commercially and were used as received.

2.1.1. Synthesis of [$HNMe_3$][7,8-Ph_2-9-I-nido-$C_2B_9H_9$] (*1*)

1,2-Ph_2-$C_2B_{10}H_{10}$ (1.000 g, 3.38 mmol) and KOH (0.430 g; 8.45 mmol) were heated to reflux in EtOH (50 ml) for 72 h. Excess KOH was removed by reaction with CO_2 and filtering off the K_2CO_3 formed. To the clear colourless solution of K[7,8-Ph_2-*nido*-7,8-$C_2B_9H_{10}$] was added I_2 (0.870 g, 3.41 mmol) in ethanol (30 ml). The reaction

mixture was heated to reflux for 2 h, during which time the solution decolourised. The volume of solution was reduced to ca. 10 ml in vacuo and distilled water (50 ml) added. Filtration and addition of aqueous $HNMe_3Cl$ (0.380 g, 4.00 mmol) gave a white precipitate which was filtered off and dried in vacuo. An alternative procedure involves extraction of the precipitate into CH_2Cl_2 (3×30 ml), drying over $MgSO_4$ and subsequent removal of the drying agents and solvents. An oily solid was recovered which was recrystallised from CH_2Cl_2/40–60 petroleum ether to give a white crystalline solid. Yield 1.000 g, (63% based on diphenylcarborane). *Anal.* Calc. for $C_{17}H_{29}B_9IN$: C, 43.3; H, 6.21; N, 2.97. Found: C, 43.3; H, 6.39; N, 2.56%. IR ν_{max} (cm^{-1}): 2537 (B–H str). ^1H NMR δ (ppm): 7.2–6.8 (m, 10H, C_6H_5), 3.1 (s, 9H, NCH_3). ^{11}B–{^1H} NMR δ (ppm): −5.70 (1B), −14.42 (4B), −20.13 (1B), −23.96 (1B), −29.73 (1B), −35.68 (1B).

2.1.2. Synthesis of [$HNMe_3$][7,8-Ph_2-9,11-I_2-7,8-*nido*-$C_2B_9H_8$] (**2**)

To a solution of K[7,8-Ph_2-*nido*-7,8-$C_2B_9H_{10}$] (1.69 mmol) in EtOH (50 ml) prepared as above, was added I_2 (1.080 g, 4.23 mmol) in ethanol (30 ml). The reaction mixture was heated to reflux for 18 h, during which time the solution decolourised. The volume of solution was reduced to ca. 10 ml in vacuo and distilled water (50 ml) added. Filtration and addition of aqueous $HNMe_3Cl$ (0.173 g, 1.80 mmol) gave a white precipitate which was filtered off and dried in vacuo. Again, an alternative work-up involves extraction of the precipitate into CH_2Cl_2 (3×30 ml), drying over $MgSO_4$ and subsequent removal of the drying agents and solvents. A white solid was recovered which was recrystallised by evaporation of a dichloromethane solution to give colourless crystals. Yield 0.230 g (23% based on diphenylcarborane). *Anal.* Calc. for $C_{17}H_{28}B_9I_2N$: C, 34.2; H, 4.73; N, 2.34. Found: C, 34.1; H, 4.76; N, 2.27%. IR ν_{max} (cm^{-1}): 2546 (B–H str). ^1H NMR δ (ppm): 7.2–6.8 (m, 10H, C_6H_5), 3.2 (s, 9H, NCH_3). ^{11}B–{^1H} NMR δ (ppm): −13.26 (3B), −16.55 (2B), −18.43 (2B, B9,11), −28.17 (1B), −35.30 (1B).

2.1.3. Syntheses of 1,8-Ph_2-2,2-(PMe_2Ph)$_2$-6,7-I_2-2,1,8-$PtC_2B_9H_7$ (**3**), 1,8-Ph_2-2,2-(PMe_2Ph)$_2$-6,12-I_2-2,1,8-$PtC_2B_9H_7$ (**4**) and 1,8-Ph_2-2,2-(PMe_2Ph)$_2$-10,12-I_2-2,1,8-$PtC_2B_9H_7$ (**5**)

Salt **2** (0.180 g; 0.30 mmol) was suspended in dry ether (30 ml) at 0 °C and ^{n}BuLi (0.24 ml of a 2.5 M solution in hexanes, 0.60 mmol) was added dropwise. The solution was stirred at room temperature for 18 h. All volatiles were removed and THF (30 ml) added. The THF solution of Li_2[7,8-Ph_2-9,11-I_2-7,8-*nido*-$C_2B_9H_7$] was added to a frozen suspension of *cis*-$PtCl_2(PMe_2Ph)_2$ (0.163 g, 0.30 mmol) in THF (25 ml) at −196 °C. The mixture was refrozen, then slowly warmed to room temperature and stirred for 18 h. All volatiles were removed in vacuo and CH_2Cl_2 (20 ml) added. The yellow suspension was filtered and evacuated to dryness to yield a yellow solid. The product was purified by TLC, eluting with 50/50 CH_2Cl_2/40–60 petroleum ether to give three yellow bands, respectively, compounds **3** ($R_f = 0.65$), **4** ($R_f = 0.56$) and **5** ($R_f = 0.45$).

3: yield 0.060 g (20%). *Anal.* Calc. for $C_{30}H_{39}B_9I_2P_2Pt$: C, 35.8; H, 3.91. Found: C, 34.9; H, 3.88%. IR ν_{max} (cm^{-1}): 2575 (B–H str). ^1H NMR δ (ppm): 7.9–6.9 (m, 20H, C_6H_5), 2.2–1.2 (m, 12H, P–CH_3). ^{11}B–{^1H} NMR δ (ppm): −3.69 (1B), −8.61 (1B), −11.70 (1B), −15.44 (3B), −19.75 (2B), −23.93 (1B). ^{31}P–{^1H} NMR δ (ppm): −15.80 (s, 1P, $^1J_{Pt-P} = 3284$ Hz), −23.95 (s, 1P, $^1J_{Pt-P} = 3227$ Hz).

4: yield 0.030 g (10%). *Anal.* Calc. for $C_{30}H_{39}B_9I_2P_2Pt$: C, 35.8; H, 3.91. Found: C, 35.1; H, 3.96%. IR ν_{max} (cm^{-1}): 2544 (B–H str). ^1H NMR δ (ppm): 8.0–6.9 (m, 20H, C_6H_5), 2.1–1.2 (m, 12H, P–CH_3). ^{11}B–{^1H} NMR δ (ppm): −3.80 (2B), −11.38 (1B), −15.39 (4B), −18.09 (1B), −23.76 (1B). ^{31}P–{^1H} NMR δ (ppm): −12.03 (s, 1P, $^1J_{Pt-P} = 3306$ Hz), −21.36 (s, 1P, $^1J_{Pt-P} = 3217$ Hz).

5: yield 0.030 g (10%). *Anal.* Calc. for $C_{30}H_{39}B_9I_2P_2Pt$: C, 35.8; H, 3.91. Found: C, 35.6; H, 3.85%. IR ν_{max} (cm^{-1}): 2581 (B–H str). ^1H NMR δ (ppm): 7.5–7.0 (m, 20H, C_6H_5), 1.8–1.1 (m, 12H, P–CH_3). ^{11}B–{^1H} NMR δ (ppm): −6.74 (3B), −13.28 (3B), −14.91 (2B), −31.11 (1B). ^{31}P–{^1H} NMR δ (ppm): −13.93 (s, 1P, $^1J_{Pt-P} = 3290$ Hz), −15.32 (s, 1P, $^1J_{Pt-P} = 3347$ Hz).

2.2. Crystallographic studies

Single crystals suitable for X-ray diffraction were grown by evaporation of a CH_2Cl_2 solution (salt **2**), from diffusion of a CH_2Cl_2 solution and 40–60 petroleum ether at −30 °C (compounds **3** and **5**) or from diffusion of a CH_2Cl_2 solution and diethylether at −30 °C (compound **4**). Salt **2** crystallises with $1\frac{1}{2}$ equivalents of CH_2Cl_2 and compound **4** with 1 equivalent of Et_2O. Data were collected at 100 K (cold N_2 gas) on a Bruker AXS *P*4 diffractometer producing graphite-monochromated Mo Kα radiation ($\lambda = 0.71069$ Å) using ω scans to $\theta_{max} = 25°$, and were corrected for absorption by psi scans. Structures were solved by direct and difference Fourier methods and refined [11] by full-matrix least-squares against F^2. Refinement was completed with all non-hydrogen atoms assigned anisotropic displacement parameters. For the anion of **2** H_{exo} atoms were refined subject to a restrained B–H distance of 1.10(2) Å, whilst the H_{endo} atom was freely refined. For **3**–**5** cage H atoms were allowed to ride on their bound boron with B–H constrained to 1.10 Å (1.12 Å for **3**). In all structures CH atoms were similarly constrained, with C–H = 0.95 (phenyl), 0.98 (CH_3) or 0.99 (CH_2) Å. H atoms except methyl H atoms were assigned displacement parameters set at 1.2 times that of the U_{eq} of their bound atom, with methyl H atoms assigned displacement parameters calculated as 1.5 times the bound carbon atom U_{eq}. H atoms were included in all molecules of solvation. For **3** the maximum and minimum residual e-density are significant but both are within 1 Å of Pt2 and thus chemically

meaningless. Table 1 contains details of the crystallographic studies.

3. Results and discussion

3.1. B-substituted carboranes

Electrophilic iodination of K[7,8-Ph_2-*nido*-7,8-$C_2B_9H_{10}$] with elemental I_2 proceeds smoothly in refluxing ethanol to generate, after metathesis with $HNMe_3Cl$, the new B-substituted nido diphenylcarboranes [$HNMe_3$][7,8-Ph_2-9-I-*nido*-7,8-$C_2B_9H_9$] (**1**) and [$HNMe_3$][7,8-Ph_2-9,11-I_2-7,8-*nido*-$C_2B_9H_8$] (**2**).

Use of one equivalent of I_2 affords a good yield of the monosubstituted 9-I species with <5% of the disubstituted 9,11-I_2 carborane also formed, as observed by ^{11}B spectroscopy. Addition of two equivalents of I_2 gives pure disubstituted compound, albeit in somewhat less good yield. Further substitution is not observed even with large excesses of I_2. The synthesis of salt **1** is analogous to that used by Hawthorne and Olsen to prepare the related species [NMe_4][9-I,-7,8-*nido*-$C_2B_9H_{11}$], although this early paper [12] does not report further substitution to the diiodo product. Both **1** and **2** are appreciably soluble in acetone and acetonitrile and sparingly soluble in halogenated solvents, but insoluble in 40/60 petroleum ether and toluene.

The compounds **1** and **2** were fully characterised by microanalysis, NMR and IR spectroscopies. In both cases the ^{1}H NMR spectra reveal signals due to cage phenyl and *N*-methyl hydrogen atoms in the correct relative integrals. ^{11}B NMR spectra are more informative. In the ^{11}B–{^{1}H} spectrum of **1** a 1:4:1:1:1:1 pattern, from high to low frequency, is observed, although the anticipated C_1 symmetry of the product requires the integral-4 signal to be a 1 + 1 + 1 + 1 coincidence. In the ^{11}B spectrum the uncoupled resonance due to the B atom bearing the iodine substituent is not obvious, and is presumed to lie within the envelope of these coincident signals. Compound **2** has a 3:2:2:1:1 pattern, its anticipated C_s symmetry requiring the highest frequency resonance to be a 2 + 1 coincidence. This time, however, the signal due to the two, symmetry equivalent, substituted B atoms is clear in the ^{11}B spectrum at δ −18.43.

Electrophilic attack on a nido carborane is expected to occur at the open face, but, to establish an unequivocal structure, a crystallographic determination of salt **2**, as its $1\frac{1}{2}CH_2Cl_2$ solvate, was undertaken.

Fig. 1 shows a perspective view of a single anion and Table 2 lists selected interatomic distances and interbond angles. The 9,11-disubstitution by iodine is confirmed. The endo H atom H10a is semi-bridging the B10–B11 edge, B10–H10a 1.17(5) Å, B11–H10a 1.56(5) Å, consistent with the optimised structure of [7,8-*nido*-$C_2B_9H_{12}$]$^-$ [13]. As anticipated [14], the (H-bridged) B10–B11 edge, 1.842(7) Å, is consequently somewhat longer that the unbridged but otherwise equivalent B9–B10 edge, 1.805(8) Å. The C7–C8 distance in **2** is 1.610(6) Å, almost identical to that in the unsubstituted analogue [7,8-Ph_2-7,8-*nido*-$C_2B_9H_{10}$]$^-$ (1.590(5) Å for the [$HNEt_3$]$^+$ salt and 1.602(3) Å in the [$C_6H_5CH_2NMe_3$]$^+$ salt) [15] and to that

Table 1
Crystallographic data for **2**–**5**[a]

Compound	**2**	**3**	**4**	**5**
Formula	$C_{17}H_{28}B_9I_2N \cdot 1\frac{1}{2}CH_2Cl_2$	$C_{30}H_{39}B_9I_2PPt$	$C_{30}H_{39}B_9I_2PPt \cdot C_2H_5O$	$C_{30}H_{39}B_9I_2PPt$
M_r	724.88	1007.73	1081.85	1007.73
Crystal size (mm)	0.60 × 0.50 × 0.30	0.42 × 0.22 × 0.20	0.30 × 0.50 × 0.40	0.40 × 0.60 × 0.50
Crystal system	triclinic	monoclinic	monoclinic	monoclinic
Space group	$P\bar{1}$	$P2_1/n$	$P2_1/n$	$P2_1/c$
a (Å)	8.7277(7)	12.003(4)	15.820(2)	10.9980(10)
b (Å)	11.0465(13)	17.308(6)	13.462(2)	25.352(3)
c (Å)	16.0255(19)	17.020(11)	20.210(2)	12.761(2)
α (°)	83.165(10)	90	90	90
β (°)	84.375(11)	93.17(4)	110.440(10)	95.950(10)
γ (°)	70.348(10)	90	90	90
U (Å^3)	1441.9(3)	3530(3)	4033.1(9)	3538.9(8)
Z	2	4	4	4
F(000)	702	1912	2080	1912
μ (Mo Kα) (mm^{-1})	2.47	5.84	5.12	5.82
Data measured	6088	7669	8597	7598
Unique data, *n*	5022	6203	7058	6209
R_{int}	0.0648	0.0404	0.0427	0.0340
R (all data)	0.0431	0.0482	0.0436	0.0378
wR_2 (all data)	0.0945	0.1056	0.1067	0.0956
S (all data)	1.074	1.063	0.735	0.953
Variables, *p*	332	397	442	398
E_{max} (e Å^{-3})	1.663	3.213	0.880	0.847
E_{min} (e Å^{-3})	−1.467	−3.252	−1.118	−1.178

[a] $R = \sum \|F_o\| - |F_c\| / \sum |F_o|$, $wR_2 = [\sum[w(F_o^2 - F_c^2)^2] / \sum w(F_o^2)^2]^{1/2}$, $(w^{-1} = [\sigma^2(F_o)^2 + (aP)^2 + bP]$ where *a* and *b* are variables and $P = [0.333(F_o)^2 + 0.667(F_c)^2])$, $S = [\sum[w(F_o^2 - F_c^2)^2/(n-p)]^{1/2}$, (where *n* is the number of data and *p* the number of parameters).

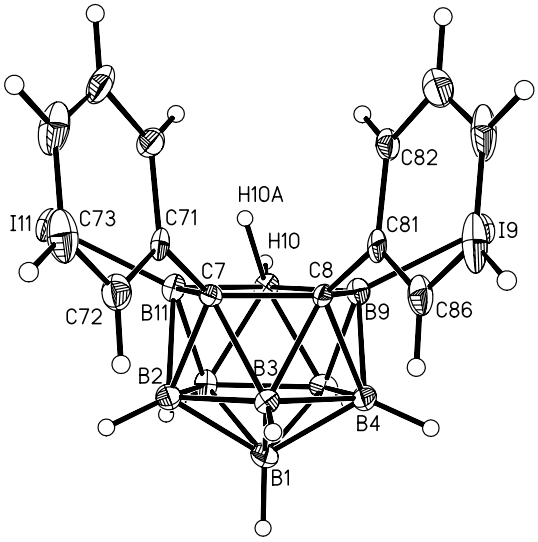

Fig. 1. Perspective view of the anion of $[HNMe_3][7,8\text{-}Ph_2\text{-}9,11\text{-}I_2\text{-}7,8\text{-}nido\text{-}C_2B_9H_{10}]$ (**2**). Atoms are drawn as 50% probability ellipsoids except for H atoms.

Table 2
Selected interatomic distances (Å) and interbond angles (°) in **2**

B1–B2	1.748(8)	B6–B11	1.770(7)
B1–B3	1.790(8)	C7–C8	1.610(6)
B1–B4	1.776(7)	C7–B11	1.620(7)
B1–B5	1.779(8)	C8–B9	1.610(7)
B1–B6	1.794(8)	B9–B10	1.805(8)
B2–B3	1.754(8)	B10–B11	1.842(7)
B2–C7	1.734(7)	C7–C71	1.510(6)
B2–B11	1.811(8)	C8–C81	1.509(6)
B2–B6	1.791(8)	B9–I9	2.210(5)
B3–B4	1.780(8)	B11–I11	2.195(5)
B3–C8	1.745(7)	B10–H10a	1.17(5)
B3–C7	1.733(7)	B11–H10a	1.56(5)
B4–C8	1.745(7)	N1–C11	1.488(7)
B4–B9	1.774(8)	N1–C12	1.492(7)
B4–B5	1.762(8)	N1–C13	1.491(6)
B5–B9	1.741(7)	C1S–C11	1.730(6)
B5–B10	1.805(8)	C1S–C12	1.764(7)
B5–B6	1.823(8)	C2S–C13	1.661(11)
B6–B10	1.800(8)	C2S–C13$^{\#1}$	1.743(11)
C71–C7–B11	121.2(4)	I9–B9–C8	121.7(3)
C71–C7–B2	121.6(4)	I9–B9–B4	117.5(3)
C71–C7–B3	116.3(4)	I9–B9–B5	121.2(3)
C71–C7–C8	117.6(4)	I9–B9–B10	121.1(3)
C81–C8–C7	116.4(4)	I11–B11–B10	123.2(3)
C81–C8–B3	115.2(4)	I11–B11–B6	120.5(3)
C81–C8–B4	120.2(4)	I11–B11–B2	116.8(3)
C81–C8–B9	121.6(4)	I11–B11–C7	121.2(3)

$^{\#1}$atom generated by the operation $1-x, -y, 1+z$.

in the substituted species $[C_6H_5CH_2NMe_3][5\text{-}I\text{-}7,8\text{-}Ph_2\text{-}7,8\text{-}nido\text{-}C_2B_9H_9]$ (1.609(10) Å) [7a]. In C-adjacent diphenylcarborane derivatives we conveniently describe the conformation of the Ph rings with respect to the cage by parameter θ_{Ph}, the modulus of the average C_{cage}–C_{cage}–C_{Ph}–C_{Ph} torsion angle [16]. The measured values in **2** are 10.0° for the ring on C7 and 8.0° for the ring on C8, these low values quantifying the clear conclusion from Fig. 1 that the Ph rings stand effectively perpendicular to the nido face of the carborane. The B–I bonds in **2** are 2.210(5) Å for B9–I9 and 2.195(5) Å for B11–I11, essentially the same as that in the anionic $[5\text{-}I\text{-}7,8\text{-}Ph_2\text{-}7,8\text{-}nido\text{-}C_2B_9H_9]^-$, 2.211 (7) Å [7a], but slightly longer than those in the neutral compounds $9,12\text{-}I_2\text{-}1,2\text{-}closo\text{-}C_2B_{10}H_{10}$, average 2.178(5) Å [17], $1,2\text{-}Ph_2\text{-}9,12\text{-}I_2\text{-}1,2\text{-}closo\text{-}C_2B_{10}H_8$, 2.175(5) Å [7a], $1,2\text{-}Ph_2\text{-}9\text{-}I\text{-}1,2\text{-}closo\text{-}C_2B_{10}H_9$, 2.178(4) Å [18], and $9,10\text{-}I_2\text{-}1,7\text{-}closo\text{-}C_2B_{10}H_{10}$, average 2.153(14) Å [19].

3.2. Platincarboranes

We have previously noted that, as is logical, metallation of asymmetrically-substituted carboranes leads to a greater number of isomerised products than does metallation of symmetrically-substituted species. Thus, we have chosen to platinate the 9,11-disubstituted carborane **2** to promote isomerisation and track its mechanism. Deprotonation of **2** was effected with ^{n}BuLi in diethyl ether to produce $Li_2[7,8\text{-}Ph_2\text{-}9,11\text{-}I_2\text{-}7,8\text{-}nido\text{-}C_2B_9H_7]$. Addition of a THF solution of this to a suspension of $cis\text{-}PtCl_2(PMe_2Ph)_2$ in the same solvent at −196 °C, followed by warming to room temperature and stirring for 18 h afforded a yellow solution. On work-up by TLC three products were isolated. The fastest moving band **3** transpired to be the major component, being approximately twice as abundant as each of the two slower bands **4** and **5**.

Compound **3** was initially characterised by microanalysis and IR and multinuclear NMR spectroscopy. As is typical of such compounds the ^{1}H NMR spectrum proved relatively uninformative in terms of detailed structural information, simply revealing signals consistent with the presence of phenyl and methyl H atoms with the correct relative integrals. ^{11}B–{^{1}H} NMR spectroscopy was also of limited use: although the chemical shift range observed, δ −4 to −24, indicates a closo species (more consistent with an isomerised $2,1,8\text{-}PtC_2B_9$ architecture that with a slipped $3,1,2\text{-}PtC_2B_9$ cage [7b,7d]), the relative broadness of the signals and the presence of significant signal overlap precludes definitive interpretation and, specifically, prevents identification of signals which remain uncoupled in the ^{11}B spectrum. The ^{31}P–{^{1}H} NMR spectrum reveals the presence of inequivalent phosphorus nuclei, each signal showing the expected ^{195}Pt satellites (average $^1J_{Pt-P} = 3256$ Hz). Careful analysis also reveals residual $^2J_{P-P}$ coupling, however the value is too small to quote accurately.

The structure of **3** was established by crystallographic study. Fig. 2 shows a perspective view of one molecule while Table 3 lists selected interatomic distances and interbond angles. The compound is thus revealed to be $1,8\text{-}Ph_2\text{-}2,2\text{-}(PMe_2Ph)_2\text{-}6,7\text{-}I_2\text{-}2,1,8\text{-}closo\text{-}PtC_2B_9H_7$, the cage having undergone a 1,2 → 1,7 C atom isomerisation (confirming the interpretation of the ^{11}B chemical shift range). The substituted (iodine-bearing) boron atoms are B6 and B7. The metal atom is bound to a CB_4 face which is folded into the usual envelope conformation (dihedral angle between B3C1B6 and B6B11B7B3 planes 14.0°) and, moreover,

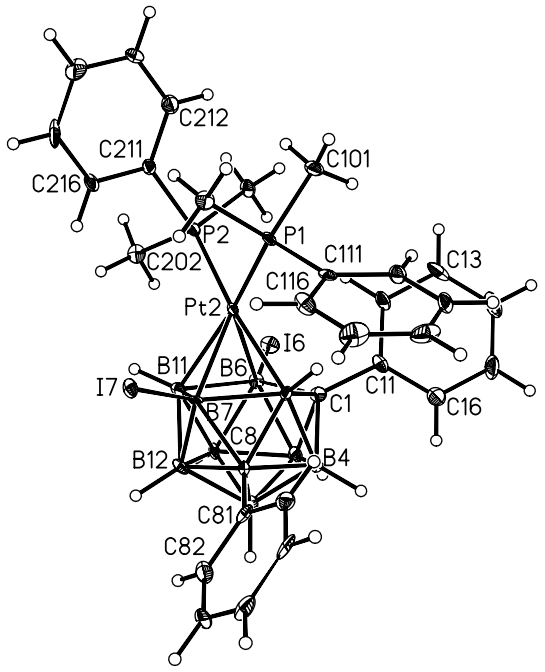

Fig. 2. Perspective view of 1,8-Ph_2-2,2-$(PMe_2Ph)_2$-6,7-I_2-2,1,8-*closo*-$PtC_2B_9H_7$ (**3**). Atoms are drawn as 50% probability ellipsoids except for H atoms.

the Pt atom is slipped away from C1 ($\Delta = 0.47$ Å) resulting in a long Pt2–C1 distance, 2.666(7) Å, emphasised by its non-inclusion in Fig. 2. The (electronic) reasons underlying these slipping and folding distortions are well documented [20] but we believe that in the present case the slipping is enhanced by a (steric) contribution arising from the orientation of the Ph ring on C1. The presence of an adjacent I atom, I6, requires the plane of this Ph ring to lie perpendicular to the metal-bonded CB_4 plane (a convenient measure of this is ζ, the modulus of the average Pt2–C1–C11–C torsion angles, $\zeta = 66.3°$) pushing back the $\{Pt(PMe_2Ph)_2\}$ fragment.

Compound **4** was similarly initially characterised by microanalysis and IR and multinuclear NMR spectroscopy, and ultimately by X-ray diffraction. The ^1H NMR spectrum was broadly similar to that of **3**, showing Ph and Me resonances with the correct relative integrals. The ^{11}B–$\{^1H\}$ NMR spectrum again revealed resonances between δ −4 and −24, indicative of a 2,1,8-*closo*-PtC_2B_9 cage. Once more the resonance(s) due to B–I could not clearly be discerned in the corresponding ^{11}B spectrum. In the ^{31}P–$\{^1H\}$ spectrum once more were two signals, each with Pt satellites (average $^1J_{Pt-Pt} = 3262$ Hz) and showing small residual J_{P-P} coupling.

The crystallographic study of **4** (Fig. 3 and Table 3) reveals a very similar molecular structure to that established for **3** except that the second substituted B atom is now B12 as opposed to B7. Thus, compound **4** is 1,8-Ph_2-2,2-$(PMe_2Ph)_2$-6,12-I_2-2,1,8-*closo*-$PtC_2B_9H_7$. The PtC_2B_9 cage of **4** resembles that of **3** in many respects: the Pt-bonded CB_4 face is envelope-folded by 15.6°, and

Table 3
Selected interatomic distances (Å) and interbond angles (°) in **3**–**5**

	3	**4**	**5**
Pt2–C1	2.666(7)	2.671(5)	2.609(5)
Pt2–B3	2.217(8)	2.234(7)	2.251(6)
Pt2–B7	2.202(7)	2.190(6)	2.217(6)
Pt2–B11	2.245(8)	2.247(7)	2.246(6)
Pt2–B6	2.365(7)	2.355(7)	2.266(6)
Pt2–P1	2.326(2)	2.3003(15)	2.3055(14)
Pt2–P2	2.298(2)	2.3105(15)	2.2887(14)
C1–B3	1.705(10)	1.705(9)	1.686(8)
C1–B4	1.647(10)	1.655(9)	1.657(8)
C1–B5	1.707(10)	1.689(9)	1.661(8)
C1–B6	1.666(10)	1.682(9)	1.733(8)
C1–C11	1.505(10)	1.507(8)	1.495(7)
B3–B4	1.821(11)	1.829(9)	1.831(8)
B3–C8	1.772(10)	1.761(8)	1.764(8)
B3–B7	1.864(11)	1.896(9)	1.871(8)
B4–B5	1.738(11)	1.733(9)	1.749(8)
B4–C8	1.747(11)	1.725(9)	1.731(8)
B4–B9	1.759(11)	1.765(9)	1.761(8)
B5–B6	1.844(11)	1.845(10)	1.829(8)
B5–B9	1.743(11)	1.742(9)	1.776(9)
B5–B10	1.775(11)	1.785(9)	1.799(9)
B6–B10	1.789(1)	1.810(9)	1.813(9)
B6–B11	1.875(11)	1.886(9)	1.879(9)
B7–C8	1.716(9)	1.710(9)	1.721(8)
B7–B12	1.790(10)	1.752(9)	1.748(8)
B7–B11	1.817(10)	1.792(9)	1.807(9)
C8–B9	1.744(10)	1.774(9)	1.767(8)
C8–B12	1.713(10)	1.745(9)	1.715(8)
C8–C81	1.496(9)	1.518(8)	1.511(7)
B9–B10	1.780(11)	1.792(9)	1.792(9)
B9–B12	1.741(11)	1.758(9)	1.788(9)
B10–B11	1.795(10)	1.783(9)	1.751(8)
B10–B12	1.774(11)	1.760(9)	1.774(9)
B11–B12	1.774(10)	1.757(9)	1.745(9)
B–I			
B6–I6	2.231(8)		
B7–I7	2.173(7)		
B6–I6		2.215(7)	
B12–I12		2.165(6)	
B10–I10			2.181(6)
B12–I12			2.169(6)
P1–Pt1–P2	93.05(7)	96.71(5)	96.61(5)

the Ph group on C1 subtends a high ζ angle, 84.8°, thus extending the slip distortion of the $\{Pt(PMe_2Ph)_2\}$ fragment to $\Delta = 0.48$ Å, Pt2–C1 = 2.666(7) Å.

The final product of the metallation, compound **5**, moves slowest on the TLC plate. ^1H NMR spectroscopy revealed the expected phenyl and methyl resonances and the ^{11}B–$\{^1H\}$ NMR spectrum showed only four peaks, δ −6 to −32, presumably reflecting significant coincidences. Once more, it was not possible to assign those resonance(s) due to the substituted B atoms. Asymmetrically disposed phosphorus atoms were again evident from the observation of two signals (with attendant Pt satellites) in the ^{31}P–$\{^1H\}$ NMR spectrum, the average $^1J_{Pt-P}$ being 3319 Hz.

The result of a crystallographic study of compound **5** is shown in Fig. 4, and Table 3 again lists key molecular parameters. This time *both* substituted B atoms (B10

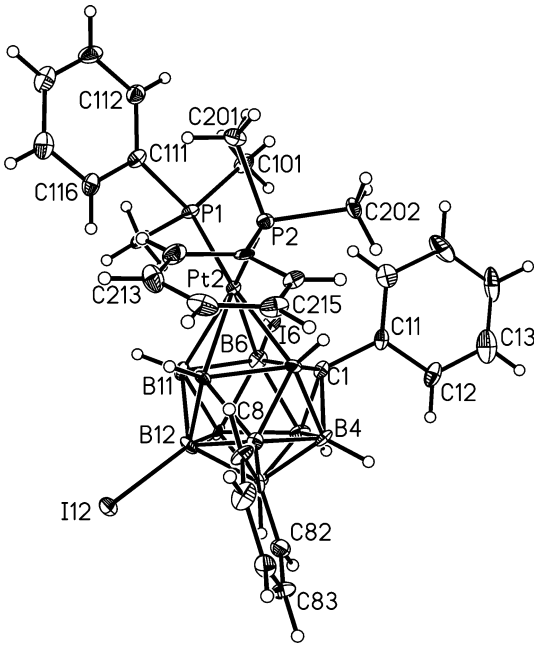

Fig. 3. Perspective view of 1,8-Ph_2-2,2-$(PMe_2Ph)_2$-6,12-I_2-2,1,8-*closo*-$PtC_2B_9H_7$ (**4**). Atoms are drawn as 50% probability ellipsoids except for H atoms.

and B12) are in the lower half of the molecule, which is thus identified as 1,8-Ph_2-2,2-$(PMe_2Ph)_2$-10,12-I_2-2,1,8-*closo*-$PtC_2B_9H_7$. Although the upper CB_4 face is still envelope-folded, this time by 15.6°, the non-adjacency of a substituted B atom to C1 means that the Ph ring on this

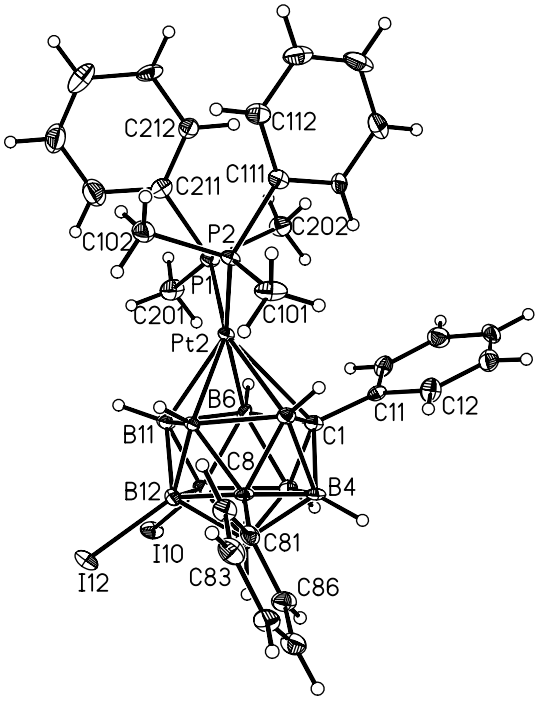

Fig. 4. Perspective view of 1,8-Ph_2-2,2-$(PMe_2Ph)_2$-10,12-I_2-2,1,8-*closo*-$PtC_2B_9H_7$ (**5**). Atoms are drawn as 50% probability ellipsoids except for H atoms.

last atom can adopt an orientation which simply minimises steric repulsion between it and the phosphine ligands. Thus, ζ is only 10.9°, as a result of which both the slip parameter Δ, 0.36 Å, and the Pt2–C1 distance, 2.609(5) Å, are reduced in **5** relative to equivalent values in **3** and **4**.

In compounds **3**–**5** collectively, the six B–I distances span the range 2.165(6)–2.231(8) Å. The two B6–I6 distances (compounds **3** and **4**) are the two longest, but it is not obvious why this should be. Certainly the four distances measured here to B7, B10 and B12, 2.169(6)–2.181(6) Å, correspond well with those, 2.169(9)–2.204(12) Å, previously found in 1,8-Ph_2-2,2-$(PMe_2Ph)_2$-X-I-2,1,8-*closo*-$PtC_2B_9H_8$, X = 7, 10, 12 [7d].

3.3. Possible mechanistic implications

In several recent contributions [7] we have interpreted the results of both 1,2 → 1,2 and 1,2 → 1,7 C atom isomerisations in B-substituted nickel- and platinacarboranes in terms of either one or two triangle face rotations (tfrs), starting from a crowded, transient, 3,1,2-MC_2B_9 species (in one case [7b] this intermediate was actually isolated).

In Scheme 1 we show how the formation of the platinacarboranes **3** could also be explained by a tfr. In Step 1 the overcrowded, transient species **I** is formed by simple complexation of the metal fragment and carborane ligand. To relieve this overcrowding, a CB_2 face in **I** undergoes a tfr (Step 2) affording the major product **3**. (note that since **I** has C_s symmetry either one of two equivalent CB_2 faces could rotate).

The formations of the minor products **4** and **5** cannot be so simply rationalised, but two factors appear relevant here. Firstly, we are fully confident that isomerisation only occurs following metallation since ^{n}BuLi deprotonation of **2** as described in Section 2.1.3 followed by reprotonation on addition of aqueous $HNMe_3Cl$ regenerates only **2** as shown by ^{11}B NMR spectroscopy. Secondly, it is likely that **3**–**5** are formed via parallel rather than sequential isomerisation steps given the mild conditions under which they are prepared and our subsequent inability to convert from one to another by heating (either nothing happens or we observe substantial decomposition).

We thus suggest Step 2′, as an alternative to Step 2, in which one of two possible B_3 triangle faces in **I** rotates to position one iodine substituent antipodal to a cage C atom, synchronous with, or followed immediately by, a CB_2 tfr analogous to that in Step 2, this overall process generating product **4**. Moreover, Step 2″, with both iodine substituents moving antipodal to cage C atoms, synchronous with or followed by CB_2 tfr, affords product **5**.

We acknowledge that above mechanism is highly speculative, and that it raises several issues. Firstly, we have previously [7d] considered rotation of a CB_2 face involving two B vertices from the lower pentagon (shown in Step 2) as less likely than one involving one upper and one lower B atom. Secondly, with regard to Step 2′, one could equally

reasonably anticipate the combination of one of the tfrs shown with the symmetry-equivalent of the other, affording a further product 1,8-Ph_2-2,2-$(PMe_2Ph)_2$-7,10-I_2-2,1,8-*closo*-$PtC_2B_9H_7$ (**II**) but this has not yet been identified.

Clearly a number of questions about the mechanism(s) of isomerisation that afford(s) compounds **3**–**5** remain, and studies designed to answer these are in hand. This is entirely consistent with the approach to chemical crystallography that Michael Hursthouse instilled in one of us as a postgraduate student – that molecular structure determination by crystallography should not be regarded simply as the end of one chemical investigation but, equally, based upon what that structure may mean in terms of chemical bonding or chemical reactivity, the beginning of another.

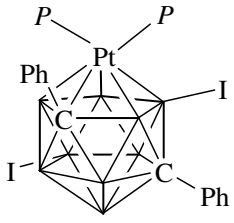

II

4. Supplementary material

Crystallographic data for the structure analyses have been deposited with the Cambridge Crystallographic Data Centre, CCDC Nos. 281522–281525 for **2**–**5**, respectively. Copies of this information may be obtained free of charge from The Director, CCDC, 12 Union Road, Cambridge CB2 1EZ, UK (fax: +44 1223 336 033; e-mail deposit@ccdc.cam.ac.uk or www: http://www.ccdc.cam.ac.uk).

Acknowledgements

We thank the Leverhulme Trust (D.E., R.M.G.) for support, C. Graham for microanalyses and Dr A.S.F. Boyd for NMR spectra.

References

[1] (a) D. Grafstein, J. Dvorak, Inorg. Chem. 2 (1963) 1128;
(b) W.N. Lipscomb, Science 153 (1966) 373;
(c) L.I. Zakharkin, V.N. Kalinin, Dokl. Akad. Nauk SSSR 169 (1966) 590;
(d) B.M. Gimarc, J.J. Ott, Inorg. Chem. 25 (1986) 83;
(e) D.J. Wales, A.J. Stone, Inorg. Chem. 26 (1987) 3845;
(f) S. Wu, M. Jones, J. Am. Chem. Soc. 111 (1989) 5373;
(g) G.M. Edvenson, D.F. Gaines, Inorg. Chem. 29 (1990) 1210;
(h) B.M. Gimarc, D.S. Warren, J.J. Ott, C. Brown, Inorg. Chem. 30 (1991) 1598;
(i) Y.V. Roberts, B.F.G. Johnson, J. Chem. Soc., Dalton Trans. (1994) 759;
(j) A.J. Welch, Steric effects in metallacarboranes, in: P. Braunstein, L.A. Oro, P.R. Raithby (Eds.), Metal Clusters in Chemistry, Wiley/VCH, New York/Weinheim, 1999, p. 69.

[2] e.g. H.D. Kaeze, R. Bau, H.A. Beall, W.N. Lipscomb, J. Am. Chem. Soc. 89 (1967) 4218.

[3] L.I. Zakharkin, V.N. Kalinin, Izv. Akad. Nauk SSSR, Ser. Khim. (1969) 607.

[4] D.R. Baghurst, R.C.B. Copley, H. Fleischer, D.M.P. Mingos, G.O. Kyd, L.J. Yellowlees, A.J. Welch, T.R. Spalding, D. O'Connell, J. Organomet. Chem. 447 (1993) C14.

[5] (a) S. Dunn, G.M. Rosair, Rh.Ll. Thomas, A.S. Weller, A.J. Welch, Angew. Chem. Int. Ed. 36 (1997) 645;
(b) S. Dunn, G.M. Rosair, A.S. Weller, A.J. Welch, Chem. Commun. (1998) 1065;
(c) S. Dunn, R.M. Garrioch, G.M. Rosair, L. Smith, A.J. Welch, Collect. Czech. Chem. Commun. 64 (1999) 1013.

[6] D.J. Wales, J. Am. Chem. Soc. 115 (1993) 1557.

[7] (a) S. Robertson, D. Ellis, T.D. McGrath, G.M. Rosair, A.J. Welch, Polyhedron 22 (2003) 1293;
(b) S. Robertson, D. Ellis, G.M. Rosair, A.J. Welch, J. Organomet. Chem. 680 (2003) 286;
(c) S. Robertson, D. Ellis, G.M. Rosair, A.J. Welch, Appl. Organomet. Chem. 17 (2003) 516;
(d) S. Robertson, R.M. Garrioch, D. Ellis, T.D. McGrath, B.E. Hodson, G.M. Rosair, A.J. Welch, Inorg. Chim. Acta 358 (2005) 1485.

[8] R.M. Garrioch, P. Kuballa, K.S. Low, G.M. Rosair, A.J. Welch, J. Organomet. Chem. 575 (1999) 57.

[9] M.M. Fein, J. Bobinski, N. Meyers, N. Schwartz, M.S. Cohen, Inorg. Chem. 2 (1963) 1111.

[10] J.M. Jenkins, B.L. Shaw, J. Chem. Soc. A (1966) 770.

[11] G.M. Sheldrick, SHELXTL version 5.1, Bruker AXS Inc., Madison, WI, 1999.

[12] F.P. Olsen, M.F. Hawthorne, Inorg. Chem. 4 (1965) 1839.

[13] M.A. Fox, A.E. Goeta, J.A.K. Howard, A.K. Hughes, A.L. Johnson, D.A. Keen, K. Wade, C.C. Wilson, Inorg. Chem. 40 (2001) 173.

[14] G.F. Mitchell, A.J. Welch, J. Chem. Soc., Dalton Trans. (1987) 1017.

[15] J. Cowie, D.J. Donohoe, N.L. Douek, A.J. Welch, Acta Crystallogr. C 49 (1993) 710.

[16] J. Cowie, B.D. Reid, J.M.S. Watmough, A.J. Welch, J. Organomet. Chem. 481 (1994) 283.

[17] A.S. Batsanov, M.A. Fox, J.A.K. Howard, A.K. Hughes, A.L. Johnson, S.J. Martindale, Acta Crystallogr. C 59 (2003) o74.

[18] T.D. McGrath, M.A. Fox, A.J. Welch, Acta Crystallogr. C 56 (2000) 487.

[19] Z. Zheng, W. Jiang, A.A. Zinn, C.B. Knobler, M.F. Hawthorne, Inorg. Chem. 34 (1995) 2095.

[20] (a) D.M.P. Mingos, M.I. Forsyth, A.J. Welch, J. Chem. Soc., Chem. Commun. (1977) 602;
(b) D.M.P. Mingos, M.I. Forsyth, A.J. Welch, J. Chem. Soc., Dalton Trans. (1978) 1363.

2.2. Crystal structure determination of $Ti(NMe_2)_4$

The capillary containing the sample was mounted onto a Stoe Stadi-4 four-circle diffractometer equipped with an Oxford Cryosystems low-temperature device [8]. After initial cooling to just below the melting point (263 K), the temperature was slowly raised until a single crystallite remained. The sample was then cooled leading to formation of a single crystal. Data were then collected at 105 K in $\omega - 2\theta$ mode to $2\theta = 60°$ using on-line profile-fitting [9]. The structure was solved by direct methods [10] and refined by full-matrix least-squares against $|F|^2$ [11]. H-atoms were located in a difference synthesis, and they were treated as freely rotating rigid groups with $r(\text{C–H}) = 0.98$ Å and $U_{iso}(\text{H}) = 1.5U_{eq}(\text{C})$. All non-H atoms were refined with anisotropic displacement parameters. The final conventional R factor [calculated using $|F|$ and 2980 data with $|F| > 4\sigma(|F|)$] was 0.0446; further data collection and refinement data are collected in Table 1. Bond distances and angles are given in Table 2, and torsion angles are listed in Table 3.

Table 1
Crystal and refinement data for $[Ti(NMe_2)_4]$

Crystal data	
Chemical formula	$[Ti(NMe_2)_4]$
M_r	224.21
Cell setting, space group	triclinic, $P\bar{1}$
a, b, c (Å)	8.277 (6), 8.407 (6), 11.167 (7)
α, β, γ (°)	105.36 (4), 97.03 (3), 116.01 (2)
V (Å^3)	647.4 (8)
Z	2
D_x (Mg m^{-3})	1.150
Radiation type	Mo Kα
μ (mm^{-1})	0.63
Temperature (K)	105 (2)
Crystal form, colour	cylinder, yellow
Crystal size (mm)	$0.28 \times 0.16 \times 0.16$
Data collection	
Absorption correction	psi-scans
T_{min}	0.816
T_{max}	0.901
Number of measured, independent and observed parameters	3599, 3599, 2985
Criterion for observed reflections	$I > 2\sigma(I)$
θ_{max} (°)	30.1
Refinement	
Refinement on	F^2
$R[F^2 > 2\sigma(F^2)]$, $wR(F^2)$, S	0.045, 0.110, 1.05
Number of reflections	3599
Number of parameters	127
Weighting scheme	calculated $w = 1/[\sigma^2(F_o^2) + (0.0446P)^2 + 0.4737P]$, where $P = (F_o^2 + 2F_c^2)/3$
$(\Delta/\sigma)_{max}$	0.001
$\Delta\rho_{max}$, $\Delta\rho_{min}$ (e Å^{-3})	0.42, −0.61
Extinction coefficient	0.004 (3)

Table 2
Experimental bond distances (Å) and angles (°) of the crystalline and the gaseous (electron diffraction) [5] $Ti(NMe_2)_4$

	Experimental value	Calculations on C_1 conformer
Distances		
Ti1–N2	1.897(2)	1.920
Ti1–N3	1.902(2)	1.926
Ti1–N4	1.908(2)	1.924
Ti1–N1	1.924(2)	1.930
Gas phase Ti–N	*1.917(3)*	
N1–C12	1.450(3)	1.449
N1–C11	1.452(3)	1.453
N2–C21	1.450(3)	1.449
N2–C22	1.451(3)	1.454
N3–C32	1.453(3)	1.451
N3–C31	1.454(3)	1.453
N4–C41	1.449(3)	1.449
N4–C42	1.451(3)	1.453
Gas phase N–C	*1.461(2)*	
Angles		
N2–Ti1–N3	105.89(9)	107.78
N2–Ti1–N4	111.74(9)	109.02
N3–Ti1–N4	109.90(9)	109.31
N2–Ti1–N1	107.03(10)	109.54
N3–Ti1–N1	110.18(9)	109.47
N4–Ti1–N1	111.89(8)	111.62
Gas phase ∠N–Ti–N	*114.2(17) (×2)* *107.2(9) (×4)*	
C12–N1–C11	111.07(18)	112.20
C21–N2–C22	111.77(18)	112.78
C32–N3–C31	111.34(18)	112.32
C41–N4–C42	111.81(19)	112.76
Gas phase ∠C–N–C	*111.4(3)*	
C12–N1–Ti1	124.97(15)	127.98
C11–N1–Ti1	123.71(14)	119.76
C21–N2–Ti1	130.90(15)	129.97
C22–N2–Ti1	117.30(15)	117.17
C32–N3–Ti1	127.06(15)	126.88
C31–N3–Ti1	121.42(15)	120.66
C41–N4–Ti1	116.88(15)	117.37
C42–N4–Ti1	131.29(15)	129.78
Gas phase C–N–Ti	*124.3(3)*	

Theoretical data were taken from PW91PW91/6-311G* calculations on the C_1 conformer found.

2.3. Structure analysis and visualisation software

Crystal structures were visualised using the programs CAMERON, DIAMOND, MERCURY and XP [12–15]. Analyses were carried out using PLATON, as incorporated in the WIN-GX suite [16,17]. Searches of the Cambridge Database were performed with the program CONQUEST and version 5.26 of the database with updates up to November 2004 [18,19].

2.4. Ab initio calculations

Calculations were carried-out to rationalise the change from a highly symmetric molecule in the gas phase (S_4 symmetry) to a less symmetric molecule in the solid state (C_1 symmetry). Geometry and frequency optimisations were performed using density functional theory (DFT)

Table 3
N–Ti–N–C torsional angles (°) in $Ti(NMe_2)_4$ in the crystal (this work), in the gas phase (electron diffraction) [5] and from DFT calculations (PW91PW91/6-311G*) of the molecule in C_1 symmetry as found in the crystal

Torsion	X-ray crystal structure	Gas phase electron diffraction	Theory DFT (C_1)
N2–Ti1–N1–C12	150.85(17)	129.0	138.9
N3–Ti1–N1–C12	−94.46(18)	−112.5	−103.1
N4–Ti1–N1–C12	28.13(19)	10.5	18.1
N2–Ti1–N1–C11	−35.51(18)	−51.0	−38.2
N3-Ti1–N1–C11	79.18(18)	−67.5	79.8
N4–Ti1–N1–C11	−158.24(16)	−169.5	−159.0
N3–Ti1–N2–C21	−1.7(2)	10.5	9.5
N4–Ti1–N2–C21	−121.31(19)	−112.5	−109.1
N1–Ti1–N2–C21	115.9(2)	129.0	128.5
N3–Ti1–N2–C22	−179.38(15)	−169.5	−166.8
N4–Ti1–N2–C22	60.98(17)	67.5	74.6
N1–Ti1–N2–C22	−61.84(17)	−51.0	−47.8
N2–Ti1–N3–C32	−110.60(19)	−67.5	−83.2
N4–Ti1–N3–C32	10.2(2)	51.0	35.2
N1–Ti1–N3–C32	133.99(18)	169.5	157.8
N2–Ti1–N3–C31	74.82(19)	112.5	101.3
N4–Ti1–N3–C31	−164.33(16)	129.0	−140.3
N1–Ti1–N3–C31	−40.58(19)	−10.5	−17.8
N2–Ti1–N4–C41	169.89(16)	169.5	−57.6
N3–Ti1–N4–C41	52.64(18)	51.0	−118.5
N1–Ti1–N4–C41	−70.11(19)	−67.5	−69.9
N2–Ti1–N4–C42	−8.7(2)	−10.5	1.3
N3–Ti1–N4–C42	−125.96(19)	−129.0	−118.5
N1–Ti1–N4–C42	111.3(2)	112.5	121.7

calculations (PW91PW91/6-311G*) starting from the geometry of the S_4 conformer determined in the gas phase. Calculations were also undertaken at the MP2 level of theory employing a basis of better than double-ζ plus polarisation quality; this comprised the standard 6-311+G* basis for Ti, the 6-31+G* basis for N and the 6-31G* basis set for C and H. The molecular geometry observed in the crystal structure (C_1 symmetry) was also optimised at the same level of theory as the DFT calculations on the S_4 conformer. All calculations were performed using the GAUSSIAN-94 or 03 program suites [20,21].

3. Results and discussion

3.1. The structure of $Ti(NMe_2)_4$ in the solid state

The crystal structure of $Ti(NMe_2)_4$ consists of monomeric $Ti(NMe_2)_4$ molecules in which the metal has approximately tetrahedral coordination (Fig. 1). The Ti–N bond distance in $Ti(NMe_2)_4$ obtained in the gas phase by electron diffraction is 1.917(3) Å [5]. In the solid state the individual Ti–N distances show some variation (Table 2): the bonds to N2, 3 and 4 span 1.897(2) to 1.908(2) Å, while Ti1–N1 measures 1.924(2) Å. At the low temperature of this data collection (105 K) the librational correction to the Ti–N distances is only 0.002 Å [15], and three of the Ti–N distances are thus significantly shortened relative to the gas phase. These are also substantially shorter than

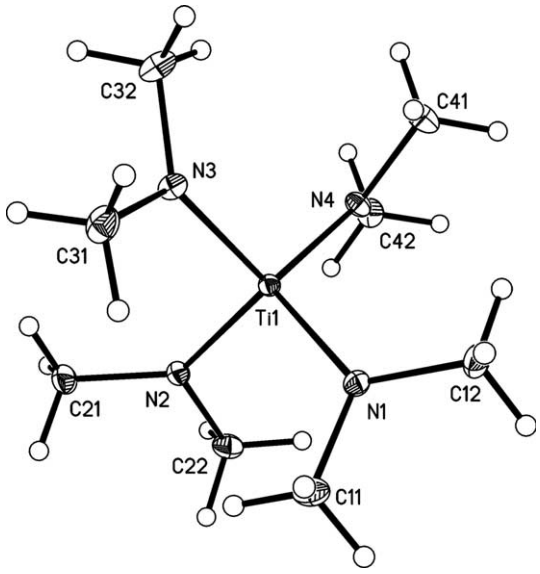

Fig. 1. The structure of $Ti(NMe_2)_4$ in the solid state. Ellipsoids enclose 30% probability surfaces, H-atoms are drawn as circles of arbitrary radius.

the Ti–N distances of 2.230(1) and 2.095(1) Å found in $Ti(ONMe_2)_4$ [22].

In the gas-phase $Ti(NMe_2)_4$ was modelled as having S_4 symmetry with two N–Ti–N angles of 114.2(17)° and four of 107.2(9)°. The distortion away from ideal tetrahedral angles has been rationalised in terms of the ligand-close-packing model by Gillespie and co-workers [23]. The structure in the solid state is reduced from S_4 symmetry to C_1 [16]. The N–Ti–N angles are less regular and span a narrower range [105.89(9)–111.89(8)°] in the solid than in the gas.

During refinement against the gas-phase electron-diffraction data the Ti–N–C angles were all constrained to be equal [124.3(3)°]. In the solid there is a significant variation in the Ti–N–C bond angles for the dimethylamido groups containing N2, N3, and N4, with one small Ti–N–C angle [116.88(15)–121.42(15)°] and one large [127.06(15)–131.29(15)°]. Since all four N–C–N angles are essentially identical [range: 111.07(18)–111.81(19)°], this corresponds to a distortion in three of the TiNC2 planes such that there is a tilting of one of the carbons towards the titanium. The larger Ti–N–C angles are all made within fragments of small N–Ti–N–C torsion angles, for example, N3–Ti1–N2–C21 is −1.7(2)°, whereas the smallest torsion angle involving C22 is 60.98(17)° (N4–Ti1–N2–C22). It seems likely that the asymmetry in the Ti–N–C angles is simply the result of ligand repulsion. Similar effects are observed in the structure of $(NMe_2)_3Zr(\mu\text{-}NMe_2)_2\text{-}Zr(NMe_2)_3$, in which the methyl groups associated with the terminal amino ligands bend away from the methyl groups associated with the bridging NMe_2 groups [6]. The Ti–N–C angles in the amino group based on N1 are more symmetrical, but here the smallest torsions involving C12 and C22 are −35.51(18)° and 28.13(19)°. In the gas phase the magnitudes of the smallest N–Ti–N–C angles

are 10.5 and 67.5 at each amido group [5], and so a similar asymmetry would be expected; the results of our ab initio calculations lend some support to this (see below).

Torsion angles are 'softer' parameters than primary bond distances and angles, and it would be anticipated that the largest differences between the solid and gas-phase structures would occur in the N–Ti–N–C angles. A superposition of the structures in the two phases is shown in Fig. 2; equivalent torsion angles are compared in Table 3. The largest differences are found at the amido group based on N3.

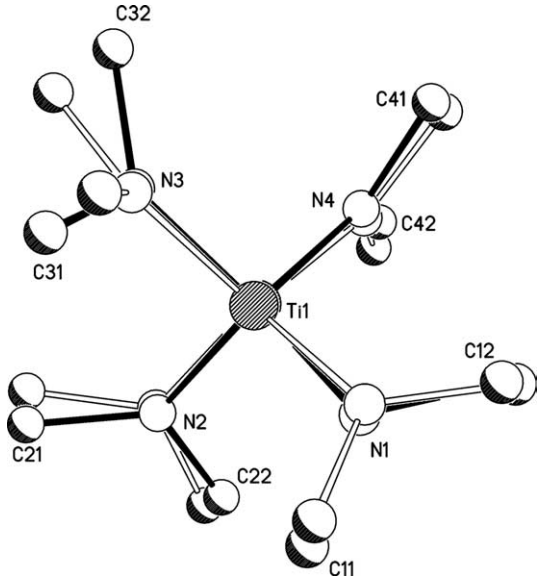

Fig. 2. Superposition of the gas phase and solid phase structures of $Ti(NMe_2)_4$. The gas-phase structure is drawn with open bonds. H-atoms have been omitted for clarity.

3.2. Intermolecular interactions

The differences between the intramolecular geometric parameters in the gas phase and crystal structures must be ascribable to crystal packing forces. There are, however, no intermolecular interactions falling within the sums of the van der Waals radii of the relevant atoms [24]. The shortest intermolecular distances comprise three contacts, each formed across inversion centres, in which Ti...Ti distances are 6.074, 6.227 and 6.650 Å (Fig. 3). These interactions form a net which is formed parallel to the (1 0 0) planes in the crystal. Successive planes are formed by lattice-repeats along [100], with Ti...Ti distances in the range 8.27–9.56 Å.

Crystal structures of essentially non-interacting, isometric molecules frequently show the same topologies as the familiar hard-sphere packings [cubic or hexagonal close-packed, or body-centred cubic (BCC)], pseudo-BCC being the most common [25]. Analysis of the Voronoi–Dirichlet polyhedron constructed on the basis of the distribution of the molecular centroids in $Ti(NMe_2)_4$ shows that each molecule is in contact with 14 others in the first coordination shell. Overall, the coordination sequence (i.e., the number of molecules in the first, second and third coordination spheres) is 14-52-114, comparing to 14-50-110 for BCC topology [26].

We have seen that optimised superposition of the gas phase and crystal molecular structures showed that while the conformations of the amido groups based on N1, N2

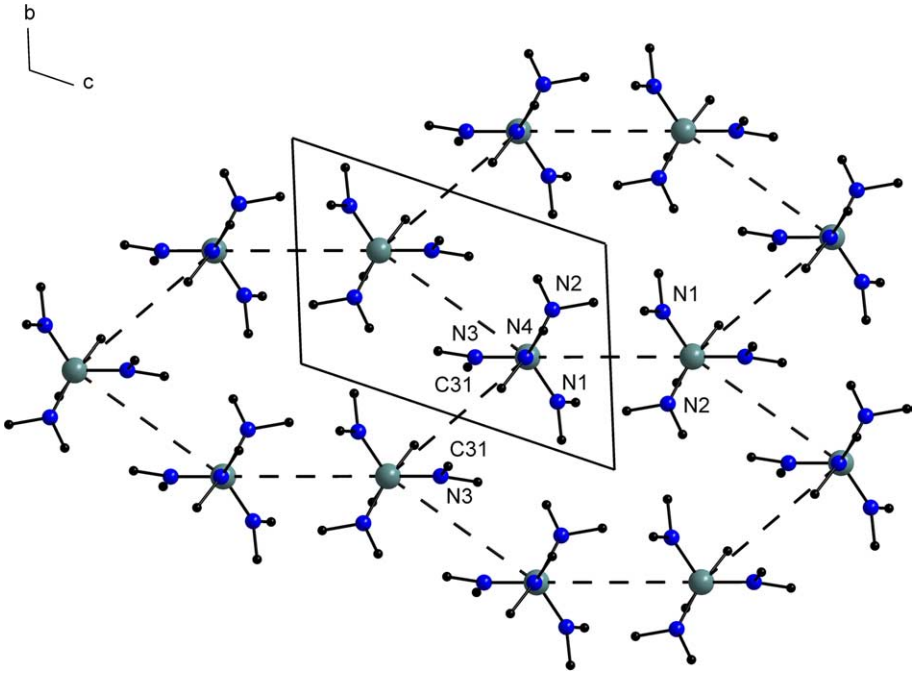

Fig. 3. Packing in the crystal structure of $Ti(NMe_2)_4$. Ti...Ti distances falling between 6 and 7 Å are shown as dashed lines. H-atoms are omitted for clarity.

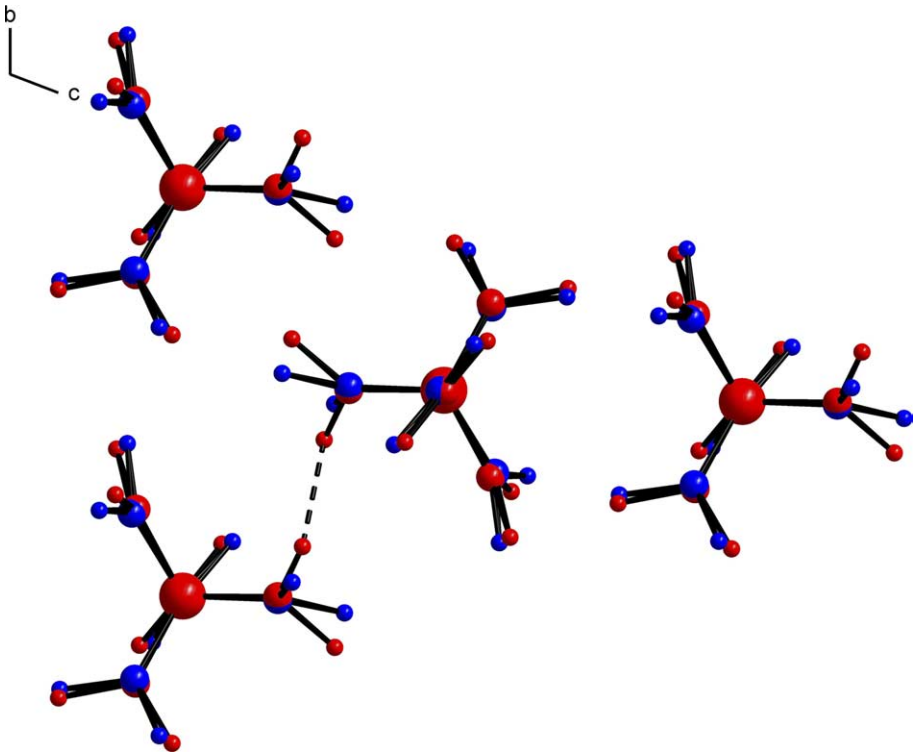

Fig. 4. Superposition of the observed crystal structure (blue) with a model structure in which the molecules have their S_4 gas-phase geometry (red). The short methyl–methyl contact referred to in the text is shown as a dashed line. (For interpretation of the references to colour in this figure legend, the reader is referred to the web version of this article.)

and N4 were similar in both phases, that of the group based on N3 was different. Fig. 3 shows that the amido groups based on N1, N2 and N4 approach one another in the crystal structure across the shortest of the Ti...Ti vectors in the (1 0 0) planes. The Ti–N bonds across this interaction are staggered with respect to each other in order to minimise repulsions between methyl groups. The shortest C···C distances formed between this pair of molecules is 3.700 Å. When the gas-phase S_4-symmetry model of $Ti(NMe_2)_4$ is positioned into the crystal structure (Fig. 4) it is clear that minimal torsional rearrangement about Ti1–N1,2 or 4 is necessary to accommodate this interaction, even though this is the closest intermolecular centroid–centroid distance in the structure.

By contrast, had the gas-phase structure been retained in the solid, the methyl group at C31 would have formed a contact across an inversion to a symmetry-equivalent methyl group measuring only 2.28 Å (Fig. 4). The twisting of the amido group based on N3 in the crystal away from its gas-phase orientation can therefore be ascribed to the avoidance of methyl–methyl close contacts; the equivalent C31···C31 contact in the crystal structure measures 3.790 Å.

3.3. Ab initio calculations

The geometry of the S_4 conformer, as observed by gas-phase electron diffraction, was optimised using MP2 and DFT methods, and the theoretical and experimental results are listed in Table 4. There is very little difference between the results of the two levels of theory. Values of bond lengths are in excellent agreement with those obtained by electron diffraction. Bond angles about the metal were calculated to be close to tetrahedral values, N–Ti–N = 109.6° or 109.4°, but were found to deviate further from tetrahedral in the GED study [N–Ti–N = 114.2(17)° or 107.2(9)°]. In the electron-diffraction refinement [5] all Ti–N–C angles were constrained to be equal, and the refined value of this parameter was 124.3(3)°. Our calculations of

Table 4
Parameters of the S_4 gas-phase molecular structure of $Ti(NMe_2)_4$ from theory (MP2 and DFT methods) and experimental gas-phase electron-diffraction data (GED) [5]

Parameter	MP2	PW91PW91/6-311G*	GED
Ti–N	1.913	1.925	1.917(3)
N–C	1.460	1.453	1.461(2)
N–C	1.455	1.450	1.461(2)
Mean C–H	109.9	110.6	112.0(4)
N–Ti–N	109.6	109.6	114.2(17)
N–Ti–N	109.4	109.4	107.2(9)
Ti–N–C	118.3	118.6	124.3(3)
Ti–N–C	129.6	128.7	124.3(3)
C–N–C	112.0	112.6	111.4
Mean N–C–H	111.1	111.4	109.3(7)
C–N–Ti–N	45.8	43.3	51(1)

Bond distances are in Å, bond angles and torsions are in °.

Ti–N–C bond angles yield an average value of 124.0° (MP2) or 123.7° (DFT), in agreement with the experiment, though the $-NMe_2$ groups are predicted to deviate noticeably from C_2 symmetry leading to Ti–N–C bond angles of 118.6° and 128.7°. The C–N–Ti–N torsion angle is calculated to be 45.8° (MP2) or 43.3° (DFT), in fair agreement with the experimental value of 51(1)°.

Examination of the predicted vibrational frequencies of Ti(NMe2)4 revealed the presence of many frequencies below 200 cm^{-1}, indicating that large amplitude motion would be expected to be present in the gas phase at ambient temperature. In particular, the four torsional motions associated with the twisting of the –NMe2 groups are predicted to lie in the region of 40–60 cm^{-1} implying that only a relatively small amount of energy is required to twist these groups from the equilibrium structure found in the gas phase to that observed in the solid phase.

The geometry of the C_1 conformer of $Ti(NMe_2)_4$ was optimised by DFT methods, starting from the structure observed in the solid state. A comparison of the calculated parameters of the C_1 conformer with those of the crystal structure showed that they were in fair agreement (Tables 2 and 3). Though the range of Ti–N bond distances is larger in the crystal structure [1.897(2)–1.924(2) Å] than in the optimised calculated structure (1.920–1.930), the shortest and longest distances are formed to the same N-atoms is each case.

The vibrational frequencies for this conformer were all real, indicating that the structure corresponds to an energy minimum, with the S_4 conformer lying only 0.2 kJ mol^{-1} lower in energy. The small energy difference between the two conformations indicates that a transition from S_4 to C_1 symmetry would be extremely facile in the gas phase. Furthermore, it suggests that distortion of the gas-phase molecular symmetry on crystallisation would only carry a minor energy penalty in terms of the intramolecular energy. This penalty would be easily overcome by alleviation of the possible intermolecular repulsion depicted in Fig. 4.

Acknowledgements

We thank the CCLRC for the computational resources used on the Columbus computer cluster at the Rutherford Appleton Laboratories, and the EPSRC and The University of Edinburgh for funding.

Appendix A. Supplementary data

Supplementary data are available free of charge on application to the Director, CCDC, 12 Union Road, Cambridge, CB2 1EZ, UK, fax: +44-1223-336033, e-mail: deposit@ccdc.cam.ac.uk or http://www.ccdc.cam.ac.uk on request, quoting the deposition number CCDC 284244. Supplementary data associated with this article can be found, in the online version, at doi:10.1016/j.poly.2005.10.019.

References

[1] D.C. Bradley, I.M. Thomas, J. Chem. Soc. (1960) 3857.
[2] R.M. Fix, R.G. Gordon, D.M. Hoffmann, Chem. Mater. 2 (1990) 235.
[3] H.-S. Hsueh, C.-T. Yang, J.I. Zink, M.H. Huang, J. Phys. Chem. B 109 (2005) 4404.
[4] E.S. Peters, C.J. Carmalt, I.P. Parkin, J. Mater. Chem. 14 (2004) 3474.
[5] A. Haaland, K. Rypdal, H.-V. Volden, R.A. Andersen, J. Chem. Soc., Dalton Trans. (1992) 891.
[6] M.H. Chisholm, C.E. Hammond, J.C. Huffman, Polyhedron 7 (1988) 2515.
[7] D.C. Bradley, M.H. Gitlitz, J. Chem. Soc. A (1969) 980.
[8] J. Cosier, A.M. Glazer, J. Appl. Cryst. 19 (1986) 105.
[9] W. Clegg, Acta Cryst. A 37 (1981) 22.
[10] G.M. Sheldrick. XS. Part of SHEXTL Suite, Ver. 6.10. University of Göttingen, Germany, and Bruker-Nonius Inc., Madison, Wisconsin, USA, 2001.
[11] G.M. Sheldrick. XL. Part of SHEXTL Suite, Ver. 6.10. University of Göttingen, Germany and Bruker-Nonius Inc., Madison, Wisconsin, USA, 2001.
[12] D.J. Watkin, L. Pearce, C.K. Prout, CAMERON – A Molecular Graphics Package. Chemical Crystallography LaborUniversity of Oxford, University of Oxford, England, 1993.
[13] Crystal Impact. DIAMOND. Version 3.0. Crystal Impact GbR, Postfach 1251, 53002 Bonn, Germany, 2004. (Available from: <http://www.crystalimpact.com/diamond>).
[14] I.J. Bruno, J.C. Cole, P.R. Edgington, M. Kessler, C.F. Macrae, P. McCabe, J. Pearson, R. Taylor, R. Acta Cryst. B 58 (2002) 389.
[15] G.M. Sheldrick. XP. Part of SHEXTL Suite, Ver. 6.10. University of Göttingen, Germany and Bruker-Nonius Inc., Madison, Wisconsin, USA, 2001.
[16] A.L. Spek, PLATON – A Multipurpose Crystallographic Tool, Utrecht University, Utrecht, The Netherlands, 2004.
[17] L.J. Farrugia, J. Appl. Cryst. 32 (1999) 837.
[18] F.H. Allen, Acta Cryst. B 58 (2002) 380.
[19] F.H. Allen, W.D.S. Motherwell, Acta Cryst. B 58 (2002) 407.
[20] M.J. Frisch, G.W. Trucks, H.B. Schlegel, P.M.W. Gill, B.G. Johnson, M.A. Robb, J.R. Cheesman, T.A. Keith, G.A. Petersson, J. AMontgomery, K. Raghavachari, M.A. Al-Laham, V.G. Zakrzewski, J.V. Ortiz, J.B. Foresman, J. Cioslowski, B.B. Stefanov, A. Nanayakkara, M. Challacombe, C.Y. Peng, P.Y. Ayala, W. Chen, M.W. Wong, J.L. Andres, E.S. Replogle, R. Gomperts, R.L. Martin, D.J. Fox, J.S. Binkley, D.J. Defrees, J. Baker, J.P. Stewart, M. Head-Gordon, C. Gonzalez, J.A. Pople, GAUSSIAN-94, Revision C.2., Gaussian Inc., Pittsburgh, PA, 1995.
[21] M.J. Frisch, G.W. Trucks, H.B. Schlegel, G.E. Scuseria, M.A. Robb, J.R. Cheeseman, J.A. Montgomery Jr., T. Vreven, K.N. Kudin, J.C. Burant, J.M. Millam, S.S. Iyengar, J. Tomasi, V. Barone, B. Mennucci, M. Cossi, G. Scalmani, N. Rega, G.A. Petersson, H. Nakatsuji, M. Hada, M. Ehara, K. Toyota, R. Fukuda, J. Hasegawa, M. Ishida, T. Nakajima, Y. Honda, O. Kitao, H. Nakai, M. Klene, X. Li, J.E. Knox, H.P. Hratchian, J.B. Cross, V. Bakken, C. Adamo, J. Jaramillo, R. Gomperts, R.E. Stratmann, O. Yazyev, A.J. Austin, R. Cammi, C. Pomelli, J.W. Ochterski, P.Y. Ayala, K. Morokuma, G.A. Voth, P. Salvador, J.J. Dannenberg, V.G. Zakrzewski, S. Dapprich, A.D. Daniels, M.C. Strain, O. Farkas, D.K. Malick, A.D. Rabuck, K. Raghavachari, J.B. Foresman, J.V. Ortiz, Q. Cui, A.G. Baboul, S. Clifford, J. Cioslowski, B.B. Stefanov, G. Liu, A. Liashenko, P. Piskorz, I. Komaromi, R.L. Martin, D.J. Fox, T. Keith, M.A. Al-Laham, C.Y. Peng, A. Nanayakkara, M. Challacombe, P.M.W. Gill, B. Johnson, W. Chen, M.W. Wong, C. Gonzalez, J.A. Pople, GAUSSIAN-03, Revision C.02, Gaussian, Inc., Wallingford CT, 2004.
[22] N.W. Mitzel, S. Parsons, A.J. Blake, D.W.H. Rankin, J. Chem. Soc., Dalton Trans (1996) 2089.

[23] G.L. Heard, R.J. Gillespie, D.W.H. Rankin, J. Mol. Struct. 520 (2000) 237.
[24] A. Bondi, J. Phys. Chem. 68 (1964) 441.
[25] E.V. Peresypkina, V.A. Blatov, Acta Cryst. B 56 (2000) 1035.
[26] V.A. Blatov, A.P. Shevchenko, TOPOS-4.0, Samara State University, Samara, Russia, 2005.

resulted in the formation of white $[SnF_4L_2]$ complexes in high yield. The solids are moisture sensitive, tenaciously retain organic solvents – clearly evident in the ^1H NMR spectra, and are only modestly soluble in chlorocarbons. Solubility is not significantly better in acetone or nitromethane and stronger donor solvents were generally avoided for spectroscopic studies since they can lead to some displacement of the neutral ligands. The complexes could be recrystallised from a large volume of anhydrous CH_2Cl_2. The complexes with Ph_3PO, Ph_3AsO and Me_3PO were briefly reported in larger compilations of their metal complexes many years ago [4–6] but characterisation was limited to microanalysis and partial IR spectra. Our IR spectra (Table 1) are generally in good agreement with those reported; where differences occur they are probably attributable to various amounts of *cis* and *trans* isomers present in the samples resulting from differences in the isolation procedures and/or solvents used [18]. Three diphosphine dioxide complexes, $[SnF_4\{o\text{-}C_6H_4(P(O)Ph_2)_2\}]$, $[SnF_4\{o\text{-}C_6H_4(P(O)Me_2)_2\}]$ and $[SnF_4\{Ph_2P(O)\text{-}CH_2P(O)Ph_2\}]$ were made similarly.

The multinuclear NMR data (Tables 1 and 2) show the presence of both *cis* and *trans* isomers in CH_2Cl_2 solution for the R_3PO and R_3AsO complexes, the approximate isomer ratios being determined from the $^{19}F\{^1H\}$ NMR spectra. For $[SnF_4(Ph_3PO)_2]$ the two isomers have similar abundance but for the other three the *trans* isomer predominates. Although resonances were observed at ambient temperatures in the ^1H, ^{31}P and ^{19}F spectra, the ^{119}Sn spectra showed broad and poorly resolved features and the samples were cooled to 273 K to improve resolution. The $^{31}P\{^1H\}$ NMR spectra show singlet resonances for each isomer with very similar chemical shifts, and no resolved coupling to ^{19}F, but with weak $^{119/117}Sn$ satellites. The $^2J(^{119/117}Sn–^{31}P)$ which lie in the range 20–65 Hz, appeared as single lines rather than as separate features for the two tin isotopes – no doubt the differences were lost in the line width, since from the magnetogyric ratios $\gamma^{119}Sn/\gamma^{117}Sn$ (1.046) the values are expected to differ by <2 Hz. The $^{19}F\{^1H\}$ spectra show singlet resonances for the *trans* isomers and two triplets for the *cis* (Table 2), with $\delta(^{19}F)$ in the range −135 to −170, and with $^1J(^{119}Sn–^{19}F)$ 1700–1950 Hz, similar to the values in substituted fluorostannates(IV) [3]. In these cases, the $^1J(^{117}Sn–^{19}F)$ satellites were also clearly resolved and although not quoted in Table 2, the magnitudes were consistent with expectation based upon $\gamma^{119}Sn/\gamma^{117}Sn$. Obtaining good quality ^{119}Sn NMR spectra proved difficult due to the modest receptivity of the tin ($D_c = 25$), poor solubilities, the presence of both isomers and also the complexity of the coupling patterns. For example, for $[SnF_4(Me_3PO)_2]$ the symmetrical quintet of triplets of the *trans* isomer was clearly evident centred at δ −781.8 Underlying this resonance is another weaker and more complex pattern centred at δ −769.0 attributed to the *cis* isomer. Based upon the various coupling constants obtained from the $^{19}F\{^1H\}$ and $^{31}P\{^1H\}$ spectra the major lines of the expected 27 line multiplet (t,t,t) were identified. The solubility of $[SnF_4(Ph_3PO)_2]$ is lower, but again two multiplets can be discerned consistent with approximately equal amounts of the two geometric isomers, although in this case the spectral quality was poor. For the $[SnF_4(R_3AsO)_2]$ complexes, the quintet due to the *trans* isomer was clearly identified in each case, but the resonance (t,t) of the less abundant *cis* form appeared near coincident and hence the chemical shift assignment less clear, although the more intense lines of the multiplets were found.

The diphosphine dioxide complexes $[SnF_4(L–L)]$ ($L–L = Ph_2P(O)CH_2P(O)Ph_2$, $o\text{-}C_6H_4(P(O)Ph_2)_2$) are, as expected, *cis* isomers showing (Table 2) two triplets in the $^{19}F\{H\}$ NMR spectra and singlets in the $^{31}P\{^1H\}$ spectra. At temperatures a little above ambient the resonances in the $^{19}F\{H\}$ NMR spectra broaden, presumably due to some dynamic process, probably chelate ring opening. On cooling the solutions the complexes precipitate which prevented low temperature studies. The $[SnF_4\{o\text{-}C_6H_4(P(O)Me_2)_2\}]$ was insoluble in chlorinated solvents, but dissolved with some decomposition (diphosphine dioxide displacement) in anhydrous *N*,*N*-dimethylformamide The $^{19}F\{H\}$ and $^{31}P\{^1H\}$ NMR spectra of the complex are given in Table 2, but the poor solubility and partial decomposition prevented a ^{119}Sn spectrum from being obtained.

Table 1
IR[a] and ^1H NMR[b] spectroscopic data

Compound	ν(P(As)O) (cm^{-1})	ν(Sn–X) (cm^{-1})	$\delta(^1H)$
$[SnF_4(Ph_3PO)_2]$	1137, 1082	580, 549, 537	7.36–7.88(m)
$[SnF_4(Me_3PO)_2]$	1085(br)	576, 559	1.855(d), $^2J_{PH} = 13.5$ Hz 1.860(d), $^2J_{PH} = 13.5$ Hz
$[SnF_4(Ph_3AsO)_2]$	877(br), 850(sh)	559(br)	7.40–7.87(m)
$[SnF_4(Me_3AsO)_2]$	865, 812(br)	550(br)	2.04(s), 2.05(s)
$[SnF_4\{o\text{-}C_6H_4(P(O)Ph_2)_2\}]$	1145, 1087(br)	585, 569, 548	7.31–7.71(m)
$[SnF_4\{Ph_2P(O)CH_2P(O)Ph_2\}]$	1145, 1092	596, 577	4.00(t), $^2J_{PH} = 13$ Hz 7.36–7.75(m)[d]
$[SnF_4\{o\text{-}C_6H_4(P(O)Me_2)_2\}]$	1147, 1093	573(br)	1.81(m) 7.49–7.85(m)[c]

[a] Nujol mull.
[b] In $CDCl_3$ at 300 MHz.
[c] In d^6-dmso.
[d] In CD_2Cl_2.

Table 2
$^{31}P\{^1H\}$, ^{119}Sn and $^{19}F\{^1H\}$ NMR spectroscopic data[a]

Compound	$\delta^{31}P\{^1H\}$[b]	$\delta^{119}Sn$[c]	$\delta^{19}F\{^1H\}$[d]	$^1J(^{19}F–^{119}Sn)$	$^2J(^{19}F–^{19}F)$	$^2J(^{31}P–^{119}Sn)$	Isomer ratio
$[SnF_4\{Me_3PO)_2]$ *trans*	65.9(s)	−781.8(q,t)	−149.2(s)	1725		50	3
cis	65.4(s)	−769.0(t,t,t)	−147.2(t)	1772	51	50	1
			−158.0(t)	1850			
$[SnF_4(Ph_3PO)_2]$ *trans*	42.5(s)	−770.0(q,t)	−149.8(s)	1704		20	1
cis	42.3(s)	−775.1(t,t,t)	−146.2(t)	1730	53	22	1
			−159.8(t)	1850			
$[SnF_4\{Me_3AsO)_2]$ *trans*		−747.7(q)	−141.6(s)	1804			3
cis		−748.4(t,t)	−140.9(t)	1827	49		1
			−148.2(t)	1818			
$[SnF_4(Ph_3AsO)_2]$ *trans*		−757.5(q)	−141.3(s)	1788			2
cis		−758.6(t,t)	−137.8(t)	1800	51		1
			−151.9(t)	1860			
$[SnF_4\{o\text{-}C_6H_4(P(O)Ph_2)_2\}]$	45.5(s)	−790.0(t,t,t)	−142.9(br)	1730	53	63	
			−167.2(t)	1923			
$[SnF_4\{Ph_2P(O)CH_2P(O)Ph_2\}]$	44.1(s)	−792.4(t,t,t)	−143.0(t)	1753	50	57	
			−167.8(t)	1930			
$[SnF_4\{o\text{-}C_6H_4(P(O)Me_2)_2\}]$[e]	62.1(s)		−143.5(t)	1740	50	57	
			−165.4(t)	1930			

[a] To obtain good resolution of the complex couplings, spectra were typically recorded at 273 K.
[b] Relative to external 85% H_3PO_4.
[c] Relative to external neat $SnMe_4$.
[d] Relative to external $CFCl_3$.
[e] *N*,*N*-Dimethylformamide solution.

2.2. Structures of *trans*-$[SnF_4(Me_3PO)_2]$, $[SnF_4\{o\text{-}C_6H_4(P(O)Ph_2)_2\}]$ and $[o\text{-}C_6H_4(P(O)Ph_2)_2]$

Colourless crystals of $[SnF_4(Me_3PO)_2]$ were grown from a sample containing both isomers by vapour phase diffusion of hexane into a CH_2Cl_2 solution. These proved on structure solution to be the *trans* isomer (Table 3 and Fig. 1). The molecule is centrosymmetric with Sn–F = 1.937(2), 1.954(2) Å, not significantly different from the values in *cis*-$[SnF_4(2,2'\text{-bipy})]$ 1.924(3)–1.948(3) Å [1]. Comparison of *d*(P–O) in the complex (1.532(3) Å) with that in Me_3PO (1.489(6) Å) [19] shows the bond is significantly lengthened upon coordination.

The crystal structures of (*cis*) $[SnF_4\{o\text{-}C_6H_4(P(O)Ph_2)_2\}]$ (Table 4, Fig. 2) and of the parent ligand, $o\text{-}C_6H_4(P(O)Ph_2)_2$ (Table 5, Fig. 3) have also been determined and the key bond lengths may be compared similarly. The *d*(Sn–F) are very similar to those in $[SnF_4(Me_3PO)_2]$, and essentially independent of the nature of the *trans* ligand. The *d*(Sn–O) at 2.088(5) and 2.071(5) Å are rather longer than in the Me_3PO complex which probably reflects the effect of the seven-membered chelate ring. As found for

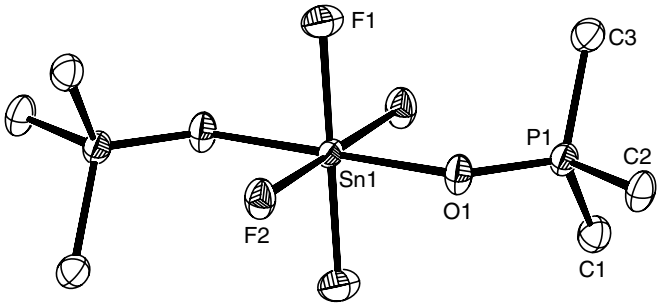

Fig. 1. Structure of *trans*-$[SnF_4(Me_3PO)_2]$ showing the atom numbering scheme. Atomic displacement ellipsoids are drawn at the 50% probability level and H atoms omitted for clarity. There is a centre of symmetry at the Sn1 atom.

Table 3
Selected bond lengths (Å) and angles (°) for *trans*-$[SnF_4(Me_3PO)_2]$[a]

Sn1–F1	1.937(2)	Sn1–F2	1.954(2)
Sn1–O1	2.045(3)	P1–O1	1.532(3)
P1–C	1.774(4)–1.782(4)		
F1–Sn1–F2	89.85(10)	F1–Sn1–O1	91.13(11)
F2–Sn1–O1	89.48(10)	P1–O1–Sn1	131.50(17)
O1–P1–C	108.4(2)–111.7(2)	C–P1–C	107.2(2)–110.2(2)

[a] The tin atom is on a centre of symmetry.

Table 4
Selected bond lengths (Å) and angles (°) for $[SnF_4\{o\text{-}C_6H_4(P(O)Ph_2)_2\}]\cdot CH_2Cl_2\cdot H_2O$

Sn1–F1	1.951(4)	Sn1–F3	1.930(4)
Sn1–F2	1.941(4)	Sn1–F4	1.940(4)
Sn1–O1	2.088(5)	Sn1–O2	2.071(5)
P1–O1	1.512(5)	P2–O2	1.525(5)
P–C	1.786(7)–1.819(7)		
F1–Sn1–F2	174.39(18)	F2–Sn1–F3	91.50(18)
F1–Sn1–F3	93.20(18)	F2–Sn1–F4	91.57(17)
F1–Sn1–F4	91.00(18)	F3–Sn1–F4	95.65(19)
F1–Sn1–O1	89.18(18)	F1–Sn1–O2	87.81(18)
F2–Sn1–O1	87.67(17)	F2–Sn1–O2	87.26(18)
F3–Sn1–O1	91.13(18)	F3–Sn1–O2	175.41(19)
F4–Sn1–O1	173.19(18)	F4–Sn1–O2	88.80(19)
O1–Sn1–O2	84.40(18)		
P1–O1–Sn1	140.5(3)	P2–O2–Sn1	133.8(3)
O–P–C	106.5(3)–112.9(3)	C–P–C	106.9(3)–109.6(3)

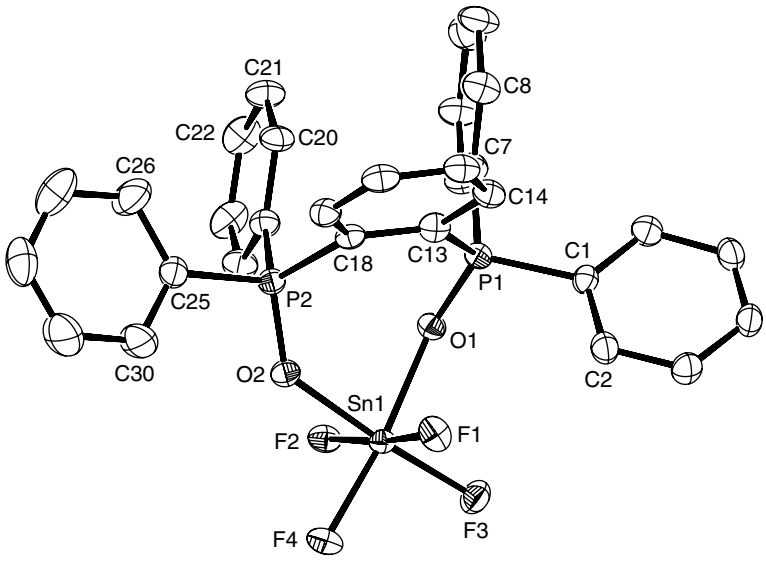

Fig. 2. Structure of the tin residue in $[SnF_4\{o\text{-}C_6H_4(P(O)Ph_2)_2\}] \cdot CH_2Cl_2 \cdot H_2O$ showing the atom numbering scheme. Atomic displacement ellipsoids are drawn at the 50% probability level and H atoms omitted for clarity.

Table 5
Selected bond lengths (Å) and angles (°) for $[o\text{-}C_6H_4(P(O)Ph_2)_2] \cdot CH_2Cl_2$

P1–O1	1.484(2)	P2–O2	1.485(2)
P1–C1	1.809(3)	P2–C18	1.838(3)
P1–C7	1.810(3)	P2–C19	1.800(3)
P1–C13	1.824(3)	P2–C25	1.815(3)
O1–P1–C1	115.74(13)	O2–P2–C18	114.46(12)
O1–P1–C7	110.22(12)	O2–P2–C19	116.22(13)
O1–P1–C13	112.88(13)	O2–P2–C25	109.84(12)
C1–P1–C7	105.49(13)	C18–P2–C19	105.81(13)
C1–P1–C13	105.77(13)	C18–P2–C25	104.88(13)
C7–P1–C13	106.02(13)	C19–P2–C25	104.60(13)

the Me_3PO case, coordination of the diphosphine dioxide to the SnF_4 results in a significant lengthening of the P–O bond, from 1.484(2), 1.485(2) in the "free" ligand to 1.512(5), 1.525(5) Å in the complex. A few poor quality crystals were also obtained from a solution of $[SnF_4\{o\text{-}C_6H_4(PMe_2)_2\}]$ in CH_2Cl_2 after several weeks. X-ray examination of these established them as the compound $[SnClF_3\{o\text{-}C_6H_4(P(O)Me_2)_2\}]$ containing a chelating diphosphine dioxide. The origin of the chlorine atom is presumably from reaction with the solvent and the oxygen in the phosphine oxide from aerial oxidation.[1]

Most interesting is the comparison with data on other tin(IV) phosphine oxides. Tudela [18] noted that in *cis*- and *trans*-$[SnBr_4(Ph_3PO)_2]$ the Sn–O (2.080(8), 2.101(9) Å) and P–O (1.515(8), 1.516(9)(av) Å) distances were the same within the usual criteria showing that the geometric isomer present has no effect, as might be expected for hard donor–acceptor interactions on a p-block metal. However, when one compares the key distances along the series $[SnX_4(R_3PO)_2]$ (Table 6) one finds that Sn–O increases with X F < Cl < Br < I. The substantially shorter Sn–O distance in the tin(IV) fluoride is clearly consistent with stronger binding of the ligand indicative of stronger Lewis acidity of the SnF_4. Moreover, studies of phosphine oxide complexes of hard early transition metals such as Y(III) or Sc(III) have shown that the metal–oxygen distances are independent of the R group (Me or Ph), although they do vary with the metal coordination number [20,21]. From Table 6 it is also notable that the P–O distance in the fluoride complex is markedly longer than in the other examples, (albeit some of the comparator data are not of high precision) which also supports stronger donation from O → Sn. The trends are replicated in $[SnF_4\{o\text{-}C_6H_4(P(O)Ph_2)_2\}]$ where the data in Table 4 can be compared with the structural data on $[SnI_4\{o\text{-}C_6H_4(P(O)Ph_2)_2\}]$ [13] (Table 6). In the iodo-complex the *d*(Sn–O) are much longer, consistent with the relative Lewis acidity of the tin centres.

2.3. $[SnX_4L_2]$ X = Cl, Br or I; L = Ph_3PO, Ph_3AsO or Me_3PO – some comparisons

These complexes have been studied on several occasions and structures have been reported for *cis*-$[SnX_4(Ph_3PO)_2]$ (X = Cl or Br) [18,23,25] and *trans*-$[SnBr_4(Ph_3PO)_2]$ [22,24]. The IR spectra have been discussed in detail [5,6,26] and our data are generally in agreement with the literature and hence not discussed further. Curiously, little NMR data have been reported previously and complete data are presented in Table 7. As can be seen, whilst both isomers are present in CH_2Cl_2 solutions of the chloro-complexes, only one isomer was present for the iodo-complexes, and only small amounts or essentially none of the second form

[1] Crystal data for $[SnClF_3\{o\text{-}C_6H_4(P(O)Me_2)_2\}] \cdot 1/2CH_2Cl_2$: $M_w = 483.77$; orthorhombic, space group *Pbcn* (no. 60), $Z = 8$, $T = 120$ K, $a = 15.290(5)°$, $b = 17.266(6)°$, $c = 13.380(3)$ Å, $V = 3532.3(19)$ Å^3; 3772 unique data gave $R_1 = 0.095$, $wR_2 = 0.173(I > 2\sigma(I))$ based on 186 independent parameters with $S = 0.95$.

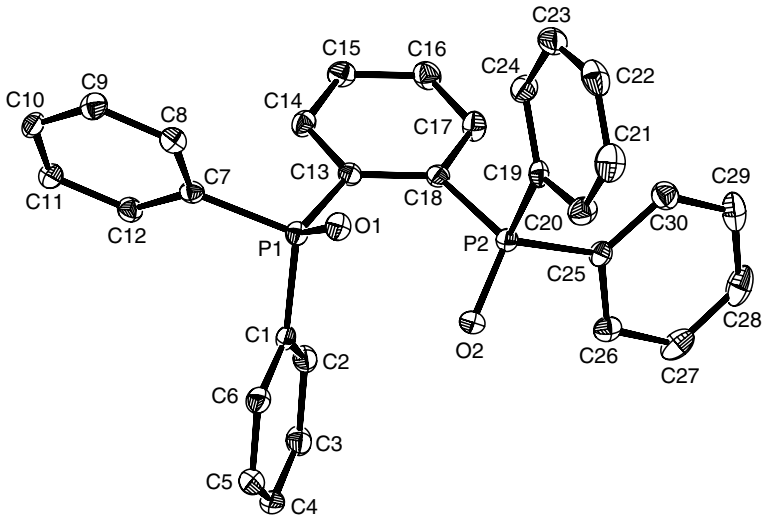

Fig. 3. Structure of $[o\text{-}C_6H_4(P(O)Ph_2)_2]\cdot CH_2Cl_2$ showing the atom numbering scheme. Atomic displacement ellipsoids are drawn at the 50% probability level and H atoms omitted for clarity.

Table 6
Selected structural data on tin(IV) phosphine oxides

Compound	*d*(Sn–O) (Å)	*d*(P–O) (Å)	Ref.
trans-$[SnF_4(Me_3PO)_2]$[a]	2.045(3)	1.532(3)	this work
cis-$[SnCl_4(Ph_3PO)_2]$[b]	2.083(2)	1.510(2)	[22]
cis-$[SnCl_4(Ph_3PO)_2]$[c]	2.086(2)	1.505(2)	[23]
trans-$[SnBr_4(Ph_3PO)_2]$[b]	2.102(9), 2.100(8)	1.504(9), 1.527(9)	[24]
cis-$[SnBr_4(Ph_3PO)_2]$[b]	2.080(8)	1.515(8)	[18]
cis-$[SnI_4(Ph_3PO)_2]$[b]	2.11(2), 2.15(2)	1.47(2), 1.50(2)	[25]
$[SnF_4\{o\text{-}C_6H_4(P(O)Ph_2)_2\}]$[a]	2.071(5), 2.088(5)	1.512(5), 1.525(5)	this work
$[SnI_4\{o\text{-}C_6H_4(P(O)Ph_2)_2\}]$[d]	2.120(5), 2.138(5)	1.509(6), 1.513(5)	[13]

[a] 120 K.
[b] 295 K.
[c] 90 K.
[d] 150 K.

in the bromo-complexes. The complexes are labile in solution and cooling the samples is necessary to observe sharp resonances and resolve couplings; the temperatures at which the presented data were obtained are given in Table 7. The trends in the spectroscopic data were also examined to see if support for the greater Lewis acidity of the SnF_4 was forthcoming. The IR data, specifically the *ν*(PO), are not useful due to the broadness of the bands and the presence of overlapping bands of the geometric isomers, but even if this were not the case, coupling with other vibrations would complicate any comparisons. The $^{31}P\{^1H\}$ NMR data are more useful (Tables 2 and 7). The chemical shift differences between the geometric isomers are small and therefore one can compare directly the changes in chemical shift simply as a function of the halide present. This shows a small but clear shift to high frequency along the series F > Cl > Br > I consistent with decreased acceptor power along this series and in agreement with the conclusions from the X-ray data above. The ^{119}Sn NMR data are not useful in this respect since the chemical shifts reflect a number of competing factors including electronegativity of the substituents, mutual ligand interactions and ligand polarisabilities [7,29]. The shift to low frequency $[SnCl_4(R_3EO)_2] > [SnF_4(R_3EO)_2] > [SnBr_4(R_3EO)_2]$ parallels that in the hexahalostannates(IV) [27–29]. Tin-119 resonances are rarely observed for iodotin species mainly due to exchange reactions in solution resulting from the weak Lewis acidity of SnI_4. The data show that SnF_4 is the strongest Lewis acid in the series SnX_4 (X = F, Cl, Br, I) towards hard bases.

3. Experimental

All compounds were made under a dinitrogen atmosphere using dry solvents and standard Schlenk and glove box techniques. SnF_2, $SnCl_4$, $SnBr_4$ and SnI_4 were obtained from Aldrich and used as received. $[SnF_4(MeCN)_2]$ and $[SnF_4(THF)_2]$ were made as described [17]. Ligands were obtained from Aldrich (Me_3PO, Ph_3PO, Ph_3AsO) and were dried by heating in vacuo before use. Other ligands were made by literature methods: $o\text{-}C_6H_4(P(O)Ph_2)_2$, $o\text{-}C_6H_4(P(O)Me_2)_2$, Me_3AsO, $Ph_2P(O)CH_2P(O)Ph_2$ [13,30,31]. IR spectra were recorded as Nujol mulls on a Perkin Elmer PE 983G spectrometer, ^1H NMR spectra in $CDCl_3$ solutions on a Bruker AV300, $^{31}P\{^1H\}$, $^{19}F\{^1H\}$ and ^{119}Sn NMR spectra on a Bruker DPX400 and referenced to 85% H_3PO_4, $CFCl_3$ and neat $SnMe_4$, respectively. Microanalytical measurements were performed by the microanalytical service, Strathclyde University.

3.1. $[SnF_4(Ph_3PO)_2]$

$[SnF_4(MeCN)_2]$ (0.277 g, 1.0 mmol) was suspended in CH_2Cl_2 (20 mL) and Ph_3PO (0.612 g, 2.2 mmol) added

Table 7
Selected NMR data on comparator complexes

Compound	$\delta^{31}P\{^1H\}$[a]	$^2J(^{31}P–^{119}Sn)$ (Hz)[b]	$\delta\ ^{119}Sn$	Ratio of isomers
$[SnCl_4(Me_3PO)_2]$	+63.4 (273 K)[c]	140	−695(t) (243 K)	4
	+62.5	106	−686(t)	1
$[SnBr_4(Me_3PO)_2]$	+61.0 (223 K)	140	−1439(t)	
$[SnI_4(Me_3PO)_2]$	+58.3 (193 K)	n.o.	n.o.[d]	
$[SnCl_4(Ph_3PO)_2]$	+40.8 (233 K)	198	−710(t) (233 K)	1
	+40.35	162	−698(t)	5
$[SnBr_4(Ph_3PO)_2]$	+38.9 (223 K)	214	−1480(t) (223 K)	
$[SnI_4(Ph_3PO)_2]$	+36.5 (183 K)	n.o.	n.o.	
$[SnCl_4(Ph_3AsO)_2]$			−639(s) (243 K)	1
			−637(s)	2
$[SnBr_4(Ph_3AsO)_2]$			−1364(s) (233 K)	
$[SnI_4(Ph_3AsO)_2]$			n.o.	
$[SnCl_4\{o\text{-}C_6H_4(P(O)Ph_2)_2\}]$[e]	+42.4 (295 K)			
$[SnBr_4\{o\text{-}C_6H_4(P(O)Ph_2)_2\}]$[e]	+41.6 (295 K)			
$[SnI_4\{o\text{-}C_6H_4(P(O)Ph_2)_2\}]$[e]	+39.8 (295 K)			

[a] In CH_2Cl_2–10% $CDCl_3$.
[b] Separate resonances for ^{119}Sn and ^{117}Sn couplings not resolved in ^{31}P NMR spectra, couplings are from ^{119}Sn spectra.
[c] Ligand chemical shifts are: Me_3PO + 38, Ph_3PO + 28, $o\text{-}C_6H_4(P(O)Ph_2)_2$ + 31.
[d] n.o., Not observed in temperature range 295–180 K.
[e] Data from [13].

and the mixture stirred at room temperature for 2 h. The white solid was filtered off, recrystallised from hot CH_2Cl_2 and dried in vacuo. Yield: 0.66 g, 88%. *Anal*. Calc. for $C_{36}H_{30}F_4O_2P_2Sn \cdot 3CH_2Cl_2$: C, 46.6; H, 3.6. Found: C, 47.1; H, 3.7%.

3.2. $[SnF_4(Ph_3AsO)_2]$

Prepared similarly from $[SnF_4(MeCN)_2]$ (0.156 g, 0.56 mmol) and Ph_3AsO (0.40 g, 1.24 mmol). Yield: 0.30 g, 64%. *Anal*. Calc. for $C_{36}H_{30}As_2F_4O_2Sn \cdot 2CH_2Cl_2$: C, 45.2; H, 3.4. Found: C, 45.3; H, 3.2%.

3.3. $[SnF_4(Me_3PO)_2]$

Prepared similarly from $[SnF_4(MeCN)_2]$ (0.28 g, 1.0 mmol) and Me_3PO (0.19 g, 2.05 mmol) and stirred for 8 h. Yield: 0.30 g, 79%. *Anal*. Calc. for $C_6H_{18}F_4O_2P_2Sn$: C, 19.0; H, 4.8. Found: C, 18.2; H, 4.7%.

3.4. $[SnF_4(Me_3AsO)_2]$

Prepared similarly from $[SnF_4(MeCN)_2]$ (0.32 g, 1.15 mmol) and Me_3AsO (0.34 g, 2.5 mmol). Yield: 0.495 g, 92%.

3.5. $[SnF_4\{o\text{-}C_6H_4(P(O)Ph_2)_2\}]$

$[SnF_4(MeCN)_2]$ (0.138 g, 0.50 mmol) and $o\text{-}C_6H_4(P(O)Ph_2)_2$ (0.239 g, 0.50 mmol) were stirred together for 0.5 h in CH_2Cl_2 (20 mL). The white precipitate was filtered off and dried in vacuo. Yield: 0.23 g, 68%. *Anal*. Calc. for $C_{30}H_{24}F_4O_2P_2Sn \cdot 0.5CH_2Cl_2$: C, 51.2; H, 3.5. Found: C, 51.2; H, 3.3%.

3.6. $[SnF_4\{Ph_2P(O)CH_2P(O)Ph_2\}]$

Powdered $Ph_2P(O)CH_2P(O)Ph_2$ (0.22 g, 0.53 mmol) and $[SnF_4(MeCN)_2]$ (0.133 g, 0.48 mmol) were dissolved in CH_2Cl_2 (10 mL) and stirred at room temperature overnight. The white precipitate was then filtered off and dried in vacuo. Yield: 0.27 g, 92%. *Anal.* Calc. for $C_{25}H_{22}F_4O_2P_2Sn \cdot 0.5CH_2Cl_2$: C, 46.9; H, 3.6. Found: C, 46.5; H, 3.7%.

3.7. $[SnF_4\{o\text{-}C_6H_4(P(O)Me_2)_2\}]$

$[SnF_4(THF)_2]$ (0.30 g, 0.88 mmol) was dissolved in CH_2Cl_2 (5 mL), $o\text{-}C_6H_4(P(O)Me_2)_2$ (0.20 g, 0.87 mmol) dissolved in CH_2Cl_2 (5 mL) was added and the mixture stirred at room temperature for 2 h. The white solid was filtered off and dried in vacuo. Yield: 0.257 g, 68%.

3.8. $[SnX_4L_2]$ (X = Cl, Br or I; L = Ph_3PO, Ph_3AsO or Me_3PO)

These were made by reaction of the anhydrous tin(IV) halide with the ligand in anhydrous CH_2Cl_2 using literature methods [6,26].

3.9. X-ray experimental

Crystals of $[SnF_4\{o\text{-}C_6H_4(P(O)Ph_2)_2\}] \cdot CH_2Cl_2 \cdot H_2O$ were obtained from CH_2Cl_2 solution layered with hexane and $o\text{-}C_6H_4(P(O)Ph_2)_2$ from CH_2Cl_2 solution. Brief details of the data collection and refinement are presented in Table 8. Data collection used a Bruker–Nonius Kappa CCD diffractometer with the crystal held at 120 K in a cold nitrogen stream. Structure solution [32] and refinement [33]

Table 8
Crystallographic data[a]

Compound	$[SnF_4(Me_3PO)_2]$	$[SnF_4\{o\text{-}C_6H_4(P(O)Ph_2)_2\}]\cdot CH_2Cl_2\cdot H_2O$	$[o\text{-}C_6H_4(P(O)Ph_2)_2]\cdot CH_2Cl_2$
Formula	$C_6H_{18}F_4O_2P_2Sn$	$C_{31}H_{28}Cl_2F_4O_3P_2Sn$	$C_{31}H_{26}Cl_2O_2P_2$
Formula weight	378.83	776.06	563.36
Crystal system	monoclinic	monoclinic	monoclinic
Space group	$P2_1/n$ (no. 14)	$P2_1/c$ (no. 14)	$P2_1/c$ (no. 14)
a (Å)	6.190(2)	17.579(3)	10.840(2)
b (Å)	11.089(4)	10.1696(15)	14.734(3)
c (Å)	9.504(3)	18.178(4)	17.576(2)
β (°)	94.32(3)	99.160(8)	104.467(12)
U (Å^3)	650.5(4)	3208.2(10)	2718.3(8)
Z	2	4	4
μ(Mo Kα) (mm^{-1})	2.24	1.12	0.38
Total no. of observations	6333	35 141	28 169
No. of unique observations (R_{int})	1486 (0.056)	7058 (0.055)	4775 (0.101)
No. of parameters, restraints	71, 0	395, 5	335, 0
R_1, wR_2 ($I > 2\sigma(I)$)[b]	0.034, 0.073	0.070, 0.183	0.046, 0.095
R_1, wR_2 (all data)	0.049, 0.079	0.082, 0.188	0.088, 0.112

[a] Other items: temperature = 120 K; wavelength (Mo Kα) = 0.71073 Å; $\theta_{max} = 27.5°$.
[b] $R_1 = \sum\|F_o| - |F_c\|/\sum|F_o|$, $wR_2 = [\sum w(F_o^2 - F_c^2)^2/\sum wF_o^4]^{1/2}$.

were routine. In $[SnF_4\{o\text{-}C_6H_4(P(O)Ph_2)_2\}]\cdot CH_2Cl_2\cdot H_2O$ the $CH_2Cl_2$was disordered with one of the chlorine atoms occupying three sites. The two remaining peaks in the difference map were interpreted as half occupancy water molecules with the O···O distance appropriate for an H-bond. No H atoms were included for these solvate molecules. Several attempts were made to grow X-ray quality crystals of $[SnF_4(Me_3AsO)_2]$ by vapour diffusion from EtOH and Et_2O. The data from the crystals obtained did not lead to a structure possibly due to twinning.

4. Supplementary data

Crystallographic data in cif format have been deposited with the Cambridge Crystallographic Data Centre (CCDC) and given numbers 278050–278052. Copies of the data can be obtained free of charge from The Director, CCDC, 12 Union Road, Cambridge, CB2 1EZ, UK, fax: +44 1223 366 033, e-mail: deposit@ccdc.ac.uk or on the web www: http://www.ccdc.cam.ac.uk.

Acknowledgements

We thank EPSRC for support (MFD), and M.J. Darmody for the preparation of some of the tin(IV) complexes in Section 3.8.

References

[1] A.D. Adley, P.H. Bird, A.R. Fraser, M. Onyszchuk, Inorg. Chem. 11 (1972) 1402.
[2] C.E. Michelson, D.S. Dyer, R.O. Ragsdale, J. Inorg. Nucl. Chem. 32 (1970) 833.
[3] P.A.W. Dean, D.F. Evans, J. Chem. Soc. A (1968) 1154.
[4] C.J. Wilkins, H.M. Haendler, J. Chem. Soc. (1965) 3174.
[5] J.P. Clark, V.M. Langford, C.J. Wilkins, J. Chem. Soc. A (1967) 792.
[6] S.H. Hunter, V.M. Langford, G.A. Rodley, C.J. Wilkins, J. Chem. Soc. A (1968) 305.
[7] P.G. Harrison, The Chemistry of Tin, Blackie & Son, London, 1989.
[8] S.J. Ruzicka, A.E. Merbach, Inorg. Chim. Acta 20 (1976) 221.
[9] S.J. Ruzicka, A.E. Merbach, Inorg. Chim. Acta 22 (1977) 191.
[10] S.E. Dann, A.R.J. Genge, W. Levason, G. Reid, J. Chem. Soc., Dalton Trans. (1996) 4471.
[11] S.E. Dann, A.R.J. Genge, W. Levason, G. Reid, J. Chem. Soc., Dalton Trans. (1997) 2207.
[12] A.R.J. Genge, W. Levason, G. Reid, J. Chem. Soc., Dalton Trans. (1997) 4549.
[13] A.R.J. Genge, W. Levason, G. Reid, Inorg. Chim. Acta 288 (1999) 142.
[14] W. Levason, M.L. Matthews, R. Patel, G. Reid, M. Webster, New J. Chem. 27 (2003) 1784.
[15] M. Bork, R. Hoppe, Z. Anorg. Allgem. Chem. 622 (1996) 1557.
[16] D. Tudela, F. Rey, Z. Anorg. Allgem. Chem. 575 (1989) 202.
[17] D. Tudela, J.A. Patron, Inorg. Synth. 31 (1997) 92.
[18] D. Tudela, J.D. Tornero, A. Monge, A.J. Sánchez-Herencia, Inorg. Chem. 32 (1993) 3928.
[19] L.M. Engelhardt, C.L. Raston, C.R. Whitaker, A.H. White, Aust. J. Chem. 39 (1986) 2151.
[20] L. Deakin, W. Levason, M.C. Popham, G. Reid, M. Webster, J. Chem. Soc., Dalton Trans. (2000) 2439.
[21] N.J. Hill, W. Levason, M.C. Popham, G. Reid, M. Webster, Polyhedron 21 (2002) 445.
[22] A.I. Tursina, L.A. Aslanov, S.V. Medvedev, A.V. Yatsenko, Koord. Khim. 11 (1985) 417.
[23] T. Szymanska-Buzar, T. Glowiak, I. Czelusniak, Main Group Met. Chem. 24 (2001) 821.
[24] A.I. Tursina, A.V. Yatsenko, S.V. Medvedev, V.V. Chernyshev, L.A. Aslanov, Zh. Strukt. Khim. 27 (1986) 157.
[25] A.I. Tursina, L.A. Aslanov, V.V. Chernyshev, S.V. Medvedev, A.V. Yatsenko, Koord. Khim. 12 (1986) 420.
[26] P.G. Harrison, B.C. Lane, J.J. Zuckerman, Inorg. Chem. 11 (1972) 1537.
[27] K.B. Dillon, A. Marshall, J. Chem. Soc., Dalton Trans. (1984) 1245.
[28] R. Colton, D. Dakternieks, Inorg. Chim. Acta 71 (1983) 101.
[29] J. Mason, Multinuclear NMR, Plenum, New York, 1987.
[30] A. Merijanian, R.A. Zingaro, Inorg. Chem. 5 (1966) 187.
[31] W. Levason, R. Patel, G. Reid, J. Organomet. Chem. 688 (2003) 280.
[32] G.M. Sheldrick, SHELXS 97, Program for Crystal Structure Solution, University of Göttingen, 1997.
[33] G.M. Sheldrick, SHELXL 97, Program for Crystal Structure Refinement, University of Göttingen, 1997.

2. Experimental

2.1. Preparation of 1–6

The preparations were carried out using 0.2 molar aqueous solutions of D,L-tartaric acid and LiOH and a second hydroxide MOH, where M = Li (**1**), Na (**2**), K (**3**), Rb (**4**), Cs (**5**) and NH_4 (**6**). A liquid handling robot was used to prepare mixtures of these solutions in the wells of a well plate. Crystals suitable for X-ray crystallography were obtained after approximately one week.

2.2. X-ray crystallography

Intensity data for structures **1**–**6** were recorded at 120 K, using a Nonius Kappa CCD area-detector diffractometer mounted at the window of a rotating anode FR591 generator with a molybdenum anode ($\lambda = 0.71073$ Å). φ and ω scans were carried out to fill the Ewald sphere [10]. An empirical absorption correction was carried out using SORTAV [11,12]. The structures were solved by direct methods and refined on F^2 by full-matrix least-squares refinements [13]. All hydrogen atoms were identified in a difference map. The positions of hydroxyl hydrogen atoms were constrained to idealised geometries. Geometrical restraints were applied to refine the positions of the water hydrogen atoms. The NH_4 hydrogen atoms in structure **6** were treated in the same manner. Details for the structure determination of **1**–**6** are listed in Table 1. Parameters of hydrogen bonds in **1**–**6** are available as supplementary data.

3. Results and discussion

3.1. $Li_2(C_4H_4O_6) \cdot 3H_2O$ (1)

Racemic dilithium tartrate trihydrate was first reported by Scacchi in 1867 [14,15]. The optical microscopic characterisation was limited by his inability to obtain the compound subsequently. It therefore represents one of the earliest examples of a disappearing form [16]. The trihydrate crystals in our hands remain unaltered, and we have been unable to obtain any other dilithium tartrate. This different behaviour is probably due to the relative purity of the chemicals available to us. Examples of disappearing forms are often related to chemical purity issues [17].

The crystal structure of **1** proved to be unusually complex. The space group is $P2_1/c$, and the unit cell contains sixteen formula units, i.e. the asymmetric unit has 24 different entities (8 Li, 12 water molecules and 4 tartrate ions). The structure is composed of two topologically different two-dimensional coordination networks $[Li_6(C_4H_4O_6)_3(H_2O)_9]_n$ (A) and $[Li_2(C_4H_4O_6)(H_2O)_3]_{2n}$ (B) which propagate parallel to the *ab*-plane. A and B are structural isomers. Both nets are shown in Figs. 1 and 2.

Table 1
Crystallographic parameters and details of the structure determination of **1**–**6**

	1	**2**	**3**	**4**	**5**	**6**
Compound	$Li_2(C_4H_4O_6) \cdot 3H_2O$	$LiNa(C_4H_4O_6) \cdot 2H_2O$	$LiK(C_4H_4O_6) \cdot H_2O$	$LiRb(C_4H_4O_6) \cdot H_2O$	$LiCs(C_4H_4O_6) \cdot H_2O$	$LiNH_4(C_4H_4O_6) \cdot H_2O$
Formula	$C_4H_{10}Li_2O_9$	$C_4H_8LiNaO_8$	$C_4H_6KLiO_7$	$C_4H_6LiO_7Rb$	$C_4H_6CsLiO_7$	$C_4H_{10}LiNO_7$
Formula weight	216.00	214.03	212.13	258.50	305.94	191.07
Crystal system	monoclinic	monoclinic	monoclinic	monoclinic	monoclinic	monoclinic
Space group	$P2_1/c$	$C2/c$	$C2/c$	$C2/c$	$C2/c$	$C2/c$
Z	16	8	8	8	8	8
a (Å)	20.8669(1)	18.384(4)	18.237(5)	18.3422(14)	18.6597(8)	18.3976(10)
b (Å)	15.0074(1)	7.9083(16)	9.682(2)	9.7710(10)	9.8643(5)	9.6130(8)
c (Å)	11.6785(1)	13.929(3)	9.5528(13)	9.6409(5)	9.7931(5)	9.7919(6)
β (°)	99.367(6)	129.25(3)	116.679(16)	115.893(4)	115.066(2)	115.118(4)
V (Å^3)	3608.45(4)	1568.2(5)	1507.2(5)	1554.4(2)	1632.80(14)	1567.99(18)
Θ range (°)	3.17–25.78	2.95–25.25	4.02–25.74	3.73–26.00	2.94–26.00	3.70–25.99
Reflections collected	22206	3915	6025	5355	4619	5672
Independent reflections	6735	1409	1339	1505	1590	1510
R_{int}	0.0641	0.0852	0.2053	0.0730	0.0375	0.0872
Data/restraints/parameters	6735/32/670	1409/0/138	1339/5/132	1505/5/137	1590/4/137	1510/14/152
Final R indices ($I > 2\sigma(I)$)[a]	$R_1 = 0.0497$ $wR_2 = 0.0903$	$R_1 = 0.0490$ $wR_2 = 0.1237$	$R_1 = 0.0614$ $wR_2 = 0.0738$	$R_1 = 0.0358$ $wR_2 = 0.0653$	$R_1 = 0.0260$ $wR_2 = 0.0552$	$R_1 = 0.0479$ $wR_2 = 0.0844$
R indices (all data)[a]	$R_1 = 0.0872$ $wR_2 = 0.0988$	$R_1 = 0.0671$ $wR_2 = 0.1321$	$R_1 = 0.2126$ $wR_2 = 0.0916$	$R_1 = 0.0673$ $wR_2 = 0.0715$	$R_1 = 0.0304$ $wR_2 = 0.0572$	$R_1 = 0.1093$ $wR_2 = 0.0972$
Crystal	colourless block	colourless plate	colourless platelet	colourless needle	colourless plate	colourless block
Crystal size (mm)	$0.50 \times 0.15 \times 0.02$	$0.15 \times 0.10 \times 0.05$	$0.07 \times 0.07 \times 0.02$	$0.12 \times 0.03 \times 0.03$	$0.1 \times 0.08 \times 0.02$	$0.07 \times 0.01 \times 0.01$

[a] $R_1 = \sum ||F_o| - |F_c|| / \sum |F_o|$; $wR_2 = \{\sum[w(F_o^2 - F_o^2)^2] / \sum[w(F_o^2)^2]\}^{1/2}$.

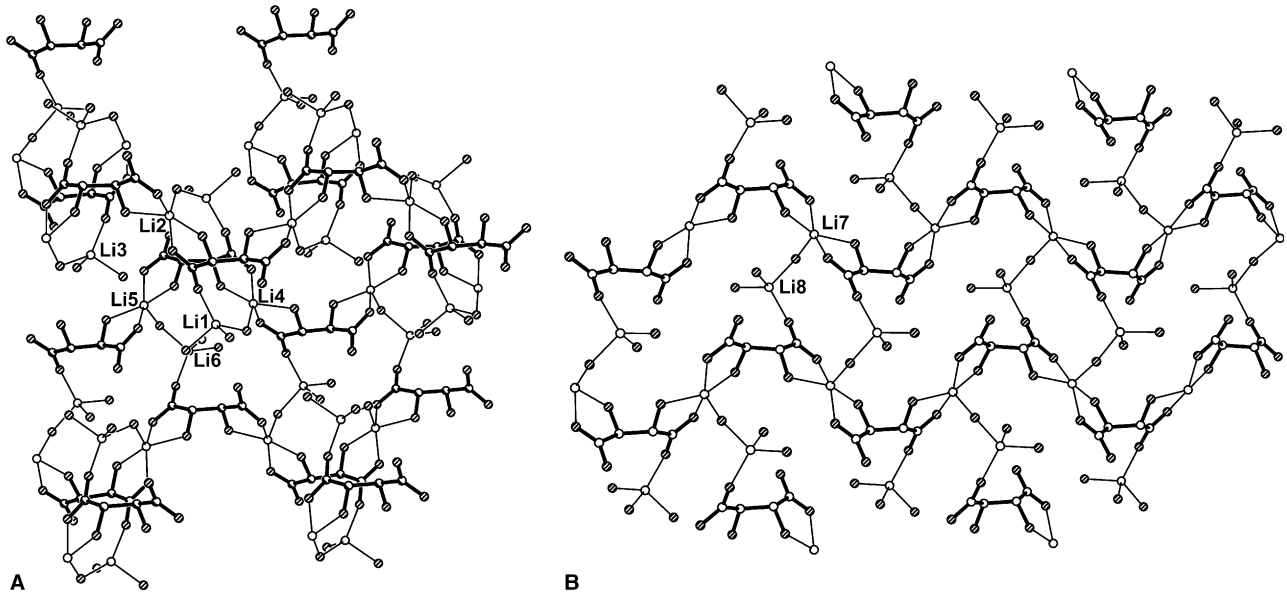

Fig. 1. Two-dimensional nets in structure **1**. Left: net $[Li_6(C_4H_4O_6)_3(H_2O)_9]_n$ (A). Right: net $[Li_2(C_4H_4O_6)(H_2O)_3]_{2n}$ (B).

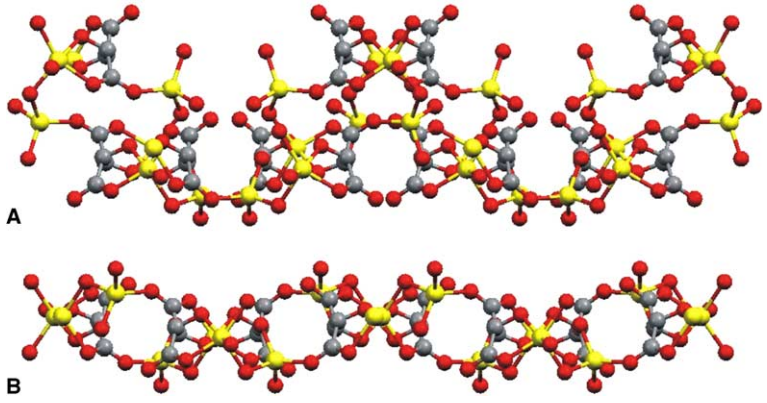

Fig. 2. Two-dimensional nets in structure **1**, viewed along *c*. Top: net $[Li_6(C_4H_4O_6)_3(H_2O)_9]_n$ (A). Bottom: net $[Li_2(C_4H_4O_6)(H_2O)_3]_{2n}$ (B).

In A, Li2, Li4 and Li5 are coordinated by oxygen in a distorted square-pyramidal fashion. The base of each pyramid is formed by two chelating tartrate ligands, while a water molecule occupies the apical position. Chelation is realised through adjacent carboxyl and hydroxyl oxygen atoms of each tartrate ion. By contrast, Li1, Li3 and Li6 are surrounded in tetrahedral fashion by three water molecules and one carboxyl oxygen. The apical water molecule in each LiO_5 unit bridges to a tetrahedral centre, Li4–O100–Li1, Li2–O102–Li3 and Li5–O105–Li6. Hence, each tetrahedral Li centre is connected to one tartrate molecule and one LiO_5 unit, while each square-pyramidal Li is linked to one Li [4] and two tartrate ions. Only one of the six oxygen sites in each tartrate ion (a carboxyl oxygen) is not involved in the coordination of Li.

Net B is centrosymmetric and contains two independent Li positions. Li7 and Li8 are surrounded by tartrate and water in a square-pyramidal and in a tetrahedral fashion, respectively, and their coordination polyhedra, linked by a Li7–O109(water)–Li8 bridge, share a common edge. The tartrate ion chelates to two Li7 centres in the same manner as described for net A. One of the remaining carboxyl oxygens additionally coordinates a Li8 centre. Hence, the Li centres, tartrate ions and water molecules are linked in a very similar fashion in nets A and B. However, the resulting two net topologies are different.

The Li–O distances in **1** lie between 1.912(4) and 2.227(4) Å, and the longest bonds are observed between the penta-coordinated Li5 and the apical water molecule. The structure of **1** is a BAABAA stack, i.e., the A:B ratio is 2:1. Adjacent A-nets are related by inversion, and there is no mutual parallel interpenetration [18] of either {A + A} or {A + B} nets. The resulting arrangement is depicted in Fig. 3. All hydrogen atoms of all water molecules and hydroxyl groups are engaged in hydrogen bonds. Fig. 4 illustrates that these interactions facilitate the intra-net stabilisation of A and B as well as the linkage of adjacent A- and B-nets into a three-dimensional hydrogen-bonded framework.

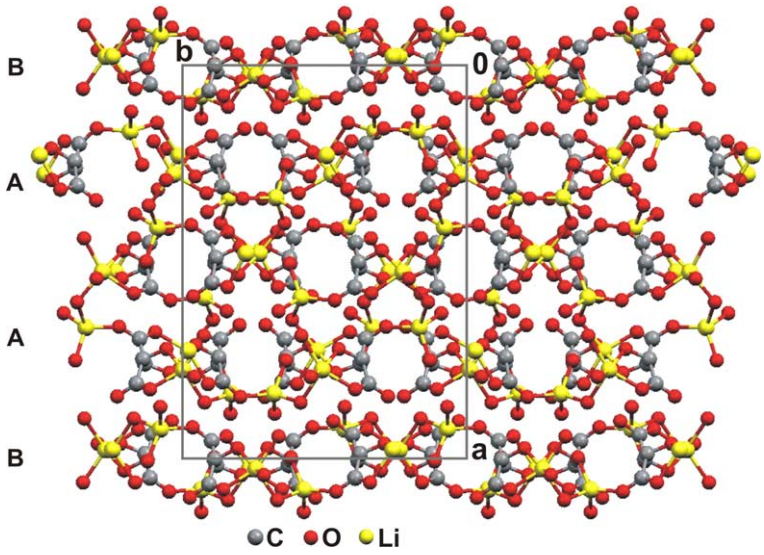

Fig. 3. BAAB sequence of two-dimensional nets in structure **1** viewed along *c*. There is no mutual interpenetration of adjacent nets.

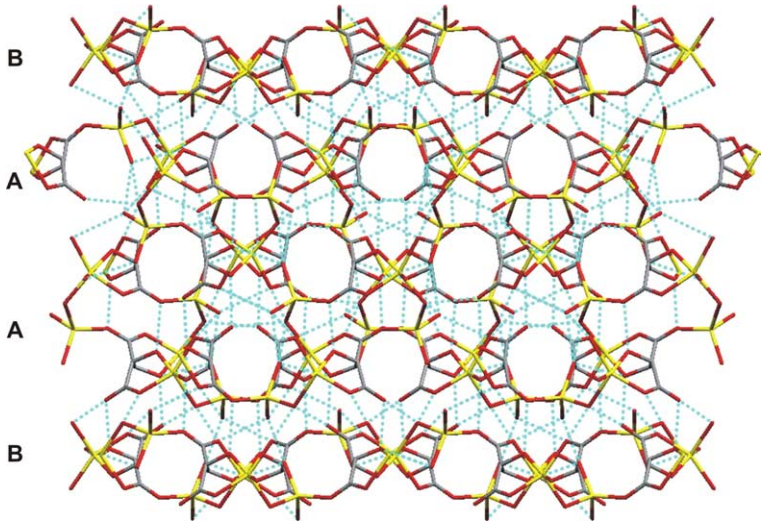

Fig. 4. Representation of **1** showing the same part of the structure, a BAAB sequence, as Fig. 3. A and B nets are connected by hydrogen bonds (indicated by dotted lines).

3.2. $LiNa(C_4H_4O_6)\cdot 2H_2O$ (**2**)

Racemic lithium sodium tartrate dihydrate crystallises in the space group *C*2/*c* with one formula unit per asymmetric unit. The structure contains two sodium atoms in special position, one on a twofold axis (Na1) and one at a centre of inversion (Na2) Na–O and Li–O bond distances for two are listed in Table 2. Li is coordinated in a distorted square-pyramidal fashion by the carboxyl and adjacent hydroxyl oxygens of two tartrate ions, and a water molecule (O8) occupies the apical position. The centrosymmetric unit $[Li(C_4H_4O_6)(H_2O)]_2$ shown in Fig. 5 is formed as a result and the Li–O lie distances between 1.940(5) and 2.192(5) Å. These units are linked via NaO_6 polyhedra.

Na1 is surrounded by four carboxyl oxygen atoms (O1, O6) of four different tartrate ions and two water molecules (*cis*, O7) in a distorted octahedral fashion, and Na1–O distances lie between 2.339(2) and 2.517(2) Å. Na2 is coordinated by two carboxyl oxygen atoms (*trans*, O6) of two different tartrate ions and four water molecules (O7 and O8) in an almost perfect octahedral fashion. Na2–O distances lie between 2.3926(19) and 2.4034(19) Å. Thus, two carboxyl oxygens (O5 and O2) do not participate in the coordination of any metal centre, while O6 coordinates Li1, Na1 as well as Na2. O1 coordinates Li1 and Na1. The Na1 octahedron shares a single edge with each of two Li and two Na2 polyhedra. Additionally, the LiO_5 polyhedron shares an edge with the octahedron around Na2. Thus, chains of edge-sharing LiO_5 and NaO_6 polyhedra are formed which run parallel to the *c*-axis. One example of such a chain is shown in Fig. 6. A diagram of the three-dimensional coordination network of **2** which is the

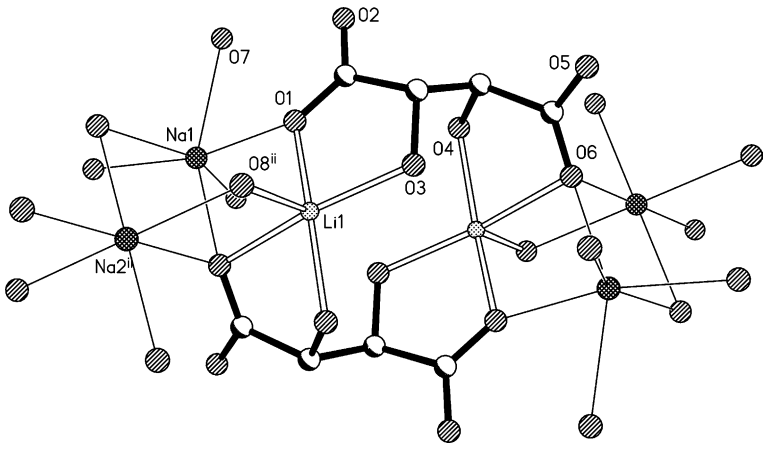

Fig. 5. Centrosymmetric $[Li(C_4H_4O_6)(H_2O)]_2$ unit in **2**, sharing oxygen atoms with four NaO_6 polyhedra.

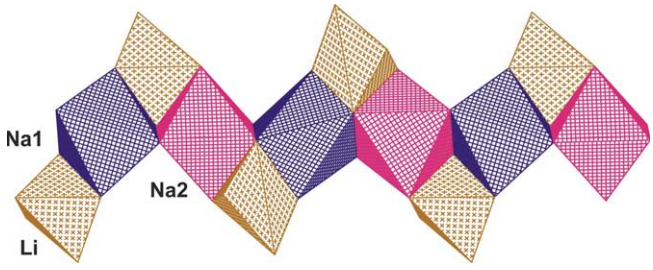

Fig. 6. Chain of edge-sharing NaO_6 and LiO_5 polyhedra in **2** running parallel to the *c*-axis.

result of the described structural features is shown in Fig. 7. This network is stabilised by hydrogen bonds in which the hydrogen atoms of all water molecules and hydroxyl groups are engaged.

*3.3. $LiM(C_4H_4O_6)\cdot H_2O$ with M = K (**3**), Rb (**4**), Cs (**5**), NH_4 (**6**)*

The racemic tartrate monohydrates **3**, **4**, **5** and **6** are isostructural. In this respect, they are similar to the series of chiral anhydrous K, Rb, Cs and NH_4 hydrogen tartrates [15–18] and their racemic counterparts [1]. Here, it was also observed that the racemic series produces mixed crystals.

3–**6** crystallise in the space group *C*2/*c*. The asymmetric unit contains one formula unit. M occupies two independent positions (M1 and M2) on a twofold axis. Each lithium centre is tetrahedrally surrounded by one water molecule and three carboxyl oxygens. Two of these oxygen atoms are related by inversion symmetry and bridge between adjacent lithium centres, so that planar Li_2O_2 rings are formed.

In the structures **3**–**5**, M1 is coordinated by 10 oxygen atoms which belong to four different tartrate ions. Two of these ligands are tridentate, and the others are bidentate. Tridentate linkage involves one carboxyl (O5) and both hydroxyl oxygen atoms (O3, O4). Bidentate linkage involves the other O of the same carboxyl group (O6) and the hydroxyl O not adjacent to it (O3). The shape of the M1 polyhedron changes considerably when the size of the alkali metal cation increases, and the relative order of the M1–O distances observed for the potassium (**3**)

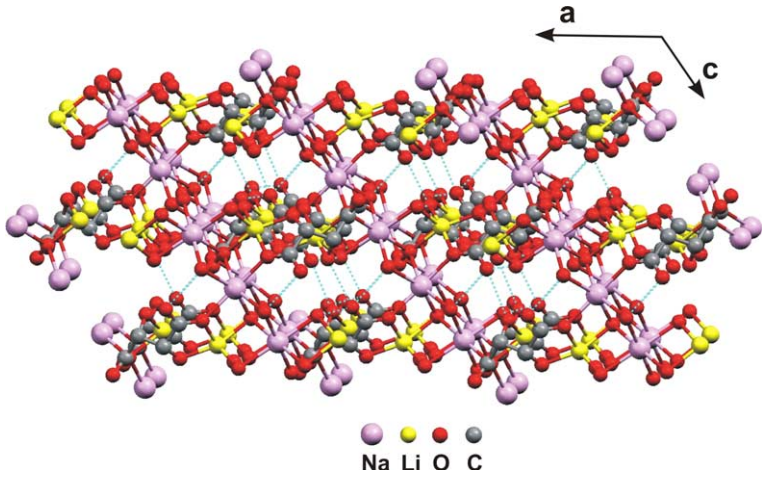

Fig. 7. Three-dimensional coordination network of **2** which is stabilised by hydrogen bonds (indicated by dotted lines).

Table 2
Selected bond distances (in Å) in **2** (c = carboxyl, h = hydroxyl, w = water oxygen)[a]

Na1–O1	c	2.339(2)
Na1–O6^{i}	c	2.371(2)
Na1–O7	w	2.517(2)
Na2–O7	w	2.3926(19)
Na2–O8	w	2.399(2)
Na2–O6^{iii}	c	2.4034(19)
Li1–O1	c	1.940(5)
Li1–O4^{i}	h	2.025(5)
Li1–O3	h	2.025(5)
Li1–O8^{ii}	w	2.06(2)
Li1–O6^{i}	c	2.192(5)

[a] Symmetry transformations: (i) $-x+1/2, -y-1/2, -z+1$; (ii) $x, -y, z+1/2$; (iii) $x-1/2, -y-1/2, z-1/2$.

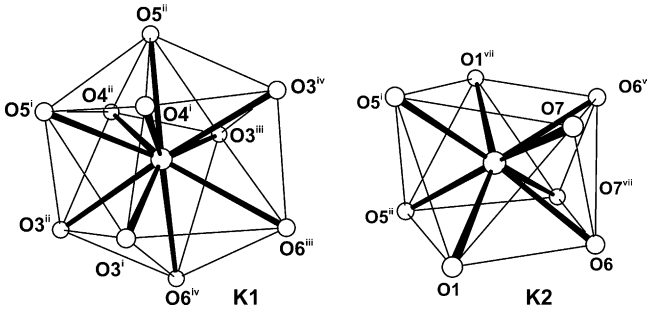

Fig. 8. Left: KO_{10} coordination polyhedron around K1 in **3**. Right: KO_8 coordination polyhedron around K2 in the same structure.

and caesium (**5**) analogues is therefore rather different (see Table 3). Fig. 8 shows the KO_{10} coordination polyhedron around K1 in structure **3**. This coordination may also be described as [8+2] since two crystallographically identical K1–O(carboxyl) bonds to bidentate ligands are considerably elongated (see K1–O6^{iii} in Table 3). In structure **5**, by contrast, the Cs1–O6^{iii} distance of 3.240 Å lies in the same range as the other four independent Cs1–O distances. Moreover, Cs1–O6^{iii} is even shorter than the corresponding K1–O6^{iii} value in **3** (3.319 Å), despite the larger radius of the metal ion.

The coordination polyhedron around M2 is a distorted square antiprism. The metal centre is surrounded by two water molecules (O7) and six carboxyl oxygens of six different tartrate molecules (O1, O5, O6). The water molecule bridges between Li and M2. All tartrate oxygens are employed in the coordination of metal centres. Of the four carboxyl oxygens, O1 is connected to M2, O2 bridges between two Li centres, O5 between M1 and M2 and O6 between M2 and two different M1 centres. One hydroxyl oxygen (O3) links two M1, while the other (O4) is only connected to M1. Thus, a three-dimensional network of edge-sharing MO_{10}, MO_8 and LiO_4 polyhedra is generated, as shown in Fig. 9.

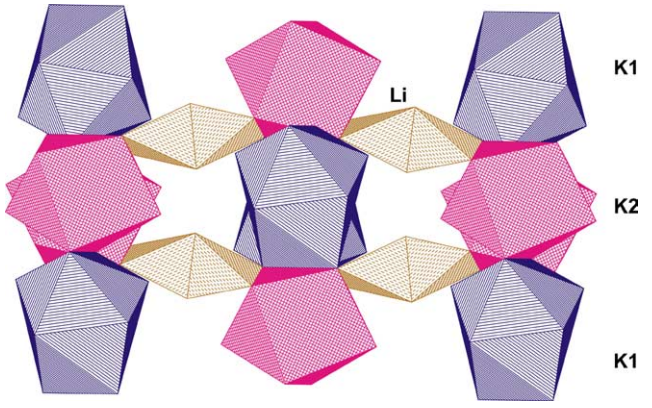

Fig. 9. The three-dimensional network in **3** generated by edge-sharing MO_{10} (K1), MO_8 (K2) and LiO_4 coordination polyhedra.

The structures of **3**–**6** may be described as stacks in which two-dimensional $[Li(C_4H_4O_6)\cdot H_2O]_n$ nets (Fig. 10) that propagate in the *ab*-plane (see Figs. 10 and 11) alternate with layers composed of M1 and M2. The three-dimensional coordination network is eventually produced

Table 3
Selected interatomic distances (in Å) in the series of **3**–**6** (c = carboxyl, h = hydroxyl, w = water oxygen)[a]

		3 (M = K)	**4** (M = Rb)	**5** (M = Cs)	**6** (M = NH_4)	
M1–O3^{i}	h	2.831(5)	2.961(3)	3.127(3)	N1···O3^{i}	3.002(2)
M1–O4^{i}	h	2.887(5)	3.048(3)	3.190(2)	N1···O4^{i}	3.058(3)
M1–O5^{i}	c	3.075(5)	3.217(3)	3.313(3)	N1···O5^{i}	3.587(4)
M1–O3^{iii}	h	3.177(4)	3.174(3)	3.221(3)	N1···O3^{iii}	3.125(2)
M1–O6^{iii}	c	3.319(5)	3.210(3)	3.240(2)	N1···O6^{iii}	3.186(4)
M2–O5^{i}	c	2.757(5)	2.883(3)	3.041(2)	N2···O5^{i}	2.796(3)
M2–O6^{v}	c	2.878(4)	2.978(3)	3.115(2)	N2···O6^{v}	2.958(3)
M2–O7	w	3.020(5)	3.184(3)	3.382(3)	N2···O7	3.343(3)
M2–O1	c	3.081(5)	3.092(3)	3.162(2)	N2···O1	3.162(2)
Li1–O7	w	1.879(11)	1.909(8)	1.937(7)	Li1–O7	1.901(5)
Li1–O6^{vi}	c	1.898(10)	1.885(7)	1.886(7)	Li1–O6^{vi}	1.893(4)
Li1–O2^{vii}	h	1.934(11)	1.944(7)	1.954(6)	Li1–O2^{vii}	1.933(5)
Li1–O2	h	1.946(10)	1.963(8)	1.963(7)	Li1–O2	1.945(5)

[a] Symmetry transformations: (i) $-x-1/2, -y+1/2, -z$; (ii) $x+1/2, -y+1/2, z+1/2$; (iii) $-x-1/2, y-1/2, -z+1/2$; (iv) $x+1/2, y-1/2, z$; (v) $x+1/2, y+1/2, z$; (vi) $-x-1/2, y+1/2, -z+1/2$; (vii) $-x-1/2, -y+3/2, -z$.

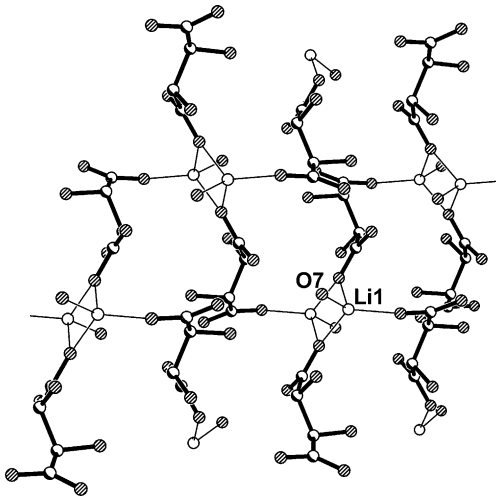

Fig. 10. Two-dimensional net $[Li(C_4H_4O_6)(H_2O)]_n$ in **3**.

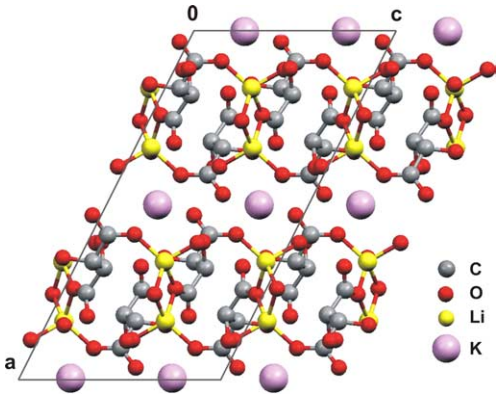

Fig. 11. Arrangement of alternating potassium (M1 + M2) and $[Li(C_4H_4O_6)(H_2O)]_n$ layers in **3** (structure viewed in the direction of the *b*-axis). K–O contacts omitted for clarity.

by coordination of M1 and M2 by the oxygens of the two neighbouring $[Li(C_4H_4O_6)(H_2O)]_n$ layers. The structures in this series contain four potential hydrogen bond donors (water molecules, hydroxyl groups) which are all engaged in H-bonding that connects adjacent $[Li(C_4H_4O_6)(H_2O)]_n$ nets. This is illustrated in Fig. 12.

In **6**, the M1 and M2 sites are occupied by NH_4. The NH_4 at the antiprismatic M2 site is hydrogen bonded to four carboxylate oxygen atoms. By contrast, NH_4 at the M1 site is linked via four bifurcated hydrogen bonds to six hydroxyl and two carboxyl oxygens.

A second product was obtained from the reaction of racemic tartaric acid with LiOH and CsOH which was subsequently shown to be the dihydrate, $LiCs(C_4H_4O_6) \cdot 2H_2O$ [19].

4. Concluding remarks

The limited set of structures considered here reinforces some of the observations noted in the previous study on racemic alkali hydrogen tartrates [2]. K, Rb, Cs and NH_4 form an isostructural set in each case. Although these two series are different with regard to the hydrogen bonding patterns they exhibit and the presence of Li and water molecules, the size difference between K and Cs is accommodated in each case by different degrees of distortion of the square antiprismatic or decahedral coordination polyhedra around the metal centre. However, the resulting Cs structures are not so well stabilised, so that an alternative Cs form was observed in each case, a polymorph in the hydrate tartrate series and the dihydrate in the present study, to be discussed elsewhere [19]. The position of the alkali metal can be adopted by NH_4 in each series under formation of hydrogen bonds NH···O. When the second cation M in LiM tartrates is a smaller Li or Na ion, then

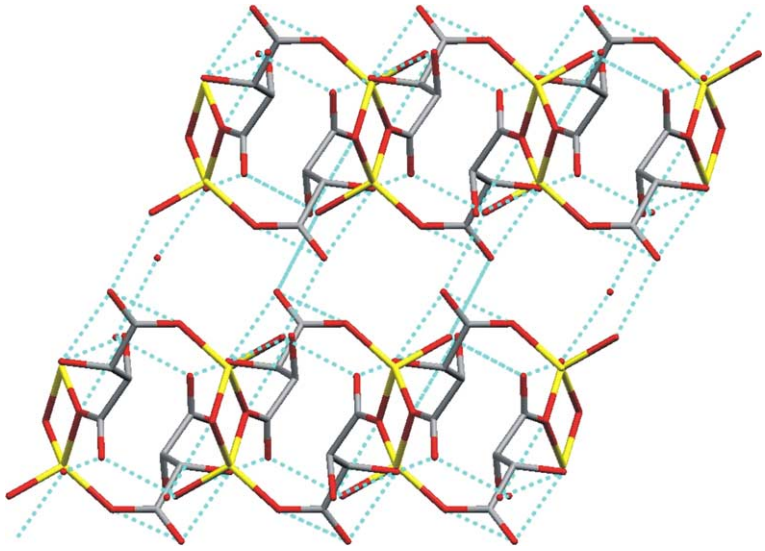

Fig. 12. Representation of **3** showing the same part of the structure as Fig. 11. Adjacent $[Li(C_4H_4O_6)(H_2O)]_n$ layers are connected by hydrogen bonds (indicated by dotted lines). K atoms omitted for clarity.

totally new structures with little similarity to their K, Rb and Cs counterparts are formed.

Appendix A. Supplementary data

Supplementary data are available from the CCDC, 12 Union Road, Cambridge CB2 1EZ, UK on request, quoting the deposition numbers CCDC 283271–283276. Supplementary data associated with this article can be found, in the online version, at doi:10.1016/j.poly.2005.10.018.

References

[1] T. Gelbrich, M.B. Hursthouse, Cryst. Eng. Commun. 7 (2005) 324.
[2] T. Gelbrich, T.L. Threlfall, S. Huth, E. Seeger, M.B. Hursthouse, Z. Anorg. Allg. Chem. 630 (2004) 1451.
[3] J. Buschmann, P. Luger, Acta Crystallogr. B 41 (1985) 206.
[4] L.K. Templeton, D.L. Templeton, Acta Crystallogr. C 45 (1989) 675.
[5] L.K. Templeton, D.L. Templeton, Acta Crystallogr. A 34 (1978) 368.
[6] A.L. Spek, Acta Crystallogr. C 43 (1987) 1633.
[7] F.H. Allen, Acta Crystallogr. B 58 (2002) 380, CSD Version 5.26 (November 2004).
[8] C. Ottenz, M. Schurmann, H. Preut, P. Bleckmann, Z. Kristallogr. – New Cyst. Struct. 213 (1998) 166.
[9] H. Hinazumi, M. Mitsui, Acta Crystallogr. B 28 (1972) 3299.
[10] D.Z. Otwinowski, W. Minor, in: C.W. Carter Jr., R.M. Sweet (Eds.), Methods in Enzymology, Macromolecular Crystallography, Part A, vol. 276, Academic Press, 1997, p. 307.
[11] R.H. Blessing, Acta Crystallogr. A 51 (1995) 33.
[12] R.H. Blessing, J. Appl. Crystallogr. 30 (1997) 421.
[13] G.M. Sheldrick, SHELXS and SHELXL97, University of Göttingen, Germany, 1997.
[14] A. Scacchi, Atti dell'accad. D. sc. fis. e mat. di Napoli 3 (1867) 24.
[15] P. GrothChemische Kristallographie, vol. 3, Engelmann, Leipzig, 1910, p. 376.
[16] J.D. Dunitz, J. Bernstein, Acc. Chem. Res. 28 (1995) 193.
[17] W. Beckmann, U. Budde, K. Nickisch, Org. Proc. Res. Dev. 2 (1998) 298.
[18] S.R. Batten, R. Robson, Angew. Chem. Int. Ed. 37 (1998) 1461.
[19] In preparation.

manner. Therefore, a systematic, consolidated and comparative discussion on complexes of this series may prove useful. In continuation of our search for new nickel(II) complexes has led to this paper in which we report synthesis of nickel(II) complexes of the types, $Ni[S_2P(OR)_2]_2$, (R = *o*-, *m*-, *p*-C_6H_4Me, Ph, CH_2Ph) and their characterization by various spectroscopic techniques. We also report on the X-ray single crystal structures of $Ni[S_2P(OC_6H_4Me\text{-}o)_2]_2$, $Ni[S_2P(OC_6H_4Me\text{-}m)_2]_2$, and $Ni[S_2P(OCH_2Ph)_2]_2$.

2. Results and discussions

Reactions of nickel(II) chloride with ammonium salts of *O*,*O*′-ditolyl/diphenyl/dibenzyl dithiophosphates in 1:2 molar ratio in aqueous solution yield nickel(II) complexes of the types, $Ni[S_2P(OR)_2]_2$

$$NiCl_2 + 2NH_4S_2P(OR)_2 \longrightarrow Ni[S_2P(OR)_2]_2 + 2NH_4Cl$$

(R = *o*-, *m*-, *p*-OC_6H_4Me, Ph and CH_2Ph).

The precipitated purple solid was separated by filtration and repeatedly washed with benzene. All of these nickel(II) complexes are purple, powdery solids, soluble in all common organic solvents and were characterized by elemental analysis, IR, UV–Vis, ^1H and ^{31}P NMR spectroscopy.

2.1. Electronic absorption spectra

The electronic spectra of the nickel(II) complexes, recorded in C_6H_6, show three bands in the region 681–690, 517–530 and 390–395 nm in the visible region with a single band at 320–322 nm in the near ultraviolet region. The first three bands can be assigned to $^1A_{1g} \rightarrow {}^1A_{2g}$, $^1A_{1g} \rightarrow {}^1B_{2g}$, and $^1A_{1g} \rightarrow {}^1E_g$ transitions, respectively. Almost identical electronic transitions for open chain and cyclic dithiophosphate complexes were observed [25,26] indicating consistent square-planar geometry.

2.2. IR spectra

The relevant assignments of the IR bands (Table 1) have been made by comparisons with the spectra of the ammonium salts of *O*,*O*′-ditolyl/diphenyl/dibenzyl dithiophosphates [27,28] and analogous nickel(II) *O*,*O*′-dialkyl dithiophosphate complexes [25,29]. The two strong intensity bands present in the 1043–985 and 835–770 cm^{-1} regions are assigned to *ν*[(P)–O–C] and *ν*[P–O–(C)] stretching vibrations, respectively. Bands due to *ν*(P═S) or $\nu(P\text{–}S)_{asym}$ and *ν*(P–S) or $\nu(P\text{–}S)_{sym}$ observed at 690–670 and 595–540 cm^{-1} in the ditolyl dithiophosphoric acids and their ammonium salts, are shifted to lower frequency by ca. 10–30 cm^{-1} in the corresponding nickel(II) complexes, indicating bidentate attachment of the ligand to the metal atom. In addition, the bands characteristic of *ortho* substitution can be seen in the region 1944–1733w cm^{-1}, 755s cm^{-1}, those of meta substitution in 1952–1809w cm^{-1}, 897, 778s cm^{-1} and those of para substitution in 1884–1745w cm^{-1}, 816s cm^{-1}. Similarly, mono substitution in complexes **4** and **5** are observed in the region 1952–1809w cm^{-1} as well as two peaks at 695, 744s cm^{-1} [30].

2.3. ^1H NMR spectra

The spectra were recorded in $CDCl_3$ solutions at room temperature. The ^1H NMR data of nickel(II) complexes are remarkably similar to those of the salts of dithiophosphoric acids [31] probably due to the large separation between the nickel and protons. Negligible shift for methyl protons is observed in complexes **1**–**3** as compared to the corresponding salts, showing a singlet in the range 2.24–2.37 ppm. The phenyl protons appear in the region 6.85–7.41 ppm in complexes **1**–**5**, undergoing slight down field shifts of ca. 0.1–0.2 ppm compared to their position in the free ligand, presumably as a consequence of the coordination of the ligand.

2.4. ^{31}P NMR spectra

The ^{31}P NMR spectra of complexes **1**–**5**, show a relatively sharp, singlet in the region 79–94 ppm, indicating that the phosphorous nuclei are equivalent and only one type of phosphorous is present in each case in solution. The ^{31}P NMR chemical shifts for these complexes are shifted approximately 20–25 ppm upfield from those of the corresponding salts of dithiophosphoric acids.

2.5. Molecular structures of $Ni[S_2P(OC_6H_4Me\text{-}o)_2]_2$, $Ni[S_2P(OC_6H_4Me\text{-}m)_2]_2$ and $Ni[S_2P(OCH_2Ph)_2]_2$

$Ni[S_2P(OC_6H_4Me\text{-}o)_2]_2$ (**1**) crystallizes in the space group $P2_1/n$ and $Ni[S_2P(OC_6H_4Me\text{-}m)_2]_2$ (**2**) and $Ni[S_2P(OCH_2Ph)_2]_2$ (**5**) crystallize in the space group $P\bar{1}$. The ORTEP diagram in Fig. 1 shows the single molecule in

Table 1
IR spectral data (cm^{-1}) for the bis[*O*,*O*′-diaryl(dibenzyl)dithiophosphate]nickel(II) complexes[a]

No.	Compound	*ν* [(P)–O–C]	*ν* [P–O–(C)]	*ν* (P═S)	*ν* (P–S)
1	$Ni[S_2P(OC_6H_4CH_3\text{-}o)_2]_2$	1043m	725m	659, 603s	560m
2	$Ni[S_2P(OC_6H_4CH_3\text{-}m)_2]_2$	1010s	718m	622, 603s	565m
3	$Ni[S_2P(OC_6H_4CH_3\text{-}p)_2]_2$	1017m	713m	665, 556s	535m
4	$Ni[S_2P(OC_6H_5)_2]_2$	1005m	723m	667, 603s	562m
5	$Ni[S_2P(OCH_2C_6H_5)_2]_2$	985s	821m	654, 603s	565m

[a] Key: s = strong, m = medium, w = weak.

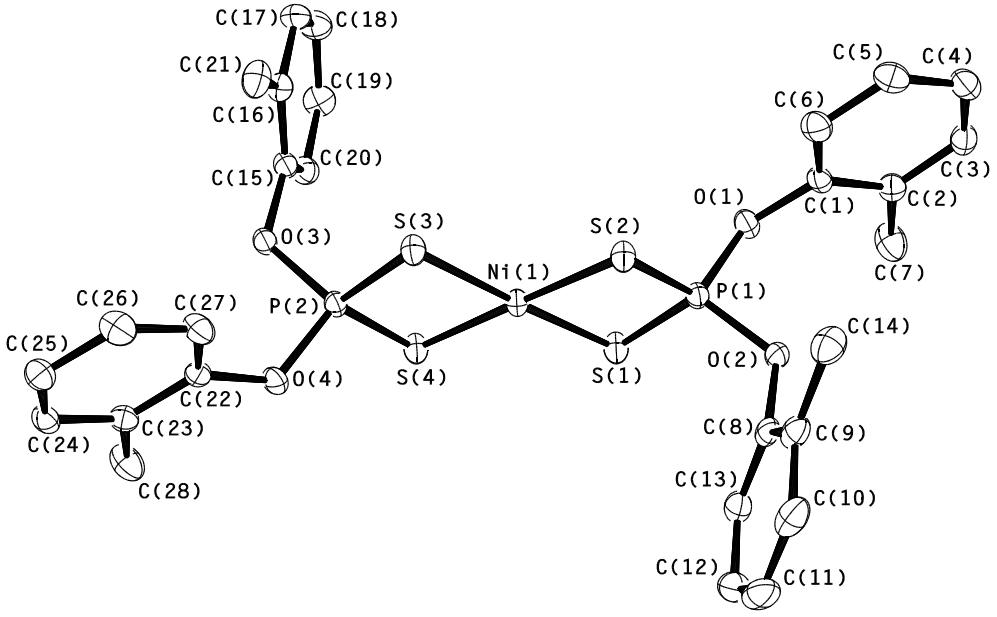

Fig. 1. ORTEP plot of $Ni\{S_2[P(OC_6H_4CH_3\text{-}o)_2]_2\}_2$. The non-hydrogen atoms are drawn with 50% probability ellipsoids. Hydrogen atoms omitted for clarity.

the asymmetric unit of **1**. In displaying the expanded two molecules of the asymmetric unit of **2** (Fig. 2) and the one and one-half molecules in the asymmetric unit of **5** (Fig. 3), the hydrogen atoms were omitted for clarity. Figs. 1–3 illustrate that the immediate environment about the Ni atom is essentially distorted square-planar and that the two dithiophosphate groups are bidentate in both complexes. The average Ni–S distance is 2.2332(6) for **1**, 2.236(6) for

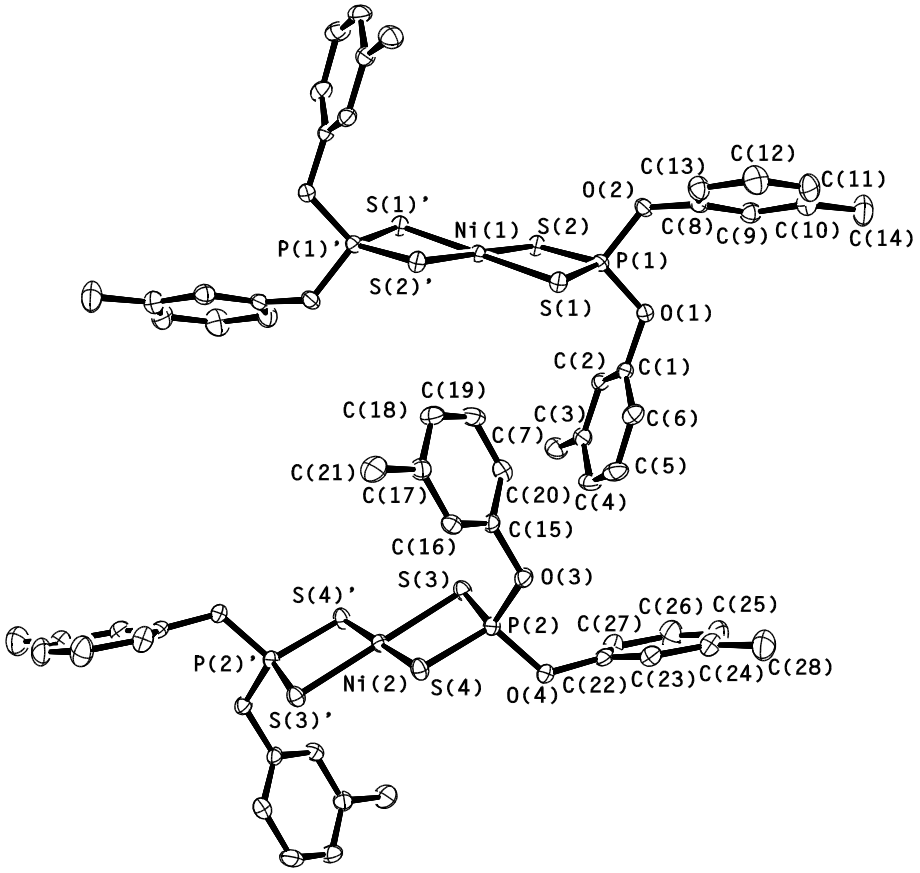

Fig. 2. ORTEP plot of the expanded two independent molecule of $Ni[S_2P(OC_6H_4CH_3\text{-}m)_2]_2$. The non-hydrogen atoms are drawn with 50% probability ellipsoids. Hydrogen atoms omitted for clarity.

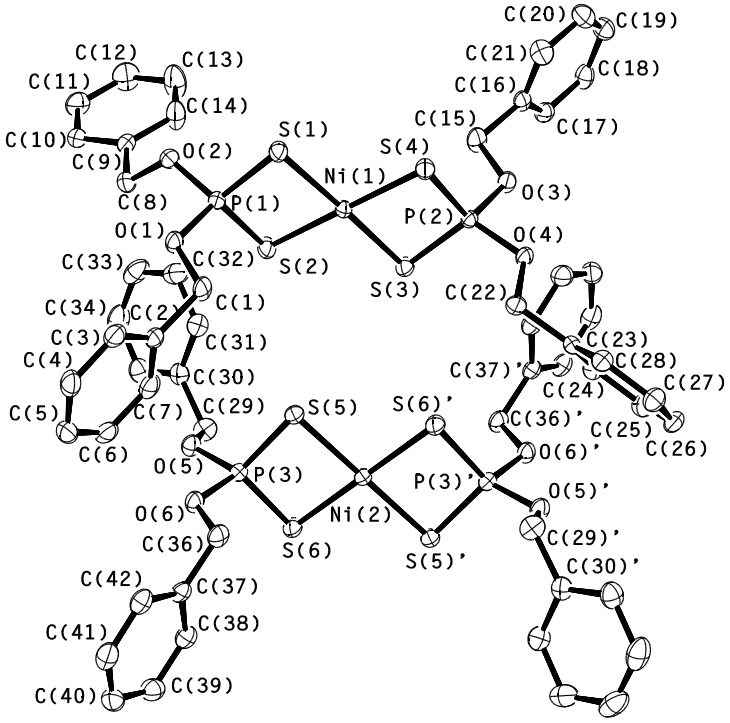

Fig. 3. ORTEP plot of the two independent molecules of $Ni[S_2P(OCH_2Ph)_2]_2$. The non-hydrogen atoms are drawn with 50% probability ellipsoids. The hydrogen atoms are omitted for clarity.

both molecules in **2** and 2.235(7) Å for those in **5**, are similar to the average value of 2.232(4) Å for $Ni[S_2P(OC_6H_4Me\text{-}p)_2]_2$ [23]. This bond length is marginally longer than found in dialkyl dithiophosphate analogue, $Ni[S_2P(OEt)_2]_2$ (2.21 Å) [32,33] and $Ni[S_2P(OPr^i)_2]_2$ (2.222(5) Å) [34]. The average S–P distances are 1.9841(7) in **1**, 1.982(7) in **2** and 1.996(5) Å in **5**, which are comparable to the values observed in $Ni[S_2P(OC_6H_4Me\text{-}p)_2]_2$ (1.976(2) Å), $Ni[S_2P(OEt)_2]_2$(1.97) and $Ni[S_2P(OPr^i)_2]_2$ (1.992(1) Å). The average P–O distances of 1.586(1) in **1**, 1.585(5) in **2** and 1.578(4) Å in **5**, lie between the values reported for the analogues, $Ni[S_2P(OEt)_2]_2$ (1.63) and $Ni[S_2P(OPr^i)_2]_2$ (1.565(1) Å) while that of **2** is identical to that of $Ni[S_2P(OC_6H_4Me\text{-}p)_2]_2$ (1.585(2) Å).

The S–Ni–S ligand bite angles are 88.39(2)° and 88.59(2)° in **1**, are 88.79(2)° and 89.18(2)° in the two molecules of **2**, and range from 87.95(3)° to 88.52(3)° in **5**; similar to the values in $Ni[S_2P(OC_6H_4Me\text{-}p)_2]_2$ (89.12(2)°) and the two analogues, $Ni[S_2P(OEt)_2]_2$ (88°) and $Ni[S_2P(OPr^i)_2]_2$ (88.10(4)°). The S–P–S bond angles vary from 103.32(3)° to 103.69(3)° in **1** and range from 104.18(4)° to 104.80(4)° in **2**, thus, having similar values as in the *para* substituted analogue, $Ni[S_2P(OC_6H_4Me\text{-}p)_2]_2$ (104.85(3)°). The values are marginally smaller in the OCH_2Ph derivative **5** (101.73(4)–102.81(4)°). The angles reported in $Ni[S_2P(OEt)_2]_2$ and $Ni[S_2P(OPr^i)_2]_2$ are 103° and 101.7(1)°, respectively. The O–P–O bond angles are 99.37(7)–99.24(7)° in **1**, range from 99.83(9)° to 100.20(9)° in **2** and are 99.39(7)° in $Ni[S_2P(OC_6H_4Me\text{-}p)_2]_2$. These values are bracketed by those in **5** ranging from 95.22(8)° to 101.04(9)°. Thus, there appear to be no significant changes or obvious trends in the distances and bond angles as the nature of R is changed in the $Ni[S_2P(OR)_2]_2$ complexes although in general the tolyl derivatives, $Ni[S_2P(OC_6H_4Me\text{-}o)_2]_2$, $Ni[S_2P(OC_6H_4Me\text{-}m)_2]_2$, $Ni[S_2P(OC_6H_4Me\text{-}p)_2]_2$, probably show the most similarities.

3. Experimental

Nickel chloride, benzyl alcohol, *o*-, *m*-, *p*-cresols were purchased from E. Merck. Solvents (benzene, *n*-hexane, diethyl ether) were dried by standard methods before use. Stringent precautions were taken to exclude moisture during experimental manipulations. Literature methods were used for the preparation of *O*,*O*′-ditolyl [27] and *O*,*O*′-diphenyl [28] dithiophosphoric acids. *O*,*O*′-dibenzyl dithiophosphoric acid was prepared by the reaction of P_2S_5 and benzyl alcohol in 1:4 molar ratio. Ammonium salts of the dithiophosphoric acids were prepared by the reaction of parent acids with an equimolar amount of ammonia in benzene.

3.1. Preparations

3.1.1. $Ni[S_2P(OC_6H_4Me\text{-}o)_2]$ (1)

Typically, to an aqueous solution of $NiCl_2 \cdot 6H_2O$ (0.287 g, 1.2073 mmol), was added an aqueous suspension of $NH_4S_2P(OC_6H_4Me\text{-}o)_2$ (0.801 g, 2.449 mmol) in 1:2 molar ratio with constant stirring. A purple solid was immediately obtained. After stirring for 3 h, the precipitated $Ni[S_2P(OC_6H_4Me\text{-}o)_2]_2$ was filtered off. The compound was purified with repeated washing with dried

benzene. Purple powdery solid. Yield: 0.768 g, 94%; m.p. 90 °C. Calc. for $C_{28}H_{28}O_4S_4P_2Ni$: Ni, 8.71; S, 18.90. Found: Ni, 8.75; S, 18.72%. ^1H NMR ($CDCl_3$): δ 2.25 (s, Me), 7.04–7.41 (m, OC_6H_4), ^{31}P NMR ($CDCl_3$): δ 84.10 ppm. UV/Vis electronic absorption spectral data [λ_{max}, nm(A)] in benzene 685, 520, 392, 322.

3.1.2. $Ni[S_2P(OC_6H_4CH_3\text{-}m)_2]_2$ (2)

Method as above gave a purple powdery solid. Yield: 0.807 g, 93%; m.p. 106 °C. Calc. for $C_{28}H_{28}O_4S_4P_2Ni$: Ni, 8.71; S, 18.90. Found: Ni, 8.60; S, 18.98%. ^1H NMR ($CDCl_3$): δ 2.38 (s, Me), 7.07–7.29 (dm, OC_6H_4), ^{31}P NMR ($CDCl_3$): δ 84.95 ppm. UV/Vis electronic absorption spectral data [λ_{max}, nm(A)] in benzene 690, 517, 394, 320.

3.1.3. $Ni[S_2P(OC_6H_4CH_3-p)_2]_2$ (3)

Method as above gave a pale purple powdery solid. Yield: 0.797 g, 89%; m.p. 171 °C. Calc. for $C_{28}H_{28}O_4S_4\text{-}P_2Ni$: Ni, 8.71; S, 18.90. Found: Ni, 8.47; S, 18.88%. ^1H NMR ($CDCl_3$): δ 2.31 (s, Me), 6.85–7.37 (m, OC_6H_4), ^{31}P NMR ($CDCl_3$): δ 79.10 ppm. UV/Vis electronic absorption spectral data [λ_{max}, nm(A)] in benzene 681, 530, 395, 322.

3.1.4. $Ni[S_2P(OPh)_2]_2$ (4)

Method as above gave a purple powdery solid. Yield: 0.759 g, 91%; m.p. 122 °C. Calc. for $C_{24}H_{24}O_4S_4P_2Ni$: Ni, 8.28; S, 18.53. Found: Ni, 8.12; S, 18.60%. ^1H NMR ($CDCl_3$): δ 7.23–7.32 (dm, OC_6H_5), ^{31}P NMR ($CDCl_3$): δ 84.59 ppm. UV/Vis electronic absorption spectral data [λ_{max}, nm(A)] in benzene 688, 525, 394, 321.

3.1.5. $Ni[S_2P(OCH_2Ph)_2]_2$ (5)

Method as above gave a purple powdery solid. Yield: 0.668 g, 86%; m.p. 125 °C. Calc. for $C_{28}H_{28}O_4S_4P_2Ni$: Ni, 8.71; S, 18.90. Found: Ni, 8.64; S, 18.78%. ^1H NMR ($CDCl_3$): δ 5.22 (s, OCH_2), 6.99–7.33 (bs, C_6H_5), ^{31}P NMR ($CDCl_3$): δ 93.66 ppm. UV/Vis electronic absorption spectral data [λ_{max}, nm(A)] in benzene 683, 527, 390, 320.

3.2. Physical measurements

Sulfur was estimated gravimetrically as barium sulfate (Messenger's method) and Nickel as dimethylglyoximate. IR spectra were recorded on a Perkin–Elmer 577 spectrophotometer in KBr pellets in the range 4000–200 cm^{-1}. Electronic spectra in the range 200–800 nm were recorded on UV visible spectrophotometer-2201 in C_6H_6. ^1H NMR spectra were recorded on a Bruker DRX300 (300MHzFT NMR) spectrometer in $CDCl_3$ using TMS as an internal standard.

Table 2
Crystal data and structure refinement for $NiS_2[P(OC_6H_4CH_3\text{-}o)_2]_2$ (**1**), $NiS_2[P(OC_6H_4CH_3\text{-}m)_2]_2$ (**2**), and $Ni[S_2P(OCH_2Ph)_2]_2$ (**5**)

Empirical formula	$C_{28}H_{28}O_4P_2S_4Ni$	$C_{28}H_{28}O_4P_2S_4Ni$	$C_{42}H_{42}O_{1.5}P_3S_6Ni_{1.5}$
Formula weight	677.39	677.39	1016.90
Temperature (K)	120(2)	120(2)	120(2)
Wavelength (Å)	0.71073	0.71073	0.71073
Crystal system	monoclinic	triclinic	triclinic
Space group	$P2_1/n$	$P\bar{1}$	$P\bar{1}$
a (Å)	9.093(2)	9.4675(4)	10.887(2)
b (Å)	13.529(2)	12.8568(5)	14.081(3)
c (Å)	23.779(4)	13.1174(6)	16.238(3)
α (°)	90.00	88.810(4)	72.70(3)
β (°)	90.17(1)	83.416(5)	76.57(3)
γ (°)	90.00	73.711(4)	72.76(3)
Volume (Å^3)	2925.3(8)	1522.4(1)	2241.4(8)
Z	4	2	2
D_{calc} (g/cm^3)	1.548	1.478	1.506
Absorption coefficient (mm^{-1})	1.099	1.049	1.069
F(000)	1400	700	1050
Crystal size (mm^3)	$0.10 \times 0.10 \times 0.05$	$0.50 \times 0.30 \times 0.14$	$0.10 \times 0.08 \times 0.08$
θ Range for data collection (°)	2.98–27.48	2.99–27.54	2.91–27.47
Index ranges	$-11 \leqslant h \leqslant 10$, $-14 \leqslant k \leqslant 17$, $-24 \leqslant l \leqslant 30$	$-12 \leqslant h \leqslant 12$, $-16 \leqslant k \leqslant 16$, $-17 \leqslant l \leqslant 17$	$-14 \leqslant h \leqslant 14$, $-18 \leqslant k \leqslant 18$, $-21 \leqslant l \leqslant 21$
Reflections collected	23640	28956	47686
Independent reflections (R_{int})	6621 (0.0418)	6973 (0.0383)	10182 (0.0536)
Maximum and minimum transmission	0.9471 and 0.8980	0.8670 and 0.6220	0.9193 and 0.9006
Refinement method	full-matrix least-squares on F^2	full-matrix least-squares on F^2	full-matrix least-squares on F^2
Data/restraints/parameters	6621/0/356	6973/0/355	10182/0/571
Goodness-of-fit on F^2	1.036	1.031	1.035
Final R indices [$F^2 > 4\sigma(F^2)$]	$R_1 = 0.0351$, $wR_2 = 0.0787$	$R_1 = 0.0354$, $wR_2 = 0.0830$	$R_1 = 0.0365$, $wR_2 = 0.0785$
R indices (all data)	$R_1 = 0.0456$, $wR_2 = 0.0843$	$R_1 = 0.0503$, $wR_2 = 0.0899$	$R_1 = 0.0545$, $wR_2 = 0.0857$
Largest difference peak and hole (e Å^{-3})	0.356 and −0428	0.563 and −0.573	0.322 and −0.467

Table 3
Bond lengths (Å) and angles (°) for Ni{S_2[P($OC_6H_4CH_3$ -*o*)$_2$]$_2$}$_2$ (**1**)

Ni(1)–S(1)	2.2415(6)	Ni(1)–S(3)	2.2353(6)
Ni(1)–S(2)	2.2241(6)	Ni(1)–S(4)	2.2318(6)
S(1)–P(1)	1.9839(7)	S(3)–P(2)	1.9854(7)
S(2)–P(1)	1.9850(7)	S(4)–P(2)	1.9820(7)
P(1)–O(1)	1.578(1)	P(2)–O(3)	1.592(1)
P(1)–O(2)	1.595(1)	P(2)–O(4)	1.579(1)
O(1)–C(1)	1.420(2)	O(3)–C(15)	1.411(2)
O(2)–C(8)	1.418(2)	O(4)–C(22)	1.419(2)
C(1)–C(6)	1.380(3)	C(15)–C(16)	1.389(3)
C(1)–C(2)	1.388(3)	C(15)–C(20)	1.390(3)
C(2)–C(3)	1.388(3)	C(16)–C(17)	1.394(3)
C(3)–C(4)	1.387(3)	C(17)–C(18)	1.375(3)
C(4)–C(5)	1.383(3)	C(18)–C(19)	1.384(3)
C(5)–C(6)	1.391(3)	C(19)–C(20)	1.383(3)
C(2)–C(7)	1.494(3)	C(16)–C(21)	1.495(3)
C(8)–C(9)	1.384(3)	C(22)–C(27)	1.372(3)
C(8)–C(13)	1.393(3)	C(22)–C(23)	1.391(3)
C(9)–C(10)	1.395(3)	C(23)–C(24)	1.394(3)
C(10)–C(11)	1.379(3)	C(24)–C(25)	1.380(3)
C(11)–C(12)	1.382(3)	C(25)–C(26)	1.380(3)
C(12)–C(13)	1.379(3)	C(26)–C(27)	1.391(3)
C(9)–C(14)	1.493(3)	C(23)–C(28)	1.498(3)
S(1)–Ni(1)–S(2)	88.39(2)	S(3)–Ni(1)–S(4)	88.59(2)
S(1)–Ni(1)–S(3)	178.51(2)	S(2)–Ni(1)–S(4)	178.00(2)
S(1)–Ni(1)–S(4)	92.04(2)	S(2)–Ni(1)–S(3)	91.03(2)
Ni(1)–S(1)–P(1)	83.86(3)	Ni(1)–S(3)–P(2)	83.57(3)
Ni(1)–S(2)–P(1)	84.30(3)	Ni(1)–S(4)–P(2)	83.74(3)
S(1)–P(1)–S(2)	103.32(3)	S(3)–P(2)–S(4)	103.69(3)
O(1)–P(1)–O(2)	99.37(7)	O(3)–P(2)–O(4)	99.24(7)
O(1)–P(1)–S(1)	108.82(6)	O(3)–P(2)–S(3)	113.64(6)
O(1)–P(1)–S(2)	116.03(6)	O(3)–P(2)–S(4)	115.39(6)
O(2)–P(1)–S(2)	114.41(6)	O(4)–P(2)–S(4)	109.03(6)
O(2)–P(1)–S(1)	115.31(6)	O(4)–P(2)–S(3)	116.29(6)
C(1)–O(1)–P(1)	126.4(1)	C(15)–O(3)–P(2)	122.1(1)
C(8)–O(2)–P(1)	123.1(1)	C(22)–O(4)–P(2)	124.3(1)
C(2)–C(1)–C(6)	123.0(2)	C(16)–C(15)–C(20)	123.4(2)
C(6)–C(1)–O(1)	120.9(2)	C(20)–C(15)–O(3)	118.3(2)
C(2)–C(1)–O(1)	116.1(2)	C(16)–C(15)–O(3)	118.1(2)
C(1)–C(2)–C(3)	116.8(2)	C(15)–C(16)–C(17)	115.7(2)
C(2)–C(3)–C(4)	121.9(2)	C(16)–C(17)–C(18)	122.6(2)
C(3)–C(4)–C(5)	119.6(2)	C(17)–C(18)–C(19)	119.8(2)
C(4)–C(5)–C(6)	120.1(3)	C(18)–C(19)–C(20)	120.2(2)
C(5)–C(6)–C(1)	118.7(2)	C(19)–C(20)–C(15)	118.4(2)
C(1)–C(2)–C(7)	121.7(2)	C(15)–C(16)–C(21)	122.1(2)
C(3)–C(2)–C(7)	121.6(2)	C(17)–C(16)–C(21)	122.2(2)
C(9)–C(8)–C(13)	122.8(2)	C(23)–C(22)–C(27)	122.9(2)
C(13)–C(8)–O(2)	117.5(2)	C(27)–C(22)–O(4)	120.6(2)
C(9)–C(8)–O(2)	119.5(2)	C(23)–C(22)–O(4)	116.4(2)
C(8)–C(9)–C(10)	116.3(2)	C(22)–C(23)–C(24)	116.9(2)
C(9)–C(10)–C(11)	121.9(2)	C(23)–C(24)–C(25)	121.4(2)
C(10)–C(11)–C(12)	120.3(2)	C(24)–C(25)–C(26)	120.1(2)
C(11)–C(12)–C(13)	119.7(2)	C(25)–C(26)–C(27)	120.1(2)
C(12)–C(13)–C(8)	119.0(2)	C(26)–C(27)–C(22)	118.8(2)
C(8)–C(9)–C(14)	122.6(2)	C(22)–C(23)–C(28)	121.4(2)
C(10)–C(9)–C(14)	121.1(2)	C(24)–C(23)–C(28)	121.8(2)

3.3. X-ray diffraction analysis

A translucent purple, block crystal of Ni[S_2P(OC_6H_4-Me-*o*)$_2$]$_2$, a brown/purple, slab crystal of NiS_2[P(OC_6H_4-Me-*m*)$_2$]$_2$ and a pink/purple block crystal of Ni[S_2-P(OCH_2-Ph)$_2$]$_2$ were mounted on glass fibres. Data were collected on a Bruker-Nonius Kappa CCD area detector

Table 4
Selected bond lengths (Å) and angles (°) for NiS_2[P($OC_6H_4CH_3$-*m*)$_2$]$_2$ (**2**)[a]

Molecule 1		Molecule 2	
Ni(1)–S(1)	2.2421(6)	Ni(2)–S(3)	2.2430(6)
Ni(1)–S(1)′	2.2421(6)	Ni(2)–S(3)″	2.2430(6)
Ni(1)–S(2)	2.2310(6)	Ni(2)–S(4)	2.2286(6)
Ni(1)–S(2)′	2.2310(6)	Ni(2)–S(4)″	2.2286(6)
S(1)–P(1)	1.9884(8)	S(3)–P(2)	1.9849(8)
S(2)–P(1)	1.9778(8)	S(4)–P(2)	1.9774(8)
P(1)–O(1)	1.589(2)	P(2)–O(3)	1.591(2)
P(1)–O(2)	1.579(2)	P(2)–O(4)	1.582(2)
O(1)–C(1)	1.418(3)	O(3)–C(15)	1.420(3)
O(2)–C(8)	1.417(3)	O(4)–C(22)	1.420(3)
C(1)–C(6)	1.375(3)	C(15)–C(20)	1.371(3)
C(1)–C(2)	1.381(3)	C(15)–C(16)	1.384(3)
C(2)–C(3)	1.394(3)	C(16)–C(17)	1.395(3)
C(3)–C(4)	1.395(4)	C(17)–C(18)	1.391(4)
C(4)–C(5)	1.388(4)	C(18)–C(19)	1.386(4)
C(5)–C(6)	1.393(4)	C(19)–C(20)	1.391(4)
C(3)–C(7)	1.504(3)	C(17)–C(21)	1.507(3)
C(8)–C(13)	1.376(3)	C(22)–C(27)	1.381(4)
C(8)–C(9)	1.379(3)	C(22)–C(23)	1.371(4)
C(9)–C(10)	1.394(3)	C(23)–C(24)	1.394(4)
C(10)–C(11)	1.385(4)	C(24)–C(25)	1.398(4)
C(11)–C(12)	1.388(4)	C(25)–C(26)	1.376(4)
C(12)–C(13)	1.387(4)	C(26)–C(27)	1.390(4)
C(10)–C(14)	1.516(4)	C(24)–C(28)	1.498(4)
S(1)–Ni(1)–S(2)	88.79(2)	S(3)–Ni(2)–S(4)	89.18(2)
S(1)′–Ni(1)–S(2)′	88.79(2)	S(3)″–Ni(2)–S(4)″	89.18(2)
S(1)–Ni(1)–S(1)′	180.00	S(3)–Ni(2)–S(3)″	180.00
S(2)–Ni(1)–S(2)′	180.00	S(4)–Ni(2)–S(4)″	180.00
S(1)′–Ni(1)–S(2)	91.21(2)	S(3)″–Ni(2)–S(4)	90.82(2)
S(1)–Ni(1)–S(2)′	91.21(2)	S(3)–Ni(2)–S(4)″	90.82(2)
Ni(1)–S(1)–P(1)	82.95(3)	Ni(2)–S(3)–P(2)	82.41(3)
Ni(1)–S(2)–P(1)	83.47(3)	Ni(2)–S(4)–P(2)	82.95(3)
S(1)–P(1)–S(2)	104.18(4)	S(3)–P(2)–S(4)	104.80(4)
O(1)–P(1)–O(2)	100.20(9)	O(3)–P(2)–O(4)	99.83(9)
O(1)–P(1)–S(1)	113.01(7)	O(3)–P(2)–S(3)	113.63(7)
O(1)–P(1)–S(2)	115.74(7)	O(3)–P(2)–S(4)	115.05(7)
O(2)–P(1)–S(2)	108.70(7)	O(4)–P(2)–S(4)	108.64(7)
O(2)–P(1)–S(1)	115.39(7)	O(4)–P(2)–S(3)	115.17(7)
C(1)–O(1)–P(1)	120.9(1)	C(15)–O(3)–P(2)	119.9(1)
C(8)–O(2)–P(1)	124.9(1)	C(22)–O(4)–P(2)	123.1(2)
C(2)–C(1)–C(6)	122.9(2)	C(16)–C(15)–C(20)	122.7(2)
C(6)–C(1)–O(1)	118.5(2)	C(20)–C(15)–O(3)	118.5(2)
C(2)–C(1)–O(1)	118.6(2)	C(16)–C(15)–O(3)	118.7(2)
C(1)–C(2)–C(3)	119.4(2)	C(15)–C(16)–C(17)	119.3(2)
C(2)–C(3)–C(4)	118.3(2)	C(16)–C(17)–C(18)	118.4(2)
C(3)–C(4)–C(5)	121.3(2)	C(17)–C(18)–C(19)	121.2(2)
C(4)–C(5)–C(6)	120.1(2)	C(18)–C(19)–C(20)	120.3(2)
C(5)–C(6)–C(1)	117.9(2)	C(19)–C(20)–C(15)	118.0(2)
C(2)–C(3)–C(7)	120.1(2)	C(16)–C(17)–C(21)	120.2(2)
C(4)–C(3)–C(7)	121.5(2)	C(18)–C(17)–C(21)	121.4(2)
C(9)–C(8)–C(13)	122.7(2)	C(23)–C(22)–C(27)	122.9(2)
C(13)–C(8)–O(2)	119.6(2)	C(27)–C(22)–O(4)	120.0(2)
C(9)–C(8)–O(2)	117.5(2)	C(23)–C(22)–O(4)	117.0(2)
C(8)–C(9)–C(10)	119.6(2)	C(22)–C(23)–C(24)	120.0(2)
C(9)–C(10)–C(11)	118.3(2)	C(23)–C(24)–C(25)	117.5(3)
C(10)–C(11)–C(12)	121.1(2)	C(24)–C(25)–C(26)	121.6(3)
C(11)–C(12)–C(13)	120.7(2)	C(25)–C(26)–C(27)	120.8(3)
C(12)–C(13)–C(8)	117.6(2)	C(26)–C(27)–C(22)	117.2(2)
C(9)–C(10)–C(14)	120.0(2)	C(23)–C(24)–C(28)	120.6(3)
C(11)–C(10)–C(14)	121.6(2)	C(25)–C(24)–C(28)	121.9(3)

[a] Symmetry equivalent positions ($x+1$, $-y+1$, $-z$) given by a prime and ($-x$, $-y$, $-z$) by a double prime.

diffractometer, with ϕ and ω scans chosen to give a complete asymmetric unit. Cell refinement [35] gave cell constants corresponding to a monoclinic for **1** and triclinic cells for **2** and **5** whose dimensions are given in Table 2 along with other experimental parameters. An absorption correction was applied [36].

The structure was solved by direct methods [37] and was refined using the WINGX version [38] of SHELXL97 [39]. All of the non-hydrogen atoms were treated anisotropically. Hydrogen atoms were included in idealized positions with isotropic thermal parameters set at 1.2 times that of the carbon atom to which they were attached. The final cycle

Table 5
Bond lengths (Å) and angles (°) for $Ni[S_2P(OCH_2Ph)_2]_2$[a]

Molecule 1				Molecule 2	
Ni(1)–S(1)	2.233(1)	Ni(1)–S(3)	2.227(1)	Ni(2)–S(5)	2.236(1)
Ni(1)–S(2)	2.2343(8)	Ni(1)–S(4)	2.2469(8)	Ni(2)–S(6)	2.2313(8)
S(1)–P(1)	1.9900(9)	S(3)–P(2)	1.9934(9)	S(5)–P(3)	2.0026(9)
S(2)–P(1)	1.999(1)	S(4)–P(2)	1.993(1)	S(6)–P(3)	1.996(1)
P(1)–O(1)	1.583(2)	P(2)–O(3)	1.577(2)	P(3)–O(5)	1.575(2)
P(1)–O(2)	1.571(2)	P(2)–O(4)	1.583(2)	P(3)–O(6)	1.579(2)
O(1)–C(1)	1.471(3)	O(3)–C(15)	1.475(3)	O(5)–C(29)	1.472(3)
O(2)–C(8)	1.466(3)	O(4)–C(22)	1.464(2)	O(6)–C(36)	1.475(3)
C(1)–C(2)	1.505(3)	C(15)–C(16)	1.502(3)	C(29)–C(30)	1.498(3)
C(2)–C(7)	1.385(3)	C(16)–C(21)	1.382(3)	C(30)–C(31)	1.383(3)
C(2)–C(3)	1.387(3)	C(16)–C(17)	1.390(3)	C(30)–C(35)	1.385(3)
C(3)–C(4)	1.390(3)	C(17)–C(18)	1.390(3)	C(31)–C(32)	1.386(3)
C(4)–C(5)	1.383(4)	C(18)–C(19)	1.381(3)	C(32)–C(33)	1.388(4)
C(5)–C(6)	1.384(4)	C(19)–C(20)	1.381(4)	C(33)–C(34)	1.374(4)
C(6)–C(7)	1.385(3)	C(20)–C(21)	1.391(3)	C(34)–C(35)	1.391(4)
C(8)–C(9)	1.507(3)	C(22)–C(23)	1.498(3)	C(36)–C(37)	1.494(3)
C(9)–C(10)	1.388(3)	C(23)–C(28)	1.388(3)	C(37)–C(38)	1.392(3)
C(9)–C(14)	1.388(3)	C(23)–C(24)	1.393(3)	C(37)–C(42)	1.394(3)
C(10)–C(11)	1.389(3)	C(24)–C(25)	1.391(3)	C(38)–C(39)	1.384(3)
C(11)–C(12)	1.380(4)	C(25)–C(26)	1.382(3)	C(39)–C(40)	1.389(4)
C(12)–C(13)	1.388(4)	C(26)–C(27)	1.382(3)	C(40)–C(41)	1.379(4)
C(13)–C(14)	1.385(3)	C(27)–C(28)	1.391(3)	C(41)–C(42)	1.388(3)
S(1)–Ni(1)–S(2)	88.52(3)	S(3)–Ni(1)–S(4)	88.00(3)	S(5)–Ni(2)–S(6)	87.95(3)
S(1)–Ni(1)–S(3)	178.39(2)	S(2)–Ni(1)–S(4)	178.24(2)	S(5)–Ni(2)–S(5)″	180.00
S(1)–Ni(1)–S(4)	92.86(3)	S(2)–Ni(1)–S(3)	90.66(3)	S(5)–Ni(2)–S(6)″	92.05(3)
Ni(1)–S(1)–P(1)	84.10(3)	Ni(1)–S(3)–P(2)	84.61(3)	Ni(2)–S(5)–P(3)	84.73(3)
Ni(1)–S(2)–P(1)	83.86(3)	Ni(2)–S(4)–P(2)	84.09(3)	Ni(2)–S(6)–P(3)	85.00(3)
S(1)–P(1)–S(2)	102.81(4)	S(3)–P(2)–S(4)	102.44(4)	S(5)–P(3)–S(6)	101.73(4)
O(1)–P(1)–O(2)	101.04(9)	O(3)–P(2)–O(4)	95.22(8)	O(5)–P(3)–O(6)	96.56(9)
O(1)–P(1)–S(1)	115.07(7)	O(3)–P(2)–S(3)	114.76(7)	O(5)–P(3)–S(5)	115.38(7)
O(1)–P(1)–S(2)	112.30(7)	O(3)–P(2)–S(4)	114.12(7)	O(5)–P(3)–S(6)	115.89(7)
O(2)–P(1)–S(2)	115.14(7)	O(4)–P(2)–S(4)	115.83(7)	O(6)–P(3)–S(6)	114.23(7)
O(2)–P(1)–S(1)	111.00(7)	O(4)–P(2)–S(3)	115.19(7)	O(6)–P(3)–S(5)	113.82(7)
C(1)–O(1)–P(1)	118.9(1)	C(15)–O(3)–P(2)	119.2(1)	C(29)–O(5)–P(3)	121.2(1)
C(8)–O(2)–P(1)	121.9(1)	C(22)–O(4)–P(2)	120.7(1)	C(36)–O(6)–P(3)	119.4(1)
O(1)–C(1)–C(2)	108.1(2)	O(3)–C(15)–C(16)	107.4(2)	O(5)–C(29)–C(30)	109.9(2)
C(7)–C(2)–C(3)	119.3(2)	C(21)–C(16)–C(17)	119.4(2)	C(31)–C(30)–C(35)	119.4(2)
C(7)–C(2)–C(1)	119.8(2)	C(21)–C(16)–C(15)	119.6(2)	C(31)–C(30)–C(29)	120.1(2)
C(3)–C(2)–C(1)	120.8(2)	C(17)–C(16)–C(15)	121.0(2)	C(35)–C(30)–C(29)	120.4(2)
C(2)–C(3)–C(4)	120.5(2)	C(18)–C(17)–C(16)	120.5(2)	C(30)–C(31)–C(32)	120.5(2)
C(5)–C(4)–C(3)	119.7(2)	C(19)–C(18)–C(17)	119.6(2)	C(31)–C(32)–C(33)	119.9(3)
C(4)–C(5)–C(6)	120.1(2)	C(18)–C(19)–C(20)	120.2(2)	C(34)–C(33)–C(32)	119.9(2)
C(5)–C(6)–C(7)	120.1(2)	C(19)–C(20)–C(21)	120.0(2)	C(33)–C(34)–C(35)	120.2(3)
C(2)–C(7)–C(6)	120.3(2)	C(16)–C(21)–C(20)	120.2(2)	C(30)–C(35)–C(34)	120.1(2)
O(2)–C(8)–C(9)	108.7(2)	O(4)–C(22)–C(23)	108.6(2)	O(6)–C(36)–C(37)	108.3(2)
C(10)–C(9)–C(14)	119.1(2)	C(28)–C(23)–C(24)	118.7(2)	C(38)–C(37)–C(42)	118.7(2)
C(10)–C(9)–C(8)	120.3(2)	C(28)–C(23)–C(22)	120.0(2)	C(38)–C(37)–C(36)	119.8(2)
C(14)–C(9)–C(8)	120.6(2)	C(24)–C(23)–C(22)	121.3(2)	C(42)–C(37)–C(36)	121.5(2)
C(9)–C(10)–C(11)	120.4(2)	C(25)–C(24)–C(23)	120.4(2)	C(39)–C(38)–C(37)	120.8(2)
C(12)–C(11)–C(10)	120.4(2)	C(26)–C(25)–C(24)	120.1(2)	C(38)–C(39)–C(40)	119.8(2)
C(11)–C(12)–C(13)	119.4(2)	C(27)–C(26)–C(25)	120.1(2)	C(41)–C(40)–C(39)	120.1(2)
C(14)–C(13)–C(12)	120.4(3)	C(26)–C(27)–C(28)	119.6(2)	C(40)–C(41)–C(42)	120.1(2)
C(13)–C(14)–C(9)	120.4(2)	C(23)–C(28)–C(27)	121.1(2)	C(41)–C(42)–C(37)	120.5(2)

[a] Symmetry equivalent positions $(-x+1, -y, -z+1)$ given by a double prime and equivalent distances and angles not listed are Ni(2)–S(5)″ 2.236(1), Ni(2)–S(6)″ 2.2313(8) Å; S(6)″–Ni(2)–S(5)″ 87.95(3)°, S(6)–Ni(2)–S(6)″ 180.00°, S(6)–Ni(2)–S(5)″ 92.05(3)°.

of full-matrix least-squares refinement was based on 6621 (for **1**), 6973 (for **2**) and 10 182 (for **5**), observed reflections (5515 (for **1**), 5651 (for **2**) and 7969 (for **5**) for $F^2 > 4\sigma(F^2)$) and 356 (for **1**), 355 (for **2**) and 571 (for **5**) variable parameters and converged (largest parameter shift was 0.001 times its esd).

Selected distances and bond angles are given in Tables 3–5 for molecules **1**, **2** and **5**, respectively, and ORTEP diagram are displayed in Figs. 1–3.

4. Concluding comments

We have successfully prepared and characterized the following complexes, $Ni[S_2P(OC_6H_4Me\text{-}o)_2]_2$, $Ni[S_2P(OC_6H_4Me\text{-}m)_2]_2$, $Ni[S_2P(OC_6H_4CH_3\text{-}p)_2]_2$, $Ni[S_2P(OC_6H_5)_2]_2$ and $Ni[S_2P(OCH_2Ph)_2]_2$. The IR, UV–Vis and ^1H NMR spectra of all of these nickel complexes are consistent with the proposed structure. The molecular structures of $Ni[S_2P(OC_6H_4Me\text{-}o)_2]_2$, $Ni[S_2P(OC_6H_4Me\text{-}m)_2]_2$ and $Ni[S_2P(OCH_2Ph)_2]_2$ were all determined to have a distorted square-planar environment around nickel, as has been found for the structures reported for the analogues, complexes $Ni[S_2P(OEt)_2]_2$ and $Ni[S_2P(OPr^i)_2]_2$.

5. Supplementary material

Additional material available from the Cambridge Crystallographic Data Centre (CCDC Nos. 280426, 280427, and 280706 for $Ni[S_2P(OC_6H_4Me\text{-}o)_2]_2$, $Ni[S_2P(OC_6H_4Me\text{-}m)_2]_2$, and $Ni[S_2P(OCH_2Ph)_2]_2$, respectively, comprises the final atomic coordinates for all atoms, thermal parameters, and a complete listing of bond distances and angles). Copies of this information may be obtained free of charge on application to The Director, 12 Union Road, Cambridge CB2 2EZ, UK (fax: +44 1223 336033; email: deposit@ccdc.cam.ac.uk or http://www.ccdc. cam.ac.uk).

Acknowledgements

One of us (M.N.) is grateful to CSIR, New Delhi for financial support. M.E.L. thanks the UK Engineering and Physical Sciences Council for support of the X-ray facilities at Southampton University. J.E.D. wishes to thank the University of Windsor for financial support. We are thankful to RSIC, CDRI, Lucknow for the spectral analyses.

References

[1] V.V. Ovchinnikov, V.I. Galkin, V.F. Toropova, R.A. Cherkasov, Zhurnal Obshchei Khimii 55 (2) (1985) 357.
[2] I.M. Oglezneva, N.V. Kirichenko, Zhurnal Strukturnoi Khimii 25 (3) (1984) 164.
[3] R. Micu-Semeniuc, L. Dumitreschu-Silaghi, I. Haiduc, Inorg. Chim. Acta 33 (1979) 281.
[4] Y. Yamada, M. Shimoi, A. Ouchi, Chem. Lett. (8) (1978) 867.
[5] W. Szczepaniak, A.S. Plaziak, Polish J. Chem. 63 (4–12) (1989) 323.
[6] E. Ciliberto, S.D. Bella, I. Fragala, G. Granozzi, N.A. Burton, I.H. Hillier, J. Kendrick, M.F. Guest, J. Chem. Soc., Dalton Trans. Inorg. Chem. (3) (1990) 849.
[7] A.A.M. Aly, A.S. El Shahawy, M. El-Zohry, A.A. Mohamed, Bull. de la Soc. Chim. de France (6) (1988) 930.
[8] G.M. Larin, G.A. Zvereva, Doklady Akademii Nauk USSR Phys. Chem. 290 (3) (1986) 649.
[9] A.S.A. Zidan, Phosphorus Sulfur Silicon Relat. Elem. 178 (3) (2003) 567.
[10] Y.P. Singh, R.C. Mehrotra, Polyhedron 5 (4) (1986) 967.
[11] R. Visalakshi, V.K. Jain, Trans. Met. Chem. 15 (4) (1990) 278.
[12] U.N. Tripathi, M.S. Singh, J. Ind. Chem. Soc. 76 (7) (1999) 360.
[13] C.P. Bhasin, G. Srivastava, R.C. Mehrotra, Ind. J. Chem., Sect. A 26A (10) (1987) 834.
[14] C.P. Bhasin, G. Srivastava, R.C. Mehrotra, Inorg. Chim. Acta 128 (1) (1987) 69.
[15] C.P. Bhasin, R.C. Mehrotra, J. Ind. Chem. Soc. 79 (4) (2002) 336.
[16] C.P. Bhasin, G. Srivastava, R.C. Mehrotra, Inorg. Chim. Acta 131 (2) (1987) 195.
[17] C.P. Bhasin, G. Srivastava, R.C. Mehrotra, Inorg. Chim. Acta 144 (2) (1988) 157.
[18] P.E. Medyantseva, A.N. Ulakhovich, G.K. Budnikov, T.A. Groisberg, Zhurnal Analiticheskoi Khimii 46 (5) (1991) 962.
[19] M. Born, J.C. Hipeaux, P. Marchand, G. Parc, Lubrication Sci. 4 (2) (1992) 93.
[20] P.I. Sanin, Rev. Inst. Franc. Petrole, et Ann. Combustibles Liquids 16 (1961) 468.
[21] S. Al-Malaika, M. Coker, G. Scott, Polym. Degrad. Stab. 22 (2) (1988) 147.
[22] F.A. Nasirov, Iran. Polym. J. 12 (4) (2003) 281.
[23] S.S. Zhang, B.Y.Y.F. Wang, X.M. Li, K. Jiao, M.B. Kassim, B.M. Yamin, Acta Crystallogr., Sect. E 60 (2004) 485.
[24] Q. Hao Fun, H. Kun, S. Chantrapromma, I. Razak, Jian Fangfang, Yang Xujie, Lu Lude, Wang Xin, Acta Crystallogr., Sect. C: Cryst. Struct. Commun. C57 (6) (2001) 717.
[25] S.E. Livingstone, A.E. Mihkelson, Inorg. Chem. 9 (11) (1970) 2545.
[26] C.P. Bhasin, G. Srivastava, R.C. Mehrotra, Inorg. Chim. Acta L131 (1983) 77.
[27] R. Ratnani, J.E. Drake, C.L.B. Macdonald, A. Kumar, S.K. Pandey, J. Chem. Crystallogr. 35 (6) (2005) 447.
[28] J.H. Fletcher, J.C. Hamilton, I. Hechenbleikner, E.I. Hoegberg, B.J. Sertl, J.T. Cassaday, J. Am. Chem. Soc. 72 (1950) 2461.
[29] K.I. Zimina, G.G. Kotova, P.I. Sanin, V.V. Sher, G.N. Kuz'mina, Neftekhimiya 5 (4) (1965) 629.
[30] R.M. Silverstein, F.X. Webster, Spectrometric Identification of Organic Compounds, 6th ed., Wiley, New York, 1998.
[31] R. Ratnani, Ph.D. Thesis, 1990.
[32] J.F. McConnell, V. Kastalsky, Acta Crystallogr. 22 (1967) 853.
[33] Q. Fernando, C.D. Green, Acta Crystallogr. 29 (1967) 647.
[34] B.F. Hoskins, E.R.T. Tiekink, Acta Crystallogr. Sect. C: Cryst. Struct. Commun. C41 (1985) 322.
[35] M. Duisenberg AJM, J. Appl. Crystallogr. 25 (1992) 92.
[36] G.M. Sheldrick, SADABS V2.10, 2003.
[37] G.M. Sheldrick, Acta Crystallogr. A46 (1990) 467.
[38] L.J. Farrugia, J. Appl. Crystallogr. 32 (1999) 837.
[39] G.M. Sheldrick, SHELXL97, University of Gottingen, Germany, 1997.

stereoisomerism [3], because the three phosphorus atoms of each cyclophosphazene ring have different substitution patterns and those that are part of the bridge, >P(N-spiro), are stereogenic, i.e., there are *R* and *S* forms. It was shown that spermine-bridged compounds such as **4** are diastereoisomeric and exist in 1:1 mixtures of meso (*RS*/*SR*) and racemic (*RR*/*SS*) forms [3]. Compound **4** was synthesised by the reaction at room temperature of 1,3-propanediol with **1** and, although a second compound was reported as the tri-spiro derivative, it was not characterized [3]; this compound is expected to be chiral and to exist as a racemic mixture.

Reaction of 1,3-propanediol with compound **1** could, in principle, give rise to a number of different derivatives; if only one functional group of the diol is used, this would give open chain forms, whilst utilisation of both functional groups of the diol can give rise to spiro, ansa and bridged derivatives. Reaction of $N_3P_3Cl_6$ with ethane-, 1,3-propane- and 1,4-butane-diols (in the presence of pyridine to neutralise the hydrochloride formed) predominantly gave spiro derivatives for all three diols, whereas ansa derivatives were rare products obtained only in small yields [9]. A bridged derivative was observed as a minor product with butanediol, indicating that chain length was a contributing factor in determining derivative-type [9]. It was also found that ansa-derivatives may be formed using sodium salts of diols as reagents in polar solvents such as THF [10]. The spiro- and ansa-derivatives of **1** should exhibit a range of stereogenic properties (achiral, meso, racemic, diastereoisomeric). The purpose of the present work is to investigate the reaction of the sodium derivative of 1,3-propanediol with compound **1** in THF under different reaction conditions, to characterize the structures and stereogenic properties of the products and to show how widespread the question of chirality should be considered in cyclophosphazene chemistry.

2. Experimental

2.1. Materials

Hexachlorocyclotriphosphazene (Otsuka Chemical Co., Ltd.) was purified prior to use by fractional crystallisation from hexane. The following chemicals were obtained from Merck; spermine (⩾97.0%), diethyl ether, dichloromethane, benzene, *n*-hexane, 1,3-propanediol (⩾99.0%), silica gel 60, sodium hydride (60% oil suspension), tetrahydrofuran, ethyl acetate, chloroform and *n*-heptane. The deuterated solvents for NMR spectroscopy were obtained from Apollo Scientific (toluene-d_8, $CDCl_3$) and the chiral solvating agent, (*S*)-(+)-2,2,2-trifluoro-1-(9-anthryl)ethanol, was obtained from Aldrich Chemical Co.

2.2. Measurements

Elemental analyses were obtained using a Carlo Erba 1106 Instrument. Mass spectrometric measurements were recorded on a VG Zab Spec GC–MS spectrometer using the fast atom bombardment (FAB) method (35 kV) with MNBA as the matrix; ^{35}Cl values were used for calculated masses. Analytical Thin Layer Chromatography (TLC) was performed on Merck silica gel plates (Merck Kieselgel 60, 0.25 mm thickness) with F_{254} indicator. Column chromatography was performed on silica gel (Merck 60, 230–400 mesh; for 3 g, crude mixture, 100 g, silica gel was used in a column of 3 cm in diameter and 60 cm in length). ^1H and ^{31}P NMR spectra were recorded in $CDCl_3$ or toluene-d_8 solutions on a Bruker DRX 500 MHz spectrometer using TMS as an internal reference for ^1H and 85% H_3PO_4 as an external reference for ^{31}P. For all new compounds both proton-coupled and proton-decoupled ^{31}P NMR spectra were recorded. Experiments involving the chiral solvating agent (CSA) were performed by addition of small aliquots of a dilute solution of CSA in the solvent used for NMR spectroscopy and the ^{31}P NMR spectrum recorded at each addition.

2.3. Synthesis

Reaction of the sodium derivative of 1,3-propanediol with compound **1** in THF at different molar ratios gave a number of spiro and ansa derivatives as summarized in Scheme 1.

2.3.1. 4:1 mole ratio

1,3-Propanediol (0.4 g, 5.3 mmol) and previously prepared [8] compound **1** (1 g, 1.33 mmol) were dissolved in 50 mL of dry THF in a 250 mL three-necked round-bottomed flask. The reaction mixture was cooled in an ice-bath and NaH (60% oil suspension, 0.42 g, 10.6 mmol) in 50 mL of dry THF was added under an argon atmosphere. The reaction mixture was stirred for 21 h at room temperature and the reaction followed to completion by TLC on silica gel plates using $CHCl_3$:ethyl acetate (3:1) as the solvent system. The reaction mixture was filtered to remove the sodium chloride formed, the THF was removed under reduced pressure and the resulting white solid subjected to column chromatography using $CHCl_3$:ethyl acetate(3:1) as eluent. Two fractions were obtained and isolated as white powders and recrystallised from chloroform:hexane (1:1). The first fraction is the dispiro-monoansa compound, **8**, (yield: 0.29 g, 25%, m.p. 147–149 °C; isolated as a chloroform adduct). *Anal*. Calc. for $C_{20}H_{41}Cl_5N_{10}P_6O_6$ requires: C, 27.27; H, 4.69; N, 15.90, M^+, 761.34. Found: C, 27.02; H, 4.20; N, 15.12% $(M + H)^+$, 761. The second fraction is the tetraspiro-derivative, **9**, whose NMR spectral data [11] and X-ray structure [12] have been characterized previously (yield: 0.33 g. 32%, mp >250 °C). *Anal*. Calc. for $C_{22}H_{46}N_{10}O_8P_6$ requires: C, 34.56; H, 6.06; N, 18.32, M^+, 764.52. Found: C, 34.35; H, 6.2; N, 17.68% $(M + H)^+$, 764.

2.3.2. 3:1 mole ratio

1,3-Propanediol (0.9 g, 11.95 mmol) and previously prepared [8] compound **1** (3 g, 3.98 mmol) were dissolved in

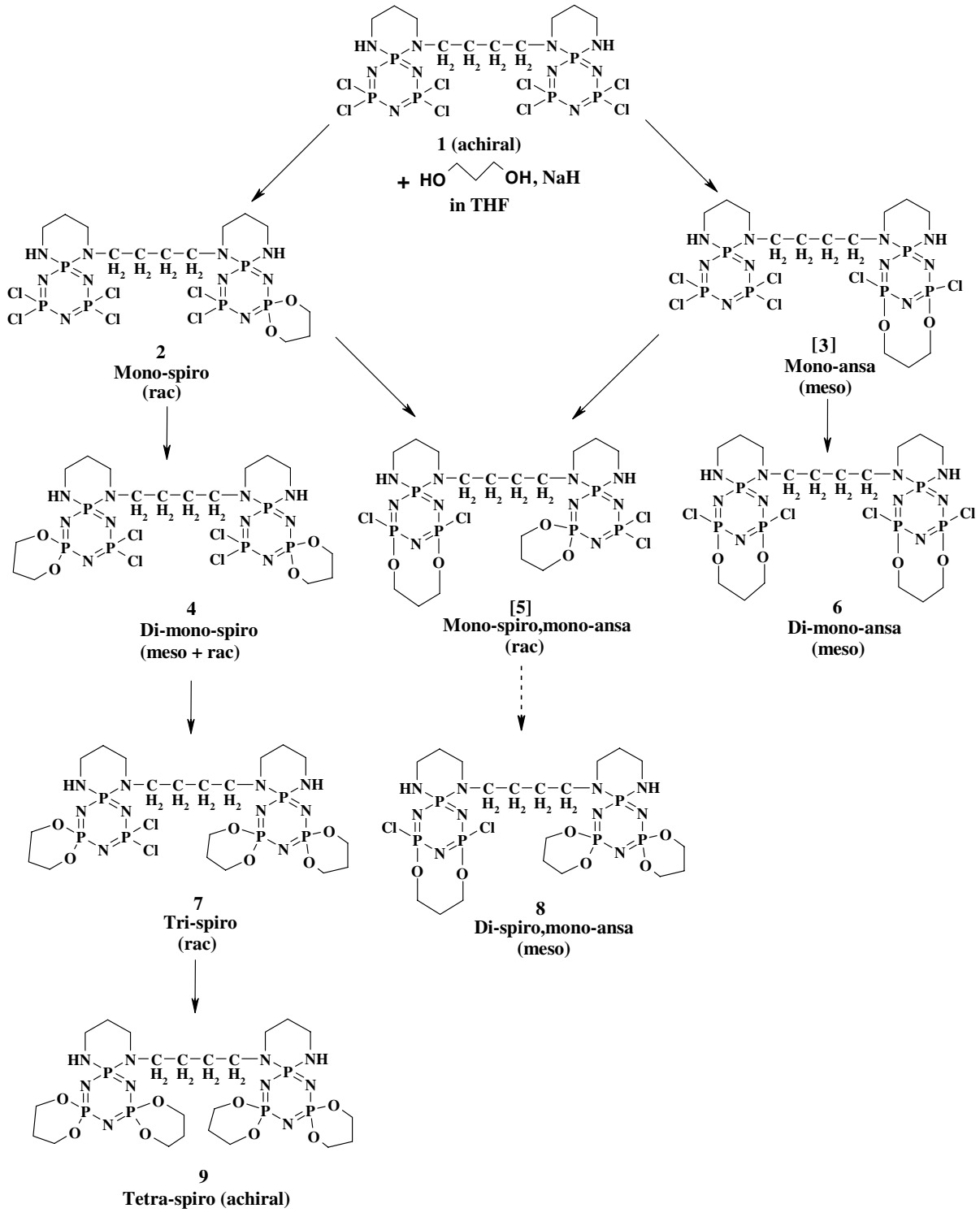

Scheme 1. Stereogenicity confirmed by X-ray (or by NMR + CSA) except for compounds with numbers in brackets.

200 mL of dry THF in a 500 mL three-necked round-bottomed flask. The reaction mixture was cooled in an ice-bath and NaH (60% oil suspension, 0.95 g, 23.9 mmol) in 50 mL of dry THF was added under an argon atmosphere. The reaction mixture was stirred for 24 h at room temperature and was followed by TLC on silica gel plates using THF:CH_2Cl_2 (5:2). The reaction mixture was filtered to remove the sodium chloride formed, the THF was removed under reduced pressure and the resulting white solid subjected to column chromatography using THF:CH_2Cl_2 (5:2) as eluent. Two fractions were obtained; the first fraction was isolated as a white powder (yield 0.22 g, 7.3%), (m.p. 84–90 °C) and characterized as the tri-spiro compound, **7**. *Anal*. Calc. for $C_{19}H_{40}Cl_2N_{10}O_6P_6$ requires: C,

30.00; H, 5.30; N, 18.40, M^+, 760. Found: C, 30.48; H, 5.14; N, 17.95%, $(M + H)^+$, 761. ^{1}H NMR, $CDCl_3$, 298 K: OCH_2 signals at 4.52m, 2H and 4.4m, 10H; 3.23m, 4H, NCH_2; 3.1m, 4H, NCH_2; 2.8m 4H, $NHCH_2$; 2.5, broad triplet, 2H, NH; O-spiro, N-spiro and bridge CCH_2 signals at 2.1m, 4H; 1.9m, 4H; 1.7, 8H. The second fraction was isolated as a white powder (yield: 0.5 g, 16.5%) (m.p. 147–149 °C), re-crystallized from CH_2Cl_2:THF:hexane (1:2:1) and characterized as the dispiro-monoansa compound, **8**. *Anal*. Calc. for $C_{19}H_{40}Cl_2N_{10}O_6P_6$ requires: C, 29.97; H, 5.30; N, 18.40, M^+, 760. Found: C, 29.30; H, 5.90; N, 17.68%. $(M + H)^+$, 760.8.

2.3.3. 2:1 mole ratio

1,3-Propanediol (1.06 g, 13.2 mmol) and previously prepared [8] compound **1** (5 g, 6.6 mmol) were dissolved in 140 mL of dry THF in a 500 mL three-necked round-bottomed flask. The reaction mixture was cooled in an ice-bath and NaH (60% oil suspension, 1.056 g, 26.4 mmol) in 100 mL of dry THF was quickly added under an argon atmosphere. The reaction was stirred for 23 h at room temperature and was followed by TLC on silica gel plates using CH_2Cl_2:ethyl acetate (6:1). The reaction mixture was filtered to remove NaCl formed, the THF was removed under reduced pressure and the resulting white solid subjected to column chromatography using CH_2Cl_2:ethyl acetate (6:1). Two fractions were obtained. The first fraction has been characterized previously as the di-monospiro derivative **4** (isomer mixture, m.p. 210–216 °C) [3] and the meso form characterized by X-ray crystallography [11]. The second major fraction was isolated as a white powder, re-crystallized from dichloromethane:hexane (1:1) and characterized as the di-monoansa derivative **6** (yield: 0.4 g, 8%) (m.p. >250 °C decomposition). *Anal*. Calc. for $C_{16}H_{34}Cl_4N_{10}O_4P_6$ requires: C, 25.35; H, 4.52; N, 18.47, M^+, 756. Found: C, 25.91; H, 4.08; N, 17.88%. $(M + H)^+$, 757. ^{1}H NMR, $CDCl_3$, 298 K: 4.48m, 4H, OCH_2 signals; 4.21m, 4H, OCH_2 signals; 3.23m, 4H, NCH_2; 3.13m, 4H, NCH_2; 2.92m 4H, $NHCH_2$; ansa CCH_2 signals at 2.2m, 2H and 1.9m, 2H; spiro and bridge CCH_2 signals at 1.75m, 4H and 1.68m, 4H.

2.3.4. 0.75:1 mole ratio

1,3-Propanediol (0.25 g, 3.2 mmol) and previously prepared [8] compound **1** (3.3 g, 4.3 mmol) were dissolved in 150 mL of dry THF in a 500 mL three-necked round-bottomed flask. The reaction mixture was cooled in an ice-bath and NaH (60% oil suspension, 0.26 g, 6.4 mmol) in 50 mL of dry THF was quickly added under an argon atmosphere. The reaction was stirred for 24 h at room temperature and was followed by TLC on silica gel plates using CH_2Cl_2–ethyl acetate (1:2) as eluent. The reaction mixture was filtered to remove the sodium chloride, the THF was removed under reduced pressure and the resulting white solid subjected to column chromatography using CH_2Cl_2:ethyl acetate (1:2). Two fractions were obtained, the first is the starting compound **1** [8], isolated as a white powder (recovery of starting material: 0.16 g, 5%) whose ^{1}H NMR has not been previously reported in detail. ^{1}H NMR, $CDCl_3$, 298 K: 3.24m, 4H, NCH_2; 3.14m, 4H, NCH_2; 2.84m 4H, $NHCH_2$; 2.67 broad quartet, 2H, NH; spiro and bridge CCH_2 signals at 1.82m, 4H and 1.56m, 4H. The second fraction was also isolated as a white powder (yield: 0.45 g, 14%), (m.p. 150–151 °C), recrystallised from CH_2Cl_2:hexane:ethyl acetate (2:1:1) and characterized as the mono-spiro compound **2**. *Anal*. Calc. for $C_{13}H_{28}Cl_6N_{10}O_2P_6$ requires: C, 20.68; H, 3.74; N, 18.55 M^+, 754. Found: C, 19.90; H, 3.50; N, 18.40% $(M + H)^+$, 754.9. ^{1}H NMR, $CDCl_3$, 298 K: 4.53m 2H, OCH_2 signals; 4.37m 2H, OCH_2 signals; 3.1–3.3m, 8H, NCH_2; 2.8–2.9m, 4H, $NHCH_2$; 2.64, broad quartet, 1H, NH; 2.52, broad triplet, 1H, NH; CCH_2 signals at 2.14m, 1H; 1.75–1.9m, 5H; 1.6m, 4H. ^{1}H NMR, toluene-d_8, 298 K: 4.53m 2H, OCH_2 signals; 4.37m 2H, OCH_2 signals; 3.25m 4H, NCH_2; 3.1–3.3m 8H, NCH_2; 3.15m 4H, NCH_2; 2.85m 4H, $NHCH_2$; 2.64, broad quartet, 1H, NH; 2.52, broad triplet, 1H, NH; CCH_2 signals at 2.14m, 1H; 1.75–1.9m, 5H; 1.6m, 4H.

2.4. X-ray crystallography

Intensity data were recorded at low temperature (120 K) on a Nonius KappaCCD diffractometer situated at the window of an FR591 rotating anode generator, driven by COLLECT [13] and DENZO [14] software. Details of data collection and refinement are given in Table 1. All structures were determined using the direct methods procedure in SHELXS-97 [15] and refined by full-matrix least-squares on F^2 using SHELXL-97 [16]. The structure of **8** exhibits a solvent of crystallisation ($CHCl_3$) and some disorder in the central chain (atom C8/C8′), which is modelled at 55:45%. Full details of data collection and structure determination have been deposited with the Cambridge Crystallographic Data Centre (CCDC).

3. Results and discussion

3.1. Formation of spiro- and ansa-substituted spermine-bridged cyclotriphosphazenes

Reaction of the sodium derivative of 1,3-propanediol with the spermine-bridged cyclophosphazene **1** in different mole ratios (4:1, 3:1, 2:1, 0.75:1) in THF gave a number of spiro- and ansa-substituted derivatives as shown in Scheme 1. In order to investigate all major reaction products, the crude reaction mixtures were routinely characterized by proton-decoupled ^{31}P NMR, as well as all major fractions isolated. Reaction of 1,3-propanediol with **1** in a 4:1 mole ratio for 21 h at room temperature gave the fully substituted dispiro-monoansa **8** and tetra-spiro **9** derivatives, whereas reaction at a 3:1 mole ratio under the same solution conditions gave the tri-spiro derivative **7** and the isomeric compound **8**. Reaction of 1,3-propanediol with **1** in a 2:1 mole ratio for 23h at room temperature gave the

Table 1
X-ray crystallographic data

	2	**6**	**8**[a]
Empirical formula	$C_{13}H_{28}Cl_6N_{10}O_2P_6$	$C_{16}H_{34}Cl_4N_{10}O_4P_6$	$C_{20}H_{41}Cl_5N_{10}O_6P_6$
Formula weight	754.97	758.15	880.70
Crystal system	monoclinic	triclinic	orthorhombic
Space group	$P2_1/c$	$P\bar{1}$	$Pna2_1$
a (Å)	9.5842(2)	8.5849(17)	15.229(3)
b (Å)	12.5090(2)	9.5425(19)	26.120(5)
c (Å)	25.3979(5)	15.6271(19)	9.2683(19)
α (°)	90	84.46(3)	90
β (°)	101.1840(10)	84.63(3)	90
γ (°)	90	75.67(3)	90
Volume (Å^3)	2987.10(10)	758.6(3)	3686.7(13)
Z	4	1	4
D_{calc} (Mg/m^3)	1.679	1.660	1.587
Absorption coefficient (mm^{-1})	0.931	0.752	0.705
$F(000)$	1536	390	1816
Crystal size (mm)	$0.55 \times 0.42 \times 0.10$	$0.28 \times 0.2 \times 0.05$	$0.45 \times 0.14 \times 0.12$
θ_{max} (°)	27.50	27.42	27.48
Reflections collected	34 810	11 470	24 873
Independent reflections ($I > 2\sigma I$)	6836	3392	7818
R_{int}	0.0779	0.0724	0.0723
Final R indices $F^2 > 2\sigma F^2$	$R_1 = 0.0607$	$R_1 = 0.0396$	$R_1 = 0.0432$
	$wR_2 = 0.1463$	$wR_2 = 0.1013$	$wR_2 = 0.0973$
$\Delta\rho$ max/min (e Å^{-3})	1.103/−0.814	0.407/−0.702	0.584/−0.389

[a] Isolated as a 1:1 adduct with chloroform.

di-monospiro **4** and di-monoansa **6** derivatives and reaction at a 0.75:1 mole ratio for 24 h at room temperature gave the mono-spiro **2** and mono-ansa **3** derivative. It is obvious from Scheme 1 that the mono-spiro derivative **2** is the precursor of the spiro-substituted compounds **4** (di), **7** (tri), and **9** (tetra), and the mono-ansa derivative **3** is a precursor of **6** (di-mono-ansa) and **8** (di-spiro/mono-ansa). The mono-spiro/mono-ansa derivative **5** could be formed from either the mono-spiro **2** or the mono-ansa compound **3** and the dispiro/mono-ansa derivative **8** should have compound **5** as precursor. Attempts were made to prepare the mono-spiro/mono-ansa compound **5**, but amounts in the reaction mixtures were too small to isolate and characterize independently. Each of the new compounds **2**, **6** and **8** was characterised by X-ray crystallography and by elemental analysis, MS and ^{31}P NMR using both proton-decoupled and proton-coupled spectra. Although crystals suitable for X-ray crystallography could not be obtained for **3** and **7**, these compounds were characterized by ^{31}P NMR spectroscopy. The ^{31}P NMR results for all of the compounds are summarised in Table 2.

3.2. X-ray crystal structures of the spiro- and ansa-derivatives (*2,6,8*) of the spermine-bridged compound, *1*

The molecular structures of compounds **2**, **6** and **8** are shown in Figs. 1–3, respectively. The crystal structures of the meso form of the di-mono-spiro compound **4** [11] and the tetra-spiro compound **9** [12] have been published previously.

3.2.1. Compound *2*

The molecular structure of the mono-spiro compound **2** in Fig. 1 depicts an asymmetrically-bridged molecule, in which one of the cyclophosphazene moieties is unsubstituted and the other exhibits a mono-spiro substituted phosphorus site. Both N_3P_3 rings of compound **2** are nearly planar, with the maximum deviations from the mean ring plane being 0.092 Å (atom P2) and 0.104 Å (atom N8) for rings 1 (spiro derivative) and 2 (un-substituted), respectively. Ring 2 exhibits slight ring compression with a shortened non-bonded separation between ring phosphorus atoms of 2.699 Å (P4···P5), whereas the expected distance surveyed from the Cambridge Structural Database [17] is about 2.78 Å. The spermine bridge introduces chirality to the molecule at the phosphorus sites linking it to the unsymmetrically-substituted cyclophosphazene ring and is found to be *S* for atom P3. The molecule is chiral and exists as a racemate. The relative conformation of the two cyclophosphazene rings around the tetra-methylene bridge is neither pure syn nor anti, but is approximately 2/3 of the way towards the latter, forming an angle of 59.5° between the two ring planes. Hydrogen-bonding occurs at the N_3P_3 moiety containing the spiro-propanedioxy group and gives rise to discreet dimers through an N–H···N interaction (N4–H4N···N2 D···A distance = 3.282 Å). Eight-membered hydrogen-bonded rings are formed, in which the two heavy atom distances are equal at 3.282 Å and result in a twist-boat conformation. At distances >3.4 Å a more complex hydrogen-bonded motif links the molecules into an infinite layer structure.

Table 2
^{31}P NMR parameters of spiro- and ansa-forms of 1,3-propanedioxy-substituted spermine-bridged cyclophosphazenes[a]

Compound: ring configuration[b]		Chemical shifts (ppm)				^{2}J(PP) (Hz)			
		>PCl_2	>P(Nspiro)	>P(Ospiro)	>P(OR)Cl	**1,2**	**1,3**	**2,3**	**2,4**
		1	**2**	**3**	**4**				
1[c]		22.1	10.4			40.5			
2		22.1	10.2			40.4			
	sp	25.0	15.5	9.0		41.1	68.0	63.6	
2[d]		21.5	11.2			40.3			
	sp	23.5	16.8	9.4		38.0	65.5	68.2	
3		22.0	10.2			40.4			
	an		16.8		30.8				46.5
4[e,f]r	sp	25.01	15.45	9.01		40.5	68.7	63.4	
m	sp	25.0	15.42	8.99		40.5	68.7	63.4	
6	an		16.4		30.4				46.3
7	sp	25.1	15.5	9.1		40.2	68.8	63.1	
	di-sp		19.8	14.6				57.9	
7[d]	sp	23.5	16.9	9.5		36.6	66.8	68.0	
	di-sp		20.8	14.9				59.9	
8	an		16.4		30.3				46.3
	di-sp		19.4	14.1				58.2	
9[e]	di-sp		19.8	14.6				58.0	

[a] 202.45 MHz ^{31}P NMR measurements in $CDCl_3$ solutions at 298 K. Chemical shifts referenced to external 85% H_3PO_4.
[b] Abbreviations: sp, spiro; an, ansa; r, racemate; m, meso.
[c] Data taken from [3].
[d] Data on toluene-d_8 at 298 K. It is noted that, in comparison of the ^{31}P NMR spectra of the mono-spiro substituted ring of both compounds **2** and **7** in toluene-d_8 and $CDCl_3$ solutions, changes occur not only in chemical shifts (as expected) but also in ^{2}J(PP) values.
[e] Data taken from [11].
[f] Unequivocal assignment of meso (m) and racemic (r) forms resulted from characterization of the meso form of the diastereoisomer by X-ray crystallography [11].

3.2.2. Compound *6*

The molecular structure of the di-monoansa compound **6** in Fig. 2 is that of a symmetrically-bridged spermine derivative, where the cyclophosphazene substituents both possess a propanedioxy ansa-bridged moiety, giving rise to a centrosymmetric structure with the centre of inversion about the central C–C bond of the spermine bridge. The cyclophosphazene ring is heavily distorted, as observed in similar ansa-bridged examples [18], with a maximum deviation from the mean ring plane of

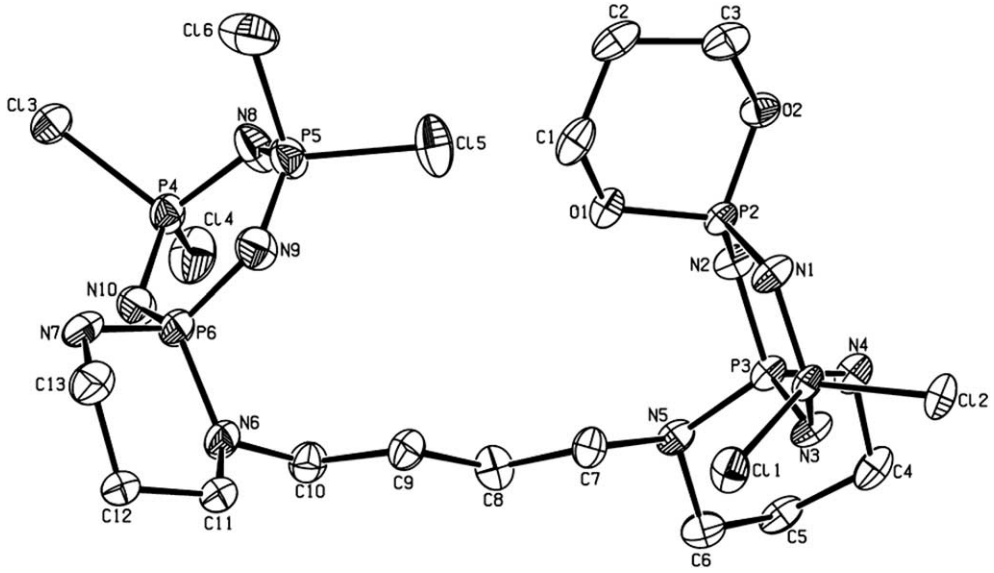

Fig. 1. Crystal structure of the mono-spiro compound **2**.

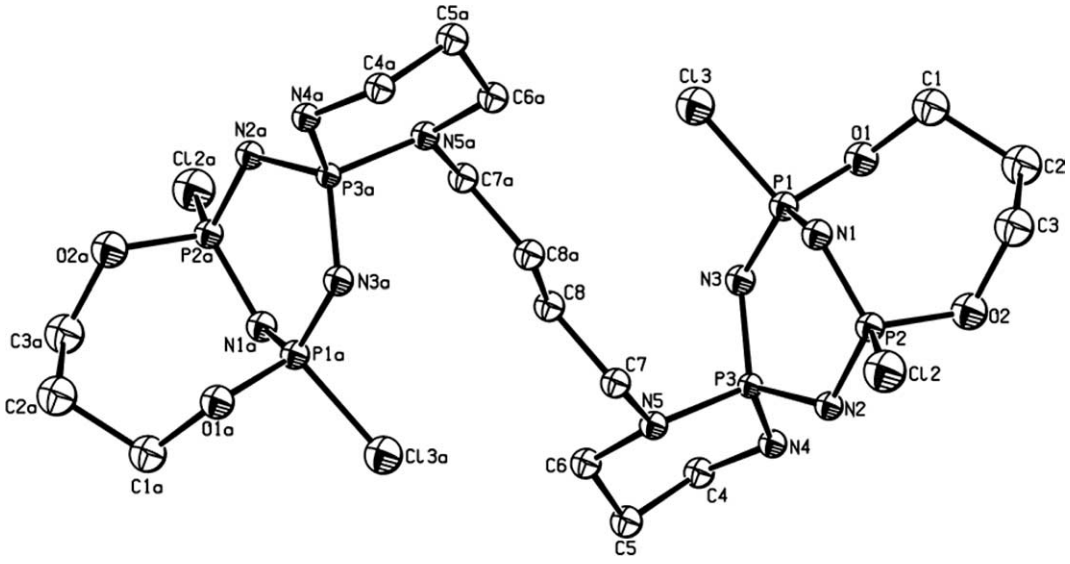

Fig. 2. Crystal structure of the di-mono-ansa compound **6**.

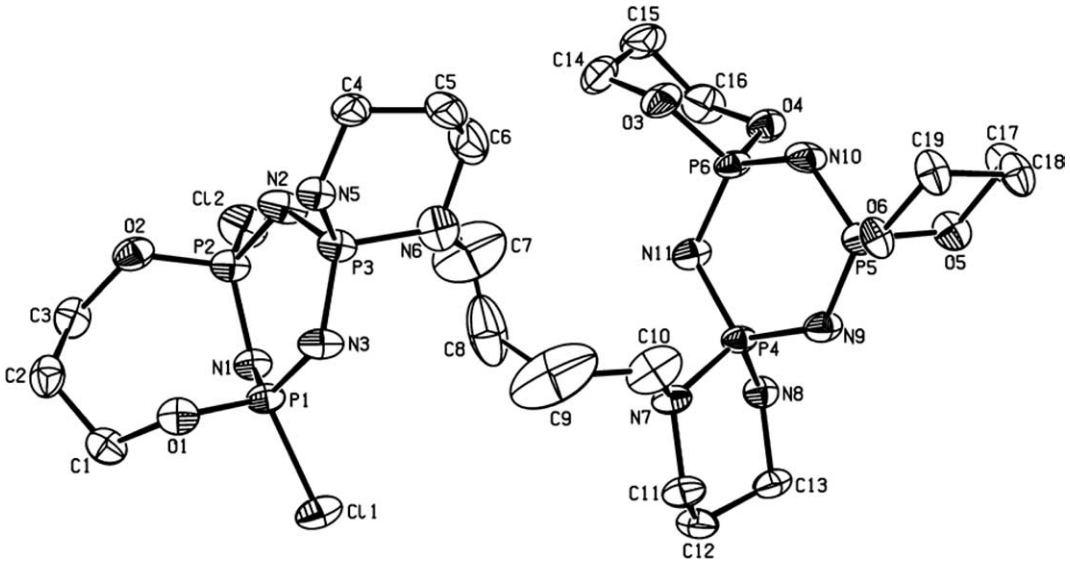

Fig. 3. Crystal structure of the di-spiro/mono-ansa compound **8**, with disorder (about atom C8) and the $CHCl_3$ solvent molecule removed for clarity.

0.328 Å for the nitrogen atom (N1) bridged by the ansa group. This give rise to compression of the cyclophosphazene ring, where the non bonded P···P separation between atoms P1 and P2 is 2.615 Å. The ansa bridge introduces chirality into the molecule such that P1 = *R* and P2 = *S*, with the symmetry generated partners having the opposite chirality due to the inversion centre resulting in **6** being a meso compound. As a result of the centrosymmetric nature of the structure, the two cyclophosphazene rings are disposed exactly syn to each other with respect to the spermine bridge. The supramolecular structure is that of a hydrogen bonded dimer, where an NH of the spermine group interacts with a cyclophosphazene ring nitrogen in a head to tail fashion (N4–H4N···N2 D···A distance = 3.154 Å). Longer range interactions arrange these dimers into an infinite sheet structure. This arrangement is similar to that of the hydrogen bonded structure of **2**, apart from the conformation of the eight-membered hydrogen-bonded ring, which forms a slightly twisted chair in the crystal structure of **6**.

3.2.3. Compound *8*

The molecular structure of the dispiro-monoansa compound **8** in Fig. 3 is that of a spermine moiety bridging two asymmetrically-substituted cyclophosphazene rings, one with an ansa propanedioxy substituent and the other with two spiro groups. As in the structure of **6** the cyclophosphazene ring of the ansa-bridged moiety is highly distorted, with the ansa-bridged cyclophosphazene ring nitrogen (N1) positioned out of the mean ring plane by 0.31 Å and with the compressed non bonded P···P

separation between atoms P1 and P2 being 2.627 Å. On the other hand, the di-spiro substituted cyclophosphazene ring is nearly planar with a maximum deviation from the mean ring plane of 0.117 Å for atom P6. Although the ansa bridge introduces chirality into the molecule such that P1 = *S* and P2 = *R*, overall the molecule is meso. The relative conformation of the two cyclophosphazene rings around the tetra-methylene bridge is in an approximate syn conformation with an angle of 26.7° between the two ring planes. As observed in structures **2** and **6** the hydrogen bonded structure of **8** is that of a dimer, formed between the NH hydrogen of the spermine group and a cyclophosphazene ring nitrogen, with the separation between donor and acceptor atoms being 3.039 and 3.140 Å. These unequal distances result in a saddle-shape hydrogen-bond ring conformation. The hydrogen-bonded motifs occur at both ends of these molecules, thus forming an infinite chain.

3.3. Characterization of the chiral configurational properties of compounds 2 and 7 by ^{31}P NMR on addition of a chiral solvating agent, (S)-(+)-2,2,2-trifluoro-1-(9-anthryl)-ethanol

It is found that one set of proton-decoupled ^{31}P NMR signals are observed for compounds **2**, **3**, **6**–**9** whereas two sets of closely-spaced signals are observed for the di-monospiro compound **4**. The latter two sets of signals correspond to the meso and racemic forms of compound **4** as shown previously for analogous spermine-bridged compounds [3]. On addition of chiral solvating agent [19], (*S*)-(+)-2,2,2-trifluoro-1-(9-anthryl)ethanol, CSA, in $CDCl_3$ or toluene-d_8 solution some of the ^{31}P NMR signals for compounds **2** and **7** separate into two signals of equal intensity characteristic of racemic mixtures. X-ray crystallography has shown that compound **2** is chiral and exists as a racemate, whereas crystals of compound **7** suitable for X-ray analysis could not be obtained. As an example, the stereogenic properties of the tri-spiro compound **7** are demonstrated by NMR spectroscopy in Fig. 4. The proton-decoupled ^{31}P NMR spectrum of compound **7** in toluene-d_8 shown in Fig. 4(a) consists of five multiplets corresponding to an AMX spin system for the mono-spiro substituted cyclophosphazene ring [signals expanded in Fig. 4(b)] and an A_2X spin system for the di-spiro-substituted ring. Assignment of the ^{31}P NMR signals of the AMX part of compound **7** to >PCl_2, >P(N-spiro) and >P(O-spiro) groups was made by comparison of proton-coupled (not shown) and proton-decoupled spectra, whereas assignment of the A_2X spin system to >P(N-spiro) and >P(O-spiro) follows simply from the triplet and doublet signals, respectively. Addition of CSA to the solution of compound **7** causes changes in chemical shifts of all signals indicating complexation and, as shown in Fig. 4(c), it also causes splitting of all peaks for the AMX part of the spectrum, which is consistent with compound **7** being chiral and existing as a racemate.

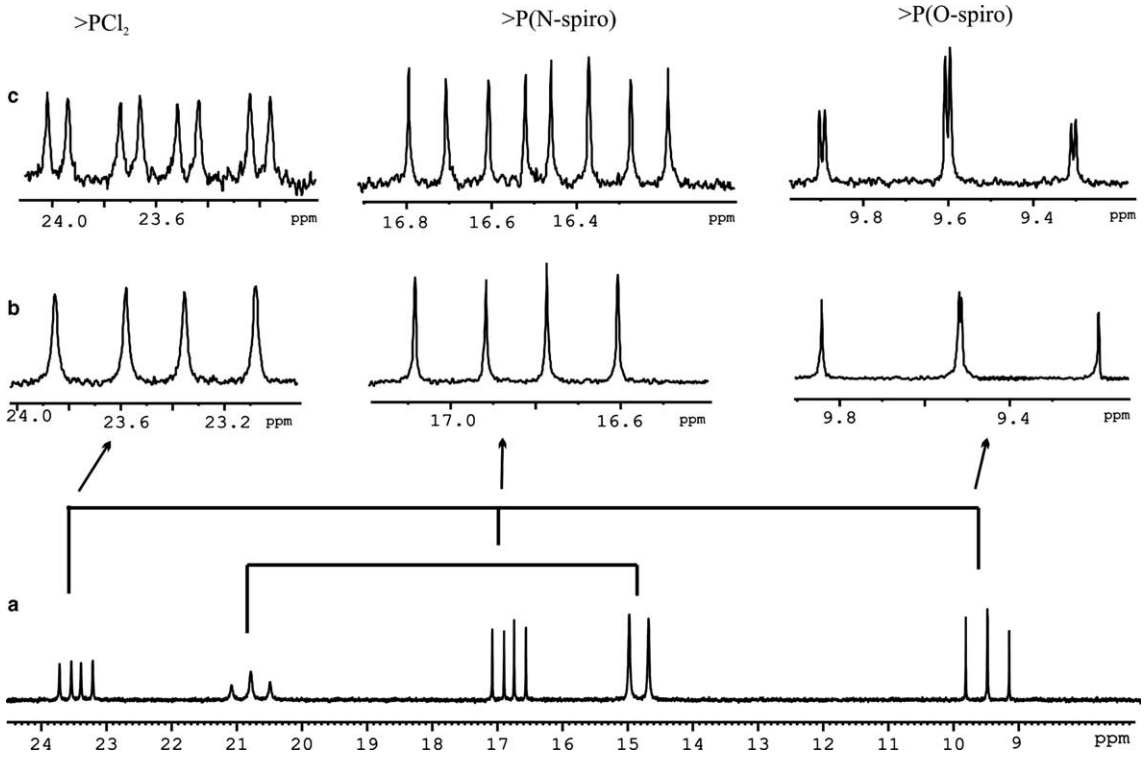

Fig. 4. 202.45 MHz proton-decoupled ^{31}P NMR spectra of the tri-spiro substituted compound **7** in toluene-d_8 solution at 298 K. (a) The AMX spin system corresponds to the mono-spiro substituted ring and the A_2X spin system corresponds to the di-spiro substituted ring. (b) Expanded signals of the AMX spin system of the mono-spiro substituted ring. (c) Addition of CSA causes each line of the AMX signals to split into two, corresponding to the two enantiomers.

The effect of addition of CSA on chemical shifts of all the spiro and ansa derivatives in either $CDCl_3$ or toluene-d_8, as appropriate, is summarised in Table 3 at a molar ratio of CSA:compound of 10:1. It is found that changes in chemical shifts occur for all compounds indicating complexation with CSA, whether the compounds are racemic, meso or achiral. Normally there is a differential effect on signals probably reflecting the mode of complexation of CSA with the compound and the proximity of the CSA to each of the groups in the complex. For example, it is found that the effect of CSA on the P(N-spiro) group of all compounds is negative (signals move to low frequency), whereas the effect on the PCl_2 and P(O-spiro) groups is smaller and can be either positive or negative. It is likely that the NH moiety of the P(N-spiro) group of all compounds is a major site of complexation of CSA, in line with previous work on many different compounds containing NH and OH groups [19]. It is also found that the effect of CSA on chemical shifts of compound **2** is greater for solutions in toluene-d_8 compared with $CDCl_3$ (Table 3), which prompted the choice of toluene-d_8 for NMR investigation of the stereogenic properties of compound **7** in solution.

It is found that care must be taken in interpreting the stereogenic properties of compounds by NMR spectroscopy on addition of CSA (or CSR) to the solution, because there are many cases of false positive results. It has already been shown [11] that the ^{31}P NMR signals of meso forms of spermine-bridged compounds such as compound **4** may exhibit doubling of peaks on addition of CSA. Another 'false positive effect' may be observed for ^{31}P NMR signals of meso compounds because the changes in chemical shifts on addition of CSA cause the spectra to change from A_2X-like to an A_2B spin system; this was observed for the 'doublet' signals of the >P(OR)Cl group of meso compound **6**, in which each resonance split into two signals of unequal and small separation (e.g., 1.8 and 2.4 Hz at an 18:1 mole ratio) that may be due to an A_2B (or even ABX) spin system rather than as a result of a stereogenic effect (Table 3). An analogous, but larger, effect has also been observed for compound **8** in this work (Table 3). On addition of CSA the 'doublet' signals of the >P(OR)Cl groups of meso compound **8** split into two signals of unequal and small separation (e.g., 3.1 and 3.8 Hz at a 17:1 mole ratio) that could be fitted as an ABX spin system, but not an A_2B spin system, which

Table 3
Effect of addition of CSA on ^{31}P NMR chemical shifts of spiro- and ansa-forms of 1,3-propanedioxy-substituted spermine-bridged cyclophosphazenes

Compound			Change in chemical shifts (ppb)[b]				Separation of signals/ppb		
No.	Type[a]		X or X_2	>PX_2	>P(bridge)	>PCl_2	>PX_2	>P(bridge)	>PCl_2
(i) CSA with symmetrically substituted spermine-bridged compounds at 10:1 mole ratio									
1[c]		ach	Cl		−21	37			
4[d]	s–s	r	$O(CH_2)_3O$	16	−140	26	13	53	25
	s–s	m	$O(CH_2)_3O$	14	−145	28	15	56	27
9[c]	ss–ss	ach.	$O(CH_2)_3O$	−48	−164				
6	a–a	m	Cl/[$O(CH_2)_3O$]0.5	11	−158		[e]		
(ii) CSA with unsymmetrically substituted spermine-bridged compounds at a 10:1 mole ratio									
2			Cl		−5	11		[f]	0[g]
	s	r	$O(CH_2)_3O$	−9	−25	4			5[h]
2[i]			Cl		−70	70	0		
	s	r	$O(CH_2)_3O$	105	−470	110	40		70
7[i]	ss		$O(CH_2)_3O$	−223	−1020		[f]	[f]	
	s	r	$O(CH_2)_3O$	74	−325	65	47	80	10
8	ss	m	$O(CH_2)_3O$	−100	−320				
	a		Cl/[$O(CH_2)_3O$]0.5	20	−184		[j]		

[a] s, spiro; a, ansa; ach, achiral, m, meso; r, racemate.
[b] $\Delta\delta = (\delta_{CSA} - \delta_{orig.})$; $\Delta\delta$ positive for high frequency shifts on addition of CSA in $CDCl_3$ unless otherwise noted.
[c] Data from [11].
[d] Although compound **4** was known to exhibit meso and racemic forms in [3], the effect of CSA (or CSR) was not reported. The effect of CSA on the meso form was reported in [11].
[e] On addition of CSA the 'doublet' signals of the >P(OR)Cl group of meso compound **6** split into two signals of unequal and small separation (e.g., 1.8 and 2.4 Hz at an 18:1 mole ratio) due to the A_2B spin system rather than as a result of a stereogenic effect; cf. [11].
[f] Signals are broad and mask any effect of CSA.
[g] Signals are sharp but no effect is observed up to 84:1 mole ratio.
[h] Approximate value derived by extrapolation of effect from higher mole ratios (between 46:1 and 84:1).
[i] In toluene-d_8 solution.
[j] On addition of CSA the 'doublet' signals of the >P(OR)Cl group of meso compound **8** split into two signals of unequal and small separation (e.g., 3.1 and 3.8 Hz at a 17:1 mole ratio) that could be fitted as an ABX spin system rather than an A_2B spin system, which probably indicates another type of example of the 'anomalous meso effect' (cf. [11]).

probably indicates another example of the 'anomalous meso effect' (as in [11]).

4. Conclusions

The chiral configurational isomers of spiro- and ansa-substituted spermine-bridged cyclophosphazene compounds have been investigated by X-ray crystallography and ^{31}P NMR spectroscopy. The symmetry of spermine-bridged cyclophosphazene compound **1** indicates that it is achiral, though it contains two potential homotopic stereogenic centres [>P(N-spiro) moiety of the two N_3P_3 units], which could lead to chiral compounds if substitution of the cyclophosphazene rings leads to asymmetry in the molecule. Substitution with 1,3-propanediol gives a series of spiro- and ansa-substituted spermine-bridged cyclo-phosphazene compounds; unsymmetrically-substituted bridged compounds are found to be chiral and exist as racemic mixtures of *R* and *S* forms, viz. mono-spiro **2** and tri-spiro **7**, whereas symmetrically-substituted bridged compounds may be meso, such as the di-mono-ansa **6** and di-spiro-mono-ansa **8** derivatives, or achiral, such as the tetra-spiro derivative **9**. Using X-ray crystallography and ^{31}P NMR spectroscopy with addition of a chiral solvating agent, (*S*)-(+)-2,2,2-trifluoro-1-(9-anthryl)ethanol, it has been shown previously that the di-mono-spiro derivative **4** exists as a 1:1 mixture of meso and racemic forms [11]. In this work, X-ray crystallographic studies have provided definitive proof of the stereogenic properties of compounds **2**, **6** and **8**, which have been confirmed using ^{31}P NMR spectroscopy and addition of a chiral solvating agent. In addition, the stereogenic properties of chiral compounds **2** and **7** have been elucidated using ^{31}P NMR spectroscopy and addition of CSA. The work demonstrates that derivatives of bridged cyclophosphazene compounds exhibit a range of stereogenic properties and that the question of chirality is an important consideration in cyclophosphazene chemistry.

5. Supplementary material

Supplementary data are available from the CCDC, 12 Union Road, Cambridge CB2 1EZ, UK on request, quoting deposition numbers CCDC 27630–276732 for compounds **2**, **6** and **8**, respectively.

Acknowledgements

We thank the Otsuka Chemical Co., Ltd. for gifts of $N_3P_3Cl_6$, the EPSRC National Crystallographic Service (Southampton, UK) and Gebze Institute of Technology Research Fund for partial support (A.K. and G.Y.C.).

References

[1] R.A. Shaw, B.W. Fitzsimmons, B.C. Smith, Chem. Rev. 62 (1962) 247.
[2] D.B. Davies, T.A. Clayton, R.J. Eaton, R.A. Shaw, A. Egan, M.B. Hursthouse, G. Sykara, I. Porwolik-Czomperlik, M. Siwy, K. Brandt, J. Am. Chem Soc. 122 (2000) 12447.
[3] S.J. Coles, D.B. Davies, R.J. Eaton, M.B. Hursthouse, A. Kılıç, T.A. Mayer, R.A. Shaw, G. Yenilmez, J. Chem. Soc. Dalton (2001) 365.
[4] I. Porwolik-Czomperlik, K. Brandt, T.A. Clayton, D.B. Davies, R.J. Eaton, R.A Shaw, Inorg. Chem. 41 (2002) 4944.
[5] I. Dez, J. Levalois-Mitjaville, H. Grützmacher, V. Gramlich, R. De Jaeger, Eur. J. Inorg. Chem. (1999) 1673.
[6] S. Beşli, S.J. Coles, D.B. Davies, R.J. Eaton, M.B. Hursthouse, A. Kılıç, R.A. Shaw, Eur. J. Inorg. Chem. (2005) 959.
[7] S. Beşli, S.J. Coles, D.B. Davies, M.B. Hursthouse, H. Ibişoglu, A. Kılıç, R.A. Shaw, Chem. Eur. J. 11 (2004) 4915.
[8] (a) J.-F. Labarre, G. Guerch, F. Sournies, R. Lahana, R. Enjalbert, J. Galy, J. Mol. Struct. 116 (1984) 75;
(b) J.-F. Labarre, Topics Curr. Chem. 129 (1985) 173;
(c) A. Kılıç, Z. Kılıç, R.A. Shaw, Phosphorus, Sulfur, and Silicon 57 (1991) 111.
[9] A.H. Alkubaisi, H.G. Parkes, R.A. Shaw, Heterocycles 28 (1989) 347.
[10] K. Brandt, T. Kupka, J. Drozd, J.C. van de Grampel, A. Meetsma, A.P. Jekel, Inorg. Chim. Acta 228 (1995) 187.
[11] S. Beşli, S.J. Coles, D.B. Davies, R.J. Eaton, M.B. Hursthouse, A. Kılıç, R.A. Shaw, G. Yenilmez Çiftçi, S. Yeşilot, J. Am. Chem. Soc. 125 (2003) 4943.
[12] S.J. Coles, D.B. Davies, M.B. Hursthouse, A. Kılıç, T.A. Mayer, R.A. Shaw, G. Yenilmez Çiftçi, Acta Cryst. B 60 (2004) 739.
[13] R. Hooft, Collect: Data Collection Software, Nonius B.V., 1998.
[14] Z. Otwinowski, W. Minor, Meth. Enzymol. 276 (1997) 307.
[15] G.M. Sheldrick, SHELXS-97, Program for Crystal Structure Solution, University of Göttingen, Germany, 1997.
[16] G.M. Sheldrick, SHELXL-97, Program for Crystal Structure Refinement, University of Göttingen, Germany, 1997.
[17] F.H. Allen, Acta Crystallogr. B 58 (2002) 380.
[18] S.R. Contractor, M.B. Hursthouse, H.G. Parkes, L.S. Shaw, R.A. Shaw, H. Yılmaz, J. Chem. Soc. Chem Commun. (1984) 675.
[19] (a) W. Pirkle, J.D. Hoover, Top. Stereochem. 13 (1982) 263;
(b) G.R. Weissman, in: J.D. Morrison (Ed.), Asymmetric Synthesis, vol. 1, Academic Press, New York, 1983, p. 153;
(c) G.R. Sullivan, Top. Stereochem. 10 (1978) 287;
(d) R.R. Fraser, in: J.D. Morrison (Ed.), Asymmetric Synthesis, vol. 1, Academic Press, New York, 1983, p. 173;
(e) P.L. Rinaldi, Progr. NMR Spectrosc. 16 (1982) 291, and references therein.

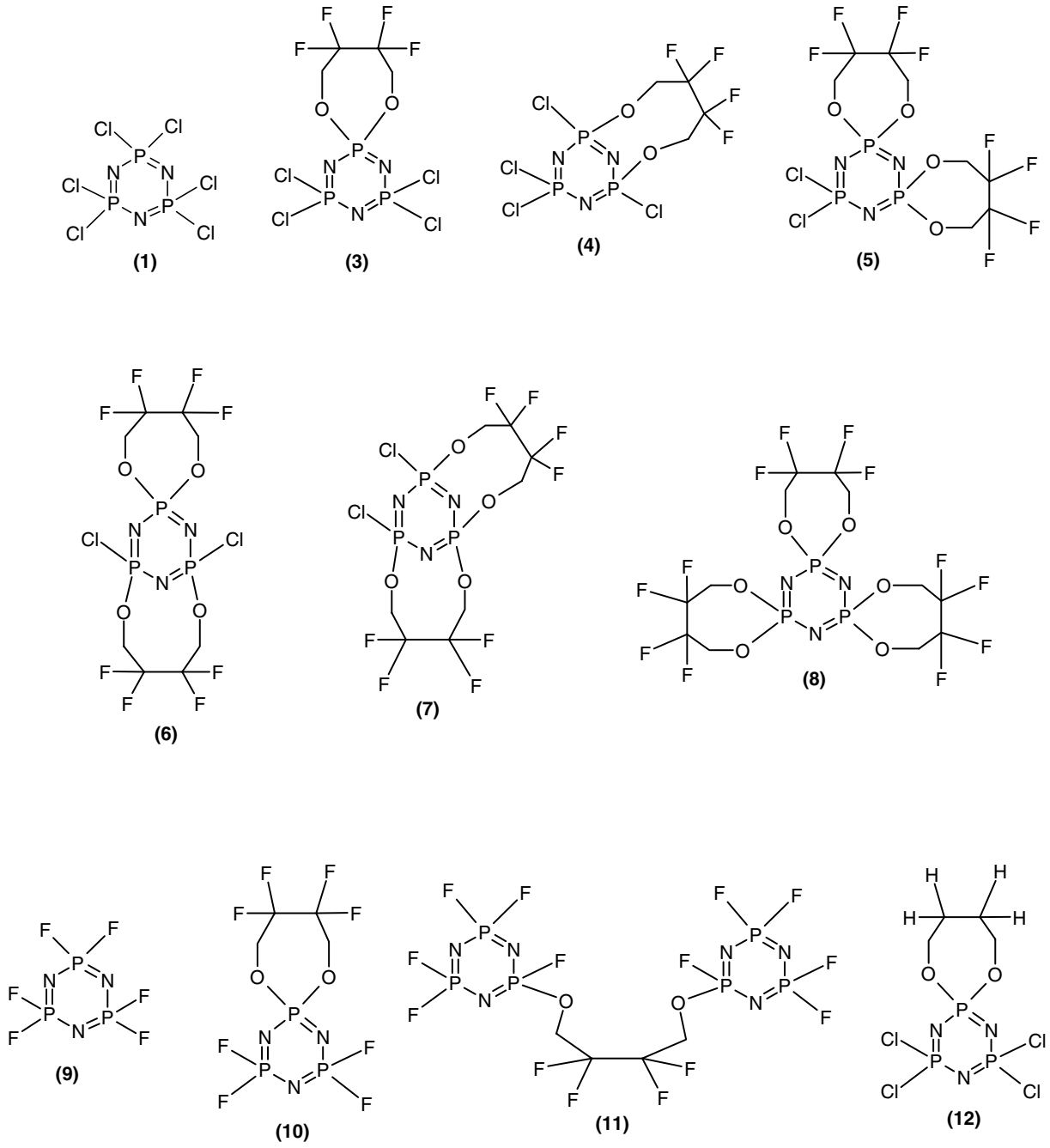

Fig. 1. Structures of compounds.

chain lengths $n > 5$ only bridged compounds were reported by Guerch et al. [4]. On the other hand, only ansa derivatives were obtained with structurally rigid di-functional reagents such as the di-lithium derivatives of ferrocene, ruthenocene and dibenzylchromium [5–8]. Herberhold and co-workers [9] reported that the reactions of the Li salt of the ferrocene (fc) diol with cyclophosphazenes (**1**) and $N_3P_3F_6$ (**9**), gave ansa derivatives, but only spiro-derivatives were obtained when the Li salts of the di-thiol or di-selenol ferrocene were used as reagents, in spite of the larger linking atoms. This mirrors the behaviour of monofunctional oxygen and sulphur nucleophiles, whose attack on the hexachloride (**1**), are predominantly non-geminal (cf. ansa with difunctional reagents) for the former [10,11] and predominantly geminal (cf. spiro with difunctional reagents) for the latter [12]. A recent report on the reactions of the hexafluoride (**9**) with sodium phenoxide again shows a non-geminal pattern [13].

Reaction of **1** with the dilithiated diol, $FcCH_2P(S)(CH_2OLi)_2$, at −80 °C yielded one spiro and two ansa (endo and exo) derivatives in the ratio ca. 1:4 [14], whereas the reaction of the silyl derivative of 2,2,3,3-tetrafluorobutane-1,4-diol (**2**), $(Me_3SiOCH_2CF_2)_2$, with **9** afforded two products; the mono-spiro derivative, $N_3P_3F_4(OCH_2CF_2CF_2CH_2O)$ (**10**), and a derivative of the singly-bridged compound, $(N_3P_3F_5)_2(OCH_2CF_2CF_2$-

CH_2O) (**11**) [15]. A second polymorph of **10** has been reported subsequently [16]. No other derivatives were observed and no reaction of the silyl reagent of **2** with the hexachloride (**1**) could be effected [15]. The purpose of the present study is to investigate the reaction of the sodium derivative of 2,2,3,3-tetrafluorobutane-1,4-diol (**2**) with hexachlorocyclotriphosphazene (**1**) and compare the results with those obtained previously for reaction with butane-1,4-diol [1] and the other related reactions [14,15].

2. Results and discussion

2.1. Reaction of hexachlorocyclotriphosphazene (1) with 2,2,3,3-tetrafluoro-1,4-butanediol (2) to form compounds (3)–(8)

We too observed no reactions between the hexachloride (**1**) and the silyl derivatives of alcohols in agreement with previous work [15], although it is known that silyl derivatives of the monophosphazene, $HN{=}PR_3$, do react with both the hexafluoride (**9**), and hexachloride (**1**), to give the analogous mono-substituted derivatives, $N_3P_3F_5(NPR_3)$ and $N_3P_3Cl_5(NPR_3)$ [17]. In the latter reaction the ease of formation of products decreased in the series [17]: $R_3 = (NMe_2)_3$, Me_3, Me_2Ph, $MePh_2$, Ph_3, $(OEt)_3$, which is in line with substituent basicity constants described and evaluated elsewhere [18]. It is clear that in addition to the driving force of formation of the Si–F (and to a lesser degree of the Si–Cl) bond, the nucleophilicity of the monophosphazene nitrogen atom plays a major role and, hence by implication, that of any other atom attached to the silyl reagent. It is also noted that silyl derivatives of alcohols should be less reactive than those of amines [17]. In order to overcome the lack of reactivity of silyl derivatives of alcohols with chlorophosphazenes, it was decided to use the sodium derivative of the fluorinated diol (**2**), as the nucleophile.

Six products were isolated from the reaction of **1** with **2** in THF at two stoichiometries (1:1.2 and 1:3). The products were the mono-spiro compound, $N_3P_3Cl_4(OCH_2CF_2CF_2CH_2O)$ (**3**), its ansa isomer (**4**), a di-spiro derivative $N_3P_3Cl_2(OCH_2CF_2CF_2CH_2O)_2$ (**5**), its spiro-ansa (**6**) and non-gem *cis* bis-ansa (**7**) isomers and a tri-spiro compound $N_3P_3(OCH_2CF_2CF_2CH_2O)_3$ (**8**). All reaction mixtures were analyzed by ^{31}P NMR spectroscopy and no other compounds were observed. The reaction of the hexachloride (**1**) with the sodium derivative of the fluorinated diol (**2**), in THF was also investigated at a stoichiometry of 1:0.4 and examination of the reaction mixture showed largely the same range of products, spiro (**3**) > ansa (**4**) > di-spiro (**5**). Reaction of **1** with **2** in THF was also effected in the presence of pyridine at room temperature; in this case, although there was evidence of the formation of spiro (**3**) and ansa (**4**) compounds as major products of the reaction, many more minor derivatives were formed, including decomposition products. All the ansa and spiro derivatives reported in this work were found to be unaffected by exposure to air and/or moisture, in contrast to previous reports [14,19] that spiro isomers are highly unstable to air and/or moisture, though their ansa isomers are stable. The reaction of the hexachloride (**1**) with the sodium derivative of the fluorinated diol (**2**) was also carried out at −78 °C, in order to compare our results most closely with those reported by Elias and co-workers [14]. The reagent **2** was added step-wise, one mole at a time and the reaction mixtures were investigated by ^{31}P NMR spectroscopy. With a stoichiometry of 1:1, examination of the reaction mixture showed largely the same range of products as the reaction at room temperature, viz. spiro (**3**) > ansa (**4**) ≈ di-spiro (**5**) > spiro-ansa (**6**) > tris-spiro (**8**). A similar range of products was formed at a stoichiometry of 1:2 though the relative proportions were changed; di-spiro (**5**) > spiro (**3**) > spiro-ansa (**6**) > ansa (**4**) > tris-spiro (**8**), whilst at a 1:3 ratio it was tris-spiro (**8**) ≫ di-spiro (**5**) > spiro-ansa (**6**). On addition of an excess of reagent only the tri-spiro compound **8** was observed. It was also found that reaction of the mono-ansa derivative **4** with an excess of reagent **2** converted it to the tri-spiro compound **8**, which was confirmed by TLC, mpt. and ^{31}P NMR.

2.2. Characterization of compounds 3–8 by ^{1}H, ^{31}P and ^{19}F NMR spectroscopy

Each of the compounds **3**–**8** was characterized by mass spectrometry and NMR spectroscopy, and the results are summarized in Table 1. The ^{31}P NMR spectra of cyclophosphazene derivatives containing the spiro moiety are observed as A_2X (or A_2B) spin systems with characteristic chemical shifts that reflects the number of spiro substituents in the compound, i.e., both the $\gtrdot PCl_2$ and $\gtrdot P(OR)_2$ chemical shifts move to high frequency (downfield) about 4.5–5.5 ppm per tetrafluorobutanedioxy moiety, as expected [20]. Similarly, the chemical shifts of the $\gtrdot P(OR)Cl$ group of the ansa derivatives move to high frequency (downfield) as the cyclophosphazene (**4**) is further substituted with spiro (**6**) or ansa (**7**) tetrafluorobutanedioxy moieties (Table 1). Whilst the chemical shifts of the PCl_2 [for isomers **3** and **4**] and $P(OR)_2$ groups [for isomers **5**, **6** and **7**] seem to be insensitive to the nature of the disposition of the P–Cl bonds (geminal or *cis*-non-geminal), the shifts of the P(OR)Cl group [for isomers **6** and **7**] show some differences. It is noteworthy that in these isomers the two P–Cl bonds of **7** represent the only example in this series, where these two bonds are in a *trans*-relationship.

The proton-decoupled ^{19}F NMR spectrum of the spiro form of the 2,2,3,3-tetrafluoro-1,4-butanedioxy moieties exists as a single line with essentially the same chemical shift (Table 1) for compounds **3**, **5**, **6** and **8**, whereas the ansa form gives rise to an AB spin system with $^{2}J(FF)$ ca. 283 Hz for compounds **4** and **6** and two AB spin systems with $^{2}J(FF)$ ca. 288 Hz for the non-gem *cis* bis-ansa compound **7**. The magnitudes of $^{2}J(FF)$ are in line with previous results on geminal coupling [21]. It should be

Table 1
MS[a] and NMR (^{1}H, ^{31}P and ^{19}F)[b] data on compounds **3**–**8**

Cpd	No.[c]	**3**	**4**	**5**	**6**	**7**	**8**
	Type[d]	sp	an	di-sp	sp-an	di-an	tri-sp
Mpt.	°C	95	145	204	120	>270	>280
M, *m*/*z*	Obs./Calc	435.9/435.8	436.0/435.8	526.0/525.9	525.9/525.9	525.8/525.9	615.9/616.0
δ (^{31}P)/ppm	$\geq PCl_2$	25.2	25.2	29.5		–	–
	$\geq P(OR)_2$	8.6	–	14.4	13.9	13.9	19.9
	$\geq P(OR)Cl$		23.6	–	28.5	31.2	–
$^{2}J_{P\text{-}P}$ (Hz)		75.0	65.0	81.5	86.5	85.4	
δ (^{19}F) (ppm)	$\geq CF_2$(sp)	−127.8	–	−127.9	−127.8	–	−127.9
	$\geq CF_2$(an)	–	−115.5/−116.6	–	−115.5/−116.7	−111.5/−115.1	–
						−117.3/−119.3	
$^{2}J_{F\text{-}F}$ (Hz)			283.5	–	282.5	288.4/288.5	
δ (^{1}H) (ppm)	$\geq CH_2$(sp)	4.39		4.35	4.36		4.24
	$\geq CH_2$(an)		4.42		4.36	4.27/4.40	
			4.75		4.74	4.62/4.75	

[a] MS (FAB + LCSIMS). Mass quoted for observed MH^+ peak and calculated for the ^{35}Cl isotopomer.
[b] 500 MHz ^{1}H NMR chemical shifts (ppm) with respect to internal TMS, 200 MHz ^{31}P NMR chemical shifts (ppm) with respect to external 85% H_3PO_4 and 470 MHz ^{19}F NMR chemical shifts (ppm) with respect to internal $CFCl_3$ observed on a Bruker 500 MHz DRX spectrometer.
[c] Structures of compounds are summarized in Fig. 1.
[d] sp = spiro and an = ansa.

noted that the line-widths of the ^{19}F NMR signals of the spiro moiety are narrower than those for the ansa moiety, which might reflect the fact that the spiro moiety is more flexible than the ansa moiety.

The ^{1}H NMR spectra of the spiro compounds **3**, **5** and **8**, are complex multiplets with similar chemical shifts (Table 1), whereas those for the mono-ansa moieties in compounds **4** and **6** are observed as two complex multiplets and for the non-gem *cis* bis-ansa compound **7** as four complex multiplets. Although analysis of these multiplets, in principle, could lead to ^{3}J(FH) and ^{3}J(PH) magnitudes and a conformational analysis of the spiro and ansa rings, in practice, this is not feasible because the appropriate Karplus-type relations for ^{3}J(FH) and ^{3}J(PH) magnitudes in such cyclophosphazene derivatives are not known. However, the conformations of the spiro and ansa rings have been determined by X-ray crystallography.

2.3. X-ray crystallographic characterization of compounds 3–8

The X-ray crystal structures are reported for compounds **3**–**8** (Figs. 2–7) and appropriate crystallographic data are summarized in Table 2.

The ($OCH_2CF_2CF_2CH_2O$) moiety forms spiro derivatives in compounds **3**, **5** and **8**, ansa derivatives in **4** and **7**, whereas compound **6** exhibits both spiro and ansa functionality. Each structure is composed of a cyclotriphosphazene core which, in all cases, exhibits no unusual deviations in geometry from either that of the parent $N_3P_3Cl_6$ structure (CSD code KAGKUY), [22] or from that observed in similar structures in the Cambridge Structural Database [23]. The cyclophosphazene rings are essentially planar, in which the deviation of individual atoms from the N_3P_3 plane in all the compounds reported here is less than 0.1 Å. However, the compounds are of structural interest

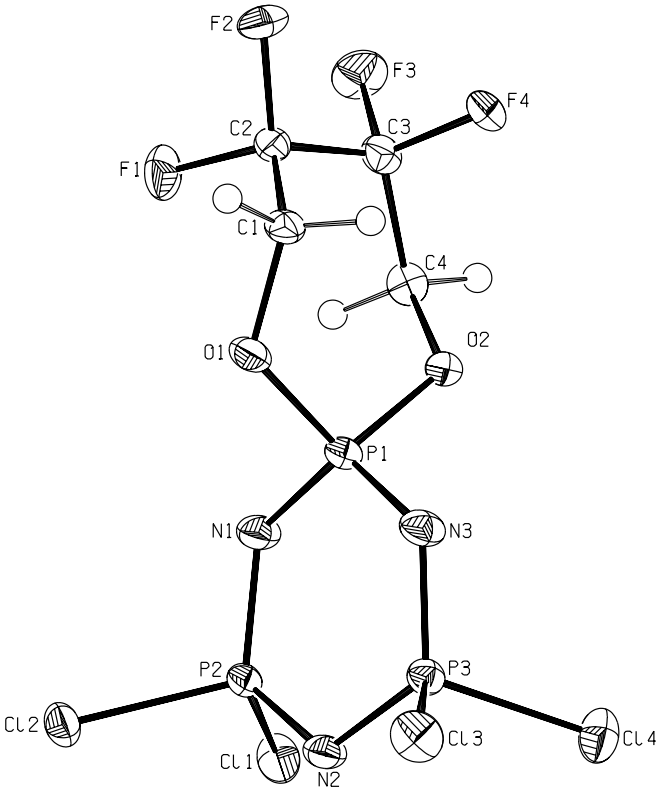

Fig. 2. The molecular structure of **3**, showing the atomic numbering scheme.

in that they are systematically substituted at the phosphorus centres by an increasing number of ($OCH_2CF_2CF_2$-CH_2O) moieties in either the spiro or ansa configurations.

The spiro rings in the spiro-substituted structures are all found to have similar twisted-chair conformations with a strictly alternating positive/negative torsion angle sequence around the ring and each ring component in a *gauche* conformation with respect to its neighbour. The twist of the

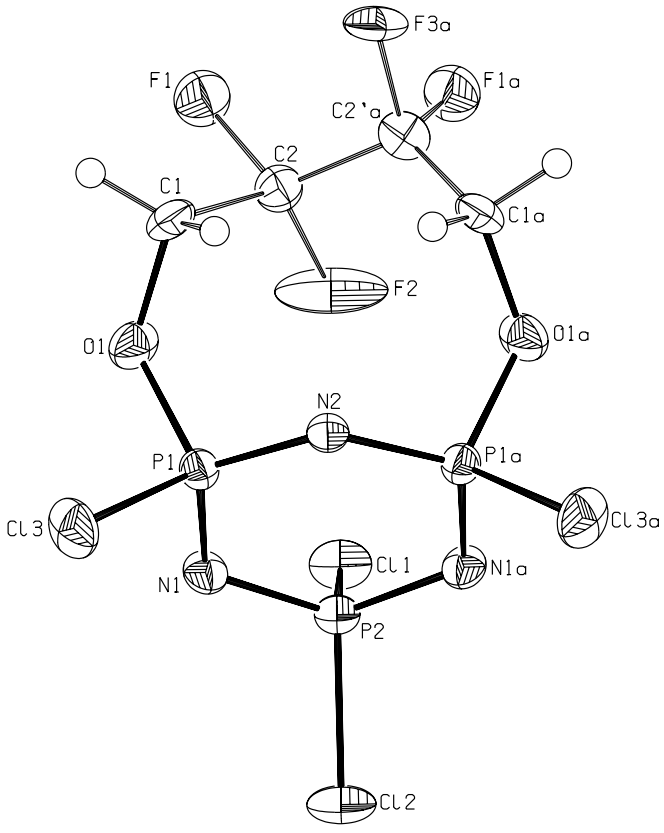

Fig. 3. The molecular structure of **4**, showing the atomic numbering scheme and with disorder omitted from the tetrafluorobutanedioxy backbone for the purposes of clarity.

7-membered P($OCH_2CF_2CF_2CH_2O$) spiro moiety gives a sense of chirality to the individual molecules which have been denoted as positive (*p*) or negative (*n*) depending on the sign of the O–P–O–C dihedral angle [16]. For the compounds measured in this work, positive twist angles are observed for the mono-spiro derivative **3** and both spiro rings of one molecule of the di-spiro compound **5**, whereas negative twist angles are observed for the spiro-ansa derivative **6** and both spiro rings of the second molecule in the unit cell of **5**. Interestingly, the tri-spiro derivative **8** has two *p* and one *n* form of twisted-chair conformation. A useful measure of ring conformation is puckering analysis [24], where calculation of the mean plane and puckering parameters afford a unique quantitative descriptor, the total puckering amplitude (Q), for a ring conformation. When subjected to ring puckering analysis the spiro substituted structures all have a total puckering amplitude, Q, in the range 0.7979–0.8359.

The spiro-containing structures exhibit intermolecular interactions, in that there are a large number of C–H···F close contacts present. Whilst not considered as 'classical' hydrogen-bonds, there is considerable evidence that interactions do exist between these moieties [25]. The range of D···A separations (some 20 in total for these 4 structures) varies from 3.073(6)Å for C1–H1A···F4 in **8** to an upper limit of 3.484(8) Å. Other notable D···A separations are: 3.102(6) Å for C8–H8B···F4 in **5**; 3.134(4) Å for C1–H1A···F4 in **3**; and 3.177(5) Å for C4–H4···F2 in **6**. Also present in structures (**5**) and (**6**) are short F···F contacts, which are currently the subject of much discussion [26], e.g., F3···F10 = 2.730(7) Å in **5** and F1···F6 = 2.885(6) Å in **6**.

The ansa-substituted structures in compounds **4**, **6** and **7** adopt the same general 9-membered ring conformation, which can best be described as a deformed crown having an anti conformation about the CH_2–CF_2 bonds. The total puckering amplitude [24] of the ansa rings is in the range 1.1878–1.1882, showing a remarkable degree of consistency. There are only a few intermolecular interactions present in these systems ranging from D···A separations for C–H···F contacts of 3.177(6) Å in **6** to 3.301(7) Å in **7**. The cyclophosphazene ring for the ansa compounds

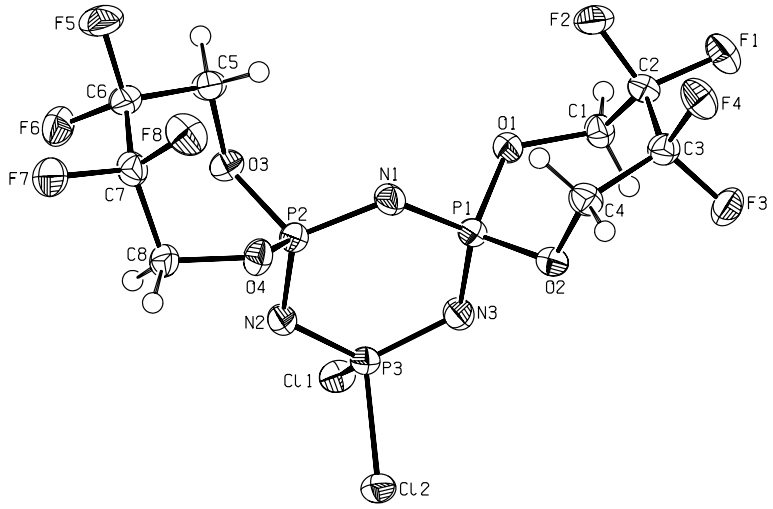

Fig. 4. The molecular structure of **5**, showing the atomic numbering scheme and only one of the two independent molecules depicted for purposes of clarity.

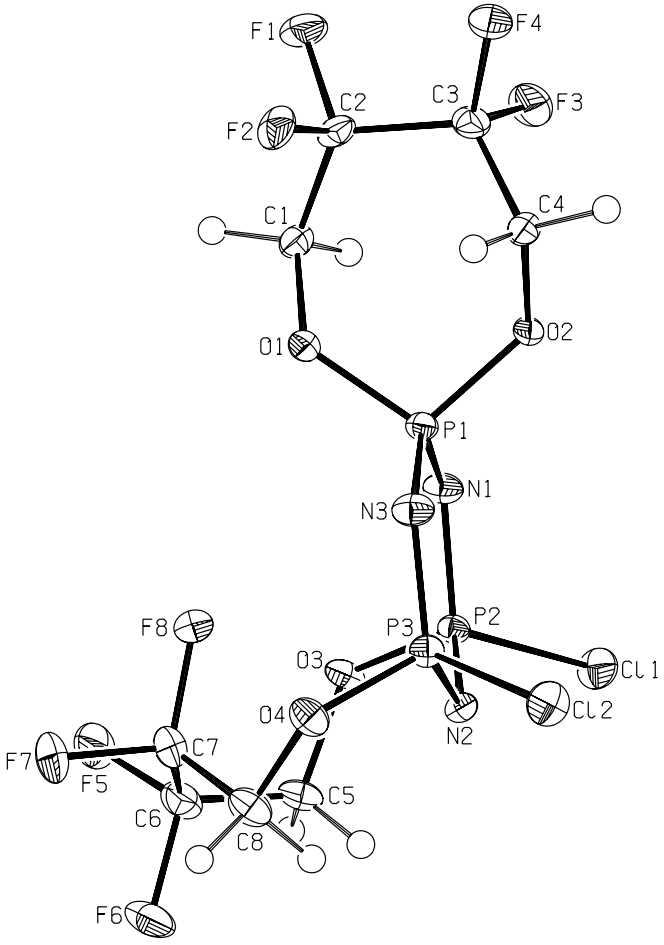

Fig. 5. The molecular structure of **6**, showing the atomic numbering scheme.

characterized in this work is essentially planar, which has also been observed for macrocyclic-phosphazene compounds having a 16-membered ansa ring [27,28]; this is in contrast to that discussed for 8-membered ansa rings (i.e., propanedioxy, propanolamino and ruthenocene) [29] and propanedioxy derivatives where the central CH_2 has been replaced by the ferrocenylCH_2P(S) moiety [14]. For the 8-membered ansa ring derivatives of cyclophosphazene, the deviation from the N_3P_3 plane of the nitrogen atom between the phosphorus atoms carrying the ansa moiety is usually greater than 0.2 Å [14,29,30]. The difference in behaviour of the ansa compounds is likely to reflect the higher degree of flexibility of the 16- and even the 9-membered rings compared to the 8-membered ansa ring system.

Whilst ansa structures of cyclophosphazenes have been known for about 20 years, ansa–ansa structures are relatively rare. There are two types of ansa–ansa structures; geminal, where the two ansa moieties share the same two phosphorus atoms, and non-geminal, where they share only one phosphorus atom. Published examples of the former all contain the tetraethyleneoxy macrocyclic group, $O(CH_2CH_2O)_4$, with the second group as either binaphthoxy [27a], ethylenediamino [27b], or another tetraethyleneoxy macrocyclic group [27c]. The ansa–ansa compound **8** reported here is only the second bis non-geminal structure in chlorocyclotriphosphazenes, the other having one tetraethyleneoxy macrocyclic ring and one binaphthoxy group [27a]. A similar structure has been proposed for a fluorocyclotriphosphazene derivative, but no crystallographic data were presented [31].

*2.4. Comparison of the electron-releasing capacity of a geminal pair of substituents for compounds derived from **1** by analysis of crystal structures*

The structure of the mono-spiro compound **3** formed from the tetrafluorobutanediol (**2**) is compared with that of its butane-1,4-diol analogue **12**, which does not have the fluorine atoms in the dioxy substituent, and also compared with a compound with an identical fluorinated spiro group, but having the 4 P–Cl bonds replaced by 4 P–F bonds, (**10**). The data are presented in Table 3 using the descriptions of bond lengths and angles shown in Fig. 8.

Comparison of the P–O bond length and POC bond angle of the butanedioxy derivative **12** with its tetrafluorobutanedioxy analogue **3** in Table 3 indicates that there is a considerably greater electron supply to the phosphazene ring of **12**, as demonstrated by a shorter P–O bond and a greater POC bond angle, resulting from the greater

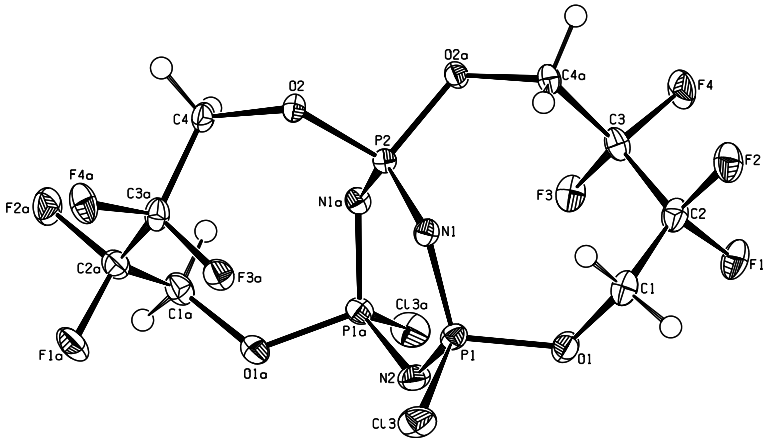

Fig. 6. The molecular structure of **7**, showing the atomic numbering scheme.

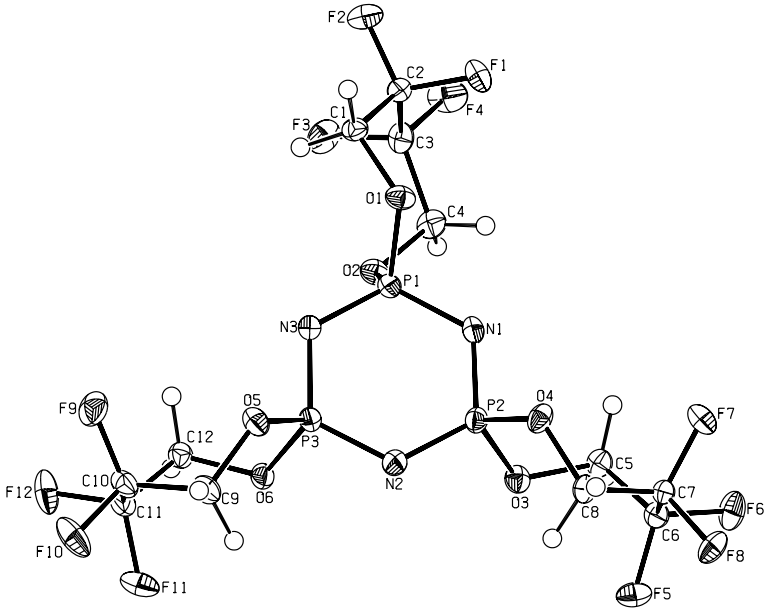

Fig. 7. The molecular structure of **8**, showing the atomic numbering scheme.

Table 2
Crystal data and refinement parameters for **3**, **4**, **5**, **6**, **7** and **8**

	3	**4**	**5**	**6**	**7**	**8**
Empirical formula	$C_4H_4Cl_4F_4N_3O_2P_3$	$C_4H_4Cl_4F_4N_3O_2P_3$	$C_8H_8Cl_2F_8N_3O_4P_3$	$C_8H_8Cl_2F_8N_3O_4P_3$	$C_8H_8Cl_2F_8N_3O_4P_3$	$C_{12}H_{12}F_{12}N_3O_6P_3$
Formula weight	436.81	436.81	525.98	525.98	525.98	615.16
Crystal system	monoclinic	orthorhombic	triclinic	monoclinic	orthorhombic	triclinic
Space group	$P2_1/n$	$Cmc2_1$	$P\bar{1}$	$C2/c$	$Pbcn$	$P\bar{1}$
a (Å)	5.89280(10)	11.3916(6)	11.4831(2)	30.6471(10)	17.0002(6)	6.6961(2)
b (Å)	13.5413(4)	11.4294(6)	12.8030(2)	6.1108(2)	11.1130(3)	10.8514(4)
c (Å)	17.6863(6	10.9340(4)	13.0505(2)	24.0233(10)	8.9716(2)	15.2892(6)
α (°)	90	90	98.4420(10)	90	90	92.1960(10)
β (°)	99.1310(10)	90	110.7170(10)	129.546(3)	90	102.5230(10)
γ (°)	90	90	100.0350(10)	90	90	107.157(3)
Volume (Å^3)	1393.42(7)	1423.60(12)	1721.29(5)	3469.3(2)	1694.94(8)	1030.00(6)
Z	4	4	4	8	4	2
D_{calc} (Mg/m^3)	2.082	2.038	2.030	2.014	2.061	1.983
Absorption coefficient (mm^{-1})	1.240	1.214	0.763	0.757	0.775	0.436
F(000)	856	856	1040	2080	1040	612
Crystal size (mm)	$0.20\times0.05\times0.02$	$0.50\times0.02\times0.02$	$0.40\times0.32\times0.05$	$0.14\times0.05\times0.05$	$0.54\times0.04\times0.03$	$0.38\times0.08\times0.02$
θ_{max} (°)	27.44	27.43	27.47	27.47	27.50	27.47
Reflections collected	12316	5884	24664	7789	9472	13843
Independent reflections	3099	1591	7674	3786	1938	4556
R_{int}	0.0490	0.0758	0.0695	0.0446	0.0743	0.0429
Final R indices $F^2>2\sigma F^2$	$R_1 = 0.0297$, $wR_2 = 0.0628$	$R_1 = 0.0364$, $wR_2 = 0.0735$	$R_1 = 0.0381$, $wR_2 = 0.1043$	$R_1 = 0.0401$, $wR_2 = 0.0780$	$R_1 = 0.0377$, $wR_2 = 0.0953$	$R_1 = 0.0376$, $wR_2 = 0.0860$
$\Delta\rho$ max/min (e Å^{-3})	0.371/−0.463	0.461/−0.389	0.587/−0.619	0.588/−0.472	0.502/−0.588	0.341/−0.434

lone-pair de-localization from the oxygen atom towards the N_3P_3 ring. Within the phosphazene ring there is also the usual pattern associated with a more electron-supplying substituent [28,32,33]: a smaller α and a larger β angle, a longer P–N bond (a) adjacent to the electron-supplying substituent, concomitant with a shorter P–N bond adjacent to it (b). This results in the Δ(P–N) value ($a-b$, as defined in Table 3) of 0.031 Å in the butanedioxy derivative **12** [32] compared to one of only 0.007 Å in its tetrafluoroalkoxy analogue **3**. Hence, there is only a very small electron-supply from the tetrafluorobutanedioxy group, which is barely distinguishable on this measure from that of a PCl_2 group.

Another approach to the electron-releasing capacity of a geminal pair of substituents is the effect this has on the average value of the P–Cl bonds in the two remaining PCl_2 groups (Table 3) compared with the value for compound **1** of 1.984 Å [22]. Although the changes are small in the sequence, (**3**) 1.990, (**12**) 1.994 [32], 1.998 Å for $N_3P_3Cl_4Ph_2$ [34] and 2.021 Å for $N_3P_3Cl_4(NPPh_3)_2$ [35], they are in keeping with the electron-supply properties

Table 3
Parameters of molecular framework of mono-spiro cyclophosphazene compounds

Structural Parameter[a]	Cyclophosphazene spiro-compound[b]		
	(**12**)[c]	(**3**)	(**10**)[d]
θ	106.1(1)	104.6(1)	104.3(2)
α	116.1(1)	117.7(1)	118.2(2)
β	122.3(1)	121.7(1)	121.2(2)
γ	119.3(1)	118.6(1)	119.5(1)
δ	120.1(2)	120.0(1)	120.1(3)
a	1.592(2)	1.577(1)	1.576(3)
b	1.561(2)	1.570(1)	1.570(3)
c	1.575(2)	1.584(1)	1.569(3)
Δ(P–N)[e]	0.031(3)	0.007(1)	0.006(4)
P–O	1.561(2)	1.579(1)	1.578(2)
POC	121.9(2)	122.7(1)	119.8(3)
P–Cl	1.994(3)	1.990(2)	

[a] Structural parameters defined in Fig. 8.
[b] Comparisons are made between spiro compounds **12**, $N_3P_3Cl_4[OCH_2CH_2CH_2CH_2O]$ and **3**, $N_3P_3Cl_4[OCH_2CF_2CF_2CH_2O]$, and between compounds **3** and **10**, $N_3P_3F_4[OCH_2CF_2CF_2CH_2O]$.
[c] Ref. [32].
[d] Ref. [14].
[e] Δ(P–N) = (*a*–*b*).

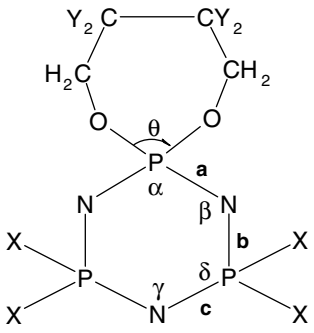

Fig. 8. Definition of bond lengths and bond angles for cyclophosphazene compounds **3**, **10** and **12**; Y = F or H, X = F or Cl.

discussed above. For the tetra-substituted compounds the P–Cl bond lengths are, as expected, rather larger: 2.002 Å for the di-spiro derivative **5** and 2.017 Å for $N_3P_3Cl_2Ph_4$ [36]. This larger effect is not surprising, because in the latter compounds the effects of 4 donor groups are spread over only 2 P–Cl bonds, whereas for the di-substituted derivatives the effects of 2 donors are spread over 4 P–Cl bonds. Nevertheless, both the changes in Δ(P–N) values and the changes in average P–Cl bond lengths demonstrate that the spiro tetrafluorobutanedioxy group has a small, but definite, electron-releasing effect relative to a PCl_2 group.

Fluorine has a much greater electronegativity than chlorine, yet comparison of the data for compound **3** with compound **10** in Table 3 shows that most of the structural parameters of the compound containing 4 P–Cl bonds are very similar to the one containing 4 P–F bonds. Perhaps the greater inductive electron-withdrawing effect of fluorine is compensated for by a more pronounced tendency to a mesomeric back-donation from its lone pairs of electrons.

2.5. Explanation of the difference in formation of spiro, ansa and bridged derivatives

It is necessary to explain the different nature of the products obtained with tetrafluorobutanediol in this work (spiro and ansa compounds) and that obtained earlier for butanediol (predominantly spiro). We also note that Shreeve and co-workers [15] reported only spiro and bridged compounds, although the same reaction solvent, THF, was used in their work as well as in ours. In both investigations the reaction mixtures were examined by NMR spectroscopy, so it can be assumed that all major products were accounted for. Shreeve and co-workers [15] found that heating the singly-bridged derivative caused partial conversion to the mono-spiro compound and it is therefore not clear how much of their spiro-derivatives are primary or secondary reaction products. Spiro derivatives are clearly the thermodynamically more stable form, which is also confirmed by the work of Elias and co-workers [30] on the transformation of fluorophosphazenes from ansa to spiro compounds in the presence of CsF. These authors also suggested that the absence of ansa compounds in the reactions with silylated reagents [15] was due to the catalytic conversion of these moieties to spiro groupings. As the PF_2 and PCl_2 groups are more electrophilic than either the PF(OR) or PCl(OR) moieties, the former would be the preferred reaction sites under kinetic control. The crystallographic data presented above show a slight, but definite, electron-supply by the spiro-tetrafluorobutanedioxy group and by implication also for the related PF(OR) and PCl(OR) groupings. However, in this work, reaction of **1** with the sodium salt of the diol (**2**) produced the ansa as well as the spiro derivative. For example, using the same molar ratio (1:0.4) of the cyclophosphazene (**1**) to the sodium salt of the diol (**2**) as used by Shreeve et al. [15], we observed by NMR spectroscopy approximately 60% unchanged $N_3P_3Cl_6$ and about 20% each of the mono-spiro (**3**) and the mono-ansa (**4**) derivatives, together with a trace of the dispiro compound **5**.

We also compared the products of the starting material, $N_3P_3Cl_6$ (**1**) with the sodium and lithium salts of the tetrafluorobutanediol (**2**) in THF using a molar ratio of 1:0.5 to confine the products to mono-substitution as much as possible. The ratio of mono-spiro (**3**):mono-ansa (**4**) was approximately 2:1 for the sodium derivative, but approximately 5:1 for the lithium reagent. As the lithium ion is smaller and its nuclear charge less shielded than that of the sodium ion, Li^+ is likely to form a stronger ion pair and hence make lithium alkoxides less reactive than their sodium analogues. THF is also probably solvating the sodium ion more strongly than the lithium ion and this too would enhance the reactivity of its alkoxide ion. Conductometric studies on the titration of alkali metal acetates with perchloric acid in acetic acid [37] and complexation studies of both the alkali metal ions with phosphazene lariat ethers by Bartsch et al. [38] indicate that ion-pairing will be stronger for lithium than for sodium alkoxides. The

counterion of the alkoxide is likely to be freer in the sodium reagent, making it more reactive than the lithium analogue, and hence proportionally more ansa derivative is obtained with the sodium alkoxide. A similar explanation can be offered for the observation that CsF acted as catalyst in the ansa to spiro transformation in fluorocyclotriphosphazenes, but LiF was reported to be inactive [14]. Reaction of **1** with the dilithiated diol, $FcCH_2P(S)(CH_2OLi)_2$, at −80 °C yielded one spiro and two ansa (endo and exo) derivatives in the ratio ca. 1:4 [14]. Reactions of the ansa isomer with the disodium salt of propane-1.3-diol indicated partial conversion of the ansa group to the spiro isomer [14], again consistent with the greater reactivity of the sodium derivative in line with the explanation above. This reaction [14] differs from the present study on the reaction of **1** with the lithium derivative of **2**, which gave significantly more spiro than ansa derivatives. The difference is likely to be a consequence of the reactions of the dilithiated diol, $FcCH_2P(S)(CH_2OLi)_2$, giving rise to spiro and ansa structures each containing one less atom than the ones reported here. The greater nucleophilic reactivity of the diol, $FcCH_2P(S)(CH_2OLi)_2$, than that of the sodium or lithium derivatives of tetrafluorobutanediol (**2**), and the low temperature of −80 °C undoubtedly also play a part. Elias and co-workers [30] have shown that for fluorophosphazenes 8-membered ansa groupings rearrange in the presence of catalysts to the thermodynamically more stable 6-membered spiro moieties and that this accelerates with increasing temperature. Whilst Elias and co-workers report that ansa derivatives of chlorocyclotriphosphazenes do not rearrange to their spiro derivatives, we infer that a similar rearrangement does take place with the 9-membered ansa groupings to 7-membered spiro moieties. We deduce this, because the plethora of ansa derivatives **4**, **6** and **7**, observed, when the molar ratio of phosphazene (**1**) to diol (**2**) was 1:1.2, whilst with an excess of the sodium derivative of **2** only the tri-spiro derivative (**8**) was observed. Clearly the ansa moiety in all three ansa carrying species rearranged at some stage to a spiro group. To prove this we treated the most abundant of these, the mono-ansa derivative **4**, with an excess of the sodium derivative of the reagent to yield the the tri-spiro derivative **8**. We cannot thus state, precisely, at which state of chlorine replacement this transformation occurred.

This raises the further question to what extent the spiro moieties observed in the reaction with a reactant ratio of 1:1.2 are primary reaction products or a result of a subsequent rearrangement. The answer was given by the NMR analysis of the low temperature reaction mixtures, which showed that the range of products and their ratios was largely the same as those observed at room temperature.

Why ansa and not bridging compounds? In the reactions of $N_3P_3Cl_6$ (**1**), with mono-functional reagents, such as secondary amines, giving rise to non-geminally di-substituted derivatives, the yields of the *trans*-isomer are generally substantially larger than that of the *cis*-isomer and steric effects were invoked to rationalize these observations [39]. However, for the reaction of **9** with NaOR [13,40,41] the reverse behaviour was observed, producing a slight predominance of the *cis* over *trans*-isomer, which was rationalized in terms of the co-ordination of the sodium ion by the lone pairs of electrons of the oxygen atom in the P–OR group already present after mono-substitution. A similar sodium ion solvation was also postulated by Brandt and co-workers [27,42] to account for the exclusive formation of *cis*-ansa macrocyclic-cyclophosphazene derivatives. Formation of such a *cis*-ansa product might be dictated by steric effects for short-chain diols, but for longer chain derivatives such as tetraethylene glycol, which were always used as sodium salts [27,42], the sodium solvation step by the existing PCl(OR) moiety may well play an important role. On the other hand, with the silylated diol no such solvation is possible and, because PF_2 is marginally more reactive than PF(OR), reaction occurs to form bridging compounds, especially as the molar ratio employed showed an excess of $N_3P_3F_6$ (**9**).

It can be seen that the nature of the products (spiro, ansa, bridged) depends, amongst other factors, on the avidity for each other of the electrophilic phosphorus-containing reagent and nucleophilic activity of the diol. The present work has shown that with an unchanged electrophile the lowered reactivity of the nucleophile favours spiro over ansa. Other work with an unchanged nucleophile has also found that a reduction in the electrophilic character of the phosphazene has the same effect, e.g., on substitution of some chlorine atoms in $N_3P_3Cl_6$ by electron-releasing substituents such as the phenyl or tertiary-butylamino groups. However, this is not the whole story, because we have observed that in the reactions of the hexachloride (**1**) with the two diols, propane-1,3-diol and 2,2-dimethylpropane-1,3-diol (using pyridine as the hydrogen halide acceptor), the former forms only traces of the ansa compound, whilst the latter does so in significant quantities [43], which has been explained in terms of the Thorpe–Ingold Effect [44]. Thus, relatively subtle changes between different nucleophiles can tilt significantly the spiro/ansa balance, which is likely to be the reason why the sodium derivative of **2** gave such a range of products that differed markedly from those obtained by the reaction of compound **12** in the presence of pyridine [1]. In case the difference was due to the diol/pyridine reagent, we have also investigated the initial stages of the same reaction using the sodium derivative of butane1,4-diol and found substantially the same range of products as with diol/pyridine reagent and most noticeably the absence of ansa-derivatives. The case of the reaction of compound **9** with the silylated derivative of **2** provides another subtle change in the nature of the nucleophile, further complicated by this reaction being largely driven by the strengths of the Si–F being formed ([17] and references therein). Much remains to be explained, such as the observation that the mono-ansa compound **4** reacts with pyrrolidine with retention of configuration [45].

3. Experimental

3.1. Materials

Hexachlorocyclotriphosphazene (Otsuka Chemical Co., Ltd) was purified by fractional crystallisation from hexane. Sodium hydride, 60% dispersion in mineral oil (Merck), the latter removed by washing with dry heptane (Merck) followed by decantation. Hexane, heptane (Merck) and 2,2,3,3-tetrafluoro-1,4-butanediol (Aldrich) were used as received. THF was distilled over a sodium–potassium alloy under an atmosphere of dry argon. All reactions were performed under a dry argon atmosphere. For column chromatography silica gel (230–400 mesh Merck) was used.

3.2. Methods

Elemental analyses were obtained using a Carlo Erba 1106 Instrument. Mass spectra were recorded on a VG Zab Spec GC–MS spectrometer using the fast atom bombardment (FAB) method (35 kV) with MNBA as the matrix; ^{35}Cl values were used for calculated masses. Analytical thin layer chromatography (TLC) was performed on Merck Silica gel plates (Merck Kieselgel 60, 0.25 mm thickness) with F_{254} indicator. Column chromatography was performed on silica gel (Merck 60, 230–400 mesh; for 3 g crude mixture, 100 g silica gel was used in a column of 3 cm in diameter and 60 cm in length). ^{1}H, ^{19}F and ^{31}P NMR spectra were recorded in $CDCl_3$ solutions on a Bruker DRX 500 MHz spectrometer using TMS as an internal reference for ^{1}H, $CFCl_3$ as an internal reference for ^{19}F and 85% H_3PO_4 as an external reference for ^{31}P. In order to assign the signals of some compounds both proton-coupled and proton-decoupled ^{19}F and ^{31}P NMR spectra were recorded.

3.3. Reaction of hexachlorocyclotriphosphazene (*1*) with 2,2,3,3-tetrafluoro-1,4-butanediol (*2*) in a 1:1.2 ratio to form compounds *3*–*7*

Hexachlorocyclotriphosphazene (**1**), (3.48 g, 10 mmol) and 2,2,3,3-tetrafluoro-1,4-butanediol (1.94 g, 12 mmol), (**2**), were dissolved in 300 mL of dry THF under an argon atmosphere in a 500 mL three-necked round-bottomed flask The reaction mixture was cooled in an ice-bath and NaH (60% oil suspension, 0.96 g, 24 mmol) in 30 mL of dry THF was quickly added to a stirred solution under an argon atmosphere. The reaction mixture was stirred for 2 h at room temperature and the reaction followed on TLC silica gel plates using hexane–dichloromethane (1:1) as eluant. Five products were observed and none of compound **1** remained. The reaction mixture was filtered to remove the sodium chloride formed and the solvent removed under reduced pressure. The resulting colorless oil was subjected to column chromatography, using hexane-dichloromethane (2:1) as eluant. The first product is the mono-spiro derivative $[N_3P_3Cl_4(OCH_2CF_2CF_2CH_2O)]$ (**3**), (1.23 g, 28%, m.p. 95 °C). *Anal.* Calc. for $C_4H_4Cl_4F_4N_3O_2P_3$: C, 11.00; H, 0.92; N, 9.62. Found: C, 10.97; H, 0.93; N, 9.52%. The second product is the isomeric mono-ansa derivative $[N_3P_3Cl_4(OCH_2CF_2CF_2CH_2O)]$, (**4**), (0.6 g, 14%, m.p. 145 °C). *Anal.* Found: C, 11.05; H, 0.93; N, 9.40%. The third product is the bis-spiro derivative $[N_3P_3Cl_2(OCH_2CF_2CF_2CH_2O)_2]$ (**5**), (0.39 g, 7%, m.p. 204 °C). *Anal.* Calc. for $C_8H_8Cl_2F_8N_3O_4P_3$: C, 18.27; H, 1.53; N, 7.99. Found: C, 18.27; H, 1.52; N, 7.65%. The fourth product is the isomeric spiro-ansa derivative $[N_3P_3Cl_2(OCH_2CF_2CF_2CH_2O)_2]$ (**6**), (0.22 g, 4%, m.p. 120 °C). *Anal.* Found: C, 18.38; H, 1.47; N, 7.64% and the fifth product is the isomeric non-gem *cis* bis-ansa derivative $[N_3P_3Cl_2(OCH_2CF_2CF_2CH_2O)_2]$ (**7**), (0.1 g, 2%, m.p. > 270 °C). *Anal.* Found: C, 18.25; H, 1.52; N, 7.89%. All of the new compounds were crystallized from hexane–dichloromethane (1:2) and obtained as colorless crystals.

3.4. Reaction of *1* with *2* in a 1:3 ratio to form compound *8*

1 (1.74 g, 5 mmol) and **2** (2.425 g, 15 mmol) were dissolved in 100 mL of dry THF under argon atmosphere in a 250 mL three-necked round-bottomed flask. The reaction mixture was cooled in an ice-bath and NaH (60% oil suspension, 1.2 g, 30 mmol) in 30 mL of dry THF was quickly added to a stirred solution under an argon atmosphere. The reaction mixture was stirred for 24 h at room temperature and the reaction followed by TLC on silica gel plates using hexane–THF (1:1). Only one product was observed and no starting material **1** was detected. The reaction mixture was filtered to remove the sodium chloride formed, the solvent removed under reduced pressure and the resulting colorless oil subjected to column chromatography, using THF as eluant. The product is the tri-spiro derivative $[N_3P_3(OCH_2CF_2CF_2CH_2O)_3]$ (**8**), (1.72, 56%, m.p. 332), a colorless solid, which was re-crystallized from THF–hexane (1:1). *Anal.* Calc. for $C_{12}H_{12}F_{12}N_3O_6P_3$: C, 23.43; H, 1.97; N, 6.83. Found: C, 23.45; H, 1.98; N, 6.81%.

3.5. Reactions of hexachlorocyclotriphosphazene (*1*) with 2,2,3,3-tetrafluoro-1,4-butanediol (*2*) at −78 °C

Hexachlorocyclotriphosphazene, (**1**), (3.48 g, 10 mmol) and 2,2,3,3-tetrafluoro-1,4-butanediol (1.62 g, 10 mmol), (**2**), were dissolved in 90 mL of dry THF under an argon atmosphere in a 100 mL three-necked round-bottomed flask at ≈−78 °C (acetone–liquid nitrogen). NaH (60% oil suspension, 0.8 g, 20 mmol) in 3 mL of dry THF was quickly added to a stirred solution under an argon atmosphere. The reaction mixture was stirred for 3 h at low temperature (−78 °C) and the reaction followed on TLC silica gel plates using hexane–dichloromethane (3:1) as eluant. 1/3 of the reaction mixture was removed for NMR analysis; 3 products **3**, **4** and **5** were observed and no starting material **1** remained. Reagent **2** and NaH were then added to achieve a 1:2 stoichiometry under the same conditions

and the reaction mixture stirred for a further 3 h. Half of this reaction mixture was removed for NMR analysis and five products (**3**, **4**, **5**, as well as **6**, **7**) were observed. Reagent **2** and NaH were again added to the remaining reaction mixture to achieve a 1:3 stoichiometry. The reaction mixture was stirred for 3 h at −78 °C, followed by 20 h at room temperature and the reaction followed on TLC silica gel plates using hexane–dichloromethane (1:1) as eluant. It was observed that all the compounds were transformed into the tri-spiro compound **8** as confirmed by TLC, mpt. and ^{31}P NMR.

3.6. Reaction of *4* with *2* in a 1:3 ratio to form compound *8*

Mono-ansa (**4**), (0.65 g, 1.5 mmol) and 2,2,3,3-tetrafluoro-1,4-butanediol (0.73 g, 4.5 mmol) (**2**), were dissolved in 10 mL of dry THF under an argon atmosphere in a 100 mL three-necked round-bottomed flask at room temperature. NaH (60% oil suspension, 0.36 g, 9 mmol) in 2 mL of dry THF was quickly added to a stirred solution under an argon atmosphere. The reaction mixture was stirred for 20 h at room temperature and the reaction followed on TLC silica gel plates using hexane-dichloromethane (1:1) as eluent. It was observed that all of compound **4** was transformed into the tri-spiro compound **8**, as was confirmed by TLC, mpt. and ^{31}P NMR.

4. X-ray structure determinations

Data were collected by means of combined phi and omega scans on a Bruker-Nonius KappaCCD area detector situated at the window of a rotating anode (λ Mo Kα = 0.71073 Å). The structures were solved by direct methods, SHELXS-97 and refined using SHELXL-97 [46]. Hydrogen atoms were included in the refinement, but thermal parameters and geometry were constrained to ride on the atom to which they are bonded. The data were corrected for absorption effects using SORTAV [47,48]. Supplementary data in the form of CIF files have been deposited with the Cambridge Crystallographic Data Centre with deposition numbers CCDC 277314–277319 inclusive.

Acknowledgements

The authors thank the Otsuka Chemical Co. Ltd for gifts of $N_3P_3Cl_6$, Professor D. Feakins for helpful discussions on the solvation of alkali metal ions, the EPSRC for funding the National Crystallographic Service (Southampton, UK) and Gebze Institute of Technology (GIT) Research Fund for partial support (S.B. and A.K.).

References

[1] A.H. Alkubaisi, H.G. Parkes, R.A. Shaw, Heterocycles 28 (1989) 347.
[2] R.A. Shaw, Phosphorus Sulfur Silicon 45 (1989) 103.
[3] G. Guerch, J.F. Labarre, R. Lahana, R. Rocques, F. Sournies, J. Galy, J. Mol. Struct. 99 (1983) 275.
[4] G. Guerch, J.F. Labarre, R. Lahana, F. Sournies, J. Galy, R. Enjalbert, J. Galy, J.P. Declercq, Inorg. Chim. Acta 83 (1984) L33.
[5] V. Chandrasekhar, K.R.J. Thomas, J. Appl. Organomet. Chem. 67 (1993) 1.
[6] P.R. Suszko, R.R. Whittle, H.R. Allcock, J. Chem. Soc., Chem. Commun. (1982) 960.
[7] H.R. Allcock, K.D. Lavin, G.H. Riding, R.R. Whittle, M. Parvez, Organometallics 5 (1989) 1621.
[8] H.R. Allcock, J.A. Dodge, I. Manners, M. Parvez, G.H. Riding, K.B. Visscher, Organometallics 10 (1991) 3098.
[9] M. Herberhold, A. Hofmann, W.Z. Milius, Anorg. Allg. Chem. 623 (1997) 1599.
[10] (a) D. Dell, B.W. Fitzsimmons, R.A. Shaw, J. Chem. Soc. (1965) 4070;
(b) S. Karthikeyan, S.S. Krishnamurthy, Z. Anorg. Allg. Chem. 513 (1984) 231.
[11] J.L. Schmutz, H.R. Allcock, Inorg. Chem. 14 (1975) 2433.
[12] A.P. Carroll, R.A. Shaw, J. Chem. Soc. (A) (1966) 914.
[13] A.S. Freund, M. Calichman, C.W. Allen, Z. Anorg. Allg. Chem. 630 (2004) 2059.
[14] K.N. Muralidharan, P. Venugopalan, A.J. Elias, Inorg. Chem. 42 (2003) 3176.
[15] A.J. Elias, R.L. Kirchmeier, J.M. Shreeve, Inorg. Chem. 33 (1994) 2727.
[16] Z. Wang, R.D. Willett, A.J. Elias, R.L. Kirchmeier, J.M. Shreeve, Acta Crystallogr. Sect. B 52 (1996) 643.
[17] D. Dahmann, H. Rose, R.A. Shaw, Z. Naturforsch. b 32 (1977) 236.
[18] (a) D. Feakins, N. Nabi, R.A. Shaw, P. Watson, J. Chem. Soc. (A) (1968) 10;
(b) D. Feakins, W.A. Last, N. Nabi, R.A. Shaw, P. Watson, J. Chem. Soc. (A) (1969) 196;
(c) D. Feakins, R.A. Shaw, P. Watson, N. Nabi, J. Chem. Soc. (A) (1969) 2468.
[19] K. Brandt, I. Porwolik, T. Kupka, A. Olejnik, R.A. Shaw, D.B. Davies, J. Org. Chem. 60 (1995) 7433.
[20] S.S. Krishnamurthy, M. Woods, Annu. Reports NMR Spectrosc. 19 (1987) 175.
[21] J.W. Emsley, L. Phillips, V. Wary, Fluorine Coupling Constants, Pergamon Press, New York, 1977.
[22] G.J. Bullen, J. Chem. Soc. B (1971) 1450.
[23] A.G. Orpen, L. Brammer, F.H. Allen, O. Kennard, D.G. Watson, R. Taylor, International Tables for Crystallography, vol. C, 1992.
[24] D. Cremer, J.A. Pople, J. Amer. Chem. Soc. 97 (1975) 1354.
[25] J.A.K. Howard, V.J. Hoy, D. O'Hagan, G.T. Smith, Tetrahedron 52 (1996) 12613.
[26] C.B. Aakeroy, A.M. Beatty, K.R. Lorimer, Struct. Chem. 10 (1999) 229.
[27] (a) K. Brandt, I. Porwolik, A. Olejnik, R.A. Shaw, D.B. Davies, M.B. Hursthouse, G.D. Sykara, J. Am. Chem. Soc. 118 (1996) 4496;
(b) K. Brandt, I. Porwolik, M. Siwy, T. Kupka, R.A. Shaw, D.B. Davies, M.B. Hursthouse, G.D. Sykara, J. Am. Chem. Soc. 119 (1997) 1143;
(c) K. Brandt, I. Porwolik-Czomperlik, M. Siwy, T. Kupka, R.A. Shaw, D.B. Davies, M.B. Hursthouse, Sykara, J. Am. Chem. Soc. 119 (1997) 12432.
[28] S. Beşli, S.J. Coles, D.B. Davies, M.B. Hursthouse, A. Kılıç, T.A. Mayer, R.A. Shaw, Acta Crystallogr. Sect. B 58 (2002) 1067.
[29] (a) S.R. Contractor, M.B. Hursthouse, H.B. Parkes, L.S. Shaw (née Gözen), R.A. Shaw, H. Yılmaz, J. Chem. Soc. Chem. Comm. (1984) 675;
(b) S.R. Contractor, M.B. Hursthouse, H.B. Parkes, L.S. Shaw (née Gözen), R.A. Shaw, H. Yılmaz, Phosphorus and Sulfur 28 (1986) 267.
[30] (a) K. Muralidharan, N.D. Reddy, A.J. Elias, Inorg. Chem. 39 (2000) 3988;
(b) N.D. Reddy, A.J. Elias, A. Vij, Inorg. Chem. Commun. 3 (2000) 29.
[31] K. Muralidharan, A.J. Elias, Inorg. Chem. 42 (2003) 7535.

[32] S.R. Contractor, M.B. Hursthouse, L.S. Shaw (née Gözen), R.A. Shaw, H. Yılmaz, Acta Crystallogr. Sect. B 41 (1985) 122.
[33] (a) R.A. Shaw, Phosphorus Sulfur 28 (1986) 99;
(b) S. Besli, S.J. Coles, D.B. Davies, M.B. Hursthouse, A. Kılıç, T.A. Mayer, R.A. Shaw, A. Uslu, Acta Crystallogr. Sect. B 58 (2002) 545.
[34] N.V. Mani, F.R. Ahmed, W.H. Barnes, Acta Crystallogr. Sect. B 19 (1965) 693.
[35] M. Krishnaiah, L. Ramamurthy, P. Ramabrahman, H. Manohar, Z. Naturforsch. b 36 (1981) 765.
[36] N.V. Mani, F.R. Ahmed, W.H. Barnes, Acta Crystallogr. Sect. B 20 (1966) 375.
[37] N. Gündüz, T. Gündüz, E. Kılıç, S.G. Öztas, M. Tüzün, L.S. Shaw (née Gözen), R.A. Shaw, J. Chem. Soc. Dalton Trans. (1987) 925.
[38] R.A. Bartsch, E.K. Lee, S. Chun, N. Elkarim, K. Brandt, I. Porwolik-Czomperlik, M. Siwy, D. Lach, J. Silberring, J. Chem. Soc. Perkin Trans. 2 (2002) 442.
[39] (a) R. Keat, R.A. Shaw, J. Chem. Soc. (1965) 2215;
(b) R. Keat, R.A. Shaw, J. Chem. Soc. (A) (1966) 908.
[40] K.C. Kumara Swamy, S.S. Krishnamurthy, Inorg. Chem. 25 (1986) 920.
[41] C.W. Allen, Chem. Rev. 91 (1991) 119.
[42] K. Brandt, M. Siwy, I. Porwolik-Czomperlik, J. Silberring, J. Org. Chem. 66 (2001) 5701.
[43] H.A. Al-Madfa, R.A. Shaw, S. Ture, Phosphorus Sulfur Silicon 53 (1990) 333.
[44] A.J. Kirby, in: V. Gold, D. Bethell (Eds.), Advances in Physical Organic Chemistry, vol. 17, Academic Press, London, New York, Toronto, 1980, p. 208.
[45] S. Beşli, S.J. Coles, D.B. Davies, R.J. Eaton, M.B. Hursthouse, H. Ibişoglu, A. Kılıç, R.A. Shaw, Chemistry – A European Journal 10 (2004) 4915.
[46] G.M. Sheldrick, SHELX Suite of Programs for Crystal Structure Solution and Refinement, University of Göttingen, Germany, 1997.
[47] R.H. Blessing, Acta Crystallogr. Sect. A 51 (1995) 33.
[48] R.H. Blessing, J. Appl. Cryst. 30 (1997) 421.

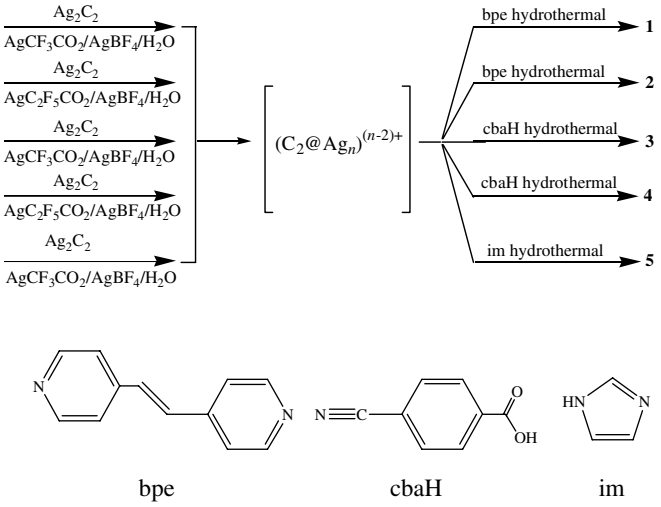

Scheme 1.

coordination sites [4]; besides this, they are capable of creating supramolecular architectures through π–π interaction and/or hydrogen bonding (involving the aromatic ring, carboxylate group of cbaH and the possible protonated forms of bpe and im) [5]. Execution of the synthetic procedure shown in Scheme 1 yielded the following five complexes, whose structures are described in the present report.

$(bpeH_2 \cdot 2H_2O)[Ag_8(C_2)(CF_3CO_2)_8(H_2O)_2] \cdot 2H_2O$ (**1**),
$[Ag_{14}(C_2)_2(C_2F_5CO_2)_{10}(H_2O)_4(bpe)] \cdot H_2O$ (**2**),
$[Ag_7(C_2)(CF_3CO_2)_2(cba)_3]$ (**3**),
$[Ag_7(C_2)(C_2F_5CO_2)_5(cbaH)(H_2O)_2]$ (**4**),
$(imH)_3[Ag_8(C_2)(CF_3CO_2)_9] \cdot H_2O$ (**5**).

2. Experimental

2.1. Synthesis

All chemicals were purchased from ACROS and Aldrich and used without further purification. Ag_2C_2 was prepared as described previously [6]. *CAUTION! Thoroughly dried Ag_2C_2 detonates easily upon mechanical shock, and only a small quantity of freshly prepared sample should be used in any chemical reaction. Excess amounts can be disposed of via slow decomposition in an alkaline solution* [7]. *To ensure safety, we used moist Ag_2C_2 in all preparations.*

2.1.1. $(bpeH_2 \cdot 2H_2O)[Ag_8(C_2)(CF_3CO_2)_8(H_2O)_2] \cdot 2H_2O$ (1)

Freshly prepared Ag_2C_2 was added to an aqueous solution (1 mL) of $AgCF_3CO_2$ (0.44 g, 2 mmol) and $AgBF_4$ (0.39 g, 2 mmol) in a plastic beaker with stirring until saturation was attained. The excess amount of Ag_2C_2 was filtered off and then *trans*-1,2-bis(4-pyridyl)ethylene (45 mg, 0.25 mmol) was added to the filtrate. The resulting suspension was placed in a 25 mL Teflon-lined stainless-steel reaction vessel and subjected to hydrothermal conditions at 115 °C for 36 h, and subsequently cooled to room temperature at 6 °C/h. Colorless block-like crystals of **1** were isolated in ~50% yield. *Anal*. Calc. for **1**: C, 17.30; H, 1.16; N, 1.34. Found: C, 17.22; H, 1.19; N 1.29%.

2.1.2. $[Ag_{14}(C_2)_2(C_2F_5CO_2)_{10}(H_2O)_4(bpe)] \cdot H_2O$ (2)

Complex **2** was synthesized in a similar manner to **1** except that $AgC_2F_5CO_2$ was used instead of $AgCF_3CO_2$. Colorless block-like crystals were obtained in ~40% yield. *Anal*. Calc. for **2**: C, 15.96; H, 0.58; N, 0.81. Found: C, 16.02; H, 0.61; N, 0.78%.

2.1.3. $[Ag_7(C_2)(CF_3CO_2)_2(cba)_3]$ (3)

The synthetic procedure for **1** was repeated using 4-cyanobenzoic acid instead of *trans*-1,2-bis(4-pyridyl)ethylene. Colorless block-like crystals of **3** were obtained in ~52% yield. *Anal*. Calc. for **3**: C, 24.96; H, 0.84; N, 2.91. Found: C, 25.02; H, 0.79; N, 2.96%.

2.1.4. $[Ag_7(C_2)(C_2F_5CO_2)_5(cbaH)(H_2O)_2]$ (4)

Complex **4** was synthesized in a similar manner to **3** except that $AgC_2F_5CO_2$ was used in place of $AgCF_3CO_2$. Colorless block-like crystals were obtained in ~65% yield. *Anal*. Calc. for **4**: C, 16.89; H, 0.51; N, 0.79. Found: C, 16.82; H, 0.48; N, 0.83%.

2.1.5. $(imH)_3[Ag_8(C_2)(CF_3CO_2)_9] \cdot H_2O$ (5)

The synthetic procedure for **1** was repeated using imidazole instead of *trans*-1,2-bis(4-pyridyl)ethylene. Colorless block-like crystals of **5** were obtained in ~48% yield. *Anal*. Calc. for **5**: C, 16.36; H, 0.80; N, 3.95. Found: C, 16.41; H, 0.79; N 3.91%.

2.2. X-ray crystallography

Selected single crystals were used for measurement on a Bruker SMART 1000 CCD diffractometer using Mo Kα radiation ($\lambda = 0.71073$ Å) at 293 K for **1**, **2**, **4** and **5**. Data collection and reduction were performed with the SMART and SAINT software [8]. An empirical absorption correction was applied using the SADABS program [9]. For complex **3**, the intensities were collected on a Rigaku AFC7R four-circle diffractometer in the variable ω-scan mode using Mo Kα radiation at 293 K. Intensity data were obtained in the range $2.3° < \theta < 25°$, and an empirical absorption correction based on ψ-scan was applied [10]. All five crystal structures were solved by direct methods and refined by full-matrix least squares on F^2 using the SHELXTL program package [11]. The crystal data and details of refinement for **1**–**5** are summarized in Table 1, and selected bond distances are listed in the legends for figures. In complex **5**, one of the three independent imH groups is orientationally disordered.

3. Results and discussion

As described before, Ag_2C_2 readily dissolves in a concentrated aqueous solution of silver(I) salts to form polyhedral

Table 1
Crystallographic data of complexes **1**–**5**

Complex	**1**	**2**	**3**	**4**	**5**
Empirical formula	$C_{15}H_{12}Ag_4F_{12}NO_{11}$	$C_{23}H_{10}Ag_7F_{25}NO_{12.5}$	$C_{30}H_{12}Ag_7F_6N_3O_{10}$	$C_{25}H_9Ag_7F_{25}NO_{14}$	$C_{14.5}H_{8.5}Ag_4F_{13.5}N_3O_{9.5}$
Formula weight	1041.71	1730.37	1443.52	1777.42	1064.71
Crystal size	$0.58\times0.47\times0.33$	$0.62\times0.56\times0.37$	$0.65\times0.52\times0.46$	$0.60\times0.42\times0.28$	$0.52\times0.46\times0.44$
Crystal system	triclinic	triclinic	triclinic	triclinic	monoclinic
Space group	$P\bar{1}$ (No. 2)	$P\bar{1}$ (No. 2)	$P\bar{1}$ (No. 2)	$P\bar{1}$ (No. 2)	$C2/c$ (No. 15)
a (Å)	8.395(2)	8.5470(5)	9.002(2)	8.586 (2)	15.5468(8)
b (Å)	11.734(2)	16.0964(9)	14.681(3)	16.614(3)	32.104(2)
c (Å)	15.234(3)	16.5655(9)	15.203(3)	16.933(4)	12.8355(7)
α (°)	68.07(3)	109.220(1)	118.74(3)	114.496(4)	90
β (°)	75.78(3)	103.807(1)	92.02(3)	98.456(5)	116.966(1)
γ (°)	75.85(3)	99.551(1)	100.89(3)	96.282(5)	90
V (Å^3)	1329.8(5)	2014.2(2)	1711.3(6)	2134.9(7)	5709.9(5)
Z	2	2	2	2	8
D_{calc} (g/cm^3)	2.587	2.845	2.801	2.765	2.475
μ(Mo Kα) (mm^{-1})	3.040	3.505	4.016	3.314	2.841
F(000)	980	1613	1352	1664	4009
Total reflections	7106	10892	6278	9419	15257
Unique reflections (R_{int})	4615 (0.0209)	7047 (0.0271)	6020 (0.0420)	7470 (0.0371)	5036 (0.0273)
Data [$I>2\ \sigma(I)$]	4077	5647	4523	5281	4307
Parameters	416	622	515	649	408
Goodness-of-fit	1.032	1.037	1.029	1.036	1.047
R_1 [$I>2\sigma(I)$][a]	0.0517	0.0617	0.0440	0.0745	0.0482
wR_2 (all data)[b]	0.1421	0.1797	0.1137	0.2142	0.1301

[a] $R_1 = \sum||F_o| - |F_c||/\sum|F_o|$.
[b] $wR_2 = \{\sum[w(F_o^2 - F_c^2)^2]/\sum[w(F_o^2)^2]\}^{1/2}$.

species of the type $[C_2@Ag_n]^{(n-2)+}$ ($n = 6$–10). The introduction of a bpe, cbaH, or im ligand to an aqueous system of this kind afforded a precipitate, which was then manipulated under hydrothermal conditions for the generation of new structural motifs. Comparison of the present work with our previous studies of the $Ag_2C_2/AgBF_4/R_fCO_2Ag$ system [12] shows that the employment of such ligands expands the scope of supramolecular assembly of new solid-state architectures.

3.1. $(bpeH_2\cdot 2H_2O)[Ag_8(C_2)\ (CF_3CO_2)_8(H_2O)_2]\cdot 2H_2O$ (*1*)

Single-crystal X-ray analysis revealed that complex **1** represents an unusual example of an inclusion complex constructed with silver(I) polyhedra each containing an encapsulated C_2^{2-} dianion. In the crystal structure of **1**, the building block is a centrosymmetric $C_2@Ag_8$ single cage in the shape of a slightly distorted cube, as shown in Fig. 1. Atoms in the face (Ag1aAg2Ag3Ag4) are coplanar within 0.0748 Å. The enclosed C_2^{2-} species retains its triple-bond character (C1–C1a = 1.24(1) Å) and binds its neighboring silver atoms via multiple σ/π Ag–C interactions in the range of 2.242(5)–2.509(5) Å.

The trifluoroacetate ligands function in μ_2- or μ_3-coordination modes, the latter further interlinking the $C_2@Ag_8$ cages into an infinite zigzag silver(I) chain along the *a* direction (Fig. 1).

Another prominent structural unit in **1** is a centrosymmetric aggregate composed of two Ag_2O_2 rhombuses connected by a pair of Ag–Ag edges. This Ag_4O_4 aggregate may be described as a distorted cube with two cleaved Ag–O edges. The relevant Ag–O (trifluoroacetate oxygen) bond distances range from 2.386(4) to 2.451(4) Å, whereas the Ag–Ag bond lengths are 2.848(1) Å. The Ag–O–Ag angles are 106.2° and 105.7° and the O–Ag–O angles are all 73.1°. The groups of atoms that form each of the six faces of the incomplete cube deviate slightly from

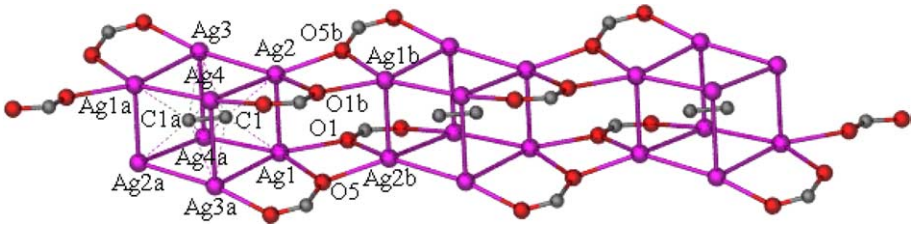

Fig. 1. A portion of polymeric chain in **1** generated from the linkage of centrosymmetric $C_2@Ag_8$ single cages via μ_3-*O*,*O*,*O*′-trifluoroacetate ligands. Selected bond distances [Å]: C1–C1a 1.24(1), C1–Ag1 2.242(5), C1–Ag2 2.244(5), C1–Ag3 2.509(5), C1–Ag4 2.420(5).

planarity, and their deviations from the respective best planes vary between 0.005 and 0.110 Å. Such a Ag_4O_4 aggregate is similar to that first found in $Ag_2C_2 \cdot 6CHF_2CO_2Ag$ [13].

The bpe molecule located at a $\bar{1}$ site is fully protonated to satisfy the charge balance. Of the three independent water molecules in **1**, O1w forms an acceptor hydrogen bond with a terminal of the $(bpeH_2)^{2+}$ dication (N1–O1w = 2.71(1) Å, H1a···O1w = 1.86, N1–H1a···O1w = 172.3°), O2w serving as an aqua ligand binds to Ag3 at 2.525(5) Å, and O3w lying on a 2-axis functions as a bridge between aqua and trifluoroacetate oxygen atoms belonging to adjacent silver(I) chains (O2w···O3w 2.661 Å and O3w···O2 2.854 Å). The resulting layer-type structure is both new and unprecedented. It is also noteworthy that hydrogen-bonded $(bpeH_2 \cdot 2H_2O)^{2+}$ moieties are accommodated between the anionic host layers, forming an inclusion complex (Fig. 2).

3.2. $[Ag_{14}(C_2)_2(C_2F_5CO_2)_{10}(H_2O)_4(bpe)] \cdot H_2O$ (2)

In the crystal structure of **2**, the building block is a centrosymmetric double cage composed of 14 silver(I) atoms, with each component single cage encapsulating an acetylenediide dianion stabilized by multiple σ- and π-interactions with silver(I) in the range of 2.124(9)–2.69(1) Å. Each single cage is in the form of a distorted triangulated dodecahedron. Atom sets, (Ag1Ag2Ag3Ag1a) and (Ag4Ag5Ag6Ag3b), are each coplanar within 0.095 and 0.144 Å, respectively, making a dihedral angle of 100.6°. The double cages are further fused together at edge Ag3Ag3b to form an infinite silver(I) column along the *a*-direction, as shown in Fig. 3.

Three kinds of pentafluoropropionate coordination modes exist in **2**, namely μ-*O*, μ_2-*O*,*O*′ and μ_3-*O*,*O*,*O*′. The μ_3-*O*,*O*,*O*′ ligand further links an additional silver atom of type Ag7 to the silver(I) column. The resulting two-dimensional network is consolidated by cross-linkage of the columns through $[Ag_2(C_2F_5CO_2)_2]$ bridging involving Ag7 (Fig. 4).

The rigid bpe ligand binds to Ag5 at 2.132(7) Å, serving as a connector that further interlinks the layers into a three-dimensional porous framework with channels running parallel to the *a*-direction, which are filled by the hydrophobic pentafluoropropyl groups (Fig. 5).

Of the three independent water molecules in **2**, one serves as an aqua ligand bound to Ag2 at O1w–Ag2 2.526(8) Å, the second functions as a bridge across Ag1 and Ag4 at O2w–Ag1 2.40(1) Å and O2w–Ag4 2.53(1) Å, and the third (with half site occupancy) is involved in donor hydrogen bonding with an oxygen atom of the pentafluoropropionate group at O3w···O10 2.402 Å.

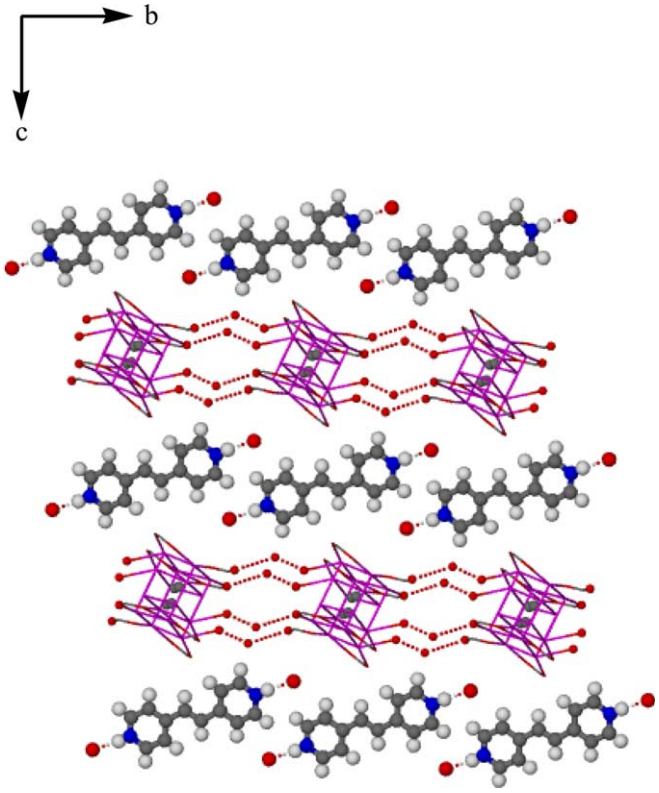

Fig. 2. Layer structure of **1** constructed from hydrogen bonds linking one-dimensional silver(I) chains viewed along the *a*-axis, with hydrogen-bonded $(bpeH_2 \cdot 2H_2O)^{2+}$ moieties accommodated between the host layers. Some $CF_3CO_2^-$ ligands, and also the CF_3 parts of the $CF_3CO_2^-$ ligands included in the figure, have been omitted for clarity.

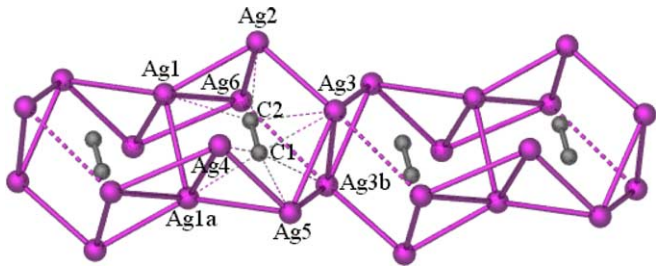

Fig. 3. A portion of silver(I) column generated from fusion of centrosymmetric double cages in **2**. Symmetry code: (a) $-x+1, -y+2, -z-1$; (b) $-x+2, -y+2, -z-1$. Selected bond distances [Å]: C1–C2 1.21(1), C2–Ag1 2.485(9), C2–Ag2 2.203(8), C1–Ag3 2.449(9), C2–Ag3 2.69(1), C1–Ag4 2.315(9), C1–Ag5 2.127(9), C2–Ag6 2.124(9).

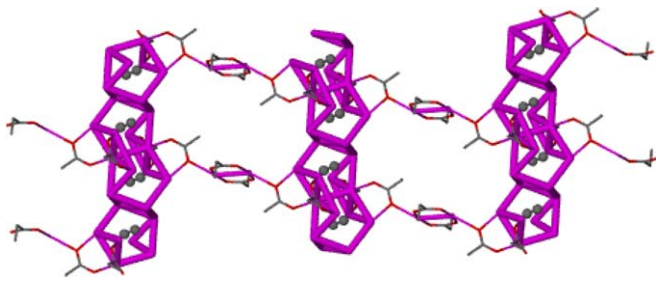

Fig. 4. Ball-and-stick representation of the two-dimensional architecture generated from the linkage of silver(I) columns by $[Ag_2(C_2F_5CO_2)_2]$ units in **2**. Some $C_2F_5CO_2^-$ ligands, and also the F atoms of the $C_2F_5CO_2^-$ ligands included in the figure, have been omitted for clarity.

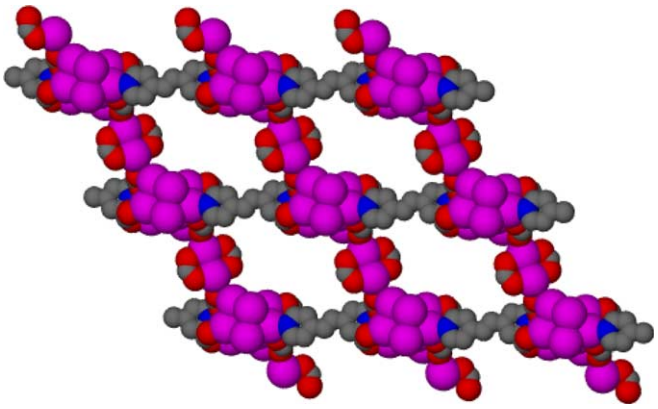

Fig. 5. Space-filling diagram showing a cross-section of the three-dimensional porous framework extending parallel to the *a*-axis in **2**. Some $C_2F_5CO_2^-$ ligands, the C_2F_5 groups of the $C_2F_5CO_2^-$ ligands included in the figure, and all hydrogen atoms have been omitted for clarity.

3.3. $[Ag_7(C_2)(CF_3CO_2)_2(cba)_3]$ (**3**)

Similar to that in **2**, the basic building block in **3** is also a centrosymmetric $(C_2)_2@Ag_{14}$ double cage. Each component single cage takes the shape of a distorted bicapped trigonal prism, in which atom sets (Ag1Ag2Ag3) and (Ag4Ag5Ag4a) constitute two triangular faces, making a dihedral angle of 8.5°. One of the silver atoms was found to exhibit positional disorder over two sites; it was represented by Ag3 with a site occupancy factor (sof) of 0.8 and Ag3′ with sof = 0.2 in structure refinement. Re-collection of a new set of intensity data using a second crystal selected from a freshly prepared sample confirmed the disordered model, but this did not result in an improvement of the *R* indices. The mean deviations of the rectangular faces capped by atoms Ag6 and Ag7 are 0.1674 and 0.2556 Å, respectively. A C_2^{2-} species is enclosed in each silver polyhedron and stabilized by mixed σ/π Ag–C interactions in the range of 2.154(8)–2.617(8) Å. Two such single cages share an edge Ag4Ag4a to form the double cage, and such double cages are connected by argentophilic interaction of the type Ag1–Ag1b (2.958(2) Å) to form an infinite chain along the *a*-direction (Fig. 6).

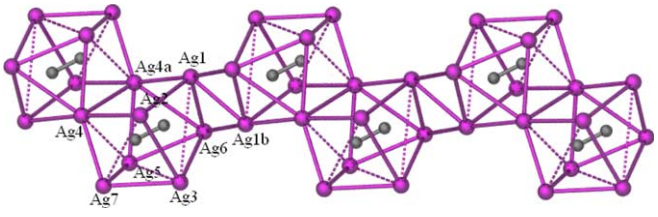

Fig. 6. Infinite silver(I) chain along the *a*-direction generated from fusion of $(C_2)_2@Ag_{14}$ double cages in **3**. Ag···Ag distances longer than 3.4 Å (twice the van der Waals radius of silver) are represented by thick broken lines. Symmetry code: (a) $-x+1, -y+2, -z+1$. Selected bond lengths [Å]: C1–C2 1.23(1), C2–Ag1 2.154(8), C1–Ag2 2.430(8), C2–Ag2 2.505(8), C2–Ag3 2.419(8), C1–Ag3 2.486(9), C1–Ag4 2.274(9), C1–Ag5 2.330(8), C2–Ag6 2.272(8), C1–Ag7 2.227(9).

There are three independent cba ligands labeled as types I, II and III around the $(C_2)@Ag_{14}$ double cage (Fig. 7(a)). The silver columns are linked via ligands I and II to form a (4,4) network (N1–Ag3 2.194(8) Å, N2–Ag2 $(-x, -y+2, -z+1)$ 2.367(8) Å, N2–Ag6 2.449(8) Å), and the nodes are further doubly bridged by III (N3–Ag7 2.285(9) Å) to form a three-dimensional coordination network (Fig. 7(b)). An alternative description is that the silver(I) columns are arranged in a hexagonal array, and each column is linked to an adjacent one by a pair of cba ligands. Every three neighboring silver columns encircle a triangular channel, and a cross-section of the three-dimensional network has the (3,6) (or 3^6) topology (Fig. 7(c)) [15]. This kind of topology is quite similar to that found in $(Ag_2C_2)(AgCF_3CO_2)_4(4\text{-pyCN})_2$ (4-pyCN = 4-cyanopyridine) [12a].

3.4. $[Ag_7(C_2)(C_2F_5CO_2)_5(cbaH)(H_2O)_2]$ (**4**)

Complex **4** was obtained in a similar manner to **3** except that $AgC_2F_5CO_2$ was used instead of $AgCF_3CO_2$ under hydrothermal conditions. The basic building unit is also a centrosymmetric $(C_2)_2@Ag_{14}$ double cage constructed from face-sharing of two $C_2@Ag_8$ single cages, each having the geometry of a distorted bicapped trigonal prism. Atom sets (Ag1Ag2Ag2a) and (Ag3Ag3aAg4) constitute two triangular faces making a dihedral angle of 167.9°. The mean deviations of the two rectangular faces capped by atom Ag6 and Ag7 are 0.0672 and 0.2777 Å, respectively. A C_2^{2-} species is enclosed in each silver polyhedron and stabilized by mixed σ/π Ag–C interactions in the range of 2.09(1)–2.59(1) Å. Two such single cages share face (Ag1Ag2Ag1aAg2a) to form the double cage, and such double cages are fused together via Ag3bAg3c edge-sharing to generate an infinite silver(I) column along the *a*-direction (Fig. 8).

Interlinkage of silver columns via neutral cbaH with bond type O12–Ag4 2.367(8) Å, N1–Ag7 2.14(1) Å generate a two-dimensional network oriented parallel to the *ab*-plane (Fig. 9). Both water molecules serve as aqua ligands bound to silver atoms (O1w–Ag7 2.34(1) Å, O2w–Ag3 2.48(1) Å).

3.5. $(imH)_3[Ag_8(C_2)(CF_3CO_2)_9]\cdot H_2O$ (**5**)

Single-crystal X-ray analysis revealed that the basic building block in **5** is a $C_2@Ag_8$ single cage in the shape of a triangulated dodecahedron located on a twofold axis. Silver cages of such type are connected by μ_3-*O*,*O*,*O*′-trifluoroacetate ligands to form a zigzag anionic silver(I) column along the *a*-direction (Fig. 10).

All three independent imidazole moieties are protonated to satisfy the overall charge balance in the crystal structure. Notably, the resulting $(imH)^+$ cations play a key role in the construction of the three-dimensional architecture. As shown in Fig. 11, the silver(I) columns are interconnected

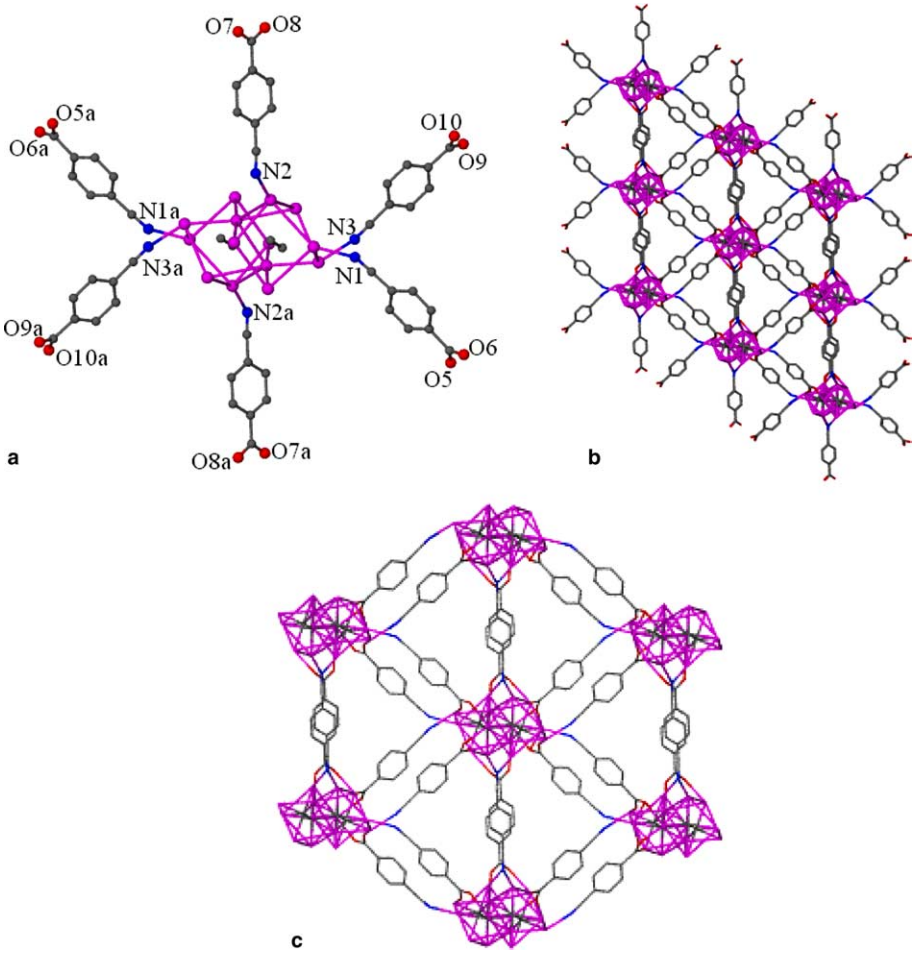

Fig. 7. (a) Various cba ligands surrounding a double silver cage in **3**. (b) Three-dimensional architecture of **3** constructed from interlinkage of silver(I) chains via cba ligands. All the $CF_3CO_2^-$ ligands and hydrogen atoms have been omitted for clarity. (c) Schematic showing the (3,6) network in **3**. All the $CF_3CO_2^-$ ligands and hydrogen atoms have been omitted for clarity.

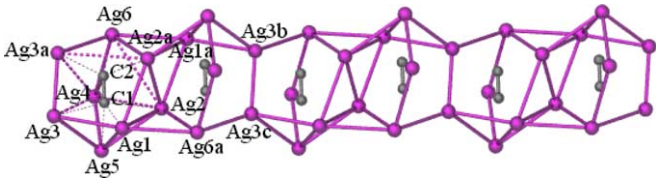

Fig. 8. A portion of the silver(I) column in **4** generated from edge sharing of centrosymmetric $(C_2)_2@Ag_{14}$ double cages. The Ag–C bonds are deleted in the other symmetry-generated cages for clarity.

by hydrogen bonding with the $(imH)^+$ cation serving as donors and *O*,*F* atoms of trifluoroacetate ligands as acceptors to form the three-dimensional architecture. The bond lengths and angles of hydrogen bonds are shown in Table 2.

The C–C bond lengths of the acetylenediide dianion in **1**–**5** are in the range 1.18(1)–1.24(1) Å, which indicate that the entrapped C_2^{2-} species retains its triple-bond character, in accordance with the previous finding in a variety of $C_2@Ag_n$ cages. In addition, the Ag···Ag distances of the silver cages in **1**–**5** lie in the ranges of 2.848(1)–3.145(1), 2.857(1)–3.288(2), 2.861(2)–3.348(3), 2.744(2)–3.258(2), 2.849(2)–3.2934(8) Å (within twice the van der Waals radius of the silver atom), respectively. This is indicative of the existence of significant argentophilic interaction [14].

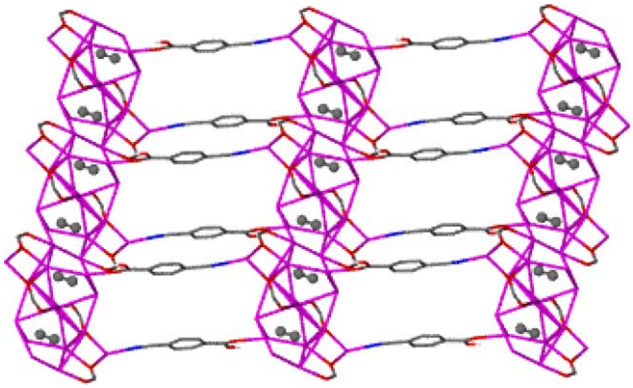

Fig. 9. Two-dimensional architecture of **4** constructed from cbaH-bridged silver(I) columns. The water molecules, some $C_2F_5CO_2^-$ ligands, and the C_2F_5 groups of the $C_2F_5CO_2^-$ ligands included in the figure have been omitted for clarity.

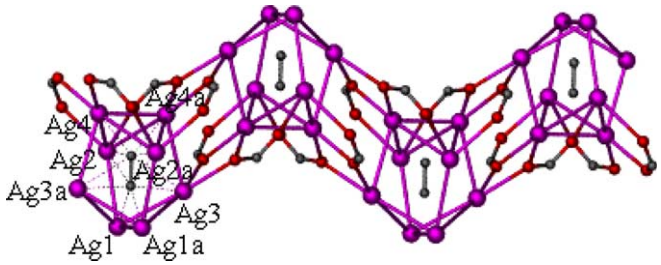

Fig. 10. A portion of the zigzag silver(I) column generated from the linkage of $C_2@Ag_8$ cages via μ_3-*O*,*O*,*O*′ coordination mode of trifluoroacetate ligands in **5**.

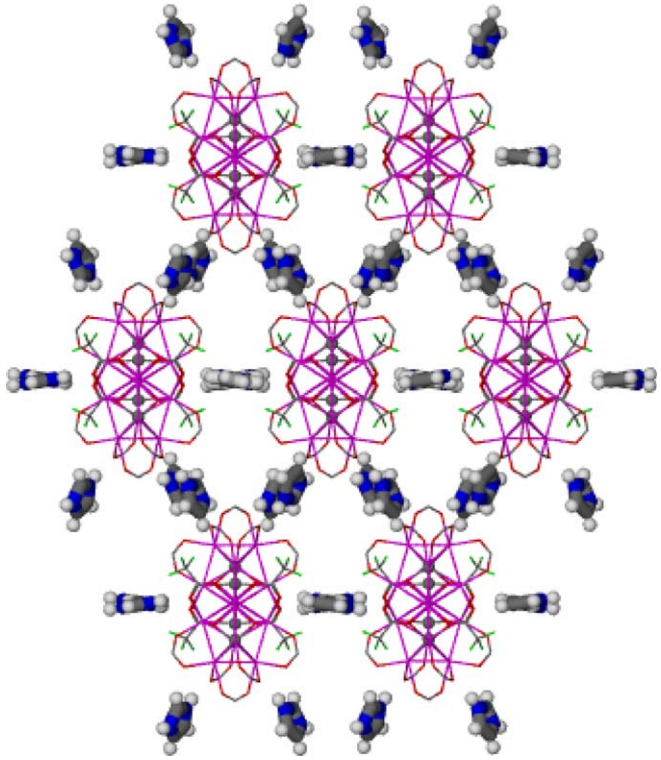

Fig. 11. Three-dimensional architecture of **5** viewed from the *c*-direction.

Table 2
Bond lengths and angles of hydrogen bonds in complex **5**

D–H···A	D···A (Å)	H···A (Å)	D–H···A (°)	Symmetry operator
N1–H1a···O8	2.830(8)	1.99	164.2	*x*, *y*, *z*
N2–H2a···O9	2.810(8)	1.96	172.6	$-x+1/2$, $-y+1/2$, $-z+1$
C15–H15a···O2	3.046	2.347	131.7	*x*, *y*, *z*
N3–H3a···O4	3.00(2)	2.26	141.4	$-x+1$, $-y$, $-z+1$
N4–H4a···O5	3.02(1)	2.18	156.6	*x*, *y*, *z*
C16–H16a···F22	3.229	2.606	122.8	$-x+1$, $-y$, $-z+1$
C18–H18a···O4	2.979	2.127	149.6	*x*, *y*, *z*
C19–H19a···F32	3.253	2.562	130.3	*x*, *y*, *z*

4. Conclusion

Through the hydrothermal reaction of potentially exobidentate ligands with $Ag_2C_2/AgR_fCO_2/AgBF_4$, we have synthesized five new $C_2@Ag_n$-containing supramolecular complexes showing unusual structure features. Complex **1** represents the first example of a hydrogen-bonded layer-type host structure containing $C_2@Ag_n$ that features the inclusion of organic guest species. This implies the possibility of introducing other cationic guest molecules between the anionic host layers, which may lead to new supramolecular materials. The slightly distorted Ag_4O_4 incomplete cube found in **1** and **5** are quite rare. Another surprising feature of **5** is the three-dimensional network constructed from $(imH)^+$-connected silver(I) columns via hydrogen bonds. The present report demonstrates that suitably chosen ancillary ligands can be used to design and construct Ag_2C_2-containing metal–organic assemblies, in which hydrogen bonding dictates the manifestation of the solid-state structures. Also, the preparation of these complexes under hydrothermal conditions demonstrates a potentially versatile approach to the construction of silver(I)-alkynyl complexes. Nevertheless, due to the presence of various subtle interactions in such supramolecular systems, the crystal engineering of Ag_2C_2-containing coordination networks is still at a primitive stage and defies predictability. Further experimentation in a systematic study of the synthesis of polynuclear silver(I) cage complexes bearing various bridging ligands is needed to shed some light on rational design and supramolecular assembly.

Acknowledgement

Financial support from the Hong Kong Research Grants Council (CERG Ref. No. CUHK 401704) is gratefully acknowledged.

Appendix A. Supplementary materials

Crystallographic data for the crystal structures reported in this paper have been deposited with the Cambridge Crystallographic Data Center (CCDC Nos. 273164–273168). This material can be obtained free of charge from the Director, CCDC, 12 Union Road, Cambridge, CB2 1EZ, UK (fax: +44 1223 336 033; e-mail: deposit@ccdc.cam.ac.uk or http://www.ccdc.cam.ac.uk). Supplementary data associated with this article can be found, in the online version, at doi:10.1016/j.poly.2005.10.026.

References

[1] (a) G.R. Desiraju, Acc. Chem. Res. 35 (2002) 565;
(b) J.Y. Lu, Coord. Chem. Rev. 246 (2003) 327;
(c) D. Braga, L. Maini, M. Polito, E. Tagliavini, F. Grepioni, Coord. Chem. Rev. 46 (2003) 53;
(d) B. Moulton, M.J. Zaworotko, Chem. Rev. 101 (2001) 1629;
(e) K.T. Holman, A.M. Pivovar, J.A. Swift, M.D. Ward, Acc. Chem. Res. 34 (2001) 107;

(f) D. Braga, F. Grepioni, Acc. Chem. Res. 33 (2000) 601.
[2] M.I. Bruce, P.J. Low, Adv. Organomet. Chem. 50 (2004) 399, 443.
[3] (a) M.P. Berthelot, Ann. (1866) 245;
(b) N.R. Thompson, in: J.C. BailarJr., H.J. Emeléus, T. Nyholm, A.F. Trotman-Dickenson (Eds.), Comprehensive Inorganic Chemistry, vol. 3, Pergamon Press, Oxford, 1973, p. 102;
(c) J.A. Shaw, E. Fisher, J. Am. Chem. Soc. 68 (1946) 2745;
(d) R. Vestin, E. Ralf, Acta Chem. Scand. 3 (1949) 101;
(e) A.D. Redhouse, P. Woodward, Acta Crystallogr. 17 (1964) 616.
[4] (a) V. Niel, M.C. Munoz, A.B. Gaspar, A. Galet, G. Levchenko, J.A. Real, Chem. Eur. J. 8 (2002) 2446;
(b) M.-C. Brandys, R.J. Puddephatt, Chem. Commun. (2001) 1508;
(c) R.-X. Yuan, R.-G. Xiong, Z.-F. Chen, X.-Z. You, S.-M. Peng, G.-H. Lee, Inorg. Chem. Commun. 4 (2001) 430;
(d) H.-Y. He, L.-G. Zhu, Acta Crystallogr., Sect. E 59 (2003) o174;
(e) R.E. LaPointe, G.R. Roof, K.A. Abboud, J. Klosin, J. Am. Chem. Soc. 122 (2000) 9560;
(f) J.-L. Pierre, P. Chautemps, S. Refaif, C. Beguin, A.E. Marzouki, G. Serratrice, E. Saint-Aman, P. Rey, J. Am. Chem. Soc. 117 (1995) 1965.
[5] (a) F.S. Delgado, J. Sanchiz, C. Ruiz-Perez, F. Lloret, M. Julve, Inorg. Chem. 42 (2003) 5938;
(b) M.-S. Wang, L.-Z. Cai, G.-W. Zhou, G.-C. Guo, J.-S. Huang, Inorg. Chem. Commun. 6 (2003) 855;
(c) J.C. MacDonald, P.C. Dorrestein, M.M. Pilley, M.M. Foote, J.L. Lundburg, R.W. Henning, A.J. Schultz, J.L. Manson, J. Am. Chem. Soc. 122 (2000) 11692;
(d) P.A. Prasad, S. Neeraj, S. Natarajan, C.N.R. Rao, Chem. Commun. (2000) 1251;
(e) R.P. Bontchev, J. Do, A.J. Jacobson, Inorg. Chem. 39 (2000) 3320.
[6] G.-C. Guo, G.-D. Zhou, Q.-G. Wang, T.C.W. Mak, Angew. Chem., Int. Ed. 37 (1998) 630.
[7] D.K. Breitinger, W.A. Herrmann (Eds.), Synthetic Methods of Organometallic and Inorganic Chemistry, vol. 5, Thieme, Stuttgart, 1999, pp. 38–39.
[8] Bruker, SMART 5.0 and SAINT 4.0 for Windows NT, Area Detector Control and Integration Software, Burker Analytical X-Ray Systems Inc., Madison, WI, 1998.
[9] G.M. Sheldrick, SADABS: Program for Empirical Absorption Correction of Area Detector Data, University of Göttingen, Göttingen, Germany, 1996.
[10] R.A. Sparks, in: F.R. Ahmed (Ed.), Crystallography, Computing Techniques, Munksgaard, Copenhagen, 1976, p. 452.
[11] G.M. Sheldrick, SHELXTL 5.1 for Windows NT: Structure Determination Software Programs, Bruker Analytical X-ray Systems, Inc., Madison, WI, 1997.
[12] (a) X.-L. Zhao, T.C.W. Mak, Dalton Trans. (2004) 3212;
(b) X.-L. Zhao, Q.-M. Wang, T.C.W. Mak, Inorg. Chem. 42 (2003) 7872;
(c) X.-L. Zhao, Q.-M. Wang, T.C.W. Mak, Chem. Eur. J. 11 (2005) 2094.
[13] Q.-M. Wang, G.-C. Guo, T.C.W. Mak, J. Organomet. Chem. 670 (2003) 235.
[14] (a) P. Pyykkö, Chem. Rev. 97 (1997) 597;
(b) M.A. Rawashdeh-Omary, M.A. Omary, H.H. Patterson, J. Am. Chem. Soc. 122 (2000) 10371.
[15] C.-Y. Su, Y.-P. Cai, C.-L. Chen, B.-S. Kang, Inorg. Chem. 40 (2001) 2210.

example of the insertion of a carbodiimide into a boron–nitrogen bond. We also report a single-crystal X-ray diffraction study of previously synthesized **4** [19].

2. Experimental

2.1. General procedures

All manipulations and reactions were performed under a dry, oxygen-free, catalyst-scrubbed argon atmosphere using a combination of standard Schlenk techniques or in an M-Braun or Vacuum Atmospheres drybox. All glassware was oven-dried and vacuum- and argon flow-degassed before use. All solvents were distilled over sodium benzophenone ketyl, except dichloromethane, which was distilled over CaH_2, and degassed prior to use. *N*,*N*,*N*′-Tris(trimethylsilyl)benzamidine [21], bis(trimethylsilyl)amido boron dichloride [22], and $[MeC\{N^iPr\}_2]BCl_2$ (**4**) [19] were prepared according to the literature procedures. The compounds 1,3-dicyclohexylcarbodiimide, 1,3-diisopropylcarbodiimide, boron halides, bis(trimethylsilyl)amidolithium, and alkyl-lithium solutions were obtained commercially and used without further purification.

2.2. Spectroscopic measurements

Low-resolution CI mass spectra were obtained on a Finnigan MAT TSQ-700 mass spectrometer and high-resolution CI mass spectra recorded on a VG Analytical ZAB-VE sector instrument. All MS analyses were performed on samples that had been sealed in glass capillaries under an argon atmosphere. ^1H, $^{13}C\{^1H\}$, and ^{11}B NMR spectra were recorded at 295 K in C_6D_6 solutions on a GE EQ-300 instrument (^1H, 300 MHz; ^{13}C, 75 MHz; ^{11}B, 96 MHz) immediately following removal of the samples from the drybox. ^1H and $^{13}C\{^1H\}$ chemical shift values are reported in parts per million (ppm) relative to $SiMe_4$ (δ 0.00), using residual solvent resonances as internal standards. ^{11}B NMR data are referenced to $BF_3{:}OEt_2$ (δ 0.00). Melting points (uncorrected) were obtained on a Fisher–Johns apparatus after flame-sealing the samples in glass capillaries under argon.

2.3. Single-crystal X-ray structure determinations

For compounds **1**, **2**, and **4**, a crystal of suitable quality was removed from a Schlenk flask under positive argon pressure, covered immediately with degassed hydrocarbon oil and mounted on a glass fiber. The X-ray diffraction data were collected at 153 K on a Nonius Kappa CCD diffractometer equipped with an Oxford Cryostream low-temperature device and a graphite-monochromated Mo Kα radiation source ($\lambda = 0.71073$ Å). Corrections were applied for Lorentz and polarization effects. All structures were solved by direct methods [23] and refined by full-matrix least-squares cycles on F^2. All non-hydrogen atoms were allowed anisotropic thermal motion, and hydrogen atoms were placed in fixed, calculated positions using a riding model (C–H 0.96 Å). Selected crystal data, and data collection and refinement parameters are listed in Table 1.

2.4. Synthesis of $[^tBuC\{N(Cy)\}_2]BCl(Ph)$ (**1**)

tert-Butyllithium (2 mL of a 2.5 M solution in diethyl ether, 5.0 mmol) was added to a cold (−78 °C) solution of 1,3-dicyclohexylcarbodiimide (1.03 g, 5.0 mmol) in 15 mL of diethyl ether. The stirred colorless reaction mixture was warmed to room temperature, then cooled to

Table 1
Selected crystal data, data collection, and refinement parameters for **1**, **2**, and **4**

Compound	**1**	**2**	**4**
Formula	$C_{23}H_{36}N_2BCl$	$C_{23}H_{36}N_2BCl$	$C_8H_{17}N_2BCl_2$
Formula weight	386.80	386.80	222.95
Crystal system	monoclinic	monoclinic	triclinic
Space group	$P2_1/n$	$P2_1/c$	$P\bar{1}$
a (Å)	8.893(5)	9.939(5)	7.409(5)
b (Å)	17.194(5)	20.598(5)	8.127(5)
c (Å)	14.511(5)	11.052(5)	10.436(5)
α (°)	90	90	94.529(5)
β (°)	92.754(5)	93.204(5)	92.529(5)
γ (°)	90	90	104.188(5)
V (Å^3)	2216.3(16)	2259.1(16)	606.0(6)
Z	4	4	2
ρ_{calc} (g cm^{-3})	1.159	1.137	1.222
$F(000)$	840	840	236
Crystal size (mm)	0.30 × 0.20 × 0.20	0.10 × 0.10 × 0.10	0.10 × 0.10 × 0.05
θ Range (°)	2.75–27.49	2.05–27.48	3.11–27.48
Number of reflections collected	9399	8308	2750
Independent reflections	5028	5147	1588
R_1 [$I > 2\sigma(I)$]	0.0432	0.0590	0.0486
wR_2 (all data)	0.1019	0.1366	0.1095
Peak and hole (e Å^{-3})	0.311 and −0.256	0.436 and −0.487	0.380 and −0.269

−78 °C following which $PhBCl_2$ (0.794 g, 5.0 mmol) was added dropwise. After being stirred at room temperature for 2 h, the reaction mixture was filtered through Celite® and the solvent was stripped from the filtrate to afford a white powder. Recrystallization of this powder from hexane solution afforded a crop of colorless crystals of **1** (1.12 g, 58% yield, mp 124–126 °C).

^{1}H NMR (C_6D_6): δ 8.02 (d, 2H, Ph); 7.35 (m, 2H, Ph); 7.26 (m, 1H, Ph); 3.53 (m, 2H, Cy); 2.07 (m, 4H, Cy); 1.62–1.53 (br m, 10H, Cy); 1.28–1.15 (m, 6H, Cy); 1.08 (s, 9H, ^{t}Bu). ^{13}C NMR (C_6D_6): δ 178.25 (N*C*N); 135.84; 135.62; 133.68; 127.83 (Ph); 56.39 (Cy–C_1); 35.08 (Cy); 34.60 (Cy); 28.49 (*C*–Me_3); 26.45; 26.43 (Cy); 25.80 (C–*Me*$_3$). ^{11}B NMR (C_6D_6): δ 6.50 (s). MS (CI^+, CH_4): *m*/*z* 386 (M+H), 351 (M−Cl). HRMS (CI, CH_4) calcd. for $C_{23}H_{36}N_2BCl$, 386.2660; found: 386.2655.

2.5. Synthesis of [^{n}BuC{N(Cy)}$_2$]BCl(Ph) (2)

Colorless crystalline **2** (mp 99–101 °C) was prepared in 63% yield from ^{n}butyllithium (2 mL of a 2.5 M solution in diethyl ether, 5.0 mmol), 1,3-dicyclohexylcarbodiimide (1.03 g, 5.0 mmol) in 15 mL of diethyl ether and $PhBCl_2$ (0.794 g, 5.0 mmol) using the procedure described above for **1**.

^{1}H NMR (C_6D_6): δ 8.08 (d, 2H, Ph); 7.39 (m, 2H, Ph); 7.26 (m, 1H, Ph); 3.19 (m, 2H); 1.98 (s, 4H); 1.83 (m, 2H); 1.57–1.28 (br m, 10H); 1.16–0.96 (br m, 10H); 0.74 (t, 3H, C*H*$_3$). ^{13}C NMR (C_6D_6): δ 166.93 (N*C*N); 133.54; 128.07; 127.99; 125.53 (Ph); 54.73 (Cy–C_1); 46.71 (*C*H$_2$CH$_2$CH$_2$-CH$_3$); 34.50 (Cy); 29.10 (Cy); 26.55; 26.45 (Cy); 25.77 (CH$_2$*C*H$_2$CH$_2$CH$_3$); 24.95 (CH$_2$CH$_2$*C*H$_2$CH$_3$); 14.03 (CH$_2$CH$_2$CH$_2$*C*H$_3$). ^{11}B NMR (C_6D_6): δ 6.47 (s). MS (CI^+, CH_4): *m*/*z* 387 (M+H), 352 (M−Cl). HRMS (CI, CH_4) calcd. for $C_{23}H_{36}N_2BCl$, 386.2660; found: 386.2660.

2.6. Synthesis of [(Me$_3$Si)$_2$NC{NCy}$_2$]BCl$_2$ (3) via metathesis

Bis(trimethylsilyl)amidolithium (0.81 g, 4.8 mmol) was added to a cold (−78 °C) solution of dicyclohexylcarbodiimide (1.00 g, 4.8 mmol) in 15 mL of hexane. The stirred colorless reaction mixture was allowed to warm to room temperature, following which it was cooled to −78 °C and BCl_3 (4.8 mL of 1.0 M solution in hexane, 4.8 mmol) was added dropwise. After being stirred at room temperature for 2 h, the reaction mixture was filtered through Celite® and the solvent was stripped from the filtrate to afford a white powder. Recrystallization from toluene at −40 °C afforded a crop of pale yellow crystals of **3** (1.63 g, 77%, mp 97–99 °C). ^{1}H NMR (C_6D_6): 3.31 (m, 2H); 2.01 (m, 4H); 1.64 (m, 8H); 1.05 (m, 8H); 0.143 (s, 18H); ^{13}C NMR (C_6D_6): 166.57 (N*C*N); 53.78 (Cy–C_1); 33.82 (Cy); 26.41 (Cy); 25.89 (Cy); 2.15 (Si*Me*$_3$); ^{11}B NMR (C_6D_6): 4.16 (s). MS (CI^+, CH_4): *m*/*z* 449 (M+H), 412 (M−Cl). HRMS (CI, CH_4) calcd. for $C_{19}H_{40}N_3BCl_2Si_2$, 447.2231; found: 447.2227.

2.7. Synthesis of [(Me$_3$Si)$_2$NC{NCy}$_2$]BCl$_2$ (3) via carbodiimide insertion

Bis(trimethylsilylamido)boron dichloride (0.589 g, 2.43 mmol) in 5 mL of hexane was added to a solution of dicyclohexylcarbodiimide (0.50 g, 2.43 mmol) in

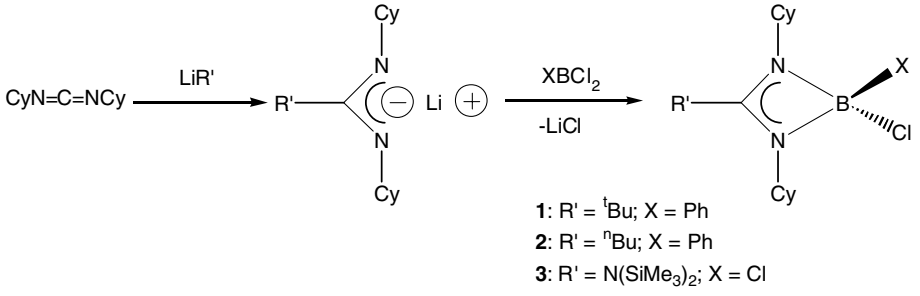

Scheme 1. Preparation of **1**–**3** by metathesis.

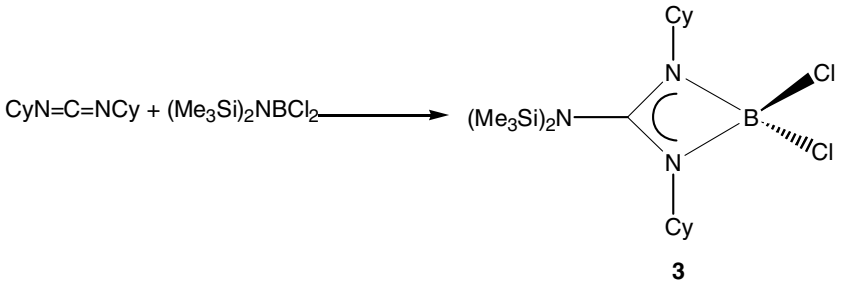

Scheme 2. Preparation of **3** by carbodiimide insertion.

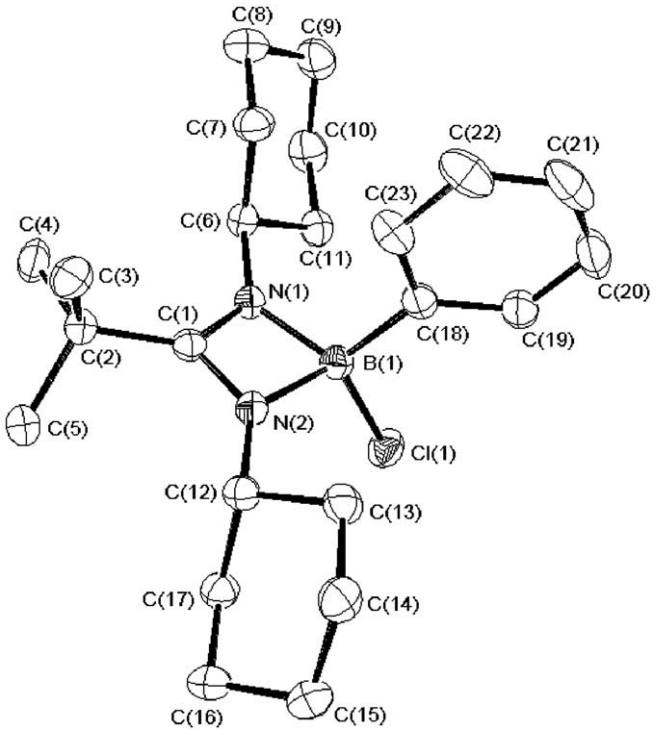

Fig. 1. ORTEP diagram of **1** with thermal ellipsoids at 40% probability. All hydrogen atoms have been omitted for clarity.

15 mL of diethyl ether at ambient temperature. A colorless reaction mixture resulted, which was stirred overnight at room temperature, following which the solvent was removed under reduced pressure to afford a white powder (0.94 g, 89% yield, mp 97–99 °C). All NMR data were identical to those obtained for **3** via the metathesis route. MS (CI^+, CH_4): *m/z* 449 (M+H), 412 (M−Cl). HRMS (CI, CH_4) calcd. for $C_{19}H_{40}N_3BCl_2Si_2$, 447.2231; found: 447.2233.

3. Results and discussion

3.1. Synthesis of boron amidinates

Alkyl-lithium insertion into carbodiimides represents a well precedented method for the synthesis of lithium amidinates (Scheme 1). In the present case, the requisite lithium reagents were prepared by treatment of 1,3-dicyclohexylcarbodiimide with ^{t}BuLi, ^{n}BuLi, or $(Me_3Si)_2NLi$ at low temperature (−78 °C). In turn, reaction of these lithium amidinates with $PhBCl_2$ or BCl_3 afforded the boron amidinates **1**, **2**, and **3** as stable crystalline solids in yields of 58%, 63% and 77%, respectively. Compound **3** can also be prepared by insertion of CyN=C=NCy into the B–N bond of $(Me_3Si)_2NBCl_2$ as summarized in Scheme 2. The yield obtained by this method is slightly higher than that obtained by the metathesis route.

In previous work, we have demonstrated that the carbodiimides will insert into the B–C bonds of both ferrocenyldibromoborane [19] and dichlorophenylborane [20]. Collectively, these represent the first examples of the synthesis of boron amidinates by means of carbodiimide insertion [24]. Intriguingly, we have found that BEt_3 and $B(NMe_2)_3$ fail to undergo carbodiimide insertion reactions. Recent theoretical studies indicate that the initial step in this insertion reaction is coordination of the carbodiimide nitrogen lone-pairs to the vacant p_z orbital of the borane [20,25,26]. Clearly, the Lewis acidity of the borane depends on the stereoelectronic characteristics of the substituents. In the case of tris(dimethylamido)borane the Lewis acidity is diminished by N → B π-bonding involving the nitrogen lone pairs and the vacant boron 2p orbital thus precluding formation of the initial donor–acceptor complex with the carbodiimide. In the case of the attempted reaction of CyN=C=NCy with BEt_3, initial formation is disfavored due to both electronic and steric effects of the C_2H_5 substituents.

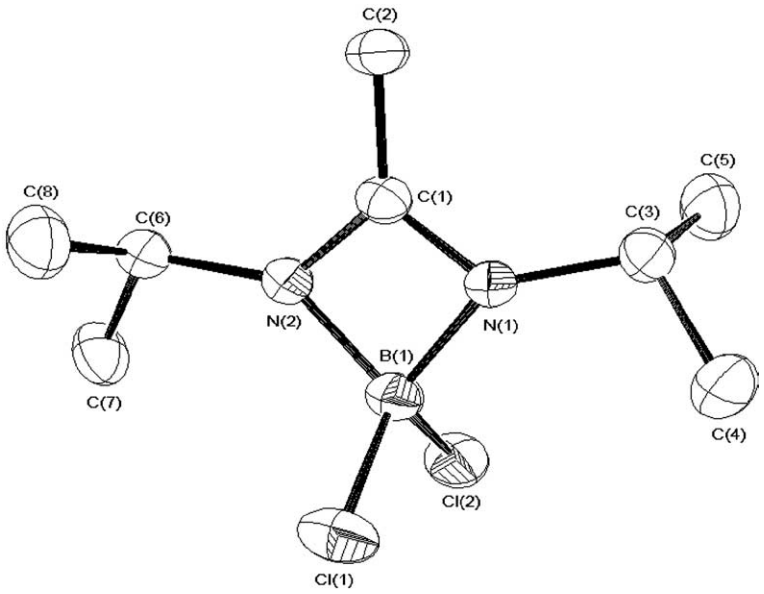

Fig. 2. ORTEP diagram of **4** with thermal ellipsoids at 40% probability. All hydrogen atoms have been omitted for clarity.

Table 2
Selected bond distances (Å) and angles (°) for **1**, **2**, and **4**

Compound **1**		Compound **2**		Compound **4**	
B(1)–Cl(1)	1.866(2)	B(1)–Cl(1)	1.862(4)	B(1)–Cl(1)	1.835(3)
B(1)–C(18)	1.595(2)	B(1)–C(18)	1.591(5)	B(1)–Cl(2)	1.842(3)
B(1)–N(1)	1.583(2)	B(1)–N(1)	1.590(4)	B(1)–N(1)	1.561(4)
B(1)–N(2)	1.572(2)	B(1)–N(2)	1.580(4)	B(1)–N(2)	1.567(4)
N(1)–C(1)	1.345(2)	N(1)–C(1)	1.333(4)	N(1)–C(1)	1.325(3)
N(2)–C(1)	1.336(2)	N(2)–C(1)	1.332(4)	N(2)–C(1)	1.334(3)
N(1)–C(6)	1.461(2)	N(1)–C(6)	1.447(4)	N(1)–C(3)	1.462(3)
N(2)–C(12)	1.463(2)	N(2)–C(12)	1.456(4)	N(2)–C(6)	1.457(3)
C(1)–C(2)	1.518(2)	C(1)–C(2)	1.485(4)	C(1)–C(2)	1.475(4)
N(1)–B(1)–N(2)	81.36(10)	N(1)–B(1)–N(2)	80.90(19)	N(1)–B(1)–N(2)	82.15(18)
N(1)–C(1)–N(2)	100.20(12)	N(1)–C(1)–N(2)	101.1(2)	N(1)–C(1)–N(2)	101.2(2)
Cl(1)–B(1)–C(18)	113.77(11)	Cl(1)–B(1)–C(18)	113.7(2)	Cl(1)–B(1)–Cl(2)	110.52(16)
N(1)–B(1)–Cl(1)	113.41(11)	N(1)–B(1)–Cl(1)	112.6(2)	N(1)–B(1)–Cl(1)	115.25(19)
N(1)–B(1)–C(18)	115.89(13)	N(1)–B(1)–C(18)	116.5(3)	N(1)–B(1)–Cl(2)	115.62(18)
N(2)–B(1)–Cl(1)	112.81(11)	N(2)–B(1)–Cl(1)	112.5(2)	N(2)–B(1)–Cl(1)	115.36(18)
N(2)–B(1)–C(18)	115.75(13)	N(2)–B(1)–C(18)	116.6(2)	N(2)–B(1)–Cl(2)	115.5(2)

3.2. Crystal structures

Single-crystal X-ray diffraction studies were carried out on both **1** and **2** to assess their structural and bonding characteristics. Compounds **1** and **2** crystallize as monomers and there are no unusually short intermolecular contacts. The molecular structure of **1** is illustrated in Fig. 1. Both molecules feature an essentially planar B–N–C–N ring and an approximately tetrahedral geometry around the boron atom. The B–N–C–N four-membered ring torsion angles are −3.35(10)° and −1.1(2)° for **1** and **2**, respectively. The B–N, B–Cl, and B–C_{Ph} bond distances are similar to those reported previously for [^{n}BuC{N(^{t}Bu)}$_2$]BCl(Ph) [27]. The C–N bond distances (averages 1.34035(19) Å for **1** and 1.3325(4) Å for **2**) are intermediate between those anticipated for single and double bonds and are indicative of delocalization at the NCN moiety. The B–N bonds in **1** and **2** are similar in length and fall in the range observed for B–N bonds in four-coordinate boron centers bound to three-coordinate nitrogen atoms [28].

The molecular structure of **4** was of interest to determine the effect, if any, of changing the steric bulk of the nitrogen and boron substituents (see Fig. 2). Overall, the metrical parameters for **4** are very similar to those for **1** and **2** (Table 2). However, the B–N–C–N ring is less distorted from planarity (0.69(18)°) than those of the cyclohexyl-substituted amidinates, presumably due to the smaller size of the diisopropyl substituent.

4. Conclusions

Three new boron amidinates have been prepared, thus adding to the short list of compounds of this type. Two of the three new compounds have been characterized by single-crystal X-ray diffraction along with a previously reported amidinate-substituted boron halide. One of the new compounds was prepared by the carbodiimide insertion reaction of CyN=C=NCy with $(Me_3Si)_2NBCl_2$. To our knowledge, this represents the first example of the insertion of a carbodiimide into a boron–nitrogen bond. Finally, since all four compounds feature boron–chlorine bonds, it is anticipated that they will prove to be useful synthons.

Acknowledgments

We gratefully acknowledge the National Science Foundation (Grant CHE-0240008) and the Robert A. Welch Foundation (Grant F-135) for support of this work.

Appendix A. Supplementary data

Full crystallographic data for the structural analyses have been deposited with the Cambridge Crystallographic Data Centre, CCDC Nos. 281291 (**1**), 281292 (**2**) and 281290 (**4**). Copies of this information can be obtained free of charge upon request from The Director, CCDC, 12 Union Road, Cambridge CB2 1EZ, UK (fax: +44 1223 336 033 or e-mail: deposit@ccdc.cam.ac.uk or www: www.ccdc.cam.ac.uk), by quoting the publication citation and the deposition number. Supplementary data associated with this article can be found, in the online version, at doi:10.1016/j.poly.2005.11.012.

References

[1] F.T. Edelmann, Coord. Chem. Rev. 137 (1994) 403.
[2] J. Barker, M. Kilner, Coord. Chem. Rev. 133 (1994) 219.
[3] A.R. Sanger, Inorg. Nucl. Chem. Lett. 9 (1973) 351.
[4] M.L. Cole, C. Jones, P.C. Junk, M. Kloth, A. Stasch, Chem. Eur. J. 11 (2005) 4482.
[5] V. Amo, R. Andres, E. de Jesus, F.J. de la Mata, J.C. Flores, R. Gomez, M.P. Gomez-Sal, J.F.C. Turner, Organometallics 29 (2005) 2331.
[6] R.T. Boere, M.L. Cole, P.C. Junk, New J. Chem. 29 (2005) 128.
[7] B. Clare, N. Sarker, R. Shoemaker, J.R. Hagadorn, Inorg. Chem. 43 (2004) 1159.

[8] H.A. Jenkins, D. Abeysekara, D.A. Dickie, J.A.C. Clyburne, J. Chem. Soc., Dalton Trans. (2002) 3919.
[9] D. Abeysekara, K.N. Robertson, T.S. Cameron, J.A.C. Clyburne, Organometallics 20 (2001) 5532.
[10] K. Kincaid, C.P. Gerlach, G.R. Giesbrecht, J.R. Hagadorn, G.D. Wheeler, A. Shafir, J. Arnold, Organometallics 18 (1999) 5360.
[11] C.C. Chang, C.S. Hsiung, H.L. Su, B. Srinivas, M.Y. Chiang, G.H. Lee, Y. Wang, Organometallics 17 (1998) 1595.
[12] M.P. Coles, D.C. Swenson, R.F. Jordan, V.G. Young, Organometallics 17 (1998) 4042.
[13] M.P. Coles, D.C. Swenson, R.F. Jordan, V.G. Young, Organometallics 16 (1997) 5183.
[14] J.T. Patton, M.M. Bokota, K.A. Abboud, Organometallics 21 (2002) 2145.
[15] S. Dagorne, R.F. Jordan, V.G. Young, Organometallics 18 (1999) 4619.
[16] J. Barker, N.C. Blacker, P.R. Phillips, N.W. Alcock, W.W. Errington, M.G.H. Wallbridge, J. Chem. Soc., Dalton Trans. (1996) 431.
[17] Y. Zhou, D.S. Richeson, Inorg. Chem. 35 (1996) 2448.
[18] Y. Zhou, D.S. Richeson, Inorg. Chem. 35 (1996) 1423.
[19] N.J. Hill, M. Findlater, A.H. Cowley, Dalton Trans. (2005) 3229.
[20] N.J. Hill, J.A. Moore, M. Findlater, A.H. Cowley, Chem. Commun. (2005) 5462.
[21] R.T. Boere, R.G. Hicks, R.T. Oakley, Inorg. Synth. 31 (1997) 94.
[22] B.L. Li, M.A. Goodman, R.H. Neilson, Inorg. Chem. 23 (1984) 1368.
[23] G.M. Sheldrick, SHELL-PC Version 5;03, Siemens Analytical X-ray Instruments Inc., Madison, WI, USA, 1994.
[24] Such insertion reactions are, however, known for aluminum, gallium and indium analogues: R. Lechler, H.-D. Hausen, J. Weidlein, J. Organomet. Chem. 359 (1989) 1.
[25] A.P. Kenney, G.P.A. Yap, D.S. Richeson, S.T. Barry, Inorg. Chem. 44 (2005) 2926.
[26] C.N. Rowley, G.A. DiLabio, S.T. Barry, Inorg. Chem. 44 (2005) 1983.
[27] P. Blais, T. Chivers, A. Downard, M. Parvez, Can. J. Chem. 78 (2000) 10.
[28] F.H. Allen, O. Kennard, D.G. Watson, L. Brammer, A.G. Orpen, R. Taylor, J. Chem. Soc., Perkin Trans. 2 (1987) S1.

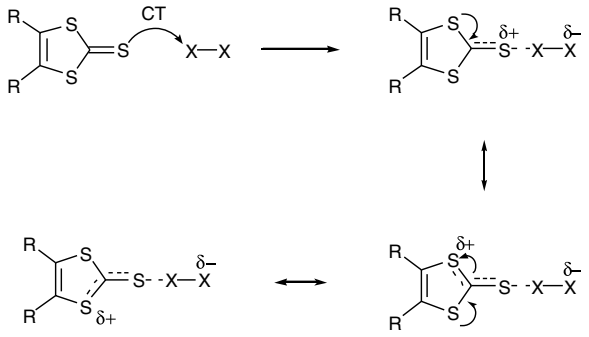

Scheme 1.

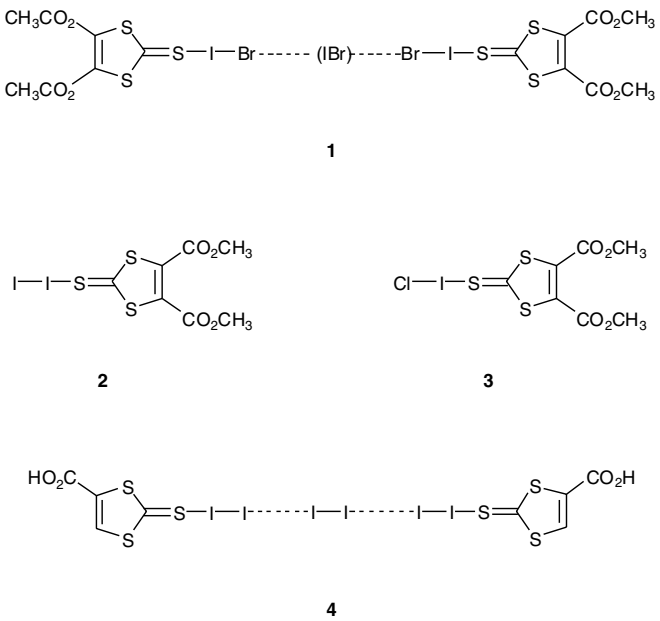

Chart 1.

derivative (**4**), which forms strong dimers through hydrogen bonding.

2. X-ray crystallography

2.1. Asymmetric units

Single crystal X-ray diffraction studies were performed on compounds **2**–**4**; the asymmetric units of each structure are illustrated in Fig. 1 and associated data given in Table 1. Throughout this paper, short intramolecular and intermolecular contacts are those in which the distance between two atoms is less than the sum of the van der Waals radii for the corresponding atoms.[1] The heterocycles bind through the thiocarbonyl functionality to the halogen species with S···I distances of 2.9122(13) Å (**2**), 2.5911(12) Å (**3**) and 2.7328(12) Å (**4**). Due to the bonding nature of the adducts (injection of electron density into the antibonding orbitals of the halogen species), we see an elongation in the bond length for diiodine (2.7899(7) Å for **2**; 2.8193(5) Å for **4**) and iodine monochloride (2.6030(11) Å), compared with the uncoordinated species in the solid state (2.715(6) Å for I_2 [13,14] and 2.446(6) Å for ICl [15]). The bond angles for S···I–I(Cl) are quasi-linear and are in the range 172–178° (Table 1). These values are typical for pnicogen–halogen and chalcogen–halogen adducts: Laurence et al. report that the mean X–Y···donor angle from 219 structures is 176.1(0.2)° [7]. In the case of **4**, the asymmetric unit consists of the expected diiodine adduct and an additional half molecule of diiodine [I(11)–I(11′) 2.7247(5) Å; symmetry code $2-x, -y, 1-z$], which is coordinated by I(1) at a bond length of I(1)···I(11) = 3.4414(6) Å.

For compounds **2**–**4**, a secondary interaction prevails between one of the sulfur atoms of the dithiole ring and the coordinated iodine atom of the dihalogen (3.55–3.62 Å, see Fig. 1 and Table 1). The bond angles between the corresponding sulfur atoms and the coordinated I_2 or ICl molecules are in the range 125–129° (Table 1). This interaction completes a four-membered ring between the coordinated iodine atoms and the two electron donating sulfurs of each structure. Each ring has a significant degree of planarity, with torsion angles of S(2)–C(1)–S(1)–I(1) = 2.4(3)° for **2**, S(2)–C(1)–S(1)–I(1) = 9.77(3)° for **3** and S(2)–C(1)–S(1)–I(2) = 2.2(3)° for **4**.

Intramolecular chalcogen–chalcogen close contacts are observed within each heterocyclic unit through oxygen atoms of the ester or acid functionalities and the sulfurs of the dithiole rings. For the esters, O(sp^3)···S interactions are in the range 2.73–3.00 Å with the shortest contacts seen for compound **2**. For compound **4**, the carbonyl oxygen is responsible for the chalcogen–chalcogen interaction with a contact distance of O(sp^2)···S = 2.88 Å. Interestingly, the latter provides a near planar four-membered ring with a torsion angle of 4.5(5)° (S(3)–C(3)–C(4)–O(2)), whereas compound **2**, which features the strongest O···S interactions but involves O(sp^3) atoms, affords less planar analogous rings with torsion angles of 12.9(5)° (S(3)–C(3)–C(6)–O(3)) and 18.1(4)° S(2)–C(2)–C(4)–O(1). The corresponding four-membered rings are further twisted in **3** (29.8(5)° for S(2)–C(2)–C(4)–O(2); 48.6(5)° for S(3)–C(3)–C(6)–O(4)).

2.2. Supramolecular structures

2.2.1. Compound 2

In the crystal structure of compound **2**, the most noticeable intermolecular interaction concerns a short contact between the thiocarbonyl sulfur and I(2) of an adjacent adduct (S(1)···I(2) = 3.5052(13) Å). This leads to polymeric

[1] The van der Waals radii (in Å) for relevant atoms are taken as: H, 1.20; O, 1.52; S, 1.80; Cl, 1.75; I, 1.98.

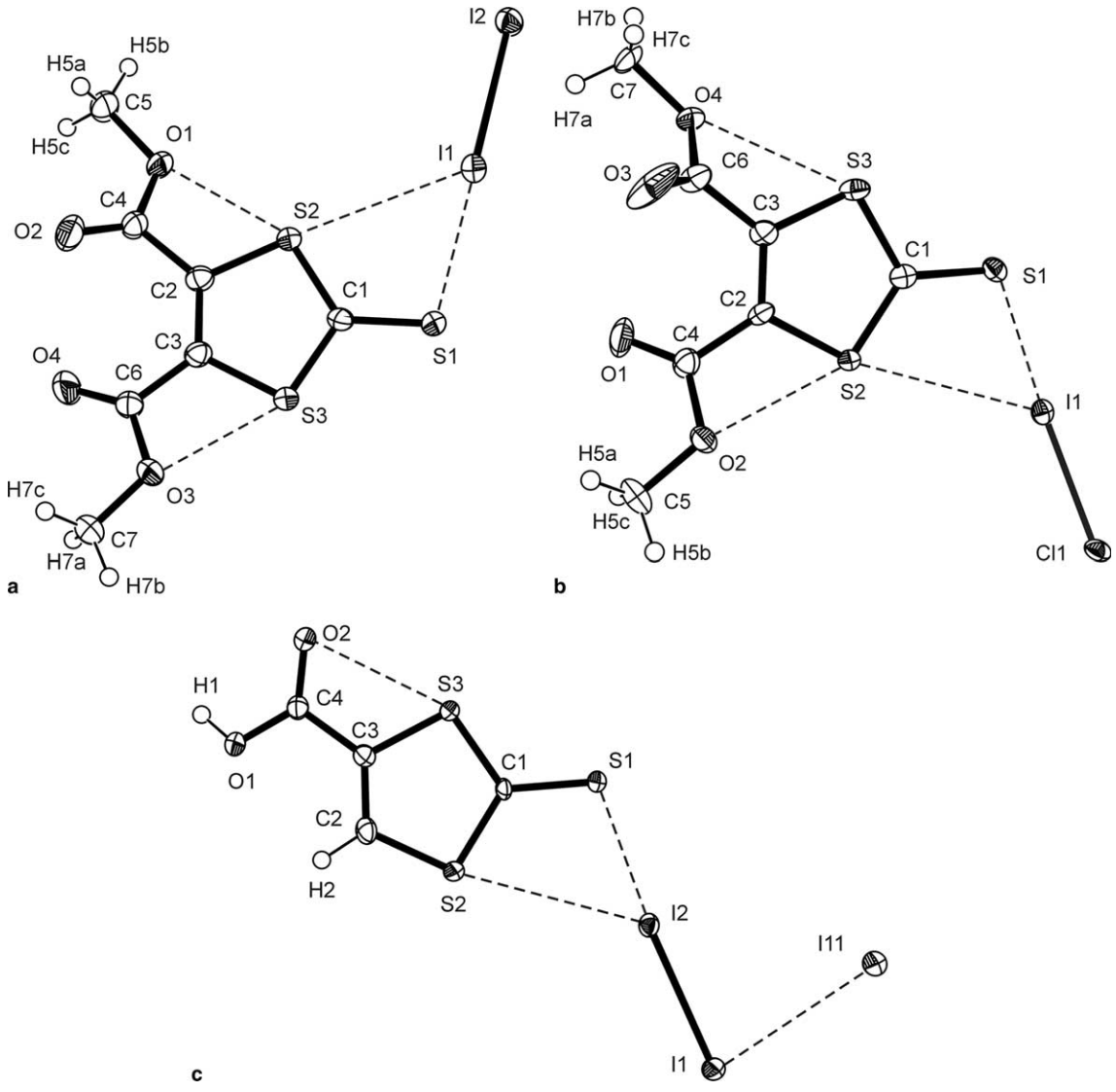

Fig. 1. Asymmetric units of compounds **2** (a), **3** (b) and **4** (c), showing intramolecular close contacts shorter than the van der Waals radii of the corresponding atoms [S, 1.80 Å; I, 1.98 Å; O, 1.52 Å].

chains of adducts in which the repeat units are linked by S(1)···I(1) and S(1)···I(2) contacts (Fig. 2(a)). The chains are held together in the perpendicular dimension by two hydrogen bonds (O(2)···H(7c) = 2.6101(11) Å; O(4)···H(5c) = 2.587(3) Å), which essentially form stacks of adducts (Fig. 2(b)). There are no further significant close contacts in the structure of **2**.

2.2.2. Compound *3*

In adduct **3**, the thione sulfur atom interacts with both atoms of the ICl molecule (S(1)···I(1) and S(1)···Cl(1), Table 1, Fig. 3(a)) in the same way that the corresponding sulfur atom binds to I_2 in **2**. Whereas the polymeric structure of **2** is essentially planar, neighbouring molecules in the chains of **3** (Fig. 3(a)) are tilted through approximately 60° with respect to one another. Within the chains, one strong (S(3)···O(2) = 3.116(3) Å) and one weak (S(2)···S(3) = 3.5956(15) Å) chalcogen–chalcogen interaction support the polymeric links of the sulfur–halogen contacts, as well as intermolecular hydrogen bonding between O(3)···H(7B) (2.450(5) Å, see Fig. 3(b)). The chains themselves form dimers through two interactions, viz. S(1)···S(1) and S(2)···I(1) (Table 1, Fig. 3(a)). Each chain of dimers is held together by three hydrogen bonds (O(1)···H(7C), O(3)···H(5A) and O(4)···H(5C), Table 1), and, together with the chalcogen and halogen based interactions, provide a network of intermolecular short contacts along the *a*-axis.

2.2.3. Compound *4*

Compound **4** incorporates an additional molecule of diiodine, positioned between two 'formal' adducts and coordinated by two I(1) atoms (Table 1, Fig. 4(a)). An intermolecular interaction between S(1) and I(1) atoms

Table 1
Summary of intramolecular and intermolecular short contacts and selected bond angles in the crystal structures of compounds **2**–**4**

Intermolecular contacts		Intramolecular contacts		Bond angles (°)	
Bond	Distance (Å)	Bond	Distance (Å)		
2					
I(2)···S(1)	3.5052(13)	I(1)···S(1)	2.9122(12)	S(1)···I(1)–I(2)	177.93(4)
O(2)···H(7c)	2.6101(11)	I(1)···S(2)	3.5588(13)	S(1)···I(2)–I(1)	172.12(4)
O(4)···H(5c)	2.587(3)	S(2)···O(1)	2.735(3)	S(2)···I(1)–I(2)	125.25(4)
		S(3)···O(3)	2.731(3)		
3					
I(1)···S(2)	3.7727(11)	I(1)···S(1)	2.5911(12)	S(1)···I(1)–Cl(1)	176.11(4)
Cl(1)···S(1)	3.3841(17)	I(1)···S(2)	3.5522(12)	S(2)···I(1)–Cl(1)	127.44(3)
S(1)···S(1)	3.4121(16)	S(2)···O(2)	2.902(3)		
S(2)···S(3)	3.5956(15)	S(3)···O(4)	2.997(4)		
S(3)···O(2)	3.116(3)	O(1)···H(5A)	2.622(4)		
O(1)···H(7C)	2.496(4)	O(1)···H(5C)	2.699(4)		
O(3)···H(5A)	2.627(5)	O(3)···H(7A)	2.691(5)		
O(3)···H(7B)	2.450(5)	O(3)···H(7C)	2.557(5)		
O(4)···H(5C)	2.630(4)				
4					
I(1)···I(11)	3.4414(6)	I(2)···S(1)	2.7328(12)	S(1)···(I2)–I(1)	175.72(3)
I(1)···S(1)	3.7186(12)	I(2)···S(2)	3.6200(12)	S(2)···(I2)–I(1)	129.64(2)
S(1)···S(1)	3.5206(16)	O(2)···S(3)	2.878(4)	I(2)–I(1)···I(11)	80.90(1)
S(2)···S(3)	3.3465(16)			I(1)···I(11)–I(11′) [2 − *x*,−*y*, 1 − *z*]	175.50(2)
O(1)···O(2)	2.648(5)				
O(2)···H(1)	1.831(5)				
O(2)···H(2)	2.617(6)				

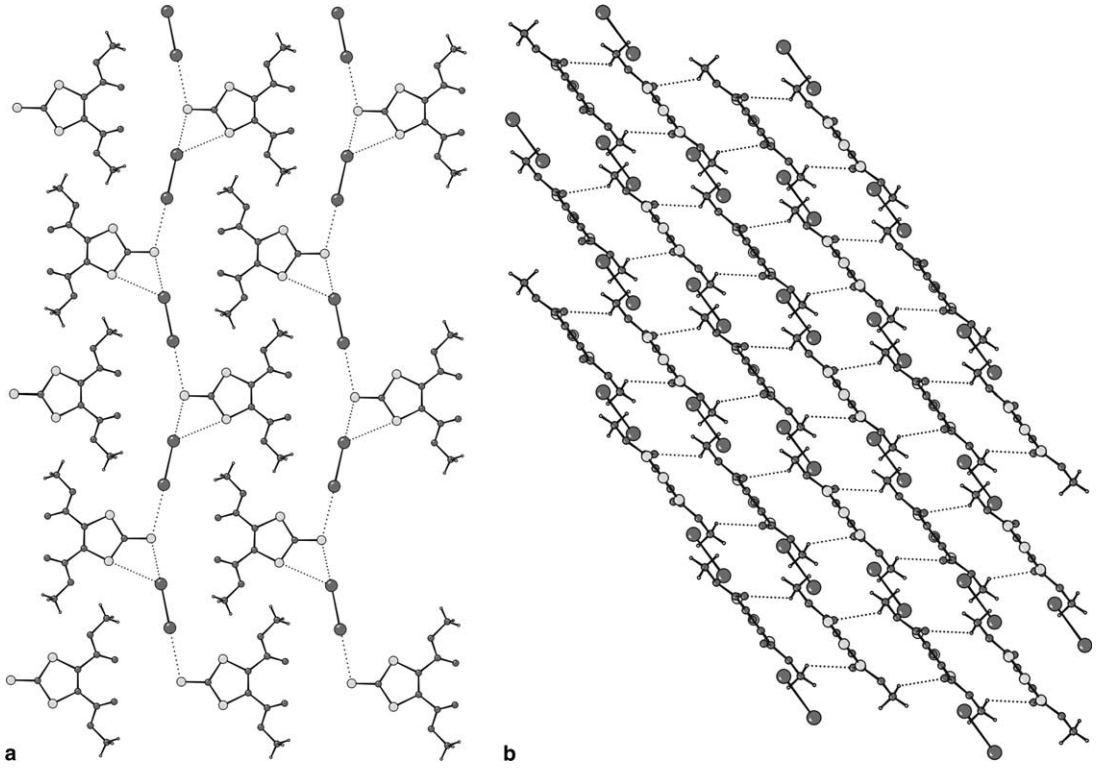

Fig. 2. Packing diagram of adduct **2** showing (a) supramolecular chains of S···I contacts, and (b) contacts between sheets through hydrogen bonding, viewed along the *b*-axis.

(3.7186(16) Å) produces a twelve membered ring of formula $I_{10}S_2$ (Fig. 4(a)). The rings are fused together with a common edge consisting of I(1)···I(11)–I(11′)···I(1′) atoms to give a ribbon-type polymeric structure (Fig. 4(b)). An additional S–I contact between adducts (S(2)···S(3), 3.3465(16) Å), affords an eight-membered ring

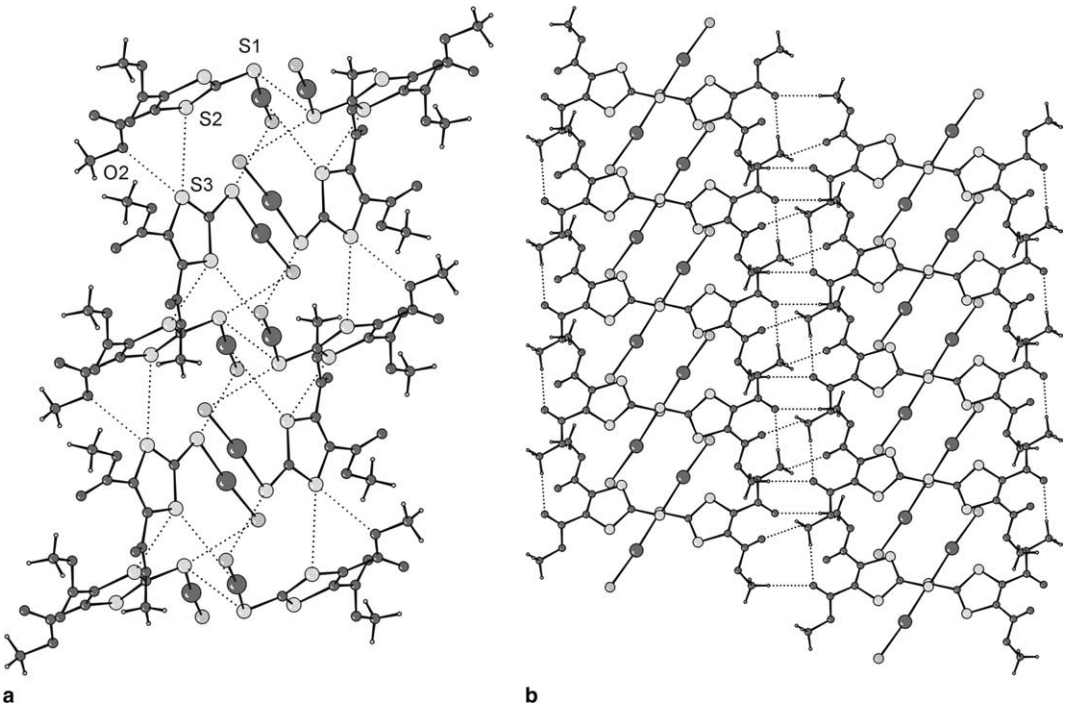

Fig. 3. Packing diagram of adduct **3** showing (a) S···I, S···Cl and chalcogen contacts, and (b) hydrogen bonding, viewed along the *b*-axis.

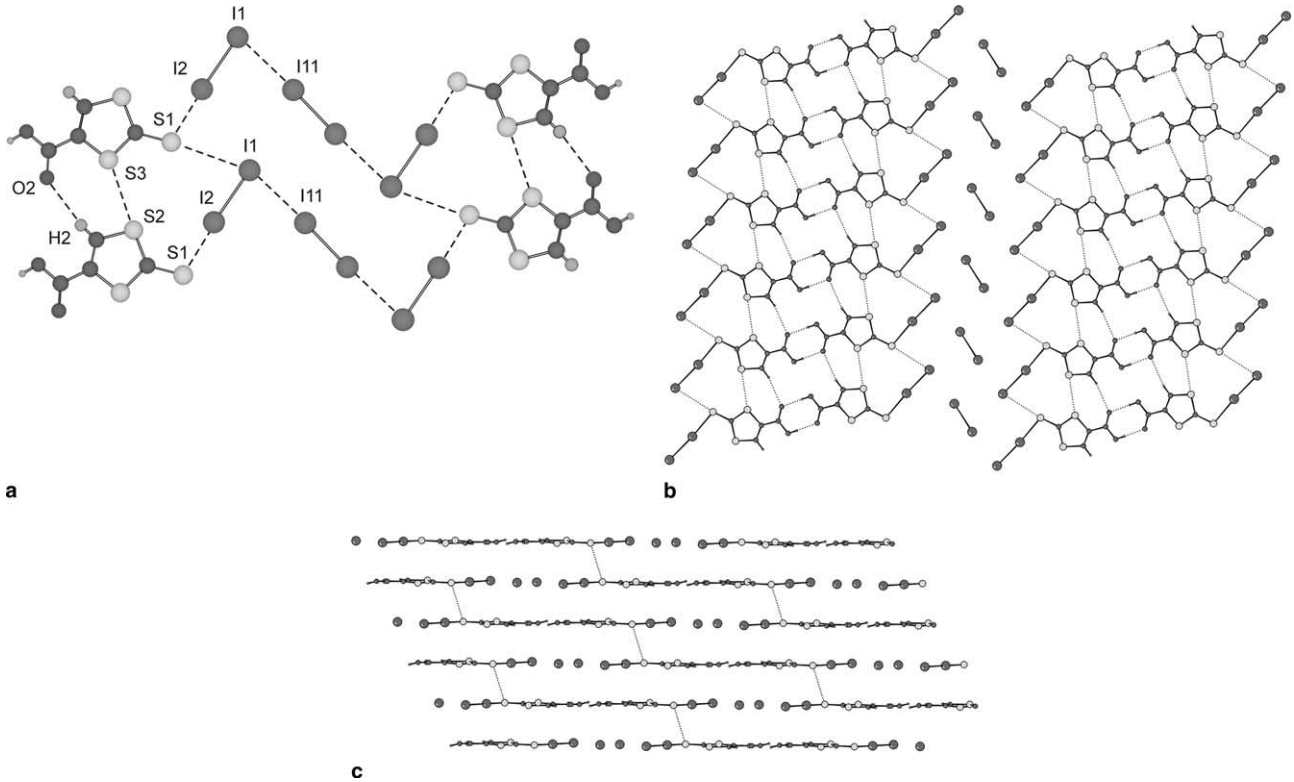

Fig. 4. (a) $I_{10}S_2$ ring of compound **4**, (b) sheets of linked adducts through S–S and S–I contacts and H-bonding, and (c) S(1)···S(1) contacts between sheets of adducts.

involving two heterocycles and one molecule of diiodine, I(1)–I(2). Classical dimerisation of the carboxylic acid groups is observed within the same plane, with an O···H distance of 1.831(5) Å. The acid functionalities are linked to the heterocyclic units by a weaker H-bond of bond length 2.617(6) Å (O(2)···H(2)). These interactions provide

planar sheets of adducts (Fig. 4(b)), which are themselves linked by sulfur–sulfur close contacts (S(1)···S(1), 3.5206(16) Å, Fig. 4(c)).

3. Experimental

3.1. Synthesis

The neutral donor molecules, 1,3-dithiole-2-thione-4-carboxylic acid and dimethyl 1,3-dithiole-2-thione-4,5-dicarboxylate, were prepared according to the literature procedures [16–18]. Formation of the adducts was achieved by refluxing the organic compounds with a two-fold excess of diiodine or iodine monochloride in acetonitrile. In each case, slow evaporation of the solvent afforded crystalline material, which was isolated by filtration. The materials slowly lose the halogen species upon standing, which hinders the characterisation of the materials by elemental analysis. Melting point determination demonstrated that the adducts rapidly decompose above 50 °C. Raman spectroscopy of the dark red/brown crystals of **2**, **3** and **4** produced very poor quality spectra consisting of a large fluorescence signal across the range 100–900 cm^{-1} which rendered meaningful analysis impossible. The IR spectra of dimethyl 1,3-dithiole-2-thione-4,5-dicarboxylate and 1,3-dithiole-2-thione-4-carboxylic acid exhibit strong bands at 1055 cm^{-1} and 1089 cm^{-1}, respectively, attributable to ν(C=S) stretching of the thiocarbonyl bond [9,19,20]. The interaction between the C=S moiety and the dihalogen/interhalogen leads to a reduction in the bond order and a shift to lower frequency of the ν(C=S) bands in the complexes, which occur at 1035 cm^{-1} in **2**, 1012 cm^{-1} in **3**, and 1039 cm^{-1} in **4**.

Table 2
Data collection and refinement parameters for compounds **2**–**4**

	2	**3**	**4**
Empirical formula	$C_7H_6I_2O_4S_3$	$C_7H_6ClIO_4S_3$	$C_4H_2I_3O_2S_3$
Formula weight	504.1	412.65	558.94
Crystal system	monoclinic	monoclinic	triclinic
Space group	$P2_1/n$	$P2_1/c$	$P\bar{1}$
a (Å)	9.807(2)	15.5564(5)	5.9723(4)
b (Å)	10.614(2)	7.3261(2)	7.9341(10)
c (Å)	13.293(3)	11.6680(3)	12.5966(15)
α (°)	90.0	90.0	99.428(11)
β (°)	100.91(3)	104.863(1)	99.050(11)
γ (°)	90.0	90.0	99.085(9)
Volume (Å^3)	1358.8(5)	1285.28(6)	571.07(11)
T (K)	150(2)	120(2)	120(2)
Z	4	4	2
D_c (Mg/m^3)	2.464	2.133	3.251
μ (mm^{-1})	5.084	3.180	8.720
Completeness, % (to θ, °)	99.2 (27.50)	99.9 (25.03)	99.6 (27.48)
Measured reflections	1470	7847	11 118
Independent reflections [$I > 2\sigma(I)$]	3093	2265	2604
R_{int}	0.0573	0.0753	0.0504
R indices [$F^2 > 2\sigma F^2$]	0.0353/0.0913	0.0340/0.0849	0.0285/0.0712
R indices (all data)	0.0490/0.1055	0.0384/0.0870	0.0322/0.0733

3.2. X-ray structure determination

Suitable single crystals were selected and data collected on a Bruker Nonius KappaCCD Area Detector at the window of a Bruker Nonius FR591 rotating anode ($\lambda_{Mo\ K\alpha} = 0.71073$ Å) driven by COLLECT [21] and DENZO [22] software at 120 K. The structure was determined in SHELXS-97 [23] and refined using SHELXL-97 [24]. Geometry calculations were performed using PLATON [25].

Further details of data collection and structure refinement are given in Table 2.

4. Conclusions

We have presented the synthesis and characterisation by X-ray crystallography of three new donor–acceptor charge transfer complexes. The diiodine and iodine monochloride adducts of 1,3-dithiole-2-thione-4-carboxylic acid and dimethyl 1,3-dithiole-2-thione-4,5-dicarboxylate provide the expected basic structure of chalcogen Lewis base–halogen adducts. The participation of all three sulfur atoms of the dithiole-thione provides a high number of supramolecular interactions. However, the carboxylic acid and ester functionalities significantly raise the dimensionality of intermolecular contacts, resulting in 3-D cross-linked structures. These functionalities could therefore be useful to 'double charge-transfer' materials in providing long range order for interesting magnetic and/or conducting properties.

5. Supplementary data

Crystallographic data (excluding structure factors) for the structures in this paper has been deposited with the Cambridge Crystallographic Data Centre as Supplementary Publication Nos. CCDC 217932, 282612 and 282613. Copies of the data can be obtained, free of charge, on application to CCDC, 12 Union Road, Cambridge CB2 1EZ, UK, www.ccdc.cam.ac.uk/conts/retrieving.html (fax: +44(0) 1223 336033 or e-mail: deposit@ccdc.cam.ac.uk).

Acknowledgement

The authors acknowledge the use of the facilities of the national X-ray crystallographic service of the EPSRC (University of Southampton).

References

[1] N. Bricklebank, S.J. Coles, S.D. Forder, M.B. Hursthouse, A. Poulton, P.J. Skabara, J. Organomet. Chem. 690 (2005) 328.
[2] M.C. Aragoni, M. Arca, F. Demartin, F.A. Devillanova, M. Garau, F. Isaia, V. Lippolis, G. Verani, J. Chem. Soc., Dalton Trans. (2005) 2252.
[3] M.C. Aragoni, M. Arca, F.A. Devillanova, M.B. Hursthouse, S.L. Huth, F. Isaia, V. Lippolis, A. Mancini, H.R. Ogilvie, G. Verani, J. Organomet. Chem. 690 (2005) 1923.

[4] N.A. Barnes, P. Bhattacharyya, S.M. Godfrey, R.T.A. Halton, I. Mushtaq, R.G. Pritchard, Phosphorus Sulfur Silicon 180 (2005) 783.
[5] For a review of earlier work see: P.D. Boyle, S.M. Godfrey, Coord. Chem. Rev. 223 (2001) 265.
[6] N. Bricklebank, Recent Res. Devel. Inorg. Organomet. Chem. 1 (2001) 25.
[7] C. Ouvrard, J.-Y. Le Questel, M. Berthelot, C. Laurence, Acta Crystallogr. B 59 (2003) 512.
[8] C. Näther, M. Bolte, Phosphorus Sulfur Silicon 178 (2003) 453.
[9] N. Bricklebank, P.J. Skabara, D.E. Hibbs, M.B. Hursthouse, K.M.A. Malik, J. Chem. Soc., Dalton Trans. (1999) 3007.
[10] D.W. Allen, R. Berridge, N. Bricklebank, S.D. Forder, F. Palacio, S.J. Coles, M.B. Hursthouse, P.J. Skabara, Inorg. Chem. 42 (2003) 3975.
[11] T. Khan, J.J.W. McDouall, E.J.L. McInnes, P.J. Skabara, P. Frère, S.J. Coles, M.B. Hursthouse, J. Mater. Chem. 13 (2003) 2490.
[12] P.J. Skabara, N. Bricklebank, R. Berridge, S. Long, M.E. Light, S.J. Coles, M.B. Hursthouse, J. Chem. Soc., Dalton Trans. (2000) 3235.
[13] F. van Bolhuis, P.B. Koster, T. Migchelsen, Acta Crystallogr. 23 (1967) 940.
[14] U. Buontempo, A. Di Cicco, A. Fillipponi, M. Nardone, P. Postorino, J. Phys. Chem. 107 (1997) 5720.
[15] G. Bernardinelli, R. Gerdil, Acta Crystallogr. 32 (1976) 1906.
[16] E. Klingsberg, J. Am. Chem. Soc. 86 (1964) 5290.
[17] B.R. O'Connor, F.N. Jones, J. Org. Chem. 35 (1970) 219.
[18] C.U. Pittman Jr., M. Narita, Y.F. Liang, J. Org. Chem. 41 (1976) 2855.
[19] F. Bigoli, P. Deplano, M.L. Mercuri, M.A. Pellinghelli, E.F. Trogu, Phosphorus Sulfur Silicon 70 (1992) 175.
[20] F. Bigoli, P. Deplano, M.L. Mercuri, M.A. Pellinghelli, E.F. Trogu, Phosphorus Sulfur Silicon 70 (1992) 65.
[21] R. Hooft, COLLECT: Data Collection Software, Nonius B.V., 1998.
[22] Z. Otwinowski, W. Minor, Methods in enzymology, in: C.W. Carter, R.M. Sweet (Eds.), Macromolecular Crystallography, Part A, vol. 276, Academic Press, New York, 1997, pp. 307–326.
[23] G.M. Sheldrick, Acta Crystallogr. A 46 (1990) 467.
[24] G.M. Sheldrick, SHELXL-97, University of Göttingen, Germany, 1997.
[25] A.L. Spek, PLATON, J. Appl. Crystallogr. 36 (2003) 7.

octahedral environment. While the discrete $[SnX_3]^-$ (X = Cl, Br) anion is observed in compounds such as $KCl \cdot KSnCl_3 \cdot H_2O$ [3] and $NH_4Br \cdot NH_4SnBr_3 \cdot H_2O$ [4], in the SnX_2 parent compounds the trigonal pyramids bridge to form infinite chains of $(SnX_2)_n$ [5]. Similar environments are seen in plumbous halides, but in these cases the distortions are often less pronounced than in the Sn(II) analogues.

In fact it is somewhat misleading to describe the non-bonding valence electrons as an *inert pair*. There are many examples where the interaction between the 5s or 6s orbitals on Sn and Pb, respectively, with empty orbitals on neighbouring anions leads to stabilisation of certain structures. Using a combination of crystallographic and simulation techniques, we have shown that layered structures of the type AB_2X_5 (A = NH_4, Rb, Cs, In; B = Sn, Pb and X = Cl, Br, I) are stabilised through the formation of cluster orbitals involving both Sn/Pb 5s/6s orbitals and empty orbitals on the halides [6]. In some cases, these interactions can lead to the complete removal of stereochemical distortion through electronic population of low-lying conduction bands, as in $CsSnBr_3$ [7].

Very little structural characterisation has been carried out on the alkaline earth metal tin(II) or lead(II) halides, the crystal structure of $Sr(SnCl_3)_2 \cdot 5H_2O$ being the only example [8]. The $Sr(MX_3)_2 \cdot 5H_2O$ (M = Sn, Pb; X = Br, Cl) system affords us the opportunity to examine the electron distribution around the $[MX_3]^-$ anion through the synergistic combination of crystallographic and electronic structure calculation techniques. While it is possible to synthesise the tin chloride, tin bromide and lead bromide analogues through conventional solution methods, the relative insolubility of $PbCl_2$ prevents synthesis of $Sr(PbCl_3)_2 \cdot 5H_2O$ in this way and we describe here how the structure of this compound can be predicted through total energy minimisation techniques.

2. Experimental

2.1. Preparation

Stoichiometric amounts of $SrCO_3$ and either $SnCl_2 \cdot 2H_2O$, $SnBr_2$ or $PbBr_2$ were weighed directly into a small beaker and the compounds dissolved in a minimum amount of dilute HX in a stream of N_2. In the cases of the tin containing compounds, a piece of tin metal was added to prevent oxidation of the product. The solution was heated to boiling and evaporated until approximately 50% of the original volume remained. Crystals appeared on cooling the solution in an ice bath and were collected by vacuum filtration. The crystals were dried in vacuo over silica gel. Attempts to synthesise the $Sr(PbCl_3)_2 \cdot 5H_2O$ analogue were unsuccessful and invariably resulted in precipitation of $PbCl_2$.

2.2. X-ray diffraction

Single-crystal X-ray diffraction data for $Sr(SnCl_3)_2 \cdot 5H_2O$, $Sr(SnBr_3)_2 \cdot 5H_2O$ and $Sr(PbBr_3)_2 \cdot 5H_2O$ were collected on an Enraf Nonius CAD-4 diffractometer at 293 K in $\omega/2\theta$ mode using graphite monochromated Mo Kα ($\lambda = 0.71073$ Å) radiation. The structures were solved by Patterson methods using SHELXS-86 and refined using SHELXL [9]. Oxygen atoms were located using difference Fourier methods. For the two tin containing compounds, the positions of the H atoms were refined in their geometric

Table 1
Crystal and refinement parameters for $Sr(MX_3)_2 \cdot 5H_2O$

	M = Sn, X = Cl	M = Sn, X = Br	M = Pb, X = Br
Formula weight	627.78	894.54	1071.54
T (K)	293(2)	293(2)	293(2)
λ (Å)	0.71073	0.71073	0.71073
Crystal system	monoclinic	monoclinic	monoclinic
Space group	*I*2/*a* (15)	*I*2/*a* (15)	*I*2/*a* (15)
Unit cell dimensions			
a (Å)	9.109(2)	9.326(2)	9.287(2)
b (Å)	12.008(2)	12.520(5)	12.317(2)
c (Å)	13.657(5)	14.213(3)	14.215(3)
β (°)	100.63	101.27	102.05
V (Å^3)	1468.2(7)	1627.5(8)	1590.2(5)
Z	4	4	4
D_{calc} (g cm^{-3})	2.840	3.651	4.476
μ (mm^{-1})	8.080	21.035	39.534
$F(000)$	1160	1592	1848
Crystal size (mm)	0.60 × 0.40 × 0.40	0.70 × 0.70 × 0.40	0.80 × 0.80 × 0.50
Number of reflections collected	1869	1931	1482
Number of independent reflections	1760	1766	1395
R_{int}	0.0159	0.0069	0.0423
Data/restraints/parameters	1760/9/85	1766/9/85	1395/0/65
Final R indices [$I > 2\sigma(I)$]	$R_1 = 0.0218$, $wR_2 = 0.0504$	$R_1 = 0.0392$, $wR_2 = 0.0766$	$R_1 = 0.0429$, $wR_2 = 0.1117$
R factors (all data)	$R_1 = 0.0293$, $wR_2 = 0.0522$	$R_1 = 0.0844$, $wR_2 = 0.0837$	$R_1 = 0.0765$, $wR_2 = 0.1292$
Maximum/minimum residual scattering density (e Å^{-3})	0.558/−0.560	0.862/−1.230	2.224/−2.401

positions. For $Sr(PbBr_3)_2 \cdot 5H_2O$, H atom positions were first optimised using density functional theory as described below and refined using geometrical constraints. Anisotropic thermal parameters were refined for all non-hydrogen atoms. All data were corrected for absorption by empirical methods (ψ-scan) [10] and subsequently corrections were applied to the isotropic models using DIFABS [11]. Molecular graphics were obtained using ORTEP-3 [12]. Material for publication was prepared using WinGX [13]. Crystal and refinement parameters are summarised in Table 1, with refined atomic coordinates in Table 2. CCDC reference numbers 415711–415713.

2.3. Electronic structure calculations

Calculations were performed using CPMD [14] with density functional theory (DFT) employed in its plane wave pseudo-potential implementation. A local density approximation (LDA) was used for the electronic exchange and correlation functional, along with Goedecker norm-conserving pseudopotentials [15,16] for each atom present in the unit cell and a plane-wave energy cut-off of 100 Ry. The electronic wave functions were transformed into their corresponding maximally localised Wannier functions using the method of Berghold et al. [17] and the centre of these Wannier functions was used to describe the positions of the electron pairs and the degree of ionicity of the chemical bonds. For $Sr(SnCl_3)_2 \cdot 5H_2O$ and $Sr(SnBr_3)_2 \cdot 5H_2O$ the electronic structure was computed at the experimental geometry as determined by X-ray diffraction. For $Sr(PbBr_3)_2 \cdot 5H_2O$, the positions of the H atoms were optimised while constraining the position of all other atoms to their experimental values. In the case of $Sr(PbCl_3)_2 \cdot 5H_2O$, the initial ionic positions were inferred by substituting Br for Cl in the optimised structure of $Sr(PbBr_3)_2 \cdot 5H_2O$ and using the $Sr(SnCl_3)_2 \cdot 5H_2O$/$Sr(SnBr_3)_2 \cdot 5H_2O$ unit cell parameter ratios to calculate the model cell parameters for the lead bromide analogue. These were calculated as $a = 9.071$ Å, $b = 11.813$ Å, $c = 13.659$ Å, $\beta = 101.41°$ in space group $I2/a$. An unconstrained (space group symmetry constraints only) optimisation of the atomic positions was then carried out followed by a Wannier analysis. The optimisations of the ionic positions were performed using a linearly scaling BFGS algorithm [18] and were terminated when the largest atomic gradient component was below 10^{-5} H bohr^{-1}. The optimised fractional coordinates of $Sr(PbCl_3)_2 \cdot 5H_2O$ are included in Table 2. All calculations were performed on a cluster of Apple X-Serve computers at Queen Mary, University of London.

Table 2
Atomic parameters for $Sr(MX_3)_2 \cdot 5H_2O$

Atom	x	y	z	U_{eqv}
(a) M = Sn, X = Cl				
Sn(1)	0.1503(1)	0.6083(1)	0.1311(1)	0.017(1)
Sr(1)	0.25(–)	0.4917(1)	0.5(–)	0.010(1)
Cl(1)	−0.1046(1)	0.6377(1)	0.1895(1)	0.022(1)
Cl(2)	0.0368(1)	0.6330(1)	−0.0555(1)	0.023(1)
Cl(3)	0.1780(1)	0.8625(1)	0.1403(1)	0.019(1)
O(1)	0.1378(3)	0.4233(2)	0.3189(2)	0.021(1)
O(2)	−0.0120(2)	0.5904(2)	0.4246(2)	0.015(1)
O(3)	0.25(–)	0.2825(3)	0.5(–)	0.021(1)
(b) M = Sn, X = Br				
Sn(1)	0.1521(1)	0.6074(1)	0.1304(1)	0.029(1)
Sr(1)	0.25(–)	0.4873(1)	0.5(–)	0.020(1)
Br(1)	−0.1108(1)	0.6356(1)	0.1905(1)	0.033(1)
Br(2)	0.0323(1)	0.6331(1)	−0.0609(1)	0.032(1)
Br(3)	0.1815(1)	0.8298(1)	0.1420(1)	0.028(1)
O(1)	0.1415(6)	0.4237(5)	0.3266(4)	0.030(2)
O(2)	−0.0113(7)	0.5871(5)	0.4284(5)	0.027(1)
O(3)	0.25(–)	0.2859(7)	0.5(–)	0.034(2)
(c) M = Pb, X = Br				
Pb(1)	0.1673(1)	0.5895(1)	0.1407(1)	0.023(1)
Sr(1)	0.25(–)	0.4857(2)	0.5(–)	0.013(1)
Br(1)	−0.1194(2)	0.6298(1)	0.1936(1)	0.020(1)
Br(2)	0.0394(2)	0.6279(1)	−0.0667(1)	0.019(1)
Br(3)	0.1844(2)	0.8344(1)	0.1459(1)	0.018(1)
O(1)	0.1359(12)	0.4216(9)	0.3254(8)	0.018(3)
O(2)	−0.0129(13)	0.5898(9)	0.4293(9)	0.020(3)
O(3)	0.25(–)	0.2817(14)	0.5(–)	0.030(4)
(d) M = Pb, X = Cl (predicted structure)				
Pb(1)	0.18694	0.60297	0.13567	
Sr(1)	0.25	0.48157	0.5	
Cl(1)	−0.09067	0.61273	0.19586	
Cl(2)	0.03980	0.63364	−0.05869	
Cl(3)	0.18844	0.83329	0.14638	
O(1)	0.12453	0.42441	0.33303	
O(2)	−0.02281	0.59825	0.43257	
O(3)	0.25	0.26971	0.5	

Estimated standard deviations are given in parentheses.

3. Results and discussion

The refined structural parameters for $Sr(SnCl_3)_2 \cdot 5H_2O$, $Sr(SnBr_3)_2 \cdot 5H_2O$ and $Sr(PbBr_3)_2 \cdot 5H_2O$ are given in Table 2 with significant contact distances in Table 3. These compounds are seen to be essentially isostructural. Only minor differences in bond lengths are seen in the structure of $Sr(SnCl_3)_2 \cdot 5H_2O$ compared to the previous determination of this structure [8]. In $Sr(SnCl_3)_2 \cdot 5H_2O$ (Fig. 1) stereochemical activity of the non-bonding valence electrons on tin is evident in the asymmetric coordination environment adopted by this atom. The primary bonding contacts from tin are to three chlorine atoms together constituting the trichlorostannate anion, $[SnCl_3]^-$. Four longer secondary contacts (3.22–3.70 Å) to chlorine atoms on neighbouring $[SnCl_3]^-$ anions complete sevenfold coordinate geometry for tin. The bond lengths and angles of the trichlorostannate anion seen in the present work are comparable with those seen in other structures where the isolated anion is found, for example $KCl \cdot KSnCl_3 \cdot H_2O$ [3] (ave. Sn–Cl = 2.57 Å, ave. Cl–Sn–Cl = 88.7°) and $NH_4Cl \cdot NH_4SnCl_3 \cdot H_2O$ [19] (ave. Sn–Cl = 2.56 Å, ave. Cl–Sn–Cl = 88.4°). In $Sr(SnCl_3)_2 \cdot 5H_2O$, Sr^{2+} exhibits ninefold coordination, with two contacts to Cl(2) of 3.05 Å and seven to oxygen atoms of water molecules. The structure of $Sr(SnBr_3)_2 \cdot 5H_2O$, like the tin chloride analogue, shows

Table 3
Significant distances (Å) and angles (°) in $Sr(MX_3)_2 \cdot 5H_2O$

	M = Sn, X = Cl	M = Sn, X = Br	M = Pb, X = Br	M = Pb, X = Cl
M–X(1)	2.614(1)	2.773(1)	2.956(2)	2.802
M–X(2)	2.584(1)	2.749(1)	2.976(2)	2.749
M–X(3)	2.633(1)	2.800(2)	3.020(2)	2.725
M···X(2)[a]	3.220(1)	3.299(1)	3.154(2)	2.900
M···X(2)[b]	3.423(1)	3.513(1)	3.334(2)	3.506
M···X(3)[c]	3.318(1)	3.395(1)	3.200(2)	3.062
M···X(1)[d]	3.700(1)	3.760(2)	3.341(2)	3.253
Sr–X(3)[c] × 2	3.054(1)	3.199(1)	3.180(2)	3.088
Sr–O(1) × 2	2.628(3)	2.600(6)	2.609(11)	2.434
Sr–O(2) × 2	2.693(2)	2.751(6)	2.756(11)	2.823
Sr–O(2)[d] × 2	2.749(2)	2.783(7)	2.765(13)	2.595
Sr–O(3)	2.512(3)	2.522(9)	2.513(17)	2.503
X(1)–M–X(2)	93.96(3)	94.41(4)	91.78(5)	89.15
X(1)–M–X(3)	86.22(3)	86.41(3)	82.63(5)	86.47
X(2)–M–X(3)	87.12(3)	87.58(3)	82.76(5)	85.21

Estimated standard deviations are given in parentheses.
Symmetry equivalents: a = 0.5 − x, y, −z; b = −x, y − 0.5, −z; c = 0.5 − x, 1.5 − y, 0.5 − z; d = 0.5 + x, 1 − y, z.

a strong stereochemically distorting influence of the non-bonding valence electron pair on tin. The tribromostannate anion $[SnBr_3]^-$ exhibits distorted trigonal pyramidal geometry, with Sn–Br bond lengths of 2.75–2.80 Å and is similar to the geometry seen in $NH_4Br \cdot NH_4SnBr_3 \cdot H_2O$ [4] (ave. Sn–Br = 2.73 Å, ave. Br–Sn–Br = 89.4°). Longer secondary contacts to a further four Br atoms at distances between 3.30 and 3.76 Å, complete seven coordination geometry for Sn. The structure of $Sr(PbBr_3)_2 \cdot 5H_2O$ is again basically isostructural with the tin bromide analogue, but appears to show less significant stereochemical distortion. Although it is possible to consider the discrete tribromoplumbate anion, $[PbBr_3]^-$ as being present in this structure, the difference between the primary bonding Pb–Br distances and secondary contacts to Br is significantly smaller than seen in the tin analogues. It is therefore more accurate to describe Pb as being located in a seven coordinate site, with three shorter (2.95–3.02 Å) and four longer contacts (3.16–3.41 Å) to Br. The evidence for stereochemical activity of the non-bonding valence electron pair on Pb in $Sr(PbBr_3)_2 \cdot 5H_2O$ is in contrast to the more regular octahedral coordination environments seen in compounds such as $KPbBr_3 \cdot H_2O$ [20] and $K_2PbBr_4 \cdot H_2O$ [21].

The predicted structure of $Sr(PbCl_3)_2 \cdot 5H_2O$ maintains the basic structure seen in the other analogues. In order to test the optimisation procedure, an unconstrained optimisation of the structure of $Sr(PbBr_3)_2 \cdot 5H_2O$ was carried out and the optimised structure was found to show a root mean square deviation of 0.201 Å from the observed crystal structure. This deviation can be attributed to the use of a local density approximation in the calculations. However, it has been shown that for lead containing inorganic systems, this functional leads to coordination geometries in generally good agreement with those experimentally observed [22]. The optimised structural parameters for $Sr(PbCl_3)_2 \cdot 5H_2O$ are given in Table 2d with significant contact distances included in Table 3. The structure of $Sr(PbCl_3)_2 \cdot 5H_2O$ differs somewhat from the lead bromide analogue in that the Pb atom has an extended coordination

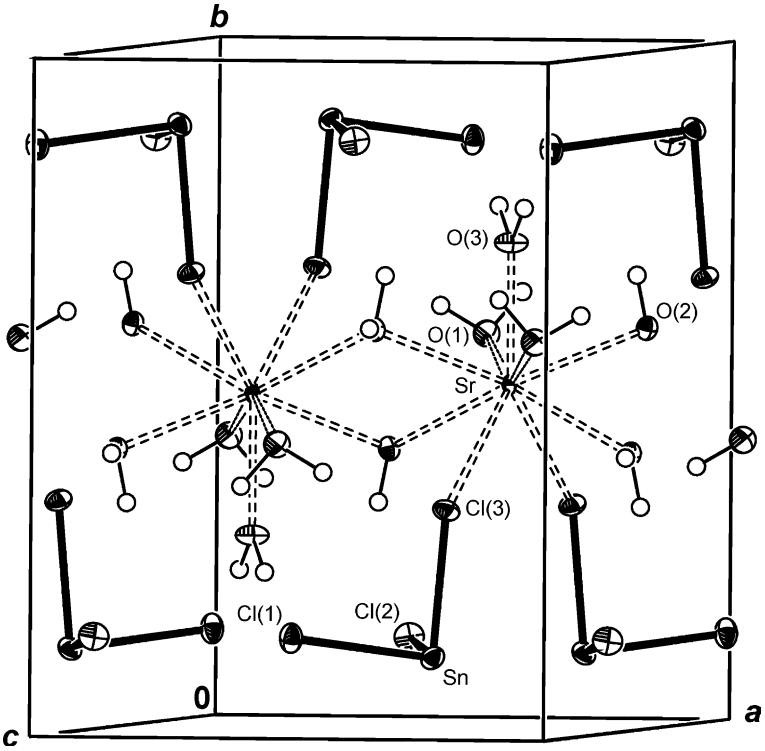

Fig. 1. Thermal ellipsoid (50% probability) plot showing part of unit cell contents of $Sr(SnCl_3)_2 \cdot 5H_2O$.

of six rather than seven and in that way is more comparable to the Sn containing analogues. Three short Pb–Cl contacts are seen with (ave. 2.76 Å). Three longer contacts ranging from 2.90 to 3.25 Å, complete distorted octahedral geometry. Interestingly, the Sr–O contacts show some significant variation, ranging from 2.43 to 2.82 Å, which may be indicative of some problems in modelling this essentially ionic interaction. However, the average Sr–O distance of 2.60 Å, is similar to the values seen in the structural analogues.

The structures of $Sr(MX_3)_2 \cdot 5H_2O$ (M = Sn, Pb; X = Br, Cl) clearly reflect the stereochemical distorting influence of the non-bonding valence electron pair on the Sn and Pb atoms. The tin chloride system has the most significant distortion, while the lead bromide system is the least distorted. The difference in electronegativity of the halide ions is evident in the difference in the degree of distortion between the tin chloride and the tin bromide structures. Similarly, the loss of distorting influence of the non-bonding valence electron pair with increase in atomic number is seen on comparing the tin bromide and lead bromide structures, the latter showing a much more spherical coordination environment.

In order to interpret the density functional results and, in particular, to focus on the position of the non-bonding valence electron pair on Sn and Pb atoms, we decided to localise the DFT orbitals obtained for each structure into a set of maximally localised Wannier functions and their corresponding centres. The Wannier functions are defined in terms of a unitary transformation of the Bloch orbitals, while requiring the total spread of the localised functions to be minimal [23–25]. The position of the Wannier centres locates the maximum density for the localised orbital concerned and can be used as a reliable indication of the centre of charge. This observation has been used to calculate successfully molecular dipole moments in ab initio molecular dynamics [26] and analyse the bonding in solid state and molecular systems [24].

The influence of both the halide X^- and the cation M^{2+} in the $[MX_3]^-$ systems, in the gas phase and in the solid state, can be compared by looking at the isosurface of the localised Wannier orbital corresponding to the non-bonding electron pair (Fig. 2). The corresponding distances between the centre of the localised Wannier orbital and the metal centre are given in Table 4. In the gas phase, we see that the non-bonding electron pair contracts toward the metal centre in both cases (Sn and Pb) when Cl^- is substituted for the larger and less electronegative Br^-, with contractions of 10% and 9%, respectively. This trend is also observed in the solid state for the two lead compounds, where a large contraction of nearly 41% is observed. However, in the case of the two Sn compounds, a small increase in this distance is observed in the solid state. The substitution of Sn for Pb results in a contraction in the distance between the metal centre to the centre of the localised Wannier orbital corresponding to the non-bonding electron pair by 24% for both halide systems in the gas phase.

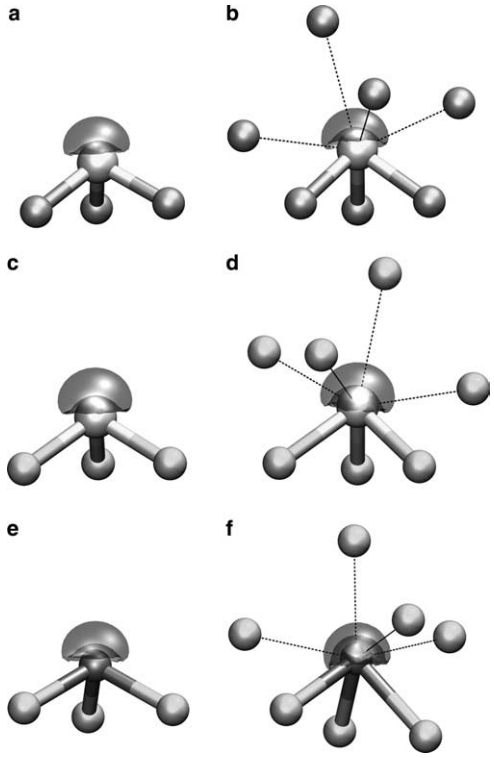

Fig. 2. Isosurfaces showing the extent of the localised Wannier function associated with the non-bonding valence electron pair of Sn and Pb in: (a) gas phase $[SnCl_3]^-$, (b) $Sr(SnCl_3)_2 \cdot 5H_2O$, (c) gas phase $[SnBr_3]^-$, (d) $Sr(SnBr_3)_2 \cdot 5H_2O$, (e) gas phase $[PbBr_3]^-$, and (f) $Sr(PbBr_3)_2 \cdot 5H_2O$.

Table 4
Distances (Å) between the metal centre and the computed maximum of the localised Wannier function (m) for the metal atom non-bonding valence electrons in gas phase $[MX_3]^-$ and $Sr(MX_3)_2 \cdot 5H_2O$

	M–m	
	$[MX_3]^-$ (gas phase)	$Sr(MX_3)_2 \cdot 5H_2O$
M = Sn, X = Cl	0.515	0.282
M = Sn, X = Br	0.467	0.287
M = Pb, X = Cl	0.390	0.138
M = Pb, X = Br	0.354	0.081

The trend is enhanced in the solid state with a contraction of this distance by 51% in the chloride and 73% in the bromide systems. Fig. 3 shows a contour plot of localised Wannier density in the Br(1)–M–Br(3) plane and clearly illustrates the contraction of the non-bonding electron pair orbital on metal substitution. These observations indicate that in a covalent environment such as the isolated $[MX_3]^-$ ion in the gas phase, the non-bonding valence electrons around lead are much closer to the metal centre than in tin and are consistent with the increased nuclear charge of lead compared to tin. In addition, the increased contraction of the non-bonding electron pair towards the Pb metal centre compared to Sn in the solid state is consistent with a decrease in stereochemical activity and directionality of the non-bonding valence electron pair orbital on Pb

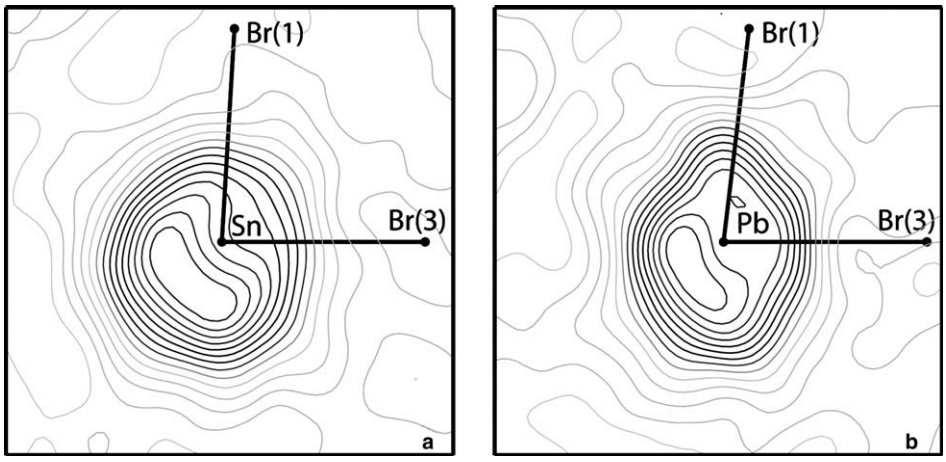

Fig. 3. Contour plots of localised Wannier density in the Br(1)–M–Br(3) plane associated with the non-bonding valence electron pair on (a) Sn in $Sr(SnBr_3)_2 \cdot 5H_2O$ and (b) Pb in $Sr(PbBr_3)_2 \cdot 5H_2O$.

compared to Sn, resulting in more regular coordination environments in the former.

Table 5 shows the distances between the maxima of the localised Wannier orbitals corresponding to all valence electrons and the M and X atom centres in $Sr(MX_3)_2 \cdot 5H_2O$. There is a clear difference observed in these distances between maxima corresponding to bonding and non-bonding electron pairs. In all cases, the maxima associated with non-bonding pairs are significantly closer to the X atom centres than those associated with bonding pairs, while the reverse is true for maxima around the metal atom centres. An indication of the degree of covalency in bonds around the Sn and Pb atoms is the percentage deviation of the charge centre maxima from the bond centre, $\%D_{cen}$ (Eq. 1). Table 6 summarises these values for the compounds under study.

$$\%D_{cen} = \frac{d_{M\text{–}m} - \frac{d_{M\text{–}X}}{2}}{d_{M\text{–}X}} \times 100\%, \quad (1)$$

Table 5
Distances between atom centres (Å) and the computed maxima (m) of the localised Wannier function in $[MX_3]^-$ units of $Sr(MX_3)_2 \cdot 5H_2O$

A–m	M = Sn, X = Cl	M = Sn, X = Br	M = Pb, X = Br	M = Pb, X = Cl
M–m(1)	2.015	2.064	2.361	2.243
M–m(2)	1.956	2.027	2.338	2.161
M–m(3)	2.035	2.138	2.414	2.151
M–m(4)	0.282	0.287	0.081	0.138
M–m(10)	2.687	2.758	2.577	2.380
X(1)–m(5)	0.443	0.497	0.516	0.443
X(1)–m(6)	0.474	0.505	0.522	0.485
X(1)–m(7)	0.476	0.516	0.551	0.490
X(1)–m(1)	0.600	0.708	0.597	0.561
X(2)–m(8)	0.464	0.497	0.503	0.464
X(2)–m(9)	0.469	0.524	0.556	0.465
X(2)–m(10)	0.475	0.542	0.579	0.526
X(2)–m(2)	0.630	0.722	0.640	0.589
X(3)–m(11)	0.460	0.516	0.526	0.467
X(3)–m(12)	0.478	0.529	0.529	0.473
X(3)–m(13)	0.480	0.536	0.579	0.515
X(3)–m(3)	0.600	0.663	0.609	0.577

Table 6
Percentage deviation of computed maxima (m) of the localised Wannier function from M–X bond centre in $Sr(MX_3)_2 \cdot 5H_2O$

m	M = Sn, X = Cl	M = Sn, X = Br	M = Pb, X = Br	M = Pb, X = Cl
m(1)	27	24	30	30
m(2)	26	24	29	29
m(3)	27	26	29	30
m(10)	33	36	32	32

where $d_{M\text{–}m}$ is the metal to maximum distance and $d_{M\text{–}X}$ is the metal to halide distance. In the case of the two tin containing compounds the more covalent interactions, Sn–X(1), Sn–X(2) and Sn–X(3) are characterised by average deviations from the bond centre of 27% and 25% for the chloride and bromide, respectively. The secondary contact to X(2a) (M–m(10)) shows a significant increase in this deviation reflecting the more electrostatic nature of this interaction. This is also reflected in the X(2)–m(10) distances in Table 5, which are similar to the other non-bonding interactions, X(1)–m(8) and X(1)–m(9) and significantly shorter than the X(2)–m(2) distances in the bonding orbital. In the case of the two lead compounds, the difference between the primary and secondary contacts is not as significant, and reflects the reduced stereochemical activity of the non-bonding electron pair.

4. Conclusions

The structures of $Sr(SnCl_3)_2 \cdot 5H_2O$, $Sr(SnBr_3)_2 \cdot 5H_2O$ and $Sr(PbBr_3)_2 \cdot 5H_2O$ are essentially isostructural. All show stereochemical activity of the non-bonding valence electron pair on Sn and Pb, with the degree of distortion less significant in the lead compound. Structure optimisation methods have allowed for prediction of optimised H atom positions in $Sr(PbBr_3)_2 \cdot 5H_2O$ and the complete structure in the case of $Sr(PbCl_3)_2 \cdot 5H_2O$.

Electronic structure calculations reveal a contraction towards the metal centre of the orbital associated with

the non-bonding valence electrons, on substitution of Sn by Pb, both in the gas phase and in the solid state. Similar contractions are observed on substitution of Cl^- by the less electronegative Br^- in the gas phase, however, this is not reflected in the solid state for the tin containing system. The relatively large deviations of the charge centre maxima from the bond centre in the M–X bonds are an indication of the degree of polarity of these bonds. While in the case of the Sn containing compounds there is a clear difference between primary and secondary M–X contacts, in the case of the Pb containing compounds this difference is less clear. This leads us to the conclusion that while the $[SnX_3]^-$ anion appears to be a discrete entity within the system $Sr(SnX_3)_2 \cdot 5H_2O$, there is less evidence for the existence of a corresponding discrete $[PbX_3]^-$ anion in lead analogues. A greater degree of polarity in the primary Pb–X interactions would be entirely consistent with the calculated contraction of the non-bonding valence electron pair orbital and the observed decrease in stereochemical distortion in the Pb coordination environment.

Appendix A. Supplementary data

Supplementary data associated with this article can be found, in the online version, at doi:10.1016/j.poly.2005.11.023.

References

[1] K.S. Pitzer, Acc. Chem. Res. 12 (1979) 271.
[2] P. Pyykko, J.-P. Desclaux, Acc. Chem. Res. 12 (1979) 276.
[3] B. Kamenar, D. Grdenic, J. Inorg. Nucl. Chem. 24 (1962) 1039.
[4] I. Abrahams, M. Christoforu, S.M. Grimes, J.D. Donaldson, J. Chem. Res. (M) (1994) 0318.
[5] I. Abrahams, D.Z. Demetriou, J. Solid State Chem. 149 (2000) 28.
[6] I. Abrahams, D.Z. Demetriou, R.T. Kroemer, H. Taylor, J. Solid State Chem. 160 (2001) 382.
[7] J.D. Donaldson, J. Silver, S. Hadjiminolis, S.D. Ross, J. Chem. Soc., Dalton Trans. (1975) 1500.
[8] H.J. Haupt, F. Huber, H.-W. Sandbote, Z. Anorg. Allg. Chem. 435 (1977) 191.
[9] G.M. Sheldrick, SHELX-97: Programs for Crystal Structure Analysis (Release 97-2), Institüt für Anorganische Chemie der Universität, Tammanstrasse 4, D-3400 Göttingen, Germany, 1998.
[10] A.C.T. North, D.C. Phillips, F.S. Matthews, Acta Crystallogr., Sect. A 24 (1968) 351.
[11] N. Walker, D. Stuart, Acta Crystallogr., Sect. A 39 (1983) 158.
[12] L.J. Farrugia, J. Appl. Crystallogr. 30 (1997) 565.
[13] L.J. Farrugia, WinGX – A Windows Program for Crystal Structure Analysis, University of Glasgow, 1998.
[14] CPMD, Copyright IBM Corp. 1990–2004, Copyright MPI für Festkörperforschung Stuttgart, 1997–2001.
[15] S. Goedecker, M. Teter, J. Hutter, Phys. Rev. B 54 (1996) 1703.
[16] C. Hartwigsen, S. Goedecker, J. Hutter, Phys. Rev. B 58 (1998) 3641.
[17] G. Berghold, C.J. Mundy, A.H. Romero, J. Hutter, M. Parrinello, Phys. Rev. B 61 (2000) 10040.
[18] S.R. Billeter, A. Curioni, W. Andreoni, Comput. Mater. Sci. 27 (2003) 437.
[19] P.C. Harrison, B.J. Haylett, T.J. King, Inorg. Chim. Acta 75 (1983) 265.
[20] H.-L. Keller, I. Jess, J. Less-Common Met. 125 (1986) 215.
[21] H.-L. Keller, J. Less-Common Met. 109 (1985) 19.
[22] R.E. Cohen, J. Phys. Chem. Solids 61 (2000) 139.
[23] G.H. Wannier, Phys. Rev. 52 (1937) 191.
[24] N. Marzari, D. Vanderbilt, Phys. Rev. B 56 (1997) 12847.
[25] P.L. Silvestrelli, N. Marzari, D. Vanderbilt, M. Parrinello, Solid State Commun. 107 (1998) 7.
[26] P.L. Silvestrelli, M. Parrinello, Phys. Rev. Lett. 82 (1999) 3308.

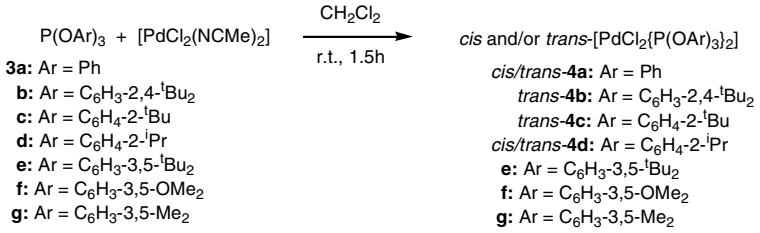

Scheme 1.

present. The IR spectrum of complex **4c** shows a single ν(Pd–Cl) at 382 cm^{-1} indicating that the chloride ligands are *trans* to one another. This value is close to that reported for the complex **4b** [9]. The *trans*-geometry was confirmed by X-ray analysis, the results of which are presented in Fig. 1.

Presumably the high steric profile of ligand **3c** in complex **4c** over-rides the electronic advantages associated with the *cis* arrangement, in which the π-acidic triarylphosphite ligands would be *trans* to the π-basic chlorides. Indeed when the 2-*tert*-butyl group is replaced with the smaller 2-isopropyl function to give complex **4d**, then a mixture of isomers is obtained. The ^{31}P NMR spectrum of complex **4d** shows two singlets at 84.4 (major) and 80.5 (minor) ppm (approximate ratio 9:1). Comparison with the ^{31}P NMR spectroscopic data for the complexes **4a**–**c** suggests that the major, higher field signal is due to the *trans* isomer. The IR spectrum indicates that in the solid state the major isomer is the *trans* complex with a single ν(Pd–Cl) at 375 cm^{-1}.

We were interested to see what the effect of steric bulk in the *meta*-positions of triarylphosphite ligands would have on the geometry of the resultant bis(phosphite) dichloropalladium complexes. To this end we synthesized the complexes **4e**–**g**. The ^{31}P NMR spectra indicate the presence of only one isomer in all cases with singlets observed at δ 76.6, 83.5 and 79.7 ppm for **4e, f, g**, respectively. In all cases the IR spectra are indicative of *cis* disposition of the chloride ligands.

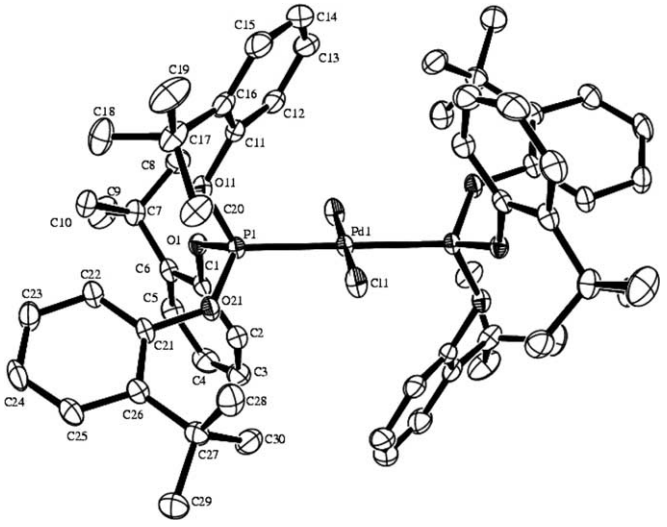

Fig. 1. The single crystal X-ray structure of *trans*-[$PdCl_2${$P(OC_6H_4$-2-^{t}Bu)$_3$}$_2$] (**4c**). Selected bond lengths (Å) and bond angles (°): Pd1–P1, 2.2895(6); Pd1–Cl1, 2.2826(5) and P1–Pd1–Cl1, 89.38(2).

2.2. Orthometallated dimeric complexes

We have previously shown that the bulky phosphite **3b** readily reacts with palladium dichloride to produce the dimeric palladacycle **1a** (Scheme 2, method **A**) [9]. By contrast, we find this method cannot be used with the much smaller ligand, triphenylphosphite, **3a**. In this case the desired complex **1b** has been synthesised previously by Albinati et al. by the reaction of the pre-formed bis-phosphite complex **4a** with one equivalent of palladium dichloride in toluene at reflux temperature (Scheme 2 method **B**) [8].

Tris(2-*tert*-butylphenyl)phosphite (**3c**) is sufficiently bulky that it is not necessary to employ method **B** (Scheme 1) for the synthesis of the orthopalladated dimer **1c**, rather it can be prepared directly by the reaction of the ligand with palladium dichloride (method **A**). Interestingly, from a synthetic perspective, tris(2-isopropyl)phosphite (**3d**) represents the cross-over point between the two methods. ^{31}P NMR spectroscopic analysis of a crude sample of the product mixture from the reaction performed using method **A** (Scheme 2) indicates that whilst the desired dimeric product **1d** is obtained, several other phosphorus containing species are also present. However, clean **1d** can be readily prepared by employing the method **B**.

The previously reported ^{31}P NMR spectra of complexes **1a** and **b** show them to be a mixture of *cis* and *trans* isomers in solution [9,8]. Complex **1d** is also obtained as a mixture of *cis* and *trans* isomers as evidenced by ^{31}P NMR spectroscopy which shows two peaks at 122.1 and 120.3 ppm, in close agreement with the value obtained for **1a** and **1b**. By contrast, the presence of only one isomer of complex **1c** in $CDCl_3$ solution is indicated by a singlet at 121.0 ppm in the ^{31}P NMR spectrum and by the lack of signals for a second isomer in the ^{1}H NMR spectrum. The single crystal X-ray structure of complex **1c** was determined and the molecule and selected data are presented in Fig. 2.

As can be seen, the molecule adopts a *trans* configuration, in line with previously reported orthopalladated triarylphosphite dimers and the related phosphinite complex **5**. The structure is grossly similar to those of complexes **1a** and **6**, with little or no significant difference between the bonds lengths about palladium [1,9]. Comparing the structure with that of the non-orthometallated complex **4c**, it can be seen that there is a slight decrease in the Pd–P bond length on orthometallation (~0.15 Å) and a slight increase in the Pd–Cl bond lengths (0.14 and 0.12 Å for the chlorides *trans* to the carbon and phosphorus donors, respectively).

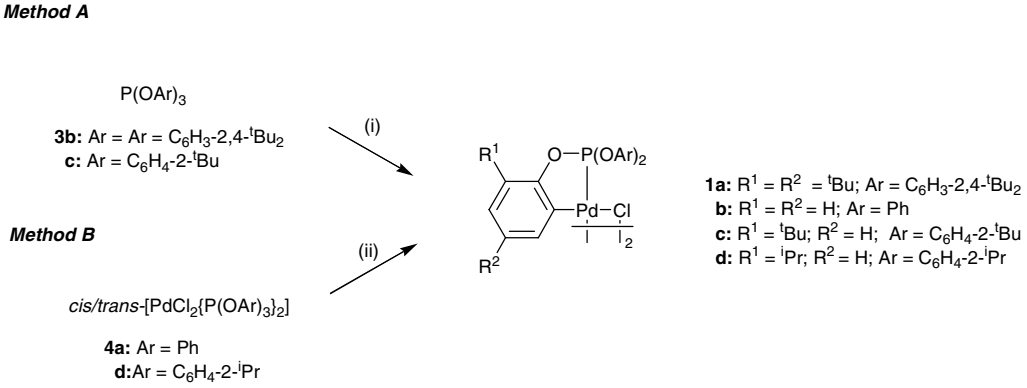

Scheme 2. Conditions: (i) 1 equiv. $PdCl_2$, 2-methoxyethanol, △, 2 h and (ii) 1 equiv. $PdCl_2$, toluene, △, 5 h.

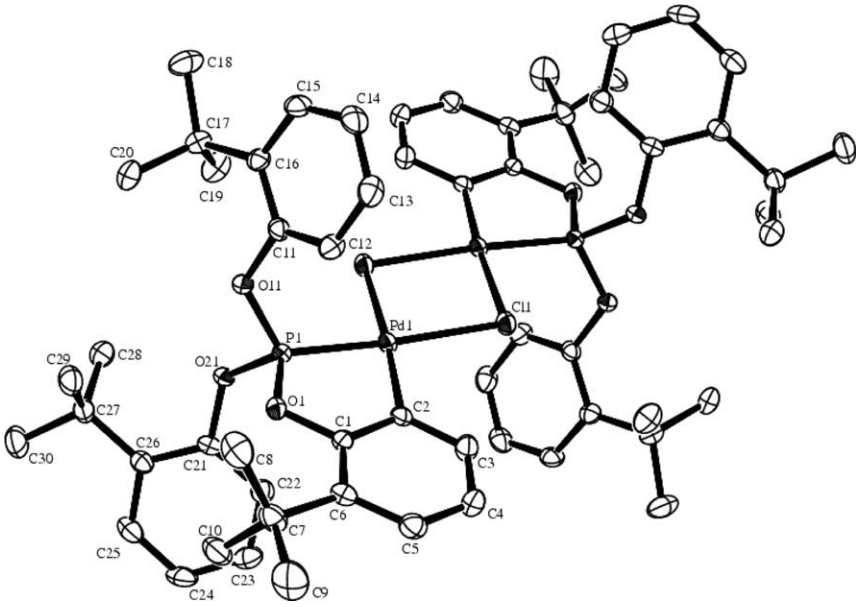

Fig. 2. The single crystal X-ray structure of *trans*-[{Pd(μ-Cl)(κ^2-*P*,*C*-P(OC_6H_3-2-^{t}Bu)(OC_6H_4-2-^{t}Bu)$_2$)}$_2$] (**1c**). Selected bond lengths (Å) and bond angles (°): Pd1–P1, 2.1425(6); Pd1–C2, 2.015(2); Pd1–Cl1, 2.4079(5); Pd1–Cl2, 2.4239(6) and P1–Pd1–C2, 80.85(6); P1–Pd1–Cl1, 172.22(2); P1–Pd1–Cl2, 95.86(2); C2–Pd–Cl1, 96.87(6); C2–Pd–Cl2, 175.32(6); Cl1–Pd–Cl2, 86.827(19).

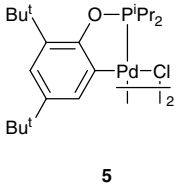

5

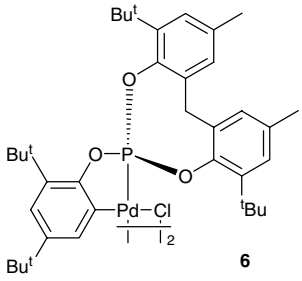

6

To the best of our knowledge, the crystal structures of all orthopalladated *triaryl*phosphite dimers – as well as the related phosphinite complex **5** – indicate that, in the solid state, the *trans* isomer crystallizes preferentially [1,9,10], although a *cis*-aryldialkylphosphite-based palladacycle has been structurally characterized [11]. Therefore, it came as a surprise that a single crystal X-ray analysis of complex **1b** shows that it adopts a *cis* configuration. The results of the structural analysis are presented in Fig. 3.

The driving force for the formation of the *cis* isomer in this case is revealed by investigating the dominant intermolecular interactions in the crystal structure, as shown in Fig. 4. From this it can be seen that adjacent molecules are arranged as head-to-tail supramolecular dimers, such that the aromatic rings are stacked in a face to face arrangement. Moreover, these supramolecular dimers are further 'locked' in position by an interaction of the ring hydrogen *para* to the oxy moiety with the orthometallated ring in a neighbouring molecule. These electrostatic interactions involving π electrons are enabled by the lack of steric bulk around the aromatic rings. The slightly offset disposition of the aromatic rings with respect to each other and the centroid–centroid separations ($\pi\cdots\pi = 4.368$ and 4.443 Å and C–H$\cdots\pi = 2.597$ and 2.717 Å) are in accordance with literature values that describe the nature of this

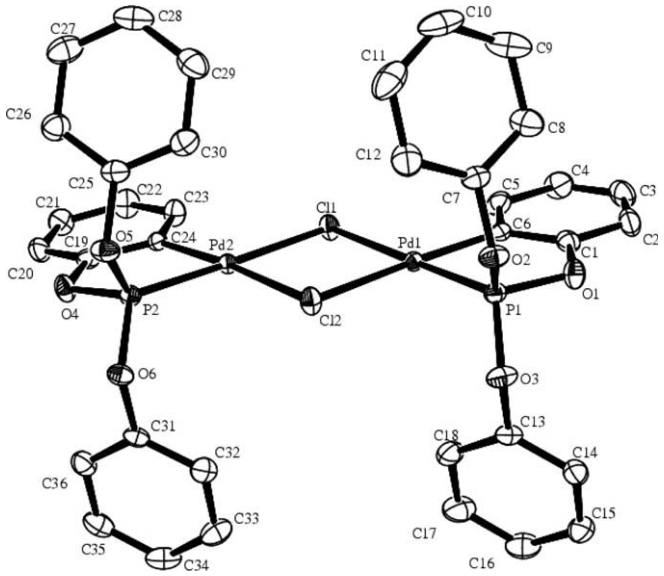

Fig. 3. The single crystal X-ray structure of *trans*-[{Pd(μ-Cl)(κ^2-*P*,*C*-P(OC$_6$H$_4$)(OPh)$_2$)}$_2$] (**1b**). Selected bond lengths (Å) and bond angles (°): Pd1–P1, 2.1499(5); Pd1–C6, 2.0105(19); Pd1–Cl1, 2.4098(5); Pd1–Cl2, 2.4099(5); Pd2–P2, 2.1516(5); Pd2–C24, 2.0096(18); Pd2–Cl1, 2.4189(5); Pd2–Cl2, 2.4179(5) and P1–Pd1–C6, 81.47(6); P1–Pd1–Cl1, 179.331(19); P1–Pd1–Cl2, 93.105(19); C6–Pd1–Cl1, 98.10(6); C6–Pd1–Cl2, 174.53(6); Cl1–Pd1–Cl2, 87.326(18); P2–Pd2–C24, 81.01(6); P2–Pd2–Cl1, 178.320(18); P2–Pd2–Cl2, 94.494(19); C24–Pd2–Cl1, 97.59(6); C24–Pd2–Cl2, 174.96(5); Cl1–Pd2–Cl2, 86.941(18).

interaction [12]. If the aromatic rings were stacked directly above each other and at a shorter separation (ca. 3.4 Å) the two π regions would repel each other, however, when they are offset and slightly further apart (in the region of ca. 4.2–4.6 Å) then the σ electrons may interact attractively with the π orbitals [13]. Due to the bidirectional configuration of the pendant aromatic groups in the molecule the crystal structure is composed of discrete tapes or ribbons. The ribbons associate with those in layers above and below through a further π···π interaction (4.034 Å).

It is easy to see that the introduction of steric bulk into both the orthometallated and non-orthometallated aryl residues would lead to a disruption in these intermolecular interactions. Presumably the preferred *trans* configuration obtained with bulky ligands results from an overall reduction of unfavourable steric interactions.

2.3. Phosphine adducts of phosphite-based palladacycles

We have previously shown that the reaction of tricyclohexylphosphine with the bulky dimeric complex **1a** in acetonitrile leads to the formation of the mononuclear adduct **2a** in which the phosphorus donors adopt a *cis* disposition (Scheme 3) [7]. By contrast, the *N*-heterocyclic carbene adducts of both the bulky complex **1a** and the smaller analogue **1b** – complexes **7** – adopt a geometry in which the carbene ligand is invariably *trans* to the phosphite ligand, regardless of the bulk of the triarylphosphite [14].

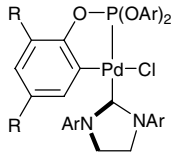

7a: R = ^{t}Bu; Ar = Mes
b: R = ^{t}Bu; Ar = C$_6$H$_3$-2,4-^{i}Pr
c: R = H; Ar = C$_6$H$_3$-2,4-^{i}Pr

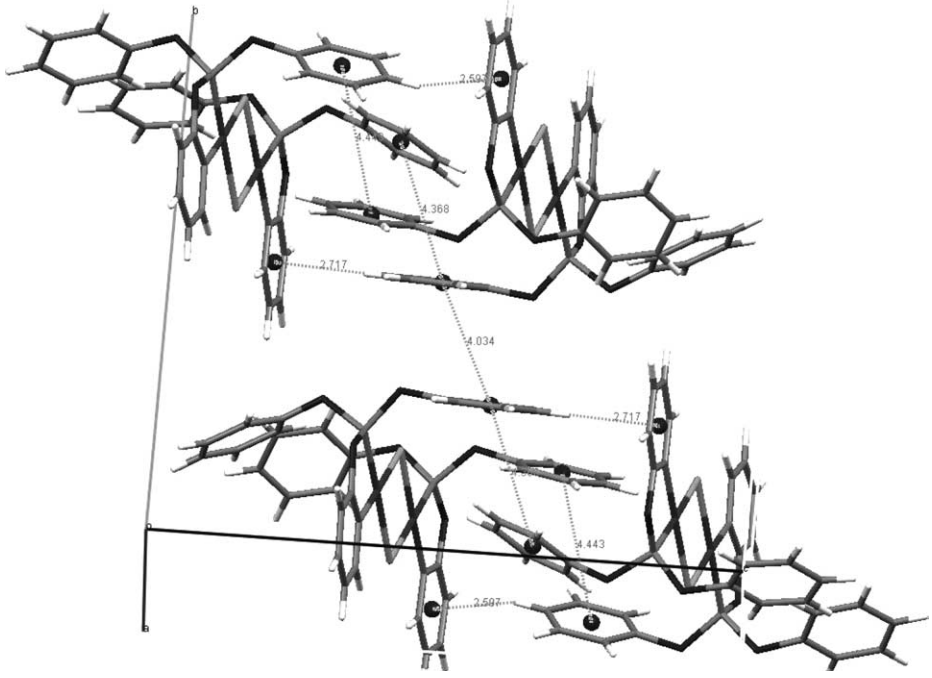

Fig. 4. Packing of complex **1c** showing major intermolecular interactions.

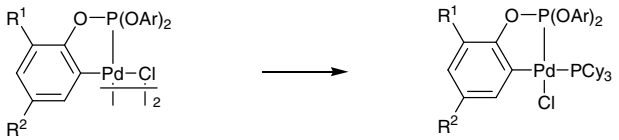

2a: $R^1 = R^2 = {}^tBu$; Ar = C_6H_3-2,4-$^tBu_2$
b: $R^1 = {}^tBu$; $R^2 = H$; Ar = C_6H_4-2-^tBu
c: $R^1 = {}^iPr$; $R^2 = H$; Ar = C_6H_4-2-^iPr
d: $R^1 = R^2 = H$; Ar = Ph

Scheme 3. Conditions: 3 equiv. PCy_3, MeCN, r.t., 5 h.

We were interested of see whether changing the bulk of the orthometallated ligand would have any bearing on the geometry of the tricyclohexylphosphine adducts. Therefore, the complexes **2b–d** were prepared in an analogous fashion to **2a**. In all cases the only product obtained is that in which the two P-donors are *cis* as evidenced by ^{31}P NMR spectroscopy. The mutual $^2J_{pp}$ couplings in complexes **2c** and **2d** (~41 Hz) are identical to that reported for complex **2a** [7], suggesting that steric bulk has very little effect on the coordination environment. By contrast complex **2b** shows a lower coupling of 36.45 Hz. We previously showed that the tri-*tert*-butylphosphine is too bulky to produce an adduct of complex **1a** [7]. Attempts to produce such adducts with the smaller complexes **1c** and **1d** gave only starting materials as adjudged by ^{31}P NMR analysis of the crude product mixtures. While the triphenylphosphite-based analogue **1b** does appear to react with P^tBu_3, this leads to a complex mixture of phosphorus-containing species.

2.4. An unusual solvolysis reaction

During the course of the synthetic studies we noticed that while complex **4g** can be prepared in the same manner as complexes **4a–f**, it is necessary to avoid the addition of methanol during work-up otherwise the isolated compound is quite obviously not the desired product. The ^{31}P NMR spectrum of the white powder precipitated over several hours in this instance shows a singlet δ 98.1 ppm, quite distinct from those of complexes of the general formula **4** which fall in the range 76.6–85.2 ppm. Furthermore, the ^1H NMR spectrum shows no aromatic signals; rather the only peak observed is a non-first-order multiplet at δ 3.83 ppm. Elemental analysis[1] is consistent with the formation of the known complex *cis*-$[PdCl_2\{P(OMe)_3\}_2]$ (**8**). Accordingly, we synthesized a genuine sample of complex **8** and found its ^1H and ^{31}P NMR spectroscopic data to be identical with those obtained above. This implies that either the complex **4g** undergoes facile methanolysis, or that the triarylphosphite ligands are labile and undergo methanolysis away from the palladium centre. The ^{31}P NMR spectrum of a $CDCl_3$/MeOH solution of ligand **3g** shows that partial methanolysis occurs within 20 h at room temperature to give an approximately 4:1 mixture of **3g** and $P(OMe)_3$ along with several other minor species. Treatment of complex **4g** with methanol under the same conditions gives a number of phosphorus-containing species as adjudged by ^{31}P NMR spectroscopy, which shows a range of peaks between 90 and 95 ppm only. While there does not appear to be any peaks corresponding to complex **8**, the lack of any signal for the starting complex **4g** and the chemical shift values for the products obtained,[2] imply that complete conversion of the starting material to partially methanolysed complexes of the form $[PdCl_2\{P(OMe)_n(OAr)_{3-n}\}\{P(OMe)_m(OAr)_{3-m}\}]$ has occurred.

While we have observed a similar alcoholysis reaction previously with a palladium–phosphinite complex [15], the facile nature of this particular reaction appears to be ligand specific; none of the other complexes **4a–f** appear to be susceptible to methanolysis under the same conditions.

3. Summary

In summary, we have shown that the stereochemistry of complexes of the type $[PdCl_2\{P(OAr)_3\}_2]$ is dependent on the size of *ortho*-substituents with bulky groups forcing the complexes to adopt the electronically less preferable *trans* configuration. In contrast, variation in the bulk of the *meta*-groups does not appear to have any significant influence on geometry. The bulk of the phosphite ligand also has implications in the choice of synthetic methodology adopted for the formation of orthopalladated dimers and their geometry in the solid state.

4. Experimental

4.1. General

All reactions were performed under nitrogen using standard schlenk techniques. All solvents were distilled from appropriate drying reagents prior to use. Ligand **3c** was prepared according to the literature method [16], while the known ligands **3d** and **3e** were prepared in a similar manner. Complexes **4a** and **8** were prepared according to the literature methods [8,17]. All other materials were obtained commercially and used as received.

[1] $[PdCl_2\{P(OMe)_3\}_2]$ requires C, 16.9; H, 4.25. Found: C, 16.9; H, 4.3%.

[2] Palladium aryldiethylphosphite complexes of the type $[PdCl_2\{P(OEt)_2(OAr)\}_2]$ show chemical shifts of ~ 90 ppm in their ^{31}P NMR spectra. See Refs. [8,11].

4.2. Synthesis of $P(OC_6H_3\text{-}3,5\text{-}OMe_2)_3$ (**3d**)

PCl_3 (0.87 ml, 10 mmol) was added to a solution of 3,5-dimethoxyphenol (4.625 g, 30 mmol) and *N*,*N*-dimethyl-*p*-toluidine (0.144 ml, 1.0 mmol) in 10 ml of xylene. The mixture was then heated at reflux, while N_2 was passed through to expel the HCl formed. After 2 h, the xylene was removed under reduced pressure and the residue was kept at 180 °C overnight in vacuo to yield the product as an orange oil that was not purified further (87% yield). *Anal.* Calc. for $C_{27}H_{33}O_3P$: C, 74.3; H, 7.6. Found: C, 73.7; H, 7.85%. NMR ($CDCl_3$): δ_H (300 MHz) 6.18 (s, 6H, aryl H2 and H6); 6.06 (s, 3H, aryl H4); 3.49 (s, 18H, Me). δ_P (121.5 MHz) 130.6.

4.3. General method for the synthesis of the complexes cis/trans-$[PdCl_2\{P(OAr)_3\}_2]$ (**4**)

A solution of $[PdCl_2(NCMe)_2]$ (0.5 mmol) and the appropriate triarylphosphite **3** (1.0 mmol) in dichloromethane (15 ml) was stirred at room temperature for 1.5 h. Methanol (20 ml) was then added and the mixture concentrated under reduced pressure to induce precipitation of the product.

4.4. trans-$[PdCl_2\{P(OC_6H_4\text{-}2\text{-}^tBu)_3\}_2]$ (**4c**)

Yellow solid (72% yield). *Anal.* Calc. for $C_{60}H_{78}Cl_2O_6P_2Pd$: C, 63.5; H, 6.9. Found: C, 63.0; H, 7.1%. NMR ($CDCl_3$): δ_H (300 MHz) 7.27 (d, 6H, $^3J_{HH} = 9$ Hz), 7.22 (d, 6H, $^3J_{HH} = 6$ Hz), 6.92 (t, 6H, $^3J_{HH} = 6$ Hz), 6.81 (t, 6H, $^3J_{HH} = 9$ Hz). δ_P (121.5 MHz) 85.20. IR (Nujol mull, polythene film): ν(Pd–Cl) 382 cm^{-1}.

4.5. cis/trans-$[PdCl_2\{P(OC_6H_4\text{-}2\text{-}^iPr)_3\}_2]$ (**4d**)

Yellow solid (63% yield). *Anal.* Calc. for $C_{54}H_{66}Cl_2O_6P_2Pd$: C, 61.75; H, 6.3. Found: C, 61.25; H, 6.2%. NMR ($CDCl_3$): δ_H (300 MHz) (most of the minor isomer peaks are coincident with or obscured by the major isomer): 7.29 (d, 6H, $^3J_{HH} = 9$ Hz), 7.10 (d, 6H, $^3J_{HH} = 9$ Hz), 7.01 (t, 6H, $^3J_{HH} = 9$ Hz), 6.93 (td, 6H, $^3J_{HH} = 9$ Hz, $^4J_{HH} = 3$ Hz), 3.22 (m, 6H), 1.00 (d, 36H, major, $^3J_{HH} = 6$ Hz), 0.93 (d, 36H, minor, $^3J_{HH} = 6$ Hz). δ_P (121.5 MHz) 84.42 (s, major isomer) and 80.46 (minor isomer). IR (Nujol mull, polythene film) ν(Pd–Cl): 375 (*trans* isomer).

4.6. cis-$[PdCl_2\{P(OC_6H_4\text{-}3,5\text{-}^tBu_2)_3\}_2]$ (**4e**)

Attempts to precipitate the product from dichloromethane solution by addition of methanol, ethanol, pentane, hexane or diethyl ether proved unsuccessful in this instance due to the high solubility of the product. Therefore, the solvent was removed in vacuo and the product was not purified further.

NMR ($CDCl_3$): δ_H (300 MHz) 7.06 (s, 6H, H4), 6.92 (s, 12H, H2 and H6), 1.06 (s, 108H, ^{t}Bu). δ_P (121.5 MHz) 76.60. IR (Nujol mull, polythene film) ν(Pd–Cl): 322 and 340 cm^{-1}.

4.7. cis-$[PdCl_2\{P(OC_6H_4\text{-}3,5\text{-}OMe_2)_3\}_2]$ (**4f**)

Pale yellow solid (26% yield). *Anal.* Calc. for $C_{48}H_{54}Cl_2O_{18}P_2Pd$: C, 49.8; H, 4.7. Found: C, 48.5; H, 4.4%. NMR ($CDCl_3$): δ_H (300 MHz) 6.35 (s, 12H, H2 and H6), 6.16 (s, 6H, H4), 3.59 (s, 36H, Me). δ_P (121.5 MHz) 83.49 ppm. IR (Nujol mull, polythene film) ν(Pd–Cl): 315 and 339 cm^{-1}.

4.8. cis-$[PdCl_2\{P(OC_6H_4\text{-}3,5\text{-}Me_2)_3\}_2]$ (**4g**)

Diethyl ether was used in place of methanol to induce precipitation. Pale yellow solid (75% yield). NMR ($CDCl_3$): δ_H (400 MHz) 6.74 (s, 12H, H2 and H6), 6.70 (s, 6H, H4), 2.10 (s, 36H, Me). δ_P (121.5 MHz, $CDCl_3$) 79.70 ppm. IR (Nujol mull, polythene film) ν(Pd–Cl): 305 and 334 cm^{-1}.

4.9. Synthesis of trans-$[\{Pd(\mu\text{-}Cl)(\kappa^2\text{-}P,C\text{-}P(OC_6H_3\text{-}2\text{-}^tBu)(OC_6H_4\text{-}2\text{-}^tBu)_2)\}_2]$ (**1c**)

A mixture of palladium dichloride (0.0745 g, 0.42 mmol) and ligand **3c** (0.200 g, 0.42 mmol) in 2-methoxyethanol (10 ml) was heated at reflux temperature for 2 h. The resultant solution was filtered through celite, ethanol (15 ml) was added and the solution concentrated in vacuo to give the product as a white solid (62% yield). *Anal.* Calc. for $C_{60}H_{78}Cl_2O_6P_2Pd_2$: C, 58.2; H, 6.2. Found: C, 57.6; H, 6.1%. NMR ($CDCl_3$): δ_H (300 MHz) 7.47 (s, 2H, orthometallated ring), 7.33 (s, 2H, orthometallated ring), 7.25 (d, 4H, free ring, $^3J_{HH} = 6$ Hz), 7.02 (d, 4H, free ring, $^3J_{HH} = 6$ Hz), 6.97–6.87 (m, 8H, free ring), 6.80 (s, 2H, orthometallated ring), 1.32 (s, 36H; free ring), 1.07 (s, 18H; orthometallated ring). δ_P (121.5 MHz) 120.96.

4.10. Synthesis of cis/trans-$[\{Pd(\mu\text{-}Cl)(\kappa^2\text{-}P,C\text{-}P(OC_6H_3\text{-}2\text{-}^iPr)(OC_6H_4\text{-}2\text{-}^iPr)_2)\}_2]$ (**1d**)

A mixture of complex **4d** (0.244 g, 0.23 mmol) and $PdCl_2$ (0.043 g, 0.24 mmol) in toluene (10 ml) was heated at reflux temperature for 5 h. The resultant solution was filtered through celite and the solvent was removed under reduced pressure. The residue was then recrystallised from CH_2Cl_2/MeOH to give the product as a white powder (98% yield). *Anal.* Calc. for $C_{54}H_{64}Cl_2O_6P_2Pd_2$: C, 56.2; H, 5.6. Found: C, 55.35; H, 5.5%. NMR ($CDCl_3$): δ_H (300 MHz) (most of the minor isomer peaks are coincident with or obscured by the broad major isomer peaks): 7.38 (d, $^3J_{HH} = 9$ Hz), 7.2 (br s) 7.13 (br m), 7.03–6.91 (br m) 6.78–6.76 (br m), 3.31 (br m, 2H, major isomer C*H*(CH_3)$_2$), 3.04 (br m, 2H, minor isomer, C*H*(CH_3)$_2$), 1.07 (Br d, CH(C*H*$_3$)$_2$). δ_P (121.5 MHz) 122.07 (major isomer), 120.29 (minor isomer).

4.11. General method for the synthesis of PCy_3 adducts of phosphite-based palladacycles (2)

A mixture of the appropriate complex **1** (0.1 mmol) and PCy_3 (0.3 mmol) in acetonitrile (10 ml) was stirred at room temperature for 5 h. The resultant solution was concentrated in vacuo and the product was precipitated by addition of an appropriate co-solvent.

4.12. [Pd(Cl){κ^2-P,C-P(OC_6H_3-2-^{t}Bu)-(OC_6H_4-2-^{t}Bu)$_2$}PCy_3] (2b)

Product precipitated as a white solid on addition of hexane (24% yield). *Anal.* Calc. for $C_{48}H_{71}ClO_3P_2Pd$: C, 64.1; H, 7.95. Found: C, 62.9; H, 8.3%. NMR ($CDCl_3$): δ_H (300 MHz) 8.42 (br m, 1H), 7.81 (br d, 2H, $^3J_{HH} = 6$ Hz), 7.285 (br d, 2H, $^3J_{HH} = 9$ Hz), 6.91 (m, 6H), 2.34 (br, 3H, Cy), 1.80 (br d, 9H, Cy), 1.49 (s, 18H, ^{t}Bu), 1.4, 1.1 and 0.8 (3 × m, 21H, Cy), 0.86 (s, 9H, ^{t}Bu). δ_P (121.5 MHz) 136.6 (d, phosphite, $^2J_{PP} = 36.5$ Hz), 28.4 (d, PCy_3, $^2J_{PP} = 36.5$ Hz).

4.13. [Pd(Cl){κ^2-P,C-P(OC_6H_3-2-^{i}Pr)-(OC_6H_4-2-^{i}Pr)$_2$}PCy_3] (2c)

This complex could not be obtained as a pure solid but as an impure oil (yield and elemental analysis were not determined). NMR ($CDCl_3$): δ_H (300 MHz) 8.20 (br dd, 2 × $J_{HH} = 6$ Hz), 7.30 (d, 2H, $J_{HH} = 9$ Hz), 2.20 (d, 2H, $J_{HH} = 6$ Hz), 7.08–6.95 (2 × m, 4H), 6.88 (m, 1H), 6.79 (m, 1H), 3.29 (m, 3H), 2.49 (m, 4H), 1.94 (m, 6H), 1.6, 1.2, 1.05 (3 × m, 32H), 0.85 (m, 3H) and 0.67 (d, $J_{HH} = 9$ Hz). δ_P (121.5 MHz) 131.43 (d, phosphite, $^2J_{PP} = 41.3$ Hz), 28.08 (d, PCy_3, $^2J_{PP} = 40.1$ Hz).

4.14. [Pd(Cl){κ^2-P,C-P(OC_6H_4)(OPh)$_2$}PCy_3] (2d)

Product precipitated as a white solid on addition of ethanol and cooling at −20 °C overnight (60% yield). *Anal.* Calc. for $C_{36}H_{47}ClO_3P_2Pd$: C, 59.1; H, 6.55. Found: C, 57.2; H, 6.4%. NMR ($CDCl_3$): δ_H (300 MHz) δ 8.42 (br d, 1H, $J_{HH} = 6$ Hz), 7.24 (m, 5H), 7.12 (m, 5H), 7.01 (m 2H), 6.72 (br s, 1H), 2.39 (br m, 3H, Cy), 1.86 (br s, 6H, Cy), 1.65 (br s, 9H) 1.49 (br m, 6H), 1.17 (br s, 9H). δ_P (121.5 MHz) 131.00 (d, phosphite, $^2J_{PP} = 41.3$ Hz), 29.00 (d, PCy_3, $^2J_{PP} = 42.5$ Hz).

5. Crystallography

Suitable single crystals were selected and data collected on a Bruker Nonius KappaCCD Area Detector at the window of a Bruker Nonius FR591 rotating anode ($\lambda_{Mo\,K\alpha} = 0.71073$ Å) driven by COLLECT [18] and DENZO [19] software at 120 K. The structure was determined in

Table 1
Crystallographic data for complexes **1b**, **1c** and **4c**

Compound	1b	1c	4c
Empirical formula	$C_{36}H_{28}Cl_2O_6P_2Pd_2$	$C_{60}H_{76}Cl_2O_6P_2Pd_2$	$C_{60}H_{78}Cl_2O_6P_2Pd_2$
Formula weight (g mol^{-1})	902.22	1238.85	1134.46
Temperature (K)	120(2)	120(2)	120(2)
Crystal system	monoclinic	triclinic	triclinic
Space group	$P2_1/c$	$P\bar{1}$	$P\bar{1}$
Unit cell dimensions			
a (Å)	12.7620(10)	8.5336(6)	10.0734(17)
b (Å)	15.5240(15)	13.3097(6)	11.1457(11)
c (Å)	17.571(2)	13.5367(8)	13.869(2)
α (°)		97.513(5)	80.124(8)
β (°)	94.053(5)	104.904(5)	74.007(10)
γ (°)		92.610(6)	86.778(9)
Volume (Å^3)	3472.5(6)	1467.98(15)	1474.6(4)
Z	4	1	1
Density (calculated) (Mg m^{-3})	1.726	1.401	1.278
Absorption coefficient (mm^{-1})	1.327	0.806	0.507
F(000)	1792	640	596
Crystal	block; colourless	blade; colourless	shard; colourless
Crystal size (mm^3)	0.60 × 0.25 × 0.25	0.52 × 0.24 × 0.07	0.19 × 0.13 × 0.07
θ Range for data collection (°)	3.03–27.50	2.98–27.48	2.93–27.48
Reflections collected	39 834	32 539	34 770
Independent reflections [R_{int}]	7945 [0.0274]	6701 [0.0423]	6731 [0.0559]
Completeness to $\theta = 27.48°$ (%)	99.6	99.8	99.8
Absorption correction	semi-empirical from equivalents	semi-empirical from equivalents	semi-empirical from equivalents
Goodness-of-fit on F^2	1.032	1.047	1.040
Final R indices [$F^2 > 2\sigma(F^2)$]	$R_1 = 0.0242$, $wR_2 = 0.0611$	$R_1 = 0.0299$, $wR_2 = 0.0637$	$R_1 = 0.0346$, $wR_2 = 0.0751$
R indices (all data)	$R_1 = 0.0319$, $wR_2 = 0.0654$	$R_1 = 0.0409$, $wR_2 = 0.0679$	$R_1 = 0.0457$, $wR_2 = 0.0802$
Largest difference in peak and hole (e Å^{-3})	0.665 and −0.683	0.552 and −0.637	0.373 and −0.698

SHELXS-97 [20] and refined using SHELXL-97 [21]. Crystallographic data for complexes **1b**, **1c** and **4c** are presented in Table 1.[3]

Acknowledgements

We thank the EPSRC (PDRA for M.B., Advanced Research Fellowship for RBB) and the Ministerio de Educación, Cultura y Deporte (MJLS) for support and Johnson Matthey for the loan of palladium salts.

References

[1] D.A. Albisson, R.B. Bedford, S.E. Lawrence, P.N. Scully, Chem. Commun. (1998) 2095.
[2] D.A. Albisson, R.B. Bedford, P.N. Scully, Tetrahedron Lett. 39 (1998) 9793.
[3] R.B. Bedford, C.S.J. Cazin, S.L. Hazelwood, Angew. Chem., Int. Ed. 41 (2002) 4120.
[4] R.B. Bedford, S.L. Hazelwood, M.E. Limmert, Chem. Commun. (2002) 2610.
[5] R.B. Bedford, C.S.J. Cazin, S.L. Hazelwood, Chem. Commun. (2002) 2608.
[6] R.B. Bedford, M.E. Blake, Adv. Synth. Catal. 345 (2003) 1107.
[7] R.B. Bedford, M. Betham, S.J. Coles, R.M. Frost, M.B. Hursthouse, Tetrahedron 61 (2005) 9663.
[8] A. Albinati, S. Affolter, P.S. Pregosin, Organometallics 9 (1990) 379.
[9] R.B. Bedford, S.L. Hazelwood, M.E. Limmert, D.A. Albisson, S.M. Draper, P.N. Scully, S.J. Coles, M.B. Hursthouse, Chem. Eur. J. 9 (2003) 3216.
[10] R.B. Bedford, S.L. Hazelwood, P.N. Horton, M.B. Hursthouse, Dalton Trans. (2003) 4164.
[11] Sokolov and co-workers found that a palladacycle based on *O*-diethoxyphosphino-(+)-estrone gives a *separable* mixture of stereoisomers. More typically the isomers of chloro-bridged phosphite-based palladacycles are in equilibrium (see for example Refs. [8,9]). See: V.I. Sokolov, L.A. Bulygina, O.Y. Borbulevych, O.V. Shishkin, J. Organometal. Chem. 582 (1999) 246.
[12] M.L. Waters, Curr. Opin. Chem. Biol. 6 (2002) 736, and references therein.
[13] C.A. Hunter, J.K.M. Sanders, J. Am. Chem. Soc. 112 (1990) 5525.
[14] R.B. Bedford, M. Betham, M.E. Blake, R.M. Frost, P.N. Horton, M.B. Hursthouse, R.-M. López-Nicolás, Dalton Trans. (2005) 2774.
[15] R.B. Bedford, S.L. Hazelwood, M.E. Limmert, J.M. Brown, S. Ramdeehul, A.R. Cowley, S.J. Coles, M.B. Hursthouse, Organometallics 22 (2003) 1364.
[16] P.W.N.M. Van Leeuwen, C.F. Roobeek, J. Organometal. Chem. 258 (1983) 343.
[17] S.M. Aucott, A.M.Z. Slawin, J.D. Woollins, Dalton Trans. (2000) 2559.
[18] R. Hooft, COLLECT: Data Collection Software, Nonius B.V., Delft, The Netherlands, 1998.
[19] Z. Otwinowski, W. Minor, Methods in enzymology, in: C.W. Carter Jr., R.M. Sweet (Eds.), Macromolecular Crystallography, Part A, vol. 276, Academic Press, New York, 1997, pp. 307–326.
[20] G.M. Sheldrick, Acta Crystallogr., Sect. A. 46 (1990) 467.
[21] G.M. Sheldrick, University of Göttingen, Germany, 1997.

[3] Crystallographic data (excluding structure factors) for the structures in this paper, has been deposited with the Cambridge Crystallographic Data Centre as Supplementary Publication Nos. CCDC 283108–283110. Copies of the data can be obtained, free of charge, on application to CCDC, 12 Union Road, Cambridge CB2 1EZ, UK (fax: +44 0 1223 336033 or e-mail: deposit@ccdc.cam.ac.uk).

and this manuscript reports on studies involving choline and triethylammonium organotriboroxinate derivatives.

2. Results and discussion

The choline tetraorganotriboroxinate salt $[Me_3NCH_2CH_2OH][Ph_4B_3O_3]$ (**1**) was prepared by the reaction in methanol solution of phenylboronic acid, diphenylborinic acid anhydride and choline hydroxide in appropriate stoichiometry (Eq. (1)). A similar procedure has been reported previously [7] for the synthesis of $[NMe_4][Ph_4B_3O_3]$. The product rapidly precipitated out of solution as an air-stable white solid which could be easily isolated by filtration, and purified by re-crystallization from acetone.

$$Ph_2BOBPh_2 + 4PhB(OH)_2 + 2[Me_3NCH_2CH_2OH][OH] \rightarrow 2[Me_3NCH_2CH_2OH][Ph_4B_3O_3](\mathbf{1}) + 5H_2O \quad (1)$$

Compound **1** was characterized by m.p. ^{11}B NMR and IR spectroscopy and gave satisfactory elemental analysis. The ^{11}B spectrum showed two signals at +29.1 and +4.2 ppm with the high frequency signal (3-coordinate B) twice the intensity of the low frequency (4-coordinate B) signal. The solid-state structure of compound **1** was obtained from a single-crystal X-ray diffraction study.

The solid-state structure of **1** reveals that the anions and cations are held together as discrete ion-pairs via a H-bond interaction between an hydroxyl O atom of the cation, O4, and a ring O atom of the anion, O3 (Fig. 1). The O4···O3 distance at 2.845(5) Å indicates a moderately strong H-bond interaction. Bond angle and bond distance data for the $[Ph_4B_3O_3]^-$ anion are summarized in the caption to Fig. 1; these data are very similar to those reported for $[Me_4N][Ph_4B_3O_4]$ [7]. It should be noted that the anion is also isoelectronic with Lewis base adducts of triorganylboroxines ($R_3B_3O_3 \cdot L$), and many of which e.g., $2(Ph_3B_3O_3) \cdot 3(p\text{-}H_2NC_6H_4NH_2)$, $2(Ph_3B_3O_3) \cdot N(CH_2CH_2)_3N$, $Ph_3B_3O_3 \cdot Me_2NCH_2CH_2NMe_2$, $Ph_3B_3O_3 \cdot py$, $(4\text{-}MeC_6H_4)_3B_3O_3 \cdot C_6H_{12}NH_2$, $(4\text{-}MeC_6H_4)_3B_3O_3 \cdot$ (4-picoline), $(4\text{-}BrC_6H_4)_3B_3O_3 \cdot$ (3-picoline), and $Me_3B_3O_3 \cdot NH_2{}^iPr \cdot MeB(OH)_2$ have been structurally characterized [9–15]. These boroxine ring structures, each of which contain one 4-coordinate and two 3-coordinate B atoms, show similar, significant, and systematic variations in BO bond lengths. This is also the case for **1** were the average BO distance involving the 4-coordinate B {1.507(5) Å} > average BO distance involving the O atom remote from the 4-coordinate B {1.396(5) Å} > the average remaining 2 BO distances {1.339(5) Å}, and reflecting the expected bond orders. The

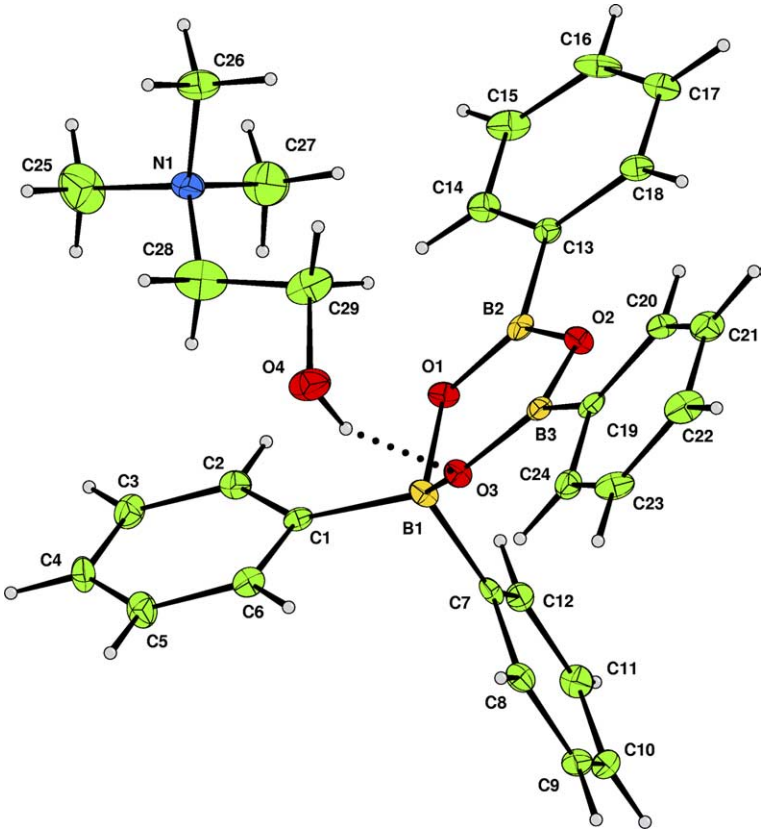

Fig. 1. Molecular structure of $[Me_3NCH_2CH_2OH][Ph_4B_3O_3]$ (**1**) showing atomic numbering scheme. Selected internuclear angles (°) and internuclear distances (Å) with esd's in parenthesis are: B1–O1 1.498(5), B1–O3 1.517(5), B1–C7 1.618(6), B1–C1 1.624(5), B2–O1 1.337(5), B2–O2 1.401(5), B2–C13 1.564(6), B3–O3 1.341(4), B3–O2 1.391(5), B3–C19 1.573(5); and O1–B1–O3 108.8(3), O1–B1–C7 110.4(3), O3–B1–C7 108.8(3), O1–B1–C1 108.6(3), O3–B1–C1 109.6(3), C7–B1–C1 110.7(3), O1–B2–O2 120.9(3), O1–B2–C13 120.9(3), O2–B2–C13 118.1(3), O3–B3–O2 121.9(3), O3–B3–C19 120.4(3), O2–B3–C19 117.7(3), B2–O1–B1 121.4(3), B3–O2–B2 118.2(3), B3–O3–B1 119.4(3). H-bond interaction: O4–H–O3 154.7, O4–H 0.84, H···O3 2.06, O4···O2 2.845(4).

B (sp^3)-C bonds {av. 1.621(6) Å} are significantly longer than the B (sp^2)-C bonds {av. 1.569(6) Å} due to π-overlap of the phenyl ring with the trigonal B centres. The ring-angle at the 4-coordinate B(1) is 108.8(3)°, whereas the 3-coordinate B(2) and B(3) centers have ring-angles averaging 121.4(3)°. The O ring-angles are in the range 118.2(3)–121.4(2)° with the angle opposite the tetrahedral B the smallest. The ring is almost planar with the rms deviation from the least squares plane being 0.128(7) Å. However, the conformation could be described as a 'shallow' boat with B1 and O2 deviating from the least squares plane of O1, B2, O3, B3 by 0.383(6) and 0.136(5) Å, respectively. The H-bond interaction is to one of the O atoms {O3} adjacent to the 4-coordinate B atom {B1}, rather than to the remote O atom {O2}. With the exception of the slight contraction of the ring angle at O3, the other bond angles and distances involving O3 are not significantly different from those of the non H-bonded, but otherwise chemically equivalent O1. The location of the H-bond acceptor site is possibly an indication of increased electron density at the O atoms adjacent to the formally negatively charged tetrahedral B atom. A H-bond interaction to this adjacent position has also been previously observed in $Me_3B_3O_3 \cdot NH_2{}^iPr \cdot MeB(OH)_2$ [14] and in that system the H-bond is essentially co-planar with the boroxine ring. This contrasts with **1** where the H-bond is at a substantial angle (such that the non-bonded angle B2 O3 H4A from the hydrogen of the donor to the cross ring vector is 118.52(4)°). It is possible that crystal-packing and steric effects play a substantial and largely unpredictable role in the H-bond location.

It was of interest to investigate whether analogous mixed-aryl anions e.g., $[(Ph_2BO)(ArBO)_2]^-$ might be prepared following a similar procedure. White solid products were obtained from reaction in methanol solution of diphenylborinic anhydride/choline hydroxide with various arylboronic acids {Ar = 4-$MeOC_6H_4$, 3-$MeOC_6H_4$, 2-$MeOC_6H_4$, 4-BrC_6H_4, $CpFe(C_5H_4)$ but these products, even when dissolved in acetone and re-precipitated with pet. ether, did not give satisfactory elemental analysis. ^{11}B NMR of these 'white products' showed the expected 3- and 4-coordinate boron signals of correct intensities, but it is likely that these materials were mixtures rather than pure compounds. From an attempted re-crystallization of a white solid isolated from the 4-$MeOC_6H_4$-$B(OH)_2/Ph_2BOBPh_2/[Me_3NCH_2CH_2OH][OH]$ (4:1:2) reaction mixture we isolated a few single-crystals of a compound which were subsequently identified by X-ray diffraction as the triarylboroxine, $(4\text{-}MeOC_6H_4)_3B_3O_3$ (**2**). This compound is well known but surprisingly its crystal structure has not been previously reported. A schematic drawing of the molecular structure of **2** is shown in Fig. 2 and pertinent bond-lengths and bond-angles are given in the

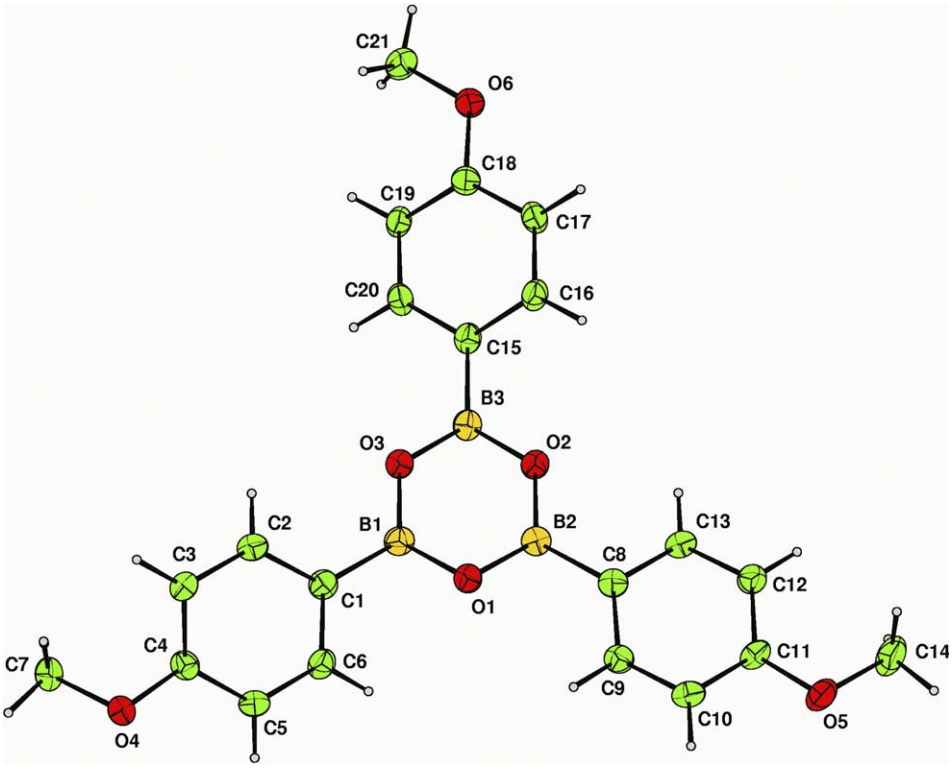

Fig. 2. Molecular structure of $(4\text{-}MeOC_6H_4)_3B_3O_3$ (**2**) showing atomic numbering scheme. Selected internuclear distances (Å) and bond angles (°) with esd's in parenthesis are: B1–O1 1.378(2), B1–O3 1.384(2), B2–O1 1.380(2), B2–O2 1.380(2), B3–O2 1.377(2), B3–O3 1.383(2), C1–B1 1.543(2), C8–B2 1.539(2), C15–B3 1.545(2); and O1–B1–O3 119.24(15), O1–B1–C1 120.46(14), O3–B1–C1 120.29(14), O1–B2–O2 119.02(14), O1–B2–C8 121.42(14), O2–B2–C8 119.55(14), O2–B3–O3 118.78(14), O2–B3–C15 120.41(14), O3–B3–C15 120.81(14), B1–O1–B2 120.74(13), B3–O2–B2 121.31(13), B3–O3–B1 120.80(13).

caption to the Figure. Previously determined single-crystal X-ray diffraction studies of boroxines include $Et_3B_3O_3$ and $Ar_3B_3O_3$, (Ar = Ph, 4-MeC_6H_4, 4-BrC_6H_4) [12,16–18]. In common with the other structurally characterized $Ar_3B_3O_3$ derivatives, the *p*-methoxyphenyl rings and the alternating B_3O_3 boroxine ring in **2** are essentially co-planar, with bond distances and angles similar to those previously reported. The B–O distances are in the range 1.377(2)–1.384(2) Å [av. 1.380(2) Å] with the boroxine ring angles close to that expected for sp^2 hybridized atoms with the B–O–B angles [120.74(13)–121.33(13)°, av. 120.96(13)°] slightly larger than the O–B–O angles [118.78(14)–119.24(15)°, av. 119.01°].

A hybrid hydroxy/triorganotriboroxinate salt, $[NEt_3H][Ph_3B_3O_3(OH)]$ (**3**), closely related to the tetraorganoboroxinate salt (**1**), was obtained in reasonable yield from the reaction of Et_3N with 3 equiv. of $PhB(OH)_2$ in anhydrous Et_2O (Eq. (2)). Compound **3** was characterized by elemental analysis, IR and ^{11}B NMR spectroscopy, and by a single-crystal X-ray diffraction study. Its ^{11}B NMR spectrum showed the expected 2 signals of relative intensity 2:1 at +29.8 and +4.6 ppm corresponding to the 3- and 4-coordinate B environments. A plausible mechanism for the formation of this novel hybrid structure might involve initial condensation of the $PhB(OH)_2$ to yield the triphenylboroxine, $Ph_3B_3O_3$, and 3 equiv. of water. Subsequent proton abstraction from the water by the Et_3N to yield the hydroxide salt $[Et_3N][OH]$ followed by addition to $Ph_3B_3O_3$ would lead to formation of the hydroxide adduct, **3**. $Ph_3B_3O_3 \cdot py$ is reported to be formed from py and $PhB(OH)_2$ under similar conditions [18] and the differing reactivity of Et_3N and py may be attributed to its increased basicity of the former.

$$Et_3N + 3PhB(OH)_2 \rightarrow [NEt_3H][Ph_3B_3O_3(OH)]\ (\mathbf{3}) + 2H_2O \quad (2)$$

A drawing of the anion and cation of **3**, showing atomic numbering scheme, is shown in Fig. 3; relevant bond angle and bond distance data are described within the caption to this figure. The solid-state dimeric structure of **3** is clearly demonstrated in Fig. 4, where short H-bond interactions (D···A, <2.9 Å) are shown. The solid-state structure has H-bond interactions between the cation and anion (N1H···O4) which exist as an ion-pair, and also anion–anion (O4H···O2) interactions which form the dimeric structure. The hydroxyl O atom, O4, is involved in both acceptor and donor H-bond interactions, with the hydroxyl hydrogen bridging across to O2 in the neighbouring anion's boroxinate ring. The heavy atoms of the dimeric anions (B3O2O4) adopt a centro-symmetric pseudo chair-like conformation with O4H···O2 angle at 166(2)°. There is also a weaker longer range H-bond interaction involving N1H and O3. Here, the N1–H···O3 angle is smaller at 122.8(1)°, and the internuclear distances are N1–H 1.04(2) Å, O3···H 2.570(19) Å, and N1···O3 3.245(18) Å. As was noted above for the tetraorganoboroxinate anion **1**, and previously for Lewis base adducts of boroxines, there is again a systematic variation of B–O bond-lengths

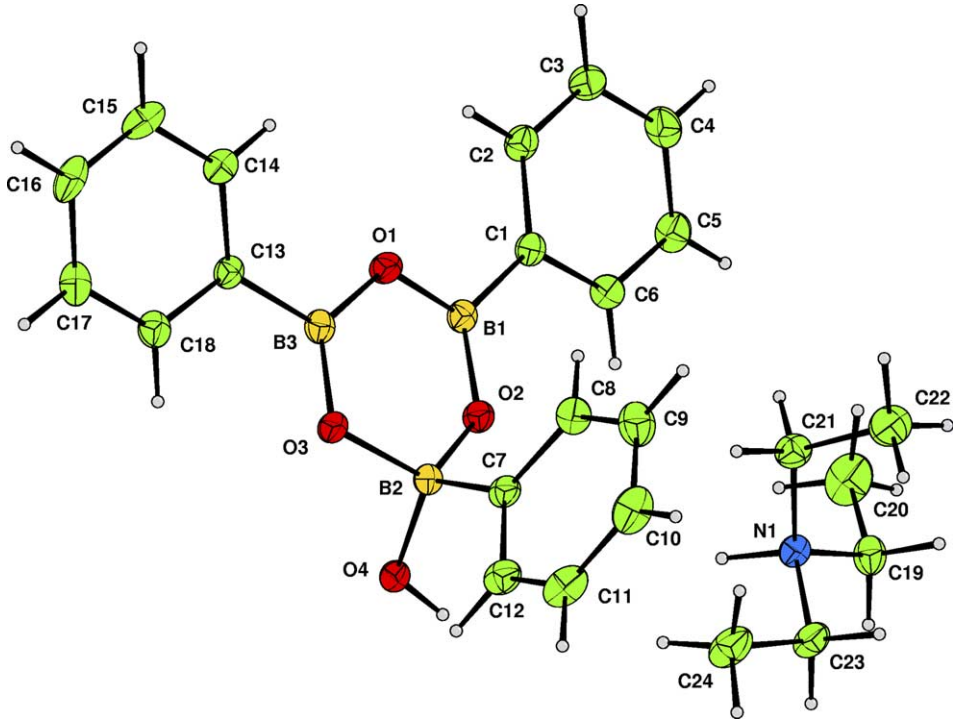

Fig. 3. Molecular structure of $[NEt_3H][Ph_3B_3O_3(OH)]$ (**3**) showing atomic numbering scheme. Selected internuclear distances (Å) and bond angles (°) with esd's in parenthesis are:B1–O2 1.344(2), B1–O1 1.396(2), B1–C1 1.567(3), B2–O4 1.456(2), B2–O3 1.490(2), B2–O2 1.507(2), B2–C7 1.617(3), B3–O3 1.337(2), B3–O1 1.391(2), B3–C13 1.571(2); and O2–B1–O1 120.80(16), O2–B1–C1 121.08(15), O1–B1–C1 118.09(16), O4–B2–O3 105.04(14), O4–B2–O2 109.48(14), O3–B2–O2 108.90(14), O4–B2–C7 113.43(14), O3–B2–C7 110.12(13), O2–B2–C7 109.71(14), O3–B3–O1 121.39(15), O3–B3–C13 120.14(15), O1–B3–C13 118.47(15), B3–O1–B1 119.07(14), B1–O2–B2 122.16(13), B3–O3–B2 122.19(14).

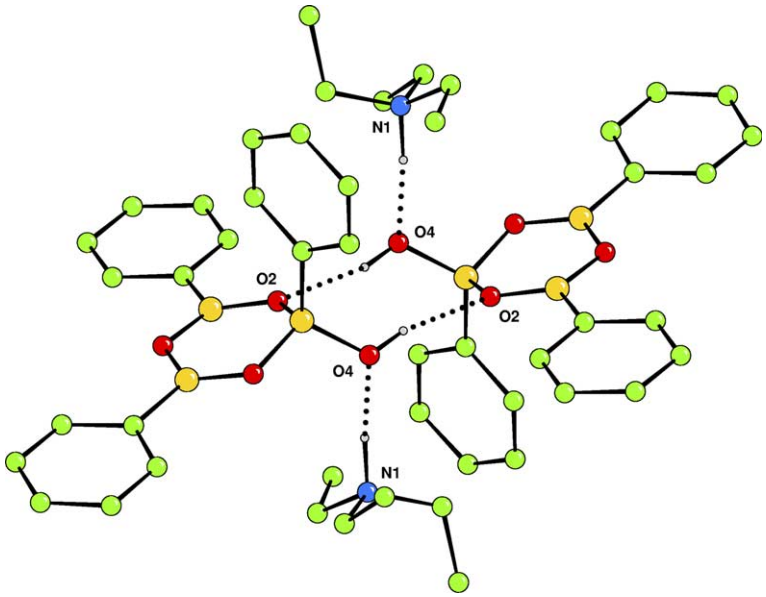

Fig. 4. Dimeric solid-state structure of **3** showing short range H-bond interactions. Internuclear angles (°) and internuclear distances (Å) with esd's in parenthesis are: O4–H–O2 166(2), O4–H 0.87(2), O2···H 1.99(2), O4···O2 2.8425(17) , and N1–H–O4 173.8(18), N1–H 1.04(2), O4···H 1.59(2), N1···O4 2.6283(19).

within the hydroxytriorganoboroxinate ring of **3**. Thus, the average BO distance involving the 4-coordinate B {1.499(2) Å} > average BO distance involving the O atom remote from the 4-coordinate B {1.394(2) Å} > the average remaining 2 BO distances {1.341(2) Å}. The *exo* ring B2–O4 distance of 1.456(2) Å is significantly shorter than the two ring O–B2 distances, indicative of a stronger bond. The B (sp^3)-C7 bond length and the B (sp^2)-C bond lengths {av. 1.569(3) Å} in **3** are not significantly different from those observed for **1**. The ring-angle at the 4-coordinate B(2) is 108.90(14)°, whereas the 3-coordinate B(1) and B(3) centers have ring-angles averaging 121.10(16)°. The O ring-angles are in the range 119.07(14)–122.19(14)°. Angles involving the B2O4 vector to O3, O2 and C7 range from 105.04(14)–113.43(14)° [av. 109.31(14)°]. The B_3O_3 ring conformation is best described as an envelope with the tetrahedrally coordinated B2 forming the flap. The rms deviation of the 5 atoms from planarity is 0.0196(7) Å and the flap of B2 is 0.334(2) Å out of the plane.

3. Experimental

3.1. General

Reactions were carried out under N_2. IR spectra were recorded on a Perkin–Elmer FT-IR 1600 spectrometer. ^{11}B NMR spectra were recorded on a Bruker 500 AVANCE spectrometer operating at 160.5 MHz. Chemical shifts are given in ppm with positive values towards high-frequency from $BF_3 \cdot OEt_2$. Elemental analysis were obtained on a Carla Erba MOD-1106 instrument using He as carrier gas. Ph_2BOPh_2 was prepared by the literature method [19] from commercially available $Ph_2BOCH_2CH_2NH_2$. The aryl boronic acids [$PhB(OH)_2$, 4-$MeOC_6H_4B(OH)_2$, 3-$MeOC_6H_4B(OH)_2$, 2-$MeOC_6H_4B(OH)_2$, 4-$BrC_6H_4B(OH)_2$, $CpFe(C_5H_4)B(OH)_2$] were obtained commercially.

3.2. Synthesis of $[Me_3NCH_2CH_2OH][Ph_4B_3O_3]$ (1)

To MeOH (5 cm^3) was added, with stirring, a methanolic solution of choline hydroxide (45% w/w, 0.31 g, 1.16 mmol), solid Ph_2BOBPh_2 (0.20 g, 0.58 mmol) and solid $PhB(OH)_2$ (0.28 g, 2.29 mmol). The solids initially dissolved to give a clear solution, and then after a few minutes the product precipitated as a white solid. The product was isolated by filtration and recrystallized from acetone. Yield: 0.28 g (52%). M.p. 189 °C. *Anal.* Calc. for $C_{29}H_{34}B_3NO_4$: C, 70.7; H, 6.9; N, 2.8. Found: C, 70.4; H, 6.6; N, 2.5%. NMR δ (^{11}B)(acetone-d_6): +4.2 (1B), +29.1 (2B). IR (ν_{max}/cm^{-1} as nujol mull, all strong): 3384, 1598, 1444, 1414, 1385, 1272, 1236, 1146, 1109, 954, 872, 706. Crystals suitable for X-ray diffraction were obtained from an acetone solution of the compound layered with pentane.

3.3. Synthesis of $[Et_3NH][Ph_3B_3O_3(OH)]$ (3)

Et_3N (0.20 g, 2.0 mmol) and $PhB(OH)_2$ (0.732, 6.0 mmol) were dissolved in Et_2O (5 cm^3). After a few minutes the solvent was evaporated and the remaining white solid recrystallized from Et_2O. Yield: 0.41 g (47%). M.p. 96 °C. *Anal.* Calc. for $C_{24}H_{32}B_3NO_4$: C, 66.9; H, 7.5; N, 3.3. Found: C, 67.2; H, 7.2 ; N, 3.0%. NMR δ (^{11}B)(acetone-d_6): +4.6 (1B), +29.8 (2B). IR (ν_{max}/cm^{-1}as nujol mull, all strong): 3424, 1600, 1446, 1377, 1252, 1175,

Table 1
Crystal data for **1**, **2**, and **3**, and their structural refinement parameters

Compound	**1**	**2**	**3**
Formula	$C_{24}H_{20}B_3O_3 \cdot C_5H_{14}NO$	$C_{21}H_{21}B_3O_6$	$C_{18}H_{16}B_3O_4 \cdot C_6H_{16}N$
Colour	colourless	colourless	colourless
Habit	shard	prism	block
Size (mm^3)	$0.14 \times 0.10 \times 0.06$	$0.40 \times 0.36 \times 0.28$	$0.15 \times 0.10 \times 0.10$
Crystal system	orthorhombic	monoclinic	orthorhombic
Space group	*Pbca*	$P2_1/c$	*Pbca*
a (Å)	16.9787(8)	8.9364(3)	19.7506(7)
b (Å)	17.2540(6)	14.2768(7)	11.0679(5)
c (Å)	18.2709(8)	16.4278(8)	22.3807(10)
β (°)		105.78°	
Z	8	4	8
Reflections	20261	17846	21379
Independent [R_{int}]	3645 [0.0741]	4402 [0.0626]	4308 [0.0823]
Completeness to $\theta = 27.48°$	$\theta = 25.02°$/77.2	$\theta = 27.45°$/95.4	$\theta = 25.03°$/99.7
Transmission maximum and minimum	0.9953 and 0.9891	0.9744 and 0.9637	0.9924 and 0.9887
Parameters	338	275	300
Final R indices [$F^2 > 2\sigma(F^2)$]	$R_1 = 0.0656$, $wR_2 = 0.1609$	$R_1 = 0.0476$, $wR_2 = 0.1131$	$R_1 = 0.0455$, $wR_2 = 0.1012$
R indices (all data)	$R_1 = 0.1088$, $wR_2 = 0.1840$	$R_1 = 0.0795$, $wR_2 = 0.1312$	$R_1 = 0.0787$, $wR_2 = 0.1161$
CCDC code	275669	275668	275667

1114, 1027, 968, 923, 750, 704. Crystals suitable for X-ray diffraction were grown from Et_2O at 6 °C.

3.4. X-ray structures of *1*, *2*, and *3*

Data for all structures were collected using Phi and omega scans on a Bruker Nonius Kappa CCD area detector diffractometer with a rotating Mo (0.71073 Å) anode following standard procedures. Data were corrected for absorption using SORTAV [20,21]. Structure solution was performed using SHELXS-97 [22] and refinement carried out on F^2 using SHELXL 97 [23]. Hydrogen atoms were placed in idealised positions and refined using a riding model. Crystal data for **1**, **2** and **3** and their structural refinement parameters are given in Table 1.

4. Supplementary material

Crystallographic data for the structure analysis has been deposited with the Cambridge Crystallographic Data Centre CCDC Nos. **1** (CCDC275669), **2** (CCDC275668), and **3** (CCDC275667). Copies of this information may be obtained free of charge from the Director, CCDC, 12 Union Road, Cambridge, CB2 1EZ (fax: +44 1223 336033) or e-mail: deposit@ccdc.cam.ac.uk or www: http://www.ccdc.cam.ac.uk.

Acknowledgements

We thank the EPSRC for funding of the X-ray crystallographic service at the University of Southampton, and for an Industrial CASE award for BMS-T. We also thank Pilkington Plc for financial support (BMS-T) and the EU Socrates scheme (L.F.).

References

[1] D.M. Schubert, M.Z. Visi, C.B. Knobler, Inorg. Chem. (2000) 2250.
[2] D.M. Schubert, R.A. Smith, M.Z. Visi, Glass Technol. 44 (2003) 63.
[3] G. Heller, J. Inorg. Nucl. Chem. 30 (1968) 2743.
[4] G.M. Wang, Y.Q. Sun, G.Y. Yang, J. Solid State Chem. 177 (2004) 4648.
[5] H.X. Zhang, S.T. Zheng, G.Y. Yang, Acta Crystallogr., Sect. C 60 (2004) O545.
[6] Y. Nishihara, K. Nara, K. Osakada, Inorg. Chem. 41 (2002) 4090.
[7] W. Kliegel, H.-W. Motzkus, S.J. Rettig, J. Trotter, Can. J. Chem. 63 (1985) 3516.
[8] E. Zeller, H. Beruda, H. Schmidbaur, Chem. Ber. 126 (1993) 2033.
[9] M. Yalpani, R. Boese, Chem. Ber. 116 (1983) 3347.
[10] G. Ferguson, A.J. Lough, J.P. Sheehan, T.R. Spalding, Acta Cryst. C 46 (1990) 2390.
[11] M.A. Beckett, G.C. Strickland, K.S. Varma, D.E. Hibbs, M.B. Hursthouse, K.M.A. Malik, Polyhedron 14 (1995) 2623.
[12] M.A. Beckett, G.C. Strickland, K.S. Varma, D.E. Hibbs, M.B. Hursthouse, K.M.A. Malik, J. Organomet. Chem. 535 (1997) 33.
[13] M.A. Beckett, D.E. Hibbs, M.B. Hursthouse, P. Owen, K.M.A. Malik, K.S. Varma, Main Group Chem. 2 (1998) 251.
[14] M.A. Beckett, D.S. Brassington, P. Owen, M.B. Hursthouse, M.E. Light, K.M.A. Malik, K.S. Varma, J. Organomet. Chem. 585 (1999) 7.
[15] J. Beckmann, D. Dakternieks, A. Duthie, A.E.K. Lim, E.R.T. Tiekink, J. Organomet. Chem. 633 (2001) 149.
[16] R. Boese, M. Plok, D. Blaser, Angew. Chem., Int. Ed. Engl. 26 (1987) 245.
[17] A.G. Avent, S.E. Lawrence, M.M. Meehan, T.G. Russell, T.R. Spalding, Collect. Czech. Chem. Commun. 67 (2002) 1051.
[18] C.P. Brock, R.P. Minton, K. Niedenzu, Acta. Cryst. C 43 (1987) 1775.
[19] G. Coates, J. Livingstone, J. Chem. Soc. (1961) 4909.
[20] R.H. Blessing, Acta Cryst. A 51 (1995) 33.
[21] R.H. Blessing, J. Appl. Cryst. 30 (1997) 421.
[22] G.M. Sheldrick, Acta Cryst. A 46 (1990) 467.
[23] G.M. Sheldrick, SHELXL 97, University of Göttingen, Germany, 1997.

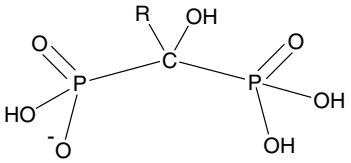

R = $(CH_2)_2NH_3^+$ (H_4L^1), $(CH_2)_3NH_3^+$(H_4L^2), $(CH_2)_5NH_3^+$(H_4L^3)

Fig. 1. Bisphosphonate structure.

2. Results and discussion

The bisphosphonic acids 4-amino-1-hydroxy-1,1-butylidenebisphosphonic acid (H_4L^2) and 6-amino-1-hydroxy-1,1-hexylidenebisphosphonic acid (H_4L^3) were synthesised as described in the patent literature [19]. We screened reactions of H_4L^2 and H_4L^3 with a range of hydrated divalent transition metal nitrates, metal = Mn, Fe, Co, Ni, Cu, Zn, Cd and vanadyl sulfate. The metal:ligand stoichiometries 0.75:1, 1:1, 1:1.5 and 1:2 were explored including reactions where the bisphosphonic acids were initially treated with 1–4 molar equivalents of NaOH. Apart from those cases employing metal:protonated ligand ratio of 0.75:1 (for, Co **1**, **6**, Ni **2**, Zn **3**, Mn **4**, and Cd **5** derivatives), the products of these reactions were otherwise very fine polycrystalline powders, not readily amenable to study by single crystal diffraction methods. The structurally characterised compounds had metal:ligand ratios of 1:2. They were insoluble in common organic solvents and water and did not melt below 290 °C.

3. X-ray crystal structures of 1–6

The structures of compounds **1**–**6** are shown in Fig. 2 along with atom numbering schemes.

The single crystal data are summarised in Section 5 while selected bond distances and angles are given in Tables 3 and 4 and selected hydrogen bonding is shown in Tables 5–11.

In common with known metal hydroxyaminoalkanebisphosphonates the ligands in compounds **1**–**6** are zwitterionic having a positively charged ammonium terminus balanced by one of the negatively charged phosphonate oxygens. In the present work further deprotonation at the second phosphonic acid group provides a bidentate dianionic ligand where each phosphonate is of the form ~P=O(O^-)(OH) with tetrahedral phosphorus and where the ligand adopts simple chelate (seen in all compounds **1**–**6**) and additionally, chelate bridging (in **4**–**6**) coordination modes. Metal coordination is roughly octahedral in all compounds **1**–**6**. Both ligand coordination modes have been reported previously for metal derivatives of H_4L, H_4L^2 (see Tables 1 and 2) but only the former for H_4L^3 [20]. The P=O (average 1.507 Å) and P–O(H) (average 1.567 Å) distances are clearly distinguished in all cases. The former are close to both chelate P–O(M) (average 1.509 Å) and bridging P–O(M) (average P–O(M) 1.499 Å). Two of the P–O(M) bonds in **4**, **5**, and **6** should be formally P=O(M) but its not possible from the data to assign these to specific bridging or chelate groups.

Compounds **1**–**3** are rare examples of mononuclear bisphosphonates with the 6-amino-1-hydroxy-1,1-hexylidene, C_6, fragment. The cupric ion derivative of H_4L^3 has previously been structurally characterised [20] and **1**–**3** are essentially isostructural with this copper compound. In the case of the Zn compound **3** we observed a doubling of the *a*-axis parameter and loss of symmetry on the molecule at 160 K (**3a**) compared to room temperature (**3b**). In **3a** the two halves of the molecule are no longer related by an inversion centre (as in **1**, **2** and **3b**). This indication of a phase transition is probably due to changes in hydrogen bonding at the lower temperature. The detail and more general occurrence of this type of phase transition in these systems requires further study but it is noteworthy that since compounds **1** and **2** are centrosymmetric at low temperature, the effect may be metal dependent.

There is an extensive network of intra and intermolecular hydrogen bonds between the molecular units, which includes lattice bound water, in all of these structures. In the mononuclear structures, for example, intramolecular H-bonds include the alkyl hydroxy group and coordinated water molecules while intermolecular bonds extend from the P–OH, P=O the terminal ammonium groups and coordinated water (see Fig. 3 and Tables 5–8). In the dinuclear structures **4** and **5** hydrogen bonding is primarily intermolecular and again extends from the P–OH, P=O, C–OH, terminal ammonium groups and coordinated water. A pair of P–OH–O=P intramolecular bonds can be seen between the bridging ligands (see Fig. 4 and Tables 9 and 10).

In contrast to **4** and **5** there is extensive intramolecular H-bonding in dinuclear compound **6** (Table 11).

This involves H–O bonds between C–OH–HO–P groups where both are part of the same bridging ligand and between C–OH–(Co)O–P groups from bridging to terminal ligands. Further intramolecular H-bonding of type NH_3^+–(Co)O–P from bridging to terminal ligands is also present.

Compounds **1** and **6** are the first examples Co^{2+} derivatives of H_4L^3 and H_4L^2 to be structurally characterised. The observed aggregation patterns, mononuclear for **1**, $[Co(H_3L^3)_2 \cdot 2H_2O]$ $2H_2O$ and dinuclear for **6**, $[Co(H_3L^2)_2 \cdot H_2O]_2$ $2H_2O$ follow those previously observed for the analogous Cu^{2+} derivatives [18,20]. This pattern is also seen in the mononuclear structure of $[Zn(H_3L^3)_2 \cdot 2H_2O]$ $2H_2O$ **3** and the previously described dinuclear compound $[Zn(H_3L^2)_2 \cdot H_2O]_2$ $2H_2O$ [18]. Others postulated that the aminoalkylidene chain length plays a role in determining aggregation [20]. The dinuclear Mn^{2+}, **4** and Cd^{2+}, **5** derivatives of H_4L^3 are apparently the first examples of dinuclear derivatives of H_4L^3. There are striking differences between the dinuclear structures derived from H_4L^3 and those derived from H_4L^2. These are discussed below in relation to dinuclear compounds

Table 1
Coordination modes exhibited by etidronate (H_4L) (taken from the CCSD Cambridge Crystallographic Structure Data Base)

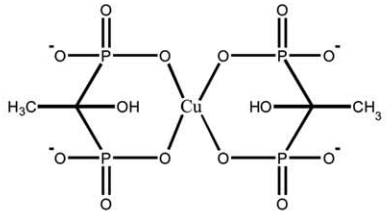

Tetrapotassium disodium bis(1-hydroxyethylidene-1,1-diphosphonate-O,O',O'')-copper(II) dodecahydrate [8]

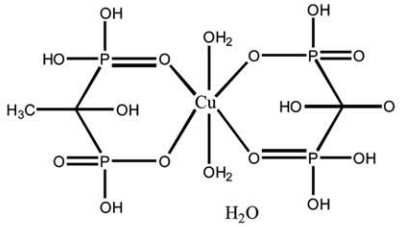

Diaqua-bis(1-hydroxyethylidene-diphosphonato)-copper(II) trihydrate [9]

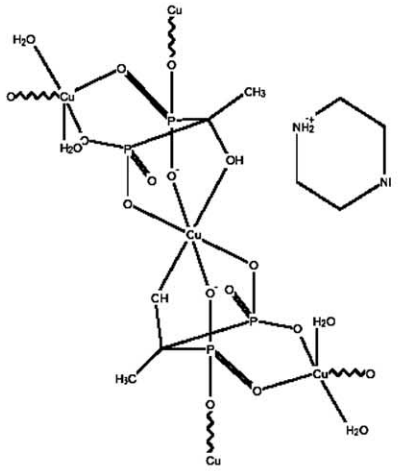

catena-(piperazinium bis(μ_3-1-hydroxyethylidene diphosphonato)-tetraaqua-tri-copper(II)) [12]

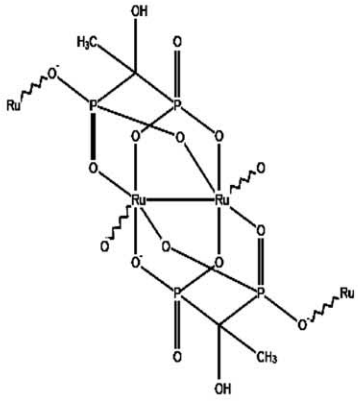

catena-(Triammonium bis(μ_3-1hydroxyethylidene diphosphonato)-diruthenium(II,III) dihydrate [13]

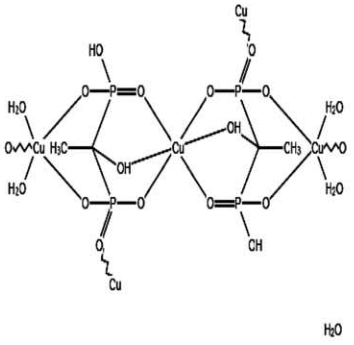

catena-(bis((μ_3-1-Hydroxyethane-1,1-diphosphonato-O,O',O'',O''',O'''',O''''')-diaqua)-tri-copper(II) dihydrate) [10]

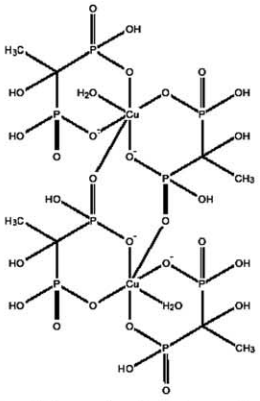

Tetra-potassium bis(aqua-(μ_2-(1-hydroxyethane-1,1-diphosphonato-O,O'))-(1-hydroxyethane-1,1-diphosphonato-O,O)-copper(II) tetrahydrate [11]

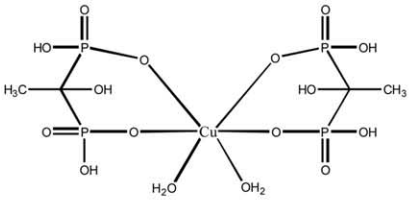

Bis(diethylammonium) diaqua-bis(1-hydroxyethylidene-1,1-diphosphonato)-cobalt(II) [14]

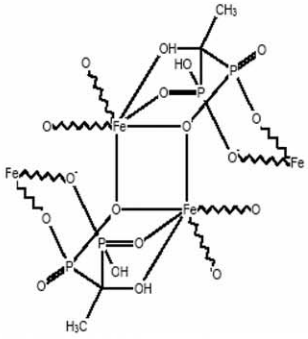

catena-(butane-1,4-diammonium bis(μ_3-1-hydroxy-1-(hydrogenphosphonate)-1-(phosphonato)ethane)-di-iron(II) dihydrate) [15]

Table 2
Coordination modes exhibited by aminohydroxyalkylidenebisphosphonate compounds

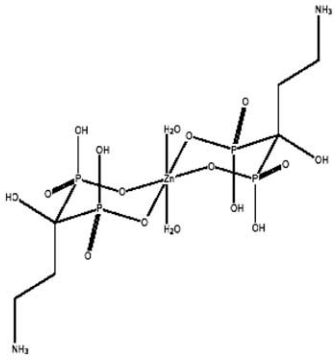

bis(3-Ammonio-1-hydroxypropylidene-1,1-bisphosphonate-O,O')-diaquazinc [17]

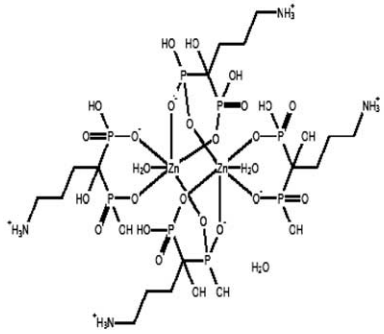

bis(μ_2-4-Amino-1-hydroxybutylidene-1,1-biphosphonite)-diaqua-bis(4-amino-1-hydroxybutylidene-1,1-biphosphonite)-di-zinc dihydrate [18]

4 and **6** with C_6 and C_4 chains, respectively. The central coordination cores are essentially the same with the pseudo-octahedral metal environments occupied by water, terminal chelating and chelate bridging bisphosphonates. The ammonium terminated C_6 and C_4 chains of the terminal ligands extend away from the dinuclear core in both cases. In the case of the bridging ligands, the C_4 chain in **6** bends in the direction of the central dinuclear core to facilitate intramolecular hydrogen bonding between the ammonium terminus and the ligating as well as non-ligating phosphonate oxygens. In contrast the C_6 chains of the bridging ligands in **4** and **5** extend away from the central dinuclear core (like the terminal ligands) so that intramolecular hydrogen bonding from the ammonium terminus is prohibited in this case (Fig. 4). However, it should be noted that there is significantly more puckering in the C_6 chains of the bridging ligands compared to those of the terminal ligands in **4** and **5**. This structural difference between dinuclear metal derivatives of L_4H^2 and L_4H^3 results in different intramolecular hydrogen bonding patterns and different overall extended structures for the hydrogen-bonded assemblies. Thus, if we consider structure directing effects of the aminoalkyl chains only, we see in **6** chain assemblies of hydrogen-bonded dimers while in **4** we see sheet-like assemblies of hydrogen bonded dimers.

The isolation of dinuclear compounds **4** and **5** with C_6 chains and extended sheet-type H-bonded structures, shows that these ligands display more versatile structure directing ability than previously seen. The different structural types, mononuclear or dinuclear, for H_4L^3 derivatives of different metals suggests the metal ions themselves may be important in determining this feature. In the present work it is noteworthy that the dinuclear structures **4** and **5** are formed by the two largest metal ions of the series used (Mn^{2+} 91pm, Cd^{2+} 103pm) while mononuclear structures were afforded by the rest (Co^{2+} 82pm, Ni^{2+} 78pm, Cu^{2+} 72pm, [20], Zn^{2+} 83pm). As mentioned earlier, divalent metal ions (Co^{2+}, this work, Cu^{2+} [20], Zn^{2+}, this work and [18]) which formed a mononuclear 1:2 derivative from H_4L^3 (C_6) gave a dinuclear 1:2 derivative with H_4L^2 (C_4). It is interesting in this context that while we report here on a dinuclear 1:2 derivative of H_4L^3 for Cd^{2+} **5**, others have reported a 1:1 complex from Cd^{2+} and H_4L^2 that has polymeric chain structure [18].

4. Conclusion

This work provides further evidence of a relationship between aggregation and alkylammonium chain length which is also linked to the size of metal ions. Additionally, the alkylammonium chain length is clearly important in determining the features of the supramolecular structures of these compounds.

5. Experimental

The compounds 4-amino-1-hydroxy-1,1-butylidenebisphosphonic acid (H_4L^2) and 6-amino-1-hydroxy-1,1-hexylidenebisphosphonic acid (H_4L^3) were prepared according to the methods described in the patent literature [19]. Reagents were purchased from Aldrich. All of the new compounds **1**–**6** displayed the infra red vibrational modes ν_{O-H} 3400, ν_{N-H} 2800, $\nu_{P=O}$ 1150, ν_{P-O-H} 980, and ν_{P-C} 770–650 cm^{-1}.

5.1. Diaqua-bis(6-hydroxyhexylidene-1,1-bisphosphonate)-cobalt dihydrate (*1*)

A bright pink solution from H_4L^3 (1.18 g, 4.23 mmol) in water 70 mL and $Co(NO_3)_2 \cdot 6H_2O$ (0.79 g, 3.08 mmol) in water 5 mL was heated in a sealed Teflon reactor held

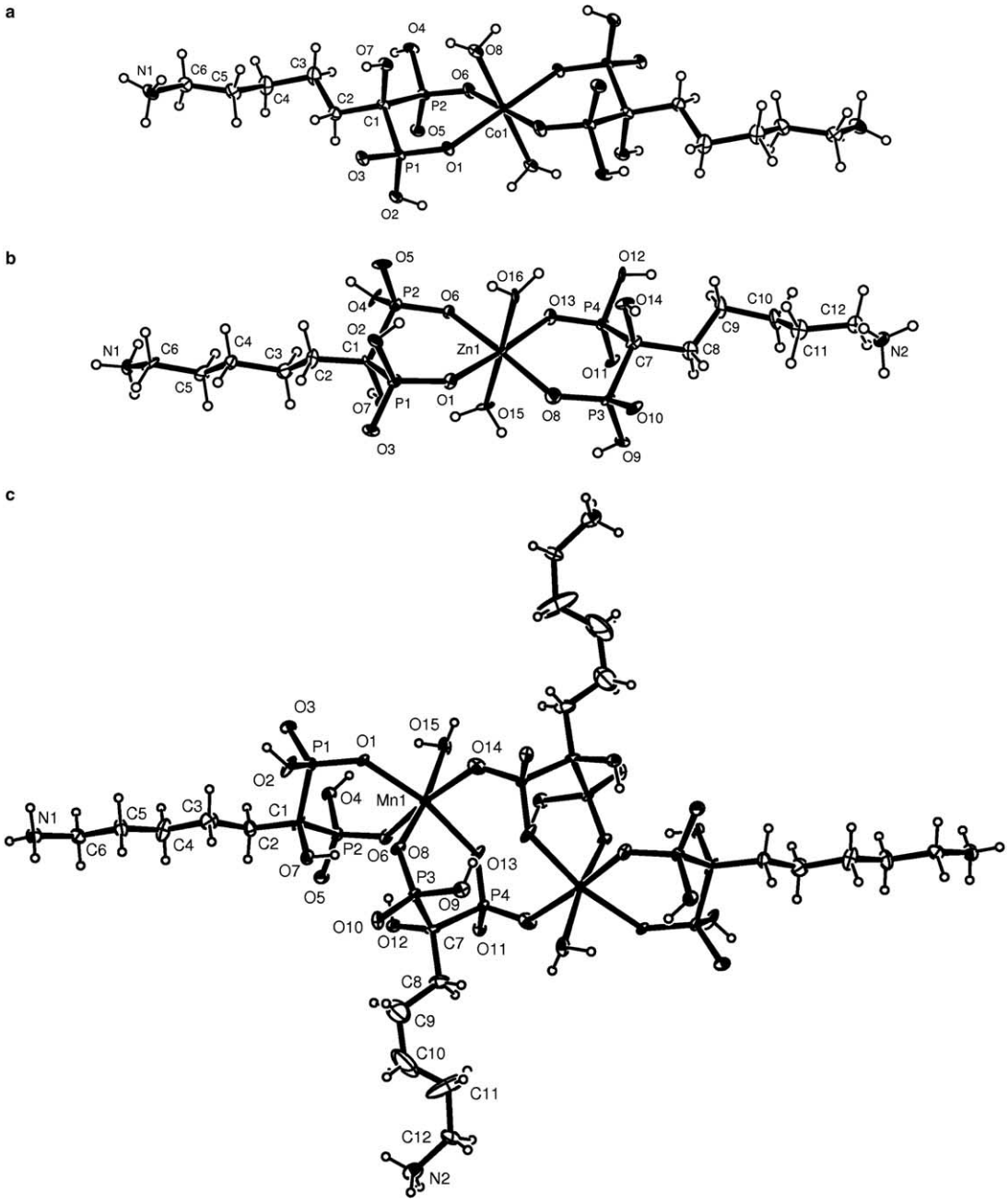

Fig. 2. Crystal structures of compounds **1**–**6**. (a) Crystal structure and atom numbering scheme for (**1**) (same scheme applies for isostructural compound (**2**) and (**3b**)). (b) Crystal structure and atom numbering scheme for (**3a**). (c) Crystal structure and atom labelling scheme for (**4**). (d) Crystal structure and atom labelling scheme for (**5**). (e) Crystal structure and atom labelling scheme for (**6**).

in an oil bath at 130 °C for 70 h and then allowed to cool to room temperature. Pink crystals of compound **1** were extracted from the walls of the Teflon reactor.

*5.2. Diaqua-bis(6-hydroxyhexylidene-1,1-bisphosphonate)-nickel dihydrate (**2**)*

Compound **2** was prepared as for **1** by combining $Ni(NO_3)_2 \cdot 6H_2O$ 1.51 mmol in 5 mL water and H_4L^3 1.98 mmol in 40 mL water at 130 °C for 130 h as pale green crystals.

*5.3. Diaqua-bis(6-hydroxyhexylidene-1,1-bisphosphonate)-zinc dihydrate (**3**)*

Compound **3** was prepared as for **1** from $Zn(NO_3)_2 \cdot 6H_2O$ 1.98 mmol in water 5 mL and H_4L^3 1.5 mmol in water 40 mL at 130 °C for 70 h and as colourless crystals.

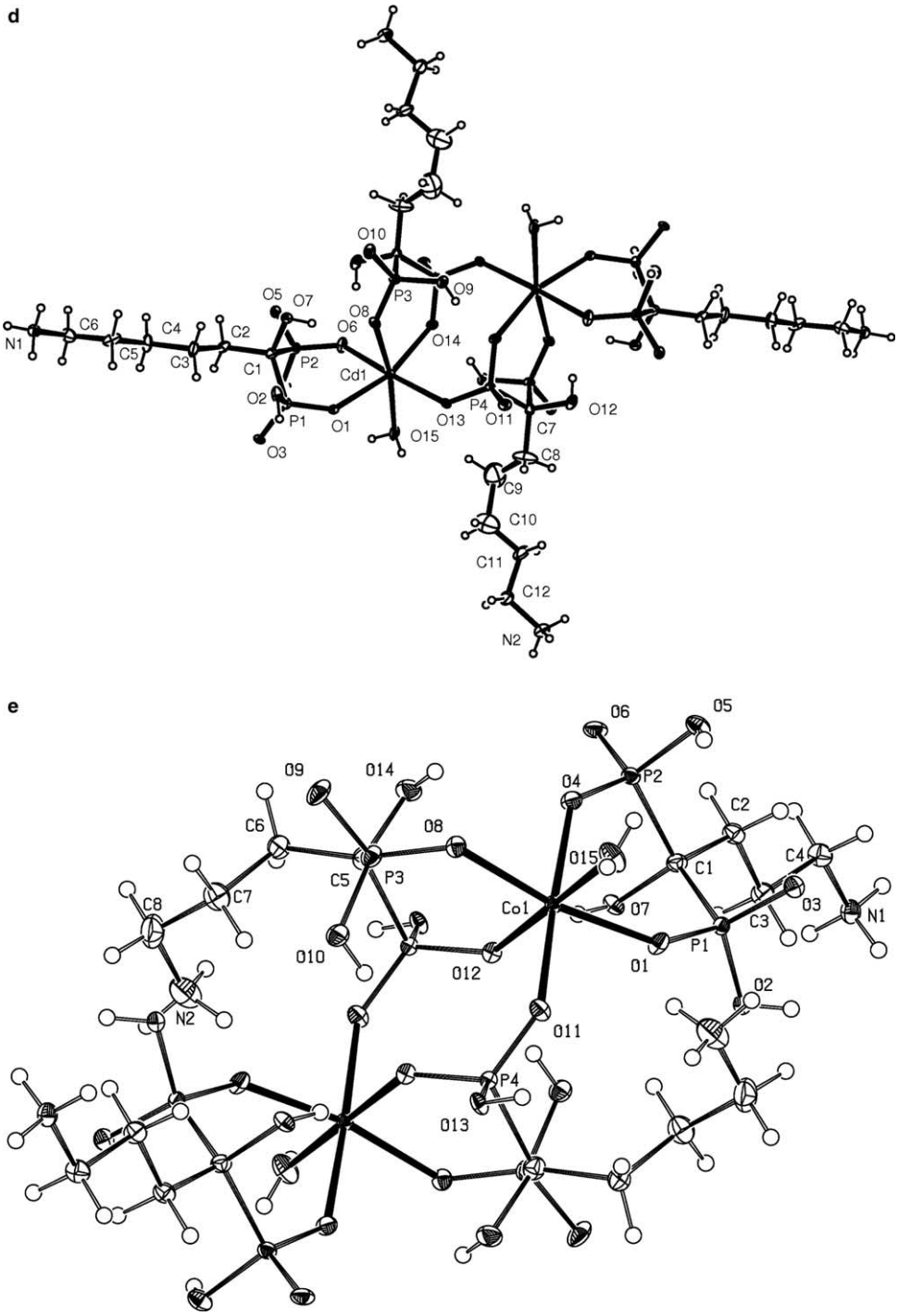

Fig. 2 (*continued*)

*5.4. Bis(μ2-6-amino-1-hydroxyhexylidene-1,1-bisphosphonate)-diaqua-bis(4-amino-1-hydroxyhexylidene-1,1-bisphosphonate)-di-manganese dihydrate (**4**)*

Compound **4** was prepared as for **1** from $Mn(NO_3)_2 \cdot 6H_2O$ 4 mmol in water 5 mL and H_4L^3 3 mmol in water 45 mL at 130 °C for 70 h as colourless crystals.

*5.5. Bis(μ2-6-amino-1-hydroxyhexylidene-1,1-bisphosphonate)-diaqua-bis(4-amino-1-hydroxyhexylidene-1,1-bisphosphonate)-di-cadmium dihydrate (**5**)*

Compound **5** was prepared as for **1** from $Cd(SO_4)$ 4.26 mmol in 10 mL H_2O and H_4L^3 3 mmol in water 80 mL at 130 °C for 70 h as colourless crystals.

Table 3
Selected bond distances Å and angles in compounds **1**, **2** and **3a**

1	**2**	**3a**	**1**	**2**	**3a**
Co–O(P)	Ni–O(P)	Zn–O(P)	O–Co–O	O–Ni–O	O–Zn–O
Co(1)–O(1) 2.101(2) Co(1)–O(6) 2.032(2)	Ni(1)–O(1) 2.014(4) Ni(1)–O(6) 2.072(4)	Zn(1)–O(1) 2.059(2) Zn(1)–O(8) 2.047(2) Zn(1)–O(13) 2.046(2)	O(1)–Co(1)–O(6) 92.38(9) O(1)–Co(1)–O(8) 87.95(8) O(6)–Co(1)–O(8) 89.81(9)	O(1)–Ni(1)–O(6) 92.87(17) O(1)–Ni(1)–O(8) 90.31(18) O(6)–Ni(1)–O(8) 91.86(18)	O(13)–Zn(1)–O(8) 93.05(9) O(13)–Zn(1)–O(1) 173.63(11) O(8)–Zn(1)–O(1) 87.92(9) O(13)–Zn(1)–O(6) 87.09(9) O(8)–Zn(1)–O(6) 175.74(10) O(1)–Zn(1)–O(6) 92.41(9)
Co–O_w	Ni–O_w	Zn–O_w			O_w–Zn–O_w
Co(1)–O(8) 2.125(2)	Ni(1)–O(8) 2.082(5)	Zn(1)–O(15) 2.127(3) Zn(1)–O(16) 2.141(3)			O(15)–Zn(1)–O(16) 177.83(9)
P–O	P–O	P–O	Co–O–P	Ni–O–P	Zn–O–P
P(1)–O(1) 1.509(2) P(1)–O(3) 1.505(2) P(1)–O(2) 1.566(2) P(2)–O(4) 1.571(2) P(2)–O(5) 1.513(2) P(2)–O(6) 1.491(2)	P(1)–O(1) 1.507(4) P(1)–O(3) 1.510(5) P(1)–O(2) 1.566(4) P(2)–O(4) 1.568(5) P(2)–O(5) 1.495(5) P(2)–O(6) 1.507(4)	O(1)–P(1) 1.502(2) O(2)–P(1) 1.554(3) O(3)–P(1) 1.512(3) O(4)–P(2) 1.558(3) O(5)–P(2) 1.507(3) O(6)–P(2) 1.497(2) O(8)–P(3) 1.493(2) O(9)–P(3) 1.561(3) O(10)–P(3) 1.520(2) O(11)–P(4) 1.514(3) O(12)–P(4) 1.555(3) O(13)–P(4) 1.507(2)	P(1)–O(1)–Co(1) 132.88(12) P(2)–O(6)–Co(1) 138.00(13)	P(1)–O(1)–Ni(1) 137.9(3) P(2)–O(6)–Ni(1) 133.3(3)	P(1)–O(1)–Zn(1) 136.89(14) P(2)–O(6)–Zn(1) 132.21(14) P(3)–O(8)–Zn(1) 136.11(14) P(4)–O(13)–Zn(1) 133.53(14)
			O–P–O	O–P–O	O–P–O
			O(3)–P(1)–O(1) 114.54(12) O(3)–P(1)–O(2) 108.65(11) O(1)–P(1)–O(2) 111.20(12) O(6)–P(2)–O(5) 115.90(13) O(6)–P(2)–O(4) 107.28(12) O(5)–P(2)–O(4) 109.89(12)	O(1)–P(1)–O(3) 116.1(3) O(1)–P(1)–O(2) 107.8(3) O(3)–P(1)–O(2) 110.1(2) O(5)–P(2)–O(6) 114.6(3) O(5)–P(2)–O(4) 108.9(3) O(6)–P(2)–O(4) 111.3(3)	O(1)–P(1)–O(2) 112.21(14) O(3)–P(1)–O(2) 107.52(14) O(1)–P(1)–C(1) 109.49(14) O(6)–P(2)–O(5) 115.31(15) O(6)–P(2)–O(4) 105.40(14) O(5)–P(2)–O(4) 113.06(15) O(8)–P(3)–O(10) 114.56(13) O(8)–P(3)–O(9) 110.03(14) O(10)–P(3)–O(9) 108.92(14) O(13)–P(4)–O(11) 114.89(14) O(13)–P(4)–O(12) 106.07(13) O(11)–P(4)–O(12) 111.35(13)
P–C	P–C	P–C	O–P–C	O–P–C	O–P–C
C(1)–P(1) 1.848(3)	P(1)–C(1) 1.853(6)	C(1)–P(1) 1.825(3) C(1)–P(2) 1.856(3) C(7)–P(3) 1.834(4) C(7)–P(4) 1.851(3)	O(3)–P(1)–C(1) 105.96(13) O(1)–P(1)–C(1) 110.31(13) O(2)–P(1)–C(1) 105.69(12) O(6)–P(2)–C(1) 108.14(13) O(5)–P(2)–C(1) 108.36(12) O(40)–P(2)–C(1) 106.91(13)	O(1)–P(1)–C(1) 107.6(3) O(3)–P(1)–C(1) 108.0(3) O(2)–P(1)–C(1) 106.9(3) O(5)–P(2)–C(1) 105.6(3) O(6)–P(2)–C(1) 110.7(3) O(4)–P(2)–C(1) 105.3(3)	O(1)–P(1)–C(1) 109.49(14) O(3)–P(1)–C(1) 107.25(15) O(2)–P(1)–C(1) 104.61(14) O(6)–P(2)–C(1) 109.64(14) O(5)–P(2)–C(1) 107.63(15) O(4)–P(2)–C(1) 105.35(15) O(8)–P(3)–C(7) 110.52(14) O(10)–P(3)–C(7) 105.12(16) O(9)–P(3)–C(7) 107.30(15) O(13)–P(4)–C(7) 108.22(14) O(11)–P(4)–C(7) 108.06(15) O(12)–P(4)–C(7) 108.03(15)
			P–C–P	P–C–P	P–C–P
			P(2)–C(1)–P(1) 113.17(16)	P(2)–C(1)–P(1) 113.0(3)	P(1)–C(1)–P(2) 111.00(17) P(3)–C(7)–P(4) 112.13(19)

*5.6. Bis(μ2-6-amino-1-hydroxybutylidene-1,1-bisphosphonate)-diaqua-bis(4-amino-1-hydroxybutylidene-1,1-bisphosphonate)-di-cobalt dihydrate (**6**)*

Compound **6** was prepared as for **1** from $Co(NO_3)_2 \cdot 6H_2O$ 4 mmol in 5 mL water and H_4L^2 3 mmol in water 45 mL at 130 °C for 70 h and isolated as pink crystals 0.67 g.

5.7. X-ray crystallography

The intensity data for **1**, **3a**, **3b**, **4** and **6** were collected on a CAD-4 diffractometer using Mo Kα radiation (λ 0.71069 Å) and ω-2θ scans at 160 or 293 K (see data for individual compounds). The unit cell parameters were determined by least-squares refinement on diffractometer angles for 25 automatically centred reflections [21]. Data

Table 4
Selected bond distances and angles in compounds **4**, **5** and **6**

4	**5**	**6**	**4**	**5**	**6**
Mn–O(P)	Cd–O(P)	Co–O(P)	O–Mn–O	O–Cd–O	O–Co–O
Mn(1)–O(1) 2.173(3)	Cd(1)–O(1) 2.305(2)	O(1)–Co(1) 2.018(4)	O(6)–Mn(1)–O(14) 168.77(11)	O(13)–Cd(1)–O(6) 170.18(9)	O(1)– O(1)–Co(1)–O(8) 170.20(14)
Mn(1)–O(6) 2.129(3)	Cd(1)–O(6) 2.242(2)	O(4)–Co(1) 2.122(4)	O(6)–Mn(1)–O(8) 89.72(10)	O(13)–Cd(1)–O(8) 99.13(9)	O(1)–Co(1)–O(11) 87.55(15)
Mn(1)–O(8) 2.150(3)	Cd(1)–O(8) 2.273(2)	O(8)–Co(1) 2.024(3)	O(14)–Mn(1)–O(8) 97.97(10)	O(6)–Cd(1)–O(8) 87.31(9)	O(8)–Co(1)–O(11) 101.07(15)
Mn(1)–O(13) 2.198(3)	Cd(1)–O(13) 2.211(2)	O(11)–Co(1) 2.062(4)	O(6)–Mn(1)–O(1) 86.76(10)	O(13)–Cd(1)–O(1) 102.87(8)	O(1)–Co(1)–O(4) 88.79(14)
Mn(1)–O(14) 2.136(3)	Cd(1)–O(14) 2.315(2)	O(12)–Co(1) 2.207(3)	O(14)–Mn(1)–O(1) 101.94(10)	O(6)–Cd(1)–O(1) 85.11(9)	O(8)–Co(1)–O(4) 82.81(14)
			O(8)–Mn(1)–O(1) 85.35(10)	O(8)–Cd(1)–O(1) 83.81(8)	O(11)–Co(1)–O(4) 175.40(14)
			O(6)–Mn(1)–O(13) 82.85(10)	O(13)–Cd(1)–O(14) 91.30(8)	O(1)–Co(1)–O(15) 87.52(16)
			O(14)–Mn(1)–O(13) 89.19(10)	O(6)–Cd(1)–O(14) 81.67(9)	O(8)–Co(1)–O(15) 87.81(15)
			O(8)–Mn(1)–O(13) 88.27(10)	O(8)–Cd(1)–O(14) 86.31(8)	O(11)–Co(1)–O(15) 90.14(15)
			O(1)–Mn(1)–O(13) 167.83(10)	O(1)–Cd(1)–O(14) 163.84(8)	O(4)–Co(1)–O(15) 92.48(15)
			O(6)–Mn(1)–O(15) 91.55(8)	O(13)–Cd(1)–O(15) 83.88(6)	O(1)–Co(1)–O(12) 92.70(14)
			O(14)–Mn(1)–O(15) 82.05(8)	O(6)–Cd(1)–O(15) 91.21(7)	O(8)–Co(1)–O(12) 91.96(13)
			O(8)–Mn(1)–O(15) 171.47(7)	O(8)–Cd(1)–O(15) 168.88(6)	O(11)–Co(1)–O(12) 90.02(14)
			O(1)–Mn(1)–O(15) 86.30(7)	O(1)–Cd(1)–O(15) 85.08(6)	O(4)–Co(1)–O(12) 87.37(13)
			O(13)–Mn(1)–O(15) 100.27(8)	O(14)–Cd(1)–O(15) 104.38(6)	O(15)–Co(1)–O(12) 179.74(15)
Mn–O_w	Cd–O_w	Co–O_w			
Mn(1)–O(15) 2.258(1)	Cd(1)–O(15) 2.373(2)	O(15)–Co(1) 2.145(4)			
P–O	P–O	P–O	Mn–O–P	Cd–O–P	Co–O–P
P(1)–O(1) 1.515(3)	P(1)–O(1) 1.498(3)	O(1)–P(1) 1.502(4)	Mn(1)–O(1)–P(1) 139.17(15)	Cd(1)–O(1)–P(1) 138.59(14)	P(1)–O(1)–Co(1) 141.1(2)
P(1)–O(2) 1.565(3)	P(1)–O(2) 1.585(3)	O(2)–P(1) 1.565(4)	Mn(1)–O(6)–P(2) 134.38(15)	Cd(1)–O(6)–P(2) 132.93(15)	P(2)–O(4)–Co(1) 134.2(2)
P(1)–O(3) 1.506(3)	O(3)–P(1) 1.510(3)	O(3)–P(1) 1.510(4)	Mn(1)–O(8)–P(3) 134.31(16)	Cd(1)–O(8)–P(3) 131.77(14)	P(3)–O(8)–Co(1) 132.0(2)
P(2)–O(5) 1.492(3)	O(4)–P(2) 1.567(3)	O(4)–P(2) 1.512(4)	P(4)–O(13)–Mn(1) 136.84(17)	P(4)–O(13)–Cd(1) 133.25(14)	P(4)#3–O(11)–Co(1) 144.2(2)
P(2)–O(6) 1.520(3)	O(5)–P(2) 1.502(3)	O(5)–P(2) 1.569(4)	P(4)–O(14)–Mn(1) 135.18(16)	P(4)–O(14)–Cd(1) 136.90(14)	P(4)–O(12)–Co(1) 134.9(2)
P(2)–O(4) 1.566(3)	O(6)–P(2) 1.515(3)	O(6)–P(2) 1.510(4)			
P(3)–O(10) 1.497(3)	O(8)–P(3) 1.521(2)	O(8)–P(3) 1.491(4)			
P(3)–O(8) 1.500(3)	O(9)–P(3) 1.571(3)	O(9)–P(3) 1.507(4)			
P(3)–O(9) 1.577(3)	O(10)–P(3) 1.513(3)	O(10)–P(3) 1.560(4)			
P(4)–O(14)#1 1.495(3)	O(11)–P(4) 1.568(3)	O(11)–P(4)#1 1.487(4)			
P(4)–O(13) 1.514(3)	O(13)–P(4) 1.508(2)	O(12)–P(4) 1.520(4)			
P(4)–O(11) 1.573(3)	O(14)–P(4)#1 1.519(2)	O(13)–P(4) 1.567(4)			

			O–P–O	O–P–O	O–P–O
			O(3)–P(1)–O(1) 115.00(16)	O(1)–P(1)–O(3) 115.00(14)	O(1)–P(1)–O(3) 115.4(2)
			O(3)–P(1)–O(2) 111.90(16)	O(1)–P(1)–O(2) 106.59(14)	O(1)–P(1)–O(2) 107.4(2)
			O(1)–P(1)–O(2) 106.85(16)	O(3)–P(1)–O(2) 111.59(14)	O(3)–P(1)–O(2) 111.02(19)
			O(5)–P(2)–O(6) 112.88(15)	O(5)–P(2)–O(6) 112.92(14)	O(6)–P(2)–O(4) 113.3(2)
			O(5)–P(2)–O(4) 108.96(16)	O(5)–P(2)–O(4) 108.72(14)	O(6)–P(2)–O(5) 108.8(2)
			O(6)–P(2)–O(4) 112.47(16)	O(6)–P(2)–O(4) 112.35(15)	O(4)–P(2)–O(5) 110.7(2)
			O(10)–P(3)–O(8) 114.24(16)	O(10)–P(3)–O(8) 113.17(15)	O(8)–P(3)–O(9) 114.5(2)
			O(10)–P(3)–O(9) 107.51(16)	O(10)–P(3)–O(9) 107.22(14)	O(8)–P(3)–O(10) 111.7(2)
			O(8)–P(3)–O(9) 111.70(15)	O(8)–P(3)–O(9) 112.27(13)	O(9)–P(3)–O(10) 106.6(2)
			O(14)#1–P(4)–O(13) 115.96(15)	O(14)#2–P(4)–O(11) 107.41(14)	O(11)#3–P(4)–O(12) 117.0(2)
			O(14)#1–P(4)–O(11) 109.94(15)	O(13)–P(4)–O(14)#2 115.67(13)	O(11)#3–P(4)–O(13) 110.8(2)
			O(13)–P(4)–O(11) 107.35(16)	O(13)–P(4)–O(11) 109.20(14)	O(12)–P(4)–O(13) 106.08(19)
P–C	P–C	P–C	O–P–C	O–P–C	O–P–C
P(1)–C(1) 1.860(3)	P(1)–C(1) 1.838(4)	C(1)–P(1) 1.837(5)	O(3)–P(1)–C(1) 110.40(15)	O(1)–P(1)–C(1) 108.55(15)	O(1)–P(1)–C(1) 107.1(2)
P(2)–C(1) 1.838(4)	P(2)–C(1) 1.853(4)	C(1)–P(2) 1.842(5)	O(1)–P(1)–C(1) 107.49(14)	O(3)–P(1)–C(1) 109.78(16)	O(3)–P(1)–C(1) 109.4(2)
P(3)–C(7) 1.853(4)	P(3)–C(7)#1 1.875(4)	C(5)–P(3) 1.843(5)	O(2)–P(1)–C(1) 104.57(16)	O(2)–P(1)–C(1) 104.79(16)	O(2)–P(1)–C(1) 106.0(2)
P(4)–C(7) 1.841(4)	P(4)–C(7) 1.841(4)	C(5) P(4) 1.852(5)	O(5)–P(2)–C(1) 108.03(16)	O(5)–P(2)–C(1) 108.03(16)	O(6)–P(2)–C(1) 106.3(2)
			O(6)–P(2)–C(1) 108.60(14)	O(6)–P(2)–C(1) 109.98(16)	O(4)–P(2)–C(1) 110.1(2)
			O(4)–P(2)–C(1) 105.53(15)	O(4)–P(2)–C(1) 104.41(15)	O(5)–P(2)–C(1) 107.4(2)
			O(10)–P(3)–C(7) 112.58(15)	O(10)–P(3)–C(7)#2 112.30(15)	O(8)–P(3)–C(5) 107.5(2)
			O(8)–P(3)–C(7) 105.22(15)	O(8)–P(3)–C(7)#2 104.79(15)	O(9)–P(3)–C(5) 108.6(2)
			O(9)–P(3)–C(7) 105.30(15)	O(9)–P(3)–C(7)#2 107.01(15)	O(10)–P(3)–C(5) 107.8(2)
			O(14)#1–P(4)–C(7) 110.35(15)	O(13)–P(4)–C(7) 111.20(15)	O(11)#3–P(4)–C(5) 111.7(2)
			O(13)–P(4)–C(7) 108.81(15)	O(14)#2–P(4)–C(7) 108.93(15)	O(12)–P(4)–C(5) 107.3(2)
			O(11)–P(4)–C(7) 103.69(16)	O(11)–P(4)–C(7) 103.69(15)	O(13)–P(4)–C(5) 102.9(2)
			P–C–P	P–C–P	P–C–P
			P(2)–C(1)–P(1) 111.85(17)	P(1)–C(1)–P(2) 113.25(19)	P(1)–C(1)–P(2) 111.0(3)
			P(4)–C(7)–P(3) 113.98(16)	P(4)–C(7)–P(3)#2 113.43(18)	P(3)–C(5)–P(4) 112.7(3)

Symmetry transformations used to generate equivalent atoms:
#1 $-x+1, -y, -z+1$;
#2 $-x, -y, -z+1$;
#3 $-x+1, -y+1, -z+1$.

Table 5
Hydrogen bonds for (**1**) [Å and °]

D–H···A	*d*(D–H)	*d*(H···A)	*d*(D···A)	∠(DHA)
N(1)–H(1A)···O(1)#2	0.91	2.04	2.895(3)	155.0
N(1)–H(1A)···O(8)#2	0.91	2.38	2.928(4)	118.5
N(1)–H(1B)···O(9)	0.91	2.09	2.982(4)	165.0
N(1)–H(1C)···O(2)#3	0.91	2.13	2.989(4)	157.7
O(2)–H(2)···O(5)#4	0.84	1.74	2.571(3)	169.1
O(4)–H(4)···O(3)#5	0.84	1.75	2.566(3)	163.5
O(7)–H(7)···O(9)#6	0.84	2.13	2.947(3)	164.1
O(8)–H(8A)···O(7)	0.889(19)	2.08(3)	2.841(3)	144(5)
O(8)–H(8B)···O(5)#7	0.870(19)	1.846(19)	2.715(3)	178(4)
O(9)–H(9A)···O(3)#2	0.89(2)	2.37(5)	2.857(3)	115(4)
O(9)–H(9A)···O(5)#8	0.89(2)	2.41(3)	3.219(4)	153(4)
O(9)–H(9B)···O(1)#9	0.89(2)	2.26(2)	3.124(3)	163(5)

Symmetry transformations used to generate equivalent atoms:
#1 $-x+1, -y, -z$;
#2 $x+1, -y+1/2, z+1/2$;
#3 $x, -y+1/2, z+1/2$;
#4 $-x+2, -y, -z$;
#5 $-x+2, y-1/2, -z+1/2$;
#6 $x-1, -y+1/2, z-1/2$;
#7 $x-1, y, z$;
#8 $-x+3, -y, -z+1$;
#9 $x+1, y, z+1$.

Table 6
Hydrogen bonds for (2) [Å and °]

D–H···A	*d*(D–H)	*d*(H···A)	*d*(D···A)	∠(DHA)
O(2)–H(2)···O(5)#2	0.84	1.77	2.593(6)	166.2
O(4)–H(4)···O(3)#3	0.84	1.74	2.558(6)	164.0
O(7)–H(7)···O(9)#1	0.84	2.14	2.962(7)	167.9
O(7)–H(7)..O(5)	0.84	2.59	3.046(6)	115.5
N(1)–H(1A)..O(4)#4	0.91	2.08	2.972(7)	165.0
N(1)–H(1B)···O(9)#5	0.91	2.11	2.985(7)	160.4
N(1)–H(1C)···O(6)#6	0.91	1.98	2.861(7)	161.2
N(1)–H(1C)···O(8)#5	0.91	2.41	2.918(7)	115.5
O(8)–H(8B)···O(7)#1	0.86(5)	2.09(6)	2.852(7)	147(6)
O(8)–H(8A)···O(3)#3	0.85(6)	1.87(6)	2.708(6)	172(7)
O(9)–H(9A)···O(6)#7	0.88(6)	2.27(7)	3.149(7)	179(8)
O(9)–H(9B)···O(5)#1	0.99(8)	1.96(9)	2.835(8)	146(12)
O(9)–H(9B)···O(3)#8	0.99(8)	2.65(14)	3.215(7)	117(9)

Symmetry transformations used to generate equivalent atoms:
#1 $-x+1, -y, -z+1$;
#2 $-x+2, y+1/2, -z+3/2$;
#3 $-x+2, -y, -z+1$;
#4 $x, -y-1/2, z+1/2$;
#5 $-x+2, y-1/2, -z+3/2$;
#6 $x+1, -y-1/2, z+1/2$;
#7 $-x+1, y+1/2, -z+1/2$;
#8 $x-1, -y+1/2, z-1/2$.

for compounds **1**, **3a**, **3b**, **4** and **6** were corrected for absorption by empirical methods (ψ scan) [22] and for Lorentz-polarization effects by XCAD4 [23]. The structures were solved by heavy-atom methods using SHELXS-97, [24] and DIRDIF-99 programs, [25] and were refined anisotropically (non-hydrogen atoms) by full-matrix least-squares on F^2 using SHELXL-97 [24]. The H atoms were calculated geometrically and refined with a riding model except for the hydrogens in the water molecules. These were taken from the difference map and the O–H distances were restrained by DFIX facility in the SHELXL-97 programme [24].

Data for **2** and **5** were collected at 120 K using a Nonius Kappa CCD area detector diffractometer mounted at the window of molybdenum rotating anode (50 kV, 90 mA, $\lambda = 0.71069$ Å). The crystal-to-detector distance was

Table 7
Hydrogen bonds for (3b) [Å and °]

D–H···A	d(D–H)	d(H···A)	d(D···A)	∠(DHA)
N(1)–H(1A)···O(1)#2	0.89	2.12	2.937(7)	151.8
N(1)–H(1A)···O(8)#2	0.89	2.35	2.927(7)	122.5
N(1)–H(1B)···O(9)	0.89	2.11	2.986(9)	169.9
N(1)–H(1C)···O(2)#3	0.89	2.20	3.017(7)	152.0
N(1)–H(1C)···O(4)#4	0.89	2.52	2.967(7)	111.6
O(2)–H(2)···O(5)#5	0.82	1.78	2.563(6)	159.0
O(4)–H(4)···O(3)#6	0.82	1.76	2.559(5)	163.4
O(7)–H(7)···O(9)#7	0.82	2.19	2.987(7)	164.6
O(8)–H(8A)···O(7)	0.90(2)	2.20(6)	2.861(6)	129(7)
O(8)–H(8B)···O(5)#8	0.89(2)	1.88(3)	2.749(6)	167(6)
O(9)–H(9A)···O(3)#2	0.89(2)	2.00(3)	2.879(8)	170(12)
O(9)–H(9B)···O(1)#9	0.90(2)	2.21(2)	3.107(8)	176(11)

Symmetry transformations used to generate equivalent atoms:
#1 $-x+1, -y, -z$;
#2 $x+1, -y+1/2, z+1/2$;
#3 $x, -y+1/2, z+1/2$;
#4 $-x+2, -y, -z+1$;
#5 $-x+2, -y, -z$;
#6 $-x+2, y-1/2, -z+1/2$;
#7 $x-1, -y+1/2, z-1/2$;
#8 $x-1, y, z$;
#9 $x+1, y, z+1$.

30 mm and ϕ and Ω scans (2.0° increments, 12 s exposure time) were carried out to fill the Ewald sphere. Data collection and processing were carried out using the COLLECT [26], DENZO [27] and maXus [28] and empirical absorption correction was applied using SORTAV [29,30]. The structure was solved by heavy-atom method using DIRDIF99 [25] and refined anisotropically (non-hydrogen atoms) by full-matrix least-squares on F^2 using the SHELXL-97 [24] program. The H atoms were calculated geometrically and refined with riding model.

The programs ORTEP-3 [31] and Platon [32] was used for diagrams and WINGX [33] was used to prepare material for publication. Crystal data and refinement details are given below.

Crystal data: (**1**) $C_{12}H_{40}CoN_2O_{18}P_4$, $M = 683.27$, monoclinic, $a = 7.365(4)$, $b = 13.087(6)$, $c = 13.449(5)$ Å, $\alpha = 90.00$, $\beta = 100.81(3)$, $\gamma = 90.00°$, $V = 1273.3(1)$ Å^3, space group $P2_1/c$, $Z = 2$, $D_{calc} = 1.782$ Mg/m^3, $\mu = 1.001$ mm^{-1}, reflections measured 2372, reflections unique 2221 with $R_{int} = 0.0124$, $T = 160(2)$ K, final R indices $I > 2(I)$] $R_1 = 0.0392$, $R_2 = 0.1028$ and for all data $R_1 = 0.0496$, $wR_2 = 0.1086$. CCDC reference number 283251.

(**2**) $C_{12}H_{40}N_2NiO_{18}P_4$, $M = 683.05$, monoclinic, $a = 7.3246(1)$, $b = 13.0353(1)$, $c = 13.480(2)$ Å, $\alpha = 90.00$, $\beta = 100.48(3)$, $\gamma = 90.00°$, $V = 1265.6(3)$ Å^3, space group $P2_1/c$, $Z = 2$, $D_{calc} = 1.792$ Mg/m^3, $\mu = 1.106$ mm^{-1}, reflections measured 6778, reflections unique 2692 with $R_{int} = 0.1675$, $T = 120(2)$ K, final R indices $I > 2(I)$] $R_1 = 0.0660$, $R_2 = 0.0936$ and for all data $R_1 = 0.2164$, $wR_2 = 0.1283$. CCDC reference number 283252.

(**3a**) $C_{12}H_{40}N_2O_{18}P_4Zn$, $M = 689.71$, monoclinic, $a = 14.618(6)$, $b = 13.036(5)$, $c = 13.842(7)$ Å, $\alpha = 90.00$, $\beta = 101.00(3)$, $\gamma = 90.00°$, $V = 2589(2)$ Å^3, space group $P2_1/c$, $Z = 4$, $D_{calc} = 1.769$ Mg/m^3, $\mu = 1.280$ mm^{-1}, reflections measured 4881, reflections unique 4553 with $R_{int} = 0.0228$, $T = 160(2)$ K, final R indices $I > 2(I)$] $R_1 = 0.0658$, $R_2 = 0.1155$ and for all data $R_1 = 0.2418$, $wR_2 = 0.1532$. CCDC reference number 283253.

(**3b**) $C_{12}H_{40}ZnN_2O_{18}P_4$, $M = 689.71$, monoclinic, $a = 7.359(2)$, $b = 13.030(3)$, $c = 13.470(3)$ Å, $\alpha = 90.00$, $\beta = 100.84(2)$, $\gamma = 90.00°$, $V = 1268.6(5)$ Å^3, space group $P2_1/c$, $Z = 2$, $D_{calc} = 1.307$ Mg/m^3, $\mu = 1.307$ mm^{-1}, reflections measured 2436, reflections unique 2243 with $R_{int} = 0.0212$, $T = 293(2)$ K, final R indices $I > 2(I)$] $R_1 = 0.0440$, $R_2 = 0.0894$ and for all data $R_1 = 0.1551$, $wR_2 = 0.1123$. CCDC reference number 283257.

(**4**) $C_{24}H_{70}Mn_2N_4O_{32}P_8$, $M = 1284.48$, monoclinic, $a = 13.761(3)$, $b = 12.885(2)$, $c = 13.134(3)$ Å, $\alpha = 90.00$, $\beta = 94.55(2)$, $\gamma = 90.00°$, $V = 2321.5(8)$ Å^3, space group $P2_1/n$, $Z = 2$, $D_{calc} = 1.838$ Mg/m^3, $\mu = 0.927$ mm^{-1}, reflections measured 4417, reflections unique 4072 with $R_{int} = 0.0219$, $T = 293(2)$ K, final R indices $I > 2(I)$] $R_1 = 0.0660$, $R_2 = 0.1518$ and for all data $R_1 = 0.2160$, $wR_2 = 0.1951$. CCDC reference number 283254.

(**5**) $C_{24}H_{70}Cd_2N_4O_{32}P_8$, $M = 1399.40$, Monoclinic, $a = 13.1520$ (5), $b = 13.2477(5)$, $c = 13.7230(5)$ Å, $\alpha = 90.00$, $\beta = 94.314(2)$, $\gamma = 90.00°$, $V = 2384.24(15)$ Å^3, space group $P2_1/n$, $Z = 2$, $D_{calc} = 1.949$ Mg/m^3, $\mu = 1.265$ mm^{-1}, reflections measured 13238, reflections unique 5359 with $R_{int} = 0.0790$, $T = 120(2)$ K, final R indices $I > 2(I)$] $R_1 = 0.0853$, $R_2 = 0.2095$ and for all data $R_1 = 0.1299$, $wR_2 = 0.2318$. CCDC reference number 283255.

(**6**) $C_{16}H_{56}Co_2N_4O_{32}P_8$, $M = 1182.27$, monoclinic, $a = 12.556(8)$, $b = 13.501$ (5), $c = 12.423(5)$ Å, $\alpha = 90.00$,

Table 8
Hydrogen bonds for (**3a**) [Å and °]

D–H···A	*d*(D–H)	*d*(H···A)	*d*(D···A)	∠(DHA)
N(1)–H(1A)···O(16)#1	0.91	2.04	2.928(4)	165.8
N(1)–H(1B)···O(17)#2	0.91	2.20	2.995(4)	145.6
N(1)–H(1B)···O(10)#1	0.91	2.29	2.968(4)	131.0
N(1)–H(1C)···O(3)#3	0.91	1.83	2.731(4)	168.4
N(2)–H(2C)···O(9)#4	0.91	2.08	2.962(4)	162.2
N(2)–H(2D)···O(18)#5	0.91	2.01	2.914(4)	171.2
N(2)–H(2E)···O(6)#6	0.91	1.97	2.856(4)	163.8
O(2)–H(2)···O(5)#7	0.84	1.74	2.569(4)	168.7
O(4)–H(4)···O(3)#1	0.84	1.73	2.548(3)	162.5
O(9)–H(9)···O(11)#8	0.84	1.80	2.629(3)	167.6
O(12)–H(12)···O(10)#9	0.84	2.04	2.507(3)	114.2
O(14)–H(14)···O(17)#5	0.84	2.04	2.872(4)	169.2
O(14)–H(14)···O(10)	0.84	2.61	3.019(4)	111.2
O(15)–H(15A)···O(7)	0.894(17)	2.082(16)	2.880(3)	148(2)
O(15)–H(15B)···O(11)#8	0.881(19)	1.915(17)	2.773(3)	164(2)
O(16)–H(16B)···O(14)	0.881(16)	2.52(2)	3.002(3)	115.1(19)
O(16)–H(16A)···O(5)#7	0.895(19)	1.778(19)	2.667(3)	171(3)
O(18)–H(18A)···N(2)#5	0.867(17)	2.419(17)	2.914(4)	116.8(17)
O(18)–H(18B)···O(2)#10	0.92(2)	2.47(3)	3.092(4)	125(2)
O(18)–H(18B)···O(6)#11	0.92(2)	2.61(2)	3.396(4)	144(3)
O(17)–H(17A)···O(11)#12	0.89(2)	2.09(2)	2.882(3)	149(3)
O(17)–H(17A)···O(10)#5	0.89(2)	2.52(3)	2.972(4)	113(2)

Symmetry transformations used to generate equivalent atoms:
#1 $-x, y+1/2, -z+3/2$;
#2 $x-1, -y+3/2, z-1/2$;
#3 $-x, -y+2, -z+1$;
#4 $x, -y+3/2, z+1/2$;
#5 $-x+1, -y+1, -z+2$;
#6 $-x+1, y-1/2, -z+5/2$;
#7 $-x, -y+2, -z+2$;
#8 $-x+1, -y+2, -z+2$;
#9 $-x+1, y+1/2, -z+5/2$;
#10 $-x, -y+1, -z+1$;
#11 $x, y-1, z-1$;
#12 $x, -y+3/2, z-1/2$.

Table 9
Hydrogen bonds for (**4**) [Å and °]

D–H···A	*d*(D–H)	*d*(H···A)	*d*(D···A)	∠(DHA)
O(2)–H(2)···O(10)#2	0.82	1.84	2.595(4)	152.9
O(4)–H(4)···O(3)#3	0.82	1.87	2.623(4)	152.4
O(9)–H(9)···O(13)#1	0.82	1.89	2.579(4)	140.6
N(1)–H(1A)···O(5)#4	0.89	2.16	2.876(4)	136.5
N(1)–H(1A)···O(14)#2	0.89	2.46	3.069(4)	126.2
N(1)–H(1B)···O(12)#4	0.89	2.00	2.791(4)	148.1
N(1)–H(1C)···O(1)#2	0.89	1.88	2.772(4)	175.1
N(2)–H(2C)···O(7)#5	0.89	2.06	2.827(5)	143.6
N(2)–H(2D)···O(15)#6	0.89	2.29	3.069(4)	145.4
N(2)–H(2E)···O(10)#5	0.89	2.17	3.019(5)	159.1
O(16)–H(16A)···O(4)#3	0.91	2.423(3)	3.321(3)	170.42(17)
O(16)–H(16B)···O(11)#7	0.90	1.996(3)	2.892(3)	170.65(12)

Symmetry transformations used to generate equivalent atoms:
#1 $-x+1, -y, -z+1$;
#2 $-x+1/2, y+1/2, -z+3/2$;
#3 $-x+1, -y+1, -z+1$;
#4 $-x, -y+1, -z+1$;
#5 $-x, -y, -z+1$;
#6 $-x+1/2, y-1/2, -z+1/2$;
#7 $x+1/2, -y+1/2, z+1/2$.

Table 10
Hydrogen bonds for (**5**) [Å and °]

D–H···A	*d*(D–H)	*d*(H···A)	*d*(D···A)	∠(DHA)
N(1)–H(1A)···O(1)#2	0.91	1.88	2.790(4)	176.7
N(1)–H(1B)···O(12)#3	0.91	1.97	2.800(4)	151.1
N(1)–H(1C)···O(5)#4	0.91	2.16	2.870(4)	134.8
N(1)–H(1C)···O(13)#2	0.91	2.41	3.076(4)	130.6
N(2)–H(2C)···O(10)#5	0.91	2.06	2.958(4)	170.8
N(2)–H(2D)···O(7)#5	0.91	2.32	2.853(4)	116.9
N(2)–H(2D)···O(2)#5	0.91	2.56	3.438(4)	161.3
N(2)–H(2E)···O(15)#6	0.91	2.14	2.991(4)	155.6
O(7)–H(7)···O(8)	0.84	1.97	2.787(3)	163.0
O(9)–H(9)···O(14)#1	0.84	1.78	2.588(3)	161.2
O(12)–H(12)···O(6)#1	0.84	1.99	2.810(4)	163.6
O(15)–H(15A)···O(3)#7	0.90	1.822(2)	2.722(2)	178.9(3)
O(15)–H(15B)···O(16)#8	0.90	1.868(4)	2.736(2)	161.3(7)
O(16)–H(16B)···N(1)#5	0.90	2.19(3)	2.731(4)	118(2)

Symmetry transformations used to generate equivalent atoms:
#1 $-x, -y, -z+1$;
#2 $-x+1/2, y+1/2, -z+1/2$;
#3 $x, y+1, z-1$;
#4 $-x, -y+1, -z$;
#5 $x, y, z+1$
#6 $x+1/2, -y+1/2, z+1/2$;
#7 $-x, -y+1, -z+1$;
#8 $-x+1/2, y-1/2, -z+3/2$.

Table 11
Hydrogen bonds for (**6**) [Å and °]

D–H···A	*d*(D–H)	*d*(H···A)	*d*(D···A)	∠(DHA)
N(1)–H(1B)···O(6)#2	0.91	1.92	2.798(6)	161.6
N(1)–H(1C)···O(13)#2	0.91	2.20	2.967(6)	141.8
N(1)–H(1C)···O(14)#2	0.91	2.55	3.285(6)	137.6
N(1)–H(1A)···O(4)#3	0.91	2.08	2.957(6)	161.9
N(2)–H(2C)···O(11)#1	0.91	2.35	3.107(7)	141.2
N(2)–H(2C)···O(1)#1	0.91	2.38	3.105(6)	137.2
N(2)–H(2D)···O(5)#4	0.91	2.16	2.912(7)	139.0
N(2)–H(2D)···O(2)#5	0.91	2.58	3.214(6)	127.6
N(2)–H(2E)···O(9)#6	0.91	2.25	3.123(8)	159.9
N(2)–H(2E)···O(10)#6	0.91	2.33	3.023(7)	133.2
O(10)–H(100)···O(12)#1	0.84	1.87	2.648(5)	153.9
O(2)–H(10)···O(6)#3	0.84	1.67	2.490(5)	164.7
O(13)–H(130)···O(9)#6	0.84	1.76	2.578(5)	165.9
O(5)–H(50)···O(3)#7	0.84	1.72	2.540(5)	166.4
O(7)–H(70)···O(12)	0.84	2.04	2.883(5)	175.5
O(14)–H(140)···O(4)	0.84	2.44	2.929(5)	118.3
O(14)–H(140)···O(8)	0.84	2.44	2.946(5)	119.3
O(15)–H(15B)···O(16)#8	0.900(11)	1.98(3)	2.862(10)	166(10)
O(15)–H(15A)···O(3)#7	0.900(11)	1.91(3)	2.797(6)	170(13)

Symmetry transformations used to generate equivalent atoms:
#1 $-x+1, -y+1, -z+1$;
#2 $-x+2, -y+1, -z+2$;
#3 $-x+2, y-1/2, -z+3/2$;
#4 $x-1, y, z$;
#5 $-x+1, y+1/2, -z+3/2$;
#6 $x, -y+3/2, z+1/2$;
#7 $-x+2, -y+1, -z+1$;
#8 $-x+1, y-1/2, -z+1/2$.

$\beta = 109.92(8)$, $\gamma = 90.00°$, $V = 1979.9(17)$ Å^3, space group $P2_1/c$, $Z = 2$, $D_{calc} = 1.983$ Mg/m^3, $\mu = 1.277$ mm^{-1}, reflections measured 3739, reflections unique 2439 with $R_{int} = 0.0162$, $T = 160(2)$ K, final R indices $I > 2(I)$] $R_1 = 0.0504$, $R_2 = 0.1360$ and for all data $R_1 = 0.0716$, $wR_2 = 0.1487$. CCDC reference number 283256.

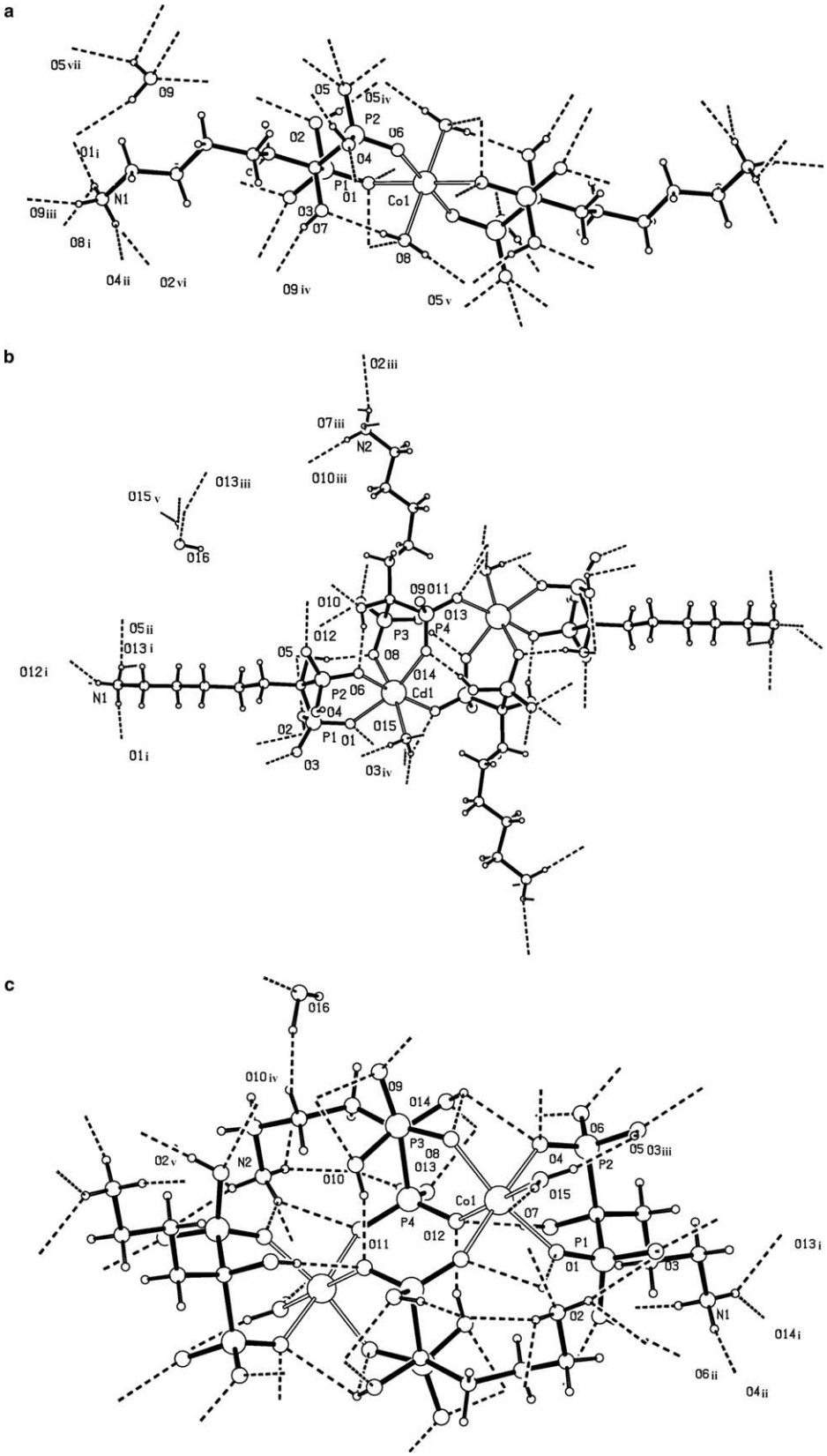

Fig. 3. Hydrogen bonding in compounds **1**, **5** and **6**. (a) Hydrogen bonding in compound **1** (symmetry codes: (i) $x+1$, $-y+1/2$, $z+1/2$; (ii) $-x$, $-y$, $-z+1$; (iii) x, $-y+1$, $z-1/2$; (iv) $x-1$, $-y+1/2$, $z-1/2$; (v) $x-1$, y, z; (vi) $-x+2$, $-y$, $-z$; (vii) $-x+3$, $-y$, $-z+1$). (b) Hydrogen bonding in compound **5** (symmetry codes: (i) x, $y+1$, $z-1$; (ii) $-x$, $-y+1$, $-z$; (iii) x, y, $z+1$; (iv) $-x$, $-y+1$, $-z+1$; (v) $-x+1/2$, $y-1/2$, $-z+3/2$). (c) Hydrogen bonding in compound **6** (symmetry codes: (i) $-x+2$, $-y+1$, $-z+2$; (ii) $-x+2$, $y-1/2$, $-z+3/2$; (iii) $-x+2$, $-y+1$, $-z+1$; (iv) $-x+1$, $-y+1$, $-z+1$; (v) $-x+1$, $y+1/2$, $-z+3/2$).

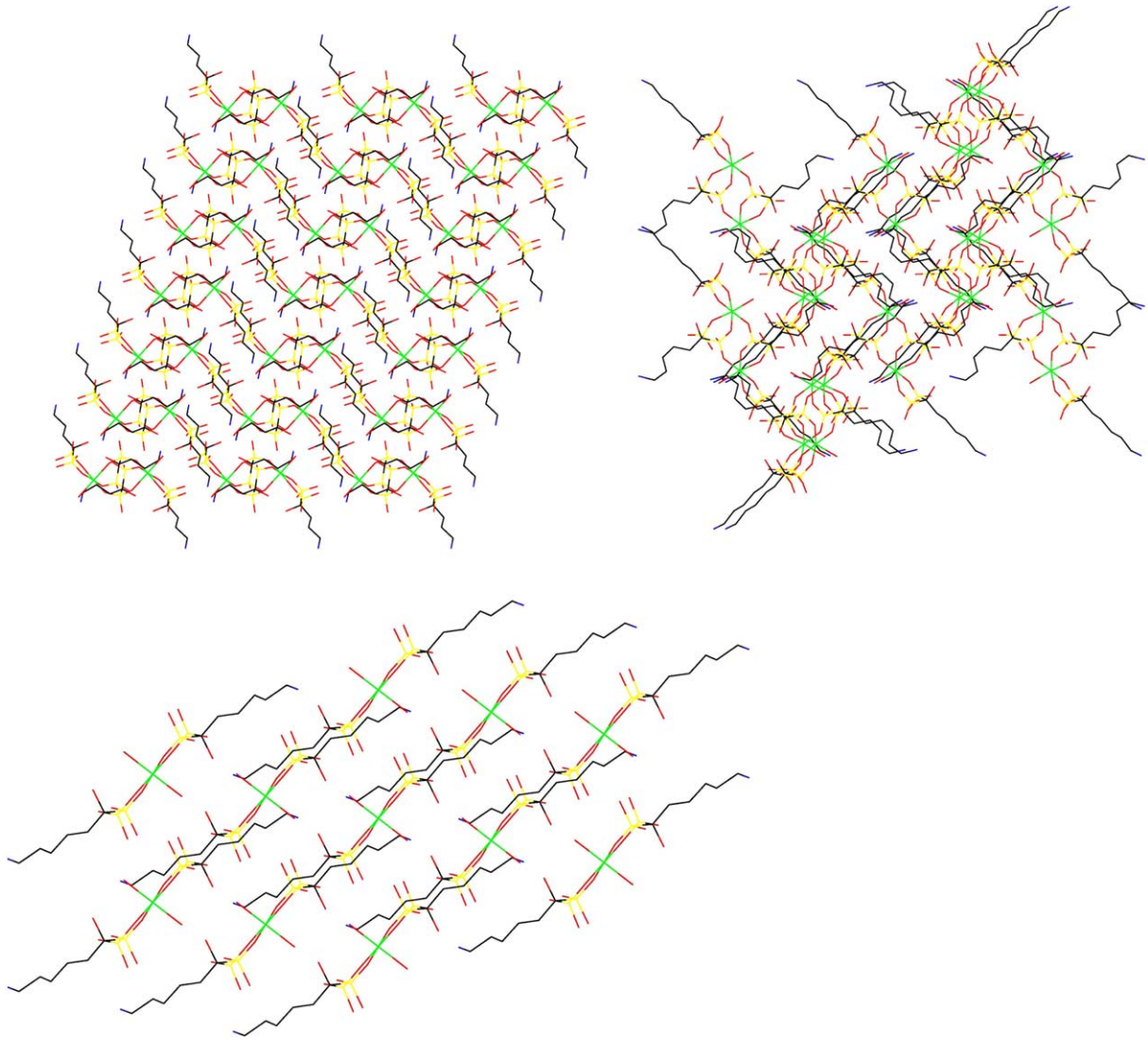

Fig. 4. Packing diagrams for compound **6** (view along *b*-axis), **4** (*c*-axis) and **3** (*b*-axis), (hydrogen, water molecules and hydrogen bonding omitted).

Acknowledgements

SPM and SG are grateful to Air Products PLC and Queen Mary University of London for support. We are grateful to EPSRC Crystallographic Service for data collection on compounds **2** and **5**.

References

[1] V.P. Kukhar, H.R. Hudson, Aminophosphinic and Aminophosphonic Acids: Chemistry and Biological Activity, Wiley, Berlin, 2000.
[2] R.G.G. Russell, M.J. Rogers, Bone 25 (1999) 97.
[3] J.-P. Silvestre, I. Bkouche-Waksman, G. Heger, N.G. Dao, New J. Chem. 14 (1990) 29.
[4] L.M. Chkolnikova, B.K. Cherbakov, N.M. Diatlova, T.A. Medved, M.I. Kabatchnik, Izvestia Akad. Nauk SSSR, Ser. Chimie (1986) 1511.
[5] J. Ohanessian, D. Avenel, D. El Manouni, M. Benramdane, Phosphorus, Sulfur Silicon 129 (1997) 99.
[6] Y. Leroux, D. El Manouni, A. Safsaf, A. Neuman, H. Gillier, Phosphorus, Sulfur Silicon 63 (1991) 181.
[7] V.M. Coiro, D. Lamba, Acta Cryst. C 45 (1989) 446.
[8] P. Zuohua, J. Xianglin, S. Meicheng, Z. Ruifang, X. Yongzhuang, Chem. J. Chin. Univ. 6 (1985) 69.
[9] K.A. Lyssenko, V.M. Akimov, M.Yu. Antipin, P.N. Abakumov, Yu.T. Struchkov, V.G. Skvortsov, M.A. Ershov, Russ. J. Inorg. Chem. 42 (1997) 1283.
[10] A. Neuman, A. Safsaf, H. Gillier, Y. Leroux, D. El Manouni, Phosphorus, Sulfur, Silicon, Relat. Elem. 70 (1992) 273.
[11] V.S. Sergienko, G.G. Aleksandrov, E.G. Russ, Coord. Chem. 25 (1999) 451.
[12] H.-H. Song, Li.-M. Zheng, X.-Q. Xin, Chin. J. Inorg. Chem. 18 (2002) 941.
[13] X.-Y. Yi, L.-M. Zheng, W. Xu, S. Feng, Inorg. Chem. 42 (2003) 2827.
[14] H.-H. Song, Z.-M. Wang, C.-H. Yan, L.-M. Zheng, X.-Q. Xin, Chin. J. Struct. Chem. 23 (2004) 202.
[15] A. Distler, F.L. Lohse, S.C. Sevov, J. Chem. Soc., Dalton Trans. (1999) 1805.
[16] V.S. Sergienko, E.O. Tolkacheva, A.B. Ilyukhin, Kristallografiya (Russ.) (Crystallogr. Rep.) 39 (1994) 1020.
[17] D. Fernandez, G. Polla, D. Vega, J.A. Ellena, Acta Crystallogr., Sect. C: Cryst. Struct. Commun. 60 (2004) m73.

[18] C. Dufau, M. Benramdane, Y. Leroux, D. El Manouni, A. Neuman, T. Prange, J.-P. Silvestre, H. Gillier, Phosphorus, Sulfur, Silicon, Relat. Elem. 107 (1995) 145.
[19] H. Blum, K.- H. Worms, US patent 4407761; G.R. Kieczykowski, D.G. Melillo; R.B. Jobson, US patent 4922007.
[20] Y. Leroux, A. Neuman, H. Gillier, D. El Manouni, Z. Abkhar, T. Prangé, Supramol. Chem. 5 (1995) 267.
[21] Enraf-Nonius CAD-4/PC Software, Version 1.5c, Enraf-Nonius, Delft, The Netherlands, 1994.
[22] A.C.T. North, D.C. Phillips, F.S. Mathews, Acta Crystallogr., Sect. A 42 (1968) 351.
[23] K. Harms, S. Wocadlo, XCAD4–CAD4 Data Reduction, University of Marburg, Marburg, Germany, 1995.
[24] G.M. Sheldrick, SHELX97 [Includes SHELXS97, SHELXL97, CIFTAB] – Programs for Crystal Structure Analysis (Release 97-2), Institüt für Anorganische Chemie der Universität, Tammanstrasse 4, D-3400 Göttingen, Germany, 1998.
[25] P.T. Beurskens, G. Beurskens, W.P. Bosman, R. de Gelder, S. Garcia-Granda, R.O. Gould, R. Israel, J.M.M. Smits, DIRDIF-99 Program system. Crystallography Laboratory, University of Nijmegen, The Netherlands. 1999.
[26] R. Hooft, B.V. Nonius, Collect Data collection and processing user interface: Collect: Data collection software, 1998.
[27] Z. Otwinowski, W. Minor, in: C.W. CarterJr, R.M. Sweet (Eds.), Denzo Data collection and processing software: Methods in Enzymology, Macromolecular Crystallography, part A, vol. 276, Academic Press, New York, 1997, pp. 307–326.
[28] S. Mackay, C.J. Gilmore, C. Edwards, M. Tremayne, N. Stewart, K. Shankland, maXus solution and refinement software suite: maXus: a computer program for the solution and refinement of crystal structures from diffraction data.
[29] SORTAV absorption correction software package: R.H. Blessing, Acta Cryst. A 51 (1995) 33.
[30] R.H. Blessing, J. Appl. Cryst. 30 (1997) 421.
[31] L.J. Farrugia, J. Appl. Crystallogr. 30 (1997) 565.
[32] A.L. Spek, PLATON, A Multipurpose Crystallographic Tool, Utrecht University, Utrecht, The Netherlands, 1998.
[33] L.J. Farrugia, J. Appl. Cryst. 32 (1999) 837.

synthesis and characterization of $\mathbf{L}^1$, related ligand $\mathbf{L}^2$ and their metal complexes (with Pt(II), Pd(II) and Hg(II)). Like platinum(II), a 20-membered metallomacrocycle is also formed by palladium(II) with $\mathbf{L}^1$. Its crystal structure is also solved and described in this paper. Moreover, macrocyclic ligands containing Te (Te/S, Te/O type) and their metal complexes are also not unknown [10b]. Metal complexes of nitrogen, oxygen, sulfur and/or phosphorus ligands containing large size chelate ring (i.e., metallomacrocycles) are well known [11–17]. The complexes $[Cu_2(\mu\text{-dppy})_3(MeCN)][BF_4]_2$ (where dppy = 2-(diphenylphosphino)pyridine) [11], *trans*-[1,8-bis(diphenylphosphino)-3,6-dioxaoctane-*P*,*P*′]carbonyl(ethanol)rhodium(I)hexaflurophosphate [12], *trans*-[1,5-bis(diphenylphosphino)-3-oxapentane-*P*,*P*′]carbonylchlororhodium(I) dimer [12], di-μ-[glutaraldehydebis(dimethylhydrazone)]-bis[dichloropalladium(II)] [13], $[\{CoCl_2Ph_2P(O)CH_2CH_2P(O)Ph_2\}_2]$ [14] and dinuclear platinum(II) complex of the dithioether ligand 1,5-bis(*n*-propylthio)pentane [15] are some examples containing 8–16-membered chelate ring. Two known examples of metallomacrocycles containing telluroether ligands are the polymeric silver(I) complex of $MeTe(CH_2)_3TeMe$ [16] and the mononuclear Hg(II) complex of 1,6-bis-2-butyltellurophenyl-2,5-diazahexa-1,5-diene [17] with 24- and 13-membered rings, respectively. Moreover, the hybrid macrocyclic ligands (P/S, P/N, P/O) and their complexes are also well document [17b].

2. Experimental

The C and H analyses were carried out with a Perkin–Elmer elemental analyzer 240 C. Tellurium was estimated by atomic absorption spectrometer. The ^1H and ^{13}C $\{^1H\}$ NMR spectra were recorded on a Bruker Spectrospin DPX-300 NMR spectrometer at 300.13 and 75.47 MHz, respectively. IR spectra in the range 4000–250 cm^{-1} were recorded on a Nicolet Protége 460 FT-IR spectrometer as KBr and CsI pellets. The conductance measurements were made in acetonitrile (concentration ~1 mM) using an ORION conductivity meter model 162. The molecular weights (concentration ~5 mM) in chloroform were determined with a Knauer vapour pressure osmometer model A0280. The melting points determined in open capillary are reported as such. 2-[3-(2-Chloroethoxy)propyl]-6-methylpyridine was prepared by chlorination of corresponding alcohol with thionyl chloride [18].

2.1. X-ray crystallography

The X-ray data for **1** was collected (at 120 K) on an Bruker Nonius Kappa CCD area detector diffractometer, with φ and ω scans chosen to give a complete asymmetric unit. An absorption correction was applied [19]. The structure was solved by direct methods [20] and was refined using the WINGX version [21] of SHELX-97 [22]. The final cycle of full-matrix least-squares refinement was based on 8483 observed reflections (6690 for $F^2 > 4\sigma(F^2)$) and 536 variable parameters and converged (largest parameter shift was 0.001 times its esd). All of the non-hydrogen atoms were treated anisotropically. Hydrogen atoms were included in idealized positions with isotropic thermal parameters set at 1.2 times that of the carbon atom to which they were attached. Table 1 lists the experimental parameters used for single crystal structure analysis and crystal data. Selected bond lengths and angles are given in Table 2. The slightly high residual electron density may ascribed to the shape of crystals (very thin plates).

2.2. Synthesis of 1-(4-methoxyphenyltelluro)-2-[3-(6-methyl-2-pyridyl)propoxy]ethane ($\mathbf{L}^1$)

Bis(4-methoxyphenyl)ditelluride (0.46 g, 1.0 mmol) was dissolved in 30 cm^3 of ethanol and the solution set to reflux under nitrogen atmosphere. A solution of sodium borohydride (0.07 g, 2.0 mmol) made in 5 cm^3 NaOH (5%) was added drop wise to the refluxing solution of the ditelluride under nitrogen atmosphere until it became colourless due to the formation of $ArTe^-$ Na^+. 2-[3-(2-Chloroethoxy)-propyl]-6-methylpyridine (0.42 g, 2.0 mmol) dissolved in 10 cm^3 of ethanol was added to this solution with constant stirring. The reaction mixture was refluxed further for 2–3 h, cooled to room temperature and poured into ice cold

Table 1
Crystal data and structure refinement for $[PdCl_2\mathbf{L}^1]_2 \cdot 1.5C_6H_6$

Empirical formula	$C_{45}H_{55}O_4N_2Cl_4Pd_2Te_2$
Formula weight	1297.71
Temperature (K)	120(2)
Wavelength (Å)	0.71073
Crystal system	triclinic
Space group	$P\bar{1}$
a (Å)	11.928(5)
b (Å)	12.793(5)
c (Å)	17.578(5)
α (°)	103.604(5)
β (°)	97.685(5)
γ (°)	108.612(5)
Volume (Å^3)	2406(2)
Z	2
D_{calc} (g/cm^3)	1.791
Absorption coefficient (mm^{-1})	2.200
F(000)	1270
Crystal size (mm^3)	0.25 × 0.10 × 0.03
θ Range for data collection (°)	2.98–25.03
Index ranges	$-14 \leqslant h \leqslant 14$, $-15 \leqslant k \leqslant 15$, $-20 \leqslant l \leqslant 20$
Reflections collected	42792
Independent reflections	8483 [$R_{int} = 0.0512$]
Maximum and minimum transmission	0.9369 and 0.6092
Refinement method	full-matrix least-squares on F^2
Data/restraints/parameters	8483/0/536
Goodness-of-fit on F^2	1.051
Final *R* indices [$F^2 > 4\sigma(F^2)$]	$R_1 = 0.0390$, $wR_2 = 0.0882$
R indices (all data)	$R_1 = 0.0579$, $wR_2 = 0.0965$
Largest differential peak and hole (e Å^{-3})	3.754 and −1.098

Table 2
Selected bond lengths (Å) and angles (°) for $[PdCl_2(\mathbf{L}^1)]_2 \cdot 1.5C_6H_6$

Te(1)–Pd(1)	2.530(1)	Te(2)–Pd(2)	2.5313(9)
Pd(1)–Cl(1)	2.313(2)	Pd(2)–Cl(3)	2.306(2)
Pd(1)–Cl(2)	2.295(2)	Pd(2)–Cl(4)	2.288(2)
Pd(1)–N(2)	2.097(4)	Pd(2)–N(1)	2.101(4)
Te(1)–C(1)	2.118(5)	Te(2)–C(19)	2.114(6)
Te(1)–C(8)	2.138(5)	Te(2)–C(26)	2.132(6)
O(2)–C(10)	1.423(6)	O(4)–C(27)	1.492(8)
O(2)–C(9)	1.431(6)	O(4)–C(28)	1.377(8)
Te(1)–Pd(1)–Cl(1)	86.12(5)	Te(2)–Pd(2)–Cl(3)	86.44(4)
Te(1)–Pd(1)–Cl(2)	94.56(5)	Te(2)–Pd(2)–Cl(4)	93.88(5)
Te(1)–Pd(1)–N(2)	176.9(1)	Te(2)–Pd(2)–N(1)	176.6(1)
N(2)–Pd(1)–Cl(1)	91.0(1)	N(1)–Pd(2)–Cl(3)	90.2(1)
N(2)–Pd(1)–Cl(2)	88.3(1)	N(1)–Pd(2)–Cl(4)	89.5(1)
Cl(1)–Pd(1)–Cl(2)	178.65(6)	Cl(3)–Pd(2)–Cl(4)	176.94(6)
C(1)–Te(1)–Pd(1)	100.1(1)	C(19)–Te(2)–Pd(2)	101.1(2)
C(8)–Te(1)–Pd(1)	104.9(2)	C(26)–Te(2)–Pd(2)	105.7(2)
C(1)–Te(1)–C(8)	95.6(2)	C(19)–Te(2)–C(26)	95.6(2)
C(13)–N(1)–C(17)	120.8(5)	C(31)–N(2)–C(35)	120.5(5)
C(13)–N(1)–Pd(2)	119.8(3)	C(31)–N(2)–Pd(1)	119.6(4)
C(17)–N(1)–Pd(2)	119.4(4)	C(35)–N(2)–Pd(1)	119.9(4)

water (100 cm^3) in which 0.1 g of NaOH was dissolved. The ligand was extracted into chloroform (4×50 cm^3) from this aqueous mixture. The extract was washed with water (2×20 cm^3) and dried over anhydrous sodium sulphate. The solvent was evaporated off under reduced pressure on a rotary evaporator, resulting in red oil, which was extracted with hexane (30 cm^3). On removing hexane from the extract under reduced pressure on a rotary evaporator ligand $\mathbf{L}^1$ was obtained as yellow viscous oil. Yield: ~70%; ^{1}H NMR ($CDCl_3$, 25 °C) (δ versus TMS): 1.91–2.01 (m, 2H, H_4), 2.52 (s, 3H, H_{11}), 2.71–2.82 (t, 2H, H_1), 2.95–3.00 (t, 2H, H_5), 3.43–3.47 (t, 2H, H_3), 3.66–3.70 (t, 2H, H_2), 3.78 (s, 3H, OCH_3), 6.73–6.76 (d, 2H, *m* to Te), 6.93–6.96 (d, 2H, H_7 and H_9), 7.43 7.48 (t, 1H, H_8), 7.65–7.70 (d, 2H, *o* to Te). ^{13}C {^{1}H} NMR ($CDCl_3$, 25 °C) (δ versus TMS) 8.1 (C_1), 24.1 (C_{11}), 28.9 (C_4), 34.5 (C_5) 54.7 (OCH_3), 69.4 (C_2), 71.8 (C_3), 99.8 (ArTe–C), 114.8 (C_9), 119.3 (ArC *m* to Te), 120.1 (C_7), 136.4 (C_8), 140.6 (ArC *o* to Te), 157.3 (C_{10}), 160.5 (ArC *p* to Te), 161.1 (C_6).

2.3. Synthesis of 2-methyl-6-{3-[2-({2-[3-(6-methyl-2-pyridyl)propoxy]ethyl}telluranyl)ethoxy]propyl}pyridine ($\mathbf{L}^2$)

Tellurium powder (0.65 g, 5.0 mmol) and sodium borohydride (0.38 g, 10.0 mmol) solution (made in 10 cm^3 of 2.0 M NaOH) were mixed in 50 cm^3 of water. The mixture was refluxed for 2 h under nitrogen atmosphere. To the resulting colourless thin slurry of Na_2Te kept under reflux, a solution of 2-[3-(6-methyl-2-pyridyl)propoxy]ethyl chloride (2.13 g, 10.0 mmol) made in 10 cm^3 of ethanol was added drop wise with constant stirring under nitrogen atmosphere. The mixture was cooled to room temperature and poured into 100 cm^3 of water. The ligand $\mathbf{L}^2$ was extracted into diethyl ether (4×30 cm^3) from the aqueous phase. The ether extract was washed with distilled water (2×15 cm^3) and dried over anhydrous sodium sulphate. On evaporating off ether under reduced pressure on a rotary evaporator $\mathbf{L}^2$ (2-methyl-6-{3-[2-({2-[3-(6-methyl-2-pyridyl)propoxy]ethyl}telluranyl)ethoxy]propyl}-pyridine) was obtained as a reddish yellow viscous liquid that was unstable as it showed the sign of decay within few days. Yield: ~75%; ^{1}H NMR ($CDCl_3$, 25 °C) (δ versus TMS) 1.96–2.00 (m, 2H, H_4), 2.51 (s, 3H, H_{11}), 2.79–2.84 (m, 4H, H_5 and H_1), 3.45–3.51 (m, 2H, H_3), 3.70–3.76 (m, 2H, H_2), 6.94–6.96 (m, 2H, H_8 and H_9), 7.427.46 (m, 1H, H_7) ^{13}C {^{1}H} NMR ($CDCl_3$, 25 °C) (δ versus TMS) 3.1 (C_1), 23.9 (C_{11}), 29.3 (C_4), 34.2 (C_5), 69.8 (C_2), 76.5 (C_3), 119.0 (C_9), 119.8 (C_7), 135.8 (C_8), 157.0 (C_6), 160.3 (C_{10}).

2.4. Synthesis of $[PdCl_2(\mathbf{L}^1)]_2$ (1)

To a solution of $\mathbf{L}^1$ (0.20 g, 0.50 mmol) made in 10 cm^3 of acetone was added $Na_2[PdCl_4]$ (0.14 g, 0.50 mmol) dissolved in 10 cm^3 of water. The resulting mixture was stirred for 2 h at room temperature and poured into 100 cm^3 of water. The complex was extracted into chloroform (4×25 cm^3). The extract was dried over anhydrous sodium sulphate, concentrated to ~5 cm^3 and mixed with hexane (20 cm^3). The resulting yellow solid was filtered, washed with hexane and dried in vacuo. The single crystals of the complex **1** were grown from benzene. The **1** crystallizes with 1.5 mol of benzene per mole. Yield: 78%; m.p. 125 °C; Λ_M (Ω^{-1} cm^2 mol^{-1}) 5.8. *Anal.* Calc. for $C_{36}H_{46}N_2O4Te_2Pd_2Cl_4$: C, 36.60; H, 3.97; N, 2.31; Te, 21.62. Found: C, 36.24; H, 3.89; N, 2.31; Te, 21.24%. Mol. wt.: 1144.6 (Calc. 1180.0). ^{1}H NMR ($CDCl_3$, 25 °C) (δ versus TMS) 2.20–2.27 (m, 2H, H_4), 3.30–3.31 (m, 4H, H_{11} and H_3), 3.54–3.66 (m, 2H, H_5 and H_3), 3.77–3.78 (m, 4H, $CH_3O + H_5$), 3.78–3.81 (t, 2H, H_2), 4.10–4.22 (m, 2H, H_1), 6.89–6.94 (m, 2H, ArH *m* to Te), 7.12–7.14 (m, 2H, H_7 and H_9), 7.36 (s, 1H, $CHCl_3$), 7.56–7.61 (m, 1H, H_8), 7.99–8.06 (m, 2H, ArH *o* to Te). ^{13}C {^{1}H} NMR ($CDCl_3$, 25 °C) (δ versus TMS) 21.8 (C_1), 27.0 (C_{11}), 29.4 (C_4), 36.6 (C_5), 55.2 (OCH_3), 66.7 (C_2), 70.3 (C_3), 103.9 (Ar–C–Te), 115.5 (C_9), 121.6 (Ar–C *m* to Te), 123.2 (C_7), 138.4 (C_8), 140.6 (Ar–C *o* to Te), 158.9 (C_{10}), 161.1 (Ar–C *p* to Te), 162.2 (C_6).

2.5. Synthesis of $[PtCl_2(\mathbf{L}^1)]_2$ (2)

A solution of $\mathbf{L}^1$ (0.20 g, 0.50 mmol) made in 10 cm^3 of acetone was added to $K_2[PtCl_4]$ (0.20 g, 0.50 mmol) dissolved in 10 cm^3 of water. The resulting mixture was stirred for 3 h at room temperature and poured into 100 cm^3 of water. The complex was extracted into chloroform (4×25 cm^3). The chloroform extract was dried over anhydrous sodium sulphate, concentrated to ~5 cm^3 on a rotary evaporator, and mixed with hexane (20 cm^3). The

resulting yellow coloured compound was filtered, washed with hexane. The single crystals suitable for diffraction were grown from chloroform:hexane (1:1) mixture. The **2** crystallizes with 2 mol of chloroform per mole. Yield: 75%; m.p. 126 °C; Λ_M (Ω^{-1} cm^2 mol^{-1}) 10.5. *Anal.* Calc. for $C_{36}H_{46}N_2O_4Te_2Pt_2Cl_4$: C, 31.82; H, 3.32; N, 2.00; Te, 18.80. Found: C, 32.91; H, 3.39; N, 2.06; Te, 18.92%. Mol. wt.: 1324.2 (Calc. 1357.3). ^{1}H NMR ($CDCl_3$, 25 °C) (δ versus TMS) 2.22–2.30 (m, 2H, H_4), 3.26–3.32 (m, 4H, H_{11} and H_3), 3.55–3.67 (m, 2H, H_5 and H_3), 3.81–3.84 (m, 4H, $CH_3O + H_5$), 3.90–3.92 (t, 2H, H_2), 4.12–4.14 (m, 1H, H_1), 4.26–4.41 (m, 1H, H_1), 6.87–6.94 (m, 2H, ArH *m* to Te), 7.10–7.13 (m, 2H, H_7 and H_9), 7.26–7.28 (s, 2H, $CHCl_3$), 7.53–7.61 (m, 1H, H_8), 7.80–7.83 (d, 1H, ArH *o* to Te), 8.00–8.06 (m, 1H ArH *o* to Te). ^{13}C {^{1}H} NMR ($CDCl_3$, 25 °C) (δ versus TMS) 18.9 (C_1), 26.8 (C_{11}), 28.0 (C_4), 36.3 (C_5), 55.3 (OCH_3), 66.9 (C_2), 70.6 (C_3), 99.8 (Ar–Te–C), 115.2 (C_9), 122.7 (Ar–C *m* to Te), 123.8 (C_7), 138.4 (C_8), 140.6 (Ar–C *o* to Te), 160.0 (C_{10}), 160.6 (Ar–C *p* to Te), 161.2 (C_6).

2.6. Synthesis of [$HgBr_2$(**L**^{1})] (**3**)

$HgBr_2$ (0.20 g, 0.55 mmol) dissolved in acetone (20 cm^3) was mixed with a solution of **L**^{1} (0.22 g, 0.55 mmol) made in chloroform (20 cm^3). The resulting mixture was stirred at room temperature until the ligand **L**^{1} was consumed (as monitored by TLC). The solvent was removed from the mixture on a rotary evaporator. The resulting residue was dissolved in 20 cm^3 of chloroform and filtered through celite. The filtrate was concentrated to 10 cm^3 and mixed with 20 cm^3 of hexane. A white complex was separated, filtered, dried in vacuo and recrystallized from acetone–hexane (2:1) mixture. Yield: 80%; m.p. 130 °C (d); Λ_M (Ω^{-1} cm^2 mol^{-1}) 7.8 *Anal.* Calc. for $C_{18}H_{23}NO_2TeHgBr_2$: C, 27.97; H, 2.97; N, 1.81; Te, 16.50. Found: C, 27.71; H, 2.91; N, 1.76; Te, 16.36%. Mol. wt.: 770.34 (Calc. 773.10). ^{1}H NMR ($CDCl_3$, 25 °C) (δ versus TMS) 1.86–1.89 (m, 2H, H_4), 2.46 (s, 3H, H_{11}), 2.71–2.75 (t, 2H, H_1), 3.37 (t, 2H, H_5), 3.46 (bs, 2H, H_3), 3.65–3.68 (m, 5H, H_2 and OCH_3), 6.74–6.77 (d, 2H, *m* to Te), 6.93–6.97 (m, 2H, H_7 and H_9), 7.47–7.52 (t, 1H, H_8), 7.68–7.71 (d, 2H, *o* to Te), ^{13}C {^{1}H} NMR ($CDCl_3$, 25 °C) (δ versus TMS) 24.4 (C_1), 24.8 (C_{11}), 28.9 (C_4), 34.8 (C_5), 55.2 (OCH_3), 66.9 (C_2), 70.4 (C_3), 99.8 (ArTe–C), 114.7 (C_9), 116.2 (Ar–C *m* to Te), 120.9 (C_7), 137.1 (C_8), 139.3 (ArC *o* to Te), 157.3 (C_{10}), 160.5 (Ar–C *p* to Te), 161.1 (C_6).

2.7. Formation of $MeOC_6H_4HgBr$ (**4**) and [RTe^+–$HgBr_2$]Br^- (R = –$CH_2CH_2OCH_2CH_2CH_2$-(2-(6-CH_3–C_5H_3N))) (**5**)

$HgBr_2$(**L**^{1}) (**3**) (0.07 g, 0.09 mmol) was dissolved in acetone–hexane (2:1) mixture and kept for slow evaporation at 25°C. After 7 days, crystals of **4** were obtained. The mother liquor was mixed with chloroform (20 ml) and refluxed for 3 h. The **5** was obtained as solid. It was filtered, washed with chloroform (2 × 5 cm^3) and dried in vacuo. **4**: Yield: 18%; m.p. 115 °C (d); Λ_M (Ω^{-1} cm^2 mol^{-1}) 6.4. *Anal.* Calc. for C_7H_7OHgBr: C, 27.70; H, 1.80. Found: C, 27.71; H, 1.82%. Mol. wt.: 379.3 (Calc. 387.6) ^{1}H NMR (DMSO-d^6, 25 °C) (δ versus TMS) 3.71 (s, 3H, OCH_3), 6.89–6.91 (d, 2H, ArH *m* to Hg), 7.34–7.37 (ArH *o* to Hg).

5: Yield: 18%; m.p. 144 °C (d); Λ_M (Ω^{-1} cm^2 mol^{-1}) 23.5. *Anal.* Calc. for $C_{11}H_{16}NOTeHgBr_3$: C, 17.70; H, 2.10; N, 1.87; Te, 17.10. Found: C, 17.30; H, 2.01; N, 1.82; Te, 17.03%. Mol. wt.: 732.1 (Calc. 745.9) ^{1}H NMR (DMSO-d^6, 25 °C) (δ versus TMS) 1.82–1.84 (t, 2H, H_4), 2.35 (s, 3H, H_{11}), 2.66–2.81 (m, 2H, H_5), 3.63–3.68 (m, 2H, H_2), 3.75–3.81 (m, 2H, H_1), 7.02–7.11 (m, 2H, H_7 and H_9), 7.68–7.78 (m, 1H, H_9).

2.8. Synthesis of [$PdCl_2$(**L**^{2})]$_2$ (**6**)

The freshly prepared sample of **L**^{2} (0.24 g, 0.50 mmol) dissolved in 10 cm^3 of acetone was added to $Na_2[PdCl_4]$ (0.14 g, 0.50 mmol) dissolved in 10 cm^3 of water. The resulting mixture was stirred for 3 h at room temperature and poured in 100 cm^3 of water. The complex was extracted with chloroform (4 × 25 cm^3). The chloroform extract was dried over anhydrous sodium sulfate and concentrated to ~10 cm^3 on a rotary evaporator, and mixed with hexane (20 cm^3). The resulting orange coloured compound was filtered, washed with hexane and recrystallized from chloroform:hexane (1:1) mixture. Yield: 79%; m.p. 139 °C (d); Λ_M (Ω^{-1} cm^2 mol^{-1}) 7.6. *Anal.* Calc. for $C_{22}H_{32}N_2O_2TePdCl_2$: C, 39.68; H, 4.84; N, 4.20; Te, 19.30. Found: C, 39.90; H, 4.53; N, 4.34; Te, 19.12%. Mol. wt.: 658.1 (Calc. 661.0). ^{1}H NMR ($CDCl_3$, 25 °C) (δ versus TMS) 1.69 (m, 2H, H_4), 2.02–2.04 (m, 2H, H'_4), 2.38–2.42 (m, 3H, H'_{11}), 2.54 (m, 3H, H_{11}), 2.84–2.97 (m, 4H, $H_5 + H'_5$), 3.35 (m, 2H, H_3), 3.53–3.65 (m, 2H, H'_3), 3.73–3.75 (m, 2 H H_2), 3.77–3.79 (m, 2H, H2′), 3.90–4.05 (m, 2H, H_1), 6.99–7.15 (m, 2H, $H_8 + H_9$), 7.47–7.52 (m, 2H, $H'_8 + H'_9$), 7.55–7.58 (m, 1H, H'_{10}) 7.60 (m, 1H, H_{10}). ^{13}C {^{1}H} NMR ($CDCl_3$, 25 °C) (δ versus TMS) 14.0 (C_1), 26.0 (C'_{11}), 26.6 (C_{11}), 28.9 (C'_4), 29.8 (C_4), 34.6 (C'_5), 35.8 (C_5), 68.2 (C'_2), 70.3 (C_2), 76.9 (C_3), 119.0 (C'_9), 120.6 (C_9), 121.0 (C'_7), 122.2 (C_7), 138.5 (C_8), 136.8 (C'_8), 159.0 (C_6), 162.9 (C_{10}) [primes indicate the pendent arm proton or carbon atoms].

2.9. Synthesis of [$PtCl_2$(**L**^{2})]$_2$ (**7**)

The freshly prepared sample of **L**^{2} (0.24 g, 0.50 mmol) dissolved in 10 cm^3 of acetone was added to $K_2[PtCl_4]$ (0.20 g, 0.50 mmol) dissolved in 10 cm^3 of water. The resulting mixture was stirred for 3 h at room temperature and poured into 100 cm^3 of water. The complex was extracted into chloroform (4 × 25 cm^3). The chloroform extract was dried over anhydrous sodium sulphate,

concentrated to ~10 cm^3 on a rotary evaporator, and mixed with hexane (20 cm^3). The resulting yellow coloured compound was filtered, washed with hexane and recrystallized from chloroform:hexane (1:1) mixture. Yield: 75%; m.p. 147 °C (d); Λ_M (Ω^{-1} cm^2 mol^{-1}) 9.0. *Anal.* Calc. for $C_{22}H_{32}N_2O_2TePtCl_2$: C, 35.21; H, 4.26; N, 3.73; Te, 17.02. Found: C, 35.12; H, 4.21; N, 3.12; Te, 16.17%. Mol. wt.: 739.2 (Calc. 749.6). ^{1}H NMR ($CDCl_3$, 25 °C) (δ versus TMS) 1.89 (m, 2H, H_4), 2.02–2.08 (m, 2H, H'_4), 2.35–2.40 (m, 3H, H'_{11}), 2.53–2.54 (m, 3H, H_{11}), 2.86–2.97 (m, 4H, $H_5 + H'_5$), 3.20–3.27 (m, 2H, H_3), 3.34–3.40 (m, 2H, H'_3), 3.56–3.62 (m, 2H, H'_2), 3.78–3.79 (m, 2H, H_2), 3.84 (m, 2H, H_1), 6.69 (m, 2H, $H_8 + H_9$), 6.99–7.15 (m, 2H, $H'_8 + H'_9$), 7.48–7.49 (m, 1H, H'_{10}), 7.50–7.58 (m, 1H, H_{10}). ^{13}C {^{1}H} NMR ($CDCl_3$, 25 °C) (δ versus TMS) 16.7 (C_1), 24.0 (C'_{11}), 27.6 (C_{11}), 28.8 (C_4), 29.3 (C'_4), 34.7 (C'_5), 36.4 (C_5), 69.7 (C'_2), 70.4 (C_2), 77.0 (C_3), 119.0 (C'_9), 120.6 (C_9), 121.6 (C'_7), 123.5 (C_7), 136.7 (C'_8), 138.4 (C_8), 161.5 (C_6), 164.0 (C_{10}) [primes indicate the pendent arm proton or carbon atoms].

2.10. Synthesis of [($PdCl_2$)$_3$(L^2)$_2$] (8)

The freshly prepared sample of L^2 (0.24 g, 0.50 mmol) dissolved in 10 cm^3 of acetone was added to $Na_2[PdCl_4]$ (0.22 g, 0.75 mmol) dissolved in 10 cm^3 of water. The resulting mixture was stirred for 3 h at room temperature and poured in to 100 cm^3 of water. The complex was extracted with 4×25 cm^3 of chloroform. The combined chloroform layer was dried over anhydrous sodium sulfate and concentrated to ~10 cm^3 on a rotary evaporator, and mixed with hexane (20 cm^3). The resulting orange colored compound was filtered, washed with hexane and recrystallized from chloroform:hexane (1:1) mixture. Yield: 72%; m.p. 141 °C (d); Λ_M (Ω^{-1} cm^2 mol^{-1}) 8.7 *Anal.* Calc. for $C_{44}H_{64}N_4O_4Te_2Pd_3Cl_6$: C, 35.21; H, 4.26; N, 3.73; Te, 17.01. Found: C, 35.16; H, 4.24; N, 3.71; Te, 17.00%. Mol. wt.: 1487.2 (Calc. 1499.4). ^{1}H NMR ($CDCl_3$, 25 °C) (δ versus TMS) 2.36–2.43 (m, 4H, H_4 and H_{11}), 3.13–3.19 (m, 2H, H_5), 3.31–3.42 (m, 1H, H_3), 3.68–3.94 (m, 5H, H_3, H_2, H_1), 7.11–7.12 (m, 2H, H_8 and H_9), 7.55–7.60 (m, 1H, H_7) ^{13}C {^{1}H} NMR ($CDCl_3$, 25 °C) (δ versus TMS) 17.3 (C_1), 27.6 (C_{11}), 28.9 (C_4), 36.4 (C_5), 69.7 (C_2), 77. 4 (C_3), 121.6 (C_9), 123.7 (C_7), 138.5 (C_8), 161.5 (C_6), 164.0 (C_{10}).

3. Results and discussion

The ligands L^1 and L^2 were prepared according to Eqs. (1) and (2) given below. The ligand L^1 was found stable for two months under ambient conditions. Thereafter, deposition of white solid starts in the oil, which is most likely a tellurium dioxide formed by its oxidative decomposition. However, on storing L^2 for only eight days at room temperature under ambient conditions TeO_2 deposits appear. In N_2 atmosphere it may be stored for one month without any sign of decomposition.

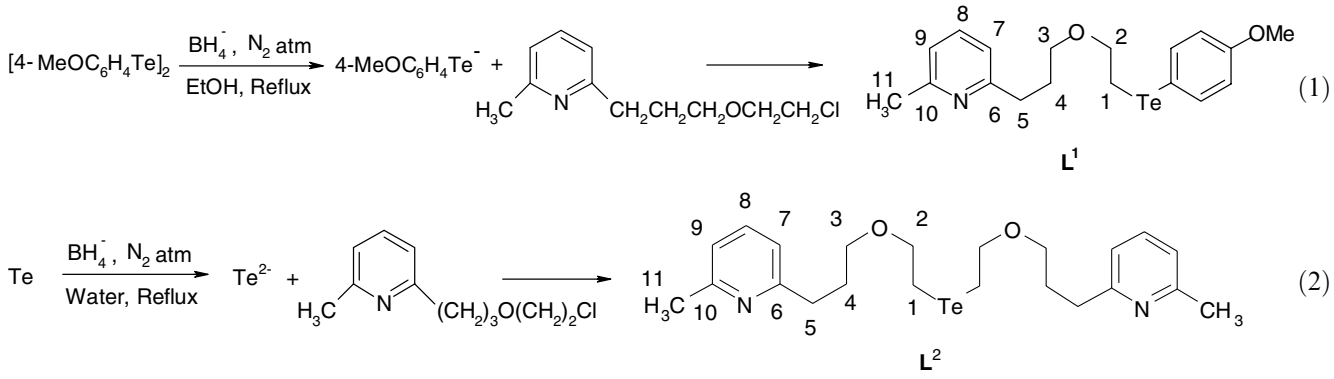

(1)

(2)

The Pd(II), Pt(II), Hg(II) complexes of L^1 and L^2 were prepared according to Eqs. (3)–(8) given below. The **1** crystallizes with 1.5 mol of benzene per mole whereas **2** with 2 mol of chloroform. The complexes **1**–**3**, **6**, **7**, and **8** can be stored at room temperature for two months easily. Single crystals of **6**–**8** suitable for X-ray diffraction could not be grown.

$$2Na_2PdCl_4 + 2L^1 \rightarrow [PdCl_2(L^1)]_2\ (\mathbf{1}) + 4NaCl \quad (3)$$

$$2K_2PtCl_4 + 2L^1 \rightarrow [PtCl_2(L^1)]_2\ (\mathbf{2}) + 4KCl \quad (4)$$

$$HgBr_2 + L^1 \rightarrow [HgBr_2(L^1)]\ (\mathbf{3}) \quad (5)$$

$$2Na_2PdCl_4 + 2L^2 \rightarrow [PdCl_2(L^2)]_2\ (\mathbf{6}) + 4NaCl \quad (6)$$

$$2K_2PtCl_4 + 2L^2 \rightarrow [PtCl_2(L^2)]_2\ (\mathbf{7}) + 4KCl \quad (7)$$

$$3Na_2PdCl_4 + 2L^2 \rightarrow [(PdCl_2)_3(L^2)_2]\ (\mathbf{8}) + 6NaCl \quad (8)$$

Both L^1 and L^2 and their complexes are highly soluble in chloroform and dichloromethane and moderately soluble in acetone. In methanol, ethanol and hexane the two ligands L^1 and L^2 are sparingly soluble. However on crystallization of **3** in acetone:hexane (2:1) mixture, the cleavage of L^1 occurs resulting in MeO C_6H_4HgBr (**4**) and [RTe^+–$HgBr_2$]Br^- (R = –$CH_2CH_2OCH_2CH_2CH_2$-(2-(6-CH_3-C_5H_3N))) (**5**) as shown in Eq. (9) given below.

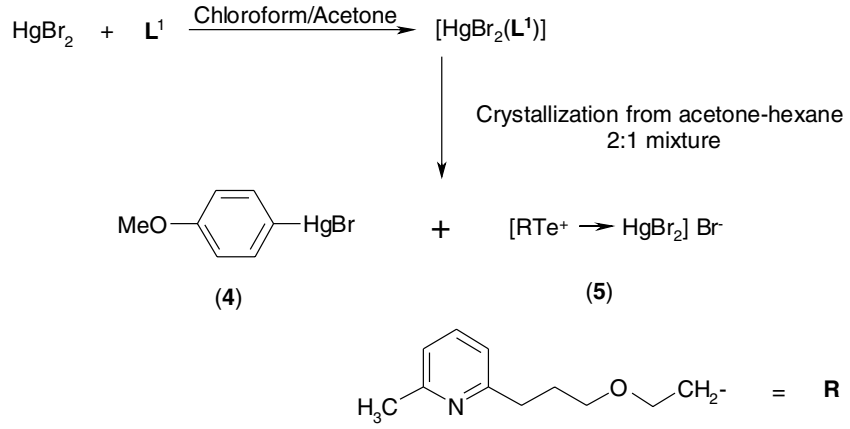

(9)

The compound **4** is soluble in common organic solvents such as chloroform, dichloromethane whereas **5** is insoluble in organic solvents. The crystal structure of **4** is solved and reported earlier [24]. The molar conductance values Λ_M of the complexes **1**–**3**, **6**, **7**, and **8** in acetonitrile at ~1 mM concentration level have been recorded. The found values are much lower than the values expected for a 1:1 electrolyte. This suggests that all the complexes **1**–**3**, **6**, **7** and **8** are non–electrolytes. The molecular weights of complexes **1**–**3**, **6**, **7** and **8** determined in chloroform by vapour pressure osmometric method were found to be very close to the values calculated from their molecular formulae. This indicates that there is no appreciable dissociation of any of these complexes in the solution. The existence of metallomacrocycles in solution may be further strengthened with ^{125}Te NMR but inadequate solubility of **1** and **2** has restricted us.

3.1. Infrared spectra

In the IR spectrum of $\mathbf{L}^1$ the bands appearing at 3060 cm^{-1} are due to C–H (aromatic) vibrations and those in the region 1456–1588 cm^{-1} due to C–C (aromatic) vibrations. The C–H (aliphatic) stretching vibrations appear at 2857–2936 cm^{-1} whereas ν(Te–C (aliphatic)) appears at 510 cm^{-1}. In IR spectrum of $\mathbf{L}^2$, the bands for C–H (aromatic) vibrations are observed at 3058 cm^{-1} while C–H (aliphatic) vibrations at 2854–2940 cm^{-1}. The band at 495 cm^{-1} seems to originate from ν(Te–C (aliphatic)). In the IR spectrum of **1**, ν(Te–C (aliphatic)) shows red shift as it appears at 478 cm^{-1}. The ν(Pd–Cl) in this spectrum appears at 357 cm^{-1} and is characteristic of a *trans* Cl–Pd–Cl system. In the IR spectrum of **2**, the bands appearing at 331 cm^{-1} may be assigned to the asymmetric stretching of *trans* Cl–Pt–Cl system. The band at 472 cm^{-1} seems to arise from Te–C (aliphatic) vibrations and show red shift of ~23 cm^{-1}. In the IR spectra of **3**, **4** and **5** a band is observed around 295 cm^{-1} which may be assigned to Hg–C/N vibrations. This indicates that in **5**, pyridine N interacts with Hg as shown for **3**. In the IR spectra of complexes **6** and **7**, the ν(M–Cl) appears at 351 and 334 cm^{-1}, respectively, indicating the presence of two *trans* M–Cl bonds (M = Pd or Pt) of a square planar complex. In the IR spectra of complexes **6** and **7** also, ν(Te–C (aliphatic)) appears at lower frequency (458 and 443 cm^{-1}, respectively) when compared to that of free ligand ($\mathbf{L}^2$). In the IR spectrum of **8**, the ν(M–Cl) due to two *trans* Pd–Cl appears at 351 cm^{-1} while the band at 481 cm^{-1} may be assigned to Te–C (aliphatic) vibrations. A red shift in this band in comparison to that of free $\mathbf{L}^2$supports the formation of M–Te bond. Similar red shifts in ν(Te–C (aliphatic)) band in the IR spectra of complexes **1**–**3** and **6** and **7** (described above) support the involvement of Te in coordination of the two ligands $\mathbf{L}^1$ and $\mathbf{L}^2$ with the metal ions.

3.2. ^{1}H NMR spectra

In the ^{1}H NMR spectrum $\mathbf{L}^1$, H_1 appears deshielded by ~1.2 ppm as compared to that of 2-[3-2-(chloroethoxy)propyl]-6-methylpyridine as the chlorine is replaced by a tellurium moiety. In the ^{1}H NMR spectrum of $\mathbf{L}^2$, H_1 protons merge with H_5 protons and appear as a multiplet with a deshielding of ~1.1 ppm as compared to 2-[3-(2-chloroethoxy)propyl]-6-methylpyridine again due to substitution of chlorine with tellurium moiety. In case of $\mathbf{L}^1$ the aromatic protons *ortho* to Te appear more deshielded as a doublet than expected as compared to *para* to Te which also appear as doublet. The pyridyl protons H_7 and H_9 in ^{1}H NMR spectrum of $\mathbf{L}^1$ appear merged as a multiplet whereas the H_8 appears as a triplet. In case of $\mathbf{L}^2$ also H_7 and H_9 appear as multiplet while H_8 appears as a triplet. The ^{1}H NMR spectrum of **1** and **2** were found to be similar and somewhat complex in the alkyl region. In the ^{1}H NMR spectrum of **2**, the two singlets at 7.26–7.28 are due to two chloroform molecules identified in the lattice of its single crystals. The H_1 proton appears to be maximum deshielded (~1.14–1.41 ppm) with respect to that of free ligand $\mathbf{L}^1$ as it coordinates through Te. Similarly, deshielding of H_5 with respect to free ligand is also large (~0.85 ppm) because

the ligand also coordinates via pyridine nitrogen, which is also reflected in the deshielding of H_{11} by ~1.1 ppm as compared to free $\mathbf{L}^1$. All other CH_2 protons also exhibit deshielding (~0.1–0.3 ppm). Some of them become non equivalent (viz. H_1, H_3 and H_5) also. Pyridine and aryl protons also appear deshielded (~0.1–0.3 ppm). In the proton NMR spectrum of **1** also maximum deshielding occurs for H_1 (~1.31–1.44 ppm) as compared to free ligand. The broad singlet at 7.24 is due to benzene molecule identified in the lattice of its single crystal. The signal for H_5 and H_{11} appear deshielded by ~0.6 and 0.3 ppm respectively, thereby indicating the binding of ligand through nitrogen pyridine also as in the case of **2**. The rigidity in the complex as compared to free ligand is probably responsible for the complexity observed in the proton NMR spectrum of complexes **1** and **2** in the alkyl region. In the proton NMR spectrum of **3**, the coordination shifts are not found to be significant as expected for a d^{10} system. Thus H_1 protons are not deshielded as expected for a d^{10} system. However H_5 protons appear to be deshielded by ~0.3 ppm as compared to that of free ligand $\mathbf{L}^1$, there by indicating the binding of pyridyl nitrogen to the metal centre. All the other protons viz. H_1, H_3, H_4 and the aromatic protons of pyridyl ring and methoxy phenyl group appear at almost the same position as that of free ligand $\mathbf{L}^1$.

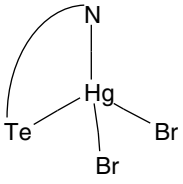

(**3**) ($\mathbf{L^1}$ = Te~N)

Most probably **3** has a tetrahedral structure given above which is corroborated by ^{13}C NMR and terminal ν(Hg–Br) bands observed in its IR spectrum.

The proton NMR spectrum of **4** and **5** are also characteristic. In the spectrum of **4** aromatic protons *ortho* and *meta* to Hg appear as doublet while OCH_3 protons appear as a singlet. In case of **5** the H_1 protons appear as multiplet and are deshielded by ~1.0 ppm as compared to those of ligand $\mathbf{L}^1$. This kind of decomposition by which **3** gives **4** and **5** is reported earlier also in tellurium chemistry [23]. The signals in the proton NMR spectra of **6** and **7** are broad in the aliphatic as well as aromatic region. Additional signals are also observed in proton NMR spectrum of **6** and **7** in the aromatic as well as aliphatic region. These additional signals are similar to those of free ligand $\mathbf{L}^2$. The multiplication of the signals may be due to free uncoordinated arm of the ligand $\mathbf{L}^2$ in **6** and **7**. The broadness of these signals may arise due to exchange between pendant and coordinated arms of $\mathbf{L}^2$. The most plausible structure of **6** and **7** may be presumed to be dimeric as shown below:

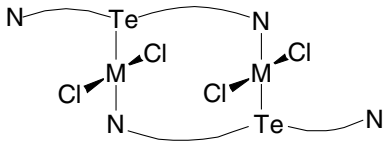

6 / 7 (M = Pd/ Pt)

On reacting $\mathbf{L}^2$ with Pd (II) according to Eq. (8), complex **8** results. The additional peaks like that of proton NMR spectra of **6** and **7** are not observed in its ^1H NMR spectrum. The spectrum not only becomes cleaner as compared to those of **6** and **7** but the signals also become sharp when compared with those of ^1H NMR spectrum of **6** and **7**. The aromatic protons show a deshielding (~0.12 ppm). These observations indicate that the free arm of ligand $\mathbf{L}^2$ present in **6/7** coordinates to third Pd atom to give a structure which is shown below.

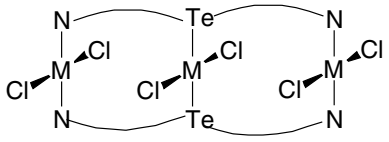

(8)

3.3. ^{13}C $\{^1H\}$ NMR spectra

The ^{13}C $\{^1H\}$ NMR for **4** and **5** could not be recorded because of their low solubilities. In the carbon-13 NMR of **1**, the C_1 signal exhibits a deshielding of ~13 ppm with respect to that of $\mathbf{L}^1$ thereby indicating the coordination through Te. In the carbon-13 NMR spectrum of **2** also, the C_1 signal shows ~10 ppm deshielding with respect to that of $\mathbf{L}^1$ while the other carbons are deshielded to a lesser extent (<4 ppm). In the spectrum of **3**, the C_1 signal appears ~16 ppm deshielded with respect to free $\mathbf{L}^1$ which may be due to the coordination of Te to the metal centre. Additional signals are observed in carbon-13 NMR spectrum of **6** in the aliphatic and aromatic regions at δ 26.0, 28.9, 34.6, 68.2, 119.0, 121.0, 130.8. Similarly in the carbon-13 NMR spectrum of **7** also, additional peaks are observed at δ 24.0, 29.3, 34.7, 69.1, 119.0, 121.6, 136.7 ppm. These extra signals are due to pendant arm of $\mathbf{L}^2$ and are corroborated by the proton NMR spectra **6/7**. The carbon-13 NMR spectrum of **8** does not have additional signals as observed in the case of **6** and **7**. This may be due to the binding of uncoordinated arm of $\mathbf{L}^2$ of **6/7** with the metal centre in **8**, which is corroborated by its ^1H NMR spectrum. However, the compounds **6**,**7** and **8** do not have adequate solubility for ^{125}Te NMR. Moreover, failure to grow their single crystals suitable for X-ray diffraction has compelled us to propose structures with limited evidences.

3.4. Crystal structure

The details of the crystal structures of **2** and **4** have already been reported by us [10,24] and their molecular structures are shown in Figs. 2 and 3 for comparative purposes. The data for crystal and structure refinement of **1** are given in Table 1, selected bond lengths and angles in Table 2 and the molecular structure in Fig. 1. The immediate environment around Pd in **1** is essentially square planar consisting of the two *trans* Cl atoms along with the Te atom of one bridging ligand and the N atom of the other. This results in the formation of a 20-membered metallomacrocycle ring as has been reported for **2** (Fig. 2).

The Pd–Cl bond lengths 2.313(2)/2.295(2) Å are comparable to those (2.131(11) ave. Å) reported for three *trans* $PdCl_2L_2$ complexes, where L represents ligands bonding to Pd through Te [25,26]. In **1**, where a pyridine nitrogen is *trans* to Te, the Pd–Te bond lengths of 2.530(1)/2.5313(9) Å are considerably shorter than the sum of the respective covalent radii of 2.63 Å [1.31 Å square planar Pd(II) and 1.32 Å (tetrahedral Te)] and also shorter than those reported earlier (2.594(8) ave. Å) for the three compounds with two *trans* Te-ligands [25,26]. Conversely, the Pd–N bond lengths of 2.097(4) and 2.101(4) Å in **1** are longer than the sum of the respective covalent radii, 2.06 Å and also longer than that reported (2.086(2) Å) for a Pd–Te bond *cis* to Te [8]; also consistent with the strong *trans* influence of tellurium. The bond angles at Te and nitrogen are as expected for trigonal pyramidal and trigonal planar geometry, respectively. The Te–C(aryl) bond lengths 2.114(6)/2.118(5) Å are shorter than Te–C(alkyl) bond lengths 2.132(6)/2.138(5) Å and close to the earlier reported values of 2.116(20) and 2.158(30) Å [27], respectively.

A distinguishing feature of the 20-membered metallomacrocycle ring can be described as an approximate rectangle (or tetragon) denoted by the four sides Te(1)···N(2), N(2)···Te(2), Te(2)···N(1), and N(1)···Te(1) with distances of 4.625(5), 8.921(5), 4.630(5), and 9.081(5) Å, respectively. However, the rectangle is twisted such that the dihedral angles for Te(1)–Pd(1)···Pd(2)–N(1) and N(1)–Pd(1)···Pd(2)–Te(2) are 31.2(2)° and 31.7(2)°, respectively, when viewed down the Pd(1)···Pd(2) vector (8.905(2) Å). The related Cl(1)–Pd(1)···Pd(2)–Cl(3) and Cl(2)–Pd(1)···Pd(2)–Cl(4) dihedral angles are 26.8(2)° and 26.0(2)°, respectively. The C_3OC_2 chain of the long sides of the macrocyclic rectangle are arranged so that the C_3O section forms a roughly regular zig-zag chain but the final C_2 section deviates from this forming a trough-like arrangement at Te. This can be expressed by looking at the torsion angle of C(9)–O(2)–C(10)–C(11) which is −77.6(6)° as opposed to that

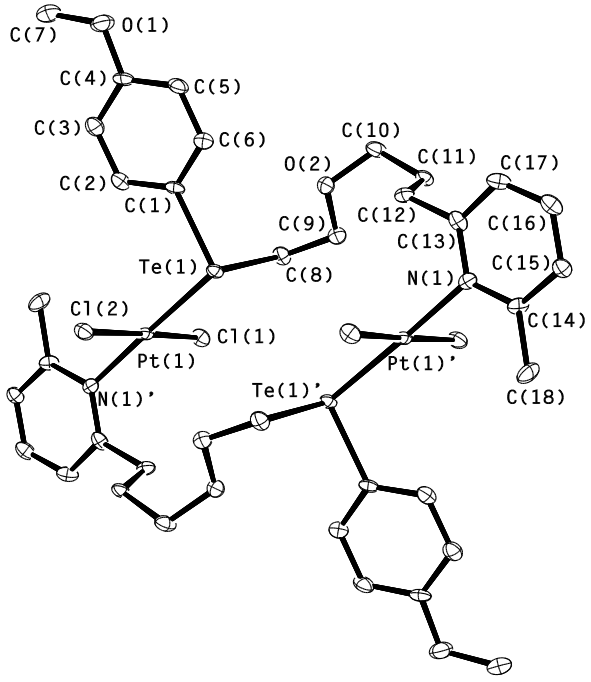

Fig. 2. Molecular structure of $[PtCl_2(\mathbf{L}^1)]_2 \cdot 2CHCl_3$ (**2**).

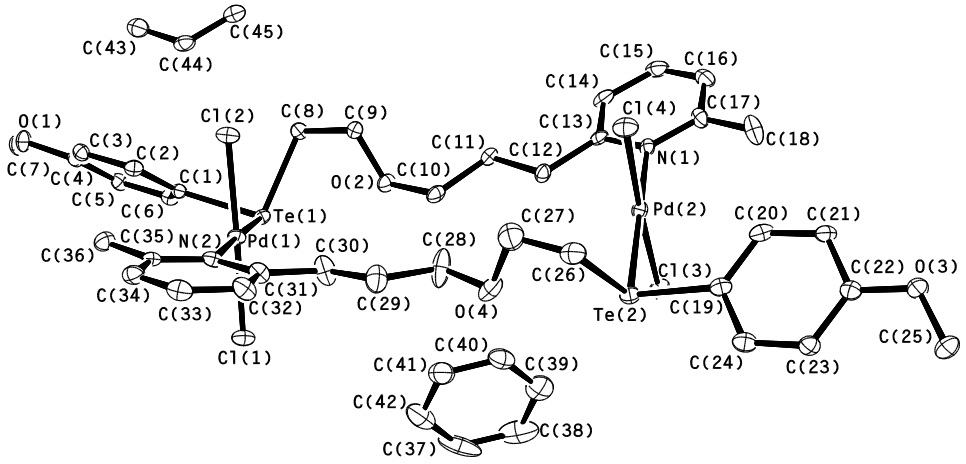

Fig. 1. Molecular structure of $[PdCl_2(\mathbf{L}^1)]_2 \cdot 1.5C_6H_6$ (**1**).

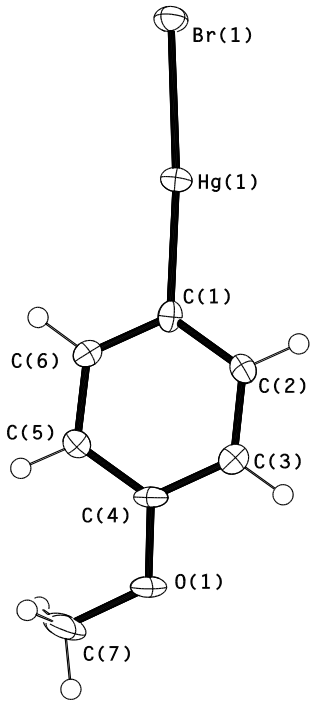

Fig. 3. Molecular structure of 4-$MeOC_6H_4HgBr$ (**4**).

of −176.7(6)° for the zig-zag section of C(12)–C(11)–C(10)–O(2). A similar geometry is observed along the other long edge with both troughs pointing in the same direction.

The relationship between the macrocycle and the solvate is such that one benzene molecule slots into the base of the macrocycle so that pairs of CH groups appear to be associated with two chlorine atoms H(39)···Cl(3), H(40)···Cl(3) and H(41)···Cl(1), H(42)···Cl(1) and also with that of an adjacent macrocycle below H(37)···Cl(1)′, H(38)···Cl(1)′. However the contact distances are all greater than 3.0 Å (CH···Cl distances being in the range 3.03–3.81 Å) and hence beyond the sum of the van der Waals radii. The other benzene molecule is sandwiched, side-on, between two phenyl (C_1–C_6) rings of adjacent macrocycles.

4. Conclusion

The potentially multidentate ligands 1-(4-methoxyphenyltelluro)-2-[3-(6-methyl-2-pyridyl)propoxy]ethane ($\mathbf{L}^1$) 2-methyl-6-{3-[2-({2-[3-(6-methyl-2-pyridyl)propoxy]ethyl}-telluranyl)ethoxy]propyl}pyridine ($\mathbf{L}^2$) have been synthesized. The $\mathbf{L}^1$ is used to design 20-membered metallomacocycles with Pd(II) and Pt(II). The **1** and **2** are the first examples of the formation of 20-membered metallomacrocycle ring by a hybrid organotellurium ligand. The decomposition of $\mathbf{L}^1$ in its mercury complex appears to be metal promoted. The **4** is the first linear ArHgX system characterized fully by X-ray diffraction on its single crystals.

5. Supplementary material

CCDC-285432 contains the supplementary crystallographic data for **1**. These data can be obtained free of charge at www.ccdc.cam.ac.uk/conts/retrieving.html [or from the Cambridge Crystallographic Data Centre, 12, Union Road, Cambridge CB2 1EZ, UK; fax: (internat.) +44 1223 336 033, e-mail: deposit@ccdc.cam.ac.uk].

Acknowledgements

A.K.S. thanks Council of Scientific and Industrial Research (India) for the Project No. 01(1849)/03/EMR-II. J.E.D. thanks the University of Windsor for financial support. We are pleased to have had the opportunity to collaborate on occasions with such a distinguished X-ray crystallographer as Professor Mike Hursthouse and on a personal note J.E.D. thanks Mike for his much valued friendship''.

References

[1] A.K. Singh, V. Srivastava, J. Coord. Chem. 27 (1992) 237.
[2] A.K. Singh, S. Sharma, Coord. Chem. Rev. 209 (2000) 49.
[3] A.K. Singh, Proc. Indian Acad. Sci. (Chem. Sci.) 114 (2002) 357.
[4] (a) E.G. Hope, W. Levason, Coord. Chem. Rev. 12 (1993) 109;
(b) W. Levason, D. Orchard, G. Reid, Coord. Chem. Rev. 225 (2002) 159;
(c) J.A. Barton, A.R.J. Genge, N.J. Hill, W. Levason, S.D. Orchard, B. Patel, G. Reid, A.J. Ward, Heteroatom Chem. 13 (2002) 550.
[5] J. Arnold, Prog. Inorg. Chem. 43 (1995) 353.
[6] P. Mathur, Adv. Organomet. Chem. 41 (1997) 243.
[7] A. Khalid, A.K. Singh, Polyhedron 16 (1997) 33.
[8] G. Singh, A.K. Singh, P. Sharma, J.E. Drake, M.B. Hursthouse, M.E. Light, J. Organomet. Chem. 688 (2003) 20.
[9] S. Bali, A.K. Singh, P. Sharma, R.A. Toscano, J.E. Drake, M.B. Hursthouse, M.E. Light, J. Organomet. Chem. 689 (2004) 2346.
[10] (a) S. Bali, A.K. Singh, P. Sharma, J.E. Drake, M.B. Hursthouse, M.E. Light, Inorg. Chem. Commun. 6 (2003) 1378;
(b) M.J. Hesford, W. Levason, M.L. Matthews, S.D. Orchard, G. Reid, J. Chem. Soc. Dalton Trans. (2003) 2434;
(c) W. Levason, S.D. Orchard, G. Reid, J. Chem. Soc. Chem. Commun. (2001) 427;
(d) M.J. Hesford, W. Levason, M.L. Matthews, G. Reid, J. Chem. Soc., Dalton Trans. (2003) 2852.
[11] E. Lastra, M.P. Gamasa, J. Gimeno, M. Lanfranchi, A. Tiripicchio, J. Chem. Soc., Dalton Trans. (1989) 1499.
[12] N.W. Alcock, J.M. Brown, J.C. Jeffery, J. Chem. Soc., Dalton Trans. (1977) 888.
[13] A.G. Constable, W.S. McDonald, B.L. Shaw, J. Chem. Soc., Dalton Trans. (1979) 1109.
[14] S.I. Al-Resayes, P.B. Hitchcock, J.F. Nixon, J. Chem. Soc., Chem. Commun. (1991) 78.
[15] J.R. Li, M. Du, R.H. Zhang, X.H. Bu, J. Mol. Struct. 607 (2002) 175.
[16] W.F. Liaw, C.H. Li, S.J. Chio, Y.C. Horng, C.C. Chou, M.C. Liaw, G.H. Lee, S.M. Peng, Inorg. Chem. 34 (1995) 3755.
[17] (a) N. Al-Salim, T.A. Hamor, W.R. McWhinnie, J. Chem. Soc., Chem. Commun. (1986) 453;
(b) P. Kommana, K.C.K. Swamy, Inorg. Chem. 39 (2000) 4384;
(c) E.P. Kyba, C.N. Clubb, S.B. Larson, V.J. Schueler, R.E. Davis, J. Am. Chem. Soc. 107 (1985) 2141;
(d) D. Colombo, A.M. Caminade, J.P. Majoral, Inorg. Chem. 30 (1991) 3365.

[18] G. Bertolini, M. Aquino, F. Ferrario, G. Pavich, A. Zaliani, A. Sala, J. Org. Chem. 61 (1996) 3358.
[19] DENZO data collection and processing software Z. Otwinowski, W. Minor, in: C.W. CarterJr., R.M. Sweet (Eds.), Methods in Enzymology, Macromolecular Crystallography, Part A, vol. 276, Academic Press, New York, 1997, p. 307.
[20] G.M. Sheldrick, Acta Crystallogr. A 46 (1990) 467.
[21] L.J. Farrugia, J. Appl. Crystallogr. 32 (1999) 837.
[22] SHELXL 97, G.M. Sheldrick, University of Gottingen, Germany.
[23] N.G. Dance, C.H.W. Jones, J. Organomet. Chem 152 (1978) 175.
[24] G. Singh, S. Bali, A.K. Singh, J.E. Drake, C.L.B. Macdonald, M.B. Hursthouse, M.E. Little, Inorg. Chim. Acta 358 (2005) 912.
[25] A.K. Singh, J. Sooriyakumar, S. Husebye, K.W. Tornroos, J. Organomet. Chem. 612 (2000) 46.
[26] A.K. Singh, J. Sooriyakumar, J.E. Drake, M.B. Hursthouse, M.E. Light, J. Organomet. Chem. 613 (2000) 244.
[27] F.H. Allen, O. Kennard, D.G. Watson, L. Brammer, A.G. Orpen, R. Taylor, J. Chem. Soc., Perkin Trans. II. (1987) S1.

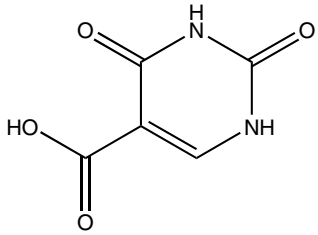

Scheme 1. Uracil-5-carboxylic acid.

sites. Additionally, it has two N–H sites which can act either protonated as hydrogen bond donor sites, or deprotonated as coordination sites. With this versatility in mind we carried out the synthesis in aqueous solution and crystallographic characterisation of alkali metal (Na–Cs) complexes of U5CAH to examine both the coordination behaviour at the metal centre and the hydrogen bonding geometries in each compound.

We succeeded in obtaining compounds for all four metal ions. By varying the reaction stoichiometry and crystallisation conditions we were able to obtain two separate rubidium compounds, one with coordinated water and one with uncoordinated but hydrogen-bonded water as solvent of crystallisation. The remaining reaction systems are unaffected by changing the method of crystallisation. In the case of potassium a neutral ligand is also coordinated. All compounds are polymeric, as would be expected with a ligand containing extensive coordination and hydrogen bonding sites. In the case of the potassium complex **2** and one of the rubidium complexes **4** the crystals were too weakly diffracting for adequate data collection using a standard laboratory X-ray source. Data for these compounds were collected at Station 9.8 of the SRS at Daresbury Laboratory, Cheshire, England, as part of the EPSRC National X-ray Crystallography Service.

The compounds presented here are: $[Na(C_5H_3N_2O_4)(H_2O)]_\infty$ (**1**); $[K(C_5H_3N_2O_4)(C_5H_4N_2O_4)]_\infty$ (**2**); $[Rb\{H(C_5H_3N_2O_4)_2\}\cdot 2H_2O]_\infty$ (**3**); $[Rb(C_5H_3N_2O_4)(H_2O)]_\infty$ (**4**); $[Cs\{H(C_5H_3N_2O_4)_2\}(H_2O)_2]_\infty$ (**5**).

2. Experimental

U5CAH monohydrate was purchased from Avocado Chemicals and used without purification. Elemental analyses were not always possible, due to the very small amount of product obtained, or due to rapid solvent loss when the crystals were separated from the mother liquor. Since the principal aim of the study was crystallographic, we developed procedures to obtain crystals of the compounds for X-ray analysis and did not attempt to optimise the synthetic methods, and therefore the yields are rather low.

2.1. Synthesis

2.1.1. $[Na(C_5H_3N_2O_4)(H_2O)]_\infty$ (1)

0.172 g (1 mmol) of U5CAH was dissolved in 20 cm^3 of distilled water. To this was added a solution of 0.05 g (0.5 mmol) Na_2CO_3 in 10 cm^3 distilled water. The mixture was boiled until around 15 cm^3 remained and the solution was then transferred to a separate vial, sealed and stored at

Table 1
Crystallographic data summary for all compounds

Compound	1	2	3	4	5
Formula	$C_5H_5N_2NaO_5$	$C_{10}H_7KN_4O_8$	$C_{10}H_{11}N_4O_{10}Rb$	$C_5H_5N_2O_5Rb$	$C_{10}H_{11}CsN_4O_{10}$
Formula weight	196.1	350.3	432.7	258.6	480.1
Radiation, λ (Å)	Mo Kα, 0.71073	synchrotron, 0.6902	Mo Kα, 0.71073	synchrotron, 0.6893	Mo Kα, 0.71073
T (K)	150	120	150	120	150
Crystal system	monoclinic	monoclinic	triclinic	monoclinic	triclinic
Space group	$P2_1/n$	Cc	$P\bar{1}$	$P2_1/c$	$P\bar{1}$
a (Å)	3.555(4)	6.816(1)	4.8838(5)	7.8301(5)	5.0620(17)
b (Å)	18.134(14)	15.400(2)	8.4124(9)	4.9937(3)	8.085(2)
c (Å)	10.635(8)	12.088(2)	10.0242(11)	18.9664(13)	9.100(2)
α (°)	90	90	112.2627(15)	90	81.43(3)
β (°)	91.39(9)	101.701(2)	101.5603(16)	98.649(1)	83.75(3)
γ (°)	90	90	93.3448(16)	90	87.99(3)
V (Å^3)	685.5(11)	1242.5(3)	369.28(7)	733.17(8)	366.02(18)
Z	4	4	1	4	1
μ (mm^{-1})	0.22	0.49	3.42	6.75	2.60
Crystal colour, habit	colourless, rod	colourless, plate	colourless, lath	colourless, plate	colourless, block
Crystal size (mm)	$0.15\times0.07\times0.05$	$0.02\times0.02\times0.01$	$0.62\times0.08\times0.04$	$0.02\times0.02\times0.01$	$0.48\times0.29\times0.24$
Diffractometer	Nonius KappaCCD	Bruker APEX2	Bruker SMART 1 K	Bruker APEX2	Nonius KappaCCD
Data collection	φ and ω scans	thin-slice ω scans	thin-slice ω scans	thin-slice ω scans	$\varphi$and ω scans
θ Range (°)	4.0–25.5	2.6–25.6	2.3–25.0	3.1–29.5	4.7–27.5°
Data collected	12248	5028	2645	7034	7421
Unique data (R_{int})	1262 (0.111)	2466 (0.028)	1289 (0.023)	2115 (0.023)	1685 (0.041)
Observed data ($F^2>2\sigma$)	880	1978	1270	1897	1644
R ($F^2>2\sigma$)	0.056	0.042	0.032	0.021	0.024
R_w (F^2, all data)	0.133	0.109	0.072	0.054	0.058
Goodness-of-fit on F^2	1.11	1.03	1.18	1.03	1.08
Difference map extremes (e Å^{-3})	0.32, −0.36	0.51, −0.34	0.73, −0.36	0.48, −0.39	1.13, −0.47

Table 2
Selected geometrical parameters (Å, °) for compounds **1**–**5**

Compound ***1***			
Na–O(2)	2.472(4)	Na–O(2a)	2.359(3)
Na–O(2b)	2.417(3)	Na–O(4a)	2.440(3)
Na–O(5)	2.457(4)	Na–O(5a)	2.326(4)
O(2a)–Na–O(2b)	89.42(12)	O(2)–Na–O(2a)	94.76(13)
O(2)–Na–O(2b)	84.93(12)	O(2a)–Na–O(4a)	72.50(11)
O(2b)–Na–O(4a)	161.57(11)	O(2)–Na–O(4a)	99.80(12)
O(2)–Na–O(5)	81.41(13)	O(2a)–Na–O(5a)	86.63(13)
O(2b)–Na–O(5a)	86.55(13)	O(2a)–Na–O(5)	171.02(12)
O(2b)–Na–O(5)	82.18(12)	O(2)–Na–O(5a)	171.36(12)
O(4a)–Na–O(5a)	88.76(13)	O(4a)–Na–O(5)	116.07(12)
O(5)–Na–O(5a)	95.97(13)		

Symmetry operators: a, $x-1$, y, z; b, $-x+1$, $-y+1$, $-z+2$

Compound ***2***			
K–O(1)	2.727(4)	K–O(3b)	2.721(4)
K–O(2a)	2.823(4)	K–O(6)	2.861(4)
K–O(5a)	2.686(4)	K–O(8a)	2.733(3)
K–O(7c)	2.734(4)		
O(1)–K–O(3b)	78.90(12)	O(1)–K–O(2a)	141.75(11)
O(1)–K–O(6)	72.35(11)	O(1)–K–O(5a)	146.32(8)
O(1)–K–O(8a)	88.00(10)	O(1)–K–O(7c)	112.06(14)
O(2a)–K–O(3b)	73.61(11)	O(2a)–K–O(5a)	70.39(12)
O(2a)–K–O(6)	76.79(7)	O(2a)–K–O(7c)	78.57(12)
O(2a)–K–O(8a)	117.72(12)	O(3b)–K–O(5a)	112.08(14)
O(3b)–K–O(6)	79.31(12)	O(3b)–K–O(7c)	144.09(7)
O(3b)–K–O(8a)	90.15(10)	O(5a)–K–O(6)	139.59(11)
O(5a)–K–O(7c)	78.36(12)	O(5a)–K–O(8a)	61.20(10)
O(6)–K–O(7c)	72.51(11)	O(6)–K–O(8a)	159.08(10)
O(7c)–K–O(8a)	123.21(10)		

Symmetry operators: a, x, $-y+1$, $z+1/2$; b, $x-1/2$, $y-1/2$, z; c, $x+1/2$, $-y+1/2$, $z+1/2$

Compound ***3***			
Rb–O(1)	3.037(3)	Rb–O(3b)	3.004(3)
Rb–O(3)	2.975(3)	Rb–O(4a)	2.973(3)
O(1)–Rb–O(3)	57.29(8)	O(3)–Rb–O(3b)	70.46(9)
O(1)–Rb–O(3b)	111.47(8)	O(3)–Rb–O(4a)	66.42(8)
O(1)–Rb–O(4a)	90.72(8)	O(3b)–Rb–O(4a)	106.66(8)

Symmetry operators: a, $-x+1$, $-y+1$, $-z$; b, $-x+1$, $-y$, $-z$

Compound ***4***			
Rb–O(1)	2.8836(12)	Rb–O(1a)	3.0095(12)
Rb–O(1b)	3.2078(14)	Rb–O(3)	2.7576(12)
Rb–O(3b)	2.9252(13)	Rb–O(3c)	3.3294(12)
Rb–O(4d)	2.7823(12)	Rb–O(6)	3.2379(14)
Rb–O(6e)	3.2176(14)	Rb–O(6f)	3.5048(14)
O(1)–Rb–O(1a)	115.84(4)	O(1)–Rb–O(1b)	99.21(3)
O(1a)–Rb–O(1b)	96.60(3)	O(1)–Rb–O(3)	60.89(4)
O(1)–Rb–O(3b)	153.43(4)	O(1a)–Rb–O(3)	71.71(4)
O(1a)–Rb–O(3b)	65.43(3)	O(1b)–Rb–O(3)	64.56(3)
O(1b)–Rb–O(3b)	55.38(3)	O(1)–Rb–O(3c)	61.69(3)
O(1a)–Rb–O(3c)	156.36(3)	O(1b)–Rb–O(3c)	62.32(3)
O(1)–Rb–O(4d)	120.33(3)	O(1a)–Rb–O(4d)	122.13(3)
O(1b)–Rb–O(4d)	87.54(3)	O(1)–Rb–O(6)	65.87(4)
O(1)–Rb–O(6e)	130.41(4)	O(1a)–Rb–O(6e)	55.47(4)
O(1b)–Rb–O(6e)	129.05(3)	O(1a)–Rb–O(6)	72.99(3)
O(1b)–Rb–O(6)	153.48(4)	O(1)–Rb–O(6f)	52.99(3)
O(1a)–Rb–O(6f)	134.18(3)	O(1b)–Rb–O(6f)	127.69(3)
O(3)–Rb–O(3c)	88.57(4)	O(3)–Rb–O(3b)	97.37(3)
O(3)–Rb–O(4d)	150.99(4)	O(3b)–Rb–O(3c)	105.77(4)
O(3c)–Rb–O(4d)	70.49(3)	O(3b)–Rb–O(4d)	70.68(3)
O(3)–Rb–O(6e)	125.52(4)	O(3)–Rb–O(6)	88.94(4)
O(3b)–Rb–O(6)	133.18(3)	O(3b)–Rb–O(6e)	73.76(4)
O(3c)–Rb–O(6)	120.78(3)	O(3c)–Rb–O(6e)	145.91(3)
O(3b)–Rb–O(6f)	146.74(3)	O(3)–Rb–O(6f)	113.74(3)
O(4d)–Rb–O(6)	118.78(4)	O(3c)–Rb–O(6f)	65.38(3)
O(6e)–Rb–O(6f)	95.85(4)	O(4d)–Rb–O(6e)	77.67(3)
O(4d)–Rb–O(6f)	76.27(3)	O(6)–Rb–O(6f)	62.02(3)
O(6)–Rb–O(6e)	65.27(3)		

Symmetry operators: a, x, $y+1$, z; b, $-x$, $y+1/2$, $-z+1/2$; c, $-x$, $y-1/2$, $-z+1/2$; d, x, $-y+3/2$, $z-1/2$; e, $-x+1$, $y+1/2$, $-z+1/2$; f, $-x+1$, $y-1/2$, $-z+1/2$

Compound ***5***			
Cs–O(1)	3.471(2)	Cs–O(3b)	3.2543(19)
Cs–O(3)	3.498(2)	Cs–O(4a)	3.1457(19)
Cs–O(5)	3.286(2)		
O(1)–Cs–O(3)	47.52(5)	O(3)–Cs–O(3b)	97.06(5)
O(1)–Cs–O(5)	50.17(5)	O(3)–Cs–O(4a)	63.64(5)
O(1)–Cs–O(3b)	60.16(5)	O(5)–Cs–O(3b)	107.36(5)
O(1)–Cs–O(4a)	79.57(5)	O(5)–Cs–O(4a)	111.64(5)
O(3)–Cs–O(5)	48.66(5)	O(3b)–Cs–O(4a)	69.44(5)

Symmetry operators: a, $-x$, $-y$, $-z+2$; b, $x+1$, y, z

approximately 5 °C. After 1 week a very small amount of crystals of **1** had formed. As a result of this it was not possible to obtain further analytical data for **1**.

2.1.2. $[K(C_5H_3N_2O_4)(C_5H_4N_2O_4)]_\infty$ (**2**)

0.184 g (1 mmol) of U5CAH was dissolved in 20 cm^3 of distilled water. To this was added a solution of 0.06 g (0.5 mmol) K_2CO_3 dissolved in 10 cm^3 distilled water. The mixture was boiled until around 15 cm^3 remained and the solution was transferred to a separate sealed vial. After 1 h of standing at room temperature a large mass of lath-shaped colourless crystals of **2** was obtained; yield 0.072 g, 20%. *Anal.* Calc. for **2**: C, 34.50; H, 2.00; N, 15.50. Found: C, 34.70; H, 2.35; N, 15.65%.

2.1.3. $[Rb\{H(C_5H_3N_2O_4)_2\}\cdot 2H_2O]_\infty$ (**3**)

0.171 g (1 mmol) of U5CAH was dissolved in 20 cm^3 of distilled water. To this was added a solution of 0.121 g (0.5 mmol) Rb_2CO_3 dissolved in 10 cm^3 distilled water. The mixture was boiled until around 15 cm^3 remained and the solution was transferred to a separate sealed vial. After 1 h of standing at room temperature a large mass of needle-shaped colourless crystals of **3** was obtained; yield 0.130 g, 31%. *Anal.* Calc. for **3**: C, 27.90; H, 2.55; N, 12.55. Found: C, 27.80; H, 2.60; N, 12.80%.

2.1.4. $[Rb(C_5H_3N_2O_4)(H_2O)]_\infty$ (**4**)

0.174 g (1 mmol) of U5CAH was dissolved in 20 cm^3 of distilled water. To this was added a solution of 0.238 g (1 mmol) Rb_2CO_3 dissolved in 10 cm^3 distilled water. The mixture was boiled until around 15 cm^3 remained and the solution was transferred to a separate sealed vial. Standing for several months at 5 °C failed to induce crystallisation, so the method of slow solvent evaporation was tried. After

around 2 weeks the solvent had evaporated to leave a very small amount of plate-shaped crystals. The amount of crystals produced was too small to enable any further analysis to be carried out.

2.1.5. $[Cs\{H(C_5H_3N_2O_4)_2\}(H_2O)_2]_\infty$ (5)

0.179 g (1 mmol) of U5CAH was dissolved in 20 cm^3 of distilled water. To this was added a solution of 0.162 g (1 mmol) $Cs(OH)\cdot H_2O$ dissolved in 10 cm^3 distilled water. The mixture was boiled until around 15 cm^3 remained and the solution was transferred to a separate sealed vial. After 1 h of standing at room temperature a large mass of small needle-shaped colourless crystals of **5** was obtained; yield 0.135 g, 29%. *Anal.* Calc. for **5**: C, 25.10; H, 2.10; N, 11.30. Found: C, 25.15; H, 2.35; N, 11.40%.

Table 3
Hydrogen bonding parameters (Å, °) for compounds **1**–**5**

D–H···A	*d*(D–H)	*d*(H···A)	*d*(D···A)	∠(DHA)
Compound ***1***				
O(5)–H(5A)···O(3c)	0.93(5)	1.86(5)	2.759(5)	160(4)
O(5)–H(5B)···O(1b)	0.88(5)	1.87(5)	2.745(4)	175(4)
N(1)–H(1N)···O(1d)	0.78(4)	2.06(4)	2.836(5)	176(4)
N(2)–H(2N)···O(4e)	0.75(4)	2.15(4)	2.898(4)	175(4)
C(3)–H(3)···O(3f)	0.95	2.43	3.364(5)	167
Symmetry operators: b, $-x+1$, $-y+1$, $-z+2$; c, $-x+1$, $-y+1$, $-z+1$; d, $x-1/2$, $-y+3/2$, $z-1/2$; e, $-x+2$, $-y+1$, $-z+1$; f, $-x+1/2$, $-y+3/2$, $z+1/2$				
Compound ***2***				
O(1)–H(1)···O(5)	0.89(4)	1.57(4)	2.448(4)	167(5)
N(1)–H(1N)···O(2e)	0.86(2)	2.00(3)	2.844(5)	165(5)
N(2)–H(2N)···O(7f)	0.84(2)	1.94(2)	2.768(5)	175(6)
N(3)–H(3N)···O(3g)	0.85(2)	2.05(3)	2.861(5)	159(5)
N(4)–H(4N)···O(6d)	0.86(2)	1.99(3)	2.800(5)	158(5)
C(8)–H(8)···O(8c)	0.95	2.30	3.175(7)	152
Symmetry operators: c, $x+1/2$, $-y+1/2$, $z+1/2$; d, $x-1/2$, $-y+1/2$, $z-1/2$; e, $x+1/2$, $-y+3/2$, $z+1/2$; f, x, $y+1$, z; g, x, $y-1$, z				
Compound ***3***				
O(2)–H(2O)···O(1c)	1.210(3)	1.210(3)	2.420(6)	180
O(5)–H(5A)···O(1d)	0.83(7)	2.16(7)	2.974(5)	170(6)
O(5)–H(5B)···O(1e)	0.82(7)	2.09(7)	2.900(5)	168(7)
N(1)–H(1)···O(4f)	0.81(3)	1.99(3)	2.805(5)	177(6)
N(2)–H(2)···O(5)	0.82(6)	1.88(6)	2.694(5)	173(5)
Symmetry operators: c, $-x$, $-y+1$, $-z+1$; d, x, $y+1$, z; e, $x+1$, $y+1$, z; f, $-x+2$, $-y+1$, $-z$				
Compound ***4***				
O(6)–H(6A)···O(1e)	0.80(3)	2.12(3)	2.904(2)	167(2)
O(6)–H(6B)···O(2a)	0.87(3)	1.83(3)	2.679(2)	164(3)
N(1)–H(1N)···O(4g)	0.78(2)	2.04(2)	2.825(2)	174(2)
N(2)–H(2N)···O(6h)	0.79(2)	2.13(2)	2.913(2)	173(3)
C(5)–H(5)···O(2i)	0.95	2.45	3.215(2)	137
Symmetry operators: a, x, $y+1$, z; e, $-x+1$, $y+1/2$, $-z+1/2$; g, $-x$, $-y+2$, $-z+1$; h, $-x+1$, $-y+1$, $-z+1$; i, $-x+1$, $-y$, $-z+1$				
Compound ***5***				
O(1)–H(1O)···O(1c)	1.232(2)	1.232(2)	2.465(4)	180
O(5)–H(5A)···O(3)	0.82(2)	2.04(2)	2.802(3)	155(3)
O(5)–H(5B)···O(2c)	0.82(2)	1.91(2)	2.719(3)	167(3)
N(1)–H(1N)···O(5d)	0.81(3)	1.88(3)	2.675(3)	166(3)
N(2)–H(2N)···O(4e)	0.83(3)	2.02(3)	2.841(3)	172(3)
C(3)–H(3)···O(2f)	0.95	2.57	3.411(3)	148
Symmetry operators: c, $-x+1$, $-y+1$, $-z+1$; d, x, y, $z+1$; e, $-x-1$, $-y$, $-z+2$; f, $-x+1$, $-y+1$, $-z+2$				

2.2. X-ray crystallography

Experimental conditions and crystallographic data parameters for all compounds are summarised in Table 1. For **1** and **5** data collection was carried out by using COLLECT [17], with cell refinement and integration using EVALCCD [18]. For **2** and **4** data collection was carried out with APEX2 [19], with cell refinement and integration by SAINT [20]. For **3** data collection was by SMART [21], with cell refinement and integration by SAINT. Semi-empirical absorption corrections, based on symmetry-equivalent and repeated reflections, were applied to all datasets using SADABS [22]. Structure solution was by direct methods using either SIR-2002 [23] (**2**, **3** and **5**) or SHELXTL [24]. For all compounds refinement was by full-matrix least-squares on F^2 using SHELXTL, with all non-hydrogen atoms refined anisotropically. All molecular diagrams were produced with DIAMOND-3 [25]. Details of hydrogen atom treatment and non-standard individual refinement strategies (where appropriate) are given below.

2.2.1. Hydrogen atom treatment

2.2.1.1. Compound ***1***. Hydrogen atoms were all located in a difference Fourier map. The C–H hydrogen atom was then constrained as riding, with a C–H bond length of 0.95 Å and $U_{iso}(H) = 1.2U_{eq}(C)$. The N–H and water hydrogen atoms were refined with $U_{iso}(H) = 1.2U_{eq}(N,O)$ but there were no constraints on the geometry.

2.2.1.2. Compound ***2***. Hydrogen atoms were all located in a difference Fourier map. The C–H hydrogen atoms were treated as above. The N–H hydrogen atoms were refined with $U_{iso}(H) = 1.2U_{eq}(N)$ and the N–H bond lengths were

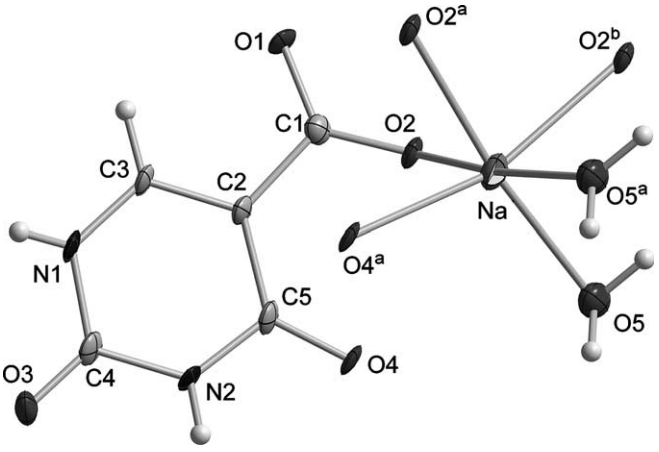

Fig. 1. The asymmetric unit of **1** (50% displacement ellipsoids) expanded to show the Na coordination sphere. Symmetry operators: a, $x-1$, y, z; b, $-x+1$, $-y+1$, $-z+2$.

restrained to 0.85(2) Å. The O–H hydrogen atom position was freely refined.

*2.2.1.3. Compounds **3** and **4**.* Hydrogen atoms were all located in a difference Fourier map. The C–H hydrogen atom was treated as above. The N–H bond lengths were restrained to 0.85(3) Å; all other parameters for these and the remaining hydrogen atoms were freely refined.

*2.2.1.4. Compound **5**.* Hydrogen atoms were all located in a difference Fourier map. The C–H hydrogen atom was treated as above. The water and N–H hydrogen atoms were refined with $U_{iso}(H) = 1.2U_{eq}(N,O)$ and the water O–H bond lengths were restrained to 0.85(1) Å with the H···H distance restrained to 1.35(2) Å. The H atom on an inversion centre was constrained to this position, but its displacement parameter was freely refined.

3. Results and discussion

The structural discussions refer to hydrogen bonding motifs described in graph set notation [26,27]. This takes the general form $R_d^a(n)$ where R = ring motif, a = number of hydrogen bonding acceptor sites, d = number of hydrogen bonding acceptor sites, and n = total number of atoms making up the motif. Selected geometrical parameters for all compounds are given in Table 2, with hydrogen bonding geometry given in Table 3.

3.1. $[Na(C_5H_3N_2O_4)(H_2O)]_\infty$ (**1**)

The asymmetric unit of **1**, expanded to show the full coordination sphere of the Na centre, is shown in Fig. 1. It consists of one Na^+ cation, one U5CA$^-$ anion and a coordinated water molecule. The Na centre is six-coordinate and has distorted octahedral geometry with only O2, O4 and O5 coordinating. In the crystal packing, O2 bridges three centres, O5 (the water molecule) bridges two centres and O4 is terminally coordinating. O1 and O3 coordinate to no Na centre but are instead involved in hydrogen bonding (discussed below). The result of this coordination is a ladder packing motif (Fig. 2) formed by dimerisation of the asymmetric unit about the crystallographic inversion centre; these dimers then extend by metal–ligand coordination in one direction only to give a polymeric chain.

There is no cross-coordination between the individual separate chains, as O1 and O3 do not coordinate, and so there is only hydrogen bonding to hold the different chains together to form the overall crystal structure. The extent of hydrogen bonding is most easily appreciated by considering two *a*-axis packing diagrams (looking along the chains), one with the hydrogen bonds omitted and a second with them included (Fig. 3). The hydrogen bonding is extensive, with O1, O3 and O4 all acting as acceptor sites (O1 and O3 are both bifurcated acceptors). An $R_2^2(8)$ motif links together the amide groups of two ligands, a very common hydrogen bonding interaction in structures featuring this type of molecule. There is also strong evidence to suggest a C–H···O interaction is present in this structure; the relevant hydrogen bonding parameters are in good agreement with typical values for a weak C–H···O interaction [28]. Finally, both hydrogen atoms of the water molecule are donor sites, but the water does not act as a hydrogen bond acceptor in this structure, since it bridges two Na centres.

Covalent bonding within the structure is unexceptional; the uracil ring is planar and the carboxylate group is twisted slightly out of the ring plane [the O2–C1–C2–C5 torsion angle is −11.3(5)°].

3.2. $[K(C_5H_3N_2O_4)(C_5H_4N_2O_4)]_\infty$ (**2**)

Despite the reasonable size of the crystals obtained of this compound, they proved to be rather weakly diffracting. Data collected using a standard X-ray tube with very long

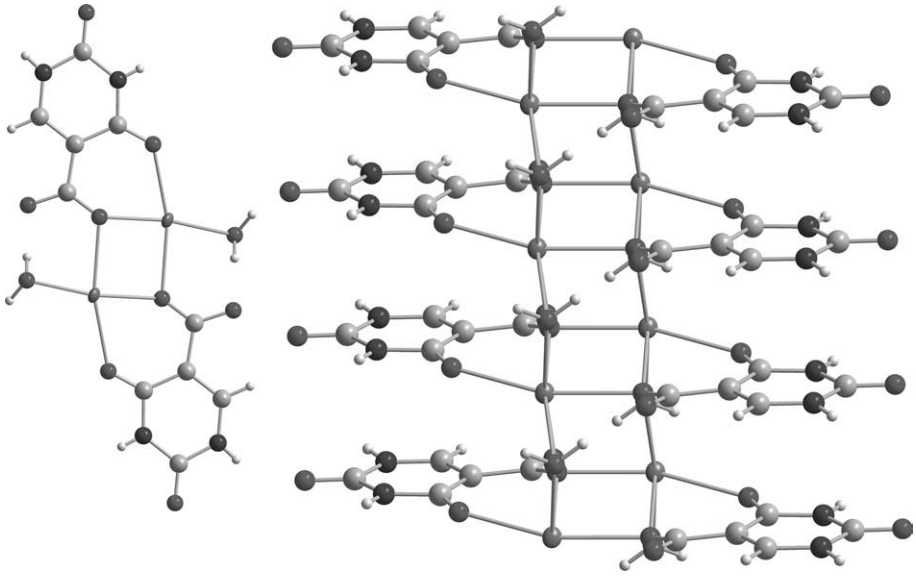

Fig. 2. The dimer and the ladder-like chain packing motif in **1**.

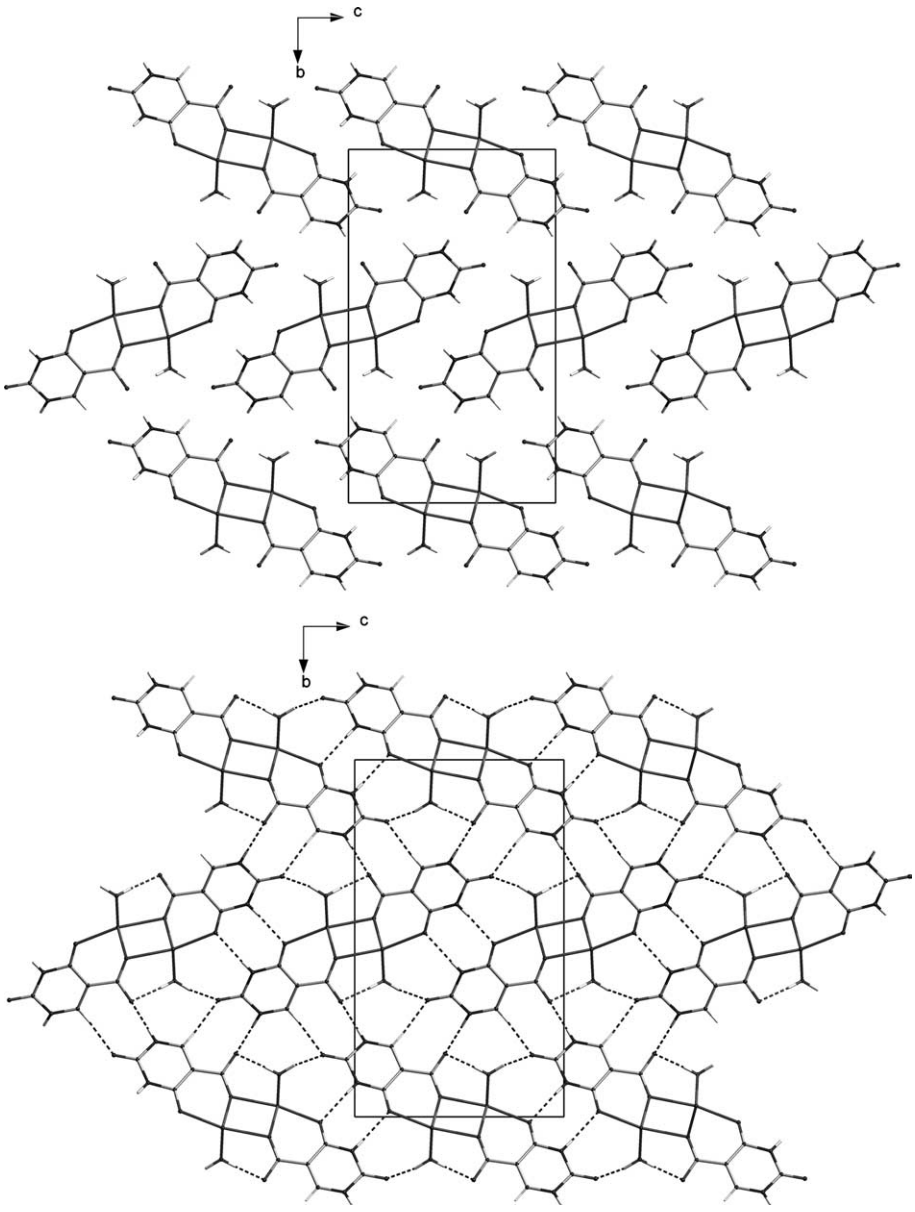

Fig. 3. Two *a*-axis packing views of **1**. The top view shows the packing without hydrogen bonding, the bottom view is identical but has the hydrogen bonding indicated by dashed lines.

exposure times (150 s per frame) were sufficient to allow structural solution and to define molecular connectivity. However, they were too weak to allow satisfactory refinement of the structure. Therefore, data were collected with synchrotron radiation, and were of much greater intensity and quality than could ever have been obtained with laboratory equipment. The structure of this compound is presented in space group *Cc*. The ADDSYM function of PLATON [29] detects a possible missed symmetry element (twofold rotation) and suggests that the true space group is actually *C*2/*c*. *Cc* and *C*2/*c* are indistinguishable from one another purely on the basis of the systematic absences in the diffraction data, so it is generally the case that an identified additional twofold rotation in space group *Cc* indicates that the true space group is *C*2/*c* [30]. However, refinement in *C*2/*c* requires that the ligand be disordered and that the K^+ ion and the O–H hydrogen atom lie on special positions in order that the charges balance. The final $R = 0.072$ in space group *C*2/*c* is much poorer than the final value in space group *Cc* (0.042), and refinement of the enantiopole parameter gives a value of 0.19(8), much closer to zero than to 0.5 [31]; these observations, combined with the fact that the structure is ordered in *Cc*, leads us to believe that, in this instance, the correct space group is *Cc*.

The asymmetric unit of **2**, expanded to show the full coordination sphere of the K centre, is shown in Fig. 4. There is no water present and the asymmetric unit consists of one K^+ cation, one $U5CA^-$ anion and one neutral U5CAH molecule. This is despite the reaction stoichiome-

try, which was deliberately kept at 1:1 K:U5CAH in an attempt to prevent an excess of unreacted ligand being incorporated into the structure. The K centre is seven-coordinate and K–O bond lengths are unexceptional. The coordination geometry is perhaps best described as being square antiprismatic (as is found with eight-coordinate complexes) with one of the vertices removed, rather than a 4:3 piano stool-type geometry which is found in seven-coordinate transition metal complexes. There is some distortion in the angles around the K centre when compared to a square antiprism, but much less than for a piano stool geometry. For example, the O6–K–O8[a] angle is 159.08(10)°, much larger than typical square antiprismatic bond angles. O5 and O8 also act together to chelate the K centre. Within each ligand molecular dimensions agree with expected values [13] and the carboxylate groups of both ligands are essentially coplanar with the uracil ring (RMS deviations of mean planes fitted through all non-H atoms are 0.041 and 0.047 Å for the neutral and deprotonated ligands, respectively).

As with compound **1** there is extensive hydrogen bonding in this structure. The crystal packing consists of roughly planar sheets of hydrogen-bonded U5CA$^-$ anions and U5CAH molecules. The sheet structure is shown in Fig. 5 and it consists of hydrogen-bonded ribbons which run parallel to the *b* and *c* axes; these ribbons are hydrogen bonded together to form the 2D grid-like arrangement in the sheet structure. Running parallel to the *b*-axis the ligands are held together by two very common hydrogen bonding motifs: the $R_2^2(8)$ motif between the amide groups and the single short strong O–H···O interaction between the carboxylate and carboxylic acid groups, a fairly common observation in hydrogen-bonded carboxylic acid structures. These are then linked by further hydrogen bonding parallel to the *c*-axis; the motifs observed in this direction are rather less common and are generally longer and weaker. The remaining amide group acts as a bifurcated donor forming two rather bent hydrogen bonds and, as was observed in **1**, there is evidence to support the presence once again of a C–H···O interaction. This is part of an $R_2^2(9)$ motif, somewhat rarer than the $R_2^2(8)$ motif observed parallel to the *b*-axis.

These hydrogen-bonded sheets are coordinated to and separated by the K$^+$ cations, which do not lie in the hydrogen-bonded plane (Fig. 6). The inter-sheet separation distance is about 3.22 Å; overlapping rings are laterally displaced by approximately half a ring diameter, as is usually found in stacked aromatic systems, so that the shortest distance between the centroids of neighbouring rings is 3.72 Å; these rings are not symmetry-related to each other, so they are not precisely parallel. These are characteristics of π stacking, which contributes to the cohesion of this structure in addition to the polymeric coordination network and the hydrogen bonding.

3.3. $[Rb\{H(C_5H_3N_2O_4)_2\}\cdot 2H_2O]_\infty$ (**3**)

There are three particularly unusual aspects of this compound in the series. The first is the sensitivity of the reaction to stoichiometry, as a second rubidium complex was also obtained and is discussed below (compound **4**). Second, the water molecule is present as hydrogen-bonded solvent of crystallisation and is not coordinated to the rubidium centre. Finally, there is peculiar behaviour of

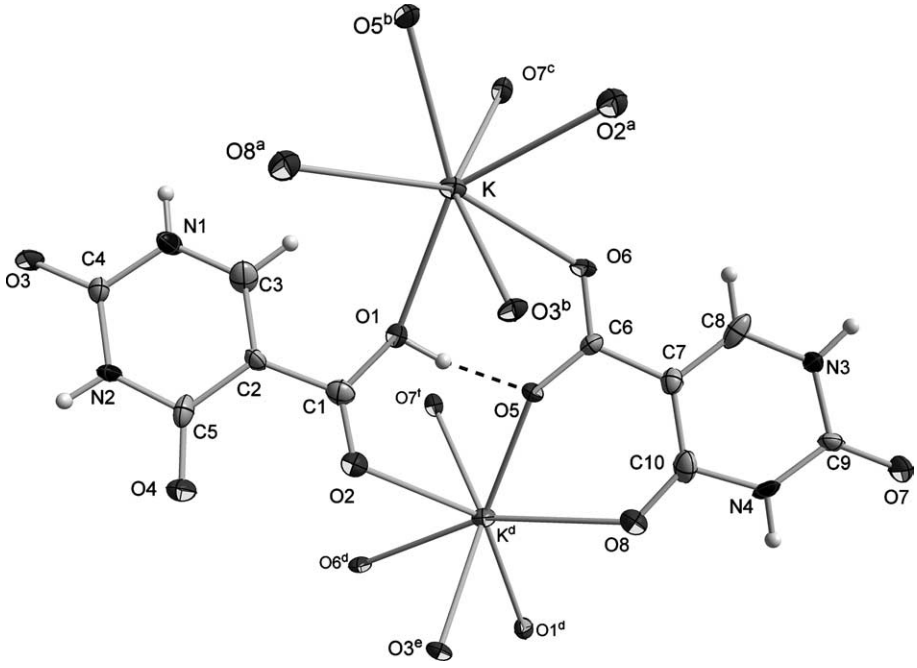

Fig. 4. The asymmetric unit of **2** (50% displacement ellipsoids) expanded to show the K coordination and the chelating nature of the UC5A$^-$ ligand. Symmetry operators: a, $x, -y+1, z+1/2$; b, $x-1/2, y-1/2, z$; c, $x+1/2, y-1/2, z+1/2$; d, $x, -y+1, z-1/2$; e, $x-1/2, -y+3/2, z-1/2$; f, $x+1/2, y+1/2, z$.

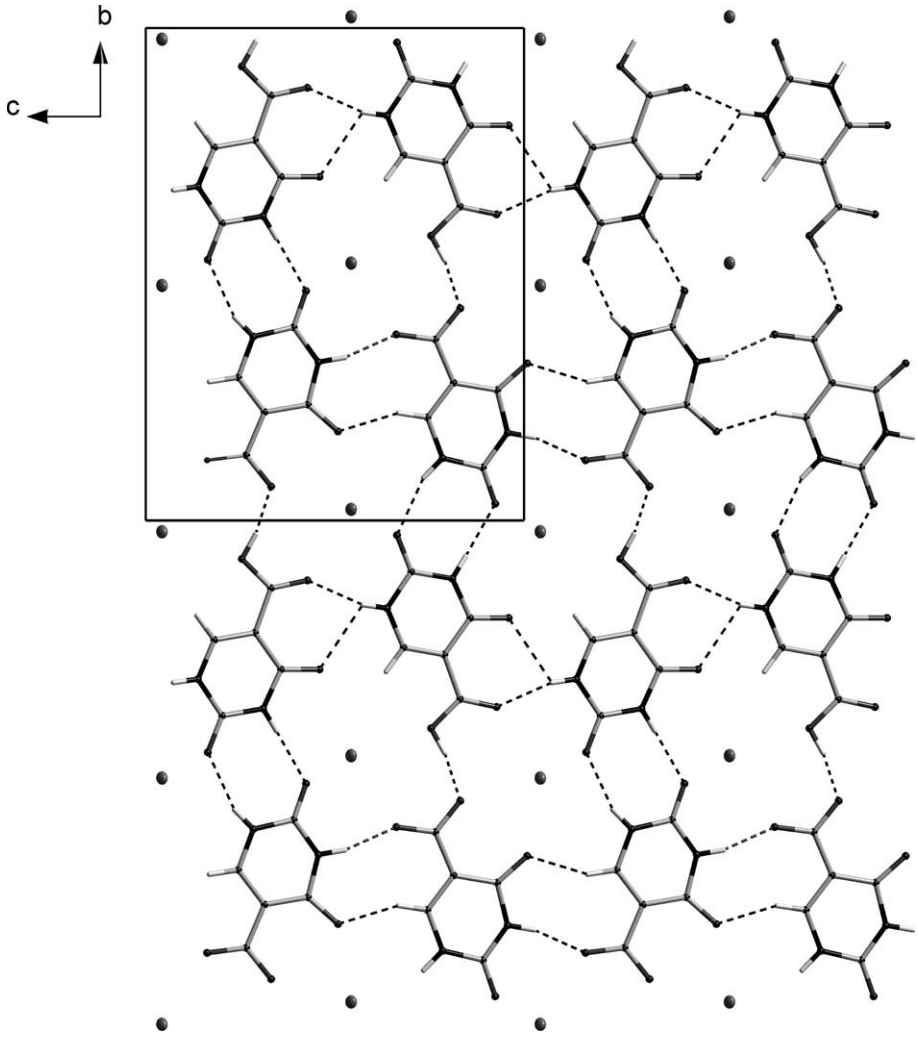

Fig. 5. The sheet structure formed by hydrogen bonding between the ligands of **2**. Coordination bonds to K have been removed for clarity of viewing and hydrogen bonding is denoted by dashed lines. It should be noted that the K^+ ions do not lie in the hydrogen-bonded plane.

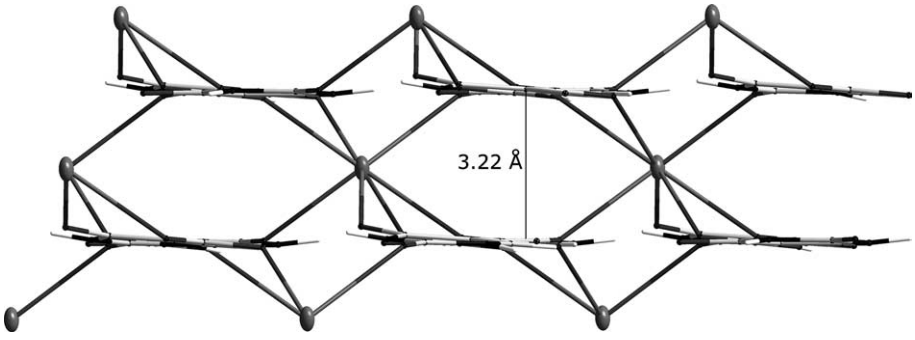

Fig. 6. The coordination of K^+ by the hydrogen-bonded ligand sheets in **2** with the short inter-sheet distance marked in Å. Note that the ligands of each sheet do not directly overlap.

the carboxylic acid group, which is only partially deprotonated and results in a hydrogen atom symmetrically shared between two carboxylate groups.

The asymmetric unit of **3**, expanded to show the full coordination of the rubidium centre, is shown in Fig. 7. The Rb centre is eight-coordinate and the eight coordinating oxygen atoms are located approximately on the eight corners of a cube with Rb at its centre, unusual in the sense that square antiprismatic geometry is more typical of an eight-coordinate complex. The ligand is chelating to the Rb centre via O1 and O3; Rb–O lengths are unexceptional, the uracil ring is essentially planar and the carboxylate group is twisted slightly out of the ring plane [the O1–C1–C2–C3 torsion angle is 6.8(5)°].

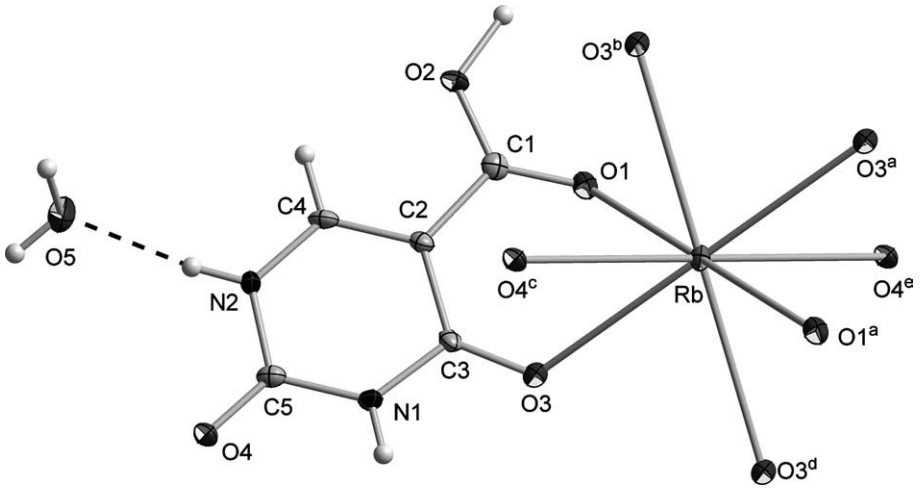

Fig. 7. The asymmetric unit of **3** (50% displacement ellipsoids) expanded to show the Rb coordination. Symmetry operators: a, $-x$, $-y$, $-z$; b, $x-1$, y, z; c, $-x+1$, $-y+1$, $-z$; d, $-x+1$, $-y$, $-z$; e, $x-1$, $y-1$, z.

The stoichiometry used in this reaction was 1:1 Rb:U5-CAH with the intention that the ligand be fully deprotonated, leaving no neutral ligand in solution. However, as was seen in **2**, this is not this case here. Unlike **2**, where separately identifiable fully deprotonated and neutral U5CAH molecules are present in the structure, here the ligands are all crystallographically equivalent. We can be certain that only partial deprotonation has occurred, since the Rb^+ cation and the O–H hydrogen atom are both located on crystallographic inversion centres. This means that both carry an effective charge of 0.5+ in the asymmetric unit, which together balance out the negative charge of the $U5CA^-$ anion. The H atom on the inversion centre is bonded symmetrically to carboxylate oxygen atoms of two ligands (Fig. 8). This gives O–H bond lengths of 1.210(2) Å, too long for a standard O–H covalent bond and shorter than an O···H hydrogen bond interaction. Such a symmetrical hydrogen bond is usually associated with a very short O···O distance, which here is 2.420 Å. Attempts to refine the hydrogen atom as disordered on either side of the inversion centre were unsuccessful; it always moved back to the inversion centre. It is always difficult to draw firm conclusions about the position of a hydrogen atom based on X-ray diffraction data alone. However, based on our other observations about the inter-oxygen distance and the hydrogen atom behaviour during refinement we can be confident about the location of this hydrogen atom and we can draw the conclusion that only partial deprotonation of U5CAH has occurred in **3**.

The crystal packing in **3** is characterised by the coordination of the ligand to the metal centre to form a 2D layer network in the *ab*-plane. Within this network is a hydrogen-bonded water molecule; both hydrogen atoms are hydrogen bond donors and the water also acts as a single hydrogen bond acceptor. A projection along the *b*-axis (Fig. 9) shows how these 2D networks are linked together. There is only one interaction and that is the O···H···O hydrogen bonding which joins the 2D networks together into an overall 3D structure. There is no other type of interaction, including any C–H···O bonding, linking the 2D networks together.

3.4. $[Rb(C_5H_3N_2O_4)(H_2O)]_\infty$ (**4**)

As was commented upon in the structural discussion of **3**, the Rb/U5CAH reaction system is sensitive to the stoichiometry used. For the synthesis of this compound the Rb:U5CAH ratio was 2:1 and this led to full deprotonation of U5CAH and not the partial deprotonation observed in **3**. The method of crystallisation was also quite different; whilst crystals of **3** grew as the reaction mixture cooled, crystals of **4** had to be obtained by subsequent solvent evaporation. The crystals were too small for analysis with a standard laboratory X-ray source so data were collected with synchrotron radiation.

Whilst having the same empirical formula as **3**, compound **4** has a rather different structure. The asymmetric unit of **4** is shown in Fig. 10 and immediately the structural

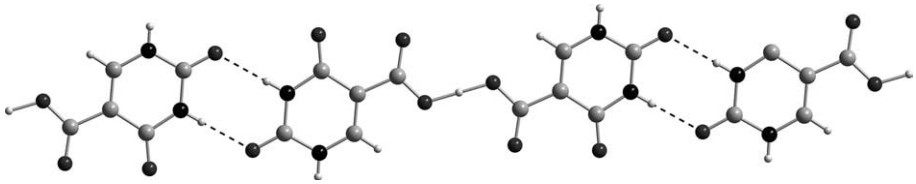

Fig. 8. The hydrogen-bonded ligand tape structure in **3**. Note the centrosymmetric hydrogen atom between the two carboxylate groups.

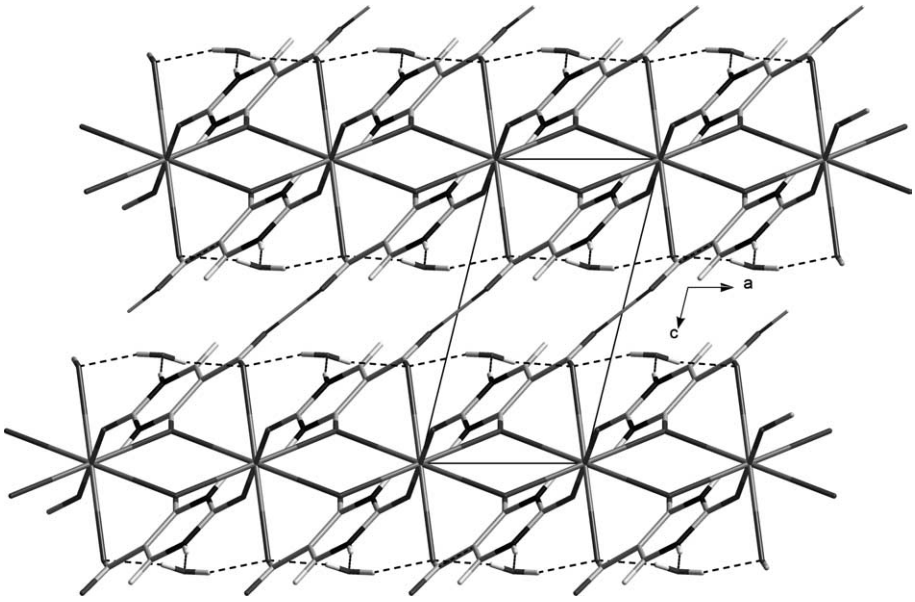

Fig. 9. A projection along the *b*-axis of **3** showing how the single centrosymmetric O···H···O interaction links the 2D networks together.

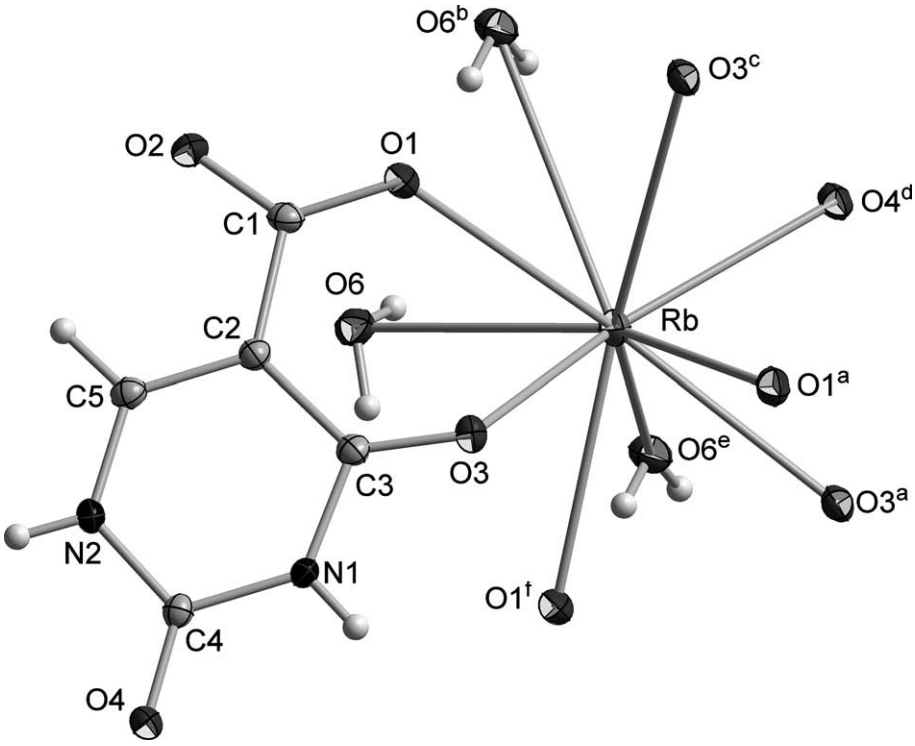

Fig. 10. The asymmetric unit of **4** (50% displacement ellipsoids) expanded to show the full coordination Rb sphere. Symmetry operators: a, $-x$, $y + 1/2$, $-z + 1/2$; b, $-x + 1$, $y - 1/2$, $z - 1/2$; c, $-x$, $y - 1/2$, $-z + 1/2$; d, x, $-y + 3/2$, $z - 1/2$; e, $-x + 1$, $y + 1/2$, $-z + 1/2$; f, x, $y + 1$, z.

differences are clear. The Rb centre is now 10-coordinate, with the water molecule also coordinated (cf. eight-coordinate and non-coordinated water in **3**). The range of Rb–O bond lengths is much wider, from the short 2.7577(12) Å to the very long 3.5046(14) Å. As seen in **2** and **3**, the ligand is chelating, with the carboxylate group essentially coplanar with the uracil ring.

Hydrogen bonding is once again extensive in the crystal packing. The ligands form hydrogen-bonded tapes (Fig. 11) with the familiar $R_2^2(8)$ motif between the amide groups again present; as with **1** and **2** there is also evidence of a weak C–H···O interaction forming part of the tape, something absent in **3**. The tapes are linked together by hydrogen bonding through the water molecule and by substantial coordination to the Rb centre. Unlike the previous examples the tapes are not coplanar and do not form sheets. Instead they pack as stacked tapes in two different orientations (Fig. 12). The angle between two mean planes fitted

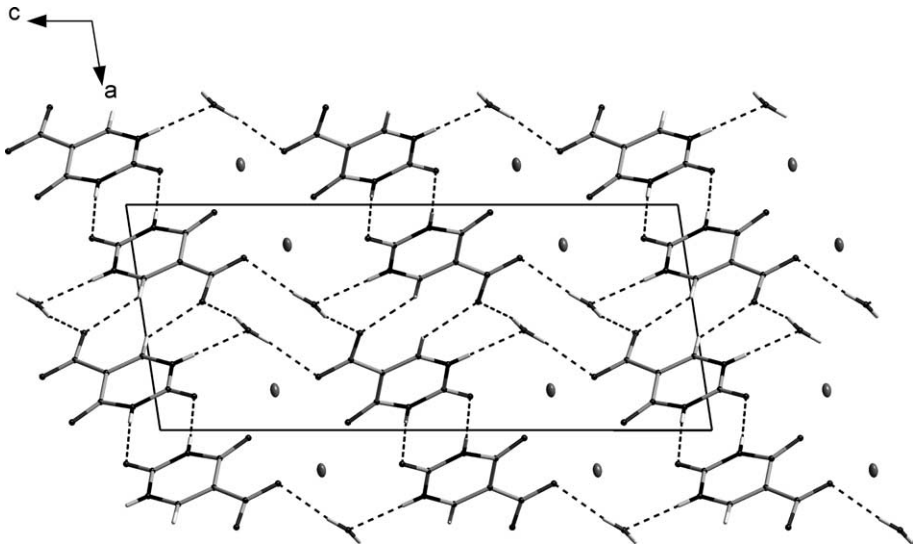

Fig. 11. A *b*-axis projection of the crystal packing of **4**. Coordination bonds to the Rb centre are not shown for clarity.

through two uracil molecules in these different orientations is approximately 74°. Fig. 12 also suggests that there are some weak stacking interactions between the uracil molecules in the stacked tapes. The distance between the tapes is approximately 3.9 Å and at this distance it is unlikely that any stacking interaction has a real influence on the crystal packing; it is probably a consequence, rather than a cause of the structure.

3.5. $[Cs\{H(C_5H_3N_2O_4)_2\}(H_2O)_2]_\infty$ (**5**)

The final compound in this series combines in one structure some of the structural motifs and features observed in previous compounds. Like **2**, the ligands take the form of hydrogen-bonded sheets and, as in **3**, we see again only partial deprotonation of the ligand, which leads to centrosymmetric hydrogen bonding between the carboxylate groups. The asymmetric unit of **5**, expanded to show the full Cs coordination sphere, is shown in Fig. 13. As with **4**, the Cs centre is 10-coordinate, although the Cs–O bond length range [3.1457(19)–3.498(2) Å] is not quite as wide as the Rb–O range in **4**. The carboxylate group is essentially coplanar with the uracil ring and the ligand again is chelating.

As with **3** the partial deprotonation of U5CAH creates a similar charge-balance issue, with the Cs^+ cation and the O···H···O hydrogen atom both located on crystallographic inversion centres. For the reasons discussed in **3**

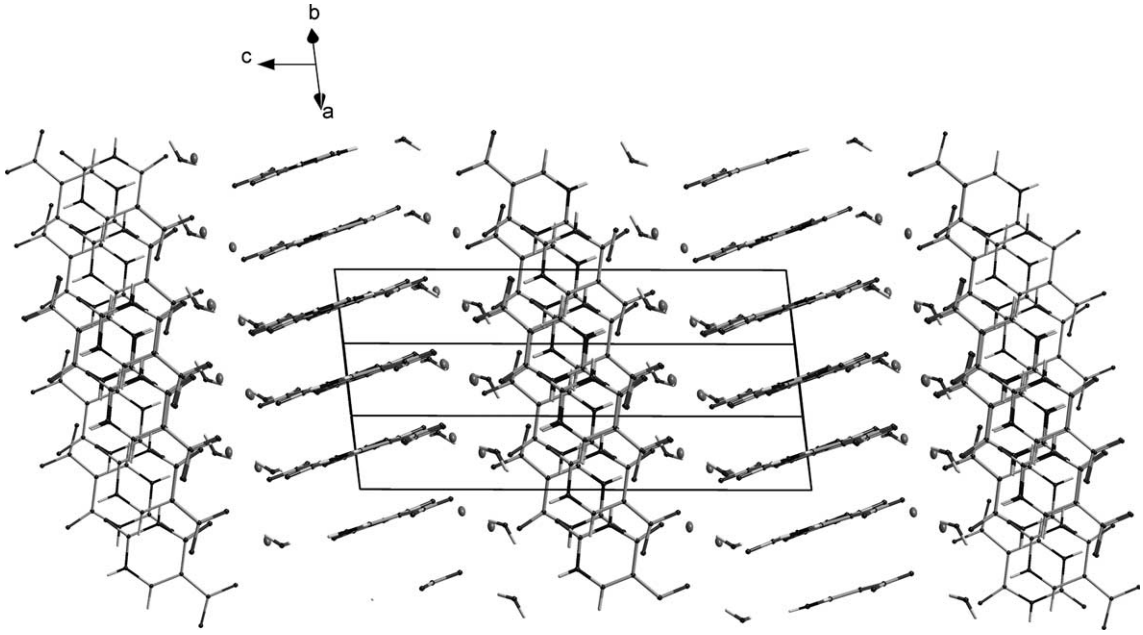

Fig. 12. An alternative view of the crystal packing of **4** showing the two different packing orientations of the hydrogen bonded tapes. Coordination to the Rb centres and hydrogen bonding interactions are not shown for clarity.

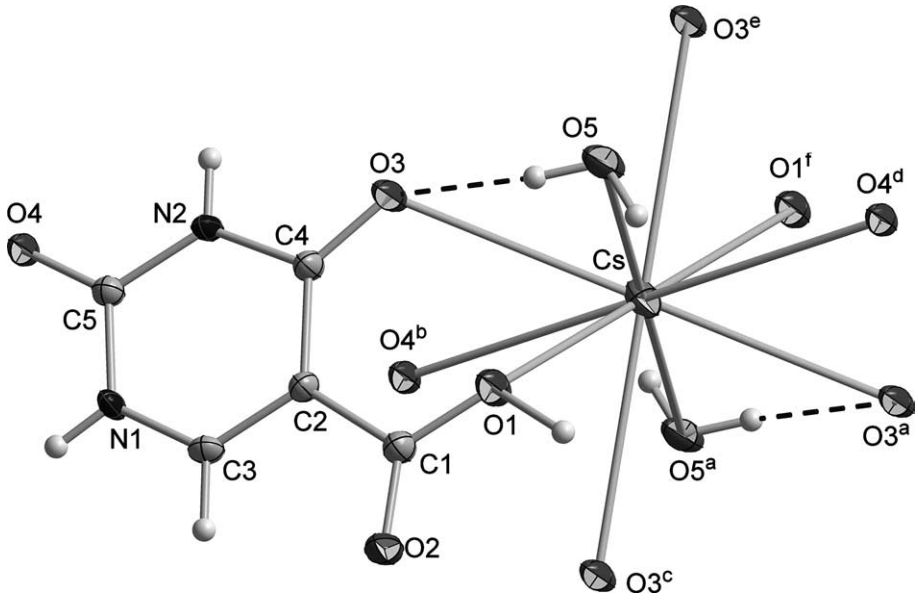

Fig. 13. The asymmetric unit of **5** (50% probability displacement ellipsoids) expanded to show the full coordination sphere of Cs. Dashed lines denote hydrogen bonds. Symmetry operators: a, $x-1, -y, z-1$; b, $-x, -y, -z+2$; c, $x+1, y, z$; d, $x+1, y, z-1$; e, $-x, -y, -1+z$; f, $-x+1, -y, -z+1$.

relating to the very short O···O distance and the behaviour of the hydrogen atom during refinement, we are satisfied that this atom is centrosymmetrically located between two carboxylate groups. The reaction stoichiometry used was Cs:U5CAH 1:1; use of an excess of base failed to give any product despite several different methods of synthesis and crystallisation.

Unlike the denser network structures formed in **3** and **4**, the crystal packing of **5** is much simpler and shares similarities with **2**. Fig. 14 gives a representation of the hydrogen bonding motifs formed between the ligand and water molecules. As we have observed throughout this study, weak C–H···O interactions play an important role in the hydrogen bonding of these compounds, and here once again we have evidence suggesting a C–H···O interaction is present. The ligand and water molecules hydrogen bond together to form approximately planar sheets featuring a quasi-rosette-shaped motif with a central cavity occupied by the Cs^+ cation. Compound **3** also features a sheet structure formed by hydrogen bonding, but the K^+ cations were situated in the inter-sheet spacing. In compound **5** the cavity formed by the rosette motif is large enough to accommodate the

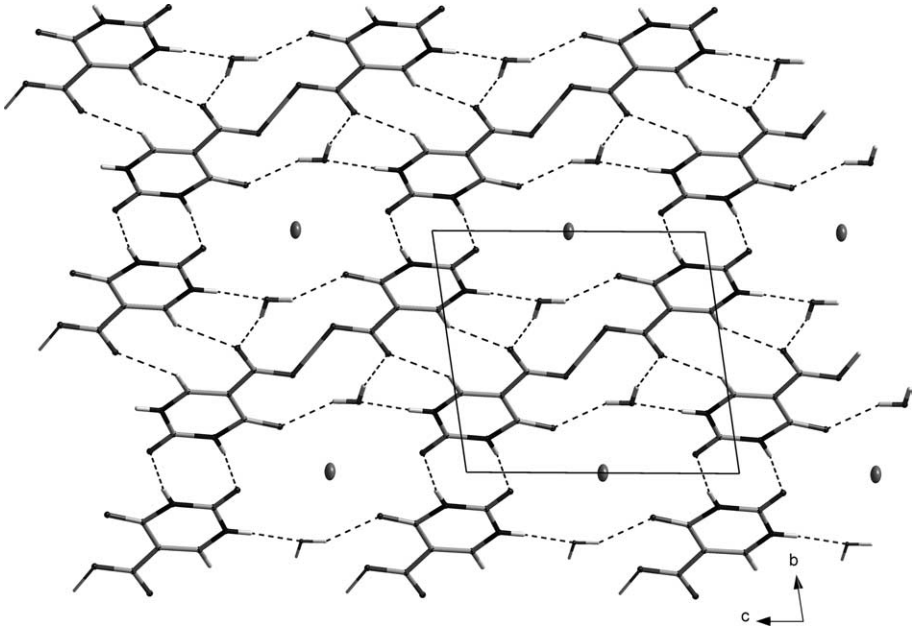

Fig. 14. The hydrogen-bonded sheet formed by the U5CA and water molecules. Note the rosette-like motif formed by the hydrogen bonding. Cs–O coordination bonds are not shown for clarity.

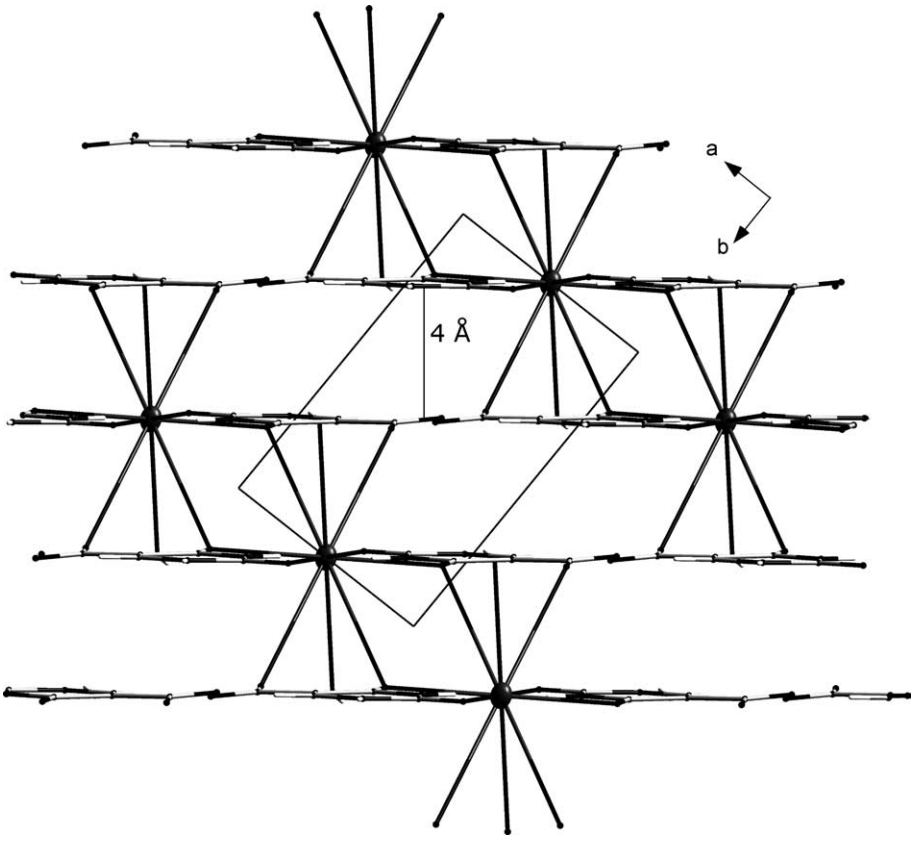

Fig. 15. A projection along the *c*-axis of **5**. The Cs^+ cations are situated in the cavities of the sheet structure created by the ligand hydrogen bonding, and are in the plane of the sheet.

Cs^+ cation neatly and it lies in the plane of the hydrogen-bonded sheet (Fig. 15). The stacking distance between the sheets is approximately 4 Å and, as was discussed for **4**, this is too long for stacking interactions to be the rational driving force behind the crystal packing.

4. Conclusion

A systematic study of alkali metal (Na–Cs) complexes of uracil-5-carboxylic acid reveals some interesting patterns in the coordination behaviour of the metal centres and hydrogen bonding of the ligands and water molecules. By using equimolar amounts of metal and ligand we were able to produce two complexes (**3** and **5**) in which the ligand was only partially deprotonated. By using an excess of base we were able to convert **3** into **4**, where the ligand is fully deprotonated; however, this synthetic behaviour could not be repeated for any of the other reaction systems.

The coordination behaviour of the different metal centres is largely unexceptional. In all cases coordination is via the oxygen atoms of the ligand and, in some cases, the water molecules. This is typical of hard centre alkali metal coordination. It was, however, surprising to note in **3** that the water molecule does not coordinate to the Rb centre but instead forms part of the hydrogen-bonded ligand network.

The hydrogen bonding between the ligands and the water molecules is of particular note, showing the versatility of U5CAH in forming different types of hydrogen bond motifs. Tapes, sheets, 2D and 3D networks are all present in these structures. The centrosymmetric sharing of a hydrogen atom between two carboxylate groups, giving a short and strong hydrogen bond, is one of the key observations in this study. Another is the observation that in four of the five compounds (not compound **3**) C–H···O hydrogen bonding interactions are observed. There is strong evidence in the H···O distances and angles to support this, and the interactions form a key part of the hydrogen bonding networks.

Acknowledgements

We thank Dr. Ross Harrington, Kathy Guille, Luca Russo and Zhanhui Yuan for assistance with data collection and processing at Station 9.8 SRS Daresbury Laboratories, Cheshire, England as part of the National X-ray Crystallography Service funded by EPSRC. We also thank the CCLRC for synchrotron beam-time allocation.

Appendix A. Supplementary data

Crystallographic data for **1**–**5** have been deposited with the Cambridge Crystallographic Data Centre, deposition

numbers 276283–276287, respectively. Copies of this information may be obtained free of charge from The Director, CCDC, 12 Union Road, Cambridge CB2 1EZ, UK (fax: +44 1223 336 033; e-mail: deposit@ccdc.cam.ac.uk or www: http://www.ccdc.cam.ac.uk). Supplementary data associated with this article can be found, in the online version, at doi:10.1016/j.poly.2005.12.013.

References

[1] D. Voet, A. Rich, Prog. Nucl. Acid Res. Mol. Biol. 10 (1970) 183.
[2] D.F. Weaver, M.B. Guillain, J.R. Carran, K. Jones, 2002, European Patent Office, Patent Number WO02083561.
[3] W.M. Kazmierski, C.J. Aquino, N. Bifulco, E.E. Boros, B.A. Chauder, P.Y. Chong, M. Duan, F. Deanda, C.S. Koble, E.W. McLean, J.P. Peckham, A.C. Perkins, J.B. Thompson, D. Vanderwall, 2004, European Patent Office, Patent Number WO2005054972.
[4] E.R. Tucci, F. Takahashi, V.A. Tucci, N.C. Li, J. Inorg. Nucl. Chem. 27 (1964) 1263.
[5] Y.D. Fridman, E.P. Tsoi, M.G. Levina, Koord. Khim. 10 (1984) 469.
[6] L. Jun-Hua, H. Mao-Chun, Z. Yin-Jun, C. Rong, W. Jia-Bao, Jiegou Huaxue 21 (2002) 392.
[7] G. Maistrallis, N. Katsaros, D. Memtzafos, A. Terzis, Acta Crystallogr., Sect. C 47 (1991) 740.
[8] F. Hueso-Urena, M.N. Moreno-Carratero, M. Quiros-Olozabel, J.M. Salas-Peregrin, R. Faure, G.A. de Cienfuegos-Lopez, Inorg. Chim. Acta 241 (1996) 61.
[9] J. Hueso-Urena, M.N. Moreno-Carretero, M.A. Remero-Molina, J.M. Sales-Peregrin, M.P. Sanchez-Sanchez, G.A.d. Cienfuegos-Lopez, R. Faure, J. Inorg. Biochem. 51 (1993) 613.
[10] E.J. Baran, R.C. Mercader, F. Hueso-Urena, M.N. Moreno-Carratero, M. Quiros-Olozabel, J.M. Salas-Peregrin, Polyhedron 15 (1996) 1717.
[11] S. Chang-Yang, J. Lin-Pei, Polyhedron 23 (2004) 2227.
[12] S. Chang-Yang, J. Lin-Pei, Polyhedron 23 (2004) 2085.
[13] G.-L. Law, L. Szeto, W.-T. Wong, Acta Crystallogr., Sect. E 60 (2004) o1072.
[14] G. Maistralis, N. Katsaros, J. Inorg. Biochem. 45 (1992) 1.
[15] K. Dobrosz-Tepak, J.C. Dobrowolski, R. Kolos, W. Lewandowski, J. Mol. Struct. 563–564 (2001) 395.
[16] C.C. Wagner, E.J. Baran, O.E. Piro, E.E. Castellano, J. Inorg. Biochem. 77 (1999) 209.
[17] Nonius, COLLECT, Nonius BV, Delft, The Netherlands, 1999.
[18] A.J.M. Duisenberg, L.M.J. Kroon-Batenburg, A.M.M. Schreurs, J. Appl. Crystallogr. 36 (2003) 220.
[19] Bruker, APEX2, Bruker AXS Inc., Madison, WI, USA, 2003.
[20] Bruker, SAINT, Bruker AXS Inc., Madison, WI, USA, 2001.
[21] Bruker, SMART, Bruker AXS Inc., Madison, WI, USA, 2001.
[22] G.M. Sheldrick, SADABS, University of Göttingen, Göttingen, Germany, 2003.
[23] M.C. Burla, M. Camalli, B. Carrozzini, G.L. Cascavano, C. Giacovazzo, G. Polidori, R. Spagna, J. Appl. Crystallogr. 36 (2003) 1103.
[24] G.M. Sheldrick, SHELXTL, Version 6, Bruker AXS Inc., Madison, WI, USA, 2001.
[25] K. Brandenburg, H. Putz, DIAMOND-3, University of Bonn, Germany, 2004.
[26] M.C. Etter, Acc. Chem. Res. 23 (1990) 120.
[27] J. Bernstein, R.E. Davis, L. Shimoni, N.-L. Chang, Angew. Chem., Int. Edn. Engl. 34 (1995) 1555.
[28] G.R. Desiraju, T. Steiner, The Weak Hydrogen Bond in Structural Chemistry and Biology, Oxford University Press, Oxford, 1999.
[29] A.L. Spek, J. Appl. Crystallogr. 36 (2003) 7.
[30] R.E. Marsh, Acta Crystallogr., Sect. B 60 (2004) 252.
[31] H.D. Flack, Acta Crystallogr. Sect. A 39 (1983) 876.

2. Experimental

Hydrated lanthanoid nitrates, 2,4,6-tri-α-pyridyl-1,3,5-triazine, and solvents were obtained as commercial products (Aldrich) and were used without purification.

2.1. Synthesis of $[Ln(tptz)(NO_3)_3(H_2O)]\cdot 2C_2H_5OH$ (4–16)

The complexes $[Ln(tptz)(NO_3)_3(H_2O)]$ were prepared essentially by the literature method [1], as is described in detail for $[Er(tptz)(NO_3)_3(H_2O)]\cdot 2C_2H_5OH$ (**14**) here. A hot solution of hydrated erbium nitrate (0.07 g., 0.18 mmol) in ethanol (5 ml) was mixed with a solution of 2,4,6-tri-α-pyridyl-1,3,5-triazine (0.05 g; 0.16 mmol) in ethanol (25 ml) and allowed to stand overnight, when well-formed pink crystals were obtained.

The other complexes were obtained similarly, with appropriate variation of lanthanoid and choice of solvent. Crystals of $[Yb(tptz)(NO_3)_3(H_2O)]\cdot 2C_2H_5OH$ (**16**) and $[Yb(tptz)(NO_3)_3\cdot C_2H_5OH]\cdot C_2H_5OH$ (**17**) were obtained from the same reaction mixture. Crystals of $[La(tptz)(NO_3)_3(H_2O)]\cdot Me_2CO$ (**2**) were obtained by recrystallisation of $[La(tptz)(NO_3)_3(H_2O)]\cdot 2C_2H_5OH$ from propanone using a microwave oven.

Analyses were obtained for a representative sample of compounds. Carbon analyses tended to be low, despite the use of oxidant.

Anal. Calc. for $[La(tptz)(NO_3)_3\cdot(MeOH)_2]$: C, 34.25; H, 2.85; N, 17.98. Found: C, 34.01; H, 2.81; N, 17.63%.

Anal. Calc. for $[La(tptz)(NO_3)_3\cdot H_2O]\cdot 2EtOH$: C, 35.35; H, 3.51; N, 16.87%. *Anal.* Calc. for $La(tptz)(NO_3)_3\cdot H_2O$: C, 32.99; H, 2.15; N, 19.24. Found: C, 33.71; H, 3.07; N, 16.92%.

Anal. Calc. for $[Pr(tptz)(NO_3)_3\cdot H_2O]\cdot 2EtOH$: C, 35.10; H, 3.48; N, 16.74%. *Anal.* Calc. for $Pr(tptz)(NO_3)_3\cdot H_2O$: C, 32.89; H, 2.15; N, 19.18. Found: C, 34.22; H, 3.15; N, 16.77%.

Anal. Calc. for $[Nd(tptz)(NO_3)_3\cdot H_2O]\cdot 2EtOH$: C, 35.10; H, 3.48; N, 16.74%. *Anal.* Calc. for $Nd(tptz)(NO_3)_3\cdot H_2O$: C, 32.73; H, 2.14; N, 19.08. Found: C, 34.26; H, 3.21; N, 16.53%.

Anal. Calc. for $[Dy(tptz)(NO_3)_3\cdot H_2O]\cdot 2EtOH$: C, 34.28; H, 3.40; N, 16.36%. *Anal.* Calc. for $Dy(tptz)(NO_3)_3\cdot H_2O$: C, 31.85; H, 2.08; N, 18.57. Found: C, 33.46; H, 3.18; N, 16.23%.

Anal. Calc. for $[Ho(tptz)(NO_3)_3\cdot H_2O]\cdot 2EtOH$: C, 34.16; H, 3.39; N, 16.30%. *Anal.* Calc. for $Ho(tptz)(NO_3)_3\cdot H_2O$: C, 31.73; H, 2.07; N, 18.50. Found: C, 33.58; H, 3.15; N, 16.18%.

Anal. Calc. for $[Er(tptz)(NO_3)_3\cdot H_2O]\cdot 2EtOH$: C, 34.06; H, 3.38%, N16.29%. *Anal.* Calc. for $Er(tptz)(NO_3)_3\cdot H_2O$: C, 31.62; H, 2.06; N, 18.44. Found: C, 32.87; H, 2.90; N, 16.20%.

Anal. Calc. for $[Yb(tptz)(NO_3)_3\cdot H_2O]\cdot 2EtOH$: C, 33.81; H, 3.35; N, 16.13%. *Anal.* Calc. for $Yb(tptz)(NO_3)_3\cdot H_2O$: C, 31.35; H, 2.05; N, 16.28. Found: C, 32.16; H, 2.60; N, 18.28%.

Anal. Calc. for $[Lu(tptz)(NO_3)_3\cdot EtOH]\cdot EtOH$ C 34.43; H, 3.42; N, 16.43%. *Anal.* Calc. for $Lu(tptz)(NO_3)_3\cdot H_2O$: C, 33.30; H, 2.79; N, 17.18. Found: C, 31.68; H, 2.39; N, 16.23%.

Anal. Calc. for $[Lu(tptz)(NO_3)_3\cdot H_2O]\cdot MeCN$: C, 32.80; H, 2.34; N, 19.12%. *Anal.* Calc. for $Lu(tptz)(NO_3)_3\cdot H_2O$: C, 31.27; H, 2.04; N, 18.23. Found: C, 32.63; H, 2.24; N, 18.80%.

2.2. X-ray crystallography

The crystal data, data collection parameters, and structure solution and refinement details for the crystal structures determined are summarised in Table 1. Data collections were carried out on a Nonius Kappa CCD diffractometer, using graphite monochromated Mo Kα radiation, except for that for $[La(tptz)(NO_3)_3(H_2O)]\cdot 2EtOH$ (**4**) which was collected on a Bruker AXS SMART diffractometer, at Station 9.8 of the CCLRC Daresbury Laboratory. Both diffractometers were equipped with an Oxford Cryostream cooling apparatus. The data sets were corrected for Lorentz and polarisation effects and for absorption using SORTAV [12] or SADABS [13] (for $[La(tptz)(NO_3)_3(H_2O)]\cdot 2EtOH$ (**4**)), except for the structures of $[Ln(tptz)(NO_3)_3(H_2O)]2EtOH$ (Ln = Eu (**9**), Ho (**13**) and Yb (**16**)) where numerical methods, based of the faces of the crystals were used. Structure solution was achieved by Patterson methods (DIRDIF-99 [14]) and refined by full-matrix least-squares on F^2 (SHELXL-97 [15]) with all ordered non-hydrogen atoms assigned anisotropic displacement parameters. Hydrogen atoms attached to carbon atoms were placed in idealised positions and allowed to ride on the relevant carbon atom. In the final cycles of refinement a weighting scheme that gave a relatively flat analysis of variance was introduced and refinement continued until convergence was reached.

3. Discussion

Reaction of the 2,4,6-tri-α-pyridyl-1,3,5-triazine (tptz) ligand with the hydrated lanthanoid nitrates in ethanolic solution gave crystals of $[Ln(tptz)(NO_3)_3(H_2O)]\cdot 2C_2H_5OH$ (Ln = La–Yb (**4**–**16**) except Pm) and $[Lu(tptz)(NO_3)_3(C_2H_5OH)]$ (**18**) that proved suitable for X-ray diffraction. In the case of ytterbium, mixtures of two crystalline compounds were obtained, $[Yb(tptz)(NO_3)_3(H_2O)]\cdot 2C_2H_5OH$ (**16**) and $[Yb(tptz)(NO_3)_3(C_2H_5OH)]$ (**17**). Microcrystals of the product of reaction using lanthanum nitrate, on recrystallisation from propanone, afforded $[La(tptz)(NO_3)_3(H_2O)]\cdot Me_2CO$ (**2**), and synthesis of the lanthanum complex in methanol afforded $[La(tptz)(NO_3)_3(CH_3OH)_2]$ (**1**). Reaction of tptz with lutetium nitrate in acetonitrile or methanol led to the formation of $[Lu(tptz)(NO_3)_3(H_2O)]\cdot MeCN$ (**19**) or $[Lu(tptz)(NO_3)_2(H_2O)_2]NO_3\cdot 3MeOH$ (**20**), respectively.

While this work was in progress, other workers reported [16] considerable difficulty in obtaining crystals of the lanthanoid nitrate complexes of tptz using MeCN as a solvent, though subsequently they reported the crystal structure of

Table 1
Crystal data, data collection parameters and refinement parameters for the complexes **1**–**20**

Identification code	**1**	**2**	**3**	**4**
Empirical formula	$C_{20}H_{20}LaN_9O_{11}$	$C_{21}H_{20}LaN_9O_{11}$	$C_{22}H_{26}N_9O_{12}Y$	$C_{22}H_{26}LaN_9O_{12}$
Formula weight	701.36	713.37	697.43	747.43
T (K)	150(2)	150(2)	150(2)	150(2)
λ (Å)	0.71073	0.71073	0.71073	0.68980
Crystal system	triclinic	triclinic	triclinic	triclinic
Space group	$P\bar{1}$	$P\bar{1}$	$P\bar{1}$	$P\bar{1}$
Unit cell dimensions				
a (Å)	9.9621(1)	9.6214(3)	9.6081(2)	9.6254(19)
b (Å)	10.4472(2)	10.4431(3)	10.8969(3)	11.041(2)
c (Å)	14.0540(2)	13.9299(5)	14.2605(3)	14.439(3)
α (°)	75.952(1)	86.856(1)	79.934(1)	79.299(3)
β (°)	74.371(1)	85.951(1)	81.857(1)	82.405(3)
γ (°)	65.434(1)	73.091(1)	86.734(1)	89.683(3)
V (Å^3)	1266.75(3)	1334.92(7)	1454.45(6)	1494.3(5)
Z	2	2	2	2
D_{calc} (Mg/m^3)	1.839	1.775	1.592	1.661
Absorption coefficient (mm^{-1})	1.765	1.676	2.081	1.504
Crystal size (mm^3)	$0.23 \times 0.20 \times 0.13$	$0.08 \times 0.05 \times 0.03$	$0.23 \times 0.14 \times 0.07$	$0.10 \times 0.10 \times 0.06$
θ Range for data collection (°)	2.98–27.42	2.93–27.45	2.91–27.37	1.82–29.24
Reflections collected	23132	27631	41591	19986
Independent reflections (R_{int})	5742 (0.0399)	6087 (0.1343)	6558 (0.1170)	8130 (0.0246)
Maximum and minimum transmission	0.8031 and 0.6870	0.9593 and 0.8776	0.8680 and 0.6461	0.9152 and 0.8642
Data/restraints/parameters	5742/0/370	6087/0/374	6558/0/405	8130/2/407
Goodness-of-fit on F^2	1.288	1.006	0.926	0.926
Final R indices [$I > 2\sigma(I)$]	$R_1 = 0.0239$, $wR_2 = 0.0652$	$R_1 = 0.0500$, $wR_2 = 0.0868$	$R_1 = 0.0450$, $wR_2 = 0.0862$	$R_1 = 0.0450$, $wR_2 = 0.0862$
R indices (all data)	$R_1 = 0.0284$, $wR_2 = 0.0888$	$R_1 = 0.1062$, $wR_2 = 0.1103$	$R_1 = 0.0911$, $wR_2 = 0.1002$	$R_1 = 0.0241$, $wR_2 = 0.0535$
Largest difference in peak and hole (e Å^{-3})	0.888 and −1.791	0.902 and −1.974	0.410 and −0.551	0.410 and −0.551

Identification code	**5**	**6**	**7**	**8**
Empirical formula	$C_{22}H_{26}CeN_9O_{12}$	$C_{22}H_{26}N_9O_{12}Pr$	$C_{23}H_{27}N_8NdO_{12}$	$C_{22}H_{26}N_9O_{12}Sm$
Formula weight	748.64	749.43	751.77	758.87
T (K)	150(2)	180(2)	150(2)	150(2)
λ (Å)	0.71073	0.71073	0.71073	0.71073
Crystal system	triclinic	triclinic	triclinic	triclinic
Space group	$P\bar{1}$	$P\bar{1}$	$P\bar{1}$	$P\bar{1}$
Unit cell dimensions				
a (Å)	9.6076(3)	9.6117(5)	9.6125(2)	9.6111(2)
b (Å)	11.0114(4)	10.9783(7)	10.9669(2)	10.9431(2)
c (Å)	14.4695(6)	14.4323(10)	14.4121(4)	14.3639(3)
α (°)	79.538(2)	79.763(3)	79.811(1)	79.933(1)
β (°)	82.414(2)	82.223(3)	82.151(1)	82.128(1)
γ (°)	88.734(2)	87.995(5)	87.590(1)	87.324(1)
V (Å^3)	1492.15(9)	1484.78(16)	1481.10(6)	1473.05(5)
Z	2	2	2	2
D_{calc} (Mg/m^3)	1.666	1.676	1.686	1.711
Absorption coefficient (mm^{-1})	1.600	1.715	1.827	2.069
Crystal size (mm^3)	$0.18 \times 0.14 \times 0.02$	$0.20 \times 0.18 \times 0.05$	$0.35 \times 0.25 \times 0.05$	$0.38 \times 0.20 \times 0.04$
θ Range for data collection (°)	3.15–27.55	1.45–25.04	3.17–27.55	3.19–30.10
Reflections collected	23722	8809	22739	45768
Independent reflections (R_{int})	6816 (0.0762)	5145 (0.0414)	6752 (0.0616)	8629 (0.0685)
Maximum and minimum transmission	0.9687 and 0.7616	0.9191 and 0.7254	0.9142 and 0.5673	0.9218 and 0.5070
Data/restraints/parameters	6816/0/405	5145/0/401	6752/0/405	8629/0/405
Goodness-of-fit on F^2	1.046	1.048	1.066	1.099
Final R indices [$I > 2\sigma(I)$]	$R_1 = 0.0484$, $wR_2 = 0.1095$	$R_1 = 0.0329$, $wR_2 = 0.0696$	$R_1 = 0.0370$, $wR_2 = 0.0882$	$R_1 = 0.0311$, $wR_2 = 0.0749$
R indices (all data)	$R_1 = 0.0865$, $wR_2 = 0.1284$	$R_1 = 0.0431$, $wR_2 = 0.0737$	$R_1 = 0.0557$, $wR_2 = 0.1006$	$R_1 = 0.0420$, $wR_2 = 0.0786$
Largest difference in peak and hole (e Å^{-3})	1.013 and −0.987	0.658 and −0.835	0.994 and −1.726	1.237 and −1.418

(*continued on next page*)

Table 1 (*continued*)

Identification code	**9**	**10**	**11**	**12**
Empirical formula	$C_{22}H_{26}EuN_9O_{12}$	$C_{22}H_{26}GdN_9O_{12}$	$C_{22}H_{26}N_9O_{12}Tb$	$C_{22}H_{26}DyN_9O_{12}$
Formula weight	760.48	765.77	767.44	771.02
T (K)	150(2)	150(2)	150(2)	150(2)
λ (Å)	0.71073	0.71073	0.71073	0.71073
Crystal system	triclinic	triclinic	triclinic	triclinic
Space group	$P\bar{1}$	$P\bar{1}$	$P\bar{1}$	$P\bar{1}$
Unit cell dimensions				
a (Å)	9.6085(2)	9.6104(1)	9.6116(2)	9.60830(1)
b (Å)	10.9303(3)	10.9186(2)	10.9088(2)	10.89760(1)
c (Å)	14.3252(3)	14.3148(2)	14.2875(3)	14.2720(2)
α (°)	79.968(1)	79.923(1)	79.930(1)	79.913(1)
β (°)	82.014(1)	81.987(1)	81.927(1)	81.855(1)
γ (°)	87.166(1)	86.966(1)	86.866(1)	86.711(1)
V (Å^3)	1466.63(6)	1463.84(4)	1459.67(5)	1455.63(3)
Z	2	2	2	2
D_{calc} (Mg/m^3)	1.722	1.737	1.746	1.759
Absorption coefficient (mm^{-1})	2.214	2.341	2.499	2.643
Crystal size (mm^3)	$0.32 \times 0.26 \times 0.04$	$0.22 \times 0.18 \times 0.05$	$0.16 \times 0.13 \times 0.03$	$0.22 \times 0.18 \times 0.04$
θ Range for data collection (°)	3.20–30.08	2.92–30.08	2.92–27.52	2.91–27.49
Reflections collected	29769	41527	27360	29839
Independent reflections (R_{int})	8519 (0.0728)	8570 (0.0620)	6691 (0.0528)	6664 (0.0431)
Maximum and minimum transmission	0.9167 and 0.5376	0.8919 and 0.6269	0.9288 and 0.6906	0.9017 and 0.5940
Data/restraints/parameters	8519/0/405	8570/0/406	6691/0/405	6664/0/405
Goodness-of-fit on F^2	0.966	0.985	1.027	1.045
Final R indices [$I > 2\sigma(I)$]	$R_1 = 0.0340$, $wR_2 = 0.0556$	$R_1 = 0.0296$, $wR_2 = 0.0587$	$R_1 = 0.0294$, $wR_2 = 0.0613$	$R_1 = 0.0285$, $wR_2 = 0.0708$
R indices (all data)	$R_1 = 0.0566$, $wR_2 = 0.0601$	$R_1 = 0.0437$, $wR_2 = 0.0623$	$R_1 = 0.0394$, $wR_2 = 0.0641$	$R_1 = 0.0323$, $wR_2 = 0.0726$
Largest difference in peak and hole (e Å^{-3})	0.968 and −0.976	0.906 and −0.883	0.775 and −1.631	0.848 and −2.045

Identification code	**13**	**14**	**15**	**16**
Empirical formula	$C_{22}H_{26}HoN_9O_{12}$	$C_{22}H_{26}ErN_9O_{12}$	$C_{22}H_{26}N_9O_{12}Tm$	$C_{22}H_{26}N_9O_{12}Yb$
Formula weight	773.45	775.78	777.45	781.56
T (K)	150(2)	150(2)	150(2)	150(2)
λ (Å)	0.71073	0.71073	0.71073	0.71073
Crystal system	triclinic	triclinic	triclinic	triclinic
Space group	$P\bar{1}$	$P\bar{1}$	$P\bar{1}$	$P\bar{1}$
Unit cell dimensions				
a (Å)	9.6090(1)	9.6004(2)	9.6124(3)	9.6053(2)
b (Å)	10.8960(1)	10.8858(3)	10.8791(3)	10.8858(2)
c (Å)	14.2560(2)	14.2428(4)	14.2273(7)	14.2006(3)
α (°)	79.860(1)	79.868(1)	79.806(1)	79.725(1)
β (°)	81.828(1)	81.767(1)	81.714(1)	81.719(1)
γ (°)	86.640(1)	86.689(1)	84.474(1)	86.510(1)
V (Å^3)	1453.50(3)	1449.36(6)	1445.20(9)	1444.84(5)
Z	2	2	2	2
D_{calc} (Mg/m^3)	1.767	1.778	1.787	1.796
Absorption coefficient (mm^{-1})	2.798	2.972	3.146	3.313
Crystal size (mm^3)	$0.25 \times 0.19 \times 0.04$	$0.48 \times 0.25 \times 0.08$	$0.26 \times 0.24 \times 0.11$	$0.23 \times 0.14 \times 0.09$
θ Range for data collection (°)	2.91–30.10	2.93–27.56	2.93–28.06	2.92–34.97
Reflections collected	51826	16734	28486	38334
Independent reflections (R_{int})	8521 (0.0412)	6639 (0.0490)	6654 (0.0589)	12630 (0.0651)
Maximum and minimum transmission	0.8963 and 0.5414	0.8079 and 0.3296	0.7235 and 0.4951	0.7547 and 0.5162
Data/restraints/parameters	8521/0/405		6654/0/405	12630/0/405
Goodness-of-fit on F^2	1.049	1.052	1.141	1.003
Final R indices [$I > 2\sigma(I)$]	$R_1 = 0.0230$, $wR_2 = 0.0511$	$R_1 = 0.0302$, $wR_2 = 0.0728$	$R_1 = 0.0375$, $wR_2 = 0.0979$	$R_1 = 0.0367$, $wR_2 = 0.0789$
R indices (all data)	$R_1 = 0.0291$, $wR_2 = 0.0529$	$R_1 = 0.0358$, $wR_2 = 0.0754$	$R_1 = 0.0458$, $wR_2 = 0.1055$	$R_1 = 0.0537$, $wR_2 = 0.0863$
Largest difference in peak and hole (e Å^{-3})	1.044 and −1.221	1.147 and −1.955	1.403 and −2.608	1.280 and −2.687

Table 1 (*continued*)

Identification code	**17**	**18**	**19**	**20**
Empirical formula	$C_{22}H_{24}N_9O_{11}Yb$	$C_{22}H_{24}LuN_9O_{11}$	$C_{20}H_{17}LuN_{10}O_{10}$	$C_{21}H_{28}LuN_9O_{14}$
Formula weight	763.54	762.45	732.41	805.49
T (K)	150(2)	150(2)	150(2)	150(2)
λ (Å)	0.71073	0.71073	0.71073	0.71073
Crystal system	triclinic	triclinic	monoclinic	triclinic
Space group	$P\bar{1}$	$P\bar{1}$	$P2_1/n$	$P\bar{1}$
Unit cell dimensions				
a (Å)	9.53830(10)	9.5290(1)	9.2814(2)	9.6852(2)
b (Å)	12.1048(2)	12.1024(1)	15.5441(4)	11.9769(2)
c (Å)	13.7600(2)	13.7520(2)	17.5975(4)	13.4392(3)
α (°)	112.323(1)	112.302(1)	90	90.460(1)
β (°)	101.8953(9)	101.911(1)	98.308(2)	107.242(1)
γ (°)	99.1145(7)	99.098(1)	90	100.531(1)
V (Å^3)	1388.06(3)	1385.87(3)	2512.17(10)	1460.58(5)
Z	2	2	4	2
D_{calc} (Mg/m^3)	1.827	1.827	1.936	1.832
Absorption coefficient (mm^{-1})	3.444	3.637	4.006	3.463
$F(000)$	754	750	1432	800
Crystal size (mm^3)	$0.33 \times 0.15 \times 0.05$	$0.33 \times 0.15 \times 0.05$	$0.25 \times 0.05 \times 0.05$	$0.20 \times 0.05 \times 0.03$
θ Range for data collection (°)	2.96–27.4	2.96–29.80	2.96–27.50	1.59–27.46
Index ranges	$-12 \leqslant h \leqslant 12$, $-15 \leqslant k \leqslant 15$, $-17 \leqslant l \leqslant 17$	$-13 \leqslant h \leqslant 13$, $-16 \leqslant k \leqslant 16$, $-19 \leqslant l \leqslant 19$	$-12 \leqslant h \leqslant 12$, $-20 \leqslant k \leqslant 20$, $-22 \leqslant l \leqslant 22$	$-12 \leqslant h \leqslant 12$, $-15 \leqslant k \leqslant 15$, $-17 \leqslant l \leqslant 17$
Reflections collected	21 318	36 103	29 333	31 549
Independent reflections (R_{int})	6352 (0.0453)	7829 (0.0572)	5729 (0.0600)	6688 (0.0627)
Maximum and minimum transmission	0.8467 and 0.3961	0.8391 and 0.3799	0.8248 and 0.4341	0.9032 and 0.5443
Data/restraints/parameters	6352/0/365	7829/0/366	5729/0/371	6688/0/412
Goodness-of-fit on F^2	1.200	1.071	1.047	1.158
Final R indices [$I > 2\sigma(I)$]	$R_1 = 0.0422$, $wR_2 = 0.1309$	$R_1 = 0.0370$, $wR_2 = 0.1051$	$R_1 = 0.0322$, $wR_2 = 0.0666$	$R_1 = 0.0293$, $wR_2 = 0.0812$
R indices (all data)	$R_1 = 0.0507$, $wR_2 = 0.1469$	$R_1 = 0.0425$, $wR_2 = 0.1081$	$R_1 = 0.0532$, $wR_2 = 0.0752$	$R_1 = 0.0431$, $wR_2 = 0.1090$
Largest difference in peak and hole (e Å^{-3})	2.427 and −2.763	1.981 and −2.829	1.044 and −1.251	0.965 and −2.700

$[Sm(tptz)(NO_3)_3(H_2O)] \cdot 2H_2O$, obtained by this route [17]. They also studied a large number of complexes of the related terdentate ligand 4-amino-bis(2,6-(2-pyridyl))1,3,5-triazine (abptz) formed by reacting the lanthanide nitrate with 1 mol of abptz in MeCN [16]. They obtained complexes with a wide range of compositions, $[La(abptz)(NO_3)_3(H_2O)_2]$ (11 co-ordinate), $[Ln(abptz)(NO_3)_3(H_2O)]$ (Ln = La, Pr–Sm; 10 co-ordinate), $[Ln(abptz)(NO_3)_3(H_2O)]$ (Ln = Yb, Y; nine co-ordinate, with one monodentate nitrate), $[Ln(abptz)(NO_3)_2(H_2O)_3]NO_3$(Ln = Nd, Sm; 10 co-ordinate) and $[Ln(abptz)(NO_3)_2(H_2O)_2]NO_3$ (Ln = Eu–Lu; nine co-ordinate), which have all been crystallographically characterised. Our fortuitous success in obtaining crystals of the tptz complexes using ethanol for the syntheses may possibly be due to a favourable hydrogen-bonding network present in the crystalline state.

Two other lanthanoid complexes of tptz have also been characterised crystallographically [18]. Tptz acts as a tridentate ligand in the structures of $[Eu(tptz)Cl_3(MeOH)_2] \cdot 2$ MeOH (eight co-ordinate) and $[Pr(tptz)(OAc)_3]_2 \cdot 2$ MeOH (10 co-ordinate). The latter features the presence of double (η^2,μ-1,1) acetate bridges increasingly familiar in other lanthanide carboxylates and their complexes [19–21].

In contrast to the situation with the abptz ligand, we have obtained isomorphous and isostructural tptz complexes covering the whole lanthanoid series, save one extreme member. This is a rarity, although both the isostructural families $[Ln(bipy)_2(NO_3)_3]$ and $[Ln(phen)_2(NO_3)_3]$ exist for La–Lu and Y (bipy = 2,2′-bipyridyl; phen = 1,10-phenanthroline) [22].

3.1. The crystal structure of $[La(tptz)(NO_3)_3(CH_3OH)_2]$ (*1*)

This compound contains 11 co-ordinate lanthanum, with three bidentate nitrate groups and two co-ordinated methanol molecules and the tridentate tptz ligand (Fig. 1). The nitrate groups are essentially planar, and the three coordinated six-membered rings of the tptz ligand are close to being co-planar, with the dihedral angle between the ring N(1)C(1)C(2)C(3)C(4)C(5) (ring A, Fig. 1) and the ring N(2)N(3)N(4)C(6)C(7)C(13) (ring B, Fig. 1) of 4.2° and that between the ring N(2)N(3)-N(4)C(6)C(7)C(13) and the ring N(5)C(14)C(15)C(16)-C(17)C(18) (ring C, Fig. 1) is 1.4°. The dihedral angle between the central triazine ring and the back, uncoordi-

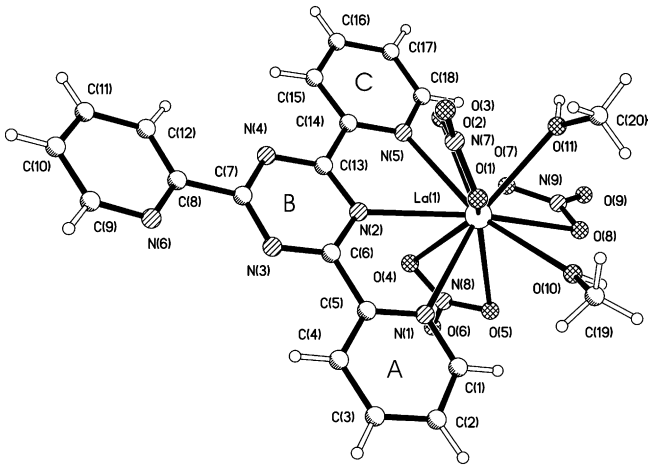

Fig. 1. The molecular structure of $[La(tptz)(NO_3)_3(CH_3OH)_2]$ (**1**) showing the atom numbering scheme.

nated pyridine ring is somewhat larger, at 10.6°. In the crystal, the molecules are linked through hydrogen bonds involving the methanolic O–H groups as hydrogen bond donors, and either a nitrate oxygen or a ring nitrogen as acceptors. The three most significant hydrogen bonds are O(10)–H(10A)···O(5) (related by $-x$, $-y+1$, $-z+1$), with parameters of H(10A)···O(5) 2.09 Å and O(10)–H(10A)···O(5) 156.6°; and a bifurcated hydrogen bond O(11)–H(11A)···N(6) (related by $x-1$, y, z), with parameters H(11A)···N(6) 2.14 Å, O(11)–H(11A)···N(6) 128.3°; and H(11A)···N(3) (related by $x-1$, y, z), with parameters H(11A)···N(3) 2.56 Å, O(11)–H(11A)···N(3) 145.1°.

Although we have not been successful in isolating the analogous $[La(tptz)(NO_3)_3(H_2O)_2]$, it is most likely that it exists in solution and the methanol complex is a surrogate for it.

The structures of two related complexes have been described in the literature, $[La(terpy)(NO_3)_3(CH_3OH)_2]$ [5] and $[La(abptz)(NO_3)_3(H_2O)_2]$ [16]. In comparison with $[La(terpy)(NO_3)_3(CH_3OH)_2]$, the tptz complex has rather longer La–N distances, averaging 2.758 Å against 2.701 Å in the case of the terpyridyl complex, whilst the La–O (CH_3OH) distances are also slightly longer, averaging 2.609 Å for $[La(tptz)(NO_3)_3(CH_3OH)_2]$ versus 2.570 Å for the terpyridyl complex. In contrast, the La–O (nitrate) distances are shorter for $[La(tptz)(NO_3)_3(CH_3OH)_2]$, they range from 2.569(2) to 2.761(2) Å, with an average of 2.636 Å, whereas for $[La(terpy)(NO_3)_3(CH_3OH)_2]$ they range from 2.596(2) to 2.926(2) Å (the last named being 0.199 Å longer than the next longest (2.727 Å)), the average La–O distance being 2.698 Å. In $[La(tptz)(NO_3)_3(CH_3OH)_2]$, the two longest La–O distances are 2.714(2) and 2.761(2) Å, a much smaller discrepancy. It is difficult to escape the conclusion that in the terpyridyl complex the congestion in the co-ordination sphere is such that it is relieved with a "sesquidentate" nitrate group, whereas in the tptz complex the co-ordination of the three nitrate groups is more symmetrical. Examining $[La(abptz)(NO_3)_3(H_2O)_2]$, the La–N distances average 2.710 Å (against 2.758 for the tptz complex) and the La–O (H_2O) distances average 2.600 Å, very similar to the value of 2.609 Å for La–O (CH_3OH) in $[La(tptz)(NO_3)_3(CH_3OH)_2]$. The shorter La–N distances in the abptz complex are counterbalanced by it having longer La–O distances involving the nitrate groups, ranging from 2.628(4) to 2.805(6) Å, averaging 2.685 Å. The longest La–O distance in the abptz complex is 0.103 Å longer than the next longest one, so again there is some suggestion of congestion being released. However, variation of the La–N distance between similar complexes of tptz and abptz having the same stoichiometry suggests that there may be some degree of steric determination in bond length.

3.2. The crystal structure of $[La(tptz)(NO_3)_3(H_2O)] \cdot Me_2CO$ (2)

This complex has 10 co-ordinate lanthanum, with a tridentate tptz ligand, three bidentate nitrates and one co-ordinated water molecule (Fig. 2), and has a geometry very similar to $[La(tptz)(NO_3)_3(H_2O)] \cdot 2C_2H_5OH$ (**4**). Comparing bond lengths in $[La(tptz)(NO_3)_3(H_2O)] \cdot Me_2CO$ (**2**) and $[La(tptz)(NO_3)_3(H_2O)] \cdot 2C_2H_5OH$ (**4**), respectively, the average La–N distances are 2.698 and 2.687 Å; the respective average La–O distances are 2.601 and 2.605 Å, whilst the corresponding Ln–O (OH_2) distances are 2.477(4) and 2.452(1) Å (Table 2). In **2** the nitrate groups are essentially planar whereas the tptz ligand shows some deviation from planarity. The pyridine ring A (as defined in Fig. 1) makes an angle of 5.2° with the central trazine ring (ring B as defined in Fig. 1) while the angle between this ring and the third coordinated pyridine ring (ring C as defined in Fig. 1 is 8.0°). As in the case of **1** the dihedral angle between the central triazine ring and the uncoordinated ring N(6)C(9)C(10)C(11)C(12)C(13) is a little greater, at 11.4°. In the crystal structure of **2** there is a relatively

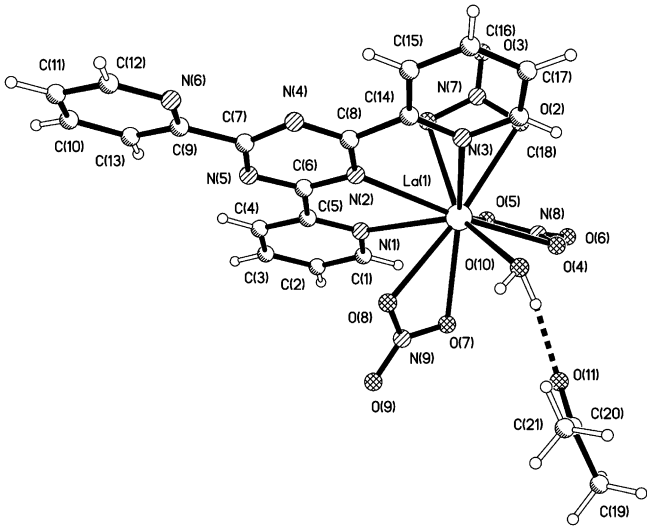

Fig. 2. The molecular structure of $[La(tptz)(NO_3)_3(H_2O)] \cdot Me_2CO$ (**2**) showing the hydrogen bonding with the acetone molecule and the atom numbering scheme.

Table 2
Bond lengths in complexes $Ln(tptz)(NO_3)_3 \cdot xH_2O$

	Y (**3**)	La (**4**)	Ce (**5**)	Pr (**6**)	Nd (**7**)	Sm (**8**)	Eu (**9**)	Gd (**10**)	Tb (**11**)	Dy (**12**)	Ho (**13**)	Er (**14**)	Tm (**15**)	Yb (**16**)
x	1	1	1	1	1	1	1	1	1	1	1	1	1	1
Co-ordination number	10	10	10	10	10	10	10	10	10	10	10	10	10	10
M–N (Å)	2.529(2)	2.667(1)	2.660(4)	2.630(3)	2.614(3)	2.593(2)	2.576(2)	2.567(2)	2.545(2)	2.534(2)	2.524(2)	2.513(2)	2.508(4)	2.490(2)
	2.539(2)	2.691(1)	2.678(4)	2.644(3)	2.629(3)	2.603(2)	2.579(2)	2.569(2)	2.555(2)	2.547(2)	2.536(2)	2.528(2)	2.508(4)	2.510(2)
	2.578(2)	2.703(1)	2.696(4)	2.668(3)	2.658(3)	2.629(2)	2.619(2)	2.607(2)	2.592(2)	2.582(2)	2.573(2)	2.562(3)	2.519(3)	2.541(2)
Average M–N (Å)	2.549	2.687	2.678	2.647	2.634	2.608	2.591	2.581	2.564	2.554	2.544	2.534	2.512	2.516
M–O (Å)	2.412(2)	2.570(1)	2.549(4)	2.524(3)	2.506(3)	2.481(2)	2.465(2)	2.456(2)	2.439(2)	2.426(2)	2.416(1)	2.401(3)	2.404(3)	2.377(2)
	2.441(2)	2.588(2)	2.565(4)	2.546(3)	2.534(3)	2.505(2)	2.490(2)	2.481(2)	2.464(2)	2.451(2)	2.441(2)	2.429(2)	2.419(3)	2.399(2)
	2.442(2)	2.595(1)	2.585(4)	2.556(2)	2.541(3)	2.511(2)	2.496(2)	2.485(2)	2.467(2)	2.453(2)	2.442(1)	2.432(2)	2.437(3)	2.413(2)
	2.505(2)	2.617(1)	2.598(4)	2.583(3)	2.568(3)	2.546(2)	2.536(2)	2.532(2)	2.520(2)	2.515(2)	2.506(2)	2.495(2)	2.520(3)	2.482(2)
	2.508(2)	2.631(1)	2.611(4)	2.592(3)	2.584(3)	2.557(2)	2.544(2)	2.538(2)	2.523(2)	2.516(2)	2.512(2)	2.503(3)	2.528(3)	2.504(2)
	2.538(2)	2.631(1)	2.618(4)	2.594(3)	2.584(3)	2.566(2)	2.558(2)	2.555(2)	2.552(2)	2.545(2)	2.544(2)	2.544(3)	2.542(3)	2.567(2)
Average M–O (Å)	2.474	2.605	2.588	2.566	2.553	2.527	2.515	2.508	2.494	2.484	2.477	2.467	2.475	2.457
M–O(NO_3) spread (Å)	0.126	0.061	0.069	0.070	0.078	0.085	0.093	0.099	0.113	0.119	0.128	0.143	0.138	0.180
M–OH_2 (Å)	2.299(2)	2.452(1)	2.424(4)	2.412(3)	2.400(3)	2.368(2)	2.349(2)	2.337(2)	2.322(2)	2.311(2)	2.303(2)	2.292(3)	2.262(3)	2.270(2)
Average M–OH_2 (Å)	2.299	2.452	2.424	2.412	2.400	2.368	2.355	2.337	2.322	2.311	2.303	2.292	2.262	2.270
M^{3+} radius in CN9		1.216	1.196	1.179	1.163	1.132	1.120	1.107	1.095	1.083	1.072	1.062	1.052	1.042
Lattice solvent	·2EtOH	·2EtOH	·2EtOH	·2EtOH	·2EtOH	·2EtOH	·2EtOH	·2EtOH	·2EtOH	·2EtOH	·2EtOH	·2EtOH	·2EtOH	·2EtOH

strong hydrogen bond between the coordinated water hydrogen and the oxygen atom of the acetone solvent molecule; the hydrogen bonding parameters are H(10B)···O(11) 1.80 Å and O(10)–H(10B)···O(11) 167.3° where O(11) is related by the symmetry operation x, $y+1$, z.

3.3. The crystal structures of $[Ln(tptz)(NO_3)_3(H_2O)] \cdot 2C_2H_5OH$ (Ln = Y (**3**), La–Yb (**4**–**16**) except Pm)

3.3.1. General points

This series of isostructural complexes is 10 co-ordinate, with a tridentate tptz ligand, three bidentate nitrates and one co-ordinated water molecule. Selected bond lengths are presented in Table 2. The lanthanum complex **4** is illustrated in Fig. 3. As has already been indicated the geometry of the complex **4** is very similar to that of complex **2**. In this case the dihedral angle between ring A and ring B is 3.9°, that between the central triazine ring (ring B) and ring C is also 3.9°, while the dihedral angle between the triazine ring and the uncoordinated pyridine ring is only 7.7°. As with the whole series the two ethanol molecules of crystallisation are hydrogen bonded to the coordinated water molecule, with the ethanolic oxygens acting as the hydrogen bond acceptors; H(10A)···O(11) 1.747(3) Å, O(10)–H(10A)···O(11) 176(3)°, H(10B)···O(12) 1.777(4) Å, O(10)–H(10B)···O(12) 173(3)°. In addition, the ethanolic O(12)–H(12A) group acts as a hydrogen bond donor to the pyridyl nitrogen N(4) of the uncoordinated pyridine ring of the tptz ligand with H(12A)···N(4) 1.95 Å and O(12)–H(12A)···N(4) 175°, with N(4) related by the symmetry operation $-x-1$, $-y$, $2-z$. There is also a short contact between the other ethanol and a nitrate group, H(11A)···O(4) 2.00 Å, O(11)–H(11A) 169.7°, with O(4) related by the symmetry operation $-x$, $-y$, $1-z$.

The same pattern is seen in the next member of the series $[Ce(tptz)(NO_3)_3(H_2O)] \cdot 2EtOH$ (**5**). The Ce–N distances vary from 2.660(4) Å [Ce(1)–N(1)] to 2.696(4) Å [Ce(1)–N(3)] for the tptz ligand, while the Ce–O distances for

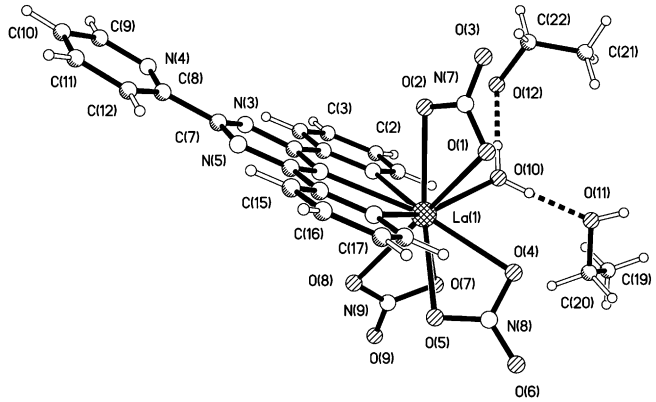

Fig. 3. The molecular structure of $[La(tptz)(NO_3)_3(H_2O)] \cdot 2EtOH$ (**4**) showing the hydrogen bonding of the hydrogen bonding of the two ethanol molecules to the complex.

the nitrate groups vary from 2.549(4) Å [Ce(1)–O(1)] to 2.618(4) Å [Ce(1)–O(6)] averaging 2.588 Å. The shortest Ce–O bond is that of the coordinated water molecule at 2.424(4) Å.

Also, the hydrogen bonding network in **5** is the same as in **4** with hydrogen bonding between the complex and the solvent molecules. In **5** the water hydrogen H(10A) forms a hydrogen bond with an ethanolic oxygen O(12) (O(10)–H(10A)···O(12)) at distances of 1.84 Å and an angle of 173°, while the other hydrogen H(10B) interacts with the other ethanolic oxygen O(11) [O(10)–H(10b)···O(11)] at a distance of 1.65 Å and an angle of 169°. Meanwhile the ethanolic hydrogen H(11A) forms an interaction with O(4) from the nitrate group [O(11)–H(11A)···O(4)] with a distance of 2.06 Å and at an angle of 154°. They are related by the symmetry operator $1 + x, y, z$. The other ethanolic hydrogen H(12A) also forms a hydrogen bond, this time with a nitrogen in the uncoordinated pyridine group [O(12)–H(12A)···N(6)] at a distance of 2.29 Å and an angle of 169° related by the symmetry operation $x, y, 1 + z$.

In the series there is also evidence for weak graphitic π–π interactions between the pyridine end groups of the tptz ligand in adjacent molecules, with centroid–centroid ring distances in the range 4.0–4.084 Å.

Comparing the family of complexes $[Ln(tptz)(NO_3)_3(H_2O)]\cdot 2EtOH$, perusal of Table 2 reveals a steady decrease in bond length with increasing atomic number, and decreasing ionic radius, of the lanthanoid ion, and the trends are illustrated in Fig. 4. Comparing the first and last members of the series, the lanthanum and ytterbium compounds, the average Ln–N distances are 2.687 Å (La) and 2.514 Å (Yb); the average Ln–O (nitrate) distances are 2.606 Å (La) and 2.457 Å (Yb); and the Ln–O (water) distances are 2.452(1) Å (La) and 2.270(2) Å (Yb). The decreases on traversing the series La–Yb are, respectively, 0.173, 0.149 and 0.182 Å. Although an ionic radius for 10 co-ordinate La^{3+} and Yb^{3+} is not given in the best literature compilation [23], ionic radii of 1.216 and 1.042 Å are given for nine co-ordinate La^{3+} and Yb^{3+}, respectively, indicating that a decrease of around 0.174 Å would be expected.

As already remarked, it is unusual for the same co-ordination number to be observed for a family of compounds across the whole lanthanide series, since there is a significant decrease of some 16% in ionic radius. The occurrence of the $[Ln(H_2O)_9]^{3+}$ ion in many solid salts of the later lanthanides (which form $[Ln(H_2O)_8]^{3+}$ ions in solution) is due to its stabilisation in the solid state by hydrogen-bonding [24], whilst many LnX_3 display decreases in co-ordination number, such as a change from 9 in $LaCl_3$ to 6 in $LuCl_3$ [25]. One feature that indicates a build-up of strain in the co-ordination environment of the lanthanide ion in these compounds is the range of Ln–O (nitrate) distances. In $[La(tptz)(NO_3)_3(H_2O)]\cdot 2C_2H_5OH$ (**4**), the La–O (nitrate) distances range from 2.570(1) to 2.631(1) Å, a spread of values of 0.061 Å, this value increasing fairly smoothly with increasing atomic number to successive values of 0.119, 0.128, 0.143 and 0.138 Å for the Dy (**12**), Ho (**13**), Er (**14**) and Tm (**15**) compounds, respectively, then *suddenly* increasing to 0.180 Å in $[Yb(tptz)(NO_3)_3(H_2O)]\cdot 2C_2H_5OH$ (**16**). The view that this reflects increasing congestion in the co-ordination sphere is supported by the fact that we were unable to isolate a lutetium member of this family, nine co-ordinate $[Lu(tptz)(NO_3)_3(C_2H_5OH)]$ (**18**) being obtained instead. Further, the isolation of crystals of $[Yb(tptz)(NO_3)_3\cdot(C_2H_5OH)]$ (**17**) (Table 3) from

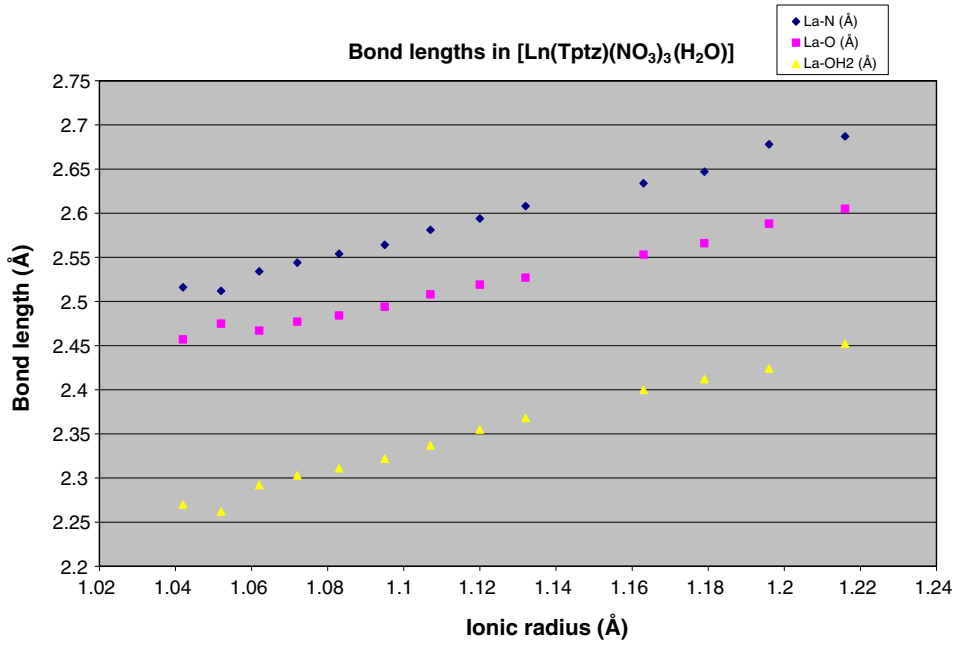

Fig. 4. A plot of the Ln–N (tptz), Ln–O (nitrate), and Ln–O (water) distances for the series $[Ln(tptz)(NO_3)_3(H_2O)]\cdot 2EtOH$ (La–Yb) showing the lanthanide contraction.

Table 3
A comparison of bond lengths in [Yb(tptz)$(NO_3)_3$(EtOH)] (**17**) and the [Lu(tptz)$(NO_3)_3$] complexes (**18**–**20**)

	17	**18**	**19**	**20**
Crystallised:	from EtOH	from EtOH	from MeCN	from MeOH
	Yb	Lu	Lu	Lu
Co-ordination number	9	9	9	9
M–N(tptz) (Å)	2.456(5)	2.453(3)	2.410(3)	2.454(4)
	2.500(5)	2.490(3)	2.46(1)	2.493(4)
	2.517(5)	2.510(3)	2.495(4)	2.518(4)
Average M–N (tptz) (Å)	2.491	2.484	2.455	2.488
M–O (NO_3) (Å)	2.273(5)	2.269(3)	2.270	2.368(3)
	2.350(5)	2.345(3)	2.370(3)	2.378(3)
	2.368(5)	2.367(3)	2.375(3)	2.411(3)
	2.406(5)	2.408(3)	2.394(3)	2.445
	2.464(5)	2.464(3)	2.447(3)	
Average M–O (NO_3) (Å)	2.3722	2.3706	2.3712	2.4005
	1 attached EtOH	1attached EtOH	1 attached H_2O	2 attached H_2O
M–OH_2 (Å)	2.271(5)	2.271(3)	2.293(3)	2.258(3), 2.274(4)
Ionic radius in CN9	1.042	1.032	1.032	1.032

the same reaction that affords [Yb(tptz)$(NO_3)_3(H_2O)]\cdot 2C_2H_5OH$ (**16**) tends to suggest that the latter compound approaches the borderline of stability.

Another way in which the co-ordinated nitrate groups can serve as an index of increasing congestion in the co-ordination sphere in these compounds can be seen in examining the asymmetry within each co-ordinated nitrate group. In the lanthanum complex (**4**), the discrepancies in La–O distance between the three pairs of bidentate nitrate groups are 0.036, 0.047 and 0.053 Å (for a symmetrically bidentate group, the values would, obviously, be zero), averaging 0.045 Å; in the cerium complex (**5**), the discrepancies in Ce–O distance between the three pairs of bidentate nitrate groups are 0.026, 0.049 and 0.053 Å, averaging 0.043 Å. In the ytterbium compound (**16**), the discrepancies are 0.069, 0.127 and 0.168 Å. Though this is not a smooth trend, the individual values for the Tm complex (**15**) being 0.091, 0.101 and 0.138 Å, yet giving a smaller total discrepancy in bond length, as befits the argument, the point is made.

A comparison is possible between bond lengths in [Nd(tptz)$(NO_3)_3(H_2O)]\cdot 2C_2H_5OH$ (**7**) (this paper) and the compounds [Nd(abptz)$(NO_3)_3(H_2O)$] [16] and [Nd(terpy)$(NO_3)_3(H_2O)$] [3]. Respective average Nd–N bond lengths are 2.634, 2.605 and 2.638 Å; Nd–O (nitrate) bonds average 2.553, 2.568 and 2.567 Å; and Nd–O (water) are 2.400, 2.470 and 2.488 Å. These values, apart from the metal–water bonds, which seem more susceptible to hydrogen-bonding forces, are closely comparable.

3.3.2. A comparison of $[Sm(tptz)(NO_3)_3(H_2O)]\cdot 2C_2H_5OH$ (*8*) and $[Sm(tptz)(NO_3)_3(H_2O)]\cdot 2H_2O$

In these complexes with identical coordination spheres, respective average Sm–N bond lengths are 2.608 and 2.615 Å [17]; Sm–O (nitrate) bonds average 2.527 and 2.533 Å; and Sm–O (water) are 2.368(2) and 2.420(2) Å. Despite the presence of different solvent molecules in the lattice, these values are in good agreement, within experimental error, apart from the metal–water bonds, which seem more susceptible to hydrogen-bonding forces.

3.4. Structures of the lutetium complexes

3.4.1. $[Lu(tptz)(NO_3)_3\cdot(C_2H_5OH)]$ (*18*)

The crystal structure of [Lu(tptz)$(NO_3)_3(C_2H_5OH)$] (**18**) shows that it is nine co-ordinate, with a tridentate tptz ligand, two bidentate nitrates, one monodentate nitrate and one co-ordinated water molecule (Fig. 5). Selected bond lengths for **18** are shown in Table 3. The initially bidentate nitrate (in the earlier elements of the series) is replaced by a monodentate nitrate and an ethanol molecule. The free ethanol molecule in the lattice (not shown in Fig. 5) is disordered over two positions. Individual atomic sites were refined with 66%:34% occupancies and the atomic coordinates and displacement parameters tied together

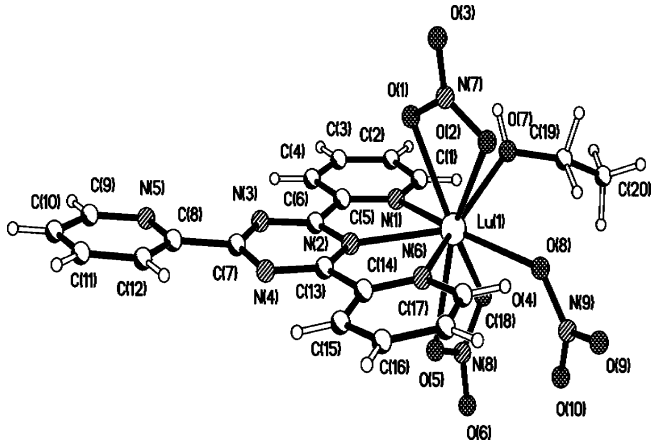

Fig. 5. The molecular structure of [Lu(tptz)$(NO_3)_3$(EtOH)] (**18**) showing the atom numbering scheme adopted. The disordered, uncoordinated EtOH solvent molecule is not shown.

and summed to unity. The oxygen atom, O(11), of the disordered lattice ethanol solvent molecule is hydrogen bonded to the OH group of the coordinated ethanol, with parameters H(7A)···O(11) 1.79 Å, O(7)–H(7A)···O(11) 172°, with O(11) related by the symmetry operation $1-x$, $-y$, $1-z$. As observed with the earlier group of lanthanoid complexes, there is also some evidence of weak graphitic packing between the coordinated pyridine rings of the tptz ligands in adjacent molecules. The centroid–centroid distances lie in the range 4.167–3.978 Å. The conformation of the tptz ligand is similar to that observed in the earlier lanthanoid complexes, **1**, **2**, and **4** with the dihedral angle between the pyridine ring (ring A) and the triazine ring (ring B) of 1.8°, that between the triazine ring and the other coordinated pyridine ring (ring C) of 8.3°, and that between the triazine ring and the uncoordinated pyridine ring of 5.9°. The complex [Yb(tptz)-$(NO_3)_3(C_2H_5OH)$] (**17**) is isostructural.

The Lu–N distances in **18** vary from 2.453(3) Å [Lu(1)–N(2)] to 2.510(3) Å [Lu(1)–N(6)] for the tptz ligand, while the Lu–O distances for the nitrate groups vary from 2.269(3) Å [Lu(1)–O(8)], the monodentate nitrate to 2.464(4) Å [Lu(1)–O(2)] averaging 2.371 Å. Comparing it with [Lu(terpy)$(NO_3)_3(C_2H_5OH)$] [2b], which it closely resembles, average bond lengths are Lu–N 2.484 and 2.457 Å (tptz complex first); Lu–O (bidentate nitrate) 2.396 and 2.414 Å; Lu–O (monodentate nitrate) 2.269(3) and 2.279(3) Å; and Lu–O (ethanol) 2.271(3) and 2.297(3) Å.

3.4.2. The structure of $[Lu(tptz)(NO_3)_3(H_2O)]\cdot MeCN$ (**19**)

The structure of [Lu(tptz)$(NO_3)_3(H_2O)]\cdot$MeCN (**19**) closely resembles that of [Lu(tptz)$(NO_3)_3(C_2H_5OH)$] (**18**) in having a tridentate tptz ligand, two bidentate nitrates, one monodentate nitrate and one co-ordinated oxygen atom from a neutral donor (Fig. 6); average bond lengths of Lu–N of 2.455 Å, Lu–O (bidentate nitrate) 2.396 Å; Lu–O (monodentate nitrate) 2.270 (3) Å; and Lu–O (H_2O) 2.293 (3) Å are closely comparable (Table 3). As in all the previous examples, hydrogen bonds contribute to the packing of the molecules in solid state with an intermolecular interaction involving O(10). The atom O(10) acts as a hydrogen bond acceptor in an interaction with the aromatic hydrogen H(16) at a distance of 1.87 Å and an angle of 151° (related by $x-1/2$, $1/2-y$, $z-1/2$). In addition, there is graphitic stacking now between the central trazine ring and the uncoordinated pyridine ring in an adjacent molecule at a centroid–centroid distance of 3.789 Å. The MeCN solvent molecule is not involved in hydrogen bonding. The ring conformations within the tptz ligand are similar to those observed in the other complexes with the dihedral angle between the coordinated pyridine ring (ring A) and the central triazine ring (ring B) of 12.8°, that between the triazine ring and the other coordinated pyridine ring (ring C) of 4.6°, and that between the triazine ring and the uncoordinated pyridine ring of 6.6°.

Two similar abptz complexes, [Ln(abptz)$(NO_3)_3(H_2O)$] (Ln = Y, Yb) have been reported [16].

3.4.3. The structure of $[Lu(tptz)(NO_3)_2\cdot(H_2O)_2]\cdot NO_3\cdot 3MeOH$ (**20**)

Isolated from the reaction of lutetium nitrate and tptz in methanol, this compound differs from the other two lutetium complexes in having an ionic structure (the cation is shown in Fig. 7), in which complete solvolysis of a co-ordinated nitrate group has occurred. The cation, containing two bidentate nitrate groups as well as two co-ordinated water molecules, strongly resembles that found in $[Lu(terpy)(NO_3)_2(H_2O)_2]NO_3\cdot 2H_2O$ [5] and terpy analogues with other heavy lanthanides. As in the case of the terpy complexes, it is the nitrate group *trans* to the terdentate N-donor that has undergone solvolysis (at least in the final product). The conformation of the tptz ligand is similar to that of the other complexes, with the dihedral angle

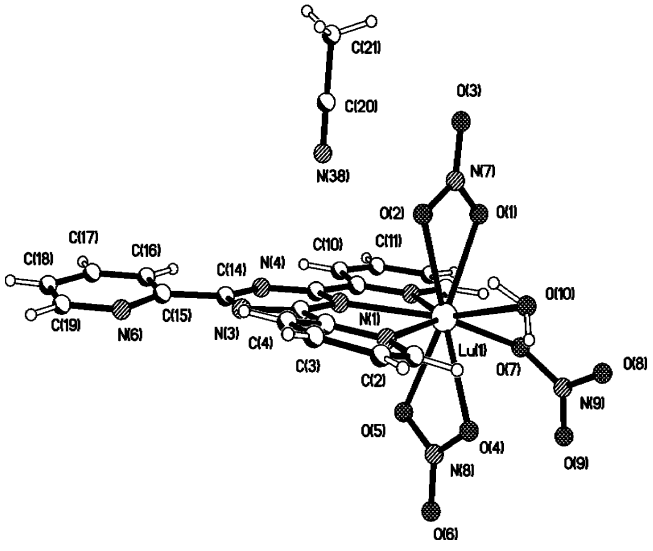

Fig. 6. The molecular structure of [Lu(tptz)$(NO_3)_3(H_2O)]\cdot$MeCN (**19**) showing that the MeCN solvent molecule is not involved in hydrogen bonding to the complex.

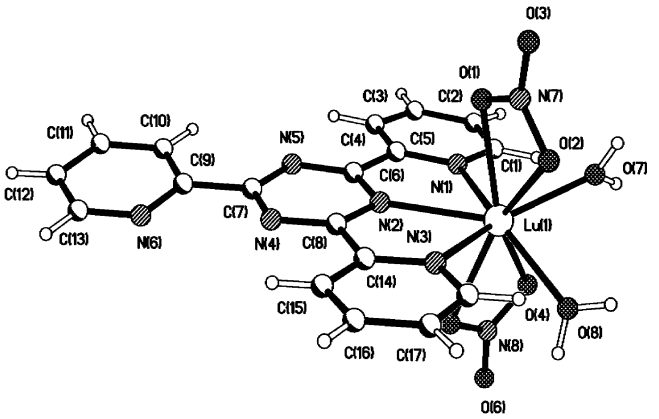

Fig. 7. The structure of the cation $[Lu(tptz)(NO_3)_2(H_2O)_2]^+$ showing the atom numbering scheme adopted.

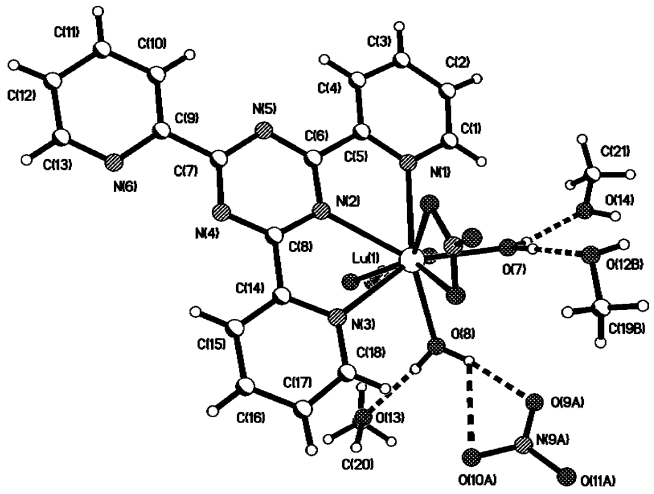

Fig. 8. The structure of $[Lu(tptz)(NO_3)_2(H_2O)_2]NO_3 \cdot 3MeOH$ (**20**) showing the hydrogen bonding network in the solid-state structure.

between ring A and the central triazine ring (ring B) being 5.1°, while that between this central ring and the other coordinated pyridine ring (ring C) is 2.8°, and the dihedral angle between the triazine ring and the uncoordinated pyridine ring is 4.3°. Corresponding average bond lengths (Table 3) (values for the tptz complex first) are: Lu–N 2.488 and 2.472 Å, Lu–O (nitrate) 2.400 and 2.411 Å and Lu–O (water) 2.266 and 2.266 Å, the latter being closely comparable to that of the other coordinated solvent molecules.

The free uncoordinated solvent molecules within the crystal lattice contribute to extensive hydrogen bonding (Fig. 8). The methanolic oxygens O(13) and O(14) both act as hydrogen bond acceptors to the coordinated water molecules. The interactions between O(13)···H(8A) and O(14)···H(7A) are 1.80 Å (O(8)–H(8A)···O(13) 163°) and 1.92 Å (O(7)–H(7A)···O(13) 153°), respectively. Meanwhile, the symmetry related nitrate anion acts as a hydrogen bond acceptor to two methanol solvent molecules. The distances between H(12A) and O(9) is 2.075 Å at an angle of 151° (related by $1-x$, $1-y$, $1-z$), while O(11) and H(14) are 2.05 Å apart, at an angle of 148.30° (related by $1-x$, $-y$, $1-z$). The hydrogen H(7B) on the coordinated O(7) acts as a hydrogen bond donor to O(12) with distances between O(12) and H(7B) at 1.81 Å and at an angle of 176° (related by x, $y-1$, z).

4. Conclusions

The structures of the complexes isolated display the expected trends in decreasing co-ordination number with decreasing ionic radius of the Ln^{3+} ion and moreover include three structural types already described for lanthanoid complexes of terpy. It has been suggested [16] that use of MeCN for syntheses can favour inclusion of nitrate in the co-ordination sphere of the metal rather than water; we note here that the same samarium complex is obtained carrying out the synthesis in ethanol or acetonitrile.

The pK_{a1} values for terpy and tptz are 4.9 and 4.5, respectively [26], showing that terpy is a stronger base [17]. For the complexes described here, Ln–N bond lengths tend in general to be greater in tptz complexes than in the terpy analogues, as noted by others [14] in some cases, which would be expected if strength as a Lewis base correlated with strength of bond in a complex, though steric factors may also operate here too.

In this study, the complex isolated for most lanthanoids is $[Ln(tptz)(NO_3)_3(H_2O)] \cdot 2C_2H_5OH$ though a species $[Ln(tptz)(NO_3)_3(C_2H_5OH)]$ is presumably present in the solutions from which it crystallises, and in the case of ytterbium and lutetium an ethanol complex $[Ln(tptz)(NO_3)_3(C_2H_5OH)]$, albeit with a lower co-ordination number, is actually isolated.

We have described structural evidence for crowding in the $[Yb(tptz)(NO_3)_3(H_2O)]$ (**17**) molecule in particular, but this does not in itself explain why crowding is not relieved by expulsion of a water molecule and why the lutetium complex isolated is not nine co-ordinate $[Lu(tptz)(\eta^2\text{-}NO_3)_3]$ with three bidentate nitrate groups, since terpyridyl analogues $[Ln(terpy)(\eta^2\text{-}NO_3)_3]$ (Ln = Yb, Lu) have been fully characterised [2b,3]. This is not a singular phenomenon as similar terpyridyl complexes $[Ln(terpy)(\eta^2\text{-}NO_3)_2(\eta^1\text{-}NO_3)(C_2H_5OH)]$ (Ln = Er, Yb, Lu) have been described [2a,2b], also aqua complexes $[Tm(terpy)(\eta^2\text{-}NO_3)_2(\eta^1\text{-}NO_3)(H_2O)]$ [3] and $[Ln(abtpz)(\eta^2\text{-}NO_3)_2(\eta^1\text{-}NO_3)(H_2O)]$ (Ln = Y, Yb) [17].

Bidentate nitrates would be favoured by the chelate effect and it would also be expected that a bidentate nitrate group would take up less space than a monodentate nitrate group and a co-ordinated ethanol (or water) molecule. Evidently this is counterbalanced by the formation of strong bonds to the monodentate donors and also by the intramolecular hydrogen bonds between an unbound oxygen of the monodentate nitrate and a hydrogen from H_2O or C_2H_5OH. In addition, an analysis of the N–Ln–N angles, for the two coordinated pyridine rings of the tptz group show a smooth increase from 120.62(4)° for the La complex (**4**) to 128.05(7)° for the Yb complex (**16**), consistent with the shortening of the Ln–N bond length across the series. This angle in **16** is slightly narrower than that found in **17** (129.47(17)°) where the Yb atom is nine coordinate instead of 10 coordinate. Thus, the tptz ligand does not seem to be sensitive to any potential strain around the lanthanoid ion centre. However, it should also be borne in mind that our conclusions are based on the species isolated in the solid state.

Ab initio quantum mechanical calculations [27] on $Ln(NO_3)_n$ and $Ln(NO_3)_n(H_2O)_m$ ($n = 1$–3, $m = 4$–6) species indicate that bidentate behaviour of the nitrate group is preferred less over monodentate binding as more nitrate groups attach themselves to the metal ion. Water binding to the lanthanide may shift binding of the nitrate group in favour of monodentate behaviour whilst bidentate binding may be favoured by entropy effects so that several different species may be present in solution. Moving to the solid state, the balance may further be altered by crystal packing

and intermolecular forces. It should also be borne in mind that the complexes obtained in the solid state are not necessarily the most abundant species in solution, as solubility is a key important factor in deciding which species is obtained in the solid state. NMR studies on the $La(NO_3)_3$/terpy system in MeCN indicated the presence of at least seven different La-containing species in the complexation process [4].

5. Supplementary material

Crystallographic supplementary data are available from The Director, CCDC, 12 Union Road, Cambridge CB2 1EZ, UK (fax: +44 1223 336 033; e-mail: deposit@ccdc.cam.ac.uk or www: http://www.ccdc.cam.ac.uk) quoting the deposition numbers CCDC 284755–284774.

Acknowledgements

We are grateful to the University of Bath for a studentship (to L.L.O.), and to the EPSRC for funding for the purchase of the X-ray diffractometer. We acknowledge the support of the CCLRC Daresbury Laboratory through the award of beamtime. We are also grateful to Mr. T.J. Spencer for microanalyses and to Professor J.C. Anderson of Nottingham University for arranging for the analyses to be carried out.

References

[1] D.A. Durham, G.H. Frost, F.A. Hart, J. Inorg. Nucl. Chem. 31 (1969) 571.
[2] (a) S.A. Cotton, P.R. Raithby, Inorg. Chem. Commun. 2 (1999) 86; (b) B. Ahrens, S.A. Cotton, N. Feeder, O.E. Noy, P.R. Raithby, S.J. Teat, J. Chem. Soc., Dalton Trans. (2002) 2027; (c) S.A. Cotton, O.E. Noy, F. Liesener, P.R. Raithby, Inorg. Chim. Acta 344 (2003) 37.
[3] M.G.B. Drew, P.B. Iveson, M.J. Hudson, J.O. Liljenzin, L. Spjuth, P.-Y. Cordier, Å. Enarsson, C. Hill, C. Madic, J. Chem. Soc., Dalton Trans. (2000) 821.
[4] M. Fréchette, C. Bensimon, Inorg. Chem. 34 (1995) 3520.
[5] L.I. Semenova, A.H. White, Aust. J. Chem. 52 (1999) 507.
[6] P.C. Leverd, M.-C. Charbonnel, J.-P. Dognon, M. Lance, M. Nierlich, Acta Crystallogr., Sect. C 55 (1999) 368.
[7] M.S. Grigoriev, C. den Auwer, C. Madic, Acta Crystallogr., Sect. C 57 (2001) 1141.
[8] A.K. Boudalius, V. Nastopoulos, A. Terzis, C.P. Raptopoulou, S.P. Perlepes, Z. Naturforsch. B 56 (2001) 122.
[9] S.A. Cotton, J. Fawcett, V. Franckevicius, Polyhedron 21 (2002) 2055.
[10] Proceedings of the 5th OECD/NEA Information Exchange Meeting on Actinide and Fission Product Partitioning and Transmutation, Mol, Belgium, 1998; Report EUR 18898 EN; Actinide and Fission Product Partitioning and Transmutation, Status and Assessment Report, Nuclear Energy Agency, OECD, Paris, 1999, pp. 119–128.
[11] C. Musikas, in: G.R. Choppin, J.D. Navratil, W.W. Schulz (Eds.), Proceedings of the International Symposium on Actinide/Lanthanide Separations, Honolulu 1984, World Scientific, Singapore, 1985, pp. 19–30.
[12] R.H. Blessing, Acta Crystallogr., Sect. A 51 (1995) 33.
[13] SADABS, version 2.03, Bruker AXS, Madison, WI, USA, 2001.
[14] P.T. Beurskens, G. Beurskens, R. de Gelder, S. Garcia-Granda, R.O. Gould, R. Israel and J.M.M. Smits, DIRDIF-99: Program for Heavy Atom Structure Solution Methods, Nijmegen, 1999.
[15] G.M. Sheldrick, SHELXL-97: A Program for Crystal Structure Refinement, University of Göttingen, Göttingen, Germany, 1996.
[16] M.G.B. Drew, M.J. Hudson, P.B. Iveson, C. Madic, M.L. Russell, J. Chem. Soc., Dalton Trans. (2000) 2711.
[17] M.G.B. Drew, M.J. Hudson, P.B. Iveson, C. Madic, Acta Crystallogr., Sect. C 56 (2000) 434.
[18] R. Wietzke, M. Mazzanti, J.-M. Latour, J. Pécaut, Inorg. Chem. 38 (1999) 3581.
[19] G. Meyer, D. Gieseke-Vollmer, Z. Anorg. Allgem. Chem. 619 (1994) 1603.
[20] A. Lossin, G. Meyer, Z. Anorg. Allgem. Chem. 620 (1994) 428.
[21] C.J. Kepert, W.-M. Lu, L.I. Semenova, B.W. Skelton, A.H. White, Aust. J. Chem. 52 (1999) 481.
[22] D.L. Kepert, L.I. Semenova, A.B. Sobolev, A.H. White, Aust. J. Chem. 49 (1996) 1005, and references therein.
[23] R.D. Shannon, Acta Crystallogr., Sect. A 32 (1976) 751.
[24] S.A. Cotton, in: R.B. King (Ed.), Encyclopedia of Inorganic Chemistry, 2nd ed., Wiley, Chichester, 2005, p. 4838.
[25] S.A. Cotton, Lanthanides and Actinides, Macmillan, New York, 1991, p. 43.
[26] I. Hagstom, L. Spjuth, A. Enarsson, J.O. Liljenzin, M. Skalberg, M.J. Hudson, P.B. Iveson, C. Madic, P.-Y. Cordier, C. Hill, N. François, Solvent Extr. Ion Exch. 17 (1999) 221.
[27] M. Dobler, P. Guilbaud, A. Dedieu, G. Wipff, New J. Chem. 25 (2001) 1458.

and **2** are previously reported [13–15]. Cation **1** and related compounds are of interest as synthons for compounds likely to be of utility in boron neutron capture therapy (BNCT) for the treatment of cancerous tumours [16–18]. Although isostructural, the two species **1** and **2** differ in the centres of their charge location: in cation **1** the positive centre resides on the alkylammonium residue and in anion **2** the negative charge is delocalised over the monocarbaborane cluster.

The $[1\text{-}(H_3NCH_2)\text{-}closo\text{-}1,2\text{-}C_2B_{10}H_{11}]^+$ cation **1** was prepared by the previously reported route from [*closo*-1,2-$C_2B_{10}H_{12}$], via the neutral (phthalimidomethy1)-*closo*-1,2-dicarborane $[1\text{-}\{C_6H_4(CO)_2NCH_3\}\text{-}closo\text{-}1,2\text{-}C_2B_{10}H_{11}]$ and isolated as its Cl^- salt **1a** [13]. The $[1\text{-}(H_3CCH_2)\text{-}closo\text{-}1\text{-}CB_{11}H_{11}]^-$ anion **2** was made by the following variant of the published procedure [19], and isolated as its $[NEt_4]^+$ salt. Thus, the $[NEt_4]^+$ salt of the [*closo*-1-$CB_{11}H_{12}]^-$ anion (made as in Ref. [19]; 1.6 g, 5.8 mmol) was dissolved in dry thf (30 ml) and a solution of *n*-BuLi in *n*-hexane (1.6 M, 12 ml, corresponding to ca. 20 mmol of *n*-BuLi) was added dropwise. After stirring for one hour at ambient temperature, CH_3CH_2I (2 ml, ca. 24 mmol) was added dropwise and the reaction was allowed to stir for three hours. H_2O (100 ml) was then added and the thf was removed by use of a rotary thin-film evaporator. The remaining aqueous solution was extracted with diethyl ether (3×30 ml), and the combined ether layers evaporated by use of a rotary thin-film evaporator. The residual colourless oil was dissolved in H_2O (50 ml), the solution filtered, and $[NEt_4]^+Br^-$ (2.1 g, 10 mmol) slowly added to the stirred filtrate. After further stirring, the white precipitate was filtered off and dried in vacuo, to yield the $[NEt_4]^+$ salt **2a** of the $[1\text{-Et-}closo\text{-}1\text{-}CB_{11}H_{11}]^-$ anion **2** (1.25 g, 4.2 mmol, 72%). Measured NMR data for [1-Et-*closo*-1-$CB_{11}H_{11}]^-$ salt **2a**, in $(CD_3)_2CO$ at 298–300 K, ordered as assignment $\delta(^{11}B)$/ppm [δ (^1H)/ppm in square brackets] are: BH(12) −10.0 [+1.61], BH(2,3,4,5,6) −13.6 [+1.56] and BH(7,8,9,10,11) −13.6 [+1.77]; additionally δ (^1H)(BEt) at +1.87 (2H, quartet), +0.89 (3H, triplet), δ (^1H)(NEt_4) at +3.51 (8H, quartet), +1.42 (12H, triplet); additionally $\delta(^{13}C)(NEt_4)$ +52.4 and +7.0, with $\delta(^{13}C)$(cluster-bound Et) +32.5 and +14.3. A sample of the $[NEt_4]^+$ salt **2a** of anion **2** (150 mg, 500 μmol) was then dissolved in aqueous nitric acid (5%, 60 ml) and extracted with Et_2O (3×20 ml). H_2O (50 ml) was then added, and then the Et_2O was removed using a rotary thin-film evaporator. The resulting aqueous solution was cooled to 0 °C, and then $AgNO_3$ (850 mg, 500 μmol) was added with stirring. The $[Ag]^+$ salt **2b** of anion **2** precipitated as a white solid (700 mg, 252 μmol, 51%). Crystals suitable for single-crystal X-ray diffraction analysis were obtained by the slow diffusion of Et_2O into a concentrated solution of **2b** (Fig. 1) in acetone. Addition of the $[Cl]^-$ salt of **1** to the $[Ag]^+$ salt **2b** in dichloromethane, followed by overnight stirring, filtration, and subsequent evaporation of the solvent, led quantitatively to the formation of the desired $[1\text{-}(H_3NCH_2)\text{-}closo\text{-}1,2\text{-}C_2B_{10}H_{11}][1\text{-}(H_3CCH_2)\text{-}closo\text{-}1\text{-}CB_{11}H_{11}]$ salt **3**. The 1:1 water solvate **3a** of the salt **3** was then identified by single-crystal X-ray diffraction analysis (Fig. 2), for which crystals were obtained by the slow diffusion of *n*-hexane into a concentrated solution of the $[1\text{-}(H_3NCH_2)\text{-}closo\text{-}1,2\text{-}C_2B_{10}H_{11}][1\text{-}(H_3CCH_2)\text{-}closo\text{-}1\text{-}CB_{11}H_{11}]$ salt **3** in dichloromethane in air. We understand that an *ortho*-dicarborane derivative with an $\{NH_3\}$ moiety has not been structurally characterised before, and, as such, the result may be of interest to chemists involved in BNCT research [16–18] (we thank a referee for pointing this out).

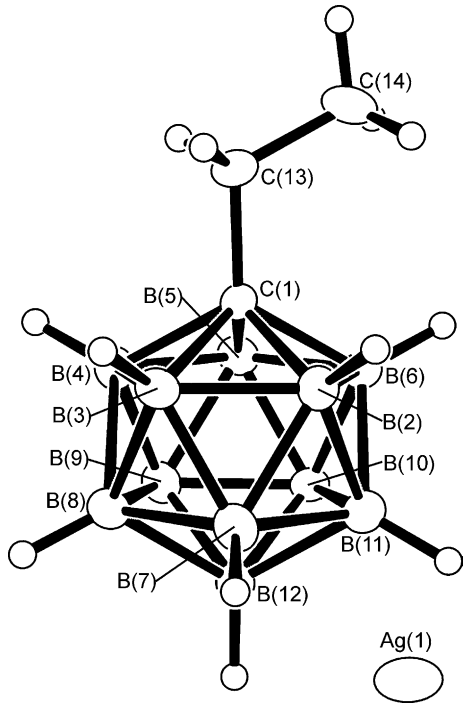

Fig. 1. ORTEP-type illustration of the basic unit of the crystallographically determined structure of $[Ag]^+[1\text{-}(H_3CCH_2)\text{-}closo\text{-}1\text{-}CB_{11}H_{11}]^-$ (species **2b**). Distances from C(1) to boron range from 1.713(2) to 1.735(2) Å; C(1)–C(13) is 1.533(1) and C(13)–C(14) is 1.509(2) Å. The $[Ag]^+$ cation is close to H(7) at 2.078 Å; the associated distance Ag(1)–B(7) is 2.666 Å. In the extended crystal lattice the $[Ag]^+$ cation is associated with three $[1\text{-Et-}closo\text{-}1\text{-}CB_{11}H_{11}]^-$ anions (Fig. 6). Crystallographic data for $Ag[1\text{-}(H_3CCH_2)\text{-}closo\text{-}1\text{-}CB_{11}H_{11}]$ species **2b**, $[Ag][1\text{-}(H_3CCH_2)\text{-}closo\text{-}1\text{-}CB_{11}H_{11}]$, $C_3H_{16}AgB_{11}$, $M = 278.94$, monoclinic ($0.26 \times 0.20 \times 0.13$ mm, colourless prism from diffusion of diethyl ether into a solution in acetone), space group $P2_1/c$, $a = 11.7166(4)$, $b = 9.8206(3)$, $c = 9.5221(3)$ Å, $\beta = 92.879(2)°$, $U = 1094.27(6)$ Å^3, $D_{calc} = 1.693$ Mg m^{-3}, $Z = 4$, Mo Kα, $\lambda = 0.71073$ Å, $\mu = 1.783$ mm^{-1}, $T = 150(2)$ K, $R_1 = 0.0947$ for 1837 reflections with $I > 2\sigma(I)$, and $wR_2 = 0.2872$ for all 2138 unique reflections; CCDC 280664, Crystallographic methods and programmes were standard; coordinates, etc., can be obtained free of charge at www.ccdc.cam.ac.uk/conts/retrieving.html [or from The Director, CCDC, 12, Union Road, Cambridge CB2 1EZ, UK (fax: +44 1223 336033; e-mail: deposit@ccdc.cam.ac.uk or http://www.ccdc.cam.ac.uk)].

We have not been able to obtain crystals of **3** without solvent. Such a solvation problem may not be a problem with the as yet unsynthesised salt $[C_3B_9H_{12}]^+$ $[CB_{11}H_{12}]^-$ because, presumably, the non-substituted spherical anions would mutually pack more efficiently, and therefore, perhaps, in their solid-state properties mimic the very high melting points of the neutral [*closo*-$C_2B_{10}H_{12}$] isomers that

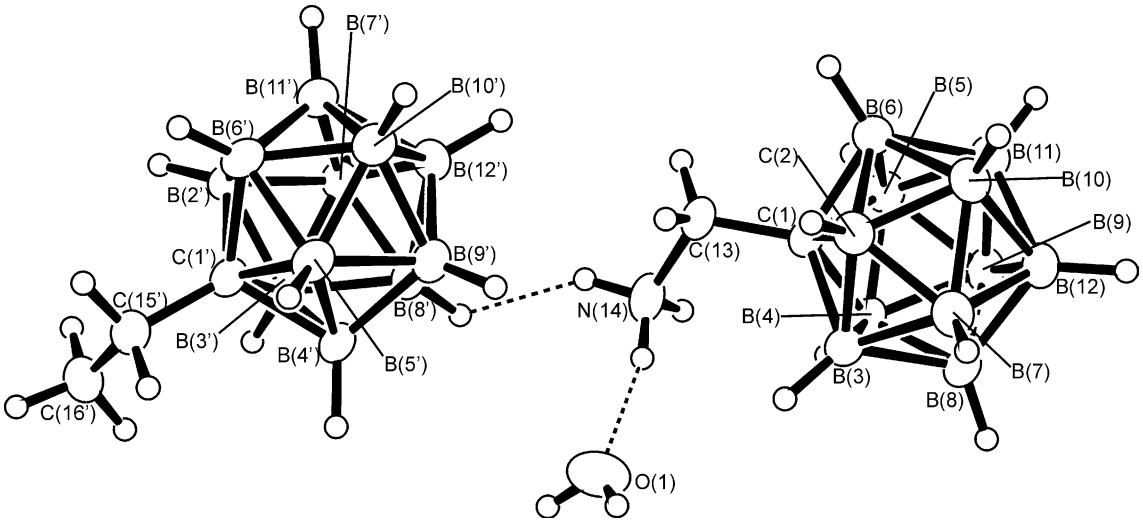

Fig. 2. ORTEP-type illustration of the basic unit of the crystallographically determined structure of $[1\text{-}(H_3NCH_2)\text{-}closo\text{-}1,2\text{-}C_2B_{10}H_{11}]^+[1\text{-}(H_3CCH_2)\text{-}closo\text{-}1\text{-}CB_{11}H_{11}]^-[H_2O]$ (species **3a**). The hatched lines represent hydrogen bonds and dihydrogen bonds. Interatomic distances associated with these bonds are C(13)–N(14) 1.471(3), N(14)–B(8′) 3.346(3), N(14)–O(1) 2.755(3), H(8′)–H(14B) 1.90 and O(1)–H(14A) 1.89 Å; N–H–H and B–H–H angles are 110° and 146° respectively. Within the $[1\text{-}(H_3CCH_2)\text{-}closo\text{-}1\text{-}CB_{11}H_{11}]^-$ anion (left) selected interatomic distances are C(1′)–C(15′) 1.532(3) and C(15′)–C(16′) 1.523(3) Å with distances from C(1′) to boron ranging from 1.705(3) to 1.729(3) Å. Angle C(1′)C(15′)C(16′) is 115.2(2)°. Within the $[1\text{-}(H_3NCH_2)\text{-}closo\text{-}1,2\text{-}C_2B_{10}H_{11}]^+$ cation (right) selected interatomic distances are C(1)–C(2) 1.640(2), C(1)–C(13) 1.517(2) and C(13)–N(14) 1.471(3) Å, with distances from C(1) to boron ranging from 1.705(3) to 1.729(3) Å. Angle C(1)C(13)N(14) is 113.5(2)°. Crystallographic methods and programmes were standard; coordinates, etc., can be obtained free of charge at www.ccdc.cam.ac.uk/conts/retrieving.html [or from The Director, CCDC, 12, Union Road, Cambridge CB2 1EZ, UK (fax: +44 1223 336033; e-mail: deposit@ccdc.cam.ac.uk or http://www.ccdc.cam.ac.uk)], Crystallographic data for $[1\text{-}(H_3NCH_2)\text{-}closo\text{-}1,2\text{-}C_2B_{10}H_{11}]$ $[1\text{-}(H_3CCH_2)\text{-}closo\text{-}1\text{-}CB_{11}H_{10.935}Cl_{0.065}]$ $[H_2O]$ **3a**: $C_6H_{33.935}B_{21}NOCl_{0.065}$, $M = 365.76$, monoclinic ($0.79 \times 0.33 \times 0.20$ mm, colourless prism from diffusion of hexane into a solution in CH_2Cl_2), space group $P2_1/c$, $a = 16.2035(3)$, $b = 10.3111(2)$, $c = 13.8135(2)$ Å, $\beta = 106.4920(10)°$, $U = 2212.95(7)$ Å^3, $D_{calc} = 1.091$ Mg m^{-3}, $Z = 4$, Mo $K\alpha$, $\lambda = 0.71073$ Å, $\mu = 0.051$ mm^{-1}, $T = 150(2)$ K, $R_1 = 0.0725$ for 3419 reflections with $I > 2\sigma(I)$, and $wR_2 = 0.2084$ for all 4325 unique reflections; CCDC 280665.

do not exhibit solvent inclusion. Another manifestation of solvent behaviour in the present system arose from the reactivity of the alkylammonium residue on the $[(H_3NCH_2)C_2B_{10}H_{11}]^+$ cation **1**. Cation **1** very readily formed the cationic iminium derivative $[(CH_3)C{=}NH\text{-}CH_2C_2B_{10}H_{11}]^+$ **4** in preliminary crystallisation attempts involving acetone as solvent. In fact, in the present system, anion **1** proved to be a relatively efficient scavenger of any acetone residues during crystallisation attempts using a variety of solvent systems if apparatus was insufficiently purged of traces of residual acetone that has been used for cleaning purposes, and salts of **4** rather than of **1** were thence often obtained as products. The phenomenon has been noted previously in the formation of the 'globule–globule assembly' $[C_2B_{10}H_{11}CH_2NH{=}CH(CH_3)_2]_4[W_{10}O_{32}][H_2O]_2[(CH_3)_2CO]_4$ [9]. Arising from this behaviour, as part of this current report we now are also able to describe the crystallographically determined structure of the $[1\text{-}(H_3CCH_2)\text{-}closo\text{-}1\text{-}CB_{11}H_{11}]^-$ salt **4a** of the iminium cation **4** (Fig. 3). Crystals suitable for single-crystal X-ray diffraction analysis were obtained by the slow diffusion of Et_2O into a concentrated solution of the $[1\text{-}(H_3NCH_2)\text{-}closo\text{-}1,2\text{-}C_2B_{10}H_{11}][1\text{-}(H_3CCH_2)\text{-}closo\text{-}1\text{-}CB_{11}H_{11}]$ salt **3** in acetone.

One reason for the developing interest in these types of species is the examination for intermolecular interactions. In this context it may be noted that cage CH···X interactions in the solid-state structures of icosahedral carbaboranes are recently reviewed [20]. It is apparent from the basic structural unit of the $[1\text{-}(H_3NCH_2)\text{-}closo\text{-}1,2\text{-}C_2B_{10}H_{11}]^+[1\text{-}(H_3CCH_2)\text{-}closo\text{-}1\text{-}CB_{11}H_{11}]^-[H_2O]$ salt **3a** (Fig. 2) that interionic interaction occurs. As mentioned above, although the cation and anion in this salt are isostructural, the two species differ in the centres of their charge location: the positive charge of the $[1\text{-}(H_3NCH_2)\text{-}closo\text{-}1,2\text{-}C_2B_{10}H_{11}]^+$ cation is located on the alkylammonium residue whereas the negative charge for the $[1\text{-}(H_3CCH_2)\text{-}closo\text{-}1\text{-}CB_{11}H_{11}]^-$ anion is delocalised over the monocarbaborane cage, albeit with some dipolar character with the more negative end of the charge distribution around the pentagonal pyramidal $\{B_6H_6\}$ cap distal from the C(1) vertex [14,21]. The positively charged alkylammonium residue contributes to the presence of the hydrogen bonding observed between the {NH} hydrogen atom in position 14B and the oxygen atom in the water molecule, as well as to the presence of the intermolecular dihydrogen bond seen between the hydrogen atoms in {BH} position 8 in the anion and in {NH} position 14A in the cation. The hydrogen bond and the dihydrogen bonds are marked in Fig. 2 as hatched lines.

The hydrogen-bond distance of 1.89 Å from the oxygen atom O(1) in the water molecule to the alkylammonium hydrogen atom, {NH} position 14A, is well within the range for typical hydrogen bonds. The distance from the

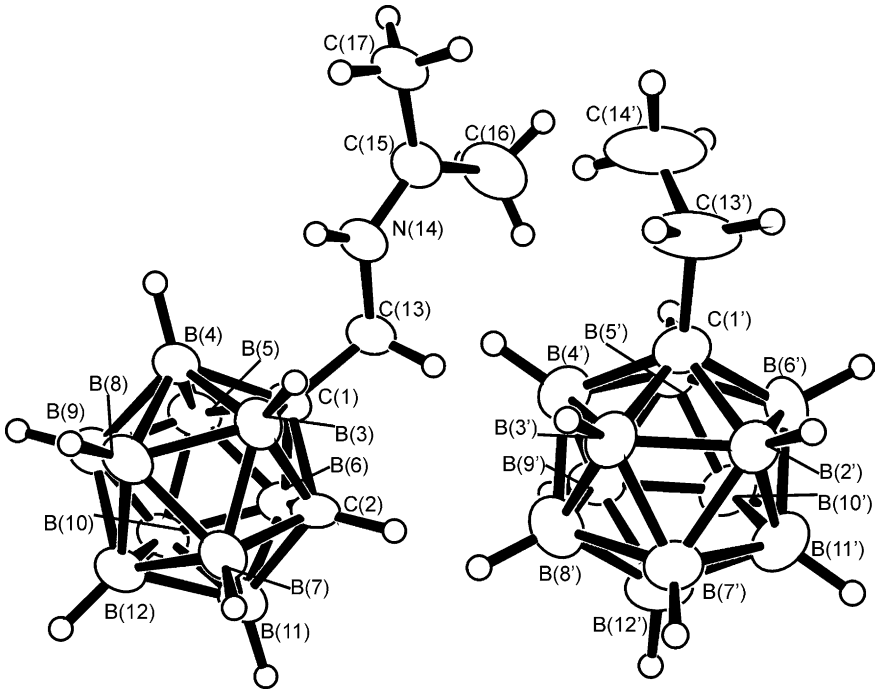

Fig. 3. ORTEP-type illustration of a basic unit of the crystallographically determined structure of [1-{$(CH_3)_2C{=}NHCH_2$}-*closo*-1,2-$C_2B_{10}H_{11}$]$^+$-[1-(H_3CCH_2)-*closo*-1-$CB_{11}H_{11}$]$^-$ (species **4a**). Within the [1-{$(CH_3)_2C{=}NHCH_2$}-*closo*-1,2-$C_2B_{10}H_{11}$]$^+$ cation (left) selected interatomic distances are C(1)–C(13) 1.498(5), C(13)–N(14) 1.457(5) and N(14)–C(15) 1.285(5) Å, with distances from C(1) to boron ranging from 1.700(6) to 1.723(6) Å. Angles C(1)C(13)N(14) C(13)N(14)C(15) are 112.5(3)° and 126.8(4)° respectively. Within the [1-Et-*closo*-1-$CB_{11}H_{11}$]$^-$ anion (right) selected interatomic distances are C(1′)–C(13′) 1.514(6) and C(13′)–C(14′) 1.421(6) Å, with distances from C(1′) to boron ranging from 1.706(6) to 1.734(7) Å. Note that in this projection the second hydrogen atom on the C(13′) {CH_2} grouping is hidden. Crystallographic methods and programmes were standard; coordinates, etc., can be obtained free of charge at www.ccdc.cam.ac.uk/conts/retrieving.html [or from The Director, CCDC, 12, Union Road, Cambridge CB2 1EZ, UK (fax: +44 1223 336033; e-mail: deposit@ccdc.cam.ac.uk or http://www.ccdc.cam.ac.uk)], Crystallographic data for [$(CH_3)C{=}NHCH_2C_2B_{10}H_{11}$][1-($H_3CCH_2$)-*closo*-1-$CB_{11}H_{11}$] **4a**: $C_9H_{36}B_{21}N$, $M = 385.4$, orthorhombic ($0.43 \times 0.13 \times 0.13$ mm, colourless prism from diffusion of diethyl ether into a solution in acetone), space group $P2_12_12_1$, $a = 7.2355(4)$, $b = 16.1780(9)$, $c = 20.4799(14)$ Å, $U = 2397.3(2)$ Å^3, $D_{calc} = 1.068$ Mg m^{-3}, $Z = 4$, Mo Kα, $\lambda = 0.71073$ Å, $\mu = 0.047$ mm^{-1}, $T = 150(2)$ K, $R_1 = 0.0607$ for 1896 reflections with $I > 2\sigma(I)$, and $wR_2 = 0.1580$ for all 3114 unique reflections; CCDC 280666.

hydrogen donor N(14) to hydrogen acceptor O(1) is 2.755 (3) Å, short when compared to a mean typical NHO hydrogen-bonded distance of 2.89 Å [22]. The positive charge associated with the alkylammonium residue will contribute to this stronger bonding; the hydrogen bonding will also be increased by the negative charge on the anion **2**, enhanced by the intracluster polarity mentioned in the previous paragraph. For similar reasons the NH–HB dihydrogen-bond distance of 1.90 Å is also towards the shorter end of the range of dihydrogen-bonding distances, typical such distances being held to range from 1.7 to 2.2 Å, with an average distance of 1.96 Å [23]. The N–H–H angle is also larger than the H–H–B angle, confirming the presence of a true dihydrogen bond, these angles being 146° and 110° respectively. A fragment of the extended solid-state structure of [1-(H_3NCH_2)-*closo*-1,2-$C_2B_{10}H_{11}$]$^+$[1-(H_3CCH_2)-*closo*-1-$CB_{11}H_{11}$]$^-$[H_2O] **3a** is illustrated in Fig. 4. There are no coordination polymers or networks as the hydrogen bonding and dihydrogen bonding only occur among the water molecule, the cation and the anion within a single asymmetric unit as in Fig. 2.

By contrast, in the extended crystal structure of the [1-{$(CH_3)_2C{=}NHCH_2$}-*closo*-1,2-$C_2B_{10}H_{11}$]$^+$[1-(H_3CCH_2)-*closo*-1-$CB_{11}H_{11}$]$^-$ salt **4a** there appear to be no significant

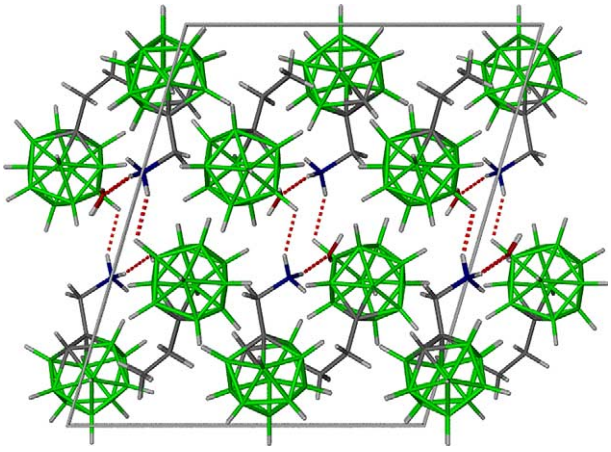

Fig. 4. Illustration of a fragment of the extended solid-state structure of [1-(H_3NCH_2)-*closo*-1,2-$C_2B_{10}H_{11}$]$^+$[1-(H_3CCH_2)-*closo*-1-$CB_{11}H_{11}$]$^-$ · H_2O (species **3a**). The view is looking directly down the *b*-axis of the unit cell. The unit cell is marked on as a grey box and the dotted red lines show the hydrogen and dihydrogen interactions. (For interpretation of the references to colour in this figure legend, the reader is referred to the web version of this article.)

specific cation–anion interionic interactions of note. The basic unit of the structure of **4a** is shown in Fig. 3 above. The lattice can be regarded as being made up of layers of

cations with the anions packed between the layers (Fig. 5, upper diagram). A referee has suggested that CH···HB interactions [20] can contribute strongly to the observed cage ordering in **4a** and also in **3a** above. It is of interest that the pattern of layer assembly in the crystallographic *bc* plane that is evident from Fig. 5 closely resembles the packing of anions within the anionic layers of on the crystal structures of the $[NEt_4]^+$ salts of several of the smaller C-phenyl monocarbaborane anions $[PhCB_nH_n]^-$. Specifically the $[NEt_4]^+$ salts of the $[PhCB_6H_6]^-$, $PhCB_7H_7]^-$ and $[PhCB_8H_8]^-$ anions crystallise with alternate layers of $[NEt_4]^+$ cations and $[PhCB_nH_n]^-$ anions [11,12]. Within the anion layers, exemplified by the structure of $[NEt_4]^+[PhCB_6H_6]^-$ (Fig. 5, lower diagram), the phenyl groups pack among the carbaborane units in a very similar manner to the $\{CH_2CH_3\}$ and $\{CH_2NH_3\}$ groups in compound **4a** (Fig. 5, upper diagram).

There is considerable contemporary interest in the interaction of the Ag^+ cation with monocarbaborane anions [14,24–35]. In this regard, aspects of the extended solid-state structure of the precursive $[Ag]^+$ salt **2b** of the $[1\text{-}(H_3CCH_2)\text{-}closo\text{-}1\text{-}CB_{11}H_{11}]^-$ anion **2** also merit brief comment. The salt **2b** crystallises in a monoclinic crystal system and is solved in space group $P2_1/c$. The basic $[Ag]^+[1\text{-}(H_3CCH_2)\text{-}closo\text{-}1\text{-}CB_{11}H_{11}]^-$ unit is shown in Fig. 1 above. In the crystal lattice the Ag^+ cation coordinates to three separate monocarbaborane anions (Fig. 6). Coordination occurs via monocarbaborane hydrogen atoms, with the first anion (the one in Fig. 1) coordinating via a single hydrogen atom in its {BH} position 7, the second anion coordinating via a hydrogen atom in its {BH} position 10, and with the third anion coordinating via two adjacent hydrogen atoms in its {BH} positions 8 and 9. These together result in a fourfold coordination sphere around the Ag^+ cation that is distorted slightly from regular tetrahedral geometry. The Ag–H interatomic distances to the first two anions, Ag(1)–H(7) at 2.078 and Ag(1)–H(10) at 1.943 Å, of which each exhibits only one such interaction to a particular Ag^+ cation, are within an atom-radius sum of 2.34 [cationic tetrahedral silver(I) at 1.14 Å and a hydrogen Van der Waals radius of, say, 1.20 Å], implying significant attractive interaction. The attractions to the doubly-coordinating anion are somewhat weaker, with the two somewhat longer distances Ag(1)–H(8) of 2.352 and Ag(1)–H(9) of 2.301 Å.

The extended solid-state structure of **2b** is characterised by layers that pack parallel to the *bc* plane of the unit cell. These layers are two asymmetric units in width and are held together by the Ag–H interactions detailed in Fig. 6 and discussed in the previous paragraph. The polar interactions between the Ag^+ cations and the monocarbaborane anions dictate each of these layers, each consisting of

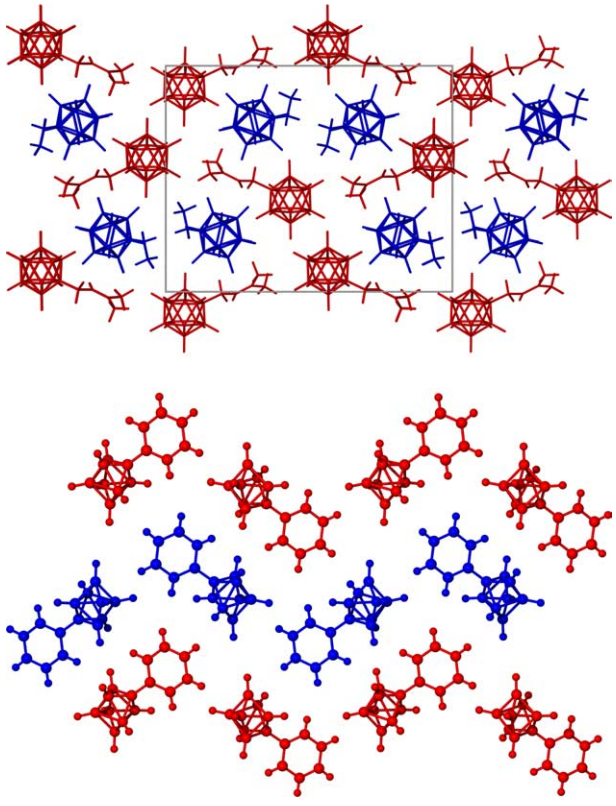

Fig. 5. *Upper diagram:* Illustration of a fragment of the extended solid-state structure of $[1\text{-}\{(CH_3)_2CNHCH_2\}\text{-}closo\text{-}1,2\text{-}C_2B_{10}H_{11}]^+$-$[1\text{-}(H_3CCH_2)\text{-}closo\text{-}1\text{-}CB_{11}H_{11}]^-$ (species **4a**). The view is looking directly down the *a*-axis of the unit cell. The unit cell is drawn as a grey box. Cations are coloured red and anions are coloured blue. *Lower diagram*: Illustration of a fragment of the extended solid-state structure of $[NEt_4]^+[PhCB_7H_7]^-$ (data from reference [11]; CCDC 164852) to illustrate the similarities in packing with species **4a**. (For interpretation of the references to colour in this figure legend, the reader is referred to the web version of this article.)

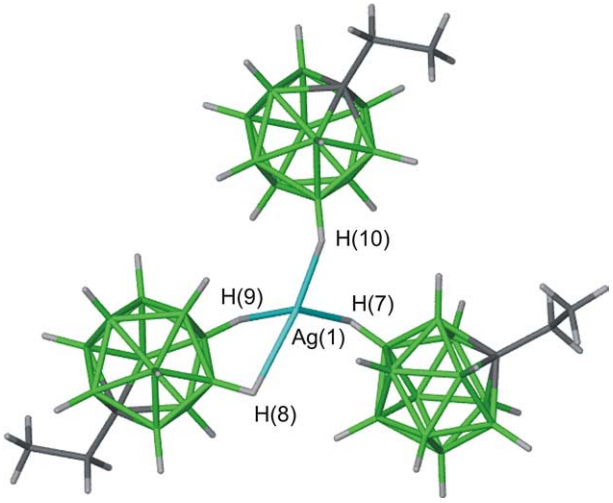

Fig. 6. Illustration to show the silver cation environment in the solid-state structure of $[Ag]^+[1\text{-}(H_3CCH_2)\text{-}closo\text{-}1\text{-}CB_{11}H_{11}]^-$ (species **2b**). The Ag^+ cation is coordinated to four hydrogen atoms in a fourfold coordination mode that is slightly distorted from regular tetrahedral geometry. Relevant interatomic distances are Ag(1)–B(7) 2.666(13), Ag(1)–B(8) 2.713(11), Ag(1)–B(9) 2.689(12), Ag(1)–B(10) 2.764(12), Ag(1)–H(7) 2.078, Ag(1)–H(8) 2.352, Ag(1)–H(9) 2.301 and Ag(1)–H(10) 1.943 Å. The H–Ag–H angles are 76.4°, 79.7°, 104.1°, 110.0°, 128.1° and 140.7°.

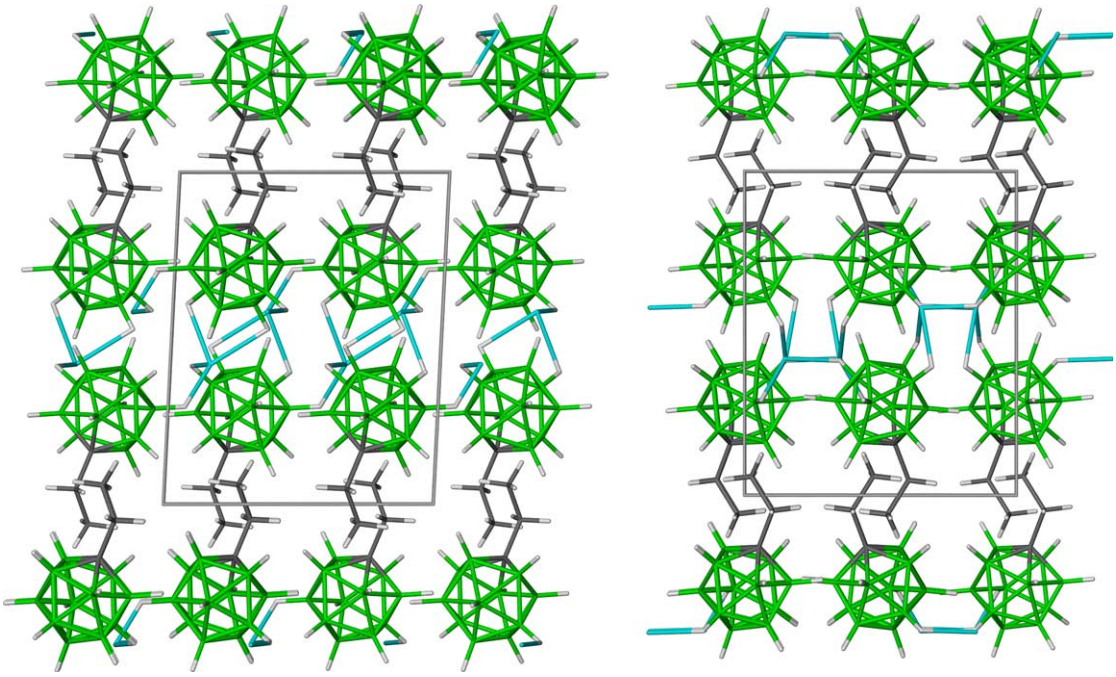

Fig. 7. Views showing fragments of the extended crystal structure for $[Ag]^+[1\text{-Et-}closo\text{-}1\text{-}CB_{11}H_{11}]^-$ (species **2b**): left, viewed down the *b*-axis, and right, viewed down the *c*-axis. The unit cell is marked on the diagrams as a grey box and the Ag^+ cations are shown in blue. The dotted red lines distinguish where the parallel double layers of anions mesh together with their lipophilic C-ethyl groups interlocking. The two-sub-layers of anions in the double layers are held together internally by B–H–Ag interaction with the central core of $[Ag]^+$ cations (see Fig. 6).

Ag^+ cations held between two sub-layers of anions. The layers then stack by means of lipophilic ethyl–ethyl interactions between ethyl groups from adjacent layers. Illustrative fragments of the extended solid-state structure are represented in Fig. 7.

Interestingly in the context of these solid-state silver-to-cluster interactions is that negative-ion electrospray mass-spectrometry results for liquid solutions of **2b** show not only an isotopomer mass-envelope with an intensity maximum of *m/z* 171.1, corresponding to the uncoordinated $\{C_3B_{11}H_{16}\}^-$ anion **2**, but also a mass-envelope with an intensity maximum of *m/z* 450.0, which corresponds to two anions **2** coordinated to the $[Ag]^+$ cation, viz. an $\{Ag(C_3B_{11}H_{16})_2\}^-$ assembly. This suggests that the associations between the $[Ag]^+$ cations and monocarbaborane anions may well persist to a significant extent in solution. We are currently examining a series of several silver salts of the monocarbaboranes for this type of anion–cation interactive behaviour.

Acknowledgements

We thank the Basque Government for financial support, and the UK DTI for support of our monocarbaborane work. We also acknowledge support from the UK EPSRC for equipment grants (J/56929, L/49505 and R/61949) and for contributions to a Research DTA for M.J.C. We also thank Ian Moss and Richard Taylor of Dow Corning Ltd. for their good offices, and Colin Kilner for assistance with X-ray crystallography.

References

[1] W.H. Knoth, J. Am. Chem. Soc. 89 (1967) 1274.
[2] W.H. Knoth, Inorg. Chem. 10 (1971) 598.
[3] B. Štíbr, Chem. Rev. 92 (1992) 225.
[4] See, for example, and references cited therein: B. Štíbr, Proc. Ind. Nat. Sci. Acad. 6 (2002) 487.
[5] B. Grüner, B. Štíbr, J. Holub, I. Císařová, Eur. J. Inorg. Chem. (2003) 1533.
[6] B. Grüner, B. Štíbr, R. Kivekäs, R. Sillanpää, P. Stopka, F. Teixidor, C. Viñas, Chem. Eur. J. (2003) 6115.
[7] B. Štíbr, J. Organomet. Chem. 690 (2005) 2694.
[8] J. Holub, B. Grüner, D.S. Perekalin, D.G. Golovanov, K.A. Lyssenko, P.V. Petrovskii, A.R. Kudinov, B. Štíbr, Inorg. Chem. 44 (2005) 1655.
[9] R. Macías, J.D. Kennedy, M. Thornton-Pett, P. Román, Cryst. Eng. Commun. 5 (2003) 93.
[10] A. Franken, C.A. Kilner, M. Thornton-Pett, J.D. Kennedy, J. Chem. Soc., Chem. Commun. (2002) 2048.
[11] S.L. Shea, J. Bould, M.G.S. Londesborough, S.D. Perera, A. Franken, D.L. Ormsby, T. Jelínek, B. Štíbr, J. Holub, C.A. Kilner, M. Thornton-Pett, J.D. Kennedy, Pure Appl. Chem. 75 (2003) 1239.
[12] S.L. Shea, S.D. Perera, J. Bould, A. Franken, T. Jelínek, J.D. Kennedy, C.A. Kilner, M.G.S. Londesborough, M. Thornton-Pett, in: Yu. Bubnov (Ed.) Boron Chemistry at the Beginning of the 21st Century Editorial URSS, Moscow, 2003, pp. 27–35.
[13] J.G. Wilson, A.K.M. Anisuzzaman, F. Alam, A.H. Soloway, Inorg. Chem. 31 (1992) 1955.
[14] T. Jelínek, P. Baldwin, W.R. Scheidt, C.A. Reed, Inorg. Chem. 32 (1993) 1982.
[15] A.S. Larsen, J.D. Holbray, F.S. Tham, C.A. Reed, J. Am. Chem. Soc. 122 (2000) 7264.
[16] J. Carlsson, L. Gedda, C. Gronvik, T. Hartman, A. Lindström, P. Lindström, H. Lundqvist, A. Lövqvist, J. Malmqvist, P. Olsson, M. Essand, J. Ponten, S. Sjöberg, B. Westermark, Int. J. Radiat. Oncol. Biol. Phys. 30 (1994) 105.

[17] A.H. Soloway, W. Tjarks, B.A. Barnum, F.G. Rong, R.F. Barth, I.M. Codogni, J.G. Wilson, Chem. Rev. 98 (1998) 1515.
[18] A.S. Batsanov, A.E. Goeat, J.A.K. Howard, A.K. Hughes, J.M. Malget, J. Chem. Soc., Dalton Trans. (2001) 1820.
[19] J. Plešek, T. Jelínek, E. Drdáková, S. Heřmánek, B. Štíbr, Collect. Czech. Chem. Commun. 49 (1984) 1559.
[20] M.A. Fox, A.K. Hughes, Coord. Chem. Rev. 248 (2004) 457.
[21] T. Jelínek, J. Plešek, S. Heřmánek, B. Štíbr, Collect. Czech. Chem. Commun. 51 (1986) 819.
[22] S.C. Wallwork, Acta Crystallogr. 15 (1962) 758.
[23] T.B. Richardson, S. Gala, R.H. Crabtree, J. Am. Chem. Soc. 117 (1995) 12875.
[24] K. Shelly, D.C. Finster, Y.J. Lee, W.R. Scheidt, C.A. Reed, J. Am. Chem. Soc. 107 (1985) 5955.
[25] Z.W. Xie, T. Jelínek, R. Bau, C.A. Reed, J. Am. Chem. Soc. 116 (1994) 1907.
[26] Z.W. Xie, R. Bau, C.A. Reed, Angew. Chem., Int. Edn. Engl. 33 (1994) 2433.
[27] S.V. Ivanov, A.J. Lupinetti, S.M. Miller, O.P. Anderson, K.A. Solntsev, S.H. Strauss, Inorg. Chem. 34 (1995) 6419.
[28] S.V. Ivanov, J.J. Rockwell, S.M. Miller, O.P. Anderson, K.A. Solntsev, S.H. Strauss, Inorg. Chem. 35 (1996) 7882.
[29] Z.W. Xie, B.M. Wu, T.C.W. Mak, J. Manning, T.C.W. Mak, C.A. Reed, J. Chem. Soc., Dalton Trans. (1997) 1213.
[30] Z. Xie, C.W. Tsang, E.T.P. Sze, Q. Yang, D.T.W. Chan, T.C.W. Mak, Inorg. Chem. 37 (1998) 6444.
[31] C.W. Tsang, Q.C. Yang, E.T.P. Sze, T.C.W. Mak, D.T.W. Chan, Z. Xie, Inorg. Chem. 39 (2000) 3582.
[32] C.-W. Tsang, Q. Yang, E.T.-P. Sze, T.C.W. Mak, D.T.W. Chan, Z. Xie, Inorg. Chem. 39 (2000) 5851.
[33] N.J. Patmore, M.F. Mahon, J.W. Steed, A.S. Weller, J. Chem. Soc., Dalton Trans. (2001) 277.
[34] D.D. Ellis, J.C. Jeffery, P.A. Jellis, J.A. Kautz, F.G.A. Stone, Inorg. Chem. 40 (2001) 2041.
[35] M.A. Fox, M.F. Mahon, N.J. Patmore, A.S. Weller, Inorg. Chem. 41 (2002) 4567.

complexes of bis(benzimidazolyl)-thioether donors with N_2S [5–7], N_2S_2 [8–12] and N_2S_3 [13–17] donor sets have been synthesized as models for the active sites in proteins and their structures, spectra and redox behaviour have been investigated with the goal of relating the electronic structure properties to the active site reactivity.

In our laboratory we have undertaken a systematic structural, spectroscopic and electrochemical study on a series of mononuclear copper(II) complexes of linear polydentate bis(benzimidazolyl)-thioether/amine/pyridine ligands [7,18–20] offering N and S donor atoms. The copper(II) complexes of nitrogen and sulfur containing Schiff base ligands have been demonstrated as valid models for blue copper proteins. Also, there is a continuing interest in investigating the relationship between the redox potentials and other electrochemical parameters and the spectral/geometrical parameters of Schiff base metal complexes, which could be the result of steric and electronic effects [21]. In this report, we describe the synthesis of copper(II) complexes of di-, tri-, tetra- and pentadentate ligands (Scheme 1) containing heterocyclic N, imine N and thioether S donors with different and varying steric demands. The 3N ligands **L1** and **L2** have been designed as they have the ability to form copper(II) complexes in a meridional rather than facial coordination mode. Two thioether sulfur atoms have been incorporated into the 3N framework of **L1/L2** to offer a N_3S_2 donor set (**L3**). The ligand **L4** has been synthesized to generate a novel CuN_2S_2 coordination geometry with steric constraints, to help in understanding the role of the central pyridine nitrogen in **L3**. The 2N ligands **L5** and **L6** are sterically constrained to impose geometric distortions in bis-complexes of copper(II). The X-ray crystal structure of the copper(II) complex of **L2** has been successfully determined. The spectral and electrochemical properties of the complexes have been studied and the results discussed.

2. Results and discussion

2.1. Synthesis

A series of systematically varied ligands have been synthesized with the aim to understand the effect of ligand electronic and steric factors upon the structure and spectra of the copper(II) complexes. The ligands **L1**, **L2** and **L3** have been synthesized using the reported procedure with slight modifications, by condensing 2,6-pyridinedicarboxaldehyde [22] with 2,4,6-trimethylaniline, 2,6-diisopropylaniline and 2-(methylthio)aniline, respectively. The ligands **L4**, **L5** and **L6** have been obtained by the condensation of isophthalaldehyde with the corresponding sterically hindered anilines. The results of elemental analyses of **L1**–**L6** were satisfactory and the ^1H and ^{13}C NMR confirmed the identity of the ligands. All the Schiff base ligands, except **L6**, readily form complexes on treating one or two equivalents of them with copper(II) salts in methanol at room temperature. The perchlorate complexes were synthesized in order to avoid the competing coordination of chloride ions to copper(II) in the presence of weakly coordinating thioether sulfur donors. Our attempt to synthesize $[Cu(L6)_2]^{2+}$ was unsuccessful and no pure solid product could be isolated from the brown solutions obtained on mixing the ligand **L6** and copper(II) perchlorate. The stoichiometries of the complexes were derived from elemental analysis and conductivity studies and that of complex **2** was confirmed by determining its X-ray crystal structure. The observed values of molar conductance suggest [23] that the complexes **1**, **2** and **4a** (30–60 Ω^{-1} cm^2 mol^{-1}) behave as neutral species, while the complexes **3**–**5** (160–205 Ω^{-1} cm^2 mol^{-1}) exist as 1:2 electrolytes in solution. The molar conductance (90 Ω^{-1} cm^2 mol^{-1}) of **3a** suggests that it behaves as 1:1 electrolyte in solution. The IR spectral data of the complexes support the coordination of the ligands to copper(II). The C=N (1700–1580 cm^{-1}) and C–S (**L3**, 690; **L6**,

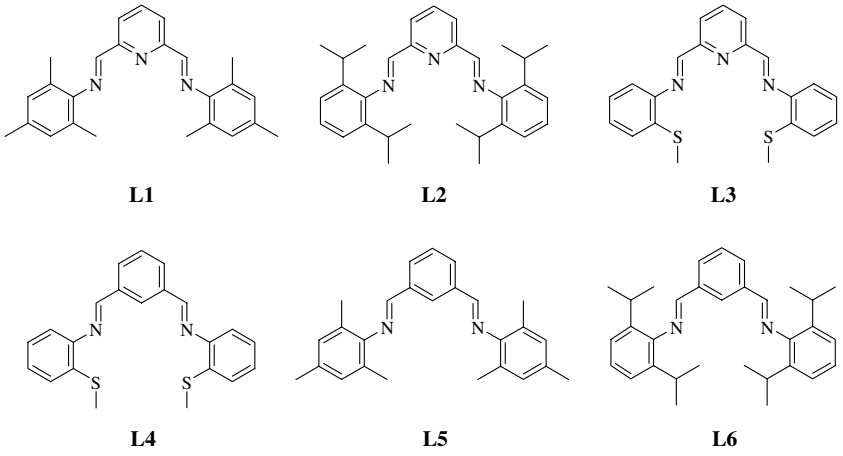

Scheme 1.

685 cm^{-1}) stretching vibrations of the ligands are shifted to lower frequencies (ν(C=N), 1600–1470 cm^{-1}; ν(C–S), 645–635 cm^{-1}) upon complex formation. The intense bands observed around 1095 and 625 cm^{-1} for the perchlorate complexes are due to ν(Cl–O) of uncoordinated perchlorate anions.

2.2. Description of the structure of [Cu(L2)Cl_2] (2)

The ORTEP representation of the structure of the complex including the atom numbering scheme is shown in Fig. 1. The crystallographic data are given in Table 1 while the bond lengths and bond angles are collected in Table 2. The structure of the complex molecule involves a five-coordinate CuN_3Cl_2 chromophore constituted by two imine (N9, N23) and one pyridine (N2) nitrogen of the tridentate ligand **L2** and two chloride ions. The geometry around copper(II) is best described as distorted square pyramidal [24], as evident from the value of the trigonal index [11] τ of 0.18 [$\tau = (\beta - \alpha)/60$, where α = N2–Cu1–Cl36 = 160.42(5)° and β = N23–Cu1–N9 = 149.63(7)°; for perfect square pyramidal and trigonal bipyramidal geometries the τ values are zero and unity, respectively]. The N9, N23 and N2 nitrogen atoms of the meridionally coordinated **L2** ligand and one of the chloride ions (Cl36) occupy the corners of the square plane. The other chloride ion (Cl37) is axially coordinated at an average angle of 99.43° to the CuN_3Cl plane. The Cu–N_{py} (1.9523 Å) and Cu–N_{imine} bond distances (2.1203, 2.1482 Å) fall in the range of values found for similar complexes [25,26]. The axial chloride ion is located at a distance (2.391 Å) longer than the equatorially located chloride ion (2.203 Å). The two phenyl rings are almost parallel to each other as in this arrangement the steric interaction between them is minimized. Also, interestingly, the bulky isopropyl substituents on the phenyl rings are pushed away from the chloride ions and hence there is no steric clash between them.

Table 1
Crystal data and structure refinement for the complex [Cu(L2)Cl_2] (**2**)

Empirical formula	$C_{31}H_{39}Cl_2CuN_3$
Formula weight	588.09
Crystal system	orthorhombic
Space group	$P2_12_12_1$
a (Å)	11.0446(2)
b (Å)	14.9386(2)
c (Å)	18.7519(3)
α (°)	90.000
β (°)	90.000
γ (°)	90.000
V (Å^3)	3093.89(9)
Z	4
D_{calc} (g cm^{-3})	1.263
Absorption coefficient (mm^{-1})	0.902
F(000)	1236
Data/restraints/parameters	7002/16/361
Goodness-of-fit on F^2	1.035
Final R indices [$I > 2\sigma(I)$]	
R^a	0.0303
wR^b	0.0755

[a] $R = \sum\|F_o| - |F_c\|/\sum|F_o|$.
[b] $wR_2 = \{\sum w[(F_o^2 - F_c^2)^2]/\sum w[(F_o^2)^2]\}^{1/2}$.

2.3. Spectral properties

The solid-state reflectance spectra of all the complexes display either one broad or two poorly separated ligand-field bands (11 900–15 800 cm^{-1}) in the visible region, which is typical of Cu(II) located in a weakly tetragonal field [27]. On dissolution in methanol or acetonitrile no

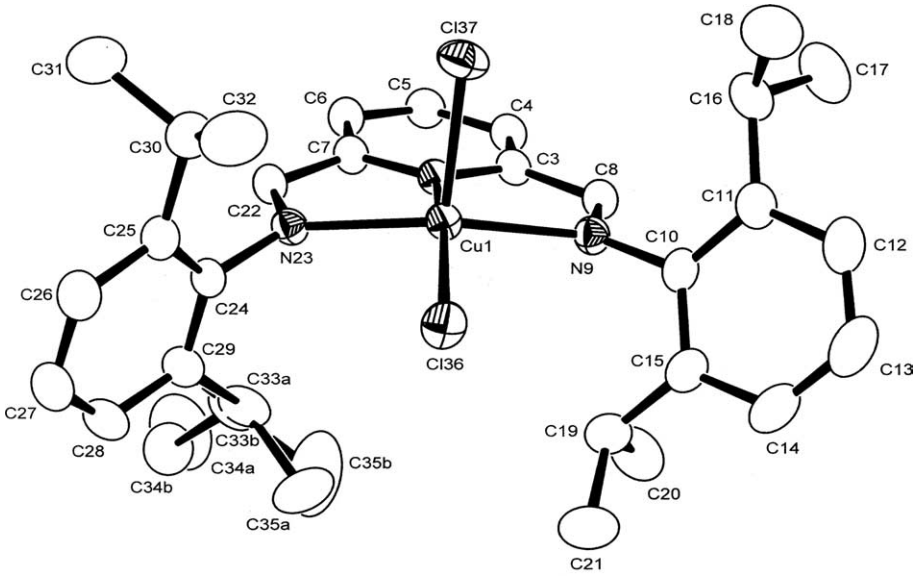

Fig. 1. ORTEP drawing of [Cu(L2)Cl_2] (**2**) showing the atom numbering scheme and thermal motion ellipsoids (50% probability level). The hydrogen atoms are omitted for clarity.

Table 2
Selected Bond lengths (Å) and angles (°) for $[Cu(L2)Cl_2]$ (**2**)

Cu(1)–N(2)	1.9523(16)
Cu(1)–N(23)	2.1203(16)
Cu(1)–N(9)	2.1482(17)
Cu(1)–Cl(36)	2.2033(5)
Cu(1)–Cl(37)	2.3905(6)
N(2)–Cu(1)–N(23)	77.39(6)
N(2)–Cu(1)–N(9)	77.44(7)
N(23)–Cu(1)–N(9)	149.63(7)
N(2)–Cu(1)–Cl(36)	160.42(5)
N(23)–Cu(1)–Cl(36)	96.82(5)
N(9)–Cu(1)–Cl(36)	101.25(5)
N(2)–Cu(1)–Cl(37)	93.66(5)
N(23)–Cu(1)–Cl(37)	101.93(5)
N(9)–Cu(1)–Cl(37)	96.36(5)
Cl(36)–Cu(1)–Cl(37)	105.88(2)

appreciable change in the ligand field bands is observed for the complexes **1**, **2** and **4** (Table 3). However, noticeable changes in the ligand field features are observed for the complexes **3** and **5**. For the complexes **1** and **2** two more absorption bands are observed at higher energies (**1**, 23 900 and 26 200 cm^{-1}; **2**, 26 300 and 28 000 cm^{-1}), which are presumably derived from nitrogen to copper(II) charge transfer (CT) transitions. Replacing the methyl groups in **1** by the more sterically demanding isopropyl groups, as in **2**, would be expected to effect distortions in the copper(II) coordination geometry and hence lower the LF energy, but no significant spectral differences are observed. Obviously, the free rotation of the phenyl rings in the complexes (cf. above) minimize the steric constraints around copper(II), which is independent of the phenyl ring substituents and hence similar LF features are observed for **1** and **2**. For complex **3**, two ligand to metal charge transfer (LMCT) bands, characteristic of $S(\sigma) \rightarrow Cu(II)$ and $N(\pi) \rightarrow Cu(II)$ transitions, are observed (33 200 and 32 700 cm^{-1}). Complex **4** in acetonitrile solution shows an absorption band (13 500 cm^{-1}) with enhanced absorptivity (2340 $M^{-1}\,cm^{-1}$) in the visible region, which may be attributed to intensity borrowing [28] from the $S(\sigma) \rightarrow Cu(II)$ LMCT band, providing strong evidence for thioether coordination to copper(II) in solution. The noteworthy observation is that the LF band energy of **4** is lower than that of **3**, with the absorptivity of **4** being 30-fold higher than that of **3** (Table 3). This suggests the presence of an axial interaction by solvent and/or distortion around copper(II) effected by the N_2S_2 donor set of the **L4** ligand, which is unfavourable for square planar coordination. The difference in electronic spectra of **3** and **4** in methanol solution indicates that complex **4** experiences partial or complete replacement of one or two weakly coordinated thioether donors by coordinating solvents. The chloride complex **4a** exhibits a spectral pattern closely similar to **4**, but with very low absorptivity (Table 3). The bis-complex **5**, which does not have a pyridine donor as in **L1**–**L3**, exhibits a broad LF band around 13 900 cm^{-1} with a shoulder around 18 900 cm^{-1}, implying a distorted square based coordination geometry. This is expected as copper(II) complexes with a N_4 donor set display a LF band in the range 14 000–19 000 cm^{-1} [7,27].

The polycrystalline EPR spectra of complexes **2**, **4a** and **5** are isotropic while those of complexes **3** and **3a** are axial. Interestingly, the complexes **1** and **4** show rhombic spectra with R values greater than unity [$R = (g_3 - g_2)/(g_2 - g_1) =$ 1.2 (**1**); 1.1 (**4**), Table 3]. The rhombicity is more likely to arise from the interaction between differently oriented Cu(II) complexes rather than a d_{z^2} ground state for copper(II) in the solid state [29,30]. The cryogenic solution EPR spectra of all the complexes are axial [$g_\parallel > g_\perp > 2.0$, $G = (g_\parallel - 2)/(g_\perp - 2) = 3.0$–4.5], suggesting the presence of a $d_{x^2-y^2}$ ground state for copper(II) located in square based geometries [31,32]. The complex $[Cu(L2)Cl_2]$ (**2**) shows $g_\parallel$ (2.254) and $A_\parallel$ ($133 \times 10^{-4}\,cm^{-1}$, Fig. 2) values, which are consistent with the '$CuN_3Cl + Cl$' chromophore as observed in the X-ray crystal structure. The complex $[Cu(L)(H_2O)_2](ClO_4)_2.(H_2O)_2$ (L = bis(benzimidazol-2-yl) methylamine) [30] with the CuN_3O_2 chromophore shows similar $g_\parallel$ (2.268) and $A_\parallel$ ($140 \times 10^{-4}\,cm^{-1}$) values. However, copper(II) complexes of tridentate ligands with a CuN_3Cl_2 coordination sphere, synthesized in our laboratory very recently [33], exhibit $g_\parallel$ and $A_\parallel$ values in the range 2.21–2.25 and 179–184 $\times 10^{-4}\,cm^{-1}$, respectively. Though the $g_\parallel$ value of complex **2** falls within this range, the very low $A_\parallel$ value observed indicates a large deviation from axial symmetry, which is evident from its crystal structure. It is interesting to compare the complexes **1** and **2**, which are expected to have similar coordination geometries. On replacing isopropyl groups in **2** by methyl groups as in **1** the $g_\parallel$ value decreases and the $A_\parallel$ value increases suggesting a decrease in geometric distortion or axial interaction with copper(II). This is supported by the lower $g_\parallel/A_\parallel$ quotient (131 cm) of complex **1**, which falls in the range 105–135 cm, as expected [34] for square-planar copper(II) complexes. The $g_\parallel$ and $A_\parallel$ values of **2**, which are higher and lower, respectively, than **1**, suggest that the former possesses a coordination geometry distorted ($g_\parallel/A_\parallel$, 169 cm) more than **1** because of the sterically demanding isopropyl groups, rather than an axial interaction [35]. This is in contrast to the similar electronic spectral parameters of **1** and **2** suggesting the usefulness of EPR spectroscopy in detecting even small differences in coordination geometries.

The copper(II) complexes containing bis(benzimidazolyl)-thioether ligands [19] offering a N_3S_2 donor set display $g_\parallel$ and $A_\parallel$ values in the range 2.24–2.29 and 138–187 $\times 10^{-4}\,cm^{-1}$, respectively. Complex **3**, also with a N_3S_2 donor set, exhibits a $g_\parallel$ value of 2.249 and an $A_\parallel$ value of $140 \times 10^{-4}\,cm^{-1}$ (Fig. 2). The relatively low $A_\parallel$ value of complex **3** supported by the relatively low value of LF band energy indicates the presence of strong geometric distortion or strong axial interaction in the square-based coordination geometry. The EPR spectral features of **3a** are very similar to that of **3**; however, a lower $g_\parallel/A_\parallel$ value is observed for **3a**. On replacing the pyridine ring in the **L3** complex by a benzene ring as in complex **4**, the $g_\parallel$ (2.382) and $A_\parallel$

Table 3
Electronic and EPR spectral data for the copper(II) complexes

Complexes	Electronic spectra[a] $\bar{\nu}_{max} \times 10^3$ cm^{-1} (ε, M^{-1} cm^{-1})			EPR spectra[b]	
	Solid	Solution		Solid	Frozen solution
		MeOH			CH_3CN
$[Cu(L1)Cl_2]$ (**1**)	11.9	12.2 (215)		g_3 2.243	$g_\parallel$ 2.192[c]
	22.3	23.9 (6070)		g_2 2.138	$A_\parallel$ 167
		26.2 (6520)		g_1 2.052	$g_\perp$ 2.091
		34.1 (15770)			$g_\parallel/A_\parallel$ 131
		MeOH			MeOH
$[Cu(L2)Cl_2]$ (**2**)	12.3	12.1 (205)		g_{ave} 2.098	$g_\parallel$ 2.254
	20.2	26.3 (2885)			$A_\parallel$ 133
		28.0 (3605)			$g_\perp$ 2.084
		34.6 (10600)			$g_\parallel/A_\parallel$ 169
		MeOH	CH_3CN		CH_3CN
$[Cu(L3)](ClO_4)_2$ (**3**)	13.5	14.0 (135)	14.5 (40)	$g_\parallel$ 2.211	$g_\parallel$ 2.249
	22.6	33.2 (10825)	29.4 (6165)	$g_\perp$ 2.072	$A_\parallel$ 140
		32.7 (4000)			$g_\perp$ 2.082
		41.7 (20340)			$g_\parallel/A_\parallel$ 161
		DMF			DMF
[Cu(L3)Cl]Cl (**3a**)	12.1	12.0 (215)		$g_\parallel$ 2.232	$g_\parallel$ 2.242
	23.6	26.6 (10560)		$g_\perp$ 2.084	$A_\parallel$ 153
		32.6 sh			$g_\perp$ 2.082
		37.2 (35890)			$g_\parallel/A_\parallel$ 146
		MeOH	CH_3CN		CH_3CN[d]
$[Cu(L4)](ClO_4)_2$ (**4**)	13.8	13.5 (1105)	13.5 (2340)	g_3 2.266	$g_\parallel$ 2.382
	23.0	15.8 sh	17.7 sh	g_2 2.138	$A_\parallel$148
		28.0 (4095)	26.4 (6025)	g_1 2.019	$g_\perp$ 2.083
		33.7 (6690)			$g_\parallel/A_\parallel$ 161
		MeOH			MeOH[e]
$[Cu(L4)Cl_2]$ (**4a**)	13.6	13.4 (400)		g_{ave} 2.078	$g_\parallel$ 2.485
	22.8	17.8 (840)			$A_\parallel$128
		28.0 (5065)			$g_\perp$ 2.105
		33.9 (15330)			$g_\parallel/A_\parallel$ 193
		MeOH			CH_3CN
$[Cu(L5)_2(H_2O)](ClO_4)_2$ (**5**)	15.8	13.9 (67)		g_{ave} 2.072	$g_\parallel$ 2.201
	19.0	18.9 sh			$A_\parallel$ 178
		29.8 (6240)			$g_\perp$ 2.069
					$g_\parallel/A_\parallel$ 124

[a] Concentration, 2×10^{-3} M for ligand field and 2×10^{-5} M for ligand based transitions.
[b] $A_\parallel$ in 10^{-4} cm^{-1}.
[c] The species $[Cu(solvent)_4]^{2+}$ is also present ($g_\parallel$ 2.418; $A_\parallel$, 148×10^{-4} cm^{-1}).
[d] Values in methanol, $g_\parallel$ 2.408; $A_\parallel$ 134×10^{-4} cm^{-1}; $g_\perp$ 2.099.
[e] Values in DMF, $g_\parallel$ 2.404; $A_\parallel$ 131×10^{-4} cm^{-1}; $g_\perp$ 2.089.

(148×10^{-4} cm^{-1}) values are enhanced (Table 3). This reveals the presence of a severely distorted square planar stereochemistry around copper(II) in **4** effected by the N_2S_2 donor atoms, the geometrical disposition of which are unfavourable for square planar coordination around Cu(II).

2.4. Redox chemistry

The electrochemical data obtained in methanol or acetonitrile solution of the present complexes using TBAP as a supporting electrolyte are collected in Table 4. For all the complexes the one electron reduction peak (E_{pc}) corresponding to Cu(II) to Cu(I) reduction occurs in the potential range 0.508–0.208 V, with a directly associated reoxidation peak (E_{pa}) in the reverse scan, whose potential values fall within the range 0.702–0.296 V (Table 4). Further, the original Cu(II) complex species undergoing reduction are completely regenerated following electrochemical oxidation (the ratio of peak currents, $i_{pa}/i_{pc} \sim 1.0$, Table 4) suggesting a chemically reversible Cu^{II}/Cu^{I} couple. However, the value of the limiting peak-to-peak separation (ΔE_p, 86–226 mV) is higher than that for the Fc/Fc^+ couple (ΔE_p, 84 mV; $E_{1/2}$, 0.414 V) under identical conditions.

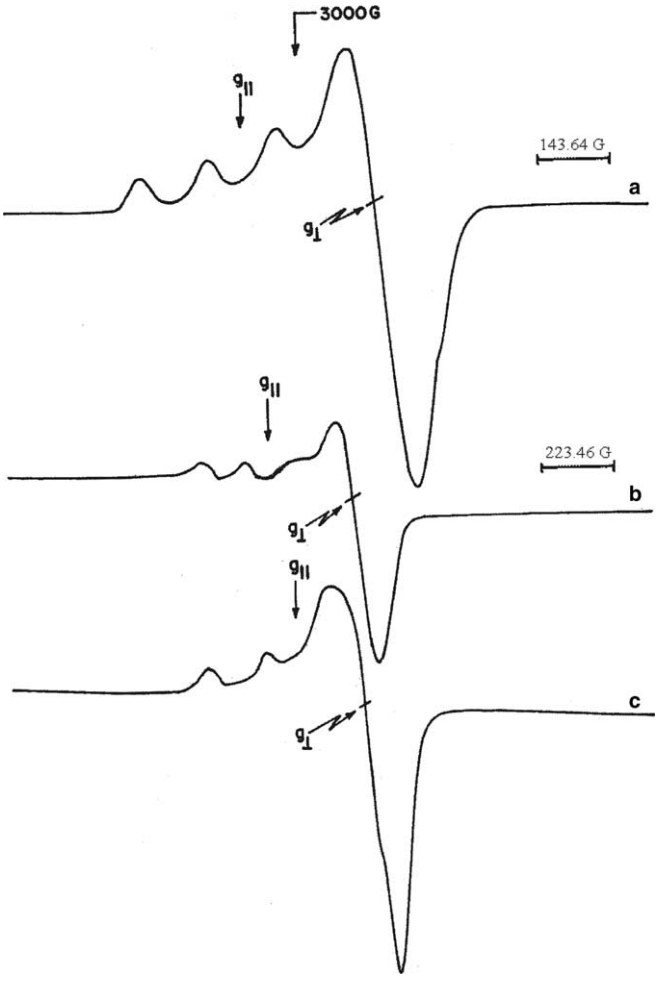

Fig. 2. X-band EPR spectra of the complexes $[Cu(L2)Cl_2]$ (**2**) (a) in methanol/acetone and $[Cu(L3)](ClO_4)_2$ (**3**) (b) and $[Cu(L5)_2](ClO_4)_2$ (**5**) (c) in acetonitrile/acetone solution at 77 K.

This suggests that the heterogeneous electron-transfer process in most of the present complexes is far from reversible and that on electron transfer considerable stereochemical reorganization of the coordination sphere occurs. However, quantitative conclusions on the extent of such reorganization are difficult to estimate [36]. Interestingly, the complexes **1** (Fig. 3) and **2** (Fig. 4(a)) have a minimal reorganizational energy barrier (ΔE_p, **1**, 88; **2**, 86; Fc/Fc^+, 84 mV) indicating that the structural reorganization between the two oxidation states is minimum and hence electron transfer in these complexes is facile. It is relevant to note that in naturally occuring electron transfer copper proteins the redox is facile because of minimal structural changes between the redox pairs.

Complex **2** exhibits a one electron reduction at 0.268 V and the corresponding oxidation occurs at 0.348 V. Interestingly, an additional anodic peak at 0.484 V is observed (Fig. 4(a)), which can be explained by assuming a square scheme (Scheme 2). As the conductance of **2** is 30 Ω^{-1} cm^2 mol^{-1} it is probable that the complex is present as a $[CuLCl]^+$ species. The additional peak may arise from the oxidation of a trigonal planar (tp) Cu(I) species. Thus, when the scan rate is increased from 50 to 500 mV the additional peak grows in height suggesting that at higher scan rates the tp Cu(I) species is preferentially formed immediately on reducing the square planar (sp) $[CuLCl]^+$ species. Further, on addition of Cl^- ions (LiCl), the height of the additional anodic peak decreases illustrating that the tp Cu(I) species combine with the Cl^- ion to form a tetrahedral Cu(I) species, decreasing its concentration. It may be noted that the tp Cu(II) species corresponding to the tp Cu(I) species could not be detected, obviously because the isopropyl substituents on the phenyl rings in the Cu(II) species would be brought closer to exhibit strong steric clashes leading to

Table 4
Electrochemical data[a] for the copper complexes at 25 ± 2 °C in methanol solution

Compound	E_{pc} (V)	E_{pa} (V)	ΔE_p (mV)[b]	$E_{1/2}$ (V)		i_{pa}/i_{pc}	$10^6 D$ (cm^2 s^{-1})
				CV	DPV[c]		
$[Cu(L1)Cl_2]$ (**1**)	0.208	0.296	88	0.252	0.274	0.9	12.3
+ LiCl	0.391	0.492	101	0.442	0.436	0.9	12.3
	0.400	0.502	102	0.451	0.474	1.0	
	0.200	0.310	110	0.255	0.266	0.8	8.9
$[Cu(L2)Cl_2]$ (**2**)	0.262	0.348[d]	86	0.305	0.316	0.8	1.1
+ LiCl	0.252	0.360	108	0.306	0.314	1.0	8.0
$[Cu(L3)](ClO_4)_2$ (**3**)	0.338	0.452	114	0.395	0.414	1.3	0.8
[Cu(L3)Cl]Cl (**3a**)	0.290[e]	0.516	226	0.403	0.398	1.1	3.0
+ LiCl	0.164	0.510	346	0.337	0.326	1.3	2.7
$[Cu(L4)](ClO_4)_2$ (**4**)	0.508	0.702	194	0.605	0.592	1.1	2.4
$[Cu(L4)Cl_2]$ (**4a**)	0.230	0.548	318	0.389	0.500[f]	0.8	13.5
+ LiCl	0.420	0.510	90	0.465	0.490	1.1	5.4
$[Cu(L5)_2(H_2O)](ClO_4)_2$ (**5**)	0.380	0.496	116	0.438	0.432	0.9	3.8

[a] Measured on a Pt working electrode vs. a non-aqueous Ag/Ag^+ reference electrode; add 544 mV [300 mV, Ag/Ag^+ to SCE; +244 mV, SCE to SHE] to convert to standard hydrogen electrode (SHE); Fc/Fc^+ couple in CH_3CN, $E_{1/2}$, 0.414 V (CV); 0.401 V (DPV); scan rate 50 mV s^{-1}; supporting electrolyte, tetra-*N*-butylammonium perchlorate (0.1 mol dm^{-3}); complex concentration, 1 mmol dm^{-3}.

[b] ΔE_p at 50 mV s^{-1} scan rate.

[c] Differential pulse voltammetry, scan rate 1 mV s^{-1}; pulse height 50 mV.

[d] Additional anodic peak appears at 0.484 V. Cathodic peak does not apppear at high scan rate.

[e] Values in DMF.

[f] Additional peak at 0.316 V.

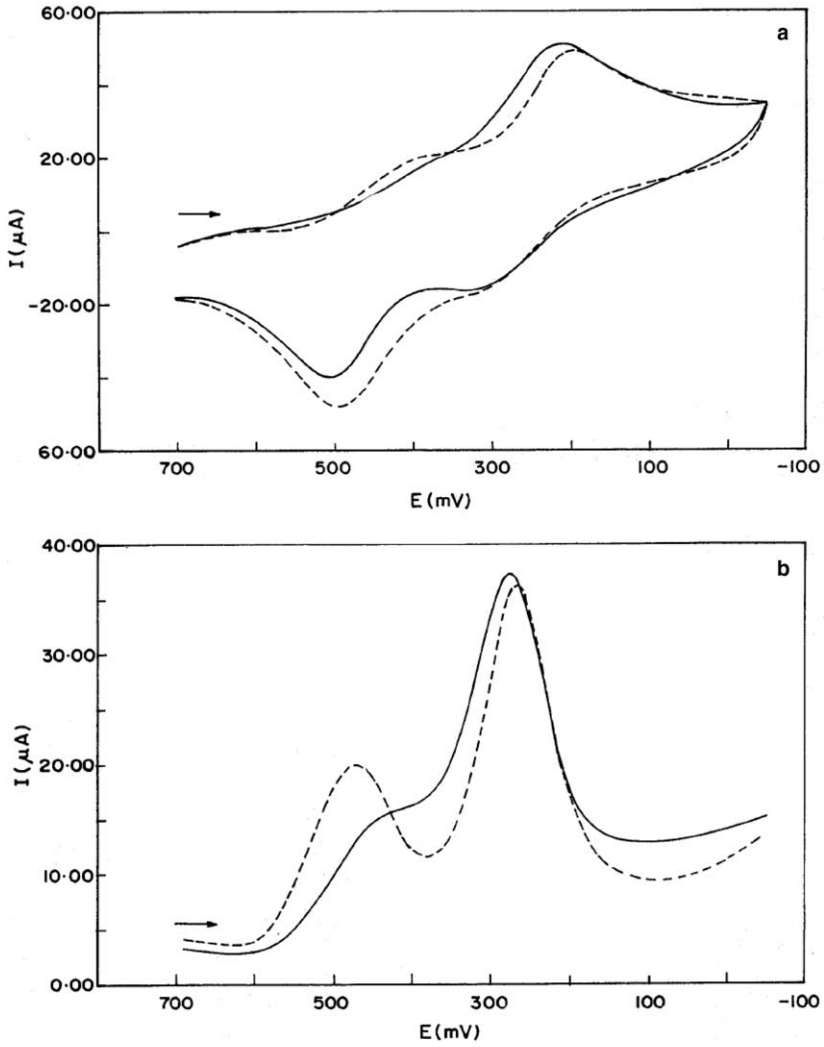

Fig. 3. Cyclic (a) and differential pulse (b) voltammograms of 0.001 M complex $[Cu(L1)Cl_2]$ (**1**) before (——) and after (-----) the addition of excess LiCl in methanol solution at 25 °C at 0.05 V s^{-1} scan rate.

its destability. Thus, in the X-ray structure of the tp Cu(I) complex $[Cu(bbtmp)](NO_3)$ [bbtmp = 2,6-bis (benzimidazol-2′-ylthiomethyl)pyridine] the benzimidazole rings are closer to each other than in the corresponding tetrahedral [Cu(bbtmp)Cl] species [17]. From the difference in E_{pa} values (ΔE_{pa}) for the oxidation of the two Cu(I) species, the $\Delta E_{1/2}$ values for the redox of [Cu(L2)Cl] and $[Cu(L2)]^+$ species was estimated assuming reversibility, from which the K_1/K_2 value was calculated [37] as 7.9×10^{-3}. The magnitude of K_1/K_2 illustrates that the tp Cu(II) species rather than the tp Cu(I) species readily combines with Cl^- ions leading to the non-detection of the tp Cu(II) species. Similarly, the tp Cu(I) species shows a reluctance to bind to the Cl^- ion illustrating the above observation that the tp Cu(I) species are directly formed from square planar $[Cu(L2)Cl]^+$ species on reduction. The decreased steric constraints in the tp Cu(II) species of **1** leads to its detection in the CV (E_{pc}, 0.391 V), in contrast to **2**. Similarly, the tp Cu(I) species for **1** will be more stable than that for **2** and hence combine with Cl^- less strongly (K_1/K_2, 1.8×10^{-3}, calculated from the two $E_{1/2}$ values (Table 4) obtained from differential pulse voltammetry (DPV)). As for **2**, an increase in scan rate leads to the formation of more tp Cu(I) species, as seen from the increase in height of the additional anodic peak with increase in scan rate. The tp Cu(II) species of **1** is more stable because the steric clash between the two phenyl rings carrying the methyl groups is less compared to the corresponding tp Cu(II) species of **2** and hence its detection in the CV.

Complex **3**, bearing a CuN_3S_2 coordination sphere, shows a positive redox potential of 0.395 V (Fig. 4(b)). The incorporation of two sulfur atoms into **1** as in complex **3** leads to a Cu(II)/Cu(I) redox potential higher than **1/2** suggesting the involvement of thioether coordination in **3** [38]. The higher $E_{1/2}$ value (0.403 V) observed for the chloro complex **3a** is almost the same as for **3** but, interestingly, the ΔE_p value of complex **3a** (226 mV) is higher than **3** (114 mV). This suggests that the chloride ion coordinates to copper(II), as shown by the lower conductance (90 Ω^{-1} cm^2 mol^{-1}) of **3a**. Further, the addition of excess LiCl shifts the cathodic peak to a more

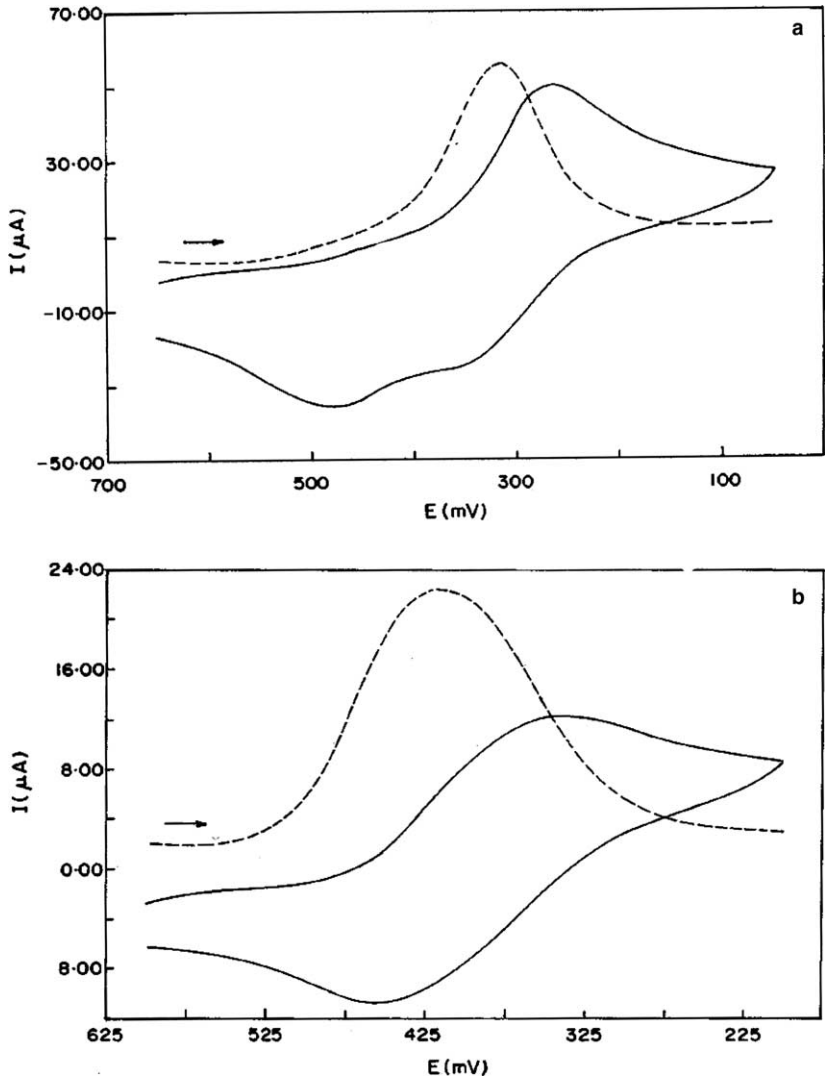

Fig. 4. Cyclic (——) and differential pulse (-----) voltammograms of the complexes $[Cu(L2)Cl_2]$ (**2**) (a) and $[Cu(L3)](ClO_4)_2$ (**3**) (b) and methanol solution at 25 °C at 0.05 V s^{-1} scan rate.

negative value confirming the coordination of the chloride ion to copper(II), which renders the reduction more difficult.

The complexes **4** and **4a** display redox potentials higher than complexes **3** and **3a**, which is expected with the incorporation of hard N donors into the CuN_2S_2 coordination sphere of **4** and **4a**. An interesting electrochemical behaviour was observed for the chloro complex **4a**, which undergoes reduction at a very low positive potential of 0.230 V with a shoulder around 0.438 V. The high ΔE_p value (318 mV) and the observation of two waves in DPV at different potentials suggest the coordination of Cl^- ion as illustrated above for **2**. A well-defined CV with a low ΔE_p value of 90 mV was obtained after the addition of excess of LiCl, supporting the dissociation of chloride ions as proposed above. It should be noted that all these proposals are only speculative in the absence of crystal structures of the complexes. The bis-complex **5** also exhibits positive redox potentials (0.438 V) because of the bulky *N*-phenyl groups, which would favour the formation of tetrahedral copper(I) species more than complex **1**, which may be

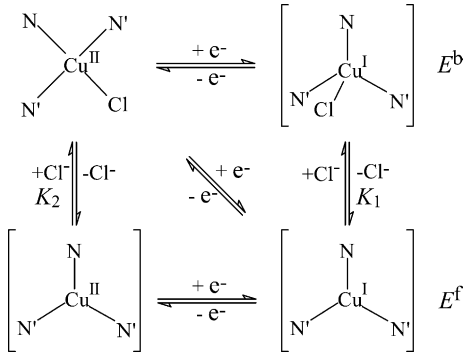

Scheme 2.

due to the presence of hard N donors in the latter complex as discussed above. The high redox potential (0.592 V versus Ag/Ag^+) for the Cu(II)/Cu(I) couple of complex **4** may be attributed to tetrahedral distortion from a regular square-based geometry.

3. Conclusions

The distinct spectral and electrochemical behaviour of copper(II) complexes of five sterically hindered Schiff base ligands have been studied. The 1:1 copper(II) complex of 2,6-bis(2,6-diisopropylphenyliminomethyl)pyridine adopts a distorted square pyramidal geometry. The replacement of isopropyl groups in this complex by the less sterically demanding methyl groups leads to a similar coordination geometry as revealed by their similar spectral and electrochemical features. However, the redox potential of the isopropyl complex is higher than the methyl complex, which is consistent with the higher $g_{\|}$ value [39] of the former complex, illustrating the importance of sterically demanding isopropyl groups in distorting the coordination geometry around copper(II). Further, the interaction of a thiolate moiety with the methyl/isopropyl complexes would be expected to generate a Cu(I) trigonal pyramidal-like or tetrahedral-like coordination geometry, which would be a better copper(II) model for the active sites of electron transfer copper proteins. Thus, Holland and Tolman [40] have recently reported four-coordinate copper(II) complexes with a thiolate and thioether containing chelating ligand and a bidentate β-diketiminate as an auxiliary ligand and these complexes are believed to be close structural mimics for the type I copper proteins. However, these complexes fail to reproduce the positive redox potential of the blue copper proteins.

The copper(II) complexes of sterically constrained ligands providing N_3S_2 and N_2S_2 donor sets, which are unfavourable for square planar coordination, have also been synthesized and characterized. The spectral and electrochemical properties of these complexes suggest the presence of thioether coordination in solution. The incorporation of a pyridine nitrogen donor into the CuN_2S_2 complexes leads to a higher LF band energy but with lower absorptivity, suggesting lesser distortion in the coordination sphere. Both the CuN_3S_2 and CuN_2S_2 complexes show positive redox potentials suggesting the coordination of at least one thioether sulfur. The bis-complex of a sterically hindering bidentate ligand also shows a positive redox potential suggesting that the distortion in the coordination sphere is significantly large.

4. Experimental

4.1. Materials

Copper(II) chloride dihydrate, copper(II) perchlorate hexahydrate, 2,6-pyridinedimethanol, 2,4,6-trimethylaniline, 2,6-diisopropylaniline, selenium dioxide (Aldrich), isophthaladehyde (Lancaster) were used without further purification.

4.2. Synthesis of ligands

4.2.1. 2,6-Bis(2,4,6-trimethylphenyliminomethyl)pyridine (*L1*)

2,6-Pyridinedicarboxaldehyde (0.68 g, 5.0 mmol) and 2,4,6-trimethylaniline (1.35 g, 10.0 mmol) were refluxed [26] in methanol (25 mL) for 2 h over molecular sieves (4 Å). The reaction mixture was filtered while hot. The yellow crystals of **L1** (1.64 g, 89%) obtained upon cooling the reaction mixture were filtered off and dried. *Anal*. Calc. for $C_{25}H_{27}N_3$: C, 81.3; H, 7.4; N, 11.4. Found: C, 81.4; H, 7.5; N, 11.4%. ^{1}H NMR ($CDCl_3$, 400 MHz): δ, ppm 8.39 (s, 2H, *H*C=N), 8.38 (d, $J = 7.8$, 2H, *H*Py), 7.97 (t, $J = 7.6$, 1H, *H*Py), 6.91 (s, 4H, *H*Ph), 2.30 (s, 6H, H_3C–PhC_4), 2.16 (s, 12H, H_3C–PhC_2). ^{13}C NMR (CDCl3, 100 MHz): δ, ppm 163.6 (*C*H=N), 155.0, 148.2, 137.7, 134.0, 129.3, 127.2, 123.0 (*C*Py, CPh), 21.2 (CH_3–C_4), 18.7 (CH_3–C_2). IR (KBr): ν, cm^{-1} 2971s, 2914s, 2914s, 1640vs, 1481s, 1205vs, 1140s, 835s, 733s.

4.2.2. 2,6-Bis(2,6-diisopropylphenyliminomethyl)pyridine (*L2*)

The ligand **L2** was synthesized by the reported procedure [41]. To a solution of 2,6-pyridinedicarboxaldehyde (0.68 g, 5.0 mmol) in ethanol (25 mL) were added 2,6-diisopropylaniline (1.77 g, 10.0 mmol) and one drop of glacial acetic acid, and the resulting mixture was refluxed over molecular sieves (4 Å). After 24 h the reaction mixture was filtered and the ligand (1.78 g, 78%) was obtained upon cooling. *Anal*. Calc. for $C_{31}H_{39}N_3$: C, 82.1; H, 8.7; N, 9.3. Found: C, 81.5; H, 8.9; N, 9.5%. ^{1}H NMR ($CDCl_3$, 400 MHz): δ, ppm 8.41 (d, $J = 7.8$, 2H, *H*Py), 8.39 (s, 2H, *H*C=N), 8.01 (t, $J = 7.8$, 1H, *H*Py), 7.21–7.10 (m, 6H, *H*Ph), 3.00 (sep, $J = 6.8$, 4H, $HC(H_3C)_2$), 1.20 (d, $J = 6.8$, 24H, $(H_3C)_2C$). ^{13}C NMR ($CDCl_3$, 100 MHz): δ, ppm 162.8 (*C*H=N), 154.6, 148.4, 137.5, 137.3, 124.7, 123.2, 122.9 (*C*Py, *C*Ph), 28.1 ($CH(H_3C)_2$), 23.6 ($(CH_3)_2C$). IR (KBr): ν, cm^{-1} 3065w, 2961vs, 1585vs, 1566w, 1456w, 1319s, 1184s, 748s.

4.2.3. 2,6-Bis(2-methylthiophenyliminomethyl)pyridine (*L3*)

A mixture of 2,6-pyridinedicarboxaldehyde (0.68 g, 5.0 mmol) and 2-(methylthio)aniline (1.47 g, 10.5 mmol) were refluxed in benzene (20 mL) for 36 h. The reaction mixture was filtered under hot conditions. Fine yellow crystals of **L3** (1.16 g, 62%) were obtained on recrystallization in benzene, which was filtered off and dried. *Anal*. Calc. for $C_{21}H_{19}N_3S_2$: C, 66.8; H, 5.1; N, 11.1. Found: C, 66.9; H, 5.1; N, 11.2%. ^{1}H NMR ($CDCl_3$, 400 MHz): δ, ppm 8.63 (s, 2H, *H*C=N), 8.41 (d, $J = 7.8$, H, *H*Py), 7.95 (t, $J = 7.8$, 1H, *H*Py), 7.36–7.11 (m, 8H, *H*Ph), 2.49 (s, 6H, H_3C). ^{13}C NMR ($CDCl_3$, 100 MHz): δ, ppm 159.7 (*C*H=N), 154.7, 147.8, 137.5, 135.1, 127.5, 125.4, 124.7, 123.6, 117.5 (*C*Py, *C*Ph), 14.9 (CH_3). IR (KBr): ν, cm^{-1} 3050w, 2978w, 2913s, 1619vs, 1570w, 1468s, 1331s, 800s, 724vs.

4.2.4. 1,3-bis(2-methylthiophenyliminomethyl)benzene (*L4*)

The ligand **L4** was synthesized by the same method adopted for **L3**, using isophthalaldehyde (0.67 g, 5.0 mmol). The yellow solid precipitated was filtered off and dried (1.43 g, 76%). *Anal*. Calc. for $C_{22}H_{20}N_2S_2$: C, 70.2; H, 5.4; N, 7.4. Found: C, 70.2; H, 5.3; N, 7.5%. ^{1}H NMR ($CDCl_3$, 400 MHz): δ, ppm 8.50 (s, 2H, *H*C=N), 8.41 (s, 1H, *H*Ph), 8.14 (d, $J = 7.8$, 1H, *H*Ph), 8.13 (d, $J = 7.6$, 1H, *H*Ph), 7.59 (t, $J = 7.6$, 1H, *H*Ph), 7.24–7.03 (m, 6H, *H*Ph), 7.01 (d, $J = 7.6$, 2H, *H*Ph), 2.48 (s, 6H, H_3C). ^{13}C NMR ($CDCl_3$, 100 MHz): δ, ppm 159.3 (*C*H=N), 148.9, 136.9, 134.3, 131.5, 130.2, 129.4, 126.8, 125.4, 124.7, 117.7 (*C*Ph), 14.9 (CH_3). IR (KBr, ν, cm^{-1}): 3050w, 2978w, 2905w, 1614vs, 1570s, 1466s, 1436s, 1351s, 1268s, 1071s, 804s, 754vs, 691s.

4.2.5. 1,3-bis(2,4,6-trimethylphenyliminomethyl)benzene (*L5*)

The ligand **L5** was prepared by refluxing isophthalaldehyde (0.67 g, 5.0 mmol) and 2,4,6-trimethylaniline (1.42 g, 10.5 mmol) in benzene (20 mL) for 36 h over molecular sieves (4 Å). The reaction mixture was filtered and the solvent removed under vacuum. The excess amine was evaporated on warming gently under high vacuum. The ^{1}H NMR spectrum of the residue showed that the product was sufficiently pure (1.62 g, 88%). *Anal*. Calc. for $C_{26}H_{28}N_2$: C, 84.7; H, 7.7; N, 7.6. Found: C, 84.8; H, 7.7; N, 7.7%. ^{1}H NMR ($CDCl_3$, 400 MHz): δ, ppm 8.36 (s, 1H, *H*Ph), 8.31 (s, 2H, *H*C=N), 8.10 (d, $J = 7.6$, 1H, *H*Ph), 8.09 (d, $J = 7.8$, 1H, *H*Ph), 7.63 (t, $J = 7.6$, 1H, *H*Ph), 6.91 (s, 4H, *H*Ph), 2.31 (s, 6H, H_3C–C_4), 2.15 (s, 12H, H_3C–C_2). ^{13}C NMR ($CDCl_3$, 100 MHz): δ, ppm 162.1 (*C*H=N); 148.6, 136.9, 133.3, 130.9, 129.4, 128.9, 128.8, 127.1 (*C*Ph), 20.9 (CH_3–C_4), 18.4 (CH_3–C_2).

4.2.6. 1,3-bis(2,6-diisopropylphenyliminomethyl)benzene (*L6*)

The ligand **L6** was prepared using the method adopted for **L5**. After the evaporation of the solvent the solid obtained was washed with hexane to yield **L6** (1.89 g, 83%). *Anal*. Calc. for $C_{32}H_{40}N_2$: C, 84.9; H, 8.9; N, 6.2. Found: C, 85.0; H, 9.0; N, 6.2%. ^{1}H NMR ($CDCl_3$, 400 MHz): δ, ppm 8.36 (s, 1H, *H*Ph), 8.32 (s, 2H, *H*C=N), 8.15 (d, $J = 7.8$, 1H, *H*Ph), 8.14 (d, $J = 7.6$, 1H, *H*Ph), 7.68 (t, $J = 7.6$, 1H, *H*Ph), 7.21–7.15 (m, 6H, *H*Ph), 3.02 (sep, $J = 6.8$, 4H, *H*C(H_3C)$_2$), 1.21 (d, $J = 6.8$, 24H, (H_3C)$_2$C). ^{13}C NMR ($CDCl_3$, 100 MHz): δ, ppm 161.8 (*C*H=N); 149.4, 137.9, 137.2, 131.5, 129.9, 129.5, 124.8, 123.5 (*C*Py, *C*Ph), 28.4 (*C*H(H_3C)$_2$), 23.9 ((*C*H_3)$_2$C). IR (KBr): ν, cm^{-1} 3057w, 2964vs, 2869s, 1636vs, 1581s, 1456w, 1361s, 1321s, 1147s, 840s, 762vs, 692s.

4.3. Synthesis of copper(II) complexes

The copper(II) complexes **1**–**4** of the ligands **L1**–**L4** were prepared by adding the corresponding copper(II) salt in methanol to a methanolic solution of the ligand in a 1:1 mole ratio. The volume of the solvent was reduced by rotary evaporation and then cooled. The product formed was filtered off, washed with small amounts of cold methanol and then dried under vacuum. Single crystals of [Cu(L2)Cl_2] (**2**) suitable for X-ray diffraction were obtained by diffusion of ether vapour into an acetonitrile solution of **2**. The complex **5** was obtained by mixing the ligand **L5** and copper(II) perchlorate hexahydrate in a 2:1 (ligand:metal) mole ratio.

*[Cu(L1)Cl_2](**1**)*. Yield: 86% (0.43 g). *Anal*. Calc. for $C_{25}H_{27}N_3Cl_2Cu$: C, 59.6; H, 5.4; N, 8.3. Found: C, 59.6; H, 5.5; N, 8.4%.

*[Cu(L2)Cl_2](**2**)*. Yield: 88% (0.52 g). *Anal*. Calc. for $C_{31}H_{39}N_3Cl_2Cu$: C, 63.3; H, 6.7; N, 7.1. Found: C, 63.4; H, 6.7; N, 7.2%.

*[Cu(L3)](ClO_4)$_2$(**3**)*. Yield: 91% (0.58 g). *Anal*. Calc. for $C_{21}H_{19}N_3O_8S_2Cl_2Cu$: C, 39.4; H, 2.9; N, 6.6. Found: C, 39.5; H, 3.0; N, 6.7%.

*[Cu(L3)Cl]Cl(**3a**)*. Yield: 76% (0.39 g). *Anal*. Calc. for $C_{21}H_{19}N_3S_2Cl_2Cu$: C, 49.3; H, 3.7; N, 8.2. Found: C, 49.3; H, 3.8; N, 8.3%.

*[Cu(L4)](ClO_4)$_2$(**4**)*. Yield: 63% (0.40 g). *Anal*. Calc. for $C_{22}H_{20}N_2O_8S_2Cl_2Cu$: C, 41.4; H, 3.2; N, 4.4. Found: C, 42.4; H, 3.4; N, 4.4%.

*[Cu(L4)Cl_2](**4a**)*. Yield: 82% (0.42 g). *Anal*. Calc. for $C_{22}H_{20}N_2S_2Cl_2Cu$: C, 51.7; H, 3.9; N, 5.5. Found: C, 51.8; H, 4.0; N, 5.5%.

*[Cu(L5)$_2$(H_2O)](ClO_4)$_2$(**5**)*. Yield: 62% (0.39 g). *Anal*. Calc. for $C_{26}H_{28}N_2O_8Cl_2Cu$: C, 48.1; H, 4.7; N, 4.3. Found: C, 48.1; H, 4.8; N, 4.3%.

4.4. Data collection and structure refinement

Single crystals of [Cu(L2)Cl_2] were chosen for X-ray data collection after careful examination under an optical microscope. The X-ray diffraction intensities were measured by ω and ϕ scans using a Nonius Kappa CCD four-circle diffractometer fitted with a CCD area detector and a graphite monochromator for the Mo Kα radiation. The unit cell parameters and the orientation matrix of the crystal were determined using all data. Data reduction was performed using the DENZO program [42], and a semi-empirical multi-scan absorption correction was applied using the program SORTAV [43]. The structures were solved by direct methods using the SHELXS-97 program [44] and refined by the full-matrix least-squares method on F^2 using SHELXL-97 [45]. While three of four isopropyl groups showed slightly higher thermal parameters, indicative of librational motion, in only one of those were the ellipsoids large enough to merit a disorder model. This was refined over two equally occupied orientations, C(33A)–C(35A) and C(33B)–C(35B). All disordered C–C bond lengths were restrained to 1.53(2) Å, and non-bonded 1,3-C$\cdots$C distances between methyl groups on each disordered orientation to 2.50(2) Å. All non-H atoms except the disordered C atoms were refined anisotropically, while all sp^2-H atoms were placed in calculated

positions and refined using a riding model. Methyl H atoms were treated as idealised groups with freely refined torsions about their C–C bonds.

5. Supplementary data

Full crystallographic data for **2** are available from the CCDC, 12 Union Road, Cambridge CB2 1EZ, UK on request, quoting the deposition number 255046.

Acknowledgements

The authors thank the Department of Science and Technology, India for financial support and the Council of Scientific and Industrial Research, India for a Senior Research Fellowship (to R.B.). One of them (M.P.) thanks the Department of Science and Technology, India and The Royal Society, UK for funding to visit Leeds. We thank Professor P. Sambasiva Rao, Pondicherry University for providing the EPR facility.

References

[1] (a) A. Volbeda, W.G.L. Hol, J. Mol. Biol. 209 (1989) 249;
(b) E.I. Solomon, M.J. Baldwin, M.D. Lowery, Chem. Rev. 92 (1992) 521;
(c) G.M. Brudvig, T.H. Stevens, S.I. Chan, Biochemistry 19 (1980) 5275;
(d) C.T. Martin, R.H. Morese, R.M. Kanne, H.B. Gray, B.G. Malmström, S.I. Chan, Biochemistry 20 (1981) 5147.

[2] (a) R.T. Jonas, T.D.P. Stack, Inorg. Chem. 37 (1998) 6615;
(b) N. Wei, N.N. Murthy, Q. Chen, J. Zubieta, K.D. Karlin, Inorg. Chem. 33 (1994) 1953;
(c) K.D. Karlin, R.W. Cruse, Y. Gultneh, A. Farooq, J.C. Hayes, J. Zubieta, J. Am. Chem. Soc. 109 (1987) 2668;
(d) N. Kitajima, T. Koda, S. Hashimoto, T. Kitagawa, Y. Moro-oka, J. Am. Chem. Soc. 113 (1991) 5664.

[3] (a) K.D. Karlin, A.D. Zuberbühler, in: J. Reedijk, E. Bouwman (Eds.), Bioinorganic Catalysis, Mercel Dekker, New York, 1999;
(b) K.D. Karlin, Z. Tyeklär (Eds.), Bioinorganic Chemistry of Copper, Chapman & Hall, New York, 1993;
(c) N. Kitajima, Y. Moro-oka, Chem. Rev. 94 (1994) 737;
(d) S. Schindler, Eur. J. Inorg. Chem. (2000) 2311.

[4] (a) D.B. Rorabacher, Chem. Rev. 104 (2004) 651;
(b) D.E. Fenton, Chem. Soc. Rev. 28 (1999) 159;
(c) N. Kitajima, Adv. Inorg. Chem. 39 (1992) 1;
(d) E.T. Adman, Adv. Protein Chem. 42 (1991) 145.

[5] A.W. Addison, P.J. Burke, K. Henrick, T. Nageswara Rao, E. Sinn, Inorg. Chem. 22 (1983) 3645.

[6] J.C. Lockhart, W. Clegg, M.N.S. Hill, D.J. Rushton, J. Chem. Soc., Dalton Trans. (1990) 3541.

[7] M. Vaidyanathan, R. Balamurugan, S. Usha, M. Palaniandavar, J. Chem. Soc., Dalton Trans. (2001) 3498.

[8] P.J.M.W.L. Birker, J. Helder, G. Henkel, B. Krebs, J. Reedijk, Inorg. Chem. 21 (1982) 357.

[9] M.J. Schilstra, P.J.M.W.L. Birker, G.C. Verschoor, J. Reedijk, Inorg. Chem. 21 (1982) 2637.

[10] F.J. Rietmeijer, P.J.M.W.L. Birker, S. Gorter, J. Reedijk, J. Chem. Soc., Dalton Trans. (1982) 1191.

[11] A.W. Addison, T. Nageswara Rao, J. Reedijk, J. van Rijn, G.C. Verschoor, J. Chem. Soc., Dalton Trans. (1984) 1349.

[12] E. Bouwman, W.L. Driessen, J. Reedijk, Coord. Chem. Rev. 104 (1990) 143.

[13] P.J.M.W.L. Birker, E.F. Godefroi, J. Helder, J. Reedijk, J. Am. Chem. Soc. 104 (1982) 7556.

[14] R.P.F. Kanters, R. Yu, A.W. Addison, Inorg. Chim. Acta 196 (1992) 97.

[15] C.R. Lucas, R.C. Hynes, J.P. Charland, Can. J. Chem. 70 (1992) 1773.

[16] A.W. Addison, P.J. Burke, J. Heterocyc. Chem. 18 (1981) 803.

[17] R. Balamurugan, M. Palaniandavar, R. Srinivasa Gopalan, Inorg. Chem. 40 (2001) 2246.

[18] S. Usha, M. Palaniandavar, J. Chem. Soc., Dalton Trans. (1994) 2277.

[19] R. Balamurugan, M. Palaniandavar, R. Srinivasa Gopalan, G.U. Kulkarni, Inorg. Chim. Acta 357 (2004) 919.

[20] M. Palaniandavar, Proc. Ind. Nat. Sci. Academy A 70 (2004) 293.

[21] (a) H. Toftlund, J. Becher, P.H. Olesen, J.Z. Pedersen, Isr. J. Chem. 25 (1985) 56;
(b) M. Gullotti, L. Casella, A. Pintar, E. Suardi, P. Zanello, S. Mangani, J. Chem. Soc., Dalton Trans. (1989) 1979;
(c) L. Casella, Inorg. Chem. 23 (1984) 2781;
(d) N. Kitajima, K. Fujisawa, M. Tanaka, Y. Moro-oka, J. Am. Chem. Soc. 114 (1992) 9232;
(e) M.A. Martinez, R.S. Aguilar, N.M. Ruvalcaba, R.C. Rosado, A.N. Vazquez, V.G. Vidales, A.Z. Dehesa, R.A. Toscano, S.H. Ortega, J.M. Fernandez, J. Chem. Soc., Dalton Trans. (2001) 2346.

[22] N.W. Alcock, R.G. Kingston, P. Moore, C. Pierpoint, J. Chem. Soc., Dalton Trans. (1984) 1937.

[23] W.J. Geary, Coord. Chem. Rev. 81 (1971) 7.

[24] (a) G. Murphy, P. Nagle, B. Murphy, B.J. Hathaway, J. Chem. Soc., Dalton Trans. (1997) 2645;
(b) G. Murphy, C. Murphy, B. Murphy, B.J. Hathaway, J. Chem. Soc., Dalton Trans. (1997) 2653;
(c) G. Murphy, C. O'Sullivan, B. Murphy, B.J. Hathaway, Inorg. Chem. 37 (1998) 240.

[25] A.W. Addison, T. Nageswara Rao, E. Sinn, Inorg. Chem. 23 (1984) 1957.

[26] J.M. Holland, X. Liu, J.P. Zhao, F.E. Mabbs, C.A. Kilner, M.T. Pett, M.A. Halcrow, J. Chem. Soc., Dalton Trans. (2000) 3316.

[27] F.J. Richardson, C.N. Payne, Inorg. Chem. 17 (1978) 2111.

[28] D.E. Nikles, P.J. Powers, F.L. Urbach, Inorg. Chem. 22 (1983) 3210.

[29] (a) W. Fitzgerald, B.J. Hathaway, J. Chem. Soc., Dalton Trans. (1981) 567;
(b) B.J. Hathaway, D.E. Billing, Coord. Chem. Rev. 5 (1970) 143.

[30] M. Palaniandavar, T. Pandiyan, M. Lakshminarayanan, H. Manohar, J. Chem. Soc., Dalton Trans. (1995) 455.

[31] M. Vaidyanathan, R. Viswanathan, M. Palaniandavar, T. Balasubramanian, P. Prabhaharan, P.T. Muthiah, Inorg. Chem. 37 (1998) 6418.

[32] A.W. Addison, in: K.D. Karlin, J. Zubieta (Eds.), Copper Coordination Chemistry: Biochemical and Inorganic Perspectives, Adenine Press, New York, 1983.

[33] A. Raja, V. Rajendiran, P. Uma Maheswari, R. Balamurugan, C.A. Kilner, M.A. Halcrow, M. Palaniandavar, J. Inorg. Biochem. 99 (2005) 1717.

[34] U. Sakaguchi, A.W. Addison, J. Chem. Soc., Dalton Trans. (1979) 600.

[35] Y. Nonaka, T. Tokh, S. Kida, Bull. Chem. Soc. Jpn. 17 (1974) 312.

[36] P. Zanello, Comment Inorg. Chem. 8 (1988) 45.

[37] (a) The relative stabilities of nitrate bound and free forms in solution were calculated from the redox potentials using the general formula, $E^{b} - E^{f} = 0.059\log(K_1/K_2)$ U. Sivagnanam, M. Palaniandavar, J. Electroanal. Chem. Interfacial Electrochem. 341 (1992) 197;
(b) Y. Ohsawa, M. Shimazaki, S. Aoyagui, J. Electroanal. Chem. 114 (1980) 235.

[38] A.W. Addison, Inorg. Chim. Acta 162 (1989) 217.

[39] H. Yokoi, A.W. Addison, Inorg. Chem. 16 (1977) 1341.

[40] P.L. Holland, W.B. Tolman, J. Am. Chem. Soc. 122 (2000) 6331.

[41] G.J.P. Britovsck, M. Bruce, V.C. Gibson, B.S. Kimberley, P.J. Maddox, S. Mastroianni, S.J. McTavish, C. Redshaw, G.A. Solan, S. Strömberg, A.J.P. White, D.J. Williams, J. Am. Chem. Soc. 121 (1999) 8728.
[42] Z. Otwinowski, W. Minor, Methods Enzymol. 276 (1997) 307.
[43] R.H. Blessing, Acta Crystallogr., Sect. A 51 (1995) 33.
[44] G.M. Sheldrick, Acta Crystallogr., Sect. A 46 (1990) 467.
[45] G.M. Sheldrick, SHELXS-97: Program for the Solution of Crystal Structure, University of Göttingen, Göttingen, Germany, 1997.

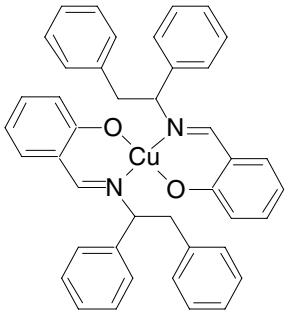

1

2 = **1** • CH_3OH

Scheme 1.

nol solvent molecules (brown form). Guest methanol molecules force the complex to adopt a more planar coordination environment in the solid state. In addition, absorption spectra in various organic solvents have been measured and a relationship is found between the features of absorption spectra and polarity of solvents as chemical external perturbations (Scheme 1).

2. Experimental

2.1. General

Chemicals of the highest commercial grade available (Aldrich and Wako) were used as received without further purification. Elemental analyses (C, H, N) were carried out on an Elementar Vario EL analyser at Keio University. Infrared spectra were recorded as KBr pellets on a JASCO FT-IR 660 plus spectrophotometer in the range of 4000–400 cm^{-1} at 298 K. Thermal analysis was performed on a SHIMADZU DSC-60 differential scanning calorimeter (DSC), where the heating rate was 10 K min^{-1} in the range 313–673 K. Diffuse reflectance spectra were measured on a JASCO V-560 spectrophotometer equipped with an integrating sphere in the range 850–220 nm at 298 K. Absorption spectra were measured on a JASCO V-560 spectrophotometer in the range 900–200 nm at 298 K. Magnetic susceptibility was measured with a Sherwood Scientific magnetic susceptibility balance at 298 K. Magnetic data were corrected for the magnetization of diamagnetic contributions, which were estimated from Pascal constants. XRD were recorded on a Rigaku RAD-C diffractometer with Cu Kα radiation ($\lambda = 1.5418$ Å). Semi-empirical molecular orbital calculations were performed the program ZINDO in a CAChe software package based on the crystal structures determined.

2.2. Synthesis

Treatment of an equimolar amount of copper(II) acetate (0.91 g, 5.00 mmol), salicylaldehyde (1.22 g, 10.0 mmol) and 1,2-diphenylethylamine (1.97 g, 10.0 mmol) in ethanol (100 mL) at 318 K for 3 h gave rise to brown crude precipitates. Recrystallization from an acetone solution at 298 K over a period of several days yielded green plate-like crystals suitable for X-ray crystallography, green form (**1**). *Anal.* Calc. for $C_{42}H_{36}CuN_2O_2$: C, 75.94; H, 5.46; N, 4.22. Found: C, 75.68; H, 5.37; N, 4.17%. IR (KBr): 1610 cm^{-1} (imine C=N stretching band). M.p. 572 K (decomposition). $\mu_{eff} = 1.52$ BM at 298 K. On the other hand, recrystallization from methanol–acetone mixed solution (1:1, v/v) at 298 K over a period of several days yielded a brown precipitate. *Anal.* Calc. for $C_{42}H_{36}CuN_2O_2$: C, 75.94; H, 5.46; N, 4.22. Found: C, 75.84; H, 5.46; N, 4.12%. IR (KBr): 1609 cm^{-1} (imine C=N stretching band). M.p. 559 K (decomposition). $\mu_{eff} = 1.43$ BM at 298 K. Well-grown brown prismatic single crystals suitable for X-ray crystallography contain methanol molecules, brown form (**2**).

2.3. X-ray crystallography

Intensity data were collected on a Rigaku AFC-7R four-circle diffractometer. The structures were solved by direct methods using SIR92 [34] and expanded by Fourier techniques. The structures were refined on F^2 anisotropically for non-hydrogen atoms by full-matrix least-squares methods with SHLEXL-97 [35] of the teXsan program package [36]. Empirical absorption corrections were applied based on ψ scans; transmission factors for **1** and **2** were 0.726–0.933 and 0.919–0.999, respectively. No significant decay in the intensity of three standard reflections was observed throughout the data collection. The hydrogen atoms were located at geometrically calculated positions, C–H = 0.950 Å, and refined isotropically. All the non-hydrogen atoms were refined anisotropically. As for **2**, C8(H6A)–C9A(H7A, H8A) and C8(H6B)–C9B(H7B, H8B) were treated as a positional disorder with 0.5 occupancy. Crystallographic data for **1** and **2** are summarized in Table 1.

3. Results and discussion

3.1. Description of structures

The molecular and crystal structures of **1** and **2** are depicted in Figs. 1–4, respectively. Selected bond distances and angles, and torsion angles of **1** and **2** are given in Tables 2 and 3, respectively.

The green form (**1**) affords a compressed tetrahedral *trans*-[CuN_2O_2] coordination geometry, in which the bidentate chelate ligands coordinate to the copper ion through phenolate oxygen atoms and imine nitrogen atoms. The Cu–N bond distances are 1.959(10) and 1.990(9) Å, while the Cu–O bond distances are 1.877(7) and 1.885(8) Å. These values are comparable to related non-planar or distorted tetrahedral complexes [16,17,19,22]. The *trans*-N–Cu–N and *trans*-O–Cu–O bond angles are 157.0(4)° and 151.1(3)°, respectively. The dihedral angle between the O1/Cu1/N1 plane and the O2/Cu1/N2 plane is 36.46(1)°,

Table 1
Crystallographic data for **1** and **2**

	1	**2**
Formula	$C_{42}H_{36}CuN_2O_2$	$C_{43}H_{40}CuN_2O_3$
Molecular weight	664.28	696.32
Crystal system	monoclinic	monoclinic
Space group	$P2_1/a$ (No. 14)	$P2_1$ (No. 4)
a (Å)	19.06(2)	20.668(5)
b (Å)	10.363(8)	9.329(2)
c (Å)	17.49(1)	9.281(4)
β (°)	103.22(7)	91.06(3)
V (Å^3)	3362(5)	1789.2(10)
Z	4	2
D_{calc} (g cm^{-3})	1.312	1.293
$F(000)$	1388	730
μ (mm^{-1})	0.689	0.652
Crystal size (mm)	$0.50 \times 0.40 \times 0.10$	$0.30 \times 0.30 \times 0.30$
Temperature (K)	298	298
θ_{min}, θ_{max} (°)	5.10, 27.55	5.05, 27.50
Wavelength (Mo Kα)	0.71073	0.71073
Total reflections	7781	4737
Observed reflections ($I > 2\sigma(I)$)	2627	3127
Number of refined parameters	425	407
R[a], R_w[b], S	0.0957, 0.3814, 1.036	0.0539, 0.1744, 0.936
Minimum and maximum residual densities (e/Å^3)	−0.82, 0.57	−0.41, 1.60

[a] $R = \sum \|F_o| - |F_c\| / \sum |F_o|$.
[b] $R_w = (\sum w(|F_o| - |F_c|)^2 / \sum w |F_o|^2)^{1/2}$, $w = 1/(\sigma^2(F_o) + (0.1469P)^2 + 10.7070P)$ for **1**, and $w = 1/(\sigma^2(F_o) + (0.102P)^2 + 0.0866P)$ for **2**, where $P = (F_o^2 + 2F_c^2|)/3$.

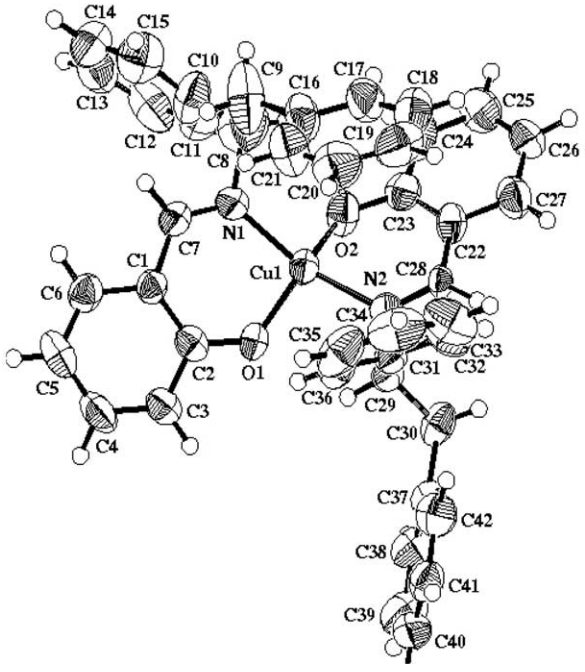

Fig. 1. The molecular structure of **1** showing the atom-labelling scheme. Displacement ellipsoids are drawn at the 50% probability level.

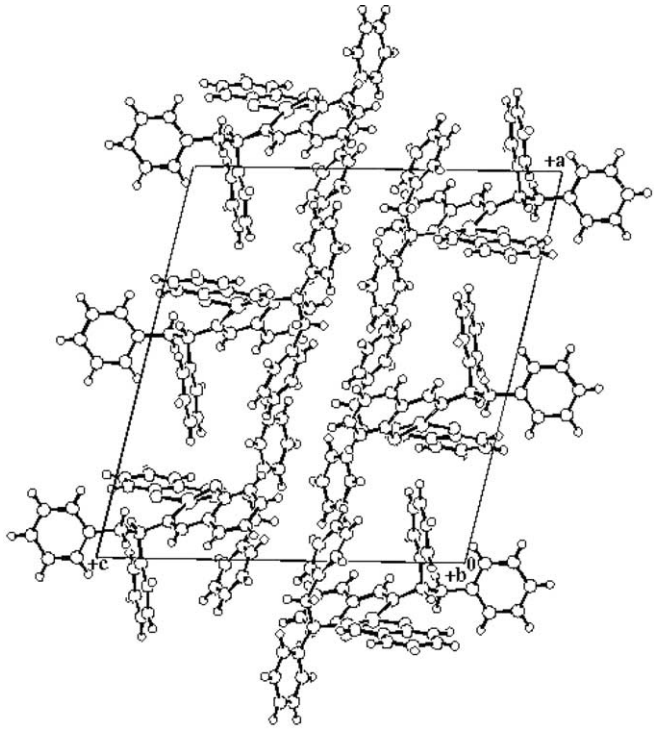

Fig. 2. Crystal packing of **1** viewed from the crystallographic b axis.

which results from two skewed ligands at opposite sides. This distorted coordination geometry is mainly ascribed to the steric hindrance of the bulky 1,2-diphenylethylamine moieties [29]. One of two 1,2-diphenylethylamine moieties of 1 is folded up, being close to the inner side of the molecule, while another one is expanded on the outside of the molecule. The corresponding torsion angles are N1–C8–C9–C16 = 65(1) and N2–C29–C30–C37 = −160.9(8)°. The imine C=N double bond lengths are 1.27(1) and

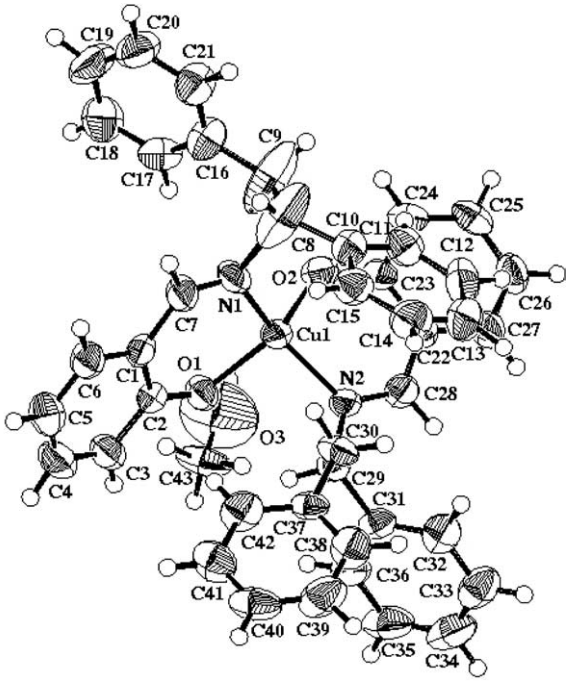

Fig. 3. The molecular structure of **2** showing the atom-labelling scheme. Displacement ellipsoids are drawn at the 50% probability level. Disordered atoms are omitted for clarity.

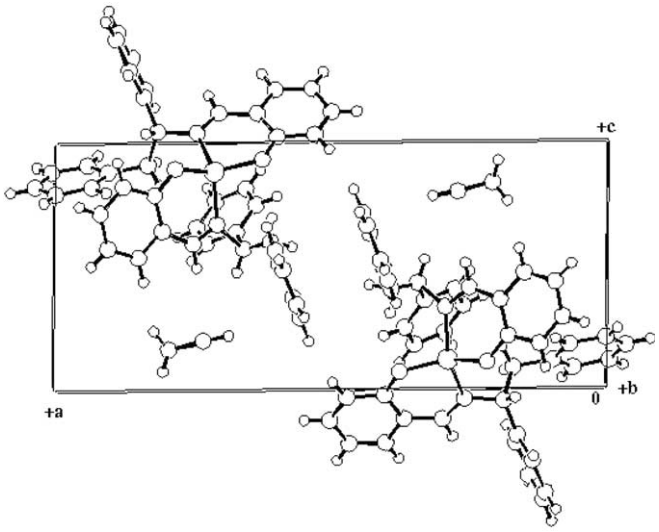

Fig. 4. Crystal packing of **2** viewed from the crystallographic *b* axis.

1.28(1) Å, which indicates that there is a sufficient decrease of the electronic distribution of dπ–pπ character through the π-conjugated system to cause distortion towards a tetrahedral environment [37]. The rest of the geometric parameters are unremarkable among analogous copper(II) complexes. No specific intramolecular hydrogen bonds could be detectable within van der Waals radii [38].

On the other hand, its crystal packing does not reveal remarkable intermolecular interactions, hence the crystals are estimated to be aggregated by weak van der Waals forces. In the crystal of **1**, the phenyl groups of one of the two 1,2-diphenylethylamine moieties face the inner side of the crystal lattice. A parallel arrangement of the molecules attribute to form molecular alignment along the crystallographic *a* axis. It should be noted that there is no space to include additional small molecules.

Table 2
Selected geometric parameters (Å, °) for **1**

Cu1–O1	1.877(7)	Cu1–O2	1.885(8)
Cu1–N1	1.959(10)	Cu1–N2	1.990(9)
N1–C7	1.27(1)	N2–C28	1.28(1)
C1–C7	1.44(1)	C22–C28	1.45(2)
O1–C2	1.31(1)	C23–O2	1.32(1)
C8–C9	1.34(3)	C29–C30	1.50(1)
C8–C10	1.56(3)	C29–C31	1.55(1)
C9–C16	1.55(2)	C30–C37	1.54(2)
O1–Cu1–O2	151.1(3)	N1–Cu1–N2	157.0(4)
O1–Cu1–N1	92.8(3)	O1–Cu1–N2	94.2(3)
O2–Cu1–N1	92.3(4)	O2–Cu1–N2	92.1(3)
Cu1–O1–C2	128.2(7)	Cu1–O2–C23	126.9(8)
Cu1–N1–C7	125.7(8)	Cu1–N1–C8	117.8(7)
C7–N1–C8	115(1)	C28–N2–C29	116.7(8)
C1–C7–N1	125(1)	C22–C28–N2	126.1(9)
N1–C8–C9–C16	65(1)	N2–C29–C30–C37	−160.9(8)
C7–N1–C8–C10	−44(1)	C28–N2–C29–C31	80.5(10)

Table 3
Selected geometric parameters (Å, °) for **2**

Cu1–O1	1.906(5)	Cu1–O2	1.875(4)
Cu1–N1	1.997(5)	Cu1–N2	1.973(5)
N1–C7	1.259(9)	N2–C28	1.286(8)
C1–C7	1.433(10)	C22–C28	1.445(8)
O1–C2	1.313(7)	C23–O2	1.303(7)
C8–C9A	1.18(2)	C29–C30	1.541(9)
C8–C10	1.54(2)	C29–C31	1.539(7)
C9A–C16	1.57(2)	C30–C37	1.519(7)
O1–Cu1–O2	139.9(2)	N1–Cu1–N2	141.3(3)
O1–Cu1–N1	92.6(2)	O1–Cu1–N2	95.9(2)
O2–Cu1–N1	101.7(2)	O2–Cu1–N2	95.6(2)
Cu1–O1–C2	127.9(4)	Cu1–O2–C23	126.9(4)
Cu1–N1–C7	123.6(5)	Cu1–N1–C8	119.6(6)
C7–N1–C8	113.3(6)	C28–N2–C29	121.3(5)
C1–C7–N1	127.4(6)	C22–C28–N2	126.9(6)
N1–C8–C9A–C16	120(1)	N2–C29–C30–C37	165.6(5)
C7–N1–C8–C10	116.0(8)	C28–N2–C29–C31	−22.9(8)

In contrast to **1**, the brown form (**2**) contains methanol molecules as crystalline solvent. Individual molecules of **2** also afford a compressed tetrahedral *trans*-[CuN_2O_2] coordination geometry. The Cu–N bond distances are 1.977(5) and 1.973(5) Å and the Cu–O bond distances are 1.906(5) and 1.875(4) Å. These values are also comparable to the related non-planar complexes [16,17,19,22]. The *trans*-N–Cu–N and *trans*-O–Cu–O bond angles are 141.3(3)° and 139.9(2)°, respectively. The dihedral angle between the O1/Cu1/N1 plane and the O2/Cu1/N2 plane is 54.46(1)°. These figures suggest that the degree of tetrahedral distortion deviated from square planar of **2** is larger than that of **1**. Although the main part of **1** and **2** is identical, the structural differences are ascribed to methanol solvent

and conformation and arrangement of the ligands, especially the 1,2-diphenylethylamine moieties. As for **2**, all phenyl groups of 1,2-diphenylethylamine moieties in the ligands are expanded outside of the molecule. The torsion angles are N1–C8–C9A–C16 = 120(1) and N2–C29–C30–C37 = 165.6(5)°. The imine C=N double bond lengths of 1.259(9) and 1.286(8) Å are similar to the corresponding values for **1** regardless of the degree of distortion [26–28].

Nevertheless, **2** contains methanol molecules as solvent, neither intramolecular nor intermolecular hydrogen bonds could be detectable in the crystals. However, a pair of phenyl groups, with a distance between them of about 4.2 Å, are faced as if they formed π–π stacking. The methanol solvent molecules are included in the void space between these quasi-stacking phenyl groups and its parent salicydenaminano moiety to stabilize crystal packing.

Recently, metal-organic frameworks for nano-scaled pores [39–43] and structural tuning by containing guest solvent molecules [44–48] have been studied widely in the field of supramolecular chemistry. In contrast to many of these metal-organic frameworks, the present complexes, **1** and **2**, are flexible mononuclear complexes without bridging ligands or intermolecular interactions. Interestingly, **1** (and **2**) may be a rare example which can vary its individual molecular structure as well as overall crystal structure to fit, or be induced by, solvent methanol molecules. The crystal lattice differences are also supported by XRD patterns for **1** and **2** (Fig. 5). The results are also consistent with simulated XRD patterns derived from the analyses of single crystal structures qualitatively.

3.2. IR and electronic spectra in the solid state

The IR spectra of **1** and **2** show bands at 1610 and 1609 cm^{-1}, respectively, which are ascribed to a stretching vibration of the imine C=N groups. The IR spectra of both complexes studied are in agreement with previous reports of analogous complexes (around 1620 cm^{-1}). However, the slight difference in distortion of coordination environment between **1** and **2** is not detectable by IR spectra.

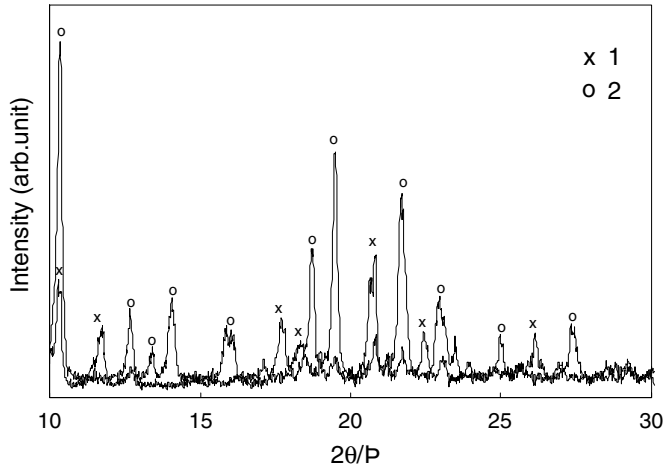

Fig. 5. XRD patterns of **1** and **2**.

The diffuse reflectance electronic spectra of **1** and **2** were recorded in the solid state. Both complexes exhibit a broad band in the region 15 000–20 000 cm^{-1} and another strong band in the region 21 000–24 000 cm^{-1}. The former broad d–d bands are attributed to a ligand field transition of the $3d^9$ copper(II) ion. In general for copper(II) complexes in C_2 symmetry, the free copper(II) ion of $3d^9$ configuration with the ^2D state splits into $^2A_1$, $^2A_2$, $^2B_1$ and $^2B_2$ levels. For this splitting, three transitions, $^2A_1 \rightarrow {}^2A_1$, $^2A_1 \rightarrow {}^2B_1$ and $^2A_1 \rightarrow {}^2B_2$, can be expected to be allowed, and the broad band is due to a combination of the three allowed transitions. A slight difference in the spectral features and apparent colors of **1** and **2** are caused by the ligand field splitting derived from the distortion of the coordination environment. Indeed, there is a tendency that tetrahedral complexes show a d–d band at lower energies, which shifts to higher energies on distorting from tetrahedral to square planar [23]. On the other hand, the strong band found at higher energies is due to overlap of a π–π* transition [49,50] and ligand (phenolate O) to copper(II) metal charge transfer (LMCT) transition. The peaks of these transitions are related to not only *trans*-$[CuN_2O_2]$ coordination geometries but also the net atomic charge on the coordinating atoms (O and N) of the ligands.

3.3. Calculations

The main results of semi-empirical calculations (ZINDO) [51,52] are summarized in Table 4. Single point calculations of heat of formation of the crystal structures determined show a difference of 5.7 kJ mol^{-1} between **1** and **2**. The fact that the energy of the green form (**1**), close to tetrahedral, is higher than that of the brown one (**2**), close to square planar. This indicates that the structural conformation of the ligands in individual molecules of **2** is more stable thermodynamically. In other words, providing external energy may be necessary to convert from the stable form **1** into the unstable form **2**.

The formal charges on the coordinating O and N atoms of the ligands and copper(II) ions have been calculated and the net atomic charges thus obtained have been averaged. The formal charges on copper(II) ions are 0.190 and 0.141 for **1** and **2**, respectively, which indicates that the more tetrahedrally distorted coordination environment prevents charge distribution through the coordination bonds. This tendency is qualitatively consistent with conventional interpretation; distortion from regular planar to tetrahedral leads to a weakening of both σ- and π-characters of coordination bonds. As the ligands of **1** and **2** are identical, the difference can be ascribed to purely coordination geometries. However, the correlation between the average negative charge of the coordinating atoms and the peaks may not be simple, because the electronic spectra consist of several types of transitions.

Table 4
Summary of calculated values of several properties for **1** and **2**

	1	**2**
Heat of formation (kJ mol^{-1})	358.1	352.4
Dipole moment (Debye)	4.96	6.96
Formal charge Cu	0.190	0.141
N	−0.173	−0.237
O	−0.477	−0.230
The lowest π–π* transition	29200	26100
Calculated (cm^{-1})	(LUMO → HOMO − 1)	(LUMO + 4 → HOMO − 1)

The dipole moments of **1** and **2** were evaluated to be 4.96 and 6.96 Debye, respectively. These values can be considered as an indication of the polarity of the molecules in their given conformations. Since **1** and **2** are distortion isomers, the larger dipole moment of **2** can be attributed to the conformation of the ligands.

3.4. Absorption spectra in various solvents

As shown in Fig. 6, the absorption spectra of **1** in the range 18000– 30000 cm^{-1} are characterized by a strong band around 27000 cm^{-1} band, and a weak shoulder-like band around 24000 cm^{-1}. The former is assigned to a π–π* transition in the ligands, while the latter is a d–d band reflecting the coordination environment. The π–π* peaks (wavenumber) and their intensity (log ε) are solvent dependent, as well as occasionally allowing the slight appearance of the shoulder-like band shape of the d–d region to shift. The shift of the π–π* region is as follows: acetone (27000 cm^{-1}, 4.16), chloroform (26900 cm^{-1}, 4.08), methanol (27100 cm^{-1}, 4.04), toluene (27000 cm^{-1}, 4.17) and DMF (26900 cm^{-1}, 4.06). The dipole moment (μ, Debye) and dielectric constant (ε) of the solvents used are: acetone (μ = 3.11, ε = 20.7), chloroform (μ = 1.11, ε = 4.81), methanol (μ = 2.97, ε = 32.6), toluene (μ = 0.37, ε = 2.44) and DMF (μ = 3.82, ε = 36.7). The π–π* bands exhibit a slight tendency of negative solvatochromism, namely the peaks of the bands shift to higher energies in solvents of increasing polarity. The results of the molecular orbital calculations above suggest that tetrahedrally distorted molecules indicate larger polarity. However, weak d–d bands are less sensitive to the polarity of solvents.

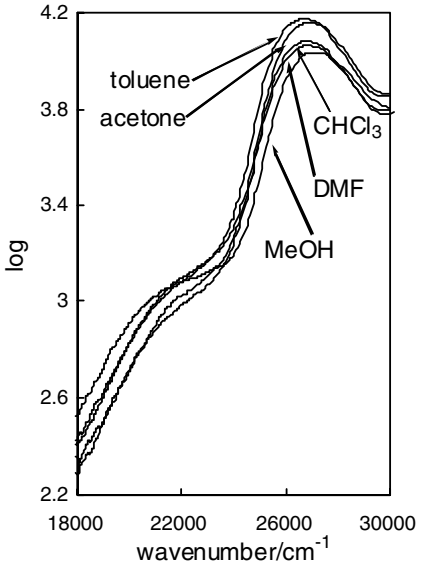

Fig. 6. Absorption electronic spectra of **1** in 1 mM solutions (acetone, chloroform, methanol, toluene and DMF) at room temperature.

In view of the theory of dielectric polarization [8], negative solvatochromism is expected for transitions from a higher dipole moment state to a smaller one. Generally, the LMCT transition moment lies antiparallel to the ground state dipole moment, when the ground state is more polar than the excited state. In this case, the ground state is stabilized by polar solvents and its transition energies are increased. On the other hand, in the cases where the peak of a band for a certain type of transition can shift in accordance with intermolecular interactions between the dipole moment of solutes and solvents, we should consider induced short-range specific interactions such as hydrogen bonds and π–π stacking.

For the present case, however, the correlation between the dipole moment of the complexes and the physical properties of solvents do not allow us to draw a conclusion that the various solvents attribute to the shift of the LMCT transitions of the complexes. We consider only the dipole–dipole part of the van der Waals solute–solvent interactions, neglecting dipole-induced dipole interactions and London's dispersion force, which is a complicated matter that we should study furthermore.

4. Concluding remarks

The syntheses, structural characterization and spectroscopic data have been reported for both the green form of solvent free and the brown form containing methanol solvent of the present copper(II) complex. It is revealed that methanol molecules as solvents in the crystals play an important role in tuning not only crystal packing but also the individual molecular conformation of this flexible mononuclear copper(II) complex without remarkable intermolecular interactions. The ZINDO calculations based on the crystal structures elucidated thermodynamical stability and difference in energy for both forms. The absorption

spectra in various solvents exhibit a relationship between molecular structures and dipole moments. Further studies on other related compounds and the development of photo-induced switching mechanisms are currently ongoing.

5. Supplementary material

Crystallographic data for the structural analyses are deposited with the Cambridge Crystallographic Data Centre, CCDC with deposition numbers 260175 and 260176 for **1** and **2**, respectively. Copies of this information can be obtained from the Cambridge Crystallographic Data Centre, 12 Union Road, Cambridge CB2 1EZ, UK (fax: +44 1223 336033; deposit@ccdc.cam.ac.uk or www: http://www.ccdc.cam.ac.uk).

Acknowledgements

This work was supported by Grant-in-Aid for the 21st Century COE program 'KEIO Life Conjugate Chemistry' form the Ministry of Education, Culture, Sports, Science and Technology, Japan. The authors thank Professor Yohru Yamada and Dr. Taketo Ikeno (Keio University) for use of the DSC apparatus.

References

[1] O. Sato, Acc. Chem. Rev. 36 (2003) 692.
[2] O. Sato, S. Hayami, Y. Einaga, Z.-Z. Gu, Bull. Chem. Soc. Jpn. 76 (2003) 443.
[3] B. Narayanan, M.M. Bhadbhade, J. Coord. Chem. 46 (1998) 115.
[4] I. Grenthe, P. Paoletti, M. Sandstrom, S. Glikberg, Inorg. Chem. 28 (1979) 2687.
[5] M.J. Riley, D. Neill, P.V. Bernhardt, K.A. Byriel, C.H.L. Kennard, Inorg. Chem. 37 (1998) 3635.
[6] K.L. Bray, H.G. Drickamer, E.A. Schmitt, D.N. Hendrickson, J. Am. Chem. Soc. 111 (1989) 2849.
[7] J. Burgess, S. Maguire, A. McGranaghan, S.A. Parsons, B. Nowicka, A. Samotus, Trans. Met. Chem. 23 (1998) 615.
[8] I. Veroni, A. Rontoyianni, C.A. Mitsopoulou, J. Chem. Soc., Dalton Trans. (2003) 255.
[9] M.M. Bhadbhade, D. Srinivas, Inorg. Chem. 32 (1993) 5458.
[10] M. Boiocchi, L. Fabbrizzi, F. Foti, M. Vazquez, J. Chem. Soc., Dalton Trans. (2004) 2616.
[11] M. Kato, A. Omura, A. Toshikawa, S. Kishi, Y. Sugimoto, Angew. Chem. Int. Ed. 41 (2002) 3183.
[12] E.J. Fernandez, J.M. Lopez-de-Luzuriaga, M. Monge, M.E. Olmos, J. Perez, A. Laguna, A.A. Mohamed, H.P. Fackler Jr., J. Am. Chem. Soc. 125 (2003) 2022.
[13] S. Yamada, Coord. Chem. Rev. 190–192 (1999) 537, and references therein.
[14] J.M. Fernandez-G, O.L. Ruiz-Tamirez, R.A. Toscano, N. Macias-Ruvalcaba, M. Aguilar-Martinez, Trans. Met. Chem. 25 (2000) 517.
[15] A. Castineiras, W. Hiller, J. Strahle, J. Romero, R. Bastida, A. Sousa, Acta Crystallogr. C 46 (1990) 770.
[16] T.P. Cheeseman, D. Hall, T.N. Waters, Nature 205 (1965) 494.
[17] P.L. Orioli, L. Sacconi, J. Am. Chem. Soc. 88 (1966) 277.
[18] H. Nozaki, H. Takaya, S. Moriuti, R. Noyori, Tetrahedron 24 (1968) 3655.
[19] G.-P. Li, Q.-C. Yang, Y.-Q. Tang, Y.-D. Guan, Z.-H. Shang, Acta Chim. Sin. 45 (1987) 421.
[20] H. Okawa, M. Nakamura, S. Kida, Inorg. Chim. Acta 120 (1986) 185.
[21] T. Akitsu, Y. Einaga, Acta Crystallogr. E 60 (2004) m1605.
[22] T. Akitsu, Y. Einaga, Acta Crystallogr. C 60 (2004) m640.
[23] P.C. Chia, D.P. Freyberg, G.M. Mockler, E. Sinn, Inorg. Chem. 16 (1977) 254.
[24] H. Tamura, K. Ogawa, A. Takeuchi, S. Yamada, Chem. Lett. (1977) 889.
[25] H. Tamura, K. Ogawa, A. Takeuchi, S. Yamada, Cryst. Struct. Commun. 9 (1980) 91.
[26] T. Akitsu, Y. Einaga, Acta Crystallogr. E 60 (2004) m436.
[27] T. Akitsu, Y. Einaga, Acta Crystallogr. E 60 (2004) m1522.
[28] T. Akitsu, Y. Einaga, Acta Crystallogr. E 60 (2004) m1555.
[29] T. Akitsu, S. Komorita, Y. Kushi, Inorg. Chim. Acta 315 (2001) 18.
[30] T. Akitsu, S. Komorita, A. Urushiyama, Bull. Chem. Soc. Jpn. 74 (2001) 851.
[31] T. Akitsu, S. Komorita, H. Tamura, Inorg. Chim. Acta 348 (2003) 25.
[32] B. Ibragimov, J. Incl. Phenom. Macrocycl. Chem. 34 (1999) 345.
[33] L.R. Nassimbeni, H. Su, Acta Crystallogr. B 58 (2002) 251.
[34] A. Altomare, G. Cascarano, C. Giacovazzo, A. Guagliardi, M.C. Brurla, G. Polidori, M. Camalli, J. Appl. Cryst. 27 (1994) 435.
[35] G.M. Sheldrick, SHELXL97, Program for the Refinement of Crystal Structures, University of Gottingen, Germany, 1997.
[36] Molecular Structure Corporation. TEXSAN, Version 1.11., MSC, 9009 New Trails Drive, The Woodlands, TX 77381-5209, USA, 2001.
[37] V. Manriquez, J. Vargas, J. Costamagna, H.G. von Schnering, K. Peters, Acta Crystallogr. C 46 (1990) 772.
[38] A. Bondi, J. Phys. Chem. 68 (1964) 441.
[39] O.M. Yaghi, H. Li, C. Davis, D. Richardson, T.L. Groy, Acc. Chem. Res. 31 (1998) 474.
[40] M. Eddaoudi, D.B. Moler, H. Li, B. Chen, T.M. Reineke, M. O'Keeffe, O.M. Yaghi, Acc. Chem. Res. 34 (2001) 319.
[41] G. Ferey, Chem. Mater. 13 (2001) 3084.
[42] M.J. Zaworotko, Chem. Commun. (2001) 1.
[43] O.R. Evans, W. Lin, Acc. Chem. Res. 35 (2002) 511.
[44] K.T. Holman, A.M. Pivovar, J.A. Swift, M.D. Ward, Acc. Chem. Res. 34 (2001) 107.
[45] V.S.S. Kumar, F.C. Pigge, N.P. Rath, Cryst. Growth Des. 4 (2004) 654.
[46] S.W. Watt, C. Dai, A.J. Scott, J.M. Burke, R.L. Thomas, J.C. Collings, C. Viney, W. Clegg, T.B. Marder, Angew. Chem. Int. Ed. 43 (2004) 3061.
[47] E. Tynan, P. Jensen, P.E. Kruger, A.C. Lees, Chem. Commun. (2004) 776.
[48] S.K. Ghosh, P.K. Bharadwaj, Inorg. Chem. 43 (2004) 5180.
[49] H. Sakiyama, H. Okawa, N. Matsumoto, S. Kida, J. Chem. Soc., Dalton. Trans. (1990) 2935.
[50] C. Evans, D. Luneau, J. Chem. Soc., Dalton. Trans. (2002) 83.
[51] M.C. Zerner, G.H. Lowe, R.F. Kirchner, U.T. Mueller-Westerhoff, J. Am. Chem. Soc. 1102 (1980) 589.
[52] J.D. Head, M.C. Zerner, Chem. Phys. Lett. 131 (1986) 359.

report also includes the analysis of the possible influence of this and other structural features on the final geometry of the complex molecule. The results are compared with those found for the previously reported Co(II) complexes of acetone *S*-methylisothiosemicarbazone [11,12] and with the similar five-coordinate bis(bidentate)–Co(II) and –Co(III) complexes containing five-membered chelate rings. In the aim of the determination of the main factors influencing the preferable geometry in these complexes, we analyzed all five-coordinate bis(bidentate)–Co complexes available in the literature. In addition to the structural determination of the complexes **1** and **2**, a study of their spectroscopic and magnetic properties has been carried out together with that of third complex with the same ligand, [CoL_2Br]Br (**3**).

2. Experimental

2.1. Synthesis of the complexes

Acetone *S*-methylisothiosemicarbazone (L) was prepared according to the procedure described in [14]. The details of the synthesis are as follows: an acetone-ethanolic solution (50 and 20 cm^3, respectively) of 23.0 g (0.1 mol) *S*-methylisothiosmicarbazide hydrogeniodide and 15 g (0.05 mol) $Na_2CO_3 \cdot 10H_2O$ were heated with refluxing. After completing the reaction (3 h), the solution was filtered and its amount reduced to a small volume by heating with warm air. The yellowish crystals of the ligand were filtered out and washed with ether and ethanol. Yield: 8.7 g.

2.1.1. [CoL_2Cl]I (**1**)

0.24 g (1 mmol) of $CoCl_2 \cdot 6H_2O$ was added with stirring to a methanolic-acetone mixture (8 and 4 cm^3, respectively) of 0.46 g (2 mmol) *S*-methylisothiosemicarbazide hydrogeniodide and 0.29 g (1 mmol) $Na_2CO_3 \cdot 10H_2O$. The mixture was heated with stirring for 15 min. The product was filtered off and the solution was allowed to stand. Violet crystals of the complex appeared after 24 h. Yield: 0.62 g, m.p. 199 °C *Anal.* Calc. for $C_{10}H_{22}ClCoIN_6S_2$ ($M = 511.74$ g mol^{-1}): C, 23.45; H, 4.30; N, 16.41; S, 12.51. Found: C, 23.21; H, 4.26; N, 16.44; S, 12.48%.

2.1.2. [$CoLBr_2$] (**2**)

0.14 g (1 mmol) of solid acetone *S*-methylisothiosemicarbazone [14] was added to a solution of 0.33 g (1 mmol) $CoBr_2 \cdot 6H_2O$ in 5 cm^3 acetone. The mixture was heated with stirring for about 15 min. After 8 h of crystallization, the product was filtered off and washed with acetone. Yield: 0.54 g, m.p. 241 °C *Anal.* Calc. for $C_5H_{11}Br_2CoN_3S$ ($M = 363.98$ g mol^{-1}): C, 16.48; H, 3.02; N, 11.54; S, 8.79. Found: C, 16.39; H, 3.05; N, 11.50; S, 8.74%.

2.1.3. [CoL_2Br]Br (**3**)

0.28 g (2 mmol) of solid acetone *S*-methylisothiosemicarbazone was added to a solution of 0.33 g (1 mmol) $CoBr_2 \cdot 6H_2O$ in 5 cm^3 ethanol. The mixture was heated with stirring for about 15 min. After 8 h of crystallization, the product was filtered off and washed with ethanol. Yield: 0.38 g, m.p. 191 °C, *Anal.* Calc. $C_{10}H_{22}CoBr_2N_6S_2$ ($M = 509.24$ g mol^{-1}): C, 23.56; H, 4.23; N, 16.50; S, 12.56. Found: C, 23.52; H, 4.18; N, 16.56; S, 12.50%.

2.2. Physical methods

Elemental (C, H, N) analysis of the air-dried compounds was carried out by standard micromethods at the Center for Instrumental Analysis, Faculty of Chemistry, Belgrade. Infrared spectra in KBr pellets (400–4000 cm^{-1}) were recorded by a FT-IR spectrophotometer. Magnetic measurements of powdered samples were carried out in the temperature range 5–200 K at an applied magnetic field of 500 Oe using a Quantum Design MPMS-XL-5 SQUID magnetometer. Diamagnetic corrections are estimated from Pascal tables.

2.3. X-ray crystallography

Crystal and structure refinement data for [CoL_2Cl]I and [$CoLBr_2$] are summarized in Table 1. The diffraction data for both complexes were collected on an Enraf-Nonius CAD4 diffractometer by using graphite-monochromated Mo Kα (0.71073 Å) radiation at 293(2) K. The data were corrected for Lorentz and polarization effects [15,16]. The absorption correction was neglected in [CoL_2Cl]I in view of the small crystal dimensions, while in the case of [$CoLBr_2$] a gaussian-type absorption correction [17,18] based on the crystal morphology was applied. Both structures were solved by heavy atom method and difference

Table 1
Crystal and structure refinement data for [CoL_2Cl]I and [$CoLBr_2$]

Empirical formula	$C_{10}H_{22}ClCoIN_6S_2$	$C_5H_{11}Br_2CoN_3S$
Formula weight	511.74	363.98
Color	violet	blue
Temperature (K)	293(2)	293(2)
Crystal size (mm)	$0.25 \times 0.14 \times 0.10$	$0.50 \times 0.16 \times 0.10$
Crystal system	monoclinic	monoclinic
Space group	$P2_1/c$	$P2_1/n$
Lattice constants		
a (Å)	9.4010(13)	8.065(15)
b (Å)	25.738(7)	10.875(10)
c (Å)	9.019(10)	13.039(8)
α (°)	90.00	90.00
β (°)	117.15(2)	91.75(10)
γ (°)	90.00	90.00
Volume (Å^3)	1941.8(10)	1143(2)
Z	4	4
D_{calc} density, ρ (g cm^{-3})	1.750	2.115
θ Range for data collection (°)	1.58–24.97	2.44–26.00
Absorption coefficient (mm^{-1})	2.828	8.631
Absorption correction	none	Gaussian
Maximum/minimum transmission		0.4626/0.2634
F(0 0 0)	1012	700
Reflections collected	3403	4011
Independent reflections [$I > 2\sigma(I)$]	1549	934
Parameters	194	112
Goodness-of-fit	0.993	1.007
R_1 [$I > 2\sigma(I)$]	0.0806	0.0903

Fourier methods and refined on F^2 by the full-matrix least-square method [19,20]. H atoms were included in the model at geometrically calculated positions with fixed C–H and N–H distances of 0.96 and of 0.86 Å, respectively, and isotropic displacement parameters equal to 1.5 and 1.2 times the equivalent isotropic displacement parameters of the C and N atoms.

3. Results and discussion

The molecular structures of $[CoL_2Cl]I$ (**1**) and $[CoLBr_2]$ (**2**) along with their crystal packing are shown in Figs. 1 and 3, respectively. The selected bond lengths and bond angles for complexes **1** and **2** are given in Tables 2 and 4, respectively. Table 3 lists the similar five coordinate bis(bidentate)–Co(II) and bis(bidentate)–Co(III) complexes containing nitrogen donating chelates, and their corresponding τ values.

3.1. Crystal structure of $[CoL_2Cl]I$ (1)

Fig. 1A shows the molecular structure of the complex molecule and the atom numbering scheme. The coordination polyhedron around Co(II) is best described in terms of the trigonal bipyramidal geometry. According to the value of 0.84 found for the geometrical parameter $\tau = (\beta - \alpha)/60$ [21], where $\alpha =$ N3a–Co–N3b and $\beta =$ N1a–Co–N1b, the structure is less than 20% distorted from an ideal trigonal bipyramid. This polyhedron comprises of one chlorine atom and two thioamide nitrogens (N3a and N3b) of the Schiff base in the equatorial positions and two terminal hydrazine nitrogens (N1a and N1b) in the axial sites. Table 2 lists selected bond lengths and angles for **1**. The interatomic Co–N and Co–Cl distances are consistent with those reported for similar Co(II) structures [11,12,22].

Table 2
Selected bond lengths (Å) and angles (°) in complex cation of $[CoL_2Cl]I$ compared with those in $[CoL_2Cl]_2[CoCl_4]$ [12]

	$[CoL_2Cl]I$		$[CoL_2Cl]_2[CoCl_4]$	
	A	B	A	B
Co–Nl	2.167(12)	2.178(12)	2.157(2)	2.181(2)
Co–N3	1.990(10)	1.999(11)	1.987(3)	1.993(3)
N1–N2	1.395(15)	1.402(14)	1.396(3)	1.413(3)
N2–C1	1.323(19)	1.308(17)	1.340(3)	1.335(2)
N3–C1	1.291(18)	1.305(17)	1.307(3)	1.299(2)
N1–C2	1.292(18)	1.298(17)	1.297(2)	1.280(3)
C2–C3	1.48(2)	1.47(2)	1.50(1)	1.48(1)
C2–C4	1.52(2)	1.50(2)	1.51(1)	1.51(1)
N3–Co–Nl	77.5(4)	77.6(5)	78.2(2)	77.6(2)
C1–N2–N1	116.6(12)	117.7(12)	115.8(2)	117.7(3)
N3–C1–N2	120.4(13)	121.2(12)	120.7(3)	121.2(2)
N2–Nl–Co	108.7(9)	108.1(8)	109.3(2)	108.1(2)
Cl–N3–Co	116.6(10)	115.9(10)	116.0(2)	115.9(3)
Co–Cl	2.337(4)		2.298(4)	
Nla–Co–Nlb	171.8(4)		168.6(1)	
N3a–Co–N3b	121.1(5)		119.9(1)	
N3a–Co–Cl	119.7(3)		119.2(2)	
N3b–Co–Cl	119.2(3)		120.8(2)	

It should be noted that depending of their carbonyl moiety, the majority of the thiosemicarbazone ligands contain more or less delocalized π electron density throughout the Schiff base, however among the over one hundred reported isothiosemicarbazide-based ligands the acetone *S*-methylisothiosemicarbazone is the only one which contains a

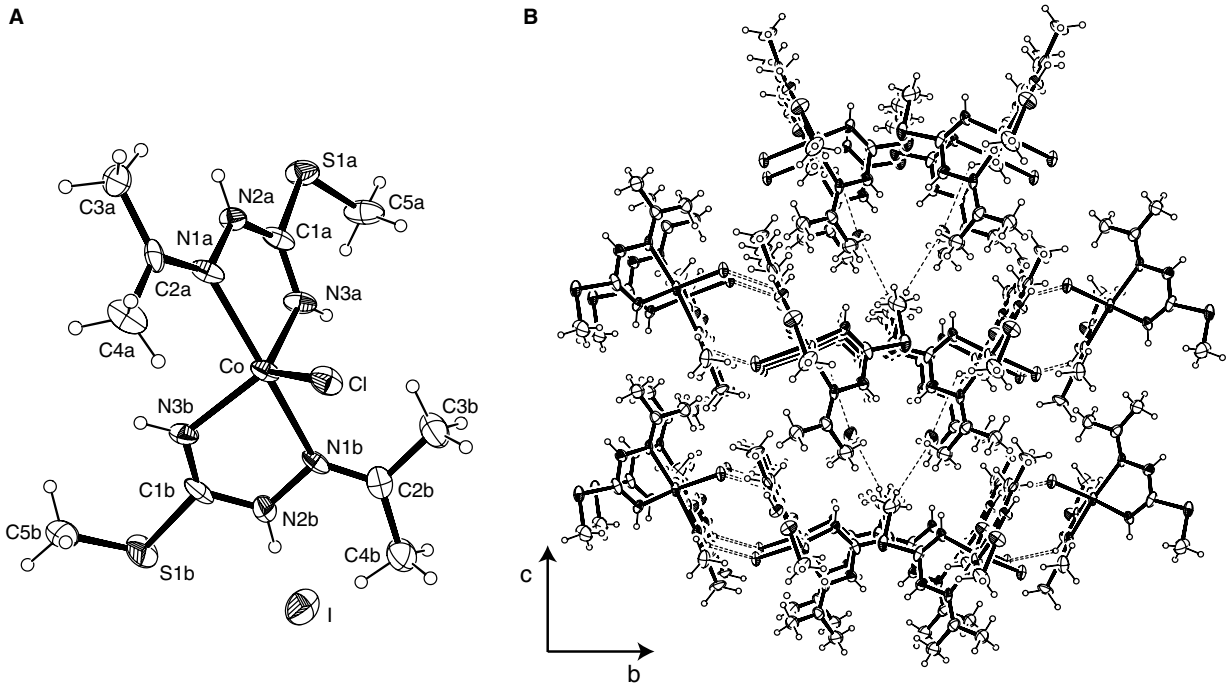

Fig. 1. (A) Molecule structure of **1**. (B) Packing arrangement (viewed down the *a*-axis) showing the N–H···Cl hydrogen bonds and C–H···I interactions.

Table 3
Five-coordinate bis(bidentate)–Co complexes with five-membered NN chelate rings

Formula	τ	Ref.	Formula	τ	Ref.
$[CoL_2Cl]I$	0.84	this work	$[Co(L^6)_2NO]\cdot PhCH_3$	0.00	[31]
$[CoL_2CH_3COO]I$	0.44	[11]	$[Co(L^7)_2Cl]$	0.17	[32]
$[CoL_2Cl]_2[CoCl_4]$	0.80	[12]	$[Co(L^8)_2I]$	0.02	[33]
$[Co(L^1)_2H_2O]\cdot H_2O$	0.78	[26]	$[Co(L^9)_2Ph_2NH_3]$	0.21	[34]
$[Co(L^2)_2H_2O]ClO_4$	0.79	[27]	$[Co(L^9)_2CNCH_3]CNCH_3$	0.17	[34]
$[Co(L^3)_2CN]\cdot H_2O$	0.08	[28]	$[Co(L^9)_2Py]CH_3COO$	0.10	[35]
	0.01				
$[Co(L^4)_2Py]$	0.02	[29]	$[Co(L^{10})_2PPh_3]\ ClO_4$	0.02	[36]
$[Co(L^5)_2NO]$	0.07	[30]	$[Co(L^{11})_2C_6H_4N_2H_2][BPh_4]$	0.08	[37]
	0.01				
	0.03				

L^1 = N-(2-chloro-6-methylphenyl)pyridine-2-carboxamide; L^2 = 2-furaldehyde *S*-methylisothiosemicarbazone; L^3 = diiminosuccinonitrile; L^4 = 3-(hydroxyamino)-3-methyl-2-butanone-oximato-*N,N′*; L^5 = dimethylglyoximato; L^6 = diphenylglyoximato; L^7 = alpha-hydroxylamino-isobutyrophenone-oximate; L^8 = *S*-methyl-1-phenylisothiosemicarbazido-*N,N′*; L^9 = N-phenyl-*o*-benzoquinone-di-imine-*N,N′*; L^{10} = *o*-benzosemiquinonedi-iminato-*N,N′*; L^{11} = 1,2-benzoquinone-diimide.

Table 4
Selected bond lengths (Å) and angles (°) of $[CoLBr_2]$

Co–N1	2.075(13)	N3–Co–N1	80.2(5)
Co–N3	1.959(13)	C1–N2–N1	117.6(13)
N1–N2	1.378(16)	N3–C1–N2	118.3(14)
N2–C1	1.339(18)	N2–N1–Co	108.9(9)
N3–C1	1.311(18)	C1–N3–Co	115.0(11)
Co–Br1	2.359(5)	N1–Co–Br1	118.4(5)
Co–Br2	2.370(5)	N3–Co–Br1	110.2(4)
C2–C3	1.48(2)	N1–Co–Br2	119.2(5)
C2–C4	1.52(2)	N3–Co–Br2	112.7(4)
		Br1–Co–Br2	111.7(2)

completely localized double bond between hydrazine N1 and carbonyl C2 atoms. This is confirmed by the corresponding bond lengths N1a–C2a = 1.292(18) Å and N1b–C2b = 1.298(17) Å and by the fact that each of the sp^2 hybridized C2 atoms bind two methyl groups through two single bonds. The localized π electron density prevents any rotation around the N1–C2 bond and favors the planarity of the ligand. The corresponding torsion angles N2–N1–C2–C3 and N2–N1–C2–C4 are 176.8° and −0.7°, −178.8° and 3.4° for branches *a* and *b*, respectively.

The hydrazine nitrogen atoms N2a and N2b are almost equivalently positioned regarding the Cl anion, however they have quite different roles in the crystal packing. The N2a–H2a moiety is involved in the hydrogen bond with the chlorine of the centrosymmetrically related complex molecule [N2a–H2a = 0.86 Å, H2a···Cl = 2.61 Å, N2a···Cl = 3.35(2) Å, N2a–H2a···Cl^{i} = 144°, (i) $-x+1$, $-y+1$, $-z+1$], while the other hydrazine moiety N2b–H2b finds the appropriate acceptor, the iodine atom, at a distance of 3.11 Å which is close to the sum of the van der Waals radii for H and I [1.20(H) + 1.98(I) = 3.18 Å] [23]. Probably as a consequence of the engagement of N2a in the hydrogen interaction, the chelate ring containing this atom shows less planarity then the other one, the corresponding N1a–N2a–C1a–N3a and N1b–N2b–C1b–N3b torsion angles are −4.4° and −0.5°, respectively. It is worth noticing that, surrounded with five methyl groups in the radius of 4 Å, the iodine atom forms contacts with both –S–CH_3 moieties where the C–H···I distances are shorter than the sum of the van der Waals radii for these two atoms H5b···I = 3.01 Å, C5a···I = 3.90(2), C5a–H5a···I^{ii} = 154°, (ii) x, y, z; H5d···I = 3.06 Å, C5b···I = 3.64(2), C5b–H5d···I^{iii} = 121°, (iii) $1+x$, y, $1+z$ (Fig. 1B).

3.2. Coordination geometry of five-coordinate bis(bidentate)–Co(II) and bis(bidentate)–Co(III) complexes containing two five-membered chelate rings

The geometrical characteristics of the complex molecules and the factors determining the degree of their deformation from the ideal geometry always deserve special attention. In the case of five coordinate complexes which could exist in two ideal geometrical forms, square pyramidal and trigonal bipyramidal, an additional problem emerges, that is to find the preferable configuration and then to search for the causes of its deformation. Considering that the nature of the complexes depends on many different factors [24], we tried to explore the effects of several, which we found most important, on the coordination geometry of the five coordinate bis(bidentate)–Co(II) and –Co(III) complexes containing two five-membered chelate rings.

3.2.1. Coordinational preference of the metal

It is well known that cobalt forms numerous complexes of various stereochemical types in both oxidation states Co(II) and Co(III), although it has been found that in complex molecules the state Co(III) is more stable relative to the state Co(II). For both oxidation states an octahedral disposition of the donor atoms around the Co ion is the most typical. The number of tetrahedral structures is also significant, particularly in the case of divalent cobalt, while the coordination number five within a trigonal bipyramidal or a square-pyramidal ligand arrangement is less common for either oxidation state [23]. Limiting our investigation to bis(bidentate)–Co(II) and –Co(III) complexes containing five-membered chelate rings with nitrogen donors we found only 15 structures whose crystal structures were reported. These compounds are listed in Table 3.

3.2.2. Bite angle of the chelating ligand

The theoretically possible arrangements of two bidentate ligands within the square pyramidal and trigonal bipyramidal complexes are represented in Scheme 1. Considering whether the ligand bridges two equatorial or equatorial and axial positions, the complexes could be distributed in four theoretically possible arrangements, (two for each geometry). However, the corresponding τ values which were calculated for each of the bis(bidentate) Co complexes (Table 3) showed that in most of the cases the geometry of the complexes is closer to square pyramidal (SP) (11 structures with τ less than 0.21) than to trigonal bipyramidal (TBP) (3 structures). Between the two possible arrangements of ligands within the SP geometry shown in Scheme 1, 1a was the only one found. This is in agreement with the fact that N–Co–N coordination angles of the small bidentate ligands, whose average value is $\langle 80.1° \rangle$, are much more in accordance with the value of 88.4°, characteristic for the equatorial part of the SP geometry than to an angle of 100° formed between the axial and equatorial sites of a SP structure (1b) [25]. The few complexes whose geometry is closer to TBP rather adopt the arrangement labelled as 2a. The angle spanned by the chelate is somewhat larger (90°) than in the previous case, which could be the reason for the smaller number of TBP structures, but it is again much more in accordance with its small bite than the case 2b where one of the bidentate ligands occupies the equatorial sites at 120°.

3.2.3. Steric and geometrical requirements of the ligands

Inspection of the tabulated square-pyramidal complexes of Co(II) and Co(III) showed two types of chelates present in their basal plane: (1) chelates without the large substituents on the donor atoms and thus without steric hindrance in the basal planes; (2) chelates which contain large substituents on the donor atoms but are able to avoid steric repulsion by the rotation of the substituents. The example for the later is the square-pyramidal complex $[CoL^8{}_2I]$, L^8 = *S*-methyl-1-phenylthiosemicarbazide [33], where the large phenyl group is attached to *S*-methylisothiosemicarbazide. However, the single bond which connects these moieties (N1–C2 = 1.43 Å) allows free rotation of the phenyl ring and formation of the basal plane of the quite regular SP structure ($\tau = 0.02$). Similarly, the corresponding N–C bonds in other SP complexes containing substitutents on the donor atoms range from 1.42 to 1.44 Å.

Among the complexes whose structure is closer to TBP, two were products of L, thus the fact that the novel complex with the same ligand also belongs to the less favorable TBP group indicates the importance of the ligand's structural features and possible steric interaction in the SP geometry. To explore this fact we analyzed the hypothetical complex molecule which contains two L ligands in the base of a SP structure (Fig. 2). The geometry of this molecule is based on the experimental data obtained for complex **1**. According to it, even in a *trans* mutual arrangement the two molecules of L, due to their steric repulsion, could not form the basal plane for a SP geometry. Since the double bond hinders the rotation of the ketone moiety around N1–C2, the hydrogen atoms of the methyl and thioamide groups are directed to each other forming too short a H···H distance of 1.46 Å (Fig. 2).

One can conclude that the final configuration of **1** is the result of the geometrical restrictions of the bidentate ligand, which besides the small bite angle also include its favored planarity caused by a pure double bond between the thiosemicarbazide and ketone moieties. The compromise between the produced steric hindrance and the maximal separations of the donor atoms eventually gives rise to the quite uniform distribution of the donor atoms within this trigonal-bipyramid [N3a–Co–N3b = 121.1 (5)°, N3a–Co–Cl = 119.7 (5)°, N3b–Co–Cl = 119.2 (5)°, N1a–Co–Cl = 94.8 (3)°, N1b–Co–Cl = 93.2 (3)°]. In the TBP complexes listed in Table 3 the corresponding N–C bonds range from 1.27 to 1.29 Å; the exception is $[Co(L^1)_2H_2O]\cdot$

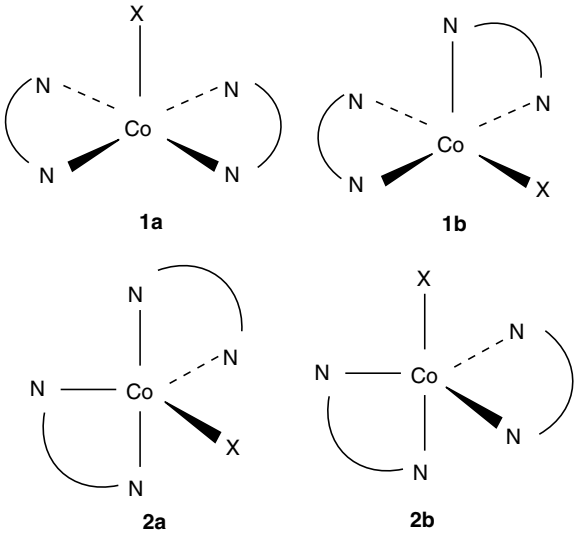

Scheme 1.

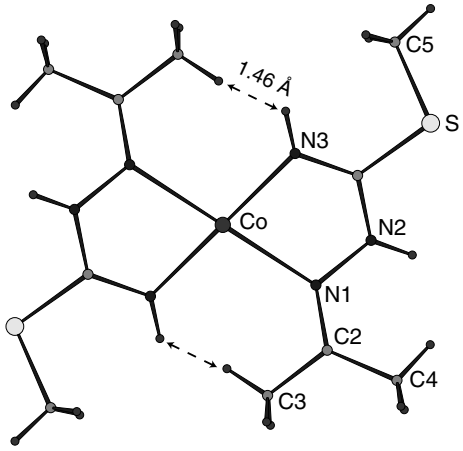

Fig. 2. The hypothetical complex molecule containing two L ligands in the base plane of a square-pyramid; the axial ligand is omitted for clarity.

H_2O [26] (N–C = 1.43 Å) whose chelate contains a phenyl group on either donor atom.

3.2.4. Interligand repulsion

According to the τ value, the geometry of the complex $[CoL_2CH_3COO]I$ [11], containing the same ligand, is almost in the middle of two terminal five coordinate structures ($\tau = 0.44$). However, viewed as SP the structure shows the less favorable distribution 1b with L bridging the axial and equatorial positions of the complex, while viewed as TBP this structure shows the common arrangement 2a in which L spans the equatorial and axial positions of the TBP structure. Similarly to **1**, the geometric requirements of the ligand prevent the formation of the basal plane of a SP geometry. On the other hand, the stronger electrostatic repulsion between the uncoordinated oxygen atom of the acetate ligand and the nitrogen donors prevents the formation of the regular TBP arrangement as found in **1**. The final geometry of $[CoL_2CH_3COO]I$ is thus markedly distorted, which can be seen from the corresponding angles: N3a–Co–N3b = 113.8°, N3a–Co–O1 = 141.1°, N3b–Co–O1 = 104.2°, N1a–Co–O1 = 105.0°, N1b–Co–O1 = 87.4°.

3.2.5. Packing considerations in the crystal lattice

Another previously reported complex of L, $[CoL_2Cl]_2$-$[CoCl_4]$ [12] contains the identical complex cation as for **1**. Comparison of their resulting geometrical parameters (Table 2) shows a considerable similarity. With N1a–Co–N1b assigned as β and N3a–Co–Cl assigned as α, the τ parameter of $[CoL_2Cl]_2[CoCl_4]$ has a value 0.80. However, since the cations of $[CoL_2Cl]_2[CoCl_4]$ and **1** are essentially identical we found it necessary to compare the τ values calculated using the same type of angles for both compounds. Thus, if we assign α to N3a–Co–N3b and β to N1a–Co–N1b we obtained the value 0.82 which is still very similar to the value of 0.84 found for **1**. The similarity of the coordination geometries of the two complexes cations is therefore evident. On the other hand the anions of the two complex molecules are rather different in size and complexity which cause considerable differences in the corresponding molecule arrangements. Since the complex cations preserve the very similar TBP geometry regardless of the different intermolecular interactions existing in the corresponding crystal structures it could be suggested that the crystal packing is not a factor of particular influence on the final geometry of these coordination polyhedrons.

3.2.6. Bidentate ligands with other donor sets

It should be mentioned that among the five coordinate bis(bidentate)–Co(II) and –Co(III) complexes with five-membered chelates containing other donor sets (NS, SS, NO and PP), the SP geometry also prevails. The TBP geometry is observed in the case of Co(II) complexes containing the bulky PPh_3 donor [38] and in the case of the thiosemicarbazide analogue of complex **1**, $[Co(TSCAc)_2Cl]Cl$, where TSCAc = acetone thiosemicarbazone [13]. Similar to L, the localized double bonds of this Schiff base (N1a–C2a = 1.29 Å N1b–C2b = 1.27 Å) prevent the rotation of the carbonyl moieties, producing steric repulsion between the planar neighboring ligands in the basal plane. The τ parameter for this complex has a value of 0.74.

According to above analysis it could be suggested that if there is no steric hindrance between the chelates in the basal plane, the SP geometry is more favorable for five coordinate Co-complexes containing two five-membered chelate rings. In these structures the bidentate ligands always coordinate in the form shown in 1a with a mutual *trans* disposition. If the steric repulsion in the basal plane cannot be avoided the coordination is TBP, and always in the form shown in 2a. This is the case described with Co(II) complexes with acetone *S*-methylisothiosemicarbazone, which due to the rigid and planar configuration of the ligand and consequent steric interactions prefer a trigonal bipyramidal arrangement.

3.3. $[CoLBr_2]$

The crystal structure of **2** consists of discrete neutral units. The Co(II) atom is placed at the center of the severely distorted tetrahedron with two Br atoms and two N atoms of the L molecule in the apices. Table 4 lists selected bond lengths and angles for **2**. Due to the different coordination geometry around the cobalt atom, the Co–N bonds in **2** are shorter than the corresponding ones in **1**, however the difference in Co–N3 bond lengths for these two complexes are less pronounced [Co–N3a = 1.987(11), Co–N3b = 1.999(11) Å in **1**, Co–N3 = 1.959(13) Å in **2**] than the difference in the corresponding Co–N1 bonds [Co–N1a = 2.167(12), Co–N1b = 2.178(12) Å in **1**, Co–N1 = 2.075(13) Å in **2**]. This is probably due to the fact that the axial and equatorial components of the pentacoordinate structure contain different contributions of p orbitals and consequently additionally longer axial bonds. In the tetrahedral structures the sp^3 orbitals are equivalent, thus the difference between the two types of Co–N bonds is less marked and it is only a consequence of the different hybridization of the nitrogen atoms. Since L keeps a constant distance between the donor atoms (2.6 Å) the resulting coordination angle is somewhat larger [N1–Co–N3 = 80.2(5)°] than in the previous five coordinate structure **1**. The distortion from the idealized stereochemistry is mainly attributed to the restricted bite angle of the Schiff base, however the other angles involving the Co atom also show marked differences from the ideal value of 109°. The largest angle in the structure is N3–Co–Br2 [119.2(5)°], while the angle between the two largest donor atoms Br1–Co–Br2 is less distorted [111.7(5)°].

The atoms of the five-membered chelate ring are practically planar with a mean plane deviation of 0.005 Å. As a consequence of the planarity, the sums of the respective internal angles is in good agreement with the ideal value of 540°. The ketone moiety slightly deviates from the plane of the chelate ring. The dihedral angle formed between the corresponding mean planes is 4.1°. On the other hand

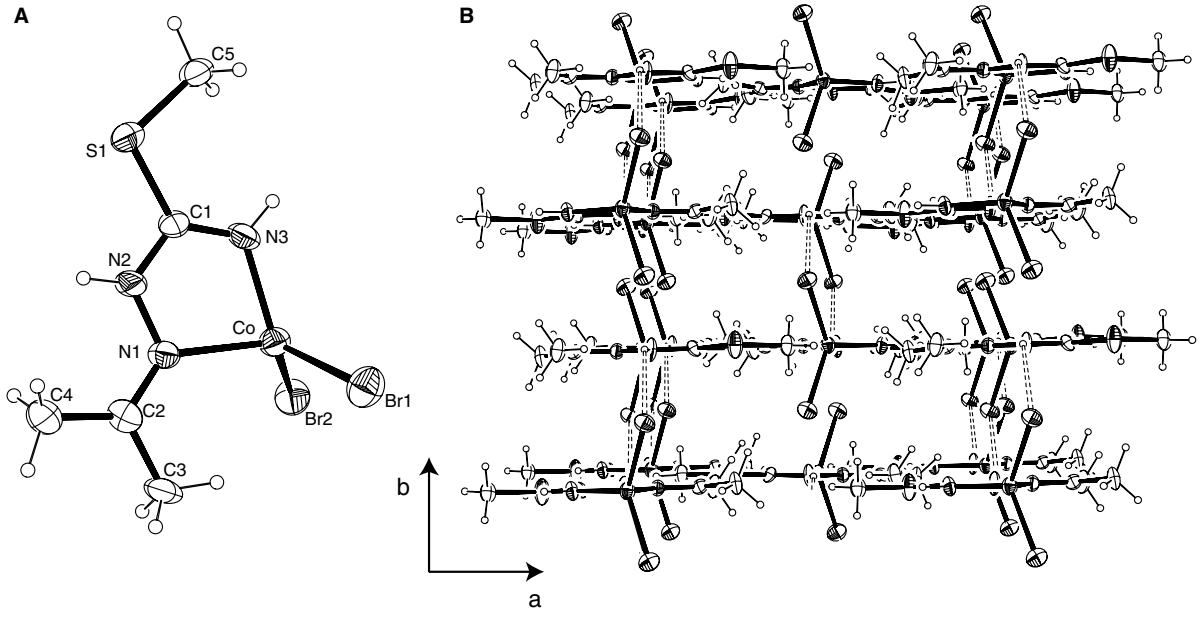

Fig. 3. (A) Molecule structure of [$CoLBr_2$]. (B) Packing arrangement as viewed down the *b*-axis.

the dihedral angle formed between least-square planes of the chelate ring and the Br1–Co–Br2 moiety is nearly orthogonal, 89.3°, thus viewing the crystal arrangement down the *b*-axis we can recognize the distinct regions containing planar isothiosemicarbazone moieties separated by the mutually crossed Br anions (Fig. 3B). The single intermolecular hydrogen bond present in the structure is formed between the hydrazine nitrogen and Br2 bromine atom, N2–H2 = 0.86 Å, N2···Br2 = 3.54(2) Å, H2···Br2 = 2.89 Å, N2–H2···$Br2^{i}$ = 133°, (i) $-x+1, -y, -z$.

3.4. Infrared spectra

The selected IR spectral assignments are listed in Table 5. The two highest energy bands found in the ligand spectrum at 3284 and 3143 cm^{-1} could be attributed to *ν*(N–H) vibrations. In the spectra of the complexes these bands are found at higher frequencies. The strong band at 1560 cm^{-1} in the spectrum of the free ligand, assigned to *ν*(C=N) vibrations, undergoes a shift from its position to lower energies in the spectra of all the metal complexes indicating coordination through the imine nitrogen. It also splits to two near bands probably as a consequence of a slightly increased energy difference between the two C=N bonds upon the ligand coordination. Absorptions in the region 1430–1300 cm^{-1} are found in the spectra of all compounds and are associated with deformation C–H vibrations of the methyl groups. A shifting of *ν*(N–N) to higher frequencies in the spectra of the complexes confirms the coordination through the azomethine nitrogen. The similar positions of the absorption bands in the spectra of [CoL_2Cl]I and [CoL_2Br]Br indicate similar structural features of these two complexes, and suggest a five coordinated geometry for [CoL_2Br]Br.

3.5. Magnetic studies

The temperature dependent magnetic susceptibilities of **1** (19.01 mg), **2** (31.27 mg) and **3** (37.66 mg) have been

Table 5
Main IR vibrations (cm^{-1})

	ν(N–H), $\nu_{a/s}(CH_3)$	*δ*(N–H), *ν*(C=N)	$\delta_{a/s}(CH_3)$	*ν*(C=N), *δ*(N–H)	*ν*(C=N), *ν*(N–N), *δ*(N–H)
L	3284		1428		1123
	3143	1619	1362	1290	1072
	2928	1560	1320		
	2909				
[$CoLBr_2$]	3419	1637	1429	1275	1160
	3254	1552	1354		1053
		1516	1312		
[CoL_2Br]Br	3376	1644	1427	1278	1149
	3179	1553	1368		1044
	2999	1518	1317		
[CoL_2Cl]I	3175	1643	1426	1279	1146
	2994	1545	1367		1056
		1521	1320		

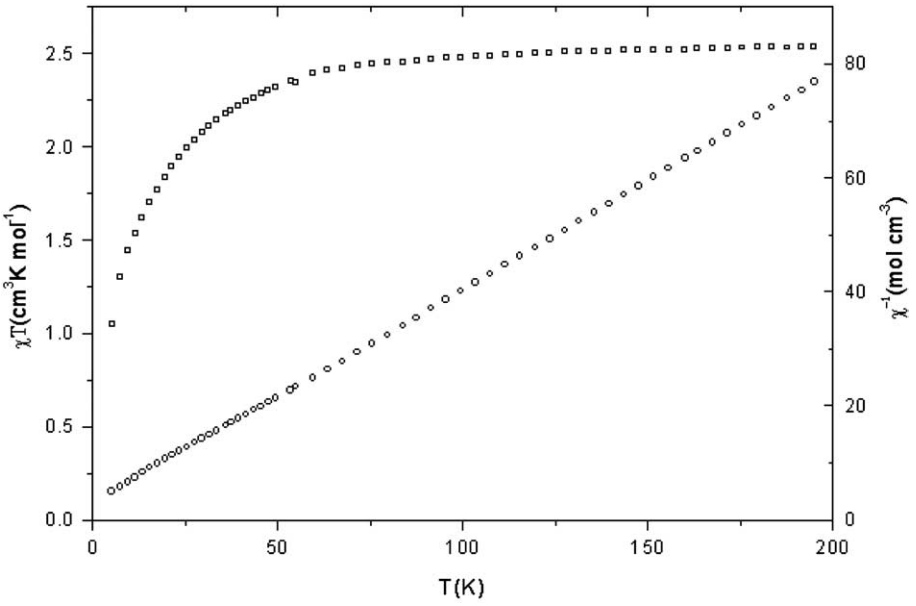

Fig. 4. χT vs. T and χ^{-1} vs. T curves for compound **2**.

Table 6
Magnetic parameters of the complexes

Compound	Cm (cm^3 K mol^{-1})	θ (K)	μ (MB)
1	2.32	−6.33	4.31
2	2.65	−7.55	4.60
3	2.38	−3.88	4.38

studied in the range of 5–200 K. The plot of the χ^{-1} and χT versus temperature (with χ being the magnetization per cobalt (II) ion) is shown in Fig. 4. A similar magnetic behavior was observed for all three Co(II) complexes and consequently only the molar susceptibility curve of compound **2** is given. In all cases the magnetic measurements obey the Curie–Weiss law. A fitting of the linear part of the χ^{-1} versus T curves resulted in the corresponding Curie constants (Cm) and Curie–Weiss temperatures (θ) which are listed in Table 6. The Curie constants correspond to g values of 2.37, 2.26 and 2.22 for compounds **1**, **2** and **3**, respectively. The values of the effective magnetic moment (μ_{eff}) [39] per cobalt (II) are slightly higher than the values expected for the spin-only $S = 3/2$ systems (3.87 μ_B) [23].

4. Conclusion

Three novel complexes of Co(II) with acetone *S*-methylisothiosemicarbazone have been synthesized and characterized by different physicochemical methods. The crystal structure analyses of compounds **1** and **2** reveal trigonal bipyramidal and tetrahedral geometries, respectively. In both structures the ligand has a planar and rigid conformation due to the prevented rotation around the localized $C^2{=}N^1$ double bond. It has been suggested that this feature of the ligand is the main reason why complex **1** adopts a trigonal bipyramidal geometry. After a full analysis of all the five coordinate bis(bidentate)–Co complexes it is clear that if there is no steric interaction in the basal plane, the SP geometry is the preferential form for this type of complex. A similar disposition of the absorption bands within the IR spectra of compounds **1** and **3** leads to the conclusion that compound **3** also adopts the less favorable trigonal bipyramidal arrangement of ligands.

Acknowledgements

The authors wish to thank Dr. Vladan Kusigerski from the Laboratory of Theoretical Physics and Condensed Matter Physics of the *VINČA* Institute for performing the magnetic measurements.

The authors are grateful to the Ministry for Science and Environmental Protection of the Republic of Serbia (Project 1318 – Physicochemical, Structural and Biological investigation of Complex Compounds).

Appendix A. Supplementary data

CCDC Nos. 271459 and 271460 contain the supplementary crystallographic data for this paper. Supplementary data associated with this article can be found, in the online version, at doi:10.1016/j.poly.2005.08.051.

References

[1] J.S. Casas, M.S. Garcia-Tasende, J. Sordo, Coord. Chem. Rev. 209 (2000) 197.
[2] M.J.M. Campbell, Coord. Chem. Rev. 15 (1975) 279.
[3] F.J. Giles, P.M. Fracasso, H.M. Kantarjian, J.E. Cortes, R.A. Brown, S. Verstovsek, Y. Alvarado, D.A. Thomas, S. Faderl, G. Garcia-Manero, et al., Leukemia Res. 27 (2003) 1077.
[4] P.N. Yadav, M.A. Demertzis, D. Kovala-Demertzi, S. Skoulika, D.X. West, Inorg. Chim. Acta 349 (2003) 30.
[5] L. Papathanasis, M.A. Demertzis, P.N. Yadav, D. Kovala-Demertzi, C. Prentjas, A. Castiñeiras, S. Skoulika, D.X. West, Inorg. Chim Acta 357 (2004) 4113.

[6] G.A. Bogdanoviić, V.M. Leovac, S.B. Novaković, V.I. Češljević, A. Spasojević-de Bire, Acta Cryst. C57 (2001) 1138.
[7] S. Blanchard, E. Bill, T. Weyhermuller, K. Wieghardt, Inorg. Chem. 43 (2004) 2324.
[8] (a) M.J.M. Campbell, R. Grzeskowiak, J. Chem. Soc. A (1967) 396;
(b) N.V. Gerbeleu, M.D. Ravenko, P.N. Bourosh, Yu.A. Simonov, V.K. Belsky, S.G. Shova, Koord. Khim. 13 (1987) 388.
[9] (a) M. Mathew, G.J. Palenik, J. Am. Chem. Soc. 91 (1969) 4923;
(b) M. Gostojić, V. Divjaković, V.M. Leovac, B. Ribar, P. Engel, Cryst. Struct. Commun. 11 (1982) 1219.
[10] (a) T.M. Allen, A.D. Burrows, M.F. Mahon, J. Chem. Soc., Dalton Trans. (1999) 215;
(b) S.B. Novaković, G.A. Bogdanović, V.M. Leovac, Inorg. Chem. Commun. 8 (2005) 9.
[11] V. Divjaković, V. Leovac, Cryst. Struct. Commun. 7 (1978) 689.
[12] W.H. Baur, E. Tillmanns, Acta Crystallogr. B42 (1986) 95.
[13] G. Dessy, V. Fares, L. Scaramuzza, Cryst. Struct. Commun. 7 (1978) 737.
[14] N.V. Gerbeleu, M.D. Revenco, V.M. Leovac, Zhur. Neorg. Khim. 22 (1977) 1858.
[15] Enraf-Nonius CAD4 Software, Version 5.0. Enraf-Nonius, Delft, The Netherlands, 1989.
[16] CAD-4 Express Software, Enraf-Nonius, Delft, The Netherlands, 1994.
[17] A.L. Spek, Acta Cryst. A46 (1990) C34.
[18] A.L. Spek, PLATON, A Multipurpose Crystallographic Tool, Utrecht University, The Netherlands, 1998.
[19] G.M. Sheldrick, SHELXS97, Program for the Solution of Crystal Structures, University of Gottingen, Germany, 1997.
[20] G.M. Sheldrick, SHELXL97, Program for the Refinement of Crystal Structures, University of Gottingen, Germany, 1997.
[21] A.W. Addison, T.N. Rao, J. Reedijak, J. van Rijn, G.C. Verschoor, J. Chem. Soc., Dalton Trans (1984) 1349.
[22] A. Garoufis, S. Kasselouri, C.P. Raptopoulou, Inorg. Chem. Commun. 3 (2000) 251.
[23] A.F. Cotton, G. Wilkinson, Advanced Inorganic Chemistry, Interscience, New York.
[24] C. Kircher, B. Krebs, Inorg. Chem. 26 (1987) 3569.
[25] B. Ferrari, G.G. Fava, C. Pelizzi, P. Tarasconi, J. Chem. Soc., Dalton Trans. (1992) 2135.
[26] A.K. Patra, M. Ray, R. Mukherjee, J. Chem. Soc., Dalton Trans. (1999) 2461.
[27] V.M. Leovac, V. Divjakovic, R. Fazlic, P. Engel, Trans. Met. Chem. 14 (1989) 139.
[28] S.M. Peng, Y. Wang, S.-L. Wang, M.C. Chuang, J. Chem. Soc., Chem. Commun. (1981) 329.
[29] Yu.A. Simonov, V.E. Zavodnik, L.P. Sharova, A.A. Dvorkin, S.A. Dyachenko, A.I. Stetsenko, Zh. Strukt. Khim. 25 (1984) 102.
[30] U. Englert, J. Strahle, Gazz. Chim. Ital. 118 (1988) 845.
[31] U. Englert, J. Strahle, Z. Kristallogr. 179 (1987) 60.
[32] S.A. Dyachenko, Yu.A. Simonov, A.I. Stetsenko, A.A. Dvorkin, T.I. Malinovskii, L.B. Volodarskii, Dokl. Akad. Nauk SSSR 244 (1979) 636.
[33] M.D. Revenko, N.V. Gerbeleu, Yu.A. Simonov, P.N. Bourosh, N.I. Vyrtosu, A.N. Sobolev, T.I. Malinovskii, Dokl. Akad. Nauk SSSR 300 (1988) 127.
[34] I.G. Fomina, A.A. Sidorov, G.G. Aleksandrov, V.N. Ikorskii, V.M. Novotortsev, S.E. Nefedov, I.L. Eremenko, Izv. Akad. Nauk SSSR (2002) 1453.
[35] Hei-Ying Cheng, Cheng-Chen Lin, Biing-Chiau Tzeng, Shie-Ming Peng, J. Chin. Chem. Soc. 41 (1994) 775.
[36] S. Nemeth, L.I. Simandi, G. Argay, A. Kalman, Inorg. Chim. Acta 166 (1989) 31.
[37] M. Zehnder, H. Loliger, Helv. Chim. Acta 63 (1980) 754.
[38] (a) Zheng-Zhi Zhang, Hsu-Kun Wang, Zhen Xi, Hung-Gen Wang, Ru-Ji Wang, J. Organomet. Chem. C22 (1988) 352;
(b) R. Ciancanelli, B.C. Noll, D.L. DuBois, M.R. DuBois, J. Am. Chem. Soc. 124 (2002) 2984.
[39] B.N. Figgis, J. Lewis, Magnetochemistry, Interscience Publ. Inc., New York, 1966.

SmI_2 reacts only in the presence of HMPA, which increases the reductive potential of the samarium salt [9].

The triorganochlorosilanes were reported [10] to react with SmI_2 in THF at room temperature to give the respective disilanes R_3SiSiR_3 in high yield, except for Me_3SiCl for which the maximum conversion was only 5%, independent of the reaction conditions.

To get more insight into the reactivity of one of the mentioned diiodides and to evaluate its advantages and limitations as a synthon compared to SmI_2 and alkali metals, we have studied the reactions of **1** with some alkyl(aryl) halides and chlorotrimethylsilane in solvating and non-solvating media.

2. Results and discussion

2.1. Reactions in THF

One of the most unusual properties found for **1** and DyI_2 is their liability to disproportionation in THF or DME solutions, caused by addition of benzene, its derivatives or some other compounds [11]. In the case of **1** this process leads to formation of NdI_3 and a mixture of NdIRR′ products (R, R′ – fragments of split solvent). The aromatic substrate is incorporated into the products to a negligible extent. The addition of phenol at −100 °C promotes similar conversions while at 20 °C the reaction proceeds as an ordinary single electron redox process to give $PhONdI_2(THF)$ [11].

In the reaction of **1** with iodobenzene in THF, independent of temperature, the main product is benzene, the yield of which reaches 84% (Table 1). Most of the benzene (73%) is formed directly in the reaction and can be separated from the non-volatile products together with the solvent by condensation in vacuum. The rest of the C_6H_6 (11%) is isolated after hydrolysis of the solid residue, indicative of the presence in the products of phenylneodymium derivatives of the type $PhNdI_2$. In addition to benzene in the reaction mixture, a small amount of biphenyl (1%) and a few unidentified products were found by HPLC. When **1** interacts

Table 1
Conditions, products and yields in the reactions of **1** with organohalides

Solvent	Substrate	Reaction temperature (°C)	Reaction time (h)	Product	Yield (%)[a]
THF	PhI	20	10	C_6H_6	84
				Ph–Ph	1
THF	PhBr	20	10	C_6H_6	59
				Ph–Ph	0.5
THF	PhCl	20	10	C_6H_6	56
				Ph–Ph	0.4
THF	$PhCH_2Cl$	20	1	$PhCH_3$	16
				$PhCH_2CH_2Ph$	82
				$PhCH_2I$	22
THF	$C_7H_{15}Br$	20	1	C_7H_{16}	22
THF	*Cyclo*-$C_6H_{11}Cl$	20	1	*Cyclo*-C_6H_{12}	23
THF	*t*-BuCl	20	1	*t*-BuH	27
				$CH_2{=}C(CH_3)_2$	63
THF	Me_3SiCl	−60	5	Me_3SiH	1
				$Me_3SiSiMe_3$	2
				$Me_3SiO(CH_2)_3CH_3$	88
THF	Me_3SiCl	20	0.5	Me_3SiH	10
				$Me_3SiSiMe_3$	8
				$Me_3SiO(CH_2)_3CH_3$	31
Benzene	PhI	80	10	No reaction	
Benzene	PhBr	80	10	No reaction	
Benzene	$PhCH_2Cl$	80	8	$PhCH_2Ph$	66[b]
Benzene	*Cyclo*-$C_6H_{11}Cl$	80	8	*cyclo*-C_6H_{11}–Ph	60[b]
				1,4-(*cyclo*-C_6H_{11})C_6H_4	62[b]
Benzene	*n*-BuCl	80	36	*sec*-BuPh	26[b]
				1,4-(*sec*-Bu)$_2C_6H_4$	29[b]
Benzene	Me_3SiCH_2Cl	80	10	No reaction	
Benzene	Me_3SiCl	80	10	No reaction	
$PhCH_2Cl$	$PhCH_2Cl$	80	3.5	$PhCH_2(C_6H_4CH_2)_{28}C_6H_4CH_2Cl$	59[c]
				$PhCH_3$	

[a] GLC or HPLC yield.
[b] Calculated for initial RCl.
[c] Conversion of $PhCH_2Cl$.

with bromobenzene, the yield of benzene, most of which is formed directly in the reaction, noticeably decreases (56%). In the case of PhCl, the yield of benzene after hydrolysis reaches 21%, but directly in the reaction only 35% of it is formed. The yield of biphenyl decreases to 0.4%.

We believe that the scheme of these reactions is similar to that of SmI_2 and includes in the first stage the electron transfer from **1** to PhX, formation of trihalide NdI_2X and phenyl radical, which splits hydrogen from THF to give benzene (Scheme 1, direction *a*) or interacts with **1** yielding the σ-complex $PhNdI_2$ (direction *b*). The latter can react with the aryl halide starting material affording biphenyl. A part of $PhNdI_2$ remains in the solution and after hydrolysis gives additional benzene.

In all the reactions after 2–3 min the mixture turned dark brown, a precipitate of neodymium trihalide deposited, and evolution of a minor amount of gas was observed. These transformations, similar to those in the reactions with benzene [11], indicate that the disproportionation of **1** mentioned above also takes place in the reactions with PhX. However in this case, such a process does not play an important role.

Unfortunately, we could not find the conditions of chromatographic analysis for consistent identification of the small amounts of benzene formed from C_6H_5F. According to the ^1H NMR spectra, fluorobenzene is also reduced in the reaction with **1,** but the yield of C_6H_6 does not exceed 8–10%. The significant amount of NdI_3 and NdIRR′ products (R, R′ = fragments of split solvent) formed in this reaction show that the halide function of C_6H_5F is negligibly involved into the transformations and that the main direction of the reaction is the same as in the reaction with benzene [11].

Unlike PhX the benzyl chloride reaction with **1** produces mainly the coupling product $PhCH_2CH_2Ph$, the yield of which reaches 82%. The yield of toluene generated directly in the reaction is 15%, but hydrolysis of the solid residue remaining after removal of volatiles affords only 1% of $PhCH_3$. Besides these products, a significant amount of $PhCH_2I$ and a few unidentified compounds were detected in the reaction mixture. These data reveal that the reaction of **1** with $PhCH_2Cl$ includes additionally I/Cl exchange beyond the stages indicated in Scheme 1. An attempt to carry out the cross-coupling reaction between PhI and benzyl chloride failed. Only benzene, toluene and bibenzyl were found in the reaction mixture formed after treatment of **1** with a mixture of iodobenzene and benzyl chloride.

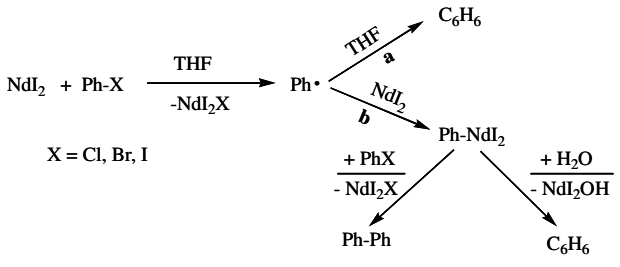

Scheme 1.

The GLC analysis of volatile products from the reactions of **1** with 1-bromoheptane and cyclohexyl chloride, which easily proceeded in THF at room temperature, revealed the presence of the respective hydrocarbons which are formed directly in the reactions in ca. 25% yield. The reaction with *tert*-butyl chloride under the same conditions afforded a mixture of isobutane and isobutylene. Coupling products also were not found in any of the three cases. Hydrolysis of the solid products remaining after separation of the volatiles from these reactions did not yield additional amounts of RH, indicative of the absence of compounds of the type $RNdI_2$ in the mixture. This is consistent with the well-known fact that σ-alkyllanthanide complexes have low stability.

In contrast to SmI_2, the iodide **1** in THF vigorously interacts with trimethylchlorosilane at room temperature. The reaction proceeds with evolution of gaseous trimethylsilane and is completed in 30 min to give 10% of Me_3SiH, hexamethyldisilane (8%) and trimethylsilylbutoxide as the main product (31%). In addition, significant amounts of organosilicon compounds were found by IR spectroscopy in the solid residue remaining after removal of the volatiles. The work on identification of this product is currently in progress. If the reaction is carried out at −60 °C, the yields of trimethylsilane and $Me_3SiSiMe_3$ drop down to 1% and 3%, respectively, but the yield of $Me_3SiO(CH_2)_3CH_3$ increases up to 88%. Formation of this product can be explained by addition of Me_3SiCl to THF in the presence of a neodymium salt (NdI_2 or NdI_2Cl) with generation of $Me_3SiO(CH_2)_3CH_2Cl$ and subsequent reduction of it by **1** like other alkyl chlorides. The similar addition of organochlorosilanes into the C–O bond of THF in the presence of $ZnCl_2$ has been described earlier [12].

2.2. Reactions in benzene

All of the above reactions of LnI_2 (Nd, Dy, Tm) were carried out in solvating media such as THF or DME in which these salts are soluble. But recently with an example of the reactions of DyI_2 with VCl_4 or vanadocene we have established that the mentioned diiodides can readily react with substrates in benzene under heterogeneous conditions [13]. This property of LnI_2 has also revealed itself in the reactions of **1** with cyclohexyl chloride, *n*-BuCl and benzyl chloride which proceed in benzene at 80 °C. However in this case, in contrast to the reactions in THF, reduction of RX is not the result. Instead, alkylation of the aromatic solvent takes place, i.e. the reactions are similar to Friedel–Crafts processes. The main organic product in the reaction with benzyl chloride is diphenylmethane, the yield of which in 8 h reaches 66%. The reactions with butyl chloride and cyclohexyl chloride result in the formation of near equal amounts of mono- and 1,4-dialkylation products. The reaction with *n*-BuCl is accompanied by isomerization of the butyl radical into the *tert*-butyl form that is characteristic

for the Friedel–Crafts alkylation. Besides the indicated products in all of the reactions, the neodymium trihalide NdI_2Cl, hydrogen and HCl are formed. The side process of I/Cl exchange and decomposition of generated HI leads as well to the isolation of a minor amount of iodine

$$NdI_2 + R\text{-}Cl \xrightarrow[-NdI_2Cl,-H_2,-HCl]{C_6H_6} R\text{-}C_6H_5 + 1,4\text{-}R_2C_6H_4$$

$$R = CH_2Ph, \textit{cyclo}\text{-}C_6H_{11}, t\text{-}Bu$$

It is known [14] that lanthanide trichlorides and tribromides catalyze the alkylation and acylation of aromatic compound similar to other Lewis acids. The sets of products of these reactions indicate that the reactions with divalent salt **1** also proceed similarly to Friedel–Crafts transformations. However in this case, the process includes an additional stage – oxidation of neodymium to the trivalent state and liberation of hydrogen. The NdI_2Cl formed in this stage evidently plays the role of catalyst in the subsequent alkylation. Catalytic transformations with **1** are less probable because of its high reductive potential, which stipulates quick oxidation of **1** by RX or HCl. It is interesting to note that the catalytic activity of NdI_3 in the benzylation of benzene is very low: only 1% of Ph_2CH_2 was obtained after heating of this iodide with benzyl chloride in benzene at 80 °C for 5 h.

In all of these reactions of **1** with RX in benzene, a significant amount of the salt was used because of its insolubility in this solvent. Therefore the yields of the products under the given conditions are rather low (20–30% calculated on **1**) and the reactions look like they are stoichiometric. Evidence that these processes can be catalytic is obtained by the reaction of **1** with benzyl chloride in the absence of solvent. The oligomers $PhCH_2(C_6H_4CH_2)_nC_6H_4CH_2Cl$ (*n* found by terminal group analysis is close to 28) were isolated in this case as a white non-crystalline solid. According to the ^1H and ^{13}C NMR data, it has mainly linear 1,4-arrangements, but 1,3-substituted fragments are also present in the product. Conversion of $PhCH_2Cl$ in 3.5 h at 80 °C was 59% where the yield of the oligomers reached 111% calculated on the amount of **1** used.

Surprisingly, both Me_3SiCl and Me_3SiCH_2Cl as well as PhI and PhBr turned out to be quite inert toward **1** in benzene.

3. Conclusion

These studies show that the reactions of neodymium diiodide **1** with alkyl(aryl) halides in THF solution are similar to those of alkali metals, but have some essential differences. The most important are: (i) formation of a significant amount of the corresponding hydrocarbons RH directly in the reaction; (ii) the reduced yield of coupling products in the case of aryl halides. In addition, the tendency of **1** to disproportionate in solvating medium in the presence of aromatic compounds causes side processes, which are not characteristic of the reactions with sodium. Probably the most substantial difference in chemical behavior between **1** and alkali metals is the ability of neodymium diiodide to catalyze the alkylation of aromatic compounds with alkyl halides when the reactions are carried out in non-solvating medium. These processes are similar to Friedel–Crafts alkylation but have an additional redox stage – oxidation of Nd(II) to Nd(III) and reduction of hydrogen.

4. Experimental

4.1. General

All the reactions were carried out in a vacuum in sealed tubes using standard Schlenk techniques. To purify and dry, THF was refluxed over NaOH and treated with **1** for 30 min before use (2 g of **1** for 100 ml THF). The solvent was collected into a reaction vessel by condensation in a vacuum from the formed solution. Benzene was dried by refluxing over sodium and treated with **1** for 30 min before use. Diiodide **1** was prepared as described in [15]. The commercial organohalides were purified according to known procedures. The ^1H and ^{13}C NMR spectra were recorded on a Bruker DPX 200 spectrometer at 20 °C. The IR spectra were recorded on a Specord M-75 spectrometer. The samples were placed as films between KBr glasses. The HPLC analysis was performed on a "Knauer" liquid chromatograph equipped with a UV-spectrophotometer ($\lambda = 254$ nm) and glass columns 150×3 mm filled with adsorbent Separon SGX C18 ("Lachema"), 5 μm granules were used. Methanol/water (80:20) solution served as an eluent at a flow-rate of 0.4 ml/min at 20 °C. Chromatographic analysis of volatile products was carried out on a "Tsvet-800" gas chromatograph equipped with a thermal conductivity detector and a stainless-steel column (3 m long and 3 mm OD). In these analysis 5% SE-30 on Chromaton N-AW (0.2–0.25 mm granules) as an adsorbent was used. A flow-rate of the carrier gas (helium) was 30 ml/min. Quantitative analysis of the reaction mixtures have been performed by the method of absolute calibration.

4.2. Reaction of *1* with PhI

To the solution of iodobenzene (0.639 g, 2.83 mmol) in 10 ml THF 0.557 g (1.5 mmol) of **1** was added at room temperature with stirring. Gradually color of the mixture changed to brown and the microcrystalline precipitate of neodymium triiodide deposited. Evolution of a small amount of gaseous products was observed. After 10 h the solvent and volatile products were removed by condensation in a vacuum and 2 ml of water was added to the residue. The obtained mixture was extracted with ether (2×7 ml) and then the extract was separated and dried with $CaCl_2$. HPLC analysis of the extract revealed the presence of 12 mg (11%) of benzene and 1 mg (1%) of biphenyl. In the volatiles 80 mg (73%) of benzene was found by GLC analysis.

The reactions of **1** with PhBr, PhCl and PhF were carried out analogously.

4.3. Reaction of *1* with $PhCH_2Cl$ in THF

A solution of benzyl chloride (2.948 g, 7.41 mmol) in 15 ml THF was added to 2.471 g (19.52 mmol) of **1**. The mixture was stirred for 1 h and left for a night at room temperature. Solvent, excess of $PhCH_2Cl$ and volatile products were removed by condensation in a vacuum and the residue was hydrolyzed by 5 ml of water. The obtained mixture was extracted with ether (2×8 ml) and then the extract was dried over $CaCl_2$ and analyzed by HPLC. Toluene (7 mg, 1%), 1.2-diphenylethane (0.56 g, 82%) and 027 g (17%) of $PhCH_2I$ were found among the products. HPLC of the volatiles revealed the presence of 0.1 g (15%) of toluene and 93 mg (6%) of benzyl iodide. The total yield of toluene was 0.107 mg (16%).

4.4. Reaction of *1* with $C_7H_{15}Br$ in THF

0.165 g (0.92 mmol) of 1-bromoheptane and 4 ml THF were condensed into an ampoule containing 0.842 g (2.11 mmol) of **1**. The mixture was stirred for 1 h at ambient temperature. Benzene and volatile products were removed by condensation in a vacuum. The solid residue was hydrolyzed by diluted HCl and the obtained solution was extracted with 4 ml of ether. GLC analysis of the ether revealed an absence of heptane or tetradecane. In the volatile fraction, besides benzene and $C_7H_{15}Br$, 20 mg (22%) of heptane was found.

The reaction of **1** with cyclohexyl chloride was carried out analogously.

4.5. Reaction of *1* with t-BuCl in THF

A mixture of *t*-BuCl (0.54 g, 5.83 mmol), **1** (0.693 g, 1.78 mmol) and 6 ml THF was stirred in a sealed ampoule for 8 h at room temperature. The solvent and volatile products were separated by condensation in a vacuum from the formed grey precipitate of NdI_2Cl. In the condensate isobutane (28 mg, 27%) and isobutylene (63 g, 63%) were found by GLC.

4.6. Reaction of *1* with Me_3SiCl in THF

At room temperature. To an evacuated 100 ml ampoule containing 3.82 g (9.6 mmol) of **1** in 5 ml THF, 0.939 g (8.6 mmol) of Me_3SiCl in 5 ml THF was added at −60 °C. The mixture was allowed to warm to room temperature and stirred for 30 min. The initial dark violet precipitate of **1** gradually disappeared but a grey precipitate of NdI_2Cl was formed. Evolution of a gaseous product and a slight warming of the mixture was observed. After completion of the reaction, THF and volatile products were transferred by condensation at 100 °C in a vacuum into an ampoule of 20 ml volume. The solution was warmed to ambient temperature and a volume of evolved gaseous Me_3SiH (16 ml, identified by GLC) was measured with a gas burette. An additional 12 mg of Me_3SiH were found in the solution by GLC. The total yield of trimethylsilane was 65 mg, (10%). In the solution 50 mg (8%) of Me_3Si-$SiMe_3$ and 0.4 g (31%) of $Me_3SiO(CH_2)_3CH_3$ were found by GLC. The butoxitrimethylsilane was isolated from the solution by distillation at normal pressure. Its characteristics, b.p. (123–125 °C), α_D^{20} (1.395), IR and ^1H NMR spectra, correspond to the literature data [16].

The low temperature reaction was carried out in the same manner but before warming to room temperature the reaction mixture was stirred at −60 °C for 5 h.

4.7. Reaction of *1* with $PhCH_2Cl$ in benzene

A mixture of 2.667 g (5.08 mmol) of **1**, 0.643 g (5.08 mmol) of benzyl chloride and 8 ml of benzene was stirred for 8 h at 80 °C in a sealed ampoule. The evolved gaseous products were released into the atmosphere, the organic layer was separated by decantation from the crystalline precipitate of neodymium trihalide and the solvent and volatile products were removed by condensation in a vacuum. The remained viscous substance was hydrolyzed by 4 ml of water and extracted with ether (2×4 ml). In the extract 0.606 g (3.6 mmol) of Ph_2CH_2, 0.015 g (0.19 mmol) of benzene, trace amounts of iodine, iodobenzene and biphenyl were found by means of HPLC and GLC.

4.8. Reaction of *1* with cyclo-$C_6H_{11}Cl$ in benzene

Under the conditions of the previous experiment, a mixture of *cyclo*-$C_6H_{11}Cl$ (1.085 g, 9.148 mmol), **1** (2.1 g, 5.269 mmol) and 5 ml of benzene was heated for 8 h. The light pink solution was separated from a grey precipitate by decantation and the precipitate was washed with benzene (2×5 ml). The reaction solution and benzene washings were combined and then washed with a diluted solution of ammonia, and dried over $CaCl_2$. Distillation of the solution afforded 0.51 g (3.18 mmol) of cyclohexylbenzene, b.p. 238–240 °C (identified by HPLC, IR, ^1H NMR). The oily non-volatile residue solidified at room temperature and was recrystallized from methanol to give 0.4 g (1.65 mmol) of 1,4-(*cyclo*-$C_6H_{11})_2C_6H_4$ with m.p. 239 °C (identified HPLC, IR, ^1H NMR). In the gaseous products H_2 and HCl were identified by GLC analysis.

4.9. Reaction of *1* with n-BuCl in benzene

To 2.97 g (7.46 mmol) of **1** a solution of *n*-BuCl (1.07 g, 11.56 mmol) in 5 ml of benzene was added. The mixture was stirred for 36 h at 80 °C. The evolved gaseous products were periodically released into the atmosphere. Then the reaction mixture was hydrolyzed with dilute HCl and extracted with ether. The extract was analyzed by HPLC and GLC. Among the products 0.4 g (2.98 mmol) of

s-BuC_6H_5 and 0.64 g (3.35 mmol) of 1,4-(*s*-Bu)$_2C_6H_4$ were found.

The reactions of **1** with PhI, PhBr, *cyclo*-$C_6H_{11}Cl$, Me_3SiCH_2Cl and Me_3SiCl were carried out using the same conditions.

4.10. Reaction of **1** with $PhCH_2Cl$ without solvent

Under the conditions of the previous experiment, a mixture of **1** (2.124 g, 5.3 mmol) and benzyl chloride (5.5 g, 43.5 mmol) was heated for 3.5 h. The reaction solution was separated from a black precipitate, the latter was washed with 5 ml of $PhCH_2Cl$ and the extract was joined to the reaction solution. Benzyl chloride and volatile products were removed by condensation in a vacuum to give a yellow-greenish oil, which gradually solidified at room temperature. Reprecipitation of the product by methanol from benzene resulted in formation of the oligomer $PhCH_2(C_6H_4CH_2)_{28}C_6H_4CH_2Cl$ as a white solid, melting above 70 °C; yield 2.353 g (conversion 59%). ^{1}H NMR (200 MHz, C_6D_6): $\delta = 3.73$ (CH_2), 4.07 (CH_2Cl), 6.99 (C_6H_4). ^{13}C NMR (50 MHz, C_6D_6) contains 28 signals, the most intensive of which are: $\delta = 141.6$, 139.3, 131.2, 131.0, 126.9, 126.3 (C_6H_4), 41.8, 41.5, 39.0 (CH_2). IR 3080w, 3050w, 3020w, 1600m, 1509m, 1493m, 1417m, 727s, 696m cm^{-1}. *Anal.* Calc. for $C_{216}H_{185}Cl$: C, 92.16; H, 6.58; Cl, 1.26. Found: C, 92.02; H, 6.75; Cl, 1.23%.

Acknowledgments

This research was supported by the Grant of President of RF for Scientific Schools (NSh-58.2003.03), Russian Foundation for Basic Researches (Grant No. 04-03-32093) and the Civilian Research and Development Foundation (CRDF) Award No. RC1-2322-NN-02.

References

[1] M.N. Bochkarev, Coord. Chem. Rev. 248 (2004) 835.
[2] W.J. Evans, P.S. Workman, N.T. Allen, Org. Lett. 5 (2003) 2041.
[3] W.J. Evans, N.T. Allen, J.W. Ziller, J. Am. Chem. Soc. 122 (2000) 2118.
[4] W.J. Evans, N.T. Allen, J.W. Ziller, J. Am. Chem. Soc. 122 (2000) 11749.
[5] N.B. Mikheev, Zh. Neorgan. Khim. 29 (1984) 450.
[6] M.N. Bochkarev, M.E. Burin, Russ. Chem. Bull. 53 (2004) 2091 (Engl. Transl.).
[7] A.N. Nesmeyanov, K.A. Kocheshkov (Eds.), Methods of Organoelement Chemistry. Lithium, Sodium, Potassium, Rubidium, Cesium, Nauka, Moscow, 1971, p. 1190.
[8] P. Girard, J.L. Namy, H.B. Kagan, J. Am. Chem. Soc. 102 (1980) 2693.
[9] (a) J. Inanaga, M. Ishikawa, M. Yamaguchi, Chem. Lett. (1987) 1485; (b) K. Otsubo, J. Inanaga, M. Yamaguchi, Tetrahedron Lett. 57 (1986) 4437; (c) R.A. Flowers, M. Shabangi, Tetrahedron Lett. 38 (1997) 1137.
[10] B.G. Zavin, A.I. Chernyavskii, Ya.S. Vygodskii, N.E. Brandukova, Dokl. Akad. Nauk. 336 (1994) 365.
[11] M.N. Bochkarev, A.A. Fagin, G.V. Khoroshenkov, Russ. Chem. Bull. 51 (2002) 1909 (Engl. Transl.).
[12] N.I. Shuikin, I.F. Bel'skii, I.E. Grushko, Zh. Obsch. Khim. (Russ.) 29 (1959) 1882.
[13] M.N. Bochkarev, M.E. Burin, V.K. Cherkasov, Russ. Chem. Bull. 53 (2004) 481 (Engl. Transl.).
[14] (a) N. Mine, Y. Fujiwara, H. Taniguchi, Chem. Lett. (1986) 357; (b) L. Hachiya, M. Morivaki, S. Kobayashi, Tetrahedron Lett. 36 (1995) 409; (c) D. Barbier-Baudry, A. Dormond, S. Richard, J.R. Desmurs, J. Mol. Catal. A 161 (2000) 23.
[15] M.A. Katkova, G.K. Fukin, A.A. Fagin, M.N. Bochkarev, J. Organomet. Chem. 682 (2003) 218.
[16] D. Brandes, A. Blaschette, J. Organomet. Chem. 73 (1974) 217.

adds to acetone yielding $C_3H_3N_2C(CH_3)_2OH$ adduct, which reacts with the starting oxo complex [14].

The factors determining the formation of the $Re_2O_3^{4+}$ complexes have not been formalised. All the reactions were carried out in a system open to the atmosphere, and water seems to be the source of the bridging oxo group. It is presumed that the formation of intermediate hydroxo-species is crucial [15,16].

This findings prompted us to explore the reactions of $[ReOCl_3(OAsPh_3)(AsPh_3)]$ and $[ReOCl_3(PPh_3)_2]$ with pyrazole in tetrahydrofurane at room temperature. In these cases the mononuclear $[ReOCl_2(pzH)_2(OAsPh_3)](ReO_4)$ (**1**) and dinuclear $[\{ReCl_2(pzH)_2\}_2(\mu\text{-}O)]$ (**2**) oxocomplexes have been isolated.

Here, we present the crystal, molecular and electronic structures of **1** and **2**. The electronic structures of **1** and **2** have been determined basing on the results of the density functional theory (DFT) calculations. The spin-allowed singlet–singlet electronic transitions of the $[ReOCl_2(pzH)_2(OAsPh_3)]^+$ cation, ReO_4^- anion and $[\{ReCl_2(pzH)_2\}_2(\mu\text{-}O)]$-complex have been calculated with the the time-dependent DFT method (TDDFT), and the UV–Vis spectra of the title compounds have been discussed on this basis.

2. Experimental

2.1. General procedure

All the reagents used to the synthesis were commercially available and were used without further purification. The $[ReOCl_3(AsPh_3)(OAsPh_3)]$ and $[ReOCl_3(PPh_3)_2]$ complexes were prepared according to the literature methods [17,18].

IR spectra were recorded on a Nicolet Magna 560 spectrophotometer in the spectral range 4000–400 cm^{-1} with the samples in the form of KBr pellets. Electronic spectra were measured on a spectrophotometer Lab Alliance UV–VIS 8500 in the range 800–200 nm in deoxygenated dichloromethane solution. ^1H NMR spectra were obtained at room temperature in $CDCl_3$ using INOVA 300 spectrometer. Magnetic susceptibilities were measured at 296 K by the Faraday method. Elemental analyses (C H N) were performed on a Perkin–Elmer CHN-2400 analyzer.

2.2. Preparation of $[ReOCl_2(pzH)_2(OAsPh_3)](ReO_4)$ (1)

$[ReOCl_3(AsPh_3)(OAsPh_3)]$ (0.5 g, 0.53 mmol) was suspended in tetrahydrofurane (30 ml) and pzH (0.14 g, 2 mmol) in THF (5 ml) was added dropwise to the stirred suspension. The mixture was stirred for 1 h at room temperature. The solvent was evaporated and the resulting residue was extracted with ethanol and diethyl ether (50 ml) was added. The blue crystals of $[ReOCl_2(pzH)_2(OAsPh_3)](ReO_4)$ were formed overnight. Yield: 30%.

IR (KBr, cm^{-1}) 3204 (m), 3134 (m), 3059 (w), 1587 (w), 1520 (w), 1480(s), 1443 (s), 1405 (m), 1342 (m), 1272 (w), 1188 (w), 1165 (w), 1121 (s) 1088 (m), 1072 (m), 1051 (s), 999 (m), 922 (vs), 906 (vs), 852 (vs), 792 (m), 769 (m), 745 (s), 689 (s), 606 (m), 480 (s), 454 (m), 415 (w). ^1H NMR ($CDCl_3$, ppm): $\delta = 6.59$, 7.78, 8.08 and 8.65 (br, 4H, C(21)–H, C(23)–H, C(31)–H and C(33)–H); 7.28 (m, 15H, C_6H_5); 7.55 and 7.69 (pseudo-triplets, 2H, C(22)–H, C(32)–H) and 13.16 ppm (s, 1H, NH). *Anal.* Calc. for $C_{24}H_{23}AsCl_2N_4O_6Re_2$: C, 29.36; H, 2.36; N, 5.71. Found: C, 29.45; H, 2.40; N, 5.80%.

2.3. Preparation of $[\{ReCl_2(pzH)_2\}_2(\mu\text{-}O)]$ (2)

$[ReOCl_3(PPh_3)_2]$ (0.83 g, 1 mmol) was suspended in tetrahydrofurane (30 ml) and pzH (0.28 g, 4 mmol) in THF (5 ml) was added dropwise to the stirred suspension. The mixture was stirred for 24 h at room temperature. The solvent was evaporated and the resulting residue was extracted with acetonitrile. The blue crystals of $[\{ReCl_2(pzH)_2\}_2(\mu\text{-}O)]$ were formed during several days. Yield: 55%.

IR (KBr, cm^{-1}) 3315 (s), 3135 (m), 2995 (w), 1610 (w,), 1515 (m), 1485 (s), 1405 (s), 1354 (s), 1277 (m), 1162 (m), 1123 (s), 1066 (s) 1051 (s), 954 (m), 771 (s, br), 742 (s, sh), 704 (s, br), 626 (w), 591 (w). *Anal.* Calc. for $C_{12}H_{16}N_8Cl_4O_3Re_2$: C, 17.27; H, 1.93; N, 13.43. Found: C, 17.40; H, 2.05; N, 13.35%.

2.4. Crystal structures determination and refinement

The X-ray intensity data of **1** and **2** were collected on a KM-4-CCD automatic diffractometer equipped with CCD detector, 55 and 20 s exposure time was used respectively and all reflections of the of Ewald sphere up to $2\theta = 50°$ was collected. The unit cell parameters were determined from least-squares refinement of the setting angles of 7336 and 6418 strongest reflections, respectively. Details concerning crystal data and refinements are given in Table 1. Lorentz, polarization and numerical absorption corrections [19] were applied. The structure were solved by the Patterson method and subsequently completed by the difference Fourier recycling. All the non-hydrogen atoms were refined anisotropically using full-matrix, least-squares technique. The hydrogen atoms were found on difference Fourier synthesis and next refined as "riding" on their parent carbon atoms [d(C–H) = 0.96 Å] and assigned isotropic temperature factors equal 1.2 times the value of equivalent temperature factor of the parent carbon atom. The crystal of 2 was racemically twinned with 7:3 participation of domains. SHELXS-97 [20], SHELXL-97 [21] and SHELXTL [22] programs were used for all the calculations. Atomic scattering factors were those incorporated in the computer programs.

3. Computational details

GAUSSIAN-03 program [23] was used in the calculations. The geometry optimisations of the $[ReOCl_2(pzH)_2(OAsPh_3)]^+$ cation, ReO_4^- anion and $[\{ReCl_2(pzH)_2\}_2(\mu\text{-}O)]$ complex were carried out with the DFT method with

Table 1
Crystal data and structure refinement for **1** and **2**

	1	**2**
Empirical formula	$C_{24}H_{23}AsCl_2N_4O_6Re_2$	$C_{12}H_{16}Cl_4N_8O_3Re_2$
Formula weight	981.68	834.53
Temperature (K)	293(2)	293(2)
Wavelength (Å)	0.71073	0.71073
Crystal system	triclinic	orthorhombic
Space group	$P\bar{1}$	$P2_12_12$
Unit cell dimensions		
a (Å)	10.0933(10)	9.5867(8)
b (Å)	11.3682(11)	15.7023(13)
c (Å)	13.5527(13)	7.6254(5)
α (°)	80.320(8)	
β (°)	74.843(8)	
γ (°)	86.133(8)	
Volume (Å^3)	1479.2(2)	1147.88(15)
Z	2	2
Density (calculated) (Mg m^3)	2.204	2.414
Absorption coefficient (mm^{-1})	9.511	11.032
$F(000)$	920	772
Crystal size (mm)	$0.15 \times 0.09 \times 0.05$	$0.25 \times 0.17 \times 0.15$
θ range for data collection (°)	2.92–25.10	3.35–25.11
Index ranges	$-12 \leqslant h \leqslant 12$	$-11 \leqslant h \leqslant 11$
	$-13 \leqslant k \leqslant 13$	$-18 \leqslant k \leqslant 17$
	$-16 \leqslant l \leqslant 16$	$-8 \leqslant l \leqslant 9$
Reflections collected	21 322	12 214
Independent reflections (R_{int})	5276 (0.0681)	2046 (0.0606)
Completeness to 2θ (%)	99.8	99.7
Maximum and minimum transmission	0.6326 and 0.3315	0.3829 and 0.1921
Data/restraints/parameters	5276/0/352	2046/0/132
Goodness-of-fit on F^2	1.036	1.102
Final R indices [$I > 2(I)$]	$R_1 = 0.0438$	$R_1 = 0.0274$
	$wR_2 = 0.0807$	$wR_2 = 0.0669$
R indices (all data)	$R_1 = 0.0700$	$R_1 = 0.0275$
	$wR_2 = 0.0887$	$wR_2 = 0.0669$
Absolute structure parameter		0.300(18)
Largest different peak and hole (e Å^{-3})	0.820 and −1.045	1.242 and −1.111

the use of B3LYP functional [24,25]. The electronic spectra the $[ReOCl_2(pzH)_2(OAsPh_3)]^+$ cation, ReO_4^- anion and $[\{ReCl_2(pzH)_2\}_2(\mu\text{-}O)]$ complex were calculated with the TDDFT method [26].

LANL2DZ basis set [27] with additional d (with exponent $\alpha = 0.3811$) and f (with exponent $\alpha = 2.033$) functions was used on the rhenium atom, 6-31G(d) on the chlorine, nitrogen, arsenic, oxygen and carbon atoms and 6-31G basis on the hydrogen atoms.

Natural bond orbital (NBO) calculations were performed with the NBO code [28] included in GAUSSIAN-03.

4. Results and discussion

4.1. Preparation of complexes

The $[ReOCl_2(pzH)_2(OAsPh_3)](ReO_4)$ complex has been isolated in the reaction of $[ReOCl_3(AsPh_3)(OAsPh_3)]$ with an excess of pyrazole in wet tetrahydrofurane at room temperature. In contrast to the analogous reactions of $[ReOX_3(AsPh_3)(OAsPh_3)]$ (X = Cl, Br) with 3,5-dimethylpyrazole (L) in acetone, dimerization and formation of dinuclear $[Re_2O_3X_4L_4]$ compounds do not occur. The presence of perrhenate anion in **1** could seem to be surprising and somewhat unexpected. However, the formation of ReO_4^- ion during synthesis of rhenium compounds has been observed previously [29].

Dimerization and formation of a dinuclear compound is observed for the reaction of $[ReOCl_3(PPh_3)_2]$ with pyrazole in tetrahydrofurane. In this case, the $[\{ReCl_2(pzH)_2\}_2(\mu\text{-}O)]$ complex has been isolated from the reaction system. However, in contrast to the previously characterised $[\{Re(O)X_2(3,5\text{-}Me_2pzH)_2\}_2(\mu\text{-}O)]$ compounds with *cis*,*cis*-ReX_2N_2 arrangement, the $ReCl_2(pzH)_2$ units in **1** are found to be *trans*,*trans*. Only two $[\{ReOX_2L_2\}_2(\mu\text{-}O)]$ complexes with a *trans* arrangement of monodentate heterocycle ligands L in the ReX_2L_2 planes have been characterised so far, $[\{ReOX_2(py)_2\}_2(\mu\text{-}O)]$ [6] and $[\{ReOX_2(1\text{-}Meim)_2\}_2(\mu\text{-}O)]$ [30].

4.2. Crystal structure of *1*

The molecular structure of **1** is shown in Fig. 1. There are no significant contacts involving either cation or anion, with the possible exception of some rather weak hydrogen bonds from the perrhenate anion to the pyrazole or phenyl

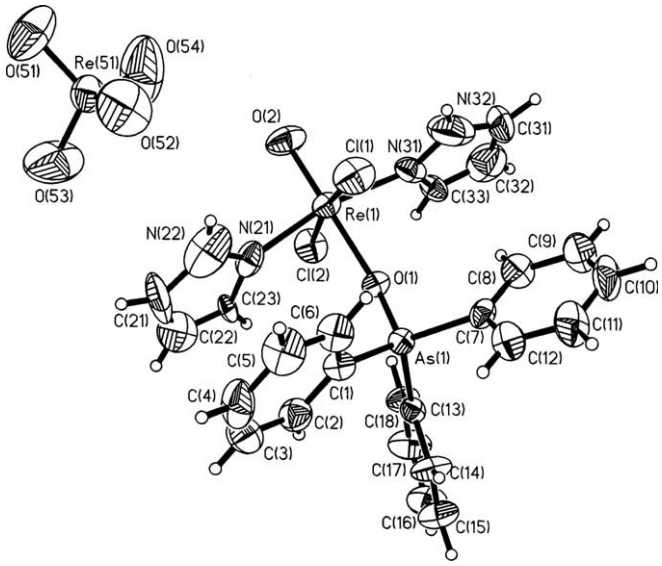

Fig. 1. The molecular structure of $[ReOBr_2(pzH)_2(OAsPh_3)](ReO_4)$.

rings. The weak intramolecular and intermolecular hydrogen bonds [31,32] of **1** are presented in Table 2.

The rhenium atom of the $[ReOCl_2(pzH)_2(OAsPh_3)]^+$ cation has a distorted octahedral environment with the *trans* arranged pyrazole ligands and oxo ion lying in *trans* position to the $OAsPh_3$ molecule. The *cis*-location of π-acid ligands (the pyrazole ligands) in relation to the oxo group seems to be dominated by electronic influence of the multiply bonded ligand, which forces the metal nonbonding d electrons to lie in the in the plane perpendicular to the M–O bond axis. This general rule appears to hold for isonitrile, carbonyl, olefin, acetylene, thioether and often phosphine ligands [33–36]. The most important bond lengths and angles for **1** are reported in Table 3. The major distortion – an increase in the O(2)–Re–Cl/N angles – appears due to the electronic factors interactions with the oxo ligand, and it is commonly observed in octahedral complexes containing a multiply bonding ligand [33,34]. The $Re–O_{oxo}$ bond in $[ReOCl_2(pzH)_2(OAsPh_3)]^+$ is a typical example of reported terminal multiple $Re–O_{oxo}$ distances in mononuclear $[ReO]^{3+}$ compounds: 1.691 Å in $[ReOCl_3(OPPh_2CH_2PPh_2)]$ [37], 1.663 Å in *trans*-$[ReOCl_3(PPh_3)_2]$ [38] and 1.673 Å in $[ReOMe_2Cl(PMe_3)_2]$ [39].

Table 2
Hydrogen bonds for **1**

D	A	H···A	D···A	D–H···A
C(18)	O(1)	2.50	2.981(9)	112.8
C(23)	Cl(2)	2.64	3.140(8)	114.7
C(33)	Cl(2)	2.52	3.093(9)	120.0
C(11)	O(52)#1	2.50	3.345(12)	150.8
C(17)	Cl(2)#2	2.76	3.469(9)	133.7
C(23)	O(53)#3	2.00	2.835(13)	148.2
C(31)	O(52)#4	2.46	3.353(14)	160.6
C(33)	O(51)#5	2.13	2.918(12)	142.1

#1 $-x+1, -y+1, -z$; #2 $-x, -y, -z+1$; #3 $-x, -y+1, -z+1$; #4 $-x, -y+1, -z$; #5 $x, y-1, z$.

Table 3
The experimental bond lengths [Å] and angles [°] for **1**

Bond lengths	
Re(1)–O(2)	1.664(5)
Re(1)–O(1)	2.018(5)
Re(1)–N(21)	2.101(7)
Re(1)–N(31)	2.105(7)
Re(1)–Cl(1)	2.391(2)
Re(1)–Cl(2)	2.375(2)
O(1)–As(1)	1.682(5)
Re(51)–O(51)	1.683(8)
Re(51)–O(52)	1.681(8)
Re(51)–O(53)	1.702(8)
Re(51)–O(54)	1.662(9)
Bond angles	
O(1)–Re(1)–O(2)	179.5(3)
O(1)–Re(1)–N(21)	84.2(2)
O(1)–Re(1)–N(31)	83.9(2)
O(2)–Re(1)–N(21)	95.8(3)
O(2)–Re(1)–N(31)	96.0(3)
N(21)–Re(1)–N(31)	168.1(2)
O(1)–Re(1)–Cl(1)	85.58(16)
O(1)–Re(1)–Cl(2)	84.84(16)
O(2)–Re(1)–Cl(1)	94.0(2)
O(2)–Re(1)–Cl(2)	95.6(2)
N(21)–Re(1)–Cl(1)	90.4(2)
N(21)–Re(1)–Cl(2)	88.6(2)
N(31)–Re(1)–Cl(1)	89.6(2)
N(31)–Re(1)–Cl(2)	89.4(2)
Cl(1)–Re(1)–Cl(2)	170.42(8)
As(1)–O(1)–Re(1)	147.0(3)
O(51)–Re(51)–O(52)	110.7(5)
O(51)–Re(51)–O(53)	110.4(5)
O(51)–Re(51)–O(54)	108.1(5)
O(52)–Re(51)–O(53)	109.5(5)
O(52)–Re(51)–O(54)	108.7(5)
O(53)–Re(51)–O(54)	109.4(7)

The $Re–OAsPh_3$ and the As–O bond lengths in $[ReOCl_2(pzH)_2(OAsPh_3)]^+$ are in good agreement with the values found for $[ReOBr_3(AsPh_3)(OAsPh_3)]$ (Re–O = 2.010(7) Å, As–O = 1.675(7) Å) and $[ReOCl_3(AsPh_3)(OAsPh_3)]$ (Re–O = 2.019(8) Å, As–O = 1.643(9) Å [17]). The bond distances and angles in the pyrazole rings are also unexceptional, and they agree well with appropriate values found previously [13,14].

4.3. Crystal structure of **2**

The molecular structure of **2** is presented in Fig. 2, and the most important bond lengths and angles are reported in Table 4. The $[\{ReCl_2(pzH)_2\}_2(\mu\text{-}O)]$ complex takes a dinuclear structure in which two rhenium atoms are bridged by the oxo ligand. The bridging oxygen atom lies in special position *a* of $P2_12_12$ space group with site symmetry 2. Each rhenium ion of **2** exhibits a distorted octahedral coordination geometry with the oxygen atoms in the axial positions and *trans* arrangement of monodentate pyrazole ligands in the $ReX_2(pzH)_2$ planes. The Re–O–Re angle is almost linear [177.5(5)°], and two halves of the dinuclear compound are rotated about 54.8° along the line linking Re···Re atoms. The torsion

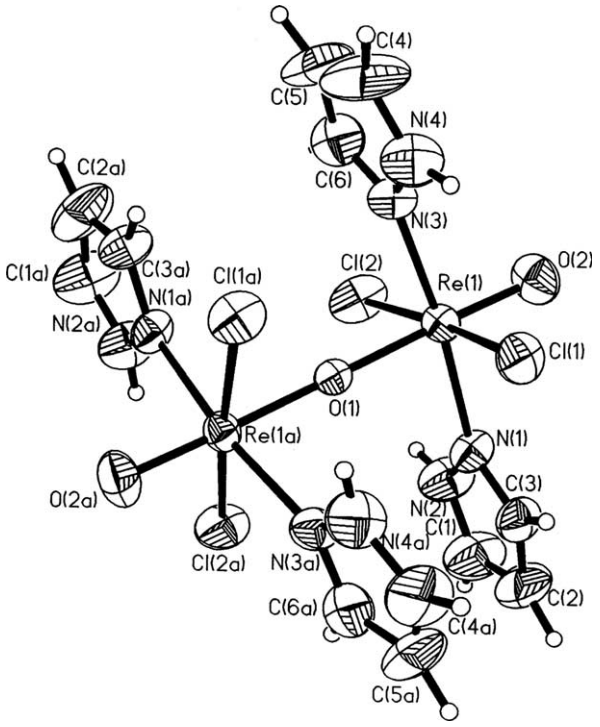

Fig. 2. The molecular structure of $[\{ReCl_2(pzH)_2\}_2(\mu\text{-}O)]$.

Cl(1)–Re(1)···Re(1#)–Cl(1#)/Cl(2#)/N(1#)/N(3#) angles are equal to 55.03(11), −125.20(8), 145.0(2) and −35.3(2)°, respectively (# indicate the $-x+2$, $-y$, z symmetry transformation). This conformation allows stacking interactions to occur between the two pairs of the heterocyclic ligands (Fig. 2; Cg···Cg# distance 4.578(15) Å, angle between Cg···Cg# vector and normal to plane Cg equal to 43.8(9)° and perpendicular distance of Cg on ring Cg# 3.538(5) Å), and succeeding intermolecular stacking interaction between pyrazole substituents indicated by N(3) atom (Cg···Cg$ distance 3.346(16) Å, angle between Cg···Cg$ vector and normal to plane Cg equal to 12.7(9)° and perpendicular distance of Cg on ring Cg$ 3.557(5) Å; $ indicate the $-x+1$, $-y$, z symmetry transformation) linking the molecules to the one dimensional chain. The structure is assembled via strong and weak hydrogen bonds (Table 5) to the three dimensional net. The Re–N, Re–Cl, Re–O_t, and Re–O_b bond lengths in **2** agree well with appropriate values found previously in similar rhenium compounds containing the O=Re–O–Re=O framework [4–12,30]. The Re–O_t bond length of **2** is slightly longer than Re–O_t distance of **1**, but it falls in the range typical of mononuclear complexes of rhenium(V) having $[ReO]^{3+}$ core. The Re–O_b bond distance is also significantly shorter than a single Re–O length. An ideal single Re–O bond distance, predicted by the use of Pauling's covalent

Table 4
The experimental bond lengths [Å] and angles [°] for **2**

Bond lengths	
Re(1)–O(1)	1.9038(4)
Re(1)–O(2)	1.692(6)
Re(1)–Cl(1)	2.421(2)
Re(1)–Cl(2)	2.414(2)
Re(1)–N(1)	2.111(7)
Re(1)–N(3)	2.106(8)
Bond angles	
O(2)–Re(1)–O(1)	178.1(3)
O(1)–Re(1)–N(1)	86.1(3)
O(1)–Re(1)–N(3)	86.1(2)
O(2)–Re(1)–N(1)	93.0(3)
O(2)–Re(1)–N(3)	94.7(3)
N(3)–Re(1)–N(1)	172.3(3)
O(1)–Re(1)–Cl(1)	86.3(2)
O(1)–Re(1)–Cl(2)	88.0(3)
O(2)–Re(1)–Cl(1)	92.0(3)
O(2)–Re(1)–Cl(2)	93.7(3)
N(1)–Re(1)–Cl(1)	89.7(2)
N(1)–Re(1)–Cl(2)	89.7(2)
N(3)–Re(1)–Cl(1)	89.9(2)
N(3)–Re(1)–Cl(2)	89.9(2)
Cl(2)–Re(1)–Cl(1)	174.31(9)
Re(1)–O(1)–Re(1)#1	177.5(5)

= $-x+2$, $-y$, z.

Table 5
Hydrogen bonds for **2**

D	A	H···A	D···A	D–H···A
N(2)	Cl(1)#1	2.62	3.296(9)	136.5
N(2)	Cl(2)	2.60	3.142(10)	122.5
N(4)	Cl(1)	2.63	3.164(9)	121.0
N(4)	Cl(2)#2	2.63	3.327(10)	139.5
C(1)	O(2)#3	2.52	3.391(14)	156.0
C(3)	Cl(1)	2.79	3.297(10)	115.4
C(6)	Cl(2)	2.74	3.254(11)	116.1

#1 x, y, $z-1$; #2 x, y, $z+1$; #3 $x+1/2$, $-y+1/2$, $-z$.

Table 6
Atomic charges from the Natural Population Analysis (NPA) for $[ReOCl_2(pzH)_2(OAsPh_3)]^+$ and **2**

Atom	Atomic charge
1	
Re(1)	1.279
Cl(1)	−0.534
Cl(2)	−0.427
O(1)	−1.096
O(2)	−0.339
N(21)	−0.332
N(22)	−0.319
N(31)	−0.333
N(32)	−0.319
As(1)	2.315
2	
Re(1)	1.281
O(1)	−0.860
O(2)	−0.405
Cl(1)	−0.502
Cl(2)	−0.502
N(1)	−0.315
N(2)	−0.308
N(3)	−0.315
N(4)	−0.308

radius for oxygen and Cotton and Lippard's value for the octahedral covalent radius of rhenium(V), should be ca. 2.04 Å [40]. It indicates some redistribution of the d_{π}–p_{π} interaction along the O_t–Re–O_b unit in the dinuclear rhenium complex.

4.4. Spectroscopic characterization

The IR spectrum of $[ReOCl_2(pzH)_2(OAsPh_3)](ReO_4)$ shows a band at 999 cm^{-1} assignable to Re=O stretching vibration of the $[ReOCl_2(pzH)_2(OAsPh_3)]^+$ cation and two intense bands at 922 and 906 cm^{-1} caused by ν(ReO) vibrations of the perrhenate ion. A strong band corresponding to the ν(As=O) vibration appears at 852 cm^{-1}. The IR spectrum of **2** shows a band at 954 cm^{-1} assignable to the symmetric Re=O stretch and a strong multicomponent ν(Re–O–Re) band at 704 $cm^{-1}$with the same shape illustrated in the article of Cotton et al. [41]. The bands of C=C and C=N stretching modes observed at ca. 1640 and 1558 cm^{-1} in uncomplexed pyrazole are shifted to considerable lower frequencies for **1** and **2** complexes. The presence of bands in the range assignable to N–H vibrations in the spectra of **1** and **2** is consistent with the coordination of pyrazole ligands in neutral monodentate form.

The protons of $OAsPh_3$ ligand are readily identified from integrations, they appear as a multiplet at 7.28 ppm. Two pseudotriplets at 7.55 and 7.69 ppm correspond to the protons bound to C(22) and C(32) atoms. Four signals in the range 6.50–8.65 ppm are associated with the other pyrazolyl CH protons, whereas the signal at 13.16 ppm is attributed to NH protons of the pyrazole ligands.

4.5. Geometry optimisation

The geometries of the $[ReOCl_2(pzH)_2(OAsPh_3)]^+$ cation, ReO_4^- anion and $[\{ReCl_2(pzH)_2\}_2(\mu\text{-}O)]$ complex were optimised in a singlet state using the DFT method with the B3LYP functional. For both compounds, a good agreement with the experimental values can be noticed for the Re–O and Re–N bond lengths. The optimised Re–N distances differs by about 0.01 Å from the experimental

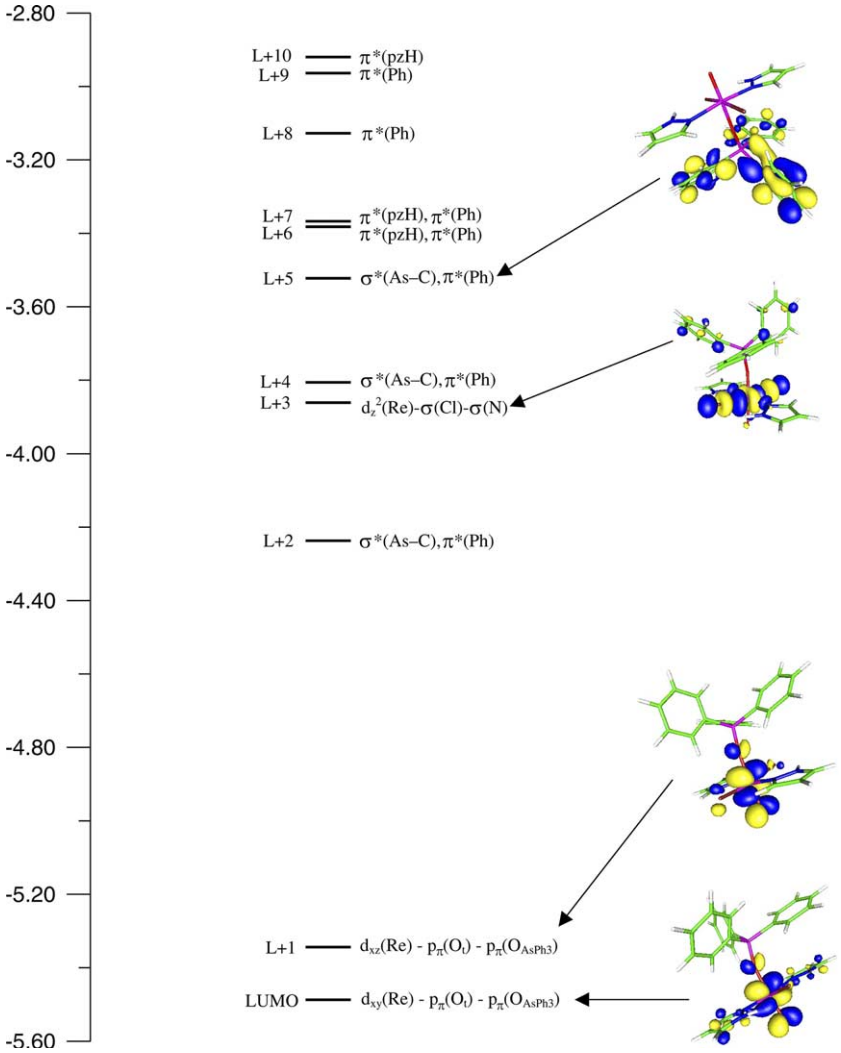

Fig. 3a. The energy (eV), character and some contours of the unoccupied molecular orbitals of $[ReOCl_2(pzH)_2(OAsPh_3)]^+$.

ones. The computed Re–O bond length of the $[ReOCl_2(pzH)_2(OAsPh_3)]^+$ cation (1.660 Å) is almost the same as the experimental value (1.664(5) Å). The optimised Re–$O_{terminal}$ distances (1.679 Å) of $[\{ReCl_2(pzH)_2\}_2(\mu\text{-}O)]$ are insignificantly shorter than the experimental values (1.692(6) Å), whereas the computed Re–$O_{bridging}$ bond lengths are little overestimated in comparison with the experimental ones. The largest differences between the experimental and optimised values are found for Re–Cl distances, the maximum deviations Re–Cl bond lengths are equal to 0.127 and 0.065 Å for **1** and **2**, respectively. Similar elongation of the rhenium–chlorine bond lengths (up to 0.25 Å) in the B3LYP with different basis sets has been found in other rhenium complexes [42]. A good agreement with the experimental values is also found for bond angles, and general trends observed in the experimental geometries are well reproduced in the calculated structures.

4.6. Charge distribution

Table 6 presents the atomic charges from the Natural Population Analysis (NPA) for **1** and **2** complexes. The calculated charges on the rhenium atoms are considerable lower than the formal charge +5. This is a result of significant charge donation from oxo ligands, chlorine ions and *N*-heterocyle molecules. For complex **2**, the considerable difference in values of charges is observed for the terminal and bridging oxo ligands – less negative are the terminal oxo ligands, which indicates the higher electron density delocalization from the terminal ligands towards the rhenium centers and corresponds to differences in the Re–O_t and Re–O_b bonds lengths.

4.7. Electronic structure

The energies, characters and contours of the selected unoccupied and occupied molecular orbitals of the $[ReOCl_2(pzH)_2(OAsPh_3)]^+$ cation are shown in Figs. 3a and 3b, respectively. The rhenium atom in $[ReOCl_2(pzH)_2(OAsPh_3)]^+$ possess the d^2 configuration, the highest MO of the cation is of d_{yz} type with an antibonding contributions from p_π chlorine orbitals. The remaining four d-type orbitals of rhenium are found among unoccupied MOs. The rhenium–oxygen interaction in the $[ReOBr_2(pzH)_2(OAsPh_3)]^+$ cation is described as a triple bond. The $\pi_{Re\equiv O}$

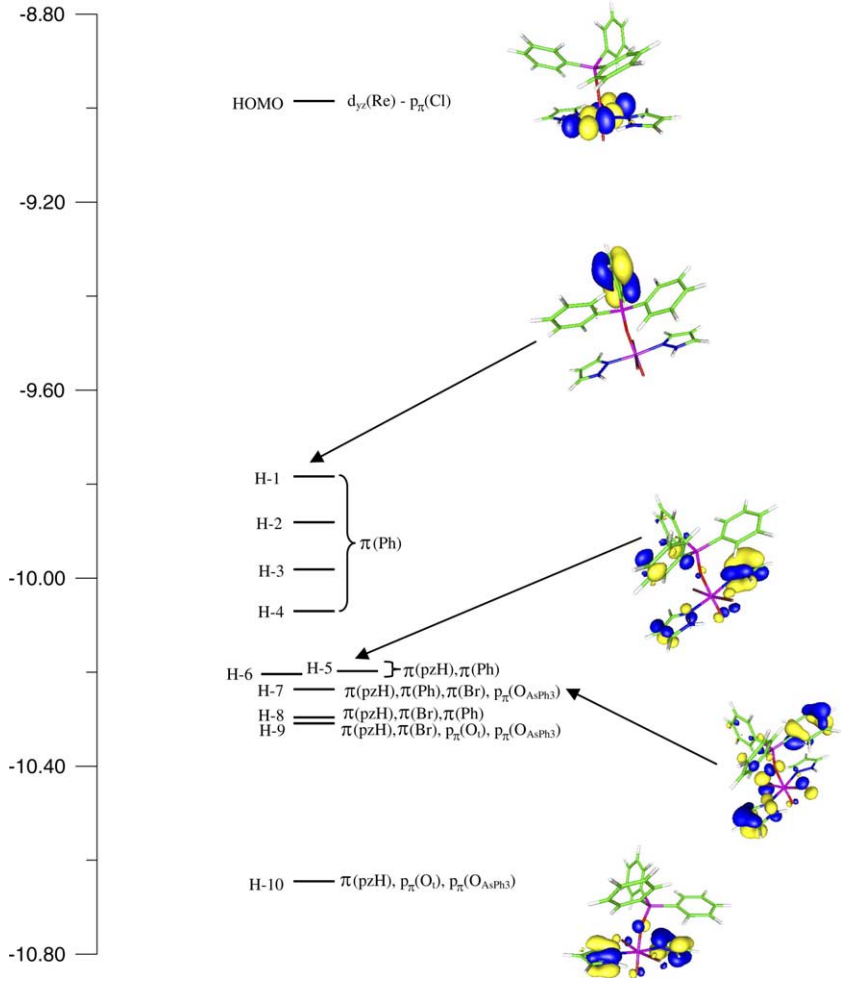

Fig. 3b. The energy (eV), character and some contours of the occupied molecular orbitals of $[ReOCl_2(pzH)_2(OAsPh_3)]^+$.

bonds arise from overlap of the two occupied oxygen p_π orbitals with the empty d_{xy} and d_{xz} metal orbitals. The LUMO and LUMO + 1 are ascribed as π-antibonding rhenium–oxygen molecular orbitals. The LUMO + 3 and LUMO + 11 of the $[ReOBr_2(pzH)_2(OAsPh_3)]^+$ cation are predominantly of d_{z^2} and $d_{x^2-y^2}$ rhenium orbital character, respectively. The LUMO + 2, LUMO + 4, LUMO + 5, LUMO + 8 and LUMO + 9 are mainly composed of π-antibonding phenyl rings, whereas π-antibonding pyrazole rings are mainly contribute to the LUMO + 6, LUMO + 7 and LUMO + 10.

The energies, characters and contours of the selected unoccupied and occupied molecular orbitals of complex **2** are presented in Figs. 4a and 4b, respectively. The rhenium atoms of **2** possess the d^2 configuration; the two highest MOs of the dinuclear complex are of d_{xz} type with an antibonding contribution from p_π chlorine orbitals. The remaining eight d-type orbitals of rhenium are found among unoccupied MOs. The d_{yz} and d_{xy} orbitals of both rhenium ions interact with the filled p_π orbitals of the terminal and bridging oxo ligands to give four π-bonding, two π-nonbonding and four π-antibonding molecular orbitals. The LUMO, LUMO + 1, LUMO + 2 and LUMO + 3 are ascribed as π-antibonding rhenium–oxygen molecular orbitals. The LUMO + 4 and LUMO + 5 are of d_{z^2}-σ_{Cl}–σ_N character. The $d_{x^2-y^2}$ rhenium orbitals make the largest contribution into the LUMO + 10 and LUMO + 11 orbitals. As the complex **2** have C_2 symmetry each molecular orbital is plus or minus combination of the symmetry equivalent d orbitals of the two Re atoms.

4.8. NBO analysis

Table 7 presents the occupancies and hybridization of the calculated natural bond orbitals (NBOs) between the rhenium and the oxo ligands for the $[ReOCl_2(pzH)_2(OAsPh_3)]^+$ cation and $[\{ReCl_2(pzH)_2\}_2(\mu\text{-}O)]$ complex. Table 8 shows the occupancies and atomic orbital compositions of the detected lone pairs (LP) orbitals of the O_b ligand, as well as the character of the acceptor orbital and stabilization energies (ΔE_{ij}) for the corresponding

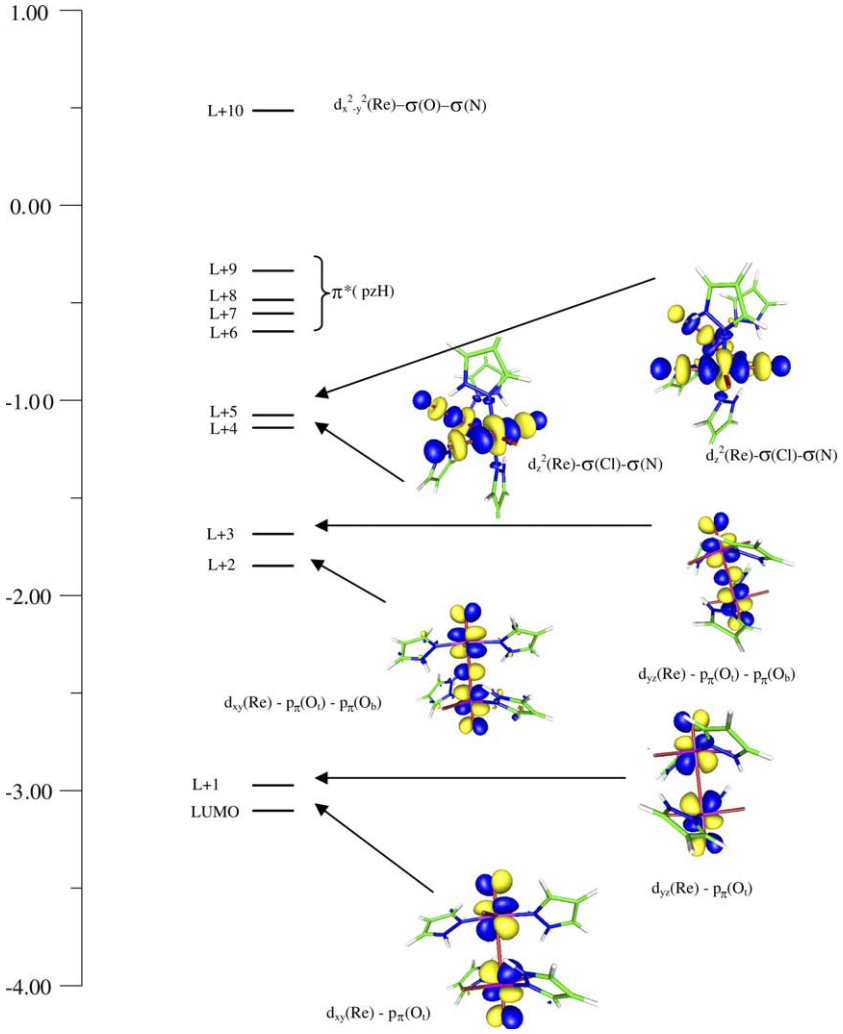

Fig. 4a. The energy (eV), character and some contours of the unoccupied molecular orbitals of **2**.

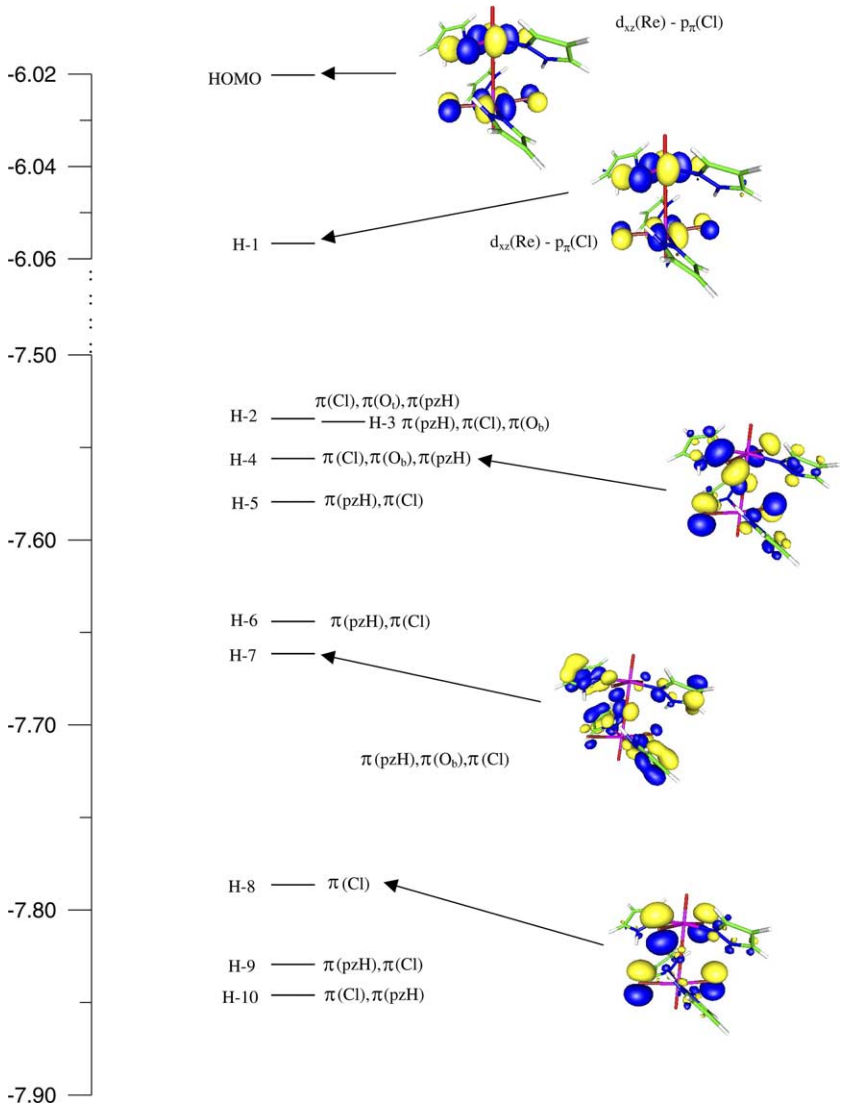

Fig. 4b. The energy (eV), character and some contours of the occupied molecular orbitals of **2**.

Table 7
The occupancies and hybridization of the calculated natural bond orbitals (NBOs) between the rhenium and the oxo ligands for $[ReOCl_2(pzH)_2(OAsPh_3)]^+$ and $[\{ReCl_2(pzH)_2\}_2(\mu\text{-}O)]$

BD	Occupancy	Hybridization of NBO
$[ReOCl_2(pzH)_2(OAsPh_3)]^+$		
Re–O_t	1.983	$0.509(sd^{14.16})_{Re} + 0.861(sp^{2.09})_O$
Re–O_t	1.993	$0.579(d)_{Re} + 0.815(p)_O$
Re–O_t	1.990	$0.572(d)_{Re} + 0.820(p)_O$
Re–O_t[a]	0.327	$0.861(sd^{14.16})_{Re} + 0.509(sp^{2.09})_O$
Re–O_t[a]	0.240	$0.815(d)_{Re} - 0.579(p)_O$
Re–O_t[a]	0.219	$0.820(d)_{Re} - 0.572(p)_O$
$[\{ReCl_2(pzH)_2\}_2(\mu\text{-}O)]$		
Re–O_t	1.959	$0.466(sd^{3.37})_{Re} + 0.885(sp^{1.75})_O$
Re–O_t	1.993	$0.574(d)_{Re} + 0.819(p)_O$
Re–O_t	1.988	$0.573(d)_{Re} + 0.820(p)_O$
Re–O_t[a]	0.288	$0.885(sd^{3.37})_{Re} - 0.466(sp^{1.75})_O$
Re–O_t[a]	0.263	$0.819(d)_{Re} - 0.574(p)_O$
Re–O_t[a]	0.237	$0.820(d)_{Re} - 0.573(p)_O$

BD denotes 2-center bond.
[a] Denotes antibond NBO.

Table 8
Stabilization energies associated with delocalisation from the lone pair orbitals of the bridging oxo ligand for $[\{ReCl_2(pzH)_2\}_2(\mu\text{-}O)]$

Donor orbital	Occupancy of donor orbital	Acceptor orbital	ΔE_{ij} (kcal/mol)
$s_{O(1)}$	1.772	$0.885(sd^{3.37})_{Re} - 0.466(sp^{1.75})_O$	83.90
$p_{O(1)}$	1.756	$0.885(sd^{3.37})_{Re} - 0.466(sp^{1.75})_O$	43.85
$p_{O(1)}$	1.660	$0.819(d)_{Re} - 0.574(p)_O$	33.75
$p_{O(1)}$	1.653	$0.820(d)_{Re} - 0.573(p)_O$	32.14

donor–acceptor interactions for complex **2**. The interactions between 'filled' (donor) Lewis-type NBOs and 'empty' (acceptor) non-Lewis NBOs lead to loss of occupancy from the localized NBOs of the idealized Lewis structure into the empty non-Lewis orbitals, and they are referred to as 'delocalization' corrections to the zeroth-order natural Lewis structure. The stabilization energy ΔE_{ij} (kcal/mol) associated with delocalization is estimated by the second-order perturbative as:

$$\Delta E_{ij} = q_i(F(i,j)^2)/(\varepsilon_j - \varepsilon_i),$$

where q_i is the donor orbital occupancy, ε_i, ε_j are diagonal elements (orbital energies) and $F(i,j)$ is the off-diagonal NBO Fock matrix element [43].

For each Re atom of **2**, three natural Re–O_t bond orbitals were detected. Due to C_2 symmetry of complex **2**, the Re(1)–O(2) and Re(2)–O(3) natural orbitals have the same character, and the values of stabilization energies (ΔE_{ij}) are equal for Re(1) and Re(2) centers. The Re–O_t bonds are all strongly polarized towards the oxygen atom. The s and p oxygen orbitals and s and d rhenium orbitals take part in the σ_{Re-Ot} bond formation, whereas the π_{Re-Ot} bond orbitals result from overlapping of the empty d_{xy} and d_{yz} rhenium orbitals with the occupied p_x and p_z orbitals of the terminal oxygen ligands. Each terminal oxo ligand of **2** has one lone pair with occupancy close to 2. The Re–O_b bonds were not detected indicating a predominant Coulomb-type interaction between the central ion and the bridging oxo ligand [44]. The bridging oxygen ligand has four lone pairs orbitals (LP) and electron density from the LP orbitals is strongly delocalized into the antibonding Re–O_t bond orbitals – the occupancy of the LP orbitals of bridging oxygen are significantly lower than ~2 (Table 8).

Three natural bond orbitals were also detected for the Re–O_t bond in the $[ReOCl_2(pzH)_2(OAsPh_3)]^+$ cation. Similar to complex **2**, the and πRe–O bonds are clearly polarized towards the oxygen end.

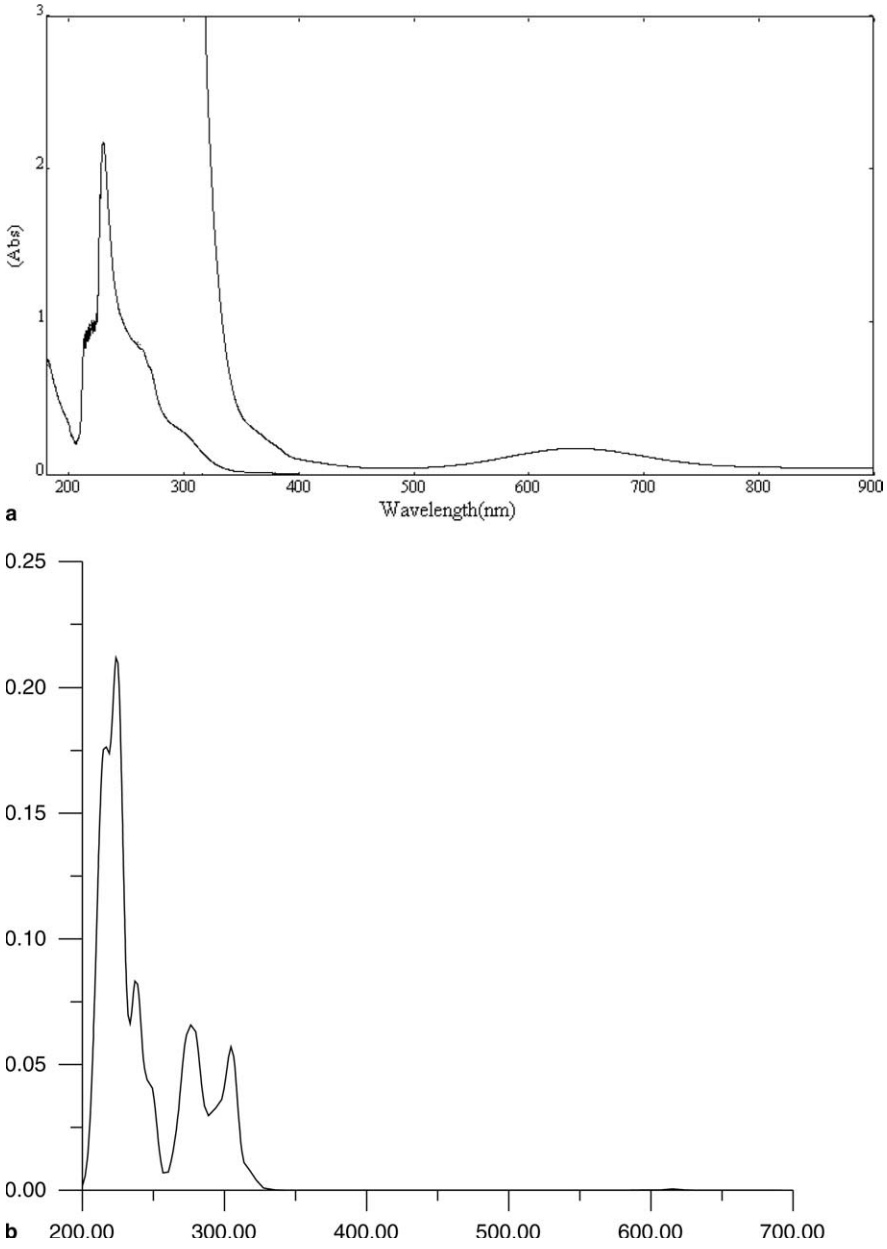

Fig. 5. The experimental (a) and calculated (b) electronic absorption spectrum of **1**.

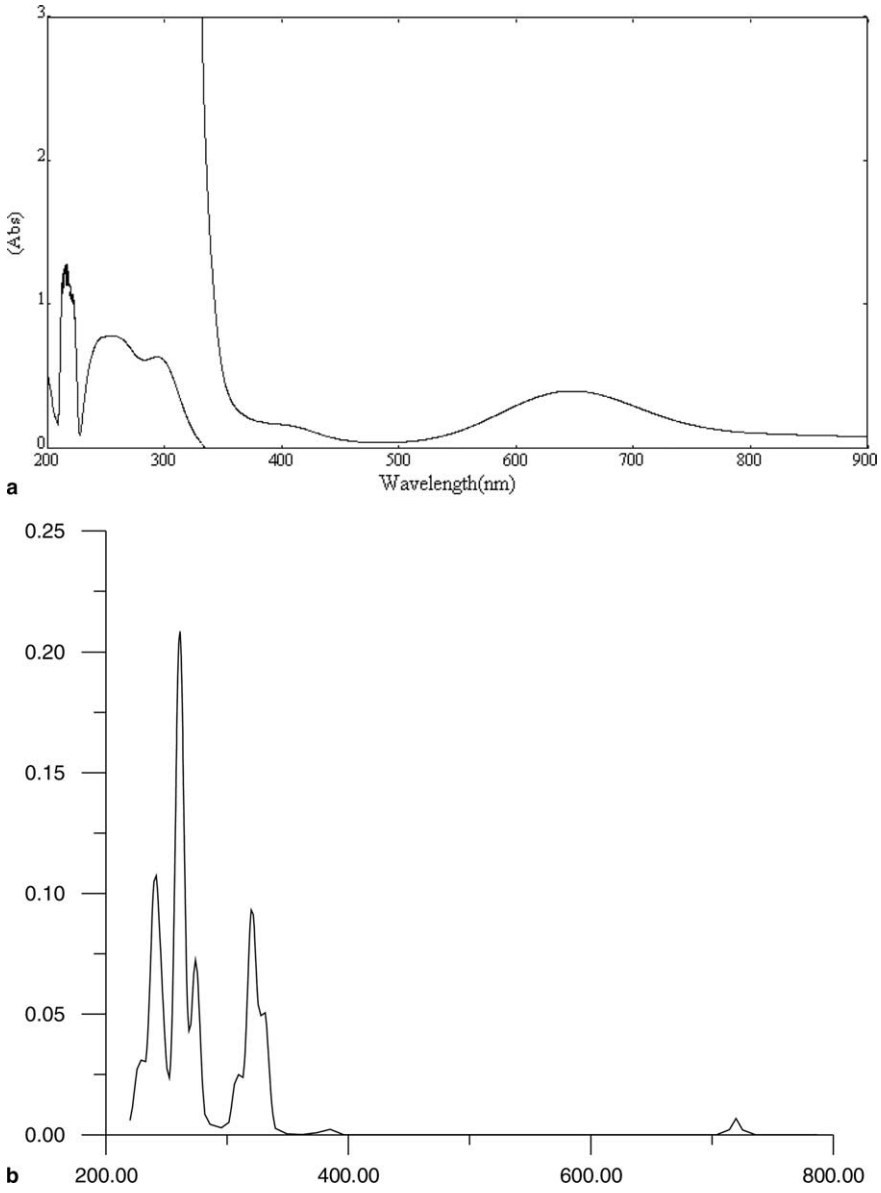

Fig. 6. The experimental (a) and calculated (b) electronic absorption spectrum of **2**.

4.9. Electronic spectra

The experimental and calculated electronic spectra of **1** and **2** are presented in Figs. 5 and 6, respectively. Each calculated transition in Figs. 5 and 6(b) was represented by a gaussian function with the height equal to the oscillator strength and width equal to 0.04.

Tables 9 and 10 present the position of the experimental absorption bands and the spin-allowed singlet–singlet electronic transitions calculated with the TDDFT method for **1** and **2**, respectively. The calculations result in many transitions with very small oscillator strengths. Except for the low energy part of the spectrum, only transitions with oscillator strengths larger than 0.010 are listed for **1** and **2**, respectively. The assignment of the calculated transitions to experimental absorption bands was based on the criterion of the energy and oscillator strength of the calculated transition. The assignment for the complex **2** is not complete. Some additional intraligand and interligand transitions are expected to be found at higher energies in the calculations for **2**.

The UV–Vis spectrum of **1** exhibits a few intense absorption bands in the range 350–200 nm and a weak absorption in the low energy range – at 651.4 nm.

The longest wavelength experimental band at 651.4 nm is attributed to the transitions of $d \rightarrow d$ character with small oscillator strengths calculated at 615.7 and 595.1 nm.

The absorption bands at 300 and 263 nm correspond mainly to the LMCT transitions that occur from the chlorine, oxygen, triphenylarsine oxide and pyrazole orbitals to the d rhenium orbitals.

Table 9
The position of experimental absorption bands and electronic transitions calculated with the TDDFT method $[ReOCl_2(pzH)_2(OAsPh_3)]^+$

The most important orbital excitations	Character	λ (nm)	E (eV)	f	Experimental Λ (nm) (E (eV))ε
H → L	d → d	615.7	2.01	0.0005	651.4 (2.01)
H → L + 1	d → d	595.1	2.08	0.0001	
H-9 → L	π(pzH)/π(Cl)/$\pi(O_t)$/$\pi(O_{AsPh3})$ → d	329.1	3.77	0.0003	382.0 (3.25)
H-1 → L	π(Ph) → d	324.3	3.82	0.0004	
H-2 → L	π(Ph) → d	318.6	3.89	0.0060	300.0 (4.13)
H-6 → L	π(pzH)/π(Ph) → d	312.4	3.97	0.0031	
H-4 → L	π(Ph) → d	306.1	4.06	0.0057	
H-9 → L	π(pzH)/π(Cl)/$\pi(O_t)$/$\pi(O_{AsPh3})$ → d	305.7	3.76	0.0381	
H-8 → L	π(pzH)/π(Cl)/π(Ph) → d				
H-6 → L	π(pzH)/π(Ph) → d	301.5	4.11	0.0145	
H-7 → L	π(pzH)/π(Ph)/π(Cl)/$\pi(O_{AsPh3})$ → d				
H-8 → L	π(pzH)/π(Cl)/π(Ph) → d	292.6	4.24	0.0180	263.2 (4.71)
H-7 → L	π(pzH)/π(Ph)/π(Cl)/$\pi(O_{AsPh3})$ → d				
H-10 → L	π(pzH)/$\pi(O_t)$/$\pi(O_{AsPh3})$ → d	281.3	4.41	0.0154	
H-11 → L + 1	π(pzH)/π(Cl)/$\pi(O_{AsPh3})$ → d	279.3	4.44	0.0223	
H-10 → L + 1	π(pzH)/$\pi(O_t)$/$\pi(O_{AsPh3})$ → d	277.0	4.48	0.0169	
H-14 → L	π(Cl)/$\pi(O_t)$/$\pi(O_{AsPh3})$ → d				
H-14 → L	π(Cl)/$\pi(O_t)$/$\pi(O_{AsPh3})$ → d	272.2	4.55	0.0425	
H-13 → L	π(pzH)/π(Br) → d				
H-14 → L + 1	π(Cl)/$\pi(O_t)$/$\pi(O_{AsPh3})$ → d	265.3	4.67	0.0106	
H-2 → L + 2	π(Ph) → π*(Ph)	247.6	5.01	0.0197	230.4 (5.38)
H → L + 9	d/π(Cl) → π*(Ph)	240.3	5.16	0.0117	
H-16 → L	π(Cl) → d	237.8	5.21	0.0510	
H-15 → L	π(Cl)/$\pi(O_t)$/$\pi(O_{AsPh3})$ → d				
H-1 → L + 4	π(Ph) → π*(Ph)	236.6	5.24	0.0140	
H-7 → L + 2	π(pzH)/π(Ph)/π(Cl)/$\pi(O_{AsPh3})$ → π*(Ph)	227.4	5.45	0.0371	
H-5 → L + 2	π(pzH)/π(Ph) → π*(Ph)	226.8	5.47	0.0152	
H-2 → L + 3	π(Ph) → d	225.1	5.50	0.0263	
H-9 → L + 2	π(pzH)/π(Cl)/$\pi(O_t)$/$\pi(O_{AsPh3})$ → π*(Ph)	225.2	5.51	0.0536	
H-2 → L + 4	π(Ph) → π*(Ph)	222.9	5.56	0.0624	
H-4 → L + 4	π(Ph) → π*(Ph)	220.0	5.63	0.0226	
H-4 → L + 4	π(Ph) → π*(Ph)	219.1	5.66	0.0114	
H-17 → L + 1	σ(Cl)/$\pi(O_t)$/$\pi(O_{AsPh3})$ → d	215.7	5.75	0.0301	
H-10 → L + 2	π(pzH)/$\pi(O_t)$/$\pi(O_{AsPh3})$ → π*(Ph)				
H-17 → L + 1	σ(Cl)/$\pi(O_t)$/$\pi(O_{AsPh3})$ → d	215.3	5.76	0.0575	
H-5 → L + 3	π(pzH)/π(Ph) → d	214.7	5.78	0.0121	
H-3 → L + 5	π(Ph) → π*(Ph)				
H-11 → L + 2	π(pzH)/π(Cl)/$\pi(O_{AsPh3})$ → π*(Ph)	213.5	5.81	0.0151	
H-7 → L + 4	π(pzH)/π(Ph)/π(Cl)/$\pi(O_{AsPh3})$ → π*(Ph)	212.7	5.83	0.0134	
H-1 → L + 7	π(Ph) → π*(Ph)/π*(pzH)	210.5	5.89	0.0104	
H-11 → L + 3	π(pzH)/π(Cl)/$\pi(O_{AsPh3})$ → d	208.4	5.95	0.0175	
H-2 → L + 6	π(Ph) → π*(Ph)/π*(pzH)	207.1	5.99	0.0137	
H-2 → L + 6	π(Ph) → π*(Ph)/π*(pzH)	206.4	6.01	0.0129	

The next band at 230 nm is assigned to the LMCT (π(O) → d) transitions calculated for perrhenate anion at ~225 nm and LLCT transitions calculated for the $[ReOCl_2(pzH)_2(OAsPh_3)]^+$ cation in the range 230–220 nm. The last ones occur from the chlorine, oxygen, triphenylarsine oxide and pyrazole orbitals to the π^*_{pzH} orbitals and π-acceptor orbitals of the arsine ligand.

Two longest wavelength experimental bands of **2** at 651.8 and 401.6 nm are attributed to the transitions of d → d character with small oscillator strengths calculated at 719.9 nm and in the range 390–365 nm, respectively.

The next experimental band at 300.0 nm corresponds to the electronic transitions calculated between 335 and 280 nm. These transitions are mainly of LMCT (π(Cl)/$\pi(O_b)$ → d and π(pzH)/π(Cl) → d character.

The transitions calculated between 275 and 230 nm are ascribed to the experimental band at 257.6 nm. They are of LMCT (π(Cl)/$\pi(O_b)$/$\pi(O_t)$/π(pzH) → d and MLCT (d → π^*_{pzH}).

5. Supplementary data

Supplementary data for $C_{24}H_{23}AsCl_2N_4O_6Re_2$ and $C_{12}H_{16}Cl_4N_8O_3Re_2$ are available from the CCDC, 12 Union Road, Cambridge CB2 1EZ, UK on request, quoting the deposition numbers 260099 and 271895.

Table 10
The position of experimental absorption bands and electronic transitions calculated with the TDDFT method for **2**

The most important orbital excitations	Character	λ (nm)	E (eV)	f	Experimental Λ (nm)(E (eV))
H → L	d → d	719.9	1.72	0.0067	651.8(1.90)
H-1 → L	d → d	711.5	1.74	0.0001	
H → L + 2	d → d	387.4	3.20	0.0004	401.6(3.09)
H-1 → L + 2	d → d	384.8	3.22	0.0019	
H → L + 3	d → d	371.1	3.34	0.0010	
H-1 → L + 3	d → d	368.8	3.36	0.0002	
H-4 → L + 1	π(Cl)/π(O_b) → d	331.9	3.74	0.0204	
H-3 → L + 1	π(Cl)/π(O_b)/π(pzH) → d				
H-5 → L	π(pzH)/π(Cl) → d	330.0	3.76	0.0311	
H-5 → L + 1	π(pzH)/π(Cl) → d	320.5	3.87	0.0143	
H-7 → L	π(pzH)/π(O_b)/π(Cl) → d	320.3	3.87	0.0538	300.0(4.13)
H-8 → L	π(Cl) → d	319.3	3.88	0.0174	
H-8 → L + 1	π(Cl) → d	308.6	4.02	0.0181	
H-16 → L	σ(Cl)/π(O_b)/π(O_t) → d	274.0	4.52	0.0710	
H-14 → L + 1	π(Cl)/π(O_b)/π(O_t) → d				
H-19 → L	π(Cl)/σ(O_t)/σ(O_b) → d	261.7	4.74	0.0168	
H-4 → L + 2	π(Cl)/π(O_b) → d	361.4	4.74	0.0149	
H-3 → L + 2	π(Cl)/π(O_b)/π(pzH) → d				
H-1 → L + 8	d → π^*(pzH)	261.3	4.75	0.0293	257.6(4.81)
H → L + 8	d → π^*(pzH)	260.6	4.76	0.1489	
H-2 → L + 3	π(Cl)/π(O_t) → d	247.9	5.00	0.0110	
H-1 → L + 9	d → π^*(pzH)	245.9	5.07	0.0119	
H-6 → L + 2	π(pzH)/π(O_b)/π(Cl) → d	240.4	5.16	0.0289	
H-2 → L + 3	π(Cl)/π(O_t) → d	239.5	5.19	0.0460	
H-11 → L + 2	π(pzH) → d	226.3	5.48	0.0110	224.0(5.54)

Acknowledgements

The GAUSSIAN-03 calculations were carried out in the Wroclaw Centre for Networking and Supercomputing, WCSS, Wroclaw, Poland under calculational grant No. 51/96.

Crystallographic part was financed by funds allocated by the Ministry of Scientific Research and Information Technology to the Institute of General and Ecological Chemistry, Technical University of Łódź.

References

[1] R.H. Holm, Chem. Rev. 87 (1987) 1401.
[2] C.C. Romão, F.E. Kühn, W.A. Hermann, Chem. Rev. 97 (1997) 3197.
[3] W.A. Hermann, F.E. Kühn, Acc. Chem. Res. 30 (1997) 169.
[4] L.G. Marzilli, M. Iwamoto, E. Alessio, L. Hansen, M. Calligaris, J. Am. Chem. Soc. 116 (1994) 815.
[5] F.E. Hahn, L. Imhof, T. Lügger, Inorg. Chim. Acta 269 (1998) 347.
[6] S. Fortin, A.L. Beauchamp, Inorg. Chim. Acta 279 (1998) 159.
[7] E. Alessio, E. Zangrando, E. Iengo, M. Macchi, P.A. Marzilli, L.G. Marzilli, Inorg. Chem. 39 (2000) 294.
[8] S. Fortin, A.L. Beauchamp, Inorg. Chem. 39 (2000) 4886.
[9] H. Sugimoto, T. Takahira, T. Yoshimura, M. Shiro, M. Yamasaki, H. Miyake, K. Umakoshi, Y. Sasaki, Inorg. Chim. Acta 337 (2002) 203.
[10] A. Lazzaro, G. Vertuani, P. Bergamini, N. Mantovani, A. Marchi, L. Marvelli, Roberto Rossi, V. Berolasi, V. Ferretti, J. Chem. Soc., Dalton Trans. (2002) 2843.
[11] T.I.A. Gerber, E. Hosten, Z.R. Tshentu, P. Mayer, E. Pérex-Carreño, S. Garcia-Granda, J.G.H. du Preez, J. Coord. Chem. 56 (2003) 1063.
[12] G. Patsis, I. Pirmettis, Ch. Tsoukalas, M. Pelecanou, C.P. Raptopoulou, A. Terzis, M. Papadopoulos, E. Chiotellis, Inorg. Chim. Acta 342 (2003) 272.
[13] B. Machura, J.O. Dzięgielewski, R. Kruszynski, T.J. Bartczak, J. Kusz, Inorg. Chim. Acta 357 (2004) 1011.
[14] B. Machura, J.O. Dzięgielewski, S. Michalik, R. Kruszynski, T.J. Bartczak, J. Kusz, Transit. Mater. Chem. 28 (2003) 939.
[15] J.L. Lock, G. Turner, Can. J. Chem. 55 (1977) 333.
[16] A.R. Middleton, A.F. Masters, G. Wilkinson, J. Chem. Soc. Dalton (1979) 542.
[17] T.J. Bartczak, W. Czurak, J.O. Dzięgielewski, B. Machura, A. Jankowska, J. Kusz, J. Warczewski, J. Coord. Chem. 52 (2001) 361.
[18] G. Rouschias, G. Wilkinson, J. Chem. Soc. A (1966) 465.
[19] STOE, Cie, X-RED, Version 1.18, STOE & Cie, GmbH, Darmstadt, Germany, 1999.
[20] G.M. Sheldrick, Acta Cryst. A 46 (1990) 467.
[21] G.M. Sheldrick, SHELXL-97, Program for the Solution and Refinement of Crystal Structures, University of Göottingen, Germany, 1997.
[22] G.M. Sheldrick, SHELXTL: release 4.1 for Siemens Crystallographic Research Systems, 1990.
[23] M.J. Frisch, G.W. Trucks, H.B. Schlegel, G.E. Scuseria, M.A. Robb, J.R. Cheeseman, J.A. Montgomery Jr., T. Vreven, K.N. Kudin, J.C. Burant, J.M. Millam, S.S. Iyengar, J. Tomasi, V. Barone, B. Mennucci, M. Cossi, G. Scalmani, N. Rega, G.A. Petersson, H. Nakatsuji, M. Hada, M. Ehara, K. Toyota, R. Fukuda, J. Hasegawa, M. Ishida, T. Nakajima, Y. Honda, O. Kitao, H. Nakai, M. Klene, X. Li, J.E. Knox, H.P. Hratchian, J.B. Cross, C. Adamo, J. Jaramillo, R. Gomperts, R.E. Stratmann, O. Yazyev, A.J. Austin, R. Cammi, C. Pomelli, J.W. Ochterski, P.Y. Ayala, K. Morokuma, G.A. Voth, P. Salvador, J.J. Dannenberg, V.G. Zakrzewski, S. Dapprich, A.D. Daniels, M.C. Strain, O. Farkas, D.K. Malick, A.D. Rabuck, K. Raghavachari, J.B. Foresman, J.V. Ortiz, Q. Cui, A.G. Baboul, S. Clifford, J. Cioslowski, B.B. Stefanov, G. Liu, A. Liashenko, P. Piskorz, I. Komaromi, R.L. Martin, D.J. Fox, T. Keith, M.A. Al-Laham, C.Y. Peng, A. Nanayakkara, M. Challacombe, P.M.W. Gill, B. Johnson, W. Chen, M.W. Wong, C. Gonzalez, J.A. Pople, GAUSSIAN-03, Revision B.03, Gaussian, Inc., Pittsburgh, PA, 2003.

[24] A.D. Becke, J. Chem. Phys. 98 (1993) 5648.
[25] C. Lee, W. Yang, R.G. Parr, Phys. Rev. B 37 (1988) 785.
[26] M.E. Casida, in: J.M. Seminario (Ed.), Recent Developments and Applications in Modern Density Functional Theory, Theoretical and Computational Chemistry, vol. 4, Elsevier, Amsterdam, 1996.
[27] P.J. Hay, W.R. Wadt, J. Chem. Phys. 82 (1985) 299.
[28] E.D. Glendening, A.E. Reed, J.E. Carpenter, F. Weinhold, NBO, version 3.1.
[29] Y.-X. He, R.J. Batchelor, F.W.B. Einstein, D. Sutton, J. Organomet. Chem. 509 (1996) 37.
[30] C. Pearson, A.L. Beauchamp, Acta Crystallogr. C 50 (1994) 42.
[31] G.A. Jeffrey, W. Saenger, Hydrogen Bonding in Biological Structures, Springer Verlag, Berlin, 1994.
[32] G.R. Desiraju, T. Steiner, The Weak Hydrogen Bond in Structural Chemistry and Biology, Oxford University Press, Oxford, 1999.
[33] G. La Monica, S. Cenini, J. Chem. Soc., Dalton Trans. (1980) 1145.
[34] D.C. Bradley, M.B. Hursthouse, K.M.A. Malik, A.J. Nielson, R.L. Short, J. Chem. Soc., Dalton Trans. (1983) 2651.
[35] V.S. Sergienko, M.A. Porai-Koshits, V.E. Mistryukov, K.V. Kotegov, Koord. Khim. 8 (1982) 230.
[36] J.M. Mayer, D.L. Thorn, T.H. Tulip, J. Am. Chem. Soc. 107 (1985) 7454.
[37] K.V. Katti, L.Ch. Barnes, Inorg. Chem. 31 (1992) 4231.
[38] A.M. Lebius, A.L. Beauchamp, Can. J. Chem. 71 (1993) 441.
[39] D.M. Hoffman, D.A. Wierda, Polyhedron 8 (1989) 959.
[40] S.R. Flechter, A.C. Skapski, J. Chem. Soc., Dalton (1972) 1073.
[41] F.A. Cotton, W.R. Robinson, R.A. Walton, Inorg. Chem. 6 (1967) 223.
[42] N. Psaroudakis, K. Mertis, D.G. Liakos, E.D. Simandiras, Chem. Phys. Lett. 369 (2003) 490.
[43] A.E. Reed, L.A. Curtiss, F. Weinhold, Chem. Rev. 88 (1988) 899.
[44] M.L. Kuznestov, A.J.L. Pombeiro, J. Chem. Soc., Dalton Trans. (2003) 738.

technique of diazo coupling reaction to incorporate Ar–N=N–$^{+}$ into imidazole backbone and have synthesized 2-(arylazo)imidazole [23]. These molecules are π-deficient and can stabilize low metal redox state and exhibit MLCT transitions in their transition metal complexes. Heterocyclic ring size, number of heteroatoms, substituents in the ring and side arm to azo function can significantly modify the physical and chemical properties of the complexes [31,32]. The exobidentate behaviour of imidazole has been eliminated by alkylation to give 1-alkyl-2-(arylazo)imidazoles. The modification of pendant aryl group may be carried out by substituting with sterically more crowded, electronically more susceptible naphthyl group to get 2-(naphthylazo)imidazoles [25]. On considering the importance of ruthenium-bipyridine system we are interested, in the present work, in developing new hetero tris-complexes of the type $[Ru(bpy)_2(L)]^{2+}$ (L = 1-alkyl-2-(naphthylazo) imidazoles). Detail synthesis, spectroscopic characterization and structural studies are reported herewith.

2. Results and discussion

2.1. The complexes

1-Alkyl-2-(naphthyl-α/β-azo)imidazoles (α/β-NaiR) (**3**, **4**; R = Me (a), Et (b), CH_2Ph (c)) are used as ligands (Scheme 1). They are unsymmetric *N*,*N*′-chelating ligands and the donor centres are abbreviated as *N*(imidazole), *N* and *N*(azo), *N*′. The complexes are isolated as perchlorate salt, $[Ru(bpy)_2(\alpha/\beta\text{-NaiR})](ClO_4)_2$, (**5**, **6**) by nucleophilic substitution of chloride from *cis*-$Ru(bpy)_2Cl_2$ by α/β-NaiR via Ag^{+}-assisted route (Eq. (1)). The synthesis may also be carried out by reacting $Ag(\alpha/\beta\text{-NaiR})_2^{+}$ with *cis*-$Ru(bpy)_2Cl_2$ (Eq. (2)).

$$Ru(bpy)_2Cl_2 + \alpha/\beta\text{-NaiR} \xrightarrow[(2)\ NaClO_4]{(1)\ Ag^{+},\ MeOH,\ reflux} [Ru(bpy)_2(\alpha/\beta\text{-NaiR})](ClO_4)_2 + 2AgCl\downarrow \quad (1)$$

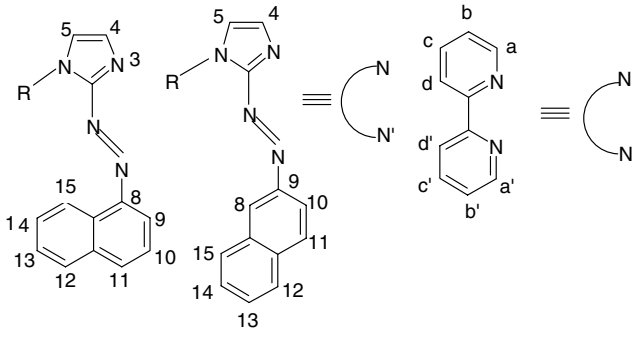

α-NaiH (**1**), α-NaiMe (**3a**), α-NaiEt (**3b**), α-NaiCH$_2$Ph (**3c**);
β-NaiH (**2**), β-NaiMe (**4a**), β-NaiEt (**4b**), β-NaiCH$_2$Ph (**4c**)

Scheme 1.

$$Ru(bpy)_2Cl_2 + [Ag(\alpha/\beta\text{-NaiR})_2]^{+} \xrightarrow[(2)\ NaClO_4]{(1)\ MeOH,\ reflux} [Ru(bpy)_2(\alpha/\beta\text{-NaiR})](ClO_4)_2 + \alpha/\beta\text{-NaiR} + 2AgCl\downarrow \quad (2)$$

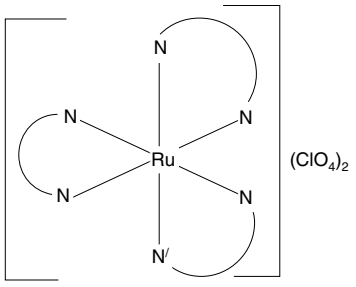

$[Ru(bpy)_2(\alpha\text{-NaiMe})](ClO_4)_2$ (**5a**), $[Ru(bpy)_2(\beta\text{-NaiMe})](ClO_4)_2$ (**6a**)
$[Ru(bpy)_2(\alpha\text{-NaiEt})](ClO_4)_2$ (**5b**), $[Ru(bpy)_2(\beta\text{-NaiEt})](ClO_4)_2$ (**6b**),
$[Ru(bpy)_2(\alpha\text{-NaiCH}_2Ph)](ClO_4)_2$ (**5c**) $[Ru(bpy)_2(\beta\text{-NaiCH}_2Ph)](ClO_4)_2$ (**6c**)

The reaction in Eq. (2) is mainly used for the synthesis of heteroleptic tris-chelates. The products were purified by chromatographic process. Tris-chelates may exist in different isomeric forms [33–35], but we have not been able to separate them by chromatography. The complexes are expectedly diamagnetic (d^6) and 1:2 electrolyte in MeCN. The composition of the compounds was formulated by elemental analyses (vide experimental section).

2.2. Spectral studies

The complexes show *ν*(N=N) and *ν*(C=N) at ca. 1360 and 1500 cm^{-1}, respectively. Very strong sharp stretching at ca. 1085 cm^{-1} is due to perchlorate (ClO_4) along with a weak band at 625 cm^{-1}.

The electronic spectra of NaiR were recorded in MeCN in the UV–VIS region (200–900 nm). Multiple transitions are observed in UV region those are referred to transitions in the coordinated ligand sites viz., bpy and NaiR. The transitions in the visible region are of typical metal-to-ligand charge transfer type (MLCT) in the range 410–480 nm with high molar extinction coefficients ($\varepsilon \sim 10^4$ dm^3 mol^{-1} cm^{-1}) (Table 1). A weak absorption is also observed ($\varepsilon \sim 10^3$ dm^3 mol^{-1} cm^{-1}) at ca. 625 nm. The spectra of the complexes are comparable to that of other $[Ru(bpy)_2(L)]^{2+}$ (L = bpy, aryl-(2-pyridylmethylene)amine [33]/2-(arylazo)pyridine [34], 1-alkyl-2-(arylazo)imidazole [35] (RaaiR′)). It is concluded that the absorption at 400–420 nm is attributed to dπ(Ru) → π*(bpy) and at 450–480 nm is assigned to dπ(Ru) → π*(NaiR) transition. The transition corresponding to 625 nm may be assigned to a state originated from mixing of singlet and triplet configuration in the excited state via spin orbit coupling in a low symmetry environment about the metal ion [36]. The MLCT transition appears at shorter wavelength in $[Ru(bpy)_2(NaiR)]^{2+}$ (λ_{max}, ca. 470 nm) compared to $[Ru(bpy)_2(RaaiR')]^{2+}$(λ_{max} ca. 500 nm). This implies that the

Table 1
UV–Vis spectral and cyclic voltammetric data of $[Ru(bpy)_2(NaiR)](ClO_4)_2$

Compound	UV–Vis spectral data[a] λ_{max}, nm ($10^{-4}\varepsilon$, $M^{-1}\,cm^{-1}$)	Cyclic voltammetric data[c] E, V (ΔE_p)			
		$E^{M}_{1/2}$	$-E^{L1}_{1/2}$	$-E^{L2}_{1/2}$	$-E^{L3}_{1/2}$
$[Ru(bpy)_2(\alpha\text{-NaiMe})](ClO_4)_2$ (**5a**)	266 (3.94), 303 (2.39)[b], 315 (2.52)[b], 398 (5.64), 455 (2.64), 630 (0.44)[b]	1.27 (120)	−0.68 (110)	−1.38 (120)	−1.75 (160)
$[Ru(bpy)_2(\alpha\text{-NaiEt})](ClO_4)_2$ (**5b**)	264 (2.75), 286 (2.17)[b], 376 (6.24), 392 (5.88), 448 (2.40), 625 (0.44)[b]	1.35 (130)	−0.68 (120)	−1.42 (140)	−1.75 (180)
$[Ru(bpy)_2(\alpha\text{-NaiCH}_2Ph)](ClO_4)_2$ (**5c**)	270 (3.48), 290 (3.15)[b], 380 (6.35), 395 (6.35), 450 (2.55), 628 (0.53)[b]	1.37 (120)	−0.62 (130)	−1.30 (140)	−1.67 (160)
$[Ru(bpy)_2(\beta\text{-NaiMe})](ClO_4)_2$ (**6a**)	241 (9.06), 280 (4.86)[b], 351 (2.31), 367 (2.63), 396 (5.70), 450 (2.02), 620 (0.420)[b]	1.24 (110)	−0.71 (130)	−1.42 (120)	−1.70 (160)
$[Ru(bpy)_2(\beta\text{-NaiEt})](ClO_4)_2$ (**6b**)	264 (2.46), 340 (3.97)[b], 376 (7.35), 392 (6.84), 450 (2.24), 626 (0.32)[b]	1.23 (110)	−0.70 (120)	−1.40 (130)	−1.75 (150)
$[Ru(bpy)_2(\beta\text{-NaiCH}_2Ph)](ClO_4)_2$ (**6c**)	260 (2.65), 348 (4.16)[b], 375 (7.55), 402 (6.45), 454 (2.40), 620 (0.28)[b]	1.26 (110)	−0.68 (120)	−1.35 (130)	−1.70 (150)

$E^{M}_{1/2} = E_{1/2}(Ru(III)/(II))$, $E^{L1}_{1/2} = E_{1/2}(azo/azo^{-})$, $E^{L2}_{1/2} = E_{1/2}(bpy/bpy^{-})$ (first chelator), $E^{L3}_{1/2} = E_{1/2}(bpy/bpy^{-})$ (second chelator).
$\Delta E_p = (E_{pc} - E_{pa})/2$, E_{pc} and E_{pa} are cathodic and anodic pick potentials.
[a] In MeCN.
[b] Shoulder.
[c] Solvent: MeCN, Platinum disk milli electrode, SCE reference, $[Bu_4N][ClO_4]$ supporting electrolyte, scan rate 50 mV s^{-1}.

LUMO which has been π*(azo) characterized is shifted to higher energy in present series of complexes than that of $[Ru(bpy)_2(RaaiR')]^{2+}$ analogue. Naphthyl group is more delocalised, polarisable, less π-acidic, sterically crowded than aryl group and may be responsible to make difference in energy and composition of MOs of the orbitals in $[Ru(bpy)_2(NaiR)]^{2+}$ and $[Ru(bpy)_2(RaaiR')]^{2+}$.

The ^1H NMR spectra were collected in CD_3CN. The proton numbering pattern is shown in the structures in Scheme 1 and the spectral data are given in Table 2. The NMR signals have been assigned by comparing with free ligand values and ruthenium-naphthylazoimidazoles [25]. The 1-Me in $[Ru(bpy)_2(NaiMe)](ClO_4)_2$ (**5a**, **6a**) signal appears at 4.1–4.2 ppm and is downfield shifted by ~0.2 ppm compared to free ligand values (free ligand δ(Me): 4.0 ppm) [25]. In $[Ru(bpy)_2(NaiCH_2CH_3)](ClO_4)_2$ (**5b**, **6b**) the 1-CH_2CH_3 show complex multiplet for $–CH_2–$ (ca. 4.5 ppm) and triplet for $–CH_3$ (1.50 ppm). The $[Ru(bpy)_2(NaiCH_2Ph)]^{2+}$ show quartet (AB type, Fig. 1(b)) for methylene protons, $–CH_2–(Ph)$, (H7a, H7b) at ca. 5.5 and 5.8 ppm ($J = 18.0$ Hz). The complexes do not possess neighbouring chiral centres but there exist a distorted coordination around the metal ion (vide supra, X-ray structure, Fig. 2). This overall distortion leads to the molecular dissymmetry [23,25]. The imidazolic 4- and 5-H protons appear at 7.4 and 7.3 ppm, respectively. The singlet nature of the proton signal may be due to rapid proton exchange with CH_3CN, which is generated by rapid hydrolysis of CD_3CN upon exposure to moisture in air. The naphthyl protons (8-H to 15-H) appear at upper field side and bpy protons (a-d –H and a′-d′-H) are observed at down field portion of the spectra.

2.3. Molecular structure of $[Ru(bpy)_2((\alpha\text{-NaiEt})](ClO_4)_2$ (**5b**)

View of the molecular unit $[Ru(bpy)_2((\alpha\text{-NaiEt})]^{2+}$ is shown in Fig. 2 and the bond parameters are given in Table 3. The distorted RuN_6 octahedron is generated by the coordination of two N-donor centres of chelated 1-ethyl-2-(naphthyl-α-azo)imidazole and four N-donor centres from two chelated bpy units. The three atomic groups Ru, N(1), C(5), C(6), N(2); Ru, N(3), C(15), C(16), N(4) and Ru, N(8), N(7), C(21), N(5) separately constitute three chelate planes (mean deviation <0.02 Å). The planes are mutually orthogonal (dihedral angle 86–90°). The chelate angles are N(1)–Ru(1)–N(8), 78.7(2); N(3)–Ru(1)–N(4) 78.0(2) and N(5)–Ru(1)–N(8), 76.3(2)°. The N–N distance is 1.287(6) Å and is slightly elongated than free azo bond length (1.266(3) Å [37]). The increase in bond length is undoubtedly due to coordination of N(azo) to ruthenium center which insists $d\pi(Ru) \rightarrow \pi^*(azo)$ charge transition. The average Ru–N(bpy) distance (av. 2.07 Å) is longer than Ru–N(imidazole) (2.036(6) Å) and Ru–N(azo) (1.987(5) Å) distances. The shortening of Ru–N(azo) distance than the Ru–N(imidazole)/Ru–N(bpy) is the indication of metal–ligand π-interaction that is localised in the

Table 2
^{1}H NMR spectra of the complexes in CD_3CN[a]

Compd	δ/ppm (J/Hz)											
	4-H[b]	5-H[b]	8-H[b]	9-H[c]	10-H[d]	11–14H[d]	15-H[c]	1-R	a,a′-H[c]	b,b′-H[e]	c,c′-H[e]	d,d′-H[c]
(**5a**)	7.42	7.32		8.00 (7.5)	7.65	7.65	7.88 (8.0)	4.12	8.98 (8.0)	7.85 (7.5)	7.85 (7.5)	8.00 (8.0)
(**5b**)	7.43	7.32		8.00 (7.5)	7.63	7.63	7.85 (8.0)	4.40, 4.55[d] 1.53 (8.0)[c]	9.00 (8.0)	7.90 (7.5)	7.90 (7.5)	8.05 (7.5)
(**5c**)	7.46	7.33		8.03 (7.5)	7.68	7.68	7.92 (8.0)	5.50, 5.75[d]	9.02 (8.5)	7.90 (7.5)	7.90 (7.5)	8.08 (7.5)
(**6a**)	7.40	7.32	8.20		8.10	7.70	7.95 (8.0)	4.20	8.98 (8.0)	7.85 (7.5)	7.85 (7.5)	8.00 (8.0)
(**6b**)	7.44	7.33	8.18		8.05	7.72	7.90 (8.0)	4.45, 4.58[d] 1.58 (8.0)	8.88 (8.0)	7.82 (7.5)	7.82 (7.5)	7.82 (8.0)
(**6c**)	7.46	7.34	8.24		8.10	7.75	8.00 (8.0)	5.45, 5.80[c]	8.98 (8.0)	7.85 (8.0)	7.85 (8.0)	8.00 (7.5)

[a] With Me_4Si as internal standard.
[b] Broad singlet.
[c] Doublet.
[d] Multiplet.
[e] Triplet.

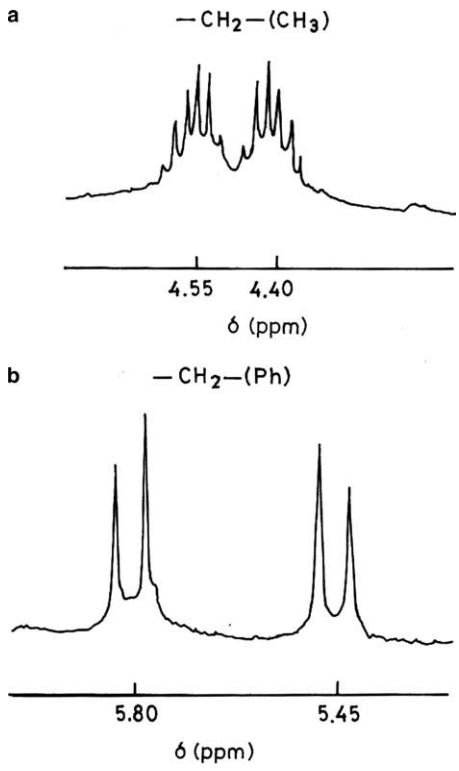

Fig. 1. ^{1}H NMR fragment of $–CH_2–$ of (a) $–CH_2–(CH_3)$ in $[Ru(bpy)_2(\alpha\text{-NaiEt})]^{2+}$ and (b) $–CH_2–(Ph)$ in $[Ru(bpy)_2(\alpha\text{-NaiCH}_2Ph)]^{2+}$ (in $CDCl_3$).

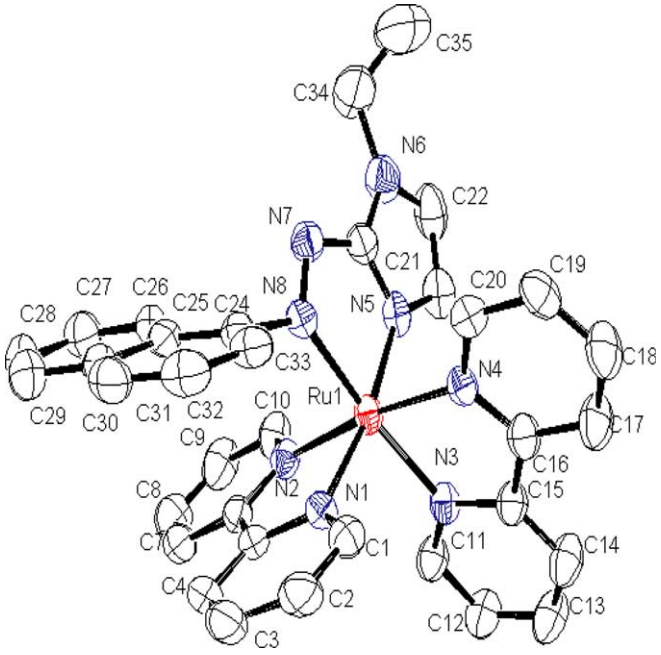

Fig. 2. ORTEP plot of $[Ru(bpy)_2(\alpha\text{-NaiEt})]^{2+}$ (30% probability ellipsoids).

M-azo fragment. The perchlorate ions hydrogen bond (C–H–O) to the ligands of the cation while at the same time forming O_3Cl–O–H–C (bpy) bonds resulting in the construction of an extended 3-D network structure (Table 4, Fig. 3). A hydrogen bonded dimer is described when naphthyl-C(26)-H–O–ClO_3 interaction is observed (Fig. 3). Each hydrogen bonded dimer then provide an opportunity to incorporate O_3Cl–O–π (Cg of N(4), C(16), C(17), C(18), C(19), C(20); 3.04 Å) interaction and forms a dimer-of-dimer.

2.4. Electrochemistry

The voltammograms display Ru(III)/Ru(II) couple at the positive side and the ligand reductions at the negative side to reference electrode, SCE. The results are given in

Table 3
Selected bond distances (Å) and angles (°) and their estimated standard deviations for $[Ru(bpy)_2(\alpha\text{-NaiEt})](ClO_4)_2$

Distances	
Ru(1)–N (1)	2.060(5)
Ru(1)–N (2)	2.066(5)
Ru(1)–N(3)	2.082(5)
Ru(1)–N (4)	2.058(5)
Ru(1)–N (5)	2.036(6)
Ru(1)–N (8)	1.987(5)
N(7)– N(8)	1.287(6)
Cl(1)–O(11)	1.439(11)
Cl(1)–O(21)	1.291(10)
Cl(1)–O(31)	1.193(5)
Cl(1)–O(41)	1.318(11)
Cl(2)–O(12)	1.412(7)
Cl(2)–O(22)	1.372(8)
Cl(2)–O(32)	1.260(9)
Cl(2)–O(42)	1.342(9)
Angles	
N(1)–Ru(1)–N(2)	78.7(2)
N(1)–Ru(1)–N(3)	89.9(2)
N(1)–Ru(1)–N(4)	97.1(2)
N(1)–Ru–N(5)	170.0(2)
N(1)–Ru(1)–N(8)	94.1(2)
N(2)–Ru(1)–N(3)	95.2(2)
N(2)–Ru(1)–N(4)	172.1(2)
N(2)–Ru(1)–N(5)	98.0(2)
N(2)–Ru(1)–N(8)	89.57(19)
N(3)–Ru(1)–N(4)	78.0(2)
N(3)–Ru(1)–N(5)	98.8(2)
N(3)–Ru(1)–N(8)	174.2(2)
N(4)–Ru(1)–N(5)	87.18(19)
N(5)–Ru(1)–N(8)	76.3(2)
O(31)–Cl(1)–O(21)	114.7(12)
O(31)–Cl(1)–O(41)	112.4(9)
O(21)–Cl(1)–O(41)	97.1(9)
O(31)–Cl(1)–O(11)	113.0(5)
O(21)–Cl(1)–O(11)	102.2(7)
O(41)–Cl(1)–O(11)	116.0(8)

Table 4
Hydrogen bonding interactions

D–H–A	D–H (Å)	H–A (Å)	D–A (Å)	∠D–H–A (°)
C(12)–H(12)–O(22)[a]	0.93	2.56	3.320(11)	139.0
C(17)–H(17)–O(21)[b]	0.93	2.39	3.251(15)	155.0
C(22)–H(22)–O(42)[b]	0.93	2.51	3.403(15)	162.0
C(26)–H(26)–O(12)[c]	0.93	2.44	3.300(11)	153.0
C(11)–H(11)–Cg(1)[d,e]	0.93	2.65(8)	3.283(8)	100.0
C(1)–H(1)–Cg(2)[d,f]	0.93	2.66(5)	3.206(8)	104.0
C(20)–H(20)–Cg(3)[d,g]	0.93	2.62(5)	3.082(7)	102.0

Symmetry – a: x, $1-y$, $1/2+z$; b: x, $1+y$, z; c: $1/2-x$, $1/2+y$, $1/2-z$; d: x, y, z; e Cg(1): Ru(1)–N(1)–C(5)–C(6)–N(2); f: Cg(2): Ru(1)–N(3)–C(15)–C(16)–N(4); g: Cg(3): Ru(1)–N(5)–C(23)–N(7)–N(8).

Table 1, and a representative voltammogram is shown in Fig. 4.

In the potential range 0.0–1.8 V at the scan rate 50 mV s^{-1} in MeCN a reversible to quasireversible (peak to-peak separation $\Delta E = 70$–120 mV) oxidative response is observed corresponding to the redox reaction (Eq. (3)).

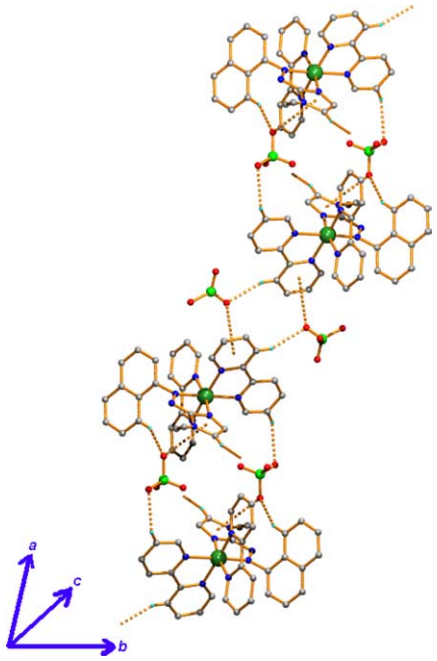

Fig. 3. Hydrogen bonded dimer-of-dimer generated by Cl–O–π interactions.

$$[Ru(bpy)_2(NaiR)]^{3+} + e \rightleftharpoons [Ru(bpy)_2(NaiR)]^{2+} \quad (3)$$

$$[Ru(bpy)_2(NaiR)]^{2+} + e \rightleftharpoons [Ru(bpy)_2(NaiR^-)]^{2+} \quad (4)$$

$$[Ru(bpy)_2(NaiR)]^{2+} + e \rightleftharpoons [Ru(bpy)(bpy^-)(NaiR^-)]^{2+} \quad (5)$$

$$[Ru(bpy)(bpy^-)(NaiR^-)]^{2+} + e \rightleftharpoons [Ru(bpy^-)(bpy^-)(NaiR^-)]^{2+} \quad (6)$$

Voltammetric profile pattern remains unchanged with in scan range 50–500 mV s^{-1}. The i_{pa}/i_{pc} ratio (i_{pa} = anodic peak current and i_{pc} = cathodic peak current) is close to 1.0, as expected for reversible couples. The Ru(III)/Ru(II) redox potential ($E^M_{1/2} = 1.2$ V, Table 1) is expectedly higher than that of $Ru(NaiR)_2Cl_2$ (0.5–0.6 V vs. SCE [25]) which

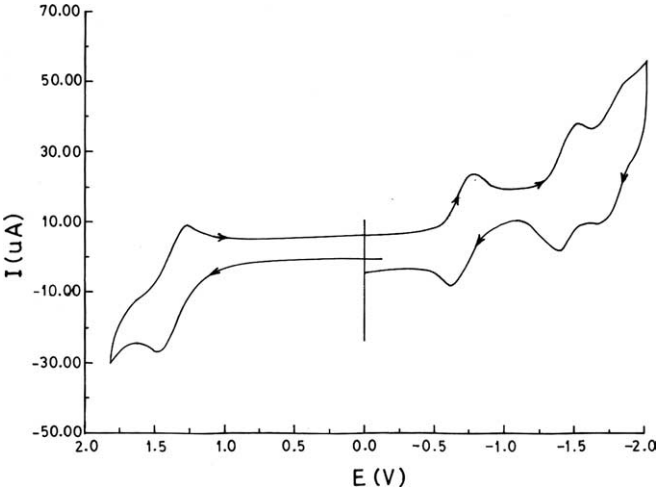

Fig. 4. Cyclic voltammogram of $[Ru(bpy)_2(\alpha\text{-NaiEt})](ClO_4)_2$ in MeCN.

are due to higher π-acidity of azoimine or diimine groups than chlorides. Some Ru(III)/Ru(II) formal potential data in tris-chelates $[Ru(bpy)_2(L)]^{2+}$ for L = *N*,*N*-bidentate neutral donor are as follows: $Ru(bpy)_3{}^{2+}$ in CH_2Cl_2 1.29 V [38]; $[Ru(bpy)_2$(2-(arylazo)pyridine)$]^{2+}$in MeCN 1.60 V [34]; $[Ru(bpy)_2$(1-alkyl-2-(arylazo)imidazole)$]^{2+}$ in MeCN 1.4 V [35]; $[Ru(bpy)_2$(*N*-phenylthiosalicylaldimine)$]^{+}$ in MeCN, 0.3 V [10]. The relative values of the potential suggest that the π-acidity order is *N*-phenylthiosalicylaldimine < bipyridine < naphthylazomidazole < arylazoimidazoles < arylazopyridines. On comparing Ru(III)/Ru(II) couple of $[Ru(bpy)_2$(1-alkyl-2-(arylazo)imidazole)$]^{2+}$ with present group of complexes it is concluded that the metal dominated redox orbital (HOMO) is less stable in present case and Ru(III)/Ru(II) couple appears at lower potential data (lowering by ~0.2 V).

In the potential range 0.0 to −2.0 V three successive reductive responses are observed under similar conditions. The interpretation of CV data may be carried out on comparison with the redox properties of *cis*-$Ru(bpy)_2Cl_2$[38], $[Ru(bpy)_2(L)]^{2+}$ (L = 2-(arylazo)pyridines [34], aryl-(2-pyridylmethylene)amine [33], 1-alkyl-2-(arylazo)imidazle [35]), and $Ru(NaiR)_2Cl_2$ [25]. These are assigned to reductions of the coordinated ligands. Redox data in Table 1 reveal that the first reduction potential of the coordinated ligand occurs at a much less negative potential than that of other two responses. The first reduction may be expected to involve the ligand having the most stable lowest unoccupied molecular orbital (LUMO) [11,23–26], which is dominated by azo function of naphthylazoimidazole than bpy (Eq. (4)). The potential of (–N=N–)/(–N=N–)$^-$ is less negative by ~0.1 V than that of data reported for $Ru(NaiR)_2Cl_2$ [25]. This may be due to coligand effect of π-acidic bpy groups. However, the (–N=N–)/(–N=N–)$^-$ couple appears at more negative value by ~0.1 V in present compounds than that of $[Ru(bpy)_2$(1-alkyl-2-(arylazo)imidazle$]^{2+}$ [35]. The presence of electron rich naphthyl group (in NaiR) may shift ligand dominated orbitals (LUMOs) to higher energy side than aryl group in RaaiR′. In the potential range −1.4 to −1.8 V two reductive responses are observed. These are referred to the reductions of bpy in $Ru(bpy)_2$–motif (Eqs. (5) and (6)). The one-electron nature of these processes was assigned from the comparison of current height with couple (3).

3. Experimental

3.1. Materials

$RuCl_3 \cdot nH_2O$ was obtained from Arrora Matthey, Calcutta and was digested thrice with concentrated HCl before use. 1-Alkyl-2-(naphthylazo)imidazoles (NaiR) and $[Ag(NaiR)_2](ClO_4)$ were synthesized as before [39]. *cis*-$Ru(bpy)_2Cl_2$ was prepared by published procedure [38]. All other chemicals and solvents used for the preparative work were of reagent grade and were used as received.

3.2. Physical measurements

Microanalytical data (C, H, N) were collected using a Perkin–Elmer 2400 CHN elemental analyser. Solution electronic spectra were recorded on a JASCO UV–VIS–NIR V-570 spectrophotometer. Infrared (IR) spectra were obtained using a JASCO 420 spectrophotometer (using KBr disks, 4000–200 cm^{-1}). The ^1H NMR spectra in CD_3CN were obtained on a Bruker 300 MHz FT NMR spectrometer using $SiMe_4$ as internal reference. Solution electrical conductivities were measured using Systronics 304 conductivity meter with solute concentration ~10^{-3} M in acetonitrile. Electrochemical work was carried out using EG & G PARC Versastat computer controlled 250 electrochemical system. All experiments were performed under a dry N_2 atmosphere at 298 K using a Pt-disk milli working electrode in the potential range +1.8 to −2.0 V. All results were referenced to a saturated calomel electrode (SCE). Reported potentials are uncorrected for junction effect.

3.3. Preparation of complexes

3.3.1. Bis(2,2′-bipyridine)[1-methyl-2-(naphthyl-α-azo)imidazole]ruthenium(II) perchlorate [Ru(bpy)$_2$(α-NaiMe)](ClO$_4$)$_2$ (**5a**)

To a suspension of $Ru(bpy)_2Cl_2$ (50 mg, 0.103 mmol) in acetone (15 ml) was added aqueous solution of $AgNO_3$ (2 mmol) and was refluxed for 15 min, AgCl so precipitated was filtered off by G-4 crucible. The acetone solution (10 ml) of α-NaiMe (25 mg, 0.106 mmol) was then added and the resulting mixture was heated to reflux for 1 h under nitrogen atmosphere. The solution volume was then evaporated to half of its original volume by N_2 bubbling and an aqueous solution of $NaClO_4$ (ca. 0.5 g in 10 ml water) was added. The reddish brown precipitate thus obtained was filtered and dried in vacuo over P_4O_{10}. The dry mass was then dissolved in minimum vol. of CH_2Cl_2 and was subjected to column chromatography on a silica gel column (60–120 mesh). A reddish brown band was eluted with C_6H_6-MeCN (3:2, v/v). It was collected and evaporated. Crystals were collected layering a solution of the complex in CH_2Cl_2 with hexane. Yield, 52 mg, 61%.

3.3.2. Reaction of Ru(bpy)$_2$Cl$_2$ with [Ag(NaiMe)$_2$](ClO$_4$)

General procedure for synthesis of $[Ru(bpy)_2$((α-*NaiMe*)$](ClO_4)_2$ is given below. To a methanolic suspension of $Ru(bpy)_2Cl_2$, (50 mg, 0.103 mmol in 10 ml MeOH) $[Ag(NaiMe)_2](ClO_4)$ (140 mg, 0,206 mmol in 25 ml in acetone) was added and refluxed for 1h under nitrogen atmosphere. Solution was filtered through a G-4 sintered glass funnel. Insoluble AgCl was filtered, the solution was evaporated to dryness and washed thoroughly with cold water (20 ml × 4). The dried mass was dissolved in methanol and an aqueous solution of $NaClO_4$ (ca. 1 g in 15 ml) was added. The reddish brown product was filtered and purified as before. Yield: 64 mg, 75%.

All other complexes were prepared similarly (yield: 70–80%).

Microanalytical data of the complexes are as follows: $[Ru(bpy)_2(\alpha\text{-NaiMe})](ClO_4)_2$, (**5a**): *Anal.* Calc. for $C_{34}H_{28}N_8O_8Cl_2Ru$: C, 48.11; H, 3.30; N, 13.21. Found: C, 48.03; H, 3.25; N, 13.26%. $[Ru(bpy)_2(\alpha\text{-NaiEt})](ClO_4)_2$, (**5b**) *Anal.* Calc. for $C_{35}H_{30}N_8O_8Cl_2Ru$: C, 48.72; H, 3.48; N, 12.99. Found: C, 48.78; H, 3.45; N, 13.06. $[Ru(bpy)_2(\alpha\text{-NaiCH}_2Ph)](ClO_4)_2$ (**5c**): *Anal.* Calc. for $C_{40}H_{32}N_8O_8Cl_2Ru$: C, 51.95; H, 3.46; N, 12.12. Found: C, 52.00; H, 3.50; N, 12.07%. $[Ru(bpy)_2(\beta\text{-NaiMe})](ClO_4)_2$, (**6a**): *Anal.* Calc. for $C_{34}H_{28}N_8O_8Cl_2Ru$: C, 48.11; H, 3.30; N, 13.21. Found: C, 48.15; H, 3.26; N, 13.27%. $[Ru(bpy)_2(\beta\text{-NaiEt})](ClO_4)_2$, (**6b**) *Anal.* Calc. for $C_{35}H_{30}N_8O_8Cl_2Ru$: C, 48.72; H, 3.48; N, 12.99. Found: C, 48.70; H, 3.53; N, 13.03%. $[Ru(bpy)_2(\beta\text{-NaiCH}_2Ph)](ClO_4)_2$ (**6c**): *Anal.* Calc. for $C_{40}H_{32}N_8O_8Cl_2Ru$: C, 51.95; H, 3.46; N, 12.12. Found: C, 52.02; H, 3.50; N, 12.18%.

Caution! Perchlorate salts of metal complexes are generally explosive. Care should be taken in handling the samples.

3.4. X-ray crystallography

Crystal suitable for X-ray work was grown by slow diffusion of hexane–benzene (1:1, v/v) into dichloromethane solution of $[Ru(bpy)_2(\alpha\text{-NaiEt})](ClO_4)_2$ (**5b**). Crystal size was $0.3 \times 0.2 \times 0.15$ mm^3. Data were collected on a Bruker SMART 1K CCD diffractometer with graphite monochromatized Mo Kα radiation ($\lambda = 0.71073$ Å) at 293(2) K. Crystal data and collection parameter are listed in Table 5. The data were corrected for absorption effects by empirical method using XPREP [40]. Systematic absences led to the identification of space group $C2/c$ in the range of 2θ of 2.16–56.6°. Of the 22,592 collected reflections 8607 were independent (3815 reflections $I > 2(I)$). The structure was solved by conventional heavy-atom method and refined by full-matrix least-squares refinements on F^2 using SHELXL-97 [41] with anisotropic displacement parameters for all non-hydrogen atoms. Hydrogen atoms were included in calculated positions with isotropic thermal parameters 1.2 times the equivalent isotopic thermal parameters of their parent carbon atoms. All calculations were carried out using SHELXS-97 [41], PLATON [42], ORTEP-32 [43].

Table 5
Crystallographic data of **5b**

Chemical formula	$C_{35}H_{30}Cl_2N_8O_8Ru$
Formula weight	862.64
T (K)	293 (2)
Crystal system	monoclinic
Space group	$C2/c$
μ (mm^{-1})	0.613
a (Å)	37.714 (5)
b (Å)	14.390(2)
c (Å)	14.0322(19)
β (°)	91.807(3)
Unit cell volume (Å^3)	7611.6(18)
Z	8
μ (cm^{-1})	6.13
ρ_{calc} (gm cm^{-3})	1.506
Measured reflections	22592
Independent reflection (R_{int})	8607 (0.0790)
R^a ($I > 2(I)$)	0.0743
wR^b	0.1770
Goodness-of-fit[c]	1.005

[a] $R = \sum|F_o - F_c|/\sum F_o$.
[b] $wR = [\sum w(F_o^2 - F_c^2)/\sum wF_o^4]^{1/2}$; $w = 1/[\sigma^2(F_o^2) + (0.0928P)^2]$, $P = (F_o^2 + 2F_c^2)/3$.
[c] GOF (Goodness-of-fit) is defined as $[w(F_o - F_c)/(n_0 - n_v)]^{1/2}$ where n_0 and n_v denote the numbers of data and variables, respectively.

4. Conclusion

In this work we have synthesised mixed tris-chelates of type $[Ru(bpy)_2(\alpha\text{-/}\beta\text{-NaiR})](ClO_4)_2$. Ligands, α-/β-NaiR (1-alkyl-(naphthyl-α-/β-azo)imidazole) belong to azoimine chelating group, –N=N–C=N–. The complexes show strong MLCT transition in the visible region. They have been characterised by spectroscopic data and in one case by single-crystal X-ray diffraction study. Cyclic voltammetry shows metal centred oxidation and ligand centred reductions.

5. Supplementary material

Crystallographic data for the structures have been deposited with the Cambridge Crystallographic data center, CCDC No. 274227. Copies of this information may be obtained free of charge from the Director, CCDC, 12 Union Road, Cambridge CB2 1EZ, UK (e-mail: deposit@ccdc.cam.ac.uk or http://www.ccdc.cam.ac.uk).

Acknowledgements

Financial support from the Council of Scientific and Industrial Research, New Delhi are gratefully acknowledged. We are also thankful to Dr. G. Mostafa, Department of Physics, Jadavpur University for his help and to National Science Council of Taiwan for financial support.

References

[1] P. Tomarik, Z. Ratajewicz, The Chemistry of Heterocyclic Compounds: part 6, Pyridine Metal Complexes, vol. 14, Wiley, New York, 1985.
[2] S. Campagna, S. Serroni, F. Puloriero, C. Di Pietro, in: V. Balzani (Ed.), Electron Transfer in Chemistry, vol. 5, VCH-Wiley, Weinheim, 2001.
[3] K. Kalyansudaram, Photochemistry of Polypyridine and Porphyrine Complexes, Academic Press, London, 1992.
[4] C. Kaes, A. Katz, M.W. Hosseini, Chem. Rev. 100 (2000) 3553.
[5] K. Pramanik, M. Shivakumar, P. Ghosh, A. Chakravorty, Inorg. Chem. 39 (2000) 195.
[6] M. Shivakumar, K. Pramanik, I. Bhattacharya, A. Chakravorty, Inorg. Chem. 39 (2000) 4332.
[7] B. Mondal, H. Paul, V.G. Puranik, G.K. Lahiri, J. Chem. Soc., Dalton Trans. (2001) 481.

[8] A.K. Deb, S. Goswami, Polyhedron 12 (1993) 1419.
[9] S. Goswami, A.R. Chakravorty, A. Chakravorty, J. Chem. Soc., Chem. Commun. (1982) 1288.
[10] D. Bhattacharyya, S. Chakraborty, P. Punshi, G.K. Lahiri, Polyhedron 18 (1999) 2951.
[11] B.K. Ghosh, A. Chakravorty, Coord. Chem. Rev. 95 (1989) 239.
[12] N. Bag, A. Pramanik, G.K. Lahiri, A. Chakravorty, Inorg. Chem. 31 (1992) 40, and references therein.
[13] H. Velders, H. Keojiman, A.L. Spek, J.G. Haasnoot, D. de Vos, J. Reedijk, Inorg. Chem. 39 (2000) 2966.
[14] A. Saha, P. Majumdar, S.-M. Peng, S. Goswami, Eur. J. Inorg. Chem. (2000) 2631, and references therein.
[15] J. Fees, H.D. Hausen, W. Kaim, Z. Naturoforsch B 50 (1995) 15.
[16] B.K. Santra, G.K. Lahiri, Proc. Indian Acad. Sci (Chem. Sci.). 11 (1999) 509, and references therein.
[17] T. Akasaka, J. Otsuki, K. Araki, Chem. Eur. J. (2002) 130.
[18] M.D. Ward, J.A. McCleverty, J. Chem. Soc., Dalton Trans. (2002) 275.
[19] H. Hartmann, T. Scheiring, J. Fiedler, W. Kaim, J. Organomet. Chem. 604 (2000) 267.
[20] W.Y. Wong, S.-H. Cheung, S.-M. Lee, S.Y. Leung, J. Organomet. Chem. 596 (2000) 36.
[21] P.K. Santra, P. Byabartta, S. Chattopadhyay, L.R. Falvello, C. Sinha, Eur. J. Inorg. Chem. (2002) 1124.
[22] P.K. Santra, D. Das, T.K. Misra, R. Ray, C. Sinha, S.-M. Peng, Polyhedron 18 (1999) 1909.
[23] T.K. Misra, D. Das, C. Sinha, P.K. Ghosh, C.K. Pal, Inorg. Chem. 37 (1998) 1672.
[24] P. Byabartta, Sk. Jasimuddin, B.K. Ghosh, C. Sinha, A.M.Z. Slawin, J.D. Woollins, New J. Chem. 26 (2002) 1415.
[25] P. Byabartta, P.K. Santra, T.K. Misra, C. Sinha, C.H.L. Kennard, Polyhedron 20 (2001) 905.
[26] P. Byabartta, S. Pal, T.K. Misra, C. Sinha, F.-L. Liao, K. Panneerselvam, T.-H. Lu, J. Coord. Chem. 479 (2002) 479, and reference therein.
[27] H. Nishihara, Coord. Chem. Rev. 249 (2005) 1468.
[28] W. Kaim, B. Schwederski, Bioinorganic Chemistry: Inorganic Elements in the Chemistry of Life, Wiley, New York, 1994.
[29] S.J. Lippard, in: I. Bertini, H.B. Gray, S.J. Lippard, J.C. Valentine (Eds.), Bioinorganic Chemistry, University Science Books, Mill Valley, 1994, p. 505.
[30] J.M. Dominguez-Vera, A. Rodriguez, R. Cuesta, R. Kivekas, E. Colacio, J. Chem. Soc., Dalton Trans. (2002) 561.
[31] E.C. Constable, Coord. Chem. Rev. 93 (1989) 205.
[32] T. Yamamoto, Z. Zhou, T. Kanbara, M. Shimura, K. Kizu, T. Kanbara, M. Shimura, K. Kizu, T. Maruyama, T. Takamura, T. Fukuida, B. Lee, N. Ooba, S. Tomaru, T. Kurihera, T. Kaino, K. Kubota, S. Sasaki, J. Am. Chem. Soc. 118 (1996) 1038.
[33] S. Choudhury, A.K. Deb, S. Goswami, J. Chem. Soc., Dalton Trans. (1994) 1305.
[34] S. Goswami, A.R. Chakravarty, A. Chakravorty, Inorg. Chem. 20 (1981) 2246.
[35] S. Pal, T.K. Misra, C. Sinha, A.M.Z. slawin, J.D. Woollins, Polyhedron 19 (2000) 1925.
[36] E. Casalbani, Q.G. Mullazzani, C.D. Clark, M.Z. Hoffmann, P.L. Orizondo, M.W. Perkovic, D.P. Rilemma, Inorg. Chem. 36 (1997) 2252.
[37] J. Dinda, K. Bag, C. Sinha, G. Mostafa, T.-H. Lu, Polyhedron 22 (2003) 1367.
[38] E.C. Johnson, B.P. Sulivan, D.J. salmon, S.A. Adeyemi, T.J. Meyer, Inorg. Chem. 17 (1978) 2211.
[39] J. Dinda, Sk. Jasimuddin, G. Mostafa, C.H. Hung, C. Sinha, Polyhedron 23 (2004) 793.
[40] G.M. Sheldrick, SHELXL-Plus, Bruker, Analytical X-Ray Instruments Inc., Madison, Wisconsin, USA, 1997.
[41] G.M. Sheldrick, SHELXL-97, Program for Crystal Structure Refinement, University of Gottingen, Germany, 1998.
[42] A.L. Spek, J. Appl. Crystallogr. 36 (2003) 7.
[43] L.J. Farrugia, J. Appl. Crystallogr. 30 (1997) 565.

strikingly different reactivity behaviors towards triarylphosphines [5]. In order to further examination of the effect of *tert*-butyl groups on the structural properties and redox reactivity of the Cu(II) salicylaldiminates we have carried out the synthesis of bis(N-3,5-Bu$^t_2$-phenyl-R-sal)copper(II) complexes, where R = H, OH, OCH_3, *t*-Bu, and their spectroscopic, structural and redox reactivity properties were studied.

In the present work, the preparation, spectroscopy, electrochemical and chemical redox properties of bis(N-3,5-Bu$^t_2$phenyl-R-sal)copper(II) complexes, (**X**), derived from 3,5-Bu$^t_2$aniline and salicylaldehyde derivatives, i.e.: bis(N-3,5-Bu$^t_2$phenyl-sal)copper(II) (**1**), bis(N-3,5-Bu$^t_2$phenyl-3-methoxy-sal)-copper(II) (**2**), bis(N-3,5-Bu$^t_2$phenyl-4-methoxy-sal)copper(II) (**3**), bis(N-3,5-Bu$^t_2$phenyl-3-hydroxy-sal)copper(II) (**4**), bis(N-3,5-Bu$^t_2$phenyl-4-hydroxy-sal)copper(II) (**5**), bis(N-3,5-Bu$^t_2$phenyl-3,5-Bu$^t_2$-sal)copper(II) (**6**) and crystal structural analysis of **1** are reported.

2. Experimental

2.1. Chemicals

All solvents, $Cu(ac)_2 \cdot H_2O$, $(NH_4)_2Ce(NO_3)_6$, n-Bu_4NClO_4, PPh_3, 3,5-di-*tert*-butylaniline, salicylaldehyde and its 3-HO, 4-HO, 3-OCH_3, 4-OCH_3 derivatives were purchased from Aldrich Chemical Co. and were used without further purification. 3,5-di-*tert*-butylsalicylaldehyde was prepared according to the procedure described by Jacobsen and his co-workers [3d].

2.2. Ligands

N-3,5-di-*tert*-butylphenyl-R-sal (**L$_x$H**) were prepared in good yields by the condensation of 3,5-di-*tert*-butylaniline and appropriate salicylaldehydes in refluxing methanol. The yellow imines were recrystallized from methanol. Yields of the **L$_x$H** are in the range 75–88%. Compound **L$_1$H**: yield % 78; m.p. 114 °C; selected IR (cm^{-1}, KBr): 1618 (CH=N), 2902–2964 (C–H, Bu^t); ^{1}H NMR (200 MHz, $CDCl_3$): δ 13.47 (s, 1H, O*H*), 8.64 (s, 1H, C*H*=N), 7.44–7.34 (m, 3H, Ar*H*), 7.13–6.91 (m, 4H Ar*H*), 1.37 (s, 18 H, *t*-Bu); ^{13}C NMR (50 MHz, $CDCl_3$): δ 162.1 (*C*H=N), 152.2, 132.9, 132.2, 121.1, 118.9, 117.3, 115.4, 35.1, 31.5; UV/Vis (EtOH): λ ($\log\varepsilon$ 1 cm^{-1} M^{-1}): 210(sh), 230(4.40), 268(4.25), 341(4.26), 438(2.36) nm; *Anal.* Calc. for $C_{21}H_{27}NO$: C, 77.50; H, 8.36; N, 4.30. Found: C, 7.71; H, 8.24; N, 4.48%. Compound **L$_2$H**: yield % 82; m.p. 144 °C; selected IR (cm^{-1}, KBr): 1624 (CH=N), 2902–2960 (C–H, Bu^t); UV/Vis (EtOH): λ ($\log\varepsilon$ cm^{-1} M^{-1}): 214(3.95), 239(4.56), 290*, 341(4.51), 416(3.88)1620. *Anal.* Calc. for $C_{22}H_{29}NO_2$: C, 77.84; H, 8.61; N, 4.12. Found: C, 77.68; H, 8.37; N, 4.23%. Compound **L$_3$H:** Yield % 85; m.p. 102 °C; Selected IR (cm^{-1}, KBr): 1626 (CH=N), 3452, 2902–2964 (C–H, Bu^t); ^{1}H NMR (200 MHz, $CDCl_3$): δ 14.04 (s, O*H*), 8.5 (s, 1H, C*H*=N), 7.39 (s, 1H, Ar*H*), 7.06–6.95 (m, 4H, Ar*H*), 6.82 (d, J = 8.0 Hz., 1H Ar*H*), 1.37 (s, 18H, *t*-Bu); ^{13}C NMR (50 MHz, $CDCl_3$): δ 161.3 (*C*H=N), 152.4, 146.3, 145.5, 122.8, 121.4, 118.5, 117.2, 115.2, 35.1, 31.5; UV/Vis (EtOH): λ ($\log\varepsilon$, cm^{-1} M^{-1}) = 222(4.45), 280(4.22), 318(4.19), 461(2.60) nm 1 cm^{-1} M^{-1}; *Anal.* Calc. for $C_{22}H_{29}NO_2$: C, 77.84; H, 8.61; N, 4.12. Found: C, 78.58; H, 9.09; N, 4.26%. Compound **L$_4$H**: Yield % 75; m.p. 163 °C; Selected IR (cm^{-1}, KBr): 1620 (CH=N), 3452 (OH), 2902–2964 (C–H, Bu^t); ^{1}H NMR (200 MHz, $CDCl_3$): δ 13,46 (s, 1H), 8.6 (s, 1H, C*H*=N), 7.39 (s, 1H, Ar*H*), 7.06–6.95 (m, 4H, Ar*H*), 6.82 (d, J = 8.0 Hz., 1H, Ar*H*), 1.37 (s, 18 H, *t*-Bu); ^{13}C NMR (50 MHz, $CDCl_3$): δ 161.3 (*C*H=N), 152.4, 146.3, 145.5, 122.8, 121.4, 118.5, 117.2, 115.2, 35.1, 31.5; UV/Vis (EtOH): λ ($\log\varepsilon$, 1 cm^{-1} M^{-1}) = 222(4.45), 280(4.22), 318(4.19), 461(2.60) nm cm^{-1} M^{-1}; *Anal.* Calc. for $C_{21}H_{27}NO_2$: C, 77.50; H, 8.36; N, 4.30. Found: C, 78.12; H, 8.43; N, 4.37%. Compound **L$_5$H**: yield % 81; m.p. 192 °C; Selected IR (cm^{-1}, KBr): 1622(CH=N), 3259 (bs, OH), 2902–2964 (C–H, Bu^t); ^{1}H NMR (200 MHz, $CDCl_3$): δ 13,75 (s, 1H), 8.4 (s, 1H, C*H*=N), 7.35 (t, 1H, Ar), 7.19 (d, J = 8.8 Hz, 1H Ar), 7.1 (d, J = 1.6 Hz, 3H, Ar), 6.9 (bs, 1H, Ar), 6.5 (s, 1H, OH), 6.4 (d, J = 8.4 Hz, 2H, CH)); ^{13}C NMR (50 MHz, $CDCl_3$): δ 159.1 (*C*H=N), 152.9, 134.8, 120.9, 114.6, 113.9, 110.3, 108.6, 104.1, 31.9 (d, J = 1.2 Hz, *C*-Bu^t); UV/Vis (EtOH): λ ($\log\varepsilon$ cm^{-1} M^{-1}): 214(3.95), 239(4.56), 290(sh), 341(4.51), 416(3.88); *Anal.* Calc. for $C_{22}H_{29}NO_2$: C, 77.50; H, 8.36; N, 4.30. Found: C, 77.68; H, 8.17; N, 4.43%. Compound **L$_6$H**: yield % 85; m.p. 119 °C; Selected IR (cm^{-1}, KBr): 1619 (CH=N), 2902–2964 (C–H, Bu^t); ^{1}H NMR (200 MHz, $CDCl_3$): δ 13.97 (s, 1H, O*H*), 8.60 (d, J = 6.0 Hz, 1H, C*H*=N), 7.49–7.15 (m, 4H, Ar*H*), 1.54–1.37 (m, 36 H, *t*-Bu); ^{13}C NMR (50 MHz, $CDCl_3$): δ 163.2 (*C*H=N), 158.3, 152.1, 148.2, 140.5, 136.9, 127.8, 126.7, 120.8, 118.5, 115.5, 35.1, 34.2, 31.6, 29.5; UV/Vis (EtOH): λ ($\log\varepsilon$ 1 cm^{-1} M^{-1}): 210(sh), 230(4.40), 268(4.25), 341(4.26), 438(2.36) nm; *Anal.* Calc. for $C_{29}H_{43}NO$: C, 82.61; H, 10.28; N, 3.32. Found: C, 82.42; H, 9.87; N, 3.42%.

2.3. Complexes

The complexes **X** were prepared by refluxing methanolic solutions of $Cu(ac)_2 \cdot H_2O$ (0.25 mmol) and **L$_x$H** (0.5 mmol) in a 1:2 molar ratio for 1.0–1.5 h. The volume of the resulting solution was reduced to one half and left at room temperature without stirring. The precipitate microcrystals were collected by filtration, washed with a small amount of cold methanol and dried on air (yields 68–85%). Recrystallization of **1** from methanol afforded X-ray suitable crystals. Yield: 76%. M.p. 196 °C. $\mu_{eff} = 1.76\mu_B$; UV/Vis ($CHCl_3$): λ ($\log\varepsilon$) = 294(4.79), 400(4.41), 500(sh), 670-(2.43); IR (KBr, cm^{-1}): ν = 1608 (CH=N), 2864–2956 (C–H in Bu^t). $C_{42}H_{52}N_2O_2Cu$: Calc.: C, 74.2; H, 7.7; N, 4.1. Found: C, 74.3; H, 7.6; N, 4.2%. Elemental analysis, physico-chemical, electronic spectral and IR data of **X** complexes are summarized in Table 1.

Table 1
Elemental analysis, physico-chemical, electronic spectral and IR data of **X** compounds

Compound	M.p. (°C)	Yield (%)	Electronic spectra, λ/nm (logε, $cm^{-1}\,M^{-1}$)	IR spectra, cm^{-1}		Found (Calc.) (%)		
				$\nu_{C=N}$	ν_{OH}	C	H	N
1	196	76	294(4.8), 400(4.4), 500[a], 660(2.2)	1608		74.3(74.2)	7.6(7.7)	4.2(4.1)
2	262	78	306(4.6), 408(4.4), 500[a] (3.2), 700[a]	1603	3488	71.2(71.4)	7.7(7.6)	3.9(3.8)
3	196	82	255, 305, 379, 480[a], 673(2.25)	1612	3438	71.2(71.4)	7.8(7.6)	3.7(3.8)
4	245	68	293, 387, 500[a], 700[a] (2.28)	1616	3432[b]	71.7(70.8)	7.5(7.4)	4.1(3.9)
5	236	75	308, 376, 450[a], 500[a], 700[a]	1603	3286[b]	70.6(70.8)	7.2(7.4)	3.7(3.9)
6	>275	85	295, 416, 500, 710[a] (2.36)	1598		86.3(86.5)	9.5(9.5)	3.2(3.1)

[a] Shoulder.
[b] Strong narrow band.

2.4. Physical measurements

Elemental analyses were carried out using a LECO CHNS 932 elemental analyzer. The magnetic susceptibilities of powdered samples were measured in a Sherwood Scientific Magnetic Susceptibility Balance (Model MK 1) magnetometer at r.t. Electronic spectra were measured on a Shimadzu 1601 UV–Vis spectrophotometer in various solvents. The IR spectra were recorded on a Perkin–Elmer FTIR spectrometer using KBr discs. ^1H and ^{13}C NMR spectra were recorded on a Bruker Spectro spin Avance DPX-400 Ultra Shield Model NMR or on a BRUKER AC 200 using TMS as an internal standard in $CDCl_3$. The ESR spectra were recorded on a Varian E-109 C model X-band spectrometer with 100 kHz modulations. The X-band EPR spectra at 300 and 113–133 K were recorded on a Varian E109 C model EPR spectrometer with 100 kHz frequency modulation using DPPH ($g = 2.0036$) as standard. Errors in g_{iso}, $g_{\|}$ and $g_{\perp}$ are ± 0.0005; errors in A_{iso}, $A_{\|}$ and $A_{\perp}$ are 0.5, 1.0 and 1.0 G, respectively.

An EcoChemie Autolab-12 potentiostat with the electrochemical software package GPES 4.9 (Utrecht, The Netherlands) was used for voltammetric measurements. A three electrode system was used: a Pt counter electrode, an Ag/AgCl reference electrode and a 2-mm sized Pt disc as working electrode. The potentiostat/galvanostat has an IR-compensation option. Therefore, the resistance due to the electrode surface was compensated throughout the measurements. Oxygen-free nitrogen was bubbled through the solution before each experiment. All experiments were carried out at room temperature.

2.5. X-ray crystallography

A suitable single crystal was mounted on a glass fiber and data collections were performed on a STOE IPDSII image plate detector using Mo Kα radiation ($\lambda = 0.710690$ Å). Intensity data were collected in the θ range 1.93–29.38° at 298 (2) K. Crystallographic data are listed in Table 2. Data collection: Stoe X-AREA [7]. Cell refinement: Stoe X-AREA [7]. Data reduction: Stoe X-RED [7]. The structure was solved by direct-methods using SIR97 [8] and anisotropic displacement parameters were applied to non-hydrogen atoms in a full-matrix least-squares refinement based on F^2 using SHELXL-97 [9]. All hydrogen atoms were positioned geometrically and refined by a riding model with U_{iso} 1.2 times that of attached atoms. Molecular drawings were obtained using ORTEP-III [10].

Table 2
Crystallographic data for the compound **1**

Formula	$C_{42}H_{52}CuN_2O_2$
Molecular weight	680.40
Temperature (K)	293(2)
Wavelength (Å)	0.71069
Crystal system	monoclinic
Space group	*C*2/*c*
Unit cell dimensions	
a (Å)	13.943(5)
b (Å)	16.413(5)
c (Å)	16.781(5)
β (°)	99.602
Volume	3786(2)
Z	4
Calculated density ($Mg\,m^{-3}$)	1.194
μ (mm^{-1})	0.613
F(000)	1452
Crystal size (mm)	$0.42 \times 0.28 \times 0.19$
θ Range	1.93–29.38
Index ranges	$-19 \leqslant h \leqslant 19$, $-22 \leqslant k \leqslant 22$, $-21 \leqslant l \leqslant 23$
Reflections collected	35857
Independent reflections	5183
Reflections observed ($>2\sigma$)	3111
Absorption correction	integration
Maximum and minimum transmission	0.7065–0.8637
Refinement method	full-matrix least-squares on F^2
Data/restrains/parameters	3111/0/224
Goodness-of-fit on F^2	0.945
Final *R* indices [$I > 2\sigma(I)$]	$R_1 = 0.0462$, $wR_2 = 0.1213$
R indices (all data)	$R_1 = 0.0772$, $wR_2 = 0.1331$
Largest difference in peak and hole ($Å^{-3}$)	0.62 and −0.54

3. Results and discussion

Except **5** (R = 4-OH) all **X** complexes are soluble in chloroform, dichloromethane, but less soluble in solvents such as alcohols, tetrahydrofuran and DMSO. The elemen-

tal analyses were satisfactory, indicating that the complexes have a ligand-to-metal ratio of 2:1.

It is well known that tetra coordinated copper(II)-Schiff base complexes derived from bidentate *N*-aryl(alkyl)-R-sal ligands with CuN_2O_2 coordination sphere usually display *trans* square planar, distorted square planar or tetrahedral arrangement [2–4c,11]. At the same time, recently reported X-ray structural studies of the solvated Cu(*N*-Ph-5-Cl-sal)$_2 \cdot 1/2CH_2Cl_2$ [3a] and Cu(*N*-*p*-CH_3Ph-sal)$_2 \cdot$ DMF [12] revealed that in these complexes the ligands are coordinated in a *cis*-N_2O_2 planar configuration. Interestingly, in the present unsolvated complex **1** the copper atom has a tetrahedrally distorted square planar geometry with two 3, 5-di-Bu$^t_2$phenyl-sal ligands in a *cis*-N_2O_2 arrangement.

3.1. Description of the structure of *1*

The molecular structure of complex **1** is illustrated in Fig. 1. Details of the crystal and data collection are outlined in Table 2. The selected bond lengths and bond angles are listed in Table 3. The X-ray diffraction analysis of **1** show that the copper ion is bonded to the oxygen and nitrogen donor atoms of the two bidentate ligand molecules in the unusual a *cis*-N_2O_2 arrangement. The geometry of **1** is distorted square planar where the dihedral angle between the two coordination planes defined by O1′Cu1N1′ and O1CuN1 is 36.91(6)° (Fig. 1). The compound has crystallographic C_2 2-fold axes passing through the copper atom. The crystal structure of **1** is built from pairs of molecules orientated in the *trans* position respect to each other and the two salicylidene groups of the neighboring mole-

Table 3
Selected bond lengths (Å) and angles (°) for complex **1**

Bond lengths	
Cu1–O1	1.8850(16)
Cu1–N1	1.9706(16)
N1–C1	1.293(3)
N1–C8	1.437(2)
O1–C7	1.293(3)
C2–C3	1.409(3)
C2–C7	1.411(3)
C3–C4	1.364(3)
C4–C5	1.388(4)
C5–C6	1.350(4)
Bond angles	
O1Cu1N1	93.73(7)
O1Cu1O1′	87.70(10)
N1Cu1N1′	97.13(9)
O1′Cu1N1′	93.73(10)
O1Cu1N1′	152.81(8)
N1C8C9	118.56(16)
N1C1C2	127.40(19)
C1N1C8	117.7(2)
C1C2C7	122.5(3)
C2C7O1	123.81(18)
Cu1N1C1	122.20(13)
Cu1O1C7	127.93(13)
Cu1N1C8	120.00(13)

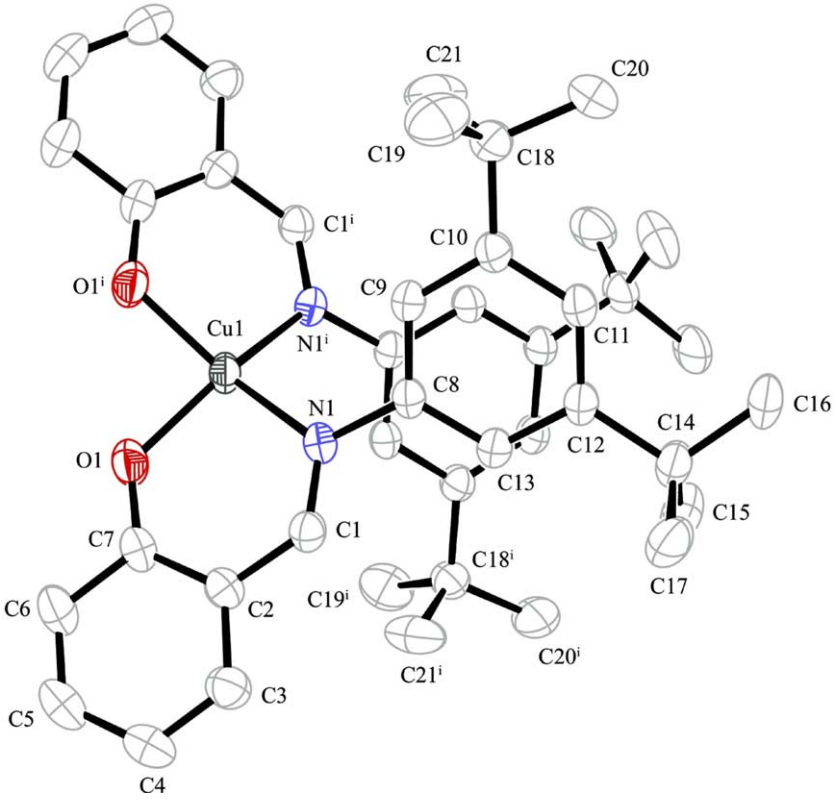

Fig. 1. An ORTER diagram of **1**. Displacement ellipsoids are drawn at the 40% probability level. H atoms are omitted for clarity.

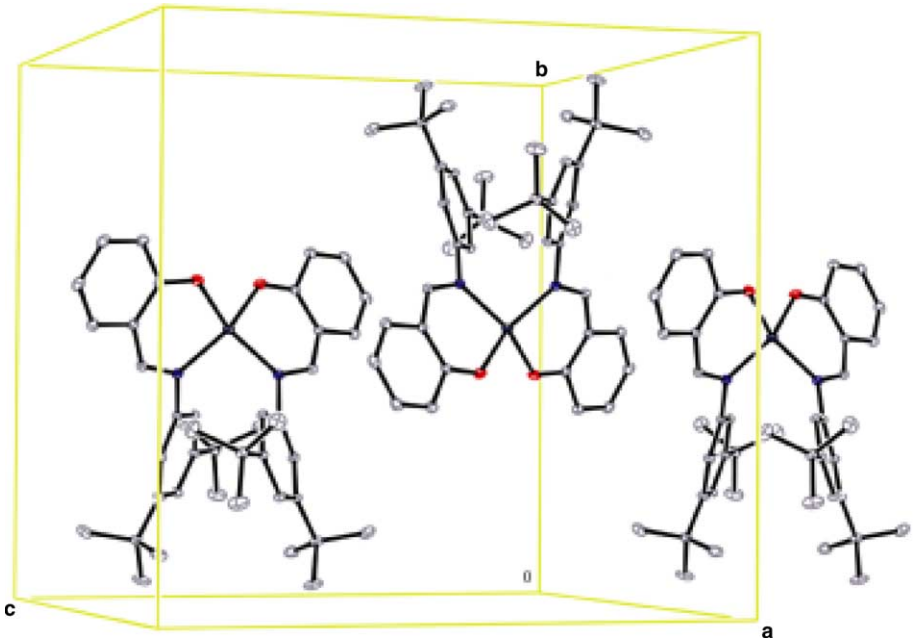

Fig. 2. View of the packing in **1** along the *a*-axis showing the possible π···π and C–H···π contacts at 10% probability displacement ellipsoids.

cules are oriented nearly parallel to each other as shown in Fig. 2. Although the centroids of the two di-tertbutylphenyl rings are indeed too far apart for any π–π interactions [the distances between the centroids of the aromatic rings of the neighboring SA molecules are 4.791(2) and 4.568(2) Å, a distances that are longer than the sum of the van der Vaals radii of two carbon atoms (3.4–3.6 Å)], the rings are not parallel, and C8···C9′ and C9···C8′ are only 3.413(3) Å, indicating quite strong interactions between these two carbons in both rings [11]. The Cu–Cu distance between the neighboring complexes units is so large (8.392 Å) that intermolecular interaction can be excluded. The copper center in **1** is in a distorted square planar environment with O1–Cu1–N1^{i}, N1–Cu1–N1^{i}, and O1–Cu1–O1^{i} (symmetry code: (i) x, y, $-z+0.5$), angles of 152.81(8)°, 97.13(9)° and 87.70(10)°, respectively. The dihedral angles between two phenyl rings and between the two salicylidene benzene rings are 27.40(9)° and 28.49(8)°, respectively. The Cu1–N1 and Cu1–O1 bond distances of 1.9706(16) and 1.8850(16) Å, respectively, agree well with the corresponding distances founded in bis(*N*-phenyl-SA)copper(II) [Cu1–N1 (1.99) and Cu1–O1 (1.88) Å [6a], bis(*N*-*p*-methylphenyl-SA)copper(II) [Cu1–N1 1.965 (3) and Cu1–O1 1.895(2) Å] [13b] and bis[*N*-*p*-$(CH_3)_2$N-phenyl-SA]copper(II) [Cu–N 1.996 (6) and Cu–O 1.885(5) Å] [6b] and in many *N*-alkyl substituted bis-SA and bis-naphthaldimine–Cu^{II} complexes [13,15,16]. Surprisingly, although, the present complex **1** differs from bis(*N*-3, 5-Bu$^{t}_{2}$-4-OCH_3-phenyl-SA)Cu^{II} (**II**) complexes [4c] only with the absence of a OCH_3 group in the 4-position of aniline ring of **1**, the latter complex has practically undistorted a *trans*-N_2O_2 square-planar geometry around Cu(II) center with Cu1–N1 and Cu1–O1 distances of 2.029 and 1.900 Å, respectively [4c]. From a chemical point of view the most significant aspect of the present structure is that it demonstrates the possibility coordination of the bidentate *N*-aryl-SA ligands to copper atom in the sterically unfavorable a *cis*-N_2O_2 arrangement configuration. The reasons that the *cis*-configuration is preferred for complex **1** are not clear.

3.2. IR, ^{1}H NMR and ^{13}C NMR spectra

In the IR spectra of the ligands along with characteristic bands in the 1619–1626 and 2550–2800 cm^{-1} regions (Section 2.2) due to ν(C=N) and intramolecularly H-bonded ν(OH), respectively, a strong narrow peak at 3452 cm^{-1} in $\mathbf{L_4H}$ and a broad strong peak at 3259 cm^{-1} in $\mathbf{L_5H}$ attributed to ν(OH) stretching of 3-OH group and intermolecularly H-bonded 4-OH, respectively, were observed.

In the spectra of **X** complexes the ν(C=N) band of the ligands undergoes small shift to lower frequencies (1598–1616 cm^{-1}), indicating that the ligands are coordinated through the imine nitrogen atoms. The disappearance of the broad band at 2600–2800 cm^{-1} and the appearance of new medium intensity bands in the region 450–600 and a strong band centered at 1523–1552 cm^{-1} which appeared only in the spectra of **X** can be assigned to ν_{Cu-N}, ν_{Cu-O} and $\nu_{C=C}$ (Table 1), respectively, as described in similar complexes [14]. The medium intensity bands detected at 3488 and 3438 cm^{-1} in the spectra of **2** and **3**, respectively, assigned to ν_{OH} of lattice water molecules.

The ^{1}H NMR and ^{13}C NMR spectral results obtained for $\mathbf{L}_x\mathbf{H}$ ligands in $CDCl_3$, with their assignments are given in Section 2. ^{1}H NMR signals were assigned on the basis of their integral intensity, spin–spin coupling patterns and chemical shift values.

3.3. Electronic spectra

Electronic spectral data of the $\mathbf{L}_x\mathbf{H}$ ligands in EtOH solution are presented in the Experimental Section. The electronic spectra of **X** in $CHCl_3$ solutions (Table 1) along with intraligand absorptions originated from $\pi \rightarrow \pi^*$ and $n \rightarrow \pi^*$ transitions also exhibited three visible bands at 400–450, 500(sh) and 660–710 nm which are assigned to the following transitions in order of decreasing energy the MLCT transition (CT band from filled d_π orbitals of Cu^{II} to the antibonding π^* orbitals of phenoate), $d_{xy} \rightarrow d_{x^2-y^2}$, and $d_{z^2} \rightarrow d_{x^2-y^2}$, respectively, in a distorted square planar geometry around copper(II) ion [17,18a].

3.4. EPR and magnetic properties

The room temperature effective magnetic moments of **1**, **5**, and **6** (1.73, 1.76 and 1.70μ_B) (Table 4) are close to the spin only value of 1.73μ_B expected for $3d^9$ systems. The similar magnetic behaviors are noticed in the magnetically dilute systems; therefore this indicates the absence of any coupling in the solid state [18a]. Indeed, our present X-ray study revealed that the nearest Cu···Cu distance in **1** is 8.386 Å. The complexes **2**, **4** and **3** exhibit magnetic moments (1.83 and 1.97μ_B) typical for square planar or pseudo-tetrahedral mononuclear copper(II) complexes with a $S = 1/2$ spin state [19,20].

The spin Hamiltonian parameters of **X** complexes is listed in Table 4. The EPR spectra of powder of all **X** at 300 and 113 K exhibit an axial signal with copper-hyperfine splitting with $g_\parallel > g_\perp > g_e$ pattern typical for a slightly distorted square planar or square planar geometries with a $d_{x^2-y^2}$ ground state [18]. Selected spectra are shown in Fig. 3. Spectral features for **1**, **4**, **5**, were significantly different from those for **2**, **3** and **6** for which in $g_\parallel$ region two [($A_\parallel = 172$ G (for **2**), 164 G (for **3**)] and three components ($A_\parallel = 119$ for **6**) of the four parallel copper hyperfine features were resolved (Fig. 3). When EPR spectra of **2**, **3** and **5** were scanned from 293 to 113 K without any changes in the line widths and *g*-factors, the linearly increasing in intensity of the high field doublet spectrum which follows the Curie law ($I = C/T$) were detected. The similar behavior is consistent with $J > 0$ (ferromagnetic coupling) or $J = 0$ [21].

The solution EPR spectra except **5** of all **X** in $CHCl_3$ at 300 K display the expected typical 4-line pattern from coupling to nuclei of ^{65}Cu ($I = 3/2$) isotopes, without ^{14}N-shfs resolutions on the high-field $m_I = 3/2$ line component. Complex **4** displays a five-line superhyperfine structure on high field copper component with $A^N_{iso} = 8.8$ G due to coupling with two ^{14}N ($I = 1$) nuclei. The resonances show m_I dependent line widths with the high field line being narrower and more intense than the low field line. According to spectral parameters obtained from frozen glass spectra of **X** (Table 4) at 133 K the complexes exhibit axial symmetry feature with $g_\parallel > g_\perp > 2.03$ indicating a $d_{x^2-y^2}$ or d_{xy} ground state in a tetragonal copper centers [18b]. The quotient $g_\parallel/A_\parallel$ value of 146–167 cm for **X**, lying between 140 and 250 cm again indicates a slightly distorted environment for Cu(II) centers [22]. It is interesting that according to $g_\parallel/A_\parallel$ value (Table 4) complex **1** prepared from unsubstituted salicylaldehyde exhibits significantly more tetrahedral distortion than **6** prepared from sterically bulky 3,5-Bu^t_2salicylaldehyde. Another interesting feature consist of significant difference between $g_\parallel/A_\parallel$ ratio for **6** determined from its powdered spectrum (192 cm) and frozen glass spectrum (146 cm), indicating changes its geometry from strongly distorted tetrahedral to a slightly distorted planar in solution.

3.5. Reduction of X complexes with PPh_3

In our early works, it has been demonstrated that some copper(II) complexes with salicylaldimine, 2-hydroxybenzylamine and β-ketoamine ligands bearing sterically hindered 2,6-di-*tert*-butylphenyl fragment unlike their unhindered analogs, undergo one-electron transfer reactions in the interactions with triarylphosphines giving corresponding metal-stabilized radical intermediates [5a,5b,5c,5d,5e]. When some copper(II) bis-chelates with *N*-2,5-di-Bu^t_2pheny-R-sal, structural isomers of the present complexes, was treated with a 2–3-fold excess of PPh_3 in various solvents the decreasing of the intensity of copper EPR signals and immediate appearance of radical signals with $g = 2.005$–2.0082 for R = 3-OH, 3-OCH_3, and 5-OH complexes were detected [23]. At the same time, no reduction process were observed for similar **II** complexes even in the interaction with 10-fold excess of PPh_3. Similar treat-

Table 4
EPR and magnetic moment data of **X** complexes

Compound	EPR parameters[a]									
	Solid			Solution ($CHCl_3$)						
X	μ_{eff} (μ_B)	$g_\parallel$	$g_\perp$	g_{iso}	$g_\parallel$	$g_\perp$	A_{iso}	$A_\parallel$	$A_\perp$	$g_\parallel/A_\parallel$ (cm)
1	1.73	2.202	2.051	2.111	2.242	2.046	66	144	27	167
2	1.83	2.186	2.063	2.129	2.245	2.071	68	156	24	155
3	1.97	2.227	2.073	2.121	2.242	2.061	68	160	22	150
4	1.83	2.142	2.046	2.127	2.217	2.082	80	192	24	124
5	1.76	2.189	2.059							
6	1.70	2.236	2.047	2.118	2.232	2.063	63	164	11	146

[a] A_{iso}, $A_\parallel$ and $A_\perp$ values are given in units of G (Gauss).

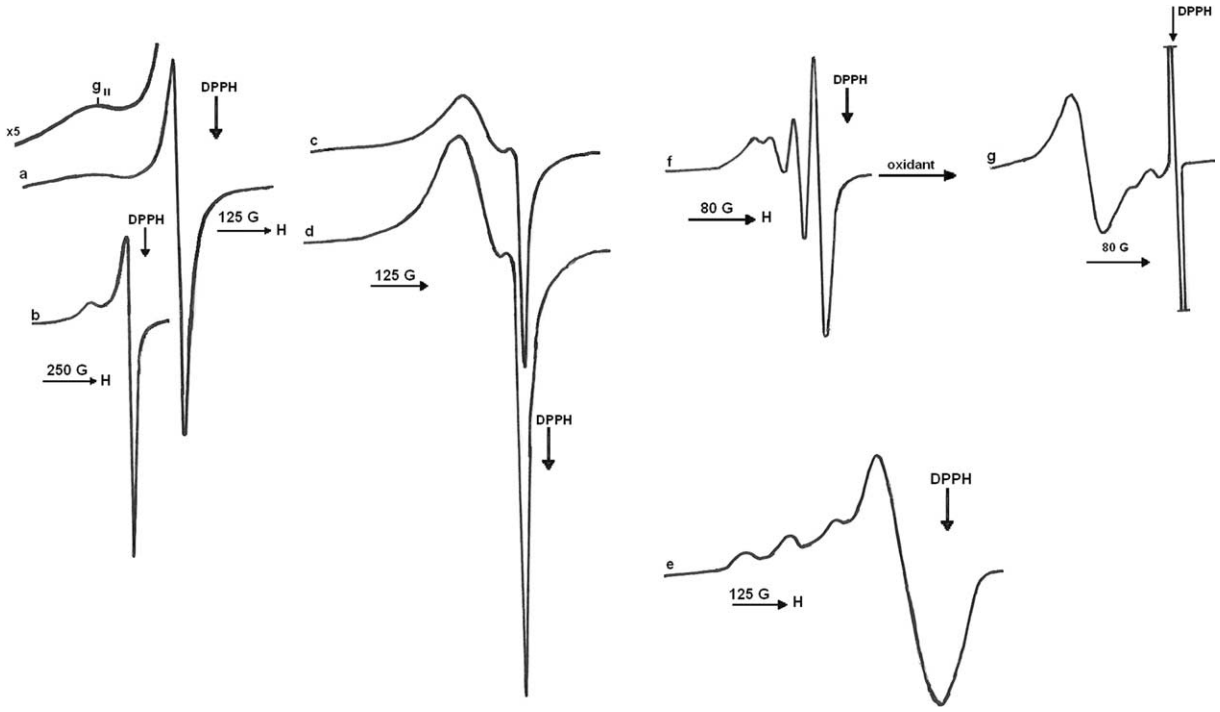

Fig. 3. ESR spectra of some **X** complexes: microcrystalline solids (a) **1** and (b) **5** at r.t., (c) powdered solid **4** at 293 K and (d) at 113 K; (e) powdered **6** at 293 K; (f) solution spectrum **6** in $CHCl_3$ and (g) oxidized **6** at r.t. under identical scanning conditions.

ment of the present **X** complexes revealed that upon addition of 3–4-fold excess of PPh_3 to $CHCl_3$ solution of **1**, **2, 4** and **6** complexes at r.t., during 3–6 h their black color changed to orange-yellow and their absorption peaks within the range of 450–700 nm were disappeared. Under similar conditions the dark brown color of **3**, during even 3 days has not changed practically [(340, 390(sh), 420(sh). 500(sh) and 670 nm(sh) (**3** + PPh_3)]. In the EPR monitoring of **X** + PPh_3 (**X** = **1**, **2**, **4**, **6**) systems during reaction process in air or in vacuum only slowly decreasing in the intensity of their spectra without appearance of any radical signals were detected.

3.6. Chemical oxidation of the complexes

Our recent studies demonstrated that in the chemical oxidation of bis[*N*-alkyl(aryl)-3, 5-Bu^t_2sal]copper(II) complexes with one-electron oxidant $(NH_4)_2[Ce(NO_3)_6]$ (CAN) in $CHCl_3$, along with decreasing of the Cu(II) signal intensity, the generation of directly coordinated phenoxyl radical complexes are also detected [23]. The present investigation of the oxidative behavior of **X** complexes at r.t. and in air conditions, revealed that when they are treated with of three to 5-fold excess amount of CAN along with color change from black or dark brown to light brown or light yellow, the disappearance of the EPR spectra of **X** and appearance new broad lines (peak-to-peak about $\Delta H = 92$–108 G) at $g = 2.169$–2.189 were detected. For complexes **5** and **6** besides broad singlets at 2.169 and 2.189 the strong radical signals at $g = 2.0055$ and $g = 2.0052$ were observed (Figs. 3(f) and (g)). The decreasing of the signal intensity of **X** + CAN system suggest that one-electron oxidation results in the generation of a Cu^{II}-phenoxyl radical complex and there is antiferromagnetic coupling between an $S = 1/2 Cu^{II}$ and an $S = 1/2$ phenoxyl radical. We suggest that the detected radical signals more probably originate from $Cu(L^{\bullet}_x)_2$ type diradical species in which one radical center is fully antiferromagnetically coupled with Cu(II).

The spectral changes for **X** + CAN systems were also monitored by UV–Vis spectroscopy during the progress of the oxidation of **X** complexes with ACN in $CHCl_3$. Since the oxidant is insoluble in $CHCl_3$ the reaction system was heterogeneous. However, the solution **X** + CAN system was mixed using a spatula for 5–6 s prior to each scanning. When three to five excess of CAN was added to the solution of **X** in $CHCl_3$ at r.t., the black solution turns to brown or light yellow with the disappearance of the original bands of visible bands at 450–700 nm.

3.7. Electrochemistry

Electrochemical properties of the complexes **X** except **5** due to its poor solubility were studied on a Pt disc electrode in dimethylsulfoxide containing 0.05 M *n*-Bu_4NClO_4 as the supporting electrolyte. Table 5 summarizes the electrode potentials for all complexes in dimethylsulfoxide. A cyclic voltammogram of **1** is given in Fig. 4. This complex displays a reduction peak at $E^1_{pc} = 0.14$ V with a corresponding oxidation peak at $E^1_{pa} = 0.26$ V. The peak separation of

Table 5
Voltammetric data for Cu(II) complexes

X	E^1_{pa}	E^1_{pc}	ΔE_p	E^2_{pa}	E^3_{pa}	E^2_{pc}	ΔE_p	E^4_{pa}	E^3_{pc}	ΔE_p	E^4_{pc}
1	0.26	0.14	0.12	0.65	−0.45	−0.59	0.14		−0.28		−1.58
2	0.26	0.17	0.11	1.08	−0.11	−0.24	0.13	−0.44	−0.59	0.15	
3	0.24	0.14	0.10	1.04	−0.16	−0.22	0.06	−0.53	−0.67	0.14	
4	0.29	0.21	0.08	0.92	0.01	−0.09	0.10	−0.35	−0.48	0.13	
5	0.37	0.20	0.17		−0.47				−0.96		

Supporting electrolyte = 0.05 M n-Bu_4NClO_4, scan rate = 100 mV/s.
Potentials are presented in volts.

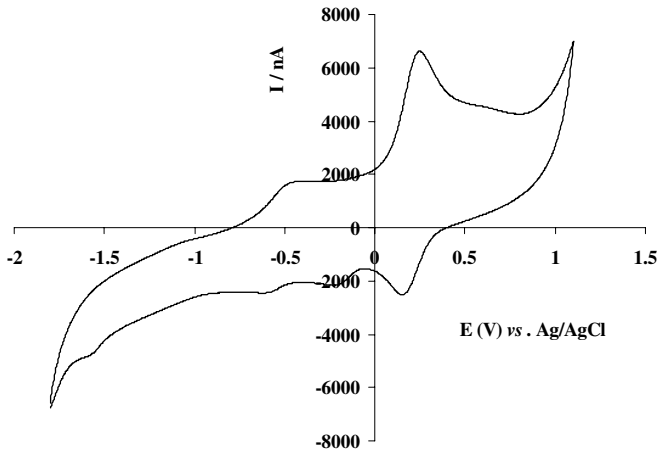

Fig. 4. A cyclic voltammogram of **1** in dimethylsulfoxide containing 0.05 M n-Bu_4NClO_4 as supporting electrolyte. Scan rate = 100 mV/s.

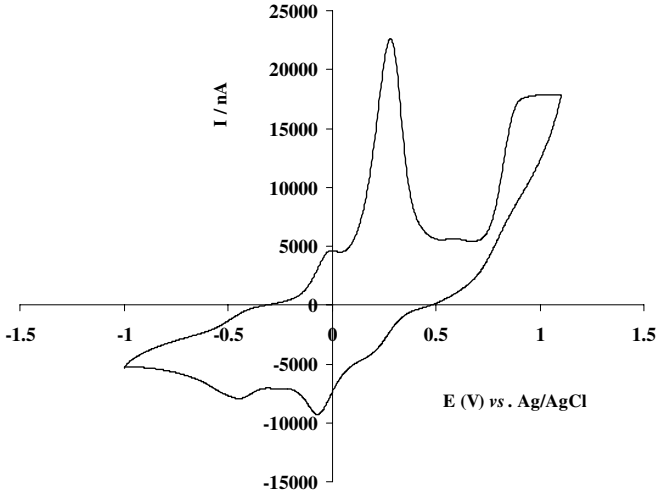

Fig. 5. A cyclic voltammogram of **4** in dimethylsulfoxide containing 0.05 M n-Bu_4NClO_4 as supporting electrolyte. Scan rate = 100 mV/s.

this couple (ΔE_p) is 0.12 V at 0.1 V/s and increases with scan rate. The most significant feature of this redox couple is the 1e-transfer electrochemical process of the formation of Cu(II)/Cu(I). The difference between forward and backward peak potentials can provide a rough evaluation of the degree of the reversibility of one electron transfer reaction. The analysis of cyclic voltammetric responses with the scan rate varying 50–300 mV/s gives the evidence for a quasi-reversible one electron oxidation. The ratio of cathodic to anodic peak height was less than one. However, the peak current increases with the increase of the square root of the scan rate. The $I_p/v^{1/2}$ value is almost constant for all scan rates. This establishes the electrode process as diffusion controlled [24]. The separation in peak potentials increases at higher scan rates. These characteristic features are consistent with the quasi-reversibility of Cu(II)/Cu(I) couple. The other oxidation or reduction peaks are listed in the Table 5 and are probably due to the ligand moiety of complex. The electrode potentials of the rest of the copper(II) complexes are given in Table 5.

A cyclic voltammogram of the complex **4** is given in Fig. 5. The complex **4** exhibits a reduction peak at $E^1_{pc} = 0.21$ V with a directly re-oxidation peak at $E^1_{pa} = 0.29$ V corresponding to the formation of Cu(II)/Cu(I) couple. The peak separation of this couple (ΔE_p) is 0.08 V. This redox couple also have quasi-reversible character as the separation in peak potentials are higher than 59 mV and the peak currents rises with increasing $v^{1/2}$. Diagnostic test for the complex **4** indicated that the electrode process is controlled by diffusion. The separation in peak potentails (ΔE_p) for complexes are in order **4** < **3** < **2** < **1** < **6**. The difference between forward and backward peak potentials can provide a rough evaluation of the degree of the reversibility. This shows that the electrochemical process of complex **4** is faster than that of the other complexes. This behavior may suggest that in complex **4**, both the Cu(II) and Cu(I) forms appear in a similar geometrical configuration, so the electron transfer does not require larger reorganization of the complex coordination geometry.

In conclusion, the present work indicates that a small changes of the substituents on the ligands of the bis(N-3, 5-Bu^t_2phenyl-R-sal)copper(II) type complexes results in striking changes both in the molecular structure of the complexes and their chemical redox reactivity. Surprisingly, in complex **1** with R = H unlike its structurally characterized bis(N-aryl(alkyl)-sal) analogs copper center exhibits a tetrahedrally distorted *cis*-N_2O_2 square planar geometry. Chemical oxidation of some complexes leads to the formation of the coordinated Cu(II)-phenoxyl radical complexes. As supported by EPR and electronic spectral studies their reduction with PPh_3 proceeded slowly without generation any radical species. The electrochemical measurements have indicated that complexes showed quasi-reversible 1e-electron transfer reduction to Cu(I) along with the reduction and oxidation of the ligand moiety of the complexes. The results also indicated that **4** has the highest

electrochemical rate assuming that the both couples have similar geometrical configuration, so the electron transfer does not require larger reorganization of the complex.

4. Supplementary data

Crystallographic data (excluding structure factors) for the structure in this paper have been deposited with the Cambridge Crystallographic Data Centre as the Supplementary Publication No. CCDC 253758. Copies of the data can be obtained, free of charge, on application to CCDC, 12 Union Road, Cambridge, CB2 1EZ, UK, fax: +44 1223 366 033, e-mail: deposit@ccdc.ac.uk or on the web www: http://www.ccdc.cam.ac.uk.

References

[1] J.W. Wittaker, in: K.D. Karlin, Z. Tyeklar (Eds.), Bioinorganic Chemistry of Copper, Chapman Hall, New York, 1993.

[2] (a) R.H. Holm, M.J. O'Connor, Prog. Inorg. Chem. 14 (1971) 329;
(b) J. Costangno, J. Vargos, R. Latorre, A. Alvardo, G. Mena, Coord. Chem. Rev. 129 (1992) 67.

[3] (a) S. Yamada, Coord. Chem. Rev. 190–192 (1999) 537;
(b) V. Casellato, P.A. Vigato, D.E. Fenton, M. Vidali, Chem. Soc. Rev. 8 (1979) 199;
(c) D.E. Fenton, Chem. Soc. Rev. 28 (1999) 159;
(d) J.F. Larrow, E.N. Jacobsen, Y. Gao, Y. Hong, X. Nie, C.M. Zeppe, J. Org. Chem. 59 (1994) 1939.

[4] (a) A.A. Medjidov, V.T. Kasumov, H.S. Mamedov, Koord. Khim. 7 (1981) 66;
(b) M.K. Guseyinova, A.A. Medjidov, V.T. Kasumov, J. Struct. Chem. 23 (1982) 114;
(c) A.A. Medjidov, V.T. Kasumov, M.K. Guseyinova, I.R. Amiraslanov, J. Struct. Chem. 22 (1981) 129.

[5] (a) V.T. Kasumov, A.A. Medjidov, Koord. Khim. 15 (1989) 1404;
(b) V.T. Kasumov, S.N. Lyubchenko, A.A. Medjidov, V.A. Kogan, A.A. Shvets, Koord. Khim. 16 (1990) 1633;
(c) V.T. Kasumov, A.A. Medjidov, Koord. Khim. 16 (1990) 1355;
(d) V.T. Kasumov, Koord. Khim. 52 (2001) 57;
(e) V.T. Kasumov, A.A. Medjidov, R.Z. Rzaev, İ.A. Golubeva, R.D. Kasumov, Koord. Khim. 19 (1993) 933;
(f) V.T. Kasumov, F. Köksal, Spectrochim. Acta Part A 58 (2002) 2199.

[6] (a) L.W. Stogsdill, E.C. Lingafelter, Acta Cryst. 17 (1964) 1058;
(b) A.N. Shnulin, Y.T. Struchkov, Kh.S. Mamedov, A.G. Bezuglaya, J. Struct. Chem. 18 (1977) 890.

[7] Stoe & Cie, X-AREA (Version 1.18) and X-RED32 (Version 1.04), Stoe & Cie, Darmstadt, Germany, 2002.

[8] A. Altomare, M.C. Burla, M. Camalli, G.L. Cascarano, C. Giacovazzo, A. Guagliardi, A.G. Moliterni, G. Polidori, R. Spagna, J. Appl. Cryst. 32 (1999) 115.

[9] G.M. Sheldrick, SHELXS-97 and SHELXL-97, University of Gottingen, Germany, 1997.

[10] M.N. Burnett, C.K. Johnson, ORTEPIII, Report ORNL-6895, Oak Ridge National Laboratory, Tennessee, USA, 1996.

[11] A. Bondi, J. Phys. Chem. 68 (1964) 441.

[12] L.T. Yıldırım, K.C. Emregül, R. Kurtaran, O. Atakol, Cryst. Res. Technol. 37 (2002) 1344.

[13] (a) J.M. Fernandez-G, R.A. Toscano, R.C. Rosado, N.M. Rubalcaba, M.A. Martinez, Polyhedron 17 (1998) 2425;
(b) J.M. Fernandez, E.A. Arauz, R.C. Rosado, R.A. Toscano, N.M. Rubalcaba, M.A. Martinez, Transition Met. Chem. 24 (1999) 18;
(c) M.A. Martinez, R.S. Aguilar, N.M. Rubalcaba, R.C. Rosado, A.N. Vazquez, V.C. Vidales, A.Z. Dehesa, R.A. Toscano, S.H. Ortega, J.M. Fernandez-G, J. Chem. Soc., Dalton Trans. (2001) 2346.

[14] J.E. Kovacic, Spectrochim. Acta 23A (1965) 183.

[15] H. Yokoi, A.W. Addison, Inorg. Chem. 16 (1977) 1341.

[16] E.C. Lingafelter, G.L. Simmons, B. Morosin, C. Scheringer, C. Freiburg, Acta Crystallogr. 14 (1961) 1222.

[17] D. Hall, S.V. Shaet, T.N. Waters, J. Chem. Soc. A (1968) 460.

[18] (a) B.J. Hathaway, D.E. Billing, Coord. Chem. Rev. 5 (1970) 1;
(b) B.A. Goodman, J.B. Raynor, Adv. Inorg. Chem. 13 (1970) 135.

[19] L. Sacconi, M. Ciampolini, J. Chem. Soc. (1964) 276.

[20] B.N. Figgs, Nature 182 (1958) 1568.

[21] D.A. Shultz, A.K. Boal, G.T. Farmer, J. Org. Chem. 63 (1998) 9462.

[22] U. Sakaguchi, A.W. Addison, J. Chem. Soc., Dalton Trans. 600 (1979).

[23] (a) V.T. Kasumov, F. Köksal, R. Köseoğlu, J. Coord. Chem. 57 (2004) 591;
(b) V.T. Kasumov, E. Taş, F. Köksal, Ş. Özalp-Yaman, Polyhedron 24 (2005) 319;
(c) V.T. Kasumov, F. Köksal, A. Sezer, Polyhedron 24 (2005) 1203.

[24] A.J. Bard, L.R. Faulkner (Eds.), Electrochemical Methods: Fundamentals and Applications, 2nd ed., Wiley, New York, 2001.

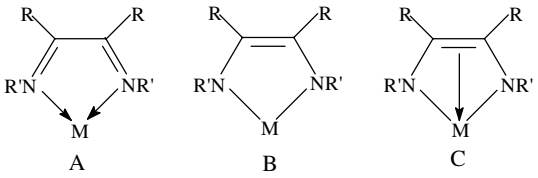

Fig. 1. Coordination modes of diazadiene ligands.

the use of sodium as the reducing agent and their octahedral geometry. These other derivatives of $MoCl_2$, however, were not structurally characterized and no details of their stereochemistry were evident from the spectroscopic studies. Therefore, an alternative synthetic methods of new diazadiene molybdenum complexes were explored.

Molybdenum complexes [**3ai**, **3bi**, **3c**] (Scheme 1) crystallize as green crystals for **3ai**, **3c**, and orange brown for **3bi** from CH_2Cl_2/*n*-hexane. All these compounds are soluble in methylene chlorid, dimethylsulfoxid, acetone and acetonitrile. They are air-sensitive and non-soluble in unpolar solvents. These compounds have been characterised by ^1H, ^{13}C NMR and IR spectroscopy.

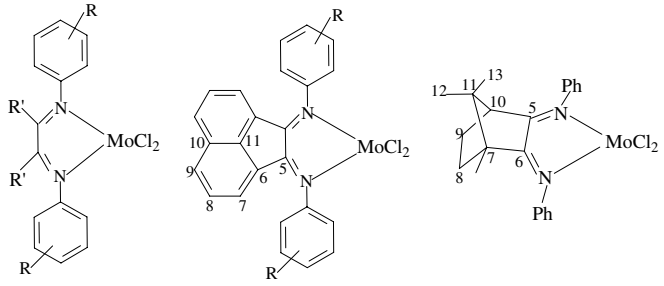

Scheme 1.

The new complexes (dad)$MoCl_2$, exhibit spectroscopic data in accord with the proposed structure.

The NMR properties unambiguously establish the diamagnetic nature of these compounds. In fact the substituent on the aryl groups of the dad ligand are all equivalent as expected for the C_{2v}-symmetric isomer. Chemical shifts of the R′N=C(R)–C(R)=NR′ subunit in the complexes [**3ai**, **3bi**, **3c**] are slightly shielded in comparison to those of the free ligands similar to other complexes [21]. The C=N carbon appears between 163 and 179 ppm.

In the IR spectra of the complexes (as KBr pellets), the C=N stretching vibration is observed at 1601–1640 cm^{-1}, i.e., shifted by 10–20 cm^{-1} to lower frequency as compared to the free ligands.

Single crystal of **3a2** was grown from a mixture of $CH_2Cl_2$and hexane solution at room temperature.

The Ortep diagram of **3a2** is shown in Fig. 2, with details of the structure determination, including unit-cell data, summarized in Table 1 and relevant bond distances and bond angles in Table 2.

The structural analysis confirms the identity of the molecule. The coordination sphere of the molybdenum center is composed of the two nitrogen atoms of the chelating diazadiene ligand and the two dichloride atoms. The coordination geometry of the molybdenum atom can be described as slightly distorted tetrahedral. This distortion is explained by the 78.17(19)° bite angle measured for the bidentate diazadiene ligand [N2–Mo–N1]. This angle are similar to the value of 72.6(3)° measured for [$W(CO)_3$(dad: R = H; R′ = *i*-Pr)(η^2-eco)] {eco = (*E*)-cyclooctene} [22].

The Mo–N distances are considerably shorter than in the structurally related complex [MoO_2Cl_2(dad: R = H; R′ = *t*-Bu)] [2.399(2) and 2.388(2) Å] [23].

The ligand and metal in this structure are essentially coplanar consistent with the π-backbonding of this ligand. The N1–C19, N2–C20 and C19–C20 bond distances of 1.267(8), 1.258(8) and 1.523(9) Å, respectively, confirm the conjugated diimine nature of this ligand and with those

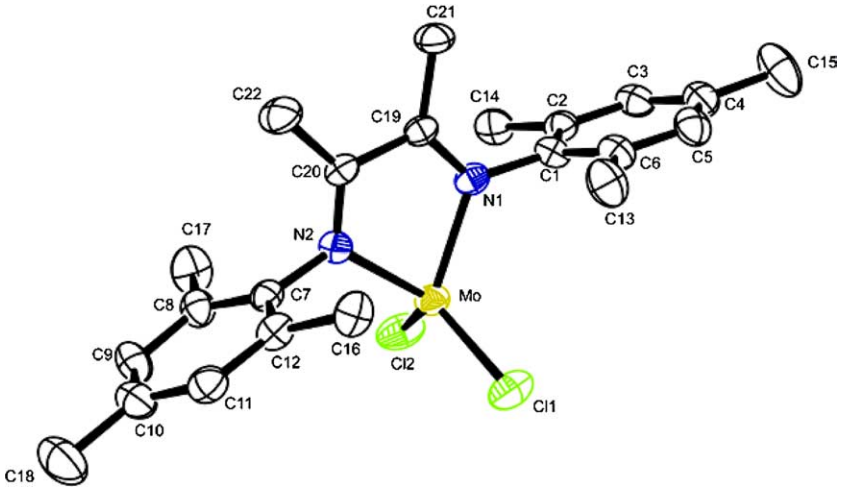

Fig. 2. ORTEP diagram of **3a2** · CH_2Cl_2. Thermal ellipsoids are at 50% probability. Hydrogen are omitted for clarity.

Table 1
Summary of crystallographic data and X-ray experimental details for **3a2**

Empirical formula	$C_{23}H_{30}Cl_4N_2Mo$
Formula weight	572.23
Crystal system	monoclinic
Space group	$P2_1/c$
Z	4
a (Å)	12.871(8)
b (Å)	14.659(9)
c (Å)	14.404(9)
α (°)	90
β (°)	90.62 (7)
γ (°)	90
V (Å^3)	2717.8(3)
ρ_{calc} (g cm^{-3})	1.399
Crystal dimensions (mm)	$0.11 \times 0.31 \times 0.64$
T (K)	293(2)
Radiation (Mo Kα) λ (Å)	0.71073
$F(000)$	1168
2θ Range (°)	2.1–26.99
Limiting indices	$-16 \leqslant h \leqslant 16$, $-18 \leqslant k \leqslant 0$, $-9 \leqslant l \leqslant 18$
Number of scanned reflections	10325
Number of independent reflections	5860
Number of observed reflections	2700
Number of parameters varied	268
Absorption correction	empirical (DIFABS)
Data reductions programs	XCAD4
Programs used	SHELX-97
R_1 (F_o), wR_2 (F_o^2) ($I > 2\sigma(I)$) (%)	8.08, 22.65
Goodness-of-fit on F^2	0.996

of complexes to with the bonding mode A can be clearly assigned (N–C: 1.26–1.30 Å; C–C: 1.40–1.55 Å) [1]. These distances are similar to those observed in $Mo(CO)_4$(dad) complex [24].

The metal-chelate ring (Mo–N2–C20–C19–N1) in complex (**3a2**) is almost flat as indicated by the torsion angles of −1.96 (0.87)°, 5.21 (0.71)° and −2.40(0.71)° for N2–C20–C19–N1, Mo–N1–C19–C20 and Mo–N2–C20–C19, respectively, which are very closer for other platinum (II) complexes [25].

Table 2
Selected interatomic distances and angles for [2,4,6-Me_3-dad]$MoCl_2$ (**3a2**)

Bond distances (Å)		Bond angles (°)	
Mo–N1	2.089(5)	N1–Mo–N2	78.17(19)
Mo–Cl1	2.204(2)	N2–Mo–Cl1	115.88(16)
N1–C19	1.267(8)	N2–Mo–Cl2	114.53(15)
N1–C1	1.464(8)	C20–N2–Mo	115.2(4)
C6–C13	1.513(11)	C20–N2–C7	121.8(6)
C2–C14	1.480(10)	C7–N2–Mo	122.9(4)
C4–C15	1.491(11)	C8–C7–N2	118.9(6)
C19–C20	1.523(9)	C12–C7–N2	117.9(6)
Mo–N2	2.087(5)	N2–C20–C19	115.7(6)
Mo–Cl2	2.220(2)	Cl1–Mo–Cl2	115.96(9)
N2–C20	1.258(8)	N1–Mo–Cl1	113.14(16)
N2–C7	1.446(8)	N1–Mo–Cl2	113.58(16)
C12–C16	1.494(10)	C19–N1–Mo	114.2(4)
C8–C17	1.497(10)	C19–N1–C1	122.2(5)
C10-C18	1.539(11)	C1–N1–Mo	123.5(4)
		C6–C1–N1	117.9(6)
		C2–C1–N1	118.5(6)
		N1–C19–C20	116.5(5)

The o-methylphenyl groups makes an angle of approximately 90° to the plane of the C=N bonds, due to the presence of the o-methyl substituents as appears from the torsion angles of 93.64 (0.79)°, −88.83 (0.76)°, 85.51 (0.84)° and −92.75 (0.79)° for C20–N2–C7–C8, C20–N2–C7–C12, C19–N1–C1–C6 and C19–N1–C1–C2, respectively.

In conclusion, we have described a convenient synthetic procedure for the preparation of the new diazadiene molybdenum (II) complexes. The application of these complexes in catalytic reactions such as oligomerization and polymerisation of alkenes (ethylene, propylene) and functional alkenes (methylacrylate) is in progress.

3. Experimental

All manipulations are carried out under an atmosphere of dry and oxygen-free argon with standard schlenck techniques. Diethylether was purified by reflux over sodium benzophenone ketyl and distilled under argon prior to use. Methylene chloride and *n*-hexane were purified from P_2O_5 and distilled under argon.

The diazadiene ligands: dab [26], Ar-BIAN, Ph-BIC [27]; $MoCl_4(thf)_2$ [19] were obtained according to the literature procedures.

All routine NMR experiments were carried out on a Bruker AM 300 and infrared spectra on a Bio-Rad FTS-6000 spectrophotometer.

3.1. General procedure for the preparation of [dad]$MoCl_2$

In an inert atmosphere, $MoCl_4(thf)_2$ (1 equiv.) was added to diazadiene ligand (3 equiv.) in 20 ml of anhydrous CH_2Cl_2. Zinc was added (5 equiv.) as a reducing agent. The solution was stirred at room temperature for two days. The supernatant was separated by filtration, and the solvent was removed under vacuum until 3 ml. Addition of hexane precipitate the product. Pure compound was isolated as a solid by crystallization from methylene chloride/hexane solution at −30 °C. Yields ranged from 52% to 83%.

3.2. [2,4,6-$(CH_3)_3$-$C_6H_2NC(H)C(H)NC_6H_2$-2,4,6-$(CH_3)_3$]$MoCl_2$ (**3a1**)

Following general procedure, from $MoCl_4(thf)_2$ (0.57 mmol, 0.22 g), [2,4,6-$(CH_3)_3$-$C_6H_2NC(H)C(H)$-NC_6H_2-2,4,6-$(CH_3)_3$] (1.7 mmol, 0.505 g). Zinc (2.85 mmol, 0.186 g) in 20 ml of methylene chloride was obtained 0.178g (yield 68%) of **3a1** as a green solid after crystallization from a mixture *n*-hexane/CH_2Cl_2 (8/2). Decomposition = 310 °C; IR ($\nu_{C=N}$ = 1615 cm^{-1}).

^{1}H NMR (300 MHz, $CDCl_3$, 25 °C, δ [ppm]): δ = 2.30 (s, 12H, *ortho*,*ortho*′-CH_3), 2.49 (6H; *para*-CH_3); 6.936 (s, 4H, Har); 8.76 (1, 2H, H–C=N).

^{13}C NMR (75.5 MHz, $CDCl_3$, 25 °C, δ [ppm]): $\delta = 19.5$ (*ortho*-CH_3); 21.5 (*para*-CH_3); 130.75 (C_{ortho}); 132 (C_{meta}); 137, 75 (C_{para}); 144 (C_{ipso}); 176.5 (C=N).

3.3. [2,4,6-$(CH_3)_3$-$C_6H_2NC(Me)C(Me)NC_6H_2$-2,4,6-$(CH_3)_3$]$MoCl_2$ (**3a2**)

Following general procedure, from $MoCl_4(thf)_2$ (0.44 mmol, 0.17 g), [2,4,6-$(CH_3)_3$-$C_6H_2NC(Me)C(Me)$-NC_6H_2-2,4,6-$(CH_3)_3$] (1.3 mmol, 0.427 g). Zinc (2.2 mmol, 0.143 g) in 20 ml of methylene chloride was obtained 0.178g (yield 83%) of **3a2** as a green solid after crystallization from a mixture *n*-hexane/CH_2Cl_2 (8/2). Decomposition = 367 °C; IR ($\nu_{C=N} = 1650$; 1607 cm^{-1}).

^{1}H NMR (300 MHz, CD_3CN, 25 °C, δ [ppm]): $\delta = 2.26$–2.36 (m, 24H, *ortho*,*ortho'*,*para*-$CH_3 + CH_3$–C=N); 7.09 (s, 4H, Har).

^{13}C NMR (75.5 MHz, CD_3CN, 25 °C, δ [ppm]): $\delta = 17.38$ (CH_3–C=N); 18.20 (*ortho*,*ortho'*-CH_3); 19.35 (*para*-CH_3); 128.43 (C_{ortho}); 129.29 (C_{meta}); 136.91 (C_{para}); 139.79(C_{ipso}); 172.16 (C=N).

3.4. [2,6-*i*-Pr_2-$C_6H_3NC(Me)C(Me)NC_6H_3$-2,6-*i*-Pr_2]$MoCl_2$ (**3a3**)

Following general procedure, from $MoCl_4(thf)_2$ (0.6 mmol, 0.23 g), [2,6-*i*-Pr_2-$C_6H_3NC(Me)C(Me)NC_6H_3$-2,6-*i*-Pr_2] (1.8 mmol, 0.731 g). Zinc (3 mmol, 0.196 g) in 20 ml of methylene chloride was obtained 0.260g (yield 67%) of **3a3** as a brown solid after crystallization from a mixture *n*-hexane/CH_2Cl_2 (9/1). Decomposition = 355 °C; IR ($\nu_{C=N} = 1654$; 1607 cm^{-1}).

^{1}H NMR (300 MHz, DMSO-d, 25 °C, δ [ppm]): $\delta = 1.16$–1.08 (m, 24H, Me); 1.98 (s, 6H, CH_3–C=N); 2.50 (sept, 4H, CH–*i*-Pr); 7.18–6.85 (m, 6H, Har).

^{13}C NMR (75.5 MHz, DMSO-d, 25 °C, δ [ppm]): $\delta = 16.63$ (CH_3–C=N); 23, 18, 23, 56 (CH_3–*i*-Pr); 27.99 (CH–*i*-Pr); 122.50 (C_{meta}); 124.15 (C_{para}); 134.76 (C_{ortho}, $C_{ortho'}$); 145.99 (C_{ipso}); 168.23 (C=N).

3.5. [2,6-*i*-Pr_2-C_6H_3-acenaphtene]$MoCl_2$: 3b1 {Ar-BIAN, Ar = 2,6-*i*-Pr_2-C_6H_3}

Following general procedure, from $MoCl_4(thf)_2$ (0.54 mmol, 0.21 g), [2,6-*i*-Pr_2-acenaphtene] (1.6 mmol, 0.785 g). Zinc (2.7 mmol, 0.176 g) in 20 ml of methylene chloride was obtained 0.262g (yield 75%) of **3b1** as orange brown solid after crystallization from a mixture *n*-hexane/CH_2Cl_2 (9/1). Decomposition = 375 °C; IR ($\nu_{C=N} = 1640$; 1601 cm^{-1}).

^{1}H NMR (300 MHz, $CDCl_3$, 25 °C, δ [ppm]): $\delta = 0.82$ (d, 12H, CH_3–*i*-Pr); 1.32 (d, 12H, CH_3–*i*-Pr); 3.26 (sept, 4H, CH–*i*-Pr); 6.65 (d, 2H; H_7); 7.55–7.3 (m, 6H, $H_{meta,meta',para}$); 8.101 (d, 2H, H_9)

^{13}C NMR (75.5 MHz, $CDCl_3$, 25 °C, δ [ppm]): $\delta =$ 24.802 (Me-*i*-Pr); 29.34 (CH–*i*-Pr); 125.43 (C_7); 126.02 (C_{meta}); 127.39 (C_{para}); 128.69 (C_8); 129.27(C_9); 131.44 (C_6); 133.12 (C_{10}); 139.87 (C_{ortho}); 140.70 (C_{11}); 145.06 (C_{ipso}); 165.63 (C=N).

3.6. [o-Me-C_6H_4-acenaphtene]$MoCl_2$ (**3b2**) {Ar-BIAN, Ar = o-Me-C_6H_4}

Following general procedure, from $MoCl_4(thf)_2$ (0.39 mmol, 0.15 g), [*o*-Me-acenaphtene] (1.1 mmol, 0.424 g). Zinc (1.95 mmol, 0.127 g) in 20 ml of methylene chloride was obtained 0.178g (yield 86%) of **3b2** as orange solid after crystallization from a mixture *n*-hexane/CH_2Cl_2 (9/1). Decomposition = 336 °C; IR ($\nu_{C=N} = 1631$, 1591 cm^{-1}).

^{1}H NMR (300 MHz, DMSO-d, 25 °C, δ [ppm]): $\delta =$ 2.18 (s, 6H, CH_3); 6.83 (d, 2H, H_7); 6.92 (d, 2H, $H_{ar\,meta}$) 7.92–7.05 (m, 10H, $6H_{ar\,9,10,11}$ and $4H_{8,9}$).

^{13}C NMR (75.5 MHz, DMSO-d, 25 °C, δ [ppm]): $\delta = 17.15$ (MeC=N); 119.75 (C_{ortho}); 120.01 (C_7); 124.55 (C_{para}); 125.43 (C_{ortho}); 126.89 (C_{meta}), 127.36 (C_8), 128,37 (C_9); 130.27 (C_{10}); 130.96 ($C_{meta'}$): 131.98 (C_6); 142.69(C_{11}); 144.30 (C_{ipso}); 163.23 (C=N).

3.7. [(Ph-Bic)]$MoCl_2$ (**3c**)

Following general procedure, from $MoCl_4(thf)_2$ (0.7 mmol, 0.28 g), [(Ph-BIC)] (2.1 mmol, 0.694 g). Zinc (3.5 mmol, 0.228 g) in 20 ml of methylene chloride was obtained 0.165g (yield 52%) of **3c** as green solid after crystallization from a mixture *n*-hexane/CH_2Cl_2 (9/1). Decomposition = 318°C; IR ($\nu_{C=N} = 1675$; 1631; 1595 cm^{-1}).

^{1}H NMR (300 MHz, acetone-d, 25 °C, δ [ppm]): $\delta = 0.68$; 0.86; 0.98 (s, 3H chacun, $H_{12,13,14}$); 1.55–1.179 (m, 4H, $H_{8,9}$); 3.15 (d, 1H, H_{10}); 7.18–7.40 (m, 10H, Har).

^{13}C NMR (75.5 MHz, acetone-d, 25 °C, δ [ppm]): $\delta = 11.37$; 17.02; 21.20 ($C_{12,13,14}$); 23, 86, 32, 69 ($C_{8,9}$); 49, 11 (C_7); 49.97 (C_{10}); 56.04 (C_{11}); 121.54, 123.14 (C_{ortho}); 127.76 (C_{para}); 129.06, 129.78 (C_{meta}); 174.13; 176.10 (C=N).

4. X-ray structure determination

A crystal ($0.11 \times 0.31 \times 0.64$ mm) suitable for X-ray intensity data collection was selected. X-ray intensity data were collected on a MACH3 Enraf Nonius diffractometer using monochromated Mo Kα radiation ($\lambda = 0.71073$ Å) at 293 K. Accurate unit cell parameters and orientation matrix were determined from 25 reflections in the range 13–15°. Intensity data were collected by using the ω–2θ scan mode with a range of $2 < \theta < 27°$. All the intensity data were corrected for Lorentz and polarization effects. The crystal structure solution carried out with direct methods from the SHELXS-97 permitted the location of all non-hydrogen atoms. After anisotropic least-squares refinement, hydrogen atoms were placed at their geometrically calculated positions and refined riding on the corresponding atoms with isotropic thermal parameters. Final refinement based on the reflections [$I > 2\sigma(I)$] converged at $R_1 = 0.0808$, $wR_2 = 0.2265$ and goodness-of-fit = 0.996.

The experimental conditions of data collection, strategy followed for the structure determination, and final results are given in Table 1.

5. Supporting information

Crystallographic data for the structural analysis have been deposited with the Cambridge Crystallographic Data Centre, CCDC No. 268891. Copies of this information may be obtained free of charge from the Director, CCDC, 12 Union Road, Cambridge CB2 1EZ, UK; fax: +44 1223 336 033 or deposit@ccdc.cam.ac.uk.

References

[1] G. Van Koten, K. Vreize, Adv. Organomet. Chem. 21 (1982) 151.
[2] M. Brookhart, D.M. Lincoln, J. Am. Chem. Soc. 110 (1988) 8719.
[3] M. Brookhart, A.F. Volpe, D.M. Lincoln, I.T. Hovarth, J.M. Millar, J. Am. Chem. Soc. 112 (1990) 5634.
[4] M. Brookhart, F.C. Rix, J.M. Desimone, J.C. Barborak, J. Am. Chem. Soc. 114 (1992) 5894.
[5] M. Brookhart, E. Hauptman, J. Am. Chem. Soc. 114 (1992) 4437.
[6] M. Brookhart, E. Hauptman, D. Lincoln, J. Am. Chem. Soc. 114 (1992) 10394.
[7] F.C. Rix, M. Brookhart, J. Am. Chem. Soc. 117 (1995) 1137.
[8] F.C. Rix, M. Brookhart, P.S. White, J. Am. Chem. Soc. 118 (1996) 4746.
[9] F.C. Rix, M. Brookhart, P.S. White, J. Am. Chem. Soc. 118 (1996) 2436.
[10] R.A. Klein, F. Hartl, C.J. Elsevier, Organometallics 16 (1997) 1284.
[11] R. Van Asselet, C.J. Elsevier, C. Amatore, A. Jutand, Organometallics 16 (1997) 317.
[12] R. Van Asselet, K. Vrieze, J.C. Elsevier, J. Organomet. Chem. 480 (1994) 27.
[13] J.H. Groen, J.G.P. Delis, W.N.M. van Leeuwen, K. Vrieze, Organometallics 16 (1997) 68.
[14] J.H. Groen, C.J. Elsevier, K. Vrieze, W.J.J. Smeets, A.L. Spek, Organometallics 15 (1996) 3445.
[15] F. Stoffelbach, R. Poli, P. Richard, J. Organomet. Chem. 663 (2002) 269.
[16] F. Stoffelbach, B. Rebiere, R. Poli, Eur. J. Inorg. Chem. (2004) 726.
[17] T. Turki, T. Guerfel, F. Bouachir, submitted.
[18] K. Fromm, M. Plaikner, E.H. Hawkins, Z. Naturforsch. B 50 (1995) 894.
[19] A.J.L. Pombeiro, R.L. Richards, Transition Met. Chem. 5 (1980) 55.
[20] A.J.L. Pombeiro, R.L. Richards, Transition Met. Chem. 6 (1981) 255.
[21] B. Bildstein, H. Kopacka, M. Fontani, M. Malaun, P. Zanello, Inorg. Chim. Acta 300–302 (2000) 16.
[22] F.W. Grevels, K. Kerpen, W.E. Klotzbuecher, K. Schaffner, R. Goddard, B. Weimann, C. Kayran, S. Oezkar, Organometallics 20 (2001) 4775.
[23] K. Dreisch, C. Andersson, C. Stalhands, Polyhedron 12 (1993) 303.
[24] R.S. Herrick, C.J. Ziegler, H. Bohan, M. Corey, M. Eskander, J. Giguere, N. McMicken, I.E. Wrona, J. Organomet. Chem. 687 (2003) 178.
[25] K.Y. Rene, J. Lachicotte, R. Eisenberg, Organometallics 16 (1997) 5234.
[26] H. Tom Dieck, I.W. Renk, Chem. Ber. 104 (1971) 92.
[27] R. Van Asselt, C.J. Elsevier, A.L. Spek, R. Benedix, Recl. Trav. Chim. Pays-Bas 113 (1994) 88.

Table 1
Ligands substituted for H_2O in $(CO)_3(dppe)Mn(OH_2)$ (* indicates atom(s) attached to Mn)

A. Monodentate ligands

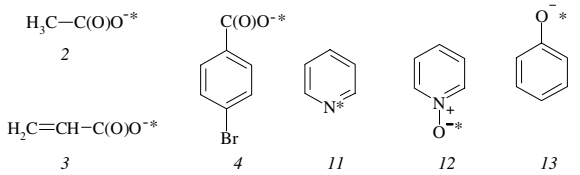

B. Polydentate ligands

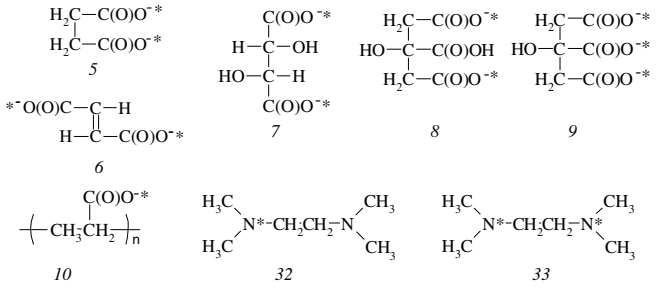

C. Ambident ligands

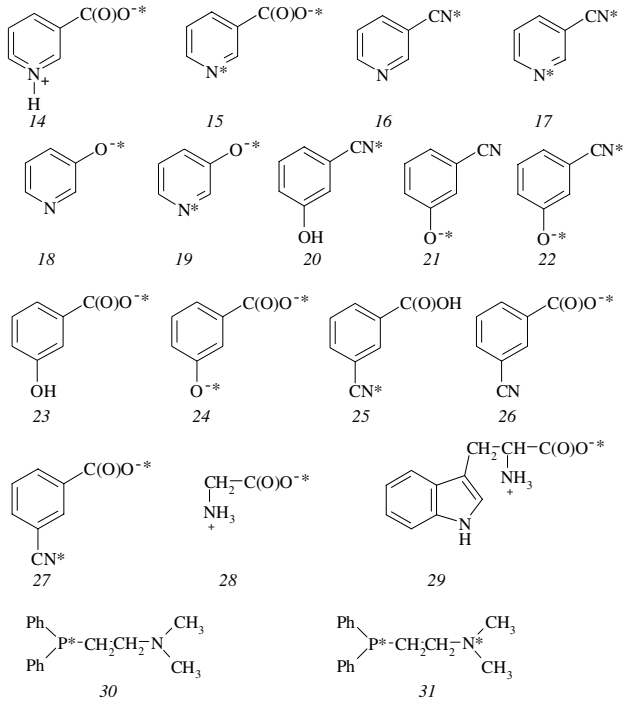

a magnetic stirrer and all involved the simple replacement of the aqua ligand of **1** by a new ligand. If the new ligand is neutral, it is used as a solution in $CHCl_3$, and if acidic, it is dissolved either in a few milliliters of water or in aqueous alkali. The general procedure was as follows: To a $CHCl_3$ solution of about 40–100 mg of **1** in about 20 mL $CHCl_3$, a solution of an equimolar quantity of the new ligand is added drop-wise. The order of addition is reversed when ambident ligands are used. After addition, stirring is continued for 10–20 min, the $CHCl_3$ solution is separated, washed with water, dried and evaporated. The resulting yellow to brown solids are thoroughly washed with hexane, dried in vacuo, collected and weighed. The yield of recovered product is 80–90%; the loss of material is incurred in handling the very small quantities involved. Only deviations form the general procedure are included in the experimental details. Our characterization of the new complexes, after ascertaining purity by TLC, relies very heavily on three techniques: high-resolution mass spectra (identification of the exact mass of the molecular ion and some significant daughter ions); close inspection of infrared spectra (carbonyl and nitrile stretching frequencies); and ^1H NMR spectra (particularly the chemical shifts of the dppe methylene protons). High-resolution mass spectra were obtained using a Kratos MS-25 high performance mass spectrometer fitted with an electrospray ionization (ESI) attachment. IR spectra were recorded on a P-E spectrum One FT-IR employing a 5-mm CaF_2 liquid cell. ^1H NMR data were obtained with $CDCl_3$ solutions using a Bruker AC-400 MHz spectrometer with the chemical shifts recorded relative to TMS $[Si(CH_3)_4]$. Ultimate analyses were not routinely determined, because, in addition to being less definitive for the characterization of pure compounds than exact mass spectra, such analyses are frequently unreliable and are further complicated by the tendency of many of these types of complexes to crystallize with non-integral molecules of solvent, which resist efforts to remove, and whose reported content must be adjusted in order to conform with results of ultimate analysis.

2.1. Reaction of *1* with monocarboxylic acids

2.1.1. Acetic acid complex, $[(CO)_3(dppe)MnOC(O)CH_3]$ (*2*)

Data ***2***: m.p.: softens at about 172 °C and decomposes above 178 °C; IR (cm^{-1}, $CHCl_3$): ν(CO) 2026, 1959 and 1910; ^1H NMR (δ, $CDCl_3$): 7.8–7.3 (m, 20H, Ph), 2.92 (m, 2H) and 2.74 (m, 2H) both from dppe, 2.18 (s, 3H, CH_3); High-resolution MS (m/z): 597.084, calc. for $[(CO)_3(dppe)MnOC(O)CH_3 + H]^+$, $C_{31}H_{28}O_5P_2Mn$, 597.079; 537.060, calc. for $[(CO)_3(dppe)Mn]^+$, $C_{29}H_{24}O_3P_2Mn$, 537.058.

The reversibility of the reaction was demonstrated by the following experiment. One drop of HBF_4 was added to the acetic acid complex **2**, dissolved in $CHCl_3$ and then stirred for 1 min. The IR of the solution showed the spectrum characteristic of the aqua complex **1**.

2.1.2. Acrylic acid complex, $[(CO)_3(dppe)MnOC(O)CH{=}CH_2]$ (*3*)

Data ***3***: m.p.: the color of the solid product changes from pale yellow at room temperature to white at 276–280 °C and decomposes at 372–378 °C; IR (cm^{-1}, $CHCl_3$): ν(CO) 2026, 1960 and 1911; ^1H NMR (δ, $CDCl_3$): 7.9–7.2 (m, 20H, Ph), 5.65 (t, 1H, CH), 4.97 (d, 2H, CH_2 attached to double bond), 2.91 (m, 2H), and 2.82 (m, 2H) both from

dppe; High-resolution MS (*m*/*z*): 609.0764, calc. for $[(CO)_3(dppe)MnOC(O)CH{=}CH_2 + H]^+$, $C_{32}H_{28}O_5P_2Mn$, 609.0792, 537.0335, calc. for $[(CO)_3(dppe)Mn]^+$, $C_{29}H_{24}O_3P_2Mn$, 537.058.

2.1.3. p-Bromobenzoic acid complex, [(CO)$_3$(dppe)MnOC(O)C$_6$H$_4$Br] (4)

The reaction was carried out using an aqueous solution of *p*-bromobenzoic acid.

Data **4**: m.p.: softens at about 192 °C and decomposes at above 225 °C; IR (cm^{-1}, $CHCl_3$): *v*(CO) 2027, 1959 and 1913; ^1H NMR (δ, $CDCl_3$): 7.9–7.2 (m, 24H, Ph), 2.99 (m, 2H) and 2.89 (m, 2H) both from dppe; High-resolution MS (*m*/*z*): 772.9814, calc. for $[(CO)_3(dppe)Mn{-}OC(O)C_6H_4Br\text{-}p + Cl]^-$, $C_{36}H_{28}O_5P_2BrClMn$, 772.9646 (Cl^- originated from the chloroform solvent used in the electrospray).

2.2. Reaction of 1 with dicarboxylic acids

Unless otherwise noted, aqueous solutions of the sodium salts of the acids were used.

2.2.1. Succinic acid complex, [(CO)$_3$(dppe)MnOC(O)CH$_2$CH$_2$C(O)OMn(dppe)(CO)$_3$] (5)

Data **5**: m.p.: softens at about 268 °C and decomposes above 298 °C; IR (cm^{-1}, $CHCl_3$): *v*(CO) 2025, 1958 and 1907; ^1H NMR (δ, $CDCl_3$): 7.9–7.2 (m, 40H, Ph), 2.86 (m, 4H, from dppe), 2.68 (m, 4H, from dppe), 2.52 (m, 2H, from succinic acid), 2.27 (m, 2H, from succinic acid); High-resolution MS (*m*/*z*): 1191.1299, calc. for $[(CO)_3(dppe)Mn{-}OC(O)CH_2CH_2C(O)O{-}Mn(dppe)(CO)_3 + H]^+$, $C_{62}H_{53}O_{10}P_4Mn_2$, 1191.135.

2.2.2. Fumaric acid complex, [(CO)$_3$(dppe)MnOC(O)CH=CHC(O)OMn(dppe)(CO)$_3$] (6)

Data **6**: m.p.: softens at about 145 °C and decomposes above 160 °C; IR (cm^{-1}, $CHCl_3$) *v*(CO) 2027, 1959 and 1914; ^1H NMR (δ, $CDCl_3$): 7.9–7.2 (m, 40H, Ph), 6.5 (s, 2H, from two CHs of fumaric acid moiety), 3.05 (m, 4H, from dppe), 2.84 (m, 4H, from dppe); High-resolution MS (*m*/*z*): 1189.200, calc. for $[(CO)_3(dppe)MnOC(O)CH{=}CHC(O)OMn(dppe)(CO)_3 + H]^+$, $C_{62}H_{51}O_{10}P_2Mn_2$, 1189.1188.

2.2.3. D-Tartaric acid complex, [(CO)$_3$(dppe)MnOC(O)(CHOH)$_2$C(O)OMn(dppe)(CO)$_3$] (7)

Data **7**: m.p.: softens at about 131 °C and decomposes above 154 °C; IR (cm^{-1}, $CHCl_3$) *v*(CO) 2029, 1962 and 1916; ^1H NMR (δ, $CDCl_3$): 7.9–7.2 (m, 40H, Ph), 2.95 (m, 4H, from dppe), 2.84 (m, 4H, from dppe); High-resolution MS (*m*/*z*): 1223.1241, calc. for $[(CO)_3(dppe)Mn{-}OC(O)(CHOH)_2C(O)O{-}Mn(dppe)(CO)_3 + H]^+$, $C_{62}H_{53}O_{12}P_2Mn_2$, 1223.1248.

2.3. Reaction of 1 with polycarboxylic acids

2.3.1. Preparation of citric acid complex, K^1(O),K^1(O)[(CO)$_3$(dppe)MnOC(O)CH$_2$–C(OH)(COOH)CH$_2$C(O)OMn(dppe)(CO)$_3$] (8)

8.2 mg (0.039 mM) of citric acid (99%, Aldrich) was suspended in a solution of **1** (75 mg, 0.117 mM) in 25 mL $CHCl_3$. After stirring for approximately 45 min, the solvent was removed by rotary evaporator. The residue was chromatographed on a column of neutral alumina gel with hexane and ethyl acetate as gradient eluents to give **8** as a yellow solid.

Data **8**: m.p.: softens at 205 °C and decomposes above 220 °C; IR (cm^{-1}, $CHCl_3$) *v*(CO) 2027, 1959 and 1916; ^1H NMR (δ, $CDCl_3$): 7.9–7.2 (m, 40H, Ph), 2.92 (m, 4H, from dppe), 2.72 (m, 4H, from dppe), 2.51 (s, 4H, CH_2); High-resolution MS (*m*/*z*): 1265.1896, calc. for $[(CO)_3(dppe)MnOC(O)CH_2C(OH)(COOH)CH_2C(O)OMn(dppe)(CO)_3 + H]^+$, $C_{64}H_{55}O_{13}P_4Mn_2$, 1265.19. *Anal.* Calc. for $C_{64}H_{54}O_{13}P_4Mn_2 \cdot 2H_2O \cdot C_6H_{14}$: C, 60.61; H, 5.23. Found: C, 59.34; H, 5.28% (NMR showed both water and hexane; the stoichiometry of the associated solvents is adjusted to conform with the hydrogen analysis). It is assumed that the manganese coordinates at the terminal carboxylic groups.

2.3.2. Preparation of citric acid complex, K^1(O),K^1(O),K^1(O)[(CO)$_3$(dppe)Mn–OC(O)CH$_2$C(OH)C(O)OMn(CO)$_3$(dppe)CH$_2$C(O)OMn(dppe)(CO)$_3$] (9)

A solution of **1** (75 mg, 0.117 mM) in 25 mL of $CHCl_3$ was added drop-wise to 3.9 mL of an aqueous solution containing 8.2 mg of citric acid (0.039 mM) and 4.68 mg of NaOH (0.117 mM). After stirring the mixture for approximately 75 min, the product was isolated in the usual manner.

Data **9**: m.p.: softens at 176 °C and decomposes above 200 °C; IR (cm^{-1}, $CHCl_3$) *v*(CO) 2026, 1955 and 1909; ^1H NMR (δ, $CDCl_3$): 7.9–7.2 (m, 40H, Ph), 2.96 (m, 6H, from dppe), 2.71 (m, 6H, from dppe), 2.51 (s, 4H, CH_2); High-resolution MS (*m*/*z*): 1802.2294 calc. for $[(CO)_3(dppe)MnOC(O)CH_2C(OH)C(O)OMn(CO)_3(dppe)CH_2C(O)OMn(dppe)(CO)_3 + H]^+$, $C_{93}H_{78}O_{16}P_6Mn_3$, 1802.19.

2.3.3. Na-polyacrlyate polymer complex, –[–CH$_2$–CH–[C(O)OMn(CO)$_3$(dppe)]]$_n$– (10)

A solution of the aqua complex, **1** (67.2 mg, 0.105 mM) in 25 mL of MeOH was placed in a round-bottom flask. A solution of sodium polyacrylate (10 mg, 0.005 mM) in 10 mL water was added drop-wise to the solution of **1** and the resulting solution was stirred for 2 h. During this time, the original clear solution became turbid. Stirring was continued overnight. The reaction mixture was evaporated to dryness with a rotary evaporator. The resulting solid was washed with 20 mL of $CHCl_3$ and 10 mL of CH_3OH leaving an orange solid, which was dried in vacuum. Yield 67%.

*Data **10***: m.p.: decomposes without melting at about 350 °C; IR (cm^{-1}, KBr): ν(CO) 2025, 1953 and 1910; *Anal*. Calc. for one unit of polymer, $C_{31}H_{27}O_5P_2Mn$: C, 62.42; H, 4.56; P, 10.38. Found: C, 60.25; H, 5.12; P, 9.86%. The calculated atomic C/P for one unit of polymer is 15.8; Found: 16.0, indicating that approximately each unit of the polyacrylate polymer is bonded to an Mn atom.

2.4. Reaction of **1** with pyridine and pyridine-N-oxide

2.4.1. Pyridine complex, $K^1(N)[(CO)_3(dppe)MnNC_5H_5]^+BF_4^-$ (**11**)

*Data **11***: m.p.: softens at about 103 °C and decomposes above 116 °C; IR (cm^{-1}, $CHCl_3$): ν(CO) 2030, 1957 and 1944; ^{1}H NMR (δ, $CDCl_3$): 7.90–6.65 (m, 20H, from Ph, 5H, from pyridine), 3.65 (m, 2H) and 3.25 (m, 2H) both from dppe; Low temperature (−53 °C) ^{1}H NMR gave the same two signals with the same intensity. High-resolution MS (*m*/*z*): 616.0856, calc. for $[(CO)_3(dppe)MnNC_5H_5]^+$, $C_{34}H_{29}NO_3P_2Mn$, 616.0921.

2.4.2. Pyridine-N-oxide complex, $K^1(O)[(CO)_3(dppe)MnONC_5H_4]^+BF_4^-$ (**12**)

*Data **12***: m.p.: softens at about 82 °C and decomposes above 90 °C; IR (cm^{-1}, $CHCl_3$): ν(CO) 2025, 1950 and 1925; ^{1}H NMR (δ, $CDCl_3$): 7.8–6.8 (m, 20H, from dppe Ph, 5H, from pyridine-*N*-oxide), 3.41 (m, 2H), 2.88 (m, 2H) both from dppe CH_2; High-resolution MS (*m*/*z*): 632.0970, calc. for $[(CO)_3(dppe)MnONC_5H_5]^+$, $C_{34}H_{29}NO_4P_2Mn$, 632.0952, 537.0581, calc. for $[Mn(dppe)(CO)_3]$, $C_{29}H_{24}O_3P_2Mn$, 537.0581.

2.4.3. Reaction of **1** with 1:1 mixture of pyridine and pyridine-N-oxide

Data: ^{1}H NMR (δ, $CDCl_3$): 7.8–6.8 (m, 40H, from dppe Ph, 5H, from pyridine and 5H, from py-*N*-oxide), 3.62 (m, 2H, from pyridine complex), 3.41 (m, 2H, from pyridine-*N*-oxide complex), 3.25 (m, 2H, from pyridine complex), 2.89 (m, 2H, from pyridine-*N*-oxide complex) These data (Table 2) for the dppe CH_2 indicate that both ligand complexes were present; from the relative intensities it was estimated that they were present in approximately equal quantities.

2.5. Reaction of **1** with phenolate anion

2.5.1. Preparation of phenol complex, $[(CO)_3(dppe)MnOC_6H_5]$ (**13**)

The reaction was carried out either by using pure phenol, or more rapidly, by adding complex **1** in $CHCl_3$ to an aqueous NaOH solution of phenol.

*Data **13***: m.p.: softens at about 128 °C and decomposes above 142 °C; IR (cm^{-1}, $CHCl_3$): ν(CO) 2017, 1942 and 1906; ^{1}H NMR (δ, $CDCl_3$): 7.8–7.1 (m, 25H, Ph), 2.97 (m, 2H) and 2.83 (m, 2H) both from dppe; High-resolution MS (*m*/*z*): 630.19, calc. for $[(CO)_3(dppe)Mn–OC_6H_5 + H]^+$, $C_{35}H_{30}O_4P_2Mn$, 630.20; 537.028, calc. for $[Mn(CO)_3\text{-}(dppe)]^+$, $C_{29}H_{24}O_3P_2Mn$, 537.058.

2.6. Reaction of **1** with ambident ligands

2.6.1. Derivatives of pyridine

2.6.1.1. $K^1(O)$ complex with pyridine-3-carboxylic acid, (nicotinic acid), $[(CO)_3(dppe)MnOC(O)C_5H_4N]$ (**14**).

*Data **14***: m.p.: softens at about 108 °C and decomposes above 135 °C; IR (cm^{-1}, $CHCl_3$): ν(CO) 2027, 1960 and 1914; ^{1}H NMR (δ, $CDCl_3$): 7.9–7.2 (m, 24H, Ph), 3.02 (m, 2H) and 2.87 (m, 2H) both from dppe; High-resolution MS (*m*/*z*): 660.105, calc. for $[(CO)_3(dppe)MnNC_5H_4\text{-}C(O)OH]^+$, $C_{35}H_{29}NO_5P_2Mn$, 660.112.

2.6.1.2. $K^1(N),K^1(O)$ dinuclear Mn complex with pyridine-3-carboxylic acid, (nicotinic acid), $[(CO)_3(dppe)MnN\text{-}C_5H_4C(O)OMn(dppe)(CO)_3]^+BF_4^-$ (**15**).

Pure **15** was obtained by column chromatography on neutral alumina using hexane and ethyl acetate as gradient eluents.

*Data **15***: m.p.: softens at 110 °C and decomposes above 150 °C; IR (cm^{-1}, $CHCl_3$): ν(CO) 2027 (broad), 1960 (broad) and 1939 (shoulder) and 1913; ^{1}H NMR (δ, $CDCl_3$): 8.73 (m), 8.35 (m, H) and 7.98 (m, H) all from nicotinic acid moiety, 7.9–7.2 (m, 40H, from Ph) 6.97 (m, H, from nicotinic acid), 3.63 (m, 2H, from dppe bonded to the Mn attached to N), 3.20 (m, 2H, from dppe bonded to the Mn attached to N), 3.01 (m, 2H, from dppe bonded to the Mn attached to the acid group), 2.85 (m, 2H, from dppe bonded to the Mn attached to the acid group); High-resolution MS (*m*/*z*): 1196.1440, calc. for $[(CO)_3\text{-}(dppe)Mn–NC_5H_4C(O)O–Mn(dppe)(CO)_3]$ $C_{64}H_{52}NO_8\text{-}P_4Mn_2$, 1196.1404; 537.0581, calc. for $[Mn(dppe)(CO)_3]$, $C_{29}H_{24}O_3P_2Mn$, 537.0581. This complex was also prepared by adding 2 molar equivalents of aqua complex to 1 mol of nicotinic acid.

2.6.1.3. $K^1(NC)$ complex with 4-cyanopyridine, $[(CO)_3\text{-}(dppe)MnNCC_5H_4N]^+BF_4^-$ (**16**).

The product was chromatographed on a column of neutral alumina with hexane and ethyl acetate as gradient eluents to give pure **16**.

*Data **16***: m.p.: softens at about 85 °C and decomposes above 108 °C; IR (cm^{-1}, $CHCl_3$): ν(CO) 2039, 1971 and 1961: ^{1}H NMR (δ, $CDCl_3$): 7.8–6.8 (m, 20H, from dppe Ph, 4H, from 4-cyanopyridine), 3.48 (m, 2H), 3.05 (m, 2H) both from dppe CH_2; High-resolution MS (*m*/*z*): 641.0930, calc. for $[(CO)_3(dppe)MnNCC_5H_4N]^+$, $C_{35}H_{28}\text{-}N_2O_3P_2Mn$, 641.0956, 537.0316, calc. for $[Mn(dppe)(CO)_3]$, $C_{29}H_{24}O_3P_2Mn$, 537.0581.

2.6.1.4. Preparation of $K^1(NC),K^1(N)$ dinuclear Mn complex with 4-cyanopyridine, $[(CO)_3(dppe)MnNCC_5H_4\text{-}N–Mn(dppe)(CO)_3]^{2+}2BF_4^-$ (**17**).

The crude product was chromatographed on neutral alumina with hexane and ethyl acetate as gradient eluents to give pure **17**.

*Data **17***: m.p.: softens at about 105 °C and decomposes above 128 °C; IR (cm^{-1}, $CHCl_3$): ν(CO) 2039, 2027

Table 2
Chemical shift of dppe CH_2 protons (ppm) and IR spectra (cm^{-1}, in $CHCl_3$) of $(CO)_3$(dppe)MnZ

Complex No.	Attached to Mn		DPPE methylene protons (δ) ppm			Stretching frequencies			
						CO			CN
	Z	Atom of	CH_2[a]	CH_2[b]	Diff.	A′	A″	A′	
1	H_2O (−53 °C)	O	3.04	2.65	0.39				
1	H_2O (25 °C)	O	2.97	2.97	0.00	2035	1965	1934	
2	Acetic acid	O	2.92	2.74	0.18	2026	1959	1910	
3	Acrylic acid	O	2.91	2.82	0.09	2026	1960	1911	
4	*p*-Bromobenzoic acid	O	2.99	2.89	0.10	2027	1959	1913	
5	Succinic acid[c]	O, O	2.86[d]	2.68[d]	0.18	2025	1958	1907	
6	Fumaric acid[c]	O, O	3.05[d]	2.84[d]	0.21	2027	1959	1914	
7	D-Tartaric Acid[c]	O, O	2.95[d]	2.84[d]	0.11	2029	1962	1916	
8	Citric acid[c]	O, O	2.92[d]	2.72[d]	0.20	2027	1959	1916	
9	Citric acid[c]	O, O, O	2.96[e]	2.71[e]	0.15	2026	1955	1909	
10	Na-Polyacrylate[c,f]					2025	1953	1910	
11	Pyridine (25 °C)	N	3.65	3.25	0.40	2030	1957	1944	
11	Pyridine (−50 °C)	N	3.53	3.20	0.33				
12[g]	Pyridine-*N*-oxide	O	3.41	2.88	0.53	2025	1950	1925	
13	Phenol	O	2.97	2.83	0.14	2017	1942	1906	
14	Nicotinic acid	O	3.02	2.87	0.15	2027	1960	1914	
15	Nicotinic acid	N	3.63	3.20	0.43	2027	1960	1939	
15	Nicotinic acid	O	3.01	2.85	0.16	2027	1960	1913	
16	4-Cyanopyridine	CN	3.48	3.05	0.43	2039	1971	1961	2259
17	4-Cyanopyridine (2)	N	3.50	3.11	0.39	2027	1961	1939	2240
		CN	3.50	3.11	0.39	2039	1971	1961	2259
18	3-Hydroxypyridine	O	3.07	2.92	0.15	2025	1948	1922	
19	3-Hydroxypyridine (2)	O	3.05	2.89	0.16	2028	1955	1918	
		N	3.59	3.23	0.36	2028	1955	1940	
20	3-Cyanophenol	N	3.39	3.04	0.35	2038	1971	1959	2257
21	3-Cyanophenol	O	2.99	2.83	0.16	2019	1945	1911	2223
22	3-Cyanophenol (2)	N	3.36	3.04	0.32	2038	1971	1958	2257
		O	3.01	2.85	0.16	2021	1947	1912	
23	3-Hydroxybenzoic acid	C(O)O	3.00	2.85	0.15	2027	1960	1911	
24	3-Hydroxybenzoic acid[c]	C(O)O, O	3.03[d]	2.85[d]	0.18	2027	1959	1916	
25	3-Cyanobenzoic acid	N	3.27	2.86	0.41	2038	1969	1960	2259
26	3-Cyanobenzoic acid	O	3.00	2.83	0.17	2028	1961	1914	2231
27	3-Cyanobenzoic acid (2)	N	3.26	2.86	0.40	2038	1969	1960	2259
		O	3.00	2.74	0.16	2027	1960	1916	
28	Glycine	O	3.03	2.87	0.16	2026	1953	1908	
29	Tryptophan	O	3.15	2.95	0.20	2026	1955	1910	
30	$Ph_2PCH_2CH_2N(CH_3)_2$	P	3.34	3.09	0.25	2027	1958	1917	
31	$Ph_2PCH_2CH_2N(CH_3)_2$ (2)	P	3.34	3.09	0.25	1931	1957	1916	
		N	2.97	2.80	0.17	1931	1957	1934	
32	$(CH_3)_2NCH_2CH_2N(CH_3)_2$	N	3.05	2.87	0.18	2025	1952	1908	
33	$(CH_3)_2NCH_2CH_2N(CH_3)_2$[c]	N, N	3.05	2.87	0.18	2025	1951	1906	
34[h]	$(CH_3)_2NCH_2CH_2N(CH_3)_2$	N	2.7	2.58	0.12	2015	1919	1895	
35	Hydride (at 25 and 100 °C)	H	2.51	2.23	0.28	1995	1915	1910	
36	Nitrato (at 25 and 100 °C)	O	2.97	2.80	0.17	2034	1968	1925	

[a] Assumed to be "*trans*" to apical CO.
[b] Assumed to be "*cis*" to apical CO.
[c] CO stretching frequencies essentially the same for each set of carbonyls.
[d] Integrates for four protons for each signal.
[e] Integrates for six protons for each signal.
[f] IR spectra of Na-polyacrylate complex was taken by using Kbr pellet.
[g] This complex is excluded from the generalizations discussed below.
[h] K^2(N) complex.

(shoulder) 1971, 1961 (broad) and 1939 shoulder; ^{1}H NMR (δ, $CDCl_3$): 7.8–6.8 (m, 40H, from dppe Ph, 4H, from 4-cyanopyridine), 3.50 (broad, m, 4H), 3.11 (broad, m, 4H) both from dppe CH_2; High-resolution MS (*m*/*z*): 1178.1601, calc. for $[(CO)_3(dppe)MnNCC_5H_4N–Mn(dppe)(CO)_3]^{2+}$, $C_{64}H_{62}N_2O_6P_4Mn_2$, 1178.1537. This complex was also prepared by adding one mole of **1** to a solution of **17**.

*2.6.1.5. Preparation of $K^1(O)$ complex with 3-hydroxypyridine, $[(CO)_3(dppe)Mn–OC_5H_4N]$ (**18**).* A solution of **1** was added drop-wise to a solution containing an equimolar

quantity of 3-hydroxypyridine dissolved in aqueous NaOH.

*Data **18***: m.p.: softens at about 75 °C and decomposes above 88 °C; IR (cm^{-1}, $CHCl_3$): ν(CO) 2025, 1948 and 1922: ^1H NMR (δ, $CDCl_3$): 7.8–6.8 (m, 20H, from dppe Ph, 4H, from 3-hydroxypyridine), 3.07 (m, 2H), 2.92 (m, 2H) both from dppe CH_2; High-resolution MS (*m*/*z*): 632.1005, calc. for $[(CO)_3(dppe)MnOC_5H_4N + H]^+$, $C_{34}H_{29}NO_4P_2Mn$, 632.0952, 537.0556, calc. for $[Mn(dppe)(CO)_3]$, $C_{29}H_{24}O_3P_2Mn$, 537.0581.

*2.6.1.6. $K^1(O),K^1(N)$ dinuclear Mn complex with 3-hydroxypyridine, $[(CO)_3(dppe)MnOC_5H_4NMn(dppe)(CO)_3]^+BF_4^-$ (**19**).* The reaction was carried out in $CHCl_3$ using an equimolar solution of **1** and **18**.

*Data **19***: m.p.: softens at about 89 °C and decomposes above 112 °C; IR (cm^{-1}, $CHCl_3$): ν(CO) 2028 (broad), 1955 (broad), 1940 (shoulder) and 1918; ^1H NMR (δ, $CDCl_3$): 7.8–6.8 (m, 40H, from dppe Ph, 4H, from 3-hydroxypyridine), 3.59 (m, 2H, from dppe bonded to the Mn attached to N), 3.23 (m, 2H, from dppe bonded to the Mn attached to N), 3.05 (m, 2H, from dppe bonded to the Mn attached to O), 2.89 (m, 2H, from dppe bonded to the Mn attached to O); High-resolution MS (*m*/*z*): 1168.1505, calc. for $[(CO)_3(dppe)MnOC_5H_4N–Mn(dppe)(CO)_3]^+$, $C_{63}H_{62}NO_7P_4Mn_2$, 1168.1454, 537.0567, calc. for $[Mn(dppe)(CO)_3]$, $C_{29}H_{24}O_3P_2Mn$, 537.0581. This complex was also prepared by using 2 molar equivalents of **1** to one of 3-hydroxypyridine.

2.6.2. Derivatives of phenol

*2.6.2.1. Preparation of $K^1(N)$ complex with 3-cyanophenol, $[(CO)_3(dppe)Mn–NCC_6H_4OH]^+BF_4^-$ (**20**).* The reaction was carried out in $CHCl_3$ using equimolar amounts of **1** and ligand.

*Data **20***: m.p.: softens at about 155 °C and decomposes above 163 °C; IR (cm^{-1}, $CHCl_3$): ν(CO) 2038, 1971 and 1959: ^1H NMR (δ, $CDCl_3$): 7.8–6.2 (m, 20H, from dppe Ph, 5H, from 3-cyanophenol), 3.39 (m, 2H), 3.04 (m, 2H) both from dppe CH_2; High-resolution MS (*m*/*z*): 656.0961, calc. for $[(CO)_3(dppe)MnNCC_6H_4OH]^+$, $C_{36}H_{29}NO_4P_2Mn$, 656.0952, 537.0461, calc. for $[Mn(dppe)(CO)_3]$, $C_{29}H_{24}O_3P_2Mn$, 537.0581.

*2.6.2.2. Preparation of $K^1(O)$ complex with 3-cyanophenol, $[(CO)_3(dppe)MnOC_6H_4CN]$ (**21**).* The reaction was carried out using a $CHCl_3$ solution of **1** and a molar equivalent of 3-cyanophenol in aqueous NaOH.

*Data **21***: m.p.: softens at about 167 °C and decomposes above 181 °C; IR (cm^{-1}, $CHCl_3$): ν(CO) 2019, 1945 and 1911; ^1H NMR (δ, $CDCl_3$): 7.8–6.2 (m, 20H, from dppe Ph, 5H, from 3-cyanophenol), 2.99 (m, 2H), 2.83 (m, 2H) both from dppe CH_2; High-resolution MS (*m*/*z*): 656.0991, calc. for $[(CO)_3(dppe)MnOC_6H_4CN + H]$, $C_{36}H_{29}$-NO_4P_2Mn, 656.0952, 537.0603, calc. for $[Mn(dppe)(CO)_3]$, $C_{29}H_{24}O_3P_2Mn$, 537.0581. In the absence of alkali but in the presence of water, **20**, and an almost equal quantity of **21** were formed.

*2.6.2.3. Preparation of $K^1(N),K^1(O)$ dinuclear Mn complex with 3-cyanophenol, $[(CO)_3(dppe)MnNCC_6H_4OMn(dpp)(CO)_3]^+BF_4^-$ (**22**).* A $CHCl_3$ solution of two molar equivalents of **1** is added to an aqueous NaOH solution of one molar equivalent of 3-cyanophenol. Compound **22** was also prepared by adding molar equivalents of **1** to either **20** or **21**.

*Data **22***: m.p.: softens at about 162 °C and decomposes above 178 °C; IR (cm^{-1}, $CHCl_3$): ν(CO) 2038, 2021, 1971, broad 1957 (1959 due to CN, and 1956 due to OH merged) and 1912; ^1H NMR (δ, $CDCl_3$): 7.8–6.2 (m, 40H, from dppe Ph, 4H, from 3-cyanophenol), 3.36 (m, 2H), 3.04 (m, 2 H) both from dppe CH_2 Mn attached to N; 3.01 (m, 2H), 2.85 (m, 2H) both from dppe CH_2 of Mn attached to O; High-resolution MS (*m*/*z*): 1192.1501, calc. for $[(CO)_3(dppe)MnNC$-$C_6H_4OMn(dppe)(CO)_3]^+$, $C_{65}H_{52}O_5P_2Mn_2$, 1192.1454, 656.0961, calc. for $[(CO)_3(dppe)MnNCC_6H_4OH]^+$, $C_{36}H_{29}NO_4P_2Mn$, 656.0952; 537.0461, calc. for $[Mn(dppe)$-$(CO)_3]$, $C_{29}H_{24}O_3P_2Mn$, 537.0581.

2.6.3. Derivatives of benzoic acid

*2.6.3.1. Preparation of $K^1(OCO)$ complex with 3-hydroxybenzoic acid, $[(CO)_3(dppe)Mn–OC(O)C_6H_4OH]$ (**23**).* The reaction was carried out by adding a $CHCl_3$ solution of **1** to an equimolar quantity of 3-hydroxybenzoic acid in aqueous $NaHCO_3$.

*Data **23***: m.p.: softens at about 114 °C and decomposes at above 124 °C; IR (cm^{-1}, $CHCl_3$): ν(CO) 2027, 1960 and 1911; ^1H NMR (δ, $CDCl_3$): 7.9–6.8 (m, 20H, from dppe Ph, 4H, from 3-hydroxybenzoic acid), 3.00 (m, 2H) and 2.85 (m, 2H) both from dppe CH_2; High-resolution MS (*m*/*z*): 673.0842, calc. for $[(CO)_3(dppe)Mn–OC_6H_4$-$COOH + H]$, $C_{37}H_{30}O_6P_2Mn$, 674.0820.

*2.6.3.2. Preparation of $K^1(OCO),K^1(O)$ complex of 3-hydroxybenzoic acid, $[(CO)_3(dppe)Mn–OC(O)C_6H_4$-$O–Mn(dppe)(CO)_3]$ (**24**).* A $CHCl_3$ solution of two molar equivalents of **1** is added to one molar equivalent of an aqueous NaOH solution of 3-hydroxybenzoic acid.

*Data **24***: m.p.: softens at about 118 °C and decomposes above 133 °C; IR (cm^{-1}, $CHCl_3$): ν(CO) 2027, 1959 and 1916; ^1H NMR (δ, $CDCl_3$): 7.9–7.2 (m, 40H, from dppe Ph, 4H, from 3-hydroxybenzoic acid), 3.03 (broad, m, 4H) and 2.85 (broad, m, 4H) both from dppe CH_2; High-resolution MS (*m*/*z*): 1211.1406, calc. for $[(CO)_3(dppe)$-$Mn–OC(O)C_6H_4O–Mn(dppe)(CO)_3 + H]^+$, $C_{65}H_{53}O_9P_4Mn_2$, 1211.1401.

*2.6.3.3. Preparation of $K^1(N)$ complex with 3-cyanobenzoic acid, $[(CO)_3(dppe)Mn–NCC_6H_4COOH]^+BF_4^-$ (**25**).* The reaction is carried out in carefully dried MeOH. The yellow solid consisted of two complexes, which were separated by chromatography on a neutral alumina column. Based on spectroscopic data, the composition of the

mixture was estimated to consist of about 85% of **25** and 15% of **26**.

*Data **25***: m.p.: softens at about 106 °C and decomposes at above 112 °C; IR (cm^{-1}, $CHCl_3$): ν(CO) 2038, 1969 and 1960; ^1H NMR (δ, $CDCl_3$): 7.9–7.2 (m, 20H, from dppe Ph, 4H, from 3-cyanobenzoic acid), 3.27 (m, 2H) and 2.86 (m, 2H) both from dppe; High-resolution MS (*m*/*z*): 684.0953, calc. for $[(CO)_3(dppe)Mn–NCC_6H_4COOH]^+$, $C_{37}H_{29}O_5P_2NMn$: 684.0901.

*2.6.3.4. Preparation of $K^1(O)$ complex with 3-cyanobenzoic acid, $[(CO)_3(dppe)Mn–O(O)CC_6H_4CN]$ (**26**).* A $CHCl_3$ solution of **1** is added to an equimolar quantity of 3-cyanobenzoic acid in aqueous NaOH.

*Data **26***: m.p.: softens at about 112 °C and decomposes at above 120 °C; IR (cm^{-1}, $CHCl_3$): ν(CO) 2028, 1961 and 1914; ^1H NMR (δ, $CDCl_3$): 7.9–7.2 (m, 20H, from dppe, 4H, from 3-cyanobenzoic acid), 3.00 (m, 2H) and 2.83 (m, 2H) both from dppe; High-resolution MS (*m*/*z*): 684.0961, calc. for $[(CO)_3(dppe)Mn–O(O)CC_6H_4CN + H]^+$, $C_{37}H_{29}O_5P_2NMn$, 684.0901.

*2.6.3.5. Preparation of $K^1(O),K^1(N)$ dinuclear Mn complex with 3-cyanobenzoic acid, $[(CO)_3(dppe)Mn–O(O)-CC_6H_4CN–Mn(dppe)(CO)_3]^+BF_4^-$ (**27**).* A $CHCl_3$ solution of two molar equivalents of **1** is added to one molar equivalent of 3-cyanobenzoic acid in aqueous NaOH solution.

*Data **27***: m.p.: softens at about 118 °C and decomposes above 124 °C; IR (cm^{-1}, $CHCl_3$): ν(CO) 2038, 2027 and 1969, cyanobenzoic acid, 3.26 (m, 2H), 2.86 (m, 2H) both from dppe CH_2 Mn attached to N; 3.00 (m, 2H), 2.74 (m, 2H) both from dppe CH_2 Mn attached to O; High-resolution MS (*m*/*z*): 3.36 (m, 2H), 3.04 (m, 2H); 3.01 (m, 2H), 2.85 (m, 2H) both from dppe CH_2 of Mn attached to O; High-resolution MS (*m*/*z*): 1220.1394, calc. for $[(CO)_3(dppe)Mn-OC(O)C_6H_4CN–Mn(dppe)(CO)_3]^+$, $C_{65}H_{62}O_8P_4NMn_2$, 1220.140.

*2.6.4. Reaction of **1** with amino acids*

*2.6.4.1. Preparation of $K^1(O)$ complex with glycine, $[(CO)_3(dppe)MnOC(O)CH_2NH_2]$ (**28**).* A $CHCl_3$ solution of **1** is added to an equimolar aqueous solution of glycine.

*Data **28***: m.p.: softens at about 130 °C and decomposes above 138 °C; IR (cm^{-1}, $CHCl_3$): ν(CO) 2026, 1953.7 and 1908; ^1H NMR (δ, $CDCl_3$): 7.9–7.2 (m, 20H, from dppe, 4H, from 3-cyanobenzoic acid), 3.03 (m, 2H) and 2.87 (m, 2H) both from dppe; High-resolution MS (*m*/*z*): 612.0921, calc. for $[(CO)_3(dppe)Mn–OC(O)CH_2NH_2 + H]^+$, $C_{31}H_{29}O_5P_2NMn$, 6121.0903.

*2.6.4.2. $K^1(O)$ complex with tryptophan, $[(CO)_3(dppe)-Mn–OC(O)CHCH_2(NH_2)C_8H_5N]$, (**29**).* The reaction is carried out in MeOH.

*Data **29***: m.p: softens at about 138 °C and decomposes above 160 °C; IR (cm^{-1}, $CHCl_3$): ν(CO) 2026, 1955 and 1910; ^1H NMR (δ, $CDCl_3$): 7.9–7.2 (m, 20H, from dppe, 4H, from 3-cyanobenzoic acid), 5.1 (broad peak due to NH_3^+ zwitter ion), 3.15 (m, 2H), and 2.95 (m, 2H) both from dppe; 2.5 (m, 2H) from CH_2 of tryptophan, 2.25 (t, H) from CH of tryptophan; High-resolution MS (*m*/*z*): 726.138, calc. for $[(CO)_3(dppe)Mn–OC(O)CHCH_2(NH_2)-C_8H_5N + H]^+$, $C_{40}H_{35}O_5P_2NMn$, 726.1372.

*2.6.5. Reaction of **1** with $Ph_2PCH_2CH_2N(CH_3)_2(pn)$*

*2.6.5.1. Preparation of $K^1(P)[(CO)_3(dppe)MnP(Ph)_2-CH_2CH_2N(CH_3)_2]^+BF_4^-$ (**30**).* The reaction is carried out by adding a $CHCl_3$ solution of **1** to a $CHCl_3$ solution of half the molar equivalent of pn.

*Data **30***: m.p.: softens at about 87 °C, decomposes above 104 °C; IR (cm^{-1}, $CHCl_3$): ν(CO) 2027, 1958 and 1917; ^1H NMR (δ, $CDCl_3$): 8.0–7.0 (m, 30H, Ph), 3.34 (m, 2H), 3.09 (m, 2H), 3.02 (m, 2H attached to P of pn), 2.72 (2H, CH_2 attached to N), 2.27 (s, 6H, CH_3 attached to N); High-resolution MS (*m*/*z*): 794.1915, calc. for $[(CO)_3Mn(dppe)P(Ph)_2CH_2CH_2\ N(CH_3)_2]$, $C_{45}H_{44}NO_3P_3Mn$, 794.1910; 537.023, calc. for $[(CO)_3Mn(dppe)]$, $C_{29}H_{24}O_3P_2Mn$, 537.058.

*2.6.5.2. $K^1(P),K^1(N)[(dppe)(CO)_3MnP(Ph)_2(CH_2)_2N-(CH_3)Mn(CO)_3(dppe)]^{2+}2BF_4^-$ (**31**).* A $CHCl_3$ solution of equimolar quantities of **1** and **30** was used.

*Data **31***: m.p.: softens at 144 °C, decomposes above 210 °C; IR (cm^{-1}, $CHCl_3$): ν(CO) 2031(broad), 1957(broad), 1913 (broad) and 1916; ^1H NMR (δ, $CDCl_3$): 8.00–7.00 (m, 50H, Ph), 3.39 (m, 2H, from dppe bonded to the Mn attached to N), 3.10 (m, 2H, from dppe, bonded to the Mn attached to P of pn), 3.01 (m, 4H, CH_2 attached to P of pn), 2.97 (m, 2H, from dppe bonded to the Mn attached to N), 2.80 (m, 2H, from dppe bonded to the Mn attached to N), 2.79 (m, 2H, CH_2 attached to N), 2.60 (s, 6H, $2CH_3$ attached to N); High-resolution MS (*m*/*z*): 1418.2647, calc. for $[(dppe)(CO)_3Mn–P(Ph)_2(CH_2)_2N(CH_3)_2–Mn(CO)_3(dppe)]^{2+}BF_4^-$, 1418.2530; 822.2166, calc. for $[(dppe)(CO)_3Mn–P(Ph)_2(CH_2)_2N-(CH_3)_2H]^{2+}BF_4$, 882.2029, 794.1882, calc. for $[(CO)_3-Mn(dppe)P(Ph)_2CH_2CH_2N(CH_3)_2]$, $C_{45}H_{44}NO_3P_3Mn$, 794.1915, 537.047, calc. for $[(CO)_3Mn(dppe)]$, $C_{29}H_{24}O_3-P_2Mn$, 537.058.

*2.7. Reaction of **1** with $(CH_3)_2NCH_2CH_2N(CH_3)_2$ (**TMED**)*

*2.7.1. $K^1(N)[(CO)_3(dppe)Mn–N(CH_3)_2CH_2CH_2N-(CH_3)_2]^+BF_4^-$ (**32**)*

A $CHCl_3$ solution of **1** is added drop-wise to a half molar equivalent of TMED in $CHCl_3$.

*Data **32***: m.p.: softened at 107 °C, decomposes at above 116 °C; IR (cm^{-1}, $CHCl_3$): ν(CO) 2025, 1952 and 1908. ^1H NMR (δ, $CDCl_3$): 7.80–7.20 (m, 20H, Ph), 3.05 (m, 2H, CH_2) and 2.87 (m, 2H, CH_2) both from dppe, 2.78 (s, 3H, CH_3 attached to quaternary N), 2.75 (s, 3H, CH_3 attached to quaternary N), 2.52 (m, 2H, CH_2 attached to quaternary N), 2.39 (m, 2H, CH_2 attached to tertiary N),

2.24 (s, 6H, CH_3 attached to tertiary N); High-resolution MS (*m/z*): 643.234, calc. for [$(CO)_3$(dppe)Mn–N$(CH_3)_2$ $CH_2CH_2N(CH_3)_2$], $C_{35}H_{38}N_2O_3P_2Mn$, 643.268, 537.042, calc. for [$(CO)_3$Mn(dppe)], $C_{29}H_{24}O_3P_2Mn$, 537.058.

2.7.2. $K^1(N)$, $K1(N)[(CO)_3(dppe)MnN(CH_3)_2$-$CH_2CH_2N(CH_3)_2Mn(CO)_3(dppe)]^{2+}2BF_4^-$ (**33**)

A $CHCl_3$ solution of TMED is added to an equimolar $CHCl_3$ solution of **1** and the product recrystallized from $CHCl_3$/hexane.

Data ***33***: m.p.: softens at about 120 °C and decomposes above 142 °C; IR (cm^{-1}, $CHCl_3$): *ν*(CO) 2025, 1951 and 1906; ^1H NMR (*δ*, $CDCl_3$): 8.00–7.00 (m, 40H, Ph), 3.07 (m, 4H, from dppe), 2.91 (m, 4H, from dppe) 2.79 (s, 6H, $2CH_3$ attached to N), 2.73 (s, 6H, $2CH_3$ attached to N), 2.52 (m, 2H, attached to N), 2.51 (s, 2H, attached to N); High-resolution MS (*m/z*): 1277.1953; calc. for [$(CO)_3$(dppe)MnN$(CH_3)_2CH_2CH_2N(CH_3)_2Mn(CO)_3$(dppe)]$^+$ BF_4^-, $C_{64}H_{64}N_2O_6P_4Mn_2BF_4$, 1277.2505, 1191.1655, calc. for [$(CO)_3$(dppe)Mn–N$(CH_3)_2CH_2CH_2N(CH_3)_2$–Mn$(CO)_3$(dppe) + H]$^+$, $C_{64}H_{65}N_2O_6P_4Mn_2$, 1191.2554.

2.7.3. $[K^2(N,N\text{-}TMED)]Mn(CO)_3Br$ (**34**)

To a solution of $Mn(CO)_5Br$ [6] (0.274 g, 1.0 mmol), in 20 mL of toluene in a round-bottom flask equipped with a condenser, 0.150 mL (1.0 mmol) of TMED dissolved in 20 mL of toluene is added drop-wise. The solution is refluxed for 3 h and the toluene is removed via rotary evaporator to give a brown solid, which is dissolved in benzene, stirred for 5 min and filtered. The filtrate is evaporated via rotary evaporator. The brown solid is recrystallized from 1:1 CH_2Cl_2/hexane, giving orange crystals of **34**. Yield 75%.

Data ***34***: m.p.: 154–158 °C, IR (cm^{-1}, CH_2Cl_2): *ν*(CO) 2015, 1919, 1893 and 1895 as a doublet; ^1H NMR (*δ*, $CDCl_3$): 2.98 (s, 6H, CH_3), 2.92 (s, 6H, CH_3), 2.7 (m, 2H), 2.58 (m, 2H); High-resolution MS (*m/z*): 333.9628, calc. for $Mn(CO)_3$(TMED)Br, 334.0189; 249.9882, calc. for [Mn(TMED)Br], 249.9877; 171.07, calc. for [Mn(TMED)], 171.0694. *Anal.* Calc. for [$Mn(CO)_3$(TMED)Br]: C, 32.26: H, 4.81. Found: C, 32.6; H, 4.85%.

3. Results and discussion

The octahedral Mn(I) complex *fac*-[$(CO)_3$(dppe)-$MnOH_2]^+BF_4^-$ (**1**) central to this study, is easily prepared in high yield by a two-step process from readily available starting materials [2,3]. Replacement of the aqua ligand is achieved by simply stirring a solution of **1** with the desired ligand, Z. Thus derivatives of **1** have been reported, where Z represents the following anions: CN; OMe; NO_3; OC(O)-CH_3; OTf; N_3 [4]; and F [6]. (In the case of the azide, further reaction of the coordinated N_3 by 1,3-dipolar addition, either to acetylenic compounds or to nitriles, gave new manganese-bonded triazoles and tetrazoles, respectively [3]). With neutral ligands [4], the corresponding ionic complexes [$(CO)_3$(dppe)MnZ]BF_4 were prepared, where Z = PhCN, CH_3CN, CH_2=CHCN, *m*-xylylNC, PPh_3 and CO [7].

We have reported [2], that the hydride, $(CO)_3$(dppe)-MnH, precursor to the corresponding aqua complex, reacts not only with HBF_4 but also with a variety of other strong acids. These reactions result in the liberation of dihydrogen and the direct formation of the neutral complex containing the anion of the acid as a new ligand. However, weaker acids such as acetic acid and phenol do not react in this fashion. We now report that such weaker acids do react with the aqua complex resulting in the replacement of the aqua ligand by the anion (conjugate base) of the weak acid thus making available a new route to the corresponding neutral complexes. Water-soluble carboxylic acids can be used in a two-phase system without added alkali, but others require the presence of base to speed the reaction. Amino acid ligands in methanol solution react in their zwitter ion form. Complexes have been prepared from both aliphatic and aromatic carboxylic acids, as well as from phenol. The reaction with succinic and fumaric acids leads to complexes containing two Mn atoms. The reaction with citric acid gives either the 2:1 complex, presumably involving the two terminal carboxyl groups, or when alkali is present, a 3:1 complex. Stirring an excess of the aqua complex with sodium acrylate polymer (Aldrich, av. mol wt. 2100) gives a product that is insoluble in all common solvents and thus resists conventional methods of characterization. The ultimate analysis of the polymer and the calculated C/P ratio from that analysis, (see supra) indicates that almost every –[–CH_2–CH–(CO_2^-)–]– unit of the acrylate polymer is attached to a separate Mn atom, giving a new polymer, **10**, of the approximate formula: –[–CH_2–CH–[C(O)OMn$(CO)_3$(dppe)]]$_n^-$. This appears to be a unique type of polymer, one highly loaded with a transition metal, and it merits further investigation. Attempts to prepare a similar polymer by initiating polymerization of [$(CO)_3$(dppe)Mn(NCCH=CH_2)]BF_4 with benzoyl peroxide or AIBN were unsuccessful.

3.1. ^1H NMR studies

3.1.1. Aqua complex *1*

The signals associated with the protons of the dppe-Mn metallacycle are of particular interest. Unlike the other related dppe complexes, which all show two signals, **1** in $CDCl_3$ at room temperature shows a single signal (*δ* 2.95, m, 4H) for these four protons. The crystal structure [3] of **1** shows a puckered metallacycle, similar to that of other dppe complexes. Apparently the rapid reversible dissociation of the aqua ligand of **1**, which may involve a concomitant rearrangement to an intermediate 5-coordinate trigonal bipyramidal structure, results in all the protons appearing equivalent on the NMR timescale. However, at −53 °C, this signal is split into two distinct methylene signals (m, *δ* 2.67, 2H; m, *δ* 3.1, 2H) owing to the slowing of dissociation of the aqua ligand at low temperature. However, even at this low temperature it appears that

axial–equatorial interconversions of the puckered structure continue, leading, on average, to an essentially planar, 5-membered ring (see Graphical Abstract). Such a planar C_s structure results in a pair of equivalent protons on adjacent carbon *cis* to the apical CO and a pair that is *trans* to this CO, giving rise to the two signals characteristic of the ^{1}H NMR of the dppe-metallacyle.

3.1.2. Hydrido and nitrato derivatives of *1*

In an attempt to obtain evidence for ligand dissociation, the ^{1}H NMR of the hydrido (the smallest ligand) and nitrato (with a long Mn–O bond) complexes [2,4] was examined in the temperature range 100 to 120 °C. However, the chemical shifts remained unchanged (m, 2H, 2.51 and m, 2H, 2.23 for hydrido, m, 2.97, 2H and m, 2.80, 2H for nitrato) indicating no dissociation under these conditions.

3.1.3. The dppe-Mn metallacycle

The chemical shifts of the methylene protons provide valuable evidence for the preferred site of mono-coordinated ambident ligands. One of the most instructive ^{1}H NMR studies [8] of this system involved the dppe complex, 6-exophenylcyclohexadienylmanganese(I), $[PhC_6H_6(dppe)Mn(NO)]PF_6$. At 25 °C, this complex showed the CH_2 protons of the dppe as two signals (δ 3.53 and 3.02) as expected. However at −75 °C four different signals were observed, which the authors ascribe to two non-equivalent axial and two non-equivalent equatorial protons, in accordance with a stable puckered C_1 structure. We examined the ^{1}H NMR of our pyridine complex, **11**, at −50 °C, but the two signals observed at room temperature remained essentially unchanged at the lower temperature.

The chemical shift data (Table 2) of the methylene protons on the dppe ligand, provide valuable diagnostic information as to the site (Table 1) of mono-coordination of ambident ligands. These data show a consistent pattern, particularly, with respect to the difference between the chemical shifts of the two sets of protons. For the 21 related complexes in which the Mn is coordinated to an oxygen atom, this difference ranges from 0.09 to 0.19 ppm or an average of 0.14 ppm. For the 10 complexes in which the Mn is attached to a nitrogen atom, either that of a pyridine or a nitrile nitrogen, this difference ranges from 0.32 to 0.43 ppm or an average of 0.39 ppm.

3.2. Infrared studies

In a previous paper [9], we analyzed the carbonyl stretching frequencies of 38 $[(CO)_3(dppe)MnZ]$ complexes. We were able to assign symmetry species A′, A″, and A′ in decreasing order of frequency, to the three carbonyl stretches in each of these related C_s complexes. The partial positive charge on the carbon atom of coordinated CO is the most important factor affecting the frequency; the more positive this charge, the larger the force constant and the higher the frequency. Data for the new complexes are shown in Table 2. These 29 complexes may be grouped into four categories (Table 3) depending on the nature of the ligand atom that is bonded to the Mn, namely cyano-nitrogen, pyridine-nitrogen, carboxyl-oxygen and phenolic-oxygen. This order is the descending order of frequencies (with one minor exception) for all three A′, A″, and A′ bonding modes. The largest difference in frequencies between the four categories of bonding types occurs with the lower A′ mode, which involves the equatorial COs moving in phase with respect to each other and out of phase with respect to the axial CO. The group of complexes with the highest frequencies of the four groups is the category in which a nitrile nitrogen atom is bonded to the Mn. The six complexes having such coordination have the relevant A′ stretching frequencies in the narrow range 1957–1961 cm^{-1} (noticeably shifted, as expected, from the values observed with ligands having free nitrile groups). The nitrile group's π* orbitals probably compete with the carbonyl π* orbitals in accepting back-donation from the Mn d-electrons, thus increasing the partial positive charge on the carbonyl carbon atoms with the net effect of increasing the carbonyl frequencies as compared to those with pyridine or oxygen-bonded ligands.

3.3. Competition for coordination sites on ambident ligands

Previous evaluations of the relative coordinating ability of some monodentate ligands have relied on the determination of equilibrium studies of substitution reactions, e.g., $(amine)W(CO)_5 + L \rightleftarrows LW(CO)_5 + amine$ [10]. The determination of the equilibrium constants by such studies is, however, rather limited and have to be carefully chosen because of analytical difficulties. The interest in unsymmetrical chelation in ambident ligands stems from their potential use in transition metal-catalyzed homogeneous reactions. The K^2 chelation of such ligands affords stability, but if one of the donor atoms is more easily dissociated than the other, the resulting vacated site on the K^1 complex may then be occupied by a substrate molecule, followed by a desired insertion reaction and a subsequent reconstitution of the original K^2 complex. One of the most frequently used ligand for such reactions is the bidentate P,N ligand,

Table 3
CO stretching frequencies from Table 2 of (various) $[(CO)_3(dppe)MnZ]$ complexes arranged according to Mn–Z bond

	Cyano "N" (**6**)		Pyridine "N" (**4**)		Carboxyl "O" (**15**)		Phenolic "O" (**3**)	
	Range	Median	Range	Median	Range	Median	Range	Median
A′	2038–2039	2038	2027–2030	2026	2025–2029	2027	2017–2021	2019
A″	1969–1971	1970	1955–1961	1959	1953–1962	1959	1942–1947	1945
A′	1958–1961	1960	1939–1944	1940	1907–1916	1913	1906–1912	1911

$(CH_3)_2NCH_2CH_2PPh_2$, (pn). It has been found, for example [11] that the rhodium-catalyzed hydroformylation of styrene gives a substantially better yield of aldehydes when pn rather than dppe is used as a chelating ligand and a similar result was found [12,13] in the case of the carbonylation of a Pt-K^2(N,P) pn complex. Studies of Ni [14], Ru [15], and heteronuclear Pt complexes [16] containing the pn ligand in its K^2(N,P) form have shown that the nitrogen site is more easily dissociated from the metal than the phosphorous atom.

Most studies involving mixed bidentate ligands, such as the ones cited above, have been devoted to investigating selective dissociation of the chelated K^2-complex to a corresponding K^1-complex. The results of such studies are generally consistent with hard-acid, soft-base (HASB) theory, with the central cationic metal acting as the hard acid, and the ligand, with two competing heteroatoms of differing hardness/softness, as the base [17]. In the case of a the K^2(N,P) pn complexes, the metal–N bond, as expected, and as the cited references show, dissociates preferentially. Although it may be reasonable to assume that preferred coordination is the reverse of preferred dissociation, it was nevertheless thought to be instructive to ascertain the preferred coordination site in the case of pn by reacting it with one mole of **1**.

Our studies show that when a solution of **1** is added dropwise to an equimolar solution of pn, the K^1(P) complex, **30**, is formed, essentially in quantitative yield. For purposes of comparing their ^{1}H NMR spectra, complexes **32** and **33** were also prepared. The difference in δ of the methyl protons attached to the trivalent and tetravalent N atoms in the complexes allows one to ascertain when and if the N is involved in the coordination of pn to the Mn. The fact that P of pn is preferred on coordination is consistent with the dissociation studies, which found that N dissociates before P in pn K^2 (P,N) complexes.

Our studies compare relative ligating ability of ambident ligands possessing combinations of carboxylate, phenolic, pyridine and nitrile groups competing for a single coordination site. When present as anions, usually in a two-phase system, the carboxylate (including the zwitter ions of amino acids) and phenolic ligands are preferred over the other type ligands. By using $NaHCO_3$ it is possible to coordinate 3-hydroxybenzoic acid exclusively at the carboxyl group, **23**, while with NaOH both functional groups are coordinated, **24**. The synthesis of **16** from 4-cyanopyridine indicates coordination at nitrile nitrogen in preference to pyridine nitrogen. In the absence of alkali or water, the nitrile group coordinates more rapidly than carboxyl of 3-hydroxybenzoic acid (**25**) or the hydroxyl of 3-cyanophenol (**20**). It would appear that a useful ambident chelating ligand for certain catalytic reactions might consist of a pyridine derivative having a suitably situated nitrile group, or one containing CN and $N(CH_3)_2$ groups. We have no plans to pursue this area of research.

Acknowledgments

We thank Prof. A. Pinhas and Dr. J.K. Bauer for valuable discussions and Drs. Tom Becker and K. Jayasimhulu for help with experimental work.

References

[1] T.M. Becker, J.A. Krause-Bauer, Acta Crystallogr., Sect. C 55 (1999), IUC 9900141.
[2] M. Orchin, S.K. Mandal, J. Feldman, Inorg. Syn. 32 (1998) 298.
[3] T.M. Becker, J.A. Bauer, C.L. Homrighausen, M. Orchin, Polyhedron 18 (1999) 2563.
[4] T.M. Becker, J.A. Bauer, C.L. Homrighausen, M. Orchin, J. Organomet. Chem. 602 (2000) 97.
[5] E.A. Deutsch, K.A. Glavan, U.S. Patent 4,489,054, (1984).
[6] T.M. Becker, J.A. Krause-Bauer, J.E. Del Bene, M. Orchin, J. Organomet. Chem. 629 (2001) 165.
[7] T.M. Becker, K. Jayasimhulu, M. Orchin, J. Organomet. Chem. 610 (2000) 118.
[8] R.D. Pike, T.J. Alavosus, W.H. Hallows, N.S. Lennhoff, W.J. Ryan, D.A. Sweigart, C.H. Bushweller, C.M. DiMeglio, J.H. Brown, Organometallics 11 (1992) 28416.
[9] B.S. Ault, T.M. Becker, G. Li, M. Orchin, Spectrochim. Acta, Part A 60 (2004) 2567.
[10] R.J. Angelici, C.M. Ingemanson, Inorg. Chem. 8 (1969) 83.
[11] C. Abu-Gnim, I. Amer, J. Mol. Catal. 85 (1993) L275.
[12] G. Anderson, G. Lumetta, Organometallics 4 (1985) 1542.
[13] G. Anderson, R. Kumar, Inorg. Chem. 23 (1984) 4064.
[14] C. Muller, R. Lachicotte, W. Jones, Organometallics 21 (2002) 1975.
[15] K. Mauthner, C. Slugove, K. Mereiter, R. Schmidt, K. Kirchner, Organometallics 16 (1997) 1956.
[16] S. Tsutsuminai, N. Komine, M. Hirano, S. Komiya, Organometallics 23 (2003) 4238, and references therein.
[17] R. Pearson, A. Scott, Survey of Progress in Chemistry, Academic Press, NY, 1969.

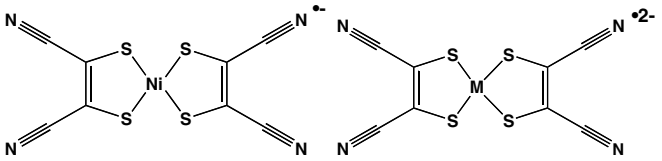

Molecule-based magnets made with $V^0(CO)_6$ are based upon its redox reaction with a neutral electron acceptor, i.e., $Ni(mnt)_2$, $\mathbf{1a}^0$. While innumerable salts of $\mathbf{1a}^n$ ($n = 1$-, 2-) have been reported, neutral $\mathbf{1}^0$ has yet to be isolated. Nonetheless, $\mathbf{1a}^0$ has been electrochemically generated in situ [20] and formation of $V[Ni(mnt)_2]_2$, **2**, was sought via

$$V^0(CO)_6 + 2Ni(mnt)_2 \rightarrow V[Ni(mnt)_2]_2\ (\mathbf{2}). \quad (1)$$

In addition to formation of **2**, we sought molecule-based magnets based on $S = 1/2$ $[M(mnt)_2]^{2-}$ [M = Co (**1b**); Cu (**1c**)]. Due **1b** and **1c** being dianions, materials of the composition of $M^{II'}[M(mnt)_2]$ (M = Co, Cu; M′ = V, Cr, Mn, Fe, Co, Ni) (**3**) were sought via

$$[M^{II'}(NCMe)_6]^{2+} + [M(mnt)_2]^{\bullet 2-} \rightarrow M^{II'}[M(mnt)_2]\ (\mathbf{3}). \quad (2)$$

2. Experimental

2.1. Synthesis

$[NBu_4][Ni(mnt)_2]$ [10a], $[NBu_4]_2[M(mnt)_2]$ (M = Co, Cu) [10e], $[M'(NCMe)_6][BF_4]_2$ (M′ = V, Mn, Fe, Co, Ni) [10g], $[Cr(NCMe)_6][B(C_6H_3(CF_3)_2)_4]_2$ [10i], and $V^0(CO)_6$ [10j] were prepared as previously reported. The supporting electrolyte, tetrabutylammonium hexafluorophosphate, was recrystallized from ethanol, which was dried and distilled under N_2. All other solvents used were also dried and distilled under nitrogen, along with the reaction being preformed under a nitrogen atmosphere. All the products are dark blue-black in color.

2.2. V[Ni(mnt)$_2$]$_2$ (2)

The $[NBu_4][PF_6]$ supporting electrolyte (1.952 g, 5.04 mmol) was dissolved in 50.0 mL of CH_2Cl_2. Twenty-five milliliters of this solution was used to dissolve $\mathbf{1a}^-$ (0.0120 g, 1.20 mmol). The solution of $\mathbf{1a}^-$, along with the $Ag/AgNO_3$ reference electrode and the Pt mesh working electrode (6.25 × 2.25 cm), were placed into one side of a two-chambered flask, and separated by sintered glass. The other side had the remainder of the electrolyte solution, along with the Pt mesh basket (1 cm diameter × 3 cm) with a 6 × 2.65 cm piece of Pt mesh rolled up inside to increase the surface area. A controlled potential electrolysis was run for 30 min at 1200 mV, following the literature procedure [20]. The electrolysis was monitored using UV–Vis spectroscopy, with the characteristic peak at 800 nm, along with the blue color of the solution, being present as early as 10 min into the electrolysis. After the complete conversion of $\mathbf{1a}^-$ to $\mathbf{1a}^0$, a solution of $V(CO)_6$ (2.5 mg, 11.4 μmol), dissolved in minimal CH_2Cl_2, was then added to the blue solution of $\mathbf{1a}^0$, turning it immediately brown and forming a precipitate. The black precipitate was filtered, and the filtrate was clear. *Anal.* Calc for $V[Ni(S_2C_2(CN)_2)_2]_2 \cdot 2.7(CH_2Cl_2) \cdot 0.36[NBu_4][PF_6]$ C, 26.76; H, 1.69; N, 10.67. Found: C, 26.68; H, 2.07; N, 10.91%. IR (KBr: cm^{-1}): $\nu_{C\equiv N}$ 2202 cm^{-1}.

2.3. Mn^{II}[Co(mnt)$_2$]

A 300-mL round bottom flask was charged with 218.3 mg (0.265 mmol) of $[NBu_4]_2[Co(mnt)_2]$, to which 200 mL of CH_2Cl_2 was added. The flask was outfitted with a stir bar, a Soxhlet extractor,[1] a double walled condensing column, and a vacuum adaptor. $[Mn(NCMe)_6][BF_4]_2$ (130.0 mg, 0.273 mmol) was placed into a thimble and then into the Soxhlet extractor. With stirring, the flask was gentled heated until refluxing, and extracted overnight. The solution was then cooled to room temperature and filtered. The fine black precipitate was dried under vacuum for one hour and then placed into a thimble and into a Soxhlet extractor with the same set-up as described above, except that 1,2-dichloroethane was the extracting solvent. The system was allowed to reflux for 2–3 days, then brought to room temperature, and the solids were collected from the thimble (yield 96%). *Anal.* Calc. for $Mn[Co(mnt)_2] \cdot 1.1(C_2H_4Cl_2)]$: C, 24.34; H, 0.94; N, 11.14. Found: C, 24.33; H, 0.99; N, 10.76%. IR (KBr: cm^{-1}): $\nu_{C\equiv N}$ 2209 cm^{-1}.

The rest of the series was made in a similar manner, taking care to keep a 1:1 molar ratio between the $[M^{III}(mnt)_2]^{2-}$ anion and the M^{II} cation {yield: ⩾95% for $[NBu_4]_{0.5}[Ni(Cu(mnt)_2)_{1.25}] \cdot 0.5MeCN$: C, 32.24; H, 2.78; N, 11.87. Found: C, 32.29; H, 2.76; N, 11.83%. IR (KBr: cm^{-1}): $\nu_{C\equiv N}$ 2238sh, 2220 cm^{-1}; $Mn[Cu(mnt)_2]$: C,

[1] Soxhlet extraction was used due to the limited solubility of some of the cations used. Although readily soluble in MeCN, along with the anions, use of MeCN could lead to possible its coordination, and undesired products. Instead, non-coordinating dichloromethane was used as the $[M(mnt)_2]^{2-}$ salts are readily soluble in it. However, the cations have different degrees of solubility; from easily soluble $[Cr(NCMe)_6][B(C_6H_3(CF_3)_2)_4]_2$ and $[Ni(NCMe)_6][BF_4]_2$ to poorly soluble for the $[V(NCMe)_6][BF_4]_2$ and $[Co(NCMe)_6][BF_4]_2$. Thus, the reaction could take a day to a week to complete, or, in the later cases of the $[V(NCMe)_6]^{2+}$ and $[Co(NCMe)_6]^{2+}$, completion does not occur. However, product was recovered from all reactions, except for the reaction of $[Co(mnt)_2]^{2-}$ with $[V(NCMe)_6][BF_4]_2$. After collecting the product via filtration, it was dried under vacuum for 1 h. Each product was cleaned by placing the solid into a Soxhlet extractor, and using dichloroethane as the solvent. This redissolves any counter-ions, but not the compound, leading to the reduction of any $[NBu_4]^+$, $[BF_4]^-$, or $[B(C_6H_3(CF_3)_2)_4]_2^-$ peaks that may have been present in the initial IR spectra.

24.09; N, 10.92. Found: C, 23.86; N, 10.76%. IR (KBr: cm^{-1}): $\nu_{C\equiv N}$ 2236sh, 2219 cm^{-1}; Fe[Cu(mnt)$_2$]: C, 24.04; N, 14.02. Found: C, 23.79; N, 14.86%. IR (KBr: cm^{-1}): $\nu_{C\equiv N}$, 2201 cm^{-1}; CoCu(mnt)$_2 \cdot 0.10MeCN \cdot 0.60C_2H_4Cl_2$: C, 24.21; H, 0.58; N, 12.32. Found: C, 24.37; H, 0.34; N, 12.30%. IR (KBr: cm^{-1}): $\nu_{C\equiv N}$ 2309sh, 2206 cm^{-1}; VCu(mnt)$_2 \cdot 0.90C_2H_4Cl_2$: C, 24.33; H, 0.75; N, 11.58. Found: C, 24.61; H, 0.73; N, 11.29%. IR (KBr: cm^{-1}): $\nu_{C\equiv N}$ 2218, 2203 cm^{-1}; $[NBu_4]_{0.2}$[Ni(Co(mnt)$_2)_{1.10}] \cdot 0.35C_2H_4Cl_2$: C, 29.60; H, 1.68; N, 12.50. Found: C, 29.63; H, 1.86; N, 12.06%. IR (KBr: cm^{-1}): $\nu_{C\equiv N}$ 2206 cm^{-1}; MnCo(mnt)$_2 \cdot 1.20C_2H_4Cl_2$: C, 24.35; H, 0.94; N, 10.92. C, 24.33; H, 0.99; N, 10.76%. IR (KBr: cm^{-1}): $\nu_{C\equiv N}$ 2209 cm^{-1}; $[NBu_4]_{0.4}$[Fe(Co(mnt)$_2)_{1.20}] \cdot 1.10MeCN \cdot 1.15C_2H_4Cl_2$: C, 31.95; H, 2.80; N, 10.67. C, 32.12; H, 3.06; N, 10.64%. IR (KBr: cm^{-1}): $\nu_{C\equiv N}$ 2201 cm^{-1}; and CrCo(mnt)$_2$: $\nu_{C\equiv N}$ 2207 cm^{-1}. Yields range from >95 % to 45–50% for V[Co(mnt)$_2$], Co[Co(mnt)$_2$], and Fe[Co(mnt)$_2$]; and 20% for V[Cu(mnt)$_2$].

2.4. Physical properties

Thermal properties were studied on a TA Instruments Model 2050 thermogravimetric analyzer (TGA) equipped with a TA-MS Fison triple filter quadrupole mass spectrometer, to identify gaseous products with masses less than 300 amu. This instrument is located in a Vacuum Atmospheres DriLab under nitrogen to protect air and moisture sensitive samples. Samples were placed in an aluminum pan and heated at 20 °C/min under a continuous 10-mL/min-nitrogen flow. The 2–300 K magnetic susceptibility was determined on a Quantum Design MPMS-5XL 5 T SQUID (sensitivity = 10^{-8} emu or 10^{-12} emu/Oe at 1 T) as previously described [21]. In addition to correcting for the diamagnetic contribution from the sample holder, core diamagnetic corrections based on summing Pascal's constants were used. Infrared spectra (600–4000 ± 1 cm^{-1}) were obtained on a Bruker Tensor 37 FT IR-40 spectrophotometer as KBr pellets. Elemental analyses were performed by Complete Analysis Laboratories Inc. of Parsippany, NJ.

3. Results and discussion

The addition of 0.5 equiv. of $V^0(CO)_6$ to in situ generated Ni(mnt)$_2^0$ results in an immediate precipitate, **2**. The IR of **2** shows a characteristic stretch of the CN group [ν_{CN} at 2202 cm^{-1}], which is broadened with respect to **1a**$^-$, indicative of coordination through the CN group. There is also an absence of a ν_{CO} absorption that would be found for a vanadium carbonyl. Peaks characteristic of $[NBu_4]^+$ as well as $[PF_6]^-$ are also present. Hence, the supporting electrolyte is occluded upon the rapid precipitation of **2**. This is also noted as the elemental analysis that fits $V^{II}\{[Ni(mnt)_2]^-\}_2 \cdot 2.7(CH_2Cl_2) \cdot 0.36[NBu_4][PF_6]$.

Evidence that the reaction products were of M′[M-(mnt)$_2$] composition were obtained from line broadening and shifts in the position of the ν_{CN} absorption. This is indicative of coordination through the nitrile on the $[M'(mnt)_2]^{2-}$. The IR spectra also showed an absence of $[BF_4]^-$, coordinated MeCN and $[B(C_6H_3(CF_3)_2)_4]^-$ peaks, indicating that these were not present in the final product, and that the desired metathesis reaction occurred.

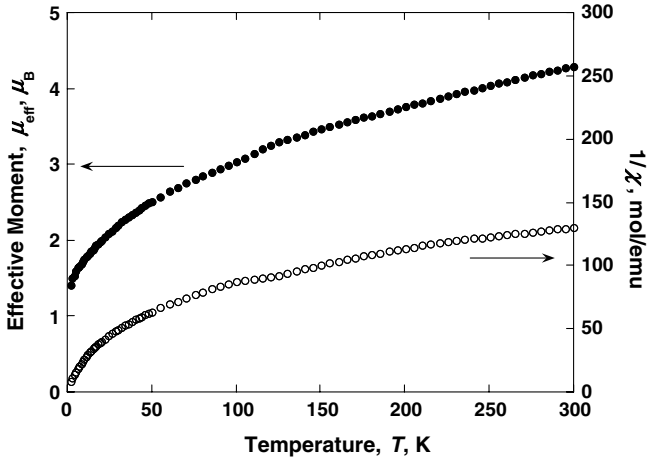

Fig. 1. The 5–300 K $\mu_{eff}(T)$ and $\chi^{-1}(T)$ for V[Ni(mnt)$_2$]$_2 \cdot 2.7(CH_2Cl_2) \cdot 0.36[NBu_4][PF_6]$ (**2**).

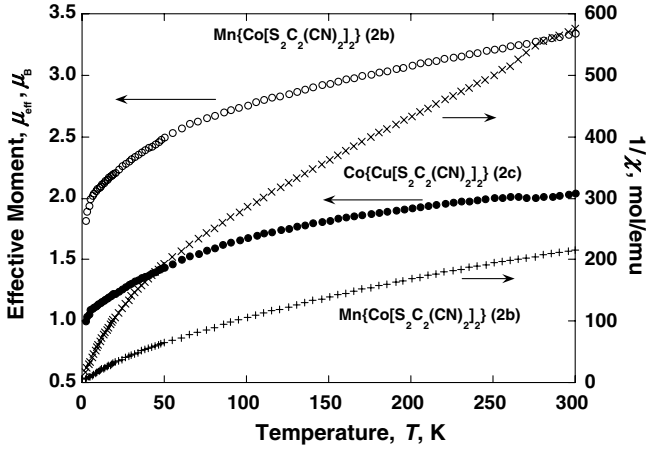

Fig. 2. The 5–300 K $\mu_{eff}(T)$ and $\chi^{-1}(T)$ for Mn[Co(mnt)$_2] \cdot 1.10(C_2H_4Cl_2)$ (○, +), and Co[Cu(mnt)$_2] \cdot 1.10(MeCN) \cdot 0.2(C_2H_4Cl_2)$ (●, ×).

The 5–300 K magnetic susceptibility, $\chi(T)$, was determined and is reported as $\mu_{eff}(T)[\equiv(8\chi T)^{1/2}]$, and $\chi^{-1}(T)$, Figs. 1 and 2, for V[Ni(mnt)$_2$]$_2$ and M′[M(mnt)$_2$] (M = Co, M′ = Mn; M = Cu, M′ = Co), respectively. For **2** $\mu_{eff}(T)$ increases with increasing temperature and at 300 K is 4.3 μ_B and still increasing. This is in accord with expected moment of 4.58 μ_B for uncoupled $S = 3/2$ V(II) and two $S = 1/2$ $[Ni(mnt)_2]^{\bullet-}$ spin sites.[2] The reduced moment is indicative of antiferromagnetic coupling that is expected. The $\mu_{eff}(T)$ above 160 K could be fit to the Curie–Weiss expression, $\chi \propto (T-\theta)^{-1}$, with $\theta \sim -400$ K indicative of strong antiferromagnetic coupling. Magnetic ordering, however, is not

[2] The alternative formulations of either $V^{III}[Ni(mnt)_2]^{2-}[Ni(mnt)_2]^-$ or $V^{IV}\{[Ni(mnt)_2]^{2-}\}_2$ would have room temperature moments of 3.31 and 1.73 μ_B, respectively. These are too low with respect to the observed value.

evident from either the magnetization, or in-phase, $\chi'(T)$, and out-of-phase, $\chi''(T)$, AC susceptibility studies.

For Mn[Co(mnt)$_2$] and Co[Cu(mnt)$_2$], $\mu_{eff}(T)$ increases with increasing temperature and is 3.36 μ_B at 300 K for Mn[Co(mnt)$_2$], and 2.00 μ_B at 250 K for Co[Cu(mnt)$_2$], and still increasing. This is in accord with uncoupled $S = 5/2$ Mn(II) and $S = 1/2$ [Co(mnt)$_2$]$^{2-}$ spins for Mn[Co(mnt)$_2$], and $S = 3/2$ Co(II) and $S = 1/2$ [Cu(mnt)$_2$]$^{2-}$ spins for Co[Cu(mnt)$_2$]. The reduced moment is indicative of antiferromagnetic coupling that is expected. The $\mu_{eff}(T)$ above 100 K for Mn[Co(mnt)$_2$] and 145 K for Co[Cu(mnt)$_2$] could be fit to the Curie–Weiss expression with $\theta \sim -115$ and -100 K, respectively, indicative of strong antiferromagnetic coupling for Mn[Co(mnt)$_2$] and Co[Cu(mnt)$_2$], respectively. None of the compounds showed evidence of magnetic ordering. Similar results are observed for the other members of these families.

Hence, unlike M[TCNE]$_x$ (M = V, Mn, Fe, Co, Ni) which magnetically order as a ferrimagnets at temperatures as high as room temperature (M = V), neither V[Ni(mnt)$_2$]$_2$ nor M$^{II'}$[M(mnt)$_2$] as well as M[Ni(mnt)$_2$]$_2${M = V, Cr, Mn, Fe, Co, Ni} [22a] magnetically order. Nonetheless, V[Ni(mnt)$_2$]$_2$ and M$^{II'}$[M(mnt)$_2$] {as well as M[Ni(mnt)$_2$]$_2$ {M = V, Cr, Mn, Fe, Co, Ni} exhibit significant antiferromagnetic coupling. We attribute the poor spin coupling of the bridging $S = 1/2$ [Ni(mnt)$_2$]$^{\bullet -}$ or [M(mnt)$_2$]$^{\bullet 2-}$ (M = Co, Cu) to the low spin density of the terminal N's (~1%) [14] for [Ni(mnt)$_2$]$^{\bullet -}$ and less for [Co(mnt)$_2$]$^{\bullet 2-}$ [22b] with respect to [TCNE]$^{\bullet -}$ (~13%) [23].

Acknowledgements

The continued partial support by the Department of Energy Division of Materials Science (Grant No. DE-FG03-93ER45504) and Army Research Office (Grant No. DAAD19-01-1-0562) is appreciated.

References

[1] (a) Conference proceedings: P. Day, A.E. Underhill, Phil. Trans. R. Soc. Lond. (A) 357 (1999) 2849;
(b) O. Kahn (Ed.), Proceedings of the 6th International Conference on Molecule-based Based Materials; Mol. Cryst., Liq. Cryst. (1999) 334;
(c) K. Itoh, J.S. Miller, T. Takui (Eds.), Proceedings of the Conference on Molecular-Based Magnets; Mol. Cryst., Liq. Cryst. (1997) 305;
(d) G. Christou (Ed.), Proceedings of the 7th International Conference on Molecule-based Magnets; Polyhedron (2001) 20;
(e) G. Christou, (Ed.), Proceedings of the 8th International Conference on Molecule-based Magnets; Polyhedron (2003) 22(#14–17).
[2] (a) Reviews: J.S. Miller, A.J. Epstein, Chem. Commun. (1998) 1319;
(b) V.I. Ovcharenko, R.Z. Sagdeev, Russ. Chem. Rev. 68 (1999) 345;
(c) W. Plass, Chem. Zeit 32 (1998) 323;
(d) J.S. Miller, A.J. Epstein, Chem. Eng. News 73 (40) (1995) 30;
(e) J.S. Miller, A.J. Epstein, Angew. Chem. Int. Ed. Engl. 33 (1994) 385;
(f) M. Kinoshita, Jpn.J. Appl. Phys. 33 (1994) 5718;
(g) J.S. Miller, A.J. Epstein, Adv. Chem. Ser. 245 (1995) 161;
(h) A. Caneschi, D. Gatteschi, Progr. Inorg. Chem. 37 (1991) 331;
(i) A.L. Buchachenko, Russ. Chem. Rev. 59 (1990) 307;
(j) J.A. Crayson, J.N. Devine, J.C. Walton, Tetrahedron 56 (2000) 7829;
(k) S.J. Blundell, F.L. Pratt, J. Phys.: Condens. Matter 16 (2004) R771.
[3] J.S. Miller, J.C. Calabrese, A.J. Epstein, R.W. Bigelow, J.H. Zhang, W.M. Reiff, J. Chem. Soc. Chem. Commun. (1986) 1026.
[4] J.S. Miller, J.C. Calabrese, H. Rommelmann, S. Chittipeddi, J.H. Zhang, W.M. Reiff, A.J. Epstein, J. Am. Chem. Soc. 109 (1987) 769.
[5] G.T. Yee, J.M. Manriquez, D.A. Dixon, R.S. McLean, D.M. Groski, R.B. Flippen, K.S. Narayan, A.J. Epstein, J.S. Miller, Adv. Mater. 3 (1991) 309.
[6] (a) J.M. Manriquez, G.T. Yee, R.S. McLean, A.J. Epstein, J.S. Miller, Science 252 (1991) 1415;
(b) J.S. Miller, G.T. Yee, J.M. Manriquez, A.J. Epstein, in: the Proceedings of Nobel Symposium #NS-81 Conjugated Polymers and Related Materials: The Interconnection of Chemical and Electronic Structure, Oxford University Press, Oxford, 1993, p. 461;
(c) La Chim. La Ind. 74 (1992) 845.
[7] J. Zhang, P. Zhou, W.B. Brinckerhoff, A.J. Epstein, C. Vazquez, R.S. McLean, J.S. Miller, ACS Symp. Ser. 644 (1996) 311.
[8] K.I. Pokhodnya, A.J. Epstein, J.S. Miller, Adv. Mater. 12 (2000) 410.
[9] E.B. Vickers, T.D. Selby, M.S. Thorum, M.L. Taliaferro, J.S. Miller, Inorg. Chem. 43 (2004) 6414.
[10] (a) H.B. Gray, R. Williams, I. Bernal, E. Billig, J. Am. Chem. Soc. 84 (1962) 3596;
(b) A. Davison, N. Edelstein, R.H. Holm, A.H. Maki, J. Am. Chem. Soc. 85 (1963) 2029;
(c) A. Davison, N. Edelstein, R.H. Holm, A.H. Maki, Inorg. Chem. 2 (1963) 1227;
(d) A. Davison, R.H. Holm, Inorg. Syn. 10 (1967) 8;
(e) E. Billig, R. Williams, I. Bernal, J.H. Walters, H.B. Gray, Inorg. Chem. 3 (1964) 663;
(f) L. Persaud, C.H. Langford, Inorg. Chem. 24 (1985) 3562;
(g) R.A. Heintz, J.A. Smith, P.S. Szalay, A. Weisgerber, K.R. Dunbar, Inorg. Synth. 33 (2002) 75;
(h) S.J. Anderson, F.J. Wells, G. Wilkinson, B. Hussain, M.B. Hursthouse, Poly 7 (1988) 2615;
(i) W.E. Buschmann, J.S. Miller, Inorg. Synth. 33 (2002) 83;
(j) X. Liu, J.E. Ellis, T.D. Selby, P. Ghalsasi, J.S. Miller, Inorg. Synth. 34 (2004) 96.
[11] P.I. Clemenson, Coord. Chem. Rev. 106 (1990) 71.
[12] N. Robertson, L. Cronin, Coord. Chem. Rev. 227 (2002) 93.
[13] A.T. Coomber, D. Deljonne, R.H. Friend, J.L. Bredas, A. Charlton, N. Robertson, A.E. Underhill, M. Kurmoo, P. Day, Nature 380 (1996) 144.
[14] L.N. Dawe, L. Turnbow, J.M. Miglioi, M.L. Taliaferro, W.W. Shum, J.N. Bagnato, L.N. Zakharov, A.L. Rheingold, A.M. Arif, M. Fourmigué, J.S. Miller, Inorg. Chem. 44 (2005) xxxx.
[15] D.K. Rittenberg, K.-i. Sugiura, B.M. Burkhart, B.G. Morin, A.M. Arif, L. Liable-Sands, A.L. Rheingold, M. Sundaralingam, A.J. Epstein, J.S. Miller, Inorg. Chem. 40 (2001) 1915.
[16] J.S. Miller, A.J. Epstein, J. Chem. Soc., Chem. Commun. (1998) 1319.
[17] G.T. Yee, J.S. Miller, in: J.S. Miller, M. Drillon (Eds.), Magnetism – Molecules to Materials, vol. 5, Wiley–VCH, Mannheim, 2004, p. 223.
[18] V. Gama, M.T. Durate, in: J.S. Miller, M. Drillon (Eds.), Magnetism – Molecules to Materials, vol. 5, Wiley–VCH, Mannheim, 2004, p. 1.
[19] W.E. Broderick, J.A. Thompson, B.M. Hoffman, Inorg. Chem. 30 (1991) 2958.
[20] W.E. Geiger, F. Barriere, R.J. LeSuer, S. Trupia, Inorg. Chem. 40 (2001) 2472.
[21] E.J. Brandon, D.K. Rittenberg, A.M. Arif, J.S. Miller, Inorg. Chem. 37 (1998) 3376.
[22] (a) J.E. Eppich, J.S. Miller, unpublished results;
(b) M.L. Taliaferro, J.S. Miller, unpublished results.
[23] A. Zheludev, A. Grand, E. Ressouche, J. Schweizer, B. Morin, A.J. Epstein, D.A. Dixon, J.S. Miller, J. Am. Chem. Soc. 116 (1994) 7243.

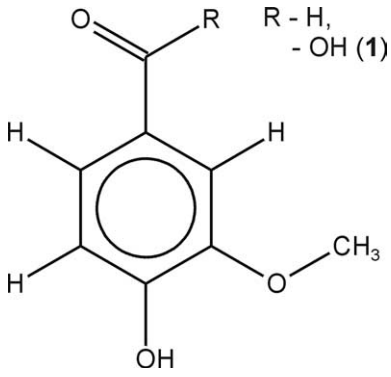

Scheme 1. Two lignin model compounds vanillin ($C_8H_8O_3$) and vanillic acid ($C_8H_8O_4$) (**1**).

on benzene ring, present in simple lignin model compounds (Scheme 1).

A dinuclear heterocarboxylate copper *paddle-wheel* compound with vanillic and acetic acid anions $[Cu_2(C_8\text{-}H_7O_4)_2(O_2CCH_3)_2(CH_3OH)_2]$ was synthesized and characterized. It was compared to a related homocarboxylate complex $[Cu_2(C_8H_7O_4)_4(H_2O)_2]$.

2. Experimental

2.1. Synthesis

All starting compounds and solvents were used as purchased, without any further purification. The single crystals of vanillic acid ($C_8H_8O_4$) (**1**), suitable for X-ray analysis, were obtained by a recrystallization from ethylacetate.

$[Cu_2(C_8H_7O_4)_2(O_2CCH_3)_2(CH_3OH)_2]$ (**2**), $[Cu_2(C_8H_7O_4)_2(O_2CCH_3)_2(H_2O)_2]$ (**2a**): Vanillic acid (0.061 g; 0.36 mmol) was added to a hot methanol solution (10.0 mL) of $[Cu_2(O_2CCH_3)_4(H_2O)_2]$ (0.040 g; 0.10 mmol). Next day, a dark green precipitate of **2** was filtered off, washed three times with methanol and then left for a day on air, yielding **2a**. Yield 80%. *Anal*. Calc. for $C_{20}H_{24}Cu_2O_{14}$ (**2a**): C, 39.0; H, 3.93; Cu, 20.7. Found: C, 38.9; H, 4.17; Cu, 20.7%. UV–Vis–NIR (DMSO) λ_{max}, 260, 290, 450(sh), 720 nm; (mull) λ_{max}, 230, 265, 290, 360(sh), 695 nm. IR, 3420 ν(O–H), 1623 $\nu_{as}(CO_2)$, 1602, 1591 $\nu_{as}(CO_2)$, 1518, 1417 $\nu_s(CO_2)$, 1398 $\nu_s(CO_2)$, 780 cm^{-1}. EPR (298 K), $g_\perp = 2.09$, $g_\parallel = 2.36$, $D = 0.329\ cm^{-1}$, $2J = 278\ cm^{-1}$; (116 K), $g_\perp = 2.07$, $g_\parallel = 2.36$, $A_{z1} = 5.6$ mT, $D = 0.326\ cm^{-1}$, $2J = 237\ cm^{-1}$. μ_{eff} (298 K), 1.48 BM. The single crystals of **2**, suitable for X-ray analysis, were obtained by a similar procedure, but at lower concentration of the starting compounds. The crystals were frozen immediately after removal from mother-liquid, to prevent their decomposition due to evaporation of methanol and its probable replacement with water molecules (elemental analysis, IR).

$[Cu_2(C_8H_7O_4)_4(H_2O)_2]$ (**3**): The starting compounds and a procedure was different as already described [8]. 0.160 g (0.40 mmol) of $[Cu_2(O_2CCH_3)_4(H_2O)_2]$ was dissolved in 10 mL of hot water. The solution was added to 0.244 g (1.45 mmol) of vanillic acid. Green crystallites were filtered off next day and then dried one day in a desiccator. Yield 80%. *Anal*. Calc. for $C_{32}H_{32}Cu_2O_{18}$ (**3**): C, 46.2; H, 3.88; Cu, 15.3. Found: C, 46.0; H, 4.18; Cu, 15.2. UV–Vis–NIR (DMSO) λ_{max}, 260, 290, 450(sh), 720 nm; (mull) λ_{max}, 230, 265, 300, 380(sh), 690 nm. IR, 3456 ν(O–H), 1615, 1596, 1570 $\nu_{as}(CO_2)$, 1518, 1455, 1426 $\nu_s(CO_2)$, 1394 $\nu_s(CO_2)$, 774 cm^{-1}. EPR (298 K), $g_x = 2.05$, $g_y = 2.06$, $g_z = 2.34$, $D = 0.306\ cm^{-1}$, $E = 0.0025\ cm^{-1}$, $2J = 241\ cm^{-1}$; (116 K), $g_x = 2.05$, $g_y = 2.06$, $g_z = 2.35$, $A_{z1} = 7.0$ mT, $D = 0.303\ cm^{-1}$, $E = 0.0030\ cm^{-1}$, $2J = 231\ cm^{-1}$. μ_{eff} (298 K), 1.56 BM. The single crystals of **3**, suitable for X-ray analysis, were obtained by a similar procedure, but at lower concentration of the starting compounds.

2.2. X-ray structure analysis

Details of the crystal data, data collection and refinement parameters for **1**, **2** and **3** are listed in Table 1. The selected distances and angles are presented in Table 2. A colorless plate of compound **1** was glued, while green prisms of compounds **2** and **3** were greased on a glass thread. The diffraction data for **1**–**3** were collected on a Nonius Kappa CCD diffractometer with graphite monochromated Mo Kα radiation. A Cryostream Cooler (Oxford Cryosystems) was used for cooling the samples of **2** and **3**. The data were processed using DENZO [13]. Structures of **1** and **2** were solved by direct methods using SIR97 [14] and refined using XTAL 3.6 [15] by a full-matrix least-squares procedure based on *F*. Structure of **3** was solved by direct methods implemented in SHELXS-97 [16] and refined by a full-matrix least-squares procedure based on F^2 (SHELXL-97) [17]. All of the non-hydrogen atoms were refined anisotropically. The positions of hydrogen atoms in **1** and **2** were obtained from the difference Fourier maps. Positional parameters of H atoms for **1**, while positional and isotropic displacement parameters of H atoms for **2**, were refined. The water hydrogen atoms in **3** were visible in the last stages of the refinement and were refined freely, while the other hydrogen atoms were included in the model at geometrically calculated positions and refined using a riding model.

2.3. Physical measurements

Metal analysis was carried out electrogravimetrically with Pt electrodes. C,H analysis was performed with a Perkin–Elmer, Elemental Analyzer 2400 CHN. The magnetic susceptibility of the substances was determined at room temperature by powdered samples with a Sherwood Scientific MSB-1 balance. Diamagnetic corrections were estimated from Pascal's constants [18]. Infrared spectra were measured on mineral mulls, using a Perkin–Elmer FT-IR 1720X spectrometer. Electronic spectra were recorded as nujol mulls and DMSO solutions with a Perkin–Elmer

Table 1
Relevant crystal data and data collection summary

	1	2	3
Formula	$C_8H_8O_4$	$C_{22}H_{28}Cu_2O_{14}$	$C_{32}H_{32}Cu_2O_{18}$
Formula weight	168.15	643.54	831.66
Crystal system	monoclinic	triclinic	monoclinic
Space group	$P2_1/c$	$P\bar{1}$	$P2_1/n$
a (Å)	3.9101(1)	8.3217(2)	8.2747(4)
b (Å)	17.3900(6)	8.9495(2)	19.5282(11)
c (Å)	11.3267(5)	9.7552(3)	10.0006(5)
α (°)	90	69.633(1)	90
β (°)	95.313(1)	76.824(1)	102.725(3)
γ (°)	90	64.165(1)	90
V (Å^3)	766.87(5)	610.52(3)	1576.31(14)
Z	4	1	2
D_{calc} (g/cm^3)	1.456	1.750	1.752
μ (mm^{-1})	0.118	1.812	1.438
T (K)	293	150	150
Crystal color	colorless	green	green
Crystal shape	plate	prism	prism
Crystal size (mm)	$0.25 \times 0.25 \times 0.10$	$0.15 \times 0.10 \times 0.09$	$0.23 \times 0.10 \times 0.10$
θ_{max} (°)	27.5	25.0	27.5
R_{int}	0.049	0.024	0.035
Refined parameters	133	172	248
Total data	10029	7267	5813
Independent data	1715	2130	3420
Observed data [$F^2 > 2\sigma(F^2)$]	981	1985	2869
R[a] (observed)	0.052	0.031	0.067
R_w[b], wR_2[c] (observed)	0.056[b]	0.026[b]	0.135[c]
$\Delta\rho_{min,max}$ (e Å^{-3})	−0.408, 0.281	−0.807, 0.555	−0.520, 1.294

[a] $R = \sum(||F_o| - |F_c||)/\sum|F_o|$.
[b] $R = \sum(w(|F_o| - |F_c|))/\sum(w|F_o|)$.
[c] $wR_2 = (\sum[w(F_o^2 - F_c^2)^2]/\sum(wF_o^2)^2)^{1/2}$.

Table 2
Selected bond distances (Å) and angles (°) in the structures **2** and **3**

2				**3**			
Cu···Cu	2.608(1)	O1–Cu–O2	169.31(5)	Cu···Cu	2.611(1)	O3–Cu–O2	169.51(16)
Cu–O1	1.960(1)	O1–Cu–O5	89.99(6)	Cu–O3	1.956(3)	O3–Cu–O5	87.06(15)
Cu–O2	1.951(1)	O1–Cu–O6	90.22(6)	Cu–O2	1.958(3)	O2–Cu–O5	90.37(15)
Cu–O5	1.965(2)	O1–Cu–O7	97.85(5)	Cu–O5	1.977(3)	O3–Cu–O4	86.93(15)
Cu–O6	1.984(2)	O2–Cu–O5	89.02(6)	Cu–O4	1.981(3)	O2–Cu–O4	93.61(15)
Cu–O7	2.160(2)	O2–Cu–O6	88.76(7)	Cu–O6	2.170(4)	O5–Cu–O4	167.67(15)
		O2–Cu–O7	92.83(5)			O3–Cu–O6	97.29(16)
		O5–Cu–O6	169.13(5)			O2–Cu–O6	93.11(16)
		O5–Cu–O7	96.87(6)			O5–Cu–O6	96.76(17)
		O6–Cu–O7	93.87(6)			O4–Cu–O6	94.68(17)
Hydrogen-bonding geometry							
O7–H7···O4 2.735(2)			169(5)[i]	O6–H1···O10 2.877(6)			167(8)[a]
				O6–H2···O9 2.959(6)			159(7)[b]
O4–H4···O6 2.751(2)			157(3)[ii]	O10–H10···O5 2.873(5)			155[c]
O4–H4···O3 2.707(2)			102(2)	O9–H9···O7 2.679(6)			114
				O10–H10···O8 2.731(6)			111

Symmetry codes: (i) $2 - x$, $1 - y$, $1 - z$; (ii) x, $1 + y$, $-1 + z$.
(a) $1/2 + x$, $1/2 - y$, $-1/2 + z$; (b) $-x$, $-y$, $1 - z$; (c) $1/2 - x$, $1/2 + y$, $5/2 - z$.

UV/Vis/NIR spectrometer Lambda 19. EPR spectra of the powdered samples were recorded by a Bruker ESP-300 spectrometer, operating at X-band (9.59 GHz) at room temperature and at 116 K. The values of parameters g, A, D, E and $2J$ were calculated directly from the signal positions in the spectra [19–21].

3. Results and discussion

3.1. The structure of free vanillic acid $C_8H_8O_4$ (1)

Two molecules of free vanillic acid are strongly H-bonded by two mutual H-bonds between their carboxylate

groups (O1–H···O2′ 2.642(3) Å), thus forming a centrosymmetrical dimeric unit (Fig. 1), as often found at carboxylic acids. Another H-bond is intramolecular, formed by the hydroxy group and the methoxy group (O4–H···O3 2.631(3) Å). A comparison to the structure of related lignin model compound vanillin (Scheme 1) [22] reveals significantly different intermolecular H-bonding, due to the aldehyde group instead of the carboxylic group. The vanillin molecules are packed in chains, where strong H-bonds connect aldehyde and phenolato groups on positions 1 and 4 of the benzene ring (O–H···O 2.712(2)–2.743(3) Å).

3.2. The structure of bis(μ-(4-hydroxy-3-methoxybenzoato-O:O′))bis(μ-(acetato-O:O′))bis(methanol) dicopper(II) (2)

The centrosymmetric *paddle-wheel* central core $[Cu_2(C_8H_7O_4)_2(O_2CCH_3)_2(CH_3OH)_2]$ (**2**) is of copper(II) acetate hydrate type, however with two different carboxylates (two acetates and two vanillic acid anions) in *trans* orientation, while methanol molecules occupy the apical positions (Fig. 2). The phenolate group is involved in all three hydrogen bonds, either intra-molecularly to methoxy oxygen atom (O4–H···O3 2.707(2) Å), or inter-molecularly to methanol molecule (O7–H···O4 2.735(2) Å) and acetate group (O4–H···O6 2.751(2) Å).

3.3. The structure of tetrakis(μ-(4-hydroxy-3-methoxybenzoato-O:O′))bis(aqua) dicopper(II) (3)

The structure of complex $[Cu_2(C_8H_7O_4)_4(H_2O)_2]$ (**3**) was already reported [8], but was redetermined due to unavailability of the atom positions from the CSD [25]. Complex **3** is of $[Cu_2(O_2CCH_3)_4(H_2O)_2]$ type with four identical carboxylate ligands. Similar pattern, as in **2**, is found in the vanillic acid anion, with the phenolate group involved in all H-bonds and an intra-molecular H-bond between hydroxy and methoxy groups. Each hydroxy group is H-bonded also inter-molecularly to axially coordinated water molecules (O6–H1···O10 2.876(6) Å, O6–H2···O9 2.958(6) Å), giving two H-bonds with each water molecule.

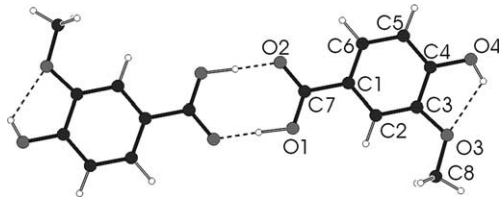

Fig. 1. The dimeric structure of free vanillic acid with two hydrogen-bonds between the carboxylic groups of the vanillic acid molecules [23,24].

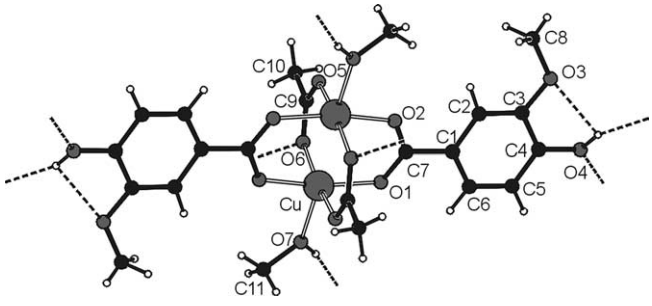

Fig. 2. Two types of carboxylate anions in a dinuclear copper(II) tetracarboxylate complex $[Cu_2(C_8H_7O_4)_2(O_2CCH_3)_2(CH_3OH)_2]$ (**2**) [23,24]. The intermolecular H-bonds are connecting the phenolate group (O4) with the acetate anion (O6) and methanol molecules (O7).

Two H-bonds (**3**) to the axial ligand instead of one (**2**) and better volatility of methanol (**2**) than water (**3**) may be the main reasons for better stability of **3** than **2** outside mother-liquid. Interestingly, only two vanillic acid anions in **3** are forming another H-bond to carboxylate oxygen atom (O10–H10···O5 2.873(5) Å), while for another two, no such connections were found, probable due to steric reasons. This is very probable reason that only two vanillic acid anions are replaced with acetates in **2**. Small acetates enable stronger (shorter) inter-molecular H-bonds, possibly due to less steric hindrance (see Table 2). Additionally, stronger stabilization in **3** than in **2** is found also in π-stacking interaction (mean inter-planar separation 3.30 Å (3.37 Å) for **3** (**2**), centroid···centroid distance 3.94 Å (4.22 Å) for **3** (**2**)). It seems that the decisive factors for the competition between the homocarboxylate (**3**) and heterocarboxylate (**2**) are inter-molecular interactions. Either weaker H-bonds, stronger π-stacking and two H-bonds to the axial ligand (**3**), or stronger H-bonds, weaker π-stacking and one H-bond to the axial ligand (**2**).

3.4. Spectroscopic and magnetic analysis

Although the compound **2** is not stable outside mother-liquid, yielding **2a**, the μ_{eff} 1.48 BM (**2a**) suggests only partial decomposition of **2** and a retainment of the dinuclear tetracarboxylate central core in the compound **2a** (1.55 BM for **3**). This is in agreement with almost identical solution or mull UV–Vis–NIR spectra for **2a** and **3**, respectively, and with EPR spectra, where typical signals (H_{z1}, $H_{\perp 2}$, H_{z2} [19], Fig. 3) for the triplet state $S = 1$ of $[Cu_2(O_2CCH_3)_4(H_2O)_2]$ type of compounds may be observed at room temperature and at 116 K (see Section 2). In the low temperature EPR spectra, the splitting of a H_{z1} signal to septet, $H_{\perp 2}$ to H_{x2} and H_{y2} and an appearance of the signal of mononuclear species H_{mono} at 330 mT were noticed. Such phenomena are often found in the low temperature spectra of the dinuclear copper(II) tetracarboxylates. Differences in the H_{z1} splitting, the hyperfine constant A_{z1} (5.6 mT; 7.0 mT), and the $H_{\perp 2}$ separation for the spectra of **2a** and **3** may be related to a different role of the bridging anions present in both complexes, and/or replacement of the apical ligand (**2** → **2a**) that might not enable full equivalency of both Cu ions in the dinuclear unit after rearrangement. Close to the H_{z1} signal in the spectra of **3**, an additional distinctive signal may be observed at 80 mT (Fig. 3). This signal is assigned as $H_{\perp 1}$ (H_{x1}, H_{y1}) that is observable, since $D < h\nu$, and may be described by the equations [19–21]:

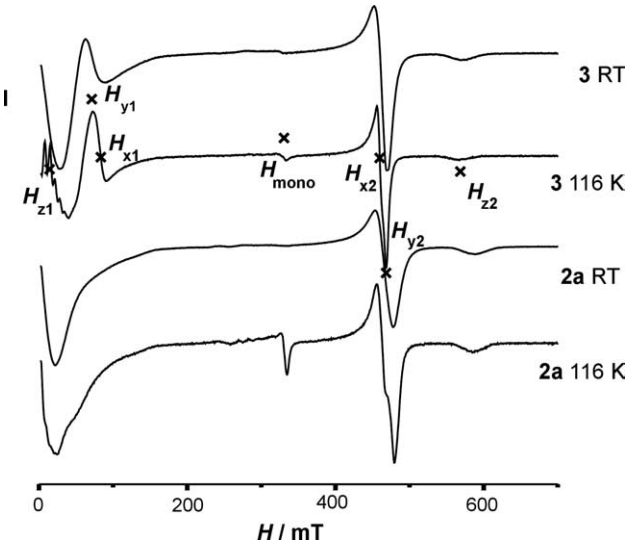

Fig. 3. Three signals H_{z1}, $H_{\perp 2}$ (H_{x2}, H_{y2}) and H_{z2}, characteristic for $[Cu_2(O_2CCH_3)_4(H_2O)_2]$ type of compounds for **2a** and **3**, and an additional signal $H_{\perp 1}$ (H_{x1}, H_{y1}) at 80 mT, in the spectra of **3** at room temperature (RT) and at 116 K.

$$H_{x1}^2 = \left(\frac{g_e}{g_x}\right)^2 (H_0 - D' + E')(H_0 + 2E'), \quad (1)$$

$$H_{y1}^2 = \left(\frac{g_e}{g_y}\right)^2 (H_0 - D' - E')(H_0 - 2E'), \quad (2)$$

$$H_0 = h\nu/g_e\beta, \quad D' = D/g_e\beta, \quad E' = E/g_e\beta.$$

Such signal and its assignment was, up to our knowledge, so far not reported for dicopper(II) tetracarboxylates, but only for $[Cu_2(O_2CCH_3)_2L_2(dmf)_2]$, with two O–C–O and two N–C–N bridges in Cu tetracarboxylate analogue [26]. Similar signal was noticed also in the spectra of copper(II) dinuclear complex with four O–C–N bridges in $[Cu_2(chp)_4]$ [27]. The partial coordination sphere in these two complexes is distorted square-planar CuO_2N_2 (only coordination atoms from bridges and without the axial ligand). The presence of the $H_{\perp 1}$ signal for these two tetracarboxylate analogues is in agreement with low D values (0.265; 0.275 $cm^{-1} \Rightarrow D < h\nu$). Structurally, the complex **3** is related to these two complexes by a relatively large torsion angle 6.0° for two *trans* O–Cu···Cu–O moieties (both O atoms are from the same carboxylate group; Fig. 4). For $[Cu_2(chp)_4]$, the O–Cu···Cu–N torsion angle is 5.1–8.6°, while for $[Cu_2(O_2CCH_3)_2L_2(dmf)_2]$, O–Cu···Cu–O 3.4° and N–Cu···Cu–N 0.9°, respectively. Comparable angles for **2** and for $[Cu_2(O_2CCH_3)_4(H_2O)_2]$ are significantly smaller (<1.2°, <2°) [28]. The Cu···Cu distances for both complexes **2** and **3** (2.608(1), 2.611(1) Å) are similar and typical for dicopper tetracarboxylates [29], therefore this distance can not be directly correlated to the appearance of the $H_{\perp 1}$ signal in the EPR spectra of **3**.

Since herein, the complex **3** is structurally characterized with **2**, and with **2a** by EPR, this correlation may not be absolutely exact. Maybe some additional information from the EPR spectra of the undecayed **2** (powder inside traces of mother solution) or from the frozen solution spectra could be obtained.

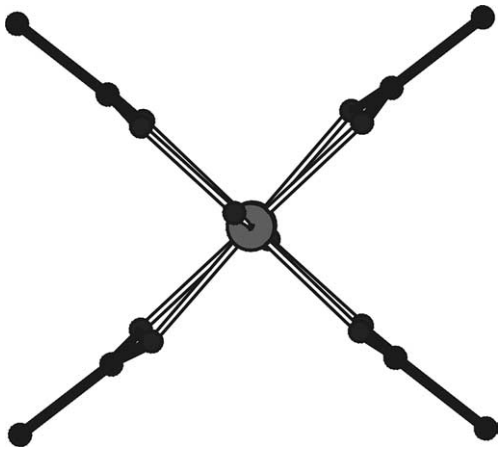

Fig. 4. Torsion in the O–Cu···Cu–O angles in **3** [23–25]. The second central copper ion is positioned behind the first one. All hydrogen atoms and aromatic rings are omitted for clarity.

A broad band at 3600–3300 cm^{-1} in the IR spectrum of **2a** agrees with the presence of water instead of methanol (a narrow band for O–H bond would be expected for **2**). One strong band in the region 1650–1550 cm^{-1} found for **3** (1570 cm^{-1}) and two strong bands in the spectrum of **2a** (1623, 1591 cm^{-1}) are probably due to the asymmetric stretching vibration [30] of one (vanillic acid anion) and two (acetate, vanillic acid anion) types of carboxylate anions in the compounds **2a** and **3**, respectively. Since in $[Cu_2(O_2CCH_3)_4(H_2O)_2]$, an acetate analogue of **3**, $\nu_{as}(CO_2)$ was observed at 1605 cm^{-1} [31], the higher energy band at 1623 cm^{-1} in the spectrum of **2a** is assigned to the acetate, while the 1591 cm^{-1} band to the vanillic acid anion.

4. Concluding remarks

The compounds $[Cu_2(C_8H_7O_4)_2(O_2CCH_3)_2(CH_3OH)_2]$ (**2**) and $[Cu_2(C_8H_7O_4)_4(H_2O)_2]$ (**3**) precipitate from the solution of the same starting compounds $[Cu_2(O_2CCH_3)_4(H_2O)_2]$ and vanillic acid, however in different polar solvent methanol or water for **2** or **3**, respectively. Heterocarboxylate compound $[Cu_2(C_8H_7O_4)_2(O_2CCH_3)_2(CH_3OH)_2]$ (**2**) is unstable outside mother-liquid. Its decomposition is partial, since the central carboxylate cage remains, however water molecules replace the apical methanol molecules. On the other hand, the homocarboxylate compound $[Cu_2(C_8H_7O_4)_4(H_2O)_2]$ (**3**) is stable also in air, probably due to two H-bonds to the axial ligand instead of one (**2**) and less volatile water (**3**) than methanol (**2**). Significant differences were found in the EPR spectra, resulting in an unexpected signal at 80 mT in the spectra of **3**, next to H_{z1}, $H_{\perp 2}$ and H_{z2}, typical for $S = 1$ spin state. This signal is assigned as $H_{\perp 1}$, due to low D axial zero field splitting parameter value ($D < h\nu$). The appearance of this signal is probably related to a relatively large torsion angle O–Cu···Cu–O, found in compound **3**, and not with the Cu···Cu distance

inside a dinuclear molecule. Coordination of the acetates, together with vanillic acid anions, in **2** and **2a**, yields stronger H-bonds and much less torsion in dicopper tetracarboxylate central core than in **3**, and seems to be an appropriate alternative to more extensive H-bonding with the axial ligand and more effective π-stacking in homocarboxylate complex **3**.

Acknowledgments

The financial support of the Ministry of Education, Science and Sport, Republic of Slovenia, through Grants MŠZŠ P-6209-124, P1-0175-103 and X-2000, is gratefully acknowledged. We thank Dr. M. Šentjurc, EPR center, 'Jožef Stefan' Institute, Ljubljana, for EPR spectra.

Appendix A. Supplementary data

The final atomic and geometrical parameters, crystal data and details concerning data collection and refinement for all three compounds have also been deposited with the Cambridge Crystallographic Data Center as supplementary material with the deposition numbers 277423 (**1**), 277424 (**2**) and 277425 (**3**), respectively. These data can be obtained, free of charge via http://www.ccdc.cam.ac.uk/const/retrieving.html. Supplementary data associated with this article can be found, in the online version, at doi:10.1016/j.poly.2005.08.031.

References

[1] M.M. Gharieb, M.I. Ali, A.A. El-Shoura, Biodegradation 15 (2004) 49.
[2] C. Xie, J.N.R. Ruddick, S.J. Rettig, F.G. Herring, Holzforschung 49 (1995) 483.
[3] J.N.R. Ruddick, C. Xie, F.G. Herring, Holzforschung 55 (2001) 585.
[4] R.J. Hobson, M.F.C. Ladd, D.C. Povey, J. Cryst. Mol. Struct. 3 (1973) 377.
[5] T.J. Greenhough, M.F.C. Ladd, Acta Crystallogr., Sect. B 34 (1978) 2619.
[6] T.J. Greenhough, M.F.C. Ladd, Acta Crystallogr., Sect. B 34 (1978) 2744.
[7] B. Kozlevčar, B. Mušič, N. Lah, I. Leban, P. Šegedin, Acta Chim. Slov. 52 (2005) 40.
[8] Z. Longguan, S. Kitagawa, H.-C. Chang, H. Miyasaka, Mol. Cryst. Liq. Cryst. 342 (2000) 97.
[9] D. Maspoch, D. Ruiz-Molina, K. Wurst, C. Rovira, J. Veciana, Chem. Commun. (2002) 2958.
[10] G. Vives, S.A. Mason, P.D. Prince, P.C. Junk, J.W. Steed, Cryst. Growth Des. 3 (2003) 699.
[11] L. Strinna Erre, G. Micera, P. Piu, F. Cariati, G. Ciani, Inorg. Chem. 24 (1985) 2297.
[12] M.A. Bañares, L. Dauphin, X. Lei, W. Cen, M. Shang, E.E. Wolf, T.P. Fehlner, Chem. Mater. 7 (1995) 553.
[13] Z. Otwinowski, W. Minor, Methods Enzymol. 276 (1997) 307.
[14] A. Altomare, M.C. Burla, M. Camalli, G. Cascarano, C. Giacovazzo, A. Guagliardi, A.G.G. Moliterni, G. Polidori, R. Spagna, J. Appl. Cryst. 32 (1999) 115.
[15] S.R. Hall, D.J. du Boulay, R. Olthof-Hazekamp (Eds.), Xtal3.6 System, University of Western Australia, 1999.
[16] G.M. Sheldrick, SHELXS-97, Program for Crystal Structure Determination, University of Göttingen, Germany, 1997.
[17] G.M. Sheldrick, SHELXL-97, Program for the Refinement of Crystal Structures, University of Göttingen, Germany, 1997.
[18] R.L. Dutta, A. Syamal, Elements of Magnetochemistry, Affiliated East-West PVT Ltd., New Delhi, 1993, pp. 6–11.
[19] S.P. Harish, J. Sobhanadri, Inorg. Chim. Acta 108 (1985) 147.
[20] T.D. Smith, J.R. Pilbrow, Coord. Chem. Rev. 13 (1974) 173.
[21] E. Wasserman, L.C. Snyder, W.A. Yager, J. Chem. Phys. 41 (1964) 1763.
[22] R. Velavan, P. Sureshkumar, K. Sivakumar, S. Natarajan, Acta Crystallogr., Sect. C 51 (1995) 1131.
[23] A.L. Spek, PLATON, University of Utrecht, The Netherlands, 2003.
[24] L.J. Farrugia, J. Appl. Cryst. 30 (1997) 565.
[25] F.H. Allen, Acta Crystallogr., Sect. B 58 (2002) 380.
[26] L. Gutierrez, G. Alzuet, J. Borras, A. Castiñeiras, A. Rodriguez-Fortea, E. Ruiz, Inorg. Chem. 40 (2001) 3089.
[27] E.J.L. McInnes, F.E. Mabbs, C.M. Grant, P.E.Y. Milne, R.E.P. Winpenny, J. Chem. Soc., Faraday Trans. 92 (1996) 4251.
[28] E.B. Shamuratov, A.S. Batsanov, Kh.T. Sharapov, Yu.T. Struchkov, T. Azizov, Koord. Khim. 20 (1994) 754.
[29] M.R. Sundberg, R. Uggla, M. Melnik, Polyhedron 15 (1996) 1157.
[30] G. Socrates, Infrared Characteristic Group Frequencies, Tables and Charts, Wiley, Chichester, 1994.
[31] Y. Mathey, D.R. Greig, D.F. Shriver, Inorg. Chem. 21 (1982) 3409.

$Ir(F_2HexO/F_2{}^tBuppy)_2(pic)$ complexes, their photophysical behaviors and redox properties, the X-ray single-crystal structure analyses of $Ir(F_2{}^tBuppy)_2(acac)$ and $Ir(F_2{}^tBuppy)_2(pic)$ and the applications of $Ir(F_2{}^tBuppy)_2(pic)$ as a dopant in the emitting layer of an EL device.

2. Experiments

2.1. Materials

$IrCl_3 \cdot 3H_2O$ was purchased from Alfa Aesar, USA, 2,4-difluoroboronic acid, picolinic acid, 1-hexanol and glycerol from Aldrich Chemicals, USA, phosphorousoxytrichloride from FERAK Laborat GMBH, Berlin (west), sodium hydride from Lancaster and the rest of the compounds from Tokyo Kasei Kogyo Co. Ltd., Japan, and all materials were used as received.

2.2. Syntheses

2-Chloropyridine-*N*-oxide, 2-chloro-4-nitropyridine-*N*-oxide and 2-chloro-4-nitro pyridine were prepared by following the methods described in the literature [3]. The synthetic routes of the ligands and the complexes are shown in Scheme 1.

2-Chloro-4-oxyhexylpyridine (yield: 53%): 2-Chloro-4-nitropyridine (1 eq) was added to a mixture of dry 1-hexanol (1.1 eq) and sodium hydride (1.5 eq) in dioxane as the solvent. The resulting solution was refluxed for 12 h. The reaction mixture was cooled to room temperature and poured into water. The organic layer separated out and the aqueous layer was washed by ethyl acetate. The combined organic extracts were dried and evaporated to dryness. The compound was purified by column chromatography. ^1H NMR (300 MHz, $CDCl_3$): δ, 8.07 (d, 1H, $J = 5.7$ Hz), 6.93 (d, 1H, $J = 3.0$ Hz), 6.71 (dd, 1H, $J = 2.1$, 6.0 Hz), 3.98 (dd, 2H, $J = 7.3$, 13.5 Hz), 1.72 (m, 2H), 1.45 (m, 2H), 1.25 (m, 4H), 0.82 (m, 3H). EIMS, m/z: 214, calc. 213.5.

2-(2′,4′-difluorophenyl)-4-oxyhexylpyridine (yield 75%): It was prepared by employing the method described in the literature [3]. 2-Chloro-4-oxyhexylpyridine was taken instead of 2-chloro-4-methoxypyridine as the starting material. ^1H NMR (300 MHz, $CDCl_3$): 8.51 (d, 1H, $J = 5.7$ Hz), 7.98 (m, 1H), 7.26 (t, 1H, $J = 2.1$ Hz), 6.94 (m, 2H), 6.78 (dd, 1H, $J = 2.4$, 5.7 Hz), 4.06 (m, 2H), 1.84 (m, 2H), 1.65 (m, 2H), 1.37 (m, 2H), 1.22 (m, 2H), 0.85 (m, 3H). EIMS, m/z: 221, calc. 221.

2-Chloro-4-*tert*-butylpyridine (yield 60%): 4-*tert*-Butylpyridine was chlorinated by the reaction with phosphorousoxytrichloride at low temperature (0–5 °C), it was stirred for 1h at 0 °C and then a further 1h at room temperature (25 °C). Then the reaction mixture was poured slowly into ice-cold water. The product was extracted by ethyl acetate and purified through column chromatography. ^1H NMR (300 MHz, $CDCl_3$): δ, 8.16 (d, 1H, $J = 6.0$ Hz), 7.27 (d, 2H, $J = 5.1$ Hz), 1.21 (s, 9H). EIMS, m/z: 170, calc. 169.5.

2-(2′,4′-Difluorophenyl)-4-*tert*-butylpyridine (yield 72%): This was prepared by a similar method to that described in the literature [3]. ^1H NMR (300 MHz, $CDCl_3$): δ, 8.60 (d, 1H, $J = 5.1$ Hz), 7.94 (dd, 1H, $J = 2.1$, 8.7 Hz), 7.72 (s, 1H), 7.25 (dd, 1H, $J = 1.8$, 5.4 Hz), 6.93 (m, 2H), 1.28 (s, 9H). EIMS, m/z: 247, calc. 247.

$(F_2{}^tBuppyppy)_2Ir(\mu\text{-}Cl)Ir(F_2{}^tBuOppyppy)_2$ (yield 70–75%): A solution of $IrCl_3 \cdot 3H_2O$ (1 mmol) and 2-(2′,4′-difluorophenyl)-4-methoxypyridine (3 mmol) in 2-ethoxyethanol (30 ml) was refluxed for 24 h. The pale green mixture was cooled to room temperature and 20 ml of 1 M HCl was added to precipitate the product. The mixture was filtered and washed with 100 ml of 1 M HCl, followed by 50 ml of methanol and then dried. The prod-

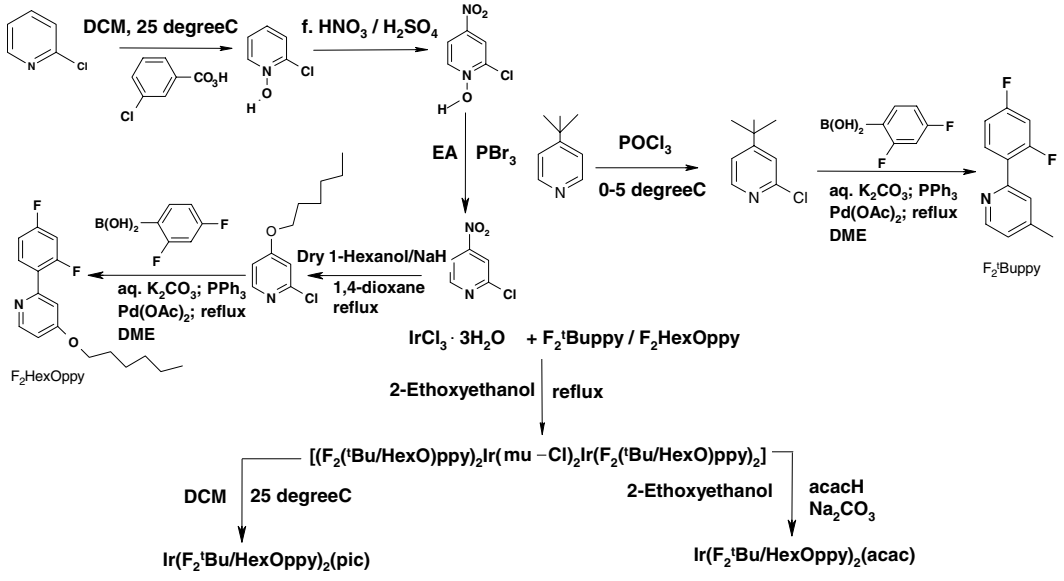

Scheme 1.

uct was obtained as a light green powder. ^{1}H NMR (300 MHz, $CDCl_3$): 9.04 (d, 4H, $J = 6.0$ Hz), 8.33 (s, 4H), 6.87 (d, 4H, $J = 6.0$ Hz), 6.32 (t, 4H, $J = 9.6$ Hz), 5.16 (d, 4H, $J = 7.2$ Hz), 1.58 (s, 36H). FABMS: *m/z*: 1439, fragmented masses, 1403 (–Cl), 1159 (–1 ligand); Calc. 1439.

$(F_2HexOppyppy)_2Ir(\mu\text{-}Cl)Ir(F_2HexOppy)_2$ (yield 70–75%): This has been synthesized by following the same method as described above. ^{1}H NMR (300 MHz, $CDCl_3$): 8.90 (d, 4H, $J = 5.7$ Hz), 7.79 (s, 4H), 6.35 (m, 8H), 5.41 (d, 4H, $J = 7.5$ Hz), 4.21 (d, 8H, $J = 6.0$ Hz), 2.05 (s, 8H), 1.69 (s, 8H), 1.31 (s, 16 H), 0.99 (s, 12H). FABMS: *m/z*: 1615, fragmented masses, 808 (–IrCl(ligand)$_2$), 773 (–Cl), calc. 1615.

$Ir(F_2HexOppy)_2(acac)$ (yield 80%) (**1a**) [1e,4]. $(F_2HexOppy)_2Ir(\mu\text{-}Cl)Ir(F_2HexOppy)_2$ (1 mmol), acetylacetone (3 mmol) and sodium carbonate (10 mmol) were mixed in 10 ml of 2-ethoxyethanol. The mixture was refluxed under nitrogen for 12 h. The reaction mixture was then cooled and the pale green precipitate was filtered off. The product was washed by methanol several times, followed by hexane. Then it was recrystallised from a mixture of dichloromethane and methanol (1:1). ^{1}H NMR (300 MHz, $CDCl_3$): 8.17 (d, 1H, $J = 6.3$ Hz), 7.73 (s, 1H), 6.73 (s, 1H), 6.32 (d, 1H, $J = 11.7$ Hz), 5.72 (d, 1H, $J = 6.0$ Hz), 5.22 (s, 1H), 4.15 (s, 2H), 1.87 (m, 8H), 1.39 (m, 6H), 0.93 (s, 3H). FABMS: *m/z*: 871, fragmented masses, 771 (–acetylacetonate); Calc. 871.

$Ir(F_2{}^tBuppy)_2(acac)$ (yield 80%) (**2a**). This has been prepared by adopting a similar method as described above. ^{1}H NMR (300 MHz, $CDCl_3$): 8.28 (m, 4H), 7.22 (d, 2H, $J = 6.0$ Hz), 6.32 (t, 2H, $J = 10.8$ Hz), 5.66 (d, 2H, $J = 8.4$ Hz), 5.24 (s, 1H), 1.81 (s, 6H), 1.44 (s, 18H), fragmented masses, 684 (–acetylacetonate); FABMS: *m/z*: 783, calc. 783.

$Ir(F_2HexOppy)_2(pic)$ (yield 88%) (**1b**) [1e,4]. 2.2 mmol of picolinic acid was added to a solution of 0.8 mmol of $(F_2{}^tBuppy)_2Ir(\mu\text{-}Cl)Ir(F_2{}^tBuppy)_2$ in 60 ml of dichloromethane at ambient temperature. The mixture was refluxed under nitrogen in an oil bath for 16 h. The reaction mixture was cooled to room temperature and a pale yellow precipitate was filtered off. The pure product was obtained by flash chromatography. ^{1}H NMR (300 MHz, $CDCl_3$): 8.44 (s, 1H), 8.30 (d, 1H, $J = 6.3$ Hz), 7.90 (s, 1H), 7.73 (m, 3H), 7.38 (s, 1H), 7.14 (s, 1H), 6.69 (s, 1H), 6.40 (m, 3H), 5.88 (d, 1H, $J = 8.4$ Hz), 5.65 (d, 1H, $J = 7.8$ Hz), 4.09 (s, 4H), 1.82 (s, 4H), 1.47 (s, 4H), 1.29 (s, 8H), 0.91 (s, 6H). FABMS: *m/z*: 894, fragmented masses, 772 (–picolinate); Calc. 894.

$Ir(F_2{}^tBuppy)_2(pic)$ (yield 92%) (**2b**). This has been synthesized by following the method as described above. ^{1}H NMR (300 MHz, $CDCl_3$): 8.59 (d, 1H, $J = 4.2$ Hz), 8.29 (m, 3H), 8.24 (s, 1H), 7.77 (s, 1H), 7.41 (s, 1H), 7.17 (d, 1H, $J = 4.2$ Hz), 7.00 (d, 1H, $J = 6.0$ Hz), 6.45 (m, 2H), 5.87 (d, 1H, $J = 9.0$ Hz), 5.57 (d, 1H, $J = 8.1$ Hz), 5.30 (s, 1H), 1.38 (s, 18H). FABMS: *m/z*: 806, fragmented masses, 685 (–picolinate), 651 (–Cl); Calc. 806.

$Ir(F_2MeOppy)_2(acac)$ (**3a**) and $Ir(F_2MeOppy)_2(pic)$ (**3b**). The syntheses of these complexes have been described in our previous paper [3].

$Ir(F_2ppy)_2(acac)$ (**4a**) and FIrpic (**4b**). The syntheses of these complexes have also been described previously [5].

2.3. Crystallography

Single-crystal diffraction data for $Ir(F_2{}^tBuppy)_2(acac)$ and $Ir(F_2{}^tBuppy)(pic)$ were collected on a Bruker SmartCCD diffractometer equipped with a normal focus, 3 kW sealed-tube X-ray source ($\lambda = 0.71073$ Å). The intensity data were collected in the ω scan mode (width of 0.3/° frame) and corrected for *Lp* and absorption effects by using the SAINT [6] program. Cell refinement and data reduction were carried out using the program Bruker SHELXTL [7] and the crystal structure was solved by direct methods using the SHELXTL [7] version 5.1 software packages. The structure was further refined by full-matrix least-square methods based on F^2 using SHELXTL version 5.1 [7]. Positions of non-hydrogen atoms were refined anisotropically, whereas the hydrogen positions were not refined.

2.4. Optical measurements and composition analyses

The ultraviolet–visible (UV–Vis) spectra of the phosphorescent iridium(III) complexes were measured on an UV–Vis spectrophotometer (Agilent Model 8453) and corrected for background due to solvent absorption. Photoluminescence (PL) spectra were carried out with a spectrophotometer (Jobin-Yvon Spex, Model Fluorolog-3). Emission quantum yields were measured by the method of Demas and Crosby [8] using *fac*-$Ir(ppy)_3$ as a reference [9]. NMR spectra were recorded on Varian 300 MHz. MS spectra (EI and FAB) were taken by micromass TRIO-2000. Cyclic voltammetry (CV) analyses were performed using CHI 2.05; dichloromethane was used as the solvent in an inert atmosphere and 0.1 M tetra(*n*-butyl)ammonium tetrafluoroborate was used as the supporting electrolyte. A glassy carbon rod was used as the working electrode, platinum was used as the counter electrode, and a silver wire was used as a pseudo-reference electrode. The TG-DTA analysis was carried out using a thermal analyzer (SEIKO 1TG/DTA Model 200). Luminescence lifetimes were obtained by exponentially fitting the emission decay curves recorded on a Continuum Model NY61 spectrofluorometer.

2.5. OLED fabrication and testing

In the fabrication of OLEDs, organic layers were thermally evaporated onto a glass substrate precoated with an indium-tin-oxide (ITO) layer with a sheet resistance of 20 Ω under high-vacuum. Prior to use, the ITO surface was ultrasonicated in a detergent solution followed by rinsing with deionized (DI) water, dipped into acetone, trichloroethylene and 2-propanol, and then degreased with a vapor of 2-propanol. After degreasing, the substrate was

oxidized and cleaned in a UV-ozone chamber before it was loaded into an evaporator. In a vacuum chamber at a pressure of 10^{-6} Torr, different layers (discussed in the EL discussion) were sequentially deposited onto the substrate to give the device structure. The current–voltage (*I–V*) profiles and light intensity characteristics for the above-fabricated devices were measured in a vacuum chamber of 10^{-6} Torr at ambient temperature using a Keithley 2400 Source Meter/2000 Multimeter coupled to a PR 650 Optical Meter.

3. Results and discussion

3.1. Syntheses

The syntheses of two new cyclometalated ligands, 2-(2′,4′-difluorophenyl)-4-oxyhexylpyridine and 2-(2′,4′-difluorophenyl)-4-*tert*-butylpyridine were carried out. The incorporation of an oxyhexyl group into the pyridyl moiety of 2-(2′,4′-difluorophenyl)-4-pyridine follows an almost similar method as described previously [3], except for step 4, where the nitro substituent was replaced by using dry 1-hexanol and sodium hydride as the base. The oxyhexyl substituent was incorporated into the pyridyl moiety of 2-(2′,4′-difluorophenyl)-4-pyridine in six steps, whereas the *tert*-butyl substituent just took two steps. Syntheses of cyclometalated complexes of iridium(III) were performed as described previously [3] using the oxyhexyl/*tert*-butyl-substituted ligands as the cyclometalated ligands and acetylacetone/picolinic acid as ancillary ligands. The thermogravimetric analysis of these complexes showed that the picolinate-Ir complexes are more stable than their corresponding acetylacetonate analogues (decomposition temperature (T_d): **1a**, 268 and **1b** 370; **2a**, 290 and **2b**, 310; **4a**, 216 and **4b** 344 °C) (Fig. 1). It is assumed that the free oxygen atom present in the picolinate of the Ir–picolinate complexes is responsible for making strong intermolecular H-bonding and hence increases the decomposition temperature. This fact is supported by the H-bonding obtained from the crystal structure of **1b**, i.e., O2···H1A′-C1A′ 2.607 Å and 120°.

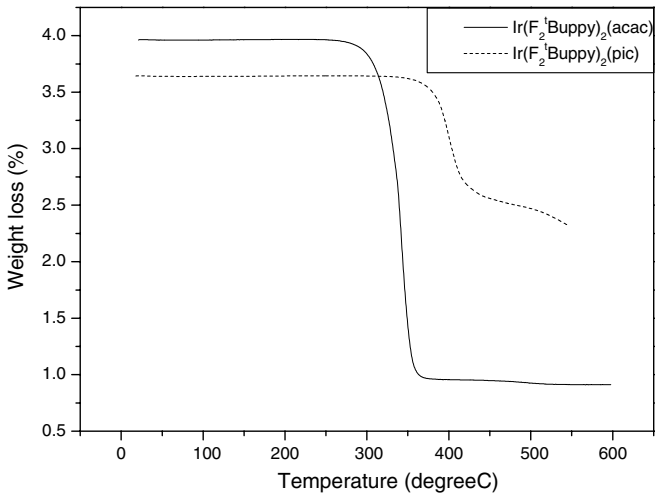

Fig. 1. Thermogravimetric analysis shows the decomposition temperature of [Ir(F_2′Buppy)$_2$(acac)] (**2a**) and [Ir(F_2′Buppy)$_2$(pic)] (**2b**).

3.2. Description of the X-ray structures

ORTEP plots of (F_2′Buppy)$_2$Ir(acac) and (F_2′Buppy)$_2$Ir(pic) molecules are shown in Fig. 2(a) and (b), respectively. Crystallographic data are given in Table 1, and selected bond lengths (Å) and angles (°) for these complexes are presented in Table 2. Single crystals of (F_2′Buppy)$_2$Ir(pic) were of lower quality than those of (F_2′Buppy)$_2$Ir(acac), which is reflected in the poor agreement factor for the (F_2′Buppy)$_2$Ir(pic) complex (Table 1). Both the complexes have octahedral geometry around iridium with *cis*-C,C *trans*-*N*,*N* chelate disposition. The Ir–C and Ir–N bond lengths are within the normal ranges expected for cyclometalated iridium(III) complexes [1b,4]. The Ir–O bond lengths are longer than the mean value of 2.088 Å reported in the Cambridge Crystallographic Database and reflect the large *trans* influence of the phenyl groups. All other bond lengths and angles within the chelate ligands are typical for cyclometalated complexes with ppy and acac/pic ligands bound to iridium(III) [2c,4,10].

3.3. Photoluminescence spectra

Fig. 3(a) and (b) shows mainly the lowest energy absorption bands for the acetylacetonate and picolinate analogues, respectively. The bands observed in the range 350–440 nm can be assigned as intraligand (IL) (π–π*) transitions (ppy^-) and metal-to-ligand charge-transfer (^{1}MLCT) (dπ (Ir) → π* (ppy^-)) transitions. Additionally, the spectra of all these complexes exhibit weaker absorption tails towards lower energy regions (440–480 nm), which may be attributed to triplet metal-to-ligand charge-transfer transitions (^{3}MLCT). As observed in Fig. 3(a) and (b), the picolinate analogues show significantly higher MLCT transitions with respect to their corresponding acetylacetonate analogues. If the comparison is confined to a particular series of complexes, either picolinate or acetylacetonate, the trend of blue-shifting of MLCT states is as follows: unsubstituted complex (FIrpic) < *tert*-butylsubstituted complex < methoxy-substituted complex ∼ oxyhexyl-substituted complex. The observed shift toward higher energy indicates an increase in energy separation between the metal d- and π*-orbitals and the strong electron-releasing effects of the substituents raise the π* orbitals of the cyclometalated ligand. These lowest excited states show solvatochromic effects and are shifted hypsochromically with increasing polarity of the solvents. As shown in Fig. 4(a), the decreasing order of maximum emission wavelength of a thin-film acetylacetonate sample is as follows: **1a** = **3a** > **2a** > **4a**. The same trend has also been observed in the picolinate thin-film analogues (Fig. 4(b)). The results reveal that the strongest electron releasing substituents, methoxy and oxyhexyl groups, shift the emission wave-

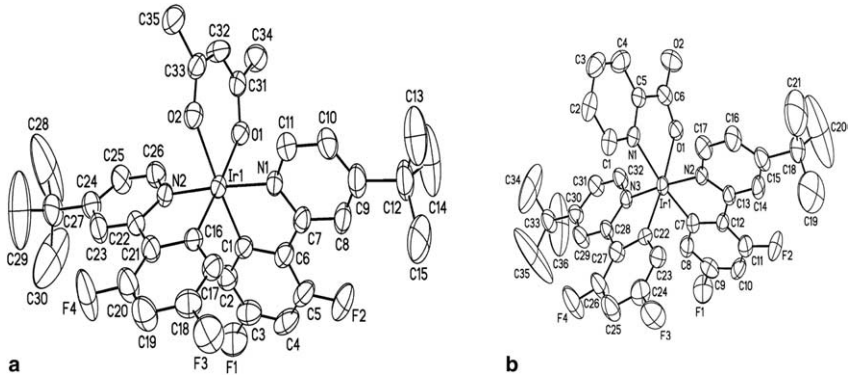

Fig. 2. ORTEP diagrams of: (a) [Ir(F_2'Buppy)$_2$(acac)] (**2a**) and (b) [Ir(F_2'Buppy)$_2$(pic)] (**2b**) (showing 50% thermal probability).

Table 1
Crystal data and structure refinement for Ir(F_2'Buppy)$_2$(acac) and Ir(F_2'Buppy)$_2$(pic)

Compound	Ir(F_2'Buppy)$_2$(acac)	Ir(F_2'Buppy)$_2$(pic)
Empirical formula	$C_{35}H_{35}F_4IrN_2O_2$	$C_{36}H_{32}F_4IrN_3O_2$
Formula weight	783.85	806.85
T (K)	294(2)	294(2)
λ (Å)	0.71073	0.71073
Crystal system	monoclinic	monoclinic
Space group	$P2_1/n$	$P2_1/n$
Unit cell dimensions		
a (Å)	13.6202(9)	13.7196(7)
b (Å)	11.7089(8)	11.6424(6)
c (Å)	20.9951(14)	21.3823(12)
β (°)	96.374(1)	95.671(1)
V (Å^3)	3327.5(4)	3398.7(3)
Z	4	4
D_{calc} (Mg m^{-3})	1.565	1.577
Absorption coefficient (mm^{-1})	4.067	3.986
F(000)	1552	1592
Crystal size (mm^3)	$0.51 \times 0.28 \times 0.20$	$0.2 \times 0.18 \times 0.1$
θ Range for data collection (°)	1.70–28.29	1.69–25.09
Index ranges	$-17 \leqslant h \leqslant 13$, $-15 \leqslant k \leqslant 15$, $-27 \leqslant l \leqslant 28$	$-8 \leqslant h \leqslant 16$, $-13 \leqslant k \leqslant 13$, $-25 \leqslant l \leqslant 25$
Reflections collected	20733	18104
Independent reflections (R_{int})	7801 (0.0360)	6031 (0.0647)
Completeness to θ (%)	94.4 (28.29 °)	99.9 (25.09 °)
Absorption correction	empirical	empirical
Maximum and minimum transmission	0.94343 and 0.50276	0.96364 and 0.75732
Refinement method	full-matrix least-squares on F^2	full-matrix least-squares on F^2
Data/restraints/parameters	7801/0/397	6031/0/415
Goodness-of-fit on F^2	1.318	1.308
Final R indices [$I > 2\sigma(I)$]	$R_1 = 0.0490$, $wR_2 = 0.0916$	$R_1 = 0.0746$, $wR_2 = 0.1328$
R indices (all data)	$R_1 = 0.0569$, $wR_2 = 0.0941$	$R_1 = 0.0956$, $wR_2 = 0.1385$
Largest difference in peak and hole (e Å^{-3})	1.403 and −2.300	1.654 and −2.643

length to the most blue region (458 nm), followed by the *tert*-butyl (462 nm) and then the unsubstituted (466 nm) complexes. This fact indirectly supports that the positions of the substituents in the ligand (pyridyl moiety) contains the LUMO states for these complexes. It also corroborate that the oxy-alkyl substituents exert stronger electronic effects relative to that of *tert*-butyl substituent. The shifting of the maximum emission wavelength is independent of the chain lengths of –OCH_3 and –O–CH_2–$(CH_2)_4$–CH_3 substituents. Solution PL emission spectra of the acetylacetonate analogues show the same trend of shifting emission wavelength (Fig. 5(a)) as is observed for the thin-film samples (Fig. 4(a)), while a different trend is observed for the solution picolinate complexes, i.e., **2b** > **4b** > **3b** > **1b** (Fig. 5(b)). The solution spectra of the oxy-alkyl substituted complexes show red-shifted and broad emission spectra relative to that of their thin-film samples. This observation prompted us to study the emissive characteristics of all the available acetylacetonate and picolinate complexes in different solvents with increasing polarities, that is systematic changes in polarity. Hence, the measurement of the solution emission spectra of these complexes were conducted in the following solvents of different polarities, toluene < chloroform < acetone < acetonitrile < methanol.

Table 2
Selected bond distances (Å) and bond angles (°) for Ir(F_2'Buppy)$_2$(acac) and Ir(F_2'Buppy)$_2$(pic)

Ir(F_2'Buppy)$_2$(acac)		Ir(F_2'Buppy)$_2$(pic)	
Ir(1)–C(16)	1.982(5)	Ir(1)–C(22)	1.987(10)
Ir(1)–C(1)	1.994(5)	Ir(1)–C(7)	2.003(10)
Ir(1)–N(2)	1.026(4)	Ir(1)–N(2)	2.032(8)
Ir(1)–N(1)	2.035(4)	Ir(1)–N(3)	2.036(8)
Ir(1)–O(1)	2.141(4)	Ir(1)–N(1)	2.146(9)
Ir(1)–O(2)	2.151(4)	Ir(1)–O(1)	2.148(7)
C(16)–Ir(1)–C(1)	91.0(2)	C(22)–Ir(1)–C(7)	89.9(4)
C(16)–Ir(1)–N(2)	80.83(19)	C(22)–Ir(1)–N(2)	96.6(4)
C(1)–Ir(1)–N(2)	96.9(2)	C(7)–Ir(1)–N(2)	79.9(4)
C(16)–Ir(1)–N(1)	96.24(19)	C(22)–Ir(1)–N(3)	80.3(4)
C(1)–Ir(1)–N(1)	81.0(2)	C(7)–Ir(1)–N(3)	98.1(4)
N(2)–Ir(1)–N(1)	176.42(17)	N(2)–Ir(1)–N(3)	176.2(3)
C(16)–Ir(1)–O(1)	176.61(18)	C(22)–Ir(1)–N(1)	97.0(4)
C(1)–Ir(1)–O(1)	89.84(18)	C(7)–Ir(1)–N(1)	172.4(4)
N(2)–Ir(1)–O(1)	95.81(16)	N(2)–Ir(1)–N(1)	95.9(3)
N(1)–Ir(1)–O(1)	87.13(16)	N(3)–Ir(1)–N(1)	86.5(3)
C(16)–Ir(1)–O(2)	91.28(18)	C(22)–Ir(1)–O(1)	173.5(4)
C(1)–Ir(1)–O(2)	176.30(18)	C(7)–Ir(1)–O(1)	96.2(3)
N(2)–Ir(1)–O(2)	86.33(16)	N(2)–Ir(1)–O(1)	86.7(3)
N(1)–Ir(1)–O(2)	95.84(16)	N(3)–Ir(1)–O(1)	96.6(3)
O(1)–Ir(1)–O(2)	88.04(14)	N(1)–Ir(1)–O(1)	77.1(3)

The solution spectra of the picolinate complexes are highly affected by the solvent polarity (Fig. 6(a)–(d)). In general, the broad and red-shifted emission is observed with increasing order of polarity. Again, the oxy-alkyl subsitituted complexes are mostly affected by solvents followed by the *tert*-butyl substituted and the unsubstituted complexes. The emission profile of the acetylacetonate complexes, however, remains almost unaffected (Fig. 7(a) and (b)). Presumably, the lowest excited state of the Ir–picolinate complexes has a significant contribution from the excited states of picolinate which is highly affected by solvent polarity. The PL quantum yields were obtained relative to [Ir(ppy)$_3$] ($\phi_{PL} = 0.4$) and the maximum value were found for the Ir(F_2'Buppy)$_2$(acac) complex (Table 3).

3.4. Cyclic voltametric studies

Analysis by cyclic voltammetry shows that all these acetylacetonates and picolinates undergo a reversible one-electron oxidation; no reduction processes were observed in chloroform. As shown in Table 3, the oxidation potentials are slightly affected by the type of ancillary ligand (acetylacetonate and picolinate; ~125 mV) for each pair of complexes, but they vary significantly between complexes with different substitutions (*tert*-butyl and oxyhexyl; ~350 mV). Oxyhexyl-substituted complexes show lower oxidation potentials with respect to their corresponding *tert*-butyl-substituted analogues, indicating the relative ease of oxidation.

3.5. Electroluminescence

The electroluminescent (EL) properties of the complex **2b** were investigated. The EL device performance was investigated by using **2b** as a dopant and CBP [4,4′-bis(9-carbazolyl)-1,1′-biphenyl] as the host in the emitting zone (D-**I**). The device structure adopted in this work is a typical multi-layer, employing indium tin oxide (ITO) as the anode, polyfluoro carbon (CF_x) as the hole injecting material, 4,4′-bis[(1-naphthyl)(phenyl)amino]-1,1-biphenyl (NPB) as the hole transporting material, **2b** as the dopant and CBP as the host, 2,6-dimethyl-4,7-diphenyl-1,10-phenanthroline (BCP) as the hole blocking material, aluminium *tris*(8-quinolinolate) (Alq_3) as the electron-transport material, LiF as the electron-injection layer and aluminum as the cathode, as shown in Fig. 8 (inset). The complex emits a greenish-blue emission in the EL spectra (Fig. 8), which are well matched to that observed in the PL spectra in solution. There are no characteristic emission peaks from Alq_3 or CBP, except a very weak emission from the NPB layer (weak emission ~425 nm in Fig. 8), indicating the emission originates from the dopant in the emitting layer. Furthermore, these results support that the effective energy transfer from the host (CBP) to the dopant (Ir complex) occurs in the emissive layer. The fabrication of another two devices

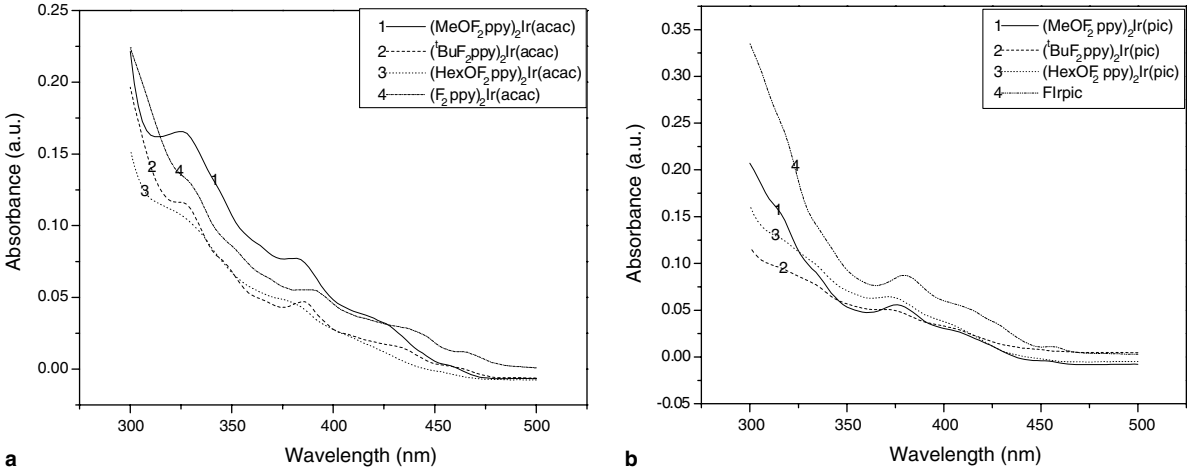

Fig. 3. Comparative absorbance spectra of the series of acetylacetonate (a) and picolinate (b) iridium(III) complexes.

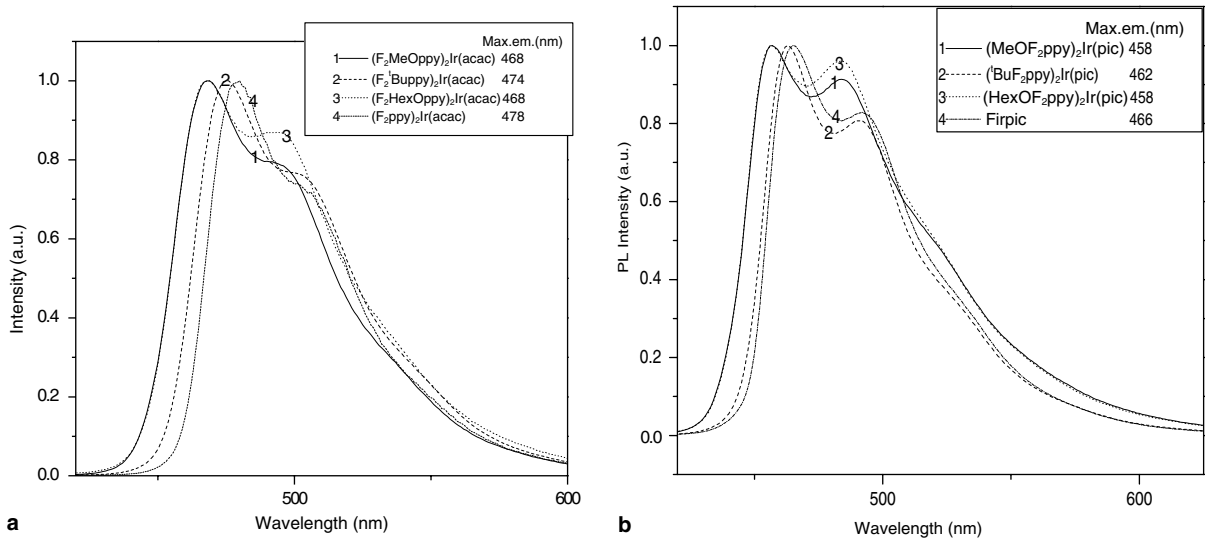

Fig. 4. Solid thin-film emission spectra of the series of acetylacetonate (a) and picolinate (b) iridium(III) complexes.

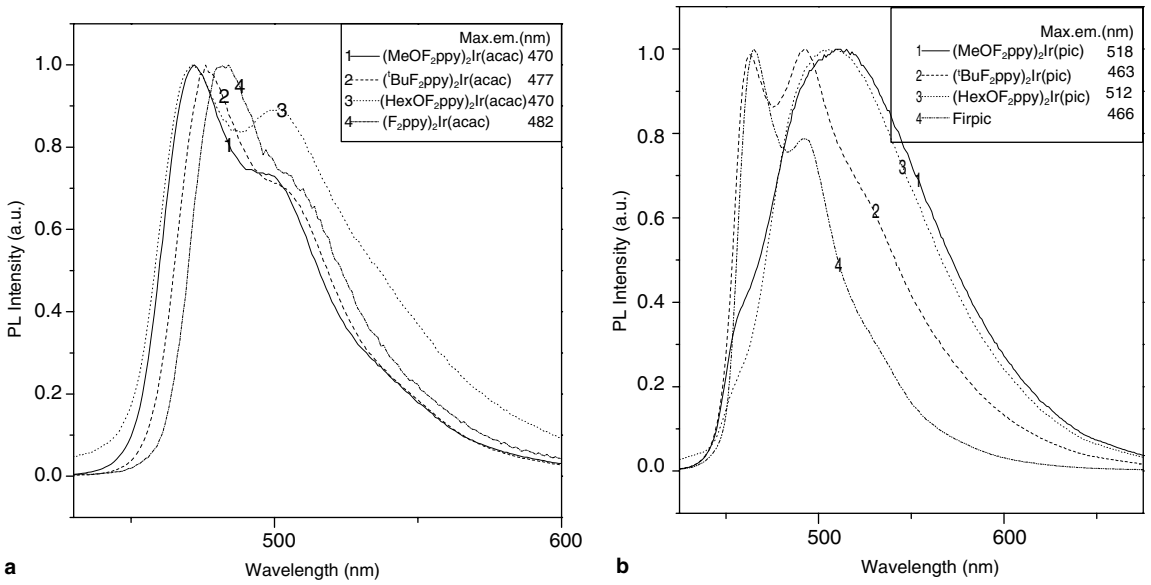

Fig. 5. Solution emission spectra (chloroform) of the series of acetylacetonate (a) and picolinate (b) iridium(III) complexes.

was also carried out, using $Ir(F_2MeOppy)_2(acac)$ [3] (D-**II**) and FIrpic (D-**III**), **3** dopants in a similar device structure as mentioned above to make a comparative study of EL performances. The lowest unoccupied molecular orbitals (LUMO) primarily lie on the pyridyl moiety [11] of the cyclometalated ligand in **2b** and it contains the electron releasing substituent *tert*-butyl (^{t}Bu). The electronic effect of the *tert*-butyl (^{t}Bu) substituent in the pyridyl moiety uplifts the LUMO state and a hypsochromically shifted emission is observed subsequently with respect to the unsubstituted Firpic complex in EL emission (472 nm → 468 nm; Fig. 8). The EL device containing the dopant $Ir(F_2MeOppy)_2(acac)$ shows the maximum emission at 472 nm, where the ancillary ligand (acac) is different from that of FIrpic and **2b**. The turn-on voltages of D-**I**, D-**II** and D-**III** are 5.6, 5.9 and 6.9, respectively (Fig. 9). The intermolecular interactions (e.g., π–π stacks in the molecular crystals) in the solid state and the ability to trap charges in the emissive layer are considered to be the most important factors in determining the operating voltage. The strong electronic coupling and intermolecular interactions in the molecular crystals contribute to effective injections and transport of charges, leading to lower operating voltages [12]. On the other hand, effective charge-trapping by the dopants gives rise to increasing driving voltages in OLEDs [13]. If the dopant material functions as a hole trap, the HOMO level of the dopant could be above that of the host material. Hence, materials having a lower oxidation potential can function as effective hole traps in OLEDs. Therefore, the observed higher operating voltages for D-**III** relative to D-**I** are predominantly caused due to effective hole trapping, which is consistent with the electro-

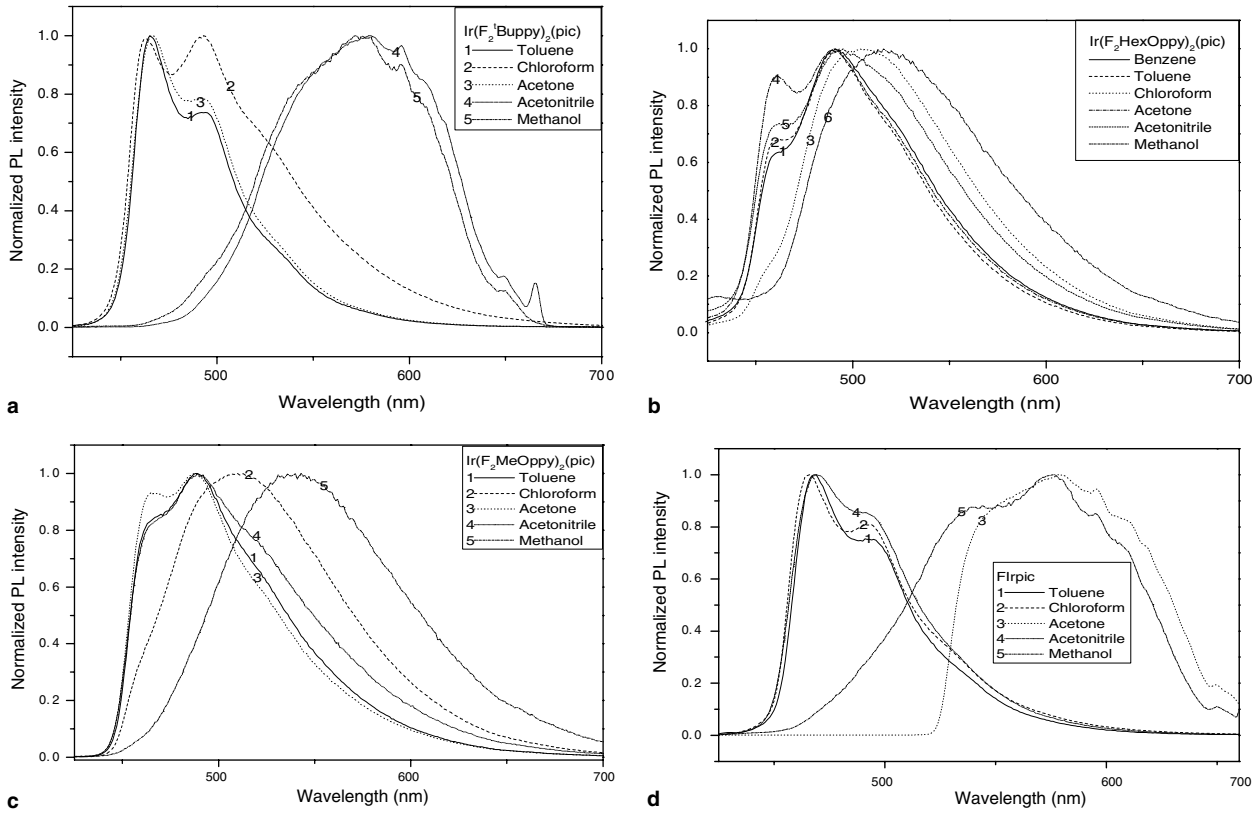

Fig. 6. Solvent dependent emission spectra of the iridium(III)-picolinate complexes: [Ir(F_2'Buppy)$_2$(pic)] (shown in a), [Ir(F_2HexOppy)$_2$(pic)] (shown in b), [Ir(F_2MeOppy)$_2$(pic)] (shown in c) and [Ir(F_2ppy)$_2$(pic)] (shown in d).

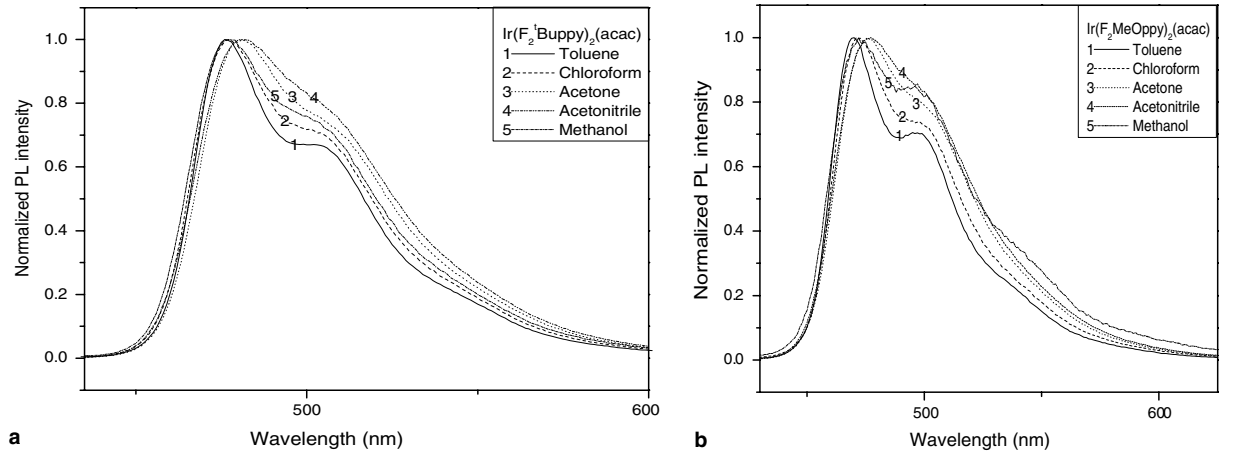

Fig. 7. Solvent dependent emission spectra of the iridium(III)-acetylacetonate complexes: [Ir(F_2'Buppy)$_2$(acac)] (shown in a) and [Ir(F_2'Buppy)$_2$(acac)] (shown in b).

chemical behavior of the dopants used in these devices (i.e., E^{ox} of **2b** (dopant in D-**I**) 0.866 V; E^{ox} of FIrpic (dopant in D-**III**) 0.586 V). The electrochemical behavior of the dopant used in D-**II** (E^{ox} of Ir(F_2MeOppy)$_2$(acac) (dopant in D-**II**) 0.506 V) is almost similar to that of D-**III**, but the observed operating voltage is significantly smaller than that of D-**III**. Presumably, the dopant used in D-**II** has relatively strong intermolecular interactions (MeO-substituent present; π–π stacks) as compared to that of the dopant used in D-**III**, which is responsible for better injection of charges and hence correspondingly lowering of driving voltages. The comparative EL performances of the devices are shown in Table 4. The luminance yield for D-**III** is superior to the remaining devices described herein. Poor solution PL luminance yield is observed (Table 3) for the substituted dopants relative to that of FIrpic, reflecting the comparatively poor EL luminance yield observed for D-**I** and **II** devices. These experiments further prompt us that there is no

Table 3
Photophysical and electrochemical data for the acetylacetonate and picolinate analogues of the iridium(III) complexes

Complex	Absorbance[a] λ (nm) ($\log\varepsilon$)	Emission λ_{max} (nm)		Quantum efficiency[a,c]	Redox $E^{ox}_{1/2}$ (V)[a]	Band gap (eV)
		Solution[a,b]	Film[b]			
$Ir(F_2{}^tBuppy)_2(acac)$	386 (4.7); 464 (4.2)	477	474	0.86	0.746	2.55
$Ir(F_2{}^tBuppy)_2(pic)$	375 (4.7); 454 (4.3)	463	462	0.78	0.866	2.77
$Ir(F_2HexOppy)_2(acac)$	379 (4.7); 456 (4.3)	470	468	0.48	0.391	2.71
$Ir(F_2HexOppy)_2(pic)$	373 (4.7); 441 (4.5)	512	458	0.71	0.504	2.72

[a] Solvent used dichloromethane.
[b] Excitations used 383, 377, 381 and 369 nm for solutions and 285, 276, 278 and 277 nm for thin films.
[c] Values are reported relative to $Ir(ppy)_3$.

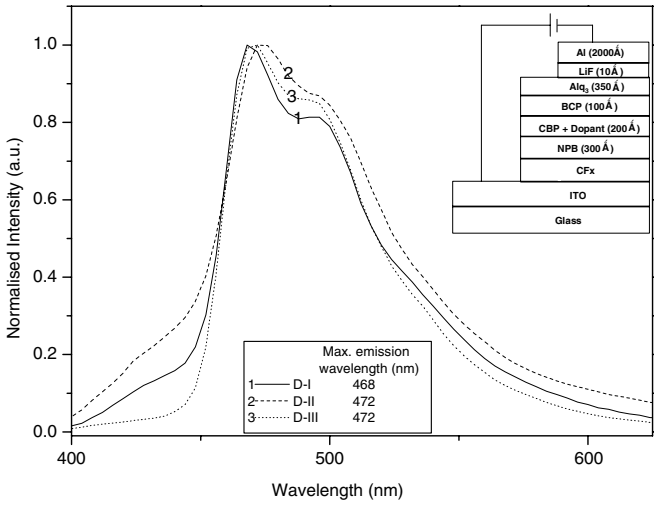

Fig. 8. Comparative EL emission spectra of the devices, D-**I**, D-**II** and D-**III**.

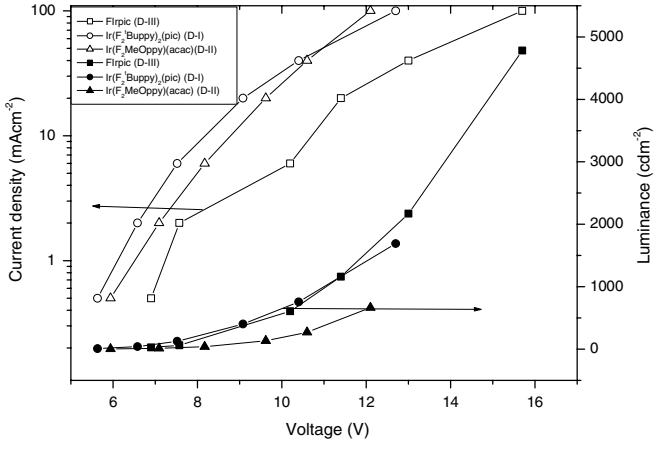

Fig. 9. Comparative current density–voltage–luminance (*I–V–L*) curves of the devices, D-**I**, D-**II** and D-**III**.

inherent tendency of the substituted dopants which results in abnormal worsening of EL performances.

Assuming that the emitting state of a complex is formed with unit efficiency, based on the $k_r = \phi_{PL}/\tau$ and $\phi_{PL} = k_r/(k_r + k_{nr})$ relationships, the calculations of radiative (k_r) and non-radiative (k_{nr}) rate constants of $Ir(F_2{}^tBuppy)_2(acac)$ ($\phi_{PL} = 0.78$; $\tau = 0.11$ μs; $k_r = 7.1 \times 10^6$; $k_{nr} = 2.0 \times 10^6$), $Ir(F_2MeOppy)_2(acac)$ ($\phi_{PL} = 0.60$; $\tau = 0.097$ μs; $k_r = 6.2 \times 10^6$; $k_{nr} = 4.0 \times 10^6$) and FIrpic ($\phi_{PL} = 0.99$; $\tau = 0.11$ μs; $k_r = 9 \times 10^6$; $k_{nr} = 9 \times 10^4$) were performed. The radiative rate constants for these complexes show almost similar order (10^6), but the non-radiative rate constants for FIrpic are less than two orders of magnitude smaller than those of substituted dopants. The non-radiative rate constant is a sum of rates for several processes that quench emission. It appears that a new luminescent quenching mechanism comes into play as the energy of the triplet states increases (for the case of substituted dopants). It may involve a self-quenching mechanism or perhaps thermal activation to a competing MLCT state on the ancillary ligand.

4. Conclusion

Syntheses of new blue-emitting iridium(III) based phosphorescent materials have been carried out. Systematic changes of emission wavelengths have been demonstrated by various ligands with different electronic properties to form a series of Ir complexes. Solution photoluminescence behavior of iridium(III)-acetylacetonate/picolinate complexes were also investigated. Comparative EL performances were also examined using three similar types of dopants described herein with the same device configuration, and the observed poor device performances for the device containing a substituted dopant with respect to the device which contains a dopant without a substituent was rationalized.

Table 4
Comparative EL performances for devices D-**I**, **II** and **III**

Dopants used (Device)	Current density (mA cm^{-2})	Drive voltage (V)	Luminance (cd m^{-2})	Luminance yield (cd A^{-1})	CIE		λ_{max} (nm)	Quantum efficiency (%)
					x	*y*		
$(F_2{}^tBuppy)_2Ir(pic)$ (D-**I**)	20	9.1	402	2.0	0.17	0.30	468	1.0
$(F_2MeOppy)_2Ir(acac)$ (D-**II**)	20	9.6	133	0.7	0.19	0.31	472	0.4
FIrpic (D-**III**)	20	11.4	1161	5.8	0.16	0.32	472	3.3

5. Supplementary material

Crystallographic data for the structural analysis have been deposited with the Cambridge Crystallographic Data Centre, CCDC Nos. 253380 and 253381 for compounds $Ir(F_2{}^tBuppy)_2(acac)$ and $Ir(F_2{}^tBuppy)(pic)$, respectively. Copies of this information may be obtained free of charge from the Director, CCDC, 12 Union Road, Cambridge, CB2 1EZ, UK (fax: +44 1223 336 033; email: deposit@ccdc.cam.ac.uk or www: http://www.ccdc.cam.ac.uk).

Acknowledgements

This research is supported by the Program for Promoting University Academic Excellence from the Ministry of Education, Taiwan, Republic of China under the Contract PPAEU 91-E-FA04-2-4-(B).

References

[1] (a) P. Coppo, E.A. Plummer, L.D. Cola, Chem. Commun. (2004) 1774;
(b) S. Jung, Y. Kang, H.-S. Kim, Y.-H. Kim, C.-L. Lee, J.-J. Kim, S.-K. Lee, S.-K. Kwon, Eur. J. Inorg. Chem. (2004) 3415;
(c) J.D. Slinker, A.a. Gorodetsky, M.S. Lowry, J. Wang, S. Parker, R. Rohl, S. Bernhard, G.G. Malliaras, J. Am. Chem. Soc. 126 (2004) 2763;
(d) S. Lamansky, P. Djurovich, D. Murphy, F. Abdel-Razzaq, H.-F. Lee, C. Adachi, P.E. Burrows, S.R. Forrest, M.E. Thompson, J. Am. Chem. Soc. 123 (2001) 4304;
(e) M.E. Thompson, S. Lamansky, P.I. Djurovich, D. Murphy, F. Abdel-Razzaq, R. Kwong, S.R. Forrest, M.A. Baldo, P.E. Burrows, Patent US 20020034656A1.

[2] (a) A. Beeby, S. Bettington, I.D.W. Samuel, Z. Wang, J. Mater. Chem. 13 (2003) 80;
(b) C.-H. Yang, K.-H. Fang, C.-H. Chen, I.-W. Sun, Chem. Commun. (2004) 2232;
(c) V.V. Grushin, N. Herron, D.D. LeClous, W.J. Marshall, V.A. Petrov, Y. Wang, Chem. Commun. (2001) 1494.

[3] I.R. Laskar, S.-F. Hsu, T.-M. Chen, Polyhedron 24 (2005) 189.

[4] S. Lamansky, P. Djurovich, D. Murphy, F. Abdel-Razzaq, R. Kwong, I. Tsyba, M. Bortz, B. Mui, R. Bau, M.E. Thompson, Inorg. Chem. 40 (2001) 1704.

[5] M.E. Thompson, S. Lamansky, V. Adamovich, P.I. Djurovich, C. Adachi, R. Kwong, S.R. Forrest, M.A. Baldo, Patent US 2002/0182441 A1.

[6] G.M. Sheldrick, SAINT: Bruker Analytical X-ray Instrument Division, Madison, WI, 1998.

[7] G.M. Sheldrick, SHELXTL Programs, version 5.1; Bruker AXS GmbH, Karlsruhe Germany, 1998.

[8] J. Demas, G.A. Crosby, J. Phys. Chem. 75 (1971) 991.

[9] K.A. King, P.J. Spellane, R.J. Watts, J. Am. Chem. Soc. 107 (1985) 1431.

[10] F.O. Graces, K. Dedian, N.L. Keder, R.J. Watts, Acta Crystallogr., Sect. C 49 (1993) 1117.

[11] P.J. Hay, J. Phys. Chem. A 106 (2002) 1634.

[12] L.S. Sapochak, A. Padmaperuma, N. Washton, F. Endrino, G.T. Schmett, J. Marshall, D. Fogarty, P.E. Burrows, S.R. Forrest, J. Am. Chem. Soc. 123 (2001) 6300.

[13] (a) P.A. Lane, L.C. Palilis, D.F. O'Brien, C. Giebeler, A.J. Cadby, D.G. Lidzey, A.J. Campbell, W. Blau, D.D.C. Bradley, Phys. Rev. B 63 (2001) 235206;
(b) D.F. O'Brien, C. Giebeler, R.B. Fletcher, A.J. Cadby, L.C. Pallilis, D.G. Lidzey, P.A. Lane, D.D.C. Bradley, W. Blau, Synth. Met. 116 (2001) 379.

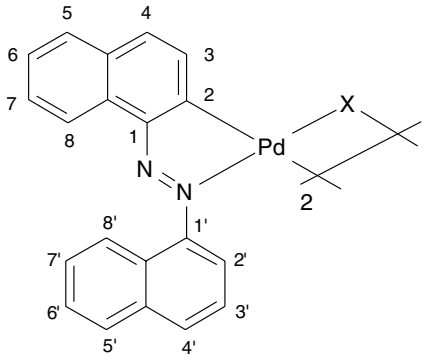

1a: X = Cl
1b: X = OAc

2. Experimental

2.1. Materials and general methods

1-(1′-Naphthylazo)naphthalene [65] were synthesised following published method with minor modifications. Thallium(I) cylopentadienide was prepared according to a reported method [66].

The IR spectra were recorded either on Perkin–Elmer 783 or on Perkin–Elmer 983 (with DS system) spectrophotometer as KBr disks. NMR spectra were obtained using either JEOL GSX 400 NB or VXR 300 S Varian Supercon spectrometer. Electronic spectra were recorded on a Shimadzu UV-240 spectrophotometer.

2.2. Di-(μ-chloro)-bis(1-(1′-naphthylazo)naphthyl-C(2), N_β)dipalladium(II) (**1a**)

A hot ethanolic solution (50 ml) of 1-(1′-naphthylazo)naphthalene (0.14 g, 0.496 mmol) was added to an ethanolic solution (20 ml) of $Na_2[PdCl_4]$ (0.14 g, 0.475 mmol). The solution was kept at room temperature for 24 h. **1a** was separated as red precipitate, thoroughly washed with water and ethanol and finally dried in vacuo. Yield: 0.157 g (75%). *Anal*. Calc. for $C_{40}H_{26}N_4Pd_2Cl_2$: C, 56.7; H, 3.1; N, 6.6. Found: C, 56.5; H, 3.0; N, 6.5%. UV/VIS (MeCN), λ/nm (ε/dm^3 mol^{-1} cm^{-1}): 500 (9250), 398 (16600), 222 (71540).

2.3. Di-(μ-acetato)-bis(1-(1′-naphthylazo)naphthyl-C(2), N_β)dipalladium(II) (**1b**)

A solution of 1-(1′-naphthylazo)naphthalene (0.25 g, 0.886 mmol) in chloroform (15 ml) was added to a solution of palladium(II)acetate (0.2 g, 0.891 mmol) in the same solvent (25 ml). The reaction mixture was kept for 48 h. at room temperature. The volume of the reaction mixture was reduced to 15 ml and was chromatographed on silica gel (60–120 mesh size). The free ligand was first eluted with benzene. **1b** was eluted as a red band by a mixture of benzene and acetonitrile (4:1 v/v) as an eluant. Removal of the solvent afforded **1b** as red crystalline powder. Yield: 0.198 g (50%). *Anal*. Calc. for $C_{44}H_{32}N_4Pd_2O_4$: C, 59.1; H, 3.6; N, 6.3. Found: C, 59.0; H, 3.6; N, 6.2%. IR (KBr; ν/cm^{-1}): 1554, 1424 (CH_3COO). UV/VIS (MeCN), λ/nm (ε/dm^3 mol^{-1} cm^{-1}): 500 (11200), 410 (18730), 280 (35100). ^{1}H NMR in DMSO-d_6 (ppm): 2.54 (s, 3H, Me), 7.34 (br s,1H, H–C(3)), 7.48–8.57 (Ar). ^{13}C {^{1}H} NMR in DMSO-d_6 (ppm):158.23 (C–2), 156.02–117.78 (Ar), 29.69 (Me).

2.4. (η^5-Cyclopentadienyl)(1-(1′-naphthylazo)naphthyl-C(2), N_β)palladium(II) (**2**)

To a suspension of **1a** (0.07 g, 0.083 mmol) in dry benzene (20 ml) was added solid TlCp (0.067 g, 0.248 mmol) with stirring. The mixture was further stirred for 4 h at room temperature. The colour of the solution became dark violet. The precipitate of TlCl was removed by filtration through a glass sintered (G-4 frit) funnel. The filtrate was evaporated to dryness in vacuo. The solid residue was taken up in CH_2Cl_2 and chromatographed on alumina column. Compound **2** was eluted as deep violet band using benzene as an eluant. Removal of the solvent afforded **2** as deep violet microcrystals. Yield: 0.045 g (60%). *Anal*. Calc. for $C_{25}H_{18}N_2Pd$: C, 66.3; H, 4.0; N, 6.2. Found: C, 66.1; H, 3.9; N, 6.1%. UV/VIS (MeCN), λ/nm (ε/dm^3 mol^{-1} cm^{-1}): 550 (8170), 470 (9600), 265 (33660), 230 (44880). ^{1}H NMR in $CDCl_3$ (ppm): 5.7 (s, 5H, Cp), 7.42–8.79 (Ar). ^{13}C {^{1}H} NMR in $CDCl_3$ (ppm): 190.08 (C–2), 155.60–121.13 (Ar), 96.66 (Cp).

2.5. Reaction of complex (**1a**) with m-chloroperbenzoic acid

Acetonitrile solution (5 ml) of *m*-chloroperbenzoic acid (0.025 g, 0.144 mmol) was added dropwise with stirring to a suspension of **1a** (0.04 g, 0.047 mmol) in acetonitrile (40 ml). The reaction mixture was further stirred for 24 h at room temperature The colour of the solution was gradually turned into violet. The solvent was removed under reduced pressure and the solid mass was repeatedly washed with aqueous ethanol (1:1, v/v) followed by Et_2O to remove the organic acids and finally it was extracted with chloroform (10 × 10 ml). Removal of the solvent in vacuo afforded **3a** as maroon microcrystals Yield: 0.018 g (45%). *Anal*. Calc. for $C_{40}H_{26}N_4O_2Pd_2$ Cl_2: C, 54.7; H, 3.0; N, 6.4. Found: C, 54.6; H, 3.0; N, 6.2%. IR (KBr;ν/cm^{-1}): 1141 ν (C–O). UV/VIS ($CHCl_3$), λ/nm (ε/dm^3 mol^{-1} cm^{-1}): 550 (30170), 510 (28640), 380 (10970), 360 (10315), 260 (59250), 240 (76150).

2.6. Reaction of complex (**1b**) with m-chloroperbenzoic acid

Acetonitrile solution (10 ml) of *m*-chloroperbenzoic acid (0.029 g, 0.168 mmol) was added dropwise with stirring to **1b** (0.05 g, 0.056 mmol) suspended in acetonitrile (35 ml). The colour of the reaction mixture was gradually turned

into violet and the stirring was continued for 3 h. The solvent was removed under reduced pressure and the residue was washed with aqueous ethanol (1:1 v/v) thrice to remove the organic acids. The residue was dissolved in chloroform (5 ml) and chromatographed on silica gel (60–120 mesh). A red violet band was eluted by a mixture of benzene and acetonitrile (25:1 v/v). Removal of the solvent afforded pure **3b**. Yield: 0.015 g (30%). *Anal*. Calc. for $C_{44}H_{32}N_4Pd_2O_6$: C, 57.1; H, 3.5; N, 6.1. Found: C, 56.9; H, 3.4; N, 5.9%. IR (KBr; ν/cm^{-1}): 1550, 1424 (CH_3COO), 1150 (C–O). UV/VIS ($CHCl_3$), λ/nm ($\varepsilon/dm^3\ mol^{-1}\ cm^{-1}$): 545 (33 180), 510 (29 550), 380 (10 160), 360 (9870), 260 (55 158), 240 (63 140). ^1H NMR in $CDCl_3$ (ppm): 2.53 (s, 3H, Me), 6.22 (d, 1H, H–C(3)), 6.51–8.63 (other aromatic protons). $^{13}C\{^1H\}$ NMR in $CDCl_3$ (ppm): 137.19 (C-2), 131.00–111.95 (Ar), 29.69 (Me).

Caution: Thallium compounds and benzene are highly hazardous chemicals. These should be handled with great care.

3. Results and discussion

3.1. Synthesis

1-(1′-Naphthylazo)naphthalene (HL) smoothly reacts with $Na_2[PdCl_4]$ in ethanol at room temperature and yields cyclopalladated chloro-bridged binuclear **1a** as red crystalline solid. Similarly palladium(II) acetate yields acetato-bridged binuclear **1b** in chloroform at room temperature. The conversion of **1b** into **1a** is readily achieved by treating **1b** with LiCl in a dioxane–water mixture. P. Rys et al. [53,54] have thoroughly studied the cyclopalladation reaction of azonaphthyl group of 1-(1′-phenylazo)naphthalene and established that the palladium–carbon bond formation occurs at C2 exclusively. The chloro-bridge of the cyclopalladated compound **1a** is cleaved by solid TlCp in benzene at room temperature to afford air stable monomeric **2**.

The IR spectrum of **1b** shows two bands at 1554 and 1424 cm^{-1} characteristic of acetato-bridged cyclopalladated compounds [67]. The strong absorption around 764 cm^{-1} of **2** is attributed to π-bonded cyclopentadienyl ring to palladium(II) centre [68].

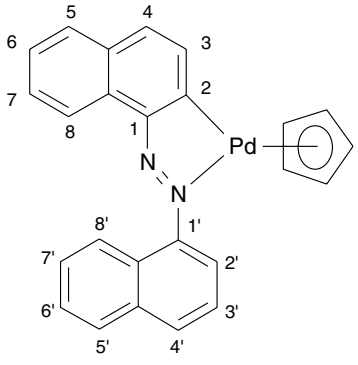

2

The strong absorption band of **1** at 500 nm is believed [36,69] to originate from $\pi \rightarrow \pi^*$ transition localised on the palladated azonaphthalene fragment L. The allowed metal to ligand charge transfer band for **2** is observed around 550 nm [61]. In contrast to the poor solubility of chloro-bridged **1a**, the acetato-bridged **1b** is suitable for ^1H and ^{13}C NMR investigations. The signal for aromatic 3-H proton of **1b** appears as broad peak at 7.34 ppm separated from other aromatic protons signals in the region of 7.48–8.57 ppm. The high field shift of H–C3 on *ortho*-metallation is well known [44,53]. The $^{13}C\{^1H\}$ NMR spectrum of **1b** exhibits the metallated carbon C(2) at 158.23 ppm and such low-field shift of aromatic carbon on metallation is well documented [53]. The ^1H NMR spectrum of **2** display a single sharp signal at ca. 5.7 ppm due to the η^5-binding of cyclopentadienyl group (Cp) to palladium(II) [70]. The equivalence of all the five carbon atoms of metal bound cyclopentadienyl group in **2** is also evident from the signal at 96.66 ppm in the $^{13}C\{^1H\}$ NMR spectrum of **2**. The signal for palladated carbon (C-2) appears at 190.08 ppm and such low field shift (31.8 ppm) of palladated carbon in presence of Cp as coligand is well known [61].

3.2. Metaloxylation Reaction of complexes (*1*) with *m*-chloroperbenzoic acid

Azoxy-naphthalene is the sole product of the reaction between 1-(1′-naphthylazo)naphthalene and *m*-chloroperbenzoic acid in non-aqueous media [65]. But the reaction of cyclopalladated complexes **1** with *m*-chloroperbenzoic acid in acetonitrile medium at room temperature results in the oxygen insertion into Pd–C(naphthyl) bond and affords **3**. The reaction virtually goes to completion within 3 h. Complexes **3** have been isolated using chromatographic technique.

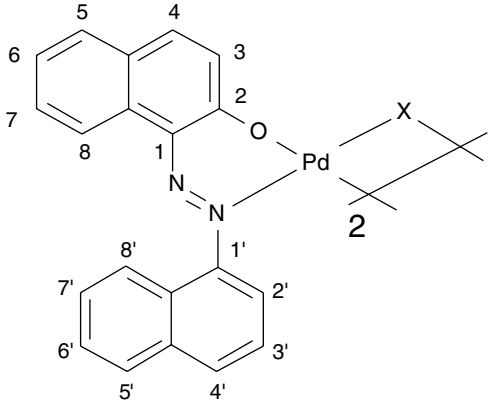

3a: X = Cl
3b: X = OAc

The strong absorptions of **3** around 545 and 515 nm are assigned [40,60] as LMCT bands. These bands appear to be a characteristic [60] of palladium(II) bound to one azonaphtholato fragment.

The IR spectrum of **3b** displays two bands at 1550 and 1424 cm^{-1} characteristic [68] of acetato-bridged compound. Both the metaloxylated **3a** and **3b** show ν(C–O) stretch [40] at ca. 1140 cm^{-1} in the IR spectra.

The ^1H NMR spectrum of **3b** shows high field shift of aromatic proton signals specially of metaloxylated ring. The effect is most dramatic in the case of H–C3 proton. The H–C3 proton of **3b** appears at 6.22 ppm. This corresponds to a high-field shift of about 1.12 ppm compared with the chemical shift of H–C3 of **1b**. This may be due to the electron releasing properties of naphtholic oxygen [36]. The $^{13}C\{^1H\}$ NMR spectrum of **3b** shows the signal for C2 at 137.19 ppm. The insertion of oxygen atom into palladium–C(naphthyl) bond shifts the signal for C2 to high field region.

3.3. Metaloxylation of (2) with m-chloroperbenzoic acid

The presence of both σ- and π-types palladium–carbon bonds [71] in **2** makes it worthy to examine its reactivity towards oxygen transfer reagent [61]. At room temperature, *m*-CPBA is added in (1:1) mole ratio to the deep violet solution of **2** in chloroform and the colour of the reaction mixture immediately turns into red violet (Fig. 1). The characteristic absorption bands of **2** at 470 and 550 nm disappear and new absorption bands develop at ca. 515 and 545 nm. The profile of the absorption spectrum with maxima at 515 and 545 nm in chloroform is very similar to those of **3** and indicates the existence [60] of one 1-(1′-naphthylazo)-2-naphtholato chelate ring per palladium(II) centre. The above reaction in $CDCl_3$ was also monitored by ^1H NMR spectroscopy. On addition of *m*-CPBA, the signal for H–C3 proton of complex **2** is shifted from 7.42 (*d*) ppm to 6.57 (*d*) ppm. The 0.85 ppm upfield shift of H–C3 is attributed to the conversion of M–C bond to M–O–C bond and the shift is due to electron releasing properties of naphtholic oxygen atoms [36]. The signal for the five protons of cyclopentadienyl ring appears at 5.7 ppm as in **2**. Therefore, the cyclopentadienyl group binds the naphthylazonaphtholato palladium(II) in η^5 fashion [70] and remains unaffected during and after metaloxylation. Chakravorty et al. [40] suggested that the metaloxylation of cyclopalladates by *m*-CPBA become more facile with the increase in the electrophillicity of palladium centres. In **2** naphthyl bound palladium centre becomes more electrophillic due to the presence of Cp as a coligand which has been reflected in the $^{13}C\{^1H\}$ NMR spectrum of **2**. The spectral studies of the reaction of **2** with *m*-CPBA establish that *m*-CPBA selectively metaloxylates the Pd–C(naphthyl) bond without affecting the cyclopentadienyl moiety in solution. The isolation of analytically pure metaloxylated compound is under progress.

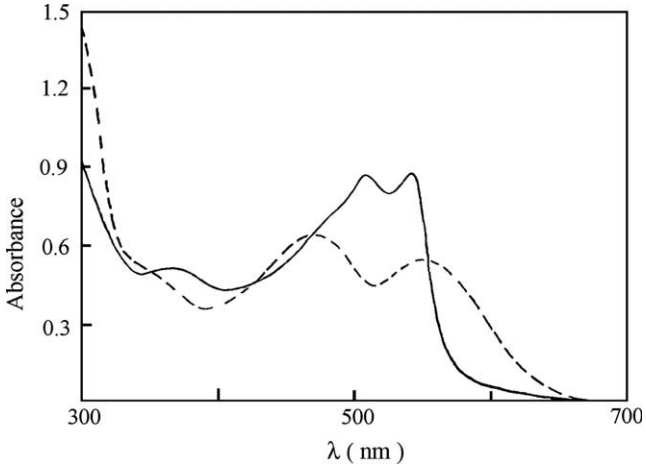

Fig. 1. Electronic spectra of pure **2** (6.68×10^{-4} M) (--------) and after metaloxylation (————) in $CHCl_3$ at 298 K.

Acknowledgements

The financial support (SR/S1/IC-10/2003) from DST, Government of India, is acknowledged. One of us (PD) thanks CSIR (India) for the award of a senior fellowship. We also thank UGC for granting Special Assistance Programme to our department.

References

[1] A.D. Ryabov, R. van Eldik, G. Le Borgne, M. Pfeffer, Organometallics 12 (1993) 1386.
[2] M. Pfeffer, J.P. Sutter, M.A. Rottvel, A. de Cian, J. Fischer, Tetrahedron 48 (1992) 2427.
[3] M. Pfeffer, Recl. Trav. Chim. Pays-Bas 109 (1990) 567.
[4] A.D. Ryabov, Synthesis (1985) 233.
[5] M. Albrecht, B.M. Cocks, A.L. Spek, G. van Koten, J. Organomet. Chem. 624 (2001) 271.
[6] J. Dupont, M. Pfeffer, J. Spencer, Eur. J. Inorg. Chem. (2001) 1917.
[7] C. Schlenk, A.W. Kleij, H. Frey, G. van Koten, Angew. Chem., Int. Ed. 39 (2000) 3445.
[8] D. Morales-Morules, R. Redon, C. Yung, C.M. Jensen, Chem. Commun. (2000) 1619.
[9] R.B. Bedford, S.M. Draper, P.N. Scully, S.L. Welch, New J. Chem. 24 (2000) 745.
[10] A.S. Gruber, D. Zim, G. Ebeling, A.L. Monteiro, J. Dupont, Org. Lett. 2 (2000) 1287.
[11] D.E. Bergbreiter, P.L. Osburn, Y.S. Liu, J. Am. Chem. Soc. 121 (1999) 9531.
[12] F. Miyazaki, K. Yamaguchi, M. Shibasaki, Tetrahedron Lett. 40 (1999) 7379.
[13] M. Ohff, A. Ohff, D. Milstein, Chem. Commun. (1999) 357.
[14] H. Weissman, D. Milstein, Chem. Commun. (1999) 1901.
[15] R.A.M. Abbenhuis, J. Boersma, G. van Koten, J. Org. Chem. 63 (1998) 4282.
[16] I. Aiello, D. Dattilo, M. Ghedini, A. Golemme, J. Am. Chem. Soc. 123 (2001) 5598.
[17] I. Aiello, D. Dattilo, M. Ghedini, A. Bruno, R. Termine, A. Golemme, Adv. Mater. 14 (2002) 1233.
[18] M.J. Baena, J. Buey, P. Espinet, C.E. García-Prieto, J. Organomet. Chem. 690 (2005) 998.
[19] L. Díez, P. Espinet, J.A. Miguel, M. Paz Rodríguez-Medina, J. Organomet. Chem. 690 (2005) 261.
[20] B.B. Eran, D. Singer, K. Praefcke, Eur. J. Inorg. Chem. (2001) 111.
[21] T. Hegmann, J. Kain, S. Diele, B. Schubert, H. Bögel, C. Tschierske, J. Mater. Chem. 13 (2003) 991.
[22] R.W. Date, E.F. Iglesias, K.E. Rowe, J.M. Elliot, D.W. Bruce, J. Chem. Soc., Dalton Trans. (2003) 1914.

[23] M. Ghedini, D. Pucci, A. Crispini, I. Aiello, F. Barigelletti, A. Gessi, O. Francescangeli, Appl. Organometal. Chem. 13 (1999) 565.
[24] A.D. Ryabov, Chem. Rev. 90 (1990) 403.
[25] J.M. Vila, G. Alberdi, M.T. Pereira, M. Marino, A. Fernández, M. López-Torres, R. Ares, Polyhedron 22 (2003) 241.
[26] A. Fernández, D. Vazquez-García, J.J. Fernández, M. López-Torres, A. Suárez, S. Castro- Juiz, J.M. Ortigueira, J.M. Vila, New J. Chem. 26 (2002) 105.
[27] A. Fernández, D. Vazquez-García, J.J. Fernández, M. López-Torres, A. Suárez, S. Castro-Juiz, J.M. Vila, New J. Chem. 26 (2002) 398.
[28] M. Gómez, J. Granell, M. Martinez, Inorg. Chem. Commun. 5 (2002) 67.
[29] J. Albert, R. Bosque, J. Granell, R. Travera, Polyhedron 20 (2001) 3325.
[30] J. Albert, A. González, J. Granell, R. Moragas, X. Solans, M. Font-Bardía, J. Chem. Soc., Dalton Trans. (1998) 1781.
[31] J. Albert, A. González, J. Granell, R. Moragas, C. Puerta, P. Valerga, Organometallics 16 (1997) 3775.
[32] J. Albert, J. Granell, R. Moragas, M. Font-Bardía, X. Solans, J. Organomet. Chem. 522 (1996) 59.
[33] J. Albert, J. Granell, A. Luque, J. Mínguez, R. Moragas, M. Font-Bardía, X. Solans, J. Organomet. Chem. 522 (1996) 87.
[34] R. Bhawmick, P. Bandyopadhyay, Trans. Met. Chem. 20 (1995) 415.
[35] P.L. Alsters, H.T. Teunissen, J. Boersma, G. van Koten, Recl. Trav. Chim. Pays-Bas 109 (1990) 487.
[36] C.R. Sinha, D. Bandyopadhyay, A. Chakravorty, Inorg. Chem. 27 (1988) 1173.
[37] P.L. Alsters, H.T. Teunissen, J. Boersma, A.L. Spek, G. van Koten, Organometallics 12 (1993) 4691.
[38] P.L. Alster, J. Boersma, G. van Koten, Organometallics 12 (1993) 1629.
[39] A.K. Mahapatra, D. Bandyopadhyay, P. Bandyopadhyay, A. Chakravorty, Inorg. Chem. 25 (1986) 2214.
[40] A.K. Mahapatra, D. Bandyopadhyay, P. Bandyopadhyay, A. Chakravorty, J. Chem. Soc., Chem. Commun. (1984) 999.
[41] C.R. Sinha, D. Bandyopadhyay, A. Chakravorty, J. Chem. Soc., Chem. Commun. (1988) 468.
[42] S.J. Tremont, H.U. Rahman, J. Am. Chem. Soc. 106 (1984) 5759.
[43] Y. Fuchita, K. Hiraki, T. Yamaguchi, T. Maruta, J. Chem. Soc., Dalton Trans. (1981) 2405.
[44] R. Bhawmick, P. Bandyopadhyay, Polyhedron 15 (1996) 2923.
[45] E.C. Constable, Polyhedron 3 (1984) 1037.
[46] J. Albert, R. Bosque, J.M. Cadena, S. Degado, J. Granell, J. Organomet. Chem. 634 (2001) 83.
[47] J. Albert, J.M. Cadena, J. Granell, G. Muller, D. Panyella, C. Sañudo, Eur. J. Inorg. Chem. (2000) 1283.
[48] J. Albert, J.M. Cadena, J. Granell, X. Solans, M. Font-Bardía, Tetrahedron Asymmetr. 11 (2000) 1943.
[49] J. Albert, J.M. Cadena, J. Granell, Tetrahedron Asymmetr. 8 (1997) 991.
[50] L. Kind, A.J. Klaus, P. Rys, V. Gramlich, Helv. Chim. Acta 81 (1998) 307.
[51] J.M. Valk, R. van Belzen, J. Boersma, A.L. Spek, G. van Koten, J. Chem. Soc., Dalton Trans. (1994) 2293.
[52] J.M. Valk, J. Boersma, G. van Koten, J. Organomet. Chem. 483 (1994) 213.
[53] A.J. Klaus, P. Rys, Helv. Chim. Acta 64 (1981) 1453.
[54] K. Gehrig, A.J. Klaus, P. Rys, Helv. Chim. Acta 66 (1984) 2603.
[55] M. Pfeffer, N. Sutter-Beydoun, A.D. Cian, J. Fischer, J. Organomet. Chem. 453 (1993) 139.
[56] I.G. Phillips, P.J. Steel, J. Organomet. Chem. 410 (1991) 247.
[57] J. Dupont, N. Beydoun, M. Pfeffer, J. Chem. Soc., Dalton Trans. (1989) 1715.
[58] J. Dupont, M. Pfeffer, J. Chem. Soc., Dalton Trans. (1990) 3193.
[59] M. Julia, D. Duteil, J.Y. Lallemand, J. Organomet. Chem. 102 (1975) 239.
[60] R. Bhawmick, H. Biswas, P. Bandyopadhyay, J. Organomet. Chem. 498 (1995) 81.
[61] R. Bhawmick, P. Bandyopadhyay, Trans. Met. Chem. 21 (1996) 187.
[62] K. Kamaraj, D. Bandyopadhyay, J. Am. Chem. Soc. 119 (1997) 8099.
[63] K. Kamaraj, D. Bandyopadhyay, Organometallics 18 (1999) 438.
[64] P. Wadhani, D. Bandyopadhyay, Organometallics 19 (2000) 4435.
[65] G.M. Badger, G.E. Lewis, J. Chem. Soc. (1953) 2151.
[66] F.A. Cotton, L.T. Reynolds, J. Am. Chem. Soc. 80 (1958) 269.
[67] H. Onoue, I. Moritani, J. Organomet. Chem. 43 (1972) 431.
[68] R.J. Cross, R. Wardle, J. Organomet. Chem. 23 (1970) C4.
[69] Y. Wakatsuki, H. Yamazaki, P.A. Grutsch, M. Santhanam, C. Kutal, J. Am. Chem. Soc. 107 (1985) 8153.
[70] P. Bandyopadhyay, A. Chakravorty, Indian J. Chem. 24A (1985) 638.
[71] K. Suzuki, A. Jindo, K. Hanaki, Inorg. Chim. Acta 210 (1993) 57.

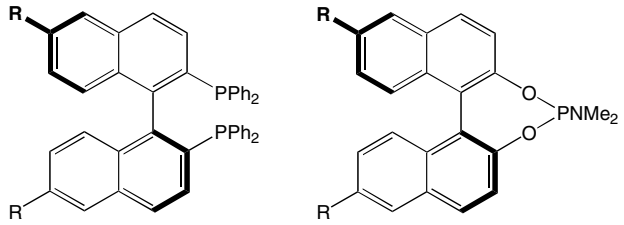

R = C_6F_{13} (**I**), CH=CHC_6F_{13} (**II**)
$CH_2CH_2C_6F_{13}$ (**III**), H (**IV**)

R = C_6F_{13} (**V**), H (**VI**)

Fig. 1. Fluoroalkylated BINAP and MonoPhos ligands.

(*R*)- and (*S*)-enantiomers of the ligands were used in the synthesis of complexes and the data obtained was identical in all cases apart from optical rotation values, which were equal in magnitude but opposite in sign; data for only the (*R*)-enantiomers is presented here.

2.1. General procedure for the formation of platinum complexes of BINAP-based ligands

cis-[$PtCl_2(MeCN)_2$] (0.033 g, 9.5×10^{-5} mol) and the BINAP ligand (9.5×10^{-5} mol) were dissolved in dry and degassed dichloromethane (35 ml) and the mixture heated to reflux under nitrogen for 3 h. Upon cooling, approximately 30 ml of the solvent was removed under reduced pressure and the product precipitated from solution by the addition of petroleum ether (b.p. 40–60 °C, 10 ml). The crude product was collected by filtration and recrystallised from dichloromethane/hexane.

2.1.1. [$PtCl_2${(*R*)-R_{f6}-BINAP}] (**VII**) (68% yield)

M.p. 186–188 °C. *m/z* (FAB) 1489 $[M-Cl]^+$ (97%), 1453 $[M-2Cl]^+$ (100%). $[\alpha]_D$ ($CHCl_3$) 264.6° ($c=1.6$). *Anal.* Calc. for $C_{56}H_{30}Cl_2F_{26}P_2Pt$: C, 44.09; H, 1.97. Found: C, 43.89; H, 1.91%. ^1H ($CDCl_3$) 6.62 (6H, m, PhH), 6.75 (4H, m, ArH), 7.22 (2H, d, $^3J_{HH}=9.0$ Hz, ArH), 7.37–7.51 (10H, m, PhH), 7.62 (2H, d, $^3J_{HH}=8.4$ Hz, ArH), 7.74 (4H, m, PhH), 7.82 (2H, s, ArH). $^{19}F\{^1H\}$ −81.12 (6F, t, $^4J_{FF}=10.4$ Hz, CF_3), −111.11 (4F, m, α-CF_2), −121.32 (4F, m, CF_2), −122.69 (4F, m, CF_2), −123.18 (4F,m, CF_2), −126.49 (4F, m, CF_2). $^{31}P\{^1H\}$ 10.79 (s, $^1J_{Pt-P}=3636$ Hz).

2.1.2. [$PtCl_2${(*R*)-R_{f6}-C_2H_2-BINAP}] (**VIII**) (69% yield)

M.p. 189–191 °C. *m/z* (FAB) 1541 $[M-Cl]^+$ (35%), 1505 $[M-2Cl]^+$ (31%). $[\alpha]_D$ ($CHCl_3$) 153.13° ($c=0.8$). *Anal.* Calc. for $C_{60}H_{34}Cl_2F_{26}P_2Pt$: C, 45.69; H, 2.16. Found: C, 45.53; H, 2.06%. ^1H ($CDCl_3$) 6.17 (2H, m, =CH), 6.65 (2H, d, $^3J_{HH}=9.0$ Hz, ArH), 6.77 (2H, m, =CH), 7.16–7.76 (22H, m), 7.50 (2H, d, $^3J_{HH}=8.8$ Hz, ArH), 7.58 (2H, s, ArH), 7.71 (2H, d, $^3J_{HH}=8.6$ Hz, ArH). $^{19}F\{^1H\}$ −80.71 (6F, t, $^4J_{FF}=9.6$ Hz, CF_3), −111.20 (4F, m, α-CF_2), −121.50 (4F, m, CF_2), −122.78 (4F, m, CF_2), −123.04 (4F, m, CF_2), −126.05 (4F, m, CF_2). $^{31}P\{^1H\}$ 10.30 (s, $^1J_{Pt-P}=3647$ Hz).

2.1.3. [$PtCl_2${(*R*)-R_{f6}-C_2H_4-BINAP}] (**IX**) (56% yield)

M.p. 181–184 °C. *m/z* (FAB) 1545 $[M-Cl]^+$ (93%), 1509 $[M-2Cl]^+$ (74%). $[\alpha]_D$ ($CHCl_3$) 198.3° ($c=0.7$). *Anal.* Calc. for $C_{60}H_{38}Cl_2F_{26}P_2Pt$: C, 45.57; H, 2.41. Found: C, 45.54; H, 2.35%. ^1H ($CDCl_3$) 2.35 (4H, m, CH_2CF_2), 2.95 (4H, m, CH_2Ar), 6.61 (6H, m, ArH and PhH), 6.75 (2H, d, $^3J_{HH}=7.3$ Hz, ArH), 6.92 (2H, d, $^3J_{HH}=9.1$ Hz, ArH), 7.27–7.42 (12H, m, PhH), 7.53 (4H, m, PhH), 7.73 (2H, d, $^3J_{HH}=6.89$ Hz, ArH), 7.77 (2H, d, $^3J_{HH}=7.1$ Hz, ArH). $^{19}F\{^1H\}$ −80.72 (6F, t, $^4J_{FF}=10.4$ Hz, CF_3), −114.16 (4F, m, α-CF_2), −121.81 (4F, m, CF_2), −122.77 (4F, m, CF_2), −123.31 (4F, m, CF_2), −126.04 (4F, m, CF_2). $^{31}P\{^1H\}$ 9.75 (s, $^1J_{Pt-P}=3665$ Hz).

2.2. General procedure for the formation of palladium complexes of BINAP-based ligands

cis-[$PdCl_2(MeCN)_2$] (0.0246 g, 9.5×10^{-5} mol) and the BINAP ligand (9.5×10^{-5} mol) were dissolved in dry and degassed dichloromethane (35 ml) and the mixture heated to reflux under nitrogen for 3 h. Upon cooling, approximately 30 ml of the solvent was removed under reduced pressure and the product precipitated from solution by the addition of petroleum ether (b.p. 40–60 °C, 10 ml). The crude product was collected by filtration and recrystallised from dichloromethane/hexane.

2.2.1. [$PdCl_2${(*R*)-R_{f6}-BINAP}] (**X**) (71% yield)

M.p. 235–237 °C (dec.). *m/z* (FAB) 1399 $[M-Cl]^+$ (9%), 1364 $[M-2Cl]^+$ (2%). $[\alpha]_D$ ($CHCl_3$) 380.8° ($c=1.0$). *Anal.* Calc. for $C_{56}H_{30}Cl_2F_{26}P_2Pd$: C, 46.83; H, 2.09. Found: C, 47.04; H, 2.14%. ^1H ($CDCl_3$) 6.71 (2H, d, $^3J_{HH}=9.1$ Hz, ArH), 6.88 (6H, m, ArH and PhH), 7.24 (2H, d, $^3J_{HH}=9.1$ Hz, ArH), 7.82 (12H, m, ArH and PhH), 7.84 (6H, m, PhH), 7.89 (2H, s, ArH). $^{19}F\{^1H\}$ −81.14 (6F, t, $^4J_{FF}=10.4$ Hz, CF_3), −111.06 (4F, m, α-CF_2), −121.32 (4F, m, CF_2), −121.71 (4F, m, CF_2), −123.13 (4F, m, CF_2), −126.47 (4F, m, CF_2). $^{31}P\{^1H\}$ 33.48 (s).

2.2.2. [$PdCl_2${(*R*)-R_{f6}-C_2H_2-BINAP}] (**XI**) (71% yield)

M.p. > 300 °C. *m/z* (FAB) 1453 $[M-Cl]^+$ (6%). $[\alpha]_D$ ($CHCl_3$) 316.4° ($c=0.6$). *Anal.* Calc. for $C_{60}H_{34}Cl_2F_{26}P_2Pd$: C, 48.42; H, 2.29. Found: C, 48.36; H, 2.19%. ^1H ($CDCl_3$) 6.21 (2H, m, =CH), 6.63 (2H, d, $^3J_{HH}=9.0$ Hz, ArH), 6.77 (2H, m, =CH), 6.89–7.70 (28H, m, PhH and ArH). $^{19}F\{^1H\}$ −80.75 (6F, t,$^4J_{FF}=9.0$ Hz, CF_3), −111.24 (4F, m, α-CF_2), −121.51 (4F, m, CF_2), −122.81 (4F, m, CF_2), −122.95 (4F, m, CF_2), −126.07 (4F, m, CF_2). $^{31}P\{^1H\}$ 32.69 (s).

2.2.3. [$PdCl_2${(*R*)-R_{f6}-C_2H_4-BINAP}] (**XII**) (55% yield)

M.p. 184–186 °C (dec.). *m/z* (FAB) 1456 $[M-Cl]^+$ (9%), 1420 $[M-2Cl]^+$ (1%). $[\alpha]_D$ ($CHCl_3$) 327.8° ($c=1.1$). *Anal.* Calc. for $C_{60}H_{38}Cl_2F_{26}P_2Pd$: C, 48.29; H, 2.55. Found: C, 48.27; H, 2.50%. ^1H ($CDCl_3$) 2.71 (4H,

m, CH_2), 3.34 (4H, m, CH_2), 6.58–7.89 (30H, m, PhH and ArH). $^{19}F\{^1H\}$ −81.31 (6F, t, $^4J_{FF} = 10.1$ Hz, CF_3), −114.52 (4F, m, α-CF_2), −122.31 (4F, m, CF_2), −123.30 (4F, m, CF_2), −123.77 (4F, m, CF_2), −126.59 (4F, m, CF_2). $^{31}P\{^1H\}$ 28.42 (s).

2.3. General procedure for the formation of platinum complexes of MonoPhos-based ligands

cis-[$PtCl_2(MeCN)_2$] (0.08 g, 2.3×10^{-4} mol) and the MonoPhos ligand (4.6×10^{-4} mol) were dissolved in dry and degassed dichloromethane (25 ml) and stirred over night under nitrogen. The solvent was removed under reduced pressure and the crude product recrystallised from dichloromethane/hexane. The precipitate was dried under vacuum to yield the product as a pale yellow solid.

2.3.1. cis-[$PtCl_2${(*R*)-MonoPhos}$_2$] (**XIII**) (53% yield)

M.p. 228–230 °C (dec). *m/z* (FAB) 949 $[M - Cl]^+$ (41%). $[\alpha]_D$ ($CHCl_3$) 119.2° ($c = 1.2$). *Anal.* Calc. for $C_{44}H_{36}Cl_2N_2O_4P_2Pt$ C, 53.65; H, 3.66; N, 2.85. Found: C, 53.46; H, 3.65; N, 2.81%. ^1H ($CDCl_3$) 2.13 (12H, d, $^3J_{PH} = 9.2$ Hz, CH_3), 7.00–7.55 (14H, m, ArH), 7.88 (4H, d, $^3J_{HH} = 8.0$ Hz, ArH), 7.93 (2H, d, $^3J_{HH} = 8.7$ Hz, ArH), 7.96 (2H, d, $^3J_{HH} = 8.5$ Hz, ArH), 8.20 (2H, d, $^3J_{HH} = 8.7$ Hz, ArH). $^{31}P\{^1H\}$ 93.22 (s, $^1J_{Pt-P} = 5604$ Hz).

2.3.2. cis-[$PtCl_2${(*R*)-R_{f6}-MonoPhos}$_2$] (**XIV**) (45% yield)

M.p. 147 °C (dec.). *m/z* (FAB) 2222 $[M - Cl]^+$ (29%). $[\alpha]_D$ ($CHCl_3$) 84.9° ($c = 1.2$). *Anal.* Calc. for $C_{68}H_{32}Cl_2F_{52}N_2O_4P_2Pt$: C, 36.17; H, 1.42; N, 1.24. Found: C, 35.94; H, 1.30; N, 1.35%. ^1H ($CDCl_3$) 2.18 (12H, d, $^3J_{PH} = 10.8$ Hz, CH_3), 7.40–7.52 (10H, m, ArH), 8.10 (2H, d, $^3J_{HH} = 8.8$ Hz, ArH), 8.18 (2H, d, $^3J_{HH} = 9.2$ Hz, ArH), 8.22 (4H, d, $^3J_{HH} = 9.1$ Hz, ArH), 8.36 (2H, d, $^3J_{HH} = 8.5$ Hz, ArH). $^{19}F\{^1H\}$ −80.75 (12F, t, $^4J_{FF} = 8.6$ Hz, CF_3), −110.35 (8F, m, α-CF_2), −121.31 (8F, m, CF_2), −121.58 (8F, m, CF_2), −122.72 (8F, m, CF_2), −126.06 (8F, m, CF_2). $^{31}P\{^1H\}$ 95.32 (s, $^1J_{Pt-P} = 5582$ Hz).

2.4. General procedure for the formation of palladium complexes of MonoPhos-based ligands

trans-[$PdCl_2(MeCN)_2$] (0.08 g, 3.1×10^{-4} mol) and the MonoPhos ligand (6.2×10^{-4} mol) were dissolved in dichloromethane (10 ml) and stirred for 1 h under nitrogen. The solvent was removed under reduced pressure and the crude product recrystallised from dichloromethane/hexane to yield a yellow solid.

2.4.1. trans-[$PdCl_2${(*R*)-MonoPhos}$_2$] (**XV**) (55% yield)

M.p. 220 °C (dec.). *m/z* (FAB) 859 $[M - Cl]^+$ (32%), 824 $[M - 2Cl]^+$ (5%). $[\alpha]_D$ ($CHCl_3$) −127.5° ($c = 1.2$). *Anal.* Calc. for $C_{44}H_{36}Cl_2N_2O_4P_2Pd$: C, 58.99; H, 4.02; N, 3.13. Found: C, 58.89; H, 3.96; N, 3.02%. ^1H ($CDCl_3$) 2.15 (12H, vt, $J_{PH} = 5.3$ Hz, CH_3), 7.23–7.48 (12H, m, ArH), 7.89 (4H, d, $^3J_{HH} = 7.5$ Hz, ArH), 7.94 (4H, d, $^3J_{HH} = 8.5$ Hz, ArH), 8.02 (2H, d, $^3J_{HH} = 8.7$ Hz, ArH), 8.28 (2H, d, $^3J_{HH} = 8.7$ Hz, ArH). $^{31}P\{^1H\}$ 118.49 (s). IR (nujol) 354 cm^{-1}.

2.4.2. trans-[$PdCl_2${(*R*)-R_{f6}-MonoPhos}$_2$] (**XVI**) (57% yield)

M.p. 145–147 °C. *m/z* (FAB) 2132 $[M - Cl]^+$ (10%). $[\alpha]_D$ ($CHCl_3$) −76.3° ($c = 1.4$). *Anal.* Calc. for $C_{44}H_{32}Cl_2F_{52}N_2O_4P_2Pd$: C, 37.66; H, 1.48; N, 1.29. Found: C, 37.51; H, 1.40; N, 1.30%. ^1H ($CDCl_3$) 2.17 (12H, vt, $J_{PH} = 5.2$ Hz, CH_3), 7.41–7.51 (10H, m ArH), 8.11 (2H, d, $^3J_{HH} = 9.1$ Hz, ArH), 8.21 (2H, m, ArH), 8.23 (4H, d, $^3J_{HH} = 9.3$ Hz, ArH), 8.42 (2H, d, $^3J_{HH} = 8.8$ Hz, ArH). $^{19}F\{^1H\}$ −80.73 (12F, t, $^4J_{FF} = 10.1$ Hz, CF_3), −110.77 (8F, m, α-CF_2), −121.79 (8F, m, CF_2), −122.20 (8F, m, CF_2), −123.18 (8F, m, CF_2), −125.90 (8F, m, CF_2). $^{31}P\{^1H\}$ 119.93 (s). IR (nujol) 356 cm^{-1}.

2.5. General procedure for the formation of rhodium complexes of MonoPhos-based ligands

[$Cp^*RhCl_2]_2$ (0.08 g, 1.3×10^{-4} mol) and the MonoPhos ligand (2.6×10^{-4} mol) were dissolved in dichloromethane and stirred for 1 h. The solvent was removed under reduced pressure and the solid obtained redissolved in a small volume of dichloromethane (3 ml). The product was precipitated from solution by addition of petroleum ether (b.p. 40–60 °C), collected by filtration and dried in vacuo to yield a red–orange solid.

2.5.1. [Cp^*RhCl_2{(*R*)-MonoPhos}] (**XVII**) (88% yield)

M.p. 228–230 °C. *m/z* (FAB) 632 $[M - Cl]^+$ (100%), 597 $[M - 2Cl]^+$ (9%). $[\alpha]_D$ ($CHCl_3$) 43.4° ($c = 3.1$). *Anal.* Calc. for $C_{32}H_{33}Cl_2NO_2PRh$: C, 57.49; H, 4.94; N, 2.10. Found: C, 57.69; H, 4.99; N, 1.99%. ^1H ($CDCl_3$) (253 K) 1.56 (15H, d, $J_{PH} = 3.9$ Hz, Cp*), 2.51 (6H, d, $^3J_{PH} = 9.8$ Hz, CH_3), 7.24 (4H, m, ArH), 7.47 (4H, m, ArH), 7.98 (1H, d, $^3J_{HH} = 9.4$ Hz, ArH), 8.00 (2H, d, $^3J_{HH} = 9.4$ Hz, ArH), 8.05 (1H, d, $^3J_{HH} = 8.9$ Hz, ArH). $^{31}P\{^1H\}$ (253 K) 141.74 (d, $^1J_{P-Rh} = 223$ Hz).

2.5.2. [Cp^*RhCl_2{(*R*)-R_{f6}-MonoPhos}] (**XVIII**) (81% yield)

M.p. 96–98 °C. *m/z* (FAB) 1269 $[M - Cl]^+$ (38%). $[\alpha]_D$ ($CHCl_3$) 15.9 ($c = 1.2$). *Anal.* Calc. for $C_{44}H_{31}Cl_2F_{26}NO_2PRh$: C, 40.49; H, 2.38; N, 1.07. Found: C, 40.37; H 2.39; N, 0.98%. ^1H ($CDCl_3$) (253 K) 1.63 (15H, d, $J_{PH} = 5.1$ Hz, Cp*), 2.54 (6H, d, $^3J_{PH} = 10.1$ Hz, CH_3), 7.30 (1H, d, $^3J_{HH} = 9.0$ Hz, ArH), 7.38 (2H, d, $^3J_{HH} = 8.6$ Hz, ArH), 7.44 (1H, d, $^3J_{HH} = 9.4$ Hz, ArH), 7.58 (1H, d, $^3J_{HH} = 9.0$ Hz, ArH), 7.60 (1H, d, $^3J_{HH} = 8.7$ Hz, ArH), 8.16 (1H, d, $^3J_{HH} = 8.9$ Hz, ArH), 8.21 (1H, d, $^3J_{HH} = 9.1$ Hz, ArH), 8.28 (1H, s, ArH), 8.31 (1H, s, ArH). $^{19}F\{^1H\}$ (253 K) −81.19 (6F, t, $^4J_{FF} = 10.6$ Hz, CF_3), −110.65 (4F, m, α-CF_2), −121.82 (4F, m, CF_2),

−121.82 (4F, m, CF_2), −123.18 (4F, m, CF_2), −126.52 (4F, m, CF_2). $^{31}P\{^1H\}$ (253 K) 143.39 (d, $^1J_{P-Rh} = 225$ Hz).

2.6. Crystal structure determination of [Cp*RhCl$_2${(R)-MonoPhos}] (XVII)

Crystals suitable for single crystal structural analysis were grown by slow evaporation from a 1:5 dichloromethane/hexane solution.

2.7. Crystal data

$C_{32}H_{33}Cl_2NO_2PRh.1/2CH_2Cl_2$, $M = 710.84$, orthorhombic, $a = 17.8135(7)$ Å, $b = 22.7127(9)$ Å, $c = 7.6566(3)$ Å, $U = 3097.8(2)$ Å^3, $1.79 < \theta < 25.00°$, $T = 150(2)$ K, space group $P2_12_12$, graphite-monochromated Mo Kα radiation, $\lambda = 0.71073$ Å, $Z = 4$, $D_{calc} = 1.524$ g cm^{-3}, $F(000) = 1452$, dimensions $0.18 \times 0.16 \times 0.11$ mm^3, μ (Mo Kα) $= 0.8933$ mm^{-1}, empirical absorption correction based on ψ scans, maximum and minimum transmission factors of 0.928 and 0.710, respectively, Bruker APEX 2000 CCD diffractometer, ω scans, data collection range $1.79 < \theta < 25.00°$, $-21 \leqslant h \leqslant 21$, $-27 \leqslant k \leqslant 26$, $-9 \leqslant l \leqslant 8$; 22 576 reflections were measured, and 5439 were unique ($R_{int} = 0.0329$). The data were corrected for Lorentz and polarisation effects.

2.8. Structure solution and refinement

Structure solution was by Patterson methods. The structure refinement on F^2 employed SHELXTL version 6.10 (SHELXTL, an integrated system for solving, refining and displaying crystal structures). For all structures hydrogen atoms were included in calculated positions (C–H = 0.96 Å) riding on the bonded atom with isotropic displacement parameters set to 1.5 U_{eq}(C) for methyl H atoms and 1.2 U_{eq}(C) for all other H atoms. All non-H atoms were refined with anisotropic displacement parameters. Final refinement cycles included one molecule of lattice CH_2Cl_2 with half occupancy. Final $R_1 = 0.0318$, $wR_2 = 0.0826$ (0.0326 and 0.0833, respectively, for all data) for 360 variables. The final residual Fourier map showed peaks of 1.038 and −0.891 e Å^{-3}.

3. Results and discussion

We have previously shown that the introduction of perfluoroalkyl substituents does not impact substantially on the application of these ligands in catalysis. However, in order to properly evaluate the electronic environment around the coordinating phosphorus centres, the air- and moisture-stable complexes *cis*-[$PtCl_2$(L)] and *cis*-[$PdCl_2$(L)] (L = R_{f6}-BINAP, R_{f6}-C_2H_2-BINAP and R_{f6}-C_2H_4-BINAP) and *cis*-[$PtCl_2$(L′)$_2$], *trans*-[$PdCl_2$(L′)$_2$] and [Cp*$RhCl_2$(L′)] (L′ = MonoPhos, R_{f6}-MonoPhos) were prepared; such complexes are well-established probes for ligand coordination chemistry and are readily prepared by displacement of weakly coordinating ligands or cleavage of halide-bridged dinuclear complexes. The ^1H and ^{19}F NMR data are unremarkable, beyond the virtual triplet for the NMe_2 protons for *trans*-[$PdCl_2$(MonoPhos)$_2$] (**XV**, **XVI**) that confirm the *trans*-arrangement for the two phosphorus(III) ligands in these complexes. The ^{31}P NMR data (Table 1) reveals, as we have shown previously, that the phosphorus chemical shift is not a particularly good probe for the electronic properties of these ligands but that, in particular, $^1J_{Pt-P}$ does reveal subtle variations in σ-donor properties. These coupling constant data reveal that even the binaphthyl rings in these ligands do not completely ameliorate the electronic influence of perfluoroalkyl substituents in the 6,6′-positions, and this is only achieved with an additional, aliphatic, C_2H_4 spacer unit. Interesting, this is equivalent to the eight-carbon unit highlighted by Gladysz et al. [13] as necessary to totally shield donor atoms, and electronic effects are even felt through a conjugated eight-carbon unit, such as in the alkenyl-binaphthyl ligand Rf-C_2H_2-BINAP.

Single crystals of [Cp*$RhCl_2${(*R*)-MonoPhos}] (**XVII**) suitable for X-ray structural determination were obtained by slow evaporation of a 5:1 hexane/dichloromethane solution. Selected bond lengths and bond angles, together with data for closely related rhodium(III) complexes, are given in Table 2 and the molecular structure shown in Fig. 2. The complex adopts the anticipated pseudo-piano stool structure in which the bond lengths and angles are consistent with the electronic properties of the phosphoramidite ligand. In particular, the Rh–P bond distance is comparable to those for Rh(III)-phosphonite complexes

Table 1
$^{31}P\{^1H\}$ NMR data

L	[$PtCl_2$L]				[$PtCl_2L_2$]		[$PdCl_2$L]				[$PdCl_2L_2$]		[Cp*$RhCl_2$L]	
	I	**II**	**III**	**IV**[a]	**V**	**VI**	**I**	**II**	**III**	**IV**[b]	**V**	**VI**	**V**	**VI**
δ_P (ppm)	10.8	10.3	9.8	9.7	95.3	93.2	33.5	32.7	28.4	27.3	119.9	118.5	143.4	141.7
Δ_P (ppm)[c]	24.6	24.8	25.4	25.2	−54.7	−55.5	47.3	47.2	43.4	42.8	−30.1	−29.5	−6.5	−7.0
$^1J_{MP}$ (Hz)	3636	3647	3666	3667	5582	5604	–	–	–	–	–	–	225	222

[a] Data taken from [15].
[b] Data taken from [16].
[c] $\Delta_P = \delta_P$(complex) − δ_P(free ligand).

Table 2
Selected bond lengths (Å) and bond angles (°) with estimated standard deviations (e.s.d.s) in parentheses for [Cp*RhCl$_2${(*R*)-MonoPhos}] (**XVII**) and related complexes

	(**XVII**)	Cp*RhCl$_2$L[a,b]	Cp*RhCl$_2$L[a,b]	Cp*RhCl$_2$L[c]	Cp*RhCl$_2$L[d]
Rh–Cp (centroid)	1.819	1.824	1.822	1.827	1.824
Rh(1)–P(1)	2.2531(10)	2.258(5)	2.254(3)	2.301(3)	2.332(3)
Rh(1)–Cl(1)	2.3935(10)	2.389(4)	2.378(3)	2.401(3)	2.179(9)
Rh(1)–Cl(2)	2.3928(10)	2.412(4)	2.391(4)	2.406(4)	2.398(3)
P(1)–Rh(1)–Cl(1)	89.63(3)	92.36(13)	92.57(12)	86.4(1)	88.28(9)
P(1)–Rh(1)–Cl(2)	87.36(3)	89.25(12)	90.99(13)	94.4(1)	86.00(9)
Cl(1)–Rh(1)–Cl(2)	93.79(4)	89.6(2)	88.4(2)	92.3(1)	93.95(9)

[a] L = PPh(OPh)$_2$. Data taken from [14].
[b] Two unique molecules in the unit cell.
[c] L = PPh$_2$(OC$_6$H$_3$F$_2$-2,6). Data taken from [14].
[d] L = P(C$_6$H$_4$C$_6$F$_{13}$-4)$_3$. Data taken from [6].

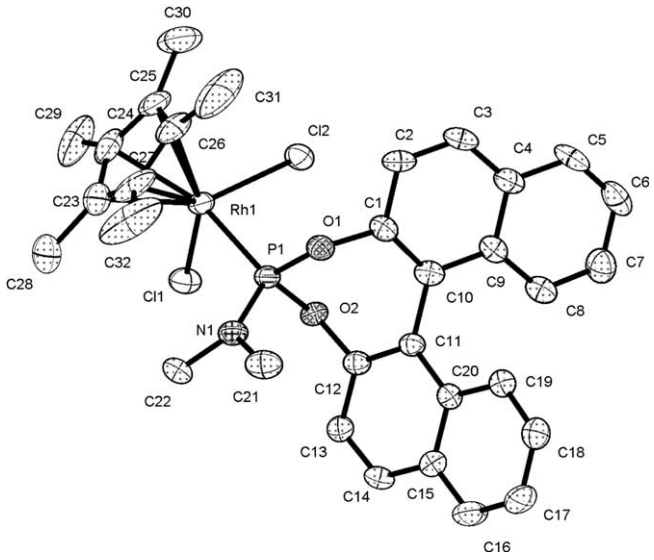

Fig. 2. Molecular structure of (**XVII**) showing the atom labelling scheme with 50% displacement probability ellipsoids. H atoms and a partial occupancy CH_2Cl_2 solvent molecule are omitted for clarity.

[14] and significantly shorter than the analogous Rh–P distances in Cp*Rh-phosphinite or -phosphine complexes [6,14]. In contrast, the steric bulk of the phosphoramidite ligand, as evidenced by the relative size of the Cl–Rh–Cl angle opposite the ligand, is much greater than that for the phosphonite ligands and more comparable to that of a phosphine.

4. Conclusions

Coordination complexes of fluoroalkylated BINAP and MonoPhos ligands have been readily prepared and characterised. Analysis of the ^{31}P NMR data for the complexes shows that the addition of perfluoroalkyl ponytails to the binaphthyl backbone has only a small effect on the electronic environment around the coordinating phosphorus centres and that this effect can be almost totally overcome by the inclusion of an extra ethyl-insulating unit.

5. Supplementary material

Crystallographic data for the structural analysis have been deposited with the Cambridge Crystallographic Data Centre, CCDC no. 269719. Copies of this information may be obtained from the Director, CCDC, 12 Union Road, Cambridge CB2 1EZ, UK (fax: + 44 1233 336033, email: deposit@ccdc.cam or www: http://www.ccdec.cam.ac.uk.

Acknowledgements

We would like to thank EPSRC (AJW), Merck (AJW) and the Royal Society (AMS) for financial support.

References

[1] P. Bhattacharyya, D. Gudmunsen, E.G. Hope, R.D.W. Kemmitt, D.R. Paige, A.M. Stuart, J. Chem. Soc, Perkin Trans. 1 (1997) 3609.
[2] E.G. Hope, R.D.W. Kemmitt, D.R. Paige, A.M. Stuart, J. Fluorine Chem. 99 (1999) 197.
[3] D.F. Foster, D.J. Adams, D. Gudmunsen, A.M. Stuart, E.G. Hope, D.J. Cole-Hamilton, Chem. Commun. (2002) 722.
[4] J.F.S. Vaughan, M.G. Pellatt, J. Sherrington, E.G. Hope, International Patent, WO 02/04120 A2, 2002.
[5] B. Croxtall, E.G. Hope, A.M. Stuart, Chem. Commun. (2003) 2430.
[6] J. Fawcett, E.G. Hope, R.D.W. Kemmitt, D.R. Paige, D.R. Russell, A.M. Stuart, J. Chem. Soc. Dalton Trans. (1998) 3751.
[7] D.J. Adams, D. Gudmunsen, J. Fawcett, E.G. Hope, A.M. Stuart, Tetrahedron 58 (2002) 3827.
[8] D.J. Birdsall, E.G. Hope, A.M. Stuart, W. Chen, Y. Hu, J. Xiao, Tetrahedron Lett. 42 (2001) 8551.
[9] D.J. Adams, W. Chen, E.G. Hope, S. Lange, A.M. Stuart, A.J. West, J. Xiao, Green Chem. 5 (2003) 118.
[10] E.G. Hope, A.M. Stuart, A.J. West, Green Chem. 6 (2004) 345.
[11] M.A. Andrews, T.C.-T. Chang, C.-W.F. Cheng, T.J. Emge, K.P. Kelly, T.F. Koetzle, J. Am. Chem. Soc. 106 (1984) 5913.
[12] T.E. Mueller, J.C. Green, D.M.P. Mingos, C.M. McPartlin, C. Whittingham, J. Organomet. Chem. 551 (1998) 313.
[13] H. Jiao, S. Le Stang, T. Soos, R. Meier, K. Kowski, P. Rademacher, L. Jafarpour, J.-B. Hamard, S.P. Nolan, J.A. Gladysz, J. Am. Chem. Soc. 124 (2002) 1516.
[14] M.J. Atherton, J. Fawcett, A.P. Hill, J.H. Holloway, E.G. Hope, D.R. Russell, G.C. Saunders, R.M.J. Stead, J. Chem. Soc. Dalton Trans. (1997) 1137.
[15] L. Kollár, P. Sándor, G. Szalontai, J. Mol. Catal. 67 (1991) 191.
[16] F. Ozawa, A. Kubo, Y. Matsumoto, T. Hayashi, Organometallics 12 (1993) 4188.

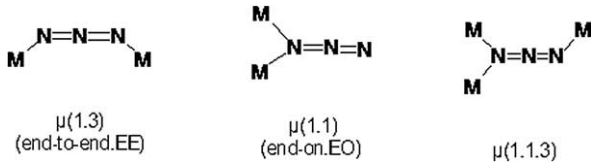

Scheme 1. Different bridging modes of the azido ion.

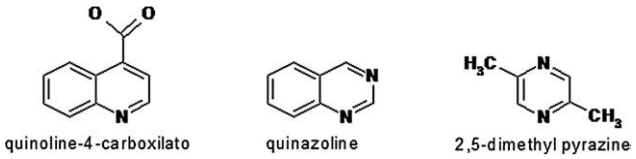

Scheme 2. Some pyridyl-based ditopic ligands.

only few known crystal structures. 2,5-dimethyl pyrazine as simultaneously bridging ligand through its μ(*N*,*N*′) atoms was found in some copper(II) complexes [7–9], nickel(II) complex [10] and silver(I) complex [11] or coordinated through only one hetero nitrogen atom as in Ru(II) complex [12]. Also quinazoline was presented as μ(*N*,*N*′) bridging in Cu(II) and Cu(I) halide complex [13]. While quinoline-4-carboxylato shows an enormous amount of complexes in the literature, although very few solved structures appear in the CCDC with Sn(II) and Re(II) [14]. Therefore, we extend our work to explore the different possible systems arising with these ligands. As part of our investigation on metal azides, we have recently reported a number of cadmium(II) azido and thiocyanato coordination polymers with some pyridine derivative ligands containing different bridging modes of $[Cd(N_3)_2]_n$ and $[Cd(NCS)_2]_n$ chains to construct coordination supramolecular frameworks [15–17]. Compared to the relatively large number of the azido-bridged polymers with Mn(II), Ni(II) and Cu(II) reported in the literature, the Cd(II) polymers are still very rare. Although diamagnetic, the cadmium systems are interesting from the structural point of view, since the systems can exhibit novel bridging networks different from other metal complexes [18]. Here, we present the reactions of cadmium(II) ions with quinoline-4-carboxylic acid, quinazoline and 2,5-dimethylpyrazine in presence of azide ions, and we isolated three complexes; 1:2:1 Cd:quinoline-4-carboxylato:H_2O (**1**), 1:2:2 Cd:quinazoline:azide (**2**) and a 1:1:2 Cd:dimethylpyrazine:azide (**3**) complexes.

2. Experimental

2.1. Material and instrumentation

Elemental analyses C, H, N were carried out using a Perkin–Elmer analyzer, Cd^{2+} was analyzed by a Perkin–Elmer Analyst 300, AAS atomic absorption spectrometer. Infrared spectra were recorded on a Bruker IFS-125 model FT-IR spectrophotometer as KBr pellets. Quinoline-4-carboxylic acid, quinazoline and 2,5-dimethylpyrazine were purchased from Aldrich Company and other chemicals were of analytical grade quality and used as received.

Caution: Metal azide complexes are potentially explosives. Only a small amount of material should be prepared and should be handled with caution.

2.2. Synthesis

The complexes **1**, **2** and **3** have been synthesized in a similar way as reported [17], where an aqueous solution (20 cm^3) of $3CdSO_4 \cdot 8H_2O$ (0.77 g, 1.0 mmol, 3 mmol in Cd^{2+}) was prepared then the organic ligand (0.34 g, 2 mmol, Qux, 0.26 g, 2 mmol, Quz or 0.22 g, 2 mmol, dmpz) dissolved in ca. 15–20 cm^3 of methanol or (methanol/water) were added, followed by a dropwise addition of aqueous solution of NaN_3 (0.65 g, 10 mmol) with continuous stirring. The turbid mixtures were heated, filtered off, boiled again and the final clear mixtures were allowed to cool gradually to room temperature then placed in a refrigerator for several days. Colourless crystals of **1** and **2** with a yield (0.14 g, ~30% and 0.23 g, ~50%), respectively and pale yellow crystals of **3** with a yield (0.49 g, ~80%) with respect to the ligand, suitable for X-ray measurements were collected and dried in air. *Anal.* Calc. for complex **1**: C, 50.60; H, 2.97; N, 5.90; Cd, 23.67. Found: C, 50.40; H, 2.88; N, 6.05; Cd, 23.59%. IR, KBr (cm^{-1}): 3573 vs, 3360 s, 2923 w, 2852 w, 2610 w, 2540 w, 2332 w, 2153 vs, 2056 w, 2038 w, 1601 s, 1577 s, 1536 w, 1458 br, 1428 w, 1403 m, 1373 m, 1340 w, 1319 s, 1227 w. 1191 br, 1110 br, 961 w, 886 br, 856 w,802 m, 683 br, 618 vs, 595 vs, 433 s, 369 s, 298 vs. *Anal.* Calc. for complex **2**: C, 42.07; H, 2.64; N, 30.66; Cd, 24.60. Found: C, 42.16; H, 2.47; N, 30.90; Cd, 24.49%. IR, KBr (cm^{-1}) (v, very; s, strong; m, medium; w, weak; br, broad): 3353 m, 2850 m, 2613 m, 2352 w, 2321 w, 2068 vs, 2036 vs, 1618 s, 1576 s, 1536 w, 1518 w, 1490 s, 1411 m, 1376 s, 1332 s, 1306 s, 1254 w, 1211 s, 1154 s, 1135 s, 1066 s, 954 s, 923 s, 867 m, 834 m, 787 s, 747 vs, 680 w, 634 s, 593 br, 522 m, 470 m, 442 br, 408 m, 387 m, 365 m, 342 m, 315 m, 293 m, 269 s, 233 s. *Anal.* Calc. for complex **3**: C, 23.66; H, 2.64; N, 36.78; Cd, 36.90. Found: C, 23.48; H, 2.72; N, 36.66; Cd, 36.43%. IR, KBr (cm^{-1}) (v, very; s, strong; m, medium; w, weak; br, broad): 3427 w, 3382 m, 3114 w, 3032 m, 2928 m, 2306 br, 2251 br, 2064 vs, 2006 w, 1838 w, 1627 w, 1552 w, 1535 w, 1502 vs, 1449 s, 1382 s, 1334 vs, 1269 br, 1159 vs, 1070 vs, 1035 s, 987 m, 896 m, 746 w, 641 m, 622 m, 594 w, 433 vs, 410 w, 387 w, 366 w, 342 w, 317 m, 290 w, 271 s, 232 s.

2.3. X-ray crystallography

All diffraction data were collected using a Siemens SMART CCD diffractometer with Mo Kα radiation ($\lambda = 0.71073$ Å, graphite monochromator). The crystals were cooled to 173(2) K by a flow of nitrogen gas using the LT-2A device. Full spheres of reciprocal lattices were scanned by 0.3° steps in ω with a crystal-to-detector

Table 1
Crystal data and structure refinement for complexes **1**, **2** and **3**

	$[Cd(Quz)_2(H_2O)]_n$ (**1**)	$[Cd(Quz)_2(N_3)_2]_n$ (**2**)	$[Cd(dmpz)(N_3)_2]_n$ (**3**)
Empirical formula	$C_{20}H_{14}Cd\ N_2O_5$	$C_{16}H_{12}Cd\ N_{10}$	$C_6H_8Cd\ N_8$
Formula weight	474.73	456.76	304.60
Temperature (K)	173(2)	173(2)	173(2)
Wavelength (Å)	0.71073	0.71073	0.71073
Crystal system	monoclinic	monoclinic	monoclinic
Space group	*C*2/*c*	*C*2/*c*	$P2_1/c$
Unit cell dimensions			
a (Å)	15.3702(1)	18.5474(1)	7.5793(1)
b (Å)	14.3612(1)	6.9516(1)	7.1152(1)
c (Å)	7.7776(1)	12.8662(1)	9.3933(2)
β (°)	92.452(1)	99.072(1)	109.699(1)
Volume (Å^3)	1715.21(3)	1638.14(3)	476.918(14)
Z	4	4	2
Density (calculated) (Mg/m^3)	1.838	1.852	2.121
Absorption coefficient (mm^{-1})	1.311	1.359	2.269
Reflections collected	14787	13557	8008
Independent reflections (R_{int})	3078 (0.0379)	2928 (0.0333)	1701 (0.0212)
Absorption correction	multi-scan	multi-scan	multi-scan
Refinement method	Full-matrix least-squares on F^2	Full-matrix least-squares on F^2	Full-matrix least-squares on F^2
Data/restraints/parameters	3078/0/139	2928/0/141	1701/0/75
Goodness-of-fit on F^2	1.019	1.018	1.062
Final *R* indices [$I > 2\sigma(I)$]	$R_1 = 0.0310$, $wR_2 = 0.0690$	$R_1 = 0.0207$, $wR_2 = 0.0496$	$R_1 = 0.0136$, $wR_2 = 0.0368$
R indices (all data)	$R_1 = 0.0474$, $wR_2 = 0.0768$	$R_1 = 0.0264$, $wR_2 = 0.0518$	$R_1 = 0.0150$, $wR_2 = 0.0377$

distance of 3.97 cm. Preliminary orientation matrices were obtained from the first frames using SMART [19]. The collected frames were integrated using the preliminary orientation matrices which were updated every 100 frames. Final cell parameters were obtained by refinement on the positions of reflections with $I > 10(I)$ after integration of all the frames using SAINT [19]. The data were empirically corrected for absorption and other effects using SADABS program [20]. The structures were solved by direct methods and refined by full-matrix least-squares on all F^2 data using SHELXTL [21]. The non-H atoms were refined anisotropically, while hydrogen atoms were refined isotropically with use of geometrical restraints. The crystallographic and refinement data are summarized in Table 1. Tables 2, 4 and 5 list the selected bond distances and angles for complexes **1**, **2** and **3**, respectively. Molecular graphics were prepared using Diamond [22].

Table 2
Selected bond lengths (Å) and bond angles (°) for complex **1**

Cd1–O11^{i}	2.2129(16)
Cd1–O11^{ii}	2.2129(16)
Cd1–O12	2.3002(16)
Cd1–O12^{iii}	2.3003(16)
Cd1–O1^{iii}	2.3566(12)
Cd1–O1	2.3566(12)
O1–Cd1^{iv}	2.3566(12)
O11^{i}–Cd1–O11^{ii}	180.0
O12–Cd1–O12^{iii}	180.0
O1^{iii}–Cd1–O1	180.0
O11^{i}–Cd1–O12	86.54(7)
O11^{ii}–Cd1–O12	93.46(7)
O11^{i}–Cd1–O12^{iii}	93.46(7)
O11^{ii}–Cd1–O12^{iii}	86.54(7)
O11^{i}–Cd1–O1^{iii}	91.87(5)
O11^{ii}–Cd1–O1^{iii}	88.13(5)
O12–Cd1–O1^{iii}	92.56(5)
O12^{iii}–Cd1–O1^{iii}	87.44(5)
O11^{i}–Cd1–O1	88.13(5)
O11^{ii}–Cd1–O1	91.87(5)
O12–Cd1–O1	87.44(5)
O12^{iii}–Cd1–O1	92.56(5)
Cd1^{iv}–O1–Cd1	111.20(8)

Symmetry transformations used to generate equivalent atoms: (i): $x, -y, z - 1/2$; (ii): $-x, y, -z + 1/2$; (iii): $-x, -y, -z$; (iv): $-x, y, -z - 1/2$.

3. Results and discussion

Three new complexes $[Cd(Qux)_2(H_2O)]_n$ (**1**), $[Cd(Quz)_2(N_3)_2]_n$ (**2**) and $[Cd(dmpz)(N_3)_2]_n$ (**3**) (Qux = quinoline-4-carboxylato anion, Quz = quinazoline, dmpz = 2,5-dimethylpyrazine) have been synthesized and found by X-ray crystallography to have 1D, 2D and 3D topologies, respectively. Although azide ion was introduced in all reactions it is present in complexes **2** and **3** but it is absent in complex **1**. These complexes are insoluble in many polar solvents, e.g., water, MeOH, and EtOH, suggesting their polymeric nature, and they are sparingly soluble in DMSO. IR spectra of these complexes confirm the coordination and the bridging nature of the azido ligand in **2** and **3** and also the carboxylato group in complex **1**.

3.1. Structures

3.1.1. $[Cd(Qux)_2(H_2O)]_n$ (1)

The structure at room temperature of complex **1** has been reported [23] but no coordinates are available. There was also no reply from authors to request for data from

CCDC (refcode XUXRUD). Thus, we present our results here. The low temperature single-crystal X-ray structure analysis of **1** indicates a 1D topology where the coordination geometry around the central Cd(II) atom is slightly distorted octahedral geometry CdO_6 as presented in Fig. 1. The two μ_2-OH_2 axially coordinated to the Cd(II) are related by a symmetry center, where the Cd(II) ion lies. Further the equatorially bonded four oxygen atoms from four different quinoline-4-carboxylato ligands at distances 2.213(2)–2.300(2) Å (see Table 2) which is very close to that of Cd–O_{carb} distances (2.283–2.284 Å) of $[Cd_3(\mu_3\text{-}OH)L_3(py)_6](ClO_4)_2$, (L = 4-[2-(4-pyridyl)ethenyl] (benzoate) [24] and $[Cd_3(nic)_4(N_3)_2(H_2O)]_n$, (nic = nicotinato anion) [17b]. Due to bridging nature of the μ_2-OH_2, the Cd–O_w distances (2.357(1) Å) in the apical positions is longer than that of Cd–O_{carb} in the equatorial position. Although the bond angles O–Cd–O are 180.0° for the atoms related by inverse center in both apical and equatorial planes, the bond angles around the Cd center range from 86.54(7) to 92.56(5)°, and deviate less than 3.5° from those expected for an ideal octahedron. This is different from the one-dimensional platinum system consisting of carboxylate-bridged *cis*-diammineplatinum dimers [25], as for compound **1** the cadmium centers are linked by triple bridges between the adjacent cadmium centers resulting in a one-dimensional linear chain Fig. 2. Each Cd(II) atom is triply bridged on both sides to two adjacent Cd atoms through two μ(O,O′)-carboxylato groups on each side and two μ_2-OH_2. The Cd···Cd distance is 3.8888(1) Å, indicative of no metal–metal interaction and distinguished from those one-dimensional metal chain complexes having infinite metal–metal interactions or bonds [26]. The structure of **1** represents a strong supramolecular interactions through the (O_w-H···N, 2.714(2) Å), where the hetero nitrogen atom of the quinoline group is hydrogen bonded to the bridging water molecules, see Fig. 3 and Table 3 for hydrogen bonding.

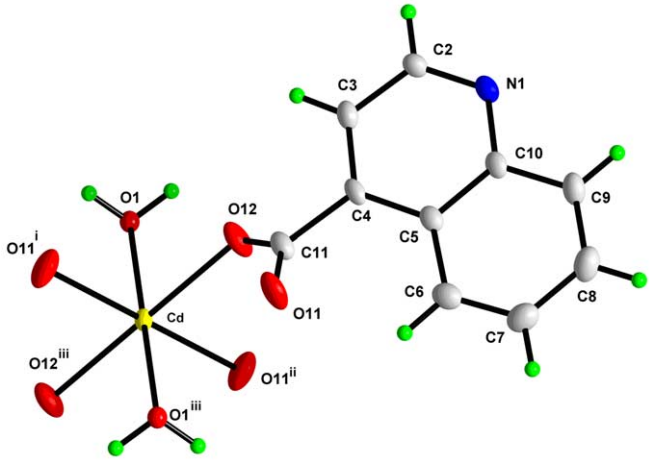

Fig. 1. Numbering scheme of $[Cd(Qux)_2(H_2O)]_n$ (**1**) and atomic displacement ellipsoids draw at 50% probability level. Symmetry codes as in Table 2.

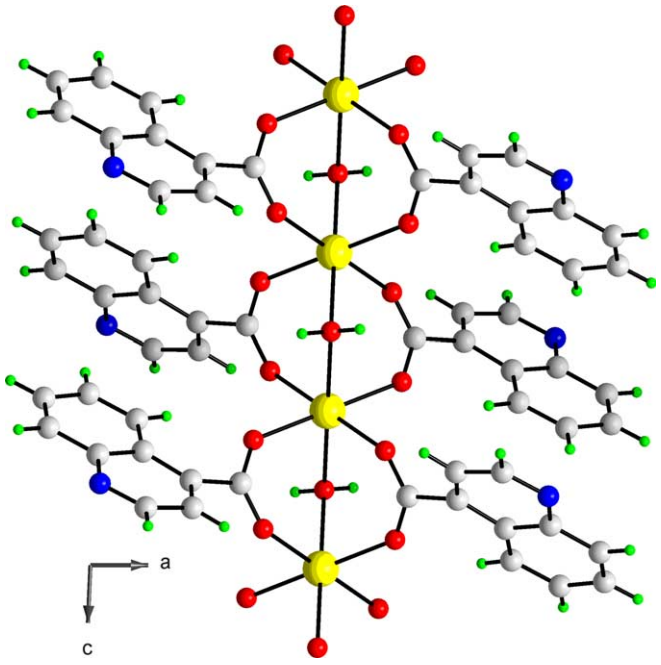

Fig. 2. 1D structure for $[Cd(Qux)_2(H_2O)]_n$ (**1**) in projection along *b*-axis.

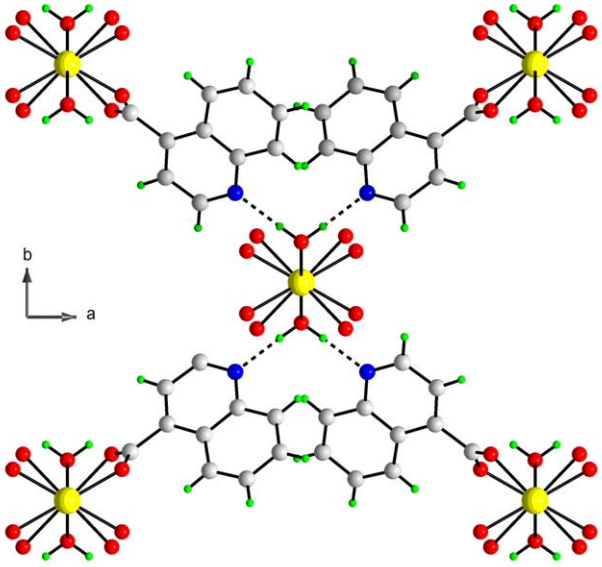

Fig. 3. Hydrogen bonds (shown as broken lines) are stabilizing the structure of $[Cd(Qux)_2(H_2O)]_n$ (**1**) in the (*a*,*b*)-plane.

Table 3
Hydrogen bonds for complex **1** [Å and °]

D–H···A	d(D–H)	d(H···A)	d(D···A)	<(DHA)
O1–H1···N1^{v}	0.87(3)	1.84(3)	2.714(2)	178(3)

Symmetry transformations used to generate equivalent atoms: (v): $-x+1/2, -y+1/2, -z$.

3.1.2. $[Cd(Quz)_2(N_3)_2]_n$ (**2**)

The low temperature X-ray single crystal structure determination for complex **2**, see numbering scheme

Fig. 4, reveals that it has a 2D structure consisting of parallel planes connected through di-EE azido groups and two terminal quinazoline ligands as shown in Fig. 5. The azide ligand bridging in *c*-direction is placed with its central atom at 2-fold axis. The azide ligands binding in *b*-direction are statistically disordered with two different positions (1:1), sharing the central N-atom at inverse center and this relative orientations differ around 30°. The cadmium atoms, positioned at 2-fold axis, are placed in a slightly distorted octahedral geometry CdN_6 linked to four azides in the equatorial plane and to two terminal quinazoline groups, coordinated through the *meta* N atoms only, in the apical positions. The distances Cd–N(azide) (see Table 4) range from 2.349(2) to 2.355(3) Å, while Cd–N(Quz) are

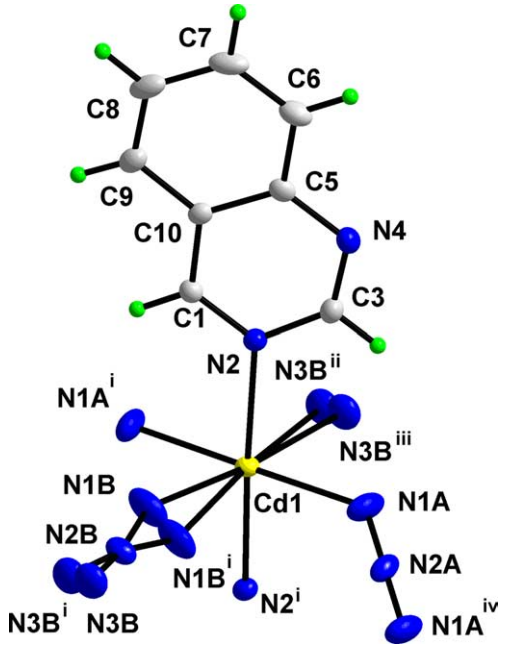

Fig. 4. Numbering scheme and atomic displacement ellipsoids of $[Cd(Quz)_2(N_3)_2]_n$ (**2**) drawn at 50% probability level. Symmetry codes as in Table 4. Note the disordered azide.

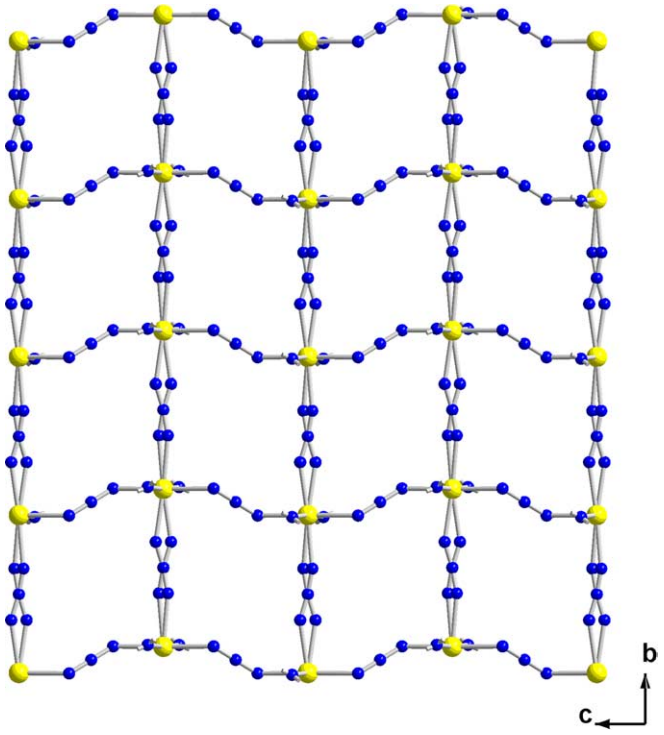

Fig. 5. Projection of the structure of $[Cd(Quz)_2(N_3)_2]_n$ (**2**) along *a*-axis. Only N-atoms of Quz are shown for simplicity.

Table 4
Selected bond lengths (Å) and bond angles (°) for complex **2**

Cd1–N2	2.3429(12)
Cd1–N2i	2.3429(12)
Cd1–N1A	2.3491(15)
Cd1–N1A^{i}	2.3491(15)
Cd1–N1B	2.355(3)
Cd1–N1B^{i}	2.355(3)
Cd1–N3B^{ii}	2.365(2)
Cd1–N3B^{iii}	2.365(2)
N1A–N2A	1.1736(14)
N2A–N1A^{iv}	1.1735(14)
N1B–N2B	1.189(3)
N2B–N1B^{i}	1.189(3)
N2B–N3B^{i}	1.149(3)
N2B–N3B	1.149(3)
N2–Cd1–N2^{i}	175.97(5)
N2–Cd1–N1B^{i}	96.49(12)
N2–Cd1–N1B	87.50(12)
N2–Cd1–N1A	87.25(5)
N2–Cd1–N1A^{i}	92.71(5)
N2–Cd1–N3B^{ii}	88.8(4)
N2–Cd1–N3B^{iii}	87.2(4)
N2^{i}–Cd1–N1B^{i}	87.50(12)
N2^{i}–Cd1–N1B	96.49(12)
N2^{i}–Cd1–N1A	92.71(5)
N2^{i}–Cd1–N1A^{i}	87.25(5)
N2^{i}–Cd1–N3B^{ii}	87.2(4)
N2i–Cd1–N3B^{iii}	88.8(4)
N1A–Cd1–N1A^{i}	179.04(8)
N1A–Cd1–N3B^{ii}	94.65(17)
N1A–Cd1–N3B^{iii}	84.39(17)
N1A^{i}–Cd1–N3B^{ii}	84.39(17)
N1A^{i}–Cd1–N3B^{iii}	94.65(17)
N1B–Cd1–N1A	97.46(11)
N1B–Cd1–N1A^{i}	83.50(11)
N1B–Cd1–N3B^{ii}	167.1(2)
N1B–Cd1–N3B^{iii}	174.3(4)
N1B^{i}–Cd1–N1A	83.50(11)
N1B^{i}–Cd1–N1A^{i}	97.46(11)
N1B^{i}–Cd1–N3B^{ii}	174.3(4)
N1B^{i}–Cd1–N3B^{iii}	167.1(2)
N1A^{iv}–N2A–N1A	180.0
N2A–N1A–Cd1	133.32(11)
N2A–N1A^{iv}–Cd1^{iv}	133.32(11)
N1B–N2B–N3B	168.8(9)
N1B^{i}–N2B–N3B^{i}	168.8(9)
N2B–N1B–Cd1	154.5(2)
N2B–N1B^{i}–Cd1	154.5(2)
N2B–N3B–Cd1^{v}	164.2(5)
N2B–N3B^{i}–Cd1^{v}	164.2(5)

Symmetry transformations used to generate equivalent atoms: (i): $-x$, y, $-z+3/2$; (ii): $-x$, $y+1$, $-z+3/2$; (iii): x, $y+1$, z; (iv): $-x$, $-y$, $-z+1$; (v): x, $y-1$, z.

2.343(1) Å. The bond angles in the equatorial plane range from 83.5(1) to 97.5(1)° and 167.1(2) to 179.04(8)°, while N(Quz)-Cd–N(azide) range from 87.2(4) to 96.5(1)° and N(Quz)-Cd–N(Quz) is 175.97(5)°. The azido ligands have Cd–N–N bond angle of 133.3(1)° for the azide placed in the 2-fold axis, while for the disordered azide placed on the inversion center, the Cd–N–N bond angles are 154.5(2) and 164.2(5)°. The Cd···Cd distances are within the 2D sheet 6.4516(1) and 6.5355(1) Å in the *b*- and *c*-directions, respectively.

3.1.3. $[Cd(dmpz)(N_3)_2]_n$ (3)

A labeled ORTEP-like plot of the structure is shown in Fig. 6, selected distances and angles are listed in Table 5. The structure of this complex can be described as a 3D network structure consisting of Cd(II) ions, each surrounded by four (EE) azido groups and two bridging μ(*N*,*N*′) dimethylpyrazine groups as shown in Figs. 7 and 8. The Cd atoms, placed at inversion center, have an octahedral slightly distorted environment CdN_6 linked to four azides in the equatorial plan with two dmpz in the apical positions. The distances Cd–N(azide) are 2.3081(9) and 2.3613(9) Å (two each), while the distances Cd–N(dmpz) are 2.407(1) Å, which is quite similar to the reported Ag–N(dmpz), 2.402(5) Å for $[Ag(CF_3CO_2)(dmpz)]_n$ [11]. The bond angles in the equatorial plane of Cd octahedra range from 83.53(4) to 96.47(4)° and from 85.73(3) to 94.26(3)° between the apical N and the equatorial ones apart from those of 180° imposed by symmetry. The azido ligands have Cd–N–N bond angle of 117.87(11)° and 133.56(8)° respectively, see Fig. 7. The dmpz ring is planar with $\chi^2 = 4.9$ and maximal departure from the mean last-square plane of 0.001(2) Å for the atoms in the ring and 0.029(1) Å for the C-methyl atoms. The Cd···Cd distances are 5.8919(1) Å via azide bridges, significantly different from the corresponding value 6.086(2) Å given for the di(EE) azide separation in the two dimensional

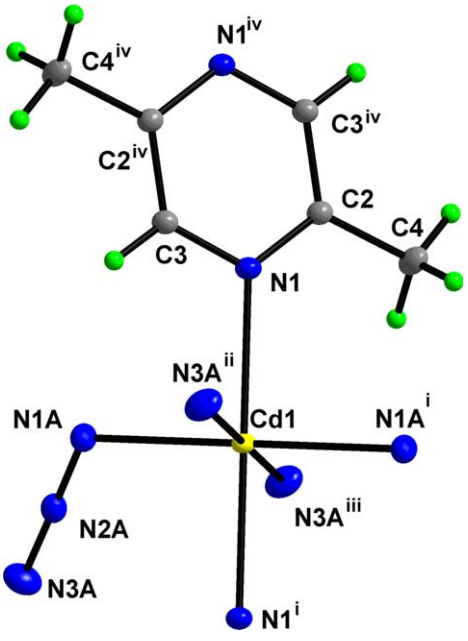

Fig. 6. Numbering scheme and atomic displacement ellipsoids of $[Cd(dmpz)(N_3)_2]_n$ (**3**) drawn at 50% probability level. Symmetry codes as in Table 5.

Table 5
Selected bond lengths (Å) and bond angles (°) for complex **3**

Cd1–N1	2.4072(10)
Cd1–N1^{i}	2.4072(10)
Cd1–N1A	2.3081(9)
Cd1–N1A^{i}	2.3081(9)
Cd1–N3A^{ii}	2.3613(9)
Cd1–N3A^{iii}	2.3614(9)
N3A–Cd1^{v}	2.3614(9)
N1A–N2A	1.1822(12)
N2A–N3A	1.1789(13)
N1–Cd1–N1^{i}	180.0
N1A–Cd1–N1	85.74(3)
N1A^{i}–Cd1–N1	94.26(3)
N3A^{ii}–Cd1–N1	88.07(3)
N3A^{iii}–Cd1–N1	91.94(3)
N1A–Cd1–N1^{i}	94.26(3)
N1A^{i}–Cd1–N1^{i}	85.73(3)
N1A^{i}–Cd1–N1A	180.0
N1Ai–Cd1–N3A^{ii}	83.53(4)
N1A–Cd1–N3A^{ii}	96.47(4)
N1Ai–Cd1–N3A^{iii}	96.47(4)
N1A–Cd1–N3A^{iii}	83.53(4)
N3A^{ii}–Cd1–N3A^{iii}	180.0
N3A^{ii}–Cd1–N1^{i}	91.94(3)
N3A^{iii}–Cd1–N1^{i}	88.06(3)
N3A–N2A–N1A	177.87(11)
N2A–N1A–Cd1	117.42(7)
N2A–N3A–Cd1^{v}	133.56(8)

Symmetry transformations used to generate equivalent atoms: (i): $-x+1$, $-y$, $-z+1$; (ii): x, $-y-1/2$, $z+1/2$; (iii): $-x+1$, $y+1/2$, $-z+1/2$; (iv): $-x$, $-y$, $-z+1$; (v): $-x+1$, $y-1/2$, $-z+1/2$.

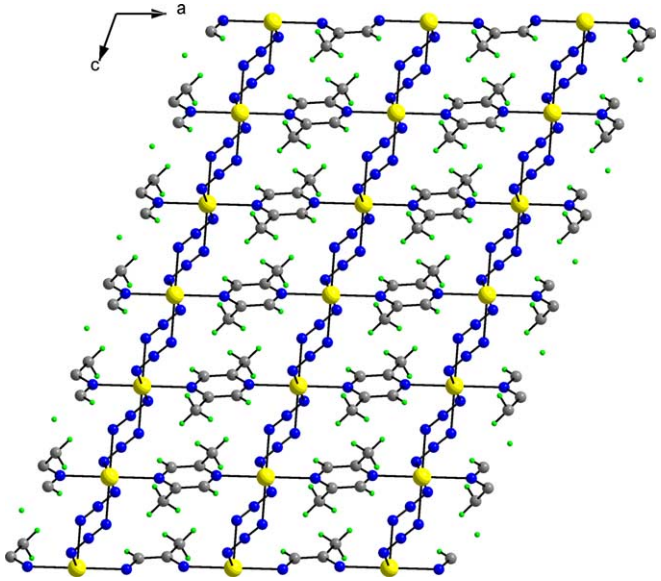

Fig. 7. Projection of $[Cd(dmpz)(N_3)_2]_n$ (**3**) viewed along *a*-direction.

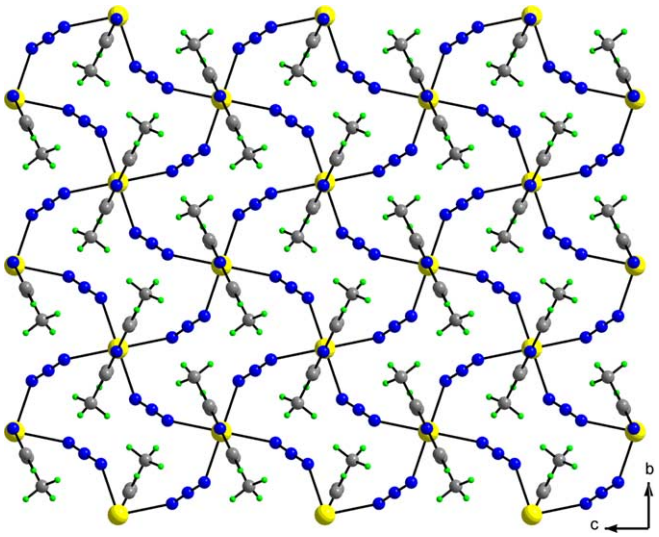

Fig. 8. Projection of $[Cd(dmpz)(N_3)_2]_n$ (**3**) viewed along *b*-direction.

complex $[Cd(4\text{-}Acpy)_2(N_3)_2]_n$ [15c], and 7.5793(1) Å via dmpz bridges in **3**.

3.2. Spectra

The room temperature IR spectrum of the crystalline complex $[Cd(Qux)(H_2O)]_n$ **1** as a KBr pellet shows no bands around 2000–2100 cm^{-1}, indicating the absence of the azide ion. The expected bands of the ν(C=O) and ν_{as}(–COO^-) around 1710–1720 and 1640–1660 cm^{-1} for the free acid are absent in the IR spectrum of **1**, instead, strong and broad bands around 1601, 1577 and 1403 cm^{-1} appeared indicating that only carboxylato anions are coordinated to the Cd(II) ion [27]. In the high energy region complex **1** exhibits a strong broad band around 3573 cm^{-1} corresponding to the water molecules coordinated to the Cd(II) ions bridging the 1D chain in complex **1**. Hydrogen bonding of the type (O–H···N) is indicated in the spectrum by the presence of broad, medium strong bands near 2450 cm^{-1} (IR) [28]. The vibration frequencies at 2068 vs, 2036 vs and 1254 w cm^{-1} for complex **2** and at 2064 vs, 2006 w and 1269 br cm^{-1} for complex **3** were assigned as (ν_{as}-N_3) and (ν_s-N_3), respectively and simply attributable to the EE bridge [29]. This is not in agreement with the symmetric nature of the bridging ($\mu_{1,3}$-N_3) groups N1A–N2A and N2A–$N1A^{iv}$ both distances are 1.1736(14) Å as imposed by symmetry. While the asymmetric disordered ($\mu_{1,3}$-N_3) group, N1B–N2B 1.189(3) and N2B–N3B 1.149(3) Å explains these bands in the spectrum of complex **2**. In complex **3** the azido groups are asymmetric [N1A–N2A, 1.1822(12) and N2A–N3A, 1.1789(13) Å] and in agreement with the experimental data. The bands related to the organic ligands, quinoline-4-carboxilato anion, quinazoline and 2,5-dimethylpyrazine in the spectra of **1**, **2** and **3** show some systematic shifts according to the coordination to the metal ion in accordance to those found for pyridine related complexes [30].

4. Supplementary material

Supplementary data are available from the CCDC, 12 Union Road, Cambridge CB2 1EZ, UK on request, quoting the deposition number(s) CCDC-280747, CCDC-280746 and CCDC-258680 (excluding structure factors) for this paper. These data can be obtained free of charge at www.ccdc.cam.ac.uk/conts/retrieving.html or fax: (internat.) +44 1223/336 033; E-mail: deposit@ccdc.cam.ac.uk.

Acknowledgements

This work was funded by the Swedish International Development Cooperation Agency under the Swedish Research Links program (Grant Nos. 348-2002-6879 and 348-2004-5473).

References

[1] (a) B.F. Hoskins, R. Robson, J. Am. Chem. Soc. 112 (1990) 1546;
(b) M. Fujita, Y.J. Kwan, S. Washizu, K. Ogurs, J. Am. Chem. Soc. 116 (1994) 1151;
(c) O.M. Yaghi, H.L. Li, J. Am. Chem. Soc. 117 (1995) 10401;
(d) P.J. Hagrman, D. Hagrman, J. Zubieta, Angew. Chem. Int. Ed. Engl. 38 (1999) 2638.

[2] (a) J.M. Lehn, Supramolecular Chemistry, VCH, Weinheim, 1985;
(b) R. Robin, B.F. Abrahms, R.R. Barten, R.W. Gable, B.F. Huskiness, J. Lieu, Supramolecular Architecture, American Chemical Society, Washington, DC, 1992;
(c) O. Kahn (Ed.), Molecular Magnetism, a Supramolecular Function, Kluwer, Dordrecht, 1996;
(d) J. Ribas, A. Escuer, M. Monfort, R. Vicente, R. Cortés, L. Lezama, T. Rojo, Coord. Chem. Rev. 193–195 (1999) 1027, and references therein.

[3] (a) A. Escuer, R. Vicente, M.A.M. Abu-Youssef, F.A. Mautner, M.A.S. Goher, L. Öhrstrom, Polyhedron 24 (2005) 557;
(b) J. Cano, Y. Journaux, M.A.S. Goher, M.A.M. Abu-Youssef, F.A. Mautner, G.J. Reiß, A. Escuer, R. Vicente, New J. Chem. 2 (2005) 306;
(c) A. Escuer, F.A. Mautner, M.A.S. Goher, M.A.M. Abu-Youssef, R. Vicente, Chem. Commun. (2005) 605.

[4] (a) A. Escuer, R. Vicente, F.A. Mautner, M.A.S. Goher, M.A.M. Abu-Youssef, J. Chem. Soc., Chem. Commun. (2002) 64;
(b) M.A.M. Abu-Youssef, M. Drillon, A. Escuer, M.A.S. Goher, F.A. Mautner, R. Vicente, Inorg. Chem. 39 (2000) 5022;
(c) M.A.M. Abu-Youssef, A. Escuer, M.A.S. Goher, F.A. Mautner, G.J. Reiß, R. Vicente, Angew. Chem. Int. Ed. Engl. 39 (9) (2000) 1624;
(d) M.A.M. Abu-Youssef, A. Escuer, D. Gatteschi, M.A.S. Goher, F.A. Mautner, R. Vicente, Inorg. Chem. 38 (1999) 5716.

[5] (a) M.A.S. Goher, J. Cano, Y. Journaux, M.A.M. Abu-Youssef, F.A. Mautner, A. Escuer, R. Vicente, Chem. Eur. J. 6 (2000) 774;
(b) M.A.S. Goher, M.A.M. Abu-Youssef, F.A. Mautner, R. Vicente, A. Escuer, Eur. J. Inorg. Chem. (2000) 1819;
(c) M.A.M. Abu-Youssef, A. Escuer, M.A.S. Goher, F.A. Mautner, R. Vicente, J. Chem. Soc., Dalton Trans. (2000) 413.

[6] (a) E.-Q. Gao, Z.-M. Wang, C.-H. Yan, Chem. Commun. (2003) 1748;
(b) E.-Q. Gao, S.-Q. Bai, Z.-M. Wang, C.-H. Yan, Dalton Trans. (2003) 1759;
(c) E.-Q. Gao, Z.-M. Wang, C.-S. Liao, C.-H. Yan, New J. Chem. 26 (2002) 1096.

[7] (a) S. Takamizawa, E. Nakata, T. Saito, H. Yokoyama, Inorg. Chem. Commun. 6 (2003) 1326;
(b) T. Otieno, J.R. Blanton, K.J. Lanham, S. Parkin, J. Chem. Cryst. 33 (2003) 335;
(c) C. Nather, J. Greve, I. Jess, C. Wickleder, Solid State Sci. 5 (2003) 1167.
[8] (a) T. Otieno, S.J. Rettig, R.C. Thompson, J. Trotter, Inorg. Chem. 32 (1993) 1607;
(b) C. Nather, J. Greve, Acta Crystallogr., Sect. C: Cryst. Struct. Commun. 57 (2001) 1388;
(c) C. Nather, J. Greve, I. Jess, Solid State Sci. 4 (2002) 813;
(d) A.W. Maverick, M.L. Ivie, J.H. Waggenspack, F.R. Fronczek, Inorg. Chem. 29 (1990) 2403.
[9] (a) D.J. Chesnut, D. Plewak, J. Zubieta, J. Chem. Soc., Dalton Trans. (2001) 2567;
(b) T. Otieno, S.J. Rettig, R.C. Thompson, J. Trotter, Can. J. Chem. 68 (1990) 1901;
(c) Wai-Fun Yeung, Song Gao, Wing-Tak Wong, Tai-Chu Lau, New J. Chem. (Nouv. J. Chim.) 26 (2002) 523.
[10] F.D. Ayres, P. Pauling, G.B. Robertson, Inorg. Chem. 3 (1964) 1303.
[11] L. Brammer, M.D. Burgard, M.D. Eddleston, C.S. Rodger, N.P. Rath, H. Adams, Cryst. Eng. Commun. 4 (2002) 239.
[12] H. Miyasaka, Ho-Chol Chang, K. Mochizuki, S. Kitagawa, Inorg. Chem. 40 (2001) 3544.
[13] (a) M. Munakata, T. Kuroda-Sowa, M. Maekawa, M. Nakamura, S. Akiyama, S. Kitagawa, Inorg. Chem. 33 (1994) 1284;
(b) J.T. Maeyer, T.J. Johnson, A.K. Smith, B.D. Borne, R.D. Pike, W.T. Pennington, M. Krawiec, A.L. Rheingold, Polyhedron 22 (2003) 419;
(c) T. Ishida, T. Nogami, M. Yasui, F. Iwasaki, H. Iwamura, N. Takeda, M. Ishikawa, Mol. Cryst. Liq. Cryst. Sci. Technol., Sect. A 279 (1996) 87;
(d) M. Yasui, Y. Ishikawa, T. Ishida, T. Nogami, F. Iwasaki, Acta Crystallogr., Sect.B: Struct. Sci. 57 (2001) 772.
[14] (a) S-.M. Kuang, P.E. Fanwick, R.A. Walton, Inorg. Chim. Acta 338 (2002) 219;
(b) R.G. Xiong, J.L. Zuo, X.Z. You, H.K. Fun, S.S.S. Raj, Organometallics 19 (2000) 4183;
(c) S-.M. Kuang, P.E. Fanwick, R.A. Walton, Inorg. Chem. 41 (2002) 405.
[15] (a) F.A. Mautner, M.A.M. Abu-Youssef, M.A.S. Goher, Polyhedron 16 (1997) 235;
(b) M.A.S. Goher, F.A. Mautner, M.A.M. Abu-Youssef, A.K. Hafez, A.M.A. Badr, J. Chem. Soc., Dalton Trans. (2002) 3309;
(c) M.A.S. Goher, F.A. Mautner, A.K. Hafez, M.A.M. Abu-Youssef, C. Gspan, A.M.A. Badr, Polyhedron 22 (2003) 975;
(d) S. Hanna, F.A. Mautner, B.B. Koppelhuber, M.A.M. Abu-Youssef, in: R Delhez, E.J. Mittelmeyer, (Eds.), Material Science Forum, 2000, pp. 321–325, 1098–1101.
[16] (a) F.A. Mautner, C. Gspan, M.A.S. Goher, M.A.M. Abu-Youssef, Monatsh. Chem. 134 (2003) 1311;
(b) M.A.S. Goher, F.A. Mautner, M.A.M. Abu-Youssef, A.K. Hafez, A.M.A. Badr, C. Gspan, Polyhedron 22 (2003) 3137;
(c) F.A. Mautner, C. Gspan, K. Gatterer, M.A.S. Goher, M.A.M. Abu-Youssef, E. Bucher, W. Sitte, Polyhedron 23 (2004) 1217;
(d) M.A.S. Goher, A.K. Hafez, M.A.M. Abu-Youssef, A.M.A. Badr, C. Gspan, F.A. Mautner, Polyhedron 23 (2004) 2349.
[17] (a) F.A. Mautner, C. Gspan, M.A.M. Abu-Youssef, M.A.S. Goher, Monatshefte für Chemie 136 (2004) 107;
(b) M.A.M. Abu-Youssef, Polyhedron 24 (2005) 1829;
(c) M.A.M. Abu-Youssef, J. Coord. Chem., in press.
[18] (a) Yan-Feng Yue, En-Qing Gao, Shi-Qiang Bai, Zheng He, Chun-Hua Yan, Cryst. Eng. Commun. 6 (89) (2004) 549;
(b) Shi-Qiang Bai, En-Qing Gao, Zheng He, Chen-Jie Fang, Chun-Hua Yan, Cryst. Eng. Commun. 6 (98) (2004) 606.
[19] SMART & SAINT: Area Detector Control and Integration Software, Siemens AXS, Madison, WI, USA, 1995.
[20] G.M. Sheldrick, SADABS. Program for Empirical Absorption Correction of Area Detectors (Version 2.03), University of Göttingen, Germany, 2002.
[21] SHELXTL: Structure Determination Programs (Version 6.10), Bruker AXS Inc., Madison, WI, USA, 2001.
[22] K. Brandenburg, Diamond: Visual Crystal Structure Information System (Version 2.1e), Impact GbR, Bonn, Germany, 2001.
[23] Zhen-Feng Chen, Pei Zhang, Ren-Gen Xiong, De-Jun Liu, Xiao-Zeng You, Inorg. Chem. Commun. 5 (2002) 35.
[24] W. Lin, Z. Wang, L. Ma, J. Am. Chem. Soc. 121 (1999) 11249.
[25] K. Sakai, M. Takeshita, Y. Tanaka, T. Ue, M. Yanagisawa, M. Kosaka, T. Tsubomura, M. Ato, T. Natano, J. Am. Chem. Soc. 120 (1998) 11353.
[26] (a) J.S. Miller (Ed.), Extended Linear Chain Compounds, Plenum Press, New York, 1982;
(b) H.J. Keller (Ed.), Chemistry and Physics of One-Dimensional Metals, Plenum Press, New York, 1977;
(c) G. Gliemann, H. Yersin, Bonding 62 (1985) 87.
[27] (a) S. Yoshida, M. Asia, Chem. Pharm. Bull. (Japan) 7 (1959) 162;
(b) I. Nakagawa, T. Shimanouchi, Spectrochim. Acta 20 (1964) 429.
[28] (a) Y. Ichida, Y. Kuroda, D. Nakamura, M. Kubo, Spectrochim. Acta A 28 (1972) 2433;
(b) R.F. Evans, W. Kynaston, J. Chem. Soc. (1962) 1005.
[29] (a) R. Cortés, M. Drillon, X. Solans, L. Lezama, T. Rojo, Inorg. Chem. 36 (1997) 677;
(b) L.-F. Tang, L. Zhang, L.-C. Li, P. Cheng, Z.-H. Wang, J.-T. Wang, Inorg. Chem. 38 (1999) 6326;
(c) S.S. Tandon, L.K. Thompson, M.E. Manuel, J.N. Bridson, Inorg. Chem. 33 (1994) 5555.
[30] N.S. Gill, R.H. Nuttall, D.E. Ecife, R.W.A. Sharp, J. Inorg. Nucl. Chem. 18 (1961) 78.

of advanced molecular materials [1]. Some proposed fields of application include molecular electronic, optronic and iono-electronic devices [1,2]. Vibrational spectroscopies have proved to be versatile methods among various techniques for characterizing thin films of phthalocyanines in solid state devices. In the past several years, the vibrational (IR and Raman) characteristics of (na)phthalocyanine in a wide range of bis[(na)phthalocyaninato] and mixed (porphyrinato)[(na)phthalocyaninato] rare earth complexes have been systematically investigated mainly by Jiang and Arnold [3,4], following the precedent studies of Aroca, Homborg, and Tran-Thi [5–7]. As summarized in our recent papers concerning the vibrational spectroscopic characteristics of sandwich tetrapyrrole rare earth complexes, several series of recently developed novel sandwich double-decker complexes with the whole series of rare earth metals, namely M(TClPP)(Pc) [4g], M(OEP)(Nc) [4d], M(TBPP)(Nc) [4e], M[Nc(tBu)$_4$]$_2$ [4c], and M(Pc)[Pc(α-OC$_5$H$_{11}$)$_4$] [4f] [M = Y, La$\cdots$Lu except Pm; H_2TClPP = 5,10,15,20-tetra(4-chloro)phenylporphyrin, H_2OEP = 2,3,7,8,12,13,7,18-octaethylporphyrin, H_2TBPP = 5,10,15,20-tetra(4-t-butyl)phenylporphyrin, H_2Nc(tBu)$_4$ = 3(4),12(13),21(22),30(31)-tetrakis(t-butyl)-2,3-naphthalocyanine, H_2Pc-(α-OC$_5$H$_{11}$)$_4$ = 1,8,15,22-tetrakis(3-pentyloxy)phthalocyanine] have been systematically studied by the Raman technique using laser excitations emitting at 633 and 785 nm, in order to achieve a complete understanding of their intrinsic properties. In contrast, investigation at the same excitation wavelengths of the Raman properties of the most common counterparts, the basic unsubstituted and peripherally octa(alkoxy)-substituted homoleptic bis(phthalocyaninato) rare earth complexes (Fig. 1), are still limited to scattered species such as M(Pc)$_2$ (M = Ce, Eu), Eu[Pc(OC$_5$H$_{11}$)$_8$]$_2$, and M[Pc(OC$_8$H$_{17}$)$_8$]$_2$ (M = Ce, Gd, Tb) (λ_{ex} = 633 nm) [4a]. It thus seems opportune to study systematically the Raman spectroscopic properties of these complexes by means of excitation with laser sources emitting at 633 and 785 nm, as for the other series mentioned above. The present work reports these studies.

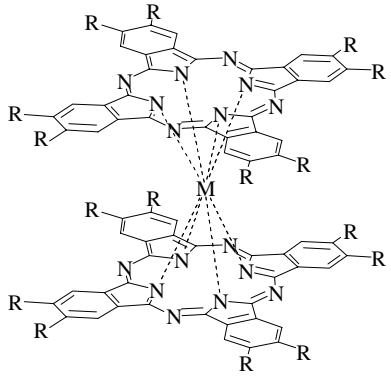

R = H, OC$_8$H$_{17}$

Fig. 1. The schematic molecular structure of bis(phthalocyaninato) rare earth sandwich complexes M(Pc′)$_2$ [Pc′=Pc, Pc(OC$_8$H$_{17}$)$_8$].

It is worth noting that we have previously recorded the Raman spectra of the bis(phthalocyaninato) compounds of Ce and Eu, namely M(Pc)$_2$ (M = Ce, Eu) and Ce[Pc(OC$_8$H$_{17}$)$_8$]$_2$, under excitation by 633 nm radiation [4a]. For the purpose of systematic comparison with those under 785 nm laser excitation, the spectra of the complete set of compounds discussed in this paper were re-measured under 633 nm excitation. Note that the Raman spectra of Ce(Pc)$_2$ and Ce[Pc(OC$_8$H$_{17}$)$_8$]$_2$ recorded this time under 633 nm excitation correspond well in band positions, but the relative intensities of some bands differ, compared with those recorded previously [4a]. Nevertheless, the results reported here are confirmed by the systematic and comparative spectra of the whole series of rare earth bis(phthalocyaninato) compounds M(Pc)$_2$ and M[Pc(OC$_8$H$_{17}$)$_8$]$_2$ (M = Y, La$\cdots$Lu except Ce and Pm), in which the one for Eu(Pc)$_2$ is in good accordance with the previous measurements [4a]. The conclusions are further reinforced by the fact that the Raman spectrum of Ce[Pc(OC$_8$H$_{17}$)$_8$]$_2$ corresponds well with that of Ce(Pc)$_2$ recorded under 633 nm excitation, the former of which is also in line with the previous measurement under excitation by 647 nm radiation [4b].

2. Experimental

Homoleptic bis(phthalocyaninato) rare earth complexes M(Pc)$_2$ and M[Pc(OC$_8$H$_{17}$)$_8$] (M = La–Lu except Pm, Y) were prepared according to published procedures [8]. Their sandwich nature has been well established through a series of spectroscopic methods including high resolution mass, UV–Vis, near-IR, and NMR techniques. Resonance Raman spectra were recorded on a few grains of the solid samples with ca. 4 cm^{-1} resolution using a Renishaw Raman Microprobe, equipped with a Spectra Physics Model 127 He–Ne laser excitation source emitting at a wavelength of 633 nm and a Renishaw diode laser emitting at 785 nm, and a cooled charge-coupled device (CCD) camera. An Olympus BHZ-UHA microscope was attached, and for these experiments the 10× objective was employed giving a spot size on the sample of about 5 μm. Laser power at the sample was approximately 0.08 mW. Spectra of excellent quality were obtained in approximately 3 min, with the exceptions noted below.

3. Results and discussion

In bis(phthalocyaninato) rare earth complexes M(Pc)$_2$, the single crystal X-ray diffraction structural data have shown that the rare earth cation is at the center of two Pc ligands facing each other in a staggered arrangement [1,2]. In the solid state, these compounds can be assumed to belong to the D_4 or D_{4d} point-groups depending on the skew angle between the two macrocyclic rings. There has been no crystallographic report on the molecular structure of peripherally octa(alkoxy)-substituted homoleptic bis(phthalocyaninato) rare earth complexes thus far. However,

according to the recently reported molecular structures of peripherally octa(hexylthio)- and 15-crown-5 ether-substituted bis(phthalocyaninato) rare earth analogues Lu[Pc(SC_6H_{13})$_8$]$_2$ and Yb[Pc(15C5)$_4$]$_2$[H_2Pc(SC_6H_{13})$_8$ = 2,3,9,10,16,17,23,24-octakis(hexylthio)phthalocyanine, H_2Pc(15C5)$_4$ = 2,3,9,10,16,17,24,25-tetrakis(15-crown-5)phthalocyanine] [9], the skew angle between the two phthalocyanine macrocyclic ligands is 42° and 42.5°, respectively, for these two compounds. The equilibrium geometry of Lu[Pc(SC_6H_{13})$_8$]$_2$ and Yb[Pc(15C5)$_4$]$_2$ is therefore D_4. This should also be true for the present alkoxy-substituted analogues M[Pc(OC_8H_{17})$_8$]$_2$.

It has been found that in the Raman spectra of Zr[Pc(*t*Bu)$_4$]$_2$, M[Nc(*t*Bu)$_4$]$_2$, and M(Pc)[Pc(α-OC_5H_{11})$_4$] [4c,4f,5], only frequencies corresponding to the characteristic fingerprint vibrations of the Pc or Nc macrocycle were observed and side chain vibrations were very weak or absent. This is also true in the present case since both laser lines used in our experiments appear to enhance modes associated with the aromatic macrocycles (see below).

Similar to other large conjugated systems, one-to-one matching of observed vibrational frequencies to the internal vibrations cannot be achieved in the vibrational spectra of homoleptic bis(phthalocyaninato) rare earth compounds due to the existence of strong couplings of some vibrational coordinates [3–7]. Therefore, the Raman spectra of these homoleptic bis(phthalocyaninato) double-decker complexes are still composed of a relatively small number of fundamentals despite the large number of Raman active vibrational modes.

3.1. Raman characteristics of M(Pc)$_2$ and M[Pc(OC_8H_{17})$_8$]$_2$ (M = Y, La–Lu except Pm) with excitation by laser line at 633 nm

The electronic absorption spectra of M(Pc)$_2$ and M[Pc(OC_8H_{17})$_8$]$_2$ (M = Pr, Tb, Tm) which are typical representatives of the UV–Vis spectra for the complexes of tervalent rare earths in each series are shown in Figs. 2 and 3, respectively [8]. All the spectra of M(Pc)$_2$ (M = Y, La–Lu except for Ce and Pm) show a typical B band at 316–325 nm with a very weak shoulder peak at the lower energy side of 342–358 nm [10]. The *Q* bands for these compounds appear as a strong absorption in the range of 658–689 nm together with the weak vibronic components at 570–596 and 595–618 nm. In addition, a weak band related with the π-radical anion at 420–458 nm is also observed. For the series of M[Pc(OC_8H_{17})$_8$]$_2$ compounds containing tervalent rare earth metal, the B absorption splits into two bands at 331–343 and 369–378 nm due to the influence of eight octyloxy groups on the phthalocyaninato rings [8d]. Their *Q* bands appear at 668–699 nm with weak vibronic absorptions at 579–601 and 604–630 nm, respectively. The weak π-radical anion band is seen at 485–513 nm. For both series of compounds, the energies of all the absorption bands mentioned above are sensitive to the metal center. In particular, along with the lanthanide contraction, the *Q* absorption band for both M(Pc)$_2$ and M[Pc(OC_8H_{17})$_8$]$_2$ blue-shifts in the same order [8d,10]. These characteristics in their electronic absorption form the basis for the fact that systematic changes are observed in both the frequencies and appearance of the Raman spectra of M(Pc)$_2$ and M[Pc(OC_8H_{17})$_8$]$_2$ along with the change in the central metal ionic size, as detailed below.

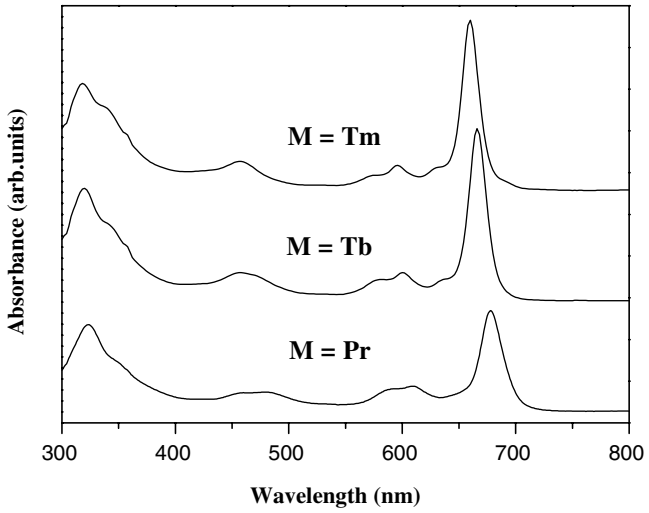

Fig. 2. The UV–Vis spectra of M(Pc)$_2$ (M = Pr, Tb, Tm) in $CHCl_3$.

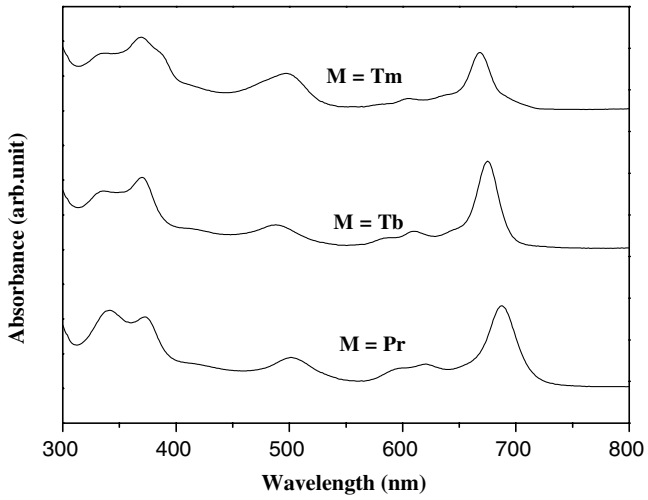

Fig. 3. The UV–Vis spectra of M[Pc(OC_8H_{17})$_8$]$_2$ (M = Pr, Tb, Tm) in $CHCl_3$.

It is worth noting that the Raman spectra of La(Pc)$_2$ and Dy[Pc(OC_8H_{17})$_8$]$_2$ with excitation at 633 nm were of poor quality due to the strong fluorescence. Figs. 4 and 5, respectively, compare the Raman spectra of three compounds M(Pc)$_2$ and M[Pc(OC_8H_{17})$_8$]$_2$ for M = Pr, Tb, and Tm under excitation by 633 nm light. As can be seen, the Raman spectra for both series of compounds M(Pc)$_2$ and M[Pc(OC_8H_{17})$_8$]$_2$ seem to be much simpler in comparison with those of M(Pc)[Pc(α-OC_5H_{11})$_4$] [4f], revealing the relatively higher molecular symmetry of these compounds than the heteroleptic analogues. In particular, the Raman

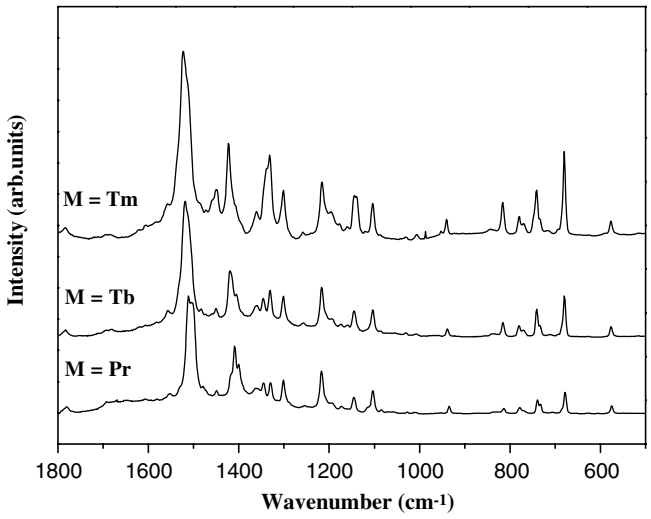

Fig. 4. Raman spectra of $M(Pc)_2$ (M = Pr, Tb, Tm) in the region of 500–1800 cm^{-1} with excitation at 633 nm.

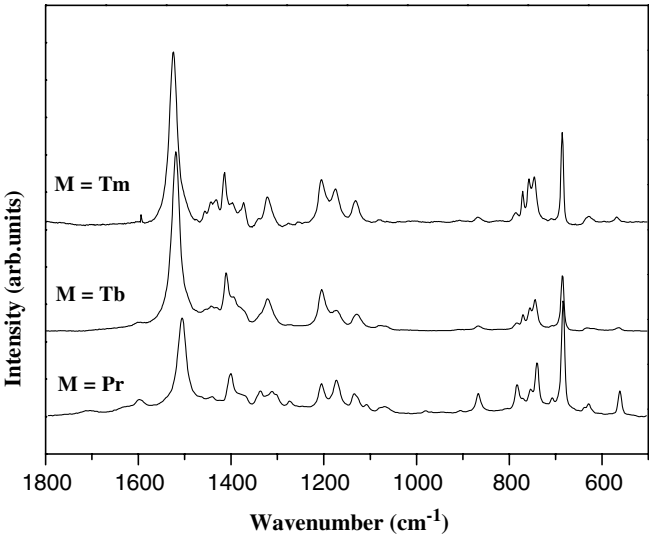

Fig. 5. Raman spectra of $M[Pc(OC_8H_{17})_8]_2$ (M = Pr, Tb, Tm) in the region of 500–1800 cm^{-1} with excitation at 633 nm.

spectra for the peripherally octa(octyloxy)-substituted bis(phthalocyaninato) rare earth complexes appear to be as simple as, or even simpler than, the corresponding unsubstituted counterparts $M(Pc)_2$, indicating again that only frequencies corresponding to the characteristic fingerprint vibrations of the Pc macrocycle in $M[Pc(OC_8H_{17})_8]_2$ were observed. Side chain vibrations were very weak or absent under excitation with laser line of 633 nm, and this is also true when using laser excitation emitting at 785 nm (see below). The observed Raman spectroscopic bands of phthalocyanine for these new homoleptic bis(phthalocyaninato) rare earths were partially assigned in Tables 1 and 2, respectively. Note that the assignments given in Tables 1 and 2 are restricted to characteristic fundamentals based on the previous description of normal modes for phthalocyaninato and especially bis(phthalocyaninato) metal derivatives [4,11]. Recent calculations on the vibrational characteristics of monomeric phthalocyanine derivatives also benefit the present assignments [12]. Due to the similar electronic structure and electronic absorption properties among the whole series of bis(phthalocyaninato) rare earth compounds, all members of each series $M^{III}(Pc)_2$ and $M^{III}[Pc(OC_8H_{17})_8]_2$ (M = Y, La–Lu except Ce and Pm) show similar Raman characteristics.

With laser excitation at 633 nm, which is nearly in resonance with the *Q* band absorptions of both series of bis(phthalocyaninato) rare earth complexes, respectively, at 658–689 and 668–699 nm, vibrational frequencies in the range of 1300–1600 cm^{-1} derived from isoindole ring stretchings and the aza group stretching are selectively intensified. For $M^{III}(Pc)_2$, the weak Raman bands at ca. 574–577 and 812–817 cm^{-1} and a band at 678–680 cm^{-1} with medium or strong intensity are attributed to phthalocyanine breathing [4,11], and the frequencies of all these modes seem to show a dependence on the rare earth size, slightly blue-shifted along with the lanthanide contraction. The medium band at ca. 740 cm^{-1} is due to aromatic phthalocyanine C–H wagging of $M(Pc)_2$ [4]. In the range of 1000–1300 cm^{-1}, there are several weak or medium bands lying at ca. 1006, 1030, 1103, 1174, 1196, 1215 and 1301 cm^{-1}, which are assigned to aromatic C–H bending. The pyrrole breathing presents two bands in the region of around 1140 and 1500 cm^{-1}. The former comprises a single peak with medium intensity at ca. 1138–1145 cm^{-1}, whereas the latter overlaps with the aza stretching vibration in the same region to form a broad band at 1495–1525 cm^{-1} for the whole series of compounds $M^{III}(Pc)_2$. For the double-deckers with early lanthanide metals, the aza stretching band appears as an unresolved shoulder on the *higher* energy side of the peak. In contrast, for the double-deckers with medium and late lanthanides, the pyrrole breathing band appears as an unresolved shoulder peak on the *lower* energy side of the more intense aza stretching peak. The intense band in the range 1409–1423 cm^{-1} and the weak band in the range 1444–1451 cm^{-1} are attributed to isoindole stretchings. The former intense band discussed above, together with the aza stretching band at 1512–1525 cm^{-1}, show dependence on the rare earth radius, shifting to higher energy along with the rare earth contraction. This is not surprising considering the blue-shifted trend of the *Q* absorptions at 658–689 nm in the same order.

As shown in Fig. 5 and organized in Table 2, the Raman spectroscopic frequencies of the phthalocyanine core in $M[Pc(OC_8H_{17})_8]_2$ have been similarly assigned by analogy with those of unsubstituted counterparts $M(Pc)_2$. The Raman spectra observed for $M[Pc(OC_8H_{17})_8]_2$ are even simpler than those of corresponding $M(Pc)_2$. This is probably due to the fact that the excitation at 633 nm is slightly further away from resonance with the main *Q* bands of $M[Pc(OC_8H_{17})_8]_2$ (668–699 nm) than with those of $M(Pc)_2$. This leads to an increased resolution in the Raman spectra of $M[Pc(OC_8H_{17})_8]_2$, which further benefits

Table 1
Characteristic Raman bands (cm^{-1}) of phthalocyanines for $M(Pc)_2$ (M = Y, Ce–Lu except Pm) ($\lambda_{ex} = 633$ nm)

Ce	Pr	Nd	Sm	Eu	Gd	Tb	Dy	Y	Ho	Er	Tm	Yb	Lu	Assignment
579w	574w	574w	574w	576w	576w	576w	576w	577w	576w	576w	577w	577w	577w	Pc breathing
677s	678m	678m	678m	678m	678m	680m	678s	680m	680s	680s	680s	680s	680s	Pc breathing
724w														
741m	739w	739m	740m	741m	741m	741m	741m	742m	741s	741s	741m	742m	741m	C–H wag
767w	771[a]	769[a]	770[a]	770[a]	770[a]	770[a]	770[a]	772[a]	769[a]	770[a]	770[a]	771[a]	770[a]	C=N aza stretching
776w	777w	779w	780w	779w	779w	780w	779w	773w	780w	779w	779w	780w	780w	C=N aza stretching
820m	814w	812w	814w	814w	814w	816w	816w	816w	816w	816w	816w	817w	817w	Pc breathing
933w	935w	935w	936w	936w	936w	939w	938w	939w	939w	939w	941w	941w	941w	
1009w	1011w	1006w	1006w	1006w	1006w	1006w	1006w	1006w	1009w	1006w	1006w	1006w	1006w	C–H bend
1026w	1027w	1027w	1029w	1029w	1029w	1031w	1029w		1029w	1031w	1031w	1031w	1031w	C–H bend
1055w														C–H bend
1103m	1104w	1103w	1104w	1103w	1103w	1104w	1103w	1104w	1103w	1103w	1104w	1104w	1103m	C–H bend
1141m	1145w	1138m	1136m	1145w	1144w	1145w	1145w	1138w	1144w	1145w	1144w	1139w	1144m	pyrrole breathing
1173w	1173w	1173w	1175w	1172w	1174w	1174w	1173w	1176w	1173w	1174w	1177w	1177w	1174w	C–H bend
1190w		1196w	1196w	1194w	1196w	1196w	1192w	1196w	1196w	1196w	1196w	1196w	1194w	C–H bend
1206w	1217m	1215m	1215w	1215m	1215m	1217m	1215m	1215w	1217m	1215m	1215m	1215m	1217m	C–H bend
	1255w			1255w	1255w	1257w	1257w			1258w	1258w	1258w	1258w	
1303w	1301m	1299m	1299m	1301m	1301m	1301m	1301m	1301w	1301w	1301w	1301w	1301w	1301w	C–H bend
1332m	1330m	1330m	1331m	1330m	1330m	1330m	1330m	1332m	1330m	1330m	1332m	1332m	1332m	C=C pyrrole and benzene stretching
1338s	1345w	1336m	1336m	1344w	1343w	1345w	1345w	1338m	1344w	1345w	1339m	1338m	1347m	isoindole stretching
1361w	1362w	1360w	1364w	1361w	1357w	1359w	1359w		1361w	1361w	1361w	1361w	1360w	isoindole stretching
1391w	1400[a]	1402[a]	1403[a]	1403[a]	1403[a]	1404[a]	1405[a]	1403[a]	1407[a]	1407[a]	1408[a]		1410[a]	isoindole stretching
1423w	1409s	1409m	1419m	1414s	1414s	1419s	1419s	1423s	1420s	1421s	1423s	1423s	1423s	isoindole stretching
1449m	1449w	1444w	1446w	1449w	1449w	1451w	1449w	1446w	1449w	1451w	1449w	1448w	1449w	isoindole stretching
1499s	1505[a]	1502s	1504s	1510[a]	1511[a]	1513[a]	1512[a]	1509s	1513[a]	1514[a]	1516[a]	1513[a]	1519[a]	coupling of pyrrole and aza stretching
	1512s	1510[a]	1513[a]	1516s	1515s	1519s	1518s		1521s	1521s	1522s	1519s	1525s	aza stretching
1556w	1553w	1553w	1557w	1554w	1554w	1556w	1556w	1561w						benzene stretching

[a] Shoulder band.

Table 2
Characteristic Raman bands (cm^{-1}) of phthalocyanines for $M[Pc(OC_8H_{17})]_2$ (M = Y, La–Lu except Pm and Dy) ($\lambda_{ex} = 633$ nm)

La	Ce	Pr	Nd	Sm	Eu	Gd	Tb	Y	Ho	Er	Tm	Yb	Lu	Assignment
561w	564w	562m	562w	562w	565w	564w	564w	568w	568w	568w	568w	568w	568w	Pc breathing
628w	625w	629w	629w	629w	634w	634w	632w	628w	629w	628w	628w	628w	636[a]	Pc breathing
683s	681s	684vs	684s	684s	684s	684s	686s	684s	684s	686s	686s	686s	686s	Pc breathing
741m	741m	741m	741m	742m	744m	744m	744w	745m	745w	745w	745w	747m	745m	C–H wag
753w	750w	755w	756w	755w	756w	756w	756w	757w	756w	756m	758m	758m	758m	
767w				771w	771w	771w	770w	771w	771w	771w	771w	771m	771w	C=N aza stretching
782w	780w	783w	783w	784w	783w	784w	784w	785w	785w	784w	787w	787w	787w	C=N aza stretching
866w	866w	867w	867w	867w	867w	867w	866w	866w	867w	867w	867w	867w	867w	coupling of isoindole deformation and aza stretching C–H bend
1067w	1073w	1069w	1064w	1075w	1080w	1078w	1080w	1080w	1081w	1081w	1081w	1080w	1078w	pyrrole breathing
1135m	1135w	1135w	1135w	1132w	1130w	1130w	1128w	1130w	1132w	1130w	1132w	1132w	1132w	C–H bend
1174m	1173s	1173m	1173m	1173w	1173w	1173w	1173w	1174w	1174w	1174w	1174w	1174w	1176w	C–H bend
1205m	1199m	1205m	1205w	1205m	1205m	1205m	1205m	1205m	1205m	1205m	1205m	1205m	1205m	C=C pyrrole and benzene stretching
1316m	1299w	1312w	1312w	1319w	1321m	1321w	1321m	1321m	1321m	1321m	1322m	1322m	1322m	isoindole stretching
1335w	1350w	1336w	1339w	1338w										isoindole stretching
								1371w	1371w	1371w	1373w	1373w	1373w	isoindole stretching
1400m	1408m	1400m	1400m	1405s	1408s	1408s	1411s	1411s	1412s	1412s	1414m	1415s	1415m	isoindole stretching
	1434m				1431w	1431w	1432w	1432w	1432w	1432w	1432w	1432w	1432w	isoindole stretching
1444w	1461w	1440w	1443w	1441w	1440w	1441w	1440w	1442w		1443w	1443w	1445w	1444w	isoindole stretching
								1457w	1457w	1457w	1457w	1457w	1457w	coupling of pyrrole and aza stretching
1504vs	1501vs	1506s	1507vs	1513vs	1515vs	1516vs	1519vs	1521vs	1521vs	1522vs	1524vs	1525vs	1527vs	benzene stretching
1600w	1599w	1599w	1597w	1599w	1597w	1596w	1594w	1597w	1596w	1594w	1597w	1599w	1590w	

[a] Shoulder band.

the assignments of the frequencies. For instance, unlike for the series of $M^{III}(Pc)_2$, a very good linear correlation can be established between the frequency of the coupled pyrrole and aza stretching modes of $M^{III}[Pc(OC_8H_{17})_8]_2$ at 1504–1527 cm^{-1} and the tervalent rare earth ionic radii, as shown in Fig. 6. In addition, the band positions of the Pc breathing modes at 561–568 and 683–686 cm^{-1}, the C=N stretch at 782–787 cm^{-1}, the coupled C=C pyrrole and benzene stretching at 1312–1322 cm^{-1} and the isoindole stretching at 1400–1415 cm^{-1} show dependence on the rare earth ionic size. They all shift to higher energy along with the rare earth contraction as for their unsubstituted analogues.

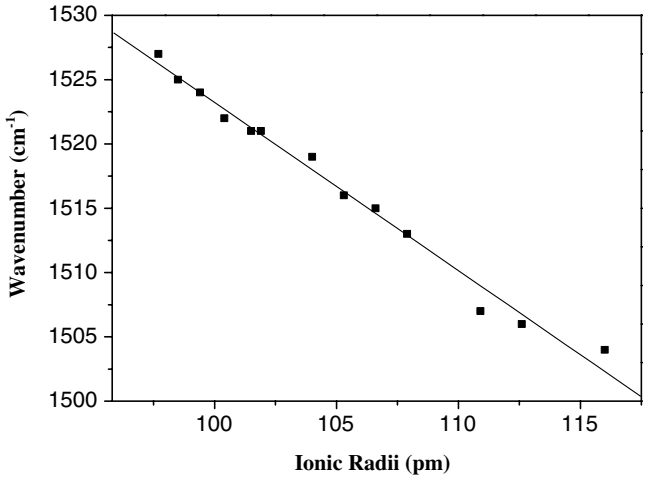

Fig. 6. Plot of wavenumber of the coupling of pyrrole and aza stretching scattering of $M[Pc(OC_8H_{17})_8]_2$ at 1504–1527 cm^{-1} with excitation at 633 nm as a function of the ionic radius of M^{III}.

The tervalent yttrium double-deckers are noteworthy. The frequencies of some above-mentioned bands for both $Y^{III}(Pc)_2$ and $Y^{III}[Pc(OC_8H_{17})_8]_2$ deviate from the linear relationship established for the other tervalent rare earth complexes (Tables 1 and 2), due probably to the intrinsic difference between yttrium and the lanthanides, namely the absence of f electrons. This is also true for these two yttrium complexes when using laser excitation emitting at 785 nm, Tables 3 and 4.

As can be expected from the previous studies [4a,4b,4d,4e,4f,8d], both $Ce(Pc)_2$ and $Ce[Pc(OC_8H_{17})_8]_2$ show different Raman spectroscopic characteristics from those of the rest of the rare earth series, which is related to the different electronic absorption spectra of these cerium complexes. As indicated by the ^1H NMR spectra, both phthalocyanine rings exist as dianions in $Ce(Pc)_2$ and $Ce[Pc(OC_8H_{17})_8]_2$, despite the XANES results that suggest a valence state intermediate between III and IV for the cerium [13]. These complexes therefore differ from other analogues that have the form $M(Pc'^{2-})Pc'^{\bullet-}$ [$Pc' = Pc, Pc(OC_8H_{17})_8$]. A comparison of the Raman spectra of $Ce(Pc)_2$ and $Ce[Pc(OC_8H_{17})_8]_2$ with those of the rest of the series shows that these cerium complexes contain most of the frequencies found for the other complexes, however the relative intensities are different. For example, a strong band appears at 1173 cm^{-1} for $Ce[Pc(OC_8H_{17})_8]_2$ (Table 2) corresponding to C–H bending, but for the other complexes, only a weak band in the same region is observed. Moreover, the marker Raman band of Pc^{2-} and $[Pc(OC_8H_{17})_8]^{2-}$ at

Table 3
Characteristic Raman bands (cm^{-1}) of phthalocyanines for $M(Pc)_2$ (M = Y, Pr–Yb except Pm) ($\lambda_{ex} = 785$ nm)

Pr	Nd	Sm	Eu	Gd	Tb	Dy	Y	Ho	Er	Tm	Yb	Assignment
572w	572w	572w	573w	573w	574w	573w	574w	575w	574w	575w	574w	Pc breathing
623w	622w	623w	622w	622w	623w	622w	623w	623w	623w	623w	623w	Pc breathing
675s	675s	676s	676s	677s	677s	678s	678s	678s	679s	678s	679s	Pc breathing
736s	737s	738s	738s	738s	738s	738s	739s	739s	739s	739s	739s	C–H wag
775w	775w	775w	776m	776m	776m	776m	777m	776m	777m	777m	777m	C=N aza stretching
810w	811w	812w	813w	813w	812w	813w	813w	814w	814w	814w	814w	Pc breathing
875w	875w	878w	877w	877w	878w	878w	879w	879w	880w	880w	880w	coupling of isoindole deformation and aza stretching
932w	932w	934w	934w	934w	935w	935w	937w	937w	937w	939w	939w	
1005w	1006w	1007w	1007w	1008w	1008w	1008w	1007w	1009w	1006w	1006w	1006w	C–H bend
1025w	1025w	1026w	1026w	1026w	1027w	1026w	1029w	1028w				C–H bend
1058w	1057w	1056m	1052m	1052m	1051m	1049m	1049s	1050s	1048s	1046s	1046s	C–H bend
1101m	1101m	1101w	1101m	1101m	1100m	1101m	1101m	1101m	1101m	1101m	1101m	C–H bend
1113w	1112w	1113w	1113w	1113w	1114w	1114w	1115w	1117w	1115w	1116w	1116w	C–H bend
1143m	1142m	1137m	1143m	1143m	1143m	1143m	1143m	1143m	1143m	1143m	1142m	pyrrole breathing
1157w	1157w	1155w	1157w	1158w	1158w	1158w	1157w	1157w	1158w	1157w	1157w	C–H bend
1172w	1172w	1172w	1172w	1173w	1172w	1172w	1174w	1174w	1175w	1175w	1175w	C–H bend
1215m	1214m	1213m	1215m	1214m	1214m	1215m	1215m	1215m	1214m	1214m	1214w	C–H bend
1299m	1299m	1298m	1299m	1299m	1299m	1300m	1300m	1299m	1300m	1300m	1300w	C–H bend
1327m	1327m	1328s	1328m	1328m	1328m	1328m	1329m	1329s	1329m	1329m	1329m	C=C pyrrole/benzene stretching
1342w	1342w	1336w	1342w	1343w	1342w	1343w	1343w	1343m	1343w	1342w	1342w	isoindole stretching
1407w	1407m	1417m	1412w	1412w	1416m	1417m	1418m	1420m	1420m	1421m	1422m	isoindole stretching
1447w	1446w	1444w	1448w	1449w	1446w	1446w	1447w	1447w	1447w	1448w	1448w	isoindole stretching
1501s	1503s											C=C pyrrole stretching
1508s	1509s	1507s	1513s	1514s	1515s	1517s	1516s	1520m	1519m	1520m	1521m	coupled pyrrole/aza stretchings

Table 4
Characteristic Raman bands (cm^{-1}) of phthalocyanines for $M[Pc(OC_8H_{17})]_2$ (M = Y, La–Lu except Pm) ($\lambda_{ex} = 785$ nm)

La	Ce	Pr	Nd	Sm	Eu	Gd	Tb	Dy	Y	Ho	Er	Tm	Yb	Lu	Assignment
558w	562w	559w	560w	560w	560w	561w	564w	562w	570w	562w	568w	568w	568w	570w	Pc breathing
626w	623w	627w	626w	627w	627w	626w	627w	630w	630w	630w	630w	627w	625w	627w	Pc breathing
682s	680w	682s	682s	682s	683s	682s	682m	687s	685m	687s	686m	686m	687m	687m	Pc breathing
707w		707w	707w	707w	707w	707w	708w	710m	709w	709w	716w	719w	716w	719w	Pc breathing
739s	740m	739m	740m	740m	741m	743s	743s	742m	746m	742m	746m	746m	748m	747m	C–H wag
751w	751w	752w	752w	751w	754w	753w	753w	757w	757w	758w	756m	757m	758m	758m	
769w	762w	769w	769w	769w	770w	769w	769w	772w	771w	773w	771w	771w	771w	771w	C=N aza stretching
780w	780w	780w	783w	783w	782w	782w	783w	786w	785w	785w	786w	786w	787w	788w	C=N aza stretching
864w	864w	865w	865w	865w	866w	866w	865w	869w	867w	869w	867w	867w	867w	863w	coupling of isoindole deformation and aza stretching
1068w	1071w	1069w	1067w	1069w	1064w	1064s	1063s	1075s	1062s	1074s	1061s	1060s	1060s	1060s	C–H bend
1132w	1132w	1131w	1132w	1133w	1132w	1130w	1129w	1135w	1135w	1136w	1134w	1135w	1137w	1136w	pyrrole stretching
1169m	1172s	1171s	1171s	1171m	1172m	1172m	1172w	1174s	1174w	1174s	1178w	1174w	1178w	1179w	C–H bend
1203m	1198w	1203m	1203m	1203m	1203m	1203m	1203m	1206m	1207w	1205m	1208w	1205w	1206w	1204w	C–H bend
1309w	1298w	1310w	1312w	1312w	1312w	1311m	1312m	1315w	1314w	1314w	1315m	1315n	1315m	1318s	C=C pyrrole and benzene stretching
1334w	1349w	1336w	1335w	1338w	1336w	1336w		1347w	1341w	1346w					isoindole stretching
1369w		1378w	1379w	1381w	1386w	1381w	1373w	1391m	1375w	1392m	1371w	1376w	1377w	1377w	isoindole stretching
1396m	1406s	1398m	1399m	1401m	1403m	1406m	1408m	1408m	1411w	1408m	1412w	1414w	1416w	1416w	isoindole stretching
1439w	1431m	1439w	1439w	1443w	1444w	1445w	1445w	1448w		1445w					isoindole stretching
	1459w														isoindole stretching
1502vs	1498vs	1505vs	1507vs	1510vs	1513vs	1514vs	1515s	1518s	1520m	1519s	1523w	1525w	1529w	1528w	coupling of pyrrole and aza stretching

1499 and 1501 cm^{-1} with contributions from pyrrole C=C, aza C=N and isoindole stretches is observed as the strongest scattering in the Raman spectra of $Ce(Pc)_2$ and $Ce[Pc(OC_8H_{17})_8]_2$. As noted above, a similar strong band due to $Pc^{\cdot-}$ and $[Pc(OC_8H_{17})_8]^{\cdot-}$ has been found to upshift to 1502–1509 and 1504–1527 cm^{-1} in the Raman spectra of $M^{III}(Pc)_2$ and $M^{III}[Pc(OC_8H_{17})_8]_2$.

3.2. Raman characteristics of $M(Pc)_2$ and $M[Pc(OC_8H_{17})_8]_2$ (M = Y, La–Lu except Pm) with excitation by laser line at 785 nm

Strong fluorescence occurred when trying to record the Raman spectra of $M(Pc)_2$ (M = La, Ce, Lu) using excitation at 785 nm, so these data do not appear in Table 3.

Using the excitation laser line at 785 nm that is far away from resonance with the *Q* absorption bands, as shown in Fig. 7 and summarized in Table 3, the macrocyclic ring deformation and ring radial vibrations between 500 and 1000 cm^{-1} in the Raman spectra of $M(Pc)_2$ are selectively intensified. This is in good accordance with the Raman characteristics of homoleptic $M(Pc)_2$ reported by Homborg [6b], especially with excitation at 1064 nm. The Pc breathing at 675–679 cm^{-1} and the aromatic C–H wagging at ca. 739 cm^{-1} are the most intense bands. The band locating at 1327–1329 cm^{-1} with medium intensity is assigned to the pyrrole C=C stretchings coupled with benzene C=C stretchings and the weak one at about 1342 cm^{-1} to the isoindole stretchings. Similar to those excited with 633 nm laser line, the frequencies of the coupled pyrrole C=C and aza C=N stretchings in the region of 1507–1521 cm^{-1} overlap to form a broad, unresolved envelope. The vibrations of $M(Pc)_2$ at 675–679 cm^{-1} assigned to the Pc breathings, at 1407–1422 cm^{-1} attributed to the isoindole stretchings, and at 1508–1521 cm^{-1} due to the coupling of aza and pyrrole stretchings are found to shift to higher energy along with the ionic radius contraction.

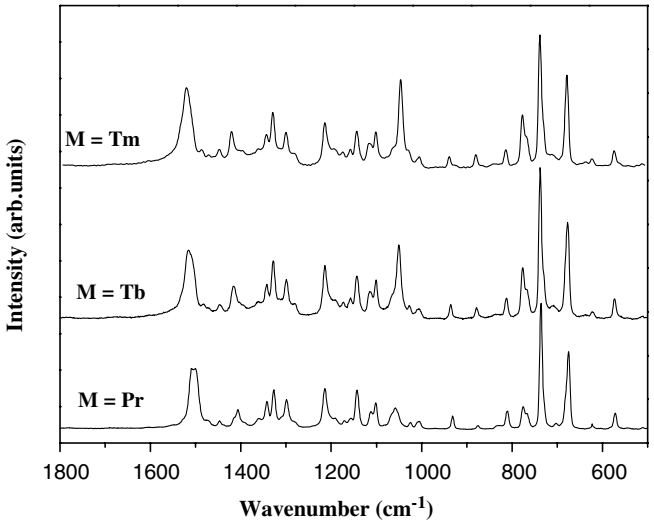

Fig. 7. Raman spectra of $M(Pc)_2$ (M = Pr, Tb, Tm) in the region of 500–1800 cm^{-1} with excitation at 785 nm.

Under the same laser line excitation of 785 nm, the Raman spectra for the octa(octyloxy)-substituted bis(phthalocyaninato) rare earth analogues $M[Pc(OC_8H_{17})_8]_2$ basically take the same spectroscopic features with corresponding unsubstituted counterparts $M(Pc)_2$. Their Raman spectroscopic frequencies with assignments are tabulated in Table 4.

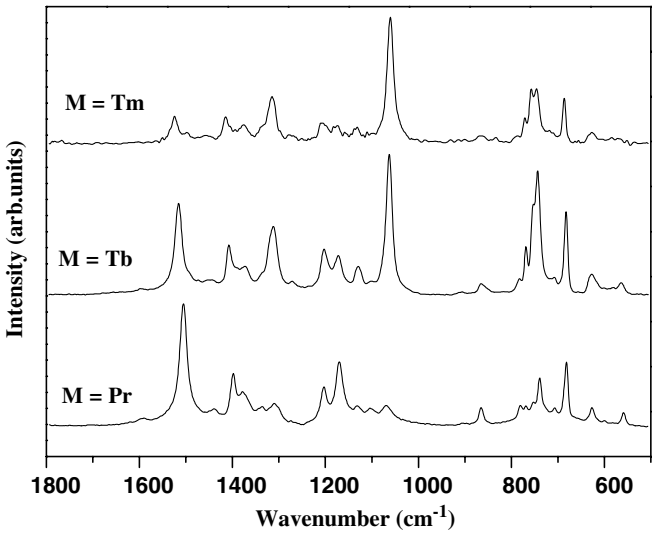

Fig. 8. Raman spectra of $M[Pc(OC_8H_{17})_8]_2$ (M = Pr, Tb, Tm) in the region of 500–1800 cm^{-1} with excitation at 785 nm.

However, this time a systematic but rather more dramatic change could be seen in the appearance of the Raman spectra across the series. Along with the decrease in the ionic size from La to Lu, the band at 1502–1528 cm^{-1} contributed from the coupling of the pyrrole and aza stretchings gradually loses some intensity, changing from a very strong scattering for the light rare earth compounds to a medium and weak one for the heavy rare earth complexes. In the same order, the band at ca. 1060 cm^{-1} assigned to the C–H bendings in contrast gradually gains some intensity to change from a weak band to an intense band. It is worth noting that similar change in the intensity of the latter band at ca. 1050 cm^{-1} due to the C–H bendings was also observed in the Raman spectra of $M^{III}(Pc)_2$ under the same laser line excitation. However, the change in the intensity of the former band for $M^{III}(Pc)_2$ was not so significant. All these results can be clearly exemplified by the Raman spectra of the Pr, Tb, and Tm complexes of the two series shown in Figs. 7 and 8.

When exciting the Raman spectrum of $Ce[Pc(OC_8H_{17})_8]_2$ with 785 nm laser line, similar to the case by means of 633 nm laser line, a Raman spectrum with different characteristics from those of the rest of the rare earth series was obtained. The intense band at 1498 cm^{-1} with contribution from both pyrrole C=C and aza C=N stretches together with isoindole stretchings is the marker Raman band of $[Pc(OC_8H_{17})_8]^{2-}$, which compares with that of $[Pc(OC_8H_{17})_8]^{\bullet-}$ at 1502–1528 cm^{-1} in the Raman spectra of $M^{III}[Pc(OC_8H_{17})_8]_2$ under the same excitation.

4. Conclusions

The Raman spectra for two series of homoleptic bis(phthalocyaninato) rare earth complexes $M(Pc)_2$ and $M[Pc(OC_8H_{17})_8]_2$ have been recorded under excitation with 633 and 785 nm laser lines. The present results are in line with those reported for related series of complexes, namely $M(Pc)[Pc(\alpha\text{-}OC_5H_{11})_4]$ and M(TClPP)(Pc), recorded under similar laser line excitations, in terms of the Raman spectroscopic characteristics of phthalocyanine ligand and the relationship between the phthalcyanine Raman characteristics and the rare earth ionic size. They also provide a good and, more importantly a systematic, experimental basis for further investigation by theoretical chemists in this field.

Acknowledgements

The authors thank the National Natural Science Foundation of China (Grant Nos. 20325105, 20431010), National Ministry of Science and Technology of China (Grant No. 2001CB6105-07), National Educational Ministry of China, Shandong University and the Science Research Centre, Queensland University of Technology for financial support.

References

[1] (a) J. Jiang, K. Kasuga, D.P. Arnold, in: H.S. Nalwa (Ed.), Supramolecular Photo-sensitive and Electro-active Materials, Academic Press, New York, 2001, p. 113;
(b) D.K.P. Ng, J. Jiang, Chem. Soc. Rev. 26 (1997) 433;
(c) J. Jiang, W. Liu, D.P. Arnold, J. Porphyrins Phthalocyanines 7 (2003) 459.

[2] J.W. Buchler, D.K.P. Ng, in: K.M. Kadish, K.M. Smith, R. Guilard (Eds.), The Porphyrin Handbook, Academic Press, New York, 1999, p. 245 (Chapter 20).

[3] (a) J. Jiang, D.P. Arnold, H. Yu, Polyhedron 18 (1999) 2129;
(b) X. Sun, M. Bao, N. Pan, X. Cui, D.P. Arnold, J. Jiang, Aust. J. Chem. 55 (2002) 587;
(c) F. Lu, M. Bao, C. Ma, X. Zhang, D.P. Arnold, J. Jiang, Spectrochim. Acta Part A 59 (2003) 3273;
(d) M. Bao, N. Pan, C. Ma, D.P. Arnold, J. Jiang, Vib. Spectrosc. 32 (2003) 175;
(e) W. Su, M. Bao, J. Jiang, Vib. Spectrosc. 39 (2005) 186.

[4] (a) J. Jiang, L. Rintoul, D.P. Arnold, Polyhedron 19 (2000) 1381;
(b) J. Jiang, U. Cornelisson, D.P. Arnold, X. Sun, H. Homborg, Polyhedron 20 (2001) 557;
(c) N. Pan, L. Rintoul, D.P. Arnold, J. Jiang, Polyhedron 21 (2002) 1905;
(d) Y. Bian, L. Rintoul, D.P. Arnold, N. Pan, J. Jiang, Vib. Spectrosc. 31 (2003) 173;
(e) X. Sun, L. Rintoul, Y. Bian, D.P. Arnold, R. Wang, J. Jiang, J. Raman Spectrosc. 34 (2003) 306;
(f) M. Bao, Y. Bian, L. Rintoul, R. Wang, D.P. Arnold, C. Ma, J. Jiang, Vib. Spectrosc. 34 (2004) 283;
(g) F. Lu, L. Rintoul, X. Sun, D.P. Arnold, X. Zhang, J. Jiang, J. Raman Spectrosc. 35 (2004) 860.

[5] (a) R. Aroca, R.E. Clavijo, C.A. Jennings, G.A. Kovacs, J.M. Duff, R.O. Loutfy, Spectrochim. Acta 45A (1989) 957;
(b) R.E. Clavijo, D. Battisti, R. Aroca, G.J. Kovacs, C.A. Jennings, Langmuir 8 (1992) 113;
(c) M.L.R. Mendez, Y. Khoussed, J. Souto, J. Sarabia, R. Aroca, J.A. de Saja, Sensors Actuators B 18–19 (1994) 89.

[6] (a) G. Ostendorp, H. Homborg, Z. Anorg. Allg. Chem. 622 (1996) 873;
(b) G. Ostendorp, H. Homborg, Z. Anorg. Allg. Chem. 622 (1996) 1222;
(c) G. Ostendorp, H. Homborg, Z. Anorg. Allg. Chem. 622 (1996) 1358;

(d) M.S. Haghighi, A. Franken, H. Homborg, Z. Naturforsch 49b (1994) 812;
(e) M.S. Haghighi, H. Homborg, Z. Anorg. Allg. Chem. 620 (1994) 1278;
(f) M.S. Haghighi, G. Peters, H. Homborg, Z. Anorg. Allg. Chem. 620 (1994) 1285.
[7] T.H. Tran-Thi, T.A. Mattioli, D. Chabach, A. De Cian, R. Weiss, J. Phys. Chem. 98 (1994) 8279.
[8] (a) J. Jiang, R.C.W. Liu, T.C.W. Mak, D.K.P. Ng, T.W.D. Chan, Polyhedron 16 (1997) 515;
(b) J. Jiang, J. Xie, M.T.M. Choi, D.K.P. Ng, J. Porphyrins Phthalocyanines 3 (1999) 322;
(c) J. Jiang, J. Xie, D.K.P. Ng, Y. Yan, Mol. Cryst. Liq. Cryst. 337 (1999) 385;
(d) W. Liu, J. Jiang, D. Du, D.P. Arnold, Aust. J. Chem. 53 (2000) 131.
[9] (a) A.G. Gurek, V. Ahsen, D. Luneau, J. Pecaut, Inorg. Chem. 40 (2001) 4793;
(b) L.A. Lapkina, Y. Gorbunova, S.E. Nefedov, A.V. Tsivadze, Russ. Chem. Bull. 52 (2003) 1.
[10] M. Bao, G. Song, F. Lu, M. Bai, J. Jiang, Chin. J. Inorg. Chem. (in Chinese) 20 (2004) 1203.
[11] H.F. Shurvell, L. Pinzuti, Can. J. Chem. 44 (1966) 125.
[12] (a) X. Zhang, Y. Zhang, J. Jiang, Vib. Spectrosc. 33 (2003) 153;
(b) X. Zhang, Y. Zhang, J. Jiang, Spectrochim. Acta Part A 60 (2004) 2195;
(c) X. Zhang, Y. Zhang, J. Jiang, J. Mol. Struct (Theochem) 673 (2004) 103.
[13] Y. Bian, J. Jiang, Y. Tao, M.T.M. Choi, R. Li, A.C.H. Ng, P. Zhu, N. Pan, X. Sun, D.P. Arnold, Z. Zhou, H.-W. Li, T.C.W. Mak, D.K.P. Ng, J. Am. Chem. Soc. 125 (2003) 12257.

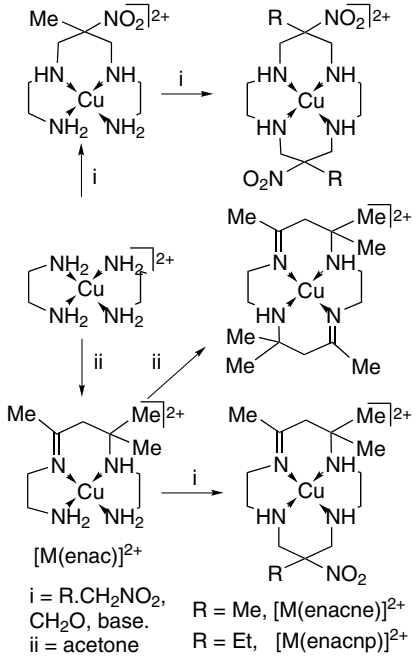

Scheme 1. Reactions of $[Cu(en)_2]^{2+}$ and $[Cu(enac)]^{2+}$ with methanal plus nitroethane [4] or nitropropane (i) or with acetone (ii) [21–25].

Terminal primary amine functions of bis(diamine) and linear tetraamine complexes of copper(II) and nickel(II) can also be linked by reaction with acetone (or related carbonyl compounds) [21]. Reactions of bis(ethane-1,2-diamine) compounds with acetone initially form compounds of the 2,3,2-tetradentate imine-triamine ligand 4,6,6-trimethyl-3,7-diazanon-3-ene-1,9-diamine, enac [22–25]. Structures of $[Cu(enac)][ZnCl_4]$ [26] and $[Ni(enac)(NO_2)]ClO_4$ have been reported [25]. Further reactions with acetone lead to hexamethyl substituted diamine diimine azamacrocycle compounds.

This communication reports reactions of $[Cu(enac)]^{2+}$ with methanal and nitroethane (or nitropropane) to form the 13-methyl-13-nitro- and 13-ethyl-13-nitro-substituted 1,8,11-tri-(secondary amine)-4-imine macrocycle cations 5,7,7,13-tetramethyl-13-nitro-1,4,8,11-tetraazacyclotetradec-4-ene, $[Cu(enacne)]^{2+}$ (or the 13-ethyl-5,7,7-trimethyl-13-nitro-homologue, $[Cu(enacnp)]^{2+}$). The structure of $[Cu(enacnp)(H_2O)](ClO_4)_2$ is reported. Structures of copper(II) compounds with 13 [5], 14 [3], 15 and 16 [5,7] membered nitro-substituted azamacrocycles formed by reaction of copper(II) compounds of linear tetraamines, methanal and nitroethane have been described. The structure of a tetracyanonickelate(II) compound of $[Cu(enacnp)]^{2+}$ has been reported [27].

An improved preparation of the $[Cu(enac)](ClO_4)_2$ starting material is reported.

2. Results

$[Cu(enac)](ClO_4)_2$ reacts with methanal plus nitroethane or nitropropane in water, or methanol, with base to form nitro-substituted imine-triamine macrocyclic products (see Scheme 1). These have properties similar to those of previously reported imine-amine azamacrocycle compounds, in particular their resistance to acid demetallation.

The macrocyclic cations form orange perchlorate salts, which also occur as blue-mauve ammine adducts and hydrates; the structural study of $[Cu(enacnp)(H_2O)](ClO_4)_2$ (below) shows an axial interaction with the water molecule. Blue-mauve colours of the tetrachlorozincate salts and of compounds $[Cu(L)(X)]ClO_4 \cdot xH_2O$ $(X^- = NCS^-, NO_2^-)$ are also indicative of axial interactions.

2.1. Structural study

The structure of $[Cu(enacnp)(H_2O)](ClO_4)_2$ was determined by X-ray diffractometry, see Section 5 for details. The cation, (Cu1), is shown in Fig. 1. The C4–N5 distance (see Table 1) and the angles about these atoms confirm the presence of the imine function. The copper(II) ion is in square-planar coordination by the imine, N4, and three secondary amine, N1, N8 and N11, nitrogen atoms of the enacnp azamacrocycle, with water oxygen O3 weakly, and perchlorate oxygen atom O11 very weakly, interacting in the axial sites.

The structure of a compound of formal composition $[Cu(enacnp)] \cdot [Ni(CN)_4] \cdot 2.5H_2O$ has been reported [26]. This has as asymmetric unit two centrosymmetric trinuclear cations $[(enacnp)Cu–\mu(NC)–Ni(CN)_2–\mu(CN)–Cu(enacnp)]^{2+}$, (Cu2), and $[(H_2O)(enacnp)Cu–\mu(NC)\text{-}Ni(CN)_2–\mu(CN)–Cu(enacnp)(OH_2)]^{2+}$, (Cu3), plus independent $[Ni(CN)_4]^{2-}$ anions and water molecules. All three $[Cu(enacnp)]^{2+}$ cations (Cu1), (Cu2) and (Cu3), have the copper(II) ion in flattened square pyramidal coordination by the imine and three secondary amine nitrogen atoms of the macrocycle, with weak axial coordination: by water and perchlorate oxygen atoms for cation (Cu1), by an isocyano bridging nitrogen atom and perchlorate oxygen atom for cation (Cu2) and by water oxygen and the isocyano bridging nitrogen atom for cation (Cu3). The principal dimensions of these three cations are shown in Table 1. The Cu–N distances for the cations are in good agreement, with the $Cu–N_{imine}$ distance ca. 0.03 Å shorter than the mean of

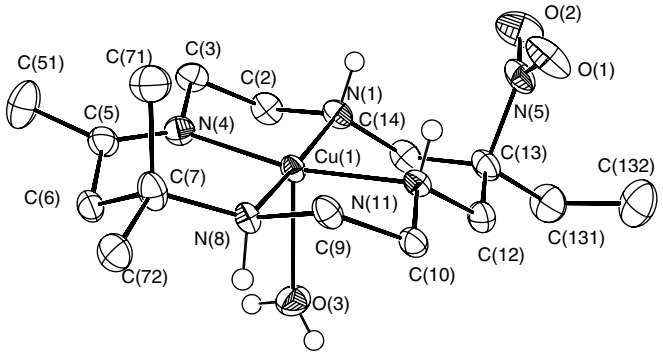

Fig. 1. The cation $[Cu(enacnp)(H_2O)]^{2+}$, drawn [28] with displacement ellipsoids at the 50% confidence level. Hydrogen atoms are shown as circles of arbitrary radius.

Table 1
Geometric parameters (Å, °) for $[Cu(enacnp)(H_2O)](ClO_4)_2$ {cation (Cu1)} and $[\{Cu(enacnp)\}_2Ni(CN)_4]$[j] $[\{Cu(enacnp)(H_2O)\}_2Ni(CN)_4]$[k] · $2[Ni(CN_4)] \cdot 8H_2O$

Dimension	Cation (Cu1)	Cation (Cu2)	Cation (Cu3)
Cu–N1	2.023(2)	2.041(3)	2.020(3)
Cu–N4	1.981(2)	1.999(4)	1.986(4)
Cu–N8	2.018(2)	2.031(3)	2.018(4)
Cu–N11	2.015(2)	2.013(3)	2.026(4)
Cu–D[a]	2.279(2)[b]	2.226(3)[c]	2.396(3)[d]
Cu–D[e]	2.905(2)[f]	3.221(3)[g]	2.677(4)[g]
N4=C5	1.295(3)	1.304(6)	1.304(6)
N1–Cu–N4	85.4(1)	85.4(2)	86.0(2)
N4–Cu–N8	95.9(1)	95.6(2)	95.9(2)
N8–Cu–N11	86.4(1)	85.9(1)	86.9(2)
N11–Cu–N1	91.3(1)	89.7(1)	91.0(2)
N1–Cu–N8	174.2(1)	166.8(2)	177.7(2)
N4–Cu–N11	168.8(1)	164.6(2)	170.7(2)
N_4 plane[h]	±0.045(2)	±0.017(2)	±0.067(2)
Cu–(N_4 plane)[i]	0.143(1)	0.246(2)	0.088(2)

[a] Distance Cu to closer donor atom in axial position.
[b] Distance to O3 of water.
[c] Distance to N of bridging cyanide.
[d] Distance to O of water.
[e] Distance Cu to further atom in axial position.
[f] Distance to O of perchlorate.
[g] Distance to O of water.
[h] Mean displacement from least squares plane of the imine and three amine N atoms.
[i] Displacement of Cu from the N_4 plane in 'mean displacement from least squares plane of the imine and three amine N atoms' towards the closer axial donor atom.
[j] {Cation (Cu2)}.
[k] {Cation (Cu3)} [26].

the Cu–N_{amine} distances. The distances and angles within the CuN_4 coordination group are consistent for the three differing axial environments, the most significant variation being in the extent of tetrahedral twisting of this group. Cations Cu(1) and Cu(2) have one closer and one very distant axial interaction, with similar closer axial donor distances {Cu–O for (Cu1) and Cu–N_{axial} for (Cu2)}. Cation (Cu3) has a more symmetrical axial environment with Cu–O and Cu–N_{axial} distances, intermediate to those of (Cu1) and (Cu2). The three cations have the same 1*RS*,8*RS*,11*SR* configuration and similar conformations of the azamacrocycles, with one methyl of the gem-dimethyl group axially oriented on the same side of the CuN_4 "plane" as the nitro-group (Table 2). The closer axial ligands for the three cations are coordinated on the other, less crowded side, of the plane.

Table 2
Displacements of atoms from CuN_2 planes for chelate rings for $[Cu(enacnp)(H_2O)](ClO_4)_2$

Atoms defining plane	Displacement (Å)
Cu,N1,N4	C2 0.480(4); C3 −0.200(4)
Cu,N8,N11	C9 −0.398(4); C10 0.332(3)
Cu,N4,N8	C5 0.082(4); C6 0.480(4); C7 −0.354(4); C51 −0.040(6); C71 −1.87(4); C72 −0.060(5)
Cu,N8,N11	C12 0.937(4); C13 0.804(4); C14 0.974(4); C131 1.834(5); C132 1.662(7); N5 −0.569(4)

Table 3
Hydrogen bonding parameters for $[Cu(enacnp)(H_2O)](ClO_4)_2$ (Å, °)

Atoms	D–H	H···A	D···A	D–H···A
N11–H11···O1	0.91	2.32	2.910(3)	123
N11–H11···O1[i]	0.91	2.33	3.068(3)	138
N1–H1···O11	0.91	2.11	3.014(3)	170
N8–H8···O22	0.91	2.44	3.201(3)	141
N11–H11···O14	0.91	2.47	3.072(3)	124
O3–H3A···O11[ii]	0.82	1.97	2.783(3)	169
O3–H3B···O21[iii]	0.81	2.04	2.810(3)	158

Symmetry operations: i: $-x+2, -y, -z+1$; ii: $x, -y+1/2, z-1/2$; iii: $-x+2, -y, -z$.

For all three cations the six-membered chelate ring including Cu,N1,N11 has a chair conformation with the NO_2 substituent axially oriented (see Table 2). The six-membered amine-imine chelate ring including Cu,N5,N8 has a half-chair conformation with one component of the gem-dimethyl group axially oriented, on the same side of the CuN_4 plane as the nitro group. The five-membered chelate rings have gauche conformations.

For $[Cu(enacnp)(H_2O)](ClO_4)_2$ the nitro-group oxygen O1 is linked to N11–H11 by an intramolecular hydrogen bond and to N11–H11 ($-x+2, -y, -z+1$) by an intermolecular hydrogen bond. All NH and water OH groups hydrogen bond to perchlorate oxygen atoms to form an H-bonding network (see Table 3).

The structure of a compound obtained from the reaction of (3,7-diazanonan-1,9-diamine)copper(II) perchlorate with methanal and nitroethane has been reported [3]. This has a chain polymeric structure, with alternating square-planar (6-methyl-6-nitro-1,4,8,11-tetraazacyclotetradecane)copper(II) and (3,7-diazanonane-1,9-diamine) copper(II) cations, linked by perchlorate ions. The Cu–N distances for the azamacrocycle cation are 2.013(6) and 2.017(5) Å (nitro-substituted chelate ring) and 1.995(6) and 1.999(6) Å (unsubstituted chelate ring), with axial Cu–O distances 2.539(7) and 2.577(6) Å.

3. Conclusions

The facile reaction of $[Cu(enac)]^{2+}$ with nitroalkyls plus methanal to form the nitro-substituted imine-triamine macrocycles completes a set of azamacrocycle compounds formed by cyclization of the bis(ethane-1,2-diamine)copper(II) cations by condensations with acetone or with methanal/nitroalkyls, as represented in the reaction scheme.

4. Experimental

4.1. Preparations of compounds

The perchlorate compounds described are potentially explosive and should be treated with caution, particularly the ethanediamine starting material. However, the enac, enacne and enacnp compounds have shown no indication of shock sensitivity and decompose non-violently if strongly heated.

4.1.1. (4,6,6-Trimethyl-3,7-diazanon-3-ene-1,9-diamine)-copper(II) perchlorate, [Cu(enac)](ClO$_4$)$_2$

Improvements have been made to the reported [21–23] preparations of [Cu(enac)](ClO$_4$)$_2$. [Cu(en)$_2$](ClO$_4$)$_2$ (20 g), 2-aminoethanol (0.5 g), methanol (50 cm^3) and acetone (50 cm^3) were heated near boiling for ca. 24 h. The solution was filtered through activated charcoal and rotary evaporated. The resulting purple gum was dissolved in water (50 cm^3), filtered through charcoal and again evaporated, to leave a purple gum. Methanol (30 cm^3) was added when the purple product slowly crystallized (nucleation with the preformed compound speeds this process). The product was filtered off and washed with ethanol, yield ca. 90%. The product so prepared was satisfactory for the preparations below but could be recrystallised from hot methanol. The use of 2-aminoethanol in the preparation of [Cu(enac)]Cl$_2$ has been reported [29].

4.2. Macrocyclic compounds

The macrocyclic cations are resistant to acid demetallation (but are rapidly oxidized by nitric acid). They are slowly degraded in alkaline solution. The infrared spectra all show ν(NH) band(s) near 3200 cm^{-1}, and sharp peaks assigned to ν(N=C) near 1665 cm^{-1} and ν(NO$_2$) (more intense) near 1550 cm^{-1}.

4.2.1. (5,7,7,13-Tetramethyl-13-nitro-1,4,8,11-tetraazacyclotetradec-4-ene)copper(II) perchlorate, [Cu(enacne)](ClO$_4$)$_2$

[Cu(enac)](ClO$_4$)$_2$ (9.26 g), nitroethane (1.6 g), methanal (formaldehyde, 3.5 cm^3 of 37% aqueous solution 1: 1.5: 3 mol ratios) and sodium hydrogen carbonate (0.5 g) were heated in water (100 cm^3) at ca. 80 °C. for 2 h. The solution was filtered while hot through activated charcoal and perchloric acid (1 g of 60% aqueous solution, sufficient to neutralise the NaHCO$_3$) was added. The product was filtered from the cold solution and washed with ethanol. The filtrate was rotary evaporated to leave a purple gum that was triturated with hot ethanol (25 cm^3) when more product crystallised. The magenta coloured *product* was recrystallised from hot acetonitrile (in which it is very soluble)/propan-2-ol or acetone: water (10:1)/propan-2-ol. Yield: 85%. *Anal.* Calc. for C$_{14}$H$_{29}$Cl$_2$CuN$_5$O$_{10}$: C, 29.9; H, 5.3; N, 12.3. Found: C, 30.0; H, 5.3; N, 12.3%. Visible spectrum in water {λ_{max}/nm (ε/dm^3 mol^{-1} cm^{-1})}: 514 (129). IR spectrum (ν_{max}/cm^{-1}): ν(NH) 3236; ν(C=N) 1663; ν(NO$_2$) 1553. A purple ammine adduct which crystallised from concd. aqueous ammonia retained the ammonia at 110 °C.

4.2.2. (13-Ethyl-5,7,7-trimethyl-13-nitro-1,4,8,11-tetraazacyclotetradec-4-ene)copper(II) perchlorate (and hydrate), [Cu(enacnp)](ClO$_4$)$_2$ and [Cu(enacnp)(H$_2$O)](ClO$_4$)$_2$

This compound was prepared as for the previous compound by using 1.9 g of nitropropane in place of the nitroethane. It crystallized in similar yield, as a mono-hydrate from solvent mixtures containing water or as the unhydrated salt from dry solvents. *Anal.* Calc. for C$_{15}$H$_{33}$Cl$_2$CuN$_5$O$_{11}$: C, 30.4; H, 5.8; N, 11.3. Found for hydrate: C, 30.4; H, 5.7; N, 11.3%. Visible spectrum in water {λ_{max}/nm (ε/dm^3 mol^{-1} cm^{-1})}, 447 (129). IR spectrum (ν_{max}/cm^{-1}): ν(NH) 3236; ν(C=N) 1663; ν(NO$_2$) 1553.

4.2.3. (5,7,7,13-Tetramethyl-13-nitro-1,4,8,11-tetraazacyclotetradec-4-ene)copper(II) tetrachlorozincate, [Cu(enacne)][ZnCl$_4$]

Zinc chloride was added to a hot solution of [Cu(enacne)](ClO$_4$)$_2$ in acetonitrile, followed by propan-2-ol. The mauve product was filtered off, washed with ethanol and recrystallised from hot methanol. *Anal.* Calc. for C$_{14}$H$_{29}$Cl$_4$CuN$_5$Zn: C, 29.5; H, 5.1; N, 12.3. Found: C, 29.6; H, 5.0; N, 12.1%.

4.2.4. (5,7,7,13-Tetramethyl-13-nitro-1,4,8,11-tetraazacyclotetradec-4-ene)thiocyanatocopper(II) Perchlorate Hydrate, [Cu(enacne)(NCS)]ClO$_4$ · H$_2$O

Sodium thiocyanate was added to a hot aqueous solution of [Cu(enacne)](ClO$_4$)$_2$. The blue product was filtered from the cold solution and recrystallised from hot methanol. *Anal.* Calc. for C$_{15}$H$_{31}$ClCuN$_6$O$_5$S: C, 35.6; H, 6.2; N, 16.6. Found: C, 35.2; H, 6.0; N, 16.8%. IR spectrum (ν_{max}/cm^{-1}): ν(OH) 3470; ν(NH) 3262, 3232; ν(C≡N) 2060vs; ν(C=N) 1662; δ (HOH) 1644; ν(NO$_2$) 1539.

4.2.5. Nitrito(5,7,7,13-tetramethyl-13-nitro-1,4,8,11-tetraazacyclotetradec-4-ene)copper(II) perchlorate, [Cu(enacne)(ONO)]ClO$_4$

This mauve coloured compound was prepared as for the thiocyanate, by using sodium nitrite. *Anal.* Calc. for C$_{15}$H$_{29}$ClCuN$_6$O$_6$: C, 33.1; H, 5.7; N, 16.5. Found: C, 33.2; H, 5.7; N, 16.6%. IR spectrum (ν_{max}/cm^{-1}): ν(NH) 3205, 3114; ν(C=N) 1669; ν(NO$_2$) 1540; ν_{as}(NO$_2^-$) 1272.

5. Crystallography

Diffraction data were collected for a dark purple plate (0.32 × 0.23 × 0.12 mm) of aqua-(13-ethyl-5,7,7-trimethyl-13-nitro-1,4,8,11-tetraazacyclotetradec-4-ene)copper(II) perchlorate, grown from water, [Cu(enacnp)(H$_2$O)](ClO$_4$)$_2$, C$_{15}$H$_{33}$Cl$_2$CuN$_5$O$_{11}$, M_r = 593.91. The crystal was monoclinic, space group $P2_1/c$, a = 11.247(3) Å, b = 15.321(5) Å, c = 14.323(6) Å, β = 97.22(2)°. Data were collected at 120(2) K, by using a SMART 1K CCD diffractometer [30] with fine focus sealed tube Mo Kα radiation (λ = 0.71073 Å) using ω scans. Multi-scan absorption corrections [31] were applied T_{min} = 0.617, T_{max} = 0.773. About 26 288 reflections (average R_{equiv} = 0.0467) were collected, $-14 < h < 14$; $-19 < k < 19$; $-18 < l < 18$; $1.83 < \theta < 27.48°$; with 5615 unique reflections, 4947 reflections with $I > 2\sigma(I)$. The structure was solved and refined on F^2 using SHELXTL [32], with H(C) and H(N) atoms in calculated positions and riding. H(O) atoms were located and their positions refined with restrained O–H distances. R_1 ($2\sigma(I)$) = 0.037, R_1 (all) = 0.043, R_w ($2\sigma(I)$) = 0.090, R_w (all) = 0.095

$(w = 1/[\sigma^2(F_o^2) + (0.0417P)^2 + (3.54P)]$ where $P = (F_o^2 + 2F_c^2)/3)$.

Appendix A. Supplementary data

Crystallographic data have been deposited with the Cambridge Crystallographic Data Centre for this structure; CCDC 277465. Copies may be obtained free of charge from the Director, CDCC, 12 Union Road, Cambridge CBZ 1EZ, UK (fax: +44 1223 336 033; e-mail: deposit@ccdc.cam.ac.uk or www: http://www.ccdc.cam.uk). Supplementary data associated with this article can be found, in the online version, at doi:10.1016/j.poly.2005.08.037.

References

[1] P.V. Bernhardt, G.A. Lawrance, Coord. Chem. Rev. 104 (1990) 297.
[2] G.A. Lawrance, M. Maeder, E.N. Wilkes, Rev. Inorg. Chem. 13 (1993) 199.
[3] P. Comba, N.F. Curtis, G.A. Lawrance, M.A. O'Leary, B.W. Skelton, A.H. White, J. Chem. Soc., Dalton Trans. (1988) 497.
[4] G.A. Lawrance, M. Rossignoli, B.W. Skelton, A.H. White, Aust. J. Chem. 40 (1987) 1441.
[5] P. Comba, N.F. Curtis, G.A. Lawrance, A.M. Sargeson, B.W. Skelton, A.H. White, Inorg. Chem. 25 (1986) 4260.
[6] P. Comba, N.F. Curtis, G.A. Lawrance, M.A. O'Leary, B.W. Skelton, A.H. White, J. Chem. Soc., Dalton Trans. (1988) 2145.
[7] G.A. Lawrance, M.A. O'Leary, Polyhedron 6 (1987) 1291.
[8] N.F. Curtis, G.J. Gainsford, A. Siriwardena, D.C. Weatherburn, Aust. J. Chem. 46 (1993) 755.
[9] P.V. Bernhardt, G.A. Lawrance, S. Luther, M. Maeder, M. Rossignoli, Inorg. Chim. Acta 306 (2000) 1.
[10] M. Rossignoli, C.C. Allen, T.W. Hambley, G.A. Lawrance, M. Maeder, Inorg. Chem. 35 (1996) 4961.
[11] G.A. Lawrance, M. Maeder, M. Napitupulu, A.L. Nolan, M. Rossignoli, V. Tiwow, P. Turner, Inorg. Chim. Acta 358 (2005) 3227.
[12] H. Xiao, G.A. Lawrance, T.W. Hambley, Aust. J. Chem. 51 (1998) 871.
[13] M. Rossignoli, P.V. Bernhardt, G.A. Lawrance, M. Maeder, J. Chem. Soc., Dalton Trans. (1997) 323.
[14] M. Rossignoli, G.A. Lawrance, M. Maeder, D.C.R. Hockless, B.W. Skelton, A.H. White, Aust. J. Chem. 49 (1996) 1307.
[15] M. Rossignoli, P.V. Bernhardt, G.A. Lawrance, M. Maeder, Aust. J. Chem. 50 (1997) 529.
[16] P.V. Bernhardt, P. Comba, B.L. Elliott, G.A. Lawrance, M. Maeder, M.A. O'Leary, G. Wei, E.N. Wilkes, Aust. J. Chem. 47 (1994) 1171.
[17] P.V. Bernhardt, K.A. Byriel, C.H.L. Kennard, P.C. Sharpe, J. Chem. Soc., Dalton Trans. (1996) 145.
[18] G.A. Lawrance, M. Maeder, M.A. O'Leary, F.H. Woon, Polyhedron 9 (1990) 2227.
[19] P.V. Bernhardt, P.C. Sharpe, Inorg. Chem. 37 (1998) 1629.
[20] L. Fabbrizzi, M. Licchelli, A.M.M. Lanfredi, O. Vassalli, F. Ugozzoli, Inorg. Chem. 35 (1996) 1582.
[21] N.F. Curtis, Coord. Chem. Rev. 3 (1968) 3.
[22] N.F. Curtis, J. Chem. Soc. (1960) 4409.
[23] M.M. Blight, N.F. Curtis, J. Chem. Soc. (1962) 3016.
[24] N.F. Curtis, J. Chem. Soc., Dalton Trans. (1972) 1357.
[25] N.F. Curtis, I.R.N. McCormick, T.N. Waters, J. Chem. Soc., Dalton Trans. (1973) 1537.
[26] N.F. Curtis, O.P. Gladkikh, Aust. J. Chem. 53 (2000) 597.
[27] N.F. Curtis, H. Puschmann, Acta Crystallogr., Sect. C. 60 (2004) m410.
[28] L.J. Farrugia, ORTEP-32, J. Appl. Crystallogr. 30 (1997) 565.
[29] M.V. Artemenko, E.S. Sereda, P.A. Suprunenko, G.I. Kal'naya, Zh. Neorg. Khim. 19 (1974) 60.
[30] Bruker SMART, (Version 5.054), SADABS (Version 2.03) and SAINT (Version 6.02A), Bruker AXS Inc., Madison, WI, USA, 1997.
[31] R.H. Blessing, Acta Crystallogr., Sect. A 51 (1995) 33.
[32] G.M. Sheldrick, SHELXTL (Version 5.10). Programs for the Solution and Refinement of Crystal Structures, 1997.

use the diamagnetic gold complex, bis(cyanoimidodithiocarbonate)aurate(III), abbreviated as $Au(cdc)_2$, which was previously used in the preparation of a molecular conductor, by combination with perylene [7].

2. Experimental

2.1. Synthesis and electrocrystallisation

Single crystals of (bedt-ttf)[$Au(cdc)_2$] were obtained by electrocrystallisation from solutions of n−Bu_4N[$Au(cdc)_2$] and bedt-ttf ($\approx 10^{-3}$ M) in different solvents: dichloromethane (A), 95% trichloroethane-5% ethanol v/v (B), trichloroethane (C) and 75% trichloroethane-25% THF (D). The gold complex of cyanoimidodithiocarbonate (also known as cyanodithiocarbimate) was prepared according to the procedure of Cotton and McCleverty [8], and recrystallised from acetone. bedt-ttf was synthesised according to the method of Larsen and Lenoir [9]. Solvents were dried and distilled following standard procedures. The electrocrystallisation was carried out in a two-compartment cell with platinum electrodes under galvanostatic conditions using a current density 15 μA cm^{-2} at 30 °C for A and with different current densities at 50 °C for the three other preparations. After ≈7 days, the dark metallic-looking plate-shaped crystals obtained on the anode were filtered off and washed with dichloromethane (trichloroethane for B, C and D). The elemental analyses of the crystalline solids obtained in all batches are within experimental error the same. In a typical elemental analysis performed in a Perkin–Elmer 240 elemental analyser at the analytical service of Instituto Tecnológico e Nuclear was found: C, 21.02; N, 6.62; H, 0.99; Au, 24.2% ($C_{14}H_8AuN_4S_{12}$ requires C, 20.66; N, 6.88; H, 0.99; Au, 24.2%).

2.2. Spectroscopy

Infrared spectra were obtained with a Nicolet SDXC spectrophotometer with FT in the range 4000–200 cm^{-1}. Most intense bands were 2192 (cdc), 1488 (bedt-ttf), 1404 (bedt-ttf), 1024 (cdc), 960 (cdc), 880 (bedt-ttf) cm^{-1}.

2.3. X-ray crystallography

A black crystal from batch A with approximate dimensions $0.25 \times 0.06 \times 0.031$ mm^3 was mounted in a glass capillary on a goniometer head. X-ray data were collected at room temperature on an Enraf-Nonius CAD-4 automatic diffractometer equipped with graphite monochromated Mo Kα radiation ($\lambda = 0.71069$ Å) in the ω-2θ scan mode. Unit cell dimensions and a crystal orientation matrix were obtained from least-square refinement of the setting angles of 25 reflections in the $8° < \theta < 10°$ range.

The unit cell was identified as monoclinic, space group $P2_1/n$. This choice was confirmed by the solution and the successful refinement of the structure. The intensities were corrected for Lorentz and polarisation effects, and an empirical absorption correction (ψ scan) was made. The structure was solved by direct methods using SIR97 [10] and refined by full-matrix least-squares methods using the program SHELXL97 [11] and the winGX software package [12]. All non-hydrogen atoms were refined anisotropically. Hydrogen atoms were placed in calculated positions. Molecular graphics were prepared with ORTEP-3 [13] and SCHAKAL-97 [14]. Crystal data and structure refinement are summarised in Table 1.

2.4. ESR measurements

All ESR signals were recorded as first derivative absorption lines in an X-band Bruker ESP300E spectrometer, equipped with an Oxford Instruments flow cryostat and a goniometer. Anisotropy was studied at room temperature, recording signals at 10° intervals for the three cartesian axis of at least two crystals from each of the four different batches. Then, for chosen orientations, signals were recorded at different temperatures in the range 4.2–300 K. However, variable temperature measurements for samples of two different batches (C and D) could not be obtained because the crystals splintered during cooling.

2.5. Magnetic susceptibility

A powdered sample of batch A was placed into a teflon bucket previously measured and magnetisation data were obtained with an Oxford Instruments Faraday balance system, at a static field of 3.5 T and a gradient of 5 T m^{-1}, in the temperature range 10–300 K

2.6. Electrical resistivity

The resistance of single crystals with four in-line gold electrodes attached to 25 μm-diameter gold wires with

Table 1
Crystal data and structure refinement of (bedt-ttf)[$Au(cdc)_2$]

Empirical formula	$C_{14}H_8N_4S_{12}Au$
Formula weight	813.93
Crystal system, space group	Monoclinic, $P2_1/n$
Unit cell dimensions	
a (Å)	6.9031(8)
b (Å)	21.3213(16)
c (Å)	7.9833(9)
β (°)	91.643(6)
V (Å^3)	1174.5(2)
Z	2
$D_{calc.}$ (Mg/m^3)	2.301
μ (mm^{-1})	7.344
$F(000)$	782
2θ, range	2.73–27.98°
h, k, l, ranges	−1/9, −1/28, −10/10
Reflections collected/unique [R_{int}]	3396/2592 [0.0363]
T maximum, minimum	0.9992, 0.6920
Data/parameters	2592/142
Goodness-of-fit on F^2	1.040
$R[I > 2\sigma(I)]$	0.0348
WR	0.0672

Demetron 308A platinum paint were measured with an Keithley 619 electrometer in the temperature range 250–350 K, with a current of 0.1 μA. On large crystals, four gold electrodes were attached in a rectangular configuration, in order to use the Montgomery method [15] to test the anisotropy of resistivity.

3. Results

3.1. Crystal structure

The unit cell belongs to the space group $P2_1/n$, with two formula units. The anionic species $[Au(cdc)_2]^-$ was centred at the origin and the bedt-ttf radical cation placed at an inversion centre located midway the central C–C double bond (Fig. 1). The gold dithiocarbimate complex is planar with average deviations from the mean plane of 0.02 Å, with a similar geometry to other complexes of the same ligand [16]. The gold atom is coordinated to four sulphur atoms in a square planar configuration with S–Au bond distances of 2.330 and 2.337 Å, and the S1–Au–S2 angles of 75.22(5)°. The four-membered ring is responsible for this angle being significantly smaller than that of almost 90° usually found in metal bisdithiolates with five-member rings, e.g., $Au(mnt)_2$, [17].

As expected for a Au(III) complex, the C–S bond lengths are typical of single carbon–sulphur bonds. In the cdc ligand, the N(1)–C(2)–N(2) is almost linear – the angle is 175.8(7)° – with bond lengths typical of triple bond for C(2)–N(2), single for C(2)–N(1) and double for C(1)–N(1) (see Table 2).

The bedt-ttf cationic species has a planar central skeleton and terminal ethylene groups deviating from this plane −0.44 Å for C(6) and 0.42 Å for C(7), as it is usual for this molecule, but without positional disorder.

The anionic and cationic species are alternately packed along the *c*-axis (Fig. 2). The bedt-ttf and $Au(cdc)_2$, units are essentially parallel and their best planes almost perpendicular to the *c*-axis, the angle with their planes being of 89.67° and 89.68°, respectively. Multiple short distance contacts between bedt-ttf and the metal complex are noticed (Table 3). Further short contacts between bedt-ttf's H atoms and the anions' N atoms (Table 4) are responsible for the absence of positional disorder of the bedt-ttf ethylene group. Between bedt-ttf units of neighbour columns there are also several short contacts along the *a* direction (Fig. 2).

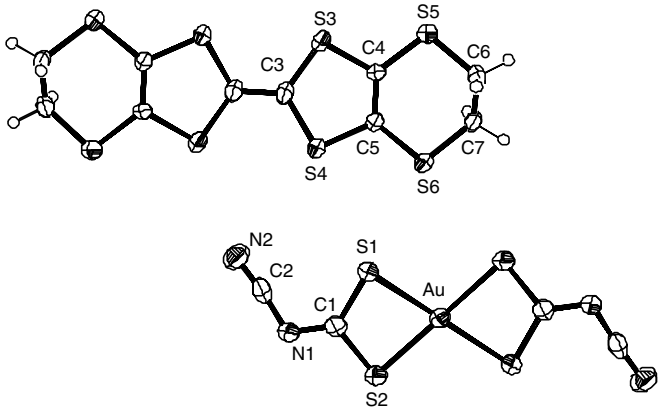

Fig. 1. The bedt-ttf (upper) and $Au(cdc)_2$ (lower) units with the adopted numbering scheme.

Table 2
Selected bond lengths (Å) angles (°) for (bedt-ttf)[$Au(cdc)_2$]

Au–S(1)	2.3300(14)	Au–S(1)[a]	2.3300(14)
Au–S(2)	2.3378(16)	Au–S(2)[a]	2.3378(16)
S(1)–C(1)	1.732(6)	S(2)–C(1)	1.732(6)
C(1)–N(1)	1.302(7)	N(1)–C(2)	1.336(8)
C(2)–N(2)	1.15(9)		
S(1)–Au–S(2)	75.22(5)	N(2)–C(2)–N(1)	175.8(7)
C(3)–C(3)[b]	1.384(10)	S(3)–C(3)	1.721(6)
S(4)–C(3)	1.725(6)	S(3)–C(4)	1.720(5)
S(4)–C(5)	1.743(5)	C(4)–C(5)	1.348(7)
S(5)–C(4)	1.747(5)	S(6)–C(5)	1.742(5)
S(5)–C(6)	1.805(6)	S(6)–C(7)	1.811(6)
C(6)–C(7)	1.529(8)		

Symmetry operations used to generate equivalent atoms: (a) $-x, -y, -z$; (b) $-x+2, -y, -z+1$.

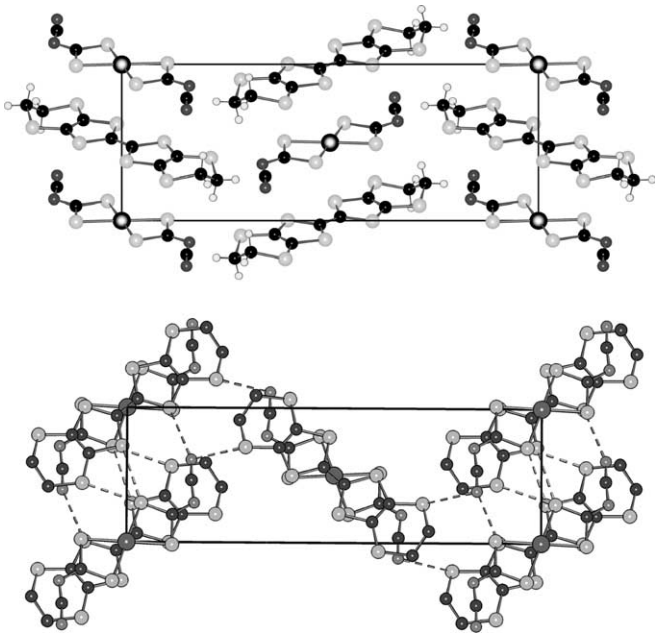

Fig. 2. The packing mode of (bedt-ttf)[$Au(cdc)_2$] viewed along *a* (top) and along *c* (bottom).

Table 3
Short contact distances (Å) between $(bedt\text{-}ttf)^+$ and $[Au(cdc)_2]^-$

Atoms	Distance
S1–S4[a]	3.656(6)
S2–S6[b]	3.441(2)
N2–S3[d]	3.290(5)
S1–S6[b]	3.341(5)
C2–S5[c]	3.408(5)
N2–S5[c]	3.274(5)

Symmetry operations used to generate equivalent atoms: (a) $x-1, y, z$; (b) $-x, -y, -z$; (c) $-x+1/2+1, y-1/2, -z+1/2$; (d) $-x+2, -y, -z+1$.

Table 4
Possible hydrogen bonds (Å, °) for (bedt-ttf)[Au(cdc)$_2$]

Donor–H distance	Donor···acceptor distance	H···acceptor distance	Donor–H···acceptor angle
C7···H7B	C7···N2(1)	H7B···N2(1)	C7–H7B···N2[a]
0.970(6)	3.358(8)	2.470(6)	151.97(36)
1.080[A]		2.374[A]	150.72[A]
C6···H6A	C6···N1(2)	H6A···N1(2)	C6–H6A···N1[b]
0.970(6)	3.642(8)	2.931(5)	131.05(37)
1.080[A]		2.860[A]	129.39[A]
C6···H6A	C6···N2(3)	H6A···N2(3)	C6–H6A ···N2[c]
0.970(6)	3.272(8)	2.796(6)	111.02(38)
1.080[A]		2.759[A]	108.89[A]
C6···H6B	C6···N1(4)	H6B···N1(4)	C6–H6B···N1[d]
0.970(6)	3.578(8)	2.626(5)	167.18(38)
1.080[A]		2.518[A]	166.62[A]

Equivalent positions: (a) $-x+1, -y, -z+1$; (b) $-x+1/2, +y+1/2, -z+1/2$; (c) $-x+1/2+1, +y+1/2, -z+1/2$; (d) $-x+1, -y, -z$.
[A] Normalised values according to [19,20].

The analysis of the bedt-ttf bond lengths in the present compound leads to a δ parameter as proposed by Guionneau et al. [18], $\delta = 0.72$, a value typical of a +1 charge, as inferred from the 1:1 stoichiometry.

3.2. Electrical resistivity

The electrical resistivity is $6.5 \times 10^3\ \Omega$ cm at room temperature and it shows a thermally activated behaviour, from which an energy gap $2\Delta = 0.51$ eV was derived. No significant conductivity anisotropy could be measured by the Montgomery method.

3.3. ESR results

First, we analyse the room temperature anisotropy of the ESR signal. Data collected from the four batches, indicated some differences in the spread of the linewidth between minimum and maximum, although obeying always to a common pattern with a shape of simple Lorentzian line. Samples from batches A and B had linewidth varying between 9 and 15 G, whereas samples from batches C and D, for some orientations, had lines wider than 20 G.

ESR is often used as a non-destructive and easy way to test different phases, which can be present even in the same preparative batch. In the case of many bedt-ttf salts different phases can be discriminated just by the linewidths [1].

To evaluate whether or not we were in the presence of two phases, samples from different batches were checked afterwards by X-ray diffraction. The automatic CAD4 routine always recognised the same unit cell parameters, although in some cases, mainly for batches C and D, the crystals were twinned. Therefore the broader absorption EPR lines are ascribed to this fact, which in turn may depend on the solvent and preparative conditions. Full determination of the crystal structure was made for a sample of batch A, showing no presence of solvent molecules, as discussed above.

As all batches yielded consistently the same elemental (C, H and N) analysis within experimental error, these differences are not attributed to solvent molecules incorporated in the structure.

Anisotropy plots of linewidth and g-value are given in Fig. 3 for rotations around three orthogonal axes indicated. The g-value anisotropy has a simple sinusoidal dependence with an 180° period, different from the linewidth dependence with two maxima in one of the 180° rotation. These two contributions became more visible upon cooling. Indeed below about 50 K at some orientations it is possible to observe two separate lines.

As expected since $Au(cdc)_2^-$ is a diamagnetic anion, the observed g-values are typical of bedt-ttf where the principal values of the g tensor in a static magnetic field are 2.011–2.012 parallel to the molecular long axis, 2.006–2.007 for the short axis and 2.002–2.003 for the normal to the molecular plane [21]. The two lines are attributed to the different orientations of the two bedt-ttf cations within the unit cell

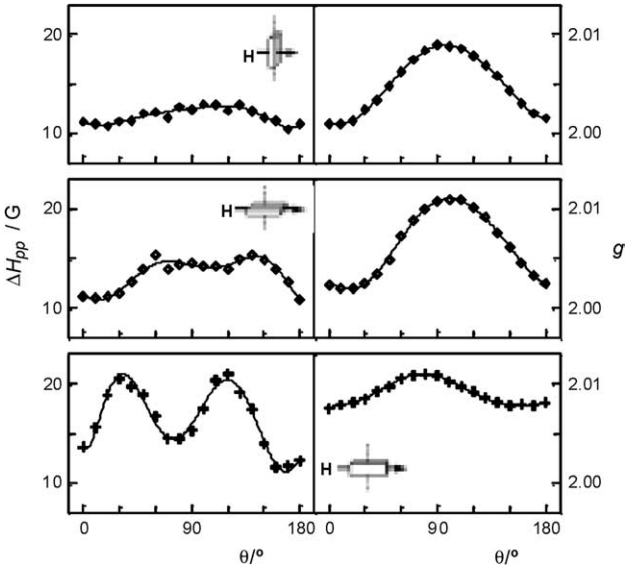

Fig. 3. Linewidth (left) and g-value (right) anisotropy of ESR signal at room temperature.

relative to the magnetic field, which become equivalent only for particular orientations.

We have chosen one orientation for which apparently only a single line is observed and recorded the signals as a function of temperature for different orientations rotated in 45° steps around the same axis. The thermal dependence of *g*-value is shown in Fig. 4 and of the linewidth in Fig. 5, where the data for (+90°) were omitted as they are within error bars coincident with those for 0°.

3.4. Magnetic susceptibility measurements

Results of paramagnetic susceptibility calculated from Faraday balance measurements assuming a diamagnetism estimated as -3.05×10^{-4} emu/mol, from tabulated Pascal's constants are displayed in Fig. 6, together with the integrated signal intensity from ESR measurements of two different crystals, from batches A and B, at the same orientation, which were normalised at room temperature as being equal to the value of the static paramagnetic susceptibility. Slightly different temperature dependences are noticed only below ~60 K. Such differences may come from a variable contributions to the Curie tail, that is larger for crystal B and the polycrystalline sample used in Faraday balance (from batch A).

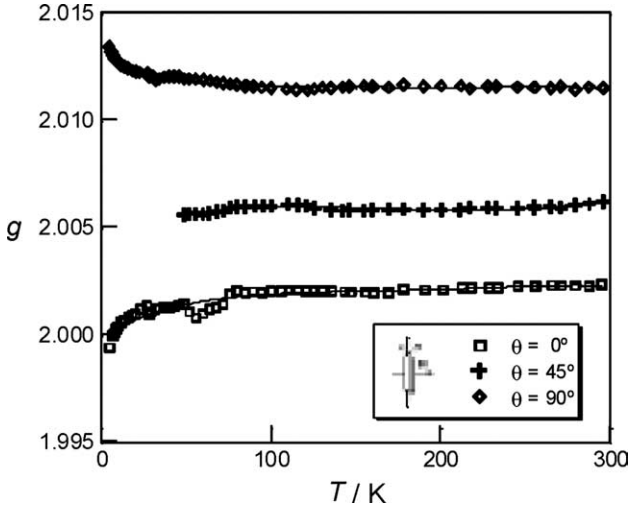

Fig. 4. Temperature dependence of the *g*-value for three different crystal orientations.

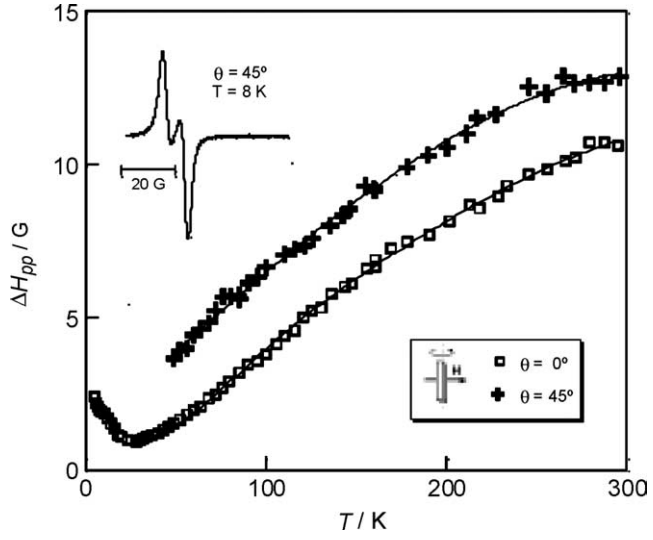

Fig. 5. Thermal dependence of ESR signal linewidth for two orientations. At 45°, two lines are observed below 50 K.

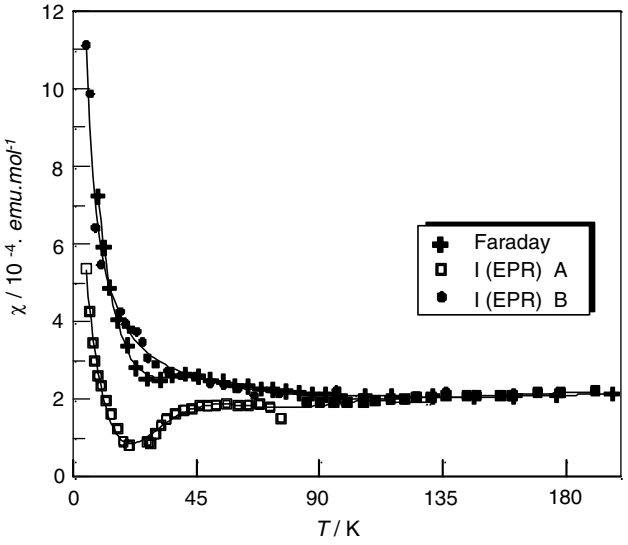

Fig. 6. The thermal dependence of the static magnetic susceptibility (crosses) compared with the ESR signal intensity (normalised) for two samples.

Assuming that the susceptibility has two contributions, one intrinsic and another a Curie tail due to impurities with different extent from sample to sample, we removed this last contribution from the different measurements and obtained for the intrinsic susceptibility always a similar behaviour with an exponential decay below 40 K corresponding to a magnetic excitation gap of $\Delta/k_B = 87 \pm 3$ K.

It is worth noting that at higher temperatures ($T > 50$ K) the paramagnetic susceptibility, is rather small ($\sim 2.5\times10^{-4}$ emu/mol at room temperature) and almost temperature independent. This is reminiscent of the Pauli contribution characteristic of conducting systems. However, the low value of the electrical conductivity ($1.5\times10^{-4}\ \Omega^{-1}\,cm^{-1}$) and its semiconducting behaviour with a large energy gap (0.51 eV) rule out such assignment. It should be also mentioned in this respect that similar high temperature behaviours were found in other non-conducting systems [22]. Amongst the bedt-ttf insulators this is a very low room temperature value of χ_p, which are mostly closer to 10^{-3} emu/mol, although a lower value of 10^{-4} emu/mol was found for (bedt-ttf)$HgBr_3$ [23].

4. Discussion and conclusions

The results show that we are in presence of a semiconducting system, and the poor electrical conductivity is

mainly a consequence of the alternated packing of bedt-ttf radical cations and bis-dithiolate anions. Even if the different short (bedt-ttf) contacts, namely along *a*, would lead to significant electronic interactions and a reasonable bandwidth, the stoichiometry makes the system half filled, a situation where an insulating regime is always expected as a consequence of the strong correlation effects dominated by large on-site Coulomb repulsions.

The metallic behaviour, sometimes with superconducting transitions at low temperatures, occurs in bedt-ttf salts where the donor molecules are partially oxidised and well segregated, usually in layers. The alternated stacking seems to stabilise the full oxidation of bedt-ttf in 1:1 salts. This is also the case of other bedt-ttf salts with metal-bis(dithiolates) such as $Ni(mnt)_2$ or $Ni(dmit)_2$, which nevertheless present differences in the packing mode. In spite of the lower symmetry of $Au(cdc)_2$, its salt is of higher symmetry (monoclinic), whereas it is triclinic in the former cases. As in the $Ni(dmit)_2$ compound, the bedt-ttf and the dithiolate species are almost parallel [24], at variance with the $Ni(mnt)_2$ compound [25] where the angle between the mean planes of radical cation and anion moieties is ca. 50°.

We have seen above that a consequence of short distance contacts between the radical cations and the anionic species through peripheral sulphur atoms inhibits the positional disorder of methylene groups characteristic of many bedt-ttf compounds. These short contacts are also responsible for the observed magnetic properties. In fact, in the absence of significant interactions, a Curie–Weiss type magnetic susceptibility due to localised $S = 1/2$ spins in each bedt-ttf cation would be expected. This is not the case and the small and almost temperature independent paramagnetism observed denotes the existence of a complex 3D network of antiferromagnetic interactions. These antiferromagnetic interactions can be either mediated through the alternating anions, mainly along *c*, and also associated with the network of short contacts between cations in neighbouring columns along *a*. There are a few cases where the antiferromagnetic interactions (J values) were estimated from the intermolecular overlap integrals [26]. This was done for 2:1 bedt-ttf salts in the Mott insulator regime. A similar study for 1:1 insulators is worth to be fulfilled, but it is beyond the scope of the present article.

The variation of the extreme *g*-values, the increase of linewidth and the exponential decay of susceptibility, all observed below 25 K can be associated with a structural modification involving small alteration of the bedt-ttf packing.

Finally, it should be mentioned that the present study shows that the small temperature independent paramagnetism in molecular compounds is not an exclusive attribute of metallic systems and it can be found also in insulators.

Supplementary crystal structure data was deposited in CCDC under No. 207760, and are available on request to CCDC, 12 Union Road, Cambridge CB2 1EZ, UK (fax: (internat.) +44 1223/336 033; e-mail: deposit@ccdc.cam.ac.uk).

Acknowledgement

Work was supported in part by FCT-Fundação para a Ciência e Tecnologia, under Contract POCTI/QUI/45108/2002 (FEDER Program, European Union).

References

[1] J.M. Williams, J.R. Ferraro, R.J. Thorn, K.D. Carlson, U. Geiser, H.H. Wang, A.M. Kini, M.-H. Whangbo, Organic Superconductors (Including Fullerenes) Synthesis, Structure, Properties and Theory, Prentice-Hall Inc., New Jersey, 1992.
[2] H. Taniguchi, M. Miyashita, K. Uchiyama, K. Satoh, N. Mori, H. Okamoto, K. Myagawa, K. Kanoda, M. Hedo, Y. Uwatoko, J. Phys. Soc. Jpn. 72 (2003) 468.
[3] H. Yamochi, T. Komatsu, N. Matsukama, G. Saito, T. Mori, M. Kusunoki, K. Sakaguchi, J. Am. Chem. Soc. 115 (1993) 11319.
[4] M. Almeida, R.T. Henriques, in: H.S. Nalwa (Ed.), Handbook of Organic Conductive Molecules and Polymers, vol. 1, Wiley, Chichester, 1997, p. 87 (Chapter 2).
[5] P. Cassoux, Coord. Chem. Rev. 185/186 (1999) 213.
[6] I.D. Parker, R.H. Friend, P.I. Clemenson, A.E. Underhill, Nature 324 (1986) 547.
[7] C.B. Dias, I.C. Santos, V. Gama, R.T. Henriques, M. Almeida, J.P. Pouget, Synth. Metals 56 (1993) 1688.
[8] F.A. Cotton, J.A. McCleverty, Inorg. Chem. 6 (1967) 229.
[9] J. Larsen, C. Lenoir, Synthesis 2 (1988) 134.
[10] A. Altomare, M.C. Burla, M. Camalli, G. Gascarano, G. Giacovazzo, A.G.G. Moliterni, G. Polidori, R. Spagna, J. Appl. Crystallogr. 32 (1999) 115.
[11] G.M. Sheldrick, SHELXL97 – A Program for Crystal Structure Determination, University of Göttingen, Germany, 1997.
[12] L.J. Ferrugia, J. Appl. Crystallogr. 32 (1999) 837.
[13] L.J. Ferrugia, J. Appl. Crystallogr. 30 (1997) 565.
[14] E. Keller, SCHAKAL-97 – A Computer Program for the Representation of Molecular and Crystallographic Models, Kristallographisches Institut der Universität Freiburg i., Br., Germany, 1997.
[15] H.C. Montgomery, J. Appl. Phys. 42 (1971) 2971.
[16] F.A. Cotton, C.B. Harris, Inorg. Chem. 10 (1968) 2140.
[17] A. Domingos, R.T. Henriques, V. Gama, M. Almeida, A. Lopes Vieira, L. Alcácer, Synth. Metals 27 (1988) B411.
[18] P. Guionneau, C.J. Kepert, G. Bravic, D. Chasseau, M.R. Turner, M. Kurmoo, P. Day, Synth. Metals 86 (1997) 1973.
[19] G.A. Jeffrey, L. Lewis, Carbohydr. Res. 60 (1978) 179.
[20] R. Taylor, O. Kennard, Acta Crystallogr. B 39 (1983) 133.
[21] T. Komatsu, H. Sato, T. Nakamura, N. Matsukawa, H. Yamochi, G. Saito, M. Kusunoki, K. Sakaguchi, S. Kagoshima, Bull. Chem. Soc. Jpn. 68 (1995) 2233.
[22] M. Fourmigué, K. Bechgaard, P. Auban, D. Jerome, K. Boubekeur, P. Batail, Synth. Metals 27 (1988) 231.
[23] N. Yoneyama, A. Miyazaki, T. Enoki, G. Saito, Bull. Chem. Soc. Jpn. 72 (1999) 639.
[24] H. Kobayashi, R. Kato, A. Kobayashi, Y. Sasaki, Chem. Lett. (1985) 191.
[25] W. Reith, K. Polborn, E. Amberger, Angew. Chem., Int. Ed. Engl. 27 (1988) 699.
[26] T. Mori, J. Solid State Chem. 168 (2002) 433.

structures containing this ligand [7]. Of these the 1,6-bridging mode, which favors the formation of the coordination polymers, is the most common. The phthalate ligand can also take part in additional weak hydrogen bonding, which stabilizes the polymeric structures by forming two- and three-dimensional networks. We have shown that a successful preparation of coordination polymers is based on a suitable choice of combinations of the phthalate bridging ligand and different amines, such as pyridine, imidazole and its derivatives, 2,2′-bipyridine, and 1,10-phenanthroline, which act as terminal ligands. Depending on both the nature of the amines and the stoichiometric ratio metal:acid:amines, infinite linear [4], zigzag [5,6] or helical [8,10] chains are formed.

Oxidation reactions have synthetic applications in both the chemical and pharmaceutical industries. The catalytic oxidation of alkenes has potentially important industrial applications since the selective oxidation products serve as starting materials for the production of many fine chemicals. Oxidation can be carried out with many different oxidants, but from an economic point of view H_2O_2 is ideally suitable. It is cheap, readily available and environmentally benign. A large effort is thus currently in progress to try to find active catalysts for the oxidation reactions using this oxidant. Several families of catalysts are known, mainly based on various transition-metal complexes as titanium, vanadium, molybdenum, manganese, tungsten and rhenium complexes [49]. The cobalt-catalyzed decomposition of hydroperoxides has also been extensively studied [50], but catalytic oxidation catalyzed by copper complexes is comparatively rare. Recently, a series of reports have been published showing that β-carbonylenolate, β-diketonate and β-ketamidate copper(II) complexes [51,52] and mixed-ligand salicylaldehyde copper(II) complex [53] can be used for catalytic oxidation cyclohexene under Mukaiyama's conditions. Some copper-based catalysts have also been reported to be active in the presence of H_2O_2 [54,55].

The present work reports the synthesis of two phthalate based copper(II) and cobalt(II) coordination polymers using imidazole (Im) as the amine, $\{[Cu(Pht)(Im)_2]\cdot 1.5H_2O\}_n$ (**1**) and $[Co(Pht)(Im)_2]_n$ (**2**), their crystal structures and presents a preliminary investigation into the catalytic activity of **1** and **2** towards the oxidation of cyclohexene using hydrogen peroxide as oxidant under aerobic conditions.

2. Experimental

2.1. Materials and methods

All the starting materials were reagent grade and used as purchased. Hydrogen peroxide (30% aqueous solution) was used as received from Acros. The infrared spectra were recorded on a Perkin–Elmer Spectrum One spectrometer using KBr pellets in the region 4000–400 cm^{-1}. Gas chromatographic analyses were carried out with a HP 5890 instrument on a RTX-5 column 30 m × 0.25 mm × 0.5 μm fitted with a flame ionization detector, and hydrogen gas pressure was 0.4 bar.

Table 1
Crystal data and structure refinement

	1	**2**
Empirical formula	$C_{28}H_{30}Cu_2N_8O_{11}$	$C_{14}H_{12}CoN_4O_4$
Formula weight	781.68	359.21
Temperature (K)	100	293(2)
Wavelength (Å)	0.71073	0.71073
Crystal size (mm)	0.38 × 0.11 × 0.02	0.3 × 0.2 × 0.5
Crystal system	orthorhombic	monoclinic
Space group	*Pbca* (No. 61)	*Pn* (No. 7)
a (Å)	19.6319(3)	8.399(2)
b (Å)	13.6365(3)	9.978(2)
c (Å)	23.4334(4)	10.011(2)
α (°)	90	90
β (°)	90	104.43(3)
γ (°)	90	90
V (Å^3)	6273.4(2)	812.5(3)
Z	8	2
D_c (g cm^{-3})	1.655	1.468
μ (mm^{-1})	1.430	1.080
F(000)	3200	366
θ Range for data collection (°)	4.59–32.56	3.65–29.18
Index ranges	$-23 \leqslant h \leqslant 29$; $-10 \leqslant k \leqslant 20$; $-31 \leqslant l \leqslant 35$	$-10 \leqslant h \leqslant 11$; $-13 \leqslant k \leqslant 13$; $-13 \leqslant l \leqslant 13$
Reflections collected	37 115	4912
Reflections unique (R_{int})	11 244 (0.1058)	2425 (0.0206)
Completeness to θ_{max}	98.6	90.5
Data/restraints/parameters	11 244/0/452	2425/2/208
Final *R* indices [$I > 2\sigma(I)$]	$R_1 = 0.0620$, $wR_2 = 0.1176$	$R_1 = 0.0281$, $wR_2 = 0.0740$
R indices (all data)	$R_1 = 0.1305$, $wR_2 = 0.1408$	$R_1 = 0.0315$, $wR_2 = 0.0787$
Goodness-of-fit on F^2	1.008	0.939
Largest difference peak and hole (e Å^{-3})	0.662 and −0.654	0.645 and −0.377

2.2. Synthesis of complexes

2.2.1. Synthesis of $\{[Cu(Pht)(Im)_2]\cdot 1.5H_2O\}_n$ (1)

Method A. To a hot suspension of *o*-phthalic acid (0.66 g, 4 mmol) and $CuCO_3\cdot Cu(OH)_2$ (0.44 g, 2 mmol) in 40 ml H_2O was added Im (0.55 g, 8 mmol). The resulting blue mixture was stirred and refluxed for 30 min and then filtered. The filtrate was allowed to stand at room temperature. Blue crystals, suitable for X-ray analysis, were filtered off the next day, washed with water, ethanol and acetone, and dried in air. Yield: 0.87 g (56%). *Anal*. Calc. for $C_{28}H_{26}Cu_2O_{11}N_8$: C, 43.02; H, 3.87; N, 14.33; Cu, 16.26. Found: C, 43.09; H, 3.71; N, 14.08; Cu, 16.20%. IR data (KBr, cm^{-1}): 3479m, 3380m, 3137s, 3067m, 2959m, 2871m, 1616vs, 1587vs, 1570vs, 1539sh, 1506sh, 1485m, 1443m, 1385vs, 1370vs, 1330m, 1263w, 1182w, 1148w, 1071s, 955w, 859m, 829m, 750s, 719m, 705m. The compound is insoluble in alcohol, acetone, acetonitrile, chloroform, and poorly soluble in water.

Method B. To a hot solution of *o*-phthalic acid (0.83 g, 5 mmol) and Im (0.69 g, 10 mmol) in 20 ml H_2O was added $Cu(CH_3COO)_2\cdot H_2O$ (0.99 g, 5 mmol). The resulting blue solution was heated for 10 min and allowed to stand at room temperature. Blue crystals formed after 1–2 days. They were filtered off, washed with water, ethanol and acetone, and dried in air. Yield: 0.82 g (42%). It was identified by comparing its IR spectrum with the crystallographically characterized precipitate from Method A, and elemental analysis. *Anal*. Found for the title compound: C, 42.69; H, 3.77; N, 13.80; Cu, 15.72%.

2.2.2. Synthesis of $[Co(Pht)(Im)_2]_n$ (2)

To a hot solution of H_2Pht (0.83 g, 5 mmol) and Im (0.69 g, 10 mmol) in water (15 ml) $Co(O_2CMe)_2\cdot 4H_2O$ (1.25 g, 5 mmol) was added. The resulting mixture was stirred and heated for 20 min. The lilac precipitate so formed was filtered off from hot solution, washed with hot water, ethanol and acetone and dried in air. Yield: 0.84 g (46.8%). *Anal*. Calc. for $C_{14}H_{12}CoN_4O_4$: C, 46.81; H, 3.37; N, 15.60; Co, 16.41. Found: C, 46.72; H, 3.32; N, 15.49; Co, 16.33%. IR data (KBr, cm^{-1}): 3137s, 3062m, 2970m, 2880m, 1612s, 1589vs, 1579sh, 1486m, 1460m, 1444m, 1394s, 1373vs, 1329m, 1267m, 1144m, 1107m, 1075vs, 957m, 914w, 840m, 752s, 702m, 656vs, 620m, 606w, 573w, 482m. Single crystals suitable for diffraction studies were obtained by recrystallization of **2** from hot aqueous solution.

2.3. Crystal structure determinations

Experimental data were collected on Bruker-Nonius KappaCCD and KUMA KM4CCD-κ-axis diffractometers using graphite monochromated Mo Kα radiation at 100 K for **1** and 293 K for**2**. The crystals were located 40 mm (**1**)/ 60 mm (**2**) from the CCD camera. 446/444 Frames were collected in 2/4 runs with a 0.5/0.5° scan width and 150 s/10 s per frame. The data were processed using the SAINT program from Bruker-Nonius (Madison, USA) and KUMA diffraction (Wroclaw, Poland) software. Crystal data, details of data collections and refinement for **1** and **2** are given in Table 1. The structures were solved by direct methods (SHELXS-97 [56]) and refined on F^2 (SHELXL-97 [57]) using anisotropic displacement parameters for non-H atoms. Except for the solute water molecules in **1**, H atoms were located from difference electron density syntheses and refined using a riding model. Selected bond distances and angles are listed in Table 2.

3. Results and discussion

3.1. Crystal structures

3.1.1. The structure of $\{[Cu(Pht)(Im)_2]\cdot 1.5H_2O\}_n$ (1)

Fig. 1 shows a view of crystallographically independent structure fragment of complex **1**. The crystal structure of **1** is characterized by $[Cu(Im)_2]$ entities linked into infinited chains by bridging phthalate anions. The observed chain structure (Fig. 2) is not unusual and has been found in the crystal structures of the catenates (μ_2-*o*-phthalato)-*bis*(pyridine)-copper(II) [16], ethylenediamine-(μ_2-*o*-phtha-

Table 2
Selected bond distances (Å) and bond angles (°) for compounds **1** and **2**

1	
Cu(1)–N(1)	1.956(3)
Cu(1)–N(3)	1.980(2)
Cu(2)–O(4)	1.971(2)
Cu(2)–O(7)*	1.972(2)
Cu(1)–O(5)	1.965(2)
Cu(1)–O(1)	1.999(2)
Cu(2)–N(5)	1.972(3)
Cu(2)–N(7)	1.978(3)
N(1)–Cu(1)–O(5)	90.50(9)
O(5)–Cu(1)–N(3)	91.31(9)
O(5)–Cu(1)–O(1)	167.34(9)
O(4)–Cu(2)–N(5)	89.38(10)
N(5)–Cu(2)–O(7)*	91.64(10)
N(5)–Cu(2)–N(7)	168.69(12)
N(1)–Cu(1)–N(3)	171.56(11)
N(1)–Cu(1)–O(1)	89.32(9)
N(3)–Cu(1)–O(1)	90.72(9)
O(4)–Cu(2)–O(7)*	176.25(10)
O(4)–Cu(2)–N(7)	91.11(10)
O(7)*–Cu(2)–N(7)	88.60(10)
2	
Co(1)–O(4)	1.952(2)
Co(1)–N(1A)	2.002(3)
Co(1)–O(1)**	1.980(2)
Co(1)–N(1B)	2.001(2)
O(4)–Co(1)–O(1)**	92.8(1)
O(1)*–Co(1)–N(1B)	116.5(1)
O(1)*–Co(1)–N(1A)	108.4(1)
O(4)–Co(1)–N(1B)	108.9(1)
O(4)–Co(1)–N(1A)	121.7(1)
N(1B)–Co(1)–N(1A)	108.3(1)

Symmetry transformations used to generate equivalent atoms: $^*x, -y+3/2, z+1/2$; $^{**}x+1/2, -y+1, z+1/2$.

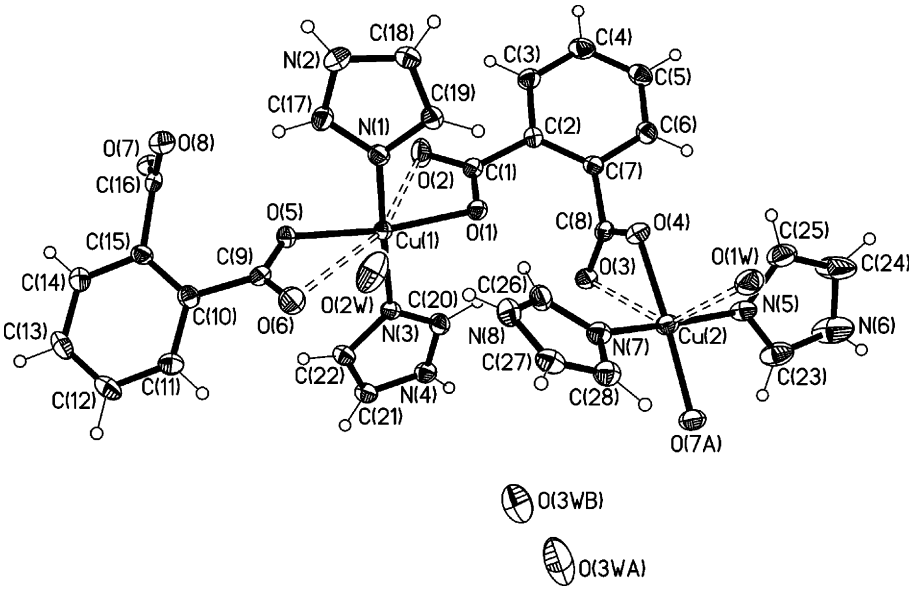

Fig. 1. Crystallographically independent structure fragment in compound **1**. Hydrogen atoms are omitted for clarity and long contacts Cu(1)–O and Cu(2)–O are indicated by double dotted lines. Atomic displacement ellipsoids are shown at the 50% probability level.

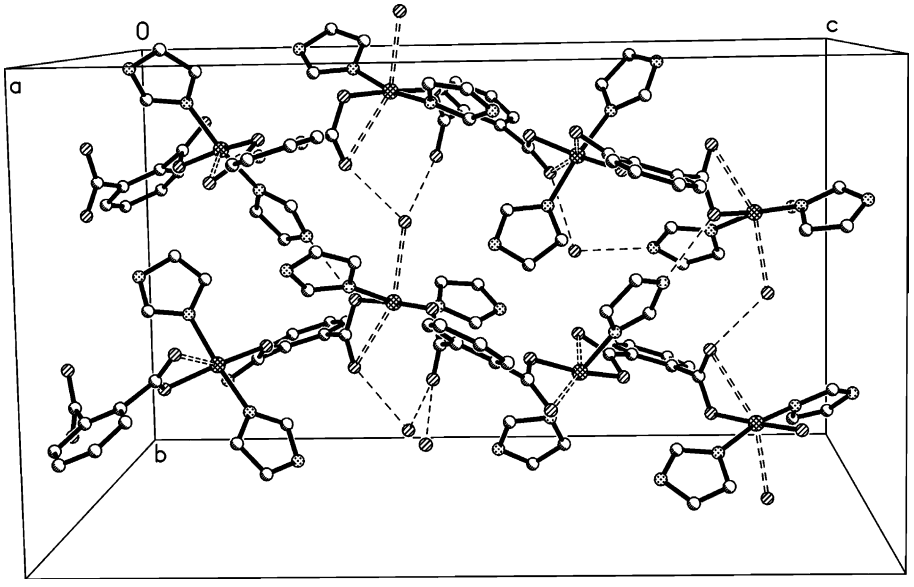

Fig. 2. The fragments of two polymeric chains in compound **1**. Hydrogen atoms are omitted for clarity. Hydrogen bonds are indicated by dotted lines and long contacts Cu–O are indicated by double dotted lines.

lato)-copper(II) [17], aqua-(1,10-phenanthroline)-(μ_2-*o*-phthalato)-copper(II) [18], (μ_2-*o*-phthalato)-*bis*(piperidine)-copper(II) [20], *bis*(μ_2-*o*-phthalato)-aqua-*tetrakis*(4-methylpyridine)-di-copper(II) [2], diammine-(μ_2-*o*-phthalato)-copper(II) [8], and (1-methylimidazole)-(μ_2-*o*-phthalato)-copper(II) [6] and aqua-(4-methylimidazole)-(μ_2-*o*-phthalato)-copper(II) [7] among others. The mode of attachment of the phthalate dianion to the metal is not always the same. In some cases, the carboxylic acid groups are attached by both oxygen atoms and in others by one oxygen atom.

There are two crystallographically independent Cu(II) centers within chains and both Cu(II) atoms have approximately square-planar N_2O_2 coordination. The O–Cu–O angles range from 167.3(1)° (O(1)–Cu(1)–O(5)) to 176.3(1)° (O(4)–Cu(2)–O(7)) and the N–Cu–N angles vary from 168.7(1)° (N(5)–Cu(2)–N(7)) to 171.6(1)° (N(1)–Cu(1)–N(3)). The different arrangement of the C=O bonds of the carboxylic acid groups relative to the coordination planes of the two independent Cu atoms indicate that the chain is relatively flexible and successive Cu···Cu distances in the chain are 6.045(1) and 6.468(1) Å. Whereas the Cu–X distances vary significantly for Cu(1) [Cu(1)–N(1) 1.956(3), Cu(1)–N(3) 1.980(2), Cu(1)–O(1) 1.999(2), Cu(1)–O(5) 1.965(2) Å], this is not the case for Cu(2) [Cu(2)–N(5) 1.972(3), Cu(2)–N(7) 1.978(3) Å, Cu(2)–O(4)

1.971(2), Cu(2)–O(7)* 1.972(2) Å]. Note, the Cu(1) and Cu(2) atoms additionally form two long contacts: Cu(1)–O(2) 2.559(2), Cu(1)–O(6) 2.894(2) Å with uncoordinated oxygen atoms of both carboxylic groups; Cu(2)–O(1w) is 2.644 and Cu(2)–O(3) is 2.861 Å. Consequently, the coordination of both Cu atoms can be described as 4 + 1 + 1.

All of the four independent imidazole ligands in **1** are involved in N–H···O hydrogen bonding interactions, of which only one is intramolecular. Thus, N(6) forms an intramolecular H bonding interaction with the free carbonyl O atom of a phthalate ligand further along the chain. The distance N(6)···O(2) is 2.793(4) Å and this is comparable to the distance N(8)···O(2w) (2.787(4) Å) between the *trans* imidazole group N–H group and a solute water molecule. There is also an additional intermolecular contact between N(2) and the water molecule O(1w) of 3.040(4) Å such that N(2) forms a bifurcated hydrogen bond to O(7) and O(1w). The remaining two independent imidazole groups, both of which are attached to Cu(1), form direct interchain N–H···O–Cu hydrogen bonds to the O atoms of the phthalate groups bonded to the Cu atoms in neighboring chains. The corresponding interatomic distances are N(4)···O(4) = 2.785(3) and N(2)···O(7) = 3.109(4) Å. This extended hydrogen bonding network stabilizes a 3D structure in complexes **1**. Fig. 2 presents a fragment of packing arrangement in **1**.

3.1.2. The structure of $[Co(Pht)(Im)_2]_n$ (2)

The structure of **2** comprises $[Co(Im)_2]$ units linked into zigzag polymeric chains by bridging phthalate anions. Fig. 3 shows a fragment of the chain in compound **2**, together with the atomic labeling scheme. The crystals are isostructural with the analogous Zn(II) complex [6]. Each Co atom adopts a tetrahedral N_2O_2 geometry, being coordinated by a pair of imidazole ligands [Co(1)–N(1a) = 2.002(3) and Co(1)–N(1b) = 2.001(2) Å] and a pair of monodentate carboxylate groups [Co(1)–O(1)* = 1.980(2) and Co(1)–O(4) = 1.952(2) Å]. The bond angles at Co(1) atom range from 92.8(1)° to 121.7(1)° (Table 2). As expected, distances and angles in coordination polyhedron agree well with those in $[Zn(Pht)(Im)_2]_n$ [6]. The nearest Co···Co distances in the chain are at 6.017(2) Å. The dihedral angles between the planes through the carboxylate groups [O(1)C(11)O(2) and O(3)C(22)O(4)] and the aromatic ring are 61.9(2)° and 33.7(2)°, respectively. For Pht ligand, the C–C bonds within the aromatic ring range from 1.373(5) to 1.404(4) Å and are similar to those in complex **1** and other Cu(II) phthalate complexes [3,7,8]. The bond distances and angles of the imidazole molecules also fall in the range of values found in other complexes, containing the coordinated imidazole [58,59].

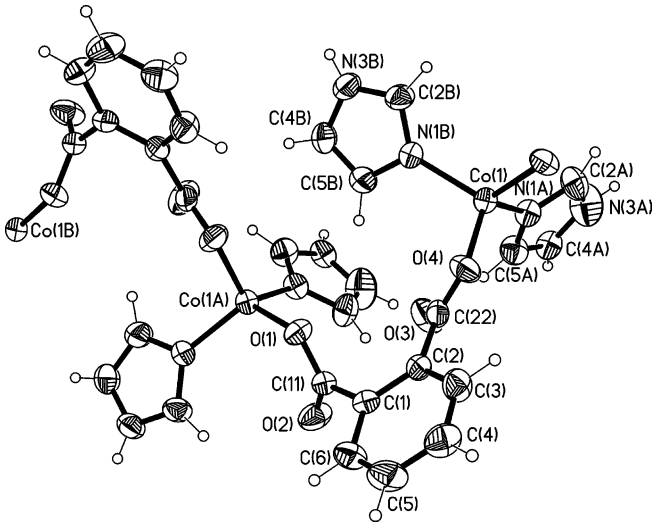

Fig. 3. Polymeric chain in compound **2** with numbering scheme. The atomic displacement ellipsoids are drawn at the 50% probability level.

The chains lie parallel along the [1 0 1] direction. The N(3b)–H(3b)···O(2) [x, $y+1$, z] = 2.754(4) Å hydrogen bonds connect the chains into layers (Fig. 4) and N(3a)–H(3a)···O(1) [$x+1$, y, z] = 2.812(4) Å interactions combine neighboring layers into a 3D network. Interestingly, in contrast to **1**, the crystal structure of **2** contains no solute water, even though the crystals of **2** were grown from hot aqueous solution.

3.2. Spectroscopic properties

IR spectra of compounds **1** and **2** showed absorptions due to N–H bond stretching of imidazole ligands and C–H bonds of aromatic rings in the range 3380–2871 cm^{-1}. Strong bands in the 1616–1570 and 1385–1370 cm^{-1} regions were assigned to the asymmetric and symmetric stretching modes of carboxylate groups, respectively [60,61]. The separations between the asymmetric and symmetric stretching frequencies, $\Delta\nu$ (ν_{asym}–ν_{sym} ranges from 246 to 185 cm^{-1}), are indicative of the fact that COO^- groups from phthalate groups have bridging O atoms [62]. Such absorptions have already been reported for other phthalate complexes with aromatic amines (1620–1520 cm^{-1}) [21,22]. IR spectrum of complex **1** also showed a strong and broad ν(O–H) stretching band around 3479 cm^{-1} confirming the presence of the water solute molecules.

3.3. Catalytic oxidation of cyclohexene

Choosing cyclohexene as a model substrate, oxidation reactions were carried out in acetone at room temperature under magnetic stirring in the presence of **1** and **2** as the catalyst using 30% H_2O_2. The evolution of the reactions was monitored by GC analysis of solution samples taken periodically to determine the concentrations of the various oxidation products. In a typical experiment, 1 ml of hydrogen peroxide (30%) was added to the reaction mixture containing cyclohexene (1 ml) and catalyst (39 mg) in 1 ml acetone. The results of the investigations are summarized in Table 3. In the case of **1** the distribution of the products was strongly dependent on the ratio of $[C_6H_{10}]$ to $[H_2O_2]$.

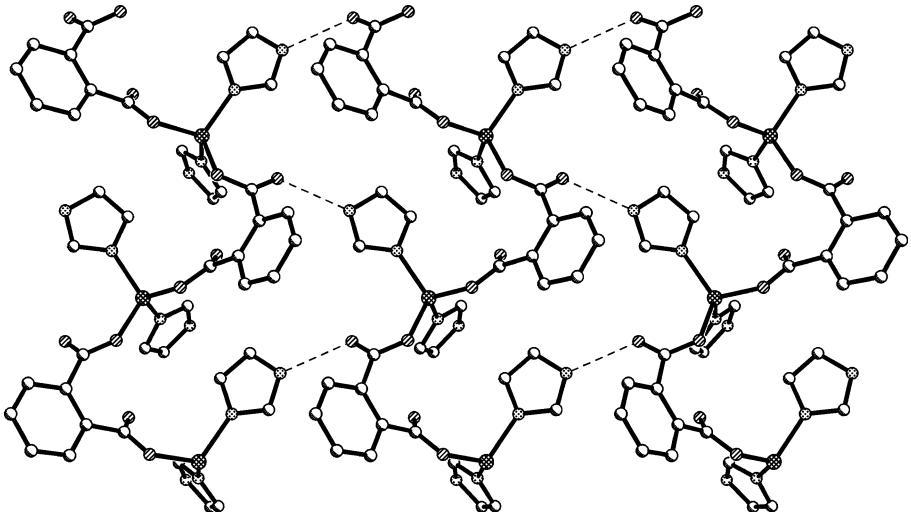

Fig. 4. Fragment of the layer formed through N–H···O interactions in structure **2**. Hydrogen atoms are omitted for clarity and hydrogen bonds are indicated by dotted lines.

Table 3
Catalytic oxidation of cyclohexene with H_2O_2[a]

Catalyst	Run	Ratio C_6H_{10}:H_2O_2	Products (%)[b]			
			Alkene	Epoxide	Alcohol	Ketone
1	1[c]	1:12	0.76	0.49	5.32	93.4
	2[c]	1:9	6.13	1.49	6.78	85.6
	3[c]	1:4.5	40.5	4.67	11.4	43.4
	4[d]	1:9	0.85	8.39	3.06	87.7
	5[e]	1:9	2.01	11.3	11.5	75.2
2	6[e]	1:9	38.8	1.94	18.7	40.6

[a] Reaction conditions: substrate (1 mmol), catalyst (0.1 mmol), temperature (22 °C).
[b] Ratio of the different products in the reaction was determined by GC analysis. Products were identified by GC–MS.
[c] Acetone – 1 ml, 48 h.
[d] Acetone – 0.5 ml, 1 h.
[e] Acetone – 1 ml, 1 h.

The largest specificity was obtained using catalyst **1** and a concentration ratio of 1:12. Under these experimental conditions the allylic hydrogen is more reactive than the C=C double bond, and the reaction proceeds to give mainly the 2-cyclohexen-1-one as the main product and cyclohexene epoxide with the lowest yield (entry 1, Table 3). In control experiments, using cyclohexene under identical experimental conditions, but excluding metal complex, or in the presence of $Cu(CH_3COO)_2 \cdot H_2O$, did not give any oxidation products.

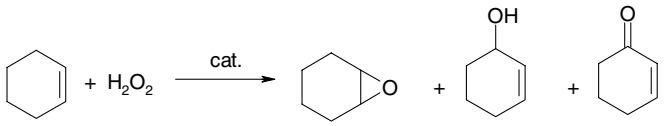

4. Conclusion

Two new copper(II) and cobalt(II) coordination polymers based on *o*-phthalic acid and imidazole have been synthesized and characterized by X-ray crystallography. The compounds have a polymeric chain structure with metal atoms linked by 1,6-bridging Pht^{2-} ligands. Preliminary catalytic investigations of the complexes for the oxidation of cyclohexene with H_2O_2 have been undertaken. The major oxidation product is 2-cyclohexen-1-one with appreciable amounts of 2-cyclohexen-1-ol depending on the reaction conditions. The yield of ketone is higher in the case of the copper complex. A systematic investigation on the use of the phthalate linker in the synthesis of 3d-metal coordination polymers and their magnetic and catalytic properties is currently underway.

5. Supplementary material

Crystallographic data for the structural analyses have been deposited with the Cambridge Crystallographic Data Centre, CCDC Nos. 271720 (**1**) and 275123 (**2**). Copies of this information may be obtained from The Director, CCDC, 12 Union Road, Cambridge, CB2 1EZ, UK (fax: +44 1233 336033; e-mail: deposit@ccdc.cam.ac.uk or http://www.ccdc.cam.ac.uk). Structure factors for **1** and **2** are available from the authors on request.

Acknowledgment

S.G.B. is grateful to DAAD for financial support to visit the Max-Planck-Institut für Kohlenforschung, Mulheim an der Ruhr, Germany.

References

[1] (a) S.R. Batten, R. Robson, Angew. Chem., Int. Ed. 37 (1998) 1460;
(b) P.J. Hagrman, D. Hargman, J. Zubieta, Angew. Chem., Int. Ed. 38 (1999) 2638;
(c) A.J. Blake, N.R. Champness, P. Hubberstey, W.-S. Li, M.A. Withersby, M. Schroder, Coord. Chem. Rev. 183 (1999) 117;
(d) R. Robson, J. Chem. Soc., Dalton Trans. (2000) 3735;
(e) M. Eddaoudi, D.B. Moler, H. Li, B. Chen, T.M. Reineke, M. O'Keeffe, O.M. Yaghi, Acc. Chem. Res. 34 (2001) 319;
(f) B. Moulton, M.J. Zaworotko, Chem. Rev. 101 (2001) 1629;
(g) B. Moulton, M.J. Zaworotko, Curr. Opin. Solid State Mater. Sci. 6 (2002) 117;
(h) Ch. Janiak, J. Chem. Soc., Dalton Trans. (2003) 2781.
[2] (a) M. Fujita, Y.J. Kwon, S. Washizu, K. Ogura, J. Am. Chem. Soc. 116 (1994) 1151;
(b) J.S. Seo, D. Whang, H. Lee, S.I. Jun, J. Oh, Y.J. Jeon, K. Kim, Nature 404 (2000) 982;
(c) J.M. Tanski, P.T. Wolczanski, Inorg. Chem. 40 (2001) 2026;
(d) O.R. Evans, H.L. Ngo, W. Lin, J. Am. Chem. Soc. 123 (2001) 10395;
(e) B. Xing, M.-F. Choi, B. Xu, Chem. Eur. J. 8 (2002) 5028;
(f) B. Gomez-Lor, E. Gutierrez-Puebla, M. Iglesias, M.A. Monge, C. Ruiz-Valero, N. Snejko, Inorg. Chem. 41 (2002) 2429;
(g) B. Kesanli, W. Lin, Coord. Chem. Rev. 246 (2003) 305.
[3] N.V. Gerbeleu, Yu.A. Simonov, G.A. Timko, P.N. Bourosh, J. Lipkowski, S.G. Baka, D.I. Saburov, M.D. Mazus, Russ. J. Inorg. Chem. 44 (1999) 1191.
[4] Yu.A. Simonov, M. Gdaniec, I.G. Filippova, S.G. Baca, G.A. Timco, N.V. Gerbeleu, Russ. J. Coord. Chem. 27 (2001) 353.
[5] S.G. Baca, Yu.A. Simonov, N.V. Gerbeleu, M. Gdaniec, P.N. Bourosh, G.A. Timco, Polyhedron 20 (2001) 831.
[6] S.G. Baca, I.G. Filippova, N.V. Gerbeleu, Yu.A. Simonov, M. Gdaniec, G.A. Timco, O.A. Gherco, Yu.L. Malaestean, Inorg. Chim. Acta 344 (2003) 109.
[7] S.G. Baca, I.G. Filippova, O.A. Gherco, M. Gdaniec, Yu.A. Simonov, N.V. Gerbeleu, P. Franz, R. Basler, S. Decurtins, Inorg. Chim. Acta 357 (2004) 3419.
[8] S.G. Baca, S.T. Malinovskii, P. Franz, Ch. Ambrus, H. Stoeckli-Evans, N.V. Gerbeleu, S. Decurtins, J. Solid State Chem. 177 (2004) 2841.
[9] Yu.A. Simonov, S.G. Baca, I.G. Filippova, M. Gdaniec, O.A. Gherco, N.V. Gerbeleu, Russ. J. Coord. Chem. 30 (2004) 727.
[10] S.G. Baca, I.G. Filippova, Ch. Ambrus, M. Gdaniec, Yu.A. Simonov, N. Gerbeleu, O.A. Gherco, S. Decurtins, Eur. J. Inorg. Chem. (2005) 3118.
[11] M.B. Cingi, C. Guastini, A. Musati, N. Nardelli, Acta Crystallogr. B 26 (1970) 1836.
[12] C.K. Prout, J.R. Carruthers, F.J.C. Rossotti, J. Chem. Soc. (1971) 3350.
[13] M.B. Cingi, A.M.M. Lanfredi, A. Tiripicchio, M.T. Camellini, Acta Crystallogr. B 33 (1977) 659.
[14] (a) M.B. Cingi, A.M.M. Lanfredi, A. Tiripicchio, M.T. Camellini, Acta Crystallogr. B 34 (1978) 134;
(b) M.B. Cingi, A.M.M. Lanfredi, A. Tiripicchio, M.T. Camellini, Acta Crystallogr. B 34 (1978) 406.
[15] M.B. Cingi, A.M.M. Lanfredi, A. Tiripicchio, M.T. Camellini, Acta Crystallogr. B 34 (1978) 412.
[16] J.W. Bats, A. Kallel, H. Fuess, Acta Crystallogr. B 34 (1978) 1705.
[17] M.B. Cingi, A.M.M. Lanfredi, A. Tiripicchio, M.T. Camellini, Acta Crystallogr. B 35 (1979) 312.
[18] M.B. Cingi, A.M.M. Lanfredi, A. Tiripicchio, M.T. Camellini, Acta Crystallogr. B 37 (1981) 2159.
[19] I. Krstanovic, L. Karanovic, D. Stojakovic, L. Golic, Cryst. Struct. Commun. 11 (1982) 1747.
[20] I. Krstanovic, Lj. Karanovic, Dj. Stojakovic, Acta Crystallogr. C 41 (1985) 43.
[21] K. Shakhatreh, E.G. Bakalbassis, I. Brudgam, H. Hartl, J. Mrozinski, C.A. Tsipis, Inorg. Chem. 30 (1991) 2801.
[22] D. Poleti, Lj. Karanovic, B.V. Prelesnik, Acta Crystallogr. C 49 (1993) 1249.
[23] E.G. Bakalbassis, A. Terzis, Inorg. Chim. Acta 218 (1994) 167.
[24] D.J. Williams, S.J. Maginn, R.J. Davey, Polyhedron 13 (1994) 1683.
[25] G. Smith, A.N. Reddy, K.A. Byriel, C.H.L. Kennard, J. Chem. Soc., Dalton Trans. (1995) 3565.
[26] J.L.L. Vaz, G. Duc, M. Petit-Ramel, R. Faure, O. Vittori, Can. J. Chem. 74 (1996) 359.
[27] D.R. Whitcomb, R.D. Rogers, Inorg. Chim. Acta 256 (1997) 263.
[28] A. Escuer, R. Vicente, F.A. Mautner, M.A.S. Goher, Inorg. Chem. 36 (1997) 1233.
[29] E.G. Bakalbassis, D.G. Paschalidis, C.P. Raptopoulou, V. Tangoulis, Inorg. Chem. 37 (1998) 4735.
[30] Z.-N. Chen, H.-X. Zhang, K.-B. Yu, B.-S. Kang, H. Cai, C.-Y. Su, T.-W. Wang, Z.-L. Lu, Inorg. Chem. 37 (1998) 4775.
[31] M.R. Bermejo, M. Fondo, A. García-Deibe, A.M. González, A. Sousa, J. Sanmartín, C.A. McAuliffe, R.G. Pritchard, M. Watkinson, V. Lukov, Inorg. Chim. Acta 293 (1999) 210.
[32] P. Lightfoot, A. Snedden, J. Chem. Soc., Dalton Trans. (1999) 3549.
[33] A.D. Burrows, R.W. Harrington, M.F. Mahon, C.E. Price, J. Chem. Soc., Dalton Trans. (2000) 3845.
[34] M. Devereux, M. McCann, V. Leon, M. Geraghty, V. McKee, J. Wikaira, Met. Based Drugs 7 (2000) 275.
[35] Y. Zhang, J. Li, Q. Su, Q. Wang, X. Wu, J. Mol. Struct. 516 (2000) 231.
[36] E. Suresh, K. Boopalan, R.V. Jasra, M.M. Bhadbhade, Inorg. Chem. 40 (2001) 4078.
[37] H.-X. Zhang, B.-S. Kang, A.-W. Xu, Z.-N. Chen, Z.-Y. Zhou, A.S.C. Chan, K.-B. Yu, C. Ren, J. Chem. Soc., Dalton Trans. (2001) 2559.
[38] Y. Wan, L. Jin, K. Wang, L. Zhang, X. Zheng, S. Lu, New J. Chem. (2002) 1590.
[39] J. Yao, W. Huang, B. Li, S. Gou, Y. Xu, Inorg. Chem. Commun. 5 (2002) 711.
[40] S. Wang, Y. Hou, E. Wang, Y. Li, L. Xu, J. Peng, S. Liu, C. Hu, New J. Chem. 27 (2003) 1144.
[41] C. Ma, C. Chen, Q. Liu, D. Liao, L. Li, L. Sun, New J. Chem. 27 (2003) 890.
[42] Y.-H. Wan, L.-P. Jin, K.-Z. Wang, J. Mol. Struct. 649 (2003) 85.
[43] L.-N. Zhu, M. Liang, Q.-L. Wang, W.-Z. Wang, D.-Z. Liao, Z.-H. Jiang, S.-P. Yan, P. Cheng, J. Mol. Struct. 657 (2003) 157.
[44] Y. Wan, L. Zhang, L. Jin, S. Gao, S. Lu, Inorg. Chem. 42 (2003) 4985.
[45] S.B. Raj, P.T. Muthianh, G. Bocelli, A. Canton, Inorg. Chem. Commun. 6 (2003) 748.
[46] X. Liu, C. Xie, X. Wang, G. Shen, D. Shen, Inorg. Chem. Commun. 6 (2003) 1433.
[47] A. Thirumurugan, S. Natarajan, J. Chem. Soc., Dalton Trans. (2004) 2923.
[48] H.-L. Liu, H.-Y. Mao, H.-Y. Zhang, Ch. Xu, Q.-A. Wu, G. Li, Y. Zhu, H.-W. Hou, Polyhedron 23 (2004) 943.
[49] B. Corain, A. Tessari, M. Zecca, J. Mol. Cat. A Chem. 96 (1995) L9.
[50] (a) W.H. Richardson, J. Am. Chem. Soc. 87 (1965) 247;
(b) W.H. Richardson, J. Am. Chem. Soc. 87 (1965) 1096;
(c) R. Hiatt, K.C. Irwin, C.W. Gould, J. Org. Chem. 33 (1968) 1430;
(d) N.A. Jonson, E.S. Gould, J. Am. Chem. Soc. 95 (1973) 5198;
(e) E.J.Y. Scott, J. Phys. Chem. 74 (1970) 1174;
(f) G. Vasvari, D. Gal, J. Chem. Soc., Faraday I 73 (1977) 399.

[51] B. Corain, E. Scanagatto, M. Basato, G. Valle, A.C. Veronese, S. Sitran, Inorg. Chim. Acta 148 (1988) 105.
[52] G. Das, R. Shukla, S. Mandal, R. Singh, P.K. Bharadwaj, Inorg. Chem. 36 (1997) 323.
[53] T. Ohta, T. Tachiyama, K. Yoshizawa, T. Yamable, T. Uchida, T. Kitagawa, Inorg. Chem. 39 (2000) 4358.
[54] T. Ohta, T. Tachiyama, K. Yoshizawa, T. Yamable, T. Uchida, T. Kitagawa, Tetrahedron Lett. 41 (2000) 2581.
[55] X. Meng, K. Lin, J. Sun, M. Yang, D. Jiang, F.-S. Xiao, Catal. Lett. 71 (3–4) (2001) 241.
[56] G.M. Sheldrick, SHELXS-97, Program for the Solution of Crystal Structures, University of Goettingen, Germany, 1997.
[57] G.M. Sheldrick, SHELXL-97, Program for the Refinement of Crystal Structures, University of Goettingen, Germany, 1997.
[58] W.D. Horrocks, J.N. Ishley, R. Whittle, Inorg. Chem. 21 (1982) 3270.
[59] X.H. Chen, B.-H. Ye, X.-Ch. Huang, Z.-T. Xu, J. Chem. Soc., Dalton Trans. (1996) 3465.
[60] K. Nakamoto, Infrared and Raman Spectra of Inorganic and Coordination Compounds, Wiley, New York, 1986, p. 236.
[61] R.C. Mehrotra, R. Bohra, Metal Carboxylates, Academic Press, New York, 1983, p. 48.
[62] G.B. Deacon, R.J. Phillips, Coord. Chem. Rev. 33 (1980) 227.

like hydroxypyridones [3,4,10] and -pyrones [10]. Calixarenes and modified calixarenes have also been prepared for uranyl extraction [1,2]. The uranyl complexes of calixarenes possess several phenolato ligands and many such complexes have been prepared and their structures have been reviewed recently [11]. It seems in many cases though, that these ligands are too rigid for optimal complex formation and more flexible ligands are required. Homoatsa and homo-oxa modified calixarenes are not as rigid as ordinary calixarenes [12,13], but the problem of the uranyl ion fitting neatly inside the cage still seems to be present. A distinct disadvantage is that the formed complexes are generally anionic and cations are required for charge balance. Homoatsacalixarenes, though, can potentially form a neutral zwitterion with uranyl ion, and an example is the ligand *p*-methyl-*N*-benzyltetrahomo-diazacalix[5]arene [13]. Open-chain, *ortho*-methylene linked di- and triphenols also form complexes with uranyl ion in a 1:2 molar ratio (U to L) in the presence of DABCO (1,4-diazabicyclo[2.2.2]octane) [14].

We have earlier used [O,N,O] type diphenoxo ligands for the complexation of W(VI) [15] and Mo(VI) ions [16]. In this work we prepared four (two are new), similar ligands for uranyl ion complexation by combining the features of the previously described ligands and we herein report the results of our studies. In this case, the ligands contain two phenol oxygens, one alcohol oxygen and one ammine nitrogen, thus there is the possibility of the ligand functioning as up to a tetradentate ligand. In Scheme 1 are depicted the ligand family in use. With these ligands we hope to offer optimal coordination conditions for the uranyl ion.

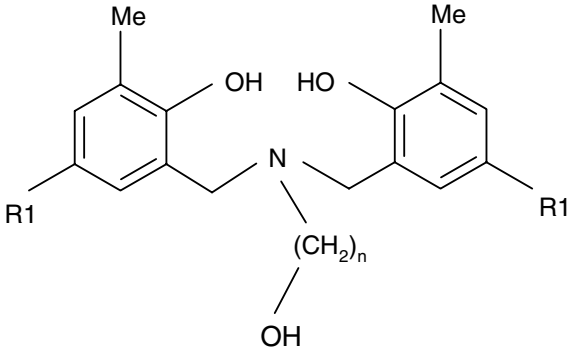

R1= methyl or *tert*-butyl

Ligand	*R1*	*n*
H_3L1	Me	2
H_3L2	*t*-Bu	2
H_3L3	Me	3
H_3L4	*t*-Bu	3

Scheme 1. The ligands under study.

2. Experimental

2.1. General information

2-Aminoethanol (Aldrich), 3-amino-1-propanol, 4-*t*-butyl-2-methylphenol (Fluka), triethylamine (Riedel), 2,4-dimethylphenol, 37% formaldehyde and uranyl nitrate hexahydrate (Merck) were used as supplied. The ligands H_3L1–H_3L4 were synthesized by following in the main a procedure for methylamino-*N*,*N*-bis(1-methylene-2-naphthol) [17]. Details of the syntheses, not optimized, are described below. NMR spectra were recorded on a Bruker AVANCE DPX 250 FT NMR spectrometer. ^{1}H and ^{13}C NMR spectra were recorded either in $CDCl_3$ or d_6-DMSO at 30 °C and chemical shifts are reported in ppm relative to $CDCl_3$ (δ 7.26, ^{1}H NMR; δ 77.0, ^{13}C NMR) or d_6-DMSO (δ 2.50, ^{1}H NMR; δ 39.50, ^{13}C NMR). Mass spectrometric measurements were performed using a Micromass LCT time of flight (TOF) mass spectrometer with electrospray ionization (ESI-MS). Elemental analysis was performed using a VarioEl III elemental analyzer.

2.2. H_3L1 {(*N*,*N*-bis(2-hydroxy-3,5-dimethylbenzyl)-2-aminoethanol) · 1/3toluene}

This compound has been earlier prepared without toluene slightly in different conditions [18a,18b]. To a solution of 2,4-dimethylphenol (2.44 g, 0.020 mol) in methanol (13 mL) was added aqueous formaldehyde (37%, 1.63 g, 0.020 mol) and 2-aminoethanol (0.61 g, 0.010 mol) with stirring. The resulting solution was refluxed for 24 h after which the solvent was evaporated off and the resulting oil left to stand at room temperature for two weeks. The small crystals that had formed in the oil were filtered off and recrystallized from toluene (8 mL) after which the white crystals were collected and washed with cold toluene (5 mL). Yield: 1.41 g (43%). Mp: 108–110 °C. ^{1}H NMR ($CDCl_3$, 250 MHz): 2.20 (d, $J = 2.3$ Hz, 12H, aryl CH_3), 2.69 (t, $J = 5.3$ Hz, 2H, NCH_2CH$_2$), 3.73 (s, 4H, NCH_2-aryl), 3.87 (t, $J = 5.3$ Hz, 2H, OCH_2CH$_2$), 6.70 (s, 2H, aryl), 6.85 (s, 2H, aryl). ^{13}C NMR ($CDCl_3$, 63 MHz): 15.9, 20.3 (aryl *C*H$_3$), 53.7, 57.0, 60.5 (N*C*H$_2$CH$_2$, N*C*H$_2$-aryl, O*C*H$_2$CH$_2$), 121.1, 124.9, 128.3, 128.5, 131.4, 151.9 (aryl). The NMR data were in agreement with the literature [18b]. ESI-MS *m*/*z*: 330.23 $[H_3L1 + H]^+$. The calculated value for H_3L1 was: $m/z = 330.21$ $[H_3L1 + H]^+$. Elemental *Anal*. Calc. for $C_{20}H_{27}NO_3 \cdot 1/3C_7H_8$: C, 74.48; H, 8.30; N, 3.89. Found: C, 74.57; H, 8.33; N, 3.75%.

2.3. H_3L2 {*N*,*N*-bis(2-hydroxy-5-t-butyl-3-methylbenzyl)-2-aminoethanol}

To a solution of 4-*t*-butyl-2-methylphenol (3.28 g, 0.020 mol) in methanol (13 mL) and water (5 mL) was added aqueous formaldehyde (37%, 1.63 g, 0.020 mol) and 2-aminoethanol (0.61 g, 0.010 mol) with stirring. The solution was refluxed for 30 h and then left to stand at

room temperature. Within a week, a white solid had formed which was separated by filtration, washed with cold methanol (5 mL) and recrystallized from methanol–water (9:1). Yield: 1.80 g (44%). Mp: 121–122 °C. ^{1}H NMR ($CDCl_3$, 250 MHz): 1.27 (s, 18H, aryl C(CH_3)$_3$), 2.23 (s, 6H, aryl CH_3), 2.72 (t, $J = 5.3$ Hz, 2H, NCH_2CH$_2$), 3.77 (s, 4H, NCH_2-aryl), 3.89 (t, $J = 5.3$ Hz, 2H, OCH_2CH$_2$), 6.89 (s, 2H, aryl), 7.05 (s, 2H, aryl).^{13}C NMR ($CDCl_3$, 63 MHz): 16.3 (aryl CH_3), 31.6 (aryl C(CH_3)$_3$), 33.9 (aryl C(CH$_3$)$_3$), 53.8, 57.1, 60.4 (NCH$_2$CH$_2$, NCH$_2$-aryl, OCH$_2$CH$_2$), 120.1, 124.4, 124.8, 127.7, 142.0, 151.9 (aryl). ESI-MS m/z: 414.29 $[H_3L2 + H]^+$. The calculated value for H_3L2 is: $m/z = 414.30$ $[H_3L2 + H]^+$. Elemental *Anal.* Calc. for $C_{26}H_{39}NO_3$: C, 75.50; H, 9.50; N, 3.39. Found: C, 74.45; H, 9.45; N, 3.45%.

2.4. H_3L3 {*N,N*-bis(2-hydroxy-3,5-dimethylbenzyl)-3-amino-1-propanol}

The preparation of the compound is reported in patent literature [18a]. To a solution of 2,4-dimethylphenol (24.5 g, 0.2 mol) in ethanol (40 mL) was added aqueous formaldehyde (37%, 17.0 g, 0.21 mol) and 3-amino-1-propanol (7.52 g, 0.1 mol) with stirring. The resulting solution was refluxed for 24 h after which most of the solvent was evaporated off and the residue taken up in toluene (15 mL) and then left to stand at −25 °C for one week. The crystals that formed were separated by filtration and the filtrate returned to cold storage for the harvesting of a second crop of crystals after a further week of storage. Total yield 1.77 g (5.2%). Mp: 126–127 °C. ^{1}H NMR ($CDCl_3$, 250 MHz): 1.88 (m, 2H, NCH$_2$CH_2CH$_2$), 2.19 (d, $J = 10.9$ Hz, 12H, aryl CH_3), 2.61 (t, $J = 6.6$ Hz, 2H, NCH_2CH$_2$), 3.63 (s, 4H, NCH_2-aryl), 3.76 (t, $J = 5.7$ Hz, 2H, OCH_2CH$_2$), 6.71 (s, 2H, aryl), 6.85 (s, 2H, aryl). ^{13}C NMR ($CDCl_3$, 63 MHz): 15.9, 20.3 (aryl CH_3), 28.6 (OCH$_2$$CH_2$), 51.6, 56.3, 61.4 (NCH$_2CH_2$, NCH$_2$-aryl, OCH$_2CH_2$), 121.6, 124.6, 128.3, 128.6, 131.0, 151.8 (aryl). ESI-MS m/z: 344.23 $[H_3L3 + H]^+$. The calculated value for H_3L3 is: $m/z = 344.22$ $[H_3L3 + H]^+$. Elemental *Anal.* Calc. for $C_{21}H_{29}NO_3$: C, 73.44; H, 8.51; N, 4.08. Found: C, 73.49; H, 8.54; N, 4.01%.

2.5. H_3L4 {(*N,N*-bis(2-hydroxy-5-t-butyl-3-methylbenzyl)-3-amino-1-propanol) · HCl}

To a solution of 4-*t*-butyl-2-methylphenol (8.21 g, 0.050 mol) in methanol (60 mL) was added aqueous formaldehyde (37%, 4.47 g, 0.055 mol) and 3-amino-1-propanol (2.10 g, 0.028 mol) with stirring. The resulting solution was refluxed for 9 h after which the solvent was removed and the resulting oil taken up in CH_3CN (10 mL) followed by the addition of 6 M HCl (6 mL, 36 mmol). The solvent was again removed and the resulting mixture of white solid and oil dissolved in CH_2Cl_2 (20 mL) with warming and left to stand at room temperature in an open vessel. The small crystals that formed during the evaporation process were separated by filtration and recrystallized from toluene. The white crystals were collected by filtration and washed with cold toluene (5 mL). Yield: 1.94 g (17%). Mp: 188–191 °C. ^{1}H NMR ($CDCl_3$, 250 MHz): 1.26 (s, 18H, aryl C(CH_3)$_3$), 2.07 (m, 2H, NCH$_2$CH_2CH$_2$) 2.40 (s, 6H, aryl CH_3), 3.26 (t, $J = 6.2$ Hz, 2H, NCH_2CH$_2$), 3.79 (t, $J = 5.7$ Hz, 2H, OCH_2CH$_2$), 4.20 (s, 4H, NCH_2-aryl), 6.96 (s, 2H, aryl), 7.19 (s, 2H, aryl). ^{13}C NMR ($CDCl_3$, 63 MHz): 17.03, 25.47, 31.47, 33.98 (aryl CH_3, aryl C(CH_3)$_3$, aryl C (CH$_3$)$_3$, NCH$_2$$CH_2$), 52.42, 56.55, 58.75 (NCH$_2$CH$_2$, NCH$_2$-aryl, OCH$_2$CH$_2$), 115.89, 125.46, 126.38, 130.39, 143.60, 151.26 (aryl). ESI-MS m/z: 428.27 $[H_3L4 + H]^+$. The calculated value for H_3L4 is: $m/z = 428.32$ $[H_3L4 + H]^+$. Elemental *Anal.* Calc. for $C_{27}H_{42}NO_3Cl$: C, 69.88; H, 9.12; N, 3.02. Found: C, 69.11; H, 9.13; N, 3.11%.

2.6. $[(UO_2)_2(H_2L1)_2(NO_3)_2]$ (**1**)

The complex **1** was prepared by dissolving together H_3L1 (0.062 g, 0.17 mmol) and $UO_2(NO_3)_2 \cdot 6H_2O$ (0.050 g, 0.10 mmol) in CH_3CN (5 mL). The resulting red solution was kept at room temperature for four days leading to the formation of crystals. The red crystals were filtered off, washed once with diethyl ether (5 mL) and then air dried. Yield: 0.025 g (38%). ^{1}H NMR (250 MHz, d_6-DMSO) 2.09, 2.15, 2.31, 2.60 (s, 24H, aryl CH_3), 2.97, 3.06 (t, 4H, NCH_2CH$_2$), 3.57, 4.19 (t, 4H, OCH_2CH$_2$), 3.65, 4.32, 4.38 (s, 8H, NCH_2-aryl), 4.83 (s, 2H, CH$_2$OH), 6.74, 6.79, 6.92, 6.98, 7.12 (s, 8H, aryl), 9.34 (s, 2H, CH$_2$NH^+). ^{13}C NMR (63 MHz, d_6-DMSO): 16.05, 16.50, 17.03, 20.07 (aryl CH_3), 51.96, 54.22, 54.82, 55.01, 57.23, 60.51 (NCH$_2$CH$_2$, NCH$_2$-aryl, OCH$_2$CH$_2$), 122.55–164.60 (aryl). Elemental *Anal.* Calc. for $C_{40}H_{52}N_4O_{16}U_2$: C, 36.37; H, 3.97; N, 4.24. Found: C, 35.73; H, 3.98; N, 4.22%. Molecular ion species were not observed by ESI-MS. Single-crystal X-ray analysis was performed on one of the crystals.

2.7. $[UO_2(H_2L1)_2] \cdot 2H_2O$ (**2**)

The complex **2** was prepared by dissolving together H_3L1 (0.054 g, 0.15 mmol), $UO_2(NO_3)_2 \cdot 6H_2O$ (0.0375 g, 0.075 mmol) and Et_3N (0.015 g, 0.15 mmol) in CH_3CN (16 mL). The resulting red solution was kept at room temperature for one week leading to the formation of crystals. The red crystals were filtered off, washed twice with diethyl ether (5 mL) and then air dried. Yield: 0.032 g (44%). ^{1}H NMR (250 MHz, d_6-DMSO): 2.09, 2.15, 2.31, 2.60 (s, 24H, aryl CH_3), 2.54, 3.06 (t, 4H, NCH_2CH$_2$), 3.56, 4.19 (t, 4H, OCH_2CH$_2$), 3.65, 4.38 (s, 8H, NCH_2-aryl), 4.83 (s, 2H, CH$_2$OH), 6.74, 6.79, 6.92, 6.98 (s, 8H, aryl), 9.34 (s, 2H, CH$_2$NH^+). ^{13}C NMR (63 MHz, d_6-DMSO): 16.03, 17.02, 20.07 (aryl CH_3), 51.97, 54.20, 54.82, 55.05, 58.23, 60.49 (NCH$_2$CH$_2$, NCH$_2$-aryl, OCH$_2$CH$_2$), 122.57–164.60 (aryl). Elemental *Anal.* Calc. for $C_{40}H_{56}N_2O_{10}U$: C, 49.89; H, 5.86; N, 2.91. Found: C,

50.16; H 5.91; N, 3.05%. ESI-MS *m/z*: 927.16 $[M + H]^+$, 949.16 $[M + Na]^+$, 965.10 $[M + K]^+$. The calculated M values for **2** are: $m/z = 927.43$ $[M + H]^+$, 949.41 $[M + Na]^+$, 965.39 $[M + K]^+$. Single-crystal X-ray analysis was performed on one of the crystals.

2.8. $[UO_2(H_2L2)_2] \cdot 2CH_3CN$ (**3**)

The complex **3** was prepared by dissolving together H_3L2 (0.038 g, 0.09 mmol), $UO_2(NO_3)_2 \cdot 6H_2O$ (0.023 g, 0.045 mmol) and Et_3N (0.009 g, 0.09 mmol) in CH_3CN (5 mL). The resulting light-red solution was kept at room temperature for two weeks leading to the formation of crystals. The light-red crystals were filtered off, washed once with diethyl ether (5 mL) and then air dried. Yield: 0.021 g (41%). ^{1}H NMR (250 MHz, d_6-DMSO): 1.22, 1.28 (s, 36H, aryl C(CH_3)$_3$), 2.13, 2.62 (s, 12H, aryl CH_3), 2.55, 3.08 (t, 4H, NCH_2CH$_2$), 3.59, 3.68, 4.14 (t, 4H, OCH_2CH$_2$), 3.68, 4.43 (s, 8H, NCH_2-aryl), 4.83 (s, 2H, CH$_2$O*H*), 6.95, 6.99, 7.12, 7.18 (s, 8H, aryl), 9.44 (s, 2H, CH$_2$NH^+). ^{13}C NMR (63 MHz, d_6-DMSO): 16.37, 17.40 (aryl CH_3), 31.38, 31.93, 33.16, 33.47 (aryl C(CH_3)$_3$), 52.41, 54.45, 54.93, 55.15, 58.33, 60.94 (NCH_2CH$_2$, NCH_2-aryl, OCH_2CH$_2$), 121.96–164.43 (aryl). Elemental *Anal*. Calc. for $C_{52}H_{76}N_2O_8U$: C, 57.03; H, 6.99; N, 2.56. Found: C, 55.39; H 6.64; N, 2.66%. Molecular ion species were not observed by ESI-MS. Single-crystal X-ray analysis was performed on one of the crystals.

2.9. $[UO_2(H_2L3)_2]$ (**4**)

The complex **4** was prepared by dissolving together H_3L3 (0.052 g, 0.15 mmol), $UO_2(NO_3)_2 \cdot 6H_2O$ (0.0375 g, 0.075 mmol) and Et_3N (0.015 g, 0.15 mmol) in CH_3CN (20 mL). The resulting red solution was kept at room temperature for two weeks allowing the formation of crystals. The red crystals were filtered off, washed once with diethyl ether (5 mL) and then air dried. Yield: 0.051 g (71%). ^{1}H NMR (250 MHz, d_6-DMSO): 1.68 (m, 4H, OCH$_2$CH_2CH$_2$), 2.09, 2.14, 2.31, 2.59 (s, 24H, aryl CH_3), 2.47, 2.92 (t, 4H, NCH_2CH$_2$), 2.98, 3.33 (t, 4H, OCH_2CH$_2$), 3.60 (s, 8H, NCH_2-aryl), 4.21 (s, 2H, CH$_2$O*H*), 6.72, 6.78, 6.90, 6.98 (aryl). ^{13}C NMR (63 MHz, d_6-DMSO): 16.09, 17.02, 20.08 (aryl CH_3), 23.12, 28.61 (OCH$_2$$CH_2CH_2$), 47.19, 50.00, 54.49, 59.21, 59.60 (NCH_2CH$_2$, NCH_2-aryl, OCH_2CH$_2$), 122.66–164.76 (aryl). Elemental *Anal*. Calc. for $C_{42}H_{56}N_2O_8U$: C, 52.83; H, 5.91; N, 2.93. Found: C, 52.86; H, 5.95; N, 3.36%. ESI-MS *m/z*: 955.23 $[M + H]^+$, 977.25 $[M + Na]^+$, 993.21 $[M + K]^+$. The calculated values for **4** were: $m/z = 955.46$ $[M + H]^+$, 977.44 $[M + Na]^+$, 993.42 $[M + K]^+$. Single-crystal X-ray analysis was performed on one of the crystals.

2.10. $[UO_2(H_2L4)_2]$ (**5**)

The complex **5** was prepared by dissolving together $H_3L4 \cdot HCl$ (0.042 g, 0.09 mmol), $UO_2(NO_3)_2 \cdot 6H_2O$ (0.0225 g, 0.045 mmol) and Et_3N (0.018 g, 0.18 mmol) in CH_3CN (5 mL). The resulting red/orange solution was kept at room temperature for two days leading to the formation of crystals. The red crystals were filtered off, washed once with diethyl ether (5 mL) and then air dried. Yield: 0.038 g (75%). ^{1}H NMR (250 MHz, d_6-DMSO): 1.22, 1.28 (aryl C(CH_3)$_3$), 1.71 (m, 4H, OCH$_2$CH_2CH$_2$), 2.13, 2.62 (s, 12H, aryl CH_3), 2.47, 2.83 (t, 4H, NCH_2CH$_2$), 2.96, 3.36 (t, 4H, OCH_2CH$_2$), 3.64 (s, 8H, NCH_2-aryl), 4.14 (s, 2H, CH$_2$O*H*), 6.93, 6.99, 7.11, 7.19 (aryl). ^{13}C NMR (63 MHz, d_6-DMSO): 16.39, 17.37 (aryl CH_3), 31.36, 31.90, 33.15, 33.45 (aryl C(CH_3)$_3$), 47.06, 50.04, 54.48, 59.19, 59.58 (NCH_2CH$_2$, NCH_2-aryl, OCH_2CH$_2$), 122.03–164.72 (aryl). Elemental *Anal*. Calc. for $C_{54}H_{80}N_2O_8U$: C, 57.74; H, 7.18; N, 2.49. Found: C, 57.72; H, 6.98; N, 2.89%. Molecular ion species were not observed by ESI-MS. Single-crystal X-ray analysis was performed on one of the crystals.

2.11. Uranyl extraction

Two-phase extraction studies were performed to determine the UO_2^{2+} cation uptake from water layer to CH_2Cl_2 layer by the ligands, H_3L1, H_3L2, H_3L3 and H_3L4. The experimental setup was following: to the bottom of a test tube was placed 3 mL of CH_2Cl_2 with ligand (0.420 mmol) and at the top of this layer was placed 2 mL of water with uranyl nitrate (c(U) = 12.5 mg/mL, n(U) = 0.105 mmol) leading to ratio of U to ligand 1:4. Furthermore, one test tube with CH_2Cl_2 containing no ligand was prepared. The samples for ICP ($V = 50$ μL, diluted to 20 mL) were taken from water layer over three days period of time. The samples were analyzed with ICP-OES at 385.958 nm using Perkin–Elmer Optima 4300DV instrument.

2.12. X-ray crystallography

Crystals suitable for single-crystal X-ray measurements were obtained directly from the reaction vessels. The crystal data for compounds **1**–**5** along with other experimental details, are summarized in Table 1. The crystallographic data were collected at 173 K on an Enraf Nonius Kappa CCD area-detector diffractometer using graphite monochromatized MoK_α radiation ($\lambda = 0.71073$ Å). Data collection was performed using φ and ω scans and the data processed using DENZO-SMN v0.93.0 [19]. SHELXA [20] absorption correction was applied to the data of **1**–**5**. The structures were solved by direct methods using the SHELXS-97 program [21] and full-matrix least-squares refinements on F^2 were performed using the SHELXL-97 program [21]. For all compounds the heavy atoms were refined anisotropically (except for C-1 in **3** and the disordered carbon atoms in **5**). The CH hydrogen atoms were included at fixed distances using fixed displacement parameters from their host atoms whilst other H atoms were refined using fixed displacement parameters. Structure figures were drawn using ORTEP-3 for Windows [22].

Table 1
Summary of crystallographic data for **1**–**5** at 173(2) K

Complex	**1**	**2**	**3**	**4**	**5**
Formula	$C_{40}H_{52}N_4O_{16}U_2$	$C_{40}H_{56}N_2O_{10}U$	$C_{56}H_{82}N_4O_8U$	$C_{42}H_{56}N_2O_8U$	$C_{54}H_{80}N_2O_8U$
Molecular weight	1320.92	962.90	1177.28	954.92	1123.24
Crystal system	monoclinic	monoclinic	triclinic	monoclinic	monoclinic
Space group (no.)	$P2_1/c$ (14)	$P2_1/c$ (14)	$P\bar{1}$ (2)	$P2_1/a$ (14)	$P2_1/c$ (14)
a (Å)	13.5841(3)	11.5007(2)	7.1860(2)	8.79500(10)	14.8509(3)
b (Å)	16.3528(4)	8.20490(10)	13.5433(5)	20.8201(4)	10.9267(4)
c (Å)	21.0204(5)	21.5198(5)	14.3965(5)	10.9669(2)	16.7848(7)
α (°)	90	90	92.854(2)	90	90
β (°)	106.354(2)	92.9907(7)	94.564(2)	99.1560(10)	102.040(2)
γ (°)	90	90	92.227(2)	90	90
V (Å^3)	4480.51(18)	2027.89(6)	1393.63(8)	1982.59(6)	2663.78(16)
Z	4	2	1	2	2
D_{calc} (g cm^{-1})	1.958	1.577	1.403	1.600	1.400
μ(MoK$_\alpha$) (cm^{-1})	72.93	40.59	29.66	41.48	30.99
Observed reflections	8454	3559	5255	4517	5409
R_{int}	0.082	0.072	0.056	0.040	0.059
Parameters	570	257	329	251	319
R_1[a]	0.077 (0.046)[b]	0.061 (0.030)	0.031 (0.029)	0.065 (0.031)	0.065 (0.033)
wR_2[c]	0.090 (0.082)	0.056 (0.050)	0.057 (0.057)	0.068 (0.060)	0.073 (0.065)
Largest difference in peak and hole (e Å^{-3})	1.42 and −1.31	0.52 and −0.54	0.72 and −1.04	0.60 and −0.57	0.59 and −0.57

[a] $R_1 = \sum\|F_o| - |F_c\|/\sum|F_o|$.
[b] Values in parentheses for reflections with $I > 2.0\sigma(I)$.
[c] $wR_2 = \{\sum[w(F_o^2 - F_c^2)^2]/\sum[w(F_o^2)^2]\}^{1/2}$ and $w = 1/[\sigma^2(F_o^2) + (aP)^2 + (bP)]$, where $P = (2F_c^2 + F_o^2)/3$.

3. Results and discussion

3.1. Syntheses of ligands and uranyl complexes

The details of the ligand syntheses are described in Section 2. Generally, the yields of the ligands were quite low. One reason for this is the fact that the solubility properties of the product and the phenol in question are quite similar and, in some cases, a crystalline adduct, containing both, was formed. Thus, the separation of the product from the sticky oil, which was generally formed at the end of the reaction, was quite difficult and as a result part of the product was lost together with the starting phenol during the separation process. The second reason for the low yield is that the reaction itself does not readily go to completion and intermediates with only one phenol moiety attached to the aminoalcohol were present. In two cases (H_3L3 and the di-*t*-butyl derivative, also prepared but not reported as it did not form solid complexes with uranyl ion), such products were able to be identified (using ^{1}H NMR) though it is likely that this happens in every case. Due to similarities in the solubilities of the product and the phenol in question, the reaction mixture of H_3L4 was treated with HCl (6 M) in order to render the product more polar with respect to the phenol. This proved to be a successful tactic as it rendered the separation process much easier.

Generally, the crystals of the complexes formed quite easily following the dissolution of the uranyl nitrate hexahydrate in acetonitrile together with an appropriate amount of the ligand. The formation of the complex was clearly indicated by the change in color of the solution from the yellow of uranyl nitrate to red. The reactions, however, were left to stand at room temperature for between two days to up to two weeks to allow the formation of crystals. The filtrates, though, were still red in color after removal of the crystals indicating that crystallization was incomplete.

H_3L1 formed solid dinuclear (**1**) or mononuclear (**2**) complexes from acetonitrile solution depending on the stoichiometry and the use of base. If the U to ligand molar ratio is 1:2 (or under 2 for ligand) complex **1** is obtained, but using the same molar ratio, 1:2, in the presence of 2 moles of triethylamine results in the formation of complex **2**. If the U to ligand molar ratio is 1:3 or more without extra base, only complex **2** forms. Complexes **1** and **2** both dissolve in DMSO and in acetone. The ^{1}H and ^{13}C NMR spectra in d_6-DMSO for compounds **1** and **2** were, accordingly, identical, so it appears that in DMSO solution compound **1** decomposes and coordinates with DMSO in the same manner as compound **2**, i.e., it forms the same species.

Ligands H_3L2, H_3L3 and H_3L4 (actually, $H_3L4 \cdot HCl$) formed complexes **3**–**5**, respectively, with $UO_2(NO)_3$ of general formula $[UO_2(H_2Lx)_2]$ (where $x = 2$, 3 or 4 and where **3** also contains two acetonitrile molecules in the unit cell). Complex **3** dissolves in DMSO, acetone, THF and CH_2Cl_2, and as such it has the best solubility properties. The acetonitrile molecules bound in the crystals of compound **3**, however, are able to escape readily from the crystalline matrix rendering the crystals prone to decay relatively soon after their removal from solution. The preparation of complex **5** using $H_3L4 \cdot HCl$ as starting material did not create any problems-the amount of the base was appropriately doubled-and this tactic of using the ligand hydrochloride seems to be a good practical method for the syntheses of these kind of complexes. The complexes

4 and **5**, though, dissolve effectively only in DMSO. For uranyl extraction studies, good solubility of the complex in organic solvents is essential, a demand which is not totally fulfilled with these present ligands. We believe, however, that these ligands can be modified accordingly such that their complex solubilities can be improved for organic, water-immiscible solvents. In order to do just this, the di-*t*-butyl ligand derivative was also prepared, but unfortunately it did not form a solid complex with uranyl ion due to the steric repulsion arising in the complex (vide infra).

3.2. Structural studies of the uranyl complexes

The solid-state structures of compounds **1**–**5** were verified by single-crystal X-ray analysis. Crystals of **1**, obtained from acetonitrile solution without the addition of base at room temperature, were comprised of neutral dinuclear UO_2 complex units in which one H_3L1 ligand binds to a UO_2^{2+} ion via one phenolato and one alkoxo oxygen donor bond (Fig. 1). The latter also forms a bond to the neighboring UO_2 unit to form a dinuclear unit. Selected bond lengths and angles for **1** are presented in Table 2. The alkoxo oxygens that bridge the two uranium ions have U–O bond lengths of 2.360(6) and 2.389(5) Å and 2.361(6) and 2.381(6) Å whilst the U–O(phenolato) bond lengths are 2.203(6) and 2.184(6) Å. The nitrate ion bonds bidentately to a single UO_2 unit and the nitrate oxygen atoms are at an average distance of 2.497 Å from the U atom. One phenol OH does not take part in bonding to U and the N atom acts as a base accepting a proton. The approximate coordination spheres around both U(VI) ions are distorted pentagonal bipyramidal with trans UO_2 groups. However, the plane of five coordinated atoms resembles a four-coordination plane if the nitrate group is taken as a single donor as the oxygen atoms of the nitrate ions and

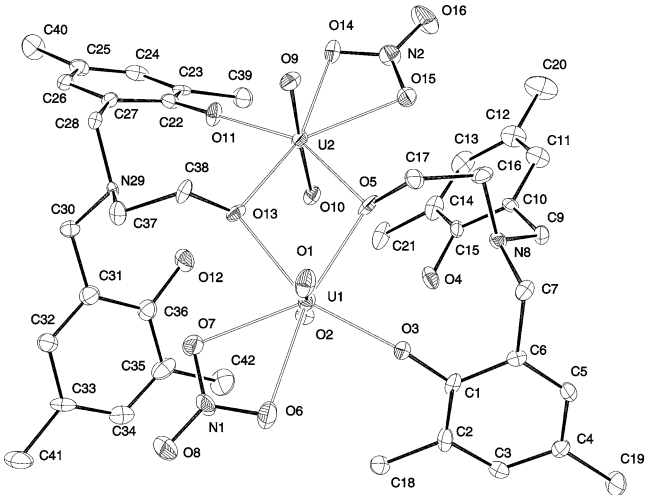

Fig. 1. Molecular structure of $[(UO_2)_2(H_2L1)_2(NO_3)_2]$ (**1**). Thermal ellipsoids have been drawn at 30% probability level. The hydrogen atoms have been omitted for clarity.

Table 2
Selected bond lengths (Å) and angles (°) for **1**

Bond lengths (Å)	
U1–O1	1.786(6)
U1–O2	1.778(6)
U1–O3	2.203(6)
U1–O5	2.360(6)
U1–O6	2.483(7)
U1–O7	2.499(6)
U1–O13	2.389(5)
U2–O9	1.783(6)
U2–O10	1.774(6)
U2–O11	2.184(6)
U2–O13	2.361(6)
U2–O14	2.503(6)
U2–O15	2.502(6)
U2–O5	2.381(6)
C1–O3	1.336(9)
C15–O4	1.385(11)
C17–O5	1.449(10)
C22–O11	1.342(10)
C36–O12	1.394(11)
C38–O13	1.420(9)
Bond angles (°)	
O1–U1–O2	177.5(3)
O3–U1–O5	85.1(2)
O3–U1–O13	155.6(2)
O5–U1–O13	70.9(2)
O7–U–O6	51.1(2)
O9-U2–O10	177.1(3)
O11–U2–O13	85.7(2)
O5–U2–O11	156.0(2)
O5–U2–O13	71.0(2)
O14–U2–O15	50.7(2)
U1–O5–U2	105.1(2)
U1–O13–U2	104.8(2)
C1–O3–U1	157.0(5)
C22–C11–U2	170.1(5)

the uranium ions (O–U–O) only form very small angles {51.1(2)° and 50.7(2)°}. The main features of this structure are the following: (1) the oxo donors are located in trans positions {the O–U–O angles are 177.5(3)° and 177.1(3)°}, (2) the O(alcoholato)–U–O(phenolato) angles are 85.1(2)° and 85.7(2)°, and (3) the bridging U–O–U angles are 105.1(2)° and 104.8(2)°. Of note, dinuclear alkoxo bridged complexes have been reported earlier [23] (see Table 2).

Red crystals of **2**–**5** were obtained from acetonitrile solution by the addition base (triethylamine). The complexes have a centrosymmetrical structure in which the uranium ion has a compressed octahedral symmetry (Figs. 2–5). The asymmetric unit of all compounds contains a UO unit with a negative H_2L^- ligand, which binds to the UO unit via two phenoxide groups. Selected bonding parameters for these four molecules are compared in Table 3. The aliphatic nitrogen atom bears an accepted proton and does not form a bond with the U(VI) ion. The proton on the nitrogen atom, however, forms weak H-bonds to O-2 and O-3 (and also to O-4 in **4**). The complexes are neutral zwitterionic units with two negative charges on oxygen atoms

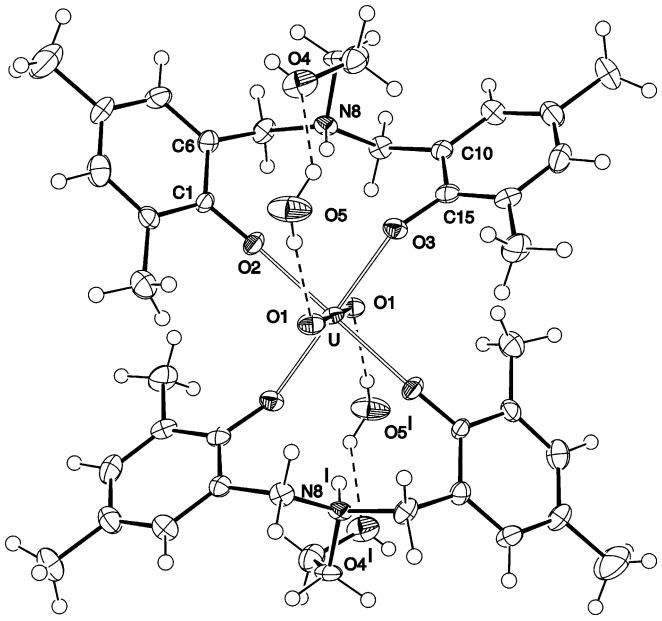

Fig. 2. Molecular structure of $[UO_2(H_2L1)_2]\cdot 2H_2O$ (**2**). Thermal ellipsoids have been drawn at 30% probability level. Symmetry operation i: $-x, -y, -z$.

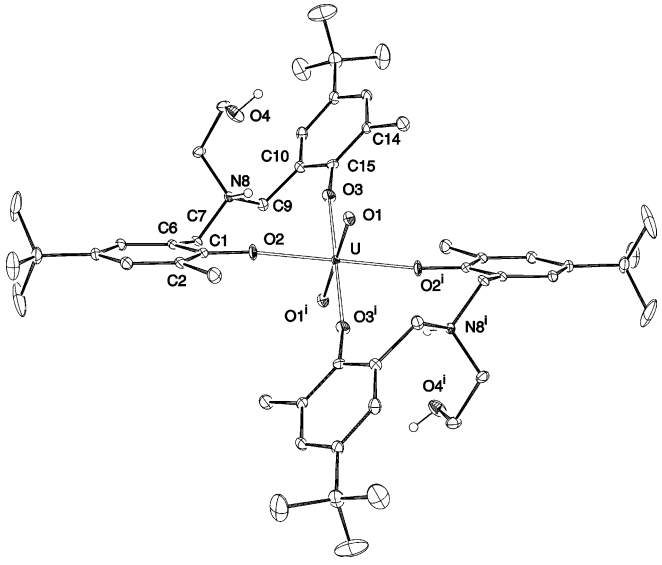

Fig. 3. Molecular structure of $[UO_2(H_2L2)_2]\cdot 2CH_3CN$ (**3**). Thermal ellipsoids have been drawn at 30% probability level. Acetonitrile molecules are not shown and the CH hydrogen atoms have been omitted for clarity. Symmetry operation i: $-x, -y, -z$.

and a positive charge on each nitrogen atom. The aliphatic alcohol groups do not take part in bonding with uranyl ion, but do form H-bonds in all compounds. The overall structure is similar to the uranyl homoazacalixarene complex [13], where the uranyl ion is located inside the cage.

The U–O(phenoxide) distances in **4** are 2.214(3) and 2.256(3) Å and in **2**–**5** they lie in the range 2.221(2)-2.241(3) Å. These bond distances are near the estimated "ideal" value of 2.2 Å found in U(VI) compounds with unrestricted, unidentate alkoxide ligands [11a]. This suggests that these ligands bind to the UO_2^{2+} ion quite effectively. The larger difference in the U–O(phenoxide) bond distances in **4** (0.04 Å) compared to **2**–**5** (0.02 Å) is possibly due to packing reasons (vide infra) and which, for example,

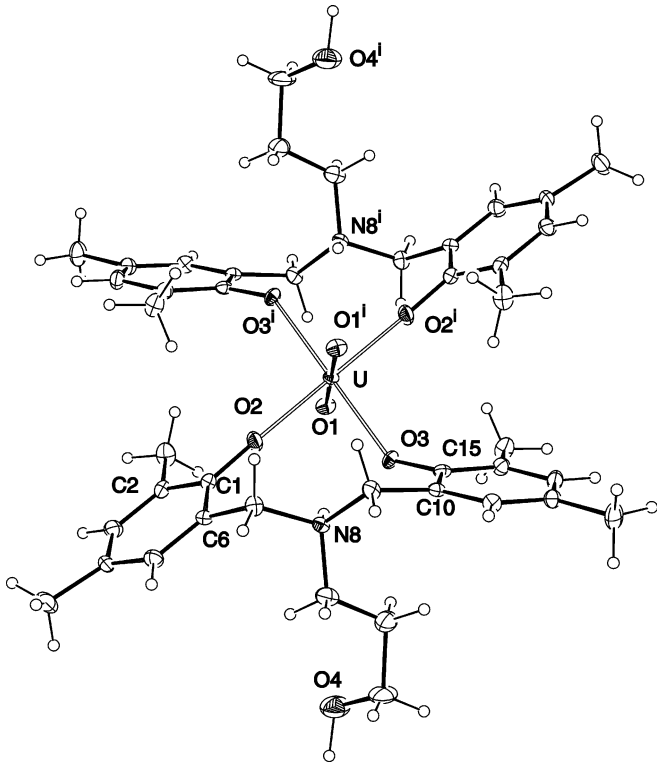

Fig. 4. Molecular structure of $[UO_2(H_2L3)_2]$ (**4**). Thermal ellipsoids have been drawn at 30% probability level. Symmetry operation i: $1-x, -1-y, -z$.

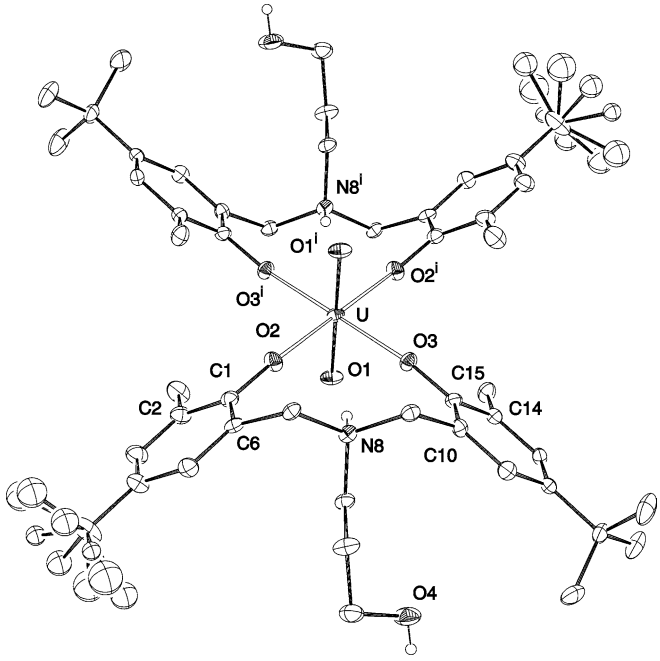

Fig. 5. Molecular structure of $[UO_2(H_2L4)_2]$ (**5**). Thermal ellipsoids have been drawn at 30% probability level and the CH hydrogen atoms have been omitted for clarity. Symmetry operation i: $-x, -1-y, 1-z$.

Table 3
Selected bond lengths (Å) and angles (°) for **2**–**5**

Complex	**2**	**3**	**4**	**5**
Bond lengths (Å)				
U–O1	1.817(3)	1.803(2)	1.808(3)	1.817(3)
U–O2	2.228(3)	2.236(2)	2.214(3)	2.232(3)
U–O3	2.241(3)	2.221(2)	2.256(3)	2.238(3)
C1–O2	1.328(5)	1.328(4)	1.330(5)	1.331(5)
C15–O3	1.344(5)	1.325(4)	1.355(5)	1.339(5)
Bond angles (°)				
O1–U–O2	89.75(13)	90.39(10)	88.88(13)	89.70(12)
O1–U–O3	89.13(13)	91.30(10)	90.40(12)	89.35(11)
O2–U–O3	84.97(12)	85.89(8)	82.38(11)	84.43(10)
O2–U–O3[a]	95.03(12)	94.11(8)	97.62(11)	95.57(10)
C1–O2–U	162.7(3)	173.4(2)	174.0(3)	160.3(3)
C15–O3–U	147.1(3)	167.0(2)	137.1(3)	158.9(3)
τ_1 vs. τ_2[b]	52.9(2)	50.0(1)	35.2(2)	66.4(1)

[a] Atom generated by inversion.
[b] Dihedral angle between the planes C1···C6 and C10···C15.

can cause distortion of the U–O–C angle. Generally, the larger the U–O–C angle is, the shorter the U–O bond distance becomes.

In all molecules, the coordination mode of aminobis(phenolate) is rather similar, but the aminoalcohol group behaves differently in its H-bond formation. In complex **2**, water molecules are present which are H-bonded to the oxo atom of the uranyl ion and the aminoalcohol oxygen atom (see Fig. 2). The hydrogen at the aminoalcohol oxygen also bonds to a water molecule. In **3**–**5**, the hydrogen of the aminoalcohol hydroxyl bonds to the uranyl oxo group. Complex **5** possesses both the shortest intermolecular O1···O4 distance {2.741(5) Å} and the longest U=O bond {1.817(3) Å} as a H-bond to the uranyl oxygen atom is known to increase the U=O bond length. But on the other hand, strong donor ligands that coordinate in an equatorial plane to the uranyl ion have been found to labilize U=O bonds [24] and thus it is not easy to distinguish between these two effects.

Conformational differences of the coordinated ligands in **2**–**5** were evident by analysis of the torsional or dihedral angles in the structures. In particular, the dihedral angles between the phenyl rings (formed by the atoms C1···C6 and C10···C15) vary and the angles between these planes in **2**–**5** are 52.9(2)°, 50.0(1)°, 35.2(2)° and 66.4(1)°, respectively. These deviations indicate that the frameworks of the ligands are flexible and that they have enough freedom to accommodate slightly different arrangements in the solid state for packing reasons.

Uranyl ion complexation with a ligand in which the methyl groups in positions 3 and 3′ of H_3L2 was replaced with *t*-butyl groups, i.e., using the ligand, *N*,*N*-bis(2-hydroxy-3,5-di-*t*-butyl-benzyl)-2-aminoethanol, was also attempted. However, a solid complex could not be crystallized out from solution although the uranyl solution did turn red indicating at least some ligand complexation. Steric constraints can account for this inability to obtain a solid complex. In the solid state of the uranyl complexes, the *t*-butyl groups at position 3 would come so close to each other that the complex is unstable (in **2** and **3**, the two relevant methyl groups are at distances of 4.013 and 4.015 Å from each other, respectively). So replacement of the methyl groups at position 3 by *t*-butyl groups simply prevents complex formation on steric hindrance grounds. Steric constraints are known, in fact, to control the formation of isomers in uranyl phenoxo complexes [25].

3.3. Uranyl ion extraction studies

The results of uranyl ion extraction studies at room temperature (22–23 °C) with the ligands H_3L1 and H_3L3 are shown in Fig. 6. The ratio of the ligand to the uranyl ion was 4:1. The concentration of the uranyl ion in the water layer of the control sample was constant during the three days follow up. The transfer of the uranyl ion from water layer to CH_2Cl_2 with H_3L_3 was 93% and with H_3L1 85% during 48 h. Already after 4 h extraction with H_3L3 84% of uranyl ions were in CH_2Cl_2 while with H_3L1 we needed 30 h to reach the same uranyl extraction level. So the H_3L3 ligand is much better extractor than H_3L1. With both ligands, H_3L1 and H_3L3, red crystals formed into and under the CH_2Cl_2 layer. These crystals were analyzed with single-crystal X-ray diffraction and they turned out to be compounds **2** and **4**, respectively. The mass% of uranyl complex **4** in CH_2Cl_2 was 78% measured from the initial level of uranyl ions in H_2O layer and 84% measured from the uranyl ions extracted to CH_2Cl_2 layer and the amount of uranyl complex **2** was 52% measured from the initial level of uranyl ions in H_2O layer and 62% measured from the uranium extracted to CH_2Cl_2 layer. The extraction system gained balance at the uranium concentration about 1 mg/mL. In order to improve the extraction of the uranyl ion, we must be able to control very complicated process in which the complexation of the uranyl ion with the ligands is one of the most important factor. The solubility of the formed

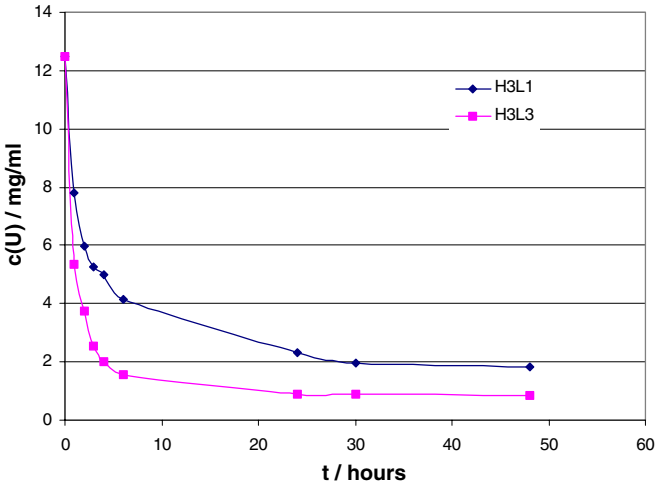

Fig. 6. The decrease of the uranium concentration as a function of time in the water layer during two-phase extraction study with ligands H_3L1 and H_3L3.

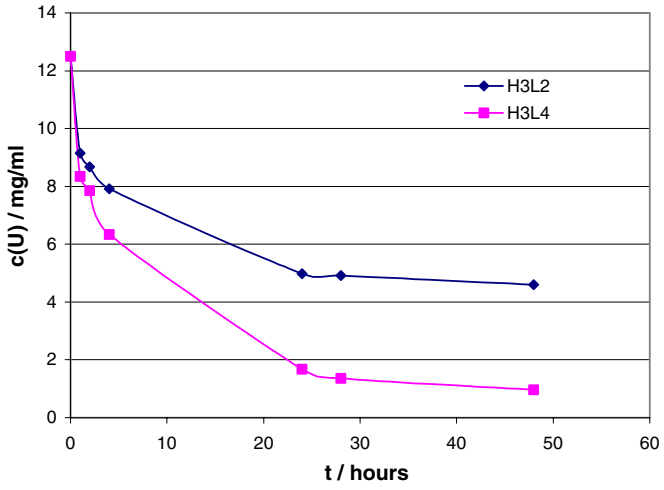

Fig. 7. The decrease of the uranium concentration as a function of time in the water layer during two-phase extraction study with ligands H_3L2 and H_3L4.

uranyl complex in the organic solvent is a second important factor and the crystallization of the uranyl complex from the organic solvent is a third one. Thus, the modification of the ligand is one of the useful ways to proceed.

The results of uranyl ion extraction studies with the ligands H_3L2 and H_3L4 are shown in Fig. 7. The uranyl ion do not crystallize with H_3L2 from dichloromethane without acetonitrile and thus the ability of H_3L2 to remove uranyl ion from water is worst. H_3L4 is slower and slightly worse than H_3L3 possibly because *t*-butyl group at position 5 increases the solubility of this uranyl complex in dichloromethane.

We are currently working in the field of the ligand modification trying to get more effective ligands for uranyl ion extraction. The pH of the water phase plays also important role during the extraction and this must also be studied. We have not yet studied how selectively this ligand family extracts the uranyl ion in the presence of other metal ions. This is an important matter, which will be also studied later.

4. Conclusion

In conclusion, we have found that $UO_2(NO_3)_2 \cdot 6H_2O$ in CH_3CN reacts with phenolic ligand precursors *N*,*N*-bis(2-hydroxy-3,5-dimethylbenzyl)-2-aminoethanol (H_3L1), *N*,*N*-bis(2-hydroxy-5-*t*-butyl-3-methylbenzyl)-2-aminoethanol (H_3L2), *N*,*N*-bis(2-hydroxy-3,5-dimethylbenzyl)-3-amino-1-propanol (H_3L3) and *N*,*N*-bis(2-hydroxy-5-*t*-butyl-3-methylbenzyl)-3-amino-1-propanol (H_3L4) to form dioxouranium(VI) complexes of the type $[UO_2(H_2L\text{-}x)_2] \cdot y$S (where $x = 1$–4, $y = 0$ or 2 and S = water or acetonitrile), and all with the similar compressed octahedral coordination spheres around U(VI). The ligand H_3L1 also formed a dinuclear complex with the uranyl ion. The neutral uranyl complexes form structures in which uranyl ion is almost ideally bonded to two ligands and the complex itself is zwitterionic. Although the yields of the ligand syntheses are poor, compared to calixarenes, these ligands are reasonably easy to prepare, and furthermore, the complexation of the new ligands mainly produce only one complex with a centrosymmetric structure.

For uranyl extraction studies, good solubility of the uranyl complexes in organic solvents is important. This is a condition that is not totally fulfilled with the present complexes, but on the other hand crystallization of the complex from the organic solvent can improve the extraction process. Thus, the ligands, H_3L1, H_3L3 and H_3L4 worked quite well in the extraction process: H_3L3 was the best one. We hope to increase our knowledge about the extraction system by preparing new ligands, which shall improve solubility of uranyl complexes in organic, water-immiscible solvents. We hope that, for example, the changing of the aminoalcohol to a simple alkyl amine will provide a solution to the problem of solubility. The selectivity of the ligands prepared in this work towards uranyl ion in the presence of other metals has not yet been studied. However, we believe that the complexes described here and their modified relatives open up new possibilities for uranyl ion extraction and the elimination of uranyl ions for ex. from biological systems.

5. Supplementary data

Crystallographic data (excluding structure factors) for the structure(s) reported in this paper have been deposited with the Cambridge Crystallographic Data Centre as supplementary publication nos. CCDC 277291–277295 for **1**–**5**. Copies of the data can be obtained free of charge on application to CCDC, 12 Union Road, Cambridge CB2 1EZ, UK (fax: (internat.) +44 1223 336 033; e-mail: deposit@ccdc.cam.ac.uk).

Acknowledgments

We are grateful to Dr. Karel D. Klika for correction of the language, to Elina Hautakangas for her help in the synthetic work and performing the elemental analysis and to Dr. Ari Väisänen for doing the ICP measurements.

References

[1] S. Shinkai, H. Koreishi, K. Ueda, T. Arimura, O. Manabe, J. Am. Chem. Soc. 109 (1987) 6371.
[2] P.D. Beer, G.D. Brindley, D.O. Fox, A. Grieve, M.I. Ogden, F. Szemes, M.G.B. Drew, J. Chem. Soc., Dalton Trans. (2002) 3101.
[3] A.E.V. Gorden, J. Xu, K.N. Raymond, P. Durbin, Chem. Rev. 103 (2003) 4207.
[4] M. Sawicki, J.-M. Siaugue, C. Jacopin, C. Moulin, T. Bailly, R. Burgada, S. Meunier, P. Baret, J.-L. Pierre, F. Taran, Chem. Eur. J. 11 (2005) 3689.
[5] J. Xu, K.N. Raymond, Inorg. Chem. 38 (1999) 308.
[6] N.N. Greenwood, A. Earnshaw, Chemistry of the Elements, Pergamon Press, Exeter, 1984, pp. 1477–1479.
[7] M.P. Wilkerson, C.J. Burns, H.J. Dewey, J.M. Martin, D.E. Morris, R.T. Paine, B.L. Scott, Inorg. Chem. 39 (2000) 5277.

[8] P.D. Wilson (Ed.), Nuclear Fuel Cycle: From Ore to Waste, Oxford Science Publications, Oxford, 1996, p. 373.
[9] K.A. Venkatesan, V. Sukumaran, M.P. Antony, P.R.V. Rao, J. Radioanal. Nucl. Chem. 260 (2004) 443.
[10] C. Drouza, V. Gramlich, M.P. Sigalas, I. Pashalidis, A.D. Keramidas, Inorg. Chem. 43 (2004) 8336.
[11] (a) J. Harrowfield, Gazz. Chim. Ital. 127 (1997) 663;
(b) P. Thuéry, M. Nierlich, J. Harrowfield, J. Vicens (Eds.), Calixarenes 2001, Kluwert Academic Publishers, Dordrecht, 2001.
[12] P. Thuéry, M. Nierlich, J. Vicens, B. Masci, H. Talemura, Eur. J. Inorg. Chem. (2001) 637.
[13] P. Thuéry, M. Nierlich, J. Vicens, H. Takemura, Polyhedron 20 (2001) 3183.
[14] (a) P. Thuéry, M. Nierlich, Z. Asfari, J. Vicens, J. Chem. Soc., Dalton Trans. (2000) 1297;
(b) P. Thuéry, Z. Asfari, M. Nierlich, J. Vicens, B. Masci, Polyhedron 21 (2002) 1949.
[15] A. Lehtonen, R. Sillanpää, Inorg. Chem. 43 (2004) 6501.
[16] A. Lehtonen, R. Sillanpää, Polyhedron 24 (2005) 257.
[17] (a) W.J. Burke, M.J. Kolbezen, C.W. Stephens, J. Am. Chem. Soc. 74 (1952) 3601;
(b) W.J. Burke, R.P. Smith, C. Weatherbee, J. Am. Chem. Soc. 74 (1952) 602.
[18] (a) W.O. Siegel, M.S. Chattha, Eur. Pat. Appl. 276073, 1988.;
(b) Y. Kim, J.G. Verkade, Organometallics 21 (2002) 2395.
[19] Z. Otwinowski, W. Minor, in: C.W. Carter, R.M. Sweet (Eds.), Macromolecular Crystallography: Part A, vol. 276, Academic Press, New York, 1997, pp. 307–326.
[20] G.M. Sheldrick, SHELX-97 (Release 97-2): A Program for Crystal Structure Refinement, University of Göttingen, Göttingen, Germany, 1998.
[21] G.M. Sheldrick, SHELXS-97 and SHELXL-97: Programs for Crystal Structure Solution and Refinement, University of Göttingen, Göttingen, Germany, 1997.
[22] L.J. Farrugia, J. Appl. Crystallogr. 32 (1999) 837.
[23] P.V. Rao, C.P. Rao, A. Sreedhara, E.K. Wegelius, K. Rissanen, E. Kolehmainen, J. Chem. Soc., Dalton Trans. (2000) 1213.
[24] D.L. Clark, S.D. Conradson, R.J. Donohoe, D.W. Keogh, D.E. Morris, P.D. Palmer, R.D. Rogers, C.D. Tait, Inorg. Chem. 38 (1999) 1456.
[25] M.P. Wilkerson, C.J. Burns, D.E. Morris, R.T. Paine, B.L. Scott, Inorg. Chem. 41 (2002) 3110.

2. Experimental

All reagents were used as purchased. $K_4Re_4S_{4-x}Te_x(CN)_{12}$ was synthesized through the reaction of $Re_4S_{4-x}Te_x(TeCl_2)_4Cl_8$ with KCN in water by technique reported for $K_4Re_4Se_4(CN)_{12}\cdot 6H_2O$ [10]. $Re_4S_{4-x}Te_x(TeCl_2)_4Cl_8$ was obtained through the reaction of $ReCl_5$ with a mixture of elemental S and Te [14]. FT-IR: Scimitar FTS 2000 – Elementary analyses: Vario EL of Elementar Analysensysteme GmbH, Z8000 (Hitachi).

2.1. Synthesis of $[\{Cu(en)_2\}_2Re_4S_{3.83}Te_{0.17}(CN)_{12}]\cdot H_2O$ (1)

A solution containing $CuSO_4\cdot 5H_2O$ (0.072 g) and en (0.03 ml) in concentrated aqueous ammonia (5 ml) was mixed with a solution of $K_4Re_4S_{4-x}Te_x(CN)_{12}$ (0.005 g) in water (5 ml). The resultant solution was kept for two weeks in a vessel covered by a watch glass. Dark red crystals formed during this time were filtered off and dried on filter paper. Yield: 0.0053 g. *Anal.* Calc. for $C_{20}H_{34}Cu_2N_{20}ORe_4S_{3.83}Te_{0.17}$: C, 30.2; H, 3.85; N, 32.8; S, 14.23. Found: C, 28.8; H, 4.11; N, 33.6; S, 14.7%. IR (KBr, cm^{-1}): $\nu_{CN} = 2154$(s), 2181(w).

2.2. Synthesis of $[\{Zn(en)_2\}_2Re_4S_{3.60}Te_{0.41}(CN)_{12}]\cdot 3.75H_2O$ (2)

A solution containing $ZnCl_2$ (0.037 g) and en (0.03 ml) in concentrated aqueous ammonia (3 ml) was mixed with a solution of $K_4Re_4S_{4-x}Te_x(CN)_{12}$ (0.005 g) in water (2 ml). The resultant solution was kept for two weeks in a vessel covered by watch glass. Dark-red crystals formed during this time were filtered off and dried on filter paper. Yield: 0.0034 g. *Anal.* Calc. for $C_{20}H_{39.50}Zn_2N_{20}O_{3.75}Re_4S_{3.60}Te_{0.41}$: C, 14.4; H, 2.39; N, 16.8; S, 6.94. Found: C, 14.9; H, 2.85; N, 16.9; S, 6.32%. IR (KBr, cm^{-1}): $\nu_{CN} = 2153$(s), 2191(w).

2.3. Synthesis of $[\{Cu(dien)(NH_3)\}Re_4S_{3.45}Te_{0.55}(CN)_{12}]\cdot 3H_2O$ (3)

A solution containing $CuSO_4\cdot 5H_2O$ (0.06 g) and dien (0.024 ml) in concentrated aqueous ammonia (3 ml) was mixed with a solution of $K_4Re_4S_{4-x}Te_x(CN)_{12}$ (0.005 g) in water (2 ml). The resultant solution was kept for one week in a vessel covered by watch glass. Dark-red plate-like crystals formed during this time were filtered off and dried on filter paper. Yield: 0.0056 g. *Anal.* Calc. for $C_{20}H_{38}Cu_2N_{20}O_3Re_4S_{3.64}Te_{0.36}$: Te, 3.02; Cu, 7.66. Found: Te, 2.80; Cu, 7.74%. IR (KBr, cm^{-1}): ν(CN) = 2170(w), 2162(w), 2154(s).

2.4. X-ray structural analyses

The structures of **1**–**3** were solved by X-ray structural analysis. Single-crystal X-ray diffraction data were collected with the use of graphite monochromatized Mo Kα radiation ($\lambda = 0.71073$ Å) at 293 K on a Bruker Nonius X8Apex diffractometer equipped with a 4K CCD area detector. The data were collected at 293 K. The φ-scan technique was employed to measure intensities. Decomposition of the crystals did not occur during data collection. Corrections were applied for Lorentz and polarization effects and for absorption [15]. The structures were solved by direct methods with employing difference Fourier

Table 1
Crystal and structure refinement data

	1	2	3
Empirical formula	$C_{20}H_{34}Cu_2N_{20}ORe_4S_{3.83}Te_{0.17}$	$C_{20}H_{39.50}N_{20}O_{3.75}Re_4S_{3.60}Te_{0.41}Zn_2$	$C_{20}H_{37}Cu_2N_{20}O_{2.50}Re_4S_{3.64}Te_{0.36}$
Formula weight	1587.03	1662.69	1632.21
Crystal size (mm)	$0.35\times0.12\times0.08$	$0.22\times0.04\times0.03$	$0.10\times0.09\times0.09$
Crystal system	orthorhombic	monoclinic	orthorhombic
Space group	$Pmn2_1$	$P2_1/n$	$Pmn2_1$
a (Å)	18.8841(3)	9.1790(3)	15.8391(8)
b (Å)	8.9767(4)	21.9702(5)	9.0423(4)
c (Å)	11.6672(7)	22.3207(6)	17.1629(9)
β (°)		95.4270(10)	
V (Å^3)	1977.79(15)	4481.1(2)	2458.1(2)
Z	2	4	2
ρ_{calc} (Mg/m^3)	2.665	2.465	2.205
μ (mm^{-1})	13.620	12.292	11.065
Index ranges	$-28\leqslant h\leqslant 27$	$-7\leqslant h\leqslant 11$	$-19\leqslant h\leqslant 16$
	$-12\leqslant k\leqslant 6$	$-26\leqslant k\leqslant 26$	$-8\leqslant k\leqslant 11$
	$-17\leqslant l\leqslant 17$	$-27\leqslant l\leqslant 27$	$-20\leqslant l\leqslant 20$
Maximum and minimum transmission	0.4087 and 0.0871	0.7093 and 0.1729	0.4041/0.4358
Reflections collected/unique, R_{int}	18237/7184, 0.0324	27740/8378, 0.0556	14544/4816, 0.0344
Data/restraints/parameters	7184/187/247	8378/30/500	14544/30/281
Final R indices [$I>2\sigma(I)$]	$R_1 = 0.0246$	$R_1 = 0.0535$	$R_1 = 0.0229$
	$wR_2 = 0.0472$	$wR_2 = 0.1258$	$wR_2 = 0.0484$
R indices (all data)	$R_1 = 0.0303$	$R_1 = 0.0915$	$R_1 = 0.0256$
	$wR_2 = 0.0484$	$wR_2 = 0.1388$	$wR_2 = 0.0490$

syntheses and refined anisotropically by full-matrix least-squares techniques on F^2 using the SHELXL-97 Release 97-2 software package [16]. Hydrogen atoms from the water molecules are not located. Hydrogen atoms from the organic ligands and ammonia are located by hydrogen bonds. ORTEP drawings were made using ORTEP III for Windows [17]. Crystallographic data as well as details of data collection and refinement for complexes **1**–**3** are listed in Table 1.

2.5. DFT calculations

Density functional theory calculations were carried out on different $[Re_4S_3Q(CN)_{12}]^{4-}$ (Q = S, Se, Te) models with full optimizations using the ADF2002 code [18]. The density functional consisted from LDA and GGA parts [19–21]. The STO basic set (TZ2P) without core-potentials was used for all atoms. The ZORA (zeroth-order relativistic approximation) method was used to account for the scalar relativistic effects [22]. The electronic binding energy (ΔE) are computed from the reaction $4Re + 3S + Q + 12C + 12N + 4e^- \rightarrow [Re_4S_3Q(CN)_{12}]^{4-}$. The atomic net charges for several $[Re_4S_3Q(CN)_{12}]^{4-}$ complexes obtained using the Hirshfeld analysis [23].

3. Results and discussion

3.1. Syntheses

$K_4[Re_4S_{4-x}Te_x(CN)_{12}]$ cluster compound has been synthesized accidentally during preparation of $K_4Re_4S_4(CN)_{12}$ cluster from $Re_4S_4(TeCl_2)_4Cl_8$ by boiling with KCN as described for $K_4Re_4Se_4(CN)_{12} \cdot 6H_2O$ [10]. According to elemental analysis the compound obtained contains the tellurium. This could be caused of sulfur shortage during the preparation of $Re_4S_4(TeCl_2)_4Cl_8$ from $ReCl_5$, S and Te [14]. Using $K_4[Re_4S_{4-x}Te_x(CN)_{12}]$, that may be described as solid solution between $K_4[Re_4S_4(CN)_{12}]$ and $K_4[Re_4S_3Te(CN)_{12}]$, copper or zinc salts and polydentate ligands, namely, ethylenediamine and diethylenetriamine, we have synthesized three new cluster compounds. All three compounds have been characterized by single-crystal X-ray diffraction method.

The two-dimensional compound **1** was synthesized by the reaction of an aqueous solution of the cluster $K_4[Re_4S_{4-x}Te_x(CN)_{12}]$ with an ammonia solution containing $CuSO_4$ and *en* in molecular ratio 1:2. The polymeric complex **2** was obtained in a similar manner using $ZnCl_2$ as a starting compound. Analogously, the molecular complex **3** was prepared using $CuSO_4$ and diethylenetriamine in ratio 1:1.

3.2. Structures

According to X-ray diffraction analysis there are two different cluster anions in compounds with compositions $[Re_4S_4(CN)_{12}]^{4-}$ and $[Re_4S_3Te(CN)_{12}]^{4-}$. The structure of $[Re_4S_4(CN)_{12}]^{4-}$ anion is similar to that in the related compounds. It contains Re_4S_4 cubane-like cluster core formed from nearly regular Re_4, with Re–Re and Re–(μ_3-S) distances in the ranges 2.7554(4)–2.7651(3) Å and 2.3497(13)–2.358(3) Å for **1**, 2.7599(7)–2.7748(8) Å and 2.345(18)–2.376(3) Å for **2**, 2.7431(13)–2.7820(14) Å and 2.34(2)–2.400(5) Å for **3**, respectively. Each Re atom is further ligated by three cyano-ligands. The structure of $[Re_4S_3Te(CN)_{12}]^{4-}$ looks like thiocyanide cluster, but one sulfur atom is substituted by the tellurium atom. The Re–(μ_3-Te) distances are in range 2.591(8)–2.654(5) Å for **1**, 2.627(5)–2.635(6) Å for **2** and 2.613(6)–2.621(4) Å for **3**. These values are similar to that found for $[Re_4Te_4(CN)_{12}]^{4-}$ anion. It is to be noted that these data are the first examples for cubane-like rhenium mixed chalcogenide cluster core Re_4S_3Te.

In structures of all three compounds, the Re_4S_4 and Re_4S_3Te cluster cores are ordered in such a way, that three position of Q_4 tetrahedron are equivalent and occupied with only sulfur atoms, but the fourth position is occupied with either sulfur or tellurium atoms.

Compound **1** has a polymeric grid structure in which the $[Re_4S_{3.83}Te_{0.17}(CN)_{12}]^{4-}$ cluster anions are situated in cross-points of this lattice and linked by $[Cu(en)_2]^{2+}$ cationic units as depicted in Fig. 1(a). Each Cu atom in the cationic part has 4 + 2 coordination environment and coordinated by four NH_2 groups of two ethylenediamine units in equatorial plane (Cu–N distances ranging from 2.008(5) to 2.028(5) Å), and by two N atoms of CN^- ligands of different cluster anions with a Cu–N distances, one of which is equal to 2.367(4) Å, and other one is longer (2.759(5) Å), but also can be considered as weak interaction.

Compound **2** also has a polymeric grid structure with $[Re_4S_{3.60}Te_{0.41}(CN)_{12}]^{4-}$ cluster anions in cross-points and $[Zn(en)_2]^{2+}$ moieties on the edges (Fig. 1(b)). However, two these lattices are differently arranged. In the case of **1** four CN^- groups of two rhenium atoms (2 + 2) take part in binding; on the other hand four CN^- ligand from three Re atoms (2 + 1 + 1) of cluster anion is in formation of polymeric structure in case of **2**. In this context, the different bridging modes have a crucial influence on the packing characteristics. The bent bridging modes in **1** resulted in the formation of wavy layers (Fig. 2(a)), whereas the tentatively flat binding of **2** generates approximately plane layers (Fig. 2(b)). There are two crystallographically independent zinc atoms in cationic part of **2**. Once again, every zinc atom has a similar environment as a copper atoms in **1**, namely, it is coordinated by amino groups of two ethylenediamines (Zn–N distances ranging from 2.093(15) to 2.143(13) Å) and by two N atoms of CN^- ligands of different cluster anions with a Zn–N with similar distances 2.221(13) and 2.334(13) Å.

In the molecular structure of compound **3**, two $[Cu(dien)(NH_3)]^{2+}$ cations are coordinated by the N atoms of CN^- ligands, that belong to one rhenium atom of the $[Re_4S_{3.45}Te_{0.55}(CN)_{12}]^{4-}$ anion (Fig. 3). Each Cu atom is coordinated by the 3N atoms of the dien ligand with

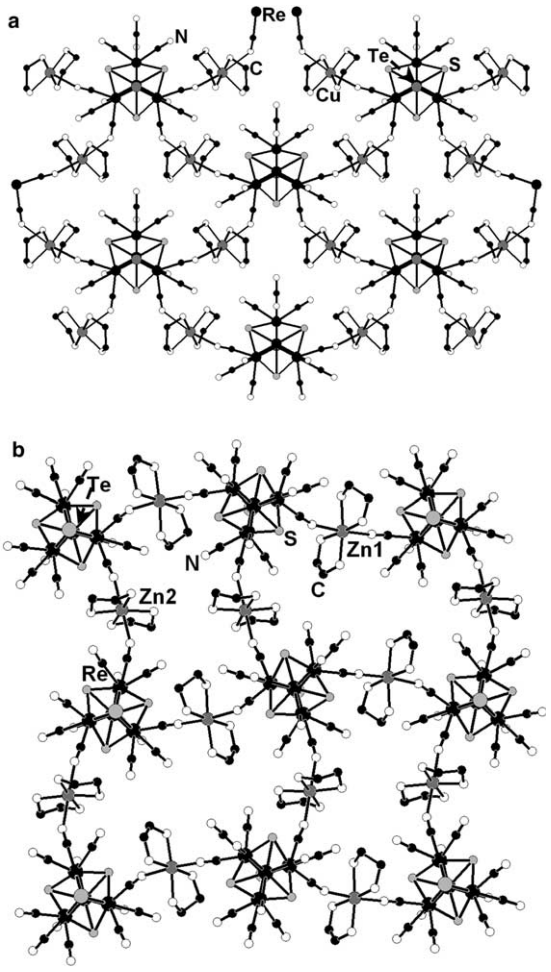

Fig. 1. Ball-and-stick representations of the $[\{M(en)_2\}_2\{cluster\}]_\infty$ layer of (a) **1** and (b) **2**. Hydrogen atoms and water molecules are omitted.

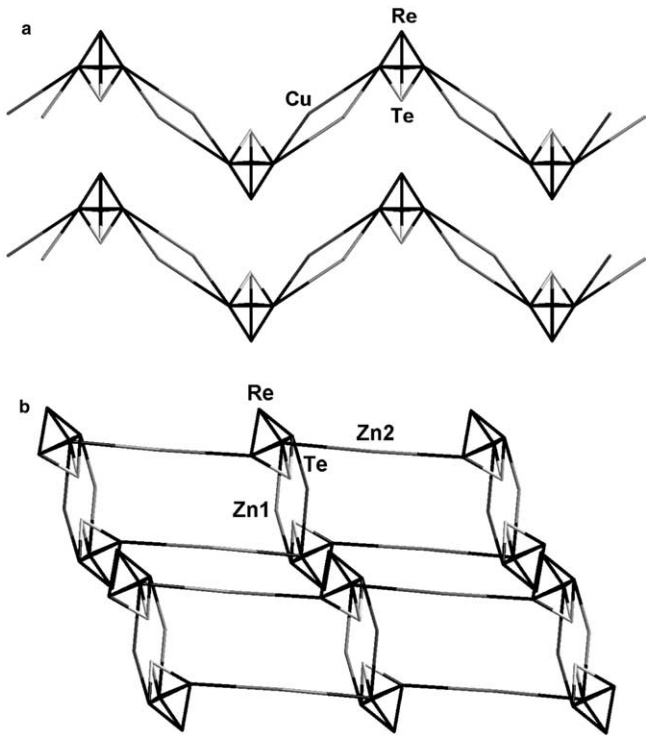

Fig. 2. Views of the stacking of layers in **1** (a) and **2** (b) using a stick model. Hydrogen, nitrogen, carbon, sulfur atoms are omitted for clarity.

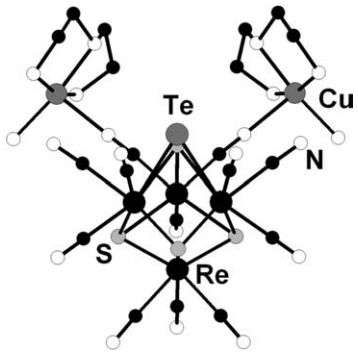

Fig. 3. View of the $[\{Cu(dien)(NH_3)\}_2Re_4S_{3.45}Te_{0.55}(CN)_{12}]$ molecule in compound **3**. Hydrogen atoms are omitted.

Cu–N distances ranging from 1.982(17) to 2.01(2) Å, by one NH_3 ligand with Cu–N distance of 1.979(19) Å and by N atom of a bridging CN^- ligand of the cluster anion with Cu–N distance 2.297(19) Å. Thus the coordination number of each Cu is equal to 5 and the copper atoms exhibit square–pyramidal coordination spheres with cyanide nitrogen in axial position.

It should be noted, that in all three structures metal cations have chosen CN groups which are the closest to tellurium atom position. To understand a reason of similar coordination the density functional theory calculations were carried out on different $[Re_4S_3Q(CN)_{12}]^{4-}$ (Q = S, Se, Te) cluster anions using ADF program. According to these calculations, there are several types of CN ligands in $[Re_4S_3Q(CN)_{12}]^{4-}$ (Q = Se, Te) cluster anions. Let's consider each Re atom to be octahedrally coordinated (without taking Re–Re bonds into account). First of all, there are three CN groups, which are bonded with ReS_3 fragment; this is the first type of ligands; remained CN ligands are coordinated to three ReS_2Q (Q = Se, Te) fragments. Within $ReS_2Q(CN)_3$ units one CN group is more distant from Q atom then another two groups (the ligands of

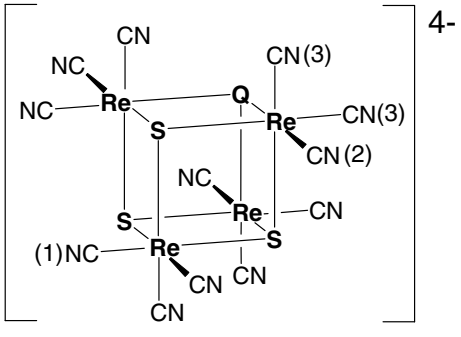

Scheme 1.

Table 2
Computed Hirshfeld charges and binding energies for $[Re_4S_3Q(CN)_{12}]^{4-}$ (Q = S, Se, Te) models

	Re	S	Q	C	N	$-\Delta E$ (eV)
$[Re_4S_4(CN)_{12}]^{4-}$	0.156 (4)	0.044 (4)		−0.069 (12)	−0.332 (12)	260.13
$[Re_4S_3Se(CN)_{12}]^{4-}$	0.147 (3); 0.156	0.039 (3)	0.122	−0.067 (3); [−0.070 (2); −0.067] {3}	−0.332 (3); [−0.336 (2); −0.332] {3}	259.55
$[Re_4S_3Te(CN)_{12}]^{4-}$	0.128 (3); 0.159	0.039 (3)	0.218	−0.066 (3); [−0.074 (2); −0.066] {3}	−0.332 (3); [−0.342 (2); −0.331] {3}	258.55

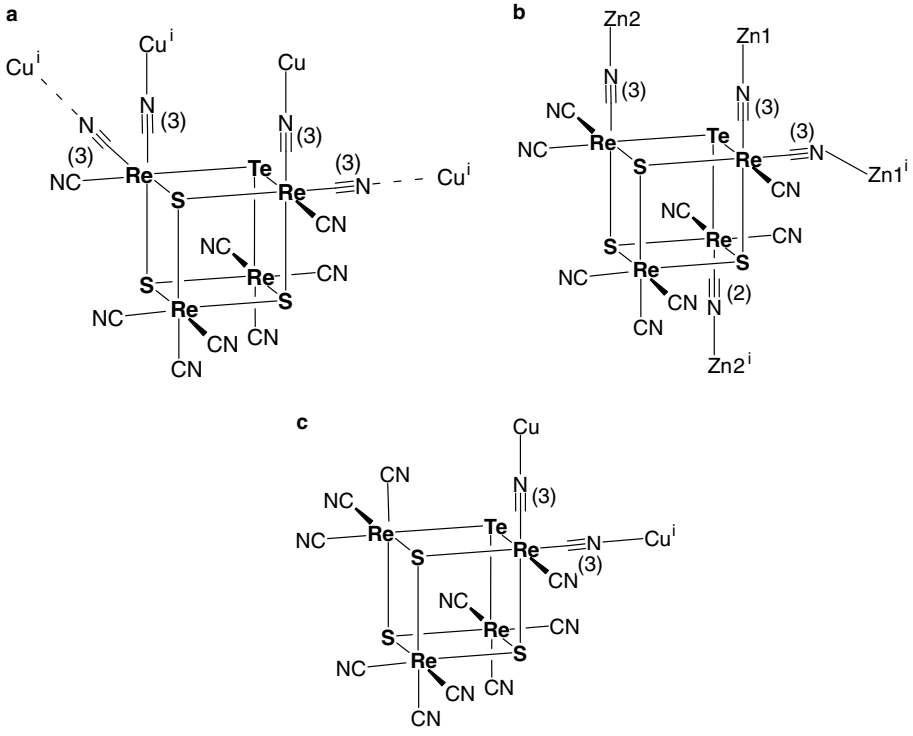

Scheme 2.

2 and 3 types, correspondingly) (Scheme 1). For CN ligands of types 1 and 2 the changes are negligible, but for six CN groups of the third type that are considerable and rise with decreasing of electronegativity of chalcogen atoms (Table 2). We propose that increasing of negative charge on N atoms of type 3 results in considerable preferences of metal ions in coordination to these atoms.

In the case of compound **1** all copper atoms are coordinated by CN groups of third type giving polymeric structure (Scheme 2a). It slightly differs from compound **2**, in which Zn1 atoms are coordinated by two CN groups of third type; whereas Zn2 cations are linked with CN groups of both second and third types. To put it another way only three of four bridged CN ligands of one cluster anion are of type 3, while the fourth one is of type 2 (Scheme 2b). In molecular compound **3**, two bridged CN groups also belong to the third type (Scheme 2c).

The received date supplement the previous research and show that substituting one sulfur atom by tellurium atom in cluster core Re_4S_4 we thus activate six CN groups of cluster anion for interaction with cation; all these groups are the nearest to Te atom.

4. Supplementary data

Supplementary data are available from the CCDC, 12 Union Road, Cambridge CB2 1EZ, UK on request, quoting the Deposition Nos. CCDC 271383 (**1**), 271384 (**2**) and 271385 (**3**).

Acknowledgement

This research was supported by the Program "The Universities of Russia" (Grant UR.05.01.208).

References

[1] T. Saito, J. Chem. Soc., Dalton Trans. (1999) 97.
[2] V.E. Fedorov, N.G. Naumov, Y.V. Mironov, S.B. Artemkina, K.A. Brylev, S.S. Yarovoi, O.A. Efremova, U-Hyon Peak, J. Struct. Chem., Engl. Transl. 43 (2002) 669.
[3] Y.V. Mironov, V.E. Fedorov, Rus. Chem. Bull., Int. Ed. 51 (2002) 569.
[4] J.-C.P. Gabriel, K. Boubekeur, S. Uriel, P. Batail, Chem. Rev. 101 (2001) 2037.
[5] Y.V. Mironov, O.A. Efremova, D.Y. Naumov, W.S. Sheldrick, V.E. Fedorov, Eur. J. Inorg. Chem. (2003) 2591.

[6] Y.V. Mironov, N.G. Naumov, K.A. Brylev, O.A. Efremova, V.E. Fedorov, K. Hegetschweiler, Angew. Chem. Int., Ed. Engl. 43 (2004) 1297.
[7] K.A. Brylev, Y.V. Mironov, N.G. Naumov, V.E. Fedorov, J.A. Ibers, Inorg. Chem. 43 (2004) 4833.
[8] Y.V. Mironov, V.E. Fedorov, C.C. McLauchlan, J.A. Ibers, Inorg. Chem. 39 (2000) 1809.
[9] Z. Zheng, T.G. Gray, R.H. Holm, Inorg. Chem. 38 (1999) 4888.
[10] Y.V. Mironov, A.V. Virovets, W.S. Sheldrick, V.E. Fedorov, Polyhedron 20 (2001) 969.
[11] Y.V. Mironov, A.V. Virovets, S.B. Artemkina, V.E. Fedorov, Angew. Chem. Int., Ed. Engl. 37 (1998) 2507.
[12] Y.V. Mironov, O.A. Efremova, V.E. Fedorov, O. Oeckler, A. Simon, C. Vicent, R. Lusar, Russ. Chem. Bull., Int. Ed. 52 (2003) 1698.
[13] Y.V. Mironov, O. Oeckler, A. Simon, V.E. Fedorov, Eur. J. Inorg. Chem. (2001) 2751.
[14] Y.V. Mironov, T.E. Albrecht-Schmitt, J.A. Ibers, Inorg. Chem. 36 (1997) 944.
[15] Bruker AXS Inc. (2004). SADABS (Version 2.11), Bruker Advanced X-ray Solutions, Madison, WI, USA.
[16] G.M. Sheldrick, SHELXTL DOS/Windows/NT. Version 5.10, Bruker Analytical X-ray Instruments, Inc., Madison, WI, 1997.
[17] L.J. Farrugia, ORTEP-3, Department of Chemistry, University of Glasgow.
[18] Amsterdam Density Functional (ADF) Program, Release 2002.02, Vrije Universteit, Amsterdam, The Netherlands, 2002.
[19] S.H. Vosko, L. Wilk, M. Nusair, Can. J. Phys. 58 (1980) 1200.
[20] A.D. Becke, Phys. Rev. A 38 (1988) 3098.
[21] J.P. Perdew, Phys. Rev. B 33 (1986) 8822.
[22] E. van Lenthe, A.E. Ehlers, E.J. Baerends, J. Chem. Phys. 110 (1999) 8943.
[23] F.L. Hirshfeld, Theor. Chim. Acta 44 (1977) 129.

structures but also make the complexes have particular characters [6]. Herein, we report the syntheses and characterizations of four new complexes, $[Cd(hpht)(phen)]_n$ (**1**), $[Cd(hpht)(2,2'\text{-bpy})]_n$ (**2**), $[Cd(hpht)(2,2'\text{-bpy})(H_2O)]_n \cdot 2nH_2O$ (**3**), and $[Cd(hpht)(4,4'\text{-bpy})]_n \cdot nH_2O$ (**4**).

2. Experimental

2.1. Materials and analyses

All chemicals are used as purchased without further purification. Thermogravimetric analyses were carried out with a NETZSCH STA 449C unit at a heating rate of 15 °C min^{-1} under nitrogen. IR spectra were recorded on a Magna 750 FT-IR spectrophotometer as KBr pallets. Elemental analyses were carried out on an Elementar Vario EL III analyzer. Fluorescence spectroscopy was performed on an Edinburgh Analytical instrument FLS920.

2.2. Syntheses

2.2.1. $[Cd(phen)(hpht)]_n$ (**1**)

H_2hpht (0.055 g, 0.3 mmol), phen (0.060 g, 0.3 mmol), and $Cd(CH_3COO)_2 \cdot 2H_2O$ (0.12 g, 0.45 mmol) were put in a mixed solution of 8 mL distilled H_2O and 2 mL ethanol, and the pH was adjusted to about 5.6 by diluent HCl aqueous solution. Then, the mixture was sealed in 25 mL Teflon-lined reactor and heated to 160 °C for 3 days, and then slowly cooled to room temperature. Colorless prism crystals of **1** were collected and washed with distilled water (yield: 67%). Complex **1** was also obtained by using $Cd(NO_3)_2 \cdot 4H_2O$ (pH 4.7, 58% yield), $CdCl_2$ (pH 5.6, 43% yield), or $CdSO_4$ (pH 5.4, 47% yield). *Anal.* Calc. for **1**: H, 3.00; C, 53.58; N, 5.95. Found: H, 3.08; C, 53.47; N, 5.98%. IR(KBr) 3067m, 3011m, 2992m, 1575vs, 1548vs, 1509vs, 1389vs, 1295s, 1146m, 1097m, 844vs, 828m, 774m, 731vs, 677vs.

2.2.2. $[Cd(hpht)(2,2'\text{-bpy})]_n$ (**2**)

The synthetic procedure of **2** is essentially the same as that for **1**, while $Cd(NO_3)_2 \cdot 4H_2O$ and 2,2′-bpy were used, and the pH was adjusted to about 5.3 by diluent NaOH aqueous solution. Colorless prism crystals of **2** were collected and washed with distilled water (yield: 76%). *Anal.* Calc. for **2**: H, 3.16; C, 51.08; N, 6.27. Found: H, 3.50; C, 50.89; N, 6.32%. IR(KBr) 3112m, 3077m, 3062m, 3027m, 2956m, 1590vs, 1544vs, 1485s, 1443vs, 1415vs, 1380vs, 1287s, 1061m, 1018s, 855m, 832m, 758vs, 723vs, 688s, 645m.

2.2.3. $[Cd(hpht)(2,2'\text{-bpy})(H_2O)]_n \cdot 2nH_2O$ (**3**)

The synthetic procedure is the same as that for **2**, and the pH was adjusted to about 5.5 by diluent NaOH aqueous solution. Colorless prism crystals of **3** were collected

Table 1
Crystallographic data for complexes **1**–**4**

	1	**2**	**3**	**4**
Empirical formula	$C_{21}H_{14}CdN_2O_4$	$C_{19}H_{14}CdN_2O_4$	$C_{19}H_{18}CdN_2O_7$	$C_{19}H_{16}N_2CdO_5$
Formula weight	470.74	446.72	498.75	464.74
T (K)	173(2)	173(2)	173(2)	173(2)
Wavelength (Å)	0.71073	0.71073	0.71073	0.71073
Crystal system	monoclinic	monoclinic	triclinic	monoclinic
Space group	$P2_1/n$	$P2_1/c$	$P\bar{1}$	$P2_1/n$
a (Å)	7.5827(9)	7.5458(2)	8.7507(18)	8.7140(9)
b (Å)	21.9042(19)	22.3825(4)	10.051(2)	9.2743(9)
c (Å)	11.2062(17)	10.2930(3)	11.637(3)	22.003(2)
α (°)	90	90	102.865(2)	90
β (°)	108.499(5)	103.088(1)	102.865(2)	92.443(6)
γ (°)	90	90	91.519(8)	90
V (Å^3)	1765.1(4)	1693.27(7)	943.6(4)	1776.6(3)
Z	4	4	2	4
D_{calc} (Mg/m^{-3})	1.771	1.752	1.755	1.738
Absorption coefficient (mm^{-1})	1.269	1.317	1.203	1.263
F(000)	936	888	500	928
Crystal size (mm)	0.40 × 0.20 × 0.04	0.52 × 0.46 × 0.12	0.40 × 0.20 × 0.10	0.80 × 0.40 × 0.30
θ Range for data collection (°)	3.02–27.48	1.82–25.00	3.06–27.48	3.21–27.47
Index ranges	$-9 \leqslant h \leqslant 9$, $-26 \leqslant k \leqslant 28$, $-10 \leqslant l \leqslant 14$	$-8 \leqslant h \leqslant 8$, $-26 \leqslant k \leqslant 23$, $-12 \leqslant l \leqslant 4$	$-11 \leqslant h \leqslant 11$, $-13 \leqslant k \leqslant 12$, $-15 \leqslant l \leqslant 13$	$-11 \leqslant h \leqslant 9$, $-12 \leqslant k \leqslant 12$, $-28 \leqslant l \leqslant 28$
Reflections collected	13489	4902	7729	12888
Refinement method	full-matrix least-squares on F^2	full-matrix least-squares on F^2	full-matrix least-squares on F^2	full-matrix least-squares on F^2
Data [$I > 2\sigma(I)$]/parameters	4024/253	2920/235	4245/274	4011/252
Goodness-of-fit on F^2	1.006	1.004	1.001	1.082
R_1 indices ($I > 2\sigma(I)$)	0.0365	0.0449	0.0350	0.0339
wR_2 indices (all data)	0.0942	0.2080	0.0946	0.0840
Largest difference peak and hole (e Å^{-3})	0.876 and −0.609	0.659 and −0.685	1.033 and −0.835	1.078 and −0.452

and washed with distilled water (yield: 28%). *Anal.* Calc. for **3**: H, 3.64; C, 45.75; N, 5.62. Found: H, 3.76; C, 45.73; N, 5.60%. IR(KBr) 3433mb, 3106w, 3079w, 3057w, 3030w, 1587vs, 15g60vs, 1543vs, 1478m, 1440s, 1391vs, 1162w, 1020m, 841w, 754s, 737s.

2.2.4. $[Cd(hpht)(4,4'\text{-bpy})]_n \cdot nH_2O$ (**4**)

The synthetic procedure is the same as that for **2**, while 4,4′-bpy was used to replace 2,2′-bpy, and the pH was adjusted to about 4.7 by diluent NaOH aqueous solution. Colorless prism crystals of **4** were collected and washed with distilled water (yield: 63%). *Anal.* Calc. for **4**: H, 3.47; C, 49.10; N, 6.03. Found: H, 3.64; C, 48.84; N, 5.99%. IR(KBr) 3416s, 3093m, 3077m, 3042m, 3019m, 1684m, 1605vs, 1548vs, 1489s, 1419s, 1380vs, 1314m, 1217s, 1151m, 1037s, 816s, 738s, 676s, 641s.

2.3. X-ray data collection and structure determination

The intensity data of **1**, **3**, **4** were collected on a Rigaku CCD diffractometer with graphite-monochromatized Mo Kα ($\lambda = 0.71073$ Å) radiation at 173 K, and the empirical absorption corrections were performed using the CRYSTALCLEAR program [7]. The intensity data of **2** were collected on a SIEMENS SMART CCD diffractometer with graphite-monochromatized Mo Kα ($\lambda = 0.71073$ Å) radiation at room temperature. The absorption correction was performed using the SADABS program [8]. The structures were solved by direct methods and refined on F^2 by full-matrix least-squares using the SHELXTL-97 program package [9]. All non-hydrogen atoms were refined anisotropically. The organic hydrogen atoms were generated geometrically (C–H = 0.95 Å). The H atoms of water were located from *E*-map, but those of the lattice water (O7) in **3** could not be located and were not taken into consideration, and the hydrogen atoms of the water in complex **4** were refined with AFIX 3 constraints on the O–H bonds. The crystallographic data for four complexes are listed in Table 1.

3. Results and discussion

3.1. Syntheses

As shown in Scheme 1, the coordination modes of $hpht^{2-}$ ligand are different in the four complexes. Andrew and co-workers have reported the second coordination mode, while the other two modes are new. As known, solvothermal reaction is complicated, and it is quite difficult to know what controls the coordination modes of $hpht^{2-}$ ligand and the formation of the complexes. In this work, we primarily studied the influence from auxiliary ligand, pH value, counter ion, and ratio of the starting materials.

The employment of terminal ligands 2,2′-bpy and 1,10-phen prevents complexes **1**–**3** from being extended to 2D or 3D architectures, but yields infinite 1-D chain structures of the three complexes. When bridging ligand 4,4′-bpy was used, 2D network **4** was obtained. Unfortunately, when 1,3-di(4-bpy)propane and piperazine were used as bridging ligands, the experiments were failed. The pH value plays a crucial role for the formation of the complexes. It is only within the specific pH range that complexes **1**–**4** can be obtained and different pH values lead to different yields of the products. More interestingly, although the starting materials and reaction conditions are quite similar, the structures of **2** and **3** are significantly different, the slightly different of the pH values of the reaction medium might play important role, although detailed reaction mechanism still remains unclear. We also studied the influence from counter ions and the mole ratio of starting materials. The results illustrate that the two factors only induce different yields of the products and may be not the key factors for the synthetic reactions.

3.2. Crystal structures

3.2.1. Crystal structures of complexes *1* and *2*

The selected bond lengths and angles of complex **1** are listed in Table 2. The asymmetric unit of **1** consists one Cd(II) ion, a phen ligand and a $hpht^{2-}$ ligand. The Cd(II) ion is six-coordinated by two nitrogen atoms from phen and four oxygen atoms from three $hpht^{2-}$ ligands in a distorted octahedron coordination geometry, as shown in Fig. 1. The Cd–O(N) bond distances are in the range 2.275–2.418 Å, with an average value of 2.350 Å. The $hpht^{2-}$ ligand links three Cd(II) ions, in which the carboxylate group chelates a Cd(II) ion and the ethylic carboxylate group bridges two Cd(II) ions (Scheme 1(a)). The two Cd(II) ions connected by two bridging ethylic carboxylate groups with interatomic distance of 4.023 Å form the basic building unit, $Cd_2(hpht)_2(phen)_2$, of the whole structure. Each two of such units are connected together through sharing the $hpht^{2-}$ ligands to form the final double chain structure. Two kinds of macrocyclic rings, one is 16-member ring (A) and the other is 8-member ring (B), are observed in the double chain (Fig. 2). Phen ligands are

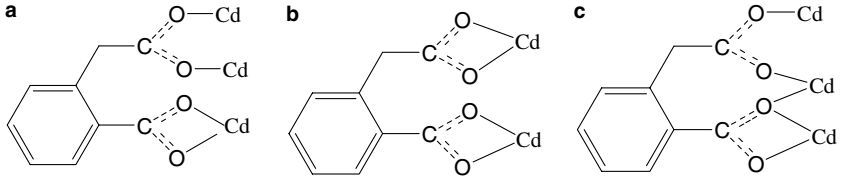

Scheme 1. The coordination modes of $hpht^{2-}$ ligands in complexes **1**–**4**.

Table 2
Selected bond lengths and angles of complex **1**

Cd(1)–O(4)#1	2.275(2)
Cd(1)–O(3)#2	2.282(2)
Cd(1)–O(2)	2.352(3)
Cd(1)–N(2)	2.382(3)
Cd(1)–N(1)	2.392(3)
Cd(1)–O(1)	2.418(3)
O(4)#1–Cd(1)–O(3)#2	111.5(3)
O(4)#1–Cd(1)–O(2)	90.0(3)
O(3)#2–Cd(1)–O(2)	135.8(3)
O(4)#1–Cd(1)–N(2)	78.1(3)
O(3)#2–Cd(1)–N(2)	82.2(3)
O(2)–Cd(1)–N(2)	141.4(3)
O(4)#1–Cd(1)–N(1)	123.0(3)
N(1)–Cd(1)–O(1)	94.0(4)
O(3)#2–Cd(1)–N(1)	109.1(3)
O(2)–Cd(1)–N(1)	87.6(3)
N(2)–Cd(1)–N(1)	69.6(3)
O(4)#1–Cd(1)–O(1)	128.2(3)
O(3)#2–Cd(1)–O(1)	83.8(3)
O(2)–Cd(1)–O(1)	53.6(3)
N(2)–Cd(1)–O(1)	153.5(3)

Symmetry transformations used to generate equivalent atoms: #1 $-x+1,-y,-z$; #2 $x-1,\ y,\ z$.

alternately attached to the two sides of the double-chain, and the vertical distance of the two adjacent phen planes at the same side is 6.897 Å. The double-chains are further stacked by π–π interaction of phen (about 3.43 Å) to form the final layer structure, and the benzene planes of $hpht^{2-}$ anions from two layers are meshed (Fig. 3). Since the previously reported homophthalate complexes are all 0-D dimmers [5], to our knowledge, **1** is the first example of homophthalate complexes with 1-D chain structure. The selected bond lengths and angles of complex **2** are listed in Table 3. The structure of **2** is quite similar to that of **1**, only 2,2′-bpy ligands replace the phen ligands. Detailed discussion of the structure will not be made here.

3.2.2. Crystal structure of complex *3*

The selected bond lengths and angles of complex **3** are listed in Table 4. The asymmetric unit of **3** consists one

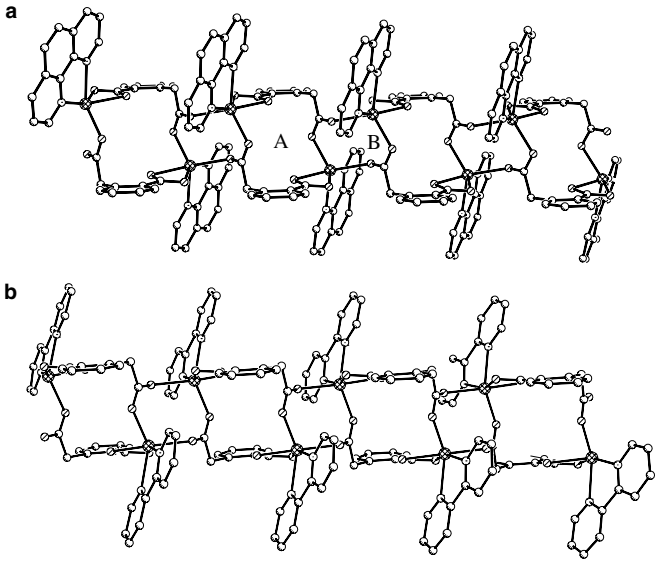

Fig. 2. View of the chains in complexes **1** (a) and **2** (b). All the H atoms are omitted for clarity.

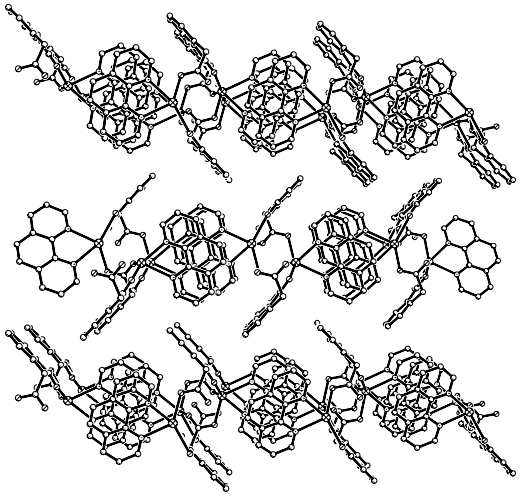

Fig. 3. View of the layer structure of complex **1** along *a*-axis. All the H atoms are omitted for clarity.

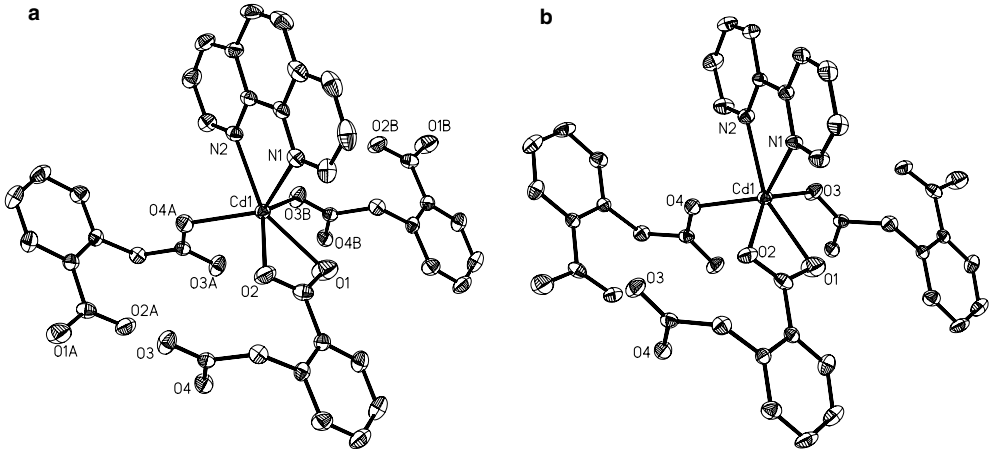

Fig. 1. Coordination environments of Cd(II) ions in complexes **1** (a) and **2** (b). All the H atoms are omitted for clarity.

Table 3
Selected bond lengths and angles of complex **2**

Cd(1)–O(4)#1	2.220(4)
Cd(1)–N(1)	2.362(4)
Cd(1)–N(2)	2.404(5)
Cd(1)–O(3)#2	2.261(4)
Cd(1)–O(1)	2.394(5)
Cd(1)–O(2)	2.411(4)
(4)#1–Cd(1)–O(3)#2	108.0 (2)
O(3)#2–Cd(1)–N(1)	107.2(2)
O(3)#2–Cd(1)–O(1)	84.5(2)
O(4)#1–Cd(1)–N(2)	80.4(2)
N(1)–Cd(1)–N(2)	68.6(2)
O(4)#1–Cd(1)–O(2)	91.1(2)
N(1)–Cd(1)–O(2)	85.8(2)
N(2)–Cd(1)–O(2)	136.5(2)
O(4)#1–Cd(1)–N(1)	129.5(2)
O(4)#1–Cd(1)–O(1)	120.5(2)
N(1)–Cd(1)–O(1)	97.7(2)
O(3)#2–Cd(1)–N(2)	84.2(2)
O(1)–Cd(1)–N(2)	158.5(2)
O(3)#2–Cd(1)–O(2)	138.2(2)
O(1)–Cd(1)–O(2)	54.2(2)
N(1)–Cd(1)–O(1)	94.0(4)

Symmetry transformations used to generate equivalent atoms: #1 $-x+1,-y+1,-z$; #2 $x-1, y, z$.

Cd(II) ion, a 2,2′-bpy ligand, a $hpht^{2-}$ ligand, a coordinated water molecule and two guest water molecules. Cd(II) ion is seven-coordinated by two nitrogen atoms from 2,2′-bpy and five oxygen atoms, four of which from two $hpht^{2-}$ ligands and one from coordinated water in a highly distorted pentagonal bipyramid coordination geometry, with O3A and N2 in the axial positions (Fig. 4). The Cd–O(N) bond distances are in the range 2.287–2.5l0 Å with an average value of 2.373 Å, slightly longer than those in complex **2**. Both carboxylate groups in $hpht^{2-}$ ligand adopt chelating coordination mode (Scheme 1(b)). The connections of Cd(II) ions and $hpht^{2-}$ ligands alternately along the *a*-axis lead to the formation of 1-D linear chain, as shown in Fig. 4. All the 2,2′-bpy ligands arrange in the same side of the chain and all the $hpht^{2-}$ ligands in the other side, which is significantly different from **1** and **2**. There are four types of hydrogen bondings in **3**. Two types of them (O5–H20···O1 and O5–H21···O4) link linear chains to form the double-chains, and the other two types (O6–H22···O2 and O6–H23···O3) link the double-chains to form the final 2-D network structure, as shown in Fig. 5. The 2-D network is corrugated because different double-chains are parallel but not in a plane. Different layers are stacked to produce the 3-D structure by the π–π weak interaction of 2,2′-bpy ligands along the *a*-axis, and the vertical distance between two 2,2-bpy ligands is about 3.467 Å. The free guest H_2O molecules are hold in the channels that formed by π–π interaction and hydrogen bonding, as shown in Fig. 6.

Table 4
Selected bond lengths and angles of complex **3**

Cd(1)–O(5)	2.287(3)
Cd(1)–O(3)#1	2.305(3)
Cd(1)–N(1)	2.346(3)
Cd(1)–O(2)	2.437(2)
Cd(1)–N(2)	2.353(3)
Cd(1)–O(1)	2.376(2)
Cd(1)–O(4)#1	2.510(2)
O(5)–Cd(1)–O(3)#1	89.6(2)
O(3)#1–Cd(1)–N(1)	107.3(2)
O(3)#1–Cd(1)–N(2)	173.8(9)
O(5)–Cd(1)–O(1)	85.6(2)
N(1)–Cd(1)–O(1)	121.9(9)
O(5)–Cd(1)–O(2)	134.9(2)
N(1)–Cd(1)–O(2)	81.6(9)
O(1)–Cd(1)–O(2)	53.2(8)
O(3)#1–Cd(1)–O(4)#1	53.78(8)
N(2)–Cd(1)–O(4)#1	120.1(9)
O(2)–Cd(1)–O(4)#1	127.0(8)
O(5)–Cd(1)–N(1)	142.3(2)
O(5)–Cd(1)–N(2)	90.5(2)
N(1)–Cd(1)–N(2)	69.2(2)
O(3)#1–Cd(1)–O(1)	101.5(9)
N(2)–Cd(1)–O(1)	84.8(2)
O(3)#1–Cd(1)–O(2)	82.7(9)
N(2)–Cd(1)–O(2)	101.6(9)
O(5)–Cd(1)–O(4)# 1	79.1(2)
N(1)–Cd(1)–O(4)# 1	84.2(9)
O(1)–Cd(1)–O(4)# 1	150.5(9)

Symmetry transformations used to generate equivalent atoms: #1 $x-1, y, z$.

3.2.3. Crystal structure of complex *4*

The selected bond lengths and angles of complex **4** are listed in Table 5. The asymmetric unit of **4** consists a Cd(II) ion, a $hpht^{2-}$ ligand, a 4,4′-bpy ligand, and a guest water molecule. Cd(II) ion is seven-coordinated by two nitrogen atoms from two 4,4′-bpy ligands and five oxygen atoms from three $hpht^{2-}$ anions in a slightly distorted pentagonal bipyramid coordination geometry (Fig. 7). Each $hpht^{2-}$ ligand links three Cd(II) ions, in which the methyl carboxylate group adopts bridging mode and the ethyl carboxylate adopts bridging-chelating mode (Scheme 1(c)). Two Cd(II) ions connected by two ethyl carboxylate groups with interatomic distance of 4.318 Å, $Cd_2(hpht)_2$, form the basic building unit of the whole structure. Each two of such units are connected together through the bridging carboxylate groups to form the 1-D chains, with benzene planes arrange on two sides of the chains reversely, which make the chain like long bench, as shown in Fig. 8. The 4,4′-bpy ligands link 1-D chains to form the final 2-D layer structure and to complete the coordination sphere of

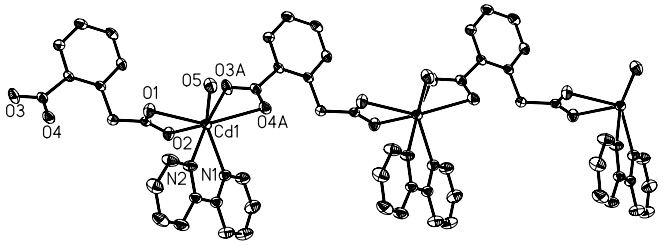

Fig. 4. View of the chain structure in complex **3**. All the H atoms are omitted for clarity.

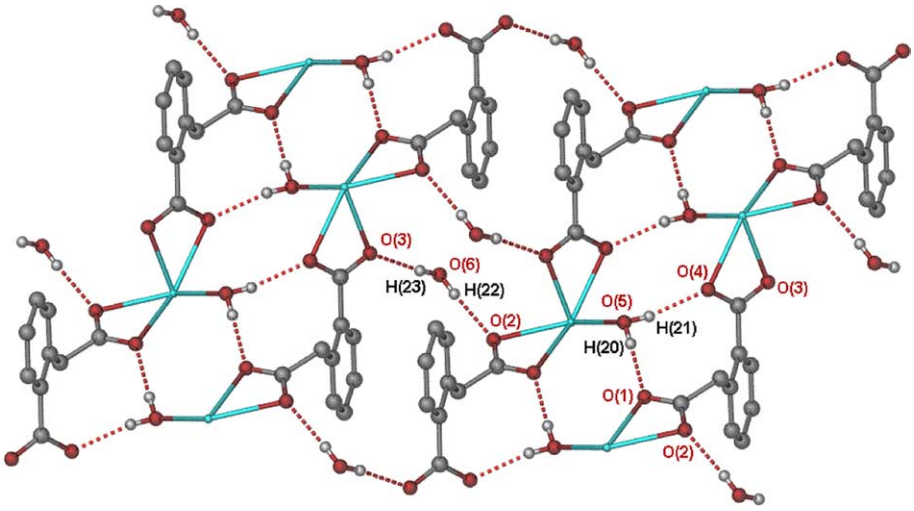

Fig. 5. View of the corrugated 2-D network in complex **3**. All the 2,2′-bpy and free guest water molecules are omitted for clarity, as well as the H atoms bonded to C atoms.

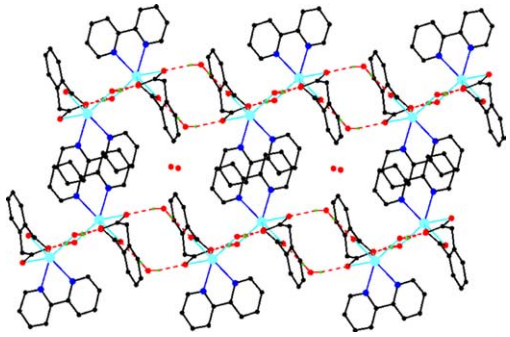

Fig. 6. View of the 3-D structure of complex **3** along *a*-axis. All the H atoms bonded to C atoms are omitted for clarity.

Cd(II) ions, and the free water molecules are hold between layers, as shown in Fig. 9.

3.3. Thermal gravimetric analysis

Thermal gravimetric analysis (TGA) diagram revealed that **1** was stable up to 317 °C, and then decomposed rapidly by the oxidation of the organic component. Complex **2** was stable up to 243 °C, and then the structure collapsed rapidly. For **3**, the first weight loss of 11.07% from 81 to 294 °C is attributed to the release of all water molecules (Calc. 10.78%). We note that the crystallization guest water is released at the same time as the coordinated water, supporting the structural evidence of hydrogen bonding in **3**. Complex **4** loses 3.78% of total weight in a range of 120–170 °C, corresponding to the loss of the free guest water (Calc. 3.87%), the framework is stable till 234 °C and then decomposed.

3.4. Fluorescence

The emission spectra of complexes **1**–**4** in the solid state at room temperature are shown in Fig. 11. It can be seen

Table 5
Selected bond lengths and angles of complex **4**

Cd(1)–N(2)# 1	2.289(2)
Cd(1)–N(1)	2.328(2)
Cd(1)–O(3)	2.428(3)
Cd(1)–O(3)#3	2.606(3)
Cd(1)–O(1)	2.328(2)
Cd(1)–O(2)#2	2.347(2)
Cd(1)–O(4)#3	2.462(3)
N(2)#1–Cd(1)–O(1)	93.7(8)
O(1)–Cd(1)–N(1)	87.6(8)
O(1)–Cd(1)–O(2)#2	85.8(8)
N(2)#1–Cd(1)–O(3)	99.4(2)
N(1)–Cd(1)–O(3)	86.6(2)
N(2)#1–Cd(1)–O(4)#3	89.8(9)
N(1)–Cd(1)–O(4)#3	87.7(9)
O(3)–Cd(1)–O(4)#3	109.1 (2)
O(1)–Cd(1)–O(3)#3	142.6(8)
O(2)#2–Cd(1)–O(3)#3	131.3(8)
O(4)#3–Cd(1)–O(3)#3	49.8(9)
N(2)#1–Cd(1)–N(1)	173.9(9)
N(2)#1–Cd(1)–O(2)#2	91.3(9)
N(1)–Cd(1)–O(2)#2	82.9(8)
O(1)–Cd(1)–O(3)	82.2(9)
O(2)#2–Cd(1)–O(3)	164.3(2)
O(1)–Cd(1)–O(4)#3	167.5(9)
O(2)#2–Cd(1)–O(4)#3	82.1(9)
N(2)#1–Cd(1)–O(3)#3	83.0(2)
N(1)–Cd(1)–O(3)#3	99.5 (2)
O(3)–Cd(1)–O(3)#3	61.9(2)

Symmetry transformations used to generate equivalent atoms: #1 $x-1/2,-y+1/2,z-1/2$; #2 $-x+1,-y+1,-z$; #3 $-x+1,-y,-z$.

that **1** exhibits an intense blue photoluminescence emission at $\lambda_{max} = 406$ nm and a very weak band at $\lambda_{max} = 524$ nm ($\lambda_{ex} = 350$ nm). The emission of **1** probably can be assigned to the intraligand fluorescent emission since very similar emissions are also observed for free H_2hpht (Fig. 10, $\lambda_{ex} = 274$ nm) and phen ligands [10].

Complex **2** exhibits an intense blue emission band ($\lambda_{max} = 422$, 498 nm, with a shoulder at 530 nm) from

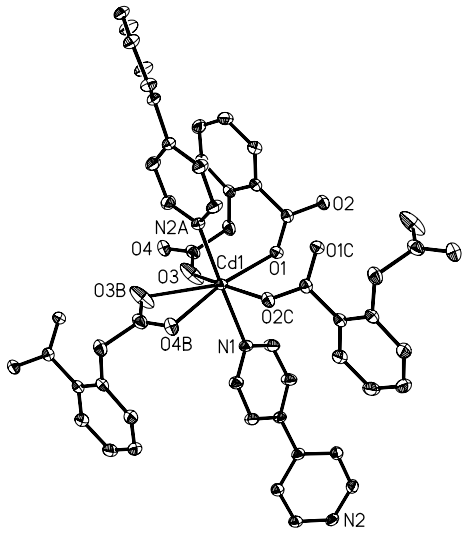

Fig. 7. Coordination environment of Cd(II) ions in complex **4**. All the H atoms are omitted for clarity.

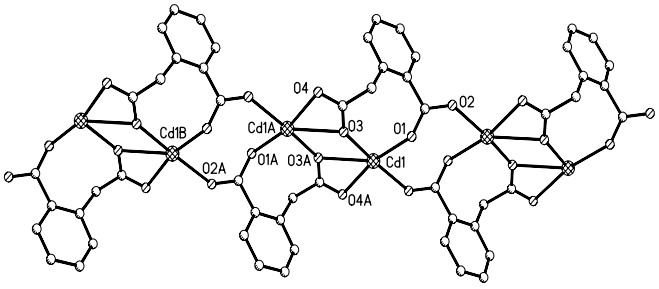

Fig. 8. View of the chain formed by Cd(II) ions and $hpht^{2-}$ ligands in complex **4**. All the H atoms are omitted for clarity.

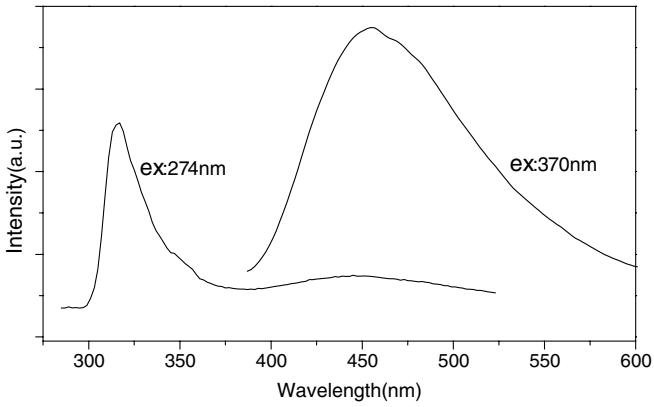

Fig. 10. Emission spectrum of homophthalic acid in the solid state.

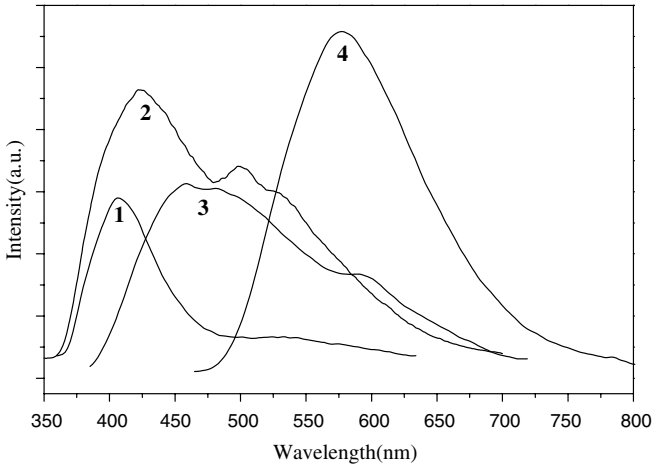

Fig. 11. Emission spectrum of complexes **1**–**4** in the solid state.

375 to 650 nm on excitation at 310 nm (Fig. 11). The peak at 422 nm can be assigned to the intraligand emission of H_2pht, since the free H_2pht ligand exhibits intense emission at $\lambda_{max} = 455$ nm upon excitation at 370 nm (Fig. 10), and the coordination of the ligand may lead to the blue-shift. The peak at 498 nm may be attributed to the intraligand emission from the 2,2′-bpy ligand [11]. It is known that the free 2,2′-bpy molecule displays a weak luminescence at ca. 535 nm. The enhancement and significant blue-shift of the photoluminescence of the coordinated 2,2′-bpy ligand compared to that of the free 2,2′-bpy molecule may, therefore, be attributed to the chelating of the 2,2′-bpy ligand to the metal ion, which effectively increases the rigidity of the ligand and reduces the loss of energy by radiationless decay of the intraligand emission excited state [12]. The shoulder emission at 530 nm may be assigned as ligand-to-metal-charge-transfer (LMCT) [13].

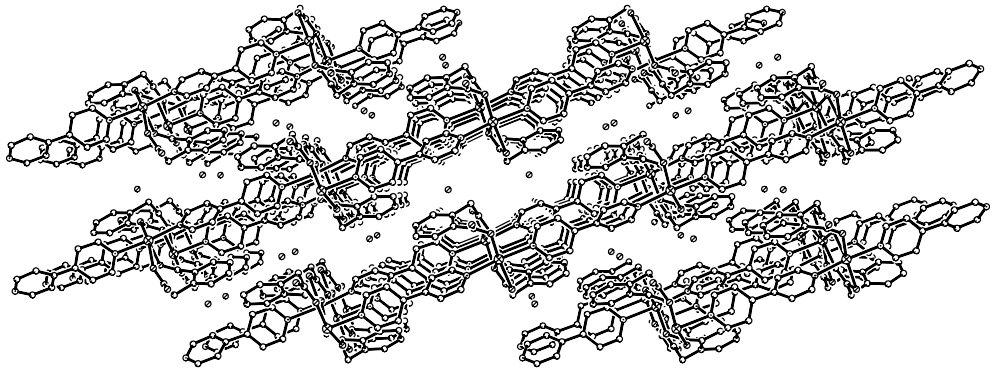

Fig. 9. View of the layer structure of complex **4** along *b*-axis. All the H atoms are omitted for clarity.

Complex **3** exhibits a broad green emission band ($\lambda_{max} = 459$, 481 nm, with a shoulder at 603 nm) from 385 to 700 nm on excitation at 372 nm (Fig. 11). We noted that the photoluminescence of **3** is similar to that of **2**, and the peaks can be assigned similarly. Compared with their analogs, both the peak at 459 nm and the shoulder red-shift and have lower intensity, which may be attributed to the different coordination mode of the ligand and different coordination environment of metal ions.

Complex **4** exhibits a very intense red photoluminescence emission at $\lambda_{max} = 577$, upon excitation at 455 nm, which has rarely been reported for cadmium complexes. While a very similar emission band of the free 4, 4′-bpy molecule with $\lambda_{max} = 432$ nm ($\lambda_{ex} = 344$ nm) is observed, the emission may be assigned to the ligand-to-metal charge transfer (LMCT) [14].

In a word, the photoluminescence properties of complexes **1**–**4** exhibit a broad range of visible light. Since complexes **1**–**4** are insoluble in common solvents and thermally stable, they may be potential candidates for photoactive materials.

4. Conclusion

In conclusion, four new complexes, **1**–**4**, have been successfully synthesized from the solvothermal reactions of cadmium salts, H_2phth and different auxiliary diimine ligands. The four complexes are stable and have particular fluorescence properties, and they may have promising application in photophysical chemistry.

5. Supplementary material

For the four complexes, full list of atomic coordinates, isotropic thermal parameters, bond lengths and angles are available from the authors on request. Crystallographic data for the structural analyses have been deposited with the Cambridge Crystallographic Data Center, CCDC Nos. 278028–278031 for complexes **1**–**4**, respectively. Copies of the data can be obtained from the Cambridge Crystallographic Data Centre, 12 Union Road, Cambridge CB2 1EZ, UK; Fax: (internet.) +44 1223 336 033; e-mail: deposit@ccdc.cam.ac.uk.

Acknowledgements

We thank the financial support from the National Natural Science Foundation of China (90206040, 20325106, and 20333070), the Natural Science Foundation of Fujian Province (E0520003), and the "one-hundred Talent" Project from CAS.

References

[1] (a) B. Moulton, M.J. Zaworotko, Chem. Rev. 101 (2001) 1629;
(b) K.T. Holman, A.M. Pivovar, J.A. Swift, M.D. Ward, Acc. Chem. Rev. 34 (2001) 107;
(c) L. Pan, X. Huang, J. Li, Y. Wu, N. Zheng, Angew. Chem., Int. Ed. 39 (2000) 527;
(d) S.H. Feng, R.R. Xu, Acc. Chem. Res. 34 (2001) 239.
[2] (a) Y.H. Wan, L.P. Zhang, L.P. Jin, S. Gao, S.Z. Lu, Inorg. Chem. 42 (2003) 4985;
(b) D.F. Sun, R. Cao, Y.C. Liang, Q. Shi, W.P. Su, M.C. Hong, J. Chem. Soc., Dalton Trans. (2001) 2335;
(c) Y.H. Wan, L.P. Jin, K.Z. Wang, J. Mol. Struct. 649 (2003) 85.
[3] (a) M.R. Cavellec, C. Lesaint, M. Noguès, J.M. Grenèche, Gérard Férey, Inorg. Chem. 42 (2003) 5669;
(b) L. Pan, K.M. Adams, H.E. Hernandez, X.T. Wang, C. Zheng, Y. Hattori, K. Kaneko, J. Am. Chem. Soc. 125 (2003) 3062.
[4] W.H. Bi, R. Cao, D.F. Sun, D.Q. Yuan, X. Li, M.C. Hong, Inorg. Chem. Commun. 6 (2003) 1426.
[5] (a) A.D. Burrows, R.W. Harrington, M.F. Mahon, C.E. Price, J. Chem. Soc., Dalton. Trans. (2000) 3845;
(b) F.A. Cotton, C. Lin, C.A. Murillo, Inorg. Chem. 40 (2001) 472;
(c) A.D. Burrows, R.W. Harrington, M.F. Mahon, S.J. Teat, Eur. J. Inorg. Chem. (2003) 766.
[6] (a) S. Ranjan, S.Y. Lin, K.C. Hwang, Y. Chi, W.L. Ching, C.S. Liu, Inorg. Chem. 42 (2003) 1248;
(b) J. Zhang, Z.J. Li, Y. Kang, J.K. Cheng, Y.G. Yao, Inorg. Chem. 43 (2004) 8085;
(c) L. Pan, H.M. Liu, X.G. Lei, X.Y. Huang, D.H. Olson, N.J. Turro, J. Li, Angew. Chem., Int. Ed. 42 (2003) 542;
(d) R. Kitaura, K. Seki, G. Akiyama, S. Kitagawa, Angew. Chem., Int. Ed. 42 (2003) 428.
[7] Rigaku, CRYSTALCLEAR, Version 13, Rigaku Corporation, Tokyo, Japan, 2001.
[8] G.M. Sheldrick, SADABS program for empirical absorption correction of area detector data, University of Göttingen, 1996.
[9] G.M. Sheldrick, SHELXS-97 program for crystal structure solution and refinement, University of Göttingen, 1997.
[10] (a) X.J. Gu, Y. Chen, J. Peng, Z.Y. Shi, E.B. Wang, N.H. Hu, J. Mol. Struct. 697 (2004) 231;
(b) L.Y. Zhang, G.F. Liu, S.L. Zheng, B.H. Ye, X.M. Zhang, X.M. Chen, Eur. J. Inorg. Chem. (2003) 2965;
(c) H. Yersin, A. Vogler (Eds.), Photochemistry and Photophysics of Coordination Compounds, Springer, Berlin, 1987.
[11] (a) G. Qian, M. Wang, Mater. Lett. 56 (2002) 71;
(b) X.M. Zhang, M.L. Tong, M.L. Gong, X.M. Chen, Eur. J. Inorg. Chem. (2003) 138.
[12] (a) L.Y. Zhang, G.F. Liu, S.L. Zheng, B.H. Ye, X.M. Zhang, X.M. Chen, Eur. J. Inorg. Chem. (2003) 2965;
(b) R.X. Yuan, R.G. Xiong, Y.L. Xie, X.Z. You, S.M. Peng, G.H. Lee, Inorg. Chem. Commun. 4 (2001) 384.
[13] X.J. Li, R. Cao, D.F. Sun, W.H. Bi, Y.Q. Wang, X. Li, M.C. Hong, Cryst. Growth Des. 4 (2004) 775.
[14] Y.F. Zhou, R.H. Wang, B.L. Wu, R. Cao, M.C. Hong, J. Mol. Struct. 697 (2004) 73.

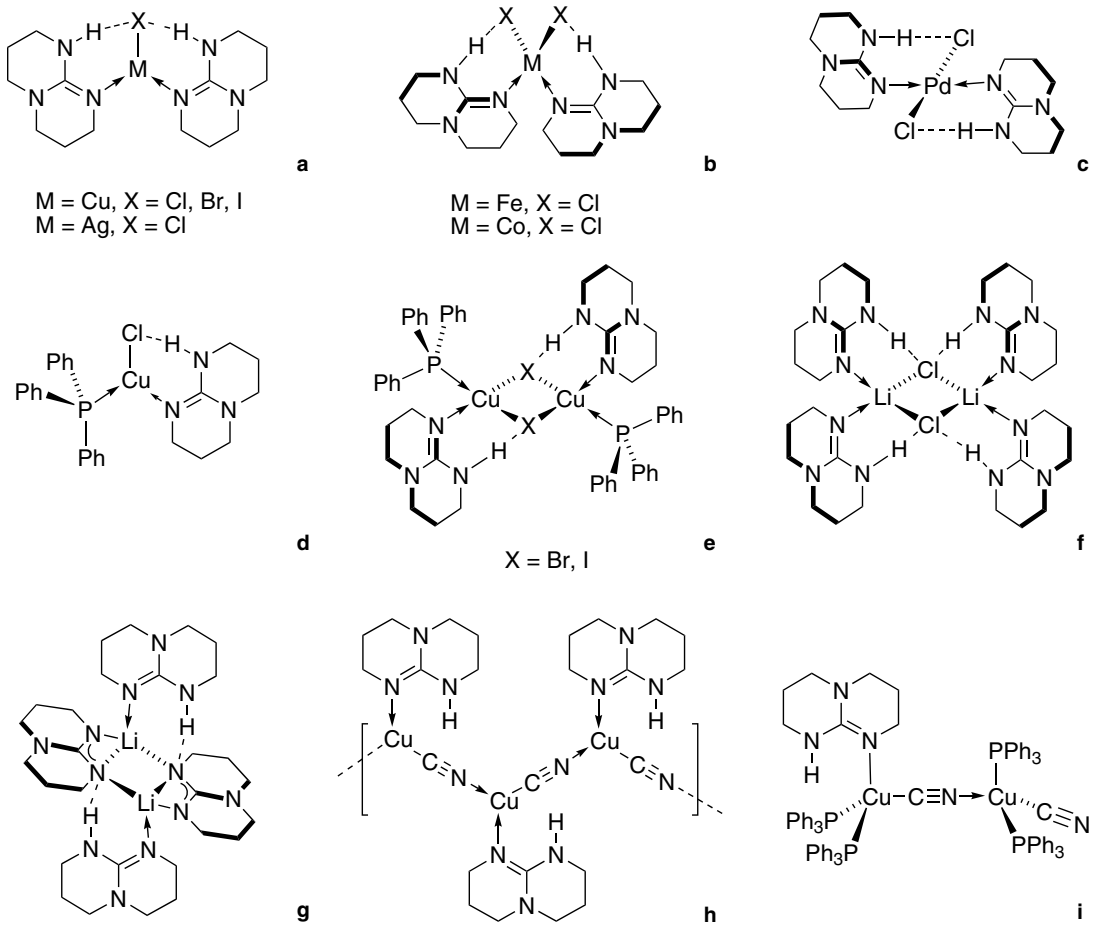

Fig. 1. Examples of compounds containing the neutral bicyclic guanidine, hppH, as a ligand.

more recently in a square-planar palladium complex (**c**) [11]. We have shown that the extent of aggregation differs in the mixed phosphine/guanidine copper(I) halides (**d**) and (**e**), where the chloride was isolated as the monomer and the heavier congeners formed μ,μ′-dihalobridged dimers [9]. In contrast to complexes of type (**a**), the bis-ligand, monovalent metal halide species formed with lithium chloride is dimeric in the solid-state, comprised of chloride bridges and tetrahedral metal centres (**f**) [9].

Hydrogen bonding between tetrasubstituted guanidines and atoms other than the halides has also been observed, albeit less frequently. The acyclic guanidine, $Me_2NC\{N^iPr\}\{NH^iPr\}$, forms intramolecular N*H*···O bonds within the monomeric zinc complexes $Zn(OAr)Me(Me_2NC\{N^iPr\}\{NH^iPr\})$ ($Ar = 2,6\text{-}^tBu_2C_6H_3$) [12] and the guanidinate/boroxide species, $Zn(OBmes_2)(Me_2NC\{N^iPr\}_2)(Me_2NC\{N^iPr\}\{NH^iPr\})$ [13]. Intramolecular hydrogen bonding by hppH to nitrogen is restricted to the mixed guanidine/guanidinate dimer, $[Li(hpp)(hppH)]_2$ (**g**) [14].

Finally, examples have been structurally characterized in which the coordinated guanidine does not undergo further interaction with the metal fragment. This situation was first noted by Bailey and co-workers with the tri-substituted guanidine, $PhN=C\{NHPh\}_2$, in the cationic silver species $Ag[PhN=C(NHPh)_2]_2[OTf]$ [15]. In this case, however, the preferential formation of *inter*molecular hydrogen bonds to the triflate anion are observed, via two S=O oxygen atoms. We have shown that the hppH ligand is monodentate in the polymeric copper(I) cyanide complex, $[CuCN(hpp)]_\infty$ (**h**), and bimetallic complex, $(Ph_3P)_2(hppH)Cu(\mu\text{-}CN)Cu(PPh_3)(CN)$ (**i**), where no readily available groups are present to interact with the N*H* atom.

In all cases discussed above, bonding occurs exclusively through donation of the imine lone pair to an orbital of suitable symmetry and energy on the metal in question. In this contribution we report the synthesis and structural analysis of series of divalent tetrahedral metal complexes of general formula $MX_2(hppH)_2$ (M = Mn, Fe, Ni, Zn; X = Cl, Br). We also report the solid-state structure of the dimeric lithium siloxide species, $[Ph_3SiOLi(hppH)(THF)]_2$, which contains an intramolecular N*H*···O hydrogen bond.

2. Experimental

2.1. General experimental procedures

All manipulations were carried out under dry nitrogen using standard Schlenk line and cannula techniques, or in a conventional nitrogen-filled glovebox operating at

<1 ppm oxygen. Solvents were dried over the appropriate drying agent and degassed prior to use. The reagents hppH (Fluka), $MnCl_2$ (Aldrich), $FeCl_2$ (Aldrich), $CoCl_2$ (Aldrich), $NiCl_2$ (Aldrich), $CuCl_2$ (Aldrich) and $ZnBr_2$ (Aldrich) were purchased from commercial sources and used as received. The compound $NiCl_2(Py)_4$ was synthesised according to literature procedures [16] and kindly donated by Dr. A.K. de K. Lewis; $(hpp)_3SiMe$ was made according to our previously reported procedure [17]. NMR spectra were recorded in $[^2H]_6$-benzene at 293 K (unless stated otherwise) using a Bruker Avance DPX 300 MHz spectrometer at 300 (^1H) and 75 ($^{13}C\{^1H\}$) MHz. Proton and carbon chemical shifts were referenced internally to residual solvent resonances. Elemental analyses were performed by S. Boyer at London Metropolitan University.

2.1.1. $MnCl_2(hppH)_2$ (1)

A solution of hppH (0.500 g, 3.59 mmol) in THF (10 mL) was added dropwise to a slurry of $MnCl_2$ (0.226 g, 1.80 mmol) in THF (10 mL). The mixture was stirred for 48 h at room temperature with gradual dissolution of the manganese dichloride and formation of a pale pink precipitate. Recrystallization from slow cooling of a warm (~70 °C) toluene solution afforded colourless crystals of **1** suitable for X-ray diffraction analysis. Yield: 0.450 g (62%). *Anal.* Calc. for $C_{14}N_6H_{26}MnCl_2$ (404.24): C, 41.60; H, 6.48; N, 20.79. Found: C, 41.72; H, 6.68; N, 20.85%.

2.1.2. $FeCl_2(hppH)_2$ (2)

Compound **2** was prepared according to the procedure described for compound **1**, using 0.500 g, hppH (3.59 mmol) and 0.228 g $FeCl_2$ (1.80 mmol). Recrystallization by slow cooling of a MeCN solution afforded light brown crystals of analytically pure **2**. Yield: 0.418 g (57%). *Anal.* Calc. for $C_{14}N_6H_{26}FeCl_2$ (405.15): C, 41.50; H, 6.47; N, 20.74. Found: C, 41.37; H, 6.65; N, 20.43%.

2.1.3. $NiCl_2(hppH)_2$ (3)

A solution of hpp_3SiMe (0.100 g, 0.22 mmol) in toluene (5 mL) was added dropwise to a slurry of $NiCl_2(Py)_4$ (0.097 g, 0.22 mmol) in toluene (10 mL) at room temperature. An immediate colour change from pale blue to purple was observed. The mixture was stirred for 24 h at room temperature and then filtered. Recrystallization from hot toluene afforded dark blue crystals of analytically pure **3**. Yield: 0.033 g (37%). *Anal.* Calc. for $C_{14}H_{26}N_6NiCl_2$ (408.02): C, 41.21; H, 6.42; N, 20.60. Found: C, 41.37; H, 6.60; N, 20.36%.

2.1.4. $ZnBr_2(hppH)_2$ (4)

Compound **4** was prepared according to the procedure described for compound **1**, using 0.500 g, hppH (3.59 mmol) and 0.400 g $ZnBr_2$ (1.78 mmol). The solid was collected after removal of the volatiles in vacuo and then washed with toluene to remove any unreacted hppH. Crystals suitable for X-ray diffraction analysis were grown from an acetonitrile solution.

^1H NMR. δ 7.44 (br, 1H, N*H*), 3.40 (m, 2H, CH_2), 2.54 (m, 2H, CH_2), 2.29 (m, $J_{HH} = 6.1$, 2H, CH_2), 2.10 (m, $J_{HH} = 6.2$, 2H, CH_2), 1.44 (m, 2H, CH_2), 0.96 (m, 2H, hpp-CH_2). $[^2H]_2$-dichloromethane: δ 6.49 (br, s, 1H, N*H*), 3.20 (m, 8H, CH_2), 1.84 (m, $J_{HH} = 5.9$, 4H, hpp-CH_2). ^{13}C NMR data were not obtained due to the low solubility of the product.

2.1.5. $hppSiPh_3$ and $[Ph_3SiOLi(hppH)(THF)]_2$ (5)

The synthesis of $hppSiPh_3$ was carried out using the procedure described for $hppSiMe_3$, [18] using 0.200 g hppH (1.44 mmol),^{n}BuLi (0.6 mL of a 2.5 M solution in hexane, 1.51 mmol) and Ph_3SiCl (0.42 g, 1.44 mmol). Removal of the volatiles afforded a white crystalline solid. Washing the solid with toluene gave two products that analyzed as $hppSiPh_3$ and $[Ph_3SiOLi(hppH)(THF)]_2$ (**5**). Crystallization of **5** from THF at 0 °C afforded crystals suitable for X-ray diffraction analysis.

$hppSiPh_3$. Anal. Calc. for $C_{25}H_{27}N_3Si$ (397.59): C, 75.52; H, 6.84; N, 10.57. Found: C, 75.71; H, 6.74; N, 10.27%. ^1H NMR: δ 8.00 (m, 6H, *o*-C_6H_5), 7.23 (m, 9H, *m,p*-C_6H_5), 2.52 (br m, 4H, CH_2), 2.23 (br m, 4H, CH_2), 1.13 (br m, 4H, CH_2).

$[Ph_3SiOLi(hppH)(THF)]_2$. Anal. Calc. for $C_{29}H_{36}N_3LiO_2Si$ (493.65): C, 70.56; H, 7.35; N, 8.51. Found: C, 70.49; H, 7.40; N, 8.44%. ^1H NMR $[^2H]_3$-acetonitrile: δ 8.00 (m, 6H, *o*-C_6H_5), 7.24 (m, 9H, *m,p*-C_6H_5), 3.64 (m, 4H, C_4H_8O), 2.97 (m, 8H, hpp-CH_2), 1.80 (m, 4H, C_4H_8O), 1.71 (br m, 4H, hpp-CH_2). ^{13}C NMR $[^2H]_3$-acetonitrile: δ 152.3 (*C*N_3), 144.6 (*C*$_6H_5$), 136.0 (*C*$_6H_5$), 128.7 (*C*$_6H_5$), 127.9 (*C*$_6H_5$), 68.2 (*C*$_4H_8O$), 48.5 (hpp-*C*H_2), 41.6 (hpp-*C*H_2), 26.2 (*C*$_4H_8O$), 23.7 (hpp-*C*H_2).

2.2. X-ray diffraction data

Crystals were covered in oil and suitable single crystals were selected under a microscope and mounted on a Kappa CCD diffractometer. The structures were refined with SHELXL-97 [19]. Details of the crystal data, intensity collection and refinement for complexes **1**–**4** are listed in Table 1 and for compound **5** in Table 3; selected bond lengths and angles for **1**–**4** in Table 2, and for **5** in Table 4. Additional features of note associated with individual data sets are listed below:

2.2.1. $MnCl_2(hppH)_2$ (1)

The molecule lies on a twofold rotation axis. The hydrogen atom on N(2) was located in the difference map and refined; other hydrogens were in riding mode. Disorder in both rings of the ligand was modeled (relative occupancies: a 0.72, b 0.75, c 0.28, d 0.25), with the lower occupancy carbon sites left isotropic.

2.2.2. $FeCl_2(hppH)_2$ (2)

As described for **1** (relative occupancies in disordered rings: a 0.72, b 0.28).

Table 1
Crystal structure and refinement data for $MnCl_2(hppH)_2$ (**1**), $FeCl_2(hppH)_2$ (**2**), $NiCl_2(hppH)_2$ (**3**) and $ZnBr_2(hppH)_2$ (**4**)

	1	**2**	**3**	**4**
Formula	$C_{14}H_{26}Cl_2MnN_6$	$C_{14}H_{26}Cl_2FeN_6$	$C_{14}H_{26}Cl_2N_6Ni$	$C_{14}H_{26}Br_2N_6Zn$
Formula weight	404.25	405.16	408.02	503.60
Temperature (K)	173(2)	173(2)	253(2)	173(2)
Wavelength (Å)	0.71073	0.71073	0.71073	0.71073
Crystal size (mm)	$0.25 \times 0.20 \times 0.20$	$0.30 \times 0.30 \times 0.30$	$0.35 \times 0.35 \times 0.30$	$0.40 \times 0.30 \times 0.20$
Crystal system	orthorhombic	orthorhombic	monoclinic	monoclinic
Space group	*Fdd*2 (No. 43)	*Fdd*2 (No. 43)	$P2_1/n$ (No. 14)	$C2/c$ (No. 15)
a (Å)	32.0384(6)	31.7631(7)	8.2851(4)	9.2893(2)
b (Å)	16.6254(3)	16.6091(4)	14.0068(7)	13.9906(3)
c (Å)	6.8663(1)	6.8574(1)	15.6742(6)	14.2981(3)
β (°)	90	90	97.259(3)	95.197(1)
V (Å^3)	3657.34(11)	3617.67(13)	1804.38(14)	1850.58(7)
Z	8	8	4	4
D_{calc} (Mg/m^3)	1.47	1.49	1.50	1.81
Absorption coefficient (mm^{-1})	1.02	1.14	1.38	5.65
θ range for data collection (°)	3.73–27.48	4.54–27.48	3.82–25.06	3.74–27.49
Reflections collected	10912	10864	18247	11000
Independent reflections (R_{int})	2022 (0.040)	1902 (0.037)	3172 (0.041)	2105 (0.055)
Reflections with $I > 2\sigma(I)$	1959	1839	2749	1892
Data/restraints/parameters	2022/1/128	1902/1/138	3172/0/216	2105/0/139
Goodness-of-fit on F^2	1.073	1.048	1.062	0.920
Final R indices [$I > 2\sigma(I)$]	$R_1 = 0.026$, $wR_2 = 0.065$	$R_1 = 0.020$, $wR_2 = 0.049$	$R_1 = 0.035$, $wR_2 = 0.093$	$R_1 = 0.029$, $wR_2 = 0.066$
R indices (all data)	$R_1 = 0.027$, $wR_2 = 0.066$	$R_1 = 0.022$, $wR_2 = 0.050$	$R_1 = 0.044$, $wR_2 = 0.098$	$R_1 = 0.035$, $wR_2 = 0.070$
Largest difference in peak and hole (e Å^3)	0.91 and −0.19	0.17 and −0.18	0.56 and −0.29	0.31 and −0.87

Table 2
Selected bond lengths (Å) and angles (°) for $MnCl_2(hppH)_2$ (**1**), $FeCl_2(hppH)_2$ (**2**), $CoCl_2(hppH)_2$, [10] $NiCl_2(hppH)_2$ (**3**) and $ZnBr_2(hppH)_2$ (**4**)

	1	**2**	**$CoCl_2(hppH)_2$**	**3**		**4**
M–N(1)	2.107(2)	2.0395(14)	2.003(4)	1.983(2)	1.977(2)	1.993(5)
M–X[a]	2.3681(5)	2.3190(4)	2.2881(13)	2.2911(8)	2.2749(8)	2.4321(4)
C=N$_{imine}$	1.319(2)	1.322(2)	1.321(6)	1.313(3)	1.316(4)	1.325(6)
C–NH	1.348(3)	1.354(3)	1.335(7)	1.354(4)	1.359(4)	1.360(6)
Δ_{CN}	0.029	0.032	0.014	0.041	0.043	0.035
C–NR$_2$	1.351(2)	1.352(2)	1.356(6)	1.355(3)	1.349(3)	1.355(3)
N$_{amine}$···X	3.28	3.30	3.23	3.24	3.21	3.40
H···X	2.46	2.52	2.57	2.45	2.47	2.59
N(1)–M–N(1′)[b]	108.68(9)	107.52(9)	107.6(2)	103.81(10)		110.8(3)
X-M-X′[b]	110.67(3)	111.63(3)	110.00(7)	116.08(3)		112.24(2)
N(1)–M-X[b]	110.77(5)	110.87(4)	109.72(12)	108.03(7)		103.92(18)
N(1)–M-X′[b]	107.97(4)	107.94(5)	109.85(11)	111.03(7)		113.11(16)
N(1′)–M-X[b]				111.12(7)		
N(1′)–M-X′[b]				106.09(7)		

[a] **1**, **2**, $CoCl_2(hppH)_2$ and **3**, X = Cl; **4**, X = Br.
[b] **3**, N(1′) = N(4); X = Cl(1) and X′ = Cl(2).

2.2.3. $ZnBr_2(hppH)_2$ (**4**)

As described for **1** (relative occupancies in disordered rings: a 0.74, b 0.26, c 0.78, d 0.22).

2.2.4. $[Ph_3SiOLi(hppH)(THF)]_2$ (**5**)

The hydrogen atom on N(2) was refined; other hydrogens were in riding mode. C(3) is disordered.

3. Results and discussion

3.1. $MX_2(hppH)_2$

The synthesis of the hppH adducts, $MnCl_2(hppH)_2$ (**1**), $FeCl_2(hppH)_2$ (**2**) and $ZnBr_2(hppH)_2$ (**4**) was achieved in a straight forward manner by combining the correct ratio of guanidine and metal salt in THF, with the exclusion of air/moisture (Scheme 1). The previously reported synthesis of **2** and the cobalt analogue, $CoCl_2(hppH)_2$, employed toluene as solvent and the mixture was refluxed to ensure complete reaction had occurred. Using our modification, each reaction proceeded with gradual dissolution of the metal starting reagent, coincident with precipitation of the product, indicating similar solubility properties. Recrystallization by slowly cooling a saturated solution (**1**, toluene; **2** and **4**, acetonitrile) to room temperature afforded analytically pure products.

Attempted synthesis of $NiCl_2(hppH)_2$ (**3**), using the direct combination of reagents analogous to the procedure

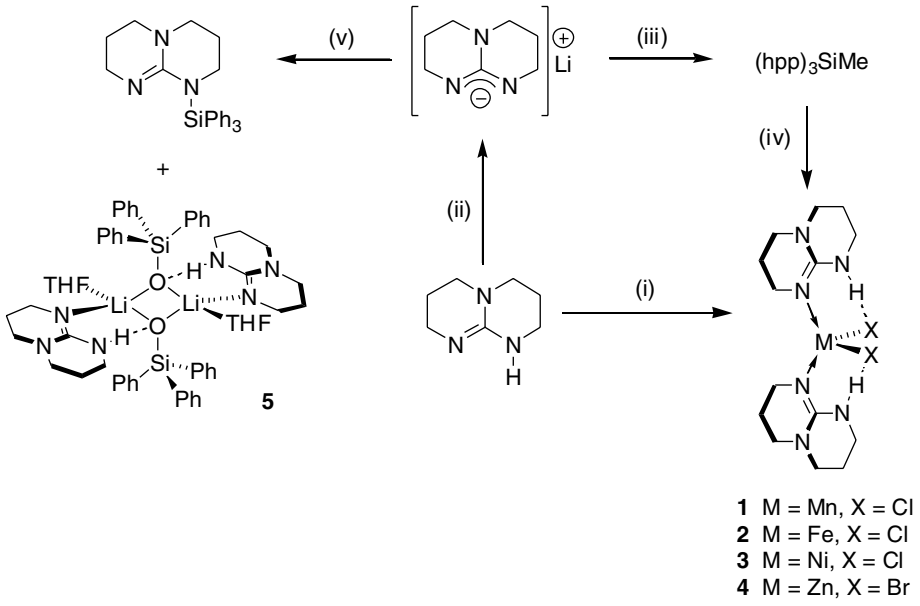

Scheme 1. (i) 1/2 MX_2, THF; (ii) ^{n}BuLi; (iii) 1/3 $SiCl_3Me$; (iv) $NiCl_2(Py)_4/H_2O$; (v) $SiPh_3Cl/H_2O$ (trace).

described above were unsuccessful. The desired product was, however, repeatedly isolated in moderate yield from the reaction between $NiCl_2(Py)_4$ and $(hpp)_3SiMe$ [17] (Scheme 1). Clearly, to give the product in this case, protonolysis of the silylated reagent must have occurred, forming the parent hppH reagent during the course of the reaction. We feel that it is unlikely that this was the result of accidental exposure to a moist atmosphere and a more likely explanation is residual water present in the nickel starting reagent (which was synthesized from the hydrate) [16].

NMR analysis of the manganese, iron and nickel complexes gave broad resonances commensurate with paramagnetic species; attempts at determining the magnetic moment using Evan's method were frustrated by limited solubility. ^{1}H NMR analysis of the diamagnetic zinc complex **4** suggested a static structure in solution, indicated by the presence of six resonances for the methylene groups within the bicyclic framework. This situation is in contrast to the three coordinate copper and silver complexes, $MCl(hppH)_2$, [8,9] in which a fluxional process occurs in solution equating the two dissimilar rings of the bicyclic framework, but has recently been noted in the palladium adduct, $PdCl_2(hppH)_2$ [11]. In the absence of further solution-state measurements for these systems, it is premature to definitively allocate the causes of these differences to purely steric or electronic factors. It does, however, suggest that intramolecular hydrogen bonding is an important feature of solution-state stability of complexes of this general type, which will become central in any proposed catalytic applications of these species in solution.

X-ray structural analyses of compounds **1**–**4** were conducted, primarily in order to acquire information about the nature of any hydrogen bonding involving the guanidine N*H* atom. The molecular structures are illustrated in Figs. 2–5; crystal structure and refinement data are given in Table 1 and selected bond lengths and angles in Table 2.

To complete the analogous series of $MCl_2(hppH)_2$ compounds where M is a metal from groups 7 to 10, the results from this study have been compared with the previously reported cobalt complex, $CoCl_2(hppH)_2$[1] [10]. Despite repeated attempts, the corresponding copper(II) chloride complex was unattainable, precluding extension of this series through to group 12. It is also noted that the presence of bromides in place of the chlorides in **4** will necessarily affect bond lengths and angles within the zinc complex and comparisons with the structure of **4** should therefore be treated accordingly.

The manganese, iron and cobalt complexes are isostructural, each crystallizing in the orthorhombic crystal system (space group *Fdd*2), whilst the nickel and zinc compounds crystallize in the monoclinic form (space groups $P2_1/n$ and $C2/c$, respectively). The former molecules each lie on a two-fold rotation axis which relates the two halves of the molecule, as does the zinc complex; the two halves of the nickel species are crystallographically distinct. The guanidine rings in compounds **1**, **2** and **4** exhibit varying degrees of disorder and were modelled accordingly (see Section 2); again due caution must therefore be exercised when discussing bond distances and angles.

In each case a monomeric, distorted tetrahedral complex forms consisting of two imine-bound guanidine ligands about the metal dihalide fragment. The metal nitrogen dis-

[1] The crystal structure of the cobalt complex, $CoCl_2(hppH)_2$, has been previously reported by Cotton and co-workers. However, the crystallographic data has not been deposited, as stated in the publication, and is therefore unavailable from the Cambridge Structural Database. We have independently synthesized and characterized the complex by X-ray diffraction studies and have deposited the data with this publication.

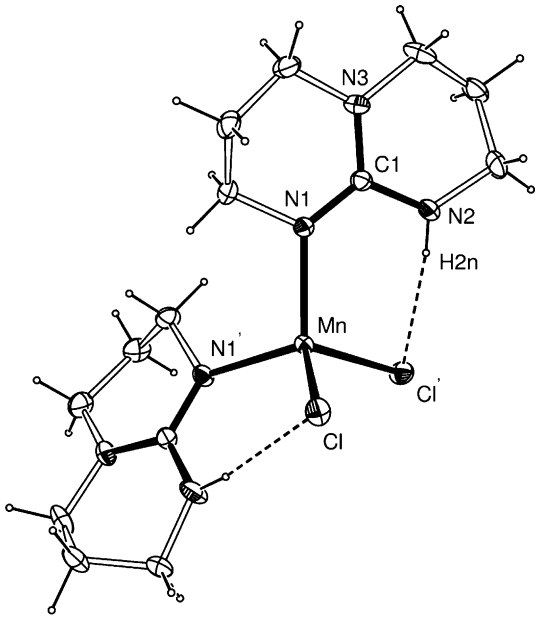

Fig. 2. ORTEP representation of the Λ isomer of $MnCl_2(hppH)_2$ (**1**) with thermal ellipsoids drawn at the 30% probability level ($-x+1$, $-y$, z).

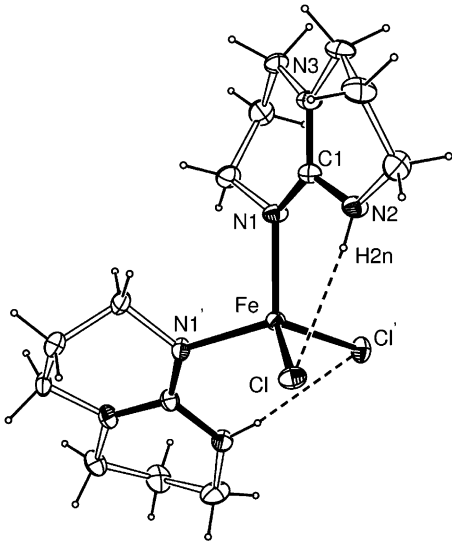

Fig. 3. ORTEP representation of the Δ isomer of $FeCl_2(hppH)_2$ (**2**) with thermal ellipsoids drawn at the 30% probability level ($'-x+3/2$, $-y+1/2$, z).

tances are, in general, shorter than in related formamidine and benzamidine complexes of the dihalides, [20–22] in agreement with greater electron donation by the guanidine. The angles about the metal in the Mn, Fe and Co compounds are not substantially distorted from the predicted tetrahedral value [ranges: **1**, 107.97(4)° to 110.77(5)°; **2**, 107.52(9)° to 111.63(3)°; $CoCl_2(hppH)_2$, 107.6(2)° to 110.00(7)°], whilst the range is appreciably greater in the nickel [103.81(10)° to 116.08(3)°] and zinc [103.92(18)° to 113.11(16)°] analogues. In the latter two examples, this distortion manifests itself further in different orientations of the neutral donor ligand and halide atoms with respect to

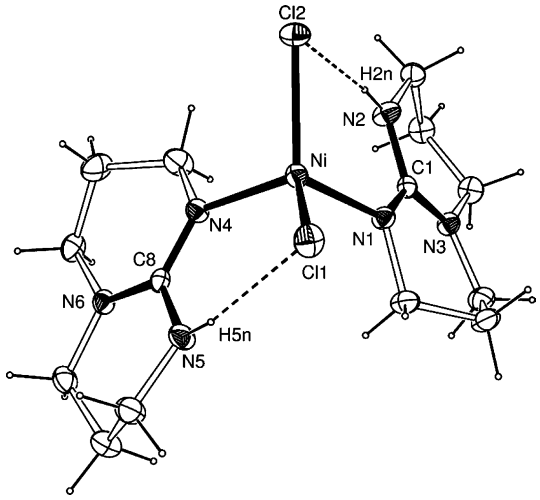

Fig. 4. ORTEP representation of the Δ isomer of $NiCl_2(hppH)_2$ (**3**) with thermal ellipsoids drawn at the 20% probability level.

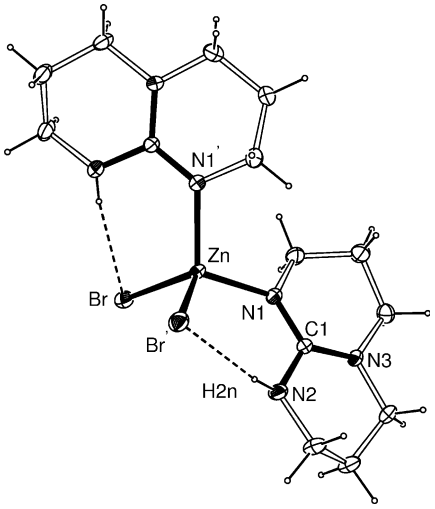

Fig. 5. ORTEP representation of the Δ isomer of $ZnBr_2(hppH)_2$ (**4**) with thermal ellipsoids drawn at the 30% probability level ($'-x$, y, $-z+1/2$).

the metal centre (illustrated in Fig. 6 for the 'CN_3' core of the Δ isomers – vide infra). Thus, the guanidine ligands are aligned almost parallel to the nickel-halide vector in **3**, while a pronounced twist between the 'Br–Zn–Br' and 'N–Zn–N' planes is observed in **4**. These observations serve to illustrate a degree of flexibility in the geometry generated at the metal upon coordination, dependant on the position of the metal in the periodic table and the nature of the halide atom present in the complex.

The carbon–nitrogen distances within the guanidine are consistent with the presence of single and double bonds in which partial delocalization has occurred (Δ_{CN} values: [23] **1**, 0.029 Å; **2**, 0.032 Å; $CoCl_2(hppH)_2$, 0.014 Å; **3**, 0.041 and 0.043 Å; **4**, 0.035 Å). The E_{anti} configuration about the amidine component of hppH, enforced by the bicyclic framework, encourages hydrogen bonding to the halide atoms (Table 2). In each complex, the amine hydrogen atoms were located and refined indicating interaction with

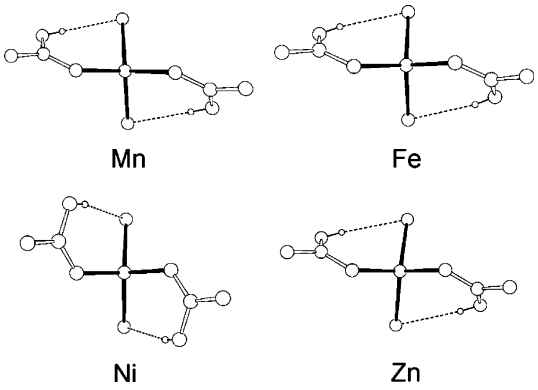

Fig. 6. Core structures of the *Δ* isomers of compounds **1**, **2**, **3** and **4** (viewed along the N–M–N plane with the guanidine ligands facing out and the halides facing into the page).

the chloride and bromide, with H···X distances in the range 2.45–2.59 Å.

The presence of these intramolecular hydrogen-bonds in the solid-state generates chiral molecules which, by analogy with D_3-tris(chelate) octahedral complexes, are assigned as the *Δ* or *Λ* isomer (Fig. 7). All of the compounds crystallise as the racemic mixture; however the way in which these molecules are arranged within the unit cell differs depending to which space group they belong. Thus, in the non-centrosymmetric space group *Fdd*2 (compounds **1**, **2** and the cobalt analogue) molecules with the *Δ* and *Λ* configuration are related by a *d*-glide perpendicular to *a*, while in the centrosymmetric space groups $P2_1/n$ (**3**) and $C2/c$ (**4**) either a centre of inversion and/or a glide plane relates the isomers.

3.2. $[Ph_3SiOLi(hppH)(THF)]_2$

During the synthesis of the triphenylsilyl-substituted guanidine, $hppSiPh_3$, using a procedure analogous to that used to generate the trimethylsilyl derivative, [18] a small amount of colourless crystalline material was isolated, identified by X-ray crystallography as the base stabilized siloxide, $[Ph_3SiOLi(hppH)(THF)]_2$ (**5**). We assume that the origin of **5** is due to the reaction between 'hppLi' with a small amount Ph_3SiOH, generated from hydrolysis of the silylchloride by adventitious water. The lithiated guanidinate is therefore a sufficiently strong base to deprotonate the silanol, with concomitant formation of the neutral guanidine which, in combination with THF solvent, stabilizes the siloxide anion, $[Ph_3SiO]^-$, in the solid-state. The product was analyzed by elemental analysis and X-ray diffraction and since one of the aims of this work is to further the understanding of intramolecular hydrogen bonding involving hppH, we feel that a brief discussion of the molecular structure of **5** is warranted (Fig. 8, Tables 3 and 4).

Compound **5** crystallizes as the symmetry related dimer in which the lithium cations and siloxide anions form a rhombohedral 'Li_2O_2' core, commonly observed with lithiated alkoxides [24,25], boroxides [25–28] and siloxides [29,30] (provided sufficient bulk is present to prevent further aggregation). Within the central ring, the angles are obtuse at lithium and acute at oxygen [99.24(15)° and 80.76(15)°, respectively], with essentially equal Li–O bond

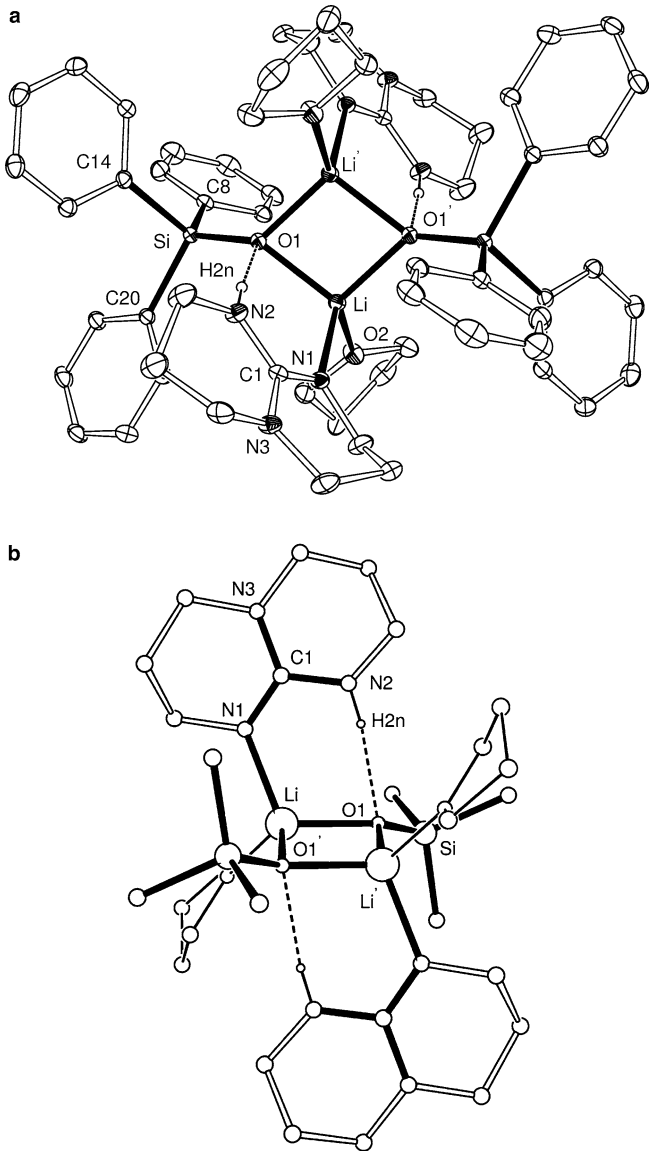

Fig. 8. (a) ORTEP representation of $[Ph_3SiOLi(hppH)(THF)]_2$ (**5**) with thermal ellipsoids drawn at the 20% probability level. (b) Core structure of **5**, emphasizing the intramolecular N*H*···O hydrogen bond. Only the *ipso*-carbon atoms of the phenyl groups shown for clarity.

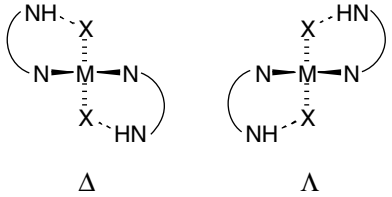

Fig. 7. Delta (*Δ*) and lambda (*Λ*) isomers of complexes **1**–**4**, viewed along the N–M–N vector.

Table 3
Crystal structure and refinement data for $[Ph_3SiOLi(hppH)(THF)]_2$ (**5**)

	5
Formula	$C_{58}H_{72}Li_2N_6O_4Si_2{\cdot}C_6H_6$
Formula weight	1065.38
Temperature (K)	173(2)
Wavelength (Å)	0.71073
Crystal size (mm)	$0.25 \times 0.20 \times 0.10$
Crystal system	monoclinic
Space group	$P2_1/n$ (No. 14)
a (Å)	12.9229(2)
b (Å)	15.7013(5)
c (Å)	14.2653(4)
β (°)	92.945(2)
V (Å^3)	2890.70(13)
Z	2
D_{calc} (Mg/m^3)	1.22
Absorption coefficient (mm^{-1})	0.12
θ range for data collection (°)	3.41–26.02
Reflections collected	30176
Independent reflections	5659 [$R_{int} = 0.053$]
Reflections with $I > 2\sigma(I)$	4499
Data/restraints/parameters	5659/0/361
Goodness-of-fit on F^2	1.020
Final R indices [$I > 2\sigma(I)$]	$R_1 = 0.053$, $wR_2 = 0.128$
R indices (all data)	$R_1 = 0.071$, $wR_2 = 0.140$
Largest difference in peak and hole (e Å^3)	0.353 and – 0.371

Table 4
Selected bond lengths (Å) and angles (°) for $[Ph_3SiOLi(hppH)(THF)]_2$ (**5**)

Li–O(1)	1.969(4)	Li–O(1′)	1.954(3)
Li–O(2)	2.011(4)	Li–N(1)	2.054(4)
Si–O(1)	1.5926(14)	C(1)–N(1)	1.302(3)
C(1)–N(2)	1.359(3)	C(1)–N(3)	1.374(3)
H(2n)···O(1)	2.04	Δ_{CN}	0.057
O(1)–Li–O(1′)	99.24(15)	O(1)–Li–O(2)	116.17(17)
O(1)–Li–N(1)	109.10(17)	O(1′)–Li–O(2)	111.23(17)
O(1′)–Li–N(1)	119.57(17)	N(1)–Li–O(2)	102.29(16)
Li–O(1)–Li′	80.76(15)	Si–O(1)–Li	139.25(13)
Si–O(1)–Li′	130.05(12)		

distances (within 3σ) to each oxygen. A similar trend has been reported in the closely related dme adduct, $[Ph_3SiO\text{-}Li(dme)]_2$ [30]. Overall, each lithium atom is distorted tetrahedral, with the coordination sphere being completed by a molecule of THF and an N_{imine} bound neutral hppH; the three coordinate siloxide oxygen atoms show significant pyramidalization [$\Sigma_{angles} = 350.06°$]. The hppH molecule is oriented approximately parallel to the Li–O vector and therefore effectively bridges this unit, with a resultant intramolecular hydrogen bond distance of 2.04 Å. This is the first reported example of an intramolecular N*H*···O bond involving the neutral hppH guanidine.

4. Summary

The series of bis-hppH adducts of the first row transition metal dihalides has been extended, showing a common bonding pattern in which intramolecular hydrogen bonding is evident. The compounds each crystallize as the racemic mixture of Δ and Λ isomers within the crystal, and it is noted that the long range order of how these isomers are arranged with respect to each other differs depending on the crystal system. The molecular structure of the lithiated siloxide $[Ph_3SiOLi(hppH)(THF)]_2$ reveals a dimer in the solid-state, in which the N*H* hydrogen bonds to the siloxide oxygen atom.

5. Supplementary material

Crystallographic data for the structural analyses have been deposited with the Cambridge Crystallographic Data Centre, CCDC nos. **1** (276689), **2** (231326) $CoCl_2(hppH)_2$ (276693), **3** (276690), **4** (276691) and **5** (276692). Copies of this information may be obtained free of charge from: The Director, CCDC, 12 Union Road, Cambridge CB2 1EZ, UK (Fax: +44 1223 336033; email: deposit@ccdc.cam.ac.uk or www: http://www.ccdc.cam.ac.uk).

Acknowledgements

We thank the University of Sussex for financial support and wish to acknowledge the use of the EPSRC's Chemical Database Service at Daresbury.

References

[1] For reviews on hydrogen-bonding and its importance in a number of key areas of chemistry, M. Meot-Ner, Chem. Rev. 105 (2005) 213.
[2] L. Kovbasyuk, R. Krämer, Chem. Rev. 104 (2004) 3161.
[3] P.R. Schreiner, Chem. Soc. Rev. 32 (2003) 289.
[4] D. Braga, L. Maini, M. Polito, E. Tagliavini, F. Grepioni, Coord. Chem. Rev. 246 (2003) 53.
[5] C.R. Bondy, S.J. Loeb, Coord. Chem. Rev. 240 (2003) 77.
[6] D. Braga, F. Grepioni, G.R. Desiraju, Chem. Rev. 98 (1998) 1375.
[7] P.J. Bailey, S. Pace, Coord. Chem. Rev. 214 (2001) 91.
[8] S.H. Oakley, M.P. Coles, P.B. Hitchcock, Inorg. Chem. 42 (2003) 3154.
[9] S.H. Oakley, D.B. Soria, M.P. Coles, P.B. Hitchcock, Dalton Trans. (2004) 537.
[10] F.A. Cotton, C.A. Murillo, D.J. Timmons, Polyhedron 18 (1999) 423.
[11] S.H. Oakley, M.P. Coles, P.B. Hitchcock, Inorg. Chem. 43 (2004) 7564.
[12] M.P. Coles, P.B. Hitchcock, Eur. J. Inorg. Chem. (2004) 2662.
[13] S.J. Birch, S.R. Boss, S.C. Cole, M.P. Coles, R. Haigh, P.B. Hitchcock, A.E.H. Wheatley, Dalton Trans. (2004) 3568.
[14] M.P. Coles, P.B. Hitchcock, Chem. Commun. (2005) 3165.
[15] P.J. Bailey, K.J. Grant, S. Pace, S. Parsons, L.J. Stewart, J. Chem. Soc., Dalton Trans. (1997) 4263.
[16] D.A. Rowley, R.S. Drago, Inorg. Chem. 6 (1967) 1092.
[17] S.H. Oakley, M.P. Coles, P.B. Hitchcock, Dalton Trans. (2004) 1113.
[18] D. Kummer, S.H.A. Halim, W. Kuhs, G. Mattern, J. Organomet. Chem. 446 (1993) 51.
[19] G.M. Sheldrick, SHELXL-97, Program for the Refinement of Crystal Structures, Göttingen, 1997..
[20] F.A. Cotton, L.M. Daniels, D.J. Maloney, J.H. Matonic, C.A. Murillo, Polyhedron 13 (1994) 815.
[21] F.A. Cotton, L.M. Daniels, C.A. Murillo, Inorg. Chim. Acta 224 (1994) 5.
[22] D.I. Arnold, F.A. Cotton, D.J. Maloney, J.H. Matonic, C.A. Murillo, Polyhedron 16 (1997) 133.

[23] G. Häfelinger, K.H. KuskeThe Chemistry of the Amidines and Imidates, vol. 2, Wiley, Chichester, 1991 (Chapter 1).
[24] J. Hvoslef, H. Hope, B.D. Murray, P.P. Power, J. Chem. Soc., Chem. Commun. (1983) 1438.
[25] G. Beck, P.B. Hitchcock, M.F. Lappert, I.A. MacKinnon, J. Chem. Soc., Chem. Commun. (1989) 1312.
[26] K.J. Weese, R.A. Bartlett, B.D. Murray, M.M. Olmstead, P.P. Power, Inorg. Chem. 26 (1987) 2409.
[27] V.C. Gibson, C. Redshaw, W. Clegg, M.R.J. Elsegood, Polyhedron 16 (1997) 2637.
[28] S.C. Cole, M.P. Coles, P.B. Hitchcock, Organometallics 23 (2004) 5159.
[29] P.B. Hitchcock, N.H. Buttrus, A.C. Sullivan, J. Organomet. Chem. 303 (1986) 321.
[30] M.J. McGeary, K. Folting, W.E. Streib, J.C. Huffman, K.G. Caulton, Polyhedron 10 (1991) 2699.

2. Experimental

2.1. Materials and synthesis

1,4,7,10-tetraazacyclododecane, $K_2[Ni(CN)_4]\cdot xH_2O$ and $K_2[Pt(CN)_4]\cdot 3H_2O$ were obtained from Strem. All chemicals and solvents were of reagent grade and were used as received.

$[Ni(cyclen)]_2[Pt(CN)_4]_2\cdot 6H_2O$ (**1**) was synthesized by a slow diffusion method. $K_2[Pt(CN)_4]\cdot 3H_2O$ (108 mg, 0.25 mmol), cyclen (86 mg, 0.5 mmol) and $Ni(CH_3COO)_2\cdot 4H_2O$ (124 mg, 0.5 mmol) contained in three separate sample tubes (10 ml) were placed together in a 200 ml beaker. The sample tubes and the beaker were then carefully filled with water such that the three sample tubes were immersed in the beaker of water but the contents were not mixed together. Purple needle-shaped crystals were obtained after leaving the beaker undisturbed at room temperature for a week. Yield: 65%. *Anal*. Calc. for $Pt_2Ni_2N_{16}C_{24}O_6H_{52}$: C, 24.67; H, 4.49; N, 19.18. Found: C, 24.55; H, 4.60; N, 19.30%. IR ν_{CN} (KBr/cm^{-1}): 2184sh, 2172s, 2138vs.

The synthesis of $[Ni(cyclen)]_2[Ni(CN)_4]_2\cdot 6H_2O$ (**2**) was similar to that of **1**. $K_2[Ni(CN)_4]\cdot xH_2O$ (120 mg, 0.5 mmol), cyclen (86 mg, 0.5 mmol) and $Ni(CH_3COO)_2\cdot 4H_2O$ (124 mg, 0.5 mmol) were used as starting materials. Purple needle-shaped crystals were obtained after one week. Yield: 65%. *Anal*. Calc. for Ni_4N_{16}-$C_{24}O_6H_{52}$: C, 32.19; H, 5.85; N, 25.02. Found: C, 32.20; H, 6.10; N, 25.05%. IR ν_{CN} (KBr/ cm^{-1}): 2165s, 2126vs.

For the synthesis of $[Mn(cyclen)]_2[Ni(CN)_4]_2\cdot 6H_2O$ (**3**), $K_2[Ni(CN)_4]\cdot xH_2O$ (60 mg, 0.25 mmol) in 5 ml H_2O was added to a solution of $Mn(ClO_4)_2\cdot 6H_2O$ (181 mg, 0.5 mmol) and cyclen (86 mg, 0.5 mmol) in 10 ml H_2O. After stirring the mixture for a few minutes, the solution was filtered to remove a white precipitate. Slow evaporation of the green filtrate in the dark gave pink crystals after one week. Yield: 10%. *Anal*. Calc. for $Mn_2Ni_2N_{16}C_{24}$-O_6H_{52}: C, 32.46; H, 5.90; N, 25.24. Found: C, 32.50; H, 6.02; N, 24.56%. IR ν_{CN} (KBr/cm^{-1}): 2157s, 2133s.

2.2. Physical measurements

Infra-red spectra (KBr pellets) were recorded on a Perkin–Elmer model 1600 FTIR spectrophotometer. Elemental analysis were performed on a Vario EL elemental analyzer. Variable-temperature magnetic susceptibility measurements were performed on crystalline samples of the title compounds in the range of 2–200 K on an Oxford Instruments Maglab2000 magnetometer. Susceptibilities were corrected for diamagnetism using Pascal's constants.

2.3. Crystallography

Crystallographic data was collected on a Rigaku AFC7R diffractometer with graphite-monochromated Mo Kα radiation ($\lambda = 0.71069$ Å) for **1** at 301 K and Bruker SMART CCD area detector with graphite monochromated Mo Kα radiation ($\lambda = 0.71069$ Å) for **2**–**3** at 298 K. The structures were solved by direct method SHELXS 86 [15] for **1** and SIR 92 [16] for **2** and **3**, and refined by full-matrix least squares technique based on F using TEXSAN crystallographic software package [17] for **1** and **2** and using CRYSTALS [18] for **3**. The intensity data were corrected

Table 1
Crystal data for $[Ni(cyclen)]_2[Pt(CN)_4]_2\cdot 6H_2O$ (**1**), $[Ni(cyclen)]_2[Ni(CN)_4]_2\cdot 6H_2O$ (**2**) and $[Mn(cyclen)]_2[Ni(CN)_4]_2\cdot 6H_2O$ (**3**)

Compound	**1**	**2**	**3**
Formula	$Pt_2Ni_2N_{16}C_{24}O_6H_{52}$	$Ni_4N_{16}C_{24}O_6H_{52}$	$Mn_2Ni_2N_{16}C_{24}O_6H_{52}$
M_r	1168.36	895.58	888.05
Crystal color, habit	red, prism	red, prism	pink, prism
Crystal dimensions (mm)	$0.43\times0.12\times0.09$	$0.45\times0.12\times0.10$	$0.12\times0.14\times0.49$
Crystal system	monoclinic	monoclinic	monoclinic
Lattice type	primitive	primitive	primitive
a (Å)	8.680(3)	8.643(2)	8.632(1)
b (Å)	14.218(3)	14.218(4)	14.177(1)
c (Å)	15.758(4)	15.542(5)	15.571(1)
β (°)	93.69(3)	93.96(1)	93.75(1)
V (Å^3)	1940.8(9)	1905.3(8)	1901.4(3)
Space group	$P21/c$ (no. 14)	$P21/c$ (no. 14)	$P21/c$ (no. 14)
Z value	2	2	2
D_{calc} (g cm^{-3})	1.999	1.561	1.551
F_{000}	1136	936	924
μ (Mo Kα) (cm^{-1})	81.70	20.05	16.83
Number of parameters refined	226	226	246
Number of reflections measured	3571	4432	4395
Number of reflections observed	2543 ($I > 3\sigma(I)$)	3645 ($I > 1.5\sigma(I)$)	3625 ($I > 1.5\sigma(I)$)
Residuals: R, R_w	0.0235; 0.0289	0.0262; 0.0355	0.047; 0.112
Goodness-of-fit	1.036	1.107	1.017
$\Delta\rho_{max}$ (e Å^{-3})	0.44	0.28	1.29
$\Delta\rho_{max}$ (e Å^{-3})	−0.73	−0.31	−0.69

for Lorentz and polarization effects. Empirical absorption corrections were also applied. All the non-hydrogen atoms were refined anisotropically. Hydrogen atoms were included but not refined. The hydrogen atoms of the water solvates for **3** were not located. The crystallographic data is collected in Table 1.

3. Results and discussion

3.1. Description of the structures

The X-ray structure of $[Ni(cyclen)]_2[Pt(CN)_4]_2 \cdot 6H_2O$ (**1**) (Fig. 1) shows that each Ni(II) centre is octahedrally coordinated to the four nitrogen atoms of a cyclen ligand and two cyano nitrogen atoms in a *cis* configuration. Two $[Ni(cyclen)]^{2+}$ units are linked by two $[Pt(CN)_4]^{2-}$ units via bridging cyano groups to produce a slightly puckered 12-membered molecular square structure. The deviation from the mean plane of the square structure is ±0.169 Å. This is because the Ni—N≡C unit is slightly bent with an Ni*–N(3)–C(3) angle of 173.1(6)° and an Ni–N(4)–C(4) angle of 166.7(6)°. Two of the Ni–N(cyclen) bonds [2.140(5) and 2.143(5) Å] are slightly longer than the other Ni–N(cyclen) bonds [2.072(5)–2.088(5) Å] and the Ni—N(≡C) bonds [2.064(5) and 2.096(6) Å]. All terminal and bridging C≡N distances are similar [1.134(7)–1.148(8) Å] and comparable to those found in $[Cu(bpy)(H_2O)Pt(CN)_4]_2 \cdot 2H_2O$ [1.114(11)–1.145(10) Å] [19] (Table 2). The intramolecular Ni···Ni separation is 7.462 Å and the closest intermolecular Ni···Ni separation is 7.943 Å. The tetranuclear square structures are arranged in a herring bone fashion, with a dihedral angle between the neighbouring square structures of 60.08°. Taking the Ni–Pt–Ni–Pt as the mean plane, the inter-planar distance between the squares is 3.752 Å and the Pt···Pt distance is 3.822 Å, indicating the presence of weak interactions between the Pt atoms. The void area of the tetranuclear square structure is capped on both sides by water solvates, O(1)/H(21)/H(22). Extensive intermolecular hydrogen bonding was observed between the tetranuclear square structures and the water solvates (Table 5 and Fig. 4).

Table 2
Selected bond lengths (Å) and bond angles (°) for $[Ni(cyclen)]_2[Pt(CN)_4]_2 \cdot 6H_2O$ (**1**)

Pt–C(1)	1.987(6)	Ni–N(6)	2.088(5)
Pt–C(2)	1.993(7)	Ni–N(7)	2.140(5)
Pt–C(3)	1.993(7)	Ni–N(8)	2.072(5)
Pt–C(4)	1.991(6)	N(1)–C(1)	1.148(8)
Ni–N(3*)	2.064(5)	N(2)–C(2)	1.134(8)
Ni–N(4)	2.096(6)	N(3)–C(3)	1.139(8)
Ni–N(5)	2.143(5)	N(4)–C(4)	1.134(7)
C(1)–Pt–C(2)	90.2(3)	N(7)–Ni–N(8)	83.3(2)
C(1)–Pt–C(3)	176.6(3)	Pt–C(1)–N(1)	176.0(6)
C(1)–Pt–C(4)	90.7(2)	Pt–C(2)–N(2)	175.5(6)
C(3)–Pt–C(4)	90.0(2)	Pt–C(3)–N(3)	174.4(6)
N(3*)–Ni–N(4)	86.5(2)	Pt–C(4)–N(4)	178.4(6)
N(5)–Ni–N(6)	80.6(2)	Ni*–N(3)–C(3)	173.1(6)
N(6)–Ni–N(7)	80.2(2)	Ni–N(4)–C(4)	166.7(6)
N(5)–Ni–N(8)	83.6(2)		

Symmetry transformation used to generate equivalent atom (*): $1-x, -y, 2-z$.

The X-ray structure of $[Ni(cyclen)]_2[Ni(CN)_4]_2 \cdot 6H_2O$ **2** (Fig. 2) shows that it is isostructural with **1**, each Ni(II) centre is octahedrally coordinated to the four nitrogen atoms of a cyclen ligand and two cyano nitrogen atoms of $[Ni(CN)_4]^{2-}$ in a *cis* configuration forming a slightly puck-

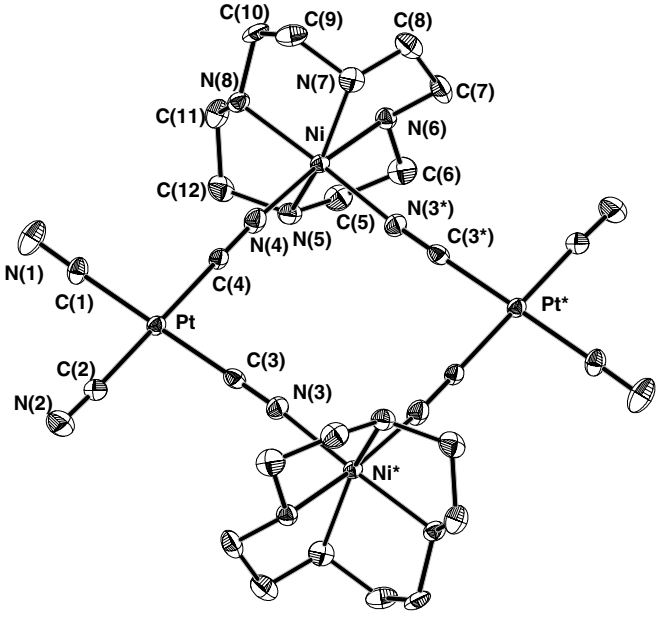

Fig. 1. An ORTEP diagram of $[Ni(cyclen)]_2[Pt(CN)_4]_2 \cdot 6H_2O$ with atom labelling scheme. The water solvates and H atoms were omitted for clarity.

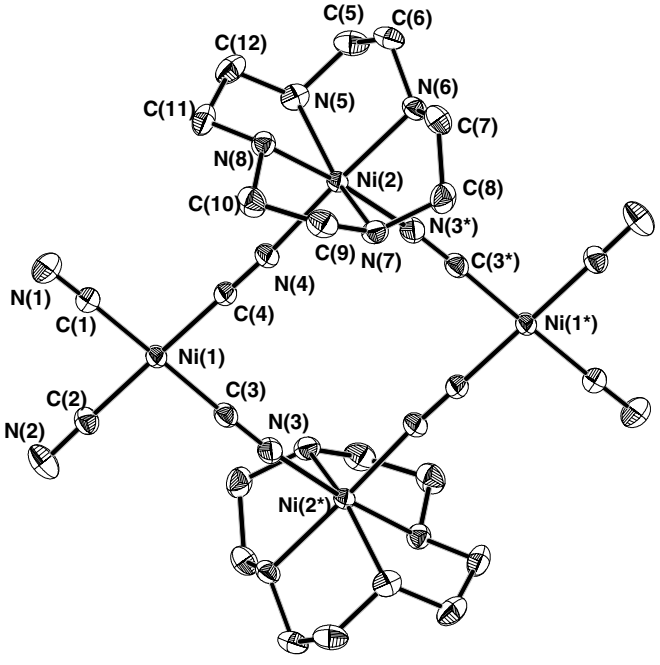

Fig. 2. An ORTEP diagram of $[Ni(cyclen)]_2[Ni(CN)_4]_2 \cdot 6H_2O$ with atom labelling scheme. The water solvates and H atoms were omitted for clarity.

ered 12-membered tetranuclear square structure. The deviation from the mean plane of the square structure is ±0.203 Å. This is because two of the Ni—N≡C units are almost linear with an Ni(2)–N(4)–C(4) angle of 176.0(2)° but the other two units are bent with an Ni(2*)–N(3)–C(3) angle of 164.0(2)°. Two of the Ni–N(cyclen) bonds [2.134(2) and 2.136(2) Å] are slightly longer than the other Ni–N(cyclen) bonds [2.070(2)–2.096(2) Å] and the Ni—N(≡C) bonds [2.064(2) and 2.091(2) Å]. All the terminal and bridging C≡N distances are similar [1.137(3)–1.152(3) Å] and comparable to those found in **1** (Table 3). The intramolecular Ni(cyclen)···Ni(cyclen) separation is 7.245 Å and the closest intermolecular Ni(cyclen)···Ni(cyclen) separation is 7.855 Å. The tetranuclear square structures are also arranged in a herring bone fashion, with a dihedral angle between the neighbouring square structures of 54.66°. Taking the four Ni atoms as the mean plane, the inter-planar distance between the squares is 3.849 Å and the shortest Ni(cyanide)···Ni(cyanide) distance is 3.944 Å, indicating the presence of weak interactions between the Ni atoms. The void area of the tetranuclear square structure is capped on both sides by water solvates, O(2)/H(23)/H(24). Extensive intermolecular hydrogen bonding is also observed in the crystal lattice (Table 6 and Fig. 5).

The X-ray structure of $[Mn(cyclen)]_2[Ni(CN)_4]_2 \cdot 6H_2O$ (**3**) (Fig. 3) shows that it is also a molecular square and is isostructural to **1** and **2**. Each Mn(II) centre is octahedrally coordinated to the four nitrogen atoms of a cyclen ligand and two cyano nitrogen atoms in a *cis* configuration forming a puckered 12-membered tetranuclear square structure. The deviation from the mean plane of the square structure is ±0.204 Å. This is because one of the Mn—N≡C unit is almost linear with a Mn(2)–N(4)–C(4) bond angle of 175.5(4)° while the other is bent with a Mn(1*)–N(3)–C(3) bond angle of 164.7(4)°. Two $[Mn(cyclen)]^{2+}$ units are linked by two $[Ni(CN)_4]^{2-}$ units via bridging cyano groups to form a molecular square. Three of the Mn–N(cyclen) bonds [2.101(4)–2.139(4) Å] are slightly longer than the other Mn–N(cyclen) bonds [2.081(4) Å] and the Mn—N(≡C) bonds [2.063(4)–2.093(4) Å]. All the bond distances of terminal and bridging cyano groups (C≡N) are similar [1.146(8)–1.150(7) Å] and comparable to those found in the structure **1** and **2** (Table 4). The intramolecular Mn···Mn separation is 7.231 Å and the closest intermolecular Mn···Mn separation is 7.871 Å. The tetranuclear square structures are also arranged in a herring bone fashion, with

Table 3
Selected bond lengths (Å) and bond angles (°) for $[Ni(cyclen)]_2[Ni(CN)_4]_2 \cdot 6H_2O$ (**2**)

Ni(1)–C(1)	1.869(2)	Ni(2)–N(6)	2.070(2)
Ni(1)–C(2)	1.864(2)	Ni(2)–N(7)	2.134(2)
Ni(1)–C(3)	1.865(2)	Ni(2)–N(8)	2.096(2)
Ni(1)–C(4)	1.864(2)	N(1)–C(1)	1.137(3)
Ni(2)–N(3*)	2.091(2)	N(2)–C(2)	1.149(3)
Ni(2)–N(4)	2.064(2)	N(3)–C(3)	1.150(3)
Ni(2)–N(5)	2.136(2)	N(4)–C(4)	1.152(3)
C(1)–Ni(1)–C(2)	89.5(1)	N(7)–Ni(2)–N(8)	80.55(7)
C(1)–Ni(1)–C(3)	176.8(1)	Ni(1)–C(1)–N(1)	175.7(3)
C(1)–Ni(1)–C(4)	89.38(10)	Ni(1)–C(2)–N(2)	176.1(2)
C(3)–Ni(1)–C(4)	90.06(9)	Ni(1)–C(3)–N(3)	178.0(2)
N(3*)–Ni(2)–N(4)	87.18(7)	Ni(1)–C(4)–N(4)	176.6(2)
N(5)–Ni(2)–N(6)	83.11(7)	Ni(2*)–N(3)–C(3)	164.0(2)
N(5)–Ni(2)–N(8)	80.56(7)	Ni(2)–N(4)–C(4)	176.0(2)
N(6)–Ni(2)–N(7)	83.27(7)		

Symmetry transformation used to generate equivalent atom (*): $1-x$, $1-y$, $2-z$.

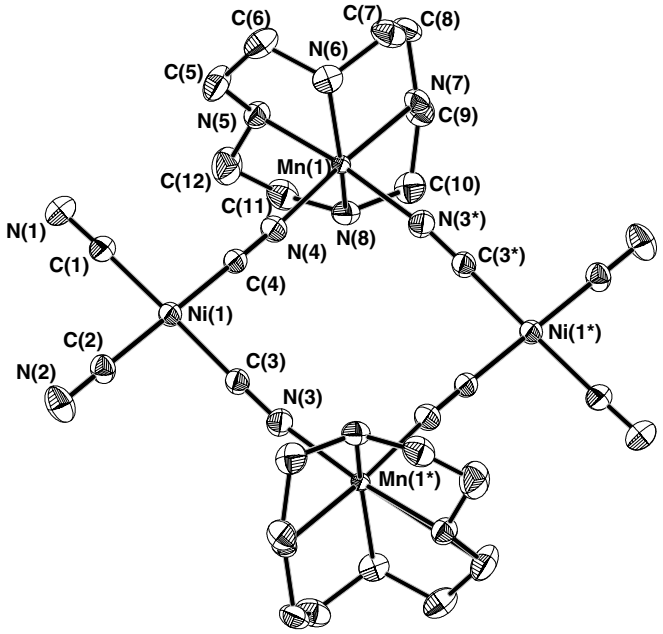

Fig. 3. An ORTEP diagram of $[Mn(cyclen)]_2[Ni(CN)_4]_2 \cdot 6H_2O$ with atom labelling scheme. The water solvates and H atoms were omitted for clarity.

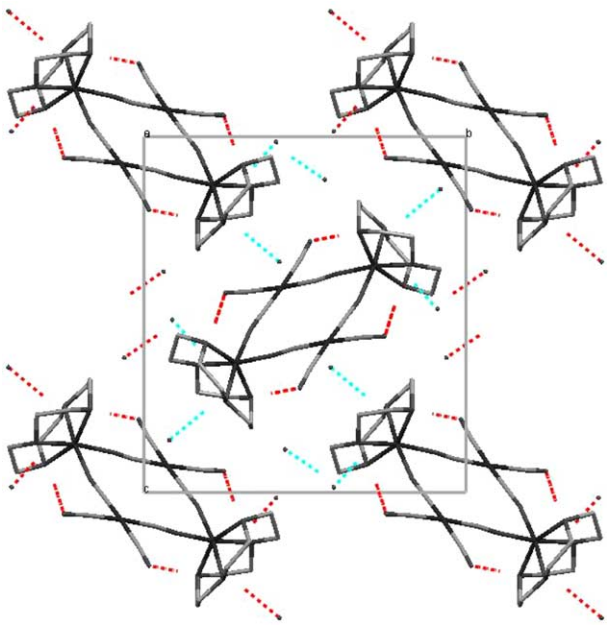

Fig. 4. Crystal packing of **1** down *a*-axis; indicating extensive intermolecular hydrogen bonding between the tetranuclear square structures and the water solvates (dotted lines); H atoms are omitted for clarity.

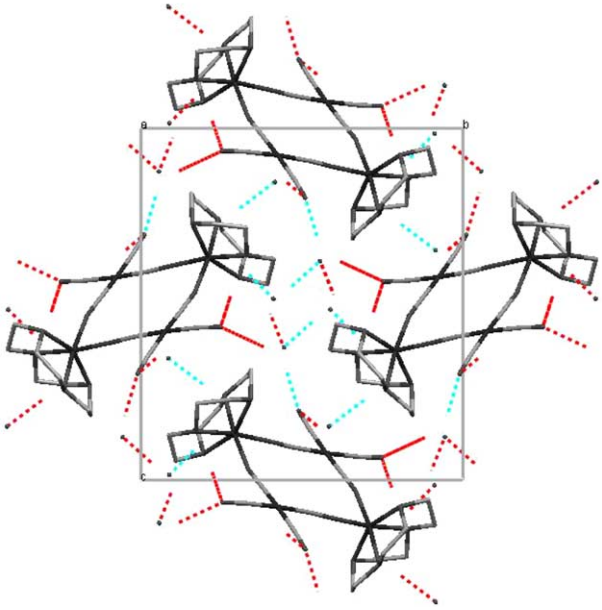

Fig. 5. Crystal packing of 2 down *a*-axis; indicating extensive intermolecular hydrogen bonding between the tetranuclear square structures and the water solvates (dotted lines); H atoms were omitted for clarity.

Table 4
Selected bond lengths (Å) and bond angles (°) for $[Mn(cyclen)]_2[Ni(CN)_4]_2 \cdot 6H_2O$ (**3**)

Ni(1)–C(1)	1.870(5)	Mn(1)–N(6)	2.139(4)
Ni(1)–C(2)	1.867(5)	Mn(1)–N(7)	2.081(4)
Ni(1)–C(3)	1.864(5)	Mn(1)–N(8)	2.139(4)
Ni(1)–C(4)	1.861(4)	N(1)–C(1)	1.146(8)
Mn(1)–N(3)	2.093(5)	N(2)–C(2)	1.150(7)
Mn(1)–N(4)	2.063(4)	N(3)–C(3)	1.149(6)
Mn(1)–N(5)	2.101(4)	N(4)–C(4)	1.148(6)
C(1)–Ni(1)–C(2)	89.9(2)	Ni(1)–C(1)–N(1)	175.4(5)
C(1)–Ni(1)–(3)	176.3(2)	Ni(1)–C(2)–N(2)	175.4(4)
C(1)–Ni(1)–(4)	89.3(2)	Ni(1)–C(3)–N(3)	178.5(4)
C(2)–Ni(1)–(3)	90.8(2)	Ni(1)–C(4)–N(4)	176.9(4)
C(2)–Ni(1)–(4)	177.0(2)	Mn(1*)–N(3)–C(3)	164.7(4)
C(3)–Ni(1)–(4)	89.8(2)	Mn(1)–N(4)–C(4)	175.5(4)
N(3*)–Mn(1)–N(4)	87.32(17)		

Symmetry transformation used to generate equivalent atom (*): $2-x$, $1-y$, $2-z$.

Table 5
Hydrogen bonding (Å and °) for **1**

D–H···A	*d*(D–H)	*d*(H···A)	*d*(D···A)	∠(DHA)
N(5)–H(1)···N(2)	0.95	2.36	3.159(9)	141
N(6)–H(6)···O(1)	0.95	2.15	3.022(9)	151
N(7)–H(11)···N(1)	0.95	2.19	3.064(8)	153
N(8)–H(16)···O(3)	0.95	2.11	2.935(8)	145
O(3)–H(25)···O(2)	0.81	2.04	2.826(10)	165

a dihedral angle between the neighbouring square structures of 58.29°. Taking the Ni–Mn–Ni–Mn as the mean plane, the inter-planar distance between the squares is 3.870 Å and the Ni···Ni distance is 3.952 Å, indicating the presence of weak interactions between the Ni atoms.

Table 6
Hydrogen bonding (Å and °) for **2**

D–H···A	*d*(D–H)	*d*(H···A)	*d*(D···A)	∠(DHA)
N(5)–H(1)···N(2)	0.95	2.25	3.120(3)	151
N(6)–H(2)···O(1)	0.95	2.10	2.913(3)	143
N(7)–H(3)···N(1)	0.95	2.45	3.233(3)	139
N(8)–H(4)···O(2)	0.95	2.12	2.988(3)	152
O(1)–H(21)···O(3)	0.88	2.25	3.071(4)	155
O(1)–H(22)···O(3)	0.89	1.92	2.790(4)	165
O(2)–H(23)···N(1)	0.89	2.24	3.061(4)	154
O(3)–H(25)···N(1)	0.95	2.08	3.017(4)	167
O(3)–H(26)···N(2)	0.81	2.11	2.936(4)	155

The void area of the tetranuclear square structure is capped on both sides by water solvates, O(2). Although the hydrogens of the water solvates were not located, it is expected that extensive intermolecular hydrogen bonding should also exist in the crystal lattice as in **1** and **2**.

3.2. Magnetic properties

The variable-temperature magnetic susceptibility of **1** was measured in the range of 2–200 K. The data obey Curie–Weiss Law $[\chi_m = C/(T-\theta)]$ with $\theta = +0.67$ K and $C = 2.36\ cm^3\ mol^{-1}\ K$ (Fig. 6). The very small positive Weiss constant suggests that there might be an overall very small ferromagnetic interaction between the Ni^{II} centres through the diamagnetic $[Pt(CN)_4]^{2-}$ bridge. The variable-temperature magnetic susceptibility of **2** was also measured in the range of 2–200 K. The data obey Curie–Weiss Law $[\chi_m = C/(T-\theta)]$ with $\theta = +0.14$ K and $C = 2.24\ cm^3\ mol^{-1}\ K$ (Fig. 7). Similar to **1**, the very small positive Weiss constant suggests that there might be an overall very weak ferromagnetic interaction between the Ni^{II} centres through the diamagnetic $[Ni(CN)_4]^{2-}$ bridge. To estimate the magnitude of the intradimer exchange coupling constant (J) and the interdimer magnetic interaction (zJ'),

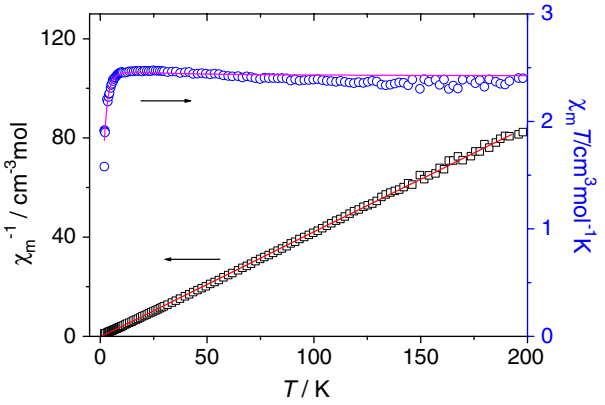

Fig. 6. Temperature dependence of χ_m^{-1} (□) and $\chi_m T$ (○) for $[Ni(cyclen)]_2[Pt(CN)_4]_2 \cdot 6H_2O$ (**1**), lines represent the fitting results using Curie–Weiss law and Ni-dimer model (see text).

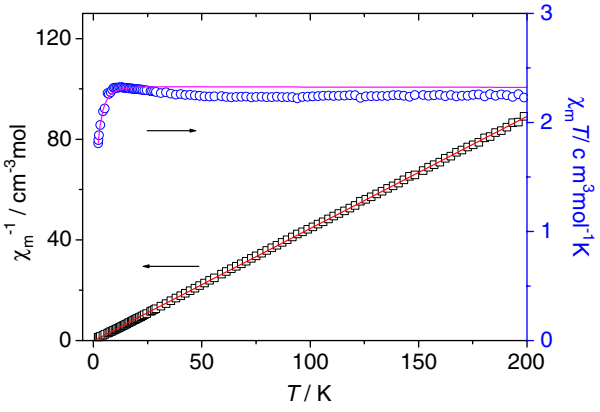

Fig. 7. Temperature dependence of χ_m^{-1} (□) and $\chi_m T$ (○) for [Ni(cyclen)]$_2$[Ni(CN)$_4$]$_2 \cdot 6H_2O$ (**2**), lines represent the fitting results using Curie–Weiss law and Ni-dimer model (see text).

the experimental data were initially fitted to a simple analytical expression based on the Hamiltonian $H = -2JS_1S_2$ with an isotropic interaction between the two Ni(II) ions and taking into account the molecular field effect. The best fit parameters are: for **1**, $J = 0.8(2)$ cm^{-1}, $zJ' = -0.33(1)$ cm^{-1}, and $g = 2.21(4)$; for **2**, $J = 0.48(4)$ cm^{-1}, $zJ' = -0.313(4)$ cm^{-1}, and $g = 2.175(6)$. When the zero-field splitting D of the Ni(II) ion was considered, a magnetic model derived by Ginsberg et al. [20] and corrected by Wen [21] has been used to fit the magnetic data, resulting in the following parameters: for **1**, $J = 0.6(1)$ cm^{-1}, $zJ' = -0.111(6)$ cm^{-1}, $D = 6$ cm^{-1}, and $g = 2.19(3)$ with $R = 2 \times 10^{-3}$; for **2**, $J = 0.23(3)$ cm^{-1}, $zJ' = -0.060(8)$ cm^{-1}, $D = 6$ cm^{-1}, and $g = 2.154(4)$ with $R = 8 \times 10^{-5}$ ($R = \sum(\chi_{obs} - \chi_{cal})^2/\sum(\chi_{obs})^2$). The fitted results suggest a very weak ferromagnetic intradimer interaction and an even weaker interdimer antiferromagnetic coupling. This is likely due to the relatively long intramolecular Ni···Ni separation (7.462 Å in **1** and 7.245 Å in **2**) and intermolecular Ni···Ni separation (7.943 Å in **1** and 7.855 Å in **2**). The magnetic behaviour of **3** was not investigated since it was expected to be similar to that of **1** and **2**.

In conclusion, we demonstrate that the use of a cyclen-capped metal complex in conjunction with a square planar tetracyanometalate $[M(CN)_4]^{2-}$ provides a general method for the synthesis of molecular squares. The 12-membered cyclen ring allows only *cis*-coordination, while the square tetracyanometalate is a good linker. This approach is potentially useful for the synthesis of other structures such as pentagons and hexagons.

4. Supplementary material

X-ray crystallographic files, in CIF format, for the structure **1**, **2** and **3** are available from the Cambridge Crystallographic Data Center, 12 Union Road, Cambridge CB2 1EZ, UK, fax: (internat.) +44 1223 336 033; e-mail: deposit@ccdc.cam.ac.uk, or via www.ccdc.cam.ac.uk/data_request/cif, by emailing data_request@ccdc.cam.ac.uk upon request, quoting the deposition numbers, CCDC-275688 (1), -275689 (2), and -275690 (3), respectively.

Acknowledgement

The work described in this paper is substantially supported by a grant from the City University of Hong Kong (7001363).

References

[1] (a) See, for example S.R. Seidel, P.J. Stang, Acc. Chem. Res. 35 (2002) 972;
(b) G.F. Swiegers, T.J. Malefetse, Coord. Chem. Rev. 225 (2002) 91;
(c) F.A. Cotton, C. Lin, C.A. Murillo, Acc. Chem. Res. 34 (2001) 759;
(d) S. Leininger, B. Olenyuk, P.J. Stang, Chem. Rev. 100 (2000) 853;
(e) D.L. Caulder, K.N. Raymond, Acc. Chem. Res. 32 (1999) 975;
(f) M. Fujita, Chem. Soc. Rev. 27 (1998) 417;
(g) R.V. Slone, K.D. Benkstein, S. Bélanger, J.T. Hupp, I.A. Guzei, A.L. Rheingold, Coord. Chem. Rev. 171 (1998) 221.
[2] (a) S.J. Lee, W. Lin, J. Am. Chem. Soc. 124 (2002) 4554;
(b) P.H. Dinolfo, J.T. Hupp, Chem. Mater. 13 (2001) 3113;
(c) K.S. Jeong, Y.L. Cho, S.Y. Chang, T.Y. Park, J.U. Song, J. Org. Chem. 64 (1999) 9459;
(d) K.-S. Jeong, Y.L. Cho, J.U. Song, H.Y. Chang, M.G. Choi, J. Am. Chem. Soc. 120 (1998) 10982;
(e) C. Müller, J.A. Whiteford, P.J. Stang, J. Am. Chem. Soc. 120 (1998) 9827;
(f) J.A. Whiteford, P.J. Stang, S.D. Huang, Inorg. Chem. 37 (1998) 5595;
(g) J.A. Whiteford, C.V. Lu, P.J. Stang, J. Am. Chem. Soc. 119 (1997) 2524;
(h) M. Fujita, J. Yazaki, K. Ogura, J. Am. Chem. Soc. 112 (1990) 5645.
[3] (a) M.L. Merlau, M.P. Mejia, S.T. Nguyen, J.T. Hupp, Angew. Chem., Int. Ed. 40 (2001) 4239;
(b) R.V. Slone, K.D. Benkstein, S. Bélanger, J.T. Hupp, I.A. Guzei, A.L. Rheingold, Coord. Chem. Rev. 171 (1998) 221.
[4] (a) F.A. Cotton, C. Lin, C.A. Murillo, J. Am. Chem. Soc. 123 (2001) 2670;
(b) A.N. Shipway, E. Katz, I. Willner, ChemPhysChem 1 (2000) 18;
(c) F.A. Cotton, L.M. Daniels, C. Lin, C.A. Murillo, J. Am. Chem. Soc. 121 (1999) 4538;
(d) M. Lahav, R. Gabai, A.N. Shipway, I. Willner, Chem. Commun. (1999) 1937.
[5] (a) S.S. Sun, A.J. Lees, Inorg. Chem. 121 (2001) 3154;
(b) J. Fan, J.A. Whiteford, B. Olenyuk, M.D. Levin, P.J. Stang, E.B. Fleischer, J. Am. Chem. Soc. 121 (1999) 2741;
(c) R.V. Slone, J.T. Hupp, C.L. Stern, T.E. Albrecht-Schmitt, Inorg. Chem. 35 (1996) 4096;
(d) R.V. Slone, D.I. Yoon, R.M. Calhoun, J.T. Hupp, J. Am. Chem. Soc. 117 (1995) 11813.
[6] A. Sautter, B.K. Kaletas, D.G. Schmid, R. Dobrawa, M. Zimine, G. Jung, I.H.M. van Stokkum, L. De Cola, R.M. Williams, F. Würthner, J. Am. Chem. Soc. 127 (2005) 6719.
[7] V.C. Lau, L.A. Berben, J.R. Long, J. Am. Chem. Soc. 124 (2002) 9042.
[8] H. Oshio, O. Tamada, H. Onodera, T. Ito, T. Ikoma, S. Tero-Kubota, Inorg. Chem. 38 (1999) 5686.
[9] H. Oshio, H. Onodera, O. Tamada, H. Mizutani, T. Hikichi, T. Ito, Chem. Eur. J. 6 (2000) 2523.
[10] H. Oshio, H. Onodera, T. Ito, Chem. Eur. J. 9 (2003) 3946.
[11] H. Oshio, M. Yamamoto, T. Ito, Inorg. Chem. 41 (2002) 5817.
[12] Y.-Z. Zhang, S. Gao, Z.-M. Wang, G. Su, H.-L. Sun, F. Pan, Inorg. Chem. 44 (2005) 4534.

[13] H.Z. Kou, S. Gao, C.H. Li, D.Z. Liao, B.C. Zhou, R.J. Wang, Y.D. Li, Inorg. Chem. 41 (2002) 4756.
[14] F. Karadas, E.J. Schelter, A.V. Prosvirin, J. Bacsa, K.R. Dunbar, Chem Commun. (2005) 1414.
[15] G.M. Shedrick, SHELXS-96, program for the solution of crystal structures, in: G.M. Sheldrick, C. Kruger, R. Goddard (Eds.), Crystallographic Computering, vol. 3, Oxford University Press, 1985, pp. 175–189.
[16] A. Altomare, M.C. Burla, M. Camalli, M. Cascarano, C. Giacovazzo, A. Guagliardi, G. Polidori, J. Appl. Crystallogr. 27 (1994) 435.
[17] TEXSAN, Crystal Structure Analysis Package, Molecular Structure Corporation, the Woodlands, TX, USA, 1992.
[18] D.J. Watkin, C.K. Prout, J.R. Carruthers, P.W. Betteridge, CRYSTALS, Chemical Crystallography Laboratory, Oxford, UK, 1996.
[19] L.R. Falvello, M. Tomás, Chem. Commun. (1999) 273.
[20] (a) A.P. Ginsberg, R.L. Martin, R.W. Brookes, R.C. Sherwood, Inorg. Chem. 11 (1972) 2884;
(b) B.W. Sun, S. Gao, B.Q. Ma, D.Z. Niu, Z.M. Wang, J. Chem. Soc., Dalton Trans. (2000) 4187.
[21] (a) T. Wen, Ph.D. thesis, Memorial University of Newfoundland, Canada, 1988;
(b) K.K. Nanda, A.W. Addison, N. Paterson, E. Sinn, L.K. Thompson, U. Sakaguchi, Inorg. Chem. 37 (1998) 1028.

Cu(II) takes place [17]. When the template is made of interconnected cylinders, long rods of copper are obtained. Slight changes in the experimental conditions induce distinct modifications of the shape and size of the nanorods [14,17].

However, despite numerous reports, as per our knowledge, this is the first report of copper nanorod synthesis without the addition of any other extra stabilizer or capping agent from outside. In this synthesis, glucose is performing multiple tasks. It not only reduces the copper(II) ions but is also responsible for the in situ stabilization of the evolved particles and acts as a capping agent to the copper metal. It is also shown that at a particular concentration of the reducing agent (glucose) well-defined nanorods were obtained. Slight changes in the experimental conditions induce distinct modifications of the shape and size of the nanorods. This reaction is very simple, reproducible and has to be carried out in alkaline medium. The morphology of the evolved particles can be controlled simply by varying its concentration but keeping other parameters constant. The evolved particles remained stable for ~7 days and were characterized by UV–Vis spectroscopy, TEM and XRD studies. Again, shape selective catalysis by the rod shaped copper nanoparticles has been demonstrated for 1,1′ coupling of 2-naphthol via oxidative phenol coupling (OPC) reaction.

2. Experimental

2.1. Reagents

All the reagents were of analytical reagent grade. Copper sulfate (Aldrich) was used as received. Aqueous solution (10^{-2} M) of the salt was used as stock solution. Glucose, anion exchange resin, Amberlite IRA 400 and sodium thiocyanate were purchased from S.D. Fine Chemicals, India, 2-naphthol was purchased from Loba Chemie, India. Milli-Q water was used throughout the experiment. Sodium hydroxide (Merck) was used as received. Aqueous solution (1.0 M) of NaOH was used as stock solution.

2.2. Instruments

The absorption spectra were recorded in a Chemito Spectrascan UV 2600 doubled beam spectrophotometer taking the solutions in a quartz cuvette of path length 1 cm. All the spectral measurements were done at room temperature. TEM measurements of the metal sols were performed in a Hitachi H-9000 NAR instrument on samples prepared by placing a drop of fresh metal sols on Cu grids precoated with carbon films, followed by solvent evaporation under vacuum. The particle size was measured using a JEOL-100CXII transmission electron microscope (TEM). X-ray diffraction (XRD) measurement was performed by PW1840 diffractometer Philips, using Co-target at working voltage 40 kV, 20 mA. The samples were centrifuged and washed with methanol. Finally, the samples were dried under vacuum and X-ray diffraction (XRD) was undertaken for all the three samples.

2.3. Preparation of samples

Three different sets of solutions namely C_1, C_2 and C_3 were prepared by dissolving 0.2, 0.3 and 0.4 g of glucose, respectively, in 5.0 ml of water. Then, 10 μL NaOH (1.0 M) was added to it and the solution was warmed to a temperature of 60 °C. Finally, 200 μL $CuSO_4$ (10^{-2} M) was introduced to each set and the final mixture was warmed for 3 min to a temperature of ~80 °C. The solutions turned light yellow in all the three sets indicating the formation of Cu(0) with the characteristic plasmon band in the visible range. The whole reaction was carried out in nitrogen atmosphere to prevent the oxidation of copper nanoparticles. The UV–Vis spectra due to the plasmon resonance arise with a significant contribution from interband transition, which produces yellow color hydrosol [18]. A drop of solution from all the three reaction mixtures was deposited on three different copper grids precoated with carbon black. To prevent surface oxidation of the Cu(0), the TEM samples were then transported to the instrument under an argon atmosphere. The TEM images indicates well-defined, nanorods (average length of ~116 nm and width 46 nm for C_2) and nanospheres (diameter for $C_1 \sim 20$ nm and for $C_3 \sim 4$ nm), respectively. The XRD analysis was carried out for the all three samples.

3. Results and discussions

3.1. UV–Vis study

In spheroidal or rod-shaped copper nanoparticles, the first distinct difference relative to spherical particle is the appearance of a surface plasmon band at lower energies [19]. Fig. 1 shows the absorption spectrum of the copper nanoparticles prepared in three different sets. The prepared spherical nanoparticles (C_1) display an absorption peak at ~499 nm which can be assigned to the absorption peak of spherical copper nanoparticles. Aqueous suspensions of the rod shaped particles (C_2) have a sharp peak at 472 nm in the UV–Vis spectra, corresponding to the transverse plasmon band of the copper nanorods and the plasmon band 740 nm is assigned to the longitudinal one. The longitudinal and transverse peak position shifted to some extent due to the dielectric constant of the medium which is again temperature dependent [20]. The solution (C_3) having higher concentration of glucose showed one peak at 463 nm (λ_{max}) only. The optical path length is 1 cm and the extinction coefficient per atom was calculated to be $1.7 \times 10^3\ l\ M^{-1}\ cm^{-1}$which is slightly lower than the literature value [13]. The whole synthetic procedure and the corresponding UV–Vis spectra is given in Scheme 1. The synthesized particles were stable for ~7 days. This kind of stabilization of Cu nanoparticles was due to the capping

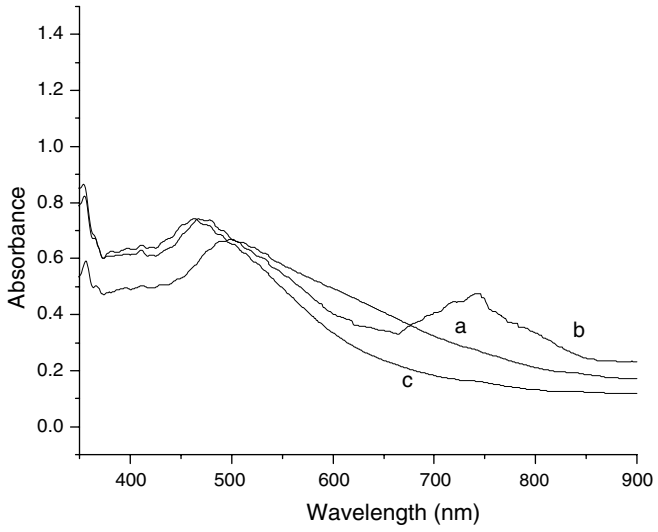

Fig. 1. UV–Vis spectra of the copper nanospheres and nanorods, (a) UV–Vis spectra of the spherical particles (C_1), (b) UV–Vis spectra of the nanorods (C_2), (c) UV–Vis spectra of the spherical particles (C_3). Conditions: $[CuSO_4] = 3.84 \times 10^{-4}$ M, $[NaOH] = 2 \times 10^{-3}$ M [glucose] = 5.78×10^{-3} M for a, 8.68×10^{-3} M for b and 1.16×10^{-2} M for c.

of particles by glucose and/or by gluconic acid in alkaline condition. The arrangement of capping agent, glucose/gluconic acid surrounding the nanoparticles is size dependent. After a few days, slow oxidation of copper particles sets in with the disappearance of absorption peaks [21] and finally the solution becomes colorless. However, the solution on a spot plate produces a distinct black coloration with ethanolic solution of rubeanic acid (0.5%) due to the formation of copper rubeanate. The test authenticates the evolution of Cu(II) ions from Cu(0).

3.2. TEM analysis

The TEM microstructures for the prepared copper nanoparticles are shown in Fig. 2(a)–(c) and the inset shows the histogram for the copper nanorods. Fig. 2(a) shows the TEM images of spherical copper particles (C_1) size of ~20 nm. Fig. 2(b) reveals the large copper nanorods (C_2) having an average length ~116 nm and diameter in the range ~46 nm with an aspect ratio of ~2.5. Fig. 2(c) describes the TEM images of the fine particles of copper having size ~4 nm (C_3) with a very few number of nanorods.

3.3. X-ray diffraction pattern

Fig. 3 shows an XRD pattern of the copper nanorods (C_2). The product exhibits a high crystallinity and no indication of impurities such as copper oxide (CuO) and cuprous oxide (Cu_2O), can be detected in the pattern. The reflection peaks at $2\theta = 43.4°$, 50.6° and 74.2° are indexed as [1 1 1], [2 0 0] and [2 2 0] planes of copper with cubic symmetry, respectively. These reflection peaks of copper nanorods have been compared with the literature values [22].

3.4. Mechanism of particle growth and the effect of OH^- ion

In presence of alkali α-glucose transforms into β-glucose through the open chain structure, which is reactive, and this phenomenon is known as mutarotation. In open chain form, the free –CHO group is available which causes the reduction of the Cu(II) to Cu(0) in the alkaline pH and at the elevated temperature. As a consequence of the reduction the –CHO group oxidizes to the corresponding –COOH which offers stability to the generated particles under alkaline condition [23]. The particle formation reaction and the mechanism are given in Scheme 2. The pH of the solution was measured at the end of the reaction. In all the three sets though the volume of added NaOH is same but the pH varies (~8.0 ± 0.5) to some extent due to the variable amount of added glucose. The base is partly neutralized by the evolved gluconic acid and hence the pH remains somewhat less than the expected value. Again, under the alkaline condition basic copper hydroxide is formed and this is responsible for nucleation and successive growth. Therefore, the OH^- ion has formidable influence

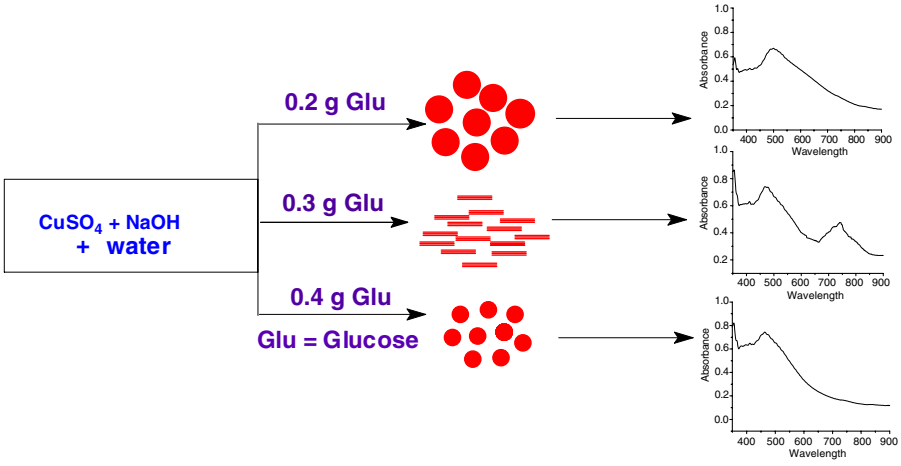

Scheme 1. The schematic representation of the synthetic procedure.

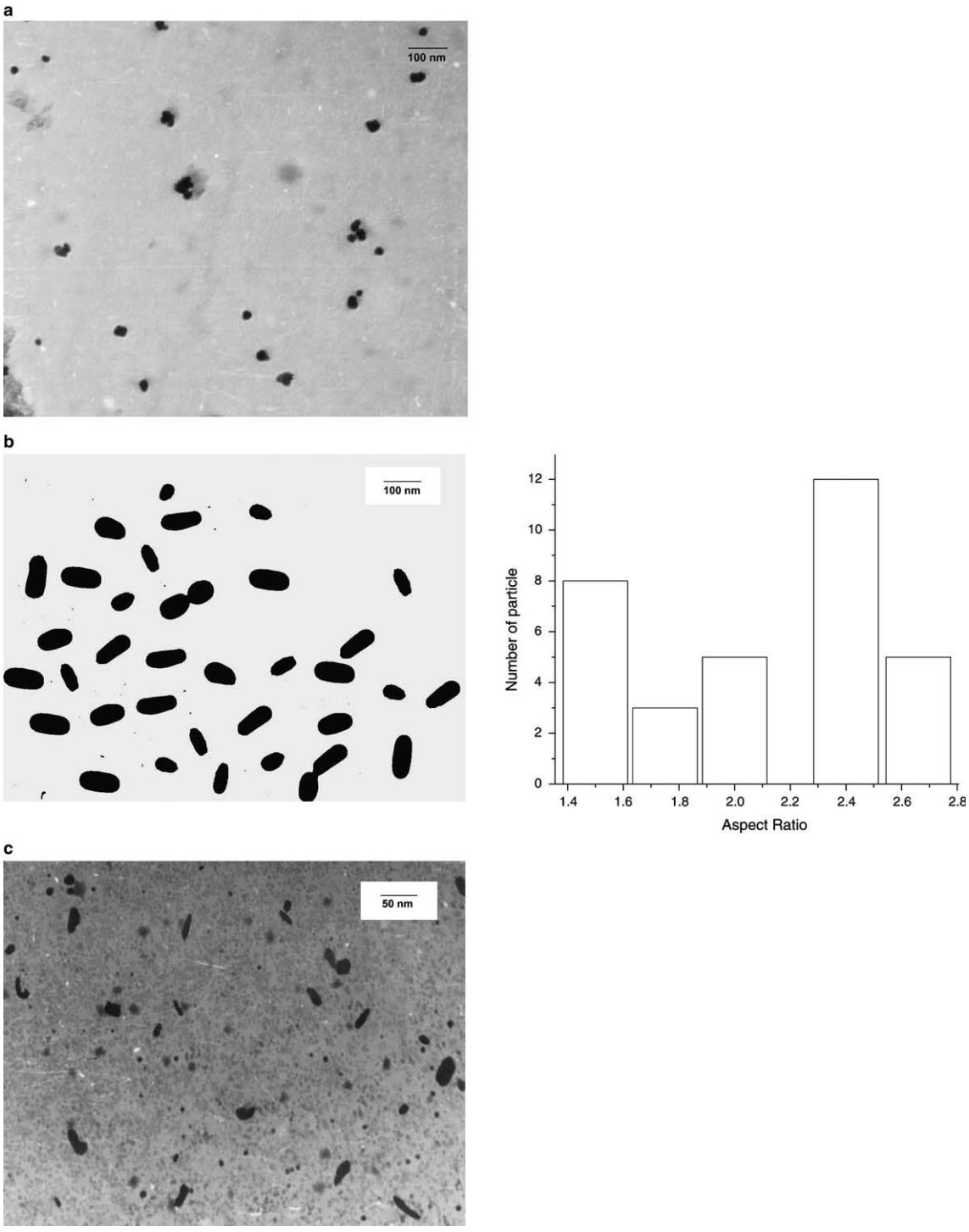

Fig. 2. TEM images of the copper nanoparticles. (a) TEM images of the spherical particles (C_1). (b) TEM images of the nanorods (C_2) and its corresponding histogram. (c) TEM images of the spherical particles (C_3). Conditions: $[CuSO_4] = 3.84 \times 10^{-4}$ M, $[NaOH] = 2 \times 10^{-3}$ M [glucose] $= 5.78 \times 10^{-3}$ M for a, 8.68×10^{-3} M for b and 1.16×10^{-2} M for c.

on the particle morphology and the directional growth as reported earlier [24].

Controlled reactions could not produce any copper nanoparticle in which no NaOH was added. Therefore, we concluded that hydroxide ion is important for particle growth. Since the concentration of NaOH is same in all the three cases so the numbers of Na^+ ions remained same but the available OH^- is different due to the variable amount of glucose for different sets. Like the previous reports [24,25] we observed that simple OH^- ions could direct the growth of Cu nanoparticles into different shapes, highlighting the importance of OH^- ions. Recently, enhanced coordination ability of the sugar molecules in alkaline medium has been well documented due to the

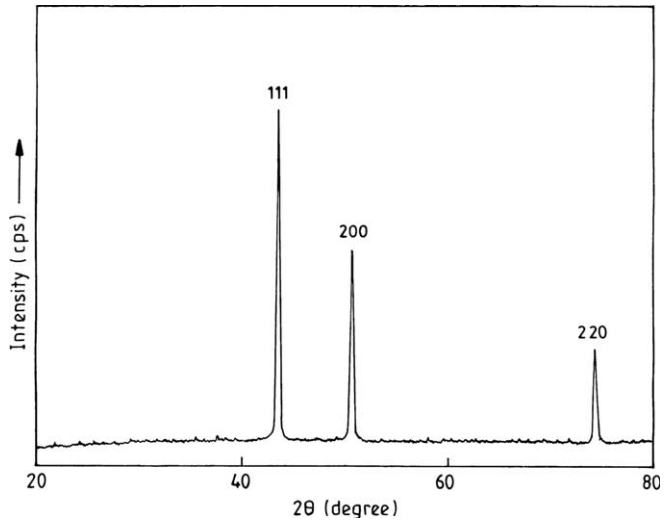

Fig. 3. X-ray diffraction pattern of the nanorods (C_2). Conditions: $[CuSO_4] = 3.84 \times 10^{-4}$ M, $[NaOH] = 2 \times 10^{-3}$ M, $[glucose] = 8.68 \times 10^{-3}$ M.

formation of deprotonated sugar anions [26,27]. In the present case, the coordinatively unsaturated surface atoms of copper particles get stabilized by the anionic sugar moiety. Furthermore, it was also observed that KOH and NH_4OH in lieu of NaOH produced similar results.

A distinct transition from the spheres to the rod shaped growth has been observed at a higher temperature (>80 °C). The evolved particles happen to be resistant to oxidation, no matter whether the produced particles are spheres or rods. Another plausible mechanism of nanorod formation lies with the stabilization of chelate of Cu(II) with the –OH groups of the glucose (at a particular concentration) that eventually produced a void space that might act as a template for particle growth. This kind of chelation of Cu(II) ions in alkaline medium and the mechanism seems analogous to the Fehling's test of glucose solution. Furthermore, gluconic acid under the experimental condition advances the stabilization process of the nanorods through effective capping [28].

3.5. Interaction with anion exchange resin

Gluconic acid, an oxidized product of glucose, produced in the reaction mixture bears a negative charge in the alkaline solution and it imparts stability to the evolved Cu(0) particles acting as a capping agent. Therefore, no extra capping agent or stabilizing agent is required and the copper nanoparticles become negatively charged. The negative charge on the surface of the evolved particles was confirmed by the ready exchange of the negatively charged copper particles with the chloride form of an anion exchange resin, Amberlite IRA 400.

3.6. Thiocyanate dissolution study: reactivity of the particles

Interaction of a diffusing ion, SCN^- with copper nanoparticles further authenticated the stability of the evolved nanorods. Same amount of SCN^- was introduced (added as NaSCN in the μM concentration) into three different sets (C_1, C_2 and C_3) of solution containing copper nanoparticles and were shaken for ~5 min considering the more diffusing nature of SCN^- ion than the capping agent, gluconic acid. From the UV–Vis spectra, 6 and 10 nm blue shift of the λ_{max} values were observed for set C_1 and C_3, respectively. Finally, increased concentration of NaSCN dissolved copper nanoparticles under ambient condition. Surprisingly, the absorption peaks of the nanorods (C_2) at lower energy region disappeared and the peak at the higher energy gradually blue shifted by the addition of aqueous SCN^- solution in portion. The corresponding

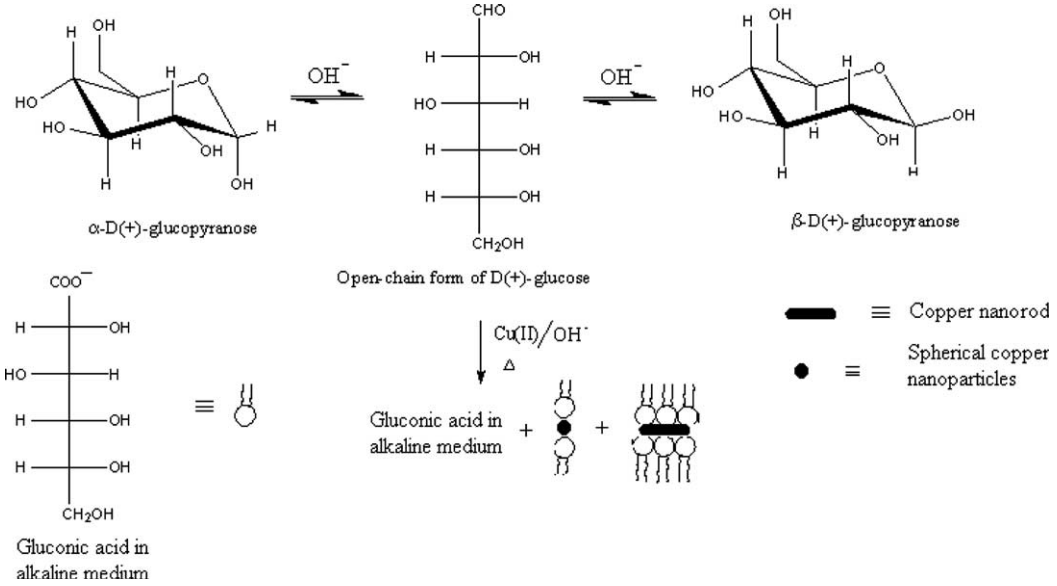

Scheme 2. The schematic presentation of the mechanism of the reaction.

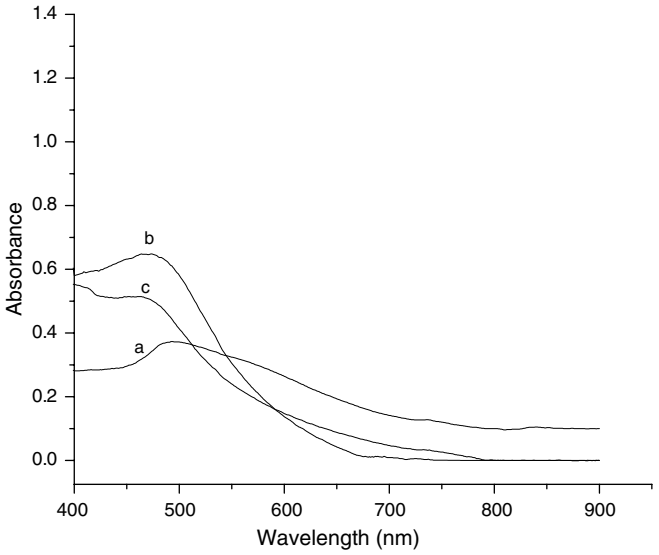

Fig. 4. The UV–Vis spectra of the evolved copper nanoparticles (rods and spheres) after addition of SCN^-. (a) UV–Vis spectra of the spherical particles after addition of SCN^- (C_1). (b) UV–Vis spectra of the nanorods after addition of SCN^- (C_2). (c) UV–Vis spectra of the spherical particles after addition of SCN^- (C_3). Conditions: $[CuSO_4] = 3.84 \times 10^{-4}$ M, $[NaOH] = 2 \times 10^{-3}$ M $[SCN^-] = 1.9 \times 10^{-6}$ M [glucose] $= 5.78 \times 10^{-3}$ M for a, 8.68×10^{-3} M for b and 1.16×10^{-2} M for c.

UV–Vis spectrum is shown in Fig. 4. On the other hand, the blue shift of the λ_{max} corroborates the shift of Fermi levels of the nanoparticles towards more negative potential and making them vulnerable to dissolution [29]. It is thus concluded that the smaller particle has greater tendency towards SCN^- attack (after pronounced blue shifting) rather than the larger one and nanorods eventually break down to the spherical particles when it reacted with the SCN^- [30,31]. Stepwise blue shifts of the λ_{max} position were noticed by the controlled addition of NaSCN solution. Again, similar shifts of λ_{max} values were noticed while $NaBH_4$ and NaCN were introduced in the μM concentrations. However, gradual increase in NaCN concentration produced a colorless solution due to the formation of $[Cu(CN)_4]^-$ species but other diffusing ions left black precipitate on standing.

3.7. Catalytic application

The evolved copper nanoparticles (rods and spheres) were individually exploited as viable catalyst for C–C bond formation via oxidative phenol coupling (OPC) between two 2-naphthol moieties [31,32]. In a round bottom flask 30 mL of the copper nanorods solution was taken and then 0.01 g of solid 2-naphthol was introduced into it. The solution was stirred at room temperature (25 °C) for ~7 days under aerated condition. Finally the product was extracted with chloroform. The product was extracted from water and separated by column chromatography using petroleum ether–EtOAc (10:1) as eluant. It was found that the rod shaped particles selectively catalyze the coupling to produce 1,1′ coupled product with a good yield (76%). The separated bi-naphthol was characterized unambiguously by TLC, UV, IR, ^1H NMR and mass spectroscopic studies. The melting point of bi-naphthol is 235 °C and the M^+ is 286. The UV–Vis spectral data shows a peak at 270 nm ($\log \varepsilon$ 4.20). IR analysis shows two broad bands at 3400 and 3500 cm^{-1} due to –OH functionality and peaks at 1620, 1600, 830, 820, 780 and 750 cm^{-1} due to the aromatic nucleus. The ^1H NMR study gives d (DMSO-d_6 + $CDCl_3$) 7.2–8.0 (12H, m, Ar–H), 8.7 (disappeared on deuteration, Ar–OH). However, we failed to detect any coupled product out of the OPC reaction involving spherical copper particles. The detailed reaction involving other phenols has been reported elsewhere [32]. It has been reported that the reactivity and stability of nanoparticles depend on the aspect ratio and spheroids are more reactive than spheres [33]. During the reaction, the spheroids transforms into spheres whereas the spheres do not react. So in our case this OPC might be due the preferential adsorption of 2-naphthol onto the copper nanorod surfaces and higher catalytic activity of the rod shaped particles are observed in comparison to spheres.

4. Conclusion

In conclusion, the novelty of this one step method for the generation of copper nanoparticles lies in its simplicity and simultaneous control of both size and shape of the particles, without employing any stabilizing agent, capping agent or any template. This surfactantless one pot synthetic procedure may be useful for producing particles of desired size and shapes. Moreover, this procedure is highly reproducible and does not involve any toxic reagents. The particles are stable for about a week at room temperature. The evolution of the copper nanorods has been unequivocally characterized. With the rapid shrinking in size in electronic devices, copper nanorods and nanowires may play an important role for connecting the future generation of electronic nanodevices and the shape selective catalyst for coupling phenols through 'C–C' bond formation.

Acknowledgments

Authors are thankful to CSIR, DST and UGC, New Delhi and IIT Kharagpur for financial assistance.

References

[1] M.A. El-Sayed, Acc. Chem. Res. 34 (2001) 257.
[2] A.M. Morales, C.M. Lieber, Science 279 (1998) 208.
[3] C.R. Martin, Science 266 (1994) 1961.
[4] M.P. Pileni, Langmuir 13 (1997) 3266.
[5] F. Kim, J.H. Song, P. Yang, J. Am. Chem. Soc. 124 (2002) 14316.
[6] C.J. Murphy, N.R. Jana, Adv. Mater. 14 (2002) 80.
[7] U. Bjoerksten, J. Moser, M. Grätzel, Chem. Mater. 6 (1994) 858.
[8] Y. Jiang, S. Decker, C. Mohs, K.J. Klabunde, J. Catal. 180 (1998) 24.
[9] S.D. Bunge, T.J. Boyle, T.J. Headly, Nano Lett. 3 (2003) 901.

[10] D. Ensign, M. Young, T. Douglas, Inorg. Chem. 43 (2004) 3441.
[11] J.L. Marignier, J. Belloni, M.O. Delcourt, J.P. Chevalier, Nature 317 (1985) 344.
[12] B.G. Ershov, N.L. Sukhov, Radiat. Phys. Chem. 36 (1990) 93.
[13] J. Khatouri, M. Mostafavi, J. Amblard, J. Belloni, Chem. Phys. Lett. 191 (1992) 351.
[14] I. Lisiecki, M.P. Pileni, J. Am. Chem. Soc. 115 (1993) 3887.
[15] I. Lisiecki, A. Filankembo, H.S. Kongehl, K. Eeiss, M.P. Pileni, J. Urban, Phys. Rev. B Condens. 61 (1999) 4968.
[16] J. Tanori, M.P. Pileni, Adv. Mater. 7 (1995) 862.
[17] T. Gao, G. Meng, Y. Wang, S. Sun, L. Zhang, J. Phys.: Condens. Matter. 14 (2002) 355.
[18] N.R. Jana, Z.L. Wang, T.K. Sau, T. Pal, Curr. Sci. 79 (2000) 1367.
[19] M.B. Mohamed, K.Z. Ismail, S. Link, M.A. El-Sayed, J. Phys. Chem. B 102 (1998) 9370.
[20] S. Link, M.B. Mohamed, M.A. El-Sayed, J. Phys. Chem. B 103 (1999) 3073.
[21] Z. Liu, Y. Bando, Chem. Phys. Lett. 378 (2003) 85.
[22] X. Cao, F. Yu, L. Li, Z. Yao, Y. Xie, J. Crystal Growth 254 (2003) 164.
[23] S.W. Han, S.W. Joo, T.H. Ha, Y. Kim, K. Kim, J. Phys. B 104 (2000) 11987.
[24] K.K. Caswell, M.B. Christopher, C.J. Murphy, Nano Lett. 3 (2003) 667.
[25] A. Filankembo, M.P. Pileni, J. Phys. Chem. B 104 (2000) 5865.
[26] S. Striegler, E. Tewes, Eur. J. Inorg. Chem. (2002) 487.
[27] S. Striegler, M. Dittel, Inorg. Chem. 44 (2005) 2728.
[28] W. Wang, S. Efrima, O. Regev, Langmuir 14 (1998) 602.
[29] N.R. Jana, T.K. Sau, T. Pal, J. Phys. Chem. B 103 (1999) 115.
[30] T. Pal, T.K. Sau, N.R. Jana, Langmuir 13 (1997) 1481.
[31] J.M. Brunel, Chem. Rev. 105 (2005) 857.
[32] T. Pal, A. Pal, Curr. Sci. 71 (1996) 106.
[33] N.R. Jana, L. Gearheart, S.O. Obare, C.J. Murphy, Langmuir 18 (2002) 922.

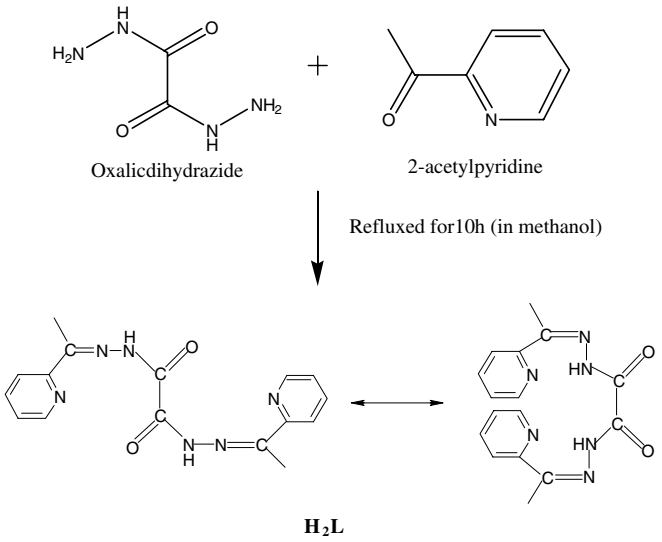

Scheme 1.

Thompson and co-workers [12] but behaves in a complete different fashion (vide infra).

In the present case, we employed copper(II) acetate and nickel(II) acetate, so that carboxylate might be able to connect the neighbouring dimeric subunits bridged by this flexidentate ligand and anticipated to get a polymeric or other architectures excluding molecular squares. From the molecular point of view, the nature of acetato bridging is magnetically very significant. For one atom acetate bridges between two paramagnetic transition metal centers, the magnetic interactions have been related to the magnitude of bridging angle (θ) and other structural features [13]. This has been especially studied for oxygen bridged metal atoms such as Cu–O–Cu. Small θ angles near 96° should lead to ferromagnetic interaction while larger value should make the interaction increasingly strongly antiferromagnetic [14,15].

Here, we use Cu(II) and Ni(II) as metal ions to observe the difference in coordination behavior of the ligand according to the geometrical preferences of the two metal centers. In case of Cu(II), we get a polymeric complex, where the ligand (**L**) in *trans* form binds two metal centers in exo fashion through the oxamido-type bridge in a bis-tridentate mode instead of the anticipated diazine bridging as observed for the ligand reported by Thompson and co-workers [12] and the dimeric subunits are connected by $\mu_{1,1}$-acetato bridges that lead to the formation of 1-D polymer. In the case of nickel(II) the ligand adopts a *cis*-conformation and binds in endo fashion as a tetradentate unit to lead to a four coordinated complex. The flexible ligand reorients itself in *trans*- and *cis*-forms by the unhindered rotation around C–C bond.

In this paper, we describe the synthesis, spectral characterization and crystal structures of two novel Cu(II) and Ni(II) complexes derived from the new flexible bistridentate ligand. The magnetic behavior for complex **1** was found to be driven by strong antiferromagnetic interactions.

2. Experimental

2.1. Materials

Oxalicdihydrazide, 2-acetylpyridine, copper(II) acetate monohydrate, nickel(II) acetate tetrahydrate were purchased from commercial sources and used as received.

2.2. Physical measurements

The infrared spectra were recorded on a Perkin–Elmer FT-IR spectrophotometer in KBr matrices. The electronic spectra were obtained as Nujol mulls as well as in acetonitrile solution on a Perkin–Elmer Lambda 40 (UV–Vis) spectrophotometer. Elemental analyses were carried out using a Perkin–Elmer 2400 II elemental analyser. Electrochemical studies were carried out with a CH600A cyclic voltammeter using tetrabutyl ammonium perchlorate as the supporting electrolyte.

Magnetic susceptibility measurement was carried out with a Quantum Design MPMS-5S SQUID magnetometer under an applied magnetic field of 5000 Oe. Diamagnetic correction was estimated from Pascal table and magnetic data were corrected for diamagnetic contribution of the sample holder. The temperature dependence of the molar magnetic susceptibility, χ_M, for the complex **1** was measured on polycrystalline sample in the temperature range 5–300 K.

2.3. Computational methodology

The computational methodology adopted in previous studies [16] on exchange-coupled dinuclear complexes has been used. For the evaluation of each coupling constant, two separate DFT calculations have been carried out, one for the highest spin state (triplet state in that case) and one for the broken symmetry state. The hybrid B3LYP functional [17] has been used as implemented in GAUSSIAN-98 [18]. For the Cu atoms a basis set of triple-ζ quality [19] was used for the valence orbitals supplemented with two p orbitals (''polarization functions''), whereas a double-ζ basis set [20] was used for C, H, N and O atoms. The J values are obtained by simply subtracting E_{HS} to E_{BS} ($J = E_{BS} - E_{HS}$) where E_{HS} and E_{BS} are the energies of high spin and broken symmetry states, respectively. Using this equation, we assume that the energy of the broken symmetry state is a good approximation of low spin state energy, following Ruiz et al. [21].

2.4. Synthesis of ligand and complexes

2.4.1. Ligand (H_2L)

Oxalic dihydrazide (1.18 g, 10 mmol) was added to a solution of 2-acetylpyridine (2.24ml, 20 mmol) in methanol (100 mL) and the mixture was refluxed for 10 h. A white solid formed which was filtered off, washed with methanol and vacuum dried (Yield: 70%). M.p. >270 °C. IR ν_{max}

cm^{-1} (KBr) 1685 (CO), 1579, 1568 (CN), 979 (pyr). *Anal* Calc. for $C_{16}H_{16}N_6O_2$: C, 59.3; H, 4.9; N, 24.9. Found: C, 59.2; H, 4.9; N, 24.8%.

2.4.2. $[\{Cu_2(L)(CH_3COO)_2\}\cdot 8H_2O]_n$ (1)

Ligand **H_2L** (0.324 g, 1 mmol) was added to a solution of $Cu(OAc)_2\cdot H_2O$ (0.398 g, 2 mmol) in 2-propanol/water (5:1) and the mixture was heated with stirring for 40 min. forming a green solution. The solution was filtered and kept in refrigerator. After five days dark green hexagonal shaped crystals suitable for X-ray diffraction were formed (Yield: 60%). IR ν_{max} cm^{-1} (KBr) 1563(CN), 455 (Cu–N), 379 (Cu–O). *Anal* Calc. for $C_{10}H_{18}N_3O_7Cu$: C, 33.7; H, 5.09; N, 11.8; Cu, 17.9. Found: C, 33.6; H, 4.9; N, 11.7; Cu, 17.7%.

2.4.3. $[Ni(L)]H_2O$ (2)

Compound **2** was prepared in a similar manner like complex **1** taking $Ni(OAc)_2\cdot 4H_2O$ instead of $Cu(OAc)_2\cdot H_2O$. After seven days red rectangular crystals suitable for X-ray diffraction were formed (Yield: 65%). IR ν_{max} cm^{-1} (KBr) 1673(CO), 1562(CN), 453 (Ni–N), 375 (Ni–O). *Anal* Calc. for $C_{16}H_{16}N_6O_3Ni$: C, 48.1; H, 4.0; N,21.0; Ni, 14.7. Found: C, 48.0; H, 3.9; N, 20.8; Ni, 14.3%.

2.5. X-ray crystallographic studies

Crystallographic data were collected on a Siemens P4 diffractometer with a Siemens SMART-CCD area detector with graphite monochromated Mo-Kα radiation ($\lambda = 0.71073$ Å) using oil-coated rapidly cooled single crystals [22]. Crystallographic parameters [23], details of data collection and refinement procedures are summarized in Table 1. The structures were solved by direct methods and refined with the software packages SHELXL-93 and SHELXL-97 [24,25]. Neutral scattering factors were taken from Cromer and Mann [26] and for the hydrogen atoms from Stewart et al. [27]. The non-hydrogen atoms were considered with a riding model under restriction of ideal symmetry at the corresponding carbon atoms.

3. Results and discussion

3.1. Description of the structures

3.1.1. $[\{Cu_2(L)(CH_3COO)_2\}\cdot 8H_2O]_n$ (1)

The molecular structure as well as the atom numbering scheme of $[\{Cu_2(L)(CH_3COO)\}\cdot 8H_2O]_n$ (**1**) illustrated in Fig. 1. Relevant bond lengths and angles are listed in Table 2. In the titled copper(II) complex **1**, one molecule of the deprotonated hexadentate ligand **L** binds two metal centers in *trans* orientation. The polynuclear complex involves distorted five coordinated copper(II) centers, each surrounded by NNO donor sets from hexadentate **L** and by two additional O-atoms from two acetate anions. For a pentacoordinated metal center, the distortion of structure from trigonal bipyramidal (TBP) to square pyramidal (SP) can be evaluated by the Addision distortion index τ [28]: $\tau = (\beta - \alpha)/60°$, α and β being the two largest angles around the central atom; values for τ are 1.0 for perfect TBP and 0.0 for perfect SP. In this complex the geometry of the Cu(II) centers are close to square pyramidal ($\tau = 0.016$) with short

Table 1
Crystallographic data for complexes **1** and **2**

Complex	**1**	**2**
Empirical formula	$C_{10}H_{18}N_3CuO_7$	$C_{16}H_{16}N_6NiO_3$
Formula weight	355.81	398.82
T (K)	193	193
Radiation	Mo Kα	Mo Kα
λ (Å)	0.71073	0.71073
Crystal system	monoclinic	monoclinic
Space group	$C2/c$	$P2_1/c$
a (Å)	16.933(1)	7.638(4)
b (Å)	12.938(1)	18.626(1)
c (Å)	13.463(1)	11.892(1)
α (°)	90	90
β (°)	102.199(1)	105.910(1)
γ (°)	90	90
Z	8	4
Crystal size (mm)	$0.10\times0.20\times0.55$	$0.4\times0.3\times0.1$
D_{calc} (Mg/m^3)	1.639	1.629
Adsorption coefficient (mm^{-1})	1.552	1.224
$F(000)$	1472	824
θ Range for data collection (°)	2.0, 23.3	2, 23.3
Reflections collected	6415	7231
Independent reflections (R_{int})	1904 (0.0212)	2086 (0.0252)
Goodness-of-fit on F^2	1.109	1.045
R indeces (all data)	$R_1 = 0.0336$, $wR_2 = 0.0913$	$R_1 = 0.0303$, $wR_2 = 0.0771$
Final R indices [$F > 4\sigma(F)$]	$R_1 = 0.0303$, $wR_2 = 0.0902$	$R_1 = 0.0270$, $wR_2 = 0.0740$
Largest difference peak and hole (e $Å^{-3}$)	0.421 and −0.312	0.278 and −0.432

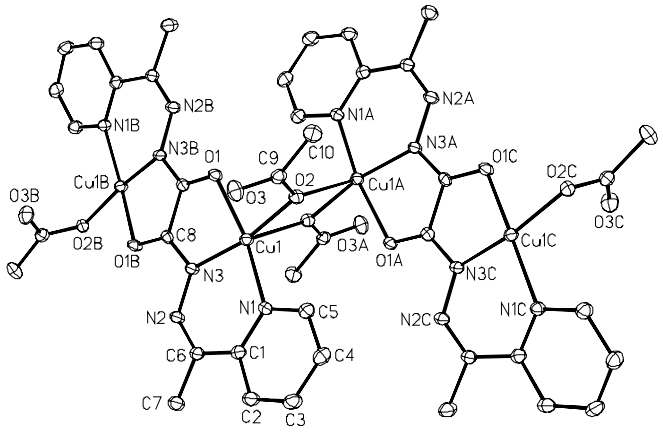

Fig. 1. ORTEP diagram of complex **1** with atom numbering scheme (thermal ellipsoids are drawn at 30% probability level). The H atoms are omitted for clarity reasons. Symmetry related atoms are marked with the letters A ($-x+1, -y+1, -z$), B ($-x+1, y, -z+1/2$) and C ($x, -y+1, z+1/2$).

Table 2
Selected bond distances (Å) and bond angles (°) for complex **1**

Cu1–N1	1.992(3)	Cu1–O2	1.950(2)
Cu1–N3	1.923(3)	Cu1–O2A	2.401(2)
Cu1–O1	2.017(2)		
O1–Cu1–O2	86.61(9)	O2–Cu1–O2A	75.59(7)
O1–Cu1–N3	83.17(9)	N1–Cu1–N3	90.25(10)
O1–Cu1–O2A	84.09(7)	O1–Cu–N1	169.44(9)
O2–Cu1–N1	99.42(10)	O2–Cu1–N3	169.36(9)
O2A–Cu1–N1	105.75(8)	O2A–Cu1–N3	106.17(8)

Symmetry operations used for equivalent atoms A: $-x+1, -y+1, -z$.

Table 3
Deviation (in Å) of the atoms for the complex **1** from the best plane calculated from O1, N3, O2, N1 and Cu1

Atoms	Deviation (Å)
Cu1	+0.246
O1	−0.033
N3	+0.034
O2	−0.033
N1	+0.034

equatorial contacts [1.993(3)–2.017(2) Å] by N_2O donor (N1, N3, O1 for Cu1) from the **L** and one acetato oxygen atom (O2 for Cu1) and a longer axial coordination [2.401(2) Å] by the oxygen atom (O2A for Cu1) of another acetate ligand. These bond lengths are comparable to the values obtained for the similar square pyramidal copper(II) systems [29]. Distortion from the square pyramidal geometry is evident from the deviation of the atoms forming the least square plane (Table 3). The two five-membered chelate rings formed by each **L** connecting two copper(II) centers are almost coplanar and make 5.229Å separation between these two centers. The diazine subunit present in the complex is tilted with respect to the mean square plane at an angle of 1.3° and the N–N diazine bond length [1.386(4) Å] is consistent with a N–N single bond [30]. The carbon–carbon bond distance (1.489(7) Å) in the coordinating ligand **L** is consistent with the C–C single bond [31]. Each of the two copper centers in one asymmetric unit is connected to neighbouring copper centers through double $\mu_{1,1}$-acetato bridges and forms an infinite polymeric network parallel to a-axis shown in Fig. 2. The non-bonding Cu–Cu separation in the double acetato bridging amounts to 3.449 Å. There are eight water molecules in the lattice for each dimeric subunit.

3.1.2. {[Ni(L)]H_2O} (**2**)

The ORTEP diagram of complex **2** with atom numbering scheme is illustrated in Fig. 3 and the relevant bond lengths and angles are listed in Table 4. Unlike **1** here, the deprotonated ligand **L** in *cis* form binds only one nickel center and forms a monomeric Ni(II) complex. The Ni(II) ion displays a distorted square planar coordination with a N_4 donor set from **L**. The square plane suffers a tetrahedral distortion as indicated by the deviation of the coordination sites from the mean plane calculated for the four N atoms

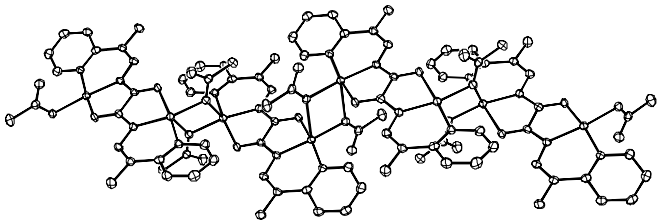

Fig. 2. Part of 1-D polymeric layer of complex **1** to show the arrangement of molecules.

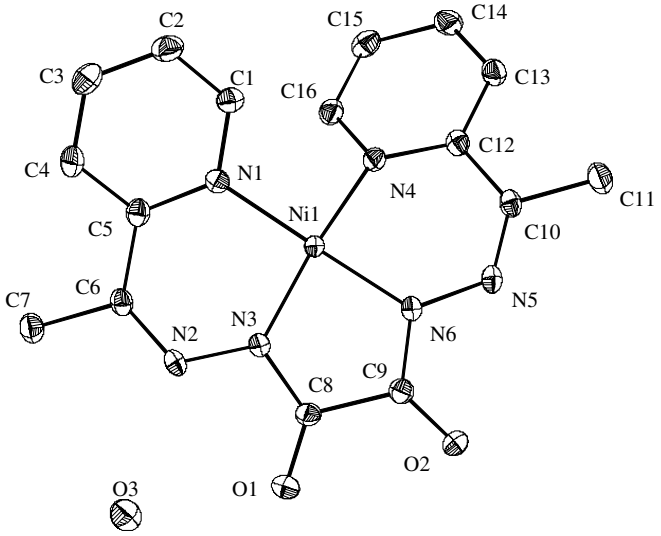

Fig. 3. ORTEP diagram of complex **2** (with water) with atom numbering scheme (thermal ellipsoids are drawn at 30% probability level). The H atoms are neglected for clarity reasons.

(N1, N3, N4 and N6) coordinated with the nickel(II) center (Table 5). This deviation from the planar arrangement of **L** is clearly seen from the torsion angle [N1–N3–N6–N4] of the coordinating Lewis bases with a value of −23.3°. The bite angles associated with six-membered rings [N1–Ni1–N3 = 91.79(8)°, N6–Ni1–N4 = 91.45(8)°] are within normal range [32]. In the title complex, the angle between the planes containing the two pyridine rings is 119.8°. The torsion angles for N1–C5–C6–N2 and N4–C12–C10–N5 with values of 20.9° and 12.4°, respectively, also show the twisting of the pyridine rings. The cause of all of these distortions (including the deviation from the planar environment of Ni1) is the steric strain induced by the hindrance of the hydrogen atoms at C1 and C16. Therefore, the pyridyl substituents are twisted away from each other thus destroying the planarity of the molecule. This fact leads to the formation of a chiral molecule, however, due to the crystallization of complex **2** in the centrosymmetric space group $P2_1/c$ the Δ and Λ isomers form a racemate in the solid state. One water molecule is present in the lattice.

The structural parameters of ligand **L** are comparable to those discussed for complex **1**. The electrical charge distribution of the ligand is symbolized by the mesomeric forms according to Fig. 4. The C8–C9 distance of 1.527(3) Å is a characteristic value for a C–C single bond [31]. This fact as well as the C5–C6 (1.480(3) Å) and C10–C12 (1.479(3) Å) bonds show that the π-systems of this ligand are well separated and a more extended delocalization of the anionic charge can clearly be excluded. The Ni1–N distances to the pyridyl groups are larger than those to the anionic nitrogen atoms N3 and N6 due to the additional electrostatic attraction of Ni1 to the latter ones. The C8–C9 single bond allows an unhindered rotation around this bond which offers the reorientation and adjustment to the copper and nickel cations.

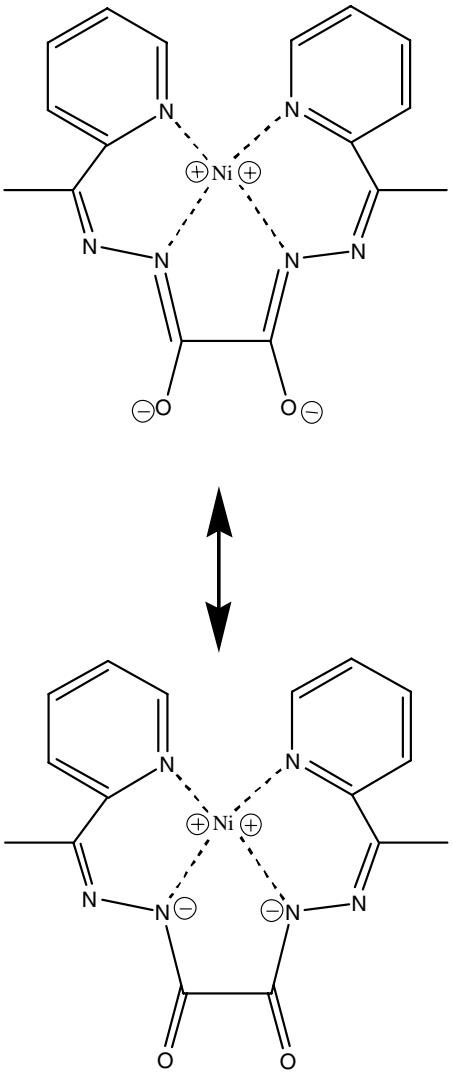

Fig. 4. Mesomeric forms of complex **2** to show the electrical charge distribution.

Table 4
Selected bond distances (Å) and bond angles (°) for complex **2**

Ni1–N6	1.850(2)	Ni1–N3	1.850(2)
Ni1–N4	1.895(2)	Ni1–N1	1.907(2)
N6–Ni1–N3	85.04(8)	N6–Ni1–N4	91.45(8)
N3–Ni1–N4	164.72(9)	N6–Ni1–N1	161.48(9)
N3–Ni1–N1	91.79(8)	N4–Ni1–N1	96.07(8)

Table 5
Deviation (in Å) of the atoms for the complex **2** from the best plane calculated from N1, N3, N4, N6, and Ni1

Atoms	Deviation (Å)
Ni1	0.029
N1	−0.275
N3	−0.275
N6	0.276
N4	0.276

3.2. Electronic spectra

Although the electronic spectra of the copper complexes with multidentate Schiff base ligands are not in general good indicators of geometry [33] but act as supporter of it. The solid-state Nujol mull absorption electronic spectrum for **1** appeared at 650, 340 and 244 nm. The broad absorption band at 650 nm is attributable to a copper ion in square pyradimal chromophore CuN_2O_3 [34]. This broad visible absorption band at 650 nm is shifted slightly to a lower energy (678 nm) in acetonitrile solution, consistent with square pyramidal geometry in solution phase. The complex displays two strong absorption bands at 340 and 244 nm in solid which are clearly charge transfer in origin and these two bands are shifted to 348 and 248 nm, respectively, in solution. The similarity in the spectrum of this complex in both solution phase and solid state indicates that the 1-D chain structure retains in the solution.

The absorption band in the solid-state Nujol mull electronic spectrum for **2** shows one band at 423 nm, which

is shifted to 432 nm in acetonitrile solution. This band corresponds to the d–d transition in square planar Ni(II) complex [35]. The solid state spectrum of this complex contains another more intense band at 310 nm, which is shifted to 316 nm in solution, is charge transfer in origin.

3.3. Electrochemical studies

The electrochemical study of the complexes **1** and **2** was performed using acetonitrile as solvent and tetrabutylammonium perchlorate as supporting electrolyte at a scan rate of 100 mV s^{-1}. Cyclic voltametry of the complex **1** shows two reductive responses on the negative side of SCE (at −0.55, −1.00 V), both of which are irreversible in nature. The observed potential gap (450 mV) between the two reductions is considerably large and is believed to be due to the effective communication between the two copper centers through the bridging ligands. One irreversible oxidation response is also observed on the positive side of SCE and which can be tentatively assigned to oxidation of the coordinated ligand.

The complex **2** exhibits an irreversible Ni(II)–Ni(III) oxidation at 1.26 V. This result suggests that Ni(III) species is unstable and undergoes rapid decomposition. One additional irreversible oxidation response is also observed on the positive side of SCE and can be tentatively assigned to oxidation of the coordinated ligand.

3.4. Magnetic studies

The magnetic behavior for complex **1** is given in Fig. 5 as χ_M versus T and $\chi_M T$ versus T, where χ_M is the magnetic susceptibility of a dinuclear unit. The rapid decrease of the $\chi_M T$ reaching very small values below 50 K and the rounded maximum exhibited by the χ_M curve around 250 K indicate that substantial antiferromagnetic interactions are operative between the Cu(II) ions. For this compound, the adjacent Cu(II) ions are linked alternatively by an oxamido-type ligand and two bridging O-atoms developing a 1-D supramolecular organization. However, considering the coordination sphere of these ions it appears that a bridging O-atom occupies an equatorial position on one Cu(II) whereas it is linked to the second center in apical position. The latter is characterized by a larger bond-length (2.399 versus 1.954 Å) due to the Jahn–Teller distortion along the z-direction. Taking into account that the unpaired electron of the Cu(II) is located in the $d_{x^2-y^2}$ orbital, no direct overlap exists between the magnetic orbitals of O-bridged Cu centers. Consequently, the exchange interaction mediated by this pathway should be weak. Conversely, it is well documented that the exchange interaction between two Cu(II) ions through the oxamido-bridge is strong [11]. A first attempt was made to analyze the experimental behavior with an alternating chain model derived from the spin Hamiltonian $\mathbf{H} = -J\sum_{i=1}^{n/2}[\mathbf{S}_{A2i}\cdot\mathbf{S}_{A2i-1} + \alpha\mathbf{S}_{A2i}\cdot\mathbf{S}_{A2i+1}]$ [11]. Best fit to the temperature dependence of $\chi_M T$ yielded $J = -330 \pm 2\ cm^{-1}$ and $\alpha J = -79\ cm^{-1}$ ($\alpha = 0.24 \pm 0.02$), $g = 2.14 \pm 0.01$, and a contribution of 0.01 mol of a $S = 1/2$ paramagnetic impurity with same molecular mass. However, the value obtained for the smallest exchange interaction, $-79\ cm^{-1}$, is not realistic if we consider it to correspond to the exchange occurring through the O-bridge. Therefore, we considered the observed magnetic behavior to result only from the strongest exchange interaction and the magnetic data have been analyzed with the Bleaney-Bowers equation [36] ($\mathbf{H} = -J\mathbf{S}_1\cdot\mathbf{S}_2$). The contribution of a paramagnetic $S = 1/2$ impurity was also taken into account. Best fit to the temperature dependence of $\chi_M T$ (Fig. 5) in the 5–310 K domain led to $J = -327 \pm 1\ cm^{-1}$, $g = 2.02$, and 0.02 mole of a paramagnetic impurity. Fitting to the variation of χ_M yielded $J = -307 \pm 2\ cm^{-1}$, $g = 1.95$. The exchange parameter found is well in the range of those reported for related oxamato- or oxalate-bridged Cu(II) ions [37,38].

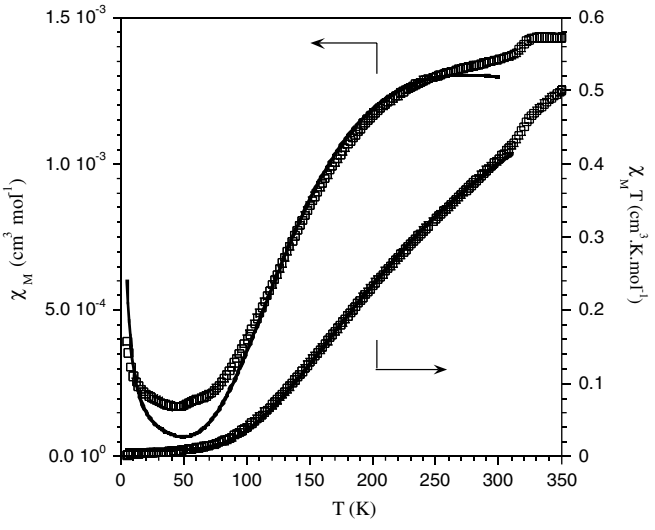

Fig. 5. Experimental (□) and calculated (——) temperature dependence of χ_M and $\chi_M T$ for complex **1**.

The magnetic behavior in the high-temperature domain deserves a short comment. Around 320 K both the $\chi_M T$ and χ_M curves exhibit a sudden slope break suggesting a modification of the magnetic behavior for the compound at this temperature. Such a disruption can be related to a structural modification occurring for a given temperature which does alter the magnetic behavior [39,40]. In the present case, the structural modification could be ascribed the water release.

3.5. DFT calculations of the exchange constants

In an effort to gain complementary information on compound **1** and in order to confirm our assumption, DFT calculations on the exchange interactions as function of the pathway were carried out. All calculations for high spin and broken symmetry states were done on dinuclear fragments with the X-ray coordinates, without any geometric optimization by theoretical methods. In order to evaluate the exchange coupling mediated by the oxamido bridge,

the calculation was done with the complete ligand set, i.e., the oxamido-ligand and the four acetates linked to the two Cu(II) centers. For the interaction through the acetate oxygen, another dinuclear cluster was extracted which contained two Cu(II) ions, two acetate ligands bridging the two copper atoms, and two shortened oxamido-ligands. These latter ligands have been shortened in the sense that the aromatic pyridine ring which is not involved in the coordination of the considered copper has been replaced by a methyl group. Both considered systems have a global charge of −2. The exchange coupling constants calculated are $J = -181$ and $+1.3\ cm^{-1}$ for oxamido- and oxygen-bridges, respectively. The main exchange interaction parameter calculated points to a somewhat smaller value than the one deduced from the experimental behavior ($J = -327\ cm^{-1}$) but the sign and the order of magnitude are correctly reproduced. More important, these calculations validate the analysis of the experimental data by a dimer model. Indeed, the computed interaction through the oxygen bridges is found to be ferromagnetic and very small compared to the antiferromagnetic interaction through the oxamido unit. In no way this weak ferromagnetic interaction can be revealed by the experimental behavior.

4. Conclusion

The design of polytopic ligand to prepare polymeric complexes is dependent on a number of factors, including the topological complexity of the ligand itself. The individual coordinating components in the ligand do not behave in a similar way for all metal ions. Here, in summary one 1-D polymeric copper(II) and one four coordinated monomeric nickel(II) complexes were assembled from copper(II) acetate and nickel(II) acetate with an easy to prepare flexible bistridentate ligand, in a rational fashion. The choice of different metal centers, in this case copper(II) or nickel(II), give rise to different products and is accomplished by the unhindered rotation of the C–C single bond, which offers the reorientation of the same ligand in *trans* and *cis*-form, respectively. This variation in the coordination behavior of the same ligand for copper(II) and nickel(II) occurred because Ni(II) has a better affinity for N-donor sites than for O ones.

5. Supplementary data

CCDC-265377 (**1**) and 265378 (**2**) contain the supplementary crystallographic data for this paper. These data can be obtained free of charge at www.ccdc.cam.ac.uk [or from Cambridge Crystallographic Data Center, 12, Union Road, Cambridge CB2 1EZ, UK; e-mail: deposit@ccdc.cam.ac.uk].

Acknowledgements

We acknowledge the financial assistance to S. Sen from the CSIR (New Delhi, India). The magnetic measurements are supported by the Centre Franco-Indien pour la promotion de la Recherche Avancée/Indo-French Centre for the Promotion of Advanced Research, Project (3108-3).

References

[1] C.C. Wang, W.C. Lo, C.C. Chou, G.H. Lee, J.M. Chen, S.M. Peng, Inorg. Chem. 37 (1998) 4059.
[2] G.A. Van Albada, I. Mutikainen, U. Turpeinen, J. Reedijk, Eur. J. Inorg. Chem. (1998) 547.
[3] P.N.W. Baxter, J.-M. Lehn, J. Fischer, M.-T. Youinou, Angew. Chem., Int. Ed. Engl. 33 (1994) 2284.
[4] C.J. Matthews, K. Avery, Z. Xu, L.K. Thompson, L. Zhao, D.O. Miller, K. Biradha, K. Poirier, M.J. Zaworotko, C. Wilson, A.E. Goeta, J.A.K. Howard, Inorg. Chem. 38 (1999) 5226.
[5] G.S. Hanan, D. Volkmer, U.S. Schubert, J.-M. Lehn, G. Baum, D. Fenske, Angew. Chem., Int. Ed. Engl. 36 (1997) 1842.
[6] P.N.W. Baxter, J.-M. Lehn, B.O. Kneisel, D. Fenske, Angew. Chem., Int. Ed. Engl. 36 (1997) 1978.
[7] Z. Xu, L.K. Thompson, C.J. Matthews, D.O. Miller, A.E. Goeta, C. Wilson, J.A.K. Howard, M. Ohba, H. Ōkawa, J. Chem. Soc., Dalton Trans. (2000) 69.
[8] R. Costa, A. Garcia, J. Ribas, T. Mallah, Y. Journaux, J. Sletten, X. Solans, V. Rodriguez, Inorg. Chem. 32 (1993) 3733.
[9] C. Mathonière, J.-P. Sutter, J.V. Yakhmi, in: J.S. Miller, M. Drillon (Eds.), Magnetism: Molecules to Materials, vol. 4, Wiley–VCH, Weinheim, 2002, p. 1.
[10] L.K. Thompson, O. Waldmann, Z. Xu, in: J.S. Miller, M. Drillon (Eds.), Magnetism: Molecules to Materials, vol. 4, Wiley–VCH, Weinheim, 2002, p. 173.
[11] O. Kahn, Molecular Magnetism, VCH, Weinheim, 1993.
[12] Z. Xu, L.K. Thompson, V.A. Milway, L. Zhao, T. Kelly, D.O. Miller, Inorg. Chem. 42 (2003) 2950.
[13] A.M. Greenaway, C.J. O'Connor, J.W. Overman, E. Sinn, Inorg. Chem. 20 (1981) 1508, and references cited there in.
[14] P.J. Hay, J.C. Thibeault, R. Hoffmann, J. Am. Chem. Soc. 97 (1975) 4884.
[15] S. Mukhopadhyay, D. Mandal, P.B. Chatterjee, C. Desplanches, J.-P. Sutter, R.J. Butcher, M. Chaudhury, Inorg. Chem. 43 (2004) 8501.
[16] E. Ruiz, P. Alemany, S. Alvarez, J. Cano, J. Am. Chem. Soc. 119 (1997) 1297.
[17] A.D.J. Becke, J. Chem. Phys. 98 (1993) 5648.
[18] M.J. Frisch, G.W. Trucks, H.B. Schlegel, G.E. Scuseria, M.A. Robb, J.R. Cheeseman, V.G. Zakrzewski, J.A. Montgomery, R.E. Stratmann, J.C. Burant, S. Dapprich, J.M. Millam, A.D. Daniels, K.N. Kudin, M.C. Strain, O. Farkas, J. Tomasi, V. Barone, M. Cossi, R. Cammi, B. Mennucci, C. Pomelli, C. Adamo, S. Clifford, J. Ochterski, G.A. Petersson, P.Y. Ayala, Q. Cui, K. Morokuma, D.K. Malick, A.D. Rabuck, K. Raghavachari, J.B. Foresman, J. Cioslowski, J.V. Ortiz, B.B. Stefanov, G. Liu, A. Liashenko, P. Piskorz, I. Komaromi, R. Gomperts, R.L. Martin, D.J. Fox, T. Keith, M.A. Al-Laham, C.Y. Peng, A. Nanayakkara, C. Gonzalez, M. Challacombe, P.M.W. Gill, B.G. Johnson, W. Chen, M.W. Wong, J.L. Andres, M. Head-Gordon, E.S. Replogle, J.A. Pople, GAUSSIAN-98: Revision A.11, Gaussian, Inc., Pittsburgh, PA, 1998.
[19] A. Schaefer, C. Huber, R. Alrichs, J. Chem. Phys. 100 (1994) 5829.
[20] A. Schaefer, H. Horn, R. Alrichs, J. Chem. Phys. 97 (1992) 2571.
[21] E. Ruiz, J. Cano, S. Alvarez, P. Alemany, J. Comput. Chem. 20 (1999) 1391.
[22] (a) T. Kottke, D. Stalke, J. Appl. Crystallogr. 26 (1993) 615;
(b) D. Stalke, Chem. Soc. Rev. 27 (1998) 171.
[23] T. Hahn (Ed.), International Tables for Crystallography, 2nd ed., Space Group Symmetry, vol. A, D. Reidel, Dordrecht, 1984.
[24] G.M. Sheldrick, SHELXL-93, Universität Göttingen, Göttingen, Germany, 1993.
[25] G.M. Sheldrick, SHELXL-97, Universität Göttingen, Göttingen, Germany, 1997.

[26] D.T. Cromer, J.B. Mann, Acta Crystallogr. 24 (1968) 321.
[27] R.F. Stewart, E.R. Davidson, W.T. Simpson, J. Chem. Phys. 42 (1965) 3175.
[28] (a) A.W. Addison, T.N. Rao, J. Reedijik, J. van Rijn, C.G. Verscoor, J. Chem. Soc., Dalton Trans. (1984) 1349;
(b) H. Miyasaka, N. Matsumoto, N. Re, E. Gallo, E. Floriani, Inorg. Chem. 36 (1997) 670.
[29] L.K. Thompson, Z. Xu, A.E. Goeta, J.A.K. Howard, H.J. Clase, D.O. Miller, Inorg. Chem. 37 (1998) 3217.
[30] Z. Xu, S. White, L.K. Thompson, O.D. Miller, M. Ohba, H. Ōkawa, C. Wilson, J.A.K. Howard, J. Chem. Soc., Dalton Trans. (2000) 1751.
[31] I.L. Finar, Organic Chemistry, 6th ed., vol.1, ELBS, p. 197.
[32] N. Mondal, S. Mitra, V. Gramlich, O.S. Ghodsi, K.M.A. Malik, Polyhedron 37 (2001) 135.
[33] M. Suzuki, A. Uehara, Bull. Chem. Soc. Jpn. 57 (1984) 3134.
[34] J.P. Costes, J.P. Laurent, J.M.M. Sanchez, J.S. Varela, M. Ahlgren, M. Sundberg, Inorg. Chem. 36 (1997) 4641.
[35] A.B.P. Lever, Inorganic Electronic Spectroscopy, 2nd ed., Elsevier, New York, 1984, p. 534.
[36] B. Bleaney, K.D. Bowers, Proc. R. Soc. London, Ser. A 214 (1952) 451.
[37] M. Julve, M. Verdaguer, A. Gleizes, M. Philoche-Levisalles, O. Kahn, Inorg. Chem. 23 (1984) 3808.
[38] A. Aukauloo, X. Ottenwaelder, R. Ruiz, Y. Journaux, Y. Pei, E. Rivière, M. Carmen Munõz, Eur. J. Inorg. Chem. (2000) 951.
[39] M. Fettouhi, B. El Ali, A.M. El-Ghanam, S. Golhen, L. Ouahab, N. Daro, J.-P. Sutter, Inorg. Chem. 41 (2002) 3705.
[40] M. Fettouhi, B. El Ali, M. Morsy, S. Golhen, L. Ouahab, B. Le Guennic, J.-Y. Saillard, N. Daro, J.-P. Sutter, E. Amouyal, Inorg. Chem. 42 (2003) 1316.

also for cobalt complexes with other types of ligands containing amino acid moieties [18].

The metal complexes with α-amino acid derivatives have been investigated extensively but less works are devoted to complexes with β-amino acid Schiff bases, particularly with β-alanine [21]. In our recent work, we have interested in the cobalt complexes of β-alanine Schiff base with 2-hydroxynaphthaldehyde and its reduced analogue. The new cobalt complexes of the Schiff base, binuclear cobalt (II) complex and trinuclear mixed-valence cobalt complex with *N*-(2-hydroxynapthalidene)-β-alanine, and cobalt complex of reduction product of the Schiff base have been synthesized; compositions and physicochemical properties of the complexes and possibilities to reduction with sodium borohydride have been studied. Crystal structure of trinuclear mixed-valence cobalt complex has been elucidated.

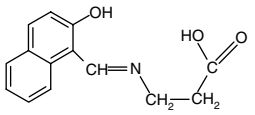

(Naphβala**H₂**) **(I)**

N-(2-Hydroxynapthalidene)-β-alanine

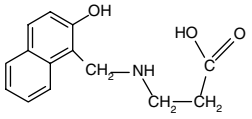

(RNaphβala**H₂**) **(II)**

N-(2-Hydroxynapthylmethyl)-β-alanine

2. Experimental

2.1. Physical and chemical measurements

UV–Vis. The electronic spectra were recorded on a Shimadzu UV–Vis 240 spectrophotometer using DMF and methanol as solvent. Kinetic measurements for reaction rates were also performed in termostated (±0.5 °C) quartz cuvettes. Optical densities were recorded at the maximum absorptivity wavelengths of the ligand (420 nm) and the complex $[Co_2(Nap\beta ala)_2 \cdot 2H_2O] \cdot H_2O$ (375 nm).

IR. Infrared spectra were recorded on a Hyper IR Shimadzu infrared spectrophotometer as KBr discs in the range of 4000–400 cm^{-1}.

Magnetic susceptibility measurements were carried out at room temperature on magnetic balance of Faraday type with $Hg[Co(SCN)_4]$ as standard.

NMR. ^1H NMR spectra of ligands were recorded on Mercury 300 BB spectrometer in DMF-d_6 solutions with TMS as internal standart at ambient temperature.

Elemental analyses. The elemental analyses were performed in the analytical laboratory, Tubitak, Ankara on LECO CHNS 932.

2.2. Synthesis of β-alanine Schiff bases with o-hydroxyaromatic aldehydes

2.2.1. Reagents

2-Hydroxynaphtaldehyde, β-alanine, sodium borohydride and the solvents used in the preparations and kinetic experiments were all Merk p.a. products.

2.2.2. N-(2-hydroxynaphtalidene)-β-alanine (NapβalaH₂) (I)

Since β-alanine is sparingly soluble in alcohols, the Schiff base formation takes long time even under the reflux conditions. To accelerate the reaction, following method was used:

The mixture of 2-hydroxynaphtaldehyde (20 mmol, 3.444 g) and β-alanine (20 mmol, 1.782 g) was milled in a porcelain mortar to obtain a homogenous mass until the release of water was observed. This mixture was added dropwise into the 200 ml of ethanol and refluxed for 1 h. The yellow crystalline compound **I** was precipitated after cooling (4.15 g, 85%). M.p.: 211–212 °C. IR (KBr, ν/cm^{-1}): 3433 (broad, OH), 3035, 3051 (broad, OH), 2476 (broad, CO*OH*), 1718 (s,C=O), 1644(C=N), 1547 (ν_{asym}(COO)), 1365 (ν_{sym}(COO)), 1268 (ν phenolic C–O). ^1H NMR (DMSO-d_6, δ): 8.96 (s, 1H, CH=N); 7.94 (d, 1H, arom. CH, $J = 7.5$ Hz); 7.65 (d, 1H, arom. CH, $J = 9.3$ Hz); 7.55 (d, 1H, arom. CH, $J = 7.5$ Hz); 7.35 (t, 1H, arom. CH, $J = 7.5$ Hz); 7.12 (t, 1H, arom. CH, $J = 7.5$ Hz); 6.63 (d, 1H, arom. CH, $J = 9.3$ Hz); 2.82 (t, 2H, CH_2, $J = 6.3$ Hz); 2.29 (t, 2H, CH_2, $J = 6.3$ Hz). *Anal*. Calc. for $C_{14}H_{13}NO_3$: C, 69.12; H, 5.39; N, 5.76. Found: C, 68.72; H, 5.34; N, 5.75%.

2.2.3. N-(2-hydroxynaphtylmethyl)-β-alanine (RNapβalaH₂) (II)

$Nap\beta alaH_2$ (10 mmol, 2.43 g) was suspended in 50 ml of ethanol and reduced by addition of excess sodium borohydride (10 mmol, 0.38 g). The solution was stirred until the yellow color of Schiff base disappeared, diluted with 8–10 times of water and the pH was adjusted to 6 by addition of 10% HCl. The white precipitate of **II** was purified by crystallization from DMF–ethanol mixture (1:1). M.p.: 198–199 °C. IR (KBr, ν/cm^{-1}): 3371 (broad, OH and NH); 2626–2700 (broad, CO*OH*), 1622 (s, C=C), 1518 (ν_{asym}(COO)), 1362 (ν_{sym}(COO)), 1273 (phenolic C–O). ^1H NMR (DMSO-d_6, δ): 7.03–7.97 (m, arom. CH); 2.83 (t, 2H, N–CH_2); 2.47 (s, 2H, Naph-CH_2) 2.29 (t, 2H, CH_2–COOH); 1.19 (s, 1H, NH). *Anal*. Calc. for $C_{14}H_{15}NO_3$: C, 68.56; H, 6.16; N, 5.71. Found: C, 68.26; H, 6.86; N, 5.70%.

2.2.4. $[Co_2(Nap\beta ala)_2 \cdot 2H_2O] \cdot H_2O$ (III)

This compound was always obtained along with trinuclear cobalt complex. It can be prepared in the yields more than 9% with water ratios higher than 9% in the solvent.

$Nap\beta alaH_2$(1 mmol, 0.243 g) was dissolved in 20 ml of hot ethanol and hot solution of cobalt acetate tetrahydrate (1 mmol, 0.249 g) in 10 ml of water was added to get

EtOH:water ratio of approximately 2:1. Immediate precipitation of fine violet-pink crystalline compound **III** was observed. The precipitate was filtered hot, washed with water, ethanol and dried in vacuo (0.22 g, 67% based on Co). M.p.: >300 °C; $\mu_{eff} = 4.87$ BM. TGA data (°C) (%) (calcd): 185 °C (5.60%) (5.70% calcd. for $-2H_2O$); 370 °C (21.0%) (21.7%, $-(3H_2O + 2CO_2)$). *Anal.* Calc. for $C_{28}H_{28}N_2O_9Co_2$: C, 51.39; H, 4.31; N, 4.28; Co, 18.01. Found: C, 51.56; H, 4.45; N, 4.55; Co, 17.18%.

2.2.5. $[Co_2(Nap\beta ala)_2 \cdot 2H_2O] \cdot H_2O$ (*III*) and $\{[Co(Nap\beta ala)_2]_2Co(H_2O)_4\} \cdot 4H_2O \cdot 2C_2H_5OH$ (*IV*)

NapβalaH$_2$(2 mmol, 0.486 g) was dissolved in 40 ml ethanol by heating and mixed with hot solution of cobalt acetate tetrahydrate (2 mmol, 0.498 g) in 4 ml water to get EtOH: water ratio of approximately 10:1. The warm solution was filtered from violet-pink fine powder (compound **III**) (0.06 g, 9% based on Co) and the filtrate was left for crystallization. The dark brown crystals (compound **IV**) were collected after 2–3 days standing (0.23 g, 25% based on Co). M.p.: >300 °C; $\mu_{eff} = 4.03$ BM; TGA Data (°C) (%) (calcd): 200 °C (17.0%) (17.1%, calcd. for $-(8H_2O + 2C_2H_5OH)$); 314 °C (23.0%) (23.5%, $-(8H_2O + 2C_2H_5OH + 2CO_2)$; 360 °C (29.0%) (29.9%, $-(8H_2O + 2C_2H_5OH + 4CO_2)$). *Anal.* Calc. for $C_{60}H_{72}N_4O_{22}Co_3$: C, 52.29; H, 5.23; N, 4.07; Co, 12.85. Found: C, 52.05; H, 5.16; N, 4.09; Co, 12.33%.

2.2.6. $Co(RNap\beta ala) \cdot 2H_2O$ (*V*)

RNapβalaH$_2$ (1 mmol, 0.245 g) in 10 ml of water containing 1 mmol NaOH was mixed with solution of cobalt acetate tetrahydrate (1 mmol, 0.249 g) in 10 ml of methanol. The deposited fine powder **V** was filtered, washed with water and ethanol and finally dried in air (0.22 g, 65% based on Co). M.p.: 335–336 °C; $\mu_{eff} = 3.67$ BM; TGA Data (°C) (%) (calcd): 111 °C (4.8%) (5.3%, calcd. for $-H_2O$); 216 °C (10.6%) (10.6%, $-2H_2O$); 310 °C (24.8%) (23.5%, $-(2H_2O + CO_2)$). *Anal.* Calc. for $C_{14}H_{17}NO_5Co$: C, 49.70; H, 5.03; N, 4.14; Co, 17.45. Found: C, 49.09; H, 4.79; N, 3.16; Co, 18.03%.

2.2.7. X-ray structural analysis

Dark brown single crystal suitable for data collection was mounted on a glass fiber and data collection was performed on a STOE IPDS 2 diffractometer with graphite monochromated Mo Kα radiation at 100 K. Details of crystal data, data collection and refinement are given in Table 1. The structure was solved by direct-methods using SHELXS-97 [30] and refined by full-matrix least-squares methods on F^2 using SHELXL-97 [34]. All non-hydrogen atoms were refined with anisotropic parameters. Hydrogen atoms bonded to carbon and ethanol hydrogens were placed in calculated positions (C–H 0.95–0.99 Å and alcohol 0.84 Å) and refined using riding model with $U = 1.2U$ of the parent atom for CH and CH$_2$ but $U = 1.5U$ for methyl and OH hydrogens). The hydrogens of the coordinated water were placed as methyl hydrogens with O–H 0.85 Å and then the one which was not involved in hydrogen bonds were deleted and refined using riding model with U 1.5 times that of attached oxygen atoms. Non-coordinated water hydrogens were found to be disordered over several positions and involved in very strong hydrogen bonding with neighboring oxygen atoms. The positions of the non-coordinated water hydrogens were not resolved. Molecular drawings were obtained using ORTEP-III [35] Geometric calculations were performed on PLATON [33]. Atomic coordinates and equivalent isotropic displacement parameters are listed in Table 2.

Table 1
Crystal data and structure refinement for $\{[Co(Nap\beta ala)_2]_2 \cdot Co(H_2O)_4\} \cdot 4H_2O \cdot 2C_2H_5OH$

Formula	$C_{60}H_{74}Co_3N_4O_{22}$
Molecular weight	1378.01
T (K)	100(2)
λ (Å)	0.71073
Crystal system	monoclinic
Space group	$P2_1/c$
Unit cell dimensions	
a (Å)	38.0567(17)
b (Å)	10.4669(4)
c (Å)	15.2160(7)
β (Å)	92.106(4)
V (Å^3)	6057.0(5)
Z	4
D_{calc} (mg/m^3)	1.511
Absorption coefficient (mm^{-1})	0.895
F(0 0 0)	2868
Crystal size (mm)	$0.55 \times 0.43 \times 0.27$
θ Range for data collection (°)	1.61–26.14
Index ranges	$-46 \leqslant h \leqslant 46$, $-12 \leqslant k \leqslant 12$, $-18 \leqslant l \leqslant 18$
Reflections collected	36 746
Independent reflections (R_{int})	11 857 (0.0986)
Reflections observed (>2σ)	7563
Data completeness	0.983
Absorption correction	numerical
Maximum and minimum transmission	0.8013 and 0.6693
Refinement method	full-matrix least-squares on F^2
Data/restraints/parameters	11 857/0/806
Goodness-of-fit on F^2	1.044
Final R indices [$I > 2\sigma(I)$]	$R_1 = 0.0735$, $wR_2 = 0.2112$
R indices (all data)	$R_1 = 0.1019$, $wR_2 = 0.2333$
Largest difference in peak and hole (e Å^{-3})	1.131 and −0.557

3. Results and discussion

N-(2-hydroxynapthalidene)-β-alanine reacts with Co(II) acetate in aqueous ethanol (1:2; v/v) to give binuclear Co(II) complex **III**, $[Co_2(Nap\beta ala)_2 \cdot 2H_2O] \cdot H_2O$, in 67% yield.

$$2Co(H_2O)_6^{2+} + 2NapHbalaH_2 + 4CH_3COO^- \rightarrow [Co_2(Nap\beta ala)_2 \cdot 2H_2O] \cdot H_2O + 9H_2O + 4CH_3COOH$$

When the water content of solution is decreased, binuclear complex formation is diminished and in aqueous ethanolic solution of 1:10 (v/v), trinuclear complex **IV** is obtained in 25% yield along with the binuclear complex **III** (9%).

Table 2
Selected bond lengths (Å) and angles (°) for the structure

Bond lengths (Å)			
Co2–O1	1.930(3)	Co3–O7	1.939(3)
Co2–O3	1.857(3)	Co3–O9	1.852(3)
Co2–O4	1.941(3)	Co3–O10	1.941(3)
Co2–O6	1.868(3)	Co3–O12	1.859(3)
Co2–N1	1.901(3)	Co3–N3	1.908(4)
Co2–N2	1.908(3)	Co3–N4	1.908(3)
Co1–O1W	2.064(3)	Co1–O3W	2.069(3)
Co1–O2W	2.110(4)	Co1–O4W	2.066(4)
Co1–O5	2.140(3)	Co1–O11	2.118(3)
C1–N1	1.303(6)	C29–N3	1.302(6)
C12–N1	1.469(6)	C40–N3	1.468(6)
C14–O1	1.249(5)	C42–O7	1.268(5)
C14–O2	1.268(6)	C42–O8	1.251(6)
C11–O3	1.312(5)	C39–O9	1.311(5)
C15–N2	1.296(5)	C43–N4	1.291(6)
C26–N2	1.456(6)	C54–N4	1.456(6)
C28–O4	1.271(5)	C56–O10	1.286(5)
C28–O5	1.257(5)	C56–O11	1.253(5)
C25–O6	1.326(5)	C53–O12	1.325(5)
Bond angles (°)			
O3–Co2–N1	91.48(14)	O9–Co3–N3	91.93(15)
O3–Co2–N2	87.51(14)	O9–Co3–N4	86.21(14)
O3–Co2–O4	88.46(13)	O9–Co3–O10	89.55(14)
O3–Co2–O6	92.02(13)	O9–Co3–O12	92.78(14)
O6–Co2–N1	86.84(14)	O12–Co3–N3	85.25(14)
O6–Co2–N2	90.86(14)	O12–Co3–N4	91.36(14)
O6–Co2–O1	90.56(13)	O12–Co3–O7	91.23(13)
N1–Co2–O1	95.06(14)	N3–Co3–O7	94.52(15)
N2–Co2–O1	86.04(14)	N4–Co3–O7	87.56(14)
N1–Co2–O4	87.86(14)	N3–Co3–O10	89.13(14)
N2–Co2–O4	94.45(14)	N4–Co3–O10	94.33(14)
O1–Co2–O4	89.57(14)	O7–Co3–O10	87.07(14)
N1–Co2–N2	177.45(16)	N4–Co3–N3	176.06(16)
O3–Co2–O1	173.09(13)	O9–Co3–O7	172.66(13)
O6–Co2–O4	174.69(12)	O12–Co3–O10	173.98(12)
O1W–Co1–O2W	91.91(14)	O3W–Co1–O5	92.41(12)
O1W–Co1–O4W	91.93(15)	O3W–Co1–O11	91.51(12)
O1W–Co1–O5	92.71(12)	O4W–Co1–O5	84.65(13)
O1W–Co1–O11	83.46(12)	O4W–Co1–O11	92.86(13)
O2W–Co1–O5	89.09(12)	O11–Co1–O5	175.37(13)
O2W–Co1–O11	93.62(12)	O4W–Co1–O2W	172.81(13)
O3W–Co1–O2W	86.26(14)	O1W–Co1–O3W	174.54(13)
O4W–Co1–O3W	90.45(16)		

$$2\mathrm{NaphβalaH_2} + \mathrm{Co_2(Naphβala)_2 \cdot 2H_2O(aq)} + \mathrm{Co(H_2O)_6^{2+}} + \tfrac{1}{2}\mathrm{O_2} + \mathrm{H_2O} + 2\mathrm{C_2H_5OH} \rightarrow [\mathrm{Co(III)(Naphβala)_2–Co(H_2O)_4^{2+}–Co(III)} \times \mathrm{(Naphβala)_2}] \cdot 4\mathrm{H_2O} \cdot 2\mathrm{C_2H_5OH} + 2\mathrm{H_3O^+}$$

Trinuclear mixed-valence complex **IV** should be formed via the oxidation of Co(II) atoms in $[\mathrm{Co_2(Naphβala)_2 \cdot 2H_2O}] \cdot \mathrm{H_2O}$ complex which is followed by the reaction with hydrated Co(II) ion.

Reduction of Schiff base by $NaBH_4$ in ethanol gives the reduced Schiff base (RNaphβala) which reacts with Co(II) to give a stable mononuclear Co(II) complex Co(RNaphβala) · $2H_2O$ (**V**). Reduction of binuclear Schiff base complex also leads to same mononuclear Co(II) complex **V**.

$$[\mathrm{Co_2(Naphβala)_2 \cdot 2H_2O}] \cdot \mathrm{H_2O}\ (\mathbf{III}) + 4\mathrm{H} + \mathrm{H_2O} \rightarrow 2\mathrm{Co(RNaphβala)} \cdot 2\mathrm{H_2O}\ (\mathbf{V})$$

3.1. Crystal structure of $\{Co(H_2O)_4[Co(Napβala)_2]_2\} \cdot 4H_2O \cdot 2C_2H_5OH$ (*IV*)

The structure of $\{\mathrm{Co(H_2O)_4[Co(Napβala)_2]_2}\} \cdot 4\mathrm{H_2O} \cdot 2\mathrm{C_2H_5OH}$ complex consist of three cobalt centre (Fig. 1). Each outer Co (Co2 and Co3) atoms are coordinated by two tridentate Naphβala ligand; but the Co(1) coordination sphere is formed from four water oxygen atoms and two oxygen atoms of carboxylate groups of Naphβala ligands which bridge the terminal (Co2 and Co3) and central (Co1) cobalt ions. Co1 atom is bridged by one $\mu_{1,3}$-OCO to Co2 and one $\mu_{1,3}$-OCO to Co3. The didepronated Naphβala ligands act as a tridentate one to the Co2 and Co3; but monodentate one to Co1. The tridentate behaviour of the Naphβala ligand results in the formation of two six membered rings in each Co2 and Co3 coordination environment having Co2–N1, Co2–N2, Co3–N3 and Co3–N4 bonds. The coordination geometry around all three cobalt atoms could be described as weakly distorted octahedron.

The stoichiometry of four dideprotonated ligands per trinuclear cobalt complex suggests a Co^{III}–Co^{II}–Co^{III} distribution of oxidation states. This can be correlated by comparing the length of the Co–O bond: since the ionic radius of Co^{II} is larger than Co^{III}, Co1–O5 and Co1–O11 bond lengths (2.140(3) and 2.118(3) Å) are noticeably longer than the Co2–O1, Co2–O4, Co3–O7 and Co3–O10 (1.930(3), 1.941(3), 1.939(3) and 1.941(3) Å). While Co^{II}–O bond lengths is around 2.1 Å, Co^{III}–O bond lengths is ~1.94 Å [18,19,24,26,27]. The absence of characteristic IR absorptions around 1700 cm^{-1} expected for the vibration of protonated carboxyl groups (COOH) also indicates that all carboxyl groups are depronated. Co^{III}–N distances are slightly shorter than Co^{II}–N distances reported earlier [18,27] but similar to Co^{II}–N distances [19,25]. All IR, UV–Vis and magnetic data supports that complex molecule has Co^{III} and Co^{II}.

In both outer coordination sphere, Co^{III}–Naph O bond lengths (~1.85 Å) are noticeably shorter than that of Co^{III}–carboxyl oxygens. These bond lengths are in good agreement with those reported for Co^{III}–Naph oxygens [19,28,29]. The coordination around Co2 and Co3 which are 3+ oxidation states coincide with each other within error limits.The oxidation state of Co1 is 2+ and coordinated by four water oxygens and two carboxyl oxygens. The distances of Co1–water oxygens and Co1–carboxyl oxygens are in good agreement with those reported for Co^{II} ions [18,19,24,31,32].

All four naphthalenolates are essentially planer with a rms deviations of ~0.06 Å. Dihedral angles between the two naphthalenolates in Co2 and Co3 environments are 28.30(8)° and 29.74(8)°, respectively. Naphthalenolates are involved in π–π, C–H–π and C–H–O interactions (Table 3).

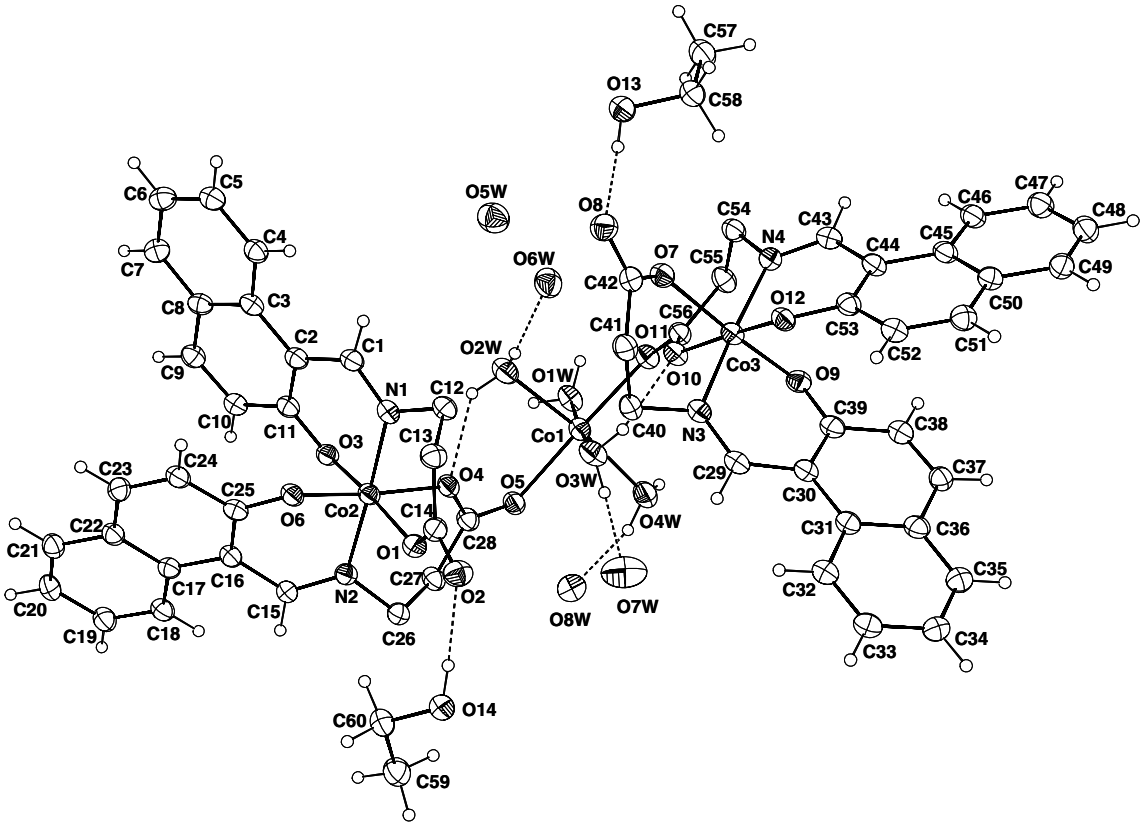

Fig. 1. A molecular view of the complex, water and ethanol solvates. The displacement ellipsoids are drawn at the 30% probability level and CH_2 hydrogens are removed for clarity.

Table 3
Intra- and intermolecular interactions

Bond	Distance (Å)	Bond	Distance (Å)
O1W···O5W^{i}	2.733(5)	O2W···O6W	2.722(5)
O1W···O14^{ii}	2.728(5)	O2W···O4	2.791(4)
O1W···O11	2.784(5)	O2W···O5	2.981(4)
O1W···O5	3.042(4)	O2W···O11	3.082(5)
O3W···O7W	2.570(6)	O4W···O13^{iii}	2.664(5)
O3W···O10	2.690(4)	O4W···O5	2.832(5)
O3W···O11	3.000(4)	O4W···O8W	2.906(5)
O3W···O5	3.039(5)	O4W···O11	3.031(5)
O5W···O7W^{v}	2.797(7)	O6W···O8W^{ii}	2.677(6)
O5W···O2^{v}	2.891(5)	O6W···O10	3.020(5)
O5W···O8	2.686(5)	O6W···O7	3.021(5)
O7W···O3W	2.570(6)	O7W···O11^{iii}	3.180(6)
O7W···O6W^{iii}	2.919(7)	O8W···O2^{i}	2.657(5)
O13···O8	2.719(4)	O8W···O5	2.740(5)
O14···O2	2.745(4)		
Non-conventional hydrogen bondings			
C33···O12^{vi}	3.321(5)	C5···O6^{v}	3.280(5)
π···π interaction			
Cg1···Cg1^{vii}	3.900(3)	Cg2···Cg2^{viii}	3.813(3)
C–H···π interaction			
C19···Cg3^{ix}	3.793(5)	C47···Cg4^{x}	3.846(5)

Symmetry codes: i: x, $1+y$, z; ii: x, $3/2-y$, $1/2+z$; iii: x, $3/2-y$, $-1/2+z$; iv: x, $-1+y$, z; v: x, $1/2-y$, $1/2+z$; vi: x, $1/2-y$, $-1/2+z$; vii: $-x$, $1-y$, $1-z$; viii: $1-x$, $1-y$, $2-z$; ix: $-x$, $1/2+y$, $3/2-z$; x: $1-x$, $1/2+y$, $3/2-z$. Cg1: C17, C18, C19, C20, C21, C22; Cg2: C45, C46, C47, C48, C49, C60; Cg3: C3, C4, C5, C6, C7, C8; Cg4: C31, C32, C33, C34, C35.

In addition to neutral coordination sphere, structure contains four water and two ethanol solvate per complex. Waters coordinated to Co1(O1W, O2W, O3W and O4W), solvate waters(O5W, O6W, O7W and O8W) and oxygen of the ethanol solvates(O14 and O14) are all involved in very strong hydrogen bonds stabilizing the three dimensional crystal structure (Table 3). Further analysis by Platon reveals that unit cell contains no residual solvent accessible void [33].

3.2. Magnetic data

The magnetic moment of binuclear cobalt complex $[Co_2(Nap\beta ala)_2 \cdot 2H_2O] \cdot H_2O$ (**III**) measured at room temperature and calculated has the value of 4.87 BM which points the presence of high spin state Co(II) in the complex.

The magnetic moment of $\{[Co(Nap\beta ala)_2]_2Co(H_2O)_4\} \cdot 4H_2O \cdot 2C_2H_5OH$ (**IV**) is 4.03 BM. This value of magnetic moment and the X-data point out undoubtly that two cobalt ions in trinuclear complex are in oxidation state 3+ and one is in oxidation state 2+.

The magnetic moment of $Co(RNap\beta ala) \cdot 2H_2O$ (**V**) is 3.67 BM which confirms the presence of Co(II) in the complex.

3.3. Spectroscopic properties

In electronic spectrum of $[Co_2(Nap\beta ala)_2 \cdot 2H_2O] \cdot H_2O$ (**III**) complex in DMF solution are the absorption bands at

$v_1 = 9000\ cm^{-1}$, $v_2 = 16400\ cm^{-1}$, $v_3 = 18200\ cm^{-1}$ which can be referred to transition from $^4A_{1g}$ ground state in $^4B_{1g}$, ^4E_g and $^4A_{2g}$ excitated states of square pyramidal Co(II) complex. The v_2 and v_3 bands are observed as shoulders on the intensive absorbtion at $26500\ cm^{-1}$, which is the charge transfer band.

In trinuclear $\{[Co(Nap\beta ala)_2]_2 \cdot Co(H_2O)_4\}$, there can be to distinguish the absorbances of $Co(Nap\beta ala)_2^{2-}$ and $Co(H_2O)_4^{2+}$ units. The relative intensive absorbance at $14200\ cm^{-1}$ ($\varepsilon = 380\ l \cdot mol^{-1} \cdot cm^{-1}$) concerns to the spin allowed $^1A_{1g} \rightarrow {}^1T_{1g}$ transition, observed usually for octahedric Co(III) complexes. The low intensive bands at 19200 and $9100\ cm^{-1}$ connect with d–d transitions in octahedric hydrate $Co(H_2O)_4^{2+}$ units.

The infrared spectra of $\{[Co(Nap\beta ala)_2]_2 \cdot Co(H_2O)_4\} \cdot 4H_2O \cdot 2C_2H_5OH$ (**IV**) show very broad intensive band at $3343\ cm^{-1}$ of hydroxyl groups. Intramolecular hydrogen bond appears as a sharp band at $3632\ cm^{-1}$. The band of azomethine group at $1619\ cm^{-1}$ is appeared at lower frequence than the band of C=N stretching in noncoordinated ligand ($1644\ cm^{-1}$). The COOH band of the ligand at $1718\ cm^{-1}$ disappears and the $v_{asym}(COO)$ band of the ligand at $1547\ cm^{-1}$ splits into two peaks at 1545 and $1569\ cm^{-1}$, which are attributed to bidentate bridge and monodentate coordinated carboxylic groups, respectively. The v_{sym} of bridge carboxylic group is at $1392\ cm^{-1}$ and monodentate carboxylic group at $1360\ cm^{-1}$, which correspond the frequence stretching differences observed in similar coordinations.

In the infrared spectra of $[Co_2(Nap\beta ala)_2 \cdot 2H_2O] \cdot H_2O$ (**III**), the absorption of hydroxyl groups at $3360\ cm^{-1}$ considerable lower compared with the trinuclear complex. Intramolecular hydrogen bond appears as a sharp band at $3633\ cm^{-1}$. The $v_{asym}(COO)$ is splitted to give peaks at 1573 and $1542\ cm^{-1}$. The $v_{sym}(COO)$ band appear at 1394 and $1362\ cm^{-1}$. The separation between these bands with the Δv value is in agreement with the value observed for the bridge bidentate carboxylates. Elemental analyses, IR, UV–Vis and magnetochemical ($\mu_{eff} = 4.87$ BM) data can be pointed out on binuclear square pyramidal structure of complex **III**.

The presence of hydrated water have been confirmed by broad absorption bands between ca. 3350 and $3450\ cm^{-1}$ in complexes.

3.4. Hydrogenation by $NaBH_4$

The hydrogenation reactions of ligand and complexes were carried out with sodium borohydride in the water containing DMF solutions at room temperature.

$$\underset{N\text{-(2-hydroxynapthalidene)-}\beta\text{-alanine (I)}}{Ar\text{–}CH{=}NCH_2\text{–}CH_2\text{–}COOH} + 2H \rightarrow \underset{N\text{-(2-hydroxynapthylmethyl)-}\beta\text{-alanine (II)}}{Ar\text{–}CH_2\text{–}NH\text{–}CH_2\text{–}CH_2\text{–}COOH}$$

$NaBH_4$ does not decompose in DMF solution even in a long time. Spectrophotometric titration of Schiff base have shown that the stoichiometric quantity of borohydride solution was spent after 24 h to achieve full hydrogenation. Thus, water-containing DMF was used in hydrogenation.

Kinetic measurements of hydrogenation have been carried out by the observation of the absorbance change at

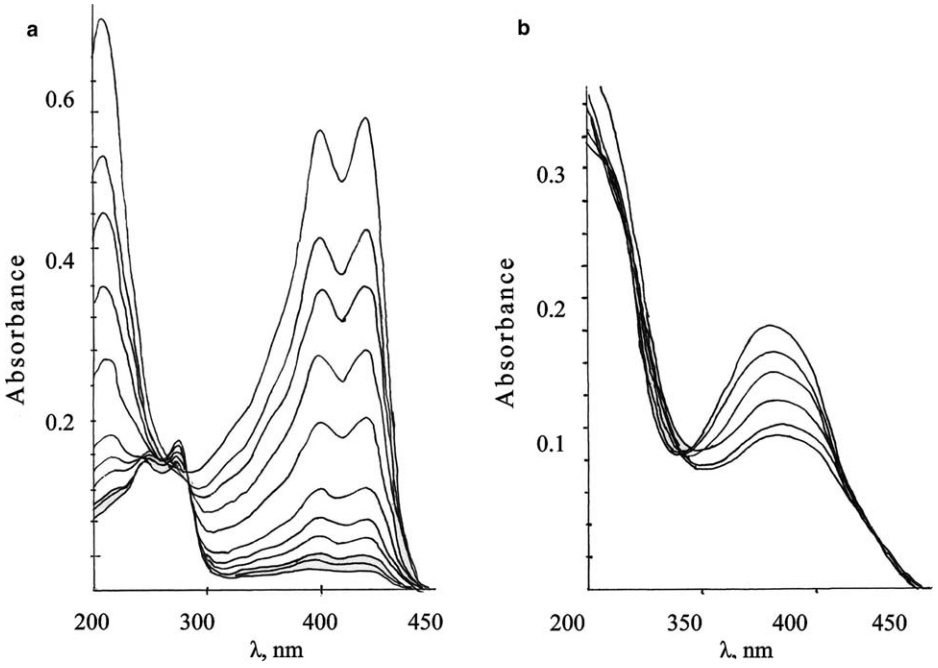

Fig. 2. (a) The absorbance change of $Nap\beta alaH_2$ (**I**) solution in DMF vs. time. Initial concentrations: $[Nap\beta alaH_2] = 10^{-4}\ mol\ L^{-1}$; $[NaBH_4] = 2 \times 10^{-3}\ mol\ L^{-1}$; $[H_2O] = 0.1\ mol\ L^{-1}$. (b) The absorbance change of $[Co_2(Nap\beta ala)_2 \cdot 2H_2O] \cdot H_2O$ (**III**) solution in DMF vs. time. Initial concentrations: $[Co_2(Nap\beta ala)_2 \cdot 2H_2O \cdot H_2O] = 9.7 \times 10^{-5}\ mol\ L^{-1}$; $[NaBH_4] = 2 \times 10^{-3}\ mol\ L^{-1}$; $[H_2O] = 0.1\ mol\ L^{-1}$.

418 nm for ligand ($NapβalaH_2$) and at 377 nm for complex **III** $[Co_2(Napβala)_2 \cdot 2H_2O] \cdot H_2O$ (Fig. 2).

Dependence of the reaction rate on the initial concentrations of ligand (or complex), sodium borohydride and water have been investigated. Reduction rates of Schiff base and the binuclear complex have been obtained by the kinetic investigations which were carried out by excess $NaBH_4$ and H_2O concentrations (about 100 times excess). In this case, the reaction can be considered as pseudo-first-order reaction

$$v = k_{\text{eff}}[\text{Sub}],$$

where k_{eff} is the reaction rate effective constant, including of initial concentrations of $NaBH_4$ and H_2O and possible intermediate active complexes formatting equilibria constants; [Sub] is the concentration of $NapβalaH_2$ or $[Co_2(Napβala)_2 \cdot 2H_2O] \cdot H_2O$.

The experimental values for k_{eff} of $NapβalaH_2$ and $[Co_2(Napβala)_2 \cdot 2H_2O] \cdot H_2O$ are 1.05×10^{-3} and 2.06×10^{-3} s^{-1} at initial concentrations of $[H_2O]_o$ and $[NaBH_4]_o$.

The obtained values

$$k'_{\text{eff}} = k_{\text{eff}}/[NaBH_4]_o[H_2O]_o,$$

are 2.0 and 3.9 l^2 mol^{-2} s^{-1} for $NapβalaH_2$ or $[Co_2(Napβala)_2 \cdot 2H_2O] \cdot H_2O$, respectively.

Trinuclear mixed-valence complex $\{[Co(Napβala)_2]_2 \cdot Co(H_2O)_4\} \cdot 4H_2O \cdot 2C_2H_5OH$ (**IV**) could not be reduced under similar conditions. Increases in sodium borohydride and water concentration did not give any results. High stability of this complex against sodium borohydride reduction can be connected with high energetic barrier reconstruction of the ligand environment around metal ion in the transition state. The presence of azomethine coordinated cobalt ions which have not contain water molecules in the coordination sphere can also be a reason for such stability against reduction.

4. Conclusions

Cobalt forms two types of complexes with *N*-(2-hydroxynaphtalidene)-β-alanine: binuclear $[Co_2(Napβala)_2 \cdot 2H_2O] \cdot H_2O$ and trinuclear mixed-valence $\{Co(H_2O)_4[Co(Napβala)_2]_2\} \cdot 4H_2O \cdot 2C_2H_5OH$. The X-ray and magnetochemical studies shows that trinuclear complex consist of two octahedrally coordinated outer cobalt ions with oxidation state 3+ and one is in oxidation state 2+. These kinds of complexations differ from the complexation with the Schiff base (LH_2) derived from 2-hydroxynaphtaldehyde and α-alanine which gives one kind of complex $Co(II)(LH)_2$ [15].

Schiff base, *N*-(2-hydroxynaphtalidene)-β-alanine, is easily reduced by $NaBH_4$ to a secondary amine which also acts as a ligand. An interesting point is observed that the binuclear complex $[Co_2(Napβala)_2 \cdot 2H_2O] \cdot H_2O$ could be reduced by sodium borohydride in water containing DMF solution into the complex **V** with hydrogenated ligand. However, according to kinetic measurements, the hydrogenation rate constant of free ligand is more noticable than the constant for complex.

It have been observed that the coordinating ligands in trinuclear complex could not be reduced under similar conditions. It connects probably with high activation energy, which is necessary for reconstruction of coordination sphere around Co^{3+} ions during the reduction reaction. Different behaviors of $[Co_2(Napβala)_2 \cdot 2H_2O] \cdot H_2O$ and $\{Co(H_2O)_4[Co(Napβala)_2]_2\} \cdot 4H_2O \cdot 2C_2H_5OH$ complexes against sodium borohydride action can be explained also by the simultaneous presence of azomethine group and water molecule in the coordination sphere of same cobalt ion, by which complex **III** is more succeptible to react with $NaBH_4$ reduction and cleaves simultaneously to give mononuclear complex of reduced ligand.

5. Supplementary material

Supplementary data are available from the Cambridge Crystallographic Data Center, CCDC, 12 Union Road, Cambridge CB2 1 EZ, UK on request quoting the deposition number 278124.

References

[1] E.E. Snell, A. Braunstein, E.S. Severin, V.M. Torchinsky, Pyridoxal Catalysis: Enzymes and Model Systems, Interscience, New York, 1968.
[2] B.M. Guirard, E.E. Snell, in: M. Florkin, E.H. Stotz (Eds.), Comprehensive Biochemistry, Elsevier, Amsterdam, 1981, p. 138.
[3] L. Casella, M. Gullotti, G. Pachioni, J. Am. Chem. Soc. 104 (1982) 2386.
[4] G.C. Percy, C. Slenton, J. Inorg. Nucl. Chem. 38 (1976) 1255.
[5] L.L. Koh, J.O. Ranford, W.T. Robinson, J.O. Svensson, A.L. Choo, D. Wu, J. Org. Chem. 35 (1996) 6466.
[6] A. Aydın, A. Üren, F. Baykut, Chim. Acta Turcica 9 (1981) 87.
[7] I. Bkouche-Waksman, J.M. Barbe, A. Kvick, Acta Crystallogr., Sect. B 44 (1988) 595.
[8] T. Ueki, T. Ashida, Y. Sasada, M. Kakudo, Acta Crystallogr. 22 (1967) 870.
[9] T. Ueki, T. Ashida, Y. Sasada, M. Kakudo, Acta Crystallogr., Sect. B 25 (1969) 328.
[10] L.J. Theriot, G.O. Carlisle, H.J. Hue, J. Inorg. Nucl. Chem. 31 (1969) 2891.
[11] G.O. Carlisle, L.J. Theriot, J. Inorg. Nucl. Chem. 35 (1973) 2093.
[12] H.M. Dawes, J.M. Waters, T.N. Waters, Inorg. Chim. Acta 66 (1982) 29.
[13] A. Garsia-Raso, J.J. Fiol, A. Lopez-Zafra, A. Cabrero, I. Mafa, E. Molins, Polyhedron 18 (1999) 871.
[14] N. Thankarajan, K. Mohanan, J. Indian Chem. Soc. 63 (10) (1986) 861.
[15] P.K. Sharma, S.N. Dubey, Proc. Indian Acad. Sci. (Chem. Sci.) 106 (1994) 23.
[16] N. Thankarajan, K. Mohanan, J. Indian Chem. Soc. 62 (1) (1985) 81.
[17] A. Fehn, T. Ederer, Sh. Mihan, W. Beck, J. Metallorg. Chem. 621 (2001) 109.
[18] J.M. Gonzales Perez, J.N. Guttierrez, Nguen-Huy Dung, B. Viossat, A. Busnot, M. Wintenberger, Inorg. Chim. Acta 184 (1991) 243.
[19] L.R. Nassimbeni, G.R. Percy, A.L. Rodgers, Acta Crystallogr., Sect. B 32 (1976) 1252.
[20] K. Korhonen, R. Hämäläinen, Acta Chem. Scand. Ser. A 33 (1979) 569.
[21] P.E. Werner, A. Valent, V. Adelskold, O. Svajlenova, Acta Chem. Scand. Ser. A 37 (1983) 51.

[22] J.E. Davies, Acta Crystallogr., Sect. C 40 (1984) 903.
[23] A. Valent, M. Melnik, D. Hudecova, B. Dudova, R. Kivekas, M.R. Sundberg, Inorg. Chim. Acta 340 (2002) 15.
[24] M. Rat, R.A. de Sousa, A. Tomas, Y. Frapart, J.P. Tuchagues, I. Artaud, Eur. J. Inorg. Chem. 4 (2003) 759.
[25] D. Radanovic, U. Ruchlewska, M.I. Duran, N.S. Draskovic, M.M. Vasojevic, I.M. Hodzic, Polyhedron 22 (2003) 2745.
[26] Y. Qi, Y. Wang, H. Fan, M. Cao, Li. Mao, Ch. Hu, E. Wang, N. Hu, H. Jia, J. Mol. Struct. 694 (2004) 73.
[27] L. Xie, L. Wei, Y. Wang, H. Hou, Y. Fan, Y. Zhu, J. Mol. Struct. 692 (2004) 201.
[28] Z.L. You, H.L. Zhu, W.S. Liu, Acta Crystallogr., Sect. E 60 (2004) 587.
[29] S.Y. Li, Z.L. You, B. Chen, Y.S. Lin, Z.D. Xiong, H.L. Zhu, Acta Crystallogr., Sect. E 60 (2004) 999.
[30] G.M. Sheldrick, Acta Crystallogr., Sect. A 46 (1990) 467.
[31] H. Icbudak, H. Olmez, O.Z. Yesilel, F. Arslan, P. Naumov, G. Jovanovski, A.R. Ibrahim, A. Usman, H-Kun Fun, S. Chantrapromma, S.W. Ng, J. Mol. Struct. 657 (2003) 255.
[32] U.P. Singh, P. Babbar, A.K. Sharma, Inorg. Chim. Acta 358 (2005) 271.
[33] A.L. Spek, PLATON: A Multipurpose Crystallographic Tool, Utrecht University, Utrecht, The Netherlands, 2005.
[34] G.M. Sheldrick, SHELXL-97: A Computer Program for Refinement of Crystal Structures, University of Göttingen, Göttingen, Germany, 1997.
[35] L.J. Farrugia, J. Appl. Crystallogr. 30 (1997) 565.

bis(L-alaninato)copper(II) with formaldehyde and acetamide, by electron impact (EI) mass spectroscopy, UV–Vis spectroscopy and magnetic susceptibility measurements. Compound **1** is soluble in water and its nucleolytic property is also described herein. The crystal structure of the insoluble compound **2**, with no lattice water molecule and slightly different from the previously synthesized compound which has one water molecule [1], has been determined.

2. Experimental

2.1. Synthesis of 1 and 2

The complexes **1** and **2** are identical or similar to those previously synthesized from the reactions of *trans*-[*bis*(L-alaninato)copper(II)], Cu(L-ala)$_2$, with formaldehyde and acetamide, as evidenced by their FTIR spectra [1]. For each reaction, a solid product crystallizes out of the reaction mixture containing Cu(L-ala)$_2$, aqueous formaldehyde and acetamide. After repeated attempts, one of the reactions finally yielded a suitable crystal of **2** for X-ray crystal structure analysis. Elemental analysis for (i) complex **1**, *Anal*. Calc. for $C_{12}H_{22}N_4O_6Cu \cdot 3H_2O$: C, 33.06; H, 6.47; N, 12.85. Found: C, 32.87; H, 6.10; N, 12.49% and (ii) complex **2**, *Anal*. Calc. for $C_{18}H_{32}N_6O_8Cu$: C, 41.26; H, 6.15; N, 16.04. Found: C, 40.74; H, 5.71; N, 15.70%.

2.2. Physical measurements

Elemental microanalysis was carried out with a Perkin–Elmer 2400. UV–Vis spectroscopic measurement was carried out on a Shimadzu UV-160 spectrophotometer on sample solutions of **1** dissolved in distilled water or dissolved in TN buffer pH 8.3 (TN = *Tris*–NaCl; *Tris* = *Tris*-(hydroxymethyl)aminomethane).

The EI mass spectra of **1** and **2** were collected on a HP 5989A mass spectrometer with a heating rate of 45 °C per minute and 70 eV electron beam. The temperature of the chamber for the insertion probe was programmed from 50 to 270 °C. Mass spectra were recorded when the ions were most abundant. The temperature range in which the mass spectra were recorded differs slightly for **1** and **2** but both are within the range 190–220 °C. The EI-MS of Cu(L-ala)$_2$ and L-alanine were similarly obtained for comparison. Infrared spectra of all compounds were recorded as KBr pellets using a Perkin–Elmer 1000 FTIR spectrometer in the frequency range 4000–600 cm^{-1}. The magnetic susceptibility measurements of **1** and **2** at room temperature were obtained with a Sherwood Magnetic Susceptibility Balance MSB Mk1 which was calibrated with Hg[Co(SCN)$_4$].

2.3. X-ray crystallography

A total of 7252 reflections for a crystal of **2** with a size of $0.48 \times 0.44 \times 0.04$ mm were collected at 293 K on a Bruker AXS area-detector diffractometer equipped with Mo Kα radiation ($\lambda = 0.71073$) using the ω-scan technique. The structure was solved by SHELXS-97 [8] and refined using SHELXL-97 [9]. The structure was refined on 2521 [$I > 2\sigma(I)$] of the 2883 reflections to $R_1 = 0.0366$ ($wR_2 = 0.0965$). Crystal data, selected bond lengths and angles and hydrogen bonding parameters are listed in Tables 1 and 2.

2.4. DNA cleavage experiments

A stock solution of complex **1** was prepared by dissolving it in Tris–NaCl buffer pH 8.3. This solution was used to react with supercoiled plasmid pBR322 DNA in the presence or absence of hydrogen peroxide. Each sample mixture was incubated with DNA (0.025 μg/μL) at 37 °C for 2 h, and then electrophoresed on 1% agarose gel. A digital

Table 1
Crystal data and structure refinement of **2**

Formula	$CuC_{18}H_{32}N_6O_8$
Formula weight	524.04
Crystal system	monoclinic
a (Å)	8.3769(5)
b (Å)	14.0830(8)
c (Å)	10.5807(6)
α (°)	90
β (°)	108.570(1)
γ (°)	90
λ (Å)	0.71073
Space group	$P2_1/a$
Z	2
V (Å^3)	1183.1(1)
D_2 (g cm^{-3})	1.471
F(000)	550
μ	0.978
Index ranges	$-10 \leqslant h \leqslant 11$; $-15 \leqslant k \leqslant 18$; $-13 \leqslant l \leqslant 11$
Data [$I_0 > 2\sigma(I_0)$]	2521
Final R indices	$R_1 = 0.0366$,
[$I_0 > 2\sigma(I_0)$]	$wR_2 = 0.0965$
R indices (all data)	$R_1 = 0.0434$, $wR_2 = 0.1005$
2θ Range (°)	4.9–56.5
Reflections	2883
Goodness-of-fit on F^2	1.061

Weighting scheme: $w = 1/[\sigma^2(F_o^2) + (0.0523P)^2 + 0.5361P$, where $P = (F_o^2 + F_c^2)/3$.

Table 2
Selected bond lengths (Å) and angles (°) of **2**

Cu1–O1	1.923(1)	O1–Cu1–O1^i	180
Cu1–N1	2.077(1)	O1–Cu1–O3	91.8(1)
Cu1–O3	2.502(2)	O1–Cu1–O3^i	88.2(1)
		O3–Cu1–O3^i	180
		O1–Cu1–N1	84.2(1)
		O1–Cu1–N1^i	95.8(1)
		O3–Cu1–N1	88.0(1)
		O3–Cu1–N1^i	92.0(1)
		N1–Cu1–N1^i	180.0
Hydrogen bonds (Å)			
N2–H2n···O2	2.895(2)		
N3–H3n···O3	2.855(2)		
N3–H3n···O1	3.026(2)		

Symmetry operation: $i = 1 - x, 1 - y, 1 - z$.

camera was used to photograph the resultant bands under UV light for each set of electrophoresis experiments.

3. Results and discussion

3.1. Characterization of 1 and 2

The FTIR of compound **1** is identical to that of *bis*[*N*-(*N*′-methylacetamido)-L-alaninato]copper(II) trihydrate which was previously synthesized [1]. Therefore, mono-acetamidomethylation of each chelated amino acid in Cu(L-ala)$_2$ by acetamide and formaldehyde has occurred. Its magnetic moment is 1.85 B.M. This value is consistent with a copper(II) complex having an octahedral coordination geometry [10–12]. The fifth and sixth coordination sites are most likely to be the carbonyl oxygen atoms of the two *N*-methylacetamido pendants. In aqueous solution, **1** has a λ_{max} value of 619 nm ($\varepsilon = 46\ M^{-1}\ cm^{-1}$) in the visible region due to a d–d transition and a λ_{max} value of 244 nm ($\varepsilon = 5055\ M^{-1}\ cm^{-1}$) in the UV region due to a LMCT transition. In TN buffer pH 8.3, **1** has the corresponding λ_{max} values of 611 nm ($\varepsilon = 49\ M^{-1}\ cm^{-1}$) and 244 nm ($\varepsilon = 5522\ M^{-1}\ cm^{-1}$). Dissolving **1** in the buffer solution has practically not affected its λ_{max} values. Aqueous solutions of *bis*(aminoacidato)copper(II) typically show a λ_{max} value of ~620 nm when two nitrogen atoms are coordinated to the copper [13]. As these values are far from that of aqueous $CuCl_2$ at 819 nm, it is reasonable to assume that at least most of complex species of **1** are not dissociated in solution.

The crystal structure of compound **2** (Fig. 1) shows that each alaninate moiety in *trans*-Cu(L-ala)$_2$ has reacted with two formaldehyde and two acetamide molecules. The resultant Mannich reaction has yielded two *N*-methylacetamido substituents at the amino nitrogen atom. One of the two *N*-methylacetamido substituents at each amino acid moiety is coordinated at an axial position via its amide carbonyl oxygen atom while the other *N*-methylacetamido group is uncoordinated. Unlike **2**, the original *trans*-Cu(L-ala)$_2$ has its axial positions occupied by the carbonyl oxygen atoms of adjacent molecules [14]. The axial bonds in **2** are stronger as evidenced by the Cu–O bond length of 2.502 Å, compared to the average Cu–O bond length of 2.8 Å in *trans*-[Cu(L-ala)$_2$]. The alaninate amino nitrogen and carboxylate oxygen atoms occupy the equatorial positions in **2**. Therefore, the copper atom has an octahedral environment. However, the octahedron is tetragonally distorted. Interestingly, the copper atom lies on a centre-of-inversion in the crystal structure. The centric nature of **2** implies racemization has occurred as L-alanine has been used to prepare the *trans*-Cu(L-ala)$_2$. This seems consistent with a previous study which shows that Cu(II) and other metal(II) ions can enhance the rate of racemization of L-alanine [15].

The two *N*-methylacetamido substituents at each amino nitrogen atom can be further distinguished by intermolecular and intramolecular hydrogen bonding. N2 of the amido nitrogen of each coordinated *N*-methylacetamido pendant

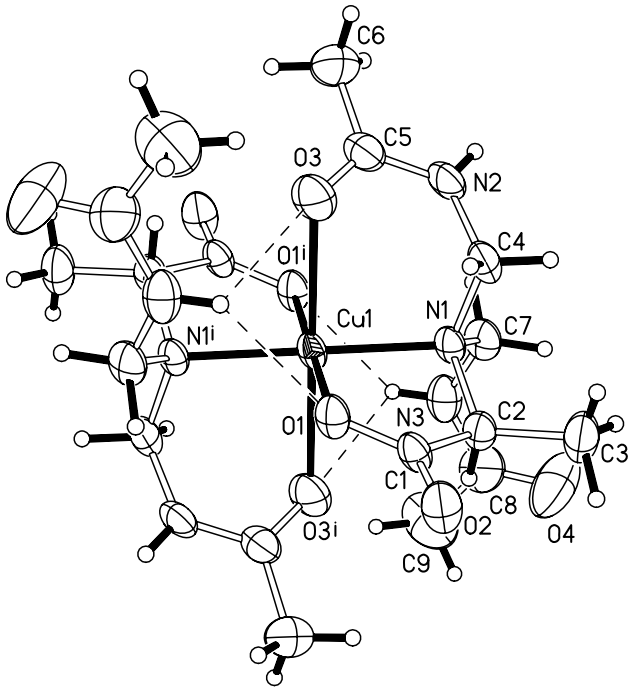

Fig. 1. ORTEP plot of **2** with the atom numbering scheme. The displacement ellipsoids are drawn at the 30% probability. Hydrogen bonding is shown by broken lines.

forms intermolecular hydrogen bonding with the amino acid carbonyl O2 of a neighbouring complex molecule. Each complex molecule thereby forms four such hydrogen bonds. On the other hand, the N3 proton of the amido nitrogen of the uncoordinated *N*-methylacetamido substituent of the *N*,*N*-di-(*N*′-methylacetamido)-L-alaninate ligand forms intramolecular hydrogen bonds with both O1 of the carboxylato oxygen atom and the amide O3 of a coordinated *N*-methylacetamido substituent of the other *N*,*N*-di-(*N*′-methylacetamido)-L-alaninate ligand (Fig. 1). Thus, four intramolecular hydrogen bonds bind together the two coordinated ligands, and this is akin to the hydrogen bonding that gives rise to the secondary structure in certain protein molecules. The prevalence of hydrogen bonding exhibited by **2** suggests a predisposition of the soluble neutral complex **1** towards hydrogen bonding as the predominant bonding mode of the complex towards DNA in the DNA grooves (see Fig. 2).

3.2. EI mass spectral analysis

The EI mass spectra of **1** and **2** show a very similar set of major fragments, viz *m*/*z* 15, 30, 41, 42, 43, 44, 59, 60, 73 and 87 (see Fig. 3 and supplementary information). Both mass spectra show close resemblance to the mass spectrum of acetamide (Wiley.1 ms library file no. 113824). In contrast, the EI-MS of Cu(L-ala)$_2$ and L-alanine (L-ala) show the absence of *m*/*z* peaks 45, 59, 60, 73 and 87. The peak at *m*/*z* 59 in both spectra of **1** and **2** can reasonably be ascribed to the molecular acetamide ion, M^+, which arises from the cleavage of the methylacetamido substituents.

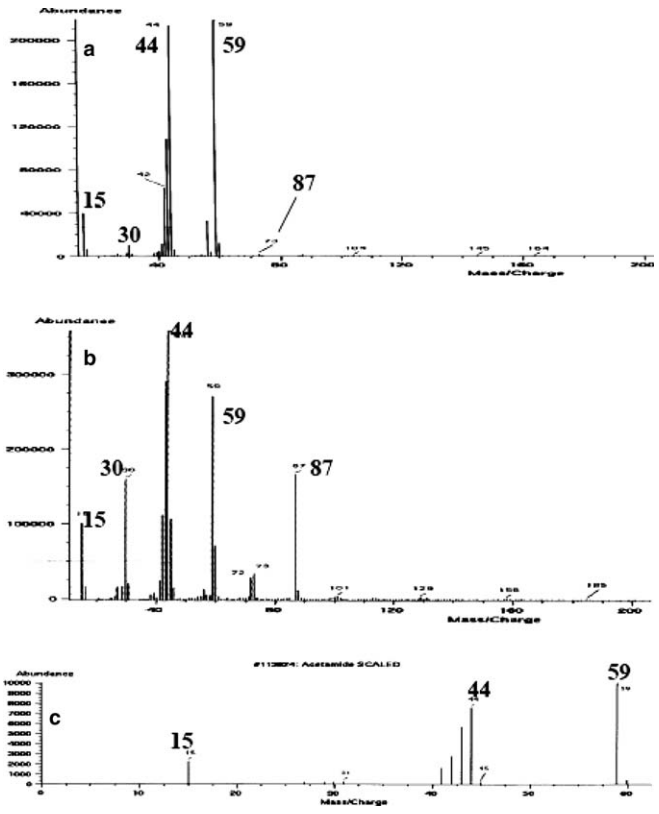

Fig. 2. Electron impact mass spectra of **1** (a), **2** (b) and acetamide (c).

The *m*/*z* 60 may be ascribed to the protonated acetamide ion while the *m*/*z* 87 is probably the immonium ion $+NH_2{=}CHNHCOCH_3$ which arises from simultaneous cleavage of the amino nitrogen from its amino acid moiety and cleavage of one of the attached acetamide moieties in **2**. Cleavage of the α-carbon – amino nitrogen bond in **2** can occur as similar cleavage has been postulated for the fragmentation of free L-alanine [16].

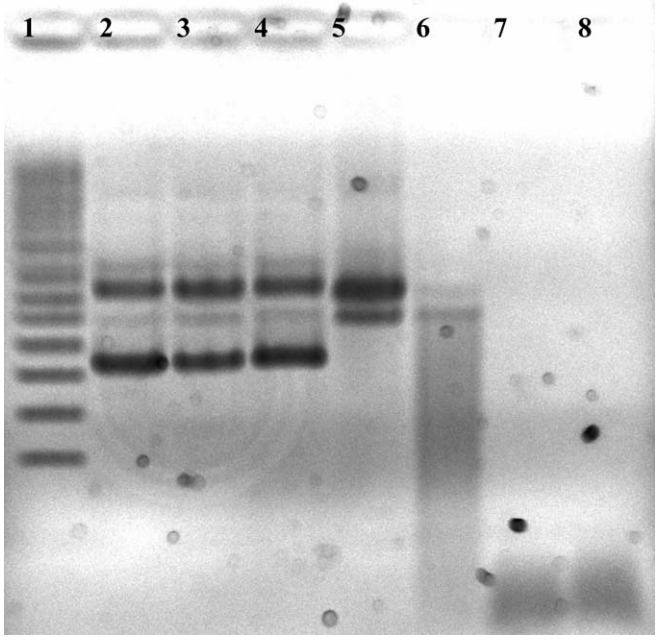

Fig. 3. Effect on the cleavage of pBR322 DNA (0.025 μg/μl) by **1** in the presence of H_2O_2 (4 mM). Lane 1, DNA marker (0.025 μg/μl), Lane 2, pBR322 alone, Lane 3, DNA + H_2O_2 (4 mM), Lane 4, DNA + **1** (6 mM), Lanes 5, 6, 7 and 8, DNA + **1** (25 μM), (50 μM), (3 mM), (6 mM) + H_2O_2, respectively.

3.3. DNA cleavage by *1*

The first set of gel electrophoresis results was obtained by reacting pBR322 DNA with an increasing complex concentration in the presence of hydrogen peroxide (4 mM). Neither incubating DNA with hydrogen peroxide alone nor DNA with 6 mM of complex alone results in any change in the DNA banding patterns (Fig. 3, lanes 3 and 4, respectively) compared to the control DNA lane (lane 2). Complex **1** (25 μM) in the presence of hydrogen peroxide caused cleavage of the DNA (Fig. 3, lane 5). Here, the entire supercoiled DNA has been converted to a more intense band of nicked DNA and a less intense band of linear DNA. The necessity of hydrogen peroxide for DNA cleavage suggests oxidative cleavage. Similar oxidative cleavage of DNA have been reported for various copper(II) complexes of other types of ligands [17,18]. At 50 μM complex concentration, all the nicked DNA has been cleaved and only a light band of linear DNA and a smear of degraded DNA are observed (Fig. 3, lane 6). Increasing the complex concentration further to 3 and 6 mM causes total degradation of the DNA. The above DNA cleavage mechanism by complex **1** is dissimilar to that of the copper(II)-L-histidine complex which is hydrolytic and where hydrogen peroxide is not needed [5].

The above electrophoresis experiment was repeated incubating a different batch of pBR322 DNA with increasing concentration of the complex in the range 15–60 μM with a lower concentration of hydrogen peroxide (2 mM; previously, the $[H_2O_2] = 4$ mM). A comparison is also made with Cu(L-ala)$_2$. Again complex **1** (60 μM) alone or hydrogen peroxide alone does not cause any change in banding patterns. This again implies that any cleavage of the DNA has to be oxidative. 15 and 35 μM of the complex are unable to cleave the DNA oxidatively (Fig. 4, lanes 5 and 6). At concentrations of 40 and 60 μM, the complex causes extensive degradation of the DNA in the presence of hydrogen peroxide via an oxidative mechanism. The precursor complex of **1** (60 μM), Cu(L-ala)$_2$, can also produce extensive oxidative cleavage of the DNA in the presence of hydrogen peroxide as a smear of DNA is observed (Fig. 4, lane 4). As lower density fragments are only present in the smear produced by 40 μM of **1** (Fig. 4, lane 7), it can be concluded that the nucleolytic ability of the complex **1** is higher than that of Cu(L-ala)$_2$. The complex **1** has an *N*-methylacetamido substituent group which has resulted from the reaction of **1** with formaldehyde and acetamide. The greater cleavage of **1** may be reasonably ascribed to the presence of these substituents.

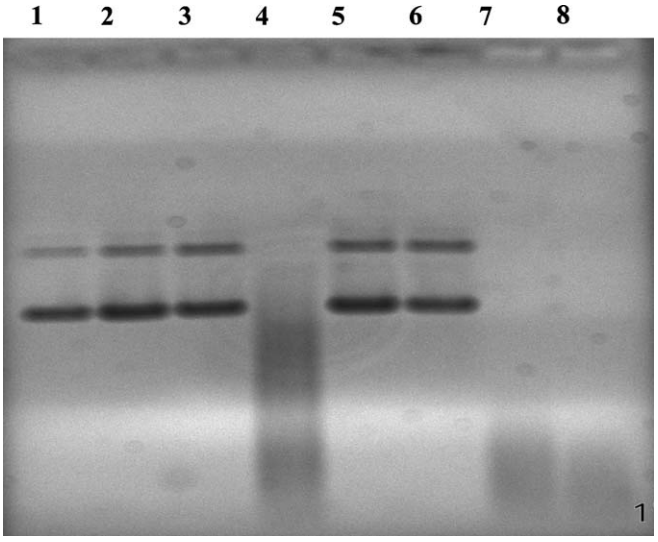

Fig. 4. Agarose (1%) gel electrophoresis banding patterns of pBR322 DNA (0.025 μg/μl) reacted with varying concentrations of **1** in the presence of H_2O_2 (2 mM). Lane 1, DNA alone, Lane 2, DNA + **1** (60 μM), Lane 3, DNA + H_2O_2, Lane 4, DNA + Cu(L-ala)$_2$ (60 μM), Lanes 5, 6, 7 and 8, DNA + **1** (15 μM), (25 μM), (40 μM) and (60 μM) + H_2O_2, respectively.

Acknowledgements

We thank Universiti Tunku Abdul Rahman, Tunku Abdul Rahman College, Universiti Sains Malaysia, and the University of Malaya for supporting this work.

Appendix A. Supplementary data

Crystallographic data for the structure in this paper have been deposited with the Cambridge Crystallographic Data Centre as the supplementary publication no. CCDC No. 240840. Copies of the data can be obtained, free of charge, on application to CCDC, 12 Union Road, Cambridge CB2 1EZ, UK, fax: +44 1223 336 033 or e-mail: deposit@ccdc.cam.ac.uk. Supplementary data associated with this article can be found, in the online version, at doi:10.1016/j.poly.2005.08.052.

References

[1] C.H. Ng, Y.T. Lim, Norhayati Moris, S.G. Teoh, Polyhedron 22 (2003) 521.
[2] C.H. Ng, T.S. Chong, S.G. Teoh, Farook Adams, S.W. Ng, J. Chem. Soc., Dalton Trans. (2002) 3361.
[3] D. Kong, J. Reibenspies, J. Mao, A. Clearfield, A.E. Martell, Inorg. Chim. Acta 342 (2003) 158.
[4] J. Liu, J. Zhou, T. Lu, L. Qu, H. Zhou, Q. Zhang, L. Ji, J. Inorg. Biochem. 91 (2002) 269.
[5] R. Ren, P. Yang, W.-J. Zheng, Z.-C. Hua, Inorg. Chem. 39 (2000) 5454.
[6] J.K. Baskin, Chem. Rev. 98 (1998) 937.
[7] M. Chikira, M. Inoue, R. Nagane, W. Harada, H. Shindo, J. Inorg. Biochem. 66 (1997) 131.
[8] G.M. Sheldrick, SHELXS-97, Program for Crystal Structure Solution, Göttingen University, Germany, 1997.
[9] G.M. Sheldrick, SHELXL97, Program for Crystal Structure Refinement, Göttingen University, Germany, 1997.
[10] S.B. Teo, S.G. Teoh, M.R. Snow, Inorg. Chim. Acta 107 (1985) 211.
[11] B.N. Figgis, J. LewisProgress in Inorganic Chemistry, vol. 6, Academic Press, New York, 1964, p. 37.
[12] C.H. Ng, S.B. Teo, S.G. Teoh, J.P. Declercq, J. Coord. Chem. 55 (2002) 909.
[13] R.P. Agarwal, D.D. Perrin, J. Chem. Soc., Dalton Trans. (1976) 82.
[14] A. Dijkstra, Acta Crystallogr. 20 (1966) 588.
[15] G.G. Smith, A. Khatib, G.S. Reddy, J. Am. Chem. Soc. 105 (1983) 293.
[16] G. Junk, H. Svec, J. Am. Chem. Soc. 85 (1963) 839.
[17] T. Kobayashi, M. Kunita, S. Nishino, H. Matsushima, T. Tokii, H. Masuda, H. Einaga, Y. Nishida, Polyhedron 19 (2000) 2639.
[18] C.P. Raptopoulou, S. Paschalidou, A.A. Pantazaki, A. Terzis, S.P. Perlepes, Th. Lialiaris, E.G. Bakalbassis, J. Mrozinski, D.A. Kyriakidis, J. Inorg. Biochem. 71 (1998) 15.

scale, and the crystal structure of newly prepared lithium bis(fluorosulfuryl)imide.

2. Results and discussion

2.1. Preparation of alkali metal bis(fluorosulfuryl)imides

Attempts to prepare lithium bis(fluorosulfuryl)imide (**LISFI**) were made in our laboratory in last years. Unfortunately, no experiments led to a crystalline product [14]. This fact can be ascribed to the extreme solubility of **LISFI** in water and polar organic solvents. Therefore we looked for such approaches that could yield crystalline **LISFI**. For example, we tried to prepare lithium salt by the reaction of $HN(SO_2Cl)_2$ with anhydrous LiF or by the reaction of $LiClO_4$ with $KN(SO_2F)_2$ in oxygen-containing solvents (tetrahydrofuran, anisole, triglyme). The utilization of these solvents was based on the assumption that they can serve as ligands for lithium atom and the formation of complexes (or only solvates) thus can enable the crystallization of the lithium salt. Unfortunately, none of above mentioned ways led to a crystalline product.

At last, we were successful in the preparation of lithium and sodium salts according to Scheme 1.

The lithium salt obtained by this reaction was crystalline and thus its molecular and crystal structures could be determined by X-ray diffraction. The last traces of water coming from $LiClO_4$ were removed by action of thionyl dichloride.

The *sodium salt* was prepared in the same manner. Though this substance was also prepared in a crystalline state we were not able to grow appropriate monocrystals for X-ray structural determinations.

However, *rubidium and cesium* salts cannot be prepared by the above-mentioned way because of negligible solubility of $RbClO_4$ and $CsClO_4$ in polar organic solvents.

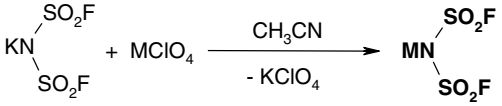

Scheme 1. Reaction of $KN(SO_2F)_2$ with $MClO_4$ (M = Li, Na) in acetonitrile.

Therefore, we had to liberate free imido-bis(sulfuric acid) difluoride from its potassium salt in nitromethane by the action of conc. $HClO_4$. The solution of free imido-bis(sulfuric) acid difluoride was filtered off from precipitated $KClO_4$ and then was converted into a corresponding salt. Salts were precipitated from the solution by addition of dichloromethane. Scheme 2 shows the preparation of Rb and Cs salts.

The products of all synthetic reactions were followed by ^{19}F NMR spectroscopy. It was found that ^{19}F NMR spectra (in tetrahydrofuran) contain only one resonance signal (singlet) that can be ascribed to a corresponding bis(fluorosulfuryl) imide ion: $LiN(SO_2F)_2$ (54.80 ppm), $NaN(SO_2F)_2$ (51.40 ppm), $RbN(SO_2F)_2$ (51.45 ppm), $CsN(SO_2F)_2$ (51.69 ppm). Therefore, ^{19}F NMR spectroscopy confirms high fluorine purity of prepared salts.

2.2. Vibrational spectra

The wavenumbers and intensities of all bands observed in infrared spectra of prepared alkali metal bis(fluorosulfuryl)imides are given in Section 3. A comparison with infrared data of potassium, rubidium, and cesium salts recorded earlier [3,4,7] in the frequency range 700–2000 cm^{-1} shows a very good agreement. The recorded Raman spectra of alkali metal salts were complemented with the spectrum of $KN(SO_2F)_2$ which was obtained according to [7] and are shown in Fig. 1. The low intensity bands occurring in the Raman spectra of $LiN(SO_2F)_2$ and $NaN(SO_2F)_2$ at 940 and 941 cm^{-1}, respectively, were assigned to the ν_1 fundamental vibration of a perchlorate impurity that is present due to the used preparation method.

The Raman spectral data and band assignments of an $N(SO_2F)_2$ group have been reported for a number of the neutral and cationic Xe(II) derivatives of bis(fluorosulfuryl)imide, $FXeN(SO_2F)_2$ [15], $Xe[N(SO_2F)_2]_2$ [16], and $XeN(SO_2F)_2^+$ [17]. Since the vibrational spectra of the $N(SO_2F)_2^-$ anion in alkali metal salts were so far not studied in a greater detail, we attempted to assign its fundamental stretching modes at least. Because the absorption bands in infrared spectra are mostly broad and exhibit numerous shoulders, only the recorded Raman spectra with much better resolved sharp lines were taken into consideration.

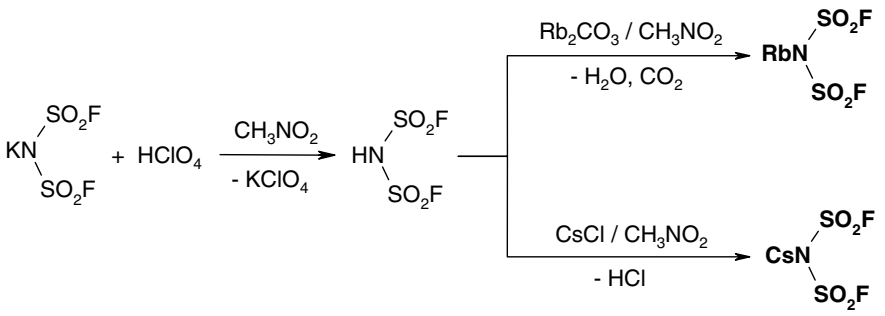

Scheme 2. The preparation of $RbN(SO_2F)_2$ and $CsN(SO_2F)_2$.

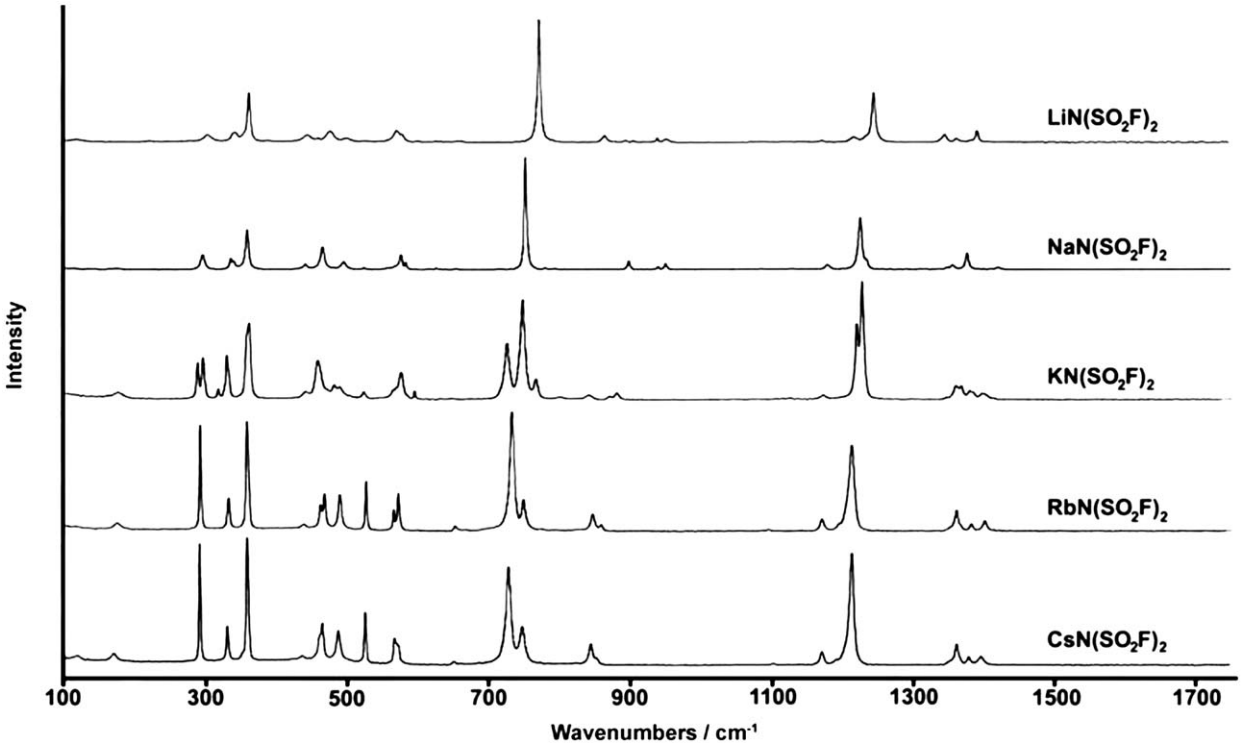

Fig. 1. Raman spectra of alkali metal bis(fluorosulfuryl)imides. K-salt was prepared according to [7].

Regardless of the actual molecular symmetry of the $N(SO_2F)_2^-$ anion in particular salts (approximately C_s for Li^+ and C_2 for Cs^+), there is eight normal stretching vibrations and all of them should be Raman and infrared active. Their tentative assignments are based mainly on previous assignments for related covalent derivatives of Xe(II) [15–17] and the isoelectronic molecule $O(SO_2F)_2$ [18], and are given in Table 1.

As follows from Fig. 1, there are four distinct groups of bands in the region of stretching vibrations above 700 cm^{-1}. Bands that occur between 1346–1421 and 1172–1246 cm^{-1} are assigned to the $\nu_{as}SO_2$ and ν_sSO_2 modes, respectively, and their average frequency is roughly invariable for the particular salts. The frequency of $\nu_{as}SO_2$ is about 100 cm^{-1} lower than for covalent compounds and indicates rather ionic character of an $N(SO_2F)_2$ group [19].

Table 1
Tentative assignments of normal stretching vibrations in Raman spectra of alkali metal bis(fluorosulfuryl)imides

Stretching mode[a]	$LiN(SO_2F)_2$	$NaN(SO_2F)_2$	$KN(SO_2F)_2$	$RbN(SO_2F)_2$	$CsN(SO_2F)_2$
ν_sSNS	774	754	727	733	728
			741	749	747
			768		
ν_{as}SNS	867 (861)[c]	(856)[c]	871 (860 + 845)[c]	(844)[c]	850 (841)[c]
νSF	897	900	843	847	845
ν'SF[b]	908	941	882	859	
	940	952			
	956				
ν_sSO_2	1174	1180	1174	1174	1172
ν'_sSO_2[b]	1219	1226	1221	1213	1213
	1246		1228		
$\nu_{as}SO_2$	1346	1357	1361	1361	1361
$\nu'_{as}SO_2$[b]	1366	1377	1370	1380	1379
	1392	1421	1381	1400	1396
		1409			

[a] Frequencies in cm^{-1}.
[b] ν In-phase motions; ν' out-of-phase motions of SO_2F groups.
[c] Values in parentheses denote infrared data.

On the other hand, the average frequencies of the two remaining band groups are not constant and exhibit a continual shift to higher wavenumbers when going from Cs^+ to Li^+ salt.

The high intensity lines in the 727–774 cm^{-1} range are assigned to the ν_s SNS mode and an increase of its average frequency from 738 cm^{-1} in $CsN(SO_2F)_2$ to 774 cm^{-1} in $LiN(SO_2F)_2$ corresponds well to the observed shortening of an average S–N bond length from 1.577(3) to 1.556(2) Å, respectively. However, the average S–N bond distances in $FXeN(SO_2F)_2$ (1.626(3) Å) [20] or $XeN(SO_2F)_2^+$ (1.69(1) Å) [17] are significantly longer than those found in alkali metal salts and, consequently, the ν_s SNS mode in these compounds should occur at lower frequency. Its reported assignment to the bands occuring in the range 797–830 cm^{-1} [16,17] therefore does not seem reasonable.

The low intensity lines, which are observed in the region 843–956 cm^{-1}, involve likely both νSF and ν_{as}SNS stretching modes. Earlier studies on the vibrational spectra of alkali metal fluorosulfates have indicated that the position of νSF in SO_3F^- is related to the polarizing power of the cation. Thus, going from the $CsSO_3F$ to $LiSO_3F$, the frequency of the νSF vibration changes quite significantly from 715 to 812 cm^{-1} [21]. Therefore, a similar set of gradually increasing Raman frequencies was chosen for the νSF stretching modes in $M^IN(SO_2F)_2$ and the remaining frequencies were attributed to the asymmetric stretch of the SNS bridge, ν_{as}SNS. Due to extremely low intensity of these bands, they were not observed in the Raman spectra of Na^+ and Rb^+ salts. For this reason, Table 1 was completed by the corresponding infrared data.

A marked increase of the frequency of ν SF and the moderate one of ν_sSNS and ν_{as}SNS in vibrational spectra of $LiN(SO_2F)_2$ and $NaN(SO_2F)_2$ is obviously related to their descending ionic character with respect to analogous salts of the heaviest alkali metals. A comparison of crystal structures of $CsN(SO_2F)_2$ [9], $KN(SO_2F)_2$ [8], and $LiN(SO_2F)_2$ indicates increasing cation–anion interactions in this order. A withdrawal of charge through the oxygen atoms of the anion by the cation therefore increases, resulting in increased pπ–dπ bonding between sulfur and fluorine and, to a smaller extent, between sulfur and nitrogen. Since a measure for the bond strengths are the internal stretching force constants, which in turn depend on vibrational frequencies, a strengthening of the S–F and S–N bonds results in a higher frequency of the corresponding stretching modes.

2.3. The crystal structure of LISFI

The basic crystal data and some details about the data collection and structure solution are given in Table 2, selected interatomic distances (Å) and angles (in degrees) in $LiN(SO_2F)_2$ and $HN(SO_2F)_2$, $KN(SO_2F)_2$, and $CsN(SO_2F)_2$ for comparison are collected in Table 3.

Table 2
Crystal data and structure refinement for $LiN(SO_2F)_2$

Identification code	**LISFI**
Empirical formula	$F_2LiNO_4S_2$
Formula weight	187.07
Temperature (K)	120(2)
Wavelength (Å)	0.71073
Crystal system	hexagonal
Space group	$P\bar{3}$
Unit cell dimensions	
a (Å)	8.4260(10)
b (Å)	8.4260(10)
c (Å)	12.682(3)
α (°)	90
β (°)	90
γ (°)	120
Volume (Å^3)	779.8(2)
Z	6
D_{calc} (Mg/m^3)	2.390
Absorption coefficient (mm^{-1})	1.015
$F(000)$	552
Crystal size (mm)	$0.35 \times 0.35 \times 0.25$
θ Range for data collection (°)	3.22–24.99
Index ranges	$-9 \leqslant h \leqslant 9$, $-10 \leqslant k \leqslant 8$, $-14 \leqslant l \leqslant 14$
Reflections collected/unique [R_{int}]	5033/904 [0.0343]
Completeness to $2\theta = 24.99$ (%)	98.7
Absorption correction	none
Maximum and minimum transmission	0.7855 and 0.7178
Refinement method	full-matrix least-squares on F^2
Data/restraints/parameters	904/0/91
Goodness-of-fit on F^2	1.132
Final R indices [$I > 2\sigma(I)$]	$R_1 = 0.0233$, $wR_2 = 0.0643$
R indices (all data)	$R_1 = 0.0268$, $wR_2 = 0.0662$
Largest difference peak and hole (e Å^{-3})	0.351 and −0.422

Table 3
Selected interatomic distances (Å) and angles (°) in $HN(SO_2F)_2$, $LiN(SO_2F)_2$, $KN(SO_2F)_2$, and $CsN(SO_2F)_2$

	$HN(SO_2F)_2$ [8]	$LiN(SO_2F)_2$	$KN(SO_2F)_2$ [8]	$CsN(SO_2F)_2$ [9]
M–O2		2.120(4)	2.637(4)	3.196(9)
M–O4		2.119(4)	2.859(4)	3.173(3)
S1–O1	1.404(3)	1.409(1)	1.413(7)	1.406(2)
S1–O2	1.403(8)	1.423(1)	1.378(5)	1.419(2)
S2–O3	1.392(2)	1.410(1)	1.395(2)	1.416(2)
S2–O4	1.413(2)	1.422(1)	1.413(8)	1.388(2)
S1–N	1.612(3)	1.556(2)	1.558(3)	1.558(2)
S2–N	1.642(1)	1.556(2)	1.577(2)	1.576(2)
S1–F1	1.511(1)	1.541(1)	1.557(3)	1.518(8)
S2–F2	1.516(4)	1.541(1)	1.569(3)	1.560(2)
O2–M–O4		82.4(5)	65.0(1)	60.4(1)
O1–S1–O2	123.2(2)	118.1(1)	118.3(2)	119.7(2)
O3–S2–O4	123.9(2)	118.1(1)	120.1(2)	119.3(1)
S1–N–S2	123.4(2)	123.0(1)	124.2(2)	120.8(2)

The structure is composed of cations and anions with strong cation–anion interactions. The asymmetric unit (Fig. 2) contains one anion in a general position and three non-equivalent Li^+ cations in special positions. Each anion is thus coordinated by three Li^+ cations and, in turn, each lithium cation is coordinated by six oxygen atoms. Li(1) is coordinated by three anions acting as

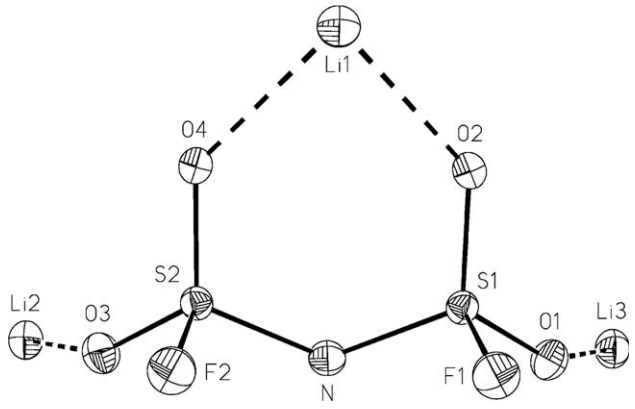

Fig. 2. Asymmetric unit of LISFI. Thermal ellipsoids are drawn on the 50% probability level.

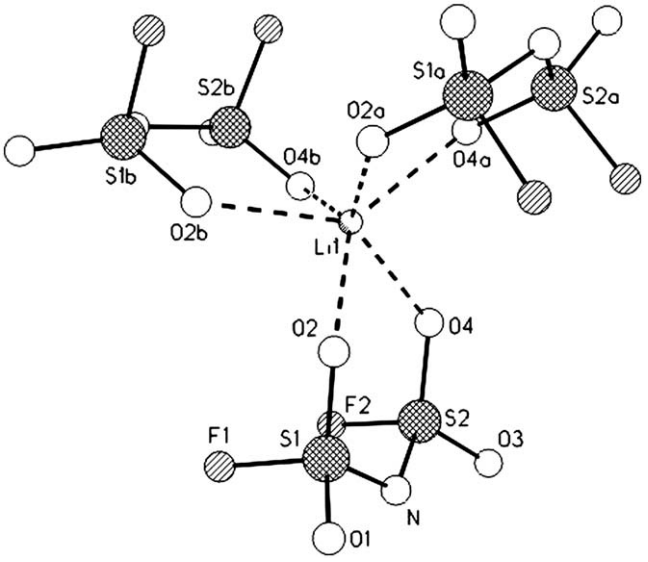

Fig. 3. Arrangement of $N(SO_2F)_2$ anions around Li1 (trigonal prismatic). Symmetry codes: O2a, O4a: $-x, 1+x-y, z$; O2b, O4b $-x+y-1, -x, z$.

bi-dentate ligands in regular trigonal prismatic arrangement (Fig. 3), while both Li(2) and Li(3) are coordinated identically by six mono-dentate anions forming distorted octahedrons (Fig. 4).

A brief search in the inorganic crystal structure database (ICSD) [22] revealed that most of Li salts of inorganic oxoacids possess tetragonal coordination of Li, e.g., carbonate, phosphate, selenate, sulfate, fluorosulfate, arsenate, etc. Octahedral coordination of Li is less common, e.g., in nitrate, perchlorate, trihydrogen bis(selenite), iodate(III). The coordination of Li in LISFI can be best compared with related compounds, $LiN(SO_2CF_3)_2$ [23] and $LiN(SO_2CF_3)_2 \cdot H_2O$ [24]. Tetrahedral coordination of Li in $LiN(SO_2CF_3)_2$ can be explained by a presence of bulky CF_3 groups which prevent anions to form chelate rings with Li and thus they serve only as bridging ligands. On the other hand, in $LiN(SO_2CF_3)_2 \cdot H_2O$ Li atoms are coordinated octahedrally by both chelating and bridging anions and water molecules.

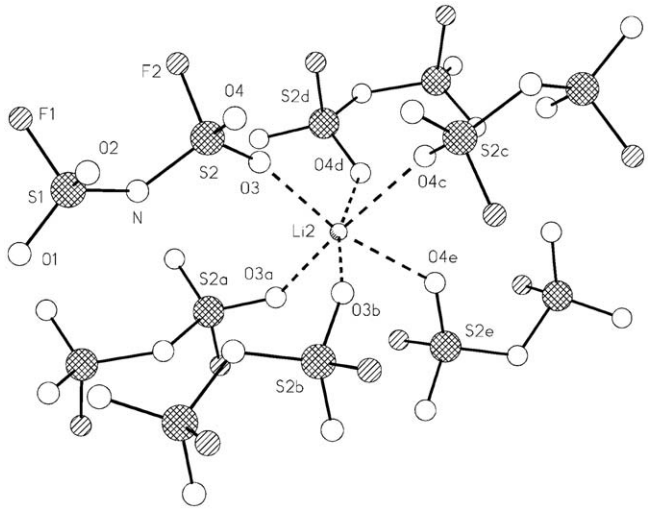

Fig. 4. Arrangement of $N(SO_2F)_2$ anions around Li2 and Li3, respectively (distorted octahedral). Symmetry codes: O3a: $1-x, 1+x-y, z$; O3b: $-x+y, 1-x, z$; O4c: $-x, 1-y, -z$; O4d: $y, -x+y, -z$; O4e: $1+x-y, 1+x, -z$.

Li–O distances in LISFI (2.020–2.201 Å) compare well with those observed in $LiN(SO_2CF_3)_2 \cdot H_2O$, 2.019–2.375 Å.

The anions in LISFI are in the "*cis*" positions having fluorine atoms on the same side of the plane defined by S–N–S bonds. This further supports previous observations that the actual configuration of $N(SO_2R)_2$ moieties depends on the character of intermolecular or cation–anion interactions [8].

A comparison of interatomic distances and angles of **LISFI** with those for free imide and K and Cs salts (Table 3) suggests that the free electron pair of the N atom is delocalized mainly in the S–N–S backbone. This fact is supported by identical bond lengths S1–N and S2–N (1.556(2) Å). Moreover, the bond order of both S–N bonds is significantly greater than 1 as compared with S–N single bond 1.775(3) in H_3NSO_3 [25].

3. Experimental

All reactions were performed under nitrogen in anhydrous conditions using conventional Schlenk techniques.

Solvents were dried by conventional methods prior to use [26]. Thionyl dichloride was supplied by Fluka and distilled with quinoline and linen oil before use [26]. Other chemicals were supplied by Lachema or Merck (p.a.).

^{19}F NMR spectra were recorded in THF using a Bruker AVANCE DRX 300 instrument.

IR and Raman spectra were recorded on a FT-IR Bruker EQUINOX IFS 55/S spectrometer with FRA 106/S equipment. IR spectra were measured as Nujol mulls between KBr windows, Raman spectra were excited by using Nd:YAG laser ($\lambda = 1064$ nm), maximal output 500 mW. Samples were measured in glass ampoules.

Intensity data were collected on a KUMA KM-4 κ-axis diffractometer equipped with CCD detector with graphite-monochromated Mo Kα radiation ($\lambda = 0.71073$ Å) at 120 K. The structure was solved by direct methods and refined anisotropically by full-matrix least-squares method. The software packages used were: Xcalibur CCD system [27] for the data collection/reduction, and SHELXTL V5.1 system [28] for the structure solution, refinement, and drawings (thermal ellipsoids are drawn at the 50% probability level).

3.1. Lithium bis(fluorosulfuryl) imide

2.5 g (23.6 mmol) dried $LiClO_4$ was dissolved in 20 ml acetonitrile in a Schlenk vessel and the solution of 5 g (22.8 mmol) $KN(SO_2F)_2$ in 5 ml acetonitrile was slowly dropwise added under stream of dry nitrogen. After the addition of the whole volume of $KN(SO_2F)_2$ solution, the reaction mixture was stirred for another 30 min. Precipitated $KClO_4$ was removed by vacuum filtration. Acetonitrile from the filtrate was then evaporated (2 kPa/40 °C) and the viscous almost colorless residue was then heated on the oil bad at 60 °C/650 Pa for 45 min. The content of the reaction vessel was left to crystallize at ambient temperature for next 24 h. The reaction mixture changed into crystalline mass containing small amount of the liquid. The desiccation of raw lithium salt was achieved by using of thionyl dichloride. The suspension of $LiN(SO_2F)_2$ in 5 ml thionyl dichloride was stirred 2.5 h at room temperature. The crystalline mass was filtered off under vacuum, washed three times by 5 ml portions of dichloromethane and dried in vacuum at 650 Pa. The product was placed into a tube and sealed. M.p. 124–128 °C. Yield: 3.8 g (88% of the theory). IR (cm^{-1}): 1378 vs, 1225 m, 1182 vs, 1121 m, 861 m, 789 m, 758 sh, 573 m.

3.2. Sodium bis(fluorosolfuryl) imide

3.5 g (28.6 mmol) dried $NaClO_4$ was dissolved in 20 ml acetonitrile in a Schlenk vessel and the solution of 6.2 g (28.3 mmol) $KN(SO_2F)_2$ in 10 ml acetonitrile was slowly dropwise added under stream of dry nitrogen. After 30 min of stirring the precipitated $KClO_4$ was filtered off under vacuum. Acetonitrile from the filtrate was evaporated (2 kPa/40 °C) and the viscous almost colorless residue was then heated on the oil bad at 50 °C/650 Pa for 60 min. The content of the vessel was left to crystallize at ambient temperature for next 24 h. The desiccation of raw sodium salt was done using thionyl dichloride. The suspension of $NaN(SO_2F)_2$ in 5 ml thionyl dichloride was stirred 1 h at room temperature. The crystalline mass was filtered off by vacuum, washed three times by 10 ml portions of dichloromethane and dried in vacuum at 650 Pa. The product was placed into a tube and sealed. M.p. 112–117 °C. Yield: 5.0 g (87% of the theory). IR (cm^{-1}): 1378 vs, 1364 s, 1229 m, 1178 m, 1124 m, 856 s, 777 m, 757 m, 654 vw, 573s, 496 w, 467 w, 442 vw.

3.3. Rubidium and cesium bis(fluorosulfuryl)imides

10.0 g (45.7 mmol) potassium bis(fluorosulfuryl) imide was dissolved in 20 ml nitromethane in a Schlenk vessel and 4.3 ml (49.9 mmol) 70% $HClO_4$ was dropwise added under cooling. The reaction mixture was stirred for 15 min. Precipitated $KClO_4$ was then filtered off under vacuum and the precipitate was twice washed by 5 ml portions of nitromethane. 6.0 g (26.0 mmol) anhydrous Rb_2CO_3 (during this reaction CO_2 is released) or 10.0 g (59.4 mmol) CsCl, respectively, was then added in small portions to combined filtrates of the $HN(SO_2F)_2$ solution under cooling. The reaction mixture was allowed to stand at room temperature for 30 min, solvent was evaporated under vacuum (ca. 2 kPa/50 °C). Crystalline raw product was pulverized and last traces of solvents were evaporated under vacuum. Rb and Cs salts were twice extracted by 20 ml portions of tetrahydrofuran, combined extracts were evaporated (2 kPa/40 °C) to 1/3 of the original volume and the isolation of solid salts was achieved by dropwise addition of dichloromethane. The IR spectra of Rb and Cs salts correspond to the published data [4]. Rb-salt: m.p. 92–96 °C, yield 10.6 g (87% of the theory), IR (cm^{-1}): 1376 vs, 1224 m, 1167 s, 1103 sh, 1092 m, 844 m, 823 sh, 768 s, 735 m, 581 m, 566 s, 491 w, 465 w, 440 w; Cs salt: m.p. 112–116 °C, yield 12.8 g (90% of the theory), IR (cm^{-1}): 1377 vs, 1221 m, 1172 s, 1100 s, 841 m, 818 sh, 764 s, 728 m, 581 m, 567 s, 489 w, 462 w, 437 w.

4. Supplementary material

Required for Ordering Data Sets, ICSD, Fachinformazionszentrum Karlsruhe.

For ordering, just send us an e-mail with the ICSD number (No. 415 618 for LISFI). It is urgently recommended to name at least the authors of the publication and the chemical formula of the compound, which will enable us to identify the record even if the CSD number was misspelled or transmitted incorrectly. The title of the deposited data set is not entirely reliable as it may be only a provisional title, and the publisher listed is the one to which the publication was to be sent at the date of deposition. E-mail: infodienste@fiz-karlsruhe.de.

References

[1] K. Xu, C.A. Angell, Inorg. Chim. Acta 298 (2000) 16.
[2] A. Růžička, L. Zatloukalová, Z. Chem. 27 (1987) 227.
[3] J.K. Ruff, M. Lustig, Inorg. Synth. 11 (1968) 138.
[4] J.K. Ruff, Inorg. Chem. 4 (1965) 1446.
[5] J.K. Ruff, Inorg. Chem. 6 (1967) 2108.
[6] M. Černík, A. Růžička, Z. Žák, V. Pevére, Ch. Michot, FR. Patent PCT/FR01/04164, WO02/053494, 2001.
[7] M. Beran, J. Příhoda, Z. Anorg. Allg. Chem. 631 (2005) 55.
[8] Z. Žák, A. Růžicka, Ch. Michot, Z. Krist. 213 (1998) 217.
[9] O. Hiemisch, D. Henschel, A. Blaschette, P.G. Jones, Z. Anorg. Allg. Chem. 623 (1997) 324.
[10] B. Krumm, A. Vij, R.L. Kirchmeier, J.M. Shreeve, Inorg. Chem. 37 (1998) 6295.

[11] S. Singh, A. Vij, M. Lal, R.D. Verma, Indian J. Chem. A 28 (1989) 890.
[12] S. Singh, D.D. DesMarteau, Inorg. Chem. 25 (1986) 4596.
[13] A. Vij, S. Singh, R.D. Verma, Bull. Soc. Chim. Fr. (1989) 331.
[14] M. Černík, MU Brno, unpublished results.
[15] R.D. LeBlond, D.D. DesMarteau, J. Chem. Soc., Chem. Commun. (1974) 555.
[16] G.A. Schumacher, G.J. Schrobilgen, Inorg. Chem. 22 (1983) 2178.
[17] R. Faggiani, D.K. Kennepohl, C.J.L. Lock, G.J. Schrobilgen, Inorg. Chem. 25 (1986) 563.
[18] J. Toužín, M. Černík, Collect. Czech. Chem. Commun. 58 (1993) 517.
[19] A. Vij, R.L. Kirchmeier, J.M. Shreeve, R.D. Verma, Coord. Chem. Rev. 158 (1997) 413.
[20] J.F. Sawyer, Inorg. Chem. 21 (1982) 4064.
[21] A. Ruoff, J.B. Milne, G. Kaufmann, M. Leroy, Z. Anorg. Allg. Chem. 372 (1970) 119.
[22] Inorganic Crystal Structure Database (ICSD), Fachinformazionszentrum Karlsruhe, release 2005/1.
[23] J.L. Nowinski, P. Lightfoot, P.G. Bruce, J. Mater. Chem. 4 (10) (1994) 1579.
[24] L.-X. Xue, C.W. Padgett, D.D. DesMarteau, W.T. Pennington, Solid State Sci. 4 (2002) 1535.
[25] J.W. Bats, P. Coppens, T.F. Koetzle, Acta Crystallogr., Sect. B 33 (1977) 37.
[26] D.D. Perrin, Purification of Laboratory Chemicals, third ed., Pergamon Press, Oxford, 1988.
[27] Xcalibur CCD System, CrysAlis Software System, Version 1.168, Oxford Diffraction Ltd., Oxford, England, 2001.
[28] Bruker, SHELXTL, Version 5.10, Bruker AXS Inc., Madison, WI, USA, 1997.

azoimidazole system and the importance of a Cu(N,S) chromophore [19] has stimulated us to design thioether functionalized azoimidazole ligands and their copper complexes. In this first report, we summarize copper(II) complexes of 1-alkyl-2-{(*o*-thioalkyl)phenylazo}imidazoles and their mixed ligand complexes. The complexes are characterized by spectroscopic and electrochemical techniques. A structure of one of the complexes has been confirmed by X-ray diffraction study.

2. Results and discussion

2.1. 1-Alkyl-2-{(*o*-thioalkyl)phenylazo}imidazoles

Imidazolylazothioether belongs to tridentate N, N′, S donor system. They are synthesized (Scheme 1) by coupling *o*-(thioalkyl)phenyldiazonium ions (**1**) with imidazole in aqueous sodium carbonate and purified by solvent extraction and a chromatographic process.

The alkylation is carried out by adding alkyliodide (MeI, EtI) in dry THF solution to the corresponding 2-{*o*-(thioalkyl)phenylazo}imidazole in the presence of sodium hydride. The ligands are new. They are abbreviated as SRaaiNR′ (**3**, **4**). The donor centers are N(imidazole) (N), N(azo) (N′) and thioether (S). The atom numbering is shown in Scheme 1. Sharp intense single bands at 1420–1430 and 1580–1600 cm^{-1} correspond to ν(N=N) and ν(C=N) + ν(C=C), respectively. The ν(N–H) in **2** appears as a medium intense sharp stretch at 3010 cm^{-1} along with multiple peaks at 2800–2900 cm^{-1} corresponding to ν(C–H). The UV–Vis spectra in methanol show two strong absorptions ($\varepsilon \sim 10^4\ M^{-1}\ cm^{-1}$) at 350–355 and 250–265 nm along with two shoulders ($\varepsilon \sim 10^3\ M^{-1}\ cm^{-1}$) in longer wavelength region, 400–415 and 450–460 nm.

The structure has been established by ^{1}H NMR spectral data. The alkylation of imidazole is supported by the disappearance of δ (N–H) at ~10.30 ppm (of **2**) and the appearance of an alkyl signal at 1.5–4.5 ppm for **3** and **4**: The N(1)–Me appears as singlet at ca. 4.00 ppm; N–CH_2–CH_3 shows a quartet for –CH_2– at ca. 4.5 (10 Hz) and a triplet at ca. 1.5 (8.0 Hz) ppm. The imidazole 4- and 5-H appear as broad singlets at 7.2–7.3 and 7.0–7.1 ppm, respectively. Broadening may be due to rapid proton exchange between these imidazolic protons. The thioalkyl group S–R also exhibits a singlet signal at 2.4 ppm for S–Me of SMeaaiNR′ (**3**). SEtaaiNEt (**4b**) shows two quartets [4.46 (9.0 Hz) and 3.00 (8.0 Hz) ppm for –CH_2– protons of N–CH_2–(CH_3) and S–CH_2–(CH_3), respectively] and two triplets [at 1.48 (8.0 Hz) and 1.33 (8.0 Hz) ppm for –(N–CH_2)CH_3 and –(S–CH_2)CH_3, respectively]. The thiophenyl protons (8-H to 11-H) have been influenced by S–R substituents. Their assignment has been done by comparing with the spectra of thioalkylazobenzene [34]. The 11-H and 8-H appear as doublets at ca. 7.8 and 7.2 ppm, respectively. The closer proximity of the electron withdrawing –N=N– group may be the reason for the higher δ of 11-H.

2.2. Copper complexes. Cu(SRaaiNR′)Cl_2 (**5**, **6**)

Copper(II) complexes of these ligands were obtained by mixing equimolar concentrations of $CuCl_2 \cdot 2H_2O$ and SRaaiNR′ in methanol. All the complexes are soluble in common organic solvents. Microanalytical data and copper analyses have confirmed the composition of the complexes as Cu(RSaaiNR′)Cl_2 (**5**, **6**). Infrared spectra of the complexes exhibit ν(N=N) and ν(C=N) at 1420–1430 and 1575–1580 cm^{-1}, respectively, and these values are red shifted by 10 cm^{-1}. This supports coordination of azo-N(N′) and imidazole-N to Cu(II).

The electronic spectra (in MeOH) of the complexes exhibit multiple high intense transitions ($\varepsilon \sim 10^4\ M^{-1}\ cm^{-1}$) (Table 1) at 500–250 nm along with a weak transition at 680–720 nm ($\varepsilon \sim 200\ M^{-1}\ cm^{-1}$). The spectra are compared with free ligand data under identical conditions. Intraligand charge transfers n–π^* and π–π^* appear at 370–380 and 250–260 nm, respectively. Other transitions at 680–720, 440–450 and 445–455 nm are new and are only observed in the complexes (Table 1). Also, the thioalkylazoimidazoles ligands possess a thioalkyl (–SR) reducing center. Copper(II) complexes containing coordinated –SR group(s) exhibit strong S (thioether) → Cu^{II} LMCT bands.

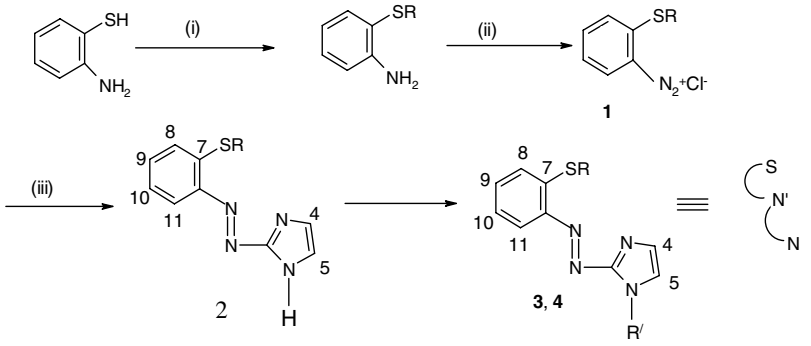

Scheme 1. (i) Dry EtOH/Na, RX; (ii) $NaNO_2$/HCl, 0–5 °C; (iii) imidazole, Na_2CO_3 solution (pH ~ 7); (iv) THF/NaH, R′X.

Table 1
UV–Vis spectral and cyclic voltammetric data

Compound	UV–Vis spectra[a] λ_{max} (nm) ($10^{-3} \times \varepsilon$ ($dm^3\ mol^{-1}\ cm^{-1}$))	Cyclic voltammetric data[c] E (V) (ΔE_p (mV))		
		Cu(II)/Cu(I)	Cu(I)/Cu(0)[d]	Ligand reductions
$Cu(SMeaaiNMe)Cl_2$ (**5a**)	685(0.21)[b], 470(5.06), 446(5.51), 376(4.86), 254(7.50)	0.21 (150)	−0.30	−0.77(140), −1.30(170)
$Cu(SMeaaiNEt)Cl_2$ (**5b**)	687(0.19)[b], 472(9.16), 445(10.14), 372(7.65), 285(5.47), 256(7.46)	0.20 (150)	−0.32	−0.82(200), −1.36(160)
$Cu(SEtaaiNMe)Cl_2$ (**6a**)	687(0.22)[b], 470(14.40), 452(14.97), 372(7.73), 290[sh](6.70), 258(7.35)	0.18 (140)	−0.30	−0.85(170), −1.32(180)
$Cu(SEtaaiNEt)Cl_2$ (**6b**)	692(0.23)[b], 470(0.85), 450(10.73), 374(9.94), 256(8.26)	0.18 (140)	−0.30	−0.81(140), −1.34(150)
$[Cu(SMeaaiNMe)(bpy)](ClO_4)_2$ (**7**)	720(0.09)[b], 522(3.75), 482(8.85), 456(10.26), 460(3.27), 380(4.05), 436(10.97), 370(22.08)	0.32 (150)	−0.25	−0.45(140), −0.70(140), −1.34(150)
$[Cu(SMeaaiNMe)(phen)](ClO_4)_2$ (**8**)	718(0.04)[b], 520(3.08), 470(1.66), 412(2.458), 358(4.33)	0.28 (150)	−0.29	−0.50(160), −0.82(170), −1.34(160)
$[Cu(SEtaaiNEt)(bpy)](ClO_4)_2$ (**9**)	722(0.12)[b], 525(4.08), 485(9.18), 450(11.49), 464(3.64), 380(4.05) 436(12.48), 362(24.14)	0.35 (140)	−0.21	−0.48(140), −0.75(140), −1.35(150)
$[Cu(SEtaaiNEt)(phen)](ClO_4)_2$ (**10**)	725(0.10)[b], 530(4.34), 481(9.44), 455(12.26), 462(5.05), 380(4.05), 440(11.54), 360(22.55)	0.33 (150)	−0.22	−0.53(150), −0.83(150), −1.36(170)

[a] Solvent, MeOH.
[b] Shoulder.
[c] Solvent, MeCN; working electrode, Pt-disk millielectrode, Pt-wire auxiliary, Ag/AgCl reference; supporting electrolyte [nBu$_4$N][ClO$_4$]; scan rate 0.05 V s^{-1}, potential $E_{1/2} = 0.5(E_{pa} + E_{pc})$, $\Delta E_p = |E_{pa} - E_{pc}|$, mV; E_{pa} = anodic peak potential, E_{pc} = cathodic peak potential.
[d] E_{pa}.

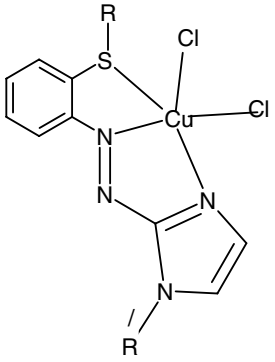

$Cu(SRaaiNR')Cl_2$; R = Me (**5**), Et (**6**); R′ = Me (**a**), Et (**b**)

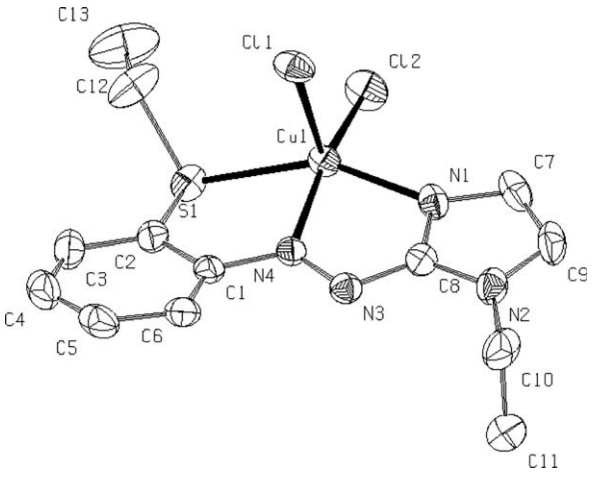

Fig. 1. ORTEP view of $Cu(SEtaaiNEt)Cl_2$ with the atom numbering scheme (30% probability ellipsoids).

Copper(II)–azoheterocycles [7,13,20,21] exhibit a strong MLCT transition involving d(Cu) → π*(arylazoheterocycle) because of efficient π-acidity of the ligands. On comparing with copper(II)-1-alkyl-2-(arylazo)imidazoles [23], pyridylthioazophenolates [35] and other pyridylthioether [19,36] based N, S donor ligands we may assign the 470–475 nm band as MLCT [d(Cu) → π*(azoimidazole)] and the 445–455 nm band as LMCT (S → Cu(II)) transitions. The very weak absorption at 680–720 nm ($\varepsilon \sim 200$ $M^{-1}\ cm^{-1}$) is undoubtedly a d–d transition [37].

2.3. Crystal structure of $Cu(SEtaaiNEt)Cl_2$

The X-ray structure of $Cu(SEtaaiNEt)Cl_2$ (**6b**) is shown in Fig. 1. The selected bond lengths and angles are listed in Table 2. The ligand serves as tridentate NN′S donor system. [N and N′ refer to N(imidazole) and N(azo) centers, respectively.] The bond parameters suggest a distorted square pyramidal geometry around the copper center. The basal plane is constituted by Cu(N,N′,S)Cl(1). One of the Cl ligands occupies an axial position (Cl(1)). The two Cu–Cl distances are different and the axial Cu–Cl(1) bond [2.4273(8) Å] is elongated by ~0.2 Å more than the Cu–Cl(2) bond [2.2296(8) Å]. There are two different N-donor centers N(imidazole)[N(1)] and N(azo) [N(4)]. The Cu–N distances do not vary significantly; Cu–N(azo) is slightly

Table 2
Bond distances and bond angles of [Cu(SEtaaiNEt)Cl_2] (**6b**)

Bond distances (Å)		Bond angles (°)	
Cu(1)–S(1)	2.3788(8)	S(1)–Cu(1)–Cl(1)	98.65(3)
Cu(1)–Cl(2)	2.2296(8)	S(1)–Cu(1)–Cl(2)	96.22(3)
Cu(1)–Cl(1)	2.4273(8)	S(1)–Cu(1)–N(1)	151.68(7)
Cu(1)–N(1)	2.014(2)	S(1)–Cu(1)–N(4)	80.93(6)
Cu(1)–N(4)	2.022(2)	Cl(1)–Cu(1)–Cl(2)	109.10(3)
N(3)–N(4)	1.272(3)	N(1)–Cu(1)–N(4)	77.88(9)
C(1)–N(4)	1.404(3)	N(1)–Cu(1)–Cl(1)	98.65(7)
C(8)–N(3)	1.374(3)	N(1)–Cu(1)–Cl(2)	99.07(7)
		N(4)–Cu(1)–Cl(1)	86.67(6)
		N(4)–Cu(1)–Cl(2)	164.23(6)

elongated (Cu(1)–N(4), 2.022(2) Å) compared to Cu–N(imidazole) (Cu(1)–N(1), 2.014(2) Å). This is contrary to the data previously reported for Cu(II)–azoimidazole complexes [23] in which N(imidazole) prefers Cu(II) to interact in stronger way than the N(azo) center. The presence of a third donor center, –SEt, may force N(azo) to chelate with Cu(II), which may be responsible for the squeezing of the Cu–N(azo) distance. The Cu–S bond distance [2.3788(8) Å] lies at the left side of the reported range of 2.3–2.8 Å [12,13,35,36]. There are two forces operating to make Cu–N(azo) a strong bond: the softening of Cu(II) on coordination to thioether–S and the structural demand of the tridentate N,N′,S system. Two chelate planes [Cu(1), S(1), C(1), C(2), N(4), deviation ⩽0.1 Å; Cu(1), N(1), C(8), N(3), N(4), mean deviation ⩽0.03 Å] are no longer planar and make a dihedral angle of 14.41(8)°. The azoimine chelated motif -Cu(-N=N-C=N-) forms a better plane than the thioazo chelating -Cu(-S -C=C -N-) unit. The large size of thioether–S may be the reason for the distortion.

2.4. Electrochemistry

The cyclic voltammogram shows a reductive response at ca. 0.2 V versus Ag/AgCl along with two couples at the negative side (Table 1 and Fig. 2). The free ligand does not show any oxidation but irreversible reductive responses appear at <−1.0 V. On comparing with the CV of Cu(RaaiR′)$_2X_2$ (X = N_3, NCS) [23], the quasireversible response at 0.2 V ($\Delta E_P > 100$ mV) may be ascribed to a Cu(II)/Cu(I) response. On traversing to the negative direction at a potential <−0.6 V, the scan reversal shows upsurge of current at av. −0.3 V followed by a Cu(II)/Cu(I) couple at av. 0.2 V. The desorption spike reflects deposition of Cu metal on the working electrode surface after reduction to copper(0). A clear Cu(I)/Cu(0) couple is not observed. To get a true picture the sweep of the CV has been started from 0.4 V in the negative direction up to −1.6 V. The reduction of Cu(II) → Cu(I) is observed at about 0.1 V and ligand reductions below −0.5 V. On scan reversal anodic peaks of the respective reductions appear at the usual positions in addition to a sharp anodic current upsurge at −0.3 V. The peak-to-peak separation of the redox couple is largely dependent on the scan rate and increases from 120 mV at 10 mV s^{-1} to 600 mV at 1000 mV s^{-1}. At slow scan rates (10–50 mV s^{-1}) ΔE_P remains almost constant as do the E_{Pa} and the E_{Pc} values. This observation suggests a low heterogeneous electron-transfer rate constant, which has been influenced by the applied potential [38]. Two quasireversible couples at −0.8 and −1.3 V are the description of [-N= N-] / [- N $\dot{-}\dot{-}$ N-] $^-$ and [-N $\dot{-}\dot{-}$ N-] $^-$ / [-N-N-] $^{=}$, respectively (Table 1).

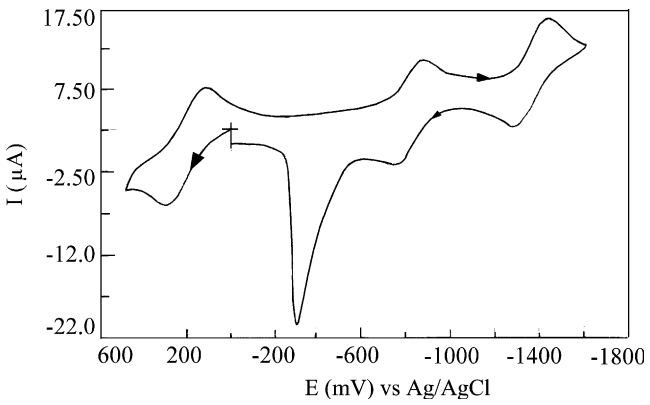

Fig. 2. Cyclic voltammogram of [Cu(SMeaaiNEt)Cl_2] in MeCN.

2.5. EPR studies

Polycrystalline spectra of Cu(SRaaiNR′)Cl_2 (**5**, **6**) at room temperature (298 K) are weakly resolved. The low resolution of the polycrystalline spectra is usual where copper centers are relatively close together, the hyperfine splitting is poor due to paramagnetic charge narrowing. However, the resolution is better in the solution, therefore the spectra (77 K) were used to determine the EPR parameters. The EPR spectra of Cu(II) complexes provide information about hyperfine and super-hyperfine structures which helps in defining the geometry and distortion of the complexes. The parallel region of the spectra is somewhat complicated compared to a single copper system and may be due to the presence of structurally different species. This means, at least in solution phase, Cu(II) may exist in geometrically different environments. The following possibilities may be considered: the existence of square pyramidal and trigonal bipyramidal geometries of Cu(NNS)Cl_2 or partial dissociation of Cl^- from the complex in MeOH forming solvento species. The conductance measurement in MeOH does not show any significant increment in molar conductivity (Λ_M = 7–9 Ω^{-1} mol^{-1}). Besides, trigonal bipyramidal Cu(II) centers give very characteristic 'inverse' EPR spectra, and no such inverse signal is present in Fig. 3. Therefore, the presence of a trigonal bipyramidal geometrical isomer of Cu(NNS)Cl_2 has been precluded. This contradiction may be explained by considering the presence of a solvated intimate ion-pair in the strongly interacting solvent MeOH, giving a mixture of different tetragonal Cu(II) species [Cu(NNS)Cl(MeOH)$^+ \cdot Cl^-$]. Mononuclear complexes show the usual four line (^{63}Cu, I = 3/2) EPR spectra and are anisotropic at higher magnetic field. The peaks of low

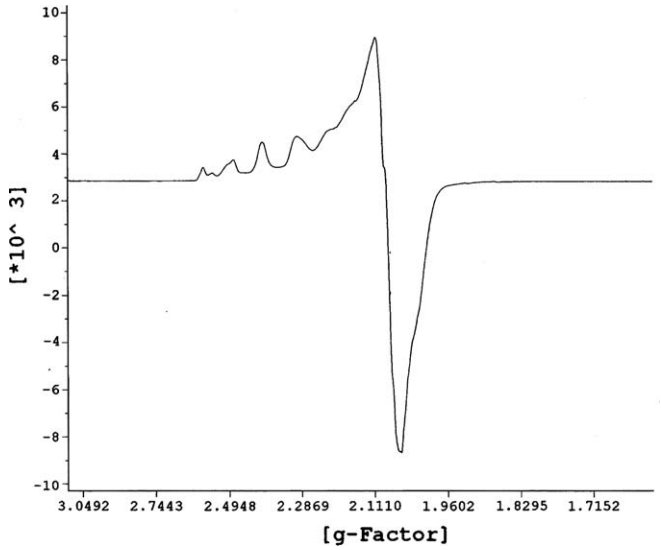

Fig. 3. EPR spectrum of Cu(SMeaaiNEt)Cl_2 (**5b**) in MeOH at 77 K.

intensity in the weaker field are considered to originate from the $g_{\|}$ component and $A_{\|}$ lies in the range 155–175 × 10^{-4} cm^{-1}. The calculated $g_{\|}$ and $g_{\perp}$ values for these complexes were 2.2–2.4 and 2.0–2.1, respectively. The relation $g_{\|} > g_{\perp} > 2.0023$ agrees with the ground state configuration of $d_{x^2-y^2}$. The super-hyperfine coupling constant $A_{\perp}$ averages to 16×10^{-4} cm^{-1} and is in the range for a Cu–N interaction [23]. For CuN_2 coordination there will be (2 × 2 + 1), 5 responses and they are observed, indeed (Fig. 3).

2.6. Ternary complexes: [Cu(NN′S)(NN/N,N′)](ClO$_4$)$_2$

To a CH_2Cl_2 solution of **5a** (**6b**) a methanolic solution of α-diimine (N,N; 2,2′-bipyridine (bpy) or 1,10-phenanthroline (phen)) was added and stirred for 2 h in air. An aqueous solution of $NaClO_4$ (saturated) was added to form a dark colored crystalline product of the composition [Cu(NN′S)(N,N)]$(ClO_4)_2$(N,N = bpy (**7**), phen (**8**))

$$Cu(NN'S)Cl_2 + N,N + 2NaClO_4 \Rightarrow [Cu(NN'S)(NN)](ClO_4)_2 + 2NaCl \quad (1)$$

Shining crystals were separated by slow diffusion of CH_2Cl_2 solution into hexane. However, these crystals were not of good enough quality to diffract X-rays for structural analysis. The characterization has been done by other physicochemical techniques. The complexes are 1:2 electrolytes in MeCN (Λ_M = 160–175 Ω^{-1} mol^{-1} cm^2). The bulk magnetic moment shows one electron paramagnetism (1.8–1.9 B.M.). The microanalytical data support the composition. Different isomers may be present and we could not separate them. The properties presented herein thus are referred to the isomer present in the compound.

Infrared spectra show a strong intense unstructured $\nu(ClO_4)$ at 1090 cm^{-1} along with a weak stretch at 625 cm^{-1}. The ν(N=N) and ν(C=N) appear at 1410–1420 and 1575–1590 cm^{-1}, respectively. The UV–Vis spectra of the complexes in CH_2Cl_2 exhibit high intense structured transitions within the wavelength range 600–250 nm along with a weak broad band >700 nm. The intraligand charge transfer transitions appear at 400–370, 300–310 and 260–270 nm, and are said to be associated with chelated diimine and azoimine functions. The intense band ($\varepsilon \sim 10^4$ mol^{-1} cm^{-1}) observed at 525–520 and 470–450 nm may be ascribed to d(Cu) → π* (azoimi/diimine), MLCT transition. The S(σ) → dπ(Cu), LMCT band has been significantly influenced by the coligands and is shifted to longer wavelength.

Cyclic voltammetry shows a reductive response at ca. 0.3 V versus Ag/AgCl along with three reductive responses at the negative side (Table 1). On comparing with the CV of Cu(NN′S)Cl_2 we may conclude that the couple is due to Cu(II)/Cu(I). Because of the better π-acidity of diimines (bpy/phen) than $2Cl^-$ the redox couple is shifted to the more positive side. Three quasireversible couples at −0.6, −0.9 and −1.3 V are the description of electron accommodation in the chelated ligands.

The complexes show four line (^{63}Cu, I = 3/2) EPR spectra and are anisotropic at higher magnetic field. The $g_{\|}$ and $g_{\perp}$ values for these complexes are 2.2–2.3 and 2.0–2.1, respectively. The relation $g_{\|} > g_{\perp} > 2.0023$ agrees with the ground state configuration of $d_{x^2-y^2}$. The $A_{\|}$ value lies in the range 160–175 × 10^{-4} cm^{-1}.

3. Experimental

3.1. Materials

$CuCl_2 \cdot 2H_2O$, *o*-(amino)thiophenol, methyl iodide (MeI), ethyl iodide (EtI), 2,2′-bipyridine (bpy), 1,10-phenanthroline (phen) were purchased from E. Marck. *o*-(Thioalkyl)-phenyldiazonium chloride was synthesized by the reported procedure [24]. Solvents were used after drying.

3.2. Measurements

Microanalyses (C, H, N) were performed using a Perkin–Elmer 2400 CHNO/S elemental analyzer. Spectroscopic measurements were carried out using the following instruments: UV–Vis spectra, reflectance spectra, JASCO UV–Vis/NIR model V-570; IR spectra (KBr disk, 4000–200 cm^{-1}), JASCO FT-IR model 420. Room temperature magnetic moments were measured using a vibrating sample 155 magnetometer at 298 K. Molar conductances (Λ_M) were measured in a Systronics conductivity meter 304 model using ca. 10^{-3} M solutions in MeCN. Electrochemical measurements were carried out with the use of a computer controlled EG&G PARC VersaStat model 250 Electrochemical instrument using a Pt-disk working electrode. The solution was IR compensated and the results were collected at 298 K. The reported results are referenced to Ag/AgCl in acetonitrile and are uncorrected for junction potential in the range +1.6 to −1.6 V. EPR spectra were measured in MeCN solution at room temperature

(298 K) and liquid nitrogen temperature (77 K) using a Bruker EPR spectrometer model EMX 10/12, X-band ER 4119 HS cylindrical resonator.

3.3. Synthesis of the ligands (SRaaiNR′)

The syntheses of the ligands were carried out following the common procedure of coupling different *o*-(thioalkyl)-phenyldiazonium ions (obtained by diazotization of *o*-(thioalkyl)aniline) with imidazole at pH 7. The procedure for the synthesis of 2-[*o*-(thiomethyl)phenylazo] (SMeaaiNH, **2a**) imidazole is as follows.

To a HCl solution (10 ml, 2 M) of *o*-(thiomethyl)aniline (1 g, 7.19 mmol), $NaNO_2$ solution (0.55 g, 7.97 mmol in 10 ml water) was added dropwise under cold conditions (cooling on an ice-salt bath, maintaining the temperature 0–5 °C). The yellow suspension thus formed was filtered through glass wool to remove tarry matter. Imidazole (0.6 g, 8.8 mmol) was dissolved in Na_2CO_3 (1.5 g in 20 ml water) solution and the diazotized solution was added in dropwise under cold conditions, and stirred with a glass rod. The initial red coloration was the indication of the diazocoupling reaction. The mixture was then kept in refrigerator for 1 h and neutralized with 2 M HCl, an orange-brown precipitate was separated. It was then filtered and dried under suction. The dry mass was redissolved in a minimum volume of 2 M HCl (volume not to exceed 20 ml) and filtered. The brown residue was rejected. The orange solution was then neutralized by adding pinch-wise finely powdered Na_2CO_3. The orange-red precipitate was filtered and dried. Yield: 0.58 g, 37%; m.p. 135 °C. UV–Vis (MeOH), λ nm (ε, $M^{-1}\,cm^{-1}$): 460 (4800) sh; 400 (7520) sh; 354 (14240); 263 (10380); 249 (9585). ^1H NMR ($CDCl_3$) (300 MHz) δ, ppm (*J*, Hz): 4-H, 7.28 bs; 5-H, 7.10 bs; 8-H, 7.25 (8.0) d; 9-H, 7.37 m; 10-H, 7.37 m; 11-H, 7.90 (8.0) d; N(1)-H, 10.30 bs; S-CH_3, 2.44.

SEtaaiNH (**2b**) was also prepared by a similar procedure with a yield of 44%; m.p. 139 °C. UV–Vis (MeOH), λ nm (ε, $M^{-1}\,cm^{-1}$): 461 (3768) sh; 403 (7976), 353 (14955); 263 (11606); 250 (10575). ^1H NMR ($CDCl_3$) (300 MHz) δ, ppm (*J*, Hz): 4-H, 7.27 bs; 5-H, 7.10 bs; 8-H, 7.23 (8.0) d; 9-H, 7.35 m; 10-H, 7.35 m; 11-H, 7.90 (8.0) d; N(1)-H, 10.30 bs; S-CH_2, 4.44 (9.0) q; (S-CH_2)-CH_3 1.54 (8.0) t [sh = shoulder; b = broad; bs = broad singlet; d = doublet; t = triplet; q = quartet; m = multiplet].

3.4. Alkylation of 2-[o-(thiomethyl)phenylazo]imidazole. Synthesis of 1-methyl-2-[o-(thiomethyl)phenylazo] imidazole (SMeaaiNMe) (**3a**)

To a dry THF solution (25 ml) of 2-[*o*-(thiomethyl) phenylazo]imidazole (0.8 g, 3.7 mmol) NaH (50% paraffin) (0.2 g) was added in small portions and stirred under cold conditions for 0.5 h. Methyl iodide (0.7 g, 4.9 mmol) was added slowly over a period of 30 min and then reaction mixture was warmed to 70 °C for an additional 1 h. The solution was evaporated, extracted with $CHCl_3$ (3 × 10 ml), washed with 15% NaOH (4 × 10 ml) and finally with distilled water (3 × 20 ml). It was chromatographed over silica gel prepared in petroleum ether (60–80 °C fraction) and the desired compound was eluted by toluene–acetonitrile (5:1 v/v). An orange-red gummy mass was separated by evaporation in vacuo (Yield: 0.35 g, 41%).

The other ligands were prepared by an identical procedure. The yield was 30–50%. The ligands are abbreviated SRaaiNR′: 1-methyl-2-[(*o*-thiomethyl)phenylazo]imidazole (SMeaaiNMe), **3a**, gum. UV–Vis (MeOH), λ nm (ε, $M^{-1}\,cm^{-1}$): 450 (3850) sh; 410 (7000) sh, 353 (12450); 260 (11150); 247 (10300). ^1H NMR ($CDCl_3$) (300 MHz) δ, ppm (*J*, Hz): 4-H, 7.25 bs; 5-H, 7.05 bs; 8-H, 7.22 (8.0) d; 9-H, 7.35 m; 10-H, 7.35 m; 11-H, 7.86 (8.0) d; 1-CH_3, 4.04 s; S-CH_3, 2.42; 1-ethyl-2-[(*o*-thiomethyl)phenylazo]imidazole (SMeaaiNEt), **3b**, gum. UV–Vis (MeOH), λ nm (ε, $M^{-1}\,cm^{-1}$): 454 (4050) sh; 405 (5565) sh, 350 (10400); 260 (9540); 250 (7500). ^1H NMR ($CDCl_3$) (300 MHz) δ, ppm (*J*, Hz): 4-H, 7.25 bs; 5-H, 7.08 bs; 8-H, 7.23 (8.0) d; 9-H, 7.40 m; 10-H, 7.40 m; 11-H, 7.85 (8.0) d; 1-CH_2, 4.50 (9.0), q; (1-CH_2)-CH_3, 1.53 (8.0) t; S-CH_3, 2.49; 1-methyl-2-[(*o*-thioethyl)phenylazo]imidazole (SEtaaiNMe), **4a**, gum. UV–Vis (MeOH), λ nm (ε, $M^{-1}\,cm^{-1}$): 455 (4205) sh; 400 (5840) sh, 350 (10580); 260 (9865); 250 (7525). ^1H NMR ($CDCl_3$) (300 MHz) δ, ppm (*J*, Hz): 4-H, 7.27 bs; 5-H, 7.07 bs; 8-H, 7.18 (8.0) d; 9-H, 7.33 m; 10-H, 7.33 m; 11-H, 7.81 (8.0) d; 1-CH_3, 4.01 s; S-CH_2, 2.97 (8.0) q, (S-CH_2)-CH_3, 1.36 (8.0), t; 1-ethyl-2-[(*o*-thioethyl)phenylazo]imidazole (SEtaaiNEt), **4b**, gum. UV–Vis (MeOH), λ nm (ε, $M^{-1}\,cm^{-1}$): 452 (4157) sh; 412 (5947) sh, 352 (11654); 263 (10188); 250 (8450). ^1H NMR ($CDCl_3$) (300 MHz) δ, ppm (*J*, Hz): 4-H, 7.29 bs; 5-H, 7.11 bs; 8-H, 7.18 (8.0) d; 9-H, 7.32 m; 10-H, 7.32 m; 11-H, 7.80 (8.0) d; 1-CH_2, 4.46 (9.0), q; (1-CH_2)-CH_3, 1.48 (8.0), t; S-CH_2, 3.00 (9.0), q; (S-CH_2)-CH_3, 1.33 (8.0), t [sh = shoulder; bs = broad singlet; d = doublet; t = triplet; m = multiplet; q = quartet; s = singlet].

3.5. Synthesis of the complexes

3.5.1. Cu(SMeaaiNMe)Cl_2 (**5a**)

1-Methyl-2-[*o*-(thiomethyl)phenylazo]imidazole (SMeaaiNMe) (0.2 g, 0.86 mmol) in methanol (10 ml) was added dropwise to a methanolic solution (10 ml) of $CuCl_2 \cdot 2H_2O$ (0.15 g, 0.88 mmol) at 298 K. The greenish brown solution was stirred for 10 min. It was then filtered and left undisturbed for a week. A dark brown crystalline compound separated. The crystals were filtered, washed with water, cold methanol and dried in vacuo. Yield was 0.21 g (66%).

All complexes were prepared by the same procedure. The yield varied from 60% to 75% and microanalytical data of the complexes are as follows: Cu(SMeaaiNMe)Cl_2 (**5a**), *Anal.* Calc. for $C_{11}H_{12}N_4SCl_2Cu$: C, 36.02; H, 3.27; N, 15.28; Cu, 17.32. Found: C, 35.94; H, 3.21; N, 15.22; Cu, 17.26%. Cu(SMeaaiNEt)Cl_2 (**5b**), *Anal.* Calc. for $C_{12}H_{14}N_4SCl_2Cu$: C, 37.80; H, 3.68; N, 14.72; Cu, 16.69. Found: C, 37.74; H, 3.62; N, 14.64; Cu, 16.58%. Cu(SEtaaiNMe)Cl_2 (**6a**), *Anal.*

Calc. for $C_{11}H_{12}N_4SCl_2Cu$: C, 37.80; H, 3.68; N, 14.72; Cu, 16.69. Found: C, 37.76; H, 3.62; N, 14.65; Cu, 16.60%. Cu(SEtaaiNEt)Cl_2 (**6b**), *Anal*. Calc. for $C_{13}H_{16}N_4SCl_2Cu$: C, 39.54; H, 4.06; N, 14.19; Cu, 16.09. Found: C, 39.48; H, 4.01; N, 14.08; Cu, 16.02%.

3.5.2. [Cu(SMeaaiNMe)(bpy)](ClO$_4$)$_2$ · H$_2$O (7)

To a CH_2Cl_2 solution (10 ml) of Cu(SMeaaiNMe)Cl_2 (0.15 g, 0.41 mmol) a methanolic solution (10 ml) of 2,2′-bipyridine (0.064 g, 0.41 mmol) was added and stirred for 3 h. The solution color turned from brown red to deep brown. It was then evaporated in air to reduce to its volume to 10 ml. A solution of $NaClO_4$ (2 ml saturated solution) was added to the methanolic suspension of the mixture and a deep brown mass immediately separated. It was filtered, washed with methanol and dried in vacuo. Slow diffusion of a CH_2Cl_2 solution of the dry mass into hexane separated shining crystals after a week. Yield was 0.198 (71%) and other yields varied from 70% to 75%. The microanalytical data of the complexes are as follows: [Cu(SMeaaiNMe)(bpy)](ClO$_4$)$_2$ · H$_2$O (**7**), *Anal*. Calc. for $C_{21}H_{22}N_6O_9SCl_2Cu$: C, 37.69; H, 3.29; N, 12.56; Cu, 9.49. Found: C, 37.58; H, 3.24; N, 12.47; Cu, 9.42%. [Cu(SMeaaiNMe)(phen)](ClO$_4$)$_2$ · H$_2$O (**8**), *Anal*. Calc. for $C_{23}H_{22}N_6O_9SCl_2Cu$: C, 39.85; H, 3.17; N, 12.13; Cu, 9.17. Found: C, 39.78; H, 3.09; N, 12.06; Cu, 9.11%. [Cu(SEtaaiNEt)(bpy)](ClO$_4$)$_2$ · H$_2$O (**9**), *Anal*. Calc. for $C_{23}H_{26}N_6O_9SCl_2Cu$: C, 39.63; H, 3.73; N, 12.06; Cu, 9.12. Found: C, 39.58; H, 3.68; N, 12.37; Cu, 9.24%. [Cu(SEtaaiNEt)(phen)](ClO$_4$)$_2$ · H$_2$O (**10**), *Anal*. Calc. for $C_{25}H_{26}N_6O_9SCl_2Cu$: C, 41.64; H, 3.33; N, 11.66; Cu, 8.81. Found: C, 41.57; H, 3.29; N, 11.75; Cu, 8.75%.

3.6. X-ray crystal structure analysis of [Cu(SEtaaiEt)Cl$_2$] (**6b**)

Data were collected with a Siemens SMART CCD diffractometer using graphite-monochromatized Mo Kα radiation ($\lambda = 0.71073$ Å) at 295(2) K. Unit cell parameters were determined from least-squares refinement of setting angles with 2θ in the range $3.8 \leqslant 2\theta \leqslant 56.6°$. Total data collected were 10661 out of which unique data were 3122. The hkl range was $-13 \leqslant h \leqslant 14$, $-19 \leqslant k \leqslant 17$, $-12 \leqslant l \leqslant 13$. A summary of the crystallographic data and structure refinement parameters are given in Table 3. Reflection data were recorded using the ω scan technique. Data were corrected for Lorentz polarization effects and for linear decay. Semi-empirical absorption corrections based on ψ-scans were applied. The structure was solved by heavy atom methods using SHELXS-97 and successive difference Fourier syntheses. All non-hydrogen atoms were refined anisotropically. The hydrogen atoms were fixed geometrically and refined using the riding model. In the final difference Fourier map the residual minima and maxima were [−0.27, 0.37 (e/Å^3) for] carried out using SHELXL-97.

Table 3
Summarized crystallographic data for [Cu(SEtaaiNEt)Cl_2] (**6b**)

	[Cu(SEtaaiNEt)Cl_2]
Empirical formula	$C_{13}H_{16}CuN_4SCl_2$
Formula weight	394.80
Temperature (K)	295(2)
Crystal system	monoclinic
Space group	$P2_1/c$
Crystal size (mm^3)	$0.15 \times 0.20 \times 0.22$
Unit cell dimensions	
a (Å)	10.7182(8)
b (Å)	14.4376(10)
c (Å)	10.7181(8)
β(°)	96.3(6)
V (Å^3)	1648.4(2)
Z	4
λ (Å)	0.71073
μ (Mo Kα) (mm^{-1})	1.773
D_{calc} (mg m^{-3})	1.591
Refine parameters	190
Reflection collected	10661
Unique data [$I > 2\sigma(I)$]	3122
R_1[a] [$I > 2\sigma(I)$]	0.0504
wR_2[b]	0.0869
Goodness-of-fit	1.137

[a] $R_1 = \sum|F_o - F_c|/\sum F_o$.
[b] $wR_2 = [\sum w(F_o^2 - F_c^2)/\sum wF_o^4]^{1/2}$, $w = 1/[\sigma^2(F^2) + (0.0416P)^2 + (0.2219P)]$.

4. Supplementary material

Crystallographic data for the structures have been deposited with the Cambridge Crystallographic data center, CCDC No. 266497. Copies of this information may be obtained free of charge from the Director, CCDC, 12 Union Road, Cambridge CB2 1EZ, UK (e-mail: deposit@ccdc.cam.ac.uk or http://www.ccdc.cam.ac.uk).

Acknowledgments

Financial support from Jadavpur University Research Grant and the Council of Scientific and Industrial Research, New Delhi are gratefully acknowledged.

References

[1] F.A. Cotton, G. Wilkinson, Advanced Inorganic Chemistry, 3rd ed., Wiley Eastern Ltd., New Delhi, 1978.
[2] G. Wilkinson, J.A. McCleverty (Eds.), Comprehensive Coordination Chemistry, vol. 5, Pergamon Press, Oxford, 1987, p. 775.
[3] J.E. Huheey, Inorganic Chemistry, 3rd ed., Harper International SI Edn, London, 1983.
[4] E.I. Solomon, in: K.D. Karlin, J. Zubieta (Eds.), Copper Coordination Chemistry: Biochemical and Inorganic Perspectives, Adenine, Guilderland, NY, 1983, p. 1.
[5] D.A. Robb, in: R. Lontie (Ed.), Copper Proteins and Copper Enzymes, vol. 2, CRC Press, Boca Raton, FL, 1984, pp. 207–241.
[6] K.D. Karlin, Z. Tyeklar, Bioinorganic Chemistry of Copper, Chapmann & Hall, New York, 1993.
[7] W. Kaim, B. Schwederski, Bioinorganic Chemistry: Inorganic Elements in the Chemistry of Life, Wiley, Chichester, New York, Brisbane, Toronto, Singapore, 1994, p. 22, 196.
[8] K. Krylova, C.P. Kulatilleke, M.J. Heeg, C.A. Salhi, L.A. Ochrymowycz, D.B. Rorabacher, Inorg. Chem. 38 (1999) 4322.

[9] M. Albrecht, K. Hubler, S. Zalis, W. Kaim, Inorg. Chem. 39 (2000) 4731.
[10] S. Chen, J.F. Richardson, R.M. Buchanan, Inorg. Chem. 33 (1994) 2376.
[11] U. Sivagnanam, M. Palaniandavar, J. Chem. Soc., Dalton Trans. (1994) 2277.
[12] P. Nagle, E. O'Sullivan, B.J. Hathaway, E. Muller, J. Chem. Soc., Dalton Trans. (1990) 3399.
[13] P.M. Bush, J.P. Whitehead, C.C. Pink, E.C. Gramm, J.L. Eglin, S.P. Watton, L.E. Pence, Inorg. Chem. 40 (2001) 1871, and references therein.
[14] H.-Y. Mao, X.-Q. Shen, G. Li, H.-Y. Zhang, C. Xu, H.-L. Liu, E.-B. Wang, Q.-A. Wu, H.-W. Hou, Y. Zhu, Polyhedron 23 (2004) 1961, and references therein.
[15] S.A. Leaver, M. Palaniandavar, C.A. Kilner, M.A. Halcrow, J. Chem. Soc., Dalton Trans. (2003) 4224.
[16] S. Dhar, P.A. Reddy, M. Nethaji, S. Mahadevan, M.K. Saha, A.R. Chakravorty, Inorg. Chem. 41 (2002) 3469.
[17] D. Sigman, T.W. Bruice, A. Majumdar, C.L. Sulton, Acc. Chem. Res. 26 (1993) 98.
[18] D.S. Sigman, A. Majumder, D.M. Perrin, Chem. Rev. 93 (1993) 2295.
[19] S. Torelli, C. Belle, C. Philouze, J.-L. Pierre, W. Rammal, E. Saint-Aman, Eur. J. Inorg. Chem. (2003) 2452.
[20] T.K. Misra, D. Das, C. Sinha, Polyhedron 16 (1997) 4163.
[21] T.K. Misra, D. Das, C. Sinha, Indian J. Chem. 37A (1998) 741.
[22] T.K. Misra, P.K. Santra, C. Sinha, Proc. Indian Acad. Sci. 110 (1998) 445.
[23] U.S. Ray, D. Banerjee, G. Mostafa, T.-H. Lu, C. Sinha, New J. Chem. 28 (2004) 1432, and references therein.
[24] U.S. Ray, B.G. Chand, G. Mostafa, J. Cheng, T.-H. Lu, C. Sinha, Polyhedron 22 (2003) 2587.
[25] D. Banerjee, U.S. Ray, J.-C. Liou, C.-N. Lin, T.-H. Lu, C. Sinha, Inorg. Chim. Acta 358 (2005) 1019.
[26] J. Dinda, P.K. Santra, C. Sinha, L.R. Falvello, J. Organomet. Chem. 629 (2001) 28.
[27] S. Pal, D. Das, C. Sinha, C.H.L. Kennard, Inorg. Chim. Acta 313 (2001) 21.
[28] Sk. Jasimuddin, P. Byabartta, G. Mostafa, T.-H. Lu, C. Sinha, Polyhedron 23 (2004) 727.
[29] P. Byabartta, Sk. Jasimuddin, G. Mostafa, T.-H. Lu, C. Sinha, Polyhedron 22 (2003) 849.
[30] Sk. Jasimuddin, G. Mostafa, C. Sinha, Inorg. Chim. Acta 357 (2004) 1975.
[31] B.G. Chand, U.S. Ray, J. Cheng, T.-H. Lu, C. Sinha, Inorg. Chim. Acta 358 (2005) 1927.
[32] B.G. Chand, U.S. Ray, G. Mostafa, T.-H. Lu, C. Sinha, J. Coord. Chem. 57 (2004) 627.
[33] B.G. Chand, U.S. Ray, G. Mostafa, T.-H. Lu, C. Sinha, Polyhedron 23 (2004) 1669.
[34] C. Sinha, Polyhedron 12 (1993) 2363.
[35] P.K. Dhara, S. Pramanik, T.-H. Lu, M.G.B. Drew, P. Chattopadhyay, Polyhedron 23 (2004) 2457.
[36] B. Adhikari, C.R. Lucas, Inorg. Chem. 33 (1994) 1376.
[37] A.B.P. Lever, Inorganic Electronic Spectroscopy, Elsevier, Amsterdam, 1984.
[38] E.A. Ambundo, M.-V. Deydier, A.J. Grall, N. Aguera-Vega, L.T. Dressel, T.H. Cooper, M.J. Heeg, L.A. Ochrymowycz, D.B. Rorabacher, Inorg. Chem. 38 (1999) 4233.

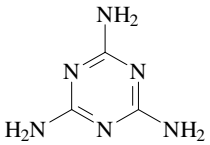

MA

2. Experimental

2.1. General procedures

All manipulations were carried out under dry, oxygen-free nitrogen by using Schlenk techniques, unless otherwise noted. Solvents were dried and deoxygenated by refluxing over the appropriate reagents before use. Diethyl ether was purified by distillation from sodium/benzophenone, and methanol from Mg/I_2. The Visible absorption spectra were recorded on a Hitachi U-2000 spectrophotometer. IR spectra were obtained from a Jasco FT/IR-460 plus spectrometer. Elemental analyses were obtained from a PE 2400 series II CHNS/O analyzer.

2.2. Materials

The reagents $CuCl_2 \cdot 2H_2O$, $Cu(OAc)_2 \cdot H_2O$ and melamine were purchased from Aldrich Chemical Co.

2.3. Preparation of the $Cu_2Cl_2(\mu\text{-}Cl)(CH_3OH)_2(\mu\text{-}OCH_3)(MA)_2$ (1)

$CuCl_2 \cdot 2H_2O$ (0.34 g, 2.00 mmol) was added to a CH_3OH solution (10 ml) containing melamine (0.25 g, 1.98 mmol). The mixture was heated to reflux for 3 h until some green-yellow solid began to precipitate. The mixture was then allowed to stir for 1 h at room temperature *T*. The solid was filtered out, washed with diethyl ether (2×10 ml) and dried under vacuum to give a green-yellow powder. Yield: 0.41 g (73%). UV–Vis (MeOH): 385 nm. *Anal.* Calc. for $C_9H_{23}Cl_3Cu_2N_{12}O_3$ (MW = 580.81): C, 18.61; H, 3.99; N, 28.94. Found: C, 18.96; H, 4.11; N, 28.77%. IR (KBr disk): 3350(m), 3150(s), 2405(s), 1718(w), 1521(m), 1498(s), 1442(w), 1040(m), 792(m), 683(m), 562(w).

2.4. Preparation of $[Cu(\eta^1\text{-}OAc)(\mu\text{-}OCH_3)(MA)]_2$ (2)

$Cu(OAc)_2 \cdot H_2O$ (0.40 g, 2.00 mmol) was added to a MeOH solution (20 ml) containing melamine (0.25 g, 1.98 mmol). The mixture was refluxed for 3 h to afford a blue solution and a blue solid. The precipitate was filtered and washed by ether (3×10 ml) and then dried under reduced pressure to give a blue solid. Yield: 0.52 g (86%). UV–Vis (MeOH): 382 nm. *Anal.* Calc. for $C_{12}H_{24}Cu_2N_{12}O_6$ (MW = 559.49): C, 25.76; H, 4.32; N, 30.04. Found: C, 25.46; H, 3.99; N, 29.88%. IR (KBr disk): 3352(s),

Table 1
Crystal data for complexes **1** and **2**

Compound	**1**	**2**
Formula	$C_{17}H_{43}Cl_3Cu_2N_{12}O_5$	$C_{12}H_{24.67}Cu_2N_{12}O_{6.33}$
Formula weight	729.06	565.52
Crystal system	orthorhombic	monoclinic
Space group	$Pna2_1$	$R\bar{3}$
a (Å)	15.3006(16)	23.2971(14)
b (Å)	13.993(2)	23.2971(14)
c (Å)	15.0662(17)	11.1490(11)
V (Å^3)	3225.7(7)	5240.5(7)
Z	4	9
D_{calc} (g/cm^3)	1.501	1.613
$F(000)$	1512	2604
Crystal size (mm)	$0.2 \times 0.3 \times 0.3$	$0.1 \times 0.2 \times 0.5$
μ(Mo Kα) (mm^{-1})	1.614	1.881
Data collection instrument	Bruker AXS P4	Bruker AXS P4
Radiation monochromated in incident beam (λ(Mo Kα), Å)	0.71073	0.71073
Range (2θ) for data collection (°)	$3.94 \leqslant 2\theta \leqslant 49.98$	$4.18 \leqslant 2\theta \leqslant 49.98$
Temperature (°C)	22	22
Limiting indices	$-1 \leqslant h \leqslant 18$, $-1 \leqslant k \leqslant 13$,$-1 \leqslant l \leqslant 17$	$-1 \leqslant h \leqslant 25$, $-27 \leqslant k \leqslant 1$, $-13 \leqslant l \leqslant 1$
Reflections collected	3485	2556
Independent reflections [R_{int}]	2967 [0.0422]	1994 [0.0224]
Refinement method	full-matrix least-squares on F^2	full-matrix least-squares on F^2
Data/restraints/parameters	2967/1/360	1994/0/183
Quality-of-fit indicator[c]	1.228	1.016
Final R indices [$I > 2\sigma(I)$][a,b]	$R_1 = 0.0719$, $wR_2 = 0.1356$	$R_1 = 0.0363$, $wR_2 = 0.0939$
R indices (all data)	$R_1 = 0.1429$, $wR_2 = 0.1654$	$R_1 = 0.0502$, $wR_2 = 0.1012$
Largest difference in peak and hole (e/Å^3)	0.923 and −0.604	0.572 and −0.368

[a] $R_1 = \sum||F_o| - |F_c||/\sum|F_o|$.

[b] $wR_2 = [\sum w(F_o^2 - F_c^2)^2/\sum w(F_o^2)^2]^{1/2}$. $w = 1/[\sigma^2(F_o^2) + (ap)^2 + (bp)]$, $p = [\max(F_o^2 \text{ or } 0) + 2(F_c^2)]/3$. $a = 0.0607$, $b = 0.1427$ for **1**; $a = 0.0244$, $b = 0.0385$ for **2**.

[c] Quality-of-fit = $[\sum w(|F_o^2| - |F_c^2|)^2/N_{observed} - N_{parameters}]^{1/2}$.

3159(s), 1742(s), 1570(s), 1442(s), 1041(s), 810(m), 679(w) , 563(w).

3. X-ray crystallography

The diffraction data for complexes **1** and **2** were collected at 22 °C on a Bruker AXS P4 diffractometer, which was equipped with a graphite-monochromated Mo Kα ($\lambda_\alpha = 0.71073$ Å) radiation. Data reduction was carried by standard methods with use of well-established computational procedures [10]. A suitable crystal of **1** was mounted on the top of a glass fiber with epoxy cement. The hemisphere data collection method was used to scan the data points at $3.94 < 2\theta < 49.98°$. The structure factors were obtained after Lorentz and polarization correction. The positions of some of the heavier atoms, including the copper atom, were located by the direct method. The remaining atoms were found in a series of alternating difference Fourier maps and least-square refinements [11]. The crystallographic procedures for **2** were similar to those for **1**. The hydrogen atoms for **1** were added by using the HADD program in SHELXTL 5.10, while those for **2** were found in a series of alternating difference Fourier maps and least-square refinements. The final residuals of the final refinement were $R_1 = 0.0719$, $wR_2 = 0.1356$. Basic information pertaining to crystal parameters and structure refinement is summarized in Table 1.

4. Results and discussion

4.1. Synthesis

The complexes $Cu_2Cl_2(\mu\text{-}Cl)(CH_3OH)_2(\mu\text{-}OCH_3)\text{-}(MA)_2 \cdot 2Et_2O$ (MA = melamine), **1**, and [Cu(η¹-OAc)-

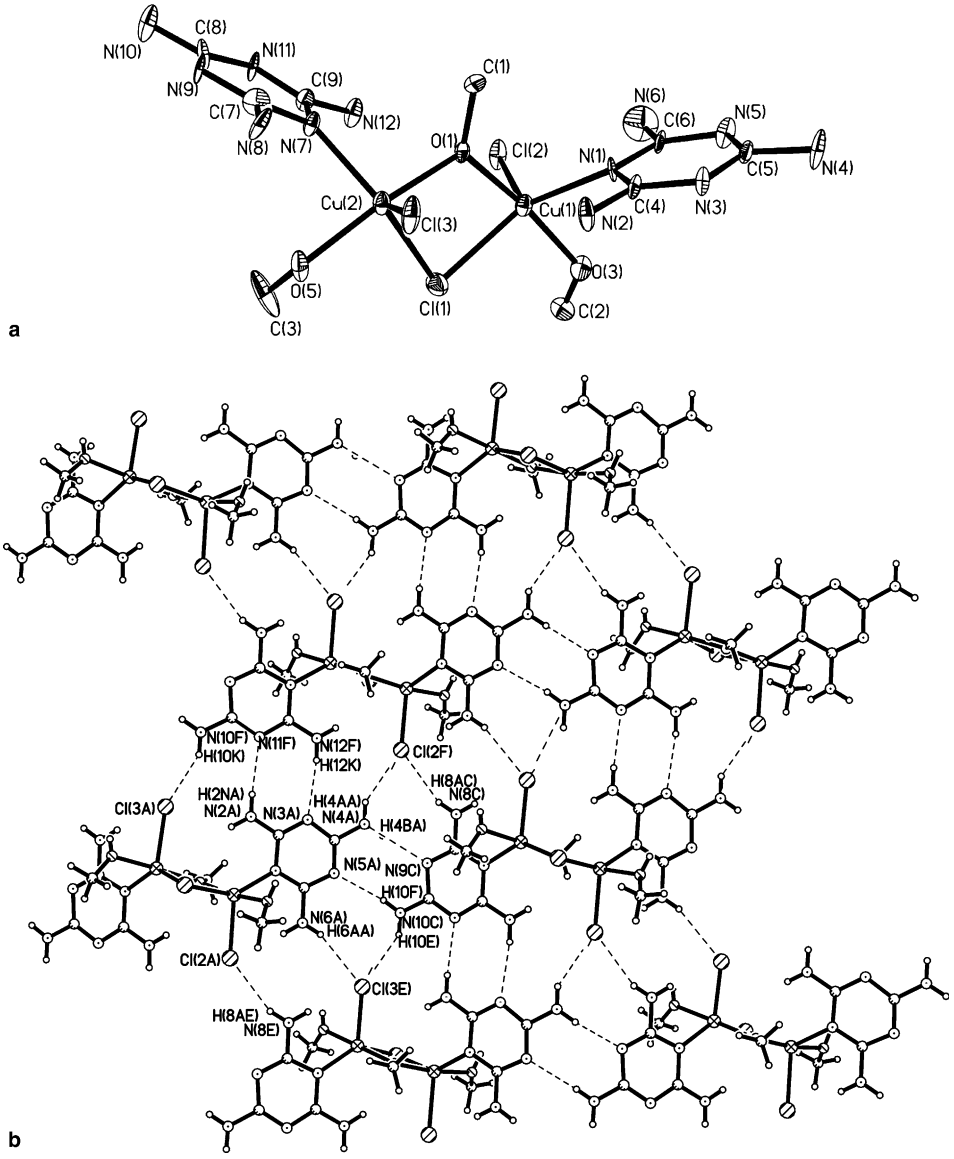

Fig. 1. (a) ORTEP drawing showing the coordination geometry of copper center of **1**. Ellipsoids are scaled to enclose 20% of the electron density. The hydrogen atoms are omitted for clarity. (b) Part of the 2-D hydrogen bonded layers of complexes present in the crystals of **1**, viewing down the *a*-axis.

(μ-OCH_3)(MA)]$_2 \cdot 0.33H_2O$, **2**, were prepared by reactions of $CuCl_2 \cdot 2H_2O$ and $Cu(OAc)_2 \cdot H_2O$, respectively, with MA in refluxing methanol. Crystals of **1** and **2** suitable for X-ray crystallography were obtained by slow diffusion of ether into a MeOH solution of **1** and **2**, respectively. Their structures have been determined by spectroscopic methods and by X-ray crystallography.

4.2. Structure of *1*

The structure of **1** was solved in the space group $Pna2_1$. Fig. 1(a) shows the local coordination of the two copper centers. Selected bond distances and angles are listed in Table 2. The copper metal center adopts slightly distorted square pyramidal coordination geometry with the bond angles significantly deviates from 90° or 180°. The basal plane comprises the bridging methoxide oxygen atom (Cu–O = 1.901(8), 1.913(7) Å), the bridging chloride atom (Cu–Cl = 2.344(3), 2.361(3)), a coordinated methanol oxygen atom (Cu–O = 1.959(9), 1.980(10) Å) and a ring nitrogen atom of a coordinated melamine ligand (Cu–N = 2.069(9), 2.077(10) Å), whereas the apical coordination site is occupied by a weakly coordinated monodentate chloride atoms (Cu–Cl = 2.447(3), 2.449(3) Å). The two copper atoms are bridged by one methoxide group and one chloride atom to form an edge-sharing bisquare pyramidal geometry and the non-bonded Cu···Cu separation in the Cu_2(μ-Cl)(μ-OCH_3) core is 3.171 Å. The dihedral angle between the two melamine planes is 44.5° and the planes of the melamine ligands are rotated by ca. 72.7° and 78.0° out of the basal coordinated planes.

The molecules of **1** are interlinked through two pairs of N–H···N self-complementary hydrogen bonds and N–H···Cl interactions (H···N = 2.15–2.34 Å, ∠N–H···N = 149.7–174.7°, H···Cl = 2.50–2.61 Å, ∠N–H···Cl = 145.4–159.0°), forming the 2-D sheets, Fig. 1(b). The diethyl ether solvents interact with the methanol groups of copper units through O–H···O hydrogen bonds (H···O = 1.84–2.61 Å, ∠O–H···O = 152.9–159.0°).

4.3. Structure of *2*

The structure of **2** was solved in the space group $R\bar{3}$. Fig. 2(a) shows the local coordination of the copper center in **2**. Selected bond distances and angles are listed in Table 2. The copper metal center adopts a slightly distorted square planar coordination geometry with the bond angles significantly deviates from 90° or 180° and the sum of the four angles about the Cu atoms is 362.37°. Complex **2** is an edge-sharing bisquare-planar complex of Cu(II) centers. The two copper centers are linked by two oxygen atoms of the methoxide groups with the non-bonded Cu···Cu separation in the Cu_2(μ-OCH_3)$_2$ core of 2.9757(9) Å. The Cu(II) atom is bonded to one nitrogen atom of the melamine ligand(Cu–N(1) = 1.986(3) Å), two *cis*-bridging methoxide oxygen atoms (Cu–O = 1.921(2)–1.924(2) Å) and one of the monodentate acetate group (Cu–O(2) = 1.938(3) Å). The dihedral angle between the two melamine planes is 0° and the planes of the melamine ligands are rotated by ca. 89.8° out of the square planar coordination planes. The molecules of **2** are interlinked through N–H···N

Table 2
Selected bond distances (Å) and angles (°) complexes for **1** and **2**

1			
Cu(1)–O(1)	1.913(8)	Cu(1)–O(3)	1.959(10)
Cu(1)–N(1)	2.069(11)	Cu(1)–Cl(1)	2.361(4)
Cu(1)–Cl(2)	2.449(4)	Cu(2)–O(1)	1.901(9)
Cu(2)–O(5)	1.980(12)	Cu(2)–N(7)	2.077(11)
Cu(2)–Cl(1)	2.344(4)	Cu(2)–Cl(3)	2.447(4)
O(1)–Cu(1)–O(3)	170.6(5)	O(1)–Cu(1)–N(1)	96.0(4)
O(3)–Cu(1)–N(1)	85.1(4)	O(1)–Cu(1)–Cl(1)	80.9(3)
O(3)–Cu(1)–Cl(1)	92.5(3)	N(1)–Cu(1)–Cl(1)	143.2(4)
O(1)–Cu(1)–Cl(2)	95.5(4)	O(3)–Cu(1)–Cl(2)	92.5(4)
N(1)–Cu(1)–Cl(2)	114.3(3)	Cl(1)–Cu(1)–Cl(2)	102.47(18)
O(1)–Cu(2)–O(5)	172.9(5)	O(1)–Cu(2)–N(7)	97.0(4)
O(5)–Cu(2)–N(7)	87.3(5)	O(1)–Cu(2)–Cl(1)	81.6(3)
O(5)–Cu(2)–Cl(1)	91.4(4)	N(7)–Cu(2)–Cl(1)	137.6(4)
O(1)–Cu(2)–Cl(3)	94.5(4)	O(5)–Cu(2)–Cl(3)	89.2(4)
N(7)–Cu(2)–Cl(3)	110.7(3)	Cl(1)–Cu(2)–Cl(3)	111.60(18)
2			
Cu–O(1)	1.921(2)	Cu–O(1A)	1.924(2)
Cu–O(2)	1.938(3)	Cu–N(1)	1.986(3)
O(1)–Cu(A)	1.924(2)		
O(1)–Cu–O(1A)	78.59(11)	O(1)–Cu–O(2)	97.63(11)
O(1A)–Cu–O(2)	166.37(11)	O(1)–Cu–N(1)	166.48(12)
O(1A)1–Cu–N(1)	94.36(11)	O(2)–Cu–N(1)	91.79(12)
Cu–O(1)–Cu(A)	101.41(11)		

Symmetry transformations used to generate equivalent atoms: (A) $-x+2$, $-y+1$, $-z$ for **2**.

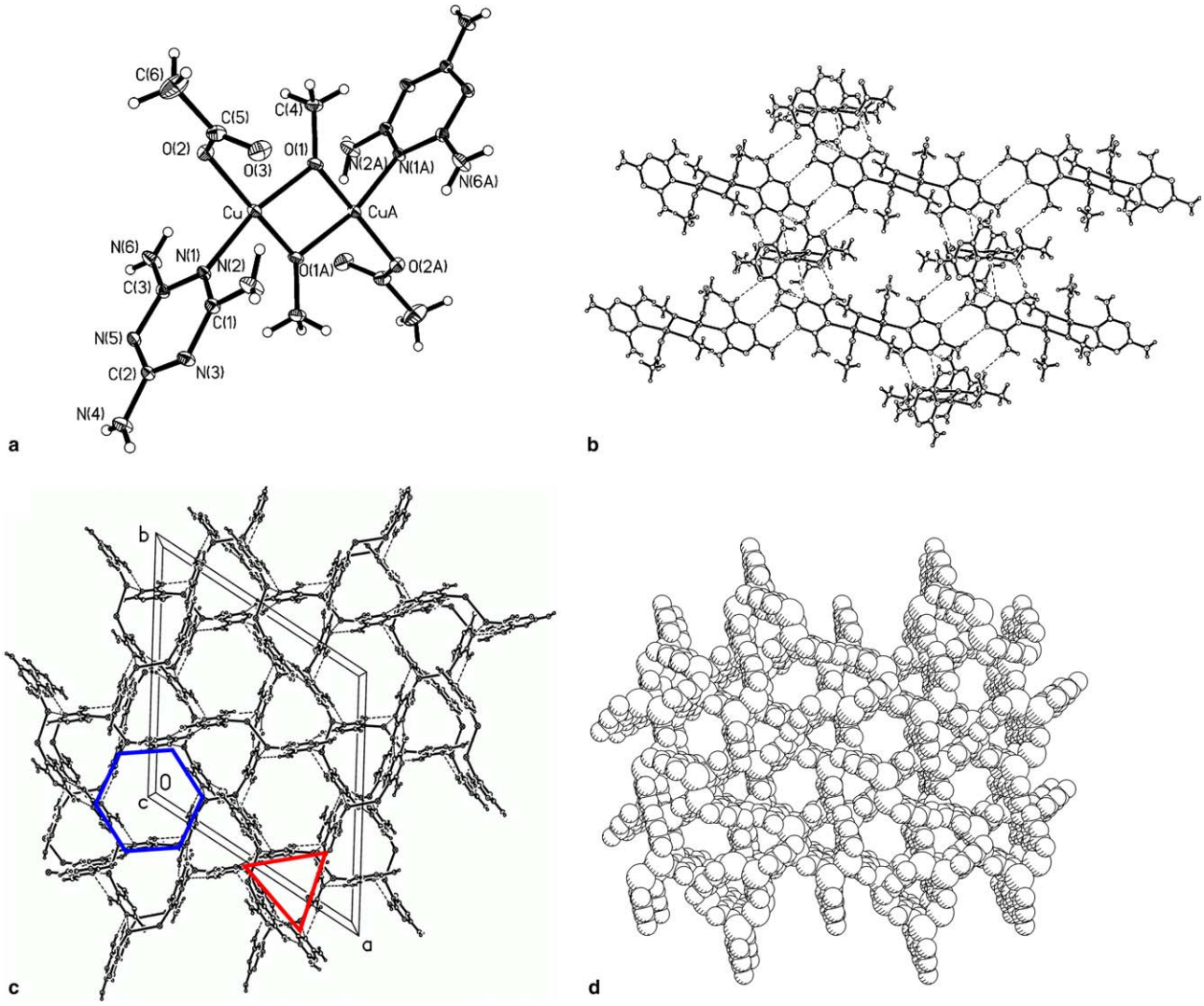

Fig. 2. (a) ORTEP drawing showing the coordination geometry of copper center of **2**. Ellipsoids are scaled to enclose 20% of the electron density. (b) Packing diagram of **2** showing the interactions among the molecules. (c) Packing diagram of **2** showing the 3-D porous supramoleculer structure with hexagonal and triangular pores. (d) A space-filling model representation for **2**. Only the Cu atoms and the melamine ligands are shown for clarity.

self-complementary hydrogen bonds and N–H···O interactions (H···N = 2.22–2.29 Å, ∠N–H···N = 155.8–177.7°, H···O = 2.02–2.29 Å, ∠N–H···O = 145.7–168.6°), Fig. 2(b), forming a 3-D porous structure with triangular and hexagonal pores, Fig. 2(c). Fig. 2(d) is a space-filling model representation for **2**, showing only metal atoms and MA ligands.

4.4. Structural comparisons for *1* and *2*

The structure of **1** is similar to the dinuclear complex $[Cu(MA)(\mu\text{-}OCH_3)(NO_3)(HOCH_3)]_2$ (Cu···Cu = 3.0016(8) Å), where the plane of the MA ligand is rotated by about 67° out of the basal coordination plane of the distorted square pyramidal geometry at the copper center, and the molecules are linked through N–H···O and N–H···N hydrogen bonds to form 2-D sheets [9]. In complex **2**, the Cu atoms adopt adopts a slightly distorted square planar coordination geometry and the planes of the melamine ligands are rotated by ca. 89.8° out of the square planar coordination planes, resulting in a 3-D porous structure with triangular and hexagonal pores. The edge length of the hexagonal pores is 5.48 Å defined as the distance between two Cu atoms of adjacent complex, while the edge length of the triangular pores is 6.98 Å defined as the distance between centers of the adjacent $Cu_2(\mu\text{-}OCH_3)_2$ cores. To our best knowledge, complex **2** shows a unique porous structure containing both hexagonal and triangular pores constrained by the N–H···N self-complementary hydrogen bonds.

4.5. Thermal properties

Complexes **1** and **2** are very stable in air at ambient temperature. Thermal gravimetric analyses (TGA) were carried out to examine the thermal stability of **1** and **2**. The samples were heated up in air at 1 atm pressure with the heating rate of 10 °C min^{-1}. The TGA curve shows that **1** is stable up to 96 °C. A total weight loss of 10.8% occurred

in the temperature range 96–295 °C, presumably due to the removal of the methanol ligands per formula unit (calcd. 11.0%). A weight loss of 43.8% occurred in the temperature range 295–372 °C, corresponding to the removal of two melamine ligands per formula unit (calcd. 43.4%). Another weight loss of 23.6% was found in the temperature range 375–420 °C, corresponding to the removal of the three chloride atoms and the bridging methoxide ligand (calcd. 23.7%). The TGA curve shows that **2** is stable up to 145 °C. A total weight loss of 56.0% occurred in the temperature range 145–310 °C, mainly corresponding to the removal of the two bridging methoxide ligands and two melamine molecules per formula unit (calcd. 56.2%). A appeasement weight loss of 21.6% occurred in the temperature range 340–410 °C, consistent with the removal of two monodentate acetate groups (calcd. 21.1%). The results indicate that a 3-D porous framework constrained by the N–H···N self-complementary hydrogen bonds is more stable than 2-D sheets.

5. Conclusions

The syntheses, structures and thermal properties of two new melamine complexes $Cu_2Cl_2(\mu\text{-}Cl)(CH_3OH)_2(\mu\text{-}OCH_3)(MA)_2 \cdot 2Et_2O$ (MA = melamine), **1**, and $[Cu(\eta^1\text{-}OAc)(\mu\text{-}OCH_3)(MA)]_2 \cdot 0.33H_2O$, **2** have been successfully accomplished. In addition to the N–H···N self-complementary hydrogen bonds, the dihedral angle between the melamine plane and the basal plane containing the metal atom of the complex may play an important role in linking the copper melamine complexes to form 2-D and 3-D architectures. The unique structure of complex **2** contains both hexagonal and triangular pores constrained by the N–H···N self-complementary hydrogen bonds.

6. Supplementary material

Crystallographic data (CIF files) for the structures **1** and **2** have been deposited with the Cambridge Crystallographic Data Centre, CCDC No. 280091–280092. Copies of this information may be obtained free of charge from The Director, CCDC, 12 Union Road, Cambridge, CB2 1EZ, UK (Fax: +44 1223 336 033; e-mail: deposit@ccdc.cam.ac.uk or on the web www: http://www.ccdc.cam.ac.uk).

Acknowledgements

We are grateful to the National Science Council of the Republic of China for support.

References

[1] (a) G.R. Desiraju, Angew. Chem., Int. Ed. Engl. 34 (1995) 2311;
(b) G.R. Desiraju, Chem. Commun. (1997) 1475;
(c) J.M. Lehn, Supramolecular Chemistry, VCH, Weinheim, 1995.
[2] (a) A.J. Blake, N.R. Champness, P. Hubberstey, W.-S. Li, M.A. Withersby, M. Schröder, Coord. Chem. Rev. 183 (1999) 117;
(b) S. Muthu, J.H.K. Yip, J.J. Vittal, Dalton Trans. (2002) 4561.
[3] (a) C.-W. Su, C.-P. Wu, J.-D. Chen, L.-S. Liou, J.-C. Wang, Inorg. Chem. Commun. 5 (2002) 215;
(b) S.-H. Liu, J.-D. Chen, L.-S. Liou, J.-C. Wang, Inorg. Chem. 40 (2001) 6499;
(c) Y.-F. Hsu, J.-D. Chen, Eur. J. Inorg. Chem. (2004) 1488.
[4] (a) R.F.M. Lange, F.H. Beijer, R.P. Sijbesma, R.W.W. Hooft, H. Kooijman, A.L. Spek, J. Kroon, E.W. Meijer, Angew. Chem., Int. Ed. Engl. 36 (1997) 969;
(b) J.P. Mathias, C.T. Seto, E.E. Simanek, G.M. Whitesides, J. Am. Chem. Soc. 116 (1994) 1725;
(c) J.A. Zerkowski, J.C. MacDonald, G.M. Whitesides, Chem. Mater. 6 (1994) 1250.
[5] (a) M.M. Chowdhry, D.M.P. Mingos, A.J.P. White, D.J. Williams, Chem. Commun. (1996) 899;
(b) M. Bicher, C. Guran, I. Jitane, Rev. Roum. Chim. 39 (1994) 1203;
(c) M.M. Chowdhry, D.M.P. Mingos, A.J.P. White, D.J. Williams, Chem. Commun. (1996) 899.
[6] (a) E.W. Hughes, J. Am. Chem. Soc. 63 (1941) 1737;
(b) A.C. Larson, D.T. Cromer, J. Chem. Phys. 60 (1974) 185.
[7] R. Dorta, H. Stoeckli-Evans, U. Bodensieck, G. Süss-FinK, J. Organomet. Chem. 553 (1998) 307.
[8] K. Sivashankar, A. Ranganathan, V.R. Pedireddi, C.N.R. Rao, J. Mol. Struct. 559 (2001) 41.
[9] D.M.L. Goodgame, I. Hussain, A.J.P. White, D.J. Williams, J. Chem. Soc., Dalton Trans. (1999) 2899.
[10] (a) XSCANS, Release, 2.1, Siemens Energy & Automation, Inc., Madison, Wisconsin, USA, 1995;
(b) SMART/SAINT/ASTRO, Release 4.03, Siemens Energy & Automation, Inc., Madison, Wisconsin, USA, 1995.
[11] SHELXTL 5.10, Bruker Analytical X-ray Instruments, Inc., Karlsruche, Germany, 1997.

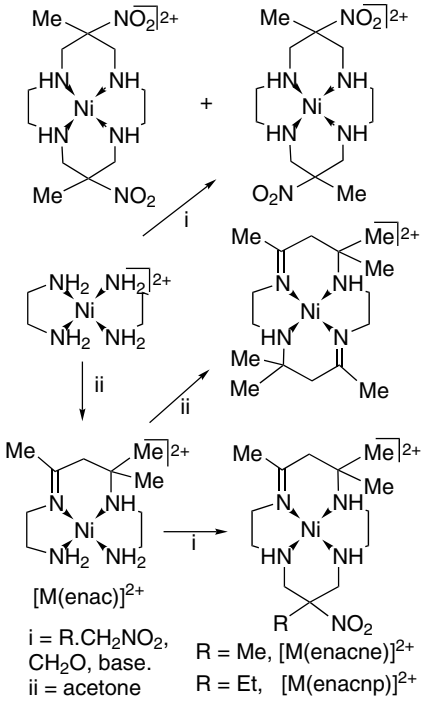

Scheme 1. Showing reactions of $[Ni(en)_2]^{2+}$ and $[Ni(enac)]^{2+}$ with methanal plus nitroethane or nitropropane: (i) [8] or with acetone (ii) [11–13].

In this communication the preparations of compounds of analogous nickel(II) cations, $[Ni(enacne)]^{2+}$ and $[Ni(enacnp)]^{2+}$, by reaction of (4,6,6-trimethyl-3,7-diazanon-3-ene-1,9-diamine)nickel(II), $[Ni(enac)]^{2+}$, with methanal and nitroethane or nitropropane are reported. The structure of $[Ni(enacne)][ZnCl_4]$ has been determined by X-ray diffractometry. An improved preparation of the $[Ni(enac)](ClO_4)_2$ starting material is reported.

2. Results

$[Ni(enac)]^{2+}$ reacts with methanal plus nitroethane (or nitropropane) in water, or methanol, plus base, to form nitro-substituted imine–triamine macrocyclic cations, see Scheme 1. These are very resistant to acid demetallation, as generally observed for azamacrocycle compounds of nickel(II), and in particular the hexamethyl-diimine–diamine azamacrocycle compounds formed by condensation of (ethane-1,2-diamine) nickel(II) compounds with acetone [12,13] and the dimethyl–dinitro cyclic tetraamine compounds formed by their condensation with methanal/nitroalkyl compounds [8]. The cations are, however, very slowly degraded in alkaline solution.

The nickel(II) cations form orange coloured singlet ground state square-planar salts with perchlorate and tetrachlorozincate anions, and blue–violet triplet ground state octahedral compounds with coordinating unidentate (NCS^- and NH_3) and bidentate $\{C_2O_4^{2-}$ (oxalato) and $C_3H_7O_2^-$ (pentan-2,4-dionato) and $NO_2^-\}$ ligands. The thiocyanato compounds show very strong singlet $\nu(C{\equiv}N)$ bands in the IR, at c. 2060 cm^{-1}, typical of *trans*-di-isothiocyanato-(tetraamine)nickel(II) compounds. The nitrite derivatives $[Ni(L)(NO_2)]ClO_4$ have properties indicative of chelate nitrito coordination, as observed for $[Ni(enac)(NO_2)]ClO_4$ [11]. The oxalato compounds $[\{Ni(L)\}_2(C_2O_4)](ClO_4)_2$ are analogous to many similar compounds in which the oxalate ion acts as a bridging bidentate ligand, coordinated with the macrocycle in a folded arrangement [14,15]. The formation of the oxalato compound is slow, and the perchlorate salt is slow to crystallise when a solution of this compound is acidified with perchloric acid. The slow interconversion between the perchlorate salt and oxalato compound suggests that a change in nitrogen configuration is occurring; as such changes are generally slow in acid. The stable configuration for the square-planar cation is 1*R*,8*R*,11*S*, as observed for the tetrachlorozincate salt (and for the copper(II) cation [9]) and folding would be expected to occur at the N1–Ni–N8 axis, for the least-strained 1*R*,8*R*,11*R*-configuration.

2.1. Structural study

The structure of $[Ni(enacne)][ZnCl_4]$ was determined by X-ray diffractometry, see Section 4.3 for details. The asymmetric unit of the compound is shown in Fig. 1. The nickel(II) ion is in square-planar coordination by the imine and three secondary amine nitrogen atoms of the 5,7,7,13-tetramethyl-13-nitro-1,4,8,11-tetraazacyclotetradec-4-ene azamacrocycle.

A persistent residual peak located axially with respect to C5 was modeled as resulting from disorder of the cation, with superposition of the 5,7,7,13-tetramethyl-4-ene and 5,5,7,13-tetramethyl-7-ene arrangements, obtained by reversal of the chelate ring –N4=C5(Me)–C6–C7(Me)$_2$–N8H– to –N4H–C5(Me)$_2$–C6–C7(Me)=N8–. The major

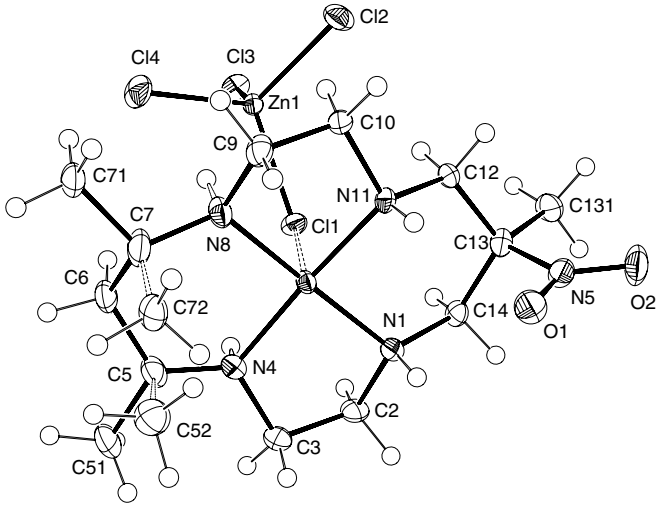

Fig. 1. The asymmetric unit of $[Ni(enacne)][ZnCl_4]$, drawn [17] with displacement ellipsoids at the 50% confidence level, with hydrogen atoms shown as circles of arbitrary radius. The site occupation factors of the C72 methyl group and H8 and of the C52 methyl group and H4 are 0.80(1) and 0.20(1), respectively.

Table 1
Selected geometric parameters for [Ni(enacne)][$ZnCl_4$][a]

Distance	Distance (Å)	Angle	Angle (°)
Ni–N1	1.934(3)	N1–Ni–N4	87.0(1)
Ni–N4	1.909(3)	N4–Ni–N8	95.0(1)
Ni–N8	1.932(3)	N8–Ni–N11	86.5(1)
Ni–N11	1.927(3)	N11–Ni–N1	91.2(1)
Ni–Cl1	2.9211(9)	N1–Ni–N8	175.8(1)
N4–C5	1.317(4)	N4–Ni–N11	174.6(1)
N8–C7	1.450(4)	N1–Ni–Cl1	86.0(1)
N5–O1	1.220(4)	N4–Ni–Cl1	88.0(1)
N5–O2	1.222(4)	N8–Ni–Cl1	97.8(1)
C13–N5	1.514(4)	N11–Ni–Cl1	97.0(1)
		O1–N5–O2	124.3(3)
		Ni–Cl1–Zn	115.9(3)

[a] Distances Zn–Cl range from 2.252(1) to 2.280(1) Å and angles Cl–Zn–Cl range from 105.87(3)° to 110.43(3)°.

component has the axial substituent on C7 (sof of $C72H_3$ and H8 = 0.80(1), 1*S*,5*S*,11*R* configuration) and the minor component has the axial substituent on C5 (sof of $C52H_3$ and H4 = 0.20(1), 1*S*,8*R*,11*R* configuration). The rest of the cation has approximate mirror symmetry.

The N_4 group is tetrahedrally twisted, with displacements of N atoms from the N_4 plane ±0.012(1) Å, with the Ni atom 0.074(1) Å from this plane {values for the copper(II) compounds [9,10] range from ±0.017(2) and 0.246(2) Å to ±0.067(2) and 0.088(2) Å}. Overall, the geometry of the cation is similar to those of the analogous copper(II) cations, but with the Ni–N distances c. 0.07 Å shorter than the corresponding Cu–N distances. The Ni–N distances (see Table 1) are similar to those of the (5,7,7,12,12,14-hexamethyl-1,4,8,11-tetraazacyclotetradeca-4,11-diene)nickel(II) perchlorate salts: for the *meso, rac*-isomers $Ni–N_{amine}$ = 1.938(2), 1.915(4); $Ni–N_{imine}$ = 1.907(2), 1.884(5) Å [16]. The six-membered diamine chelate ring including Ni,N1,N11 has a chair conformation with the nitro group axially oriented (on the same side of the NiN_4 plane as the axial methyl substituent), the five-membered chelate rings including Ni,N1,N4 and NiN8,N11 have unsymmetrical gauche conformations and the amine– imine chelate ring including Ni,N5,N8 has a twisted conformation (see Table 2 for displacements of atoms from NiN_2 planes for chelate rings). The distance N4–C5 and angles about these atoms reflect the predominant imine character of this bond.

For [Ni(enacne)][$ZnCl_4$] the nitro group is approximately aligned with C13···Ni, with O1 hydrogen-bonded to both N1–H1 and N11–H11 (see Table 3), whereas for the copper(II) compounds the nitro group is aligned approximately normal to this direction {for [Cu(enacnp)(H_2O)](ClO_4)$_2$ both these N–H groups hydrogen bond to perchlorate ion oxygen atoms [9] and for [Cu(enacnp)][$Ni(CN)_4$]·H_2O only one of these NH groups hydrogen bonds to a nitro group oxygen atom [10]}.

Table 3
Hydrogen bonding parameters (Å, °) for [Ni(enacne)][$ZnCl_4$]

Atoms	H···A	D···A	DH···A
N1–H1···O1	2.39	2.935(3)	117
N1–H1···Cl3[i]	2.58	3.348(3)	140
N4–H4···Cl1	2.72	3.432(3)	136
N8–H8···Cl4	2.74	3.658(3)	134
N11–H11···O1	2.27	2.885(4)	123
N11–H11···O1[ii]	2.22	3.100(4)	157

Symmetry operations: i, $-x+1/2$, $y+1/2$, $-z+1/2$; ii, $-x+1$, $-y+1$, $-z+1$.

The tetrachlorozincate ion is located on the side of the NiN_4 plane remote from the nitro and methyl groups, with one chloride ion located approximately axially with respect to the nickel(II) ion, with Ni1–Cl1 = 2.921(1) Å, which indicates a weak interaction. The closest axial approach on the other side of the plane is Ni···Cl3 ($-x+1$, $-y+1$, $-z+1$) = 3.598(1) Å. Intermolecular hydrogen bonds link partial occupancy N4–H4···Cl1 and N8–H8···Cl4 to the tetrachlorozincate ion, while intramolecular hydrogen bonds form a network, see Table 3.

3. Conclusions

The facile reaction of $[Ni(enac)]^{2+}$ with nitroalkyl compounds plus methanal to form the nitro-substituted imine–triamine macrocycles completes a set of azamacrocycle compounds formed by cyclization of the bis(ethane-1,2-diamine)nickel(II) cations by condensations with acetone (diimine macrocycles) or with methanal/nitroalkyls (dinitro–tetraamine macrocycles), shown in the Reaction Scheme 1. The cations have properties similar to those of the hexamethyl-diimine–diamine macrocycle cation formed with acetone [12,13] and the dimethyl–dinitro–tetraamine cations formed with methanal/nitroalkyl compounds [5]. However, the "mixed substituent" cations more readily form triplet ground state compounds, with both planar and folded-macrocycle, than either of the symmetrical cations, indicating less hindrance of the axial coordination

Table 2
Displacements of atoms from NiN_2 planes for chelate rings for [Ni(enacne)][$ZnCl_4$]

Atoms defining plane	Displacement (Å)
Ni,N1,N4	C2 −0.386(5); C3 0.204(5)
Ni,N8,N11	C9 0.425(5); C10 0.0.274(5)
Ni,N4,N8	C5 −0.010(5); C6 −0.326(6); C7 0.458(6); C51 −0.006(8); C71 0.298(8); C52 1.68(1); C72 1.996(6)
Ni,N8,N11	C12 −0.964(5); C13 −0.867(5); C14 −0.880(5); C131 −2.070(7); N5 0.423(7), O1 1.446(6); O2 0.370(8)
Ni,N4,N8	C5 0.082(4); C6 0.480(4); C7 −0.354(4); C51 −0.040(6); C71 −1.87(4); C72 −0.060(5)

sites by axial substituents. The cations are resistant to acid demetallation, but in base are slowly degraded by reversal of the Mannich reaction by which they are formed.

4. Experimental

4.1. Preparations of compounds

The perchlorate compounds described are potentially explosive and should be treated with caution, particularly the ethane-1,2-diamine starting materials. However, the enac, enacne and enacnp perchlorate compounds have shown no indication of shock sensitivity and decompose non-violently when strongly heated. The macrocyclic cations are resistant to acid demetallation (but are rapidly oxidized by nitric acid). They are slowly degraded in alkaline solution. The infrared spectra all show ν(NH) bands near 3200 cm^{-1}, and sharp peaks assigned to ν(N=C) near 1665 cm^{-1} and $\nu(NO_2)$ (more intense) near 1550 cm^{-1}.

4.1.1. (4,6,6-Trimethyl-3,7-diazanon-3-ene-1,9-diamine)nickel(II) perchlorate, [Ni(enac)](ClO4)2

Improvements have been made to the reported [11] preparation of $[Ni(enac)](ClO_4)_2$. $[Ni(en)_3](ClO_4)_2 \cdot H_2O$ (20 g) was added to a solution of $[Ni(H_2O)_6](ClO_4)_2$ (8.14 g) in methanol (100 cm^3), 2:1 mol ratio, producing a solution of "$[Ni(en)_2]^{2+}$". Acetone (100 cm^3) and 2-aminoethanol (2 g) were added and the solution was heated near boiling for 48 h. The solution was then rotary evaporated; the resulting orange gum dissolved in hot water (100 cm^3), treated with decolourising charcoal, filtered and again rotary evaporated to leave an orange gum. This was dissolved in ethanol (200 cm^3) by heating and stirring and the solution allowed to stand for 24 h. The orange product that slowly crystallised (nucleation with the preformed compound speeds this process) was filtered off, washed with ethanol and recrystallised from hot methanol, or by dissolving in hot acetone, adding an equal volume of ethanol and allowing the solution to evaporate. Yield 20 g, 75%.

4.1.2. (5,7,7,13-Tetramethyl-13-nitro-1,4,8,11-tetraazacyclotetradec-4-ene)nickel(II) perchlorate, [Ni(enacne)](ClO4)2

4.1.2.1. Preparation from [Ni(enac)](ClO4)2. $[Ni(enac)](ClO_4)_2$ (10 g) was dissolved in water (100 cm^3), nitroethane (1.8 g), paraformaldehyde (2.5 g) and $NaHCO_3$ (0.5 g) added and the solution heated at c. 75 °C. for 2 h. then filtered through charcoal while hot. Sodium oxalate (2 g) was added, and the solution heated near boiling for 2 h, then stood for 24 h. while blue violet $[\{Ni(enacne)\}_2(C_2O_4)](ClO_4)_2 \cdot 2H_2O$ crystallised. The solid was filtered off, washed well with hot water, then acetone (yield 8.6 g, 80%). This material was added to a hot aqueous solution of calcium perchlorate (prepared by dissolving 2 g of $CaCO_3$ in just sufficient perchloric acid in 50 cm^3 of water), adding "filter aid" or a further 1 g of $CaCO_3$ to facilitate later filtration and the suspension heated and stirred until the blue–violet starting material had all reacted to leave a white suspension in an orange solution. An equal volume of acetone was added and the solid filtered off and washed with hot 1:1 acetone water. The orange product crystallised as this solution evaporated.

The product was recrystallised from hot acetonitrile (in which it is extremely soluble)/propan-2-ol or from hot 10:1 acetone:water/ethanol. The compound tends to separate from water as an orange gum that only slowly crystallises. The orange *product* was filtered off and washed with ethanol. Yield c. 70%. *Anal.* Calc. for $C_{14}H_{29}Cl_2N_5NiO_{10}$: C, 30.2; H, 5.2; N, 12.6. Found: C, 29.9; H, 5.2; N, 12.5%. Visible spectrum in water {λ_{max}/nm (ε/dm^3 mol^{-1} cm^{-1}), 448 (76). IR spectrum (ν_{max}/cm^{-1}): ν(NH) 3236; ν(C=N) 1663; $\nu(NO_2)$ 1553.

4.1.2.2. Preparation from [Ni(enac)][ZnCl4]. [Ni(enac)]-$[ZnCl_4]$ [11] (10.1 g) was dissolved in water (100 cm^3) and $NaHCO_3$ (4.2 g) added. Effervescence occurred and $ZnCO_3$ precipitated. This was filtered off, nitroethane (1.8 g) and paraformaldehyde (2.5 g) added and the solution treated as for the previous preparation. Perchloric acid (4 g, 60%), sodium oxalate (2 g) then $NaHCO_3$ (2 g) (effervescence) were added, and the preparation continued as for the previous preparation, with similar yield of product.

4.1.3. (13-Ethyl-5,7,7-trimethyl-13-nitro-1,4,8,11-tetraazacyclotetradec-4-ene)nickel(II) Perchlorate, [Ni(enacnp)](ClO4)2

This orange compound was prepared and recrystallised as for the previous compound by using 1.9 g of nitropropane in place of the nitroethane, with similar yield of *product*. *Anal.* Calc. for $C_{15}H_{31}Cl_2N_5NiO_{10}$: C, 30.2; H, 5.2; N, 12.6. Found: C, 29.9; H, 5.2; N, 12.5%. Visible spectrum in water {λ_{max}/nm (ε/dm^3 mol^{-1} cm^{-1}) 447 (76). IR spectrum (ν_{max}/cm^{-1}): ν(NH) 3236; ν(C=N) 1663; $\nu(NO_2)$ 1553.

4.2. Other compounds

Compounds of $[Ni(enacne)]^{2+}$ and/or $[Ni(enacnp)]^{2+}$ were prepared from the perchlorate salts, with procedures for $[Ni(enacnp)]^{2+}$ compounds analogous to those described for the $[Ni(enacne)]^{2+}$ compound.

4.2.1. Ammine adducts

Sparingly soluble purple ammine adducts crystallised when the perchlorate salts were stirred under concd. aqueous ammonia. These slowly lost ammonia on exposure to the atmosphere, or when stirred with methanol, to reform the orange perchlorate salts.

4.2.2. trans-Dithiocyanato-(5,7,7,13-tetramethyl-13-nitro-1,4,8,11-tetraazacyclotetradec-4-ene)nickel(II), trans-[Ni(enacne)(NCS)2]

Sodium thiocyanate was added to a hot, concentrated aqueous solution of $[Ni(enacne)](ClO_4)_2$. Pale lavender coloured crystals of the *product* were filtered from the cold

solution and recrystallised from hot water. *Anal.* Calc. for $C_{16}H_{29}N_7NiO_2S_2$: C, 40.5; H, 6.2; N, 20.7. Found: C, 40.4; H, 6.0; N, 20.6%. IR spectrum (ν_{max}/cm^{-1}): ν(NH) 3302, 3217; ν(C≡N) 2066vs, ν(C=N) 1671; ν(NO_2) 1545.

4.2.3. trans-Dithiocyanato-(13-Ethyl-5,7,7-trimethyl-13-nitro-1,4,8,11-tetraazacyclotetradec-4-ene)nickel(II), trans-[Ni(enacnp)(NCS)$_2$]

Anal. Calc. for $C_{17}H_{31}N_7NiO_2S_2$: C, 42.1; H, 6.5; N, 20.2. Found: C, 41.8; H, 6.4; N, 20.1%. IR spectrum (ν_{max}/cm^{-1}): ν(NH) 3297, 3229; ν(C≡N) 2049vs; ν(C=N) 1671; ν(NO_2) 1543.

4.2.4. (5,7,7,13-Tetramethyl-13-nitro-1,4,8,11-tetraazacyclotetradec-4-ene)nickel(II) tetrachlorozincate, [Ni(enacne)][ZnCl$_4$]

Zinc chloride was added to a solution of [Ni(enacne)](ClO_4)$_2$ in acetonitrile, followed by propan-2-ol until turbid. The orange *product* was filtered off and recrystallised from hot methanol containing a few drops of concd. HCl. *Anal.* Calc. for $C_{14}H_{29}Cl_4N_5NiO_2Zn$: C, 29.7; H, 5.2; N, 12.4. Found: C, 29.9; H, 5.2; N, 12.2%. IR spectrum (ν_{max}/cm^{-1}): ν(NH) 3217, 3153; ν(C=N) 1650; ν(NO_2) 1550.

4.2.5. μ-Oxalato-bis{(5,7,7,13-Tetramethyl-13-nitro-1,4,8,11-tetraazacyclotetradec-4-ene)nickel(II)} perchlorate dihydrate, [{Ni(enacne)}$_2$(C$_2$O$_4$)](ClO$_4$)$_2$·2H$_2$O

Sodium oxalate was added to a hot aqueous solution of [Ni(enacne)](ClO_4)$_2$ and the solution heated for c. 30 min. The insoluble blue *product* was filtered from the cold solution and washed with water, then ethanol. *Anal.* Calc. for $C_{15}H_{33}ClN_5NiO_8$: C, 35.6; H, 6.6; N, 13.9. Found: C, 35.6, 35.8; H, 5.9, 5.7; N, 13.8, 13.9%. IR spectrum (ν_{max}/cm^{-1}): ν(NH) 3284, 3264; ν(C=N)+ν(C=O) 1650vs, complex; ν(NO_2) 1545.

4.2.6. (Pentane-2,4-dionato κ^2 O,O′)(5,7,7,13-tetramethyl-13-nitro-1,4,8,11-tetraazacyclotetradec-4-ene κ^4)nickel(II) perchlorate [Ni(enacne)(acac)]ClO$_4$

Pentane-2,4-dione (acetyl acetone, 0.5 g) was added to a hot aqueous solution of [Ni(enacne)](ClO_4)$_2$ (2 g), followed by dilute aqueous ammonia. The sparingly soluble blue *product* crystallised as the solution cooled. This was filtered off, washed with water then ethanol and was recrystallised from hot acetone/propan-2-ol. *Anal.* Calc. for $C_{19}H_{36}ClN_5NiO_8$: C, 41.0; H, 6.5; N, 12.6. Found: C, 41.2; H, 6.6; N, 12.6%. IR spectrum (ν_{max}/cm^{-1}): ν(NH) 3326, 3267; ν(C=N) 1656; ν(NO_2) 1549; (acac$^-$) 1600, 1520.

4.2.7. Nitrito κ^{2}O,O′(5,7,7,13-tetramethyl-13-nitro-1,4,8,11-tetraazacyclotetradec-4-ene κ^4)nickel(II) perchlorate, [Ni(enacne)(NO$_2$)]ClO$_4$

[Ni(enacne)](ClO_4)$_2$ was dissolved in a hot methanol solution containing a small excess of $NaNO_2$. The grey–green *product* that crystallised as the solution cooled was recrystallised from hot methanol/propan-2-ol. *Anal.* Calc. for $C_{14}H_{29}ClN_6NiO_8$: C, 33.4; H, 5.8; N, 16.7. Found: C, 33.9; H, 5.9; N, 16.6%. IR spectrum (ν_{max}/cm^{-1}): ν(NH) 3294, 3252; ν(C=N) 1658; ν(NO_2) 1540; ν_{as}(NO_2^-) 1203.

4.2.8. Nitrito κ^2 O,O′(13-ethyl-5,7,7-trimethyl-13-nitro-1,4,8,11-tetraazacyclotetradec-4-ene κ^4)nickel(II) perchlorate, [Ni(enacnp)(NO$_2$)]ClO$_4$

Anal. Calc. for $C_{15}H_{31}ClN_5NiO_4$: C, 33.4; H, 5.8; N, 16.6. Found: C, 33.6; H, 5.7; N, 16.6%. IR spectrum (ν_{max}/cm^{-1}): ν(NH) 3294, 3252; ν(C=N) 1658; ν(NO_2) 1540; ν_{as}(NO_2^-) 1203.

4.3. Crystallography

Diffraction data was collected for an orange plate ($0.80 \times 0.33 \times 0.03$ mm) grown from water of (5,7,7,13-tetramethyl-13-nitro-1,4,8,11-tetraazacyclotetradec-4-ene)-nickel(II) tetrachlorozincate, [Ni(enacne)][ZnCl$_4$], $C_{14}H_{29}Cl_4N_5NiO_2Zn$, $M_r = 565.3$.

The crystal was monoclinic, space group $P\,2_1/n$, a 9.3111(6), b 18.479(1), c 13.2900(8) Å, β 108.644(1)°. 7589 Reflections ($2.4 < \theta < 26.3°$) were used to determine cell parameters at 93(2) K.

Data was collected at 93(2) K, by using a SMART 1K CCD diffractometer [18] with fine focus sealed tube Mo Kα radiation (λ 0.71073 Å) using ω scans. Multi-scan absorption corrections [19] were applied, T_{min} 0.675. T_{max} 0.928. 17337 Reflections (avge. $R_{equiv} = 0.0322$) were collected ($-10 < h < 11$; $-22 < k < 22$; $-16 < l < 15$; $2.36 < \theta < 26.37°$) with 4341 unique reflections and 3475 reflections with $I > 2\sigma(I)$.

The structure was solved and refined on F^2 using SHELXTL [20], with H(C) and H(N) atoms in calculated positions and riding. A persistent residual peak near the axial substitution position on C5 was accommodated by assuming superposition of the 1*R*,8*R*,11*S* and 1*S*,8*S*,11*R* arrangements of the cation, effectively reversing the N4–N8 chelate ring, and thus shifting the position of the axial methyl substituent from site C72 to site C52. Independently refined sof of (methyl group C72 and H8) and of (methyl group C52 and H4) had a combined value close to 1. Refinement with the combined sof fixed at 1 gave values for sof (C72 methyl and H4) = 0.80(1) and for sof (C52 methyl and H8) = 0.20(1). The bond C5–C52 was restrained (1.56 Å, with default parameters), but remained long. Because of the low sof for C52 and the 1.68(1) Å C5–C52 distance, C52 was refined with isotropic parameters.

Final R_1 ($2\sigma(I)$) = 0.0352, R_1 (all) = 0.0503, R_w ($2\sigma(I)$) = 0.0848, R_w (all) = 0.0887; $(w = 1/[\sigma^2(F_o^2) + (0.0559P))^2]$, where $P = (F_o^2 + 2F_c^2)/3$.

5. Supplementary material

Crystallographic data has been deposited with the Cambridge Crystallographic Data Centre for this structure; CCDC 281480. Copies of this information may be obtained

free of charge on application to The Director, 12 Union Road, Cambridge CB2 2EZ, UK (fax: +44 1223 336033; e-mail: deposit@ccdc.cam.ac.uk or http://www.ccdc.cam.ac.uk).

References

[1] P.V. Bernhardt, G.A. Lawrance, Coord. Chem. Rev. 104 (1990) 297.
[2] G.A. Lawrance, M. Maeder, E.N. Wilkes, Rev. Inorg. Chem. 13 (1993) 199.
[3] P. Comba, N.F. Curtis, G.A. Lawrance, A.M. Sargeson, B.W. Skelton, A.H. White, Inorg. Chem. 25 (1986) 4260.
[4] G.A. Lawrance, M. Rossignoli, B.W. Skelton, A.H. White, Aust. J. Chem. 40 (1987) 1441.
[5] P. Comba, N.F. Curtis, G.A. Lawrance, M.A. O'Leary, B.W. Skelton, A.H. White, J. Chem. Soc., Dalton Trans. (1988) 2145.
[6] P. Comba, N.F. Curtis, G.A. Lawrance, M.A. O'Leary, B.W. Skelton, A.H. White, J. Chem. Soc., Dalton Trans. (1988) 497.
[7] G.A. Lawrance, M.A. O'Leary, Polyhedron 6 (1987) 1291.
[8] N.F. Curtis, G.J. Gainsford, A. Siriwardena, D.C. Weatherburn, Aust. J. Chem. 46 (1993) 755.
[9] N.F. Curtis, H. Puschmann, Polyhedron (POLY-D-05-00105).
[10] N.F. Curtis, H. Puschmann, Acta Crystallogr., Sect. C 60 (2004) m410.
[11] N.F. Curtis, H.K.J. Powell, H. Puschmann, C.E.F. Rickard, J.M. Waters, Inorg. Chim. Acta 355 (2003) 25.
[12] N.F. Curtis, Coord. Chem. Rev. 3 (1968) 3.
[13] N.F. Curtis, J. Chem. Soc., Dalton Trans. (1972) 1357.
[14] N.F. Curtis, J. Chem. Soc. (1963) 4109.
[15] N.F. Curtis, I.R.N. McCormick, T.N. Waters, J. Chem. Soc., Dalton Trans. (1973) 1537.
[16] L.J. Farrugia, ORTEP-32, J. Appl. Cryst. 30 (1997) 565.
[17] D.J. Szalda, E. Fujita, Acta Crystallogr., Sect. C 48 (1992) 1767.
[18] Bruker SMART (Version 5.054), SADABS (Version 2.03) and SAINT (Version 6.02A), Bruker AXS Inc., Madison, Wisconsin, USA, 1997.
[19] R.H. Blessing, Acta Crystallogr., Sect. A 51 (1995) 33.
[20] G.M. Sheldrick, SHELXTL (Version 5.10). Programs for the solution and refinement of crystal structures, 1997.

GSK-3beta is a regulatory serine/threonine kinase that has many cellular targets. So, selecting small molecule inhibitors of GSK-3beta may have a variety of therapeutic uses including the treatment of neurodegenerative diseases, type II diabetes and cancer. This inhibition occurs on the edge of its ATP-binding-site [4].

Activation of the energy-sensing enzyme AMP-activated protein kinase (AMPK) has been shown to increase insulin-independent glucose transport in skeletal muscle in response to such stimuli as exercise and hypoxia. The concentration of malonyl CoA was increased and acetyl CoA carboxylase phosphorylation at serine 79 was decreased as the medium glucose was raised [5].

DNA damage can be induced by aminoacetone, a metabolite of threonine and glycine but this only occurs in the presence of Cu(II) [6].

Calcineurin is a serine/threonine phosphatase involved in cellular responses to calcium-mobilizing signals. Mutations of the antioxidant enzyme Cu, Zn superoxidismutase can be associated to calcineurin [7].

Since it is difficult to unravel all possible interactions in living systems due to the great number of existing potential ligands and metal ions involved in the biological processes, we have attempted to study the metals and ligands of interest in separate. The work here described intended to assess the interactions of a phosphorylated ligand, an amino acid containing an hydroxyl group and the metal ion Cu(II).

The present paper reports the results of aqueous solution equilibria and spectral studies of binary and ternary copper(II) ion complexes with ATP or PCr with the amino acids glycine, serine, tyrosine and threonine (Fig. 1). Although all these binary systems but Cu(II)–PCr were already studied, they were repeated in order to use the same conditions for the binary and ternary systems.

The phosphorylated ligands chosen were ATP and PCr. ATP is responsible for most of the energy-consuming activities in a cell. When the third phosphate group of ATP is removed by hydrolysis, resulting in the formation of ADP and Pi, free energy is released. PCr is an organic compound found in muscle tissue capable of storing and providing energy for muscular contraction. Creatine kinase, an enzyme present in muscle, brain, and other tissues of vertebrates, catalyses the reversible conversion of ADP and PCr into ATP and creatine [8].

The amino acids selected were serine, tyrosine, threonine and glycine. Glycine is the only amino acid of the four under study that does not have a hydroxyl group, and was used for comparison with the others in order to establish possible hydroxyl-phosphate interactions.

Glycine is a very important amino acid present in collagen and synthesized from serine [9]. Serine is involved in the synthesis of sphingol and therefore in the formation of sphingomyelins (phospholipids) in the brain. In the phosphoproteins, serine is present as phosphoserine [9]. It is part of the active center in the enzyme acetylcholinesterase. Acetylcholine synthesis is made through the choline–acetylase enzyme in the presence of ATP. PCr can replace ATP in this reaction [10]. Threonine's behavior and importance is similar to serine's. Tyrosine presents a third basic substituent in the aromatic ring, a hydroxy phenol group. This third group is not spatially favored for a direct complexation to a metal ion, but it is prone to participate in a complex of 5 or 6 linked rings [11]. Tyrosine is the precursor of the thyroid hormones and of melanin [8].

2. Experimental

2.1. Materials

ATP, PCr, Gly, Ser, Thr and Tyr were purchased from Sigma–Aldrich Chem. Co., USA and were used as received. Copper(II) sulfate pentahydrate, potassium nitrate, standard solutions of carbonate-free potassium hydroxide (Titrisol®) 0.1 mol/L, EDTA $c = 0.1$ mol/L and the buffer solutions of pH 4.0 and 7.0 were purchased from Merck (Germany), p.a. reagents. All other chemicals used were of analytical grade. All solutions and experiments were made with double distilled, deionized and carbonate-free water.

2.2. pH titrations

2.2.1. Reagents

A carbonate-free potassium hydroxide 0.1 mol/L solution was prepared from Titrisol ampoules. A copper(II) sulfate solution (0.01 mol/L) was prepared by dissolving copper(II) sulfate pentahydrate in deionized and bidistilled water and was standardized against a standard solution of EDTA $c = 0.1$ mol/L (Titriplex). All solutions were prepared with doubly distilled, deionized and carbonate-free water.

2.2.2. Apparatus

The titrimetric data were obtained using an E485 Methrom Herisau Multi-hand semiautomatic microburette, a B375 Micronal pH meter and a combined glass electrode. The glass electrode was calibrated before each titration with two Merck standard buffer solutions in a nitrate medium: first with the pH 7.0 solutions (the same in the bulb) followed by a pH 4.0 solution. All titrations were performed at 25.0 ± 0.1 °C by coupling the titration cell with a thermostatic bath set at this temperature.

2.2.3. Procedure

For the determination of the acid dissociation constants of all ligands (Gly, Ser, Thr, Tyr, ATP and PCr), aqueous solutions (1×10^{-3} mol/L) of the ligands were titrated with 0.1 mol/L KOH at 25.0 °C under ionic strength of 0.1 mol/L using a 1.2 mol/L solution of KNO_3. The amino acid solutions were protonated by the proper addition of strong acid. For the determination of the binary systems (one ligand and Cu(II)), solutions containing either the amino acids (aa), or PCr or ATP and Cu(II) ion were titrated at 1:1 metal to ligand ratios. For the ternary systems (Cu(II), one of the aa and either ATP or PCr), the

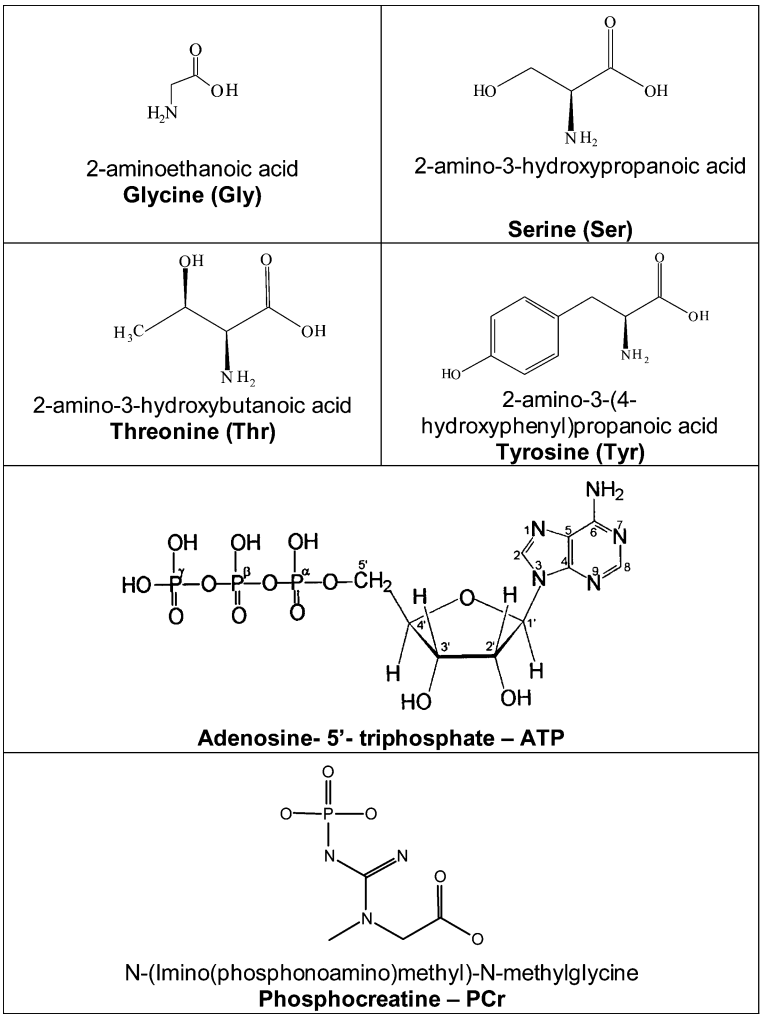

Fig. 1. Structures of ligands.

ratio used was 1:1:1 Cu(II):aa:ATP or PCr. The concentration of the stock solution of Cu(II) ion was 1×10^{-2} mol/L for all binary and ternary systems. The concentration of all studied ligands was always the same and equal to 1×10^{-3} mol/L. All binary and ternary systems were titrated with 0.1 mol/L KOH under the same experimental conditions mentioned above. Each set of titrations was performed at least thrice in order to check the repeatability of the data.

All the dissociation and the complex formation constants were determined using the HYPERQUAD program, and the speciation as a function of pH using the HYSS program [12].

The hydrolysis constants for the metal ion copper(II) were taken from the literature [13] and were fully employed in the calculations.

2.3. Spectral analysis

Cu(II) complexes were studied in aqueous solution at 25 °C by UV–Vis spectroscopy. These solutions were prepared in the same way as previously done for the potentiometry. The same metal:ligand ratio solutions were prepared and analyzed in a wide range of pH values, adjusted by adding small increments of 0.1 mol/L KOH solution in order to obtain the maximum absorbance of each predominant species, as was previously determined in the species distribution diagrams of all the binary and ternary systems. The ionic strength was 0.1 mol/L using a KNO_3 1.2 mol/L solution. A double-beam Perkin–Elmer Lambda 19 spectrophotometer was used with a quartz cell and 1 cm path length.

The solutions for EPR determinations were prepared by adding appropriate volumes of the ligand and the metal solutions in order to achieve a ratio of Cu(II):ligand 1:1 in the binary systems (where L = aa or ATP or PCr) and of Cu(II):aa:ATP or Cu(II):aa:PCr 1:1:1 in the ternary systems, in a previously acidified solution, pH < 2.0 (solution of HNO_3 0.1 mol/L). The pH was then adjusted with a solution of KOH (1.0 and 0.1 mol/L) according to the values in which the maximum percentage of one species was found in the species distribution diagrams and following the maximum absorbance values of the d–d transitions of the complexed species in the UV spectra, for each set of ligands and the copper(II) ion.

The EPR spectra of the aqueous solutions were obtained at room temperature (300 K) in a quartz flat cell. An ESP 300E EPR spectrometer (Bruker, Germany) was operated at a frequency of ≈9.7 GHz (X-band), with 100 kHz of modulation frequency, 10.145 G of modulation amplitude and approximately 20 mW microwave power.

It was not possible to obtain the spectrum of ATP and Cu(II) in solution because substantial insoluble products were formed in the pH where the 1:1 complex is formed.

3. Results and discussion

The stability of binary and ternary complexes may be evaluated by the following equilibria (charges were omitted for simplicity):

$$pM + qH + rA \text{ (or B)} \Longleftrightarrow M_pH_qA_r \text{ (or } B_r\text{)}, \quad \beta_{M_pH_qA_r} \text{ (or Br)}, \tag{1}$$

$$pM + qH + rA + sB \Longleftrightarrow M_pH_qA_rB_s, \quad \beta_{M_pH_qA_rB_s}, \tag{2}$$

where M is the metal ion, H is the proton, A is one of the aa and B is ATP or PCr.

The stability constant of the binary and ternary complexes may be represented by:

$$\log \beta_{pqr} = [M_pH_qA_r]/[M]^p[H]^q[A]^r, \tag{3}$$

$$\log \beta_{pqrs} = [M_pH_qA_rB_s]/[M]^p[H]^q[A]^r[B]^s. \tag{4}$$

It is also possible to define the stability constants of ternary complexes in relation to their corresponding binary ones [11], represented by the equilibria (5) and (6):

$$M + B \Longleftrightarrow MB, \quad K^M_{MB} = [MB]/[M][B], \tag{5}$$

$$MA + B \Longleftrightarrow MAB, \quad K^{MA}_{MAB} = [MAB]/[MA][B]. \tag{6}$$

The difference between the stability of the ternary and the two correspondent binary complexes shows the tendency of the formation of ternary species [14]. This is expressed by the following equation:

$$\Delta \log K = \log \beta_{MAB} - (\log \beta_{MA} + \log \beta_{MB}). \tag{7}$$

In order to verify the tendency of the formation of complexes with intramolecular interactions, the difference between the stability constants of the ternary and the binary complexes was calculated using Eq. (7).

3.1. Potentiometric studies

By using the potentiometric titration data, the protonation constants of the ligands and the complexation constants of the binary and ternary systems were refined using the HYPERQUAD program [12].

3.1.1. Dissociation constants of the ligands

Although data of all ligands can be found in the literature, all of them were refined in this study in order to obtain all values based on the same experimental conditions. The values found in this study (Table 1) are in good agree with the ones reported [15–17].

Table 1
Protonation constants ($\log\beta$) of Gly, Ser, Thr, Tyr, PCr and ATP at 25 °C, $I = 0.1$ mol/L (KNO_3) (the SDs are given in parenthesis)

Species	$\log\beta$ (this work)	$\log\beta$ [Ref.]
H_2Gly	12.44 (0.01)	11.70–12.29 [15]
HGly	9.62 (0.01)	9.30–9.80 [15]
H_2Ser	11.77 (0.01)	11.14–11.70 [15]
HSer	9.12 (0.01)	9.05–9.30 [15]
H_2Thr	11.69 (0.01)	11.13–11.27 [15]
HThr	8.98 (0.01)	8.93–9.52 [15]
H_2Tyr	11.73 (0.01)	10.91–11.32 [15]
HTyr	9.05 (0.01)	9.03–9.30 [15]
H_2ATP	11.05 (0.01)	10.75 [16]
HATP	6.81 (0.01)	6.50 [16]
H_2PCr	15.29 (0.01)	15.70 [17]
HPCr	11.04 (0.02)	11.20 [17]

PCr has four acidic groups: the first protonation constant refers to the guanidine group, the second to the hydroxyl group of the phosphoric group, the third to the carboxylic acid portion and the fourth to another hydroxyl group of the phosphoric terminal group. The obtained values refer to the guanidine group ($\log\beta_1$) and to the hydroxyl group of the phosphoric group ($\log\beta_2$) [17].

3.1.2. Cu(II):aa, Cu(II):ATP and Cu(II):PCR binary systems

The values of the formation constants of all binary species are listed in Table 2.

The only system for which no literature data could be found is Cu:PCr, but anyhow all systems were refined in this study so that all values would be based on the same experimental conditions.

It can be seen in Table 2 that the values for all Cu:aa systems studied are very similar. Since Gly does not have the hydroxyl group and behaves like the other aa, they are all

Table 2
Stability constants of binary systems Cu(II):aa (aa = Gly, Ser, Thr and Tyr), Cu(II):ATP and Cu(II):PCr at 25 °C, $I = 0.1$ mol/L (KNO_3) (the SDs are given in parenthesis)

Species	$\log\beta$ (this work)	$\log\beta$ [Ref.]
CuGly	8.23 (0.01)	8.23 [18]
$CuGlyH_{-1}$	1.42 (0.01)	
$CuGlyH_{-2}$	−9.13 (0.01)	
CuSer	8.10 (0.01)	7.95 [19]
$CuSerH_{-1}$	0.85 (0.01)	
$CuSerH_{-2}$	−9.42 (0.01)	
CuThr	8.13 (0.01)	8.02 [19]
$CuThrH_{-1}$	1.21 (0.01)	
$CuThrH_{-2}$	−8.92 (0.01)	
CuTyr	7.87 (0.01)	7.82 [20]
$CuTyrH_{-1}$	1.26 (0.01)	
$CuTyrH_{-2}$	−8.20 (0.01)	
CuATPH	10.36 (0.01)	10.24 [21]
CuATP	6.40 (0.01)	6.51 [21], 6.42 [22]
$CuATPH_{-1}$	−1.40 (0.01)	−1.21 [21]
$CuATPH_{-2}$	−10.52 (0.01)	
CuPCrH	14.41 (0.01)	
CuPCr	7.89 (0.01)	
$CuPCrH_{-1}$	1.97 (0.01)	

probably bound through the amino and the carboxylic groups, leaving the hydroxyl group free. The values here obtained were compared with the reported ones [18–20].

In all Cu:aa species distribution diagrams, ML species are formed early (pH around 3) due to the great affinity between Cu(II) and the amino group, which has its proton displaced in order to complexate. In Fig. 2 the species distribution diagram of Cu:Ser is shown as example.

The values of the formation constants of the Cu:ATP system are shown in Table 2 and compared with those already determined [21–23]. In Fig. 3, it can be seen that the Cu:ATP species is formed in higher pH than the Cu:aa species.

Although there is the possibility that PCr may act as a tridentate ligand, this hypothesis is not probable because the value of $\log \beta_{CuPCr}$ (7.89), Table 2, is much lower than the value for the correspondent complex with phosphoserine (9.38), where it acts as tridentate [24]. If the correspondent values of $\log \beta_{CuL}$ where L = diisopropylphosphorylguanidine (DPG), which does not have the carboxylate group, or creatine (Cr), which does not have the phosphate group ($\log \beta_{CuDPG} = 8.63$ [25] and $\log \beta_{CuCr} = 7.20$ [15]) are compared, it can be concluded that the value of $\log \beta_{CuPCr}$ can be either for the coordination through the oxygen atom of the phosphate group and through the nitrogen atom of the guanidine group, or through the oxygen atom of the carboxylate group and through the nitrogen atom of the guanidine group.

In Fig. 4, the species distribution can be seen as a function of pH for the species for which the constants were here determined, besides the hydrolysis constants of Cu(II) and the protonation constants of PCr. It can be observed that CuHPCr predominates until pH approximately 6, and afterwards, as the deprotonation begins to occur, the hydrolysis of the complex begins.

3.1.3. Cu:ATP:aa and Cu:PCr:aa ternary systems

The formation constants of the ternary systems (Cu:ATP or PCr:aa 1:1:1) involving Cu(II) and one of the aa and ATP or one of the aa and PCr are presented in Tables 3 and 4.

All ternary species in the systems Cu:ATP:aa have almost coincidental curves. This coincidental pH profile behavior explains the very similar stability constants calculated and presented in Table 3. The value of the formation constant of the CuATPTyr species was compared with an already determined value (12.86) [26].

The same occurs with the systems Cu:PCr:aa, as can be seen in Table 4.

From the species distribution diagram it can be concluded that the binary species prevail at acidic pH values for all Cu:ATP:aa systems and the ternary complexes only

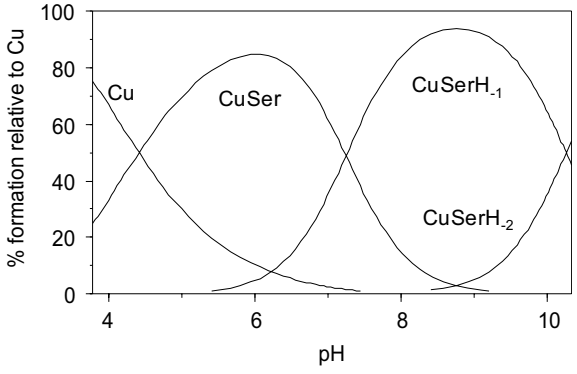

Fig. 2. Species distribution as a function of pH of 1:1 Cu:Ser.

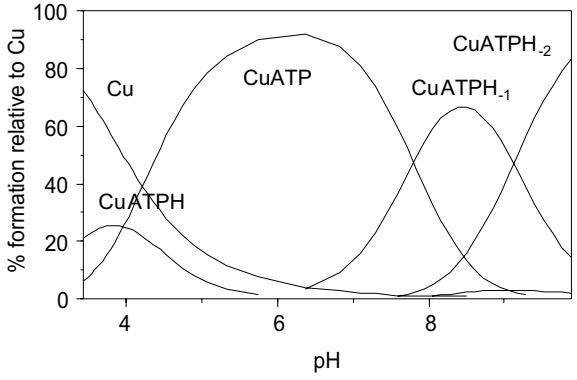

Fig. 3. Species distribution as a function of pH of 1:1 Cu:ATP.

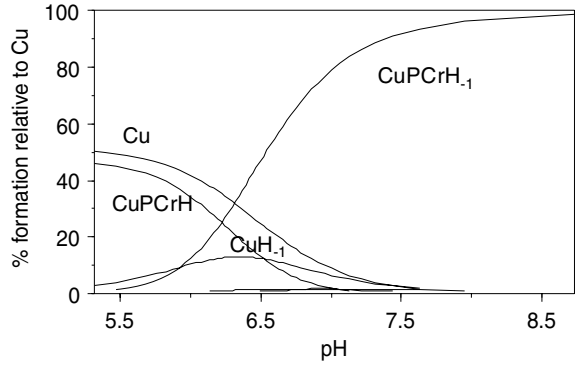

Fig. 4. Species distribution as a function of pH of 1:1 Cu:PCr.

Table 3
Stability constants of ternary systems Cu(II):ATP:aa (aa = Gly, Ser, Thr and Tyr) at 25 °C, $I = 0.1$ mol/L (KNO_3) (the SDs are given in parenthesis)

Species	$\log \beta$ (this work)
CuATPGlyH	18.86 (0.02)
CuATPGly	13.24 (0.01)
$CuATPGlyH_{-1}$	4.38 (0.01)
CuATPSerH	18.05 (0.03)
CuATPSer	13.10 (0.01)
$CuATPSerH_{-1}$	4.20 (0.01)
CuATPThrH	18.24 (0.03)
CuATPThr	13.22 (0.01)
$CuATPThrH_{-1}$	4.28 (0.01)
CuATPTyrH	18.16 (0.03)
CuATPTyr	13.08 (0.01)
$CuATPTyrH_{-1}$	4.25 (0.01)

Table 4
Stability constants of ternary systems Cu(II):PCr:aa (aa = Gly, Ser, Thr and Tyr) at 25 °C, $I = 0.1$ mol/L (KNO_3) (the SDs are given in parenthesis)

Species	$\log\beta$ (this work)
$CuPCrGlyH_2$	27.30 (0.03)
CuPCrGlyH	22.45 (0.01)
CuPCrGly	15.81 (0.02)
$CuPCrSerH_2$	27.84 (0.02)
CuPCrSerH	22.69 (0.02)
CuPCrSer	16.09 (0.03)
$CuPCrThrH_2$	27.66 (0.02)
CuPCrThrH	22.83 (0.02)
CuPCrThr	16.02 (0.03)
$CuPCrTyrH_2$	27.77 (0.02)
CuPCrTyrH	22.77 (0.02)
CuPCrTyr	16.06 (0.02)

at pH higher than 6. In Fig. 5, the species distribution diagram of Cu:ATP:Ser can be seen as an example.

As in the ternary systems where ATP was the second ligand, all profiles for the systems Cu:PCr:aa had coincidental behavior. The species distribution diagram of Cu:PCr:Ser is shown in Fig. 6. As the stability constants of the ternary systems are very similar, so are the species distribution diagrams. In these cases the ternary species predominate in all the pH range. In acidic pH values the protonated species prevail and after, pH 7, the species Cu:PCr:aa is the most abundant.

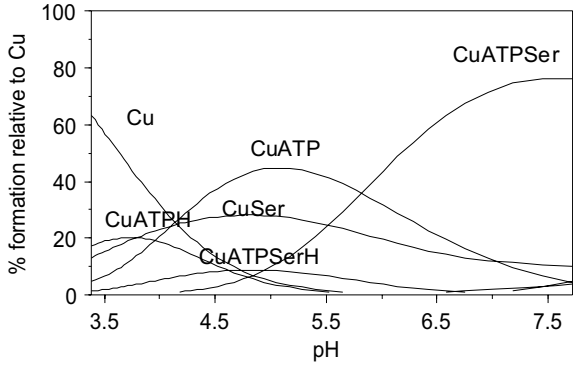

Fig. 5. Species distribution as a function of pH of 1:1 Cu:ATP:Ser.

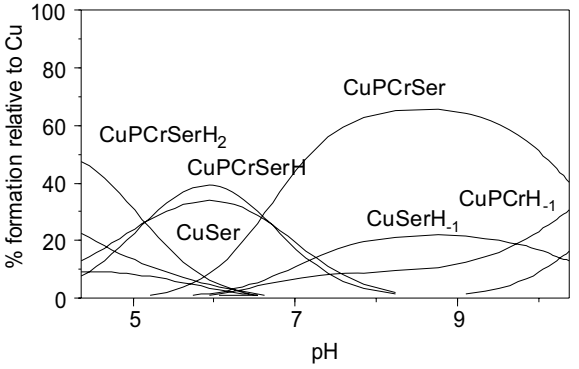

Fig. 6. Species distribution as a function of pH of 1:1 Cu:PCr:Ser.

Table 5
Assessment of intramolecular interactions: values of experimental $\log\beta$ and $\Delta\log K$

Species	$\log\beta$ CuATPaa or $\log\beta$ CuPCraa	($\log\beta$ CuATP or $\log\beta$ CuPCr) + $\log\beta$ Cuaa	$\Delta\log K$
CuATPGly	13.24	14.63	−1.39
CuATPSer	13.10	14.50	−1.40
CuATPThr	13.22	14.27	−1.31
CuATPTyr	13.08	14.53	−1.19
CuPCrGly	15.81	16.12	−0.31
CuPCrSer	16.09	15.99	0.19
CuPCrThr	16.02	16.02	0.00
CuPCrTyr	16.06	15.76	0.30

3.1.4. Intramolecular interactions in ternary systems

The possibility of intramolecular interactions between ATP or PCr and the aa in the ternary systems was investigated. These interactions can occur through hydrogen bonds between the OH group of the amino acid and the negatively charged oxygen atoms of the ATP's phosphate or the PCr's phosphate or carboxylate group. The evaluation of the possibility of intramolecular aa–ATP or aa–PCr interaction, shown in Table 5, was done by calculating the experimental values of $\log\beta$ with $\log K$ (Eq. (7)).

The values of $\Delta\log K$ for the ternary complexes formed with ATP do not indicate any additional stabilization of the complexes. If the Δ of the other complexes are compared with the glycinato one, the differences are −0.01, +0.08 and +0.2, therefore, interactions in CuATPTyr and CuATPThr complexes cannot be entirely rejected.

For the ternary complexes with PCr, the complexes Cu:PCr:Ser and Cu:PCr:Tyr show values of $\Delta\log K$ higher than zero, which can be justified by the presence of any kind of interaction between the ligands. As PCr acts as a bidentate ligand, there is one non-coordinated position (carboxylate or phosphate) and both Ser and Tyr have an OH group free. Since the possibility of interaction does not occur when the amino acid is Gly, which does not have an OH group, it may be assumed that the interaction in the ternary complexes of PCr with Ser and Tyr is between a phosphate or carboxylate of PCr and the OH group of the amino acids. In the case of Thr, this amino acid has an OH group in the β carbon, similarly to Ser, but it has an additional terminal methyl group that can make the interaction with PCr difficult. If the same comparison of Δ with the glycinato compound is done, the values obtained are +0.5, +0.31 and +0.6 which reinforce the probability of interactions.

3.2. Ultraviolet visible spectral analysis

In all systems studied, two distinct bands could be observed: a very intense band in the UV region that corresponds to LMTC and another one, less intense, in the visible region corresponding to a d–d transition band [27].

The wide band observed in the visible region, in all systems, is characteristic of the d^9 configuration of the copper(II) ion, which originates only one term of the free ion,

^{2}D, that has its energy levels shifted by the octahedral field. Both shifted levels belong to the same ^{2}D term and must have the same electronic repulsion [28].

In all the systems studied the donor atoms are either oxygen or nitrogen. For this reason, it is interesting to recognize when only oxygen or nitrogen is bonded to Cu(II). When oxygen atoms are replaced by nitrogen ones in a tetragonal geometry in a cupric ion, the maximum absorption wavelength value shifts to smaller values, indicating a formation of a stronger ligand field, and the molar absorptivity usually increases [28]. Generally speaking, when the maximum wavelength (λ_{max}) is greater than or equal to 720 nm, the chelating atom is oxygen; when λ_{max} is near 620 nm, the chelating atom is the nitrogen; and for values between 620 and 720 nm, both atoms are chelating the metal ion.

3.2.1. Binary systems

3.2.1.1. Cu:ATP system. This system was already studied by us [23]. As can be seen in Table 6, the maximum wavelengths of the d–d bands shift from 818.4 to 720.4 nm as the pH rises. These values suggest that Cu(II) is bound only to oxygen atoms, that is, to two phosphate groups.

3.2.1.2. Cu:PCr system. As can be seen in Table 6, the maximum wavelengths of the d–d bands in the Cu:PCr system shift from 754.0 to 692.4 nm. This indicates that the donor atoms are one oxygen (phosphate or carboxylate) and one nitrogen (guanidine group).

3.2.1.3. Cu:aa. For all aa, the maximum wavelength of the d–d bands shift from 802 nm at lower pHs to 620 nm at more basic pHs, as can be seen in Table 6 for the Cu:Ser system. This indicates that the amino acids bind first to Cu(II) through the oxygen of the carboxylate and, as the pH rises, the nitrogen atom of the amine group is also bound.

3.2.2. Ternary systems

3.2.2.1. Cu:ATP:aa systems. In all systems it can be observed that at low pHs all the maximum wavelengths are above 720 nm. This suggests that the predominating species is not bound to a nitrogen atom. This confirms that in the ternary systems with ATP, the Cu(II) ion binds firstly to ATP, then to the oxygen atom of the amino acid and only when the pH is higher than 7 the nitrogen is coordinated. At this moment the maximum wavelength is lower than 720 nm. The values for Cu:ATP:Ser can be seen in Table 6.

3.2.2.2. Cu:PCr:aa systems. For the ternary systems Cu:PCr:aa, it is also possible to make some generalizations (see Table 6). At lower pHs, the predominant species does not have a nitrogen atom of the aa bounded, which justifies the value of $\lambda_{max} > 720$ nm. As the pH rises the amino groups of the ligands begin to deprotonate and the λ_{max} shifts to smaller values, indicating the participation of nitrogen in the coordination.

Table 6
UV spectra data at different pH values of the binary systems Cu(II):ATP, Cu:PCr and Cu:aa in a 1:1 ratio and ternary systems Cu(II):ATP:aa and Cu(II):PCr:aa in a 1:1:1 ratio at 25 °C, $I = 0.1$ mol/L (KNO_3) (aa = Gly, Ser, Thr and Tyr)

Systems	pH	λ_{max} (nm)	ε (mol^{-1} L cm^{-1})
Cu:ATP	3.55	818.4	20.88
	4.24	813.2	24.81
	6.28	782.0	30.94
	7.22	769.2	35.42
	8.46	746.8	37.33
	10.19	720.4	39.31
CuPCr	5.70	754.0	33.24
	6.31	726.8	51.94
	6.48	718.8	58.45
	6.91	700.4	70.90
	7.39	692.4	74.06
Cu:ser	3.92	766.0	20.88
	5.37	724.0	29.11
	6.30	714.0	32.07
	7.10	692.0	39.89
	8.94	634.4	59.64
	9.59	633.0	62.80
Cu:ATP:ser	3.56	794.0	22.92
	4.13	780.4	27.83
	5.37	753.2	35.38
	7.70	704.2	42.12
	8.90	695.6	44.55
Cu:PCr:ser	4.62	746.8	26.04
	6.10	710.4	39.45
	7.11	667.9	49.25
	8.13	652.4	54.46
	9.95	649.2	56.68

3.3. EPR spectral analysis

The EPR analysis was performed for the binary systems Cu:PCr and Cu:aa and for the ternary systems Cu:ATP:aa and Cu:PCr:aa. The isotropic EPR parameter A_0 of the corresponding species is shown in Table 7.

Table 7
Isotropic EPR parameter A_0 and the corresponding pH of the binary systems species Cu:aa and Cu:PCr in a 1:1 ratio and of the ternary systems Cu:ATP:aa and Cu:PCr:aa in a 1:1:1 ratio (aa = Gly, Ser, Thr and Tyr)

Predominant species	pH	A_0 ($\times 10^{-4}$), cm^{-1}
CuGly	5.82	57.5
CuSer	6.46	60.71
CuTyr	5.40	61.22
CuThr	6.23	61.5
CuATP	n.d.	n.d.
CuPCr	6.53	61.5
CuATPGly	8.21	64.0
CuATPSer	7.70	64.0
CuATPTyr	7.86	64.0
CuATPThr	7.89	64.0
CuPCrGly	9.47	64.0
CuPCrSer	8.80	64.0
CuPCrTyr	8.83	68.0
CuPCrThre	8.87	68.0

It can be observed that the A_0 parameter, which is associated to the ligand field, has lower values for the binary systems (57.5–61.5) and greater values for the ternary systems (64.0–68.0), indicating that more donor atoms are coordinated to Cu(II), which means that the ternary compounds were formed.

4. Conclusions

There are many possibilities regarding the bonding sites of ATP in Cu(II) complexes but from the values here obtained we can suggest that the donor atoms in the Cu:ATP complex are probably two oxygen atoms of phosphates [23].

The PCr molecule has three possible donor atoms: one oxygen of the phosphate group, the nitrogen atom of the guanidine group and the oxygen of the carboxylate group. Although there is the possibility of PCr acting as a tridentate ligand, this hypothesis is not probable because the value of $\log\beta_{\mathrm{CuPCr}}$ (7.89) is much lower than the value for the correspondent complex with phosphoserine (9.38) where it acts as tridentate [24]. If we compare the correspondent values of $\log\beta_{\mathrm{CuI}}$ where L = diisopropylphosphorylguanidine (DPG), which does not have the carboxylate group, or creatine (Cr), which does not have the phosphate group ($\log\beta_{\mathrm{CuDPG}} = 8.63$ [25] and $\log\beta_{\mathrm{CuCr}} = 7.20$ [15]), it can be concluded that the value of $\log\beta_{\mathrm{CuPCr}}$ can be either for coordination through the oxygen atom of the phosphate group and the nitrogen atom of the guanidine group, or through the oxygen atom of the carboxylate group and the nitrogen atom of the guanidine group. Since NMR analysis is very difficult for Cu(II) ion and far IR spectra cannot differentiate a M–O band corresponding to an oxygen of the phosphate and an oxygen of the carboxylate, we decided to study these complexes in the solid state. We synthesized a complex with Cu(II), PCr and Tyr and after its characterization we concluded that it was a complex Cu:Tyr:$PO_3H_2 \cdot H_2O$ [29] where PCr lost the creatine molecule. So it is more probable that the oxygen atom bound to Cu(II) in the Cu–PCr complex is that of the phosphate.

The values of the stability constants of the ternary Cu(II) complexes with the amino acid polyamines and ATP or PCr indicate that these are stable complexes. This behavior was confirmed by the increase of the maximum wavelength in the absorption spectra and the increase of the A_0 parameter of the EPR analyses when we compare them with the binary complexes. $\Delta\log K(\log\beta_{\mathrm{CuaaL}} - (\log\beta_{\mathrm{Cuaa}} + \log\beta_{\mathrm{CuLATP}}))$, aa = Gly, Ser, Tyr and Thr, and L = ATP or PCr, showed that in all cases but when aa = Ser or Tyr and L = PCr, the ternary complexes are less stable than the binary ones, suggesting that in most cases no interaction occurs between the ligands in the ternary complexes. This probably only occurs when L = PCr and aa = Ser or Tyr. Since PCr acts as a bidentate ligand, there is one non-coordinated position and both Ser and Tyr have an OH group free. Since the possibility of interaction does not occur when the amino acid is Gly, which does not have an OH group, it seems that the interaction in the ternary complexes of PCr with Ser and Tyr is between a phosphate or carboxylate (probably carboxylate) of PCr and the OH group of the amino acids. These results can help understand biological interactions among a phosphorylated ligand, an amino acid containing an hydroxyl group and the metal ion Cu(II).

Appendix A. Supplementary data

Supplementary data associated with this article can be found, in the online version, at doi:10.1016/j.poly.2005.09.016.

References

[1] S. Johnson, Med. Hypotheses 53 (5) (1999) 407.
[2] C.R. Zhao, L. Shang, W. Wang, D.O. Jacobs, J. Surg. Res. 105 (1) (2002) 10.
[3] S.M. Vanderwerf, M.J. Cooper, I.V. Stetsenko, S. Lutsenko, J. Biol. Chem. 266 (39) (2001) 36289.
[4] J.A. Bertrand, S. Thieffine, A. Vulpetti, C. Crisitiane, B. Valasina, S. Knapp, H.M. Kalisz, M. Flocco, J. Mol. Biol. 333 (2) (2003) 393.
[5] S.I. Itani, A.K. Saha, T.G. Kurowski, H.R. Coffin, K. Tornheim, N.B. Ruderman, Diabetes 52 (7) (2003) 1635.
[6] Y. Hiraku, J. Sugimoto, T. Yamaguchi, S. Kawanishi, Arch. Biochem. Biophys. 365 (1) (1999) 62.
[7] A. Ferri, R. Gabbianelli, A. Casciati, F. Celsi, G. Rotilio, M.T. Carri, J. Neurochem. 79 (3) (2001) 531.
[8] W. Kaim, B. Schwederski, Bioinorganic Chemistry: Inorganic Elements in the Chemistry of Life, Wiley, Chichester, 1994.
[9] W.H. Elliot, D.C. Elliot, Biochemistry and Molecular Biology, 2nd ed., Oxford University Press, Oxford, 2002, p. 296.
[10] D.L. Nelson, M.M. Cox, Lehniger Principles of Biochemistry, 3rd ed., Worth Publishers, New York, 2004, p. 510.
[11] T. Kiss, in: K. Burger (Ed.), Biocoordination Chemistry, Ellis Horwood, Nova York, 1990.
[12] P.S. Gans, A.J. Vacca, J. Chem. Soc., Dalton Trans. (1985) 1195.
[13] R. Sylva, M.J. Davidson, Chem. Soc., Dalton Trans (1979) 232.
[14] H. SigelMetal Ions in Biological Systems: Mixed Ligand Complexes, vol. 2, Marcel Dekker, New York, 1973, p. 3.
[15] IUPAC Stability Constants Database, Release 3, Version 3.02, 1998; compiled by L.D. Pettit, H.K.J. Powell, Academic Software, Timble, Otley, West Yorkshire, UK, 1998.
[16] M.J. Khalil, Chem. Eng. Data 45 (2000) 70.
[17] W.D. Kumler, J.J.J. Eiler, Am. Chem. Soc. 65 (1943) 2355.
[18] G. Andreregg, S. Khileif, Talanta 42 (1995) 1067.
[19] C. Rondgi, L. Huakuan, Acta Chim. Sinica (1988) 808.
[20] L. Gasque, R. M-Esorza, L.J. Ramiriz, Inorg. Biochem. 48 (1992) 121.
[21] R. Cini, A. Cinquantini, R. Seeber, Inorg. Chim. Acta 123 (1986) 69.
[22] R. Smith, A.E. Martell, Y. Chen, Pure Appl. Chem. 63 (1991) 1015.
[23] J.A. da Silva, J. Felcman, A.L.R. Mercê, A.S. Mangrich, R.S.C. Lopes, C.C. Lopes, Inorg. Chim. Acta 356 (2003) 155.
[24] E.H. Abbot, M.S. Mohan, Inorg. Chem. 17 (1978) 2203.
[25] C.C.N. Lopes, Doctorade Dissertation, Department of Chemistry, PUC-Rio, Brazil, 2001.
[26] G. Arena, R. Calì, V. Cucinotta, S. Musumeci, E.R.S. Sammartano, Thermochim. Acta 74 (1984) 77.
[27] R.S.J. Phillips, J. Annu. Rev. (1966) 501.
[28] B. Pullman, Eletronic Aspects of Biochemistry, Academic Press Inc., New York, 1964, p. 519.
[29] I.G. Silva, Master Thesis, Department of Chemistry, PUC-Rio, Brazil, 2003.

with a Nicolet Avatar 360 FT-IR spectrometer using the KBr pellet technique. Thermogravimetric analyses were conducted on a SDT Q600 Thermal Analyzer using a heating rate of 5 °C/min from room temperature to 900 °C.

2.2. Synthesis

2.2.1. [Zn(cca)(phen)]$_n$ (1)

A mixture of H_2cca (0.020 g, 0.1 mmol), $Zn(Ac)_2 \cdot 2H_2O$ (0.022 g, 0.1 mmol), phen · H_2O (0.020 g, 0.1 mmol), NaOH aqueous solution (0.3 ml, 0.65 mol l^{-1}) and deionized water (5 ml) was sealed in a Teflon-lined stainless vessel (25 ml), and heated at 140 °C for 72 h under autogenous pressure, then cooled slowly to room temperature. Colorless single crystals were obtained by filtration, washed with water and ethanol, and dried in air. Yield: 0.038 g (87.2%). *Anal*. Calc. for $C_{22}H_{14}N_2O_4Zn$: C, 60.59; H, 3.21; N. 6.43. Found: C, 60.34; H, 3.59; N, 6.38%. IR data (KBr pellet, cm^{-1}): 3442m, 1640m, 1625m, 1599s, 1555m, 1518m, 1428s, 1383s, 1355s, 1237w, 1142w, 1105w, 982w, 869w, 845w, 789m, 725s.

2.2.2. [Co(cca)$_{0.5}$(Hcca)(phen)(H_2O)] (2)

The synthesis of complex **2** followed the similar procedure as for complex **1**, but using $CoCl_2 \cdot 6H_2O$ and heated at 120 °C. Yield: 0.015 g (27.6%). *Anal*. Calc. for $C_{27}H_{20}N_2O_7Co$: C, 59.65; H, 3.68; N, 5.15. Found: C, 59.43; H, 3.39; N, 4.77%. IR data (KBr pellet, cm^{-1}): 3440s, 1689m, 1608m, 1427s, 1384s, 984w, 841w, 789m, 726m, 685w.

2.2.3. [Cu(cca)(phen)]$_n \cdot nH_2O$ (3)

The synthesis of complex **3** followed the similar procedure as for complex **1**, but using $CuCl_2 \cdot 2H_2O$. Yield: 0.036 g (79.7%). *Anal*. Calc. for $C_{22}H_{16}N_2O_5Cu$: C, 58.42; H, 3.54; N, 6.20. Found: C, 58.34; H, 3.29; N, 6.19%. IR data (KBr pellet, cm^{-1}): 3425s, 1640m, 1590s, 1551m, 1517m, 1425s, 1360s, 1235w, 1175w, 1106w, 1049w, 985w, 854m, 787m, 724s, 648w.

2.2.4. [Mn(cca)(phen)(H_2O)]$_n \cdot 0.25nH_2O$ (4)

The synthesis of complex **4** followed the similar procedure as for complex **1**, but using $Mn(Ac)_2 \cdot 2H_2O$. Yield: 0.02 g (44.7%). *Anal*. Calc. for $C_{22}H_{16.5}N_2O_{5.25}Mn$: C, 58.96; H, 3.68; N, 6.25. Found: C, 59.07; H, 3.52; N, 6.52%. IR data (KBr pellet, cm^{-1}): 3439s, 1650s, 1597m, 1553m, 1511w, 1425m, 1379s, 1345m, 1241w, 1098w, 1042w, 987w, 852w, 789w, 730w, 712w.

2.3. X-ray diffraction determination

Diffraction intensities for the four complexes were collected at 293 K on a Bruker SMART 1000 CCD area detector diffractometer employing graphite monochromatized Mo Kα radiation ($\lambda = 0.71073$ Å) in ϕ and ω scan modes. Semi-empirical absorption correction was applied on the four complexes using the SADABS program [25]. The structures were solved by direct methods [26] and refined by full-matrix least-squares method on F^2 using SHELXS 97 and SHELXL 97 programs, respectively [26,27]. Non-hydrogen atoms were refined anisotropically. Hydrogen atoms were placed in geometrically calculated positions. The crystallographic data for complexes **1**–**4** are listed in Table 1, selected bond lengths (Å) and bond angles (°) in Table 2.

3. Results and description

3.1. Description of the structures

In complexes **1**–**4**, the ligands derived from H_2cca proligand adopt three kinds of coordination modes, as shown in Scheme 1. The coordination mode Scheme 1a has been reported [24].

Table 1
Crystal data and structure refinement parament for complexes **1**–**4**

	1	2	3	4
Chemical formula	$C_{22}H_{14}N_2O_4Zn$	$C_{27}H_{20}N_2O_7Co$	$C_{22}H_{16}N_2O_5Cu$	$C_{22}H_{16.50}N_2O_{5.25}Mn$
Formula weight	435.71	543.37	451.91	447.80
Crystal system	monoclinic	triclinic	monoclinic	monoclinic
Space group	$C2/c$	$P\bar{1}$	$C2/c$	$C2/c$
a (Å)	21.859(3)	10.016(2)	5.139(1)	18.326(2)
b (Å)	11.665(2)	11.087(2)	18.853(4)	14.053(1)
c (Å)	7.375(2)	12.435(2)	20.981(4)	16.289(2)
α (°)	90	73.898(3)	90	90
β (°)	100.301(3)	89.221(3)	90.066(4)	103.642(2)
γ (°)	90	65.777(3)	90	90
V (Å^3)	1850.3(6)	1202.0(4)	2033.1(7)	4076.6(8)
Z	4	2	4	8
$F(000)$	880	558	924	1836
D_{calc} (Mg/m^3)	1.557	1.499	1.476	1.453
θ Range (°)	1.99–25.00	2.24–25.01	2.16–25.00	1.85–25.01
Goodness-of-fit	1.125	1.039	1.063	1.050
Final R indices, [$I > 2\sigma(I)$]	$R_1 = 0.0697$, $wR_2 = 0.2158$	$R_1 = 0.0527$, $wR_2 = 0.1301$	$R_1 = 0.0586$, $wR_2 = 0.0787$	$R_1 = 0.0751$, $wR_2 = 0.1934$

Table 2
Selected bond distances (Å) and angles (°) for complexes **1**–**4**

Complex ***1***			
Zn(1)–O(1)	2.088(4)	Zn(1)–N(1)	2.318(5)
Zn(1)–O(2)#2	2.198(4)		
O(1)–Zn(1)–O(1)#1	113.4(2)	O(2)#2–Zn(1)–O(2)#3	168.3(2)
O(1)–Zn(1)–O(2)#2	100.4(2)	O(2)#2–Zn(1)–N(1)	84.9(2)
O(1)–Zn(1)–O(2)#3	86.1(2)	O(2)#3–Zn(1)–N(1)	85.5(2)
O(1)–Zn(1)–N(1)	88.2 (2)	O(2)#2–Zn(1)–N(1)#1	85.5(2)
O(1)–Zn(1)–N(1)#1	157. 8(2)	O(2)#3–Zn(1)–N(1)#1	84.9(2)
O(1)#1–Zn(1)–O(2)#2	86.1(2)	N(1)–Zn(1)–N(1)#1	70.9(2)
O(1)#1–Zn(1)–O(2)#3	100.4(2)		
Complex ***2***			
Co(1)–O(1)	1.988(3)	Co(1)–N(1)	2.205(3)
Co(1)–O(3)	2.012(3)	Co(1)–N(2)	2.079(3)
Co(1)–O(7)	1.975(3)		
O(1)–Co(1)–O(3)	96.1(1)	O(3)–Co(1)–N(1)	168.7(1)
O(1)–Co(1)–O(7)	127.1(1)	O(3)–Co(1)–N(2)	92.2(1)
O(1)–Co(1)–N(1)	92.4(1)	O(7)–Co(1)–N(1)	85.7(1)
O(1)–Co(1)–N(2)	118.4(1)	O(7)–Co(1)–N(2)	112.5(1)
O(3)–Co(1)–O(7)	95.1(1)	N(2)–Co(1)–N(1)	77.1(1)
Complex ***3***			
Cu(1)–O(1)	1.93(3)	Cu(1)–N(1)	2.012(4)
Cu(1)–O(3)#3	1.95(3)		
O(1)–Cu(1)–O(1)#1	96.3(2)	O(3)#3–Cu(1)–N(1)	165.8(7)
O(1)–Cu(1)–O(3)#3	93.1(3)	O(3)#3–Cu(1)–N(1)#1	93.8(9)
O(1)–Cu(1)–N(1)	90.6(8)	N(1)–Cu(1)–N(1)#1	82.5(3)
O(1)–Cu(1)–N(1)#1	173.1(8)		
Complex ***4***			
Mn(1)–O(1)	1.946(5)	Mn(1)–N(1)	2.173(6)
Mn(1)–O(3)	1.984(5)	Mn(1)–N(2)	2.094(6)
Mn(1)–O(5)	2.057(5)		
O(1)–Mn(1)–O(3)	108.8(3)	O(3)–Mn(1)–N(1)	86.0(2)
O(1)–Mn(1)–O(5)	106.1(2)	O(3)–Mn(1)–N(2)	139.8(2)
O(1)–Mn(1)–N(1)	98.1(2)	O(5)–Mn(1)–N(1)	155.4(2)
O(1)–Mn(1)–N(2)	109.4(2)	O(5)–Mn(1)–N(2)	90.9(2)
O(3)–Mn(1)–O(5)	90.2(2)	N(2)–Mn(1)–N(1)	76.9(2)

Symmetry transformations used to generate equivalent atoms: (#1) $-x$, y, $-z+3/2$; (#2) $-x$, $-y$, $-z+2$ and (#3) x, $-y$, $z-1/2$ for **1**, (#1) $-x+1$, y, $-z+1/2$; (#2) $-x+1/2$, $-y+1/2$, $-z$ and (#3) $x+1/2$, $-y+1/2$, $z+1/2$ for **3**.

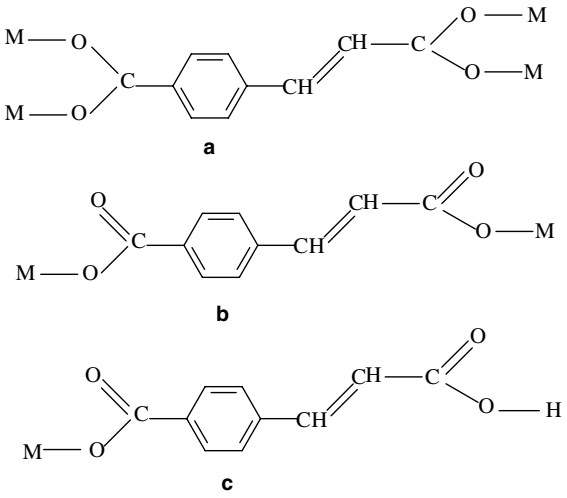

Scheme 1. The coordination modes of the ligands derived from H_2cca proligand in complexes **1**–**4**.

3.1.1. *[Zn(cca)(phen)]$_n$ (**1**)*

There is only one metal ion environment in complex **1**. As shown in Fig. 1, Zn(II) ion is placed in a distorted octahedron, which is completed by four oxygen atoms of four cca^{2-} anions and two nitrogen atoms of one phen ligand with the same Zn–N distance. In complex **1**, each cca^{2-} anion adopts a bis(bridging-bidentate) mode, bridging four Zn(II) ions (see Scheme 1a). All Zn(II) ions are linked by cca^{2-} anions into a three-dimensional MOF with channels of 12.388×13.381 Å (defined by the separation between two adjacent zinc atoms, see Fig. 2). Chelating phen ligand occupies the diagonal position, which greatly decreases the dimensions of the cavities. All phen rings in complex **1** are parallel to each other, and the nearest face-to-face distance is 3.29 Å, indicating the presence of π–π stacking interaction, which stabilizes the structure.

3.1.2. *[Co(cca)$_{0.5}$(Hcca)(phen)(H$_2$O)] (**2**)*

Complex **2** is a three-dimensional supramolecular structure constructed by coordination bonds, hydrogen bonds and π–π stacking interactions. Not all H_2cca ligands are completely deprotonated. Two types of coordination modes for anions of H_2cca ligands are present in the structure: (a) each carboxylate group of cca^{2-} anion adopts a monodentate mode, bridging two Co(II) ions (see Scheme 1b); (b) H_2cca ligand is partially deprotonated, forming $Hcca^-$ anion, which coordinates with Co(II) ions in monodentate mode (see Scheme 1c). The coordination environment of Co(II) ion is shown in Fig. 3. Each Co(II) ion is coordinated by two nitrogen atoms of one phen ligand and three oxygen atoms, one of which comes from a $Hcca^-$ anion, one from a cca^{2-} anion, and one from a water molecule. The coordination geometry of Co(II) ion can be described as trigonal bipyramid. Two Co(II) ions connected by a cca^{2-} anion constitute the basic building block, as shown in Fig. 3. Different kinds of hydrogen bonds are observed between the building blocks: (a) hydrogen bonds between the undeprotonated carboxylate groups and uncoordinated carboxylate oxygen atoms (O···O

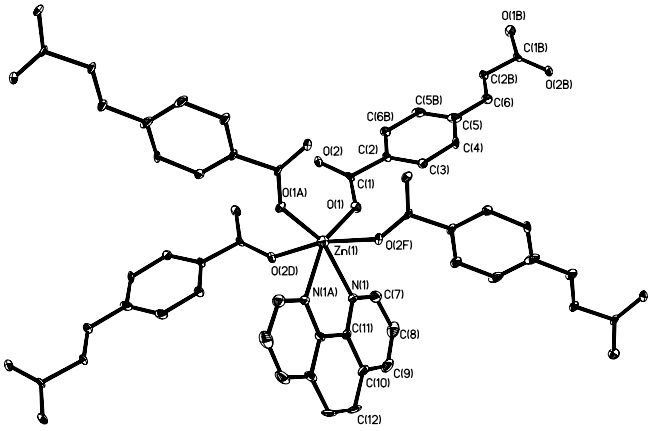

Fig. 1. The coordination environment of Zn(II) ion in complex **1** with 30% thermal ellipsoids, all hydrogen atoms are omitted for clarity.

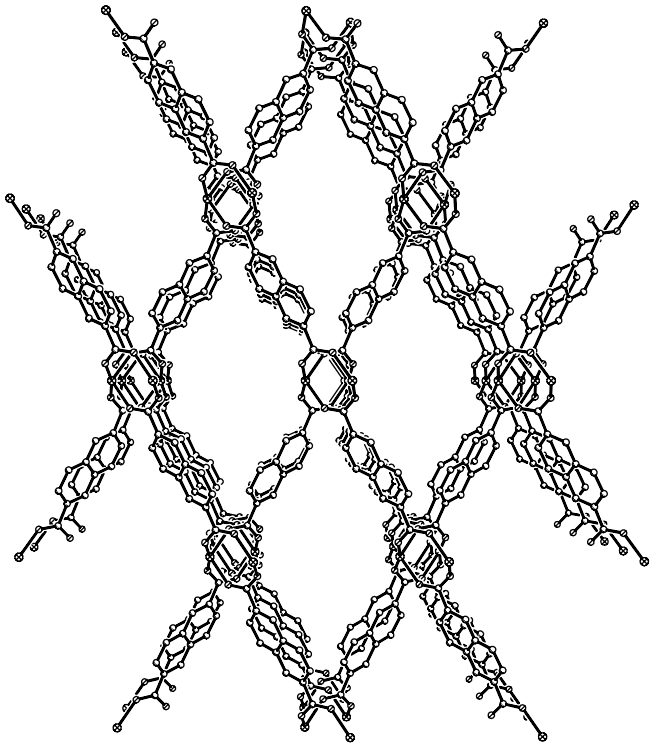

Fig. 2. The three-dimensional network of complex **1** viewed along the *c*-axis, phen molecules and all hydrogen atoms are omitted for clarity.

distance: 2.617 Å); (b) hydrogen bonds between the coordinated water molecules and uncoordinated carboxylate oxygen atoms (O···O distance: 2.713, 2.584 Å). These hydrogen bonds bring the building blocks into a layer structure with cavities of 13.626 × 15.861 Å (see Fig. 4). Chelating phen ligands lie at the diagonal lines, just the same as that in complex **1**. There are π–π stacking interactions between the phen rings (face-to-face distance: 3.29 Å), which causes the formation of a three-dimensional supramolecular network.

3.1.3. $[Cu(cca)(phen)]_n \cdot nH_2O$ (**3**)

The coordination environment of Cu(II) ion in complex **3** is shown in Fig. 5. Each Cu(II) ion is four-coordinated by two oxygen atoms of two cca^{2-} anions and two nitrogen atoms of one phen molecule with the same Cu–N bond length. The coordination geometry can be described as planar square. In complex **3**, cca^{2-} anions adopt bis(monodentate) mode (see Scheme 1b), linking Cu(II) ions into one-dimensional zigzag chains. There are hydrogen bonds between the crystal water molecules and the uncoordinated carboxylate oxygen atoms (O···O distance: 2.811 Å), which brings the chains into layers. All phen rings are parallel to each other and the nearest separation is 3.50 Å along the *a*-axis, showing the presence of π–π stacking interaction. It is the hydrogen bonds and the π–π stacking

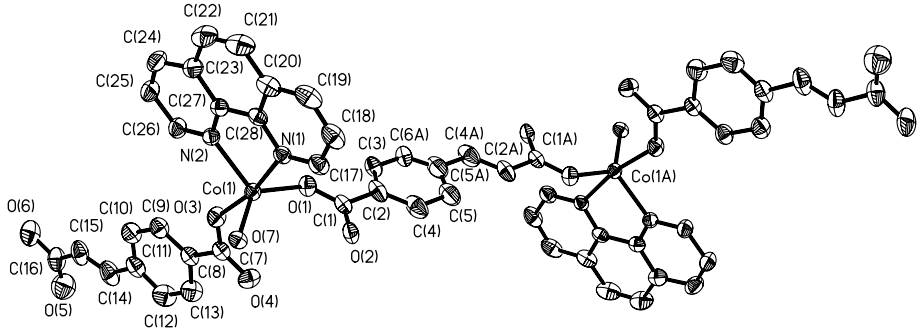

Fig. 3. The coordination environment of Co(II) ion in complex **2** with 30% thermal ellipsoids, all hydrogen atoms are omitted for clarity.

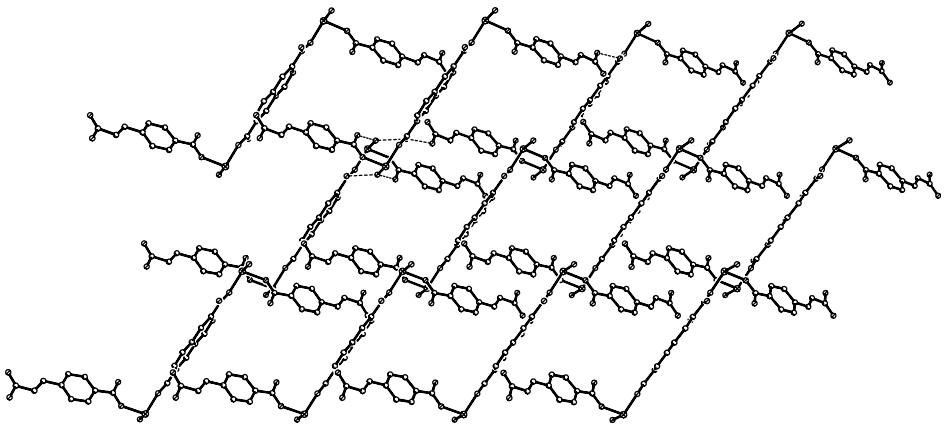

Fig. 4. Layer structure of complex **2** viewed along the *a*-axis, all phen molecules are omitted for clarity.

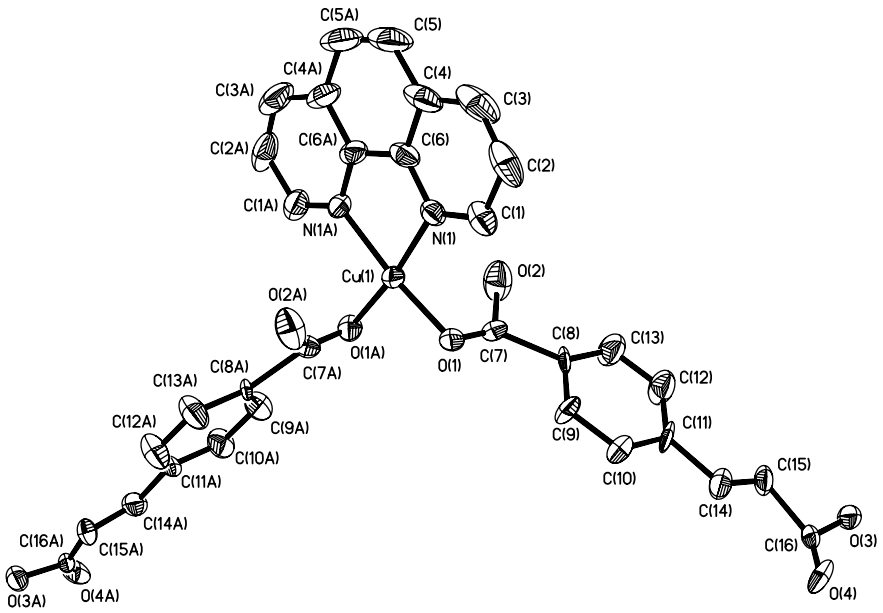

Fig. 5. The coordination environment of Co(II) ion in complex **3** with 30% thermal ellipsoids, all hydrogen atoms are omitted for clarity.

interactions that makes the formation of a three-dimensional supramolecular network, and crystal water molecules are enclosed, as shown in Fig. 6.

3.1.4. $[Mn(cca)(phen)(H_2O)]_n \cdot 0.25nH_2O$ (**4**)

There is only one type of metal ion environment in complex **4**. As shown in Fig. 7, each Mn(II) ion is placed in a distorted trigonal bipyramid, which is completed by two oxygen atoms of two cca^{2-} anions, one oxygen atom of one water molecule and two nitrogen atoms of one phen molecule. In complex **4**, each cca^{2-} anion adopts a bis(monodentate) mode (see Scheme 1b), bridging two Mn(II) ions. All Mn(II) ions are linked by cca^{2-} anions into one-dimensional zigzag chains, as shown in Fig. 8. There are hydrogen bonds between coordinated water molecules and uncoordinated carboxylate atoms (O···O distance: 2.922 Å) and π–π stacking interactions (face-to-face distance: 3.58 Å), which results in the formation of a three-dimensional structure.

From the above descriptions, it can be seen that although with same ligands H_2cca and phen, complexes **1**–**4** have different structures. In complex **1**, each cca^{2-} anion adopts a bis(bridging-bidentate) mode. Zn(II) ions are six-coordinated and linked by cca^{2-} anions into a three-dimensional structure; In complex **2**, each cca^{2-} anion adopts a bis(monodentate) mode and each $Hcca^{-}$ anion adopts a

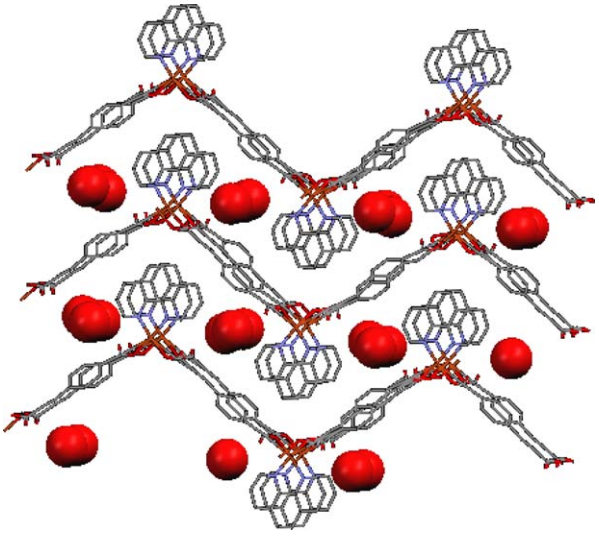

Fig. 6. Three-dimensional structure of complex **3** viewed along the *a*-axis, all hydrogen atoms are omitted for clarity, red balls represent the free water molecules.

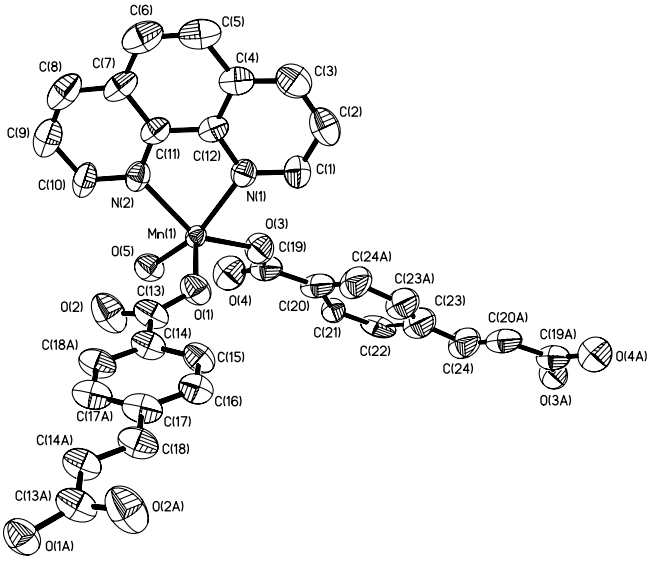

Fig. 7. The coordination environment of Mn(II) ion in complex **4** with 30% thermal ellipsoids, all hydrogen atoms are omitted for clarity.

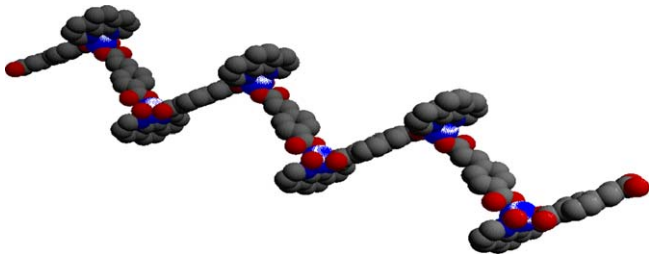

Fig. 8. The one-dimensional zigzag chain in complex **4** viewed along the *b*-axis.

monodentate mode. Co(II) ions are five-coordinated and constitute a dinuclear structure; In complexes **3** and **4**, each cca^{2-} anion adopts a bis(monodentate) mode. Metal(II) ions are all linked by cca^{2-} anions into one-dimensional zigzag chains. However, Cu(II) ions are four-coordinated, while Mn(II) ions are five-coordinated, in which one water molecule occupies the fifth coordination site. So we can conclude that the coordination number/or coordination geometry of the metal center, coordination modes of ligands, hydrogen bonds and π–π stacking interactions have profound influences on the supramolecular network.

3.2. Thermal analyses

Thermogravimetric analyses of complexes **2**–**4** were carried out to examine their water loss and thermal stabilities. For complex **2**, the first weight loss of 3.1% from 226 to 270 °C corresponds to the loss of coordinated water molecules (calc. 3.3%). Increasing temperature led to further decomposition above 370 °C. For complex **3**, the first weight loss of 3.7%, which occurred from 35 to 143 °C, corresponds to the loss of crystal water molecules (calc. 4.0%). The further decomposition of complex **3** occurred above 243 °C. While for complex **4**, it lost its crystal water molecules from 75 to 168 °C and further decomposed above 345 °C.

4. Supplementary data

Crystallographic data for the structural analysis have been deposited with the Cambridge Crystallographic Data Centre, CCDC Nos. 278646–278649 for **1**–**4**, respectively. Copies of this information may be obtained free of charge from the CCDC, 12 Union Road, Cambridge, CB2 1EZ, UK (fax:+44 1223 336 033; e-mail: deposit@ccdc.cam.ac.uk or www: http://www.ccdc.cam.ac.uk).

Acknowledgment

This project is supported by National Nature Science Foundation of China (20331010).

References

[1] J.S. Seo, D. Whang, H. Lee, S.I. Jun, J. Oh, Y.J. Jeon, K. Kim, Nature 404 (2000) 982.
[2] B. Gomez-Lor, E. Gutiérrez-Puebla, M. Iglesias, M.A. Monge, C. Ruiz-Valero, N. Snejko, Inorg. Chem. 41 (2002) 2429.
[3] K.P. Mörtl, J.P. Sutter, S. Golhen, L. Ouahab, O. Kahn, Inorg. Chem. 39 (2000) 1626.
[4] Z.L. Huang, M. Drillon, N. Masciocchi, A. Sironi, J.T. Zhao, P. Rab, P. Panissod, Chem. Mater. 12 (2000) 2805.
[5] M. Riou-Cavellec, C. Albinet, J.M. Grenèche, G. Férey, J. Mater. Chem. 11 (2001) 3166.
[6] J. Guilhem, L. Tchertanov, K. Nakatani, J. Am. Chem. Soc. 122 (2000) 9444.
[7] T.M. Reineke, M. Eddaoudi, M. Fehr, D. Kelley, O.M. Yaghi, J. Am. Chem. Soc. 121 (1999) 1651.
[8] C. Reinhard, H.U. Güdel, Inorg. Chem. 41 (2002) 1048.
[9] J. Lehn, Angew. Chem. Int. Ed. 29 (1990) 1304.
[10] M. Eddaoudi, D.B. Moler, H. Li, B. Chen, T.M. Reineke, M. O'Keeffe, O.M. Yaghi, Acc. Chem. Res. 34 (2001) 319.
[11] C. Ruiz-Pérez, P. Lorenzo-Luis, M. Hernández-Molina, M.M. Laz, F.S. Delgado, P. Gili, M. Julve, Eur. J. Inorg. Chem. (2004) 3873.
[12] M. Oh, G.B. Carpenter, D.A. Sweigart, Angew. Chem., Int. Ed. 42 (2003) 2025.
[13] F.A.A. Paz, J. Klinowski, Inorg. Chem. 43 (2004) 3882.
[14] B.Q. Ma, P. Coppens, Chem. Commun. (2003) 2290.
[15] M. Liang, Q.L. Wang, L.H. Yu, D.Z. Liao, Z.H. Jiang, S.P. Yan, P. Cheng, Polyhedron 23 (2004) 2203.
[16] E. Coronado, J.R. Galán-Mascarós, C.J. Gómez-García, E. Martínez-Ferrero, S.V. Smaalen, Inorg.Chem. 43 (2004) 4808.
[17] J. Tao, M.L. Tong, X.M. Chen, J. Chem. Soc., Dalton Trans. (2000) 3669.
[18] S.A. Bourne, J. Lu, A. Mondal, B. Moulton, M.J. Zaworotko, Angew. Chem., Int. Ed. 40 (2001) 2111.
[19] J. Sun, L. Weng, Y. Zhou, J. Chen, Z. Chen, Z. Liu, D. Zhao, Angew. Chem., Int. Ed. 41 (2002) 4471.
[20] J.F. Ma, J. Yang, G.L. Zheng, L. Li, J.F. Liu, Inorg. Chem. 42 (2003) 7531.
[21] D.N. Dybtsev, H. Chun, K. Kim, Angew. Chem., Int. Ed. 43 (2004) 5033.
[22] C.B. Liu, C.Y. Sun, L.P. Jin, S.Z. Lu, New J. Chem. 28 (2004) 1019.
[23] Y.B. Wang, X.J. Zheng, W.J. Zhuang, L.P. Jin, Eur. J. Inorg. Chem. (2003) 3572.
[24] H. Kumagai, Y. Oka, K. Inoue, M. Kurmoo, J. Chem. Soc., Dalton Trans. (2002) 3442.
[25] G.M. Sheldrick, SADABS, Program for Empirical Absorption Correction of Area detector Data, University of Göttingen, Germany, 1997.
[26] G.M. Sheldrick, SHELXS 97, Program for Crystal Structure Solution, University of Göttingen, Germany, 1997.
[27] G.M. Sheldrick, SHELXS 97, Program for Crystal Structure Refinement, University of Göttingen, Germany, 1997.

show only a singlet. δP values are −51.171, 67.665, and 13.640 ppm, respectively. $[Pd(L\text{-}L)(dppmS_2)](ClO_4)_2$ complexes were prepared by mixing of solution of $Pd(L\text{-}L)CI_2$ complexes in CH_2CI_2 and $dppmS_2$ ligand in $(CH_3)_2CO$ and in the presence of $NaClO_4 \cdot H_2O$ salt.

Analytical data of three yellow complexes are in accordance with the proposed formulation. Solid state IR spectra of the complexes **1**–**3** showed the characteristic absorption of P═S group at 585, 585 and 577 cm^{-1}, respectively. This bond in each complex is displaced towards lower frequencies as compared with the free ligand and corresponds to the coordinated P═S group. It clearly shows that $dppmS_2$ is coordinating to Pd(II) metal center via S donor atoms. ClO_4^- group vibrations give rise to two bands in 1100 and 620 cm^{-1} region. These values are consisted with the literature values [10].

In the case of $[Pd(dppe)(dppmS_2)](ClO_4)_2$ (**2**) and $[Pd(dppp)(dppmS_2)](ClO_4)_2$ (**3**), the resonances due to the dppe and dppp phosphorus atoms appear at 78.50 and 14.04 ppm, respectively. In the case of $[Pd(dppm)(dppmS_2)](ClO_4)_2$ (**1**), the chemical shift of dppm is −43.40 ppm. It has been seen that the signals of chelated diphosphine ligands are shifted to the down field relative to the starting complexes. Phosphorus chemical shifts of $dppmS_2$ are 40.50; 40.60 and 38.00 ppm in complexes **1**–**3**, respectively. These values have shown a small increase on coordination, relative to the free $dppmS_2$ ligand (34.5 ppm). In most of the present cases, the phosphorus of the P═S groups experiences a small increase in shielding on coordination. The range for $\Delta\delta$ is +2 to −11 ppm [11]. This might be expected since the metal is attached a site remote from the NMR active phosphorus nuclei (see Fig. 1).

Complex **1** was recrystalized from acetone–ether and includes one molecule acetone, and complex **3** was recrystalized from acetonitrile–ether for X-ray crystallography. The perspective views of complexes **1a** and **3** are given in Figs. 2 and 3, respectively. The selected bond distances and angles are listed in Table 1.

Both complexes adopt a monoclinic crystal system. $(CH_3)_2CO$ lies in the lattice as a non-bonded molecule in complex **1a**.

Palladium atoms in complex **1a** and **3** are distorted square planar environments (sum of the angles are 360.06 and 360.57) with from P(3)Pd(1)S(2) and P(4)Pd(1)S(1) angles of 93.80(5)° and 92.25(4)° for complex **1a**; P(4)Pd(1)S(2) and P(3)Pd(1)S(1) angles of 172.42(4)° and 173.43(4)° for complex **3**. There is a small difference in bite angles of diphosphine disulphide, [S(1)Pd(1)S(2); 102.05(4)° for complex **1a** and 97.19(4)° for complex **3**]. This difference should be related with the diphosphines bite angles [P(3)Pd(1)P(4); 71.96(5)° for complex **1a** and P(4)Pd(1)P(3); 88.97(4)° for complex **3**].

Pd–S bond lengths are slightly different from each other. Pd(1)–S(1) and Pd(1)–S(2) are 2.3850(12) and 2.4069(13) Å

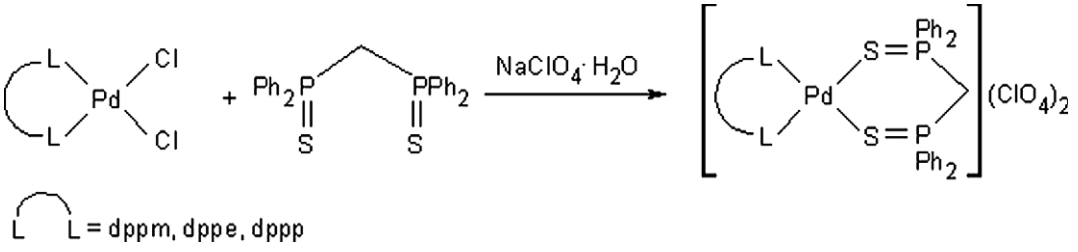

Fig. 1. Synthetic pathway of complexes $[Pd(L\text{-}L)(dppmS_2)]$ $(ClO_4)_2$.

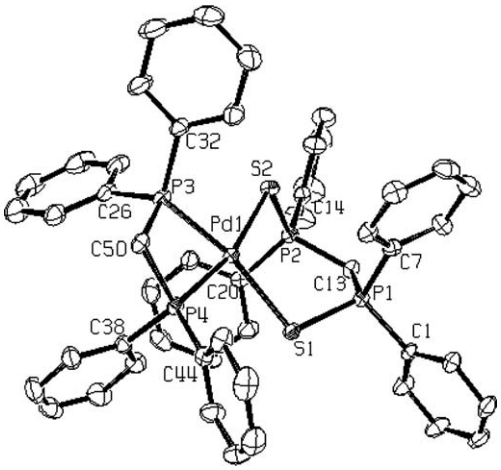

Fig. 2. The perspective view of **1a** (20% thermal probability). Hydrogen atoms, anions and solvent molecule are omitted for clarity.

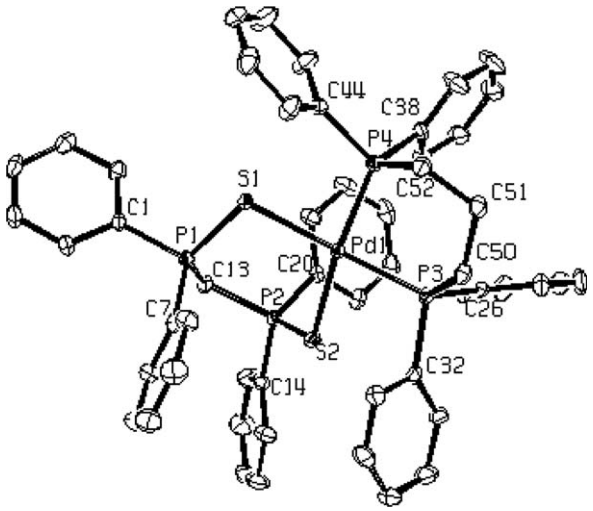

Fig. 3. The perspective views of **3** (20% thermal probability). Hydrogen atoms, anions are omitted for clarity.

Table 1
Selected bond angles (°) and distances (Å) for $[Pd(dppm)(dppmS_2)](ClO_4)_2 \cdot (CH_3)_2CO$ (**1a**) and $[Pd(dppp)(dppmS_2)](ClO_4)_2$ (**3**)

	1a	3
Bond distances		
Pd(1)–S(1)	2.3850(12)	2.3878(10)
Pd(1)–S(2)	2.4069(13)	2.3960(10)
P(1)–S(1)	2.0026(18)	1.9994(14)
P(2)–S(2)	2.0064(17)	1.9966(14)
Pd(1)–P(3)	2.2601(13)	2.2888(10)
Pd(1)–P(4)	2.2620(13)	2.2859(10)
Bond angles		
S(1)–Pd(1)–S(2)	102.05(4)	97.19(4)
P(4)–Pd(1)–S(2)	165.60(5)	172.42(4)
P(3)–Pd(1)–P(4)	71.96(5)	88.97(4)
P(3)–Pd(1)–S(1)	164.07(5)	173.43(4)
P(3)–Pd(1)–S(2)	93.80(5)	86.65(4)
P(4)–Pd(1)–S(1)	92.25(4)	87.76(4)

for complex **1a**. Pd(1)–S(1) and Pd(1)–S(2) are 2.3878(10) and 2.3960(10) Å for complex **3**. These are comparible with *cis*-$[Pd(\eta^1\text{–}S\text{–}C_5H_4NS)_2(dppe)]$ [12] and $Ni[N(SPPh_2)_2\text{–}SS^1]_2$ [13] complexes reported in the literatures.

In complex **3**, six membered dppp chelate ring has a chair conformation with Pd(1)–P(3)–C(50)–C(51) and Pd(1)–P(4)–C(52)–C(51) torsion angles of −59.4(4)° and 57.4(4)°, respectively, and with Pd(1) and C(51) atoms located 0.768 Å below and 0.818 Å above the plane defined by atoms P(3)–P(4)–C(50)–C(52). $dppmS_2$ rings are twist–boat and boat conformations in both complexes, respectively [14].

P–S bond lengths are 2.0026(18) and 2.0064(17) Å for complex **1a**; 1.9994(14) and 1.9966(14) Å for complex **3**. These values are agreement with $[Te_2(\mu\text{-}CI)_2\{(SPPh_2)_2N\}_2]$ complex reported in the literature [15].

Pd–P bond distances [2.2601(13) and 2.2620(13) for complex **1a**; 2.2859(10) and 2.2888(10) Å for **3**] are consisted with the mean Pd–P distance observed in the complex *cis*-$[Pt(\eta^1\text{–}S\text{–}C_5H_4NS)_2(dppe)]$ [12] but shorter than $[Pt(dppe)(PPh_3)(CHNMe_2)]^{2+}$ complex reported by Ferguson et al. [16].

3. Experimental

Solvents were dried according to the methods given in the literature and were purified under inert conditions [17]. All synthesis were carried using standard Schlenk tube techniques under inert atmosphere.

dppm, dppe, dppp, $NaClO_4 \cdot H_2O$ and acetone were purchased from Merck Chemical; dichloromethane, toluene, methanol, hexane and diethylether were purchased from Lab-Scan. The starting complexes, $[PdCl_2(COD)]$ (COD = 1,5-cyclooctadiene)[18], which is used for preparing the $[PdCI_2(L\text{-}L)]$ complexes [L-L = dppm ($Ph_2PCH_2PPh_2$), dppe ($Ph_2PCH_2CH_2PPh_2$), dppp ($Ph_2PCH_2CH_2CH_2PPh_2$)] [19], $dppmS_2$ ($Ph_2P(S)CH_2P(S)Ph_2$) [20] were synthesized according to the methods given in the literature.

$^{31}P\{^1H\}$ NMR spectra were recorded on Varian AS 400+Mercury instruments, chemical shifts, in ppm, related to external 85% H_3PO_4. Coupling constants are in Hz. IR spectra were recorded from 4000 to 400 cm^{-1} with a Perkin–Elmer 1600 FT-IR instrument. Melting points were determined by electrothermal melting point detection apparatus. Elemental analyses were performed by the Midwest Microlab in Indianapolis, USA.

3.1. $[Pd(dppm)(dppmS_2)](ClO_4)_2$ (1)

$PdCl_2(dppm)$ (0.18 mmol, 0.10 g) and $dppmS_2$ (0.18 mmol, 0.08 g) were placed in 30 mL CH_2Cl_2 and stirred. The solution of $NaClO_4 \cdot H_2O$ (0.71 mmol, 0.10 g) in 20 mL acetone was added dropwise to the stirring solution. Stirring was continued for 24 h at room temperature. After that, the solution was removed in vacuo and yellow solid was washed with water and diethyl ether. Complex **1** was recrystallized from acetone/diethyl ether (1:3 v/v) to give yellow crystals. (0.90 g, 80% yield). Data for **1**: $^{31}P\{^1H\}$ NMR (DMSO): −43.40 ppm (s), 40.50 ppm (s). Selected IR data (KBr): $\nu_{(P=S)}$ 585 cm^{-1}, 1100 (s) and 620 (m) cm^{-1} (ClO_4^-). *Anal.* Calc. for $C_{50}H_{44}Cl_2O_8P_4PdS_2$: C, 52.75; H, 3.90; S, 5.63. Found: C, 52.40; H, 4.10; S, 5.08%.

3.2. $[Pd(dppe)(dppmS_2)](ClO_4)_2$ (2)

$[PdCl_2(dppe)]$ (0.35 mmol, 0.20 g), $dppmS_2$ (0.35 mmol, 0.16 g) were placed together in 30 mL CH_2CI_2 and stirred. The solution of $NaClO_4 \cdot H_2O$ (1.40 mmol, 0.20 g) in 20 mL acetone was added dropwise to the stirring solution. The stirring was continued for 3 h and then solution was refluxed for 48 h. Then, the solution was removed in vacuo and yellow solid was washed with water and diethylether. Complex **2** was recrystallized from methanol/diethyl ether (1:3 v/v). (0.81 g, 71% yield). Data for **2**: $^{31}P\{^1H\}$ NMR (DMSO): 78.50 ppm (s), 40.60 ppm (s). Selected IR data (KBr): $\nu_{(P=S)}$ 585 cm^{-1}, 1100 (s) and 620 (m) cm^{-1} (ClO_4^-). *Anal.* Calc. for $C_{51}H_{46}Cl_2O_8P_4PdS_2$: C, 53.15; H, 4.02; S, 5.56. Found: C, 53.06; H, 4.44; S, 6.67%.

3.3. $[Pd(dppp)(dppmS_2)](ClO_4)_2$ (3)

A similar method was used for the preparation of $[Pd(dppm)(dppmS_2)](ClO_4)_2$ by using $[PdCl_2(dppp)]$ (0.33 mmol, 0.20 g), $dppmS_2$ (0.33 mmol, 0.15 g) and $NaClO_4 \cdot H_2O$ (1.30 mmol, 0.19 g). After 24 h, the yellow solution was removed in vacuo and the yellow solid was washed with water and diethylether. Complex **3** was recrystallized from acetonitrile/diethyl ether (1:3 v/v). (0.84 g, 72% yield). Data for **3**: $^{31}P\{^1H\}$ NMR (DMSO): 14.04 ppm (s), 38.00 ppm (s). Selected IR data (KBr): $\nu_{(P=S)}$ 577 cm^{-1}, 1100 (s) and 620 (m) cm^{-1} (ClO_4^-). *Anal.* Calc. for $C_{52}H_{48}Cl_2O_8P_4PdS_2$: C, 53.55; H, 4.15; S, 5.50. Found: C, 52.67; H, 4.17; S, 2.87%.

Table 2
Crystal data, data collection and structure-refinement parameters for complexes **1a** and **3**

	1a	**3**
Empirical Formula	$C_{50}H_{44}Cl_2O_8P_4PdS_2 \cdot (CH_3)_2CO$	$C_{52}H_{48}Cl_2O_8P_4PdS_2$
Color	Yellow	Yellow
Crystal size (mm)	$0.39 \times 0.34 \times 0.29$	$0.26 \times 0.26 \times 0.25$
Crystal system	monoclinic	monoclinic
Space group	$P21/n$	$P21/c$
Unit cell dimensions		
a (Å)	20.7657(15)	18.6851(11)
b (Å)	11.7784(9)	13.6907(8)
c (Å)	23.0224(17)	20.7791(12)
α (°)	90	90
β (°)	107.480(1)	103.585(1)
γ (°)	90	90
Volume (Å^3)	5370.9(7)	5166.8(5)
Z	4	4
D_{calc} (Mg m^{-3})	1.479	1.499
Formula weight	1196.23	1166.20
Absorption coefficient (mm^{-1})	0.697	0.721
$F(000)$	2448	2384
Index ranges	$-25 \leqslant h \leqslant 25$ $-14 \leqslant k \leqslant 14$ $-28 \leqslant l \leqslant 28$	$-23 \leqslant h \leqslant 23$ $-17 \leqslant k \leqslant 17$ $-25 \leqslant l \leqslant 25$
θ range (°)	1.16–26.37	1.12–26.37
Number of data measured	10994	10546
Number of data with $[I > 2\sigma(I)]$	9943	9372
$R_1[I > 2\sigma(I)]$	0.0710	0.0571
$wR_2[I > 2\sigma(I)]$	0.1513	0.1263

3.4. X-ray crystallographic study of *1a* and *3*

X-ray crystallographic data collection and processing was carried out using a Bruker AKS XMART APEX system; with graphite-monochromated Mo Kα radiation at 297 K. The structures were solved by direct methods SHELXTL [21]. The hydrogen atoms were placed in geometrically calculated positions using a riding model with U_{iso} constrained at 1.2 for non-methyl groups and 1.5 for methyl groups times U_{eq} of the carrier carbon atoms. Crystal data of **1a** and **3** are listed in Table 2.

4. Supplementary material

Crystallographic data for $C_{50}H_{44}Cl_2O_8P_4PdS_2 \cdot (CH_3)_2CO$ and $C_{52}H_{48}Cl_2O_8P_4PdS_2$ have been deposited with the Cambridge Crystallographic Data Center. Copies of available materials can be obtained, free of charge, on application to the Director, CCDC, 12 Union Road, Cambridge CB2 1EZ, UK (Fax: +44 1223 336-033 or E-mail: deposit@ccdc.cam.ac.uk). Deposition numbers are CCDC 279019 and CCDC 271253, respectively.

Acknowledgements

We thank the University of Babes Bolyai for X-ray crystallography support and the Research Foundation of Ege University (2002 FEN 072) for funding..

References

[1] C.J. Carmalt, N.C. Norman, Polyhedron 14 (11) (1995) 1405.
[2] S.O. Grim, E.D. Walton, Inorg. Chem. 19 (1980) 1982.
[3] T.S. Tarlok, M.K. Sandhu, J. Chem. Soc., Dalton Trans. (1988) 1401.
[4] P.K. Baker, A.I. Clark, M.G.B. Drew, M.C. Durrant, R.L. Richards, Polyhedron 17 (9) (1998) 1407.
[5] T.S. Lobana, R. Verma, A. Singh, M. Shikha, A. Castineiras, Polyhedron 21 (2002) 205.
[6] H. Schumann, J. Organomet. Chem. 320 (1987) 145.
[7] M. Valderrama, R. Contreras, M. Bascunan, S. Alegria, Polyhedron 14 (15) (1995) 2239.
[8] B. Alvarez, E.J. Fernandez, M.C. Gimeno, P.G. Jones, A. Laguna, J.M. Lopez-de-Luzuriaga, Polyhedron 17 (11–12) (1998) 2029.
[9] G.P. Suranna, P. Mastrorilli, C.F. Nobile, W. Keim, Inorg. Chim. Acta 305 (2000) 151.
[10] A. Laguna, M. Laguna, A. Rojo, M.N. Fraile, J. Organomet. Chem. 315 (1986) 269.
[11] D.E. Berry, J. Browning, K.R. Dixon, R.W. Hilts, A. Pidcock, Inorg. Chem. 31 (1992) 1479.
[12] T.S. Lobana, R. Verma, G. Hundal, A. Castineiras, Polyhedron 19 (2000) 899.
[13] P. Bhattacharyya, J. Novasad, J. Phillips, A.M.Z. Slawin, D.J. Williams, J.D. Woollins, J. Chem. Soc., Dalton Trans. (1995) 1607.
[14] D. Cremer, J.A. Pople, J. Am. Chem. Soc. 97 (1975) 1354.
[15] J. Novasad, K.W. Törnroos, M. Necas, A.M.Z. Slawin, J.D. Woollins, S. Husebye, Polyhedron 18 (1999) 2861.
[16] G. Ferguson, Y. Li, A.J. McAlees, R. McCrindle, E. Zong, J. Organomet. Chem. 617 (2001) 671.
[17] W.L. Jolly, The Synthesis and Characterization of Inorganic Compounds, Prentice-Hall, Englewood Cliffs, 1970, 116.
[18] J. Chatt, L.M. Vallarino, L.M. Venanzi, J. Chem. Soc. (1957) 3413.
[19] W.L. Steffen, G.J. Palenik, Inorg. Chem. 15 (10) (1976) 2432.
[20] A. Davison, D.L. Reger, Inorg. Chem. 10 (9) (1971) 1967.
[21] G.M. Sheldrick, SHELXTL: Program for the Refinement of Crystal Structures, University of Göttingen, Göttingen, Germany, 1997 (Bruker AXS, Madison, WI, USA).

coordinated methanol molecules is sometimes critical for the catalytic activity of such compounds [7,12–15], while the *cis*-MoO_2^{2+} moiety can target to free methanol molecules and oxidize them to formaldehyde [16]. The presence of intramolecular C–H···O bond is important when referring to models proposed for C–H bond activation in the oxidation of methanol to formaldehyde [7,12].

The bioinorganic consideration of DHBAs originates from their ability to act as non-toxic and effective chelating agents for ions with high charge to ionic radius ratio. DHBAs were used in the chelation therapy [17], are the basic neurotransmitter metabolites and take part in glucose metabolism [18] and in trace elements uptake by microorganisms [19]. Their redox multiplicity and antioxidant capability are of great interest for bioinorganic chemistry [20], particularly for modeling molybdenum hydroxylases [1]. They can easily coordinate as bidentate ligands with metals either through the two-hydroxyl oxygen atoms of the benzoic ring or through the hydroxyl oxygen atom of the carboxyl group [21–24]. The crystal structure of Zn(2,5-DHBA)$_2 \cdot 4H_2O$ suggests monodentate coordination, only through one carboxylic oxygen [25].

The ligands 2,3-DHBA and 2,5-DHBA (Scheme 1) are well known hydroxylation products of salicylic acid (they are indicators for the presence of hydroxyl radicals) and are used as models for organic compounds of larger molecular weight. They are found in plants, fruits and vegetables [26]. Their metal complexes can act as radical scavengers and are potential antiparalytic drugs [27]. Enzymes such as 2,3-dihydroxybenzoate dehydrogenase or ligase, catalyze the production or activation of 2,3-DHBA [28]. 2,3-DHBA can be found in the human body as an intermediate of many biological reactions [29,30], providing considerable antitumor and anti-inflammatory activity [31]. It is also used as a marker of in vivo oxidative stress [32]. 2,5-DHBA or gentisic acid is a well known second line metabolite of aspirin [33]. Gentisate 1,2-dioxygenase is the enzyme that catalyzes the degradation of gentisic acid [34]. The crystal form of this ligand is a necessary material in MALDI applications due to its ability to constrain peptides, carbohydrates or glycolipids via strong hydrogen bonds [35,36].

Although a molybdenum complex of 2,3-DHBA has been structurally characterized [29], no 2,5-DHBA complex with this metal has ever been referred. Zubieta et al. [7] have carried out extensive studies on polyoxomolybdate complexes including $(n\text{-}Bu_4N)_2 \cdot [Mo_4O_6(\mu\text{-}O)_4(\mu_3\text{-}OMe)_2(OC_6H_4O)_2]$, a structurally characterized tetrameric molybdenum complex of catechol. Complexes with the same metallic core $[Mo_4O_6(\mu\text{-}O)_4(\mu_3\text{-}OMe)_2]^{2+}$ and catechol derivatives (2,3-dihydroxynaphthalene [37] and phenanthraquinone [38]) have been structurally characterized. The core is structurally characterized even without an organic ligand, but with chloride ions as ligand [39]. A tetrameric complex with 3-hydroxy-picolinic acid having only oxo-bridges has also been structurally characterized [8]. For trinuclear oxomolybdenum complexes with catechol derivatives, there are no literature reports, while a trimetallic core has been investigated [40].

We have reported the isolation and characterization of a 2,3-DHBA complex with Fe(III) [41], the interaction of 2,3-DHBA with Mn(II) [42] or Ni(II) [21] and recently, the isolation from aqueous solution and characterization of Mo(VI) complexes with this ligand [22]. Moreover, we have worked on the synthesis and characterization of Mo(VI) complexes of 2,5-DHBA [23] or 3,4-DHBA [24] isolated from aqueous solution.

In the present study, we demonstrate two molybdenum complexes of 2,3- and 2,5-DHBA prepared by reaction with $(PPh_4)_4Mo_8O_{26}$ in the same solvent system, under aerobic conditions and at room temperature. The oligomeric tetra- and trinuclear molybdenum complexes were further investigated using IR and ESR in solid state, UV–Vis and NMR spectroscopy, as well as elemental, thermogravimetric analysis and cyclic voltammetry.

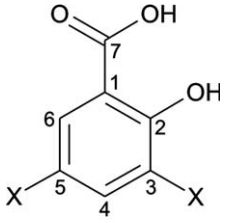

3-OH, 5-H: 2,3-DHBA
3-H, 5-OH: 2,5-DHBA

Scheme 1. 2,3- and 2,5-dihydroxybenzoic acids.

2. Experimental

2.1. Materials and methods

All chemicals were purchased from Aldrich and used without further purification. Elemental analyses were performed using a Perkin–Elmer 240B elemental analyzer. IR spectra were recorded using a KBr pellet on a Perkin–Elmer 880 IR spectrophotometer. Thermogravimetric and differential thermal analysis were carried out on a Mettler Toledo S R apparatus in N_2 atmosphere (temperature range: 40–1200 °C; heating rate: 20 °C/min). ESR spectra in solid state (298 and 10 K) were recorded on a Bruker ER-200D-SRC X-band spectrometer interfaced to a personal computer and equipped with an Oxford ESR 900 cryostat, an Anritsu MF76A frequency counter and a Bruker 035N NMR gaussmeter. UV–Vis spectra were recorded with 1-cm cuvette on a Hitachi U-2000 spectrophotometer. ^1H, ^{13}C and 2D (COSY, HSQC, HMQC) NMR spectra were recorded on a Varian UNITYplus operating at 300 MHz spectrometer or a Bruker Avance operating at 500 MHz, in CD_3OD solution with TMS as internal standard and DMSO-d_6 using the solvent peak as an internal reference (2.50 ppm). Cyclic voltammograms were recorded on an AFCBP1 Biopotentiostat (Pine Instrument Company) and a standard three-electrode assembly

(working: Pt disk, auxiliary: platinum wire, reference: SCE, scan rate: 100 mV s^{-1}).

2.2. Synthesis

2.2.1. Synthesis of $(PPh_4)_4Mo_8O_{26}$

An aqueous solution (15 ml) of PPh_4Br (209.7 mg, 0.5 mmol) was added to a solution of $(NH_4)_2MoO_4$ (98 mg, 0.5 mmol) in water (15 ml) and a white solid was produced. The solid was filtered and dried overnight in vacuum over $CaCl_2$, giving $(PPh_4)_4Mo_8O_{26}$ (solid **A**) as reported in analogous preparations [43,44].

2.2.2. Synthesis of $(PPh_4)_2 \cdot [Mo_4O_6(\mu\text{-}O)_4(\mu_3\text{-}OMe)_2\text{-}(2,3\text{-}DHBA)_2]$ (**1**)

2,3-DHBA (34.5 mg, 0.22 mmol) was added to 7 ml of an acetonitrile:methanol (7:3) stirred solution, and left until it was completely dissolved. Upon the addition of solid **A** (71.6 mg, 0.03 mmol), a deep red-brown solution was formed. After 5 h of stirring, the solution was filtrated and the filtrate was layered with Et_2O giving deep red-brown crystals. Yield: 82%. *Anal.* Calc. for $C_{64}H_{54}Mo_4O_{20}P_2$: C, 48.12; H, 3.41. Found: C, 48.42; H, 3.52%. UV–Vis (CH_3CN; λ_{max}, nm (ε, $cm^{-1}\,M^{-1}$)): 330 (20×10^3), 270 (27×10^3), 220 (185×10^3).

2.2.3. Synthesis of $(PPh_4)_2 \cdot [Mo_3O_6(\mu\text{-}O)_2\text{-}(2,5\text{-}DHBA)_2] \cdot CH_3CN$ (**2**)

2,5-DHBA (34.5 mg, 0.22 mmol) was added to 7 ml of an acetonitrile:methanol (7:3) stirred solution, and left until it was completely dissolved. After the addition of solid **A** (71.6 mg, 0.03 mmol), a yellow solution was formed. Without any further stirring, the layering with Et_2O produced orange crystals suitable for X-ray determination. Yield: 46%. *Anal.* Calc. for $C_{64}H_{51}Mo_3NO_{16}P_2$: C, 53.15; H, 3.56; N, 0.97. Found: C, 52.94; H, 3.51; N, 0.84%. UV–Vis (CH_3CN; λ_{max}, nm (ε, $cm^{-1}\,M^{-1}$)): 324 (13×10^3), 261 (24×10^3), 225 (131×10^3).

2.3. X-ray crystallography

The orange crystals of **1** and **2** were mounted in air. Diffraction measurements were made on a Crystal Logic dual goniometer diffractometer using graphite monochromated Mo Kα radiation. Unit cell dimensions were determined by the angular settings of 25 automatically centered reflections in the range $11° < 2\theta < 23°$ and they appear in Table 1. Three standard reflections monitored every 97 reflections showed less than 3% variation and no decay. Lorentz, polarization corrections were applied using Crystal Logic software. Further crystallographic details for **1**: $2\theta max = 50°$; scan speed 5°/min; scan range 1.6° plus $\alpha_1\alpha_2$ separation; reflections collected/unique/used, 5749/5512 ($R_{int} = 0.0136$)/5512; 514 parameters refined; $(\Delta/\rho)max = 0.002$; $(\Delta\rho)max/(\Delta\rho)min = 0.688/-0.572$ e/Å^3; R/R_w (all data) = 0.0350/0.0805. Further crystallographic details for **2**: $2\theta max = 50°$; scan speed 6°/min; scan range 1.6° plus $\alpha_1\alpha_2$ separation; reflections collected/unique/used, 9752/9344 ($R_{int} = 0.0138$)/9344; 960 parameters refined; $(\Delta/\rho)max = 0.008$; $(\Delta\rho)max/(\Delta\rho)min = 0.332/-0.284$ e/Å^3; R/R_w (all data) = 0.0220/0.0557.

Table 1
Crystallographic data summaries for complexes $(PPh_4)_2 \cdot [Mo_4O_6\text{-}(\mu\text{-}O)_4(\mu_3\text{-}OMe)_2(2,3\text{-}DHBA)_2]$ (**1**) and $(PPh_4)_2 \cdot [Mo_3O_6(\mu\text{-}O)_2(2,5\text{-}DHBA)_2] \cdot CH_3CN$ (**2**)

Empirical formula	$C_{64}H_{54}Mo_4O_{20}P_2$ (**1**)	$C_{64}H_{51}Mo_3NO_{16}P_2$ (**2**)
Formula weight	1588.78	1439.82
Crystal size	$0.20 \times 0.30 \times 0.80$	$0.20 \times 0.35 \times 0.70$
T (K)	293(2)	293(2)
Crystal system	triclinic	monoclinic
Space group	$P\bar{1}$	$P2_1$
Unit cell dimensions		
a (Å)	9.071(3)	12.719(5)
b (Å)	12.797(4)	17.655(7)
c (Å)	14.814(5)	14.706(6)
α (°)	108.41 (1)	90
β (°)	100.84 (1)	114.700(1)
γ (°)	97.93 (1)	90
V (Å^3)	1566.2(9)	3000(2)
Z	1	2
D_{calc} (g/cm^3)	1.685	1.594
μ(Mo Kα) (mm^{-1})	0.909	0.742
$F(000)$	796	1452
Reflections collected	5749	9752
Independent reflections (R_{int})	5512 (0.0136)	9344 (0.0138)
Goodness-of-fit (on F^2)	1.034	1.045
R[a]	0.0299[c]	0.0211[d]
R_w[b]	0.0767[c]	0.0550[d]

[a] $R = \Sigma||F_o| - |F_c||/\Sigma|F_o|$.
[b] $R_w = [\Sigma w(|F_o|^2 - |F_c|^2)^2/\Sigma w(|F_o|^2)^2]^{1/2}$.
[c] For 4885 reflections with $I > 2\sigma(I)$.
[d] For 9130 reflections with $I > 2\sigma(I)$.

The structures were solved by direct methods using SHELX-86 and refined in full-matrix least-squares procedure on F^2 with SHELX-97 [45]. All non-H atoms in the structures of **1** and **2** · MeCN were refined anisotropically. All hydrogen atoms in both structures were located by difference maps and were refined isotropically. The acetonitrile solvent molecule in **2** was found disordered over two positions and it was refined isotropically with occupation factors summing one (no H-atoms for the MeCN molecule were included in the refinement). Selected atomic distances and bond angles are presented in Tables 2 and 3.

3. Results and discussion

The general reactions of $(PPh_4)_4Mo_8O_{26}$ with the ligands are presented in Scheme 2. The ligand amount is in excess ($(PPh_4)_4Mo_8O_{26}/L = 1/8$), but the metal-to-ligand ratio is 1:1. It is notable that in the case of 2,5-DHBA, a long reaction under stirring leads to the formation of $(PPh_4)_2Mo_6O_{19}$ crystals. The crystals obtained were identified by X-ray crystallography with no further interest for presentation. Methanol seems to play an important role

Table 2
Selected atomic distances (Å) and bond angles (deg) for complex **1**[a]

Mo1–O14	1.678(2)	Mo2–O15	1.693(2)
Mo1–O11′	1.829(2)	Mo2–O16	1.687(3)
Mo1–O12	1.818(2)	Mo2–O11	1.974(2)
Mo1–O3	2.051(2)	Mo2–O12	1.986(2)
Mo1–O4	1.975(2)	Mo2–O13′	2.263(2)
Mo1–O13	2.404(2)	Mo2–O13	2.228(2)
C7–O1	1.208(5)	C2–O3	1.343(4)
C7–O2	1.325(5)	C3–O4	1.342(4)
O4–Mo1–O3	76.40(9)	O12–Mo2–O13	74.91(7)
O11′–Mo1–O3	83.78(9)	O11–Mo2–O13	82.62(8)
O12–Mo1–O4	90.47(10)	O15–Mo2–O12	95.95(11)
O14–Mo1–O3	99.60(12)	O16–Mo2–O13	94.53(10)
O14–Mo1–O4	100.79(12)	O16–Mo2–O11	95.62(12)
O14–Mo1–O11′	102.26(13)	O16–Mo2–O12	100.07(12)
O14–Mo1–O12	103.07(13)	O16–Mo2–O15	105.69(13)
O14–Mo1–O13	174.12(11)	O16–Mo2–O13′	161.61(10)
C2–O3–Mo1	115.75(18)	O1–C7–O2	119.1(4)
C3–O4–Mo1	119.18(19)	O1–C7–C2	117.6(3)
C2–C1–C7	122.0(3)	O1–C7–C2	123.3(4)

[a] Primed atoms are generated through the symmetry transformation: $1-x, 1-y, -z$.

Table 3
Selected atomic distances (Å) and bond angles (deg) for complex **2**

Mo1–O23	1.693(2)	Mo1–O24	1.726(2)
Mo2–O25	1.694(2)	Mo2–O26	1.701(2)
Mo3–O27	1.700(2)	Mo3–O28	1.709(2)
Mo1–O21	1.896(2)	Mo2–O22	1.908(2)
Mo1–O1	2.309(2)	Mo3–O1	2.367(2)
Mo2–O11	2.287(2)	Mo3–O11	2.362(2)
Mo1–O12	2.329(2)	Mo2–O2	2.359(2)
Mo1–O3	1.945(2)	Mo2–O13	1.955(2)
C7–O2	1.238(4)	C17–O12	1.248(4)
C7–O1	1.303(3)	C17–O11	1.299(3)
C2–O3	1.353(4)	C12–O13	1.348(4)
C5–O4	1.381(5)	C15–O14	1.359(4)
O23–Mo1–O24	103.93(12)	O27–Mo3–O28	104.77(14)
O21–Mo1–O1	73.69(8)	O22–Mo3–O11	71.94(8)
O3–Mo1–O1	80.07(8)	O21–Mo3–O11	80.69(9)
O23–Mo1–O21	102.04(10)	O27–Mo3–O21	100.32(12)
O23–Mo1–O1	162.87(9)	O27–Mo3–O22	100.40(12)
O24–Mo1–O12	168.66(10)	O28–Mo3–O1	162.92(11)
O25–Mo2–O26	104.40(12)	Mo1–O21–Mo3	122.64(11)
O13–Mo2–O11	81.41(8)	Mo2–O22–Mo3	122.41(11)
O25–Mo2–O13	98.16(10)	Mo1–O1–Mo3	91.59(7)
O25–Mo2–O22	100.98(10)	Mo2–O11–Mo3	91.94(7)
O25–Mo2–O11	164.83(9)	C7–O1–Mo1	126.55(17)
O26–Mo2–O2	166.13(10)	C7–O2–Mo2	131.29(18)
O1–C7–O2	124.2(3)	O11–C17–O12	124.4(3)
O2–C7–C2	118.9(3)	O12–C17–C11	118.2(2)
O1–C7–O2	116.9(3)	O11–C17–C11	117.4(2)

in the production of the tetranuclear complex of 2,3-DHBA, probably via an intermediate with bridged and terminal methanol molecules (Scheme 3).

The structure of complex **1** anion (Fig. 1) shows that 2,3-DHBA prefers, under these particular experimental conditions, the coordination to molybdenum via the two hydroxyl oxygen atoms rather than the participation of the carboxyl group. The structure consists of four distorted MoO_6 octahedra with two *cis*-MoO_2^{2+} units and two molybdenum atoms having each ligand coordinated and one terminal oxygen atom. There is a symmetry center in the molecule between the four molybdenum atoms. For the *cis*-MoO_2^{2+} unit, the Mo=O bond lengths (1.687(3) and 1.693(2) Å) as well as the O=Mo=O angles are in agreement with those mentioned in the literature [20,21]. The O4–Mo1–O3 angle (76.40(9)°) as well as the average O14–Mo1–O (101.43°) angle involving O3, O4, O11 and O12 atoms show this distortion. The two ligand molecules are in *trans* position to the metallic core, with strong hydrogen bonding between the carboxylic hydrogen and O3

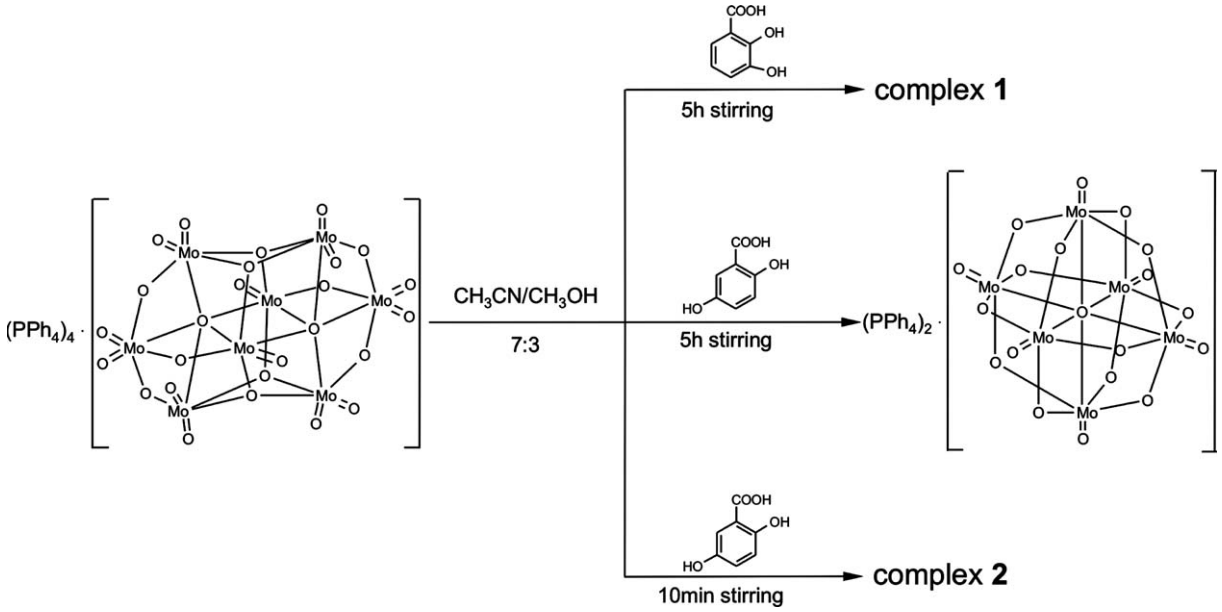

Scheme 2. Reaction diagram of the complexes.

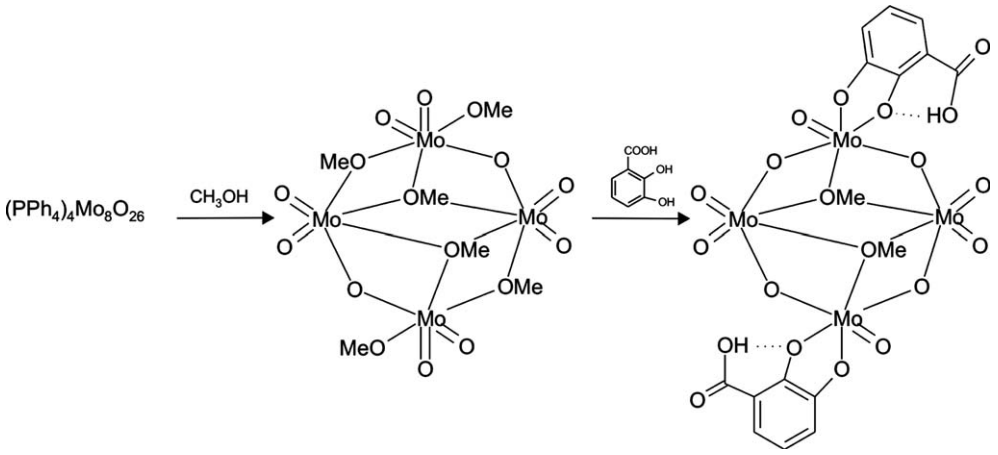

Scheme 3. The participation of methanol in the formation of complex **1**.

[HO2···O3 = 1.951 Å, O2···O3 = 2.618 Å, O2–HO2···O3 = 150.49°]. The hydrogen bond affects the C2–O3–Mo1 angle (115.75(18)°) relatively to the C3–O4–Mo1 one (119.18(19)°). The existence of the carboxyl-group does not dramatically change the metallic core configuration, as it is concluded from the comparison of our structure with the corresponding tetranuclear molybdenum complex of catechol [7].

The structure of complex **2** anion (Fig. 2) consists of three distorted MoO_6 octahedra. Each molybdenum atom has the *cis*-MoO_2^{2+} unit, with a Mo–O distance range of 1.693–1.726 Å and an average O=Mo=O angle of 104.37°. The structure of complex **2** is characterized as unusual, because of the rarity of trinuclear oxomolybdenum complexes and the fact that each of the two ligands coordinates with all three molybdenum atoms, due to a unique tridentating binding of gentisic acid that differs from the usual salicylate (bidentate) coordination type [46]. For each ligand, the hydroxyl-oxygen of the carboxylate group acts as a bridge between two molybdenum atoms, while the third molybdenum atom coordinates with the carbonyl-oxygen. The C–O (1.299(3) and 1.303(3) Å) and C=O (1.238(4) and 1.248(4) Å) bond lengths are obviously affected by the participation of the carboxylate group, in contrast to the respective bond lengths of a non-coordinated one, as for complex **1** (C–O 1.325(5), C=O 1.208(5) Å). The two hydroxyl non-bonded groups of the ligands are in *trans* position to the metallic core, and participate in hydrogen bonding interactions [HO4···O24′ $(2-x,-0.5+y,1-z)$ = 2.069 Å, O4···O24′ = 2.758 Å, O4–HO4···O24′ = 175.9°; HO14···O28″ $(1-x,-0.5+y,-z)$ = 2.142 Å, O14···O28″ = 2.717 Å, O14–HO14···O28″ = 162.4°] giving rise to a 2D polymeric network extended parallel to the [10−1] plane (Fig. 3).

The characteristic bands in the IR spectra of the complexes are presented in Table 4. For complex **1**, two medium sharp peaks at 2920 and 2818 cm^{-1} are indicative of the C–H stretch of methoxy groups [47] and the ν(C–O) vibration of the methoxo bridge is found at 1283 cm^{-1}.

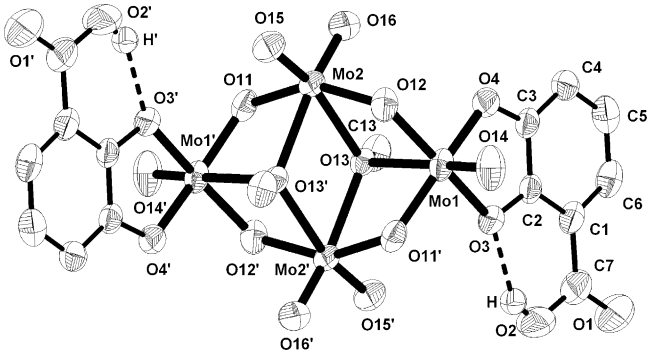

Fig. 1. The molecular structure of the complex **1** anion showing the atomic labeling (40% thermal probability ellipsoids). The intramolecular H-bonds are shown as dashed lines. Primed atoms are generated through the symmetry transformation $1-x$, $1-y$, $-z$.

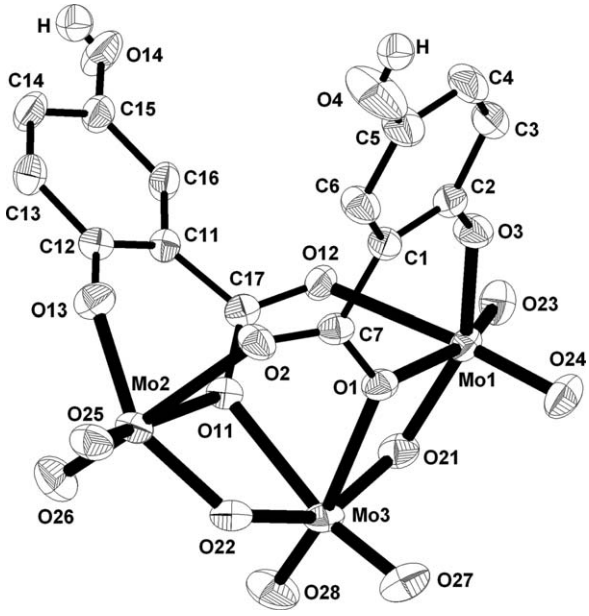

Fig. 2. The molecular structure of the complex **2** anion showing the atomic labeling (40% thermal probability ellipsoids).

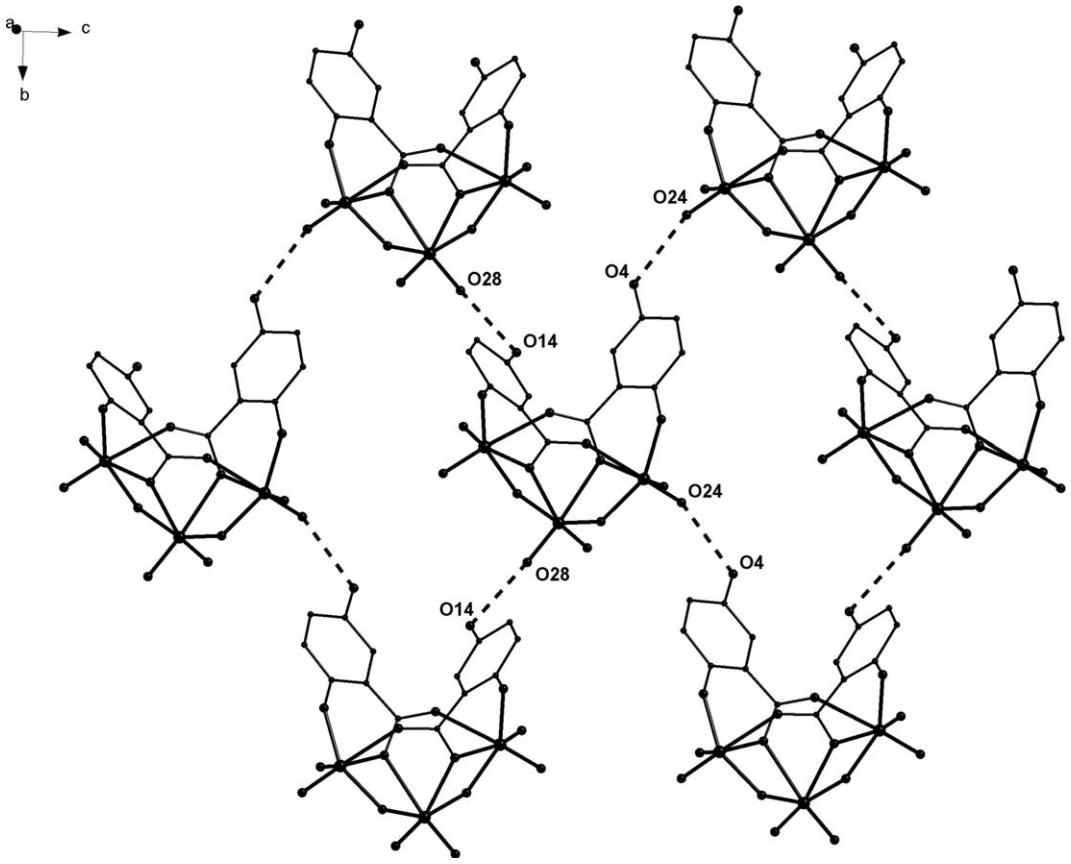

Fig. 3. The 2D polymeric network of complex **2** anion, extended in parallel to the [10−1] plane (H-bonds are shown as dashed lines).

The position of the carbonyl asymmetric stretching band at 1720 cm^{-1} and the broad symmetric one at 1379 cm^{-1} are indicative of the strong hydrogen bond in the carboxylic group. The intense characteristic doublet at 956 and 916 cm^{-1} is due to the *cis*-MoO_2^{2+} group and corresponds to the ν_{sym} and ν_{asym} of O=Mo=O bond, respectively. Approximately, the same vibration energy (936 cm^{-1}) is expected for the ν(Mo=O) stretch of the two molybdenum centers, connected with only one terminal oxygen. The bands appearing at 738, 662, 632 and 555 cm^{-1} are indicative of the Mo–O–Mo bridges, through oxygen or methanol. Moreover, the Mo–O bond types are attributed to the vibration observed at 337 cm^{-1} [7,8,24,46,48]. For complex **2**, the carbonyl asymmetric stretching band of the ligand's carboxylic group is observed at 1588 cm^{-1}, while two bands represent the symmetric one at 1379 and 1352 cm^{-1} showing two non-symmetric ligand molecules. The $\Delta\nu$ between the symmetric and asymmetric carboxylate vibration bands is equal to 218 cm^{-1}, in contrast to what is expected for such carboxylate coordination modes [49]. The two sets of bands for the vibration energy of the *cis*-MoO_2^{2+} group (940–881 and 908–854 cm^{-1}) indicate the geometrical differentiation of Mo(3) from the other two molybdenum atoms. The band attributed to the Mo–O–Mo bridges appears at 640 cm^{-1}, while the Mo–O bond vibration types at 337 cm^{-1}.

Table 4
Characteristic IR data (cm^{-1}) of complexes **1** and **2**

Assignment	**1**	**2**
ν C–H methoxo	2920m, 2818m	
ν_{as} COOH	1720vs (1669vs)[a]	1588vs (1667vs)
ν_s COOH	1379m,b (1298vs)	1369vs, 1352vs (1380s)
ν C–O methoxo	1283m	
ν C–O catechol	1252s, 1222s (1233vs)	1476vs, 1435vs (1438vs)
ν_s *cis*-MoO_2^{2+}	956vs	940vs, 908vs
ν Mo=O	937s	
ν_{as} *cis*-MoO_2^{2+}	916vs	881s, 854s
ν_{as} Mo–O–Mo	779vs, 750vs	640vs
ν_s Mo–O–Mo	555m	564m
ν Mo–O methoxo	337s	

vs, very strong signal; s, strong signal; m, medium signal; b, broad signal; ν_s, symmetric vibration; ν_{as}, asymmetric vibration.
[a] Free ligand's vibration in parentheses.

Table 5
Thermogravimetry data of complex **1**

Temperature range (°C)	Experimental mass loss (%)	Eliminated species	Calculated mass loss (%)	Residue
190–260	2.9	Ether $O(CH_3)_2$	2.9	$Mo_4C_{62}H_{48}O_{19}P_2$
300–500	46.9	C, H $C_{58}H_{48}$	46.9	$Mo_4C_4O_{19}P_2$
800–960	16.5	P_2O_5, 4CO $C_4O_9P_2$	16.0	Mo_4O_{10} ($\mathbf{2}\cdot Mo_2O_5$)

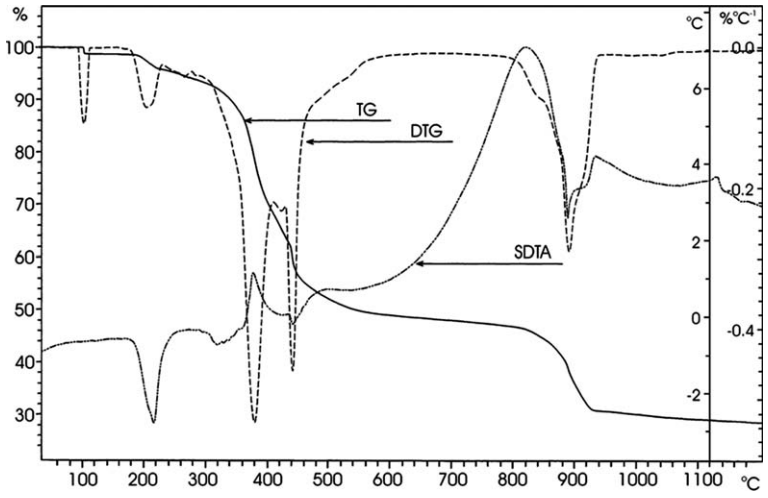

Fig. 4. TG, DTG and SDTA curves for complex **1** (the first peak observed in the DTG without any signal change in the energy flow corresponds to instrument noise).

Thermogravimetric data of complex **1** are summarized in Table 5. The extraction of the two methoxo triple-bridges (exp. 2.9%, calc. 2.9%) is observed with an endothermic reaction at the temperature of 217 °C (Fig. 4), producing $O(CH_3)_2$. In general, bridged methanol molecules are extracted in this temperature range, while terminal methanol molecules are extracted at lower temperatures [47]. The experimental organic loss (C, H from the ligand and the counter ion) occurred in the region between 300 and 500 °C having two main maximum values at 383 and 443 °C (DTG curve, Fig. 4). The weight loss at 383 °C involves an exothermic decomposition reaction of the complex, while the second involves an endothermic process (SDTA curve, Fig. 4). The organic loss is difficult to be confirmed by the corresponding theoretical value, because of the complicated reaction steps that take place [50], including partial structural fragmentation [51]. Experiments of combined TG analysis and IR identification confirm the tetraphenylphosphonium decomposition at temperatures of 350–400 °C, at metal complexes with this counter ion. The exothermic reaction can be related to the simultaneous strong reaction of phosphorus atom with oxygen, after the P–C bond breaking [52]. The ligand decomposition (443 °C) is an endothermic process that occurs at higher temperatures than that for the free ligand, because of its coordination with the metal [53]. A total mass loss of 46.9%, in this region, is required for the total carbon and hydrogen extraction (calc. 46.9%), while structural fragmentation also takes place. The next loss occurs at a much higher temperature value (891 °C) and corresponds to the extraction of P_2O_5 [54] and CO that are formed by the ligand decomposition (exp. 16.5%, calc. 16.0%) [24], while the metal oxides are formed [55]. So, the final residue at 1200 °C is free of phosphorus atoms and only consists of the dimeric molybdenum oxide, Mo_2O_5 (exp. 32.5%, calc. 34.2%).

The ESR spectra of both complexes in solid state at ambient temperature or at 10 K, did not give any signal characteristic of DHBAs in their semi-oxidized form (semiquinones) or Mo(V). A Mo(VI)-catecholate to Mo(V)-semiquinonate interconversion could be expected especially when a molybdenum atom does not contain a *cis*-MoO_2^{2+} moiety but only one terminal oxygen atom. The color of the crystal could also be an indication of an electronic transition for this interconversion.

The electronic absorptions of the complexes in CH_3CN showed no significant difference between the complexes in their absorption area but only in their ε values. The ligand-to-metal charge transfer band appears at 330 nm for **1** and 324 nm for **2**. The bands at 270 nm for **1** and 261 nm for **2** are characteristic of the $n \rightarrow \pi^*$ and $\pi \rightarrow \pi^*$ transition bands attributed to catechol [43]. The $Mo{=}O^{4+}$ chromophore band appears at 220 nm for **1** and 225 nm for **2** [24]. For each band, the molar coefficient of **1** is bigger than **2**, calculated per one molybdenum atom.

The ^1H NMR spectrum of complex **1** in CD_3OD (Fig. 5), demonstrates one group of ligand peaks with ppm values at 7.04 (doublet, correlated to H^6), 6.60

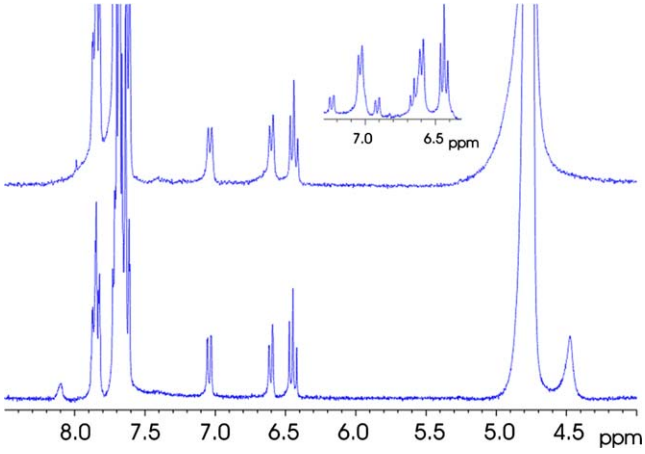

Fig. 5. ^1H NMR spectrum of complex **1** freshly diluted in CD_3OD (bottom), after 27 days (upper) and three months later (inset).

Table 6
^{1}H NMR data of complexes **1** and **2**

Solvent	Ligand protons (ppm)							
	1				**2**			
	H_{COOH} (s)	H^6 (d)	H^4 (d)	H^5 (tr)	$H_{OH\text{-}5}$ (s)	H^6 (s)	H^4 (d)	H^3 (d)
CD_3OD		7.04	6.60	6.45		6.77	6.54	6.67
		7.23[a]	6.92	6.65				
DMSO-d_6	13.08	7.00	6.84	6.76	8.94	6.85	6.49	6.69
	14.19[b]	6.91	6.55	6.38–6.35				

[a] Peaks due to degradation.
[b] Peaks due to isomerization.

(doublet, correlated to H^4) and 6.45 ppm (triplet, correlated to H^5). This only type of the ligand peaks and their infinitesimal splitting are indicative of its absolute intramolecular symmetry in the electronic environment of each atom, even when the complex is dissolved in this particular solvent. The integral quotient of the PPh_4^+ protons to the ligand ones equals to 1 (1.14), as expected. The methoxo triple-bridged protons appear with a single broad peak at 4.5 ppm, while the integral value confirms their 1:1 ratio with the ligand and the counter ion. Remarkable at the spectrum is the presence of a single broad peak at 8.1 ppm. This peak is lost after about one month (27 days) as well as the one at 4.5 ppm indicating a connection between them. Particularly, the methoxo groups seem to be displaced and the peak at 8.1 ppm represents an intermediate in this reaction. After approximately three months, a new group of peaks at 7.23 (doublet, H^6), 6.92 (doublet, H^4) and 6.65 ppm (triplet, H^5) appears. Since these peaks are in the same region, it is considered that the benzoic ring did not break (another metallic core or ligand oxidation state or decarboxylation). This conversion corresponds to 33%. The ^{1}H NMR spectrum of complex **2** in CD_3OD (Table 6) is more complicated giving no distinct peaks corresponding to the ligand peaks and this is due to the non-symmetrical conformation of the two ligand molecules.

In the ^{1}H NMR spectrum of complex **1** in DMSO-d_6 (Fig. 6) three groups of peaks are observed (also confirmed by the COSY experiment, Fig. 7) with the main peaks at 13.08 (–COO*H*), 7.00 (doublet, H^6), 6.84 (doublet, H^4) and 6.76 ppm (triplet, H^5). The corresponding proton shifts from the free ligand, show that H^6 (0.24 ppm downfield) and H^4 (0.16 ppm downfield) are more affected by the coordination. The secondary group exists in a 33% with peaks at 14.19 (–COO*H*), 6.91 (doublet, H^6), ~6.55 (two doublets, H^4) and 6.38–6.35 ppm (two triplets close, H^5). The peak partition of H^4 and especially H^5 indicates isomerization. For the third group, peaks at 13.59 (–COO*H*), 7.08 (doublet, H^6) and 6.43 ppm (triplet, H^5) are observed, in about 12% compared with the main group. So, in DMSO-d_6, complex **1** does not seem to be stable giving at 33% percentage a group of peaks having the same chemical shifts with the dimeric complex of molybdenum with 2,3-DHBA isolated from aqueous solution [22]. In the ^{13}C NMR spectrum of complex **1** in DMSO-d_6 (Table 7), the most characteristic shifts of the main group (as the secondary group carbons are not observed), compared with the free ligand, are focused on the carbons that are closer to the coordination area, while the only methoxo group peak at the area between 40 and 70 ppm appears at

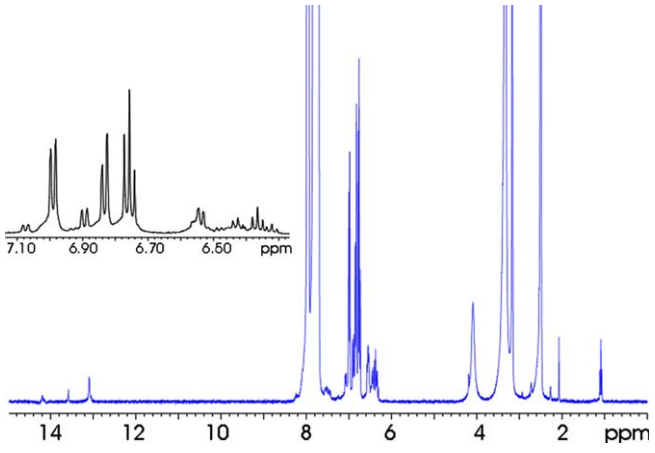

Fig. 6. ^{1}H NMR spectrum of complex **1** in DMSO-d_6.

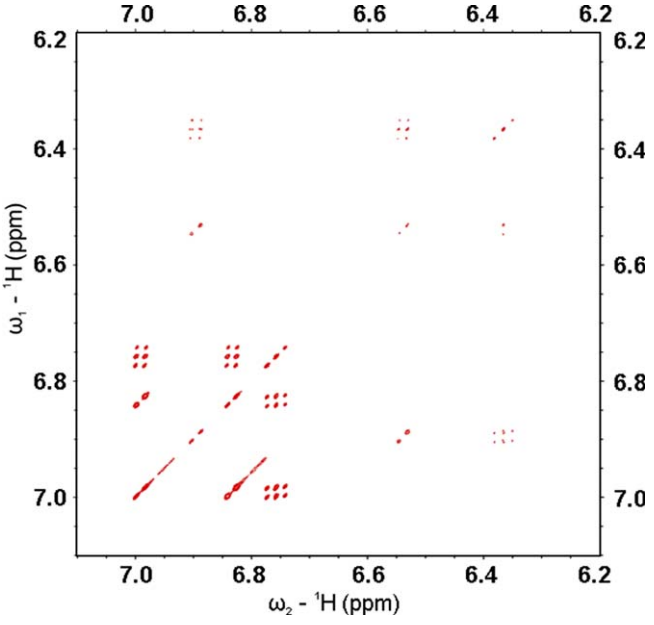

Fig. 7. COSY spectrum of complex **1** in DMSO-d_6.

Table 7
^{13}C NMR data (ppm) of complexes **1** and **2** in DMSO-d_6

	Ligand carbons							CH_3OH
	C^1	C^2	C^3	C^4	C^5	C^6	C^7	
1	120.06 (113.20)	156.10 (150.49)	153.65 (145.99)	118.38 (120.05)	116.36 (118.65)	120.67 (120.80)	165.49 (172.58)	48.56
2	123.55 (112.66)	155.74 (154.21)	119.34 (117.84)	119.96 (123.84)	149.23 (149.47)	113.81 (114.64)	173.10 (171.83)	

Free ligand corresponding shifts in parentheses.

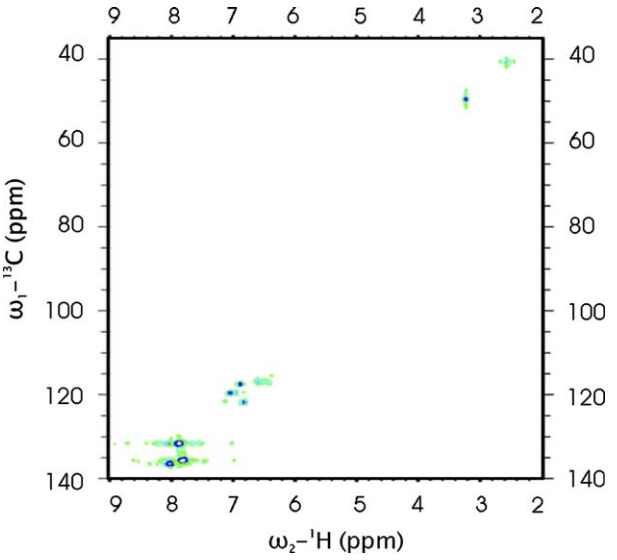

Fig. 8. HSQC spectrum of complex **1** in DMSO-d_6.

48.56 ppm (corresponding proton signal at 3.2 ppm), indicating that the bridged methanol molecules are extracted (Fig. 8). The ^1H NMR spectrum of complex **2** in DMSO-d_6 (Fig. 9), demonstrates one group of peaks at 8.94 (–O*H*), 6.84 (singlet, H^6), 6.69 (doublet, H^4) and 6.49 ppm (doublet, H^3). The integral ratio of the PPh_4^+ protons to the ligand ones equals to 1 (1.09), as expected. Comparing with the corresponding free ligand peaks, the peak of H^6 is more affected ($\Delta\delta = 0.33$ ppm) than those

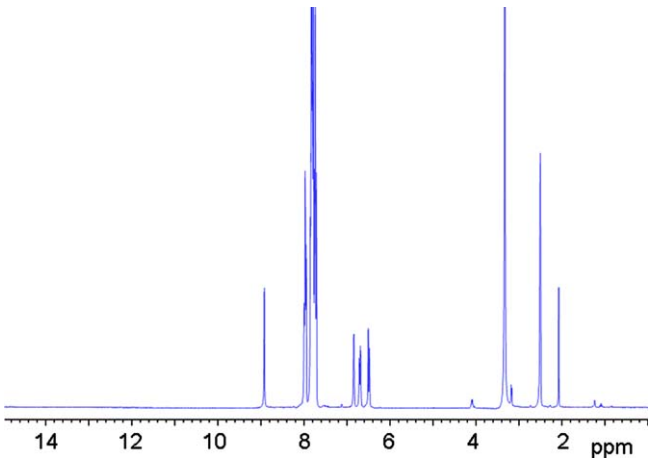

Fig. 9. ^1H NMR spectrum of complex **2** in DMSO-d_6.

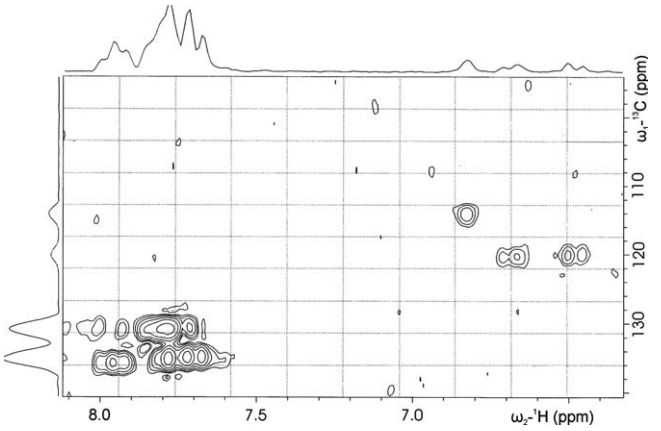

Fig. 10. HSQC spectrum of complex **2** in DMSO-d_6.

of H^4 ($\Delta\delta = 0.27$ ppm) or H^3 ($\Delta\delta = 0.29$ ppm). In the ^{13}C NMR spectrum of complex **2** in DMSO-d_6, the most affected by the coordination carbon atom is C^1 ($\Delta\delta = 11$ ppm), with a smaller shift for C^4 ($\Delta\delta = 4$ ppm) and surprisingly no important shift for C^2 (Fig. 10).

The cyclic voltammogram of complex **1** in CH_3CN, between −2 and +2 V vs. SCE, reveals the stabilization of the semi-oxidized form of the ligand when coordinated (Fig. 11). For the unbounded 2,3-DHBA, an oxidation at −0.67 V corresponds to the conversion of the reduced to the semi-oxidized form of the ligand (semiquinone), while one anodic peak at +0.53 V is due to the conversion of

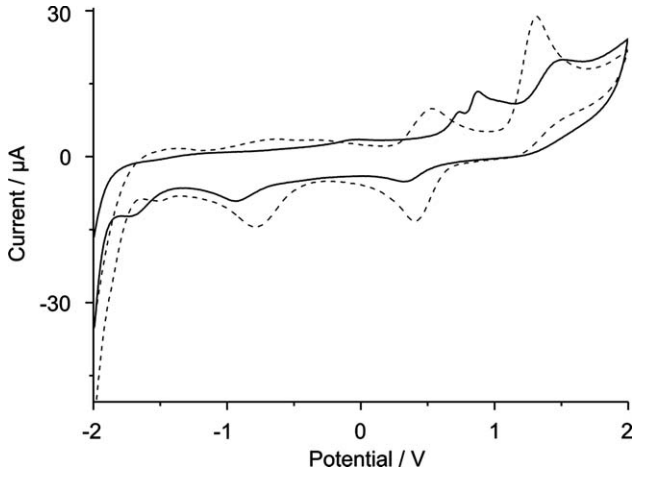

Fig. 11. Cyclic voltammograph of complex **1** (—) and 2,3-DHBA (-----), in CH_3CN. Supporting electrolyte: $TBNPF_6$; reference electrode: SCE.

the semi-oxidized to the fully oxidized form (quinone) [56]. The anodic peak at +1.30 V corresponds to the quinone polymerization [57]. For the complex, the first oxidation step of the catecholate to the semiquinonate form of the ligand occurs at −0.04 V and the second one that is due to the conversion to the quinonate form, at +0.74 V. In addition, a peak at +0.88 V corresponds to the decarboxylation of the ligand [58], while polymerization happens at 1.49 V [59,22].

4. Conclusions

In summary, the results reported in this paper are: (i) The reaction of the isomeric catechol derivatives 2,3- and 2,5-DHBA with an octanuclear molybdenum cluster in analogous conditions, lead to different polyooxomolybdate complexes. (ii) The tetranuclear molybdenum complex of 2,3-DHBA with two triple bridged methanol molecules was investigated for its reactivity by thermal decomposition studies yielding methyl ether, as happens in analogous complexes. The information collected by multinuclear NMR experiments in protolytic and complexing solvents indicates the degradation of the complex via the extraction of the methoxo bridges. The reductive form of the ligand was confirmed by solid state ESR and cyclic voltammetry. Further studies of a possible catalytic activity of complex **1** are in progress. (iii) To our knowledge the structure of the trinuclear molybdenum complex of 2,5-DHBA is the first example for polydentate coordination type of this ligand. Especially, the tridentate binding mode of gentisic acid differs from the usual salicylate with the participation of both carboxylate oxygen atoms. (iv) Complex **2** is less stable than **1** at the stirring time in their parent solutions, with ligand release and the formation of the polyoxometalate complex $(PPh_4)_2[Mo_6O_{19}]$.

5. Supplementary material

Crystallographic data for the structural analysis have been deposited with the Cambridge Crystallographic Data Centre, CCDC Nos. 282204 and 282205 for **1** and **2**, respectively. Copies of this information may be obtained free of charge on application to CCDC, 12 Union Road, Cambridge CB2 1EZ, UK (fax: +44 1223 336 033; e-mail: deposit @ccdc.cam.ac.uk or www: http://www.ccdc.cam.ac.uk).

Acknowledgements

This work was supported by the European Community and the Greek Ministry of Education and Religion and especially the research program HERAKLEITOS (EPEAEK II). The authors are grateful to Dr. A. Moutsatsou for her help in thermogravimetric measurements, Dr. N. Psaroudakis for the cyclic voltammetry experiments and the reviewers for their useful comments.

References

[1] (a) S.C. Liu, S.N. Shaikh, J. Zubieta, Inorg. Chem. 28 (1989) 723;
(b) S.C. Liu, S.N. Shaikh, J. Zubieta, J. Chem. Soc., Chem. Commun. (1988) 1017;
(c) S. Lincoln, S.A. Koch, Inorg. Chem. 25 (1986) 1594.
[2] (a) E-I. Ochiai, General Principles of Biochemistry of the Elements, Plenum Press, New York, 1987;
(b) E.I. Stiefel, in: S.J. Lippard (Ed.), Progress in Inorganic Chemistry, Wiley, New York, 1977 (Chapter 2);
(c) R. Hille, Chem. Rev. 96 (1996) 2757;
(d) A. Sigel, H. Sigel, Metal Ions in Biological Systems: Molybdenum and Tungsten. Their Roles in Biological Processes, vol. 39, Marcel Dekker Inc., New York, 2002;
(e) R.S. Pilato, E.I. Stiefel, in: J. Reedijk, E. Bouwman (Eds.), Bioinorganic Catalysis, 2nd ed., Marcel Dekker, New York, 1999 (Chapter 6).
[3] (a) G. Peng, J. Nicholli, E. McCullorgh, J. Spence, Inorg. Chem. 33 (1994) 2857;
(b) A. Thapper, R.J. Deeth, E. Nordlander, Inorg. Chem. 38 (1999) 1015;
(c) J.A. Gray, R.H. Holm, J. Am. Chem. Soc. 111 (1989) 2111;
(d) P. Tsao, C.J. Fritchie, H.A. Levy, J. Am. Chem. Soc. 100 (13) (1978) 4089;
(e) M.S. Reynolds, J.M. Berg, R.H. Holm, Inorg. Chem. 23 (1984) 3057.
[4] B.A. Reul, D.J. Becker, L.N. Ongemba, C.J. Bailey, J.-C. Henquin, S.M. Brichard, J. Endocrinol. 155 (1997) 55.
[5] (a) M.J. Morris, Coordin. Chem. Rev. 172 (1998) 181;
(b) M.I. Khan, J. Zubieta, Prog. Inorg. Chem. 43 (1995) 1.
[6] (a) A.J. Bridgeman, G. Cavigliasso, Inorg. Chem. 41 (2002) 1761;
(b) T. Yamase, H. Fujita, K. Fukushima, Inorg. Chim. Acta 151 (1988) 15;
(c) J. Rhule, C. Hill, D. Judd, Chem. Rev. 98 (1998) 327.
[7] H.K. Kang, S.C. Liu, S.N. Shaikh, T. Nicholson, J. Zubieta, Inorg. Chem. 28 (1989) 920.
[8] S.M.O. Quintal, H.I.S. Nogueira, H.M. Carapuca, V. Felix, M.G.B. Drew, J. Chem. Soc., Dalton Trans. (2001) 3196.
[9] L. Lisnard, P. Mialane, A. Dolbecq, J. Marrot, F. Secheresse, Inorg. Chem. Commun. 6 (2003) 503.
[10] B. Modec, J.V. Brencic, E.M. Burkholder, J. Zubieta, J. Chem. Soc., Dalton Trans. (2003) 4618.
[11] R. Villanneau, R. Delmont, A. Proust, P. Gouzerh, Chem. Eur. J. 6 (2000) 1184.
[12] E.M. McCarron III, R.L. Harlow, J. Am. Chem. Soc. 105 (1983) 6179.
[13] E.M. McCarron Jr., R.L. Harlow, Z.G. Li, C. Suto, Y. Yuen, J. Solid State Chem. 136 (1998) 247.
[14] S. Liu, S.N. Shaikh, J. Zubieta, Inorg. Chem. 26 (26) (1987) 4303.
[15] R.K. Grasselli, J.D. Burrington, Adv. Catal. 30 (1981) 133.
[16] J.N. Allison, W.A. Goddard, J. Catal. 92 (1) (1985) 127.
[17] (a) R.C. Scarrow, K.N. Raymond, Inorg. Chem. 27 (1988) 4140, and references cited therein;
(b) W. Kiggen, F. Vogtle, Angew. Chem., Int. Ed. 23 (1984) 714;
(c) A.E. Martell, W.F. Anderson, D.G. Badman, Development of Iron Chelators for Clinical Use, Elsevier North Holland, Amsterdam, 1981.
[18] C. Pierpont, R. Buchanan, Coordin. Chem. Rev. 38 (1981) 45.
[19] C. Bianchini, P. Frediani, F. Laschi, A. Meli, F. Vizza, E. Zianello, Inorg. Chem. 29 (1990) 3402.
[20] Z. Sroka, W. Cisowski, Food Chem. Toxicol. 41 (2003) 753.
[21] V. Aletras, A. Karaliota, M. Kamariotaki, D. Hatzipanayioti, N. Hadjiliadis, Inorg. Chim. Acta 312 (2001) 151.
[22] A. Lymberopoulou-Karaliota, D. Hatzipanayioti, M. Kamariotaki, M. Potamianou, C. Litos, V. Aletras, Inorg. Chim. Acta 358 (2005) 2975.
[23] A. Karaliota, V. Aletras, D. Hatzipanayioti, M. Kamariotaki, M. Potamianou, J. Mass Spectrom. 37 (2002) 760.

[24] A. Karaliota, M. Kamariotaki, D. Hadjipanagioti, V. Aletras, J. Inorg. Biochem. 69 (1998) 79.
[25] G. Micera, L.S. Erre, P. Piu, F. Cariati, G. Ciani, A. Sironi, Inorg. Chim. Acta 107 (1985) 223.
[26] K. Zhang, Y.G. Zuo, J. Agric. Food Chem. 52 (2004) 222.
[27] (a) G. Cohen, R.A. Greenwald, Oxy radicals and their scavenger system: Molecular Aspects, vol. I, Elsevier Science Publishing Co., New York, 2000, p. 95;
(b) M. Xang, P.Y. Du, K. Wang, J. Beig. Med. Univ. 19 (1987) 183.
[28] (a) A. Sakaitani, F. Rusnak, N.R. Quinn, C. Tu, T.B. Frigo, G.A. Berctold, C.T. Walsh, Biochemistry 29 (1990) 6789;
(b) F. Rusnak, W.S. Fataci, C.T. Walsh, Biochemistry 28 (1989) 6827.
[29] W.P. Griffith, H.I.S. Nogueira, B.C. Parkin, R.N. Sheppard, A.J.P. White, D.J. Williams, J. Chem. Soc., Dalton Trans. (1995) 1775.
[30] H.K. Chae, W.G. Klemperer, T.A. Marquart, Coordin. Chem. Rev. 128 (1993) 209.
[31] (a) C.A. Tyson, S.E. Levalley, R. Chan, P.D. Hobbs, M.I. Dawson, J. Pharmacol. Exp. Ther. 228 (1984) 676;
(b) V.P. Kotsaki-Kovatsi, A.J. Vafiadou, G. Koehler-Samuilidou, A. Kovatsis, Vet. Hum. Toxicol. 39 (1997) 211;
(c) E.P. Kable, P.G. Parsons, Biochem. Pharmacol. 37 (1988) 1711;
(d) G.E. Marak, N.A. Rao, A. Sevanian, V. Zdravkovich, G.O. Till, P.A. Wood, Ophthalmic Res. 19 (1987) 120.
[32] A. Ghiselli, O. Laurenti, G. De Mattia, G. Maiani, A. Ferro-Luzzi, Free Radical Biol. Med. 13 (1992) 621.
[33] W.E. Wallace, M.A. Arnould, R. Knochenmuss, Int. J. Mass Spectrom. 242 (2004) 19.
[34] C.C. Yeo, M.V.M. Wong, Y.M. Feng, K.P. Song, C.L. Poh, Gene 312 (2003) 239.
[35] N. Mano, J. Goto, Anal. Sci. 19 (2003) 3.
[36] A. Mele, L. Malpezzi, J. Am. Soc. Mass Spectrom. 11 (3) (2000) 228.
[37] X.M. Lu, H.J. Zhu, H.Z. Yuan, X.A. Mao, Spectrosc. Spectr. Anal. 22 (2002) 36.
[38] X.M. Lu, H.J. Zhu, S.C. Liu, Chem. J. Chinese Univ. – Chinese 17 (1996) 183.
[39] N. Strukan, M. Cindric, T. Kajfez, B. Kamenar, G. Giester, Acta Crystallogr. C 56 (2000) E443.
[40] E. Gumaer, K. Lettko, L. Ma, D. Macherone, J. Jubieta, Inorg. Chim. Acta 179 (1991) 47.
[41] M. Kamariotaki, A. Karaliota, D. Stabaki, T. Bakas, V. Papaefthymiou, S.P. Perlepes, N. Hadjiliadis, Transit. Metal Chem. 19 (1994) 241.
[42] D. Hatzipanayioti, A. Karaliota, M. Kamariotaki, A. Veneris, P. Falaras, Transit. Metal Chem. 23 (1998) 407.
[43] X.M. Lu, S.C. Liu, X. Mao, X.H. Bu, J. Mol. Struct. 562 (2001) 89.
[44] M. Filowitz, R.K.C. Ho, W.G. Klemperer, W. Shum, Inorg. Chem. 18 (1979) 93.
[45] (a) G.M. Sheldrick, SHELXS-86, Structure Solving Program, University of Gottingen, Germany, 1986;
(b) G.M. Sheldrick, SHELXL-97, Program for the Refinement of Crystal Structures from Diffraction Data, University of Gottingen, Germany, 1997.
[46] C.F. Edwards, W.P. Griffith, A.J.P. White, D.J. Williams, J. Chem. Soc., Dalton Trans. (1993) 3813.
[47] E.M. McCarron III, R.H. Staley, A.W. Sleight, Inorg. Chem. 23 (1984) 1043.
[48] S.M. Malinak, D.T. Rosa, D. Coucouvanis, Inorg. Chem. 37 (1998) 1175.
[49] G.B. Deacon, R.J. Phillips, Coordin. Chem. Rev. 33 (1980) 227.
[50] J.T. Wrobleski, D.B. Brown, Inorg. Chem. 18 (2) (1979) 498.
[51] J. Lu, Y. Xu, Chem. Mater. 10 (1998) 4141.
[52] H. Rijnberk, C. Nather, W. Bensch, Z. Anorg. Allg. Chem. 625 (1999) 1172.
[53] B.R. Srinivasan, S.C. Sawant, Thermochim. Acta 402 (2003) 45.
[54] I. Szczygiel, Thermochim. Acta 417 (2004) 75.
[55] A.A. Soliman, W. Linert, Thermochim. Acta 338 (1999) 67.
[56] J.P. Wilshire, L. Leon, P. Bosserman, D.T. Sawyer, J. Am. Chem. Soc. 101 (1979) 3379.
[57] S.M. Golabi, D. Nematollahi, J. Electroanal. Chem. 430 (1997) 141.
[58] D. Nematollahi, H. Goodarzi, J. Org. Chem. 67 (2002) 5036.
[59] (a) M. Bodini, C. Osorio, A. Del Valle, V. Arancibia, G. Munoz, Polyhedron 14 (1995) 2933;
(b) M.E. Bodini, V. Arancibia, Transit. Metal Chem. 22 (1997) 150.

method. The recent calculations with the TD-DFT method for open- and closed-shell of 5d-metal complexes (including rhenium complexes) have supported the TD-DFT method to be applicable for such systems giving good assignment of experimental spectra [13–19].

2. Experimental

2.1. General procedure

The reactions were carried out under argon atmosphere. All solvents were of reagent grade and were used as received. Ammonium perrhenate, Ph_3P, pzH and pyz were purchased from Aldrich and used as received. $[ReCl_4(PPh_3)_2]$ was prepared according to the literature method [20].

IR spectra were recorded on a Nicolet Magna 560 spectrophotometer in the spectral range 4000–400 cm^{-1} with the samples in the form of KBr pellets. Electronic spectra were measured on a spectrophotometer Lab Alliance UV–VIS 8500 in the range 900–200 nm in deoxygenated dichloromethane solution. Elemental analyses (C H N) were performed on a Perkin–Elmer CHN-2400 analyzer.

2.2. Preparation of *[ReCl$_4$(pzH)(PPh$_3$)]* (*1*)

$[ReCl_4(PPh_3)_2]$ (1 g, 1.15 mmol) and pzH (0.30 g, 4.4 mmol) in chloroform (100 cm^3) were refluxed overnight. The colour of the reaction mixture changed slowly from dark red to brown. The volume was condensed to 10 cm^3 and orange microcrystalline solid was formed by an addition of 100 cm^3 of ethanol. The product was washed with EtOH and cold ether, and dried in vacuo. The crystals of **1** suitable for X-ray investigation were obtained by recrystallization from $CHCl_3$–EtOH. Yield 80%.

IR (KBr, cm^{-1}) 3342 (s), 3140 (m) 3062 (w), 1580 (w) 1517 (m) 1486 (s), 1444 (s), 1405 (m), 1350 (s), 1268 (m), 1150 (m), 1128 (s) 1093 (s), 1058 (s), 1008 (w), 778 (s), 755 (s), 700 (s), 582 (m), 531 (s), 494 (s).

Anal. Calc. for $C_9H_{15}N_6Cl_4ORe$: C, 38.31; H, 2.91; N, 4.25. Found: C, 38.53; H, 3.0; N, 4.30%.

2.3. Preparation of *[ReCl$_4$(pyz)(PPh$_3$)]* (*2*)

A procedure similar to that for **1** was used with $[ReCl_4(PPh_3)_2]$ (1 g, 1.15 mmol) and pyz (0.3 g, 3.7 mmol). An orange crystalline precipitate of **2** was collected in 80% yield.

IR (KBr, cm^{-1}) 3093 (w) 3059 (w), 1581 (w) 1512 (w) 1481 (s), 1434 (s), 1414 (m), 1339 (w), 1318 (w), 1188 (w), 1149 (s) 1120 (s), 1090 (s), 1053 (s), 1028 (w), 807 (s), 746 (s), 691 (vs), 524 (s), 502 (s), 465 (m), 450 (sh).

Anal. Calc. for $C_9H_{15}N_6Cl_4ORe$: C, 39.42; H, 2.86; N, 4.18. Found: C, 39.63; H, 2.92; N, 4.31%.

2.4. Crystal structures determination and refinement

The X-ray intensity data of **1** and **2** were collected on a KM-4-CCD automatic diffractometer equipped with CCD detector, 20 and 29 s exposure time was used receptively and all reflections of Ewald sphere was collected up to $2\theta = 50°$. The unit cell parameters were determined from least-squares refinement of the setting angles of 7903 and 12323 strongest reflections, respectively, for **1** and **2**. Details concerning crystal data and refinement are given in Table 1. Lorentz, polarization and numerical absorption corrections [21] were applied. The structure were solved by the Patterson method and subsequently completed by the difference Fourier recycling. All the non-hydrogen atoms were refined anisotropically using full-matrix, least-squares technique. The carbon bonded hydrogen atoms were founded on difference Fourier synthesis and they were refined as ''riding'' on their parent carbon atoms [d(C–H) = 0.96 Å] and assigned isotropic temperature factors equal 1.2 times the value of equivalent temperature

Table 1
Crystal data and structure refinement for **1** and **2**

	1	**2**
Empirical formula	C_{21} $H_{19}Cl_4N_2PRe$	$C_{22}H_{19}Cl_4N_2PRe$
Formula weight	658.35	670.36
Temperature (K)	293(2)	293(2)
Wavelength (Å)	0.71073	0.71073
Crystal system	triclinic	monoclinic
Space group	$P\bar{1}$	$P2_1/c$
Unit cell dimensions		
a (Å)	10.5796(7)	17.5845(5)
b (Å)	11.0495(7)	9.05250(10)
c (Å)	11.3454(8)	15.7452(6)
α (°)	78.276(6)	
β (°)	86.039(5)	109.002(2)
γ (°)	65.089(6)	
Volume (A^3)	1177.58(14)	2369.80(12)
Z	2	4
Density (calculated) (Mg/m^3)	1.857	1.879
Absorption coefficient (mm^{-1})	5.692	5.659
F(0 0 0)	634	1292
Crystal size (mm)	$0.55 \times 0.45 \times 0.35$	$0.39 \times 0.30 \times 0.09$
θ Range for data collection	3.53–25.10°	3.09–25.11°
Index ranges	$-12 \leqslant h \leqslant 12$	$-20 \leqslant h \leqslant 20$
	$-13 \leqslant k \leqslant 13$	$-10 \leqslant k \leqslant 10$
	$-13 \leqslant l \leqslant 11$	$-13 \leqslant l \leqslant 18$
Reflections collected	11470	23594
Independent reflections	4172 ($R_{int} = 0.0291$)	4222 ($R_{int} = 0.0190$)
Completeness to 2θ (%)	99.5	99.8
Maximum and minimum transmission	0.198 and 0.083	0.639 and 0.217
Data/restraints/parameters	4172/0/262	4222/0/271
Goodness-of-fit on F^2	1.096	1.143
Final R indices [$I > 2\sigma(I)$]	$R_1 = 0.0240$	$R_1 = 0.0176$
	$wR_2 = 0.0602$	$wR_2 = 0.0350$
R indices (all data)	$R_1 = 0.0247$	$R_1 = 0.0194$
	$R_1 = 0.0607$	$wR_2 = 0.0355$
Largest difference peak and hole (e A^{-3})	0.981 and −1.183	0.751 and −0.701

factor of the parent carbon atom. SHELXS97 [22], SHELXL97 [23] and SHELXTL [24] programs were used for all the calculations. Atomic scattering factors were those incorporated in the computer programs.

2.5. Computational details

GAUSSIAN03 program [25] was used in the calculations. The geometry optimization was carried out with the DFT method with the use of B3LYP functional [26,27]. The electronic spectra were calculated with the TDDFT method [28]. The calculations were performed by using ECP basis set on the rhenium atom, the standard 6-31+g** basis for chlorine, oxygen and nitrogen, 6-31+g* for carbon and 6-31G basis for hydrogen atoms. The Xe core electrons of Re were replaced by an effective core potential and DZ quality Hay and Wadt Los Alamos ECP basis set (LANL2DZ) [29] was used for the valence electrons. Additional *d* function with exponent $\alpha = 0.3811$ and *f* function with exponent $\alpha = 2.033$ on the rhenium atom were added.

2.6. Magnetic measurement

The magnetic measurements of the powdered samples was measured over the temperature range 1.8–300 K using a Quantum Design SQUID – based MPMSXL – 5-type magnetometer. The superconducting magnet was generally operated at a field strength ranging from 0 to 5 T measurements. Measurements sample of compounds were made at magnetic field 0.5 T.

The SQUID magnetometer was calibrated with the palladium rod sample. Corrections are based on subtracting the sample – holder signal and contribution χ_D estimated from the Pascal constants [37] and equal -257×10^{-6} cm^3 mol^{-1} for complex [$ReCl_4(pzH)(PPh_3)$] (**1**) and -263×10^{-6} cm^3 mol^{-1} for complex [$ReCl_4(pyz)(PPh_3)$] (**2**). The t.i.p. per Re^{4+} center was assumed to be 70×10^{-6} cm^3 mol^{-1}. The effective magnetic moment was calculated from the equation, $\mu_{eff} = 2.83(\chi_M T)^{1/2}$(B.M.).

3. Results and discussion

The [$ReCl_4(pzH)(PPh_3)$] (**1**) and [$ReCl_4(pyz)(PPh_3)$] (**2**) complexes have been obtained in high yield in the reactions of [$ReCl_4(PPh_3)_2$] with pyrazole and pyrazine, respectively

$$[ReCl_4(PPh_3)_2] + pzH \rightarrow [ReCl_4(pzH)(PPh_3)] + PPh_3 \quad (R.1)$$

$$[ReCl_4(PPh_3)_2] + pyz \rightarrow [ReCl_4(pyz)(PPh_3)] + PPh_3 \quad (R.2)$$

The excess of pzH and pyz ensures the maximum yield of the products.

The elemental analysis of the complexes is in good agreement with their formulation. The presence of the strong band in the range assignable to N–H vibrations in the spectrum of **1** confirms the coordination of pyrazole in a neutral monodentate form. The absorption bands at ~1580 and ~1515 cm^{-1} are typical of mono-coordinated diaza ligands [30].

3.1. X-ray structures

Perspective drawings of **1** and **2** are given in Figs. 1 and 2, respectively. The rhenium atom of the both complexes is in a distorted octahedral environment with four chlorine

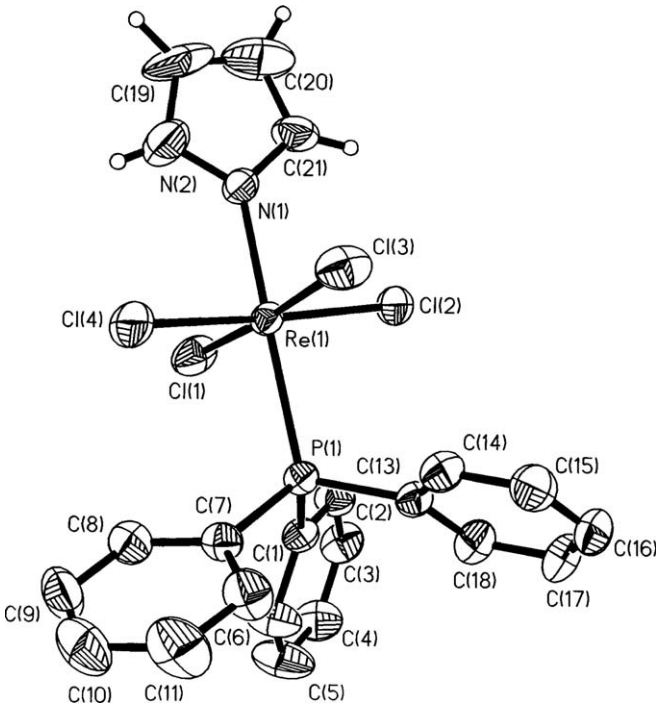

Fig. 1. The molecular structure of **1**. The hydrogen atoms of the phenyl rings are omitted for clarity.

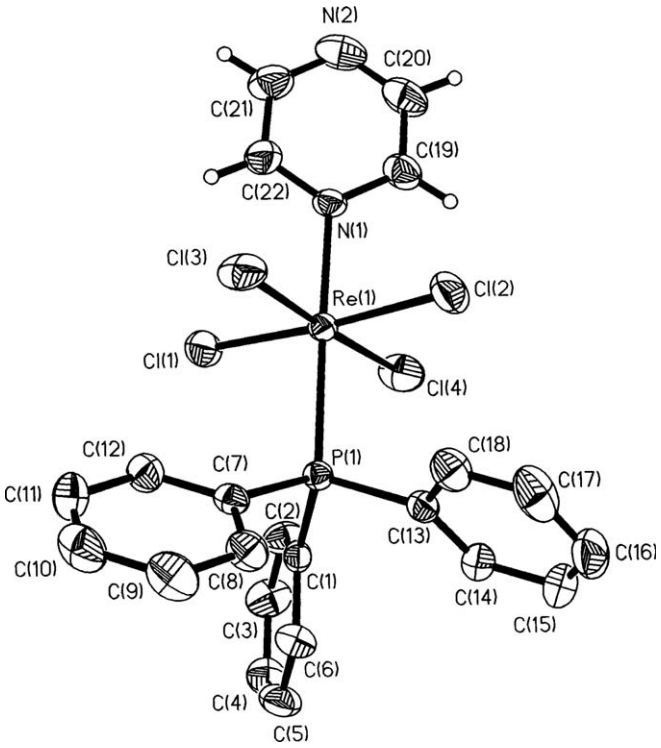

Fig. 2. The molecular structure of **2**. The hydrogen atoms of the phenyl rings are omitted for clarity.

ions in the equatorial plane, and N-donor ligand and PPh_3 molecule in axial positions. Table 1 presents crystal data and structural refinement for **1** and **2**. The most important experimental bond lengths and angles for **1** and **2** are reported in Tables 2 and 3, respectively. The Re–N, Re–Cl and Re–P bond lengths are unexceptional, they agree well with appropriate values found previously in similar rhenium compounds [7–12]. The weak C–H···Cl and medium strength N–H···Cl intra- and intermolecular hydrogen bonds [31,32] of **1** and **2** are presented in Table 4. Via these interactions a hydrogen bonded dimer (in **1**) and infinite hydrogen bonded chains along crystallographic *b* axis (in **2**) are created. The shortest Re···Re distance is 6.670 and 7.753 Å, respectively, for **1** and **2**.

The bond valences were computed as $v_{ij} = \exp[(R_{ij} - d_{ij})/b]$ [33–36], where R_{ij} is the bond-valence parameter (in the formal sense the R_{ij} parameter value can be considered as an idealized single-bond length between *i* and *j* atoms). The R_{Re-N}, R_{Re-P}, R_{Re-Cl} were taken as 2.06, 2.46 and 2.23 [35], respectively, and *b* was taken as 0.37 [33]. The computed bond valences of rhenium are $v_{Re-N} = 0.761$; $v_{Re-P} = 0.840$; $v_{Re-Cl} = 0.775$, 0.758, 0.730, 0.764 v.u. (valence units) for **1** and $_{Re-N} = 0.666$; $v_{Re-P} = 0.871$; $v_{Re-Cl} = 0.758$, 0.763, 0.784, 0.751 v.u. (valence units) for **2**. These means that the triphenylphosphine groups are strongest bonded substituents, the strength of Re–Cl bonds are comparable to the strength of $Re–N_{(pyrazole)}$ bond, and the pyrazine is the weakest bonded substituent (the bond is about 15% weaker in comparison to $Re–N_{(pyrazole)}$).

3.2. Optimized geometries

The geometries of **1** and **2** were optimized in quartet and doublet states using the DFT method with the B3LYP functional. The energies of the doublet states are of 15.8 and 16.3 kcal higher for **1** and **2**, respectively. The optimized geometric parameters of the quartet states are

Table 2
The experimental and optimized bond lengths (Å) and angles (°) for **1**

	Bond lengths			Bond angles	
	Experimental	Optimized		Experimental	Optimized
Re(1)–Cl(1)	2.3245(11)	2.383	N(1)–Re(1)–Cl(3)	88.10(9)	87.69
Re(1)–Cl(2)	2.3323(10)	3.371	N(1)–Re(1)–Cl(2)	88.62(9)	90.17
Re(1)–Cl(3)	2.3464(11)	2.369	Cl(3)–Re(1)–Cl(2)	88.48(4)	89.35
Re(1)–Cl(4)	2.3296(11)	2.405	N(1)–Re(1)–Cl(1)	88.41(9)	88.84
Re(1)–N(1)	2.161(3)	2.173	Cl(3)–Re(1)–Cl(1)	176.30(4)	176.00
Re(1)–P(1)	2.5245(9)	2.586	Cl(2)–Re(1)–Cl(1)	92.67(4)	92.73
			N(1)–Re(1)–Cl(4)	89.29(9)	88.10
			Cl(3)–Re(1)–Cl(4)	88.96(5)	88.18
			Cl(2)–Re(1)–Cl(4)	176.74(4)	176.96
			Cl(1)–Re(1)–Cl(4)	89.77(5)	89.73
			N(1)–Re(1)–P(1)	175.87(9)	178.56
			Cl(3)–Re(1)–P(1)	95.02(4)	93.74
			Cl(2)–Re(1)–P(1)	88.76(3)	89.67
			Cl(1)–Re(1)–P(1)	88.52(4)	89.74
			Cl(4)–Re(1)–P(1)	93.46(4)	92.12

Table 3
The experimental and optimized bond lengths (Å) and angles (°) for **2**

	Bond lengths			Bond angles	
	Experimental	Optimized		Experimental	Optimized
Re(1)–Cl(1)	2.3323(7)	2.386	N(1)–Re(1)–Cl(3)	89.74(6)	88.81
Re(1)–Cl(2)	2.3300(8)	2.368	N(1)–Re(1)–Cl(2)	86.59(6)	87.53
Re(1)–Cl(3)	2.3202(7)	2.368	Cl(3)–Re(1)–Cl(2)	88.45(3)	88.96
Re(1)–Cl(4)	2.3359(7)	2.380	N(1)–Re(1)–Cl(1)	89.00(6)	87.99
Re(1)–N(1)	2.2106(19)	2.2265	Cl(3)–Re(1)–Cl(1)	90.78(3)	90.16
Re(1)–P(1)	2.5111(6)	2.577	Cl(2)–Re(1)–Cl(1)	175.53(2)	175.46
			N(1)–Re(1)–Cl(4)	88.76(6)	88.79
			Cl(3)–Re(1)–Cl(4)	177.25(3)	176.74
			Cl(2)–Re(1)–Cl(4)	89.16(3)	88.74
			Cl(1)–Re(1)–Cl(4)	91.49(3)	91.96
			N(1)–Re(1)–P(1)	178.47(5)	178.38
			Cl(3)–Re(1)–P(1)	91.70(2)	92.16
			Cl(2)–Re(1)–P(1)	92.93(2)	93.78
			Cl(1)–Re(1)–P(1)	91.50(2)	90.71
			Cl(4)–Re(1)–P(1)	89.78(2)	90.29

gathered in Tables 2 and 3 for **1** and **2**, respectively. In general, the predicted bond lengths and angles are in good agreement with the values based upon the X-ray crystal structure data.

3.3. Charge distribution

Table 5 presents the atomic charges from the natural population analysis (NPA) for **1** and **2** complexes. The calculated charges on the rhenium atoms are considerable lower than the formal charge +4. It results from charge donation from the chloride ions and triphenylphosphine ligand. There is large positive charge on the P atom, and the charges on the chloride ions are significantly smaller than −1. The populations of the d_{xy}, d_{xz}, d_{yz}, $d_{x^2-y^2}$ and d_z^2 orbitals of the central atoms in **1** and **2** are following: complex **1** – 1.235, 1.239, 1.046, 1.130 and 1.228; complex **2** – 1.246, 1.233, 1.116, 1.124 and 1.186.

Table 4
Hydrogen bonds for **1** and **2**

D	A	H···A	D···A	D–H···A
1				
N(2)	Cl(4)	2.75	3.212(5)	115.2
N(2)	Cl(4)[a]	2.63	3.340(5)	140.1
C(2)	Cl(2)	2.66	3.497(4)	149.7
C(4)	Cl(3)	2.75	3.300(4)	118.7
C(21)	Cl(2)	2.62	3.149(5)	116.5
2				
C(2)	Cl(1)	2.78	3.456(3)	130.7
C(2)	Cl(4)	2.72	3.389(3)	129.1
C(19)	Cl(2)	2.73	3.188(3)	111.1
C(20)	Cl(4)[b]	2.72	3.580(3)	153.3

[a] $-x, 1-y, 1-z$.
[b] $-x, y+0.5, -z-0.5$.

Table 5
Atomic charges from the natural population analysis (NPA) for **1** and **2**

Atom	**1**	**2**
Re(1)	0.558	0.535
Cl(1)	−0.345	−0.352
Cl(2)	−0.323	−0.317
Cl(3)	−0.320	−0.323
Cl(4)	−0.371	−0.339
P(1)	1.395	1.408
N(1)	−0.343	−0.474
N(2)	−0.340	−0.412

3.4. Molecular orbitals

The energies and characters of the selected MOs for **1** and **2** are presented in Tables 6 and 7, respectively. The rhenium atoms in **1** and **2** compounds possess $(d_{xz})^1(d_{yz})^1(d_{xy})^1$ configuration. For **1** and **2** complexes, the rhenium d_{xz}, d_{yz} and d_{xy} orbitals make main contributions into the HOMO − 2, HOMO − 1 and HOMO with α spin and HOMO, LUMO and LUMO + 1 with β spin. In all these molecular orbitals, the rhenium d_{xz}, d_{yz} and d_{xy} orbitals bear antibonding character towards the p_π orbitals of the chloride ligands. For complex **1**, the LUMO with α spin and the LUMO + 9 with β spin are of d_z^2-σ_{Cl}-σ_P character. The $d_{x^2-y^2}$ rhenium orbital has a significant contribution in the LUMO + 1 with α spin and the LUMO + 6 with β spin.

Table 6
The energies and characters of the selected molecular orbitals with α and β spins for **1**

	α MO		β MO	
	E (eV)	Character	*E* (eV)	Character
HOMO − 12	−7.849	π(Cl), π(pzH)	−7.990	π(pzH), π(Cl)
HOMO − 11	−7.771	π(Cl)	−7.898	π(pzH), π(Cl)
HOMO − 10	−7.662	π(pzH), π(Cl)	−7.735	π(Cl)
HOMO − 9	−7.401	π(Ph)	−7.637	π(Cl), n(P), n(N)
HOMO − 8	−7.323	π(Cl)	−7.581	π(pzH), π(Cl)
HOMO − 7	−7.113	π(Ph), d_{xz}(Re)	−7.572	π(Cl)
HOMO − 6	−7.093	π(Ph), π(Cl), d_{yz}(Re)	−7.371	π(Ph)
HOMO − 5	−6.985	π(Ph), d_{yz}	−7.133	π(Cl), π(Ph)
HOMO − 4	−6.944	π(Ph), n(P)	−7.073	π(Ph)
HOMO − 3	−6.908	π(Ph), π(Cl), d_{xz}	−7.007	π(Cl), π(Ph)
HOMO − 2	−6.696	d_{yz}(Re), π(Cl), π(Ph)	−6.936	π(Ph)
HOMO − 1	−6.455	d_{xz}(Re), π(Cl)	−6.894	π(Ph), π(Cl)
HOMO	−6.275	d_{xy}(Re), π(Cl)	−6.788	π(Ph), n(P)
LUMO	−1.556	d_{z^2}(Re)-σ(P)-σ(N)	−3.500	d_{yz}(Re), π(Cl)
LUMO + 1	−1.358	$d_{x^2-y^2}$(Re)-σ(Cl)	−3.349	d_{xz}(Re), π(Cl)
LUMO + 2	−1.020	π*(Ph), σ*(P–C)	−2.914	d_{xy}(Re), π(Cl)
LUMO + 3	−0.825	π*(Ph), σ*(P–C)	−1.103	π*(Ph), σ*(P–C), d_{z^2}(Re)
LUMO + 4	−0.625	π*(pzH)	−1.011	π*(Ph), σ*(P–C), d_{z^2}(Re)
LUMO + 5	−0.455	π*(Ph)	−0.793	π*(Ph), σ*(P–C)
LUMO + 6	−0.436	π*(Ph), d_{z^2}(Re)	−0.690	$d_{x^2-y^2}$(Re)-σ(Cl)
LUMO + 7	−0.170	π*(Ph)	−0.543	π*(pzH)
LUMO + 8	−0.113	π*(Ph)	−0.441	π*(Ph)
	0.351		−0.254	d_{z^2}(Re), π*(Ph)

Table 7
The energies and characters of the selected molecular orbitals with α and β spins for **2**

	α MO		β MO	
	E (eV)	Character	*E* (eV)	Character
HOMO − 12	−7.988	π(Cl)	−8.409	π(pyz), π(Cl)
HOMO − 11	−7.986	π(Cl), n(P), n(N)	−8.072	n(N)
HOMO − 10	−7.905	π(Cl)	−7.874	π(Cl), π(pyz)
HOMO − 9	−7.507	π(Ph)	−7.817	π(Cl), n(P), n(N)
HOMO − 8	−7.438	π(Cl)	−7.793	π(Cl)
HOMO − 7	− 7.223	π(Ph), d_{yz}	−7.722	π(Cl)
HOMO − 6	−7.195	π(Ph)	−7.467	π(Ph), π(Cl)
HOMO − 5	−7.080	π(Ph), d_{xz}	−7.244	π(Cl), π(Ph)
HOMO − 4	−7.029	π(Ph), n(P)	−7.171	π(Ph)
HOMO − 3	−6.964	π(Ph), d_{xz}, n(P), n(N)	−7.132	π(Cl), π(Ph)
HOMO − 2	−6.734	d_{yz}(Re), π(Cl)	−7.027	π(Ph)
HOMO − 1	−6.698	d_{xz}(Re), π(Cl)	−6.978	π(Ph), π(Cl)
HOMO	−6.392	d_{xy}(Re), π(Cl)	−6.885	π(Ph), n(P)
LUMO	−2.471	π^*(pyz)	−3.727	d_{yz}(Re), π(Cl), π^*(pyz)
LUMO + 1	−1.736	d_{z^2}(Re)-σ(P)-σ(N)	−3.538	d_{xz}(Re), π(Cl)
LUMO + 2	−1.454	$d_{x^2-y^2}$(Re)-σ(Cl), π^*(pyz)	−3.040	d_{xy}(Re), π(Cl)
LUMO + 3	−1.351	π^*(pyz), $d_{x^2-y^2}$-σ(Cl)	−2.276	π^*(pyz), d_{xz}
LUMO + 4	−1.147	π^*(Ph), σ^*(P–C)	−1.354	π^*(pyz)
LUMO + 5	−0.882	π^*(Ph), σ^*(P–C)	−1.264	d_{z^2}(Re)-σ(P)-σ(N), π^*(Ph)
LUMO + 6	−0.587	π^*(Ph), σ^*(P–C), d_{z^2}(Re)	−1.128	π^*(Ph), σ^*(P–C), d_{z^2}(Re)
LUMO + 7	−0.506	π^*(Ph)	−0.840	π^*(Ph), σ^*(P–C), d_{xz}(Re)
LUMO + 8	−0.298	π^*(Ph)	−0.757	$d_{x^2-y^2}$(Re)-σ(Cl)
LUMO + 9	−0.168	π^*(Ph)	−0.508	π^*(Ph)

For complex **2**, the LUMO orbital with α-spin has predominantly π* (pyz) character. The d_z^2 rhenium orbital has a significant contribution in the LUMO + 1 with α spin and the LUMO + 5 with β spin, whereas the LUMO + 2 with α spin and the LUMO + 8 with β have predominantly $d_{x^2-y^2}$-σ_{Cl} character. A contribution of σ* (P–C) phosphine orbitals is visible in several unoccupied molecular orbitals with α and β spins of **1** and **2** compounds. These orbitals are involved in the π-back bonding between metal center and phosphine ligand. In classical concepts empty phosphorous 3d orbitals are used for this purpose. Now, it is generally recognized that the d orbitals, which are very high in energy play only a minor role in the π_{M-PR3} bond formation [33].

3.5. Electronic spectrum from the TDDFT calculations

The electronic spectra of **1** and **2** exhibit two intense absorption bands below 300 nm and some weaker absorptions in the low energy range. The experimental and calculated electronic spectra of **1** and **2** are presented in Figs. 3 and 4, respectively. Each calculated transition was represented by a gaussian function with the height equal to the oscillator strength and width equal to 0.04.

Tables 8 and 9 show the energies and molar absorption coefficients of the experimental absorption bands and the spin-allowed quartet–quartet electronic transitions calculated with the TDDFT method for **1** and **2**, respectively. The assignment of the calculated transitions to the experimental absorption bands was based on the criterion of the energy and oscillator strength of the calculated transition.

The investigated complexes are of large size; the number of basis functions is equal 532 and 546 for **1** and **2**, respectively. Ninety electron transitions calculated by the TDDFT method do not comprise all the experimental absorption bands. The shortest wavelength experimental band of **2** is not assigned to the calculated transitions, and the assignment for the complex **1** is not complete. As the solution spectra of PPh_3, pyrazole and pyrazine exhibit intense absorption bands in 270–200 nm region, some additional intraligand and interligand transitions are expected to be found at higher energies in the calculations for **1** and **2**.

The longest wavelength weak experimental bands at 752 nm for **1** and 761 nm for **2** correspond to the spin-forbidden transitions $^4A_{1g} \rightarrow {}^2E_g$.

For **1** and **2** complexes, the experimental absorption bands between 500 and 250 nm result from d–d and ligand–metal charge transfer (LMCT) transitions. The last ones occur from chloride, phosphine and pyrazole or pyrazine ligand orbitals to the d rhenium orbitals. The d → d transitions calculated in this range have small oscillator strengths. Consequently, they do not contribute significantly to the overall shape of these bands.

3.6. Magnetic properties

The magnetic properties of $[ReCl_4(pzH)(PPh_3)]$ (**1**) complex under the form χ_M versus T and $\chi_M T$ versus T (χ_M being the molar magnetic susceptibilities) are shown in Fig. 5. The effective magnetic moment of 3.40 B.M. ($\chi_M T = 1.44\ cm^3\ mol^{-1}\ K$) at 300 K corresponding three

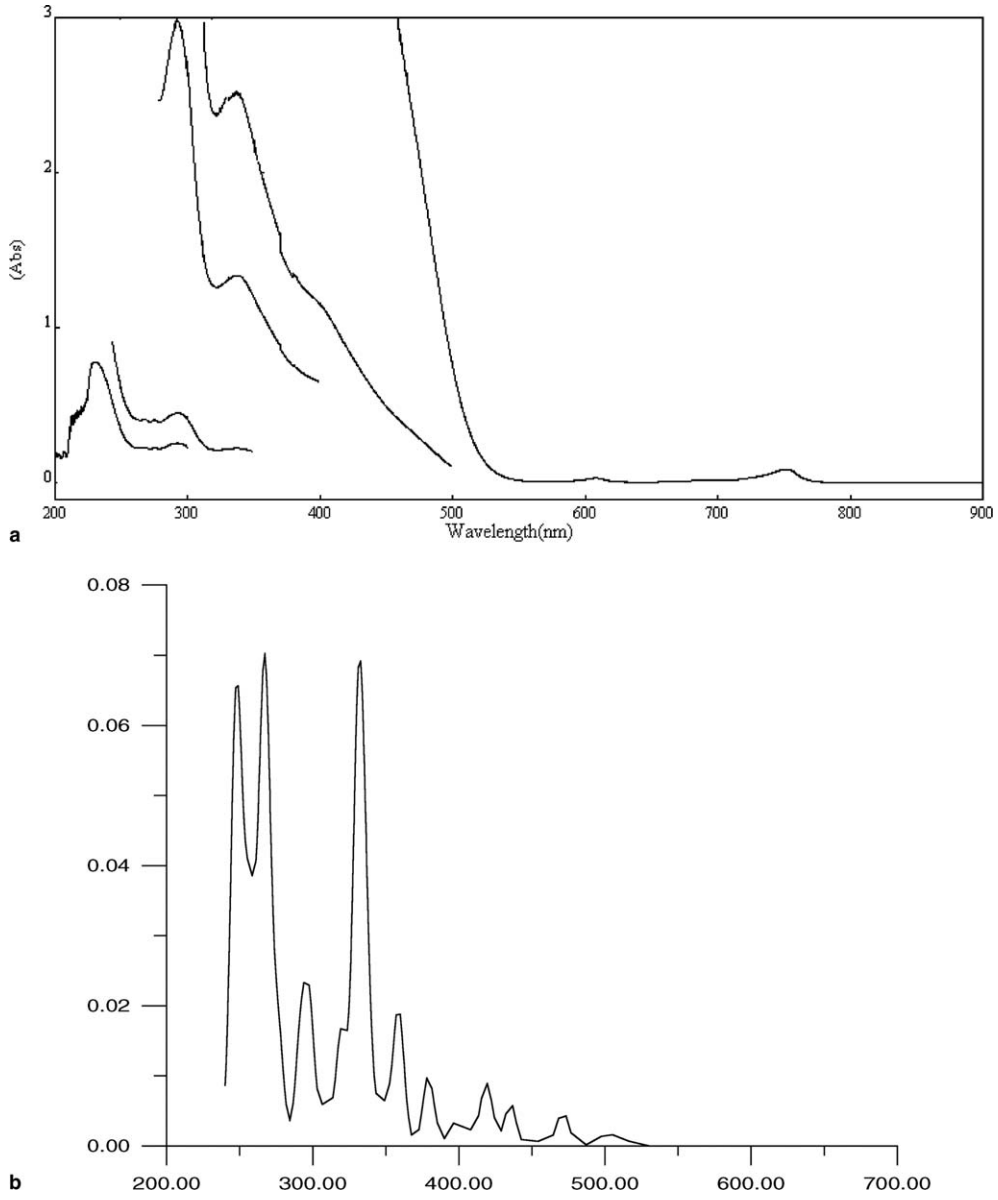

Fig. 3. The experimental (a) and calculated (b) electronic absorption spectrum of **1**.

unpaired electrons. The reduction of magnetic moments in comparison with the spin-only value (3.87 B.M.) can be explained on the basis of depopulation of spin–orbit coupled excited states and/or zero-field effects. The magnetic susceptibilities of other rhenium(IV) salts have been reported elsewhere [38–42]. The value of $\chi_M T$ product decreases only slightly with temperature lowering. In the low-temperature range (below 50 K), a more evident decrease of the value of $\chi_M T$ is observed with continuous decrease of the temperature to 0.04 $cm^3\ mol^{-1}$ K (0.57 B.M.) at 1.8 K.

The susceptibility curves exhibit the maximum at 8 K, indicating the presence the antiferromagnetic 3D ordering in the crystal lattice with the ratio of the Curie–Weiss Θ to the Neel's temperature $\Theta/T_N \approx 1$.

The values of the Curie and Weiss constants determined from the relation $1/\chi_M = f(T)$ over temperature range 80–300 K are equal to 1.50 $cm^3\ mol^{-1}$ and −10.1 K, respectively. A negative value of Weiss constant suggests the antiferromagnetic coupling of the rhenium(IV) centers in the crystal lattice.

To interpret quantitatively the susceptibility data, we used the approaches in which we considered that magnetic susceptibility of this complex might be described by the susceptibility of $^4A_{2g}$ term with the zero-field splitting [43].

Zero-field splitting and ligand field of symmetry lower than cubic lead to the anisotropy of magnetic properties of an ion. The relevant spin Hamiltonian is defined by the following equation:

$$H = D\left[S_z^2 - \frac{1}{3}S(S+1)\right] + g_{II}\beta H_z S_z + g_{\perp}\beta(H_x S_x + H_y S_y), \quad (1)$$

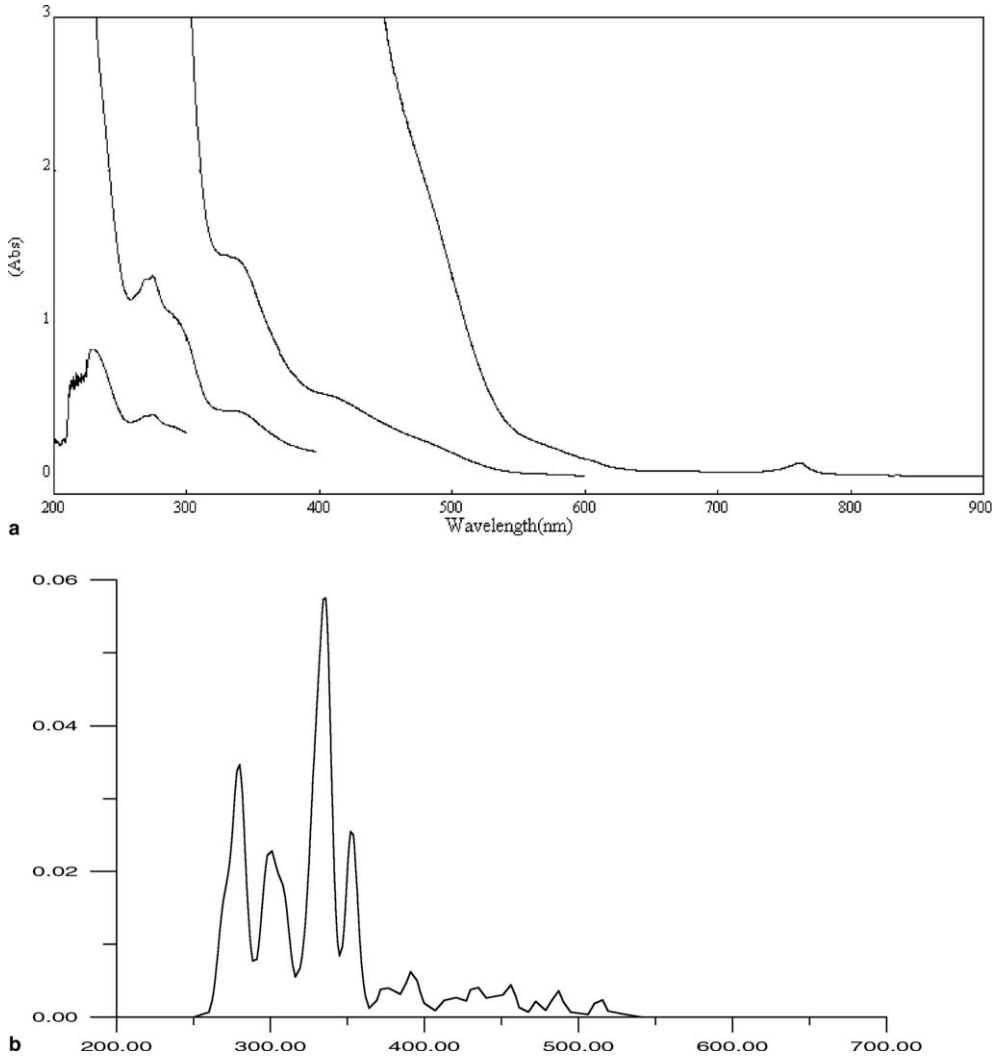

Fig. 4. The experimental (a) and calculated (b) electronic absorption spectrum of **2**.

where DS_z^2 represents the splitting into two Kramers doublets in the absence of magnetic field. The parallel and perpendicular zero field susceptibilities for $S = \frac{3}{2}$ (Eqs. (2) and (3)) were corrected by the factor predicted from the molecular field (Eq. (4)) [42,44]:

$$\chi_{\mathrm{II}} = \frac{N\beta^2 g_{\mathrm{ReII}}^2}{4kT} \cdot \frac{1 + 9\exp\left(-\frac{2D}{kT}\right)}{1 + \exp\left(-\frac{2D}{kT}\right)}, \tag{2}$$

$$\chi_{\perp} = \frac{N\beta^2 g_{\mathrm{Re}\perp}^2}{4kT} \cdot \frac{4 + 6\frac{kT}{2D}\left[1 - \exp\left(-\frac{2D}{kT}\right)\right]}{1 + \exp\left(-\frac{2D}{kT}\right)}, \tag{3}$$

where D is the zero-field splitting parameter, N is the Avogadro's number, g is the spectroscopic splitting factor, β is the Bohr magneton, k is the Boltzmann constant and T is the absolute temperature.

$$\chi_{\mathrm{av}} = \frac{\chi_{\mathrm{av}}}{1 - \left(\frac{2zJ'}{Ng_{\mathrm{av}}^2\beta^2}\right)\chi_{\mathrm{av}}}, \tag{4}$$

where zJ' is the exchange parameter and was applied to calculate magnetic exchange effect by means of a molecular field.

Since our data concern powdered sample, the average magnetic susceptibility is equal to $\chi_{\mathrm{av}} = 1/3\chi_{\mathrm{II}} + 2/3\chi_{\perp}$. The least-squares fit of the experimental data using this equation was limited to the 9–300 K range and leads to $D = 20.8\ \mathrm{cm}^{-1}$, $g_{\mathrm{II}} = 1.10$, $g_{\perp} = 2.03$ and $zJ' = -4.18\ \mathrm{cm}^{-1}$. The agreement factor R defined as $R = \Sigma_{i=1}^{n}\left(\chi_m^{\mathrm{exp}} - \chi_m^{\mathrm{calc}}\right)^2/\Sigma_{i=1}^{n}\left(\chi_m^{\mathrm{exp}}\right)^2$ is 2.93×10^{-5}.

The magnetic properties of $[ReCl_4(pyz)(PPh_3)]$ (**2**) complex under the form χ_M versus T and $\chi_M T$ versus T (χ_M being the molar magnetic susceptibilities) are plotted in Fig. 6. The effective magnetic moment of 3.35 B.M. ($\chi_M T = 1.40\ \mathrm{cm}^3\ \mathrm{mol}^{-1}\ \mathrm{K}$) at 300 K corresponding three unpaired electrons. The magnetic curve show that the $\chi_M T$ values remain nearly constant in a wide range and smoothly decrease at low temperatures. The slight decrease of $\chi_M T$ at low temperatures could be attributed to zero-field splitting effect [45].

Generally, the complex **2** shows linear χ_M^{-1} vs. T behavior in the 80–300 K interval, with $C = 1.44\ \mathrm{cm}^3\ \mathrm{mol}^{-1}$ and $\Theta = -7.9$ K.

Table 8
The energy and molar absorption coefficients of absorption bands and the electronic transitions calculated with the TDDFT method for **1**

The most important orbital excitations	Character	λ (nm)	E (eV)	f	Experimental λ (nm) (E [eV]) ε
H − 5(β) → L(β)	π(Cl)/π(Ph) → d	513.0	2.42	0.0011	470.0(2.64)780
H(β) → L(β)	π(Ph)/n(P) → d				
H(β) → L(β)	π(Ph)/n(P) → d	501.6	2.47	0.0025	
H − 5(β) → L(β)	π(Cl)/π(Ph) → d				
H(β) → L + 1(β)	π(Ph)/n(P) → d	471.1	2.63	0.0052	
H − 1(β) → L(β)	π(Ph)/π(Cl) → d	459.3	2.70	0.0017	
H − 1(β) → L + 1(β)	π(Ph)/π(Cl) → d	435.6	2.85	0.0054	409.0(3.03)2420
H − 4(β) → L(β)	π(Ph) → d	423.7	2.93	0.0013	
H − 2(β) → L + 1(β)	π(Ph) → d	419.6	2.95	0.0063	
H − 7(β) → L + 1(β)	π(Cl) → d	415.9	2.98	0.0032	
H − 5(β) → L + 1(β)	π(Cl)/π(Ph) → d				
H − 10(β) → L(β)	π(Cl) → d	406.2	3.05	0.0015	
H(α) → L + 1(α)	d → d	402.9	3.08	0.0005	
H(α) → L + 1(α)	d → d	401.1	3.09	0.0007	
H − 7(β) → L + 1(β)	π(Cl) → d	397.1	3.12	0.0024	370.0(3.35)4560
H − 10(β) → L + 1(β)	π(Cl) → d	379.3	3.27	0.0068	
H − 8(β) → L + 1(β)	π(pzH)/π(Cl) → d				
H − 9(β) → L(β)	π(Cl), n(P), n(N) → d	377.4	3.28	0.0028	
H − 1(α) → L(α)	d → d	362.8	3.42	0.0008	
H − 1(α) → L + 1(α)					
H − 11(β) → L(β)	π(pzH)/π(pCl) → d	359.5	3.45	0.0045	
H − 10(β) → L + 1(β)	π(Cl) → d	358.6	3.46	0.0091	
H − 8(β) → L + 1(β)	π(pzH)/π(Cl) → d				
H − 8(β) → L + 1(β)	π(pzH)/π(Cl) → d	357.1	3.47	0.0058	
H − 4(β) → L+2(β)	π(Ph) → d				
H − 2(α) → L(α)	d → d	350.9	3.53	0.0005	338.0(3.67)6850
H − 1(α) → L + 1(α)					
H − 4(β) → L+2(β)	π(Ph) → d	349.5	3.55	0.0040	
H − 2(α) → L(α)	d → d	350.0	3.56	0.0002	
H − 7(β) → L+2(β)	π(Cl) → d	334.8	3.71	0.0277	
H − 9(β) → L+2(β)	π(Cl), n(P), n(N) → d	331.2	3.74	0.0298	
H − 8(β) → L+2(β)	π(pzH)/π(Cl) → d				
H − 12(β) → L + 1(β)	π(pzH)/π(Cl) → d	330.1	3.76	0.0230	
H − 10(β) → L+2(β)	π(Cl) → d	319.3	3.88	0.0152	
H − 8(β) → L+2(β)	π(pzH)/π(Cl) → d				
H − 2(α) → L + 1(α)	d → d	314.2	3.95	0.0004	
H − 13(β) → L + 1(β)	π(Cl) → d	297.5	4.17	0.0187	293.2(4.23)18,515
H − 14(β) → L(β)	π(Cl) → d	291.6	4.25	0.0134	
H − 4(α) → L(α)	π(Ph), n(P) → d	276.5	4.48	0.0133	
H − 3(α) → L(α)	π(Ph)/π(Cl) → d				
H − 8(α) → L(α)	π(Cl) → d	267.2	4.64	0.0285	
H − 16(β) → L + 1(β)	π(Cl)/σ(Cl) → d				
H − 16(β) → L + 1(β)	π(Cl)/σ(Cl) → d	266.4	4.65	0.0217	
H − 8(α) → L + 1(α)	π(Cl) → d	257.2	4.82	0.0170	
H − 4(α) → L(α)	π(Ph), n(P) → d				
H − 1(α) → L(α)	d → π*(Ph)	247.7	5.01	0.0294	231.6(5.35)54,400
H(β) → L+4(β)					
H − 2(α) → L+2(α)	d → π*(Ph)	246.5	5.03	0.0114	

The experimental magnetic data of complex **2** were fitted to the empirical relations proposed earlier [46]. The parallel and perpendicular zero field susceptibilities (Eqs. (5) and (6)) were corrected by the factor predicted from the molecular field (Eq. (4)) [42,44]:

$$\chi_{\mathrm{II}} = \frac{N\beta^2 g_{\mathrm{II}}^2}{4kT} \cdot \frac{1 + 9\exp\left(-\frac{2D}{kT}\right)\exp\left(\frac{J}{kT}\right)}{1 + \exp\left(-\frac{2D}{kT}\right)} \tag{5}$$

$$\chi_{\mathrm{I}\perp} = \left\{ \left[\frac{N\beta^2 g_{\perp}^2}{kT}\right]\left[1 + 9\exp\left(-\frac{2D}{kT}\right)\right]^{-1} + 3N\beta^2 g_{\perp}^2 \tanh\left(\frac{D}{kT}\right) \Big/ 4D \right\} \times \left\{ \left(\frac{kT}{J}\right)\tanh\left(\frac{J}{2kT}\right) + \left[\sec h^2\left(\frac{J}{2kT}\right)\right] \Big/ 2 \right\} \tag{6}$$

Table 9
The energy and molar absorption coefficients of absorption bands and the electronic transitions calculated with the TDDFT method for **2**

The most important orbital excitations	Character	λ (nm)	E (eV)	f	Experimental λ (nm) (E [eV]) ε
H − 5(β) → L(β)	π(Cl)/π(Ph) → d	527.1	2.35	0.0005	490.0(2.53)1650
H(β) → L(β)	π(Ph)/n(P) → d				
H(β) → L(β)	π(Ph)/n(P) → d	513.6	2.41	0.0028	
H(β) → L + 1(β)	π(Ph)/n(P) → d	486.4	2.55	0.0037	
H − 1(β) → L(β)	π(Ph)/π(Cl) → d	473.0	2.62	0.0022	
H − 2(β) → L(β)	π(Ph) → d	456.1	2.72	0.0043	
H − 1(β) → L + 1(β)	π(Ph)/π(Cl) → d	447.5	2.77	0.0025	408.4(3.04)2180
H − 4(β) → L(β)	π(Ph) → d	438.3	2.83	0.0015	
H − 2(β) → L + 1(β)	π(Ph) → d	432.1	2.87	0.0042	
H − 7(β) → L + 1(β)	π(Cl) → d	420.1	2.95	0.0014	
H − 5(β) → L + 1(β)	π(Cl)/π(Ph) → d				
H − 8(β) → L(β)	π(Cl) → d	413.6	3.00	0.0014	
H(α) → L+2(α)	d → d	393.6	3.15	0.0002	382.0(3.25)2715
H − 8(β) → L + 1(β)	π(Cl) → d	393.1	3.15	0.0030	
H − 9(β) → L(β)	π(Cl), n(P), n(N) → d	390.1	3.18	0.0031	
H(α) → L + 1(α)	d → d	383.5	3.23	0.0003	
H − 10(β) → L(β)	π(Cl)/π(pyz) → d	374.2	3.31	0.0023	
H − 1(α) → L + 1(α)	d → d	361.4	3.43	0.0003	339.0(3.66)6150
H − 2(α) → L + 1(α)	d → d	358.5	3.46	0.0004	
H − 2(α) → L(α)	D → π*(pyz)	352.4	3.52	0.0218	
H − 7(β) → L+2(β)	π(Cl) → d	336.2	3.69	0.0379	
H − 8(β) → L+2(β)	π(Cl) → d	334.9	3.70	0.0131	
H − 10(β) → L+2(β)	π(Cl)/π(pyz) → d	329.9	3.70	0.0194	
H − 6(β) → L+2(β)	π(Ph)/π(Cl) → d				
H − 1(α) → L+2(α)	d → d	328.8	3.77	0.0046	
H − 2(α) → L+2(α)	d → d	326.1	3.80	0.0054	
H − 14(β) → L + 1(β)	π(Cl)/d → d	308.5	4.02	0.0119	275.2(4.51)22,715
H − 15(β) → L(β)	π(Cl)/σ(Cl) → d	297.8	4.16	0.0126	
H − 3(α) → L + 1(α)	π(Ph) → d	279.6	4.43	0.0261	
					230.2(5.39)58,225

Since our data concern powdered sample, the experimental magnetic susceptibility is equal $\chi_{av} = 1/3\chi_{II} + 2/3\chi_{\perp}$. The least-squares fit of the experimental data using this equation was limited to the whole temperature range and leads to $D = -21.3\ cm^{-1}$, $J = -1.19\ cm^{-1}$, $zJ' = -0.58\ cm^{-1}$ and $g_{av} = 1.72$. The agreement factor R defined as $R = \Sigma_{i=1}^{n}(\chi_m^{exp} - \chi_m^{calc})^2/\Sigma_{i=1}^{n}(\chi_m^{exp})^2$ is 1.14×10^{-4}. A negative value of the exchange parameter suggests the presence of weak antiferromagnetic interactions between Re^{IV} ions at crystal lattice.

The occurrence of a bulky ligands result in the diamagnetic dilution due to increasing distance between the paramagnetic Re^{IV} centers, the magnetic interaction might be transmitted by hydrogen bonds.

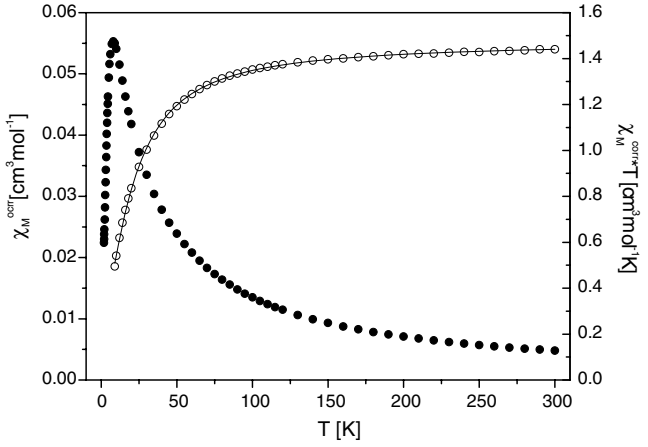

Fig. 5. Thermal dependence of χ_M (●) and $\chi_M T$ (○) for $[ReCl_4(pzH)(PPh_3)]$ (**1**) χ_M (●). The solid line is the calculated curve.

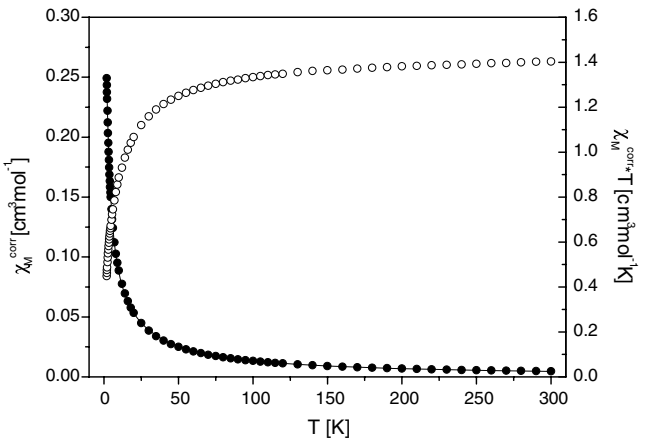

Fig. 6. Thermal dependence of χ_M (●) and $\chi_M T$ (○) for $[ReCl_4(pyz)(PPh_3)]$ (**2**). The solid line is the calculated curve.

4. Conclusions

Two novel Re(IV) compounds – $[ReCl_4(pzH)(PPh_3)]$ (**1**) and $[ReCl_4(pyz)(PPh_3)]$ (**2**) – have been prepared and structurally as well as spectroscopically characterized. The geometries of **1** and **2** were optimized in quartet and doublet states using the DFT method with the B3LYP functional. The energies of the doublet states of **1** and **2** complexes are higher, which is consistent with the results of magnetic measurements. The values of effective magnetic moments of **1** and **2** complexes at 300 K correspond to three unpaired electrons and confirm $(d_{xz})^1(d_{yz})^1(d_{xy})^1$ configuration of the rhenium atoms in **1** and **2**.

5. Supplementary data

Supplementary data for $C_{21}H_{19}Cl_4N_2PRe$ and $C_{22}H_{19}Cl_4N_2PRe$ are available from the CCDC, 12 Union Road, Cambridge CB2 1EZ, UK on request, quoting the deposition numbers: 276935 for **1** and 276936 for **2**.

Acknowledgments

The GAUSSIAN03 calculations were carried out in the Wrocław Centre for Networking and Supercomputing, WCSS, Wrocław, Poland. Crystallographic part was financed by funds allocated by the Ministry of Scientific Research and Information Technology to the Institute of General and Ecological Chemistry, Technical University of Łódź.

References

[1] J.R. Dilworth, S.J. Parrott, Chem. Soc. Rev. 27 (1998) 43.
[2] S.S. Jurisson, J.D. Lydon, Chem. Rev. 99 (1999) 2205.
[3] S. Liu, D.S. Edwards, Chem. Rev. 99 (1999) 2235.
[4] W.Y. Lin, C.P. Lin, S.J. Yeh, B.T. Hsieh, Z.T. Tsai, G. Tinbg, T.C. Yen, S.J. Wang, F.F. Knapp Jr., M.G. Stabin, J. Nucl. Med. 24 (1997) 590.
[5] J. Sattigeri, A.L. Rodriguez, J.A. Katzenellenbogen, Bioorg. Med. Chem. 10 (2002) 1381.
[6] E.S. Mull, V.H.R. Maxon, L.E. Schroder, L.C. Washburn, S.R. Thomas, R.C. Samaratunga, D. Biniakiewicz, J.S. Moulton, D.D. Cummings, G.J. Ehrhardt, V. Morris, J. Nucl. Med. 39 (1998) 659.
[7] B. Machura, J.O. Dzięgielewski, R. Kruszynski, T.J. Bartczak, J. Kusz, Inorg. Chem. Commun. 6 (2003) 1436.
[8] B. Machura, J.O. Dzięgielewski, S. Michalik, R. Kruszynski, T.J. Bartczak, J. Kusz, Transition Met. Chem. 28 (2003) 939.
[9] B. Machura, M. Jaworska, R. Kruszynski, Polyhedron 23 (2004) 1819.
[10] B. Machura, M. Jaworska, R. Kruszynski, Polyhedron 23 (2004) 2523.
[11] B. Machura, M. Jaworska, R. Kruszynski, Polyhedron 23 (2004) 2005.
[12] B. Machura, M. Jaworska, R. Kruszynski, Polyhedron 24 (2005) 267.
[13] M.C. Aragoni, M. Arca, T. Cassano, C. Denotti, F.A. Devillanova, F. Isaia, V. Lippolis, D. Natali, L. Niti, M. Sampietro, R. Tommasi, G. Verani, Inorg. Chem. Commun. 5 (2002) 869.
[14] P. Romaniello, F. Lelj, Chem. Phys. Lett. 372 (2003) 51.
[15] P. Norman, P. Cronstrand, J. Ericsson. Chem. Phys. 285 (2002) 207.
[16] J. Bossert, N.B. Amor, A. Strich, C. Daniel, Chem. Phys. Lett. 342 (2001) 617.
[17] C.E. Powell, M.P. Cifuentes, A.M. McDonagh, S.K. Hurst, N.T. Lucas, C.D. Delfs, R. Stranger, M.G. Humphrey, S. Houbrechts, I. Asselberghs, A. Persoons, D.C.R. Hockless, Inorg. Chim. Acta 352 (2003) 9.
[18] J.P. Morral, C.E. Powell, R. Stranger, M.P. Cifuentes, M.G. Humphrey, G.A. Heath, J. Organomet. Chem. 670 (2003) 248.
[19] P. Romaniello, F. Lelj, J. Mol. Struct. Theochem. 636 (2003) 23.
[20] G. Rouschias, G. Wilkinson, J. Chem. Soc. A 993 (1967).
[21] STOE & Cie, X-RED. Version 1.18, STOE & Cie GmbH, Darmstadt, Germany, 1999.
[22] G.M. Sheldrick, Acta Crystallogr. A 46 (1990) 467.
[23] G.M. Sheldrick, SHELXL97. Program for the Solution and Refinement of Crystal Structures, University of Göttingen, Germany, 1997.
[24] G.M. Sheldrick, SHELXTL: Release 4.1 for Siemens Crystallographic Research Systems, 1990.
[25] M.J. Frisch, G.W. Trucks, H.B. Schlegel, G.E. Scuseria, M.A. Robb, J.R. Cheeseman, J.A. Montgomery Jr., T. Vreven, K.N. Kudin, J.C. Burant, J.M. Millam, S.S. Iyengar, J. Tomasi, V. Barone, B. Mennucci, M. Cossi, G. Scalmani, N. Rega, G.A. Petersson, H. Nakatsuji, M. Hada, M. Ehara, K. Toyota, R. Fukuda, J. Hasegawa, M. Ishida, T. Nakajima, Y. Honda, O. Kitao, H. Nakai, M. Klene, X. Li, J.E. Knox, H.P. Hratchian, J.B. Cross, C. Adamo, J. Jaramillo, R. Gomperts, R.E. Stratmann, O. Yazyev, A.J. Austin, R. Cammi, C. Pomelli, J.W. Ochterski, P.Y. Ayala, K. Morokuma, G.A. Voth, P. Salvador, J.J. Dannenberg, V.G. Zakrzewski, S. Dapprich, A.D. Daniels, M.C. Strain, O. Farkas, D.K. Malick, A.D. Rabuck, K. Raghavachari, J.B. Foresman, J.V. Ortiz, Q. Cui, A.G. Baboul, S. Clifford, J. Cioslowski, B.B. Stefanov, G. Liu, A. Liashenko, P. Piskorz, I. Komaromi, R.L. Martin, D.J. Fox, T. Keith, M.A. Al-Laham, C.Y. Peng, A. Nanayakkara, M. Challacombe, P.M.W. Gill, B. Johnson, W. Chen, M.W. Wong, C. Gonzalez, J.A. Pople, Gaussian 03, Revision B. 03, Gaussian, Inc., Pittsburgh, PA, 2003.
[26] A.D. Becke, J. Chem. Phys. 98 (1993) 5648.
[27] C. Lee, W. Yang, R.G. Parr, Phys. Rev. B 37 (1988) 785.
[28] M.E. Casida, in: J.M. Seminario (Ed.), Recent Developments and Applications in Modern Density Functional Theory, Theoretical and Computational Chemistry, vol. 4, Elsevier, Amsterdam, 1996.
[29] P.J. Hay, W.R. Wadt, J. Chem. Phys. 82 (1985) 299.
[30] J.P. Collman, J.T. McDevitt, C.R. Leidner, G.T. Yee, J.B. Torrance, W.A. Little, J. Am. Chem. Soc. 109 (1987) 4606.
[31] G.A. Jeffrey, W. Saenger, Hydrogen Bonding in Biological Structures, Springer, 1994.
[32] G.R. Desiraju, T. Steiner, The Weak Hydrogen Bond in Structural Chemistry and Biology, Oxford University Press, 1999.
[33] A. Vogler, H. Kunkely, Coord. Chem. Rev. 230 (2002) 243.
[34] I.D. Brown, Acta Crystallogr. B 48 (1992) 553.
[35] I.D. Brown, Acta Crystallogr. B 53 (1997) 381.
[36] M. O'Keeffe, N.E. Brese, J. Am. Chem. Soc. 113 (1991) 3226.
[37] E. König, Magnetic Properties of Coordination and Organometallic Transition Metal Compounds, Springer, Berlin, 1966.
[38] J. Mroziński, Bull. Acad. Polon. Sci. Ser. Chim. 7 (1980) 559.
[39] J. Mroziński, Bull. Acad. Polon. Sci. Ser. Chim. 10 (1980) 789.
[40] J. Małecka, L. Jager, Ch. Wagner, J. Mroziński, Polish J. Chem. 72 (1998) 1879.
[41] A. Tomkiewicz, T.J. Bartczak, R. Kruszyński, J. Mroziński, J. Mol. Struct. 595 (2001) 225.
[42] A. Tomkiewicz, F. Villain, J. Mroziński, J. Mol. Struct. 555 (2000) 383.
[43] B.N. Figgis, Trans. Faraday Soc. 56 (1960) 1553.
[44] R. Chiozzone, R. González, C. Kremer, G. De Munno, J. Cano, F. Lloret, M. Julve, J. Faus, Inorg. Chem. 38 (1999) 4745.
[45] J.S. Griffith, Trans. Faraday Soc. 56 (1960) 193.
[46] P.A. Reynolds, Ch.D. Delfs, D.N. Figgis, N.J. Henderson, B. Maubaraki, K.S. Murray, J. Chem. Soc., Dalton Trans. (1992) 2309.

possible coordination modes because the four carboxylate groups may be completely or partially deprotonated. These structural features render H_4BTEC an important ligand that yields various networks for coordination polymers [12]. The use of H_4BTEC in combination with the aromatic chelate ligand phen results in the formation of a 2-D uranyl-containing polymeric compound **2**.

2. Experimental

2.1. Synthesis

Compounds **1** and **2** were synthesized through a hydrothermal route. All reagents were of analytical grade and commercially available. The syntheses were carried out in 20 mL Telfon-lined stainless steel vessels under autogenous pressures with a filling capacity of approximately 70%.

2.1.1. $[(UO_2)_3O(OH)_3(NA)_2]^- \cdot H_3O^+$ (1)

A typical mixture of $UO_2(OAc)_2 \cdot 2H_2O$ (214 mg), H_2QA (120 mg), 2,2′-bipyridine (bipy, 168 mg) and water (10 mL) in a molar ratio of 1:2:2:1110 was stirred for 1 h in air, the final solution was transferred to and sealed in a Teflon-lined autoclave which was subsequently heated at 160 °C for 3 days. Pale-yellow block crystals of **1** were obtained after washing with water and drying in air, and the yield of the product was about 75% on the basis of U. Main IR features (KBr): $v = 3557$w, 3507w, 3120w, 3060w, 1634s, 1596s, 1558w, 1334s, 1147s, 1010m, 922s, 843m, 760s, 697s, 647s, 540s, 430s cm^{-1}.

2.1.2. $(UO_2)_2(phen)_2(BTEC)$ (2)

A mixture of $UO_2(Ac)_2 \cdot H_2O$ (220 mg), H_4BTEA (120 mg), phen (196 mg) and water (10 mL) in a molar ratio of 1:1:2:1100 was stirred for 1 h. The resulting solution was sealed in an autoclave and heated at 160 °C for 3 days under autogenous pressure. After cooling to room temperature, the yellow columnar crystals were washed several times with distilled water and dried in air at room temperature. The yield of the product was about 80% on the basis of U. Main IR features (KBr): $v = 3419$w, 3058w, 1627s, 1550s, 1501m, 1452m, 1400s, 1333s, 1215w, 1135m, 1097w, 933s, 840s, 771w, 712s, 663m, 544s, 440m cm^{-1}.

2.2. Physical measurements

The powder X-ray diffraction (XRD) patterns (Cu Kα radiation, $\lambda = 1.5418$ Å) were recorded on a Siemens D5005 diffractometer with a graphite monochromator at room temperature. The FT-IR spectra of the samples dispersed in KBr pellets were obtained on a Bruker IFS 66V/S FT-IR spectrometer. IR absorptions are described as follows: strong (s), medium (m) and weak (w). The thermogravimetric (TG) and the differential thermal analysis (DTA) were conducted on a Netzsch STA 449C thermal analyzer under a flow of dry air at a heating rate of 20 K min^{-1}. The solid state diffuse-reflectance UV–Vis spectra for powder samples were recorded on a Perkin–Elmer Lambda 20 UV–Vis spectrometer equipped with an integrating sphere, using $BaSO_4$ as white standard. The as-prepared powder samples were mounted on a Perkin–Elmer LS55 fluorescence spectrophotometer to measure the photoluminescent (PL) property.

2.3. X-ray crystal structure analyses

Single-crystal X-ray data for both **1** and **2** were collected at 293(2) K on a Bruker Smart-CCD diffractometer (Mo Kα, $\lambda = 0.71073$ Å). The structures were solved by direct methods (SHELXS-97), and refined with the full-matrix least-squares on F^2 method using the SHELXTL-97 program together with an empirical absorption correction. All non-hydrogen atoms were refined anisotropically and the aromatic hydrogen atoms were calculated ($d_{C-H} = 0.93$ Å) and fixed with thermal parameters based on the carbon atoms to which they are bonded. The H atoms attached to the oxygen atoms (Ow) of the lattice water and coordinating water molecules were not located. The experimental crystallographic data for **1** and **2** are listed in Table 1; selected bond lengths and angles of **1** and **2** are listed in Table 2.

3. Results and discussion

3.1. Syntheses

In the hydrothermal reaction process for compound **1**, H_2QA was transformed into HNA via decarboxylation. Decarboxylation of quinolinic acid is common under hydrothermal conditions [11a,11d,13a]. The electron-withdrawing effect of the N atom in the pyridine ring results in lower electron density on the *ortho*-C atom so

Table 1
Crystal data and structure refinement for **1** and **2**

Compound	**1**	**2**
Formula	$C_{12}H_{14}N_2O_{15}U_3$	$C_{17}H_9N_2O_6U$
Formula weight	1140.34	575.29
T (K)	293(2)	293(2)
Crystal system	monoclinic	monoclinic
Space group	$P2_1/n$	$P2_1/c$
a (Å)	12.819(2)	8.503(1)
b (Å)	12.506(2)	17.277(2)
c (Å)	13.201(3)	10.389(1)
α (°)	90	90
β (°)	91.670(1)	94.322(8)
γ (°)	90	90
V (Å^3)	2115.46(7)	1521.9(3)
Z	4	4
ρ (Mg/m^3)	3.580	2.511
μ (mm^{-1})	22.988	10.706
Reflections collected/unique	11 703/3732	10 728/3761
Data/parameters	3732/289	3761/235
Goodness-of-fit on F^2	1.060	1.061
R_1[a]/wR_2[b] [$I > 2\sigma(I)$]	0.0333/0.0890	0.0274/0.0694
R_1/wR_2 (all data)	0.0373/0.0913	0.0361/0.0726

[a] $R_1 = \sum\|F_o| - |F_c\|/\sum|F_o|$.
[b] $wR_2 = [\sum[w(F_o^2 - F_c^2)^2]/\sum[w(F_o^2)^2]]^{1/2}$.

Table 2
Selected bond lengths (Å) and angles (°) for **1**[a] and **2**[b]

*Compound **1***			
U(1)–O(8)	1.779(6)	U(1)–O(9)	1.791(7)
U(1)–O(5)	2.231(6)	U(1)–O(6)	2.354(6)
U(1)–O(1)	2.421(7)	U(1)–O(7)	2.449(5)
U(1)–O(12A)	2.567(6)	U(2)–O(10)	1.769(7)
U(2)–O(5)	2.214(6)	U(2)–O(11)	1.793(7)
U(2)–O(12A)	2.492(6)	U(2)–O(2A)	2.401(7)
U(2)–O(3)	2.413(6)	U(2)–O(7A)	2.535(6)
U(3)–O(14)	1.755(6)	U(3)–O(13)	1.774(6)
U(3)–O(5)	2.240(5)	U(3)–O(4A)	2.395(7)
U(3)–O(6)	2.405(6)	U(3)–O(12)	2.429(6)
U(3)–O(7A)	2.527(6)		
O(8)–U(1)–O(9)	173.9(3)	O(5)–U(1)–O(6)	69.7(2)
O(6)–U(1)–O(1)	77.3(2)	O(7)–U(1)–O(12A)	68.9(2)
O(5)–U(1)–O(12A)	67.5(2)	O(10)–U(2)–O(11)	176.3(3)
O(5)–U(2)–O(12A)	69.2(2)	O(3)–U(2)–O(12A)	74.6(2)
O(5)–U(2)–O(7A)	68.4(2)	O(2A)–U(2)–O(7A)	74.5(2)
O(14)–U(3)–O(13)	174.7(3)	O(5)–U(3)–O(6)	68.7(2)
O(5)–U(3)–O(7A)	68.2(2)	O(4A)–U(3)–O(6)	75.0(2)
O(12)–U(3)–O(7A)	69.9(2)		
*Compound **2***			
U(1)–O(6)	1.757(4)	U(1)–O(5)	1.760(4)
U(1)–O(4)	2.419(3)	U(1)–O(2)	2.469(3)
U(1)–O(1)	2.482(3)	U(1)–O(3)	2.546(4)
U(1)–N(1)	2.616(4)	U(1)–N(2)	2.688(4)
O(6)–U(1)–O(5)	179.3(2)	O(4)–U(1)–O(3)	52.1(1)
O(2)–U(1)–O(1)	52.8(1)	N(1)–U(1)–N(2)	61.2(1)
O(1)–U(1)–O(3)	67.2(1)	O(1)–U(1)–N(1)	119.6(1)
O(4)–U(1)–N(2)	67.6(1)		

[a] Symmetry transformations used to generate equivalent atoms: (A) $-x+5/2, y+1/2, -z-1/2$; (B) $-x+5/2, y-1/2, -z-1/2$.

[b] Symmetry transformations used to generate equivalent atoms: (A) $-x+1, y+1/2, -z+3/2$; (B) $x, -y+1/2, z-1/2$; (C) $x, -y+1/2, z+1/2$; (D) $-x+1, y-1/2, -z+3/2$.

that the *ortho*-COOH group gets lost more easily than the *meta*-COOH. When we replaced H_2QA with HNA under the same synthetic conditions, a powder form of compound **1**, which was not suitable for single-crystal structure analysis, was also obtained and the product yield was lower. The crystallization temperature is also important for the hydrothermal synthesis of **1**. If the reaction temperature is below 160 °C (e.g. 150 or 140 °C), the decarboxylation of the ligand does not occur, and an unknown crystalline phase appears. At temperatures distinctly above 160 °C (e.g. 170 or 180 °C), the reactant is carbonized and no proper crystals of **1** are formed. The presence of bipy is critical for the growth of the crystals of **1** although this ligand is not incorporated in the structure of **1**. In the absence of bipy, no crystals of **1** are observed in the final product of the reaction system either. A pH value of about 7.0 (i.e., the reaction system is neutral) favors the formation of compound **1**, and it is believed that in the synthesis of **1**, bipy acts as both an auxiliary reagent and a pH adjuster.

In contrast, the single crystals of compound **2** are obtained easily. However, the reaction time affects the crystal size of **2**, and a crystallization time of 3 days is the best for the formation of high quality single crystals of **2** for structure analysis. If the reaction time is shorter than 3 days, the crystals are smaller, whereas a reaction time longer than 3 days leads to apparent defects on the crystals of **2**.

3.2. Thermal properties

The two compounds are stable in air and insoluble in water and common organic solvents such as ethanol, acetonitrile and acetone. Thermogravimetric curves have been obtained in air for crystalline samples of **1** and **2** in the temperature range of 37–800 °C. From the TG curves, the decomposition of **1** can be described as a two-step process. The first has an initial weight loss of about 4.7% from 37 to 300 °C, corresponding to the removal of the lattice water and hydroxyl groups (calculated value 4.6%) that accompanies a distinct endothermic effect at around 209 and 284 °C, respectively. For the second stage, the weight loss of 19.0% in the range of 300–500 °C is assigned to the removal of NA groups from the structure (calculated value 20.1%), as indicated by a strong exothermic effect at 460 °C. The total weight loss is 23.7%, in agreement with the calculated result based on the single-crystal structure (24.7%). Compound **2** is thermally stable up to approximately 450 °C on the basis of powder XRD patterns. The rapid decomposition of the compound starting at about 470 °C is followed by a distinct exothermic effect at around 570 °C. The total weight loss of **2** (56.1%), attributable to removal of the total organic component, is in agreement with the calculated value based on the single-crystal structure of **2** (53.7%).

3.3. Crystal structures

For both compounds **1** and **2**, the peak positions of the experimental powder X-ray diffraction patterns correspond well with those simulated on the basis of the single-crystal structures, confirming that the two compounds are single phases. The asymmetric units for **1** and **2** are depicted in Fig. 1.

3.3.1. $[(UO_2)_3O(OH)_3(NA)_2]^- \cdot H_3O^+$ (**1**)

Single-crystal X-ray diffraction analysis has revealed that the crystal structure of **1** consists of one-dimensional single-stranded helical ribbons with a composition of $[(UO_2)_3O(OH)_3]_n^{n+}$. The ribbons are coordinated with NA ligands at both sides. Compound **1** crystallizes in the monoclinic space group $P2_1/n$. In each independent crystallographic unit of **1**, there are two chelating NA ligands, one lattice water molecule and a $[(UO_2)_3O(OH)_3]^+$ species consisting of three interconnected uranyl sub-structures which join together through a common vertex (Fig. 1(a)). Each uranium center is seven-coordinated by two oxygen atoms in the axial positions and another five O atoms in the equatorial plane of the pentagonal bipyramid. The axial U=O bond distances range from 1.755(6) to 1.793(7) Å with an average value of 1.777(5) Å, whereas the equatorial U–O distances vary from 2.214(6) to 2.567(6) Å with an average value of 2.405(5) Å. These values are in accordance with

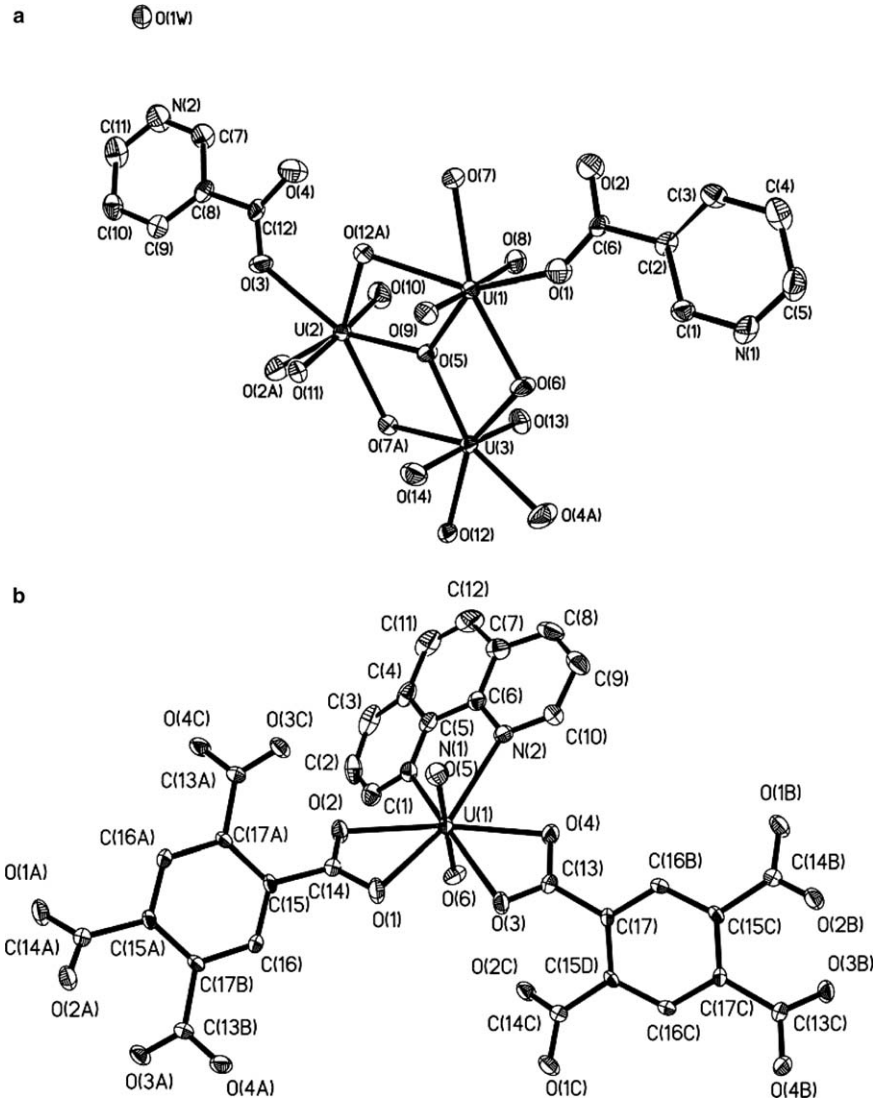

Fig. 1. (a) ORTEP drawing of the asymmetric unit of **1**. Thermal ellipsoids are shown at 50% probability. (b) ORTEP drawing of the asymmetric unit of **2**. Thermal ellipsoids are shown at 40% probability. All hydrogen atoms are omitted for clarity.

those observed for other uranium-containing compounds in the literature [3,7,11]. In addition, for the ribbons of **1**, there are three protons in each asymmetric unit, which are attached to O atoms to form hydroxyls. In total, there are four bridging O atoms in one asymmetric unit of **1** besides those from the NA ligands and from the axial O atoms of the U=O bonds. Among the four bridging O atoms, O(5) adopts a μ_3 binding mode in the center of the trinuclear-uranium unit, with the distance of U–O(5) for each UO_7 bipyramid being significantly shorter than those of other U–O bonds due to the stronger interactions in its environment. Bond-valence analysis [14a,14b] can be used to distinguish the O atoms and the OH groups. Bond valence sum calculations using the parameters derived by Burns et al. [14c] for seven-coordinate U(VI) give rise to a value of 2.13 for O(5). However, the bond valence sums for O(6), O(7) and O(12) are 1.06, 1.28 and 1.26, respectively, suggesting that these three O atoms have enough residual strength to seize protons. Therefore, it is reasonable that O(6), O(7) and O(12) are assigned as hydroxo O atoms. Similar calculation leads to bond valence sums of 5.92, 5.92 and 6.06 for U(1), U(2) and U(3), respectively. It is interesting to note that a trinuclear $[(UO_2)_3O(OH)_3]^+$ unit similar to that for our compound has also been observed previously by Åberg [13b].

The trinuclear $[(UO_2)_3O(OH)_3]^+$ units in **1** share edges to form infinite one-dimensional helical ribbons. A representation of the ribbon structure is depicted in Fig. 2(a). The central axis of each helical ribbon running along the *b*-axis is a twofold screw axis (Fig. 2(b)) and the ribbons are coordinated with NA ligands at both sides. The carboxyl groups of the NA ligands are deprotonated and adopt a bidentate bridging coordination fashion, establishing bridges between adjacent metal centers with distances of 3.894 Å for U(1)···U(2) and 3.873 Å for U(2)···U(3). The composition of the uranium oxide ribbon can be described as $[(UO_2)_3O(OH)_3]_n^{n+}$ which is in accord with the structural formula of the extensive polyhedral

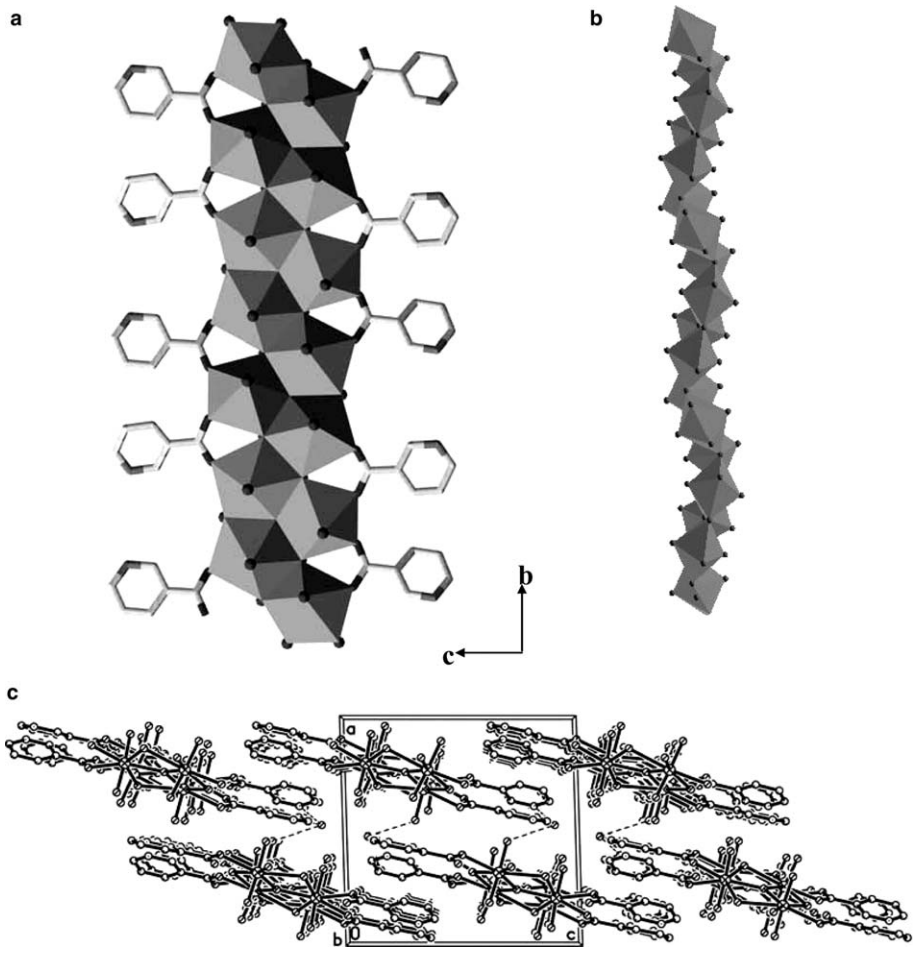

Fig. 2. (a) A polyhedral representation of the uranium ribbons built from edge-sharing pentagonal bipyramids along the *a*-axis; (b) the single-stranded helical ribbon with NA groups being omitted for clarity, and (c) view of the structure along the *b*-axis for **1**. The dotted lines show the Ow···N/O hydrogen bonding interactions.

$(UO_2)_kO_l(OH)_m$ chains or layers formed by uranyl units linked with oxo or hydroxo groups [15]. Burns et al. summarized the structural chemistry of uranyl oxides and systematically classified uranium minerals and inorganic phases based on the polymerization of uranyl polyhedra. The topological structure of the uranium oxide ribbon in **1** has not been observed in the uranyl compounds reported previously.

Taking into account of the attached NA ligands, the ribbons of $[(UO_2)_3O(OH)_3(NA)_2]_n^{n-}$ become negatively charged. The negative charges in the anionic NA-coordinated ribbons are compensated by H_3O^+ cations residing between adjacent ribbons. Although the H atoms of the water molecule could not be located from the difference Fourier map, the observed Ow···N/O contact distances (2.756/2.917 Å) in **1** suggest the presence of H-bondings involving the water molecules. In the crystal structure of **1**, each ribbon within the unit cell is surrounded by the nearest four ribbon neighbors. As illustrated in Fig. 2(c), the polyoxouranium ribbons in **1** are held together to form 2D layers in the *ab*-plane by packing forces of the H-bonds. These layers are further extended into a 3D architecture through offset face-to-face stacking interaction between the π-systems of the NA ligands from adjacent layers along the *a*-axis (the shortest C···C distance is about 3.45 Å) [16].

3.3.2. $(UO_2)_2(phen)_2(BTEC)$ (2)

The crystal structure of **2** comprises a layer with the composition of $UO_2(BTEC)_{0.5}$, which is coordinated by phen ligands above and below the layer plane. The uranium atom in **2** axially binds two oxygen atoms (Fig. 1(b)) to form a linear uranyl unit with an O=U=O angle of 179.3(2)° and U=O distances of 1.757(4) and 1.760(4) Å. Equatorially, each uranium atom is coordinated with four oxygen atoms from two chelating carboxylate groups of two different BTEC (mean U–O bond length 2.479(3) Å) ligands. These bond distances are typical of uranyl complexes [3,7,11]. On the other hand, the uranium atom is also coordinated by two nitrogen atoms of a single phen ligand, with U–N distances of 2.688(4) and 2.616(4) Å. The U–N distance of 2.688(4) Å is a little longer than those reported in the literature (2.371–2.633 Å) [4]. The phen ligand is twisted through the rotation of the whole molecule with a dihedral angle of 23° between the phen molecule and the equatorial plane, and as a result, the two coordinating N atoms are located above and below the uranyl equatorial plane,

respectively. The longer U–N bond distances and the tilt of the phen molecule minimize the repulsion between the phen group and the equatorial or axial O atoms, resulting in the location of the uranium atom in a distorted hexagonal bipyramid environment.

The connection of uranyl units with the BTEC ligands gives rise to a layer in which four uranyl and four BTEC units form a rectangular ring (Fig. 3(a)). All the carboxyl groups of each BTEC ligand, which is shared by four rings in the layer, are deprotonated and adopt a bidentate chelating mode. The phen units coordinate to the U atoms alternately from above and below the ring-containing layer. There exist edge-to-face π–π stacking interactions between the adjacent two phen rings with the shortest C···C

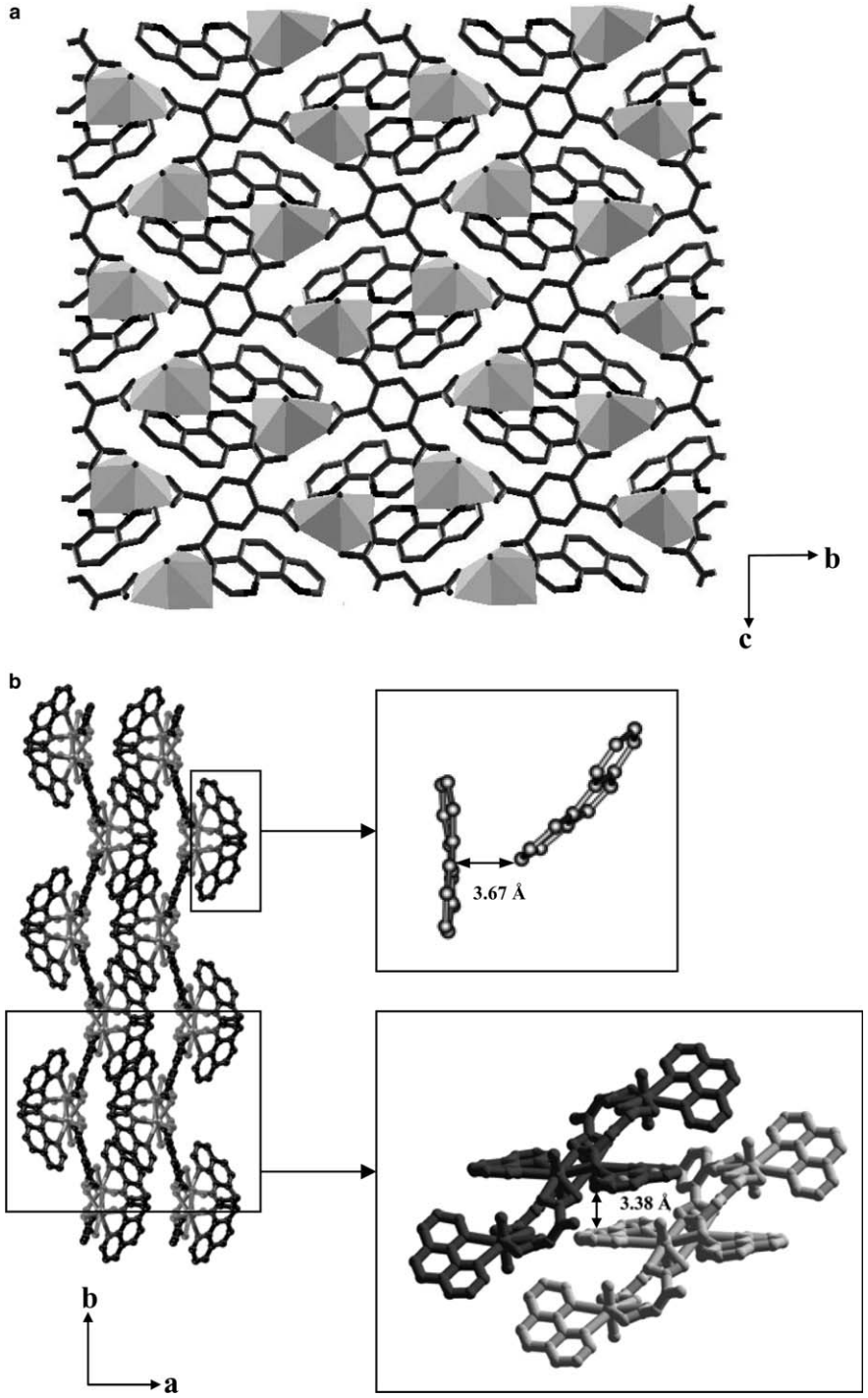

Fig. 3. (a) View of the connection of the BTEC ligand and uranyl ion along the *a*-axis and (b) the arrangement of the layers along the *a*-axis for **2.** Perspective views in the right part of (b) show the edge-to-face π–π interactions between adjacent phen rings of the same layers (top) and the π–π interactions between phen rings of adjacent layers (bottom).

distance being about 3.67 Å (Fig. 3(b)) [16]. Fig. 3(b) also displays the arrangement of the layers along the *a*-axis. The void space between two chelating phen groups on one side of the layer is filled with a phen group from the other side of an adjacent layer. There exists an offset face-to-face π–π stacking interaction between the interplanar phen rings, the shortest C···C distance being about 3.38 Å (Fig. 3(b)) [16]. Because of the two types of π–π interactions (edge-to-face and face-to-face), the crystals of **2** are insoluble in water.

3.4. Photoluminescent properties

Compounds **1** and **2** exhibit intense PL emissions in the solid state at room temperature. The emission spectrum of **1** is characterized by a broad band from 480 to 600 nm centered at 515 and 534 nm and two shoulders at 558 and 585 nm upon excitation at 434 nm. The solid-state emission spectrum of **2** under excitation at 341 nm appears somewhat different from that of **1** with the main emission peaks at 491, 511, 534 nm and two weak peaks at 560 and 586 nm. The PL spectra of **1** and **2** show typical emission features of uranyl compounds [8,7c,7d]. It is reasonable that the emission bands of **1** and **2** ranging from 500 to 600 nm are related to the transitions from the first excited electronic level to the symmetric and antisymmetric vibrational levels of the uranyl ion [17,18], and the relatively strong emission of **2** at 491 nm is attributable to uranyl ion emission from a triplet to a singlet state [18]. The excitation wavelengths (434 nm for **1** and 341 nm for **2**), under which the emission spectra were monitored, are much longer than the maximum absorption wavelengths of the ligands (283 nm for HNA, 322 nm for phen and 300 nm for H_4BTEC). This demonstrates that there is no intramolecular energy transfer from the ligand to uranium and the uranyl ion is excited directly.

The excitation spectra of **1** obtained by monitoring the emissions at 515 and 534 nm are rather similar and consist of several asymmetric broad bands ranging from 300 to 500 nm with the maximal excitation wavelengths being at 347, 434 and 476 nm. When the excitation wavelength is varied from 434 to 347 nm, the general feature of the emission spectra of **1** remains the same, but the emission intensities are slightly lower. When monitoring the emission at 511 nm for **2**, the excitation spectrum shows the most intense peak at 341 nm and contains fine structures with about 15-nm separations ranging from 300 to 500 nm. The fine structures correlate with the O=U=O symmetric stretching frequency in the excited state [19]. Obviously, the excitation behavior of **2** is different from that of **1**. This difference in excitation feature is coincident with the UV–Vis absorptions for **1** and **2** (Fig. 4(c)). For **2**, the broad UV–Vis absorption band in the 400–500 nm region contains fine structures with about 15-nm separations. In contrast, the absorption fine structures of **1** are not clear. The absorption bands from 400 to 500 nm arise from the electronic transitions from the bonding orbitals to the non-bonding orbitals. This transition is forbidden, and as a result, the absorption intensity in the visible region is lower than that of the absorption in the UV region arising from the transitions from the bonding orbitals to the anti-bonding orbitals [20].

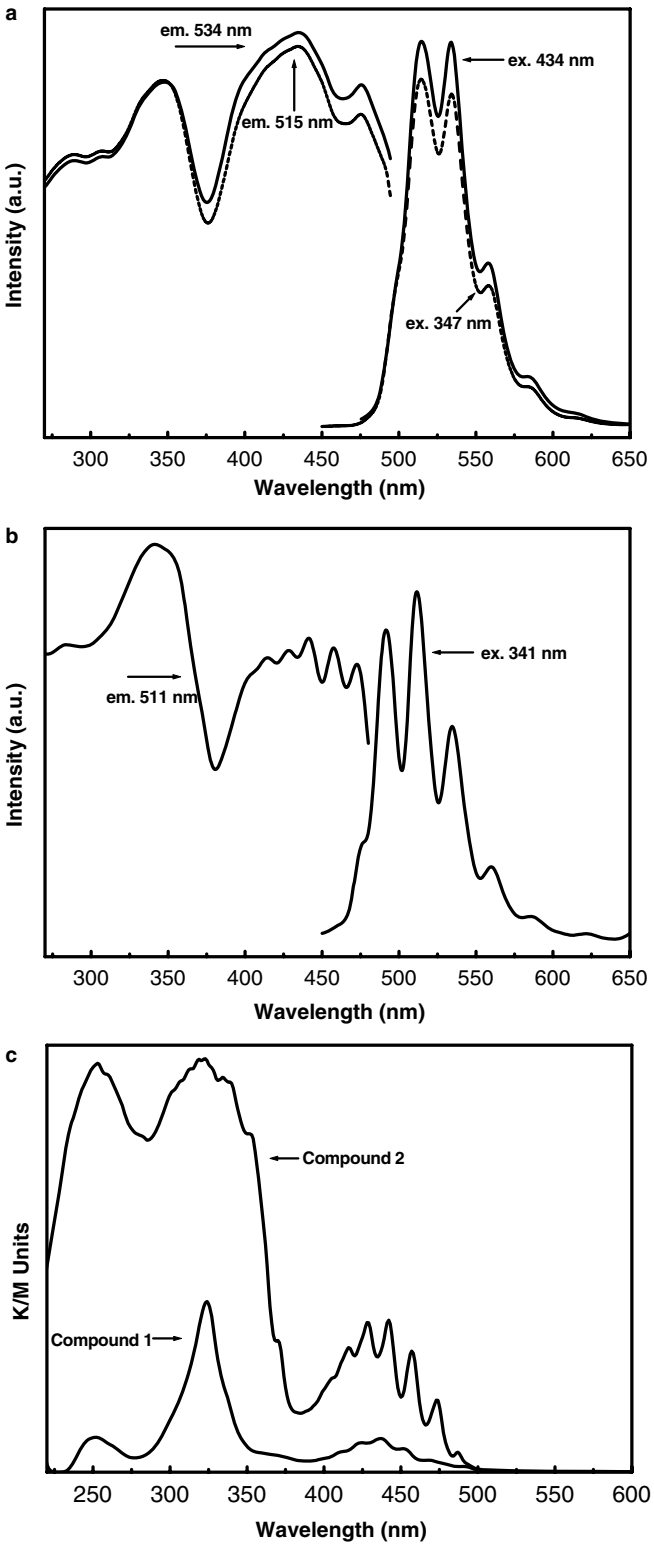

Fig. 4. Photoluminescent emission spectra of **1** with excitation at 354 and 434 nm, and excitation spectra of **1** with emission at 534 and 515 nm (a); emission spectrum of **2** with excitation at 341 nm, and excitation spectrum of **2** with emission at 511 nm (b); UV–Vis diffuse reflectance spectra of compounds **1** and **2** (c).

4. Conclusions

Two new uranium–organic compounds crystallize from hydrothermal reaction systems. Compound **1** is composed of unique one-dimensional helical chains $[(UO_2)_3O(OH)_3]_n^{n+}$ coordinated with nicotinate groups. The formation of **1** may prelude rich structures of uranyl ribbon in the presence of organic ligands. In the coordination polymer compound **2**, the O-donor (H_4BTEC) and N-donor ligands (phen) coordinate with the uranyl centers simultaneously. As a result, a layer is formed by the connection of uranyl units and BTEC ligands, with the chelating phen ligands decorating both sides of the layer. Both compounds emit intense yellow light under the excitation of UV rays.

Acknowledgements

We gratefully acknowledge the financial support of the National Natural Science Foundation of China and the Education Ministry of China.

Appendix A. Supplementary data

Crystallographic data for the structures reported in this paper have been deposited with the Cambridge Crystallographic Data Centre. The CCDA reference numbers are 218125 and 270812, respectively, for compounds **1** and **2**. These data can be obtained free of charge at www.ccdc.cam.ac.uk/conts/retrieving.html [or from the Cambridge Crystallographic Data Centre, 12 Union Road, Cambridge CB2 1EZ, UK; fax: +44 1223 336 033; e-mail: deposit@ccdc.cam.ac.uk]. Electronic supporting information (ESI) available with this article includes TG–DTA curves and powder X-ray diffraction patterns (PDF). These materials are available free of charge via the Internet at http://www.scincedirect.com. Supplementary data associated with this article can be found, in the online version, at doi:10.1016/j.poly.2005.09.018.

References

[1] (a) G. Férey, C. Mellot-Draznieks, C. Serre, F. Miliange, Acc. Chem. Res. 38 (2005) 217;
(b) C.N.R. Rao, S. Natarajan, R. Vaidhyanathan, Angew. Chem., Int. Ed. Engl. 43 (2004) 1466;
(c) M. Eddaoudi, D.B. Moler, H. Li, B. Chen, T.M. Reineke, M. O'keeffe, O.M. Yaghi, Acc. Chem. Res. 34 (2001) 319;
(d) S.L. James, Chem. Soc. Rev. 32 (2003) 276.

[2] (a) L. Pan, K.M. Adams, H.R. Hernandez, X. Wang, C. Zheng, Y. Hattor, K. Kaneko, J. Am. Chem. Soc. 125 (2003) 3062;
(b) Y.F. Zhou, F.L. Jiang, D.Q. Yuan, B.L. Wu, R.H. Wang, Z.Z. Lin, M.C. Hong, Angew. Chem., Int. Ed. Engl. 43 (2004) 5665;
(c) B. Zhao, P. Cheng, Y. Dai, D.Z. Liao, S.P. Yan, Z.H. Jiang, F.L. Wang, Angew. Chem., Int. Ed. Engl. 42 (2003) 934;
(d) D.L. Long, A.J. Blake, N.R. Champness, C. Wilson, M. Schröder, J. Am. Chem. Soc. 123 (2001) 3401.

[3] (a) P. Thuéry, C. Villiers, J. Jaud, M. Ephritikhine, B. Masci, J. Am. Chem. Soc. 126 (2004) 6838;
(b) J.-C. Berthet, M. Nierlich, M. Ephritikhine, Angew. Chem., Int. Ed. Engl. 42 (2003) 1952;
(c) L. Salmon, P. Thuéry, E. Rivière, J.-J. Girerd, M. Ephritikhine, J. Chem. Soc., Dalton Trans. (2003) 2872;
(d) L. Salmon, P. Thuéry, E. Rivière, J.-J. Girerd, M. Ephritikhine, Chem. Commun. (2003) 762.

[4] (a) M.J. Sarsfield, M. Helliwell, J. Am. Chem. Soc. 126 (2004) 1036;
(b) J.-C. Berthet, M. Nierlich, M. Ephritikhine, Chem. Commun. (2003) 1660;
(c) M.J. Sarsfield, H. Steele, M. Helliwell, S.J. Teat, J. Chem. Soc., Dalton Trans. (2003) 3443;
(d) J.-C. Berthet, M. Nierlich, M. Ephritikhine, J. Chem. Soc., Dalton Trans. (2004) 2814.

[5] D. Rose, Y.-D. Chang, Q. Chen, J. Zubieta, Inorg. Chem. 33 (1994) 5167.

[6] F.A. Cotton, G. Wilkinson, Advanced Inorganic Chemistry, 5th ed., Wiley, New York, 1988, p. 992 (Chapter 21).

[7] (a) P. Thuéry, M. Nierlich, B.W. Baldwin, N. Komatsuzaki, T. Hirose, J. Chem. Soc., Dalton Trans. (1999) 1047;
(b) L.A. Borkowski, C.L. Cahill, Inorg. Chem. 42 (2003) 7041;
(c) Y.R. Xie, H. Zhao, X.S. Wang, Z.R. Qu, R.G. Xiong, X. Xue, Z. Xue, X.Z. You, Eur. J. Inorg. Chem. (2003) 3712;
(d) M. Frisch, C.L. Cahill, J. Chem. Soc., Dalton Trans. (2005) 1518;
(e) J.-Y. Kim, A.J. Norquist, D. O'Hare, J. Chem. Soc., Dalton Trans. (2003) 2813.

[8] A.C. Bean, S.M. Peper, T.E. Albrecht-Schmitt, Chem. Mater. 13 (2001) 1266.

[9] P.B. Duval, C.J. Burns, D.L. Clark, D.E. Morris, B.L. Scott, J.D. Thomopsom, E.L. Werkema, L. Jia, R.A. Andersen, Angew. Chem., Int. Ed. Engl. 40 (2001) 3358.

[10] (a) G.J. Hutching, C.S. Heneghan, I.D. Hundson, S.H. Tayor, Nature 384 (1996) 341;
(b) T.M. McCleskey, C.J. Burns, W. Tumas, Inorg. Chem. 38 (1999) 5924.

[11] (a) W. Chen, H.M. Yuan, J.Y. Wang, Z.Y. Liu, J.J. Xu, M. Yang, J.S. Chen, J. Am. Chem. Soc. 125 (2003) 9266;
(b) Z.T. Yu, Z.L. Liao, Y.S. Jiang, G.H. Li, G.D. Li, J.S. Chen, Chem. Commun. (2004) 1814;
(c) Z.T. Yu, Z.L. Liao, Y.S. Jiang, G.H. Li, J.S. Chen, Chem. Eur. J. 11 (2005) 2642;
(d) Z.T. Yu, G.H. Li, Y.S. Jiang, J.J. Xu, J.S. Chen, J. Chem. Soc., Dalton Trans. (2003) 4219.

[12] (a) N. Snejko, E. Gutiérrez-Puebla, J.L. Martínez, M.A. Monge, C. Ruiz-Valero, Chem. Mater. 14 (2002) 1879;
(b) R. Cao, D. Sun, Y. Liang, M. Hong, K. Tatsumi, Q. Shi, Inorg. Chem. 41 (2002) 2087;
(c) L.J. Zhang, J.Q. Xu, Z. Shi, W. Xu, T.G. Wang, J. Chem. Soc., Dalton Trans. (2003) 1148.

[13] (a) A.R. Katritzky, D.A. Nichols, M. Siskin, R. Murugan, M. Balasubramanian, Chem. Rev. 101 (2001) 837;
(b) M. Åberg, Acta Chem. Scand. A 32 (1978) 101.

[14] (a) N.E. Brese, M. O'Keeffe, Acta Crystallogr., Sect. B 47 (1991) 192;
(b) I.D. Brouwn, D. Altermatt, Acta Crystallogr., Sect. B 41 (1985) 244;
(c) P.C. Burns, R.C. Ewing, F.C. Hawthorne, Can. Mineral. 35 (1997) 1551.

[15] P.C. Burns, M.L. Miller, R.C. Ewing, Can. Mineral. 34 (1996) 845.

[16] C. Janiak, Dalton Trans. (2000) 3885.

[17] R.S. Addleman, C.M. Wai, Phys. Chem. Chem. Phys. 1 (1999) 783.

[18] A.F. Leung, L. Hayashibara, J. Spadaro, J. Phys. Chem. Solids 60 (1999) 299.

[19] (a) P.M. Almond, T.E. Albrecht-Schmitt, Inorg. Chem. 41 (2002) 1177;
(b) A.J. Gaunt, I. May, R. Copping, A.I. Bhatt, D. Collison, O.D. Fox, K.T. Holman, M.T. Pope, J. Chem. Soc., Dalton Trans. (2003) 3009.

[20] (a) R.S. Addleman, M. Carrott, C.M. Wai, T.E. Carleson, B.W. Wenclawiak, Anal. Chem. 73 (2001) 1112;
(b) J. Huang, X. Wang, A.J. Jacobson, J. Mater. Chem. 13 (2003) 191;
(c) V.A. Volkovich, T.R. Griffiths, D.J. Fray, R.C. Thield, Phys. Chem. Chem. Phys. 3 (2001) 5182.

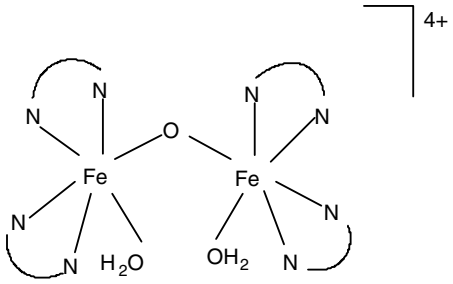

Fig. 1. Graphical structure of **1** drawn on the basis of its crystal structure.

2. Experimental

2.1. Materials

Crystals of $[Fe_2^{III}(\mu\text{-}O)(phen)_4(H_2O)_2](NO_3)_4 \cdot 5H_2O$ were prepared by a known method [24]. The prepared samples gave satisfactory electronic spectra [24] and elemental analyses (*Anal.* Calc. for $C_{48}H_{32}Fe_2O_{13}N_{12} \cdot 7H_2O$: C, 47.15; H, 3.8; Fe, 9.1; N, 13.75. Found: C, 47.1; H, 3.7; Fe, 9.0; N, 13.7%.). Stock solution of ascorbic acid was prepared by dissolving L-ascorbic acid (H_2A, G.R., E. Merck) in freshly boiled water and was stored in the dark. 1,10-Phenanthroline monohydrate (Sigma) was used as received. Solution of recrystallised $NaNO_3$ (G.R., E. Merck) was standardized by passing through a Dowex 50W 8-X strong cation exchange resin in the H^+ form and titrating the liberated acid with standard NaOH to a phenolphthalein end point. This solution of $NaNO_3$ was used for maintaining the ionic strength of the reaction mixtures. All other reagents used were of reagent grade. Doubly distilled freshly boiled water was used throughout. Reported kinetic data are in excess phenanthroline at 25.0 °C and $I = 1.0$ mol dm^{-3}.

2.2. Equilibrium measurements

Acid dissociation constants of **1** were determined by pH-metric titration of 15.0 ml of 1.0 mmol dm^{-3} solution of **1** with standard NaOH solution using a Metrohm (736 GP Titrino) autotitrator at 25.0 °C [30]. The ionic strength of the titrating medium was kept at 1.0 mol dm^{-3}. The built-in program of the autotitrator yielded two pK values.

2.3. Physical measurements and kinetics

Absorbance and electronic spectra were recorded with a Shimadzu (1601 PC) spectrophotometer using 1.00 cm quartz cells. Kinetics was monitored at 510 nm, the visible maximum of the reaction product $[Fe(phen)_3]^{2+}$ ($\varepsilon = 11\,100$ mol^{-1} dm^3 cm^{-1}) [25] in situ in the 'kinetic mode' of the instrument in the electrically controlled thermostated (25.0 ± 0.1 °C) cell housing (CPS-240A). At this wavelength only $[Fe(phen)_3]^{2+}$ absorbs appreciably. A large excess of C_{phen} (3.0 mmol dm^{-3}) over the complex (0.025 mmol dm^{-3}) was used. For all reactions, reagent solution (adjusted to desired pH by using dilute nitric acid and sodium hydroxide solutions) was directly injected into the spectrophotometer cell containing other components of the reaction mixture kept at same pH. Excess phenanthroline acted as buffer for the reaction mixtures. The pH of the experimental solutions was measured with a combined Ag/AgCl glass electrode of Metrohm (736 GP Titrino) autotitrator before and after the reaction. The linearity of measurements using the electrode was established using pH 4, 7 and 9 buffers. The electrode was calibrated to read $-\log[H^+]$ directly using a series of acid solutions at the ionic strength used for kinetic experiments. The $[H^+]$ in these solutions was determined by titration against NaOH solutions [26].

2.4. Stoichiometry and reaction products

Reaction stoichiometry was determined by spectrophotometric titration ($\lambda = 510$ nm) of a 0.05 mmol dm^{-3} solution of **1** with different amounts of reducing agent under the same condition at which kinetics were studied.

3. Results and discussion

3.1. Equilibrium studies

The built-in program of Metrohm 736 GP Titrino autotitrator yielded two pK_a values for the title complex (**1**) from the pH titration curve, $pK_{a1} = 3.71 \pm 0.11$ and $pK_{a2} = 5.28 \pm 0.10$, respectively. The difference ($pK_{a1} - pK_{a2}$) for the binuclear complex **1** is quite different from those for the dinuclear iron(III)-hydroxamic acid complexes ($pK_{a1} = 8.80 \pm 0.15$; $pK_{a2} = 9.40 \pm 0.18$) [27]. A prominent electronic interaction of the two M^{III} centers via the oxo-bridge in **1** is thus indicated and is indeed expected from the antiferromagnetic coupling well known in several μ-oxo bridged complexes of Fe^{III} [28].

In weakly acidic solution, viz. the pH interval chosen for our study, the oxo-bridge in **1** is stable. However, at pH < 2, **1** slowly cleaves to $[Fe(phen)_3]^{2+}$, identified spectrophotometrically.

We used excess 1,10-phenanthroline in all our kinetic measurements to suppress any possible phen releasing equilibrium and thereby minimized the number of kinetically active iron(III) species under investigation. Excess C_{phen} used in kinetic runs also buffers the reacting solution to within ±0.04 (but mostly within ±0.02) pH units. Use of excess C_{phen} was essential also to ensure quantitative formation of the tris(phenanthroline) complex $[Fe(phen)_3]^{2+}$.

3.2. Stoichiometry and reaction products

The break point in the absorbance versus total concentration of ascorbic acid (T_A) was observed at [complex]: $T_A = 1{:}1$ (Fig. 2; Table 1). The UV–Vis spectra of product solutions indicate quantitative formation of $[Fe(phen)_3]^{2+}$

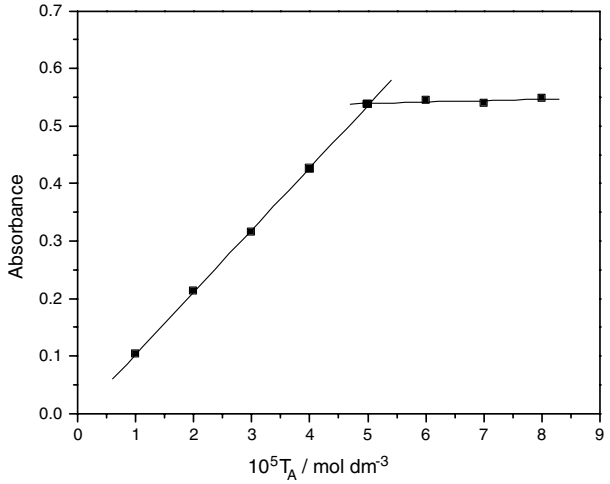

Fig. 2. Stoichiometry of the reaction between **1** and ascorbic acid. [**1**] = 0.050 mM, [Cl^-] = 1.0 M, I = 1.0 M, T = 25.0 °C, C_{phen} = 3.0 mM, pH 4.2, T_A = (0.010–0.080) mM, λ = 510 nm.

Table 1
Stoichiometry of reduction of **1**[a] by ascorbic acid

pH	$10^5 \times T_A$ (M)	Absorbance (λ = 510 nm)
4.2	1.0	0.104
	2.0	0.213
	3.0	0.315
	4.0	0.426
	5.0	0.538
	6.0	0.545
	7.0	0.540
	8.0	0.548

[a] Concentration of complex used = 0.050 mM, [Cl^-] = 1.0 M, I = 1.0 M, T = 25.0 °C, C_{phen} = 3.0 mM.

as the sole iron product. These results suggest the occurrence of reaction (1) in the entire redox process to produce $[Fe(phen)_3]^{2+}$ along with dehydroascorbic acid.

$$[Fe_2^{III}(\mu\text{-}O)(phen)_4(H_2O)_2]^{4+} + H_2A + 2phen \rightarrow 2[Fe(phen)_3]2^+ + 3H_2O + A \quad (1)$$

3.3. Kinetics and mechanism

In weakly acidic solutions, the oxo-bridge in **1** is thermodynamically stable. Unidentate ligands such as SCN^- rapidly substitute [17] the aqua ligands in **1**, thus indicating their labile nature [29]. Under the experimental conditions used, **1** and its H_2O acid dissociated derivatives **1a** and **2a** coexist in rapid equilibria (Eqs. (2) and (3)).

$$\mathbf{1} \overset{K_{a1}}{\rightleftharpoons} \underset{\mathbf{1a}}{[Fe_2^{III}(\mu\text{-}O)(phen)_4(H_2O)(OH)]^{3+}} + H^+ \quad (2)$$

$$\mathbf{1a} \overset{K_{a2}}{\rightleftharpoons} \underset{\mathbf{2a}}{[Fe_2^{III}(\mu\text{-}O)(phen)_4(OH)_2]^{2+}} + H^+ \quad (3)$$

In the experimental pH range, free ascorbic acid (H_2A) and its monodeprotonated conjugate base (HA^-) co-exist in solution. The dideprotonated form is negligible in the pH range of this study (pH 3.95–5.09), as expected from the pK_2 value [31,32]. In the presence of excess reducing agent, the reaction followed excellent first-order kinetics for at least 90% reaction. Fig. 3 shows the change in UV–Vis spectra of the complex solution and the reaction mixture after complete reaction. Fig. 4 demonstrates some first-order curves with different reagent concentrations. The final absorbance (A_{inf}) was in full agreement with the quantitative formation of $Fe(phen)_3^{2+}$. At a fixed pH, the first-order rate constant k_0 increases with increasing the total ascorbic acid concentration (T_A) (Table 2) and plot of k_0 versus T_A is an excellent straight line (r = 0.993) (Fig. 5) with no significant intercept. The observed linear dependence on T_A suggests that the reaction path involves one reagent molecule. At a fixed T_A, the observed

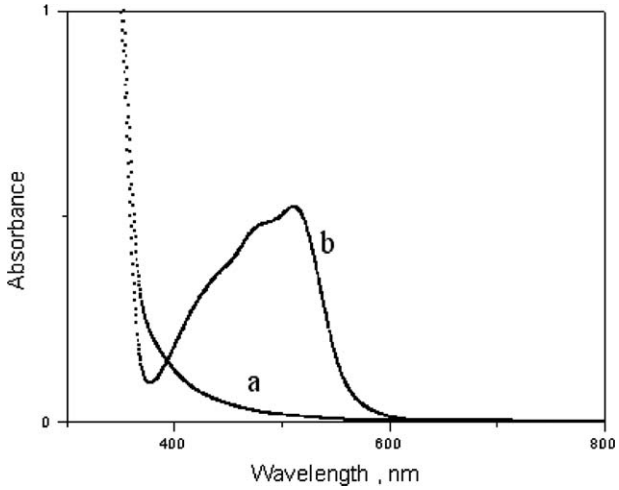

Fig. 3. Spectral changes observed by mixing **1** with ascorbic acid at: [**1**] = 0.025 mM, [Cl^-] = 1.0 M, pH 4.05, I = 1.0 M, T = 25.0 °C, C_{phen} = 3.0 M, T_A = 0.50 mM, Spectra noted at t = 0 s (a), t = 300 s (b).

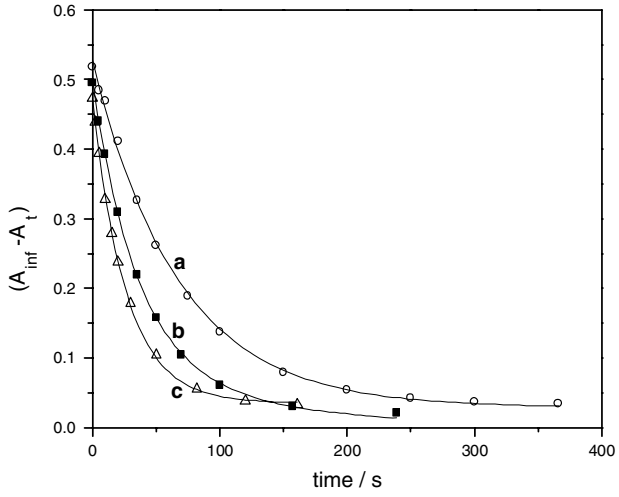

Fig. 4. The ($A_{inf} - A_t$) vs. time (t) data for the reduction of **1** by ascorbic acid. [**1**] = 0.025 mM, [Cl^-] = 1.0 M, pH 4.05, I = 1.0 M, T = 25.0 °C, C_{phen} = 3.0 mM, T_A = 0.50 (a); 0.75 (b) 1.0 (c) mM. The points indicate experimental data and the lines indicate the best-fitting first-order exponential decay.

Table 2
First-order rate constants[a] at 25.0 °C, $I = 1.0$ M ($NaNO_3$)

pH	$[Cl^-]$ (M)	$10^4 \times T_A$ (M)	$10^2 k_0$ (s^{-1})
4.05	1.0	5.0	1.6 (1.5)
		7.5	2.1 (2.2)
		10	3.0 (3.0)
		12	4.1 (3.7)
		20	5.9 (5.9)
		22	6.4 (6.6)
		25	6.9 (7.4)
3.95		5.0	1.5 (1.2)
4.00			1.3 (1.3)
4.17			2.0 (1.9)
4.39			2.5 (2.8)
4.74			4.0 (4.2)
5.09			4.8 (4.8)
4.2	0.90	2.5	1.4 (1.4)
	0.80		1.6 (1.6)
	0.70		1.8 (1.8)
	0.60		2.1 (2.0)
	0.50		2.3 (2.3)
	0.40		2.5 (2.6)
	0.30		2.7 (2.8)
	0.20		3.1 (3.0)

[a] Concentration of complex used 0.025 mM. $C_{phen} = 3.0$ mM. Calculated k_0 are given in parentheses.

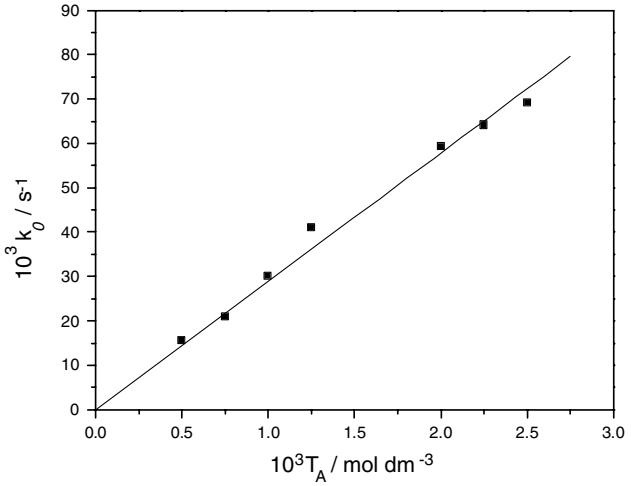

Fig. 5. Plot of $10^3 k_0$ vs. $10^3 \times T_A$. [**1**] = 0.025 mM, $[Cl^-] = 1.0$ M, $I = 1.0$ M, $T = 25.0$ °C, $C_{phen} = 3.0$ mM, $T_A = (0.50–2.5)$ mM. pH 4.05. The points indicate experimental data and the line indicates the best-fitting straight line.

pseudo-first-order rate constant increases with increasing pH (Table 2, Fig. 6), probably indicating kinetic inactivity of diprotonated form of the reducing agent, which is in accordance with some earlier studies [33]. The first-order rate constants show an inverse square dependence on the chloride ion concentration. Plot of $1/k_0$ versus $[Cl^-]^2$ is an excellent straight line (Fig. 7). No significant change in observed rate constant was noticed by varying C_{phen}. Varying C_{phen} in the range 3.0–10 mmol dm^{-3} at $T_A =$ 0.50 mmol dm^{-3}, $[Cl^-] = 1.0$ mol dm^{-3} and pH 4.05 yielded $k_0 = (1.6 \pm 0.1) \times 10^{-2}\ s^{-1}$. This observation

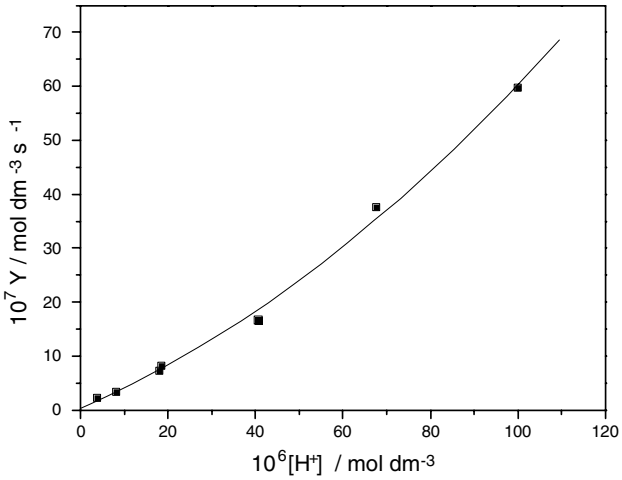

Fig. 6. Plot of $10^7 \times Y$ vs. $10^6 \times [H^+]$, where $Y = k_0([H^+] + K_a)(A + C[Cl]^2)/T_A K_a$. [**1**] = 0.025 mM, $[Cl^-] = 1.0$ M, $I = 1.0$ M, $T = 25.0$ °C, $C_{phen} = 3.0$ mM, $T_A = 0.50$ mM, pH 3.95–5.09. The points indicate experimental data and the line indicates the best-fitting second order polynomial curve.

$$\mathbf{1} \overset{K_{a1}}{\rightleftharpoons} \mathbf{1a} + H^+ \quad (4)$$

$$\mathbf{1a} \overset{K_{a2}}{\rightleftharpoons} \mathbf{2a} + H^+ \quad (5)$$

$$\mathbf{H_2A} \overset{K_a}{\rightleftharpoons} \mathbf{HA^-} + H^+ \quad (6)$$

$$\mathbf{1} + Cl^- \overset{K_1}{\rightleftharpoons} [Fe^{III}{}_2(\mu\text{-}O)(phen)_4(H_2O)Cl]^{3+} \quad (7)$$
2

$$\mathbf{2} + Cl^- \overset{K_2}{\rightleftharpoons} [Fe^{III}{}_2(\mu\text{-}O)(phen)_4Cl_2]^{2+} \quad (8)$$
3

$$\mathbf{1} + \mathbf{HA^-} \xrightarrow{k_1} \text{Products} \quad (9)$$

$$\mathbf{1a} + \mathbf{HA^-} \xrightarrow{k_2} \text{Products} \quad (10)$$

$$\mathbf{2a} + \mathbf{HA^-} \xrightarrow{k_3} \text{Products} \quad (11)$$

Scheme 1.

suggests that no phen-releasing equilibrium is important in the reaction media. Considering all these, Scheme 1 is proposed to account for the observed kinetics. We assume all the equilibria to be relatively rapid. Scheme 1 leads to the following equation:

$$k_0 = \frac{T_A K_a (k_1[H^+]^2 + k_2 K_{a1}[H^+] + k_3 K_{a1} K_{a2})}{([H^+] + K_a)(A + B[Cl] + C[Cl]^2)}, \quad (12)$$

where

$$A = [H^+]^2 + K_{a1}[H^+] + K_{a1}K_{a2}, \quad (13)$$

$$B = K_1[H^+]^2, \quad (14)$$

$$C = K_1 K_2 [H^+]^2. \quad (15)$$

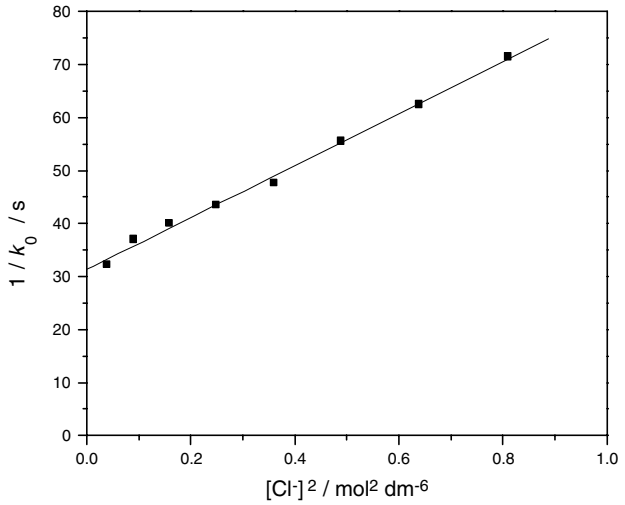

Fig. 7. Plot of $1/k_0$ vs. $[Cl^-]^2$. [**1**] = 0.025 mM, $[Cl^-] = (0.20–1.0)$ M, $I = 1.0$ M, $T = 25.0$ °C, $C_{phen} = 3.0$ mM, $T_A = 0.25$ mM, pH 4.2. The points indicate experimental data and the line indicates the best-fitting straight line.

As the plot of $1/k_0$ versus $[Cl]^2$ is an excellent straight line ($r = 0.995$) with an intercept, we neglect the terms which are first-order with respect to chloride ion concentration. Thus, Eq. (12) is transformed to the following equation:

$$k_0 = \frac{T_A K_a (k_1[H^+]^2 + k_2 K_{a1}[H^+] + k_3 K_{a1} K_{a2})}{([H^+] + K_a)(A + C[Cl]^2)}. \quad (16)$$

The straight line plot of $1/k_0$ versus $[Cl]^2$ at a fixed pH (=4.2) and fixed T_A (=0.25 m mol dm^{-3}) (Fig. 7) has slope = $([H^+] + K_a)C/(T_A K_a(k_1[H^+]^2 + k_2 K_{a1}[H^+] + k_3 K_{a1} K_{a2})) = (49 \pm 1)$ mol^{-1} dm^3 s and intercept $([H^+] + K_a) A/(T_A K_a(k_1[H^+]^2 + k_2 K_{a1}[H^+] + k_3 K_{a1} K_{a2})) = (31 \pm 1)$ mol dm^{-3} s. Hence, from intercept, $k_1[H^+]^2 + k_2 K_{a1}[H^+] + k_3 K_{a1} K_{a2} = 3.8 \times 10^{-6}$ s^{-1} at pH 4.2. Putting this value in the expression of slope, we get $K_1 K_2 = 7.0$ mol^{-2} dm^6 at 25.0 °C and $I = 1.0$ mol dm^{-3}. These calculations were done using the value of K_a ($pK_a = 4.03$) obtained from the literature [31]. Again, plot of k_0 versus T_A at fixed pH (=4.05) and fixed [Cl] (=1 mol dm^{-3}) is an excellent straight line with slope = $K_a(k_1[H^+]^2 + k_2 K_{a1}[H^+] + k_3 K_{a1} K_{a2})/(([H^+] + K_a)(A + C[Cl]^2)) = (29 \pm 1)$ mol^{-2} dm^6 s^{-1}. So, $k_1[H^+]^2 + k_2 K_{a1}[H^+] + k_3 K_{a1} K_{a2} = 5.1 \times 10^{-6}$ mol^{-1} dm^3 s^{-1} at pH 4.05. Plot of $k_0([H^+] + K_a)(A + C[Cl]^2)/T_A K_a$ versus $[H^+]$ is a good second-order polynomial fit ($r = 0.996$) (Fig. 6) which gives $k_1 = 2.5 \times 10^2$ mol^{-2} dm^6 s^{-1}, $k_2 = 1.8 \times 10^2$ mol^{-2} dm^6 s^{-1} and $k_3 = 33$ mol^{-2} dm^6 s^{-1}. Values of $(k_1[H^+]^2 + k_2 K_{a1}[H^+] + k_3 K_{a1} K_{a2})$ calculated for pH 4.2 and 4.05 using these values of k_1, k_2 and k_3 match well with the values obtained from the chloride plot and the reagent plot, respectively. The calculated first-order rate constants using Eq. (16) are in close proximity (10–15%) of the experimental values (Table 2).

The rate of the whole reaction is very much slowed down in presence of chloride ion. We have observed no rate saturation with increasing $[Cl^-]$. Eq. (16) explains the observed kinetics well and also implies that k_0 should tend to zero at very high chloride concentration. Hence, it seems reasonable to assume that an inner-sphere mechanism is operating. Ascorbate ion replaces the coordinated aquo or hydroxo moieties to form inner-sphere bond with Fe^{III} centers and then the electron transfers take place. The inhibition by chloride ions can be explained in terms of its competition with ascorbate to form the inner sphere bonds by replacing aquo or hydroxo ligands. Our experimental data show an inverse square dependence of k_0 on $[Cl^-]$ and thus allow us to neglect the terms which are first-order with respect to $[Cl^-]$. The implication is that incorporation of one chloride ion in the complex molecule does not inhibit the reaction. A possible explanation to this is that as long as there is one replaceable aquo or hydroxo group present in the complex molecule, reaction proceeds via its replacement by ascorbate ion. The presence of two chloride ions in the coordination sphere is necessary to block the reaction.

The order of magnitude $k_1 > k_2 > k_3$ indicates that the diaquo species is the most reactive form and the dihydroxo species is the least reactive. This is in accordance with the results found in the oxidation of hydrazine by **1** [30]. The diaquo species has the highest positive charge and interacts with the negative ascorbate ion more readily than the other two forms of the complex. The lowest activity of the dihydroxo form is due to its low charge. The order of activity can also be explained in terms of number of easily replaceable water molecules present in the coordination sphere. The diaquo has two water molecules, the monoaquo has one and the dihydroxo none and hence their order of reactivity. A similar trend of reactivity was found in the oxidation of thiosulfate ion by a dinuclear $Mn^{IV,IV}$ complex [34], where reactivity increased with increasing number of coordinated water molecules.

The steps (9)–(11) can occur either via an initial slow one-electron transfer followed by another rapid one-electron transfer, or by a two electron transfer mechanism, leading to $[Fe(phen)_3]^{2+}$ and dehydroascorbic acid. There are examples where formation of radical species HA$^{\cdot}$ have been proposed as a result of oxidation by iron(III) species [35–37]. In our case, the oxidant is a two electron acceptor and a two-electron transfer mechanism similar to the case of ferriporphyrin dimer [23] can also work. However, a choice between these two possibilities cannot be made from our results.

Acknowledgements

We gratefully acknowledge the financial help provided by the Department of Science and Technology (New Delhi, India) for the present work. One of he authors (B.B.D.) is grateful to UGC, India, for the senior research fellowship provided to him.

References

[1] D.M. Kurtz Jr., J. Biol. Inorg. Chem. 2 (1997) 159.
[2] (a) J.B. Vincent, G.L. Olivier-Lilley, B.A. Averill, Chem. Rev. 90 (1990) 1447;

(b) S.Y. Choi, P.E. Eaton, D.A. Kopp, S.J. Lippard, M. Newcomb, R. Shen, J. Am. Chem. Soc. 121 (1999) 12198.
[3] E.I. Solomon, Inorg. Chem. 40 (2001) 3656.
[4] R.E. Stenkamp, L.C. Sieker, L.H. Jensen, J. Am. Chem. Soc. 106 (1984) 618.
[5] R.E. Stenkamp, L.C. Sieker, L.H. Jensen, J. Sanders-Loehr, Nature (London) 291 (1981) 263.
[6] W.A. Hendrickson, in: J. Lamy, J. Lamy (Eds.), Invertebrate Oxygen Binding Proteins: Structure, Active Site and Function, Marcell-Dekker, New York, 1981, p. 503.
[7] W.T. Elam, E.A. Sterrn, J.D. McCallum, J. Sanders-Loehr, J. Am. Chem. Soc. 104 (1982) 6369.
[8] A. Hendrickson, M.S. Co, J.L. Smith, K.O. Hodgson, G.L. Klippenstein, Proc. Natl. Acad. Sci. USA 79 (1982) 6255.
[9] K. Garbett, D.W. Darnall, I.M. Koltz, R.J.P. Williams, Arch. Biochem. Biophys. 135 (1969) 419.
[10] H.B. Gray, H.J. Schugar, in: G.L. Eichharn (Ed.), Inorganic Biochemistry, Elsevier, Amsterdam, 1973, p. 102.
[11] J. Sanders-Loehr, T.M. Loehr, A.G. Mauk, H.B. Gray, J. Am. Chem. Soc. 102 (1980) 6992.
[12] D.M. Kurtz Jr., D.F. Shriver, I.M. Koltz, Coord. Chem. Rev. 24 (1977) 145.
[13] S.M. Freier, L.L. Duff, D.F. Shriver, I.M. Koltz, Arch. Biochem. Biophys. 205 (1980) 449.
[14] A.K. Shiemke, T.M. Loehr, J. Sanders-Loehr, J. Am. Chem. Soc. 106 (1984) 4951.
[15] B.M. Sjoberg, T.M. Loehr, J. Sanders-Loehr, Biochemistry 21 (1982) 96.
[16] B. Chaudhuri, R. Banerjee, Can. J. Chem. 76 (1998) 350.
[17] B. Chaudhuri, R. Banerjee, J. Chem. Soc., Dalton Trans. (1998) 3451.
[18] E. Adams, L. Frank, Annu. Rev. Biochem. 49 (1980) 1005.
[19] E. Cadenas, Annu. Rev. Biochem. 58 (1989) 79.
[20] G.M. Brown, B.S. Brunschwig, C. Creutz, J.F. Endicott, N. Sutin, J. Am. Chem. Soc. 101 (1979) 1298.
[21] R.A. Rickman, R.L. Sorenso, K.O. Witkins, G. Davies, Inorg. Chem. 16 (1977) 1570.
[22] J.J. Jwo, A. Haim, J. Am. Chem. Soc. 98 (1976) 1172.
[23] F.L. Harris, D.L. Toppen, Inorg. Chem. 17 (1978) 74.
[24] J.E. Plowman, T.M. Loehr, C.K. Schauerand, O.P. Anderson, Inorg. Chem. 23 (1984) 3553.
[25] G. Nord, B. Pedersen, E. Bjergbakke, J. Am. Chem. Soc. 105 (1983) 1913.
[26] S. Mukhopadhyay, R. Banerjee, J. Chem. Soc., Dalton Trans. (1993) 933.
[27] M.T. Caudle, C.D. Caldwell, A.L. Crumbliss, Inorg. Chim. Acta 240 (1995) 519.
[28] (a) G. McLendon, R.J. Motekaitis, A.E. Martell, Inorg. Chem. 15 (1976) 2306;
(b) S. Chardon-Noblat, O. Horner, B. Chabut, F. Avenier, N. Debaecker, P. Jones, J. Pecaut, L. Dubois, C. Jeandey, J.-L. Oddou, A. Deronzier, J.-M. Latour, Inorg. Chem. 43 (2004) 1638, Though in this article no acidity constant was determined, but it was clearly established that the deprotonation results from the metal bound water molecule in a diferric complex.
[29] A.F.M. Nazer, C.F. Wells, J. Chem. Soc., Dalton Trans. (1980) 1532.
[30] J. Bhattacharyya, K. Dutta, S. Mukhopadhyay, Dalton Trans. (2004) 2910.
[31] E. Pelizzetti, E. Mentasti, E. Pramauro, Inorg. Chem. 15 (1976) 1898.
[32] J. Xu, R.B. Jordan, Inorg. Chem. 29 (1990) 4180.
[33] (a) A. McAuley, L. Spencer, P.R. West, Can. J. Chem. 63 (1985) 1198;
(b) D. Dixon, T.P. Dasgupta, N.P. Sadler, J. Chem. Soc., Dalton Trans. (1997) 1903.
[34] A.K. Bhattacharya, A.B. Mondal, R. Banerjee, J. Chem. Soc., Dalton Trans. (1997) 2351.
[35] U.S. Mehrotra, M.C. Agrawal, S.P. Mushran, J. Phys. Chem. 73 (1996) 1996.
[36] E. Pelizzetti, E. Mentasti, E. Pramauro, Inorg. Chem. 15 (1976) 2898.
[37] M.J. Hynes, D.F. Kelly, Chem. Commun. (1988) 849.

2. Results and discussion

2.1. Synthesis

The two complexes $Be[(Me_2N)_2P(O)F]_4(ClO_4)_2$ (**1**) and $Be[(Et_2N)_2P(O)F]_4(ClO_4)_2$ (**2**) were prepared by a method well-known in the literature [16]. They are soluble in nitromethane, acetonitrile and dichloromethane. The complexes prepared were characterised by elemental analysis and particularly by their NMR data and comparison with the corresponding data for the free ligands (see Table 1).

2.2. Spectroscopic studies

The infrared spectra show strong bands within the range 1295–1300 cm^{-1} attributed to $\nu_{P=O}$. The P=O stretching vibration is shifted towards lower wave numbers on coordination to the beryllium atom compared with its value for the free ligands. The coordination shift is about 20 cm^{-1} and is consistent with phosphoryl coordination to the beryllium atom. Absorption bands at 638 and 614 cm^{-1} were observed in the IR spectra of the two complexes and are assigned to metal–ligand stretching (Be–O bond), in agreement with literature results [17].

The NMR spectra of the two complexes prepared are quite similar and the data obtained from these spectra are summarised in Table 1. The ^{31}P and ^{19}F NMR resonances of bound ligands are shifted to higher field compared with those of the free ligands. The difference in the ^{31}P chemical shift between free and bound ligands is more important than that observed in ^{19}F NMR spectra, confirming coordination of the fluorophosphoramide ligand through the oxygen atom.

The $^{31}P\{^1H\}$ spectrum for the free ligand showed a doublet due to coupling with ^{19}F atom; a similar doublet shifted to higher field was observed for each of the two complexes prepared. In the latter, each signal of the doublet appears as a 1:1:1:1 quartet owing to coupling with ^9Be atom ($I = 3/2$) (Fig. 1). The coupling constants $^1J_{P-F}$ are larger for the bound ligand than for the free one (Table 1). The upfield shift of the bound ligand signals compared to that of the free ligand is indicative of disruption of the PO π interaction as a result of complex bond formation, in agreement with IR data [18]. This relatively small upfield shift (see Table 1) is perhaps demonstrative of a sizeable N → P inductive effect by means of π donation from the nitrogen centres of NMe_2 to compensate the loss of electron density around phosphorus following complexation. The same dichotomy has been observed with HMPA as ligand [19].

The ^9Be NMR spectrum of each of the two complexes prepared, at room temperature, consists of a 1:4:6:4:1 quintuplet (see Fig. 2) with $^2J_{P-Be}$ coupling constant of ~5 Hz comparable to that previously found for the HMPA derivative [10]. The sharpness of all the signals, which is consistent with a cubic symmetry around the quadrupolar metal centre, suggests, for the two complexes prepared, a tetrahedral geometry. The $^2J_{P-Be}$ coupling constant for complex **1** is 4.8 Hz versus 6 Hz for the complex $Be[HMPA]_4(ClO_4)_2$ [10]. The difference may be explained by the fact that the movement of the nitrogen lone pair towards phosphorus upon complex formation is more important in the case of HMPA than that of $(Me_2N)_2P(O)F$ due to a deficiency of a Me_2N group in the latter.

The two bonds spin coupling of beryllium with phosphorus is consistent with a 'covalent' Be–OP bond, similar to that observed for beryllium with the very hard fluoride anion [20]. In the absence of X-ray data, the use of theoretical calculations is particularly informative [21,22]. We have thus performed DFT calculations on complex **1**.

2.3. Theoretical calculations

The geometries of the $Be[(Me_2N)_2P(O)F]_4^{2+}$ cation of complex **1** and its ligand, $(Me_2N)_2P(O)F$, were optimised by means of the DFT B3LYP/6-31G* method. The optimised structure of complex **1** is shown in Fig. 3. The complex and its ligand have been identified as local minima on the singlet potential energy surfaces (PES). Optimised values of selected geometrical parameters are listed in Table 2. The ^{31}P, ^{19}F and ^9Be NMR chemical shifts calculated by the same method are collected in Table 3. The beryllium ion is considered to be coordinated by four ligand molecules. The tetrahedral geometry around the beryllium is shown with O–Be–O angles at the metal from 107° to 109°. The values of the Be–O distance, 1.620–1.635 Å, as well as the other bond distances and angles are in good agreement with the values reported for similar molecules using X-ray diffraction [23]. Interestingly, the P–O distance of 1.519 Å is very identical to that of 1.517 Å obtained by the crystal structure of the complex $[\{N(CH_2PPh_2O)_3\}Be(OH_2)](ClO_4)_2$ [12].

In complex **1**, the coordination mode is thus confirmed by a lengthening of the P=O bond of the complex compared to that of the free ligand (1.481 Å) calculated at the same level of theory. This lengthening is equal to 8.6% and is consistent with the low stretching frequency observed in the IR spectra and may also explain the differences observed in the ^{31}P NMR chemical shifts between the

Table 1
NMR data of the complexes **1** and **2** and their ligands in a mixture of nitromethane and dichloromethane

Compound	δ_{31P} (ppm)	δ_{19F} (ppm)	δ_{9Be} (ppm)	$^1J_{P-F}$ (Hz)	$^2J_{P-Be}$ (Hz)
$(Me_2N)_2P(O)F$	17.3	79.1		948	
$(Et_2N)_2P(O)F$	16.3	79.7		949	
$Be[(Me_2N)_2P(O)F]_4(ClO_4)_2$ (**1**)	15.0	78.0	−5.07	952	4.8
$Be[(Et_2N)_2P(O)F]_4(ClO_4)_2$ (**2**)	15.6	78.3	−5.30	958	4.9

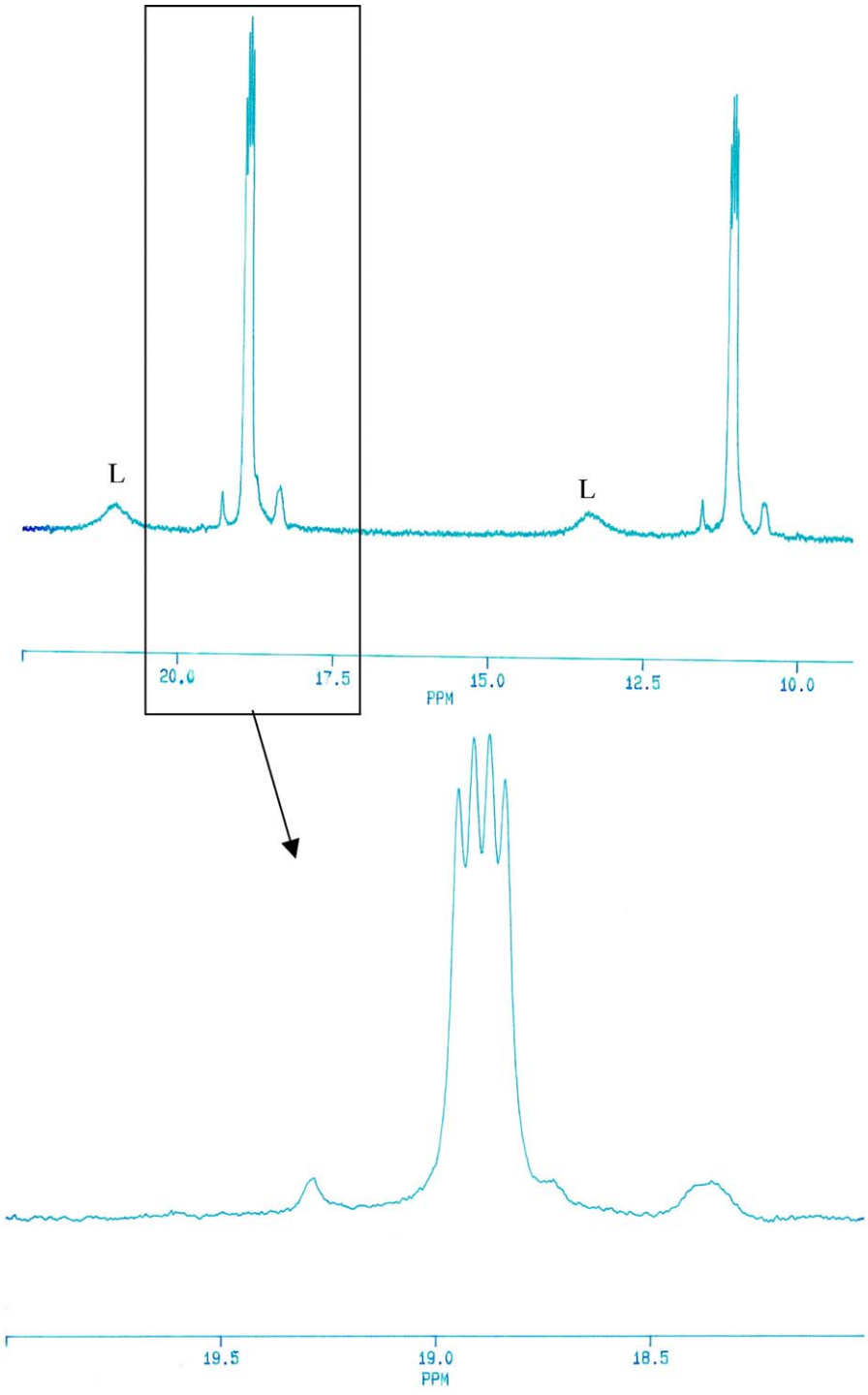

Fig. 1. $^{31}P\{^{1}H\}$ NMR spectrum of complex **1** at −35 °C in dichloromethane (L: dissociated ligand signals).

free and bound ligands in solution. The slight shortening of the P–F bond is in good agreement with the small increase of the $^{1}J_{P-F}$ coupling constant values found for the complexes compared with that of the free ligands in solution (see Table 1). The angle of the F–P–O in the free ligand (∼112°) is narrowed to ∼107° in the complex. This may be interpreted in terms of steric effects due to the coexistence of four ligand molecules around the beryllium atom in a tetrahedral geometry and may also explain the differences in $^{1}J_{P-F}$ coupling constants observed for the complex compared with the free ligand.

For complex **1** and its ligand, the overall agreement between theory and experiment is satisfactory. In particular, the small difference between the ^{31}P chemical shifts of bound and free ligands (Table 3) is in good agreement with that observed in solution. This small shift may be again explained by the N → P inductive effect compensating the loss of electron density around phosphorus following complexation.

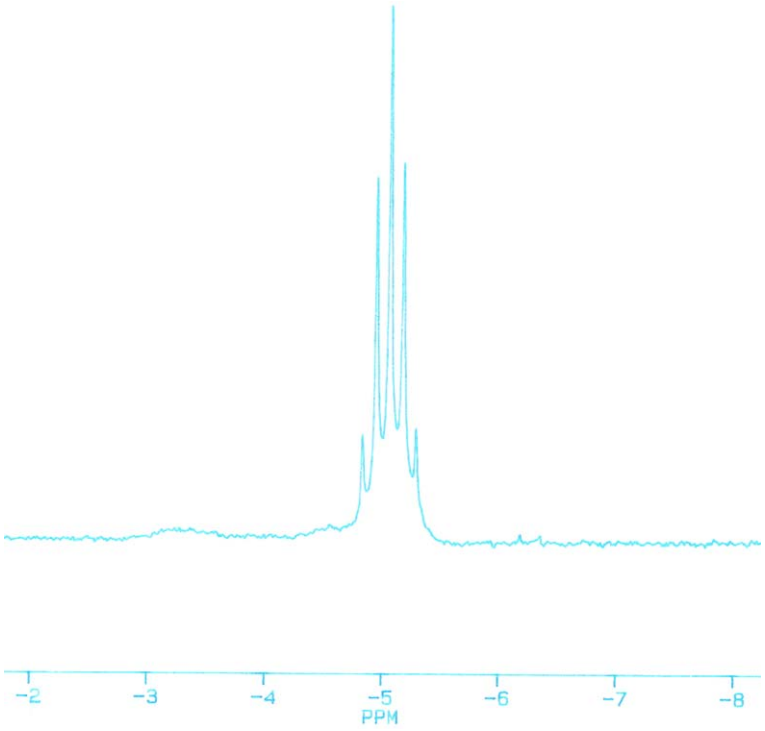

Fig. 2. ^{9}Be NMR spectrum of complex **1** at 25 °C in CD_3NO_2–CD_2Cl_2.

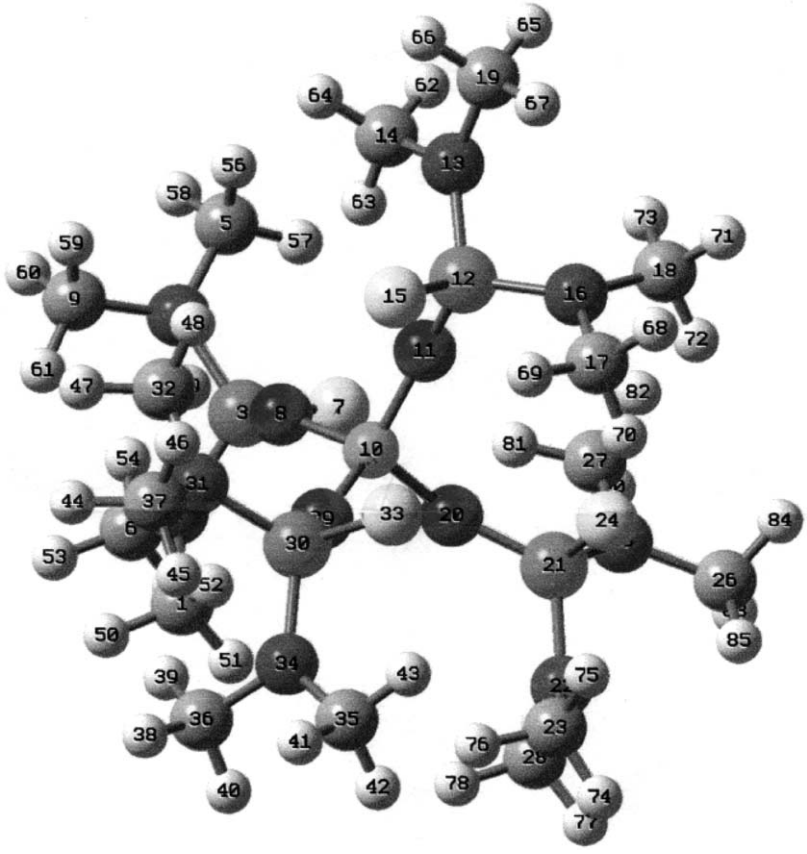

Fig. 3. DFT/B3LYP optimised structure of complex **1**.

Table 2
Selected optimised geometrical parameters[a] for complex **1**[b] and its ligand, $(Me_2N)_2P(O)F$

	Complex **1**	Ligand
P12–O11	1.514	
P3–O8	1.519	1.481
P30–O29	1.513	
P21–O20	1.519	
Be10–O8	1.632	
Be10–O29	1.635	
Be10–O11	1.620	
Be10–O20	1.632	
P21–F24	1.598	
P12–F15	1.594	1.604
P3–F7	1.593	
P30–F33	1.592	
Be10–O20–P21	142.26	
Be10–O11–P12	158.08	
Be10–O8–P3	145.68	
Be10–O29–P30	153.68	
F15–P12–O11	106.13	
F24–P21–O20	106.61	112.06
F33–P30–O29	107.47	
F7–P3–O8	106.90	
O11–Be10–O8	109.08	
O20–Be10–O8	108.61	
O29–Be10–O8	107.47	

[a] Distances in angstrom (Å) and angles in degrees (°).
[b] See Fig. 3 for labelling of the atoms.

Table 3
Theoretical ^9Be, ^{31}P and ^{19}F NMR chemical shifts for complex **1**[a] and its ligand

	Complex **1**	ligand
Be10	−0.10	
P3	27.16	
P12	24.38	24.57
P21	28.21	
P30	22.13	
F7	95.86	
F15	93.52	
F24	97.91	94.48
F3	92.88	

[a] See Fig. 3 for labelling of the atoms.

It is satisfying to remark that the theoretical chemical shifts (Table 3) are in fair agreement with the experimental values. This leads further support to the structural characterisation discussed above.

In this context, it is also worth to note that the difference between the theoretical and experimental (solvent dependent) chemical shift values may be explained by the fact that no solvent effect was taken into account in the DFT calculations.

3. Experimental

3.1. Toxicity

Beryllium and its compounds are highly toxic [24,25] and should be handled with extreme care [26]. Experiments were conducted in a well ventilated fumehood. Spillages and especially ones of particular nature were washed down well with water. Transportation of samples outside the fumehood were minimised and NMR measurements were carried out with extreme caution.

3.2. Preparation

All preparations were carried out under a nitrogen atmosphere in solvents dried by standard techniques [27] and stored over molecular sieves. NMR spectra were recorded on a Bruker Ac-300 instrument in a mixture of CD_2Cl_2–CD_3NO_2; ^{31}P at 121 MHz (85% H_3PO_4), ^{19}F at 282 MHz ($CFCl_3$), and ^9Be at 42.17 MHz ($Be(H_2O)_4^{2+}$). IR spectra: Perkin–Elmer Paragon 1000 PC. The ligands $(R_2N)_2P(O)F$ were prepared according to methods described in the literature (R = Me [28]; R = Et [29]).

The two complexes **1** and **2** were prepared following a method described by Van Leeuwen et al. [16]. The hydrated beryllium(II) perchlorate (0.28 g, 1 mmol) was dissolved in ethanol and an appropriate amount of triethylorthoformate was added. After 2 h the ligand (4 mmol) was added, the solution was then concentrated by distilling off the solvent at reduced pressure. Addition of anhydrous ether led to the precipitation of the complex as a white solid. This was filtered washed with ether and dried in vacuum. ((**1**): 75% and (**2**): 80% yield). *Anal.* Calc. for complex $C_{16}H_{48}N_8O_{12}P_4F_4BeCl_2$ (**1**): C, 23.33; H, 5.83; N, 13.60. Found: C, 22.94; H, 6.13; N, 13.58%. *Anal.* Calc. for complex $C_{32}H_{80}N_8O_{12}P_4F_4BeCl_2$ (**2**): C, 36.67; H, 7.64; N, 10.69. Found: C, 36.45; H, 7.88; N, 10.62%.

3.3. Computational details

Density functional theory (DFT) calculations were carried out on the complex **1** using the suite of programs GAUSSIAN-03W [30], with the non-local hybrid functional denoted as B3LYP [31]. A double-ζ polarisation basis set 6-31G* [32–36] was employed for each atom. The geometries of both the complex **1** and the ligand were optimised using analytical gradient. The harmonic vibrational frequencies of the different stationary points of the PES have been calculated at the same level of theory in order to identify the local minima as well as to estimate the corresponding zero-point vibrational energy (ZPE).

The ^9Be, ^{31}P and ^{19}F NMR absolute shielding constants (δ values) were calculated at the B3LYP/DFT level with the Gauge-Independent Atomic Orbital (GIAO) method [37–41] using the same basis set. The calculated magnetic shieldings were converted into δ chemical shifts by noting that at the same level of theory the ^9Be (in $Be(H_2O)_4$), ^{31}P (in H_3PO_4) and ^{19}F (in $CFCl_3$) absolute shieldings are 114.24, 378.43 and 179.39, respectively.

4. Conclusions

We have shown that the ligands $(R_2N)_2P(O)F$ (R = Me or Et) form stable complexes with the beryllium(II) ion,

comparable to that obtained with HMPA. This indicates that the substitution of one NMe_2 group by a fluorine atom has little effect on the basicity (donor ability) of the ligands used. The results also show:

1. The remarkable affinity of the beryllium(II) ion toward the PO functionalities.
2. That the ^{9}Be NMR spectroscopy is a potential technique for the study of phosphoryl-containing beryllium complexes.
3. That the DFT calculations are a useful supporting tool for such a study since a combination of empirical and theoretical studies can, in favourable cases, overcome the limitations of each.

Acknowledgements

The authors wish to thank Professor A. Baklouti of the Department of Chemistry, Faculty of Sciences of Tunis, University of Tunis El Manar for his valuable help and discussions of this work.

References

[1] J.V. Dunworth (Ed.), International Series of Monographs on Nuclear Energy, vol. 1, MacMillan, New York, 1963.
[2] M.D. Rossman, O.P. Preus, M.B. Powers, Beryllium: Biomedical and Environmental Aspects, Williams and Wilkens, Baltimore, 1991.
[3] C.Y. Wong, J.D. Woollins, Coord. Chem. Rev. 130 (1994) 243.
[4] H.G. Schmidbaur, Be-Org. 1 (1987) 155.
[5] D.N. Skilleter, Chem. Br. 26 (1990) 26.
[6] L. Alderighi, P. Gans, S. Midollini, A. Vacca, in: A.G. Sykes (Ed.), Advances in Inorganic Chemistry, Academic Press, New York, 2000, p. 109.
[7] O. Kumberger, H. Schmidbaur, CHUIZ 27 (1993) 310.
[8] N.M. Karayannis, E.E. Bradshaw, L.L. Pytlewsky, M.M. Labes, J. Inorg. Nucl. Chem. 32 (1970) 1079.
[9] J.J. Delpuech, A. Peguy, P. Rubini, I. Steinmetz, Nouv. J. Chim. 1 (1977) 133.
[10] J.J. Delpuech, A. Peguy, M.R. Khaddar, J. Magn. Reson. 6 (1972) 325.
[11] J.J. Delpuech, A. Peguy, M.R. Khaddar, J. Electroanal. Chem. 29 (1971) 31.
[12] F. Cecconi, C.A. Ghilardi, S. Midollini, A. Orlandini, Inorg. Chem. Commun. 3 (2000) 350, and references therein.
[13] J.L. Bock, D.E. Ash, J. Inorg. Biochem. 13 (1980) 105.
[14] D.J. Price, J.G. Joshi, J. Biol. Chem. 258 (1983) 108.
[15] M.A.M. Khouna, M.T. Ben Dhia, M.R. Khaddar, Phosphorus, Sulfur, Silicon 178 (2003) 2309.
[16] P.W.N.M. Van Leeuwen, W.L. Groeneveld, Inorg. Nucl. Chem. Lett. 3 (1967) 145.
[17] M.W.G. De Bolster, Z. Anorg. Allg. Chem. 434 (1977) 78.
[18] E. Linder, R. Lehner, H. Scheer, Chem. Ber. 100 (1967) 1331.
[19] S.R. Wade, G.R. Willey, J. Inorg. Nucl. Chem. 42 (1980) 1133.
[20] M. Schmidt, H. Schmidbaur, Z. Naturforsh. b 53 (1998) 1294.
[21] Z. Lin, Chem. Soc. Rev. 31 (2002) 239.
[22] F. Maseras, A. Lledos, E. Colt, O. Ensenstein, Chem. Rev. 100 (2000) 601.
[23] F. Cecconi, C.A. Ghilardi, S. Midollini, A. Orlandini, Inorg. Chem. 37 (1998) 146, and references therein.
[24] W.K. Robins, J.H. Runnels, B. Marryfield, Anal. Chem. 47 (1975) 2095.
[25] D.A. EverestBeryllium Comprehensive Inorganic Chemistry, vol. 1, Pergamon Press, Oxford, 1973, p. 531.
[26] D.A. Everest, The chemistry of berylliumTopics in Inorganic Chemistry and General Chemistry, vol. I, Elsevier, Amsterdam, 1964.
[27] D.D. Perrin, W.L.F. Armarego, D.R. Perrin, Purification of Laboratory Chemicals, Pergamon Press, Oxford, 1966.
[28] E.A. Robinson, D.S. Lavery, Spectrochim. Acta A 28 (1972) 1099, and references therein.
[29] G. Schrader, Monographie No. 62 zu "Angewandte Chemie" und "Chemie – Ingenieur –Technik", Verlag Chemie, Weinheim/Bergstrasse, 1951.
[30] M.J. Frisch, G.W. Trucks, H.B. Schlegel, G.E. Scuseria, M.A. Robb, J.R. Cheeseman, J.A. Montgomery Jr., T. Vreven, K.N. Kudin, J.C. Burant, J.M. Millam, S.S. Iyengar, J. Tomasi, V. Barone, B. Mennucci, M. Cossi, G. Scalmani, N. Rega, G.A. Petersson, H. Nakatsuji, M. Hada, M. Ehara, K. Toyota, R. Fukuda, J. Hasegawa, M. Ishida, T. Nakajima, Y. Honda, O. Kitao, H. Nakai, M. Klene, X. Li, J.E. Knox, H.P. Hratchian, J.B. Cross, C. Adamo, J. Jaramillo, R. Gomperts, R.E. Stratmann, O. Yazyev, A.J. Austin, R. Cammi, C. Pomelli, J.W. Ochterski, P.Y. Ayala, K. Morokuma, G.A. Voth, P. Salvador, J.J. Dannenberg, V.G. Zakrzewski, S. Dapprich, A.D. Daniels, M.C. Strain, O. Farkas, D.K. Malick, A.D. Rabuck, K. Raghavachari, J.B. Foresman, J.V. Ortiz, Q. Cui, A.G. Baboul, S. Clifford, J. Cioslowski, B.B. Stefanov, G. Liu, A. Liashenko, P. Piskorz, I. Komaromi, R.L. Martin, D.J. Fox, T. Keith, M.A. Al-Laham, C.Y. Peng, A. Nanayakkara, M. Challacombe, P.M.W. Gill, B. Johnson, W. Chen, M.W. Wong, C. Gonzalez, J.A. Pople, GAUSSIAN-03, Revision B.05, Gaussian, Inc., Pittsburgh, PA, 2003.
[31] (a) A.D. Becke, J. Chem. Phys. 98 (1993) 5648;
(b) C. Lee, W. Yang, R.G. Parr, Phys. Rev. B. 37 (1988) 785.
[32] W.J. Hehre, R. Ditchfield, J.A. Pople, J. Chem. Phys. 56 (1972) 2257.
[33] G.A. Petersson, A. Bennett, T.G. Tensfeldt, M.A. Al-Laham, W.A. Shirley, J. Mantzaris, J. Chem. Phys. 89 (1988) 2193.
[34] G.A. Petersson, M.A. Al-Laham, J. Chem. Phys. 94 (1991) 6081.
[35] P.C. Hariharan, J.A. Pople, Theoret. Chim. Acta 28 (1973) 213.
[36] V.A. Rassolov, M.A. Ratner, J.A. Pople, P.C. Redfern, L.A. Curtiss, J. Comp. Chem. 22 (2001) 976.
[37] K. Wolinski, J.F. Hilton, P. Pulay, J. Am. Chem. Soc. 112 (1990) 8251.
[38] J.L. Dodds, R. McWeeny, A.J. Sadlej, Mol. Phys. 41 (1980) 1419.
[39] R. Ditchfield, Mol. Phys. 27 (1974) 789.
[40] R. McWeeny, Phys. Rev. 126 (1962) 1028.
[41] F. London, J. Phys. Radium, Paris 8 (1937) 397.

occurrence and mechanical separation is often needed. In this case, conglomerate crystallization arising from a racemizing solution (molten state) or mechanical stirring can be used to give high enantiomeric excess [10].

In this paper, we describe the preparations and single-crystal structures of two enantiomerically pure crystals, formulated as $[Ru(phen)(bpy)_2](PF_6)_2$ (**1** for Δ-enantiomer and **2** for Λ-enantiomer), crystallizing in the chiral $P4_1$ and $P4_3$ space groups, which means that some spontaneous resolution process takes place. To the best of our knowledge, this work is the first example of conglomerate crystallization for Ru(II) complexes. Additionally, three similar hexa-coordinate Ru(II) complexes, i.e., $[Ru(phen)(bpy)_2](BF_4)_2$ (**3**), $[Ru(phen)_2(bpy)](PF_6)_2$ (**4**) and $[Ru(bpy)_2(dmbpy)](PF_6)_2$ (**5**) with different bidentate chelating ligands and counterions, which pack into the centrosymmetric space groups, are also involved by contrast.

2. Experimental

2.1. Materials and measurements

All reagents and solvents were of analytical grade and used without further purification. UV/Vis spectra were recorded with a Shimadzu UV-3150 double-beam spectrophotometer. Infrared spectra (IR, 4000–400 cm^{-1}) were determined in a Horiba FT-700 spectrophotometer. Analyses for carbon, hydrogen and nitrogen were performed on a Perkin–Elmer 1400C analyzer. ^1H NMR spectra were collected on a Varian Unit 500 MHz spectrometer and a JEOL GSX 270 MHz spectrometer. Fast atom bombing mass spectra (FAB-MS) were measured with a JEOL JMS-777V spectrometer.

2.2. Syntheses of bis(2,2′-bipyridine)(1,10-phenanthroline)ruthenium(II) hexafluorophosphorate (*1* and *2*) and bis(2,2′-bipyridine)(1,10-phenanthroline)-ruthenium(II) tetrafluoroborate (*3*)

A solution of 1,10-phenanthroline monohydrate (0.180 g, 1.0 mmol) in methanol (20 mL) was added to a solution of *cis*-bis(2,2′-bipyridine) dichlororuthenium(II) hydrate (0.484 g, 1.0 mmol) in 100 mL methanol. This mixture was refluxed for 1 h, and then divided into two halves after cooled to room temperature. Excess saturated aqueous NH_4PF_6 and $NaBF_4$ solutions were added, respectively. The resulting two mixtures were concentrated to ca. 10 mL by a rotatory evaporator and the red precipitates were filtered, washed by water and dried in vacuo. Racemic mixture of **1** and **2**; Yield: ~60%. Main IR (KBr pellets, cm^{-1}): 3434s, 2925m, 2855w, 1637s, 1467m, 1447m, 1428m, 1067m, 840vs, 763m, 558m. ^1H NMR (500 MHz, CD_3COCD_3, ppm, TMS): 8.86 (d, 2H, $J = 8.05$ Hz, H_7), 8.83 (d, 2H, $J = 7.88$ Hz, H_3), 8.81 (d, 2H, $J = 7.67$ Hz, H_{13}), 8.45 (d, 2H, $J = 5.15$ Hz, H_{11}), 8.41 (s, 2H, H_{14}), 8.26–8.25 (m, 2H, H_8), 8.18 (d, 2H, $J = 5.85$ Hz, H_{10}), 8.14–8.13 (m, 2H, H_4), 7.95–7.92 (d, d, 2H, H_{12}), 7.89 (d, 2H, $J = 5.05$ Hz, H_6), 7.64–7.63 (m, 2H, H_9), 7.39–7.38 (m, 2H, H_5). *Anal.* Calc. for $RuC_{32}H_{24}N_6P_2F_{12} \cdot C_2H_5OH$: C, 43.93; H, 3.25; N, 9.04. Found: C, 43.84; H, 3.31; N, 8.89%. FAB-MS: 739 $[Ru(bpy)_2(phen)(PF_6)]^+$. UV–Vis ($\lambda_{max}$, methanol, nm): 449.0 (MLCT), 286.0 ($\pi \rightarrow \pi^*$), 264.5 (MLCT). **3**; Yield: 76%. Main IR (KBr pellets, cm^{-1}): 3065w, 1635m, 1618m, 1600m, 1544m, 1064vs, 848s, 773s and 719m. *Anal.* Calc. for $RuC_{32}H_{24}N_6B_2F_8$: C, 50.09; H, 3.15; N, 10.95. Found: C, 50.01; H, 3.30; N, 10.87%. FAB-MS: 680 $[Ru(bpy)_2(phen)(BF_4)]^+$.

2.3. Synthesis of bis(1,10-phenanthroline)(2,2′-bipyridine) ruthenium(II) hexafluorophosphorate (*4*)

The synthesis of **4** is similar to **1** and **2** except that 0.360 g (2.0 mmol) 1,10-phenanthroline monohydrate was added and refluxed for 12 h. Yield: 67%. Main IR: 3406b, 2923m, 2853w, 1605m, 1467m, 1447m, 1428m, 838vs, 759m, 557s. ^1H NMR: 8.90 (d, 2H, $J = 8.95$ Hz, bpy), 8.85 (d, 2H, $J = 4.65$ Hz, phen), 8.83 (d, 2H, $J = 3.90$ Hz, phen), 8.46 (d, 2H, $J = 5.15$ Hz, phen), 8.42 (d, 2H, $J = 2.85$ Hz, phen), 8.28 (d, 2H, $J = 6.55$ Hz, phen), 8.20 (d, 2H, $J = 5.20$ Hz, phen), 8.16–8.14 (m, 2H, bpy), 7.96 (d, 2H, $J = 2.85$ Hz, bpy), 7.91–7.89 (m, 2H, phen), 7.67–7.64 (m, 2H, phen), 7.42–7.39 (d, d, 2H, bpy). *Anal.* Calc. for $RuC_{34}H_{24}N_6P_2F_{12}$: C, 44.99; H, 2.67; N, 9.26. Found: C, 44.93; H, 2.81; N, 9.22%. FAB-MS: 763 $[Ru(bpy)(phen)_2(PF_6)]^+$. UV–Vis ($\lambda_{max}$, methanol, nm): 449.0 (MLCT), 286.0 ($\pi \rightarrow \pi^*$), 264.5 (MLCT).

2.4. Synthesis of bis(2,2′-bipyridine)(4,4′-dimethyl-2,2′-bipyridine) ruthenium(II) hexafluorophosphorate (*5*)

The synthetic method of **5** is similar to that of **1** and **2** except that 4,4′-dimethyl-2,2′-bipyridine (0.184 g, 1.0 mmol) was added instead of 1,10-phenanthroline monohydrate. Yield: 82%. Main IR (KBr pellets, cm^{-1}): 3397b, 2923w, 1620s, 1604w, 1466s, 1447s, 1424m, 844vs, 763s, 557s. ^1H NMR: 8.82 (d, 2H, $J = 3.10$ Hz, bpy), 8.80 (d, 2H, $J = 3.40$ Hz, bpy), 8.69 (s, 2H, dmbpy), 8.21–8.18 (m, 4H, bpy) 8.06 (m, 4H, bpy), 8.03 (m, 2H, dmbpy) 7.59–7.54 (m, 4H, bpy), 7.41 (d, $J = 5.65$ Hz, 2H, dmbpy), 2.56 (s, 6H, Me). *Anal.* Calc. for $RuC_{32}H_{28}N_6P_2F_{12} \cdot 2C_2H_5OH$: C, 44.13; H, 4.12; N, 8.58. Found: C, 44.22; H, 4.29; N, 8.47%. FAB-MS: 743 $[Ru(bpy)_2(dmbpy)(PF_6)]^+$.

2.5. X-ray data collection and solution

X-ray single-crystal diffraction data of complexes **1**–**5** were collected on a Rigaku Mercury CCD area-detector at 293(2) K using graphite mono-chromated Mo Kα radiation ($\lambda = 0.71073$ Å). All the diffraction data were reduced by the program CRYSTALCLEAR [11] and empirical absorption corrections were done [12]. The original data files generated by CRYSTALCLEAR were transformed to SHELXTL97 format by TEXSAN program [13], and then all five structures

Table 1
Crystal and refinement data for Ru(II) complexes **1**–**5**

Complex	**1**	**2**	**3**	**4**	**5**
Empirical formula	$RuC_{34}H_{32}N_6O_2P_2F_{12}$	$RuC_{34}H_{30}N_6OP_2F_{12}$	$RuC_{32}H_{24}N_6O_2B_2F_8$	$RuC_{34}H_{24}N_6P_2F_{12}$	$RuC_{36}H_{40}N_6O_2P_2F_{12}$
Formula weight	947.67	929.65	799.26	907.60	979.75
Crystal size (mm)	$0.40 \times 0.20 \times 0.20$	$0.50 \times 0.20 \times 0.10$	$0.40 \times 0.30 \times 0.20$	$0.30 \times 0.20 \times 0.10$	$0.30 \times 0.20 \times 0.20$
Crystal system	tetragonal	tetragonal	monoclinic	monoclinic	monoclinic
Space group	$P4_1$	$P4_3$	$P2_1/c$	$C2/c$	$C2/c$
a (Å)	17.808(3)	17.796(3)	20.550(4)	24.976(5)	11.915(2)
b (Å)	17.808(3)	17.796(3)	13.613(3)	10.691(2)	27.638(6)
c (Å)	12.400(3)	12.384(3)	24.775(5)	17.205(3)	13.099(3)
α (°)	90	90	90	90	90
β (°)	90	90	109.60(3)	132.43(3)	105.77(3)
γ (°)	90	90	90	90	90
V (Å^3)	3932.4(11)	3922.0(13)	6529(2)	3390.8(12)	4151.4(14)
Z, D_{calc} (Mg/m^3)	4, 1.601	4, 1.574	8, 1.626	4, 1.778	4, 1.573
$F(000)$	1904	1864	3200	1808	1984
μ (mm^{-1})	0.577	0.575	0.567	0.661	0.549
Temperature (K)	293(2)	293(2)	293(2)	293(2)	293(2)
h_{min}/h_{max}	−21/19	−21/21	−24/22	−30/27	−14/12
k_{min}/k_{max}	−20/21	−21/21	−16/16	−12/12	−31/32
l_{min}/l_{max}	−14/13	−13/15	−29/29	−18/20	−15/15
Parameters	509	579	958	303	339
Flack value	0.02(5)	0.01(5)			
Absorption correction	multi-scan	multi-scan	multi-scan	multi-scan	multi-scan
Final R indices [$I > 2\sigma(I)$]	$R_1 = 0.0628$, $wR_2 = 0.1566$	$R_1 = 0.0610$, $wR_2 = 0.1371$	$R_1 = 0.0965$, $wR_2 = 0.2395$	$R_1 = 0.0575$, $wR_2 = 0.1306$	$R_1 = 0.0626$, $wR_2 = 0.1559$
R indices (all data)	$R_1 = 0.0652$, $wR_2 = 0.1583$	$R_1 = 0.0636$, $wR_2 = 0.1390$	$R_1 = 0.1114$, $wR_2 = 0.2506$	$R_1 = 0.0620$, $wR_2 = 0.1329$	$R_1 = 0.0679$, $wR_2 = 0.1590$
Goodness-of-fit on F^2	1.038	1.026	1.113	1.163	1.154

$R_1 = \sum \| F_o| - |F_c \| / \sum |F_o|$, $wR_2 = [\sum [w(F_o^2 - F_c^2)^2] / \sum w(F_o^2)^2]^{1/2}$.

were solved by direct methods and refined by least-squares method on F^2_{obs}. All non-H atoms were anisotropically refined and all hydrogen atoms were inserted in the calculated positions assigned fixed isotropic thermal parameters and allowed to ride on their respective parent atoms. All calculations and molecular graphics were carried out with the SHELXTL PC program package on a PC computer [14]. The summary of the crystal data, experimental details and refinement results for complexes **1**–**5** is listed in Table 1.

3. Results and discussion

3.1. Preparation and characterization

All the complexes reported in this paper were synthesized by refluxing stoichiometric amounts of *cis*-bis(2, 2′-bipyridine)dichlororuthenium(II) hydrate and phen monohydrate for **1**–**4** and dmbpy for **5**, respectively, in methanol, and then treated in situ anion exchange by adding excess NH_4PF_6 or $NaBF_4$ in order to precipitate the complexes from their mother solutions (Scheme 1). They all have satisfactory analytic results of IR, EA, UV–Vis and MS, and their single-crystal samples suitable for X-ray diffraction determination were grown from the mixtures of methanol/water or ethanol/water by slow evaporation in air at room temperature. Three sets of data for **1** and **2** were recorded and solved, respectively, to verify the repeatability of conglomerate crystallization, however, only the best ones were reported herein.

3.2. Structural description of Ru(II) complexes

According to the X-ray single-crystal diffraction analysis, **1** and **2** crystallize in the tetragonal system of chiral space groups $P4_1$ and $P4_3$, while **3**, **4** and **5** crystallize in the monoclinic centrosymmetric space groups $P2_1/c$ (**3**) and $C2/c$ (**4** and **5**). Each asymmetric unit of **3** contains two crystallographically unequivalent molecules (a pair of Δ and Λ enantiomers), and there is half of the crystallographically unique molecule in the asymmetric units of **4** and **5**. For complex **4**, a reduced unit cell [$a = 17.205(3)$, $b = 10.691(2)$, $c = 18.438(4)$ Å, $\beta = 91.10(3)°$] with smaller

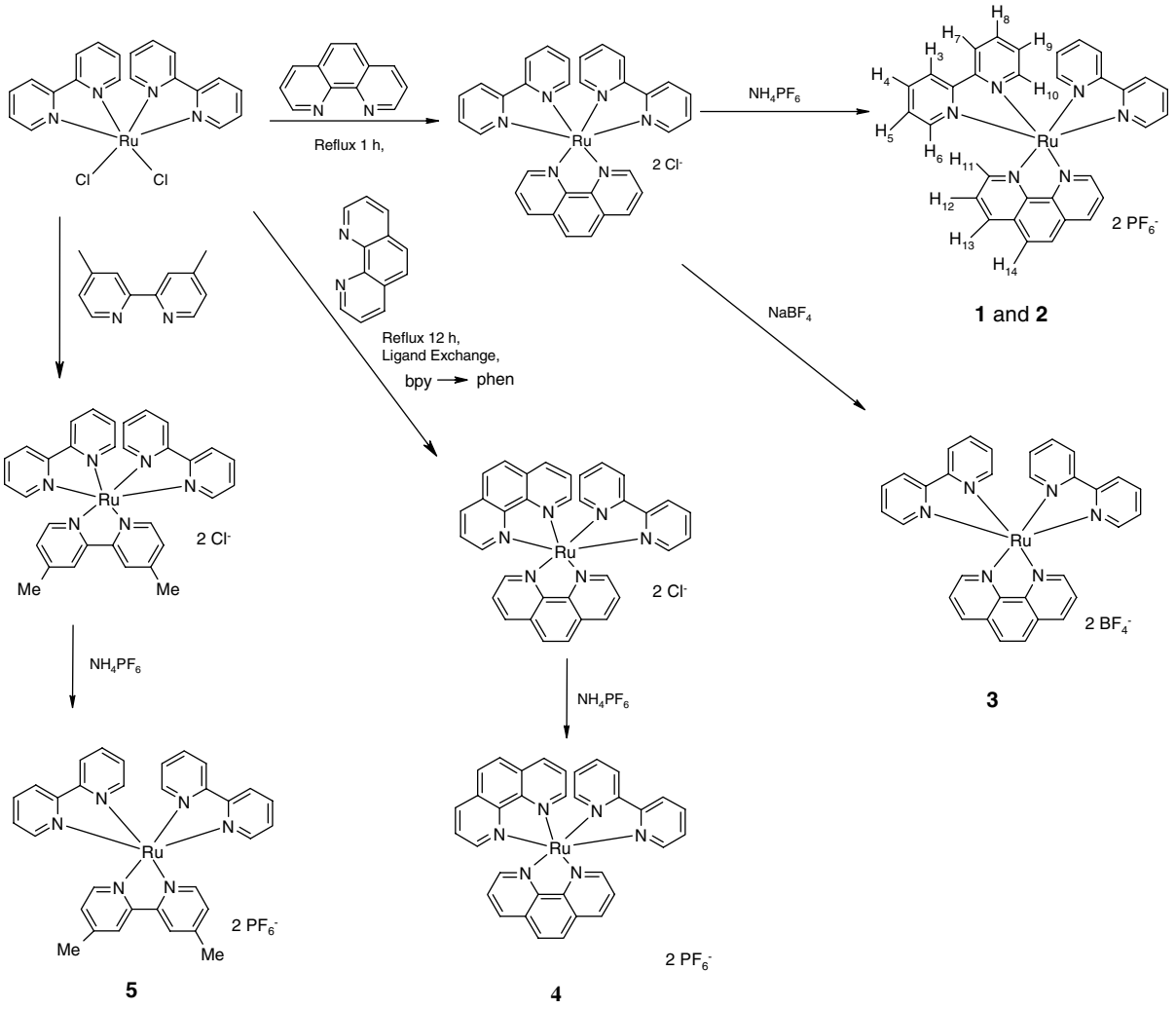

Scheme 1. Schematic illustration for the preparation of Ru(II) complexes **1**–**5**.

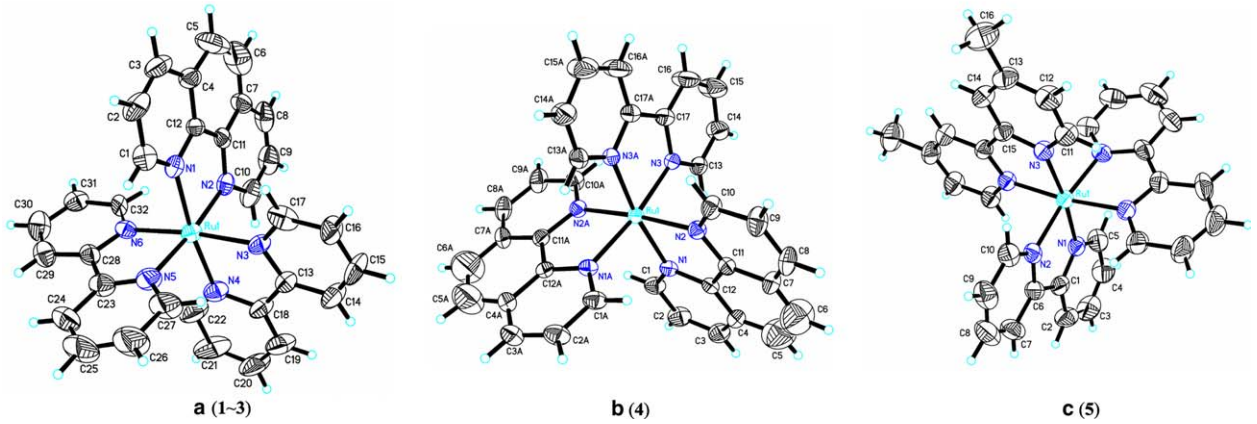

Fig. 1. ORTEP views of molecular structures of **1**–**5** with the atom-numbering scheme. Displacement ellipsoids are drawn at the 30% probability level and anions are omitted for clarity.

β angle and $I2/a$ space group can be obtained by performing the unit cell transformation (the matrix used is 0 0 1, 0 1 0, −1 0 −1). In view of the non-standard setting of space group $C2/c$ generated in this case, the initial unit cell is retained.

As illustrated in Fig. 1, all of five ruthenium(II) centers are coordinated by six nitrogen atoms from three bidentate phen, bpy or dmbpy ligand, adopting distorted octahedron configurations. The geometries (bond lengths, bond angles and dihedral angles) around all the Ru(II) centers are in the normal range, and some of PF_6^- and BF_4^- counterions are found to be disordered over two positions with different site occupancy factors.

Typical π–π stacking interactions are found between phen ligands of adjacent units in the packing structures of **1**, **2** and **3** with the separations of 3.52(1) Å for **1** and **2**, and 3.62(1) Å for **3** because phen has better delocalized π-system in comparison with bpy. π–π Stacking interactions are also observed in **4** between two neighboring phen molecules with the distance at 3.56(1) Å. Offset π–π stacking interactions are found in **5** between two vicinal bpy ligands with the shortest separation of 3.65(2) Å as well as the ones between two contiguous dmbpy ligands with the shortest separation of 3.68(2) Å. In **1** and **2**, it is worthwhile to mention that the phen rings are perpendicular to the screw c-axis in their crystal structures (Fig. 2), which may contribute to the formation of chiral packing.

The absolute configuration of crystals can be verified by the Flack parameters [15] of their single-crystal structures. In our case, the Flack absolute structure parameter of **1** has a value of 0.02(5), while the inverted stereochemistry gives a high value of 0.96(6). As for **2**, the value is 0.01(5) for right space group but 0.97(5) for the inverted one. The low Flack parameters indicate that the absolute configurations of **1** and **2** are correct. In fact, spontaneous resolution is a well-documented phenomenon. However, it is not the case for the system where six-coordinate metal complexes with three bidentate ligands are involved. There have been many crystallographic reports about similar complexes, but most of them crystallize in the centrosymmetric space groups [16]. To the best of our knowledge, this is the first report on the spontaneous resolution for Ru(II) complexes that may be interesting on the research for obtaining enantiomerically pure coordination complexes [17].

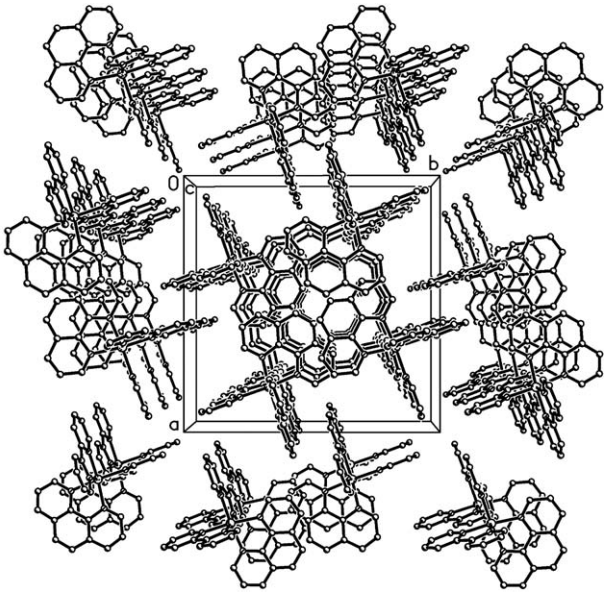

Fig. 2. Perspective view of packing structure of **2** down the 4-fold screw c-axis, hydrogen atoms and PF_6^- anions are omitted for simplicity.

In our experiment, single-crystal sample of **2** is obtained first, however, we do not know it crystallizes in a chiral space group ($P4_3$) until the structure is successfully solved. At that time we think the result is uncommon because no obvious symmetry breakage is present and no related report for this Ru(II) complex. If it is true, there should be another crystal packed into the other enantiomorphic space group ($P4_1$) with the same unit cell within the experimental errors. After repeating the experiment many times, we do obtain the expected crystal of **1** but racemic crystal has never been found. Further studies hint that both of the needle-like

crystals can be controlled by seeding with preformed chiral crystals. In their absence, the chirality of crystals is sometimes $P4_1$ and sometimes $P4_3$ but almost equiprobable. This is also true when the same beaker and the same mother liquid are used for repeated crystallization. Actually, **1** and **2** grow radially as a single colony from the first-appearing nucleus, which makes the mechanical separation of them possible. This could be the reason why a single chirality is preserved during the whole crystal growth. In this way, **1** and **2** can afford enantiomerically pure chiral coordination complexes simply upon self-resolution crystallization. Thus, it is concluded that the chirality is essentially governed by the chirality that happens to the first-separating nucleus acting as the seed for subsequent crystal growth.

Kondepudi et al. [18] have discussed the kinetics of symmetry breakage in the process of seeding or in the presence of chiral autocatalysis and competition for solute (direct or indirect) between the two enantiomers. However, it is still difficult for us to specify why only either Δ or Λ configuration can be obtained (Fig. 3). It is believed that PF_6^- anions and hydrogen bonding interactions found in the solid-state play key role in the process of crystal growth, because experimental results tell us that neither BF_4^- nor ClO_4^- with the same cationic structure can crystallize in the chiral space group under the same condition [19].

A ligand exchange reaction is found between bpy and phen ligands when 2-fold 1,10-phenanthroline monohydrate was treated with *cis*-bis(2,2′-bipyridine)dichlororuthenium(II) hydrate by refluxing for 12 h. Crystalline solids **4** can be obtained in a moderate yield, other than $[Ru(phen)_3][PF_6]_2$, $[Ru(bpy)_3][PF_6]_2$ or starting $[Ru(bpy)_2(phen)][PF_6]_2$, but only in the racemic form. It is suggested that the symmetry breaking process may be destroyed when both Δ and Λ enantiomers undergo the ligand exchange reaction. Hesek et al. [20] reported the crystal structure of the Δ-enantiomer for **5** using a stereoretentive synthesis from the predetermined Δ-$[Ru(bpy)_2(Me_2SO)Cl]Cl$, which crystallizes in the orthorhombic space group $P2_12_12_1$ with obviously different unit cell: $a = 13.731(11)$, $b = 20.496(9)$, $c = 13.521(8)$ Å, $V = 3805$ Å^3. In our case, only racemic complex can be crystallized because of the lack of symmetric breakage, which is supposed to be normal for general Ru(II) complexes.

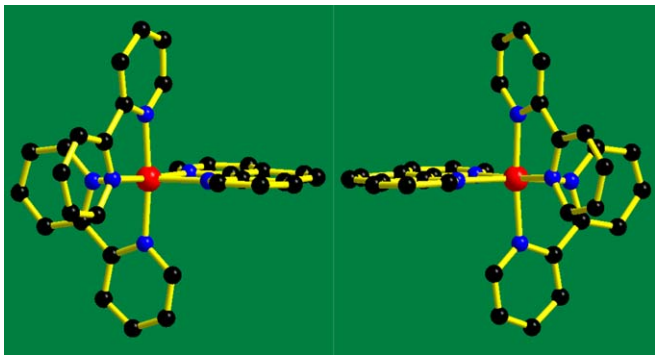

Fig. 3. Ball-and-stick view of the enantiomeric pair of **1** (Δ-enantiomer, left) and **2** (Λ-enantiomer, right) with mirror symmetry (sphere colors: black – C; blue – N; red – Ru). Hydrogen atoms and PF_6^- anions are omitted for clarity.

4. Conclusion

In summary, we reported herein a pair of chiral ruthenium(II) complexes crystallizing in $P4_1$ and $P4_3$ space groups, which were obtained by crystallization-induced single-colony crystal growth from the racemic alcohol–water solution under ambient condition. Their absolute configurations were verified by the Flack parameters and interactions at the supramolecular level may dominate the spontaneous resolution process. A ligand exchange between phen and bpy was found if long time refluxing was performed but only the racemic product **4** could be yielded. To extend our study, another counterion (BF_4^-) and ligand (dmbpy) were selected to prepare similar hexa-coordinate Ru(II) complexes. However, the X-ray single-crystal diffraction studies demonstrated that racemic crystals could only be obtained in these experiments, which could be in agreement with the results in most cases.

5. Supplementary material

CCDC Nos. 271355–271359 (complexes **1**–**5**) contain the supplementary crystallographic data for this paper. These data can be obtained free of charge at www.ccdc.cam.ac.uk/conts/retrieving.html [or from the Cambridge Crystallographic Data Centre, 12, Union Road, Cambridge CB2 1EZ, UK; fax: (internat.) +44 1223 336 033; e-mail: deposit@ccdc.cam.ac.uk].

Acknowledgment

This work was supported by a Grant-in-Aid for Scientific Research (Nos. 15201028 and 14654135) from the Ministry of Culture, Education, Science Sports, and Technology of Japan. W.H. also acknowledges the support of the National Natural Science Foundation of China (No. 20301009).

References

[1] (a) V. Balzani, F. Scandola, Supramolecular Photochemistry, Ellis Horwood, Chichester, 1991;
(b) M.K. Nazeeruddin, A. Kay, I. Rodicio, R. Humphry-Baker, E. Mueller, P. Liska, N. Vlachopoulos, M. Graetzel, J. Am. Chem. Soc. 115 (1993) 6382;
(c) E. Baranoff, J.P. Collin, J. Furusho, Y. Furusho, A.-C. Laemmel, J.-P. Sauvage, Inorg. Chem. 41 (2002) 1215;
(d) K. Araki, H. Endo, G. Masuda, T. Ogawa, Chem. Eur. J. 10 (2004) 3331.
[2] For reviews, see the following: (a) K. Kalyanasundaram, Coord. Chem. Rev. 46 (1982) 159;
(b) A. Juris, S. Barigelletti, S. Campagna, V. Balzani, P. Belser, A. von Zelewsky, Coord. Chem. Rev. 84 (1988) 85;
(c) V. Balzani, A. Juris, M. Venturi, S. Campagna, S. Serroni, Chem. Rev. 96 (1996) 759.
[3] V.W.-W. Yam, B. Li, N. Zhu, Adv. Mater. 14 (2002) 719.

[4] A. von Zelewsky, O. Mamula, J. Chem. Soc., Dalton Trans. (2000) 219.
[5] L. Ademi, E.C. Constable, C.E. Housecroft, M. Neuburger, S. Schaffner, J. Chem. Soc., Dalton Trans. (2003) 4565.
[6] (a) T.J. Rutherford, M.J. Quagliotto, F.R. Keene, Inorg. Chem. 34 (1995) 3857;
(b) K. Warnmark, O. Heyke, J.A. Thomas, J.M. Lehn, Chem. Commun. (1996) 2603;
(c) D. Tzalis, Y. Tor, J. Am. Chem. Soc. 119 (1997) 852.
[7] (a) B. Bosnich, F.P. Dwyer, Aust. J. Chem. 19 (1966) 2229;
(b) H.U. Blaser, Chem. Rev. 92 (1992) 835.
[8] (a) T. Ezuhara, K. Endo, Y. Aoyama, J. Am. Chem. Soc. 121 (1999) 3279;
(b) O. Hamelin, J. Pécaut, M. Fontecave, Chem. Eur. J. 10 (2004) 2548.
[9] (a) T. Suzuki, T. Fukushima, Y. Yamashita, T. Miyashi, J. Am. Chem. Soc. 116 (1994) 2793;
(b) I. Azumaya, D. Uchida, T. Kato, A. Yokoyama, A. Tanatani, H. Takayanagi, T. Yokozawa, Angew. Chem., Int. Ed. 43 (2004) 1360.
[10] See for reviews: (a) D.K. Kondepudi, K. Asakura, Acc. Chem. Res. 34 (2001) 946;
(b) L. Perez-Garcia, D.B. Amabilino, Chem. Soc. Rev. 31 (2002) 342.
[11] Molecular structure Coorporation & Rigaku Coorporation, 2001. CRYSTALCLEAR, Version 1.3. MSC, 9009 New Trails Drive, The Woodlands, TX 77381-5209, USA, and Rigaku, Toyko, Japan.
[12] R. Jacobson, REQAB, Private communication, 1998.
[13] Molecular structure Coorporation & Rigaku Coorporation, 2000. TEXSAN, Version 1.11. MSC, 9009 New Trails Drive, The Woodlands, TX 77381-5209, USA, and Rigaku, Toyko, Japan.
[14] Bruker, SHELXTL (Version 6.10), Bruker AXS Inc., Madison, WI, USA, 2000.
[15] H.D. Flack, Acta Crystallogr. Sect. A 39 (1983) 876.
[16] (a) I. Dance, M.J. Scudder, Chem. Soc., Dalton Trans. (1998) 1341;
(b) J. Breu, C. Kratzer, H. Yersin, J. Am. Chem. Soc. 122 (2000) 2548, and references cited therein.
[17] (a) H.D. Flack, Helv. Chim. Acta 86 (2003) 905;
(b) H.D. Flack, G. Bernardinelli, Cryst. Eng. 6 (2003) 213.
[18] D.K. Kondepudi, K.L. Bullock, J.A. Digits, J.K. Hall, J.M. Miller, J. Am. Chem. Soc. 115 (1993) 10211.
[19] B.H. Ye, X.M. Chen, T.X. Zeng, L.N. Ji, Inorg. Chim. Acta 240 (1995) 5.
[20] D. Hesek, Y. Inoue, S.R.L. Everitt, H. Ishida, M. Kunieda, M.G.B. Drewb, Chem. Commun. (1999) 403.

of (μ-Se)[CpFe(CO)$_2$]$_2$ with alkyl or aryl chloroformates [31].

Based on our previous reactions of the iron selenide with electrophiles [29–31] this paper describes its reaction with chlorothionoformates (ROC(S)Cl). This reaction was found to give the expected selenothiocarbonates, CpFe(CO)$_2$SeC(S)OR. These complexes can be converted to the chelated complexes CpFe(CO)(κ^2*Se*,*S*-SeC(S)OR) upon photolysis.

2. Experimental

All manipulations were performed under an inert atmosphere of nitrogen using standard Schlenk line techniques. Diethyl ether, hexane and benzene were distilled from sodium/benzophenone ketyl under nitrogen. Dichloromethane was refluxed over P_2O_5 and distilled under nitrogen. The complex (μ-Se)[CpFe(CO)$_2$]$_2$ was prepared by literature method [23]. The reagents: chlorothionoformates, iron dimer [CpFe(CO)$_2$]$_2$, and selenium were obtained from Acros and were used as received.

Nuclear magnetic resonance (NMR) spectra were recorded on a Bruker 200 MHz spectrometer. Chemical shifts are in ppm relative to TMS at 0 ppm. Infrared (IR) spectra were recorded on a Nicolat Nexus FT-IR spectrometer using NaCl solvent cells. Elemental analyses were done in Laboratoire d'Analyse Elémentaire, Université de Montréal, Montréal, Que., Canada. Melting points were reported on a Staurt Melting point apparatus (SMP3) and are uncorrected. The photolytic reactions were carried out in a medium pressure mercury lamp (150 W) with a quartz immersion cell.

2.1. General procedure for the preparation of CpFe(CO)$_2$SeC(S)OR (**1**)

The complex (μ-Se)[CpFe(CO)$_2$]$_2$ (0.22 g, 0.50 mmol) dissolved in diethyl ether (70 mL) was stirred under N_2 and chlorothionoformate (0.55 mmol) was added. After stirring overnight, the volatiles were removed under reduced pressure and the resulting solid was redissolved in a minimum amount of CH_2Cl_2 and introduced to a silica gel column made up in hexane. Elution with hexane removes the unreacted chlorothionoformates. Elution with hexane/dichloromethane solution (1:1 v:v ratio) gave a red-brown band which was collected and identified as CpFe(CO)$_2$SeC(S)OR, followed by a red band which was also collected and identified as CpFe(CO)$_2$Cl. The CpFe(CO)$_2$SeC(S)OR were recrystallized from dichloromethane/hexane.

2.1.1. [CpFe(CO)$_2$SeC(S)OC$_6$H$_5$] (**1a**)

Yield: 72%. m.p. 159–160 °C. ^{1}H NMR ($CDCl_3$) δ 4.95 (s, 5H, C_5H_5); 7.41 (m, 5H, C_6H_5). IR (CH_2Cl_2, cm^{-1}) ν_{CO} 2035s, 1985s. Calc. for $C_{14}H_{10}FeO_3SSe$: C, 42.78; H, 2.56; S, 8.16. Found: C, 42.70; H, 2.44; S, 7.88%.

2.1.2. [CpFe(CO)$_2$SeC(S)O-4-C$_6$H$_4$Cl] (**1b**)

Yield: 82%. m.p. 99–100 °C. ^{1}H NMR ($CDCl_3$) δ 5.06 (s, 5H, C_5H_5); 7.02 (d, 2H, C_6H_4); 7.37 (d, 2H, C_6H_4). IR (CH_2Cl_2, cm^{-1}) ν_{CO} 2037s, 1992s. Calc. for $C_{14}H_9ClFeO_3SSe$: C, 39.33; H, 2.12; S, 7.50. Found: C, 39.02; H, 1.96; S, 7.00%.

2.1.3. [CpFe(CO)$_2$SeC(S)O-4-C$_6$H$_4$F] (**1c**)

Yield: 80%. m.p. 136–137 °C. ^{1}H NMR ($CDCl_3$) δ 5.06 (s, 5H, C_5H_5); 7.06 (d, 2H, C_6H_4); 7.20 (d, 2H, C_6H_4). IR (CH_2Cl_2, cm^{-1}) ν_{CO} 2036s, 1991s. Calc. for $C_{14}H_9FFeO_3SSe$: C, 40.90; H, 2.21; S, 7.80. Found: C, 39.98; H, 2.18; S, 7.11%.

2.1.4. [CpFe(CO)$_2$SeC(S)OC$_6$F$_5$] (**1d**)

Yield: 87%. m.p. 133–134 °C. ^{1}H NMR ($CDCl_3$) δ 5.08 (s, H's, C_5H_5). IR (CH_2Cl_2, cm^{-1}) ν_{CO} 2041s, 1997s. Calc. for $C_{14}H_5F_5FeO_3SSe$: C, 34.81; H, 1.04; S 6.64. Found: C, 34.34; H, 1.08; S, 5.98%.

2.1.5. [CpFe(CO)$_2$SeC(S)O-4-C$_6$H$_4$Me] (**1e**)

Yield: 89%. m.p. 148–149 °C. ^{1}H NMR ($CDCl_3$) δ 2.33 (s, 3H, CH_3); 5.03 (s, 5H, C_5H_5); 6.93 (d, 2H, C_6H_4); 7.22 (d, 2H, C_6H_4). IR (CH_2Cl_2, cm^{-1}) ν_{CO} 2036s, 1991s. Calc. for $C_{15}H_{12}FeO_3SSe$: C, 44.25; H, 2.97; S, 7.88. Found: C, 44.46; H, 2.77; S, 7.50%.

2.2. General procedure for the preparation of CpFe(CO)(κ^2Se,S-SeC(S)OR) (**2**)

A THF solution (30 mL) of CpFe(CO)$_2$SeC(S)OR (0.25 mmol) was irradiated under a stream of N_2 for 30 min. The volatiles were removed by vacuum and the resulting solid was dissolved in a minimum amount of dichloromethane and transferred to a silica gel column. The column was eluted with CH_2Cl_2/hexane (1:2 v:v ratio) to separate the products as an orange-brown band which were recrystallized from hexane.

2.2.1. [CpFe(CO)(κ^2Se,S-SeC(S)OC$_6$H$_5$)] (**2a**)

Yield: 85%. m.p. 102–103 °C. ^{1}H NMR ($CDCl_3$) δ 4.65 (s, 5H, C_5H_5); 7.10 (m, 5H, C_6H_5). IR (CH_2Cl_2, cm^{-1}) ν_{CO} 1954s. Calc. for $C_{13}H_{10}FeO_2SSe$: C, 42.77; H, 2.76; S 8.78. Found: C, 42.54; H, 2.66; S, 8.47%.

2.2.2. [CpFe(CO)(κ^2Se,S-SeC(S)O-4-C$_6$H$_4$Cl)] (**2b**)

Yield: 90%. m.p. 79–80 °C. ^{1}H NMR ($CDCl_3$) δ 4.65 (s, 5H, C_5H_5); 7.07 (d, 2H, C_6H_4); 7.35 (d, 2H, C_6H_4). IR (CH_2Cl_2, cm^{-1}) ν_{CO} 1947s. Calc. for $C_{13}H_9ClFeO_2SSe$: C, 39.08; H, 2.27; S, 8.03. Found: C, 39.60; H, 2.47; S, 7.38%.

2.2.3. [CpFe(CO)(κ^2Se,S-SeC(S)O-4-C$_6$H$_4$F)] (**2c**)

Yield: 78%. m.p. 95–96 °C. ^{1}H NMR ($CDCl_3$) δ 4.65 (s, 5H, C_5H_5); 7.11 (d, 2H, C_6H_4); 7.25 (d, 2H, C_6H_4). IR (CH_2Cl_2, cm^{-1}) ν_{CO} 1952s. Calc. for $C_{13}H_9FFeO_2SSe$: C, 40.77; H, 2.37; S, 8.37. Found: C, 40.34; H, 2.09; S, 7.95%.

2.2.4. [CpFe(CO)(κ^2Se,S-SeC(S)OC$_6$F$_5$)] (**2d**)

Yield: 65%. m.p. 72–73 °C. ^{1}H NMR ($CDCl_3$) δ 4.69 (s, H's, C_5H_5). IR (CH_2Cl_2, cm^{-1}) ν_{CO} 1959s. Calc. for

Table 1
Selected crystal data and refinement parameters for $CpFe(CO)_2SeC(S)O$-4-C_6H_4Cl (**1b**)

Empirical formula	$C_{14}H_9ClFeO_3SSe$
Formula weight	427.53
Crystal size (mm)	$0.13 \times 0.10 \times 0.08$
Crystal system	monoclinic
Space group	$P2_1/c$
Unit cell dimensions	
a (Å)	6.9410(10)
b (Å)	13.4830(10)
c (Å)	16.5320(10)
α (°)	90.00
β (°)	98.27(5)
γ (°)	90.00
V (Å^3)	1531.1(3)
Z	4
Index ranges	$-9 < h < 9$, $0 < k < 18$, $0 < l < 23$
D_{calc} (Mg m^{-3})	1.855
Radiation type	Mo Kα
μ (mm^{-1})	3.677
λ (Å)	0.71069
θ Range (°)	1.96–30.04
$R[F^2>2\sigma(F^2)]$	0.0621
$wR(F^2)$[a]	0.036

[a] $w = 1/[\sigma^2(F_o^2) + (0.0426P)^2]$, where $P = (F_o^2 + 2F_o^2)/3$.

$C_{13}H_5F_5FeO_2SSe$: C, 34.32; H, 1.11; S, 7.05. Found: C, 33.71; H, 1.00; S 6.77%.

2.2.5. *[CpFe(CO)(κ²Se,S-SeC(S)O-4-C₆H₄Me)] (**2e**)*

Yield: 92%. m.p. 88–89 °C. ^{1}H NMR ($CDCl_3$) δ 2.36 (s, 3H, CH_3); 4.66 (s, 5H, C_5H_5); 7.02 (d, 2H, C_6H_4); 7.20 (d, 2H, C_6H_4). IR (CH_2Cl_2, cm^{-1}) ν_{CO} 1950s. Calc. for $C_{14}H_{12}FeO_2SSe$: C, 44.35; H, 3.19; S, 8.46. Found: C, 44.85; H, 3.07; S, 8.46%.

2.3. X-ray structure analysis

Single crystal of **1b** was obtained from CH_2Cl_2/hexane mixture. Intensity data were collected on a KappaCCD diffractometer with graphite monochromated Mo Kα radiation at 173 K. The crystallographic data are shown in Table 1. The cell parameters were determined from 5095 reflections collected in the range $1.96 \leqslant \theta \leqslant 30.04°$. There were 4473 independent reflections with 3717 observed reflections ($>2\sigma(I)$). The structure was solved by direct method using SHELXS-97 [32] and DIFMAP synthesis using SHELXTL-96 [33].

3. Results and discussion

3.1. Synthesis and characterization of *1*

The selenothiocarbonate complexes $CpFe(CO)_2SeC(S)OR$ [R = Ph (**1a**), 4-C_6H_4Cl (**1b**), 4-C_6H_4F (**1c**), C_6F_5 (**1d**), 4-C_6H_4Me (**1e**)] were readily synthesized by stirring a diethylether solution of chlorothionoformates and (μ-Se)$[CpFe(CO)_2]_2$ (Scheme 1) at room temperature.

To the best of my knowledge, complexes **1** are the first selenothiocarbonate of iron to be reported. The analogues ethyl-dithiocarbonate complexes, $Cp'Fe(CO)_2SC(S)OEt$ ($Cp' = C_5H_5$, C_5Me_5) are reported by the reaction of $[Cp'Fe(CO)_2]_2$ and $[EtOC(S)S]_2$. Substitution reactions of these dicarbonyl complexes with phosphine or phosphite ligands gave $Cp'Fe(CO)(L)SC(S)OEt$ ($L = PPh_3$, PBu_3, $P(OEt)_3$, $P(OPh)_3$) [34,35]. Complexes **1** are air stable as solids and in solutions. They are soluble in most common organic solvents such as THF, CH_2Cl_2 but sparingly soluble in hydrocarbons. These complexes were isolated as red-brown solids and characterized by elemental analysis, IR and ^{1}H NMR spectroscopy. The solution IR spectra of **1** (in CH_2Cl_2) exhibited two strong absorbances in the carbonyl region at 2035–2041 and 1985–1997 cm^{-1}. These ν_{CO} stretches are comparable to those of $CpFe(CO)_2SeSO_2R$ (2038–2043 and 1993–1999 cm^{-1}) [29] and of $CpFe(CO)_2SeCO_2R$ (2036–2043 and 1988–1993 cm^{-1}) [31] but higher than those of selenocarboxylates, $CpFe(CO)_2SeCOR$

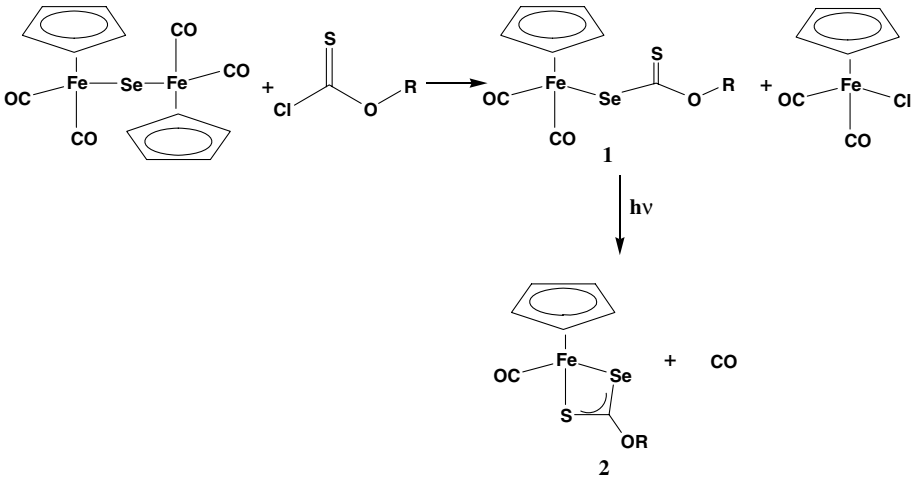

R= Ph (**a**), 4-C_6H_4Cl (**b**), 4-C_6H_4F (**c**), C_6F_5 (**d**), 4-C_6H_4Me (**e**)

Scheme 1.

(2030–2035 and 1965–1973 cm^{-1}) [23]. These results show that the ligands: selenosulfonates, selenocarbonates and selenothiocarbonates are of comparable basicity, and they all have higher basicity than the selenocarbxylate ligands.

The ^1H NMR spectra for complexes **1** are in accordance with their formulation. Their spectra display a singlet in the range 4.95–5.08 ppm for their cyclopentadienyl ring protons. This peak falls within the same range observed for selenocarbonates $CpFe(CO)_2SeCO_2R$ (4.98–5.09 ppm) [12]. However, this peak is lower than that observed for selenosulfonate, $CpFe(CO)_2SeSO_2R$ (5.19–5.24 ppm) [29] and of selenocarboxylate complexes, $CpFe(CO)_2SeCOR$ (5.08–5.11 ppm) [23]. The resonances for the protons of the R-groups are observed in the expected values and multiplicity.

3.2. Synthesis and characterization of 2

Photolytic reaction of a THF solution of complexes **1** in the absence of added ligand leads to the generation of the chelate complexes $CpFe(CO)(\kappa^2 Se,S\text{-}SeC(S)OR)$ (**2**). The selenocarbonate ligands in **2** are bonded to the metal through both the sulfur and the selenium atoms. These dark red complexes are soluble in most organic solvents including hydrocarbons. Solutions of **2** are quite air sensitive even under inert atmosphere. Upon exposure to air, they decompose within few minutes.

Complexes **2** are characterised by IR, ^1H NMR spectroscopy as well as elemental analysis. The IR spectra of **2** show the characteristic ν_{CO} absorption in the range 1947–1959 cm^{-1}. This absorption is similar to those of $CpFe(CO)(EPh_3)SeCOR$ (1941–1957 cm^{-1}) and are lower than those of the starting complexes **1**. These differences might be attributed to the weak π-acid character of the chelate selenothiocarbonate ligand compared to that of carbonyl ligand. The ^1H NMR spectra of **2** show the Cp-peak in the range 4.65–4.69 ppm. This peak is lower than that of the corresponding Cp-peak of complexes **1** and within the same range observed for $CpFe(CO)(EPh_3)$-SeCOR (4.61–4.77 ppm).

3.3. Crystal structure

The structure of $CpFe(CO)_2SeC(S)O\text{-}4\text{-}C_6H_4Cl$ (**1b**) was determined crystallographically and is shown in Fig. 1. The relevant bond parameters are listed in Table 2. The complex adopts the geometry of a three-legged pianostool, with Cp as the base and the two carbonyls and the Se-coordinated selenothiocarbonate ligand as the legs. The Cp ligand is bound to the metal in an η^5-fashion with Fe–C bond distances ranging between 2.081(3) and 2.112(3) Å. The Fe–C bond distances (of carbonyl ligands) of 1.785(3) and 1.769(3) Å are in normal range for $CpFe(CO)_2X$ complexes. The Fe–Se bond length of 2.3958(5) Å is close to the range of Fe–Se bond lengths found in related iron complexes such as $CpFe(CO)_2SeSO_2C_6H_5$ [29] and $CpFe(CO)_2$-$SeCO_2C_2H_5$ [30]. The C=S bond distance of 1.633(3) Å is similar to that observed for $(PPh_3)_2Pt(CS_3)$ and $(dppe)PtCS_3$ [36].

Table 2
Selected bond length (Å) and angles (°) of $CpFe(CO)_2SeC(S)O\text{-}4\text{-}C_6H_4Cl$ (**1b**)

Fe–Se	2.3985(2)	C8–Se–Fe	107.80(7)
Fe–C1	1.785(3)	C1–Fe–Se	88.51(9)
Fe–C2	1.769(3)	C2–Fe–Se	90.10(9)
Fe–C3	2.081(3)	C2–Fe–C1	95.12(13)
Fe–C4	2.098(3)	C8–O3–C9	119.71(19)
Fe–C5	2.112(3)	O3–C8–S	124.98(19)
Fe–C6	2.100(3)	O3–C8–Se	112.99(17)
Fe–C7	2.083(3)	S1–C8–Se	122.03(14)
Se–C8	1.881(2)		
S1–C8	1.633(3)		
C1–O1	1.131(3)		
C2–O2	1.145(3)		
C8–O3	1.351(3)		

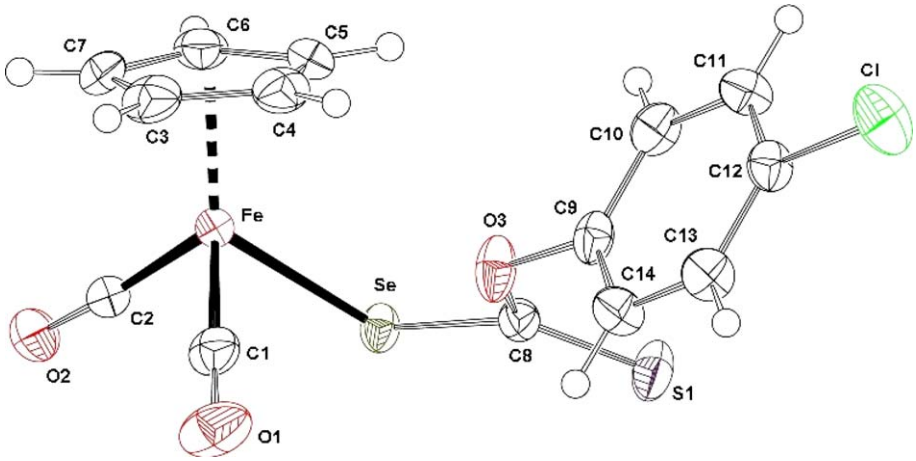

Fig. 1. ORTEP drawing of $CpFe(CO)_2SeC(S)O\text{-}4\text{-}C_6H_4Cl$ (**1b**).

4. Supplementary materials

Crystallographic data for the structural analysis have been deposited with the Cambridge Crystallographic Data Centre, CCDC No. 277847 for compound **1b**. Copies of this information may be obtained free of charge from The Director, CCDC, 12 Union Road, Cambridge, CB2 1EZ, UK (fax: +44 1233 336 033; e-mail: deposit@ccdc.cam.ac.uk or www:http://www.ccdc.cam.ac.uk).

Acknowledgments

The author thanks the Deanship of Research, Jordan University of Science and Technology for financial support, Grant No. 119/2003. He also thanks Prof. Richard Welter (University of Strasburg, France) for determining the X-ray structure.

References

[1] S. Narayan, V.K. Jain, K. Panneerselvam, T.H. Lu, S.F. Tung, Polyhedron 18 (1999) 1253.
[2] A. Singhal, V.K. Jain, R. Misra, B. Varghese, J. Mater. Chem. (2001) 1121.
[3] S. Dey, V.K. Jain, S. Chaudhury, A. Knoedler, F. Lissner, W. Kaim, J. Chem. Soc., Dalton Trans. (2001) 723.
[4] S. Dey, V.M. Jain, A. Knoedler, W. Kaim, Inorg. Chim. Acta 349 (2003) 104.
[5] S. Dey, V.M. Jain, S. Chaudhury, A. Knoedler, W. Kaim, Polyherdon 22 (2002) 489.
[6] P. Arsenyan, K. Oberte, K. Rubina, S. Belyakov, Tett. Lett. (2005) 1001.
[7] J.R. Dilworth, N. Wheatley, Coord. Chem. Rev. 119 (2000) 89.
[8] J. Real, M. Pages, A. Polo, J.F. Pinella, A. Alvarez-Larena, Chem. Commun. (1999) 277.
[9] W.A. Jones, M.R. Chim, J. Am. Chem. Soc. 116 (1994) 198.
[10] M. Misono, N. Nojiri, Appl. Catal. 64 (1990) 1.
[11] D.A. Gaul, W.S. Rees Jr., Adv. Mater. 12 (2000) 1029.
[12] H. Ando, H. Inuzuka, K. Takahashi, J. Appl. Phys. 58 (1985) 802.
[13] E.G. Hope, W. Levason, Coord. Chem. Rev. 122 (1993) 109.
[14] C.M. Goldman, M.M. Olmstead, P.K. Mascharak, Inorg. Chem. 35 (1996) 2752.
[15] C.A. Grapperhaus, M.Y. Darensbourg, L.W. Sumner, D.J. Russell, J. Am. Chem. Soc. 118 (1996) 1791.
[16] C. Zhou, L. Cai, R.H. Holm, Inorg. Chem. 35 (1996) 2767.
[17] A. Volbeda, E. Garcin, C. Piras, A.L. de Lacey, V.M. Fernandez, E.C. Hatchikian, M. Frey, J.C. Fontecilla-Camps, J. Am. Chem. Soc. 118 (1996) 12989.
[18] M.K. Eidsness, R.A. Scott, B.C. Prickril, D.V. DerVartanian, J. LeGall, I. Moura, J.J.G. Moura, H.D. Peck, Proc. Natl. Acad. Sci. USA 86 (1989) 147.
[19] G. Voordouw, N.K. Menon, J. LeGall, E.S. Chai, H.J. Peck, A.E. Przybyla, J. Bacteriol. 171 (1989) 2894.
[20] C. Zirngibl, W. van Dongen, B. Scworer, R. Von Bunau, M. Richter, A. Klein, R.K. Thaner, Eur. J. Biochem. 208 (1992) 511.
[21] M. Teceira, G. Frnque, I. Moura, P.A. Lespinat, Y. Berlier, B. Prickril, H.J. Peck, A.V. Xavier, J. LeGall, J.J. Moura, J. Biochem. 167 (1987) 47.
[22] M.K. Eidsness, R.A. Scott, B.C. Prickill, D.V. DerVartanian, J. LeGall, I. Moura, J.J.G. Moura, H.D. Peck Jr., Proc. Natl. Acad. Sci. USA 86 (1989) 147.
[23] I. Jibril, O. Abu-Nemrih, Synth. Reac. Inorg. Met. Org. Chem. 26 (1996) 1409.
[24] W.A. Herman, J. Rohrmann, H. Hecht, J. Organomet. Chem. 290 (1985) 53.
[25] I. Jibril, F.T. Esmadi, H. El-Masri, L. Zsolnai, G. Huttner, J. Organomet. Chem. 510 (1996) 109.
[26] L.-C. Song, H.W. Cheng, Q.-M. Hu, Organometallics 23 (2004) 1072.
[27] L.-C. Song, H.W. Cheng, Q.-M. Hu, J. Organomet. Chem. 689 (2004) 1849.
[28] P.G. Jones, C. Thöne, Inorg. Chem. 35 (1996) 6625.
[29] M. El-khateeb, T. Obidate, Polyhedron 20 (2001) 2393.
[30] M. El-khateeb, A. Lataifeh, I. Jibril, Trans. Met. Chem. 28 (2003) 85.
[31] M. El-khateeb, Inorg. Chim. Acta 357 (2004) 4341.
[32] G.M. Sheldrick, SHELXS-97, Program for the Solution of Crystal Structures, University of Göttingen, Germany, 1997.
[33] G.M. Sheldrick, SHELXL-96, Program for the Refinment of Crystal Structures, University of Göttingen, Germany, 1996.
[34] M. Moran, I. Cuadrado, J.R. Masaguer, J. Losada, J. Organomet. Chem. 335 (1987) 255.
[35] M. Moran, I. Cuadrado, C. Munoz-Reja, J.R. Masaguer, J. Losada, J. Chem. Soc., Dalton Trans. (1988) 149.
[36] S.A. Aucott, A.M.Z. Alexander, J.D. Woolins, Polyhedron 19 (2000) 499.

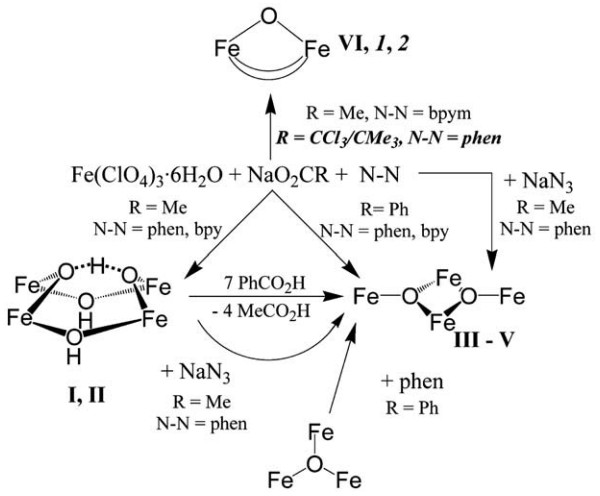

Scheme 1. The various preparations/transformations and the cores of the isolated clusters resulting from our synthetic efforts in the $Fe^{III}/RCO_2^-/N–N$ chemistry. The results described in this work are presented in bold italics.

and $[Fe_4(OHO)(OH)_2(O_2CMe)_4(bpy)_4](ClO_4)_3$ (**II**) were synthesized [7]. It was then found that when R = Ph and N–N = phen, we invariably obtained the tetranuclear butterfly-shaped complex $[Fe_4O_2(O_2CPh)_7(phen)_2](ClO_4)$ (**III**). This metal core persisted even when perchlorates were eliminated from the reaction mixture by reacting basic iron(III) benzoate with phen in MeCN, leading to complex $[Fe_4O_2(O_2CPh)_8(phen)_2]$ (**IV**) [8]. When R = Me, N–N = phen and NaN_3 was added to the reaction mixture, the butterfly tetranuclear cluster $[Fe_4O_2(O_2CMe)_6(N_3)_2(phen)_2]$ (**V**) was obtained, instead of the rectangular core [9]. Finally, when R = Me, N–N = bpym, intermolecular hydrogen-bonds between coordinated bipyrimidine with aquo ligands of adjacent molecules influenced the structure of the final product leading to hydrogen-bonded chains of $[Fe_2O(O_2CMe)_2(bpym)_2(H_2O)_2](ClO_4)_2$ (**VI**) [10]. All these reactions and transformations are summarized in Scheme 1.

A key observation is that the R group has the most important influence upon the identity of the final product when N–N is either phen or bpy. Being intrigued by this observation, we decided to further explore the parameter space of this reaction system with respect to that particular degree of freedom, the R group. We herein report the syntheses, structural and physical studies of complexes $[Fe_2O(O_2CR_3)_2(phen)_2(H_2O)_2](ClO_4)_2$ (**1**: R = CCl_3, **2**: R = CMe_3).

2. Experimental

2.1. Materials

All reagents and solvents were of analytical grade and used as received, except for sodium carboxylates, which were synthesized from reaction of their respective acids with sodium hydrogen carbonate at a 1:1 ratio. The syntheses were carried out under aerobic conditions. *Warning*: Although no such tendency was observed during the present work, perchlorate salts are potentially explosive and should be handled with caution in small quantities.

2.2. Syntheses

2.2.1. $[Fe_2O(O_2CCCl_3)_2(phen)_2(H_2O)_2](ClO_4)_2 \cdot 0.5MeCN \cdot 1.5H_2O$ (**1** · 0.5MeCN · 1.5H_2O)

A solution of phen · H_2O (0.238 g, 1.20 mmol) in MeCN (5 mL) was added to a solution of $Fe(ClO_4)_3 \cdot 9H_2O$ (0.620 g, 1.20 mmol) and NaO_2CCCl_3 (0.389 g, 4.10 mmol) in MeCN (5 mL). Upon addition the color of the solution turned from deep red to very dark green-brown. Parallelepiped green-brown crystals formed after ca. 5 days. These were collected by filtration, washed with a small amount of MeCN and dried in vacuo over silica gel (Yield: 0.35 g, ~46%). The dried sample analysed as solvent-free. *Anal*. Calc. for $C_{28}H_{16}Cl_8Fe_2N_4O_{13}$: C, 32.24; H, 1.59; N, 5.54. Found: C, 32.15; H, 1.68; N, 5.43%.

2.2.2. $[Fe_2O(O_2CCMe_3)_2(phen)_2(H_2O)_2](ClO_4)_2 \cdot MeCN$ (**2** · MeCN)

A solution of phen · H_2O (0.397 g, 2.00 mmol) in MeCN (8 mL) was added to a solution of $Fe(ClO_4)_3 \cdot 9H_2O$ (1.033 g, 2.00 mmol) and NaO_2CCMe_3 (0.435 g, 3.50 mmol) in MeCN (7 mL). Upon addition the color of the solution turned from deep red to very dark green-brown. The solution was allowed to slowly evaporate until its volume had reached ~3 mL. Then the solution was capped, and parallelepiped green crystals formed after ca. 5 days. These were collected by filtration, washed with a small amount of chilled MeCN and dried in vacuo over silica gel (Yield: 0.23 g, ~31%). The dried sample analysed as solvent-free. *Anal*. Calc. for $C_{34}H_{34}Cl_2Fe_2N_4O_{13}$: C, 45.92; H, 3.85; N, 6.30. Found: C, 45.79; H, 3.97; N, 6.21%.

2.3. Physical measurements

Elemental analysis for carbon, hydrogen, and nitrogen was performed on a Perkin–Elmer 2400/*II* automatic analyzer. Infrared spectra were recorded as KBr pellets in the 4000–400 cm^{-1} range on a Bruker Equinox 55/S FT-IR spectrophotometer. Variable-temperature (4.2–300 K) Mössbauer spectra were collected with a constant acceleration spectrometer using a ^{57}Co (Rh) source and a variable temperature Oxford cryostat. Home-written routines were used to fit the Mössbauer parameters and determine their standard deviations of statistical origin (given in parentheses). Isomer shift values (δ) are reported relative to iron foil at 300 K. Variable-temperature magnetic susceptibility measurements were carried out on a polycrystalline sample of **1** over the 5–300 K temperature range using a Quantum Design MPMS SQUID susceptometer under a magnetic field of 1 T. Diamagnetic corrections for the complex were estimated from Pascal's constants. The magnetic susceptibility has been computed by analytical calculation of the energy levels associated with the spin Hamiltonian.

Least-squares fittings were accomplished with an adapted version of the function-minimization program MINUIT [11]. The error factor R is defined as $R = \sum \frac{(x_{exp}-x_{calc})^2}{Nx_{exp}^2}$, where N is the number of experimental points. X-band EPR spectra at liquid helium temperatures were recorded with an ER200D Bruker spectrometer equipped with an Oxford ESR-900 cryostat and an Anritsu frequency counter.

2.4. X-ray crystallography

A green-brown prismatic crystal of **1** ($0.18 \times 0.38 \times 0.78$ mm) was mounted on a glass fiber and covered with epoxy glue, and a green prismatic crystal of **2** ($0.06 \times 0.30 \times 0.30$ mm) was mounted in capillary with drops of mother liquid. Diffraction measurements were made on a Crystal Logic Dual Goniometer diffractometer using graphite monochromated Mo radiation. Important crystal data and parameters for data collection for **1** and **2** are reported in Table 1. Unit cell dimensions were determined and refined by using the angular settings of 25 automatically centered reflections in the range $11° < 2\theta < 23°$. Intensity data were recorded using a θ–2θ scan. Three standard reflections, monitored every 97 reflections showed less than 3% intensity fluctuation and no decay. Lorentz polarization and psi-scan absorption corrections (only for **1**) were applied using Crystal Logic software. The structures were solved by direct methods using SHELXS-97 [12] and refined by full-matrix least-squares on F_o^2 with SHELXL-97 [13]. Further experimental crystallographic details for **1**: $2\theta_{max} = 50°$, scan speed 5.0 °/min; scan range $1.6 + \alpha_1\alpha_2$ separation; reflections collected/unique/used, 7459/7150 [$R_{int} = 0.0190$]/7150; 643 parameters refined; $(\Delta/\sigma)_{max} = 0.000$; $(\Delta\rho)_{max}/(\Delta\rho)_{min} = 0.850/-0.774$ e Å^{-3}; R/R_w (for all data), 0.0611/0.1253. All hydrogen atoms were located by difference maps and were refined isotropically, except those of the MeCN and partially occupied H_2O solvent molecules which were not included in the refinement. All non-hydrogen atoms were refined anisotropically. Further experimental crystallographic details for **2**: $2\theta_{max} = 48°$, scan speed 1.5°/min; scan range $1.6 + \alpha_1\alpha_2$ separation; reflections collected/unique/used, 7114/6794 [$R_{int} = 0.0364$]/6794; 631 parameters refined; $(\Delta/\sigma)_{max} = 0.000$; $(\Delta\rho)_{max}/(\Delta\rho)_{min} = 0.777/-0.496$ e Å^{-3}; R/R_w (for all data), 0.1074/0.1991. All hydrogen atoms were located by difference maps and were refined isotropically, except those of the methyl groups, which were introduced at calculated positions as riding on bonded atoms. All non-hydrogen atoms were refined anisotropically.

Table 1
Crystallographic data for complexes **1** · 0.5MeCN · 1.5H_2O and **2** · MeCN

	1 · 0.5MeCN · 1.5H_2O	**2** · MeCN
Formula	$C_{29}H_{24.5}Cl_8Fe_2N_{4.5}O_{16.5}$	$C_{36}H_{41}Cl_2Fe_2N_5O_{15}$
Formula weight	1095.33	966.34
Space group	*C*2/*c*	$P\bar{1}$
Unit cell dimensions		
a (Å)	14.761(6)	13.570(10)
b (Å)	18.002(8)	13.06(2)
c (Å)	31.99(1)	14.51(2)
α (°)		81.90(4)
β (°)	99.08(1)	88.38(3)
γ (°)		86.86(4)
V (Å^3)	8394(6)	2165(5)
Z	8	2
T (°C)	25	25
λ(Mo Kα) (Å)	0.71073	0.71073
ρ_{calc} (g/cm^3)	1.733	1.483
μ (mm^{-1})	1.275	0.865
R_1[a]	0.0455[b]	0.0653[c]
wR_2[a]	0.1135[b]	0.1710[c]

[a] $w = 1/[\sigma^2(F_o^2) + (aP)^2 + bP]$ and $P = [\max(F_o^2, 0) + 2(F_c^2)]/3$; $R_1 = \sum(|F_o| - |F_c|)/\sum(|F_o|)$ and $wR_2 = \{\sum[w(F_o^2 - F_c^2)^2]/\sum[w(F_o^2)^2]\}^{1/2}$.
[b] For 5751 reflections with $I > 2\sigma(I)$.
[c] For 4581 reflections with $I > 2\sigma(I)$.

3. Results and discussion

3.1. Synthesis

The syntheses of the complexes were based upon the syntheses of other complexes of the $Fe^{III}/RCO_2^-/N$–N reaction system. Previous investigations involved the variations of carboxylates (R = Me or Ph), aromatic N-donor ligands (phen, bpy, bpym), or anions (elimination of perchlorates, or the inclusion of azides). In all previous studies, R groups were electron donating and no investigations had been carried out with electron withdrawing groups. We therefore decided to carry out a comparative study between two different carboxylates, one with electron withdrawing substituents and one with electron donating ones. For purposes of comparison, we have chosen two substituents with comparable steric hindrances, $R = CCl_3$ (trichloroacetates) and CMe_3 (pivalates).

Similar to previous investigations, an effort was made to minimize the degrees of freedom, by keeping the $Fe^{III}/RCO_2^-/N$–N stoichiometry constant to 1:1.75:1, respectively, and by carrying out the reactions in MeCN, without the use of solvent mixtures to induce crystallization. The reactions that led to **1** and **2** can be summarized by the following reaction:

$$2Fe(ClO_4)_3 \cdot 6H_2O + NaO_2CR + 2phen \cdot H_2O \xrightarrow[20\ °C]{MeCN} \underset{\mathbf{1}:R=CCl_3;\ \mathbf{2}:R=CMe_3}{[Fe_2O(O_2CR)_2(phen)_2(H_2O)_2](ClO_4)_2} + 2NaClO_4 + 2HClO_4 + 11H_2O \quad (1)$$

The close resemblance of the two structures, despite the very different acidities of the RCO_2^- ligands, leads us to assume that this is not a factor noticeably affecting the product of the reaction. It may rather be the steric hindrances of the R groups, similar for both carboxylates, which regulate the product identity. Of course, we should note that in solution a variety of species may be present, of which the least soluble will precipitate. Therefore, it would be more precise to state that the bulkiness of the ligand has a simultaneous effect both on the relative stabilities of the species

in solution *and* their relative solubilities. It is those two parameters together that define the final product, with solubility possibly being preponderate, without us being able to distinguish their individual contributions. This has been beautifully illustrated by Caneschi et al. [14], who have managed to isolate and characterize three different complexes from the same reaction mixture.

One final synthetic detail concerns the high propensity of **1** and **2** to form supersaturated solutions. Indeed, very concentrated solutions were employed for precipitation to occur, and despite the rapid colour changes, indicative of product formation, no crystallization occurred until after several days. In the case of **2** in particular, slow evaporation of the reaction solution had to be additionally employed to induce crystallization. Once crystallization was initiated however, important yields of both complexes precipitated very rapidly, as is the case for supersaturated solutions.

3.2. Description of the structures

Complex **1** crystallizes in the monoclinic $C2/c$ space group. A partially labelled ORTEP plot is shown in Fig. 1. It consists of $[Fe_2O(O_2CCCl_3)_2(phen)_2(H_2O)_2]^{2+}$ cations containing the typical $\{Fe_2(\mu_2\text{-}O)(\mu_2\text{-}O_2CCCl_3)_2\}^{2+}$ metal core.

The coordination environment around the Fe atoms is octahedral, with O_4N_2 donor atom sets. The cation of the complex is similar in structure with the cation of complex **VI** previously reported [10], with a difference being that whereas in **1** the two aqua ligands are in *cis* positions with respect to the Fe–O–Fe plane, in **VI** they are in *trans* positions with respect to that plane (see Table 2).

Complex **2** crystallizes in the triclinic $P\bar{1}$ space group. Its overall structure is very similar to that of **1**, with the two iron atoms forming a $\{Fe_2(\mu_2\text{-}O)(\mu_2\text{-}O_2CCMe_3)_2\}^{2+}$ metal core. A partially labelled ORTEP plot is shown in Fig. 2. The main difference of the two structures is that in **2** the aqua ligands are in *trans* positions with respect to the Fe–O–Fe plane, similar to complex **VI** (see Table 3).

Table 2
Selected bond lengths (Å) and angles (°) for complex **1**

Fe(1)–O(1)	1.791(3)	Fe(2)–O(1)	1.787(3)
Fe(1)–O(6)	2.054(3)	Fe(2)–O(7)	2.045(4)
Fe(1)–O(2)	2.060(3)	Fe(2)–O(3)	2.048(3)
Fe(1)–O(4)	2.094(3)	Fe(2)–O(5)	2.079(3)
Fe(1)–N(1)	2.134(3)	Fe(2)–N(4)	2.133(3)
Fe(1)–N(2)	2.196(3)	Fe(2)–N(3)	2.173(3)
Fe(1)···Fe(2)	3.150		
O(1)–Fe(1)–O(6)	93.63(15)	O(1)–Fe(2)–O(7)	94.85(15)
O(1)–Fe(1)–O(2)	100.12(11)	O(1)–Fe(2)–O(3)	99.30(12)
O(6)–Fe(1)–O(2)	88.37(14)	O(7)–Fe(2)–O(3)	89.77(14)
O(1)–Fe(1)–O(4)	92.41(11)	O(1)–Fe(2)–O(5)	92.99(11)
O(6)–Fe(1)–O(4)	173.91(14)	O(7)–Fe(2)–O(5)	171.83(14)
O(2)–Fe(1)–O(4)	91.34(12)	O(3)–Fe(2)–O(5)	91.24(11)
O(1)–Fe(1)–N(1)	97.06(12)	O(1)–Fe(2)–N(4)	97.87(12)
O(6)–Fe(1)–N(1)	91.32(14)	O(7)–Fe(2)–N(4)	90.84(14)
O(2)–Fe(1)–N(1)	162.80(12)	O(3)–Fe(2)–N(4)	162.71(12)
O(4)–Fe(1)–N(1)	87.16(12)	O(5)–Fe(2)–N(4)	85.80(12)
O(1)–Fe(1)–N(2)	173.29(12)	O(1)–Fe(2)–N(3)	174.90(12)
O(6)–Fe(1)–N(2)	84.64(15)	O(7)–Fe(2)–N(3)	85.69(15)
O(2)–Fe(1)–N(2)	86.32(11)	O(3)–Fe(2)–N(3)	85.77(12)
O(4)–Fe(1)–N(2)	89.28(11)	O(5)–Fe(2)–N(3)	86.30(11)
N(1)–Fe(1)–N(2)	76.53(12)	N(4)–Fe(2)–N(3)	77.05(12)
Fe(2)–O(1)–Fe(1)	123.36(14)		

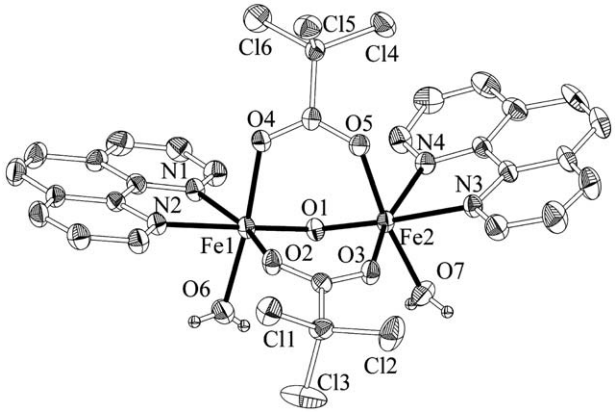

Fig. 1. Partially labelled ORTEP plot of the cation of **1** with ellipsoids drawn at the 30% probability level. All hydrogen atoms, except those of the aquo ligands, were omitted for clarity.

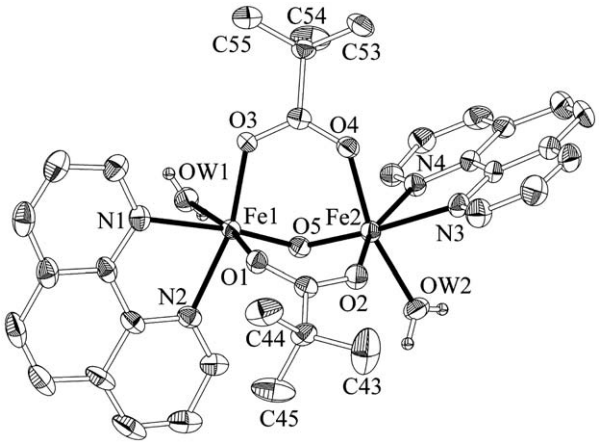

Fig. 2. Partially labelled ORTEP plot of the cation of **2** with ellipsoids drawn at the 30% probability level. All hydrogen atoms, except those of the aquo ligands, were omitted for clarity.

Hydrogen bonding interactions between the coordinated water molecules, the perchlorate counterions and the solvent molecules lead to the formation of polymeric networks in the crystal structures of **1** and **2** stabilizing the lattice structures of both compounds (Table 4).

3.3. IR spectroscopy

In the $\nu(OH)_{water}$ region, the spectra of dried **1** and **2** show medium, broad bands at 3355 and 3386 cm^{-1}, respectively, assignable to coordinated water [15]. The spectrum of **1** presents two strong bands at 1626 and 1361 cm^{-1},

Table 3
Selected bond lengths (Å) and angles (°) for complex **2**

Fe(1)–O(5)	1.798(5)	Fe(2)–O(5)	1.791(4)
Fe(1)–O(3)	2.001(4)	Fe(2)–O(2)	2.009(5)
Fe(1)–O(1)	2.046(5)	Fe(2)–O(4)	2.033(5)
Fe(1)–O(W1)	2.100(6)	Fe(2)–O(W2)	2.113(6)
Fe(1)–N(2)	2.155(5)	Fe(2)–N(4)	2.146(5)
Fe(1)–N(1)	2.216(6)	Fe(2)–N(3)	2.205(6)
Fe(1)···Fe(2)	3.087		
O(5)–Fe(1)–O(3)	99.34(19)	O(5)–Fe(2)–O(2)	98.2(2)
O(5)–Fe(1)–O(1)	97.47(18)	O(5)–Fe(2)–O(4)	95.72(19)
O(3)–Fe(1)–O(1)	95.66(19)	O(2)–Fe(2)–O(4)	98.11(19)
O(5)–Fe(1)–O(W1)	93.3(2)	O(5)–Fe(2)–O(W2)	96.6(2)
O(3)–Fe(1)–O(W1)	87.4(2)	O(2)–Fe(2)–O(W2)	88.2(2)
O(1)–Fe(1)–O(W1)	168.2(2)	O(4)–Fe(2)–O(W2)	165.2(2)
O(5)–Fe(1)–N(2)	96.3(2)	O(5)–Fe(2)–N(4)	99.5(2)
O(3)–Fe(1)–N(2)	164.14(19)	O(2)–Fe(2)–N(4)	161.67(19)
O(1)–Fe(1)–N(2)	85.0(2)	O(4)–Fe(2)–N(4)	85.0(2)
O(W1)–Fe(1)–N(2)	89.0(2)	O(W2)–Fe(2)–N(4)	85.0(2)
O(5)–Fe(1)–N(1)	170.89(19)	O(5)–Fe(2)–N(3)	174.82(19)
O(3)–Fe(1)–N(1)	88.3(2)	O(2)–Fe(2)–N(3)	86.5(2)
O(1)–Fe(1)–N(1)	86.61(18)	O(4)–Fe(2)–N(3)	81.4(2)
O(W1)–Fe(1)–N(1)	82.1(2)	O(W2)–Fe(2)–N(3)	85.7(2)
N(2)–Fe(1)–N(1)	75.9(2)	N(4)–Fe(2)–N(3)	76.1(2)
Fe(2)–O(5)–Fe(1)	118.7(2)		

attributed to the antisymmetric and symmetric stretching vibrations of the carboxylate group, respectively [16,17]. The respective bands for the pivalato ligands in **2** appear at 1536 and 1427 cm^{-1}. The differences $\Delta = \nu_{as}(COO) - \nu_s(COO)$ between the asymmetric and symmetric stretching vibration frequencies are equal to 265 cm^{-1} for **1** and 109 cm^{-1} for **2**, lower than that of NaO_2CCl_3 ($1675 - 1354 = 321\ cm^{-1}$) and NaO_2CMe_3 ($1552 - 1413 = 139\ cm^{-1}$), as expected for the crystallographically established bidentate bridging mode of the trichloroacetate and pivalate ligation, respectively [17].

Of the ν(C=C) and ν(C=N) stretching vibrations of free 1,10′-phenanthroline between 1200 and 1600 cm^{-1}, all are known to shift to slightly higher frequencies upon complexation, except the one at 1586 cm^{-1}, which is virtually unaffected [18]. However, due to overlaps with the carboxylate asymmetric and symmetric stretching vibrations some of those are unobserved. Thus, in the spectrum of **1** we can identify some of those bands having shifted to 1585, 1519, 1427 and 1226 cm^{-1} and in the spectrum of **2** to 1625, 1583, 1484, 1520, 1226 cm^{-1}. A band at 1627 cm^{-1} in **1** is masked by the asymmetric stretching of the trichloroacetates, whereas a band at 1427 cm^{-1} in **2** is masked by the symmetric stretch of the pivalates. Bands of free phen in the 1050–700 cm^{-1} region shift to lower frequencies in the spectra of the complexes with splitting to the strong bands at ca. 730 cm^{-1} (only for **1**) and 850 cm^{-1} (only for **2**) [19].

The Fe–O–Fe antisymmetric and symmetric stretching vibrations [20] occur at 727 (**1**)/728 cm^{-1} (**2**) and 527 (**1**)/539 cm^{-1} (**2**), respectively. Finally, the strong and broad band around 1100 cm^{-1} and the medium band at 625 cm^{-1} are attributed to the $\nu_3(F_2)$ and $\nu_4(F_2)$ modes of the uncoordinated T_d perchlorate anions [16]. The broad character and signs of splitting of the band at ~1100 cm^{-1} both indicate the involvement of the ClO_4^- ions in hydrogen bonding [21].

3.4. Mössbauer spectroscopy

Mössbauer spectra from powder samples of **1** and **2** were collected between 4.2 and 300 K. Representative spectra of both complexes recorded at 78 K are shown in Fig. 3. These consist of symmetric quadrupole-split doublets, over the whole temperature regime, as predicted by the crystal structures, which reveal the existence of two iron sites in each complex with similar coordination spheres and geometries. Mössbauer parameters are presented in Table 5.

An increase of the isomer shifts of **1** and **2** upon cooling from 300 to 78 K is attributed to a second-order Doppler effect [22]. The quadrupole splitting does not exhibit significant temperature dependences, as is expected for high-spin iron(III). The lines are quite narrow and perfectly symmetric, indicating on the one hand, samples of high purity and on the other hand, iron sites of very similar Mössbauer parameters in both complexes. Thus, the different

Table 4
Hydrogen bonding interactions in **1** and **2**

Interaction	D···A (Å)	H···A (Å)	D–H···A (°)	Symmetry operation
*Compound **1***				
O(6)–H(O6A)···O(W2)	2.626	2.006	144.8	x, y, z
O(6)–H(O6A)···N(S1)	2.810	2.129	158.4	$0.5 - x, 0.5 + y, 0.5 - z$
O(6)–H(O6B)···O(10)	2.831	2.038	176.6	$-0.5 + x, -0.5 + y, z$
O(7)–H(O7A)···O(W1)	2.675	1.914	171.9	x, y, z
O(7)–H(O7B)···O(12)	2.690	1.997	177.2	$0.5 - x, 0.5 + y, 0.5 - z$
O(W1)–H(W1A)···O(11)	2.675	2.114	172.9	$0.5 - x, -0.5 + y, 0.5 - z$
O(W1)–H(W1B)···O(13)	2.811	1.949	170.1	x, y, z
*Compound **2***				
O(W1)–H(W1A)···O(10)	2.715	1.941	155.8	$1 - x, 2 - y, 1 - z$
O(W1)–H(W1B)···O(13)	2.808	2.150	162.6	x, y, z
O(W2)–H(W2A)···N(S1)	2.844	1.951	167.1	$1 - x, 1 - y, -z$
O(W2)–H(W2B)···O(6)	2.878	2.067	162.9	$x, y, -1 + z$

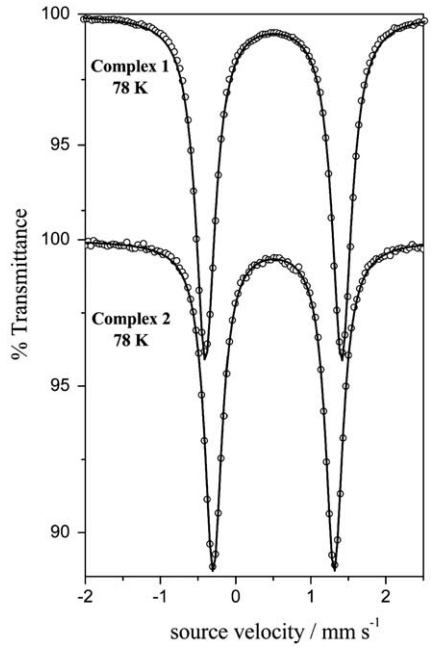

Fig. 3. Zero-field Mössbauer spectra from powder samples of **1** and **2** at 78 K.

Table 5
Mössbauer parameters for **1** and **2**

Complex	T (K)	δ (mm s^{-1})	ΔE_Q (mm s^{-1})	$\Gamma_{1/2}$ (mm s^{-1})
1	4.2	0.521(1)	1.806(1)	0.161(1)
	78	0.505(1)	1.812(1)	0.155(1)
	294	0.396(1)	1.848(1)	0.152(1)
2	4.2	0.513(1)	1.602(1)	0.144(1)
	78	0.506(1)	1.608(1)	0.140(1)
	294	0.398(2)	1.640(2)	0.157(3)

orientations of the aqua ligands (see Section 3.2) do not have any significant effect from the view of Mössbauer spectroscopy. The quadrupole splitting for both compounds is relatively large for ferric species, as found in other ferric sites of spin-coupled diiron oxo-bridged complexes encountered in proteins and model compounds [23]. A similar large quadrupole splitting has been observed for the ferric site of a (μ-oxo)-bis(carboxylato) Fe^{III}–Cr^{III} heterometallic complex [24]. This large value has been considered to arise from two sources. First, a large EFG arises from the asymmetry of the charge of the ligand sphere which is enhanced by the short Fe–O_{oxo} distance, and second, from covalency effects, that perturb the valence electron configuration of Fe^{III}.

Both complexes exhibit almost identical isomer shifts over the entire temperature range, which is in line with their similar donor atom sets (O_4N_2 for both complexes) and coordination geometries. However, there exists an interesting difference in their quadrupole splitting; complex **1** shows a quadrupole splitting of ~1.8 mm s^{-1}, significantly larger than that exhibited by **2** (~1.6 mm s^{-1}). All ferric sites exhibit O_4N_2 donor atom sets so these differences should not arise from varying inhomogeneities in the coordination spheres. A close inspection of the two structures reveals that bond length dispersions for all iron atoms fall in almost identical limits [**1**: Fe(1), 1.791–2.196; Fe(2), 1.787–2.173; **2**: Fe(1), 1.798–2.216; Fe(2), 1.791–2.205]. Thus, geometrical deviations from ideal octahedral geometries may as well be excluded from influencing the quadrupole splitting, since these deviations are remarkably similar for both complexes. Thus, the only other factor that can be held responsible for the observed differences are the different carboxylate ligands in **1** and **2**. Specifically, we observe that whereas trichloroacetates contain an electron withdrawing Cl_3C group, pivalates contain an electron donating Me_3C group attached to the carboxyl function. This correlates with the differences in the pK_a values of the respective acids (0.70 for Cl_3CCO_2H and 5.03 for Me_3CCO_2H). Comparisons with strictly similar complexes are difficult, since there are no examples of $[Fe_2O(O_2CR)_2(phen)_2(H_2O)_2]^{2+}$ complexes characterized by Mössbauer spectroscopy. However, a similar complex, $[Fe_2O(O_2CCH_2Cl)_2(bpy)_2(H_2O)_2](NO_3)_2$ was reported [25] to exhibit an isomer shift of 0.52 mm s^{-1} and a quadrupole splitting of 1.89 mm s^{-1} at 4.2 K. This high quadrupole splitting coincides with the presence of a ligand with an electron-withdrawing side group (–CH_2Cl). However, more examples would be required in order to make a valid correlation between those factors. We also conclude from the above that such simple systems are ideally suited for the study of physical phenomena at a fundamental level, without the complications encountered on larger systems.

3.5. Magnetic properties

Variable-temperature magnetic susceptibility data (5–300 K) for **1** are shown in Fig. 4.

The $\chi_M T$ product at 300 K is 1.66×10^{-3} cm^3 mol^{-1} K, much lower than the spin-only value expected for two

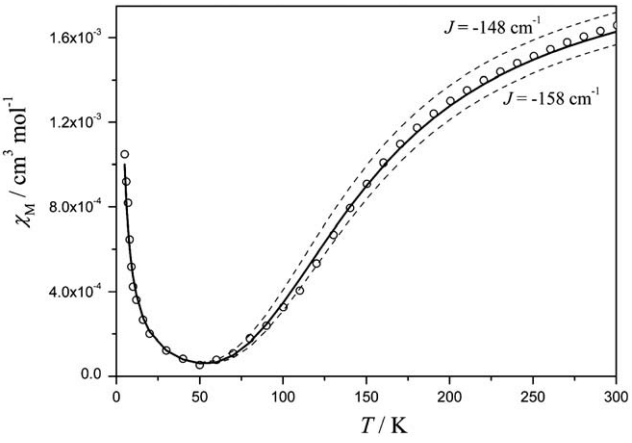

Fig. 4. χ_M vs. T plot for complex **1**. The solid line represents the best fit to the experimental data (open circles) according to the respective Hamiltonian. The dashed lines represent simulations with J values fixed to ± 5 cm^{-1} with respect to the best-fit value.

non-interacting $S = 5/2$ ions ($8.76\ cm^3\ mol^{-1}\ K$), and decreases rapidly upon cooling, indicating strong antiferromagnetic interactions (Fig. S1). This is corroborated by the constant drop of the magnetic susceptibility upon cooling, down to a minimum of $5.39 \times 10^{-5}\ cm^3\ mol^{-1}$ at ~50 K, indicating a diamagnetic ground state. An increase of χ_M below that temperature is attributed to a small fraction of high-spin ferric paramagnetic impurities. The presence of such impurities is also evident in X-band EPR spectra recorded at 4.2 K (Fig. S2) giving rise to characteristic derivative signal at $g \sim 4.3$ and weaker absorption peaks for $g \leqslant 9.0$. The overall magnetic behaviour of the complex is typical of oxo-bridged diferric complexes. The spin Hamiltonian describing the coupling within the system is

$$\hat{H} = -2J\hat{S}_1\hat{S}_2 \quad (2)$$

with $S_1 = S_2 = 5/2$.

Fitting the experimental data with the above-mentioned model and allowing for a small fraction ρ of ferric impurities yields best-fit parameters $J = -153\ cm^{-1}$, $g = 2.0$ (fixed), $\rho = 0.3\%$ with $R = 4.2 \times 10^{-3}$. The J value is well defined within a narrow range, as can be seen by simulations carried out with theoretical values differing by $\pm 5\ cm^{-1}$ (~±3%) from the best-fit value. The coupling strength falls beyond the upper limit (more negative value) of the range previously reported for (μ-oxo)bis(μ-carboxylato) bridged [23,26] diferric complexes, which is $-140\ cm^{-1}$ in $[Fe_2O(O_2CMe)_2(metpen)_2](ClO_4)_4$ (where metpen = *N*-methyl-*N*,*N*,*N*′,*N*′-tetrakis(2-pyridylmethyl)-1,2-ethanediamine) [27]. Taking into account the structural parameters of **1**, the empirical relation proposed by Gorun and Lippard [28] yields a calculated value of $-127\ cm^{-1}$, whereas the semiempirical one proposed by Weihe and Güdel [29] yields a J value of $-118\ cm^{-1}$ (using the $-2J$ Hamiltonian formalism), both of which are lower than the experimentally derived value. More recent theoretical studies, employing density functional theory, have correctly predicted the order of magnitude of the exchange interaction in μ-oxo and μ-hydroxo bis(acetato) complexes and have elucidated the 10-fold decrease of the coupling upon protonation of the oxo bridge [30,31]. In the Fe^{III}–O–Fe^{III} dimers the dominant pathway dictating the magnitude of the exchange coupling was found to be through the oxo bridge. A pathway mediated by the bridging acetates was also found [30] albeit of lesser importance. As in the case of quadrupole splitting (see above) this may suggest that the nature of the bridging carboxylates may be responsible for the variations of the exchange couplings [23] in the various (μ-oxo)bis(carboxylato) diferric complexes.

4. Conclusions

The use of two bulky carboxylates in the well-studied Fe^{III}/RCO_2^-/phen system has yielded two new dinuclear complexes containing the $\{Fe_2O(O_2CR)_2\}^{2+}$ metal core. The important differences in the electron withdrawing (or donating) strengths of the alkyl groups of the carboxylate ligands were not found to greatly influence the structures of the final products, both of which are dinuclear and contain the same metal core; it was rather concluded that it is the steric hindrances of the RCO_2^- ligands that mostly affect the identities of the final products. On the other hand, however, despite the close structural resemblance of the two complexes, their Mössbauer spectra exhibit important differences in their quadrupole splitting. This has been attributed to the different electron withdrawing potentials of the R substituents. The magnetic behaviour of **1** is typical of oxo-bridged diferric complexes, and the antiferromagnetic coupling is the strongest reported for complexes containing the $\{Fe_2O(O_2CR)_2\}^{2+}$ core.

Acknowledgements

A.K.B. thanks the Greek State Scholarship Foundation (IKY) for support through a postdoctoral grant. We thank the Greek General Secretariat of Research and Technology for a grant within the frame of the Competitiveness EPAN 2000–2006, Centers of Excellence #25.

Appendix A. Supplementary data

Full crystallographic details have been deposited in CIF format with the Cambridge Crystallographic Data Centre. Copies of the data can be obtained free of charge on request from the CCDC, 12 Union Road, Cambridge CB2 1EZ, UK (fax: +44 1223 3360 033; e-mail: deposit@ccdc.cam.ac.uk or www at http://www.ccdc.cam.ac.uk) quoting the deposition number CCDC 282415 for **1** and 282416 for **2**. Fig. S1 showing the EPR spectrum of **1** and Fig. S2 showing the $\chi_M T$ vs. T curve for **1**. Supplementary data associated with this article can be found, in the online version, at doi:10.1016/j.poly.2005.09.021.

References

[1] M. Cavallini, J. Gomez-Segura, D. Ruiz-Molina, M. Massi, C. Albonetti, C. Rovira, J. Veciana, F. Biscarini, Angew. Chem. Int. Ed. 44 (2005) 888.
[2] M.N. Leuenberger, D. Loss, Nature 410 (2001) 789.
[3] (a) Although the literature is abundant for various first-row metal complexes, for recent representative examples involving iron complexes, see: J. Legros, C. Bolm, Chem. Eur. J. 11 (2005) 1086;
(b) F. Avenier, L. Dubois, P. Dubourdeaux, J.-M. Latour, Chem. Commun. (2005) 480;
(c) L. Bénisvy, J.-C. Chottard, J. Marrot, Y. Li, Eur. J. Inorg. Chem. (2005) 999.
[4] S.J. Lippard, J.M. Berg, Principles of Bioinorganic Chemistry, University Science Book, Mill Valley, CA, 1994.
[5] S. Mukhopadhyay, S.K. Mandal, S. Bhaduri, W.H. Armstrong, Chem. Rev. 104 (2004) 3981.
[6] X. Zhang, H. Furutachi, S. Fujinami, S. Nagamoto, Y. Maeda, Y. Watanabe, T. Kitagawa, M. Suzuki, J. Am. Chem. Soc. 127 (2005) 826.
[7] A.K. Boudalis, N. Lalioti, G.A. Spyroulias, C.P. Raptopoulou, A. Terzis, V. Tangoulis, S.P. Perlepes, J. Chem. Soc., Dalton Trans. (2001) 955.

[8] A.K. Boudalis, N. Lalioti, G.A. Spyroulias, C.P. Raptopoulou, A. Terzis, A. Bousseksou, V. Tangoulis, J.-P. Tuchagues, S.P. Perlepes, Inorg. Chem. 41 (2002) 6474.
[9] A.K. Boudalis, V. Tangoulis, C.P. Raptopoulou, A. Terzis, J.-P. Tuchagues, S.P. Perlepes, Inorg. Chim. Acta 357 (2004) 1345.
[10] A.K. Boudalis, C.P. Raptopoulou, A. Terzis, S.P. Perlepes, Polyhedron 23 (2004) 1271.
[11] F. James, M. Roos, Comput. Phys. Commun. 10 (1975) 345.
[12] G.M. Sheldrick, SHELXS-97: Program for Crystal Structure Solution, University of Göttingen, Göttingen, Germany, 1997.
[13] G.M. Sheldrick, SHELXL-97: Program for the Refinement of Crystal Structures from Diffraction Data, University of Göttingen, Göttingen, Germany, 1997.
[14] R. Ruiz, C. Sangregorio, A. Caneschi, P. Rossi, A.B. Gaspar, J.A. Real, M.C. Muñoz, Inorg. Chem. Commun. 3 (2000) 361.
[15] L.S. Gelfand, F.J. Iaconiani, L.L. Pytlewski, A.N. Speca, C.M. Mikulski, N.M. Karayannis, J. Inorg. Nucl. Chem. 42 (1980) 377.
[16] K. Nakamoto, Infrared and Raman Spectra of Inorganic and Coordination Compounds, 4th ed., Wiley, New York, 1986.
[17] G.B. Deacon, R.J. Phillips, Coord. Chem. Rev. 33 (1980) 227.
[18] M.M. Campos-Valette, R.E. Clavijo, F. Mendizabal, W. Zamudio, R. Baraona, G. Diaz, Vib. Spectrosc. 12 (1996) 37.
[19] A.K. Boudalis, V. Nastopoulos, S.P. Perlepes, C.P. Raptopoulou, A. Terzis, Transition Met. Chem. 26 (2001) 276.
[20] J. Sanders-Loehr, W.D. Wheeler, A.K. Shiemke, B.A. Averill, T.M. Loehr, J. Am. Chem. Soc. 111 (1989) 8084.
[21] V. Tangoulis, C.P. Raptopoulou, A. Terzis, S. Paschalidou, S.P. Perlepes, E. Bakalbassis, Inorg. Chem. 36 (1997) 3996.
[22] N.N. Greenwood, T.C. Gibbs, Mössbauer Spectroscopy, Chapman & Hall, New York, 1971, pp. 9–11, 50–53.
[23] D.M. Kurtz Jr., Chem. Rev. 90 (1990) 585.
[24] J.H. Rodriguez, Y.-M. Xia, P.G. Debrunner, P. Chaudhuri, K. Wieghardt, J. Am. Chem. Soc. 118 (1996) 7542.
[25] K.L. Taft, A. Masschelein, S. Liu, S.J. Lippard, D. Garfinkel-Shweky, A. Bino, Inorg. Chim. Acta 198–200 (1992) 627.
[26] K.S. Murray, Coord. Chem. Rev. 12 (1974) 1.
[27] K.B. Jensen, C.J. McKenzie, O. Simonsen, H. Toftlund, A. Hazell, Inorg. Chim. Acta 257 (1997) 163.
[28] S.M. Gorun, S.J. Lippard, Inorg. Chem. 30 (1991) 1625.
[29] H. Weihe, H.U. Güdel, J. Am. Chem. Soc. 119 (1997) 6539.
[30] J.H. Rodriguez, J.K. McCusker, J. Chem. Phys. 116 (2002) 6253.
[31] M. Shoji, Y. Nishiyama, Y. Maruno, K. Koizumi, Y. Kitagawa, S. Yamanaka, T. Kawakami, M. Okumura, K. Yamaguchi, Int. J. Quantum Chem. 100 (2004) 887.

can mimic the active site of those metalloenzymes which are known to contain imidazole groups from histidine, bound to the metal centre in the active site [18]. This is the case of hydrotris(pyrazolyl)borates, that have been employed to modelize metalloproteins thanks to their ability to mimic the multiple coordination of histidine to metal ions [19].

Taking into account the afore-mentioned, during last years we have carried out a systematic investigation on the coordination chemistry of thiazoline derivatives with transition metal ions [20–27]. As a continuation of this research, we have recently initiated a study about the coordination behaviour of thiazoline derivatives that contain the pyrazole ring in their structure. In this paper, results are reported on the structural characterization of 2-(pyrazol-1-yl)-2-thiazoline (PyTn), as well as a study through elemental analysis, IR, UV–Vis–NIR diffuse reflectance, X-ray diffraction, and magnetic susceptibility of the solid phases obtained by reaction of PyTn with Co(II) and Cu(II), as well as electronic paramagnetic resonance (EPR) of the latter.

2. Experimental

2.1. Preparation of 2-(pyrazol-1-yl)-2-thiazoline (PyTn)

The preparation of PyTn has been carried out as it is described by Haugwitz et al. [28]. The resulting oil was crystallized from 1:2 diethyl ether–petroleum ether mixture. *Anal*. Calc. for $C_6H_7N_3S$: C, 47.04; H, 4.61; N, 27.43; S, 20.93. Found: C, 46.82; H, 4.73; N, 27.08; S, 20.54%. UV–Vis (EtOH): λ_{max}, nm (ε, L mol^{-1} cm^{-1}) 242 (32364), 268 (7409). ^{1}H NMR (deuteriochloroform): δ 8.21 (d, $J = 2.6$ Hz, 1H, C(5)H), 7.68 (s, 1H, C(6)H), 6.42 (s, 1H, C(4)H), 4.34 (t, $J = 8.2$, 2H, CH_2–N), 3.50 ppm (t, $J = 8.2$, 2H, CH_2–S); ^{13}C NMR (deuteriochloroform): δ 158.68 C(1), 142.60 C(4), 128.07 C(6), 108.72 C(5), 61.18 C(3), 34.05 ppm C(2).

2.2. Preparation of $[CoCl_2(PyTn)_2]\cdot 2H_2O$ (1)

This complex was isolated from a freshly prepared 96% ethanol solution (2.5 mL) of $CoCl_2\cdot 6H_2O$ (77.6 mg, 0.3 mmol) that was added to a 96% ethanol solution (5 mL) of PyTn (100 mg, 0.6 mmol). The resulting solution was allowed to evaporate slowly at room temperature. After a few days, red crystals were isolated from the solution (99.4 mg, 67%). Crystals were separated by filtration, washed with cold ether and air-dried. *Anal*. Calc. for $C_{12}H_{18}Cl_2CoN_6O_2S_2$: C, 30.52; H, 3.84; N, 17.79; S, 13.58. Found: C, 30.51; H, 3.73; N, 17.61; S, 13.59%.

2.3. Preparation of $[\{CuCl(PyTn)\}_2(\mu\text{-}Cl)_2]$ (2)

This complex was prepared by reacting a 96% ethanol solution (2.5 mL) of $CuCl_2\cdot 2H_2O$ (111.3 mg, 0.6 mmol) with a 96% ethanol solution (5 mL) of PyTn (100 mg, 0.6 mmol), being obtained a green powder that was filtered and crystallized from distilled water (165.1 mg, 88%). Crystals were filtered and washed with cold ether and air-dried. *Anal*. Calc. for $C_6H_7Cl_2CuN_3S$: C, 25.05; H, 2.45; N, 14.61; S, 11.15. Found: C, 25.00; H, 2.49; N, 14.45; S, 11.18%.

2.4. Instrumental procedures

Chemical analyses of carbon, hydrogen, nitrogen and sulphur were performed by microanalytical methods using a FISONS EA-1108 microanalyser. IR spectra were recorded on a Perkin–Elmer FT-IR 1720 spectrophotometer, from KBr pellets in the 4000–370 cm^{-1} range and on a Perkin–Elmer FT-IR 1700X spectrophotometer, from polyethylene pellets in the 500–150 cm^{-1} range. Electronic spectra of the ligand in ethanol solution and the copper(II) complex in DMSO solution were measured on a Shimadzu UV-3101 PC using a 10 mm quartz cell. UV–Vis–NIR reflectance spectra for complexes in the 200–2500 nm range were obtained from pellets of the samples, using a Shimadzu UV-3101 PC spectrophotometer and $BaSO_4$ as a reference. Magnetic susceptibility measurements were performed on polycrystalline samples using a magnetometer with pendulum MANICS DSM8, equipped with helium continuous-flow cryostat and a electromagnetometer DRUSCH EAF 16 UE. Data were corrected for temperature independent paramagnetism and diamagnetic contributions, which were estimated from the Pascal constants. The EPR spectrum was recorded at room temperature on a BRUKER ESP-300E spectrometer using the X band of microwave. ^{1}H and ^{13}C NMR spectra were obtained with a Bruker AM 400 instrument at 400 and 100 MHz, respectively, in $CDCl_3$ using Me_4Si as internal standard.

2.5. Crystal structures determination

Crystal data, data collection and refinement details for PyTn, **1** and **2** are given in Table 1. X-ray diffraction measurements were performed using a Bruker SMART CCD diffractometer. The first 50 frames were recollected at the end of data collection to monitor for decay. All data were corrected for Lorentz and polarization effects, while absorption corrections were performed by means of SADABS program [29]. The structures of PyTn and **2** were solved by direct methods and subsequent Fourier differences, while **1** structure was solved using Patterson method and subsequent Fourier differences. For these structure solutions, the WinGX package [30] was employed, and all the structures were refined by full-matrix least-squares. The H atoms attached to C atoms were positioned geometrically, with U_{iso} values derived from U_{eq} values of the corresponding C atom. The hydrogen atoms from water molecules were directly located from successive Fourier differences syntheses and included in the calculation with estimated isotropic displacement parameters without refinement, with the O–H and H···H distances restrained (DFIX) to 0.957(3) and 1.513(3) Å, respectively, in order

Table 1
Crystal data, data collection and refinement details for PyTn, $[CoCl_2(PyTn)_2]\cdot 2H_2O$ (**1**) and $[\{CuCl(PyTn)\}_2(\mu\text{-}Cl)_2]$ (**2**)

	PyTn	1	2
Crystal shape	block	prism	prism
Colour	colourless	red	green
Size (mm)	$0.54\times0.36\times0.31$	$0.37\times0.36\times0.10$	$0.30\times0.20\times0.16$
Chemical formula	$C_6H_7N_3S$	$C_{12}H_{18}Cl_2CoN_6O_2S_2$	$C_{12}H_{14}Cl_4Cu_2N_6S_2$
Crystal system	monoclinic	triclinic	triclinic
Space group	$P2_1/c$	$P\bar{1}$	$P\bar{1}$
Unit cell dimensions			
a (Å)	8.847(1)	7.157(1)	7.502(2)
b (Å)	7.077(1)	7.769(1)	7.828(2)
c (Å)	11.774(1)	8.538(1)	8.675(2)
α (°)		98.92(1)	82.61(1)
β (°)	94.27(1)	94.05(1)	75.53(1)
γ (°)		91.96(1)	82.25(1)
V (Å^3)	735.1(1)	467.3(1)	486.4(2)
Z	4	1	1
T (K)	293(2)	293(2)	293(2)
D_{calc} (g cm^{-3})	1.384	1.678	1.964
μ (mm^{-1})	0.361	1.447	2.961
$F(000)$	320	241	286
Diffractometer	Bruker SMART CCD	Bruker SMART CCD	Bruker SMART CCD
Radiation	Mo Kα ($\lambda = 0.71073$ Å)	Mo Kα ($\lambda = 0.71073$ Å)	Mo Kα ($\lambda = 0.71073$ Å)
Collection method	ϕ–ω	ϕ–ω	ϕ–ω
2θ range (°)	4.6–56.4	4.8–56.6	5.3–52.2
Index ranges	$-9 \leqslant h \leqslant 11$, $-9 \leqslant k \leqslant 9$, $-12 \leqslant l \leqslant 15$	$-9 \leqslant h \leqslant 9$, $-10 \leqslant k \leqslant 10$, $-11 \leqslant l \leqslant 11$	$-9 \leqslant h \leqslant 8$, $-9 \leqslant k \leqslant 9$, $-10 \leqslant l \leqslant 9$
Independent reflections	1748	2108	1796
Observed reflections	1398 [$F > 4.0\sigma(F)$]	1970 [$F > 4.0\sigma(F)$]	1690 [$F > 4.0\sigma(F)$]
Maximum/minimum transmission	0.8962/0.8288	0.8688/0.6166	0.6487/0.4704
Number of refined parameters	92	115	118
R [$I > 2\sigma(I)$][a]	0.039	0.0368	0.0262
wR (all data)[b]	0.1005	0.106	0.0676
Goodness-of-fit (GOF)[c]	1.005	1.038	1.093
ρ_{max} and ρ_{min} (e Å^{-3})	0.369 and −0.337	0.522 and −0.467	0.269 and −0.395

[a] $R = \sum\|F_o| - |F_c\|/\sum|F_o|$.
[b] $wR = \{\sum[w(F_o^2 - F_c^2)^2]/\sum[w(F_o^2)^2]\}^{1/2}$.
[c] $\text{GOF} = \{\sum[w(F_o^2 - F_c^2)^2]/(N_{rflns} - N_{params})\}^{1/2}$.

to ensure a chemically reasonable geometry for these molecules.

3. Results and discussion

3.1. Description of the structures

3.1.1. PyTn

The X-ray study of PyTn reveals that crystals are made of monoclinic unit cells, each one containing four PyTn molecules. A diagram of the molecular structure and the atom numbering system used are shown in Fig. 1. Selected bond lengths and angles are given in Table 2.

In the S–C(1)–N(1)–C(2)–C(3) ring, the short C(1)–N(1) bond [1.257(2) Å], together with a high S–C(1)–N(1) bond angle [120.8(1)°] and a relatively long S–C(1) bond distance [1.750(2) Å], indicates that it deals with a thiazoline ring [31].

Regarding to pyrazole ring, bond distances and angles are the normal ones for a ring of this nature [32].

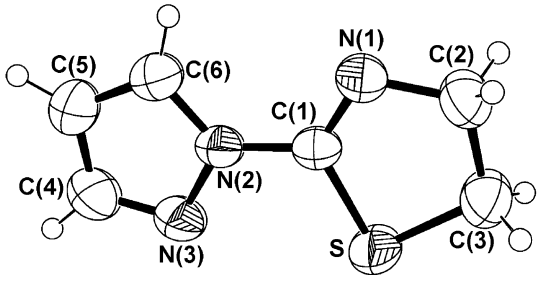

Fig. 1. Crystal structure of PyTn, showing the atom-numbering scheme. The thermal ellipsoids are drawn at a 50% level.

From the examination of the least squares planes, it is deduced that both heterocyclic rings are plane, with a maximum deviation with respect to the rings mean plane of 0.004(2) Å for C(3) from thiazoline ring and 0.006(2) Å for C(6) from pyrazole ring. The dihedral angle between thiazoline and pyrazole rings [2.9(0)°] indicates that both heterocycles are nearly coplanar.

Table 2
Selected bond lengths (Å) and angles (°) for PyTn

S–C(1)	1.750(2)	N(2)–N(3)	1.365(2)
S–C(3)	1.796(2)	N(3)–C(4)	1.316(3)
N(1)–C(1)	1.257(2)	C(6)–C(5)	1.349(3)
N(1)–C(2)	1.461(2)	C(2)–C(3)	1.517(3)
C(1)–N(2)	1.396(2)	C(5)–C(4)	1.397(3)
N(2)–C(6)	1.358(2)		
C(1)–S–C(3)	89.0(1)	N(3)–N(2)–C(1)	119.6(1)
C(1)–N(1)–C(2)	110.9(2)	C(4)–N(3)–N(2)	103.7(2)
N(1)–C(1)–N(2)	122.0(2)	C(5)–C(6)–N(2)	106.7(2)
N(1)–C(1)–S	120.8(1)	N(1)–C(2)–C(3)	111.9(2)
N(2)–C(1)–S	117.2(1)	C(6)–C(5)–C(4)	105.4(2)
C(6)–N(2)–N(3)	111.9(2)	N(3)–C(4)–C(5)	112.3(2)
C(6)–N(2)–C(1)	128.4(1)	C(2)–C(3)–S	107.5(1)

3.1.2. $[CoCl_2(PyTn)_2]\cdot 2H_2O$ (1)

The X-ray diffraction study of $[CoCl_2(PyTn)_2]\cdot 2H_2O$ shows that crystals are made up of triclinic unit cells, each one containing one complex molecule and two crystallization water molecules. A diagram of the molecular structure is shown in Fig. 2, while selected bond lengths, angles and hydrogen-bond parameters are given in Table 3.

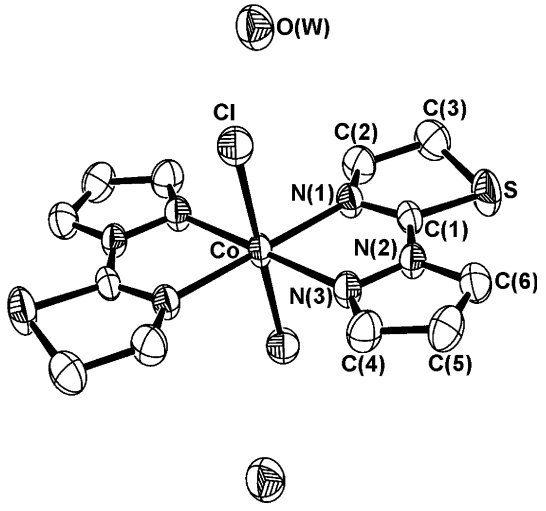

Fig. 2. Molecular structure of the $[CoCl_2(PyTn)_2]\cdot 2H_2O$ molecule, showing the atom-numbering scheme. The ellipsoids are drawn at a 50% level.

The cobalt(II) atom is hexa-coordinate, showing a distorted octahedral environment with the ligand–metal–ligand bite angles being comprised within 77.2(1)° [N(1)–Co–N(3)] and 102.8(1)° [N(1)–Co–N(3a)]. It is linked to two thiazoline N atoms and two pyrazole N atoms from two PyTn ligands that behave as didentate, constituting the equatorial plane, as well as to two chloride ions in the axial positions.

The Co–Cl distances [Co–Cl = 2.472(1) Å] are in accordance with the calculated average value [2.308(143) Å] for 129 hexa-coordinate cobalt(II) complexes with a chromophore group CoN_4Cl_2 obtained from the Cambridge Structural Database (CSD) [33] using CONQUEST software [34]. Likewise, the Co–N distances [Co–N(1) = 2.097(2) Å, Co–N(3) = 2.157(2) Å] are similar and comparable to the mean value [2.004(155) Å] calculated for 129 cobalt(II) complexes in which the metal ion is hexa-coordinate and has such chromophore group, found in a survey using CSD.

The two five-membered chelate rings are essentially planar, with a maximum deviation in relation to the corresponding mean plane of 0.039 Å for C(1).

In the case of PyTn ligands, the 2-thiazoline heterocycles lose their planar conformation, adopting a conformation near to envelope with the apex at C(3), deviating 0.339 Å from the plane formed by S, C(1), N(1) and C(2) [maximum mean-plane deviation for C(1) = 0.013 Å], which is in accord with their puckering parameters [$q = 0.217$ Å, $\phi = 140.1°$] [35].

Meanwhile, pyrazole ring remains planar, as was to be expected for an aromatic ring, with a maximum deviation with respect to the mean plane of 0.004 Å for C(6).

As it can be seen in Fig. 2, the thiazoline ring rotates around C(1)–N(2) bond in such a way that pyrazole and 2-thiazoline rings arrange their N atoms [N(1) and N(3)] to the same side in order to coordinate. Thus, the torsion angle N(1)–C(1)–N(2)–N(3) possesses a value of 7.3(3)° in the cobalt(II) complex, while in the free ligand, is 176.4(2)°.

The crystal structure is stabilized by a hydrogen-bond network, in which chlorine atoms act as acceptors of hydrogen and water molecules act as donors of hydrogen. A diagram showing this network is given in Fig. 3.

Table 3
Selected bond lengths (Å), angles (°) and hydrogen-bond parameters for $[CoCl_2(PyTn)_2]\cdot 2H_2O$ (**1**)

Co–Cl	2.472(1)	Co–N(1)	2.097(2)
Co–N(3)	2.157(2)	N(1)–C(1)	1.271(3)
C(1)–N(2)	1.392(3)	N(2)–N(3)	1.356(3)
N(1)–Co–N(3)	77.2(1)	N(2)–N(3)–Co	110.5(1)
N(3)–N(2)–C(1)	117.7(2)	N(1)–C(1)–N(2)	119.6(2)
C(1)–N(1)–Co	114.6(2)	N(1)–Co–Cl	92.8(1)
N(1)–Co–N(3a)	102.8(1)	N(3)–Co–Cl	89.1(1)
N(1)–Co–Cl(a)	87.2(1)	N(3)–Co–Cl(a)	90.9(1)
Bond A···H–D	Position of A	A···D (Å)	A···H–D (°)
Cl(1)···H(1W)–O(1W)	x, y, z	3.229(3)	170.7(2.4)
Cl(1)···H(2W)–O(1W)	$-x+1, -y+1, -z+1$	3.297(2)	170.2(2.0)

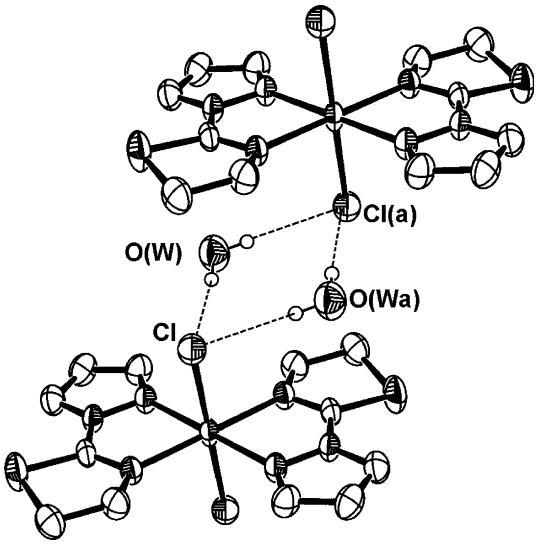

Fig. 3. View of the hydrogen-bond network of $[CoCl_2(PyTn)_2]\cdot 2H_2O$.

3.1.3. [{CuCl(PyTn)}$_2$(μ-Cl)$_2$] (2)

The molecular structure of the copper(II) complex is shown in Fig. 4. Selected interatomic distances and angles are listed in Table 4.

The structure consists of centrosymmetric dimeric $[\{CuCl(PyTn)\}_2(\mu\text{-}Cl)_2]$ units, in which two chloro ligands bridge the copper atoms forming a four-membered ring; a terminal chloro ligand and a didentate chelating molecule of PyTn completing five-coordination at each metal. The bridging Cu_2Cl_2 unit is strictly planar by the presence of the crystallographic inversion centre in the middle of the dimer.

The five donor atoms do not define a regular polyhedron around copper. The approach of Reedijk et al. [36] has been used to assign a specific coordination geometry. Analysis of the shape determining angles, α and β (the two largest angles around the central atom) yields a value for the trigonality index, τ [$\tau = (\alpha - \beta)/60$], of 0.05. According to it ($\tau = 0$ and 1 for perfect square pyramidal and trigonal bipyramidal geometries, respectively), the geometry around copper can be described as a slightly distorted tetragonal pyramid. In this structure, the basal plane is made up of one thiazoline nitrogen atom N(1), one pyrazole nitrogen atom N(3), the bridging chloro ligand Cl(2) and the terminal chloro ligand Cl(1), while the apical site is occupied by the other bridging chloro ligand Cl(2a). The Cl(2a)–metal–basal ligand angles differ from the ideal value for a square pyramid (90°), ranging between 106.1(1)° [for Cl(1)–Cu–Cl(2a)] and 83.3(1)° [N(1)–Cu–Cl(2a)]. Likewise, the basal ligand–metal–basal ligand angles differ from the ideal value of 90°, ranging between 96.2(1)° [Cl(1)–Cu–Cl(2)] and 78.9(1)° [N(3)–Cu–N(1)].

Table 4
Selected bond lengths (Å) and angles (°) for $[\{CuCl(PyTn)\}_2(\mu\text{-}Cl)_2]$ (2)

Cu–Cl(2)	2.217(1)	Cu–Cl(1)	2.254(1)
Cu–N(1)	2.012(2)	Cu–N(3)	1.995(2)
Cu–Cl(2a)	2.906(1)	C(1)–N(1)	1.260(3)
C(1)–N(2)	1.373(3)	N(3)–N(2)	1.374(3)
C(2)–N(1)	1.442(3)	C(1)–S	1.743(2)
C(6)–N(2)	1.366(3)	C(4)–N(3)	1.306(3)
Cl(1)–Cu–Cl(2)	96.2(1)	N(3)–Cu–Cl(2)	170.4(1)
N(3)–Cu–N(1)	78.9(1)	N(1)–Cu–Cl(1)	167.5(1)
N(1)–Cu–Cl(1)	91.5(1)	N(3)–Cu–Cl(1)	93.0(1)
Cl(2)–Cu–Cl(2a)	91.4(1)	Cl(1)–Cu–Cl(2a)	106.1(1)
N(1)–Cu–Cl(2a)	83.3(1)	N(3)–Cu–Cl(2a)	88.6(1)

The terminal Cu–Cl(1) distance [Cu–Cl(1) = 2.254(1) Å] is slightly shorter than the calculated average value [2.268(35) Å] for 90 copper(II) complexes with a chromophore group $CuCl_3N_2$ and short Cu–$Cl_{terminal}$ bond distances (<2.4 Å) according to Orpen et al. [37]. These bond distances have been obtained by means of CONQUEST software [34] from the CSD [33]. Likewise, the bridging Cu–Cl(2) distance [Cu–Cl(2) = 2.217(1) Å] is comparable

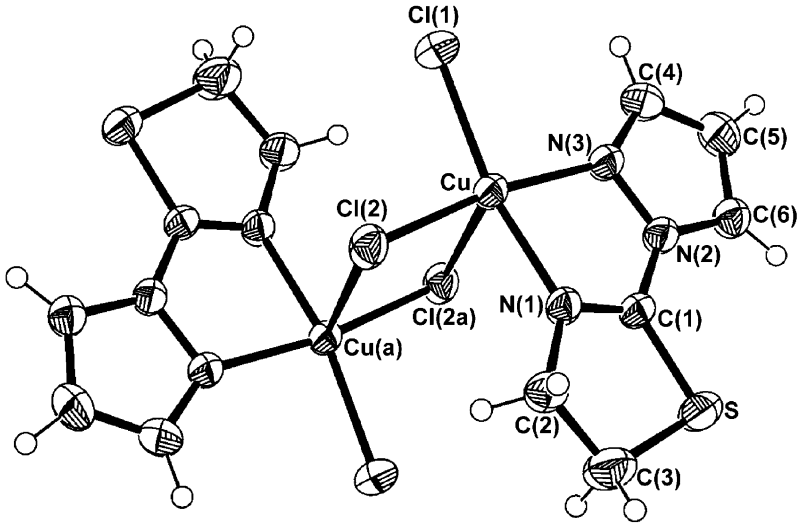

Fig. 4. Molecular structure of $[\{CuCl(PyTn)\}_2(\mu\text{-}Cl)_2]$, showing the atom-numbering scheme. The ellipsoids are drawn at a 50% level.

to the calculated average value [2.309(53) Å] for short Cu–$Cl_{bridging}$ bond distances (<2.43 Å) [37] of 56 five-coordinated copper(II) complexes collected in CSD [33]. On the other hand, the Cu–Cl(2a) distance [Cu–Cl(2a) = 2.906(1) Å] is considerably larger than the calculated average value [2.554(100) Å] for 11 copper(II) complexes with Cu–$Cl_{bridging}$ bond distances considered long (>2.50 Å) [37]. The Jahn–Teller distortion, often seen in Cu(II) complexes, causes the substantial elongation of Cu–Cl(2a) bond compared with in-plane bonds. The angle Cu–Cl(2)–Cu(a) [88.6(1)°] is slightly shorter than the average 89.40(5)° in CSD. Likewise, the Cu–Cu distance [3.612(1) Å] is larger than the average value found for 188 dinuclear copper(II) complexes containing two chloro bridging ligands [3.499(133) Å] in CSD. Likewise, the Cu–$N_{pyrazole}$ bond distance [Cu–N(3) = 1.995(2) Å] is in good agreement with the calculated average value [1.987(16) Å] found for [$CuCl_2(pdmp)_2$] [pdmp = 1-phenyl-3,5-dimethylpyrazole] [38,39], [$CuCl_2(DPEP)_2$] [DPEP = P,P-diphenyl-2-(3,5-dimethylpyrazol-1-yl)ethylphosphinate-N] [40], *trans*-bis(4-bromopyrazole-N)-dichloro-copper (II) [41] and [$CuCl_2(Pz_2CPh_2)$] [Pz_2CPh_2 = diphenyl dipyrazolylmethane-*N*,*N*′] [42]. Finally, the Cu–$N_{thiazoline}$ bond distance [Cu–N(1) = 2.012(2) Å] is comparable to the calculated mean value [1.952(38) Å] for 12 copper(II) complexes collected in CSD, and to the Cu–$N_{thiazoline}$ bond length in [$CuCl_2$(TzHy)] [Cu–N(1) = 1.969(3) Å] [TzHy = (4,5-dihydro-1,3-thiazol-2-yl)hydrazine] [27].

The five-membered chelate ring Cu–N(1)–C(1)–N(2)–N(3) shows a conformation near to envelope with the apex at Cu. This atom is 0.263 Å out of the plane formed by N(1), C(1), N(2) and N(3) [maximum mean-plane deviation for C(1) = 0.014 Å]. This geometry is proved by the puckering parameters $q = 0.128$ Å and $\phi = 350.5°$ [35].

As was to be expected, the pyrazole ring N(2)–N(3)–C(4)–C(5)–C(6) is essentially planar with maximum mean-plane deviation for C(4) [0.004 Å]. Nevertheless, the puckering parameters calculated for the thiazoline ring S–C(1)–N(1)–C(2)–C(3) [$q = 0.187$ Å; $\phi = 138.8°$], according to Cremer and Pople [35], indicate a conformation between half-chair and envelope with the C(2) and C(3) atoms deviating above (0.107 Å) and below (0.181 Å), respectively, from the plane formed by S, C(1) and N(1).

As it happens in the case of **1**, the thiazoline ring rotates around C(1)–N(2) bond, disposing N(1) and N(3) atoms to the same side with the aim of coordinating, which leads to a torsion angle N(1)–C(1)–N(2)–N(3) of 2.7(3)°, much lower compared with the value for PyTn [176.4(2)°].

3.2. Magnetic susceptibility measurements

The observed molar magnetic susceptibility for **1** was corrected for diamagnetism and temperature-independent paramagnetism to provide the fully corrected magnetic moment at room temperature, 4.61 BM. The value of the fully corrected magnetic moment obtained for complex **1** can be considered in the range 4.7–5.2 BM characteristic of complexes with the octahedral environment around cobalt(II) [43].

Variable temperature (7.5–300 K) magnetic susceptibility data were collected for polycrystalline sample of the complex **2**. Susceptibility values per mole of dimer as a function of the temperature have been plotted in Fig. 5. This behaviour is typical for ferromagnetic interaction between the two Cu(II) centres of the dimer. The experimental data were fitted using the following Bleaney–Bowers equation [44] for a binuclear compound with a total spin $S = 1$ containing the J' term

$$\chi_M = \frac{2N\beta^2 g^2}{kT - (6J' + \exp(-J/kT))}[3 + \exp(-J/kT)]^{-1}.$$

In this expression, χ_M represents the susceptibility per mole of dimer, corrected for diamagnetism and temperature independent paramagnetism, J is the exchange coupling constant, J' is the interdimers exchange coupling constant and the other symbols have their usual meaning. The average value got from EPR spectrum (2.148) has been taken as g value. The parameters J and J' were determined as adjustable parameters, in a least-squares fitting procedure that led to the values $J = 13.73\ cm^{-1}$ and $J' = -6.04\ cm^{-1}$.

The agreement factor R, defined as $\sum(\chi_{exp} - \chi_{calc})^2/(\chi_{exp})^2$ is then equal to 7.91×10^{-6}.

The positive J parameter implies intradimer ferromagnetic interaction.

Dinuclear copper(II) complexes with a Cu(μ-Cl)$_2$Cu motif containing chloro bridging ligands have been studied in order to draw meaningful magneto-structural correlations. In these complexes, the local geometry around the metal centre is usually a square pyramid with a different degree of distortion towards a trigonal bipyramid. The global arrangement of the two square pyramids gives rise to three types of geometries: square pyramids sharing one base-to-apex edge with the two bases nearly perpendicular to one another (type I), square pyramids sharing one base-to-apex

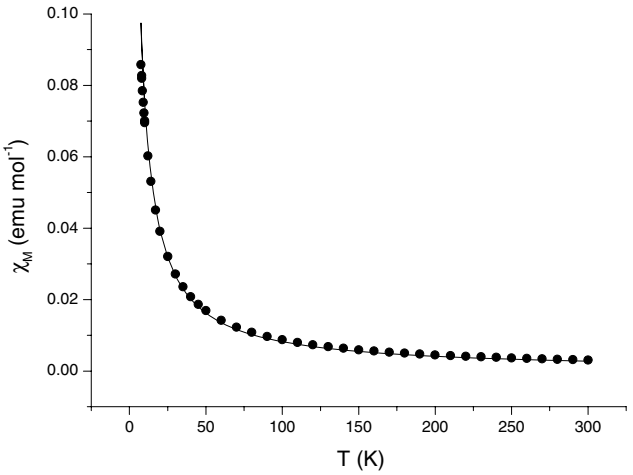

Fig. 5. Variation of the susceptibility as a function of the absolute temperature for [{CuCl(PyTn)}$_2$(μ-Cl)$_2$].

edge but with parallel basal planes (type II) and square pyramids sharing a basal edge with coplanar basal planes (type III). The extended Hückel calculations performed by Rodríguez et al. [45,46] show that the super exchange pathway with the metal centres will take place mainly through a π* type interaction between the $d_{x^2-y^2}$ orbitals of Cu(II) ions and the p orbitals of chloro bridging ligands for type II complexes, as it is the case of $[\{CuCl(PyTn)\}_2(\mu\text{-}Cl)_2]$. For an ideal geometry with a square core, the overlap integral between the former orbitals would be zero, and therefore, there would not be any magnetic coupling between the copper centres. As above, these type II complexes present very small J values, which are due to structural deviations from the ideal square Cu_2Cl_2 core. The small calculated J value for $[\{CuCl(PyTn)\}_2(\mu\text{-}Cl)_2]$ is therefore consistent with the calculations performed by the aforementioned authors.

3.3. Spectroscopic studies

The cobalt(II) complex exhibits a typical spectrum for octahedral species in the solid state [47]. Two multicomponent absorptions are observed in the 6800–11 000 and 15 000–21 000 cm^{-1} ranges, which are assigned to the $^4T_{1g}(F) \rightarrow {}^4T_{2g}(F)$ and $^4T_{1g}(F) \rightarrow {}^4T_{1g}(P)$ transitions, respectively.

The ν_3 and ν_1 bands are splitted into two components of almost equal intensities, that together with the lower magnetic moment value, can be due to the presence of a low symmetry of the crystal field, C_i.

Moreover, the spectrum shows one intense band at 34 020 cm^{-1} which is assigned to the $\pi \rightarrow \pi^*$ transition of the organic ligand.

Ligand field parameters, $10Dq$ and B, were calculated on the basis of octahedral geometry from the averaged values of the ν_1 and ν_3 bands taking the centre of gravity of the total intensity by using the Konig's equations [48]

$$\nu_1 = 1/2(10Dq - 15B) + 1/2[(10Dq + 15B)^2 - 12B \cdot 10Dq]^{1/2},$$
$$\nu_3 = [(10Dq + 15B)^2 - 12B \cdot 10Dq]^{1/2}.$$

The calculated values of the ligand field parameters $10Dq = 9500\ cm^{-1}$ and $B = 740\ cm^{-1}$ are in good agreement with the predicted values for octahedral complexes and are consistent with the presence of a chromophore group $[CoCl_2N_4]$.

The electronic reflectance spectrum of the copper(II) complex displays two strong bands at 34 250 and 27 860 cm^{-1} which can be assigned to organic ligand → Cu and Cl → Cu charge transfer transitions, respectively.

Furthermore, this spectrum consists of a broad d–d asymmetric band centred at about 14 000 cm^{-1} (12 870 cm^{-1} in DMSO solution). Presumably, all four d–d transitions ($^2A[(d_{x^2-y^2})^1] \rightarrow {}^2A[(d_{z^2})^1]$, $^2A[(d_{xy})^1]$, $^2A[(d_{xz})^1]$, $^2A[(d_{yz})^1]$) of the square-pyramidal geometry [49] are responsible to this band.

The EPR spectra of a polycrystalline sample at 298 K (Fig. 6) and at 77 K in DMSO solution (Fig. 7) of complex **2** were recorded in the X-band, using the 100 kHz field modulation.

The EPR parameters of copper(II) complex are presented in Table 5.

The spectrum of **2** at 298 K is typically axial with well-defined $g_\parallel$ and $g_\perp$ values. The geometric parameter $G = (g_\parallel - 2)/(g_\perp - 2)$ value is found to be in the range 3.5–5.0 and $g_\parallel > g_\perp > 2.0023$, which is consistent with a $d_{x^2-y^2}$ ground state having a negligible exchange coupling [49,50].

With regard to the EPR spectrum in frozen DMSO (77 K), it shows four hyperfine lines, characteristic of monomeric copper(II) complexes.

Kivelson and Neiman have shown that $g_\parallel$ is a moderately sensitive function for indicating covalency;

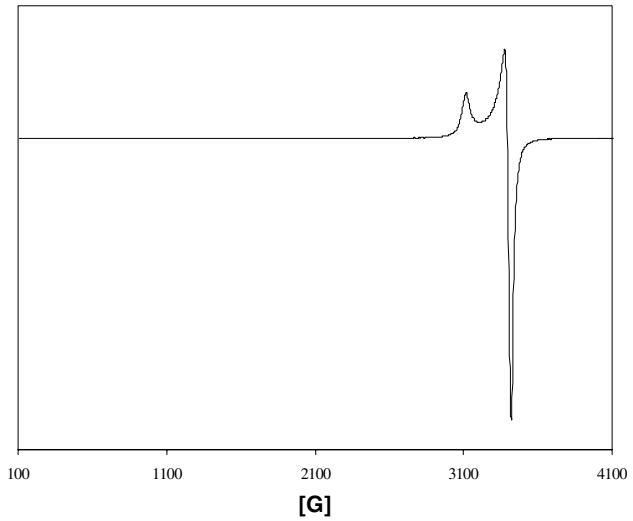

Fig. 6. EPR spectrum of $[\{CuCl(PyTn)\}_2(\mu\text{-}Cl)_2]$ in the polycrystalline state at 298 K.

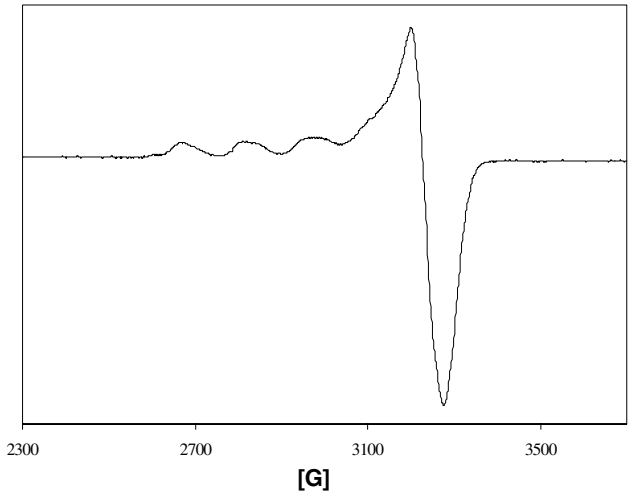

Fig. 7. EPR spectrum of $[\{CuCl(PyTn)\}_2(\mu\text{-}Cl)_2]$ in DMSO solution at 77 K.

Table 5
EPR parameters of $[\{CuCl(PyTn)\}_2(\mu\text{-}Cl)_2]$ (**2**)

Compound	Solid (298 K)		DMSO (77 K)			
	$g_\parallel$	$g_\perp$	$g_\parallel$	$g_\perp$	$A_\parallel$[a]	G
$[CuCl_2(PyTn)]$	2.2437	2.0483	2.2422	2.0499	143.49	4.85

[a] Units: $\times 10^{-4}$ cm^{-1}.

Table 6
Bonding parameters and orbital reduction parameters of $[\{CuCl(PyTn)\}_2(\mu\text{-}Cl)_2]$ (**2**)

Compound	α^2	β^2	γ^2	$K_\parallel$	$K_\perp$
$[\{CuCl(PyTn)\}_2(\mu\text{-}Cl)_2]$	0.6990	0.9768	0.8709	0.6828	0.6088

for an ionic environment, $g_\parallel$ is normally greater than 2.3 and for covalent environment, it is less than 2.3. The $g_\parallel$ value of this compound is found to be less than 2.3, which indicates covalent character of M–L bond [51].

The EPR parameters $g_\parallel$, $g_\perp$, $A_\parallel$ and the energy of the d–d transition band were used to evaluate the bonding parameters α^2, β^2 and γ^2, which may be regarded as measures of the in-plane σ bonds, in-plane π bonds and out-of-plane π bond covalency, respectively (Table 6) [52].

The value of the in-plane σ bonding parameter α^2 was calculated using the following expression [51,53]:

$$\alpha^2 = -A_\parallel/0.036 + (g_\parallel - 2.0023) + 3/7(g_\perp - 2.0023) + 0.04.$$

The orbital reduction factors, $K_\parallel = \alpha^2\beta^2$ and $K_\perp = \alpha^2\gamma^2$ were calculated using the following expressions:

$$K_\parallel^2 = (g_\parallel - 2.0023)E_{d\text{–}d}/8\lambda_0,$$
$$K_\perp^2 = (g_\perp - 2.0023)E_{d\text{–}d}/2\lambda_0,$$

where λ_0 is the spin–orbit coupling constant, with a value of -828 cm^{-1} for a copper(II) system.

According to Hathaway [49], for pure σ bonding, $K_\parallel \approx K_\perp \approx 0.77$, and for in-plane π bonding, $K_\parallel < K_\perp$, while for out-of-plane π bonding, $K_\perp < K_\parallel$. In this complex, it is observed that $K_\parallel > K_\perp$ which indicates the presence of significant out-of-plane π bonding. This is further confirmed by the bonding parameters α^2, β^2 and γ^2, which are less than 1.0, expected for pure ionic character of the bonds, and decrease with increasing covalent nature of the bonding.

Therefore, the evaluated α^2, β^2 and γ^2 values are consistent with both in-plane σ and out-of-plane π bonding.

The IR spectrum of PyTn in the 4000–370 cm^{-1} range presents bands attributable to thiazoline ring vibrations at 1641 (W_1), 991 (W_2), 904 (W_3), 773 (W_4), 677 (W_5), 649 (W_6), 615 (W_8), 575 (W_7) and 428 cm^{-1} (Γ_1) [54,20–27].

Moreover, characteristic bands of pyrazole ring vibrations are detected at 1514 (ν_6), 1392 (ν_{10}), 1350 (ν_{11}), 991 (ν_{17}), 914 (ν_{18}), 674 (ν_{19}) and 649 cm^{-1} (ν_{27}), and likewise, a typical band of N-substituted pyrazoles is found at 1263 cm^{-1} (ν_{12}) [55–57].

Table 7
Infrared bands (cm^{-1}) due to thiazoline and pyrazole rings vibrations of PyTn, $[CoCl_2(PyTn)_2]\cdot 2H_2O$ (**1**) and $[\{CuCl(PyTn)\}_2(\mu\text{-}Cl)_2]$ (**2**)

Assignment	PyTn	**1**	**2**
Thiazoline			
W_1	1641 s	1626 s	1621 s
W_2	991 m	949 m	958 w
W_3	904 s	906 s	902 m
W_4	773 m	760 m	755 sh
W_5	677 w	689 m	681 w
W_6	649 w	654 w	644 w
W_8	615 m	608 s	602 m
W_7	575 w	587 m	575 w
Γ_1	428 w	473 m	420 w
Pyrazole			
ν_6	1514 w	1533 s	1524 s
ν_{10}	1392 s	1401 s	1396 s
ν_{11}	1350 m	1360 s	1364 s
ν_{12}	1263 w	1273 m	1263 m
ν_{17}	991 m	949 m	958 w
ν_{18}	914 m	934 s	934 m
ν_{19}	674 w	669 w	671 sh
ν_{27}	649 w	654 w	644 w

The IR spectra of $[CoCl_2(PyTn)_2]\cdot 2H_2O$ (**1**) and $[\{CuCl(PyTn)\}_2(\mu\text{-}Cl)_2]$ (**2**) in the 4000–370 cm^{-1} region show the presence of bands due to organic moiety rings vibrations, as it is shown in Table 7.

Other relevant bands in the spectrum of **1** are the ones assignable to symmetric and antisymmetric H_2O stretchings at 3495 and 3423 cm^{-1} [23,58]. Moreover, the librational mode of water molecules, due to rotational oscillations, is observed at 553 and 508 cm^{-1} [59], whereas the band attributable to HOH bending and a third librational mode band are hindered by the bands due to W_1 and Γ_1 vibrations.

In the low frequency (500–150 cm^{-1}) region, the C_i symmetry of the cobalt(II) complex predicts the appearance of three bands assignable to metal–ligand stretching vibrations. Thus, the far-infrared spectrum of this complex shows three bands due to this type of vibrations at 303, 283 and 210 cm^{-1}. From these, the band at 303 cm^{-1} could be assigned to ν(Co–Cl) [22,60], the band at 283 cm^{-1} may correspond to $\nu(Co\text{–}N_{Pyrazole})$, according to the literature data [60], while the band at 210 cm^{-1} can be tentatively attributed to ν $(Co\text{–}N_{Thiazoline})$ [21,25].

In the case of the dimer **2**, the appearance of four bands is observed, from which the one at 388 cm^{-1} may be attributed to $\nu(Cu\text{–}N_{Pyrazole})$ vibration [61], whereas the band at 319 cm^{-1} could be assigned to $\nu(Cu\text{–}Cl_{terminal})$ [27,59,62–64]. The band at 295 cm^{-1} may comprise the two $\nu(Cu\text{–}Cl_{bridging})$ vibrations [27,59,62–64], and finally, $\nu(Cu\text{–}N_{Thiazoline})$ vibration is found at 249 cm^{-1} [24].

4. Supplementary material

CCDC Nos. 259316, 272078 and 259315 corresponding to PyTn, $[CoCl_2(PyTn)_2]\cdot 2H_2O$ and $[\{CuCl(PyTn)\}_2(\mu\text{-}Cl)_2]$ contain the supplementary crystallographic data

for this paper. These data can be obtained free of charge via www.ccdc.cam.ac.uk/conts/retrieving.html (or from the CCDC, 12 Union Road, Cambridge CB2 1EZ, UK; fax: +44 1223 336 033; e-mail: deposit@ccdc.cam.ac.uk).

Acknowledgements

We thank the Junta de Extremadura and the FEDER [Projects 2PR02A098 and 2PR04A011] for financial support. A.M. Lozano-Vila thanks the Spanish Ministerio de Ciencia y Tecnología for her Ph.D. fellowship.

References

[1] H.R. Hoveyda, V. Karunaratne, C. Orvig, Tetrahedron 48 (1992) 5219.
[2] C.G. Bonde, N.J. Gaikwad, Bioorg. Med. Chem. 12 (2004) 2151.
[3] S.H. Kim, H. Son, G. Nam, D.Y. Chi, J.H. Kim, Bioorg. Med. Chem. Lett. 10 (2000) 1143.
[4] L.M. Cañedo, J.A. de la Fuente, C. Gesto, M.J. Ferreiro, C. Jiménez, R. Riguera, Tetrahedron Lett. 40 (1999) 6841.
[5] C.G. van Kralingen, J. Reedijk, A.L. Spek, Inorg. Chem. 19 (1980) 1481.
[6] C.A. Bolos, K.T. Papazisis, A.H. Kortsaris, S. Voyatzi, D. Zambouli, D.A. Kyriakidis, J. Inorg. Biochem. 88 (2002) 25.
[7] K. Schmidt, M. Jung, R. Keilitz, B. Schnurr, R. Gust, Inorg. Chim. Acta 306 (2000) 6.
[8] A. Ino, A. Murabayashi, Tetrahedron 55 (1999) 10271.
[9] A. Ino, Y. Hasegawa, A. Murabayashi, Tetrahedron 55 (1999) 10283.
[10] R.J. Boyce, G.C. Mulqueen, G. Pattenden, Tetrahedron Lett. 35 (1994) 5705.
[11] F.J. Schmitz, M.B. Ksebati, J.S. Chang, J.L. Wang, M.B. Hossain, D. van der Helm, J. Org. Chem. 54 (1989) 3463.
[12] Z. Chang, N. Sitachitta, J.V. Rossi, M.A. Roberts, P.M. Flatt, J. Jia, D.H. Sherman, W.H. Gerwick, J. Nat. Prod. 67 (2004) 1356.
[13] J.-Y. Lai, J. Yu, B. Mekonnen, J. Falck, Tetrahedron Lett. 37 (1996) 7167.
[14] Z.-X. Huang, P.M. May, D.R. Williams, M. Gozálvez, Inorg. Chim. Acta 56 (1981) 41.
[15] L.S. Goodman, A. Gilman, The Pharmacological Basis of Therapeutics, Macmillan, New York, 1980.
[16] H. Yakamoto, Y. Eikyu, S. Okuda, K. Kawabata, H. Takasugi, H. Tanaka, S. Matsumoto, Y. Matsumoto, S. Tawara, Bioorg. Med. Chem. 10 (2002) 1535.
[17] A.A. Bekhit, T. Abdel-Aziem, Bioorg. Med. Chem. 12 (2004) 1935.
[18] F. Mani, Coord. Chem. Rev. 120 (1992) 325.
[19] N. Kitajima, W.B. Tolman, Prog. Inorg. Chem. 43 (1995) 419.
[20] A. Bernalte-García, F.J. García-Barros, F.J. Higes-Rolando, A.M. Pizarro-Galán, C. Valenzuela-Calahorro, Thermochim. Acta 339 (1999) 95.
[21] A. Bernalte-García, F.J. García-Barros, F.J. Higes-Rolando, F. Luna-Giles, Polyhedron 18 (1999) 2907.
[22] A. Bernalte-García, F.J. García-Barros, F.J. Higes-Rolando, F. Luna-Giles, Polyhedron 20 (2001) 3315.
[23] F.J. Barros-García, A. Bernalte-García, F.J. Higes-Rolando, F. Luna-Giles, R. Pedrero-Marín, E. Viñuelas-Zahínos, Inorg. Chim. Acta 357 (2004) 1457.
[24] F.J. Barros-García, A. Bernalte-García, F.J. Higes-Rolando, F. Luna-Giles, M.A. Maldonado-Rogado, E. Viñuelas-Zahínos, Inorg. Chim. Acta 357 (2004) 3574.
[25] F.J. Barros-García, A. Bernalte-García, A.M. Lozano-Vila, F. Luna-Giles, E. Viñuelas-Zahínos, Polyhedron 24 (2005) 129.
[26] F.J. Barros-García, A. Bernalte-García, F. Luna-Giles, M.A. Maldonado-Rogado, E. Viñuelas-Zahínos, Polyhedron 24 (2005) 1125.
[27] F.J. Barros-García, A. Bernalte-García, F.J. Higes-Rolando, F. Luna-Giles, A.M. Pizarro-Galán, E. Viñuelas-Zahínos, Z. Anorg. Allg. Chem. 631 (2005) 1898.
[28] R.D. Haugwitz, B.V. Maurer, A.J. Martínez, G.A. Jacobs, V.L. Narayanan, Synthesis (1976) 336.
[29] G.M. Sheldrick, SADABS: Program for Empirical Absorption Correction, University of Göttingen, Göttingen, Germany, 1996.
[30] L.J. Farrugia, J. Appl. Crystallogr. 32 (1999) 837.
[31] C. Cohen-Addad, Acta Crystallogr., Sect. B 38 (1982) 1753.
[32] T. La Cour, S.E. Rasmussen, Acta Chem. Scand. 27 (1973) 1845.
[33] I.J. Bruno, J.C. Cole, P.R. Edgington, M. Kessler, C.F. Macrae, P. McCabe, J. Pearson, R. Taylor, Acta Crystallogr., Sect. B 58 (2002) 389.
[34] F.H. Allen, Acta Crystallogr., Sect. B 58 (2002) 380.
[35] D. Cremer, J.A. Pople, J. Am. Chem. Soc. 97 (1975) 1354.
[36] A.W. Addison, T.N. Rao, J. Reedijk, J. Van Rijn, G.C. Verschorr, J. Chem. Soc., Dalton Trans. (1984) 1349.
[37] A.G. Orpen, L. Brammer, F.H. Allen, O. Kennard, D.G. Watson, R. Taylor, J. Chem. Soc., Dalton Trans. (1989) S1.
[38] R.H.P. Francisco, J.R. Lechat, A.C. Massabni, C.B. Melios, M. Molina, J. Coord. Chem. 10 (1980) 149.
[39] A.J. Costa-Filho, C.E. Munte, C. Barberato, E.E. Castellano, M.P.D. Mattioli, R. Calvo, O.R. Nascimento, Inorg. Chem. 38 (1999) 4413.
[40] S. Kingsley, V. Chandrasekhar, C.D. Incarvito, M.K. Lam, A.L. Rheingold, Inorg. Chem. 40 (2001) 5890.
[41] G. Valle, R. Ettorre, V. Peruzzo, Acta Crystallogr., Sect. C 51 (1995) 1293.
[42] J.L. Shaw, T.B. Cardon, G.A. Lorigan, C.J. Ziegler, Eur. J. Inorg. Chem. (2004) 1073.
[43] B.N. Figgis, J. Lewis, Prog. Inorg. Chem. 6 (1964) 37.
[44] B. Bleaney, K.D. Bowers, Proc. R. Soc. London Ser. A 214 (1952) 451.
[45] M. Rodríguez, A. Llobet, M. Corbella, A.E. Martell, J. Reibenspies, Inorg. Chem. 38 (1999) 2328.
[46] M. Rodríguez, A. Llobet, M. Corbella, Polyhedron 19 (2000) 2483.
[47] A.B.P. Lever, Inorganic Electronic Spectroscopy, 2nd ed., Elsevier, Amsterdam, 1984.
[48] D.K. Rastogi, K.C. Sharma, S.K. Dua, M.P. Teotia, J. Inorg. Nucl. Chem. 37 (1975) 685.
[49] B.J. Hathaway, in: G. Wilkinson, R.D. Gillard, J.A. McCleverty (Eds.), Comprehensive Coordination Chemistry, vol. 5, Pergamon Press, Oxford, 1987.
[50] B.J. Hathaway, J. Chem. Soc., Dalton Trans. (1972) 1196.
[51] D. Kivelson, R.R. Neiman, J. Chem. Phys. 35 (1961) 149.
[52] M. Joseph, V. Suni, M.R. Prathapachandra Kurup, M. Nethaji, A. Kishore, S.G. Bhat, Polyhedron 23 (2004) 3069.
[53] A.H. Maki, B.R. McGarvey, J. Chem. Phys. 29 (1958) 35.
[54] G. Mille, J.L. Meyer, J. Chouteau, J. Mol. Struct. 50 (1978) 247.
[55] G. Zerbi, C. Alberti, Spectrochim. Acta 18 (1962) 407.
[56] J.R. Durig, M. Mamula Bergana, W.M. Zunic, J. Raman Spectrosc. 23 (1992) 357.
[57] J.M. Orza, O. Mó, M. Yánez, J. Elguero, Spectrochim. Acta Part A 53 (1997) 1383.
[58] F.J. Barros-García, A. Bernalte-García, F.J. Higes-Rolando, F. Luna-Giles, R. Pedrero-Marín, Polyhedron 23 (2004) 1453.
[59] K. Nakamoto, Infrared and Raman Spectra of Inorganic and Coordination Compounds. Part B: Applications in Coordination, Organometallic and Bioinorganic Chemistry, 5th ed., Wiley, New York, 1997.
[60] A. Chadghan, J. Pons, A. Caubet, J. Casabó, J. Ros, A. Álvarez-Larena, J.F. Piniella, Polyhedron 19 (2000) 855.
[61] J. Pons, A. Chadghan, J. Casabó, A. Álvarez-Larena, J.F. Piniella, J. Ros, Polyhedron 20 (2001) 2531.
[62] B. De Castro, C. Freire, D. Domínguez, J. Gomes, Polyhedron 10 (1991) 2541.
[63] A. Bernalte-García, F.J. García-Barros, F.J. Higes-Rolando, F. Luna-Giles, R. Pedrero-Marín, J. Inorg. Biochem. 98 (2004) 15.
[64] Y.J. Weaver, J.A. Weaver, J. Nucl. Inorg. Chem. 37 (1975) 1309.

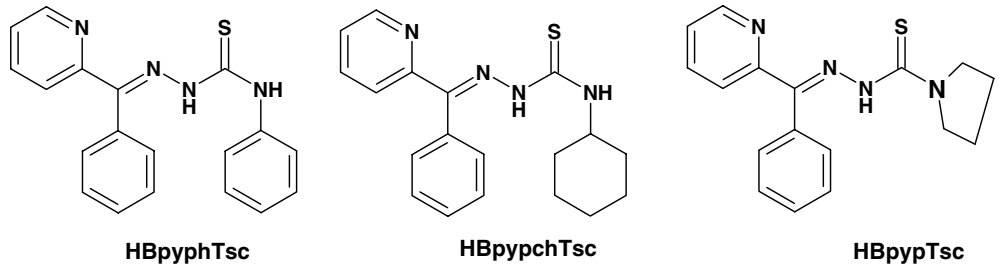

Fig. 1. Structures of thiosemicarbazones.

2 mmol) in chloroform. The reaction mixture was refluxed for 20 min and cooled. Deep brown shining microcrystals of compound **1** separated out, which were filtered, washed thoroughly with ether and dried over P_4O_{10} in vacuo. X-ray quality single crystals were grown from a solution of chloroform in 6 days.

*2.2.2. Synthesis of [Mn(BpychTsc)$_2$] · H_2O (**2**)*

Manganese acetate (0.2449 g, 1 mmol) dissolved in 20 ml ethanol and HBpychTsc (0.676 g, 2 mmol) dissolved in 30 ml hot ethanol were mixed and stirred for 3 h. The yellow colored solid, which separated on cooling, were filtered, washed with hot ethanol and ether and dried over P_4O_{10} in vacuo.

*2.2.3. Synthesis of [Mn(BpyphTsc)$_2$] (**3**)*

Manganese sulphate (0.169 g, 1 mmol) dissolved in a mixture of hot water and methanol and HBpyphTsc (0.664 g, 2 mmol) dissolved in 30 ml hot methanol were mixed and stirred for 3 h. The yellow colored solids, which separated, were filtered, washed with hot ethanol and ether and dried over P_4O_{10} in vacuo.

2.3. Physical measurements

Elemental analyses were carried out using a Heraeus elemental analyzer at CDRI, Lucknow, India. Molar conductance measurements of the complexes of the solutions in dimethylformamide (10^{-3} M) at room temperature were measured using a digital conductivity meter. The magnetic susceptibility measurements were carried out at Indian Institute of Technology, Roorkee, India, at room temperature in the polycrystalline state on a PAR model 155 vibrating sample magnetometer at 5 K Oersted field strength.

The IR spectra were recorded on a Shimadzu DR 8001 series FTIR instrument using KBr pellets. The solid-state reflectance spectra of the ligand and the complexes were recorded on Ocean Optics, Inc. SD2000 Fibre Optic Spectrometer. The EPR spectra of the complexes were recorded in a Varian E-112 Spectrometer using TCNE as the standard at SAIF, IIT, Bombay, India.

2.4. X-ray crystallography

Single crystals of compound **1** for X-ray analysis were grown by slow evaporation of the complex in chloroform/methanol mixture. A deep brown shining crystal of compound **1** was mounted on a glass fiber with epoxy cement. The crystallographic data and structure refinement parameters for the compound are given in Table 1. The data were collected using a Bruker Smart Apex CCD diffractometer equipped with graphite monochromated Mo Kα ($\lambda = 0.71073$ Å) radiation at temperature 293 K. The trial structure was solved using SHELXS-97 and refinement was carried out by full-matrix least squares on F^2 (SHELXTL) [7]. Molecular graphics employed was ORTEP-III and PLATON [8].

3. Results and discussion

3.1. Synthesis of complexes

Colors, elemental analyses and stoichiometries of the three Mn(II) complexes are presented in Table 2. All the

Table 1
Crystal refinement parameters of compound **1**

Empirical formula	$C_{34}H_{34}MnN_8S_2$
Formula weight	673.75
Temperature (K)	293(2)
Wavelength (Å)	0.71073
Crystal system, space group	monoclinic, $P21/c$
Unit cell dimensions	
a (Å)	10.7790(7)
b (Å)	20.4342(13)
c (Å)	14.9354(9)
α (°)	90
β (°)	94.895(1)
γ (°)	90
Volume (Å^3)	3277.7(4)
Z, calculated density (Mg/m^3)	4, 1.365
Absorption coefficient (mm^{-1})	0.568
$F(000)$	1404
Crystal size (mm)	$0.40 \times 0.32 \times 0.10$
θ Range for data collection (°)	2.42–25.00
Limiting indices	$-12 \leqslant h \leqslant 12$, $-16 \leqslant k \leqslant 24$, $-17 \leqslant l \leqslant 14$
Reflections collected/unique	13145/5719 [$R_{(int)} = 0.0964$]
Completeness to $\theta = 25.00$	99.2%
Absorption correction	Empirical
Maximum and minimum transmission	0.9454 and 0.8047
Refinement method	Full-matrix least-squares on F^2
Data/restraints/parameters	5719/0/406
Goodness-of-fit on F^2	1.057
Final R indices [$I > 2\sigma(I)$]	$R_1 = 0.0966$, $wR_2 = 0.2006$
R indices (all data)	$R_1 = 0.1791$, $wR_2 = 0.2369$
Largest difference peak and hole (e Å^{-3})	0.458 and −0.449

Table 2
Stoichiometries and partial elemental analyses of the complexes

Compound	Empirical formula	Colour	Found (calculated) %			Λ_M[1] (in DMF)	μ B.M.
			C	H	N		
$[Mn(BpypTsc)_2]$ (**1**)	$C_{34}H_{34}MnN_8S_2$	Brown	60.60 (60.63)	5.01 (5.05)	16.63 (16.64)	3.2	6.01
$[Mn(BpychTsc)_2]\cdot H_2O$ (**2**)	$C_{38}H_{44}N_8S_2OMn$	Yellow	61.78 (61.15)	5.96 (5.88)	14.92 (14.95)	1.8	5.94
$[Mn(BpyphTsc)_2]$ (**3**)	$C_{38}H_{30}N_8S_2Mn$	Yellow	63.27 (63.70)	4.30 (4.17)	15.46 (15.57)	5.02	5.79

[1] Molar conductivity of 10^{-3} M solution, in ohm^{-1} cm^2 mol^{-2}.

compounds are soluble in polar organic solvents like chloroform, DMF, DMSO, etc. The three complexes synthesized using the three ligands have the same stoichiometry $[ML_2]$, i.e. a structure in which two anionic ligands are coordinated to the Mn(II) ion.

Conductivity measurements of the three complexes in DMF (10^{-3} M) indicate that all complexes are nonelectrolytes in DMF. The magnetic moments of the three Mn(II) complexes were calculated from the magnetic susceptibility measurements and using the diamagnetic corrections. The magnetic moments of the three complexes $[Mn(BpypTsc)_2]$, $[Mn(BpychTsc)_2]\cdot H_2O$, and $[Mn(BpyphTsc)_2]$ are 6.01, 5.94 and 5.79 B.M., respectively, indicating the presence of five unpaired electrons and hence these are high spin complexes [9,10].

3.2. Crystal structure of $[Mn(BpypTsc)_2]$

The single crystal X-ray diffraction studies indicate a distorted octahedral geometry for the compound. A list of selected bond parameters of the Mn complex (1) is presented in Table 3. The Mn(II) center is coordinated in an N_4S_2 meridional manner by two monodeprotonated ligand moieties using pairs of *cis* pyridyl-*N*, *trans* azomethine-*N* and *cis* thiolate-*S* atoms and form four five membered chelate rings. Of these, sulfur involving rings are somewhat planar and slightly puckered, while the other two are almost planar. From the bond angles, it is observed that the coordination geometry is quite far from a perfect octahedron. The dihedral angle formed by the mean planes of the bicyclic chelate systems of each of the ligands is 86.36°. The planes containing Mn1, S1, N5, N1, S2 and Mn1, N2, N5, N6, S2 are deviated from the mean plane by −0.7280(1) Å (N5) and −0.2915(1) Å (N6), respectively, whereas Mn1, S1, N2, N1, N6 plane deviated from the mean plane by 0.1392(1) Å (Mn1). However, the N5–Mn1–S2 angle is only 148.0(1) Å. Fig. 2 shows the molecular structure of the compound along with atom numbering scheme.

On coordination to the metal ion, the ligand undergoes structural reorientation as the configuration about the N2–C6 changes from Z to E. This suggests that a possible rotation about the azomethine double bond occurs on coordination and pyridyl nitrogen is now in a position to coordinate as NNS manner. The two thiolate sulfur atoms are observed to be deviated farthest from the central Mn(II) atom, at distances of 2.523(2) Å {Mn1–S1} and 2.499(2) Å {Mn1–S2}, while the Mn–N bonds are observed

Table 3
Selected bond lengths and angles of the compound **1**

Bond lengths (Å)		Bond angles (°)	
Mn(1)–N(2)	2.227(6)	N(2)–Mn(1)–N(6)	155.5(2)
Mn(1)–N(1)	2.307(6)	N(2)–Mn(1)–N(5)	95.2(2)
Mn(1)–S(2)	2.499(2)	N(6)–Mn(1)–N(5)	71.9(2)
Mn(1)–S(1)	2.523(2)	N(2)–Mn(1)–N(1)	71.9(2)
Mn(1)–N(6)	2.232(6)	N(6)–Mn(1)–N(1)	87.1(2)
Mn(1)–N(5)	2.265(6)	N(5)–Mn(1)–N(1)	90.6(2)
S(1)–C(13)	1.705(8)	N(2)–Mn(1)–S(2)	116.4(2)
S(2)–C(30)	1.727(8)	N(6)–Mn(1)–S(2)	76.9(2)
N(3)–C(13)	1.336(9)	N(5)–Mn(1)–S(2)	148.0(2)
N(7)–C(30)	1.341(9)	N(1)–Mn(1)–S(2)	94.9(2)
N(2)–N(3)	1.358(8)	N(2)–Mn(1)–S(1)	76.3(2)
N(6)–N(7)	1.367(8)	N(6)–Mn(1)–S(1)	123.6(2)
N(2)–C(6)	1.296(9)	N(5)–Mn(1)–S(1)	91.6(2)
N(6)–C(23)	1.304(9)	N(1)–Mn(1)–S(1)	148.2(2)
		S(2)–Mn(1)–S(1)	99.7(1)
		C(13)–S(1)–Mn(1)	96.7(3)
		C(30)–S(2)–Mn(1)	96.9(3)

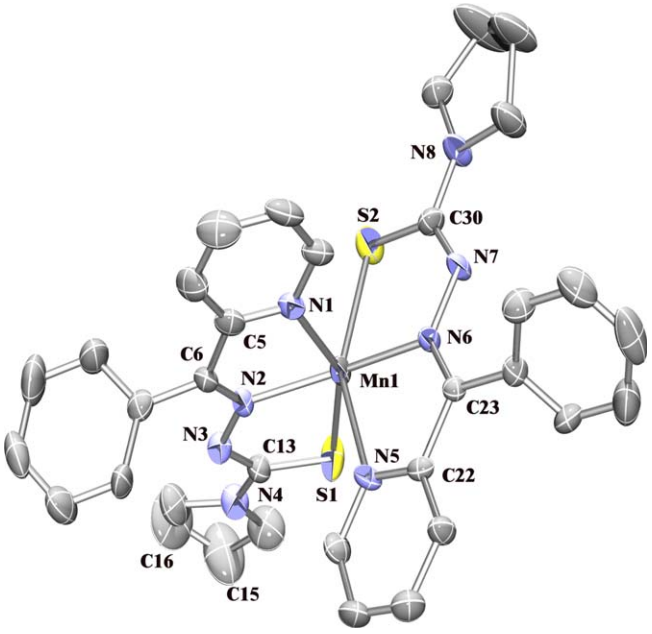

Fig. 2. ORTEP diagram for the compound $Mn(BpypTsc)_2$ (**1**) in 50% probability ellipsoids. Hydrogen atoms are omitted for clarity.

at an average distance of 2.3 Å. The Mn–$N_{azomethine}$, Mn–N_{py}, and Mn–S bond lengths are comparable with the previously reported manganese complexes [11,12]. These comparatively larger bond lengths are indicative of weak bonding of the ligand to the metal. The C13–N3–N2 bond angle reduced from 121.1(2)° of metal free ligand to 113.1(6)° in the complex as a consequence of bonding. Coordination lengthens the thiosemicarbazone moiety's C13–S1 bond length by 0.024(8) Å and C30–S2 by 0.046(8) Å. The decrease in bond length of N3–C13 and N7–C30 by 0.024(10) and 0.019(10) Å, respectively, on coordination confirms the deprotonation after enolization. Ring puckering analysis shows that the N4 containing pyrrolydine ring is closest to a twist form on C15 and C16, and N8 containing ring is in a half chair form [13]. Interestingly, there are no classic hydrogen bonds seen in crystal structure. However, some weak hydrogen bonding and C–H...π interactions including that between metal containing chelate rings Cg(1) and Cg(2) with pyridyl ring protons (Table 4) are seen in the crystal lattice. The orientation in the close packing (Fig. 3) is in such a way that the symmetry related molecules are reinforced by very weak π...π interactions involving phenyl and pyridyl rings (Table 4).

Table 4
H-bonding and C–H...π and π...π interactions in compound (**1**)

D–H...A	H...A (Å)	D...A (Å)	D–H...A (°)
C1–H1A...N7[a]	2.812	3.589	141.73
C10–H10A...S1[d]	2.944	3.729	142.97
C20–H20A...N1[e]	2.944	3.820	157.53
C33–H33B...N4[f]	2.938	3.870	161.68
C33–H33B...N3[f]	2.866	3.740	150.42
C–H...π	**H...Cg (Å)**	**X...Cg (Å)**	**X–H...Cg (°)**
C(1)–H(1A)...Cg(2)[a]	2.75	3.2378	113
C(2)–H(2A)...Cg(1)[b]	2.67	3.4235	139
C(18)–H(18A)...Cg(1)[a]	2.87	3.860	117
C(20)–H(20A)...Cg(7)[c]	2.69	3.6173	175
π...π	**Cg–Cg (Å)**	**α (°)**	**B (°)**
Cg(7)–Cg(8)[a]	5.1707	88.43	45.48
Cg(7)–Cg(8)[c]	4.9968	88.43	7.72
Cg(8)–Cg(7)[a]	5.1707	88.43	42.95
Cg(8)–Cg(8)[c]	3.8715	0.00	24.07
Cg(8)–Cg(9)[g]	5.3681	32.34	38.71
Cg(8)–Cg(10)[c]	5.9712	66.16	53.22
Cg(9)–Cg(8)[d]	5.3681	32.34	57.36
Cg(9)–Cg(10)[d]	5.1362	68.33	6.28
Cg(10)–Cg(7)[g]	5.0802	31.68	38.79
Cg(10)–Cg(8)[c]	5.9712	66.16	38.40
Cg(10)–Cg(9)[c]	5.5928	68.33	36.50
Cg(10)–Cg(9)[h]	5.9144	51.26	52.74

Cg(1) = Mn1, S1, C13, N3, N2; Cg(2) = Mn1, S2, C30, N7, N6; Cg(7) = N1, C1, C2, C3, C4, C5.
Cg(8) = N5, C18, C19, C20, C21, C22; Cg(9) = C7, C8, C9, C10, C11, C12; Cg(10) = C24, C25, C26, C27, C28, C29.
D, donor; A, acceptor; Cg, centroid; α, dihedral angle between planes *I* and *J*; angle Cg(I)–Cg(J).
Equivalent position codes: (a) *x*, *y*, *z*; (b) *x*, 1/2 − *y*, 1/2 + *z*; (c) 2 − *x*, −*y*, 1 − *z*; (d) *x* − 1, +*y*, +*z*; (e) −*x*, −*y*, −*z* + 1; (f) −*x*, +*y* + 1/2, −*z* + 1/2; (g) 1 + *x*, *y*, *z*; (h) 1 + *x*, 1/2 − *y*, 1/2 + *z*.

3.3. Infrared spectra

The infrared spectral assignments (cm^{-1}) of ligands HBpypTsc, HBpychTsc and HBpyphTsc and their Mn(II) complexes are presented in Table 5. The bonding sites of the thiosemicarbazones to the metal ion have been deduced by comparing the spectra of the complexes with the spectra of the ligands.

The *ν*(C=N) bands of thiosemicarbazones are found to be shifted to higher frequencies in **2** and **3** and to lower frequency in **1** indicating the coordination via the azomethine nitrogen [14–16]. The involvement of this nitrogen in bonding is also supported by a shift in *ν*(N–N) to higher frequencies. The appearance of a new band at 1450 cm^{-1} in the IR spectra of compound **1** and bands at ≈1510 cm^{-1} in compounds **2** and **3** due to the newly formed *ν*(N=C) support the above observation. The bands observed at ca. 1370 and 830 cm^{-1}, which are assigned to *ν*(C=S) and *δ*(C=S) vibrations in the free ligands are shifted to lower wavenumbers in the complexes suggesting the change of bond order and strong electron-delocalization. This large negative shift of the *ν*(C=S) band indicates the coordination of the ligand via the thiolate sulfur to the manganese atom. The coordination of the nitrogen atom of the pyridine ring to the Mn(II) ion in the complexes is indicated by the shifting of the pyridine ring vibrations of the ligands to higher frequencies in their manganese complexes [17–19]. In the far IR spectra of the complexes, the bands at ca. 470, 424 and 310 cm^{-1} are assigned to the *ν*(Mn–$N_{azomethine}$), *ν*(Mn–S) and *ν*(Mn–N_{py}) modes [20] respectively.

3.4. Electronic spectra

The diffuse reflectance spectra of the three Mn(II) complexes were recorded in MgO matrix and the spectral data are given in Table 6. The ground state of the high spin octahedrally coordinated Mn^{2+} ion is $^6A_{1g}$. Since there are no other terms of sextet spin multiplicity, all the d–d transitions in high spin d^5 complexes are not only Laporte forbidden but also spin forbidden [21]. The d^5 configuration gives rise to the ^4G, ^4D and ^4P excited states. The diffuse reflectance spectra of the Mn(II) complexes exhibit weak absorption bands at ca. 18 000, 23 000 and 25 974 cm^{-1}. The three lowest energy bands are assigned to $^6A_{1g} \rightarrow {}^4T_{1g}(G)$, $^6A_{1g} \rightarrow {}^4T_{2g}(G)$ and $^6A_{1g} \rightarrow {}^4Eg(G)$, $^4A_{1g}(G)$ transitions. The pair of transitions $^6A_{1g} \rightarrow {}^4Eg(G)$, $^4A_{1g}(G)$, are degenerate in octahedral symmetry whose energies are given by $10B + 5C$. These assignments are obtained by fitting the observed spectrum to the Tanabe Sugano diagram [22]. The energies corresponding to the above transitions and the values of Racah parameters *B* and *C* and *D*q calculated are given in Table 6. The extent of covalence in the metal–ligand bond may be evaluated from the electronic spectrum by estimating $\beta = B/B_0$. The value of B_0 for Mn^{2+} is 860 cm^{-1} [23]. The absorption bands observed for $n \rightarrow \pi^*$ and $\pi \rightarrow \pi^*$ transitions of the ligands are slightly shifted in the complexes.

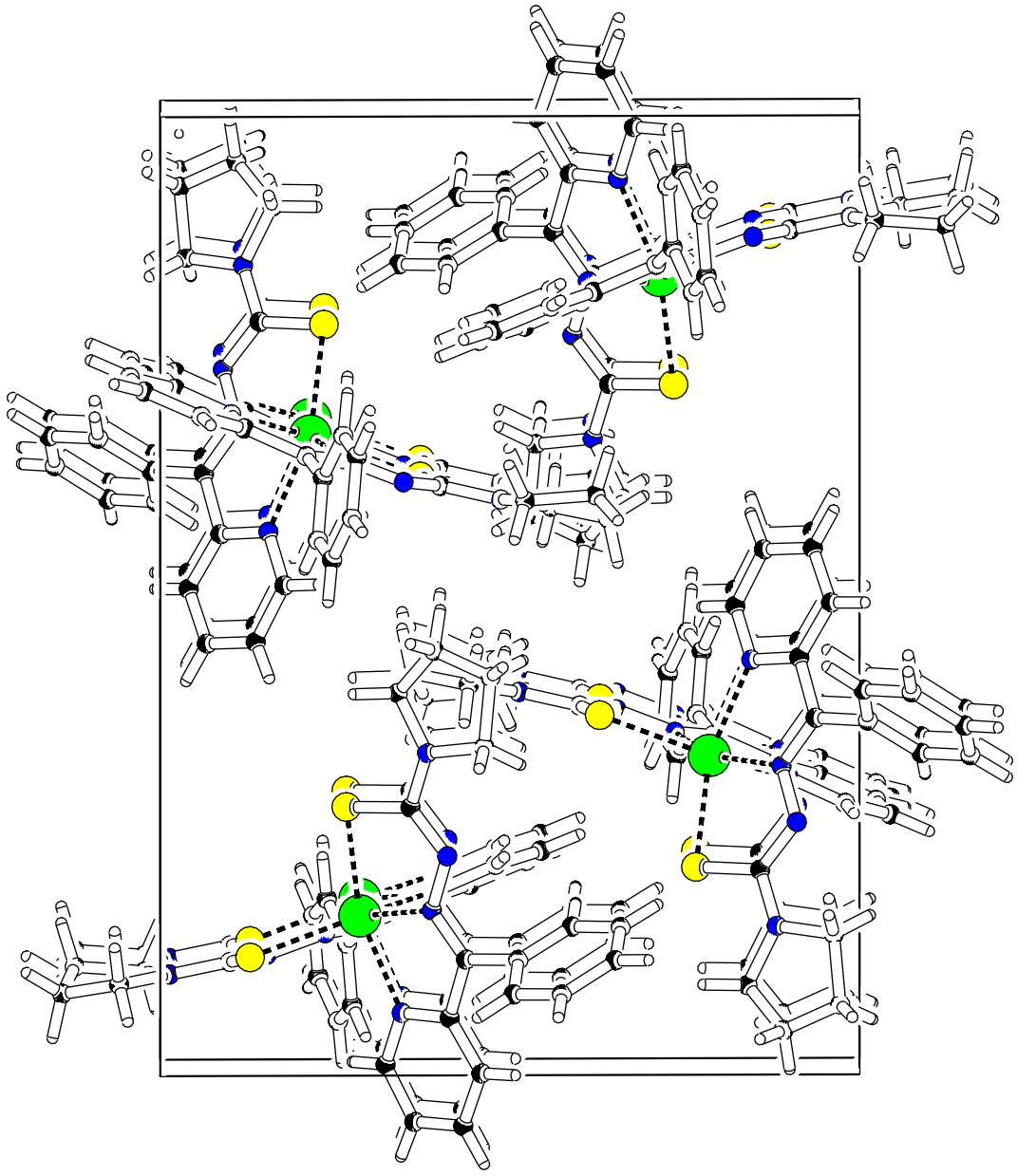

Fig. 3. Packing diagram of compound **(1)** viewing along the '*a*'-axis.

3.5. Electron paramagnetic resonance spectra

The spin Hamiltonian used to represent the EPR spectra of Mn(II) is given by $\mathscr{H} = g\beta Hs + D[S_z^2 - S(S+1)/3] + E(S_x^2 - S_y^2)$, where H is the magnetic field vector, g is the spectroscopic splitting factor, β the Bohr magneton, D is the axial zero field splitting term, E is rhombic zero field splitting parameter and S is the electron spin vector [24]. If D and E are very small compared to $g\beta Hs$, five EPR transitions are expected viz., $|+5/2> \leftrightarrow |+3/2>$, $|+3/2> \leftrightarrow |+1/2>$, $|+1/2> \leftrightarrow |-1/2>$, $|-1/2> \leftrightarrow |-3/2>$ and $|-3/2> \leftrightarrow |-5/2>$.

In the X band, CW-EPR spectra of the polycrystalline samples of the three manganese(II) complexes, a broad signal is observed with g value ~2.19. In polycrystalline samples, at room temperature, Mn(II) complexes give very broad signals, which are due to dipolar interactions and enhanced spin lattice relaxation [25].

The EPR spectra of the three compounds in DMF solution at 298 K are almost similar exhibiting a six line manganese hyperfine pattern centered at $g = 2.015$, 1.993 and 2.008, respectively. A sextet is observed in the spectra of the compound **2** and **3** in solution at room temperature due to electron spin nuclear spin coupling. This hyperfine spectrum of six lines corresponds to $m_I = \pm 5/2$, $\pm 3/2$, $\pm 1/2$, resulting from allowed transitions ($\Delta m_s = \pm 1$, $\Delta m_I = 0$). These hyperfine lines are not clearly resolved in the spectrum of compound **1**, due to poor glass formation.

In addition to this a pair of low intensity forbidden lines lying between each of the two main hyperfine lines is

Table 5
IR spectral assignments of Mn(II) complexes

Compound	ν(C=N)	ν(N–N)	ν(C–S)	$\delta_{(C=S)}$	ρ(py)	ν(Mn–N)	ν(Mn–S)	ν(Mn–N)
HBpypTsc	1630s	1118s	1342s	842m	649m			
[Mn(BpypTsc)$_2$] (**1**)	1611s	1123m	1321s	785m	661m	521w	416s	318w
HBpychTsc	1582s	1118s	1370s	833m	607m			
[Mn(BpychTsc)$_2$]·H$_2$O (**2**)	1632m	1149m	1313s	786s	643w	459s	418s	303s
HBpyphTsc	1591s	1102s	1369s	835m	622m			
[Mn(BpyphTsc)$_2$] (**3**)	1625m	1128s	1325s	782m	630s	489s	428m	316s

Table 6
Electronic spectral data of Mn(II) complexes (cm^{-1})

Compound	$^6A_{1g} \rightarrow {}^4T_{1g}$(G)	$^6A_{1g} \rightarrow {}^4T_{2g}$(G)	$^6A_{1g} \rightarrow {}^4$Eg, $^4A_{1g}$(G)	$n \rightarrow \pi^*$	$\pi \rightarrow \pi^*$	B	10Dq (cm^{-1})	C (cm^{-1})	$\beta = B/B_0$
HBpypTsc				29240, 29760	43300				
[Mn(BpypTsc)$_2$] (**1**)	18083	22471	25164	31545	36100	694	8584	2232	0.8069
HBpychTsc				28735	38610				
[Mn(BpychTsc)$_2$]·H$_2$O (**2**)	18181	22883	25906	29940	36900	692	8060	3058	0.8046
HBpyphTsc				29410	37313				
[Mn(BpyphTsc)$_2$] (**3**)	18083	23094	25706	30395	36100	667	8000	2948	0.7756

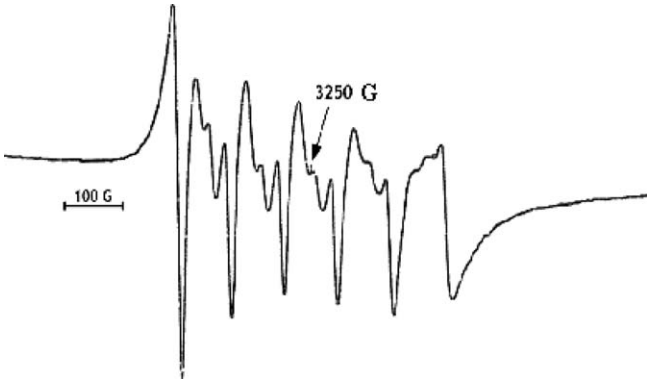

Fig. 4. EPR spectrum of compound **2** in DMF at 77 K.

observed in the frozen solution spectra of the complexes **2** (Fig. 4) and **3** in DMF at 77 K. The forbidden lines in the spectrum arise due to the mixing of the nuclear hyperfine levels by the zero-field splitting factor of the Hamiltonian [26,27]. The ^{55}Mn hyperfine coupling constant for the complexes are estimated to be approximately $A = 270$, 253 and 247 MHz, respectively. The average separation of the forbidden hyperfine lines in the spectrum is approximately 70 MHz.

The observed g values are very close to the free electron spin value of 2.0023 indicating the absence of spin–orbit coupling in the ground state, $^6A_1$. It is seen that the A values are somewhat lower than those of the pure ionic compounds. The A_{iso} values are consistent with the octahedral coordination [28]. Based on the spectral studies an octahedral structure can be assigned to the Mn(II) complexes.

4. Supplementary information

Crystallographic data for the structural analysis has been deposited with the Cambridge Crystallographic Data center, CCDC 222664 for compound Mn(BpypTsc)$_2$ (**1**). The data can be obtained free of charge at www.ccdc.cam.ac.uk/conts/retrieving.html (or from Cambridge Crystallographic Data Centre (CCDC), 12 Union Road, Cambridge CB2 1EZ, UK; fax: +44 0 1223-336033; e-mail: deposit@ccdc.cam.ac.uk).

Acknowledgements

One of the authors A.S. is thankful to the Cochin University of Science and Technology, Kochi, India, for a Junior Research Fellowship. M. Joseph thanks the University Grant Commission for financial support. M.R.P. Kurup is thankful to DST, New Delhi for financial support. The authors thank the Malaysian Government and Universiti Sains Malaysia for research grant R&D No. 305/PFIZIK/610961.

References

[1] K. Wieghardt, Angew. Chem., Int. Ed. 28 (1989) 1153.
[2] N.N. Greenwood, A. Earnshaw, Chemistry of the Elements, 2nd ed., Reed Educational and Professional, Oxford, 1997.
[3] A. Sreekanth, M.R.P. Kurup, Polyhedron 23 (2004) 969.
[4] M. Joseph, V. Suni, C.R. Nayar, M.R.P. Kurup, H.-K. Fun, J. Mol. Struct. 705 (2004) 63.
[5] M. Joseph, V. Suni, M.R.P. Kurup, M. Nethaji, A. Kishore, S. Bhat, Polyhedron 23 (2004) 3069.
[6] M. Joseph, M. Kuriakose, M.R.P. Kurup, M. Nethaji, A. Kishore, S. Bhat, Polyhedron (in press).
[7] G.M. Sheldrick, SHELXS-97 Program for the Solution of Crystal Structures, University of Göttingen, Göttingen, Germany, 1997.
[8] A.L. Spek, PLATON, A Multipurpose Crystallographic Tool, Utrecht, Netherlands, 1999.
[9] B.N. Figgis, Introduction to Ligand fields, Wiley Eastern Limited, New Delhi, 1976.
[10] B.N. Figgis, J. Lewis, Prog. Inorg. Chem. 6 (1964) 37.
[11] V. Philip, V. Suni, M.R.P. Kurup, M. Nethaji, Spectrochim. Acta A (in press).
[12] A. Usman, I.A. Razak, S. Chantrapromma, H.-K. Fun, A. Sreekanth, S. Sivakumar, M.R.P. Kurup, Acta Cryst. C 58 (2002) m461.
[13] D. Cremer, J.A. Pople, J. Am. Chem. Soc. 97 (1975) 1354.

[14] A. Sreekanth, M.R.P. Kurup, Polyhedron 22 (2003) 3321.
[15] M.J.M. Campbell, Coord. Chem. Rev. 15 (1975) 279.
[16] B.S. Garg, M.R.P. Kurup, S.K. Jain, Y.K. Bhoon, Transit. Met. Chem. 16 (1991) 111.
[17] E. Bayer, C.G. Witte, J. Coord. Chem. 7 (1977) 13.
[18] D.F. Little, C.J. Long, Inorg. Chem. 7 (1968) 3401.
[19] M. Canadas, E. Lopez-Torres, A. Martinez-Arias, M.A. Mendiola, M.T. Sevilla, Polyhedron 19 (2000) 2059.
[20] K. Nakamoto, Infrared and Raman Spectra of Inorganic and Coordination Compounds, 3rd ed., Wiley, New York, 1978.
[21] J.E. Huheey, E.A. Keiter, R.L. Keiter, Inorganic Chemistry, 4th ed., Addison-Wesley, New York, 1993.
[22] A.B.P. Lever, Inorganic Electronic Spectroscopy, 2nd ed., Elsevier Science Publishing Company, Amsterdam, 1984.
[23] R.L. Dutta, A. Syamal, Elements of Magnetochemistry, 2nd ed., ISBN publication, 1993.
[24] D.J.E. Ingram, Spectroscopy at Radio and Microwave frequencies, 2nd ed., Butterworth, London, 1967.
[25] B.S. Garg, M.R.P. Kurup, S.K. Jain, Y.K. Bhoon, Transit. Met. Chem. 13 (1988) 92.
[26] B. Bleany, R.S. Rubins, Proc. Phys. Soc. Lond. 77 (1961) 103.
[27] W. Linert, F. Renz, R. Boca, J. Coord. Chem. 40 (1996) 293.
[28] R. Singh, I.S. Ahuja, C.L. Yadava, Polyhedron 1 (1981) 327.

IR spectra were recorded on a Pye Unicam SP3-300 spectrophotometer over the spectral range 4000–200 cm^{-1} in the solid state using KBr/CsI Pellets. ^{1}H, ^{19}F and ^{13}C NMR spectra were recorded on Jeol JNM-400 NMR spectrometer using TMS, CF_3COOH and $CDCl_3$ as references, respectively. Antimony was determined according to a literature method [11]. Molecular weights were determined cryoscopically in nitrobenzene using a Beckman thermometer of ±0.01 accuracy. The molar conductance of 10^{-3} M solution of the compounds was determined at 25 °C with a Khera DC610 Digital conductivity meter in methanol.

The FAB mass spectra were recorded on Jeol SX 102 mass spectrometer using DA-6000 data analysis system. Argon was used as bombarding gas at 6 kV, 10 mA. The accelerating voltage was kept at 10 kV. *m*-nitrobenzyl alcohol (NBA) was used as matrix.

2.2. Representative synthetic procedures

2.2.1. Synthesis of $(C_6F_5)_2SbCH_3$

A solution of iodomethane (2.839 g, 0.02 mol) in dry diethyl ether was added drop wise to magnesium turnings (0.486 g, 0.02 mol) embedded in diethyl ether under nitrogen atmosphere at 0 °C. The resulting Grignard solution was cooled upto −10 °C and a solution of $(C_6F_5)_2SbCl$ (9.826 g, 0.02 mol) in dry diethyl ether was slowly added with constant stirring. The mixture was stirred for an additional 1 h at room temperature and subsequently refluxed for 1 h more. The mixture was then cooled to 0 °C and treated with ice water containing NH_4Cl and subsequently followed by the addition of 4 N HCl (1 ml) and stirred to make the solution acidic. The ether layer was separated and the aqueous brownish layer was further extracted with chloroform. The organic layers were then mixed and kept over anhydrous Na_2SO_4 overnight. The organic layer was filtered and the filtrate was distilled on an oil-bath to remove the solvent. The residue was crystallized by petroleum–ether (40–60 °C) to afford pale yellow crystals of $(C_6F_5)_2Sb(CH_3)$ (**1**), yield 6.87 g (73%), m.p. 98–99 °C.

2.2.2. Synthesis of $(C_6F_5)_2Sb(C_6H_4CH_3$-*p*)

p-Bromotoluene (3.421 g, 0.02 mol), dissolved in dry diethyl ether was added drop wise to magnesium turnings (0.486 g, 0.02 mol) embedded in diethyl ether under nitrogen atmosphere at 0 °C. This Grignard solution was cooled upto −10 °C and a solution of $(C_6F_5)_2SbCl$ (9.826 g, 0.02 mol) in dry diethyl ether was slowly added with constant stirring. The mixture was stirred for 2 h at room temperature and subsequently refluxed for 1 h more. The mixture was then cooled to 0 °C and treated with ice water containing NH_4Cl and subsequently followed by the addition of 4 N HCl (1 ml) and stirred to make the solution acidic. The ether layer was separated and the aqueous brownish layer was further extracted with chloroform. The organic layers were then mixed and kept over anhydrous Na_2SO_4 overnight. The organic layer was filtered and the filtrate was distilled on an oil-bath to remove the solvent. The residue was crystallized by petroleum–ether (40–60 °C) to afford $(C_6F_5)_2Sb(C_6H_4CH_3$-*p*) (**2**), yield 7.548 g (69%), m.p. 93 °C.

2.2.3. Synthesis of $(C_6F_5)_2Sb(C_6H_5)$

A solution of bromobenzene (3.140 g, 0.02 mol) in dry diethyl ether was added drop wise to magnesium turnings (0.486 g, 0.02 mol) embedded in diethyl ether under nitrogen atmosphere at 0 °C. The resulting Grignard solution was cooled upto −10 °C and a solution of $(C_6F_5)_2SbCl$ (9.826 g, 0.02 mol) in dry diethyl ether was slowly added with constant stirring. The mixture was stirred for an additional 1 h at room temperature and subsequently refluxed for 1 h more. The mixture was then cooled to 0 °C and treated with ice water containing NH_4Cl and subsequently followed by the addition of 4 N HCl (1 ml) and stirred to make the solution acidic. The ether layer was separated and the aqueous brownish layer was further extracted with chloroform. The organic layers were then mixed and kept over anhydrous Na_2SO_4 overnight. The organic layer was filtered and the filtrate was distilled on an oil-bath to remove the solvent. The residue was crystallized by petroleum–ether (40–60 °C) to afford $(C_6F_5)_2Sb(C_6H_5)$ (**3**), yield 7.035 g (66%), m.p. 89–90 °C.

Similarly the $(C_6F_5)Sb(C_6H_5)_2$ (**4**) was prepared by using Grignard reagent (C_6H_5MgBr) and $(C_6F_5)SbCl_2$.

$(C_6F_5)_2Sb(C_6H_5)$ and $(C_6F_5)Sb(C_6H_5)_2$ were also prepared by the reaction of C_6F_5MgBr with $C_6H_5SbCl_2$ and $(C_6H_5)_2SbCl$, respectively, and the yields were 47% and 26%, respectively. These compounds were synthesized in the same reaction conditions as described earlier for other compounds.

2.2.4. Reaction of $(C_6F_5)_2Sb(C_6H_5)$ and Cl_2 gas

Dry chlorine gas (generated by reaction of $KMnO_4$ and conc. HCl) was bubbled in a solution of $(C_6F_5)_2Sb(C_6H_5)$ (5.33 g, 10 mmol) in petroleum–ether (60–80 °C) at 0 °C under moisture free and nitrogen atmosphere with constant stirring. White precipitate was started to settle down and the bubbling of Cl_2 gas was stopped as soon as pale yellow colour in the solution persist and the reaction mixture was further stirred for 30 min at room temperature, afterwards the solvent was filtered off. The precipitate was washed thrice with petroleum–ether (60–80 °C) to remove unreacted $(C_6F_5)_2Sb(C_6H_5)$. The precipitate was characterized as $(C_6F_5)_2(C_6H_5)SbCl_2$ (**9**), m.p. 207 °C, yield 4.89 g (81%).

Similarly the dichlorides of $(C_6F_5)_2Sb(CH_3)$, $(C_6F_5)_2Sb(C_6H_4CH_3$-*p*) and $(C_6F_5)Sb(C_6H_5)_2$ were obtained.

2.2.5. Reaction of $(C_6F_5)_2Sb(C_6H_5)$ and liquid Br_2

Solution of liquid bromine (1.6 g, 10 mmol) in petroleum–ether (60–80 °C) was added drop wise into a precooled (0 °C) solution of $(C_6F_5)_2Sb(C_6H_5)$ (5.3 g, 10 mmol) in petroleum–ether (60–80 °C) (100 ml) under nitrogen atmosphere with constant stirring. After each drop of addition of liquid bromine, yellow colour disappeared, as soon as the colour of bromine persists, the addition was stopped.

After allowing the temperature to rise slowly to room temperature the petroleum–ether was distilled (50 ml) and solution was cooled overnight to obtain a solid mass. The solid mass was washed thrice with petroleum–ether (60–80 °C) to remove unreacted $(C_6F_5)_2Sb(C_6H_5)$. The residue was characterized as $(C_6F_5)_2(C_6H_5)SbBr_2$ (**10**), m.p. 193–194 °C, yield 5.27 g (76%).

Similarly the dibromides of $(C_6F_5)_2Sb(CH_3)$, $(C_6F_5)_2$-$Sb(C_6H_4CH_3$-*p*) and $(C_6F_5)Sb(C_6H_5)_2$ were obtained.

3. Results and discussion

In our previous publications, we have reported the synthesis of mono- and bis(pentafluorophenyl)antimony(III) chlorides and their oxidative-addition and displacement reactions [5]. So, continuing our interest in the synthesis, reactions and spectroscopic studies of pentafluorophenylantimony derivatives, in the present investigation some new mixed triorganoantimony(III) compounds bearing pentafluorophenyl and hydrocarbon based organic groups, i.e., methyl and aryl, were synthesized by Grignard reaction using methyl- or arylmagnesium halide and pentafluorophenyl antimony(III) chloride in diethylether as shown below (Scheme 1).

Compounds **3** and **4** were also synthesized alternatively by the reaction of pentafluorophenylmagnesium bromide and arylantimony halide (Scheme 2).

It has been observed that earlier method (Scheme 1) is more satisfactory and the yields of the products were high and also the reactions proceeded more smoothly.

The oxidative-addition reactions of these mixed triorganoantimony(III) compounds were also studied and it has been observed that the dihalides could be formed very easily like other triorganoantimony(III) compounds by passing dry chlorine gas or adding a solution of liquid Br_2 in petroleum–ether to a solution of mixed triorganoantimony(III) compounds in petroleum–ether, respectively (Scheme 3).

The molar conductance values of the compounds were evaluated in methanol (10^{-3} M solution), which were in the range of 15–45 Ω^{-1} mol^{-1} cm^2, showing their non-conducting behaviour in solution [12]. The molecular weights and thus van't Hoff factor '*i*' (0.98–1.02) determined cryoscopically in nitrobenzene showed their monomeric nature.

$$nRMgX + (C_6F_5)_{3-n}SbCl_n \longrightarrow (C_6F_5)_{3-n}SbR_n$$

n = 1, X = I, R = CH_3 **1**, X = Br, R = $C_6H_4CH_3$-*p* **2**, C_6H_5 **3**

n = 2, X = Br, R = C_6H_5 **4**

Scheme 1.

$$nC_6F_5MgBr + R_{3-n}SbCl_n \longrightarrow R_{3-n}Sb(C_6F_5)_n$$

R = C_6H_5, n = 1 **3** or 2 **4**

Scheme 2.

$$R_2R'Sb + X_2 \longrightarrow R_2R'SbX_2$$

X = Cl, R = C_6F_5, R′ = CH_3 **5**, $C_6H_4CH_3$-*p* **7**, C_6H_5 **9**

R = C_6H_5, R′ = C_6F_5 **11**

X = Br, R = C_6F_5, R′ = CH_3 **6**, $C_6H_4CH_3$-*p* **8**, C_6H_5 **10**

R = C_6H_5, R′ = C_6F_5 **12**

Scheme 3.

The elemental analysis were also found satisfactory and within permissible limits (Table 1).

3.1. Infrared spectra

IR spectra of the compounds **1**–**12** were recorded in solid state using KBr/CsI pellets in the range of 4000–200 cm^{-1}. Some of the characteristic absorption bands of the synthesized mixed pentafluorophenylantimony(III and V) compound are given in Table 2.

In all derivatives characteristic ν(C–C) bands of C_6F_5 group were appeared at ~1640 (s), 1515 (vs) and 1480 (vs) cm^{-1} as well as ν(C–F) absorption band at ~1380 (s), 1275 (m), 1080 (vs) and 980 (vs) cm^{-1} and comparable to reported values [13].

In compounds **1**, **2** and **5**–**8** aliphatic ν(C–H) stretching vibrations for CH_3 group appeared at ~2900 cm^{-1} and δ(C–H) bending vibrations at 1415–1390 cm^{-1}.

The C_6H_5 group in compounds **2**–**4** and **7**–**12** showed aromatic ν(C–H) stretching vibrations at ~3040-3000 cm^{-1} and ring stretching vibrations ν(C–C) at ~1440 (m) cm^{-1}. In these derivative ring stretching vibrations due to C_6H_5 (except at ~1440 cm^{-1}) [14] and C_6F_5 (except at ~1645 cm^{-1}) [13] groups overlapped at ~1520–1470 cm^{-1} due to close proximities of these absorption bands, hence could not be separately assignable. Further the characteristic out of plane (C–H) bending vibrations δ(C–H) appeared at ~735 (m) cm^{-1}, gave an additional information for the formation of these compounds.

The spectra of all the chlorides show a band at 332 ± 7 cm^{-1} and the spectra of all the bromides show a strong band at 232 ± 5 cm^{-1}, which may be assigned to antimony-chlorine and -bromine stretching vibrations, respectively.

3.2. ^1H NMR spectra

The ^{1}H NMR spectra of compounds **1**–**12** were recorded in $CDCl_3$ using TMS as the reference at 400 MHz instrument. The chemical shift values are tabulated in Table 3.

The signals for CH_3 protons in compound **1**, **5** and **6** appeared at δ 2.65 ± 0.08 ppm as singlet and in compounds **2**, **7** and **8** appeared at δ 2.31 ± 0.04 ppm as singlet. The aryl protons of the compounds **2**–**4** and **7**–**12** appeared at δ 7.15–7.80 ppm as multiplet and do not allow any clear interpretation.

Table 1
Some physical and analytical data of mixed triorganoantimony(III and V) compounds

Comp. No.	Empirical formula (molecular weight)	M.p. (°C)	Yield (%)	Λ_M (Ω^{-1} mol^{-1} cm^2) 10^{-3} M solution in methanol	Analysis: Found (%) (Calculated) (%)		
					C	H	Sb
1	$C_{13}H_3F_{10}Sb$ (470.89)	98–99	73	28.32	33.14 (33.16)	0.62 (0.64)	25.84 (25.86)
2	$C_{19}H_7F_{10}Sb$ (546.99)	93	69	21.08	41.74 (41.72)	1.31 (1.29)	22.29 (22.26)
3	$C_{18}H_5F_{10}Sb$ (532.97)	89–90	66	26.70	40.57 (40.56)	0.93 (0.95)	22.86 (22.84)
4	$C_{18}H_{10}F_5Sb$ (443.02)	34–35	59	24.82	48.78 (48.80)	2.30 (2.27)	27.47 (27.48)
5	$C_{13}H_3F_{10}Cl_2Sb$ (541.80)	104–105	79	34.08	28.80 (28.82)	0.59 (0.56)	
6	$C_{13}H_3F_{10}Br_2Sb$ (630.70)	115–116	72	33.29	24.75 (24.76)	0.46 (0.48)	
7	$C_{19}H_7F_{10}Cl_2Sb$ (617.90)	175	68	30.36	36.90 (36.93)	1.12 (1.14)	
8	$C_{19}H_7F_{10}Br_2Sb$ (706.80)	185	76	29.86	32.32 (32.29)	1.00 (0.99)	
9	$C_{18}H_5F_{10}Cl_2Sb$ (603.87)	207	81	31.67	35.83 (35.80)	0.85 (0.83)	
10	$C_{18}H_5F_{10}Br_2Sb$ (692.78)	193–194	76	29.80	31.20 (31.21)	0.75 (0.73)	
11	$C_{18}H_{10}F_5Cl_2Sb$ (513.92)	201	75	32.09	42.05 (42.07)	1.94 (1.96)	
12	$C_{18}H_{10}F_5Br_2Sb$ (602.83)	211	68	33.13	35.84 (35.86)	1.64 (1.67)	

Table 2
Characteristic IR absorption bands (cm^{-1}) for mixed triorganoantimony(III and V) compounds

Comp. No.	Molecular formula	ν(C–H)	ν(C–C)	δ(C–H)	ν(C–F)	ν(Sb–C)	ν(Sb–Cl)/ν(Sb–Br)
1	$(C_6F_5)_2Sb(CH_3)$	2925, 2910	1641 (s), 1513 (vs), 1487 (vs)	1415 (w), 1393 (m)	1373 (m), 1282 (m), 1079 (vs), 970 (vs)	615 (m)	
2	$(C_6F_5)_2Sb(C_6H_4CH_3$-*p*)	3020, 3012, 2918, 2876	1637 (s), 1514 (vs), 1467 (vs), 1440 (m)	1405 (m), 1395 (w), 786 (m), 749 (m)	1370 (m), 274 (m), 1078 (vs), 968 (vs)	610 (m)	
3	$(C_6F_5)_2Sb(C_6H_5)$	3040, 3009	1638 (s), 1525 (vs), 1490 (vs), 1436 (m), 1432 (m)	789 (w), 734 (m)	1375 (s), 1275 (m), 1078 (vs), 994 (vs)	603 (m)	
4	$(C_6F_5)Sb(C_6H_5)_2$	3043, 3015	1637 (s), 1512 (vs), 1471 (vs), 1432 (m)	784 (m), 731 (s)	1371 (s), 1274 (m), 1076 (vs), 998 (vs)	609 (m)	
5	$(C_6F_5)_2(CH_3)SbCl_2$	2927, 2911	1643 (s), 1515 (vs), 1488 (vs)	1417 (w), 1386 (m)	1396 (m), 1284 (m), 1084 (vs), 972 (vs)	617 (m)	338
6	$(C_6F_5)_2(CH_3)SbBr_2$	2925, 2910	1639 (s), 1513 (vs), 1482 (vs)	1415 (m), 1383 (m)	1393 (m), 1281 (m), 1081 (vs), 969 (vs)	615 (m)	235
7	$(C_6F_5)_2(C_6H_4CH_3$-*p*)$SbCl_2$	3019, 2920, 2836	1639 (s), 1517 (vs), 1470 (vs), 1438 (m)	1410 (m), 1376 (m), 785 (m), 745 (m)	1397 (m), 1272 (m), 1082 (vs), 970 (vs)	615 (m)	334
8	$(C_6F_5)_2(C_6H_4CH_3$-*p*)$SbBr_2$	3017, 2920, 2885	1637 (s), 1519 (vs), 1470 (vs), 1437 (m)	1410 (m), 1375 (w), 787 (m), 740 (m)	1395 (s), 1272 (m), 1080 (vs), 974 (vs)	610 (m)	230
9	$(C_6F_5)_2(C_6H_5)SbCl_2$	3042, 3010	1641 (s), 1530 (vs), 1495 (vs), 1438 (m)	787 (m), 734 (m)	1391 (s), 1288 (m), 1090 (vs), 997 (vs)	610 (m)	335
10	$(C_6F_5)_2(C_6H_5)SbBr_2$	3040, 3010	1638 (m), 1525 (s), 1489 (vs), 1436 (m)	780 (m), 732 (m),	1389 (s), 1286 (m), 1095 (vs), 995 (vs)	605 (m)	232
11	$(C_6F_5)(C_6H_5)_2SbCl_2$	3045, 3015	1640 (s), 1513 (vs), 1494 (vs), 1435 (m)	775 (m), 734 (m)	1391 (s), 1288 (m), 1090 (vs), 996 (vs)	613 (m)	325
12	$(C_6F_5)(C_6H_5)_2SbBr_2$	3040, 3015	1632 (s), 1515 (vs), 1488 (vs), 1430 (m)	766 (m), 731 (w)	1391 (m), 1286 (s), 1092 (vs), 994 (vs)	608 (m)	237

In these mixed triorganoantimony(V) halides **5**–**12**, due to halogens no significant shifting was observed in proton NMR signals compared to parent compounds as only one signal due to methyl protons is observed which indicates that organyl functionalities are present in one plane and halogens acquire apical position. Thus, it may be assigned that these compounds bear trigonal bipyramidal structure.

3.3. ^{19F}NMR spectra

All these compounds showed invariably the signals due to $F_{2,6}$, F_4 and $F_{3,5}$ at δ −121.00 to −129.91 ppm, −147.21 to −150.20 ppm and −157.63 to −160.90 ppm, respectively. The resonance of F_4 was easily recognizable in each spectrum being half of the intensity compared to $F_{2,6}$ and $F_{3,5}$. The F_4 signal appeared as triplet due to $F_{3,5}$ coupling. The $F_{2,6}$ signals appeared as doublet in all these derivatives and the $F_{3,5}$ signals as triplet. The $F_{3,5}$ signals appeared at higher field as compared to the $F_{2,6}$ and F_4 chemical shift, indicating that the electron density has been withdrawn from these centers ($F_{2,6}$ and F_4) to antimony and attached halogens, which may be attributed to a combined effect of electron donor abilities of pentafluorophenyl ring [15] as well as electrophilic nature of the antimony in these compounds. This observation is in accordance to previous studies that the C_1 carbon of perfluorinated benzene ring feels high electron density due to diminished inductive effect of fluorine atom and donation of electron density from the unshared p electron of fluorine to the π system of the ring (p–π interaction) [7,16]. A marginal yet distinct

Table 3
^{1}H and ^{19}F NMR data of mixed triorganoantimony(III and V) compounds

Comp. No.	^{1}H NMR δ (ppm)		^{13}C NMR δ (ppm)	^{19}F NMR δ (ppm)		
	Ph	CH_3		$F_{3,5}$ [$J_{3,4}$ (Hz)]	$F_{2,6}$ [$J_{2,3}$ (Hz)]	F_4
1		2.73 (s)	27.6 (CH_3), 153 ($C_{2,6}$), 149 (C_4), 143.7 ($C_{3,5}$), 140.4 (C_1)	−158.00 (t) [19.54]	−128.00 (d) [20.54]	−148.00 (t)
2	7.16–7.53 (m)	2.35 (s)	21.47 (CH_3), 140 (C_4), 136 (C_1), 134 ($C_{2,6}$), 130 ($C_{3,5}$)	−160.00 (t) [19.53]	−121.00 (d) [20.53]	−150.00 (t)
3	7.31–7.62 (m)		146.6 (C_1), 136.2 ($C_{2,6}$), 130.2 (C_4), 129.4 ($C_{3,5}$)	−160.90 (t) [19.53]	−121.10 (d) [20.54]	−150.10 (t)
4	7.29–7.79 (m)		145.4 (C_1), 136.5 ($C_{2,6}$), 130.4 (C_4), 129.1 ($C_{3,5}$)	−160.80 (t) [19.53]	−121.30 (d) [20.53]	−150.20 (t)
5		2.59 (s)		−157.81 (t) [19.53]	−129.91(d) [20.53]	−147.21 (t)
6		2.68 (s)		−157.63 (t) [19.53]	−128.80 (d) [20.53]	−147.64 (t)
7	7.16–7.60 (m)	2.27 (s)		−159.91 (t) [19.53]	−123.22 (d) [20.54]	−149.81 (t)
8	7.15–7.56 (m)	2.30 (s)		−159.71 (t) [19.53]	−122.71 (d) [20.53]	−149.61 (t)
9	7.28–7.60 (m)			−159.22 (t) [19.54]	−125.90 (d) [20.55]	−149.82 (t)
10	7.30–7.65 (m)			−159.12 (t) [19.54]	−124.78 (d) [20.54]	−149.63 (t)
11	7.25–7.80 (m)			−159.13 (t) [19.53]	−123.82 (d) [20.53]	−148.91 (t)
12	7.30–7.75 (m)			−158.82 (t) [19.53]	−122.91 (d) [20.53]	−149.73 (t)

effect on chemical shift has been noticed due to electronegativity difference of halogens (Cl, Br) attached to antimony. The additive effects of halogens and pentafluorophenyl rings seem to be negligible.

3.4. ^{13}C NMR spectra

In compounds **1** and **2**, ^{13}C signals for CH_3 appeared at δ 27.6 and 21.47 ppm, respectively. Chemical shifts for C_6F_5 group in compound **1**, appeared as very weak signals at δ 140.4 (C_1), 153 ($C_{2,6}$), 143.7 ($C_{3,5}$) and 149 (C_4) ppm, which indicate that C_1 position is more shielded than $C_{3,5}$, $C_{2,6}$ or C_4 centers and the order of chemical shift is $C_1 > C_{3,5} > C_4 > C_{2,6}$.

In compound **2**–**4** the ^{13}C signals due to C_6F_5 group were not prominent thus could not be assigned and only signals for C_6H_5 group were assigned which appeared at δ 129.1–146.6 ppm.

3.5. Mass spectrometry

The FAB mass spectra have been measured for two compounds $(C_6F_5)_2Sb(C_6H_4CH_3\text{-}p)$ (**2**) and $(C_6F_5)_2Sb(C_6H_5)$ (**3**). The FAB mass spectrum of compound **2** showed parent ion peak at m/z 546 (19.1%) for $[(C_6F_5)_2Sb(C_6H_4CH_3)]^+$, but the highest mass fragment was $[(C_6F_5)Sb(C_6H_4CH_3)]^+$ at m/z 379 (100%). Other important peaks at m/z 455 (18.7%), 288 (42.3%) and 212 (32.6%) corresponds to $[(C_6F_5)_2Sb]^+$, $[(C_6F_5)Sb]^+$ and $[(C_6H_4CH_3)Sb]^+$, respectively.

The parent ion peak in the FAB spectrum of compound **3** was $[(C_6F_5)_2Sb(C_6H_5)]^+$ at m/z 532 (36.1%). Two other important peaks for $[(C_6F_5)Sb(C_6H_5)]^+$ at m/z 365 (22.3%) and $[(C_6F_5)Sb]^+$ m/z 288 (53.4%) were also appeared in the spectrum.

4. Conclusion

Hydrocarbon based Grignard reagent found more favourable for the synthesis of such mixed triorganoantimony(III) derivatives and the reactions of these derivatives with halogens took place in similar manner as in case of other triorganoantimony(III) derivatives (Fig. 1).

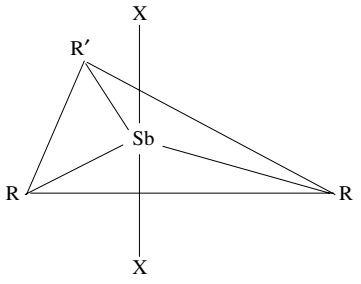

$R \neq R' = C_6F_5$, CH_3, $C_6H_4CH_3\text{-}p$, C_6H_5 and X = Cl or Br

Fig. 1. Configuration of mixed triorganoantimony(V) halides.

Spectroscopic studies revealed that the pentavalent compounds **5**–**12** bear trigonal bipyramidal structure having organyl functionalities in one plane.

Acknowledgements

One of the authors (SKS) is thankful to DRDO, New Delhi for the award of Senior Research Fellowship. Thanks are also due to Mr. N. Ahmed of IIT, Kanpur for extending NMR facilities and RSIC, Lucknow for providing Mass spectra.

References

[1] S.M. Sze (Ed.), Physics of Semiconductor Devices, second ed., Wiley, New York, 1981.
[2] C.R.M. Grovenor (Ed.), Microelectronics Materials, Adam Hilger, Philadelphia, PA, 1989.
[3] R. Tyagi, R.K. Purohit, S.K. Agarwal, A.K. Shreedhar, Mater. Res. Bull. 27 (1992) 623.
[4] S.C. Cohen, A.G. Massey, Advances in Fluorine Chemistry 6 (1970) 83.
[5] P. Raj, A.K. Saxena, K. Singhal, A. Ranjan, Polyhedron 4 (1985) 251, and references therein.
[6] P. Raj, A.K. Aggarwal, A.K. Saxena, J. Fluorine Chem. 42 (1989) 163.
[7] A.K. Saxena, A. Ranjan, K. Misra, P.S. Venkataramani, Indian J. Chem. A 37 (1998) 736.
[8] (a) S.K. Shukla, A. Ranjan, A.K. Saxena, J. Fluorine Chem. 122 (2003) 165;

(b) S.K. Shukla, A. Ranjan, A.K. Saxena, J. Phosphorus Sulfur Silicon 178 (2003) 785;
(c) S.K. Shukla, A. Ranjan, A.K. Saxena, J. Fluorine Chem. 113 (2002) 155;
(d) S.K. Shukla, A. Ranjan, A.K. Saxena, Synth. React. Inorg. Met.-Org. Chem. 30 (50) (2000) 909.
[9] A.I. Vogel, Practical Organic Chemistry, third ed., Longmans, London, 1971.
[10] M. Nunn, D.B. Sowerby, D.M. Wesolek, J. Organomet. Chem. 251 (3) (1983) C45.
[11] T.R. Crompton, Comprehensive Organometallic Analysis, Plenum Press, New York, 1987, p. 27.
[12] W.J. Geary, Coord. Chem. Rev. 7 (1) (1971) 81.
[13] B.A. Nevett, A. Perry, Spectrochim. Acta Part A 31 (2) (1975) 101.
[14] E. Maslowsky Jr., Vibrational Spectra of Organometallic Compounds, Wiley–Interscience, New York, 1977.
[15] M. Fild, O. Glemser, in: P. Tarrant (Ed.), Fluorine Chemistry Reviews, vol. 3, Marcel Dekker, Inc., New York, 1969, pp. 129–144.
[16] W.A. Sheppard, C.M. Sharts, Organic Fluorine Chemistry, W.A. Benjamin Inc., New York, 1969, pp. 33.

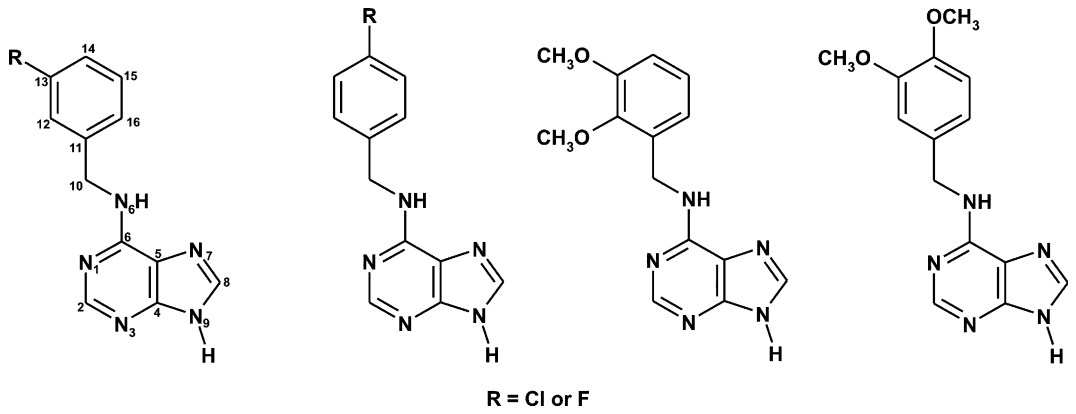

Scheme 1.

be increased by coordination of cytokinin-derived compounds to a suitable transition metal. Recently, we have focused our interest on the preparation of Pt(II), Pd(II), Cu(II), Ni(II) and Co(II) complexes with the above-mentioned organic derivatives [4–8].

To date, only a few of cobalt complexes with purine and adenine derivatives as ligands have been structurally characterized and deposited at Cambridge Crystallographic Data Centre (CCDC) [9]. The coordination variability both the purine and adenine moieties, relating to their four or five nitrogen-donor atoms, can be shown, among others, on the following examples. In 1D-polymeric chain octahedral cobalt complexes of formulae $[Co^{II}(\mu\text{-ox})(H_2O)(purH\text{-}N9)]_n$, $[Co^{II}(\mu\text{-ox})(H_2O)(purH\text{-}N9)_{0.76}(adeH\text{-}N9)_{0.24}]_n$ (ox = oxalate(2−), purH = purine, adeH = adenine), purine and/or adenine are coordinated to cobalt through the *N*9 atom of an imidazole ring [10]. The same manner of the ligand coordination was found in monomeric complexes *cis*-$[Co^{III}(ade\text{-}N9)Cl(en)_2]Br \cdot H_2O$ (en = 1,2-diaminoethane) [11] and $(adeH^+)_2[Co^{II}(H_2O)_4(adeH\text{-}N9)_2](SO_4)_2 \cdot 6H_2O$ [12]. On the other hand, the adenine can be also bound via *N*3 as determined in $\{[Co^{II}(\mu\text{-ox})(H_2O)(adeH\text{-}N3)] \cdot 2(adeH) \cdot (H_2O)\}_n$ [10]. From general point of view, other nitrogen atoms of purine (i.e., *N*1 and *N*7) and adenine (i.e., *N*1, *N*6 and *N*7) derivatives can be also used for coordination to cobalt. This was found in some Co(III) complexes which X-ray structures were determined. For example, the coordination through *N*7 was found in $[Co(acac)_2(NO_2)(tca\text{-}N7)] \cdot H_2O \cdot DMF$ (acacH = acetylacetone, tca = tricanthine) [13], $[Co(acac)_2(NO_2)(1,9\text{-dimethyl-ade}H^+\text{-}N7)][Co(acac)_2(NO_2)_2]$ [14] and $[Co(3\text{-benzyl-ade-}N7)(dmg)_2(dmp)] \cdot H_2O \cdot EtOH$ (dmg = dimethylglyoximate, dmp = dimethylphosphonate) [15]. Moreover, in the tetrahedral $[Co^{II}(ade\text{-}N6,N7)Cl(H_2O)] \cdot H_2O$ complex, adenine acts probably as a bidentate ligand through *N*6 and *N*7 atoms [16]. Unfortunately, the conclusion relating to a mode of coordination in the latter complex is not supported by results following from a single crystal X-ray analysis and was deduced from IR data only.

In our previous work, we have published the first preparation and biological activity of mononuclear tetrahedral high-spin Co(II) complexes bearing the cytokinin-derived compounds as ligands [8]. Herein, we describe the preparation, characterization and cytotoxicity of the Co(II) complexes with 6-(3-chlorobenzylamino)purine (HL_1), 6-(4-chlorobenzylamino)purine (HL_2), 6-(2,3-dimethoxybenzylamino)purine (HL_3), 6-(3,4-dimethoxybenzylamino)purine (HL_4), 6-(3-fluorobenzylamino)purine (HL_5) and 6-(4-fluorobenzylamino)purine (HL_6) (see Scheme 1).

2. Experimental

2.1. Materials

$CoCl_2 \cdot 6H_2O$, 6-chloropurine, 3-chlorobenzylamine, 4-chlorobenzylamine, 2,3-dimethoxybenzylamine, 3,4-dimethoxybenzylamine, 3-fluorobenzylamine, 4-fluorobenzylamine and the solvents {dimethyl sulfoxide (DMSO), *N*,*N*-dimethylformamide (DMF), etc.} were purchased from Aldrich Co. and were used as received.

2.2. Syntheses

2.2.1. 6-(3-Chlorobenzylamino)purine (HL_1), 6-(4-chlorobenzylamino)purine (HL_2), 6-(2,3-dimethoxybenzylamino)purine (HL_3), 6-(3,4-dimethoxybenzylamino)purine (HL_4), 6-(3-fluorobenzylamino)purine (HL_5), 6-(4-fluorobenzyl amino)purine (HL_6) and $[H^{2+}L_2](ClO_4)_2 \cdot 2H_2O$

Compounds HL_1–HL_6 were prepared by the reaction of 6-chloropurine with an appropriate benzylamine in *n*-butanol with the addition of triethylamine by the procedure similar to that as described previously [17]. Yields ranged from 65% to 70%. The purity and composition of the compounds were proved by elemental analyses, ^1H and ^{13}C NMR spectra, thin-layer chromatography using a Silica gel 60 F_{254} (Merck) precoated aluminum plates with $CHCl_3$:CH_3OH:conc. NH_4OH (8:2:0.2, v/v/v) as a mobile phase, and melting points (data shown in Doležal et al., Bioorg. Med. Chem. 2005, submitted). Crystals of $[H^{2+}L_2](ClO_4)_2 \cdot 2H_2O$ were obtained by recrystallization of HL_2 from 2 M $HClO_4$.

HL_1. *Anal*. Calc. for $C_{12}H_{10}N_5Cl$: C, 55.5; H, 3.9; N, 27.0. Found: C, 55.3; H, 4.0; N, 27.2%. IR (cm^{-1}): 3429m, 3260m, 3077m, 2939m, 1622vs, 1538w, 1485w, 1158w. ^1H NMR (DMF-d_7, ppm): δ 13.00 (s, 1H, N9H), 8.24 (s, 1H, C2H), 8.20 (s, 1H, C8H), 7.50 (s, 1H, C12H), 7.42 (d, 1H, C16H), 7.36 (t, 1H, C15H), 7.24 (d, 1H, C14H), 4.90 (s, 2H, C10H). ^{13}C NMR (DMF-d_7, ppm): 155.02 (C6), 152.96 (C2), 150.58 (C4), 143.53 (C11), 139.67 (C8), 133.80 (C13), 130.50 (C12), 127.63 (C16), 127.13 (C15), 126.44 (C14), 119.51 (C5), 43.33 (C10). ES+ MS: *m/z* 261 $[HL_1]^+$. HL_2. *Anal*. Calc. for $C_{12}H_{10}N_5Cl$: C, 55.5; H, 3.9; N, 27.0. Found: C, 55.5; H, 4.1; N, 26.8%. IR (cm^{-1}): 3430m, 3261w, 3048w, 2997w, 1626vs, 1567m, 1491w, 1155w. ^1H NMR (DMF-d_7, ppm): δ 12.98 (s, 1H, N9H), 8.23 (s, 1H, C2H), 8.19 (s, 1H, C8H), 8.11 (s, 1H, N6H), 7.48 (dd, 2H, C12H, C16H), 7.38 (dd, 2H, C13H, C15H), 4.88 (s, 2H, C10H). ^{13}C NMR (DMF-d_7, ppm): δ 155.41 (C6), 153.25 (C2), 152.79 (C4), 140.41 (C11), 139.69 (C8), 132.32 (C14), 129.94 (C12, C16), 128.91 (C13, C15), 119.69 (C5), 43.59 (C11). ES+ MS: *m/z* 261 $[HL_2]^+$. HL_3. *Anal*. Calc. for $C_{14}H_{15}N_5O_2$: C, 58.9; H, 5.3; N, 24.5. Found: C, 58.5; H, 5.2; N, 24.7%. IR (cm^{-1}): 3422w, 3262w, 3067w, 2995w, 2835w, 1623vs, 1539w, 1480s, 1274m. ^1H NMR (DMF-d_7, ppm): δ 13.01 (s, 1H, N9H), 8.24 (s, 1H, C2H), 8.20 (s, 1H, C8H), 7.83 (s, 1H, N6H), 6.98 (t, 1H, C15H), 6.97 (dd, 2H, C14H, C16H), 4.92 (s, 2H, C10H), 3.87 (d, 6H, C17H, C18H). ^{13}C NMR (DMF-d_7, ppm): 155.00 (C6), 152.71 (C2), 149.63 (C4), 149.35 (C14), 148.43 (C13), 139.64 (C8), 132.70 (C11), 121.93 (C12), 120.31 (C5), 119.89 (C16), 111.96 (C15), 56.81 (C17), 48.89 (C18), 43.23 (C10). MS: *m/z* 286 $[HL_3]^+$. HL_4. *Anal*. Calc. for $C_{14}H_{15}N_5O_2$: C, 58.9; H, 5.3; N, 24.5. Found: C, 58.7; H, 5.2; N, 24.7%. IR (cm^{-1}): 3430m, 3288w, 3072w, 2992w, 2834w, 1623vs, 1515s, 1464w, 1255m. ^1H NMR (DMF-d_7, ppm): δ 12.92 (s, 1H, N9H), 8.25 (s, 1H, C2H), 8.18 (s, 1H, C8H), 7.95 (s, 1H, N6H), 7.13 (s, 1H, C12H), 6.95 (d, 1H, C16H), 6.91 (d, 1H, C15H), 4.81 (s, 2H, C10H), 3.79 (d, 6H, C17H, C18H). ^{13}C NMR (DMF-d_7, ppm): 155.00 (C6), 152.71 (C2), 149.63 (C4), 149.35 (C14), 148.43 (C13), 139.64 (C8), 132.70 (C11), 121.93 (C12), 120.31 (C5), 119.89 (C16), 111.96 (C15), 56.81 (C17), 48.89 (C18), 43.23 (C10). ES+ MS: *m/z* 286 $[HL_4]^+$. HL_5. *Anal*. Calc. for $C_{12}H_{10}N_5F$: C, 59.3; H, 4.1; N, 28.8. Found: C, 59.1; H, 3.9; N, 28.4%. IR (cm^{-1}): 3456vs, 3267s, 3085w, 2941m, 1630vs, 1567w, 1485w, 1253w. ^1H NMR (DMF-d_7, ppm): δ 12.99 (s, 1H, N9H), 8.25 (s, 1H, C2H), 8.21 (s, 1H, C8H), 8.17 (s, 1H, N6H), 7.36 (qui, 1H, C12H), 7.29 (d, 1H, C16H), 7.26 (t, 1H, C15H), 7.04 (1H, C14H), 4.92 (s, 2H, C10H). ^{13}C NMR (DMF-d_7, ppm): 163.41 (C13), 155.31 (C6), 153.23 (C2), 151.01 (C4), 144.46 (C11), 139.89 (C8), 130.77 (C15), 123.98 (C16), 119.75 (C5), 114.64 (C12), 113.97 (C14), 43.66 (C10). ES+ MS: *m/z* 244 $[HL_5]^+$. HL_6. *Anal*. Calc. for $C_{12}H_{10}N_5F$: C, 59.3; H, 4.1; N, 28.8. Found: C, 59.2; H, 4.0; N, 28.3%. IR (cm^{-1}): 3447s, 3259m, 3044s, 2950m, 1630vs, 1568vs, 1489s, 1256m. ^1H NMR (DMF-d_7, ppm): δ 12.95 (s, 1H, N9H), 8.26 (s, 1H, C2H), 8.21 (s, 1H, C8H), 8.13 (s, 1H, N6H), 7.50 (q, 2H, C12H, C16H), 7.13 (t, 2H, C13H, C15H), 4.89 (s, 2H, C10H). ^{13}C NMR (DMF-d_7, ppm): 162.32 (C14), 155.11 (C6), 153.22 (C2), 151.66 (C4), 139.94 (C8), 137.43 (C11), 130.13 (C12), 130.01 (C16), 119.20 (C5), 115.64 (C13), 115.35 (C15), 43.48 (C10). MS: *m/z* 244 $[HL_6]^+$.

2.2.2. $[Co(L_1)Cl(H_2O)_2]\cdot H_2O$ (1), $[Co(L_2)Cl(H_2O)_2]\cdot 2H_2O$ (2), $[Co(L_3)Cl(H_2O)_2]\cdot H_2O$ (3), $[Co(L_4)Cl(H_2O)_2]\cdot H_2O$ (4), $[Co(L_5)Cl(H_2O)_2]\cdot H_2O$ (5), $[Co(L_6)Cl(H_2O)_2]\cdot H_2O$ (6) and $[Co_6(\mu\text{-}L_6)_4Cl_8(DMSO)_{10}]\cdot 4DMSO$ (7)

Co(II) complexes **1**–**6** were synthesized by the following general method: a solution of an appropriate organic ligand (1 mmol) in EtOH (15 cm^3) and triethylamine (0.14 cm^3) were mixed with stirring. Then, a solution of $CoCl_2\cdot 6H_2O$ (0.24 g, 1 mmol) was added. The pale blue precipitate formed immediately. This reaction mixture was refluxed at 70 °C and stirred for 5 h. All the synthetic steps proceeded under nitrogen atmosphere. Then, the precipitate was filtered off, washed with EtOH (3×10 cm^3), Et_2O (2×10 cm^3) and dried under an infrared lamp at 40 °C. Yields ranged from 60% to 75%.

Crystals of $[Co_6(\mu\text{-}L_6)_4Cl_8(DMSO)_{10}]\cdot 4DMSO$ (**7**) suitable for single crystal X-ray analysis were obtained by recrystallization of the complex **6** from DMSO. In more details, complex **6** was dissolved in DMSO and dark green crystals were obtained by slow evaporation of the solvent after several months.

$[Co(L_1)Cl(H_2O)_2]\cdot H_2O$ (**1**). *Anal*. Calc. for $CoC_{12}H_{15}N_5O_3Cl_2$: C, 35.4; H, 3.7; N, 17.2; Co, 14.5. Found: C, 35.1; H, 3.7; N, 16.9; Co, 14.2%. IR (KBr) (cm^{-1}): 3397s, 1621vs, 1532w, 1474m, 1170m. IR (Nujol) (cm^{-1}): 449, 315, 303. ^1H NMR (DMF-d_7, ppm): δ 8.77 (s, 1H, C8H), 8.21 (s, 1H, C2H), 7.56 (s, 1H, C12H), 7.50 (s, 1H, C16H), 7.41 (s, 1H, C15H), 7.34 (s, 1H, C14H), 5.01 (s, 2H, C11H). ^{13}C NMR (DMF-d_7, ppm): 155.62 (C6), 152.69 (C2), 147.10 (C4), 142.82 (C11), 145.70 (C8), 134.71 (C13), 131.65 (C12), 127.39 (C16), 127.41 (C15), 125.45 (C14), 119.20 (C5), 42.37 (C10). ES+ MS: *m/z* 391 $[Co(L_1)Cl(H_2O)_2]^+$, 354 $[Co(L_1)Cl]^+$, 260 $[HL_1]^+$. $[Co(L_2)Cl(H_2O)_2]\cdot 2H_2O$ (**2**). *Anal*. Calc. for $CoC_{12}H_{17}N_5O_4Cl_2$: C, 33.9; H, 4.0; N, 16.5; Co, 13.9. Found: C, 33.5; H, 3.9; N, 16.4; Co, 13.5%. IR (KBr) (cm^{-1}): 3409m, 1620vs, 1540w, 1473w, 1171w. IR (Nujol) (cm^{-1}): 435, 315, 303. ^1H NMR (DMF-d_7, ppm): δ 8.61 (s, 1H, C8H), 8.46 (s, 1H, C2H), 7.49 (s, 2H, C12, C16), 7.33 (s, 2H, C13, C15), 5.01 (s, 2H, C10H). ^{13}C NMR (DMF-d_7, ppm): δ 155.65 (C6), 153.09 (C2), 148.70 (C4), 141.82 (C11), 145.98 (C8), 134.09 (C14), 131.21 (C12, C16), 129.30 (C13, C15), 118.72 (C5), 45.31 (C10). ES+ MS: *m/z* 391 $[Co(L_2)Cl(H_2O)_2]^+$, 354 $[Co(L_2)Cl]^+$, 260 $[HL_2]^+$. $[Co(L_3)Cl(H_2O)_2]\cdot H_2O$ (**3**). *Anal*. Calc. for $CoC_{14}H_{20}N_5O_5Cl$: C, 38.9; H, 4.7; N, 16.2; Co, 13.6. Found: C, 38.6; H, 4.5; N, 16.0; Co, 13.3%. IR (KBr) (cm^{-1}): 3414s, 1622vs, 1541w, 1479m, 1275m IR (Nujol) (cm^{-1}): 430, 315, 303. ^1H NMR (DMF-d_7, ppm): δ 8.62 (s,

1H, C8H), 8.36 (s, 1H, C2H), 7.86 (s, 1H, N6H), 7.05 (s, 1H, C15H), 7.01 (s, 2H, C14H, C16H), 5.01 (s, 2H, C10H), 3.90 (d, 6H, C17H, C18H). ^{13}C NMR (DMF-d_7, ppm): 155.78 (C6), 153.70 (C13), 154.15 (C2), 148.52 (C4), 147.63 (C12), 145.38 (C8), 133.12 (C11), 125.01 (C16), 121.48 (C15), 119.12 (C5), 111.92 (C14), 62.81 (C17), 55.24 (C18), 41.00 (C10). ES+ MS: *m/z* 414 $[Co(L_3)Cl(H_2O)_2]^+$, 379 $[Co(L_3)Cl]^+$, 286 $[HL_3]^+$. $[Co(L_4)Cl(H_2O)_2]\cdot H_2O$ (**4**). *Anal.* Calc. for $CoC_{14}H_{20}N_5O_5Cl$: C, 38.9; H, 4.7; N, 16.2; Co, 13.6. Found: C, 38.7; H, 4.6; N, 15.9; Co, 13.2%. IR (KBr) (cm^{-1}): 3429s, 1621vs, 1516s, 1465m, 1266m. IR (Nujol) (cm^{-1}): 436, 314, 303. ^{1}H NMR (DMF-d_7, ppm): δ 8.61 (s, 1H, C8H), 8.35 (s, 1H, C2H), 8.25 (s, 1H, N6H), 7.28 (s, 1H, C12H), 7.04 (s, 1H, C16H), 6.96 (s, 1H, C15H), 4.98 (s, 2H, C10H), 3.81 (6H, C17H, C18H). ^{13}C NMR (DMF-d_7, ppm): 155.33 (C6), 151.15 (C2), 145.68 (C4), 149.23 (C14), 148.46 (C13), 145.21 (C8), 132.62 (C11), 121.36 (C12), 120.98 (C5), 120.01 (C16), 112.57 (C15), 56.01 (C17), 47.53 (C18), 43.91 (C10). ES+ MS: *m/z* 414 $[Co(L_4)Cl(H_2O)_2]^+$, 379 $[Co(L_4)Cl]^+$, 286 $[HL_4]^+$. $[Co(L_5)Cl(H_2O)_2]\cdot H_2O$ (**5**). *Anal.* Calc. for $CoC_{12}H_{15}N_5O_3ClF$: C, 36.9; H, 3.9; N, 17.9; Co, 15.1. Found: C, 36.5; H, 3.6; N, 18.2; Co, 15.0%. IR (KBr) (cm^{-1}): 3409m, 1621vs, 1537w, 1474w, 1250w. IR (Nujol) (cm^{-1}): 441, 324, 307. ^{1}H NMR (DMF-d_7, ppm): δ 8.80 (s, 1H, C8H), 8.63 (s, 1H, C2H), 7.38 (m, 3H, C12H, C15H, C16H), 7.07 (t, 1H, C14H), 5.02 (s, 2H, C10H). ^{13}C NMR (DMF-d_7, ppm): 156.00 (C6), 153.70 (C2), 148.23 (C4), 145.02 (C11), 146.12 (C8), 129.16 (C15), 125.01 (C16), 120.13 (C5), 115.16 (C12), 112.57 (C14), 44.28 (C10). MS: *m/z* 337 $[Co(L_5)Cl]^+$, 244 $[HL_5]^+$. $[Co(L_6)Cl(H_2O)_2]\cdot H_2O$ (**6**). *Anal.* Calc. for $CoC_{12}H_{15}N_5O_3ClF$: C, 36.9; H, 3.9; N, 17.9; Co, 15.1. Found: C, 36.6; H, 3.5; N, 17.6; Co, 14.8%. IR (KBr) (cm^{-1}): 3416m, 1622vs, 1510m, 1474w, 1272w. IR (Nujol) (cm^{-1}): 436, 317, 310. ^{1}H NMR (DMF-d_7, ppm): δ 8.59 (s, 1H, C8H), 8.38 (s, 1H, C2H), 7.56 (s, 2H, C12H, C16H), 7.16 (s, 2H, C13H, C15H), 4.95 (s, 2H, C10H). ^{13}C NMR (DMF-d_7, ppm): 156.45 (C6), 154.28 (C2), 146.23 (C4), 144.13 (C8), 136.20 (C11), 130.30 (C12), 128.12 (C16), 120.50 (C5), 114.31 (C13), 113.78 (C15), 43.14 (C10). MS: *m/z* 337 $[Co(L_6)Cl]^+$, 244 $[HL_6]^+$.

2.3. Physical measurements

All compounds were characterized by elemental analyses (C, H, N) using a ThermoFinnigan Flash EA-1121 Elemental Analyser. The cobalt content was determined by a chelatometric (EDTA) titration on murexide as an indicator. IR spectra of all compounds were recorded on a ThermoNicolet Nexus 670 FT-IR spectrometer as KBr pellets (400–4000 cm^{-1}) and using Nujol (150–500 cm^{-1}) and DRIFT (4000–10 000 cm^{-1}) techniques (only in case of the complexes). ^{1}H and ^{13}C NMR data of the ligands and Co(II) complexes in DMF-d_7 were collected on a Bruker 300 MHz NMR spectrometer Avance 600 with tetramethylsilane as an internal standard. Electronic absorption spectra of DMF solutions of the complexes were obtained on a Perkin–Elmer Lambda40 spectrometer in the 11 000–25 000 cm^{-1} range. Diffuse-reflectance spectra were recorded using a Perkin–Elmer Lambda35 spectrometer in the same range. Magnetic susceptibilities were measured by the Faraday method at room temperature using $Hg[Co(SCN)_4]$ as a calibrant, corrections for diamagnetism were calculated from Pascal's constants [18]. ES+ mass spectra of the ligands and complexes were recorded on a Waters ZMD 2000 mass spectrometer using a flow injection mode in mass monitoring interval 30–900 *m/z*. The spectra were collected using 3.0 s cyclical scans with cone voltage 20 and 40 V, at the source block temperature 80 °C, desolvation temperature 150 °C and desolvation gas flow rate 200 l/h. Conductances of 10^{-3} M solutions of the complexes in DMF were measured using a WTW Cond340i/SET conductometer at 25 °C. Thermogravimetric (TG) measurements were made in the temperature range of 20–1000 °C using a THASS TGA XP-10 thermal analyser. Melting points of the ligands used were determined on a Büchi Melting point B-540 apparatus and were uncorrected.

2.4. X-ray structure determinations

Diffraction data for $[H^{2+}L_2](ClO_4)_2\cdot 2H_2O$ and $[Co_6(\mu\text{-}L_6)_4Cl_8(DMSO)_{10}]\cdot 4DMSO$ (**7**) were collected on an Oxford Diffraction Xcalibur2 diffractometer equipped with Sapphire2 CCD detector at 100 K. The CRYSALIS software package (Version 1.171.24) was used for data collection and reduction. Both structures were solved by the SIR97 program [19] incorporated in the WINGX system (Version 1.70.00) [20]. All non-hydrogen atoms were refined anisotropically by the full-matrix least-squares procedure SHELXL-97 [21] on F^2 with weight: $w = 1/[\sigma^2(F_o)^2 + (0.0869P)^2 + 1.9024P]$ for $[H^{2+}L_2](ClO_4)_2\cdot 2H_2O$ and $w = 1/[\sigma^2(F_o)^2 + (0.1875P)^2 + 8.3404P]$ for **7**, where $P = (F_o^2 + 2F_c^2)/3$. In $[H^{2+}L_2](ClO_4)_2\cdot 2H_2O$, H-atoms attached to C and N atoms were found from difference Fourier maps and refined using a 'riding' model with C–H distances of 0.95 and 0.99 Å, the N–H distances of 0.88 Å with U_{iso} values derived from U_{eq} of the corresponding C and N atoms, respectively. $U_{iso}(H) = 1.2U_{eq}$ (CH, CH_2 and NH). The H-atoms of water molecules were refined freely. The largest peak and hole on the final difference map were 0.632 [0.90 Å from O(4)] and −0.606 [0.87 Å from Cl(2)] e Å^{-3}, respectively. In **7**, H-atoms belonging to all ligands, except for those of disordered DMSO molecules, were positioned theoretically and H-atoms of solvated DMSO were not included into calculation. In connection with overall bad crystal data quality [$R_{int} = 0.1333$], statistical data relating to this structure are not satisfactory. Nevertheless, the molecular structure of **7** was determined unambiguously from chemical point of view. The crystal data and structure refinements for $[H^{2+}L_2](ClO_4)_2\cdot 2H_2O$ and **7** are given in Table 1.

Table 1
Crystal data and structure refinements for $[H^{2+}L_2](ClO_4)_2 \cdot 2H_2O$ and $[Co_6(\mu\text{-}L_6)_4Cl_8(DMSO)_{10}] \cdot 4DMSO$ (**7**)

	$[H^{2+}L_2](ClO_4)_2 \cdot 2H_2O$	(**7**)
Empirical formula	$C_{12}H_{16}Cl_3N_5O_{10}$	$C_{76}H_{90}Cl_8Co_6F_4N_{20}O_{17}S_{14}$
Formula weight	496.65	2717.70
Temperature (K)	100(2)	100(2)
Wavelength (Å)	0.71073	0.71073
Crystal system, space group	triclinic, $P\bar{1}$	monoclinic, $P2_1/n$
Unit cell dimension		
a (Å)	8.273(5)	13.559(5)
b (Å)	8.306(5)	25.212(5)
c (Å)	14.798(5)	17.437(5)
α (°)	78.721(5)	90
β (°)	80.048(5)	100.820(5)
γ (°)	75.441(5)	90
Volume (Å^3)	957.0(9)	5855(3)
Z, Calculated density (Mg m^{-3})	2, 1.724	2, 1.542
Absorption coefficient (mm^{-1})	0.544	1.333
F(000)	580	2760
Crystal size (mm)	$0.30 \times 0.30 \times 0.25$	$0.30 \times 0.30 \times 0.25$
θ range for data collection (°)	2.57–25.00	2.70–25.00
Index ranges	$-9 \leqslant h \leqslant 9$, $-9 \leqslant k \leqslant 6$, $-17 \leqslant l \leqslant 17$	$-16 \leqslant h \leqslant 14$, $-28 \leqslant k \leqslant 29$, $-20 \leqslant l \leqslant 20$
Reflections collected/unique	6920/3237 [$R_{int} = 0.0806$]	42 659/10 293 [$R_{int} = 0.1333$]
Data/restraints/parameters	3237/4/288	10 293/2/664
Goodness-of-fit on F^2	1.101	1.141
Final R indices [$I > 2\sigma(I)$]	$R_1 = 0.0481$, $wR_2 = 0.1221$	$R_1 = 0.1111$, $wR_2 = 0.2889$
R indices (all data)	$R_1 = 0.0586$, $wR_2 = 0.1498$	$R_1 = 0.1458$, $wR_2 = 0.3231$
Largest difference peak and hole (e Å^{-3})	0.632 and −0.606	2.189 and −1.650

2.5. Cytotoxicity testing

Cytotoxicity of the starting compounds (i.e., HL_1–HL_6 and $CoCl_2 \cdot 6H_2O$) and complexes **1**–**6** was assessed by a Calcein AM assay. The following human tumour cell lines were used: malignant melanoma (*G361*), chronic myelogenous erythroleukemia (*K562*), osteogenic sarcoma (*HOS*) and breast adenocarcinoma (*MCF7*). IC_{50} values, i.e., the drug concentration lethal to 50% of the tumour cells, were estimated. Our experimental setup relating to the cytotoxicity testing was described previously in greater details [7].

3. Results and discussion

3.1. Magnetic, conductivity data, electronic spectra

Magnetic, conductivity and electronic spectral data of the prepared complexes are given in Table 2. The effective magnetic moment values vary from 4.4 to 4.7 μ_{eff}/μ_B, which correspond with the values expected for tetrahedral high-spin (d^7) Co(II) complexes [22–25] (see Scheme 2). The molar conductivity values of the complexes (10^{-3} M in DMF) at 25 °C range from 11.0 to 18.7 S cm^2 mol^{-1} and show on their non-ionic character [26].

Both absorption (DMF solutions) and diffuse-reflectance (solid state) electronic spectra of all the complexes are similar and exhibit three maxima at ca. 15 700, 16 100 and 18 700 cm^{-1}, and 15 600, 16 000 and 18 100 cm^{-1}. The electronic spectra of compound **2** are shown in Fig. 1. As it is generally known, regular tetrahedral Co(II) complexes should have only one d–d transition in the visible region. In the case of described complexes, a band centered at ca. 16 000 cm^{-1} is splitted into two peaks what is probably due to the interaction with the doublet state through spin–orbit coupling and may be attributed to the ν_3 transition, i.e., $^4A_2 \rightarrow {}^4T_1(P)$ [27–31]. The calculated values of molar absorption coefficients range from 103 to 527 M^{-1} cm^{-1} and correspond to d–d transitions [32]. Additionally, the next two d–d transitions were observed in the NIR region. The broadbands at ca. 7560 cm^{-1} can be attributed to the spin allowed transition $^4A_2 \rightarrow {}^4T_1(F)$ (ν_2) [33], while weak peaks near 4450 cm^{-1} were assigned to the ν_1 transition, i.e. $^4A_2 \rightarrow {}^4T_2(F)$. The curve shapes and maxima positions both in the solution and solid-state spectra are almost identical, and so, it can be expected that the prepared complexes are sufficiently chemically inert and do not change their coordination spheres in the solvent used. The ligand field parameters *10Dq* and the Racah parameters *B* were calculated from Tanabe–Sugano matrices described in the literature [34,35]. To calculate *10Dq* and *B* values, the maximal intensity of the relevant ν_2 and ν_3 bands were used. Calculated values for degree of covalent binding of ligands β (≈ 0.69) and ligand field strength *10Dq* (4420–4430 cm^{-1}) as well as Racah parameters *B* (668–671 cm^{-1}) are comparable for all the complexes. However, these values differ to those described for some tetrahedral complexes in the literature, e.g., [Co(Th4DM)(OH)(H$_2$O)] (*10Dq* = 4110 cm^{-1}, *B* = 709 cm^{-1} and $\beta = 0.73$), where HTh4DM = 4-acetamidobenzaldehyde-N(4)-dimethyl-thiosemicarbazone [36], and [$CoCl_2$(TdTn)] (*10Dq* = 4861 cm^{-1}, *B* = 754 cm^{-1} and $\beta = 0.78$), where TdTn = 2-(3,4-dichlorophenyl)imino-*N*-

Table 2
Magnetic, conductivity and electronic spectral data of the complexes **1**–**6**

Compound	μ_{eff}/μ_B (293 K)	λ_M[a] (S cm^2 mol^{-1})	Absorption maxima (cm^{-1})/ε (M^{-1} cm^{-1})		$10Dq$ (cm^{-1})	B (cm^{-1})	β
			DMF solution	Solid state			
1	4.4	18.7	7570		4430	668	0.69
			15710/470	15420			
			16090/454	15960			
			18640/125	18030			
2	4.4	12.1	7570		4430	669	0.69
			15710/464	15460			
			16100/449	15910			
			18660/127	18000			
3	4.6	11.0	7560		4420	671	0.69
			15700/445	15450			
			16090/439	15970			
			18660/130	18050			
4	4.6	13.0	7550		4420	670	0.69
			15700/414	15500			
			16100/405	15920			
			18650/103	18130			
5	4.7	14.4	7570		4430	670	0.69
			15720/527	15710			
			16100/518	16190			
			18720/144	18070			
6	4.7	11.2	7550		4420	670	0.69
			15730/515	15740			
			16100/502	16110			
			18690/137	18070			

[a] Measured in 10^{-3} M DMF solutions.

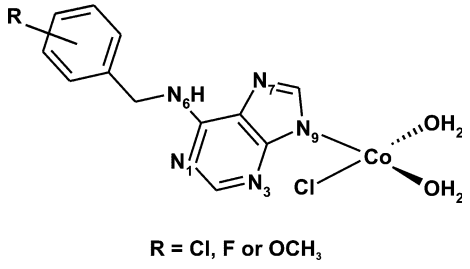

Scheme 2.

(2-thiazolin-2-yl)thiazolidine [37]. The difference of spectral parameters is caused by dissimilarity of chromophores, i.e. $CoNClO_2$ versus $CoNSO_2$ or CoN_2Cl_2. Thus, the results following from electronic spectral data are in agreement with the conclusions from magnetic measurements.

3.2. NMR measurements

The ^{1}H and ^{13}C NMR spectra of the free cytokinin derivatives as well as the complexes were measured in DMF-d_7 and the chemical shifts are summarized in Section 2.2. Differences between NMR spectra of the complexes and free ligands provide circumstantial evidence on a complex formation. The largest coordination shifts $\Delta\delta$ ($\Delta\delta = \delta_{complex} - \delta_{ligand}$) were observed in ^{1}H NMR spectra for the H8 protons, which were shifted downfield by 0.38–0.59 ppm. The largest coordination shifts were also found for C8 and C4 signals in ^{13}C NMR spectra. The C8 signals were shifted downfield by ca. 6.29 ppm, while the C4 signals were shifted upfield by ca. 4.09 ppm. On the basis of this fact, we can conclude that the ligands are deprotonated at the *N*9 position of an imidazole ring and moreover, the coordination of the cytokinin derivatives to cobalt proceeds

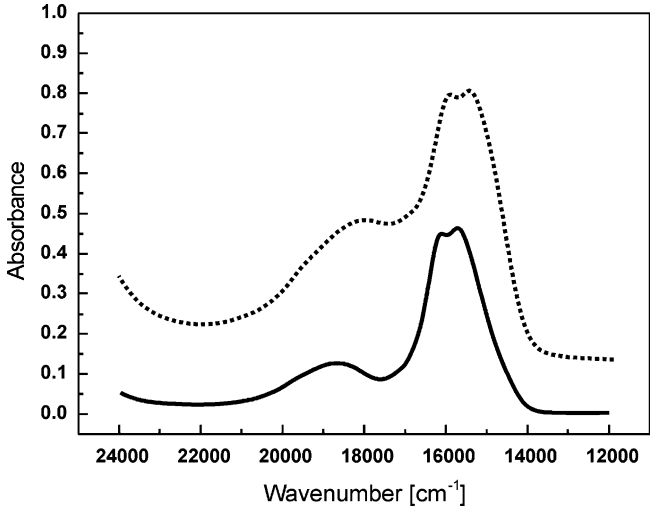

Fig. 1. Absorption electronic solution (—) and diffuse-reflectance spectra (···) of complex **2**.

via the same atom in all the complexes (see Scheme 2). The similar conclusion can be made in case of the measurement in methanol-d_4. However, the interpretation of the spectra is somewhat complicated due to limited solubility of the complexes as well as free ligands in methanol-d_4. We have also measured NMR spectra in DMSO-d_7 and acetone-d_6. Unfortunately, reproducible NMR data in DMSO-d_7 and acetone-d_6 have not been obtained, probably in connection with the decomposition of the complexes in these solvents. This conclusion was proved in the case of **6** by a single crystal X-ray analysis, where the recrystallization of the complex from DMSO led to formation of complex **7** (see Section 3.8).

3.3. Computational analysis

Theoretical calculations using the DFT (B3LYP) approach were performed with the aim to suggest a possible coordination mode of the studied 6-benzylaminopurine derivatives to the cobalt(II) ion. This approach partially substitutes the absence of crystallographic data of any of the studied Co(II) complexes. All calculations were done using the GAUSSIAN03 program [38]. As a model system, complex **2** was chosen. Preliminary optimized data were prepared on the HF/6-31* level of the theory. Then, the obtained geometries were fully optimized at the B3LYP level with 6-311++G** (for ligands) and 6-311+G* (for complexes) basis sets. Harmonic-frequency analysis was used to verify the nature of found stationary points as the minima as well as for the calculation of zero-point vibrational energies. Calculated infrared frequencies of the ligands, as shown in Table 3, were not scaled. Natural-bond orbital analysis (NBO) was used for investigation of the electron distribution in the studied complexes [39].

From general point of view, each of the 6-benzylaminopurine derivatives used in this study offers several possible binding sites for the cobalt complex formation, e.g., *N*1, *N*3, *N*7 or *N*9 for the monodentate binding, *N*6–*N*7 for bidentate one, and *N*7–*N*9 or *N*3–*N*9 for bridging coordination [9,16]. The *N*1 binding site is strongly sterically hindered by the methylene hydrogens of the benzylamino group, and complex **2** is not probably formed by this way. The optimized geometries of complex **2** with the possible monodentate coordination modes of the 6-(4-chlorobenzylamino)purine ligand are shown in Fig. 2. Similar to the *N*1 coordination, the benzyl functional group partially hinders the bidentate coordination to cobalt(II) ion via the *N*6 and *N*7 donor atoms. Mutual orientation of purine ring and benzylamino group leads to the different spatial orientation of the lone electron pairs of *N*6 and *N*7 atoms. This arrangement makes impossible effective a bidentate binding of the organic ligand to cobalt(II) ion. On the other hand, the *N*3 and *N*9 positions are in essence equivalent from both the geometrical and sterical perspectives, and moreover, both donor atoms are well uncovered for the coordination with the cobalt ion.

The electron distribution within the purine skeleton of anion L_2^- gives preference rather to the coordination via the *N*7 atom with highest negative partial charge. The remaining three nitrogen atoms (i.e., *N*1, *N*3 and *N*9) have comparable charges. On the other hand, the greatest changes in the charge distribution have been observed in case of the coordination via the *N*9 atom (for details, see Table 3).

Bond distances between the corresponding nitrogen and cobalt atoms are nearly identical in all three studied systems (Table 4). All three suggested models also offer the strong hydrogen bond interaction between one water molecule coordinated to the cobalt(II) ion and the corresponding adjacent nitrogen atom, i.e., *N*3 for the *N*9-coordinated complex, *N*9 for the *N*3-coordinated complex and *N*6 for the *N*7-coordinated complex (see Fig. 2). Selected calculated hydrogen bond parameters are also summarized in Table 3.

Difference between ΔSCF energies of the *N*3 and *N*9 coordinated complexes is 1.01 kcal mol^{-1} in favour of the *N*9 coordination. The energy of the *N*7 complex is higher by 15.7 kcal mol^{-1}, also in comparison with the *N*9 complex. It is supposable that the L_2^- anion is coordinated to cobalt via *N*9 or *N*3 atom in complex **2**, and some dynamic equilibrium should be expected in the solution.

Table 3
Selected calculated partial charges and geometrical parameters of the complex **2**

Coordination site	Partial charges (Mulliken/NBO)				Interatomic parameters (Å, °)				
	N1	N3	N7	N9	Co–N	Co–Cl	Co–O	O–H···N[b]	∠DHA[c]
N7	−0.07/−0.54	−0.08/−0.47	−0.01/−0.77	−0.10/−0.50	1.98	2.23	2.10 2.02[a]	2.67	154.3
N3	−0.09/−0.56	0.11/−0.70	−0.18/−0.53	−0.50/−0.66	2.02	2.23	2.09 2.01[a]	2.54	155.3
N9	−0.15/−0.57	−0.50/−0.62	−0.17/−0.52	0.19/−0.74	1.99	2.22	2.09 2.06[a]	2.62	155.5
Free L_2^-	−0.19/−0.61	−0.16/−0.53	−0.27/−0.60	−0.20/−0.59					

[a] The value belongs to the Co–O bond with oxygen atom participating in the HO(H)···N hydrogen bond.
[b] The distance between donor (D) and acceptor (A) atoms.
[c] The O–H···N angle.

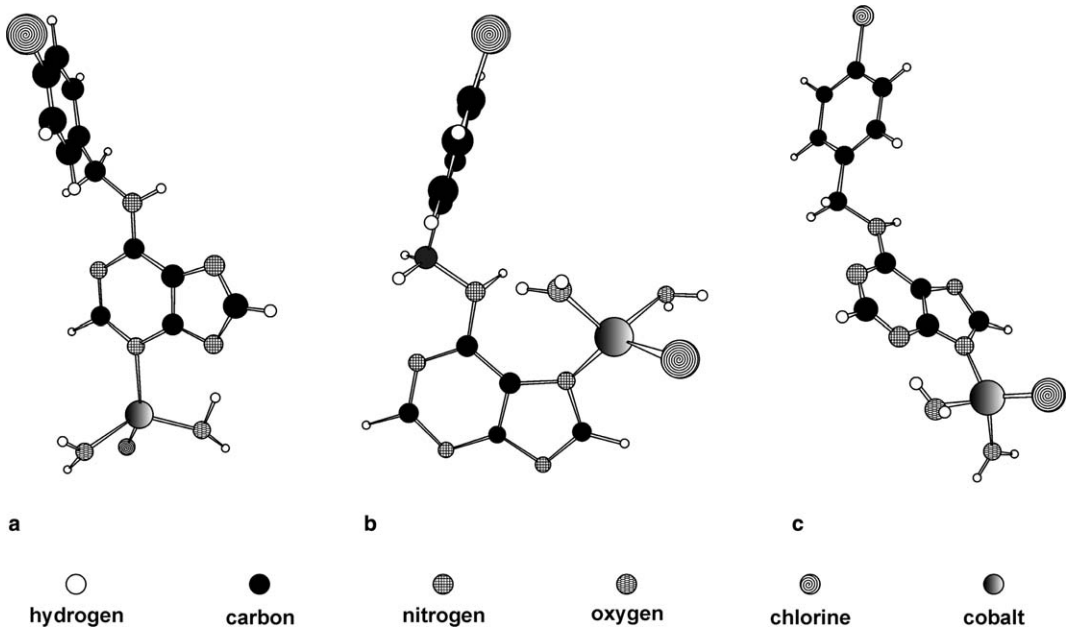

Fig. 2. Optimized geometries of possible structures of complex **2**. The most probable structure is depicted in a variant *c*.

Table 4
Comparison of calculated and experimental infrared frequencies (cm^{-1}) of the ligands HL_1–HL_6 and their assignment

HL_1		HL_2		HL_3		HL_4		HL_5		HL_6		Assignment
Calcd.	Exp.	Calcd.	Exp.	Calcd.	Exp.	Calcd.	Exp.	Calcd.	Exp.	Calcd.	Exp.	
3648		3648		3650		3649		3648		3648		$\nu(N_9–H)$
3612	3429	3613	3430	3609	3422	3619	3430	3612	3455	3613	3447	$\nu(N_6–H)$
3241	3260	3240	3261	3239	3262	3240	3288	3240	3267	3240	3259	$\nu(C_8–H)$
3091	3077	3093	3048	3137	3067	3081	3072	3092	3085	3096	3082	$\nu_{as}(CH_2)$
3017	2985	3019	2997	3046	2995	3014	2992	3018	2941	3016	2950	$\nu_s(CH_2)$
1630	1622	1630	1626	1629	1623	1629	1623	1632	1630	1630	1630	$\nu(C{=}N)$
1636	1538	1614	1567	1622	1539	1615	1515	1626	1567	1636	1568	$\nu(C{=}C)_{ar}$
				1240	1274	1292	1255					$\nu(C_{ar}–O)$
1099	1157	1100	1155					1269	1253	1240	1256	$\nu(C_{ar}–X)$

3.4. IR spectra

In the IR spectra of all the ligands as well as the complexes, the maxima belonging to the ν(C=N) vibration appeared in the 1620–1630 cm^{-1} region, while the bands at 1465–1491 and 1510–1568 cm^{-1} belong to ν(C=C) vibration. The broadbands between 3339 and 3447 cm^{-1} are associated with the ν(N–H) vibration. The characteristic bands of the C_{ar}–Cl, C_{ar}–F and C_{ar}–O groups are observed in the 1155–1174, 1250–1272, and 1255–1275 cm^{-1} regions, respectively. All the bands discussed above confirm the presence of the ligands in complexes **1**–**6** [40]. The far-IR spectra of the complexes revealed absorptions in the 430–449 and 314–324 cm^{-1} ranges, which may be assigned to the ν(Co–N), and ν(Co–O) stretching bands, respectively. The bands between 303 and 310 cm^{-1} can be attributed to the ν(Co–Cl) stretching vibration [41–45].

The comparison of measured frequencies with calculated values is given in Table 4. Because of the fact that calculations were carried out in vacuum, and thus interactions among molecules were ignored, differences between experimental and theoretical values appeared. In spite of this, values correspond sufficiently.

3.5. Mass spectroscopy

The ES+ mass spectra of complexes **1** and **2** showed a peak at 260 *m*/*z* identifying the presence of HL_1 and HL_2 molecule in these complexes. The presence of HL_3 and HL_4 in compounds **3** and **4** is obvious from the maximum at 286 *m*/*z*. The maxima observed at 244 *m*/*z* confirmed the presence of the ligands HL_5 and HL_6 in compounds **5** and **6**. The peaks observed at 136 and 121 *m*/*z* correspond to the fragments of adenine and purine, respectively. The peaks for fragments $[Co(L_1)Cl(H_2O)_2]^+$ and $[Co(L_2)Cl(H_2O)_2]^+$ appeared at 391 *m*/*z*, while peaks observed at 414 *m*/*z* belong to fragments $[Co(L_3)Cl(H_2O)_2]^+$ and $[Co(L_4)Cl(H_2O)_2]^+$. The peaks observed at 354 *m*/*z* for compounds **1** and **2** are associated with fragments $[Co(L_1)Cl]^+$ and $[Co(L_2)Cl]^+$, respectively. The peaks

appeared at 379 *m/z* correspond with fragments $[Co(L_3)Cl]^+$ and $[Co(L_4)Cl]^+$. In case of the complexes **5** and **6**, the maxima appeared at 337 *m/z* agree with the fragments $[Co(L_5)Cl]^+$ and $[Co(L_6)Cl]^+$.

3.6. Thermal analyses

Thermal decomposition of all complexes is very similar. TG curves showed that compounds **1** and **3**–**6** are monohydrates while the complex **2** exists as a dihydrate. The curves of thermal degradation of compounds **2** and **4** are shown in Fig. 3. In the case of **2**, the first weight loss is apparent between 40 and 138 °C and can be attributed to the loss of one crystal water molecule (found/calc. 4.1/4.2%) and the existence of the compound having formula of $[Co(L_2)Cl(H_2O)_2]\cdot H_2O$, which is stable between 138 and 196 °C. The weight loss connected with the elimination of the second crystal water molecule can be observed between 196 and 280 °C. A plateau occurs on the TG curve in the 280–305 °C temperature interval and it can be associated with formation of an anhydrous complex $[Co(L_2)Cl(H_2O)_2]$ (found/calc. 8.7/8.5%). It is evident from the TG curves of **1** and **3**–**6** that the weight loss between ca. 35 and 140 °C is connected with the release of one crystal water molecule. Thermal decomposition of all complexes is finished at ca. 960 °C, giving Co_3O_4/CoO mixture in ratio 4:1 which was determined by means of X-ray powder diffraction analysis and PDF2 database [46] in the case of **3** and **6**.

3.7. X-ray structure of 6-(4-chlorobenzylamino)purin-di-ium diperchlorate dihydrate, $[H^{2+}L_2](ClO_4)_2\cdot 2H_2O$

The crystal structure of 6-(4-chlorobenzylamino)purin-di-ium diperchlorate dihydrate is composed of 6-(4-chlorobenzylamino)purin-di-ium cation, two perchlorate anions and two water molecules of crystallization. The molecular structure together with the atom numbering scheme is shown in Fig. 4. The cation is clearly protonated at the *N*7 and *N*9 positions, and a combination of *N*1 and *N*3

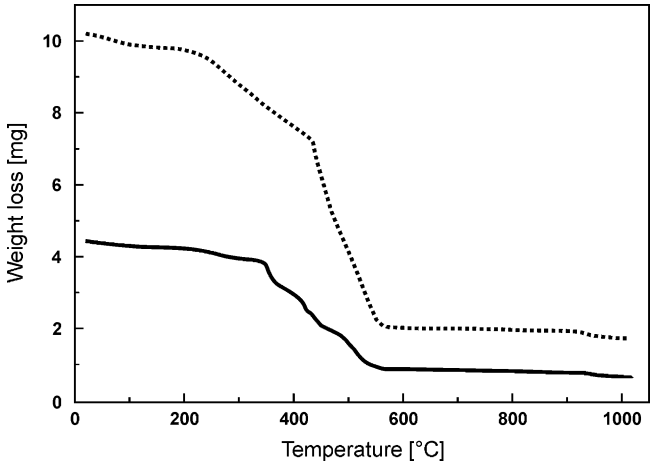

Fig. 3. Thermogravimetric curves of the complexes **2** (—) and **4** (···).

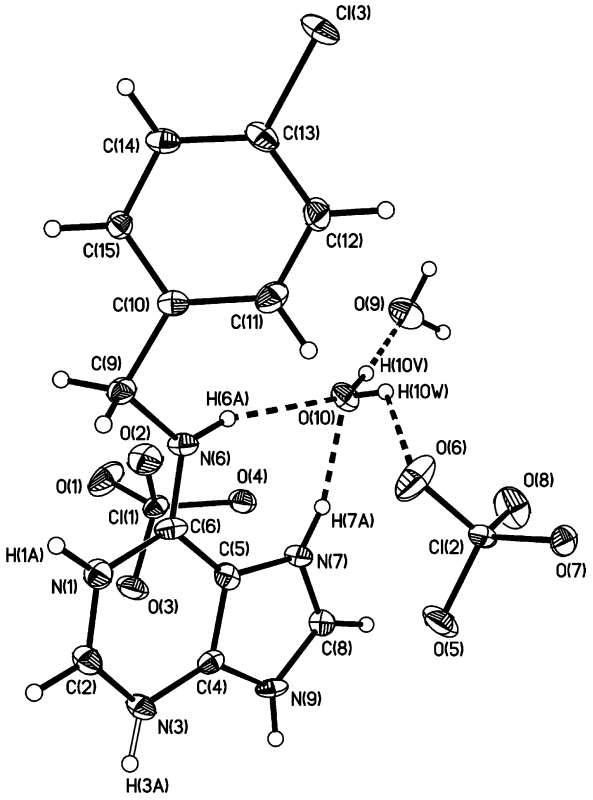

Fig. 4. The molecular structure of $[H^{2+}L_2](ClO_4)_2\cdot 2H_2O$ with the atom labelling scheme. The non-H atoms are drawn as displacement ellipsoids at the 50% probability level and H atoms are shown as small spheres at arbitrary radii. Dashed lines indicate possible hydrogen bonds. The H1A and H3A positions belong to the identical hydrogen atom, which is disordered over two positions with the probability of 34% for the H1A position and 66% for the H3A one.

ones. However, the positions of the latter proton are statistically disordered over two positions with probability of 34% (for N(1)–H), and 66% (for N(3)–H), respectively. The position of the hydrogen atoms differs from free bases, where the protonation occurs only at the *N*9 position. The molecular structure of $[H^{2+}L_2](ClO_4)_2\cdot 2H_2O$ represents the (*N*1, *N*3), *N*9-protonated *N*7 tautomer. There are significant deviations from planarity in both purine and phenyl rings [47]. Maximum deviation from the LSQ-plane is 0.0119(3) Å for C2 of the purine ring and 0.0077(3) Å for C14 of the phenyl ring. The dihedral angle between the above-mentioned rings is equal to 53.45(1)°. It is significantly lower in comparison to that found for 6-(2-chlorobenzylamino)purine dihydrate [79.5(2)°] [5], 6-(4-chlorobenzylamino)purinium perchlorate [86.19(1)°] [6] and 6-(4-methoxybenzylamino)purin-3-ium chloride [77.46(5)°] [48]. Selected bond lengths and angles are given in Table 5, while hydrogen bond parameters are summarized in Table 6. The C2–N3–C4, C8–N7–C5 and C8–N9–C4 bond angles in a purine skeleton of $[H^{2+}L_2](ClO_4)_2\cdot 2H_2O$ are 116.1(3)°, 108.3(3)° and 107.5(3)° and are slightly different from the values obtained for the above-mentioned compounds. All the above-discussed differences are probably caused by a degree of

Table 5
Selected bond lengths (Å) and angles (°) for $[H^{2+}L_2](ClO_4)_2 \cdot 2H_2O$

Bond lengths		Bond angles	
N(1)–C(2)	1.307(5)	C(2)–N(1)–C(6)	120.1(3)
N(1)–C(6)	1.359(5)	N(1)–C(2)–N(3)	126.2(3)
C(2)–N(3)	1.334(5)	C(2)–N(3)–C(4)	116.1(3)
N(3)–C(4)	1.357(5)	N(3)–C(4)–C(5)	121.2(3)
C(4)–N(9)	1.358(5)	N(9)–C(4)–C(5)	108.1(3)
C(4)–C(5)	1.370(5)	C(4)–C(5)–N(7)	106.0(3)
C(5)–N(7)	1.381(4)	C(4)–C(5)–C(6)	119.8(3)
C(5)–C(6)	1.415(5)	N(1)–C(6)–C(5)	116.7(3)
N(6)–C(6)	1.310(4)	C(8)–N(7)–C(5)	108.3(3)
N(7)–C(8)	1.313(4)	N(7)–C(8)–N(9)	110.2(3)
C(8)–N(9)	1.335(5)	C(8)–N(9)–C(4)	107.5(3)

Table 6
Hydrogen bonds for $[H^{2+}L_2](ClO_4)_2 \cdot 2H_2O$ (Å, °)

D–H···A	*d*(D–H)	*d*(H···A)	*d*(D···A)	∠(DHA)
N(3)–H(3A)···O(4)^{i}	0.88	2.16	2.919(4)	143.5
N(3)–H(3A)···O(7)^{ii}	0.88	2.31	2.910(4)	125.2
N(6)–H(6A)···O(10)	0.88	2.09	2.943(4)	161.8
N(7)–H(7A)···O(10)	0.88	1.87	2.680(4)	153.1
N(9)–H(9A)···O(4)^{iii}	0.88	2.09	2.862(4)	145.3
N(9)–H(9A)···O(7)^{ii}	0.88	2.34	2.900(4)	121.3
N(9)–H(9A)···O(7)^{iv}	0.88	2.46	3.009(4)	120.8
O(9)–H(9V)···O(5)^{v}	0.85(3)	2.17(4)	2.953(5)	153(5)
O(9)–H(9V)···O(5)^{vi}	0.85(3)	2.34(4)	3.009(4)	136(5)
O(9)–H(9W)···O(1)^{vii}	0.88(3)	2.08(3)	2.874(4)	150(4)
O(10)–H(10V)···O(9)	0.89(3)	1.80(3)	2.684(4)	170(6)
O(10)–H(10W)···O(6)	0.85(3)	2.38(4)	2.995(4)	130(4)
O(10)–H(10W)···O(3)^{vii}	0.85(3)	2.55(3)	3.243(4)	139(4)

Symmetry transformations used to generate equivalent atoms: (i) $x+1, y, z$; (ii) $x, y+1, z$; (iii) $-x+1, -y+1, -z+2$; (iv) $-x+2, -y, -z+2$; (v) $-x+1, -y, -z+2$; (vi) $x-1, y, z$; (vii) $x, y-1, z$.

protonation and substitution of the whole 6-benzylaminopurine moiety. The $C_g1\cdots C_g2$, $C_g1\cdots C_g3$ and $C_g2\cdots C_g3$ distances are 6.311(2), 7.0208(21) and 2.1086(7) Å, respectively, where C_g1, C_g2 and C_g3 are the centroids of benzene, purine and imidazole rings. Torsion angles of C9–N6–C6–C5, C6–N6–C9–C10 and N6–C9–C10–C15 are 178.8(3)°, 157.6(3)°, and 138.7(3)°, respectively.

3.8. X-ray structure of $[Co_6(\mu\text{-}L_6)_4Cl_8(DMSO)_{10}] \cdot 4DMSO$ (7)

The interatomic and geometrical parameters of complex **7** are not discussed in detail in connection with the overall bad crystal data quality and consequently with the low quality of the refinement. Thus, the discussion regarding to the molecular structure of **7** is focused on the description of the stereochemistry in the vicinity of the central Co(II) ions and on the manner of coordination of organic ligands only. The molecular structure of the centrosymmetric hexanuclear complex $[Co_6(\mu\text{-}L_6)_4Cl_8(DMSO)_{10}] \cdot 4DMSO$ is depicted in Fig. 5. Four of the six central atoms, Co(1), Co(1A), Co(2) and Co(2A), are surrounded by six atoms in a distorted octahedral arrangement, while the geometry around Co(3) and Co(3A) atoms is tetrahedral. Thus, HL_6, i.e., 6-(4-fluorobenzylamino)purine, acts as a tridentate bridging ligand in this complex. There is a direct metal–metal interaction between Co(1) and Co(1A) atoms with the bond length of 2.667(2) Å. Furthermore, these two cobalt atoms are connected with four bridging organic ligands HL_6, which are coordinated via *N*3 and *N*9 donor atoms. One chlorine atom is bonded to Co(2) and Co(2A), respec-

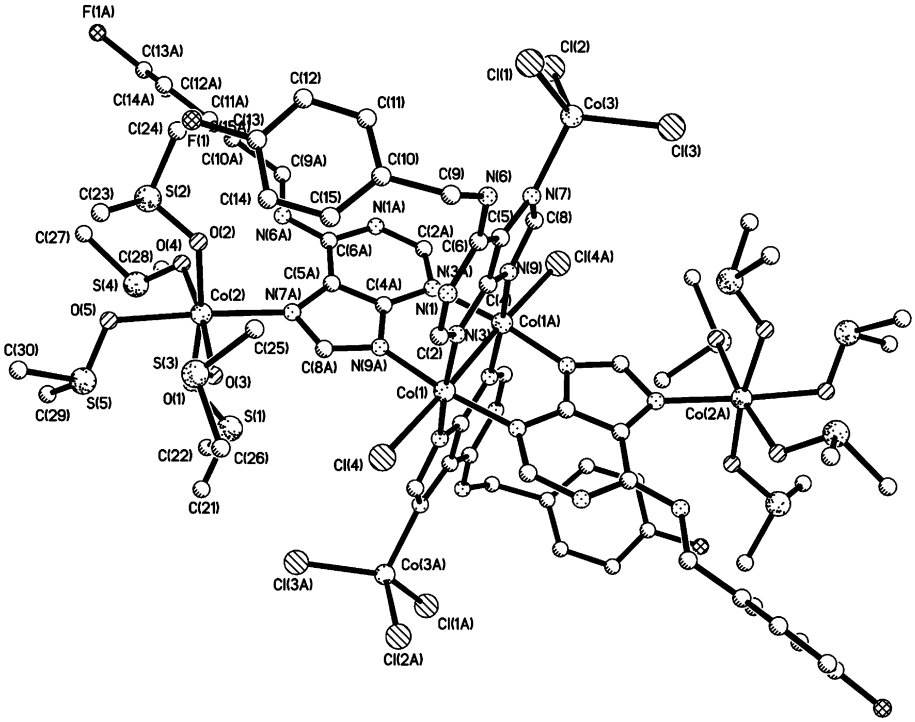

Fig. 5. The molecular structure of $[Co_6(\mu\text{-}L_6)_4Cl_8(DMSO)_{10}] \cdot 4DMSO$ (**7**). Hydrogen atoms and solvated DMSO molecules were omitted for clarity.

Table 7
Selected bond lengths (Å) and angles (°) for $[Co_6(\mu\text{-}L_6)_4Cl_8(DMSO)_{10}]\cdot 4DMSO$ (**7**)

Co(1)–N(9A)	1.926(7)	Co(3)–Cl(1)	2.255(3)
Co(1)–N(3A)^{i}	1.933(7)	Co(3)–Cl(2)	2.267(3)
Co(1)–N(3)	1.938(7)	Co(3)–Co(3A)^{i}	12.757(3)
Co(1)–N(9)^{i}	1.932(7)	N(9A)–Co(1)–N(3A)^{i}	172.2(3)
Co(1)–Cl(4)	2.456(2)	N(3)–Co(1)–N(9)^{i}	172.6(3)
Co(1)–Co(1A)^{i}	2.667(2)	Cl(4)–Co(1)–Co(1A)^{i}	175.45(9)
Co(1)–Co(2)	5.9575(19)	O(2)–Co(2)–O(1)	171.7(3)
Co(1)–Co(3)	7.0505(19)	O(4)–Co(2)–O(3)	172.3(3)
Co(2)–O(4)	2.079(7)	N(7A)–Co(2)–O(5)	176.9(3)
Co(2)–O(2)	2.079(6)	N(7)–Co(3)–Cl(3)	110.6(2)
Co(2)–O(1)	2.092(7)	N(7)–Co(3)–Cl(1)	111.4(2)
Co(2)–O(3)	2.103(7)	Cl(3)–Co(3)–Cl(1)	112.56(15)
Co(2)–N(7A)	2.137(6)	N(7)–Co(3)–Cl(2)	103.9(2)
Co(2)–O(5)	2.144(6)	Cl(3)–Co(3)–Cl(2)	110.07(15)
Co(2)–Co(3)	9.838(2)	Cl(1)–Co(3)–Cl(2)	107.93(14)
Co(2)–Co(2A)^{i}	12.877(3)		
Co(3)–N(7)	2.027(7)		
Co(3)–Cl(3)	2.237(3)		

Symmetry transformations used to generate equivalent atoms: (i) $-x+1$, $-y+1$, $-z+2$.

tively, and it appears as a terminal ligand. Each of the Co(2) and Co(2A) atoms are coordinated by five oxygen atoms of DMSO and the *N*7 atom of the purine moiety. Coordination spheres of Co(3) and Co(3A) are formed by three chlorine atoms and the *N*7 atom originating from 6-(4-fluorobenzylamino)purine. Selected bond lengths and angles are given in Table 7. It is evident, that the octahedral surrounding of Co(1) atom is slightly deformed as can be obvious from angle values in the vicinity of the central atom, i.e., N(9A)–Co(1)–N(3A), N(3)–Co(1)–N(9) and Cl(4)–Co(1)–Co(1A), which were found to be 172.2(3)°, 172.6(3)° and 175.45(9)°, respectively. As for the Co(2) atom, the O(2)–Co(2)–O(1), O(4)–Co(2)–O(3) and N(7A)–Co(2)–O(5) bond angles are 171.7(3)°, 172.3(3)° and 176.9(3)°, respectively. A tetrahedral surrounding of the Co(3) atom is slightly deformed which can be seen from the bond angle values N(7)–Co(3)–Cl(3) [110.6(2)°], N(7)–Co(3)–Cl(1) [111.4(2)°], Cl(3)–Co(3)–Cl(1) [112.56(15)°], N(7)–Co(3)–Cl(2) [103.9(2)°], Cl(3)–Co(3)–Cl(2) [110.07(15)°] and Cl(1)–Co(3)–Cl(2) [107.93(14)°].

3.9. Testing for cytotoxicity

The cytotoxicity of the prepared complexes as well as the starting compounds, i.e., $CoCl_2\cdot 6H_2O$ and ligands HL_1–HL_6, was tested against malignant melanoma (*G361*), chronic myelogenous erythroleukemia (*K562*), osteogenic sarcoma (*HOS*) and breast adenocarcinoma (*MCF7*) human cancer cell lines. As can be seen from Table 8, *G361*, *K562* and *MCF7* cell lines were insensitive to all the assayed compounds in tested concentrations. *HOS* cell line was insensitive to starting compounds and **2**, whereas complexes **1** and **3**–**6** showed increased cytotoxic activity against this cell line. IC_{50} values of these compounds range from 7 to 28 μM and are close to that for similar Co(II) complexes we had described previously [8]. Moreover,

Table 8
The cytotoxicity of the studied compounds, expressed as IC_{50} values (μM) assessed by a Calcein AM assay

Compound	Cell line[a]			
	G361	*HOS*	*K562*	*MCF7*
HL_1	>50	>50	>50	>50
HL_2	>50	>50	>50	>50
HL_3	>50	>50	>50	>50
HL_4	>50	>50	>50	>50
HL_5	>50	>50	>50	>50
HL_6	>50	>50	>50	>50
1	>50	28	>50	>50
2	>50	>50	>50	>50
3	>50	27	>50	>50
4	>50	22	>50	>50
5	42	10	>50	>50
6	>50	7	>50	>50
$CoCl_2\cdot 6H_2O$	>50	>50	>50	>50

[a] *G361* – human malignant melanoma, *K562* – human chronic myelogenous erythroleukemia, *HOS* – human osteogenic sarcoma, *MCF7* – human breast adenocarcinoma.

these values are comparable and even better than those obtained for Roscovitine (CYC202) (20 μM) [7], a cytokinin-derived compound, currently undergoing Phase IIb clinical trials for lung cancer and cancer from a group of B-cell hematological malignancies [49]. The obtained IC_{50} values in the case of all complexes, except for **2**, in connection with the HOS cell line show that higher cytotoxicity of the Co(II) complexes as compared to free cytokinins is probably caused by the complex formation.

4. Supplementary material

Crystallographic data of the structural analysis have been deposited with the Cambridge Crystallographic Data Centre as supplementary publication numbers CCDC: 269650 {for $[H^{2+}L_2](ClO_4)_2\cdot 2H_2O$} and 269651 {for **7**}. Copies of this information may be obtained free of charge from The director, CCDC, 12 Union Road, Cambridge, CB2 1EZ, UK (fax: +44 1223-336-033; e-mail: deposit @ccdc.cam.ac.uk or http://www.ccdc.cam.ac.uk).

Acknowledgements

This financial support from The Ministry of Education, Youth and Sports (MSM6198959218) and the Grant Agency of the Czech Republic (203/04/1168) is acknowledged. The authors thank Dana Vychodilová and Eva Hirnerová for technical assistance and Dr. Zdeněk Šindelář for magnetochemical measurements.

References

[1] C.O. Miller, F. Skoog, M.H. Von Saltza, F.M. Strong, J. Am. Chem. Soc. 78 (1955) 1392.
[2] M. Strnad, Physiol. Plant. 100 (1997) 170.
[3] J. Veselý, M. Havlíček, M. Strnad, J.J. Blow, A. Donella-Deana, L. Pinna, D.S. Leatham, J.Y. Kato, L. Detivaud, S. Leclerc, L. Meijer, Eur. J. Biochem. 224 (1994) 771.

[4] Z. Trávníček, M. Maloň, Z. Šindelář, K. Doležal, J. Rolčík, V. Kryštof, M. Strnad, J. Marek, J. Inorg. Biochem. 84 (2001) 23.
[5] M. Maloň, Z. Trávníček, M. Maryško, R. Zbořil, M. Mašláň, J. Marek, K. Doležal, J. Rolčík, V. Kryštof, M. Strnad, Inorg. Chim. Acta 323 (2001) 119.
[6] M. Maloň, Z. Trávníček, M. Maryško, J. Marek, K. Doležal, J. Holub, J. Rolčík, M. Strnad, Transition Met. Chem. 27 (2002) 580.
[7] Z. Trávníček, M. Maloň, M. Zatloukal, K. Doležal, M. Strnad, J. Marek, J. Inorg. Biochem. 94 (2003) 307.
[8] Z. Trávníček, A. Klanicová, I. Popa, J. Rolčík, J. Inorg. Biochem. 99 (2005) 776.
[9] F.H. Allen, Acta Crystallogr. Sect. B 58 (2002) 380.
[10] J.P. García-Terán, O. Castillo, A. Luque, U. García-Couceiro, P. Román, F. Lloret, Inorg. Chem. 43 (2004) 5761.
[11] T.J. Kistenmacher, Acta Crystallogr., Sect. B: Struct. Crystallogr. Cryst. Chem. 30 (1974) 1610.
[12] P. de Meester, A.C. Skapski, J. Chem. Soc., Dalton Trans. (1973) 1596.
[13] T. Sorrell, L.A. Epps, T.J. Kistenmacher, L.G. Marzilli, J. Am. Chem. Soc. 100 (1978) 5756.
[14] C.C. Chiang, L.A. Epps, L.G. Marzilli, T.J. Kistenmacher, Inorg. Chem. 18 (1979) 791.
[15] P.J. Toscano, C.C. Chiang, T.J. Kistenmacher, L.G. Marzilli, Inorg. Chem. 20 (1981) 1513.
[16] M.S. Masoud, A.A. Soayed, A.E. Ali, Spectrochim. Acta A 60 (2004) 1907.
[17] S.M. Hecht, N.J. Leonard, R.Y. Schmitz, F. Skoog, Phytochemistry 9 (1970) 1173.
[18] O. Kahn, Molecular Magnetism, Wiley, New York, 1993.
[19] A. Altomare, M.C. Burla, M. Camalli, G.L. Cascarano, C. Giacovazzo, A. Guagliardi, A.G.G. Moliterni, G. Polidori, R. Spagna, J. Appl. Crystallogr. 32 (1999) 115.
[20] L.J. Farrugia, J. Appl. Crystallogr. 32 (1999) 837.
[21] G.M. Sheldrick, SHELX-97. Programs for Crystal Structure Analysis (Release 97-2), University of Göttingen, Germany, 1997.
[22] S.G. Vulfson, Molecular Magnetochemistry, Gordon and Breach Science Publishers, Amsterdam, 1998.
[23] F.A. Cotton, G. Wilkinson, C.A. Murillo, M. Bochmann, Advanced Inorganic Chemistry, 6th ed., Wiley, New York, 1999.
[24] F. Téllez, A. Flores-Parra, N. Barba-Behrens, R. Contreras, Polyhedron 23 (2004) 2481.
[25] C.M. Mikulski, L. Mattucci, L. Weiss, N.M. Karayannis, Inorg. Chim. Acta 107 (1985) 81.
[26] W.J. Geary, Coord. Chem. Rev. 7 (1971) 110.
[27] F.A. Cotton, D.M.L. Goodgame, M. Goodgame, J. Am. Chem. Soc. 83 (1961) 4690.
[28] A. Maslejova, S. Uhrinova, J. Mrozinski, B. Zurowska, M.C. Munoz, M. Julve, Inorg. Chim. Acta 255 (1997) 343.
[29] M. Amirnasr, A.H. Mahmoudkhani, A. Gorji, S. Dehghanpour, H. Reza Bijanzadeh, Polyhedron 21 (2002) 2733.
[30] C.A. Otter, S.M. Couchman, J.C. Jeffery, K.L.V. Mann, E. Psillakis, M.D. Ward, Inorg. Chim. Acta 278 (1998) 178.
[31] S.S. Konstantinović, B.C. Radovanović, Ž. Cakić, V. Vasić, J. Serb. Chem. Soc. 68 (2003) 641.
[32] A.B.P. Lever, Inorganic Electronic Spectroscopy, 2nd ed., Elsevier, Amsterdam, 1984.
[33] E. Slyk, A. Wojtczak, M. Jaskólski, M. Gilski, J.G. Haasnoot, J. Reedijk, Inorg. Chim. Acta 260 (1997) 145.
[34] E. König, Struct. Bond. 9 (1971) 175.
[35] M. Nowak, H. Keppler, Am. Mineral. 83 (1998) 43.
[36] D.X. West, H. Beraldo, A.A. Nassar, Transition Met. Chem. 24 (1999) 595.
[37] F.J. Barros-García, A. Bernalte-García, A.M. Lozano-Vila, F. Luna-Giles, E. Viñuelas-Zahínos, Polyhedron 24 (2005) 129.
[38] M.J. Frisch, G.W. Trucks, H.B. Schlegel, G.E. Scuseria, M.A. Robb, J.R. Cheeseman, J.A. Montgomery Jr., T. Vreven, K.N. Kudin, J.C. Burant, J.M. Millam, S.S. Iyengar, J. Tomasi, V. Barone, B. Mennucci, M. Cossi, G. Scalmani, N. Rega, G.A. Petersson, H. Nakatsuji, M. Hada, M. Ehara, K. Toyota, R. Fukuda, J. Hasegawa, M. Ishida, T. Nakajima, Y. Honda, O. Kitao, H. Nakai, M. Klene, X. Li, J.E. Knox, H.P. Hratchian, J.B. Cross, V. Bakken, C. Adamo, J. Jaramillo, R. Gomperts, R.E. Stratmann, O. Yazyev, A.J. Austin, R. Cammi, C. Pomelli, J.W. Ochterski, P.Y. Ayala, K. Morokuma, G.A. Voth, P. Salvador, J.J. Dannenberg, V.G. Zakrzewski, S. Dapprich, A.D. Daniels, M.C. Strain, O. Farkas, D.K. Malick, A.D. Rabuck, K. Raghavachari, J.B. Foresman, J.V. Ortiz, Q. Cui, A.G. Baboul, S. Clifford, J. Cioslowski, B.B. Stefanov, G. Liu, A. Liashenko, P. Piskorz, I. Komaromi, R.L. Martin, D.J. Fox, T. Keith, M.A. Al-Laham, C.Y. Peng, A. Nanayakkara, M. Challacombe, P.M.W. Gill, B. Johnson, W. Chen, M.W. Wong, C. Gonzalez, J.A. Pople, GAUSSIAN 03, Revision C.02, Gaussian, Inc., Wallingford, CT, 2004.
[39] A.E. Reed, L.A. Curtiss, F. Weinhold, Chem. Rev. 88 (1988) 899.
[40] C.J. Pouchert, The Aldrich Library of Infrared Spectra, 3rd ed., Aldrich Chemical Company Press, Milwaukee, 1981.
[41] P. Kamalakannan, D. Venkappayya, J. Inorg. Biochem. 90 (2002) 22.
[42] E. Szlyk, A. Surdykowski, M. Barwiolek, E. Larsen, Polyhedron 21 (2002) 2711.
[43] K. Nakamoto, Infrared and Raman Spectra of Inorganic and Coordination Compounds, Part B: Applications in Coordination, Organometallic, and Bioinorganic Chemistry, 5th ed., Wiley, New York, 1997.
[44] J.R. Anacona, M. Azocar, O. Nusetti, C. Rodriguez-Barbarin, Trans. Met. Chem. 28 (2003) 24.
[45] A.N. Speca, C.M. Mikulski, F.J. Iaconianni, L.L. Pytlewski, N.M. Karayannis, Inorg. Chim. Acta 37 (1979) 551.
[46] PDF-2 Database Sts 1-47, (1997). ICDD, 12 Campus Boulevard, Newton Square, Pennsylvania 19073-3273, USA.
[47] M. Nardelli, J. Appl. Crystallogr. 28 (1995) 659.
[48] Z. Trávníček, I. Popa, K. Doležal, Acta Crystallogr., Sect. C 60 (2004) 662.
[49] J.A. Alvi, B. Austen, V.J. Weston, C. Fegan, D. Mac Callum, A. Gianella-Borradori, D.P. Lane, M. Hubank, J.E. Powell, W. Wei, A.M. Tailor, P.A. Moss, T. Stankovic, Blood 105 (11) (2005) 4484.

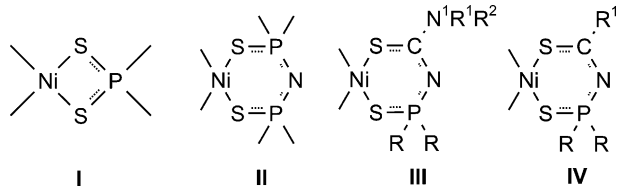

Scheme 1. Ni(II) complexes with thiophosphorus ligands containing NiS_4 core.

The complexes III and IV – with thiophosphoryl thioureas and thioamides – are the most suitable for investigation owing to convenient methods of synthesis of the ligands available in the literature [18–20] and the ease of variation of the substituents at phosphorus, carbon, and exocyclic nitrogen N^1 for alteration of steric environment around the nickel atom. Thus *bis*-bidentate ureas $[(i\text{-PrO})_2P(S)NHC(S)]_2Z$ with Z equal to open-chain substituents $[NH(CH_2)_2NH$, $NH(CH_2)_7NH$, $NH(CH_2)_2O(CH_2)_2NH$, $NH(CH_2)_2O(CH_2)_2O(CH_2)_2NH]$, crown (diaza-18-crown-6), or piperazine fragment are known [2,21,22].

To date complexes of type III have been described for $R = Ph$, $R^1 = H$, $R^2 = H$ [23,24], $R = Ph$, $R^1 = H$, $R^2 = Me$ **6** [23,25,26], $R = Ph$, $R^1 = H$, $R^2 = Ph$ [1,24,26], $R = Ph$, $R^1 = H$, $R^2 = C_6H_4Me$-3 [1], $R = Ph$, $R^1 = H$, $R^2 =$ Napht-1 [1], $R = Ph$, $R^1 = H$, $R^2 =$ Napht-2 **7** [1], $R = Ph$, $R^1 = H$, $R^2 = C_6H_4(OMe)$-4 [27]; $R = Ph$, $R^1 = R^2 = Me$ [23], $R = Ph$, $R^1 = R^2 = Et$ [24,26]; $R = Ph$, $R^1 = R^2 =$ Bu **8** [24]; $R = Ph$, $N^1R^1R^2 =$ Piperidine **9** [1]; $R = OPr^i$, $R^1 = H$, $R^2 = Ph$ **10** [28]; $R = OPh$, $R^1 = R^2 = Pr^i$ **11** [29]; $R = OPr^i$, $N^1R^1R^2 =$ Monoaza-18-crown-6 **12** [30]. The only complex of the type IV is known for $R = OPr^i$, $R^1 = Ph$ **13** [31,32].

We report here the structure of the complex $[Ni\{PhNHC(S)NP(S)(OPr^i)_2\text{-}S,S\}_2]$ **10** determined by X-ray single crystal diffraction and its behavior in dichloromethane solution investigated by NMR ^{31}P spectroscopy.

2. Results and discussion

X-ray structural analysis of the title molecule shows that the nickel atom is positioned in the symmetry center of a distorted square-planar arrangement with *trans*-disposition of the ligands; the S(2)Ni(1)S(1) and S(1)Ni(1)S(2)$(2 - x; 1 - y; 1 - z)$ angles are equal to 98.13(3) and 81.87(3)°, respectively (Fig. 1).

The six-membered cycle Ni(1)S(1)P(1)N(1)C(1)S(2) has a form of the asymmetric boat; the P(1)N(1)C(1)S(2) fragment is essentially planar within the limits of 0.011(4) Å while the S(1) and Ni(1) atoms deviate by 0.2039 and 1.1232(9) Å, respectively, from the plane. The exocyclic N(2) atom is located practically in the base plane of the heterocycle [the N(2) atom deviation is 0.012(4) Å]. No any strong inter- or intramolecular hydrogen bonding has been found in the solid state.

The geometry of the thiourea N(1)C(1)N(2) fragment indicates sp^2 hybridization of the N(2) atom with the valence angles sum being equal to 360°. The lone electron pair on N(2) is in a conjugation with the endocyclic N(1)=C(1) bond; the torsion angle N(1)C(1)N(2)C(3) is 5.1(6)°. The bond lengths distribution in the planar N(1)C(1)N(2) fragment supports the existence of such conjugation. Actually, the C(1)–N(1) bond length [1.291(4) Å] is somewhat elongated in comparison with the average C=N distance in Schiff bases of 1.27 Å [33] and the standard C=N bond length measures 1.279 Å [34]. On the other hand, the C(1)–N(2) bond [1.357(4) Å] is intermediate between double and ordinary bonds (the C–N distance in amines is 1.469 Å [34] and the standard N–C(sp^2) bond length is 1.452 Å [35]). The Ni(1)–S(1) and Ni(1)–S(2) distances of 2.2174(9) and 2.2073(9) Å, respectively, are close, suggesting electron density delocalization between the S(1) and S(2) atoms of the ligand. The C(1)–S(2) bond length [1.740(3) Å] indicates also such delocalization; this distance

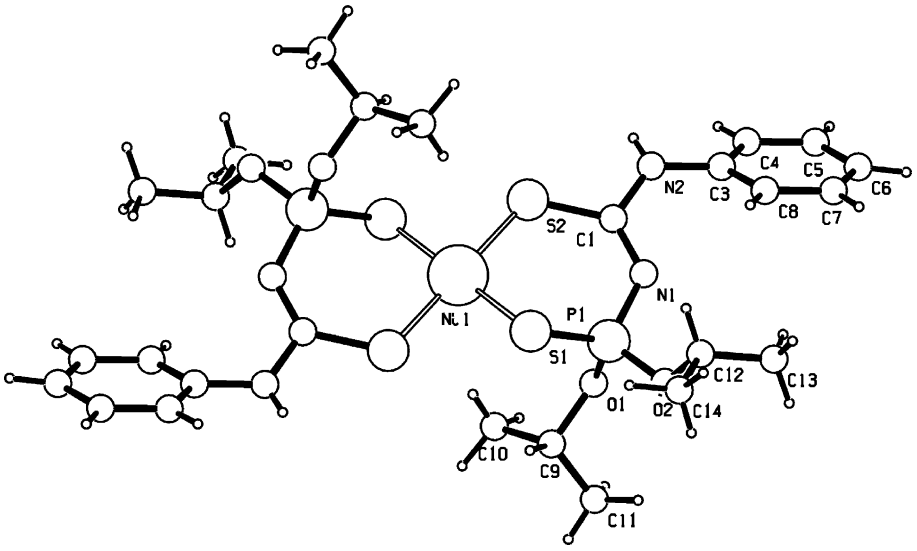

Fig. 1. Molecular structure of the $[Ni\{PhNHC(S)NP(S)(OPr^i)_2\text{-}S,S\}_2]$ complex.

differs significantly from the C=S bond length in thioureas (1.681 Å) and C–S bond length in sulfides (1.819 Å) [34]. The C(1)–S(2) and P(1)–S(1) distances in **10** are close to those in **6** [25], **11** [29], and **12** [30]. The basic geometrical parameters of these compounds are compared in Table 1. As it is evident from the data in this Table 1, the close similarity of the bond parameters between the compounds indicate that they are not influenced by the different nature of substituents attached to the phosphorus (Ph, OPr^i, or OPh) and exocyclic nitrogen N(2) atoms (H and Me, H and Ph, or Alk and Alk). Conformations of the complexes **10**, **11**, **12**, and **6** are also essentially identical.

2.1. Behavior of the [Ni{PhNHC(S)NP(S)(OPr^i)$_2$-S,S}$_2$] complex in dichloromethane solution

Aside from compounds **7** and **9** almost all the rest complexes above mentioned are diamagnetic both in the solid state and in solution, consistent with a square-planar environment. The complexes **7** and **9** are reported [1] to possess square-planar coordination geometry only in solution but in the solid state there are present both square-planar and tetrahedral forms. The authors [29] note an upfield ^{31}P NMR shift for the complex **11** in comparison with the free ligand: −11 and 53.3 ppm, respectively. Unfortunately, the absence of information about the conditions of the spectra recording (concentrations, solvent, etc.), makes the interpretation of this fact difficult. However in our opinion it is the tetrahedral distortion of the nickel environment of the complex in solution that gives rise to this considerable shift.

These results made us investigate the behavior of the complex **10** in solution. Solid state MAS NMR data (^{31}P and ^{13}C) of complex **10** reveal the only diamagnetic form which was found to be *trans*-square-planar isomer with C_i symmetry. NMR ^{31}P and UV–Vis spectroscopy data for solutions show the following picture.

In the electronic absorption spectra of complex **10** (Fig. 2) two bands at ~640 and ~530 nm, two "shoulders"

Table 1
Selected interatomic distances (Å) and angles (°) for **10**, **6** [25], **11** [29], and **12** [30]

	10	6	11	12
Ni(1)–S(1)	2.2174(9)	2.216	2.226	2.219
Ni(1)–S(2)	2.2073(9)	2.214	2.205	2.211
C(1)–S(2)	1.740(3)	1.760	1.745	1.754
P(1)–S(1)	1.990(1)	2.016	1.978	2.000
P(1)–N(1)	1.594(3)	1.610	1.574	1.584
C(1)–N(1)	1.291(4)	1.294	1.321	1.302
C(1)– N(2)	1.357(4)	1.347	1.337	1.349
S(2)–Ni(1)–S(1)	98.13(3)	98.10	97.65	97.80
Ni(1)–S(2)–C(1)	117.6(1)	118.5	118.1	117.6
S(1)–P(1)–N(1)	117.4(1)	116.7	119.8	116.3
S(2)–C(1)–N(1)	130.3(3)	129.0	127.4	127.5
P(1)–N(1)–C(1)	125.8(2)	125.6	127.5	128.0
Ni(1)–S(1)–P(1)	102.20(5)	101.10	101.36	100.41

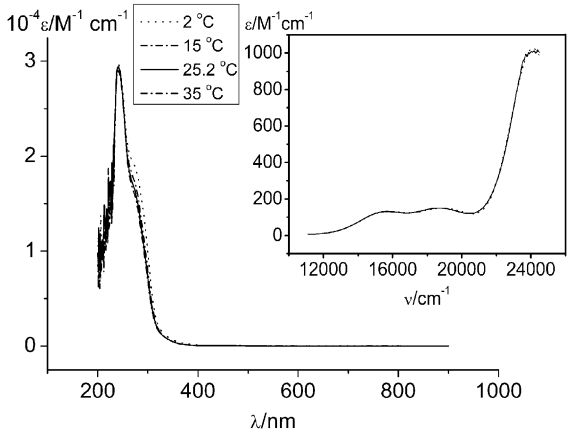

Fig. 2. Electronic absorption spectra of complex **10** in dichloromethane solutions at 2, 15, 25.2, and 35 °C ($c_{Ni(II)} = 1.0 \times 10^{-4}$ M); in the right insert the long-wave part of experimental spectrum at 25.2 °C ($c_{Ni(II)} = 3.49 \times 10^{-3}$ M) (solid line) and that reconstructed on Gaussian components (dot line) are shown.

at ~410 and ~275 nm, as well as band at 242 nm are observed at 298 K. The spectra exhibit weak temperature dependence. The latest high-energy intensive transitions ($\nu_{sh} = 36400$ cm^{-1}, $\varepsilon_{sh} = 16000$ mol dm^{-3} cm^{-1} and $\nu_{max} = 41332$ cm^{-1}, $\varepsilon_{max} = 29500$ mol dm^{-3} cm^{-1}) fall obviously into ligand–ligand and ligand-to-metal transitions [36]. From the long-wave spectrum part three Gaussian components were reconstructed (see Fig. 2) with the spectral parameters $\nu_{max} = 15411$ cm^{-1} ($\varepsilon_{max} = 130$ mol dm^{-3} cm^{-1}), $\nu_{max} = 19078$ cm^{-1} ($\varepsilon_{max} = 160$ mol dm^{-3} cm^{-1}), and $\nu_{max} = 24132$ cm^{-1} ($\varepsilon_{max} = 1190$ mol dm^{-3} cm^{-1}).

The three bands reported for the absorption spectra of the square-planar species Ni[S_2CNEt$_2$-*S,S*]$_2$ (at 15900, 19000, and 21000 cm^{-1}) [37] and **13** Ni[PhC(S)NP(S)(OPr^i)$_2$-*S,S*]$_2$ (at 16530, 18920, and 21960 cm^{-1}) [32] were assigned, respectively, to the d–d transitions $^1A_{1g} \rightarrow {}^1B_{1g}$ ($d_{x^2-y^2} \rightarrow d_{xy}$), $^1A_{1g} \rightarrow {}^1B_{3g}$ ($d_{xz} \rightarrow d_{xy}$), and $^1A_{1g} \rightarrow {}^1B_{1g}$ ($d_{z^2} \rightarrow d_{xy}$) at the local D_{2h} symmetry. Thus the bands at 15411 and 19078 cm^{-1} for compound **10** can be assigned to the corresponding $^1A_{1g} \rightarrow {}^1B_{1g}$ and $^1A_{1g} \rightarrow {}^1B_{3g}$ transitions respectively with the same D_{2h} symmetry of square-planar isomers. The reconstructed band at 24132 cm^{-1} may be assigned to the remaining $^1A_{1g} \rightarrow {}^1B_{1g}$ transition with its high intensity deriving from activation by the ligand-to-metal transition [32,37]. Bands in the range of 700–800 nm, which are inherent features of tetrahedral or pseudo-tetrahedral complexes with the $Ni^{II}S_4$ core [13,38], were not observed in the electronic spectra of complex **10** (Fig. 2), indicating negligible contribution for pseudo-tetrahedral isomers in the solutions.

In dichloromethane solutions of the compound **10** four signals which were denoted by A_1, A_2, B, and C have been detected by ^{31}P–{^{1}H} NMR method (Fig. 3). The dominant C signal refers to the monocrystal *trans*-isomer **C** (with anti-disposition of two ligands in boat conformations) because its ^{31}P chemical shift in solution at −80 °C (55.41 ppm) coincides very closely with that in the MAS

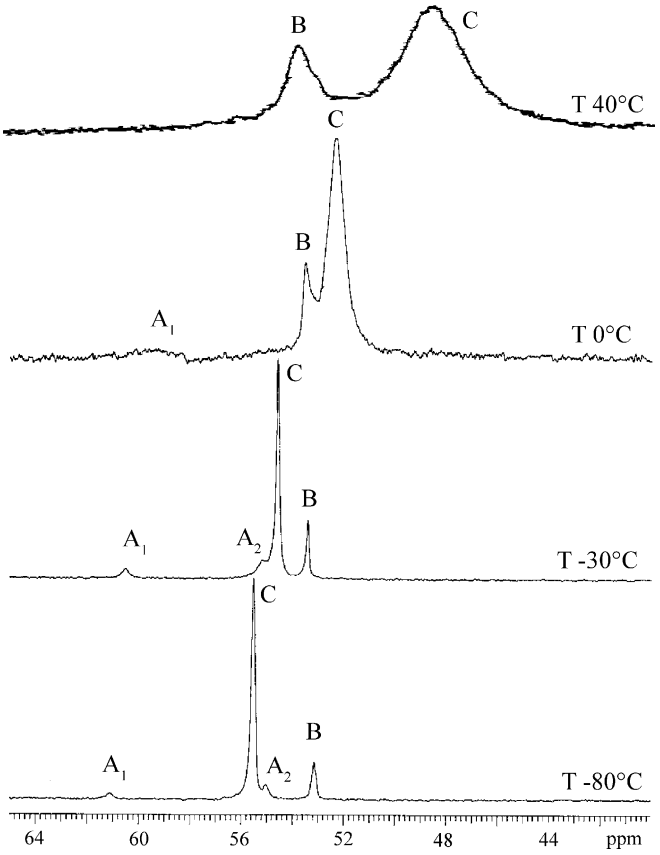

Fig. 3. The NMR $^{31}P–\{^1H\}$ spectrum of the complex **10** solutions in dichloromethane at different temperatures ($c_{Ni(II)} = 2.5 \times 10^{-2}$ M) and 121.4 MHz.

NMR $^{31}P–\{^1H\}$ spectrum of the polycrystals (56.2 ppm). As can be seen from the 2D-NMR $^{31}P–\{^1H\}$ spectra (Fig. 4), the cross-peaks are evidence for exchange between signals – A_1–C, A_2–C, and B–C. The absence of exchange between A_1 and A_2 implies, in view of alike intensity and line-width of the A_1 and A_2 signals, that they are diastereotopic and assigned to nonequivalent ligand conformations (boat and chair) of the same complex isomer (**A**). A rather small displacement of the B signal (53.03 ppm at −80 °C) from the C signal suggests to the same ligand conformations in the isomers (boat) but with different disposition (*cis*- instead of *trans*-) in the plane of the NiS_4 core. In accordance with this the A_1 signal at 54.93 ppm (−80 °C) relates to the boat ligand conformation whereas the A_2 signal at 61.02 ppm (−80 °C) belongs to the chair one of the complex form (**A**). Taking into account that in all studied crystals of related complexes, **6**, **10**, **11**, and **12**, two ligands are in anti-orientation about the NiS_4 core plane (see above) and based on reported electronic and NMR spectra, the three signal groups ($A_1 + A_2$, B, and C) can be related respectively to the three following diamagnetic square-planar isomers with different dispositions and conformations of two ligands in anti-orientation: *trans*-chair–boat (**A**) [39], *cis*-boat–boat (**B**), and *trans*-boat–boat (**C**) in equilibrium (Fig. 5).

One more possible conformation isomer **D** (*cis*-chair–boat) is instable and consequently may be unobserved considering that for steric reasons the *cis*-disposition of the ligands should be energy unfavorable and chair-conformation is not realized in the crystal. However the signals of all of four possible isomers (**A**, **B**, **C**, and **D**), including two weak diastereotopic phosphorus signals D_1 and D_2, are observed in the ^{31}P NMR spectra of the allied complex [Ni{*t*-BuNHC(S)NP(S)(OPr^i)$_2$-*S*,*S*}$_2$] [40] (**14**) (Fig. 6). This is not surprising, since line-widths of all the ^{31}P NMR signals for **14** are several times narrower than those for **10** in the whole temperature range studied. In keeping with the above assignment, the lack of visible exchange between A_1 or A_2 and B signals (Fig. 4) is due to the low probability of simultaneous change of the ligand conformation and disposition at the **A**–**B** interconversion and the latter process is carried out in two stages through slow *cis*–*trans*-isomerisation with **C** (see below).

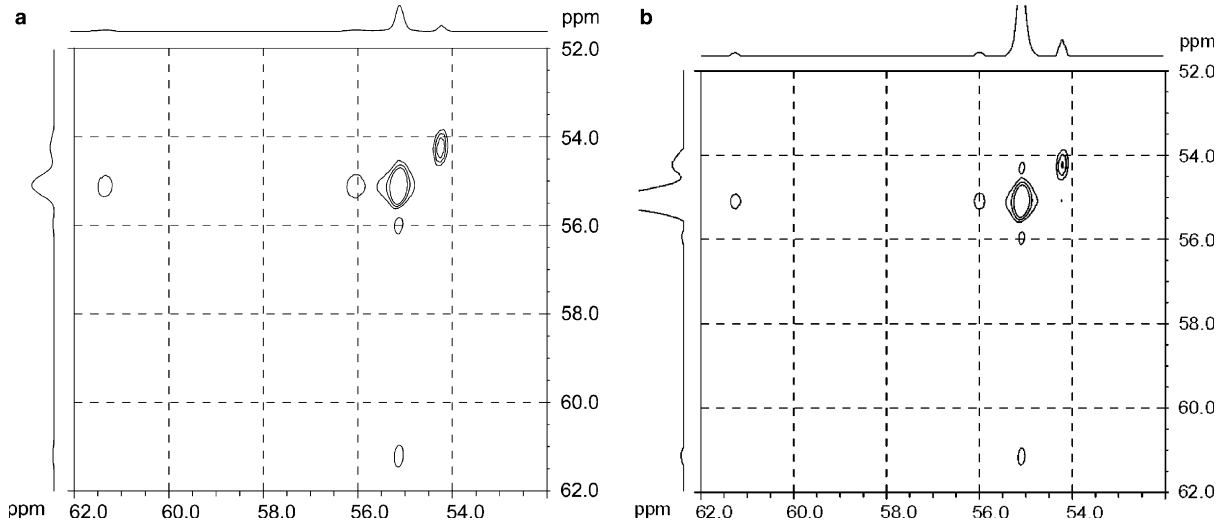

Fig. 4. The 2D-NMR NOESY $^{31}P–\{^1H\}$ spectra of the complex **10** solution in dichloromethane-d_2 at −20 °C and 161.9 MHz with mixing time 130 ms (a) and 500 ms (b).

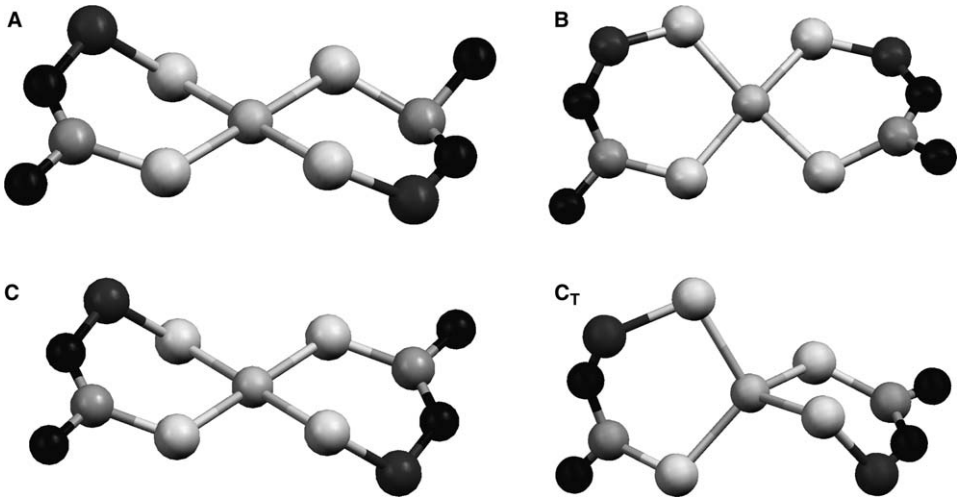

Fig. 5. Proposed structures of isomers of the **10** complex in dichloromethane solutions: **A** (*trans*-chair–boat), **B** (*cis*-boat–boat), **C** (*trans*-boat–boat), and, as an example, $\mathbf{C_T}$ (pseudo-tetrahedral). In all square-planar forms two ligands are in anti-orientation about the NiS_4 core. Only chelate backbones shown.

From the relative integral intensities of signal C to $A_1 + A_2$, the equilibrium constant $K_{AC} = [\mathbf{C}]/[\mathbf{A}]$ values were calculated for the temperature range from −80 to 0 °C. Likewise the equilibrium constant $K_{BC} = [\mathbf{C}]/[\mathbf{B}]$ values were determined at different temperatures (from −80 to 40 °C). Then from the $\log K_{AC(BC)} - 1/T$ dependences (Fig. 7) the enthalpy (ΔH) and entropy (ΔS) of corresponding equilibria were calculated by:

$$2.303R \log K = \Delta S/R - (\Delta H/R) \cdot 1/T, \quad (1)$$

with $\Delta H_{AC} = -6.3 \pm 0.4$ kJ mol^{-1} and $\Delta S_{AC} = -12.5 \pm 1.9$ J K^{-1} mol^{-1} (whence it follows $K_{AC} = 2.83$ at 25 °C), $\Delta H_{BC} = -6.0 \pm 0.4$ kJ mol^{-1} and $\Delta S_{BC} = -14.2 \pm 1.7$ J K^{-1} mol^{-1} ($K_{BC} = 2.07$ at 25 °C). With regard to the above K_{AC} and K_{BC} values the magnitude of the K_{AB} constant (Scheme 2) can be estimated as $K_{AB} = K_{AC}/K_{BC}$ (for example, $K_{AB} = 1.37$ at 25 °C).

It should be particularly emphasized that in the 2D-NMR ^{31}P–{^1H} spectra (Fig. 4) cross-peaks between $A_{1(2)}$ and C signals have rather high intensity at both mixing time, 130 and 500 ms, intensity of cross-peaks between B and C signals is detectable only at mixing time 500 ms and negligible (minor) at 130 ms, while cross-peaks between $A_{1(2)}$ and B signals are completely absent. From the dependence of integral intensities of the exchange cross-peaks on mixing time in NOESY ^{31}P–{^1H} spectra (Fig. 4), the rate constants for the **A**–**C** exchange can be only roughly estimated [41] at about several s^{-1} whereas those for the **B**–**C** exchange are many times smaller. Low rates of the **B**–**C** exchange and unobserved **A**–**B** exchange confirm above-made assignment of **B** form to *cis*-isomer with slow *cis*–*trans*-isomerisation rate. In any case the roughly estimated rate constant values for any exchange processes between **A**, **B**, and **C** forms are too small to

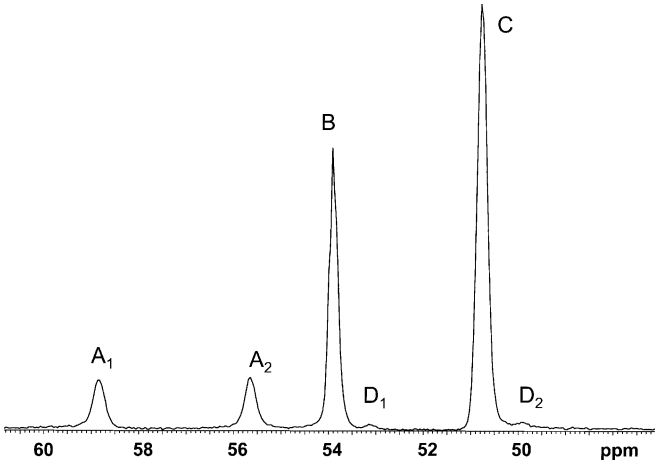

Fig. 6. The NMR ^{31}P–{^1H} spectrum of the complex [Ni{*t*BuNHC(S)-NP(S)(OPr^i)$_2$-*S*,*S*}$_2$] solution in dichloromethane-d_2 at 25 °C and 121.4 MHz [40].

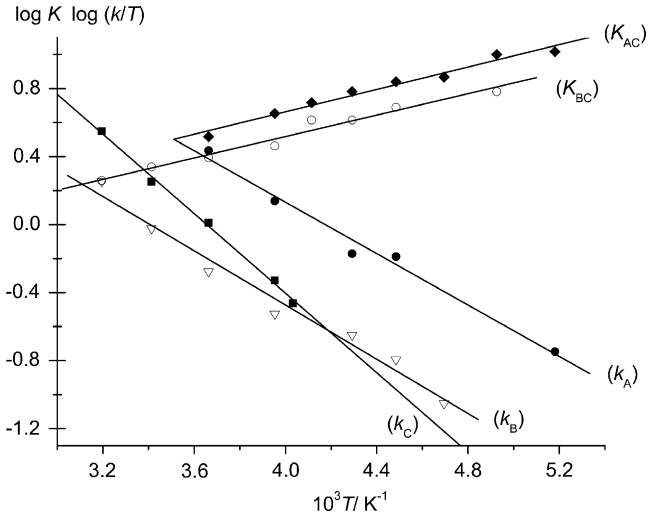

Fig. 7. Dependences of $\log K_{AC}$, $\log K_{BC}$, $\log(k_A/T)$, $\log(k_B/T)$, and $\log(k_C/T)$ on $1/T$ for the complex **10** solutions in dichloromethane.

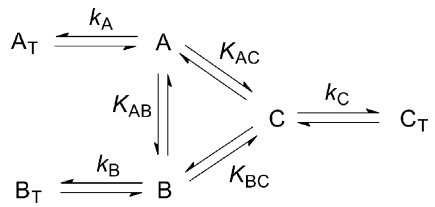

Scheme 2. Conformation equilibria realized in the complex **10** solutions in dichloromethane.

explain the observed line-width spreading of all signals when temperature is increased (Fig. 3). The increasing of the line-width at half height ($\Delta\nu_{1/2}$) with increasing temperature for diamagnetic species **A**, **B**, and **C** (Fig. 3) is explicable only through acceleration of "slow" chemical exchange between them and respective minor (unobserved) pseudo-tetrahedral forms of D_{2d} symmetry ($\mathbf{A_T}$, $\mathbf{B_T}$, and $\mathbf{C_T}$). According to well-known relations [41] such exchange provides also an explanation for marked upfield shift of the A_1, A_2, and C signals with increased temperature (Fig. 3). Indeed, on the one hand, the equilibrium square-planar-pseudo-tetrahedral isomers for nickel(II) complexes are commonly shifted with temperature to the latter [13,38,42,43]. On the other hand, large upfield ^{31}P NMR shift is typical for paramagnetic nickel(II) species [13,29,32]. As an example, the upfield ^{31}P NMR shifts are −86 and −424 ppm (at 298 K), respectively, for mono-adduct and bis-adduct of [Ni{PhC(S)NP(S)(OPr^i)$_2$-*S*,*S*}$_2$] with pyridine [32] and ∼−500 ppm for [Ni{(SPPh$_2$)$_2$N-*S*,*S*}$_2$] in organic solvents [13]. (The very slight temperature dependence of the B signal shift (Fig. 3) will be explained below). Hence the equilibria realized in studied solutions can be presented by Scheme 2.

In the "slow-exchange" limit Eq. (2) [41] applies to the line-width ($\Delta\nu_{1/2}$) or spin-spin relaxation rate (T_2^{-1}) of the **A** or **B** or **C** form.

$$\pi\Delta\nu_{1/2} = T_2^{-1} = T_{2A(B,C)}^{-1} + \tau_{A(B,C)}^{-1}. \quad (2)$$

In this expression $T_{2A(B,C)}^{-1}$ is the spin–spin relaxation rate of the **A**(**B**,**C**) form in the absence of chemical exchange and $\tau_{A(B,C)}$ is the life time of this form associated with the pseudo-first-order rate constants for transitions $\mathbf{A} \rightarrow \mathbf{A_T}$, $\mathbf{B} \rightarrow \mathbf{B_T}$, and $\mathbf{C} \rightarrow \mathbf{C_T}$, respectively, $\tau_{A(B,C)}^{-1} = k_{A(B,C)}$, see Scheme 2. In such a manner the k_A, k_B, and k_C values at different temperatures were estimated by Eq. (2) including the $T_{2A(B,C)}^{-1} = \pi \cdot 8$ Hz contribution and then the activation enthalpy ($\Delta H_A^{\neq}$, $\Delta H_B^{\neq}$, and $\Delta H_C^{\neq}$) and entropy ($\Delta S_A^{\neq}$, $\Delta S_B^{\neq}$, and $\Delta S_C^{\neq}$) of the $\mathbf{A} \rightarrow \mathbf{A_T}$, $\mathbf{B} \rightarrow \mathbf{B_T}$, and $\mathbf{C} \rightarrow \mathbf{C_T}$ reactions were evaluated from the $\log(k_{A(B,C)}/T) - 1/T$ dependencies (Fig. 7) using the Eyring equation (3).

$$k = (k_B T)/h \cdot \exp(\Delta S^{\neq}/R)\exp(-\Delta H^{\neq}/RT). \quad (3)$$

The results obtained are $\Delta H_A^{\neq} = 14.5 \pm 1.1$ kJ mol^{-1} and $\Delta S_A^{\neq} = -137.2 \pm 4.6$ J K^{-1} mol^{-1} (with $k_A = 1.2 \times 10^3$ s^{-1} at 25 °C), $\Delta H_B^{\neq} = 15.3 \pm 1.1$ kJ mol^{-1} and $\Delta S_B^{\neq} = -145.6 \pm 4.2$ J K^{-1} mol^{-1} (with $k_B = 3.3 \times 10^2$ s^{-1} at 25 °C), and $\Delta H_C^{\neq} = 22.5 \pm 0.9$ kJ mol^{-1} and $\Delta S_C^{\neq} = -115.4 \pm 3.3$ J K^{-1} mol^{-1} (with $k_C = 6.7 \times 10^2$ s^{-1} at 25 °C).

Above-mentioned absence of high-field shift with increasing temperature for the B signal in comparison with A and C signals can be then explained by slower $\mathbf{A} \rightarrow \mathbf{A_T}$ exchange relative to the $\mathbf{B} \rightarrow \mathbf{B_T}$ and $\mathbf{C} \rightarrow \mathbf{C_T}$ exchange, $k_A < k_B$, k_C (see [41]). In this case the slight temperature upfield shift of the B signal that is responsible for exchange may be canceled by own downfield temperature shift of the B_T signal due to Fermi-contact interaction (cf. [32]).

The above-mentioned low rates of the exchange processes between square-planar **A** and **B** or **B** and **C** forms are due to need of *cis–trans*-isomerisation. The latter can be only slow because it calls for conversion of pseudo-tetrahedral D_{2d} isomers ($\mathbf{A_T}$ and $\mathbf{B_T}$) to high-energy tetrahedral T_d transition state. It is necessary to note small accumulation fractions of the pseudotetrahedral isomers and the higher rates of their interconversion with the square-planar forms for the compound **10** in reference to the nickel(II) complexes with Schiff bases [42–44]. The minor accumulation of the pseudotetrahedral forms can be explained by a high degree of covalency of the Ni–S bonds (similar to the Cu–S σ and π bonds [45]) providing higher crystal field stabilization energy (CFSE) for the square-planar isomers with low-spin d^8 configuration in comparison with high-spin D_{2d} isomers.

3. Experimental

3.1. General procedures

Infrared spectrum was recorded in Nujol in the range 250–4000 cm^{-1} on a Bruker-Vector 22 Fourier-transform spectrometer. Electronic absorption spectra of solutions were recorded in the range 200–900 nm on a Perkin–Elmer Lambda 35 spectrophotometer. The NMR ^{31}P–{^{1}H} spectra were obtained at 121.4 MHz using a Varian Unity-300 NMR spectrometer with a standard VTC 4 variable temperature unit. Spectra were recorded with complete ^{1}H noise decoupling. Normal conditions were as follows: sweep width 400 ppm; pulse consisting 7 μs (45°), number of accumulations 250–7000 and a repetition rate of 1–5 s. The 2D-NMR NOESY ^{31}P–{^{1}H} spectra were obtained on the Bruker AVANCE-400 NMR spectrometer (9.4 T) at 161.9 MHz for ^{31}P with mixing time 10–500 msec. NOESY spectra were acquired in the phase sensitive TPPI mode, with 1 K × 64 complex FIDs, spectral width of 2500 Hz, recycling delay of 2 s, 64 scans, at −20 °C. The high-resolution solid-state NMR experiments were acquired using a Bruker DSX-400 spectrometer (9.4 T) and 4 mm Bruker probe head. Room temperature ^{31}P MAS spectra were acquired using single-pulse consisting of 0.5 μs (π/12) pulse widths of 300 kHz, and pulse delays of 5 s, with collection of 256 transients and spinning rate of 10 kHz. The ^{31}P chemical shifts are referenced to 85% phosphoric acid (0 ppm). Transverse relaxation times (T_2)

were evaluated from the NMR $^{31}P–\{^1H\}$ line-widths ($\Delta\nu_{1/2}$) by relation $T_2^{-1} = \pi(\Delta\nu_{1/2})$ with an accuracy of 3–5%. ^{13}C chemical shifts were measured relative to adamantane as external standard. Spinning rate was 12 kHz. The electronic spectra reconstruction and thermodynamic and kinetic parameters computations were carried out by means of Microcal Origin 6.1 programs. Electrospray mass spectrum was obtained on a Micromass Q-TOF Ultima3 instrument.

3.2. *[Ni{PhNHC(S)NP(S)(OPr^i)$_2$-S,S}$_2$] (**10**)*

This complex was prepared according to the established literature method [28]. M.p. 127–129 °C (*Anal.* Calc. for $C_{26}H_{40}N_4NiO_4P_2S_4$: C, 43.29; H, 5.52; Ni, 8.14; P, 8.60. Found: C, 43.65; H, 5.53; Ni, 8.01; P, 8.45%.). IR ν/cm^{-1} (Nujol mull) 3403m [ν(NH)], 1590m [δ(Ph)], 1523s [ν(SPNCS)], 1033s, 1001s, 979s [ν(POC)], 573m [ν(P=S)] and 403w, 370w [ν(Ni–S)]. {Lit.: ν/cm^{-1} (CCl_4, $c = 0.10$ mol dm^{-3}) 3400 (NH), 1525 (S–C=N), 1005 (P–N), 1030, 980 (POC), 575 (P=S); $^{31}P–\{H\}$ NMR: δ 52 (s) [28]}. ESI-MS ($CHCl_3$) {*m*/*z* (%) [assignment]}: 743 (41) $[NiL_2 + Na]^+$, 1111 (100) $[2Ni + 3L]^+$, 1465 (88) $[2(NiL_2) + Na]^+$, 1831 (8) $[3Ni + 5L]^+$. MAS NMR $^{31}P–\{^1H\}$, 56.2 ppm. MAS NMR $^{13}C–\{^1H\}$, ppm: 177.0 (CS), 135.8, 129.4, and 125.6 (all 3 peaks – Ph), 73.1 and 71.8 (OCH_2), 25.8 and 24.6 (CH_3).

3.3. *X-ray crystallography*

Crystal data for **10**: $C_{26}H_{40}N_4NiO_4P_2S_4$, monoclinic, space group $P2_1/c$, $Z = 2$ (molecule in a special position), $a = 8.4637(2)$, $b = 21.3625(2)$, $c = 9.3263(3)$ Å, $\beta = 100.68(2)°$, $V = 1691.2(5)$ Å^3 (at 20 °C), $D_{calc} = 1.42$ g cm^{-3}. Data were collected on an Enraf-Nonius CAD-4 diffractometer in the $\omega/2\theta$-scan mode, $\theta \leqslant 26.9°$, using graphite monochromated MoKα radiation. An empirical absorption correction based on ψ-scans was applied (μMo 9.41 cm^{-1}). The structure was solved by direct method using the SIR [46] program and refined by the full-matrix least-squares using SHELXL97 [47] program. All non-hydrogen atoms were refined anisotropically. Hydrogen atoms were located from a subsequent difference map and refined isotropically in the final cycles. The final residuals were $R(F_o^2) = 0.036, R_w(F_o^2) = 0.073$. All calculations were performed on PC using WINGX [48] program. Cell parameters, data collection and data reduction were performed on Alpha Station 200 computer using MOLEN [49] program. All figures were made using the program PLATON [50].

CCDC-262044 contains the supplementary crystallographic data for this paper. These data can be obtained free of charge from The Cambridge Crystallographic Data Centre via www.ccdc.cam.ac.uk/data_request/cif. X-ray crystallographic file, in CIF format, for [Ni{PhNHC(S)NP(S)(OPr^i)$_2$-S,S}$_2$] **10**. This material is available free of charge via the Internet at http://pubs.acs.org.

Acknowledgements

The support of the Russian Foundation for Basic Research (Grant Nos. 03-03-32372-a and 03-03-96225-r2003tatarstan_a) is gratefully acknowledged. We are grateful to Dr. Alexander Yu. Verat for measuring of the electronic spectra.

References

[1] A. Ziegler, V.P. Botha, I. Haiduc, Inorg. Chim. Acta 15 (1975) 123, and refs. therein.
[2] R. Rosler, C. Silvestru, G. Espinosa-Perez, I. Haiduc, R. Cea-Olivares, Inorg. Chim. Acta 241 (1996) 47, and refs. therein.
[3] V. Kastalsky, J.F. McConnell, Acta Crystallogr. Sect. B 25 (1969) 909.
[4] J.F. McConnell, V. Kastalsky, Acta Crystallogr. Sect. B 22 (1967) 853.
[5] P.E. Jones, G.B. Ansell, L. Katz, Acta Crystallogr. Sect. B 25 (1969) 1939.
[6] P.S. Shetty, Q. Fernando, Acta Crystallogr. Sect. B 25 (1969) 1294.
[7] P. Porta, A. Sgamellotti, N. Vinciguerra, Inorg. Chem. 7 (1968) 2625.
[8] M.R. Churchill, J. Cooke, J.P. Fennessey, J. Wormald, Inorg. Chem. 10 (1971) 1031.
[9] D. Cupertino, R. Keyte, A.M.Z. Slawin, D.J. Williams, J.D. Woollins, Inorg. Chem. 35 (1996) 2695.
[10] P. Bhattacharyya, J. Novosad, J. Phillips, A.M.Z. Slawin, D.J. Williams, J.D. Woollins, Dalton Trans. (1995) 1607.
[11] R. Beckett, B.F. Hoskins, J. Chem. Soc., Dalton Trans. (1974) 622.
[12] S. Seiler, R. Richter, U. Braun, L. Beyer, O. Lindqvist, L. Andersen, Z. Anorg. Allg. Chem. 528 (1985) 107.
[13] E. Simon-Manso, M. Valderrama, D. Boys, Inorg. Chem. 40 (2001) 3647.
[14] The present work had been started and preliminary results had been presented on ICCC 34 {V.V. Brusko, A.I. Rakhmatullin, V.G. Shtyrlin, D.B. Krivolapov, I.A. Litvinov, N.G. Zabirov, in: 34th International Conference on Coordination Chemistry (ICCC34). Edinburgh (UK). 2000. Abstracts. P. 0782} before [13] was published.
[15] S. Yamada, A. Takeuchi, Coord. Chem. Rev. 86 (1982) 187.
[16] C. Papadimitriou, P. Veltsistas, J. Novosad, R. Cea-Olivares, A. Toscano, P. Garcia-Garcia, M. Lopez-Cardosa, A.M.Z. Slawin, J.D. Woollins, Polyhedron 16 (1997) 2727.
[17] A. Davison, L. Reger, Inorg. Chem. 10 (1971) 1967.
[18] T.Q. Ly, J.D. Woollins, Coord. Chem. Rev. 176 (1998) 451.
[19] R.M. Kamalov, M.G. Zimin, A.N. Pudovik, Uspekhi Khimii 54 (1985) 2044.
[20] N.G. Zabirov, F.M. Shamsevaleev, R.A. Cherkasov, Uspekhi Khimii 60 (1991) 2189.
[21] N.G. Zabirov, N.I. Galyautdinov, V.A. Shcherbakova, R.A. Cherkasov, J. Gen. Chem. USSR (Engl. Transl.) 60 (1990) 1112.
[22] N.G. Zabirov, V.V. Brus'ko, S.V. Kashevarov, F.D. Sokolov, V.A. Shcherbakova, A.Yu. Verat, R.A. Cherkasov, Russ. J. Gen. Chem. 70 (2000) 1214.
[23] H. Groeger, A. Schmidpeter, Chem. Ber. 100 (1967) 3216.
[24] E. Uhlemann, R. Schulz, A. Friedrich, Z. Chem. 27 (1987) 225.
[25] T. Iwamoto, F. Ebina, H. Nakazawa, C. Nakatsuka, Bull. Chem. Soc. Jpn. 52 (1979) 1857.
[26] L. Ojima, T. Onishi, T. Iwamoto, N. Inamoto, K. Tamaru, Bull. Chem. Soc. Jpn. 44 (1971) 2150.
[27] J. Bodeker, Z. Chem. 11 (1971) 463.
[28] G.A. Lazareva, M.G. Zimin, R.G. Islamov, R.M. Kamalov, V.F. Toropova, Organophosphorus Compounds and Polymers, Chuvash State University, Cheboksary, 1983, p. 54.
[29] Z. Zak, T. Gloviak, N.T.T. Chau, E. Herrmann, Z. Anorg. Allg. Chem. 586 (1990) 136.

[30] F.D. Sokolov, N.G. Zabirov, V.V. Brusko, D.B. Krivolapov, I.A. Litvinov, Mend. Comm. 13 (2003) 72.
[31] V.F. Toropova, G.A. Lazareva, F.M. Batyrshina, M.G. Zimin, Zh. Anal. Khim. 37 (1982) 1739.
[32] V.V. Brusko, A.I. Rakhmatullin, V.G. Shtyrlin, N.G. Zabirov, Russ. J. Gen. Chem. 70 (2000) 1521.
[33] L.V. Vilkov, V.S. Mastrukov, N.I. Sadova, Determination of the Geometrical Structure of Free Molecules, Mir, Moscow, 1983.
[34] F.H. Allen, O. Kennard, D.G. Watson, L. Brammer, A.G. Orpen, R. Taylor, J. Chem. Soc., Perkin Trans. II (1987) S1.
[35] H.L. Ammon, P.H. Mazzocchi, M.C. Regan, E. Colicelli, Acta Crystallogr. Sect. B 35 (1979) 1722.
[36] A.B.P. Lever, Inorganic Electronic Spectroscopy, second ed., Elsevier, Amsterdam, 1984.
[37] R.H. Dingle, Inorg. Chem. 10 (1971) 1141.
[38] A. Davison, E.S. Switkes, Inorg. Chem. 10 (1971) 837.
[39] Such a kind of square planar isomer with two different chelate ring conformations was shown by X-ray for Pd[$(EtO)_2P(S)NP(S)Ph_2$-*S*,*S*]$_2$: D.C. Cupertino, R.W. Keyte, A.M.Z. Slawin, J.D. Woollins, Polyhedron 18 (1998) 311.
[40] V.V. Brusko, S.V. Baranov, Unpublished data.
[41] (a) J.A. Pople, W.G. Schneider, H.I. Bernstein, High-Resolution Nuclear Magnetic Resonance, McGraw-Hill Book Company, New York, 1959;
(b) R.R. Ernst, G. Bodenhausen, A. Wokaun, Principles of Nuclear Magnetic Resonance in One and Two Dimentions, Claredon Press, Oxford, 1987, and references therein.
[42] R.H. Holm, G.W. Everett Jr., A. Chakravorty, Progr. Inorg. Chem. 7 (1966) 83.
[43] L. Sacconi, Coord. Chem. Rev. 1 (1966) 126.
[44] R.H. Holm, M.J. O'Connor, Progr. Inorg. Chem. 14 (1971) 241.
[45] A.L. Kon'kin, V.G. Shtyrlin, N.G. Zabirov, A.V. Aganov, L.E. Zapechel'nyuk, S.V. Kashevarov, A.V. Zakharov, Zh. Neorg. Khim. 41 (1996) 1156.
[46] A. Altomare, G. Cascarano, C. Giacovazzo, D. Viterbo, Acta Crystallogr. Sect. A 47 (1991) 744.
[47] G.M. Sheldrick, SHELXL97 A Computer Program for Crystal Structure Determination, University for Göttingen, Göttingen, 1997.
[48] L.J. Farrugia, J. Appl. Crystal. 32 (1999) 837.
[49] L.H. Straver, A.J. Schierbeek, MOLEN. Structure Determination System, vols. 1 and 2. Nonius B.V. Delft. Netherlands, 1994.
[50] A.L. Spek, Acta Crystallogr. Sect. A 46 (1990) S34.

2. Results and discussion

In search of new group 6 metal catalysts, we endeavor to prepare carbonyl complexes of tungsten with a silyl anion such as Ph_3Si^-, Ph_2SiH^-, Et_3Si^-, and Et_2SiH^- in their coordination sphere. We envisage a viable route to such complexes from $W(CO)_6$, whose carbonyl ligands could be replaced by the desired anion in photochemical oxidative addition reaction with the corresponding hydrosilanes. The activation of the Si—H bond by tungsten(0) carbonyls and the formation of a W—H bond can be followed by ^1H NMR spectroscopy due to the appearance of a high-field signal with the corresponding satellite signals caused by the coupling with the ^{183}W atom (14% ^{183}W abundance; $I = 1/2$).

2.1. Activation of the Si—H bond of diphenylsilane

In a previous paper, we showed that the photochemical reaction of $W(CO)_6$ with H_2SiPh_2 leads to the formation of the μ-diphenylsilylene complex $[(\mu\text{-}SiPh_2)\{W(CO)_5\}_2]$ (**1**) [28]. This reaction probably occurs via the formation of an intermediate silyl complex containing a W—H bond, e.g., $[WH(SiHPh_2)(CO)_5]$ (Scheme 1).

However, the pentacarbonyl tungsten(II) compound is very unstable, making direct observation difficult. To utilize the activation of the Si—H bond of diphenylsilane by tungsten carbonyls, the reaction of H_2SiPh_2 with $W(CO)_6$ in the presence of ketones was investigated (Scheme 2).

2.1.1. Photochemical reaction of $W(CO)_6$ with H_2SiPh_2 in the presence of $Me_2C{=}O$ and ^iPrOH in the NMR tube

The photochemical reaction of $W(CO)_6$ with H_2SiPh_2 and acetone (6:6:1 molar ratio) in cyclohexane-d_{12} occurs very smoothly to give alkoxysilane, $Ph_2SiH(O^iPr)$ (**I**), as a major product (Scheme 3). The formation of compound **I** is revealed by the characteristic proton signals in the ^1H NMR spectrum, i.e., a singlet at δ_H 5.48 (Si—H, $^1J_{Si-H} = 210$ Hz), a heptet at δ_H 4.12 (CH), and a doublet at δ 1.19 (2Me), in the intensity ratio 1:1:6, respectively (Fig. 1(b)–(d)).

Several small portions of acetone were consumed and transformed almost completely to **I**. The very low-intensity proton signal observed at δ_H 5.64 (Si—H, $^1J_{Si-H} = 220$ Hz) is due to disiloxane, $Ph_2HSiOSiHPh_2$ (**II**) [6b,22,27] identified by GC–MS analysis ($M_r = 382.60$) in the post-reaction mixture. Disiloxane **II** is formed in reaction of H_2SiPh_2 with water, which initially gives a silanol, Ph_2HSiOH (δ_H 5.60, $^1J_{Si-H} = 220$ Hz), which can then react as an alcohol, producing the dehydrosilylation product **II**. The dehydrocondensation of siloxane **I** and diphenylsilanol gives $Ph_2SiHOSiPh_2(O^iPr)$ (**III**), whose Si—H bond was observed by ^1H NMR at δ_H 5.71 ($^1J_{Si-H} = 218$ Hz) (Fig. 1). An alternative route to **III**, which cannot be excluded, is the hydrosilylation of acetone by disiloxane **II**. The formation of compound **III** was also established by GC–MS analysis ($M_r = 440.68$). In order to determine whether the photochemically generated catalyst is also capable of effecting dehydrosilylation after the decay of acetone, 2-propanol was added to the same NMR tube (Fig. 1(d)). Irradiation led to the alcoholysis of H_2SiPh_2, and monoalkoxysilane (**I**) as well as dialkoxysilane $Ph_2Si(O^iPr)_2$ (**IV**) [22,24,25,29] were produced (Fig. 1(e)). The formation of compound **IV** is manifested by characteristic proton signals in the ^1H NMR spectrum, i.e., a heptet at δ_H 4.18 (CH) and a doublet at δ_H 1.18 (Me), in the intensity ratio 1:6. Furthermore, the formation of compound **IV** was proved by GC–MS analysis ($M_r = 300.47$). These spectral results suggest a mechanism for the activation of the Si—H bond of silane in which the coordinatively unsaturated tungsten(0) carbonyl compound activates the silane for backside nucleophilic attack at the silicon by the oxygen atom of ketone, alcohol, or water resulting in the formation of a silicon–oxygen bond. Subsequent reductive elimination of the hydrosilylation or dehydrosilylation product releases the coordinatively unsaturated tungsten(0) carbonyl compound able to activate the Si—H bond of silane.

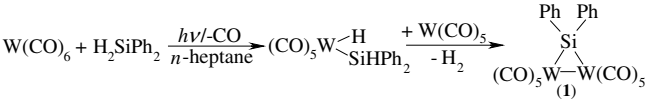

Scheme 1. Photochemical reaction of H_2SiPh_2 with $W(CO)_6$.

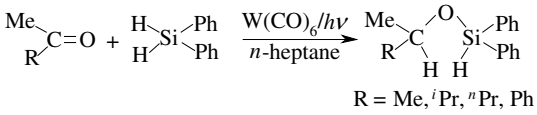

Scheme 2. Hydrosilylation of ketones by H_2SiPh_2.

2.1.2. Hydrosilylation of acetone with H_2SiPh_2 in the presence of catalytic amounts of $W(CO)_6$

Irradiation of $W(CO)_6$, H_2SiPh_2, and an excess of acetone (1:50:150 molar ratio) in *n*-heptane gives hydrosilylation product **I** (42%), and disiloxane (**II**) (7.5%) and **III** (1%) (Table 1). However, under these photochemical conditions, acetone can be transformed to 4-hydroxo-4-methyl-2-pentanone, $Me_2C(OH)CH_2COMe$, which undergoes dehydrosilylation by H_2SiPh_2 to give $Ph_2SiH(OCMe_2CH_2COMe)$ as the intermediate dehydrosilylation product and next the cyclization product, 4,6-trimethyl-2,2-diphenyl-1,3-dioxa-2-silacyclohexane $Ph_2Si(OCMe_2CH_2CHMeO)$ (**V**) (13.5%) ($M_r = 298.45$). In the ^1H NMR spectrum of the above reaction mixture, the methine proton of **V** was detected at δ 4.45 as a pseudo sextet, i.e. a quartet of triplets with an average $^3J_{H-H}$ value of 5.2 Hz. Similar dioxasilacycloalkanes have been reported by Bedard and Corey [22] from the reaction of secondary silanes with diols. Although conversion of acetone reached ca. 70% after 10 min of photolysis, in the post-reaction mixture unchanged H_2SiPh_2 was detected by GC–MS in ca. 36% (Table 1).

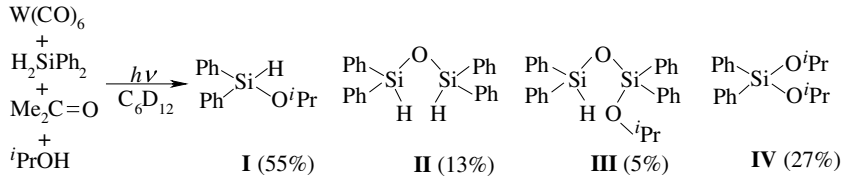

Scheme 3. Results of GC–MS analysis of silicon compounds formed as a result of H_2SiPh_2 transformation by acetone, 2-propanol, and water in the presence of photochemically activated $W(CO)_6$ in cyclohexane-d_{12} solution.

2.1.3. Dehydrogenative silylation of ^{i}PrOH with H_2SiPh_2 in the presence of $W(CO)_6$

After 2.5 h photolysis of *n*-heptane solution of $W(CO)_6$, H_2SiPh_2, and ^{i}PrOH (1:50:50 molar ratio) the conversion of 2-propanol reached 25% and the formation of silicon compounds **I** (35%), **II** (14%), **III** (10%), and **IV** (7%) was observed by GC–MS analysis (Table 1). Unchanged H_2SiPh_2 was present in 34%, and the formation of biphenyl (<1%) was also detected. This experiment proved that the activation of hydridosilanes by the tungsten atom also plays a key role in alcoholysis of H_2SiPh_2 by 2-propanol.

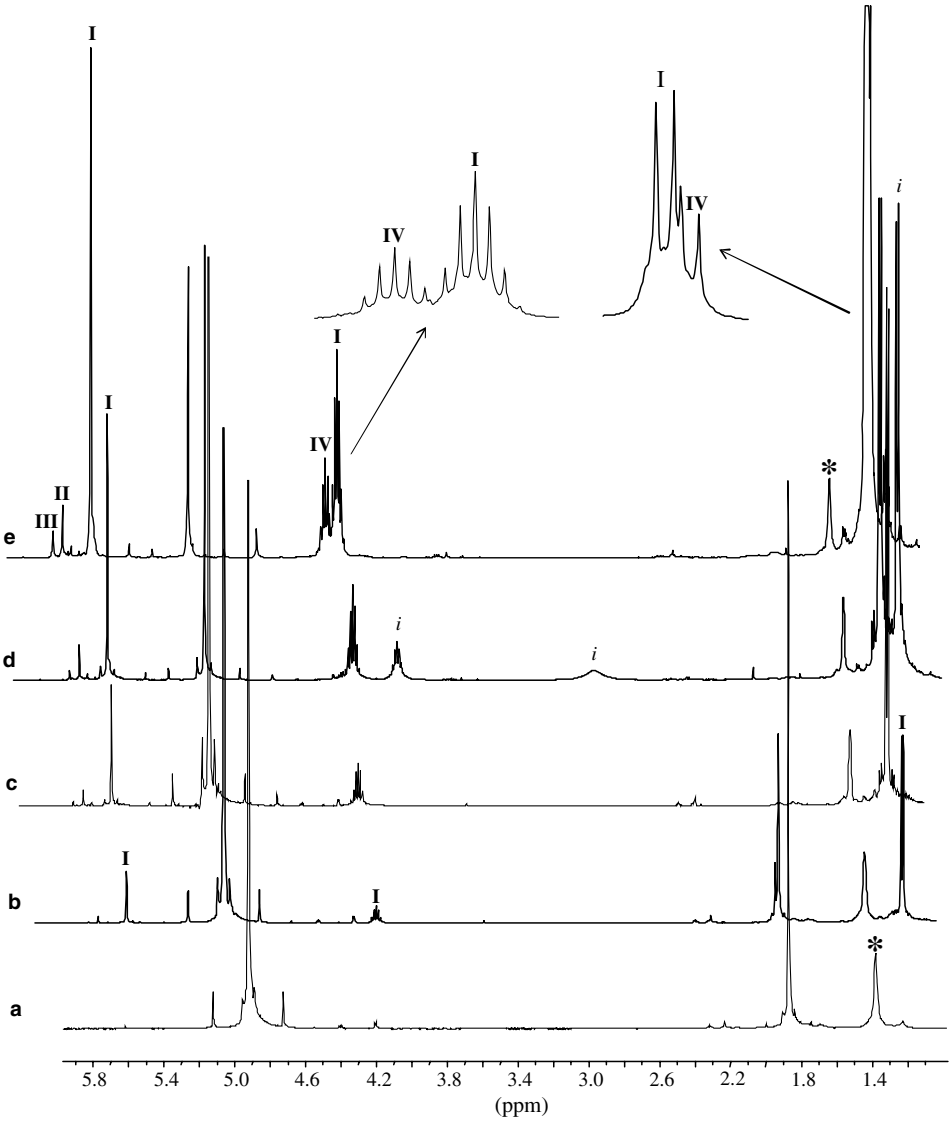

Fig. 1. ^{1}H NMR spectral changes during photolysis of $W(CO)_6$, acetone, and H_2SiPh_2 in cyclohexane-d_{12} (*): (a) prior to photolysis; (b)–(c) after continued photolysis; (d) after addition of ^{i}PrOH (*i*); (e) after photolysis. The peaks at 1.89 and 1.12 ppm represent methyl resonances for acetone and $Ph_2SiH(O^iPr)$ (**I**), respectively. The peaks at 5.48 and 4.94 ppm are due to Si—H proton resonances for **I** and H_2SiPh_2, respectively. Two heptets at 4.18 and 4.12 ppm are due to the methine proton resonances of $Ph_2Si(O^iPr)_2$ (**IV**) and **I**, respectively.

Table 1
Organosilicon compounds detected by GC–MS analysis of the post-reaction mixture obtained from photochemical reaction of $W(CO)_6$, H_2SiPh_2, ketones RMeC=O, R = Me, ^{i}Pr, ^{n}Pr, Ph and/or ^{i}PrOH

Distribution of compounds (%)	R = Me[a]	R = Me[b]	^{i}PrOH[c]	R = ^{i}Pr[a]	R = ^{n}Pr[a]	R = Ph[a]
$Ph_2HSi(OCHRMe)$ (**I**, **VI**, **VII**, **VIII**)	42	50	35	32	29	61
$Ph_2Si(OCHRMe)_2$ (**IV**)		24	7			
$Ph_2Si(OCHMeCH_2CMe_2O)$ (**V**)	13.5					
$Ph_2HSiOSiHPh_2$ (**II**)	7.5	12	14	8	7	20
$Ph_4Si_4O_3$ (**IIa**)				2		
$Ph_2HSiOSi(OCHRMe)Ph_2$ (**III**)	1	5	10			1
Ph_2SiH_2	36	9	34	58	64	18

[a] Photochemical reaction (1 h) carried out in *n*-heptane.
[b] Photochemical reaction carried out in cyclohexane-d_{12} with Me_2C=O and ^{i}PrOH.
[c] Photochemical reaction (2.5 h) of ^{i}PrOH without of ketone.

2.1.4. Hydrosilylation of ^{i}PrMeC=O with H_2SiPh_2 in the presence of $W(CO)_6$

In photochemical reaction (1 h) of $W(CO)_6$, H_2SiPh_2, and ^{i}PrMeC=O (1:50:150 molar ratio) in *n*-heptane the formation of the hydrosilylation product $Ph_2SiH(OCHMe^iPr)$ (**VI**) ($M_r = 270.44$) was observed by GC–MS (Table 1). However, tetraphenyldisiloxane (**II**) was also produced. Some times, the further products of hydrolysis such as $Ph_4Si_4O_3$ (**IIa**) ($M_r = 468.05$) were also detected in small amounts (ca. 1%). The conversion of ^{i}PrMeC=O reached only ca. 20%, but unchanged H_2SiPh_2 was present in 58% in the residue obtained after evaporation of volatile substances.

2.1.5. Hydrosilylation of ^{n}PrMeC=O with H_2SiPh_2 in the presence of $W(CO)_6$

In photochemical reaction (1 h) of $W(CO)_6$, H_2SiPh_2, and ^{n}PrMeC=O (1:50:150 molar ratio) in *n*-heptane the conversion of ^{i}PrMeC=O reached only ca. 30%. The formation of the hydrosilylation product $Ph_2SiH(OCHMe^nPr)$ (**VII**) ($M_r = 270.44$) was observed by GC–MS with 29% yield (Table 1).

2.1.6. Hydrosilylation of acetophenone with H_2SiPh_2 in the presence of $W(CO)_6$

Photochemical reaction (1 h) of $W(CO)_6$, H_2SiPh_2, and MePhC=O (1:50:150 molar ratio) in *n*-heptane leads to the low (ca. 10%) conversion of acetophenone. In the post-reaction mixture, the hydrosilylation product $Ph_2SiH(OCHMePh)$ (**VIII**) ($M_r = 304.46$) was present in 61% and disiloxane **II** in 20% (Table 1).

2.1.7. Photochemical reaction of $W(CO)_6$ with H_2SiPh_2 in the presence of water

The photochemical reaction (3.5 h) of $W(CO)_6$, H_2SiPh_2, and water (1:50:50 molar ratio) in *n*-heptane selectively provided disiloxane **II** [6b,22,27], probably through the intermediate formation of diphenylsilanol. In spite of the fact that the formation of $HOSiHPh_2$ was observed (δ_H 5.60, $^1J_{Si-H} = 220$ Hz) in all reactions monitored by ^{1}H NMR, its high reactivity precluded its isolation and full characterization. This experiment proved very well that the reaction of H_2SiPh_2 with water is concurrent to the hydrosilylation of ketones or dehydrogenative silylation of alcohols.

2.2. Photochemical reaction of $W(CO)_6$ with $HSiPh_3$

During the photochemical reaction of $W(CO)_6$ and $HSiPh_3$ in *n*-heptane solution, the η^6-coordination of the phenyl ring of triphenylsilane to the tungsten atom and the formation of the compound $[W(CO)_3(\eta^6\text{-}PhSiHPh_2)]$ (**2**) as the major product and no oxidative addition of the Si—H bond to the tungsten atom was observed (Scheme 4) [30].

In an attempt to reveal the reactivity of compound **2** we treated its cyclohexane-d_{12} solution with acetone. Proton NMR analysis showed the immediate decay of the proton signal characteristic for the Si—H bond of **2** and the appearance of new proton signals at 3.47 and 1.17 ppm in an intensity ratio of 1:6. Such results suggested a strong interaction between the C=O linkage of acetone and the Si—H bond of **2**. However, the evaporation of acetone returned the chemical shift values for compound **2** to their original position in the absence of acetone. In an attempt to activate compound **2** for further reaction, we irradiated its solution in C_6D_{12} containing $HSiPh_3$ and ca. 15 equiv. of acetone. ^{1}H NMR monitoring of proton signals indicates that acetone could not be hydrosilylated by $HSiPh_3$ in the presence of **2**. The appearance of a proton signal at 2.34 ppm indicates rather the coordination of an acetone molecule to the tungsten atom in place of the CO ligand, lost during the irradiation. The η^6-coordination of silane to the tungsten atom does not activate the Si—H bond of **2** for the 1,2 addition of the carbonyl group of acetone.

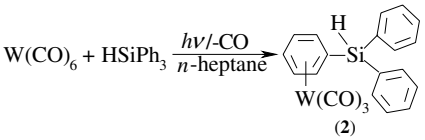

Scheme 4. η^6-arene compound **2** formed in photochemical reaction of $HSiPh_3$ with $W(CO)_6$ in *n*-heptane solution.

2.3. Photochemical reaction of $W(CO)_6$ with $HSiEt_3$

Upon irradiation of $W(CO)_6$ and $HSiEt_3$ in cyclohexane-d_{12} the η^2-coordination of the Si—H bond to the tungsten atom was detected by ^1H NMR spectroscopy due to a high-field shift for the hydrogen bound to silicon from δ_H 3.71 (heptet, $^3J_{H-H} = 3.2$ Hz, $^1J_{Si-H} = 179$ Hz) to $\delta_H - 8.58$ (heptet, $^3J_{H-H} = 1.6$ Hz, $^1J_{W-H} = 35$ Hz, $^1J_{Si-H} = 89$ Hz) (Fig. 2). Although the value of the tungsten–hydrogen coupling constant is typical for the W—H bond, the magnitude of the silicon–hydrogen coupling constant indicates substantial retention of the Si—H bond and the formation of an η^2–silane complex. A similar $^1J_{Si-H}$ value of ca. 80 Hz was earlier observed for chromium compounds formed in photochemical reaction of [$Cr(CO)_3(\eta^6$-arene)] and H_2SiPh_2 [6a]. These NMR data support the existence of a three-centre, two-electron Si—H···W bond (Scheme 5).

Such agostic interactions between C—H bonds and transition metal centres have been detected in numerous electronically unsaturated transition metal alkyl and alkylidene complexes and have been shown to play a key role in many catalytic processes involving the C—H bond activation [31–36]. As was shown by a ^1H NMR experiment, the addition of acetone to the NMR tube containing the Si—H bond of $HSiEt_3$ activated by η^2-coordination to the tungsten atom leads to the formation of the hydrosilylation product $Et_3Si(O^iPr)$ (**IX**) [24]. The formation of compound **IX** is indicated by the characteristic proton signals, i.e., a heptet at δ_H 3.99 (CH) and a doublet at δ_H 1.13 (2Me) in an intensity ratio of 1:6, respectively. The proton signals of the ethyl groups of compound **IX** are very close to those of free silane and are observed at δ_H 0.97 (t, Me) and 0.57 (q, CH_2).

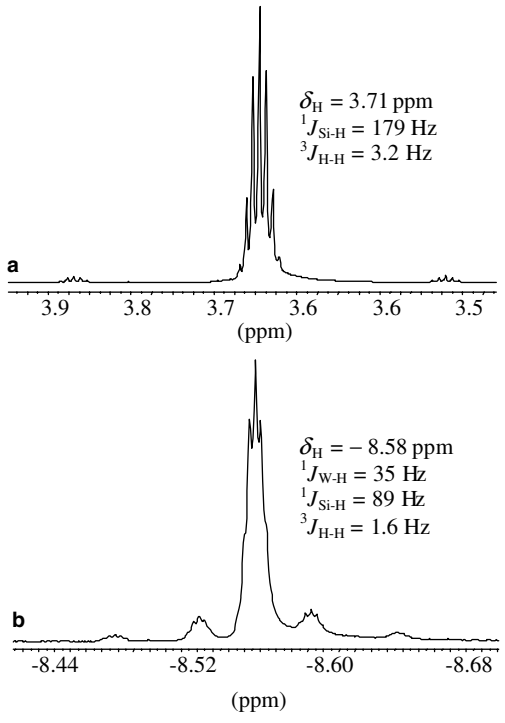

Fig. 2. (a) The Si—H region of the ^1H NMR spectrum of $HSiEt_3$ in C_6D_{12}. (b) Proton signal at δ_H −8.58 generated during the photolysis of $HSiEt_3$ in the presence of $W(CO)_6$ at 279 K showing the η^2-interaction of the Si—H bond with the tungsten atom.

$$W(CO)_6 + HSiEt_3 \xrightarrow[C_6D_{12}]{h\nu/-CO} (CO)_5W \leftarrow \begin{matrix} H \\ | \\ SiEt_3 \end{matrix}$$

Scheme 5. Activation of Si—H bond of $HSiEt_3$.

The monitoring of photochemical reaction between $W(CO)_6$ and $HSiEt_3$ in *n*-heptane solution by IR spectroscopy revealed the decay of the ν(CO) frequency due to $W(CO)_6$ and the appearance of three ν(CO) bands characteristic for a pentacarbonyltungsten moiety with a local C_{4v} symmetry at 2083 (vw), 1951 (vs), and 1938 (s) cm^{-1}. A week band simultaneously observed at 1914 cm^1 may be due to a ν(CO) frequency of a subsequently formed $W(CO)_4$ moiety. However, isolation of the pure reaction product failed. Evaporation of the solvent gave a compound whose IR spectrum in the carbonyl region (2098 (vw), 2069 (w), 2006 (s), 1912 (vs)) was rather similar to the binuclear compound **1** [28].

2.4. Photochemical reaction of $W(CO)_6$ with H_2SiEt_2

The photochemical reaction between $W(CO)_6$ and H_2SiEt_2 in *n*-heptane solution was monitored by IR spectroscopy, which showed the decay of the ν(CO) frequency due to $W(CO)_6$ and the appearance of three ν(CO) bands characteristic for the pentacarbonyltungsten moiety at 2086 (w), 1958 (vs), and 1944 (s) cm^{-1}. A very weak band observed at 2098 cm^{-1} may be due to the ν(CO) frequency of a simultaneously formed binuclear compound. However, isolation of the pure reaction product failed. Evaporation of the solvent gave a mixture of compounds whose IR spectrum in the carbonyl region (ν(CO): 2098 (vvw), 2070 (w), 2010 (s), 1959 (vs), and 1944 (vs)) is rather similar to the binuclear compound **1** with ν(CO) bands at 2098 (s), 2056 (vs), 2032 (s), 2020 (w), 2007 (s), 1975 (vs), and 1956 (vs) [28] and [{W(μ-SiI_2)$(CO)_5$}$_2$] obtained by Schmid and Boese (ν(CO): 2065, 1995, 1935) [37]. The ^1H NMR spectrum (toluene-d_8, 243 K) of this crude product revealed three hydride resonances at δ_H −8.98 ($^1J_{W-H} = 40$ Hz), −9.32 ($^1J_{W-H} = 37$ Hz), and −10.18 ($^1J_{W-H} = 44$ Hz) in an intensity ratio of 1:10:1, respectively. The hydride signal at −9.32 ppm has comparable intensity to proton signal at 4.80 ppm, on which 29-silicon satellites are observed (Fig. 3). This NMR spectrum indicates the presence of a H—W—$SiHEt_2$ unit. The IR and NMR data suggest the formation of a mixture of pentacarbonyl and tetracarbonyl hydride compounds also containing a binuclear compound such as [{W(μ-$SiEt_2$)H$(CO)_4$}$_2$] characterized by the X-ray diffraction study by Bennett and Simpson [38]; however, none was isolated from the reaction mixture in a pure state.

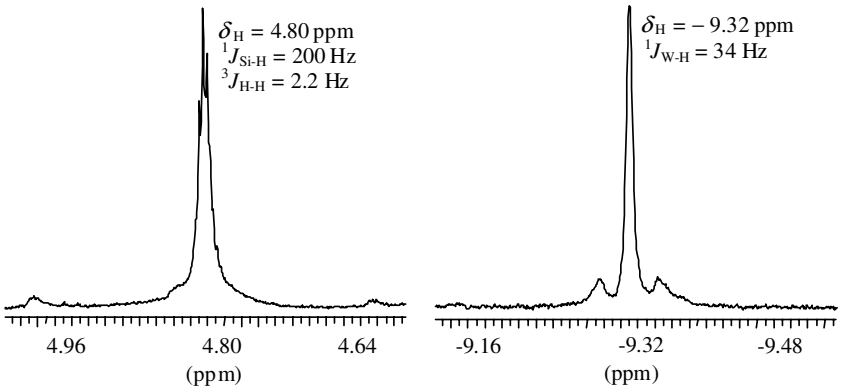

Fig. 3. The Si—H and W—H region of the ^{1}H NMR spectrum (C_7D_8, 500 MHz), showing the formation of a H—W—SiHEt$_2$ unit in photochemical reaction of W(CO)$_6$ with H_2SiEt_2.

3. Conclusions

Photochemical reactions of W(CO)$_6$ create a coordinatively unsaturated d^6 species which interacts with the Si—H bond of hydridosilanes such as H_2SiPh_2, H_2SiEt_2, and $HSiEt_3$. The η^2-interaction of the Si—H bond with the tungsten atom and the existence of a three-centre, two-electron Si—H···W bond was detected by ^{1}H NMR during the photochemical reaction of W(CO)$_6$ with $HSiEt_3$ in cyclohexane-d_{12} ($\delta_H - 8.58$, heptet, $^3J_{H-H} = 1.6$ Hz, $^1J_{W-H} = 35$ Hz, $^1J_{Si-H} = 89$ Hz). This spectral result is consistent with a mechanism where a tungsten(0) compound activates the Si—H bond of silane for backside nucleophilic attack by the oxygen atom of ketone, alcohol, or water at the silicon atom, resulting in the formation of a silicon–oxygen bond.

The photochemical activation of W(CO)$_6$ has been found effective for both the hydrosilylation of ketones as well as the dehydrosilylation of 2-propanol and water by H_2SiPh_2. In reaction with water H_2SiPh_2 transforms very easily to silanol and next to disiloxane. The reaction of H_2SiPh_2 with water is concurrent to the hydrosilylation of ketones or dehydrosilylation of alcohols.

It must be noted that the activation of Si—H bond by tungsten(0) carbonyls can be observed only in non-coordinating solvents such as alkanes, which proves that silanes are activated by the coordinatively unsaturated complex of tungsten(0). We continue to investigate the scope and mechanistic details of these tungsten-catalyzed processes.

Further efforts to explore the photochemical reaction of W(CO)$_6$ with hydrosilanes in catalytic hydrosilylation of C=C bonds of cyclic olefins (norbornene and norbornadiene) are currently in progress.

4. Experimental

4.1. General information

The synthesis and manipulation of all chemicals was carried out under an atmosphere of nitrogen using the standard Schlenk technique. Solvents and liquid reagents were predried with CaH_2 and vacuum-transferred into small storage flasks prior to use. Other chemicals (W(CO)$_6$, H_2SiPh_2, $HSiPh_3$, H_2SiEt_2, and $HSiEt_3$) were obtained from commercial suppliers and used as received. IR spectra were measured with a Nicolet-400 FT-IR instrument. NMR spectra were obtained on a Bruker AMX 500 MHz spectrometer (^{1}H NMR, 500.13 MHz; ^{13}C{^{1}H} NMR, 125.76 MHz; ^{29}Si{^{1}H} 99.36 MHz). The chemical shifts for ^{1}H NMR spectra were referenced to the residual protons in $CDCl_3$ at δ_H 7.24 and in cyclohexane-d_{12} at δ_H 1.40 or to the proton signal of the Si—H bond of H_2SiPh_2 at δ_H 4.93. ^{13}C NMR spectra were calibrated to the natural abundance of ^{13}C in $CDCl_3$ at δ_C 77.00 and in cyclohexane-d_{12} at δ_C 27.8. ^{29}Si{^{1}H} NMR spectra were calibrated to $SiMe_4$ or to the signal of H_2SiPh_2 at δ_{Si} −37.08. The photolysis source was an HBO 200 W high-pressure Hg lamp. The analysis of the organic products was carried out on a Hewlett–Packard GC–MS system.

4.2. Photochemical reaction of W(CO)$_6$ with silanes

A solution of W(CO)$_6$ (0.1 g, 0.28 mmol) and silanes (H_2SiPh_2 [28], $HSiPh_3$ [30], H_2SiEt_2, $HSiEt_3$) (ca. 0.28 mmol) in freshly distilled *n*-heptane (60 cm^3) was irradiated through quartz at 283 K or at room temperature (H_2SiPh_2 and $HSiPh_3$). Generally, the color of the solution changed from yellow to brown during the course of the reaction, which was monitored by IR measurements in solution. Photolysis was stopped when the IR band of W(CO)$_6$ reached its minimum intensity (ca. 1–4 h). The volatile materials were then stripped from the reaction mixture under reduced pressure at room temperature. The residue was analyzed by IR and NMR spectroscopy. In reaction of H_2SiPh_2 and $HSiPh_3$ analytically pure compounds **1** [28] and **2** [30] were isolated, but in other cases isolation of pure compounds was not possible due to substantial decomposition even in strictly anhydrous conditions.

4.3. Reactions in a NMR tube

A solution of W(CO)$_6$ (0.01 g, 0.028 mmol) and silane in cyclohexane-d_{12} or toluene-d_8 (0.7 cm^3) was irradiated in a

NMR tube at 283 K or 243 K and periodically analyzed by ^{1}H NMR at an appropriate temperature. Reactions with acetone and 2-propanol subsequently added via syringe to the NMR tube were carried out under the same conditions.

4.4. Procedure for testing the catalytic activity of $W(CO)_6$ and characterization of silicon compounds

Hydrosilylation experiments were carried out in a photoreactor containing *n*-heptane solution (10 cm^3) of $W(CO)_6$ (0.01 g, 0.028 mmol), H_2SiPh_2 (0.26 cm^3, 1.4 mmol), ketone (4.2 mmol), and cyclopentane, hexane, or undecane as the internal chromatographic standard. In reaction of 2-propanol and water, the molar ratio of H_2SiPh_2 and the reagents was 1:1. The reaction mixture was irradiated (1 h) through quartz at room temperature, and the conversion was monitored by gas chromatography. The solvent was then removed under reduced pressure at room temperature, and the residue was analyzed by GC–MS and NMR spectroscopy.

4.5. Identification of silicon compounds detected during the hydrosilylation and dehydrogenative silylation reactions

$Ph_2SiH(O^iPr)$ (**I**) ($C_{15}H_{18}OSi$, $M_r = 242.39$). GC–MS: *m*/*z* (relative intensity): 242 (M^+, 4), 199 (24), 183 (50), 164 (100), 122 (96), 105 (38), 78 (50). ^{1}H NMR ($CDCl_3$, 298 K): δ_H 7.6–7.2, (m, 10H, Ph), 5.48 (s, $^1J_{Si-H} = 210$ Hz, 1H, Si—H), 4.14 (heptet, $^3J_{H-H} = 6$ Hz, 1H, CH), 1.20 (d, $^3J_{H-H} = 6$ Hz, 6H, Me). $^{13}C\{^1H\}$ NMR ($CDCl_3$, 298 K): δ_C 67.25 (1C, CH), 25.11 (2C, Me). $^{29}Si\{^1H\}$ NMR (cyclohexane-d_{12}, 298 K): δ_{Si} − 18.56.

$Ph_2HSiOSiHPh_2$ (**II**). ($C_{24}H_{22}OSi_2$, $M_r = 382.60$) [6b,22,27]. GC–MS: *m*/*z* (relative intensity): 382 (M^+, 2), 303 (31), 226 (100), 181 (34), 105 (27), 78 (19), 51 (5). IR (KBr pellet, *v*, cm^{-1}): 3068 (w), 3054 (vw), 3022 (w), 3001 (w), 2122 (w,br, Si—H), 1589 (w), 1484 (w), 1430 (vs), 1331 (vw), 1262 (vw), 1158 (m), 1119 (vs), 1095 (vs) 1065 (m), 1027 (m), 997 (w), 865 (w), 836 (vs), 809 (vs), 742 (s), 728 (vs), 697 (vs), 499 (s), 461 (s), 430 (w). ^{1}H NMR ($CDCl_3$, 298 K): δ_H 7.57 (d, $^3J_{H-H} = 7.3$ Hz, 8H, HC_2-Ph), 7.35 (t, $^3J_{H-H} = 7.3$, 4H, HC_4-Ph), 7.25 (t, $^3J_{H-H} = 7.3$ Hz, 8H, HC_3-Ph), 5.64 (s, $^1J_{Si-H} = 219$ Hz, 2H, Si—H). $^{13}C\{^1H\}$ NMR ($CDCl_3$, 298 K): δ_C 134.90 ($^1J_{Si-C} = 80$ Hz, 4C, C_1-Ph), 134.29 (8C, C_2-Ph), 130.22 (4C, C_4-Ph), 127.94 (8C, C_3-Ph). $^{29}Si\{^1H\}$ NMR ($CDCl_3$, 298 K): δ_{Si} −22.92 ($^1J_{Si-C} = 79$ Hz).

$Ph_4Si_4O_3$, (**IIa**) ($C_{24}H_{20}O_3Si_4$, $M_r = 468.76$). GC–MS: *m*/*z* (relative intensity): 468 (M^+, 5), 425 (78), 397 (10), 381 (27), 319 (80), 303 (100), 257 (24), 243 (51), 181 (66) 151 (25), 105 (56), 78 (27), 43 (39).

$Ph_2HSiOSi(O^iPr)Ph_2$ (**III**). ($C_{27}H_{28}O_2Si_2$, $M_r = 440.68$). GC–MS: *m*/*z* (relative intensity): 440 (M^+, 18), 319 (100), 303 (18), 243 (48), 199 (11), 181 (17), 105 (6), 77 (6). ^{1}H NMR ($CDCl_3$, 298 K): δ_H 7.7–7.2 (m, 20H, Ph), 5.71 (s, $^1J_{Si-H} = 218$ Hz, 1H, Si—H), 4.21 (heptet, $^3J_{H-H} = 6$ Hz, 1H, CH), 1.11 (d, $^3J_{H-H} = 6$ Hz, 6H, Me).$^{13}C\{^1H\}$ NMR ($CDCl_3$, 298 K): δ_C 65.56 (1C, CH), 25.54 (2C, Me).

$Ph_2Si(O^iPr)_2$ (**IV**) ($C_{18}H_{26}O_2Si$, $M_r = 300.47$) [22,24,25,29]. GC–MS: *m*/*z* (relative intensity): 300 (M^+, 2), 285 (10), 241 (48), 222 (90), 199 (73), 181 (39), 164 (25), 139 (100), 118 (12), 105 (12), 77 (26), 45 (15). ^{1}H NMR ($CDCl_3$, 298 K): δ_H 7.7–7.3 (m, 10H, Ph), 4.18 (heptet, $^3J_{H-H} = 6$ Hz, 2H, CH), 1.18 (d, $^3J_{H-H} = 6$ Hz, 12H, Me). $^{13}C\{^1H\}$ NMR ($CDCl_3$, 298 K): δ_C 65.88 (2C, CH), 25.63 (4C, Me). $^{29}Si\{^1H\}$ NMR ($CDCl_3$, 298 K): δ_{Si} − 24.64.

$Ph_2\overline{Si(OCMe_2CH_2CHMeO)}$ (**V**). ($C_{18}H_{24}O_2Si$, $M_r = 298.45$). GC–MS: *m*/*z* (relative intensity): 298 (M^+, 23), 283 (59), 239 (59), 199 (100), 181 (73), 139 (74), 123 (35), 105 (29). ^{1}H NMR ($CDCl_3$, 298 K): δ_H 7.6–7.2 (m, 10H, Ph), 4.45 (qt, $^3J_{H-H} = 5.2$ Hz, 1H), 1.33 (s, 6H, Me), 1.28 (d, $^3J_{H-H} = 6$ Hz, 3H, Me), 1.11 (d, $^3J_{H-H} = 6$ Hz, 1H, CH_2), 1.06 (d, $^3J_{H-H} = 6$ Hz, 1H, CH_2).

$Ph_2SiH(OCHMe^iPr)$ (**VI**) ($C_{17}H_{22}OSi$, $M_r = 270.44$). GC–MS: *m*/*z* (relative intensity): 270 (M^+, 0.9), 255 (1), 227 (69), 199 (15), 183 (100), 123 (72), 105 (35), 78 (11), 45 (10). ^{1}H NMR ($CDCl_3$, 295 K): δ_H 7.6–7.2 (m, 10H, Ph), 5.49 (s, $^1J_{Si-H} = 211$ Hz, 1H, Si—H), 3.74 (q,$^3J_{H-H} = 6$ Hz, 1H, *H*CMe), 1.69 (m, 1H, *H*CMe$_2$), 1.12 (d, $^3J_{H-H} = 6.3$ Hz, 3H, Me), 0.90 (d, $^3J_{H-H} = 6.7$ Hz, 3H, Me), 0.88 (d, $^3J_{H-H} = 6.7$ Hz, 3H, Me). $^{13}C\{^1H\}$ NMR ($CDCl_3$, 298 K): δ_C 134.67 (4C, C_2-Ph), 130.12 (2C, C_4-Ph), 127.90 (4C, C_3-Ph), 75.46 (1C, *C*HMe), 35.16 (1C, *C*HMe$_2$), 19.78 (1C, *Me*CH), 18.25 (1C, *Me*CHMe) 18.01 (1C, *Me*CHMe). $^{29}Si\{^1H\}$ NMR ($CDCl_3$, 298 K): δ_{Si} −17.89.

$Ph_2SiH(OCHMe^nPr)$ (**VII**) ($C_{17}H_{22}OSi$, $M_r = 270.44$). GC–MS: *m*/*z* (relative intensity): 270 (M^+, 0.7), 269 (1), 227 (41), 199 (21), 183 (100), 123 (68), 105 (27), 78 (15), 45 (15). ^{1}H NMR ($CDCl_3$, 295 K): δ_H 7.6–7.2 (m, 10H, Ph), 5.50 (s, $^1J_{Si-H} = 211$ Hz, 1H, Si—H), 3.96 (qt, $^3J_{H-H} = 6$ Hz, 1H, *H*CMe), 1.57 (m, 1H, CH_2), 1.41 (m, 2H, CH_2), 1.31 (m., 1H, CH_2), 1.17 (d, $^3J_{H-H} = 6.2$ Hz, 3H, Me), 0.83 (t,$^3J_{H-H} = 7$ Hz, 3H, Me). $^{13}C\{^1H\}$ NMR ($CDCl_3$, 298 K): δ_C 134.62 (4C, C_2-Ph), 130.13 (2C, C_4-Ph), 127.91 (4C, C_3-Ph), 70.66 (1C, *C*HMe), 41.48 (1C, *C*H$_2$CH), 23.27 (1C, *Me*CH), 18.86 (1C, *C*H$_2$Me), 14.05 (1C, *Me*CH$_2$). $^{29}Si\{^1H\}$ NMR ($CDCl_3$, 298 K): δ_{Si} −17.07.

$Ph_2SiH(OCHMePh)$ (**VIII**) ($C_{20}H_{20}OSi$, $M_r = 304.46$). GC–MS: *m*/*z* (relative intensity): 304 (M^+, 0.3), 289 (3), 259 (4), 226 (12), 199 (100), 183 (28), 148 (3), 105 (26), 77 (15), 45 (6). ^{1}H NMR ($CDCl_3$, 295 K): δ_H 7.8–7.2 (m, 15H, Ph), 5.46 (s, $^1J_{Si-H} = 213$ Hz, 1H, Si—H), 4.99 (q,$^3J_{H-H} = 6$ Hz, 1H, CH), 1.49 (d, $^3J_{H-H} = 6$ Hz, 3H, Me). $^{13}C\{^1H\}$ NMR ($CDCl_3$, 298 K): δ_C 72.61 (1C, CH), 26.18 (2C, Me). $^{29}Si\{^1H\}$ NMR ($CDCl_3$, 298 K): δ_{Si} −17.09 ($^1J_{Si-C} = 79$ Hz).

$Et_3Si(O^iPr)$ (**IX**). ^{1}H NMR (cyclohexane-d_{12}, 298 K): δ_H 3.99 (heptet, $^3J_{H-H} = 6$ Hz, 1H, CH), 1.13 (d, $^3J_{H-H} = 6$ Hz, 6H, 2Me), 0.97 (t, $^3J_{H-H} = 7.8$ Hz, 9H, Me), 0.57 (q, $^3J_{H-H} = 7.8$ Hz, 6H, CH_2).

Acknowledgements

Support of this work was generously provided by the Polish State Committee for Scientific Research (Grant No. 3T09A 067 28). We are also grateful to S. Baczyński for the measurement of NMR spectra and M. Hojniak for GC–MS analysis.

References

[1] H.G. Kuivila, C. Warner, J. Org. Chem. 29 (1964) 2845.
[2] M.A. Schroeder, M.S. Wrighton, J. Am. Chem. Soc. 96 (1974) 6235.
[3] I. Ojima, T. Kogure, Tetrahedron Lett. 22 (1974) 1889.
[4] M.A. Schroeder, M.S. Wrighton, J. Organomet. Chem. 128 (1977) 345.
[5] A. Albinati, W.R. Caseri, P.S. Pregosin, Organometallics 6 (1987) 788.
[6] (a) E. Matarasso-Tchiroukhine, G. Jaouen, Can. J. Chem. 66 (1988) 2157;
(b) E. Matarasso-Tchiroukhine, J. Chem. Soc., Chem. Commun. (1990) 681.
[7] H. Brunner, U. Obermann, Chem. Ber. 122 (1989) 499.
[8] J.Y. Corey, X.-H. Zhu, Organometallics 11 (1992) 672.
[9] Y. Nishibayashi, K. Segawa, K. Ohe, S. Uemura, Organometallics 14 (1995) 5486.
[10] J.B. Baruah, K. Osakada, T. Yamamoto, J. Mol. Catal. A: Chem. 101 (1995) 17.
[11] W. Abdelgader, D. Chmielewski, F.-W. Grevels, S. Özkar, N.B. Peynircioglu, Organometallics 15 (1996) 604.
[12] S.U. Son, S.-J. Pail, Y.K. Chung, J. Mol. Catal. A: Chem. 151 (2000) 87.
[13] H. Brunner, M. Weber, M. Zabel, J. Organomet. Chem. 684 (2003) 6.
[14] G. Zanoni, F. Castronovo, M. Franzini, G. Vidari, E. Giannini, Chem. Soc. Rev. 32 (2003) 115.
[15] C.G. Arena, R. Pattacini, J. Mol. Catal. A: Chem. 222 (2004) 47.
[16] Z. Foltynowicz, B. Marciniec, J. Organomet. Chem. 376 (1989) 15.
[17] Y. Wakatsuki, H. Yamazaki, M. Nakano, Y. Yamamoto, J. Chem. Soc., Chem. Commun. (1991) 703.
[18] K.J. Ivin, J.C. Mol, Olefin Metathesis and Metathesis Polymerization, Academic Press, San Diego, CA, 1997.
[19] B. Marciniec, B. Pietraszuk, Curr. Org. Chem. 7 (2003) 691.
[20] C. Pietraszuk, B. Marciniec, H. Fischer, Tetrahedron Lett. 44 (2003) 7121.
[21] B. Marciniec, D. Chadyniak, S. Krompiec, J. Mol. Catal. A: Chem. 224 (2004) 111.
[22] T.C. Bedard, J.Y. Corey, J. Organomet. Chem. 428 (1992) 315.
[23] F. Le Bideau, T. Coradin, J. Hénigue, E. Samuel, Chem. Commun. (2001) 1408.
[24] A. Purkayshtha, J.B. Baruah, J. Mol. Catal. A: Chem. 198 (2003) 47.
[25] L.D. Field, B.A. Messerle, M. Rehr, L.P. Soler, T.W. Hambley, Organometallics 22 (2003) 2387.
[26] (a) J.Y. Corey, J. Braddock-Wilking, Chem. Rev. 99 (1999) 175;
(b) Z. Lin, Chem. Soc. Rev. 31 (2002) 239.
[27] D.A. Straus, C. Zang, G.E. Quimbita, S.D. Grumbine, R.H. Heyn, T.D. Tilley, A.L. Reingold, S.J. Geib, J. Am. Chem. Soc. 112 (1990) 2673.
[28] A. Gądek, A. Kochel, T. Szymańska-Buzar, Organometallics 24 (2003) 4869.
[29] C.C. Chappelow, R.J. Elliot, J.T. Goldwin, J. Org. Chem. 25 (1960) 435.
[30] A. Gądek, A. Kochel, T. Szymańska-Buzar, J. Organomet. Chem. 690 (2005) 685.
[31] M. Brookhart, M.L.H. Green, L.-L. Wong, Prog. Inorg. Chem. 36 (1988) 1.
[32] R. Bau, S.A. Mason, B.O. Patrick, C.S. Adams, W.B. Sharp, P. Legzdins, Organometallics 20 (2001) 4492.
[33] R.J. Goddard, R. Hoffmann, E.D. Jemmis, J. Am. Chem. Soc. 102 (1980) 7667.
[34] J.H. Wengrovius, R.R. Schrock, M.R. Churchill, H.J. Wasserman, J. Am. Chem. Soc. 104 (1982) 1739.
[35] M.R. Churchill, H.J. Wasserman, Inorg. Chem. 22 (1983) 1574.
[36] C.M. Bastos, K.S. Lee, M.A. Kjelsberg, A. Mayr, D. Van Engen, S.A. Koch, J.D. Franolic, W.T. Klooster, T.F. Koetzle, Inorg. Chim. Acta 279 (1998) 7.
[37] G. Schmid, R. Boese, Chem. Ber. 105 (1972) 3306.
[38] M.J. Bennett, K.A. Simpson, J. Am. Chem. Soc. 93 (1971) 7156.

[C(sp^2/aryl or sp^3), N, X] terdentate ligands are well known and many examples have been reported with X = N [14], S [15], O [16], mainly due to the potential hemilability of the Pd–X bond in these systems, which plays an important role in homogeneous catalysis. Nevertheless all the examples reported for those complexes containing terdentate [C(sp^2/ferrocene), N, X] ligands are scarce, and to the best of our knowledge only compounds with X = N [17] and S [17b,17d,18] have been described, and recently ferrocene-based pincer complexes of palladium have been reported, bearing a terdentate [P, C, P] ligand [19]. Ferrocene-based cyclometallated complexes with [C, N, S] ligands are mainly with thioethers, and the unique examples derived from thiosemicarbazones have been recently reported by us [20]. As a continuation of our studies related to ferrocenylthiosemicarbazone ligands, herein we report the synthesis and characterization of new polynuclear organometallic and coordination compounds, the latter being generated after unusual σPd–C bond cleavage in the starting material.

2. Results and discussion

2.1. Synthesis and characterization

The thiosemicarbazones (η^5-C_5H_5)Fe(η^5-C_5H_4)C(H)=NN(H)C(=S)NHR (R = H, **a**; R = Me, **b**) were obtained by reaction of ferrocenecarboxaldehyde with thiosemicarbazide or with 4-methylthiosemicarbazide, respectively, in H_2O in the presence of HCl at room temperature. The NH_2 protons gave rise to two characteristic resonances at 6.33 and 7.10 ppm in the ^{1}H NMR spectrum of ligand **a** which were attributed to the restricted rotation of the NH_2 group about the C(=S)NH_2 axis. The NH protons showed resonances at 9.79 (**a**), 7.34 (N*H*Me, **b**) and 9.41 ppm (N*H*, **b**). A singlet ca. 7.80 ppm was assigned to the HC=N proton, and two apparent triplets ca. 4.50 ppm were ascribed to the H2/H5 and H3/H4 protons of the substituted ferrocenyl ring, as a simplification of the expected 20 lines of the theoretical spectrum for an AA′XX′ spin system. The C_5H_5 resonance appeared as a singlet at 4.20 ppm. The resulting new complexes derived from **a** and **b** are shown in Scheme 1. Preparative details, characterising microanalytical, IR, ^{1}H and ^{31}P–{^{1}H} NMR data are in Section 4.

Thus, treatment of a suspension of K_2PdCl_4 in EtOH/H_2O with the corresponding thiosemicarbazone afforded the cyclometallated complexes [Pd{(η^5-C_5H_5)Fe(η^5-C_5H_3)C(H)=NN=C(S)NHR}]$_4$ (R = H, **1a**; R = Me, **1b**), with the ligand in the *E*/*Z* configuration for which an octanuclear structure is proposed following the trend for these and other related compounds of tridentate [C, N, S] ligands [21]; the FAB mass spectra of **1a** and **1b** showed clusters of peaks, centred at 1566 and 1622 amu, which correspond to $[M]^+$, supporting the proposed formulation. The sulfur atom of each cyclometallated moiety displaying two different coordination modes: chelating, as part of the Pd*N*NC(NHR)*S* coordination ring, and bridging, linking two cyclometallated moieties through the metal atoms.

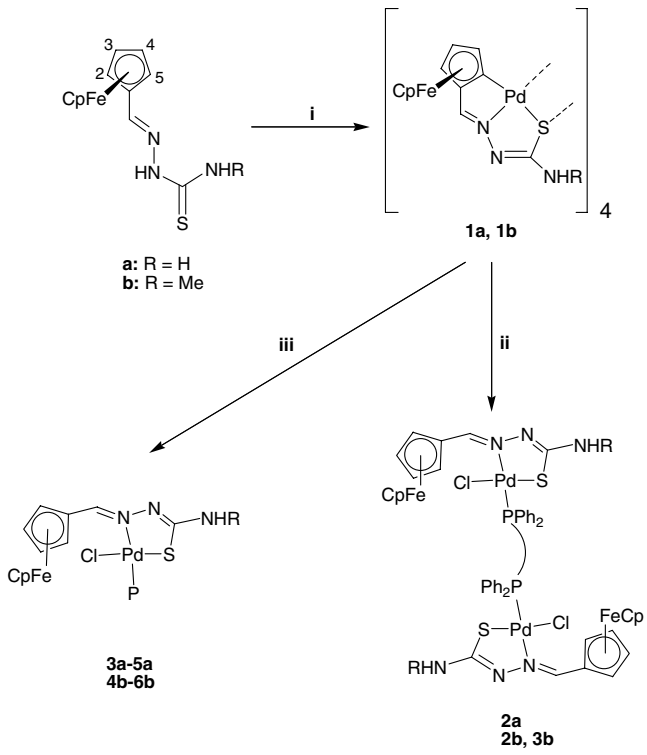

Scheme 1. (i) K_2PdCl_4, ethanol/water; (ii) $Ph_2P(CH_2)_nPPh_2$ (*n* = 1, **2b**; *n* = 4, **2a**, **3b**) 1:2 molar ratio, acetone, CH_2Cl_2/hexane; (iii) $P(PPh_3$, **3a**, **4b**; PPh_2Et, **4a**, **5b**; $P(C_6D_5)_3$, **5a**, **6b**) 1:4 molar ratio, acetone, CH_2Cl_2/hexane.

The absence of the signal for the NH group in the ^{1}H NMR spectra was in agreement with deprotonation [22]. The NH_2 (**1a**) and N*H*Me (**1b**) resonances appeared as a singlet (5.34 ppm) and a broad signal (5.37 ppm), respectively, shifted to lower frequency with respect to the spectra of the free ligands. Metallation of the ligand was clear from the absence of the AA′XX′system of the C_5H_4 ring; three proton resonances were assigned to the new C_5H_3 ring (see Section 4). In the IR spectra, the presence of the *ν*(N–H) band ca. 3420 cm^{-1} indicated the NHR group was not coordinated, and absence of the *ν*(N–H) band for the NNH group confirmed deprotonation of the latter [23]. The *ν*(C=N) band was shifted to lower wavenumbers upon complex formation [24] in an opposite trend to that observed in other thiosemicarbazones complexes [23], which can be attributed to the C,N moiety being part of the five-membered metallacycle [25]. The band assigned to the *ν*(C=S) stretching vibration ca. 870 cm^{-1} in the free ligands disappeared in the spectra of the complexes, in accordance with loss of the C=S double bond character upon deprotonation of the NH group.

Treatment of complexes **1a** and **1b** with tertiary diphosphines (1:2 molar ratio) or monophosphines (1:4 molar ratio) in acetone at room temperature and ulterior recrystallization from CH_2Cl_2/*n*-C_6H_{14} gave rise to tetranuclear or dinuclear complexes, respectively, with loss of the metallated ring upon cleavage of the σPd–C bond, as opposed to the case of similar complexes with ferrocenylthiosemicarbazones obtained by us earlier [21b], where

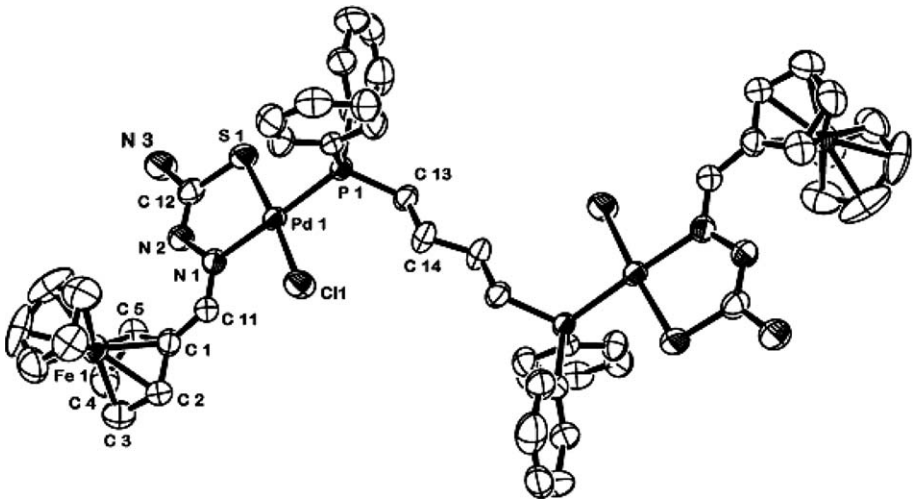

Fig. 1. Molecular structure of [{Pd[(η^5-C_5H_5)Fe(η^5-C_5H_4)C(H)=NN=C(S)NH_2](Cl)}$_2${μ-$Ph_2P(CH_2)_4PPh_2$}] (**2a**), with labelling scheme. Hydrogen atoms have been omitted for clarity.

the metal–carbon bond was retained. These results, together with our most recent findings[1], allow us to anticipate possible reasons for the behaviour of these complexes: (a) the absence of the MeC=N methyl group in the present complexes seems to favour demetallation of the cyclopentadienyl ring; (b) under the reaction conditions employed the source of chlorine should be either dichloromethane, which would put forward the non-spectator character of this solvent, or possibly traces of acid in the solvent; (c) it is also noteworthy to point out that the latter could account for the proton source and act as catalyst in the process [26]. Thus, reaction of **1a** and **1b** with tertiary diphosphines ($Ph_2PCH_2PPh_2$, $Ph_2P(CH_2)_4PPh_2$, 1:2 molar ratio) or with tertiary monophosphines (PPh_3, PPh_2Et, $P(C_6D_5)_3$, 1:4 molar ratio) gave the tetranuclear complexes [{Pd[(η^5-C_5H_5)Fe(η^5-C_5H_4)C(H)=NN=C(S)NHR]-(Cl)}$_2$(μ-PP)] (**2a**, **3b**: PP = $Ph_2P(CH_2)_4PPh_2$; **2b**, PP = $Ph_2PCH_2PPh_2$; see Scheme 1) and the dinuclear complexes [Pd{(η^5-C_5H_5)Fe(η^5-C_5H_4)C(H)=NN=C(S)-NHR}(Cl)(P)] (**3a**, **4b**: P = PPh_3; **4a**, **5b**: P = PPh_2Et; **5a**, **6b**, P = $P(C_6D_5)_3$; see Scheme 1), respectively; with the diphosphine acting as a bridging ligand between the two palladium atoms in the former case. In the IR spectra, the absence of the *ν*(C=S) stretching vibration and of the *ν*(N–H) band for the NNH group, as well as the shift to lower wavenumbers of the *ν*(C=N) band was in accordance with [N,S] coordination of the deprotonated ferrocenylthiosemicarbazone ligands to the palladium atom. A band ca. 310 cm^{-1} was assigned to the *ν*(Pd–Cl) vibration, in accordance with the now present terminal Pd–Cl bonding. In the ^{1}H NMR spectra, two apparent triplets assigned to the H2/H5 and H3/H4 protons (AA′XX′ system) confirmed the regeneration of the substituted ferrocene ring, whilst absence of the –NH resonance suggested the hydrazynic nitrogen atom remained deprotonated. The *H*C=N resonance ca. *δ* 8.30 ppm appeared as a doublet due to coupling with the ^{31}P nucleus [^4J(PHi) ca. 4.0 Hz], thereby indicating a phosphorus *trans* to nitrogen geometry, within the terms of the "transphobic effect" [27]; in the case of complexes **2a**, **2b**, **3b**, the ^{1}H NMR spectra showed only one set of signals putting forward the symmetric nature of these complexes. The ^{31}P–{^{1}H} NMR spectra showed a singlet, shifted to higher frequency from the spectrum of the free phosphine, in agreement with phosphorus coordination to metal center; for complexes **2a**, **2b**, **3b**, this showed that the two phosphorus nuclei were equivalent [28] as might be expected from the ^{1}H NMR data (vide supra).

2.2. Molecular structures of compounds *2a* and *2b*

Suitable crystals of **2a** and **2b** were grown by slowly evaporating CH_2Cl_2/*n*-C_6H_{14} solutions. The molecular structure of each neutral compound with the numbering scheme is illustrated in Figs. 1 and 2, respectively. Selected bond lengths and angles are listed in Table 1. The structures consist in discrete molecules separated by van der Waals distances (Table 2).

The crystal structures comprise a half molecule per asymmetric unit, and exhibit C_2 symmetry about the PCH_2CH_2–CH_2CH_2P bond (**2a**) or the central PCH_2P group (**2b**). The four-coordinated palladium(II) atoms are bonded to an iminic nitrogen atom and a thioamide sulphur atom of the deprotonated thiosemicarbazone ligand, and to a chlorine atom (*trans* to S). A phosphorus atom from the diphosphine ligand, which bridges the two palladium atoms, completes the metal coordination sphere. The sum of angles about palladium are 360.28° (**2a**) and 360.05°

[1] Recently, we have found that related ligands with five-membered rings, such as pyrrol, furane and thiophene thiosemicarbazones, are difficult to metallate or they do not undergo cyclometallation at all when the imine carbon, C=N, is bonded to hydrogen (for pyrrol derivatives see J.M. Vila et al., Z. Anorg. Allg. Chem., 635 (2005) 2197); however, ligands with alkyl substituted C=N groups readily undergo cyclometallation (A. Amoedo, Ph.D. Dissertation, Universidad de Santiago de Compostela, Santiago).

(**2b**), with the distortion most noticeable in the somewhat reduced "bite" angle of the thiosemicarbazone moiety consequent upon chelation (83.37(15)° for **2a**, 83.1(3)° for **2b**). The geometry around the palladium atom is slightly distorted square-planar, the mean deviation from the least squares plane (plane 1: Pd(1), N(1), S(1), P(1), Cl(1) are 0.0783 (**2a**) and 0.0731 (**2b**)). The metallated rings (plane 2: Pd(1), S(1), C(12), N(1), N(2), r.m.s. 0.0261 (**2a**), 0.0433 (**2b**)) are also planar and coplanar with the palladium coordination plane (angles between planes: 1/2 3.83(0.12)° (**2a**), 4.56(0.10)° (**2b**)).

The palladium–nitrogen bond lengths (2.107(5) Å, **2a**; 2.079(9) Å, **2b**) are longer than the predicted single bond value of 2.011 Å, based on the sum of covalent radii for nitrogen(sp^2) and palladium, 0.701 and 1.31 Å, respectively [29] and reflects the *trans* influence of the phosphorus atom

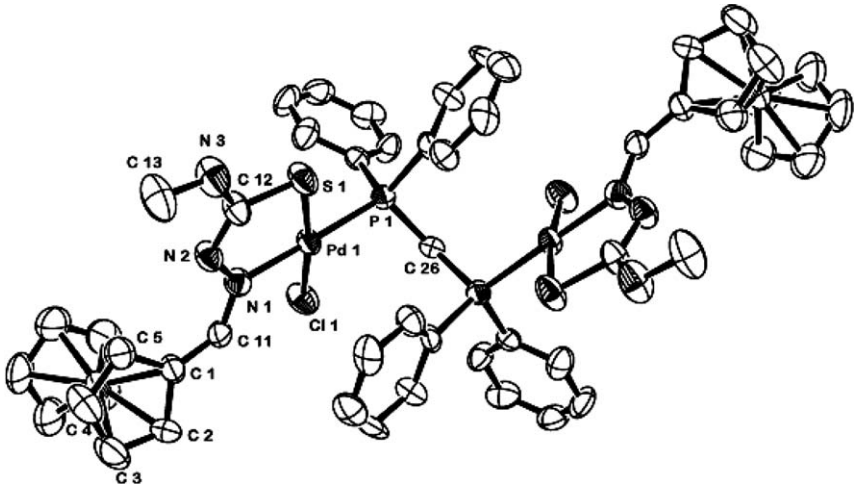

Fig. 2. Molecular structure of [{Pd[(η^5-C_5H_5)Fe(η^5-C_5H_4)C(H)=NN=C(S)NHMe](Cl)}$_2$(μ-$Ph_2PCH_2PPh_2$)] (**2b**), with labelling scheme. Hydrogen atoms have been omitted for clarity.

Table 1
Crystal and structure refinement data

	2a	**2b**
Formula	$C_{52}H_{52}Cl_2Fe_2N_6P_2Pd_2S_2$	$C_{53}H_{52}Cl_8Fe_2N_6P_2Pd_2S_2$
Formula weight	1282.46	1507.17
Temperature (K)	293(2)	293(2)
Wavelength (Å)	0.71073	0.71073
Crystal system	monoclinic	monoclinic
Space group	*P*2(1)/*c*	*P*2/*c*
a (Å)	10.339(3)	15.408(4)
b (Å)	17.785(5)	8.750(2)
c (Å)	13.894(4)	22.489(5)
α (°)	90	90
β (°)	93.389(5)	94.400(5)
γ (°)	90	90
V (Å^3)	2550.4(12)	3023.0(12)
Z	2	2
D_{calc} (Mg/m^3)	1.670	1.656
Absorption coefficient (mm^{-1})	1.544	1.572
F(000)	1292	1508
Crystal size (mm^3)	0.34 × 0.29 × 0.09	0.36 × 0.33 × 0.31
θ Range for data collection (°)	1.86–26.43	1.33–26.44
Index ranges	−5/2, −12/22, −17/16	−14/19, −10/10, −28/28
Reflections collected	13790	16756
Independent reflections [R_{int}]	5209 [0.0621]	6147 [0.1091]
Completeness to $\theta = 26.43°$	99.3%	98.9%
Absorption correction	SADABS	SADABS
Refinement method	full-matrix least-squares on F^2	
Data/restraints/parameters	5209/0/307	6147/0/339
Goodness-of-fit on F^2	0.955	0.881
Transmissions	0.870, 0.600	0.6414, 0.6014
Final *R* indices [$I > 2\sigma(I)$]	$R_1 = 0.0457$, $wR_2 = 0.0762$	$R_1 = 0.0550$, $wR_2 = 0.1196$
R indices (all data)	$R_1 = 0.1219$, $wR_2 = 0.0883$	$R_1 = 0.2005$, $wR_2 = 0.1851$
Largest difference in peak and hole (e Å^{-3})	0.748 and −0.502	0.635 and −0.686

Table 2
Selected bond distances (Å) and angles (°) for **2a** and **2b**

2a			
Pd(1)–N(1)	2.107(5)	Pd(1)–S(1)	2.2436(17)
Pd(1)–P(1)	2.2543(16)	Pd(1)–Cl(1)	2.3397(16)
S(1)–C(12)	1.776(6)	N(1)–N(2)	1.390(6)
N(2)–C(12)	1.280(7)	N(3)–C(12)	1.344(7)
N(1)–C(11)	1.281(6)	C(1)–C(11)	1.436(7)
P(1)–C(13)	1.825(6)	C(14)–C(13)	1.518(7)
N(1)–Pd(1)–S(1)	83.37(15)	N(1)–Pd(1)–P(1)	175.04(14)
S(1)–Pd(1)–P(1)	92.54(6)	N(1)–Pd(1)–Cl(1)	94.47(15)
S(1)–Pd(1)–Cl(1)	173.41(6)	P(1)–Pd(1)–Cl(1)	89.90(6)
C(11)–N(1)–N(2)	115.9(5)	C(11)–N(1)–Pd(1)	124.2(4)
N(2)–N(1)–Pd(1)	119.9(4)	C(12)–N(2)–N(1)	113.3(5)
C(12)–S(1)–Pd(1)	96.6(2)	N(2)–C(12)–S(1)	126.6(5)
2b			
Pd(1)–N(1)	2.079(9)	Pd(1)–S(1)	2.242(3)
Pd(1)–P(1)	2.257(3)	Pd(1)–Cl(1)	2.350(3)
S(1)–C(12)	1.773(11)	N(1)–C(11)	1.285(12)
N(1)–N(2)	1.401(10)	N(2)–C(12)	1.296(13)
N(3)–C(12)	1.313(12)	N(3)–C(13)	1.485(13)
C(1)–C(11)	1.425(13)	P(1)–C(26)	1.815(7)
N(1)–Pd(1)–S(1)	83.1(3)	N(1)–Pd(1)–P(1)	178.0(3)
S(1)–Pd(1)–P(1)	94.89(11)	N(1)–Pd(1)–Cl(1)	94.2(3)
S(1)–Pd(1)–Cl(1)	171.99(11)	P(1)–Pd(1)–Cl(1)	87.86(10)
C(12)–S(1)–Pd(1)	97.3(4)	C(11)–N(1)–N(2)	114.5(9)
C(11)–N(1)–Pd(1)	124.1(7)	N(2)–N(1)–Pd(1)	121.0(6)
C(12)–N(2)–N(1)	112.5(9)	N(2)–C(12)–S(1)	125.6(8)

[30,31]. The palladium–sulfur bond lengths, (2.2436(17) Å, **2a**; 2.242(3) Å, **2b**) are shorter than the expected value of 2.33 Å (based on the sum of the covalent radii for sulfur and palladium, 1.02 and 1.31 Å, respectively). The Pd–P bond distances, 2.2543(16) (**2a**) and 2.257(3) (**2b**) are shorter than the sum of the single bond radii for palladium and phosphorus (2.41 Å), whilst the Pd–Cl bond lengths, 2.3397(16) (**2a**) and 2.350(3) Å (**2b**), are slightly longer than the sum of the covalent radii (2.30 Å). The S–C and C–N bond lengths in the chelate ring [S(1)–C(12), 1.776(6), N(2)–C(12), 1.280(7) Å, **2a**; S(2)–C(39), 1.773(11), N(5)–C(39), 1.296(13) Å, **2b**] are consistent with increased single and double bond character, respectively.

3. Conclusions

The results reported in the present paper show that ferrocenyl thiosemicarbazones are readily metallated to give the corresponding cyclopalladated octanuclear complexes. However, reaction of the latter with tertiary mono- and diphosphines yields products with cleavage of the Pd–C bond, protonation of the cyclopentadienyl ring, and Pd–Cl bond formation. These results, together with very recent findings from our laboratory, allow us to point out several factors responsible for this behaviour such as are the absence of an alkyl group on the imine carbon atom, the presence of traces of acid in CH_2Cl_2, and the not so negligible reactivity of this solvent. We are currently undertaking the research of related chemistry aimed at providing further proof for our proposal, which shall be communicated in the near future.

4. Experimental

Solvents were purified by standard methods [32], chemicals were reagent grade. Microanalyses were carried out at the Servicio de Análisis Elemental at the University of Santiago using a Carlo Erba Elemental Analyzer, Model 1108. IR spectra were recorded on a Perkin–Elmer 1330 and on a Mattson spectrophotometer. NMR spectra were obtained as $CDCl_3$ solutions and referenced to $SiMe_4$ (^1H) or 85% H_3PO_4 (^{31}P–{^1H}) and were recorded on Bruker WM250 and AMX-300 spectrometers (only selected data is presented for compounds containing phosphine). All chemical shifts are reported downfield from standards. The FAB mass spectra were recorded with a Fisons Quatro mass spectrometer with a Cs ion gun; 3-nitrobenzyl alcohol was used as the matrix.

4.1. (η^5-C_5H_5)Fe(η^5-C_5H_4)C(H)=NN(H)C(=S)NH_2 (**a**)

To a stirred suspension of thiosemicarbazide (0.213 g, 2.336 mmol) in water (40 cm^3) a few drops of HCl 36% and ferrocenecarboxaldehyde (0.5 g, 2.336 mmol) were added. The resulting mixture was stirred for 4 h at r.t., filtered off, washed with water and dried in vacuo to yield an orange solid.

Yield: 91.4%. *Anal*. Calc. for $C_{12}H_{13}N_3FeS$: C, 50.2; H, 4.6; N, 14.7; S, 11.2. Found: C, 49.7; H, 4.4; N, 14.2; S, 11.1%. IR: ν(N–H) 3431m, 3151w, ν(C=N) 1592m, ν(C=S) 876 cm^{-1}. ^1H NMR (δ ppm, J Hz): 4.20 (s, 5H, C_5H_5), 4.32 (t, 2H, H3/H4, $N = 3.4$), 4.58 (t, 2H, H2/H5, $N = 3.4$), 6.33, 7.10 (s, 2H, NH_2), 7.80 (s, 1H, *H*C=N), 9.79 (s, 1H, N*H*).

Ligand **b** was prepared as an orange air-stable solid following a similar procedure.

4.2. (η^5-C_5H_5)Fe(η^5-C_5H_4)C(H)=NN(H)C(=S)NHMe (**b**)

Yield: 93.5%. *Anal*. Calc. for $C_{13}H_{15}N_3FeS$: C, 51.8; H, 5.0; N, 14.0; S, 10.6. Found: C, 51.5; H, 5.0; N, 13.5; S, 10.1%. IR: ν(N–H) 3430m, 3143w, ν(C=N) 1609m, ν(C=S) 873 cm^{-1}. ^1H NMR (δ ppm, J Hz): 3.24 (d, 3H, NH*Me*, ^3J(HMe) = 4.8 Hz), 4.20 (s, 5H, C_5H_5), 4.40 (at, 2H, H3/H4, $N = 3.8$), 4.57 (at, 2H, H2/H5, $N = 3.8$), 7.34 (b, 1H, N*H*Me), 7.69 (s, 1H, *H*C=N), 9.41 (s, 1H, N*H*).

4.3. [Pd{(η^5-C_5H_5)Fe(η^5-C_5H_3)C(H)=NN=C(S)-NH_2}]$_4$ (**1a**)

To a stirred solution of K_2PdCl_4 (200 mg, 0.613 mmol) in EtOH (40 cm^3) and H_2O (6 cm^3), (η^5-C_5H_5)Fe(η^5-C_5H_4)C(H)=NN(H)C(=S)NH_2 (**a**) (193 mg, 0.674 mmol) were added. The mixture was stirred for 24 h at r.t. and the resulting precipitate filtered off, washed with cold ethanol and dried in vacuo.

Yield: 53.3%. *Anal.* Calc. for $C_{48}H_{44}Fe_4N_{12}Pd_4S_4$: C, 36.8; H, 2.8; N, 10.7; S, 8.2. Found: C, 36.3; H, 2.8; N, 10.3; S, 8.3%. IR: ν(N–H) 3428m, ν(C=N) 1525w. ^{1}H NMR (δ ppm, J Hz): 3.88 (b, 1H, H4), 4.06 (s, 5H, C_5H_5), 4.23 (b, 1H, H3), 4.35 (b, 1H, H2), 5.34 (s, 2H, NH_2), 7.59 (s, 1H, *H*C=N).

Compound **1b** was prepared as a red air-stable solid following a similar procedure.

*4.4. [Pd{(η^5-C_5H_5)Fe(η^5-C_5H_3)C(H)=NN=C(S)-NHMe}]$_4$ (**1b**)*

Yield: 56.5%. *Anal.* Calc. for $C_{52}H_{52}Fe_4N_{12}Pd_4S_4$: C, 38.5; H, 3.2; N, 10.4; S, 7.9. Found: C, 38.1; H, 3.1; N, 10.5; S, 7.5%. IR: ν(N–H) 3417m, ν(C=N) 1601m. ^{1}H NMR (δ ppm, J Hz): 2.95 (d, 3H, NH*Me*, ^3J(HMe) = 4.8), 3.90 (d, 1H, H4, ^3J(H3H4) = 1.2), 4.08 (s, 5H, C_5H_5), 4.33 (b, 1H, H3), 4.40 (b, 1H, H2), 5.37 (b, 1H, N*H*Me), 7.63 (s, 1H, *H*C=N).

*4.5. [{Pd[(η^5-C_5H_5)Fe(η^5-C_5H_4)C(H)=NN=C(S)NH$_2$]-(Cl)}$_2${μ-Ph$_2$P(CH$_2$)$_4$PPh$_2$}] (**2a**)*

To a stirred solution of compound **1a** (30 mg, 0.018 mmol) in acetone (15 cm^3) 1,4-bis(diphenylphosphino)butane (dppb) (16 mg, 0.038 mmol) was added. The mixture was stirred for 24 h at r.t., filtered off and the solvent removed under reduced pressure. The red residue was recrystallized from CH_2Cl_2/*n*-C_6H_{14}.

Yield: 66.9%. *Anal.* Calc. for $C_{52}H_{52}Cl_2Fe_2N_6P_2Pd_2S_2$: C, 48.7; H, 4.1; N, 6.6; S, 5.0. Found: C, 48.5; H, 4.0; N, 6.2; S, 4.9%. IR: ν(N–H) 3457m, ν(C=N) 1533m, ν(Pd–Cl) 305m cm^{-1}. ^{1}H NMR (δ ppm, J Hz): 4.22 (s, 5H, C_5H_5), 4.45 (t, 2H, H3/H4, $N = 3.4$), 4.93 (t, 2H, H2/H5, $N = 3.4$), 4.68 (s, 2H, NH_2), 8.31 (d, 1H, *H*C=N, ^4J(PH) = 4.2). ^{31}P–{^{1}H} NMR (δ ppm) 19.1s.

Compounds **2b** and **3b** were prepared as red air-stable solids following a similar procedure.

*4.6. [{Pd[(η^5-C_5H_5)Fe(η^5-C_5H_4)C(H)=NN=C(S)-NHMe](Cl)}$_2$(μ-Ph$_2$PCH$_2$PPh$_2$)] (**2b**)*

Yield: 61.7%. *Anal.* Calc. for $C_{51}H_{50}Cl_2Fe_2N_6P_2Pd_2S_2$: C, 48.3; H, 4.0; N, 6.6; S, 5.1. Found: C, 48.0 H, 4.2; N, 6.8; S 4.9%. IR: ν(N–H) 3440m, ν(C=N) 1596m, ν(Pd–Cl) 302m cm^{-1}. ^{1}H NMR (δ ppm, J Hz): 2.94 (d, 3H, NH*Me*, ^3J(HMe) = 4.9), 4.14 (s, 5H, C_5H_5), 4.19 (t, 2H, H3/H4, $N = 3.8$), 4.40 (t, 2H, H2/H5, $N = 3.8$), 5.39 (b, 1H, N*H*Me), 8.21 (d, 1H, *H*C=N, ^4J(PH) = 4.5). ^{31}P–{^{1}H} NMR (δ ppm) 23.5s.

*4.7. [{Pd[(η^5-C_5H_5)Fe(η^5-C_5H_4)C(H)=NN=C(S)NHMe](Cl)}$_2${μ-Ph$_2$P(CH$_2$)$_4$PPh$_2$}] (**3b**)*

Yield: 56.5%. *Anal.* Calc. for $C_{56}H_{54}Cl_2Fe_2N_6P_2Pd_2S_2$: C, 49.5; H, 4.3; N, 6.4; S, 4.9. Found: C, 49.1; H, 4.0; N, 6.4; S, 4.4%. IR: ν(N–H) 3417m, ν(C=N) 1596m, ν(Pd–Cl) 323m cm^{-1}. ^{1}H NMR (δ ppm, J Hz): 2.97 (b, 3H, NH*Me*), 4.23 (s, 5H, C_5H_5), 4.87 (t, 2H, H3/H4, $N = 3.8$), 5.04 (t, 2H, H2/H5, $N = 3.8$), 5.48 (b, 1H, N*H*Me), 8.33 (d, 1H, *H*C=N, ^4J(PH) = 4.1). ^{31}P–{^{1}H} NMR (δ ppm) 23.7s.

*4.8. [Pd{(η^5-C_5H_5)Fe(η^5-C_5H_3)C(H)=NN=C(S)NH$_2$}-(Cl)(PPh$_3$)] (**3a**)*

To a stirred solution of compound **1a** (30 mg, 0.019 mmol) in acetone (15 cm^3) triphenylphosphine (20 mg, 0.077 mmol) was added. The mixture was stirred for 24 h at r.t., filtered off, dried in vacuo and the orange residue recrystallized from CH_2Cl_2/*n*-C_6H_{14}. Yield: 52.1%. *Anal.* Calc. for $C_{30}H_{27}ClFeN_3PPdS$: C, 52.2; H, 3.9; N, 6.1; S, 4.6. Found: C, 52.0; H, 3.8; N, 6.4; S, 4.7%. IR: ν(N–H) 3449m, ν(C=N) 1533m, ν(Pd–Cl) 304m cm^{-1}. ^{1}H NMR (δ ppm, J Hz): 4.24 (s, 5H, C_5H_5), 4.46 (t, 2H, H3/H4, $N = 3.4$), 4.96 (t, 2H, H2/H5, $N = 3.4$), 4.63 (s, 2H, NH_2), 8.41 (d, 1H, *H*C=N, ^4J(PH) = 4.0). ^{31}P–{^{1}H} NMR (δ ppm) 26.2s.

Compounds **4a**, **5a** and **4b**–**6b** were prepared as air-stable solids following a similar procedure.

*4.9. [Pd{(η^5-C_5H_5)Fe(η^5-C_5H_3)C(H)=NN=C(S)NH$_2$}-(Cl)(PPh$_2$Et)] (**4a**)*

Yield: 56.9%. *Anal.* Calc. for $C_{26}H_{27}ClFeN_3PPdS$: C, 48.6; H, 4.2; N; 6.5; S, 5.0. Found: C, 48.3; H, 4.1; N, 6.2; S, 4.9%. IR: ν(N–H) 3437m, ν(C=N) 1535m, ν(Pd–Cl) 303m cm^{-1}. ^{1}H NMR (δ ppm, J Hz): 4.22 (s, 5H, C_5H_5), 4.45 (t, 2H, H3/H4, $N = 3.4$), 4.95 (t, 2H, H2/H5, $N = 3.4$), 4.65 (s, 2H, NH_2), 8.34 (d, 1H, *H*C=N, ^4J(PH) = 4.2). ^{31}P–{^{1}H} NMR (δ ppm) 26.5s.

*4.10. [Pd{(η^5-C_5H_5)Fe(η^5-C_5H_3)C(H)=NN=C(S)NH$_2$}-(Cl){P(C_6D_5)$_3$}] (**5a**)*

Yield: 59.5%. *Anal.* Calc. for $C_{30}H_{12}D_{15}ClFeN_3PPdS$: C, 51.1; H, 6.0; N, 6.0; S, 4.6. Found: C, 51.4; H, 5.9; N, 5.4; S, 4.9%. IR: ν(N–H) 3445m, ν(C=N) 1534m, ν(Pd–Cl) 302m cm^{-1}. ^{1}H NMR (δ ppm, J Hz): 4.24 (s, 5H, C_5H_5), 4.46 (t, 2H, H3/H4, $N = 3.4$), 4.96 (t, 2H, H2/H5, $N = 3.4$), 4.69 (s, 2H, NH_2), 8.41 (d, 1H, *H*C=N, ^4J(PH) = 4.2). ^{31}P–{^{1}H} NMR (δ ppm) 26.0s.

*4.11. [Pd{(η^5-C_5H_5)Fe(η^5-C_5H_3)C(H)=NN=C(S)NH-Me}(Cl)(PPh$_3$)] (**4b**)*

Yield: 61.3%. *Anal.* Calc. for $C_{31}H_{29}ClFeN_3PPdS$: C, 52.9; H, 4.2; N, 6.0; S, 4.6. Found: C, 53.4; H, 3.9; N, 5.6; S, 4.3%. IR: ν(N–H) 3422m, ν(C=N) 1596m, ν(Pd–Cl) 324m cm^{-1}. ^{1}H NMR (δ ppm, J Hz): 2.97 (d, 3H, NH*Me*, ^3J(HMe) = 4.9), 3.95 (b, 1H, N*H*Me), 4.22 (s, 5H, C_5H_5), 4.45 (t, 2H, H3/H4, $N = 3.8$), 5.00 (t, 2H, H2/H5, $N = 3.8$), 3.95 (b, 1H, N*H*Me), 8.41 (d, 1H, *H*C=N, ^4J(PH) = 4.1). ^{31}P–{^{1}H} NMR (δ ppm) 23.3s.

4.12. [Pd{(η^5-C_5H_5)Fe(η^5-C_5H_3)C(H)=NN=C(S)NHMe}(Cl)(PPh_2Et)] (**5b**)

Yield: 63.8%. *Anal*. Calc. for $C_{27}H_{29}ClFeN_3PPdS$: C, 49.4; H, 4.5; N, 6.4; S, 4.9. Found: C, 50.0; H, 4.7; N, 6.1; S, 5.1%. IR: ν(N–H) 3423m, ν(C=N) 1592m, ν(Pd–Cl) 299m cm^{-1}. ^1H NMR (δ ppm, J Hz): 3.00 (d, 3H, NH*Me*, ^3J(HMe) = 4.6), 3.88 (b, 1H, N*H*Me), 4.20 (s, 5H, C_5H_5), 4.44 (t, 2H, H3/H4, $N = 3.8$), 4.99 (t, 2H, H2/H5, $N = 3.8$), 8.34 (d, 1H, *H*C=N, ^4J(PH) = 3.7). ^{31}P–{^1H} NMR (δ ppm) 26.5s.

4.13. [Pd{(η^5-C_5H_5)Fe(η^5-C_5H_3)C(H)=NN=C(S)NHMe}(Cl){$P(C_6D_5)_3$}] (**6b**)

Yield: 57.4%. *Anal*. Calc. for $C_{31}H_{14}D_{15}ClFeN_3PPdS$: C, 51.8; H, 6.2; N, 5.8; S, 4.5. Found: C, 51.8; H, 5.9; N, 5.6; S, 3.9%. IR: ν(N–H) 3428s, ν(C=N) 1593m, ν(Pd–Cl) 278w cm^{-1}. ^1H NMR (δ ppm, J Hz): 2.85 (d, 3H, NH*Me*, ^3J(HMe) = 5.1), 4.21 (s, 5H, C_5H_5), 4.31 (t, 2H, H3/H4, $N = 3.8$), 4.53 (t, 2H, H2/H5, $N = 3.8$), 5.02 (b, 1H, N*H*Me), 8.78 (d, 1H, *H*C=N, ^4J(PH) = 2.2). ^{31}P–{^1H} NMR (δ ppm) 25.7s.

4.14. X-ray crystallographic study[2]

Three-dimensional, room temperature X-ray data were collected in the range $1.86 < \theta < 26.43°$ (**2a**), $1.33 < \theta < 26.44°$ (**2b**) on a Bruker CCD diffractometer by the omega scan method. Reflections were measured from a hemisphere of data collected of frames each covering 0.3 degrees in omega. The 13790 (**2a**), 16756 (**2b**) reflections measured were corrected for Lorentz and polarisation effects and for absorption using a semi-empirical correction based on symmetry-equivalent and repeated reflections. The structure was solved by direct methods and refined by full matrix least unique data, 307 (**2a**) 339 (**2b**) parameters, with allowance for the thermal anisotropy of all non hydrogen atoms. Hydrogen atoms were included in calculated positions and refined in riding mode. The refinement was carried out taking into account the minor components of the disorder. Minimum and maximum final electron density 0.748 and −0.502 (**2a**), 0.635 and −0.686 (**2b**) e $Å^{-3}$. The structure solution and refinement were carried out using the program package SHELX-97 [33].

Acknowledgements

We thank the DGESIC (Ministerio de Ciencia y Tecnología) Proyecto BQU2002-04533-C02-01 for financial support, and the Xunta de Galicia, incentive PGIDIT03PXIC20912PN, for financial support.

Appendix A. Supplementary data

Crystallographic data (excluding structure factors) for the structures reported in this paper have been deposited with the Cambridge Crystallographic Data Centre as supplementary publication numbers 279562 (**2a**) and 279563 (**2b**). Copies of the data can be obtained free of charge on application to CCDC, 12 Union Road, Cambridge CB2 1EZ, UK. Supplementary data associated with this article can be found, in the online version, at doi:10.1016/j.poly.2005.10.003.

References

[1] (a) I. Omae, Organometallic Intramolecular Coordination Compounds, Elsevier, Amsterdam, 1986;
(b) O.A. Dunina, V.M. Zalewskaya, V.M. Potapov, Russ. Chem. Rev. 57 (1988) 250;
(c) I. Omae, Coord. Chem. Rev. 83 (1988) 137, and references therein;
(d) A.D. Ryabov, Chem. Rev. 90 (1990) 403;
(e) J. Dupont, C.S. Consorti, J. Spencer, Chem. Rev. 105 (2005) 2527.
[2] (a) L. Main, B.K. Nicholson, Adv. Met.-Org. Chem. 3 (1994) 1;
(b) J. Spencer, M. Pfeffer, Adv. Met.-Org. Chem. 6 (1998) 103.
[3] (a) J. Dupont, M. Pfeffer, J. Spencer, Eur. J. Inorg. Chem. (2001) 1917;
(b) L. Botella, C. Najera, Angew. Chem., Int. Ed. 41 (2002) 179.
[4] S.B. Wild, Coord. Chem. Rev. 166 (1997) 291.
[5] C.M. Che, W.F. Fu, S.W. Lai, Y.J. Hou, Y.I. Liu, Chem. Commun. (2003) 118.
[6] (a) V.W.W. Yam, K.M.C. Wong, N.J. Zhu, J. Am. Chem. Soc. 124 (2002) 6506;
(b) W. Lu, B.X. Mi, M.C.W. Chan, Z. Hul, N. Zhu, S.T. Lee, C.M. Che, Chem. Commun. (2002) 206;
(c) C. Adachi, M.A. Baldo, S.R. Forrest, S. Lamanski, M.L. Thompson, R.C. Kwong, Appl. Phys. Lett. 78 (2001) 1622.
[7] (a) T.J. Kealy, P.L. Pauson, Nature 186 (1951) 1039;
(b) G. Wilkinson, M. Rosenblum, M.C. Whiting, R.B. Woodward, J. Am. Chem. Soc. 74 (1952) 2125;
(c) E.O. Fischer, W. Pfab, Z. Naturfosch. B 7 (1952) 377.
[8] (a) For a comprehensive overview of ferrocene and metallocene chemistry, see: A. Togni, R.L. Halterman (Eds.), Metallocenes, Wiley–VCH, Weinheim, Germany, 1998;
(b) N.J. Long, Metallocenes: An Introduction to Sandwich Complexes, Blackwell, Oxford, 1998.
[9] (a) A. Togni, T. Hayashi (Eds.), Ferrocenes: Homogeneus Catalysis. Organic Synthesis. Materials Science, VCH, Weinheim, Germany, 1995;
(b) C.S. Slone, D.A. Weinberger, C.A. Mirhin, Prog. Inorg. Chem. 48 (1999) 233;
(c) R.C.J. Atkinson, V.C. Gibson, N.J. Long, Chem. Soc. Rev. 33 (2004) 313.
[10] (a) For recent advances in cyclometallated [C(sp2/ferrocene),N] ligands see, for instance: C. López, R. Bosque, J. Arias, E. Evangelio, X. Solans, M. Font-Bardía, J. Organomet. Chem. 672 (2003) 34;
(b) J.M. Vila, E. Gayoso, T. Pereira, M. Mariño, J. Martínez, J.J. Fernández, A. Fernández, M. López-Torres, J. Organomet. Chem. 637–639 (2001) 577;
(c) V.V. Dunina, O.N. Gorunova, M.V. Livantsov, Y.K. Grishin, L.G. Kuz'mina, N.A. Kataeva, A.V. Churakov, Tetrahedron: Asymm. 11 (2000) 3967.

[2] Crystallographic data (excluding structure factors) for the structures reported in this paper have been deposited with the Cambridge Crystallographic Data Centre as supplementary publication numbers 279562 (**2a**) and 279563 (**2b**). Copies of the data can be obtained free of charge on application to CCDC, 12 Union Road, Cambridge CB2 1EZ, UK [fax: (internat.) +44 1223/336 033; e-mail: deposit@ccdc.cam.ac.uk].

[11] (a) Y. Wu, J. Hou, H. Yun, X. Cui, R. Yuan, J. Organomet. Chem. 637–639 (2001) 793;
(b) F. Yang, Y. Zhang, R. Zheng, J. Tang, M. He, J. Organomet. Chem. 651 (2002) 146.
[12] L.E. Overwan, T.P. Remarchuk, J. Am. Chem. Soc. 124 (2002) 12.
[13] X.L. Cui, Y.J. Wu, L.R. Yang, Chin. Chem. Lett. 10 (1999) 127.
[14] (a) L. Xu, Q.S. Li, X. Jia, X. Huang, R. Wang, Z. Zhou, Z. Lin, A.S.C. Chen, Chem. Commun. (2003) 1666;
(b) J. Bravo, C. Cativela, R. Navarro, E.P. Urriolabeitia, J. Organomet. Chem. 650 (2002) 157;
(c) A. Fernández, P. Uría, J.J. Fernández, M. López-Torres, A. Suárez, D. Vázquez-García, M.T. Pereira, J.M. Vila, J. Organomet. Chem. 620 (2001) 8.
[15] (a) C. López, A. Caubet, S. Pérez, X. Solans, M. Font-Bardiá, J. Organomet. Chem. 681 (2003) 82;
(b) I. Pal, S. Dutta, F. Basuli, S. Goverdhan, S.M. Peng, G.H. Lee, S. Bhattacharya, Inorg. Chem. 42 (2003) 4338;
(c) A. Fernández, D. Vázquez-García, J.J. Fernández, M. López-Torres, A. Suárez, S. Castro-Juiz, J.M. Vila, New. J. Chem. 26 (2002) 398.
[16] (a) C. López, S. Pérez, X. Solans, M. Font-Bardiá, J. Organomet. Chem. 650 (2002) 258;
(b) X. Riera, A. Caubet, C. López, V. Moreno, E. Freisinger, M. Willermann, B. Lippert, J. Organomet. Chem. 629 (2001) 97;
(c) A. Fernández, D. Vazquez-Garcia, J.J. Fernández, M. Lopez-Torres, A. Suarez, S. Castro-Juiz, J.M. Ortigueira, J.M. Vila, New. J. Chem. 26 (2002) 105.
[17] (a) C. López, S. Pérez, X. Solans, M. Font-Bardiá, J. Organomet. Chem. 690 (2005) 228;
(b) A. González, J.R. Granell, C. López, J. Organomet. Chem. 637–639 (2001) 116;
(c) C. López, A. Caubet, S. Pérez, X. Solans, M. Font-Bardiá, J. Organomet. Chem. 651 (2002) 105;
(d) S. Pérez, C. López, A. Caubet, X. Solans, M. Font-Bardiá, J. Organomet. Chem. 689 (2004) 3184.
[18] (a) C. López, A. Caubet, R. Bosque, X. Solans, M. Font-Bardiá, J. Organomet. Chem. 645 (2002) 146;
(b) S. Pérez, C. López, A. Caubet, R. Bosque, X. Solans, M. Font-Bardiá, A. Roig, E. Molins, Organometallics 23 (2004) 224.
[19] A.A. Koridze, S.A. Kuklin, A.M. Sheloumov, F.M. Dolgushin, V.Y. Lagunova, I.I. Petukhova, M.C. Ezernitskaya, A.S. Peregudov, P.V. Petrovskii, E.V. Vorontsov, M. Baya, R. Poli, Organometallics 23 (2004) 4585.
[20] J.M. Vila, E. Gayoso, M.T. Pereira, J.M. Ortigueira, G. Alberdi, M. Mariño, R. Alvarez, A. Fernández, Eur. J. Inorg. Chem. (2004) 2937.
[21] (a) J.M. Vila, M.T. Pereira, J.M. Ortigueira, M. Graña, D. Lata, A. Suarez, J.J. Fernández, A. Fernández, M. López-Torres, H. Adams, J. Chem. Soc., Dalton Trans. (1999) 4193;
(b) A. Amoedo, M. Graña, J. Martínez, T. Pereira, M. López-Torres, A. Fernández, J.J. Fernández, J.M. Vila, Eur. J. Inorg. Chem. (2002) 613;
(c) A.G. Quiroga, J.M. Pérez, I. López-Solera, J.R. Masaguer, A. Luque, P. Román, A. Edwards, C. Alonso, C. Navarro-Ranninger, J. Med. Chem. 41 (1998) 1399.
[22] J.S. Casas, M.V. Castaño, M.C. Cifuentes, A. Sánchez, J. Sordo, Polyhedron 21 (2002) 1651.
[23] T.S. Lobana, A. Sánchez, J.S. Casas, A. Castiñeiras, J. Sordo, M.S. Gracía-Tasende, E.M. Vázquez-López, J. Chem. Soc. Dalton Trans. (1997) 4289.
[24] D.X. West, J.S. Ives, G.A. Bain, A.L. Liberta, J. Valdés-Martínez, K.H. Ebert, S. Hernández-Ortega, Polyhedron 16 (1997) 1995.
[25] H. Onoue, I. Moritani, J. Organomet. Chem. 43 (1972) 431.
[26] J.M. Vila, B.L. Shaw, J. Chem. Soc., Chem. Comm. (1987) 1778.
[27] J. Vicente, J.A. Abad, A.D. Frankland, M.C. Ramirez de Arellano, Chem. Eur. J. 5 (1999) 3067.
[28] R. Ares, M. López-Torres, A. Fernández, M.T. Pereira, G. Alberdi, D. Vázquez-García, J.J. Fernández, J.M. Vila, J. Organomet. Chem. 665 (2003) 76.
[29] F.H. Allen, O. Kennard, D.G. Watson, R. Taylor, J. Chem. Soc., Dalton Trans. (1989) S1.
[30] T. Suzuki, A. Morikawa, K. Kashiwabara, Bull. Chem. Soc. Jpn. 69 (1996) 2539.
[31] A. Habtemariam, B. Watchman, B.S. Potter, R. Palmer, S. Parsons, A. Parkin, P.J. Sadler, J. Chem. Soc. Dalton Trans. (2001) 1306.
[32] W.L.F. Armarego, C. Chai, Purification of Laboratory Chemicals, fifth ed., Butterworth–Heinemann, Oxford, 2003.
[33] G.M. Sheldrick, SHELX-97, An Integrated System for Solving and Refining Crystal Structures from Diffraction Data, University of Gottingen, Germany, 1997.

totpy = 4′-(4-tolyl)-2,2′:6′,2″-terpyridine); their spectral, electrochemical and catalytic properties were studied. The ability of the complexes to act as catalysts for electrooxidations of benzyl alcohol, cyclohexanol, cyclohexene, ethylbenzene, 1,2-butanediol and 1,4-butanediol were studied in homogeneous solution and with the complexes immobilized in carbon paste electrodes and within Nafion® films on electrodes.

2. Experimental

2.1. Materials

Water was doubly distilled from alkaline potassium permanganate. $RuCl_3 \cdot xH_2O$, 1,2-bis(dichlorophosphine)-ethane and 1,2-bis(dimethylphosphine) ethane were purchased from Aldrich Chemical Co. Methylene chloride and acetonitrile were kept in an alumina column before use. All other reagents and solvents were of reagent quality and were used without further purification.

2.2. Instrumentation and measurements

Routine UV–Vis spectra were obtained in 1-cm quartz cells by using a Hewlett–Packard 8453 spectrophotometer. Electrochemical experiments were conducted by using a PAR Model 273A Potentiostat/Galvanostat. Cyclic voltammetric and differential pulse voltammetric experiments were performed in a one-compartment cell using a carbon working electrode, a platinum wire auxiliary electrode and a saturated calomel (SCE) or a Ag/AgCl reference electrode. The $E_{1/2}$ values for reversible couples were calculated from half the difference between E_p values for the cathodic and anodic waves. The catalytic tests were performed at 25 ± 1 °C. The pH values of aqueous solutions were buffered at an ionic strength of 0.25 mol L^{-1} by HNO_3 and $NaNO_3$ (pH 2.0), potassium hydrogen phthalate, HNO_3 and $NaNO_3$ (pH 3.0), potassium hydrogen phthalate, NaOH and $NaNO_3$ (pH 4.0–5.5), Na_2HPO_4 and NaH_2PO_4 (pH 6.0–8.0), $Na_2B_4O_7 \cdot 10H_2O$ and $NaNO_3$ (pH 9.0) and $Na_2B_4O_7 \cdot 10H_2O$ and NaOH (pH 10.0–10.8). Elemental analyses were performed using a CHNS-O CE Instruments Model EA 1110 elemental analyzer. Ruthenium analyses were performed with a Model V-85 B Braun ICP-AES-atomic emission spectrometer. EPR spectra of the solid complexes were recorded at room temperature on a Bruker EP 200D spectrometer. ^{1}H NMR spectra were obtained with a Bruker AC-80 spectrometer. Mass spectra were obtained with a Hewlett–Packard gas chromatograph/MS system 5988A.

2.3. Preparation of the ligand 4′-(4-tolyl)-2,2′:6′,2″-terpyridine (totpy)

The 4′-(4-tolyl)-2,2′:6′,2″-terpyridine ligand was prepared analogously to the literature procedure [24,25]; a 2:1 ratio of 2-acetylpyridine:*p*-tolualdehyde was used. The solid was recrystallized from ethanol to obtain 1.01 g (54%) of light green crystals, identified as 4′-(4-tolyl)-2,2′:6′,2″-terpyridine (totpy) (Fig. 1). ^{1}H NMR: m, 8.65–8.85 ($H_{3,3''}$; $H_{6,6''}$; $H_{3',5'}$); m, 7.80–8.00 ($2H_o$; $H_{4,4''}$); m, 7.35–7.45 ($2H_m$; $H_{5,5''}$); s, 2.47 ($-CH_3$). ESI MS: *m*/*z* 323.20. *Anal.* Calc. for $C_{22}H_{17}N_3$: C, 81.71; H, 5.30; N, 12.99. Found: C, 82.09; H, 5.28; N, 13.38%.

2.4. Preparation of the complexes

$[RuCl_3(totpy)]$ was prepared according to the literature procedure [1,2]. Yield: 85%. *Anal.* Calc. for $C_{22}H_{17}N_3Cl_3Ru$: C, 49.78; H, 3.23; N, 7.92. Found: C, 48.95; H, 3.28; N, 7.67%.

2.4.1. [Ru(L)(totpy)Cl](PF$_6$) (L = 1,2-bis(dimethylphosphino)ethane)

A mixture of $[RuCl_3(totpy)]$ (0.38 g, 0.71 mmol) and 1,2-bis(dimethylphosphino)ethane (0.15 g, 1.00 mmol) were heated to reflux, under a N_2 atmosphere, in 115 mL of 3:2 ethylene glycol:water in the presence of NEt_3 (0.5 mL) and LiCl (0.15 g, 3.55 mmol) for 2.5 h. The hot solution was filtered and 2.0 mL of a saturated aqueous solution of NH_4PF_6 was added to the filtrate. The resulting red-brown crystals were washed with cold water and dried under vacuum. The product was recrystallized by dissolution in acetone and precipitated by adding diethyl ether. Yield: 0.32 g (60%). The complex is pure enough to be used in the synthesis of the aqua complex described in Section 2.4.3.

2.4.2. [Ru(L′)(totpy)Cl](PF$_6$) (L′ = 1,2-bis(dichlorophosphino)ethane)

The complex was prepared analogously to that described in the above section, except that a 4:1 ratio of acetonitrile:water and *N*-ethylmorpholine (30 drops) were used. Yield: 0.40 g (68%). The complex is pure enough to be used in the synthesis of the aqua complex described in Section 2.4.4.

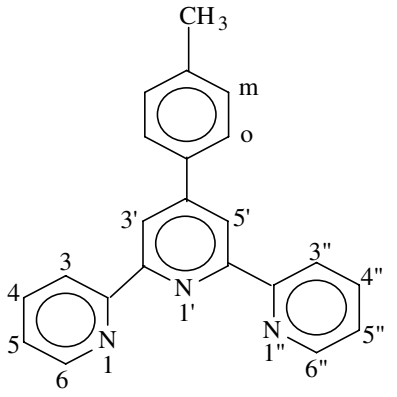

Fig. 1. 4′-(4-Tolyl)-2,2′:6′,2″-terpyridine (totpy).

2.4.3. [Ru(L)(totpy)(OH$_2$)](PF$_6$)$_2$ (L = 1,2-bis(dimethylphosphino)ethane) (**1**)

One hundred and seventy milligrams (0.23 mmol) of [Ru(L)(totpy)Cl](PF$_6$) and 0.07 g (0.27 mmol) of silver *p*-toluenesulfonate were heated to reflux in 46 mL of 1:1 acetone:water under a N_2 atmosphere for 1 h; the hot solution was filtered and 3.0 mL of a saturated aqueous solution of NH_4PF_6 was added to the filtrate. The volume was reduced to 20 mL in a rotatory evaporator. The brown crystals were collected by filtration, washed twice with cold water and dried under vacuum. The complex was reprecipitated twice from acetone–diethyl ether. Yield: 0.14 g (69%). *Anal.* Calc. for $C_{28}H_{35}N_3OP_4F_{12}Ru$: C, 39.11; H, 4.00; Ru, 11.47. Found: C, 39.44; H, 4.29; Ru, 11.46%.

2.4.4. [Ru(L′)(totpy)(OH$_2$)](PF$_6$)$_2$ (L′ = 1,2-bis(dichlorophosphino)ethane) (**2**)

The complex was prepared analogously to **1**, except that a 1:2 ratio of acetone:water was used. Yield: 0.10 g (43%). *Anal.* Calc. for $C_{24}H_{23}ON_3Cl_4P_4F_{12}Ru$: C, 29.90; H, 2.40; Cl, 14.7; Ru, 10.48. Found: C, 31.40; H, 2.39; Cl, 14.2; Ru, 10.27%.

2.5. Modified electrodes

2.5.1. Carbon paste electrodes

Carbon paste electrodes [7,20] containing 3:2 by weight of carbon powder: mineral oil were used for cyclic voltammetric studies. The modified electrodes contained 3:22 by weight of complex:paste. The carbon paste holder was constructed of a thick-walled Teflon tube with 0.3 cm i.d. A copper sleeve equipped with a copper wire plunger was mounted at the top of the Teflon tube. By rotating the sleeve, the plunger could be made to extrude a used paste layer which was sliced off to form a fresh paste surface.

2.5.2. Nafion® transparent ITO modified electrode [21–23]

Sixty microliters of Nafion® ethanolic solution (2.5%) was cast on the ITO electrode surface (effective area = 1.0 cm^2); the solvent was air evaporated at room temperature; the coated electrode was dipped in pure water for 1 h and then soaked in an aqueous solution of the complex (2.0 mmol L^{-1}) for 30 min.

3. Results and discussion

3.1. Spectroscopic and redox properties of the aqua complexes in solution

Fig. 2 shows the absorption spectrum of **1** in methylene chloride. Cyclic and differential pulse voltammograms of **2** in methylene chloride are shown in Fig. 3. Table 1 shows spectroscopic and redox data for the complexes. The aqua complexes have similar spectra. Both aqua complexes exhibit several very intense bands in the UV region, assignable to polypyridyl ligand $\pi \rightarrow \pi^*$ excitations; in the visible region the bands at $\lambda_{max} = 490$ nm ($\varepsilon =$

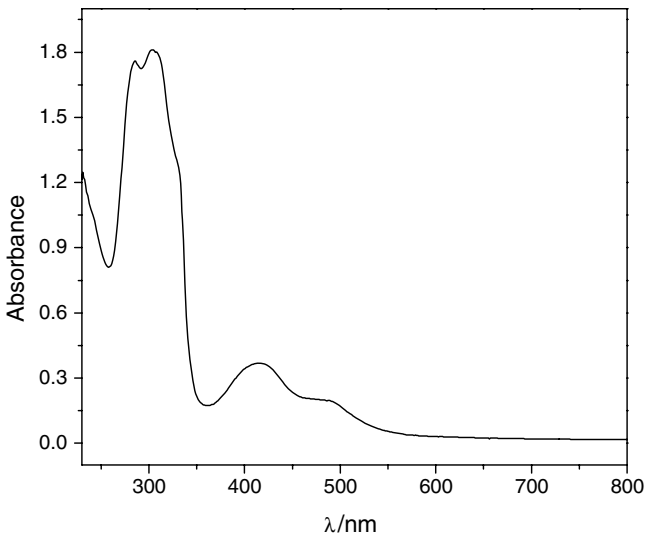

Fig. 2. UV–Vis spectrum of 1.0×10^{-4} mol L^{-1} [Ru(L)(totpy)(H$_2$O)](PF$_6$)$_2$ (**1**) (L = 1,2-bis(dimethylphosphino)ethane) in CH_2Cl_2.

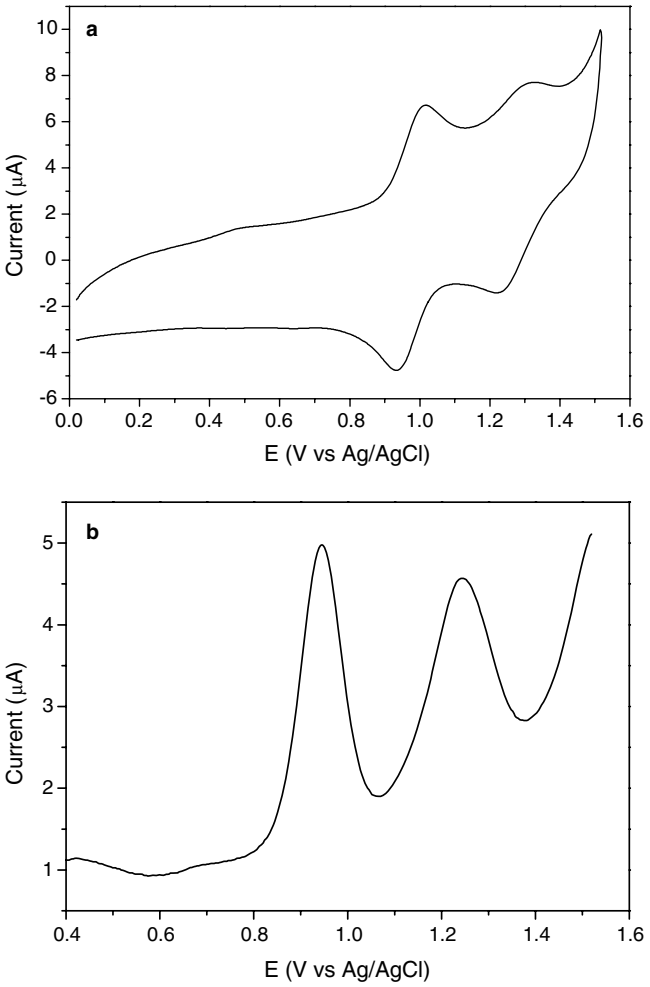

Fig. 3. (a) Cyclic voltammogram and (b) differential pulse voltammogram of 1.0×10^{-3}mol L^{-1} [Ru(L′)(totpy)(H$_2$O)](PF$_6$)$_2$ (**2**) (L′ = 1,2-bis(dichlorophosphino) ethane) in CH_2Cl_2 + 0.1 mol L^{-1} TBAP, glassy carbon working electrode; (a) $v = 100$ mV s^{-1}; (b) 10 mV s^{-1}.

Table 1
Electrochemical and spectral data for the complexes

Complexes	$E_{1/2}$ (V)		λ_{max}/nm ($\varepsilon_{max} \times 10^3$/mol^{-1} L cm^{-1})
	$Ru^{III/II}$	$Ru^{IV/III}$	
$[RuCl_3(totpy)]$	+0.05[a]		226 (17), 285 (16), 310 (13), 406 (4.7)[b]
$[Ru(L)(totpy)(H_2O)](PF_6)_2$ (**1**)	+0.85	+1.02[c]	285 (17), 305 (18), 414 (3.7), 490 (1.9)[e]
	+0.46	+0.66[d]	
$[Ru(L')(totpy)(H_2O)](PF_6)_2$ (**2**)	+0.96	+1.26[c]	285 (39), 310 (41), 475 (7.9)[e]
	+0.57	+0.77[d]	

[a] MeCN + 0.1 mol L^{-1} TBAP; glassy carbon working electrode; $v = 100$ mV s^{-1}.
[b] CH_3CN.
[c] CH_2Cl_2 + 0.1 mol L^{-1}; glassy carbon working electrode; $v = 100$ mV s^{-1}.
[d] In 7:3 phosphate buffer ($\mu = 0.20$ mol L^{-1}): *tert*-butyl alcohol solution, pH 6.8.
[e] CH_2Cl_2.

1.9×10^3 mol L^{-1} cm^{-1}) and 475 nm ($\varepsilon = 7.9 \times 10^3$ mol L^{-1} cm^{-1}) for **1** and **2**, respectively, can be attributed to metal-to-ligand $d\pi(Ru) \rightarrow \pi^*$ (diphosphine) transitions. One additional band is observed for **1** at 414 nm ($\varepsilon = 3.7 \times 10^3$ mol L^{-1} cm^{-1}) and can be attributed to metal-to-ligand $d\pi(Ru) \rightarrow \pi^*$ (polypyridyl) transitions [26]. For **1**, the MLCT band appears at higher wavelength; this reflects the electron-donation effect of the methyl substituents on the phosphine ligand, which destabilize the $d\pi(Ru)$ electrons, causing the $d\pi(Ru) \rightarrow \pi^*$ (diphosphine) transitions to occur at lower energy. On the other hand, for **2**, the MLCT band appears at higher energy, due to the electron-withdrawing effect of the chloro substituents on the phosphine ligand; similar effects were observed for a substituted bipyridine ligand [10]. It can be observed that the MLCT bands are shifted to higher energies upon substitution of the anionic chloride ligand for the neutral aqua ligand.

The cyclic voltammograms for both **1** and **2** in methylene chloride exhibit two reversible redox waves corresponding to the $Ru^{III/II}$ and $Ru^{IV/III}$ couples (0.85/1.02 and 0.96/1.26 V versus Ag/AgCl, respectively). The oxo-aqua ligands allow rapid proton transfer to be concomitant with electron transfer, permitting the accessibility of several oxidation states via gain or loss of protons (Scheme 1). The redox potentials of **1** are less positive, reflecting the electron-donation effect of the methyl substituents on the phosphine ligand. The observed potentials in methylene chloride are more positive than those obtained in aqueous solution (Table 1); for **2**, the separation between the two couples (mV) is larger than in water. This behavior can be due to a very slow deprotonation of the first oxidized species; the deprotonation of the aqua ligand to form Ru^{III}–OH is facilitated in aqueous solution but not in methylene chloride (low protic and polar solvent).

EPR spectra of ruthenium(III) complexes show *g* tensor values [27] that can be used to derive ground states. The

$$[\overset{II}{Ru}\text{-}OH_2]^{2+} \underset{+e,\,+H^+}{\overset{-e,\,-H^+}{\rightleftharpoons}} [\overset{III}{Ru}\text{-}OH]^{2+} \underset{+e,\,+H^+}{\overset{-e,\,-H^+}{\rightleftharpoons}} [\overset{IV}{Ru}{=}O]^{2+}$$

Scheme 1.

1 and **2** aqua complexes show no EPR signals, indicating the oxidation state Ru(II).

3.2. $E_{1/2}$ versus pH of the aqua complexes

The potentials of the $Ru^{IV/III}$ couple of **1** and the potentials of the $Ru^{III/II}$ couple of **2** vary with the pH of the solution, resulting in the $E_{1/2}$ versus pH variations shown in Fig. 4 for **2**. Within the $8.3 > pH > 2.0$ region, the plot for **1** is a straight line, with slope −0.062; for **2**, within the $9.6 > pH > 2.0$ region, the straight line has slope −0.059; the slopes are very close and coincident with the Nernstian prediction of −0.059 V/pH unit, indicative of one-electron oxidation accompanied by the dissociation of one proton [7,28] (Schemes 2 and 3).

For **1**, the potentials become pH independent at $pH > 8.3$, indicating that, in this region, $[Ru^{III}(L)(totpy)(O)]^+$ is the dominant species (Scheme 4).

The same behavior is shown for **2** at $pH > 9.6$; in this case $[Ru^{II}(L')(totpy)(OH)]^+$ is the dominant species (Scheme 5):

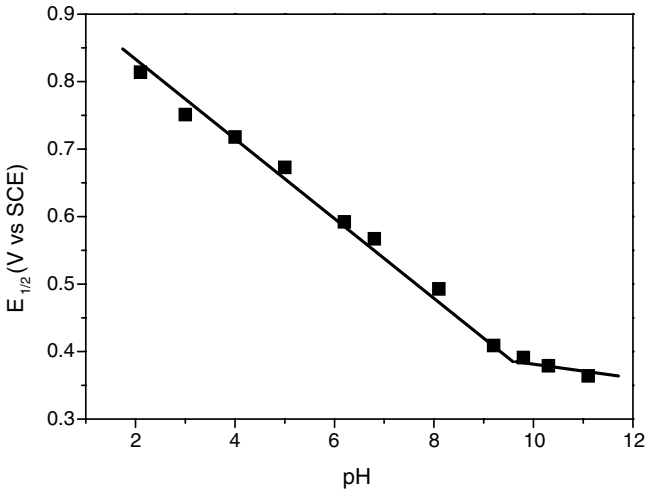

Fig. 4. Plot of $E_{1/2}$ vs. pH for the $Ru^{III/II}$ redox couple of $[Ru(L')(totpy)(H_2O)](PF_6)_2$ (**2**) (L′ = 1,2-bis(dichlorophosphino)ethane); glassy carbon working electrode.

$$[Ru^{III}(L)(totpy)(OH)]^{2+} \underset{+e^-,+H^+}{\overset{-e^-,-H^+}{\rightleftharpoons}} [Ru^{IV}(L)(totpy)(O)]^{2+}$$

Scheme 2.

$$[Ru^{II}(L')(totpy)(OH_2)]^{2+} \underset{+e^-,+H^+}{\overset{-e^-,-H^+}{\rightleftharpoons}} [Ru^{III}(L')(totpy)(OH)]^{2+}$$

Scheme 3.

$$[Ru^{III}(L)(totpy)(O)]^{+} \underset{+e^-}{\overset{-e^-}{\rightleftharpoons}} [Ru^{IV}(L)(totpy)(O)]^{2+}$$

Scheme 4.

3.3. Electrocatalytic oxidations of organic substrates in homogeneous solution

The catalytic activities of **1** and **2** for the oxidation of organic substrates were investigated by cyclic voltammetric experiments in 7:3 phosphate buffer (pH 6.8):*tert*-butyl alcohol solutions. Mixed solvent systems have been used by other groups for similar experiments with no adverse effects [12]. In the presence of a 50-fold excess of substrate, the cyclic voltammograms of **1** and **2** show an enhancement of the oxidation peaks and a decrease of the reduction peaks upon reversal potential scan. This is indicative of catalytic activity [7].

Catalytic tests can give the reactivity order for the electrooxidations: for **1**, benzyl alcohol > 1,4-butanediol > cyclohexanol > cyclohexene > ethylbenzene > 1,2-butanediol; for **2**, 1,4-butanediol > benzyl alcohol > cyclohexanol > cyclohexene > 1,2-butanediol > ethylbenzene. The oxidation products were identified in bulk electrolyses experiments using polypyridyl and phosphine ruthenium complexes described previously [6–10]: benzyl alcohol was oxidized to benzaldehyde and benzoic acid, 1-4 butanediol to δ-butyrolactone, 1-2-butanediol to 1-hydroxy-2-butanone, cyclohexanol to cyclohexanone, cyclohexene → 2-cyclohexen-1-one, and ethylbenzene to acetophenone. The proposed mechanism for oxidations using ruthenium oxo complexes suggests the formation, in the transition state, of an electron-deficient carbon [29]. A substituent can decrease the activation energy, inducing delocalization of the positive charge by hyperconjugation, inductive or resonance effects. In this way, the benzyl alcohol has a higher reactivity than cyclohexene: the resonance effect in the benzyl alcohol aromatic ring is responsible by positive charge delocalization; in cyclohexene, the allylic carbocation formed at C-3 before the water molecule attack (S_N2 reaction) induces a stabilization by resonance with a conjugated unsaturation at the carbon ring. Nevertheless, as cyclohexene has fewer canonic structures than benzyl alcohol, the lower positive charge delocalization decreases the reactivity. The higher reactivity of a primary alcohol compared to a secondary one was also observed in homogeneous catalysis by using $[Ru(tpy)(bpy)(H_2O)]^{2+}$ [8].

A generalization can be made: benzyl alcohol and 1,4-butanediol are more reactive than cyclohexanol; cyclohexene has an intermediate reactivity; ethylbenzene and 1,2-butanediol have the lowest reactivities.

$$[Ru^{II}(L')(totpy)(OH)]^{+} \underset{+e^-}{\overset{-e^-}{\rightleftharpoons}} [Ru^{III}(L')(totpy)(OH)]^{2+}$$

Scheme 5.

3.4. Electrocatalytic oxidation of organic substrates at a carbon paste electrode (CPE) containing *1* and *2*

The cyclic voltammetric behavior of the CPE containing **1** and **2** in 7:3 phosphate buffer (pH 6.8):*tert*-butyl alcohol solutions, in the presence of benzyl alcohol, cyclohexanol, 1,4-butanediol, 1,2-butanediol and ethylbenzene shows pronounced enhancement of the anodic currents. The observed reactivity order for **1** is benzyl alcohol > cyclohexanol > 1,4-butanediol > 1,2-butanediol > cyclohexene > ethylbenzene and for **2** is benzyl alcohol > ethylbenzene > cyclohexanol > 1,4-butanediol cyclohexene > 1,2-butanediol. The reactivities of CPE containing **1** and **2** were somewhat different from those of homogeneous catalysis; surprisingly, high reactivity in the oxidation of ethylbenzene by **2** was observed. Higher reactivity of the primary alcohol was also observed in homogeneous catalysis by using **1** and **2**. The high reactivity of benzyl alcohol can be due to its higher permeability into the active surface of the carbon paste electrode.

For quantitative evaluation of the electrocatalysis surface, the dependence of the peak height on the benzyl alcohol concentration and on the potential scan rate was studied [30]. The peak height was linearly dependent (Fig. 5) (correlation coefficient 0.998, with plot intercept near zero) on the concentration of benzyl alcohol, indicating that the electrocatalysis is *pseudo-first-oder* in this

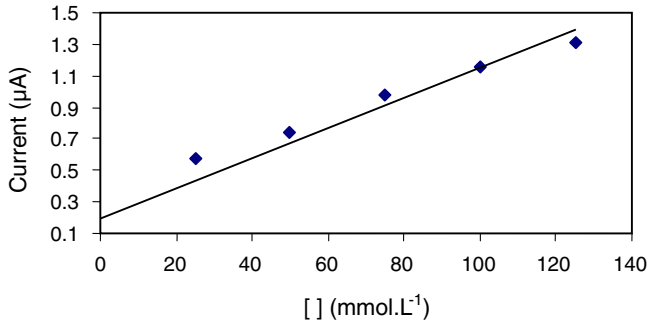

Fig. 5. Plot of the oxidation peak currents of the CPE containing $[Ru(L)(totpy)(H_2O)](PF_6)_2$ (**1**) (L = 1,2-bis(dimethylphosphino)ethane) against benzyl alcohol concentrations; in 7:3 phosphate buffer (pH 6.8):*tert*-butyl alcohol solution, $v = 100\ mV\ s^{-1}$.

benzyl alcohol concentration range. The anodic peak currents change linearly with the square root of the scan rate; this is characteristic of surface electrocatalysis with the catalyst confined to the electrode surface under diffusion control of the substrates.

3.5. Electrocatalytic oxidation of organic substrates at a ITO/Nafion®/complex electrode

The cyclic voltammogram of **1** in the ITO/Nafion® transparent electrode shows the $Ru^{IV/III}$ redox couple only ($E_{1/2} = +0.74$ V versus SCE). This is probably due to the sluggishness of the $Ru^{III/II}$ couple observed in modified electrodes [18b].

The reactivity of $Ru^{IV}{=}O^{2+}$ complexes has been explored with ITO electrodes [31]. The cyclic voltammogram in the presence of 50 mmol L^{-1} of benzyl alcohol shows a decrease of the anodic current, as a consequence of the dissolution of the aqua complex adsorbed in the Nafion® polymer film. The dissolution of the aqua complex is clearly noticed when the solution changes from colorless to yellow. Therefore, benzyl alcohol being a polar substrate can dissolve the Nafion® film. When the substrate is cyclohexene, that which has a low polarity, the catalytic activity is noticed by the significant increase of the anodic current and the decrease of the cathodic current (Fig. 6).

The dependence of the anodic peak current with scan rate was studied from 50 to 500 mV s^{-1}, in the presence cyclohexene (Fig. 7(a)). The plot of I_{pa} versus $v^{1/2}$ (Fig. 7(b)) shows that the anodic peak current varies linearly with the square root of the scan rate (correlation coefficient 0.998), indicating that the reaction is also controlled by diffusion of the substrate [7].

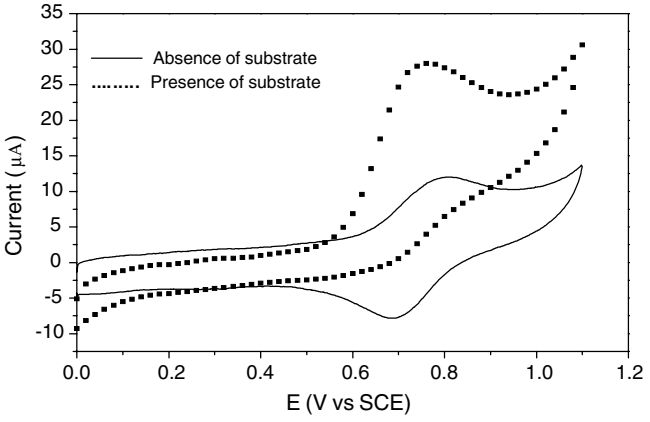

Fig. 6. Cyclic voltammograms of ITO electrode, modified by Nafion® containing $[Ru(L)(totpy)(H_2O)](PF_6)_2$ (**1**) (L = 1,2-bis(dimethylphosphino)ethane) in 4:1 $HNO_3/NaNO_3$ buffer (pH 2.3):*tert*-butyl alcohol solution (——), and in the presence of 50 mmol L^{-1} of cyclohexene (■■■), $v = 100$ mV s^{-1}.

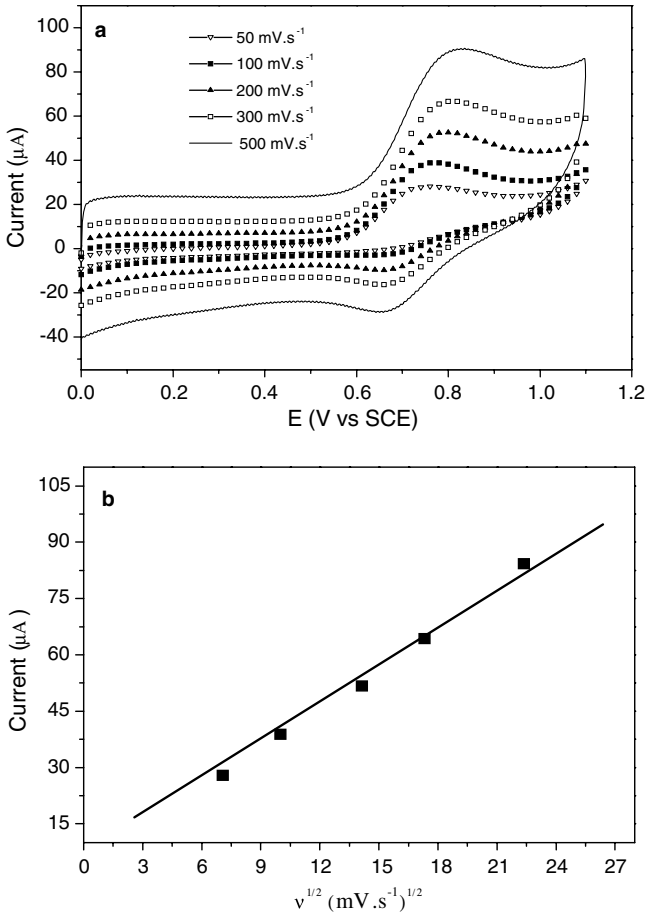

Fig. 7. (a) Cyclic voltammograms of ITO electrode, modified by Nafion® containing $[Ru(L)(totpy)(OH_2)](PF_6)_2$ (**1**) (L = 1,2-bis(dimethylphosphino)ethane), in 4:1 $HNO_3/NaNO_3$ buffer (pH 2.3):*tert*-butyl alcohol solution, in the presence of 50 mmol L^{-1} of cyclohexene, several scan rates. (b) Plot I_{pa} vs. $v^{1/2}$.

4. Conclusions

The results obtained in this work show that the complexes $[Ru(L)(totpy)(OH_2)](PF_6)_2$ (L = 1,2-bis(dimethylphosphino)ethane) (**1**) and $[Ru(L')(totpy)(OH_2)](PF_6)_2$ (L′ = 1,2-bis(dichlorophosphino)ethane) (**2**) can be used in electrooxidations of organic substrates containing different functional groups. The phosphine–ruthenium(IV)-oxo complexes have the advantage of being mild oxidants, since more powerful oxidants usually cause undesirable side reactions.

The preparations of carbon paste and ITO/Nafion® electrodes are simple and straightforward and the characteristics of the mediators are preserved upon transfer from solution to the immobilized state.

Acknowledgements

The authors thank Fundação de Amparo a Pesquisa do Estado de São Paulo (FAPESP) for financial support.

References

[1] J.P. Santos, M.E.D. Zaniquelli, C. Batalini, W.F. De Giovani, J. Phys. Chem. B 105 (2001) 1780.
[2] J.P. Santos, M.E.D. Zaniquelli, C. Batalini, W.F. De Giovani, Thin Solid Films 349 (1999) 238.
[3] (a) C.A. Bessel, P. Aggarwal, A.C. Marschilok, K.J. Takeuchi, Chem. Rev. 101 (2001) 1031;
(b) T.J. Meyer, H.V. Huynh, Inorg. Chem. 42 (2003) 8140.
[4] M.E. Marmion, K.J. Takeuchi, J. Am. Chem. Soc. 110 (1988) 1472.
[5] J.G. Muller, J.H. Acquaye, K.J. Takeuchi, Inorg. Chem. 31 (1992) 4552.
[6] M. Navarro, W.F. De Giovani, J.R. Romero, J. Mol. Catal. A 135 (1998) 249.
[7] E.C. Lima, P.G. Fenga, J.R. Romero, W.F. De Giovani, Polyhedron 17 (1998) 313.
[8] M. Navarro, W.F. De Giovani, J.R. Romero, Synth. Commun. 20 (1990) 399.
[9] J.M. Madurro, G. Chiericato Jr., W.F. De Giovani, J.R. Romero, Tetrahedron Lett. 29 (1988) 765.
[10] M. Navarro, S.E. Galembeck, J.R. Romero, W.F. De Giovani, Polyhedron 15 (9) (1996) 1531.
[11] (a) E.L. Lebeau, T.J. Meyer, Inorg. Chem. 38 (1999) 2174;
(b) L.K. Stultz, M.H.V. Huynh, R.A. Binstead, M. Curry, T.J. Meyer, J. Am. Chem. Soc. 122 (2000) 5984.
[12] (a) V.J. Catalano, R.A. Heck, A. Öhman, M.G. Hill, Polyhedron 19 (2000) 1049;
(b) V.J. Catalano, R. Kurtaran, R.A. Heck, A. Öhman, M.G. Hill, Inorg. Chim. Acta 286 (1999) 181.
[13] A. Llobet, Inorg. Chim. Acta 221 (1994) 125.
[14] J.M. Mayer, Acc. Chem. Res. 31 (1998) 441.
[15] S.A. Trammell, J.C. Wimbish, F. Odobel, L.A. Gallagher, P.M. Narula, T.J. Meyer, J. Am. Chem. Soc. 120 (1998) 13248.
[16] B.A. Moyer, B.K. Sipe, T.J. Meyer, Inorg. Chem. 20 (1981) 1475.
[17] L.A. Gallagher, T.J. Meyer, J. Am. Chem. Soc. 123 (2001) 5308.
[18] (a) W.F. De Giovani, A. Deronzier, J. Electroanal. Chem. 337 (1992) 285;
(b) W.F. De Giovani, A. Deronzier, J. Chem. Soc., Chem. Commun. (1992) 1461.
[19] M. Rodríguez, I. Romero, C. Senz, A. Llobet, A. Deronzier, Electrochim. Acta 48 (2003) 1047.
[20] (a) F. Tobalina, F. Pariente, L. Hernández, H.D. Abruña, E. Lorenzo, Anal. Chim. Acta 395 (1999) 17;
(b) W.J. Vining, T.J. Meyer, J. Electroanal. Chem. 237 (1987) 191.
[21] M. Yagi, M. Kaneko, Chem. Rev. 101 (2001) 21.
[22] M. Yagi, M. Kasamastu, M. Kaneko, J. Mol. Catal. A 151 (2000) 29.
[23] M. Shi, F.C. Anson, Lagmuir 12 (1996) 2068.
[24] C. Chamchoumis, P.G. Potvin, Chem. Res. (S) (1998) 180.
[25] E.C. Constable, P. Harverson, D.R. Smith, L.A. Whall, Tetrahedron 50 (1994) 7799.
[26] A. Dovletoglou, S.A. Adeyemi, T.J. Meyer, Inorg. Chem. 35 (1996) 4120.
[27] H.A.S. Silva, R.M. Carlos, A.J. Camargo, C.M.C. Picchi, R.H.A. Santos, B.R. McGarvey, D.W. Franco, Inorg. Chim. Acta 357 (2004) 3147.
[28] K.J. Takeuchi, M.S. Thompson, D.W. Pipes, T.J. Meyer, Inorg. Chem. 23 (1984) 1845.
[29] M.S. Thompson, T.J. Meyer, J. Am. Chem. Soc. 104 (1982) 4106.
[30] W. Kutner, J.A. Gilbert, A. Tomaszewski, T.J. Meyer, R.W. Murray, J. Electroanal. Chem. 205 (1986) 185.
[31] M. Navarro, M.N. Collomb, A. Deronzier, J. Electroanal. Chem. 520 (2002) 150.

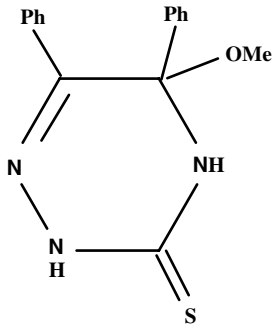

Scheme 1. Drawing of LH_2OCH_3.

particular ligand can show different coordination behaviour, as we have established in previous works [14]. In fact, we have characterized complexes of the title ligand acting as bidentate NS giving monomeric complexes with some organotin (IV) derivatives [15], as well as with nickel and cobalt salts. With other metals, as cadmium, acts also as bidentate bridging via the sulphur atom, giving dinuclear structures [16].

The most usual type of coordination in compounds of Hg(II) is a distorted octahedron with two bonds much shorter than the other four. In extreme, this results in a linear-2 coordination in which case bonds are largely covalent. This situation usually takes place with S-donor ligands. The complexes [Hg(5-CF_3-pyS_2)] and [Hg(5-CF_3-MepyS_2)] are examples of this type of coordination, where the Hg(II) ion is bonded to two ligands via the sulphur atoms, giving a linear SS disposition [17,18].

The aim of this work is the synthesis and characterization of mercury complexes derived of 5-methoxy-5,6-diphenyl-4,5-dihydro-2H-[1,2,4]triazine-3-thione LH_2OCH_3 (Scheme 1), in order to get new complexes and to explore their potential capability as modifiers of a carbon paste electrode for mercury determination and kinetic speciation in water samples. In this paper, we report the synthesis and structural characterisation of two mercury compounds with this cyclic ligand. In both complexes, and induced by the metal structural preferences, the triazine acts as monodentate through the sulphur atom, behaviour that has not been observed previously.

2. Experimental

2.1. Physical measurements

IR spectra in the 4000–400 cm^{-1} range were recorded as KBr pellets on a Jasco FT/IR-410 spectrophotometer. ^1H and ^{13}C NMR spectra were recorded on a spectrophotometer Bruker AMX-300 using $CDCl_3$ and DMSO-d_6 as solvents and TMS as reference. Fast atom bombardment (FAB) mass spectra were recorded on a VG Auto Spec instrument using Cs as the fast atom and *m*-nitrobenzilalcohol (*m*NBA) as the matrix. Conductivity data were measured using freshly prepared DMF solutions (ca. 10^{-3} M) at 25 °C with a Metrohm Herisau model E-518 instrument. Electrochemical measurements were performed with a BAS CV 27 voltammograph and a BAS A-4 XY register using a glassy carbon (∅ 5 mm) as working electrode, a platinum wire as auxiliary, and a double junction, with porous ceramic wick, Ag/AgCl as reference electrode, standardized for the redox couple ferricinium/ferrocene ($E_{1/2} = +0.400$ V, $\Delta E_p = 60$ mV). Cyclic voltammetry studies of LH_2OCH_3 and complexes were carried out on 0.01 M solutions in dimethylformamide containing 0.1 M [NBu_4][PF_6] as supporting electrolyte. The range of potential studied was between +1.0 and −2.2 V. All solutions were purged with nitrogen steam for 5 min before measurement and the working electrode was polished before each experiment with diamond paste. The procedure was performed at room temperature and nitrogen atmosphere was maintained over the solution during the measurements.

2.2. Crystallography

Crystals were mounted on a glass fibre and transferred to a Bruker SMART 6K CCD area-detector three-circle diffractometer with a MAC Science Co., Ltd. Rotating Anode (Cu Kα radiation, $\lambda = 1.54178$ Å) generator equipped with Goebel mirrors at settings of 50 kV and 110 mA. X-ray data were collected with a combination of six runs at different φ and 2θ angles, 3600 frames. The data were collected using 0.3° wide ω scans and crystal-to-detector distance of 4.0 cm. Empirical absorption corrections (SADABS) [19] were applied using multiple measurements of symmetry-equivalent reflections (ratio of minimum to maximum apparent transmission: 0.373482 for complex **1** and 0.556564 for complex **2**). The unit cell parameters were obtained by full-matrix least-squares refinements of 5528 and 7730 reflections for complexes **1** and **2**, respectively. The raw intensity data frames were integrated with the SAINT [20] program, which also applied corrections for Lorentz and polarization effects. The software package SHELXTL [21] version 6.10 was used for space group determination, structure solution and refinement. The space group determination was based on a check of the Laue symmetry and systematic absences and was confirmed using the structure solution. The structure was solved by direct methods (SHELXS-97) [22], completed with difference Fourier syntheses, and refined with full-matrix least squares using SHELXL-97 [23] minimizing $\omega(F_o^2 - F_c^2)^2$. Weighted R factors (R_w) and all goodness of fit (S) are based on F^2; conventional R factors (R) are based on F. All non-hydrogen atoms were refined with anisotropic displacement parameters. All scattering factors and anomalous dispersions factors are contained in the SHELXTL [24] 6.10 program library. H atoms were found in a difference map, but were then positioned geometrically and included as riding, with C–H = 0.95 and 0.99 Å, and $U_{iso}(H) = 1.2\,U_{eq}(C)$. The coordinates were refined as riding on the parent atom and the occupancy and U_{ij} were fixed.

2.3. Syntheses

All reagents and other solvents were obtained from standard commercial sources and were used as received.

2.4. 5-Methoxy-5,6-diphenyl-4,5-dihydro-2H-[1,2,4]triazine-3-thione, LH_2OCH_3

The characterisation of the ligand LH_2OCH_3 was previously published [24], although it was synthesised according to a modified procedure [25].

Selected spectroscopic data: IR (KBr, cm^{-1}): 3184s and 3131s (NH), 1608w (C=N), 1550s (NCS), 846w (CS). ^1H NMR (300 MHz, $CDCl_3$, 25 °C): 3.4 (s, 3H, OCH_3), 6.9 (d, 1H, NH), 7.1–7.3 (m, 6H, Ph), 7.4 (m, 2H, Ph), 7.6 (m, 2H, Ph), 9.5 (d, 1H, NH), ^{13}C NMR (300 MHz, $CDCl_3$, 25 °C): 169.7 (CS), 142.4 (CN), 141.7, 133.7, 129.3, 126.5, (Ph), 83.2 (CR_4), 50.7 (CH_3O).

2.5. [HgL_2] (**1**)

This complex was prepared as previously reported [26].

M.p. 218 °C (D). Λ_M (DMF, $\Omega^{-1}\,cm^2\,ml^{-1}$): 25. *m/z* ($FAB^+$): 731 ($[HgL_2+1]^+$, 30%). Selected spectroscopic data: IR (KBr, cm^{-1}): 1601w, 1581w (C=N), 1491s (NCS), 815w (CS). ^1H NMR (300 MHz, DMSO, 25 °C): 7.4–7.1 (m, Ph). ^{13}C NMR (300 MHz, DMSO-d_6, 25 °C): 174.7 (CS), 154.3, 153.2 (CN), 135.2, 134.4, 130.9, 129.5, 129.4, 129.0, 128.6, 128.1 (Ph). Single crystals of complex **1** suitable for X-ray analysis, were grown by slow evaporation of a solution of the complex in acetonitrile.

2.6. [HgMeL] (**2**)

Over a solution of LH_2OCH_3 (0.32 g, 1.1 mmol) and $LiOH\cdot H_2O$ (0.05 g, 1.1 mmol) in 50 ml of methanol was drop wise added a solution of HgMeCl (0.27 g, 1.1 mmol) in the same solvent. The solution was stirred at room temperature for 6 h. Then it was evaporated until a yellow solid appeared, which was filtered off and vacuum dried. Yield 73%. m.p 140 °C. Λ_M (DMF, $\Omega^{-1}\,cm^2\,ml^{-1}$): 9. *m/z* (FAB+): 482.0 ($[HgMeL+1]^+$, 100%). 696.0 ($[Hg_2MeL+1]^+$, 30%), 945 ($[Hg_2Me_2L_2]^+$, 4%), 961.1 ($[Hg_2Me_2L_2]^+$, 2%). IR (KBr, cm^{-1}): 1598w, 1578w (C=N), 1483s (NCS), 816w (CS). ^1H NMR (300 MHz, DMSO-d_6, 25 °C): 7.3–7.5 (m, 10H, Ph), 0.89 (s, 3H, CH_3, $J^2(^{199}Hg–^1H) = 186$ Hz). ^{13}C NMR (300 MHz, DMSO-d_6, 25 °C): 176.5 (CS), 154.6, 153.1 (CN), 135.6, 135.4, 130.7, 129.6, 129.2, 129.1, 128.6, 128.5 (Ph), 9.4 (CH_3). Single crystals suitable for X-ray analysis were obtained by slow evaporation of a solution of the complex in DMF.

3. Results and discussion

In the synthesis of both complexes takes place the loss of the methoxy group as a methanol molecule, probably due to acid–base reaction with the relatively high acidic N–H bond, yielding LH, according to a mechanism previously published. Reaction with mercury nitrate does not need the presence of lithium hydroxide, which is necessary in the reactions studied with other metal salts [15,16].

Conductivity measurements in DMF indicate the presence of non-ionic species in this solvent [27]. The mass spectrometry indicates the different mercury/ligand ratio. Mass spectrum of complex **1** shows a peak corresponding to $[HgL_2+1]^+$, which indicates the presence of a specie containing one mercury ion and two deprotonated ligands. However, mass spectrum of complex **2** shows a peak at 482.0 amu, which is attributed to $[HgMeL+1]^+$ and corresponds to the molecular ion. The other peaks observed are probably due to molecular associations produced during the experiment.

The X-ray analysis shows that the crystal structure of complex **1** is made up of discrete centrosymmetric molecules of [HgL_2] (Fig. 1), which agrees with the spectroscopic data, but rules out the structure previously proposed for this complex [26]. The mercury atom is bonded to two sulphur atoms of two thiosemicarbazone ligands in a linear disposition (S–Hg–S = 180.0°). Complex **2** consists of [HgMeL] entities (Fig. 2), where the mercury is also in a linear disposition, bonded to the sulphur atom of a triazine ligand and the methyl group (S–Hg–C = 175.7°). Crystallographic data and selected bond distances and angles are given in Tables 1–3.

In both complexes, the triazine rings can be considered planar with a maximum deviation of 0.0498 Å for C(3) in complex **1** and 0.0571 Å for C(1) in complex **2**. The sulphur atom is 0.260 Å above this plane in complex **1** and 0.3385 Å under in complex **2**. The mercury atom is 0.5938 Å above this plane and 0.2791 Å under in complexes **1** and **2**, respectively. The aromatic rings form with respect to this plane dihedral angles of 44.9° for C(10)–C(15) and 36.95° for C(4)–C(9) in complex **1** and 47.22° and 31.92°, respectively, in complex **2**. An important change is observed with respect to LH_2OCH_3, where the dihedral angles are 95.07° and 36.94°, respectively, [24]. This change in one of the phenyl rings could be explained by the loss of the methoxy group, although it also could be attributed to crystal packing. Owing to deprotonation, there is a considerable electronic delocalisation through the thiosemicarbazone backbone, which is slightly larger in complex **2**. As a consequence all the C–N bonds have almost the same length, which does not occur in LH_2OCH_3 (1.28–1.459 Å). In the complexes, the thione bonds distances (1.755 and 1.763 Å for complexes **1** and **2**) are longer than in the precursor ligand (1.628 Å) and they are closer to the value expected for a single bond (1.82 Å) [28]. In addition the N(3)–C(2)–C(3) angles are close to 120°, as would be expected for sp^2 hybridisation, while in LH_2OCH_3 is 108°, corresponding to sp^3 hybridisation.

Although there is no covalent bond between the mercury atom and N(1) in complex **1** and N(3) in complex **2**, there is some interaction, because N–Hg distances are

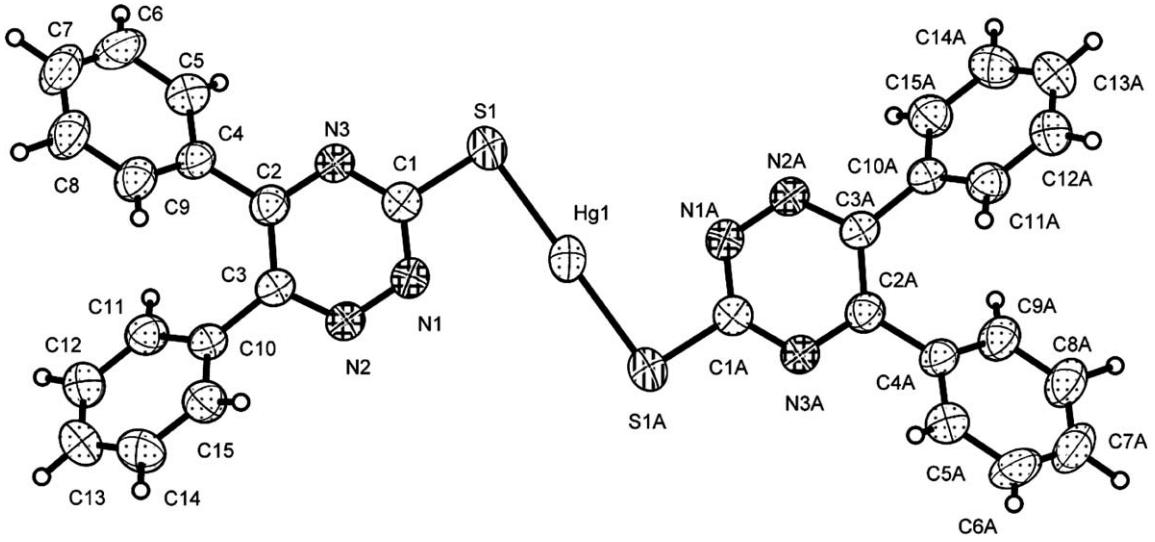

Fig. 1. Molecular structure of complex [HgL_2] **1**. Thermal ellipsoids are shown at 50% probability.

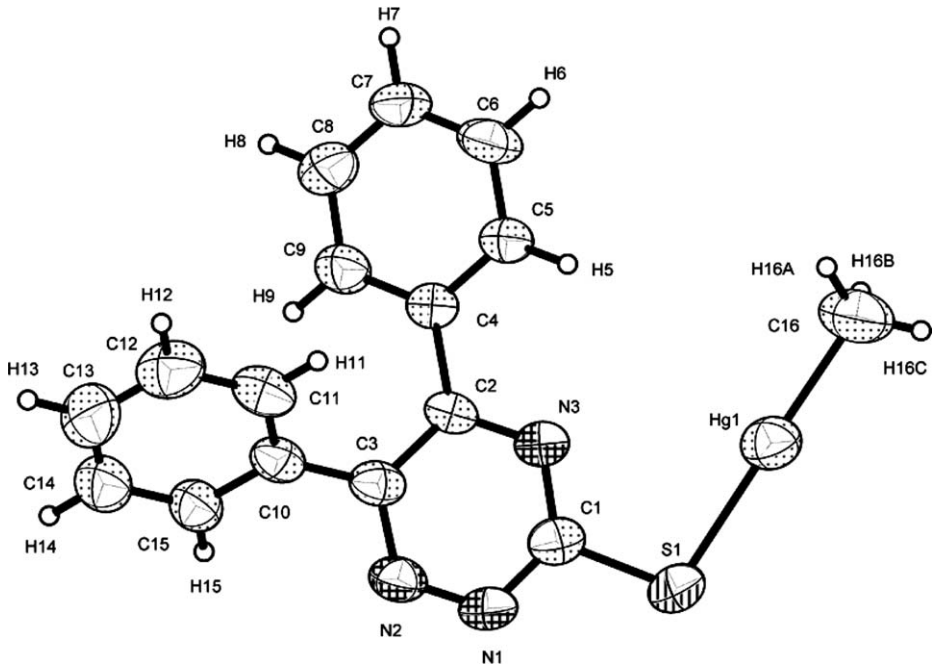

Fig. 2. Molecular structure of complex [HgMeL] **2**. Thermal ellipsoids are shown at 50% probability.

2.806 and 3.146 Å, respectively, which are larger than the sum of the covalent radii (2.25 Å), but shorter than the sum of the Van der Waals radii (3.23 Å). Some authors assume that if the Hg–N distance is lower than the sum of the Van der Waals radii there is covalent bond [29]. The non-existence of a Hg–N bond in both complexes is supported by the S–Hg–S angle, which is perfectly linear. If the mercury ion would have to accommodate an additional bond with the nitrogen atom, there must be a change in the sp hybridisation, which will be reflected in a deviation of the angle [13].

There are π–π interactions between the phenyl rings, with a distance of 3.817 Å in complex **1** and 3.846 Å in complex **2**.

The crystal structure of complex **1** belongs to the monoclinic system. In the crystal packing the mercury atoms are placed in the eight corners and in the middle of a cube, giving a body-centred cubic packing.

The absence of any band in the 2600-cm^{-1} region in the IR spectra of both complexes suggests the absence of any thiol tautomer [30]. In the spectra, there are no bands in the 3000–3300-cm^{-1} region, which indicates the absence of N–H bonds. Moreover bands attributable to the nitrate group in complex **1** are not observed [31]. The absence of these bands confirms that the ligand acts as a monoanion L in this complex. The band corresponding to the CS moiety is shifted to lower frequencies, indicating coordination of the sulphur to the metal ion. The presence of two bands

Table 1
Crystal data and structure refinement for complexes **1** and **2**

	1	**2**
Formula	$C_{30}H_{20}N_6S_2Hg$	$C_{16}H_{13}N_3SHg$
M	729.23	479.94
Crystal system	monoclinic	orthorhombic
Space group	$P2(1)/n$	$P2(1)2(1)2(1)$
a (Å)	10.3574(2)	5.9923(10)
b (Å)	11.5451(2)	14.0288(3)
c (Å)	11.5016(3)	18.5810(3)
α (°)	90	90
β (°)	98.9730(10)	90
γ (°)	90	90
U (Å^3)	1358.50(5)	1562.01(5)
Z	2	4
D_{calc} (Mgm^{-3})	1.783	2041
Absorption coefficient (mm^{-1})	11.850	18.882
$F(000)$	708	904
Goodness-of-fit on F^2	1.002	1.064
Reflections collected	8487	9395
Independent reflections [R_{int}]	2469 [0.0443]	2872 [0.0539]
Completeness to $\theta = 70.53°$ (%)	95.1	96.9
Absorption correction	SADABS v. 2.03	SADABS v. 2.03
Refinement method	full-matrix least-squares on F^2	full-matrix least-squares on F^2
Final R_1 and wR_2 [$I > 2\sigma(I)$]	$R_1 = 0.0286$, $wR_2 = 0.0719$	$R_1 = 0.0316$, $wR_2 = 0.0783$
R indices (all data)	$R_1 = 0.0346$, $wR_2 = 0.0756$	$R_1 = 0.0335$, $wR_2 = 0.0800$

Table 2
Selected bond distances (Å) for complexes [HgL_2] **1** and [HgMeL] **2**

	[HgL_2] **1**	[HgMeL] **2**
Hg(1)–S(1)	2.3362(10)	2.3703(16)
Hg(1)–C(16)		2.086(8)
N(1)–N(2)	1.334(4)	1.335(8)
N(1)–C(1)	1.336(4)	1.312(9)
N(2)–C(3)	1.338(4)	1.343(7)
N(3)–C(1)	1.326(4)	1.341(7)
N(3)–C(2)	1.334(4)	1.326(8)
S(1)–C(1)	1.755(3)	1.763(7)
C(2)–C(3)	1.413(4)	1.430(8)

Table 3
Selected angles (°) for complexes [HgL_2] **1** and [HgMeL] **2**

	[HgL_2] **1**	[HgMeL] **2**
N(2)–N(1)–C(1)	118.1(3)	117.5(5)
N(1)–N(2)–C(3)	119.6(3)	120.5(5)
C(1)–N(3)–C(2)	116.5(3)	117.1(5)
N(3)–C(1)–N(1)	125.6(3)	125.9(6)
N(3)–C(1)–S(1)	116.6(2)	119.9(5)
N(1)–C(1)–S(1)	117.8(2)	114.2(4)
N(3)–C(2)–C(3)	119.6(3)	118.6(5)
N(3)–C(2)–C(4)	115.8(3)	117.6(5)
C(3)–C(2)–C(4)	124.6(3)	123.8(5)
N(2)–C(3)–C(2)	119.8(3)	119.1(6)
N(2)–C(3)–C(10)	115.2(3)	115.9(5)
C(2)–C(3)–C(10)	125.1(3)	125.0(5)
C(1)–S(1)–Hg(1)	94.01(11)	102.0(2)
S(1)#1–Hg(1)–S(1)	180.00(2)	
C(16)–Hg(1)–S(1)		175.7(3)

attributable to C=N bonds could indicate the formation of a new imine group, due to the loss of the methoxy group of the ligand LH_2OCH_3, although the great electronic delocalisation in the ring probably leads to there being only one C=N band and the new band could be due to the hydrazinic CN. These imine nitrogen atoms are non-coordinate to the metal ion.

The ^{1}H NMR spectra of both complexes show a multiplet in the aromatic region, corresponding to the phenyl rings of the ligand. In complex **2** a signal at 0.89 ppm, corresponding to the CH_3 group, can also be observed. The absence of any signal corresponding to amine protons supports the ligand deprotonation. The absence of the singlet attributable to the methoxy group at 3.4 ppm confirms the loss of the inserted methoxy group. In the spectrum of complex **2**, the singlet corresponding to the methyl group shows the satellites corresponding to the coupling with the mercury ion with $J^2 = 186$ Hz.

In the ^{13}C NMR spectra the signals corresponding to the methoxy group (50.7 ppm) and the tetrasubstituted carbon atom (83.2 ppm) of LH_2OCH_3 have disappeared and a new signal corresponding to an imine group is observed. The imine groups are not bonded to the metal ion, as the X-ray diffraction has established for complexes **1** and **2**. In addition the signal corresponding to the thione group is deshielded, suggesting the presence of metal–sulphur bonds. In complex **2**, the signal of the methyl group bonded to the mercury atom appears at 9.4 ppm.

Cyclic voltammetry of the ligand LH_2OCH_3 and complex **1** have been previously published [26]. Complex **1** shows a reversible redox couple at $E_{1/2} = -0.492$ V. On scanning from +1.0 to −2.2 V cyclic voltammogram of complex **2** shows a redox couple at $E_{1/2} = -0.275$ V, corresponding to a Hg(II)/Hg(I) process (Fig. 3) and two irreversible cathodic peaks corresponding to ligand reduction processes at −1.325 and −1.825 V. Analysis of the redox couple in the interval 25–800 mV s^{-1} shows a lineal variation of i_{pc} versus

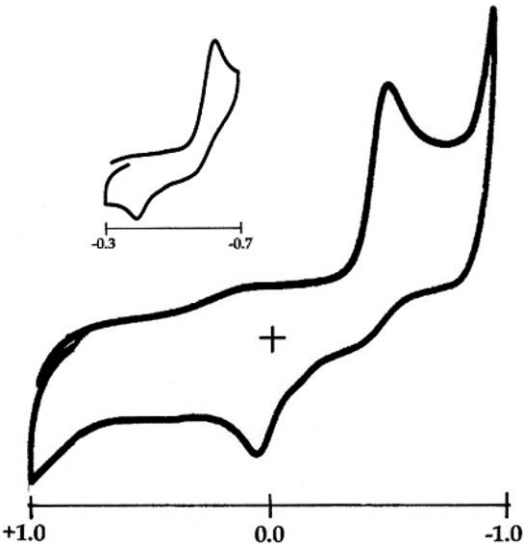

Fig. 3. Cyclic voltammogram of complex [HgMeL] **2** in DMF; $v = 100$ mV/s. Inset the redox couple.

$v^{1/2}$. Small dependence of the potential peak with the scan rate is observed, and the i_{pa}/i_{pc} ratio is close to the unity. These results suggest a diffusion controlled quasirreversible process [32]. The reduction process Hg(II)/Hg(I) is more difficult in complex **1**, where the mercury atom is bonded to two sulphur atoms due to the fact that electronic density over the metal ion is bigger than when the environment is formed by one sulphur and one carbon atom, as occurs in complex **2**.

4. Conclusions

Reactions of the ligand LH_2OCH_3 with two mercury salts lead to the formation of the corresponding coordination compounds, where the ligand has lost the methoxy group and acts as a monoanion. The methylmercury derivative is only obtained in the presence of basic medium.

In both complexes the ligand acts as monodentate and binds to the mercury ion through the sulphur atom, giving a linear disposition around the metal. This coordination mode is usually observed in mercury complexes, although coordination only via the sulphur atom is not frequent in triazines and it is observed for the first time in this particular ligand.

The results obtained confer good prospects for compound **2** to be used to prepare new sensors for the highly toxic $HgMe^+$ ion. Development of these sensors is very important due to alkyl mercury derivatives are great environmental pollutants and could affect food and soils (some compounds are used as pesticides in the treatment of seeds and can be introduced in natural waters).

5. Supplementary material

CCDC 256950 for complex **1** and 269350 for complex **2** contain the supplementary crystallographic data for this paper. These data can be obtained free of charge at www.ccdc.cam.ac.uk/conts/retrieving.html [or from the Cambridge Crystallographic Data Centre, 12 Union Road, Cambridge, CB2 1EZ, UK, fax: +44 1223 366 033, e-mail: deposit@ccdc.ac.uk or on the web www: http://www.ccdc.cam.ac.uk.

Acknowledgements

We thank DGICYT (Project BQU2001-0151) for financial support.

References

[1] D.X. West, A.E. Liberta, S.B. Padhye, R.C. Chikate, P.B. Sonawane, A.S. Kumbhar, R.G. Yeranda, Coord. Chem. Rev. 123 (1993) 49, and refs. therein.
[2] A.E. Liberta, D.X. West, Biometals 5 (1992) 121.
[3] D.X. West, S.B. Padhye, P.B. Sonawane, Struct. Bond. 76 (1991) 1.
[4] J.G. Cory, A.H. Cory (Eds.), International Encyclopaedia of Pharmacology and Therapeutics, Pergamon Press, New York, 1989.
[5] J. Ruipérez, M.A. Mendiola, M.T. Sevilla, J. Rodríguez-Procopio, L. Hernández, Electroanalysis 14 (2002) 532.
[6] M.J. Gismera, M.A. Mendiola, J. Rodríguez-Procopio, M.T. Sevilla, Anal. Chim. Acta 385 (1999) 143.
[7] M. Colilla, M.A. Mendiola, J.R. Procopio, M.T. Sevilla, Electroanalysis 17 (2005) 933.
[8] E. Palomares, R. Villar, J. Durrant, Chem. Commun. (2004) 362.
[9] R.K. Mahajan, I. Kaur, T.S. Lobana, Talanta 59 (2003) 101.
[10] G. Giacomelli, A. Porcheddu, L. Luca, Curr. Org. Chem. 8 (2004) 1497.
[11] Z. Brzozowski, F. Saczewski, M. Gdaniec, Eur. J. Med. Chem. 35 (2000) 1053.
[12] J.S. Casas, A. Castiñeiras, M.C. Rodríguez-Argüelles, A. Sánchez, J. Sordo, A. Vázquez-López, E.M. Vázquez-López, J. Chem. Soc., Dalton Trans. (2000) 2267.
[13] J.S. Casas, M.S. Tasende, J. Sordo, Coord. Chem. Rev. 209 (2000) 197.
[14] E. López-Torres, M.A. Mendiola, C.J. Pastor, B. Souto Pérez, Inorg. Chem. 43 (2004) 5222, and references therein.
[15] E. López-Torres, M.A. Mendiola, C.J. Pastor, J.R. Procopio, Eur. J. Inorg. Chem. (2003) 2711.
[16] E. López-Torres, M.A. Mendiola, Polyhedron 24 (2005) 1435.
[17] A. Sousa-Pedrares, J. Romero, J.A. García-Vázquez, M.L. Durán, I. Casanova, A. Sousa, J. Chem. Soc., Dalton Trans. (2003) 1379.
[18] A. Rodríguez, A. Sousa-Pedrades, J.A. García-Vázquez, J. Romero, A. Sousa, Eur. J. Inorg. Chem. (2005) 2242.
[19] G.M. Sheldrick, SADABS version 2.03, Program for Empirical Absorption Correction, Universität Göttingen, 1997–2001.
[20] G.M. Sheldrick, SAINT + NT (version 6.04) *SAX* Area-Detector Integration Program, Bruker AXS, Madison, WI, 1997–2001.
[21] Bruker AXS SHELXTL (version 6.10) Structure Determination Package, Bruker AXS, Madison, WI, 2000.
[22] SHELXS-97, Program for Structure Solution: G.M. Sheldrick, Acta Crystallogr. Sect. A 46 (1990) 467.
[23] SHELXL-97, Program for Crystal Structure Refinement, Universität Göttingen, 1997.
[24] A. Arquero, M. Cañadas, M. Martínez-Ripoll, M.A. Mendiola, A. Rodríguez, Tetrahedron 54 (1998) 11271.
[25] E. Franco, E. López-Torres, M.A. Mendiola, M.T. Sevilla, Polyhedron 19 (2000) 441.
[26] M.A. Blanco, E. López-Torres, M.A. Mendiola, E. Brunet, M.T. Sevilla, Tetrahedron (2002) 1525.
[27] W.J. Geary, Coord. Chem. Rev. 7 (1971) 81.
[28] E. Sutton, Tables of Interatomic Distances, Configuration in Molecules and Ions (Supplement), The Chemical Society, London, 1965.

[29] T.S. Lobana, A. Sánchez, J.S. Casas, A. Castiñeiras, J. Sordo, M.S. García-Tasende, Polyhedron 17 (1998) 3701.
[30] D.E. Fenton, D.H. Cook, I.W. Nowell, J. Chem. Soc., Chem. Commun. (1977) 274.
[31] K. Nakamoto, Infrared and Raman Spectra of Inorganic and Coordination Compounds, 5th ed., Wiley, New York, 1997.
[32] B.W. Rossiter, J.F. Hamilton, 2nd ed.Electrochemical Methods, vol. II, Wiley, New York, 1986.

suitable matrix [1e–g]. One potentially interesting approach is to encapsulate the complexes in cyclodextrins (CDs) [6]. In these host–guest systems, the CDs are acting as second-sphere ligands non-covalently attached to the first-sphere ligands [7]. As well as modifying the mechanical and thermal stabilities of the guest, the inclusion in CDs can also affect the photophysical behavior. Thus, the encapsulation of the complex $Eu(NTA)_3 \cdot 2H_2O$ in β-CD induces emission from the singlet excited state of the ligands, with the corresponding inefficiency of the ligand-to-metal energy transfer step [6b]. In contrast, encapsulation of the same complex in γ-CD, which has a cavity diameter of 7.9 Å compared with 6.2 Å for β-CD, actually induces a more efficient ligand-to-metal ion energy transfer pathway [6c].

The presence of coordinated water molecules in complexes with the general formulae $Eu(\beta\text{-diket})_3 \cdot 2H_2O$ is usually a disadvantage because the luminescence can be quenched by the nonradiative dissipation of energy on the high-energy O–H vibrations. As a result, many complexes of the type $Eu(\beta\text{-diket})_3 \cdot L$ have been prepared in which the solvent molecules are replaced by a Lewis base organic ligand. $Eu(NTA)_3$ complexes are now known with L = bipy [4f], phen [4j,8], 1,4-diaza-1,3-butadienes [9] and pyrazolylpyridine [10]. Binuclear complexes $[Ln(NTA)_3]_2 \cdot bpym$ (Ln = Eu, Gd; bpym = 2,2′-bipyrimidine) have also been obtained [8]. The photoluminescence properties of these complexes, such as the $^5D_0$ quantum efficiency, vary considerably according to the nature of the adducting molecule. In the present work, we report on the encapsulation of the complex $Eu(NTA)_3 \cdot bipy$ in β-CD. The photoluminescence properties of the resultant inclusion compound have been studied and compared with those of the "free" complex. We also describe the single-crystal X-ray structure of the solvated compound $Eu(NTA)_3 \cdot bipy \cdot 0.44CHCl_3$.

2. Experimental

2.1. Materials and methods

Microanalyses were performed at the Instituto de Tecnologia Química e Biológica (ITQB), Lisbon. Thermogravimetric analysis (TGA) studies were performed using a Shimadzu TGA-50 system at a heating rate of 5 K min^{-1} under air. IR spectra were obtained as KBr pellets using a FT-IR Mattson-7000 infrared spectrophotometer. Raman spectra were recorded on a Bruker RFS100/S FT instrument (Nd:YAG laser, 1064 nm excitation, InGaAs detector). ^{13}C solid-state NMR spectra were recorded at 100.62 MHz on a Bruker Avance 400 P spectrometer. ^{13}C CP MAS NMR spectra were acquired with a 3.5 μs 90° proton pulse and 2 ms contact time with spinning rates of 7–8.5 kHz and 4 s recycle delays. The photoluminescence measurements were recorded between 10 and 300 K on a modular double grating excitation spectrofluorimeter with a TRIAX 320 emission monochromator (Fluorolog-3, Jobin Yvon-Spex) coupled to a R928 Hamamatsu photomultiplier, using the front face acquisition mode. All of the photoluminescence spectra were corrected for optical and detection spectral response.

The complex $Eu(NTA)_3 \cdot 2H_2O$ was prepared using the literature method [11]. β-CD was kindly donated by La Roquette (France) and used as received.

2.2. $Eu(NTA)_3 \cdot bipy$ (**1**)

A solution of 2,2′-bipyridine (0.055 g, 0.35 mmol) in $CHCl_3$ (5 mL) was added to a solution of $Eu(NTA)_3 \cdot 2H_2O$ (0.344 g, 0.35 mmol) in $CHCl_3$ (15 mL) at room temperature, and the reaction mixture was stirred for 3 h at room temperature. The solvent was then removed and the resulting solid washed with *n*-hexane. After drying in vacuum, a light orange powder was obtained (0.31 g, 80%). *Anal.* Calc. for $EuC_{52}H_{32}F_9N_2O_6$ (1103.8): C, 56.58; H, 2.92; N, 2.54. Found: C, 56.50; H, 2.59; N, 3.10%. IR (ν_{max}/cm^{-1}): 2977w, 2911w, 1640s, 1621s, 1614vs, 1568s, 1530s, 1509s, 1472m, 1463m, 1384m, 1299vs, 1198s, 1189s, 1135s, 1123s, 793s, 763m, 684m, 568m. Raman (ν_{max}/cm^{-1}): 3059m, 2990m, 1622s, 1595s, 1570w, 1466s, 1430w, 1386vs, 1356w, 1312m, 1292m, 1218m, 1201m, 1015m, 771m, 517m, 346w, 228w. ^1H NMR (300 MHz, $CDCl_3$): $\delta = 12.95$ (br, 2H, bipy), 10.43 (d, $J = 7$ Hz, 2H, bipy), 9.74 (br, 2H, bipy), 8.52 (d, $J = 8$ Hz, 2H, bipy), 7.91 (d, $J = 8$ Hz, 3H, naphth), 7.79, 7.76 (s + d, 9H, naphth), 7.55 (d, $J = 8$ Hz, 6H, naphth), 7.42 (d, $J = 8$ Hz, 3H, naphth), 3.45 (s, 3H, COC*H*CO).

2.3. β-CD:$Eu(NTA)_3 \cdot bipy$

A solution of β-CD (245 mg, 0.181 mmol) in water (10 mL) and ethyl acetate (2.5 mL) was treated with a solution of $Eu(NTA)_3 \cdot bipy$ (**1**) (200 mg, 0.181 mmol) in ethyl acetate (1.0 mL), and the mixture was stirred at 65 °C for 4 h. The resulting pale yellow precipitate was isolated by centrifugation and dried in air at room temperature (53 mg). *Anal.* Calc. for $C_{42}H_{70}O_{35} \cdot 0.5(C_{52}H_{32}F_9N_2O_6Eu) \cdot 8H_2O$ (1831.0): C, 44.61; H, 5.62; N, 0.76. Found: C, 44.46; H, 5.00; N, 0.86%. TGA up to 150 °C revealed a sample weight loss of 8.1% (calcd: for loss of $8H_2O$, 7.9%). IR (ν_{max}/cm^{-1}): 3383s, 2934m, 1675w, 1631sh, 1611m, 1595m, 1570m, 1532m, 1509m, 1461m, 1438w, 1385w, 1368w, 1355w, 1335w, 1301s, 1254w, 1199s, 1185sh, 1156s, 1134sh, 1099sh, 1079s, 1053sh, 1033vs, 1004sh, 947m, 937m, 863w, 845sh, 794m, 761m, 738w, 707w, 684m, 644w, 608m, 579m, 530w, 523sh, 474w, 453vw, 411vw. ^{13}C CP MAS NMR: $\delta = 194.0$–184.1 (very broad, guest CO), 136.6–114.6 (very broad, guest bipy/naphth), 102.4 (β-CD C-1), 84.0, 81.0, 78.3 (β-CD C-4), 73.1 (β-CD C-2,3,5), 63.7, 59.5 (β-CD, C-6).

2.4. Crystal structure determination of **1** (chloroform solvate)

Crystals suitable for X-ray diffraction were obtained by slow diffusion of diethyl ether into a solution of the crude

product in chloroform. The structure was determined at 120 K using graphite monochromatized radiation. Data were collected on a Siemens SMART diffractometer and corrected for Lorentz-polarization effects and for absorption [12]. Crystal data and experimental parameters are presented in Table 1. The structure was solved by direct methods using SIR-97 [13] and refined by least-squares techniques using programs from the KRYSTAL package [14]. Hydrogen atoms were kept fixed in calculated positions with C–H = 0.95 Å and with isotropic displacement factors 20% larger than U_{eq} for the atoms to which they were bonded. The europium chelate complex crystallized together with chloroform molecules, which were constrained to have threefold symmetry [15]. The chloroform site was not fully occupied. The CF_3 groups at C40 and C60 were both orientationally disordered over two sites; all C–F distances were constrained to be equal. Atomic scattering factors were taken from elsewhere [16]. Selected bond distances and angles are listed in Table 2.

Table 1
Crystal data and structure refinement

Molecular formula	$Eu(NTA)_3 \cdot bipy \cdot 0.44(CHCl_3)$
Empirical formula	$C_{52.44}H_{32.44}Cl_{1.32}EuF_9N_2O_6$
Formula weight	1156.38
Crystal system	monoclinic
Space group	*P*2/*c*
a (Å)	21.813(3)
b (Å)	11.353(2)
c (Å)	20.550(3)
β (°)	110.238(2)
V (Å^3)	4775(1)
Z	4
D_{calc} (g cm^{-1})	1.608
T (K)	120
Reflections collected	60626
Independent (R_{int})	14551 (0.039)
Observed [$I > 3\sigma(I)$]	10995
R indices[a] [$I > 3\sigma(I)$] R_1	0.026
wR_2	0.033
$\Delta\rho_{max}$ and $\Delta\rho_{min}$ (e Å^{-3})	1.29(9) and −0.93(3)

[a] $R_1 = \sum||F_o| - |F_c||/\sum|F_o|$; $wR_2 = (\sum||F_o| - |F_c||)^2/\sum w|F_o^2|^{1/2}$, $w = 1/\{((\sigma F_o^2) + B + (1 + A)F_o^2)^{1/2} - |F_o|\}^2$.

Table 2
Selected bond distances (Å) and angles (°) for $Eu(NTA)_3 \cdot bipy \cdot 0.44CHCl_3$

Eu–N1	2.569(2)
Eu–N2	2.572(2)
Eu–O20	2.375(2)
Eu–O21	2.375(2)
Eu–O40	2.437(2)
Eu–O41	2.315(2)
Eu–O60	2.340(2)
Eu–O61	2.365(2)
N1–Eu–N2	62.88(7)
O20–Eu–O21	71.18(5)
O40–Eu–O41	70.25(5)
O60–Eu–O61	72.13(6)

3. Results and discussion

The compound $Eu(NTA)_3 \cdot bipy$ (**1**) was prepared by the reaction of $Eu(NTA)_3 \cdot 2H_2O$ with 2,2′-bipyridine in a 1:1 ratio in chloroform. The ^1H NMR spectrum of **1** (recrystallized) in $CDCl_3$ was in accordance with a NTA:bipy ratio of 3:1. Only one set of signals was observed for the protons of the bipy ligand between 8.5 and 13.0 ppm (two doublets and two broad peaks), considerably downfield shifted with respect to the analogous signals in the spectra of the free ligand (7.2–8.7 ppm [17]). The observed shifts are comparable with those measured for other 1:1 adducts of bipy with tris(β-diketonate)europium(III) complexes [17,18]. No evidence was found for the dissociation of the complex in solution. The NMR signals of the NTA groups appear as a sharp singlet at 3.45 ppm for the methine protons and several sharp peaks between 7.4 and 7.9 ppm for the aromatic protons. Single crystals suitable for X-ray diffraction analysis were obtained by slow diffusion of diethyl ether into a solution of the crude product in chloroform. The molecular structure is shown in Fig. 1. The molecule crystallized together with chloroform. $Eu(NTA)_3 \cdot bipy \cdot 0.44CHCl_3$ is monomeric, with the Eu ion being coordinated to the nitrogen atoms of the bipyridine group (Eu–N = 2.57 Å) and the oxygen atoms of the three NTA groups (Eu–O = 2.315–2.437 Å, Table 2). These distances are similar to those for unsolvated $Eu(NTA)_3 \cdot bipy$ [4f], $Eu(NTA)_3 \cdot bipy \cdot 0.5CH_3CH(OH)CH_3$ [4f], and the corre-

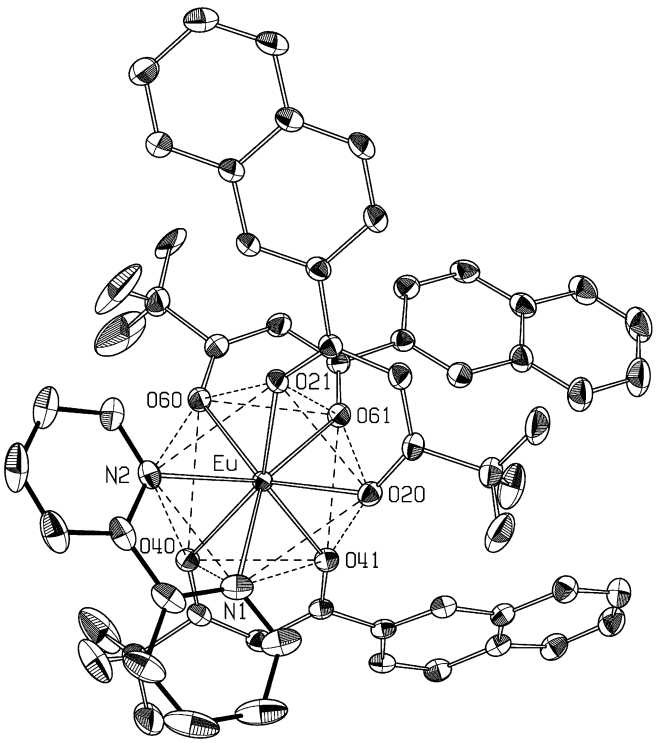

Fig. 1. Molecular structure of $Eu(NTA)_3 \cdot bipy$ in $Eu(NTA)_3 \cdot bipy \cdot 0.44CHCl_3$ with atom numbering scheme. Thermal ellipsoids are drawn at the 50% probability level and hydrogen atoms have been omitted for clarity.

sponding 1,10-phenanthroline and 2,2′-bipyrimidine adducts [8]. The coordination polyhedron is a distorted square antiprism, with the bidentate ligands spanning opposite sides of the 'square' faces. These faces are defined by N1,N2,O20,O21 and by O40,O41,O60,O61. In the ideal square antiprism, these would be planar but here the faces are creased about the diagonals N1···O21 and O40···O61 with angles of 9.0(1)° and 3.3(1)° (cf. 0°, 0° for a square antiprism, 0°, 21.8° for a bicapped trigonal prism and 29.5°, 29.5° for a dodecahedron [19]). In the unsolvated complex $Eu(NTA)_3 \cdot bipy$, there are two crystallographically independent molecules both having coordination polyhedra which are well-defined square antiprisms, whereas in the isopropanol solvate the polyhedron is a distorted bicapped trigonal prism [4f].

Addition of a solution of **1** in ethyl acetate to a solution of β-CD in water and ethyl acetate gave a pale yellow precipitate which was isolated by centrifugation and air-dried at ambient temperature. The product, designated as β-CD:$Eu(NTA)_3 \cdot bipy$, was characterized by elemental analysis, powder XRD, TGA, ^{13}C CP MAS NMR, FT-IR and photoluminescence spectroscopy. Although a 1:1 molar ratio of β-CD and complex **1** was used, elemental analysis of the product (together with TGA – see below) was more consistent with a final stoichiometry of about 2:1. Powder XRD analysis of the product showed the formation of a new poorly crystalline phase (not shown), different from either of the starting components β-CD or complex **1**. This was an initial indication for the isolation of a true inclusion compound.

Fig. 2 shows the TGA results for β-CD:$Eu(NTA)_3 \cdot bipy$ compared with those for the pure components β-CD hydrate and complex **1**, and also a physical mixture of β-CD and **1** in a 2:1 molar ratio. TGA of β-CD shows loss

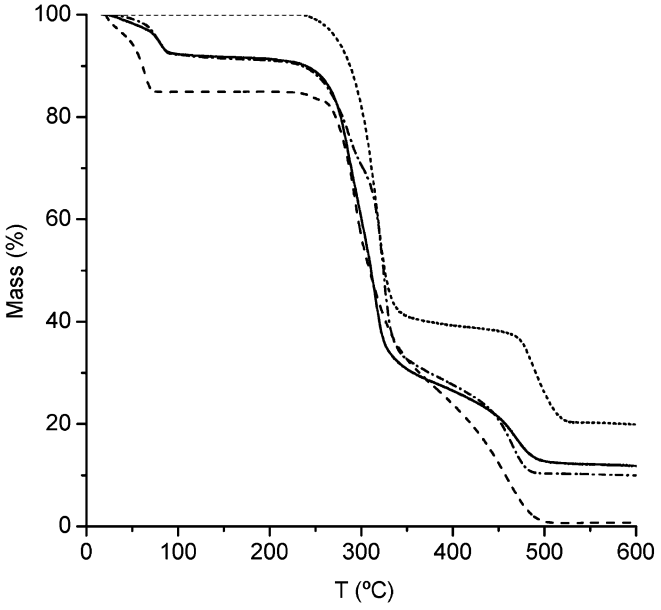

Fig. 2. TGA traces for β-CD (– – –), $Eu(NTA)_3 \cdot bipy$ (**1**) (· · · · · ·), a 2:1 physical mixture of β-CD and **1** (– · –), and the compound β-CD:$Eu(NTA)_3 \cdot bipy$ (——).

of hydrated water up to 80 °C (15%, 10 water molecules per β-CD molecule). There is no further change until about 230 °C when the compound starts to melt and decompose. At 500 °C, 100% mass loss is complete. The europium chelate **1** is devoid of hydration waters since the thermogram does not show any weight loss up to 250 °C. The compound then decomposes in two steps up to 530 °C, leaving a residual mass of 20%. Even though β-CD and complex **1** start decomposing at nearly the same temperature, we can clearly distinguish the two overlapping processes in the TG curve for the physical mixture, which demonstrates that the two components behave independently. In contrast, compound β-CD:$Eu(NTA)_3 \cdot bipy$ starts decomposing at about the same point as β-CD (230 °C), but there is no overlapping step towards slightly higher temperature for the degradation of the europium chelate **1**. The fact that the decomposition of the two components cannot be distinguished is an additional support for the successful isolation of a true inclusion compound, because it suggests that the $Eu(NTA)_3 \cdot bipy$ molecules are isolated from one another by complexation with the host β-CD molecules.

^{13}C MAS NMR spectroscopy is often useful for the recognition of inclusion complex formation between organic or metallo-organic guests and cyclodextrins [6b,20]. The spectrum of pristine β-CD hydrate exhibits multiple resonances for each type of carbon atom [21]. This has been mainly correlated with different torsion angles about the (1 → 4) linkages for C-1 and C-4 [21a,21b], and with torsion angles describing the orientation of the hydroxyl groups [21c]. The different carbon resonances are assigned to C-1 (101–104 ppm), C-4 (78–84 ppm), C-2,3,5 (71–76 ppm), and C-6 (57–65 ppm). In the spectrum of the compound β-CD:$Eu(NTA)_3 \cdot bipy$ (not shown), the β-CD resonances are broader, becoming almost single peaks for C-1 and C-2,3,5. The broadening of the peaks could be induced by the paramagnetic Eu^{3+} ions of encapsulated guest molecules. However, it is more likely that conformational changes of the β-CD macrocycle are responsible. Thus, the inclusion of bulky guest molecules in β-CD compels the ring to adopt a more symmetrical conformation, with each glucose unit in a more similar environment [20]. By comparison with previous experimental and theoretical studies on the interaction of the complex $Eu(NTA)_3 \cdot 2H_2O$ with β-CD and γ-CD [6b,6c], and also crystallographic studies of inclusion compounds of naphthalene or naphthalene derivatives in CDs [22], we propose that the host–guest interaction in the compound β-CD:$Eu(NTA)_3 \cdot bipy$ involves the partial inclusion of the naphthoyl moieties of the guest within the β-CD cavities. The ^{13}C CP MAS NMR spectrum of the compound β-CD:$Eu(NTA)_3 \cdot bipy$ also contained resonances due to the europium chelate molecule, but these were broad and weak. The presence of structurally intact $Eu(NTA)_3 \cdot bipy$ molecules was confirmed by the IR spectrum, which contained strong peaks due to the europium complex (e.g., 1614, 1299 and 793 cm^{-1}) and β-CD (e.g., 1157, 1079 and 1029 cm^{-1}). These bands were essentially unshifted

and with equal relative intensities compared with the corresponding bands for the pure components (complex **1** and pristine β-CD hydrate).

Fig. 3 compares the excitation spectrum of the complex **1** with that of the inclusion compound β-CD:Eu(NTA)$_3$ · bipy, monitored around the $^5D_0 \rightarrow {}^7F_2$ lines. The spectrum of the complex shows a large broad band ascribed to the triplet levels of the ligands and a series of lines corresponding to intra-4f^6 lines. The inclusion of the complex into β-CD induces an enlargement of the ligands excited levels, suggesting an effective interaction between β-CD and the NTA ligands of the complex, and a decrease of the intensity of the Eu^{3+} lines with respect to that of the large broad band. This intensity decrease of the intra-4f^6 lines indicates an enhancement of the Eu^{3+} sensitized process due to encapsulation of the Eu(NTA)$_3$ · bipy molecules. Moreover, the sensitized spectral region of the inclusion compound covers a larger UV-A-B range, compared with that for non-included **1**.

Fig. 4 shows the emission of Eu(NTA)$_3$ · bipy (**1**) and the inclusion compound β-CD:Eu(NTA)$_3$ · bipy for the excitation wavelengths that maximize the Eu^{3+} emission intensities. The spectra consist of the typical Eu^{3+} emission lines ascribed to the intra-4f^6 $^5D_0 \rightarrow {}^7F_{0-4}$ transitions. For both compounds only one line is observed for the non-degenerate $^5D_0 \rightarrow {}^7F_0$ transition and no changes are detected in the emission spectra upon variation of the excitation wavelength, suggesting, therefore, that the Eu^{3+} ions occupy the same average local environment within each compound. However, changes are observed in the energy and number of Stark components due to the encapsulation of the complex. In particular, a higher ligand field splitting is evident for the $^5D_0 \rightarrow {}^7F_{1,2}$ transitions: 2 and 3 Stark components for bulk **1**, and 3 and 4 Stark components for the inclusion compound. The increase in the number

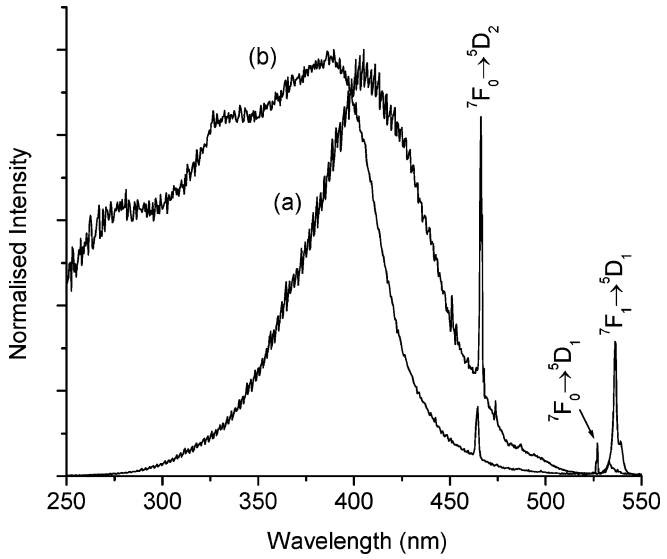

Fig. 3. Room-temperature excitation spectra for: (a) the complex Eu(NTA)$_3$ · bipy (**1**) and (b) the inclusion compound β-CD:Eu(NTA)$_3$ · bipy, monitored around 613 and 615 nm, respectively.

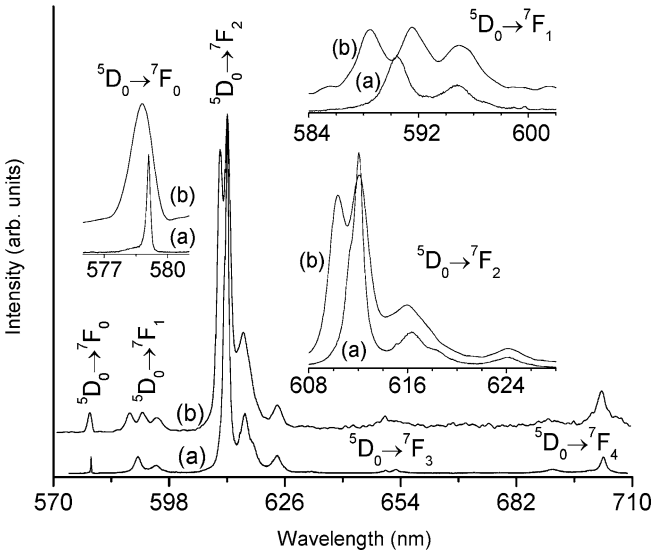

Fig. 4. Room-temperature emission spectra for: (a) the complex Eu(NTA)$_3$ · bipy (**1**) and (b) the inclusion compound β-CD:Eu(NTA)$_3$ · bipy, excited around 405 and 398 nm, respectively.

of Stark components indicates a decrease in the Eu^{3+}-local symmetry. We may speculate that the change in the Eu^{3+} coordination polyhedron makes the NTA ligands more geometrically accessible for inclusion in the host cavities. For both the complex **1** and the inclusion compound, no emission from the ligands triplet states could be observed, suggesting an efficient energy transfer between them and the Eu^{3+} levels. The non-observation of excited states of the ligands in the inclusion compound suggests a better accommodation of the luminescent complex within the cyclodextrin cavity, as has been reported for the 1:1 inclusion compound comprising β-cyclodextrin and Eu(NTA)$_3$ · 2H$_2$O [6b].

4. Conclusions

Powder XRD, TGA, ^{13}C CP MAS NMR and photoluminescence spectroscopy indicate that an inclusion compound comprising β-cyclodextrin and the adduct Eu(NTA)$_3$ · bipy can be prepared by co-precipitation from a solvent mixture. The photophysical properties of the europium complex are modified by the introduction of the second-sphere ligand (β-CD) non-covalently attached to the first-sphere ligands (NTA and bipy). This may be due, in part, to a change in the Eu^{3+} coordination polyhedron. The reorganization of the ligands may be necessary for the formation of an inclusion complex with a 2:1 (host:guest) stoichiometry, in which the naphthoyl moieties of the guest species are partially encapsulated within the β-CD cavities. Such a change would not be surprising since we now know that at least three different polyhedra are possible for the adduct Eu(NTA)$_3$ · bipy simply by recrystallizing the compound from different solvents. Thompson et al. [4f] already showed that two of these crystalline forms have different luminescence spectra.

5. Supplementary data

Crystallographic data for the structural analysis have been deposited with the Cambridge Crystallographic Data Centre, CCDC No. 279710. These data can be obtained free of charge at www.ccdc.cam.ac.uk/conts/retrieving.html [or from the Cambridge Crystallographic Data Centre, 12 Union Road, Cambridge CB2 1EZ, UK; fax: (internat.) +44 1223 336 033; e-mail: deposit@ccdc.cam.ac.uk].

Acknowledgements

The authors are grateful to FCT, POCTI and FEDER for financial support (Project POCTI/CTM/46780/2002). We also thank the University of Aveiro (J.A.F.) and the FCT (J.A.F., S.S.B) for research grants. A.H. is indebted to the Carlsberg Foundation for the diffractometer. We are grateful to Prof. João Rocha for access to research facilities and Paula Esculcas for assistance in the NMR experiments.

References

[1] (a) G.F. de Sá, O.L. Malta, C. de Mello Donegá, A.M. Simas, R.L. Longo, P.A. Santa-Cruz, E.F. da Silva, Coord. Chem. Rev. 196 (2000) 165;
(b) K.C. Joshi, V.N. Pathak, Coord. Chem. Rev. 22 (1977) 37;
(c) L. Thompson, J. Legendziewicz, J. Cybinska, Li Pan, W. Brennessel, J. Alloys Compd. 341 (2002) 312, and references cited therein;
(d) L.N. Sun, H.J. Zhang, Q.G. Meng, F.Y. Liu, L.S. Fu, C.Y. Peng, J.B. Yu, G.L. Zheng, S.B. Wang, J. Phys. Chem. B 109 (2005) 6174;
(e) P. Lenaerts, K. Driesen, R. Van Deun, K. Binnemans, Chem. Mater. 17 (2005) 2148;
(f) M.R. Robinson, J.C. Ostrowski, G.C. Bazan, M.D. McGehee, Adv. Mater. 15 (2003) 1547;
(g) D. Sendor, U. Kynast, Adv. Mater. 14 (2002) 1570.

[2] (a) L.R. Melby, N.J. Rose, E. Abramson, J.C. Caris, J. Am. Chem. Soc. 86 (1964) 5117;
(b) H. Bauer, J. Blanc, D.L. Ross, J. Am. Chem. Soc. 86 (1964) 5125.

[3] F.A. Hart, in: G. Wilkinson, R.D. Gillard, J.A. McCleverty (Eds.), Comprehensive Coordination Chemistry, vol. 3, Pergamon Press, Oxford, 1987, p. 1059.

[4] (a) A. Bellusci, G. Barberio, A. Crispini, M. Ghedini, M. La Deda, D. Pucci, Inorg. Chem. 44 (2005) 1818;
(b) D.R. van Staveren, G.A. van Albada, J.G. Haasnoot, H. Kooijman, A.M.M. Lanfredi, P.J. Nieuwenhuizen, A.L. Spek, F. Ugozzoli, T. Weyhermüller, J. Reedijk, Inorg. Chim. Acta 315 (2001) 163;
(c) A.K. Trikha, L.B. Zinner, K. Zinner, P.C. Isolani, Polyhedron 15 (1996) 1651;
(d) D.F. Moser, L.C. Thompson, V.G. Young Jr., J. Alloys Compd. 303–304 (2000) 121;
(e) H.J. Batista, A.V.M. de Andrade, R.L. Longo, A.M. Simas, G.F. de Sá, N.K. Ito, L.C. Thompson, Inorg. Chem. 37 (1998) 3542;
(f) L.C. Thompson, F.W. Atchison, V.G. Young, J. Alloys Compd. 275–277 (1998) 765;
(g) K. Iftikhar, M. Sayeed, N. Ahmed, Inorg. Chem. 21 (1982) 80;
(h) L.C. Thompson, S. Berry, J. Alloys Compd. 323–324 (2001) 177;
(i) V. Tsaryuk, J. Legendziewicz, L. Puntus, V. Zolin, J. Sokolnicki, J. Alloys Compd. 300–301 (2000) 464;
(j) M. Uekawa, Y. Miyamoto, H. Ikeda, K. Kaifu, T. Nakaya, Bull. Chem. Soc. Jpn. 71 (1998) 2253;
(k) O.L. Malta, M.A. Couto dos Santos, L.C. Thompson, N.K. Ito, J. Lumin. 69 (1996) 77;
(l) R.C. Holz, L.C. Thompson, Inorg. Chem. 32 (1993) 5251.

[5] (a) O.L. Malta, H.F. Brito, J.F.S. Menezes, F.R. Gonçalves e Silva, C. de Mello Donegá, S. Alves Jr., Chem. Phys. Lett. 282 (1998) 233;
(b) O.L. Malta, H.F. Brito, J.F.S. Menezes, F.R. Gonçalves e Silva, S. Alves Jr., F.S. Farias Jr., A.V.M. de Andrade, J. Lumin. 75 (1997) 255;
(c) L.D. Carlos, C. de Mello Donegá, R.Q. Albuquerque, S. Alves Jr., J.F.S. Menezes, O.L. Malta, Mol. Phys. 101 (2003) 1037.

[6] (a) H.F. Brito, C.A.A. Carvalho, O.L. Malta, J.J. Passos, J.F.S. Menezes, R.D. Sinisterra, Spectrochim. Acta A 55 (1999) 2403;
(b) S.S. Braga, R.A. Sá Ferreira, I.S. Gonçalves, M. Pillinger, J. Rocha, J.J.C. Teixeira-Dias, L.D. Carlos, J. Phys. Chem. B 106 (2002) 11430;
(c) S.S. Braga, R.A. Sá Ferreira, I.S. Gonçalves, P. Ribeiro-Claro, M. Pillinger, J. Rocha, J.J.C. Teixeira-Dias, L.D. Carlos, J. Incl. Phenom. Macrocycl. Chem. 44 (2002) 261.

[7] E. Fenyvesi, L. Szente, N.R. Russel, M. McNamara, in: J. Szejtli, T. Osa (Eds.), Comprehensive Supramolecular Chemistry, vol. 3, Pergamon Press, Oxford, 1996 (Chapter 10).

[8] J.A. Fernandes, R.A. Sá Ferreira, M. Pillinger, L.D. Carlos, J. Jepsen, A. Hazell, P. Ribeiro-Claro, I.S. Gonçalves, J. Lumin. 113 (2005) 50.

[9] J.A. Fernandes, R.A. Sá Ferreira, M. Pillinger, L.D. Carlos, I.S. Gonçalves, P.J.A. Ribeiro-Claro, Eur. J. Inorg. Chem. (2004) 3913.

[10] S. Gago, J.A. Fernandes, J.P. Rainho, R.A. Sá Ferreira, M. Pillinger, A.A. Valente, T.M. Santos, L.D. Carlos, P.J.A. Ribeiro-Claro, I.S. Gonçalves, Chem. Mater. 17 (2005) 5077.

[11] R.G. Charles, A. Perrotto, J. Inorg. Nucl. Chem. 26 (1964) 373.

[12] Siemens SMART, SAINT and XPREP: Area-Detector Control and Integration Software, Siemens Analytical X-ray Institute Inc., Madison, WI, USA, 1995.

[13] A. Altomare, G. Cascarano, C. Giacovazzo, A. Guagliardi, A.G.G. Moliterni, M.C. Burla, G. Polidori, M. Camalli, R. Spagna, SIR-97, University of Bari, Italy, 1997.

[14] A. Hazell, KRYSTAL: An Integrated System of Crystallographic Programs, Aarhus University, Denmark, 1995.

[15] G.S. Pawley, Adv. Struct. Res. Diffr. Methods 4 (1971) 1.

[16] International Tables for X-ray Crystallography, vol IV, Kynoch Press, Birmingham, 1974 (present distributor: Kluwer, Dordrecht).

[17] K. Iftikhar, Polyhedron 15 (1996) 1113.

[18] N.S. Bhacca, J. Selbin, J.D. Wander, J. Am. Chem. Soc. 94 (1972) 8719.

[19] M.A. Porai-Koshits, L.A. Aslanov, Struct. Chem. 13 (1972) 244.

[20] H. Okumura, Y. Kawaguchi, A. Harada, Macromolecules 36 (2003) 6422.

[21] (a) M.J. Gidley, S.M. Bociek, J. Am. Chem. Soc. 110 (1988) 3820;
(b) S.J. Heyes, N.J. Clayden, C.M. Dobson, Carbohydr. Res. 233 (1992) 1;
(c) R.P. Veregin, C.A. Fyfe, R.H. Marcessault, M.G. Tayler, Carbohydr. Res. 160 (1987) 41.

[22] A. Kokkinou, K. Yannakopoulou, I.M. Mavridis, D. Mentzafosa, Carbohydr. Res. 332 (2001) 85, and references cited therein.

like tetrahedral, square pyramidal or trigonal-bipyramidal of comparable stability and this often leads to significant differences in the metal–ligand geometry and overall molecular shape. This metal ion also finds significant use in bioinorganic chemistry [7] and magnetism [8]. Using $[Cd(NCS)_6]^{4-}$ as a building block in conjunction with $[Cu(tren)(OH_2)]^{2+}$, results in a bimetallic trinuclear complex of the type $[Cu_2Cd(tren)_2(NCS)_6]$ (**1**) with *trans*-$[Cd(NCS)_4(SCN)_2]^{4-}$ instead of covalently bonded polymeric $[Cu_2Cd(tren)_2(NCS)_6]_n$ with *cis*/*trans*-$[Cd(NCS)_2(SCN)_4]^{4-}$ as molecular ions. X-ray crystallography study shows the presence of hydrogen bonded trinuclear entities to form a 3D supramolecular continuum. Although the magnetic behaviour of this complex is less important, its structure establishes the fact that the coordination nature of the metal ions plays a vital role in structure determination as well as on the coordination matrix of the molecular ion. The details of synthesis, structure and properties are described below.

2. Experimental

2.1. Materials

High purity tris(2-aminoethyl)amine (Fluka, Germany), copper nitrate trihydrate (E. Merck, India), cadmium nitrate tetrahydrate (E. Merck, India) and ammonium thiocyanate (E. Merck, India) were purchased from the respective concerns and used as received. All other chemicals and solvents were AR grade and were used as received.

2.2. Physical measurements

Elemental analyses (carbon, hydrogen and nitrogen) were performed on a Perkin–Elmer 2400 CHNS/O elemental analyzer. IR spectra (KBr discs, 4000–300 cm^{-1}) were recorded using a Perkin–Elmer model RX 1 spectrometer. Molar conductance was measured using a Systronics conductivity meter where the cell constant was calibrated with 0.01 M KCl solution and dry MeOH was used as the solvent. Ground state absorption measurements were made with a Jasco model V-530 UV–Vis spectrophotometer. Magnetic susceptibilities at room temperature were measured with a PAR 155 vibrating sample magnetometer with $Hg[Co(SCN)_4]$ as the reference. Measurements on powdered samples were performed in the temperature range 2–300 K using a Quantum Design MPMS-7 SQUID magnetometer in a magnetic field of 0.1 T. The experimental susceptibilities were corrected for the diamagnetism of the constituent atoms (Pascal tables).

2.3. Preparation of the complex

The trinuclear complex **1** was prepared as a bluish green crystalline product through three different methods. These are described below.

2.3.1. Method A

An aqueous solution (5 cm^3) of NH_4NCS (0.457 g, 6 mmol) was added to a solution of $Cd(NO_3)_2 \cdot 4H_2O$ (0.311 g, 1 mmol) in the same solvent (10 cm^3) giving rise to a colourless solution. In another container $Cu(NO_3)_2 \cdot 3H_2O$ (0.483 g, 2 mmol) and tren (0.293 g, 2 mmol) were mixed together in an aqueous solution (10 cm^3) producing a bluish green solution. This bluish green solution was slowly added to the above colourless solution. During addition a colour change was not distinct but the intensity of the bluish green colour increased indicating complexation. The final mixture was filtered and left for slow evaporation in air. Bluish green rectangular crystals suitable for X-ray diffraction formed after a week. Yield, 0.69 g (75%). *Anal*. Calc. for $C_{18}H_{36}N_{14}S_6CdCu_2$ (**1**): C, 24.56; H, 4.12; N, 22.27. Found: C, 24.59; H, 4.09; N, 22.29%. IR (KBr, cm^{-1}): *v* (NCS) 2129, 2064. Λ_M (DMF, $ohm^{-1}\,cm^2\,mol^{-1}$): 10. UV–Vis (λ, nm): 885, 670, 260.

2.3.2. Method B

$Cd(NO_3)_2 \cdot 4H_2O$ (0.311 g, 1 mmol), $Cu(NO_3)_2 \cdot 3H_2O$ (0.483 g, 2 mmol), tren (0.293 g, 2 mmol) and NH_4NCS (0.457 g, 6 mmol) were mixed in water (20 cm^3) in a container resulting in a bluish green solution. The mixture was filtered and left for slow evaporation. Bluish green crystals were formed after few days. Yield, 0.55 g (60%).

2.3.3. Method C

An NH_4NCS (0.457 g, 6 mmol) solution in water (10 cm^3) was added to a solution of $Cu(NO_3)_2 \cdot 3H_2O$ (0.242 g, 1 mmol) in a container resulting in a brown mixture. $Cd(NO_3)_2 \cdot 4H_2O$ (0.622 g, 2 mmol) in water (10 cm^3) was mixed with tren (0.293 g, 2 mmol) in a separate container producing a colourless solution. The brown solution was added dropwise to the colourless solution giving a bluish green coloration. This was filtered and left for slow evaporation in air. Bluish green rectangular crystals were formed after two weeks. Yield, 0.36 g (40%).

2.4. X-ray crystallography

Single crystals were obtained by slow evaporation of an aqueous solution of the reaction mixture. The crystal data and data collection parameters are listed in Table 1. Bluish green crystals suitable for X-ray crystallographic analyses were selected following examination under a microscope. Diffraction data were collected on a Bruker-AXS SMART APEX/CCD diffractometer using Mo Kα radiation, and were corrected for Lorentz and polarization effects and for absorption using the SADABS program [9]. The structure was solved by direct methods and the structure solution and refinement were based on $|F|^2$. All non-hydrogen atoms were refined with anisotropic displacement parameters whereas hydrogen atoms were placed in calculated positions when possible and given isotropic *U* values 1.2 times that of the atom to which they are bonded. The

Table 1
Crystal data and structure refinement parameters for **1**

Empirical formula	$C_{18}H_{36}N_{14}S_6CdCu_2$
Formula weight	880.45
Temperature (K)	200(2)
Wavelength (Å)	0.71073
Crystal system, Space group	monoclinic, $C2/c$
a (Å)	15.8068(14)
b (Å)	11.2946(10)
c (Å)	19.7608(18)
β (°)	107.863(2)
V (Å^3)	3357.9(5)
Z	4
ρ (Mg m^{-3})	1.742
μ (mm^{-1})	2.291
$F(000)$	1776
Crystal size (mm)	$0.20 \times 0.20 \times 0.20$
θ Range for data collection (°)	2.17–28.28
Limiting indices	$-19 \leqslant h \leqslant 20$, $-14 \leqslant k \leqslant 11$, $-24 \leqslant l \leqslant 25$
Reflections collected	10263
Independent reflections	3962 [$R_{int} = 0.0275$]
Completeness to $\theta = 28.32°$	95.3%
Refinement method	full-matrix least-squares on F^2
Data/restraints/parameters	3962/0/187
Goodness-of-fit on F^2	1.056
Final R indices [$I > 2\sigma(I)$]	$R_1 = 0.0360$, $wR_2 = 0.0911$
R indices (all data)	$R_1 = 0.0482$, $wR_2 = 0.0966$
Largest different peak and hole (e Å^{-3})	0.764 and −0.695

crystallographic calculations were conducted with the SHELXTL v.6.1 program package [10].

3. Results and discussion

3.1. Synthesis and formulation

The trinuclear $[Cu_2Cd(tren)_2(NCS)_6]$ (**1**) compound was prepared using three different routes (Methods A–C; see Section 2). In Method A, the building units $[Cu(tren)(OH_2)]^{2+}$ and $[Cd(NCS)_6]^{4-}$ were generated in solutions separately. The molecular ion, $[Cd(NCS)_6]^{4-}$, was obtained by addition of six moles of ammonium thiocyanate to one mole of cadmium(II) nitrate tetrahydrate (Eq. (1)). The complementary unit $[Cu(tren)(OH_2)]^{2+}$ was prepared by dropwise addition of two moles of tren to a two molar copper(II) nitrate trihydrate in a separate container (Eq. (2)). The trinuclear **1** resulted through union of *trans*-$[Cd(NCS)_4(SCN)_2]^{4-}$ and $[Cu(tren)(OH_2)]^{2+}$ in a 1:1 ratio of these building blocks (Eq. (3)).

$$Cd(NO_3)_2 \cdot 4H_2O + 6NH_4NCS \rightarrow (NH_4)_4[Cd(NCS)_6] + 2NH_4NO_3 + 4H_2O \quad (1)$$

$$2Cu(NO_3)_2 \cdot 3H_2O + 2tren \rightarrow 2[Cu(tren)(OH_2)](NO_3)_2 + 4H_2O \quad (2)$$

$$(NH_4)_4[Cd(NCS)_6] + 2[Cu(tren)(OH_2)](NO_3)_2 \rightarrow [Cu_2Cd(tren)_2(NCS)_6] + 4NH_4NO_3 + 2H_2O \quad (3)$$

The principle involved is the union of two complementary units $[Cd(NCS)_6]^{4-}$ and $[Cu(tren)(OH_2)]^{2+}$, which results in the trinuclear compound instead of the polymers of the type **2** and **3** [4]. **1** was also achieved in good yield by a single-pot [11] reaction (Method B, see Section 2) using a 1:2:2:6 molar ratio of $Cd(NO_3)_2 \cdot 4H_2O$, $Cu(NO_3)_2 \cdot 3H_2O$, tren and NH_4NCS. A 1:2 molar ratio of alternate building units $[Cu(NCS)_6]^{4-}$ and $[Cd(tren)(OH_2)_2]^{2+}$ leads to the same trinuclear complex showing a inherent tendency towards its formation (Method C, see Section 2). A change in metal ion arouses a change in the coordination matrix of the molecular ion as well as in the dimensionality compared to that of **2** and **3** [4].

The complex was characterised by elemental (C, H and N) analyses, solution electrical conductivity and magnetic susceptibility measurements and spectroscopic (IR and UV–Vis) properties and X-ray results. It is moderately soluble in common organic solvents like, methanol, ethanol, acetonitrile, dimethylformamide and dimethylsulfoxide. In methanol it behaves as a non-electrolyte as is evident from its low conductivity value [12]. The trinuclear complex, $[Cu_2Cd(tren)_2(NCS)_6]$ (**1**) shows bands at 3355 and 3265 cm^{-1} due to N–H stretching of the NH_2 group and bands at 2890 cm^{-1} can be assigned to the aliphatic C–H stretching vibration. Two well resolved peaks at 2129 and 2064 cm^{-1} attributed to the ν(NCS) stretching mode of thiocyanate [13] are distinctly seen. Presence of more than one band confirm both *N*- and *S*-coordination of thiocyanates in a bridging motif as well as terminals. The band corresponding to the stretching frequency ν(CS) appears at 770 cm^{-1}. The complex displays multiple absorption bands and shoulders in the 200–1000 nm range in MeOH solution. A band at 885 nm is assignable to a d–d transition ($d_{x^2-y^2}$, $d_{xy} \rightarrow d_{z^2}$) of copper(II) moieties in a trigonal bipyramidal (tbp) geometry [14]. A higher energy shoulder is observed at 670 nm which is typical of copper(II) complexes with tbp geometry. An absorption at 260 nm may be assigned to a ligand based transition. The solid state reflectance spectrum shows a good correspondence to the solution spectrum indicating similar gross geometric and electronic structure in the solid state and in solution.

3.2. Structure

The structural analysis shows that trinuclear **1** consists of 3D supramolecular continuum by multiple weak intra- and intermolecular N–H···S hydrogen bondings. An ORTEP diagram of the trinuclear unit and perspective view of the hydrogen bonded 3D network structure are shown in Figs. 1 and 2, respectively. Selected interatomic bond distances and bond angles relevant to the cadmium(II) and copper(II) coordination spheres are given in Table 2. The significant hydrogen bonding parameters are set in Table 3.

Each *trans*-$[Cd(NCS)_4(SCN)_2]^{4-}$ is connected to two $[Cu(tren)]^{2+}$ units through 1,3-thiocyanate bridges leading to a trinuclear unit and the cadmium atom is at the inversion centre. The geometry around the 4d ion, Cd(1), is a distorted octahedron with a relatively hard *trans*-CdN_4S_2 instead of the relatively soft *cis*/*trans*-CdN_2S_4 matrix

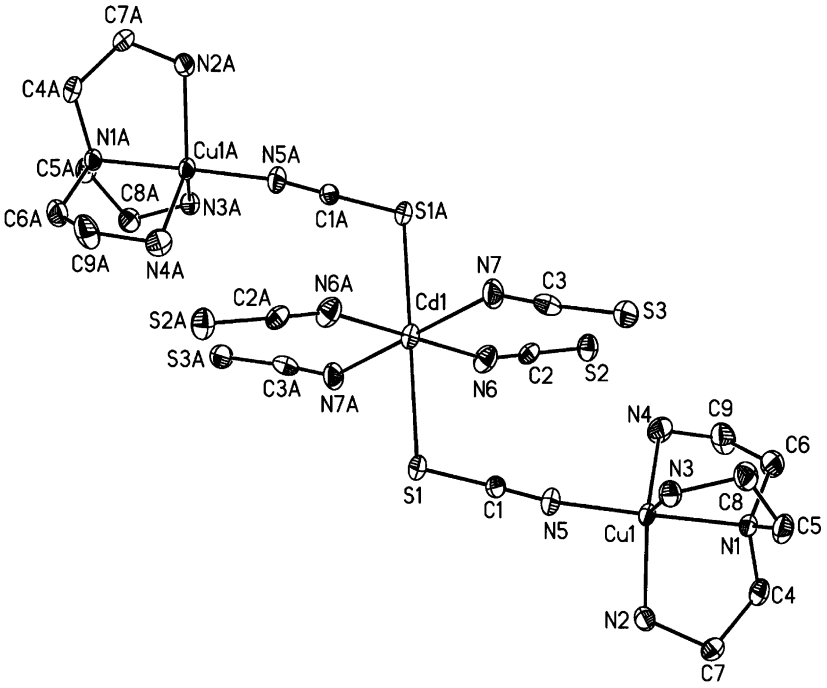

Fig. 1. ORTEP representation of $[Cu_2Cd(tren)_2(NCS)_6]$ (**1**).

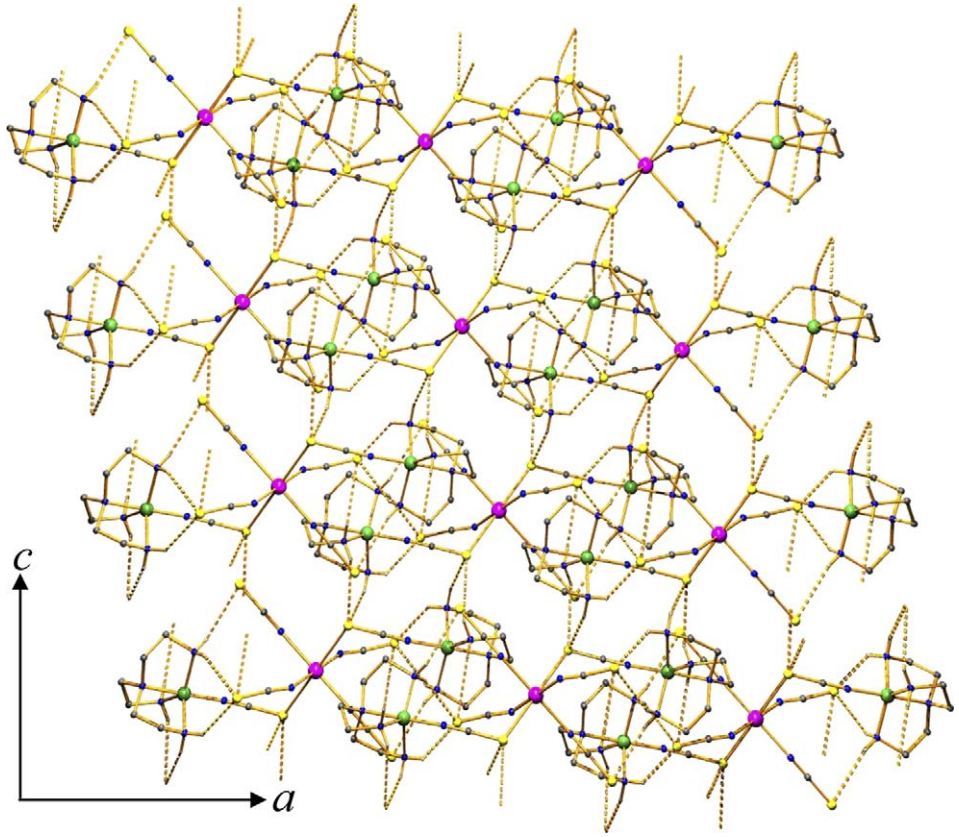

Fig. 2. 3D network in **1** formed by N–H···S hydrogen bondings.

present in **2** and **3** [4]. The *trans*-CdN_4S_2 chromophore is formed by two S atoms of two different bridging NCS^- and four N atoms of the four terminal pseudohalides. Cu(1) of $[Cu(tren)]^{2+}$ is in a distorted trigonal bipyramidal environment with a hard CuN_5 chromophore produced through attachment of four N atoms of the tripodal amine

Table 2
Selected bond distances (Å) and angles (°) for **1**

Bond distances			
Cu(1)–N(1)	2.047(2)	Cd(1)–N(6A)	2.273(3)
Cu(1)–N(2)	2.057(3)	Cd(1)–N(7)	2.373(3)
Cu(1)–N(3)	2.115(3)	Cd(1)–N(7A)	2.373(3)
Cu(1)–N(4)	2.047(3)	Cd(1)–S(1)	2.7805(8)
Cu(1)–N(5)	1.960(3)	Cd(1)–S(1A)	2.7805(8)
Cd(1)–N(6)	2.273(3)		
Bond angles			
N(6A)–Cd(1)–N(6)	180.0(2)	S(1)–Cd(1)–S(1A)	180.00(3)
N(6A)–Cd(1)–N(7)	90.79(12)	N(6)–Cd(1)–S(1A)	85.64(8)
N(6)–Cd(1)–N(7)	89.21(12)	N(2)–Cu(1)–N(3)	115.07(11)
N(6A)–Cd(1)–N(7A)	89.21(12)	N(5)–Cu(1)–N(4)	94.86(12)
N(6)–Cd(1)–N(7A)	90.79(12)	N(5)–Cu(1)–N(1)	178.73(12)
N(7A)–Cd(1)–N(7)	180.00(15)	N(4)–Cu(1)–N(1)	84.01(11)
N(6A)–Cd(1)–S(1)	85.64(8)	N(5)–Cu(1)–N(2)	96.23(12)
N(6)–Cd(1)–S(1)	94.36(8)	N(4)–Cu(1)–N(2)	129.55(12)
N(7)–Cd(1)–S(1)	89.58(8)	N(1)–Cu(1)–N(2)	84.95(10)
N(7A)–Cd(1)–S(1)	90.42(8)	N(1)–Cu(1)–N(3)	83.55(10)
N(6A)–Cd(1)–S(1A)	94.36(8)	N(5)–Cu(1)–N(3)	96.35(12)
N(7)–Cd(1)–S(1A)	90.42(8)	N(4)–Cu(1)–N(3)	112.31(12)
N(7A)–Cd(1)–S(1A)	89.58(8)		

Table 3
Hydrogen bond distances (Å) and angles (°) for **1**

D–H···A	D–H	H···A	D···A	∠D–H···A
N(2)–H(2B)···S(3)[a]	0.9200	2.7900	3.557(3)	141.00
N(3)–H(3A)···S(3)	0.9200	2.6600	3.398(3)	137.00
N(3)–H(3B)···S(1)[b]	0.9200	2.7600	3.606(3)	153.00
N(4)–H(4C)···S(2)	0.9200	2.7500	3.492(3)	139.00
N(4)–H(4D)···S(3)	0.9200	2.8000	3.617(3)	149.00
N(2)–H(2A)···S(1)[b]	0.9200	2.7500	3.592(3)	152.00
C(9)–H(9A)···S(3)[a]	0.9900	2.8400	3.636(5)	138.00

Symmetry code: [a] $1/2 - x$, $1/2 + y$, $1/2 - z$; [b] $1 - x$, y, $1/2 - z$.

and one N atom of a bridging NCS^-. The sequence in the bridge is represented as Cu(1A)–N(5A)–C(1A)–S(1A)–Cd(1)–S(1)–C(1)–N(5)–Cu(1) (Fig. 1).

The equatorial plane of Cd(1) consists by four terminal N-coordinated thiocyanates [N(6), N(6A), N(7), N(7A)] and the two S atoms of the bridging pseudohalide [S(1), S(1A)] lie in the axial positions. The Cd(1)–S bond length [2.7805(8) Å] is much longer than the Cd(1)–N lengths which lie within the range 2.273(3)–2.373(3) Å. Ranges of *cisoid* angles [85.64(8)°–94.36(8)°] reflect the deviation of the chromophore from an ideal octahedron. *Transoid* angles on the other hand are 180.00°. Two bridging thiocyanate nitrogens [N(5), N(5A)] of *trans*-$[Cd(NCS)_4(SCN)_2]^{4-}$ coordinate to the adjacent $[Cu(tren)]^{2+}$ forming the trinuclear unit. The three primary amine nitrogens [N(2), N(3), N(4)] of the tripod form the equatorial plane around copper(II) with the tertiary amine [N(1)] and thiocyanate nitrogen [N(5)] placed at the axial sites. Cu–N distances within the equatorial plane lie within a close range [2.047(3)–2.115(3) Å] while the axial distances show a significant difference [Cu(1)–N(1), 2.047(3) Å; Cu(1)–N(5), 1.960(3) Å]. Angles of the equatorial plane [N(2)–Cu(1)–N(3), 115.07(11)°; N(2)–Cu(1)–N(4), 129.55(12)°; N(3)–Cu(1)–N(4), 112.31(12)°] show deviation from the ideal 120° whereas the *trans* axial angle N(1)–Cu(1)–N(5), 178.73(12)° is close to the ideal 180°. The mean deviation of the copper(II) atom from the basal plane is 0.209 Å. Cu···Cd and Cu···Cu distances within the same unit are 5.975 and 11.949 Å, respectively and the Cu···Cu distance between two adjacent layers is 9.714 Å. All the Cd–S/N and Cu–N/S bond lengths and angles are similar to the reported ones [15,16].

An interesting feature of **1** is the interionic hydrogen bonds which play an important role in the crystal packing and the stability of the trinuclear complex. Adjacent trinuclear units are cross-linked by three intramolecular and three intermolecular N–H···S hydrogen bondings [17] with involvement of all the S atoms of the pseudohalides. The range of the donor–acceptor distances lie within a range of 3.40–3.64 Å and this is slightly greater than the usual 3.35 Å as reported in several works [18,19]. Trinuclear entities are so placed that a copper(II) coordination moiety of one unit lies very close to another copper(II) moiety of the adjacent trimer. One terminal sulfur [S(3)] of CdN_2S_4 is engaged in trifurcated N–H···S hydrogen bonding. Of them, two are intramolecular with the H's of the two amine nitrogens [N(2), N(3)] of tren from the same unit (Table 3) and the other one is an intermolecular hydrogen bonding between the amine nitrogen [N(4)] of tren belonging to the adjacent unit. The other terminal sulfur atom [S(2)] participates in intramolecular hydrogen bonding with the remaining amine nitrogen [N(4)] of tren bound to copper(II) of the same unit. Presence of four such types of N–H···S bondings (three-intra and one-inter) leads to the formation of supramolecular layers of the trinuclear units. The bound S(1) of cadmium(II) participates in intermolecular bifurcated hydrogen bonding with amine nitrogens [N(2), N(3)] of the adjacent layers leading to an extended three-dimensional network (Fig. 2).

3.3. Magnetism

Variable-temperature magnetic susceptibility measurements have been performed in the range 2–300 K. The thermal variation of molar susceptibility χ_M together with a plot of $\chi_M T$ versus T of complex **1** is shown in Fig. 3. The magnetic moment (μ_{eff}) per copper(II) centre is the same as that expected for an isolated paramagnetic system with $S = 1/2$ ($\mu_{eff} = 1.732$ BM) for copper(II) [20]. **1** consists of two copper(II) ions as its basic unit. For each copper(II), $\chi_M T$ is, as indicated, close to 0.4 $cm^3\,mol^{-1}\,K$ – thus a total of 0.8 $cm^3\,mol^{-1}\,K$ is the result. The experimental value of 0.82 $cm^3\,mol^{-1}\,K$ is almost constant throughout the temperature range (Fig. 3). This shows coupling between the paramagnetic centres is negligible. Each magnetic centre behaves as a discrete unit which implies that the long –NCS–Cd–SCN– bridge inhibits magnetic exchange.

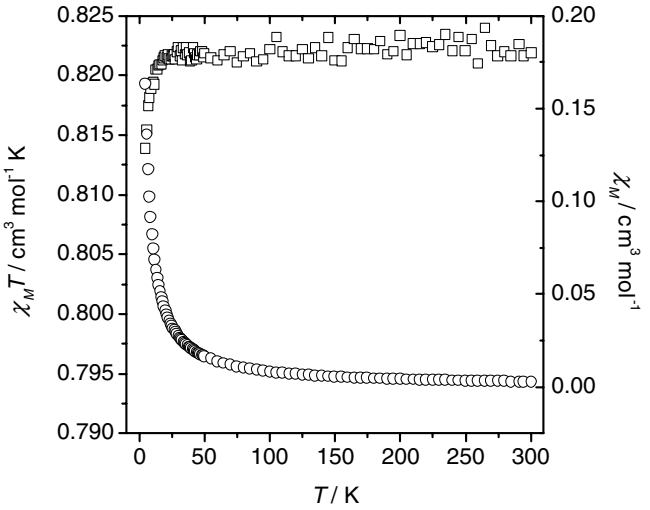

Fig. 3. Plots of $\chi_M T$ vs. T and χ_M vs. T in **1**.

4. Conclusion

A new trinuclear based supramer is synthesised through reactions of the building components $[Cu(tren)(OH_2)]^{2+}$ and $[Cd(NCS)_{6-n}(SCN)_n]^{4-}$ with a preassigned ratio. Use of copper(II) with lower coordination affords the heterotrinuclear ensemble $[Cu_2Cd(tren)_2(NCS)_6]$ instead of polymeric $[Cu_2Cd(tren)_2(NCS)_6]_n$ like that of **2** and **3** [4]. Presence of the diamagnetic $[Cd(NCS)_{6-n}(SCN)_n]^{4-}$ molecular ion hinders magnetic coupling between the paramagnetic centres in this complex. This prompts us to extend our work with a paramagnetic ion based molecular ion to find its effect on magnetic interactions in different complexes.

5. Supplementary data

Crystallographic data for the structural analysis have been deposited with the Cambridge Crystallographic Data Centre, CCDC No. 211745 (**1**). Copies of this information can be obtained free of charge from the Director, CCDC, 12 Union Road, Cambridge, CB2 IEZ, UK (Fax: +44 1223 336033; e-mail: deposit@ccdc.cam.ac.uk or www.ccdc.cam.ac.uk).

Acknowledgements

Financial support from the Department of Science and Technology (DST) and Council of Scientific and Industrial Research (CSIR), New Delhi, India is gratefully acknowledged.

References

[1] (a) M.S. El Falah, E. Rentchler, A. Caneschi, R. Sessoli, D. Gatteschi, Angew. Chem. Int. Ed. 35 (1996) 1947;
(b) K.V. Langenberg, S.R. Batten, K.J. Berry, D.C.R. Hockless, B. Moubaraki, K.S. Murray, Inorg. Chem. 36 (1997) 5006;
(c) H. Miyasaka, H. Ieda, N. Matsumoto, N. Re, R. Crescenzi, C. Floriani, Inorg. Chem. 37 (1998) 255.

[2] (a) M. Ohba, N. Usuki, N. Fukita, H. Okawa, Inorg. Chem. 37 (1998) 3349;
(b) S. Ferlay, T. Mallah, R. Ouahes, P. Veillet, M. Verdaguer, Inorg. Chem. 38 (1999) 229;
(c) T. Lu, H. Xiang, C. Su, P. Cheng, Z. Mao, L. Ji, New J. Chem. 25 (2001) 216.

[3] (a) R.J. Parker, L. Spiccia, K.J. Berry, G.D. Fallon, B. Moubaraki, K.S. Murray, Chem. Commun. (2001) 333;
(b) M. Clemente-Leon, E. Coronado, J.R. Galan-Mascaros, C.J. Gomez-Garcia, T. Woike, J.M. Clemente-Juan, Inorg. Chem. 40 (2001) 87;
(c) R.J. Parker, L. Spiccia, S.R. Batten, J.D. Cashion, G.D. Fallon, Inorg. Chem. 40 (2001) 4696;
(d) J. Larinova, R. Clerac, J. Sanchiz, O. Kahn, S. Golhen, L. Ouahab, J. Am. Chem. Soc. 120 (1998) 13088.

[4] D. Bose, Sk.H. Rahaman, R. Ghosh, G. Mostafa, J. Ribas, C.-H. Hung, B.K. Ghosh, Polyhedron, in press. Available online: 6 September 2005.

[5] (a) Y.-H. Li, X.-S. Wang, H. Zhao, R.-X. Yuan, J. Zhang, R.-G. Xiong, X.-Z. You, H.-X. Ju, Z.-L. Xue, Inorg. Chem. 43 (2004) 712;
(b) M. Kawahara, M.K. Kabir, K. Yamada, A. Adachi, H. Kumagai, Y. Narumi, K. Kindo, S. Kitagawa, S. Kawata, Inorg. Chem. 43 (2004) 92;
(c) Y.Z. Zhang, S. Gao, H.L. Sun, G. Su, Z.M. Wang, S.W. Zhang, Chem. Commun. (2004) 1906.

[6] (a) Y.S. You, C.S. Hong, K.M. Kim, Polyhedron 24 (2005) 249;
(b) J.K. Clegg, L.F. Lindoy, J.C. McMurtie, D. Schilter, J. Chem. Soc., Dalton Trans. (2005) 857;
(c) Z.-K. Chan, Y.-Y. Wu, J.-D. Chen, C.-Y. Yeh, C.-C. Wang, Y.-F. Tsai, J.-C. Wang, J. Chem. Soc., Dalton Trans. (2005) 985.

[7] A.K. Patra, S. Dhar, M. Nethaji, A.R. Chakravarty, J. Chem. Soc., Dalton Trans. (2005) 896.

[8] G.-Y. Hsu, C.-W. Chen, S.-C. Cheng, S.-H. Lin, H.-H. Wei, C.-J. Lee, Polyhedron 24 (2005) 487.

[9] SADABS v2.02: Area-Detector Absorption Correction, Siemens Industrial Automation, Inc., Madison, WI, 1996.

[10] SHELXTL 6.1, Bruker AXS Inc., Madison, WI, 2001.

[11] (a) Special issue on Focus on Self-Assembly, Acc. Chem. Res. 32 (1999) No. 4;
(b) B.J. Holliday, C.A. Mirkin, Angew. Chem. Int. Ed. 40 (2001) 2022.

[12] W.J. Geary, Coord. Chem. Rev. 7 (1971) 81.

[13] K. Nakamoto, Infrared and Raman Spectra of Inorganic and Coordination Compounds, Part B, fifth ed., Wiley, New York, 1997, p. 116.

[14] (a) A.B.P. Lever, Inorganic Electronic Spectroscopy, second ed., Elsevier Science, New York, 1984;
(b) H.-Y. Mao, X.-Q. Shen, G. Li, H.-Y. Zhang, C. Xu, H.-L. Liu, E.-B. Wang, Q.-A. Wu, H.-W. Hou, Y. Zhu, Polyhedron 23 (2004) 1961.

[15] (a) A. Mondal, G. Mostafa, A. Ghosh, I.R. Laskar, N.R. Chaudhuri, J. Chem. Soc., Dalton. Trans. (1999) 9;
(b) F.H. Liu, W.Z. Chen, X.Z. You, J. Solid State Chem. 169 (2002) 199;
(c) J.H. Zhou, Y.F. Peng, Y.P. Zhang, B.L. Li, Y. Zhang, Inorg. Chem. Commun. 7 (2004) 1181.

[16] (a) K.-Y. Choi, Y.-M. Jeon, H. Ryu, J.-J. Oh, H.-H. Lim, M.-W. Kim, Polyhedron 23 (2004) 903;
(b) E.M. Jouad, M. Allain, M.A. Khan, G.M. Bonet, Polyhedron 24 (2005) 327.

[17] D. Bose, J. Banerjee, Sk.H. Rahaman, G. Mostafa, H.-K. Fun, R.D.B. Walsh, M.J. Zaworotko, B.K. Ghosh, Polyhedron 23 (2004) 2045.

[18] J.L. Seela, M.J. Knapp, K.S. Kolack, H.-R. Chang, J.C. Huffman, D.N. Hendrickson, G. Christou, Inorg. Chem. 37 (1998) 516.

[19] C.-K. Lam, T.C.W. Mak, Chem. Commun. (2003) 2660.

[20] (a) Y.-B. Jiang, H.-Z. Kou, R.-J. Wang, A.-L. Cui, J. Ribas, Inorg. Chem. 44 (2005) 709;
(b) F. Bonadio, M.-C. Senna, J. Ensling, A. Sieber, A. Neels, H.-S. Evans, S. Decurtins, Inorg. Chem. 44 (2005) 969.

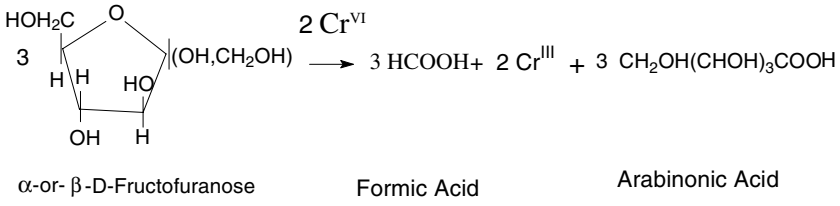

Scheme 1.

to occur in most oligo- and polysaccharides, probably because of the greater stability of this form of the sugar as compared with its pyranose form [14]. The mechanism of oxidation of ketohexoses by transition-metal ions in acid media has been little studied [15–18]. Being D-Fru present at animal and vegetal level, the chromic interaction of this ketose was considered of great importance to be studied, in order to compare its reactivity with aldoses, deoxyaldoses, aminoaldoses, aldonic acids and the respective lactones. In this paper, results on the chromic oxidation of D-Fru (Scheme 1) and structural evidences of the intermediate Cr^{V} complexes formed in acid and neutral aqueous solutions are described.

2. Experimental

2.1. Materials

D-Fructose, potassium dichromate, acrylonitrile, perchloric acid, and sulfuric acid were commercial products of highest available purity. Aqueous solutions were prepared in double-destilled, deionized, water. For experiments performed in the pH range 1–7, the pH of the solutions was adjusted by addition of 0.5 M $HClO_4$ and NaOH 0.5 M. In experiments performed at constant ionic strength ($I = 1.0$ M) and different $[H^+]$, mixtures of $NaClO_4$ and $HClO_4$ solutions were prepared. The concentration of stock solutions of $HClO_4$ was determined by titration by standard analytical methods [19].

The stability of the organic substrate under conditions used in the kinetic studies was tested by paper chromatography (PC) at a given $[H^+]$ and by HPLC.

2.2. Spectrophotometry

Spectrophotometric measurements were made by monitoring absorbance changes at 350 and 570 nm on a Jasco-V-530-UV/Vis spectrophotometer with fully thermostated cell compartments (±0.2 °C). Each kinetic run was performed under pseudo-first-order conditions using excess of [D-Fru] over $[Cr^{VI}]$. A mixture containing appropriate amounts of all reactants (except oxidant) was thermally equilibrated at the desired temperature and this was rapidly added to a measured amount of the oxidant solution (pre-equilibrated at the same temperature). The reaction was followed until at least 80% conversion. Experiments were performed at 33° unless otherwise mentioned and mixtures of sodium perchlorate were used to maintain a constant ionic strength (I) of a 1.00 M.

The Cr^{VI} consumption was followed spectrophotometrically at 350 nm. In all experiments, the concentration of Cr^{VI} was kept constant at 8.0×10^{-4} M while ketose concentration was varied from 0.02 to 0.1 M. The observed pseudo-first-order rate constants (k_{obs}), determined from the slopes of the linear part of plots of $\ln(Abs_{350})$ versus time, were deduced from multiple determinations and were within ±5% of each other.

The formation of Cr^{III} was monitored at 570 nm, $[Cr^{VI}] = 6.0 \times 10^{-3}$ M in the presence of excess ketose and $[HClO_4] = 1.0$ M.

Chromate esters were investigated by UV/Vis spectrophotometry in the 300–500 nm region in which these esters show characteristic absorption bands. An excess of organic substrate maximized ester formation while minimizing successive oxidation steps. Reactions were performed at pH 4.0, to ensure that ester formation was not rate limiting; at higher pH the overall reduction of Cr^{VI} is much slower than at pH 1.0. The instrument was zeroed to an arrangement of the reference and sample beams passing through matched cuvettes, both containing Cr^{VI} in H_2O at pH 4.0. The solution in the sample cell was replaced with the reaction solution containing 6×10^{-4} M Cr^{VI} and 0.06–0.33 M ketose at pH 4.0, $I = 1.0$ M and $T = 33$ °C.

The formation of CrO_2^{2+} was examined by periodic scanning of O_2-saturated solutions containing 0.125 M Fru and 0.045 mM Cr^{VI} in $HClO_4$.

2.3. Product analysis

2.3.1. General

HPLC was employed to detect the reaction products under the conditions used in the kinetic measurements (excess of ketose over Cr^{VI}). The chromatograms were obtained on a KNK-500 A chromatograph provided with a 7125 HPLC pump. The separation was carried out on a supelcogel C-610 H HPLC column (300.0 × 7.8 mm, Bio-Rad Laboratories), using 0.1% v/v H_3PO_4 as eluent, and a flow rate of 0.5 ml/min, at 30 °C. The samples were filtered through at 0.2-μm membrane prior to the injection into the chromatographic system. The effluent was monitored with refractive index (ERC-7522, ERMA INC) and 115 UV Gilson ($\lambda = 220$ nm) detectors.

Standard solutions of the D-Fru, D-arabinonic acid, D-formic acid were prepared individually in 0.2 M $HClO_4$

and chromatographed separately to determine the retention time (t_R) of each sample.

2.4. EPR measurements

All of the EPR experiments were carried out at room temperature with a Bruker ESP-300 E spectrometer. The microwave frequency was generated with a Bruker 04-ER (9–10 GHz) and measured with a Racal-Dana frequency meter. The magnetic field was measured with a Bruker NMR-probe gaussmeter. All the EPR experiments were carried out at 20 °C. EPR spectra were simulated by means of the program PEST WinSIM [20] with 100% Lorentzian lineshapes. The spectral parameters for each Cr^V species were consistent within all simulations.

2.5. Free-radicals test

Upon addition of 0.5 ml acrylonitrile (0.20 M in 0.20 M $HClO_4$) to a reaction mixture: 2.5×10^{-2} M $K_2Cr_2O_7$ and 5.0×10^{-2} M D-Fru in 2 ml of 0.20 M $HClO_4$, at 33 °C. After 10 min, a white precipitate of a polymer appeared slowly. Blank experiments with either Cr^{VI} or D-Fru gave no detectable white precipitates. The possible reaction of Cr^V or Cr^{IV} with acrylonitrile was excluded based on the absence of a precipitate one day after mixing [Cr^VO-(ehba)]K [21] or [Cr^{IV}O(ehba)]K [22] (ehba = 2-ethyl-2-hydroxybutanoic acid) and acrylonitrile under the same reaction conditions than before.

3. Results and discussion

3.1. Rate studies

The absorbance versus times curves at 350 nm exhibit a monotonic decrease of absorbance which cannot be described by a single exponential decay.

Under the present experimental conditions, no induction period was detected as Kabir-ud-Din et al. [18] observed in their study of Influence of sodium dodecil sulfate/Triton X-100 micelles on the oxidation of the D-fructose by chromic acid in presence of perchloric acid.

At this wavelength, kinetics traces show an initial deviation from first-order decay over short time periods. These kinetics profiles could be adequately described by the set consecutive first-order reactions of Scheme 2.

It is known that Cr^V species absorb strongly at 350 nm and may superimpose Cr^{VI} absorbance yielding the wrong interpretation of spectrophotometric absorbance decay values [23] . Thus considering the Cr^V absorption superimposition, the absorbance at 350 nm, at any time during the reaction, is given by:

$$Abs_{350} = \varepsilon^{VI}[Cr^{VI}] + \varepsilon^{V}[Cr^{V}]. \quad (1)$$

Combining Eq. (1) with rate expressions [24] derived from Scheme 2 yields:

$$S + Cr^{VI} \xrightarrow{k_6} I^o \xrightarrow{k_5} Cr^V \rightarrow Cr^{III}$$

$$+ \quad S$$

$$Cr^{III}$$

S= organic substrate I^o = intermediate

Scheme 2.

$$Abs_{350} = Abs_0\, e^{-2k_6 t} + k_6 \varepsilon^V [Cr^{VI}]_0 (e^{-k_5 t} - e^{-2k_6 t})/(2k_6 - k_5). \quad (2)$$

In this equation, ε^V refers to the molar absorptivity of Cr^V at 350 nm. Values of ε^V depend of pH and were assumed to be the same as for the complex $[Cr^V(O)(ehba)_2]^-$ [21] in the same [H^+] range (ε^V 900–1000 $M^{-1}\,cm^{-1}$). Parameters k_6 and k_5 refer to the rate of disappearance of Cr^{VI} and Cr^V, respectively, and were evaluated from a non-linear iterative computer fit of Eq. (2). It must be noted that in Eq. (2), k_6 appears in the numerator of the pre-exponential term and $2k_6$ appears in the denominator and in the exponential terms because, according to the proposed reaction scheme, only half of the Cr^{VI} reaches Cr^{III} throughout a Cr^V intermediate.

Unlike that observed for the chromic oxidation of D-gluconic acid [25], in the present case, Cr^V was not detected spectrophotometrically at 750 nm under conditions used in the EPR kinetic experiments. Fortunately, it could be easily detected by EPR measurements.

The reaction of D-Fru and Cr^{VI} was performed at [H^+] lower than used in the kinetic measurements in order to obtain information of the structure of Cr^V species formed as intermediates in the reduction of Cr^{VI} to Cr^{III}.

In 0.2 M $HClO_4$, the EPR spectra consist of the one signal at $g_{iso} = 1.9791$. At this [H^+], the superhyperfine (shf) pattern of the EPR signal (the ^1H shift splitting (a_H) for Cr^V-alcoholato species is usually < 1 G) could not be resolved.

When the pH > 1, the redox reaction becomes slow and Cr^V species remain in solution for a long time and the distribution and structure of these intermediates may be analyzed from the EPR spectral features.

In the 3–7 pH range and D-Fru:Cr^{VI} ratio 19/1 at 25 °C, the EPR spectrum is composed (signals were deconvoluted by fitting the spectra by lorentzian derivatives) of two triplet at $g_{iso1} = 1.9800$ ($a_H = 0.79 \times 10^{-4}\,cm^{-1}$), $g_{iso2} = 1.9797$ ($a_H = 0.71 \times 10^{-4}\,cm^{-1}$) and one doublet at $g_{iso3} = 1.9792$ ($a_H = 0.58 \times 10^{-4}\,cm^{-1}$), each with the four weak ^{53}Cr (9.55% abundance, $I = 3/2$) hyperfine peaks at 17.7 G spacing, typical of five-coordinate oxochromate (V) complexes (see Fig. 1) [26,27].

In order to rule out the possibility to assign one of the three Cr^V species to chelates formed with the oxidation products; a reaction of chromate with glutatione (1:1 ratio) in the presence of a 20 times excess of D-Fru was performed

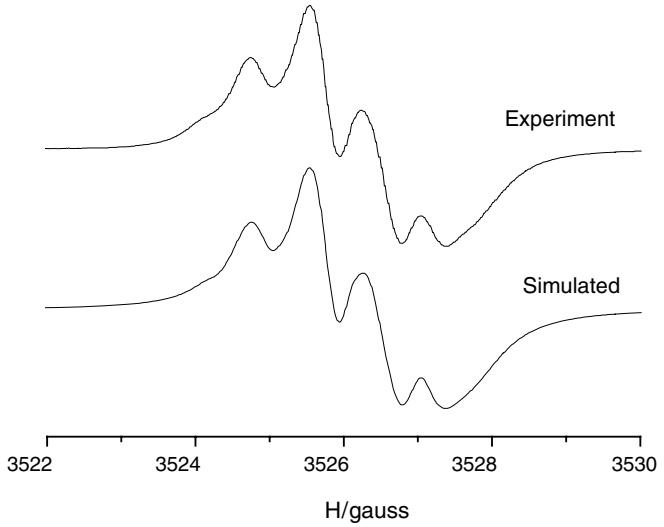

Fig. 1. Experimental and simulated X-band EPR spectra of mixtures of $[Cr^{VI}] = 0.015$ M, [D-Fru] = 0.28 M, $T = 24$ °C, $I = 1$ M, pH 5, $t = 24$ h, frequency ≈ 9.7 GHz, mod. amp. = 0.4 G.

and afforded Cr^{V} EPR spectra identical to those obtained by direct reaction of D-Fru with Cr^{VI}.

The different shf coupling constants of the two triplets indicate that they may correspond to the two geometric isomers of the Cr^{V} bischelate ($[Cr(O)(O^{2(4)}, O^{3(5)}$-β-D-fructopyranose$)_2]^-$).

The doublet at g_{iso3} indicates that, in this oxo-Cr^{V}-D-Fru species, only one carbinolic proton is coupled to the electronic spin and can be assigned to the Cr^{V} bischelate $[Cr(O)(O^{ring},O_2$-β-D-fructofuranose$)$ $(O^{2(4)},O^{3(5)}$-β-D-fructopyranose$)]^-$ with one D-Fru molecule acting as bidentate through the α-hydroxodiolate moiety of the piranosic form and the second D-Fru molecule bound to Cr^{V} at the α-hydroxodiolate group, and the ring oxygen atom of the furanosic form (see Scheme 3).

Fig. 2 shows a curve for peak-to-peak heights of Cr^{V} EPR signals versus time obtained on a reacting solution. Values of the rates of disappearance of Cr^{VI} (k_6) and Cr^{V} (k_5), respectively, may be calculated by Eq. (3) [25,28] which fits well the experimentally observed Cr^{V} intermediate growth and decay curve in Fig. 2

$$h = Ak_6\{\exp(-k_5t) - \exp(-2k_6t)\}/(2k_6 - k_5). \quad (3)$$

In Eq. (3), h is the peak-to-peak height and A depends on the spectrometer settings and is adjusted by the fitting program [29].

For conditions stated in Fig. 2, the values of k_6 and k_5 were: $k_6 = 1.4 \times 10^{-4}$ s^{-1}, $k_5 = 1.37 \times 10^{-3}$ s^{-1} and the time of maximum Cr^{V} concentration, $T_{max} \approx 17$ min.

To verity if this assignment of the rate constant values was correct, k_{obs} ($2k_6$) was evaluated spectrophotometrically at 25 °C under conditions used in the EPR experiments and the k_{obs} ($2k_6$) value was reproduced.

For several runs at different D-fructose/chromium(VI) ratios, k_5 values were at least six times larger than k_6 values [27].

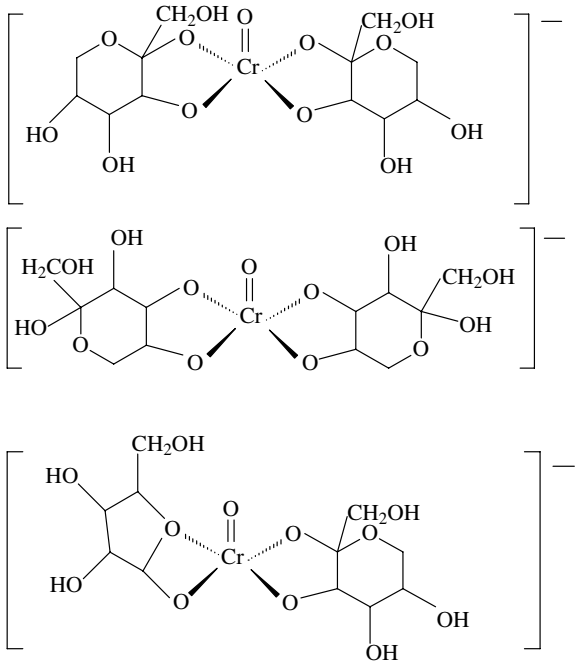

Scheme 3.

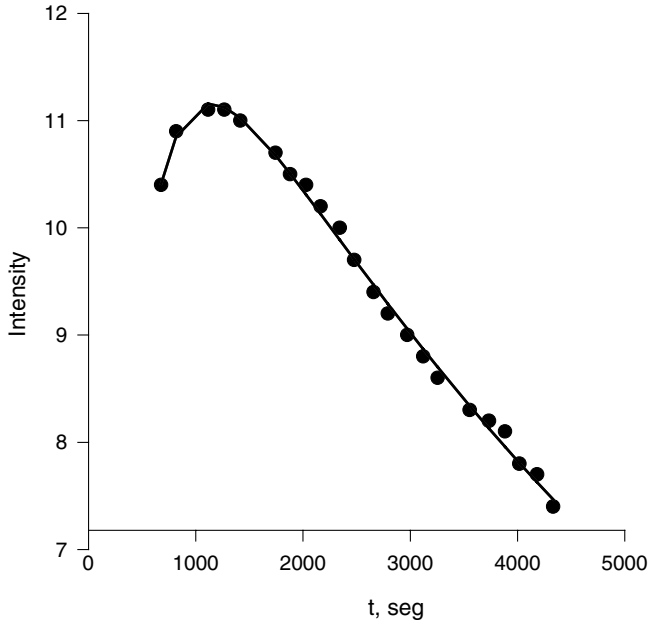

Fig. 2. Peak-to-peak heights of Cr^{V} EPR signals vs. time. $[Cr^{VI}] = 0.44$ M, [D-Fru] = 0.83 M, $[HClO_4] = 0.2$ M, $T = 24$ °C, $I = 1$ M.

The reactions were carried out at various fixed [oxidant] keeping other variables, viz. [D-Fru], $[H^+]$, I and temperature constant. Pseudo-first-order rate constants obtained from Eq. (2) ($2k_6$) were coincident with values obtained from the slope of the linear part of the ln absorbance versus time curves, therefore, most of the k_{obs} were calculated through the last approach.

The independence of k_{obs} over a range of $[Cr^{VI}]_0$ (Table 1) was in agreement with a first-order dependence on $[Cr^{VI}]_T$. The rate law was, therefore, given as:

Table 1
Observed first-order rate constant for different $[Cr^{VI}]_0$, [D-Fru] = 0.025 M, $[H^+]$ = 1 M, I = 1 M, T = 33 °C, λ = 350 nm

$10^4[Cr^{VI}]_0$ (M)	4.0	5.0	6.0	7.0	8.0	10.0
$10^4\ k_{obs}$ (s^{-1})	4.50 ± 0.01	4.90 ± 0.01	5.20 ± 0.01	5.10 ± 0.01	5.20 ± 0.01	5.00 ± 0.02

$$-d[Cr^{VI}]/dt = k_{obs}[Cr^{VI}].$$

The observed rate constants were calculated from the absorbance data obtained at 350 nm.

The first-order-dependence of the rate upon $[Cr^{VI}]$ was verified, and k_{obs} was obtained following the Cr^{III} growth at 570 nm. Initial reaction rates were obtained by fitting the absorbance at 570 nm/time data to a polynomial expression [30] and calculating the slope of the tangent at time zero (r_i). First-order rate constants were obtained from these initial rates by means of the equation $-r_i/(A_0 - A_t)$ and were coincident with those obtained at 350 nm.

This is consistent with the observation of the isosbestic point at 527 nm (Fig. 3). At the end of the reaction, the two d–d bands ascribed to Cr^{III} were observed at $\lambda_{max} = 411$ nm ($\varepsilon = 17.5\ mol^{-1}\ cm^{-1}$) and $\lambda_{max} = 570$ nm ($\varepsilon = 15.2\ mol^{-1}\ cm^{-1}$). We found no shift toward shorter wavelength with those observed to the $^4A_{2g} \rightarrow {}^4T_{1g}$ and $^4A_{2g} \rightarrow {}^4T_{2g}$ transitions of $[Cr(OH_2)_6]^{3+}$ ion [31] at the same $[H^+]$.

Thus, it was confirmed that chromium(III) aqua ion was the product under the present experimental conditions.

Table 2 summarizes values of k_{obs} for various concentrations of D-Fru at fixed concentrations of perchloric acids. Plots of k_{obs} versus [D-Fru] (Fig. 4) gave good straight lines with a positive intercept from which values of k_1 and k_2 were determined (Table 3).

Dependence of k_1 and k_2 with $[HClO_4]$ are shown in Figs. 5 and 6 and may be expressed by the following equation:

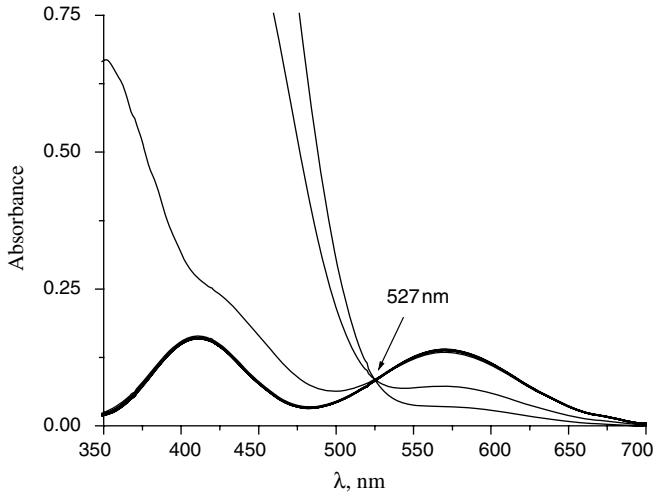

Fig. 3. Time evolution of the UV/Vis spectrum of a mixture of $[Cr^{VI}] = 9.00 \times 10^{-3}$ M, [D-Fru] = 0.20 M, $[HClO_4]$ = 1.00 M, T = 33 °C, I = 1 M over a period of ca. 240 min.

$$k_{obs} = k_1 + k_2\ [S],$$
$$k_1 = a\ [H^+]^2, \quad (4)$$
$$k_2 = b\ [H^+]^2,$$

where $a = 1.66 \times 10^{-4} \pm 3.56 \times 10^{-6}\ M^{-2}\ s^{-1}$ and $b = 1.79 \times 10^{-2} \pm 5.63 \times 10^{-4}\ M^{-3}\ s^{-1}$.

The complete rate law is then given by:

$$-d[Cr^{VI}]/dt = (a + b[\text{D-Fru}])[H^+]^2[Cr^{VI}]_T, \quad (5)$$

where $[Cr^{VI}]_T$ represents the total chromium(VI) concentration.

The oxidation of D-Fru by Cr^{VI} should occur through two parallel slow steps leading to the redox products.

3.2. Detection of the intermediate Cr^{VI} ester

Differential UV–Vis spectra obtained within 5 min after mixing revealed a distinctive absorption at 374 nm (Fig. 7) consistent with that ascribed to Cr^{VI}-oxy-esters [32,33]. Fig. 7 showed that the absorbance at 374 nm increased with increasing the concentration of D-Fru, probably as a result of a shift toward the ester in the esterification equilibrium.

The formation of Cr^{IV} is consistent with the observation of CrO_2^{2+}, the product of the reaction of Cr^{II} with O_2, which is taken as an indirect evidence of Cr^{IV} formation [34].

The band at 350 nm decreased in intensity over a period of 4 h, while new peaks at 293 and 248 nm grew in and then decreased (Fig. 8). The observed peaks were those of CrO_2^{2+}[35], formed as a long-lived intermediate. The CrO_2^{2+} absorbance at 249 nm ($Abs_{249}(CrO_2^{2+})$) was estimated by subtracting the $Abs_{249}(Cr^{VI})$ – the contribution of Cr^{VI} species to the absorbance at 249 nm, which concentrations could be calculated at 350 nm – from the total Abs_{249}, and the rate constant for the formation of $Abs_{249}(CrO_2^{2+})$ versus time curve (inset in Fig. 8).

Under all experimental conditions (large to moderate excess of D-ketose over Cr^{VI}), CO_2 was never observed as a reaction product, but the presence of HCOOH acid was detected through the $HgCl_2$ reaction [36], indicating that degradation to the lower homologues occurred. Formic acid was also detected by HPLC.

A reaction mixture obtained from 9.6×10^{-3} M Cr^{VI} and 0.24 M ketose in 0.2 M $HClO_4$ acid was submitted to HPLC: two products appearing at t_r 13.32 and 17.01 min were detected besides the peak corresponding to the starting D-Fru at t_r = 15.52 min. The retention time of the reaction products was coincident with of the standard solution of D-arabinonic acid and formic acid, respectively. The

Table 2
Observed pseudo-first-order rate constant for different concentrations of $HClO_4$ and D-Fru. $T = 33$ °C; $[Cr^{VI}]_0 = 8.00 \times 10^{-4}$ M, $I = 1$ M

[S] (M)	$[HClO_4] = 0.10$ M $10^6 k_{obs}$ (s^{-1})	$[HClO_4] = 0.20$ M $10^5 k_{obs}$ (s^{-1})	$[HClO_4] = 0.50$ M $10^5 k_{obs}$ (s^{-1})	$[HClO_4] = 0.75$ M $10^4 k_{obs}$ (s^{-1})	$[HClO_4] = 1.00$ M $10^4 k_{obs}$ (s^{-1})
0.02	9.00 ± 0.01	3.00 ± 0.01	14.50 ± 0.0	2.55 ± 0.01	4.30 ± 0.01
0.04		7.00 ± 0.01	25.50 ± 0.05	5.05 ± 0.01	8.50 ± 0.01
0.06	20.00 ± 0.04	8.50 ± 0.01	35.50 ± 0.05	7.05 ± 0.01	11.90 ± 0.03
0.08	30.00 ± 0.05	10.00 ± 0.03	46.50 ± 0.07	9.30 ± 0.02	14.80 ± 0.04
0.10	40.00 ± 0.06	12.50 ± 0.06	58.50 ± 0.10	10.40 ± 0.02	18.50 ± 0.05

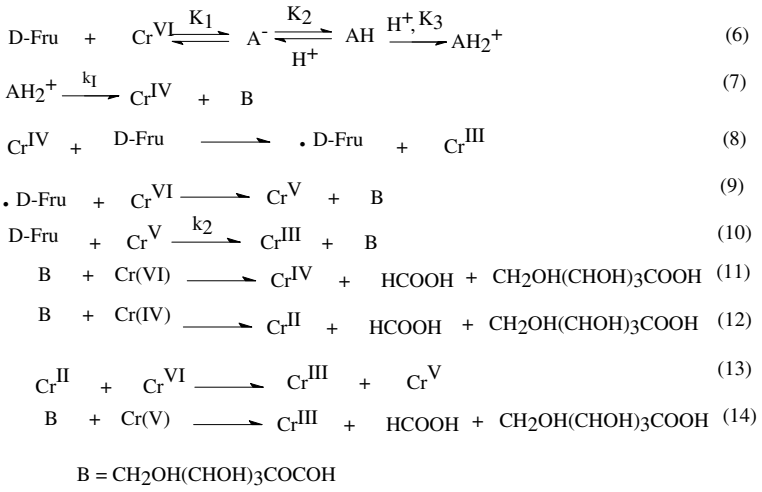

Scheme 4.

presence of D-arabinonic acid as the reaction product was further confirmed by paper chromatography using BuOH/AcOH/H_2O (4:1:5) as eluent. Paper chromatogram was visualized by two kinds of development reagents: a three stage dip of silver nitrate, sodium hydroxide and sodium thiosulfate [37] an *p*-anisidine reagent [38].

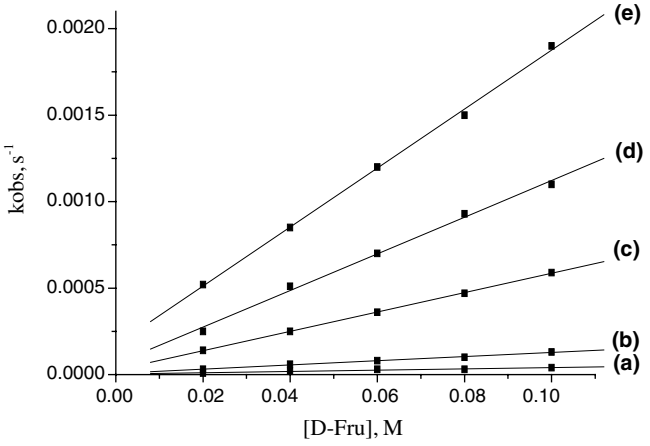

Fig. 4. Effect of [D-Fru] on k_{obs} at 33 °C, $I = 1$ M and [$HClO_4$] (M) = (a) 0.10 M, (b) 0.20 M, (c) 0.50 M, (d) 0.75 M and (e) 1.00 M.

In Scheme 4, a complex multistep mechanism that takes into account all the previous results detailed above (a) kinetic results, (b) polymerization of acrylonitrile added to the reaction mixture, (c) detection of an intermediate Cr^{VI} ester and oxocromate(V) species, (d) observation of CrO_2^{2+} and (e) identification of oxidation and reduction products is being proposed.

According to the above mechanism, the full rate law for the oxidation of D-Fru by Cr(VI), under the kinetic measurements, can be written as:

$$-d[Cr^{VI}]/Dt = (k_I + k_{II}[D\text{-Fru}])K_1K_2K_3[D\text{-Fru}] \times [H^+]^2\,[Cr^{VI}]. \quad (15)$$

Since

$$[Cr^{VI}]_T = [Cr^{VI}](1 + K_1[D\text{-Fru}] + K_1K_2[D\text{-Fru}][H^+] + K_1K_2K_3[D\text{-Fru}][H^+]^2). \quad (16)$$

Table 3
Values of k_1 and k_2 for different [$HClO_4$]

[$HClO_4$] (M)	0.100	0.200	0.500	0.750	1.000
$10^4 k_1$ (s^{-1})	0.024 ± 0.005	0.067 ± 0.009	0.40 ± 0.05	0.90 ± 0.09	1.7 ± 0.3
$10^4 k_2$ (M^{-1} s^{-1})	3.7 ± 0.4	11.0 ± 0.5	55.0 ± 0.7	106.2 ± 4.0	174.0 ± 4.0

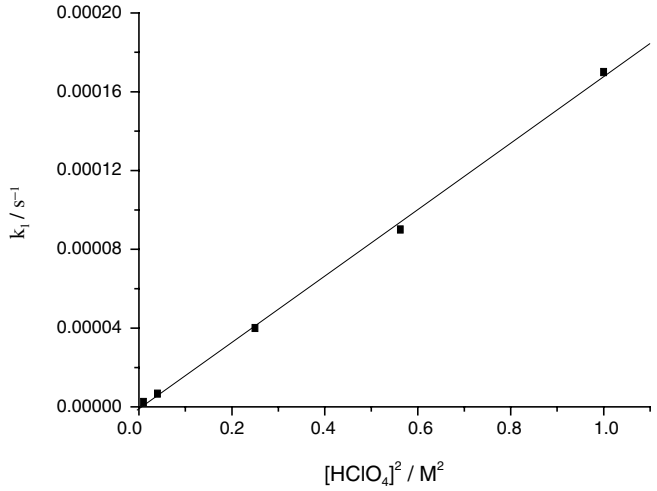

Fig. 5. Effect of acidity on k_1.

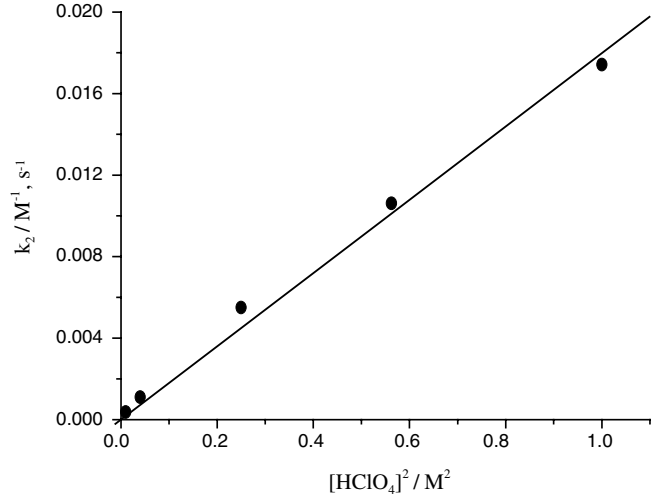

Fig. 6. Effect of acidity on k_2.

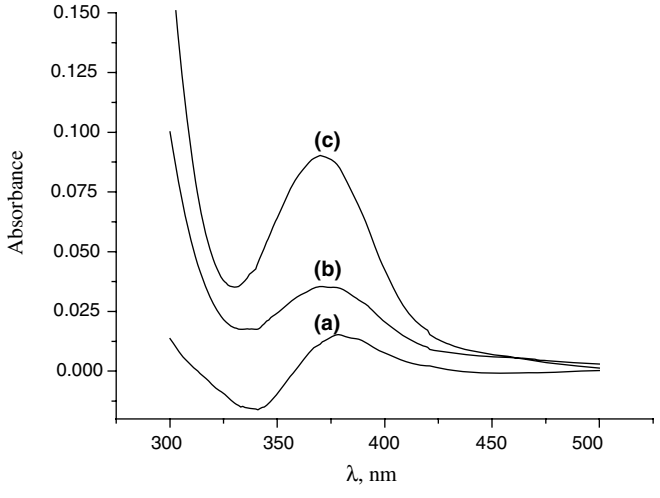

Fig. 7. UV–Vis difference spectra of Cr^{VI}/D-Fru solutions at pH 4.00, showing the increasing band at 374 nm with increasing [D-Fru] = (a) 0.06 M, (b) 0.18 M, (c) = 0.33 M; $[Cr^{VI}] = 6.00 \times 10^{-4}$ M, $T = 33$ °C, $I = 1$ M. Spectra taken after 5 min.

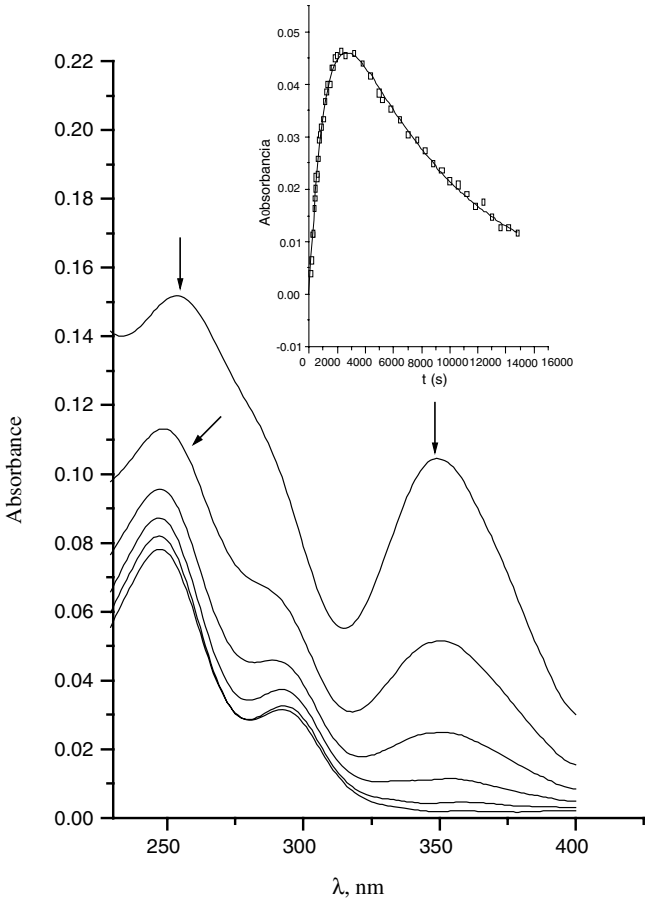

Fig. 8. Formation of CrO_2^{2+} ($\lambda_{max} = 293, 248$ nm) from the reaction between 0.125 M D-Fru, 1.26 mM O_2 and 4.5×10^{-2} mM Cr^{VI} in 1 M $HClO_4$. Inset: Experimental (□) and simulated (—) curves for the variation of the CrO_2^{2+} absorbance with time.

Replacing $[Cr^{VI}]$ in Eq. (15)

$$-\mathrm{d}[Cr^{VI}]/\mathrm{d}t = \frac{(k_I + k_{II}[\text{D-Fru}])K_1K_2K_3[\text{D-Fru}][H^+]^2[Cr^{VI}]_T}{1 + K_1[\text{D-Fru}] + K_1K_2[\text{D-Fru}][H^+] + K_1K_2K_3[\text{D-Fru}][H^+]^2}. \quad (17)$$

Thus, if K_1 [D-Fru] is the largest term in the denominator, Eq. (17) will be simplified to the experimentally observed form (see Eq. (5)).

Since

$$a = k_I K_2 K_3,$$
$$b = k_{II} K_2 K_3.$$

In this mechanism, we have assumed that the β-D-fructopyranose form is the reactive form of the organic substrate because this form is the most plentiful in aqueous solutions, with the two furanose forms also being present in quantifiable amounts. The remaining two tautomers are present only in trace amounts [39]. This assumption is based on the detection of HCOOH and D-arabinonic acid in the reaction mixture, which implies that the chromic ester is produced between the hemiacetal hydroxyl group

and the hydroxyl in *cis* position as has been observed for chromic oxidation of D-aldoses [40] with the concomitant C_1–C_2 breaking bond. In any case, a possible mechanism involving the open chain or the furanose forms may not be discarded.

Acknowledgments

We thank the National Research Council of Argentina (CONICET), the Third World Academy of Sciences (TWAS), the National University of Rosario (UNR), the International Foundation for Science (IFS), the National Agency for Science Promotion, the ALFA Program (CRO-CON Network, Project 7-0064-9), ANTORCHAS Foundation for financial support, the SEPCYT- Hungarian conmimment Grant HU/A98-EVI/07. Our thank is extensively to Dr. Sandra Signorella for revising the present manuscrit and to Miss Ana Tioni for helpful technical assistance.

References

[1] R.M. Stern, in: S. Langård (Ed.), Biological and Environmental Aspects of Chromium, Elsevier, Amsterdam, 1982, p. 5.
[2] IARC Monographs on the Evaluation of the Carcinogenic Risk of Chemicals to Humans, International Agency for Research on Cancer, Lyon, France, 1990, p. 49.
[3] X. Shi, A. Chiu, C.T. Chen, B. Halliwell, V. Castranova, V.J. Vallyathan, Toxicol. Environ. Health B (1999) 87.
[4] A. Yassi, E. Nieboer, in: J.O. Nriagu, E. Nieboer (Eds.), Chromium in the Natural and Human Environments, Wiley–Interscience, New York, 1988, p. 443.
[5] M. Cieslak-Golonka, Polyhedron 15 (1996) 3667.
[6] (a) A. Kortenkamp, M. Casadevall, P. da Cruz Fresco, R.O.J. Shayer, NATO ASI Series, Series w, 1997, p. 5.;
(b) D.M. Stearns, K.E. Wetterhahn, NATO ASI Series, Series 2, 1997, p. 55.
[7] D.M.L. Goodgame, P.B. Hayman, D.E. Hathway, Polyhedron 1 (1982) 497.
[8] M. Rizzotto, V. Moreno, S. Signorella, V. Daier, L.F. Sala, Polyhedron 19 (2000) 417.
[9] S. Signorella, M. Santoro, C. Palopoli, C. Brondino, J.M. Salas Peregrin, M. Quiroz, L.F. Sala, Polyhedron 17 (1998) 2739.
[10] L.F. Sala, C. Palopoli, S. Signorella, Polyhedron 14 (1995) 1725.
[11] S. Signorella, M.I. Frascaroli, S. García, M. Santoro, J.C. Gonzalez, C. Palopoli, V. Daier, N. Casado, L.F. Sala, J. Chem. Soc., Dalton Trans. (2000) 1617.
[12] S. Signorella, R. Lafarga, V. Daier, L.F. Sala, Carbohyd. Res. 324 (2000) 127.
[13] S. Signorella, V. Daier, S. García, R. Cargnello, J.C. Gonzalez, M. Rizzotto, L.F. Sala, Carbohyd. Res. 316 (1999) 14.
[14] L.M.J. Werstraeten, Adv. Carbohyd. Chem. Biochem. 22 (1964) 229.
[15] T.A. Turney, Oxidation Mechanism, Butterworth, London, 1965, p. 102.
[16] K.K. Sengupta, S. Nath Basu, S. Sen Gupta, Carbohyd. Res. 97 (1981) 1.
[17] X. Shi, N.S. Dalal, Arch. Biochem. Biophys. 277 (1990) 342.
[18] Kabir-ud-Din, A.m.A. Morshed, Z. Khan, Carbohyd. Res. 337 (2002) 1573.
[19] I.M. Kolthoff, E.B. Sandell, E.J. Meehan, S. Bruckenestein, in: Análisis Químico Cuantitativo (Ed.), S.R.L Buenos Aires, Sexta Edición , 1988, p. 806.
[20] WinSIM EPR Calculations for MS Windows, Version 0.96, National Institute of Environmental Health Sciences, 1995.
[21] M. Krumpolc, J. Rocek, Inorg. Synth. 20 (1980) 63.
[22] M.C. Ghosh, E.S. Gould, Inorg. Chem. 30 (1991) 491.
[23] G. Haight, G. Jursich, M. Kelso, P. Merril, Inorg. Chem. 24 (1985) 2740.
[24] R.G. Wilkins, The Study of Kinectics and Mechanism of Reactions of Transition Metal Complexes, Allyn and Bacon, Boston, 1974, p. 20.
[25] R. Bramley, J. Ji, R. Rudd, P. Lay, Inorg. Chem. 29 (1990) 3089.
[26] G. Barr-David, M. Charara, R. Codd, R.P. Farrell, J.A. Irwin, P.A. Lay, R. Branley, J.Y. Ji, G.R. Hanson, J. Chem. Soc., Faraday Trans. 91 (1995) 1207.
[27] S. Signorella, S. García, L.F. Sala, Polyhedron 11 (1992) 1391.
[28] S. Signorella, M. Santoro, M. Mulero, L.F. Sala, Can. J. Chem. 72 (1994) 398.
[29] J. Moore, P. Pearson, Kinetics and Mechanism, third ed., Wiley, New York, 1981, p. 295.
[30] W. Chandler, E. Lee, D. Lee, J. Chem. Ed. 64 (1987) 878.
[31] A.B.P. Lever, Inorganic Electronic Spectroscopy, second ed., Elsevier, Amsterdam, 1984, p. 419.
[32] J.K. Beattie, G.P. Haight, in: J.O. Edwards (Ed.), Inorganic Reaction Mechanism Part II, Wiley, New York, 1972.
[33] M. Mitewa, P. Bontchev, Coord. Chem. Rev. 61 (1985) 241.
[34] S. Scott, A. Bakac, J. Espenson, J. Am. Chem. Soc. 114 (1992) 4205.
[35] S.L. Scott, A. Bakac, J.H. Espenson, J. Am. Chem. Soc. 113 (1991) 7787.
[36] (a) A.G. Fadnis, S.K. Kulshrestha, Rev. Roumaine Chim. 2 (1983) 99;
(b) F. Fiegal, Spot Test Inorganic Chemistry, Elsevier, Amsterdam, London, 1963, p. 434.
[37] W. Travelyan, D. Proctor, J. Harrison, Nature 166 (1950) 44.
[38] L. Haugh, J. Jones, N. Wadman, J. Chem. Soc. (1950) 1702.
[39] A.E. Flood, Carbohydr. Res. 288 (1996) 45.
[40] L.F. Sala, S. Signorella, M. Rizzotto, M. Frascaroli, F. Gandolfo, Can. J. Chem. 70 (1992) 2046.

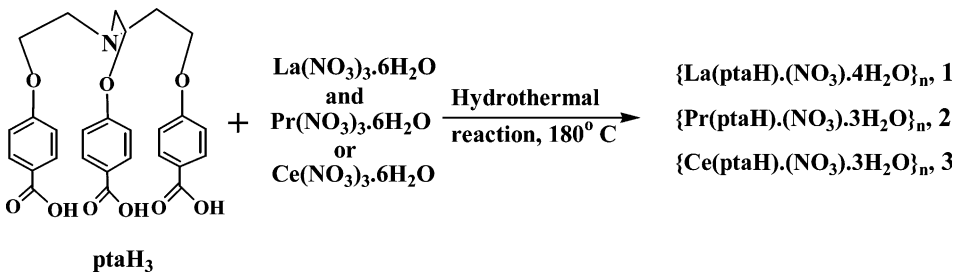

Scheme 1. Synthetic scheme for **1**, **2** and **3**.

2. Experimental

2.1. Chemicals and reagents

The metal salts were obtained from Aldrich and used as received. All other chemicals were procured from S.D. Fine Chemicals, India. The solvents were purified prior to use by standard procedure. All hydrothermal syntheses were performed at 180 °C for 48 h in Teflon-lined stainless steel autoclaves under autogenous pressure.

2.1.1. Synthesis of the ligand $ptaH_3$

The synthesis and characterization of the podand was achieved as described earlier [12].

2.1.2. $\{[La(ptaH)(NO_3)]\cdot 4H_2O\}_n$ (**1**)

A mixture of the tripodal ligand $ptaH_3$ (0.13 g; 0.25 mmol) and $La(NO_3)_3\cdot 6H_2O$ (0.16 g; 0.37 mmol) taken in 4 ml of water, was placed in a Teflon-lined stainless steel autoclave. The vessel was sealed and heated to 180 °C for 48 h and then cooled to room temperature at a rate of 1 °C per min. Colorless rectangular parallelepiped crystals were collected in ~50% yield from the reaction mixture. *Anal.* Calc. for $C_{27}H_{33}N_2O_{16}La$: C, 41.55; H, 4.26; N, 3.59. Found: C, 41.44; H, 4.47; N, 3.49%.

Crystals of **1** were heated in an oven for 3 h at 150 °C to obtain **1′**.

2.1.3. $\{[Pr(ptaH)(NO_3)]\cdot 3H_2O\}_n$ (**2**)

Compound **2** was prepared following a similar procedure as above, by treating $ptaH_3$ with $Pr(NO_3)_3\cdot 6H_2O$ in 1:1.5 molar ratio. Faintly purple crystals in the form of rectangular parallelepiped were collected from the reaction mixture in ~45% yield. *Anal.* Calc. for $C_{27}H_{31}N_2O_{15}Pr$: C, 42.42; H, 4.08; N, 3.66. Found: C, 42.33; H, 4.16; N, 3.39%.

Table 1
Crystal data and structure refinement parameters of the compounds

Compound	**1**	**1′**	**2**	**3**
Empirical formula	$C_{27}H_{33}N_2O_{16}La$	$C_{27}H_{33}N_2O_{16}La$	$C_{27}H_{31}N_2O_{15}Pr$	$C_{27}H_{31}N_2O_{15}Ce$
Formula weight	780.46	780.46	764.45	763.66
Temperature (K)	100(1)	100(1)	100(1)	100(1)
Radiation	Mo Kα	Mo Kα	Mo Kα	Mo Kα
Wavelength (Å)	0.71069	0.71069	0.71069	0.71069
Crystal system	triclinic	triclinic	triclinic	triclinic
Space group	$P\bar{1}$	$P\bar{1}$	$P\bar{1}$	$P\bar{1}$
a (Å)	11.334(5)	11.012(5)	11.133(5)	11.116(5)
b (Å)	12.128(5)	11.970(5)	11.834(5)	11.843(5)
c (Å)	12.363(5)	12.369(5)	12.299(5)	12.319(5)
α (°)	78.53(5)	79.84(5)	80.37(5)	99.50(5)
β (°)	65.26(5)	67.17(5)	67.17(5)	112.37(5)
γ (°)	87.87(5)	89.64(5)	89.92(5)	90.02(5)
V (Å^3)	1510.6(7)	1475.6(7)	1468.8(6)	1475.6(7)
Z	2	2	2	2
ρ_{calc} (Mg/m^3)	1.716	1.757	1.728	1.719
μ (mm^{-1})	1.495	1.530	1.737	1.621
F(000)	788	788	772	770
Reflections collected	10105	9913	9834	9913
Independent reflections	6805	5120	6793	6686
Refinement method	full-matrix least-squares on F^2	full-matrix least-squares on F^2	full-matrix least-squares on F^2	full-matrix least-squares on F^2
GOF	1.118	1.049	1.080	1.042
Final R indices [R_1]	0.031	0.066	0.025	0.028
[$I > 2\sigma(I)$] [wR_2]	0.080	0.142	0.065	0.070
R indices [R_1]	0.032	0.098	0.026	0.030
(All data) [wR_2]	0.081	0.156	0.066	0.071

Table 2
Selected bond distances (Å) and bond angles (°) of the compounds

1			
La(1)–O(6)	2.468(2)	La(1)–O(10)	2.628(2)
La(1)–O(5)	2.518(2	La(1)–O(9)	2.629(2)
La(1)–O(8)	2.529(2)	La(1)–O(12)	2.679(3)
La(1)–O(3)	2.531(2)	La(1)–OW(4)	2.640(2)
O(6)–La(1)–O(5)	136.21(8)	O(3)–La(1)–O(9)	97.70(6)
O(6)–La(1)–O(8)	80.58(7)	O(3)–La(1)–O(9)	151.75(7)
O(5)–La(1)–O(8)	141.54(8)	O(10)–La(1)–O(9)	113.23(7)
O(6)–La(1)–O(3)	67.57(7)	O(6)–La(1)–OW(4)	116.94(8)
O(5)–La(1)–O(3)	75.80(8)	O(5)–La(1)–OW(4)	70.84(8)
O(8)–La(1)–O(3)	141.33(7)	O(8)–La(1)–OW(4)	105.98(7)
O(6)–La(1)–O(3)	78.31(8)	O(3)–La(1)–OW(4)	72.13(7)
O(5)–La(1)–O(3)	69.07(7)	O(3)–La(1)–OW(4)	132.44(7)
O(8)–La(1)–O(3)	121.28(7)	O(10)–La(1)–OW(4)	108.71(8)
O(3)–La(1)–O(3)	74.14(7)	O(9)–La(1)–OW(4)	66.04(7)
O(6)–La(1)–O(10)	131.44(7)	O(6)–La(1)–O(12)	150.74(7)
O(5)–La(1)–O(10)	73.49(9)	O(5)–La(1)–O(12)	72.88(8)
O(8)–La(1)–O(10)	71.58(8)	O(8)–La(1)–O(12)	72.05(7)
O(3)–La(1)–O(10)	146.75(7)	O(3)–La(1)–O(12)	131.50(7)
O(3)–La(1)–O(10)	83.21(7)	O(3)–La(1)–O(12)	124.89(7)
O(6)–La(1)–O(9)	73.64(7)	O(10)–La(1)–O(12)	48.12(7)
O(5)–La(1)–O(9)	136.18(7)	O(9)–La(1)–O(12)	81.03(7)
O(8)–La(1)–O(9)	50.86(7)	OW(4)–La(1)–O(12)	63.11(8)
1′			
La(1)–O(6)	2.467(5)	La(1)–O(9)	2.560(4)
La(1)–O(5)	2.482(5)	La(1)–O(12)	2.586(5)
La(1)–O(3)	2.486(4)	La(1)–O(10)	2.627(6)
La(1)–O(8)	2.536(4)	La(1)–OW(4)	2.935
O(6)–La(1)–O(5)	136.10(16)	O(8)–La(1)–O(10)	72.54(16)
O(6)–La(1)–O(3)	68.56(16)	O(9)–La(1)–O(10)	74.99(15)
O(5)–La(1)–O(3)	76.11(16)	O(12)–La(1)–O(10)	49.13(16)
O(6)–La(1)–O(8)	82.73(15)	O(6)–La(1)–O(3)	77.48(15)
O(5)–La(1)–O(8)	140.61(16)	O(5)–La(1)–O(3)	69.08(15)
O(3)–La(1)–O(8)	138.15(14)	O(3)–La(1)–O(3)	75.76(14)
O(6)–La(1)–O(9)	77.49(15)	O(8)–La(1)–O(3)	128.00(14)
O(5)–La(1)–O(9)	129.97(15)	O(9)–La(1)–O(3)	154.74(15)
O(3)–La(1)–O(9)	91.97(13)	O(12)–La(1)–O(3)	90.62(15)
O(8)–La(1)–O(9)	51.21(13)	O(10)–La(1)–O(3)	130.25(15)
O(6)–La(1)–O(12)	136.34(18)	O(6)–La(1)–OW(4)	121.7(4)
O(5)–La(1)–O(12)	72.84(18)	O(5)–La(1)–OW(4)	62.7(3)
O(3)–La(1)–O(12)	148.83(17)	O(3)–La(1)–OW(4)	67.5(3)
O(8)–La(1)–O(12)	71.94(16)	O(8)–La(1)–OW(4)	107.0(3)
O(9)–La(1)–O(12)	109.96(15)	O(9)–La(1)–OW(4)	67.8(3)
O(6)–La(1)–O(10)	150.80(16)	O(12)–La(1)–OW(4)	99.8(4)
O(5)–La(1)–O(10)	71.30(16)	O(10)–La(1)–OW(4)	54.8(4)
O(3)–La(1)–O(10)	121.67(16)	O(3)–La(1)–OW(4)	124.4(3)
2			
Pr(1)–O(2)	2.4055(19)	Pr(1)–O8	2.4839(17)
Pr(1)–O(9)	2.4406(18)	Pr(1)–O5	2.5303(19)
Pr(1)–O(3)	2.4669(18)	Pr(1)–O12	2.5531(19)
Pr(1)–O(6)	2.4695(18)	Pr(1)–O(10)	2.629(2)
O(2)–Pr(1)–O(9)	71.09(6)	O(2)–Pr(1)–O(12)	140.13(6)
O(2)–Pr(1)–O(3)	138.16(6)	O(9)–Pr(1)–O(12)	146.14(6)
O(9)–Pr(1)–O(3)	74.84(6)	O(3)–Pr(1)–O(12)	71.46(7)
O(2)–Pr(1)–O(6)	83.93(6)	O(6)–Pr(1)–O(12)	71.65(6)
O(9)–Pr(1)–O(6)	137.28(6)	O(8)–Pr(1)–O(12)	68.20(6)
O(3)–Pr(1)–O(6)	137.88(6)	O(5)–Pr(1)–O(12)	108.14(6)
O(2)–Pr(1)–O(8)	77.41(6)	O(2)–Pr(1)–O(10)	149.58(6)
O(9)–Pr(1)–O(8)	123.98(6)	O(9)–Pr(1)–O(10)	113.75(5)
O(3)–Pr(1)–O(8)	103.22(6)	O(3)–Pr(1)–O(10)	67.90(6)
O(6)–Pr(1)–O(8)	81.08(6)	O(6)–Pr(1)–O(10)	72.85(5)
O(2)–Pr(1)–O(5)	78.39(6)	O(8)–Pr(1)–O(10)	116.78(6)
O(9)–Pr(1)–O(5)	88.07(5)	O(5)–Pr(1)–O(10)	71.95(5)

Table 2 (*continued*)

2			
O(3)–Pr(1)–O(5)	124.19(6)	O(12)–Pr(1)–O(10)	49.21(5)
O(6)–Pr(1)–O(5)	52.47(5)		
O(8)–Pr(1)–O(5)	129.26(6)		
3			
Ce(1)–O(2)	2.422(2)	Ce(1)–O(8)	2.5053(18)
Ce(1)–O(9)	2.4575(19)	Ce(1)–O(5)	2.545(2)
Ce(1)–O(3)	2.4846(18)	Ce(1)–O(10)	2.5769(19)
Ce(1)–O(6)	2.4868(18)	Ce(1)–O(12)	2.6545(12)
O(2)–Ce(1)–O(9)	70.88(6)	O(8)–Ce(1)–O(5)	129.33(6)
O(2)–Ce(1)–O(3)	137.78(6)	O(2)–Ce(1)–O(10)	140.32(6)
O(9)–Ce(1)–O(3)	74.75(6)	O(9)–Ce(1)–O(10)	146.06(6)
O(2)–Ce(1)–O(6)	84.60(6)	O(3)–Ce(1)–O(10)	71.46(7)
O(9)–Ce(1)–O(6)	137.78(6)	O(6)–Ce(1)–O(10)	71.25(6)
O(3)–Ce(1)–O(6)	137.58(6)	O(8)–Ce(1)–O(10)	67.86(7)
O(2)–Ce(1)–O(8)	77.97(7)	O(5)–Ce(1)–O(10)	107.86(6)
O(9)–Ce(1)–O(8)	123.82(6)	O(2)–Ce(1)–O(12)	149.96(4)
O(3)–Ce(1)–O(8)	102.43(7)	O(9)–Ce(1)–O(12)	114.14(4)
O(6)–Ce(1)–O(8)	81.42(6)	O(3)–Ce(1)–O(12)	68.05(5)
O(2)–Ce(1)–O(5)	78.48(6)	O(6)–Ce(1)–O(12)	72.43(4)
O(9)–Ce(1)–O(5)	88.71(6)	O(8)–Ce(1)–O(12)	116.13(5)
O(3)–Ce(1)–O(5)	124.75(6)	O(5)–Ce(1)–O(12)	72.20(4)
O(6)–Ce(1)–O(5)	52.17(5)	O(10)–Ce(1)–O(12)	48.84(4)

Table 3
Nonbonding distances (Å) and angles (°) for the water clusters in the compounds

1			
Ow1···Ow2	2.789	Ow1···Ow2···Ow3	133.38
Ow2···Ow3	2.770	Ow2···Ow3···Ow4	134.56
Ow3···Ow4	2.681	Ow2–H···Ow1	170.40
Ow1···O2	2.988	Ow3–H···Ow2	166.24
Ow1···O8	2.714	Ow4–H···Ow3	169.44
Ow2···O11	2.861	Ow1–H···O2	137.38
		Ow2–H···O8	164.04
1′			
Ow1···Ow2	2.659	Ow1···Ow2···Ow3	141.95
Ow2···Ow3	2.711	Ow2···Ow3···Ow4	130.12
Ow3···Ow4	2.081	Ow1–H···Ow2	146.32
Ow1···O8	2.834	Ow2–H···Ow3	141.27
Ow3···O5	2.812	Ow1–H···O8	146.60
		Ow3–H···O5	155.33
2			
Ow1···Ow2	2.719	Ow1···Ow2···Ow3	139.60
Ow2···Ow3	2.773	Ow2–H···Ow1	151.60
Ow1···O6	2.816	Ow3–H···Ow2	163.92
Ow2···O11	2.856	Ow1–H···O6	160.72
Ow3···O3	2.884	Ow2–H···O11	155.84
		Ow3–H···O3	165.60
3			
Ow1···Ow2	2.751	Ow1···Ow2···Ow3	139.32
Ow2···Ow3	2.777	Ow1–H···Ow2	170.97
Ow1···O6	2.822	Ow3–H···Ow2	149.57
Ow3···O3	2.875	Ow1–H···O6	170.70
		Ow3–H···O3	168.88

2.1.4. $\{[Ce(ptaH)(NO_3)]\cdot 3H_2O\}_n$ (**3**)

This was synthesized as above treating $ptaH_3$ with $Ce(NO_3)_3\cdot 6H_2O$ in 1:1.5 molar ratio. Colorless rectangular crystals were isolated from the reaction mixture in

~39% yield. *Anal.* Calc. for $C_{27}H_{31}N_2O_{15}Ce$: C, 42.46; H, 4.09; N, 3.66. Found: C, 42.31; H, 4.14; N, 3.78%.

2.2. Physical measurements

Spectroscopic data were collected as follows: IR (KBr disk, 400–4000 cm^{-1}) Perkin–Elmer Model 1320; X-ray powder pattern (CuK_α radiation at a scan rate of 3°/min, 293 K) Siefert ISODEBYEFLEX-2002 X-ray generator; thermogravimetric analysis (heating rate of 5 °C/min) Perkin–Elmer Pyris 6. Microanalyses for the compounds were obtained from the Central Drug Research Institute, Lucknow, India.

2.3. X-ray crystallography

Single crystal X-ray data at 100 K were collected on a Bruker SMART APEX CCD diffractometer using graphite-monochromated Mo Kα radiation ($\lambda = 0.71073$ Å). Data reduction, structure solution and structure refinement were carried out as described earlier [12]. The crystal and refinement data are collected in Table 1 while selected bond distances and angles are given in Table 2. The H-bonding distances and angles pertaining to the water clusters are listed in Table 3.

3. Results and discussion

All the compounds are stable in air and insoluble in common organic solvents. Each shows strong infrared absorption bands between 1350 and 1550 cm^{-1} that are diagnostic [13] of coordinated carboxylates.

The structure (Fig. 1) of **1** consists of La(III) ions, partially deprotonated $ptaH^{2-}$ ligand, nitrate anions and water molecules. Each metal is bonded to four carboxylates from four different ligand units. One carboxylate donates both its O atoms, two carboxylates donate one O atom each (the other O atom in each case is

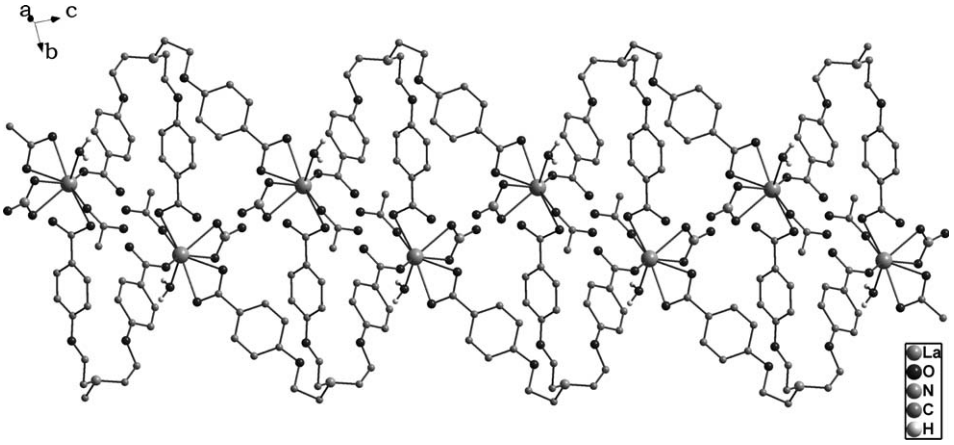

Fig. 1. A perspective view of the metallomacrocycle in **1**. For clarity, only metal bound water H atoms are shown.

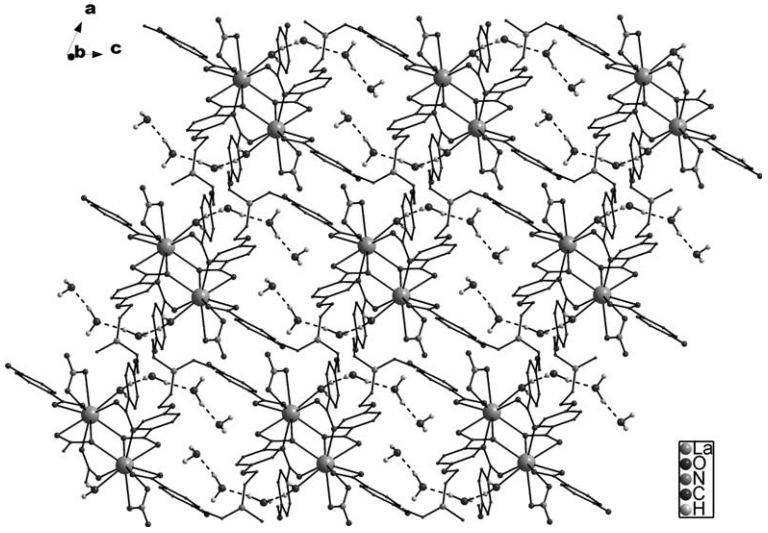

Fig. 2. A view showing water tetramers occupying the voids of the interlinked metallocycles along crystallographic *c*-axis in **1**.

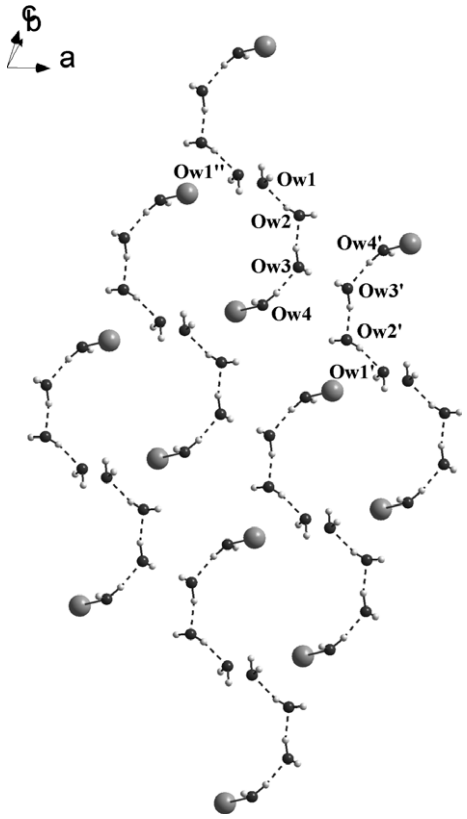

Fig. 3. A close view of the water tetramer present in **1** showing the atom numbering scheme.

donated to a different La(III)) while the fourth carboxylate is protonated and donates a single O atom. Each metal ion is also bound to two O atoms of the nitrate anion and one water molecule (Ow4) showing eight coordination. The overall structure looks like (Fig. 1) an array of metallocycles joined via the bridgehead N atom of the podand extending along the crystallographic *c*-axis. In the metallocyclic units, the two La(III) ions show a distance of either 9.24 or 10.78 Å while the distance between the bridgehead N atoms is 17.42 Å forming an oval-shaped cavity. The bond distances and bond angles involving the metal ions (Table 2) are within normal [10,12] statistical errors.

An interesting feature of **1** is that the La(III)-bound water (Ow4) is H-bonded to three more water molecules forming an acyclic tetramer (Fig. 2). These tetramers extend to the middle of the void spaces of the metallocycles. The four water O atoms in the cluster are coplanar to within ±0.03 Å. Both theoretical and experimental studies of tetrameric water clusters indicated [14–17] a quasi-planar cyclic minimum energy structure with an S_4 symmetry where each water molecule forms two hydrogen bonds. Thus, the existence of high energy acyclic tetramer in **1** is a consequence of the MOF structure which does not have enough room to accommodate a cyclic structure. The average O···O distance in the cyclic structure was estimated to be 2.79 Å in the gas phase while those found in crystal lattices [16,17] show a wide ranging O···O distances (2.77–3.00 Å). In **1**, the water molecules are quite strongly bonded to each other as evident from the O···O distances (range 2.681(4)–2.789(6) Å) and O···H–O angles (range 166.24(3)–169.44(4)°). The atom Ow1 is close to Ow1″ (2.923(4) Å) although the positions of hydrogen atoms are such that Ow1 is not hydrogen-bonded to Ow1″ (Fig. 3). Instead, Ow1 is hydrogen-bonded to a nearby carboxylate O atom. Other water molecules of the cluster act as H-bond donors to available carboxylate O or nitrate anions with an O···O distance in the range 2.714–2.861 Å further reinforcing the structure.

The robustness of the framework is reflected in the thermogravimetric analysis of **1** which shows negligible weight loss till about 150 °C and the loss of 9.3% corresponding to all of the water (calculated 9.22%) takes place above 260 °C. However, complete breakdown of the complex takes place at ~270 °C. The macroscopic crystal shape and color of **1** remain unchanged after heating the crystals at 150 ± 1 °C for 3 h at atmospheric pressure. A new X-ray data are collected every hour after the heat treatment. The X-ray crystal structure of **1**′ reveal that the porous framework is retained with slight changes in La(III)-carboxylate bonding (Table 2). However, the metal-bound water tetramer slowly moves away from the metal (Scheme 2) showing La–Ow4 bond distance of 2.935(13) Å from the original 2.640(6) Å. This experiment shows that each La(III) ion is strongly bonded to the carboxylate. Also, supramolecular interactions between the water molecules and between the water molecules and the MOF are strong enough to resist escape of water. To the best of our knowledge, it is the first example where the movement of a water cluster is monitored after applying heat and the passage of time in the crystalline state.

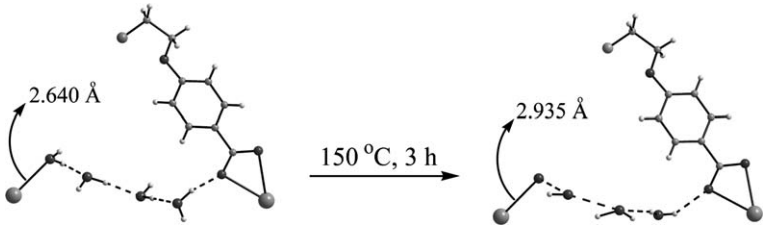

Scheme 2. A shematic view illustrating the movement of metal bound water cluster away from the La(III) atom upon heating in **1**.

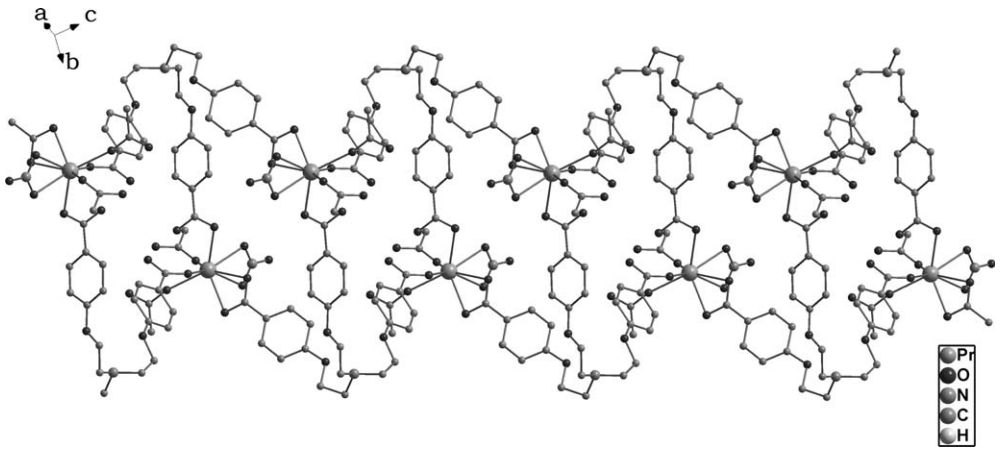

Fig. 4. A perspective view of the metallomacrocycle in **2**. All H atoms are omitted for clarity.

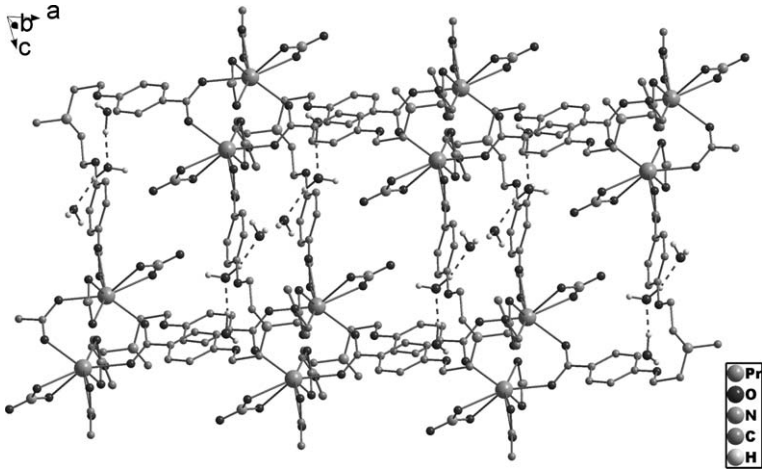

Fig. 5. View of the metal-organic framework structure along *a* crystallographic axis in **2** containing water trimer in the metallocyclic cavity.

As **2** and **3** have the identical structure, the structure of **2** is only described here. The structure consists of a partially deprotonated $ptaH^{2-}$ ligand, nitrate anion, one Pr(III) ion and three water molecules in the asymmetric unit. Each metal is bonded to five carboxylates from five different ligand units (Fig. 4) where one carboxylate donates both its O atoms, three carboxylates donate one O atom each (the other O atom in each case is donated to a different Pr(III)) while the fifth carboxylate is protonated and donates a single O atom. Each metal ion is also bonded to two O atoms of a nitrate anion assuming overall eight coordination. The bridging carboxylates propagate the MOF as an array of metallocycles extending along the crystallographic *c*-axis. In the metallocycles, the two Pr(III) ions show a distance of either 9.43 or 10.03 Å while the distance between the bridgehead N atoms is 17.58 Å. The bond distances and angles involving the metal ion (Table 2) are similar to the ones found in the carboxylate complexes of the metals [10,12]. The three water molecules form a bent $(H_2O)_3$ cluster (Fig. 5) occupying the voids in the metallocycles. Theoretical studies [18] on water trimers predicted the existence of several cyclic and two acyclic structures. However, to the best of our knowledge, only one acyclic water trimer has been found [19,20] in a crystal host till date. The water molecules in **2** are quite strongly bonded to each other (Table 3) as evident from the O···O distances (range 2.719–2.773 Å) and O···H–O angles (range 151.60–163.92°). These water molecules act as H-bond donors to the available carboxylate or nitrate O atoms with the O···O distances in the range 2.816–2.884 Å maintaining strong water–MOF interactions.

Thermogravimetric analyses show that in **2** or **3**, weight-loss occurs in stages beginning above 70 °C and the loss of 7.1% corresponding to all of the water (calculated 7.07%) takes place above 250 °C. The FTIR spectra of **1**–**3** show a broad band centered around 3420 cm^{-1} attributable [13] to the O–H stretching frequency pertaining to the water cluster. This broad band significantly reduces on heating the compounds under vacuum (0.1 mm) at 260 °C for 3 h suggesting escape

of the water molecules from the lattice. The IR spectrum of ice shows the O–H stretching at 3220 cm^{-1} while this stretching vibration in liquid water [21] appears at 3490 and 3280 cm^{-1}. Thus, the water clusters in **1**, **2** and **3** shows O–H stretching vibration similar to that of liquid water. Once water is expelled from the lattice by heating, no re-absorption is observed upon deliberate exposure to water vapor for 3 days as monitored by FTIR spectroscopy. Powder X-ray diffraction patterns corroborate the thermal behavior of **1**, **2** and **3** showing major changes in peak positions as well as their intensities before and after water expulsion.

4. Conclusion

In conclusion, we have characterized La(III)-bound acyclic water tetramer in **1** and bent acyclic water trimer in **2** and **3** in the porous coordination polymers of lanthanide ions with the podand. The water clusters gains stability from strong hydrogen-bonding interactions with the available carboxylate O atoms as well with metal bound nitrate anion. The metal bound water cluster in **1** slowly moves away upon heating. The MOFs are quite robust and maintain their crystallinity on heating at ~150 °C in normal atmosphere up to 4 h. We are presently engaged in building porous framework structures using this ligand with different metal ions including lanthanides with guests other than water.

Acknowledgments

We gratefully acknowledge the financial support received from the Department of Science and Technology, New Delhi, India (to P.K.B.) and a SRF (from the CSIR) to S.N. We thank Prof. V. Chandrasekhar for the TGA data.

Appendix A. Supplementary data

Crystallographic data for the structural analysis have been deposited with the Cambridge Crystallographic Data Centre, CCDC No. for **1**, **1′**, **2** and **3** are 238353, 247658, 273126 and 273127, respectively. These data can be obtained online free of charge via www.ccdc.cam.ac.uk/conts/retrieving.html (or from Cambridge Crystallographic Data Centre, 12, Union Road, Cambridge CB21EZ, UK, fax: +44 1223 336 033; or e-mail: deposit@ccdc.cam.ac.uk). IR, TGA, and X-ray powder diffraction patterns of complexes **1**–**3**. Supplementary data associated with this article can be found, in the online version, at doi:10.1016/j.poly.2005.08.003.

References

[1] M. Eddaoudi, J. Kim, N. Rosi, D. Vodak, J. Wachter, M. O'Keeffee, O.M. Yaghi, Science 295 (2002) 469.
[2] R. Kitaura, K. Seki, G. Akiyama, S. Kitagawa, Angew. Chem., Int. Ed. 42 (2003) 428.
[3] B. Moulton, M.J. Zaworotko, Chem. Rev. 101 (2001) 1629.
[4] J.S. Seo, D. Whang, H. Lee, S.I. Jun, J. Oh, Y. Jin, Y.J. Jeon, K. Kim, Nature 404 (2000) 982.
[5] (a) F. Millange, C. Serre, G. Ferey, Chem. Commun. (2002) 822; (b) P. Ayyappan, O.R. Evans, W. Lin, Inorg. Chem. 40 (2001) 4627.
[6] T.E. Gier, X. Bu, P. Feng, G.D. Stucky, Nature 395 (1998) 154.
[7] R. Robson, J. Chem. Soc., Dalton Trans. (2000) 3735.
[8] J.-C. Bünzli, C. Piguet, Chem. Rev. 102 (2002) 1897.
[9] D.-L. Long, A.J. Blake, N.R. Champness, C. Wilson, M. Schröder, Angew. Chem., Int. Ed. 40 (2001) 2444.
[10] (a) K.M. Buschbaum, C.C. Quitmann, Inorg. Chem. 42 (2003) 2742;
(b) S. Neogi, G. Savitha, P.K. Bharadwaj, Inorg. Chem. 43 (2004) 3771;
(c) S.K. Ghosh, P.K. Bharadwaj, Inorg. Chem. 44 (2005) 3156.
[11] (a) J. Xu, E. Radkov, M. Zeigler, K.N. Raymond, Inorg. Chem. 39 (2000) 4156;
(b) S. Aime, A. Barge, M. Botta, A. Casnati, M. Fragai, C. Luchinat, R. Ungaro, Angew. Chem., Int. Ed. 40 (2001) 4737.
[12] S. Neogi, P.K. Bharadwaj, Inorg. Chem. 44 (2005) 816.
[13] K. Nakamoto, Infrared and Raman Spectra of Inorganic and Coordination Compounds, 5th ed., Wiley, New York, 1997.
[14] J.D. Cruzan, L.B. Braly, K. Liu, M.G. Brown, J.G. Loeser, R.J. Saykally, Science 271 (1996) 59.
[15] (a) M. Masella, N. Gresh, J.-P. Flament, J. Chem. Soc., Farady Trans. 94 (1998) 2745;
(b) S.X. Xantheas Jr., T.H. Dunning, J. Chem. Phys. 99 (1993) 8774.
[16] S. Pal, N.B. Sankaran, A. Samanta, Angew. Chem., Int. Ed. 42 (2003) 1741.
[17] S. Supriya, S. Manikumari, P. Raghavaiah, S.K. Das, New J. Chem. 27 (2003) 218, and references cited therein.
[18] (a) F.N. Keutsch, J.D. Cruzan, R.J. Saykally, Chem. Rev. 103 (2003) 2533;
(b) E.M. Mas, R. Bukowski, K. Szalewicz, J. Chem. Phys. 118 (2003) 4386.
[19] L.R. MacGillivray, J.L. Atwood, J. Am. Chem. Soc. 119 (1997) 2592.
[20] S.K. Ghosh, P.K. Bharadwaj, Inorg. Chem. 44 (2005) 0000.
[21] D. Eisenberg, W. Kauzmann, The Structure and Properties of Water, Oxford University Press, Oxford, 1969.

in which $[Mn(\eta^5\text{-}C_5H_5)_2]$ was reacted with carbon monoxide at elevated temperatures and pressures [4,8]. Reactions analogous to those used for the preparations of $[Mn(\eta^5\text{-}C_5Me_5)(CO)_3]$ and $[Mn(\eta^5\text{-}C_5Bz_5)(CO)_3]$ were also not suitable due to the very low solubility of C_5Ph_5H [9–12]. For instance, the purple radical, $C_5Ph_5^{\bullet}$, generated from the mixture of C_5Ph_5Br, zinc dust and $Mn_2(CO)_{10}$ in refluxing tetrahydrofuran, was not sufficiently reactive to cleave the Mn–Mn bond even though the reaction was continued for four days. In most reactions involving $Mn_2(CO)_{10}$ as a precursor, metal–metal bond cleavage has been shown to be the initial step [13]. $[Mn(CO)_3Br]$, $[Mn(CO)_3(CH_3CN)_3]Br$ and $[Mn(CO)_3(CH_3CN)_2Br]$ are readily prepared and are the most commonly used precursors for substitution reactions as a consequence of the lability of the CH_3CN and Br^- ligands.

Both (**1**) and (**3**) are air stable in solid and in solution. Their inertness parallels that of other substituted cyclopentadienyl complexes. The kinetic inertness of $[Mn(\eta^5\text{-}C_5RH_4)(CO)_3]$ (R = H, Me) is well known; no carbonyl exchange with ^{14}CO occurs in toluene at 32 °C over several weeks, no reaction occurs between PPh_3 and $[Mn(\eta^5\text{-}C_5H_5)(CO)_3]$ even in refluxing decalin and substitution of CO is only possible either by ultraviolet irradiation or by using Me_3NO to actively remove CO [13].

Similarly, $[Mn(\eta^5\text{-}C_5Me_5)(CO)_3]$ undergoes monosubstitution either under ultraviolet irradiation or by oxidative substitution [12,14]. There are many reports of cyclopentadienyl manganese derivatives with one or more ligands substituted for CO [13,15]. Recently, a study on the monosubstitution of $[Mn(\eta^5\text{-}C_5R_5)(CO)_3]$ (R = H, Me or Et) in *n*-heptane solution under ultraviolet irradiation showed that the bulkier ligand, C_5Et_5, better stabilised the formation of the solvated intermediate, $[Mn(\eta^5\text{-}C_5R_5)(CO)_2(n\text{-heptane})]$ than did the other two ligands [16]. Substitution of one CO in $[Mn(\eta^5\text{-}C_5Ph_5)(CO)_3]$ (**1**) by PMe_2Ph was readily achieved by refluxing a THF solution in the presence of Me_3NO to give $[Mn(\eta^5\text{-}C_5Ph_5)(CO)_2(PMe_2Ph)]$ (**2**). Using an analogous procedure, it was possible to introduce a range of other substituents (including phosphines and isonitriles).

$[Mn(\eta^5\text{-}C_5Ph_5)(CO)_3]$ (**1**) is not oxidised by reactants such as Br_2, I_2 or $NOBF_4$, even in the presence of CH_3CN. Recently, it has been found that monosubstitution of a carbonyl ligand proceeded smoothly when $[Ru(\eta^5\text{-}C_5Ph_5)(CO)_2Br]$ or $[Os(\eta^5\text{-}C_5Ph_5)(CO)_2Br]$ were reacted with other ligands in the presence of Me_3NO [17,18].

However, compounds (**1**) and (**3**) each undergo a reversible, one-electron cyclic voltametric oxidation in CH_2Cl_2 at 0.98 V for (**1**) and 0.89 V for (**3**) (both versus $Fc^{+/0}$).

$$[Mn(\eta^5\text{-}C_5Ar_5)(CO)_3] \rightleftharpoons [Mn(\eta^5\text{-}C_5Ar_5)(CO)_3]^+ + e^-$$

The reversibility of these oxidations confirms that complexes of the penta-*p*-tolylcyclopentadienyl ligand, $C_5(p\text{-tol})_5^-$, are easier to oxidise than are those of the $C_5Ph_5^-$ ligand. These oxidation potentials are much higher than that for $[Mn(\eta^5\text{-}C_5H_5)(CO)_3]$ which undergoes a reversible oxidation at ca. 0.29 V [19]. In general, the value of the redox couple for a pentaphenylcyclopentadienyl complex is shifted 0.25–0.30 V more positively than that of its cyclopentadienyl analogue [20,21].

In addition, $[Mn(\eta^5\text{-}C_5H_5)(CO)_3]$ exhibits a second irreversible oxidation at 1.48 V detected in CF_3CO_2H at a platinum electrode [19], an electrochemically reversible reduction, coupled to a follow-up chemical reaction at −2.46 V [22] and a second irreversible reduction at −3.32 V observed in tetrahydrofuran at a platinum electrode [23]. The first reduction has been shown by preparative electrolysis to generate red $[Mn(\eta^5\text{-}C_5H_5)(CO)_3]^-$. However, chemical reduction of $[Mn(\eta^5\text{-}C_5H_5)(CO)_3]$ in HMPA yields predominantly first $[Mn(CO)_5]^-$ and then $[Mn(CO)_4]^{3-}$ by poorly defined ligand redistribution reactions [24]. We have observed no additional oxidations, nor corresponding reductions of $[Mn(\eta^5\text{-}C_5Ar_5)(CO)_3]$.

Table 1
Selected average interatomic distances and angles in $[Mn(\eta^5\text{-}C_5Ph_5)(CO)_3]$ (**1**)

Atoms	Average dimension
Mn–C (C_5)	2.16(1) Å
Mn–CO	1.78(1) Å
C–O	1.17(1) Å
C–C (C_5 ring)	1.42(2) Å
C(C_5)–*ipso*-C (C_6)	1.50(2) Å
CO–Mn–CO	90.3(5)°
Mn–C–O	175(1)°
C–C–C (C_5 ring)	107.7(1)°

2.1. Crystal structure determinations

2.1.1. $[Mn(\eta^5\text{-}C_5Ph_5)(CO)_3]$ (1)

An air-stable crystal of $[Mn(\eta^5\text{-}C_5Ph_5)(CO)_3]$ (**1**) was grown by slow vapour diffusion of pentane into a dichloromethane solution of (**1**) and the crystal structure was determined at room temperature. A single crystal X-ray diffraction study of (**1**) was undertaken for comparison with that of (**2**). Compound (**1**) crystallises in the monoclinic space group $P2_1/n$ (#14). The crystal structure of (**1**) consists of discrete molecules in the solid state and no intermolecular contacts of significance were observed in the solid. The closest intermolecular contact is 3.46 Å between C(33) on molecule (x, y, z) and C(34) on molecule $(-x, -y, -z)$. The closest intermolecular non-bonding approaches to manganese are greater than 4 Å. Final atomic positional coordinates, with estimated standard deviations, bond lengths and angles and anisotropic thermal parameters are deposited.[1] Selected interatomic bond distances and angles, with standard

[1] The atomic coordinates and thermal parameters have been submitted as supplementary material for deposition at the Cambridge Crystallographic Data Centre with deposition number CCDC 284608 (see Deposition of crystallographic data).

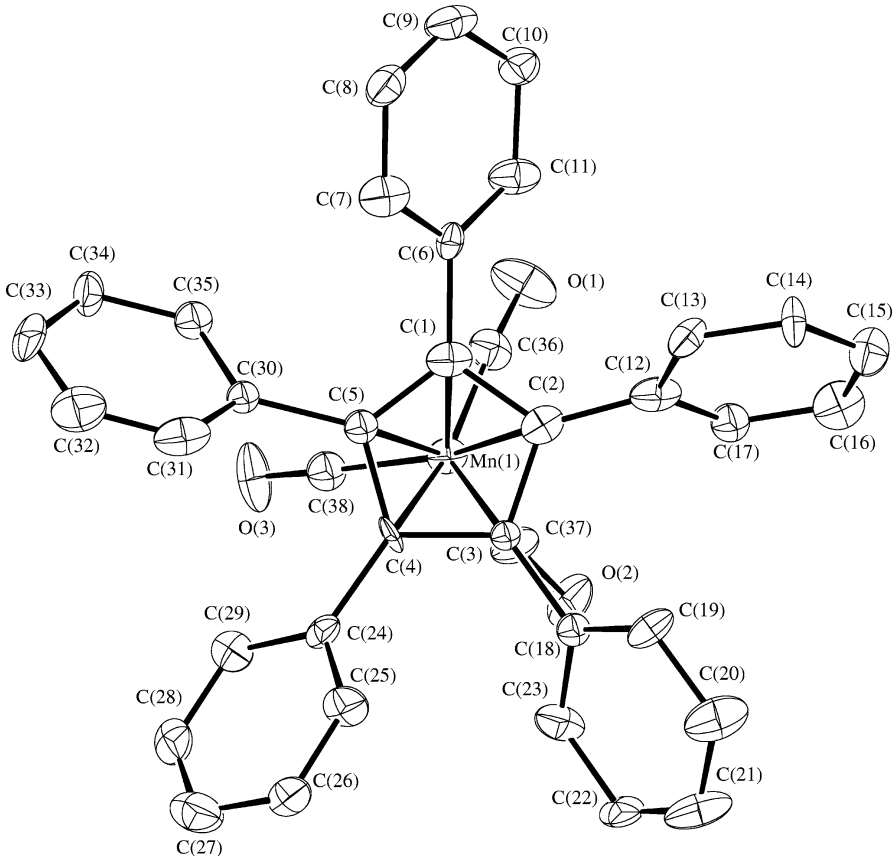

Fig. 1. ORTEP [39] illustration of $[Mn(\eta^5\text{-}C_5Ph_5)(CO)_3]$ (**1**), viewed perpendicular to the C_5 ligand plane, showing the atom numbering scheme.

deviations derived from the refinement, are given in Table 1. The atomic nomenclature is defined in Fig. 1. Figs. 1 and 2 illustrate the molecular geometry viewed along, and perpendicular to, the normal to the C_5 plane of the $C_5Ph_5^-$ ligand, respectively.

2.1.2. The $[Mn(\eta^5\text{-}C_5Ph_5)(CO)_3]$ molecule

Coordination by the η^5-pentaphenylcyclopentadienyl group and the three carbonyl groups creates a "three-legged piano stool" environment about the manganese atom. The Mn–(C_5 centroid) distance is 1.784 Å and the average Mn–C distance of 2.16 Å may be compared with the mean of nearly 147 structures of $[Mn(C_5R_5)(CO)_3]$ compounds of 1.775(1) and 2.142(2) Å. The Mn–CO distances (1.74(1), 1.77(1) and 1.83(1) Å) are indistinguishable and may be compared, for example, with the mean bond length of 1.784(2) in the $[Mn(C_5R_5)(CO)_3]$ compounds. The C=O bond lengths in (**1**) are the same within experimental error. The Mn–(C_5 centroid) distance is relatively long; there being only 42 compounds with Mn–(C_5 centroid) distances of 1.785 Å or longer. There appears to be no simple correlation between Mn–(C_5 centroid) distance and other parameters – whilst many of these 42 compounds do have bulky cyclopentadienyl ligands and the longest Mn–(ring centroid) distance reported to date is the exceptionally long (at $R = 0.0979$) 1.912 Å of $[\{Os_3(\mu\text{-}H)(CO)_8(PPh_3)_2\}(\mu\text{-}O_2C\text{-}\{(\eta^5\text{-}C_5H_4)Mn(CO)_3\}]$[2]) [25], that of $[Mn(\eta^5\text{-}C_5H_5)(CO)_3]$ is 1.794 Å.

The C_5 nucleus of the pentaphenylcyclopentadienyl ligand is planar to within 0.014 Å. The C–C bond lengths of the C_5 ring range from 1.39(2) to 1.46(1) Å, the average C–C bond length being 1.42 Å, which is consistent with C_5Ph_5 rings in other metal complexes. The *ipso*-carbon atoms of each of the phenyl rings are displaced slightly from the C_5 plane by between 0.09 and 0.20 Å, with the average distance being 0.16 Å. The *ipso*-carbon atoms of all phenyl rings are on the opposite side of the C_5 plane to the manganese atom. The phenyl rings are all also planar to within a mean deviation from the plane of 0.02 Å and are canted at between 46.2° and 61.9° (average 51.6°) to the C_5 ring in a paddle wheel arrangement. The average angle between the planes of adjacent phenyl rings of the $C_5Ph_5^-$ ligand is 54.9°.

2.1.3. $[Mn(\eta^5\text{-}C_5Ph_5)(CO)_2(PMe_2Ph)]$ (**2**)

$[Mn(\eta^5\text{-}C_5Ph_5)(CO)_2(PMe_2Ph)]$(**2**) also crystallises in the monoclinic space group $P2_1/n$ (#14). The crystal structure of (**2**) consists of discrete molecules in the solid state and no

[2] This distance is a considerable outlier in Mn–(C_5 centroid) distances, d, of $[Mn(\eta^5\text{-}C_5R_5)(CO)_3]$ compounds – the next 7 longest distances are in the range $1.812 \leqslant d \leqslant 1.823$ Å.

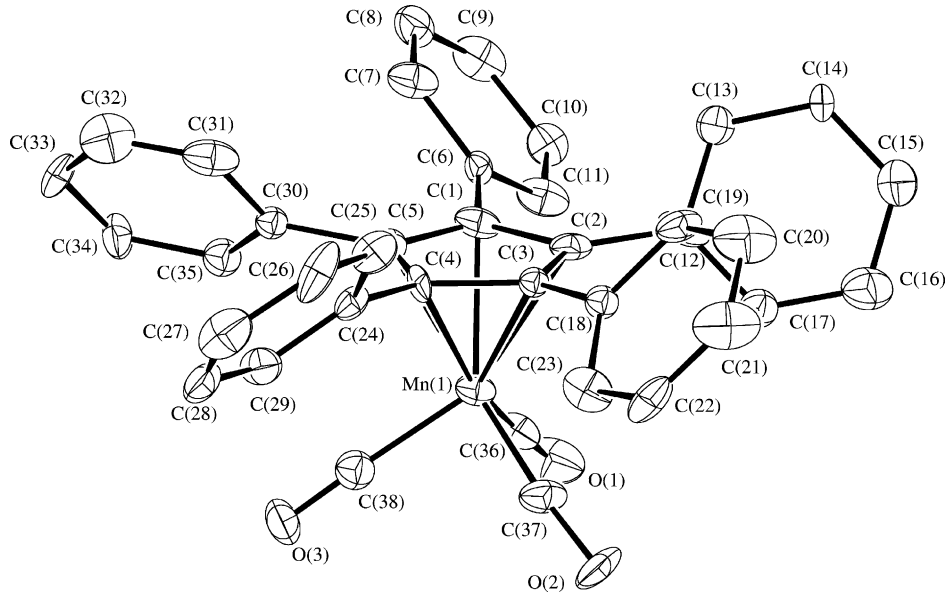

Fig. 2. ORTEP [39] illustration of $[Mn(\eta^5\text{-}C_5Ph_5)(CO)_3]$ (**1**), viewed parallel to the C_5 ligand plane, showing the atom numbering scheme.

intermolecular contacts of significance were observed in the solid. The closest intermolecular contact is 3.332(5) Å between O(1) on molecule (x, y, z) and C(41) on molecule $(1/2 - x, 1/2 + y, 1/2 - z)$. The closest intermolecular non-bonding approaches to manganese are greater than 4 Å. Final atomic positional coordinates, with estimated standard deviations, bond lengths and angles and anisotropic thermal parameters are deposited.[3] Selected interatomic bond distances and angles, with standard deviations derived from the refinement, are given in Table 2. The atomic nomenclature is defined in Fig. 3. Figs. 3 and 4 illustrate the molecular geometry viewed along, and perpendicular to, the normal to the C_5 plane of the $C_5Ph_5^-$ ligand, respectively.

The Mn–(C_5 centroid) distance is 1.809 Å and the average Mn–C(C_5) distance of 2.178(4) Å are both slightly longer than those of (**1**). The Mn–(C_5 centroid) distance is at the upper end of such distances in $[Mn(C_5R_5)(CO)_3]$ compounds, with only 8 compounds with longer Mn–(C_5 centroid) distances. It is easily the longest such distance in $[Mn(\eta^5\text{-}C_5R_5)(CO)_2(PX_3)]$ ($X \neq M$, P) compounds, as are, therefore, the Mn–C(C_5) distances.[4] That is, *on average*, the Mn–cyclopentadienyl distance of $[Mn(C_5R_5)(CO)_3]$ compounds *contracts* on phosphine substitution, but has increased in this case. The Mn–CO distances (1.757(4), 1.773(4) Å) are indistinguishable and similar to those in (**1**), but relatively long

Table 2
Selected average interatomic distances and angles in $[Mn(\eta^5\text{-}C_5Ph_5)(CO)_2PMe_2Ph]$ (**2**)

Atoms	Average dimension
Mn–C (C_5)	2.178(4) Å
Mn–P	2.264(1) Å
Mn–CO	1.765(4) Å
C–O	1.158(4) Å
C–C (C_5 ring)	1.427(5) Å
C(C_5)–*ipso*-C (C_6)	1.492(5) Å
CO–Mn–CO	91.2(2)°
Mn–C–O	178.9(3)°
C–C–C (C_5 ring)	108.0(3)°

for $[Mn(\eta^5\text{–}C_5R_5)(CO)_2(PX_3)]$ ($X \neq M$, P) compounds. As in (**1**), the C=O bond lengths in (**2**) are the same within experimental error. The Mn–P distance of 2.264(1) Å is again easily the longest in the 31 $[Mn(\eta^5\text{-}C_5R_5)(CO)_2(PX_3)]$ ($X \neq M$, P) compounds reported to date (range $2.126 \leqslant d \leqslant 2.359$, mean 2.215 Å). These distances easily exceed those of the $[Mn(\eta^5\text{-}C_5R_5)(CO)_2(PX_3)]^+$ ($X \neq M$, P) cations, which are included in the above analyses.

The C_5 nucleus of the pentaphenylcyclopentadienyl ligand is planar to within 0.006 Å. The C–C bond lengths of the C_5 ring range from 1.415(5) to 1.432(5) Å, the average C–C bond length being 1.427(5) Å, which is consistent with C_5Ph_5 rings in other metal complexes. The *ipso*-carbon atoms of each of the phenyl rings are displaced slightly from the C_5 plane by between 0.158 and 0.268 Å, with the average distance being 0.202 Å. This is a greater displacement than in $[Mn(\eta^5\text{-}C_5Ph_5)(CO)_3]$ (mean 0.161 Å). The *ipso*-carbon atoms of all phenyl rings are on the opposite side of the C_5 plane to the manganese atom. The phenyl rings are all also planar to within a mean deviation from the plane of

[3] The atomic coordinates and thermal parameters have been submitted as supplementary material for deposition at the Cambridge Crystallographic Data Centre with deposition number CCDC 284609 (see Deposition of crystallographic data).

[4] 41 observables from 31 compounds, ranges: Mn–(C_5 centroid) $1.744 \leqslant d \leqslant 1.791$, mean 1.774 Å; Mn–C($C_5$) $2.113 \leqslant d \leqslant 2.211$, mean 2.140 Å.

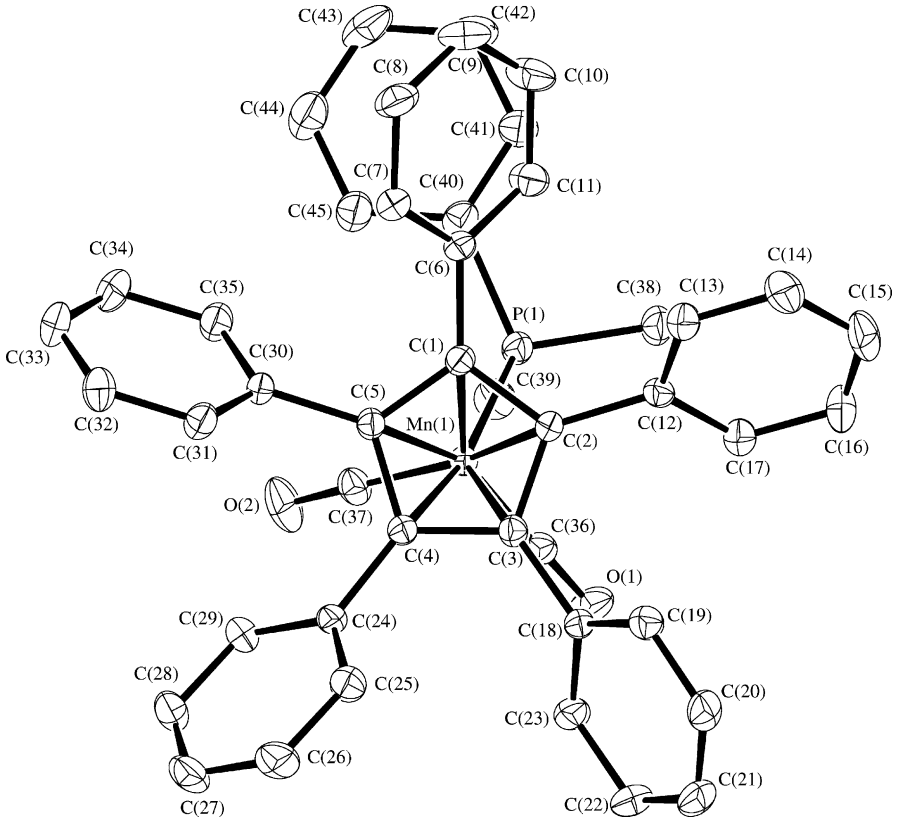

Fig. 3. ORTEP [39] illustration of $[Mn(\eta^5\text{-}C_5Ph_5)(CO)_2PMe_2Ph]$ (**2**), viewed perpendicular to the C_5 ligand plane, showing the atom numbering scheme.

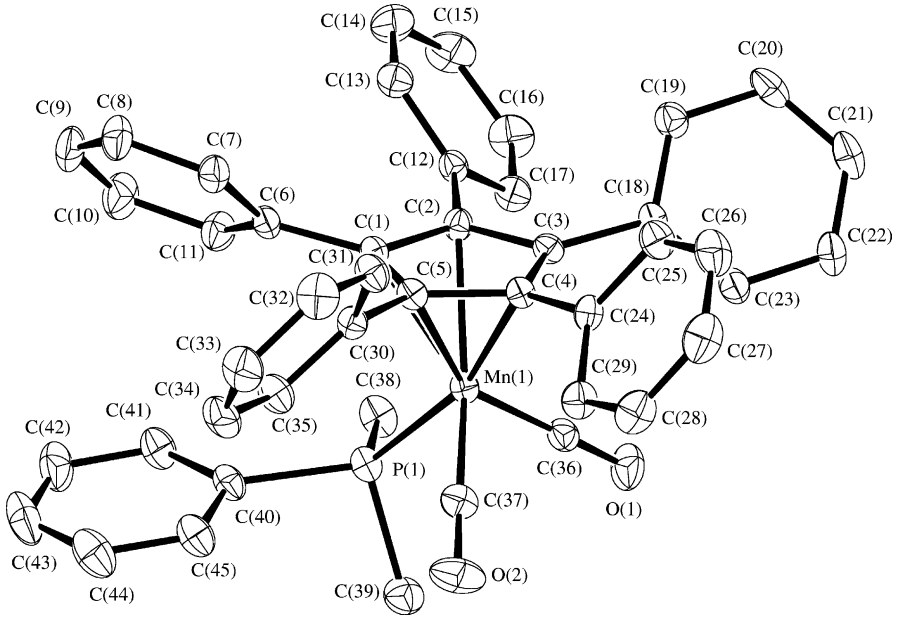

Fig. 4. ORTEP [39] illustration of $[Mn(\eta^5\text{-}C_5Ph_5)(CO)_2PMe_2Ph]$ (**2**), viewed parallel to the C_5 ligand plane, showing the atom numbering scheme.

0.012 Å and are canted at between 47.06° and 56.87° (average 51.5°) to the C_5 ring in a paddle wheel, or propeller, arrangement. The average angle between the planes of adjacent phenyl rings of the $C_5Ph_5^-$ ligand is 52.6°.

2.1.4. The $[Mn(\eta^5\text{-}C_5Ph_5)(CO)_2(PMe_2Ph)]$ molecule

A similar "three-legged piano stool" environment about the manganese atom results from coordination by the η^5-pentaphenylcyclopentadienyl group, the two carbonyl groups and the phosphine.

The most remarkable feature of the structure is the near parallel orientations of the C_5 and the PMe_2Ph phenyl planes. The angle between the phosphine phenyl and C_5 planes is only 7.55°, a consequence of the need to minimise intramolecular interferences between the phosphine methyl and cyclopentadienyl phenyl substituents. This steric pressure is also reflected in the slightly longer Mn-(C_5 centroid) distance in (**2**) by comparison with (**1**), and the considerably longer dimensions than in all $[Mn(\eta^5\text{-}C_5R_5)(CO)_2(PX_3)]$ ($X \neq M$, P) compounds reported to date.

With the chiral $C_5Ph_5^-$ phenyl propeller, and the chirality at the manganese atom, molecule (**2**) is diastereotopic in the solid state. However, the phenyl propellers and the phosphine substituents appear to rotate freely on the NMR time-scale at room temperature in solution, as there are no unexpected multiplicities in the ^1H, ^{13}C or ^{31}P NMR spectra, and, unlike $[Ru(\eta^5\text{-}C_5Ph_5)(CO)_2(PPh_3)Br]$ [26], the diastereomers are not resolved in solution.

3. Conclusions

Manganese derivatives of $C_5Ar_5^-$ ligands are readily accessible in high yield from easily available starting materials. The compounds $[Mn(\eta^5\text{-}C_5Ar_5)(CO)_3]$ undergo reversible one-electron oxidations at potentials more positive than the cyclopentadienyl analogue. Substitution of one of the CO ligands by P- and C-donor ligands is conveniently effected via the intermediacy of Me_3NO. The Mn-(C_5 centroid) distances of $[Mn(\eta^5\text{-}C_5Ph_5)(CO)_3]$ and $[Mn(\eta^5\text{-}C_5Ph_5)(CO)_2(PMe_2Ph)]$ are relatively long for compounds of these types. In particular, the Mn-ligand distances in $[Mn(\eta^5\text{-}C_5Ph_5)(CO)_2(PMe_2Ph)]$ are considerably longer than those reported for $[Mn(\eta^5\text{-}C_5R_5)(CO)_2(PX_3)]$ ($X \neq M$, P) compounds to date. Although the phosphine and cyclopentadienyl phenyl substituents of $[Mn(\eta^5\text{-}C_5Ph_5)(CO)_2(PMe_2Ph)]$ adopt configurations minimising steric interferences in the solid state, these substituents appear to be freely rotating (on the NMR time-scale) in solution at room temperature.

4. Experimental

All manipulations were performed at atmospheric pressure under an atmosphere of dinitrogen by using conventional Schlenk techniques. Chlorobenzene (Merck) was dried, distilled and stored over calcium hydride. Tetrahydrofuran (thf) (Merck) was pre-dried over sodium wire and distilled from sodium benzophenone ketyl. *n*-Hexane (BDH) was distilled from sodium wire. Dichloromethane (Ajax) was distilled from calcium hydride. C_5Ph_5Br [27], and $C_5(p\text{-}MeC_6H_4)_5Br$ [28] were prepared as described previously. $Mn_2(CO)_{10}$ (Aldrich), PMe_2Ph (Fluka) and ^tBuNC (Aldrich) were used as received. $[Mn(CO)_5Br]$, $[Mn(CO)_3(CH_3CN)Br]_2$ and $[Mn(CO)_3(CH_3CN)_3]Br$ were prepared according to literature procedures [29–31]. Trimethylamine *N*-oxide dihydrate (Aldrich) was dehydrated by sublimation prior to use. Flash silica (240–400 mesh) was obtained from Merck. Melting points were recorded on a Reichert hot platform in air and are uncorrected. ^1H and ^{13}C NMR spectra were recorded on Bruker AC200F (^1H NMR 200.13 MHz, ^{13}C NMR 50.33 MHz) or Bruker AMX400 (^1H NMR 400.21 MHz) spectrometers. The spectra were referenced internally to TMS or to residual solvent resonances (CD_2Cl_3, ^1H δ 5.30 ppm, ^{13}C δ 53.8 ppm). ^{31}P NMR spectra were recorded on a Bruker AMX400 spectrometer operating at 162.0 MHz and were referenced to external neat trimethylphosphite (taken to be δ 140.85 ppm from 85% H_3PO_4). Electron impact mass spectra were obtained using a Kratos MS 9 geometry mass spectrometer with a direct insertion probe, a 280 °C source temperature, 70 eV ionisation voltage and 4 kV acceleration voltage.

Melting points were determined using a Gallenkamp melting point apparatus in air and are uncorrected.

Elemental analyses were carried out by one of the following departments: the Australian Microanalytical Service in Melbourne, the Microanalytical Service at the Australian National University or at the JEAF in The University of Sydney.

Infrared spectra were recorded on a Digilab FTS-40 infrared spectrophotometer either as a solution or as a suspension in a potassium bromide matrix. The resolution used was 4 cm^{-1} and the number of scans was 16.

Electrochemical experiments were performed using a BAS 100W Electrochemical Analyser. The sample cell was fitted with a plastic top that could be sealed almost air-tight. A three-electrode configuration was used. The working electrode was a BAS glassy carbon disc (3 mm diameter) which was polished with an alumina (0.25 mm grade) suspension on a velvet polishing cloth, then rinsed with distilled water and acetone, and then dipped in the solvent of use for one minute before each cyclic voltammogram was recorded. The auxiliary electrode was a platinum wire (0.5 mm diameter, 4 cm length) which did not need cleaning between voltammograms but was cleaned by rinsing with 5 M aqueous HNO_3, distilled water and the solvent used prior to each set of experiments. The reference electrode was a BAS Ag/AgCl/NaCl (3 M) electrode with a vycor frit. All samples were thoroughly degassed with high purity argon (CIG) which was passed through a scrubber and a drying tower to remove any traces of oxygen and water, respectively. All potentials are quoted relative to the ferrocenium/ferrocene redox couple, which was observed at ca. 500 mV against the reference electrode [Ag/AgCl/NaCl (3 M)]. Samples were prepared as approximately 1 mM solutions with tetra(*n*-butyl)ammonium tetrafluoroborate (TBATFB ca. 0.1 M) as the supporting electrolyte. TBATFB was prepared either from aqueous HBF_4 (35% v/v, Merck) and $(n\text{-}C_4H_9)NOH$ (40% w/w, Aldrich) or by recrystallisation of TBATFB (Aldrich) three times from ethyl acetate/diethyl ether in air, then drying in vacuo. Full *iR* (100%) compensation was employed in each scan. Except as otherwise stated, all measurements were carried out in dichloromethane

solution with 0.1 M TBATFB as the supporting electrolyte and a scan rate of 100 mV s^{-1}.

4.1. Preparation of [$Mn(\eta^5$-$C_5Ph_5)(CO)_3$] (1)

4.1.1. Method A: reaction of [$Mn(CO)_3(CH_3CN)_3$]Br with LiC_5Ph_5

A solution of LiC_5Ph_5 (1.0 mmol) in tetrahydrofuran (10 mL) was added to a solution of $[Mn(CO)_3(CH_3CN)_3]Br$ (0.34 g, 1.0 mmol) in tetrahydrofuran (10 mL). The solution was refluxed with stirring for 16 h, then the solvent was removed under reduced pressure. The orange/yellow solid was extracted into CH_2Cl_2, and chromatographed on a hexane/alumina column under N_2. Elution with CH_2Cl_2/hexane (1:3) gave a light yellow band which was collected. The solvent was removed under vacuum to yield [$Mn(\eta^5$-$C_5Ph_5)(CO)_3$] (**1**) as a pale yellow solid (0.40 g, 68%).

4.1.2. Method B: reaction of [$Mn(CO)_5Br$] with LiC_5Ph_5

A solution of LiC_5Ph_5 (1.0 mmol) in tetrahydrofuran (10 mL) was added to a solution of $[Mn(CO)_5Br]$ (0.27 g, 1.0 mmol) in tetrahydrofuran (10 mL) and the resultant solution was refluxed with stirring for 16 h. The product was purified chromatographically as in Method A (0.22 g, 38%).

4.1.3. Method C: reaction of [$Mn(CO)_3(CH_3CN)_2Br$] with C_5Ph_5Br and Zn

A mixture of $[Mn(CO)_3(CH_3CN)_2Br]$ (0.15 g, 0.50 mmol), C_5Ph_5Br (0.26 g, 0.50 mmol) and zinc dust (0.033 g, 0.50 mmol) in tetrahydrofuran (15 mL) was refluxed with stirring for 16 h. The product was purified chromatographically as in Method A (0.17 g, 59%). M.p. 287–289 °C. *Anal*. Calc. for $C_{38}H_{25}MnO_3$: C, 78.08; H, 4.31. Found: C, 78.0; H, 4.3%. ^{1}H NMR (ppm, 200 MHz, CD_2Cl_2): δ 7.06 (br, m, 25 H, Ar-*H*). IR ν_{max} (cm^{-1}, KBr): 3060 w, 2007 vs, 1934 vs, 1923 vs, 1503 w, 1445 w, 746 w, 739 w, 699 m sh, 665 m, 636 m, 559 w, ν_{max} (CO) (cm^{-1}, CH_2Cl_2): 2015 s, 1934 s. MS (EI) (*m*/*z*%): 584 (M^+, 12), 528 ($M^+ - 2CO$, 17), 500 ($M^+ - 3CO$, 100), 446 ($C_5Ph_5H^+$, 33).

4.2. Preparation of [$Mn(\eta^5$-$C_5Ph_5)(CO)_2(PMe_2Ph)$] (2)

$PPhMe_2$ (0.22 mL, 0.70 mmol) and trimethylamine oxide (0.045 g, 0.60 mmol) were added to a solution of $[Mn(C_5Ph_5)(CO)_3]$ (0.295 g, 0.51 mmol) in tetrahydrofuran (30 mL) and the resulting reaction mixture was heated at reflux for 16 h. The solvent was removed in vacuo to afford an orange oil and the crude product was purified by column chromatography on alumina eluting with CH_2Cl_2/hexane (20/80 *v*/*v*). The product was recrystallised from CH_2Cl_2/hexane to give [$Mn(\eta^5$-$C_5Ph_5)(CO)_2(PMe_2Ph)$] (**2**) as an orange crystalline solid (0.285 g, 81%). M.p. 287–289 °C. *Anal*. Calc. for $C_{45}H_{36}MnOP$: C, 77.80; H, 5.22. Found: C, 77.4; H, 4.9%. ^{1}H NMR ($CDCl_3$): δ 7.55–6.75 (br m, 30H, (C_6H_5)C_5 and P(C_6H_5)), 1.59 (br s, 6H, $2 \times PCH_3$) ppm. $^{31}P\{^1H\}$ NMR ($CDCl_3$): δ 45.86 (s) ppm. I.R. (KBr): *v* 1850 (vs), 1918 (vs) cm^{-1}.

4.3. Preparation of [$Mn(\eta^5$-$C_5(p\text{-}tol)_5)(CO)_3$] (3)

4.3.1. Method A: reaction of [$Mn(CO)_3(CH_3CN)_3$]Br with $LiC_5(p\text{-}tol)_5$

A solution of $LiC_5(p\text{-tol})_5$ (0.87 mmol) in tetrahydrofuran (10 mL) was added to a solution of $[Mn(CO)_3(CH_3CN)_3]Br$ (0.30 g, 0.86 mmol) in tetrahydrofuran (10 mL). The resultant solution was refluxed with stirring for 16 h, then the solvent was removed under reduced pressure. The orange/yellow solid was extracted into CH_2Cl_2, and chromatographed on a hexane/alumina column under N_2. Elution with CH_2Cl_2/hexane (1:5) gave a light yellow band which was collected. The solvent was then removed to yield [$Mn(\eta^5$-$C_5(p\text{-tol})_5)(CO)_3$] (**3**) as a pale yellow solid (0.19 g, 34%).

4.3.2. Method B: reaction of [$Mn(CO)_3(CH_3CN)_3$]Br with $C_5(p\text{-tol})_5Br$ and Zn

Tetrahydrofuran (15 mL) was added to a solid mixture of $[Mn(CO)_3(CH_3CN)_3]Br$ (0.34 g, 1.0 mmol), $C_5(p\text{-tol})_5Br$ (0.59 g, 1.0 mmol) and zinc dust (0.075 g, 1.1 mmol). The resultant solution was refluxed with stirring for 16 h. The product was purified chromatographically as in Method A (0.45 g, 69%).

M.p. 255–257 °C. *Anal*. Calc. for $C_{43}H_{35}MnO_3$: C, 78.89; H, 5.39. Found: C, 78.1; H, 5.2%. ^{1}H NMR (ppm, 200 MHz, CD_2Cl_2): δ 7.09–6.83 (m, 20H, Ar-*H*) 2.26–2.17 (m, 15H, CH_3). IR ν_{max} (cm^{-1}, KBr): 3020 w, 2922 w, 2008 vs, 1932 vs, 1926 vs, 1520 m, 1187 w, 1020 w, 838 w, 820 w, 805 w, 728 w, 666 m, 630 m, 538 m sh. MS (EI) (*m*/*z*%): 654 (M^+, 4.4), 598 ($M^+ - 2CO$, 2), 570 ($M^+ - 3CO$, 100), 526 ($C_5Ph_5H^+$, 34).

4.4. Structure determinations

[$Mn(\eta^5$-$C_5Ph_5)(CO)_3$] (**1**): a yellow blade like crystal having approximate dimensions of $0.47 \times 0.20 \times 0.12$ mm was attached to a thin glass fibre, and mounted on an Enraf-Nonius CAD4 diffractometer employing graphite monochromated Mo Kα radiation. Primitive monoclinic cell constants were obtained from a least-squares refinement using the setting angles of 25 reflections in the range $16.02 < 2\theta < 24.24°$. Diffraction data were collected at a temperature of 21 ± 1 °C using ω scans to a maximum 2θ value of 49.9°. The intensities of three representative reflections measured every 60 min, decreased by 53.2% and a polynomial correction factor was accordingly applied to the data. An analytical absorption correction was applied and the data were also corrected for Lorentz and polarisation effects.

All calculations were undertaken with the TEXSAN [32] crystallographic software package. Neutral atom scattering factors were taken from Cromer and Waber [33]. Anomalous dispersion effects were included in Fcalc [34] and the

values for $\Delta f'$ and $\Delta f''$ were those of Creagh and McAuley [35]. The values for the mass attenuation coefficients were those of Creagh and Hubbell [36]. The structure was solved in the space group $P2_1/n$ (#14) by heavy-atom Patterson methods [37] and expanded using Fourier techniques [38]. In general non-hydrogen atoms were modelled anisotropically, however C(3), C(5), C(17), C(18), C(30) and C(35) were refined with isotropic thermal parameters. Hydrogen atoms were included in the model at calculated positions with group thermal parameters. ORTEP projections of the molecule are provided in Figs. 2 and 3 [39].

4.5. Crystal data for $[Mn(\eta^5\text{-}C_5Ph_5)(CO)_3]$ (1)

Formula $C_{38}H_{25}MnO_3$, M 584.52, monoclinic, space group $P2_1/n$ (#14), a 16.929(4), b 8.928(2), c 20.054(4) Å, β 106.04(2), V 2913.0(11) Å^3, D_c 1.333 g cm^{-3}, Z 4, crystal size 0.47 by 0.20 by 0.12 mm, colour yellow, habit blade, temperature 294(2) K, λ(Mo Kα) 0.71073 Å, μ(Mo Kα) 0.4900 mm^{-1}, T (Analytical)$_{min,max}$ 0.8984, 0.9489, $2\theta_{max}$ 49.98, hkl range −20 19, −1 10, −1 10, N 4061, N_{ind} 3167-(R_{merge} 0.0738), N_{obs} 2058($I > 2\sigma(I)$), N_{var} 344, residuals[5] $R_1(F)$ 0.0967, $wR_2(F^2)$ 0.2971, GoF(all) 1.274, $\Delta\rho_{min,max}$ −1.516, 1.455 e$^-$ Å^{-3}.

[Mn(η^5-C_5Ph_5)(CO)$_2$(PMe_2Ph)] (**2**): a yellow blade like crystal having approximate dimensions of $0.28 \times 0.25 \times 0.11$ mm was attached to a thin glass fibre, and mounted on a Rigaku AFC7R diffractometer employing graphite monochromated Cu Kα radiation from a rotating anode generator. Primitive monoclinic cell constants were obtained from a least-squares refinement using the setting angles of 21 reflections in the range $68.01 < 2\theta < 91.99°$. Diffraction data were collected at a temperature of 21 ± 1 °C using ω–2θ scans to a maximum 2θ value of 130.2°. Omega scans of several intense reflections made prior to data collection, had an average width at half-height of 0.18°, and scans of $(1.73 + 0.35 \tan\theta)°$ were made at a speed of 16.0°/min (in omega). The weak reflections ($I < 15.0\sigma(I)$) were rescanned up to 10 times. Stationary background counts were recorded on each side of the reflection, with a 2:1 ratio of peak to background counting time. The intensities of three representative reflections measured every 150 reflections, did not change significantly during the data collection. An analytical absorption correction was applied and the data were also corrected for Lorentz and polarisation effects.

All calculations were undertaken with the TEXSAN [32] crystallographic software package. Neutral atom scattering factors were taken from Cromer and Waber [33]. Anomalous dispersion effects were included in Fcalc [34] and the values for $\Delta f'$ and $\Delta f''$ were those of Creagh and McAuley [35]. The values for the mass attenuation coefficients were those of Creagh and Hubbell [36]. The structure was solved in the space group $P2_1/n$ (#14) by direct methods [40] and expanded using Fourier techniques [38]. Non-hydrogen atoms were modeled with anisotropic thermal parameters and hydrogen atoms were included in the model at calculated positions with group thermal parameters. ORTEP projections of the molecule are provided in Figs. 1 and 2 [39].

4.6. Crystal data for $[Mn(\eta^5\text{-}C_5Ph_5)(CO)_2(PMe_2Ph)]$ (2)

Formula $C_{45}H_{33}MnO_2P$, M 691.62, monoclinic, space group $P2_1/n$(#14), a 15.251(4), b 13.804(3), c 17.682(4) Å, β 106.39(2), V 3571.2(15) Å^3, D_c 1.286 g cm^{-3}, Z 4, crystal size 0.28 by 0.25 by 0.11 mm, colour yellow, habit blade, temperature 294(2) K, λ(Cu Kα) 1.5418 Å, μ(Cu Kα) 3.714 mm^{-1}, T(Analytical)$_{min,max}$ 0.420, 0.698, $2\theta_{max}$ 130.20, hkl range 0 17, 0 16, −20 19, N 6028, N_{ind} 6027 (R_{merge} 0.05469), N_{obs} 4016($I > 2\sigma(I)$), N_{var} 443, residuals[6] $R_1(F)$ 0.0472, $wR_2(F^2)$ 0.1356, GoF(all) 1.189, $\Delta\rho_{min,max}$ −0.383, 0.495 e$^-$ Å^{-3}.

Acknowledgement

We thank the Australian Research Council for financial support.

References

[1] K. Ziegler, B. Schnell, Justus Liebigs Ann. Chem. 445 (1925) 266.
[2] K. Ziegler, F.A. Fries, Ber. 59B (1926) 242.
[3] W. Hübel, R. Merenyi, J. Organomet. Chem. 2 (1964) 213.
[4] T.S. Piper, F.A. Cotton, G. Wilkinson, J. Inorg. Nucl. Chem. 1 (1955) 165.
[5] A.F. Berndt, R.E. Marsh, Acta Crystallogr. 16 (1963) 118.
[6] P.J. Fitzpatrick, Y. Le Page, J. Sedman, I.S. Butler, Inorg. Chem. 20 (1981) 2852.
[7] J. Cowie, E.J.M. Hamilton, J.C.V. Laurie, A.J. Welch, J. Organomet. Chem. 394 (1990) 1.
[8] E.O. Fischer, R. Jira, Z. Naturforsch. 9B (1954) 618.
[9] M.D. Rausch, W.-M. Tsai, J.W. Chambers, R. Rogers, H.G. Alt, Organometallics 8 (1989) 816.
[10] R.B. King, A. Efraty, J. Am. Chem. Soc. 94 (1972) 3773.
[11] R.B. King, M.Z. Iqbal, A.D. King, J. Organomet. Chem. 171 (1979) 53.
[12] I. Bernal, J.D. Korp, W.A. Herrmann, R. Serrano, Chem. Ber. 117 (1984) 434.
[13] G. Wilkinson, F.G.A. Stone, E.W. Abel (Eds.), Comprehensive Organometallic Chemistry, vol. 4, Pergamon, 1982, p. 1.
[14] R.B. King, A. Efraty, W.M. Douglas, J. Organomet. Chem. 56 (1973) 345.
[15] G. Wilkinson, F.G.A. Stone, E.W. Abel (Eds.), Comprehensive Organometallic Chemistry, vol. 6, Pergamon, 1995, p. 109.
[16] F.P.A. Johnson, M.W. George, V.N. Bagratashvili, L.N. Vereshchagina, M. Poliakoff, Mendeleev Commun. (1991) 26.
[17] N.G. Connelly, I. Manners, J. Chem. Soc., Dalton Trans. (1989) 283.
[18] L.D. Field, T.W. Hambley, P.A. Humphrey, A.F. Masters, P. Turner, Polyhedron 17 (1998) 2587.

[5] $R_1 = \sum ||F_o| - |F_c|| / \sum |F_o|$ for $F_o > 2\sigma(F_o)$; $wR_2 = (\sum w(F_o^2 - F_c^2)^2 / \sum (wF_c^2)^2)^{1/2}$ all reflections $w = 1/[\sigma^2(F_o^2) + (0.10P)^2 + 15.0P]$ where $P = (F_o^2 + 2F_c^2)/3$.

[6] $R_1 = \sum ||F_o| - |F_c|| / \sum |F_o|$ for $F_o > 2\sigma(F_o)$; $wR_2 = (\sum w(F_o^2 - F_c^2)^2 / \sum (wF_c^2)^2)^{1/2}$ all reflections $w = 1/[\sigma^2(F_o^2) + (0.05P)^2 + 1.0P]$ where $P = (F_o^2 + 2F_c^2)/3$.

[19] C.J. Pickett, D. Pletcher, J. Chem. Soc., Dalton Trans. (1976) 636.
[20] K. Broadley, G.A. Lane, N.G. Connelly, W.E. Geiger, J. Am. Chem. Soc. 105 (1983) 2486.
[21] N.G. Connelly, W.E. Geiger, G.A. Lane, S.J. Raven, P.H. Rieger, J. Am. Chem. Soc. 108 (1986) 6219.
[22] S.M. Sawtelle, R.F. Johnston, C.C. Cook, Inorg. Chim. Acta 221 (1994) 85.
[23] T. Wurminghausen, D. Sellmann, J. Organomet. Chem. 199 (1980) 77.
[24] J.E. Ellis, R.A. Faltynek, S.G. Hentges, J. Organomet. Chem. 120 (1976) 389.
[25] N.V. Podberezskaya, V.A. Maksakov, I.V. Slovokhotova, S.P. Babailov, A.V. Virovets, V.P. Kirin, J. Struct. Chem. (Translation of Zhurnal Strukturnoi Khimii) (2000) 40 (1999) 914.
[26] H. Adams, N.A. Bailey, A.F. Browning, J.A. Ramsden, C. White, J. Organometal. Chem. 387 (1990) 305.
[27] L.D. Field, K.M. Ho, C.M. Lindall, A.F. Masters, A.G. Webb, Aust. J. Chem. 43 (1990) 281.
[28] L.D. Field, A.F. Masters, M. Gibson, D.R. Latimer, T.W. Hambley, I.E. Buys, Inorg. Chem. 32 (1993) 211.
[29] M.H. Quick, R.J. Angelici, in: D.F. Shriver (Ed.), Inorganic Syntheses, vol. 19, Wiley, New York, 1979, p. 160.
[30] J.G. Dunn, D.A. Edwards, J. Organomet. Chem. 27 (1971) 73.
[31] R.H. Reimann, E. Singleton, J. Chem. Soc., Dalton Trans. (1974) 808.
[32] Molecular Structure Corporation, TEXSAN: Single Crystal Structure Analysis Software, Version 1.6, Molecular Structure Corporation, The Woodlands, TX, USA, 1993.
[33] D.T. Cromer, J.T. Waber, in: J.A. Ibers, W.C. Hamilton (Eds.), International Tables for X-Ray Crystallography, vol. IV, Kynock Press, Birmingham, England, 1974, p. 71.
[34] J.A. Ibers, W.C. Hamilton, Acta Crystallogr. 17 (1964) 781.
[35] D.C. Creagh, W.J. McAuley, in: A.J.C. Wilson (Ed.), International Tables for Crystallography, vol. C, Kluwer Academic Publishers, Boston, 1992, p. 219.
[36] D.C. Creagh, J.H. Hubbell, in: A.J.C. Wilson (Ed.), International Tables for Crystallography, vol. C, Kluwer Academic Publishers, Boston, 1992, p. 200.
[37] P.T. Beurskens, G. Admiraal, G. Beurskens, W.P. Bosman, S. Garcia-Granda, R.O. Gould, J.M.M. Smits, C. Smykalla, PATTY The DIRDIF program system. Technical Report of the Crystallography Laboratory, University of Nijmegen, The Netherlands, Version Nijmegen, 1992.
[38] P.T. Beurskens, G. Admiraal, G. Beurskens, W.P. Bosman, R. de Gelder, R. Israel, J.M.M. Smits, The DIRDIF-94 Program System. Technical Report. Crystallography Laboratory, University of Nijmegen, The Netherlands, DIRDIF-94, Nijmegen, 1994.
[39] C.K. Johnson, ORTEPII, a Thermal Ellipsoid Plotting Program, Report ORNL-5138, Version Oak Ridge National Laboratories, Oak Ridge TN, 1976.
[40] A. Altomare, M. Cascarano, C. Giacovazzo, A. Guagliardi, J. Appl. Crystallogr. 26 (1993) 343.

many nucleophilic and electrophilic reactions [16,17], so it was reasonable to examine metallosurfactants in this content. It is argued that the high charge and size of the head group of complexes having long paraffin tails, detergent-like characteristics are able to penetrate biological membranes and destabilize the exterior membrane of the organism [18]. Moreover, transition metal ions complexes with lipophilic ligands in micellar or vesicular aggregates have attracted considerable attention as catalysts for the cleavage of esters and amides and as biomimetic models of hydrolytic metalloenzymes [19,20]. Recently, there has been increasing interest in the use of these organized media to study the fundamental photochemical reactions of metal complexes with relevance to the conversion of solar energy into other useful forms of energy through photochemical reactions [21,22]. As a part of our studies on transition metal-based surfactants [3,4] in this paper we report the synthesis, characterization and determination of critical micelle concentration values of some more novel cobalt(III) surfactant complexes.

2. Experimental

2.1. Chemicals and reagents

All the reagents were of analytical grade (Aldrich and Merck). Ultra pure water, obtained by deionising distilled water using a Milli-Q Reagent Grade water system, was used for preparative work and to make up solutions for all physical measurements.

2.2. Synthesis of metallosurfactants of cobalt(III) complexes

The surfactant cobalt(III) complexes synthesized here were prepared by a similar method to those complexes reported in the literature [23], by replacing the lower amine groups by long-chain amine ligands as follows.

2.2.1. *cis*-$[Co(en)_2(C_{12}H_{25}NH_2)Cl](ClO_4)_2$ and *cis*-$[Co(en)_2(C_{16}H_{33}NH_2)Cl](ClO_4)_2$

trans-$[Co(en)_2Cl_2]Cl$ [24], (3.0 g, 10.5 mmol) was dissolved in water (20 mL). To this solution slightly more than the calculated amount of dodecylamine (3 mL), where the amine used was not sufficiently miscible with (soluble in) water, was first mixed with ethanol (2 mL) and then added drop by drop over a period of 30 min. The green solution gradually became red during the reaction. The mixture was set aside at 313 K for 2 days until no further change was observed. Afterwards a saturated solution of sodium perchlorate in very dilute perchloric acid was added. Slowly a pasty solid mass separated out and it was filtered off, washed with small amounts of alcohol followed by acetone, and then it was dried over air. The semi-dried solid was further dried in a drying pistol over fused calcium chloride and stored in a vacuum desiccator. For the complex *cis*-$[Co(en)_2(C_{16}H_{33}NH_2)Cl](ClO_4)_2$ cetylamine was used instead in the place of dodecylamine.

2.2.2. *cis*-$[Co(en)_2(C_{12}H_{25}NH_2)Br](ClO_4)_2$ and *cis*-$[Co(en)_2(C_{16}H_{33}NH_2)Br](ClO_4)_2$

This complex was synthesized by adopting the same method as described for the synthesis of the complex *cis*-$[Co(en)_2(C_{16}H_{33}NH_2)Cl](ClO_4)_2$ except that in place of *trans*-$[Co(en)_2Cl_2]Cl$, *trans*-$[Co(en)_2Br_2]Br$ [23] (3.0 g, 7.16 mmol) was used. The same procedure was followed for the complex *cis*-$[Co(en)_2(C_{16}H_{33}NH_2)Br](ClO_4)_2$, but in the place of dodecylamine, cetylamine was used.

Complexes *cis*-$[Co(en)_2(C_{12}H_{25}NH_2)NO_2](NO_3)_2$, *cis*-$[Co(en)_2(C_{16}H_{33}NH_2)NO_2](NO_3)_2$, *cis*-α-$[Co(trien)(C_{12}H_{25}NH_2)NO_2](NO_3)_2$ and *cis*-α-$[Co(trien)(C_{16}H_{33}NH_2)NO_2](NO_3)_2$ were prepared by the ligand substitution method by replacing the chloride ion with dodecylamine/cetylamine from the corresponding *cis*-$[Co(en)_2(NO_2)Cl](NO_3)_2$ [25] and *cis*-α-$[Co(trien)(NO_2)Cl](NO_3)_2$ [26].

Complexes *cis*-α-$[Co(trien)(C_{12}H_{25}NH_2)Cl]^{2+}$ and *cis*-α-$[Co(trien)(C_{12}H_{25}NH_2)Br]^{2+}$ were prepared as reported in the literature [4], the same procedure was followed for complexes *cis*-α-$[Co(trien)(C_{16}H_{33}NH_2)Cl]^{2+}$ and *cis*-α-$[Co(trien)(C_{16}H_{33}NH_2)Br]^{2+}$, but in the place of dodecylamine, cetylamine was used as a coordinating ligand.

Safety note! Perchlorate salts of metal complexes with organic ligands are potentially explosive. Only small amounts of materials should be prepared, and these should be handled with caution.

2.3. Instrumentation

Infrared (IR) spectra were recorded on a Jasco 460 plus spectrometer using the potassium bromide discs method. ^1H NMR spectra were recorded in the appropriate deuteriated solvents using a Bruker AC 300F (300 MHz) spectrometer with TMS as internal reference. Electronic absorption spectra were taken in 10^{-3} M perchloric acid medium recorded on a Varian Cary 500 Scan UV–Vis–NIR spectrophotometer. C, H and N were estimated using a Perkin–Elmer 2400 CHN instrument. Conductivity studies were done in aqueous solutions of the complexes with an Elico conductivity bridge type CM 82 and a dip-type cell with a cell constant of 1.0.

2.4. Determination of CMC

The critical micelle concentration values of these complexes were determined conductometrically using a specific conductivity meter (Elico CM 82). The conductivity cell (dip-type with a cell constant of 1.0) was calibrated with KCl solutions in the appropriate concentration range. The cell constant was calculated using molar conductivity data for KCl published by Shedlovsky [27] and Chambers [28]. Various concentrations of cobalt(III)-surfactant complexes were prepared in the range 10^{-5}–10^{-1} mol dm^{-3} in aqueous solution. The conductivity of these solutions was measured at 303, 308 and 313 K. The temperature of the thermostat was maintained constant to within ±0.01 K. At least a set of 50 specific conductance readings for 50

different concentrations of complex was noted in order to get the critical micelle concentration values for each system.

3. Results and discussion

The cobalt(III)-surfactant complexes synthesized in the present study were characterized by UV–Vis, IR and NMR spectra and checked by comparing the spectra with those for the corresponding ordinary complexes where one of the ligands is butylamine instead of dodecylamine/cetylamine, reported earlier [3,4,29–34]. The purity of the complexes was checked by cobalt [35], elemental and halide analyses, which were found to be in good agreement with those of the calculated ones (Table 1).

The uniqueness of the cobalt(III)-surfactant coordination complexes lies in the fact that the bond between the head group and the tail part of the surfactant-cobalt(III) complex is a coordinate bond and the surfactant contains a higher charge on the head group unlike common surfactants (sodium dodecyl sulfate). At the same time like the common surfactants, these cobalt(III)-surfactant coordination compounds form foam in aqueous solution when mechanically disturbed like shaking, and these complexes dissolve slowly in water, though sometimes we have to sonicate the solution to get a homogeneous solution (see Fig. 1).

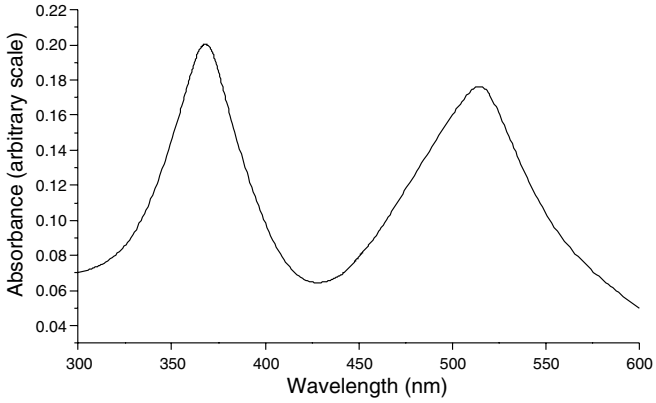

Fig. 1. Visible absorption spectra of *cis*-[Co(en)$_2$($C_{12}H_{25}NH_2$)Cl](ClO$_4$)$_2$.

3.1. Spectroscopic characterization

Several attempts have been made to relate differences in infrared spectra to the structure of the geometrical configuration of complexes [29–34]. The IR spectra of a number of Co(III) complexes were determined and were recorded in Tables 2 and 3. For the assignment of a geometrical configuration to these complexes, infrared spectroscopy was used. Various workers have employed [29–34] the NH_2 deformation mode in the 1700–1500 cm^{-1} region, CH_2 rocking mode in the 900–850 cm^{-1} region and Co–N stretching mode in the 610–500 cm^{-1} region to distinguish between the *cis* and *trans* isomers of cobalt(III)-ethylenediamine complexes. Baldwin [31] suggested that the most consistent variations between the spectra of *cis* and *trans* isomers were found in the CH_2 rocking region (900–850 cm^{-1}). The *cis* isomers always show two peaks, whereas the *trans* isomers usually have only one. Hughes and McWhinnie [30] studied the infrared absorption spectra of several bis(ethylenediamine)cobalt(III) complexes and obtained a satisfactory correlation in the 610–500 cm^{-1} region, where Co–N stretching modes of the chelate ring occur. Here, no *trans* isomers had more than three strong bands, while all *cis* isomers had at least four, sometimes occurring as shoulders. The bands for the *trans* isomers were generally evenly distributed, while those for *cis* complexes occurred in two groups with a wide separation between them. The data in Tables 2 and 3, indicate that generally the complexes studied followed the previous trends. Because of lower symmetry in the present study (Fig. 2), the *cis* isomers show two bands for the NH_2 deformation, two bands for the NH_2 wagging modes, two bands for the CH_2 rocking mode and four bands occurring as groups of two with a wide separation for the Co–N stretching mode. The complex of the type *cis*-α-[Co(trien)XCl]$^{n+}$ of the present study shows two bands for the NH_2 deformation in the region 1630–1580 cm^{-1}, two bands for the

Table 1
Microanalysis and visible spectra of metallosurfactant cobalt(III) complexes

	Surfactants	λ_{max} (ε)[a]	Yield (%)	% Found (Calc.)				
				Co	C	H	N	Cl/Br
1	*cis*-[Co(en)$_2$($C_{12}H_{25}NH_2$)Cl](ClO$_4$)$_2$	515 (90)	67	9.8 (9.9)	32.1 (32.3)	6.2 (6.4)	11.5 (11.7)	6.1 (5.9)
2	*cis*-[Co(en)$_2$($C_{12}H_{25}NH_2$)Br](ClO$_4$)$_2$	523 (91)	64	9.1 (9.2)	30.0 (30.1)	5.10 (5.9)	10.8 (10.9)	12.3 (12.5)
3	*cis*-[Co(en)$_2$($C_{12}H_{25}NH_2$)NO$_2$](NO$_3$)$_2$	460 (94)	57	11.3 (11.4)	37.2 (37.4)	7.4 (7.4)	21.9 (21.8)	
4	*cis*-[Co(en)$_2$($C_{16}H_{33}NH_2$)Cl](ClO$_4$)$_2$	512 (96)	65	9.2 (9.2)	37.4 (37.5)	5.5 (5.6)	10.5 (10.9)	5.2 (5.5)
5	*cis*-[Co(en)$_2$($C_{16}H_{33}NH_2$)Br](ClO$_4$)$_2$	520 (97)	60	8.6 (8.6)	35.0 (35.1)	5.3 (5.2)	9.9 (10.2)	11.4 (11.6)
6	*cis*-[Co(en)$_2$($C_{16}H_{33}NH_2$)NO$_2$](NO$_3$)$_2$	459 (99)	52	10.4 (10.5)	42.8 (42.9)	6.2 (6.4)	19.8 (20.0)	
7	*cis*-α-[Co(trien)($C_{12}H_{25}NH_2$)Cl](ClO$_4$)$_2$	485 (103)	65	9.0 (9.1)	37.2 (37.2)	6.3 (6.5)	10.9 (10.8)	5.6 (5.4)
8	*cis*-α-[Co(trien)($C_{12}H_{25}NH_2$)Br](ClO$_4$)$_2$	490 (104)	60	8.4 (8.5)	34.7 (34.8)	6.0 (6.1)	9.8 (10.1)	11.3 (11.5)
9	*cis*-α-[Co(trien)($C_{12}H_{25}NH_2$)(NO$_2$)](NO$_3$)$_2$	448 (106)	50	10.3 (10.4)	42.5 (42.4)	7.2 (7.4)	19.7 (19.8)	
10	*cis*-α-[Co(trien)($C_{16}H_{33}NH_2$)Cl](ClO$_4$)$_2$	483 (108)	63	8.3 (8.3)	40.9 (41.0)	6.9 (7.1)	9.6 (9.9)	4.7 (5.0)
11	*cis*-α-[Co(trien)($C_{16}H_{33}NH_2$)Br](ClO$_4$)$_2$	487 (109)	59	7.7 (7.8)	38.7 (38.6)	6.4 (6.7)	9.3 (9.4)	10.5 (10.7)
12	*cis*-α-[Co(trien)($C_{16}H_{33}NH_2$)(NO$_2$)](NO$_3$)$_2$	445 (111)	55	9.3 (9.4)	46.1 (46.3)	7.9 (8.1)	17.8 (18.0)	

[a] λ in nm; ε in M^{-1} cm^{-1}.

Table 2
IR spectral data of metallosurfactant bis(ethylenediamine)cobalt(III) complexes

Complexes	Frequencies (cm^{-1})
cis-$[Co(en)_2(C_{12}H_{25}NH_2)Cl](ClO_4)_2$	3200 (s), 3100 (s), 2909–2875 (w), 1635 (s), 1580 (s), 1475 (m), 1390 (m), 1288 (w), 1221 (m), 1170 (sh), 1148 (w), 1120 (w), 1110 (w), 1090 (m), 1054 (m), 1000 (w), 890 (m), 880 (m), 819 (m), 800 (w), 670 (w), 591 (m), 581 (w), 561 (w), 519 (w), 510 (w)
cis-$[Co(en)_2(C_{12}H_{25}NH_2)Br](ClO_4)_2$	3181 (s), 3094 (s), 2894–2850 (w), 1627 (s), 1577 (s), 1471 (w), 1386 (w), 1283 (m), 1220 (s), 1163 (w), 1150 (s), 1124 (w), 1104 (w), 1084 (m), 1060 (m), 1007 (w), 889 (m), 880 (m), 820 (w), 803 (m), 760 (sh), 664 (w), 577 (m), 553 (w), 520 (w), 514 (w)
cis-$[Co(en)_2(C_{12}H_{25}NH_2)NO_2](NO_3)_2$	3204 (s), 3103 (s), 2942–2870 (m), 1610 (s), 1570 (s), 1453 (m), 1330(m), 1290 (w), 1281 (m), 1214 (w), 1159 (w), 1143 (m), 1126 (w), 1053 (w), 1004 (w), 894 (m), 888 (w), 875 (m), 860 (m), 643 (sh), 584 (w), 560 (m), 521 (w), 507 (w)
cis-$[Co(en)_2(C_{16}H_{33}NH_2)Cl](ClO_4)_2$	3234 (s), 3110 (s), 2912–2850 (w), 1630 (s), 1595 (s), 1470 (m), 1393 (m), 1280 (w), 1228 (m), 1176 (sh), 1140 (w), 1108 (w), 1092 (w), 1056 (m), 1010 (w), 885 (m), 880 (w), 824 (m), 807 (m), 682 (s), 580 (w), 560 (m), 523 (w), 504 (w)
cis-$[Co(en)_2(C_{16}H_{33}NH_2)Br](ClO_4)_2$	3227 (s), 3103 (s), 2900–2860 (m), 1623 (s), 1584 (s), 1467 (w), 1395 (w), 1283 (m), 1220 (s), 1173 (w), 1135 (w), 1120 (m), 1110 (w), 1053 (w), 1007 (sh), 890 (m), 874 (m), 817 (w), 800 (w), 670 (m), 574 (m), 555 (w), 517 (w), 503 (w)
cis-$[Co(en)_2(C_{16}H_{33}NH_2)NO_2](NO_3)_2$	3226 (s), 3112 (s), 2907–2862 (w), 1617 (s), 1582 (s), 1447 (w), 1392 (m), 1290 (w), 1281(w), 1207 (m), 1193 (w), 1140 (m), 1123 (w), 1060 (s), 1000 (w), 890 (m), 886 (w), 872 (m), 853 (m), 664 (sh), 591 (s), 580 (w), 553 (w), 514 (w), 500 (w)

s, strong; m, medium; sh, shoulder; w, weak.

Table 3
IR spectral data of metallosurfactant (triethylenetetramine)cobalt(III) complexes

Complexes	Frequencies (cm^{-1})
cis-α-$[Co(trien)(C_{12}H_{25}NH_2)Cl](ClO_4)_2$	3253 (s), 3180 (s), 3110 (m), 3051 (m), 1580 (s), 1492 (w), 1480 (m), 1453 (s), 1443 (w), 1390 (m), 1370 (m), 1360 (m), 1327 (m), 1300 (w), 1294 (s), 1275 (w), 1245 (s), 1200 (m), 1160 (w), 1153 (s), 1125 (w), 1050 (m), 1010 (w), 980 (w), 905 (w), 870 (m), 800 (s), 745 (w), 700 (m), 680 (w), 665 (w), 642 (w), 582 (m), 563 (m)
cis-α-$[Co(trien)(C_{12}H_{25}NH_2)Br](ClO_4)_2$	3232 (s), 3154 (s), 3090 (m), 3055 (m), 1572 (s), 1487 (m), 1476 (w), 1450 (m), 1437 (sh), 1392 (m), 1374 (m), 1363 (w), 1330 (m), 1302 (m), 1295 (s), 1270 (m), 1240 (m), 1200 (w), 1153 (s), 1120 (m), 1045 (sh), 1004 (m), 976 (sh), 900 (w), 871 (s), 800 (m), 764 (m), 740 (m), 674 (w), 660 (w), 637 (w), 580 (m), 560 (w)
cis-α-$[Co(trien)(C_{12}H_{25}NH_2)NO_2](NO_3)_2$	3227 (s), 3176 (s), 3107 (m), 3055 (m), 1580 (m), 1490 (sh), 1481 (m), 1432 (w), 1390 (m), 1375 (w), 1361 (w), 1330 (m), 1302 (w), 1290 (s), 1274 (m), 1240 (m), 1205 (w), 1162 (w), 1150 (s), 1120 (m), 1050 (w), 1007 (w), 981 (m), 906 (m), 862 (s), 802 (m), 767 (w), 740 (w), 678 (s), 660 (w), 640 (w), 580 (w), 562 (w)
cis-α-$[Co(trien)(C_{16}H_{33}NH_2)Cl](ClO_4)_2$	3264 (s), 3189 (s), 3114 (m), 3050 (m), 1585 (s), 1493 (m), 1480 (m), 1440 (w), 1387 (s), 1370 (m), 1365 (w), 1334 (w), 1300 (w), 1285 (s), 1276 (m), 1239 (m), 1205 (w), 1170 (w), 1150 (m), 1127 (s), 1058 (s), 1012 (w), 984 (w), 912 (w), 867 (s), 808 (m), 769 (m), 747 (w), 680 (w), 660 (w), 637 (m), 584 (w), 560 (m)
cis-α-$[Co(trien)(C_{16}H_{33}NH_2)Br](ClO_4)_2$	3257 (s), 3173 (s), 3104 (m), 3051 (m), 1577 (m), 1491 (m), 1480 (m), 1437 (w), 1380 (sh), 1365 (w), 1330 (w), 1280 (m), 1275 (s), 1240 (m), 1205 (m), 1175 (m), 1153 (s), 1130 (w), 1060 (w), 1010 (w), 980 (w), 911 (m), 860 (s), 805 (m), 770 (w), 750 (w), 683 (w), 665 (s), 640 (m), 580 (m), 564 (w)
cis-α-$[Co(trien)(C_{16}H_{33}NH_2)NO_2](NO_3)_2$	3260 (s), 3176 (s), 3103 (m), 3048 (m), 1575 (m), 1483 (m), 1456 (sh), 1442 (w), 1431 (w), 1397 (s), 1377 (sh), 1360 (w), 1336 (w), 1324 (m), 1307 (m), 1294 (s), 1260 (m), 1240 (w), 1212 (m), 1198 (m), 1164 (w), 1150 (s), 1125 (w), 1100 (w), 1057 (m), 1040 (m), 1000 (w), 981 (w), 904 (w), 879 (s), 802 (m), 783 (m), 760 (w), 674 (w), 641 (s), 567 (w), 579 (w)

s, strong; m, medium; sh, shoulder; w, weak.

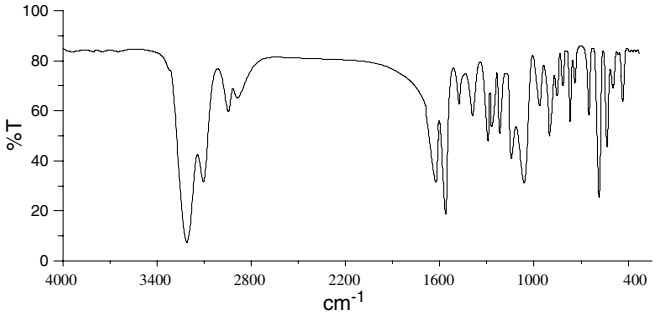

Fig. 2. Infrared spectra of *cis*-$[Co(en)_2(C_{16}H_{33}NH_2)Cl](ClO_4)_2$.

CH_2 or NH_2 twist mode in the region 1150–980 cm^{-1}, and the CH_2 rock mode in the region 940–860 cm^{-1} appeared as two bands. The spectroscopic data collected in Tables 2 and 3, therefore clearly indicate a *cis* configuration for the cobalt(III)-ethylenediamine and *cis*-α configuration for the cobalt(III)-triethylenetetramine type of surfactant complexes.

The ^1H NMR spectrum offers conclusive proof of the configuration of the isomers in solution. The *cis* and *trans* isomers of $[Co(en)_2X_2]^+$ ions have different symmetry properties, and this factor appears to govern the difference in their NMR spectra. The *cis* isomers possess C_2-symmetry with the twofold axis in the plane of the cobalt and the two X groups, and this makes the $–CH_2CH_2–$ groups

equivalent provided that the cobalt–ethylenediamine rings have the same conformation. Moreover, in complexes of the type *cis*-$[Co(en)_2X_2]^{n+}$ there are four pairs of equivalent nitrogen protons, but in complexes of the type *cis*-$[Co(en)_2XY]^{n+}$, although some protons are similarly orientated, no two protons are in identical situations. In complexes of the type *trans*-$[Co(en)_2X_2]^{n+}$ all the protons are equivalent, but in complexes of the type *trans*-$[Co(en)_2XY]^{n+}$ the protons on one side of the plane of the ethylenediamine ring all will experience a different field from those on the other side. It is possible that if the ligands X and Y differed greatly in size, inversion of the chelate ring would be hindered or even inhibited. In the case of *trans* complexes, two separate proton resonances of equal area would be observed if inversion was inhibited, while with *cis* complexes a most complex pattern would result. In *trans* isomers, however, with D_{2h} symmetry, the amine protons and methylene protons of ethylenediamine appear as a singlet at 3 ppm. In the present study, for the *cis* complexes (Fig. 3), due to the lower symmetry, the methylene protons of ethylenediamine show a more complex absorption around 2.8–2.7 ppm. The methylene protons of the long chain moieties (dodecylamine/cetylamine) give rise to a multiplet usually at 1.25–1.8 ppm, whereas the terminal methyl group of the hydrocarbon chain substituent gives a triplet at 0.84 ppm. The ^{1}H NMR spectral data for the cobalt(III)-triethylenetetramine complexes exhibit signals in the region 2.6–3.0 ppm attributable to the $-CH_2$ group of the triethylenetetramine chelate ring, thus confirming the *cis* structure of the complex.

The wavelength of the first absorption maximum in aqueous perchlorate medium for each complex is given in Table 1. It has been observed that the absorption spectra [33,34] of the *cis* and *trans* forms of $[Co(en)_2(NH_3)Y]^{n+}$ cations (Y = Cl or H_2O) showed some differences in the longest-wavelength absorption band (d–d transition). The *trans* form showed a lower intensity band ($\varepsilon < 50\ M^{-1}\ cm^{-1}$) whereas the *cis* form showed a higher intensity band ($\varepsilon > 70\ M^{-1}\ cm^{-1}$). This observation can be used to determine the geometrical configuration of the present cations, whose longest-wavelength absorption maxima are shown in Table 1. By comparing the spectra of the corresponding butylamine complexes [23], it reveals that both the ordinary and the surfactant complexes have the same structure and the replacement of lower aliphatic amine ligands by long chain aliphatic amine ligands does not affect the symmetry of the surfactant complexes (Fig. 1).

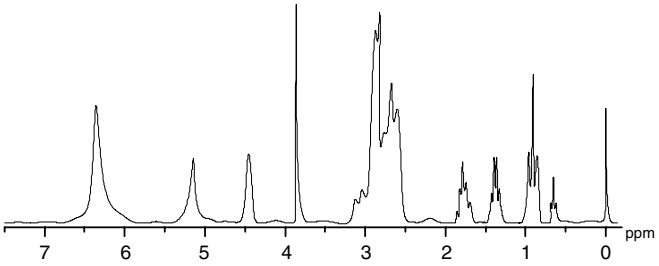

Fig. 3. ^{1}H NMR spectrum of *cis*-$[Co(en)_2(C_{16}H_{33}NH_2)Cl](ClO_4)_2$.

3.2. Critical micelle concentration values (CMC)

The CMC values were computed from the slope of [Co(III)] versus specific conductance data. The complex concentration at which the micellization starts was evident from the change in the slope of the plot and that particular concentration is the CMC under the experimental conditions. The CMC values were determined at three different temperatures (303, 308 and 313 K). At all temperatures a break in the conductance versus concentration plots, characteristic of micelle formation was observed. The CMC values were determined by fitting the data points above and below the break to two equations of the form $y = mx + c$ and solving the two equations simultaneously to obtain the point of intersection. Least-squares analysis was employed and correlation coefficients were greater than 0.98 in all the cases. The conductivity measurements at three different temperatures have been repeated three times and the accuracy of the CMC values was found with in ±3% error. Fig. 4 illustrates the plot for the complex *cis*-$[Co(en)_2(C_{12}H_{25}NH_2)Cl](ClO_4)_2$; similar plots (not shown) were obtained for all the remaining complexes. Tables 4 and 5 show the values of the CMCs of cobalt(III)-ethylenediamine surfactant and Cobalt(III)-triethylenetetramine surfactant respectively, as a function of temperature. It was found that CMC values increase on increasing the temperature for a given system. This behavior may be related to two competitive effects. Firstly, a temperature increase causes a decrease in hydration in the hydrophilic group, which favors micellization. Secondly, a temperature increase also causes a disruption of the water surrounding the hydrophobic group, and this retards micellization. The relative magnitude of these two opposing effects will determine the CMC behavior. It is observed that by changing

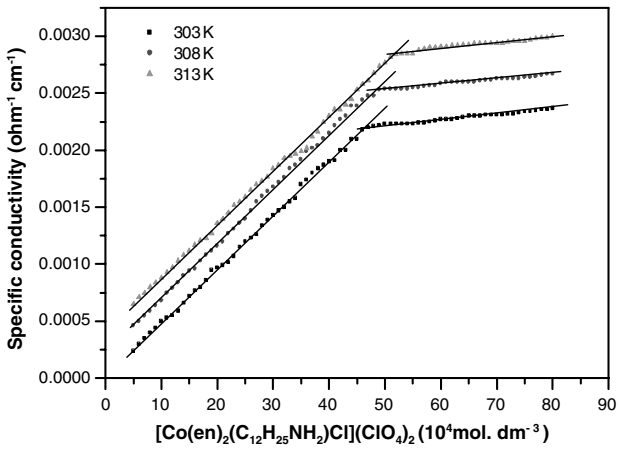

Fig. 4. Electrical conductivity vs. cobalt(III) concentration for aqueous $Co(en)_2(C_{12}H_{25}NH_2)Cl^{2+}$ solutions.

Table 4
CMC values of bis(ethylenediamine)cobalt(III) surfactant complexes in aqueous solution

Complexes	CMC (mol dm^{-3})			ΔG^0_m (kJ mol^{-1})	ΔH^0_m (kJ mol^{-1})	$T\Delta S^0_m$ (kJ mol^{-1})
	303 K	308 K	313 K			
cis-$[Co(en)_2(C_{12}H_{25}NH_2)Cl](ClO_4)_2$	4.60×10^{-3}	4.91×10^{-3}	5.23×10^{-3}	-25.1 ± 0.5	-18.3 ± 0.2	6.8 ± 0.1
cis-$[Co(en)_2(C_{12}H_{25}NH_2)Br](ClO_4)_2$	4.03×10^{-3}	4.42×10^{-3}	4.72×10^{-3}	-26.4 ± 0.7	-23.2 ± 0.1	3.2 ± 0.2
cis-$[Co(en)_2(C_{12}H_{25}NH_2)NO_2](NO_3)_2$	3.90×10^{-3}	4.14×10^{-3}	4.63×10^{-3}	-25.4 ± 0.5	-19.7 ± 0.2	5.7 ± 0.2
cis-$[Co(en)_2(C_{16}H_{33}NH_2)Cl](ClO_4)_2$	8.24×10^{-5}	10.34×10^{-5}	10.93×10^{-5}	-42.0 ± 0.1	-31.3 ± 0.3	10.6 ± 0.1
cis-$[Co(en)_2(C_{16}H_{33}NH_2)Br](ClO_4)_2$	8.01×10^{-5}	9.76×10^{-5}	10.07×10^{-5}	-42.4 ± 0.1	-37.9 ± 0.2	4.4 ± 0.1
cis-$[Co(en)_2(C_{16}H_{33}NH_2)NO_2](NO_3)_2$	7.72×10^{-5}	8.42×10^{-5}	9.10×10^{-5}	-41.8 ± 0.4	-33.1 ± 0.1	8.7 ± 0.2

Table 5
CMC values of (triethylenetetramine)cobalt(III) surfactant complexes in aqueous solution

Complexes	CMC (mol dm^{-3})			ΔG^0_m (kJ mol^{-1})	ΔH^0_m (kJ mol^{-1})	$T\Delta S^0_m$ (kJ mol^{-1})
	303 K	308 K	313 K			
cis-α-$[Co(trien)(C_{12}H_{25}NH_2)Cl](ClO_4)_2$	1.0×10^{-3}	1.50×10^{-3}	1.82×10^{-3}	-32.0 ± 0.4	-13.0 ± 0.1	18.9 ± 0.4
cis-α-[Co(trien) $(C_{12}H_{25}NH_2)Br](ClO_4)_2$	1.1×10^{-3}	1.42×10^{-3}	1.64×10^{-3}	-31.5 ± 0.3	-14.2 ± 0.3	17.3 ± 0.1
cis-α-$[Co(trien)(C_{12}H_{25}NH_2)(NO_2)](NO_3)_2$	0.80×10^{-3}	1.21×10^{-3}	1.43×10^{-3}	-32.3 ± 0.7	-13.2 ± 0.1	19.1 ± 0.2
cis-α-$[Co(trien)(C_{16}H_{33}NH_2)Cl](ClO_4)_2$	8.26×10^{-5}	8.51×10^{-5}	9.02×10^{-5}	-43.5 ± 0.4	-27.7 ± 0.4	15.8 ± 0.3
cis-α-$[Co(trien)(C_{16}H_{33}NH_2)Br](ClO_4)_2$	8.04×10^{-5}	8.43×10^{-5}	8.91×10^{-5}	-43.5 ± 0.5	-31.8 ± 0.2	11.7 ± 0.4
cis-α-$[Co(trien)(C_{16}H_{33}NH_2)(NO_2)](NO_3)_2$	8.45×10^{-5}	8.72×10^{-5}	9.17×10^{-5}	-42.6 ± 0.6	-28.1 ± 0.1	14.5 ± 0.2

the ion from Cl^- to Br^-, the CMC decreases. It may be due to the increase in the size of the ion in the coordination sphere, which makes it more weakly hydrated. Weakly hydrated ions can be adsorbed more readily in the micellar surface which decreases the charge repulsion between the polar groups and thus facilitates the micellization. Further with an increase in the alkyl chain on the polar head group, the CMC again shows a decrease. This may be due to an increase in hydrophobic character of the molecule in the coordination sphere with that of dodecyl/cetylamine.

3.3. Thermodynamics of micellization

The change in the CMC with temperature is generally analyzed in terms of the phase separation or the equilibrium model for micelle formation [36–38]. According to these models, the standard Gibbs free energy of micelle formation per mole of monomer, ΔG^0_m, is given by

$$\Delta G^0_m = RT(2-\alpha_{ave})\ln \mathrm{CMC}, \quad (1)$$

where R, T and α_{ave} are gas constant, absolute temperature and average degree of micellar ionization, respectively.

The enthalpy of micelle formation can be obtained by applying the Gibbs–Helmholtz equation to Eq. (1)

$$\Delta H^0_m = -RT^2(2-\alpha_{ave})\mathrm{d}\ln \mathrm{CMC}/\mathrm{d}T. \quad (2)$$

Once the Gibbs free energy and the enthalpy of micelle formation are obtained, obviously, the entropy of micelle formation can be determined by

$$\Delta S^0_m = (\Delta H^0_m - \Delta G^0_m)/T. \quad (3)$$

The thermodynamic parameters of micellization for the cationic surfactant with variable head group polarity were compiled in Tables 4 and 5. The observed more negative Gibbs free energy of micellization for the surfactants with increasing head polarity indicates more favored micellization. Moreover, since the changes of CMC with temperature are small, the value of ΔH^0_m and ΔS^0_m must be rather inaccurate and should be considered as only approximate. Negative values of enthalpy (ΔH^0_m) of micellization indicate an exothermic nature of the micellization process. Nuselder and Engberts [39] have suggested that for the negative ΔH^0_m the London-dispersion forces play major role in the micelle formation. The positive values of ΔS^0_m clearly indicate that the micellization of the studied surfactants in aqueous solution is governed mainly by hydrophobic interactions between the surfactant cations resulting in the breakdown of the structured water surrounding the hydrophobic groups, and indicates that the cationic surfactants are entropy driven. The observed increase in the entropy values indicates that increasing the head group polarity favors the micellization process.

4. Conclusion

As mentioned in our previous reports [3,4], the critical micelle concentration values of cobalt(III)-surfactant coordination complexes in the present study are also very low compared to that of the simple organic surfactant, dodecylammonium chloride (CMC = 1.5×10^{-2} mol dm^{-3}). Thus, it is concluded that these metal surfactant complexes have more capacity to associate themselves, forming aggregates, compared to those of ordinary synthetic organic surfactants. This suggests that the introduction of a metal complex to the hydrophilic part of the amphiphile can remarkably enhance the ability of aggregation.

Acknowledgement

Sponsorship of this work by the University Grants Commission (No. F.12-9/2001/SR-I) is gratefully acknowledged.

References

[1] G.W. Walker, R.J. Geue, A.M. Sargeson, C.A. Behm, J. Chem. Soc., Dalton Trans. 15 (2003) 2992.
[2] D.A. Jaeger, M.F. Peacock, D. Scott Bohle, Langmuir 19 (2003) 4859.
[3] M.N. Arumugam, K. Santhakumar, N. Kumaraguru, S. Arunachalam, Asian J. Chem. 15 (2003) 191, and 991.
[4] M.N. Arumugam, S. Arunachalam, Ind. J. Chem. A 36 (1997) 84, and 315.
[5] M. Iida, A. Sakamoto, T. Yamashita, K. Shundoh, S. Ohkawa, K. Yamanari, Bull. Chem. Soc. Jpn. 73 (2000) 2033.
[6] D.A. Jaeger, V.B. Reddy, D. Scott Bohle, Tetrahedron Lett. 40 (1999) 649.
[7] D.A. Jaeger, V.B. Reddy, N. Arulsamy, D. Scott Bohle, Langmuir 14 (1998) 2589, and references therein.
[8] M.E. Karaman, R.M. Pashley, N.K. Bolonkin, Langmuir 11 (1995) 2872.
[9] D.W. Bruce, I.R. Denby, G.J.T. Tiddy, J.M. Watkins, J. Mater. Chem. 3 (1993) 911.
[10] M. Yashiro, K. Matsumoto, N. Seki, S. Yoshikawa, Bull. Chem. Soc. Jpn. 66 (1993) 1559.
[11] M. Yashiro, K. Matsumoto, S. Yoshikawa, Chem. Lett. (1992) 1429.
[12] M. Yashiro, K. Matsumoto, S. Yoshikawa, Chem. Lett. (1989) 985.
[13] C.A. Behm, I.I. Creaser, B. Korybut-Daszkiewicz, R.J. Geue, A.M. Sargeson, G.W. Walker, J. Chem. Soc., Chem. Commun. 24 (1993) 1844.
[14] C.A. Behm, P.F.L. Boreham, I.I. Creaser, B. Korybut-Daszkiewicz, D.J. Maddalena, A.M. Sargeson, G.M. Snowdown, Aust. J. Chem. 48 (1995) 1009.
[15] G. Ghirlanda, P. Scrimin, P. Tecilla, A. Toffoletti, Langmuir 14 (1998) 1646.
[16] J.H. Fendler, E.J. Fendler, Catalysis in Micellar and Macromolecular Systems, Academic Press, Newyork, 1975.
[17] J.H. Fendler, Membrane Mimetic Chemistry, Wiley, Newyork, 1982.
[18] A.M. Sargeson, Coord. Chem. Rev. 151 (1996) 89.
[19] J. Qing, S. Qing Cheng, B. Ying Jiang, J. Du, C. Wei Hu, X. Cheng Zeng, Colloids Surf. A 235 (2004) 137.
[20] J. Song Yu, X. Qi Yu, X. Yu Su, T. Wang, Q.X. Xiang, M. Yang, R. Gang Xie, J. Mol. Catal. A 202 (2003) 17.
[21] S.A. Sapp, C.M. Eillott, C. Contado, S. Caramori, C.A. Bignozzi, J. Am. Chem. Soc. 124 (2002) 11215.
[22] P.J. Cameron, L.M. Peter, S.M. Zakeeruddin, M. Gratzel, Coord. Chem. Rev. 248 (2004) 1447.
[23] S.C. Chan, F. Leh, J. Chem. Soc. (1966) 760.
[24] M. Krishnamurthy, J. Inorg. Nucl. Chem. 34 (1972) 3915.
[25] W. Rindermann, R. van Eldik, Inorg. Chim. Acta 64 (1982) L203.
[26] F. Basolo, J. Am. Chem. Soc. 70 (1948) 2634.
[27] T. Shedlovsky, J. Am. Chem. Soc. 54 (1932) 1411.
[28] J.F. Chambers, J.M. Stokes, R.H. Stokes, J. Phys. Chem. 60 (1956) 985.
[29] D.A. Buckingham, D. Jones, Inorg. Chem. 4 (1965) 1387.
[30] M.N. Hughes, W.R. Mcwhinnie, J. Inorg. Nucl. Chem. 28 (1966) 1659.
[31] M.E. Baldwin, J. Chem. Soc. (1960) 4369.
[32] M.L. Morris, D.H. Busch, J. Am. Chem. Soc. 82 (1960) 1521.
[33] Y. Yasui, Y. Shimura, Bull. Chem. Soc. Jpn. 36 (1963) 1286.
[34] R.S. Nyholm, M.L. Tobe, J. Chem. Soc. (1956) 1707.
[35] R.G. Linck, Inorg. Chem. 9 (1970) 2529.
[36] P. Mukerjee, J. Phys. Chem. 66 (1962) 1375.
[37] J.J. Galan, A. Gonzalez-Perez, J.R. Rodriguez, J. Therm. Anal. Calorim. 72 (2003) 465.
[38] A. Gonzalez-Perez, J.C. Del Castillo, T. Czapkiewicz, J.R. Rodrigue, Colloid Polym. Sci. 280 (2002) 503.
[39] J.J.H. Nusselder, J.B.F.N. Engberts, J. Colloid Interf. Sci. 148 (1992) 353.

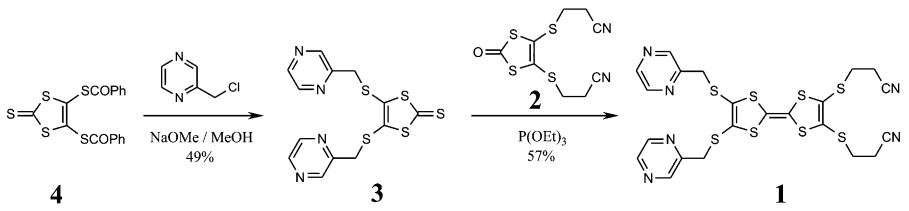

Scheme 1. Synthetic pathway to the target compound **1** via the triethylphosphite mediated coupling reaction.

2. Experimental

2.1. Materials

The compounds 4,5-bis(cyanoethylthio)-1,3-dithiole-2-one (**2**) [13], 4,5-bis(benzoylsulfanyl)-1,3-dithiole-2-thione (**4**) [13] and 2-chloromethylpyrazine [14] were prepared according to the literature procedures. All other chemicals and solvents were purchased from commercial sources and were used without further purification.

2.2. Preparation of *3*

Compound **4** (4.27 g, 10.5 mmol) was suspended in 25 ml of dry MeOH under Ar. Na (0.63 g, 27.4 mmol) was dissolved in 52 ml of dry MeOH. The NaOMe solution was then added dropwise over a period of 15 min to the suspension of **4**. The resulting dark red solution was stirred for another 30 min. Freshly prepared 2-chloromethylpyrazine (2.70 g, 21.0 mmol) was added at once and the resulting brownish yellow mixture was stirred overnight. The reaction mixture was then extracted twice with $CHCl_3$ and CH_2Cl_2. The organic phases were collected, dried over $MgSO_4$ and the filtrate was evaporated under reduced pressure. Purification of the brownish oil by column chromatography eluting with a gradient of 0–100% EtOAc in CH_2Cl_2 yielded compound **3** as brownish oil. Yield: 0.85 g (49%). *Anal.* Calc. for $C_{13}H_{10}N_4S_5$: C, 40.81; H, 2.63; N, 14.64. Found: C, 40.67; H, 2.54; N, 15.42%. ^{1}H NMR (ppm): δ 4.12 (s, 4H), 8.53 (m, 6H). ^{13}C NMR (ppm): δ 39.6, 137.0, 143.9, 144.3, 144.5, 151.8, 210.4. Selected IR data (cm^{-1}, KBr pellet): 3038, 3006, 2974, 1665, 1577, 1527, 1473, 1401, 1308, 1217, 1186, 1115, 1065, 1018, 887, 837, 763, 516. Mass spectrum (FAB) *m*/*z*: 383 $(\mathbf{3})^+$.

2.3. Preparation of *1*

Compound **1** was synthesized according to the literature procedure for the preparation of the pyridyl analogue [15].

Compounds **3** (0.99 g, 2.6 mmol) and **2** (1.31 g, 5.1 mmol) were refluxed for 2 h in 25 ml of $P(OEt)_3$ at 110 °C under Ar. The mixture was then cooled to 0 °C and the orange precipitate was filtrated off and washed with cold MeOH. The precipitate was dried over P_4O_{10} under vacuum and purified by column chromatography eluting with a gradient of 0–100% EtOAc in CH_2Cl_2. Yield: 0.92 g (57%). *Anal.* Calc. for $C_{22}H_{18}N_6S_8$: C, 42.42; H, 2.91; N, 13.49. Found: C, 42.39; H, 2.96; N, 13.04%. ^{1}H NMR (ppm): δ 2.75 (t, $J = 7$ Hz, 4H), 3.09 (t, $J = 7$ Hz, 4H), 4.04 (s, 4H), 8.50 (m, 6H). ^{13}C NMR (ppm): δ 18.9, 31.3, 39.5, 109.2, 113.0, 117.4, 128.1, 129.3, 143.5, 144.4, 144.6, 152.3. Selected IR data (cm^{-1}, KBr pellet): 2925, 2855, 2250 (CN), 1731, 1668, 1527, 1474, 1401, 1307, 1282, 1216, 161, 1113, 1056, 1018, 888, 838, 772. Mass spectrum (ESI) *m*/*z*: 621.94 $(\mathbf{1})^+$, 528.83 (**1**-methylpyrazyl)$^+$.

2.4. Preparation of the CT compound $(\mathbf{1}_2)^{2+}[(I_2)_{3/2}I^-]_2 \cdot 2CH_2Cl_2$

The black crystals of the charge-transfer salt of **1** with I_2 were obtained by layer diffusion. 5 ml of a 2 mM clear solution of **1** in CH_2Cl_2 were successively superposed by layers of 2 ml of pure CH_2Cl_2, 2 ml of pure hexane and 5 ml of a 4 mM solution of I_2 in hexane. Crystals were grown within 2 days at 5 °C. *Anal.* Calc. for $C_{22}H_{18}I_4N_6S_8 \cdot CH_2Cl_2$: C, 22.73; H, 1.66; N, 6.91. Found: C, 22.38; H, 1.53; N, 6.75%.

2.5. Physical measurements

All ^{1}H NMR and ^{13}C NMR spectra were measured in $CDCl_3$ at 300 and 75.5 MHz, respectively. FT-IR data were collected on a Perkin–Elmer Spectrum One spectrometer at a resolution of 1 cm^{-1}. Elemental analyses were performed on an EA 1110 Elemental Analyzer CHN Carlo Erba Instruments. Cyclic voltammetric measurements were conducted on a Metrohm VA-Stand 663 electrochemical analyser. Conductivity measurements were made with the standard four-probe technique. Mass spectra were recorded on a Micromass AutoSpec spectrometer using FAB or ESI. Magnetic susceptibility data of the polycrystalline sample were collected with a Quantum Design SQUID magnetometer (XL5S) equipped with a 50 kG magnet and operating in the temperature range 1.8–300 K. Pascal's constants were used for the diamagnetic correction.

2.6. X-ray structural analyses

A single crystal ($0.36 \times 0.80 \times 0.04$ mm) of the title compound $(\mathbf{1}_2)^{2+}[(I_2)_{3/2}I^-]_2 \cdot 2CH_2Cl_2$ was mounted on a Nonius four circle diffractometer equipped with a CCD camera and a graphite monochromated Mo Kα radiation source

($\lambda = 0.71073$ Å). Effective absorption correction was performed (SCALEPACK) [16]. The structure was solved with direct method using SHELXS-97 and refined with full-matrix least-squares method on F^2 using SHELX-97 programs [17]. Crystallographic data: Triclinic, space group $P\bar{1}$, $a = 10.9642(3)$ Å, $b = 11.6722(4)$ Å, $c = 16.4413(8)$ Å, $\alpha = 91.690(1)°$, $\beta = 98.031(1)°$, $\gamma = 113.591(3)°$, $V = 1900.9(1)$ Å^3, $Z = 2$, $T = 293(2)$ K, μ(Mo Kα) = 3.816 mm^{-1}, $D_{calc} = 2.10$ g cm^{-3}, 12426 reflections measured of which 6302 unique ($R_{int} = 0.0319$), $R(F^2) = 0.0604$ [4467 data with $I > 2\,\sigma(I)$], $wR(F^2) = 0.1784$. Complete crystal structure results as CIF files including bond lengths, bond angles and atomic coordinates are deposited as Supplementary materials.

3. Results and discussion

3.1. Synthesis and characterization

For the synthesis of the asymmetrically functionalized donor ligand **1**, the generally adopted strategy via the triethylphosphite mediated coupling of two appropriate chalcogenone precursors was used, as depicted in Scheme 1. The precursor **3** was prepared according to the procedure for the preparation of 4,5-bis(2-pyridylmethylsulfanyl)-1,3-dithiole-2-thione [18]. Compared to the pyridyl analogue, the slightly lower yield of **3** is mainly due to the thermal instability of 2-chloromethylpyrazine which slowly decomposes at room temperature [14] and thus should be freshly prepared prior to use. Although the coupling reaction frequently suffers from disadvantages such as low yield or tedious separations [19], the target compound **1** could be prepared from its corresponding precursors in reasonable yield comparable to other typical phosphite mediated coupling reactions [15,20]. All compounds have been characterized by ^{1}H NMR, ^{13}C NMR, elemental analysis and mass spectrometry and are in agreement with the proposed structures (Scheme 1). In the IR spectrum of **1** the intense absorption band at 2250 cm^{-1}, corresponding to CN vibrations, is clearly visible. Due to the good solubility in chloroform even the quaternary C atoms of the inner (109.2 and 113.0 ppm) and outer double bonds (128.1 and 129.3 ppm) of the TTF core could be detected in the ^{13}C NMR spectrum.

Although the neutral donor is very soluble in common organic solvents, no single crystals of X-ray quality have been obtained yet. Nevertheless, compound **1** can readily be oxidized by iodine, affording the CT complex $(\mathbf{1}_2)^{2+}$-$[(I_2)_{3/2}I^-]_2 \cdot 2CH_2Cl_2$ which crystallizes as black rod-like crystals.

3.2. Electrochemical measurements

The solution redox properties of the new donor ligand **1** were investigated in dichloromethane by cyclic voltammetry (CV). The CV data are presented in Table 1 together with those of bis(ethylenedithio)tetrathiafulvalene (ET) [21] and 4,5-bis(cyanoethylthio)-4′,5′-(ethylenedithio)tetrathiafulvalene (BCET-ET) [20] for comparison. In each case the two typical reversible single-electron redox couples are observed, corresponding to the sequential formation of the stable TTF radical cation and the dication. Compared to ET and BCET-ET, attachment of the cyanoethyl protection groups and the pyrazine units in compound **1** increases mainly the first redox potential due to the electron-withdrawing effect of these groups [21]. The second potential remains almost unaffected.

Table 1
Cyclic voltammetric data[a]

Compound	$E_1^{1/2}$ (V)	$E_2^{1/2}$ (V)	ΔE (mV)
ET	0.52	0.94	420
BCET-ET	0.60	0.98	380
1	0.69	0.97	280

[a] All oxidation potentials were determined under N_2 in CH_2Cl_2 vs. Ag/AgCl at room temperature. Measurements have been done at a scan rate of 100 mV s^{-1} using 0.1 M Bu_4NPF_6 as electrolyte and Pt as working electrode.

3.3. Crystal structure

The ORTEP drawing of the asymetric unit of compound $(\mathbf{1}_2)^{2+}[(I_2)_{3/2}I^-]_2 \cdot 2CH_2Cl_2$, which crystallizes in the triclinic space group $P\bar{1}$, is shown in Fig. 1(a). The asymmetric unit

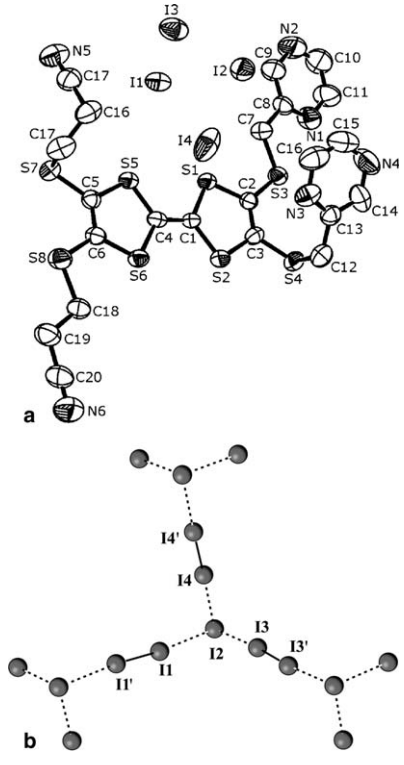

Fig. 1. (a) ORTEP representation of the asymmetric unit of $(\mathbf{1}_2)^{2+}$-$[(I_2)_{3/2}I^-]_2 \cdot 2CH_2Cl_2$, ellipsoids are drawn at 50% probability; C1–C4 1.37(1), C1–S1 1.726(8), C1–S2 1.721(8), C2–S1 1.750(9), C3–S2 1.740(9), C4–S6 1.743(8), C4–S5 1.710(9), C5–S5 1.732(9), C6–S6 1.725(9), C2–C3 1.33(1), C5–C6 1.34(1) Å; (b) iodine connectivity, I2–I1 3.427(1), I2–I3 3.448(1), I2–I4 3.467(2), I1–I1′ 2.768(1), I3–I3′ 2.789(2), I4–I4′ 2.830(3) Å. Hydrogen atoms and solvent molecules are omitted for clarity.

contains one donor molecule $\mathbf{1}^{\cdot+}$, 3/2 molecules I_2, one I^- and one solvent molecule. The donor molecule exhibits no unusual structural parameters (for selected bond distances see Fig. 1(a)). Nevertheless, it is worth mentioning that the central C=C bond length (1.37(1) Å) of the TTF unit is slightly larger than that of the neutral pyridyl analogue (1.34(1) Å) [15] which, however, is in accordance with its oxidized state.

The crystal structure is built up by layers of head-to-tail dimers of $\mathbf{1}^{\cdot+}$ which are embedded in a 2D polyiodide network, as illustrated in Fig. 2. Disordered solvent molecules (dichloromethane) are located inbetween the layers.

The 2D polyiodide network exhibits an interesting topology. Four crystallographically independent iodine atoms form a trigonal pyramid with I2 as vertex and I1, I3, I4 as the triangular base. The distances between the vertex (I2) and the other three atoms (I1, I3, I4) are in the range of 3.42–3.47 Å (Fig. 1(b)). These trigonal pyramids are connected through the iodine atoms of the bases to form a 2D grid of 18-membered hexagonal rings in chair conformation parallel to the *ab*-plane (Fig. 2). The I–I distances between two adjacent pyramids range from 2.77 to 2.83 Å (Fig. 1(b)). This particular iodine arrangement can also be described as aggregates consisting of I_2 units (I1–I1′, I3–I3′ and I4–I4′) and iodide $(I2)^-$. Consequently, per formula unit, the overall iodine/iodide stoichiometry can be given as $[(I_2)_{3/2}I^-]_2$ and regarded as a special case of an octaiodide I_8^{2-} which usually consists of two I_3^- units connected through an I_2 molecule [22]. Indeed, the structure looks very similar to the one found in $[Co(urea)_6]I_8$ where distinguishable Z-shaped octaiodides with contact distances of 3.75 and 3.93 Å build up an analogous hexagonal honeycomb structure [23]. However, in the present case all contact distances are in the range of secondary I···I bonds (3.4–3.7 Å) [22] and are symmetrically arranged so that specific I_8^{2-} units cannot be recognized and the overall structure is best described as an infinite two-dimensional polyiodide network [11].

The dimers of $\mathbf{1}^{\cdot+}$ are located inside the hexagonal meshs (Fig. 3(a)). The S–S contacts between the donor molecules of a dimer (3.41–3.55 Å) are shorter than the sum of the van der Waals radii (3.60 Å) [24], reflecting the formation of spin-paired π-dimers [25] (Fig. 3(b)). This is confirmed by a magnetic measurement of the CT compound which shows only a diamagnetic behaviour corresponding to a total $S = 0$ spin state. Finally, a conductivity measurement revealed that the resistivity was too high (>1.5 GΩ cm) to be measured by the specific instrumental set-up. This is in a good agreement with the large distances (more than 7 Å) between neighbouring dimers as determined by X-ray structure analysis.

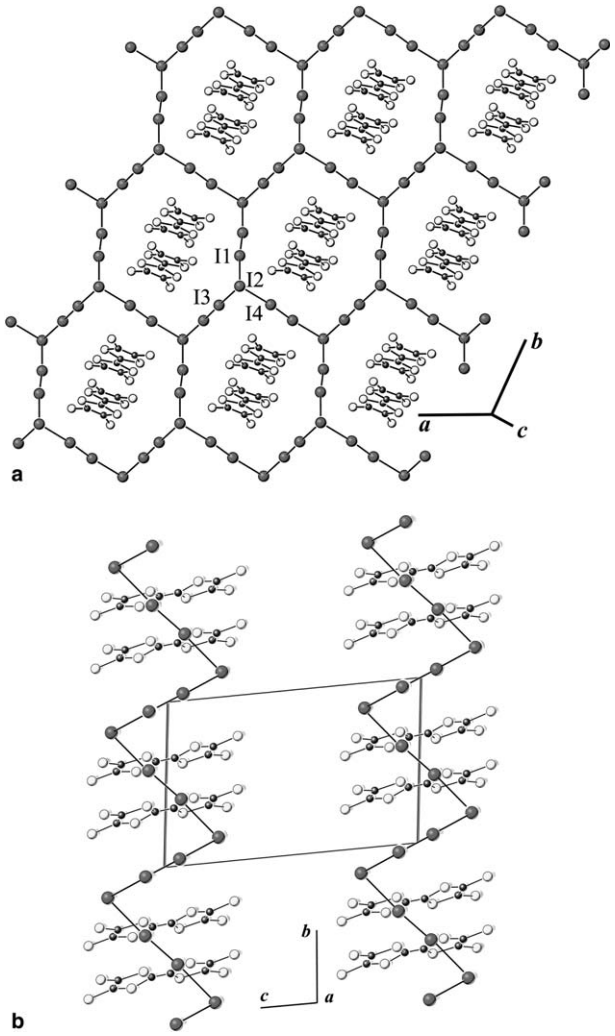

Fig. 2. (a) 2D iodide grid with embedded dimers of oxidized compound $\mathbf{1}^{\cdot+}$; (b) crystal packing of $(\mathbf{1}_2)^{2+}[(I_2)_{3/2}I^-]_2 \cdot 2CH_2Cl_2$. Hydrogen atoms, solvent molecules, methylpyrazine and $-(CH_2)_2CN$ groups are omitted for clarity.

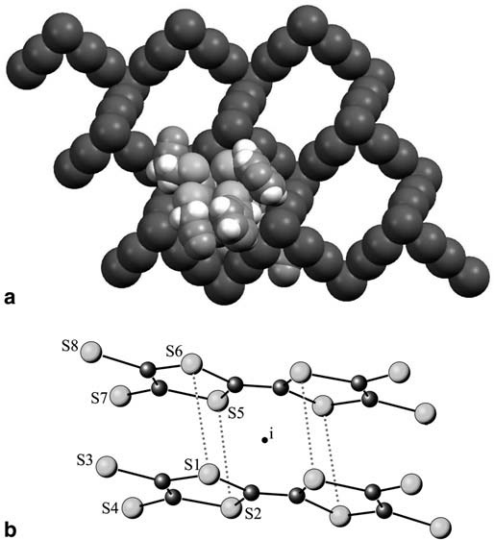

Fig. 3. (a) Space filling representation of the hexagonal polyiodide meshs with embedded dimer of $\mathbf{1}^{\cdot+}$; (b) intradimer S···S contacts: S1–S6 3.542(3), S2–S5 3.412(3) Å.

4. Conclusion

The oxidation of the new donor ligand **1** with iodine resulted in the formation of a CT-compound where the radical cations of **1** form spin-paired π-dimers. The embedding of these dimers in layers of regular 2D honeycomb like grids formed by the unique $[(I_2)_{3/2}I^-]$ units is responsible for the insulating property of this compound.

The ability to bind transition metal ions and the formation of charge transfer complexes and radical salts of this new donor **1** are currently under investigation in our laboratory.

Acknowledgements

This work was supported by the Germaine de Staël foundation and the Swiss National Science Foundation (Project No. 200020-107589) as well as by the ESF programme – SONS (NANOSYN). We are also grateful to Prof. L. Kloo (Royal Institute of Technology, Stockholm) for the help with the description of the polyiodide structure.

Appendix A. Supplementary material

Crystallographic data for the structural analysis have been deposited with the Cambridge Crystallographic Data Centre as supplementary publication no. CCDC 266943. Copies of the data can be obtained free of charge on application to CCDC, 12 Union Road, Cambridge CB21EZ, UK (fax +44 1223 336 033, e-mail: deposit@ccdc.cam.ac.uk). Supplementary data associated with this article can be found, in the online version, at doi:10.1016/j.poly.2005.10.033.

References

[1] H. Tanaka, Y. Okano, H. Kobayashi, W. Suzuki, A. Kobayashi, Science 291 (2001) 285.
[2] M.N. Jayaswal, H.N. Peindy, F. Guyon, M. Knorr, N. Avarvari, M. Fourmigué, Eur. J. Inorg. Chem. 13 (2004) 2646.
[3] T. Devic, N. Avarvari, P. Batail, Chem. Eur. J. 10 (2004) 3697, and references therein.
[4] T. Devic, P. Batail, M. Fourmigue, N. Avarvari, Inorg. Chem. 43 (2004) 3136.
[5] F. Le Derf, M. Mazari, N. Mercier, E. Levillain, G. Trippé, A. Riou, P. Richomme, J. Becher, J. Garín, J. Orduna, N. Gallego-Planas, A. Gorgues, M. Sallé, Chem. Eur. J. 7 (2001) 447.
[6] L. Ouahab, T. Enoki, Eur. J. Inorg. Chem. 5 (2004) 933.
[7] F. Iwahori, S. Golhen, L. Ouahab, R. Carlier, J.P. Sutter, Inorg. Chem. 40 (2001) 6541.
[8] F. Setifi, L. Ouahab, S. Golhen, Y. Yoshida, G. Saito, Inorg. Chem. 42 (2003) 1791.
[9] S.-X. Liu, S. Dolder, A. Neels, H. Stoeckli-Evans, S. Decurtins, Inorg. Chem. 42 (2003) 4801.
[10] N. Le Narvor, N. Robertson, E. Wallace, J.D. Kilburn, A.E. Underhill, P.N. Bartlett, M. Webster, J. Chem. Soc., Dalton Trans. 6 (1996) 823.
[11] A.J. Blake, F.A. Devillanova, R.O. Gould, W.-S. Li, V. Lippolis, S. Parsons, C. Radek, M. Schröder, Chem. Soc. Rev. 27 (1998) 195.
[12] R.P. Shibaeva, E.B. Yagubskii, Chem. Rev. 104 (2004) 5347.
[13] N. Svenstrup, J. Becher, Synthesis 3 (1995) 215.
[14] G.R. Newkome, G.E. Kiefer, Y.-J. Xia, V. Gupta, Synthesis 8 (1984) 676.
[15] S. Dolder, S.-X. Liu, G. Labat, S. Decurtins, J. Phys. IV France 114 (2004) 683.
[16] Z. Otwinowski, W. Minor, in: C.W. CarterJr., R.M. Sweet (Eds.), Methods in Enzymology: Macromolecular Crystallography, Part A, vol. 276, Academic Press, London, 1997, pp. 307–326.
[17] G.M. Sheldrick, SHELX 97: Program for the Refinement of Crystal Structures, University of Göttingen, Göttingen, Germany, 1997.
[18] J. Becher, A. Hazell, C.J. McKenzie, C. Vestergaard, Polyhedron 19 (2000) 665.
[19] A.J. Moore, M.R. Bryce, J. Chem. Soc., Chem. Commun. 22 (1991) 1638.
[20] K.B. Simonsen, N. Svenstrup, J. Lau, O. Simonsen, P. Mørk, G.J. Kristensen, J. Becher, Synthesis 3 (1996) 407.
[21] S.-X. Liu, S. Dolder, E.B. Rusanov, H. Stoeckli-Evans, S. Decurtins, C.R. Chimie 6 (2003) 657.
[22] P.H. Svensson, L. Kloo, Chem. Rev. 103 (2003) 1649.
[23] N.E. Kuzmina, K.K. Palkina, E.V. Savinkina, I.A. Kozlova, N.T. Kuznetzov, Zh. Neorg. Khim. 45 (2000) 10.
[24] A. Bondi, J. Phys. Chem. 68 (1964) 441.
[25] P. Frère, P.J. Skabara, Chem. Soc. Rev. 34 (2005) 69.

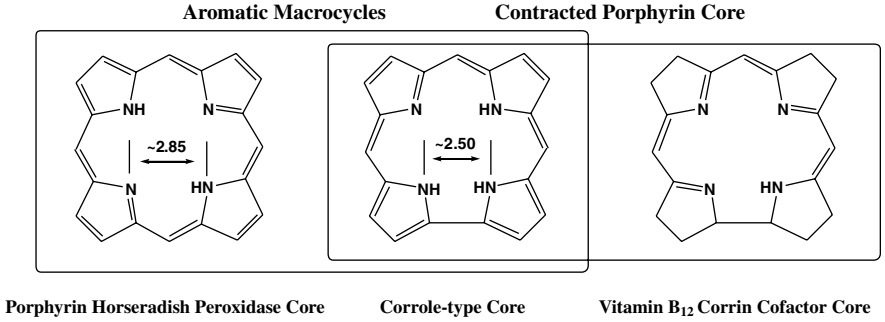

Fig. 1. A comparison of porphyrin derivative metal binding cores.

pentafluorophenyl group substitution at the *meso* positions of the corrole. Metalloporphyrins bearing thienyl substituents on all *meso* groups (tetrathienyl-substituted) have been reported in which the metal is copper [30,31] or cobalt [32]. Thus, studying metallocorroles with thienyl substitution allows us to probe the steric and electronic effects at the metal site [28,33]. Presence of peripheral sulfur groups may furthermore open the possibility for subsequent metal ion binding and allow for supramolecular assemblies.

Thienyl group substituents are comparable to phenyl substitution and are far removed from the electron withdrawing capacity of the pentafluorophenyl group. However, this can be evaluated by electrochemical studies and a consideration of Hammett parameters. We have recently reported the synthesis and crystallographic structures of both 5-(thienyl)dipyrromethane isomers [34]. Thus, herein we describe the synthesis and full characterization of new 5,10,15-tris(thienyl)metallocorroles by techniques that include single-crystal X-ray diffraction, spectroscopy, mass spectrometry, and cyclic voltammetry. Importantly, the molecular structures of 2-thienyl metallocorrole complexes of copper and cobalt, and the 3-thienyl cobalt corrole have been obtained (see Scheme 1).

2. Results and discussion

2.1. Synthesis

Both free base thienyl corroles were prepared from the respective dipyrromethanes and aldehydes using general conditions previously developed for sterically unhindered dipyrromethanes [35]. In particular, the reaction between 5-(2-thienyl)dipyrromethane or 5-(3-thienyl)dipyrromethane [34] and thiophene carboxyaldehyde occurs with the addition of a catalytic amount of TFA; subsequent addition of DDQ gives the green fluorescent 5,10,15-tris(2-thienyl)corrole and 5,10,15-tris(3-thienyl)corrole, respectively (Scheme 1). Both copper complexes **3** and **4** were obtained by the reaction of the corresponding 5,10,15-tris(thienyl)corrole with excess $Cu(OAc)_2 \cdot H_2O$ in pyridine solution at room temperature. This synthetic step is very low yielding in the overall scheme providing ca. 3%

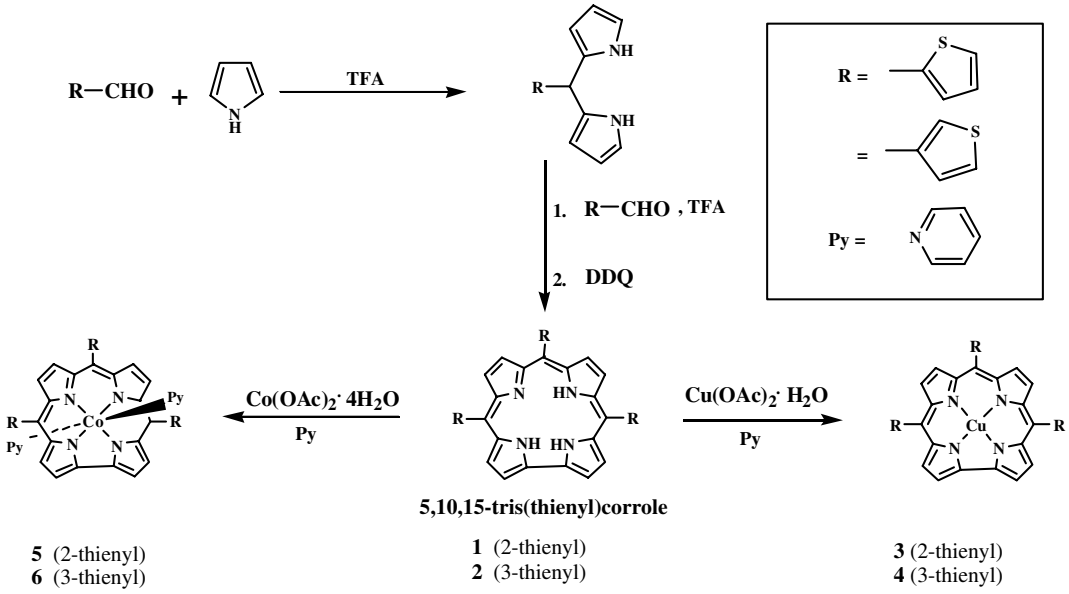

Scheme 1. Preparation of 5,10,15-tris(thienyl)corroles and their corresponding copper complexes and cobalt bis-pyridine complexes.

of free base. The direct synthesis of such corroles from aldehydes and pyrrole was not achievable in our hands.

Metallation occurs rapidly and accompanied by a visible color change. The corresponding reddish-brown copper complexes were obtained within 20 min with yields of ca. 90%. Both cobalt complexes **5** and **6** were obtained by the reaction of the corresponding 5,10,15-tris(thienyl)corrole with excess $Co(OAc)_2 \cdot 4H_2O$ in a refluxing pyridine solution for an overall yield of ca. 90%.

The stability of complexes **3**–**6** are notable in contrast to some related copper and cobalt systems with the electron withdrawing $-C_6F_5$ groups at the three *meso* positions [8,11]. For the copper species, there is no green component in the reaction mixture as in the tris-pentafluorophenyl-substituted corrole reported by Gross and coworkers [8]. The solution containing the copper complexes remains reddish-brown after one week at RT and in the absence of light. This points to an enhanced stability towards C–C coupling compared to the trispentafluorophenyl corroles and has furthered our interest in these derivatives [8,11]. Thus, CV data and diffraction studies have been obtained and are presented and discussed below to attempt to understand the unique properties of thienyl substitution.

2.2. Structural studies

We have conducted single-crystal X-ray diffraction studies of Cu(T2TC) (**3**), Co(T2TC)$(Py)_2$ (**5**) and Co(T2TC)$(Py)_2$ (**6**) (Tables 1 and 2). Complex **3** was found to crystallize in the monoclinic space group $C2/c$ with the cell parameters: $a = 10.374(13)$ Å, $b = 23.21(3)$ Å, $c = 20.625(17)$ Å, $\beta = 95.53(5)°$, $V = 4942(9)$ Å^3, and contained no solvent of crystallization. The cell parameters for the analogous tris-substituted 3-thienyl derivatives **5** and **6** are as follows: (**5**), triclinic, $P\bar{1}$, $a = 11.6509(13)$ Å, $b = 12.4878(14)$ Å, $c = 15.4676(18)$ Å, $\alpha = 98.237(2)°$, $\beta = 105.613(2)°$, $\gamma = 106.376(2)°$, $V = 2020.1(4)$ Å^3; (**6**) triclinic, $P\bar{1}$, $a = 9.705(4)$ Å, $b = 11.745(5)$ Å, $c = 16.401(6)$ Å, $\alpha = 101.298(7)°$, $\beta = 95.059(7)°$, $\gamma = 112.872(7)°$ and $V = 1661.0(11)$ Å^3, $Z = 2$. The solution for **5** and **6** contained two axial pyridine ligands and a benzene solvent of crystallization in the case of **5**. The molecular structures and packing diagrams for compound **3** are provided in Figs. 2 and 3; these diagrams for compounds **5** and **6** are found in Figs. 5–8. The crystallographic data for **3**, **5** and **6** is summarized in Table 3.

Table 1
Selected bond distances and angles in Cu(T2TC) (**3**)

Distances	
Cu–N(3)	1.886(4)
Cu–N(1)	1.888(5)
Cu–N(4)	1.889(4)
Cu–N(2)	1.891(4)
C(1)–C(19)	1.446(7)
Angles	
N(3)–Cu–N(4)	90.76(18)
N(1)–Cu–N(4)	82.60(19)
N(3)–Cu–N(2)	97.46(16)
N(1)–Cu–N(2)	91.18(18)

Table 2
Selected bond distances and angles for Co(T2TC)$(Py)_2$ (**5**) and Co(T3TC)$(Py)_2$ (**6**)

Co(T2TC)(Py_2)		Co(T3TC)(Py_2)	
Co–N(1)	1.861(5)	Co(1)–N(1)	1.866(3)
Co–N(2)	1.894(5)	Co(1)–N(4)	1.871(3)
Co–N(3)	1.898(5)	Co(1)–N(3)	1.892(3)
Co–N(4)	1.863(5)	Co(1)–N(2)	1.904(3)
Co–N(5)	2.004(5)	Co(1)–N(6)	1.998(3)
Co–N(6)	1.981(4)	Co(1)–N(5)	1.998(3)
N(1)–Co–N(4)	82.5(2)	N(1)–Co(1)–N(4)	82.12(13)
N(1)–Co–N(2)	91.5(2)	N(1)–Co(1)–N(3)	173.47(12)
N(4)–Co–N(2)	173.8(2)	N(4)–Co(1)–N(3)	91.41(13)
N(1)–Co–N(3)	173.0(2)	N(1)–Co(1)–N(2)	91.27(12)
N(4)–Co–N(3)	90.5(2)	N(4)–Co(1)–N(2)	173.39(13)
N(2)–Co–N(3)	95.5(2)	N(3)–Co(1)–N(2)	95.20(13)
N(1)–Co–N(6)	90.16(19)	N(1)–Co(1)–N(6)	91.07(13)
N(4)–Co–N(6)	91.79(19)	N(4)–Co(1)–N(6)	89.14(13)
N(2)–Co–N(6)	90.00(19)	N(3)–Co(1)–N(6)	89.69(12)
N(3)–Co–N(6)	89.96(19)	N(2)–Co(1)–N(6)	90.97(12)
N(1)–Co–N(5)	90.8(2)	N(1)–Co(1)–N(5)	88.35(12)
N(4)–Co–N(5)	90.9(2)	N(4)–Co(1)–N(5)	88.26(12)
N(2)–Co–N(5)	87.42(19)	N(3)–Co(1)–N(5)	90.60(12)
N(3)–Co–N(5)	89.4(2)	N(2)–Co(1)–N(5)	91.59(12)
N(6)–Co–N(5)	177.3(2)	N(6)–Co(1)–N(5)	177.39(12)

The *meso* aryl groups are often found approximately normal to the corrole plane. For the thienyl groups, there is a wide range of $C_{pyrrolyl}$–C_{meso}–C_{ipso}–$C_{thienyl}$ dihedral values. For the copper compound, the angles were ca. 26°, 43° and 53° showing great flexibility of the thienyl moiety. Additionally, these angles for the cobalt complex **5** were ca. 52°, 86° and 87° and for **6** were ca. 55°, 60° and 80°, showing that the thienyl group may contribute partially to corrole core conjugation. Rotational fluxionality is further supported by NMR studies provided below.

The measurements of copper corrole cores of those structurally characterized to date are compared in Fig. 4. All examples lack axial substituents, in contrast to the cobalt complexes presented hereafter.

As illustrated in Fig. 4, copper corrole core measurements are similar, irrespective of peripheral substitution and define a Cu sitting between the four nitrogens that are in a distorted square with all Cu–N bonds 1.87–1.89 Å. The short N···N distance in the distorted square is 2.46 Å and the opposing side is 2.83 Å – a difference of ca. 0.4 Å that is accommodated by the sides of ca. 2.70 Å. These geometric similarities suggest differences that lead to dinuclear products as in the *meso*-5,10,15-trispentafluorophenylcorrole may be mainly electronic in nature.

Molecular structures of cobalt corrole compounds number 14 to date in which almost all of these structures have been characterized as a complex containing a central cobalt of formal oxidation state III. There are structural examples in which the cobalt oxidation state has been assigned as IV

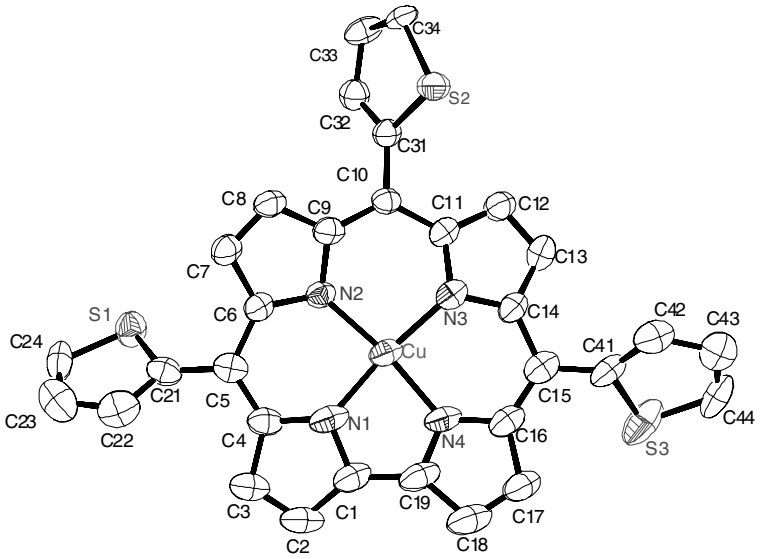

Fig. 2. Molecular structure of Cu(T2TC) (**3**). Thermal ellipsoids are shown at the 50% level. Hydrogen atoms have been removed for clarity.

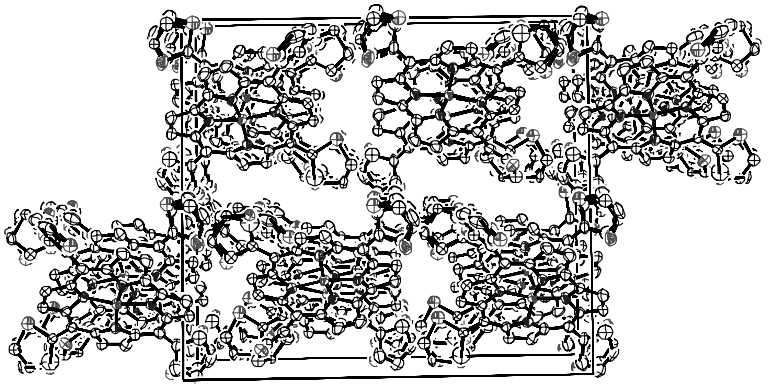

Fig. 3. The crystallographic packing array of Cu(T2TC) (**3**) when looking down the *b*-axis. Both disordered thienyl groups are present and hydrogens are omitted for clarity.

and V [36,37]. Interestingly, the axial pyridine groups in Figs. 5 and 7 are nearly orthogonal to each other. Structures in which orthogonality and near coplanarity have been previously reported [11,38,39].

2.3. NMR spectroscopy

To probe the dynamics of our systems, variable temperature NMR spectra have been obtained for complexes **3** and **4**. Variable temperature stack plotted ^{1}H NMR data are provided below, obtained between the temperatures of −50 and 60 °C (Figs. 9 and 10). Noteworthy is the difference in spectral signal broadening over this range. This is thought to be due exclusively to the different rotational conformations in the metallocorroles of the thienyl groups whose rotations are on the time scale of NMR at the temperature of the studies, not due to the change in electronics of the Cu core [6]. ^{1}H NMR spectra, below room temperature feature broad signals. This same shifting is apparent in the free corrole base. Upon complexation, there is a slight degree of up-field shifting with respect to metal free corroles. High temperature ^{1}H NMR spectra of the Cu complexes appear more resolved [40]. These data indicate that the diamagnetic square planar d^8 complexes with low spin Cu(III) ions coordinated by closed-shell corroles. Our studies in $CDCl_3$ solvent precluded examining beyond these minimum and maximum temperatures.

In the cobalt complex, the proton signals of the *trans* axial pyridines in a 2:4:4 ratio are all up-field shifted perhaps due to the formation of diamagnetic current-effect of the corroles in the complexes [11]. With the common $-C_6F_5$ substituent, there is greater bulk and greater symmetry which does give rise to broadening, but the proton spectrum of the species is simplified.

In addition to these obtaining NMR, all compounds were characterized by UV–vis spectra. Porphyrinoids and corresponding metal complexes give rise to a Soret band, the strong ligand based π–π^* electron transition. These bands for compounds **1**–**6** appear in Table 4. The sulfur atom that is changed from the α-(2-thienyl) to the β-(3-thi-

Table 3
Crystal data for Cu(T2TC) (**3**), $Co(T2TC)(Py)_2 \cdot C_6H_6$ (**5**), and $Co(T3TC)(Py)_2$ (**6**)

Compound	Cu(T2TC) (**3**)	$Co(T2TC)(Py)_2 \cdot C_6H_6$ (**5**)	$Co(T3TC)(Py)_2$ (**6**)
CCDC deposit no.	273811	273812	277370
Empirical formula	$C_{31}H_{17}CuN_4S_3$	$C_{47}H_{27}CoN_6S_3$	$C_{41}H_{27}CoN_6S_3$
Formula weight	605.21	830.86	758.80
Temperature (K)	293(2)	293(2)	293(2)
Radiation (λ), Å	0.71073	0.71073	0.71073
Crystal system	monoclinic	triclinic	triclinic
Space group	$C2/c$	$P\bar{1}$	$P\bar{1}$
a (Å)	10.374(13)	11.6509(13)	9.705(4)
b (Å)	23.21(3)	12.4878(14)	11.745(5)
c (Å)	20.625(17)	15.4676(18)	16.401(6)
α (°)	90	98.237(2)	101.298(7)
β (°)	95.53(5)	105.613(2)	95.059(7)
γ (°)	90	106.376(2)	112.872(7)
V (Å^3)	4942(9)	2020.1(4)	1661.0(11)
Z	8	2	2
Calculated density (Mg/m^3)	1.627	1.366	1.517
Absorption coefficient (mm^{-1})	1.169	0.622	0.748
F(000)	2464	852	780
θ Range for data collection (°)	1.75–28.02	1.41–28.04	1.29–28.06
Limiting indices	$-12 \leqslant h \leqslant 13$, $-24 \leqslant k \leqslant 30$, $-26 \leqslant l \leqslant 26$	$-15 \leqslant h \leqslant 15$, $-15 \leqslant k \leqslant 16$, $-19 \leqslant l \leqslant 19$	$-12 \leqslant h \leqslant 12$, $-14 \leqslant k \leqslant 15$, $-21 \leqslant l \leqslant 20$
Reflections collected/unique	14655/5658 [$R_{int} = 0.0774$]	22713/8931 [$R_{int} = 0.0987$]	19070/7487 [$R_{int} = 0.0715$]
Completeness to theta	94.4%	91.1%	92.8%
Absorption correction	SADABS	SADABS	SADABS
Refinement method	full-matrix least-squares on F^2	full-matrix least-squares on F^2	full-matrix least-squares on F^2
Data/restraints/parameters	5658/85/463	8931/42/503	7487/60/571
Goodness-of-fit on F^2	1.027	1.017	1.008
Final R indices [$I > 2\sigma(I)$]	$R_1 = 0.0608$, $wR_2 = 0.1088$	$R_1 = 0.0793$, $wR_2 = 0.1818$	$R_1 = 0.0528$, $wR_2 = 0.1095$
R indices (all data)	$R_1 = 0.1584$, $wR_2 = 0.1280$	$R_1 = 0.1998$, $wR_2 = 0.2138$	$R_1 = 0.1169$, $wR_2 = 0.1314$

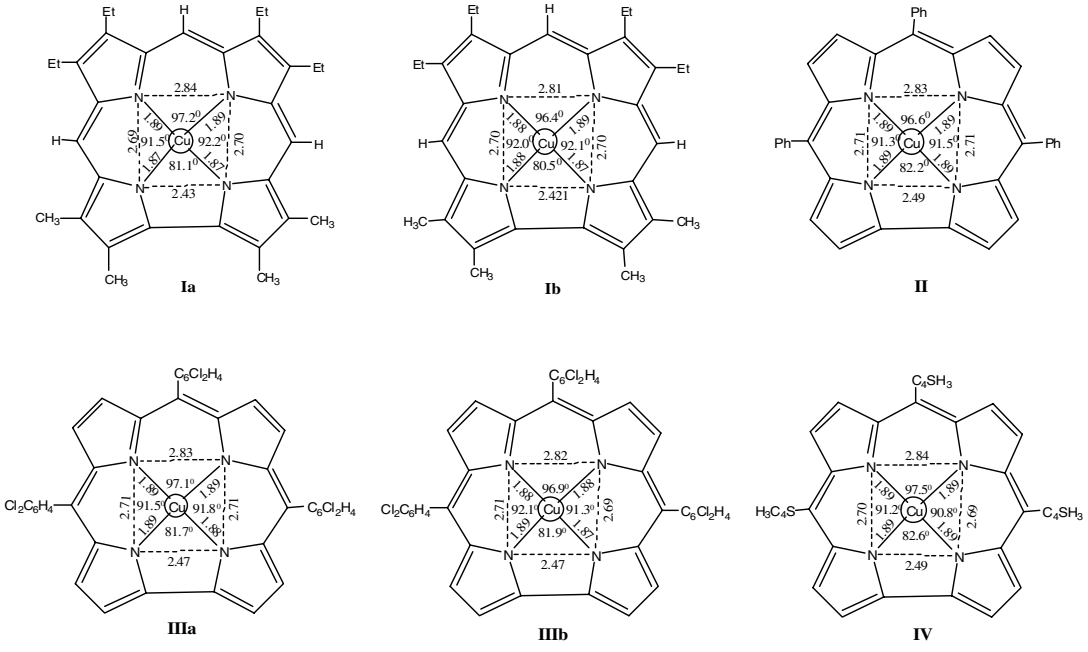

Fig. 4. Comparison of the cores of known Cu corrole complexes. **Ia**, **Ib** [36]; **II**, [29]; **IIIa,b**; [8]; **IV**, this work.

enyl) position in the *meso* substitution gives rise to a band that is always comparatively higher in energy. When the cobalt complex is in solution with excess pyridine, it too becomes blue shifted. This suggests a mono-pyridine derivative forms [11]. A small but measurable difference of 9 nm is detected towards higher energy from 425 in **1** to 416 in **2**.

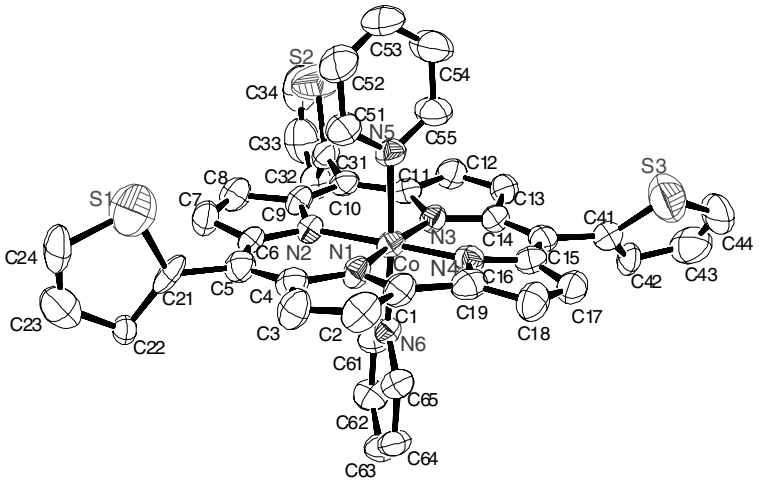

Fig. 5. Molecular structure of Co(T2TC)(Py)$_2$ (**5**). Thermal ellipsoids are shown at the 50% level. Hydrogen atoms and the benzene molecule are omitted for clarity.

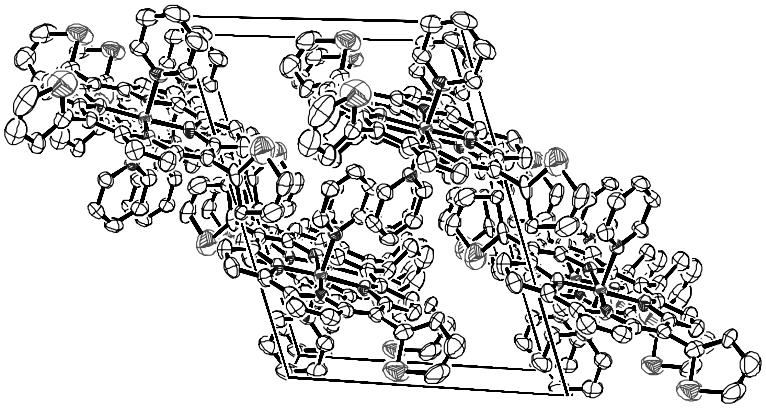

Fig. 6. The crystallographic packing array of Co(T2TC)(Py)$_2$ (**5**) when looking down the *b*-axis. Hydrogens are omitted for clarity.

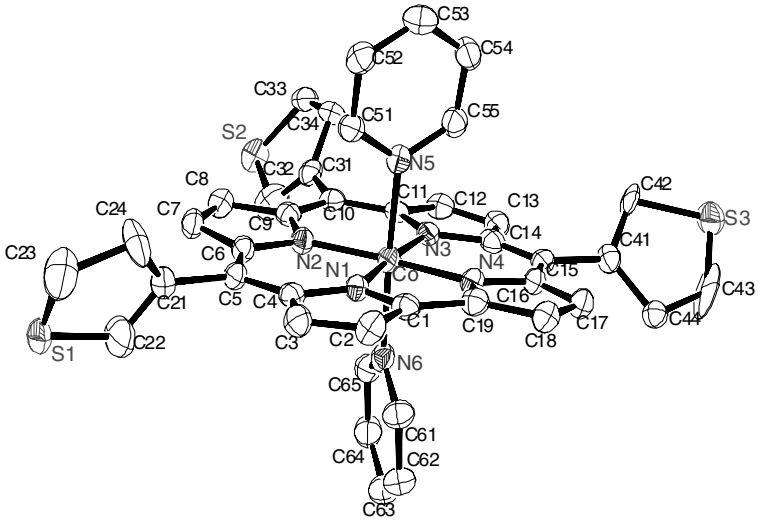

Fig. 7. Molecular structure of Co(T3TC)(Py)$_2$ (**6**). Thermal ellipsoids are shown at the 50% level. Hydrogen atoms have been removed for clarity.

The values for the porphyrins exhibit the same trend at H_2(T2TP): 426 (5.59) and H_2(T3TP) 421 (5.76) [30]. Upon copper complexation, the bands are red shifted keeping an isomeric separation of 21 nm; the corresponding porphyrin system yields a separation of 3 nm [30]. The cobalt metallocorrole isomeric difference is 8 nm.

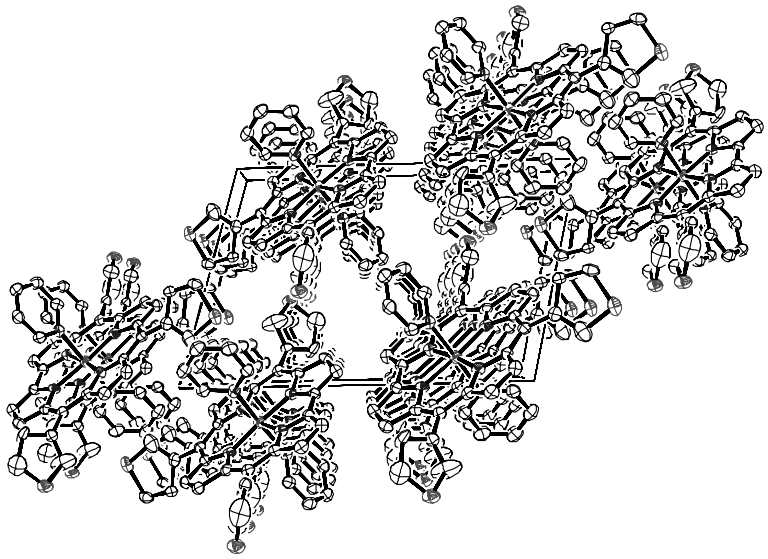

Fig. 8. The crystallographic packing array of Co(T3TC)$(Py)_2$ (**6**) when looking down the *b*-axis. Hydrogens are omitted for clarity. Thermal ellipsoids are shown at the 50% level.

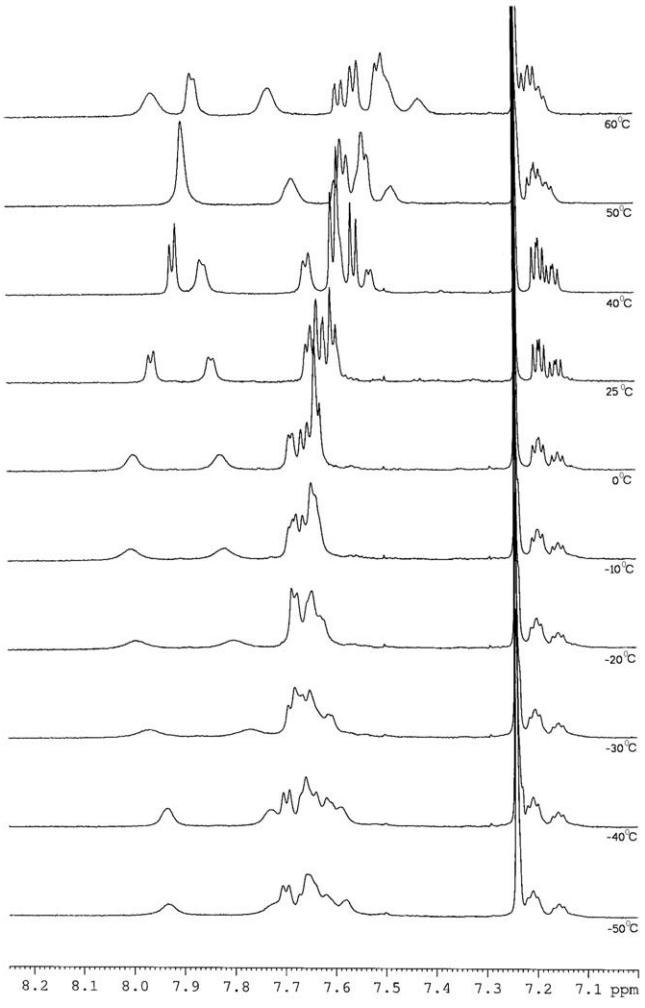

Fig. 9. Aromatic region (7–8 ppm range) of the ^{1}H NMR spectra for Cu(T2TC) (**3**) from −50 °C (bottom) to 60 °C (top).

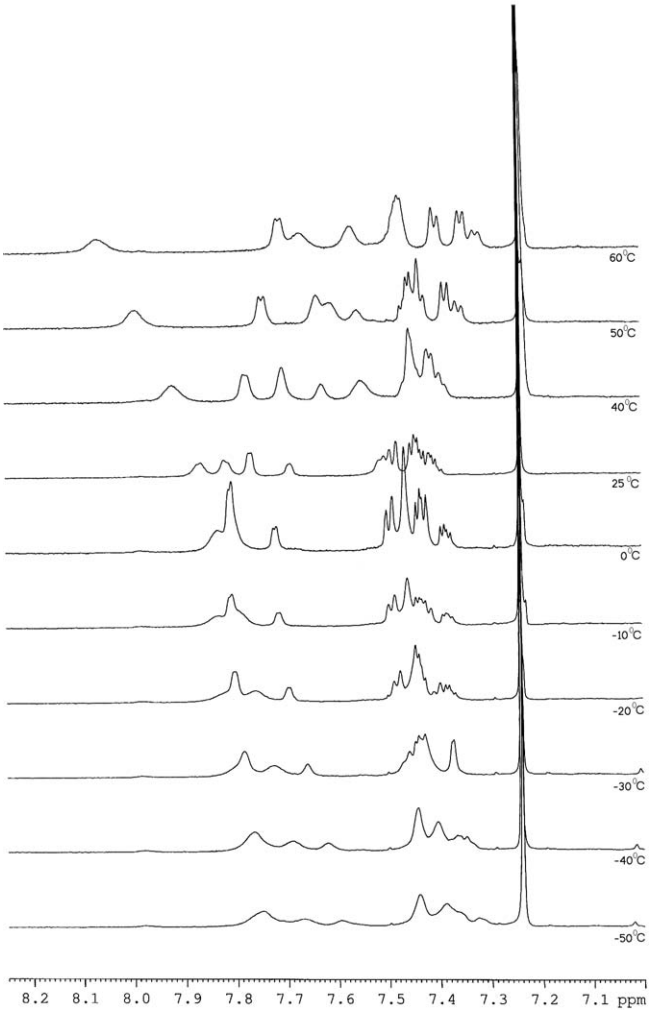

Fig. 10. Aromatic region (7–8 ppm range) of the ^{1}H NMR spectra for Cu(T3TC) (**4**) from −50 °C (bottom) to 60 °C (top).

Table 4
Soret band assignments for corroles and metallocorroles

Compound	λ_{max} (nm), (log ε/($M^{-1}.cm^{-1}$))
H_3(T2TC) (**1**)	425 (5.17)
H_3(T3TC) (**2**)	416 (4.78)
Cu(T2TC) (**3**)	442 (4.82)
Cu(T3TC) (**5**)	421 (5.05)
Co(T2TC)$(Py)_2$ (**4**)	446 (4.96)[a]
	411 (4.97)[b]
Co(T3TC)$(Py)_2$ (**6**)	438 (4.85)[a]
	397 (4.99)[b]

[a] In the presence of excess pyridine.
[b] In the absence of excess pyridine.

2.4. Mass spectrometry

Further data have been obtained to support the enhanced stability of metallocorrole compounds **3**, **4**, **5** and **6** towards C–C coupling, as compared to the $–C_6F_5$ substituted systems. The mass spectra of the copper isomer complexes **3** and **4** show no degree of C–C dinuclear coupling, and the isolated material for the Co isomers shows small observable peaks by high resolution mass spectrometry (see mass spectra provided in the Supporting Information). The monomers seem markedly more stable at room temperature than the corresponding $–C_6F_5$ systems. The [$(\mathbf{3})_2$-2H] products that these signals suggest were not isolated, but only characterized by mass spectrometry but thought to be the same C–C coupling species as those seen by Gross and coworkers [8]. Compared to the $–C_6F_5$ substituted systems, coordinating solvents for these systems were not required. The cobalt compound was further purified by preparative TLC before performing the cyclic voltammetry studies provided below. Material for these studies was made possible through the recrystallization of cobalt crystals with a DCM and *n*-heptane mixture.

2.5. Electrochemistry

The cyclic voltammograms (CVs) of the 5,10,15-tris(thienyl)corrole ligands (**1** and **2**) and their corresponding complexes (**3**, **4**, **5** and **6**) have been obtained and are presented below. Their redox potentials are also provided (Fig. 11).

The reversible half-wave potentials ($E_{1/2}$) for Cu(T2TC) are −0.57 and 0.27 V. The potential at 0.27 V, compares to the oxidation potential of metal-free corrole [$E_{1/2} = 0.15$ V] and has been assigned to corrole-centered oxidation, while the reduction potential at −0.57 V has been assigned to the metal center. The difference in this redox couple ($E_{1/2(ox)} - E_{1/2(red)}$; 0.84 V) also indicates that the two different centers are involved for reduction and oxidation processes (see Table 5).

$$(T2TC)Cu^{II} \underset{-e^-}{\overset{+e^-}{\rightleftharpoons}} (T2TC)Cu^{III} \underset{+e^-}{\overset{-e^-}{\rightleftharpoons}} (T2TC^{\bullet+})Cu^{III} \quad (1)$$

The one-electron oxidation of the 5,10,15-tris(2-thienyl)corrole ligands (**1**) is similar to that of the 5,10,15-tris(3-thienyl)corrole ligands (**2**). The 5,10,15-tris(2-thienyl)corrole ligand (**1**) and its metal complexes (**3** and **5**) have more positive redox potentials than those of the corresponding 3-thienyl ligand (**2**) and its metal complexes (**4** and **6**) because of the greater electron-withdrawing power of 5,10,15-tris(2-thienyl)corrole ligands. This is further supported by a consideration of Hammett and Modified Swain-Lupton Constants (Table 6). Sulfur oxidation has not fully been ruled out in this case. Lastly, these systems are not directly analogous to the corresponding tetrathienyl porphyrin derivatives in that the porphyrin systems undergo two oxidations and two reductions each [30].

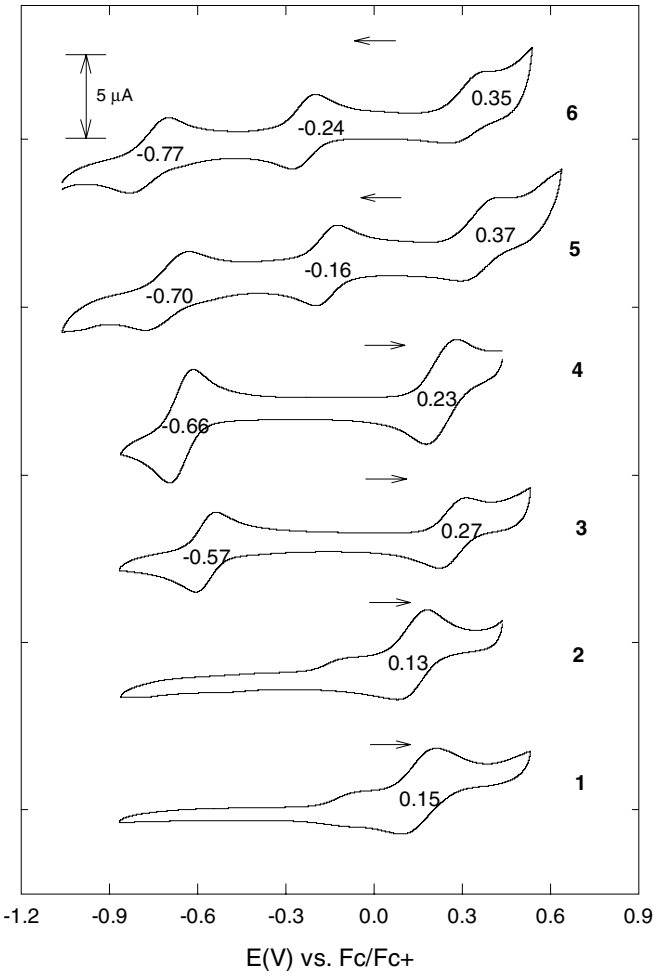

Fig. 11. The cyclic voltammograms of 1 mM 5,10,15-tris(thienyl)corrole ligands (**1** and **2**), 1 mM copper(III) 5,10,15-tris(thienyl)corrole (**3** and **4**), and 1 mM cobalt(III) 5,10,15-tris(thienyl)corrole (**5** and **6**) in benzonitrile solution, 0.1 M TBAP at a scan rate of 100 mV/s (second scans are provided only). $E_{1/2}$ (V) values are provided for each species.

As compared with the copper corroles, the species Co(T2TC)$(py)_2$ (**5**) and Co(T3TC)$(py)_2$ (**6**) have two reduction steps (Fig. 11). This is in contrast to the previously reported Co(tpfc)PPh_3 derivative which exhibits an irreversible reduction process [11]. Co(tpfc)PPh_3 loses a PPh_3 group during the reduction process and then changes to a bis-pyridine coordinated complex. In the case of **5** and **6**, there is an absence of phosphine, and there is excess pyridine; thus, the pyridines present at the outset of the

Table 5
Half-wave potentials ($E_{1/2}$, vs. SCE or Fc/Fc^+) of known copper corrole compounds[a]

Compounds	Oxidation (V) vs.		Reduction (V) vs.		Solvent	Reference
	SCE	Fc/Fc^+	SCE	Fc/Fc^+		
(T2TC)Cu^{III}		0.27		−0.57	C_6H_5CN	this work
(T3TC)Cu^{III}		0.23		−0.66	C_6H_5CN	this work
[(TPC)Cu^{III}]	0.76	0.45[b]	−0.20	−0.51[b]	CH_2Cl_2	[28]
[(TPFC)Cu^{III}]	1.13	0.82[b]	0.19	−0.16[b]	CH_2Cl_2	[28]
	1.01		0.22		C_6H_5CN	[8]
[(TDCC)Cu^{III}]		0.92		0.06	C_6H_5CN	[8]
[{T(*p*-CH_3-P)C}Cu^{III}]	0.70	0.39[b]	−0.23	−0.54[b]	CH_2Cl_2	[28]
[{T(*p*-OCH_3-P)C}Cu^{III}]	0.65	0.34[b]	−0.24	−0.55[b]	CH_2Cl_2	[28]
[{T(*p*-CF_3-P)C}Cu^{III}]	0.89	0.58[b]	−0.08	−0.39[b]	CH_2Cl_2	[28]

SCE values are provided and have been converted into Fc/Fc^+ values where possible.
[a] TPC = 5,10,15-triphenylcorrole; TPFC = 5,10,15-tris(pentafluorophenyl)corrole; TDCC = 5,10,15-tris(2,6-dichlorophenyl)corrole.
[b] Literature values are reported as V vs. SCE (CH_2Cl_2, 0.1 M TBAP) but have been converted to V vs. Fc/Fc^+ using a related value for the estimated standard potential [$E_{1/2}(Fc/Fc^+) = E_{1/2}(SCE) - 0.31$ V] with these conditions: MeCN, 0.2 M $LiClO_4$ which may not be precise for the conditions used herein: CH_2Cl_2, 0.1 M TBAP [41].

Table 6
A comparison of Hammett and Modified Swain-Lupton constants [33]

X	σ_m (σ_3)	σ_p	R^+	R^-	F	R
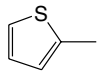	0.09	0.05	-0.56	0.06	0.13	-0.08
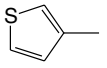	0.03	-0.02	-0.46	0.05	0.08	-0.10
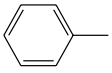	0.06	-0.01	-0.30	-0.10	0.12	-0.13
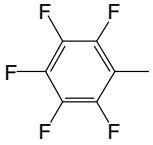	0.26	0.27	-0.09	0.11	0.27	0.00
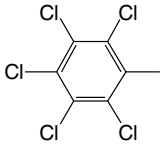	0.25	0.24			0.27	-0.03
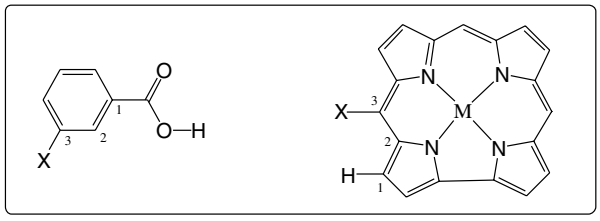						

voltammetric measurement are believed to be retained throughout the course of the experiment. As compared with the copper corrole complexes (**3** and **4**), the cobalt corrole complexes (**5** and **6**) have a more positive oxidation and more negative metal-centered reduction. That means corrole-centered oxidation and metal-centered reduction of cobalt corrole complexes is more difficult than their corresponding copper corrole complexes.

Firstly, *meso* substituents in metallocorroles exert a strong influence on the half-wave potential for one-electron oxidation and this potential is shifted from 820 mV to ca. 270 mV, when the *meso* substituents vary from pentafluorophenyl to thienyl groups. This large decrease in potential shift ca. 550 mV suggests that the removal of an electron is from the corrole "HOMO" [28]. It is easier for thienyl-substituted corroles to be oxidized than the pentaflurophenylphenyl analogs (Table 5) [28].

C–C bond coupling of metallocorroles through the β-carbon in solution has been considered an electronic effect when comparing like tris-*meso*-substituted metallocorroles. Again we see less evidence for corrole oxidation in these thienyl-substituted systems than for tris-pentafluoro derivatives. Thus, Hammett parameters for the various substituents can be discussed. The values for both 2- and 3-thienyl systems are quite similar and can be discussed in connection to electrochemical differences. The Hammett constants (σ) for pentafluorophenyl (pfp)/pentachlorophenyl (pcp) groups are higher than that of 2-thienyl/3-thienyl groups in terms of the ionizations of benzoic acid and *meta*-substituted benzoic acid. Furthermore the electronic effects, i.e. field effects (F) and resonance effects (R) of pfp and pcp substituents are higher than those of both thienyl substituents. By comparing electronic effects with metallocorrole, pfp/pcp groups at the 3-position are more electron withdrawing than the thienyl groups. The 2,6-dichlorophenyl group, though of greater bulk than the thienyl groups, has a greater electron withdrawing effect. C–C coupling is prominent for electron withdrawing substituents at the *meso* positions of metallocorroles but is not necessarily due to the bulkiness of the groups.

3. Conclusions

We have reported novel *meso*-substituted thienyl corroles and the respective metallocorroles for copper and

cobalt. These new derivatives allow for the investigation of compounds electrochemically for coordination and thiophene–thiophene coupling to form macromolecular arrays. Cu(T2TC), Co(T2TC)$(Py)_2$ and Co(T3TC)$(Py)_2$ have been structurally characterized. Dimerization of metallocorroles in solution depends on the electronic effects of the substituents at *meso* positions which are revealed through cyclic voltammetry, NMR and UV–vis spectroscopic data. More electron withdrawing groups tend to give coupling through β-carbons. The bulkiness of the aromatic group is thought to be important. But the thienyl groups are less electron withdrawing than the commonly studied pentafluorophenyl substitutions. Our cyclic voltammetric data support a single oxidation/reduction, devoid of C–C coupling dinuclear products. UV data allow for Soret bands for all ligands and complexes to be measured and indicate red shifting upon metal complexation. One of our strong research motivations involves exploring peroxidase reactivity in related iron systems.

4. Experimental

4.1. General considerations

All solvents and chemicals used in the following synthetic steps were of analytical grade and were used as received: i.e., 2-thiophene carboxyaldehyde, 3-thiophene carboxyaldehyde, pyrrole, $Cu(OAc)_2 \cdot H_2O$, $Co(OAc)_2 \cdot 4H_2O$, pyridine, and C_6H_5CN (Aldrich), dichloromethane, hexane, $MgSO_4$, EtOAc (Merck) and TBAP (Fluka). TBAP was dried overnight under vacuum at 70 °C prior to use. All solvents used for NMR spectral analysis were purchased commercially and were of spectroscopic grade. Infrared spectra were recorded with a Bruker Equinox 55 spectrophotometer and UV–vis spectra were with JASCO V-503 UV–vis spectrometer. A Vario EL III CHNS elemental analyzer was used for microanalysis. High-resolution MALDI mass spectrometry was performed by the staff of the research supporting team at KAIST on a VG AUTOSPEC ULTIMA with a trisector double focusing magnetic sector analyzer at a resolution of 80 000.

^1H spectra were measured in $CDCl_3$ with Bruker Avance 300 and Bruker Avance 400 spectrometers. Variable temperature ^1H NMR spectra were performed in $CDCl_3$ at temperatures between and including −50 and 60 °C. At each temperature, thermal equilibration time was monitored automatically. Spectral signals were calibrated by the protio impurity of the $CDCl_3$ solvent. The synthetic details for the preparation of 5(2-thienyl)dipyrromethane and 5(3-thienyl)dipyrromethane have been reported previously [34,42].

4.2. Physical methods

Cyclic voltammetry was carried out with a BAS 100B (Bioanalytical Systems, Inc.). A three-electrode system was used and consisted of a gold disk working electrode, a platinum wire counter electrode, and a Ag/Ag^+ electrode (MF-2062 kit, Bioanalytical Systems, Inc.) as the reference electrode. The Ag/Ag^+ contained 0.1 M tetrabutylammonium perchlorate (TBAP) and 0.01 M $AgNO_3$ in benzonitrile. In 0.1 M TBAP, the $E_{1/2}$ of the ferrocene/ferrocenium ion couple was taken to be 0.067 V vs. Ag/Ag^+ in benzonitrile. The values in electrochemical experiments are reported versus the ferrocene/ferrocenium ion redox couple.

4.3. X-ray crystallography of Cu(T2TC), Co(T2TC)$(Py)_2$ and Co(T3TC)$(Py)_2$

Crystals of **3**, **5** and **6** suitable for diffraction were grown by slow evaporation of dichloromethane (**3**) and benzene solution, (**5**, **6**), at room temperature. The single-crystal sizes **3**, **5** and **6** were $0.30 \times 0.03 \times 0.20\ mm^3$, $0.50 \times 0.40 \times 0.30\ mm^3$, and $0.3 \times 0.2 \times 0.2\ mm^3$, respectively. Reflection data for **3**, **5**, and **6** were collected on a Bruker 1 K SMART CCD-based diffractometer with graphite-monochromated Mo Kα radiation ($\lambda = 0.7107$ Å). The hemisphere of reflection data was collected as ω scan frames with 0.3°/frame and an exposure time of 5 s/frame under room temperature conditions. Cell parameters were determined and refined by the SMART program [43]. Data reduction was performed using SAINT software [44]. The data were corrected for Lorentz and polarization effects. An empirical absorption correction was applied using the SADABS program [45]. The structures of the compounds were solved by direct methods and refined by full matrix least-squares methods using the SHELXTL program package with anisotropic thermal parameters for all non-hydrogen atoms. Early into the crystallographic solution it was established that each of the three thienyl moieties in compounds **3** and **6** were disordered by ca. 180° rotation about the C_{meso}–$C_{thienyl}$ vector as evidenced by distortions in the atomic thermal parameters upon least-squares refinement. Thiophene fluxionality was evident from VT NMR data provided below, and thus crystallographic disorder was anticipated and has been observed also in the structural solutions for the dipyrromethane precursors [34]. To obtain the molecular structures of **3** and **6** satisfactorily, modeling of this disorder was undertaken and involved creating atomic coordinates for a second thienyl group; both parts were refined to nearly half occupancy. Additionally, the carbon atoms in the benzene solvent molecule of crystallization (in the crystallographic solution for **4**) were refined with the ISOR command in which a given standard deviation is assigned and allows the atomic thermal parameters to approximate isotropic behavior.

4.4. Preparation of 5,10,15-tris(2-thienyl)corrole [H_3(T2TC)]

A sample of 5(2-thienyl)dipyrromethane (1.00 g; 4.38 mmol) and 2-thiophene carboxyaldehyde (0.245 g; 2.19 mmol) were added to 150 mL of a dichloromethane solution of TFA (0.13 mM). The reaction mixture was

standing for 6 h at room temperature. The colour of the solution changed from yellow to pink-red. DDQ (1.0 g, 4.4 mmol) in 50 mL toluene was added during a 10 min period with vigorous stirring. Stirring was continued for an additional 15 min. The reaction mixture was then concentrated and filtered twice through a pad of silica gel using CH_2Cl_2 as the eluent, followed by preparative TLC separation (CH_2Cl_2/hexane 1:1). A broad dark green band was collected as pure corrole (71 mg, 3.0%). *m/z* ($M + H^+$): 545.08 Calc. 545.11 Obs. IR (KBr; cm^{-1}): 3436; 3361 [ν_{N-H}]. ^1H NMR (δ; $CDCl_3$): 9.10 [br, 2H], 8.87 [br, 2H], 8.72 [br, 4H], 7.96 [br, 2H], 7.83 [br, 4H], 7.54 [br, 3H] at 25 °C. 9.10 [br, 2H], 8.73 [br, 2H], 8.46 [br, 4H], 7.91 [br, 4H], 7.86 [br, 1H], 7.81 [br, 1H], 7.58 [br, 2H], 7.52 [br, 1H] at −50 °C. UV–vis: λ_{max} ($\log\varepsilon/(M^{-1}\,cm^{-1})$) 627 nm (4.25); 588 nm (4.29); 425 nm (5.17) [Soret band]; 286 nm (4.43).

4.5. Preparation of 5,10,15-tris(3-thienyl)corrole [H_3(T3TC)]

The synthetic procedure of H_3(T3TC) is similar to that of H_3(T2TC) using 5(3-thienyl)dipyrromethane and 3-thiophene carboxyaldehyde as a replacement of 5(2-thienyl)dipyrromethane and 2-thiophene carboxyaldehyde, respectively. The yield was 83.5 mg (3.5%). *m/z* (M^+): 544.08 (calc); 544.19 (obs). IR (KBr; cm^{-1}): 3436; 3373 (ν_{N-H}). ^1H NMR (δ; $CDCl_3$): 8.95 [br, 2H], 8.82 [br, 2H], 8.64 [br, 2H], 8.48 [br, 2H], 8.20 [br, 2H], 8.17 [br, 2H], 8.09 [br, 2H], 7.82 [br, 2H], 7.76 [s, 1H] at 25 °C. λ_{max} ($\log\varepsilon/(M^{-1}\,cm^{-1})$) 622 nm (3.84); 581 nm (3.82); 416 nm (4.78) [Soret band]; 281 nm (4.18).

4.6. Preparation of Cu(T2TC)

Copper(II) acetate monohydrate (excess) was added to a 5 mL pyridine solution of H_3(T2TC) (**1**) (33 mg, 0.63 mmol). The reaction mixture was stirred for 30 min at room temperature during which the colour of the solution changed from green to reddish-brown. The volatiles were then removed by reduced pressure using a vacuum line. The crude product was then dissolved in a minimum volume of dichloromethane and purified by silica gel column chromatography. A reddish-brown fraction containing Cu(T2TC) was collected by using a dichloromethane–hexane (1:1 v/v) eluant. Yield 33.4 mg. (91%). *m/z* ($M + H^+$): 605.00 (calc); 605.97 (obs). ^1H NMR (δ; $CDCl_3$): 7.95 [br; 2H], 7.88 [d; 2H; $J = 3.7$ Hz], 7.72 [br, 2H]; 7.58 [d; H; $J = 5.1$ Hz]; 7.55 [d; 2H; $J = 4.6$ Hz], 7.50 [d; 4H; $J = 4.2$ Hz], 7.42 [br, H], 7.22–7.17 [m; 3H] at 60 °C. λ_{max} ($\log\varepsilon/(M^{-1}\,cm^{-1})$) 521 nm (3.80); 442 nm (4.82) [Soret band]; 312 nm (3.91); 270 nm (4.20).

4.7. Preparation of Cu(T3TC)

The synthetic procedure reported above for Cu(T2TC) was used to generate Cu(T3TC), in which H_3(T3TC) was used in place of H_3(T2TC). Yield 33 mg. (90%). *m/z* (M^+): 604.00 (calc); 604.09 (obs). ^1H NMR (δ; $CDCl_3$): 8.06 [br; 2H], 7.71 [d; 2H; $J = 3.71$ Hz]; 7.67 [br; 2H], 7.57 [br, 2H], 7.47 [m, 4H], 7.40 [d, $J = 4.7$ Hz, 2H], 7.35 [d, $J = 4.2$ Hz, 2H]; 7.32 [d, $J = 4.3$ Hz, H] at 60 °C. λ_{max} ($\log\varepsilon/(M^{-1}\,cm^{-1})$) 565 nm (3.71); 539 nm (3.98); 421 nm (5.05) [Soret band]; 268 nm (4.53).

4.8. Preparation of Co(T2TC)(Py)$_2$

An approximate threefold excess of $Co(OAc)_2 \cdot 4H_2O$ was added to a hot pyridine solution of H_2(T2TC) (33 mg; 0.06 mmol) and this reaction mixture was refluxed for 1 h. After this time, the reaction mixture was cooled to room temperature and the solvent and volatiles were removed by rotary evaporation. The green crude product was dissolved in a minimum volume of dichloromethane and then isolated by vacuum-filtration. A large volume of diethyl ether was added to the filtrate and a brown precipitate formed after a 30-min period which was then separated by vacuum filtration. The green filtrate was collected and pure crystalline Co(T2TC)$(Py)_2$ was obtained slow diffusion of dichloromethane into *n*-heptane solvent. Yield 40.05 mg. (87%). *m/z* ($M^+ - 2Py$): 599.99 (calc.); 600.98 (obs). ^1H NMR (δ; $CDCl_3$): 9.21 [d, $J = 4.7$ Hz, 2H] 9.1 [d, $J = 4.3$ Hz, 2H], 8.94 [br, 1H], 8.89 [br, 2H], 7.92 [br, 2H], 7.79 [d, $J = 4.7$ Hz, 2H], 7.74 [br, 1H], 7.70 [d, $J = 4.7$ Hz, 2H], 7.49–7.52 [m, 2H], 7.40–7.43 [m, 1H], 6.08 [t, 2H; *para*-H of pyridine], 5.28 [br, 4H; *meta*-H of pyridine], 2.13 [b, 4H; *ortho*-H of pyridine]. λ_{max} ($\log\varepsilon/(M^{-1}\,cm^{-1})$) 629 nm (4.48); 588 nm (4.20); 549 nm (4.04); 446 nm (4.96) [Soret band]; 418 nm (4.72); 314 nm (4.43) (in the presence of excess Py).

4.9. Preparation of Co(T3TC)(Py)$_2$

The synthetic procedure of Co(T3TC) $\cdot$ $(Py)_2$ is similar to that of Co(T2TC)$(Py)_2$ using H_3(T3TC) as a replacement of H_3(T2TC). A yield of 42 mg (91%) was obtained. *m/z* ($M^+ - 2Py$): 599.99 (calc); 600.09 (obs). ^1H NMR (δ, $CDCl_3$ RT): 9.32 [2H]; 9.22 [2H]; 9.11 [2H]; 9.07 [2H]; 8.09 [2H]; 7.92 [3H]; 7.82 [1H]; 7.21–7.27 [m, 3H]; 4.81 [b, 2H; *para*-H of pyridine], 4.39 [b, 4H; *meta*-H of pyridine], 2.54 [b, 4H; *ortho*-H of pyridine]. λ_{max} ($\log\varepsilon/(M^{-1}\,cm^{-1})$) 629 nm (4.49); 584 nm (4.04); 543 nm (3.87); 455 nm (4.78); 438 nm (4.85) [Soret band]; 400 nm (4.57); 309 nm (4.33) (in the presence of excess Py).

5. Supporting information

(i) Cif files of the crystallographic determinations of **3**, **5** and **6**: files CCDC-273811, CCDC-273812, and CCDC-277370 are included. These data are available without cost at www.ccdc.cam.ac.uk/conts/retrieving.html or from the Cambridge Crystallographic Data center (CCDC), 12 Union Road, Cambridge CB2 IEZ, United Kingdom; fax +44(0)1223 336033; e-mail: deposit@ccdc.cam.ac.kr.

(ii) Mass spectrometric data. (iii) Photo of a preparative TLC plate prior to isolation of the purified H3(T3TC) material.

Acknowledgement

DGC gratefully acknowledges financial support from KAIST and the BK 21 Project. YD gratefully acknowledges financial support from the CMDS and the BK 21 Project. J.K. gratefully acknowledges financial support from the BK 21 Project and the MICROS project. Professors Sukbok Chang and Iwan Cho are appreciated for their donations of various chemicals. Hack Soo Shin is gratefully acknowledged for his technical assistance in obtaining ^{13}C and Variable temperature NMR spectra. Teresa Lindstead is thanked for her assistance in depositing our crystallographic data to the CCDC.

References

[1] L. Simkhovich, N. Galili, I. Saltsman, I. Goldberg, Z. Gross, Inorg. Chem. 39 (2000) 2704.
[2] Z. Gross, G. Golubkov, L. Simkhovich, Angew. Chem., Int. Ed. 39 (2000) 4045.
[3] L. Simkhovich, A. Mahammed, I. Goldberg, Z. Gross, Chem.-Eur. J. 7 (2001) 1041.
[4] J. Bendix, H.B. Gray, G. Golubkov, Z. Gross, Chem. Commun. (2000) 1957.
[5] L. Simkhovich, I. Goldberg, Z. Gross, Inorg. Chem. 41 (2002) 5433.
[6] L. Simkhovich, I. Luobeznova, I. Goldberg, Z. Gross, Chem.-Eur. J. 9 (2003) 201.
[7] G. Golubkov, Z. Gross, Angew. Chem., Int. Ed. 42 (2003) 4507.
[8] I. Luobeznova, L. Simkhovich, I. Goldberg, Z. Gross, Eur. J. Inorg. Chem. (2004) 1724.
[9] L. Simkhovich, Z. Gross, J. Inorg. Biochem. 86 (2001) 433.
[10] G. Golubkov, J. Bendix, H.B. Gray, A. Mahammed, I. Goldberg, A.J. DiBilio, Z. Gross, Angew. Chem., Int. Ed. 40 (2001) 2132.
[11] A. Mahammed, I. Giladi, I. Goldberg, Z. Gross, Chem.-Eur. J. 7 (2001) 4259.
[12] L. Simkhovich, P. Iyer, I. Goldberg, Z. Gross, Chem.-Eur. J. 8 (2002) 2595.
[13] E. Vogel, S. Will, A.S. Tilling, L. Neumann, J. Lex, E. Bill, A.X. Trautwein, K. Wieghardt, Angew. Chem. 106 (1994) 771.
[14] Z. Gross, L. Simkhovich, N. Galili, Chem. Commun. (1999) 599.
[15] L. Simkhovich, Z. Gross, Tetrahedron Lett. 42 (2001) 8089.
[16] J. Grodkowski, P. Neta, E. Fujita, A. Mahammed, L. Simkhovich, Z. Gross, J. Phys. Chem. A 106 (2002) 4772.
[17] R.A. Eikey, S.I. Khan, M.M. Abu-Omar, Angew. Chem., Int. Ed. 41 (2002) 3592.
[18] Z. Gross, H.B. Gray, Adv. Synth. & Catalysis 346 (2004) 165.
[19] Z. Gross, N. Galili, L. Simkhovich, Tetrahedron Lett. 40 (1999) 1571.
[20] A. Mahammed, I. Goldberg, Z. Gross, Organic Lett. 3 (2001) 3443.
[21] I. Saltsman, A. Mahammed, I. Goldberg, E. Tkachenko, M. Botoshansky, Z. Gross, J. Am. Chem. Soc. 124 (2002) 7411.
[22] I. Saltsman, I. Goldberg, Z. Gross, Tetrahedron Lett. 44 (2003) 5669.
[23] Z. Gross, N. Galili, I. Saltsman, Angew. Chem., Int. Ed. 38 (1999) 1427.
[24] Z. Gross, J. Biolog. Inorg. Chem. 6 (2001) 733.
[25] B. Andrioletti, E. Rose, J. Chem. Soc.,Perkin Trans. 1 (2002) 715.
[26] D. Aviezer, S. Cotton, M. David, A. Segev, N. Khaselev, N. Galili, Z. Gross, A. Yayon, Cancer Res. 60 (2000) 2973.
[27] A. Mahammed, H.B. Gray, J.J. Weaver, K. Sorasaenee, Z. Gross, Bioconjugate Chem. 15 (2004) 738.
[28] I.H. Wasbotten, T. Wondimagegn, A. Ghosh, J. Am. Chem. Soc. 124 (2002) 8104.
[29] C. Bruckner, P.R. Brinas, J.A.K. Bauer, Inorg. Chem. 42 (2003) 4495.
[30] P. Bhyrappa, P. Bhavana, Chem. Phys. Lett. 349 (2001) 399.
[31] Y. Diskin-Posner, S. Balasubramanian, G.K. Patra, I. Goldberg, Acta Crystallogr., Sect. E E57 (2001) m346.
[32] Z.-F. Li, S.-W. Wang, W.-S. Song, H.-N. Deng, Y.-Q. Wang, Y.-X. Wang, Youji Huaxue 23 (2003) 588.
[33] C. Hansch, A. Leo, R.W. Taft, Chem. Rev. 91 (1991) 165.
[34] N. Maiti, J. Lee, Y. Do, D.G. Churchill, H.S. Shin, J. Chem. Cryst. (2005) 949.
[35] D.T. Gryko, K. Jadach, J. Org. Chem. 66 (2001) 4267.
[36] S. Will, J. Lex, E. Vogel, H. Schmickler, J.-P. Gisselbrecht, C. Haubtmann, M. Bernard, M. Gross, Angew. Chem., Int. Ed. Eng. 36 (1997) 357.
[37] S. Will, J. Lex, E. Vogel, V.A. Adamian, E. Van Caemelbecke, K.M. Kadish, Inorg. Chem. 35 (1996) 5577.
[38] J.-M. Barbe, F. Burdet, E. Espinosa, C.P. Gros, R. Guilard, J. Porph. Phthalocyan. 7 (2003) 365.
[39] R. Guilard, C.P. Gros, F. Bolze, F. Jerome, Z. Ou, J. Shao, J. Fischer, R. Weiss, K.M. Kadish, Inorg. Chem. 40 (2001) 4845.
[40] Y.S. Balazs, I. Saltsman, A. Mahammed, E. Tkachenko, G. Golubkov, J. Levine, Z. Gross, Mag. Res. Chem. 42 (2004) 624.
[41] A.J. Bard, L.R. Faulkner, Electrochemical Methods: Fundamentals and Applications, second ed., John Wiley & Sons, Inc., New York, 2001.
[42] B.J. Littler, M.A. Miller, C.H. Hung, R.W. Wagner, D.F. O'Shea, P.D. Boyle, J.S. Lindsey, J. Org. Chem. 64 (1999) 1391.
[43] SMART, version 5.0, Data Collection Software, Bruker AXS, Inc., Madison, WI, 1998.
[44] SAINT, version 5.0, Data Integraton Software, Bruker AXS Inc., Madison, WI, 1998.
[45] G.M. Sheldrick, SADABS, Program for absorption correction with the Bruker SMART system, Universitat Göttingen, Germany, 1996.

2.1. Preparation of the complexes

2.1.1. $[Co(2,3\text{-}L)_2(N_3)_2][Na_3(H_2O)_{10}]$ (1)

A mixture of cobalt(II) chloride pentahydrate (0.73 g, 3 mmol) in 15 cm^3 water and NaN_3 (0.78 g, 7 mmol) in 5 cm^3 water. To this mixture an aqueous/ethanolic solution of 20 cm^3 of 2,3-H_2L (1.0 g, 6 mmol) was added, followed by addition of 150 cm^3 acetone, the final mixture was stirred for about 2 h, and filtered. The filtrate was allowed to stand in an open beaker over several days to deposit deep green crystal of the complex. Good quality complexes were obtained by mixing cobalt(II) chloride pentahydrate in acetone, NaN_3 in water and 2,3-H_2L in water/ethanol in the above molar ratio. To this mixture, an excess amount of solid $K_2S_2O_8$ was added with vigorous stirring for about 2 h. The final mixture was filtered and the filtrate allowed to stand over several days, to produce 60% yield. *Anal.* Calc. for $C_{14}H_{26}CoN_8Na_3O_{18}$: C, 23.3; H, 3.6; N, 15.5; Co, 8.4. Found: C, 23.27; H, 3.32; N, 15.47; Co, 8.4%.

2.1.2. $[Co(2,5\text{-}L)_2(N_3)_2][Na_3(H_2O)_8](H_2O)_2$ (2)

This complex was prepared by the procedures given for **1**, except that 2,5-pyridine dicarboxylic acid used instead of 2,3-H_2L. Good quality dark green crystals of **2**, were obtained upon using a large excess solid $K_2S_2O_8$ yield 45%. *Anal.* Calc. for $C_{14}H_{26}CoN_8Na_3O_{18}$: C, 23.3; H, 3.6; N, 15.5; Co, 8.4. Found: C, 23.22; H, 3.32; N, 15.55; Co, 8.5%.

2.2. Physical measurements

Elemental analyses were carried out using a Perkin–Elmer analyzer. Infrared spectra were recorded in a Bruker IFS-125 model FT-IR spectrophotometer as Nujol mulls. Electronic spectra were obtained using Shimadzu UV-3101 PC Scanning spectrophotometer. The experimental procedures and instruments used for other measurements are as described previously [7].

Caution. Metal azide complexes are potential explosives. Only a small amount of material should be prepared and handled with caution.

2.3. X-ray crystallography

Single crystal X-ray data were measured at 99(2) K on a modified STOE four circle diffractometer using graphite crystal-monochromatized Mo Kα radiation ($\lambda = 0.71069$ Å). The intensities were corrected for Lorentz-polarization effects, intensity decay and for absorption. Crystallographic data and processing parameters are given in Table 1. The structures were solved by direct methods and subsequent Fourier analyses. Anisotropic displacement parameters were applied to non-hydrogen atoms in full-matrix least-squares refinements based on F^2. The hydrogen atoms were located from difference Fourier maps, assigned with isotropic displacement factors and included in the final refinement cycles on calculated positions. Analytical expressions of neutral-atom scattering factors were employed, and anomalous dispersion corrections were incorporated. Occupancy of 0.5 was assigned for atoms Na(2) in case of **1**; for Na(2) and the hydrogen atoms bonded to O(6) and O(7) atoms in case of **2**, respectively. The SHELXTL/PC program package [8] and program DIFABS [9] were used for computations. Selected bond parameters are given in Tables 2 and 3, for complexes **1** and **2**, respectively.

Table 1
Crystallographic data and processing parameters

Compound	1	2
Empirical formula	$C_{14}H_{26}CoN_8Na_3O_{18}$	$C_{14}H_{26}CoNa_3N_8O_{18}$
Formula mass	722.33	722.33
System	triclinic	triclinic
Space group	$P\bar{1}$	$P\bar{1}$
a (Å)	7.522(3)	6.879(3)
b (Å)	8.600(3)	8.398(3)
c (Å)	11.011(4)	12.229(4)
α (°)	88.20(3)	78.28(3)
β (°)	80.66(3)	76.70(3)
γ (°)	83.95(3)	89.89(3)
V (Å^3)	698.9(4)	672.4(4)
Z	1	1
μ(Mo Kα) (mm^{-1})	0.755	0.785
D_{calc} (Mg/m^3)	1.716	1.784
Approximate crystal size (mm)	$0.27 \times 0.22 \times 0.15$	$0.26 \times 0.14 \times 0.10$
θ Range (°)	2.76–26.00	3.05–27.00
Reflections collected	3164	3354
Independent reflections/R_{int}	2719/0.0232	2934/0.0283
Parameters	210	210
Goodness-of-fit on F^2	1.056	1.073
R_1/wR_2 [$I > 2\sigma(I)$]	0.0402/0.0980	0.0412/0.0840
R_1/wR_2 (all data)	0.0449/0.1046	0.0514/0.0948
Largest peak/hole (e/Å^3)	0.571/−0.543	0.353/−0.420

3. Results and discussion

Despite the many trials for preparation of cobalt(III) azido complexes of 2,3-, 2,4-, 2,5-, 2,6-, 3,4- and 3,5-pyridine dicarboxylic acids ligands, we isolated only solid complexes for 2,3 and 2,5-pyridine dicarboxylic acids. In the case of other acids, we could not isolate the solid complexes although green colors were obtained upon addition of $K_2S_2O_8$ to an aqueous/acetone solutions of the contents. The electronic spectra (vide infra) of these solutions are similar to those of the isolated solid complexes dissolved in water, suggesting the formation of respective complexes in solutions. In fact the change of the red to green colored solution takes place only if the ratio of acetone to water exceeds 6:1. In aqueous solution, no such change to green whatever the amount of $K_2S_2O_8$ added to the mixture. That we isolated solid cobalt(III) azido complexes of 2,3- and 2,5-pyridine dicarboxylic acids only but not with other acids, is in contrast with the result of similar reactions with dimethyl pyridine, also known as lutidines. In case of these latter ligands, cobalt(III) azido complexes have been isolated for 3,4-, and 3,5-dimethyl pyridines only whereas

Table 2
Selected bond lengths (Å) and angles (°) for **1**

Co(1)–O(1)	1.893(2)	Co(1)–N(1)	1.927(2)
Co(1)–N(11A)	1.966(2)	N(11)–N(12)	1.200(3)
N(12)–N(13)	1.146(4)	O(1)–C(6)	1.298(3)
O(2)–C(6)	1.229(3)	O(3)–C(7)	1.248(3)
O(4)–C(7)	1.253(3)	O(2)–Na(1)	2.388(2)
Na(1)–O(5)	2.339(2)	Na(1)–O(9)	2.385(3)
Na(1)–O(6)	2.402(2)	Na(1)–O(7)	2.407(2)
Na(1)–O(8)	2.439(3)	O(7)–Na(2B)	2.415(3)
O(7)–Na(2)	2.502(3)	O(8)–Na(2B)	2.037(4)
O(9)–Na(2)	2.223(3)	Na(2)–O(8B)	2.037(4)
Na(2)–O(7B)	2.415(3)	Na(2)–N(13C)	2.421(4)
Na(1)···Na(2B)	3.244(3)	Na(1)···Na(2)	3.430(3)
Na(2)···Na(2B)	3.835(4)	O(5)···O(3F)	2.716(3)
O(5)···O(1E)	3.060(3)	O(5)···O(2E)	3.181(3)
O(6)···O(4F)	2.851(3)	O(6)···O(3)	2.740(3)
O(7)···O(5E)	2.870(3)	O(8)···O(6G)	2.748(4)
O(8)···N(13E)	3.181(4)	O(9)···O(4C)	2.710(4)
O(9)···N(11A)	3.042(4)		
O(1A)–Co(1)–N(1)	95.59(8)	O(1)–Co(1)–N(11)	92.38(9)
N(1)–Co(1)–N(11)	90.81(9)	N(12)–N(11)–Co(1)	116.4(2)
N(13)–N(12)–N(11)	177.7(3)	N(12)–N(13)–Na(2D)	162.8(2)
O(5)–Na(1)–O(9)	168.42(8)	O(5)–Na(1)–O(2)	82.43(8)
O(9)–Na(1)–O(2)	91.45(9)	O(5)–Na(1)–O(6)	91.45(8)
O(9)–Na(1)–O(6)	98.72(9)	O(2)–Na(1)–O(6)	93.17(8)
O(5)–Na(1)–O(7)	84.81(8)	O(9)–Na(1)–O(7)	86.65(9)
O(2)–Na(1)–O(7)	100.41(8)	O(6)–Na(1)–O(7)	165.28(8)
O(5)–Na(1)–O(8)	87.26(9)	O(9)–Na(1)–O(8)	99.96(11)
O(2)–Na(1)–O(8)	167.22(10)	O(6)–Na(1)–O(8)	79.49(11)
O(7)–Na(1)–O(8)	86.10(11)	Na(1)–O(7)–Na(2B)	84.56(9)
Na(1)–O(7)–Na(2)	88.65(9)	Na(2B)–O(7)–Na(2)	102.51(10)
Na(2)–O(9)–Na(1)	96.18(11)	O(8B)–Na(2)–O(9)	165.6(2)
O(8B)–Na(2)–O(7B)	95.60(12)	O(9)–Na(2)–O(7B)	89.18(12)
O(8B)–Na(2)–N(13C)	90.6(2)	O(9)–Na(2)–N(13C)	98.6(2)
O(7B)–Na(2)–N(13C)	120.99(13)	O(8B)–Na(2)–O(7)	79.86(12)
O(9)–Na(2)–O(7)	87.99(10)	O(7B)–Na(2)–O(7)	77.49(10)
N(13C)–Na(2)–O(7)	160.22(13)		

Symmetry codes: (A) $-x+1$, $-y+1$, $-z+1$; (B) $-x+2$, $-y+1$, $-z$; (C) $x+1$, y, z; (D) $x-1$, y, z; (E) $-x+1$, $-y+1$, $-z$; (F) $-x+1$, $-y$, $-z$; (G) $-x+2$, $-y$, $-z$.

Table 3
Selected bond lengths (Å) and angles (°) for **2**

Co(1)–O(1)	1.898(2)	Co(1)–N(1)	1.905(2)
Co(1)–N(11)	1.958(2)	N(11)–N(12)	1.203(3)
N(12)–N(13)	1.154(3)	C(6)–O(2)	1.227(3)
C(6)–O(1)	1.286(3)	C(7)–O(4)	1.252(3)
C(7)–O(3)	1.255(3)	Na(1)–O(2)	2.329(2)
Na(1)–O(5)	2.358(2)	Na(1)–O(8)	2.368(3)
Na(1)–O(5B)	2.394(2)	Na(1)–O(6)	2.406(2)
Na(1)–O(7)	2.465(2)	O(3)–Na(2)	2.277(3)
O(6)–Na(2)	2.425(3)	O(8)–Na(2)	2.243(3)
Na(2)–O(7C)	2.184(3)	Na(2)–O(6C)	2.199(3)
Na(1)···Na(2C)	3.202(2)	Na(1)···Na(2)	3.296(3)
Na(1)···Na(1B)	3.461(2)	O(5)···O(3F)	2.837(3)
O(5)···O(4D)	2.724(3)	O(6)···O(9A)	2.818(3)
O(7)···O(2B)	3.023(3)	O(7)···N(13G)	3.137(4)
O(8)···O(3D)	2.866(3)	O(8)···O(9E)	2.850(3)
O(9)···N(11E)	2.950(4)	O(9)···O(4H)	2.780(4)
O(1)–Co(1)–N(1)	95.18(8)	O(1A)–Co(1)–N(11)	92.03(9)
N(1A)–Co(1)–N(11)	91.89(9)	N(12)–N(11)–Co(1)	116.0(2)
N(13)–N(12)–N(11)	177.3(3)	O(2)–C(6)–O(1)	125.8(2)
O(2)–C(6)–C(1A)	120.4(2)	O(1)–C(6)–C(1A)	113.8(2)
C(6)–O(1)–Co(1)	114.9(2)	C(6)–O(2)–Na(1)	127.5(2)
O(4)–C(7)–O(3)	125.8(2)	O(4)–C(7)–C(4)	116.3(2)
O(3)–C(7)–C(4)	117.9(2)	O(2)–Na(1)–O(5)	92.05(8)
O(2)–Na(1)–O(8)	102.67(9)	O(5)–Na(1)–O(8)	92.55(8)
O(2)–Na(1)–O(5B)	90.93(7)	O(5)–Na(1)–O(5B)	86.54(8)
O(8)–Na(1)–O(5B)	166.39(9)	O(2)–Na(1)–O(6)	98.17(8)
O(5)–Na(1)–O(6)	168.68(8)	O(8)–Na(1)–O(6)	89.96(8)
O(5B)–Na(1)–O(6)	88.43(8)	O(2)–Na(1)–O(7)	169.09(8)
O(5)–Na(1)–O(7)	83.11(8)	O(8)–Na(1)–O(7)	87.35(9)
O(5B)–Na(1)–O(7)	79.06(8)	O(6)–Na(1)–O(7)	85.99(9)
Na(1)–O(5)–Na(1B)	93.46(8)	O(7C)–Na(2)–O(6C)	98.55(11)
O(7C)–Na(2)–O(8)	166.92(13)	O(6C)–Na(2)–O(8)	91.79(12)
O(7C)–Na(2)–O(3)	83.08(11)	O(6C)–Na(2)–O(3)	107.33(11)
O(8)–Na(2)–O(3)	101.52(11)	O(7C)–Na(2)–O(6)	79.46(10)
O(6C)–Na(2)–O(6)	90.60(10)	O(8)–Na(2)–O(6)	92.52(10)
O(3)–Na(2)–O(6)	156.65(12)		

Symmetry codes: (A) $-x$, $-y+1$, $-z+1$; (B) $-x$, $-y+2$, $-z$; (C) $-x$, $-y+1$, $-z$; (D) $-x+1$, $-y+1$, $-z$; (E) $-x+1$, $-y+1$, $-z+1$; (F) x, $y+1$, z; (G) x, y, $z-1$; (H) $-x+1$, $-y$, $-z+1$.

2,*x*-dimethyl pyridines form cobalt(III) azido complexes in solution only. This difference is definitely due to the different nature of the di-substituents in both cases. For dimethyl pyridines, the presence of a methyl group in the 2-position in the pyridine ring which is not interacting with cobalt atom, causes a steric hindrances and prevents the formation of such complexes. In case of dicarboxylic acid, the carbonyl group in position 2 in the pyridine ring takes part in the coordination of cobalt center thus forming solid cobalt(II) azido complexes whereas the carbonylate groups in 3,4- or 3,5- are far from the hetero N atom and could not form N, O chelate rings with the metal center. For 2,4-pyridine dicarboxylic acid, it may be an electronic reason that prevents the formation of solid cobalt(III) azido complex.

3.1. Structures

Perspective views of compounds **1** which is formulated as $[Co(2,3\text{-}L)_2(N_3)_2][Na_3(H_2O)_{10}]$ and **2** as $[Co(2,5\text{-}L)_2(N_3)_2][Na_3(H_2O)_8](H_2O)_2$ are given in Figs. 1 and 2 and selected bond parameters are summarized in Tables 2 and 3, respectively. Both complexes **1** and **2** are similar and crystallize in the triclinic space group $P\bar{1}$ with $Z=1$. The trivalent Co(1), located at the inversion center, is six-coordinated with *trans*-octahedral geometry. The CoN_4O_2 chromophore is formed by N(1) and O(1) in **1** and N(1) and O(1A) in **2**, respectively, donor atoms of two chelating 2,3- or 2,5-pyridine dicarboxylato anions, two (N11) atoms of mono dentate azido ligands [Co(1)–N(1) = 1.927(2), Co(1)–O(1) = 1.893(2) and Co(1)–N(11) = 1.966(2) Å for **1** and Co(1)–N(1) = 1.905(2), Co(1)–O(1A) = 1.898(2) and Co(1)–N(11) = 1.958 (2) Å for **2**]. In both complexes the chelating –COO group in position 2 is asymmetric [Δ(C–O) = 0.069(3) Å for **1** and Δ(C–O) = 0.059(3) Å for **2**], and coplanar to central pyridine ring [torsion angle N(1)–C(1)–C(6)–O(1) = 1.6(3)° (**1**) and N(1)–C(1)–C(6A)–O(1A) = 5.5(4)° (**2**)]. The non-chelating –COO groups in position 3 in complex **1** has symmetric C–O bonds and is almost perpendicular to the aromatic ring [torsion angle C(1)–C(2)–C(7)–O(3) = −89.4(3)°] whereas for that in

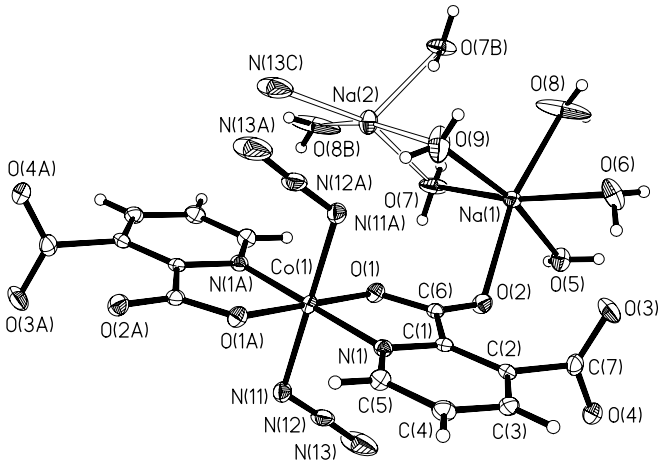

Fig. 1. Perspective view and atom labeling scheme of (**1**). Na(2) has occupancy of 0.5.

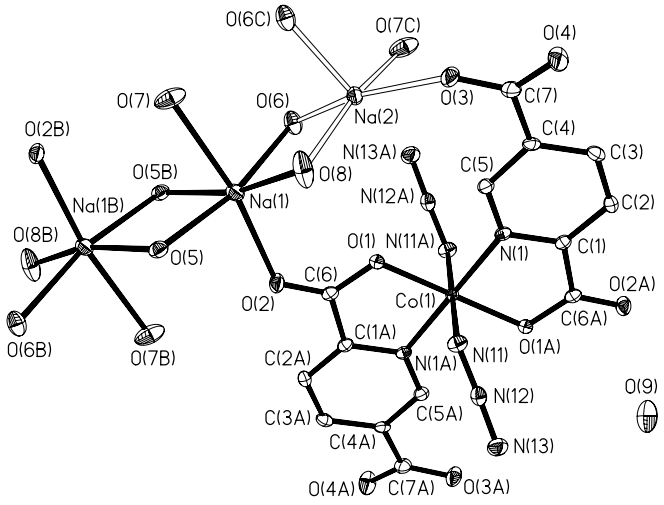

Fig. 2. Perspective view and atom labeling scheme of (**2**). Na(2) has occupancy of 0.5.

position 5 in **2** which has also symmetric C–O bonds the torsion angle C(3)–(C4)–C(7)–O(3) is −10.4(4)°. The bond parameters of the asymmetric mono-dentate azido ligand [N(11)–N(12) = 1.200(3), N(12)–N(13) = 1.146(4) Å; N(11)–N(12)–N(13) = 177.7(3)°, Co(1)–N(11)–N(12) = 116.4(2)°] in **1**, are comparable with corresponding parameters in **2** [N(11)–N(12) = 1.203(3), N(12)–N(13) = 1.154(4) Å; N(11)–N(12)–N(13) = 177.3(3)°, Co(1)–N(11)–N(2) = 116.0(2)°] and in good agreement with values reported for *mer*-[$Co(L_3)(N_3)_3$] (L = py or 4-picolinic) [10], (L = 3,4-lutidine or 3,5-lutidine) [11] or bis(ethylenediamines)cobalt(III) complexes [12]. The Co···Co separation of the monomeric $[Co(2,3\text{-}L)_2(N_3)_2]^{3-}$ complex anion is 6.879(3) Å and that of the monomeric $[Co(2,5\text{-}L)_2(N3)_2]^{3-}$ is 7.522(3) Å, Na(1), and Na(2) with occupancy 0.5, act as counter ions in both complexes. Na(1) is octahedrally coordinated by O(2) of chelating –COO groups and O atoms of five water molecules with Na(1)–O distances from 2.339(3) to 2.439(3) Å in **1** and from 2.184(3) to 2.415(3) Å in **2**. In complex **1**, the distorted tetragonal pyramids of the Na(2) are formed by N(13C) of azide group and O atoms of four water molecules with Na(2)–N(13C) = 2.421(4) Å, Na(2)–O from 2.037(4) to 2.502(3) Å. In contrast to **1**, the tetragonal pyramids of Na(2) in **2** are formed by five O atoms, O(3) of non-chelating COO^- group and O atoms of four water molecules [Na(2)–O distances from 2.184(3) to 2.425(3) Å] and two centro symmetrically related octahedra of Na(1) have a common edge [O(5) and O(5B)], thus O(9) is not coordinated to Na and acts as a lattice water molecule. Hydrogen bonds of the types O–H–O and O–H···N (Tables 2 and 3) connected the complex anions, the Na polyhedra for **1** and additionally lattice water for **2** to form supramolecular network structures.

3.2. Electronic spectra

The electronic spectra of the solid complex **1** and **2** in Nujol mull exhibited two split bands as given in Table 4. These spectra are similar to those of six-coordinate *mer*-$[CoL_3(N_3)_3]$ complexes [10,11]. The band in the range 28 000–25 000 cm^{-1} is due to $^1A_{1g} \rightarrow {}^1T_{2g}$ in a low spin octahedral cobalt(III) complexes which is not affected by lowering of the symmetry. Owing to the high intensity of this band it may be mixed with a change transfer transition. The low energy absorption band $^1A_{1g} \rightarrow {}^1T_{1g}$ in an octahedron is expected to be less intense and split to a very much greater extent in the spectra of *trans*-$[CoL_4X_2]$ than in the *cis*-isomers. The spectrum of $Co(en)_2(H_2O)$ complex shows two components for the $^1T_{1g}$ state (in O_h) [13]. Similar split is observed here with the band around 17 000–16 000 cm^{-1} due to $^1A_{1g} \rightarrow {}^1A_{2g}$ [14]. The spectra of aqueous solution of **1** and **2** exhibit also two split bands (Table 4), which are more or less similar to those of solid complexes suggesting that they retain their identity in aqueous solutions. The electronic spectra of aqueous solution of **1** and **2** are similar to that of a green filtrate obtained from the reaction

Table 4
Electronic spectral data[a]

Complex	λ_{max} (ξ)	
	NM[b]	H_2O
1	28 570vs[c,f]	28 650vbr[c,d] (14 559)
	25 136vs	24 875brs[d,f] (1586)
	16 667	17 361 (278)
	15 106sh[e]	14 970 (130)
2	26 316vs	28 500 (14 000)
		24 875 (1300)
	17 301	17 206 (230)
	15 106	14 970 (120)

[a] In cm^{-1}.
[b] Nujol mull.
[c] v = very.
[d] br = broad.
[e] sh = shoulder.
[f] s = strong.

mixture of cobalt(II) in azide ions and 3,4-pyridine dicarboxylic acid in water–acetone (2:12) solution to which a sufficient amount of solid $K_2S_2O_8$ was added and the final mixture allowed to stand one day. This observation suggests that the cobalt(III) azide complex is also formed in case of other pyridine dicarboxylic acids in acetone solutions.

3.3. IR spectra

The IR spectra (Table 5) of free acid ligands show several bands in the range 3400–1900 cm^{-1}, very similar to those observed in spectra of free pyridine mono carboxylic acids [15]. No carbonyl stretch bands are observed around 1700 cm^{-1} suggesting that the two –COOH groups are involved in strong inter- and intra-hydrogen bonds. Several ν_{as} COO^- bands in the range 1680–1600 cm^{-1} in free ligands are shifted to lower frequencies (1645–1600 cm^{-1}) in complexes confirming the coordination of the least one of the two carboxylate groups. The shift of the lower frequency bands related to pyridine nucleus evidences that the nitrogen atoms are involved in complexation of both ligands in **1** and **2**. The $\nu_{as}N_3$ appears as a very strong sharp band at 2031 and 2038 cm^{-1} for **1** and **2**, respectively. The position of this band is consistent with terminal azides in other cobalt(III) complexes [16], and the appearance for the asymmetric nature of the terminal azido ligands in **1** and **2**.

3.4. Thermal analysis

First step of decomposition of **1** from 20 to 100 °C is due to emission of H_2O, followed by a second step with further emission of H_2O up to 235 °C (3 or more superimposed peaks in MS and DTA signal). At 250 °C rapid, exothermic decomposition of sample occurs with emission of N_2 and CO_2 (step 3). An undetermined amount of solid sample was last during deflagration. For complex **2**, heating to $T > 225$ °C was avoided in order to prevent deflagration of azide (contamination of furnace and sample holder). First step is due to emission of H_2O up to 116 °C (several superimposed peaks in MS and DTA signal), followed by further emission of H_2O up to 225 °C. MS signal shows no significant emission of N_2 up to 225 °C.

Table 5
IR spectral data (cm^{-1})

2,3-H2L	1	2,5H2L	2	Assignment
3420m	3600vs	3448	3600	[νO–H···O and
3100vs	3000vs	2500s	3000	νO–H···N]
2800		1898m		
1700sh	1680	1680vs	1646	$\nu_{as}COO^-$
1571vs	1638	1628ms	1617	
	1589	1590	1595	
641	698	632m	683m	[pyridine ring]
565s	571	538		
	2031vs		2038vs	$\nu_{as}N_3$
	1339s		1337s	ν_sN_3

v = very, s = strong, m = medium, sh = shoulder.

4. Conclusion

Of six pyridine dicarboxylic acids; 2,3-, 2,4-, 2,5-, 2,6-, 3,4-, and 3,5-H_2L, we isolated only two solid cobalt(III) azido complexes of 2,3- and 2,5-H_2L. Although the other acids form cobalt(III) complexes in acetone solutions it is still questionable why no solid complex of any stoichiometry has been isolated, particularly for 2,4- and 2,6-H_2L acids. Both complexes **1** and **2** are found to contain sodium ion. Although the Na ions in **1** and **2** are surrounded by aqua molecules, there is a link between Na and one or more oxygen atoms of the carboxylato groups of H_2L acids, thus, the two metal centers are connected via the organic ligand while the azide ligand bridges only the cobalt(III) centers. Thus, alkali metal and transition metal atoms can be connected via an azido ligand or organic ligand or both azido and organic ligand. Investigations with other pseudo halides as well as other metals are in progress.

5. Supplementary material

Crystallographic data in CIF format have been deposited with the Cambridge Crystallographic Data Centre as CCDC-278125 and CCDC-278126 for **1** and **2**, respectively. Copies of the data can be obtained free of charge on application to CCDC, 12 Union Road, Cambridge, CB2 1EZ, UK (fax: +44 1233 336033; e-mail: deposit@ccdc.cam.ac.uk or http://www.ccdc.cam.ac.uk).

Acknowledgments

M.A.S. Goher thanks the Swedish International Development Cooperation Agency under the Swedish Research Links program (Grant 348-2004-5473). F.A. Mautner thanks Professor Belaj and Professor Kratky (Universität Graz), and Professor Sitte and Dr. Bucher (Montanuniversität Leoben) for assistance.

References

[1] M.A.S. Goher, M.A.M. Abu-Youssef, F.A. Mautner, Z. Naturforsch. 47b (1992) 139.
[2] M.A.S. Goher, M.A.M. Abu-Youssef, F.A. Mautner, H.P. Fritzer, Z. Naturforsch. 47b (1992) 1754.
[3] M.A.S. Goher, F.A. Mautner, A. Popitsch, Polyhedron 12 (1993) 2557.
[4] M.A.S. Goher, F.A. Mautner, Polyhedron 13 (1994) 2148.
[5] M.A.S. Goher, F.A. Mautner, Polyhedron 14 (1995) 1439.
[6] M.A.S. Goher, M.A.M. Abu-Youssef, F.A. Mautner, Z. Naturforsch. 48b (1993) 1795.
[7] M.A.M. Abu-Youssef, A. Escuer, R. Vicente, F.A. Mautner, L. Öhrstrom, M.A.S. Goher, Polyhedron 24 (2005) 557.
[8] SHELXTL/PC 5.03, Siemens Analytical Automation Inc., Madison, WI, 1995.
[9] H. Walker, D. Stuart, Acta Crystallogr. A39 (1983) 158.
[10] M.A.S. Goher, R.-J. Wang, T.C.W. Mak, Polyhedron 11 (1992) 829.

[11] M.A.S. Goher, N.A. Al-Salem, F.A. Mautner, Polyhedron 16 (1997) 3747.
[12] M.E. Kastner, D.A. Smith, A.G. Kuzmission, J.N. Cooper, T. Tyree, M. Yearick, Inorg. Chim. Acta 158 (1989) 185.
[13] M.A. Couldwell, D.A. House, J. Inorg. Nucl. Chem. 33 (1971) 2583.
[14] J. Fujita, Y. Shimura, Bull. Chem. Soc. Jpn. 36 (1963) 281.
[15] A.R. Gainsford, D.A. House, J. Inorg. Nucl. Chem. 32 (1970) 688.
[16] A.B.P. Lever, Inorganic Electronic Spectroscopy, 2nd ed., Elsevier, New York, 1984, p. 477.

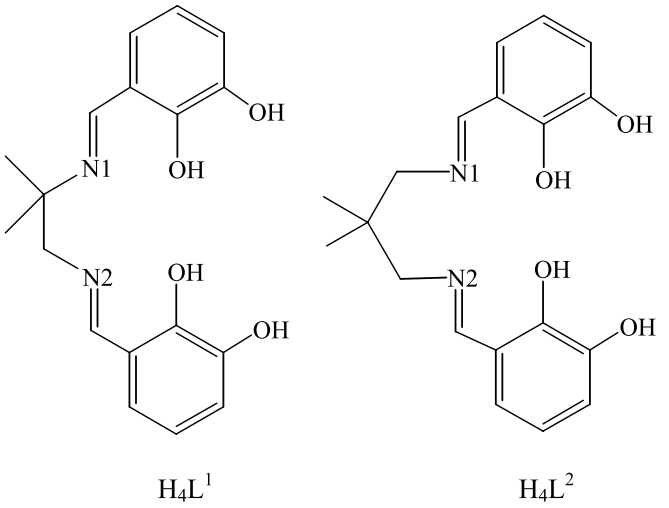

H_4L^1 H_4L^2

Scheme 1. The Schiff bases H_4L^1 and H_4L^2.

We report herein the crystal structure of two new examples of polynuclear complexes in the first category, obtained with the ligands *N*,*N*′-bis(3-hydroxysalicylidene)-2-methyl-1,2-propanediamine] (H_4L^1) and *N*,*N*′-bis(3-hydroxysalicylidene)-2,2-dimethyl-1,3-propanediamine (H_4L^2), represented in Scheme 1.

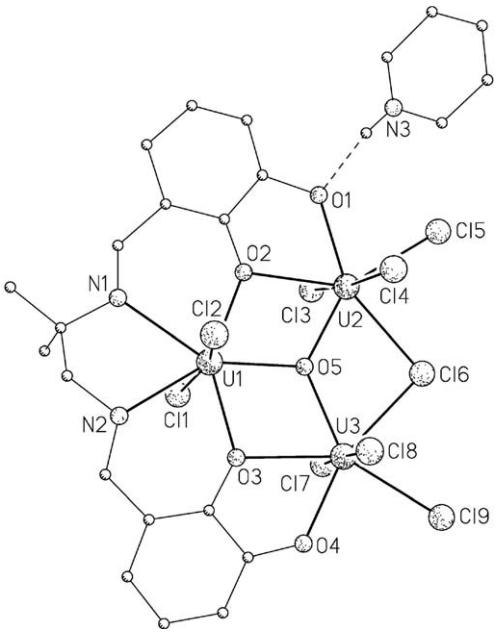

Fig. 1. View of the dianionic $\{[Hpy][U_3L^1Cl_9O]\}^{2-}$ complex in **1**. Other counter-ions, solvent molecules and hydrogen atoms are omitted for clarity. Atoms are represented as spheres, the carbon ones being arbitrarily reduced. The hydrogen bond is shown as a dashed line.

2. Results and discussion

The trinuclear compound $[Hpy]_3[U_3L^1Cl_9O] \cdot HpyCl \cdot 2py$ crystallizes in the monoclinic space group $P2_1/n$, with one complete molecule in the asymmetric unit (Fig. 1). The complex is trianionic and its charge is compensated by three pyridinium ions (a fourth pyridinium being associated with a non-coordinated chlorine atom). The atom U1 is bound to the two oxygen atoms O2 and O3 [mean value 2.292(4) Å] and the two nitrogen atoms N1 and N2 [mean value 2.53(5) Å] defining the inner site of the Schiff base. Two chlorine atoms [mean U–Cl bond length 2.653(2) Å] and the μ_3-oxo atom O5 complete the environment of U1 (Table 1). The resulting uranium hepta-coordinated environment is pentagonal bipyramidal with the two chlorine atoms Cl1 and Cl2 in apical positions. U1 is located at 0.019(8) Å from the mean plane defined by the five atoms O2, O3, O5, N1, N2 [maximum deviation 0.11(1) Å]. Atoms U2 and U3 are also hepta-coordinated, in pentagonal bipyramidal environments; both atoms are linked to two oxygen atoms of the outer site of the Schiff base (O1 and O2 for U2, O3 and O4 for U3) and they are positioned at −0.12(2) and 0.07(2) Å, respectively, from the mean plane defined by these four oxygen atoms [maximum deviation 0.139(9) Å]. Three terminal chlorine atoms (Cl3, Cl4, Cl5 for U2; Cl7, Cl8 and Cl9 for U3), the μ_2-chloro atom Cl6 [U2–Cl6–U3 90.75(18)°] and the μ_3-oxo atom O5 complete their coordination spheres. The mean planes defined by the five donor atoms in the pentagonal environment of the three uranium atoms [maximum deviation 0.15(1) Å for U2 and 0.25(1) Å for U3; displacement of the metal atom 0.001(6) Å for U2 and 0.025(6) Å for U3] define dihedral angles in the range 1.7(6)–7.5(6)°. The whole assembly, including the three uranium atoms, the N_2O_4 donor set of the Schiff base, the μ_3-oxo ion and the Cl5, Cl6 and Cl9 chlorine atoms is thus not far from planarity, as can be seen in Fig. 2 [maximum deviation 0.265(8) Å for Cl9]. The Schiff base conformation is of the *stepped* type with the two aromatic rings defining a very small dihedral angle of 9(1)° with each other and being nearly coplanar with the mean N_2O_2 inner site plane [dihedral angles 6(1)° and 14.1(9)°]. The core of the complex is made of a nearly equilateral triangle of U^{4+} ions around the central O^{2-} ion [U1···U2 3.7954(12), U1···U3 3.8119(11), U2···U3 4.0198(12) Å, U1–O5–U2 117.1(6)°, U1–O5–U3 115.0(7)°, U2–O5–U3 127.8(7)°]. A search of the Cambridge Structural Database [6] gives a mean value of 2.24(7) Å for U–O bond lengths involving μ_3-oxo groups, which is in agreement with the present value of 2.24(4) Å. One pyridinium ion is involved in a hydrogen bond with the oxygen atom O1 of the ligand [N3···O1 2.74(3), N3–H 0.86, H···O1 1.89 Å, N3–H···O1 167°] and two other ones with pyridine molecules [N4···N5 2.82(3), N4–H 0.86, H···N5 1.97 Å, N4–H···N5 171°; N7···N8 2.82(3), N7–H 0.86, H···N8 1.98 Å, N7–H···N8 167°]. A fourth pyridinium ion, associated with a chlorine atom, is also present as an independent group [N6···Cl 10 3.00(3), N6–H 0.86, H···Cl 10 2.14 Å, N6–H···Cl 10 176°].

The compound $[U_4(L^2)_2(H_2L^2)_2(py)_2O][CF_3SO_3]_2$ (**2**) crystallizes in the monoclinic space group $C2/c$, with only half a molecule in the asymmetric unit, the other half being

Table 1
Environment of the uranium atoms in compounds **1** and **2**: selected bond lengths (Å) and angles (°)

1							
U1–O2	2.296(15)	O2–U1–N1	75.9(6)	U2–O1	2.262(14)	O1–U2–O2	65.5(5)
U1–O3	2.287(13)	N1–U1–N2	67.1(6)	U2–O2	2.489(14)	O2–U2–O5	67.6(5)
U1–O5	2.247(15)	N2–U1–O3	73.8(5)	U2–O5	2.203(15)	O5–U2–Cl6	72.3(4)
U1–N1	2.580(18)	O3–U1–O5	73.1(5)	U2–Cl3	2.633(6)	Cl6–U2–Cl5	78.2(2)
U1–N2	2.479(17)	O5–U1–O2	70.4(5)	U2–Cl4	2.680(6)	Cl5–U2–O1	77.1(4)
U1–Cl1	2.655(6)	Cl1–U1–Cl2	164.27(19)	U2–Cl5	2.725(6)	Cl3–U2–Cl4	172.5(2)
U1–Cl2	2.651(6)			U2–Cl6	2.762(6)		
U3–O3	2.547(14)	O3–U3–O4	64.3(5)				
U3–O4	2.211(14)	O3–U3–O5	67.9(5)				
U3–O5	2.273(13)	O5–U3–Cl6	69.0(4)				
U3–Cl6	2.885(7)	Cl6–U3–Cl9	77.23(17)				
U3–Cl7	2.627(6)	Cl9–U3–O4	83.4(4)				
U3–Cl8	2.650(6)	Cl7–U3–Cl8	177.6(2)				
U3–Cl9	2.682(5)						
2							
U1–O2A	2.307(11)	O2A–U1–N1A	73.8(4)	U2–O1A	2.188(11)	O1B–U2–O2B	64.2(4)
U1–O3A	2.291(9)	N1A–U1–N2A	73.1(5)	U2–O2A	2.574(10)	O2B–U2–O3B	69.6(3)
U1–O3A′	2.553(10)	N2A–U1–O3A	74.0(4)	U2–O1B	2.619(10)	O3B–U2–O4B	65.7(4)
U1–O4A′	2.209(10)	O3A–U1–O2A	140.3(4)	U2–O2B	2.367(10)	O4B–U2–O1B	65.8(3)
U1–O1B′	2.370(11)	O4A′–U1–O3A′	65.4(3)	U2–O3B	2.367(9)	O1A–U2–N1	79.9(4)
U1–N1A	2.554(12)	O3A′–U1–O1	64.9(3)	U2–O4B	2.502(10)	N1–U2–O1	96.4(4)
U1–N2A	2.526(13)	O1–U1–O1B′	71.5(3)	U2–O4B′	2.404(10)	O1–U2–O4B′	70.3(3)
U1–O1	2.369(8)	O1B′–U1–O4A′	156.9(4)	U2–O1	2.335(8)	O4B′–U2–O1A	86.6(4)
				U2–N1	2.732(14)		

Symmetry code: $' = -x, y, 0.5 - z$.

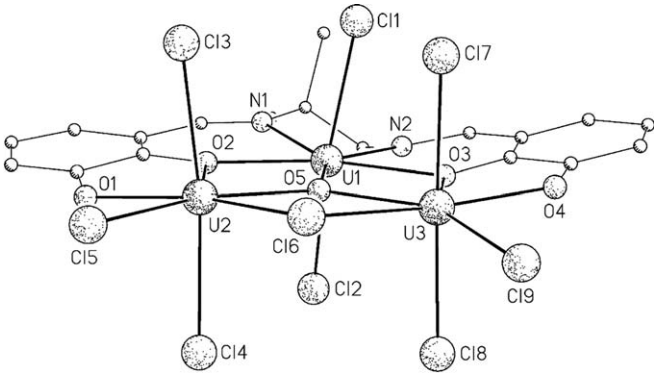

Fig. 2. View along the plane of the Schiff base of the trianionic $[U_3L^1Cl_9O]^{3-}$ moiety in **1**. Counter-ions, solvent molecules and hydrogen atoms are omitted for clarity. Atoms are represented as spheres, the carbon ones being arbitrarily reduced.

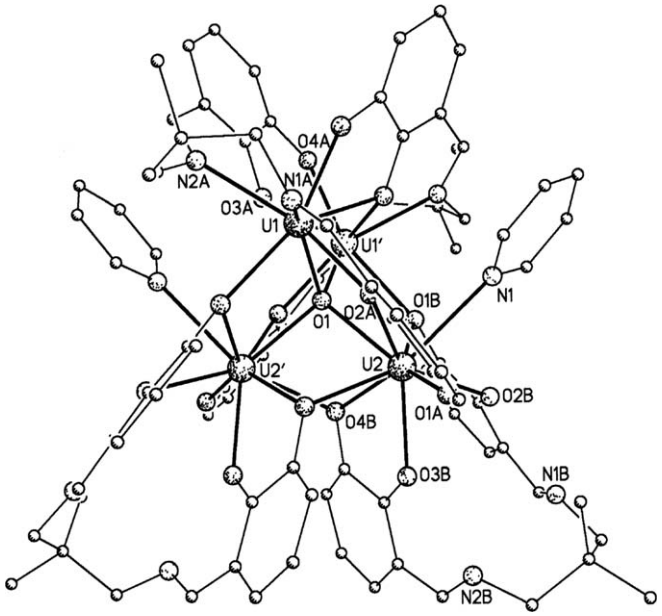

Fig. 3. View of the dicationic $[U_4(L^2)_2(H_2L^2)_2(py)_2O]^{2+}$ complex in **2**. Hydrogen atoms and counter-ions are omitted for clarity. Atoms are represented as spheres, the carbon ones being arbitrarily reduced. Symmetry code: $' = -x, y, 0.5 - z$.

generated by the binary axis (Fig. 3). The complex itself is dicationic, which, considering the presence of a central μ_4-oxo ion, implies that four protons are still attached to the Schiff bases. The two independent uranium atoms are in different environments, as shown in Fig. 4. The atom U1 is bound to the two oxygen atoms O2A and O3A and two nitrogen atoms N1A and N2A defining the inner site of the Schiff base labelled A, whereas the atom U2 is bound to the four oxygen atoms O1B–O4B defining the outer site of the second Schiff base, labelled B. The Schiff base A and the symmetry related molecule A′ ensure the assembly of U1 and U1′ through the bridging oxygen atoms O3A and O3A′ and the terminal hydroxy groups O4A and O4A′ which are linked to U1′ and U1, respectively. The uranium atoms U2 and U2′ are associated by the Schiff bases B and B′ via the bridging oxygen atoms O4B and O4B′. Both Schiff bases A and B are involved in the association of U1, U1′, U2 and U2′, with the bridging oxygen atoms

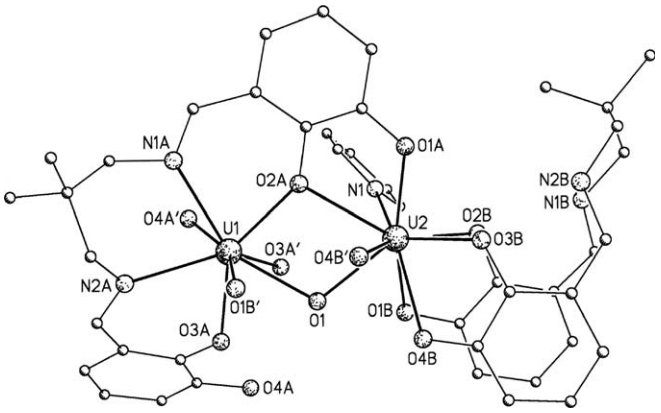

Fig. 4. View of the environment of the uranium atoms in the asymmetric unit in **2**. Atoms are represented as spheres, the carbon ones being arbitrarily reduced. Symmetry code: $' = -x, y, 0.5 - z$.

O2A and O1B, the terminal hydroxy group O1A and their symmetry equivalents. Finally, the four uranium atoms are linked by the μ_4-oxo atom O1. The eight-coordinate U1 atom adopts a dodecahedral configuration [7] defined by the two nearly orthogonal trapezia O2A, N1A, N2A, O3A and O4A′, O3A′, O1, O1B′ [dihedral angle 88.3(2)°]. Because of the coordination of an extra pyridine molecule, U2 is nine-coordinate and its environment can be described as a capped square antiprism with the two sets of atoms O1B, O2B, O3B, O4B and O1A, N1, O1, O4B′ defining the bases [dihedral angle 5.6(7)°] and O2A in capping position [7]. The mean U1–N and the U2–N1 (pyridine) bond lengths, 2.54(2) and 2.732(14) Å respectively, are unexceptional. The U1–O4A′ and U2–O1A bond lengths, which involve non-bridging oxygens, are typically short [mean value 2.199(15) Å] while U2–O2B and U2–O3B [2.367(10) Å] are significantly longer, indicating that the remaining protons are likely to be located on these two oxygen atoms. The bridging oxygen atoms are all involved in dissymmetric bonds, one of them shorter than the other, with the corresponding ranges 2.291(9)–2.404(10) and 2.502(10)–2.619(10) Å; such differences have been observed in some of the structures reported previously [2b,2c]. Finally, the bond lengths involving the μ_4-oxo atom O1 [mean value 2.35(2) Å] are similar to those of the other two reported cases [2.40(9) and 2.36(10) Å] [2a,4c] while the U–O1–U angles span the range 102.7(5)–113.67(2)°. It may be noted that a μ_6-oxo group is present in the U(V) hexanuclear isopolyoxometalate complex reported by Duval et al. with a mean U–O bond length of 2.6(1) Å [4b].

The two Schiff bases in **2** present very different conformations. Molecule A does not match exactly the usual *boat* (*umbrella*) or *stepped* conformations [8] since the mean plane defined by the aromatic ring bearing O1A and O2A is close to the N_2O_2 mean plane defined by the four donor atoms of the inner site [maximum deviation 0.237(7) Å] with a dihedral angle of 13.4(7)°, while the other aromatic ring, bearing O3A and O4A, is more tilted, with a dihedral angle of 39.8(6)°. However, this conformation is not far from that generally observed when the inner site-coordinated uranium atom is close to the N_2O_2 mean plane [out-of-plane displacement 0.113(6) Å in **2**], the distorsions being likely due to the distinct attachment of the four oxygen atoms O1–O4 to the metal centres. The second ligand presents a more unusual conformation which is a borderline case of the *umbrella* shape, in which the two aromatic rings are facing each other, with a dihedral angle of 24.8(6)°. The Schiff base, which roughly admits a pseudo-mirror plane, thus appears as if folded around its middle line. As a result, the four oxygen atoms of the outer site define a mean plane with a maximum deviation of 0.138(5) Å. but, at variance with U1 and ligand A, atom U2 is expelled at a distance of 1.561(5) Å from this plane; the two nitrogen atoms of this molecule are the only ones among all the donor atoms of both ligands to be un-coordinated. The centroids of the two aromatic rings facing each other are separated by 3.89 Å, which could indicate the presence of a weak π–π interaction. The Cambridge Structural Database [6] gives several examples of such conformations, with different kinds of folding around the diimino bridge, leading to inter-centroid distances lower than 4 Å, some of them for triatomic diimino bridges comparable to that in **2** [9], but the largest number for longer bridges [10]. As a further difference between molecules A and B, it may be noted that the non-bridging oxygens are the external ones in A and the internal ones (protonated) in B. The four uranium centres are arranged so as to form a slightly distorted tetrahedron encompassing the central μ_4-oxo atom (Fig. 5), with U···U distances and U···U···U angles in the range 3.6465(14)–3.9373(9) Å and 55.44(2)–62.774(16)°, respectively. The edges of the tetrahedron cor-

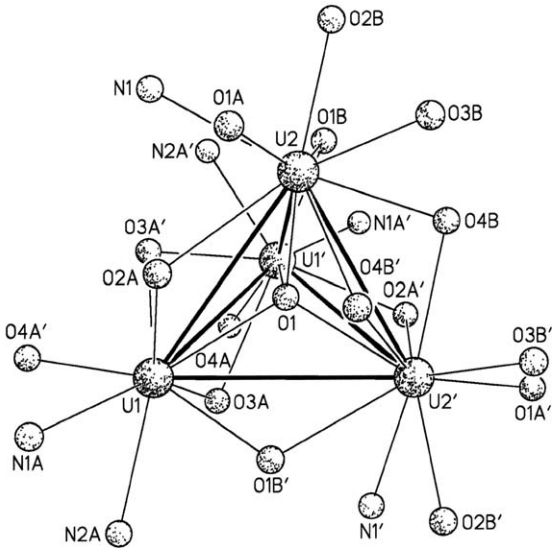

Fig. 5. View of the uranium atoms and their environment in **2**. The μ_4-oxo-centered U_4 tetrahedron is highlighted. Symmetry code: $' = -x, y, 0.5 - z$.

respond either to double (U1···U1′ and U2···U2′) or simple (all other edges) oxygen bridging.

In contrast with the symmetric or pseudo-symmetric elongated tetra- or hexanuclear complexes which are built from di- or trinuclear subunits [2b,2c], respectively, the more compact arrangement associated with convergent Schiff bases leads to more tightly packed uranium assemblages with unusual geometries, since a cubane-type U_4O_4 motif was present in the octa-nuclear complex aforementioned (in which the eight uranium centres were arranged as four edge-sharing, oxo-centered tetrahedra) [2a] whereas a single triangle or tetrahedron is observed in the present cases. It is to be noted that, in these cases and in contrast with the elongated assemblages, these globular polyuranium assemblies are held by μ_3-oxo or μ_4-oxo groups resulting from adventitious traces of water and/or oxygen present during the synthesis, which are effective in promoting these architectures containing tightly packed uranium assemblages.

3. Experimental

3.1. Synthesis

[Hpy]$_3$[U$_3$L^{1}Cl$_9$O] · HpyCl · 2py (***1***). UCl_4 was synthesized as reported in the literature [11]. H_4L^1 was mixed in a 1:1 ratio with UCl_4 in pyridine. Adventitious traces of oxygen and/or water probably entered the reaction flask during prolonged heating at 110 °C, which resulted in the formation of yellow crystals of the trinuclear U^{IV} compound $[Hpy]_3[U_3L^1Cl_9O] \cdot HpyCl \cdot 2py$ (**1**).

[U$_4$(L^2)$_2$(H$_2$L^2)$_2$(py)$_2$O][CF$_3$SO$_3$]$_2$ (***2***). $U(OTf)_3$, where OTf is trifluoromethanesulfonate, was synthesized as reported in the literature [12]. The copper complex CuH_2L^2 was synthesized by reaction of H_4L^2 with 1 mol equiv. of $Cu(acac)_2$ in tetrahydrofuran. This mononuclear metal complex was mixed in a 1:1 ratio with $U(OTf)_3$ in pyridine. Adventitious traces of oxygen and/or water probably entered the reaction flask during prolonged heating at 80 °C, which resulted in the formation of red crystals of the tetranuclear U^{IV} compound $[U_4(L^2)_2(H_2L^2)_2(py)_2O][CF_3SO_3]_2$ (**2**) following the substitution of Cu for U. Attempts to prepare this complex in a controlled way, by introducing measured quantities of water into the reaction mixture, were unsuccessful.

3.2. Crystallography

Data were collected at 100(2) K on a Nonius Kappa-CCD area detector diffractometer [13] using graphite monochromated Mo Kα radiation ($\lambda = 0.71073$ Å) and processed with DENZO-SMN [14]. The structures were solved by direct methods with SHELXS-97 and refined by full-matrix least-squares on F^2 with SHELXL-97 [15]. Absorption effects were empirically corrected with the program DELABS from PLATON [16]. All non-hydrogen atoms were refined with anisotropic displacement parameters.

Table 2
Crystal data and structure refinement details

	1	**2**
Empirical formula	$C_{48}H_{50}Cl_{10}N_8O_5U_3$	$C_{88}H_{86}F_6N_{10}O_{23}S_2U_4$
M (g mol^{-1})	1887.55	2781.91
Crystal system	monoclinic	monoclinic
Space group	$P2_1/c$	$C2/c$
a (Å)	18.5136(16)	26.622(3)
b (Å)	14.2363(9)	27.442(3)
c (Å)	22.8774(14)	20.187(2)
α (°)	90	90
β (°)	95.202(5)	118.238(4)
γ (°)	90	90
V (Å^3)	6004.9(7)	12992(2)
Z	4	4
D_{calc} (g cm^{-3})	2.088	1.422
μ (Mo Kα) (mm^{-1})	8.565	5.067
$F(000)$	3520	5288
Crystal size (mm)	$0.17 \times 0.12 \times 0.08$	$0.12 \times 0.10 \times 0.05$
Reflections collected	34 542	41 703
Independent reflections	9678	11 982
Observed reflections [$I > 2\alpha(I)$]	6775	4762
R_{int}	0.152	0.080
Parameters refined	645	604
R_1	0.092	0.073
wR_2	0.196	0.163
S	1.071	0.915
$\Delta\rho_{min}$ (e Å^{-3})	−1.23	−1.06
$\Delta\rho_{max}$ (e Å^{-3})	1.42	0.74

Due to the rather low quality of the crystals, and hence the data, for compound **1**, some restraints on displacement parameters had to be applied for several badly behaving atoms, particularly in the pyridinium ions and pyridine solvent molecules. Some restraints on displacement parameters were also applied for the O, C and F atoms of the CF_3SO_3 moiety in compound **2**. The hydrogen atoms were introduced at calculated positions (except the phenolic ones in compound **2**, which were not found on Fourier-difference maps) and were treated as riding atoms with an isotropic displacement parameter equal to 1.2 (CH, CH_2) or 1.5 (CH_3) times that of the parent atom. The molecular plots were drawn with SHELXTL [17]. Crystal data and structure refinement details are given in Table 2.

4. Supplementary material

Crystallographic data for the structural analysis have been deposited with the Cambridge Crystallographic Data Centre, CCDC Nos. 285357 and 285358. Copies of this information may be obtained free of charge from The Director, CCDC, 12 Union Road, Cambridge CB2 1EZ, UK (fax: +44 1223 336033; e-mail: deposit@ccdc.cam.ac.uk or www: http://www.ccdc.cam.ac.uk).

References

[1] (a) J. Sanmartín, M.R. Bermejo, A.M. García-Deibe, A.L. Llamas-Saiz, Chem. Commun. (2000) 795;
(b) J. Sanmartín, M.R. Bermejo, A.M. García-Deibe, I.M. Rivas, A.R. Fernández, J. Chem. Soc., Dalton Trans. (2000) 4174.

[2] (a) L. Salmon, P. Thuéry, M. Ephritikhine, Polyhedron 23 (2004) 623;
(b) L. Salmon, P. Thuéry, M. Ephritikhine, J. Chem. Soc., Dalton Trans. (2004) 1635;
(c) L. Salmon, P. Thuéry, M. Ephritikhine, J. Chem. Soc., Dalton Trans. (2004) 4139.
[3] (a) T. Le Borgne, E. Rivière, J. Marrot, P. Thuéry, J.J. Girerd, M. Ephritikhine, Chem. Eur. J. 8 (2002) 774;
(b) L. Salmon, P. Thuéry, E. Rivière, J.J. Girerd, M. Ephritikhine, Chem. Commun. (2003) 762;
(c) L. Salmon, P. Thuéry, E. Rivière, J.J. Girerd, M. Ephritikhine, J. Chem. Soc., Dalton Trans. (2003) 2872;
(d) L. Salmon, P. Thuéry, E. Rivière, M. Ephritikhine, Inorg. Chem. (in press).
[4] (a) J. Rebizant, M.R. Spirlet, C. Apostolidis, Acta Crystallogr., Section C 48 (1992) 452;
(b) L.M. Mokry, N.S. Dean, C.J. Carrano, Angew. Chem., Int. Ed. 35 (1996) 1497;
(c) P.B. Duval, C.J. Burns, D.L. Clark, D.E. Morris, B.L. Scott, J.D. Thompson, E.L. Werkema, L. Jia, R.A. Andersen, Angew. Chem., Int. Ed. 40 (2001) 3358;
(d) L. Moisan, T. Le Borgne, P. Thuéry, M. Ephritikhine, Acta Crystallogr., Section C 58 (2002) 98;
(e) J.C. Berthet, M. Nierlich, Y. Miquel, C. Madic, M. Ephritikhine, Dalton, Trans. (2005) 369.
[5] (a) A. Immirzi, G. Bombieri, S. Degetto, G. Marangoni, Acta Crystallogr., Section B 31 (1975) 1023;
(b) A.J. Zozulin, D.C. Moody, R.R. Ryan, Inorg. Chem. 21 (1982) 3083;
(c) P. Charpin, M. Lance, M. Nierlich, D. Vignier, J. Livet, C. Musikas, Acta Crystallogr., Section C 42 (1986) 1691;
(d) G. Van Den Bossche, M.R. Spirlet, J. Rebizant, J. Goffart, Acta Crystallogr., Section C 43 (1987) 837;
(e) D. Rose, Y.D. Chang, Q. Chen, J. Zubieta, Inorg. Chem. 33 (1994) 5167;
(f) P. Thuéry, M. Nierlich, B. Souley, Z. Asfari, J. Vicens, J. Chem. Soc., Dalton Trans. (1999) 2589;
(g) P. Thuéry, M. Nierlich, B.W. Baldwin, N. Komatsuzaki, T. Hirose, J. Chem. Soc., Dalton Trans. (1999) 1047;
(h) M.P. Wilkerson, C.J. Burns, H.J. Dewey, J.M. Martin, D.E. Morris, R.T. Paine, B.L. Scott, Inorg. Chem. 39 (2000) 5277;
(i) P. Thuéry, B. Masci, Supramol. Chem. 15 (2003) 95;
(j) P. Thuéry, B. Masci, Polyhedron 22 (2003) 3499;
(k) P. Thuéry, C. Villiers, J. Jaud, M. Ephritikhme, B. Masci, J. Am. Chem. Soc. 126 (2004) 6838;
(l) B. Masci, P. Thuéry, New J. Chem. 29 (2005) 493.
[6] A.F.H. Allen, Acta Crystallogr., Section B 58 (2002) 380.
[7] (a) M.G.B. Drew, Coord. Chem. Rev. 24 (1977) 179;
(b) D.L. Kepert, Inorganic Stereochemistry, Heidelberg, Springer-Verlag, 1982.
[8] G. Bandoli, D.A. Clemente, U. Croatto, M. Vidali, P.A. Vigato, J. Chem. Soc., Dalton Trans. (1973) 2331.
[9] (a) N.A. Bailey, D.E. Fenton, P.B. Roberts, A.M. Walford, J. Chem. Soc., Dalton Trans. (1987) 1865;
(b) S.S. Tandon, V. McKee, J. Chem. Soc., Dalton Trans. (1989) 19;
(c) A.J. Atkins, A.J. Blake, M. Schröder, Chem. Commun. (1993) 353;
(d) H. Aneetha, C.R.K. Rao, K.M. Rao, P.S. Zacharias, X. Feng, T.C.W. Mak, B. Srinivas, M.Y. Chiang, J. Chem. Soc., Dalton Trans. (1997) 1697;
(e) M. Sánchez, H. Höpfl, M.E. Ochoa, N. Farfán, R. Santillan, S. Rojas, Inorg. Chem. 40 (2001) 6405.
[10] (a) P.D. Cradwick, M.E. Cradwick, G.G. Dodson, D. Hall, T.N. Waters, Acta Crystallogr., Section B 28 (1972) 45;
(b) E.M. Holt, S.L. Holt, M. Vlasse, Cryst. Struct. Commun. 8 (1979) 645;
(c) A. Nishinaga, H. Tomita, K. Nishizawa, T. Matsuura, S. Ooi, K. Hirotsu, J. Chem. Soc., Dalton Trans. (1981) 1504;
(d) E.G. Alyea, T.D. Dee, G. Ferguson, J. Crystallogr. Spectrosc. Res. 15 (1985) 29;
(e) U. Casellato, P. Guerriero, S. Tamburini, P.A. Vigato, R. Graziani, Inorg. Chim. Acta 119 (1986) 75;
(f) M.N. Tahir, D. Ulku, H. Nazir, O. Atakol, Acta Crystallogr., Section C 53 (1997) 181.
[11] J.A. Hermann, J.F. Suttle, Inorg. Synth. 5 (1957) 143.
[12] J.C. Berthet, M. Lance, M. Nierlich, M. Ephritikhine, Eur. J. Inorg. Chem. (1999) 2005.
[13] Kappa-CCD Software, Nonius BV, Delft, 1998.
[14] Z. Otwinowski, W. Minor, Methods Enzymol. 276 (1997) 307.
[15] G.M. Sheldrick, SHELXS-97 and SHELXL-97, University of Göttingen, Göttingen, 1997.
[16] A.L. Spek, PLATON, University of Utrecht, 2000.
[17] G.M. Sheldrick, SHELXTL, Version 5.1, Bruker AXS Inc., Madison, WI, 1999.

for the difference in affinity of ruthenium for hydrogen sulfide and dimethyl sulfide ligands, this effect has been elegantly applied to explain some unusual features of sulfur based metal complexes including the questions related to the competitive catalysts for metal sulfur enzymes [10].

The 1,4-dithiane (1,4-dt) ligand can bind to a metal center via a variety of bonding modes. This versatility of 1,4-dt is attributed to the presence of two S atoms and its proximity. The large size of the S atom makes it easier to adopt different angles at this atom in complexes, which is necessary for different geometries. The 1,4-dithiane can function as a chelating ligand for a single metal center, as a monodentate or yet as bridged ligand in binuclear species [11]. The literature reports that the chair conformation of the 1,4-dt species is preferred [12,13]. Probably, this is the reason why a very few X-ray structures of compounds containing the 1,4-dt molecule as a bidentate ligand are noticed [14–17].

In this work, we present the first example of a metal center system that form complexes with the 1,4-dithiane acting as bidentate, monodentate and bridged ligand. The electrochemical, spectroscopic and crystallographic data of such complexes highlights the conformational versatility of this ligand towards the coordination chemistry.

2. Experimental

2.1. Materials

All manipulations were carried out under argon atmosphere using Schlenk techniques. The solvents were purified according to standard procedures [18]. The water used throughout was purified by a Milli-Q system (Millipore Co.). The *mer*-[$Ru^{III}Cl_3$(dppb)H_2O] and [$Ru^{II}Cl_2$(dppb)-PPh_3] (dppb = 1,4-bis(diphenylphosphino)butane, PPh_3 = triphenylphosphine) complexes were prepared according to the literature [19,20]. Tetrabutylammonium perchlorate (TBAP) was purchased from Fluka, recrystallized twice from absolute ethanol solution, filtered and dried under vacuum. All other chemicals of reagent grade were used as received.

2.1.1. *trans*-[$RuCl_2$(dppb)(1,4-dt)]

trans-[$RuCl_2$(dppb)(1,4-dt)] complex was synthesized from the [$RuCl_2$(dppb)PPh_3] (0.100 g, 0.12 mmol) and 1,4-dt (0.014 g, 0.12 mmol) at room temperature in 5 mL of dichloromethane. The mixture was stirred under argon during 30 min and the resulting solution was reduced to near 1 mL volume. The product was precipitated by the addition of diethyl ether, separated by filtration, washed with diethyl ether and dried under vacuum. Yield: 40.0 mg, 80%. *Anal.* Calc. for $C_{32}H_{36}Cl_2P_2S_2Ru$, fw.: 718.69; C, 53.48; H, 5.05; S, 8.92. Found: C, 53.27; H, 5.06; S, 8.87%.

Recrystallization of *trans*-[$RuCl_2$(dppb)(1,4-dt)] from dichloromethane/diethyl ether solution yielded yellow crystals suitable for single crystal X-ray analysis. Crystal data and structure refinement for this complex are summarized in Table 1.

Table 1
Crystal data and structure refinement for the *trans*-[$RuCl_2$(dppb)(1,4-dt)] complex

Empirical formula	$C_{32}H_{36}Cl_2P_2S_2Ru$
Formula weight	718.69
Temperature (K)	120(2)
Wavelength (Å)	0.71073
Crystal system	monoclinic
Space group	$P2_1/c$
Unit cell dimensions	
a (Å)	10.7020(1)
b (Å)	12.0660(1)
c (Å)	26.5840(3)
β (°)	99.57(1)
Volume (Å^3)	3385.06(6)
Z	2
D_c (Mg m^{-3})	1.577
Absorption coefficient (mm^{-1})	1.021
F(000)	1640
Crystal size (mm^3)	$0.20 \times 0.04 \times 0.04$
θ Range for data collection (°)	1.55–25.00
Index ranges	$-12 \leqslant h \leqslant 12$, $-14 \leqslant k \leqslant 14$, $-31 \leqslant l \leqslant 31$
Reflections collected	11 543
Independent reflections [R_{int}]	5957 [0.0215]
Completeness to $\theta = 25.00°$	100.0%
Maximum and minimum transmission	0.9603 and 0.8219
Refinement method	full-matrix least-squares on F^2
Data/parameters	5957/406
Goodness-of-fit on F^2	1.171
Final R indices [$I > 2\sigma(I)$]	$R_1 = 0.0373$, $wR_2 = 0.1077$
R indices (all data)	$R_1 = 0.0581$, $wR_2 = 0.1534$
Largest difference peak and hole (e Å^{-3})	1.104 and −2.421

2.1.2. *mer*-[$RuCl_3$(dppb)(1,4-dt)]

mer-[$RuCl_3$(dppb)(1,4-dt)] complex was prepared from *mer*-[$RuCl_3$(dppb)H_2O] (0.100 g, 0.15 mmol) and 1,4-dt (0.039 g, 0.32 mmol) dissolved in CH_2Cl_2 (10 mL) with stirring for 12 h, at room temperature. The resulting red dark solution was reduced to near 1 mL volume, by rotary evaporation. A red solid was obtained by the addition of diethyl ether, which was separated by filtration, washed with diethyl ether, and dried and stored under vacuum. Yield: 98.0 mg, 85%. *Anal.* Calc. for $C_{32}H_{36}Cl_3P_2RuS_2$, fw. 754.16; C, 50.96; H, 4.81; S, 8.50. Found: C, 50.85; H, 4.86; S, 8.54%.

2.1.3. [{$RuCl_3$(dppb)}$_2$(μ-(1,4-dt))]

The [{$RuCl_3$(dppb)}$_2$(μ-(1,4-dt))] binuclear complex was obtained from stoichiometric amounts (1:1) of *mer*-[$RuCl_3$(dppb)H_2O] (0.100 g, 0.15 mmol) and *mer*-[$RuCl_3$-(dppb)(1,4-dt)] (0.115 g, 0.15 mmol) dissolved in CH_2Cl_2 (10 mL), with stirring for 12 h, at room temperature. The solution was then reduced to near 3 mL volume, followed by the addition of diethyl ether (10 mL) to form of a red-violet precipitate that was collected, washed with diethyl ether, dried and stored under vacuum in the absence of light. Yield: 190.0 mg, 89%. *Anal.* Calc. for $C_{60}H_{64}Cl_6P_4$-Ru2S_2, fw. 1388.08; C, 51.92; H, 4.65; S: 4.62. Found: C, 51.89; H, 4.68; S, 4.59%.

2.2. Apparatus

Single crystals were used for data collection and cell parameter determination on an Enraf–Nonius Kappa-CCD diffractometer, using Mo Kα radiation ($\lambda = 0.71073$ Å). Data collection was made by using the COLLECT program [21]; integration and scaling of the reflections were performed with the HKL Denzo-Scalepack system of programs [22]. Absorption corrections were carried out by using the multi-scan method [23]. The structure was solved by direct methods with SHELXS-97 [24]. The models were refined by full-matrix least-squares on F^2 with SHELXL-97 [25]. All the hydrogen atoms were stereochemically positioned and refined with the riding model [26]. The NMR spectra were obtained in a T BRUKER DRX400 spectrometer at 298 K, using H_3PO_4 85% as external reference for $^{31}P\{^1H\}$ (161 MHz). Elemental analyses were performed on a Fison equipment, EA 1108 model. The electrochemical experiments were carried out at room temperature in freshly distilled dichloromethane containing 0.1 mol L^{-1} TBAP under argon atmosphere. These measurements were performed by using an electrochemical analyzer from Bioanalytical Systems Inc. (BAS), model 100BW, at 25 ± 0.2 °C. A conventional electrochemical glass cell of one compartment containing three electrodes and two gas inlets was used in these experiments. A platinum foil and a pseudo-reference Ag/AgCl electrode prepared at the working day, 1 h before the experiments beginning, were used as working and auxiliary electrodes, respectively. The electrochemical potentials reported in this study were all converted to the normal hydrogen electrode (NHE), based on the ferrocene/ferrocenium ($Fc^{+/0}$) redox couple in CH_2Cl_2, as reported by Koelle et al. [27]. The transmission infrared spectra of the isolated species dispersed in CsI were obtained by using a BOMEM MICHELSON instrument, model 102. The electronic spectra, acquired on a HP8452A spectrophotometer, were obtained in CH_2Cl_2 solutions.

3. Results and discussion

The characterization of the *trans*-[$RuCl_2$(dppb)(1,4-dt)], *mer*-[$RuCl_3$(dppb)(1,4-dt)] and [{$RuCl_3$(dppb)}$_2$(μ-(1,4-dt))] complexes was carried out by cyclic voltammetry, electronic, infrared, NMR and EPR spectroscopies and X-ray diffraction when it was possible.

The very intense infrared absorption of the free 1,4-dt molecule at 664 cm^{-1}, which is assigned to the C–S stretching mode [12], shifts to lower frequency (650 cm^{-1}) and dramatically decreases in intensity in the spectra of the *trans*-[$RuCl_2$(dppb)(1,4-dt)] and [{$RuCl_3$(dppb)}$_2$(μ-(1,4-dt))] complexes. Similar behavior was observed for some similar systems [28,29]. These downshifts would suggest that in these complexes the 1,4-dithiane ligand is coordinated through both sulfur atoms to the metal center. On the other hand, the IR spectrum of the *mer*-[$RuCl_3$(dppb)-(1,4-dt)] complex shows two bands at 668 and 655 cm^{-1} assigned to the C–S stretching modes of the 1,4-dt non-coordinated and coordinated to the Ru(III) ion, respectively [12]. Based on similar systems, these observations suggest that the 1,4-dt is coordinated through only one sulfur atom to the ruthenium in the *mer*-[$RuCl_3$(dppb)(1,4-dt)] complex [28]. For the *trans*-[$RuCl_2$(dppb)(1,4-dt)] complex, the Ru–Cl stretching frequency (*ν*Ru–Cl) is observed at 260 cm^{-1}. The presence of only one *ν*Ru–Cl band suggests the *trans* configuration for this complex. Conversely, two *ν*Ru–Cl bands would be expected for the *cis* configuration [30].

The X-ray structure of the *trans*-[$RuCl_2$(dppb)(1,4-dt)] complex clearly shows that the 1,4-dt ligand is coordinated in a bidentate mode to the ruthenium atom, in a distorted octahedron with the metal on a twofold axis with a *trans* configuration of the Cl atoms with the sulfur atoms necessarily *trans* to the phosphorous atoms (Fig. 1). The 1,4-dt molecule normally exists in a C_{2h} conformation similar to the chair form of cyclohexane [13]. The D_2 form of this molecule, similar to a boat, has not been detected in any appreciable amount of complexes since it has a relative unstable energy level, 5 kcal mol^{-1} higher than the C_{2h} form [12]. Despite the energy difference between the C_{2h} and D_2 configurations, the crystallographic data point for the 1,4-dt D_2 conformer in the *trans*-[$RuCl_2$(dppb)(1,4-dt)] complex, where 1,4-dt acts as a bidentate ligand. The relevant interatomic bond lengths and angles are listed in Table 2.

As expected for a relatively soft Ru (II) center, the Ru–P distances (2.297(1) and 2.317(1) Å) are shorter than the Ru–S distances (2.404(1) and 2.444(1) Å). The Ru–S, Ru–P and Ru–Cl bond lengths (Table 2) are within the well established range for Ru(II) complexes [31,32]. The S–C distances (ca. 1.824 Å) of the coordinated ligand are slightly elongated compared with the free 1,4-dt molecule (ca. 1.811 Å) [12]. The C–C bonds of the coordinated

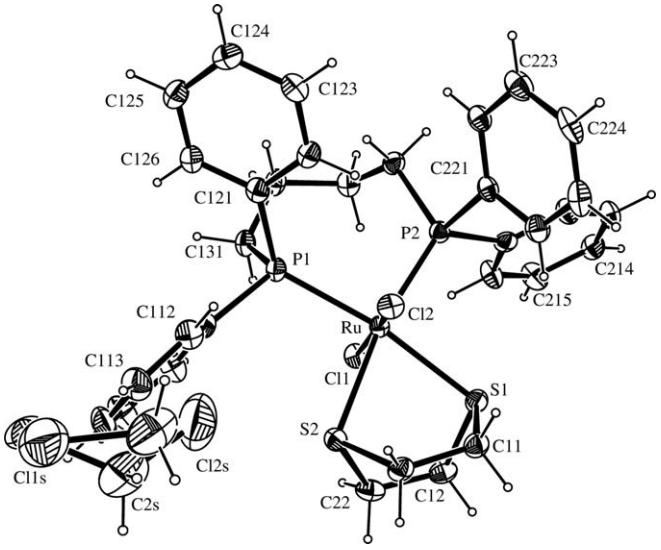

Fig. 1. ORTEP view of the *trans*-[$RuCl_2$(dppb)(1,4-dt)] complex, showing the atoms labeling and the 50% probability ellipsoids.

Table 2
Selected bond lengths (Å) and angles (°) for the *trans*-[$RuCl_2$(dppb)(1,4-dt)] complex

Bond length (Å)			
Ru–P(2)	2.297(1)	P(1)–C(111)	1.828(4)
Ru–P(1)	2.317(1)	P(1)–C(121)	1.844(4)
Ru–S(1)	2.404(1)	P(1)–C(131)	1.845(4)
Ru–Cl(2)	2.414(9)	P(2)–C(221)	1.836(4)
Ru–Cl(1)	2.439(9)	P(2)–C(231)	1.840(4)
Ru–S(2)	2.444(1)	P(2)–C(211)	1.855(4)
S(1)–C(11)	1.821(4)	C(11)–C(21)	1.540(5)
S(1)–C(12)	1.825(4)	C(12)–C(22)	1.537(6)
S(2)–C(22)	1.822(4)	C(111)–C(112)	1.392(6)
S(2)–C(21)	1.828(4)	C(111)–C(116)	1.393(6)
Bond angle (°)			
P(2)–Ru–P(1)	93.88(4)	S(1)–Ru–S(2)	74.80(3)
Cl(2)–Ru–S(2)	83.63(3)	P(1)–Ru–S(1)	171.32(4)
Cl(1)–Ru–S(2)	88.62(3)	P(1)–Ru–S(2)	96.79(4)
P(2)–Ru–Cl(2)	93.96(3)	C(11)–S(1)–C(12)	95.42(19)
P(1)–Ru–Cl(2)	87.73(3)	C(11)–S(1)–Ru	101.40(13)
S(1)–Ru–Cl(2)	93.35(3)	C(12)–S(1)–Ru	103.09(13)
P(2)–Ru–Cl(1)	94.44(3)	C(22)–S(2)–C(21)	94.97(19)
P(1)–Ru–Cl(1)	89.02(3)	C(22)–S(2)–Ru	101.31(14)
S(1)–Ru–Cl(1)	88.65(3)	C(21)–S(2)–Ru	101.49(13)
Cl(2)–Ru–Cl(1)	171.18(3)	C(111)–P(1)–C(121)	100.65(18)
P(2)–Ru–S(2)	168.95(4)	C(111)–P(1)–C(131)	101.97(18)

1,4-dt (average value of 1.54 Å) are elongated comparatively with the free species, 1.490(18) Å [12].

The angles of the bonds involving the ruthenium atom indicate that the chloride atoms are in the *trans* configuration (see Table 2). The observation that the C–S–C angles of the 1,4-dt change from ca. 99.0° (6) in the free molecule to 95.42° (19) in the coordinated ligand [13], strongly suggests that electronic density of the sulfur atoms was withdrawn upon coordination. The S–M–S angle is smaller for the ruthenium complex, 74.80(3)°, comparatively to the [PtI_2(1,4-dt)] compound, 79.74 (8)° [15]. This result is attributed to the size difference between these atoms, i.e. 134 pm for ruthenium and 138 pm for platinum [33].

The $^{31}P\{^1H\}$ spectrum of the *trans*-[$RuCl_2$(dppb)(1,4-dt)] complex showed one single signal, at δ 33.0 ppm, indicating that the symmetrical arrangement of the two phosphorous atoms is maintained in solution [30]. This signal presents a downshift in comparison with similar complexes in which the metal centers are bonded to a nitrogen atoms where the $^{31}P\{^1H\}$ NMR chemical shifts are close to 42 ppm [30].

The electronic absorption spectrum data are shown in the Table 3. Apart from the transitions involving the phosphine ligands, observed at 240 nm [34], the UV/Vis spectrum of the *trans*-[$RuCl_2$(dppb)(1,4-dt)] complex, presents one band at 452 nm ($\varepsilon = 290$ L mol^{-1} cm^{-1}), in CH_2Cl_2 solution. This absorption band is sensitive toward solvent changes (425 nm in *N*,*N*′-dimethylformamide) and was assigned to the metal-to-ligand charge transfer transition, (1,4-dt) $\pi \leftarrow d\pi$ (Ru). Charge transfer transitions of low extinction coefficients were also observed for the $[Ru(NH_3)_5L]^{2+}$ type complexes, where L = dithioether ligands (see Table 3) [4].

Table 3
Electronic absorptions data, λ (nm), ε (L mol^{-1} cm^{-1}), and $Ru^{III/II}$ half-wave formal potential, $E_{1/2}$ (*V* vs. NHE), for some ruthenium complexes

Complex	λ	$\varepsilon \times (10^{-3})$	$E_{1/2}$	Reference
mer-[$RuCl_3$(dppb)(1,4-dt)]	530	2.0	0.45	this work
	420	1.6		
	347	2.2		
[{$RuCl_3$(dppb)}$_2$(μ-(1,4-dt))]	530	3.8	0.45	this work
	420	3.2		
	347	4.2		
mer-[$RuCl_3$(dppb)H_2O]	533	1.6	0.34	[19]
	420	1.3		
	350	1.7		

For the *mer*-[$RuCl_3$(dppb)(1,4-dt)] complex, the absorption at 530 nm is observed with higher intensity ($\varepsilon = 2.0 \times 10^3$ L mol^{-1} cm^{-1}) when compared with the band at 533 nm for the *mer*-[$RuCl_3$(dppb)H_2O] complex ($\varepsilon = 1.6 \times 10^3$ L mol^{-1} cm^{-1}), in the same experimental conditions [19]. The band at 533 nm in the spectrum of *mer*-[$RuCl_3$-(dppb)H_2O] complex has been assigned as a ligand-to-metal charge transfer (LMCT), (Ru^{III}) $d\pi \leftarrow p\pi$ (Cl) [12]. For the *mer*-[$RuCl_3$(dppb)(1,4-dt)] and [{$RuCl_3$(dppb)}$_2$-(μ-(1,4-dt))] complexes, the absorption bands at 530 nm occur with higher intensity than that of *mer*-[$RuCl_3$-(dppb)H_2O] complex probably due to the contribution of the (Ru^{III}) $d\pi \leftarrow p\pi$ (S) LMCT [26]. As expected, for the [{$RuCl_3$-(dppb)}$_2$(μ-(1,4-dt))] binuclear complex the extinction coefficient of the band at 530 nm is almost two times more intense ($\varepsilon = 3.8 \times 10^3$ L mol^{-1} cm^{-1}) than that observed for the *mer*-[$RuCl_3$(dppb)(1,4-dt)] mononuclear complex.

The EPR spectrum of the *mer*-[$RuCl_3$(dppb)(1,4-dt)] complex, in CH_2Cl_2, differently of that acquired for the aqua-complex that presents zero field signals [14], shows three *g*-values in 2.87, 2.15 and 1.73. This result is typical of Ru(III) species with rhombic distortions [35], suggesting that the 1,4-dt is coordinated in a monodentate mode.

The EPR spectrum of the binuclear [{$RuCl_3$(dppb)}$_2$(μ-(1,4-dt))] complex, in CH_2Cl_2, shows a large signal ($g =$ 2,31) which is characteristic of complexes with exchange interaction between the ruthenium atoms [36].

The cyclic voltammograms obtained for the *trans*-[$RuCl_2$(dppb)(1,4-dt)] complex in CH_2Cl_2 evidenced a redox process with half-wave formal potential, $E_{1/2} =$ 0.77 V. This value was observed to be independent of the sweep rate from 0.05 to 0.5 V s^{-1}. In addition, it was observed that the ratio between the anodic and cathodic currents is almost unit, the difference between the anodic and cathodic potentials, ΔE, is approximately equals to 0.07 V, and plots of ip versus $v^{1/2}$ are linear. These results indicate that the Ru^{III}/Ru^{II} redox process of this complex is reversible, involving one-electron transfer and diffusion-controlled [37]. The $E_{1/2}$ value observed for this complex is 0.11 V higher than that observed for the *trans*-[$RuCl_2$-(dppb)(bipy)], $E_{1/2} = 0.66$ V, where bipy = 2,2′-bipyridine, in the same experimental conditions [30]. This difference reflects the stronger π-acid property of the 1,4-dt compared

Table 4
$E_{1/2}$ values (in V vs. NHE) for Ruthenium complexes.

System	L	$E_{1/2}$	Reference
$[RuCl_2(dppb)(L)]$	NH_3 [a]	0.59	[23]
	Pyridine[b]	0.68	[23]
	Bipy	0.66	[23]
	1,4-Dithiane	0.77	this work
$[Ru(NH_3)_5(L)]^{2+}$	Pyridine	0.30	[38]
	4,4′-Dithiodipyridine	0.40	[39]
	Dimethyl sulfide	0.50	[40]
	1,4-Dithiane	0.52	[4]
	1,3-Dithiane	0.55	[4]
	1,2-Dithiane	0.66	[4]

[a] $[RuCl_2(dppb)(NH_3)_2]$.
[b] $[RuCl_2(dppb)(py)_2]$, where py = pyridine.

with bipy ligand, when bonded to Ru(II) in the *trans*-$[RuCl_2(dppb)(LL)]$ type complexes. For comparison, the electrochemical data for a series of $[Ru(NH_3)_5(L)]^{2+}$ and *trans*-$[RuCl_2(dppb)(LL)]$ type complexes are displayed in Table 4.

For both type of complexes, the $E_{1/2}$ values show the stability enhancement of the reduced Ru(II) state when the metal center is coordinated through sulfur instead of nitrogen pyridine ring atom [41,42]. This data reflect the pronounced π-acid effect of the sulfur atom, especially for the dithiane isomers (see Table 4). In these cases, the higher values are assigned to the extra interaction between the coordinated and noncoordinated sulfur atoms which decreases as the S–S distance increases [4].

4. Conclusion

The data collected in this work for the *trans*-$[RuCl_2$-(dppb)(1,4-dt)], *mer*-$[RuCl_3(dppb)(1,4\text{-dt})]$ and $[\{RuCl_3$-$(dppb)\}_2(\mu\text{-}(1,4\text{-dt}))]$ complexes where the 1,4-dithiane ligand acts as bidentate, monodentate and ambidentate forms, respectively, exemplify the conformational versatility of this ligand towards the coordination chemistry. The *trans*-$[RuCl_2(dppb)(1,4\text{-dt})]$ complex consists in the first example of an hexacoordinated ruthenium complex with 1,4-dithiane as a bidentate ligand, in a D_2 conformation.

5. Supplementary material

Crystallographic data for the structural analysis have been deposited with the Cambridge Crystallographic Data Center, CCDC No. 279648. Copies of this information may be obtained free of charge from The Director, CCDC, 12 Union Road, Cambridge, CB2 1EZ, UK (fax: +44 1223 336033; e-mail: deposit@ccdc.cam.ac.uk or http://www.ccdc.cam.ac.uk).

Acknowledgements

We are grateful for the financial support by CAPES, FAPESP and CNP Brazilian agencies.

References

[1] H. Beinert, Eur. J. Biochem. 267 (2000) 5657.
[2] E.I. Stiefel, In: Transition Metal Sulfur Chemistry, Biological and Industrial Significance, ACS Symposium Series, Washington, 1996.
[3] C.A. Stein, H. Taube, J. Am. Chem. Soc. 100 (1978) 1635.
[4] C.G. Kuehn, S.S. Isied, Prog. Inorg. Chem. 27 (1979) 153.
[5] A. Streitweiser Jr., S.P. Ewing, J. Am. Chem. Soc. 97 (1975) 190.
[6] A. Streitweiser Jr., J.G. Williams, J. Am. Chem. Soc. 97 (1975) 191.
[7] S. Oae, T.D. Joyce, Organic Sulfur Chemistry: Structure and Mechanism, CRC Press Inc., London, 1991.
[8] S. Wolfe, F. Bernardi, I.G. Csizmadia, A. Mangini, Organic Sulfur Chemistry, Elsevier, Amsterdam, 1985, pp. 133.
[9] C.G. Kuehn, H. Taube, J. Am. Chem. Soc. 98 (1976) 689.
[10] D. Sellmann, J. Sutter, Acc. Chem. Res. 30 (1997) 460.
[11] J.C. Bayo'n, C. Claver, A.M. Masdeu-Bultó, Coord. Chem. Rev. 193 (1999) 73.
[12] T.E. Rosso, M.W. Ellzy, J.O. Jensen, H.F. Hameka, D. Zeroka, Spectrochim. Acta A 55 (1999) 121.
[13] R.E. March, Acta Crystallogr. 8 (1955) 91.
[14] R.D. Adams, L. Chen, J.H. Yamamoto, Inorg. Chim. Acta 229 (1995) 47.
[15] M.H. Johansson, H.P. Engelbrecht, Acta Crystallogr. E 57 (2001) m114.
[16] M. Green, M. Draganjac, Y. Jiang, P.M. Nave, A.W. Cordes, C.D. Bryan, J.K. Dixon, S.L. Folkert, C.-H. Yu, J. Chem. Crystallogr. 33 (2003) 473.
[17] U. Frey, S. Elmroth, B. Moullet, L.I. Elding, A.E. Merbach, Inorg. Chem. 30 (1991) 5033.
[18] D.D. Perrin, W.L.F. Armarego, Purification of Laboratory Chemicals, 3rd ed., Pergamon Press, Oxford, 1988.
[19] L.R. Dinelli, A.A. Batista, K. Wohnrath, M.P. de Araujo, S.L. Queiroz, M.R. Bonfadini, G. Oliva, O.R. Nascimento, P.W. Cyr, K.S. MacFarlane, B.R. James, Inorg. Chem. 38 (1999) 5341.
[20] C.W. Jung, P.E. Garrou, P.R. Hoffman, K.G. Caulton, Inorg. Chem. 23 (1984) 726.
[21] Enraf-Nonius, COLLECT, Nonius BV, Delft, The Netherlands, 1997–2000.
[22] Z. Otwinowski, W. Minor, HKL Denzo and Scalepack, in: C.W. CarterJr., R.M. Sweet (Eds.), Methods in Enzimology, vol. 276, Academic Press, New York, 1997, p. 307.
[23] R.H. Blessing, Acta Crystallogr. A 51 (1995) 33.
[24] G.M. Sheldrick, SHELXS-97. Program For Crystal Structure Resolution, University of Göttingen, Göttingen, Germany, 1997.
[25] G.M. Sheldrick, SHELXL-97. Program for Crystal Structures Analysis, University of Göttingen, Göttingen, Germany, 1997.
[26] L.J. Farrugia, J. Appl. Cryst. 30 (1997) 565.
[27] U. Koelle, F. Khouzami, Angew. Chem., Int. Ed. 19 (1980) 640.
[28] S.S.S. Borges, A.L. Coelho, I.S. Moreira, M.A.B. Araujo, Polyhedron 13 (1994) 1015.
[29] S.R. Wade, G.R. Willey, Inorg. Chim. Acta 72 (1983) 201.
[30] S.L. Queiroz, A.A. Batista, G. Oliva, M.T.P. Gambardella, R.H.A. Santos, K.S. MacFarlane, S.J. Rettig, B.R. James, Inorg. Chim. Acta 267 (1998) 209.
[31] D.T.T. Yapp, S.J. Rettig, B.R. James, K.A. Skov, Inorg. Chem. 36 (1997) 5635.
[32] D.C. Mudalige, E.S. Ma, S.J. Rettig, B.R. James, W.R. Cullen, Inorg. Chem. 36 (1997) 5426.
[33] S.-X. Xiao, W.C. Trogler, D.E. Ellis, Z. Berkovitch-Yellin, J. Am. Chem. Soc. 105 (1983) 7033.
[34] A.A. Batista, E.A. Polato, S.L. Queiroz, O.R. Nascimento, B.R. James, S.J. Rettig, Inorg. Chim. Acta 230 (1995) 111.
[35] Q.A. Paula, A.A. Batista, O.R. Nascimento, A.J. Costa-Filho, M.S. Schultz, M. Bonfadini, G. Oliva, J. Braz. Chem. Soc. 11 (2000) 530.
[36] A.J. Bard, L.R. Faulkner, Electrochemical Methods, Fundamentals and Applications, Wiley, New York, 1980.

[37] T. Matsubara, P.C. Ford, Inorg. Chem. 15 (1976) 1107.
[38] D.W. Franco, I.S. Moreira, Inorg. Chem. 33 (1994) 1607.
[39] C.G. Kuehn, S.S. Isied, J. Am. Chem. Soc. 98 (1976) 689.
[40] D. Sellmann, J. Sutter, Acc. Chem. Res. 30 (1997) 460.
[41] A. Wu, D.C. Kennedy, B.O. Patrick, B.R. James, Inorg. Chem. Comm. 6 (2003) 996.
[42] M.O. Santiago, C.L. Donnici, I.S. Moreira, R.M. Carlos, S.L. Queiroz, A.A. Batista, Polyhedron 22 (2003) 3205.

of the electronic and steric properties of the triarylphosphines on the synthesis, spectroscopical properties and structure of mononuclear Rh(I)–chloride complexes.

2. Experimental

2.1. Chemicals and physical measurements

Phosphines PR_3 with $R = 4\text{-}(OCH_3)C_6H_4$, $3\text{-}(OCH_3)C_6H_4$, $2\text{-}(OCH_3)C_6H_4$, $4\text{-}(CH_3)C_6H_4$, $3\text{-}(CH_3)C_6H_4$, $2\text{-}(CH_3)C_6H_4$, $4\text{-}ClC_6H_4$, $3\text{-}ClC_6H_4$, $4\text{-}FC_6H_4$, $4\text{-}(CF_3)C_6H_4$, C_6H_5, and $R_3 = (C_6H_5)_2(C_6F_5)$, $(C_6H_5)(C_6F_5)_2$ and $(C_6F_5)_3$ and $RhCl_3 \cdot 3H_2O$ were purchased from Strem Chemicals and used as received. The complex $[\{Rh(\mu\text{-}Cl)(\eta^4\text{-}COD)\}_2]$ was prepared as previously reported [11]. Solvents were dried and degassed prior to use. All manipulations were carried out under dry nitrogen atmospheres using Schlenk techniques. Thin layer chromatography (Merck, 5×7.5 cm^2 Kiesegel 60 F_{254}) was used to monitor the progress of the reactions. Elemental analyses were determined by Galbraith Labs. Inc., USA. NMR spectra were recorded by Spectral Data Services (IL, USA) on a SDS-360 spectrometer working at 360 MHz (^{1}H), 282 MHz (^{19}F) and 202 MHz (^{31}P) in $CDCl_3$ solutions at ambient temperature. Chemical shifts are given in ppm relative to TMS (^{1}H, $\delta = 0$), H_3PO_4 (^{31}P, $\delta = 0$) and $CFCl_3$ (^{19}F, $\delta = 0$). Since all reactions were conducted similarly, only a general procedure is described.

2.2. General procedure

To a solution of the complex $[\{Rh(\mu\text{-}Cl)(\eta^4\text{-}COD)\}_2]$ (200 mg, 0.406 mmol) in acetone (10 cm^3) were added two equivalents of the corresponding phosphine. The color of the solution quickly changed from orange to yellow. The mixture was stirred at room temperature and checked for completion by TLC. After that the solvent was removed in vacuo. All complexes were isolated as crystalline solids.

2.3. Compounds characterization

2.3.1. $[RhCl(\eta^4\text{-}COD)(P(4\text{-}OCH_3C_6H_4)_3)]$ (**1**)

Yield 89%; orange-yellow. *Anal.* Calc. for $C_{29}H_{33}ClO_3PRh$: C, 58.16; H, 5.55. Found: C, 58.06; H, 5.17%. ^{1}H NMR, $CDCl_3$ δ (ppm); 7.64 (m, 6H, C*H*-phosphine) 6.89 (m, 6H, C*H*-phosphine), 5.53 (m, 2H, COD-C*H trans*-P), 3.81 (s, 9H, phosphine-OCH_3), 3.12 (m, 2H, COD-C*H trans*-Cl), 2.20 (m, 4H, COD-CH_2), 2.10–1.90 (m, 4H, COD-CH_2). ^{31}P NMR, $CDCl_3$ $\delta = 27.7$ ppm, d, $^1J_{Rh-P} = 148.7$ Hz.

2.3.2. $[RhCl(\eta^4\text{-}COD)\{P(4\text{-}CH_3C_6H_4)_3\}]$ (**2**)

Yield 99%; yellow. *Anal.* Calc. for $C_{29}H_{33}ClPRh$: C, 63.23; H, 6.04. Found: C, 64.00; H, 6.07%. ^{1}H NMR, $CDCl_3$ δ (ppm); 7.71 (m, 6H, C*H*-phosphine), 7.53 (m, 6H, C*H*-phosphine), 5.54 (m, 2H, COD-C*H trans*-P), 3.13 (m, 2H, COD-C*H trans*-Cl), 2.40 (m, 4H, COD-CH_2), 2.35 (s, 9H, phosphine-CH_3), 2.10–1.90 (m, 4H, COD-CH_2). ^{31}P NMR, $CDCl_3$ $\delta = 29.3$ ppm, d, $^1J_{Rh-P} = 149.3$ Hz.

2.3.3. $[RhCl(\eta^4\text{-}COD)\{P(C_6H_5)_3\}]$ (**3**)

Yield 94%; yellow. *Anal.* Calc. for $C_{26}H_{27}ClPRh$: C, 61.41; H, 5.36. Found: C, 61.74; H, 5.33%. ^{1}H NMR, $CDCl_3$ δ (ppm); 7.75 (m, 6H, C*H*-phosphine), 7.40 (m, 9H, C*H*-phosphine), 5.58 (m, 2H, COD-C*H trans*-P), 3.15 (m, 2H, COD-C*H trans*-Cl), 2.40 (m, 4H, COD-CH_2), 2.15–1.85 (m, 4H, COD-CH_2). ^{31}P NMR, $CDCl_3$ $\delta = 31.3$ ppm, d, $^1J_{Rh-P} = 150.1$ Hz.

2.3.4. $[RhCl(\eta^4\text{-}COD)\{P(4\text{-}FC_6H_4)_3\}]$ (**4**)

Yield 93%; yellow. *Anal.* Calc. for $C_{26}H_{24}ClF_3PRh$: C, 55.49; H, 4.30. Found: C, 55.84; H, 4.29%. ^{1}H NMR, $CDCl_3$ δ (ppm); 7.70 (m, 6H, C*H*-phosphine), 7.10 (m, 6H, C*H*-phosphine), 5.60 (m, 2H, COD-C*H trans*-P), 3.08 (m, 2H, COD-C*H trans*-Cl), 2.45 (m, 4H, COD-CH_2), 2.20–1.90 (m, 4H, COD-CH_2). ^{31}P NMR, $CDCl_3$ $\delta = 29.5$ ppm, d, $^1J_{Rh-P} = 152.6$ Hz. ^{19}F NMR, $CDCl_3$, $\delta = -109.4$ ppm.

2.3.5. $[RhCl(\eta^4\text{-}COD)\{P(4\text{-}CF_3C_6H_4)_3\}]$ (**5**)

Yield 97%; yellow. *Anal.* Calc. for, $C_{29}H_{24}ClF_9PRh$: C, 48.86; H, 3.39. Found: C, 48.56; H, 3.08%. ^{1}H NMR, $CDCl_3$ δ (ppm); 7.84 (m, 6H, C*H*-phosphine), 7.68 (m, 6H, C*H*-phosphine), 5.69 (m, 2H, COD-C*H trans*-P), 3.11 (m, 2H, COD-C*H trans*-Cl), 2.44 (m, 4H, COD-CH_2), 2.20–1.95 (m, 4H, COD-CH_2). ^{31}P NMR, $CDCl_3$ $\delta = 32.2$ ppm, d, $^1J_{Rh-P} = 154.1$ Hz. ^{19}F NMR, $CDCl_3$, 4-CF_3C$_6$H$_4$, $\delta = -63.6$ ppm, s.

2.3.6. $[RhCl(\eta^4\text{-}COD)\{P(4\text{-}ClC_6H_4)_3\}]$ (**6**)

Yield 82%; yellow. *Anal.* Calc. for $C_{26}H_{24}Cl_4PRh$: C, 51.01; H, 3.95. Found: C, 51.62; H, 4.06%. ^{1}H NMR, $CDCl_3$ δ (ppm); 7.65 (m, 6H, C*H*-phosphine), 7.38 (m, 6H, C*H*-phosphine), 5.61 (m, 2H, COD-C*H trans*-P), 3.07 (m, 2H, COD-C*H trans*-Cl), 2.42 (m, 4H, COD-CH_2), 2.20–1.90 (m, 4H, COD-CH_2). ^{31}P NMR, $CDCl_3$ $\delta = 30.3$ ppm, d, $^1J_{Rh-P} = 152.8$ Hz.

2.3.7. $[RhCl(\eta^4\text{-}COD)\{P(3\text{-}OCH_3C_6H_4)_3\}]$ (**7**)

Yield 87%; orange-yellow. *Anal.* Calc. for $C_{29}H_{33}ClO_3PRh$: C, 58.16; H, 5.55. Found: C, 58.66; H, 5.57%. ^{1}H NMR, $CDCl_3$ δ (ppm); 7.40 (m, 3H, C*H*-phosphine), 7.25 (m, 6H, C*H*-phosphine), 6.70 (m, 3H, C*H*-phosphine), 5.57 (m, 2H, COD-C*H trans*-P), 3.77 (s, 9H, phosphine-OCH_3), 3.21 (m, 2H, COD-C*H trans*-Cl), 2.40 (m, 4H, COD-CH_2), 2.15–1.85 (m, 4H, COD-CH_2). ^{31}P NMR, $CDCl_3$ $\delta = 32.8$ ppm, d, $^1J_{Rh-P} = 149.9$ Hz.

2.3.8. $[RhCl(\eta^4\text{-}COD)\{P(3\text{-}CH_3C_6H_4)_3\}]$ (**8**)

Yield 90%; orange-yellow. *Anal.* Calc. for $C_{29}H_{33}ClPRh$: C, 63.23; H, 6.04. Found: C, 62.90; H, 5.95%. ^{1}H NMR, $CDCl_3$ δ (ppm); 7.54 (m, 6H, C*H*-phosphine), 7.25 (m, 6H, C*H*-phosphine), 5.56 (m, 2H, COD-C*H trans*-P), 3.14

(m, 2H, COD-C*H trans*-Cl), 2.40 (m, 4H, COD-CH_2), 2.35 (s, 9H, phosphine-CH_3), 2.15–1.85 (m, 4H, COD-CH_2). ^{31}P NMR, $CDCl_3$ $\delta = 30.8$ ppm, d, $^1J_{Rh-P} = 149.4$ Hz.

*2.3.9. [RhCl(η⁴-COD){P(3-ClC₆H₄)₃}] (**9**)*

Yield 83%; yellow. *Anal.* Calc. for $C_{26}H_{24}Cl_4PRh$: C, 51.01; H, 3.95. Found: C, 50.65; H, 4.02%. ^{1}H NMR, $CDCl_3$ δ (ppm); 7.63 (m, 6H, C*H*-phosphine), 7.40 (m, 6H, C*H*-phosphine), 5.66 (m, 2H, COD-C*H trans*-P), 3.11 (m, 2H, COD-C*H trans-Cl*), 2.45 (m, 4H, COD-CH_2), 2.20–1.95 (m, 4H, COD-CH_2). ^{31}P NMR, $CDCl_3$ $\delta = 32.4$ ppm, d, $^1J_{Rh-P} = 153.2$ Hz.

*2.3.10. [RhCl(η⁴-COD){P(2-OCH₃C₆H₄)₃}] (**10**)*

Yield 87%; yellow. *Anal.* Calc. for, $C_{29}H_{33}ClO_3PRh$: C, 58.16; H, 5.55. Found: C, 57.89; H, 5.48%. ^{1}H NMR, $CDCl_3$ δ (ppm); 7.38 (m, 3H, C*H*-phosphine), 7.20 (m, 3H, C*H*-phosphine), 6.90 (m, 3H, C*H*-phosphine), 6.81 (m, 3H, C*H*-phosphine), 5.23 (m, 2H, COD-C*H trans*-P), 3.84 (m, 2H, COD-C*H trans*-Cl), 3.52 (s, 9H, phosphine-OCH_3), 2.35 (m, 4H, COD-CH_2), 1.98 (m, 4H, COD-C**H**$_2$). ^{31}P NMR, $CDCl_3$ $\delta = 16.6$ ppm, d, $^1J_{Rh-P} = 147.2$ Hz.

*2.3.11. [RhCl(η⁴-COD){P(2-CH₃C₆H₄)₃}] (**11**)*

Yield 95%; yellow. *Anal.* Calc. for $C_{29}H_{33}ClPRh$: C, 63.23; H, 6.04. Found: C, 63.41; H, 5.92%. ^{1}H and ^{31}P NMR, not observed in solution, see text.

*2.3.12. [RhCl(η⁴-COD){P(C₆H₅)₂(C₆F₅)}] (**12**)*

Yield 64%; yellow. *Anal.* Calc. for $C_{26}H_{22}ClF_5PRh$: C, 52.15; H, 3.70. Found: C, 52.97; H, 3.72%. ^{1}H NMR, $CDCl_3$ δ (ppm); 7.75 (m, 4H, C*H*-phosphine), 7.45 (m, 6H, C*H*-phosphine), 5.55 (m, 2H, COD-C*H trans*-P), 3.38 (m, 2H, COD-C*H trans*-Cl), 2.40 (m, 4H, COD-CH_2), 2.15–1.80 (m, 4H, COD-CH_2). ^{31}P NMR, $CDCl_3$ $\delta = 22.5$ ppm, d, $^1J_{Rh-P} = 151.9$ Hz. ^{19}F NMR, $CDCl_3$, $\delta = -124.9$ (m, 2F, *ortho*), −149.4 (dd, 1F, *para*), −160.3 (m, 2F, *meta*).

2.4. X-ray crystallography

Single crystals of **11** were obtained by slow evaporation of a saturated acetone solution. X-ray diffraction data were measured at 298 K on a Siemens P4 diffractometer using common procedures [12] and were corrected for absorption effect by means of ψ-scans data. The structure was solved and refined using standard procedures [13] without restraints or constraints. H atoms were placed on idealised positions and refined using a riding model with fixed isotropic U. Crystal data are collected in Table 1.

Table 1
Crystal data for [RhCl(η⁴-COD){P(2-CH₃C₆H₄)₃}] (**11**)

Empirical formula	$C_{29}H_{33}ClPRh$
Formula weight	550.88
Color, habit	yellow regular prism
Crystal size (mm)	$0.5 \times 0.2 \times 0.1$
Space group	$P2_1/n$
a (Å)	8.2231(11)
b (Å)	17.575(3)
c (Å)	17.058(2)
β (Å)	91.334(11)
V (Å^3)	2464.5(6)
Z	4
Absorption coefficient (mm^{-1})	0.882
Radiation	Mo Kα ($\lambda = 0.71073$ Å)
2θ Range (°)	4.64–45.98
Reflections collected	4650
Independent reflections[a]	3417 ($R_{int} = 3.01\%$)
Transmission factors (minimum, maximum)	0.804, 0.917
Final R indices [2610 $I > 2\sigma(I)$] (%)[a]	$R_1 = 4.09$, $wR_2 = 8.47$
Final R indices [all data] (%)[a]	$R_1 = 6.49$, $wR_2 = 9.43$
Goodness-of-fit, S[a]	1.026
Data-to-parameters ratio	3417/289

[a] R_{int}, R_1, wR_2 and S are defined as follows:

$$R_{int} = \frac{\sum |F_o^2 - \langle F_o^2 \rangle|}{\sum F_o^2},\quad R_1 = \frac{\sum ||F_o| - |F_c||}{\sum |F_o|},\quad wR_2 = \sqrt{\frac{\sum w(F_o^2 - F_c^2)^2}{\sum w(F_o^2)^2}},$$

$$S = \sqrt{\frac{w(F_o^2 - F_c^2)^2}{m - n}}.$$

3. Results and discussion

3.1. Synthesis and characterization

The reactions of the chloro-bridged complex [{Rh(μ-Cl)(η⁴-COD)}$_2$] with 12 different triarylphosphines in acetone solutions afforded the mononuclear complexes [RhCl(η⁴-COD)(PR$_3$)], with R = 4-(OCH$_3$)C$_6$H$_4$ (**1**), 4-(CH$_3$)C$_6$H$_4$ (**2**), C$_6$H$_5$ (**3**), 4-FC$_6$H$_4$ (**4**), 4-(CF$_3$)C$_6$H$_4$ (**5**), 4-ClC$_6$H$_4$ (**6**), 3-(OCH$_3$)C$_6$H$_4$ (**7**), 3-(CH$_3$)C$_6$H$_4$ (**8**), 3-ClC$_6$H$_4$ (**9**), 2-(OCH$_3$)C$_6$H$_4$ (**10**), 2-(CH$_3$)C$_6$H$_4$ (**11**) and R$_3$ = (C$_6$H$_5$)$_2$(C$_6$F$_5$) (**12**) (Scheme 1).

An equilibrium between mononuclear and dinuclear species is rapidly achieved, with the mononuclear complex existing as the predominant species [14].

Compounds **1**–**12** are yellow or orange-yellow, stable crystalline solids which are soluble in common solvents – acetone, chloroform and dichloromethane. Analytical data and NMR parameters are consistent with the given formulae. IR spectra show absorptions characteristic of the 1,5-cyclooctadiene and the substituted triarylphosphines although they are not significant to the following discussion. A summary of spectroscopic data for complexes **1**–**12** is presented in Table 2.

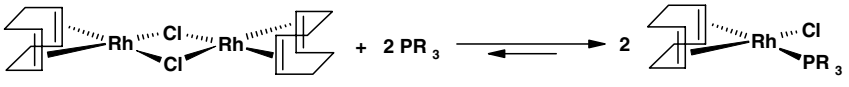

Scheme 1. Reaction between [{Rh(μ-Cl)(η⁴-COD)}$_2$] and PR$_3$.

Table 2
Summary of spectroscopic data for complexes **1**–**12**

Complex	Phosphine	^{1}H δ (ppm) CH	^{31}P δ (ppm)	$^1J_{Rh-P}$ (Hz)
1	P(4-$OCH_3C_6H_4$)$_3$	5.53, 3.12	27.7	148.7
2	P(4-$CH_3C_6H_4$)$_3$	5.54, 3.13	29.3	149.3
3	P(C_6H_5)$_3$	5.58, 3.15	31.3	150.1
4	P(4-FC_6H_4)$_3$	5.60, 3.08	29.5	152.6
5	P(4-$CF_3C_6H_4$)$_3$	5.69, 3.11	32.2	154.1
6	P(4-ClC_6H_4)$_3$	5.61, 3.07	30.3	152.8
7	P(3-$OCH_3C_6H_4$)$_3$	5.57, 3.21	32.8	149.9
8	P(3-$CH_3C_6H_4$)$_3$	5.56, 3.14	30.8	149.4
9	P(3-ClC_6H_4)$_3$	5.66, 3.11	32.4	153.2
10	P(2-$OCH_3C_6H_4$)$_3$	5.23, 3.84	16.6	147.2
11	P(2-$CH_3C_6H_4$)$_3$	[a]	[a]	[a]
12	P(C_6H_5)$_2$(C_6F_5)	5.55, 3.38	22.5	151.9

[a] Not observed in solution.

Equivalent experiments using P(C_6H_5)(C_6F_5)$_2$ or P(C_6F_5)$_3$ failed to react, even when a reflux or excess of phosphine were used, probably reflecting a considerable reduction of the basicity of the phosphorous atom impairing its ability to act as a base (see Table 3).

Proton NMR spectra of compounds **1**–**12** show the expected different resonances for methine (CH) and methylene (CH_2) protons of the cyclooctadiene ring, the aromatic protons and, for complexes **1**, **2**, **7**, **8** and **10**, the methyl protons of the phosphine.

Two different sets for the CH protons of the cyclooctadiene were observed, arising from two different *trans* substituents at the metallic centre [15]. The overall range for complexes **1**–**12** is $\Delta\delta = 3.84$–3.07 ppm for the *trans*-Cl CH absorptions and $\Delta\delta = 5.69$–5.23 ppm for the *trans*-P. However, these resonances are rather insensitive to the nature of the phosphine in *trans* position.

Fluorine NMR spectra of compounds **4** (P(4-FC_6H_4)$_3$ with a AA′BB′X magnetic system), and **5** (P(4-$CF_3C_6H_4$)) exhibit single absorptions. ^{19}F NMR spectrum of [RhCl(η^4-COD)(P(C_6H_5)$_2$(C_6F_5))] (**12**), show three signals of a AA′BB′C magnetic system corresponding to *ortho*, *meta* and *para* fluorine nuclei of the PC_6F_5 moiety.

Table 3
Summary of electronic and steric parameters for the triphenylphosphines employed in this study [6]

Phosphine	χ	θ (°)
P(4-$OCH_3C_6H_4$)$_3$	10.5	145
P(4-$CH_3C_6H_4$)$_3$	11.5	145
P(C_6H_5)$_3$	13.3	145
P(4-FC_6H_4)$_3$	15.7	145
P(4-$CF_3C_6H_4$)$_3$	20.5	145
P(4-ClC_6H_4)$_3$	16.8	145
P(3-$OCH_3C_6H_4$)$_3$	[a]	[a]
P(3-$CH_3C_6H_4$)$_3$	11.3	148
P(3-ClC_6H_4)$_3$	19.6	148
P(2-$OCH_3C_6H_4$)$_3$	[a]	[a]
P(2-$CH_3C_6H_4$)$_3$	10.7	178
P(C_6H_5)$_2$(C_6F_5)	20.4	158
P(C_6H_5)(C_6F_5)$_2$	27.6	171
P(C_6F_5)$_3$	34.8	184

[a] Data not available.

^{31}P NMR spectra of compounds **1**–**12** exhibit signals with chemical shifts spanning over ca. 5 ppm from 27.7 to 32.8 ppm except for compounds **10** ($\delta = 16.63$ ppm) and **12** ($\delta = 22.50$ ppm). Each signal is a doublet due to ^{103}Rh–^{31}P coupling with $^1J_{Rh-P}$ between 147.7 and 154.05 Hz.

Although all complexes studied display expected similarities, there is a feature which is worth noting. Despite the close resemblance among the series of phosphines bearing 4-, 3- and 2-$OCH_3C_6H_4$ and 4-, 3- and 2-$CH_3C_6H_4$ substituents, only [RhCl(η^4-COD)(P(2-$CH_3C_6H_4$)$_3$)$_2$] (**11**) seems unable to remain as stable mononuclear complex in solution and rearranges to the starting materials [{Rh(μ-Cl)(η^4-COD)}$_2$] and P(2-$CH_3C_6H_4$)$_3$. The difference between both *ortho*-substituted phosphines with 2-$CH_3C_6H_4$ and 2-$OCH_3C_6H_4$, seems the larger flexibility of the methoxy group compared with the methyl moiety. Molecular models indicate a considerable steric hindrance with 2-$CH_3C_6H_4$ which is released when the methyl group is free to rotate around the oxygen atom. A previous work has proved the difference in reactivity between iridium complexes when two of these phosphines are bounded to the metal centre [16].

3.2. ^{31}P NMR spectroscopic analysis

Correlations between experimental $^1J_{Rh-P}$ or ^{31}P chemical shifts from the coordination compounds and electronic properties of the phosphine ligands could be useful to analyse the metallic environment of these complexes. Chemical shifts of free phosphines P(4-XC_6H_4)$_3$ (X = OCH_3, CH_3, H, F, Cl and CF_3) show a tendency almost parallel to the corresponding ^{31}P δ in their rhodium compounds, suggesting that electronic shielding is affected similarly in all compounds upon complexation.

As shown in Fig. 1, isosteric phosphines, according to their cone angle ($\theta = 145°$), show an inverse relation between their electronic properties, as accounted by Giering's electronic parameter χ, and the experimental magnetic coupling constant $^1J_{P-Rh}$. This is a similar behaviour to the previously reported for Pt(II)–P [9], and Pt(0)–P complexes [10], and it can be rationalized in terms of a reduction on the phosphorus covalent radius upon the addition of electron-withdrawing groups on the phenyl rings, considering these triarylphosphines as exclusively σ-donors [6a].

3.3. Crystal structure

Relevant bond distances and angles for complex **11** are displayed in Table 4. The asymmetric unit contains one molecule with all atoms on general positions (Fig. 2). Considering the COD molecule as a bidentate ligand, the metallic center displays a slightly distorted square planar coordination geometry found in numerous 16-electrons Rh(I) complexes. The COD ligand approximates a tub

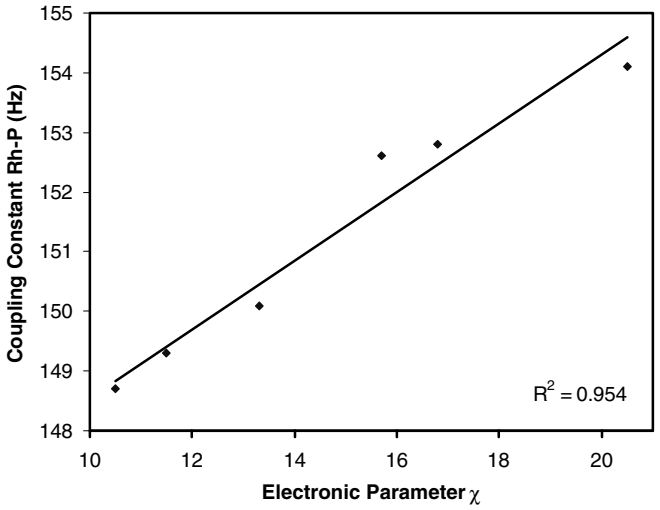

Fig. 1. Graph of the electronic parameter χ for the isosteric phosphines $P(4\text{-}XC_6H_4)_3$ ($X = OCH_3$, CH_3, H, F, Cl, and CF_3) and $^1J_{P-Rh}$ of $[RhCl(\eta^4\text{-}COD)(P(4\text{-}XC_6H_4)_3)]$ (**1**–**6**).

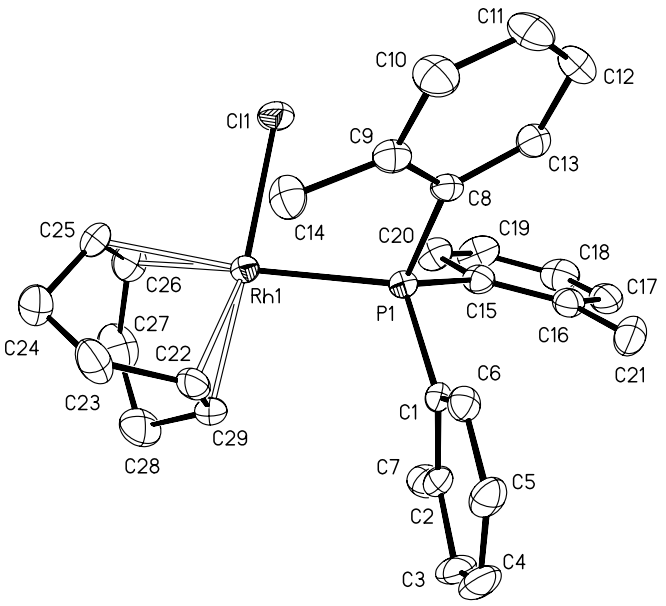

Fig. 2. X-ray structure of **11**, showing displacement ellipsoids at the 30% probability level. H atoms have been omitted for clarity.

Table 4
Selected bond lengths (Å) and angles (°) for $[RhCl(\eta^4\text{-}COD)(P(2\text{-}CH_3C_6H_4)_3)]$ (**11**)

Bond length (Å)			
Rh1–C22	2.124(5)	Rh1–C29	2.138(5)
Rh1–C26	2.182(5)	Rh1–C25	2.206(6)
Rh1–P1	2.3607(14)	Rh1–Cl1	2.3773(14)
P1–C15	1.838(5)	P1–C1	1.840(5)
P1–C8	1.849(5)	C22–C29	1.384(8)
C25–C26	1.362(8)		
Bond angle (°)			
C22–Rh1–C29	37.9(2)	C22–Rh1–C26	95.6(2)
C29–Rh1–C26	80.5(2)	C22–Rh1–C25	79.8(2)
C29–Rh1–C25	87.6(2)	C26–Rh1–C25	36.2(2)
C22–Rh1–P1	95.32(16)	C29–Rh1–P1	98.40(16)
C26–Rh1–P1	160.13(19)	C25–Rh1–P1	163.37(17)
C22–Rh1–Cl1	155.73(18)	C29–Rh1–Cl1	164.61(18)
C26–Rh1–Cl1	88.64(17)	C25–Rh1–Cl1	90.02(16)
P1–Rh1–Cl1	88.15(5)		

conformation (D_{2d} local symmetry) also found in the vast majority of COD-containing complexes. The geometry for the tri-*o*-tolylphosphine is unaffected by coordination and remains very close to that of the free ligand [17]. The main structural feature for the solid state structure of **11** is the significant *trans* influence of the phosphine: Rh–C bond lengths *trans* to the P atom are lengthened by ca. 0.06 Å by comparison of Rh–C bond lengths *trans* to the Cl atom (see Table 4). This effect also induces non-equivalent double bonds in the COD moiety, the shortest bond length, C25–C26 = 1.362(8) Å, being *trans* to the phosphine, while the C22–C29 bond, 1.384(8), which is located *trans* to the chloride. However, both double bonds are still shorter than in free COD [18].

A similar behaviour was previously observed in two directly related structures, namely those containing triphenylphosphine, complex **3** [19], and tri(*p*-fluorophenyl)phosphine, complex **4** [20]. In the former case, the *trans* influence induced by the triphenylphosphine is characterized by a lengthening of coordination of ca. 0.10 Å for Rh–C *trans* to the phosphine, and for the latter, the calculated effect is of ca. 0.11 Å. These strong *trans* influences yield, as in the previous case, unbalanced double bond lengths for the COD moiety, for example 1.363 and 1.440 Å in **4**.

The bulkiness of the phophine is evident from the Rh–P distance, significantly larger in the case of **11** [2.3607(14) Å] compared to **3** and **4** [2.308 and 2.297 Å, respectively]. It is obvious that **3** and **4** present similar Tolman's cone angles, $\theta \approx 145°$, while **11**, for which includes an *ortho* substituent, should have a significantly larger cone angle ($\theta \approx 178°$). Assuming, from purely steric considerations, that a smaller cone angle should result in a better ligand, a stronger phosphine coordination is expected for **3** and **4** compared to **11**, as actually observed in Rh–P bond distances. This also explains the lability of complex **11** in solution, which rapidly reorganizes to the dinuclear complex and the free phosphine.

4. Conclusions

The addition of two equivalents of twelve different triarylphosphines to solutions of the dinuclear complex $[\{Rh(\mu\text{-}Cl)(\eta^4\text{-}COD)\}_2]$ affords the mononuclear species $[RhCl(\eta^4\text{-}COD)(PR_3)]$. However, no mononuclear species could be detected in solution when electron-poor phosphines, like $P(C_6H_5)(C_6F_5)_2$ and $P(C_6F_5)_3$, or bulky phosphines, such as $P(2\text{-}CH_3C_6H_4)_3$, were employed. The solid state structure for the complex $[RhCl(\eta^4\text{-}COD)(P(2\text{-}CH_3C_6H_4)_3)]$ (**11**) displays a long Rh–P bond distance, compared to $[RhCl(\eta^4\text{-}COD)\{P(C_6H_5)_3\}]$ (**3**) and

[RhCl(η^4-COD){P(4-FC_6H_4)$_3$}] (**4**), which accounts for the lability of this complex in solution. Solution ^{31}P NMR data for complexes with isosteric phosphines **1**–**6**, reveals that electron-withdrawing groups on the phenyl rings increases the $^1J_{P-Rh}$, in a similar fashion to that observed for Pt compounds indicating comparable bonding characteristics.

5. Supplementary data

Crystallographic data for compound **11** has been deposited with the Cambridge Crystallographic Data Centre; CCDC 273550. Copy of this information can be obtained free of charge from The Cambridge Crystallographic Data Centre via www.ccdc.cam.ac.uk/data_request/cif.

Acknowledgements

We are grateful to DGAPA-UNAM-IN116001 for financial support. J.T. thanks CONACYT-México for a scholarship.

References

[1] (a) C.P. Mehnert, R.A. Cook, N.C. Dispenziere, E.J. Mozeleski, Polyhedron 23 (2004) 2679;
(b) A. Roodt, S. Otto, G. Steyl, Coord. Chem. Rev. 245 (2003) 121;
(c) J. Vicente, J. Gil-Rubio, D. Bautista, Inorg. Chem. 40 (2001) 2636;
(d) S. Jääskeläinen, P. Suomalainen, M. Haukka, H. Riihimäki, J.T. Pursiainen, T.A. Pakkanen, J. Organomet. Chem. 633 (2001) 69;
(e) G.K. Anderson, R. Kumar, Inorg. Chim. Acta 146 (1988) 89.
[2] (a) M.T. Reetz, X. Li, Angew. Chem., Int. Ed. 44 (2005) 2962;
(b) I. Angurell, G. Muller, M. Rocamora, O. Rossell, M. Seco, Dalton Trans. (2003) 1194;
(c) B. Richter, A.L. Spek, G. van Koten, B.-J. Deelman, J. Am. Chem. Soc. 122 (2000) 3945;
(d) D.R. Palo, C. Erkey, Organometallics 19 (2000) 81.
[3] (a) M.L. Clarke, D. Ellis, K.L. Mason, A.G. Orpen, P.G. Pringle, R.L. Wingad, D.A. Zaher, R.T. Baker, Dalton Trans. (2005) 1294;
(b) V. Circu, M.A. Fernandes, L. Carlton, Polyhedron 22 (2003) 3293;
(c) S.A. Serron, L. Luo, C. Li, M.E. Cucullu, E.D. Stevens, S.P. Nolan, Organometallics 14 (1995) 5290;
(d) C.J. Elsevier, B. Kowall, H. Kragtn, Inorg. Chem. 34 (1995) 4836.
[4] T. Allman, R.G. Goel, Can. J. Chem. 60 (1982) 716.
[5] C.A. Tolman, Chem. Rev. 77 (1977) 313.
[6] (a) H.-Y. Liu, K. Eriks, A. Prock, W.P. Giering, Organometallics 9 (1990) 1758;
(b) M.R. Wilson, H. Liu, A. Prock, W.P. Giering, Organometallics 12 (1993) 2044;
(c) M.R. Wilson, A. Prock, W.P. Giering, A.L. Fernandez, C.M. Haar, S.P. Nolan, B.M. Foxman, Organometallics 21 (2002) 2758.
[7] S. Joerg, R.S. Drago, J. Sales, Organometallics 17 (1998) 589.
[8] L. Gonsalvi, H. Adams, G.J. Sunley, E. Ditzel, A. Haynes, J. Am. Chem. Soc. 124 (2002) 13597.
[9] D.W. Allen, B.F. Taylor, J. Chem. Soc., Dalton Trans. (1982) 51.
[10] C.J. Cobley, P.G. Pringle, Inorg. Chim. Acta 265 (1997) 107.
[11] (a) J. Chatt, L.M. Venanzi, J. Chem. Soc. (1957) 4735;
(b) G. Giordano, R.H. Crabtree, Inorg. Synth. 28 (1990) 88.
[12] XSCAnS Users Manual, Siemens Analytical X-ray Instruments Inc., Madison, WI, USA, 1991.
[13] G.M. Sheldrick, SHELXTL-Plus, Release 5.10, Siemens Analytical X-ray Instruments Inc., Madison, WI, USA, 1998.
[14] (a) C.A. Ogle, T.C. Masterman, J.L. Hubbard, J. Chem. Soc., Chem. Commun. (1990) 1733;
(b) B. Denise, G. Pannetier, J. Organomet. Chem. 99 (1975) 455;
(c) B. Denise, G. Pannetier, J. Organomet. Chem. 148 (1978) 155.
[15] (a) K. Vrieze, H.C. Volger, J. Organomet. Chem. 11 (1968) P17;
(b) K. Vrieze, H.C. Volger, A.P. Praat, J. Organomet. Chem. 14 (1968) 185;
(c) K. Vrieze, H.C. Volger, A.P. Praat, J. Organomet. Chem. 15 (1968) 447.
[16] R. Brady, W.H. De Camp, B.R. Flynn, M.L. Schneider, J.D. Scott, L. Vaska, M.F. Werneke, Inorg. Chem. 14 (1975) 2669.
[17] T.S. Cameron, B. Dahlèn, J. Chem. Soc., Perkin Trans. 2 (1975) 1737.
[18] I. Garneau, S. Raymond, F. Brisse, Acta Cryst. C 51 (1995) 538.
[19] Q.L. Horn, D.S. Jones, R.N. Evans, C.A. Ogle, T.C. Masterman, Acta Cryst. E 58 (2002) m51.
[20] M. Iglesias, C. Del Pino, A. Corma, S. Garcia-Blanco, S. Martinez Carrera, Inorg. Chim. Acta 127 (1987) 215.

silanethiols. We have undertaken a structural study of ammonium tri-*tert*-butoxysilanethiolates, derivatives of various amines. It is known that primary ammonium tri-*tert*-butoxysilanethiolates form adducts with a cubane-like core [7]. In this paper, we describe syntheses and structures of selected secondary ammonium salts of tri-*tert*-butoxysilanethiol.

2. Experimental

General remarks: All synthetic procedures were carried out under argon, using standard Schlenk techniques. Tri-*tert*-butoxysilanethiol [13] was prepared according to the literature. The solvents and amines were dried by standard methods, and distilled under argon prior to use. Elemental analyses were performed on Elemental Analyser Ea 1108 (Carlo Erba Instruments). Melting points were determined on SMP3 apparatus (Stuart Scientific, UK) and are uncorrected.

*[(Bu^{t}O)$_3$SiS$^{(-)(+)}$NH$_2$(C$_2$H$_5$)$_2$]$_2$ (**1**):* Diethylamine (0.2 mL, 2 mmol) was added to a solution of (Bu^{t}O)$_3$SiSH (0.56 g, 2 mmol) in benzene (5 mL). Small, transparent crystals separated after one day at room temperature. They were collected and recrystallised from cold hexane giving small, good quality crystals with a sharp m.p. 92–94 °C. Calc. for $C_{16}H_{39}NO_3SSi$: C, 54.3; H, 11.1; N, 4.0; S, 8.9. Found: C, 54.2; H, 11.3; N, 3.7; S, 8.9%.

*[(Bu^{t}O)$_3$SiS$^{(-)(+)}$NH$_2$(C$_2$H$_4$)$_2$O]$_2$ (**2**):* (Bu^{t}O)$_3$SiSH (0.84 g, 3 mmol) was dissolved in benzene (10 mL). To the solution of tri-*tert*-butoxysilanethiol a portion of morpholine (0.26 mL, 3 mmol) was added. After standing for one week at room temperature, crystals of **2** formed and were suitable for X-ray analysis; m.p. 93–95 °C. Calc. for $C_{16}H_{37}NO_4SSi$: C, 52.3; H, 10.1; N, 3.8; S, 8.7. Found: C, 53.0; H, 10.5; N, 3.8; S, 8.5%.

*[(Bu^{t}O)$_3$SiS$^{(-)(+)}$NH$_2$(C$_6$H$_{11}$)$_2$]$_2$ (**3**):* To a solution of (Bu^{t}O)$_3$SiSH (0.56 g, 2 mmol) in acetonitrile (5 mL) dicyclohexylamine (0.4 mL, 2 mmol) was added. The crystals used for X-ray measurements were prepared by recrystallisation of the crude product from hot acetonitrile; m.p. 89–90 °C. Calc. for $C_{24}H_{51}NO_3SSi$: C, 62.4; H, 11.2; N, 3.0; S, 6.9. Found: C, 62.1; H, 11.2; N, 3.0; S, 6.9%.

*[(Bu^{t}O)$_3$SiS$^{(-)(+)}$NH$_2$C$_5$H$_6$Me$_4$]$_2$ (**4**):* 2,2,6,6-tetramethylpiperidine (0.3 mL, 2 mmol) was added to a solution of (Bu^{t}O)$_3$SiSH (0.56 g, 2 mmol) in propanol-2 (8 mL). Crystals (m.p. 104–106 °C) separated from the solution after 2 weeks at 0–5 °C. Calc. for $C_{21}H_{47}NO_3SSi$: C, 59.8; H, 11.2; N, 3.3; S, 7.6. Found: C, 59.6; H, 11.5; N, 3.3; S, 7.4%.

2.1. X-ray crystallographic study

Diffraction data were recorded on a KUMA KM4 diffractometer with graphite-monochromated Mo Kα radiation

Table 1
Crystallographic data and structure refinement details for: [(Bu^{t}O)$_3$SiS$^{(-)(+)}$NH$_2$(C$_2$H$_5$)$_2$]$_2$ (**1**), [(Bu^{t}O)$_3$SiS$^{(-)(+)}$NH$_2$(C$_2$H$_4$)$_2$O]$_2$ (**2**), [(Bu^{t}O)$_3$SiS$^{(-)(+)}$NH$_2$(C$_6$H$_{11}$)$_2$]$_2$ (**3**), [(Bu^{t}O)$_3$SiS$^{(-)(+)}$NH$_2$C$_5$H$_6$(Me)$_4$]$_2$ (**4**)

	1	**2**	**3**	**4**
Empirical formula	$C_{16}H_{39}NO_3SSi$	$C_{16}H_{37}NO_4SSi$	$C_{24}H_{51}NO_3SSi$	$C_{21}H_{47}NO_3SSi$
M_r (g mol^{-1})	353.63	367.62	461.81	421.75
Temperature (K)	200(2)	200(2)	200(2)	200(2)
Wavelength (Å)	0.71073 (Mo Kα)	0.71073 (Mo Kα)	0.71073 (Mo Kα)	0.71073 (Mo Kα)
Crystal system	monoclinic	monoclinic	triclinic	monoclinic
Space group	$P2_1/n$	$P2_1/c$	$P\bar{1}$	$P2_1/c$
a (Å)	9.547(2)	14.644(3)	10.013(2)	15.315(2)
b (Å)	15.375(3)	9.331(2)	11.235(2)	15.396(3)
c (Å)	15.246(3)	16.723(3)	13.369(3)	11.296(2)
α (°)			102.16(3)	
β (°)	91.54(3)	103.45(3)	95.37(3)	102.34(2)
γ (°)			98.06(3)	
V (Å^3)	2237.1(8)	2222.4(8)	1443.9(6)	2601.9(8)
Z	4	4	2	4
Calculated density (Mg m^{-3})	1.050	1.099	1.060	1.077
Crystal size (mm)	0.4 × 0.3 × 0.3	0.4 × 0.3 × 0.3	0.6 × 0.5 × 0.5	0.5 × 0.3 × 0.2
θ Range (°)	1.88–25.00	1.43–25.00	1.57–26.5	1.36–30.00
Limiting indices	$-11 \leqslant h \leqslant 11$; $0 \leqslant k \leqslant 18$; $0 \leqslant l \leqslant 18$	$-16 \leqslant h \leqslant 16$; $0 \leqslant k \leqslant 11$; $0 \leqslant l \leqslant 19$	$-12 \leqslant h \leqslant 12$; $0 \leqslant k \leqslant 13$; $-16 \leqslant l \leqslant 16$	$-21 \leqslant h \leqslant 0$; $-21 \leqslant k \leqslant 0$; $-15 \leqslant l \leqslant 15$
Reflections collected/unique (R_{int})	4091/3920 (0.0205)	5276/3886 (0.0197)	6295/5972 (0.0092)	7736/7484 (0.0441)
Completeness to θ_{max} (%)	99.5	99.4	99.8	95.2
Refinement method	full-matrix least-squares on F^2	full-matrix least-squares on F^2	full-matrix least-squares on F^2	full-matrix least-squares on F^2
Data/restraints/parameters	3920/0/233	3886/3/265	5972/0/314	7484/0/265
Goodness-of-fit on F^2	1.051	1.064	1.060	1.010
Final R indices [$I > 2\sigma(I)$]	$R_1 = 0.0392$; $wR_2 = 0.1094$	$R_1 = 0.0459$; $wR_2 = 0.1215$	$R_1 = 0.0487$; $wR_2 = 0.1436$	$R_1 = 0.0396$; $wR_2 = 0.0936$
R indices (all data)	$R_1 = 0.0587$; $wR_2 = 0.1210$	$R_1 = 0.0672$; $wR_2 = 0.1363$	$R_1 = 0.0678$; $wR_2 = 0.1661$	$R_1 = 0.0983$; $wR_2 = 0.1115$
Largest difference in peak and hole (e Å^{-3})	0.442 and −0.414	0.556 and −0.394	1.092 and −0.314	0.354 and −0.519

using Sapphire-2 CCD detector. The apparatus was equipped with an open flow thermostat (Oxford Cryosystems) which enabled experiments at 200 K. The stream of nitrogen also prevented the specimen from contact with moist and oxygen. The structures were solved with direct methods and refined with the SHELX-97 program package [14] with the full-matrix least-squares refinement based on F^2. No absorption corrections were applied. All non-hydrogen atoms were refined anisotropically. Hydrogen atoms were refined in geometrically idealised position with isotropic temperature factors 1.2 times the equivalent isotropic temperature factors U_{eq} of their attached atoms (1.5 for CH_3 groups). Hydrogen atoms of ammonium groups were found in the electron density Fourier map and refined without constraints. Disordered Bu^t groups: C12–C14 in **1** (s.o.f. 0.693(10)/0.307(10)); C31–C34 in **2** (s.o.f. 0.547(16)/0.453(16)); C22–C24 in **3** (s.o.f. 0.507(9)/0.493(9)). Basic crystal data, description of the diffraction experiment, and details of the structure refinement are given in Table 1.

3. Results and discussion

Tri-*tert*-butoxysilanethiol reacts readily with secondary amines. All the ammonium salts, described below, were obtained according to the general reaction scheme:

$$(Bu^tO)_3SiSH + R_2NH = (Bu^tO)_3SiS^{(-)}H_2N^{(+)}R_2$$

We decided to use diethylamine, morpholine, dicyclohexylamine and 2,2,4,4-tetramethylpiperidine to study the influence of an additional acceptor oxygen atom and steric hindrance in the vicinity of amine group on the pattern of the hydrogen bond network.

The reaction of tri-*tert*-butoxysilanethiol with the amines yields transparent crystals of: diethylammonium tri-*tert*-butoxysilanethiolate (**1**), morpholinium tri-*tert*-butoxysilanethiolate (**2**), dicyclohexylammonium tri-*tert*-butoxysilanethiolate (**3**) and 2,2,4,4-tetramethylpiperidinium tri-*tert*-butoxysilanethiolate (**4**). The products are hygroscopic and slowly oxidise in the air. Salt **1** was crystallised from hexane, **2** from benzene, **3** from acetonitrile and **4** from propanol-2. It is worthy to note, that none of the last two "hydrogen bond-active" solvents has been found in the solid state.

Molecular structures of the four salts, determined by X-ray diffraction analyses, are shown in Figs. 1–4.

X-ray structural analysis of the four ammonium tri-*tert*-butoxysilanethiolates **1**–**4** points to unexpected similarity of the compounds. It is apparent that the donor O atom of morpholinium salt **2** does not participate in bonding and does not change the hydrogen bonds pattern. The increase of steric hindrance around of the nitrogen atom in compounds **3** and **4** also has no impact on the type of hydrogen bonding.

Hydrogen bond parameters for compounds **1**–**4** are given in Table 2.

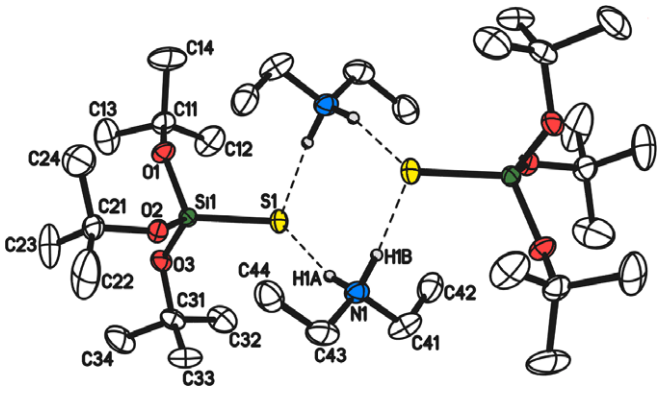

Fig. 1. The structure of $[(Bu^tO)_3SiS^{(-)}H_2N^{(+)}Et_2]_2$ (**1**). Thermal ellipsoids 30%, C–H hydrogen atoms omitted.

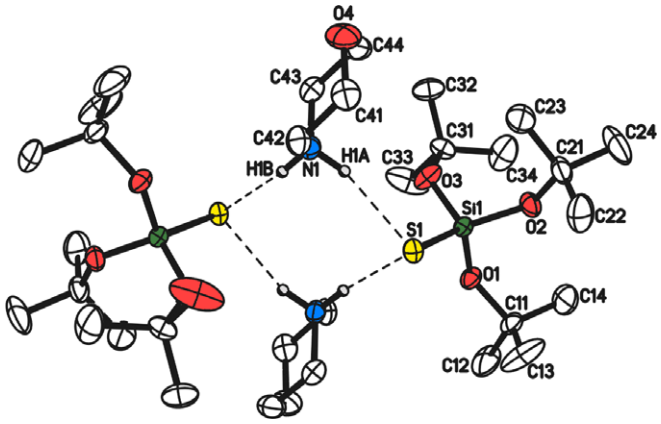

Fig. 2. Structure of $[(Bu^tO)_3SiS^{(-)}H_2N^{(+)}(C_2H_4)_2O]_2$ (**2**). Thermal ellipsoids 30%, C–H hydrogen atoms omitted.

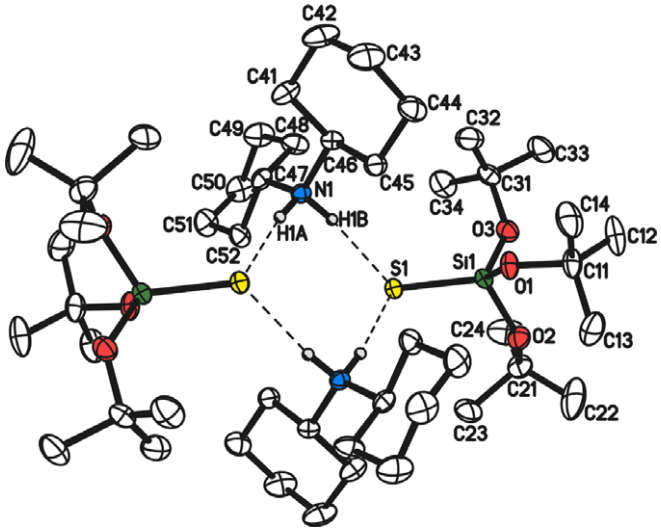

Fig. 3. Structure of $[(Bu^tO)_3SiS^{(-)}H_2N^{(+)}(C_6H_{11})_2]_2$ (**3**). Thermal ellipsoids 30%, C–H hydrogen atoms omitted.

The N···S distances of 3.16–3.34 Å are within the range typical for $N^{(+)}$–H···$^{(-)}$S hydrogen bond type observed in ammonium dithiocarbamates [2,3], aromatic thiolates [4,5,28] or silanethiolates [6,7].

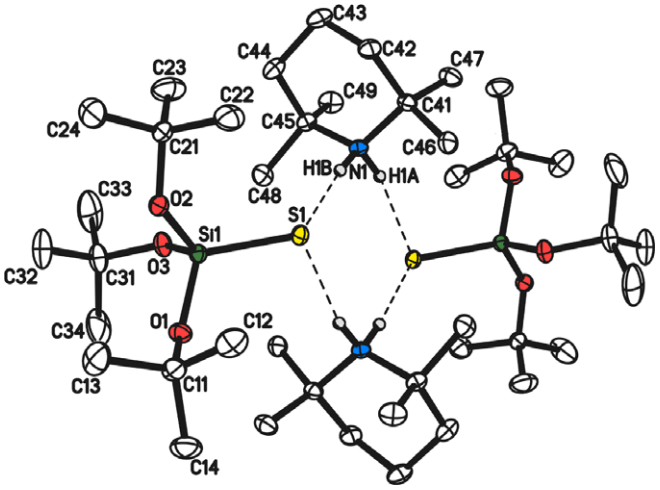

Fig. 4. Structure of $[(Bu^tO)_3SiS^{(-)}H_2N^{(+)}C_5H_6Me_4]_2$ (**4**). Thermal ellipsoids 30%, C–H hydrogen atoms omitted.

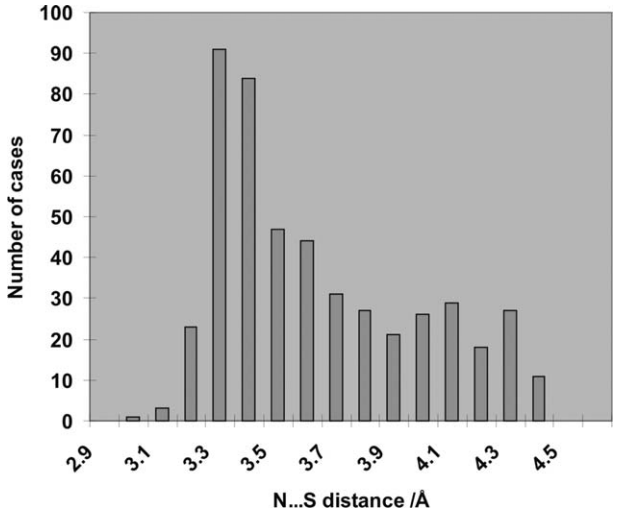

Fig. 5. Histogram of N···S distances reported in the CCDC database.

Table 2
Hydrogen bonds in compounds **1**–**4**

D–H···A	*d*(D–H) (Å)	*d*(H···A) (Å)	*d*(D···A) (Å)	∠(DHA) (°)
1				
N(1)–H(1A)···S(1)	0.90(3)	2.30(3)	3.189(2)	168(2)
N(1)–H(1B)···S(1)$^{\#1}$	0.99(3)	2.17(3)	3.155(2)	172(3)
2				
N(1)–H(1A)···S(1)	0.92(3)	2.34(3)	3.217(2)	160(2)
N(1)–H(1B)···S(1)$^{\#2}$	0.92(3)	2.27(4)	3.176(2)	168(3)
3				
N(1)–H(1A)···S(1)$^{\#1}$	0.97(3)	2.26(3)	3.221(2)	171(2)
N(1)–H(1B)···S(1)	0.94(3)	2.32(3)	3.246(2)	170(2)
4				
N(1)–H(1B)···S(1)	0.91(2)	2.44(2)	3.341(1)	173(2)
N(1)–H(1A)···S(1)$^{\#3}$	0.93(2)	2.34(2)	3.248(1)	167(2)

Symmetry codes: #1: $-x+1, -y+1, -z+1$; #2: $-x+1, -y, -z+1$; #3: $-x+1, -y+1, -z$.

For comparison purposes, we performed a CCDC search, looking for compounds with N···S distances of hydrogen bonds shorter than 4.5 Å. Results of the search are shown in the form of histogram in Fig. 5. Maximum population lies between 3.3 and 3.5 Å and corresponds mainly to charge-assisted hydrogen bonds. Compounds with aliphatic mercapto groups, forming weak S–H···N hydrogen bonds, can be found in the 3.60–4.00 Å range of distances [5].

We assume that hydrogen bonding in the studied compounds **1**–**4** is relatively strong as acceptor–donor distances are short compared to the whole set of considered structures. The high strength of the bonding can be justified by complete proton transfer from silanethiol to the amine. There are several evidences of such a process. First, ammonium hydrogen atoms have been found in the electron density map close to the nitrogen atom. Second argument is based on positions of heavy atoms. In all cases Si–S bond length is short, which is typical for ionic silanethiolates. Covalent silanethiolates have Si–S bond lengths usually ca. 0.05 Å longer (see Table 3). Similar proton transfer is also assumed for 4-aminothiophenol [5], perhaps better described as "zwitterion" or internal ammonium thiophenolate.

All of the studied ammonium silanethiolates comprise a dimer $[(Bu^tO)_3SiS^{(-)}H_2N^{(+)}R_2]_2$, in which four charge-assisted $N^{(+)}$–H···$^{(-)}$S hydrogen bonds form a stable, repeatable core. This pattern of eight-membered ring with four donors and two acceptors is known as R4,2(8) in the graph theory [25,26] (see Fig. 6).

Dimeric unit [thiol-amine]$_2$ is a characteristic feature for all studied ammonium salts. The dimers are packed in crystal as separate units with no hydrogen bonds between them (only van der Waals forces). Exemplary packing diagram of **2** is presented in Fig. 7.

Table 3
Mean Si–S bond lengths – literature data

Si–S bond length (Å)	Compound	Reference
Covalent		
2.169	$[\{(Bu^tO)_3SiSAu\}_4]$	[15]
2.143	$[\{(\{Bu^tO\}_3SiS)_2Pb\}_2]$	[16]
2.136	$[\{(Bu^tO)_3SiS\}_4Sn_2S_2]$	[17]
2.132	$\{(Bu^tO)_3SiS\}_2$	[18]
2.120	$HOOC–C_6H_4–HgSSi(OBu^t)_3$	[19]
2.119	$\{(Bu^tO)_3Si\}_2S$	[20]
Ionic		
2.066	$2(Bu^tO)_3SiS^{(-)}$, $C_{10}H_{28}N_4{}^{(+)}\cdot 2C_3H_7OH$	[21]
2.066	$(Bu^tO)_3SiS^{(-)}$, $C_9H_{18}NH_2{}^{(+)}$	this work
2.064	$Li_8\{(Bu^tO)_3SiS\}_6(OH)_2(H_2O)_2$	[22]
2.063	$[Li_2\{(Bu^tO)_3SiS\}_2(C_4H_{10}O_2)]$	[23]
2.062	$(i\text{-}PrO)_3SiS^{(-)}H_3N^{(+)}Bu^t$	[7]
2.061	$(Bu^tO)_3SiS^{(-)}$, $(C_2H_5)_2NH_2{}^{(+)}$	this work
2.059	$(Bu^tO)_3SiS^{(-)}H_2N^{(+)}(C_2H_4)_2O$	this work
2.056	$(Bu^tO)_3SiS^{(-)}$, $(C_6H_{11})_2NH_2{}^{(+)}$	this work
2.052	$[Li_2\{(Bu^tO)_3SiS\}_2(C_4H_8O)_2]$	[23]
2.013	$[Cl_3SiS^{(-)(+)}NEt_4]\cdot 0.5CCl_4$	[24]

Standard deviations are of 2–3 units in the last digit.

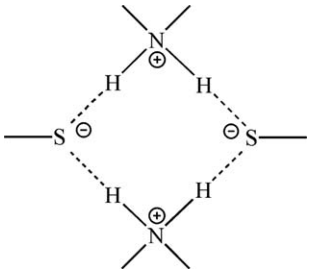

Fig. 6. Schematic drawing of R4,2(8) motif.

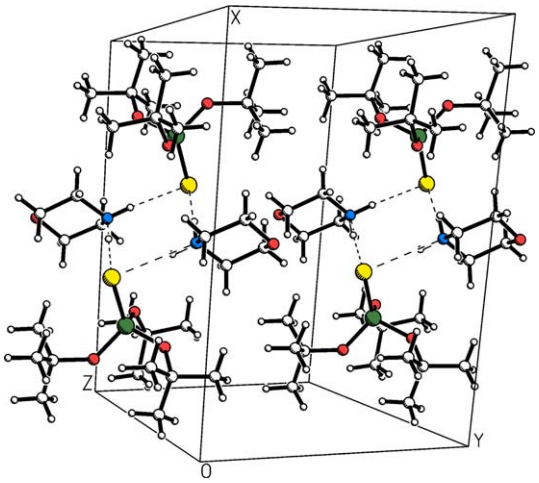

Fig. 7. Packing diagram for $(Bu^tO)_3SiS^{(-)}H_2N^{(+)}(C_2H_4)_2O$ (**2**).

Pattern R4,2(8), although rare, has already been found in ammonium dithiocarbamate [2] and amine-ketone dimers [27]. In the first case only the anionic sulfur atom from $–CS_2^-$ group (with the longer C–S bond) takes part in hydrogen bonding and the doubly bonded S atom is passive. Another example of this motif is present in study by Carmalt et al. [28], where anionic sulfur is donated by $C_6F_5S^{(-)}$ anion.

Some preliminary results [29] on salts of tri-*tert*-butoxysilanethiol with amines bearing hydroxyl groups also point to the robustness of the dimeric synthon.

Our earlier studies on salts of **primary** amines with silanethiols [7] have shown that cubane-like structures are formed. The cubanes can be regarded as combined dimers of two motifs R4,2(8) (see Fig. 8). The connection between

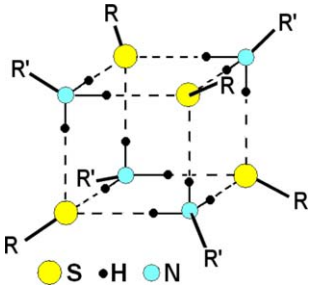

Fig. 8. Structure of primary ammonium silanethiolates.

dimers is also built from charge-assisted $N^{(+)}–H\cdots S^{(-)}$ hydrogen bonds. In other words, every face of the cube is formed by the ring R4,2(8). Final cubic structure is just the result of fact, that $–NH_3^{(+)}$ cation and $–S^{(-)}$ anion are perfect vertexes for the cube, being a triple donor and a triple acceptor, respectively.

When a less demanding thiophenolate anion is combined with dicyclohexylammonium cation an infinite chain structure of hydrogen bonds can be alternatively formed [4].

Crystal engineering scientists make wide use of supramolecular hydrogen bond motif R2,2(8) (eight-membered ring containing two donors and two acceptors) often observed in dimers of carboxylic acids. Although less abundant than R2,2(8), motif R4,2(8) shows also some universality and can be realised by several chemically different atomic arrangements (Fig. 9):

(a) $N^{(+)}–H\cdots O$ for antimony [30] or nickel [31] compounds, containing protonated amine as counter-cation,
(b) $N^{(+)}–H\cdots S^{(-)}$ for several classes of compounds, mainly metallothiolates [32–36,28,37]. All known ammonium silanethiolates belong to this class,
(c) $N^{(+)}–H\cdots O^{(-)}$ for some ammonium monothiooxalates [38,39]
(d) $O–H\cdots S^{(-)}$ for structures with water molecule as a donor [40,41].

The pattern can be seen, in some cases, only when less rigorous criteria for maximum hydrogen- acceptor distance, e.g., sum of van der Waals radii plus 0.1 A, are applied.

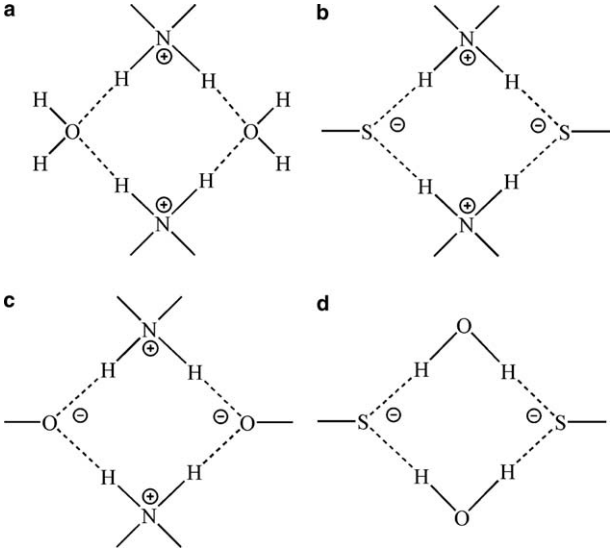

Fig. 9. Isographic functional groups of the R4,2(8) motif, (a) protonated amine–water, (b) protonated amine–anionic sulfur, (c) protonated amine–anionic oxygen, (d) anionic sulfur–water.

4. Conclusion

Eight-membered ring with four donors and two acceptors, R4,2(8), is characteristic for adducts of all studied amines with tri-*tert*-butoxysilanothiol. Oxygen atom of morpholinium salt **2** and the steric hindrance around of the nitrogen atom in compounds **3** and **4** have no impact on the hydrogen bond pattern.

5. Supplementary data

CCDC Nos. 237890–237893 (for compounds **1**, **2**, **3** and **4**, respectively) contain the supplementary crystallographic data for this paper. These data can be obtained free of charge on request, quoting the deposition number, at www.ccdc.cam.ac.uk/conts/retrieving.html (or from the Cambridge Crystallographic Data Centre, 12 Union Road, Cambridge CB2 1EZ, UK; fax: (international) +44 1223 336 033; e-mail: deposit@ccdc.cam.ac.uk).

Acknowledgements

Financial support for KB from the Polish State Committee of Scientific Research (Project No. 3 T09A 120 28) is gratefully acknowledged. Authors thank Dr. Anna Dolega for helpful discussion during preparation of the manuscript.

References

[1] G.R. Desiraju, T. Steiner, The weak hydrogen bond in structural chemistry and biologyIUCr Monographs on Crystallography, vol. 9, Oxford University Press, Oxford, 1999.
[2] A. Wahlberg, Acta Crystallogr. B34 (1978) 3479.
[3] A. Wahlberg, Acta Crystallogr. B35 (1979) 485.
[4] K. Baranowska, J. Chojnacki, B. Becker, W. Wojnowski, Acta Crystallogr. E59 (2003) o765.
[5] R.K.R. Jetti, R. Boese, T.S. Thakur, V.R. Vangala, G.R. Desiraju, Chem. Commun. (2004) 2526.
[6] K. Baranowska, J. Chojnacki, W. Wojnowski, B. Becker, Acta Crystallogr. E59 (2003) o2022.
[7] B. Becker, K. Baranowska, J. Chojnacki, W. Wojnowski, Chem. Commun. (2004) 620.
[8] S. Suh, J.H. Hardesty, T.A. Albright, D.M. Hoffman, Inorg. Chem. 38 (1999) 1627.
[9] G.M. Kapteijn, D.M. Grove, W.J.J. Smeets, H. Kooijman, A.L. Spek, G. van Koten, Inorg. Chem. 35 (1996) 534.
[10] S. Daniel, D.M. Hoffman, Inorg. Chem. 41 (2002) 3843.
[11] W.P. Chung, J.C. Dewan, M.A. Walters, Inorg. Chem. 30 (1991) 4280.
[12] W. Wojnowski, A. Herman, Z. Anorg. Allg. Chem. 425 (1976) 91.
[13] R. Piękoś, W. Wojnowski, Z. Anorg. Allg. Chem. 318 (1962) 212.
[14] G.M. Sheldrick, SHELX-97. Programs for the Solution and the Refinement of Crystal Structures from Diffraction Data, University of Göttingen, Göttingen, Germany, 1997.
[15] W. Wojnowski, B. Becker, J. Saßmannshausen, E.M. Peters, K. Peters, H.G. von Schnering, Z. Anorg. Allg. Chem. 620 (1994) 1417.
[16] W. Wojnowski, M. Wojnowski, K. Peters, E.-M. Peters, H.G. von Schnering, Z. Anorg. Allg. Chem 535 (1986) 56.
[17] K. Peters, E.-M. Peters, H.G. von Schnering, W. Wojnowski, S. Tamulewicz, Z. Kristallogr. NCS 213 (1998) 347.
[18] W. Wojnowski, M. Wojnowska, B. Becker, M. Noltemeyer, Z. Anorg. Allg. Chem. 561 (1988) 167.
[19] J. Chojnacki, A. Wałaszewska, E. Baum, W. Wojnowski, Acta Crystallogr. E59 (2003) m125.
[20] W. Wojnowski, W. Bocheńska, K. Peters, E.-M. Peters, H.G. von Schnering, Z. Anorg. Allg. Chem. 533 (1986) 165.
[21] B. Becker, A. Zalewska, A. Konitz, W. Wojnowski, Z. Anorg. Allg. Chem. 627 (2001) 271.
[22] K. Baranowska, J. Chojnacki, W. Wojnowski, I. Krossing, Acta Crystallogr. E58 (2002) m569.
[23] E. Jesionka, A. Ciborska, J. Chojnacki, W. Wojnowski, Acta Crystallogr. C61 (2005) m321.
[24] U. Mueller, V. Krug, Z. Naturforsch. 40b (1985) 1015.
[25] M.C. Etter, Acc. Chem. Res. 23 (1990) 120.
[26] J. Bernstein, R.E. Davis, L. Shimoni, N.-L. Chang, Angew. Chem., Int. Ed. Engl. 34 (1995) 1555.
[27] C.B. Aakeroy, A.M. Beatty, Aust. J. Chem. 54 (2001) 409.
[28] C.J. Carmalt, C.W. Dinnage, I.P. Parkin, A.J.P. White, D.J. Williams, J. Chem. Soc., Dalton Trans. (2001) 518.
[29] K. Baranowska, Unpublished results.
[30] L. Engelke, C. Nather, W. Bensch, Eur. J. Inorg. Chem. (2002) 2936.
[31] T.J. Podesta, A.G. Orpen, CrystEngComm 4 (2002) 336.
[32] T. Jiang, A. Lough, G.A. Ozin, R.L. Bedard, J. Mater. Chem. 8 (1998) 733.
[33] M. Schur, A. Gruhl, C. Nather, I. Jess, W. Bensch, Z. Naturforsch. 54 b (1999) 1524.
[34] K. Tani, S. Hanabusa, S. Kato, S. Mutoh, S. Suzuki, M. Ishida, J. Chem. Soc., Dalton Trans. (2001) 518.
[35] P. Roman, J.I. Beitia, A. Luque, J.M. Gutierrez-Zorrilla, Mater. Res. Bull. 27 (1992) 339.
[36] M.C. Aragoni, M. Arca, F. Demartin, F.A. Devillanova, C. Graiff, F. Isaia, V. Lippolis, A. Tiripicchio, G. Verani, Eur. J. Inorg. Chem. (2000) 2239.
[37] O.V. Shishkin, N.N. Kolos, V.D. Orlov, V.P. Kuznetsov, E.E. Lakin, Acta Crystallogr. C51 (1995) 2643.
[38] B. Krzyzanowska, W.J. Stec, M.W. Wieczorek, J. Blaszczyk, Heteroatom Chem. 5 (1994) 533.
[39] P. Roman, J.I. Beitia, A. Luque, C. Guzman-Miralles, Polyhedron 15 (1996) 1071.
[40] C. Nather, S. Scherb, W. Bensch, Acta Crystallogr. E59 (2003) m280.
[41] M. Wang, W. Chen, L. Cai, G. Zhou, G. Guo, J. Huang, J. Cluster Sci. 14 (2003) 495.

structure where 3-pyridylmethanol is terminal ligand coordinated through nitrogen atom of pyridine rings. The complexes $[CuX_2(\mu\text{-}3PM)_2]_n$ (where X = salicylate [13] (sal), flufenamate [14] (fluf) or clofibriate [15] (clof)) are two-dimensional coordination polymers, where Cu atoms are linked by bridged 3-pyridylmethanol ligand. On the other hand, the complex $[CuX_2(\mu\text{-}3PM)_2]_n$ (X = trichloroacetate [16], dichloroacetate [16], 3-nitrobenzoate [17], 3,5-dinitrobenzoate [11] and niflumate (nif) [18]) is one-dimensional coordination polymer, where Cu atoms are linked by bridged 3-pyridylmethanol ligand. The crystal structure of zinc(II) complex $[Zn(benzoate)_2(\mu\text{-}3PM)_2]_n$ consists also of one-dimensional coordination polymers, where Zn atoms are linked by bridged 3-pyridylmethanol ligand [19].

In this report, we describe the synthesis and spectral properties as well as X-ray structure analysis of coordination polymers with formulas: $[Cu(2\text{-}MeSnic)_2(\mu\text{-}3PM)_2]_n$ (**1**), where 2-MeSnic = 2-methyltionicotinate; $[Cu(2\text{-}Clbz)_2(\mu\text{-}3PM)_2]_n$ (**2**), where 2-Clbz = 2-chlorobenzoate and $[Cu_3(2\text{-}Clnic)_6(\mu\text{-}3PM)_4(3PM)_2]_n$ (**3**), where 2-Clnic = 2-chloronicotinate.

2. Results and discussion

2.1. Structure of complex *1*

The molecule of **1** lies about an inversion centre and the molecular structure of **1** is shown in Fig. 1. Selected bond lengths and bond angles are summarized in Table 1. Coordination environment of the copper(II) atom is tetragonal bipyramidal. The tetragonal plane is built up by a pair of unidentate 2-methylnicotinate anions using carboxylate oxygen atoms [Cu–O1 = 1.956(2) Å] and a pair of neutral 3-pyridylmethanol molecules using nitrogen atoms of pyridine ring [Cu–N2 = 2.010(2) Å] in *trans* positions. The axial positions are occupied by two hydroxyl oxygen atoms

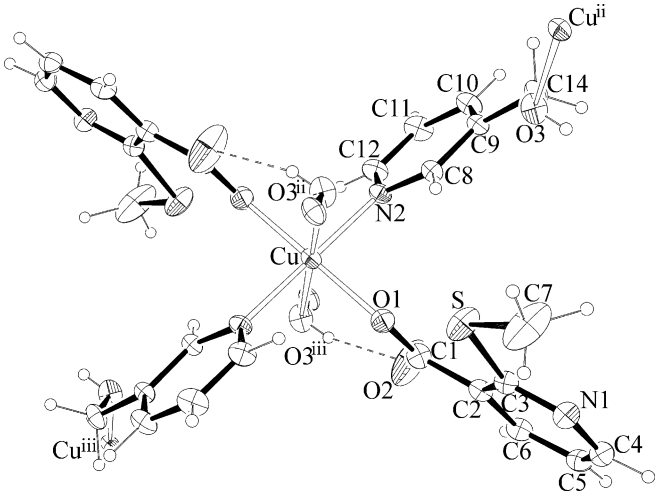

Fig. 1. Perspective view of complex $[Cu(2\text{-}MeSnic)_2(\mu\text{-}3\text{-}PM)_2]_n$ (**1**), with the atom numbering scheme. Thermal ellipsoids are drawn at the 50% probability level.

Table 1
Selected bond lengths (Å) and angles (°) for **1**, **2** and **3**[a]

1			
Cu–O1	1.956(2)	Cu–N2	2.010(2)
Cu–O3^{ii}	2.707(2)	Cu–O3^{iii}	2.707(2)
O1–Cu–N2	90.19(6)	O1–Cu–N2^{i}	89.81(6)
O1–Cu–O3^{iii}	88.21(6)	O1–Cu–O3^{ii}	91.79(6)
N2–Cu–O3^{ii}	95.68(6)	N2–Cu–O3^{iii}	84.32(6)
2			
Cu–O1	1.964(1)	Cu–N1	2.017(1)
Cu–O3^{v}	2.4668(9)	Cu–O3^{vi}	2.4668(9)
O1–Cu–N1	89.30(4)	O1–Cu–N1^{iv}	90.70(4)
O1–Cu–O3^{v}	89.28(4)	O1–Cu–O3^{vi}	90.72(4)
N1–Cu–O3^{v}	92.34(4)	N1–Cu–O3^{vi}	87.66(4)
3			
Cu1–O1	1.982(4)	Cu1–N2	2.025(4)
Cu1–O8^{viii}	2.418(4)	Cu1–O8^{vii}	2.418(4)
Cu2–O4	1.958(4)	Cu2–O6	1.964(4)
Cu2–N5	2.019(6)	Cu2–N6	2.025(5)
Cu2–O3	2.338(4)	O4–Cu2–O6	178.4(2)
O1–Cu1–N2	89.5(2)	N6–Cu2–O3	89.6(2)
O1–Cu1–O8^{viii}	87.4(2)	N2–Cu1–O8^{viii}	84.7(2)
O1–Cu1–O8^{vii}	92.6(2)	N2–Cu1–O8^{vii}	95.2(2)
O4–Cu2–N5	91.3(2)	O4–Cu2–N6	90.5(2)
O6–Cu2–N6	89.9(2)	O6–Cu2–N5	88.1(2)
O4–Cu2–O3	87.7(2)	O6–Cu2–O3	93.9(2)
N5–Cu2–O3	99.5(2)		

[a] Symmetry code: (i) $-x, -y, -z+1$; (ii) $x+1, y, z$; (iii) $-x-1, -y, -z+1$; (iv) $-x, -y, -z$; (v) $x, -y+1/2, z+1/2$; (vi) $-x, y-1/2, -z-1/2$; (vii) $x-1, y, z$; (viii) $-x+1, -y+1, -z+1$.

[Cu–O3^{ii} = 2.707(2) Å] from adjacent two molecules of 3-pyridylmethanol ($x+1$, y, z and $-x-1$, $-y$, $-z+1$). The intramolecular hydrogen bonds O3–H3···O2 (Table 2) create six membered metalocyclus and stabilize the molecular structure.

The crystal structure of **1** consists of 1-D chains (Fig. 2). The 1-D chains consist of copper(II) centers linked by bridges of neutral 3-pyridylmethanol molecules. The weak hydrogen bonds [C8–H8···O3 ($-x-1$, $-y$, $-z+1$) and C12–H12···O1 ($-x$, $-y$, $-z+1$)] (Table 2) stabilize 1-D coordination polymers. The 1-D chains of **1** are connected by face-to-face π···π stacking interactions [20] between two

Table 2
Parameters in (Å) and (°) of hydrogen bonds within the structure **1**, **2** and **3**

D–H···A		*d*(D···A)	∠(DHA)
1			
O3–H3···O2	$x-1, y, z$	2.609(2)	119.1
C8–H8···O3	$-x-1, -y, -z+1$	3.110(2)	114.6
C12–H12···O1	$-x, -y, -z+1$	3.059(3)	101.1
2			
O3–H7···O2	$-x, y+1/2, -z-1/2$	2.668(2)	165.5
3			
O3–H10···O7		2.649(6)	154(8)
O8–H23···O2	$x+1, y, z$	2.674(7)	156(7)
O9–H30···O5	$x-1, y, z$	2.721(8)	159(9)
C28–H19···O9	$-x+1, -y+1, -z+2$	3.229(8)	127.4
C35–H27···O4	$x+1, y, z$	2.909(8)	112.4
C33–H25···N4	$x, y-1, z$	3.490(9)	156.6
C(33)–H(25)···N(4)	$x, y-1, z$	3.490(9)	156.6

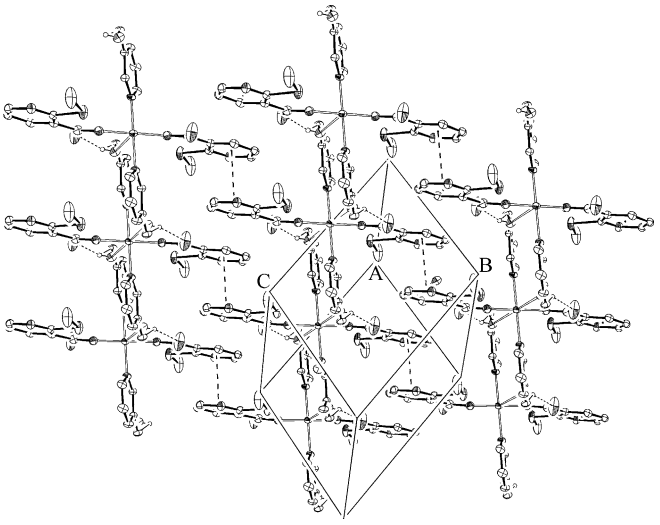

Fig. 2. View of the packing of $[Cu(2\text{-}MeSnic)_2(\mu\text{-}3\text{-}PM)_2]_n$ (**1**) in the crystal structure; hydrogen atoms are omitted for clarity.

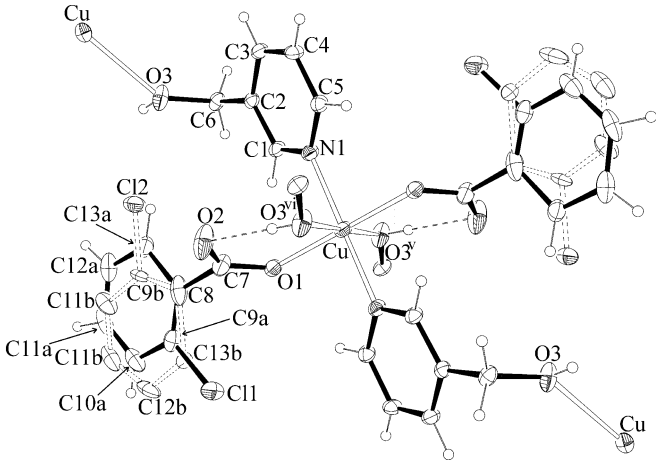

Fig. 3. Perspective view of complex $[Cu(2\text{-}Clbz)_2(\mu\text{-}3\text{-}PM)_2]_n$ (**2**), with the atom numbering scheme. Thermal ellipsoids are drawn at the 50% probability level.

pyridine rings of 2-methyltionicotinate anions ($-x-1$, $-y-1$, $-z+2$) of complex **1** and a weak hydrogen bond interaction. The plane–plane and centroid–centroid distances of $\pi\cdots\pi$ stacking interactions are 3.34 and 3.47 Å, respectively.

2.2. Structure of complex 2

The molecule of **2** lies about an inversion centre and the molecular structure of **2** is shown in Fig. 3. Selected bond lengths and bond angles are summarized in Table 1. The coordination environment of the copper(II) atom is tetragonal bipyramidal. The tetragonal plane is built up by a pair of unidentate 2-chlorobenzooate anions using carboxylate oxygen atoms [Cu–O1 = 1.964(1) Å] and a pair of neutral 3-pyridylmethanol molecules using nitrogen atoms of the pyridine ring [Cu–N1 = 2.017(1) Å] in *trans* positions. The axial positions are occupied by two hydroxyl oxygen atoms [$Cu\text{–}O3^{v} = Cu\text{–}O3^{vi}$ = 2.4668(9) Å] from adjacent two molecules of 3-pyridylmethanol ($-x$, $y+1/2$, $-z-1/2$ and x, $-y-1/2$, $z+1/2$). The intramolecular hydrogen bonds O3–H7···O2 (Table 2) create six membered metalocyclus and stabilize the molecular structure.

The crystal structure of **2** consists of 2-D sheets (Fig. 4). The layers are situated in *bc* plane and consist of two zigzag chains crossing at the Cu(II) atom as shown in Fig. 4.

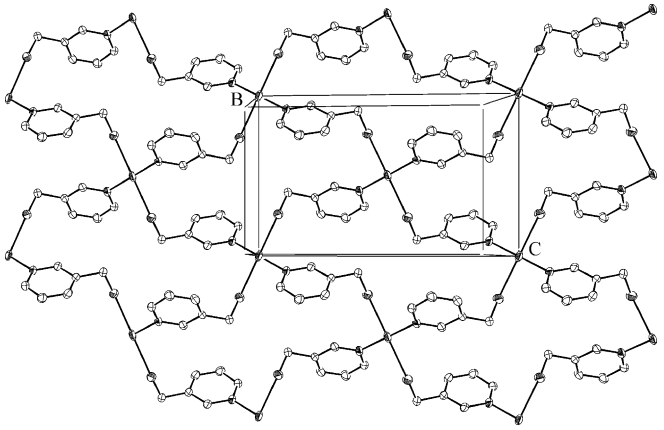

Fig. 4. View of the packing of $[Cu(2\text{-}Clbz)_2(\mu\text{-}3\text{-}PM)_2]_n$ (**2**) in the crystal structure; hydrogen atoms and 2-chlorbenzoate groups are omitted for clarity.

2.3. Structure of complex 3

The crystal structure of **3** consists of 1-D coordination polymers. The 1-D chains consist of two chemical by different copper(II) centers bridged by 3-pyridylmethanol ligands. The molecular structure of **3** is shown in Fig. 5 Selected bond lengths and bond angles are summarized in Table 1. The copper(II) atom Cu1 lies at the inversion centre [0, 0.5, 0.5]. The coordination environment of the Cu1 atom is tetragonal bipyramidal (Fig. 5). The tetragonal plane is built up by a pair of unidentate 2-chloronicotinate anions using carboxylate oxygen atoms [Cu1–O1 = 1.982(4) Å] and a pair of neutral bridging 3-pyridylmethanol molecules using nitrogen atoms of pyridine ring [Cu1–N2 = 2.025(4) Å] in *trans* positions. The axial positions are occupied by two hydroxyl oxygen atoms from adjusted bridging two molecules of 3-pyridylmethanol [$Cu1\text{–}O8^{viii} = Cu1\text{–}O8^{vii}$ = 2.418(4) Å ($-x+1$, $-y+1$, $-z+1$ and $x-1$, y, z)]. Atoms Cu2 lie in general crystallographic position. The coordination environment of the Cu2 atoms is tetragonal pyramidal (Fig. 5). The tetragonal plane is built up by a pair of unidentate 2-chloronicotinate anions using carboxylate oxygen atoms [Cu2–O4 = 1.958(4) and Cu2–O6 = 1.964(4) Å], one bridging and one terminal neutral 3-pyridylmethanol molecules using nitrogen atoms of the pyridine ring [Cu2–N5 = 2.019(5) and Cu2–N6 = 2.025(5) Å, respectively]. The axial position is occupied by the hydroxyl oxygen atom

of adjacent bridging molecule of 3-pyridylmethanol [Cu2–O3 = 2.338(4) Å]. The Cu2 atom is 0.092(3) Å above the equatorial plane O4–N5–O6–N6 toward water oxygen atom O3. For such five coordinated structures, the parameter τ ($\tau = \alpha - \beta/60$, where α and β are the longest angles) was introduced [21]. Value τ is 0 for perfectly tetragonal geometry and 1 for perfectly trigonal-bipyramidal geometry. In this case $\tau = 0.027$.

The crystal structure of **3** consists of 1-D "accordion" chains, which lie in *ac* plane (Fig. 6). As can be seen, the strong intramolecular O–H···O hydrogen bonds [O3–H10···O7; O8–H23···O2 ($x+1$, y, z)] (Table 2) create six membered metalocycles and stabilize with intermolecular O–H···O hydrogen bonds [O9–H30···O5 ($x-1$, y, z)] the 1-D "accordion" chains. In Fig. 6 a view of the packing of **3** perpendicular to *bc* plane is shown. The "accordion" chains are only connected by various weak hydrogen bond interactions C–H···O [C28–H19···O9 ($-x+1$, $-y+1$, $-z+2$); C35–H27···O4 ($x+1$, y, z)] and C–H···N [C33–H25···N4 (x, $y-1$, z)] (Table 2).

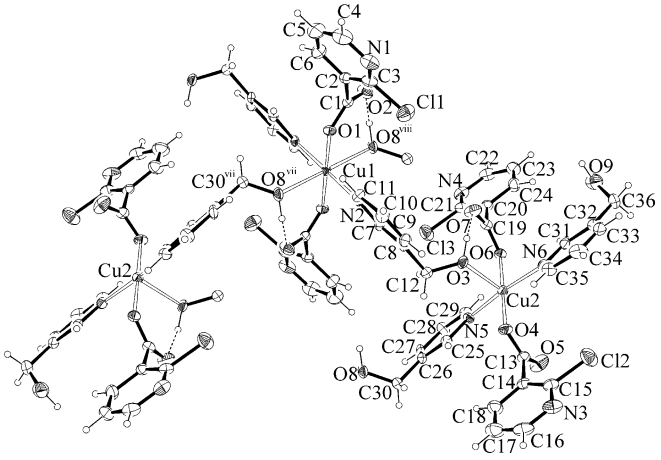

Fig. 5. Perspective view of complex $[Cu_3(2\text{-Clnic})_6(\mu\text{-3-PM})_4(3\text{-PM})_2]_n$ (**3**), with the atom numbering scheme. Thermal ellipsoids are drawn at the 30% probability level.

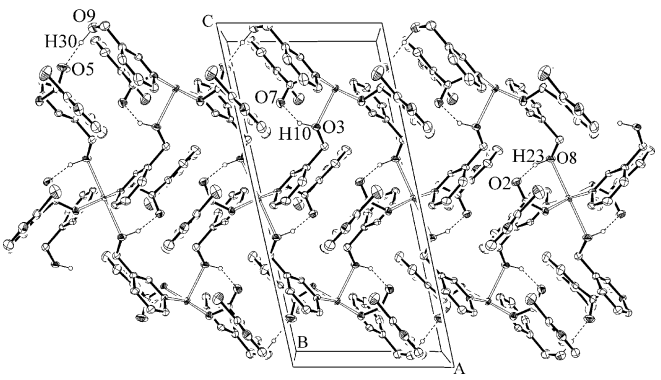

Fig. 6. View of the packing of $[Cu_3(2\text{-Clnic})_6(\mu\text{-3-PM})_4(3\text{-PM})_2]_n$ (**3**) in the crystal structure; hydrogen atoms are omitted for clarity.

2.4. EPR spectra

The EPR spectra of all complexes under study were measured in powder state at room temperature and were interpreted by computer simulation using spin Hamiltonian

$$\hat{H} = B \cdot \bar{g} \cdot \hat{S} + \hat{S} \cdot \bar{A} \cdot \hat{I}, \quad (1)$$

where the symbols have their usual meaning [22]. All three EPR spectra exhibit axial monomeric type of signal with values of the *g* factors (see Table 3) typical for compounds with tetragonal distorsion around the Cu(II) atom [23]. The order of $g_\perp < g_\parallel$ indicates $d_{x^2-y^2}$ ground state. In addition, the EPR spectrum of **2** also exhibits features of hyperfine splitting in parallel part of signal ($I^{Cu} = 3/2$) with a value of $A_\parallel = 174$ Gauss (see Fig. 7).

3. Experimental

3.1. Preparation of the complexes

3.1.1. *[Cu(2-MeSnic)$_2$(μ-3PM)$_2$]$_n$ (**1**)*

The complex **1** was prepared by adding 3PM (5 cm^3) in excess to methanol solutions (20 cm^3) of appropriate Cu(2-Mesnic)$_2 \cdot H_2O$ (1.25 mmol). The fine blue microcrystals produced on standing were separated, washed and dried in vacuo, yield 85%. *Anal*. Calc. for **1**: C, 50.52; H, 4.24; N, 9.06; S, 10.37; Cu, 10.28. Found: C, 50.4; H, 4.4; N, 9.1; S, 10.5; Cu, 10.15%. IR (KBr) cm^{-1}: 1607 $\nu_{as}(COO^-)$;

Table 3
EPR spin Hamiltonian parameters for studied complexes[a]

	$g_\perp$	$g_\parallel$	$A_\parallel$/Gauss
1	2.068	2.241	174
2	2.053	2.275	
3	2.088	2.288	

[a] The EPR spectra were measured in polycrystalline form at room temperature.

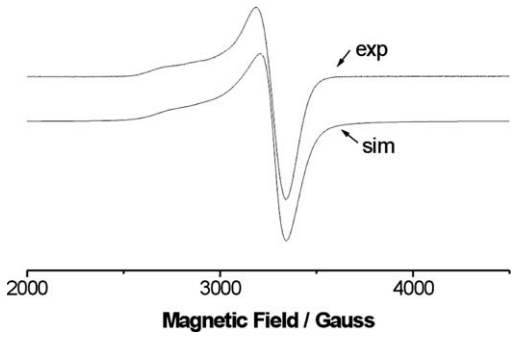

Fig. 7. EPR powder spectrum of **2** at room temperature and its computer simulation.

1377 $\nu_s(COO^-)$; 1072 ν(C–O). IR (PE) cm^{-1}: 435 γ(py); 421 γ(py); 402 γ(py). VIS cm^{-1}: 16900, 13500.

3.1.2. [Cu(2-Clbz)$_2$(3PM)$_2$]$_n$ (2)

The complex **2** was prepared by adding 3PM (5 cm^3) in excess to methanol–acetone solutions (4 cm^3 methanol + 1 cm^3 acetone) of Cu(2-Clbz)$_2 \cdot H_2O$ (1.25 mmol). The fine blue microcrystals produced on standing were separated, washed and dried in vacuo. Well-shaped single crystals of [Cu(2-Clbz)$_2$(μ-3PM)$_2$]$_n$ **2** suitable for structure determination were obtained by recrystallizing in a mixture methanol–acetone (4 + 1), yield 80%. *Anal*. Calc. for **2**: C, 42.16; H, 2.95; N, 8.19; Cu, 9.29. Found: C, 42.2; H, 2.8, N, 8.2, Cu, 9.35%. IR (KBr) cm^{-1}: 1602 $\nu_{as}(COO^-)$; 1386 $\nu_s(COO^-)$; 1029 ν(C–O). IR (PE) cm^{-1}: 462 γ(py); 424 γ(py); 384 γ(py). VIS cm^{-1}: 16140.

3.1.3. [Cu$_3$(2-Clnic)$_6$(μ-3PM)$_4$(3PM)$_2$]$_n$ (3)

The complex **3** was prepared by adding 3PM (5 cm^3) in excess to methanol solutions (20 cm^3) of appropriate Cu(2-Clnic)$_2 \cdot H_2O$ (1.25 mmol). The fine blue microcrystals produced on standing were separated, washed and dried in vacuo. Well-shaped single crystals of [Cu$_3$(2-Clnic)$_6$(μ-3PM)$_4$(3PM)$_2$]$_n$ suitable for structure determination were obtained by recrystallizing in methanol, yield 80%. *Anal*. Calc. for **3**: C, 48.46; H, 3.39; N, 9.42; Cu, 10.68. Found. C, 48.2; H, 3.4; N, 9.4; Cu, 10.57%. IR (KBr) cm^{-1}: 1629 $\nu_{as}(COO^-)$; 1605 $\nu_{as}(COO^-)$; 1382 $\nu_s(COO^-)$; 1065 ν(C–O). IR (PE) cm^{-1}: 462 γ(py); 424 γ(py); 385 γ(py). VIS cm^{-1}: 15750.

3.2. Chemical reagents, analysis and spectral studies

All the chemicals used were of analytical grade (Aldrich or Sigma) and were used without further purification.

Copper was determined by electrolysis after mineralization of the complexes; carbon, hydrogen, nitrogen and sulfur were determined by microanalytical methods (Carlo Erba Instruments EA 1108). Besides the elemental analysis, the water content in hydrates was determined from thermogravimetrical curves.

Electronic spectra of the powdered samples in Nujol mulls were recorded at room temperature on a Specord M40 and Specord 200, respectively. IR spectra were recorded on a Nicolet Magna 750 spectrophotometer at room temperature. Spectra of solid samples were obtained in nujol mulls, KBr and polyethylene pellets at a resolution of 1 cm^{-1}. EPR spectra of powder samples were measured on a Bruker 200D SRC X-band (9.4 GHz) at room temperature. The simulations of the EPR spectra were performed using the commercially available program SIMFONIA (Bruker) [24].

3.3. Structure determination

Data collection and cell refinement were carried out using a κ-axis diffractometer Kuma KM-4 CCD with graphite monochromated Mo Kα radiation, using CRYSALIS software package [25]. The diffraction intensities were corrected for Lorentz and polarization factors. The structures were solved by direct methods using SHELXS-97 [26] or SIR-97 [27]. The numerical absorption correction

Table 4
Crystallographic data for compounds **1**, **2** and **3**

	1	**2**	**3**
Empirical formula	$C_{13}H_{13}N_2O_3SCu_{0.5}$	$C_{13}H_{11}NO_3ClCu_{0.5}$	$C_{36}H_{30}N_6O_9Cl_3Cu_{1.5}$
M	309.08	296.45	892.32
T (K)	170(2)	100(2)	293(2)
Crystal size (mm^3)	0.40 × 0.25 × 0.20	0.18 × 0.15 × 0.10	0.20 × 0.16 × 0.15
Crystal system	triclinic	monoclinic	triclinic
Space group	$P\bar{1}$	$P2_1/c$	$P\bar{1}$
a (Å)	7.5003(9)	10.9140(9)	8.656(2)
b (Å)	9.7682(9)	8.4720(8)	11.947(2)
c (Å)	10.4550(9)	13.6580(9)	19.014(4)
α (°)	67.415(5)		101.98(3)
β (°)	70.174(5)	102.920(3)	101.98(3)
γ (°)	86.450(5)		90.43(3)
U ($Å^3$)	663.3(1)	1230.9(2)	1878.9(7)
Z	2	4	2
D_{calc} ($Mg\,m^{-3}$)	1.548	1.600	1.577
μ (Mo Kα) (mm^{-1})	1.030	1.151	1.133
F(000)	319	606	909
θ Range (°)	2.90–27.99	3.62–28.00	2.87–28.00
$h/k/l$	−9,9/−12,12/−13,13	−14,14/−11,11/−17,17	−11,6/−15, 15/−24,24
Reflections collected	4296	8257	14492
Unique reflections (R_{int})	3064 (0.0194)	2926 (0.0380)	8620 (0.0251)
Data/restraints/parameters	3064/0/178	2926/0/220	8620/3/514
S	1.065	0.976	1.077
R_1, wR_2 (observed reflections)	0.0346, 0.0902	0.0370, 0.0899	0.0520, 0.1390
R_1, wR_2 (all reflections)	0.0361, 0.0920	0.0539, 0.0992	0.0520, 0.1390
$-\Delta_\rho/-\Delta_\rho$ ($e^{-1}Å^{-3}$)	−0.420/0.360	−0.410/0.292	−0.630/1.306

was made by using CRYSALIS. Geometrical analysis was performed using SHELXL-97 [28]. The structure of the complexes **1**, **2** and **3** was drawn by ORTEP-3 for Windows [29]. The Single Crystal Suite WINGX was used as an interface system for all the crystallographic programs and as software for preparing material for publication [30]. Crystal data and conditions of data collection and refinement are reported in Table 4.

The 2-chlorophenyl group of compound **2** is disordered occupying two statistical positions, represented by atoms C9a, C10a, C11a, C12a, C13a, Cl1 and atoms C9b, C10b, C11b, C12b, C13b, Cl2 with site occupancy factors of 0.647 and 0.353, respectively.

4. Conclusion

Three novel coordination polymers formed by copper(II) carboxylate with 3-pyridylmethanol have been prepared and characterized. The crystal structure of **1** consists of 1-D chains, which are linked by face-to-face $\pi\cdots\pi$ stacking interactions. The crystal structure of **2** consists of 2-D sheets. The crystal structure of **3** is a new type of coordination polymer and consists of 1-D "accordion" chains. Analysis of the packing of coordination polymers in the crystal structure shows that strong O–H$\cdots$O hydrogen bonds play a role in stabilization of polymeric chains.

5. Supplementary material

Crystallographic data (excluding structure factors) for the structure reported in this paper have been deposited with the Cambridge Crystallographic Data Centre as supplementary publication nos. CCDC-282782 (**1**), CCDC-282783 (**2**) and CCDC-282784 (**3**). Copies of the data can be obtained free of charge on application to the CCDC, 12 Union Road, Cambridge CB2 1EZ, UK [fax: (internat.) +44 1223/336033; e-mail:deposit@ccdc.cam.ac.uk].

Acknowledgements

We thank Scientific Grant Agency of the Ministry of Education of Slovak Republic and the Slovak Academy of Sciences for financial support (1/2452/05 and 1/2450/05) and Research and Development Support Agency for financial support (APVT-20-005504).

References

[1] (a) A. Erxleben, Coord. Chem. Rev. 246 (2003) 203;
(b) L. Carlucci, C. Ciani, D.M. Proserpio, Coord. Chem. Rev. 246 (2003) 247;
(c) S.R. Batten, R. Robson, Angew. Chem., Int. Ed. Engl. 37 (1998) 1461;
(d) H.W. Roesky, M. Andruh, Coord. Chem. Rev. 236 (2003) 91;
(e) B. Moulton, M.J. Zaworotko, Chem. Rev. 101 (2001) 1629;
(f) S.R. Barnett, N.R. Champness, Coord. Chem. Rev. 246 (2003) 145;
(g) C. Janiak, Dalton Trans. (2003) 2781.
[2] M. Eddaoudi, H. Li, O.M. Yaghi, J. Am. Chem. Soc. 122 (2000) 1391.
[3] H. Li, C.E. Davis, T.L. Groy, D.G. Kelley, O.M. Yaghi, J. Am. Chem. Soc. 120 (1998) 2186.
[4] M. Fujita, Y.J. Kwon, S. Washizu, K.J. Ogura, J. Am. Chem. Soc. 116 (1994) 1151.
[5] W. Lin, Z. Wang, L. Ma, J. Am. Chem. Soc. 121 (1999) 11249.
[6] S.-L. Zheng, X.-M. Chen, Aust. J. Chem. 57 (2004) 703.
[7] J. Kim, D. Vodak, A. Sudik, J. Wachter, M. O'Keeffe, O.M. Yaghi, Proc. Natl. Acad. Sci. 99 (2002) 4900.
[8] D. Maspoch, D. Ruiz-Molina, J. Veciana, J. Mater. Chem. 14 (2004) 2713.
[9] M. Melnik, K. Smolander, P. Sharrock, Inorg. Chim. Acta 103 (1985) 187.
[10] J. Moncol, M. Mudra, P. Lonnecke, M. Koman, M. Melnik, J. Chem. Crystallogr. 34 (2004) 423.
[11] (a) P. Stachova, M. Korabik, M. Koman, M. Melnik, J. Mrozinski, M. Mazur, D. Valigura, in: M. Melnik, J. Sima, M. Tatarko (Eds.), Advanced in Coordination, Bioinorganic and Inorganic Chemistry, Slovak Technical University Press, Bratislava, 2005, p. 386;
(b) P. Stachova, M. Korabik, M. Koman, M. Melnik, J. Mrozinski, T. Glowiak, M. Mazur, D. Valigura, Inorg. Chim. Acta in press, doi:10.1016/j.ica2005.10.040.
[12] I. Ondrejkovicova, S. Galkova, M. Koman, T. Lis, in: M. Melnik, J. Sima, M. Tatarko (Eds.), Advanced in Coordination, Bioinorganic and Inorganic Chemistry, Slovak Technical University Press, Bratislava, 2005, p. 280.
[13] N.N. Hoang, F. Valach, L. Macaskova, M. Melnik, Acta Crystallogr. C 48 (1992) 1933.
[14] S. Lörinc, M. Koman, M. Melnik, J. Moncol, D. Ondrusova, Acta Crystallogr. E 60 (2004) M590.
[15] J. Moncol, M. Koman, M. Melnik, T. Glowiak, CrystEngComm. 3 (2001) 262.
[16] M. Mudra, J. Moncol, J. Svorec, M. Melnik, P. Lönnecke, T. Glowiak, R. Kirmse, Inorg. Chem. Commun. 6 (2003) 1259.
[17] P. Stachova, D. Valigura, M. Koman, T. Glowiak, Acta Crystallogr. E 61 (2005) M994.
[18] F. Valach, M. Tokarcik, P. Kubinec, M. Melnik, L. Macaskova, Polyhedron 16 (1997) 1461.
[19] V. Zelenak, I. Cisarova, M. Sabo, P. Llewellyn, K. Gyoryova, J. Coord. Chem. 57 (2004) 87.
[20] C. Janiak, J. Chem. Soc., Dalton Trans. (2000) 3885.
[21] A.W. Adison, T.N. Rao, J. Reedijk, J. van Rijn, G.C. Verschoor, J. Chem. Soc., Dalton Trans. (1984) 1349.
[22] F.E. Mabbs, D. Collison, in: Electron Paramagnetic Resonance of d-Transition Metal Compounds, Elsevier, Amsterdam, 1992, pp. 1–1326.
[23] B.J. Hathaway, D.E. Billing, Coord. Chem. Rev. 3 (1970) 143.
[24] SIMFONIA, Simulation Program for EPR Data, Shareware, Bruker, 1996.
[25] Xcalibur CCD system, CRYSALIS Software system, Version 1.170, Oxford Diffraction Ltd., Oxford, UK, 2003.
[26] G.M. Sheldrick, Acta Crystallogr. A 46 (1990) 467.
[27] A. Altomare, M.C. Burla, M. Camalli, G.L. Cascarano, C. Giacovazzo, A. Guagliardi, A.G.G. Moliterni, G. Polidori, R. Spagna, J. Appl. Crystallogr. 32 (1999) 328.
[28] G.M. Sheldrick, T.R. Schneider, Meth. Enzymol. 277 (1997) 319.
[29] L.J. Farrugia, J. Appl. Crystallogr. 30 (1997) 105.
[30] L.J. Farrugia, J. Appl. Crystallogr. 32 (1999) 837.

of 0.5 g (0.27 mmol) $H_3PMo_{12}O_{40}$. The yellow solution was allowed to stand for several days and the yellow crystals were collected. Yield: 35%. *Anal*. Calc. for $H_3PMo_{12}O_{40}$: C, 8.00; H, 1.73; N, 1.86. Found: C, 8.30; H, 1.60; N, 1.79%.

2.3. X-ray crystallography

Experimental parameters pertaining to single-crystal X-ray analysis of **I** are given in Table 1. Data were collected on a Siemens SMART 1000 CCD platform diffractometer with graphite monochromated Mo Kα radiation ($\lambda = 0.71073$ Å). The final unit cell was determined from 999 reflections in the range of $2.3° < \theta < 23.3°$. The data were integrated using the SAINT suite of software and corrected for the effects of absorption using SADABS. The structure was solved by direct methods and refined iteratively via full-matrix least-squares on F_o^2 and difference Fourier analysis using the SHELX-97 [17] suite of software, with the assistance of X-Seed [18]. All non-hydrogen atoms were refined with anisotropic displacement parameters. The hydrogen atoms of the proline moieties were placed in idealized positions and refined with a riding model whereas those of included water molecules were not modeled. There is some evidence of minor positional disorder of one of the proline moieties and two of the included water molecules which could not be successfully modeled.

Table 1
Crystal data and refinement parameters for **I**

Compound	$[C_5H_{10}NO_2]_3[PMo_{12}O_{40}]\cdot 4.5H_2O$ (**I**)
Formula	$C_{15}H_{37}N_3O_{50.5}PMo_{12}$
Formula weight	2249.73
Crystal size	$0.26 \times 0.22 \times 0.20$
Crystal system	monoclinic
Space group	$P2_1$
T (K)	173(2)
a (Å)	12.4387(17)
b (Å)	13.1472(18)
c (Å)	15.685(2)
β (°)	96.850(2)
V (Å^3)	2546.8(6)
Z	2
ρ_{calc} (g cm^{-3})	2.934
μ(Mo Kα) (mm^{-1})	3.008
$2\theta_{max}$ (°)	56
Number of measured reflections	22882
Number of unique reflections	11372
Number of reflections with $[I > 2\sigma(I)]$	10900
Number of parameters	742
R_{int}	0.0256
R_1, wR_2 $[I > 2\sigma(I)]$	0.0256, 0.0637
R_1, wR_2 (all data)	0.0274, 0.0631
Flack parameter, χ	0.01(3)
Maximum and minimum residual (e Å^{-3})	1.687 (proline) and −0.852

3. Result and discussion

3.1. IR spectrum

Comparing the IR spectrum of **I**, with that of $H_3PMo_{12}O_{40}$, we can see that the vibrational bands of the $P–O_{a(\text{the central oxygens bonded to P})}$ and the $Mo–O_{d(\text{terminal or skin oxygen atoms})}$ have red-shifted from 1063.1 and 962.4 cm^{-1} to 1061.2 and 959.7 cm^{-1}, respectively. The vibrational bands of the $Mo–O_{b(\text{corner-shared oxygens})}$ and the $Mo–O_{c(\text{edge-shared oxygens})}$ have blue-shifted from 875.1 and 786.8 cm^{-1} to 880.5 and 789.2 cm^{-1}, respectively. The results indicate that the $P–O_a$ and $Mo–O_d$ bonds were weakened and $Mo–O_b$ and $Mo–O_c$ were strengthened in the title compound **I**. These observations suggest some interactions between the proline nitrogen atom and the oxygen atoms of the $[PMo_{12}O_{40}]^{3-}$ anion [19]. The peaks at 1391–1734 cm^{-1} and the peaks at 2950–2919 cm^{-1} are characteristic of $C_5H_{10}NO_2{}^{1+}$, the 1453.1 cm^{-1} feature is characteristic of the N–H vibration, and the features at 1615.4 and 1643.8 cm^{-1} are associated with N–H and C=O symmetric stretching vibration, respectively. The other bands at 2919 and 2950 cm^{-1} are attributed CH_2 group of the proline.

3.2. ^{13}C NMR spectrum

According to the ^{13}C NMR spectrum the lines at 170.980 ppm; 59.367 ppm; 46.026 ppm; 28.311 ppm; 23.602 ppm are assigned to C1, C2, C5, C3 and C4 of proline, respectively. These patterns are, generally, what one expects of protonated proline and there does not seem to be any striking clue that would require further analysis.

3.3. ^1H NMR spectrum

^1H NMR (ppm): 4.269 (T, 1H, C2H); 3.190 (T, 2H, C5H); 2.1–2.4 (Q, 2H, C3H); 1.7–2.1 (M, 2H, C4H). These shifts and patterns are consistent with the seven hydrogen atoms that are covalently bonded to the carbon atoms of the proline.

3.4. X-ray crystallography

The crystal structure of $[C_5H_{10}NO_2]_3[PMo_{12}O_{40}]\cdot 4.5H_2O$ (Fig. 1) consists of $[PMo_{12}O_{40}]^{3-}$ units linked together by $[C_5H_{10}NO_2]^{1+}$ ions through electrostatic interactions. The ratio of anion to proline is 1–3 and the prolines in the structure, having been protonated by the acidic hydrogens of $H_3PMo_{12}O_{40}$, function as cations and balance the charge.

In the Keggin-type $[PMo_{12}O_{40}]^{3-}$ polyoxoanion, the Mo centers exhibit a distorted $[MoO_6]$ octahedral environment, with all the Mo–O distances being within the 1.664(10)–2.453(7) Å. The MoO_6 octahedra are somewhat distorted and the Mo–O distances can be divided into several

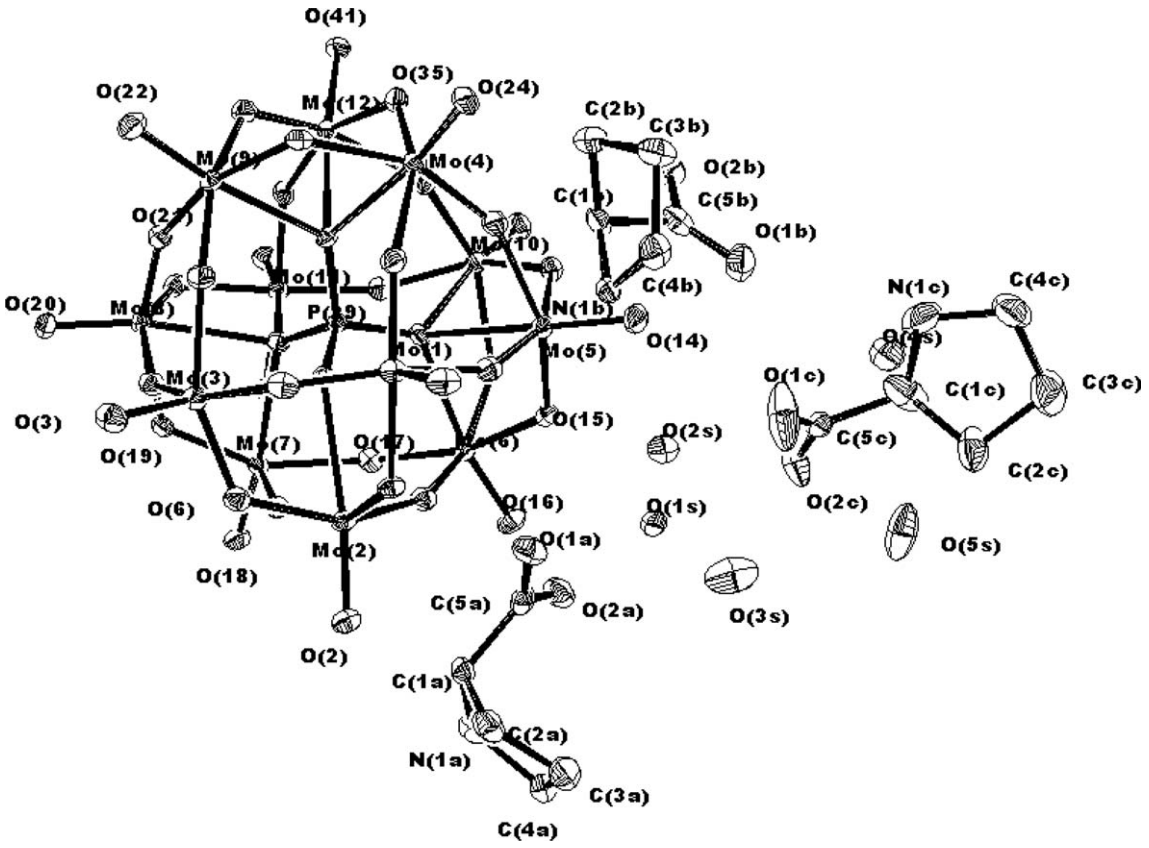

Fig. 1. Molecular structure unit with atom labeling of the title compound and ellipsoids are at 30% probability. The hydrogen atoms are omitted for clarity.

different groups according to the type of oxygen atoms, O_d, O_a, O_b and O_c, where O_d represents the terminal oxygen atoms, O_a represents those coordinated to P and to Mo atoms, O_b represents those coordinated to the Mo atoms whose MoO_6 octahedra are corner-shared and O_c represents those coordinated to the Mo atoms whose octahedra are edge-shared. As observed in many other polyoxomolybdates [20,21], the Mo–$O_{b/c}$ bonds fall into two well-resolved categories: the long pairs of Mo–O bonds and the short pairs of Mo–O bonds with the two bonds in a pair being in the *cis* positions. These are summarized in Table 2 with those of $H_3[PMo_{12}O_{40}]\cdot(29–31)H_2O$ for comparison [22]. This kind of distortion generates an interesting result. The Mo–$O_{b/c}$ bond lengths are alternately short and long, so that the distances of Mo–O–Mo are alternately short and long in the four rings around the structure (Fig. 2). The mean distance of Mo–Mo in four groups of edge-shared octahedra Mo_3O_{13} is 3.423 Å, 3.406 Å, 3.410 Å and 3.410 Å as compared with the analogue structure, i.e, $H_3[PMo_{12}O_{40}]\cdot(29–31)H_2O$, that is 3.42 Å with no significant alternating long/short bond lengths. The repulsion of Mo–Mo [23] may have brought about the alternative bond lengths in the prolinium 12-molybdophosphate but other major factors are effective to this evidence.

The proline structures bond distances and angles have standard values, thus there is no need to report them. In addition to intermolecular interactions between them, there

Table 2
Comparision of bond distances (Å and °) ([ ], average; ( ), difference)

	$H_3[PMo_{12}O_{40}]\cdot(29–31)H_2O$	$[C_5H_{10}NO_2]_3[PMo_{12}O_{40}]\cdot 4.5H_2O$
Mo–O_d	1.676(4)–1.680(6) [1.678] (0.004)	1.664(4)–1.696(4) [1.680] (0.032)
Mo–O_b	1.910(4)–1.914(4) [1.912] (0.004)	1.808(4)–2.028(4) [1.917] (0.220)
Mo–O_c	1.922(2)–1.924(4) [1.923] (0.002)	1.815(4)–2.038(4) [1.926] (0.223)
Mo–O_a	2.434(5)–2.436(3) [2.435] (0.002)	2.406(3)–2.453(3) [2.430] (0.047)

are intramolecular interactions that force the carboxylate group of one proline in the opposite direction (with respect to the pentagonal ring to which they are attached) of the carboxylate groupe of the neighboring proline. This spatial orientation is indicated by the torsion angle: O(5B)–C(1B)–N(1B)–C(4B) = 87.56°, C(5A)–C(1A)–N(1A)–C(4A) = 85.30° and C(5C)–C(1C)–N(1C)–C(4C) = 149.78°.

Another interesting feature of the crystal structure is evident from the view along the *z*-axis. POMs and prolines construct a network not dissimilar to the DNA strands. In the zig-zag arrangement of the polyoxometalate-proline

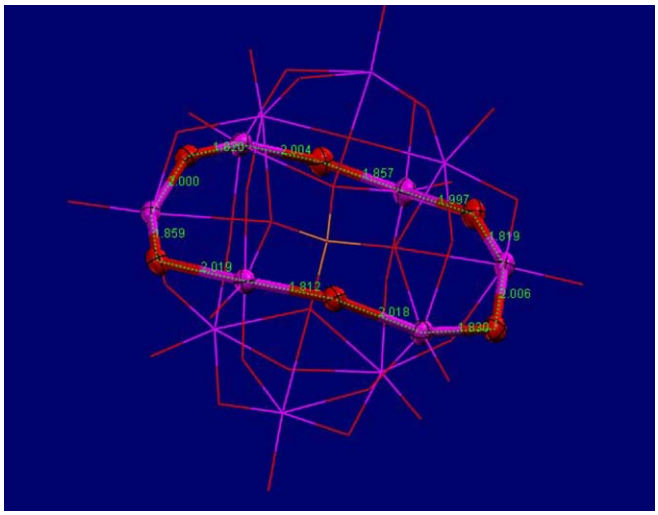

Fig. 2. Rings of alternative bonds in $[PMo_{12}O_{40}]^{-3}$ (show two rings and prolines omitted for clarity).

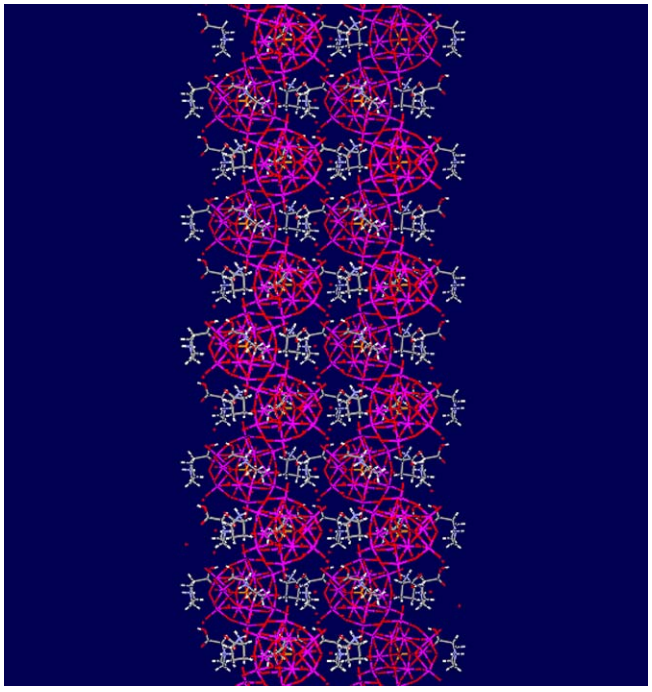

Fig. 3. View of the $[C_5H_{10}NO_2]_3[PMo_{12}O_{40}] \cdot 4.5H_2O$ along the *z*-axis.

chains, a directional orientationis is maintained that is, likely, caused by the noncovalent interactions among the constituents of the lattice (Fig. 3).

4. Conclusion

The synthesis and characterization of this new organic–inorganic salt, $(C_5H_{10}NO_2)_3PMo_{12}O_{40} \cdot 4.5H_2O$, is an important continuous step to incorporate organic molecules of biological significance into the network of inorganic cluster-compounds.

A combination of electrostatic forces and hydrogen bonding keeps this "adduct" stable in the solid state. The fact that in the solution phase the compound is also stable makes it a viable candidate for applications as homogeneous catalysis [24]. There may be potential pharmaceutical benefits that are yet to be explored.

5. Supplementary data

Crystallographic data for the structure reported in this paper have been deposited with the Cambridge Crystallographic Data Center as supplementary publication no. CCDC-280411. Copies of the data can be obtained free of charge an application to the CDCC, 12 Union Road, Cambridge CB2 1EZ, UK (e-mail: deposit@ccdc.cam.ac.uk).

References

[1] M.T. Pope, A. Muller, Angew. Chem., Int. Ed. Engl. 30 (1991) 34.
[2] M.H. Alizadeh, H. Eshtiagh-Hosseini, R. Khoshnavazi, J. Mol. Struct. 688 (2004) 33.
[3] M.H. Alizadeh, Hossein Razavi, F. Mohammadi Zonoz, M.R. Mohammadi, Polyhedron 22 (2003) 933.
[4] M.H. Alizadeh, S.P. Harmalker, Y. Jeanenin, J. Martin-Frere, M.T. Pope, J. Am. Chem. Soc. 107 (1985) 2662.
[5] M.H. Alizadeh, Hossein Razavi, F.F. Bamoharram, K. Daneshvar, J. Mol. Catal. A 206 (2003) 89.
[6] N. Yamamoto, D. Schols, E.D. de Clercg, et al., Mol. Pharmacol. 42 (1992) 1109.
[7] Y. Inouge, Y. Tokutake, T. Yoshida, et al., Antivirus Res. 20 (1993) 317.
[8] J.T. Rhule, C.L. Hill, D.A. Judd, Chem. Rev. 98 (1998) 327.
[9] E.B. Wang, C.W. Hu, L. Xu, Introduction of Polyoxometalates Chemistry, Chemical Industry Press, Beijing, 1998.
[10] L.C.W. Baker, D.C. Glick, Chem. Rev. 98 (1998) 3.
[11] J.H. Liu, J. Peng, E.B. Wang, J. Mol. Struct. 525 (2000) 71.
[12] D.C. Crans, M. Mahroof-Tahir, O. Aderson, Inorg. Chem. 33 (1994) 5586.
[13] D. Attanasio, M. Bonamico, V. Fares, J. Chem. Soc., Dalton Trans. (1990) 3221.
[14] J. Peng, E.B. Wang, Y.S. Zhou, J. Chem. Soc., Dalton Trans. (1998) 3865.
[15] E. You, E.B. Wang, Q.L. He, J. Mol. Struct. 524 (2000) 133.
[16] X. Wu, J. Biol. Chem. 43 (1920) 189.
[17] G.M. Sheldrick, SHELX-97, University of Göttingen, Göttingen, Germany, 1997.
[18] L.J. Barbour, J. Supramol. Chem. 1 (2001) 189. Available from: <http://x-seed.net/>.
[19] J.Y. Niu, X.Z. You, C.Y. Duan, Inorg. Chem. 35 (1996) 4211.
[20] M.T. Pope, Inorg. Chem. 15 (1976) 2008.
[21] R. Strandberg, Acta Crystallogr., Sect. B 33 (1977) 3090.
[22] R. Strandberg, Acta Chem. Scand. A 29 (1975) 359.
[23] J.F. Garvey, M.T. Pope, Inorg. Chem. 17 (1978) 1115.
[24] Yi-Yuan Peng, Qiu-Ping Ding, et al., Tetrahedron Lett. 44 (2003) 3871.

data were obtained using the following instruments: UV–Vis spectra, JASCO UV–Vis–NIR model V 570; IR spectra (KBr disk, 4000–200 cm^{-1}), FTIR JASCO model 420; ^1H NMR spectra, Bruker (AC) 300 MHz FTNMR spectrometer. Electrochemical measurements were performed using computer-controlled PAR model 270 VERSASTAT electrochemical instruments with Pt-disk electrodes. All measurements were carried out under a nitrogen environment at 298 K with reference to saturated calomel electrode (SCE) in acetonitrile using $[n\mathrm{Bu_4N}][\mathrm{ClO_4}]$ as supporting electrolyte. The reported potentials are uncorrected for junction potential.

2.2. Materials

2-(Arylazo)pyrimidines were prepared by the reported procedure [10]. $H_2PtCl_6 \cdot xH_2O$ was purchased from Arrora Matthey, Kolkata, India. K_2PtCl_4 was prepared from the reported method [8]. Aniline, *o*-toluidine, *m*-toluidine, *p*-toluidine, *p*-chloroaniline were received from Sisco Research Lab (SRL). The purification of acetonitrile and preparation of *n*-tetra butylammonium perchlorate $[n\mathrm{Bu_4N}][\mathrm{ClO_4}]$ for electrochemical work were done as before [10]. Dinitrogen was purified by bubbling through an alkaline pyrogallol solution. All other chemicals and solvents were of reagent grade and were used without further purification. Commercially available SRL silica gel (60–120 mesh) was used for column chromatography.

2.3. Preparation of complexes

2.3.1. Dichloro[2-(phenylazo)pyrimidine]platinum(II), Pt(papm)Cl_2 (**4a**)

2-(Phenylazo)pyrimidine (papm) (0.2 g, 1.09 mmol) in MeCN–H_2O (15 ml) was added to an MeCN–H_2O (1:1, v/v, 40 ml) solution of K_2PtCl_4 (0.4 g, 0.96 mmol) and the mixture was refluxed for 24 h. On slow evaporation, a brown precipitate gradually appeared; it was filtered and washed with cold MeCN–H_2O (1:1, v/v, 3 × 5 ml). The dried mass was dissolved in a minimum volume of CH_2Cl_2 and chromatographed over a silica gel column. The desired compound was eluted by C_7H_9–MeCN (2:1, v/v) as an orange-red band; yield, 0.3 g (50%). Other complexes were prepared under identical conditions and yield varied in the range 45–50%. Calc. for $C_{10}H_8N_4Cl_2Pt$ (**4a**): C, 26.66; H, 1.77; N, 12.44. Found: C, 26.55; H, 1.69; N, 12.35%. Calc. for $C_{11}H_{10}N_4Cl_2Pt$ (**4b**): C, 28.44; H, 2.15; N, 12.07. Found: C, 28.55; H, 2.08; N, 11.99%. Calc. for $C_{10}H_7N_4Cl_2Pt$ (**4c**): C, 24.76; H, 1.44; N, 11.56. Found: C, 24.62; H, 1.37; N, 11.42%.

2.3.2. Chloro[(2-(8-imidophenyl)phenylazo)pyrimidine-N,N′,N″]platinum(II), Pt(papm-N–C_6H_5)Cl, (**5a**)

To an acetonitrile solution (15 ml) of Pt(papm)Cl_2 (90.3 mg, 0.67 mmol) was added slowly aniline (0.1 g, 1.08 mmol) in the same solvent (10 ml). The reaction mixture was stirred and refluxed continuously for 4 h. The colour of the solution changed gradually from orange-red to brown. The solution was evaporated in air, and the residue was washed thoroughly first with water (2 × 5 ml) and then with 50% aqueous-ethanol (3 × 5 ml). The residue was dissolved in dichloromethane (10 ml) and the solution was chromatographed over silica gel column (60–120 mesh). An orange-brown band was eluted by C_7H_9–MeCN (9:1) mixture. The eluted solution on evaporation in vacuo gave pure compound. Orange-brown compound was isolated in 45% yield.

The greenish-brown product is the coupled product, Pt(papm-N-C_6H_5)Cl. All other complexes were prepared similarly; yield, 40–55%. Calc. for $C_{16}H_{12}N_5ClPt$ (**5a**): C, 38.05; H, 2.38; N, 13.87. Found: C, 38.12; H, 2.31; N, 13.73%. Calc. for $C_{17}H_{14}N_5ClPt$ (**6a**): C, 39.34; H, 2.70; N, 13.50. Found: C, 39.23; H, 2.61; N, 13.41%. Calc. for $C_{17}H_{14}N_5ClPt$ (**7a**): C, 39.34; H, 2.70; N, 13.50. Found: C, 39.24; H, 2.62; N, 13.40%. Calc. for $C_{17}H_{14}N_5ClPt$ (**8a**): C, 39.34; H, 2.70; N, 13.50. Found: C, 39.20; H, 2.60; N, 13.39%. Calc. for $C_{17}H_{14}N_5OClPt$ (**9a**): C, 38.16; H, 2.62; N, 13.09. Found: C, 38.00; H, 2.56; N, 13.20%. Calc. for $C_{16}H_{11}N_5Cl_2Pt$ (**10a**): C, 35.62; H, 2.04; N, 12.98. Found: C, 35.48; H, 2.11; N, 12.86%. Calc. for $C_{17}H_{14}N_5ClPt$ (**5b**): C, 39.34; H, 2.70; N, 13.50. Found: C, 39.22; H, 2.66; N, 13.42%. Calc. for $C_{18}H_{16}N_5ClPt$ (**6b**): C, 40.56; H, 3.00; N, 13.14. Found: C, 40.43; H, 2.94; N, 13.02%. Calc. for $C_{18}H_{16}N_5ClPt$ (**7b**): C, 40.56; H, 3.00; N, 13.14. Found: C, 40.37; H, 2.84; N, 13.05%. Calc. for $C_{18}H_{16}N_5ClPt$ (**8b**): C, 40.56; H, 3.00; N, 13.14. Found: C, 40.41; H, 2.89; N, 13.00%. Calc. for $C_{18}H_{16}N_5OClPt$ (**9b**): C, 39.38; H, 2.91; N, 12.76. Found: C, 39.15; H, 2.82; N, 12.64%. Calc. for $C_{17}H_{13}N_5Cl_2Pt$ (**10b**): C, 36.88; H, 2.35; N, 12.65. Found: C, 36.74; H, 2.28; N, 12.54%. Calc. for $C_{16}H_{11}N_5Cl_2Pt$ (**5c**): C, 35.62; H, 2.04; N, 12.98. Found: C, 35.53; H, 2.10; N, 12.77%. Calc. for $C_{17}H_{13}N_5Cl_2Pt$ (**6c**): C, 36.88; H, 2.35; N, 12.65. Found: C, 36.75; H, 2.31; N, 12.53%. Calc. for $C_{17}H_{13}N_5Cl_2Pt$ (**7c**): C, 36.88; H, 2.35; N, 12.65. Found: C, 36.69; H, 2.28; N, 12.54%. Calc. for $C_{17}H_{13}N_5Cl_2Pt$ (**8c**): C, 36.88; H, 2.35; N, 12.65. Found: C, 36.74; H, 2.29; N, 12.52%. Calc. for $C_{17}H_{13}N_5OCl_2Pt$ (**9c**): C, 35.85; H, 2.28; N, 12.30. Found: C, 35.71; H, 2.20; N, 12.19%. Calc. for $C_{16}H_{10}N_5Cl_3Pt$ (**10c**): C, 36.47; H, 1.74; N, 12.20. Found: C, 36.55; H, 1.81; N, 12.23%.

2.4. X-ray structure determination

The X-ray quality single crystal of Pt(papm-N–C_6H_4–Me-*m*)Cl (**7a**) was grown by slow diffusion of hexane into dichloromethane solution of the complex at 298 K. The crystal size was $0.25 \times 0.11 \times 0.08\ mm^3$. X-ray diffraction data were collected at 293(2) K with the Siemens SMART CCD using graphite-monochromatized Mo Kα radiation ($\lambda = 0.71073$ Å). Unit cell parameters were determined from least-squares refinement of setting angles with 2θ in the range 4–57°. A summary of the crystallographic data and structure refinement parameters are given in Table 1.

Table 1
Crystallographic data of Pt(papm-N–C_6H_4–Me-*m*)Cl (**7a**)

Chemical formula	$C_{17}H_{14}ClN_5Pt$
Formula weight	517.88
Crystal size (mm^3)	$0.25 \times 0.11 \times 0.08$
Crystal system	monoclinic
Space group	$P2_1/n$
a (Å)	7.459(1)
b (Å)	16.899(2)
c (Å)	13.117(18)
β (°)	92.497(3)
V ($Å^3$)	1652.0(4)
Z	4
T (K)	295(2)
λ (Å)	0.71073
2θ Range (°)	4–57
Reflection collected	9981
Unique reflections [a]	2522
hkl Range	$-9 \leqslant h \leqslant 9$, $-21 \leqslant k \leqslant 20$, $20 \leqslant l \leqslant -15$
ρ_{calc} (g cm^{-3})	2.082
μ (Mo Kα) (mm^{-1})	8.662
R[b]	0.0303
wR[c]	0.0569
Goodness-of-fit[d]	0.904

[a] $I > 2\sigma(I)$%.
[b] $R = \sum|F_o - F_c|/\sum F_o$.
[c] $wR = \left[\sum(F_o^2 - F_c^2)^2/\sum w(F_o^4)\right]^{1/2}$, $w = 1/[\sigma^2(F_o)^2 + (0.0283P)^2]$, where $P = (F_o + 2F_c^2)/3$.
[d] Goodness-of-fit is defined as $[w|F_o - F_c|/(n_o - n_v)]^{1/2}$, where n_o and n_v denotes the numbers of data and variables, respectively.

Of 9981 collected reflections 2522 unique reflections were recorded using ω-scan technique. Data were corrected for L_p effects and for linear decay. Semi-empirical absorption corrections based on ψ-scans were applied. The structure was solved by direct method using SHELX-97 and successive difference Fourier syntheses [11]. All non-hydrogen atoms were refined anisotropically. The hydrogen atoms were fixed geometrically and refined using riding model. In the final difference Fourier maps the residual maximum and minimum were 1.312 and -0.627 e $Å^{-3}$. All calculations were carried out using the SHELX-97.

2.5. Molecular orbital calculations

Extended Huckel molecular orbital calculation [12,13] was performed using the ICON software package originally developed by Hoffmann. The atomic parameters were taken from the crystallographic data (Table 1). For drawing figures and graphic package 'cacao' was used.

3. Results and discussion

3.1. Synthesis and formulation

2-(Arylazo)pyrimidines (aapm, **3**) are *N*,*N*′-chelators. The reaction of aapm with K_2PtCl_4 in MeCN–H_2O (1:1, v/v) has yielded orange-red crystalline product, Pt(aapm)Cl_2 (**4**), in the yield of 45–50%.

The reaction between Pt(aapm)Cl_2 and $ArNH_2$ in 1:1 ratio in MeCN suspension under refluxing condition has yielded greenish brown product (Eq. (1)). This has been identified as amine coupled product abbreviated Pt(aapm-N–C_6H_4-R′Cl) [where, R′ = H (**5**), *o*-Me (**6**) *m*-Me (**7**), *p*-Me (**8**), *p*-OMe (**9**), *p*-Cl (**10**)].

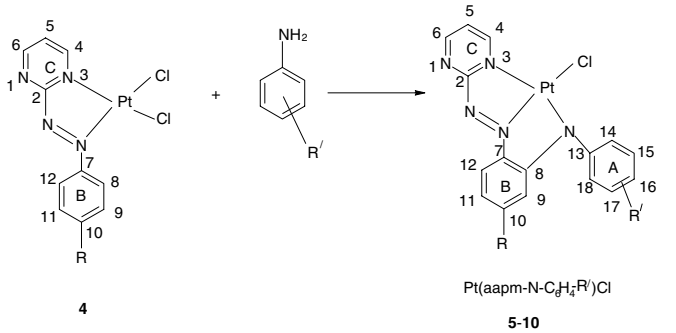

4 **5-10**

(1)

The arylamination takes place at the *ortho* position (at the C(8)–H bond) to azo function in the pendant aryl ring (B-ring) of aapm and forms platinum(II) complex of tridentate *N*,*N*′,*N*″-chelating ligand (*N*,*N*′,*N*″ refer to *N*(pyrimidine), *N*(azo) and *N*(arylamine), respectively). Microanalytical data support the composition of the complexes (see Section 2).

3.2. Molecular structure of Pt(papm-N–C_6H_4–Me-*m*)Cl (*7a*)

A molecular view of Pt(papm-N–C_6H_4–Me-*m*)Cl is shown in Fig. 1 and the selected bond parameters are listed in Table 2. The crystallographic asymmetry unit contains 24 non-hydrogen atoms of which 17 lie in a plane nearly perpendicular to crystallographic *c*-axis. These atoms comprise the two chelate rings, the aromatic groups fused to them and the Pt and Cl-atoms. The atomic groups Pt, N(1), C(4), N(3), N(4), and Pt, N(4), C(5), C(10), N(5) constitute two chelate planes (mean deviation <0.04 Å) and they are nearly planar (dihedral angle 1.8°). The chelate bite angles are N(1)–Pt–N(4), N(4)–Pt–N(5), 79.3°(4) and 81.8°(8). The Pt atom lies within the square plane defined by N_3Cl donor centers (deviation, <0.01). The pendant *m*-tolyl ring is inclined at an angles of 64.35° with the principal plane of 17 atoms. There are three types of Pt–N bonds: Pt–N(pyrimidine) [Pt–N(1)], 2.013(3) Å; Pt–N(azo) [Pt–N(4)], 1.919(9) Å and longest Pt–N(arylamine) [Pt–N(5)], 2.014(9) Å. The shortest Pt–N bond length is Pt–N(1) and longest Pt–N distance is Pt–N(5). The N=N bond length is 1.312(1) Å. The free ligand value of N=N bond is not available but the literature data available in some free arylazoheterocycles suggest that it is nearly 1.25(1) Å [14]. The elongation of N=N azo distance is consistent with electron delocalization from metal to ligand fragment [5,6]. A significant back-bone conjugation is also observed in the coordinated anionic ligand. This is viewed from the difference in N(azo)–C(phenyl-B/pyrimidine-C), distances. The N(azo)–C(pyrimidine-C) (N(3)–C(4)), 1.381(4) Å;

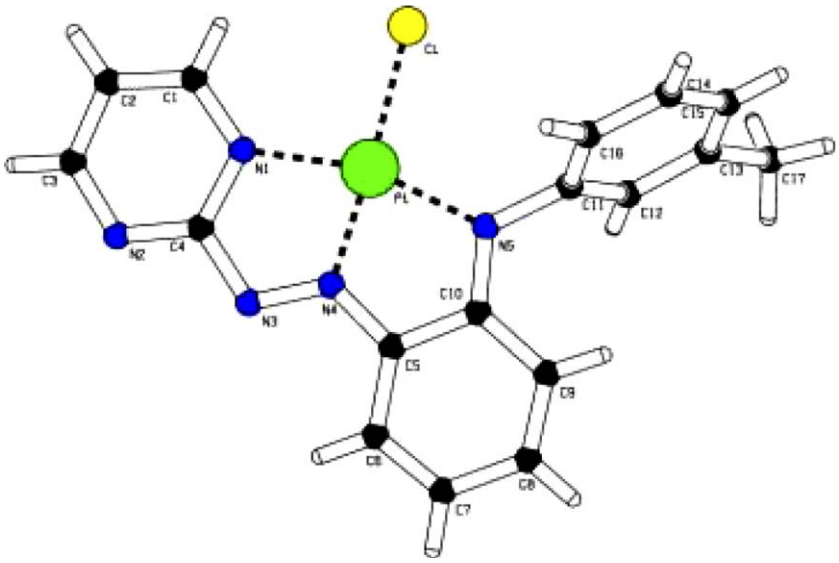

Fig. 1. Molecular structure of [Pt(papm-N–C_6H_4–Me-*o*)Cl] (**7a**).

Table 2
Selected bond lengths (Å) and angles (°) of Pt(papm-N–C_6H_4–Me-*m*)Cl (**7a**)

Bonds	Distances (Å)	Angles	Value (°)
Pt–N(1)	2.013(3)	N(1)–Pt–N(4)	79.3(4)
Pt–N(4)	1.919(9)	N(4)–Pt–N(5)	81.8(8)
Pt–N(5)	2.014(9)	N(1)–Pt–Cl(1)	97.0(4)
N(3)–N(4)	1.381(6)	N(5)–Pt–Cl(1)	101.7(4)
C(4)–N(1)	1.381(6)	N(1)–Pt–N(5)	161.1(8)
C(4)–N(3)	1.381(6)	N(4)–Pt–Cl(1)	176.3(8)
Pt–Cl(1)	2.291(2)	Pt–N(1)–C(4)	110.2(6)
C(5)–N(4)	1.346(6)	Pt–N(5)–C(10)	111.3(50)
C(10)–N(5)	1.332(8)	Pt–N(4)–C(5)	116.4(1)
C(11)–N(5)	1.441(1)		
N(1)–C(1)	1.332(8)		
N(2)–C(4)	1.322(1)		
N(2)–C(3)	1.333(3)		
C(2)–C(3)	1.361(9)		
C(1)–C(2)	1.353(8)		
C(5)–C(6)	1.411(7)		
C(6)–C(7)	1.350(8)		
C(7)–C(8)	1.419(9)		
C(8)–C(9)	1.367(6)		
C(9)–C(10)	1.435(1)		

N(azo)–C(phenyl-B) (N(4)–C(5)), 1.346(6) Å are noticeably shorter than that of N(imino)–C(phenyl-A) (N(5)–C(11)), 1.441(1) Å. More interesting feature is the ring C–C distance in B-ring C(5)–C(10); they have been elongated by 0.02–0.1 Å from that of ring-A and ring-C parameters. This leads us to conclude that the ring-B is more efficiently involve in back bone conjugation than that of other rings (A and C) with the coordinated Pt(II). This is also supported by the shortening of Pt–N(4) distance (1.919(9) Å) with reference to Pt–N(1), 2.013(3) and Pt–N(5), 2.014(9) Å. The bond parameters and backbone conjugation are also comparable with the literature data [5,6].

A hydrogen bonded cyclic dimmer is observed through C(12)–H(12)···N(3) C(12)–H, 0.93 Å; H(12)···N(3), 2.598(7) Å; C(12)···N(3), 2.598(7) Å and ∠C(12)–H(12)–N(3), 165.53°. Dimers are then arranged compactly to provide a platform for π–π interaction between pyrimidine (acceptor) of one unit with azophenyl ring (donor) of adjacent unit (distance between Cg(4) of pyrimidine···Cg(3) of azophenyl equals to 3.735(5) Å) and a supramolecular ladder is formed (Fig. 2).

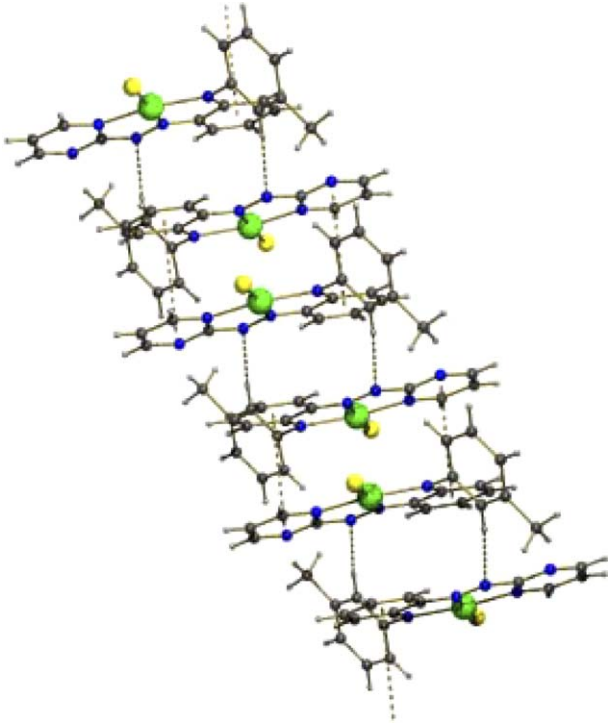

Fig. 2. Supramolecular ladder constituted via π···π interaction between pyrimidine and azoaryl in hydrogen-bonded cyclic dimers.

3.3. Spectra and bonding

The presence of two ν(Pt–Cl) stretches at 340 and 300 cm^{-1} in Pt(aapm)Cl_2 is in agreement with *cis*-$PtCl_2$ configuration [15] while a single transmission at 300–320 cm^{-1} is observed in the amine coupled products (**5**–**10**). The sharp single band at 1400–1415 cm^{-1} in free ligand is referred to ν(N=N) [5]. This has been shifted to lower frequency, 1360–1375 cm^{-1} in Pt(aapm)Cl_2 and supports the coordination of azo-N to Pt(II). In Pt(aapm-N–Ar)Cl (**5**–**10**) the ν(N=N) appears at 1260–1290 cm^{-1}; this significant reduction in azo frequency may be due to charge delocalization from N–Ar fragment (ring A) to the azo function intramolecularly (vide infra).

In chloroform solution of Pt(aapm)Cl_2 the absorption bands are observed at 250–550 nm. On comparison with free ligand data we may conclude that the transitions <400 nm are intraligand charge transfer transitions [10]. The spectral pattern have changed abruptly in Pt(aapm-N–Ar)Cl (**5**–**10**) and exhibit multiple transitions in the visible to NIR region (500–1250 nm). The spectral data are collected in Table 3 and a representative figure is shown in Fig. 3. The low energy spectral band in Pt(aapm-N–Ar)Cl, is associated with HOMO → LUMO (62a → 63a) charge transfer [5,6]. The MOs are calculated by EHMO approximation using X-ray crystallographic parameter of Pt(papm-N–C_6H_4–Me-*m*)Cl (**7a**). The HOMO (62a) receives 68% azoaryl group and 26% metal orbitals and

Table 3
Solution spectral [a] and cyclic voltammetric [b] data

Compounds	UV–Vis–NIR spectra λ_{max}/nm($10^{-3}\varepsilon$/dm^3 mol^{-1} cm^{-1})	Cyclic voltammetric data[b] $E_{1/2}/V$ (ΔE_p/mV)			
		$E^1_{1/2}$	$-E^2_{1/2}$	$-E^3_{1/2}$	$-E^4_{1/2}$
Pt(papm)Cl_2 (**4a**)	541(1.10), 408(4.40), 324(2.97)		0.12(100)	1.14(180)	
Pt(*p*-tapm)Cl_2 (**4b**)	528(1.42), 405(4.82), 328(3.08)		0.17(120)	1.20(200)	
Pt(*p*-Clpapm)Cl_2 (**4c**)	546(0.97), 415(3.82), 335(4.52)		0.09(100)	1.05(200)	
Pt(papm-N-C_6H_5)Cl (**5a**)	1222(0.86)[c], 1046(1.93), 902(2.11) 806(1.58)[c], 736(0.88)[c], 550(1.18)[c], 472(4.39), 412(6.03), 358(8.91)	1.113(100)	0.314(70)	0.778(170)	1.085(180)
Pt(papm-N-C_6H_4-Me-*o*)Cl (**6a**)	1216(1.08)[c], 1038(2.46), 900(2.74), 804(2.66), 758(2.06)[c], 688(1.15)[c], 474(5.02)[c], 418(7.46), 358(11.66)	1.047(150)	0.375(105)	0.898(140)	1.264(190)
Pt(papm-N-C_6H_4-Me-*m*)Cl (**7a**)	1224(1.40)[c], 1050(2.90), 906(3.44), 808(2.50)[c], 738(1.25)[c], 470(6.16)[c], 414(8.68), 356(13.15)	1.018(100)	0.388(95)	0.935(160)	1.269(160)
Pt(papm-N-C_6H_4-Me-*p*)Cl (**8a**)	1220(1.55), 1052(3.49), 918(3.84), 807(2.79), 740(1.45), 474(6.99)[c], 420(10.06), 358(15.05)	1.052(76)	0.325(140)	0.870(100)	1.294(170)
Pt(papm-N-C_6H_4-OMe-*p*)Cl (**9a**)	1216(1.08)[c], 1054(3.18), 914(3.47), 811(2.55)[c], 734(1.24)[c], 510(3.80)[c], 456(7.98), 428(8.38), 356(12.85)	1.009(95)	0.413(100)	0.945(170)	1.448[d]
Pt(papm-N-C_6H_4-Cl-*p*)Cl (**10a**)	1220(1.08)[c], 1060(3.05), 892(3.29), 800(2.50)[c], 732(1.20)[c], 540(1.10)[c], 470(4.21), 410(5.96), 356(10.43)	1.127(100)	0.304(120)	0.746(160)	1.018(180)
Pt(*p*-tapm-N-C_6H_5)Cl (**5b**)	1160(0.92)[c], 1050(2.05), 928(1.23)[c], 840(2.60)[c], 738(1.89), 556(1.23)[c]	1.018(90)	0.409(110)	0.904(140)	1.236(175)
Pt(*p*-tapm-N-C_6H_4-Me-*o*)Cl (**6b**)	1164(1.07)[c], 1020(2.15), 920(1.35)[c], 830(2.22), 730(1.42), 520(5.62)	1.011(90)	0.438(100)	0.930(120)	1.227(190)
Pt(*p*-tapm-N-C_6H_4-Me-*m*)Cl (**7b**)	1156(1.22), 1018(2.24), 906(1.56), 828(2.19)[c], 732(1.40), 518(5.08)[c]	1.010(95)	0.430(100)	0.925(130)	1.240(190)
Pt(*p*-tapm-N-C_6H_4-Me-*p*)Cl (**8b**)	1166(0.97), 1055(1.88), 933(2.39)[c], 852(1.70), 746(0.91), 560(1.50), 485(4.61)	1.007(80)	0.450(100)	0.923(120)	1.253(170)
Pt(*p*-tapm-N-C_6H_4-OMe-*p*)Cl (**9b**)	1154(0.94)[c], 1016(1.53), 912(1.69)[c], 872(2.45)[c], 736(1.09), 442(6.39)	0.968(90)	0.474(110)	0.938(140)	1.532[d]
Pt(*p*-tapm-N-C_6H_4-Cl-*p*)Cl (**10b**)	1174(1.08), 1032(2.10), 910(1.45)[c], 830(2.45), 755(1.57), 530(5.36),	1.086(100)	0.383(100)	0.801(95)	1.208(160)
Pt(*p*-Clpapm-N-C_6H_5)Cl (**5c**)	1198(0.62)[c], 1028(1.32)[c], 908(1.46), 729(1.40), 740(1.51), 768(1.99)[c], 482(4.53)[c]	1.117(85)	0.405(100)	0.749(120)	1.159(150)
Pt(*p*-Clpapm-N-C_6H_4-Me-*o*)Cl (**6c**)	1198(0.64), 1044(1.19), 930(1.45), 745(1.40), 568(1.95), 500(3.64), 445(8.95)	1.026(90)	0.375(110)	1.040(100)	1.136(190)
Pt(*p*-Clpapm-N-C_6H_4-Me-*m*)Cl (**7c**)	1200(0.79), 1048(1.35), 935(1.55), 740(1.50), 570(2.00), 500(3.50), 440(9.05)	1.031(80)	0.368(120)	1.048(90)	1.127(170)
Pt(*p*-Clpapm-N-C_6H_4-Me-*p*)Cl (**8c**)	1208(0.71)[c], 1040(1.40), 920(1.66), 740(1.50), 572(2.03), 490(4.85)	1.026(100)	0.375(100)	1.040(130)	1.136(160)
Pt(*p*-Clpapm-N-C_6H_4-OMe-*p*)Cl (**9c**)	1200(0.68), 1060(2.04), 950(2.89), 805(2.83), 745(1.65[c]), 565(1.34), 475(5.32)	0.938(90)	0.394(110)	0.823(130)	1.359[d]
Pt(*p*-Clpapm-N-C_6H_4-Cl-*o*)Cl (**10c**)	1224(1.06), 1066(2.10), 910(3.05), 810(2.42), 740(1.22)[c], 560(1.26), 480(5.42)	1.122(90)	0.300(100)	0.728(110)	1.048(140)

[a] Solvent $CHCl_3$.
[b] Solvent MeCN, supporting electrolyte [$n$$Bu_4$N][$ClO_4$], Pt-disk milli working electrode, Pt-wire auxiliary electrode, reference electrode SCE, at 298 K.
[c] Shoulder.
[d] E_{pc}.

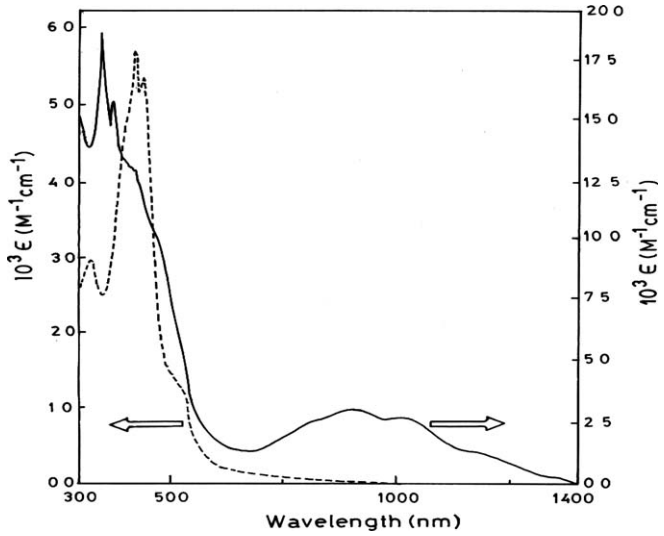

Fig. 3. Electronic spectra of Pt(*p*-tapm)Cl_2 (**4b**) (.....) and Pt(*p*-tapm–N–C_6H_4–Me-*m*) (**7b**) (—) in $CHCl_3$.

the LUMO (63a) shares 33% azo and 31% azoaryl character. Other transitions may be characterized to HOMO − 1 (61a) → LUMO (63a), HOMO − 2 (60a) → LUMO (63a), HOMO (62a) → LUMO + 1 (64a) etc. The effect of substituent R (at B-ring of arylazopyrimidine) and R′ (at A-ring of N–Ar) are also observed. Both steric and electronic effects of X influence the energy of HOMOs. The electron donating substituents destabilize the MOs and thus energy of HOMO is increased. The *o*-Me provides greater steric effect compared to other and influences the HOMO. The substituent R (at B-ring) influences more prominently to the LUMOs and the band maxima (λ_{max}) follow the sequence *p*-Clpapm < papm < *p*-tapm. This is expected in view of the electronic property of *p*-Me and *p*-Cl groups.

In the ^{1}H NMR spectra the signals were assigned on the basis of chemical shifts, spin–spin interaction and their effect on substitution and on comparison with the spectra of Pd(aapm)Cl_2 [5]. The spectral data are given in Table 4. The downfield portion of the spectra corresponds to pyrimidine-H (4-H–6-H, C-ring) [10] and upperfield portion refers to azo–aryl-protons, 8-H–12-H (B-ring). The binding of aapm with Pt(II) is supported by the appearance of spin–spin coupling [16] of ^{1}H (4-H) and ^{195}Pt (33.1%) and the coupling constant is $^3J_{Pt-H}$ is 20–24 Hz.

The NMR spectra of **5**–**10** resemble those of their Pd-containing analogues, Pd(aapm-N–Ar)Cl, [5] and are consistent with their proposed structures. A strong ^{195}Pt–^{1}H (J = 21–27 Hz) was observed to the pyrimidine 4H resonance (Fig. 4). The effect of substituents R′ (R′-C_6H_4–N–) on the signal movement is in accordance with the electronic effect of the group [16,17]. A significant observation is that azo–aryl protons (B-ring) (9-H–12-H) in Pt(aapm-N–C_6H_4-R′Cl) are up field shifted by 0.5–1.2 ppm relative to Pt(aapm)Cl_2 while pyrimidine protons (C-ring protons, 4-H–6-H) are shifted to up field side by 0.2–0.5 ppm compared to the parent complex, Pt(aapm)Cl_2. Azopyrimidine function is electron deficient while *N*-aryl ring (ring A) is σ-donor and may support intramolecular charge transfer transition. This may be reason for up field shifting of arylazopyrimidine protons (4-H–12-H) in the fused compound.

Table 4
^{1}H NMR spectral data of Pt(aapm)Cl_2 (**4**) and Pt(aapm-N–Ar)Cl (**5**–**10**) in $CDCl_3$

Compound	δ/ppm (*J*/Hz)														
	4-H[a]	5-H[b]	6-H[a]	8-H[a]	9-H	10-H	11-H	12-H[a]	14-H[a]	15-H	16-H	17-H	18-H[a]	R	R′
4a	8.41(6.0)	7.63(7.0)	8.19(7.0)	7.26(7.0)	7.12[c]	7.12[c]	7.12[c]	7.26[c]							
4b	8.36(6.0)	7.60(7.0)	8.17(7.0)	7.11(7.0)	6.86[a](7.0)		6.86[a](7.0)	7.11(7.0)						2.44	
4c	8.44(6.0)	7.60(7.0)	8.28(7.0)	7.34(7.0)	7.44[a](8.0)		7.44[a](8.0)	7.34(7.0)							
5a	8.04(6.0)	6.80(7.0)	8.29(6.0)		6.21[a](7.0)	6.99[c]	6.99[c]	6.69(8.0)	7.28(8.0)	6.62[c]	6.62[c]	6.62[c]	7.28(8.0)		
6a	8.02(6.0)	6.74(7.0)	8.26(6.0)		6.18[a](7.0)	6.93[c]	6.93[c]	6.67(8.0)		6.40[a](7.0)	6.58[c]	6.58[c]	7.22(8.0)		2.67
7a	8.04(6.0)	6.74(7.0)	8.27(6.0)		6.19[a](7.0)	6.90[c]	6.90[c]	6.67(8.0)	6.92[d]		6.39[c]	6.39[c]	7.20(7.0)		2.56
8a	8.00(6.0)	6.72(7.0)	8.25(6.0)		6.17[a](7.0)	6.88[c]	6.88[c]	6.65(8.0)	7.20(9.0)	6.39[a](8.0)		6.39[a](8.0)	7.20(9.0)		2.31
9a	8.00(6.0)	6.73(6.0)	8.24(6.0)		6.14[a](7.0)	6.86[c]	6.86[c]	6.63(8.0)	7.15(9.0)	6.34[a](9.0)		6.34[a](9.0)	7.15(9.0)		3.81
10a	8.07(6.0)	6.81(7.0)	8.33(6.0)		6.30[a](7.0)	7.06[c]	7.06[c]	6.77(7.0)	7.38(8.0)	6.82[a](7.0)		6.82[a](7.0)	7.38(8.0)		
5b	8.03(6.0)	6.77(7.0)	8.20(6.0)		6.04[a]		6.71[a](9.0)	6.60(7.0)	7.35(8.0)	6.60[c]	6.60[c]	6.60[c]	7.35(8.0)	2.42	
6b	8.04(6.0)	6.76(7.0)	8.18(6.0)		6.02[d]		6.69[a](7.0)	6.58(7.0)		6.37[a](7.0)	6.60[c]	6.60[c]	7.20(8.0)	2.44	2.60
7b	8.05(6.0)	6.75(7.0)	8.16(6.0)		6.04[d]		6.70[a](7.0)	6.60(7.0)	6.90[d]		6.38[c]	6.38[c]	7.18(7.0)	2.42	2.50
8b	8.04(6.0)	6.70(7.0)	8.22(7.0)		6.00[d]		6.68[a](7.0)	6.60(7.0)	7.24(7.0)	6.42[a](7.0)		6.42[a](7.0)	7.24(7.0)	2.42	2.33
9b	8.00(6.0)	6.71(7.0)	8.20(7.0)		6.03[d]		6.70[a](7.0)	6.62(7.0)	7.19(8.0)	6.35[a](9.0)		6.35[a](9.0)	7.19[a](8.0)	2.44	3.84
10b	8.05(6.0)	6.80(6.0)	8.35(6.0)		6.08[d]		6.66[a](7.0)	6.60(7.0)	7.42(8.0)	6.35[a](9.0)		6.78[a](7.0)	7.42[a](8.0)	2.45	
5c	8.08(6.0)	6.88(7.0)	8.35(6.0)		6.42[d]		7.20[a](8.0)	7.07(7.0)	6.88(7.0)	6.54[c]	6.54	6.54[c]	6.88(7.0)		
6c	8.06(6.0)	6.86(7.0)	8.33(6.0)		6.40[d]		7.17[a](8.0)	7.09(7.0)		6.44[a](7.0)	6.60	6.60[c]	7.38(8.0)		2.69
7c	8.06(6.0)	6.87(7.0)	8.32(6.0)		6.40[d]		7.79[a](7.0)	7.06(7.0)	7.23[d]		6.46	6.46[c]	7.34(8.0)		2.58
8c	8.09(6.0)	6.82(6.0)	8.31(6.0)		6.39[d]		7.16[a](7.0)	7.09(7.0)	6.69(7.0)	6.17[a](7.0)		6.17[a](7.0)	6.69(7.0)		2.33
9c	8.05(6.0)	6.80(7.0)	8.36(6.0)		6.33[d]		7.13[a](7.0)	7.01(7.0)	6.65(7.0)	6.12[a](7.0)		6.12[a](7.0)	6.65(7.0)		3.82
10c	8.10(6.0)	6.84(7.0)	8.35(6.0)		6.37[d]		7.16(7.0)	7.05(7.0)	7.22(7.0)	6.80[a](7.0)		6.80[a](7.0)	7.22(7.0)		

[a] Doublet.
[b] Triplet.
[c] Multiplet.

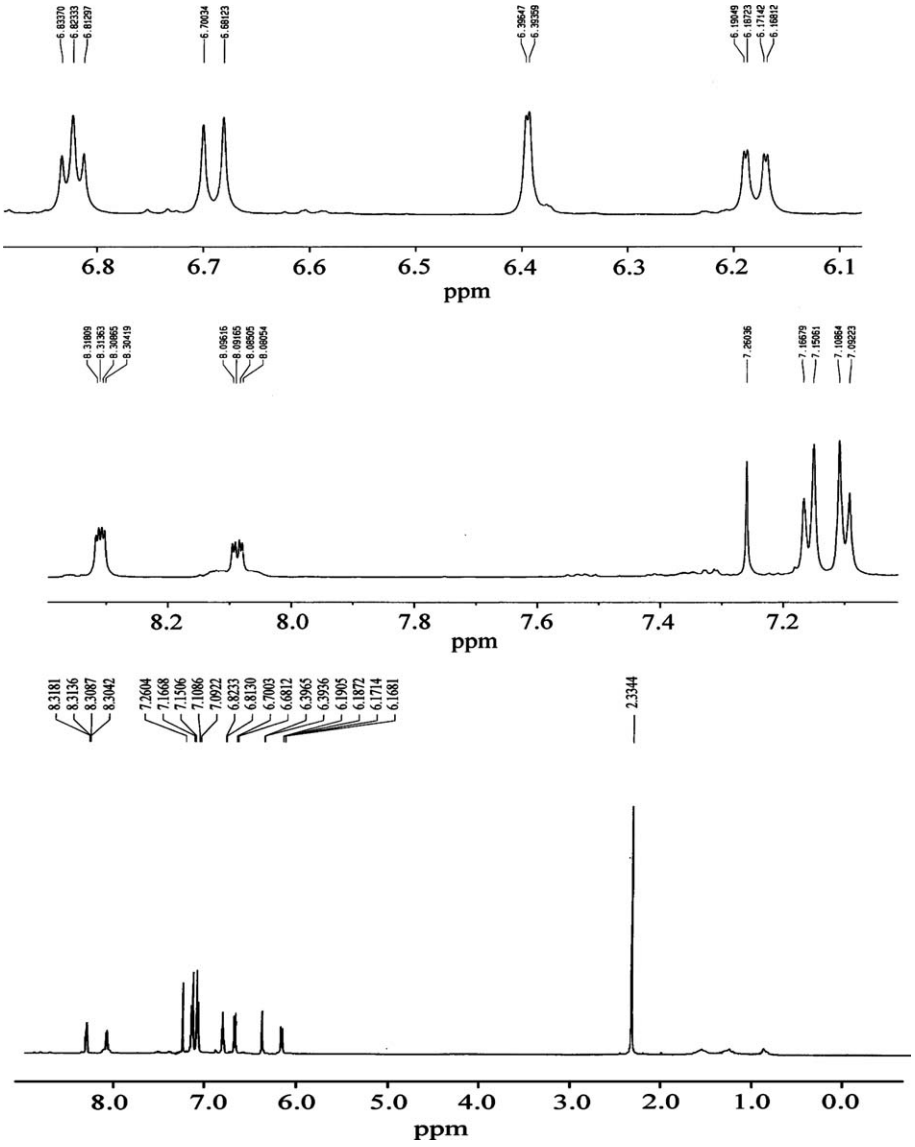

Fig. 4. ^{1}H NMR spectrum of Pt(*p*-Clpapm–N–C_6H_4–Me-*p*)Cl (**8c**) in $CDCl_3$ at 298 K.

3.4. Electrochemistry

The electrochemical properties of Pt(aapm)Cl_2 (**4**) and Pt(aapm-N–Ar)Cl (**5**–**10**) have been investigated by cyclic voltammetry. The results are given in Table 3 and a representative voltammogram is shown in Fig. 5. Pt(aapm)Cl_2 exhibit two quasireversible ($\Delta E_p > 100$ mV) reduction couples at negative to SCE and have assigned to reduction of azo group [13,18,19]. Pt(aapm-N–Ar)Cl show four successive redox couples. One redox couple appears at positive side to SCE in the potential range 0.8–1.1 V and oxidative in nature. This redox response is quasireversible in nature which is supported from $\Delta E_p \geqslant 80$ mV ($\Delta E_p = [E_{pa} - E_{pc}]$, peak-to-peak separation). One electron nature of the redox couple is supported from i_{pa}/i_{pc} ($\approx$1.0) and differential pulse voltammetry (DPV). Platinum(II) unlike palladium

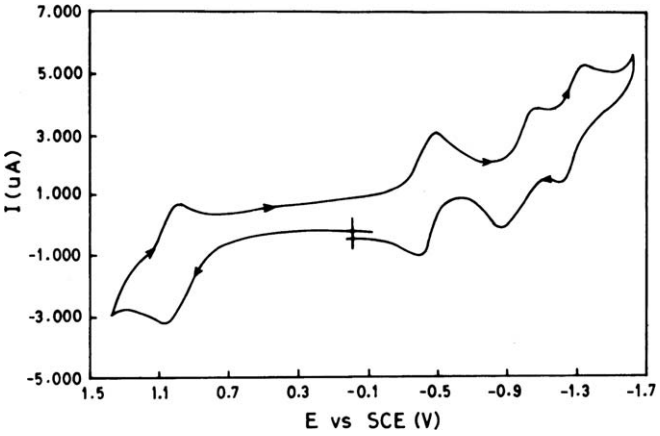

Fig. 5. Cyclic voltammogram of Pt(*p*-tapm–N–C_6H_4–Me-*m*)Cl (**7b**) in MeCN.

is irreversibly oxidized to platinum(IV) by 2e stoichiometry [6,18]. The redox responses at positive potential to SCE may be corresponding to electron extraction from HOMO (62a), which has major share from N–Ar group (68%). Thus Eq. (2) is justified.

Three redox responses at negative to SCE are reductive in nature. The reductions correspond to sequential electron feeding at LUMOs. There are four successive redox accessible levels in –N=N–C=N– group (Eqs. (3)–(6)). The LUMO (63a) shares 33% azo (–N=N–) contribution and thus electron may be localized at azo center. So the reductions may be ascribed by Eqs. (3)–(6).

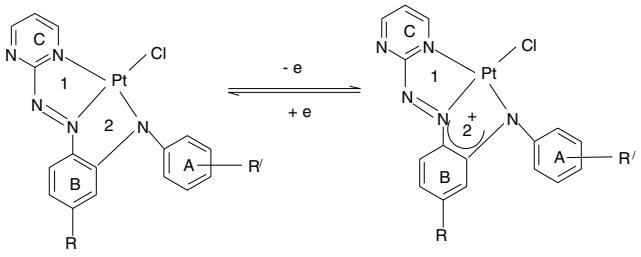

(2)

$$[\text{–N=N–C=N–}] \overset{+e}{\rightleftharpoons} [\text{–N=N–C}^{\cdot-}\text{–N–}]^{-} \quad (3)$$

$$[\text{–N=N–C}^{\cdot-}\text{–N–}]^{-} \overset{+e}{\rightleftharpoons} [\text{–N}^{\cdot-}\text{–N–C}^{\cdot-}\text{–N–}]^{2-} \quad (4)$$

$$[\text{–N}^{\cdot-}\text{–N–C}^{\cdot-}\text{–N–}]^{2-} \overset{+e}{\rightleftharpoons} [\text{–N–N–C}^{\cdot-}\text{–N–}]^{3-} \quad (5)$$

$$[\text{–N–N–C}^{\cdot-}\text{–N–}]^{3-}\,1 \overset{+e}{\rightleftharpoons} [\text{–N–N–C–N–}]^{4-} \quad (6)$$

4. Conclusion

Pt(arylazopyrimidinie)Cl_2 have been reacted with arylamine ($ArNH_2$). The coupled products have been characterized by spectroscopic and electrochemical studies. In one case the structural confirmation has been carried out by X-ray diffraction study. Crystallographic parameters have been used to EHMO calculation. The spectral and electrochemical results have been correlated with MO calculation and compared with the results of palladium complexes.

5. Supplementary materials

Crystallographic data for the structure Pt(papm-N–C_6H_4–Me-*m*)Cl (**7a**) have been deposited with the Cambridge Crystallographic Data center, CCDC No. 184679. Copies of this information may be obtained free of charge from the Director, CCDC, 12 Union Road, Cambridge CB2 1EZ, UK, e-mail: deposit@ccdc.cam.ac.uk or www: htpp://www.ccdc.cam.ac.uk.

Acknowledgments

Financial support from the University Grants Commission and Department of Science and Technology, New Delhi are gratefully acknowledged.

References

[1] E.C. Constable, Metal and Ligand Reactivity, VCH, Weinheim, 1996.
[2] R.A. Helon, J.K. Kochi, Metal Catalysed Reactions of Organic Compounds, Academic Press, New York, 1981.
[3] C.K. Pal, S. Chattopadhyay, C. Sinha, D. Bandhyopadhyay, A. Chakravorty, Polyhedron 13 (1994) 999.
[4] P.K. Santra, R. Roy, C. Sinha, Proc. Indian Acad. Sci. (Chem. Sci.) 112 (2000) 523.
[5] P.K. Santra, P. Byabratta, S. Chattopadhyay, C. Sinha, L.R. Falvello, Eur. J. Inorg. Chem. (2002) 1124.
[6] M. Panda, S. Das, G. Mostafa, A. Castineiras, S. Goswami, Dalton Trans. (2005) 1249.
[7] B.K. Santra, P. Munshi, G. Das, P. Bharadwaj, G.K. Lahiri, Polyhedron 18 (1999) 617.
[8] S. Pal, D. Das, C. Sinha, C.H.L. Kennard, Inorg. Chim. Acta 313 (2001) 21.
[9] G.K. Routh, S. Pal, D. Das, C. Sinha, A.M.Z. Slawin, J.D. Woollins, Polyhedron 20 (2001) 363.
[10] P.K. Santra, D. Das, T.K. Misra, R. Roy, C. Sinha, S.-M. Peng, Polyhedron 18 (1999) 1909.
[11] G.M. Sheldrick, SHELXS-97, Program for the Solution of Crystal Structure, University of Gottingen, Germany, 1997.
[12] M. Haga, E.S. Dodsworth, A.B.P. Lever, Inorg. Chem. 25 (1986) 447.
[13] C.K. Pal, S. Chattopadhyay, C. Sinha, A. Chakravorty, Inorg. Chem. 33 (1994) 6140.
[14] T. Mathur, U.S. Ray, J.-C. Liou, T.-H. Lu, C. Sinha, Polyhedron 24 (2005) 739.
[15] S. Pal, D. Das, P. Chattopadhyay, C. Sinha, K. Panneerselvam, T.-H. Lu, Polyhedron 19 (2000) 1263.
[16] L.M. Jackman, S. Sternhell, Applications of Nuclear Magnetic Resonance Spectroscopy in Organic Chemistry, second ed., Pergamon Press, Oxford, 1969.
[17] C. Sinha, Polyhedron 12 (1993) 2363.
[18] S. Chattopadhyay, C. Sinha, P. Basu, A. Chakravorty, Organometallics 10 (1991) 1135.
[19] P. Santra, Ph.D. thesis, Burdwan University, Burrdwan, 2001.

with propane-1,3-diamine compounds of nickel(II) and copper(II) yield $[M(cis\text{-}Me_6[15]diene)]^{2+}$ compounds [13] and the structure of *N-rac*-$[Cu(cis\text{-}Me_6[15]diene)]Cl(ClO_4)_3$ {*cis*-Me_6[15]diene = 6,8,8,13,13,15-hexamethyl-1,5,9,12-tetraazacyclotpentadeca-5,15(1)-diene} has been reported [16]. Analogous reactions with butane-1,4-diamine complexes yield homologous *cis*-Me_6[16]diene complexes [17], which have not been structurally characterized. Reaction of tris(propane-1,3-diamine)nickel(II) perchlorate with acetone yields $[Ni(trans\text{-}Me_6[16]diene)](ClO_4)_2$ [18] for which the structures of cyclic amine reduction products have been reported [19]. Reaction of bis(propane-1,3-diamine)-copper(II) perchlorate with acetone yields both *cis* and *trans* isomers of $[Cu(Me_6[16]diene)]^{2+}$; the structures of *N-rac*-$[Cu(cis\text{-}Me_6[16]diene)][ZnCl_4]$ and of co-crystallised *N-rac*-$[Cu(trans\text{-}Me_6[16]diene)]$ *N-meso*-$[Cu(cis\text{-}Me_6[16]\text{-}diene)](ClO_4)_4$ have been determined [20]. Reaction of hexane-1,6-diamine hydroperchlorate with acetone yields $[H_2(trans\text{-}Me_6[22]diene)](ClO_4)_2$, from which copper(II) and nickel(II) compounds were prepared. The compound $[Cu_2(trans\text{-}Me_6[22]diene)(OMe)_2](ClO_4)_2$ has a dinuclear structure with each copper(II) ion coordinated by one amine and one imine group of the macrocycle and two bridging methoxy groups [21,22].

The structure of *N-rac*-$[Cu(cis\text{-}Me_6[14]diene)](ClO_4)_2$ is now reported, permitting comparison of the structures of the series of copper(II) *cis*-hexamethyl-tetraaza-cyclo-diene macrocycle compounds with fourteen to eighteen ring-members (see the Scheme 1).

Cations related to $[Cu(cis\text{-}Me_6[14]diene)]^{2+}$ often form very water-insoluble precipitates with tetracyanonickelate(II), but for $[Cu(cis\text{-}Me_6[14]diene)]^{2+}$ the product was sufficiently water-soluble to permit growth of crystals suitable for a structural study.

A number of compounds with amine cations and cyanometallate anions have been structurally characterized [23]. These frequently have bridging cyano groups with a variety of multi-nuclear groupings. For (tetraamine)copper(II) cations chain-polymeric structures are usual, as for the bis(ethane-1,2-diamine)copper(II) compound $[-(en)_2Cu\text{–}NC\text{–}Ni(CN)_2\text{–}CN\text{-}]_n$ [24,25] (and analogous compounds of other tetraaminecopper(II) cations), with *trans* axially-coordinated tetracyanonickelate anions. Related structures are present for *C-meso*-(5,5,7,12,12,14-hexamethyl-1,4,8,11-tetraazacyclotetradecane)copper(II) compounds with $[Fe(CN)_6]^{3-}$ [26] and $[Cr(CN)_6]^{3-}$ [27]. For the (13-ethyl-5,7,7-trimethyl-13-nitro-1,4,8,11-tetraazacyclotetradec-4-ene)copper(II) cation, $[Cu(L)]^{2+}$, a trinuclear tetracyanonickelate-bridged compound with cations $[(L)Cu\text{–}NC\text{–}Ni(CN)_2\text{–}CN\text{–}Cu(L)]^{2+}$ and independent $[Ni(CN)_4]^{2-}$ anions is formed [28]. The structure of a tetracyanonickelate(II) compound of $[Cu(cis\text{-}Me_6[14]diene)]^{2+}$ is now reported.

2. Results

2.1. N-rac-(5,7,7,12,12,14-hexamethyl-1,4,8,11-tetraazacyclotetradeca-4,14(1)-diene)copper(II) perchlorate

The structure of *N-rac*-$[Cu(cis[14]diene)](ClO_4)_2$ was determined by X-ray diffractometry, see Section 4 for details.

The compound is isostructural with the Ni(II) analogue [4]. The asymmetric unit consists of half the $[Cu(cis[14]\text{-}diene)]^{2+}$ cation and one perchlorate ion, see Fig. 1. The cation lies on a twofold axis, through Cu and the mid-points of bonds C2–C3, C9–C10, establishing the *N-rac*-configuration, with one NH group and one axially oriented methyl substituent on each side of the CuN_4 plane. The copper(II) ion is in slightly tetrahedrally twisted planar coordination by the four N-atoms (*trans* N–Cu–N angles = 176.67(5)°), see below and Table 1 for other significant dimensions. The Cu–N bond is, as is usual, slightly shorter for the imine nitrogen than for the secondary amine nitrogen. The N4–C5 distance of 1.284(2) Å and the bond angles about these atoms confirm the location of the imine function. The five-membered chelate rings have symmetrical, but different, gauche conformations, and the six-membered chelate ring has a twist conformation [angle N–Cu–N and displacements of atoms from relevant CuN_2 planes/°, Å: Cu,N4,$N4^i$ (diimine chelate): 85.62(7), C3, 0.339(1); Cu,N8,$N8^i$ (diamine chelate): 86.60(7), C9, −0.385(1); Cu,N4,N8 (amine–imine chelate): 93.98(5), C5, 0.070(1), C51, 0.433(3), C6, −0.170(3), C7, −0.841(2), C71, −0.873(3); C72, −2.258(1)].

A well-ordered perchlorate ion lies on each side of the planar cation, with the closest oxygen atom O1 {and $O1^i$} lying off the tetragonal axis, with O1–Cu–$O1^i$ = 174.3°, with Cl1 "above" $N4^i$, with Cu–O1 = 3.017(1) Å, indicating very weak interactions. Hydrogen bonds N8–H8···$O4^i$ [H···O, N–O, N–H···O/Å, °: 2.50, 3.211(2), 136] and N8–H8···$O1^{ii}$ [2.53, 3.168(2),

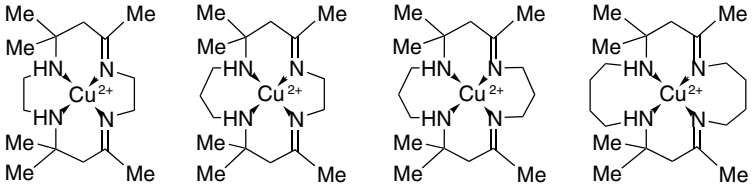

Scheme 1. The formulae of *cis*-(diamine–diimine) azamacrocycle copper(II) cations which have been structurally characterised.

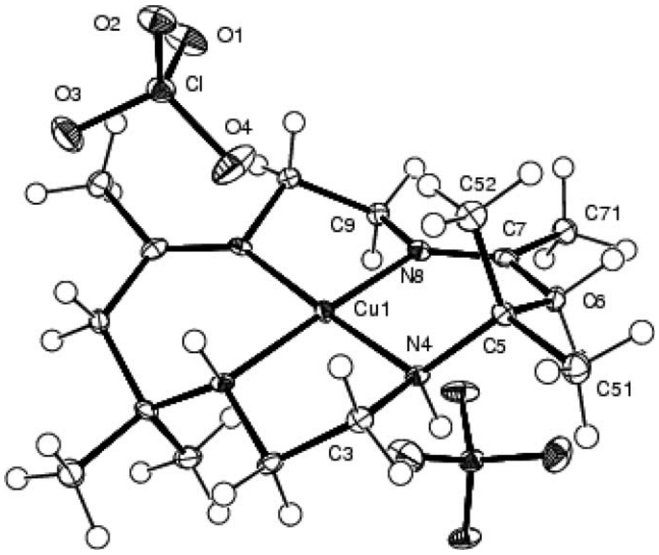

Fig. 1. *N-rac*-(5,7,7,12,12,14-hexamethyl-1,4,8,11-tetraazacyclotetradeca-4,14(1)-diene)copper(II) perchlorate, drawn [29] with displacement ellipsoids at the 50% confidence level, with hydrogen atoms shown as circles of arbitrary radius.

127] link the cation and perchlorate ions; symmetry operations i = $-x$, y, $-z + 1/2$; ii = $x + 1/2$, $y + 1/2$, $-z + 1/2$.

2.2. Di-μ-cyano-1:2κ^2 C:N;1:3κ^2 C:N-dicyano-1κ^2 C-bis(*N-rac*-5,7,7,12,12,14-hexamethyl-1,4,8,11-tetraazacyclotetradeca-4,14(1)-diene)copper(II)–nickel(II) tetra(cyano-κ^1C) nickelate(II)

The structure of [{*N-rac*-Cu(*cis*[14]diene)}$_2${Ni(CN)$_4$}]·[Ni(CN)$_4$] was determined by X-ray diffractometry, see Section 4.2 for details.

The crystal has an asymmetric unit including the (tetraazamacrocycle)copper(II) cation and halves of two independent centrosymmetrical tetracyanonickelate(II) ions [Ni2(N21–C21)(N22–C22)] and [Ni3(N30–C30)(N31–C31)], see Fig. 2. The tetracyanonickelate(II) ion including Ni3 links two (tetraazamacrocycle)copper(II) units to form symmetrical trinuclear cations, see Fig. 3. The bridging tetracyanonickelate ion is coordinated axially with Cu–N30 = 2.298(2), Cu···Cu = 9.918(2) Å, see Fig. 3. The second tetracyanonickelate(II) ion, including Ni2, which is inclined to the first at 8.3(1)°, does not interact with the copper(II) cation, other than by the hydrogen bond N11–H11···N33^{i} {N11–N33^{i} = 3.000(3), H11···N33^{i} = 2.26 Å, N11–H11···N33^{i} = 136°, symmetry operation i = $-x$, $-y$, $-z$.

The (5,7,7,12,14,14-hexamethyl-1,4,8,11-tetraazacyclotetradeca-4,11-diene)copper(II) cation is present in the *N-rac* configuration, with dimensions (see Table 1) similar to those of the perchlorate salt, except that the CuN$_4$ group is bent along the N1–Cu–N8 axis {N1–Cu–N8 = 178.25(7)°, N4–Cu–N11 = 160.30(7)°} with the Cu displaced towards the axially interacting cyano nitrogen atom N30 (see Fig. 4) {displacements of atoms from best N$_4$ plane: N1 −0.163(1), N4 0.159(1), N8 −0.156(1), N11

Table 1
Comparison of dimensions of (*cis*-tetraazacyclic-diene)copper(II) and related cations

Compound	Mean Cu–N$_{amine}$	Mean Cu–N$_{imine}$	Twisting of N$_4$ group	Displ. of Cu from N$_4$ plane	Axial interactions	Ref.
N-rac-[Cu(*cis*-Me$_6$[14]diene)](ClO$_4$)$_2$	1.994(1)	1.969(1)	±0.056(1)	0	Cu–O 3.017(1)	[a]
N-rac-[{Cu(*cis*Me$_6$[14]diene)}$_2${Ni(CN)$_4$}][Ni(CN)$_4$]	2.009(3)	1.974(3)	±0.16(1)	0.18	Cu–NC 2.298(2)	[a]
N-rac-[Cu(*cis*-Me$_6$[15]-diene)]$_2$Cl(ClO$_4$)$_3$[b]	2.02(1)	1.99(1)	±0.30(1)	0.09(1)	Cu–Cl 2.83(1), Cu–O 2.94(1)	[16]
N-rac-[Cu(*cis*-Me$_6$[16]-diene)][ZnCl$_4$]	2.026(1)	2.006(1)	±0.559(1)	0.149(1)	Cu–Cl 3.34(1)	[20]
N-meso-[Cu(*cis*-Me$_6$[16]diene)](ClO$_4$)$_2$[c]	2.03(1)	2.02(1)	±0.019(6)	0.047(6)	Cu–O 3.3	[20]
N-rac-[Cu(*trans*-Me$_6$[16]diene)](ClO$_4$)$_2$[c]	2.05(1)	2.02(1)	±0.094(7)	0.175(7)	Cu–O 2.5	[20]
N-meso-[Cu(*cis*-Me$_6$[18]diene)](ClO$_4$)$_2$	2.018(7)	1.987(6)	±0.13(1)	0.04(1)		[11]
C-meso-[Cu(*cis*-Me$_6$[14]ane)](ClO$_4$)$_2$	2.028(6)		0	0	Cu–O 2.657(5), Cu–O 2.697(5)	[5]
N-meso-[Cu(*trans*-Me$_6$[14]diene)](ClO$_4$)$_2$	2.027(7)	1.974(5)	0	0		[4]
N-rac-[Ni(*cis*-Me$_6$[14]diene)](ClO$_4$)$_2$[d]	1.927(6)	1.891(6)	±0.007	0	Ni–O 3.21	[9]

[a] This work.
[b] *N-rac*-{6,8,8,13,15-hexamethyl-1,5,9,13-tetraazacyclotpentadeca-5,15(1)-diene)copper(II)}.
[c] Co-crystallised.
[d] Isostructural with the Cu analogue.

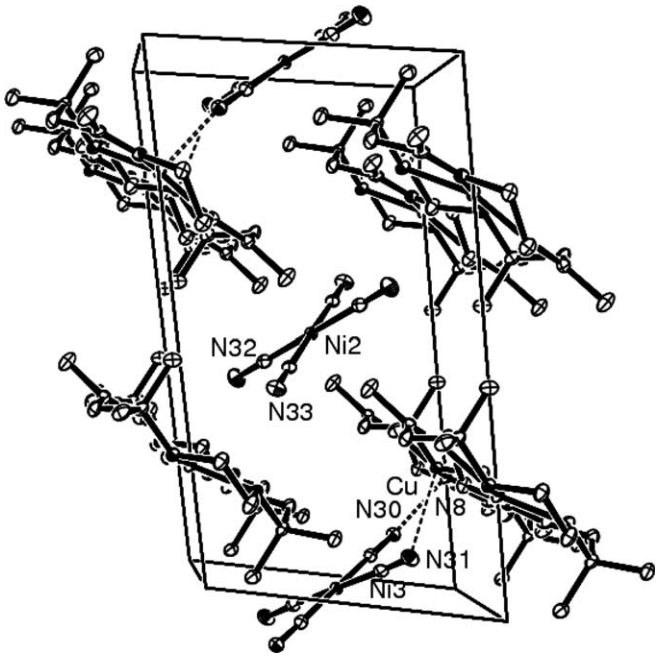

Fig. 2. The unit cell of $[\{N\text{-}rac\text{-}Cu(cis[14]diene)\}_2\{Ni(CN)_4\}]\cdot[Ni(CN)_4]$, viewed normal to (0 1 0), drawn as for Fig. 1, with hydrogen atoms omitted for clarity.

0.161(1) Cu −0.181(1) Å}. The Cu–N distances {Cu–N1 = 1.964(2), Cu–N4 = 1.987(2), Cu–N8 = 2.016(2), Cu–N11 = 2.002(2) Å} are slightly longer than the values for the perchlorate salt, again with Cu–N distances slightly shorter for imine than for amine nitrogen. These increased Cu–N distances with increased coordination number, together with the appreciable folding of the macrocycle in response to the axial coordination of the tetracyanonickelate group indicate the flexibility of these azamacrocycles.

The cyano nitrogen atom N30 is near the tetragonal axis of the tetraaza cation {angles N–Cu–N30 range from 85.0(1)° to 109.2(1)° with Cu–N30≡C30 = 142.1(2)°}. The plane of the $[Ni3(CN)_4]^{2-}$ ion is inclined to the best N_4 plane of the cation at 72.98(4)°, angled away from the axially oriented methyl group C121 and oriented such that the closest approach is N31 to N8, with a hydrogen bond N8–H8···N31 {N8···N31 = 3.328(3), H8···N31 = 2.53 Å. N8–H8···N31 = 145°}.

Both tetracyanonickelate ions are slightly distorted from D_{4h} symmetry, the bridging ion including Ni3 more so than the independent ion including Ni2, with the largest affects associated with the coordinated N30 atom. The bond C30≡N30 = 1.849(2) Å is slightly shorter than the other C≡N distances {all 1.861(2) Å}, and the coordinated cyano group Ni3–C30≡N30 more bent {bond angle = 174.6(2)°} than the others {Ni3–C31≡N31 = 176.2(2)°, Ni2–C32≡N32 179.2(2)° and Ni2–C33≡N33 = 178.7(2)°}.

3. Discussion

3.1. The perchlorate salt

Fourteen membered 1,4,8,11-tetraazacyclotetradecane macrocycles have the optimal (minimal strain energy) configurations for coordination to copper(II) ions, shown for $[Cu(cis[14]diene)](ClO_4)_2$ by the optimal Cu–N distances, near coplanarity of the CuN_4 group and near optimal ring bond and torsion angles. Like its nickel(II) analogue, $[Cu(cis[14]diene)](ClO_4)_2$ is most stable in the *N-rac* configuration.

Increasing the ring size for homologous metal-free tetraazamacrocycles leads to increasing "hole-size" and tetrahedral twisting of the N_4 group. However, the copper(II) cations of the *cis*-diene tetrazamacrocycles from 14 to 18 ring-members show little increase in Cu–N distance with increasing ring-size; the increasing strain being accommodated by a combination of increasing puckering of the ring and by increasing tetrahedral twisting of the CuN_4 group. The $[Cu(cis\text{-}Me_6[16]diene)]^{2+}$ cation has the CuN_4 group near co-planar for the perchlorate salt (with *N-meso* configuration) and appreciably twisted for the tetrachlorozincate

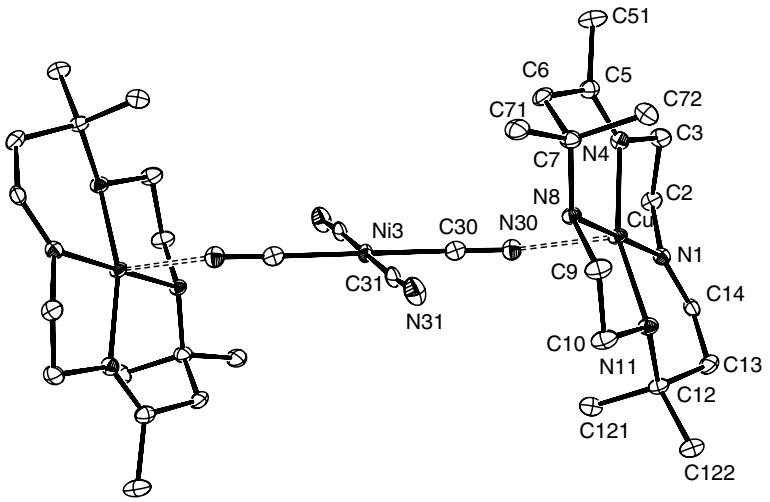

Fig. 3. The $[\{N\text{-}rac\text{-}Cu(cis[14]diene)\}_2\{Ni(CN)_4\}]^{2+}$ trinuclear cation, drawn as for Fig. 1.

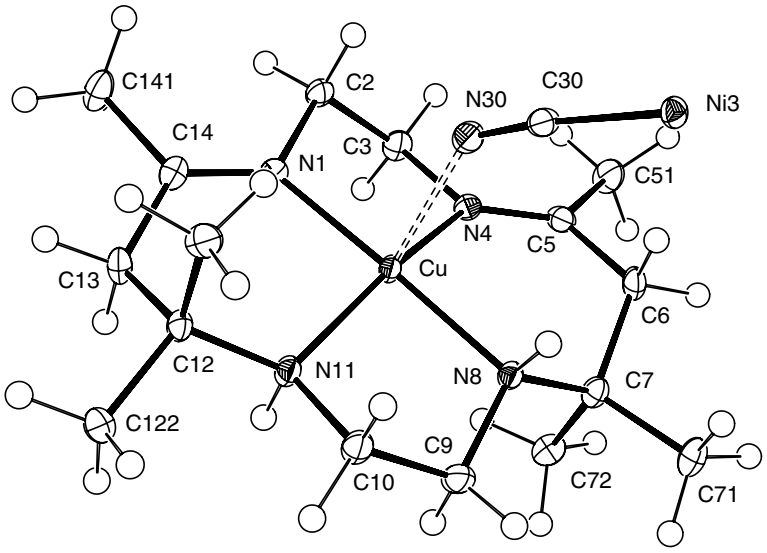

Fig. 4. The $[\{N\text{-}rac\text{-}Cu(cis[14]diene)\}_2\{Ni(CN)_4\}]^{2+}$ cation, showing the axial interaction with the bridging cyano group, drawn as for Fig. 1.

salt (with *N-rac* configuration), showing the influence of configuration on geometry [20]. For the perchlorate salts the *N-meso*-$[Cu(cis\text{-}Me_6[18]diene)]^{2+}$ cation has marginally shorter Cu–N distances and little (±0.007 Å) tetrahedral twisting of the N_4 group, but has a highly puckered ring, while the *N-rac*-$[Cu(trans\text{-}Me_6[18]diene)]^{2+}$ cation has a very twisted macrocycle, with ±0.13(1) Å displacements of the N_4 group.

3.2. The tetracyanonickelate(II) compound

The cation $[Cu(cis\text{-}Me_6[14]diene)]^{2+}$, like many similar cations, forms a compound with tetracyanonickelate(II) which is sparingly water-soluble (an analogous compound formed by $[Cu(trans\text{-}Me_6[14]diene)]^{2+}$ is much less soluble). A number of such compounds with metal–amine cations and cyanometallate anions have been structurally characterized [23]. These frequently have bridging cyano groups with a variety of multi-nuclear groupings, commonly chain-polymeric, which generally show some degree of antiferromagnetic spin coupling. A structurally similar compound, formed by (13-ethyl-5,7,7-trimethyl-13-nitro-1,4,8,11-tetraazacyclotetradec-4-ene)copper(II), has one trinuclear cation similar to that here described {Cu–N_{cyano} = 2.226(3) Å, Cu–N≡C = 168.2(3)°} and another with a water molecule coordinated *trans* to the bridging cyano group {Cu–N_{cyano} = 2.677(4), Cu–O = 2.396(3) Å and Cu–N≡C = 137.7(3)°}, and also has independent $[Ni(CN)_4]^{2-}$ ions [28].

The nickel(II) analogue of the compound now reported occurs as the singlet ground state salt with non-interacting ions $[Ni(cis\text{-}Me_6[14]diene)][Ni(CN)_4]\cdot H_2O$, while the *trans* isomeric cation occurs as both a singlet ground state salt *N-rac*-$[Ni(trans\text{-}Me_6[14]diene)][Ni(CN)_4]\cdot 3H_2O$ and as a triplet ground state linear polymer *N-meso*-$[\text{-}Ni(trans\text{-}Me_6[14]diene)NC\text{–}Ni(CN)_2\text{–}CN\text{–}]_\infty$, with Ni–$C_{cyano}$ = 2.207(1) Å [30].

4. Experimental

4.1. Preparation of compounds

4.1.1. N-rac-5,7,7,12,12,14-Hexamethyl-1,4,8,11-tetraazacyclotetradeca-4,1(14)-diene)copper(II) Perchlorate

Orange *N-rac*-$[Cu(cis[14]diene)](ClO_4)_2$ was prepared by reaction of tris(ethane-1,2-diamine)copper(II) perchlorate with acetone, separating the *cis*- and *trans* isomeric products by fractional crystallisation from water, as reported in [1]. The crystal used for the structural study was obtained by allowing a hot saturated solution in water to cool slowly.

4.1.2. Di-μ-cyano-1:2κ^2 C:N;1:3κ^2 C:N-dicyano-1κ^2 C-bis-(N-rac-5,7,7,12,12,14-hexamethyl-1,4,8,11-tetraazacyclo- tetra deca-4,1(14)-diene)copper(II)-nickel(II) tetra(cyano-κ^1C)nickelate(II)

A solution of $Na_2[Ni(CN)_4]\cdot 3H_2O$ in hot water was added to a solution of *N-rac*-$[Cu(cis[14]diene)](ClO_4)_2$ (equimolar amounts) in hot water. The sparingly soluble dark blue product was filtered from the cold solution, washed with cold water and air-dried. A crystal for the structural study was obtained by slow cooling of a hot aqueous solution. *Anal.* Calc. for $C_{20}H_{32}N_8CuNi$: C, 47.4; H, 6.4; N, 22.1. Found: C, 47.2; H, 6.2; N, 22.1%. IR spectrum: sharp bands were assignable to ν(NH) 3232 and ν(C=N) 1667 cm^{-1} of the $[Cu(cis[14]diene]^{2+}$ cation and a single sharp band at 2113 cm^{-1} to ν(C≡N) of the $Ni(CN)_4]^{2-}$ anions (although there are four structurally distinct cyanide ions in the structure.

4.1.3. Magnetic susceptibility

The magnetic susceptibility of $[\{Cu(cis\text{-}Me_6[14]diene)\}_2\{Ni(CN)_4\}][Ni(CN_4)]$, measured by the Gouy method at 293 K, was 1.32×10^{-8} m^3 (mol of Cu)$^{-1}$ which after correction for diamagnetism using Pascal's constants gives

an effective magnetic moment of 1.75 μ_B, indicating that little, if any, spin coupling is present.

4.2. Structural study for N-rac-(5,7,7,12,12,14-hexamethyl-1,4,8,11-tetraazacyclotetradeca-4,14(1)-diene)copper(II) perchlorate

4.2.1. Crystal data

$C_{16}H_{32}Cl_2CuN_4O_8$, $M_r = 542.91$, orange block grown from water, $0.36 \times 0.11 \times 0.10$ mm, orthorhombic, space group *P bcn*, $a = 10.483(1)$, $b = 10.934(1)$, $c = 19.195(3)$, $Z = 4$, $T = 273(2)$ K, cell from 7963 reflections, θ_{min} 2.69°, θ_{max} 32.85°.

Bruker SMART 1K CCD area detector diffractometer, φ and ω scans, Mo Kα radiation ($\lambda = 0.71073$ Å), $T =$ 88(2) K, multi-scan absorption correction (based on symmetry-related measurements, Bruker SADABS 2004/1) [31], $T_{min} = 0.695$, $T_{max} = 0.879$, 20617 measured reflections (average $R_{eqiv.}$ 0.0371), $h - 15 \rightarrow 12$, $k - 12 \rightarrow 16$, $l - 29 \rightarrow 8$, θ_{min} 2.12, θ_{max} 32.82°, 3763 independent reflections, 2956 reflections with $I > 2\sigma(I)$.

4.2.2. Solution and refinement [32]

Refinement on F^2, all H-atoms are in calculated positions and riding, 144 parameters. $R_1 = 0.0303$, $wR =$ 0.0708 $\{I > 2\sigma(I)\}$, R_1 0.0478, $wR = 0.0783$ {all reflections}, $\{w = 1/[\sigma^2(F_o^2) + (0.0375P)^2 + 1.2441P]$ where $P = (F_o^2 + 2F_c^2)/3)\}$.

4.3. Structural study for di-μ-cyano-1:2κ^2 C:N;1:3κ^2 C:N-dicyano-1κ^2 C-bis(N-rac-5,7,7,12,12,14-hexamethyl-1,4,8,11-tetraazacyclotetradeca-4,14(1)-diene)copper(II)-nickel(II) tetra(cyano-κ^1 C)nickelate(II)

4.3.1. Crystal data

$C_{40}H_{64}Cu_2N_{16}Ni_2$, $M_r = 1013.58$, violet block grown from water, $0.34 \times 0.16 \times 0.05$ mm, triclinic, space group $P\bar{1}$, $a = 8.5092(9)$, $b = 9.675(1)$, $c = 15.227(2)$ Å, $\alpha =$ 104.705(2)°, $\beta = 94.856(2)$°, $\gamma = 113.002(2)$°, Z 1, $T =$ 93(2) K, cell from 4208 refl., θ_{min} 2.90, $2\theta_{max}$ 25.65°.

4.3.2. Data collection

As for previous compound; $T = 88(2)$ K, $T_{min} = 0.8334$, $T_{max} = 1.000$ (as for the first compound), 6442 measured reflections (average $R_{eqiv.}$ 0.0205), $h - 10 \rightarrow 10$, $k - 10 \rightarrow 12$, $l - 19 \rightarrow 16$, θ_{min} 2.38°, θ_{max} 26.38°, 4792 independent reflections, 3713 reflections with $I > 2\sigma(I)$.

4.3.3. Refinement [32]

Refinement on F^2, all H-atoms are in calculated positions and riding, 282 parameters. $R_1 = 0.028$, $wR_2 =$ 0.069 $\{I > 2\sigma(I)\}$, $R_1 = 0.035$, $wR_2 = 0.072$ {all reflections} $\{w = 1/[\sigma^2(F_o^2) + ((0.0428P))^2]$ where $P = (F_o^2 + 2F_c^2)/3)\}$.

Appendix A. Supplementary data

Crystallographic data has been deposited with the Cambridge Crystallographic Data Centre; perchlorate salt CCDC 277925 and tetracyanonickelate compound CCDC 277926. Copies of this information may be obtained free of charge on application to The Director, CCDC, 12 Union Road, Cambridge CB2 2EZ, UK (fax: +44 1223 336033; e-mail: deposit@ccdc.cam.ac.uk or http://www.ccdc.cam.ac.uk). Supplementary data associated with this article can be found, in the online version, at doi:10.1016/j.poly.2005.10.025.

References

[1] N.F. Curtis, J. Chem. Soc., Dalton Trans. (1972) 1357.
[2] M.M. Blight, N.F. Curtis, J. Chem. Soc. (1962) 3016.
[3] T.H. Lu, T.J. Lee, B.F. Liang, C.S. Chung, J. Inorg. Nucl. Chem. 43 (1981) 2333.
[4] T.J. Lee, T.H. Lu, C.S. Chung, T.Y. Lee, Acta Cryst. Sect. C 40 (1984) 70.
[5] E. Ochiai, S.J. Rettig, J. Trotter, Can. J. Chem. 56 (1978) 267.
[6] N.F. Curtis, Y.M. Curtis, H.K.J. Powell, J. Chem. Soc., Sect. A (1966) 1015.
[7] M.F. Bailey, I.E. Maxwell, J. Chem. Soc., Dalton Trans. (1972) 938.
[8] B.T. Kilbourn, R.R. Ryan, J.D. Dunitz, J. Chem. Soc., Sect. A (1969) 2407.
[9] D.J. Szalda, E. Fujita, Acta Crystallogr., Sect. C 48 (1992) 1767.
[10] J.W.L. Martin, J.H. Timmons, A.E. Martell, C.J. Willis, Inorg. Chem. 19 (1980) 2328.
[11] J.H. Timmons, P. Rudolf, A.E. Martell, J.W.L. Martin, A. Clearfield, Inorg. Chem. 19 (1980) 2331.
[12] N.F. Curtis, D.A. House, J. Chem. Soc., Sect. A (1967) 537.
[13] N.F. Curtis, G.J. Gainsford, Aust. J. Chem. 39 (1986) 1509.
[14] J.L. Love, H.K.J. Powell, J. Chem. Soc., Chem. Commun. (1968) 39.
[15] N.F. Curtis, Inorg. Chim. Acta 59 (1982) 171.
[16] O.P. Gladkikh, N.F. Curtis, Acta Cryst., Sect. C 52 (1996) 1418.
[17] J.W.L. Martin, J.H. Timmons, A.E. Martell, J. Coord. Chem. 10 (1980) 251.
[18] D.A. House, N.F. Curtis, J. Am. Chem. Soc. 86 (1964) 223.
[19] N.F. Curtis, O.P. Gladkikh, Aust. J. Chem. 53 (2000) 727.
[20] N.F. Curtis, W.T. Robinson, J.M. Waters, Unpublished work.
[21] M. Yamashita, H. Ito, T. Ito, Inorg. Chem. 22 (1983) 2101.
[22] R.W. Hay, M.P. Pujari, Inorg. Chim. Acta 99 (1985) 75.
[23] J. Cernak, M. Orendac, I. Potocnak, A.J. Chomic, A. Orendacova, J. Skorsepa, A. Feher, Coord. Chem. Rev. 224 (2002) 51.
[24] J.-H. Luo, M.-X. Wu, Y.-M. Wang, D.-S. Gao, D. Li, C.-Z. Cheng, Jiegou Huaxue 19 (2000) 187.
[25] J. Lokaj, K. Gyerova, A. Sopkova, J. Sivy, V. Kettmann, V. Vrabel, Acta Cryst., Sect. C 47 (1991) 2447.
[26] H.Z. Kou, D.Z. Liao, Z.H. Jiang, S.P. Yan, Q.J. Wu, S. Gao, G.L. Wang, Inorg. Chem. Commun. 3 (2000) 151.
[27] M.S. El Fallah, J. Ribas, X. Solans, M. Font-Bardia, J. Chem. Soc., Dalton Trans. (2001) 247.
[28] N.F. Curtis, H. Puschmann, Acta Cryst., Sect. C 60 (2004) m410.
[29] L.J. Farrugia ORTEP3.2, J. Appl. Cryst. 30 (1997) 565.
[30] N.F. Curtis, G.J. Gainsford, Aust. J. Chem. 37 (1984) 1799.
[31] R.H. Blessing, Acta Cryst., Sect. A 51 (1995) 33.
[32] G.M. Sheldrick, SHELXS and SHELXL-97, programs for the solution and refinement of crystal structures, University of Gottingen, Germany, 1997.

and excited state [43]. These bands emerge as consequence of the presence of donor and acceptor groups that could also act as binding centres. Transduction of the coordination events are based on selective guest interaction with either the donor or acceptor groups in the signalling framework. Those systems are of interest from either a photophysical point of view and as suitable scaffoldings for building up selective chromogenic chemosensors. Carbonyl groups are good acceptors in charge transfer bands. As donor groups nitrogen atoms are especially common due to their ability to delocalise their lone pair in the molecule. In fact there are a number of chemosensors based on charge transfer transitions containing amines as donor and carbonyls as acceptor groups, which have been employed as cations and anion sensors [44–47].

As part of our interest in the development of chromogenic chemosensors, we report here a study on the use of naphthoquinone derivatives as receptors for the chromogenic sensing of metal cations and anions in acetonitrile.

2. Results and discussion

Products L^1 and L^2 (see Scheme 1) have been synthesised following the process described by Yoshida et al. [48] by condensation reaction of the corresponding aniline derivate with the sodium salt of 1,2-naphthoquinone-4 sulphonate in acetic acid at 30 °C using nickel acetate as reaction promoter. The reaction proceeds via nickel coordination to the carbonyl groups increasing the sulphonate capacity as leaving group favouring the reaction. The products were purified by column chromatographic. The ^{1}H MNR spectrum of L^2 shows a broad unresolved signal centred at 3.7 ppm attributed to protons from the macrocycle, whereas L^1 shows a singlet at 3.07 ppm due to CH_3 groups. Both L^1 and L^2 compounds show a singlet at 6.4 ppm, and signals in the 7.4–8.2 range from the naphthoquinone framework and two doublets at 6.7 and 7.4 from the 1,4-disubstituted anilinium ring. ^{13}C NMR displayed the expected signals in the aliphatic region and signals in aromatic zone in the 111–157 ppm range. Resonances at 180.10 and 180.26 ppm were attributed to two nonequivalent carbonyl groups. The visible spectrum of these compounds shows a broad band centred at 534 ($\log\varepsilon = 3.80$) and 532 nm ($\log\varepsilon = 3.86$), for L^1 and L^2, respectively, attributed to an intra-ligand charge transfer band (ICT) form the amine to the carbonyl groups.

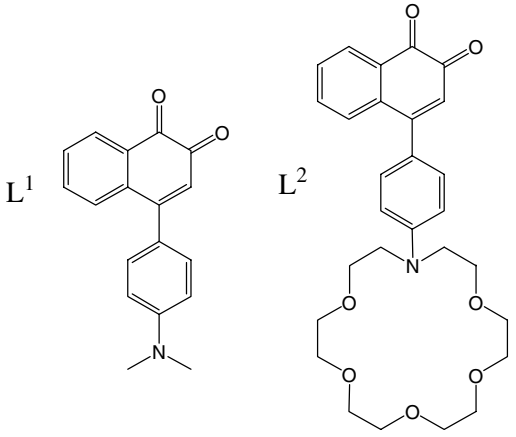

Scheme 1. Chemical structures of L^1 and L^2.

3. Cation sensing properties of L^1 and L^2

As stated above, the electronic transition of lower energy for both L^1 and L^2, is a broad band at ca. 532 nm attributed to an internal charge transfer transition. Changes observed in this band by the presence of alkaline (Li^+, Na^+, and K^+), alkaline earth (Mg^{2+}, Ca^{2+}, and Ba^{2+}) and transition metal cations (Fe^{3+}, Hg^{2+}, Cu^{2+}, Pb^{2+}, Zn^{2+}, Co^{2+}, Cd^{2+}, Ni^{2+}, and Ag^+) have been studied.

In a first experiment with these cations in acetonitrile it was evident that whereas the colour of acetonitrile solutions of L^2 were affected by the presence of Fe^{3+}, Hg^{2+}, Cu^{2+}, Pb^{2+} and Ba^{2+}, only the cations Fe^{3+}, Hg^{2+} and Cu^{2+}, induced a colour change for L^1. In the presence of the remaining metal cations, both L^1 and L^2 remained silent. The different behaviour observed for L^1 and L^2 in the presence of Pb^{2+} and Ba^{2+} should clearly be attributed to the presence of the 18-crown-6 macrocycle coordination unit in L^2 [49].

In a more detailed study with L^2, it was observed, however, that the behaviour found for Ba^{2+} was somewhat different to that found for Pb^{2+} (see Fig. 1). Thus, while the presence of Pb^{2+} resulted in a complete deactivation of the charge transfer band, the Ba^{2+} is only able to produce a partial decrease of the intensity of the band at 532 nm. This might be attributed to a stronger covalent Pb^{2+}–N interaction that could result in a more efficient capture the electron pair of the nitrogen [50]. On the contrary, the interaction of Ba^{2+} with L^2 is expected to have a stronger electrostatic character and, at least partially, the interaction with the nitrogen atoms is due to the charge of the cation that would additionally be coordinating the oxygen atoms from the macrocycle. This stronger preference of L^2 for Pb^{2+} over Ba^{2+} can also be observed when compared the stability constants obtained for the L^2–Pb^{2+} and L^2–Ba^{2+} systems which resulted to be near two order of magnitude larger for the former (see Table 1). In fact, visible titration experiments of acetonitrile solutions of L^2 with the metal cations Ba^{2+} or Pb^{2+} were indicative of the formation of 1:1 metal-to-ligand species in agreement with the coordination of the metal cations in the aza-oxa macrocycle. The $\log K$ for the formation of the corresponding $[M(L^2)]^{2+}$ ($M = Ba^{2+}$, Pb^{2+}) complexes were determined from nonlinear least-squares treatment of the titration profiles [51]. The results are shown in Table 1. Fig. 2 shows the titration curve of the system L^2–Ba^{2+}. From similar titration experiments, the stability constants for the formation of complexes of the ligands L^1 and L^2 with the metal cations Fe^{3+}, Hg^{2+}, Ba^{2+} and Pb^{2+} were also obtained and are shown in Table 1. As stated above, Ba^{2+} and Pb^{2+}

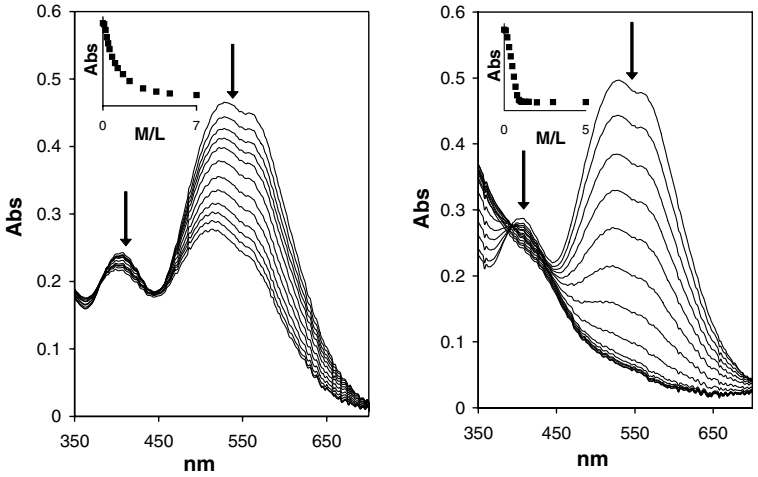

Fig. 1. UV–Vis absorption spectra of compound L^2 (6.4×10^{-5} mol dm^{-3}) in acetonitrile with different concentrations of metals. Left: Ba^{2+}, right: Pb^{2+}. The inset shows the corresponding titration curve at 534 nm.

Table 1
Logarithm of the stability constants for the formation of complexes with receptors L^1 and L^2

	L^1	L^2
$Fe^{3+} + 2L \leftrightarrow [L_2Fe]^{3+}$	10.20(4)	9.67(7)
$Hg^{2+} + 2L \leftrightarrow [L_2Hg]^{2+}$	13.12(8)	14.71(7)
$Pb^{2+} + L \leftrightarrow [LPb]^{2+}$		7.99(3)
$Ba^{2+} + L \leftrightarrow [LBa]^{2+}$		4.58(5)

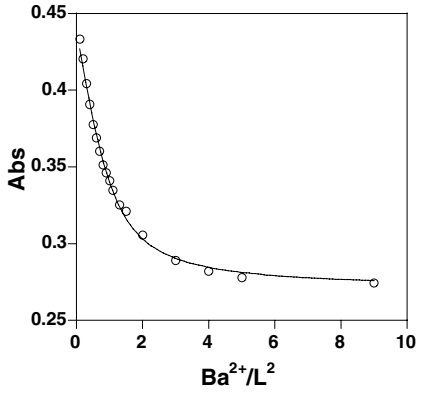

Fig. 2. Titration curve of the system L^2–Ba^{2+}.

are the only metal cations that produce optical changes with receptor L^2 but not with L^1, suggesting that they are coordinated through the aza-oxa macrocyclic unit. The coordination mode of Ba^{2+} and Pb^{2+} with L^2, was also followed by ^{1}H NMR. These studies were in agreement with cation coordination through the macrocycle. Thus, for instance, addition of Ba^{2+} to CD_3CN solutions of L^2 induced two significant variations in the resonances of the uncoordinated ligand, (i) a shift of the multiplet of the aliphatic zone from 3.5–3.8 to 3.6–4 ppm and (ii) a shift of the doublets of the aryl ring of the aniline subunit from 6.90 and 7.45 to 7.44 and 7.64 ppm, respectively, while the other aromatic signals showed unremarkable shifts in the presence of this cation.

The changes observed upon addition of increasing amount of Cu^{2+}, Hg^{2+} and Fe^{3+} to acetonitrile solutions of L^1 are shown in Figs. 3 and 4. In this case, a very similar behaviour was also found for ligand L^2 in the presence of these metal cations (not shown). As it can be seen in the Fig. 3, the Cu^{2+} cation induced the appearance of a new band at 420 nm, which resulted in a colour change of the solution form purple to yellow. Fe^{3+} and Hg^{2+} showed a somewhat different behaviour to that for Cu^{2+}. They both produce the bleaching of the solution upon addition of 0.5 equiv. but, in this case, the band at 420 nm does not appear and the solution remains colourless (see Fig. 4). This behaviour is somewhat similar to that found for Pb^{2+} with L^2, with the difference that 1 equiv. of Pb^{2+} is necessary to produce the complete bleaching. In fact, titration experiments strongly suggested that the Hg^{2+} and

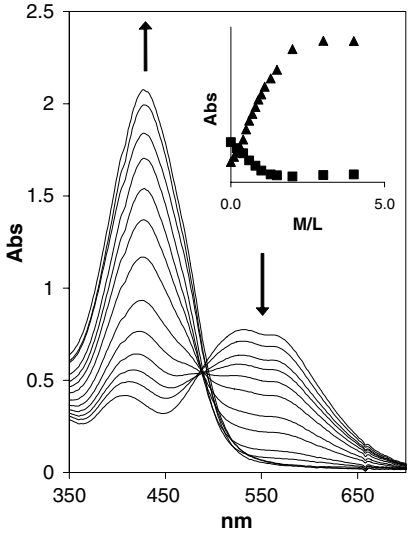

Fig. 3. UV–Vis titrations of compound L^1 (1.2×10^{-4} mol dm^{-3}) in acetonitrile with different concentrations of Cu^{2+}. The inset shows the titration curves at 534 and 420 nm.

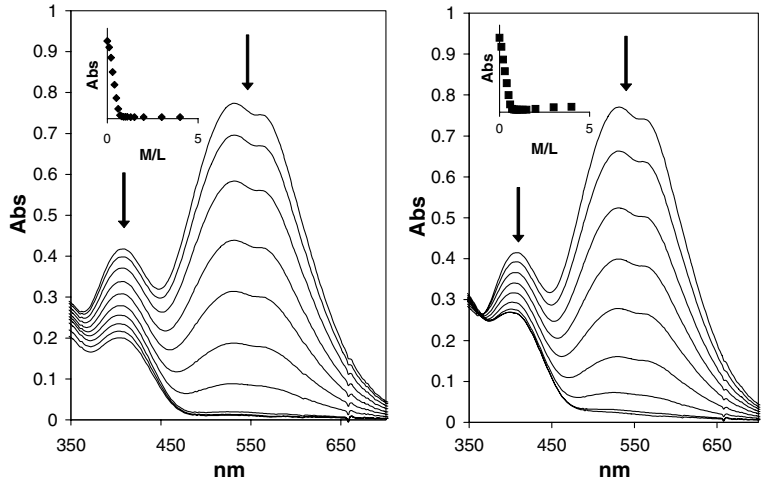

Fig. 4. UV–Vis titrations of compound L^1 (1.2×10^{-4} mol dm^{-3}) in acetonitrile with different concentrations of metals. Left: Hg^{2+}, right: Fe^{3+}. The inset shows the corresponding titration curve at 534 nm.

Fe^{3+} cations form 2:1 ligand-to-metal complexes with both L^1 and L^2. Additionally, the binding constants, obtained from titration profiles with Hg^{2+} or Fe^{3+}, are approximately the same for both L^1 and L^2 ligands (see Table 1) suggesting that the presence of the macrocycle in L^2 has no significant influence in the coordination process with these metals. This low influence of the macrocycle in the coordination and the partial positive charge in the nitrogen in the excited state might suggest a coordination mode through the carbonyls groups. However, all the remaining experimental results point towards coordination through the nitrogen. Thus, the interaction of the cations with the acceptor groups of molecules such L^1 and L^2 would result in a bathochromic shift of the absorbance as it has been reported for similar compounds in EtOH solutions in the presence of large amounts of the metal cations Cu^{2+} or Ni^{2+} [52]. However, we have not observed such a bathochromic shift in acetonitrile with L^1 or L^2 with any of the metal cations studied even in the presence of an excess of cation. This is indicative that the coordination through the nitrogen atom is relatively weaker in solvents with ability to form hydrogen bonds such as EtOH. In fact, in the presence of water no changes are observed in the absorbance spectra of L^1 and L^2 upon addition of metal cations. In contrast, in our case, we observed changes in the absorbance spectra of the systems L^2–Hg^{2+} and L^2–Fe^{3+} similar to those found for L^2–Pb^{2+}. This suggests that there is a similar coordination mode in the three cases and that this coordination occurs via the nitrogen atom as indicated the inhibition of the charge transfer band. Finally, we have performed ^{1}H NMR studies of L^1 in CD_3CN in the presence of Hg^{2+}. Fig. 6 (for H numbering scheme see Fig. 5) shows the evolution of the aromatic signals upon addition of Hg^{2+}. The most significant shifts are observed for Ha and Hb protons. Ha shifts from 6.9 to 7.8 and Hb from 7.45 to 7.8 ppm, indicating a decrease of the electronic density due to the coordination of the metal to the nitrogen. A

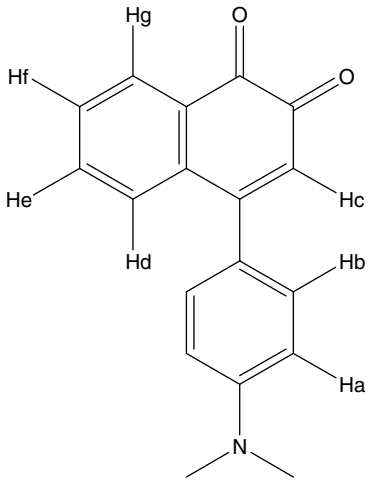

Fig. 5. Numbering scheme for protons of L^1.

similar behaviour was found for NMR titrations for the L^2–Hg^{2+} system. These shifts happen in the same direction than in the case of Ba^{2+}. Additionally, we can correlate the changes in the absorption spectra with the ^{1}H NMR shifts and the bonding strength. Thus, while Hg^{2+} induced $\Delta\delta$ of the Ha and Hb protons of 0.9 and 0.35, the cation Ba^{2+} gave $\Delta\delta$ of 0.65 and 0.15 ppm for the same protons, indicating that in the later the coordination to the nitrogen is less effective than with the Hg^{2+} metal cation. This is also in agreement with the observed optical behaviour; whereas, Hg^{2+} induced a complete elimination of the charge transfer band of L^2, the Ba^{2+} cation bring on only a decrease of the band intensity.

Due to its somewhat different behaviour, Cu^{2+} is discussed separately. Addition of increasing amounts of Cu^{2+} to either L^1 or L^2 induced the disappearance of the charge transfer band and the apparition of a new transition at 420 nm that turns yellow the solution. The decrease of the band at 534 nm and the increase of the band at

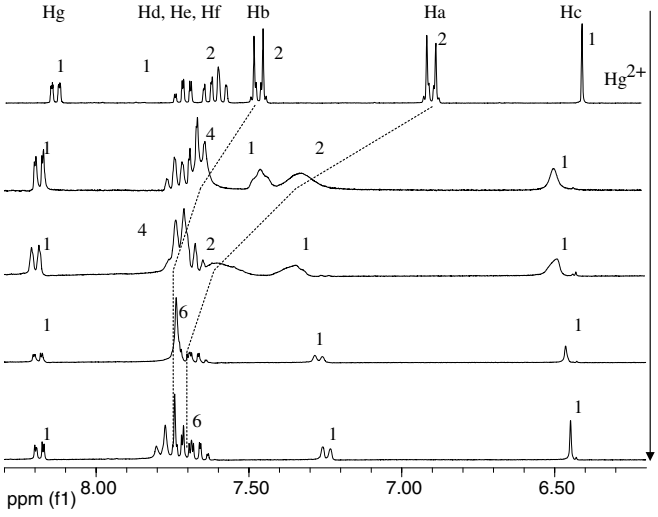

Fig. 6. ^{1}H NMR of L^1, aromatic protons, from up to down absence of Hg^{2+}, and 0.4, 1, 3 and 5 equiv. Numbers next to the signals indicate the amount of hydrogen atoms deduced from the integration.

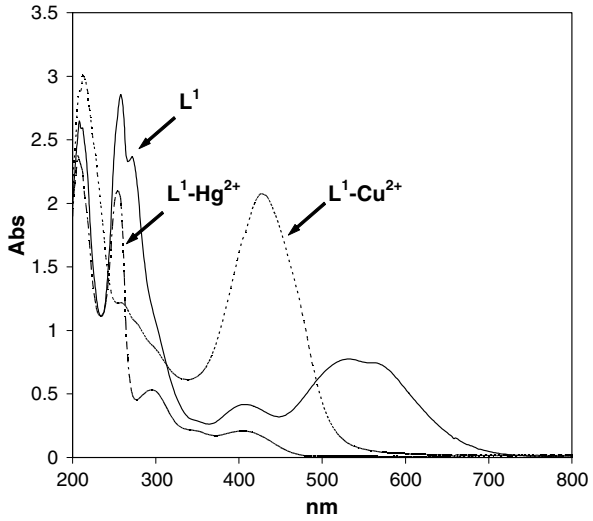

Fig. 7. Changes in the UV–Vis spectra of L^1 (1.2×10^{-4} mol dm^{-3}) upon addition of equimolar amounts of Hg^{2+} and Cu^{2+} in acetonitrile.

420 nm in the titration experiments with Cu^{2+}, did not evolve together. The apparition of the band at 420 nm needs a higher amount of Cu^{2+} and continues growing when the 534 nm band has disappeared. That suggested that there are more than two spices at the same time in solution, and more than a complex is statistically formed at the same time. In order to obtain more information of the system, we carried out some studies using as models both parts of the L^1–L^2 molecules, the *N*,*N*-dimethylaniline and the 1,2-naphthoquinone frameworks. The dimethylaniline group shows an absorption band at 253 nm ($\log\varepsilon = 4.18$) and the naphthoquinone at 250 nm ($\log\varepsilon = 4.37$). L^1 and L^2 showed a band at approximately at 260 nm with a shoulder at longer wavelength which can tentatively be assigned to a mixture of the two original bands of the *N*,*N*-dimethylaniline and the 1,2-naphthoquinone groups. Fig. 7 shows the UV–Vis spectrum of L^1 and the changes observed upon addition of 2 equiv. of the corresponding metal cation. The cations Fe^{3+}, Hg^{2+}, Pb^{2+} and Ba^{2+}, induced the disappearance of the shoulder but the band at shorter wavelength remain unaltered. This suggested a change in the electronic structure of the aniline whereas the naphthoquinone moiety remains basically unaffected in agreement with coordination through the nitrogen of the aniline. On the contrary, Cu^{2+} shows a special behaviour and not only the shoulder, but also the band assigned to the naphthoquinone group disappeared (see Fig. 7). This might indicate a double coordination of the Cu^{2+} cation through the amine and the carbonyl groups.

4. Interaction with anions

Addition of the tetrabutylammonium salts of the anions F^-, Cl^-, Br^-, NO_3^-, I^-, $H_2PO_4^-$ or HSO_4^- to acetonitrile solutions of L^1 or L^2 did not induce any change in the optical properties of the receptors, even in the presence of large amounts of anions (10 equiv.). This is a quite expected behaviour because receptors L^1 and L^2 do not have anion coordination sites. However, it has been known that metallic complexes of chromoionophores can also act as anion chemosensors as they could be very sensible to electronic changes induced by anions [53–59]. Therefore, we carried additional studies on the optical variation observed by addition of the anions F^-, Cl^-, Br^-, I^-, NO_3^-, HSO_4^- or $H_2PO_4^-$ to metal complexes of L^1 and L^2 and different behaviours were observed. In general there was found a partial recovery of the absorption bands of the original dye. This is, specially the case in the presence of the anions F^-, Cl^-, Br^-, I^- and NO_3^- that induced the recovery of the dye band in some extents for the L–M^{2+} systems when $M^{2+} = Pb^{2+}$, Hg^{2+}, Fe^{3+} and Ba^{2+}. This general behaviour is attributed to a debilitation of the M–N bond induced by coordination of the anions to the metal cation that induced a partial retrieving of the original charge transfer band of the dye. In some cases, the retrieving on the band intensity at 530 nm is complete suggesting that the metal cation is completely displaced. Additionally, the anions HSO_4^- or $H_2PO_4^-$ showed a different behaviour in their interaction with certain metal complexes. Thus, for instance, the addition of HSO_4^- to acetonitrile solutions of the L^2–Ba^{2+} complex resulted in a bleaching of the solution. On the other hand, the addition of HSO_4^- or $H_2PO_4^-$ to acetonitrile solutions of L^2 with of Pb^{2+}, Hg^{2+} or Fe^{3+} did not result in any remarkable optical variation. Fig. 8 shows the observed colour changes upon addition of 1 equiv. of the corresponding anion to acetonitrile solution of the Ba–L^2 system. As it can be observed there is a complete elimination of the band at 534 nm in the case of HSO_4^- and a partial bleaching in the presence of $H_2PO_4^-$.

The interaction of Ba^{2+} with the sulphate is widely known and, for example, it has been employed as a suitable method for the sulphate determination in aqueous

Fig. 8. L^2 in acetonitrile ($[L^1] = 1.06 \times 10^{-4}$ M) in presence of 1 equiv. of Ba^{2+} and 1 equiv. of the corresponding anion, from left to right, NO_3^-, HSO_4^-, $H_2PO_4^-$, F^-, Cl^-, Br^-, I^- and no anion.

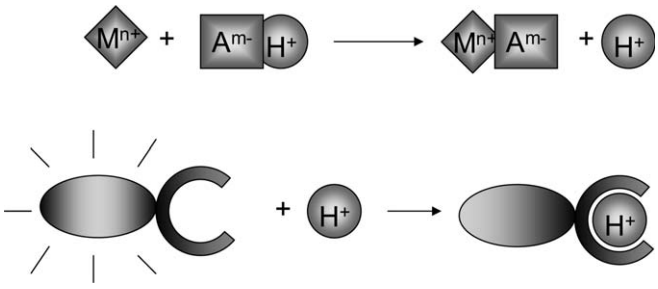

Fig. 9. Scheme of the coupled reactions.

environments, due to the formation of an insoluble precipitate. Although in our case, there was not evidence of precipitate formation, the interaction between Ba^{2+} and HSO_4^- is probably the origin of this significant variation. Most likely, the absorption changes can be due to the coordination of HSO_4^- with Ba^{2+} to form a short of ion pair. Additionally, the coordination increases the acidity of the sulphate that is then acid enough to protonate L^1 or L^2 inducing bleaching of the solution. In this case the anion, through the interaction with the metal, is "transformed" into a cation (H^+) which is the responsible of induce the change in the spectroscopic properties of the chromophore (see Fig. 9). The anion is then recognised via an indirect way, by a combination of metal coordination and dye protonation. This was confirmed by the effects observed upon addition of different acids (such as $HClO_4$, H_2SO_4 and *p*-toluensulphonic acid) to acetonitrile solutions of L^1 or L^2; a complete bleaching was observed upon addition of 1 equiv. of H^+.

5. Conclusions

We have reported here a study of the behaviour of naphthoquinone derivatives as receptors for the chromogenic sensing of metal cations and anions in acetonitrile. Both L^1 and L^2 showed a charge transfer band at ca. 530 nm that is hypochromically shifted upon addition of the metal cations Cu^{2+}, Fe^{3+} and Hg^{2+}. Additionally, the metal cations Pb^{2+} and Ba^{2+} also induced bleaching of acetonitrile solutions of L^2. In all cases, the results obtained suggested that the interaction with the receptor occurs via coordination with the nitrogen atom from the anilinium group. Studies in the presence of anions were also carried out. A chromogenic sensing of the anion HSO_4^- in acetonitrile was observed using the metal complex $[Ba(L^2)]^{2+}$.

6. Experimental

6.1. General remarks

All commercially available reagents were used without further purification. Air/water-sensitive reactions were performed in flame dried glassware under argon. Acetonitrile and CH_2Cl_2 were dried with CaH_2 and distilled prior to use. 16-Phenyl-16-aza-1,4,7,10,13-pentaoxacycloheptadecane, was prepared following known procedures.

6.2. Physical measurements

The NMR spectra were recorded with a Varian Gemini 300 spectrometer. Chemical shifts are reported in ppm downfield from the TMS signal. Spectra taken in $CDCl_3$ were referred to the residual $CHCl_3$.

6.3. Preparation of 4-(4-dimethylamino-phenyl)-[1,2]naphthoquinone (L^1)

The synthetic process was firstly reported by Yoshida et al. [48]. To 30 mL of glacial acetic acid containing 260 mg (1 mmol) of 1,2-naphthoquinone-4-sulfonate sodium salt and 249 mg (1 mmol) of nickel acetate, 10 mL of acetic acid containing 127 μL (1 mmol) of *N*,*N*-dimethylaniline were added. The reaction mixture was stirred at 30 °C for 5 h, mixed with 25 mL of water and extracted with CH_2Cl_2. The organic phase was washed several times with an aqueous solution of sodium carbonate until neutrality. Then the organic phase was dried and the solvent removed to dryness. The blue solid was purified by silica gel column chromatography with CH_2Cl_2:EtOH mixtures as eluent, obtaining 90.3 mg (32.3%) ^{1}H NMR: ($CDCl_3$) $\delta = 3.04$ (s, 6H, NCH_3), 6.37 (s, 1H, C=C*H*), 6.74 (d, 2H, Ar*H*), 7.35 (d, 2H, Ar*H*), 7.4–7.6 (m, 3H, Ar*H*), 8.13 (d, 1H, Ar*H*). ^{13}C NMR: ($CDCl_3$)$\delta = 40.11$, 111.63, 123.35, 125.66, 129.78, 129.87, 130.19, 130.39, 131.86, 134.69, 135.24, 151.57, 157.36, 180.10, 180.26. High resolution EI$^+$ mass spectra: Calc. for $C_{18}H_{15}NO_2$: 277.1102. Found: *m*/*z* 277.1078%.

6.4. Preparation of 4-[4-(1,4,7,10,13-pentaoxa-16-aza-cyclooctadec-16-il)-phenyl]-[1,2]naphthoquinone (L^2)

To 40 mL of glacial acetic acid containing 345 mg (1.3 mmol) of 1,2-naphthoquinone-4-sulfonate sodium salt and 330 mg (1.3 mmol) of nickel acetate, 15 mL of acetic acid containing 450 mg (1.3 mmol) of 16-phenyl-16-aza-1,4,7,10,13-pentaoxacycloheptadecane were added. The reaction mixture was stirred at 30 °C for 24 h, and then mixed with 40 mL of water and extracted with CH_2Cl_2. The organic phase was washed several times with an aqueous solution of sodium carbonate until neutrality. Then the

organic phase was dried and the solvent removed to dryness. The blue solid was purified by silica gel column chromatography with CH_2Cl_2:EtOH mixtures as eluent, obtaining 52.8 mg (8.2%) ^1H NMR: ($CDCl_3$)$\delta = 3.5$–3.9 (m, 24H, CH_2), 6.42 (s, 1H, C=C*H*), 6.81 (d, 2H, Ar*H*), 7.32 (d, 2H, Ar*H*), 7.4–7.6 (m, 3H, Ar*H*), 8.18 (d, 1H, Ar*H*). High resolution FAB^+ mass spectra: Calc. for $C_{28}H_{33}NO_7$: 495.2257. Found: *m*/*z* 495.2188%.

Acknowledgements

We thank the Ministerio de Ciencia y Tecnología (Projects REN2002-04237-C02-01, MAT2003-08568-C03-02) and the Generalitat Valenciana (GRUPOS03/035) for support. J.V.R.L. thank the Ministerio de Educación, Cultura y Deporte for a Doctoral Fellowship.

References

[1] R. Martínez-Máñez, F. Sancenon, Chem. Rev. 103 (2003) 4419.
[2] M. Vazquez, L. Fabbrizzi, A. Taglietti, R.M. Pedrido, A.M. Gonzalez-Noya, M.R. Bermejo, Angew. Chem., Int. Ed. 43 (2004) 1962.
[3] P.D. Beer, D.P. Cormode, J.J. Davis, Chem. Commun. (2004) 414.
[4] J.L. Sessler, E. Katayev, G.D. Pantos, Y.A. Ustynyuk, Chem. Commun. (2004) 1276.
[5] R. Martínez-Máñez, F. Sancenón, J. Fluoresc. 15 (2005) 267.
[6] M. Takagi, H. Nakamura, K. Ueno, Anal. Lett. 19 (1977) 1115.
[7] J.P. Dix, F. Vögtle, Angew. Chem., Int. Ed. 17 (1978) 857.
[8] Z.H. Wang, T. Hirose, B.W. Baldwin, Y. Yang, Chem. Commun. (1977) 297.
[9] T. Hirose, B.W. Baldwin, Z.H. Wang, K. Kasuga, T. Uchimaru, A. Yliniemelä, Chem. Commun. (1996) 391.
[10] D. Jiménez, R. Martínez-Máñez, F. Sancenón, J. Soto, Tetrahedron Lett. 45 (2004) 1257.
[11] A.B. Descalzo, R. Martíñez-MáñezRadeglia, R. Radeglia, K. Rurack, J. Soto, J. Am. Chem. Soc. 125 (2003) 3418.
[12] J.V. Ros-Lis, R. Martínez-Máñez, K. Rurack, F. Sancenón, J. Soto, M. Spieles, Inorg. Chem. 43 (2004) 5183.
[13] D. Jiménez, R. Martínez-Máñez, F. Sancenón, J.V. Ros-Lis, J. Soto, A. Benito, E. García-Breijo, Eur. J. Inorg. Chem. (2005) 2393.
[14] H. Mohindra Chawia, K. Srinivas, J. Chem. Soc., Chem. Commun. (1994) 2593.
[15] S. Zhao, J.H. Luong, J. Chem. Soc., Chem. Commun. (1995) 663.
[16] K. Tsubaki, H. Tanaka, H. Morikawa, K. Fuji, Tetrahedron 59 (2003) 3195.
[17] T.D. James, P. Linnane, S. Shinkai, Chem. Commun. (1996) 281.
[18] H. Cao, M.D. Heagy, J. Fluoresc. 14 (2004) 569.
[19] J.V. Ros-Lis, R. Martínez-Máñez, J. Soto, Org. Lett. 7 (2005) 2337.
[20] D. Jiménez, R. Martínez-Máñez, F. Sancenon, J. Soto, Tetrahedron Lett. 43 (2002) 2823.
[21] F. Sancenon, R. Martínez-Máñez, J. Soto, Chem. Commun. (2001) 2262.
[22] D.A. Jose, D.K. Kumar, B. Ganguly, A. Das, Org. Lett. 6 (2004) 3445.
[23] J. Morey, M. Orell, M.A. Barcelo, P.M. Deya, A. Costa, P. Ballester, Tetrahedron Lett. 45 (2004) 1261.
[24] S.L. Wiakur, P.N. Floriano, E.V. Anslyn, J.T. McDevitt, Angew. Chem., Int. Ed. 42 (2003) 2070.
[25] Z. Zhong, E.V. Anslyn, Angew. Chem., Int. Ed. 42 (2003) 3005.
[26] M.S. Han, D.H. Kim, Tetrahedron 690 (2004) 11251.
[27] G.J. Mohr, Sensor Actuator B 107 (2005) 2.
[28] J.D. Winkler, C.M. Bowen, V. Michelet, J. Am. Chem. Soc. 120 (1998) 3237.
[29] J.V. Ros-Lis, R. Martínez-Máñez, J. Soto, Chem. Commun. (2002) 2248.
[30] J.V. Ros-Lis, B. Garcia, D. Jimenez, R. Martínez-Máñez, F. Sancenon, J. Soto, F. Gonzalvo, M.C. Valldecabres, J. Am. Chem. Soc. 126 (2004) 4064.
[31] D. Jiménez, R. Martínez-Máñez, F. Sancenon, J.V. Ros-Lis, A. Benito, J. Soto, J. Am. Chem. Soc. 125 (2003) 9000.
[32] F. García, J.M. García, B. García-Acosta, R. Martínez-Máñez, F. Sancenón, J. Soto, Chem. Commun. (2005) 2790.
[33] J.V. Ros-Lis, R. Martínez-Máñez, J. Soto, Chem. Commun. (2005) 5260.
[34] A.B. Descalzo, D. Jiménez, M.D. Marcos, R. Martínez-Máñez, J. Soto, J. El Haskouri, C. Guillem, D. Beltrán, P. Amorós, M.V. Borrachero, Adv. Mater. 14 (2002) 966.
[35] M. Comes, G. Rodriguez-Lopez, M.D. Marcos, R. Martínez-Máñez, F. Sancenon, J. Soto, L.A. Villaescusa, P. Amoros, D. Beltran, Angew. Chem., Int. Ed. 44 (2005) 2918.
[36] M. Comes, M.D. Marcos, R. Martínez-Máñez, F. Sancenon, J. Soto, L.A. Villaescusa, P. Amoros, D. Beltran, Adv. Mater. 16 (2004) 1783.
[37] A.B. Descalzo, K. Rurack, H. Weisshoff, R. Martínez-Máñez, M.D. Marcos, P. Amoros, K. Hoffmann, J. Soto, J. Am. Chem. Soc. 127 (2005) 184.
[38] H. Itoh, K. Naka, Y. Chujo, J. Am. Chem. Soc. 126 (2004) 3026.
[39] D. Aldakov, P. Anzenbacher, J. Am. Chem. Soc. 126 (2004) 4752.
[40] P. Anzenbacher, K. Jursikova, D. Aldakov, M. Marquez, R. Pohl, Tetrahedron 60 (2004) 11163.
[41] Y.-H. Kim, J.-I. Hong, Chem. Commun. (2002) 512.
[42] H. Miyaji, S.R. Collinson, I. Prokes, J.H.R. Tucker, Chem. Commun. (2003) 64.
[43] K. Rurack, M. Sczepan, N. Spieles, U. Resch-Genger, W. Rettig, Chem. Phys. Lett. 320 (2000) 87.
[44] A.P. de Silva, H.Q.N. Gunaratne, T. Gunnlaugsson, A.J.M. Huxley, C.P. McCoy, J.T. Rademacher, T.E. Rice, Chem. Rev. 97 (1997) 1515.
[45] H.G. Löhr, F. Vötgle, Acc. Chem. Res. 18 (1985) 65.
[46] K. Rurack, Spectrochim. Acta, Part A 57 (2001) 2161.
[47] B. Valeur, I. Leray, Coord. Chem. Rev. 205 (2000) 3.
[48] K. Yoshida, T. Koujiri, N. Oga, M. Ishiguro, Y. Kubo, J. Chem. Soc., Chem. Commun. (1989) 708.
[49] R.D. Rogers, A.H. Bond, Inorg. Chim. Acta 192 (1992) 163.
[50] H. Mrozek, H. Nikol, A. Vogler, F. Vögtle, J. Photochem. Photobiol. A: Chem. 84 (1994) 227.
[51] J. Bourson, J. Pouget, B. Valeur, J. Phys. Chem. 97 (1993) 4552.
[52] K. Yoshida, N. Oga, T. Koujiri, M. Ishiguro, Y. Kubo, J. Chem. Soc., Perkin. Trans. 1 (1990) 1891.
[53] D.H. Lee, J.H. Im, S.U. Son, Y.K. Chung, J.I. Hong, J. Am. Chem. Soc. 125 (2003) 7752.
[54] V. Amendola, E. Bastianello, L. Fabbrizzi, C. Mangano, P. Pallavicini, A. Perotti, A. Manotti-Lanfredi, F. Ugozzoli, Angew. Chem., Int. Ed. 39 (2000) 2917.
[55] L. Fabbrizzi, P. Pallavicini, L. Parodi, A. Perotti, A. Taglietti, J. Chem. Soc., Chem. Commun. (1995) 2439.
[56] L. Fabbrizzi, P. Pallavicini, L. Parodi, A. Taglietti, Inorg. Chim. Acta 238 (1995) 5.
[57] V. Amendola, L. Fabbrizzi, C. Mangano, P. Pallavicini, M. Zema, Inorg. Chim. Acta 337 (2002) 70.
[58] Y.H. Kim, J.I. Hong, Chem. Commun. (2002) 512.
[59] B. García-Acosta, X. Albiach-Martí, E. García, L. Gil, R. Martínez-Máñez, K. Rurack, F. Sancenón, J. Soto, Chem. Commun. (2004) 774.

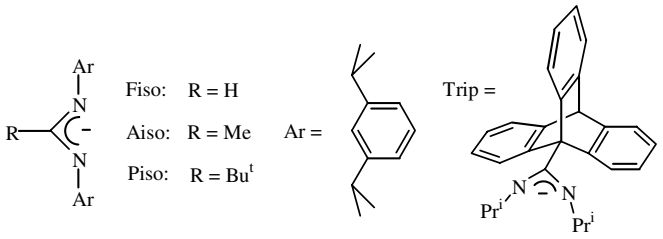

Fig. 1. Bulky amidinate ligands used in this study.

that its κ^2-N,N-chelated isomer is more stable than the η^1-N,η^3-arene ligated form by 37.9 kJ/mol. In this paper we detail further attempts to form complexes of the type, [:M{κ^2-*N*,*N*-*N*(R)C(R′)N(R)}]. Although unsuccessful, these have led to the formation of a number of novel group 13-amidinate and amidine complexes.

2. Results and discussion

2.1. Syntheses

The synthesis of group 13 metal(I)-amidinate complexes using metal halides as precursors could potentially be achieved via two main routes, viz. metathesis reactions between an amidinate salt and a low oxidation state metal halide, or the reduction of a amidinato-metal(III) halide complex. In the first instance, the treatment of 'GaI' [7] with an in situ prepared solution of the lithium formamidinate, [Li(Fiso)], was carried at low temperature. Although the a Ga(I)-amidinate complex did not result, colourless crystals of an approximately 50:50 mixture of the gallium(II) and (III) complexes, [{GaI(Fiso)}$_2$] (**7**) and [GaI(Fiso)$_2$] (**8**), were obtained (Scheme 1). The mechanism of this reaction presumably involves a series of disproportionation reactions, as evidenced by the deposition of gallium metal. An intentional, moderately yielding synthesis of the Ga(II) complex, **7**, was devised whereby [Li(Fiso)] was treated at low temperature in Et_2O/toluene with the Ga(II) halide complex, [{$GaI_2(NHCy_2)$}$_2$] (Cy=cyclohexyl) [8]. The related reaction of [{$GaI_2(NHCy_2)$}$_2$] with the bulkier pivamidinate salt, [Li(Piso)], afforded the analogous dimeric complex, [{GaI(Piso)}$_2$] (**9**), though only in a trace yield. The only other products of the reaction that were identifiable were gallium metal, LiI, $NHCy_2$ and PisoH. It is noteworthy that when the potassium salt of the formamidinate, [K(Fiso)], was treated with [{$GaI_2(NHCy_2)$}$_2$] under similar conditions to the preparation of **7**, only the gallium(III) complex, **8**, was isolated in moderate yield (Scheme 1).

In an attempt to form an indium(I)-amidinate complex, [Li(Fiso)] was reacted with InCl in diethyl ether. This, however, led to indium metal deposition and the isolation of [InCl(Fiso)$_2$] (**10**) in moderate yield via a disproportionation process (Scheme 2). It is worthy of note that similar disproportionation reactions, but giving indium(II) complexes, have been observed in the reactions of bulky lithium β-diketiminates with InCl [9].

In the case of aluminium there is no known stable aluminium(I) halide that can be used as a precursor for metathesis reactions. To circumvent this problem we decided to synthesise suitable amidinato-aluminium(III) iodide complexes and attempt their reduction to four-membered aluminium(I) heterocycles. This seemed appropriate as six-membered aluminium(I) heterocycles have previously been prepared by this methodology [4a]. Therefore, we treated the known aluminium alkyl and hydride complexes, [$AlMe_2$(Aiso)] (**11**) [2c] and [{AlH_2(Piso)}$_2$] (**4**) [3], with iodine in toluene (Scheme 3). In both cases the expected complexes, **12** and **14**, resulted, but the AlI_3 adduct, **13**, was also formed in the former reaction. Reaction of [$AlMe_2$(Piso)] (**15**) [2c] with I_2 also yields **14**, however the hydride route allows a faster reaction, a higher yield and a cleaner product. Moreover, both iodine atoms of the I_2 reactant can be transferred to the Al centre because the in situ formed HI subsequently reacts with

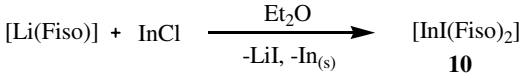

Scheme 2.

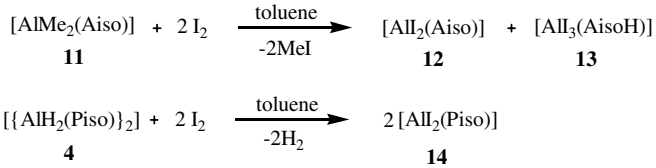

Scheme 3.

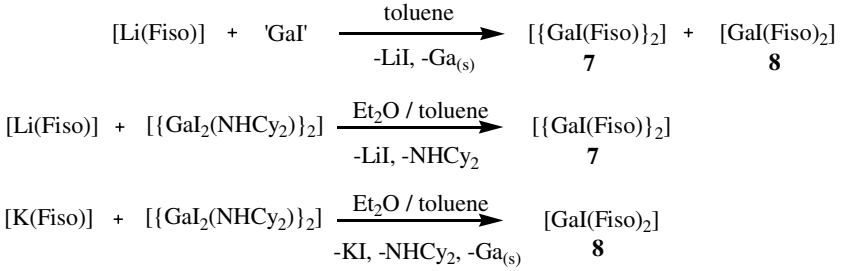

Scheme 1.

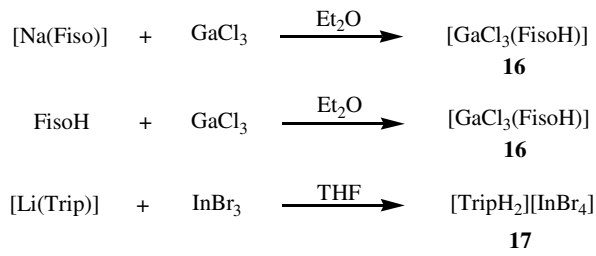

Scheme 4.

another hydride ligand, while the initially formed MeI in the alkyl route is less reactive and needs to be separated from the reaction mixture. Unfortunately, all attempts to reduce **12** or **14** to the corresponding aluminium(I) heterocycles using potassium metal, KC_8 or sodium have so far met with failure.

A number of attempts were made to prepare amidinatogallium(III) and indium(III) halide complexes as it was thought their reduction to metal(I) complexes would be more facile than for their aluminium counterparts. Little success has been had here as, for example, the only identifiable product from the reaction of [Na(Fiso)] with $GaCl_3$ was the adduct, **16**, formed in low yield (Scheme 4). Although not useful for reduction reactions, compound **16** was intentionally prepared in moderate to good yield by treating FisoH with $GaCl_3$ (Scheme 4). Similarly, when the very bulky lithium amidinate, [Li(Trip)] [10], was treated with $InBr_3$ and the reaction mixture recrystallised from chloroform, the only crystalline product obtained was the amidinium salt, **17** (Scheme 4). The protons of the cation presumably originate from either residual moisture in the reagents ($InBr_3$ or reaction solvents), or hydrogen abstraction from chloroform. The latter seems more likely as **17** was formed when the reaction and work-up was repeated under rigorous exclusion of moisture. Attempts to recrystallise the reaction product from THF instead of chloroform did not lead to a crystalline product.

2.2. Crystal structures

The crystal structure of **7** contains one full dimeric molecule in the asymmetric unit which is depicted in Fig. 2. Each of its gallium centres form essentially planar four-membered rings with the chelating amidinate unit (Ga–N: 2.012 Å average), and each is further coordinated by an iodine atom (Ga–I: 2.542 Å average). The distorted tetrahedral environments of the gallium centres are completed by a Ga–Ga bond with a length of 2.4304(10) Å, which is in the normal range for Ga–Ga bonds in compounds of the type [{LGaI}$_2$] [11].[1] The two N_2CGa planes are approximately parallel to each other and almost perpendicular to the nearly planar Ga_2I_2 fragment. The structure of compound **9** (Fig. 3) is similar to that of **7** but the molecule

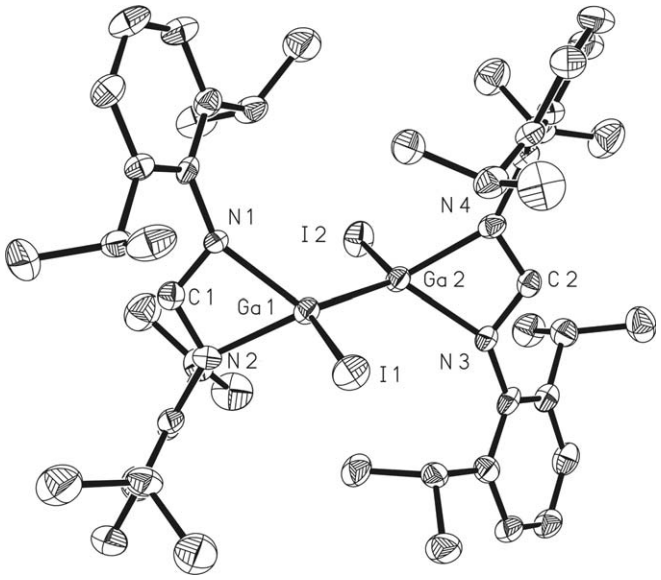

Fig. 2. Molecular structure of **7** (ORTEP, 50% thermal ellipsoids). Hydrogen atoms have been omitted for clarity. Selected bond lengths (Å) and angles (°): Ga1–Ga2 2.4304(10), Ga1–I1 2.5437(9), Ga2–I2 2.5396(9), Ga1–N1 2.009(4), Ga1–N2 2.019(4), Ga2–N3 2.011(4), Ga2–N4 2.008(4), C1–N1 1.313(6), C1–N2 1.316(6), C2–N3 1.331(6), C2–N4 1.322(6); N1–Ga1–N2 66.36(15), N3–Ga2–N4 66.75(16), Ga2–Ga1–I1 119.48(3), Ga1-Ga2-I2 121.19(3), N1–C1–N2 114.0(4), N3–C2–N4 112.9(4).

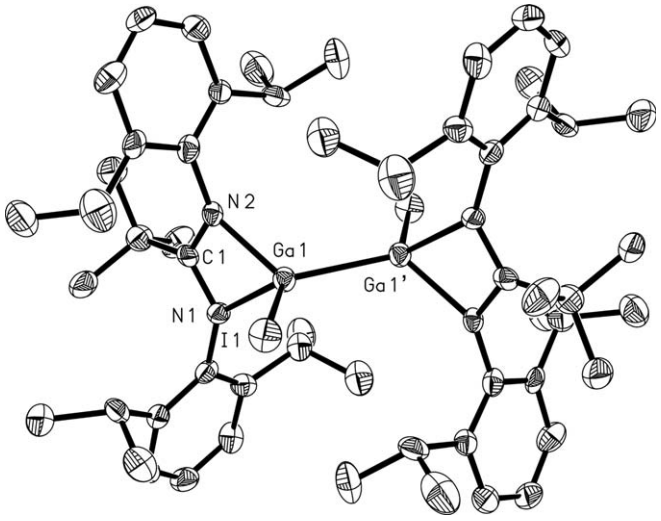

Fig. 3. Molecular structure of **9** (ORTEP, 50% thermal ellipsoids). Hydrogen atoms have been omitted for clarity. Selected bond lengths (Å) and angles (°): Ga1–Ga1′ 2.4521(15), Ga1–I1 2.5537(10), Ga1–N1 2.006(5), Ga1–N2 1.996(5), C1–N1 1.337(8), C1–N2 1.342(8); N1–Ga1–N2 66.2(2), Ga1'–Ga1–I1 115.56(5), N1–C1–N2 109.3(6). Symmetry operation ′: $-x+2, -y, -z+1$.

sits on an inversion centre and thus only half a molecule occupies the asymmetric unit. The bulkier substituent in the backbone of the amidinate unit in **9** leads to a slightly more acute NCN angle [109.3(6)°] compared with those of **7** [112.9(4)° and 114.0(4)°]. In both compounds, the C–N bond lengths within their four-membered rings are indicative of considerable delocalisation over the NCN

[1] As determined from a survey of the Cambridge Crystallographic Database, September, 2005.

fragments. It is noteworthy that compounds **7** and **9** represent the first examples of gallium(II) complexes bearing an amidinate group, though Uhl et al. [12] have reported a related gallium(II) complex bearing a 1,3-diphenyltriazenido group which is isoelectronic to formamidinates.

Compounds **8** and **10** are isomorphous with the group 13 hydride complexes $[MH(Fiso)_2]$ **1**–**3** [3], and display similar structural features to each other, though the quality of the data for **8** is too poor to allow comment on its structure here. The indium centre of **10** (Fig. 4) is five coordinate with two chelating amidinate units and one Cl atom [In–Cl: 2.3574(10) Å] giving it a heavily distorted trigonal bipyramidal coordination geometry with N(3) and N(1) in apical positions. As a result, these N-centres are significantly more distant from In(1) than equatorial N(2) and N(4). In addition, there appears to be a lesser degree of delocalisation over the amidinate backbones of **10** compared with those of **7** and **9**, as evidenced by the significantly different N–C distances within each NCN fragment of the former. The structural parameters of **10** compare well with those of the only other structurally characterised bis(amidinato) indium halide complex, $[InCl\{[N(Cy)]_2CBu^t\}_2]$ [13].

Both compounds **13** and **16** (Figs. 5 and 6, respectively) are adducts of a neutral amidine with a group 13 trihalide. The main difference between their structures is the configuration at the C(1)–N(1) bond which is *Z* for **13** and *E* for **16**. This difference most likely results from the greater steric influence of the methyl group on C(1) in **13** compared to the hydrogen at C(1) in **16**. The NCNM fragments of both **13** and **16** are essentially planar and the M–N bond lengths [**13** 1.935(6) Å, **16** 1.941(3) Å] are in the normal range, as are the metal–halide distances.[1] Surprisingly, an examination of the C–N distances within the NCN fragment of **16** suggests significant delocalisation over that fragment,

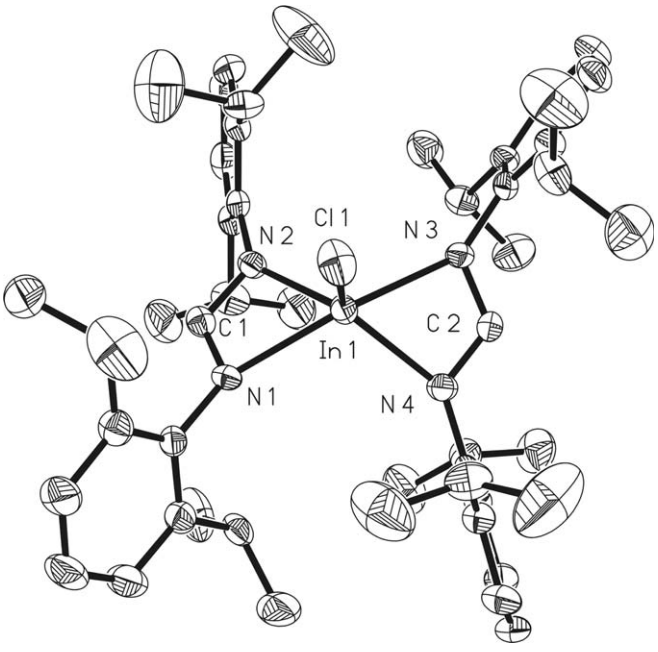

Fig. 4. Molecular structure of **10** (ORTEP, 50% thermal ellipsoids). Hydrogen atoms have been omitted for clarity. Selected bond lengths (Å) and angles (°): In1–Cl1 2.3574(11), In1–N1 2.244(3), In1–N2 2.181(3), In1–N3 2.270(3), In1–N4 2.168(3), C1–N1 1.309(5), C1–N2 1.327(5), C2–N3 1.304(5), C2–N4 1.326(5); N1–In1–N2 60.30(11), N3–In1–N4 60.35(11), N2–In1–N3 105.72(11), N1–In1–N4 109.18(11), N1–In1–Cl1 101.45(8), N1–C1–N2 115.0(4), N3–C2–N4 116.1(3).

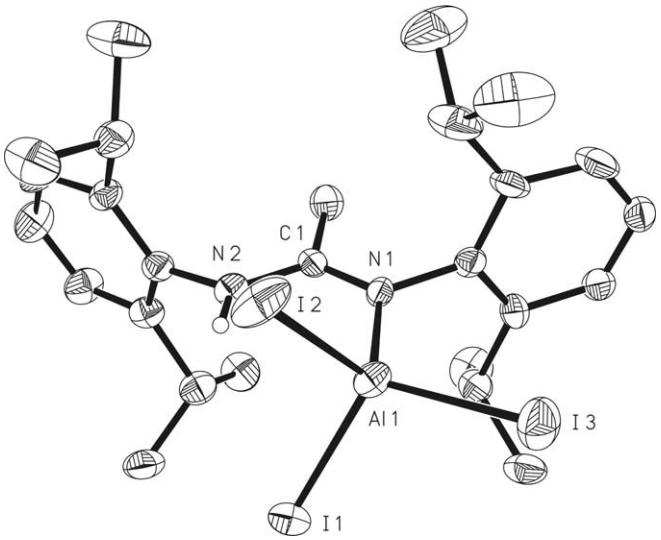

Fig. 5. Molecular structure of **13** (ORTEP, 50% thermal ellipsoids). Hydrogen atoms have been omitted for clarity. Selected bond lengths (Å) and angles (°): Al1–I1 2.530(2), Al1–I2 2.531(2), Al1–I3 2.473(2), Al1–N1 1.935(6), C1–N1 1.327(9), C1–N2 1.306(9); I1–Al1–I3 111.41(9), I1–Al1–I2 107.27(18), I2–Al1–I3 112.18(8), C1–N1–Al1 126.2(5), N1–C1–N2 120.0(6).

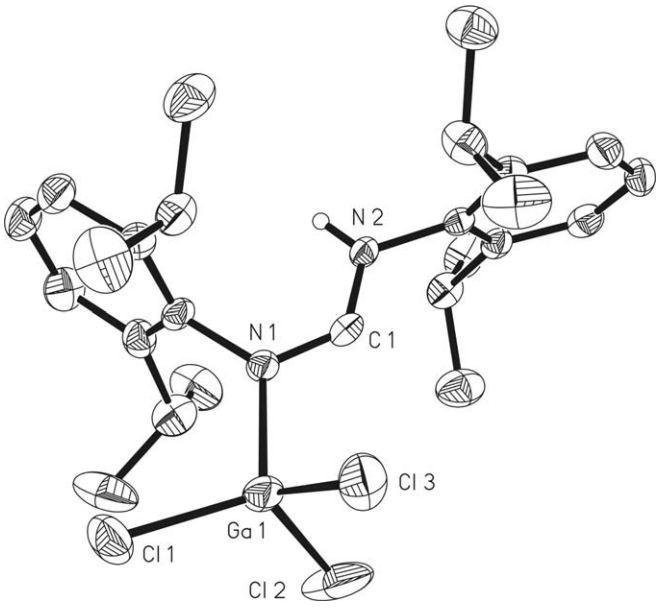

Fig. 6. Molecular structure of **16** (ORTEP, 50% thermal ellipsoids). Hydrogen atoms, except on N(2), have been omitted for clarity. Selected bond lengths (Å) and angles (°): Ga1–N1 1.941(3), Ga1–Cl1 2.1397(11), Ga1–Cl2 2.1683(14), Ga1–Cl3 2.1676(13), C1–N1 1.306(4), C1–N2 1.309(4); Cl1–Ga1–Cl2 114.75(5), Cl1–Ga1–Cl3 114.57(4), Cl2–Ga1–Cl3 107.29(6), C1–N1–Ga1 116.1(2), N1–C1–N2 128.6(3).

whereas the same fragment in **13** appears to be more localised, though both its amidine N–C bond lengths lie between those expected for single and double bonded distances.[1]

The molecular structure of **14** is depicted in Fig. 7 and is comparable with that of the corresponding methyl derivative [$AlMe_2$(Piso)] (**15**) [2c] in that its metal centre is chelated by the Piso ligand and has a distorted tetrahedral geometry. Its Al–N (1.886 Å average) and Al–I (2.460 Å average) distances lie in the expected regions[1]. The structure of the amidinium salt, **17**, (Fig. 8) shows the compound to consist of separate ions which have no significant contacts. The tetrahedral $[InBr_4]^-$ anion has been structurally characterised in salts on previous occasions [14]. The geometry of the amidinium cation closely resembles that of the neutral amidine [10], though the amidine exhibits largely localised backbone NC bonds, whereas those in **17** appear to be delocalised. In addition, the amidinium cation has a slightly more acute NCN angle [127.0(4)°] relative to that of the amidine, TripH [129.91(18)°].

2.3. Spectroscopic properties

The NMR spectra for the majority of the compounds reported here are consistent with their solid-state structures and will be only briefly discussed. For example, the ^{1}H NMR spectrum of [{GaI(Fiso)}$_2$] (**7**) displays two methyl doublet resonances and a virtual septet for the methine protons. The ^{1}H NMR spectra for the compounds [$MX(Fiso)_2$] (**8**: M = Ga, X = I; **10**: M = In, X = Cl) are less symmetrical and exhibit overlapping multiplet resonances for the protons of the methyl groups. Compounds [AlI_2(Aiso)] (**12**) and [AlI_3(AisoH)] (**13**) can be easily distinguished by their ^{1}H NMR spectra. As expected, the spectrum of the higher symmetry compound, **12**, shows two isopropyl methyl doublet signals and one methine virtual septet resonance, while the spectrum of **13** displays four isopropyl methyl doublets and two methine septets. Contrastingly, both the ^{1}H and ^{13}C NMR spectra of [$GaCl_3$-(FisoH)] (**16**) are indicative of a more symmetrical molecule than the solid-state structure suggests. This observation implies a fluxional exchange of the $GaCl_3$ fragment and amidine proton between N-centres, which is rapid on the NMR timescale. Cooling solutions of **16** did not lead to a resolution of the spectra. The N*H* proton of **13** resonates at δ 8.98 ppm (IR: N–H stretch 3295 cm^{-1}) and that for **16** appears at δ 8.67 ppm (IR: N–H stretch 3313 cm^{-1}), cf. **17** ^{1}H NMR: δ 5.42 ppm (NH); IR: 3358 cm^{-1} (N–H str.).

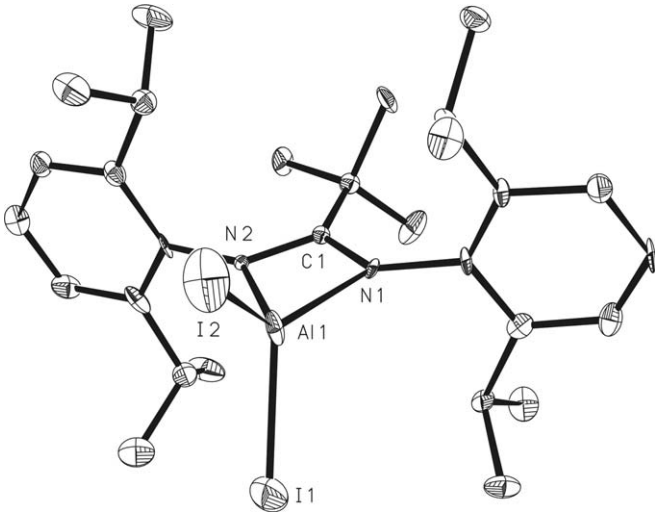

Fig. 7. Molecular structure of **14** (ORTEP, 50% thermal ellipsoids). Hydrogen atoms have been omitted for clarity. Selected bond lengths (Å) and angles (°): Al1–N1 1.884(7), Al1–N2 1.889(8), Al1–I1 2.481(3), Al1–I2 2.438(3), C1–N1 1.363(12), C1–N2 1.350(11); I1–Al1–I2 107.21(11), N1–Al1–N2 70.3(3), N1–C1–N2 106.4(7).

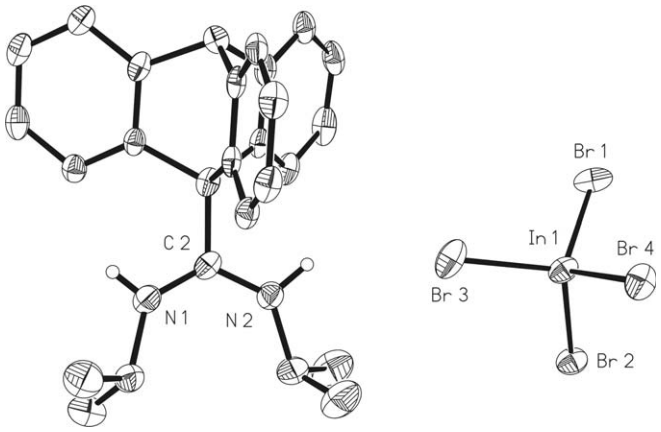

Fig. 8. Molecular structure of **17** (ORTEP, 50% thermal ellipsoids). Hydrogen atoms, except on nitrogen atoms, have been omitted for clarity. Selected bond lengths (Å) and angles (°): In1–Br1 2.5043(7), In1–Br2 2.5096(6), In1–Br3 2.4945(7), In1–Br4 2.4934(6), C2–N1 1.316(6), C2–N2 1.322(6); Br1–In1–Br2 105.20(2), Br3–In1–Br1 111.73(2), N1–C2–N2 127.0(4).

3. Conclusions

Attempts have been made to synthesise amidinato-group 13 metal(I) complexes, either by methathesis reactions between amidinate salts and metal(I) halides, or by reduction of amidinato-metal(III) halide complexes. Although no metal(I) complexes have been formed, the former route has led to a range of amidinato-metal(II) and (III) complexes via disproportionation processes. These include the first examples of gallium(II) amidinate complexes. Metathesis reactions between amidinate salts and metal(III) halides have afforded a series of amidinato-metal(III) halide complexes, amidine-metal(III) halide adducts and one amidinium salt. In general, and like our previous findings with amidinato-group 13 hydride complexes [3b], syntheses employing the Fiso ligand normally lead to complexes bearing two amidinate ligands (except the Ga(II) compound **7**), whereas only one Piso group could be transferred to a metal atom. This is probably because the bulky Bu^t group on the backbone of Piso, compared to the

hydrogen backbone atom of Fiso, gives a more rigid and sterically demanding amidinate unit. Further investigations using bulky amidinate and related ligands to stabilise low oxidation state group 13 complexes by metathesis or reduction pathways are underway in our laboratory.

4. Experimental

4.1. General

All manipulations were carried out using standard Schlenk line and glove box techniques under an inert atmosphere (argon or nitrogen). Hexane, toluene, THF and D_6-benzene were distilled over potassium, whilst diethyl ether was distilled over Na/K alloy. Infrared spectra were obtained as Nujol mulls using a Perkin–Elmer 1600 Series FTIR spectrometer with NaCl plates. NMR spectroscopy was carried out using either Jeol Eclipse 300, Bruker WM 250 or Bruker DPX 400 spectrometers, and were referenced to the residual ^{1}H or ^{13}C resonances of the solvent used. Mass spectra were recorded using a VG Fisons Platform II instrument operating under APCI conditions, or were obtained from the EPSRC Mass Spectrometry Service, Swansea. Melting points were obtained under argon in sealed capillaries and are not corrected. The compounds FisoH [15], PisoH [16], 'GaI' [17] and [AlMe$_2$(Aiso)] [2c] were synthesised by literature procedures. [K(Piso)][2] was obtained by treating PisoH with 1.05 eq. of K[N(SiMe$_3$)$_2$] in toluene (reflux, 2 h), then removing all volatiles in vacuo and drying the residue at 50 °C under vacuum for several hours. [AlMe$_2$(Piso)] was synthesised by treatment of PisoH with 1.05 eq of AlMe$_3$ in toluene (−78 °C to room temperature), removing all volatiles and drying the product under vacuum. The product was obtained almost quantitatively as a colourless crystalline material and the spectroscopic data were compared with the literature values [2c].

4.2. [{GaI(Fiso)}$_2$] (7)

Bu^{n}Li (0.743 ml of a 1.6 M solution in hexanes, 1.19 mmol) was added to solution of FisoH (0.433 g, 1.19 mmol) in diethyl ether (30 mL) at −20 °C. The resultant solution was warmed to room temperature and stirred overnight. It was then cooled to −50 °C and a solution of [{GaI$_2$(NHCy$_2$)}$_2$] (0.60 g, 0.59 mmol) in toluene (30 mL) added over 5 min. The resultant solution was stirred for 2 h and slowly warmed to room temperature overnight. Volatiles were then removed in vacuo and the residue was extracted into hexane (50 mL) and filtered. The filtrate was concentrated to ca. 30 mL and placed at −30 °C overnight giving colourless crystals of **7**. Yield: 0.30 g, 42%; m.p. >300 °C; ^{1}H NMR (250 MHz, C$_6$D$_6$, 298 K): δ 1.20 (d, $^3J_{HH} = 6.8$ Hz, 24 H, CH(CH_3)), 1.48 (d, $^3J_{HH} = 6.8$ Hz, 24 H, CH(CH_3)), 3.92 (v. sept, $^3J_{HH} = 6.8$ Hz, 8 H, CH(CH$_3$)), 7.10–7.30 (m, 12 H, Ar–H), 7.55 (s, 2H, NC(H)N); ^{13}C NMR (100.6 MHz, C$_6$D$_6$, 298 K): δ 25.0 (CH(*C*H$_3$)), 26.0 (CH(*C*H$_3$)), 29.2 (*C*H(CH$_3$)), 124.4 (*m*-Ar*C*), 127.4 (*p*-Ar*C*), 138.0 (*ipso*-Ar*C*), 145.4 (*o*-Ar*C*), 166.6 (N*C*N); MS/EI, *m*/*z* (%): 365.3 (FisoH$^+$, 12), 176.0 (ArNH$^+$, 100); IR ν/cm^{-1} (Nujol): 1668 m, 1636 m, 1585 m, 1260 s, 1097 m, 1055 m, 933 m, 799 m, 753 m. N.B. [{GaI(Piso)}$_2$] (**9**) was prepared by an equivalent procedure but was only obtained in trace amounts. As a result, no spectroscopic data were obtained for this compound.

4.3. [GaI(Fiso)$_2$] (8)

A solution of [{GaI$_2$(NHCy$_2$)}$_2$] (0.88 g, 0.87 mmol) in toluene (20 mL) and Et$_2$O (10 mL) was added at −80 °C to a slurry of [K(Fiso)] (0.77 g, 1.91 mmol) in toluene (20 mL) and Et$_2$O (10 mL). The mixture was warmed to room temperature overnight, filtered, concentrated to ca. 30 mL and placed at −30 °C overnight to yield colourless crystals of **8**. Yield: 0.33 g, 41%; m.p. 275–277 °C; ^{1}H NMR (400 MHz, C$_6$D$_6$, 298 K): δ 1.10–1.35 (m, 48 H, CH(CH_3)$_2$), 3.54 (br. v. sept, $^3J_{HH}$ = ca. 6.7 Hz, 8 H, CH(CH$_3$)$_2$), 6.97–7.30 (m, 12 H, Ar–H), 7.63 (s, 2 H, NCHN); ^{13}C NMR (100.6 MHz, C$_6$D$_6$, 298 K): δ 23.8 (CH(*C*H$_3$)), 24.5 (CH(*C*H$_3$)), 25.1 (CH(*C*H$_3$)), 25.5 (CH(*C*H$_3$)), 28.5 (*C*H(CH$_3$)), 28.6 (*C*H(CH$_3$)), 123.4 (*m*-Ar*C*), 125.6 (*p*-Ar*C*), 141.2 (*ipso*-Ar*C*), 144.0 (*o*-Ar*C*), 160.2 (N*C*N); MS/APCI *m*/*z* (%): 365 (FisoH$_2^+$, 100); IR ν/cm^{-1} (Nujol): 1668 m, 1560 m, 1260 s, 1200 m, 1176 m, 799 m, 751 m.

4.4. [InCl(Fiso)$_2$] (10)

Bu^{n}Li (2.50 ml of a 1.6 M solution in hexanes, 4.00 mmol) was added at room temperature to a solution of FisoH (1.39 g, 3.80 mmol) in Et$_2$O (70 mL) and the mixture stirred for 3 h. The resultant solution was added dropwise at to a slurry of InCl (1.20 g, 7.99 mmol) in Et$_2$O (20 mL) at −80 °C. The reaction mixture was slowly warmed to room temperature overnight in the absence of light. It was then filtered, volatiles removed from the filtrate in vacuo and the residue was extracted into hexane (40 mL). Placement of the extract at −30 °C overnight gave colourless crystals of **10**. Yield 0.42 g, 25%; m.p. 200–205 °C (dec.); ^{1}H NMR (400 MHz, C$_6$D$_6$, 298 K): δ 1.00–1.80 (m, 48 H, CH(CH_3)$_2$), 3.71–4.00 (m, 8 H, CH(CH$_3$)$_2$), 6.90–7.28 (m, 12 H, Ar–H), 7.47 (s, 2 H, NC(H)N); ^{13}C NMR (100.6 MHz, C$_6$D$_6$, 298 K): δ 24.0 (CH(*C*H$_3$)), 24.5 (CH(*C*H$_3$)), 25.3 (CH(*C*H$_3$)), 25.5 (CH(*C*H$_3$)), 28.3 (*C*H(CH$_3$)), 28.6 (*C*H(CH$_3$)), 123.5 (*m*-Ar*C*), 126.3 (*p*-Ar*C*), 139.3 (*ipso*-Ar*C*), 143.6, (*o*-Ar*C*), 158.1 (N*C*N); MS/APCI, *m*/*z* (%): 365 (FisoH$_2^+$, 100); IR ν/cm^{-1} (Nujol): 1668 m, 1636, 1585 m, 1260 s, 1097 m, 1055 m, 933 m, 799 m.

[2] THF adducts of [K(Piso)] have been previously obtained, see [15].

4.5. [AlI_2(Aiso)] (**12**) and [AlI_3(AisoH)] (**13**)

A solution of I_2 (3.85 g, 15.2 mmol) in toluene was added to a cooled solution (−80 °C) of [$AlMe_2$(Aiso)] (3.00 g, 6.90 mmol, 1.0 eq) in toluene (35 mL). The mixture was then warmed to room temperature and stirred for 2 d. Volatiles were removed in vacuo, the residue extracted with hexane (40 mL) and the extract placed at −30 °C overnight to give yellow crystals of **13**. Volatiles were removed from the mother liquor and the residue dissolved in toluene/hexane (2:1, 60 mL) and placed at −30°C overnight to give crystals of **13** in a first crop and a mixture of **12** and **13** in a second crop. The crystals were manually separated.

12: Yield 0.74 g, 16%; m.p. 186–187 °C; ^{1}H NMR (400 MHz, C_6D_6, 298 K): δ 1.02 (d, $^3J_{HH} = 6.8$ Hz, 12 H, CH(CH_3)), 1.17 (s, 3 H, CCH_3), 1.19 (d, $^3J_{HH} = 6.8$ Hz, 12 H, CH(CH_3)), 3.50 (v. sept, $^3J_{HH} = 6.8$ Hz, 4 H, CH(CH_3)), 6.82–7.08 (m, 6 H, Ar–H); ^{13}C NMR (100.6 MHz, C_6D_6, 298 K): δ 14.5 (H_3CC), 24.3 (CH(CH_3)), 25.8 (CH(CH_3)), 28.9 (CH(CH_3)), 124.6 (*m*-Ar*C*), 129.2 (*p*-Ar*C*), 135.1 (*ipso*-Ar*C*), 145.4 (*o*-Ar*C*), 172.0 (N*C*N); MS/EI *m*/*z* (%): 378.3 (AisoH$^+$, 22), 335.3 (AisoH$^+$ − Pr^i, 26), 202.2 (AisoH$^+$ − ArNH, 100), 177.2 ($ArNH_2^+$, 24); IR ν/cm^{-1} (Nujol): 1636 m, 1596 m, 1260 s, 1097 m, 934 m, 864 m, 799 m, 746 m.

13: Yield 1.20 g, 22%; m.p. 220–222 °C (dec.); ^{1}H NMR (400 MHz, C_6D_6, 298 K): δ 1.10 (d, $^3J_{HH} = 6.8$ Hz, 6 H, CH(CH_3)), 1.13 (d, $^3J_{HH} = 6.8$ Hz, 6 H, CH(CH_3)), 1.22 (d, $^3J_{HH} = 6.8$ Hz, 6 H, CH(CH_3)), 1.34 (s, 3 H, CCH_3), 1.60 (d, $^3J_{HH} = 6.8$ Hz, 6 H, CH(CH_3)), 3.54 (v. sept, $^3J_{HH} = 6.8$ Hz, 2 H, CH(CH_3)), 3.63 (v. sept, $^3J_{HH} = 6.8$ Hz, 2 H, CH(CH_3)), 7.00–7.24 (m, 6 H, Ar–H), 8.98 (s, 1 H, NH); ^{13}C NMR (100.6 MHz, C_6D_6, 298 K): δ 14.5 (H_3CC), 24.6 (CH(CH_3)), 24.8 (CH(CH_3)), 24.9 (CH(CH_3)), 25.1 (CH(CH_3)), 29.0 (CH(CH_3)), 29.1 (CH(CH_3)), 125.3 (*m*-Ar*C*), 129.3 (*p*-Ar*C*), 139.0 (*ipso*-Ar*C*), 144.8 (*o*-Ar*C*), 186.0 (N*C*N); MS/EI *m*/*z* (%): 785.7 (M$^+$, <5), 742.7 (M$^+$ − Pr^i, <5), 659.0 (M$^+$ − I, 100), 379.3 ($AisoH_2^+$, 19), 335.2 (AisoH$^+$ − Pr^i, 26), 202.2 (AisoH$^+$ − ArNH, 100); IR ν/cm^{-1} (Nujol): 3295 (NH), 1641 m, 1570 m, 1321 m, 1260 s, 1170 m, 1096 m, 934 m, 870 m; Acc. mass. EI for M$^+$ − I: found: 659.0926; calculated: 659.0934.

4.6. [AlI_2(Piso)] (**14**)

A solution of I_2 (0.54 g, 2.13 mmol) in toluene (30 mL) was added dropwise to a slurry of [{AlH_2(Piso)}$_2$] (0.91 g, 1.02 mmol) in toluene (15 mL) at −20 °C until gas evolution had ceased. The solution was then warmed to room temperature and stirred for 30 min. Volatiles were removed in vacuo and the residue dissolved in toluene (30 mL), filtered and concentrated under reduced pressure to give **14** as a light yellow crystalline solid after placement at −30°C overnight. Yield 1.25 g, 88%; m.p. 238–240 °C (no dec. until >300 °C); ^{1}H NMR (400 MHz, C_6D_6, 298 K): δ 0.94 (s, 9 H, C(CH_3)$_3$), 1.39 (d, $^3J_{HH} = 6.8$ Hz, 12 H, CH_3), 1.48 (d, $^3J_{HH} = 6.8$ Hz, 12 H, CH_3), 3.83 (v. sept, $^3J_{HH} = 6.8$ Hz, 4 H, CH), 7.06–7.26 (m, 6 H, Ar–H), ^{13}C NMR (100.6 MHz, C_6D_6, 298 K): δ 21.8 (CH(CH_3)), 28.0 (CH(CH_3)), 28.3 (CH(CH_3)), 28.7 (C(CH_3)$_3$), 41.2 (C(CH_3)$_3$), 123.2 (*m*-Ar*C*), 129.2 (*p*-ArC), 135.0 (*ipso*-Ar*C*), 144.1 (*o*-Ar*C*), 185.9 (N*C*N); MS/APCI *m*/*z* (%): 421 (PisoH$^+$, 100), 244 (PisoH$^+$ − ArNH, 71); IR ν/cm^{-1} (Nujol): 1641 m, 1590 m, 1542 m, 1323 m, 1257 s, 1200 m, 1178 m, 1098 m, 803 m, 756 m.

4.7. [$GaCl_3$(FisoH)] (**16**)

A solution of FisoH (0.50 g, 1.37 mmol) in Et_2O (20 mL) was added to a solution of $GaCl_3$ (0.25 g, 1.37 mmol) in Et_2O (10 mL) at −80 °C. The mixture was slowly warmed to room temperature, filtered and the solvent removed in vacuo. The residue was extracted into toluene (8 mL) and the extract cooled to −30 °C to give colourless crystals of **16**. Yield 0.48 g, 65%; m.p. 158–160 °C; ^{1}H NMR (300 MHz, C_6D_6, 298 K): δ 1.13 (br. d, $^3J_{HH} = 6.8$ Hz, 24 H, CH(CH_3)), 3.27 (br. sept, $^3J_{HH} = 6.8$ Hz, 4 H, CH(CH_3)), 7.02–7.09 (m, 6 H, Ar–H), 7.83 (s, 1 H, HCN_2), 8.67 (s, 1 H, NH); ^{13}C NMR (100.6 MHz, C_6D_6, 298 K): δ 22.5 (CH(CH_3)), 27.3 (CH(CH_3)), 122.6 (*m*-Ar*C*), 122.9 (*p*-Ar*C*), 124.9 (*ipso*-Ar*C*), 127.5 (*o*-Ar*C*), 146.6 (N*C*N); MS (APCI), *m*/*z* (%): 365 ($FisoH_2^+$, 100); IR ν/cm^{-1} (Nujol): 3313 (NH), 1586 m, 1327 m, 1175 m, 1058 m, 806 m.

4.8. [$TripH_2$][$InBr_4$] (**17**)

A solution of [Li(Trip)] (0.25 g, 65 mmol) in THF (15 mL) was added over 5 min to a solution of $InBr_3$ (0.23 g, 0.65 mmol) in THF (10 mL) at −50°C. The mixture was slowly warmed to room temperature and stirred for 2 d. Volatiles were removed in vacuo and the residue washed with hexane (20 mL) and Et_2O (15 mL). The residue was then recrystallised from chloroform at −30 °C giving colourless crystals of **17** overnight. Yield 0.09 g, 15%; m.p. 233–235 °C; ^{1}H NMR (300 MHz, $CDCl_3$, 298 K): δ 1.37 (d, $^3J_{HH} = 6.8$ Hz, 6 H, CH(CH_3)$_2$), 1.65 (d, $^3J_{HH} = 6.8$ Hz, 6 H, CH(CH_3)$_2$), 3.42 (v. sept, $^3J_{HH} = 6.8$ Hz, 2 H, CH(CH_3)$_2$), 3.55 (s, 1 H, CH), 5.42 (s, 2 H, NH), 6.97–7.18 (m, 3 H, ArH), 7.22–7.29 (m, 3 H, ArH), 7.33–7.43 (m, 3 H, ArH), 7.52–7.68 (m, 3 H, ArH); ^{13}C NMR (100.6 MHz, C_6D_6, 298 K): δ 22.1 (CH(CH_3)), 23.4 (CH(CH_3)), 24.7 (CH(CH_3)), 50.6 (CAr_3), 121.3 (*ArC*), 125.7 (*ArC*), 125.9 (*ArC*), 126.6 (*ArC*), 127.8 (*ArC*), 140.2 (*ArC*), 146.0 (N*C*N); MS/APCI *m*/*z* (%): 381 ($TripH_2^+$, 100); IR ν/cm^{-1} (Nujol): 3358 (NH), 1640 m, 1457 m, 1376 m, 1260 s, 1093 m, 911 m, 801 m, 750 m.

4.9. Crystallographic studies

Crystals of **7**, **9**, **10**, **13**, **14**, **16** and **17** suitable for X-ray crystal structure determination were mounted in

Table 1
Crystal data and refinement details for **7**, **9**, **10**, **13**, **16** and **17**.$CHCl_3$

Compound	**7**	**9**	**10**	**13**	**14**	**16**	**17** · $CHCl_3$
Formula	$C_{50}H_{70}Ga_2I_2N_4$	$C_{58}H_{86}Ga_2I_2N_4$	$C_{50}H_{70}ClInN_4$	$C_{26}H_{38}AlI_3N_2$	$C_{29}H_{43}AlI_2N_2$	$C_{25}H_{36}Cl_3GaN_2$	$C_{28}H_{30}Br_4Cl_3InN_2$
Molecular weight	1120.34	1232.55	877.37	786.26	700.43	540.63	935.35
Crystal system	triclinic	orthorhombic	monoclinic	monoclinic	orthorhombic	monoclinic	triclinic
Colour, habit	colourless needle	colourless block	colourless plate	yellow block	yellow block	colourless block	colourless needle
Crystal size/mm	$0.12 \times 0.06 \times 0.04$	$0.25 \times 0.25 \times 0.20$	$0.40 \times 0.10 \times 0.06$	$0.10 \times 0.10 \times 0.10$	$0.15 \times 0.15 \times 0.10$	$0.10 \times 0.10 \times 0.10$	$0.10 \times 0.03 \times 0.03$
Space group	$P\bar{1}$	*Pbca*	$P2_1/c$	$P2_1/n$	$Pna2_1$	$P2_1/c$	$P\bar{1}$
a (Å)	10.782(2)	14.479(3)	14.490(3)	11.697(2)	18.034(4)	10.434(2)	8.2810(2)
b (Å)	11.471(2)	19.212(4)	16.575(3)	19.694(4)	10.165(2)	19.992(4)	13.2880(4)
c (Å)	21.861(4)	20.302(4)	21.288(4)	13.437(3)	16.981(3)	14.054(3)	15.6340(5)
α (°)	79.37(3)	90	90	90	90	90	89.5200(10)
β (°)	83.10(3)	90	109.28(3)	92.39(3)	90	108.53(3)	75.8270(10)
γ (°)	74.18(3)	90	90	90	90	90	85.8670(10)
V (Å^3)	2549.7(9)	5647(2)	4826.3(17)	3092.7(11)	3113.1(11)	2779.6(10)	1663.55(8)
Z	2	4	4	4	4	4	2
T (K)	150	150	150	150	150	123	150
ρ_{calc} (Mg m^{-3})	1.459	1.450	1.207	1.689	1.494	1.292	1.867
μ (mm^{-1})	2.303	2.087	0.581	3.076	2.067	1.293	5.776
F(000)	1132	2520	1856	1520	1400	1128	904
Θ (°) for data collection	3.04–27.47	2.92–27.50	3.00–27.47	3.03–26.37	3.02–26.00	2.95–25.02	3.08–25.00
Completeness to θ (%)	99.1	99.7	99.7	99.6	99.6	99.2	98.4
Reflections collected/unique	44 851/11 551	40 722/6470	34 974/11 026	21 192/6317	20 063/5188	13 527/4873	9750/5770
R_{int}	0.1437	0.1167	0.1097	0.0760	0.1208	0.0685	0.0369
Goodness-of-fit on F^2	1.019	1.011	1.015	1.039	1.038	1.055	1.034
Parameters varied	540	310	533	299	319	296	356
Largest peak/hole (e^{-1}/Å^3)	0.63/−0.89	0.63/−0.69	0.53/−0.71	1.96 (near I1)/−2.26 (near I3)	1.66 (near I1)/−1.59 (near I1)	0.99/−0.91	0.65/−0.83
Final R indices $[I > 2\sigma(I)]$	$R_1 = 0.0563$, $wR_2 = 0.0950$	$R_1 = 0.0715$, $wR_2 = 0.1026$	$R_1 = 0.0626$, $wR_2 = 0.1011$	$R_1 = 0.0571$, $wR_2 = 0.1439$	$R_1 = 0.0670$, $wR_2 = 0.1599$	$R_1 = 0.0483$, $wR_2 = 0.0993$	$R_1 = 0.0382$, $wR_2 = 0.0774$

$R_1(F) = \{\sum(|F_o|-|F_c|)/\sum|F_o|\}$. $wR_2(F^2) = \{\sum w(|F_o|^2 - |F_c|^2)^2 / \sum w|F_o^2|^2\}^{1/2}$, where w is the weight given each reflection.

silicone oil. Crystallographic measurements were made using a Nonius Kappa CCD diffractometer. The structures were solved by direct methods and refined on F^2 by full matrix least squares (SHELX-97) [18] using all unique data. Data were corrected for absorption using a SORTAV multi-scan absorption correction [19]. The R_{int} values for several of the compounds were high due to poor crystal quality, though this has not led to any ambiguity regarding the molecular connectivity of these compounds. The Flack parameter of −0.05(5) for **14** confirms that it has been refined as its correct absolute configuration. Crystal data, details of data collections and refinement are given in Table 1.

5. Supplementary material

Crystallographic data (excluding structure factors) have been deposited with the Cambridge Crystallographic Data Centre. CCDC-283677 (**7**), CCDC-283672 (**9**), CCDC-283678 (**10**), CCDC-283673 (**13**), CCDC-283674 (**14**), CCDC-283675 (**16**) and CCDC-283676 (**17**) contain the supplementary crystallographic data for this paper. These data can be obtained free of charge via www.ccdc.cam.ac.uk/conts/reteiving.html (or from the Cambridge Crystallographic Data Centre, 12 Union Road, Cambridge, CB2 1EZ, UK; fax: +44 1223 336033; e-mail: deposit@ccdc. cam.ac.uk).

Acknowledgements

We thank The Leverhulme Trust for funding (postdoctoral fellowship for A.S.) and the EPSRC (partial studentship for M.K.). The EPSRC National Mass Spectrometry Service at Swansea University is also gratefully acknowledged.

References

[1] (a) J. Barker, M. Kilner, Coord. Chem. Rev. 133 (1994) 219;
(b) F.T. Edelmann, Coord. Chem. Rev. 137 (1994) 403, and references therein.
[2] (a) J. Barker, N.C. Blacker, P.R. Phillips, N.W. Alcock, W. Errington, M.G.H. Wallbridge, J. Chem. Soc., Dalton Trans. (1996) 431;
(b) M.P. Coles, D.C. Svenson, R.F. Jordan, V.G. Young, Organometallics 16 (1997) 5183;
(c) M.P. Coles, D.C. Svenson, R.F. Jordan, V.G. Young, Organometallics 17 (1998) 4042;
(d) S. Dagorne, R.F. Jordan, V.G. Young, Organometallics 18 (1999) 4619;
(e) G. Talarico, P.H.M. Budzelaar, Organometallics 19 (2000) 5691;
(f) S. Dagorne, I.A. Guzei, M.P. Coles, R.F. Jordan, J. Am. Chem. Soc. 122 (2000) 274;
(g) D. Abeysekera, K.N. Robertson, T.S. Cameron, J.A.C. Clyburne, Organometallics 20 (2001) 5532;
(h) H.A. Jenkins, D. Abeysekera, D.A. Dickie, J.A.C. Clyburne, Dalton Trans. (2002) 3919;
(i) J.A.R. Schmidt, J. Arnold, Organometallics 21 (2002) 2306;
(j) R.T. Boere, M.L. Cole, P.C. Junk, New. J. Chem. 29 (2005) 128.
[3] (a) R.J. Baker, C. Jones, P.C. Junk, M. Kloth, Angew. Chem. Int. Ed. 43 (2004) 3852;
(b) M.L. Cole, C. Jones, P.C. Junk, M. Kloth, A. Stasch, Chem. Eur. J. 11 (2005) 4482.
[4] (a) C. Cui, H.W. Roesky, H.-G. Schmidt, M. Noltemeyer, H. Hao, F. Cimpoesu, Angew. Chem. Int. Ed. 29 (2000) 4274;
(b) N.J. Hardman, B.E. Eichler, P.P. Power, Chem. Commun. (2000) 1991;
(c) M.S. Hill, P.B. Hitchcock, Chem. Commun. (2004) 1818;
(d) M.S. Hill, P.B. Hitchcock, R. Pongtavornpinyo, Dalton Trans. (2005) 273;
(e) Y. Cheng, P.B. Hitchcock, M.F. Lappert, M. Zhou, Chem. Commun. (2005) 752;
(f) M.S. Hill, P.B. Hitchcock, R. Pongtavornpinyo, Angew. Chem. Int. Ed. 44 (2005) 4231.
[5] R.J. Baker, C. Jones, Coord. Chem. Rev. 249 (2005) 1857, and references therein.
[6] C. Jones, P.C. Junk, J.A. Platts, D. Rathmann, A. Stasch, Dalton Trans. (2005) 2497.
[7] R.J. Baker, C. Jones, Dalton Trans. (2005) 1341, and references therein.
[8] R.J. Baker, H. Bettentrup, C. Jones, Eur. J. Inorg. Chem. (2003) 2446.
[9] M. Stender, P.P. Power, Polyhedron 21 (2002) 525.
[10] R.J. Baker, C. Jones, J. Organomet. Chem. (in press).
[11] (a) For example, R.J. Baker, R.D. Farley, C. Jones, M. Kloth, D.M. Murphy, Dalton Trans. (2002) 3844;
(b) N.J. Hardman, R.J. Wright, A.D. Phillips, P.P. Power, J. Am. Chem. Soc. 125 (2003) 2667;
(c) W. Uhl, A. El-Hamdan, M. Prott, P. Spuhler, G. Frenking, Dalton Trans. (2003) 1360.
[12] W. Uhl, I. Hahn, R. Wartchow, Chem. Ber. 130 (1997) 417.
[13] Y. Zhou, D.R. Richeson, Inorg. Chem. 35 (1996) 2448.
[14] For example, D.E. Hibbs, M.B. Hursthouse, C. Jones, N.A. Smithies, Main Group Chem. 2 (1998) 293.
[15] M.L. Cole, P.C. Junk, J. Organomet. Chem. 666 (2003) 55.
[16] A. Xia, H.M. El-Kaderi, M.J. Heeg, C.H. Winter, J. Organomet. Chem. 682 (2003) 224.
[17] M.L.H. Green, P. Mountford, G.J. Smout, S.R. Peel, Polyhedron 9 (1990) 2763.
[18] G.M. Sheldrick, SHELX-97, University of Göttingen, 1997.
[19] R.H. Blessing, Acta Crystallogr. A 51 (1995) 33.

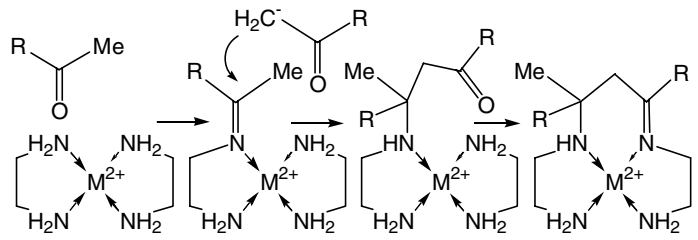

Scheme 1.

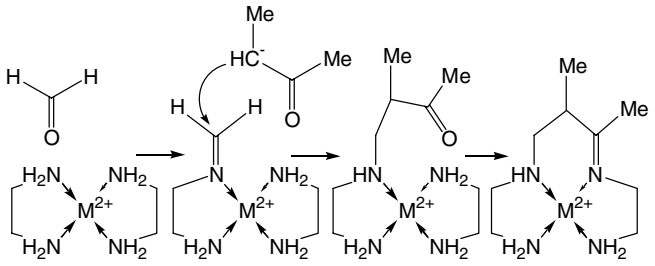

Scheme 2.

ligand (see Scheme 2). It was suggested that the methanal was formed by aerial oxidation of methanol, catalysed by other ingredients present in the reaction mixture.

If this reaction occurred as proposed, it seemed likely that the same product could be more easily formed by a conventional reaction of ethane-1,2-diamine complexes, butanone and methanal, in the presence of zinc chloride to provide the tetrachlorozincate anion which facilitates crystallisation of many related cations. This communication reports such reactions for nickel(II) and copper(II), and structural studies of the products formed by reactions of ethane-1,2-diamine complexes of nickel(II) with butanone, and with butanone plus methanal.

Alternative preparations of [Ni(enmekf)][$ZnCl_4$] by reactions of [$Ni(en)_3$][$ZnCl_4$] with preformed 3-methyl-4-hydroxybutan-2-one or 3-methylbut-3-ene-2-one have been reported, see Scheme 3 [6]. The formation of azamacrocycle compounds incorporating ethane-1,2-diamine and butanone has been reported [7] and structures of copper(II) and nickel(II) compounds of 5,7,12,14-tetraethyl-7,14-dimethyl-1,4,8,11-tetraazacyclotetradeca-4,11-diene have been reported [8–10].

The formation of compounds of 5,7,7-trimethyl-3,7-diazanon-3-ene-1,9-diamine (enac) by reaction of ethane-1,2-diamine compounds of nickel(II) or copper(II) with

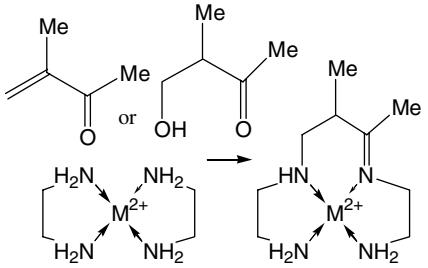

Scheme 3.

acetone have been reported [1,3,11,12], and the structures of [Cu(enac)][$ZnCl_4$] [13] and [Ni(enac)(NO_2)]ClO_4 [12], have been reported.

Shevenko et al. have reported reactions of elemental metals, ethane-1,2-diamine dihydrochloride {or its *N*-(2-hydroxyethyl) derivative} and acetone to form [Cu(enac)][$MnCl_4$], [Ni(enac)][$MnCl_4$], [Cu(L)][$MnCl_4$] and [Ni(L)][$MnCl_4$], L = 1,15-dihydroxy-7,9,9-trimethyl-3,6,10,13-tetraazapentadeca-6-ene [14]. Structures were reported for [Ni(enac)][$MnCl_4$] and [Cu(L)][$MnCl_4$].

2. Results

Tris(ethane-1,2-diamine)nickel(II) and bis(ethane-1,2-diamine)copper(II) tetrachlorozincates react over a period of days in refluxing methanol/butanone to form the (4,6-diethyl-6-methyl-3,7-diazadecan-3-ene-1,9-diamine)-nickel(II) or -copper(II) tetrachlorozincate salts, [M(enmek)][$ZnCl_4$]. The structure of [Ni(enmek)][$ZnCl_4$] is reported below.

When the reactions were repeated in the presence of methanal (formaldehyde, as paraformaldehyde) more rapid reactions occurred, with products [M(enmekf)][$ZnCl_4$] formed, for which analysis indicated formulae [Ni($C_9H_{22}N_4$)][$ZnCl_4$] and [Cu($C_9H_{22}N_4$)][$ZnCl_4$]·H_2O, in agreement with a tetradentate ligand formed by combination of two ethane-1,2-diamine, one butanone and one methanal residue, with elimination of 2 mol of water. The structure of [Ni(enmekf)][$ZnCl_4$], reported below, shows the presence of the tetradentate ligand 4,5-dimethyl-3,7-diazanon-3-ene-1,9-diamine, the same as for the copper(II) compound described by Shevchenko et al. [5].

2.1. Structural studies

The structures of (4,6-diethyl-6-methyl-3,7-diazanon-3-ene-1,9-diamine)nickel(II) tetrachlorozincate and (4,5-dimethyl-3,7-diazanon-3-ene-1,9-diamine)nickel(II) tetrachlorozincate were determined by X-ray diffractometry, see Section 3.2 and Table 1 for crystallographic details.

2.1.1. 6SR,7RS-(4,6-diethyl-6-methyl-3,7-diazanon-3-ene-1,9-diamine)nickel(II) tetrachlorozincate, [Ni(enmek)][$ZnCl_4$]

The asymmetric unit contains discrete square planar (4,6-diethyl-6-methyl-3,7-diazadecan-3-ene-1,9-diamine)-nickel(II) cations and tetrachlorozincate anions, see Fig. 1,

Table 1
Crystallographic data

Compound	[Ni(enmek)][$ZnCl_4$]	[Ni(enmekf)][$ZnCl_4$]
Formula	$C_{12}H_{28}Cl_4N_4NiZn$	$C_9H_{22}Cl_4N_4NiZn$
M_r	494.26	452.19
Space group	tetragonal, $P4_12_12$	orthorhombic, $Pna2_1$
a (Å)	11.1100(3)	15.3465(6)
b (Å)	11.1100(3)	8.9305(4)
c (Å)	31.905(1)	12.5401(4)
Z	8	4
Crystal dimensions (mm)	$0.60 \times 0.60 \times 0.30$	$0.30 \times 0.10 \times 0.10$
Reflections (for cell parameters)	5356	5136
θ Range (for cell parameters)	2.59–32.52	2.64–34.16
T (K)	273(2)	273(2)
θ_{max} (°)	32.8	34.5
hkl	$-16 \leqslant h \leqslant 16$; $-16 \leqslant k \leqslant 8$; $-46 \leqslant l \leqslant 46$	$-22 \leqslant h \leqslant 22$; $-13 \leqslant k \leqslant 13$; $-17 \leqslant l \leqslant 19$
T_{min}, T_{max}	0.325, 0.443	0.499, 0.730
Measured reflections	39499	19423
Independent reflections	6682	5559
Reflections with $I > 2\sigma(I)$	6594	5208
R_{int}	0.025	0.025
Flack parameter [16]	0.077(9)	−0.012(7)
$R[F^2 > 2\sigma(F^2)]$	0.031	0.024
$wR(F^2)$	0.066	0.057
S	1.27	1.03
Parameters	202	159

Table 2 for selected dimensions, Table 3 for displacements of atoms from selected planes and Table 4 for hydrogen bonding interactions.

The N_4 group is slightly tetrahedrally twisted (displacements of N atoms from the N_4 plane ±0.014(1) Å), with the Ni displaced by 0.018(1) Å from the plane. Chloride ions of tetrachlorozincate ions are located in approximately axial positions. The C62 methyl substituent is axially oriented, on the opposite side of the N_4 plane as the N7–H group (configuration C6, *S*; N7, *R*). The C41 and C61 methylene groups are equatorially oriented, with the C42 and C63 methyl groups displaced on opposite sides of the N4 plane, with C42 on the same side as C62.

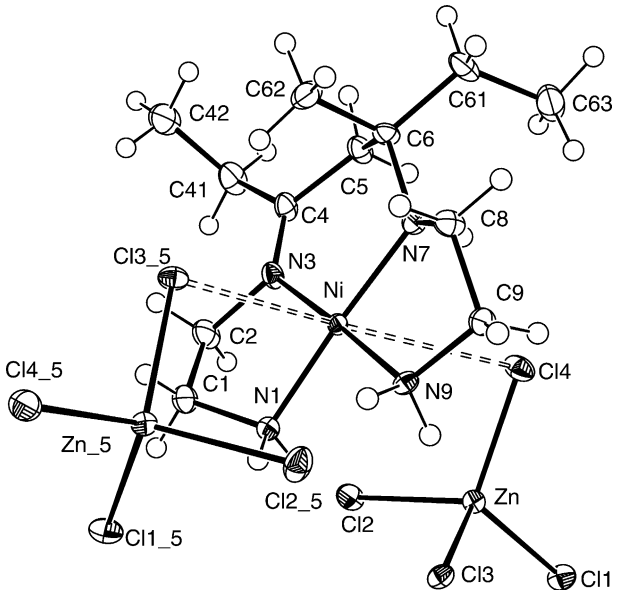

Fig. 1. [Ni(mek)][$ZnCl_4$] drawn [15] with displacement ellipsoids at the 50% confidence level, with hydrogen atoms shown as circles of arbitrary radius. The symmetry operation 5 = $-x + 1/2$, $y + 1/2$, $-z + 1/4$.

2.1.2. 5SR,7RS-(4,5-dimethyl-3,7-diazanon-3-ene-1,9-diamine)nickel(II) tetrachlorozincate, [Ni(enmekf)][$ZnCl_4$]

The asymmetric unit contains discrete square planar (4,6-dimethyl-3,7-diazanon-3-ene-1,9-diamine)nickel(II) cations and tetrachlorozincate anions, see Fig. 2, Table 2 for selected dimensions, Table 3 for displacements of atoms from selected planes and Table 5 for hydrogen bonding interactions.

The N_4 group has slight tetrahedral twisting (displacements of N atoms from N_4 plane ±0.006(1) Å), with the Ni displaced by 0.004(1) Å from the plane. Chloride ions of tetrachlorozincate ions are located in approximately axial positions. The C51 methyl substituent is axially oriented, on the same side of the N_4 plane as the N7–H group (configuration C5, *S*; N7, *R*).

2.1.3. Comparison of structures of (3-azanon-3-ene-1,9-diamine)metal(II) tetrachlorometalate salts

The structures of [Ni(enmekf)][$ZnCl_4$] and [Cu(enmekf)][$ZnCl_4$] are very similar, though they are not isostructural, with similar conformations of the ligands. In particular, both have the C5 methyl substituent axially oriented (see Table 3 for displacements of atoms from chelate (MN_2) planes). The M–N bond lengths are ca. 0.1 Å shorter for the singlet ground state nickel(II) compounds [Ni(enmek)][$ZnCl_4$], [Ni(enmekf)][$ZnCl_4$] and [Ni(enac)][$MnCl_4$] than for the copper(II) compounds [Cu(enmekf)][$ZnCl_4$] and [Cu(enac)][$ZnCl_4$], with the bond to the imine nitrogen only marginally shorter than the bonds to primary and secondary amine nitrogen atoms. The compounds have similar ligand conformations, though [Cu(enac)][$ZnCl_4$] has the CuN_4 group appreciably folded, whereas for the other cations it is near coplanar. The five-membered chelate rings all have asymmetric gauche conformations, with the pair having approximate C_2 symmetry. The six-membered chelate rings have C6 most displaced from the MN_2 plane, on the same side as the axial substituent for the enmekf compounds, on the opposite side for the other compounds.

For [Ni(enmek)][$ZnCl_4$], [Ni(enmekf)][$ZnCl_4$], [Ni(enac)][$MnCl_4$] and [Cu(enmek)][$ZnCl_4$] the cations are linked into chains by tetrachlorozincate ions, with chloride ions near both tetragonal axes, with unequal M–Cl distances (see Table 1). These M–Cl distances increase in the order $[Cu(enmek)]^{2+} < [Ni(enmekf)]^{2+} < [Ni(enmek)]^{2+}$, $[Ni(enac)]^{2+}$, though for the nickel(II) compounds, only Ni–Cl1 for [Ni(enmekf)][$ZnCl_4$] is significantly less than

Table 2
Selected dimensions for (3-azanon-3-ene-1,9-diamine)metal(II) tetrachlorometalate salts (Å, °)

Dimension	[Ni(enmek)][$ZnCl_4$][a]	[Ni(enmekf)][$ZnCl_4$][b]	[Cu(enmekf)][$ZnCl_4$][c,f]	[Ni(enac)][$MnCl_4$][d,f]	[Cu(enac)][$ZnCl_4$][e,f]
M–N1	1.904(2)	1.916(2)	1.997(4)	1.928(6)	2.001(4)
M–N3	1.907(2)	1.898(2)	1.998(4)	1.888(5)	1.988(4)
M–N7	1.912(2)	1.920(2)	1.998(4)	1.894(6)	2.011(4)
M–N9	1.925(2)	1.922(2)	2.018(4)	1.899(5)	2.007(4)
N3–C4	1.275(3)	1.289(3)	1.280(6)	1.289(8)	1.261(7)
N1–M–N3	86.4(1)	86.73(7)	85.7(2)	85.3(2)	85.3(2)
N1–M–N7	176.7(1)	177.93(7)	178.3(2)	176.7(2)	167.5(2)
N1–M–N9	91.1(1)	91.63(7)	94.6(2)	91.6(2)	95.9(2)
N3–Ni–N7	96.2(1)	95.25(7)	94.5(2)	96.1(2)	93.5(2)
N3–Ni–N9	177.5(1)	178.36(7)	178.7(2)	175.8(3)	178.8(2)
N7–M–N9	86.3(1)	86.39(7)	85.2(2)	86.9(2)	85.6(2)
M–Cl	3.339(2)[g]	3.087(2)[i]	2.876(4)[k]	3.348(6)[m]	2.697(1)
M–Cl	3.346(2)[h]	3.427(2)[j]	3.189(4)[l]	3.656(6)[n]	
Cl–M–Cl	164.5(2)	170.8(2)	172.2(2)	156.4(3)	

[a] (4,6-Diethyl-6-methyl-3,7-diazanon-3-ene-1,9-diamine)nickel(II) tetrachlorozincate. Zn–Cl distances range from 2.235(1) Å for Zn–Cl1 to 2.308(1) Å for Zn–Cl2 and Cl–Zn–Cl angles range from 105.17(2)° for Cl2–Zn–Cl4 to 117.75(2)° for Cl2–Zn–Cl3.
[b] (4,5-Dimethyl-3,7-diazanon-3-ene-1,9-diamine)nickel(II) tetrachlorozincate. Zn–Cl distances range from 2.258(1) Å for Zn–Cl1 to 2.304(1) Å for Zn–Cl3 and Cl–Zn–Cl angles range from 102.42(2)° for Cl2–Zn–Cl4 to 114.91(3)° for Cl1–Zn–Cl4.
[c] (4,5-Dimethyl-3,7-diazanon-3-ene-1,9-diamine)copper(II) tetrachlorozincate, from [5]; space group $Pna2_1$; $a = 15.305(3)$ Å, $b = 9.060(2)$ Å, $c = 12.452(3)$ Å.
[d] (5,7,7-Trimethyl-3,7-diazanon-3-ene-1,9-diamine)nickel(II) tetrachloromanganate, from [11]. Mn–Cl distances range from 2.2336(2) to 2.2.384(2) Å and Cl–Mn–Cl angles range from 102.86(2)° to 115.36(7)°.
[e] (5,7,7-Trimethyl-3,7-diazanon-3-ene-1,9-diamine)copper(II) tetrachlorozincate, from [12].
[f] Atom labels adjusted for comparability.
[g] Cl3 ($-x + 1/2$, $y + 1/2$, $z + 1/4$).
[h] Cl4.
[i] Cl2.
[j] Cl1 ($-x$, $-y$, $z + 1/2$).
[k] Cl2.
[l] Cl1 ($-x$, $-y$, $z + 1/2$).
[m] Cl1.
[n] Cl3 ($-x$, $-y$, $z + 1/2$).

Table 3
Displacements of atoms from mean MN_2 planes for chelate rings for (3-azanon-3-ene-1,9-diamine)metal(II) tetrachlorometalate salts[a]

Chelate ring	Atom	[Ni(enmek)][$ZnCl_4$]	[Ni(enmekf)][$ZnCl_4$]	[Ni(enac)][$MnCl_4$][a]	[Cu(enmekf)][$ZnCl_4$][b]	[Cu(enac)][$ZnCl_4$][b]
M, N1, N3	C1	0.638(4)	−0.573(3)	0.735	−0.492	0.217
	C2	0.086(4)	0.065(3)	0.150	0.155	−0.461
M, N3, N7	C4	−0.126(4)	−0.086(3)	−0.133	0.116	−0.073
	C5	−0.344(5)	0.014(3)	−0.234	0.047	0.067
	C6	0.439(4)	−0.695(3)	0.625	−0.710	0.774
	C41	−0.086(6)	0.297(5)	−0.269	0.370	−0.362
	C42	1.331(7)				
	C51		1.423(4)		1.440	
	C61	0.138(6)		0.481		2.213
	C62	1.942(4)		2.194		0.820
	C63	−1.300(6)				
M, N7, N9	C8	0.621(4)	0.514(3)	0.568	0.538	−0.364
	C9	−0.083(4)	−0.201(3)	−0.064	−0.199	0.358

[a] Positive displacements are in the direction of the axial substituents.
[b] Atom labels adjusted for comparability.

the sum of the van der Waals radii. In contrast [Cu(enac)][$ZnCl_4$] has a "molecular" structure with a close interaction of the cation with a single tetrachlorozincate ion, with one, much shorter, Cu–Cl interaction.

For all these compounds there is a network of N–H···Cl hydrogen bonds (see Tables 4 and 5).

3. Experimental

3.1. Synthesis of compounds

Preparations of Ni(enmek)][$ZnCl_4$] [2,4,6] and [Cu(enmekf)][$ZnCl_4$] [5] have been reported.

Table 4
Hydrogen bonding for [Ni(enmek)][$ZnCl_4$]

Atoms	H···Cl (Å)	N–H···Cl (°)	N···Cl (Å)
N1–H1C···Cl2	2.56	152.7	3.387
N1–H1C···Cl3	2.87	121.8	3.425
N1–H1D···Cl1^{i}	2.72	136.8	3.431
N7–H7···Cl4	2.64	138.1	3.372
N9–H9C···Cl2^{i}	2.40	164.3	3.274
N9–H9D···Cl3	2.44	160.4	3.305

Symmetry operation i = $-x - 1/2$, $y - 1/2$, $-z + 1/4$.

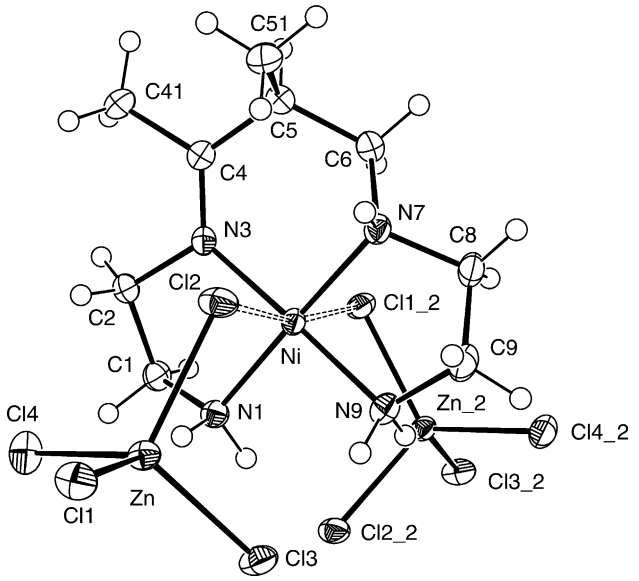

Fig. 2. [Ni(mekf)][$ZnCl_4$], drawn as for Fig. 1. The symmetry operation 2 = $-x$, $-y$, $z + 1/2$.

Table 5
Hydrogen bonding for [Ni(enmekf)][$ZnCl_4$]

Atoms	H···Cl (Å)	N–H···Cl (°)	N···Cl (Å)
N1–H1C···Cl2^{i}	2.39	159.6	3.251
N1–H1D···Cl4	2.63	153.7	3.457
N7–H7···Cl2	2.83	123.9	3.417
N9–H9C···Cl3	2.42	167.9	3.303
N9–H9D···Cl4^{i}	2.77	140.6	3.509
N9–H9D···Cl2^{i}	2.94	137.9	3.661

Symmetry operation i = $-x + 1$, $-y$, $z + 1/2$.

[Ni(enmekf)][$ZnCl_4$] and [Cu(enmekf)][$ZnCl_4$]·H_2O have now been prepared by refluxing [$Ni(en)_3$][$ZnCl_4$] or [$Cu(en)_2$][$ZnCl_4$] in 2:1 methanol:butanone plus 2 mol proportion of paraformaldehyde until the starting material had all reacted (ca. 6 h). This was obvious for the nickel compound as the sparingly soluble mauve coloured starting material was slowly converted to the sparingly soluble orange product. Reaction in the absence of the paraformaldehyde was much slower, taking several days under reflux to form [M(enmek)][$ZnCl_4$].

The compounds were recrystallised from hot 1:1 methanol:water by addition of propan-2-ol until turbid. The initial products were contaminated by small amounts of [M(enmek)][$ZnCl_4$], which was lost on recrystallisation. The copper(II) compound crystallised as a mono-hydrate, while the unhydrated compound for which the structure was reported [5] was crystallised from methanol.

[Ni(enmekf)][$ZnCl_4$]. Anal. Calc. for $C_9H_{22}Cl_4N_4NiZn$: C, 23.9; H, 4.9; N, 12.4. Found: C, 24.2; H, 4.9; N, 12.3%. IR (cm^{-1}): ν(NH) 3251, 3204, 3121w; ν(C=N) 1643; δ(NH2) 1583, 1572.

[Cu(enmekf)][$ZnCl_4$]·H_2O. Anal. Calc. for $C_9H_{24}Cl_4CuN_4OZn$: C, 22.8; H, 5.0; N, 12.0. Found: C, 22.8; H, 4.8; N, 12.3%. IR (cm^{-1}): ν(OH) 3480br; ν(NH) 3889, 3236, 3133w; ν(C=N) 1652; δ(NH2) 1584.

3.2. Structural determinations

The structures of [Ni(enmek)][$ZnCl_4$] and [Ni(enmekf)][$ZnCl_4$] were determined by X-ray diffractometry, by using a Bruker SMART 1K CCD area detector diffractometer, Mo Kα radiation (fine focus, sealed tube with graphite monochromator, $\lambda = 0.71073$ Å) with ϕ and ω scans [17] (see Table 1 for data). The data were corrected for absorption by multi-scans using SADABS v2.03 [18].

The structures were solved and refined on F^2 by using SHELXS97 and SHELXL97 [19], with hydrogen atoms in calculated positions and riding.

Appendix A. Supplementary data

Crystallographic data have been deposited with the Cambridge Crystallographic Data Centre; [Ni(enmek)][$ZnCl_4$] CCDC 283179 and [Ni(enmekf)][$ZnCl_4$] CCDC 283178. Copies may be obtained free of charge from The Director, CCDC, 12 Union Road, Cambridge, CBZ 1EZ, UK (fax: +44 1223 336 033; e-mail: deposit @ccdc.cam.ac.uk or http://www.ccdc.cam.ac.uk). Supplementary data associated with this article can be found, in the online version, at doi:10.1016/j.poly.2005.10.030.

References

[1] M.M. Blight, N.F. Curtis, J. Chem. Soc. (1962) 3016.
[2] D.A. House, N.F. Curtis, J. Am. Chem. Soc. 86 (1964) 1331.
[3] N.F. Curtis, Coord. Chem. Rev. 3 (1968) 3.
[4] N.F. Curtis, J. Chem. Soc., Dalton Trans. (1974) 347.
[5] D.V. Shevchenko, S.R. Petrusenko, V.N. Kokozay, I. Svoboda, J. Kozisek, Inorg. Chem. Commun. 8 (2005) 665.
[6] T.E. MacDermott, D.H. Busch, J. Am. Chem. Soc. 89 (1967) 5780.
[7] N.F. Curtis, Aust. J. Chem. 27 (1974) 71.
[8] T.J. Lee, T.H. Lu, B.F. Liang, C.S. Chung, T.Y. Lee, J. Chin. Chem. Soc. (Taipei) 28 (1981) 191.
[9] T.J. Lee, T.Y. Lee, W.B. Juang, C.S. Chung, Acta Crystallogr., Sect. C 41 (1985) 1745.
[10] T.H. Lu, T.J. Lee, T.Y. Lee, B.F. Liang, C.S. Chung, Proc. Natl. Sci. Counc., Repub. China, Part A 8 (1984) 217.
[11] N.F. Curtis, J. Chem. Soc., Dalton Trans. (1972) 1357.
[12] N.F. Curtis, O.P. Gladkikh, Aust. J. Chem. 53 (2000) 597.
[13] N.F. Curtis, H.K.J. Powell, H. Puschmann, C.E.F. Rickard, J.M. Waters, Inorg. Chim. Acta 355 (2003) 25.
[14] D.V. Shevchenko, S.R. Petrusenko, V.N. Kokozay, B.W. Skelton, J. Coord. Chem. 57 (2004) 1287.

[15] L.J. Farrugia, ORTEP3.2, J. Appl. Crystallogr. 30 (1997) 565.
[16] H.D. Flack, Acta Crystallogr., Sect. A 39 (1983) 876.
[17] Bruker, SMART (Version 5.054), SADABS (Version 2.03) and SAINT (Version 6.02A), Bruker AXS Inc., Madison, WI, USA, 1997.
[18] R.H. Blessing, Acta Crystallogr., Sect. A 51 (1995) 33.
[19] G.M. Sheldrick, SHELXS and SHELXL, Programs for the Solution and Refinement of Crystal Structures, University of Gottingen, Germany, 1997.

detail by cyclic voltammetry (CV) [29,30]. Consistent with previous reports, the electroreduction of **2** in the absence of MesBr occurs in two successive, reversible electron-transfer steps (Eqs. (1) and (2), Fig. 1(a)).

$$[\underset{\mathbf{2}}{NiBr_2(bpy)}] + 2e^- \rightleftharpoons [Ni(bpy)] + 2Br^- \quad E_p^{C_1} \tag{1}$$

$$[Ni(bpy)] + e^- \rightleftharpoons [Ni(bpy)]^{\bullet -} \quad E_p^{C_2} \tag{2}$$

MesBr is electrochemically inactive in the range of potentials corresponding to the reduction of nickel(II) complexes. Indeed, the electrochemical reduction of MesBr on the glassy carbon electrode, which involves the transfer of two electrons, takes place at more negative potentials than −2.5 V, in the region of the supporting electrolyte discharge.

In agreement with previously reported data [4,22,23], the anodic component of the first cathodic wave (C_1) of **2** disappeared in the presence of MesBr, and two new reduction waves (C_3 and C_4), showing anodic components, appeared at more negative potentials (Fig. 1(b); Table 1).

Waves C_3 and C_4 are due to the reduction of organo-nickel(II) products formed upon oxidative addition of MesBr to a nickel(0) species [4,22,23]. Indeed, wave C_3 corresponds to the reduction of the σ complex **1** formed by oxidative addition of MesBr to [Ni(bpy)] generated at potential C_1, while wave C_4 corresponds to the reduction of another intermediate, probably the bis-mesityl complex $[Ni(Mes)_2(bpy)]$ (**3**) formed by reaction of MesBr with the reduced form of **1**, generated at C_3, as previously reported (Eq. (3)) [4–6].

$$[\underset{\mathbf{1}}{NiBr(Mes)(bpy)}] + 2e^- + MesBr \xrightarrow{C_3} [\underset{\mathbf{3}}{Ni(Mes)_2(bpy)}] + 2Br^- \tag{3}$$

Unfortunately, we were unable to isolate compound **1** as a pure product as it was invariably contaminated by traces of solvent and of the supporting electrolyte salt. Analytically pure **1** was, however, obtained by extraction with toluene after electrolysis, which also allowed the recovery of the electrolyte. The electrochemically synthesized nickel complex **1** was authenticated by various methods, including a single-crystal X-ray analysis that showed the nickel center to be coordinated in a distorted square-planar environment by a chelating bpy ligand and a mesityl and a bromo ligand in a *cis* arrangement (Fig. 2). The mesityl ring is perpendicular to the N,N,Ni plane, apparently due to steric interaction of the methyl groups with the *cis* bromo ligand and the *ortho* hydrogen atom of bpy. The molecular structure is very similar to that previously reported for the same complex obtained by recrystallization from THF [17,21]. However, the two X-ray analyses differ crystallographically; the crystals of **1** obtained here exhibit a triclinic cell with two molecules of **1** and one toluene molecule in the unit cell, whereas the previously reported compound crystallized in the orthorhombic system with eight molecules of **1** and eight THF molecules in the unit cell (two independent molecules of each in the asymmetric unit) [21].

Table 1
Peak potentials and currents from the CV curves of the investigated nickel complexes[a]

Complex	Waves	E_p (V)	I_p (μA)	Number of electrons
$[NiBr_2(bpy)]$	C_1	−1.55	64	2
	A_1	−1.38	41	2
	C_2	−2.28	26	1
	A_2	−2.16	19	1
$[NiBr_2(bpy)]$ + MesBr	C_1	−1.55	63	2
	C_3	−1.80	18	
	A_3	−1.77	16	
	C_4	−2.01	17	
	A_4	−1.90	12	
[NiBr(Mes)(bpy)]	C_3	−1.78	29	1
	A_3	−1.71	19	1

[a] C – cathodic wave (reduction), A – anodic wave (oxidation).

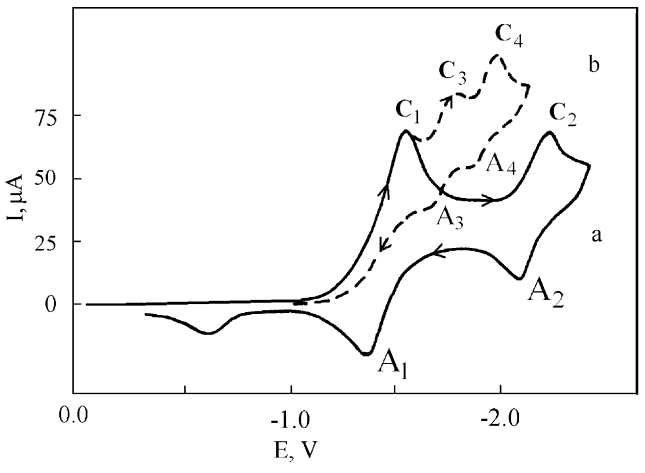

Fig. 1. Cyclic voltammograms in DMF of $[NiBr_2(bpy)]$ (10^{-2} M) in the absence (a) and in the presence (b) of MesBr (2×10^{-2} M) (CV curves were recorded at the first scan: curve a – from 0.00 to −2.40 V and back to 0.00 V; curve b – from 0.00 to −2.15 V and back to 0.00 V).

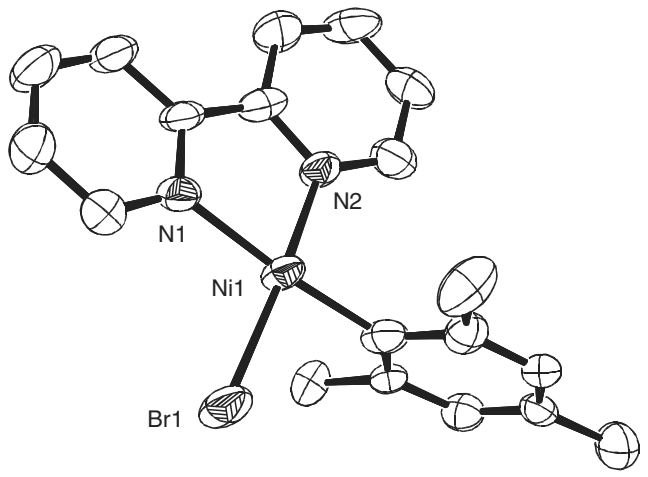

Fig. 2. ORTEP view of the electrochemically synthesized nickel complex **1** (hydrogen atoms are omitted for clarity).

The use of traditional reducing agents to prepare **1** from **2** and MesBr is not feasible, as other products, for example, **3** (Eq. (4)) and the homocoupling product Mes-Mes (Eq. (5)), are invariably formed.

$$[\underset{\mathbf{1}}{\mathrm{NiBr(Mes)(bpy)}}] + [\mathrm{Ni(bpy)}] + \mathrm{MesBr} \longrightarrow [\underset{\mathbf{2}}{\mathrm{NiBr_2(bpy)}}] + [\underset{\mathbf{3}}{\mathrm{Ni(Mes)_2(bpy)}}] \quad (4)$$

$$[\underset{\mathbf{3}}{\mathrm{Ni(Mes)_2(bpy)}}] \longrightarrow [\mathrm{Ni(bpy)}] + \mathrm{Mes\text{-}Mes} \quad (5)$$

Electrolysis of **2** in the presence of an equivalent amount of MesBr at the potential of the working electrode E_p^{Cl} (−1.48 to −1.55 V) is therefore the cleanest and most efficient method of preparing **1** (Eq. (6)).

$$[\underset{\mathbf{2}}{\mathrm{NiBr_2(bpy)}}] + 2e^- \xrightarrow[-2Br^-]{E_p^{Cl}} [\mathrm{Ni(bpy)}] \xrightarrow{\mathrm{MesBr}} [\underset{\mathbf{1}}{\mathrm{NiBr(Mes)(bpy)}}] \quad (6)$$

The σ-aryl complex **1** was also successfully prepared by treating [Ni(bpy)(COD)] [31], prepared in situ from [Ni(COD)$_2$] and bpy, with MesBr in toluene (Eqs. (7) and (8)):

$$[\mathrm{Ni(COD)_2}] + \mathrm{bpy} \longrightarrow [\mathrm{Ni(COD)(bpy)}] + \mathrm{COD} \quad (7)$$

$$[\mathrm{Ni(COD)(bpy)}] + \mathrm{MesBr} \longrightarrow [\mathrm{NiBr(Mes)(bpy)}] + \mathrm{COD} \quad (8)$$

The preparation of Ni^{II} σ-aryl complexes by oxidative addition of aromatic halides to nickel(0) complexes has been studied in detail by Tsou and Kochi [32]. In particular, several σ-organyl Ni^{II} complexes have been synthesized by oxidative addition of organic halides to [Ni(COD)$_2$] in the presence of various ligands, generally phosphines [33], while complexes with bpy, which are generally synthesized from the corresponding Ni^{II} phosphine complexes by ligand-exchange reactions, are less common [34,35].

Complex **1** was examined as catalyst precursor for the oligomerization of ethylene after activation with MAO in toluene at low ethylene pressure (5 bar) at an initial temperature of 25 °C. Under these conditions, **1** generated an active catalyst for the oligomerization of ethylene to even-numbered olefins in the C_4–C_{26} range with a Schulz–Flory distribution [36]. No solid material was obtained. Selected data (average values over three identical runs) are given in Table 2.

Excellent turnover frequencies, close to 10^5 moles of C_2H_4 converted (mol of Ni × h)$^{-1}$, were obtained, whereas no catalytic activity was observed in the absence of MAO. The selectivity for α-olefins was rather modest due to the occurrence of a fast isomerization process, which is typical for Ni^{II} oligomerization catalysts [37]. Increasing the ethylene pressure resulted in an appreciable increase of the selectivity for α-olefins, whereas the α value remained constant (entries 1–3). In a control experiment (entry 4), the oligomerization reaction was carried out in the presence of *n*-undecene, and the oligomeric mixture showed only a small amount of C_{11} internal olefins (<5%), which suggests that chain transfer occurs mainly from an internal olefin hydride nickel species rather than from an α-olefin hydride complex. In a second independent experiment (entry 5), the precatalyst concentration was reduced to one tenth while leaving the MAO concentration unchanged. As a result, an appreciable decrease in the catalytic activity was observed, probably due to a smaller increase in the temperature, and the α value increased slightly. Finally, **1** was replaced by **2** (entry 6). Under comparable experimental conditions, the dibromide precursor was significantly less active (also evidenced by a much less exothermic reaction), but showed a similar selectivity for α-olefins and a slightly higher α value.

The oligomerization of ethylene by **2**/MAO has been previously investigated by Brookhart and coworkers [7]. Scheme 1 shows the mechanisms of oligomerization, propagation, chain transfer and olefin isomerization proposed for a variety of Ni^{II} catalysts containing chelating nitrogen ligands [37]. The results obtained by using **1** as catalyst precursor nicely fit the overall mechanism illustrated in Scheme 1.

Indeed, after MAO has created a free coordination site at nickel, the first ethylene insertion(s) into the Ni-mesityl bond, followed by β-H elimination, would give a [(bpy)-NiH] moiety. The fact that both the activity and the α factor do not change on increasing the ethylene pressure is actually

Table 2
Ethylene oligomerization with **1** and **2**[a]

Run	Catalysis procedure[b]	Precatalyst	Amount (μmol)	MAO (equiv)	Pressure (bar)	$T_{initial}$ (°C)	ΔT (°C)	TOF[c,d] ($\times 10^3$)	α[c,e]	α-Olefin selectivity[c] (%)
1	A	**1**	12	300	5	25	15	82.5	0.36	31
2	A	**1**	12	300	12	24	17	87.3	0.37	39
3	A	**1**	12	300	20	24	19	89.2	0.37	45
4[f]	A	**1**	12	300	5	25	14	73.0	0.38	33
5	B	**1**	1.2	3000	5	24	4	66.2	0.40	38
6	A	**2**	12	300	5	24	8	33.6	0.43	35

[a] Reaction conditions: 100 mL toluene, 15 min.
[b] See Section 4.
[c] Determined by GC (average value C_{14}/C_{16}).
[d] Moles of C_2H_4 converted (mol of Ni × h)$^{-1}$.
[e] Schulz–Flory parameter α = rate of propagation/(rate of propagation + rate of chain transfer) = moles C_{n+2}/moles C_n.
[f] In the presence of 0.01 mol *n*-undecene.

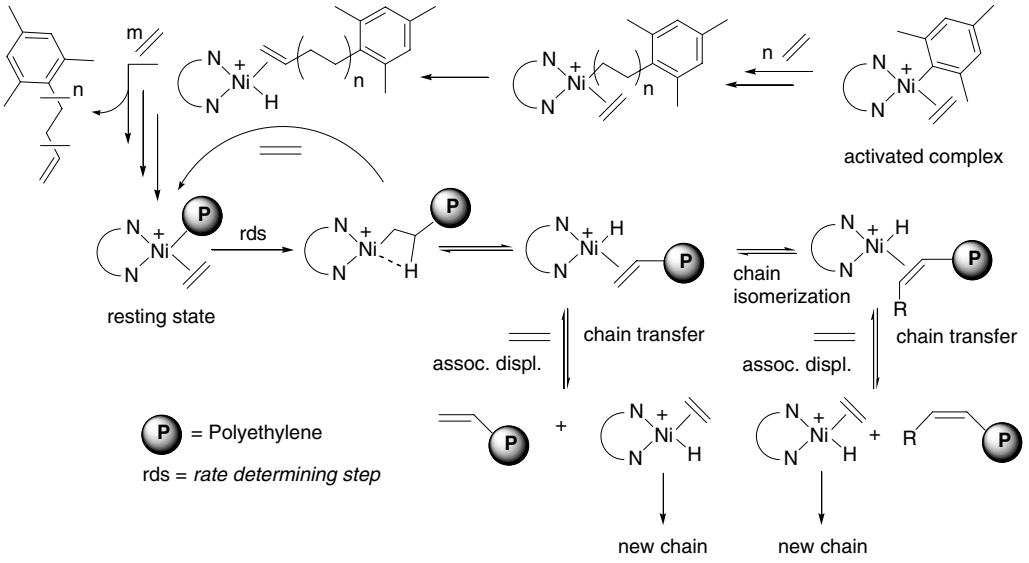

Scheme 1.

consistent with a Ni alkyl resting state, while the increase in α-olefin selectivity with monomer pressure can be explained by chain transfer occurring via an associative displacement. Finally, the absence of isomerization of added *n*-undecene (entry 4) indicates that chain transfer from an internal olefin hydride nickel complex is faster than chain transfer from an α-olefin hydride species [7].

Assuming that **1** and **2** exhibit the same mechanism of ethylene oligomerization, the lower activity of the dibromide complex **2** may be rationalized in terms of the different solubility of the two precursors in toluene. The dibromide complex **2** is much less soluble than the monobromide derivative **1**, and its reaction with MAO is initially heterogeneous. A shorter induction period for **1**, evidenced by a rapid exotherm, may also be caused by the presence of a metal–carbon bond in this precursor, which would favor the insertion of the monomer.

3. Conclusions

We have shown that preparative electrochemistry can be an effective, high-yield, and selective method for the generation of σ-organyl metal complexes. Using the synthetic protocol described in this paper a variety of (N-N)Ni σ-aryl complexes could be prepared and successfully employed in catalytic processes, where they show improved activity as compared to traditional precursors [4–7].

4. Experimental

4.1. General procedures

All manipulations and reactions were carried out under an atmosphere of dry nitrogen. All solvents were purified and dried prior to use. DMF was dried with calcium hydride and purified by distillation. [$NiBr_2$(bpy)] [38], [Ni(COD)$_2$] [39] and [Ni(COD)(bpy)] [31] were synthesized according to the literature procedures; $(NBu_4)BF_4$, bpy, MesBr and a 10% solution of methylalumoxane in toluene were commercial products. The electrolyte $(NBu_4)BF_4$ was dried by melting in vacuum and stored under nitrogen. Cyclic voltammograms were recorded at a glassy carbon electrode (working surface 3.14 mm^2) in a thermostatically controlled (20 °C) three-electrode electrochemical cell under N_2 in the presence of $(NBu_4)BF_4$ (0.1 M). A silver electrode $Ag/AgNO_3$ (0.01 mol L^{-1} solution in CH_3CN) was used as a reference electrode and a platinum wire served as an auxiliary electrode. Curves were recorded at a constant potential scan rate of 50 mV s^{-1}. The preparative electrolyses were carried out at room temperature in galvanostatic regime [potential of the working electrode −1.48 to −1.55 V, ref. $Ag/AgNO_3$ (0.01 mol · L^{-1} solution in CH_3CN)], using an EG&G Princeton Applied Research potentiostat/galvanostat model 273A in an electrochemical cell (three-electrode cell, 40 mL) with separation of anodic and cathodic compartments. Glassy carbon electrode with a surface area of 60 cm^2 was used as a cathode. Nitrogen was bubbled through the stirred electrolyte during the electrolysis. A solution of $(NBu_4)BF_4$ (0.1 M) in DMF was used as electrolyte. The NMR spectra were recorded on Bruker 400 spectrometers. Melting points were measured on Electrothermal IA9000 SERIES Digital Melting Point Apparatus in capillary tubes. The nickel content was determined by atomic absorption spectrometry using a Carl Zeiss AAS1 spectrometer. GC analyses were performed on a Shimadzu GC-17A equipped with a flame ionization detector and a 30 m (0.25 mm i.d., 0.25 mm film thickness) SPB-1 Supelco fused silica capillary column. GC/MS analyses were performed on a Shimadzu QP 5000 apparatus equipped with a column identical with that used for GC analysis. Infrared spectra were recorded on a Perkin–Elmer FT-IR Spectrum BX instrument.

4.2. Electrochemical synthesis of [NiBr(Mes)(bpy)]

A solution for electrolysis was prepared by mixing [$NiBr_2$(bpy)] (0.188 g, 0.5 mmol), MesBr (0.075 mL, 0.5 mmol), and $(NBu_4)BF_4$ (0.987 g, 3.0 mmol) in DMF (30 mL). A constant current of 26.8 mA was passed through the solution for 1 hour. After the electrolysis was completed, the solution was transferred to a flask, the solvent was evaporated in vacuum and the residue was extracted with toluene (three times). Toluene was partly evaporated and decanted to remove residual supporting electrolyte salt. The product was recrystallized from hot toluene; cooling to −20 °C gave 0.18 g (87%) of bright red crystals of **1**; m.p. 148 °C (decomp 186 °C). The compound **1** was dried in vacuum at room temperature prior to the NMR studies. ^{1}H NMR (400 MHz, [D_6]acetone, 25 °C): $\delta = 9.47$ (dd, $^3J(H^6–H^5) = 5.7$ Hz, $^4J(H^6–H^4) = 1.2$ Hz, 1H, H_{bpy}-6), 8.41 (d, $^3J(H^3–H^4) = 7.8$ Hz, 1H, H_{bpy}-3), 8.37 (d, $^3J(H^{3'}–H^{4'}) = 8.1$ Hz, 1H, H_{bpy}-3′), 8.24 (ddd, $^3J(H^4–H^5) = 7.5$ Hz, $^3J(H^4–H^3) = 7.8$ Hz, $^4J(H^4–H^6) = 1.2$ Hz, 1H, H_{bpy}-4), 8.21 (ddd, $^3J(H^{4'}–H^{5'}) = 7.5$ Hz, $^3J(H^{4'}–H^{3'}) = 8.1$ Hz, $^4J(H^{4'}–H^{6'}) = 1.2$ Hz, 1H, H_{bpy}-4′), 7.76 (ddd, $^3J(H^5–H^6) = 5.7$ Hz, $^3J(H^5–H^4) = 7.5$ Hz, $^4J(H^5–H^3) = 1.2$ Hz, 1H, H_{bpy}-5), 7.40 (ddd, $^3J(H^{5'}–H^{6'}) = 5.7$ Hz, $^3J(H^{5'}–H^{4'}) = 7.5$ Hz, $^4J(H^{5'}–H^{3'}) = 1.2$ Hz, 1H, H_{bpy}-5′), 7.26 (dd, 1H, $^3J(H^{6'}–H^{5'}) = 5.7$ Hz, $^3J(H^{6'}–H^{4'}) = 1.2$ Hz, 1H, H_{bpy}-6′), 6.51 (s, 2H, *m*-H in Mes), 3.10 (s, 6H, *o*-CH_3), 2.24 (s, 3H, *p*-CH_3) ppm. ^{13}C NMR (100 MHz, [D_6]acetone, 25 °C): $\delta = 157.6$ (C_{bpy}-2), 154.4 (C_{bpy}-2′), 152.0 (C_{bpy}-6), 151.3 (C_{bpy}-6′), 145.0 (C_{Mes}-1), 142.9 (C_{Mes}-2), 140.8 (C_{bpy}-4), 140.0 (C_{bpy}-4′), 133.0 (C_{Mes}-4), 128.4 (C_{bpy}-3), 127.9 (C_{bpy}-3′), 127.0 (C_{Mes}-3), 123.5 (C_{bpy}-5), 122.8 (C_{bpy}-5′), 26.6 (*o*-CH_3), 21.3 (*p*-CH_3) ppm. IR (KBr): 3103 (w), 3027 (w), 2907 (br, s), 1603 (s), 1515 (s), 1443 (br, s), 1312 (w), 1261 (w), 1241 (w), 1156 (w), 1062 (w), 1029 (s), 877 (w), 846 (s), 800 (w), 767 (s), 650 (w), 637 (w), 563 (w), 418 (w) cm^{-1}. $C_{19}H_{19}BrN_2Ni$ ($M = 413.98$ g mol^{-1}): Calc.: C, 55.12; H, 4.63; N, 6.77. Found: C, 55.37; H, 4.8; N, 6.76.

4.3. Synthesis of [NiBr(Mes)(bpy)] from [Ni(COD)$_2$]

A solution of bpy (0.390 g, 2.5 mmol) in toluene (5 mL) was added to a cooled (−30 °C) suspension of [Ni(COD)$_2$] (0.690 g, 2.5 mmol) in toluene (20 mL). Then, MesBr (3.8 mL, 25.4 mmol) was added to this mixture at −30 °C. The reaction mixture was slowly warmed to room temperature (over 3 h) and stirred at r.t. for 6 h. The resulting solution was filtered, the solvent evaporated in vacuum, and the product extracted from the residue with diethyl ether. Evaporation of diethyl ether gave **1** as a dark red powder (0.76 g, 73%); m.p. 144–146 °C. The NMR data (^{1}H and ^{13}C) were in agreement with those given above.

4.4. Crystal data for 1

Space group $P\bar{1}$, $Z = 2$, $a = 8.689(4)$ Å, $b = 9.292(4)$ Å, $c = 13.053(5)$ Å, $\alpha = 89.000(8)°$, $\beta = 77.600(8)°$, $\gamma = 84.730(8)°$. Data were collected with a Siemens CCD (SMART) diffractometer (ω-scans). Data reduction with SAINT, including SADABS, a program for empirical absorption correction. The structure was solved by direct methods and non-hydrogen atoms were refined anisotropically (SHELX97) with exception of toluene (solvent), which was located disordered on a special position and refined only isotropically. All H atoms were calculated on idealized positions. Pictures were generated with ORTEP for Windows [40]. Due to the small size of the crystal ($0.1 \times 0.06 \times 0.04$ mm^3) the structure parameters are of inferior quality.

4.5. Ethylene oligomerization reactions

A 500 mL stainless steel reactor was heated at 60 °C under vacuum overnight and then cooled to room temperature under a nitrogen atmosphere

Procedure A. The solid precatalyst (12 μmol) was charged into the reactor, which was sealed and placed under vacuum. An oxygen-free toluene solution of MAO (3600 μmol), prepared by adding 100 mL of a solution of MAO (2.37 mL) in toluene (97.63 mL), was then introduced into the reactor by suction. The reaction mixture was stirred at room temperature for a few seconds. The reactor was then pressurized with ethylene to 5 bar and stirred at 1500 rpm.

Procedure B. Oxygen-free toluene (97.63 mL) and a solution of MAO (2.37 mL) were introduced into the reactor. The system was then pressurized with ethylene (5 bar final pressure) and stirred at 1500 rpm for 5 min. In a separate Schlenk flask, the solid precatalyst (12 μmol) was dissolved in oxygen-free toluene (50 mL). The autoclave was slowly depressurized to 1 bar and the precatalyst solution (5 mL) was added by syringe. The system was repressurized to the appropriate pressure and stirred at 1500 rpm.

Irrespective of the procedure, ethylene was continuously fed to maintain the ethylene pressure at the desired value. After 15 min, the reactions were quenched by cooling the system to 10 °C, depressurizing, and then introducing acidic MeOH (2 mL, 5% HCl); a certain amount of pentadecane (C_{15} internal standard) was also injected into the reactor. The reaction mixtures were stirred at 1500 rpm for 10 min. The solutions were analyzed by GC and GC–MS. The mass and the α-olefin content of the C_{12}, C_{14}, and C_{16} fractions were determined by GC using calibration curves with standard solutions. The Schulz–Flory constant α was determined by the molar ratio of the C_{12}, C_{14}, and C_{16} fractions.

5. Supplementary material

CCDC No. 264389 (**1**) contains the supplementary crystallographic data for this paper. These data can be obtained free of charge via www.ccdc.cam.ac.uk/conts/retrieving.html (or from the Cambridge Crystallographic

Data Centre, 12 Union Road, Cambridge CB2 1EZ, UK; fax: +44 1223 336 033; or deposit@ccdc.cam.uk).

Acknowledgements

Two of us thank the *Deutsche Forschungsgemeinschaft* (DFG – D.G.Y., ref. no. 436 RUS 17/53/03) and the *Sächsisches Ministerium für Wissenschaft und Kunst* (SMWK – T.D.I., ref. no. 4-7531.50-04-0361-03/21) for financial support of their stay in Leipzig, Germany. Financial support from the *Research and Educational Center of the Kazan State University – REC 007* (Y1-C-07-06), *Tatarstan Academy of Science* (07-7.1-291) and *European Community* (NANOHYBRID STREP project No. 516972) is gratefully acknowledged.

References

[1] Technology Vision 2020, The US Chemical Industry, American Chemical Society, Washington, 1996, p. 75.
[2] J.J. Eisch, S.R. Sexsmith, Res. Chem. Intermed. 13 (1990) 149.
[3] J.-Y. Nedelec, J. Perichon, M. Troupel, Organic electroreductive coupling reactions using transition metal complexes as catalysts, in: E. Steckhan (Ed.), Topics in Current Chemistry, vol. 185, Springer-Verlag, Berlin, Heidelberg, 1997, p. 141.
[4] Yu.H. Budnikova, J. Perichon, D.G. Yakhvarov, Yu.M. Kargin, O.G. Sinyashin, J. Organomet. Chem. 630 (2001) 185.
[5] D.G. Yakhvarov, Yu.G. Budnikova, O.G. Sinyashin, Elektrokhimiya 39 (2003) 1407.
[6] D.G. Yakhvarov, Yu.G. Budnikova, O.G. Sinyashin, Russ. J. Electrochem. 39 (2003) 1261.
[7] (a) C.M. Kilian, L.K. Johnson, M. Brookhart, Organometallics 16 (1997) 2005;
(b) M.D. Leatherman, S.A. Svejda, L.K. Johnson, M. Brookhart, J. Am. Chem. Soc. 125 (2003) 3068.
[8] C.M. Kilian, D.J. Tempel, L.K. Johnson, M. Brookhart, J. Am. Chem. Soc. 118 (1996) 11664.
[9] L.K. Johnson, C.M. Kilian, M. Brookhart, J. Am. Chem. Soc. 117 (1995) 6414.
[10] C. Wang, S. Friedrich, T.R. Younkin, R.T. Li, R.H. Grubbs, D.A. Bansleben, M.W. Day, Organometallics 17 (1998) 3149.
[11] A. Held, F.M. Bauers, S. Mecking, J. Chem. Soc., Chem. Commun. (2000) 301.
[12] C. Geyer, S. Schindler, Organometallics 17 (1998) 4400.
[13] P.T. Matsanuga, J.C. Mavrapoulos, C.R. Hess, G.L. Hillhouse, Polyhedron 14 (1995) 175.
[14] P.T. Matsanuga, C.R. Hess, G.L. Hillhouse, J. Am. Chem. Soc. 116 (1994) 3665.
[15] P.T. Matsanuga, G.L. Hillhouse, A.L. Rheingold, J. Am. Chem. Soc. 115 (1993) 2075.
[16] G. Wilke, G. Hermann, Angew. Chem. Int. Ed. Engl. 5 (1966) 581; Angew. Chem. 78 (1966) 591.
[17] J. Chatt, B.L. Shaw, J. Chem. Soc. 4 (1960) 1718.
[18] W. Siedel, Z. Chem. 25 (1985) 411.
[19] J.M. Coronas, G. Muller, M. Rocamora, C. Miravitlles, X. Solans, J. Chem. Soc., Dalton Trans. (1985) 2333.
[20] A. Klein, Z. Anorg. Allg. Chem. 627 (2001) 645.
[21] M.P. Feth, A. Klein, H. Bertagnolli, Eur. J. Inorg. Chem. (2003) 839.
[22] D.G. Yakhvarov, E.G. Samieva, D.I. Tazeev, Yu.G. Budnikova, Izv. Akad. Nauk., Ser. Khim. 51 (2002) 734.
[23] D.G. Yakhvarov, E.G. Samieva, D.I. Tazeev, Yu.G. Budnikova, Russ. Chem. Bull. 51 (2002) 796.
[24] D.G. Yakhvarov, Yu.H. Budnikova, O.G. Sinyashin, Izv. Akad. Nauk., Ser. Khim. 52 (2003) 545.
[25] D.G. Yakhvarov, Yu.H. Budnikova, O.G. Sinyashin, Russ. Chem. Bull. 52 (2003) 567.
[26] D.R. Fahey, B.A. Baldwin, Inorg. Chim. Acta 36 (1979) 269.
[27] M. Cusumano, V. Ricevuto, J. Chem. Soc., Dalton Trans. (1978) 1682.
[28] J.R. Moss, B.L. Shaw, J. Chem. Soc. A (1966) 1793.
[29] Yu.G. Budnikova, D.G. Yakhvarov, V.I. Morozov, Yu.M. Kargin, A.V. Il'yasov, Yu.N. Vyakhireva, O.G. Sinyashin, Zh. Obshch. Khim. 72 (2002) 184.
[30] Yu.G. Budnikova, D.G. Yakhvarov, V.I. Morozov, Yu.M. Kargin, A.V. Il'yasov, Yu.N. Vyakhireva, O.G. Sinyashin, Russ. J. General Chem. 72 (2002) 168.
[31] E. Dinjus, I. Gorski, E. Uhlig, H. Walther, Z. Anorg. Allg. Chem. 422 (1976) 75.
[32] T.T. Tsou, J.K. Kochi, J. Am. Chem. Soc. 101 (1979) 6319.
[33] (a) See for example: J.S. Brown, P.R. Sharp, Organometallics 22 (2003) 3604;
(b) M.I. Sladek, T. Braun, B. Neumann, H.-G. Stammler, New J. Chem. 27 (2003) 313;
(c) Y.-J. Kim, R. Sato, T. Maruyama, K. Osakada, T. Yamamoto, J. Chem. Soc., Dalton Trans. (1994) 943;
(d) J. Campora, E. Gutierrez, M.L. Poveda, C. Ruiz, E. Carmona, J. Chem. Soc., Dalton Trans. (1992) 1769;
(e) J. Campora, E. Carmona, E. Gutierrez, P. Palma, M.L. Poveda, C. Ruiz, Organometallics 11 (1992) 11.
[34] E. Wenschuh, R. Zimmering, Z. Chem. 27 (1987) 448.
[35] W. Seidel, L. Raupach, Z. Chem. 28 (1988) 414.
[36] (a) B.L. Small, M. Brookhart, A.M. Bennett, J. Am. Chem. Soc. 120 (1998) 4049;
(b) G.J.P. Britovsek, M. Bruce, V.C. Gibson, B.S. Kimberley, P.J. Maddox, S. Mastroianni, S.J. McTavish, C. Redshaw, G.A. Solan, S. Stromberg, A.J.P. White, D.J. Williams, J. Am. Chem. Soc. 121 (1999) 8728;
(c) B.L. Small, M. Brookhart, J. Am. Chem. Soc. 120 (1998) 7143;
(d) G.J.P. Britovsek, S. Mastroianni, G.A. Solan, S.P.D. Baugh, C. Redshaw, V.C. Gibson, A.J.P. White, D.J. Williams, M.R.J. Elsegood, Chem. Eur. J. 6 (2000) 2221;
(e) Y. Chen, R. Chen, C. Qian, X. Dong, J. Sun, Organometallics 22 (2003) 4312;
(f) M.E. Bluhm, C. Folli, M. Doring, J. Mol. Catal. A 212 (2004) 13;
(g) Y. Chen, C. Qian, J. Sun, Organometallics 22 (2003) 1231.
[37] (a) S.D. Ittel, L.K. Johnson, M. Brookhart, Chem. Rev. 100 (2000) 1169;
(b) B.C. Gibson, S.K. Spitzmesser, Chem. Rev. 103 (2003) 283;
(c) B. Rieger, L.S. Baugh, S. Kacker, S. Striegler, Late Transition Metal Polymerization Catalysis, Wiley-VCH, 2003, p. 331.
[38] M. Troupel, Y. Rollin, O. Sock, G. Meyer, J. Perichon, Nov. J. Chim. 10 (1986) 593.
[39] D.J. Krysan, P.B. Mackenzie, J. Org. Chem. 55 (1990) 4229.
[40] (a) SMART: Area-Detector Software Package, Siemens Industrial Automation, Inc., Madison, WI, 1993.;
(b) SAINT: Area-Detector Integration Software. Version 6.01, Siemens Industrial Automation, Inc., Madison, WI, 1999.;
(c) G.M. Sheldrick, SADABS, Program for Scaling, Correction of Area-detector Data, Göttingen, 1997;
(d) SHELX97 [Includes SHELXS97, SHELXL97]: G.M. Sheldrick, SHELX97. Programs for Crystal Structure Analysis (Release 97-2), University of Göttingen, Germany, 1997;
(e) ORTEP3 for Windows:L.J. Farrugia, J. Appl. Crystallogr. 30 (1997) 565.

[6]. In such hybrid systems, it has been found that the crystal packing pattern and charge state of the organic cations greatly depend on the combination of the organic cation and complex anions, resulting in a remarkable influence on the magnetic interaction between the anionic transition metal complexes via the organic cations [7,8]. Consequently, it is still a challenge for chemists to construct dual-property materials, seeking to establish for instance a coupling between the conduction electrons and the magnetic spin moments.

Therefore, intense investigations are devoted to the chemical modification of the donor atoms (S) of tetrathiafulvalene (TTF) series [9,10] or the attachment of functional groups to the core of the donor framework [11–18] for an enhancement of the intermolecular interactions among electron donors and acceptors (or counter anions) which is essential to stabilize the conducting and superconducting states (suppressing the Peierls distortions) at low temperature. Moreover, it is well known that cyano groups are able to engage in weak intermolecular interactions such as hydrogen bonding and halogen bonding with halogenated anions. In this context, a new organic donor tetracyanodibenzotetrathiafulvalene (TCN-DBTTF) has now been synthesized via triethyl phosphite mediated coupling reaction of 5,6-dicyanobenzene-1,3-dithiole-2-one; the synthesis of the latter has been published in Ref. [19].

In this paper, we describe the synthesis of the donor molecule TCN-DBTTF and also the crystal structure, electrical and magnetic properties of its charge transfer salt (TCN-DBTTF)[Fe(H_2O)$_6$][$FeBr_4$]$_3$ (**1**).

2. Experimental

2.1. Materials and equipments

Unless stated otherwise, all chemicals were purchased from commercial sources and used as received. Infrared spectra were obtained on a Perkin–Elmer SYSTEM 2000 FT-IR spectrometer. ^{1}H NMR (300 MHz) spectra were recorded on a Bruker AC-300 NMR spectrometer using TMS as an internal standard. Mass spectra were measured on an AutoSpec Q MS spectrometer. Elemental analyses were performed on a Carlo-Erba-1106 instrument. Tetraethylammonium iron(III) tetrabromide (TEA · $FeBr_4$) was prepared as described in the literature [6].

2.2. Synthesis of TCN-DBTTF

The compound 5,6-dicyanobenzene-1,3-dithiole-2-one (1 g, 4.6 mmol) was suspended in the mixture of triethyl phosphite (10 ml) and toluene (10 ml). The mixture was heated up to 120 °C under argon atmosphere and stirred for 3 h. During the reaction, a red precipitate was formed. After cooling to room temperature, 20 ml of methanol was added to the reaction mixture to complete precipitation. The product was isolated by filtration as a red powder and washed with methanol (0.74 g, 80%): m.p. >250 °C; EI-MS: 404(M^+); ^{1}H NMR (300 MHz, DMSO-d_6): $\delta = 8.33$ (s, 2H); IR (KBr, cm^{-1}): $\nu = 2232$ (s), 1566 (w), 1354 (s), 1218 (m), 891 (w). *Anal.* Calc. for $C_{18}H_4N_4S_4$: C, 53.40; H, 1.00; N, 13.80. Found: C, 53.10; H, 0.80; N, 13.60%.

2.3. Synthesis of (TCN-DBTTF)[Fe(H_2O)$_6$][$FeBr_4$]$_3$ (1)

In a two-compartment H-shaped cell, single crystals of **1** were grown by electrochemical oxidation in CH_2Cl_2 in the presence of TCN-DBTTF and TEA · $FeBr_4$ under a constant current of 1.5 μA with Pt electrodes. The anodic and cathodic chambers are separated by a porous frit. Brown block-shaped crystals were observed on the bottom of the anodic chamber after 20 days. The crystals were collected and washed with CH_2Cl_2. IR (KBr cm^{-1}): 2244 (m), 1616 (m), 1359 (w), 1222 (w), 892 (m). *Anal.* Calc. for $C_{18}H_{16}Br_{12}Fe_4N_4O_6S_4$: C, 12.80; H, 0.95; N, 3.30. Found: C, 13.07; H, 0.97; N, 3.16%.

2.4. Crystallography

A brown crystal of **1** was mounted on a Stoe Mark II-Imaging Plate Diffractometer System (Stoe & Cie, 2002) equipped with a graphite-monochromator. Data collection was performed at −120 °C using Mo Kα radiation ($\lambda = 0.71073$ Å). One hundred and ninety-seven exposures (3 min per exposure) were obtained at an image plate distance of 100 mm, 180 frames with $\varphi = 0°$ and $0 < \omega < 180°$, and 17 frames with $\varphi = 90°$ and $0 < \omega < 17°$, with the crystal oscillating through 1.5° in ω. The resolution was D_{min}–D_{max}: 17.78–0.72 Å. The structure was solved

Table 1
Crystallographic data for **1**

	1
Molecular formula	$C_{18}H_{16}Br_{12}Fe_4N_4O_6S_4$
Molecular weight	1694.91
Crystal dimensions (mm^3)	0.20 × 0.167 × 0.10
Temperature (K)	153(2)
Crystal system	monoclinic
Space group	*C2/c*
Unit cell dimensions	
a (Å)	35.759(3)
b (Å)	9.9966(6)
c (Å)	12.1129(10)
β (°)	98.350(7)
V (Å^3)	4284.1(6)
Z	4
Density calculated (g cm^{-3})	2.628
Absorption coefficient (mm^{-1})	12.752
R_{int}	0.0854
Measured reflections	22492
Independent reflections	5952
Reflections with $I > 2\sigma(I)$	3968
R_1 (observed data)	0.0620
wR_2 (all data)	0.1492
GOF	1.008

Table 2
Selected bond lengths (Å) and bond angles (°) for **1**

Bond lengths (Å)					
S(1)–C(1)	1.721(8)	S(1)–C(2)	1.744(7)	S(2)–C(1)	1.718(7)
S(2)–C(3)	1.743(8)	C(2)–C(3)	1.391(9)	C(8)–N(1)	1.140(10)
C(9)–N(2)	1.137(11)	C(1)–C(1)^{i}	1.381(15)	C(5)–C(8)	1.435(10)
Fe(1)–Br(1)	2.3283(11)	Fe(1)–Br(2)	2.3340(12)	Fe(1)–Br(1)^{ii}	2.3283(11)
Fe(1)–Br(2)^{ii}	2.3340(12)	Fe(2)–Br(3)	2.3648(14)	Fe(2)–Br(4)	2.3281(13)
Fe(2)–Br(5)	2.3316(14)	Fe(2)–Br(6)	2.3082(14)	Fe(3)–O(3)	2.089(5)
Fe(3)–O(3)^{iii}	2.089(5)	Fe(3)–O(2B)	2.09(2)	Fe(3)–O(2B)^{iii}	2.09(2)
Fe(3)–O(1B)	2.14(13)	Fe(3)–O(1A)	2.139(9)	Fe(3)–O(2A)	2.106(9)
Bond angles (°)					
S(1)–C(1)–S(2)	116.6(4)	C(1)–S(1)–C(2)	95.9(3)	C(1)–S(2)–C(3)	95.2(3)
C(4)–C(5)–C(8)	121.4(6)	C(7)–C(6)–C(9)	120.5(6)	C(5)–C(8)–N(1)	177.7(10)
C(6)–C(9)–N(2)	178.1(8)				

Symmetry transformations used to generate equivalent atoms: i, $-x+2$, $-y+1$, $-z$; ii, $-x+2$, y, $-z+1/2$; iii, $-x+5/2$, $-y-1/2$, $-z$.

by direct methods using the program SHELXS-97 [20] and refined by full matrix least squares on F^2 with SHELXL97 [21]. The hydrogen atoms were included in calculated positions and treated as riding atoms using SHELXL-97 default parameters. All non-hydrogen atoms were refined anisotropically. Four of the six water molecules in the $[Fe(H_2O)_6]^{2+}$ cation were disordered over two positions and refined with half occupations; no H-atoms were found for the water molecules in reasonable positions. A semi-empirical absorption correction was applied using MULABS (PLATON03 [22], $T_{min} = 0.146$, $T_{max} = 0.266$).

Crystallographic data of **1** are collected in Table 1. Selected bond lengths and angles are given in Table 2.

2.5. Physical measurements

Magnetic susceptibility data of a crystalline sample of **1** were collected on a MPMS Quantum Design SQUID magnetometer (XL-5) in the temperature range of 300–1.8 K at a field of 1000 G. The sample was wrapped in a saran bag and put into a straw, which served as sample holder. The molar magnetic susceptibility has been corrected for the diamagnetic contributions of the sample holder and of the sample, the latter is calculated from Pascal's constants.

3. Results and discussion

3.1. Structure of (TCN-DBTTF)[Fe(H$_2$O)$_6$][FeBr$_4$]$_3$ (1)

The compound crystallizes in a monoclinic space group ($C2/c$) and an ORTEP plot of the molecular structure with the atomic numbering scheme is shown in Fig. 1. The unit cell contains four oxidized TCN-DBTTF molecules, four $[Fe(H_2O)_6]^{2+}$ cations and 12 $[FeBr_4]^-$ anions.

In the crystal structure, the donor molecule shows approximate D_{2h} symmetry, whereby only a center of inversion at the midpoint of the C(1)=C(1b) bond is imposed by the exact space group symmetry. The TCN-DBTTF molecule is nearly planar (the dihedral angle between the benzene ring and the central TTF plane is 1.5°), and the four peripheral cyano groups lie also in the plane of the dibenzotetrathiafulvalene skeleton, which is quite similar to other dibenzotetrathiafulvalene derivatives [23]. One $[FeBr_4]^-$ anion (Fe(1)) is located on a site with a twofold rotation axis and one $[FeBr_4]^-$ anion (Fe(2)) lies on a general position. The Fe–Br bond lengths of the $[FeBr_4]^-$ anions, 2.3283(11)–2.3340(12) Å for Fe(1) and 2.3082(14)–2.3648(14) Å for Fe(2), are similar to other $[FeBr_4]^-$ salts [24]. The Fe(3) center of the $[Fe(H_2O)_6]^{2+}$ cation lies on an inversion center. Four of the six water molecules of the $[Fe(H_2O)_6]^{2+}$ cations are disordered over two positions and refined with half occupations and the Fe–O bond lengths of $[Fe(H_2O)_6]^{2+}$ are in the range of range of 2.089–2.14 Å.

Importantly, the bond lengths of the central C=C bond, the C–S bonds near the molecular center and the outer C=C bonds within the TTF molecule are related to the degree of ionicity of the donor molecule. The central C=C bond length of TCN-DBTTF moiety of **1** is 1.381(15) Å. Thus, it can be inferred that the TCN-DBTTF moiety in **1** is essentially fully oxidized according to the correlation between the oxidation states of TTF derivatives and bond lengths of central C=C bonds [25], which is fully in accordance with the stoichiometry of **1**.

In the crystal lattice of **1** (Fig. 2), the donor molecules are arranged in layers parallel to the *bc* plane. Along the *c*-axis, the direction of the molecular planes of two adjacent TCN-DBTTF molecules alternate with a dihedral angle of 77.4°. They are separated from each other by tetrahedral $[FeBr_4]^-$ anions; no specific CN···Br short contacts can be identified. However, weak intermolecular interactions of S···Br [3.566–3.741 Å], Br···C [3.487–3.533 Å] and Br···Br [3.651–3.871 Å] as well as hydrogen bonds C–H···Br [C···Br 3.742 Å; C–H···Br 178°] are observed. Along the *b*-direction, the donor molecules are parallel and coplanar to each other forming a columnar arrangement with S···S distances of 10 Å. In addition, $[Fe(H_2O)_6]^{2+}$ cations are located in-between the donor

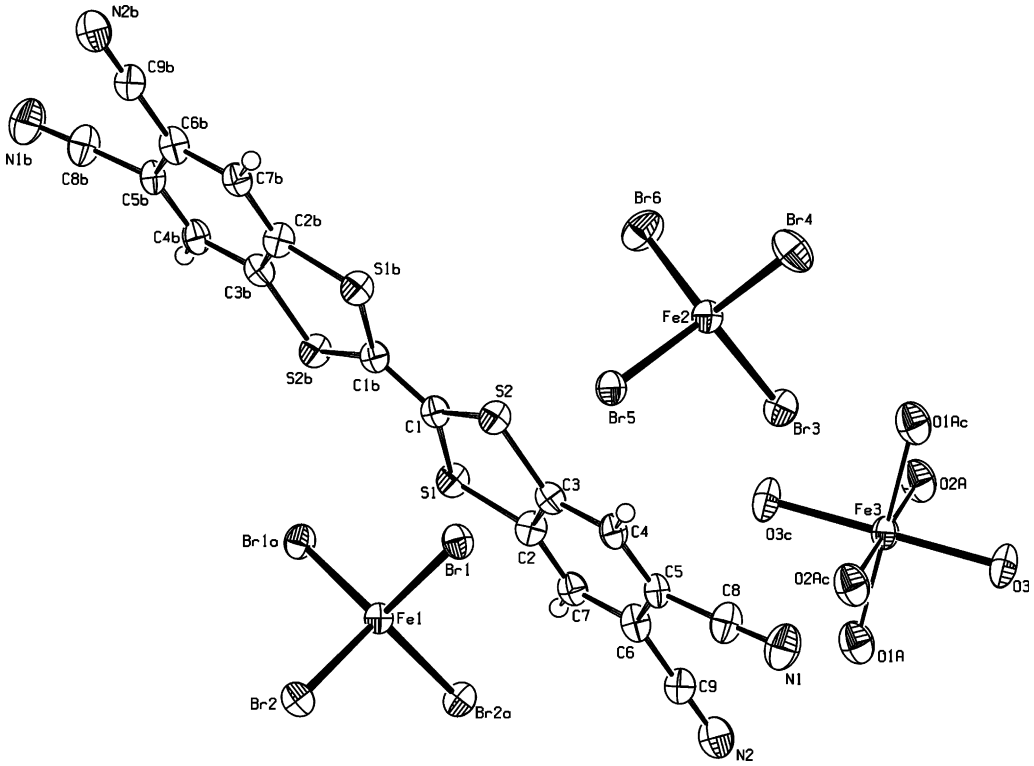

Fig. 1. ORTEP plot (50% probability ellipsoids) of **1**.

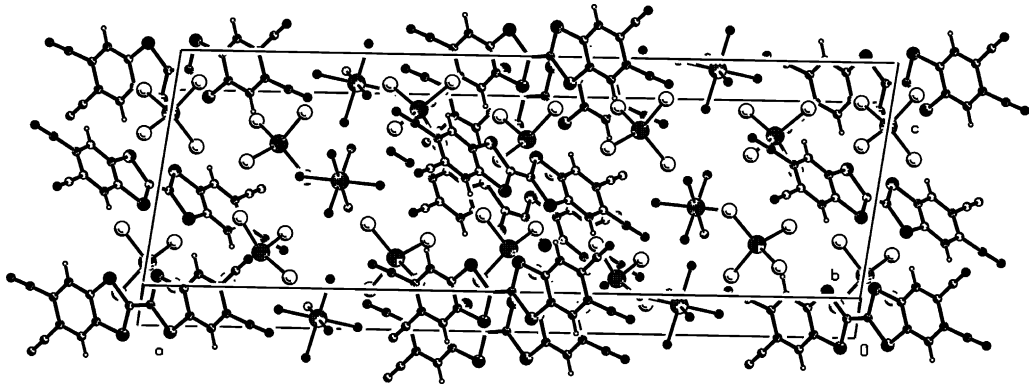

Fig. 2. Projection of the crystal structure of **1**. Hydrogen atoms are omitted for clarity.

molecule assemblies and there are CN···O [2.881–3.025 Å] and O···Br [3.316 Å] short contacts.

3.2. Electrical conductivity

The compound **1** shows a low electrical conductivity with a room temperature value $\sigma = 4.3 \times 10^{-7}$ S cm^{-1}. This observation corresponds to its structural feature of the crystal packing which does not show any specifically close stacking arrangements of the donor and acceptor units.

3.3. Magnetic properties

The compound **1** is composed of three types of paramagnetic spin carriers: oxidized TCN-DBTTF radicals ($S = 1/2$), $[Fe(H_2O)_6]^{2+}$ cations ($S = 2$) and $[FeBr_4]^-$ anions ($S = 5/2$), the latter ones are located on two crystallographically different sites. The thermal dependence of the magnetic susceptibility of **1** is shown in form of a $\chi_M T$ versus T plot (Fig. 3). The calculated $\chi_M T$ value is 17.9 emu K/mol per stoichiometric formula unit, with g (rad) = 2; g (Fe^{2+}) = 2.2 which is typical for HS Fe^{2+}; g (Fe^{3+}) = 2.06 [16]. This $\chi_M T$ value compares fairly well with the experimental $\chi_M T$ value at room temperature of 16.9 emu K/mol. With decreasing temperature, the $\chi_M T$ values decrease continuously, indicating overall antiferromagnetic interactions among these different paramagnetic centers. Clearly, the whole crystal structure is rather complex so that many different magnetic exchange pathways, extended in all three directions, are present. This situation

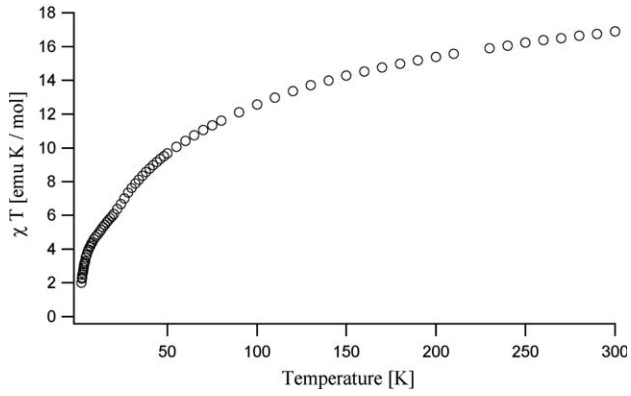

Fig. 3. Temperature dependence of $\chi_M T$ for compound **1**.

renders a meaningful analysis with the assignment of specific exchange coupling parameters as impossible. Additionally, there is no signature of a magnetically ordered phase down to 1.8 K.

4. Conclusions

A charge transfer salt (TCN-DBTTF)$[Fe(H_2O)_6][FeBr_4]_3$ (**1**) based on the new donor TCN-DBTTF was synthesized by electrocrystallization. In the crystal lattice, intermolecular CN···O interactions are observed rather than otherwise favorable CN···Br interactions. As a result of the specific crystal packing, the compound shows a low electrical conductivity in the order of 10^{-7} S cm^{-1} and the magnetic measurements exhibit overall antiferromagnetic exchange interactions among the three different spin carriers.

Acknowledgments

This work was supported by the Swiss National Science Foundation (Grant No. 200020-107589) as well as by the ESF Programme – SONS (NANOSYN).

Appendix A. Supplementary data

Crystallographic data for the structure reported in this paper have been deposited with the Cambridge Crystallographic Data Centre, CCDC No. 271519 for **1**. Copies of the data can be obtained free of charge on application to CCDC, 12 Union Road, Cambridge CB2 1EZ, UK (fax: +44 1223 336033; e-mail: deposit@ccdc.cam.ac.uk or on the web www: http//www.ccdc.cam.ac.uk). Supplementary data associated with this article can be found, in the online version, at doi:10.1016/j.poly.2005.10.037.

References

[1] J.M. Williams, J.R. Ferraro, R.J. Thorn, K.D. Carlson, U. Geiser, H.H. Wang, A.M. Kini, M.-H. Whangbo, Organic Superconductors (Including Fullerenes), Prentice Hall, Englewood Cliffs, 1992.
[2] E. Coronado, P. Day, Chem. Rev. 104 (2004) 5419.
[3] T. Enoki, A. Miyazaki, Chem. Rev. 104 (2004) 5449.
[4] L. Ouahab, T. Enoki, Eur. J. Inorg. Chem. (2004) 933, and references therein.
[5] A.W. Graham, M. Kurmoo, P. Day, J. Chem. Soc., Chem. Commun. (1995) 2061.
[6] H. Fujiwara, E. Fujiwara, Y. Nakazawa, B.Zh. Narymbetov, K. Kato, H. Kobayashi, M. Tokumoto, P. Cassoux, A. Kobayashi, J. Am. Chem. Soc. 123 (2001) 306.
[7] E. Fujiwara, H. Fujiwara, H. Kobayashi, T. Otsuka, A. Kobayashi, Adv. Mater. 14 (2002) 1376.
[8] M. Katsuhara, M. Aragaki, T. Mori, Y. Misaki, K. Tanaka, Chem. Mater. 12 (2000) 3186.
[9] D. Jérome, A. Mazaud, M. Ribault, K. Bechgaard, J. Phys. Lett. (France) 41 (1980) 95.
[10] D. Jérome, Science 252 (1991) 1509.
[11] S.-X. Liu, S. Dolder, M. Pilkington, S. Decurtins, J. Org. Chem. 67 (2002) 3160.
[12] C.Y. Jia, D.Q. Zhang, Y. Xu, W. Xu, H.M. Hu, D.B. Zhu, Synth. Met. 132 (2003) 249.
[13] A. Dolbecq, A. Guirauden, M. Fourmigué, K. Boubekeur, P. Batail, M.-M. Rohmer, M. Bénard, C. Coulon, M. Sallé, P. Blanchard, J. Chem. Soc., Dalton Trans. (1999) 1241.
[14] A.S. Batsanov, A.J. Moore, N. Roberston, A. Green, M.R. Bryce, J.A.K. Howard, A.E. Underhill, J. Mater. Chem. 7 (1997) 387.
[15] B. Domercq, T. Devic, M. Fourmigué, P. Auban-Senzier, E. Canadell, J. Mater. Chem. 11 (2001) 1570.
[16] T. Devic, J.N. Bertran, B. Domercq, E. Canadell, N. Avarvari, P. Auban-Senzier, M. Fourmigue, New J. Chem. 25 (2001) 1418.
[17] G. Cooke, A.K. Powell, S.L. Heath, Synthesis 11 (1995) 1411.
[18] N. Terkia-Derdra, R. Andreu, M. Sallé, E. Levillain, J. Orduna, J. Garín, E. Ortí, R. Viruela, R. Pou-Amérigo, B. Sahraoui, A. Gorgues, J.-F. Favard, A. Riou, Chem. Eur. J. 6 (2000) 1199.
[19] C. Loosli, C.Y. Jia, S.-X. Liu, M. Haas, M. Dias, E. Levillain, A. Neels, H.S. Evans, A. Hauser, S. Decurtins, J. Org. Chem. 70 (2005) 4988.
[20] G.M. Sheldrick, Acta Crystallogr., Sect. A 46 (1990) 467.
[21] G.M. Sheldrick, SHELXL-97, Program for Crystal Structure Refinement, University of Göttingen, Germany, 1997.
[22] A.L. Spek, J. Appl. Cryst. 36 (2003) 7.
[23] T. Inayoshi, I. Ono, Synth. Met. 110 (2000) 153.
[24] T. Mallah, C. Hollis, S. Bott, M. Kurmoo, P. Day, M. Allan, R.H. Friend, J. Chem. Soc., Dalton Trans. (1990) 859.
[25] M.B. Inoue, M. Inoue, M.A. Bruck, Q. Fernando, J. Chem. Soc., Chem. Commun. (1992) 515.

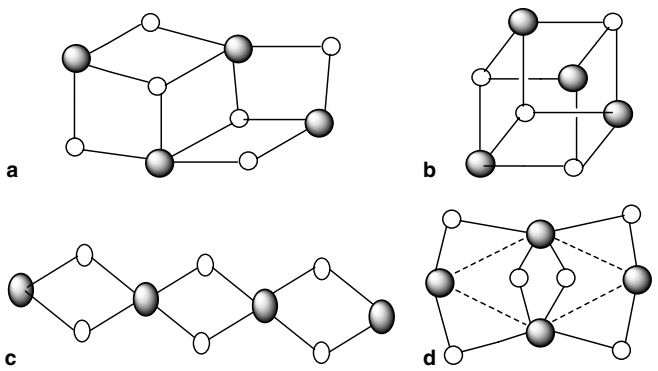

Scheme 1. (a) Dicubane-like; (b) cubane-like; (c) string; (d) rhomb-like.

of our knowledge, only one case doubly acetato-bridged dicubane Cu(II) complex with dpd-H has ever been documented, which is octanuclear [12].

2. Experimental

Caution: Perchlorate complexes of metal ions are potentially explosive. Only a small amount of material should be prepared and it should be handled with caution.

2.1. Synthesis

All chemicals were used as purchased with reagent grade. Infrared spectra were recorded on a Nicolet magna 750 FT-IR spectrophotometer using KBr pellets in the range of 400–4000 cm^{-1}. Elemental analyses were performed by the elemental analysis laboratories in our institute. UV–Vis spectra measurements were made at room temperature range from 330 to 1100 nm with Perkin–Elmer Lambda-35 UV/VIS spectrophotometer. Magnetic measurements for **1** were carried out on a PPMS60000 magnetometer.

2.1.1. [{Cu_4(dpd-H)$_4$(ClO_4)$_2$(H_2O)$_2$}(ClO_4)$_2$ · $2H_2O$] (*1*)

A 20 ml MeOH/H_2O solution (1:1, v/v) of $Cu(ClO_4)_2 \cdot 6H_2O$ (0.74 g, 2 mmol), di-2-pyridylketone (0.1843 g, 1 mmol) and 3-amino-1,2-propanediol (0.0936 g, 1 mmol) was refluxed for 1 h with stirred. The blue solution was left at ambient temperature for several days to obtain blue crystals. Yield: 34.2% (0.52 g) (based on dpk) (*Anal.* Calc. for $C_{44}H_{44}Cl_4Cu_4N_8O_{28}$: C, 34.57; H, 2.90; N 7.33. Found: C, 34.20; H, 3.07; N 7.25%). IR (KBr pellet, cm^{-1}): ν(OH) 3435, ν(C–O) 1607,ν(C=N, C=C) 1476, 1446, 1385, $\nu(ClO_4^-)$ 1084, 623.

2.1.2. [{Ni_4(dpd-H)$_4$(H_2O)$_4$}(ClO_4)$_4$ · $4H_2O$] (*2*)

Green crystals of **2** were obtained with the similar procedure to that of **1** except for the replacement of $Cu(ClO_4)_2 \cdot 6H_2O$ with $Ni(ClO_4)_2 \cdot 6H_2O$. Yield: 39.0% (0.61 g) (based on dpk) (*Anal.* Calc. for $C_{44}H_{52}Cl_4N_8Ni_4O_{32}$: C, 33.42; H, 3.31; N, 7.09. Found: C, 33.76; H, 3.32; N, 7.01%). IR (KBr pellet, cm^{-1}): ν(OH) 3434, ν(C–O) 1608, ν(C=N, C=C) 1475, 1443, 1384, $\nu(ClO_4^-)$ 1087, 626.

2.1.3. [{Ni_4(dpd-H)$_4$(OAc)$_2$(H_2O)$_2$}(ClO_4)$_2$] (*3*)

A 20 ml methanol solution of $Ni(OAc)_2 \cdot 4H_2O$ (0.4980 g, 2 mmol) and di-2-pyridylketone (0.1846 g, 1 mmol) was refluxed for 1 h with stirred. After cooled, $NaClO_4 \cdot H_2O$ (0.42 g, 3 mmol) was added. And the green solution was left at ambient temperature for several days to obtain green block crystals. Yield: 46.9% (0.65 g) (based on dpk) (*Anal.* Calc. for $C_{48}H_{46}Cl_2N_8Ni_4O_{22}$: C,41.40; H, 3.33; N, 8.05. Found: C, 41.03; H, 3.34; N, 7.92%) IR (KBr pellet, cm^{-1}): ν(OH) 3436, ν(C–O) 1605, $\nu(COO^-)$ 1573, 1337, ν(C=N, C=C) 1473, 1442, 1385, $\nu(ClO_4^-)$ 1089, 624.

2.2. X-ray crystallography

X-ray single crystal data were collected at 130.15 K (for **1**) and 293(2) K (for **3**) on a MERCURY-CCD area-detector diffractometer, and at 293(2) K on a Simens SMART-CCD area-detector diffractometer (for **2**) with Mo Kα radiation ($\lambda = 0.71073$ Å). Data reductions and absorption corrections of **1** and**3** were made with Multi-scan type, while those of **2** were performed with SMART and SADABS software. These structures were solved by direct methods and were refined by full matrix least-squares methods using SHELXL-97 [13]. Anisotropic displacement parameters were refined for all non-hydrogen atoms. And hydrogen atoms were added in the riding model and not refined. The crystal data and refinement details for the three complexes are listed in Table 1. Selected bond distances and bond angles are listed in Tables S1–3 (supplementary).

3. Results and discussion

3.1. Synthesis

Our previous attempt to prepare **1** and **2** without the use of 3-amino-1,2-propandiol was unsuccessful, and mononuclear Cu(II) and Ni(II) complexes [14,15] were obtained. Hence we infer that 3-amino-1,2-propandiol may act as a buffer in the course of the present reaction.

3.2. Description of the crystal structure of the complex *1*

The complex **1** is made up of the cation $[Cu_4(dpd\text{-}H)_4(ClO_4)_2(H_2O)_2]^{2+}$ (Fig. 1), two isolated ClO_4^- and two free H_2O. Within each $[Cu_4(dpd\text{-}H)_4(ClO_4)_2(H_2O)_2]^{2+}$, the cubane-like Cu_4O_4 core is dominated, constructed by four copper atoms and four oxygen atoms from four dpd-H ligands each at alternating corners. Four Cu(II) atoms are not crystallographically equivalent but all in distorted $[CuN_2O_4]$ octahedral geometries. Each Cu(II) atom is surrounded by two nitrogen donors and two oxygen atoms from dpd-H with the Cu–N and Cu–O bond lengths

Table 1
Crystal data and refinement details for complexes **1**, **2** and **3**

	1	**2**	**3**
Empirical formula	$C_{44}H_{44}Cl_4Cu_4N_8O_{28}$	$C_{44}H_{52}Cl_4N_8Ni_4O_{32}$	$C_{48}H_{46}Cl_2N_8Ni_4O_{22}$
Crystal size (mm)	$0.25 \times 0.08 \times 0.05$	$0.54 \times 0.50 \times 0.28$	$0.30 \times 0.25 \times 0.22$
Crystal system	triclinic	monoclinic	monoclinic
Space group	$P\bar{1}$	$C2/c$	$C2/c$
Unit cell dimensions			
a (Å)	11.1124(1)	21.9000(3)	23.040(8)
b (Å)	12.731	12.8052(1)	12.101(4)
c (Å)	21.1887(3)	21.3072(2)	21.148(7)
α (°)	75.208(6)	90	90
β (°)	78.861(6)	90.576(1)	116.489(6)
γ (°)	72.626(6)	90	90
V (Å^3)	2743.81(5)	5974.96(11)	5277(3)
Z	2	4	4
Formula weight	1528.83	1581.58	1392.67
D_c (g/cm^3)	1.850	1.758	1.753
$F(000)$	1544	3232	2848
θ Range (°)	3.01 to 27.48	1.84 to 25.00	3.15 to 27.48
Reflections measured	21390	8341	19649
hkl Range	−14 to 14, −13 to 16, −27 to 27	−26 to 25, −13 to 15, −25 to 12	−16 to 29, −15 to 15, −27 to 27
Independent reflections	12403	5144	6029
R_{int}	0.0271	0.0216	0.0287
Observed reflections [$I > 2\sigma(I)$]	10211	4136	5132
Parameters refined	793	416	374
R[a]	0.0497	0.0783	0.0629
Rw[b]	0.1086	0.2005	0.1767
Goodness-of-fit	1.081	1.096	1.074
Maximum/mean shift in final cycle	0.001/0.000	0.002/0.000	0.000/0.000
Maximum/minimum $\Delta\rho$ (e/Å^3)	0.852/−0.747	1.301/−0.851	1.396/−0.951

1, $a = 0.0455$, $b = 6.24$; **2**, $a = 0.1351$, $b = 38.12$; **3**, $a = 0.1056$, $b = 15.7662$.
[a] $R = \sum(||F_o| - |F_c||)/\sum|F_o|$.
[b] $Rw = \{\sum w[(F_o^2 - F_c^2)^2]/\sum w[(F_o^2)^2]\}^{1/2}$, $w = 1/[\sigma^2(F_o^2) + (aP)^2 + bP]$, $P = (F_o^2 + 2F_c^2)/3$.

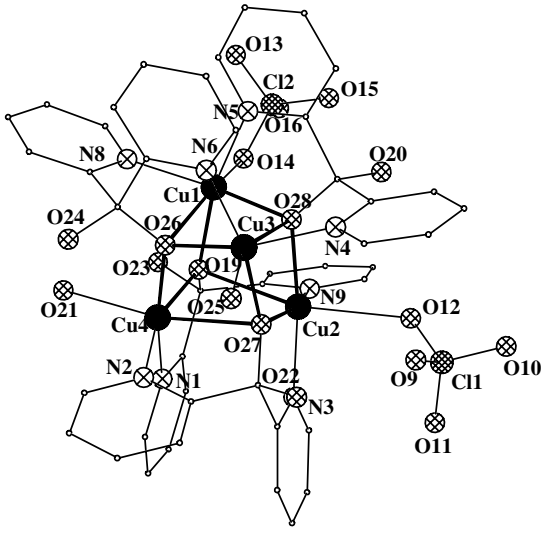

Fig. 1. View of the cation $[Cu_4(dpd\text{-}H)_4(ClO_4)_2(H_2O)_2]^{2+}$ in **1**. Hydrogen atoms are omitted for clarity.

in the range of 1.970(3)–2.030(3) and 1.934(2)–2.010(2) Å. In addition, Cu(1) and Cu(2) atoms are weakly bonded to the other two oxygen atoms from dpd-H and ClO_4^- (Cu–O = 2.405(3)–2.503(3) Å) while Cu(3) and Cu(4) atoms are weakly coordinated by the other two oxygen atoms from dpd-H and H_2O (Cu–O = 2.246(3)–2.582(3) Å). Obviously, the axial bond lengths are longer than the corresponding equatorial bond distances, which may be ascribed to Jahn–Teller distortion. As is shown in Scheme 2, all dpd-H ligands adopt the same coordination way (μ_3:η_1:η_3:η_1), which are also observed in other compounds [7,16]. Each ligand uses one deprotonated alkoxo oxygen atom to bridge three metal atoms and another alkoxo oxygen atom remains protonated and unbound to metal ions. Furthermore, each ligand also uses two nitrogen atoms of the pyridine rings to coordinate to two Cu(II)

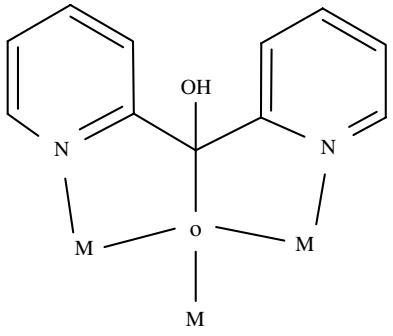

Scheme 2.

ions, respectively. The Cu···Cu separations are about 3.129–3.307 Å. In addition, there is a complex hydrogen-bonding network among H_2O molecules, the ClO_4^- counterion and hydroxyl group of dpd-H, with the distances in the range of about 2.684–3.056 Å.

To the best of our knowledge, only two compounds containing tetranuclear Cu(II) and dpd-H which show zigzag chain and rhombic coplanar structures have been reported [17]. In addition, one octanuclear complex $[Cu_8(dpk \cdot OH)_8(O_2CMe)_4](ClO_4)_4 \cdot 9H_2O$ have been reported, which presents the configuration two tetranuclear cubane cores connected by acetate [12].

3.3. Description of the crystal structure of the complexes 2 and 3

The structures of **2** and **3** are almost similar (Figs. 2 and 3), a little difference being that complex **2** contain lattice water molecules besides containing isolated perchlorate anions. Both of them contain the cubane-type $Ni_4(dpd\text{-}H)_4$ species. Each Ni_4O_4 cubane core is constructed by four nickel atoms and four oxygen atoms from four dpd-H ligands at alternating corners. All Ni(II) atoms are in distorted octahedral geometries. Ni1 and Ni1A atoms in **2** (A: $-x+1,\ y,\ -z+1/2$) or **3** (A: $-x+1,\ y,\ -z+3/2$) are coordinated by three nitrogen donors and three oxygen atoms from different dpd-H ligands, while the Ni2 and Ni2A centers are enclosed by one nitrogen donor from one dpd-H ligand and five oxygen atoms. Besides three μ_3-alkoxo oxygen atoms from three different dpd-H ligands and one oxygen atom from one H_2O molecule, the fifth oxygen atom is from one H_2O molecule and one monodentate CH_3COO^- group for **2** and **3**, respectively. Similar to those in **1**, another oxygen atom of each dpd-H ligand remains protonated and unbound to metal ions, and each dpd-H ligand adopts μ_3:η_1:η_3:η_1 coordination way. The Ni–N bond lengths are about 2.029–2.089 Å, while Ni–O bond distances are about 2.002–2.131 Å, of which Ni–O(CH_3COO^-) distances are shorter than Ni–O(H_2O) and Ni–O(dpd-H). The Ni···Ni separations are about 3.031–3.271 Å. Compound **2** exhibits a complex hydrogen-bonding network among the water molecules, ClO_4^- counterion and hydroxyl group of dpd-H (O···O 2.634–3.044 Å). And in compound **3**, there is also a complex hydrogen-bonding network among the water molecules, ClO_4^- counterion, hydroxyl group of dpd-H and CH_3COO^- group (O···O 2.637–3.040 Å). Thus, the present cubane-type $Ni_4(dpd\text{-}H)_4$ skeleton resembles that found in $[\{Ni_4(dpd\text{-}H)_4(OAc)_3(H_2O)\}(ClO_4) \cdot 8.25H_2O]$ and $[Ni_4(OAc)_2\{N(CN)_2\}_2(dpd\text{-}H)_4] \cdot 10H_2O$ [7a,7b,7c].

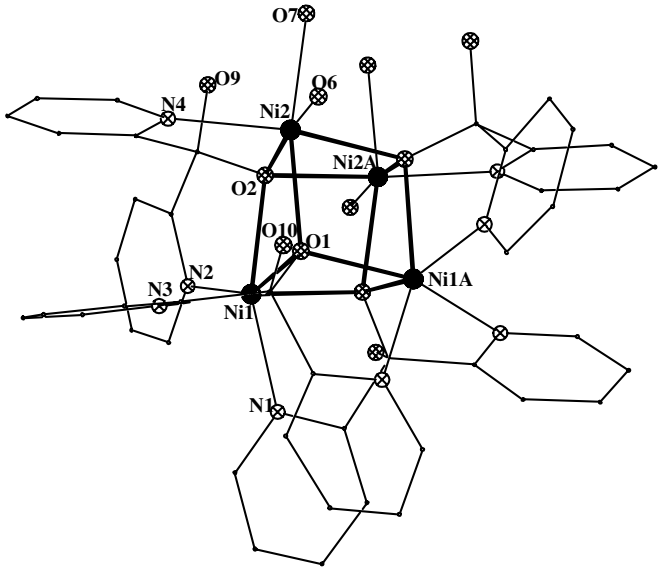

Fig. 2. View of the cation $[Ni_4(dpd\text{-}H)_4(H_2O)_4]^{2+}$ in **2**. (Symmetry codes: (A): $-x+1,\ y,\ -z+1/2$). Hydrogen atoms are omitted for clarity.

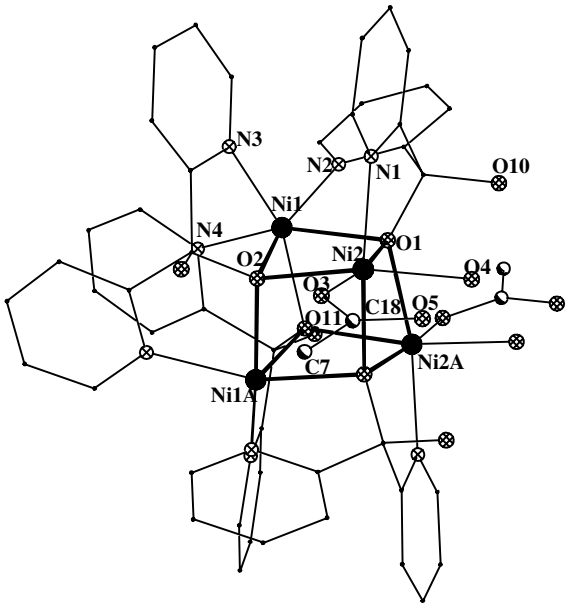

Fig. 3. View of the cation $[Ni_4(dpd\text{-}H)_4(OAc)_2(H_2O)_2]^{2+}$ in **3** (Symmetry codes: (A): $-x+1,\ y,\ -z+3/2$). Hydrogen atoms are omitted for clarity.

3.4. IR and UV/Vis spectroscopy

IR spectra of **1**, **2** and **3** are similar for their structural similarity. We analyze them with **3** as an example. The peak at about 1605 cm^{-1} is corresponding to single C–O bond from the ligand dpd-H. Additionally, the peaks at about 1473, 1442, 1385 cm^{-1} are attributed to the pyridyl ring stretching, 683 cm^{-1} for the pyridyl ring C–H in-plane vibration and 755, 770, 804 cm^{-1} for the pyridyl ring C–H out-of-plane vibration. In contrast with **1** and **2**, **3** have a CH_3COO^- group. Because two C–O bonds occur resonance, the typical strong C=O stretching vibration disappear. So the two spectral bands at about 1573 and 1337 cm^{-1} are, respectively, from asymmetrical and symmetrical vibrations of the COO^- group.

The UV/Vis spectroscopies of **1**, **2** and **3** are also similar. The $\pi \rightarrow \pi^*$ transition of **1**, **2** and **3** occur at 209, 210 and 216 nm, respectively, while the $n \rightarrow \pi^*$ transition of them appear at 264, 264 and 261 nm, respectively.

3.5. Magnetic property of *1*

Temperature dependent magnetic susceptibility of **1** was measured in the range of 2–300 K at 10 kG and shown in Fig. 4. At room temperature, the $\chi_m T$ values per Cu_4 unit is 1.66 $cm^3\,mol^{-1}\,K$, compared with the expected values (1.5 $cm^3\,mol^{-1}\,K$) for four spin only Cu^{II} ions ($S = 1/2$, $g = 2$). Upon cooling, **1** shows a continuous decreasing of $\chi_m T$, suggesting an overall antiferromagnetic coupling, as confirmed by the negative Weiss constant (−20.8 K).

Taking into account the compound topology, we group into two exchange parameters J and J' ($J = J_{13} = J_{24}$, $J' = J_{12} = J_{14} = J_{23} = J_{34}$). The corresponding network of exchange pathways is shown in Scheme 3. The magnetic behavior of such cubane-like cluster can be described by the Hamiltonian given in Eq. (1):

$$H = -J(S_1S_3 + S_2S_4) - J'(S_1S_2 + S_1S_4 + S_2S_3 + S_3S_4). \quad (1)$$

Which leads to Eq. (2):

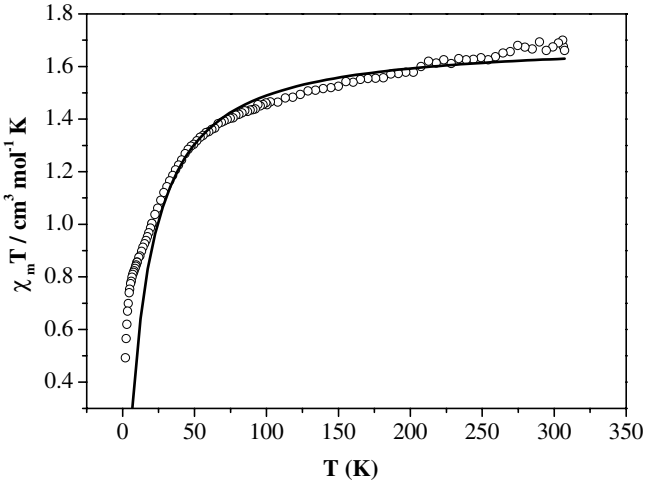

Fig. 4. Plot of $\chi_m T$ vs. T for **1**. Solid line, fit of Eq. (2); ∘, experimental data.

The best fit was obtain with $J_1 = -6.4\ cm^{-1}$, $J_2 = -10.9\ cm^{-1}$, $g = 2.119$, $\theta = 1.4$ K and $R = 4 \times 10^{-5}$. The above two results demonstrate antiferromagnetic coupling of **1**.

Strong dependence of the exchange integral magnitude versus the Cu–O–Cu angle is well documented in dimeric dibridged complexes. The exchange interaction is ferromagnetic for the Cu–O–Cu angles less than 97° and antiferromagnetic for larger angles [18]. However, the interaction within our tetranuclear Cu(II) complex is

$$\chi = \frac{2Ng^2\beta^2}{kT} \frac{2\exp(J/kT) + \exp[(2J - J')/kT] + 5\exp[(2J + J')/kT]}{1 + 6\exp(J/kT) + \exp[(2J - 2J')/kT] + 3\exp[(2J - J')/kT] + 5\exp[(2J + J')/kT]}. \quad (2)$$

The fit was reached with the parameters $J = J' = -12.1\ cm^{-1}$, $g = 2.13$ and $R = 9.2 \times 10^{-4}$. In fact, adopting one exchange parameter J can obtain the similar results.

In addition, we also adopt another model to fit the curve. (Fig. 5) Without regard to the weaker Cu–O (Cu(4)–O(27), Cu(2)–O(19), Cu(3)–O(28)) interaction, we take on the compound exchange pathways as butterfly topology, and simplify them to two exchange parameters J_1 and J_2 ($J_1 = J_{12} = J_{23} = J_{34} = J_{14}$, $J_2 = J_{13}$), as is shown in Scheme 4. The exchange interaction can be described by the reduced Hamiltonian

$$H = -J_1(S_1S_2 + S_2S_3 + S_3S_4 + S_1S_4) - J_2(S_1S_3). \quad (3)$$

Hence, the 2–300 K experimental data were fitted next, by using the following resulting theoretical expression for the magnetic susceptibility:

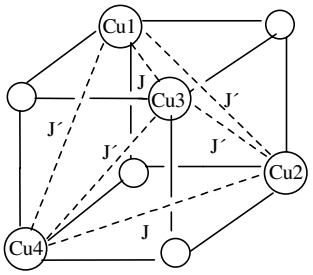

Scheme 3.

$$\chi = \frac{Ng^2\beta^2}{3k(T-\theta)} \times \frac{30[\exp(2J_1 + 0.5J_2)/kT] + 6[\exp(-2J_1 + 0.5J_2)/kT] + 6\exp(0.5J_2/kT) + 6\exp(-1.5J_2/kT)}{5\exp[(2J_1 + 0.5J_2)/kT] + 3\exp[(-2J_1 + 0.5J_2)/kT] + \exp[(-4J_1 + 0.5J_2)/kT] + 3\exp(0.5J_2/kT) + 4\exp(-1.5J_2/kT)}. \quad (4)$$

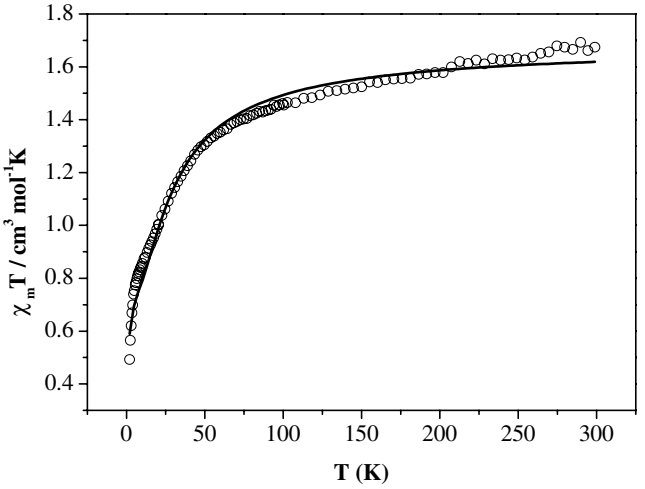

Fig. 5. Plot of $\chi_m T$ vs. T for **1**. Solid line, fit of Eq. (4); ○, experimental data.

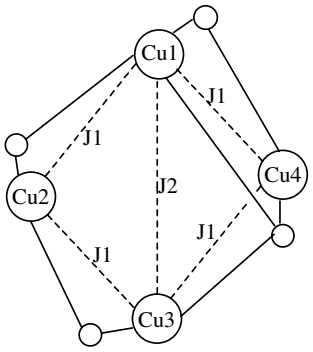

Scheme 4.

antiferromagnetic with the Cu–O–Cu angles in the range of 86.2–112.1°. It is reported in the literature that the ferromagnetic interaction occurs in the tetranuclear copper system with the Cu–O–Cu angles of 139.2–140.5° [19] while the antiferromagnetic interaction presents with Cu–O–Cu angles of 95.7–103.4° [20]. Apparently, the structure–exchange-interactions are complicated in the tetranuclear copper system and different from those in the dimeric copper complexes.

4. Conclusion

In summary, we have prepared three new tetranuclear cubane-like complexes constructed from multidentate ligand dpd-H. These compounds were characterized with X-ray single crystal diffraction as well as elemental analysis, IR and UV/Vis spectroscopy. The magnetic property of **1** was also studied.

5. Supplementary material

CCDC numbers 277929, 277930 and 277931 are for compounds **1–3**, respectively. These crystallographic data for this paper can be obtained free of charge via www.ccdc.cam.ac.uk/conts/retrieving.html or on application to The Director, CCDC, 12 Union Road, Cambridge CB2 2EZ, UK (fax: +44 1223 336033; e-mail: deposit@ccdc.cam.ac.uk or http://www.ccdc.cam.ac.uk).

Acknowledgements

This research was supported by the State Key Laboratory of Structural Chemistry, the National Science and Technology of China (001CB1089), the Chinese Academy of Sciences (CAS), the National Science Foundation of China (20273073, 20333070, 90206040) and the Science Foundation of CAS and Fujian Province (2004HZ01-1, 2003J042, 2004J041 and Z0513022).

Appendix A. Supplementary data

Supplementary data associated with this article can be found, in the online version, at doi:10.1016/j.poly.2005.11.002.

References

[1] T. Afrati, C. Dendrinou-Samara, C.P. Raptopoulou, A. Terzis, V. Tangoulis, D.P. Kessissoglou, Angew. Chem. Int. Ed. 41 (2002) 2148.
[2] M. Du, X.-H Bu, Y.-M. Guo, J. Ribas, Chem. Eur. J. 10 (2004) 1345.
[3] E.C. Sanudo, W. Wernsdorfer, K.A. Abboud, G. Christou, Inorg. Chem. 43 (2004) 4137.
[4] S.L. Castro, Z. Sun, C.M. Grant, J.C. Bellinger, D.N. Hendrickson, G.J. Christou, J. Am. Chem. Soc. 117 (1998) 2365.
[5] (a) P.J. Steel, C.J. Sumby, J. Chem. Soc., Dalton Trans. (2003) 4505; (b) S.L. Wang, J.W. Richardson Jr., S.J. Briggs, R.A. Jacobson, Inorg. Chim. Acta. 111 (1986) 67.
[6] (a) C. Hemmert, M. Renz, H. Gornitzka, S. Soulet, B. Meunier, Chem. Eur. J. 5 (1999) 1766;
(b) E. Katsoulakou, N. Lalioti, C.P. Raptopoulou, A. Terzis, E.M. Zoupa, S.P. Perlepes, Inorg. Chem. Commun. 5 (2002) 719.
[7] (a) M.-L. Tong, S.-L. Zheng, J.-X. Shi, Y.-X. Tong, H.K. Lee, X.-M. Chen, J. Chem. Soc., Dalton Trans. (2002) 1727;
(b) M.-L. Tong, H.K. Lee, S.-L. Zheng, X.-M. Chen, Chem. Lett. (1999) 1087;
(c) G.S. Papaefstathiou, A. Escuer, F.A. Mautner, C. Raptopoulou, A. Terzis, S.P. Perlepes, R. Vicente, Eur. J. Inorg. Chem. (2005) 879;
(d) A. Tsohos, S. Dionyssopoulou, C.P. Raptopoulou, A. Terzis, E.G. Bakalbassis, S.P. Perlepes, Angew. Chem. Int. Ed. 38 (1999) 983.
[8] G.S. Papaefstathiou, A. Escuer, R. Vicente, M.F. Bardia, X. Solans, S.P. Perlepes, Chem. Commun. 23 (2001) 2414.
[9] (a) M.G. Barandika, Z. Serna, R. Cortés, L. Lezama, T. Rojo, M.K. Urtiaga, M.I. Arriortua, T. Rojo, Chem. Commun. 1 (2001) 45;
(b) Z.E. Serna, L. Lezama, M.K. Urtiaga, M.I. Arriortua, M.G. Barandika, R. Cortes, T. Rojo, Angew. Chem. Int. Ed. 39 (2000) 344.
[10] A.K. Boudalis, F. Dahan, A. Bousseksou, J.P. Tuchagues, S.P. Perlepes, J. Chem. Soc., Dalton Trans. 17 (2003) 3411.
[11] V. Tangoulis, C.P. Raptopoulou, S. Paschalidou, A.E. Tsohos, E.G. Bakalbassis, A. Terzis, S.P. Perlepes, Inorg. Chem. 36 (1997) 5270.
[12] V. Tangoulis, C.P. Raptopoulou, A. Terzis, S. Paschalidou, S.P. Perlepes, E.G. Bakalbassis, Inorg. Chem. 36 (1997) 3996.
[13] G.M. Sheldrick, SHELXL-97, Program for X-ray Crystal Structure Refinement, University of Göttingen, Göttingen, Germany, 1997.
[14] G. Yang, M.-L. Tong, X.-M. Chen, S.W. Ng, Acta Crystallogr. Sect., C: Cryst. Struct. Commun. 54 (1998) 732.
[15] The work has not been published.

[16] G.S. Papaefstathiou, A. Escuer, C.P. Raptopoulou, A. Terzis, S.P. Perlepes, R. Vicente, Eur. J. Inorg. Chem. (2001) 1567.
[17] (a) S.R. Breeze, S. Wang, J.E. Greedan, N.P. Raju, Inorg. Chem. 35 (1996) 6944;
(b) V. Tangoulis, C.P. Raptopoulou, S. Paschalidou, A.E. Tsohos, E.G. Bakalbassis, A. Terzis, S.P. Perlepes, Inorg. Chem. 36 (1997) 5270.
[18] V.H. Crawford, H.W. Richardson, J.R. Wasson, D.J. Hodgson, W.E. Hatfield, Inorg. Chem. 15 (1976) 2107.
[19] Z.-Q. Xu, L.K. Thompson, D.O. Miller, J. Chem. Soc., Dalton Trans. (2002) 2462.
[20] J.W. Hall, W.E. Estes, E.D. Estes, R.P. Scaringe, W.E. Hatfield, Inorg. Chem. 16 (1977) 1572.

behaviour of alkali metal amides derived from three commonly used chiral secondary amines; *S*-(α-methylbenzyl)benzylamine, *R*,*R*-bis-α-methylbenzylamine, and *S*-*N*-(α-methylbenzyl)allylamine, shown in Fig. 1 [21,22]. The lithium complexes are known to be extremely useful in enantioselective deprotonation reactions with prochiral ketones and epoxides, and in Michael addition reactions to α,β-unsaturated esters, producing high ee values [23–40]. Since both reactivity and structure are inextricably linked with selectivity then it is of interest to exam the structures of the chiral amine adducts of Me_3M, the aluminium amides formed from thermal elimination of MeH from these complexes and ultimately the complexes formed on reaction with unsaturated substrates. This is key to the future rational design of highly effective and selective reagents.

As the first part of this study we now report the synthesis and solid state characterisation of (*S*,*R*)-[$Me_3Al \cdot HN(CHMePh)(CH_2Ph)$] (**1**), [(*S*,*R*)-$Me_3Ga \cdot HN(CHMePh)(CH_2Ph)$] (**2**), $Me_3Al \cdot HN(CHMePh)_2$ (**3**), $Me_3Ga \cdot HN(CHMePh)_2$ (**4**), (*S*,*S*)-]$Me_3Al \cdot HN(CHMePh)(CH_2CH{=}CH_2)$] (**5**) and (*S*,*S*)-[$Me_3Ga \cdot HN(CHMePh)(CH_2CH{=}CH_2)$] (**6**), as well as the unusual solution behaviour observed for **1** in comparison with its gallium analogue **2**, and with the other complexes.

2. Results and discussion

2.1. Synthesis

Under inert conditions, each amine was added slowly to a hexane solution of Me_3M (M = Al, Ga) at −78 °C and allowed to warm slowly to room temperature. Following reduction of the solvent in vacuo, colourless crystals suitable for X-ray diffraction were readily obtained at −20 °C over 48 h. The crystals were all isolated and washed with cold hexane prior to further analysis. Whilst compounds **1**–**6** are stable at room temperature under inert atmosphere, crystals of the Me_3Ga adduct incorporating (*S*)-*N*-(α-methylbenzyl)allylamine (**6**) are highly soluble in trace amounts of solvent and have a melting point below room temperature. Due to the unusual NMR data obtained for complex **1** it was synthesised four times under differing conditions: (i) addition of amine to Me_3Al at −78 °C; (ii) addition of amine to Me_3Al at room temperature; (iii) addition of Me_3Al to amine at −78 °C, and, (iv) addition of Me_3Al to amine at room temperature. Irrespective of the mode of synthesis of the colourless crystals, similar NMR spectra and crystal structures were obtained.

2.2. NMR analysis

NMR data were collected on all six compounds in C_6D_6 at room temperature. While compounds **2**–**6** produced ^1H spectra with expected chemical shift patterns compound **1** gave an interesting spectrum of very broad signals which seemed to indicate the presence of two complexes in a ratio of approximately 2:1. The benzylic CH_2 protons in **1** are also diastereotopic appearing at δ3.80 and δ3.44, which is in contrast to that of the Ga analogue, **2**, for which there is only one signal attributable to these protons. Also, all the signals in the spectrum of **2** are significantly sharper, as are those of all the other complexes **3**–**6**. Indeed this was observed for four sets of crystals of **1**, all synthesised under different conditions as described above. We fully expected the two possible diastereomers for all complexes to be present in a 1:1 ratio expecting little discrimination over the way the N–Al dative bond formed and little restriction to rotation around the C–N bonds, and therefore, our first assumption was that the spectrum represented the possibility that there was an equilibrium between four and five coordinate Al species, [$Me_3Al \cdot L$] and [$Me_3Al \cdot L_2$], and free $AlMe_3$. However, there was no evidence in either the ^1H or ^{13}C spectra of differing AlMe signals. The ^{13}C NMR though also revealed two possible isomers. The second possibility was that there had been hydrolysis and that we were seeing both free and bound amine. However, this was ruled out by successive NMR measurements which showed a similar pattern for **1** but no sign of this occurring for all the other complexes. To examine this phenomenon more closely, variable temperature spectra were obtained in d_8-toluene on all complexes. While the others are unremarkable the spectra of **1** resolved into two species as the temperature was lowered and a comparison of **1** and **2** are shown in Figs. 2 and 3, respectively. That two distinct AlMe signals are now apparent at −60 °C suggests it could be possible that what is being observed is an equilibrium between the four coordinate monomeric species, [$Me_3Al \cdot L$], and the Me bridged dimer, [$Me_3Al \cdot L]_2$; an equilibrium which is not common for Ga given its lower Lewis acidity and reluctance to form five coordinate complexes. Such an equilibrium would give four and five coordinate Al centres, however, ^{27}Al NMR seemed to indicate that by far the only complex present in any substantial amount contains four coordinate Al, though the signal is quite broad (at −60 °C, δ 71.7, half-height line width 3448 Hz). Also, there was almost no change in the chemical shift value over the temperature range 30 to −60 °C, suggesting that the system is far from dynamic

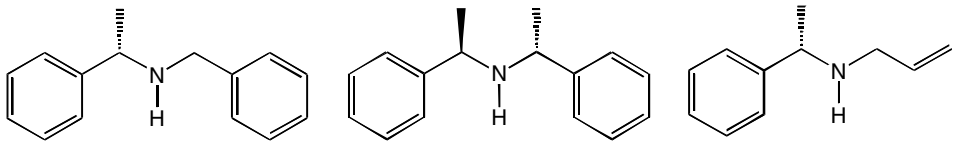

Fig. 1. Three common chiral secondary amines used in this study: *S*-(α-methylbenzyl)benzylamine, *R*,*R*-bis-α-methylbenzylamine, and *S*-*N*-(α-methylbenzyl)allylamine.

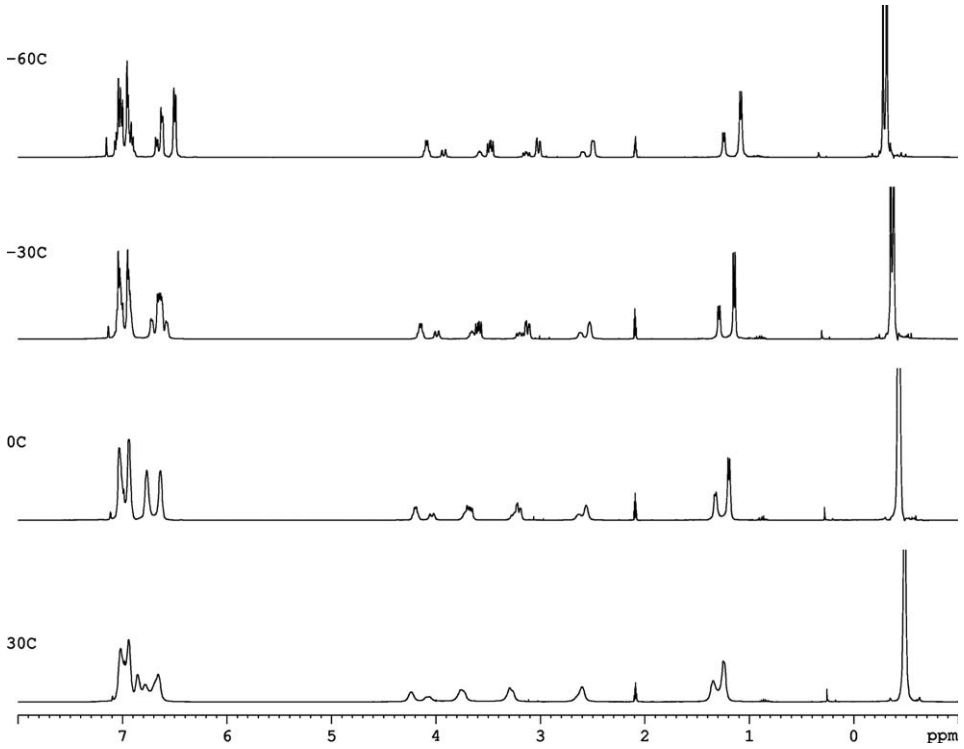

Fig. 2. Variable temperature ^{1}H NMR spectra in d_8-toluene of $Me_3Al \cdot HN(CHMePh)(CH_2Ph)$ (**1**).

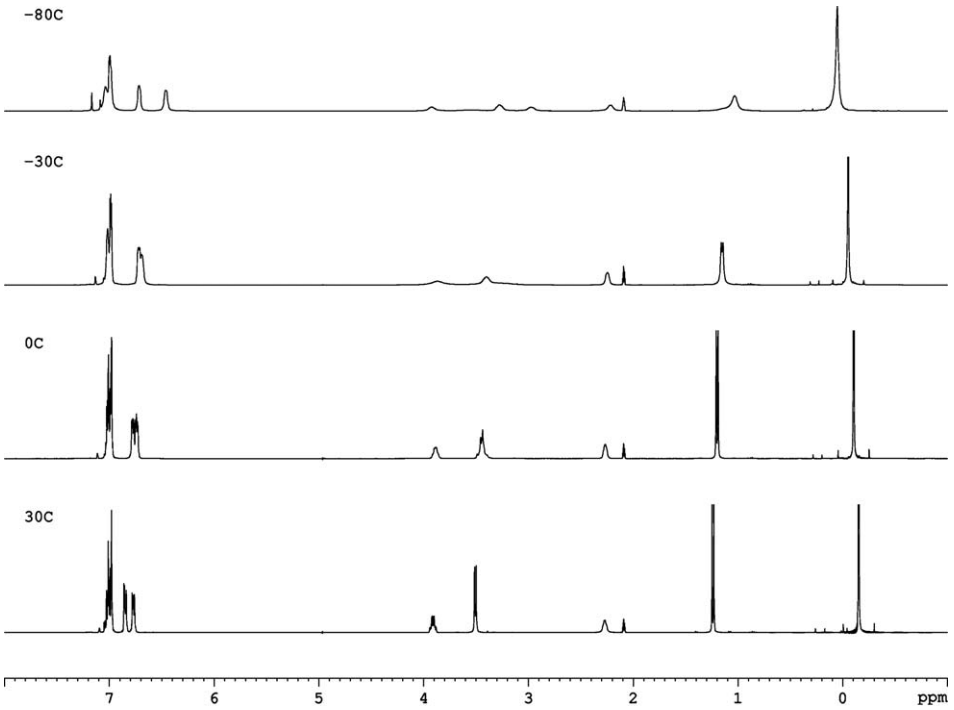

Fig. 3. Variable temperature ^{1}H NMR spectra in d_8-toluene of $Me_3Ga \cdot HN(CHMePh)(CH_2Ph)$ (**1**).

[41]. The other alternative is, of course, that the two diastereomers (*S*,*S* and *S*,*R*) are quite distinct and form in relative amounts of 2:1. Why this should be the case for **1** and not for the other complexes, which seems to negate an argument involving the relative coordination abilities of Al over Ga, we have, as yet, no explanation. Some exploratory ab initio calculations on the two diastereomers revealed the *S*,*R* conformation to be more stable than the *S*,*S* but by only 11 kcal mol^{-1} and it would be difficult to see this energy difference as significant. In assuming an

equilibrium situation sample **1** was also heated to 80 °C to induce possible rearrangement of the two species through inversion at the N centre before being allowed to cool again to 30 °C. However, no difference in the respective amounts of the two species was observable.

Despite this a comparison of the NMR data for this series of chiral amine adducts dissolved in d_6-benzene is useful as it gives insight into the influence of factors such as increasing steric demands by the amino group and the nature of the metal on the chemical shift values. This data is listed in Table 1. Information obtained on compounds **1**–**6** is compared with that already reported for the $AlMe_3$ and $GaMe_3$ adducts of the dibenzylamine ligand, **7** and **8**, respectively [16,17].

With the exception of **4**, all ^1H and ^{13}C chemical shift values for the methyl groups attached to the metal centre are upfield from TMS and appear dependant on both the amine moiety and the metal. It is clear that the Ga adducts display higher chemical shift values than each of the corresponding Al compounds. Moreover, each of the chiral adducts experiences greater deshielding than that shown by dibenzylamine in **7** and **8** resulting in a slight downfield shift in both the ^1H and ^{13}C methyl peaks. This pattern is consistent in both the Al and Ga adduct series and suggests that increasing steric bulk around the nitrogen centre affects the chemical shift positioning. Such an analysis concords with previous studies [16,17] which hypothesise that such shift changes may be due to the increasing *p* character of the M–C bond as the C–M–C bond angles decrease to accommodate larger amine ligands. In particular, ^{13}C shifts are known to be very sensitive to steric effects. This is evidenced by the consistent increase in chemical shift from the less hindered **7** and **8** (δ −8.06 ppm, δ −5.10 ppm) to the more bulky structures of **1** and **2** (δ −6.18 ppm, δ −3.57 ppm) and **3** and **4** (δ −5.51 ppm, δ 0.46 ppm). Notably, the replacement of one methyl-benzyl group with a less bulky allyl component in **5** and **6** appears to reduce the steric effects thereby lowering the chemical shift (δ −6.82 ppm, δ −3.84 ppm).

2.3. Structural analysis

Each of the crystal structures obtained for **1**–**6** were found to be monomeric and crystallise under an orthorhombic crystal system in the $P2_12_12_1$ space group. Data on complex **1** was collected four times on each occasion producing the (*S*,*R*) diastereomer. Consequentially, a direct structural comparison of these adducts is likely to produce meaningful results. The molecular structures of **1**, **4** and **5** are shown in Figs. 4–6. Table 2 contains a summary of the crystallographic data for **1**–**6** whilst Table 3 provides

Table 1
Me_3M ^1H and ^{13}C data for the Me_3-M-amine adducts of **1**–**8** (M = Al, Ga)

Amine	Adducts			
	^1H (ppm)		^{13}C (ppm)	
	M = Al	M = Ga	M = Al	M = Ga
Dibenzylamine[a]	−0.38	−0.10	−8.06	−5.10
(*S*)-(α-methylbenzyl)benzylamine	−0.34	−0.07	−6.18	−3.57
(*R*,*R*)-bis-α-methylbenzylamine	−0.27	0.05	−5.51	0.46
(*S*)-*N*-(α-methylbenzyl)allylamine	−0.33	−0.02	−6.82	−3.84

[a] Data obtained from [16].

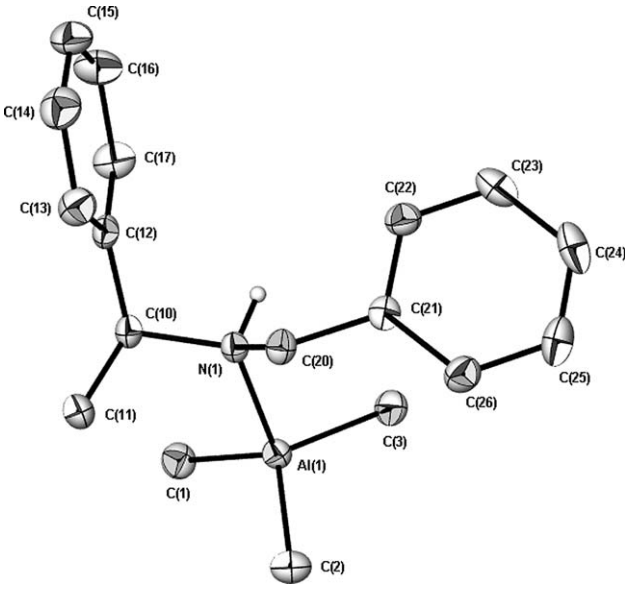

Fig. 4. Molecular structure of (*S*,*R*)-$Me_3Al \cdot HN(CHMePh)(CH_2Ph)$ (**1**). Thermal ellipsoids shown at 50% probability. All H except on N and chiral C omitted for clarity. The Ga complex, **2**, is isostructural.

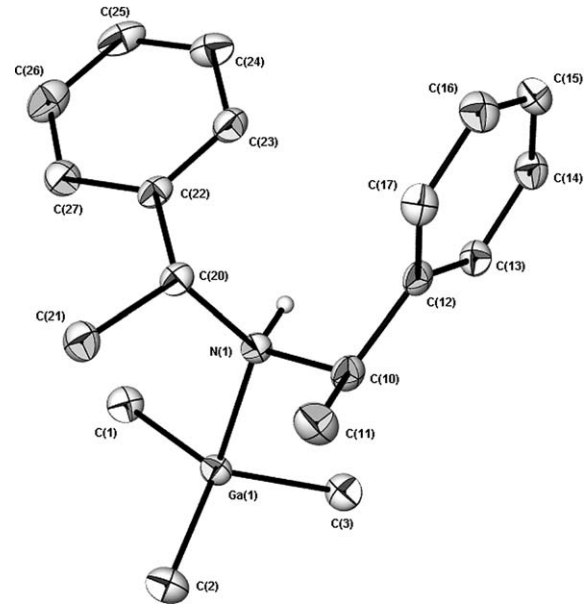

Fig. 5. Molecular structure of $Me_3Ga \cdot HN(CHMePh)_2$ (**4**). Thermal ellipsoids shown at 50% probability. All H except on N and chiral C omitted for clarity. The Al complex, **3**, is isostructural.

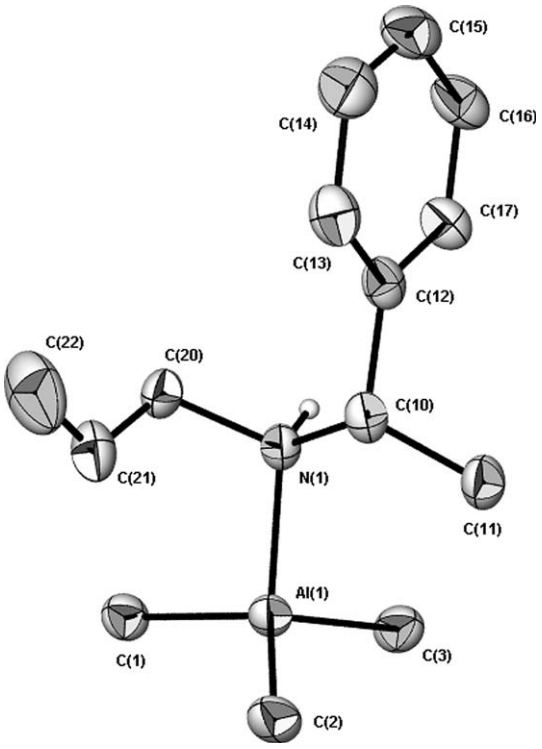

Fig. 6. Molecular structure of (*S*,*S*)-$Me_3Al \cdot HN(CHMePh)(CH_2CH{=}CH_2)$ (**5**). Thermal ellipsoids shown at 50% probability. All H except on N and chiral C omitted for clarity.

a listing of selected bond lengths and angles for **1**–**6** with comparison to **7** and **8**.

All six structures are comparable with those of the dibenzylamine adducts previously reported for Me_3Al, **7**, and Me_3Ga, **8**. The structural solutions show the nitrogen on each amine to be bound to the *tris*-alkylated metal centre giving each metal a highly distorted tetrahedral geometry. The bond lengths between the metal and N donors (av. 2.064 Å, Al adducts; 2.160 Å, Ga adducts) are typical of these adduct complexes (ca. ~2.0 Å) [16,17] containing datively bonded nitrogen and metal atoms. As expected, the M–N bond distances of each amine adduct increase by approximately 0.1 Å with the heavier metal. The greater charge to radius ratio about the Ga nucleus and therefore weaker polarisability when compared to Al explains this trend. This hypothesis also serves to support the greater ^{13}C and ^{1}H NMR chemical shifts downfield of the free amine in the Me_3Ga adducts over the Me_3Al congeners.

The C–M–C angles for the Al adducts are more acute than those found for the analogous Ga structure which can be attributed to the greater size of the Ga(III) metal centre. The greater ionic radius provides an improved ability to reduce any geometric distortion caused by the proximity of the amine.

Increased steric hindrance created by the addition of α-methyl groups about the N centre causes a slight elongation of the M–N bond, as would be expected, though once established there is only a minimal effect on the bond distance whether there is one or two methyl groups or whether there is one or two benzyl groups. Thus, the N–Al bond distances for **1**, **3** and **5** (2.065(1), 2.068(1) and 2.066(2) Å, respectively) are longer than that observed in **7** (2.058(2) Å), though are strikingly similar to each other. The same pattern is observed for the N–Ga bond distances in **2**, **4** and **8** (2.162(1), 2.168(2) and 2.151(8) Å, respectively). So, even in **5** where one bulky benzyl group is replaced by a more flexible and less sterically demanding allyl tail there is no significant difference in bond length. Interestingly, there were no intra- or intermolecular electrostatic contacts between the allyl groups and the Al metal centres.

It would be expected that as methyl groups are added to the benzylic carbons on dibenzylamine there would be an increase in the relevant M–N–C bond angles. There would be firstly an observable decrease in symmetry when one is added (as in **1**, **2** and in **5**, **6** by analogy) and a re-establishment of higher symmetry on addition of two (as in **3** and **4**).

Table 2
Summary of crystallographic data for **1**–**6**

Compound	**1**	**2**	**3**	**4**	**5**	**6**
Formula	$C_{18}H_{26}NAl$	$C_{18}H_{26}NGa$	$C_{19}H_{28}NAl$	$C_{19}H_{28}NGa$	$C_{14}H_{24}NAl$	$C_{14}H_{24}NGa$
M_w	283.4	326.1	297.4	340.1	233.3	276.1
Crystal system	orthorhombic	orthorhombic	orthorhombic	orthorhombic	orthorhombic	orthorhombic
Space group	$P2_12_12_1$	$P2_12_12_1$	$P2_12_12_1$	$P2_12_12_1$	$P2_12_12_1$	$P2_12_12_1$
a (Å)	8.845(2)	8.860(2)	6.712(1)	6.699(1)	6.172(1)	6.172(1)
b (Å)	11.613(2)	11.612(2)	14.684(3)	14.730(3)	12.491(3)	12.513(3)
c (Å)	17.101(3)	17.068(3)	18.655(4)	18.633(4)	19.750(4)	19.733(4)
V (Å^3)	1757.22(4)	1755.9(6)	1838.4(6)	1838.8(6)	1522.5(5)	1523.8(5)
Z	4	4	4	4	4	4
$2\theta_{max}$ (°)	56.6	59.2	56.6	56.6	56.6	56.6
D_{calc} (g cm^{-3})	1.072	1.234	1.075	1.229	1.018	1.203
μ (cm^{-1})	1.07	15.59	1.05	14.91	1.12	17.84
T (K)	123	123	123	123	123	123
N_{ind}	4350	4849	4560	4554	3753	3737
N_o	3633	4509	4156	3804	2970	3260
R_w	0.076	0.053	0.077	0.073	0.089	0.079
R_1 [$I > 2\sigma(I)$]	0.038	0.024	0.032	0.033	0.039	0.032
Goodness-of-fit (F^2)	1.03	1.06	1.03	0.83	1.04	0.92

Table 3
Selected bond lengths (Å) and angles (°) for **1**–**8**

M = Al, Ga	1	2	3	4	5	6	7[a]	8[a]
M(1)–N(1)	2.065(1)	2.162(1)	2.068(1)	2.168(2)	2.066(2)	2.160(2)	2.058(2)	2.151(3)
M(1)–C(1)	1.981(2)	1.987(2)	1.981(1)	1.985(2)	1.983(2)	1.999(2)	1.966(3)	1.981(4)
M(1)–C(2)	1.982(2)	1.987(2)	1.984(1)	1.990(3)	1.990(2)	1.989(3)	1.977(3)	2.000(4)
M(1)–C(3)	1.978(2)	1.987(2)	1.971(1)	1.982(3)	1.976(2)	1.988(2)	1.961(2)	1.975(5)
N(1)–C(10)	1.521(2)	1.500(2)	1.531(2)	1.522(3)	1.511(2)	1.498(3)	1.499(2)	1.485(6)
N(1)–C(20)	1.508(2)	1.515(2)	1.522(2)	1.514(3)	1.508(2)	1.502(3)	1.495(3)	1.491(4)
N(1)–M(1)–C(1)	103.2(2)	104.7(1)	102.9(1)	100.6(1)	104.1(1)	104.3(1)	102.1(1)	100.4(1)
N(1)–M(1)–C(2)	103.1(2)	101.5(1)	100.3(1)	98.8(1)	105.8(1)	102.2(1)	103.97(1)	102.1(1)
N(1)–M(1)–C(3)	106.6(1)	101.5(1)	110.4(1)	108.7(1)	103.1(1)	101.8(1)	106.39(1)	104.8(1)
C(1)–M(1)–C(2)	113.9(1)	115.3(1)	112.3(1)	113.8(1)	116.0(1)	117.0(1)	114.5(1)	115.4(2)
C(1)–M(1)–C(3)	114.1(1)	115.5(1)	117.2(1)	118.4(1)	111.9(1)	115.3(1)	118.0(1)	119.3(2)
C(2)–M(1)–C(3)	114.4(1)	115.4(1)	111.9(6)	113.4(1)	114.2(1)	113.4(1)	110.2(1)	111.8(2)
M(1)–N(1)–C(10)	115.6(1)	114.9(1)	112.4(1)	112.1(1)	118.0(1)	118.0(1)	111.3(1)	111.4(2)
M(1)–N(1)–C(20)	113.7(1)	113.4(1)	121.9(1)	121.9(1)	112.2(1)	111.4(1)	114.7(1)	114.3(2)
C(10)–N(1)–C(20)	112.1(1)	112.8(1)	113.8(1)	114.2(2)	111.4(2)	111.7(2)	110.8(2)	111.1(3)

[a] Data obtained from [16].

Table 4
Non-bonding methyl–metal distances (Å) for **1**–**6**

M = Al, Ga	1	2	3	4	5	6
C11–M	3.518	3.565	3.326	3.384	3.250	3.305
C21–M			3.732	3.790		

However, this is not the case. Within **7** and **8** the two M–N–C internal angles are different though they show an identical pattern to each other (cf. 114.7(2)°, 111.4(2)° in **7** and 114.3(2)° and 111.3(2)° in **8**). The marginal effect evident here on changing the metal is true for all the compounds under examination. In **1** and **2**, despite the introduction of the methyl group, the bond angles actually become closer (115.6(1)°, 113.6(1)° in **1** and 114.9°, 113.4(1)° in **2**), which contrasts with **5** in which a more substantial asymmetry in observed (117.9(1)°, 112.2(1)°) These values are closer to the angles observed in **3** and **4** which rather than being more symmetrical around the N–M bond are dramatically different (121.9(1)°, 112.4(1)° in **3** and 121.9(1)°, 112.1(1)° in **4**). The same pattern is also observed in the methyl–metal distances (Table 4).

One further point of interest in the structures of **3** and **4** is the staggered orientation of the benzylmethyl groups. These are arranged such that both methyl groups are located on the same side of the molecule though there is by necessity a positional interchange of Ph and H on one moiety. The Me groups in Me_3M are then positioned in the most sterically favourable orientation between the benzylic methyls. However, this is not completely symmetrical and the closest Me···Me interactions, as defined by the dihedral angles for C21(11)–C20(10)–M–C2, are 18° and 35.7° in **3** and 15° and 35.6° in **4**. This gives some indication of why there are significant differences in the C–N–M angles described above. This staggered orientation of the benzylmethyl groups is not unique and has been observed in other crystallographically characterised compounds which contain the bis-(α-methylbenzyl)amido moiety [42–46].

3. Conclusion

We have synthesised and structurally characterised, by NMR and X-ray diffraction, six chiral amine complexes of Me_3Al and Me_3Ga and demonstrated that in solid state they are all monomeric and found in the same space group, $P2_12_12_1$. The Me_3Al complex of (PhMeCH)($PhCH_2$)NH appears to form two distinct isomers in solution which is in contrast to the analogous Ga complex or other Al complexes studied. Whether this is the formation of two different distereoisomers has not been definitively answered but does not appear to result from varying coordination environments at the Al centre or hydrolysis. In general, increased steric effects caused by the presence of Me groups on the benzylic carbons of the amine causes a downfield shift in observed ^1H and ^{13}C chemical shift values of the Me groups in the alkylmetal moiety. The C_2 symmetrical amine $(PhMeCH)_2NH$ produces a structure which has both methyl groups on the amine located on the same side of the molecule but actually shows a reduced symmetry, with regards to the bond angles at the M–N bond, in comparison with the complexes derived from the less symmetrical amines, (PhMeCH)($PhCH_2$)NH and (PhMeCH)($CH_2CH{=}CH_2$)NH.

4. Experimental

4.1. General procedures

Owing to the highly air and moisture sensitive nature of the compounds investigated, syntheses and manipulation of all adducts were performed under Argon (CIG, high purity) through the use of standard Schlenk, vacuum line and dry box techniques. Amine reagents were dried and stored over molecular sieves whilst all solvents were dried over a NaK alloy, distilled under an atmosphere of nitrogen and stored over molecular sieves. Me_3Al and Me_3Ga, as neat liquids, were purchased from Strem Chemicals Inc. and used without further purification. C, H and N

elemental analyses were obtained for all new compounds from Chemical and Micro Analytical Services Pty Ltd., Belmont, Australia. NMR spectra were obtained on Brucker DRX-300 spectrometer with chemical shifts referenced to deuterated benzene. Melting points were determined in sealed capillaries using a Thomas Hoover melting point apparatus and were not corrected.

4.2. Structure determinations

Crystallographic data were collected on an Enraf Nonius KappaCCD with graphite monochromated MoKα ($\lambda_0 = 0.71073$ Å) radiation. Single crystals of compounds **1**–**6** of suitable quality for X-ray analysis were mounted on a glass fibre under oil. Data were collected at 123 K and processed using Nonius Software. Structures were solved refined by full matrix least-squares on F^2 and expanded using direct methods with all calculations performed by the SHELXS 97 software [47] and XSEED interface [48]. All H atoms were placed in calculated positions (C–H 0.95 Å) and included in the final least-squares refinement. All other atoms were located and refined anisotropically.

4.3. General synthesis of $Me_3Al \cdot$ amine adducts

In a typical synthesis, 12.5 mmol of the respective amine was added dropwise to a solution of $AlMe_3$ (12.5 mmol, 0.9 g) in hexane (15 ml) at −78 °C. The colourless solution was allowed to stir and warm to room temperature before filtration and reduction of the solvent under vacuum. Large colourless crystals which were suitable for crystallographic determination formed at −20 °C within 48 h. The crystals were washed with cold hexane, dried in vacuo and stored in a dry box.

4.4. General synthesis of $Me_3Ga \cdot$ amine adducts

In a typical synthesis, 17.4 mmol of the respective amine was added drop-wise to a solution of $GaMe_3$ (2 ml) in hexane (20 ml) at −78 °C. The colourless solution was allowed to stir and warm to room temperature before filtration and reduction of 70% of the solvent under vacuum. Large colourless crystals formed at −20 °C over 48 h which were suitable for crystallographic determination. The crystals were washed with cold hexane, dried in vacuo and stored in a dry box. In the case of adduct **6**, the crystals are highly sensitive to traces of solvent and have a melting point close to room temperature. If the crystals are subjected to any reduction in pressure they immediately melt.

4.4.1. $Me_3Al \cdot HN(CHMePh)(CH_2Ph)$ (**1**)

Yield 81%, m.p. 69–70 °C, ^{1}H NMR (300 MHz, C_6D_6, 25 °C) δ 6.96 (b, *ortho*-H); δ 6.83 (b, *meta*-H); δ 6.74 (b, *para*-H); δ 4.20 and δ 4.05 (s, H, CH); δ 3.75 and δ 3.30 (s, H, CH_2); δ 2.58 (s, H, NH); δ 1.21 (s, 3H, CH_3); δ −0.34 (s, 9H, $Al(CH_3)_3$), ^{13}C NMR (75 MHz, C_6D_6): δ 141.0 (*ipso*-C); δ 137.3 (*ipso*-C); δ 129.8, δ 129.6, δ 129.5 and δ 128.9 (*Ar*-C); δ 57.5 (CH); δ 51.9 and δ 47.3 (CH_2); δ 18.8 and δ 16.6 (CH_3); δ 6.2 ($AlCH_3$). *Anal*. Calc. for $C_{18}H_{26}NAl$: C, 76.14; H, 9.35; N, 5.02. Found: C, 76.32; H, 9.19; N, 4.95%.

4.4.2. $Me_3Ga \cdot HN(CHMePh)(CH_2Ph)$ (**2**)

Yield 67%, m.p. 58–59 °C, ^{1}H NMR (300 MHz, C_6D_6, 25 °C) δ 7.01 (b, *ortho*-H); δ 6.86 (b, *meta*-H); δ 6.81 (b, *para*-H); δ 3.87 (s, H, CH); δ 3.52 (s, 2H, CH_2); δ 2.20 (s, H, NH); δ 1.20 (d, 3H, CH_3, $J^2 = 6.9$ Hz); δ −0.08 (s, 9H, $Ga(CH_3)_3$), ^{13}C NMR (75 MHz, C_6D_6): δ 141.4 (*ipso*-C); δ 137.8 (*ipso*-C); δ 128.9, δ 128.8 (*ortho*-C), δ 128.7 and δ 128.0 (*meta*-C); δ 127.9 and δ 127.7 (*para*-C); δ 56.8 (CH); δ 49.2 (CH_2); δ 18.2 (CH_3); δ −3.6 ($GaCH_3$). *Anal*. Calc. for $C_{18}H_{26}NGa$: C, 66.31; H, 8.02; N, 4.34. Found: C, 66.20; H, 7.98; N, 4.31%.

4.4.3. $Me_3Al \cdot HN(CHMePh)_2$ (**3**)

Yield 74%, m.p. 85–86 °C, ^{1}H NMR (300 MHz, C_6D_6, 25 °C) δ 6.91 (b, 2H *para*-H); δ 6.89 (b,4H, *meta*-H); δ 6.64 (b, 4H, *ortho*-H); δ 4.18 (s, 2H, CH); δ 2.84 (s, H, NH); δ 1.40 (d, 6H, CH_3, $J^2 = 7.0$ Hz); δ −0.28 (s, 9H, $Al(CH_3)_3$), ^{13}C NMR (75 MHz, C_6D_6): δ 141.2 (*ipso*-C); δ 128.4 (*ortho*-C), δ 127.6 (*meta*-C); δ 126.9 (*para*-C); δ 54.4 (CH); δ 17.7 (CH_3); δ −5.5 ($AlCH_3$). *Anal*. Calc. for $C_{19}H_{27}NAl$: C, 77.03; H, 9.12; N, 4.73. Found: C, 76.95; H, 9.21; N, 4.65%.

4.4.4. $Me_3Ga \cdot HN(CHMePh)_2$ (**4**)

Yield 46%, m.p. 61 °C, ^{1}H NMR (300 MHz, C_6D_6, 25 °C) δ 7.07 (m, *para*-H, *meta*-H); δ 6.99 (b, 4H, *ortho*-H); δ 3.71 (q, 2H, CH, $J^2 = 6.1$ Hz); δ 1.73 (s, b, H, NH); δ 1.21 (d, 6H, CH_3, $J^2 = 6.8$ Hz); δ −0.05 (s, 9H, $Ga(CH_3)_3$), ^{13}C NMR (75 MHz, C_6D_6): δ 144.6 (*ipso*-C); δ 129.0 (*ortho*-C), δ 128.6 (*meta*-C); δ 127.6 (*para*-C); δ 55.8 (CH); δ 23.6 (CH_3); δ 0.46 ($GaCH_3$). *Anal*. Calc. for $C_{19}H_{27}NGa$: C, 77.03; H, 9.12; N, 4.73. Found: C, 76.95; H, 9.21; N, 4.65%.

4.4.5. $Me_3Al \cdot HN(CHMePh)(CH_2CH{=}CH_2)$ (**5**)

Yield 49%, m.p. 34–36 °C, ^{1}H NMR (300 MHz, C_6D_6, 25 °C) δ 7.02 (b, 3H, *para*, *meta*-H); δ 6.72 (b, *ortho*-H); δ 5.65 (s, 1H, $CH_2CH{=}CH_2$); δ 4.82 (d, 1H, $J^1 = 9.55$ Hz, $CH_2CH{=}CH_2^a$); δ 4.70 (d, 1H, $J^1 = 17.14$ Hz, $CH_2CH{=}CH_2^b$); δ 3.85 (broad, s, H, CH); δ 3.07 (m, H, $CH_2^a CH{=}CH_2$); δ 2.75 (m, H, $CH_2^b CH{=}CH_2$); δ 1.99 (m, H, NH); δ 1.23 (s, 3H, CH_3); δ −0.33 (s, 9H, $Al(CH_3)_3$), ^{13}C NMR (75 MHz, C_6D_6): δ 140.2 (*ipso*-C); δ 132.7 ($CH_2CH{=}CH_2$); δ 128.4 (*ortho*-C), δ 127.9 (*meta*-C), δ 126.6 (*para*-C); δ 119.2 ($CH_2CH{=}CH_2$); δ 55.5 (CH); δ 49.3 (NCH_2); δ 21.9 (CH_3); δ −6.8 ($AlCH_3$). *Anal*. Calc. for $C_{14}H_{24}NAl$: C, 70.25; H, 10.5; N, 5.5. Found: C, 72.1; H, 10.4; N, 6.0%.

4.4.6. $Me_3Ga \cdot HN(CHMePh)(CH_2CH{=}CH_2)$ (**6**)

Yield 52%, m.p. <20 °C, ^{1}H NMR (300 MHz, C_6D_6, 25 °C) δ 7.02 (m, 3H, *para*, *meta*-H); δ 6.68 (b, 2H, *ortho*-H); δ 5.65 (m, 1H, $CH_2CH{=}CH_2$); δ 4.84 (dp, 1H,

$J^1 = 8.85$ Hz, $CH_2CH{=}CH^a_2$); δ 4.69 (dp, 1H, $J^1 = 14.18$ Hz, $CH_2CH{=}CH^b_2$); δ 3.78 (p, H, CH, $J^1 = 6.87$ Hz, $J^2 = 14.46$ Hz); δ 3.02 (m, H, CH_2 $^aCH{=}CH_2$); δ 2.68 (m, H, CH_2 $^bCH{=}CH_2$); δ 1.81 (s, H, NH); δ 1.15 (d, 3H, CH_3, $J^1 = 6.90$ Hz); δ −0.02 (s, 9H, $Ga(CH_3)_3$), ^{13}C NMR (75 MHz, C_6D_6): δ 141.7 (*ipso*-C); δ 133.4 ($CH_2CH{=}CH_2$); δ 128.4 (*ortho*-C), δ 127.5 (*meta*-C), δ 126.7 (*para*-C); δ 118.6 ($CH_2CH{=}CH_2$); δ 56.6 (CH); δ 48.4 (NCH_2); δ 20.6 (CH_3); δ −3.8 ($GaCH_3$). Satisfactory elemental analysis was not obtained most likely as a result of decomposition.

5. Supplementary material

Crystallographic data (excluding structure factors) have been deposited with the Cambridge Crystallographic Data Centre as supplementary publication numbers CCDC Nos. 178829–178833 (**1**–**5**), 216079 (**6**). Copies of the data can be obtained free of charge on application to CCDC, 12 Union Road, Cambridge CB2 1EZ, UK, fax: +44 1223 336 033; email deposit@ccdc.cam.ac.uk.

Acknowledgements

We thank the Australian Research Council and Monash University for financial support. We also thank Dr. John McGrady (York University) for some ab initio calculations (6-31G*) on the two diastereomers of compounds **1** and **2**.

References

[1] M.C. Carreño, M.J. Sanz-Cuesta, F. Colobert, G. Solladié, Org. Lett. 6 (2004) 3537.
[2] M. d'Augustin, L. Palais, A. Alexakis, Angew. Chem., Int. Ed. 44 (2005) 1376.
[3] P.K. Fraser, S. Woodward, Chem. Eur. J. 9 (2003) 776.
[4] L. Liang, A.S.C. Chan, Tetrahedron: Asymmetry 13 (2002) 1393.
[5] O. Pamies, G. Net, A. Ruiz, C. Claver, S. Woodward, Tetrahedron: Asymmetry 11 (2000) 871.
[6] D. Polet, A. Alexakis, Tetrahedron Lett. 46 (2005) 1529.
[7] J.J. Eisch, in: E.W. Abel, F.G.A. Stone, G. Wilkinson (Eds.), Comprehensive Organometallic Chemistry, vol. 11, Elsevier Science Inc., 1995 (Chapter 6).
[8] A.J. Downs (Ed.), Chemistry of Aluminium, Gallium, Indium, and Thallium, first ed., Blackie Academic & Professional, London, 1993.
[9] K. Maruoka, H. Yamamoto, Tetrahedron 44 (1988) 5001.
[10] K. Maruoka, H. Yamamoto, Angew. Chem., Int. Ed. Engl. 24 (1985) 668.
[11] S. Saito, in: H. Yamamoto, K. Oshina (Eds.), Main Group Elements in Organic Synthesis, vol. 1, Wiley–VCH, 2004 (Chapter 6).
[12] H. Schumann, J. Kaufmann, S. Dechert, Z. Anorg. Allg. Chem. 630 (2004) 1999.
[13] M.F. Lappert, P.P. Power, A.R. Sanger, R.C. Srivastava, Metal and Metalloid Amides, Ellis Horwood/Wiley, New York, 1980.
[14] G.E. Coates, M.L.H. Green, K. Wade, third ed.Organometallic Compounds, vol. 1, Methuen, London, England, 1967.
[15] G.H. Robinson (Ed.), Coordination Chemistry of Aluminium, VCH, New York, 1993.
[16] S.J. Schauer, C.L. Watkins, L.K. Krannich, R.B. Gala, E.M. Gundy, C.B. Lagrone, Polyhedron 14 (23) (1995) 3505.
[17] C.H. Lake, S.J. Schauer, L.K. Krannich, C.L. Watkins, Polyhedron 18 (1999) 879.
[18] F.C. Sauls, L.V. Interrante, Coord. Chem. Rev. 128 (1993) 193.
[19] D.C. Bradley, Polyhedron 18 (1994) 1111.
[20] M.G. Gardiner, C.L. Raston, Coord. Chem. Rev. 128 (1997) 1.
[21] P.C. Andrews, P.J. Duggan, G.D. Fallon, T.D. McCarthy, A.C. Peatt, J. Chem. Soc., Dalton Trans. (2000) 1937.
[22] P.C. Andrews, P.J. Duggan, G.D. Fallon, T.D. McCarthy, A.C. Peatt, J. Chem. Soc., Dalton Trans. (2000) 2505.
[23] S.G. Davies, D.R. Fenwick, Chem. Commun. (1997) 565.
[24] S.G. Davies, D.R. Fenwick, O. Ichicara, Tetrahedron: Asymmetry 8 (1997) 3387.
[25] S.G. Davies, G.D. Smyth, Perkins Trans. I (1996) 2467.
[26] S.G. Davies, O. Ichihara, Tetrahedron: Asymmetry 7 (1996) 1919.
[27] S.G. Davies, D.J. Dixon, Chem. Commun. (1996) 1797.
[28] S.G. Davies, G. Bhalay, Tetrahedron: Asymmetry 7 (1996) 1959.
[29] S.G. Davies, A.S.I. Walters, Perkins Trans. I (1994) 1129.
[30] K. Koga, Pure Appl. Chem. 66 (1994) 1487.
[31] P.J. Cox, A. Persad, N.S. Simpkins, Synlett 57 (1992) 5438.
[32] T. Honda, N. Kimura, M. Tsubuki, Tetrahedron: Asymmetry 4 (1993) 21.
[33] T. Honda, N. Kimura, M. Tsubuki, Tetrahedron: Asymmetry 4 (1993) 1475.
[34] K. Aoki, H. Naguchi, K. Koga, K. Tomioka, Tetrahedron Lett. 34 (1993) 5105.
[35] B.J. Bunn, N.S. Simpkins, J. Org. Chem. 58 (1993) 533.
[36] M. Bunnage, S.G. Davies, C.J. Goodwin, Perkins Trans. I (1993) 1375.
[37] S.G. Davies, O. Ichihara, Tetrahedron: Asymmetry 2 (1991) 183.
[38] P.J. Cox, N.S. Simpkins, Tetrahedron: Asymmetry 2 (1991) 1.
[39] C.M. Cain, R.P.C. Cousins, G. Coumbarides, N.S. Simpkins, Tetrahedron 46 (1990) 523.
[40] R.S. Ward, Chem. Soc. Rev. 19 (1990) 1.
[41] M.R.P. van Vliet, P. Buysingh, G. van Koten, K. Vrieze, Organometallics 4 (1985) 1701.
[42] D.R. Armstrong, F.J. Craig, A.R. Kennedy, R.E. Mulvey, Chem. Ber. 129 (1996) 1293.
[43] P. Wyatt, C.P. Butts, V. Patel, B. Voysey, Perkin Trans. 1 (2000) 4222.
[44] A. Kawachi, H. Maeda, K. Mitsudo, K. Tamao, Organometallics 18 (1999) 4530.
[45] W. Clegg, M. Ranelli, R.F.W. Jackson, Acta Crystallogr., Sect. C 51 (1995) 1604.
[46] M.B. Eleveld, H. Hogeveen, Tetrahedron Lett. 25 (1984) 5187.
[47] G.M. Sheldrick, SHELXS97, Program for the Solution of Crystal Structures, Göttingen, Germany, 1997.
[48] L.J. Barbour, XSEED: A graphical interface for use with the SHELXS program suite, University of Missouri, 1999.

development of new complexes having the ability to target specific tissues and physiological states [4,5,16,17]. Some chelating agents have been developed for metal intoxication, e.g., water soluble phosphine chelating agents are designed for chelating metals such as technetium, rhenium, platinum and gold [18–20]. Many organic compounds used in medicine do not have a purely organic mode of action; some are activated or biotransformed by metal ions including metalloenzyme, others have a direct or indirect effect on metal ion metabolism [4].

The pharmacological activities of these metal compounds depend on the metal ion, its ligands and the structure of the compounds. These factors are responsible for reaching them at the proper target site in the body [21]. Biologically relevant metal complexes have several requirements in terms of their synthetic design. First, a biologically active metal complex should have a sufficiently high thermodynamic stability to deliver the metal to the active site. The metal-ligand binding should be hydrolytically stable. The kinetics with which the metal ion undergoes ligation or deligation reactions is of great importance. The molecular weight of the metal complex is also critical. The compounds of low molecular weight with neutral charge and some water solubility are soluble in almost any medium and may slip through biological membranes by passive diffusion [22].

This article focuses on the chemistry and some recent developments on metal complexes relating to gold antiarthritic, silver antimicrobial, vanadium antidiabetic and bismuth antiulcer, drugs.

2. Gold antiarthritic and antitumor agents

Gold(I) drugs, such as gold(I) thiomalate [myocrisin $(Autm)_n$], gold(I) thioglucose [solganol $(Autg)_n$] and auranofin [2,3,4,6-tetra-*o*-acetyl-1-thio-β-D-glucopyranosato-(S)-triethylphosphine gold(I)] have been successfully used over many years for the treatment of rheumatoid arthritis [11,12,23]. Besides treating arthritis, a large number of phosphine gold(I) complexes especially, auranofin and $[Au(dppe)_2]Cl$ (dppe = 1,2-bis(diphenylphosphino) ethane) are also known to exhibit promising antitumor properties [24–28]. $[Au(CN)_2]^-$ and gold(I) thiocyanate complexes have also been investigated as chemotherapeutic agents, including mainly studies of the antitumor and anti-HIV activity, and cytotoxicity of several tertiary phosphine complexes of AuSCN [27,29,30]. Structures of some important gold drugs with their trade names are shown in Fig. 1.

The crystal structure of auranofin shows that gold is linearly coordinated by the sulfur atom of thioglucose and phosphorus of Et_3P to give a discrete monomeric molecular species [31]. Gold thiolates are polymeric in nature [32–34] (by sulfur bridging) with a gold–gold interaction (Fig. 2).

Since gold(I) is extremely labile, these gold(I) complexes after their administration, undergo several ligand exchange reactions in the body with biofluids, cells and proteins [32,35–38]. In the body gold(I) binds to the SH and S–S

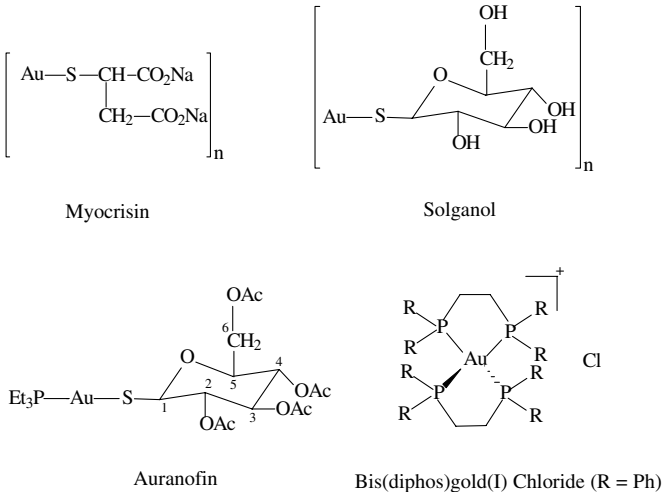

Fig. 1. Structures of some important gold drugs.

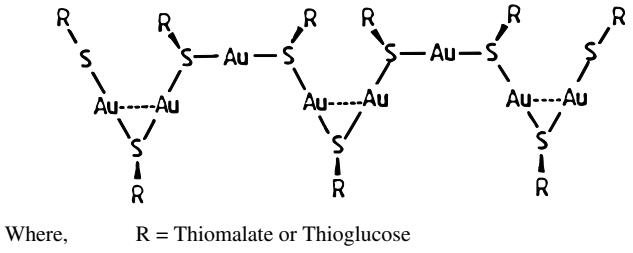

Fig. 2. Polymeric structure of gold(I) thiolates.

units of proteins such as blood serum albumin, which transport gold compounds throughout the body [39]. Gold(I) thiolates, (Gold(I), thiomalate and thioglucose) being polymers cannot enter red blood cells (RBCs) [40,41], while auranofin being monomeric does enter into RBCs immediately after its absorption and binds to glutathione (GSH) and hemoglobin (Hb) [42,43]. The RBCs, which contain thiol and thione ligands, e.g., GSH, Hb and ergothionine (ErS), can form stable complexes with gold drugs [44–46]. Gold has no known biological function in the body and hence there are no natural mechanisms for gold in the body. Therefore toxic effects may arise by the use of gold drugs [32].

Gold(I) thiolates because of their chain structure can undergo rapid ligand exchange reactions with the incoming ligands [11,12]. When excess thiols (RSH) such as cysteine and glutathione are added to $(Autm)_n$ polymers, they usually eject thiomalate by forming $[Au(thiolate)_2]^-$ species [47–49]. The kinetic analysis of these reactions shows that they proceed through associative mechanism. ^{13}C NMR studies suggest that thiols with the lowest pK_a values bind most strongly to gold(I) [47]. Thus binding of gold drugs with cysteine ($pK_a = 8.5$) will be thermodynamically more favored over glutathione ($pK_a = 8.9$). The phosphine gold(I) thiolate complexes undergo oxidation resulting in disulfide and tetragold clusters with bridging thiolate ligands [50].

$$2R_3PAuSR + Cp_2Fe^+ \rightarrow Cp_2Fe + 0.5(SR)_2 + 0.5[(R_3PAu)_2(\mu\text{-}SR)]_2^{2+} \quad (1)$$

The reaction of thiones such as ergothionine [46], Imt (imidazolidine-2-thione) [51], Diaz (1,3-diazinane-2-thione) [52] and mercaptopurines [53] with $(Autm)_n$ solution, usually results in the formation of a ternary complex of the type [>C=S–Au-tm], without ejecting thiomalate. Recently, it has been proposed that $(Autg)_n$ upon interaction with thiones does not form [>C=S–Au-tg], which suggests that the Au–S bond in $(Autg)_n$ is stronger compared to that in $(Autm)_n$ [54].

In auranofin ($Et_3PAuSATg$) both triethylphosphine and thioglucose ligands are strongly bound to gold(I), therefore, the ligand exchange reactions of auranofin are comparatively slower [32,42,44]. Several studies have shown that during the exchange reactions of auranofin ($Et_3PAuSATg$) with various biological sulfur containing ligands, e.g., bovine serum albumin and red blood cells, the $SATg^-$ ligand of auranofin is readily displaced while the gold bound phosphine is displaced slowly [36–38,44]. The presence of Et_3P bound to Au(I) appears to enhance the thiol exchange rates because of the high trans influence of phosphines [32].

Serum albumin is the most abundant plasma protein and principal extracellular source of sulfhydryl groups in the circulatory system [56]. Auranofin ($Et_3PAuSATg$) reacts rapidly with mercaptalbumin (AlbSH) via a ligand exchange reaction to form AlbS–Au–PEt_3 with gold binding to Cys-34 [36,57]

$$AlbSH + Et_3PAuSATg \rightleftarrows\rightleftarrows\rightleftarrows AlbS\text{–}Au\text{–}PEt_3 + HSATg \quad (2)$$

The albumin–gold complex, AlbS–Au–PEt_3 has been characterized by ^{31}P NMR [32,36,58], ^1H NMR [59,60] and chromatography [56,61]. The methyl and isopropyl analogues of auranofin ($R_3PAuSATg$; R = Me/*i*Pr) undergo similar reactions as (2) [62,63]. The AlbS–Au–PEt_3 complex further reacts with thiols leading to the oxidation of the phosphine moiety to Et_3PO [55]. The principal oxidants are albumin disulfide bonds and water is the major source of oxygen for the formation of Et_3PO [64].

$$AlbS\text{–}Au\text{–}PEt_3 + RSH \rightleftarrows\rightleftarrows\rightleftarrows AlbSH\text{–}Au\text{–}SR + Et_3PO + H^+ \quad (3)$$

The rate of phosphine oxidation increases as the affinity of thiol for gold increases, for example the ability of various thiols to cause Et_3PO formation from AlbS–Au–PEt_3 is; ATgSH > TgSH > GSH, as expected from their basicity [55]. The rate of formation of R_3PO decreases as the affinity of phosphine towards gold(I) in $R_3PAuSATg$ increases. For example, Me_3P is displaced to form the corresponding Me_3PO more readily than is Et_3P from auranofin, while *i*-Pr_3PO is formed only in small quantities from *i*-$Pr_3PAuSATg$ [62,63].

In addition to binding with mercaptalbumin, auranofin can also bind with disulfide sites of albumin as described by

$$AlbSSR + Et_3PAuSATg \rightleftarrows\rightleftarrows\rightleftarrows AlbSSR\text{–}Et_3PAuSATg \quad (4)$$

The AlbSSR–$Et_3PAuSATg$ complex is weakly bound and readily dissociates during separation by conventional gel chromatography [56]. Hemoglobin (Hb) and glutathione (GSH) in RBCs does not compete effectively with serum albumin for gold(I). The high affinity of albumin compared to Hb and GSH towards gold suggests that the accumulation/transfer of gold metabolites of auranofin in RBCs is thermodynamically not favored [43].

The kinetic analysis of the reaction between auranofin and serum albumin shows that the reaction is first order in albumin and zero order with respect to auranofin, with a rate constant, $k_1 = 3.4 \pm 0.3 \times 10^{-2}\ s^{-1}$ for Eq. (2). However, under physiological conditions, where auranofin concentration is low, 10–25 μM ([albumin] = ~400 μM) the reaction is suggested to follow the second order kinetics with a rate constant of $8 \pm 2 \times 10^2\ M^{-1}\ s^{-1}$ [56]. This high value of rate constant corresponding to a rapid ligand exchange reaction of auranofin with albumin explains the very strong affinity of Cys-34 for gold(I). A multistep mechanism was suggested [56] which can be explained as follow:

$$AlbSH \underset{k_{-1}}{\overset{k_1}{\rightleftharpoons}} {}^*AlbSH \quad (5)$$

$${}^*AlbSH + R_3PAuSATg \underset{k_{-2}}{\overset{k_2}{\rightleftharpoons}} {}^*AlbSAuPR_3 + AtgSH \quad (6)$$

$${}^*AlbSAuPR_3 \underset{k_{-3}}{\overset{k_3}{\rightleftharpoons}} AlbSAuPR_3 \quad (7)$$

where $^*AlbSH$ and $^*AlbSAuPR_3$ are conformationally altered albumin molecules in which cys-34 is accessible to other solute molecules. The rate law corresponding to this mechanism is:

$$\frac{d[AlbSAuPR_3]}{dt} = \frac{k_1k_2[R_3PAuSATg][AlbSH]}{k_{-1} + k_2[R_3PAuSATg]} = k_{obs}[AlbSH] \quad (8)$$

where

$$k_{obs} = \frac{k_1k_2[R_3PAuSATg]}{k_{-1} + k_2[R_3PAuSATg]}$$

In the interaction of auranofin with thiones such as thiourea and ergothionine, a simultaneous replacement of both Et_3P and $SATg^-$ ligands was observed, forming [>C=S–Au–SATg] and [Et_3P–Au–S=C<] type complexes [65,66]. These ligands are consequently oxidized to Et_3PO and $(SATg)_2$, respectively. Some of the liberated E_3P also reacts with thiones forming Et_3P–S=C< species. The Et_3PO resonance in ^{31}P NMR and $(SATg)_2$ resonances in ^{13}C NMR appeared after several (4–19) days showing that the exchange reactions are very slow. With thiols, the Et_3PO resonance was observed in the ^{31}P NMR after 24–72 h. A comparison of the rate of formation of Et_3PO from auranofin with various thiones demonstrates that their order of reactivity is Tu > Diaz > ErS > Imt [66].

The dicyanoaurate(I) anion, $[Au(CN)_2]^-$ has been identified as a common metabolite of the gold drugs in the blood and urine of chrysotherapy patients [67,68]. Model studies show that $[Au(CN)_2]^-$ is formed in vitro when CN^- reacts with the gold drugs or with the gold–protein metabolites such as the albumin–gold–triethylphosphine complex, AlbS–Au–PEt_3 [44,69]. As a result of this interaction, the intermediates $[RS–Au–CN]^-$ and $[Et_3P–Au–CN]$ are formed, which undergo disproportionation generating $[Au(CN)_2]^-$ that is readily taken up by red blood cells (RBCs) [44,69–73]. Several studies describe the formation of $[Au(CN)_2]^-$ by disproportionation of L–Au–CN complexes in solution [23,74–78] according to the following equilibrium;

$$2\,[L–Au–CN] \rightleftarrows\rightleftarrows\rightleftarrows [AuL_2]^+ + [Au(CN)_2]^- \quad (9)$$

Although the concentration of cyanide in RBCs is very low (0.3–1 μM) [79], the very large formation constant of $[Au(CN)_2]^-$ ($\log\beta = 36$) [80] favors its formation. Cyanide is produced in the body by oxidation of SCN^- by the enzyme myeloperoxidase in polymorphonuclear leukocytes [70,71]. The formation of aurocyanide is dependent on thiocyanate and occurs both by the myeloperoxidase dependent oxidation of thiocyanate and by a secondary reaction of hypochlorous acid with thiocyanate [71]. The aurocyanide formed inhibits the oxidative burst of polymorphonuclear leukocytes and inhibition of the oxidative burst of PMN may decrease the progression of the arthritis disease [71,81]. The level of $[Au(CN)_2]^-$ is higher for smokers than for nonsmokers because of inhalation of HCN from tobacco smoke [82,83]. Thus cyanide acts as a shuttle to carry gold into red blood cells, because of inhalation of HCN from tobacco smoke [84]. The most convincing mechanism by which $[Au(CN)_2]^-$ is transported through the cell membrane is the one, in which $[Au(CN)_2]^-$ undergoes ligand exchange reactions to bind to sulfhydryl groups immobilized on or in the membrane [79]. A series of such exchange reactions then passes the gold across the membrane and into the cells, where it may react with molecules containing sulfhydryl groups such as glutathione [79]. The displacement of CN^- from $[Au(CN)_2]^-$ by thiols in the model systems have already been studied [44], where the reaction may be written as:

$$[Au(CN)_2]^- + RSH \rightarrow [RSAuCN]^- + HCN \quad (10)$$

The replacement of cyanide from $[Au(CN)_2]^-$ depends on the strength of incoming ligand and stability of the resulting complex [23].

Gold compounds have been shown to possess antitumor and antibacterial activity, analogous to that of cisplatin [85]. In the light of close chemical similarity between the compounds of Pt and Au, there is a possibility that both may use DNA as a target site. Au(I) and Au(III) complexes can bind to DNA in vitro and can cleave DNA in cell culture [86]. Both gold(I) and gold(III) coordination compounds exhibit cytotoxic properties towards several tumor lines and both types of complexes are also effective on cells resistant to cisplatin [87–90]. In addition to a direct action on DNA, these complexes might also interact with other cellular sites and mitochondria appear as likely candidates [89]. Auranofin is cytotoxic to p388 leukaemia cells and inhibits DNA polymerases. Triethylphosphine gold(I) chloride reacts with DNA and inhibits oxidative phosphorylation [89]. $[Au(CN)_2]^-$ and Et_3PAuCN are also known to possess antitumor activity [27,33]. The tetrahedral chelate complex, $[Au(dppe)_2]Cl$ is active against certain types of cancer cells [91] and combination of $[Au(dppe)_2]Cl$ with cisplatin provided greater activity compared with either agent given alone [92]. Gold(I) complexes of bidentate pyridyl phosphines, $[Au(dpype)_2]Cl$ have shown promising in vitro and in vivo antitumor properties against B16 melanomia and p388 leukemia cells [93]. Another gold complex containing a monophosphine and a diphosphine instead of having both chelating phosphines, has been reported as potential antitumor agent [94]. Being structurally different, the linear two coordinate and tetrahedral gold(I) phosphine complexes may follow different mechanisms. Reactions with sulfhydryl groups are likely to be involved for auranofin and Et_3PAuCl, whereas lipophilic cationic properties of $[Au(dppe)_2]Cl$ and $[Au(dpype)_2]Cl$ may be important [89].

Auranofin and other gold complexes inhibited DNA replication but only at high concentrations compared with those that inhibited colony formation [95]. Et_3PAuCl appeared to interact with DNA under certain conditions (pH 9.5, borate buffer) but this compound did not produce DNA interstrand crosslinks and DNA breakage. The DNA reactivity of Et_3PAuCl was significantly less than that of cisplatin [96]. The high concentrations required for the cytotoxic effect suggested that DNA polymerases might not be a critical factor for the cytotoxic and antitumor actions of auranofin. Inhibition of DNA replication may have occurred via an interaction between auranofin and sulfhydryl groups on DNA polymerases [95]. Cisplatin-resistant cell lines with altered mitochondria were hypersensitive to auranofin and $[Au(dppe)_2]Cl$ along with a number of other antimitochondrial agents [87]. The results of various studies suggest that mitochondria are the primary intracellular targets for cytotoxic effects of auranofin and Et_3PAuCl [87,95–98].

The cationic tetrahedral complexes as $[Au(dppe)_2]^+$ are more stable with respect to ligand exchange reactions rather than the linear complexes and an important difference is that $[Au(dppe)_2]Cl$ is much less reactive towards thiols [99]. Lipophilicity of tetrahedral complexes plays a key role in determining their cellular uptake, cytotoxicity, host toxicity and in vivo antitumor activity [100]. In contrast to auranofin, inhibition of tumor colony formation by $[Au(dppe)_2]Cl$ was associated with preferential inhibition of protein synthesis compared to DNA and RNA synthesis and the production of DNA protein crosslinks [92]. Mitochondria were also suggested as potential targets involved in the antitumor and cytotoxic activity of $[Au(dppe)_2]Cl$.

$[Au(dppe)_2]Cl$ induced a rapid dissipation of the inner mitochondrial membrane potential, increased mitochondrial respiration, mitochondrial swelling and increased permeability of the inner membrane to cations and protons in isolated mitochondria [87,89,101].

In mitochondria, thioredoxin reductase appears as very specific target and both gold(I) and gold(III) complexes are highly specific inhibitors of mitochondrial thioredoxin reductase [90]. Thioredoxin reductase is a selenium enzyme with a selenol group present in the active site at the carboxy terminus of the enzyme [102]. Gold compounds preferentially interact with this site since selenol displays a greater affinity towards heavy metals [103]. Glutathione reductase, a protein, structurally and functionally closed to thioredoxin reductase but lacking selenol at the catalytic site requires concentrations of auranofin and other gold compounds orders of magnitude greater to be inhibited [104]. Both gold(I) and gold(III) markedly inhibit the activity of thioredoxin reductase, mitochondrial respiration to alter mmembrane potential and finally to induce swelling [90].

Gold(III) complexes, $(C_2H_5)_3P$-$AuBr_3$ [105], $[Au(PPh_3)L]$ (L = imidazole) [106], $[AuCl_2(dmamp)]$, (dmamp = 2-(dimethylaminomethyl) phenyl) [85], RAu(III)L (L = thiosalicylate) [107] and a number of amine–gold(III) complexes [108] are known to exhibit antibacterial and antitumor activity. Gold(III) complexes of aminoquinolines were also found to possess DNA binding properties and cytotoxicity against melanoma and lung tumor cells [109]. Gold(III) tetraaryl porphyrins are known to exert high potency than cisplatin in killing human cancer cells including drug resistant variants [110]. The cytotoxicity of gold(III) complexes is associated with the presence of gold(III) center, e.g., $[Au(en)_2]Cl_3$ and $[Au(dien)Cl]Cl_2$ are more cytotoxic than the corresponding platinum complexes [108]. Gold(III) compounds appear less effective than auranofin in stimulating mitochondrial swelling and this might depend on the different permeability characteristics of these compounds [90]. The development of gold(III) complexes as potential antitumor agent has been hampered by their poor stability under physiological conditions. The stability of gold(III) center may be enhanced by coordination to multidentate ligand. However, the excessive stabilization results into the loss of biological activity [108].

Although gold drugs have been in clinical use for over 70 years, their exact mechanisms of action are still unknown. This is because the specific cellular targets for gold are unclear. Gold(I) has a high affinity for thiolate sulfur, hence proteins containing cysteine thiolate groups (albumin, glutathione) are possible target sites for gold(I). Several metabolites of these drugs have been characterized; $[Au(CN)_2]^-$ has been identified as a common metabolite of all gold drugs. The antitumor properties of posphine–gold complexes are probably due to their antimitochondrial activity. Optimization of their hydrophilic–lipophilic balance may be a key to improving their selectivity for tumor mitochondria.

3. Silver antimicrobial agents

Silver and its compounds have long been used as antimicrobial agents in medicine. Silver is active at low concentrations and has a low toxicity. Silver sulfadiazine is a widely used broad-spectrum antibiotic ointment, effective against a broad range of bacteria and some yeasts. It is used to prevent and treat skin infections on the areas of burnt skin [4].

Silver complexes of oxygen donor ligands such as, $[Ag(hino)]_2$ (where hino = 4-isopropyltopolone) [111] and water-soluble silver(I) complexes of (*R*)-(+)- and (*S*)-(−)-2-pyrollidone-2-carboxylic acid [112] displayed wide ranging and effective activities against some bacteria, yeasts and moulds. It has been found that the silver–oxygen bonding properties rather than the chiral helical or achiral polymer structure play a role in exhibiting antimicrobial activities. The antimicrobial activities of the silver(I)–oxygen bonding complexes are independent of whether the ligand itself possesses antimicrobial activities. Examples of such complexes are; $\{[Ag(L\text{-}Hasp)]_2\}$ and $\{[Ag(L\text{-}Hasp)]_2\}_n$, where the ligand showed no activity [113]. Similarly, salicylic acid (salH) did not prevent the growth of a fungal pathogen, while the silver complexes, $[Ag(salH)]_2$ and $[Ag(NH_3)(salH)]_2$ greatly inhibited cell reproduction. These complexes also produced a cytotoxic response against human cancer cells [114].

The biological action of the silver(I) oxygen complexes comes from a weaker bonding property of the Ag–O bond. In the biological system, the ease of ligand replacement of the silver(I) complexes would result in further replacement with biological ligands [113,115–117]. The Ag–O bonding complexes can readily undergo ligand replacement with O-, N- or S-donor atoms. The antimicrobial activities by silver(I)–oxygen bonding complexes are due to the silver(I) ion itself, i.e., due to a direct interaction between the silver(I) ion and biological ligands such as protein, enzymes and membrane. The coordinating ligands of the silver(I) complexes play the role of carrier for the silver(I) ion to the biological system [111]. The magnitude of antimicrobial properties of silver complexes is related to the ease with which they participate in ligand exchange reactions [118]. For example, it has been speculated that the weak Ag–O [113] and Ag–N [115] bond strengths might play an important role in exhibiting wider spectrum of antimicrobial and antifungal activities and that the potential target sites for inhibition of bacterial and yeast growth by silver complexes might be the sulfur containing residues of proteins [119]. Generally, Ag–S complexes have been shown to have a narrower spectrum of antibacterial activity than Ag–N complexes but no antifungal activity [120]. In contrast, the compounds with Ag–P bonds have shown no activity against bacteria, yeast or molds [115,121].

A sulfur coordinated, water soluble silver(I) complex of thiomalic acid showed remarkable antimicrobial activity against some bacteria, yeast and moulds. Although aqueous silver nitrate itself has similar activities for bacteria, the complexation of silver(I) with thiomalate leads to

appreciably high activities for some moulds [122,123]. Antimicrobial activities have been observed for sulfur bonded silver complexes of 2-mercaptonicotinic acid, $[Ag(Hmna)]_6 \cdot 4H_2O$ [119] and 2-mercaptobenzoic acid, $[Ag(Hmba)]_n$ and $[Na\{Ag(Hmba)\} \cdot H_2O]_n$ [121]. The spectra of antimicrobial activities observed in Ag–S bonded compounds have so far been narrower than those in the Ag–N bonded compounds such as $[Ag(im)]_n$ (im = imidazole) and $[Ag(triaz)]_n$ (triaz = 1,2,4-triazole) [120,124]. The key factor determining the spectra of antimicrobial activity is the nature of atom coordinated to the silver(I) atom and its bonding properties, (i.e., the ease of ligand replacement), rather than the solid state structure, solubility, charge and degree of polymerization of the complexes [118,120].

4. Vanadium antidiabetic agents

The discovery of vanadium's insulin behavior (stimulate glucose uptake and oxidation as well as glycogen synthesis) during 1975–1980 has stimulated the renewed interest in vanadium coordination chemistry [125,126]. Vanadium compounds mimic most of the metabolic effects of insulin on different cellular types [127–129]. Vanadium compounds modify glucose and lipid metabolism in adipose tissue, muscle, liver and several cultured cell lines, which may contribute to the glucose-regulating effects of vanadium [127,129]. The antidiabetic action of vanadium may be attributed to the inhibition of several enzymes involved in the carbohydrate and fat metabolism, such as phosphodiesterase and tyrosine phosphatases [127,129,130]. During the years 1980–90, the insulin like actions of vanadium salts were examined in a large variety of insulin responsive cells and tissues. Vanadium salts activate hexose transport in adipose and muscle tissues [127]. Vanadium activates glycogenesis and inhibits glycogenolysis in liver and diaphragm [131]. It inhibits several key metabolic enzyme systems in liver, muscle and adipose tissues, all of which act collectively towards utilizing or storing cell entered glucose as well as blocking the actions of hormones that oppose insulin actions [132]. It also serves as an electron acceptor, which could stimulate enzymatic and nonenzymatic oxidation of NAD and NADPH into their oxidized forms NAD^+ and $NADP^+$ [133,134]. Besides the antidiabetic effects for which it is now so well known, vanadium also exhibits a number of other therapeutic effects including anti-tumor and anti-inflammatory activities [135,136].

Vanadium possesses various oxidation states, e.g., +3, +4 and +5, all of which can interact with biomolecules containing negatively charged oxygen donors such as carboxylate, phenolate, phosphate, phosphonate and hydroxamate groups [137]. Under physiological conditions vanadium exists predominantly in the anionic form as vanadate, VO_4^{3-} (oxidation state +5) and in the + 4 oxidation state as vanadyl cation (VO^{2+}) [127]. In experimental diabetic animals, both vanadyl and vanadate ions have been found to have an insulin mimetic effects on glucose metabolism. However, vanadyl is less toxic than the vanadate ion [138]. Vanadium complexes with organic ligands are often less toxic and can have improved aqueous solubility and lipophilicity [4]. The chelated vanadium complexes have the property of increasing permeation into tissues by passive diffusion and corresponding increased insulin mimetic efficacy. The most effective ligands are those having nearly the same binding affinity for the vanadyl (+4) cation and the vanadate (+5) anion at physiological pH values [127,139].

In recent decades, some vanadyl complexes with several types of organic ligands such as maltol have been proposed for clinical use in humans [135,140–143]. Maltol (3-hydroxy-2-methyl-4-pyrone) and its derivatives like kojic acid (3-hydroxy-2-hydroxymethyl-4-pyrone) possess moderate intrinsic bioactivity and low toxicity profile. They can act as anionic and chelating *O*,*O*′ ligands forming neutral oxovanadium complexes [135,144–146]. Coordination complexes of oxovanadium(IV) with maltol and ethylmaltol (which are under clinical trials) have proven especially suitable for enhancing vanadium's insulin mimetic activity in experimental diabetic animals in recent years [144,147]. The orally active complex bis(maltolato)oxovanadium(IV) {BMOV} is three times more effective in vivo as insulin mimetic agent than $VOSO_4$ [148–150]. The insulin-enhancing properties of BMOV has been investigated thoroughly [140,143,144,150,151]. Several analogues of BMOV have been synthesized and tested for bioactivity as potential insulin enhancing agents [144,152]. Substitution of nitrogen for oxygen in the maltolato heterocycle lowers the solubility of complex rendering it unfit for therapeutic utility [144]. Vanadium complexes with thio derivatives of maltol also did not lower the blood glucose levels, possibly because of the rapid dissociation and excretion [153].

BMOV possesses several advantages over inorganic vanadium compounds in terms of its oral administration, low toxicity and enhanced tissue uptake [154]. The complex BMOV has a five coordinate square pyramidal geometry with the oxo ligand in the axial position and trans maltolato ligands (Fig. 3) [4]. In aqueous solutions or in alcohol, BMOV, V(IV) undergoes reversible oxidation to form the V(V) maltol complexes, $[VO_2(ma)_2]^-$ or $[VO(OR)(ma)_2]$, respectively. The oxidation kinetics being second order; substitution reactions of BMOV showed that oxygen must bind for the oxidation to $[VO_2(ma)_2]^-$ to take place [154]. The reaction in water is pH dependent and it has been

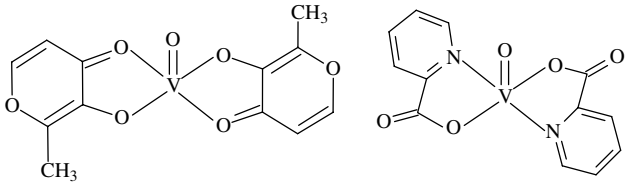

BMOV $VO(pic)_2$

Fig. 3. Structures of insulin mimetic vanadium complexes.

shown that both $[VO(H_2O)(ma)_2]$ and $[VO(OH)(ma)_2]^-$ can be oxidized by molecular oxygen [154]. A recent study shows that V(V)-dipicolinato complex is the more effective insulin enhancing agent compared to BMOV, which is so far considered as the most effective. The compound's acid stability or its redox chemistry may be key to the ability of the V(V) complex to lower the elevated glucose levels in the diabetic wistar rat during oral treatment [155].

β-Diketonato complexes such as $VO(acac)_2$ have been considered as potential insulin mimetic agents [156,157]. Recently, a new orally active complex, bis(α-furancarboxylato) oxovanadium(IV) has shown the glucose lowering ability comparable to BMOV, and possesses high water solubility and less toxicity when orally administered in diabetic rats [158]. Vanadium complexes of pyridine carboxylic acids are particularly interesting molecular model systems because they are potential agents for treating insulin dependent diabetes mellitus in rats by injection or oral administration [159]. Several oxovanadium complexes with substituted picolinic acid have been reported [137,160–165]. The picolinato complexes, for example bis(pyridine-2-carboxylato) oxovanadium(IV), $VO(pic)_2$ (Fig. 3) exerted a higher insulin mimetic activity than that of $VOSO_4$ [166]. For the oxovanadium complexes of 3-hydroxypyridine-2-carboxylic acid, mono as well as tetranuclear species are formed. The mononuclear complex exhibits relatively higher insulin mimetic activity than $VOSO_4$, while the tetranuclear complex shows significantly lower activity [167]. Some vanadyl complexes of anti-inflammatory drugs containing carboxylate ligands have been reported [168]. The oxovanadium picolinato system possesses satisfactory hydrolytic stability as well as disfavors interconversion between the oxovanadium(IV) and dioxovanadium(V) complexes, a property desired in insulin-mimetic drug.

Peptide bound complexes with one tetradentate ligand in place of two bidentate ligands may increase the stability constants of resulting complexes via the chelate effect. Hydrated oxovanadium complexes of *N*-alkylated derivatives of various amino acids, $[VO(XeX)(H_2O)]$ where XeX = *N*,*N*′-ethylene bis-α-amino acid have been synthesized and were observed to possess insulin mimetic effect [169–171]. Recently, some vanadyl complexes with amino acid derivatives containing an imidazole group have been reported [172].

A few V(V) complexes [155,173,174] and V(III)-hydroxypyrone and -pyridinone complexes [175] have been reported as having glucose lowering effects. V(III) complexes have been shown to lower diabetic hyperglycemia after acute treatment, but they are not usually considered as potential therapeutic agents because they readily oxidize to V(IV) and V(V) compounds under physiological conditions [175].

Several factors such as the electronic properties of the substituent, its position on the ligand and the hydrophobic nature of the complex alter the biological activity of the complex. The introduction of electron donating substituents in the pyridine ring of picolinato ligand alters the activity of the resulting complex. The picolinato complexes possessing iodo group $[VO(ipa)_2]^-$ and methyl groups $[VO(3\text{-}mpa)_2]$ and $[VO(6\text{-}mpa)_2]$ provided higher activities than $[VO(pa)_2]$ [159]. The complexes having electron withdrawing Cl^- groups $[VO(4\text{-}Clpa)_2]$ exhibits lower in vivo activity than $[VO(pa)_2]$ [176]. Moreover, the in vitro activity of $[VO(3\text{-}mpa)_2]$ is higher than that of $[VO(6\text{-}mpa)_2]$ [159]. The hydrophobicity of a complex also affects its biological activity. The insulin mimetic activity of $[VO(6mpa)_2]$ with the higher partition coefficient than $[VO(pa)_2]$ in the *n*-octanol/saline system was higher [177].

An important property of synthetic vanadium containing insulin-mimetic compounds is their varying patterns of tissue uptake. Vanadyl species were distributed in peripheral tissues and gradually eliminated from the circulating blood, depending on their chemical structures [159]. The slower elimination of vanadyl species from the circulating blood of rats given vanadyl–picolinato complexes was closely related with their interaction with the blood components such as serum proteins or erythrocytes [177]. The organ distribution of $VO(pic)_2 \cdot H_2O$ indicates a preferential accumulation in bone vs kidney, which is twice than that seen with BMOV. The ratio of vanadium in kidney vs liver was also far greater for BMOV (7.4: 1.0 compared to 1.4:1.0), which may be less suitable for an insulin mimetic [163,178]. Distribution studies indicated that vanadium distribution in the body was not homogeneous [178,179]. Vanadium was detected in almost all body tissues after drug administration with the following order of magnitude: bone > kidney ⩾ liver ⩾ spleen > heart > testes > lung > pancreas > blood ∼ muscle > brain. Residence time was short for blood, longer for kidney, testes and liver, and very long for bone. Vanadium concentration in bone, kidney and liver 24 h after oral administration of BMOV were two to three times higher than those of $VOSO_4$, which is consistent with the increased glucose lowering potency of BMOV compared with $VOSO_4$ [178,179].

Vanadium compounds show the insulin mimetic effect through an inhibition of protein tyrosine phosphatases (PTPases) [129,180–182]. Because PTPases are considered to be negative regulators of the insulin-signalling pathway, it was suggested that vanadium can enhance insulin signaling and action by virtue of its capacity to inhibit PTPase activity and increase tyrosine phosphorylation of substrate proteins [129,183–187]. The PTPase inhibition by vanadium prevents dephosphorylation of tyrosine phosphorylated insulin receptor substrate (IRS) and increases the tyrosine phosphorylation level [129]. Recent findings demonstrate that BMOV inhibited intracellular PTP1B activity and enhanced the autophosphorylation of the insulin receptor in vivo, supporting that PTP inhibition as the mechanism of insulin sensitization [180,181]. NMR and X-ray studies of the interaction of BMOV with two phosphatases, HCPTA (human low molecular wt cytoplasmic protein tyrosine phosphatase) and PTP1B (protein tyrosine phosphatase 1B) demonstrated that uncomplexed

vanadium (VO_4) is the active component of BMOV. The crystal structure of PTP1B soaked with BMOV reveals that VO_4 is coordinated to serine 215 through a complex network of hydrogen bonds. The chelating maltol ligands were not observed in the structure, suggesting that ligand dissociation and oxidation to VO_4 may be required for efficient phosphatase inhibition. The presence of uncomplexed VO_4 at the active site further suggests that the organic ligand plays no role at the enzyme except perhaps as a delivery vehicle for vanadium [180]. In addition, based on kinetics of ligand substitution, it has been proposed that maltol would be readily replaced by stronger ligands in biological fluids [188].

Another target of vanadium could be the lipid phosphatase, phosphatase and tensin homologue (PTEN), which can dephosphorylate PIP_3 (phosphatidylinositol 3,4,5-triphosphate) [129,189]. The PETN inhibition prevents dephosphorylation of PIP_3, which is important for the activation of phospholipid-dependent kinase (PDK) and related serine/threonine protein kinases responsible for phosphorylation and stimulation of several downstream signaling protein kinases, such as protein kinase B (PKB) [190,191]. Activation of these protein serine/threonine kinases has been implicated in many of the physiological responses of insulin at the level of glucose transport, glycogen and protein synthesis [192].

Despite their impressive antidiabetic properties, vanadium compounds have been associated with several toxic effects. The most common are diarrhea, decreased fluid and food uptake, dehydration and reduced body weight gain, which could be corrected by decreasing the dose level [129,193,194]. Organic vanadium compounds are much safer as antidiabetic agents than inorganic vanadium salts. Administration of the chelator iron was also found to minimize vanadate toxicity without altering its antidiabetic actions [195]. In addition to gastrointestinal discomfort, other toxic effects of vanadium salts include hepatotoxicity, nephrotoxicity and tetratogenicity as well as reproductive toxicity [194]. Further detailed investigations are needed to evaluate the toxicity of various vanadium compounds before undertaking long-term clinical trials in humans.

5. Bismuth antiulcer agents

Bismuth compounds are most commonly used for treating gastrointestinal disorders [196]. The effectiveness of bismuth has been attributed to its bactericidal action against the gram-negative bacterium *Helicobacter pylori* (the bacterium associated with the mucus layer of ulcers) [197]. The roles of colloidal bismuth citrate (CBS) and bismuth subsalicylate (BSS) in gastric and duodenal ulcer therapy and the eradication of Helicobacter pylori have been studied extensively [198–202]. Among the bismuth containing pharmaceuticals, bismuth subsalicylate (Pepto-Bismol), colloidal bismuth citrate (De-Nol) and ranitidine bismuth citrate (Pylorid) are the most widely used for the treatment of diarrhea, dyspepsia and peptic ulcers [196,203–205]. Recently, a bismuth single–triple capsule containing CBS, metroindazole and tetracycline has been approved for the eradication of *H. pylori* [206,207]. Several other bismuth salts such as $Bi(NO_3)_2 \cdot 5H_2O$, $BiCl_3$ and BiOCl are also employed in medicine. Elemental bismuth has also been found in natural medicinal plants. The diversity of bismuth compounds in medicine extends to the treatment of syphilis and tumors, in radioisotope therapies, in the reduction of renal toxicity of cisplatin and pharmacy [196]. Citrate (3-carboxy-3-hydroxypentane-1,5-dioic acid) salts of bismuth represent the most extensively studied series of bismuth compounds by virtue of their widespread medicinal use. Bismuth citrate is essentially insoluble in water, but a dramatic increase in solubility with increasing pH has been exploited as a bioready source of soluble bismuth, a material referred to as "Colloidal Bismuth Subcitrate" (CBS) [196]. Ranitidine bismuth citrate is a new water soluble therapy for peptic ulcer disease, which is obtained from the reaction of ranitidine hydrochloride (*N*,*N*-dimethyl-5-(3-nitromethylene-7-thia-2,4-diaaoctyl)furan-2-methamine) with bismuth citrate [153]. [^{1}H, ^{13}C] HSQC NMR has shown that a wide range of types of bound citrate in aqueous solutions of Ranitidine bismuth citrate at pH 7.4. The identification of cluster species in solution is particularly important since they may be taken up by cells by a different mechanism compared to low molecular mass complexes [208].

The coordination chemistry of Bi(III) with carboxylates and amino carboxylates is dominated by intermolecular interactions, which leads to polymeric structures [207]. The X-ray structures of Bi(III) citrate complexes are complicated and contain chains and sheets of dimeric $[Bi_2(Cit)_2]^{2-}$ units. The $[Bi_2(Cit)_2]^{2-}$ dimer contains strong Bi(III)-alkoxide bonds and a double carboxylate bridge (Fig. 4) [4,209]. ^{1}H and ^{13}C NMR studies indicate rapid exchange of citrate moieties at low concentration and the existence oligomeric and polymeric units at higher concentration [208,210–212]. Recently, the structure of colloidal bismuth subcitrate was determined under acidic conditions. X-ray crystallography revealed the presence of three types of Bi-citrate dinuclear unit $[Bi(cit)_2Bi]^{2-}$, which function as building blocks, assembling into a three dimensional polymer. CBS may rearrange from colloidal particles such as $[Bi_6O_4(cit)_4]^{6-}$ and $[Bi_{12}O_8(cit)_8]^{12-}$ at neutral pH value, to sheets and 3D polymers under acidic conditions (e.g., in stomach) due to rapid ligand exchange. Because the complex has significant resistance to acid (HCl), it can be regarded as the potential active species of the antiulcer

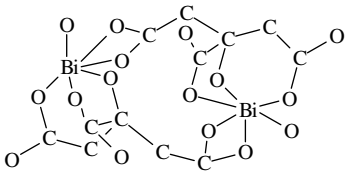

Fig. 4. Bismuth citrate dimer.

drug CBS in stomach and is thus a possible candidate for the tiny crystals found on the ulcer craters [213].

Despite its popular use, bismuth exhibits only modest antibacterial activity. Bismuth therapy provides short-term effects requiring administration of relatively large, frequent doses, which increase the chances of toxicity. The limited antibacterial effect of bismuth is attributed to the poor solubility of bismuth in water [214]. Chelation of bismuth with certain thiol compounds significantly enhanced its solubility and lipophilicity, thereby enhancing its potency and versatilely as an antimicrobial agent. The lipid aspect of bismuth-thiols facilitates transport into and through lipid membranes in bacteria [215]. Certain chemical features on thiols are necessary for the biological activity of Bi–S compounds. It has been observed that the addition of one or more carbon atoms to the chelate ring abolished the biological activity, whereas, the addition of a sulfur atom to the ring but not the addition of oxygen restored the biological activity [216]. Alcohols, amines and especially, acid group substitutions on thiols diminished activity, likely through their influence on lipophilicity. Dithiols are generally more active than monothiols, as they are better chelators [215]. Bismuth is likely the antibacterial moiety, since it is known to exchange with thiols and inactivate membrane-bound enzymes involved in respiration, such as the F_1-ATPase of *H. pylori* [217]. When bismuth is replaced with arsenic and antimony, the compound's antibacterial activities are reduced [215], which confirms that antibacterial activities are attributed to the bismuth contents.

The biological effects of Bi(III) are due to binding to proteins and enzymes [203]. Sulfur-based biomolecules represent the primary targets for Bi pharmaceuticals, such as CBS and BSS [218,219]. Bismuth compounds of such ligands have been characterized by ^{13}C NMR [197,220–222], mass spectrometry [218,219,223,224] and X-ray crystallography [223–225]. Bi(III) binds strongly to both oxygen and sulfur ligands. Cysteine and glutathione may play a role in the transport of Bi(III) in cells and biofluids. Bi(III)-thiolate adducts are kinetically labile, which allows rapid translocation of Bi(III) inside cells [203]. Animal studies have shown that simultaneous oral administration of bismuth salts and thiols produces a significant rise in bismuth concentration in blood plasma. The sulfur-based ligands are speculated to achieve *tris*-substitution in Bi(methionine)$_3$ and Bi(cysteine)$_3 \cdot 5H_2O$. The glutathione complex, [Bi(SG)$_3$] is very stable over a wide range of pH (2–10), with binding through sulfur atom only. The binding of bismuth with proteins of exposed ulcer tissue and the formation of a protective coating is proposed as a mode of action for the antiulcer behavior of some bismuth compounds [220]. A recent study shows that BSS reacts not only with thiol containing substrates but also with some common foods to produce soluble bismuth products and these products have excellent against the bacterium *Clostridium difficile* [226].

The antimicrobial activity of bismuth complexes towards gram-negative bacteria has been reported to be dependent on the iron uptake system, as iron is essential for the growth of *H. pylori*. Efficient iron acquisition is thought to be an important virulence factor for this bacterium [222]. Bismuth is primarily present in red blood cells, possibly binding to glutathione with the remainder in serum or plasma [227–229]. Previous investigations showed that albumin may be the major target for Bi(III) in plasma especially since albumin has a free thiolate group at cys-34 [227]. But recently, it has been demonstrated that binding of Bi(III) to transferrin (hTF) is much stronger than human albumin (HAS) in blood plasma [230]. Most of the Bi^{3+} was associated with transferrin in the presence of a large excess of albumin. Moreover, the binding constant for Bi^{3+} to HAS, log$K$ was calculated to be 11.2, which is much lower than that for Bi^{3+} to hTF ($\log K_1 = 19.9$ and $\log K_2$ 18.6) [230]. This suggests that transferrin is the major target for bismuth in blood plasma. Lactroferrin (hLF) is another major iron-binding protein in the transferrin family. Lactoferrin is present in significant amounts in the stomach secretions of patients with gastritis. Bi(III) binds to human lactoferrin into the two specific iron sites in the presence of either carbonate or oxalate. The presence of ATP facilitates the release of Bi(III) from the lactoferrin complex. The Bi_2-hLF complex blocked the iron uptake to intestinal cells. Bi(III) may be released inside the cells and inhibit target enzymes, in the case of bacteria, including enzymes essential for their survivals [222].

Bi(III) ions inhibits the biological activity of glycine-extended gastrin-17, a gastrointestinal hormone. The biological activity of gastrin-17 is associated with its binding to high affinity Fe(III) ions. Bi(III) ions inhibit the action of gastrin by blocking its effects on cell proliferation and cell migration in the gastrointestinal tract [231].

Bi(III) binds strongly to metallothionein (MT) with a stoichiometry Bi_7MT and can readily replace Zn^{2+} and Cd^{2+} ions. NMR studies suggest that Zn^{2+} is displaced faster than Cd^{2+}. Bi–S bonds in metallothionein are remarkably stable even down to pH values near 1.0, in contrast to Zn^{2+} and Cd^{2+}, which are 50% dissociated at pH 4.6 and 3.05, respectively. The high stability of Bi-MT suggests that it could play an important role in the pharmacological activity of bismuth antiulcer drugs [232]. Metallothionein may also play a role in cellular resistance to Pt anticancer drugs [232,233]. Bismuth is known to induce the synthesis of renal metallothionein [234]. Administration of bismuth can induce the synthesis of metallothionein in kidney but not in tumor tissue. This reduces the renal toxicity of cisplatin without compromising its antitumor activity [235,236]. The protection probably involves platinum binding to Bi-induced metallothionein. Therefore it has been suggested bismuth compounds are ideal for clinical application has adjuncts in chemotherapy with cisplatin [232]. Bismuth compounds themselves are known to possess antitumor activity and DNA-binding property [237].

Bismuth therapy is associated with several side effects. The most common consequence of overdose is neurological

dysfunction [238]. Neurotoxicity of bismuth drugs is generally diagnosed by the detection of bismuth in blood, plasma or serum [239]. In experimental animals bismuth overdose results in lowered serum testosterone levels suggesting that reproductive dysfunction may be an additional component of bismuth toxicity [238]. Bismuth toxicity is reversible over several week or months, when bismuth intake is stopped [240].

6. Conclusions

In this review, various structural and mechanistic aspects of some metallodrugs have been explained. Although the exact mechanism of these drugs is not completely understood, there have been many developments in understanding of the factors that control metal binding to possible biological target such as thiols. Further studies are required to explore their actual mechanism of action. For gold complexes, which exhibit promising antitumor properties, there is a need to study the interactions between gold complexes and mitochondrial enzymes and other cellular targets that could lead to cell death. The kinetics of metal–ligand interactions are crucial to all properties related to biological activity, therefore metallokinetics of these drugs should be investigated. For vanadium complexes however, several systematic kinetic studies have been reported. Understanding the nature of interactions of metallodrugs with cell membrane and the biological targets like DNA and proteins is also important. Such informations are useful in development of new compounds that comprise the efficient transport properties and possess minimum side effects.

References

[1] S.J. Lippard, M.J. Berg, Principles of Bioinorganic Chemistry, University Science Books, Mill Valley, CA, 1994.
[2] C. Orvig, M.J. Abrams, Chem. Rev. 99 (1999) 2201.
[3] C.D. Garner, J. Chem. Soc., Dalton Trans. (1997) 3903.
[4] Z. Guo, P.J. Sadler, Angew. Chem., Int. Ed. 38 (1999) 1512.
[5] P.J. Blower, Annu. Rep. Prog. Chem., Section A 96 (2000) 645.
[6] C.X. Zhang, S.J. Lippard, Curr. Opin. Chem. Biol. 7 (2003) 481.
[7] R.A. Sanchez-Delgado, A. Anzellotti, Mini. Rev. Med. Chem. 4 (2004) 23.
[8] E.R. Jamieson, S.J. Lippard, Chem. Rev. 99 (1999) 2467.
[9] T.W. Hambley, J. Chem. Soc., Dalton Trans. (2001) 2711.
[10] M.A. Fuertes, J. Castilla, C. Alonso, J.M. Perez, Curr. Med. Chem. 10 (2003) 257.
[11] C.F. Shaw III, Chem. Rev. 99 (1999) 2589.
[12] S.L. Best, P.J. Sadler, Gold Bull. 29 (1996) 87.
[13] W.A. Volkert, T.J. Hoffman, Chem. Rev. 99 (1999) 2269.
[14] S. Liu, D.S. Edwards, Chem. Rev. 99 (1999) 2235.
[15] H. Breitz, D.R. Fisher, B.W. Wessels, J. Nucl. Med. 39 (1998) 234P.
[16] M. Woods, Z. Kovacs, A.D. Sherry, J. Supramol. Chem. 2 (2002) 1.
[17] P. Caravan, J.J. Ellison, T.J. McMurrey, R.B. Lauffer, Chem. Rev. 99 (1999) 2293.
[18] O. Andersen, Chem. Rev. 99 (1999) 2683.
[19] O. Andersen, Mini. Rev. Med. Chem. 4 (2004) 11.
[20] K.V. Katti, H. Gali, C.J. Smith, D.E. Berning, Acc. Chem. Res. 32 (1999) 9.
[21] P.J. Sadler, Z. Guo, Pure Appl. Chem. 70 (1998) 863.
[22] K.H. Thompson, V.G. Yuen, J.H. McNeill, C. Orvig, in: A.S. Tracey, D.C. Crans (Ed.), Vanadium Compounds; Chemistry, Biochemistry and Therapeutic Applications, ACS Symposium Series, vol. 711, 1998, p. 329.
[23] S. Ahmad, Coord. Chem. Rev. 248 (2004) 231.
[24] P.J. Sadler, R.E. Sue, Met. Based Drugs 1 (1994) 107.
[25] S.J. Berners-Price, P.J. Sadler, Struct. Bond. 70 (1988) 27.
[26] (a) T.M. Simon, D.H. Kunishima, G.J. Vibert, A. Lorber, Cancer 44 (1979) 1965;
(b) T.M. Simon, D.H. Kunishima, G.J. Vibert, A. Lorber, Cancer Res. 41 (1981) 94.
[27] C.K. Mirabelli, R.K. Johnson, D.T. Hill, L. Faucette, G.R. Girard, G.Y. Kuo, C.M. Sung, S.T. Crooke, J. Med. Chem. 29 (1986) 218.
[28] K.C. Agrawal, K.B. Bears, D. Marcus, H.B. Jonassen, Proc. Am. Assoc. Cancer Res. 69 (1978) 110.
[29] C.F. Shaw III, in: H. Schmidbaur (Ed.), Gold-Progress in Chemistry, Biochemistry and Technology, Wiley, New York, 1999, pp. 259–308.
[30] D. Schneider, S. Nogai, A. Schier, H. Schmidbaur, Inorg. Chim. Acta 352 (2003) 179.
[31] D.T. Hill, B.M. Sutton, Cryst. Stuct. Commun. 9 (1980) 679.
[32] S.J. Lippard (Ed.), Platinum, Gold and Other Metal Chemotherapeutic Agents, ACS Symposium Series, vol. 209, 1983, p. 356.
[33] R. Bau, J. Am. Chem. Soc. 120 (1998) 9380.
[34] R.C. Elder, K. Ludwig, J.N. Cooper, M.K. Eidness, J. Am. Chem. Soc. 107 (1985) 5024.
[35] A.A. Isab, P.J. Sadler, J. Chem. Soc,. Dalton Trans. (1982) 135.
[36] M.T. Coffer, C.F. Shaw III, M.K. Eidsness, J.W. Watkins, R.C. Elder, Inorg. Chem. 25 (1986) 333.
[37] D.J. Ecker, J.C. Hemple, B.M. Sutton, R. Krisch, S.T. Crook, Inorg. Chem. 25 (1986) 3139.
[38] C.F. Shaw III, A.A. Isab, M.T. Coffer, C.K. Mirabelli, Biochem. Pharmacol. 40 (1990) 1227.
[39] R.C. Elder, Chem. Rev. 87 (1987) 1027.
[40] D.H. Brown, G. McKlinlay, W.E. Smith, J. Chem. Soc., Dalton Trans. (1977) 1874.
[41] A.A. Isab, P.J. Sadler, J. Chem. Soc., Dalton Trans. (1981) 1657.
[42] A.P. Intoccia, T.L. Flanagan, D.T. Walz, L. Gutzait, J.E. Swagzdis, J. Flagillano Jr., B.Y. Hwang, R.H. Dewey, H. Noguchi, in: B.M. Sutton (Ed.), Bioinorg. Chem. of Gold Coord. Comp., Smith Kline and French Laboratories, Philadelphia, 1983, p. 21.
[43] C.F. Shaw III, M.T. Coffer, J. Klingbeil, C.K. Mirabelli, J. Am. Chem. Soc. 110 (1988) 729.
[44] A.A. Isab, A.L. Hormann, M.T. Coffer, C.F. Shaw III, J. Am. Chem. Soc. 110 (1988) 3278, and references therein.
[45] G. Lewis, C.F. Shaw III, Inorg. Chem. 25 (1986) 58.
[46] A.A. Isab, J. Inorg. Biochem. 45 (1992) 261.
[47] A.A. Isab, P.J. Sadler, J. Chem. Soc., Dalton Trans. (1982) 135.
[48] D.T. Hill, B.M. Sutton, A.A. Isab, M.T. Razi, P.J. Sadler, J.M. Trooster, G.M. Callis, Inorg. Chem. 22 (1983) 2936.
[49] A.P. Arnold, K.S. Tan, D.L. Rabenstein, Inorg. Chem. 25 (1986) 2433.
[50] A.A. Mohamed, H.E. Abdou, J. Chen, A.E. Bruce, M.R.M. Bruce, Comm. Inorg. Chem. 23 (2002) 321.
[51] A.A. Isab, J. Chem. Soc., Dalton Trans. (1986) 1049.
[52] A.A. Isab, Inorg. Chim. Acta 135 (1987) 19.
[53] S. Ahmad, A.A. Isab, J. Coord. Chem. 55 (2002) 189.
[54] A.A. Isab, S. Ahmad, A.R. Al-Arfaj, M.N. Akhtar, J. Coord. Chem. 56 (2003) 95.
[55] M.T. Coffer, C.F. Shaw III, A.L. Horman, C.K. Mirabelli, S.T. Crooke, J. Inorg. Biochem. 30 (1987) 177.
[56] J.R. Roberts, J. Xaio, B. Schliesman, D.J. Parsons, C.F. Shaw III, Inorg. Chem. 35 (1996) 424.
[57] C.F. Shaw III, Comm. Inorg. Chem. 8 (1989) 233.
[58] J. Xiao, C.F. Shaw III, Inorg. Chem. 31 (1992) 3706.
[59] O.M.N. Dhubhghaill, P.J. Sadler, A.J. Tucker, J. Am. Chem. Soc. 114 (1992) 1118.

[60] J. Christodoulou, P.J. Sadler, A.J. Tucker, Eur. J. Biochem. 225 (1994) 363.
[61] D.J. Ecker, J.C. Hemple, B.M. Sutton, R. Kirsch, S.T. Crooke, Inorg. Chem. 25 (1986) 3139.
[62] A.A. Isab, C.F. Shaw III, J.D. Hoeschele, J. Locke, Inorg. Chem. 27 (1988) 3588.
[63] C.F. Shaw III, A.A. Isab, J.D. Hoeschele, M. Starich, J. Locke, P. Schulteis, J. Xiao, J. Am. Chem. Soc. 116 (1994) 2254.
[64] A.A. Isab, C.F. Shaw III, J. Locke, Inorg. Chem. 27 (1988) 3406.
[65] S. Ahmad, A.A. Isab, J. Inorg. Biochem. 88 (2002) 44.
[66] A.A. Isab, S. Ahmad, J. Inorg. Biochem. 88 (2002) 53.
[67] A.J. Canumalla, N. Al-Zamil, M. Philips, A.A. Isab, C.F. Shaw III, J. Inorg. Biochem. 85 (2001) 67.
[68] R.C. Elder, Z. Zhao, Y. Zhang, J.G. Dorsey, E.V. Hess, K. Tepperman, J. Rheumatol. 20 (1993) 268.
[69] G.G. Graham, J.R. Bales, M.C. Gtootveld, P.J. Sadler, J. Inorg. Biochem. 25 (1985) 163.
[70] G.G. Graham, M.M. Dale, Biochem. Pharm. 39 (1990) 1697.
[71] G.G. Graham, A.J. Kettle, Biochem. Pharm. 56 (1998) 307.
[72] A.J. Canunumalla, S. Schraa, A.A. Isab, C.F. Shaw III, E. Gleichman, L. Dunemann, M. Turfeld, J. Biol. Inorg. Chem. 3 (1998) 9.
[73] A.A. Isab, J. Inorg. Biochem. 46 (1992) 145.
[74] A.L. Hormann, C.F. Shaw III, D.W. Bennett, W.M. Reiff, Inorg. Chem. 25 (1986) 3953.
[75] A.L. Hormann, C.F. Shaw III, Inorg. Chem. 29 (1990) 4683.
[76] A.A. Isab, M.S. Hussain, M.N. Akhtar, M.I.M. Wazeer, A.R. Al-Arfaj, Polyhedron 18 (1999) 1401.
[77] S. Ahmad, A.A. Isab, H.P. Perzanowski, Can. J. Chem. 80 (2002) 1279.
[78] S. Ahmad, A.A. Isab, A.R. Al-Arfaj, A.P. Arnold, Polyhedron 21 (2002) 2099.
[79] Y. Zhang, E.V. Hess, K.G. Pyrhuber, J.G. Dorsey, K. Tepperman, R.C. Elder, Inorg. Chim. Acta 229 (1995) 271.
[80] R.D. Hancock, N.P. Finnkelstein, A. Avers, J. Inorg. Nucl. Chem. 34 (1972) 3747.
[81] R. Rudkowski, G.G. Graham, G.D. Champion, J.B. Ziegler, Biochem. Pharm. 39 (1990) 1687.
[82] G.G. Graham, T.M. Haavisto, P.M. McNaught, C.D. Browne, G.D. Champion, J. Rheum. 9 (1982) 527.
[83] D.W. James, N.W. Ludvigsen, L.G. Cleland, J. Rheum. 9 (1982) 532.
[84] G.G. Graham, T.M. Haavisto, H.M. Jones, G.D. Champion, Biochem. Pharm. 33 (1984) 1257.
[85] R.V. Parish, J. Mack, L. Hargreaves, J.P. Wright, J. Chem. Soc. Dalton. Trans. (1996) 69.
[86] C.F. Blank, J.C. Dabrowiak, J. Inorg. Biochem. 21 (1984) 21.
[87] Y. Dong, S.J. Berners-Price, D.R. Thorburn, T. Antalis, J. Dickinson, T. Hurst, L. Qiu, S.K. Khoo, P.G. Parsons, Biochem. Pharmacol. 53 (1997) 1673.
[88] G. Marcon, S. Carotti, M. Coronnello, L. Messori, E. Mini, P. Orioli, T. Mazzei, M.A. Cinellu, G. Minghetti, J. Med. Chem. 45 (2002) 1672.
[89] M.J. Mckeage, L. Maharaj, S.J. Berners-Price, Coord. Chem. Rev. 232 (2002) 127.
[90] M.P. Rigobello, L. Messori, G. Marcon, M.A. Cinellu, M. Bragadin, A. Folda, G. Scutari, A. Bindoli, J. Inorg. Biochem. 98 (2004) 1634.
[91] S.P. Frickler, Gold Bull. 29 (1996) 53.
[92] S.J. Berners-Price, C.K. Mirabelli, R.K. Johnson, M.R. Mattern, F.L. McCabe, L.F. Faucette, C.M. Sung, S.M. Mong, P.J. Sadler, S.T. Crooke, Cancer Res. 46 (1986) 5486.
[93] S.J. Berners-Price, G.R. Girard, D.T. Hill, B.M. Sutton, P.S. Jarrett, L.F. Faucette, R.K. Johnson, C.K. Mirabelli, P.J. Sadler, J. Med. Chem. 33 (1990) 1386.
[94] F. Caruso, M. Ross, J. Tanski, C. Pettinari, F. Marchetti, J. Med. Chem. 46 (2003) 1737.
[95] H.S. Allaudeen, R.M. Snyder, M.H. Whitman, S.T. Crooke, Biochem. Pharmacol. 34 (1985) 3243.
[96] C.K. Mirabelli, J.P. Zimmermann, H.R. Bartus, C. Sung, S.T. Crooke, Biochem. Pharmacol. 35 (1986) 1435.
[97] G.F. Rush, P.F. Smith, G.D. Hoke, D.W. Alberts, R.M. Snyder, C.K. Mirabelli, Toxicol. Appl. Pharmacol. 90 (1987) 391.
[98] P.A. Andrews, K.D. Albright, Cancer Res. 52 (1992) 1895.
[99] S.J. Berners-Price, P.J. Sadler, Struct. Bond. (Berlin) 70 (1988) 27.
[100] M.J. Mckeage, S.J. Berners-Price, P. Galettis, R.J. Bowen, W. Brouwer, L. Ding, L. Zhuang, B.C. Baguley, Cancer Chemother. Pharmacol. 46 (2000) 343.
[101] P.F. Smith, G.D. Hoke, D.W. Alberts, P.J. Bugelski, S. Lupo, C.K. Mirabelli, G.F. Rush, J. Pharmacol. Exp. Therap. 249 (1989) 944.
[102] T. Sandalova, L. Zhong, Y. Lindqvist, A. Holmgren, G. Schneider, Proc. Natl. Acad. Sci. USA 98 (2001) 9533.
[103] D.L. Klayman, in: D.L. Klayman, W.H.H. Gunther (Eds.), Organic Selenium Compounds: Their Chemistry and Biology, Wiley, New York, 1973, pp. 67–172.
[104] S. Gromer, L.D. Arscott, C.H. Williams Jr., R.H. Schirmer, K. becker, J. Biol. Chem. 273 (1998) 20096.
[105] B. Ward, J.C. Dabrowiak, J. Am. Chem. Soc. 109 (1987) 3810.
[106] K. Nomiya, R. Noguchi, K. Ohsawa, K. Tsuda, M. Oda, J. Inorg. Biochem. 78 (2000) 363.
[107] T. Yang, C. Tu, J. Zhang, L. Lin, X. Zhang, Q. Liu, J. Ding, Q. Xu, Z. Guo, J. Chem. Soc., Dalton Trans. (2003) 3419.
[108] L. Messori, F. Abbate, G. Marcon, P. Orioli, M. Fontani, E. Mini, T. Mazzei, S. Carotti, T. O'Connell, P. Zanello, J. Med. Chem. 43 (2000) 3541.
[109] W. Henderson, L.J. McCaffery, B.K. Nicholson, J. Chem. Soc., Dalton Trans. (2000) 2753.
[110] C.M. Che, R.W. Sun, W.Y. Yu, C.B. Ko, N. Zhu, H. Sun, Chem. Commun. (2003) 1718.
[111] K. Nomiya, A. Yoshizawa, K. Tsukagoshi, N.C. Kasuga, S. Hirakawa, J. Watanabe, J. Inorg. Biochem. 98 (2004) 46.
[112] K. Nomiya, S. Takahashi, R. Noguchi, J. Chem. Soc. Dalton Trans. (2000) 4369.
[113] K. Nomiya, H. Yokoyama, J. Chem. Soc. Dalton Trans. (2002) 2483.
[114] B. Coyle, M. McCann, K. Kavanagh, M. Devereux, V. Mckee, N. Kayal, D. Egan, C. Deegan, G.J. Finn, J. Inorg. Biochem. 98 (2004) 1361.
[115] K. Nomiya, S. Takahashi, R. Noguchi, S. Nemoto, T. Takayama, M. Oda, Inorg. Chem. 39 (2000) 3301.
[116] K. Nomiya, S. Takahashi, R. Noguchi, J. Chem. Soc. Dalton Trans. (2000) 1343.
[117] K. Nomiya, S. Takahashi, R. Noguchi, J. Chem. Soc. Dalton Trans. (2000) 4369.
[118] I. Tsyba, B.B. Mui, R. Bau, R. Noguchi, K. Nomiya, Inorg. Chem. 42 (2003) 8028.
[119] K. Nomiya, H. Yokoyama, J. Chem. Soc. Dalton Trans. (2000) 2091.
[120] K. Nomiya, K. Tsuda, T. Sudoh, M. Oda, J. Inorg. Biochem. 68 (1997) 39.
[121] K. Nomiya, Y. Kondoh, K. Onoue, N.C. Kasuga, H. Nagano, M. Oda, T. Sudoh, S. Sakuma, J. Inorg. Biochem. 58 (1995) 255.
[122] K. Nomiya, K. Onoue, Y. Kondoh, N.C. Kasuga, Polyhedron 14 (1995) 1359.
[123] K. Nomiya, Y. Kondoh, H. Nagano, M. Oda, J. Chem. Soc. Chem. Commun. (1995) 1679.
[124] K. Nomiya, K. Tsuda, N.C. Kasuga, J. Chem. Soc. Dalton Trans. (1998) 1653.
[125] T.J.B. Simons, Nature (London) 281 (1979) 337.
[126] I.G. Macara, Trends Biochem. Sci. 5 (1980) 92.
[127] Y. Shechter, I. Goldwaser, M. Mironchik, M. Frikin, D. Gefel, Coord. Chem. Rev. 237 (2003) 3.
[128] K.H. Thompson, J.H. McNeill, C. Orvig, Chem. Rev. 99 (1999) 2561.
[129] A.K. Srivastava, M.Z. Mehdi, Diabetic Med. 22 (2004) 2.

[130] H. Sakura, Y. Kojima, Y. Yoshikawa, K. Kawabe, H. Yasui, Coord. Chem. Rev. 226 (2002) 187.
[131] S.M. Brichard, J.C. Henquin, Trend Pharmacol. Sci. 16 (1995) 265.
[132] Y. Shecter, Diabetes 39 (1990) 1.
[133] T. Takino, H. Yasui, A. Yoshitake, Y. Hamajima, R. Matsushita, J. Takada, H. Sakurai, J. Biol. Inorg. Chem. 6 (2001) 133.
[134] G. Micera, D. Sanna, E. Kiss, E. Garribba, T. Kiss, J. Inorg. Biochem. 75 (1999) 303.
[135] K.H. Thompson, C. Orvig, Coord. Chem. Rev. 219–221 (2001) 1033.
[136] P. Noblia, M. Vieites, B.S. Parajon-Costa, E.J. Baran, H. Cerecetto, P. Draper, M. Gonzalez, O.E. Piro, E.E. Castellano, A. Azqueta, A.L. de Cerain, A.M. Vega, D. Gambino, J. Inorg. Biochem. 99 (2005) 443.
[137] Y.H. Xing, K. Aoki, F.Y. Bai, J. Coord. Chem. 57 (2004) 157.
[138] J.M. Llobet, J.L. Domingo, Toxicol. Lett. 23 (1984) 227.
[139] I. Goldwaser, J. Li, E. Gershonov, M. Armoni, E. Karnieli, M. Fridkin, Y. Shechter, J. Biol. Chem. 274 (1999) 26617.
[140] J.H. McNeil, V.G. Yuen, H.R. Hoveyda, C. Orvig, J. Med. Chem. 35 (1992) 1489.
[141] H. Sakurai, Y. Kojima, Y. Yoshikawa, K. Kawabe, H. Yasui, Coord. Chem. Rev. 226 (2002) 187.
[142] I.J. Goldwaser, E. Gershonov, M. Armoni, E. Karnieli, M. Fridkin, Y. Shechter, J. Biol. Chem. 274 (1999) 26627.
[143] P. Caravan, L. Celmini, N. Glover, F.G. Herring, H. Li, J.H. McNeill, S.J. Rettig, I.A. Setyawati, E. Shuter, Y. Sun, A.S. Tracey, V.G. Yuen, C. Orvig, J. Am. Chem. Soc. 117 (1995) 12759.
[144] K.H. Thompson, B.D. Liboiron, Y. Sun, K.D. Bellman, I.K. Setyawati, B.O. Patrick, V. Karunaratne, G. Rawji, J. Wheeler, K. Sutton, S. Bhanot, C. Cassidy, J.H. McNeill, V.G. Yuen, C. Orvig, J. Biol. Inorg. Chem. 8 (2003) 66.
[145] M.A. Barrand, B.A. Callingham, R.C. Hider, J. Pharm. Pharmacol. 39 (1987) 203.
[146] M.M. Finnegan, S.J. Rettig, C. Orvig, J. Am. Chem. Soc. 108 (1986) 5033.
[147] K.H. Thompson, C. Orvig, J. Chem. Soc., Dalton Trans. (2000) 2885.
[148] V.G. Yuen, C. Orvig, J.H. McNeill, Can. J. Physiol. Pharmacol. 73 (1995) 55.
[149] V.G. Yuen, C. Orvig, J.H. McNeill, Can. J. Physiol. Pharmacol. 71 (1993) 263.
[150] V.G. Yuen, C. Orvig, K.H. Thompson, J.H. McNeill, Can. J. Physiol. Pharmacol. 71 (1993) 270.
[151] S. Dai, V.G. Yuen, C. Orvig, J.H. McNeill, Pharmacol. Commun. 3 (1993) 311.
[152] K. Saatchi, K.H. Thompson, B.O. Patrick, M. Pink, V.G. Yuen, J.H. McNeill, C. Orvig, Inorg. Chem. 44 (2005) 2689.
[153] V. Monga, K.H. Thompson, V.G. Yuen, V. Sharma, B.O. Patrick, J.H. McNeill, C. Orvig, Inorg. Chem. 44 (2005) 2678.
[154] Y. Sun, B.R. James, S.J. Rettig, C. Orvig, Inorg. Chem. 35 (1996) 1667.
[155] P. Buglyo, D.C. Crans, E.M. Nagy, R.L. Lindo, L. Yang, J.J. Smee, W. Jin, L. Chi, M.E. Godzala III, G.R. Willsky, Inorg. Chem. 44 (2005) 5416.
[156] S.S. Amin, K. Cryer, B. Zhang, S.K. Dutta, S.S. Eaton, O.P. Anderson, et al., Inorg. Chem. 39 (2000) 406.
[157] M.M. Tahir, D. Brezina, N. Fatima, M.I. Choudhary, A. Rahman, J. Inorg. Biochem. 99 (2005) 589.
[158] M. Xie, L. Gao, L. Li, W. Liu, S. Yan, J. Inorg. Biochem. 99 (2005) 546.
[159] H. Yasui, A. Tamura, T. Takino, H. Sakurai, J. Inorg. Biochem. 91 (2002) 327.
[160] T. Takino, H. Yasui, A. Yoshitake, Y. Hamajima, R. Matsushita, J. Takada, H. Sakurai, J. Biol. Inorg. Chem. 6 (2001) 133.
[161] E. Kiss, K. Petrohan, D. Sanna, E. Garriba, G. Micera, T. Kiss, Polyhedron 19 (2000) 55.
[162] T. Sasagawa, Y. Yoshikawa, K. Kawabe, H. Sakurai, Y. Kojima, J. Inorg. Biochem. 88 (2002) 108.
[163] M. Melchior, K.H. Thompson, J.M. Jong, S.J. Rettig, E. Shutter, V.G. Yuen, et al., Inorg. Chem. 38 (1999) 2288.
[164] H. Sakurai, K. Fujii, H. Watanabe, H. Tamura, Biochem. Biophys. Res. Commun. 214 (1995) 1095.
[165] T. Takino, H. Yasui, A. Yoshitake, Y. Hamajima, R. Matsushita, J. Tanaka, H. Sakurai, J. Biol. Inorg. Chem. 6 (2001) 133.
[166] Y. Adachi, H. Sakurai, Chem. Pharm. Bull. 52 (2004) 428.
[167] M. Nakai, M. Obata, F. Sekiguchi, M. Kato, et al., J. Inorg. Biochem. 98 (2004) 105.
[168] S.B. Etcheverry, D.A. Barrio, A.M. Cortizo, P.A.M. Williams, J. Inorg. Biochem. 88 (2002) 94.
[169] M.M. Aly, J. Coord. Chem. 43 (1998) 89.
[170] K. Kawabe, M. Tadokoro, Y. Kojima, Y. Fujisawa, H. Sakurai, Chem. Lett. (1998) 9.
[171] K. Kawabe, M. Tadokoro, A. Ichimura, Y. Kojima, T. Takino, H. Sakurai, J. Am. Chem. Soc. 121 (1999) 7937.
[172] K. Kawabe, T. Sasagawa, Y. Yoshikawa, et al., J. Biol. Inorg. Chem. 8 (2003) 893.
[173] K. Kanamori, K. Nishida, N. Miyata, K. Okamoto, Y. Miyoshi, A. Tamura, H. Sakurai, J. Inorg. Biochem. 86 (2001) 649.
[174] B. Song, N. Aebischer, C. Orvig, Inorg. Chem. 41 (2002) 1357.
[175] M. Melchior, S.J. Rettig, B.D. Liboiron, K.H. Thompson, V.G. Yuen, J.H. McNeill, C. Orvig, Inorg. Chem. 40 (2001) 4686.
[176] H. Sakurai, A. Tamura, T. Takino, K. Ozutsumi, K. Kawabe, Y. Kojima, Inorg. React. Mech. 2 (2000) 69.
[177] H. Yasui, K. Takechi, H. Sakurai, J. Inorg. Biochem. 78 (2000) 185.
[178] I.A. Setyawati, K.H. Thompson, V.G. Yuen, Y. Sun, M. Battell, D.M. Lyster, C. Vo, T.J. Ruth, S. Ziesler, J.H. McNeill, C. Orvig, J. Appl. Physiol. 94 (1998) 569.
[179] J. Azay, J. Bres, M. Krosniak, P.L. Teissedre, J.C. Cabanis, J.J. Serrano, G. Cros, Fund. Clin. Pharmacol. 15 (2001) 313.
[180] K.G. Peters, M.G. Davis, B.H. Howard, M. Pokross, V. Rastogi, C. Diven, K.D. Greis, E. Eby-Wilkens, M. Maier, A. Evdokimov, S. Soper, F. Genbauffe, J. Inorg. Biochem. 96 (2003) 321.
[181] A. Mohammad, J. Wang, J.H. McNeill, Mol. Cell. Biochem. 229 (2002) 125.
[182] S.K. Pandey, J.-F. Theberge, M. Bernier, A.K. Srivatava, Biochemistry 38 (1999) 14667.
[183] G. Palmer, J.P. Bonjour, J. Caverzasio, Endocrinology 137 (1996) 4699.
[184] F. Ahmad, J.L. Azevedo, R. Cortright, G.L. Dohm, B.J. Goldstein, J. Clin. Invest. 100 (1997) 449.
[185] M.F. White, C.R. Kahn, J. Biol. Chem. 269 (1994) 1.
[186] R.H. van Huijsduijnen, W.H.B. Sauer, A. bombrun, D. Swinnen, J. Med. Chem. 47 (2004) 4142.
[187] I.G. Fantus, E. Tsiami, Mol. Cell. Biochem. 182 (1998) 109.
[188] E. Kiss, I. Fabian, T. Kiss, Inorg. Chim. Acta 340 (2002) 114.
[189] T. Maehama, J.E. Dixon, J. Biol. Chem. 273 (1998) 13375.
[190] P.R. Shepherd, D.J. Withers, K. Siddle, Biochem. J. 333 (1998) 471.
[191] L.Q. Dong, R.B. Zhang, P. Langlais, H. He, M. Clark, L. Zhu, et al., J. Biol. Chem. 274 (1999) 8117.
[192] M.F. White, Am. J. Physiol. Endocrinol. Metab. 283 (2002) E413.
[193] J.L. Domingo, M. Gomez, D.J. Sanchez, J.M. Llobet, C.L. Keen, Mol. Cell. Biochem. 153 (1995) 233.
[194] J.L. Domingo, Biol. Trace Elem. Res. 88 (2002) 97.
[195] B.A. Reul, S.S. Amin, J.P. Buchet, L.N. Ongemba, D.C. Crans, S.M. Brichard, Br. J. Pharmacol. 126 (1999) 467.
[196] G.G. Briand, N. Burford, Chem. Rev. 99 (1999) 2601.
[197] H. Sun, H. Li, A.B. Mason, R.C. Woodworth, P.J. Sadler, J. Biol. Chem. 276 (2001) 8829.
[198] G.F. Baxter, Pharm. J. 243 (1989) 805.
[199] G.F. Baxter, Chem. Br. (1992) 445.
[200] Y. Glupczynski, A. Buret, Am. J. Gastroenterol. 85 (1990) 1545.
[201] B.J. Marshall, Am. J. Gastroenterol. 86 (1991) 16.
[202] B.J. Marshall, J. Infec. Dis. 153 (1986) 650.
[203] P.J. Sadler, H. Li, H. Sun, Coord. Chem. Rev. 185–186 (1999) 689.
[204] H. Sun, P.J. Sadler, Top. Biol. Inorg. Chem. 2 (1999) 159.
[205] S. Suerbaum, P. Michetti, New. Eng. J. Med. 347 (2003) 1175.

[206] C. O'Morain, T. Borody, A. Faley, W.A. deBoer, C. Dallaire, et al., Aliment. Pharmacol. Ther. 17 (2003) 415.
[207] W.A. deBoer, Expert Opin. Invest. Drugs 10 (2001) 1559.
[208] J.A. Parkinson, H. Sun, P.J. Sadler, Chem. Commun. (1998) 881.
[209] P.J. Barrie, M.I. Djuran, M.A. Mazid, M. McPartlin, P.J. Sadler, I.J. Scowen, H. Sun, J. Chem. Soc. Dalton Trans. (1996) 2417.
[210] E. Asato, K. Kastura, M. Mikuriya, U. Turpeinen, I. Mutikainen, J. Reedijk, Inorg. Chem. 34 (1995) 2447.
[211] E. Asato, K. Kastura, M. Mikuriya, T. Fugii, J. Reedijk, Inorg. Chem. 32 (1993) 5322.
[212] E. Asato, W.L. Driessen, R.A.G. deGraaff, F. Hulsbergen, J. Reedijk, Inorg. Chem. 34 (1991) 4210.
[213] W. Li, L. Jin, N. Zhu, X. Hou, F. Deng, H. Sun, J. Am. Chem. Soc. 125 (2003) 12408.
[214] B.J. Marshall, Rev. Infect. Dis. 12 (1990) S87.
[215] P. Domenico, R.J. Salo, S.G. Novick, P.E. Schoch, K.V. Horn, B.A. Cunha, Antimicrob. Agents Chemother. 41 (1997) 1697.
[216] D.E. Mahony, S. Lim-Morrison, L. Bryden, G. Faulkner, P.S. Hoffman, L. Agocs, G.G. Briand, N. Burford, H. Maguire, Antimicrob. Agents Chemother. 43 (1999) 582.
[217] W.C. Beil, C. Birkholz, S. Wagner, K.F. Sewing, Pharmacology 50 (1995) 337.
[218] N. Burford, M.D. Eelman, D.E. Mahony, M. Morash, Chem. Commun. (2003) 146.
[219] G.G. Briand, N. Burford, M.D. Eelman, N. Aumeerally, L. Chen, T.S. Cameron, K.N. Robertson, Inorg. Chem. 43 (2004) 6495.
[220] G. Alonzo, N. Bertazi, M. Cosiglio, Inorg. Chim. Acta 85 (1984) L35.
[221] H. Sun, H. Li, P.J. Sadler, J. Inorg. Biochem. 59 (1995) 190.
[222] L. Zhang, K.Y. Szeto, W.B. Wong, T.T. Loh, P.J. Sadler, H. Sun, Biochemistry 40 (2001) 13281.
[223] N. Burford, M.D. Eelman, T.S. Cameron, Chem. Commun. (2002) 1402.
[224] G.G. Briand, N. Burford, M.D. Eelman, T.S. Cameron, K.N. Robertson, Inorg. Chem. 42 (2003) 3136.
[225] G.G. Briand, N. Burford, T.S. Cameron, Chem. Commun. (2000) 13.
[226] D.E. Mahony, A. Woods, M.D. Eelman, N. Burford, S.J.O. Veldhuyzen van Zanten, Antimicrob. Agents Chemother. 49 (2005) 431.
[227] N. Rao, S. Feldman, Pharm. Res. 7 (1990) 188.
[228] N. Rao, S. Feldman, Pharm. Res. 7 (1990) 237.
[229] P.J. Sadler, H. Sun, H. Li, Chem. Eur. J. 2 (1996) 701.
[230] H. Sun, K.Y. Szeto, J. Inorg. Biochem. 94 (2003) 114.
[231] J. Pannequin, S. Kovac, J.P. Tantiongco, R.S. Norton, A. Shulkes, K.J. Barnham, G.S. Baldwin, J. Biol. Chem. 279 (2003) 2453.
[232] H. Sun, H. Li, I. Harvey, P.J. Sadler, J. Biol. Chem. 274 (1999) 29094.
[233] D.C. Lemkuil, D. Nettesheim, C.F. Shaw III, D.H. Petering, J. Biol. Chem. 269 (1994) 24792.
[234] R.A. Disilvestro, J. Liu, C.D. Klaassen, Res. Commun. Mol. Path. Pharmacol. 93 (1996) 163.
[235] A. Naganuma, M. Satoh, N. Imura, Cancer Res. 47 (1987) 983.
[236] M. Satoh, Y. Aoki, C. Tohyama, Cancer Chemother. Pharmacol. 40 (1997) 358.
[237] X. wang, X. Zhang, J. Lin, J. Chen, Q. Xu, Z. Guo, Dalton Trans. (2003) 2379.
[238] J.C. Hutson, J. Appl. Toxicol. 25 (2005) 234.
[239] A. Slikkerveer, F.A. deWolff, Med. Toxicol. Adv. Drug Exp. 4 (1989) 303.
[240] M.F. Gordon, R.I. Abrams, D.B. Rubin, W.B. Barr, D.D. Correa, Movement Disord. 10 (2004) 220.

important characteristics of the Schiff-base ligands is that even a small modification of the ligand structure can significantly change key properties of the corresponding iron complex. For instance, after introducing several electron-withdrawing nitro groups to iron complexes with H_2salen type of ligands, effective catalysts for hydrocarbon oxidations with dioxygen as the oxidant were obtained [18–20]. In a similar manner, concerning both the iron(II) and iron(III) coordination chemistry with Schiff-base ligands, much emphasis has been focused on the understanding of the factors which control the spin state of the metal ion, as well as the intermolecular solid-state effects that induce or influence the spin-crossover phenomenon [9,10,21]. It has been reported that the replacement of a methoxo group with an ethoxo group in a hexadentate N_4O_2 Schiff-base ligand results in dramatic changes of the magnetic properties of the corresponding iron(II) complexes, due to small alterations in the intermolecular interactions and crystal packing [21]. In addition, a small number of iron(III) complexes with Schiff-base ligands can exhibit both high-spin and low-spin electronic configuration and a thermal low-spin ⇆ high-spin transition has been observed for these spin-crossover complexes [12,15,22–27].

In this contribution we report on the synthesis, structural, spectroscopic and magnetic characterization of new examples of iron(III) complexes with dianionic N_4O_2 Schiff-base ligands (Chart 1): $[Fe(L_1)](ClO_4)$ (**1**), $[Fe(L_1)](BF_4)$ (**2**), $[Fe(L_2)](ClO_4)$ (**3**) and $[Fe(L_2)](BF_4)$ (**4**). Although the synthesis of the ligands H_2L_1 and H_2L_2 has been reported earlier [28], only one iron(III) complex of the ligand H_2L_1 has been reported so far [26].

2. Experimental

2.1. Synthesis

All chemicals and reagents used for the preparation of ligands and complexes were commercial products (Merck) and were used without purification. All reactions were carried out in air, unless stated otherwise.

Caution. Perchlorate salts are highly explosive, and should be handled with care and in small amounts.

2.1.1. General synthesis of the ligands dihydrogen [N,N′,N″,N‴-1,5,8,12-tetraazadodecane-bis(salicylaldiminato)] [H_2L_1] and dihydrogen [N,N′,N″,N‴-1,5,8,12-tetraazadodecane-bis(3-methoxysalicylaldiminato)] [H_2L_2]

1,5,8,12-Tetraazadodecane (0.01 mol) was dissolved in ethanol (10 ml) and then added to a stirred ethanol solution of the corresponding aldehyde (0.02 mol). The reaction mixture was heated to reflux over night. After cooling to room temperature, the solvent was removed under reduced pressure. The final viscous residue was kept under vacuum for 5 days and the ligands have been purified by repeated crystallizations in methanol.

H_2L_1. Nature: yellow solid. Yield: (2.678 g, 81%); m.p.: (28–30 °C). $C_{22}H_{30}N_4O_2$ (382.51); Calc.: C, 69.08; H, 7.90; N, 14.65. Found: C, 65.96; H, 7.80; N, 13.69%. IR: 1630 cm^{-1} (C=N). ^1H NMR (in CD_3OD): 8.18 (s, 2H, imine-H), 7.16 (m, 2H), 6.92 (m, 2H), 6.72 (m, 2H), 6.55 (m, 2H), 4.85 (s, 2H, b, N-H), 3.53 (t, 4H), 2.49 (m, 4H), 1.78 (m, 4H), 1.27 (m, 4H). ESI-MS, *m/z*: 383.

H_2L_2. Nature: yellow liquid. Yield: (3.5 g, 79%). $C_{24}H_{34}N_4O_4$ (442.56); Calc.: C, 65.14; H, 7.74; N, 14.46%. IR: 1629 cm^{-1} (C=N). ^1H NMR (in CD_3OD); 8.28 (s, 2H, imine-H), 6.83 (m, 2H), 6.78 (m, 2H), 6.52 (m, 2H), 4.79 (s, 2H, b, N-H), 3.70 (s, 6H OCH_3), 3.49 (m, 4H), 2.57 (m, 4H), 1.75 (m, 4H), 1.08 (m, 4H). ESI-MS, *m/z*: 443.

2.1.2. General synthesis of [$Fe^{III}L$]X ($X = ClO_4^-$ and BF_4^-) complexes

A methanol solution of $Fe(ClO_4)_2 \cdot 6H_2O$ or $Fe(BF_4)_2 \cdot 6H_2O$ (0.001 mol, 5 ml) was added dropwise to a stirred solution of the Schiff-base ligand (H_2L_1 and H_2L_2) (0.001 mol, 30 ml). The resulting solution was stirred for 3 h and then it was filtrated. The slow evaporation at room temperature of the resulting filtrates allows obtaining the solid compounds **1**–**4**. All four compounds were recrystallized from hot methanol. X-ray quality light green crystals for (**1**) and purple crystals for (**3** and **4**) were obtained by vapor diffusion of diethyl ether into CH_3OH: $CHCl_3$ mixture over 15 days. Numerous attempts to obtain crystals of **2** failed.

*[$Fe(L_1)$]ClO_4 (**1**)*. Yield: (0.256 g, 58%), $C_{22}H_{28}N_4O_6ClFe$ (535.78): Calc. C, 49.31; H, 5.26; N, 10.45. Found:

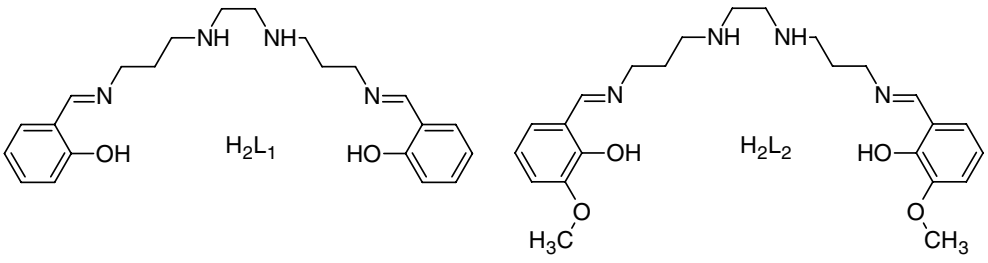

Chart 1.

C, 49.97; H, 5.53; N, 10.44%. IR (ν/cm^{-1}): 3260 (N-H), 1608 (C=N) and 1027, 620 ClO_4^-. UV/Vis/NIR, λ_{max}/nm: 564, 399, 320.

*[Fe(L$_1$)](BF$_4$) (**2**)*. Yield: (0.237 g, 54%), $C_{22}H_{28}N_4O_2F_4BFe$ (523.14): Calc.: C, 50.51; H, 5.39; N, 10.70. Found: C, 49.39; H, 5.06; N, 10.03%. IR (ν/cm^{-1}): 3263 (N-H), 1607 (C=N) and 1066, 630 BF_4^-. UV/Vis/NIR, λ_{max}/nm: 575, 402, 345, 236.

*[Fe(L$_2$)](ClO$_4$) (**3**)*. Yield: (0.413 g, 83%). $C_{24}H_{32}N_4O_8ClFe$ (597.83): Calc.: C, 48.54; H, 5.41; N, 9.40. Found: C, 47.66; H, 5.51; N, 9.32%. IR (ν/cm^{-1}): 3236 (N-H), 1631 (C=N) and 1070, 621 ClO_4^-. UV/Vis/NIR, λ_{max}/nm: 602, 373.

*[Fe(L$_2$)](BF$_4$) (**4**)*. Yield: (0.264 g, 53%). $C_{24}H_{32}N_4O_4F_4BFe$ (583.20): Calc.: C, 49.42; H, 5.33; N, 9.60. Found: C, 49.95; H, 5.55; N, 8.72%. IR (ν/cm^{-1}): 3252 (N-H), 1651 (C=N) and 1068, 636 BF_4^-. UV/Vis/NIR, λ_{max}/nm: 605, 369.

2.2. Physical measurements

C, H and N analyses were performed with a Perkin–Elmer 2400 series II analyzer. Infrared spectra (4000–300 cm^{-1}) were recorded on a Perkin–Elmer Paragon 1000 FTIR spectrometer equipped with a Golden Gate ATR device, using the reflectance technique. ^{1}H NMR spectra were recorded on a Bruker 300 DPX MHz spectrometer in $CDCl_3$ solution, using TMS as the internal standard. Diffuse reflectance spectra were obtained on a Perkin–Elmer Lambda 900 spectrophotometer using MgO as a reference. The solution UV/Vis spectra of the compounds were recorded in the range of 200–800 nm with a Cary 50 Varian UV/Vis/NIR spectrometer. Electrospray mass spectra (ESI–MS) in CH_3CN were recorded on a Thermo finnigan AQA apparatus. The cyclic voltammetry measurements were performed with an Autolab PGstat10 potentiostat controlled by GPES4 software. A three-electrode system was used, consisting of a glassy carbon (GC) working electrode, a platinum (Pt) auxiliary electrode and an Ag/AgCl reference electrode. All potentials are given versus Ag/AgCl. The experiments were carried out in acetonitrile at room temperature under argon with tetrabutylammonium hexafluorophosphate as the electrolyte. The phenoxy ligands showed no redox activity between +2.00 and −2.00 V. Magnetic susceptibility measurements (5–300 K) were carried out at 0.1 T using a Quantum Design MPMS-5 5T SQUID magnetometer. Data were corrected for magnetization of the sample holder and for diamagnetic contributions, which were calculated from the Pascal constants. X-band electron paramagnetic resonance (EPR) measurements were performed at room temperature and at 77 K for polycrystalline samples, as well as at 77 K for frozen CH_3CN solutions on a JEOL RE2X electron spin resonance spectrometer, using DDPH ($g = 2.0036$) as a standard.

2.3. X-ray crystallography and data collection

Crystals suitable for structure determination were mounted on Lindemann-glass capillaries and transferred into the cold nitrogen stream of a Nonius KappaCCD diffractometer on a rotating anode (Mo Kα radiation, graphite monochromator, $\lambda = 0.71073$). The intensity data were corrected for Lorentz and polarization effects and for absorption. The structure was solved by direct methods. The programs COLLECT [29] SHELXS-97 [30] SHELXL-97 [31] were used for data reduction, structure solution and structure refinement, respectively. The plots were obtained using

Table 1
Crystal data and details of the structure determination for **1**, **3** and **4**

	1	**3**	**4**
Formula	$C_{22}H_{28}ClFeN_4O_6$	$C_{24}H_{32}ClFeN_3O_9$	$C_{24}H_{32}FeN_4O_4BF_4$
Formula weight	535.78	597.83	583.20
Crystal system	monoclinic	monoclinic	monoclinic
Space group	$P2_1/c$	$P2_1$	$P2_1$
a (Å)	7.5450(15)	7.5680(15)	7.507(3)
b (Å)	15.272(3)	17.694(4)	17.539(10)
c (Å)	20.776(4)	10.308(2)	10.262(18)
β (°)	94.12(3)	106.26(3)	106.46(4)
V (Å^3)	2387.8(8)	1325.1(5)	1296(2)
Z	4	2	2
D_{calc} (Mg m^{-3})	1.490	1.498	1.495
μ(Mo Kα) (mm^{-1})	0.789	0.727	0.649
Crystal size (mm)	0.30 × 0.30 × 0.30	0.04 × 0.08 × 0.20	0.03 × 0.15 × 0.22
T (K)	173	173	173
Data collected	35050	17290	17926
Unique data	5501	5883	5846
R_{int}	0.108	0.087	0.072
$R(F)$ [$I > 2\sigma(I)$]	3100	4335	4338
$R_w(F^2)$	0.0543	0.0495	0.0503
S	1.03	0.98	1.04
$\Delta\rho_{min}$, $\Delta\rho_{max}$ (e Å^{-3})	−0.52, 0.42	−0.56, 0.43	−0.75, 0.47

the PLATON package [32]. All non-hydrogen atoms were refined anisotropically. Hydrogen atoms were placed at idealized positions and allowed to ride on the connecting atom. Crystallographic data of the compounds are listed in Table 1.

3. Results and discussions

3.1. Synthesis and spectroscopic characterization

The Schiff-base ligands H_2L_1 and H_2L_2 were synthesized by small modification of the original procedure [28] and serve as hexadentate ligands in all four complexes (**1**–**4**) reported in this account. As shown in Chart 1, the ligands employ two secondary amine nitrogens, two imine nitrogens and two phenoxo oxygens to bind iron(III) in these complexes. The ether oxygen in H_2L_2 is unlikely to bind to metals. The complexes **1**–**4** were synthesized in good yield by the reaction of $Fe(ClO_4)_2 \cdot 6H_2O$ or $Fe(BF_4)_2 \cdot 6H_2O$ with H_2L_1 or H_2L_2 in a molar ratio 1:1, using methanol as solvent and at room temperature. Analytically pure compounds were obtained in all cases as indicated by elemental and mass analysis. Crystals suitable for single-crystal X-ray diffraction studies were obtained by slow diffusion of diethyl ether into methanol–chloroform solutions of complexes **1**, **3** and **4**. Attempts to similarly obtain single crystals of the complex **2** have remained unsuccessful, despite the large variety of solvents used.

The infrared spectra of the complexes **1**–**4** are dominated by the characteristic bands of the ligands L_1^{2-} and L_2^{2-}. In all cases, the absence of the ν_{O-H} stretching vibration in the range 3300–3600 cm^{-1} indicates that the phenolic group is dehydronated by the coordination to iron(III) ion. A sharp peak centered at 3230–3260 cm^{-1} is most likely due to the N–H stretching vibration of the secondary amine groups. The phenolic ν_{C-O} stretching vibration in the free Schiff bases is observed in the range of 1240–1270 cm^{-1} [33], which is shifted to 1297 cm^{-1} thus indicating coordination of the phenolic oxygen. The $\nu_{C=N}$ stretching vibration appears near 1630 cm^{-1} in the free Schiff base ligands [34]. In the present complexes, one strong band with a resolved doublet ($\Delta\nu_{C=N} < 50\ cm^{-1}$) is present around 1607–1615 cm^{-1} and it has been attributed to the $\nu_{C=N}$, shifted to lower energies by coordination to iron(III) ion. The multiplicity observed for the $\nu_{C=N}$ stretching vibration appears to be due to the crystal packing effects involving the counter anions ClO_4^- and BF_4^-, as also indicated by the X-ray crystal structures discussed below [35]. The presence of the perchlorate counter ion is indicated by the bands at 1072, 620 cm^{-1} (**1**) and 1070, 621 cm^{-1} (**3**). Apparently, a doublet was observed for the tetrafluoroborates at 1068, 997 cm^{-1} (**2**) and 1066, 994 cm^{-1} (**4**) for the analogues containing tetrafluoroborate counter ion. In fact, we observed subtle differences in the IR spectrum of repeated preparations of the complex **2**; this behaviour may perhaps be due to different wrapping environment of donor atoms (nitrogen and oxygen) to an iron(III) center.

In the solid state, the ligand field spectra of **1**–**4** display a single low-energy band with a maximum in the range of 593–649 nm, which is ascribed to the charge-transfer transition from the p_π orbitals of the phenolic oxygens to the d^*_π orbitals of the iron(III) ions. A second charge-transfer band occurs in the range 350–400 nm and it has been assigned to a $p_\pi \rightarrow d^*_\sigma$ type transition [33]. The absence of any other bands in the visible region suggests that the spin allowed d–d transitions are obscured by the tail of the charge-transfer band.

3.2. Description of crystal structures

Fig. 1 shows the molecular structures of the complex **1** along with the atomic numbering scheme used for all non-carbon and non-hydrogen atoms. Selected bond distances and angles are listed in Table 2. The lattice of **1** is made up of $[Fe(L_1)]^+$ cations and uncoordinated perchlorate anions. In the cationic complex, the coordination environment around the iron(III) center is a distorted octahedron built from two phenoxo oxygens, two imine nitrogens, and two secondary-amine nitrogens. The molecular entity shown in Fig. 1 exemplifies how the dianionic hexadentate ligand L_1^{2-} enfolds the iron(III) center in a *trans* coordination mode for the phenolic groups. The iron(III) ion lies within the plane defined by the four nitrogen atoms of the ligand L_1^{2-} and it is 0.006(1) Å out of this plane. The largest deviation from the octahedral geometry of the FeN_4O_2 chromophore is defined by the angle N(18)–Fe(1)–N(212) = 174.04(10)°. The iron to phenoxo oxygen bonds are *trans* to each other with O(10)–Fe(1)–O(20) = 174.43(9)°. The average Fe–N(imine) bond lengths is shorter than the Fe–N(amine) bond lengths (1.954(2) and 1.961(2) Å against 2.023(2) and 2.032(2) Å) and both are consistent with the reported bond lengths for similar

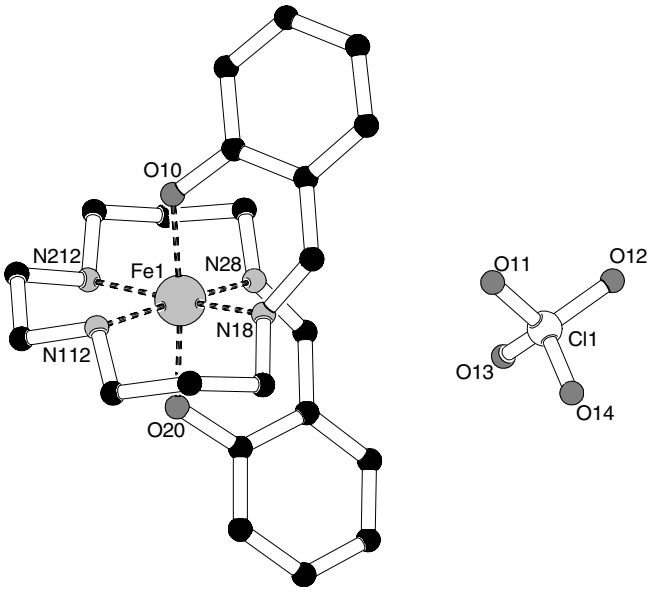

Fig. 1. Pluton projection of the molecular structure of **1**. Hydrogen atoms are omitted for clarity.

Table 2
Selected bond lengths (Å) and angles (°) for **1**, **3** and **4**

Bond lengths (Å)		Bond angles (°)			
1					
Fe(1)–O(10)	1.874(2)	O(10)–Fe(1)–O(20)	174.43(9)	O(20)–Fe(1)–N(212)	89.81(9)
Fe(1)–O(20)	1.8792(19)	O(10)–Fe(1)–N(18)	89.59(10)	N(18)–Fe(1)–N(28)	93.59(10)
Fe(1)–N(18)	1.961(2)	O(10)–Fe(1)–N(28)	93.88(10)	N(18)–Fe(1)–N(112)	90.97(10)
Fe(1)–N(28)	1.954(2)	O(10)–Fe(1)–N(112)	89.93(10)	N(18)–Fe(1)–N(212)	174.04(10)
Fe(1)–N(112)	2.032(2)	O(10)–Fe(1)–N(212)	86.18(10)	N(28)–Fe(1)–N(112)	174.08(10)
Fe(1)–N(212)	2.023(2)	O(20)–Fe(1)–N(18)	94.11(10)	N(28)–Fe(1)–N(212)	90.88(10)
		O(20)–Fe(1)–N(28)	90.05(9)	N(112)–Fe(1)–N(212)	84.84(10)
		O(20)–Fe(1)–N(112)	85.85(9)		
3					
Fe(1)–O(10)	1.893(3)	O(10)–Fe(1)–O(20)	176.13(13)	O(20)–Fe(1)–N(214)	90.72(13)
Fe(1)–O(20)	1.882(3)	O(10)–Fe(1)–N(110)	90.00(13)	N(110)–Fe(1)–N(114)	90.24(14)
Fe(1)–N(110)	1.946(3)	O(10)–Fe(1)–N(114)	91.84(13)	N(110)–Fe(1)–N(210)	94.36(14)
Fe(1)–N(210)	1.944(4)	O(10)–Fe(1)–N(210)	92.85(13)	N(114)–Fe(1)–N(210)	173.43(15)
Fe(1)–N(114)	2.025(4)	O(10)–Fe(1)–N(214)	86.26(13)	N(214)–Fe(1)–N(110)	174.48(14)
Fe(1)–N(214)	2.023(4)	O(20)–Fe(1)–N(110)	92.84(13)	N(214)–Fe(1)–N(114)	85.83(15)
		O(20)–Fe(1)–N(114)	85.53(13)	N(214)–Fe(1)–N(210)	89.88(15)
		O(20)–Fe(1)–N(210)	89.55(13)		
4					
Fe(1)–O(10)	1.881(4)	O(10)–Fe(1)–O(20)	176.34(14)	O(20)–Fe(1)–N(214)	91.22(14)
Fe(1)–O(20)	1.876(4)	O(10)–Fe(1)–N(110)	89.24(13)	N(110)–Fe(1)–N(114)	90.34(14)
Fe(1)–N(110)	1.940(5)	O(10)–Fe(1)–N(114)	90.63(14)	N(110)–Fe(1)–N(210)	94.09(15)
Fe(1)–N(210)	1.949(5)	O(10)–Fe(1)–N(210)	92.70(14)	N(110)–Fe(1)–N(214)	173.61(16)
Fe(1)–N(114)	2.011(5)	O(10)–Fe(1)–N(214)	86.08(15)	N(114)–Fe(1)–N(210)	174.49(15)
Fe(1)–N(214)	2.040(5)	O(20)–Fe(1)–N(110)	93.26(13)	N(114)–Fe(1)–N(214)	85.37(14)
		O(20)–Fe(1)–N(114)	86.68(13)	N(210)–Fe(1)–N(214)	90.48(15)
		O(20)–Fe(1)–N(210)	89.79(14)		

iron(III) low-spin complexes with Schiff-base ligands [15,16]. The average Fe–O bond length is known to be insensitive to the spin state of the iron(III) [9,10,12,24–27,36]. In the case of **1**, the iron to oxygen bond lengths are almost constant with Fe(1)–O(10) = 1.874(2) Å and Fe(1)–O(20) = 1.879(3) Å.

In the crystal lattice, the mononuclear entities of **1** are organized into infinite 1D chains due to the hydrogen-bonding interactions involving the secondary amine functions and one oxygen atom of a perchlorate anion (Fig. 2 and Table 3). The establishment of hydrogen bonds seems to be aiding crystallization, since their strength and directionality play a decisive role in the intermolecular interaction. Each molecule is chiral and both enantiomers occur in the crystal lattice.

The molecular structure of **3** consists of $[Fe(L_2)]^+$ cations and well separated perchlorate anions (Fig. 3). The coordination geometry around the iron(III) ion is distorted octahedral, and the coordination mode of L_2^{2-} is similar to that observed for the ligand L_1^{2-} in the complex **1**. Introduction of the methoxo groups in the ligand L_2^{2-} coordinated to the iron(III) ion induces only little changes in the metric parameters of **3** compared to **1** (Table 2). As a result, the Fe–O and Fe–N bond lengths are again consistent with the presence of an iron(III) low-spin complex (Table 2). The largest distortion from the octahedral geometry is determined by the angle N(114)–Fe(1)–N(210) = 173.43(15)°. As compared with the complex **1**, the iron to phenoxo-oxygen bonds are slightly longer and the angle O(10)–Fe(1)–O(20) = 176.13(13)° is less deviating from linearity. The hydrogen-bonding network that connects the cation complex $[Fe(L_2)]^+$ and the perchlorate ions is an important feature of **3** (Table 3). Although the individual molecules are connected into one-dimensional infinite chains via hydrogen-bonding interactions in a similar manner to that observed for **1**, the hydrogen contacts with the facial amine are weaker in **2** as compared with **1**.

The cation complex **4** is isostructural with that in complex **3**, as also seen in the almost identical infrared spectra; the structure again consisting of $[Fe(L_2)]^+$ cations and uncoordinated tetrafluoroborate anions. Necessarily, the geometric features of the complex are substantially similar to those of the complex **3** as can be seen from Table 2. In the crystal lattice, hydrogen bonds interactions are established between the $[Fe(L_2)]^+$ cations and tetrafluoroborate anions (Table 3).

Both compounds **3** and **4** are chiral in the solid and spontaneously crystallize as pure enantiomers; the absolute structure based on Flack's parameter has been determined, which was possible due to the presence of a heavy element. The fact that **3** and **4** have different lattice structures compared to **1** and **2** is ascribed to their different hydrogen bond patterns.

3.3. Solution chemistry and redox behaviour

Ligand field spectra of the complexes **1**–**4** have also been recorded in acetonitrile solution and all show spectroscopic

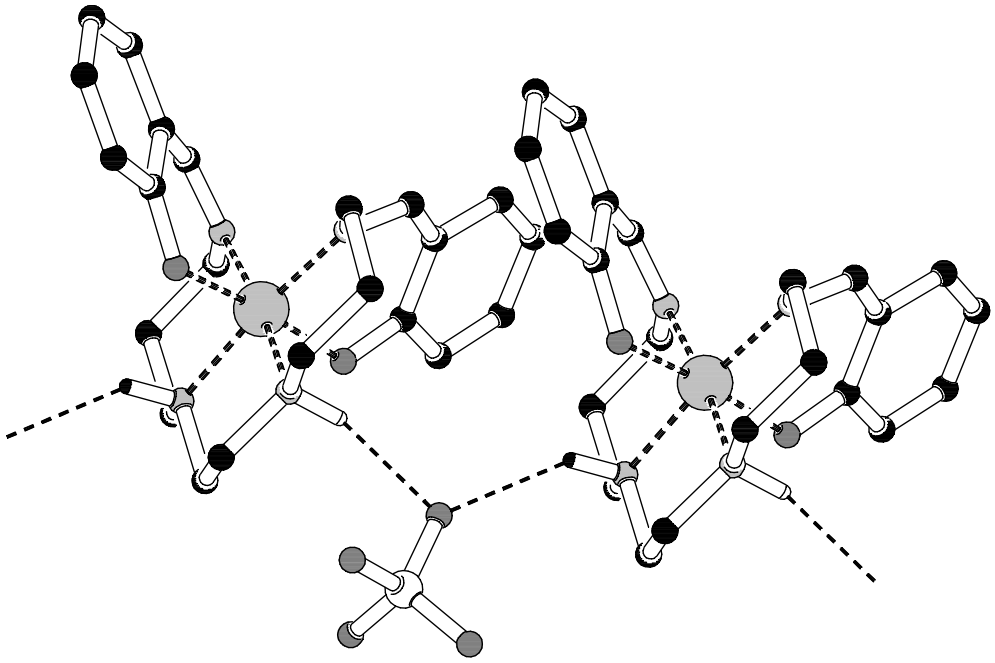

Fig. 2. The hydrogen bond network involving the ClO_4^- anion and the complex cation $[Fe(L_1)]^+$ of **1**.

Table 3
Hydrogen bond details (distances [Å] and angles [°]) for **1**, **3** and **4**

Donor–H···acceptor	D–H	H···A	D···A	D–H···A
1				
N(112)–H(11)···O(12)	0.9302	2.2509	2.998(5)	136
N(212)–H(21g)···O(12)	0.9301	2.3869	3.150(5)	139
3				
N(114)–H(11i)···O(13)	0.93	2.41	3.306(13)	160
N(214)–H(21i)···O(13)	1	2.15	3.079(13)	153
4				
N(114)–H(11i)···F(14)	0.93	2.21	3.050(12)	150
N(214)–H(21i)···F(14)	0.93	2.35	3.252(13)	164

features that are similar to that in the solid state consisting of two absorption bands with maxima in the range 565–605 and 365–402 nm. Notably, the maximum of the LMCT band due to the $p_\pi \rightarrow d_\pi^*$ is shifted from ~560 nm in the compounds **1** and **2** to ~600 nm in **3** and **4**. This behaviour reflects changes in the Lewis acidity of the iron(III) center due to the presence of the OCH_3 donating group in the ligand L_2^{2-} (complexes **3** and **4**) which decreases the degree of any iron to ligand π bonding. The features discussed above suggest that geometry of the iron(III) core is similar in both solid and solution states. This property is further supported by the positive ESI-MS spectra of all complexes that exhibit a major peak at $m/z = 436.3$ for **1** and **2** or $m/z = 496.3$ for **3** and **4**.

Cyclic voltammograms of all four complexes were recorded in acetonitrile in the potential range −1.6 to +0.6 V versus Ag/AgCl reference electrode. In all cases, the cyclic voltammogram presents a quasi-reversible one-electron wave with the half-wave potential value, $E_{1/2}$, of 500 mV versus Ag/AgCl for the reduction of iron(III) to iron(II). Fig. 4 presents the cyclic voltammogram of the complex **3**. The phenoxy ligands showed no redox activity between +2.0 and −1.8 V. As a result, the electrochemical behaviour indicates that all four complexes are stable in acetonitrile solution and the coordination environment of iron(III) ion is similar.

3.4. EPR and Magnetic Susceptibility measurements

Temperature dependent magnetic susceptibility measurements for **1**–**4** were performed on polycrystalline samples in the range 5–300 K using SQUID magnetometer. In all cases the χ_M values have been corrected for diamagnetism [37]. At room temperature, the product of molar susceptibility times temperature ($\chi_M T$) of the $[Fe(L_1)](ClO_4)$ (**1**), $[Fe(L_1)](BF_4)$ (**2**), $[Fe(L_2)](ClO_4)$ (**3**), and $[Fe(L_2)](BF_4)$ (**4**) complexes is 0.453, 0.459, 0.456, and 0.454 $cm^3\ K\ mol^{-1}$, respectively. The observed $\chi_M T$ values are slightly higher than the spin-only value of 0.375 $cm^3\ K\ mol^{-1}$ expected for one unpaired electron

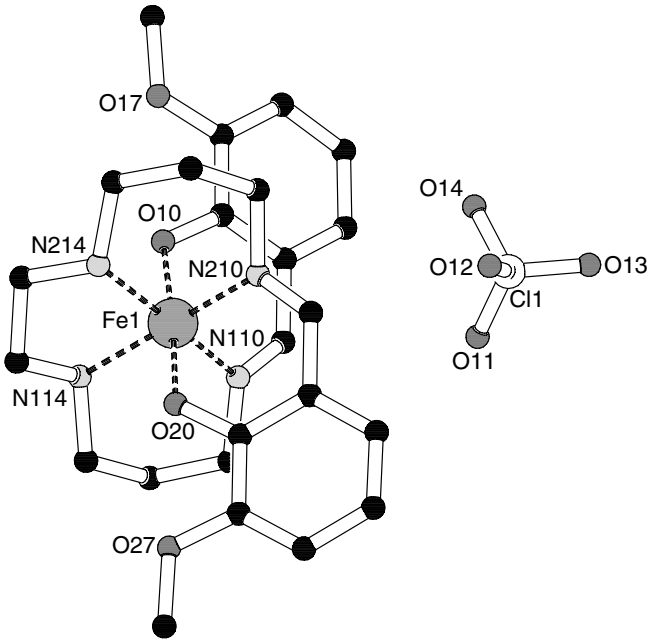

Fig. 3. Pluton projection of the molecular structure of **3**. Hydrogen atoms are omitted for clarity.

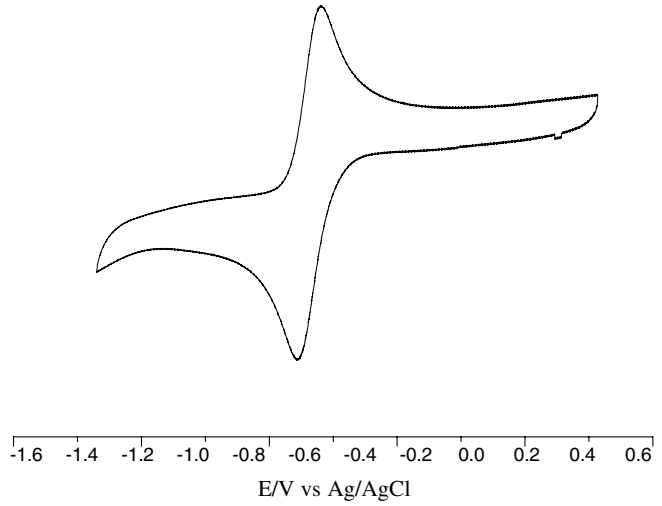

Fig. 4. Cyclic voltammogram of 1 mM $[Fe(L_2)](ClO_4)$ (**3**) in CH_3CN at room temperature and recorded at 100 mV/s scan rate.

($S = 1/2$) and this characteristic is due to the orbital contribution. The electronic ground state of the octahedral iron(III) complexes is orbitally degenerate ($^2T_{2g}$) and little to moderate orbital contribution to the $\chi_M T$ values is often observed for low-spin iron(III) complexes with Schiff-base ligands [26,37,38]. The $\chi_M T$ versus T curves follow a Curie law, in agreement with the presence of independent coordination sites.

The low-spin electronic configuration ($S = 1/2$) of the iron(III) centers in the complexes **1**–**4** is further confirmed by the EPR spectra at room temperature for solid-state samples and at 77 K for acetonitrile frozen solutions (Table 4). The EPR spectra of the complex **3** are displayed in Figs. 5 and 6. The results presented in Table 4 demonstrate that the iron(III) ions remains low-spin ($S = 1/2$) at both temperatures. Other six-coordinate iron(III) Schiff-base complexes with N_XO_Y donor sets like $[Fe(N_4O_2)]^+$, $[Fe(N_2O_2)L_2]^+$, $[Fe(N_3O_2)L]^+$ and $[Fe(N_4O_2)]^+$ are either high-spin ($S = 5/2$) or exhibit spin equilibrium [39,40]. Even closely related hexadentate Schiff-base ligands with N_4O_2 donor set do not afford low-spin ($S = 1/2$) iron(III) complexes [21]. Only in very few complexes the coordination of hexadentate ligands to iron(III) ion leads to low-spin electronic configuration [38]. Conversely, all four complexes are low-spin iron(III) compounds from room temperature down to 5 K. From Table 4, all the g matrix values are closely comparable to each other, this indicating that all four complexes are strict in their geometry with subtle distortion around iron(III) center.

The complexes **1**–**4** all have an N_4O_2 donor atom set forming a distorted octahedral coordination geometry around the iron(III) ion, with the oxygen donor atoms occupying *trans*-positions. In all four complexes, the crystallographic, spectroscopic and magnetic studies agree with the presence of a low-spin electronic configuration for the iron(III) ion. The previous studies on hexacoordinated iron(III) complexes with a N_4O_2 donor set have revealed that the *cis* positions of the oxygen donor atoms can provoke drastic changes on the spin state of the iron(III) complexes and high-spin or spin-crossover behaviors were observed, depending on the relative orientation of the additional ligands [15,25]. In addition, the intermolecular hydrogen-bonding interactions involving the amines bound to the iron(III) increase the donor strength of the ligand and favor the low-spin electronic configuration of the metal ion [21].

4. Conclusions

The synthesis and characterization of four new iron(III) complexes with hexadentate Schiff-base ligands with N_4O_2 donor sets is reported. The crystal structures of the

Table 4
EPR spectral data for the complexes **1**–**4**

Complexes	RT, solid samples in Q band			Frozen solutions at 77 K, CH_3CN		
	g_{xx}	g_{yy}	g_{zz}	g_{xx}	g_{yy}	g_{zz}
$[Fe(L_1)](ClO_4)$ (**1**)	2.28	2.13	2.05	2.35	2.12	1.94
$[Fe(L_1)](BF_4)$ (**2**)	2.29	2.18	2.06	2.35	2.12	1.94
$[Fe(L_2)](ClO_4)$ (**3**)	2.25	2.13	2.03	2.34	2.10	1.94
$[Fe(L_2)](BF_4)$ (**4**)	2.26	2.14	2.08	2.35	2.11	1.95

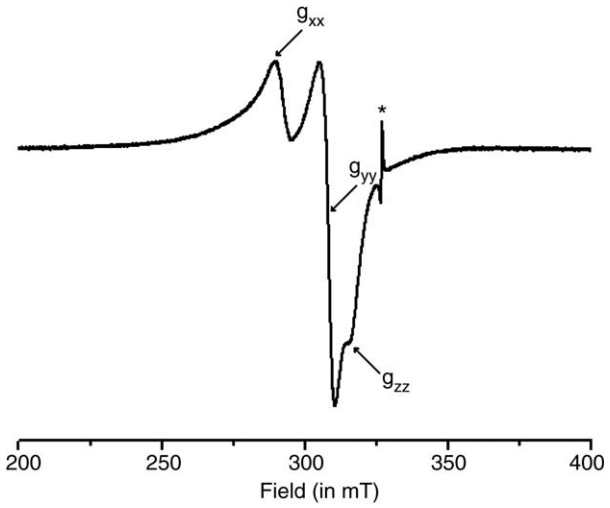

Fig. 5. X-band EPR spectrum of the polycrystalline sample of $[Fe(L_2)](ClO_4)$ (**3**) at room temperature.

complexes **1**, **3** and **4** indicate the presence of $[Fe(L_1)]^+$ or $[Fe(L_2)]^+$ cations and well-separated perchlorate or tetrafluoroborate anions. The coordination geometry around iron(III) center is pseudo-octahedral with the two phenolic oxygen atoms in *trans* configurations. The crystal lattices are stabilized through extended hydrogen-bonding interactions. The structural, spectroscopic and magnetic studies indicate that the *trans* configuration and the hydrogen-bonding interactions play important role in the stabilization of the low-spin electronic state of the iron(III). The ligand field spectra, electrochemistry and ESI-MS studies suggest that the mononuclear $[Fe(L_1)]^+$ or $[Fe(L_2)]^+$ entities are retained in solution. The temperature dependent magnetic susceptibility studies as well as electron paramagnetic resonance indicate that all four iron(III) complexes remain in low-spin electronic configuration at room temperature as well as 77 K.

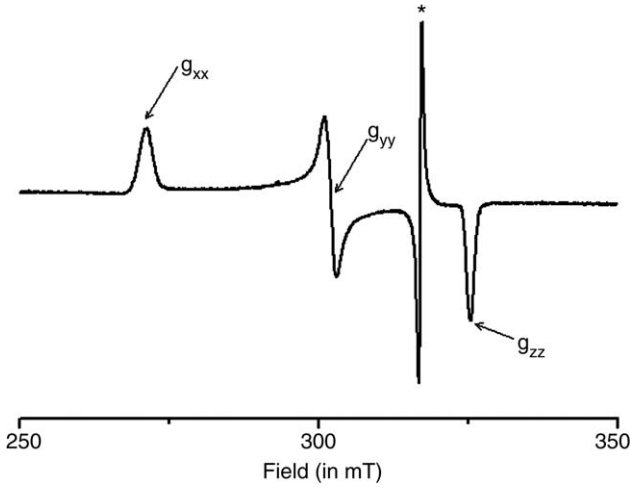

Fig. 6. X-band EPR spectrum of $[Fe(L_2)](ClO_4)$ (**3**) in CH_3CN at 77 K.

5. Supplementary material

Crystallographic data (excluding structure factors) have been deposited with the Cambridge Crystallographic Data Centre as supplementary publication Nos. CCDC 267399–267401. Copies of the data can be obtained free of charge on application to The Director, CCDC, 12 Union Road, Cambridge CB2 1EZ, UK (fax: +44 1223 336 033; e-mail: deposit@ccdc.cam.ac.uk or www: http//www.ccdc.cam.ac. uk).

Acknowledgements

This work has been financially supported in part by the Netherlands Technology Research Foundation (STW) applied science division of The Netherlands Organization for Scientific Research. This work was also supported by the Dutch Economy, Ecology, Technology (EET) programme, a joint programme of the Ministry of Economic Affairs, the Ministry of Education, Culture and Science, and the Ministry of Housing, Spatial Planning and the Environment.

References

[1] S. Fujii, H. Ohyanishiguchi, N. Hirota, A. Nishinaga, Bull. Chem. Soc. Jpn. 66 (1993) 1408.
[2] V.K. Sivasubramanian, M. Ganesan, S. Rajagopal, R. Ramaraj, J. Org. Chem. 67 (2002) 1506.
[3] H. Fujii, T. Kurahashi, T. Ogura, J. Inorg. Biochem. 96 (2003) 133.
[4] R.B. Bedford, D.W. Bruce, R.M. Frost, J.W. Goodby, M. Hird, Chem. Commun. (2004) 2822.
[5] K.P. Bryliakov, E.P. Talsi, Angew. Chem., Int. Edit. 43 (2004) 5228.
[6] T. Katsuki, Chem. Soc. Rev. 33 (2004) 437.
[7] S.K. Edulji, S.T. Nguyen, Organometallics 22 (2003) 3374.
[8] H. Fujii, Y. Funahashi, Angew. Chem., Int. Edit. 41 (2002) 3638.
[9] M.M. Bhadbhade, D. Srinivas, Polyhedron 17 (1998) 2699.
[10] S. Hayami, K. Inoue, Y. Maeda, Mol. Cryst. Liq. Cryst. 334 (1999) 1285.
[11] W. Chiang, D. Vanengen, M.E. Thompson, Polyhedron 15 (1996) 2369.
[12] C.T. Brewer, G. Brewer, G.B. Jameson, P. Kamaras, L. May, M. Rapta, J. Chem. Soc., Dalton Trans. (1995) 37.
[13] P.J. Nichols, G.D. Fallon, K.S. Murray, B.O. West, Inorg. Chem. 27 (1988) 2795.
[14] R.N. Mukherjee, A.J. Abrahamson, G.S. Patterson, T.D.P. Stack, R.H. Holm, Inorg. Chem. 27 (1988) 2137.
[15] B.J. Kennedy, A.C. McGrath, K.S. Murray, B.W. Skelton, A.H. White, Inorg. Chem. 26 (1987) 483.
[16] B.J. Kennedy, G. Brain, E. Horn, K.S. Murray, M.R. Snow, Inorg. Chem. 24 (1985) 1647.
[17] L. Canali, D.C. Sherrington, Chem. Soc. Rev. 28 (1999) 85.
[18] A. Bottcher, M.W. Grinstaff, J.A. Labinger, H.B. Gray, J. Mol. Catal. A – Chem. 113 (1996) 191.
[19] A. Bottcher, E.R. Birnbaum, M.W. Day, H.B. Gray, M.W. Grinstaff, J.A. Labinger, J. Mol. Catal. A – Chem. 117 (1997) 229.
[20] M.W. Grinstaff, M.G. Hill, J.A. Labinger, H.B. Gray, Science 264 (1994) 1311.
[21] L. Salmon, A. Bousseksou, B. Donnadieu, J.P. Tuchagues, Inorg. Chem. 44 (2005) 1763.
[22] P.J. van Koningsbruggen, Y. Maeda, H. Oshio, Spin Crossover in Transition Metal Compounds I, vol. 233, 2004, pp. 259–324.

[23] Y. Ikuta, M. Ooidemizu, Y. Yamahata, M. Yamada, S. Osa, N. Matsumoto, S. Iijima, Y. Sunatsuki, M. Kojima, F. Dahan, J.P. Tuchagues, Inorg. Chem. 42 (2003) 7001.
[24] R. Boca, Y. Fukuda, M. Gembicky, R. Herchel, R. Jarosciak, W. Linert, F. Renz, J. Yuzurihara, Chem. Phys. Lett. 325 (2000) 411.
[25] R. Hernandez-Molina, A. Mederos, S. Dominguez, P. Gili, C. Ruiz-Perez, A. Castineiras, X. Solans, F. Lloret, J.A. Real, Inorg. Chem. 37 (1998) 5102.
[26] S. Hayami, T. Matoba, S. Nomiyama, T. Kojima, S. Osaki, Y. Maeda, Bull. Chem. Soc. Jpn. 70 (1997) 3001.
[27] Y. Maeda, M. Miyamoto, Y. Takashima, H. Oshio, Inorg. Chim. Acta 204 (1993) 231.
[28] U. Casellato, P. Guerriero, S. Tamburini, P.A. Vigato, R. Graziani, J. Chem. Soc., Dalton Trans. (1990) 1533.
[29] Nonius, Nonius Collect Software BV, Delft, The Netherlands, 2002.
[30] G.H. Sheldrick, SHELXS-97. Program for Crystal Structure Solution, University of Gottingen, Gottingen, Germany, 1997.
[31] G.H. Sheldrick, SHELXL-97. Program for Crystal Structure Refinement, University of Gottingen, Gottingen, Germany, 1997.
[32] A.L. Spek, J. Appl. Crystallogr. 36 (2003) 7.
[33] S. Tanase, E. Bouwman, G.J. Long, A.M. Shahin, A.M. Mills, A.L. Spek, J. Reedijk, Eur. J. Inorg. Chem. (2004) 4572.
[34] H. Keypour, S. Salehzadeh, R.V. Parish, Molecules 7 (2002) 140.
[35] P. Pascal, Ann. Chim. Phys. 19 (1910) 5.
[36] C.T. Brewer, G. Brewer, L. May, J. Sitar, R. Wang, J. Chem. Soc., Dalton Trans. (1993) 151.
[37] M.F. Tweedle, L.J. Wilson, J. Am. Chem. Soc. 98 (1976) 4824.
[38] J.C. Noveron, R. Herradora, M.M. Olmstead, P.K. Mascharak, Inorg. Chim. Acta 285 (1999) 269.
[39] J.P. Costes, F. Dahan, J.P. Laurent, Inorg. Chem. 29 (1990) 2448.
[40] K. Ramesh, R. Mukherjee, J. Chem. Soc., Dalton Trans. (1992) 83.

particular, we report the synthesis of {[3,5-(i-Pr)$_2$Pz]Ag}$_3$, {[3,5-(i-Pr)$_2$,4-(Br)Pz]Ag}$_3$, and {[3,5-(i-Pr)$_2$,4-(NO_2)Pz]-Ag}$_3$ via a very convenient route using silver(I) oxide and the corresponding pyrazoles, and their spectroscopic and solid-state structural data.

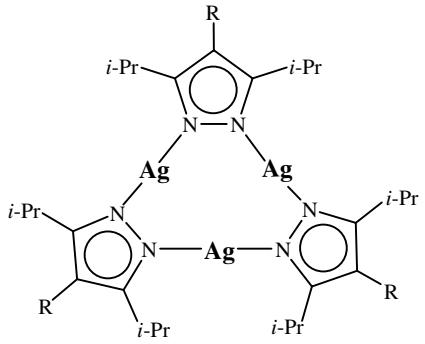

{[3,5-(i-Pr)$_2$,4-(R)Pz]Ag}$_3$

R = H, Br, NO_2

2. Experimental

2.1. General procedures

All manipulations were carried out under an atmosphere of purified nitrogen using standard Schlenk techniques. Solvents were purchased from commercial sources, distilled from conventional drying agents and degassed by the freeze–pump–thaw method twice prior to use. The glassware was oven-dried at 150 °C overnight. NMR spectra were recorded at 25 °C on a JEOL Eclipse 500 spectrometer (^{1}H, 500.16 MHz, ^{13}C, 125.78 MHz). Proton and carbon chemical shifts are reported in ppm versus Me_4Si. Infrared spectra were recorded on a JASCO FT-IR 410 spectrometer. Melting points were obtained on a Mel-Temp II apparatus and were not corrected. Elemental analyses were performed using a Perkin–Elmer Model 2400 CHN analyzer. Ag_2O and [3,5-(i-Pr)$_2$Pz]H were purchased from commercial sources. [3,5-(i-Pr)$_2$,4-(Br)Pz]H and [3,5-(i-Pr)$_2$,4-(NO_2)-Pz]H were prepared by published methods [35,36].

2.2. {[3,5-(i-Pr)$_2$Pz]Ag}$_3$

Ag_2O (0.42 g, 1.82 mmol) and [3,5-(i-Pr)$_2$Pz]H (0.50 g, 3.30 mmol) were mixed in benzene (20.0 mL). The resulting mixture was protected from light using aluminum foil and refluxed overnight. After cooling, the solution was filtered through a bed of celite to remove some insoluble black material. The filtrate was collected and the solvent was removed under reduced pressure to obtain crude {[3,5-(i-Pr)$_2$Pz]Ag}$_3$ as a colorless solid. X-ray quality crystals were grown from hexane at room temperature. Yield: 95% M.p.: 220 °C (dec.) ^{1}H NMR ($CDCl_3$): δ 1.33 (d, 36H, $J = 7.0$ Hz, CH_3), 2.96 (septet, 6H, $J = 7.0$ Hz, CH), 5.98 (s, 3H, Pz-H$_4$); ^{13}C{^{1}H} NMR ($CDCl_3$): δ 23.6 (CH_3), 28.8 (CH), 95.6 (Pz–CH), 160.6 (Pz–C$_{3,5}$). IR (Nujol): 3853, 2920, 1734, 1541, 1518, 1364, 1297, 1173, 1132, 1103, 1045, 918, 893, 721, 674. *Anal.* Calc. for $C_{27}H_{45}Ag_3N_3$: C, 41.72; H, 5.84; N, 10.81. Found: C, 41.51; H, 5.90; N, 10.80%.

2.3. {[3,5-(i-Pr)$_2$,4-(Br)Pz]Ag}$_3$

A mixture of Ag_2O (0.21 g, 0.91 mmol) and [3,5-(i-Pr)$_2$,4-(Br)Pz]H (0.38 g, 1.65 mmol) in benzene (15.0 mL) was protected from light using aluminum foil, and refluxed overnight. After cooling, the solution was filtered through a bed of celite and the filtrate was collected. The solvent was removed under reduced pressure to obtain crude {[3,5-(i-Pr)$_2$,4-(Br)Pz]Ag}$_3$ as a colorless solid. X-ray quality crystals were grown from hexane at 5 °C. Yield: 92% m.p.: 196–198 °C. ^{1}H NMR ($CDCl_3$): δ 1.40 (d, 36H, $J = 7.5$ Hz, CH_3), 3.14 (septet, 6H, $J = 7.5$ Hz CH); ^{13}C{^{1}H} NMR ($CDCl_3$): δ 22.0 (CH_3), 28.4 (CH), 89.0 (C–Br), 156.6 (Pz–C$_{3,5}$). IR (Nujol): 2920, 1653, 1276, 1168, 1141, 1103, 1088, 1037, 893, 665. *Anal.* Calc. for $C_{27}H_{42}Ag_3Br_3N_3$: C, 31.98; H, 4.17; N, 8.29. Found: C, 31.90; H, 4.00; N, 8.31%.

2.4. {[3,5-(i-Pr)$_2$,4-(NO_2)Pz]Ag}$_3$

Ag_2O (0.21 g, 0.91 mmol) and [3,5-(i-Pr)$_2$,4-(NO_2)Pz]H (0.32 g, 1.65 mmol) were mixed in benzene (15.0 mL). The resulting mixture was protected from light using aluminum foil and refluxed overnight. After cooling, the solution was filtered through a bed of celite to remove some insoluble black material. The filtrate was collected and the solvent was removed under reduced pressure to obtain crude {[3,5-(i-Pr)$_2$,4-(NO_2)Pz]Ag}$_3$ as a yellowish-white solid. X-ray quality crystals were grown from dichloromethane/hexane at 5 °C. Yield: 88% m.p.: >265 °C. ^{1}H NMR ($CDCl_3$): δ 1.47 (d, 36H, $J = 7.0$ Hz, CH_3), 3.67 (septet, 6H, $J = 7.0$ Hz, CH); ^{13}C{^{1}H} NMR ($CDCl_3$): δ 21.4 (CH_3), 28.6 (CH), 129.0 (C–NO_2), 158.5 (Pz–C$_{3,5}$). IR (Nujol): 2924, 2361, 1653, 1558, 1521, 1342, 1187, 1173, 1108, 1083, 1052, 1034, 833, 775, 665. *Anal.* Calc. for $C_{27}H_{42}Ag_3N_9O_6$: C, 35.55; H, 4.64; N, 13.82. Found: C, 35.40; H, 4.42; N, 13.73%.

2.5. X-ray structure determination

X-ray quality crystals of {[3,5-(i-Pr)$_2$Pz]Ag}$_3$ and {[3,5-(i-Pr)$_2$,4-(Br)Pz]Ag}$_3$ were obtained from hexane at room temperature and at 5 °C, respectively. A mixture of hexane and dichloromethane was used to obtain crystals of {[3,5-(i-Pr)$_2$,4-(NO_2)Pz]Ag}$_3$ at 5 °C. The X-ray intensity data were measured on a Bruker SMART APEX CCD area detector system equipped with a Low Temperature device, a graphite monochromator, and a Mo Kα fine-focus sealed tube ($\lambda = 0.71073$ Å). The data frames were integrated with the Bruker SAINT-PLUS software package. Data were corrected for absorption effects using the multi-scan technique (SADABS). All the structures were solved and refined using

Table 1
X-ray crystallographic data for $\{[3,5\text{-}(i\text{-}Pr)_2Pz]Ag\}_3$, $\{[3,5\text{-}(i\text{-}Pr)_2,4\text{-}(Br)Pz]Ag\}_3$, and $\{[3,5\text{-}(i\text{-}Pr)_2,4\text{-}(NO_2)Pz]Ag\}_3$

	$\{[3,5\text{-}(i\text{-}Pr)_2Pz]Ag\}_3$	$\{[3,5\text{-}(i\text{-}Pr)_2,4\text{-}(Br)Pz]Ag\}_3$	$\{[3,5\text{-}(i\text{-}Pr)_2,4\text{-}(NO_2)Pz]Ag\}_3 \cdot 0.8(CH_2Cl_2)$
Empirical formula	$C_{27}H_{45}Ag_3N_6$	$C_{27}H_{42}Ag_3Br_3N_6$	$C_{27.80}H_{43.60}Ag_3Cl_{1.6}N_9O_6$
Formula weight	777.30	1014.01	980.25
Temperature (K)	100(2)	100(2)	100(2)
Wavelength (Å)	0.71073	0.71073	0.71073
Crystal system	monoclinic	tetragonal	monoclinic
Space group	*P*2(1)/*c*	*I*4(1)/*a*	*P*2(1)
Unit cell dimensions			
a (Å)	26.8604(17)	43.4831(15)	13.4019(5)
b (Å)	13.8362(9)	43.4831(15)	13.0266(5)
c (Å)	16.9719(11)	14.7045(5)	21.9982(8)
α (°)	90	90	90
β (°)	98.3620(10)	90	103.8310(10)
γ (°)	90	90	90
Volume (Å^3)	6240.5(7)	27803.0(17)	3729.1(2)
Z	8	32	4
Density (calculated) (Mg/m^3)	1.655	1.938	1.746
R_1, wR_2 [$I > 2\sigma(I)$]	0.0319, 0.0724	0.0311, 0.0587	0.0369, 0.0982
R_1, wR_2 (all data)	0.0380, 0.0756	0.0441, 0.0573	0.0384, 0.0997

the Bruker SHELXTL software package. Table 1 shows the unit cell dimensions and important structural parameters for the compounds $\{[3,5\text{-}(i\text{-}Pr)_2Pz]Ag\}_3$, $\{[3,5\text{-}(i\text{-}Pr)_2,4\text{-}(Br)Pz]Ag\}_3$, and $\{[3,5\text{-}(i\text{-}Pr)_2,4\text{-}(NO_2)Pz]Ag\}_3$. The asymmetric unit of each of these compounds contains two trimer units. The $\{[3,5\text{-}(i\text{-}Pr)_2,4\text{-}(NO_2)Pz]Ag\}_3$ also crystallizes with 1.6 molecules of CH_2Cl_2 in the asymmetric unit. Crystallographic data (cif files) for these compounds have been deposited with the Cambridge Crystallographic Data Center, CCDS Nos. 281063–281065.

3. Results and discussion

Trimeric, silver(I) pyrazolates could be obtained using several methods. Fackler and co-workers reported the synthesis of $\{[3,5\text{-}(Ph)_2Pz]Ag\}_3$ from CuCl and $[3,5\text{-}(Ph)_2Pz]Na$ in the presence of $AgNO_3$ [16,23] or using $[3,5\text{-}(Ph)_2Pz]Na$ and $Ag(THT)NO_3$ [24]. Syntheses of several other trimeric silver(I) pyrazolates were reported during past two decades following closely related synthetic procedures [22,26]. Masciocchi et al. reported the synthesis of trimeric $\{[Pz]Ag\}_3$ by removing PPh_3 from dimeric silver(I) pyrazolate, $\{(PPh_3)Ag[Pz]\}_2$ [21]. Synthesis of the trimeric Ag(I) complex, $\{[3,5\text{-}(CF_3)_2Pz]Ag\}_3$ using a mixture of silver(I) oxide and 3,5-bis(trifluoromethyl) pyrazole was reported by our group in 2000 [15]. A very similar method was followed by Chi et al. to obtain $\{[3\text{-}(t\text{-}Bu),5\text{-}(CF_3)Pz]Ag\}_3$ and $\{[3,5\text{-}(t\text{-}Bu)_2Pz]Ag\}_3$ [27]. Trimeric $\{[Pz(IN)]Ag\}_3$ was synthesized by Ishida et al. by a reaction of [Pz(IN)]H (3-pyrazolyl imino nitroxide), $AgClO_4$, and 1,8-diazabicyclo[5.4.0]-7-undecene in acetonitrile [25].

The synthetic route established for $\{[3,5\text{-}(CF_3)_2Pz]Ag\}_3$ was utilized for the preparation of trimeric silver(I) complexes described in this paper. In particular, $\{[3,5\text{-}(i\text{-}Pr)_2Pz]Ag\}_3$, $\{[3,5\text{-}(i\text{-}Pr)_2,4\text{-}(Br)Pz]Ag\}_3$, and $\{[3,5\text{-}(i\text{-}Pr)_2,4\text{-}(NO_2)Pz]Ag\}_3$ were synthesized by reacting silver(I) oxide with $[3,5\text{-}(i\text{-}Pr)_2Pz]H$, $[3,5\text{-}(i\text{-}Pr)_2,4\text{-}(Br)Pz]H$, and $[3,5\text{-}(i\text{-}Pr)_2,4\text{-}(NO_2)Pz]H$, respectively. All these complexes are colorless, crystalline, and air stable solids. They are readily soluble in most of the common organic solvents such as hexane, methylene chloride, tetrahydrofuran, diethyl ether, and toluene. $\{[3,5\text{-}(i\text{-}Pr)_2Pz]Ag\}_3$, $\{[3,5\text{-}(i\text{-}Pr)_2,4\text{-}(Br)Pz]Ag\}_3$, and $\{[3,5\text{-}(i\text{-}Pr)_2,4\text{-}(NO_2)Pz]Ag\}_3$ were characterized by X-ray diffraction, IR and NMR spectroscopy data.

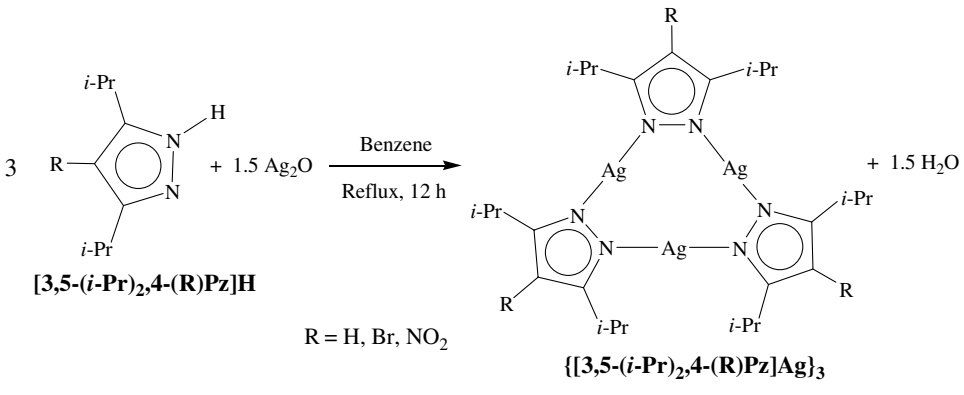

^{1}H and ^{13}C NMR spectral data of compounds $\{[3,5\text{-}(i\text{-}Pr)_2Pz]Ag\}_3$, $\{[3,5\text{-}(i\text{-}Pr)_2,4\text{-}(Br)Pz]Ag\}_3$, and $\{[3,5\text{-}(i\text{-}Pr)_2,4\text{-}(NO_2)Pz]Ag\}_3$ are fairly straightforward. In all three compounds, the ^{1}H and ^{13}C NMR chemical shift values are very close to those observed for their corresponding free ligands. However, as expected, the proton NMR spectra of the three silver adducts lack the broad peak corresponding to the N–H proton of the free pyrazole ligands.

X-ray crystallographic data show that the three complexes feature nine-membered Ag_3N_6 metallacycles. They show the presence of a trinuclear cyclic array of three linearly coordinated silver ions (N–Ag–N bond angles range from 168.61(16)° to 178.20(18)°) and three bridging pyrazolates, similar to the triangular framework found in several pyrazolate complexes of the coinage metal ions such as $\{[3,5\text{-}(Ph)_2Pz]Au\}_3$ [23], $\{[3,5\text{-}(CF_3)_2Pz]Ag\}_3$ [15], and $\{[3,5\text{-}(CH_3)_2Pz]Cu\}_3$ [12]. The Ag–N bond lengths are not unusual (range from 2.048(3) to 2.128(5) Å) (see Table 2).

The compound $\{[3,5\text{-}(i\text{-}Pr)_2Pz]Ag\}_3$ crystallizes in the $P2(1)/c$ space group with two chemically similar but crystallographically different trimer units in the asymmetric unit. The most notable feature of $\{[3,5\text{-}(i\text{-}Pr)_2Pz]Ag\}_3$ is that these trimers exist in pairs resulting in Ag–Ag bonded dimers of trimers as illustrated in Fig. 1. Each of these

Table 2
Bond distances (Å) and bond angles (°) for $\{[3,5\text{-}(i\text{-}Pr)_2Pz]Ag\}_3$, $\{[3,5\text{-}(i\text{-}Pr)_2,4\text{-}(Br)Pz]Ag\}_3$, and $\{[3,5\text{-}(i\text{-}Pr)_2,4\text{-}(NO_2)Pz]Ag\}_3$

	$\{[3,5\text{-}(i\text{-}Pr)_2Pz]Ag\}_3$	$\{[3,5\text{-}(i\text{-}Pr)_2,4\text{-}(Br)Pz]Ag\}_3$	$\{[3,5\text{-}(i\text{-}Pr)_2,4\text{-}(NO_2)Pz]Ag\}_3$
Ag–N (range)	2.048(3)–2.088(3)	2.053(4)–2.094(4)	2.101(5)–2.128(5)
Ag···Ag (intra, range)	2.324–3.489	3.413–3.489	3.296–3.529
Ag···Ag (inter, shortest)	2.9870(4)	3.0438(5)	
N–Ag–N (range)	170.21(13)–177.68(13)	168.61(16)–172.89(16)	170.52(19)–178.20(18)

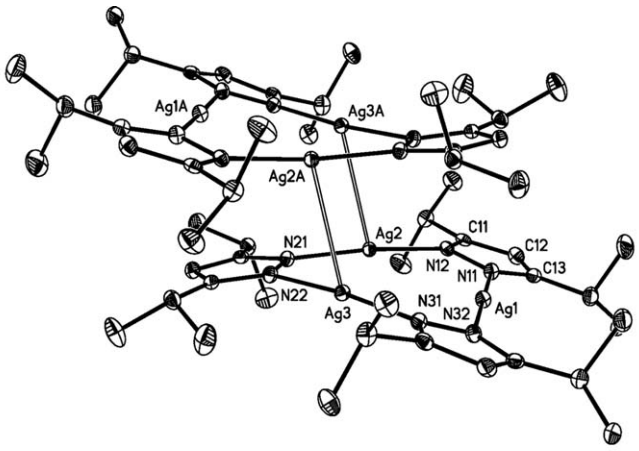

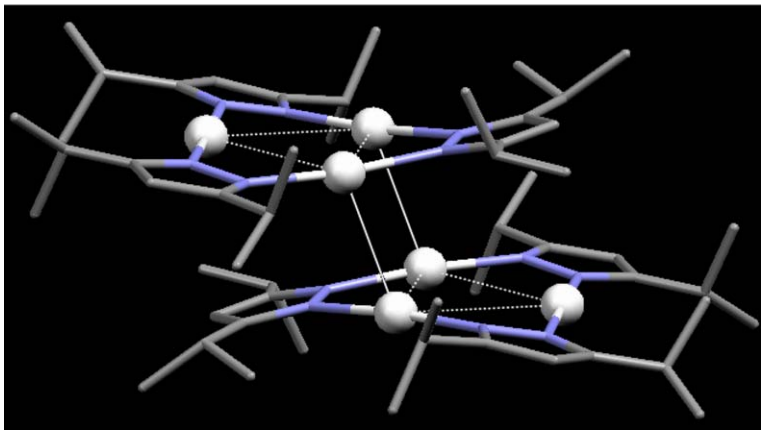

Fig. 1. Two views of the molecular structure of $\{[3,5\text{-}(i\text{-}Pr)_2Pz]Ag\}_3$. Hydrogen atoms have been omitted for clarity. Selected bond lengths (Å) and bond angles (°): Ag(1)–N(32) 2.048(3), Ag(1)–N(11) 2.053(3), Ag(2)–N(21) 2.070(3), Ag(2)–N(12) 2.073(3), Ag(3)–N(31) 2.075(3), Ag(3)–N(22) 2.088(3), Ag(4)–N(62) 2.057(3), Ag(4)–N(41) 2.062(3), Ag(1)–Ag(2) 3.3628(4), Ag(2)–Ag(3A) 2.9870(4), Ag(3)–Ag(2A) 2.9870(4), Ag(4)–Ag(5) 3.3245(5), Ag(5)–Ag(6A) 2.9952(5), Ag(6)–Ag(5A) 2.9952(5), N(11)–N(12) 1.375(4), N(21)–N(22) 1.383(4), N(31)–N(32) 1.370(4), N(11)–C(13) 1.338(5), N(21)–C(23) 1.346(5), N(22)–C(21) 1.346(5), N(32)–Ag(1)–N(11) 177.68(13), N(21)–Ag(2)–N(12) 173.00(12), N(31)–Ag(3)–N(22) 174.23(12), N(62)–Ag(4)–N(41) 172.90(13), N(42)–Ag(5)–N(51) 174.50(13), N(61)–Ag(6)–N(52) 170.21(13).

Table 3
Closest inter-trimer Ag–Ag distances (Å) for selected trimeric silver(I) pyrazolates

Compound	Closest inter-trimer Ag···Ag separation	Ref.
$\{[3,5\text{-}(Ph)_2Pz]Ag\}_3$ (from CH_2Cl_2)	2.971(1)	[24]
$\{[3,5\text{-}(i\text{-}PrSCH_2)_2Pz]Ag\}_3$	3.041(1)	[18]
$\{[Pz(IN)]Ag\}_3$	3.179(8)	[25]
$\{[2\text{-}(3(5)\text{-}Pz)Py]Ag\}_3$	3.227(2)	[20]
$\{[3,5\text{-}(Me)_2Pz]Ag\}_3$	3.230(13)	[22]
$\{[3,5\text{-}(CF_3)_2Pz]Ag\}_3$ (from CH_2Cl_2)	3.2037(4)	[2]
$\{[3,5\text{-}(CF_3)_2Pz]Ag\}_3$ (from hexane)	3.307(13)	[15]
$\{[Pz]Ag\}_3$	3.431(4)	[21]

dimer of trimers sits on a center of inversion. The Ag_6 units adopt a chair conformation. The third silver atom of each trimer unit does not show close inter-trimer Ag–Ag contacts. The Ag–Ag distances (of the two crystallographically different dimer of trimers) are 2.9869(4) and 2.9953(5) Å. These distances are significantly smaller than the sum of the van der Waals radii (3.40 Å) of silver. To our knowledge, $\{[3,5\text{-}(i\text{-}Pr)_2Pz]Ag\}_3$ has the second shortest Ag–Ag intermolecular distance (2.9869(4) Å) reported for a trimeric silver(I) pyrazolate. $\{[3,5\text{-}(Ph)_2Pz]Ag\}_3$ crystals obtained from CH_2Cl_2, which exist as dimer of trimers, has a slightly shorter Ag–Ag contact at 2.971(1) Å [24].

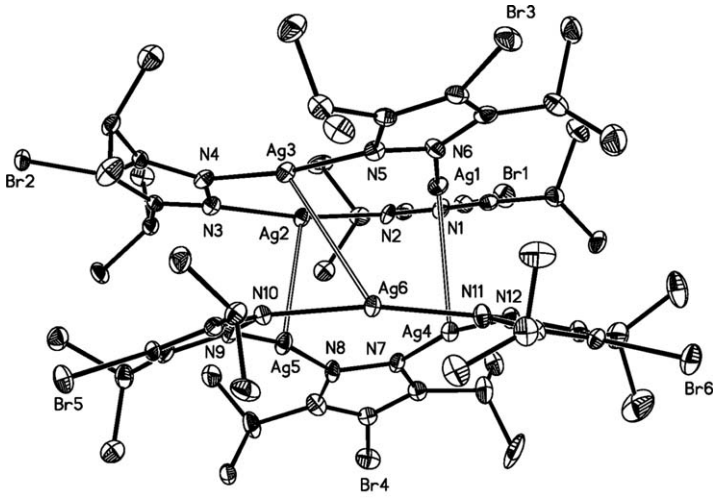

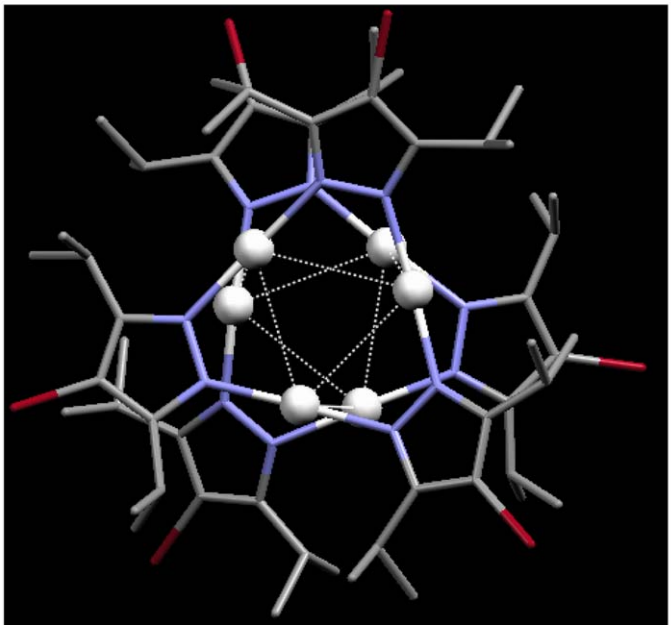

Fig. 2. Two views of the molecular structure of $\{[3,5\text{-}(i\text{-}Pr)_2,4\text{-}(Br)Pz]Ag\}_3$. Hydrogen atoms have been omitted for clarity. Selected bond lengths (Å) and bond angles (°): Ag(1)–N(6) 2.053(4), Ag(1)–N(1) 2.062(4), Ag(2)–N(3) 2.080(4), Ag(2)–N(2) 2.080(4), Ag(3)–N(4) 2.093(4), Ag(3)–N(5) 2.094(4), Ag(4)–N(12) 2.072(4), Ag(4)–N(7) 2.080(4), Ag(5)–N(8) 2.068(4), Ag(1)–Ag(4) 3.0438(5), Ag(2)–Ag(5) 3.2460(5), N(1)–N(2) 1.366(5), N(3)–N(4) 1.373(5), N(5)–N(6) 1.380(6), Br(1)–C(2) 1.899(5), Br(2)–C(11) 1.881(5), Br(3)–C(20) 1.884(5), N(1)–C(3) 1.351(7), N(2)–C(1) 1.350(6), N(4)–C(10) 1.348(6), N(6)–Ag(1)–N(1) 172.89(16), N(3)–Ag(2)–N(2) 171.02(16), N(4)–Ag(3)–N(5) 171.89(15), N(12)–Ag(4)–N(7) 171.89(15), N(8)–Ag(5)–N(9) 169.02(16), N(10)–Ag(6)–N(11) 169.98(16).

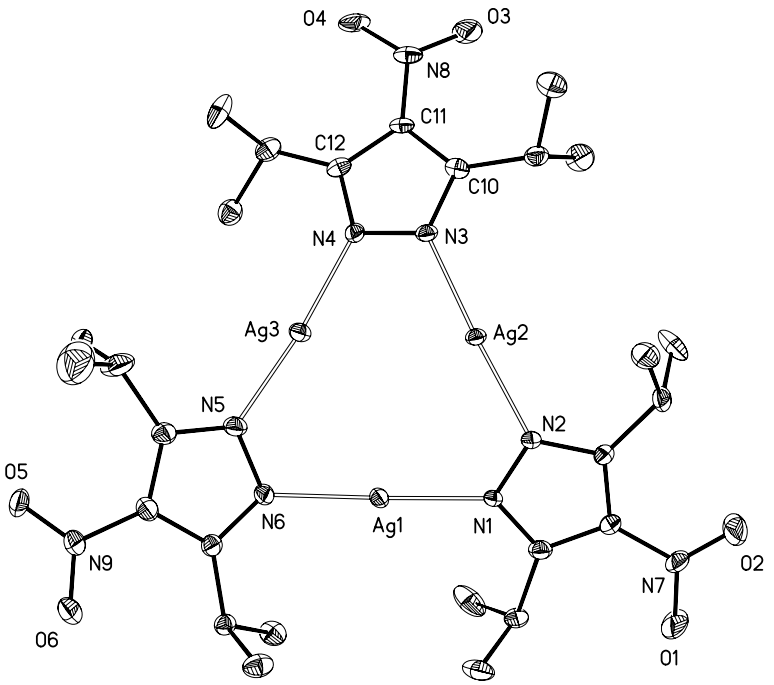

Fig. 3. Molecular structure of and $\{[3,5\text{-}(i\text{-}Pr)_2,4\text{-}(NO_2)Pz]Ag\}_3$. Only one of the trimers present in the asymmetric unit is shown. Hydrogen atoms and the dichloromethane molecules have been omitted for clarity. Selected bond lengths (Å) and bond angles (°): Ag(1)–N(1) 2.104(4), Ag(1)–N(6) 2.128(5), Ag(2)–N(3) 2.120(5), Ag(3)–N(4) 2.098(5), Ag(3)–N(5) 2.109(5), Ag(4)–N(15) 2.119(5), Ag(4)–N(10) 2.123(5), Ag(5)–N(12) 2.072(5), Ag(2)–Ag(3) 3.2962(6), Ag(4)–Ag(5) 3.3409(6), N(1)–C(1A) 1.343(8), N(2)–C(3) 1.344(7), N(3)–C(10) 1.334(7), N(4)–C(12) 1.344(7), N(5)–C(19) 1.323(8), N(1)–Ag(1)–N(6) 178.20(18), N(3)–Ag(2)–N(2) 171.28(19), N(4)–Ag(3)–N(5) 170.52(19), N(15)–Ag(4)–N(10) 173.8(2), N(15)–Ag(4)–N(10) 173.8(2).

We note however that $\{[3,5\text{-}(Ph)_2Pz]Ag\}_3$ has one short inter-trimer Ag–Ag contact whereas $\{[3,5\text{-}(i\text{-}Pr)_2Pz]Ag\}_3$ dimerizes with the formation of two Ag–Ag links. Solvents used in the crystallization could also affect the structures. For example, work by Fackler et al. showed that $\{[3,5\text{-}(Ph)_2Pz]Ag\}_3$ crystallizes from THF/Et_2O as well separated trimers with no close Ag–Ag contacts [23]. We have observed similar solvent effects on $\{[3,5\text{-}(CF_3)_2Pz]Ag\}_3$. In addition to $\{[3,5\text{-}(i\text{-}Pr)_2Pz]Ag\}_3$, $\{[3,5\text{-}(Ph)_2Pz]Ag\}_3$, and $\{[3,5\text{-}(CF_3)_2Pz]Ag\}_3$, silver(I) complexes such as $\{[3,5\text{-}(i\text{-}PrSCH_2)_2Pz]Ag\}_3$, $\{[2\text{-}(3(5)\text{-}Pz)Py]Ag\}_3$, and $\{[Pz(IN)]Ag\}_3$, reported by Meyer et al. [18], Stavropoulos et al. [20], and Ishida et al. [25], respectively, also display dimer of trimer structures with inter-trimer Ag–Ag distances in the range of the sum of the van der Waals radii of silver (Table 3). The copper(I) analog $\{[3,5\text{-}(i\text{-}Pr)_2Pz]Cu\}_3$ is known [19], and it also shows isolated dimer of trimers like the silver adduct $\{[3,5\text{-}(i\text{-}Pr)_2Pz]Ag\}_3$.

The trimer moieties in $\{[3,5\text{-}(i\text{-}Pr)_2,4\text{-}(Br)Pz]Ag\}_3$ form dimers leading to a pseudo octahedral Ag_6 unit (Fig. 2). All three silver atoms of the $\{[3,5\text{-}(i\text{-}Pr)_2,4\text{-}(Br)Pz]Ag\}_3$ moiety show close inter-trimer Ag–Ag interactions, which are less than or very close (from 3.044(5) to 3.408(5) Å) to the sum of the van der Waals radii of silver. The trimer units deviate from planarity and adopt bowl shaped structures facilitating these Ag–Ag contacts. The packing diagram of $\{[3,5\text{-}(i\text{-}Pr)_2,4\text{-}(Br)Pz]Ag\}_3$ shows that there are several inter-trimer Ag–Br links (at about 3.5 Å range) as well. Interestingly, the copper(I) analog of $\{[3,5\text{-}(i\text{-}Pr)_2,4\text{-}(Br)Pz]Ag\}_3$ adopts a tetrameric structure in the solid state forming $\{[3,5\text{-}(i\text{-}Pr)_2,4\text{-}(Br)Pz]Cu\}_4$ [37].

Unlike $\{[3,5\text{-}(i\text{-}Pr)_2Pz]Ag\}_3$ or $\{[3,5\text{-}(i\text{-}Pr)_2,4\text{-}(Br)Pz]Ag\}_3$, the 4-nitro analog $\{[3,5\text{-}(i\text{-}Pr)_2,4\text{-}(NO_2)Pz]Ag\}_3$ does not form dimer of trimers with Ag–Ag contacts. The asymmetric unit contains two trimer units and 1.6 molecules of dichloromethane. The $\{[3,5\text{-}(i\text{-}Pr)_2,4\text{-}(NO_2)Pz]Ag\}_3$ units exists as isolated trimers (Fig. 3). However, there are close inter-trimer Ag–O contacts (closest at 2.732 Å) between the silver atoms and the oxygen atoms of the nitro groups. This may be a reason for the non-existence of even weak inter-trimer Ag–Ag interactions. The H-atoms of the dichloromethane molecules present in the crystals also show close contacts with some of the oxygen atoms of the nitro groups.

Overall, we describe the synthesis and characterization of three new silver pyrazolates containing 3,5-isopropyl groups, and different substituents on the pyrazolyl ring 4-positions. They can be synthesized using silver(I) oxide as the Ag(I) source. They show different packing patterns with notable differences in inter-trimer Ag–Ag distances. We are currently carrying out studies on photochemical and physical properties of these silver adducts.

4. Supplementary material

Crystallographic data for $\{[3,5\text{-}(i\text{-}Pr)_2Pz]Ag\}_3$, $\{[3,5\text{-}(i\text{-}Pr)_2,4\text{-}(Br)Pz]Ag\}_3$, and $\{[3,5\text{-}(i\text{-}Pr)_2,4\text{-}(NO_2)Pz]Ag\}_3$ have been deposited with the Cambridge Crystallographic Data

Center, CCDS Nos. 281063–281065. Copies of this information may be obtained free of charge from the Director, Cambridge Crystallographic Data Centre (CCDC), 12 Union Road, Cambridge, CB2 1EZ (fax: +44 1223 336033; e-mail: deposit@ccdc.cam.ac.uk; or http://www.ccdc.cam.ac.uk).

Acknowledgments

We thank The Robert A. Welch Foundation (Y-1289) and National Science Foundation (CHE-0314666) for support of this work.

References

[1] G. La Monica, G.A. Ardizzoia, Prog. Inorg. Chem. 46 (1997) 151.
[2] M.A. Omary, M.A. Rawashdeh-Omary, M.A.W. Gonser, O. Elbjeirami, T. Grimes, T.R. Cundari, H.V.K. Diyabalanage, C.S. Palehepitiya Gamage, H.V.R. Dias, Inorg. Chem. 44 (2005) 8200.
[3] G. Yang, R.G. Raptis, Inorg. Chem. 42 (2003) 261.
[4] G.A. Ardizzoia, S. Cenini, G. La Monica, N. Masciocchi, M. Moret, Inorg. Chem. 33 (1994) 1458.
[5] G.A. Ardizzoia, M.A. Anagaroni, G. La Monica, F. Cariati, S. Cenini, M. Moret, N. Masciocchi, Inorg. Chem. 30 (1991) 4347.
[6] M. Enomoto, A. Kishimura, T. Aida, J. Am. Chem. Soc. 123 (2001) 5608.
[7] A. Kishimura, T. Yamashita, T. Aida, J. Am. Chem. Soc. 127 (2005) 179.
[8] H.V.R. Dias, H.V.K. Diyabalanage, M.A. Rawashdeh-Omary, M.A. Franzman, M.A. Omary, J. Am. Chem. Soc. 125 (2003) 12072.
[9] M.A. Omary, M.A. Rawashdeh-Omary, H.V.K. Diyabalanage, H.V.R. Dias, Inorg. Chem. 42 (2003) 8612.
[10] H.V.R. Dias, H.V.K. Diyabalanage, M.G. Eldabaja, O. Elbjeirami, M.A. Rawashdeh-Omary, M.A. Omary, J. Am. Chem. Soc. 127 (2005) 7489.
[11] G.A. Ardizzoia, G. La Monica, Inorg. Synth. 31 (1997) 299.
[12] M.K. Ehlert, S.J. Rettig, A. Storr, R.C. Thompson, J. Trotter, Can. J. Chem. 68 (1990) 1444.
[13] M.K. Ehlert, S.J. Rettig, A. Storr, R.C. Thompson, J. Trotter, Can. J. Chem. 70 (1992) 2161.
[14] M.K. Ehlert, A. Storr, R.C. Thompson, Can. J. Chem. 70 (1992) 1121.
[15] H.V.R. Dias, S.A. Polach, Z. Wang, J. Fluor. Chem. 103 (2000) 163.
[16] R.G. Raptis, J.P. Fackler Jr., Inorg. Chem. 27 (1988) 4179.
[17] G.A. Ardizzoia, S. Cenini, G. La Monica, N. Masciocchi, A. Maspero, M. Moret, Inorg. Chem. 37 (1998) 4284.
[18] F. Meyer, A. Jacobi, L. Zsolnai, Chem. Ber./Recueil. 130 (1997) 1441.
[19] K. Fujisawa, Y. Ishikawa, Y. Miyashita, K.-i. Okamoto, Chem. Lett. 33 (2004) 66.
[20] K. Singh, J.R. Long, P. Stavropoulos, J. Am. Chem. Soc. 119 (1997) 2942.
[21] N. Masciocchi, M. Moret, P. Cairati, A. Sironi, G.A. Ardizzoia, G. La Monica, J. Am. Chem. Soc. 116 (1994) 7668.
[22] N. Masciocchi, P. Cairati, A. Sironi, Powder Diffr. 13 (1998) 35.
[23] H.H. Murray, R.G. Raptis, J.P. Fackler, Inorg. Chem. 27 (1988) 26.
[24] A.A. Mohamed, L.M. Perez, J.P. Fackler, Inorg. Chim. Acta 358 (2005) 1657.
[25] S. Yamada, T. Ishida, T. Nogami, Dalton Trans. 6 (2004) 898.
[26] M.C. Torralba, P. Ovejero, M.J. Mayoral, M. Cano, J.A. Campo, J.V. Heras, E. Pinilla, M.R. Torres, Helv. Chim. Acta 81 (2004) 250.
[27] Y. Chi, E. Lay, T.-Y. Chou, Yi-Hwa Song, A.J. Carty, Chem.Vap. Deposit. 11 (2005) 206.
[28] G. Banditelli, A.L. Bandini, F. Bonati, R.G. Goel, G. Minghetti, Gazz. Chim. Ital. 112 (1982) 539.
[29] B. Bovio, F. Bonati, G. Banditelli, Inorg. Chim. Acta 87 (1984) 25.
[30] S.J. Kim, S.K. Kang, K.-M. Park, W.-C. Zin, M.-G. Choi, K. Kim, Chem. Mater. 10 (1998) 1889.
[31] J. Barbera, A. Elduque, R. Gimenez, F.J. Lahoz, J.A. Lopez, L.A. Oro, J.L. Serrano, Inorg. Chem. 37 (1998) 2960.
[32] G. Minghetti, G. Banditelli, F. Bonati, Inorg. Chem. 18 (1979) 658.
[33] A. Kishimura, T. Yamashita, M. Enomoto, T. Aida, J. Am. Chem. Soc. 127 (2005) 179.
[34] E. Buchner, Berichte 22 (1889) 842.
[35] Y. Takahashi, M. Akita, S. Hikichi, Y. Moro-oka, Organometallics 17 (1998) 4884.
[36] L.E. Ochando, J.M. Amigo, D. Louer, C. Fontenas, J. Elguero, J. Mol. Struct. 562 (2001) 11.
[37] H.V.R. Dias, H.V.K. Diyabalanage, Unpublished results.

Based on the strong coordinative behavior of the 2-aminobenzothiazole which is a molecular model for complex biological molecules, we decided to add supplementary coordination sites rich in lone pairs by substituting the NH protons by PPh_2 and $P(OEt)_2$ and their oxides (O, S and Se) and to study their structure, preferred conformations, intra- and intermolecular sulfur donor and acceptor interactions and cooperative hydrogen bonds.

The aim of our research was also to study the preferred conformers and the tautomeric preference of the N–H and the geometric isomers of N–P bonds, in order to understand the influence of hydrogen bonds and acid/base contacts and to know if groups like PY_2 (Y = Ph and OEt) or $Y_2P{=}E$ (E = O, S, Se) could favor the homodimerization through multiple hydrogen bonds. Labile N–H bonds favor intermolecular cooperative hydrogen bonds with electronic lone pairs (N, O, S and Cl) or aromatic π electrons. Hydrogen bond is a fundamental element for catenation of organic, inorganic or mixed molecular units to give a variety of complex structures [18,19]. N–H coordination networks are biologically important due to the molecular recognition of hydrogen bonds [20].

Our research has been focused on the exploration of supramolecular assemblies formed by double, triple and quadruple hydrogen bonds, these supramolecular units with multiple hydrogen bonds are scarcely reported and they have been only observed in organic systems as cianuric acid–melamina complex, dimers of diaminotriazines, diaminopirimidines, ureidopirimidone and dicarboxylic acids [21].

Another interest of our research is the study of weak donor acceptor interactions at sulfur and selenium atoms which determines preferred conformers and conglomerates. It is recognized that sulfur presents coordinating contacts at distances lesser than 3.70 Å, sulfur (Lewis base) is donor in the axis perpendicular to the plane depicted by the bonds X–S–Z or acceptor (Lewis acid) following the directions of S–X or Z–S bonds [8,9,22–29].

2. Experimental

2.1. Materials

All synthetic work and the handling of samples were carried out under inert atmosphere (N_2), using carefully dried glassware and dry solvents. $P(C_6H_5)_2Cl$, 2-aminobenzothiazole, NEt_3, Se and S powders were commercially available. Bis(trimethylsilyl)peroxide was prepared at the laboratory [30]. NEt_3 was dried according to established procedures, and freshly distilled before use. 2-Aminobenzothiazole was sublimated at low pressure before use.

2.2. Synthesis of the compounds **2**–**11**. General procedure

2.2.1. 2-Aminobenzothiazole-diphenylphosphane (**2**)

To a stirred solution of 2-aminobenzothiazole (2.0 g; 13.3 mmol) and NEt_3 (2.7 g; 26.7 mmol) in THF (125 mL) at −78 °C was added dropwise a solution of $P(C_6H_5)_2Cl$ (2.94 g; 13.3 mmol) in THF (20 mL) under nitrogen atmosphere. The mixture was warmed to r.t. and kept stirring for 2 h. Then, insoluble material was filtered off and the solvent removed at 0.1 torr. Compound **2** was obtained as a white powder, dried at 0.05 torr during 8 h and recrystallized from hot toluene or benzene. Colorless crystals were suitable for diffraction analysis. Yield: 4.27 g, 96%, m.p. 132–136 °C. *Anal.* Calc. for $C_{19}H_{15}N_2SP$: C, 68.26; H, 4.49; N, 8.38; S, 9.58. Found: C, 68.57; H, 4.81; N, 8.82; S, 8.99%. MS, *m/z* (%): 334(100) M^+, 257(23), 183(54), 150(8). FAB+ [335]. IR (ν cm^{-1}): NH 3448, C=N 1540, P–C 1445 and 1096, C–S 1391 and 639, P–N 1067 and 926. ^1H NMR (400 MHz; THF-d_8), δ (ppm): 7.30 [d, H4, $^3J(^1H{-}^1H)$ 8.0], 7.18 [dd, H5, $^3J(^1H{-}^1H)$ 8.0, 7.7], 7.06 [dd, H6, $^3J(^1H{-}^1H)$ 8.0, 7.7], 7.64 [d, H7, $^3J(^1H{-}^1H)$ 8.0], 7.55 [m, H_o], 7.35 [m, H_m, H_p].

2.2.2. 2-Aminobenzothiazole-diethylphosphite (**3**)

It was synthesized following the same procedure as for **2** using 1.0 g (6.7 mmol) of **1**, 1.35 g (13.3 mmol) of NEt_3 and 1.0 g (6.7 mmol) of $PCl(EtO)_2$ in 150 mL of THF. Compound **3** is a white solid. Yield: 1.67 g, 93%, m.p. 70–72 °C. *Anal.* Calc. for $C_{11}H_{15}N_2SO_2P$: C, 48.89; H, 5.55; N, 10.37; S, 11.85. Found: C, 49.33; H, 5.75; N, 10.86; S, 11.58%. MS, *m/z* (%): 270(68) M^+, 242(6), 226(19), 197(24), 180(18), 150(46), 121(91), 93 (100), 65(82). IR (ν cm^{-1}): NH (3323, 3235), C=N (1618, 1599), P–C (1450), C–S (1391, 618), P–N (1102, 922), P–O (1043, 1026), PO–C (1160). ^1H NMR (400 MHz; THF-d_8), δ (ppm): 7.54 [d, H4, $^3J(^1H{-}^1H)$ 7.8], 7.25 [dd, H5, $^3J(^1H{-}^1H)$ 7.8, 7.5], 7.08 [dd, H6, $^3J(^1H{-}^1H)$ 7.8, 7.5], 7.62 [d, H7, $^3J(^1H{-}^1H)$ 7.8], 3.94 [7.8] [dq, CH_2, $^3J(^1H{-}^1H)$ 7.0], 1.24 [t, CH_3, $^3J(^1H{-}^1H)$ 7.0].

2.2.3. 2-Aminobenzothiazole-diphenylphosphane oxide (**4**)

Bis(trimethylsilyl)peroxide (0.53 g, 3 mmol) was added dropwise at r.t. to a stirred suspension of **2** (1.0 g; 3 mmol) in 100 mL of toluene under nitrogen atmosphere. After stirring for 24 h, a white precipitate was filtered and dried at low pressure (0.05 Torr) during 8 h. Compound **4** is a white solid. Yield 0.89 g, 85%, m.p. 240–242 °C. *Anal.* Calc. for $C_{19}H_{15}N_2SPO$: C, 65.13; H, 4.32; N, 8.00; S, 8.15. Found: C, 65.25; H, 4.33; N, 8.01; S, 8.79%. MS, *m/z* (%): 350(100), 273(33), 226(21), 201(34). IR (ν cm^{-1}): NH 3578, 1266, C=N 1581, P–C 1435, 1125, C–S 1411, 626, P–N 1062, 954, P=O 1168. ^1H NMR (400 MHz; THF-d_8), δ (ppm): 7.20 [d, H4, $^3J(^1H{-}^1H)$ 7.7], 7.19 [dd, H5, $^3J(^1H{-}^1H)$ 7.7, 7.5], 7.04 [dd, H6, $^3J(^1H{-}^1H)$ 7.7, 7.5], 7.37 [d, H7, $^3J(^1H{-}^1H)$ 7.7], 7.84 [m, H_o], 7.37 [m, H_m, H_p].

2.3. General Method for compounds **5**–**8**

2.3.1. 2-Aminobenzothiazole-diphenylphosphane sulfide (**5**)

Compound **5** was obtained as a white solid prepared with the same procedure as described for compound **4**

using 1.0 g (3 mmol) of **2** and 0.96 g (3 mmol) of S powder. Yield: 0.89 g, 81%, dec. at 268–270 °C. *Anal.* Calc. for $C_{19}H_{15}N_2S_2P$: C, 62.28; H, 4.13; N, 7.64; S, 17.50. Found: C, 62.13; H, 4.26; N, 7.39; S, 17.43%. MS, *m*/*z* (%): 366(74) M^+, 289(7), 257(100), 217(38), 179(21), 139(33). IR (*v*, cm^{-1}): NH 3554, 1251, C=N 1583, P–C 1432, 1181, C–S 1400, P–N 1024, 952, P=S 673. ^1H NMR (400 MHz; THF-d_8), δ (ppm): 7.13 [d, H4, $^3J(^1H–^1H)$ 8.0], 7.19 [dd, H5, $^3J(^1H–^1H)$ 8.0, 7.5], 7.04 [dd, H6, $^3J(^1H–^1H)$ 8.0, 7.5], 7.44 [d, H7, $^3J(^1H–^1H)$ 8.0], 7.94 [m, H_o], 7.33 [m, H_m, H_p].

2.3.2. 2-Aminobenzothiazole-diphenylphosphane selenide (*6*)

Compound **6** was prepared with the same procedure as described for compound **4** using 1.0 g (3 mmol) of **2** and 0.24 g (3 mmol) of Se powder. The reaction mixture was kept stirring for 48 h at r.t., and then was heated at 115 °C for 6 h. Compound **6** is a white solid. Yield 0.90 g, 73%, dec. at 270–274 °C. *Anal.* Calc. for $C_{19}H_{15}N_2SPSe$: C, 55.21; H, 3.66; N, 6.58; S, 7.49. Found: C, 55.53; H, 3.64; N, 6.81; S, 7.25%. MS, *m*/*z* (%): 414(73) M^+, 334(23), 257(100), 179(29). IR (*v* cm^{-1}): NH 3468, 1250, C=N 1587, P–C 1431, 1098, C–S 1398, P–N 1023, 951, P=Se 438, 418. ^1H NMR (400 MHz; THF-d_8), δ (ppm): 7.17 [d, H4, $^3J(^1H–^1H)$ 8.0], 7.22 [dd, H5, $^3J(^1H–^1H)$ 8.0, 7.5], 7.07 [dd, H6, $^3J(^1H–^1H)$ 8.0, 7.5], 7.48 [d, H7, $^3J(^1H–^1H)$ 8.0], 7.96 [m, H_o], 7.34 [m, H_m, H_p].

2.3.3. 2-Aminobenzothiazole-diethylphosphate sulfide (*7*)

It was synthesized following the same procedure as described for compound **4** using 1.0 g (3 mmol) of **3** and 0.95 g (3.7 mmol) of S powder. Compound **7** gave colorless monocrystals from benzene suitable for diffraction analysis. Yield: 0.9 g, 79%, m.p. 159–162 °C. *Anal.* Calc. for $C_{11}H_{15}N_2S_2O_2P$: C, 43.70; H, 5.00; N, 9.27; S, 21.21. Found: C, 44.22; H, 4.89; N, 9.51; S, 21.39%. MS, *m*/*z* (%): 302(51) M+, 257(21), 225(24), 197(21), 150(100). IR (υ cm^{-1}): NH 3449, C=N 1599, 1580, P–C 1411, C–S 1389, P–N 978, 955, P–O 1052, 1028, POC 1158, P=S 659. ^1H NMR (400 MHz; THF-d_8), δ (ppm): 7.28 [d, H4, $^3J(^1H–^1H)$ 7.7], 7.27 [dd, H5, $^3J(^1H–^1H)$ 7.7, 7.5], 7.13 [dd, H6, $^3J(^1H–^1H)$ 7.7, 7.5], 7.54 [d, H7, $^3J(^1H–^1H)$ 7.7], 4.06 [$J(^1H–^{31}P)$ 9.5] [dq, CH_2, $^3J(^1H–^1H)$ 7.1], 1.26 [t, CH_3, $^3J(^1H–^1H)$ 7.1].

2.3.4. 2-Aminobenzothiazole-diethylphosphate selenide (*8*)

It was synthesized following the previous procedure using 1.0 g (3 mmol) of **3** and 0.29 g (3.7 mmol) of selenium. Compound **8** is a white solid. Yield: 1.06 g, 82%, m.p. 152–155 °C. *Anal.* Calc. for $C_{11}H_{15}N_2SO_2PSe \cdot 1/15C_7H_8$: C, 38.75; H, 4.41; N, 7.88; S, 9.02. Found: C, 38.74; H, 4.40; N, 8.32; S, 8.83%. MS, *m*/*z* (%): 350 (26) M^+, 241(32), 213(69), 197(31), 162(26), 150(100). IR (*v* cm^{-1}): NH 3418, C=N 1573, P–C 1449, C–S 1390, P–N 950, P–O 1047, 1020, POC (1159), P=Se 429. ^1H NMR (400 MHz; THF-d_8), δ (ppm): 7.23 [d, H4, $^3J(^1H–^1H)$ 8.0], 7.23 [dd, H5, $^3J(^1H–^1H)$ 8.0, 7.7], 7.11 [dd, H6, $^3J(^1H–^1H)$ 8.0, 7.7], 7.54 [d, H7, $^3J(^1H–^1H)$ 8.0], 4.04 [$J(^1H–^{31}P)$ 9.8] [dq, CH_2, $^3J(^1H–^1H)$ 7.0], 1.24 [t, CH_3, $3J(^1H–^1H)$ 7.0].

2.3.5. Lithium 2-aminobenzothiazolide-diphenylphosphane (*9*)

A solution of **2** (0.25 g; 0.75 mmol) and 1, 4, 7, 10, 13, 16-hexaoxaciclooctadecane (0.24 g; 0.89 mmol) in THF (80 mL) was cooled at −50 °C and under nitrogen atmosphere was added slowly *n*-BuLi [0.75 mmol; 1.5 M]. The mixture was warmed at r.t. and the solvent was eliminated at 0.05 Torr. Compound **9** is a pale yellow solid. Yield: quantitative. *Anal.* Calc. for $C_{27}H_{30}LiN_2O_2PS$: C, 66.93; H, 6.24; N, 5.78; S, 6.62. Found: C, 66.30; H, 6.52; N, 5.35; S, 6.90%. FAB(+): 485 ($C_7H_5SN_2P(C_6H_5)_2Li \cdot 2THF$), 341 ($C_7H_5SN_2P(C_6H_5)_2$-Li). IR (KBr) *v* ($cm^{-1}$): 1646, 1444, 1122, 1125, 627, 1021. ^1H RMN (400 MHz; THF-d_8), δ (ppm): 7.11 [d, H4, $^3J(^1H–^1H)$ 7.9], 7.04 [dd, H5, $^3J(^1H–^1H)$ 7.9, 7.5], 6.78 [dd, H6, $^3J(^1H–^1H)$ 7.9, 7.5], 7.36 [d, H7, $^3J(^1H–^1H)$ 7.9], 7.60 [m, H_o], 7.19 [m, H_m, H_p]. ^7Li NMR (155.4 MHz; THF-d_8), δ: +1.3.

2.3.6. Lithium 2-aminobenzothiazolide-diphenylphosphane oxide (*10*)

Compound **10** was obtained as colorless single crystals from a solution of **9** 200 mg (0.33 mmol) in THF (1.0 mL) and hexane (5.0 mL) and let aside for two months. Yield: 16 mg, 8%, m.p. 145 °C. X-ray diffraction analysis was performed.

2.3.7. Bis-(2-aminothiazolium) tetrachloro-diphenyl plumbate (*11*)

Compound **11** was obtained as colorless crystals from the equimolar mixture of compounds **2** and $Pb(NO_3)_2$, in THF and in the presence of $NHEt_3Cl$. No reaction was detected by NMR in the following hours and even after a few days at room temperature. The solution in an NMR tube was let aside for three months, few crystals were formed in THF-d_8 that were analyzed by X-ray diffraction.

2.4. Physical measurements

NMR spectra were recorded in DMSO-d_6 and THF-d_8 dried with sodium spheres, on a Jeol GSX-270, Jeol Eclipse 400 and Bruker 300 Avance spectrometers. Chemical shifts are given in ppm and referred to Me_4Si or H_3PO_4 (aq., 85 %) [$\delta^{31}P = 0$ with $\Xi(^{31}P) = 40.480747$ MHz, neat Me_2Se [$\delta^{77}Se = 0$ with $\Xi(^{77}Se) = 19.071513$ MHz] and $MeNO_2$ neat $\Xi(^{15}N) = 10.136767$ MHz. Assignment of ^1H and ^{13}C NMR data were supported by 2D $^1H/^{13}C$ HETCOR and $^1H/^{13}C$ HMBC experiments. NMR data are given in Tables 1 and 2. Electron impact (EI) mass spectra at 20 eV were performed in a Hewlett–Packard HP 5989A spectrometer with direct inlet. Melting points (uncorrected) were measured using a MeITemp II equipment in a closed capillar tube. Elemental Analyses were carried out in a Flash 1112 Thermo Finnigan analyzer. IR spectra were

Table 1
^{13}C NMR data (DMSO-d_6) and [$^nJ(^{13}C–^{31}P)$, Hz] for compounds **2–9**

Compd.	Benzothiazolyl ring							Y = Ph				Y = OEt	
	C2	C4	C5	C6	C7	C8	C9	C_i	C_o	C_m	C_p	O–C	CH_3
1	167.2	118.2	125.4	121.0	120.5	131.5	153.1						
2	169.6 [33.0]	119.2	125.5	121.9	120.7	132.1 [12.3]	152.5	138.7 [9.2]	131.4 [20.8]	128.5 [6.9]	129.4		
3	169.0 [23.0]	119.5	125.5	122.2	120.6	131.6 [9.3]	151.6					59.6 [10.4]	16.6 [5.2]
4	168.5 [3.0]	115.2	125.5	121.0	121.2	130.1	147.2	137.9 [127.6]	131.6 [9.2]	128.4 [12.3]	130.8		
5	167.8	114.5	125.8	121.2	121.7	129.6	145.0	139.4 [105.9]	131.2 [10.4]	128.5 [12.4]	130.8		
6	167.7	114.1	125.3	120.8	121.2	129.0	144.0	138.4 [96.0]	130.8 [10.9]	127.9 [12.4]	130.3 [2.8]		
7	165.5 [9.3]	113.0	126.1	122.2	121.8	127.1	138.8					62.1 [5.2]	15.5 [7.3]
8	166.1 [11.4]	112.1	126.2	122.8	122.0	126.3	137.2					62.6 [4.6]	15.4 [9.2]
9	180.0	114.8	124.9	118.6	120.9	132.5 [14.6]	153.3	133.0 [18.6]	131.5 [19.8]	127.9 [6.3]	127.7		

Table 2
^1H and ^{31}P NMR data for **1–9**

Compd.	$\delta^{31}P$	$\delta^1(NH)$[a]		$\Delta\delta/\Delta T$[b]
		+20 °C	−100 °C	
1		7.15		
2	+41.7[c]	8.65	9.63	8.2
3	+131.0	9.61		
4	+16.9	11.20	12.24	8.7
5	+44.7	11.08	11.96	7.3
6	+38.6	11.23	12.07	6.8
7	+67.2	10.95	12.15	10.0
8	+68.5	11.07	12.03	8.0
9	+53.9			

[a] In THF-d_8, δ (N–H) in **2** and **3** is exocyclic and for **4–8** is endocyclic.
[b] $\Delta\delta$ of ^1H NMR; $\times 10^{-3}$ ppm/K.
[c] DMSO-d_6.

taken in KBr disc (4000–400 cm^{-1}) in a FT spectrum GX Perkin–Elmer spectrometer. FAB (fast atom bombardment) spectrum was recorded using a Jeol SX-102A spectrometer.

2.5. X-ray crystallographic study

Suitable single crystals of compounds **2**, **7**, **10** and **11** were submerged in perfluoro ether oil and mounted in a capillary tube (0.5 mm). Crystal data and information about the data collection and structure refinement details are given in Tables 3–6. X-ray diffraction studies were performed with Siemens SMART Area-detector, CAD4, Kappa-CCD diffractometer using Mo radiation ($\lambda = 0.71073$ Å) at 293 K. The WINGX software was used. The crystal structures were determined and refined with the SHELXTL-97 $[x, y]$ system. Hydrogen atoms were found by Fourier difference in **2** and **10**.

3. Results and discussion

Phosphoramides **2** and **3** were prepared by the condensation of 2-aminobenzothiazole and the corresponding phosphorus halides in the presence of NEt_3. Their oxidation afforded compounds **4–8** P=E (E = O, S, Se), Scheme 1. Even though, that the synthesis of **2** and **4** was previously reported by Henning [31], where the characterization of **4** was only based on the melting point and IR spectrum.

Table 3
Selected values of bond lengths (Å) and angles (°) for **2**

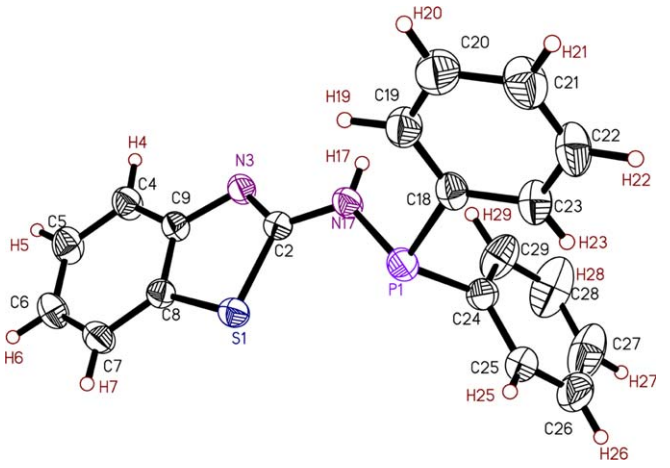

S1–C2	1.752(2)	S1–C8	1.729(2)
P1–N17	1.689(2)	P1–C18	1.801(3)
P1–C24	1.807(3)	N3–C2	1.287(3)
N3–C9	1.390(3)	N17–C2	1.347(3)
C8–C9	1.383(3)		
C8–S1–C2	88.2(1)	N17–P1–C18	101.1(1)
N17–P1–C24	104.4(1)	C18–P1–C24	103.6(1)
C2–N3–C9	110.3(2)	C2–N17–P1	120.9(2)
N3–C2–S1	116.3(2)	N3–C2–N17	124.5(2)
N17–C2–S1	119.1(2)	C9–C8–S1	110.2(2)
C8–C9–N3	115.0(2)		

Compounds **2–8** were prepared in good yield, they are white solids very reactive to moisture and oxygen, partially soluble in DMSO and THF, and insoluble in $CHCl_3$, CH_2Cl_2, acetone and hydrocarbons. They were characterized by NMR, IR, mass spectrometry, elemental analyses and X-ray diffraction (**2** and **7**). The reaction of **2** with *n*-BuLi in THF, at −78 °C and in the presence of 1,4,7,10,13,16-hexa-oxacyclooctadecane, was performed in order to obtain the lithium amide **9**, which was characterized in solution. After two months, suitable monocrystals were obtained from a solution of **9** in THF:hexane (1:5). X-ray diffraction study showed that a new compound **10** was formed in solution, which was the lithium coordination compound of the oxidized 2-aminobenzothiazole-diphenylphosphane.

Table 4
Selected values of bond lengths (Å) and angles (°) for **7**

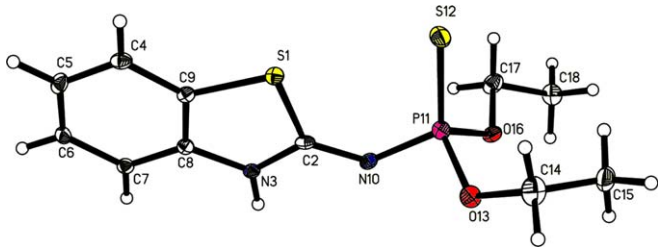

P11–O13	1.581(3)	N10–C2	1.312(4)
P11–O16	1.588(2)	O13–C14	1.460(4)
P11–N10	1.633(3)	O16–C17	1.444(4)
P11–S12	1.926(1)	C4–C5	1.373(5)
S1–C9	1.747(4)	C4–C9	1.393(5)
S1–C2	1.770(4)	C5–C6	1.393(5)
N3–C2	1.344(4)	C6–C7	1.387(5)
N3–C8	1.400(4)	C8–C9	1.389(5)
N3–C2–S1	109.9(3)	N10–P11–S12	119.0(1)
N10–C2–N3	121.3(3)	C9–S1–C2	90.8(2)
N10–C2–S1	128.8(3)	C2–N3–C8	116.2(3)
O13–P11–O	99.8(1)	C2–N10–P11	125.2(3)
O13–P11–N10	102.1(1)	C14–O13–P11	122.6(2)
O16–P11–N10	103.8(1)	C17–O16–P11	122.4(2)
O13–P11–S12	115.7(1)	C8–C9–S1	111.4(3)
O16–P11–S12	113.9(1)	C9–C8–N3	111.5(3)

Table 5
Selected values of bond lengths (Å) and angles (°) for **10**

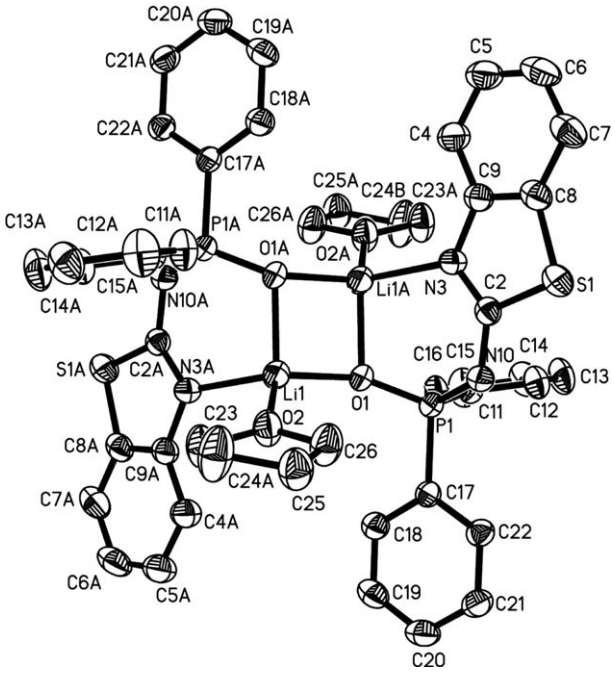

C2–N3	1.326(3)	C2–N10	1.331(3)
C2–S1	1.783(3)	C8–S1	1.732(3)
C8–C9	1.408(4)	C11–C16	1.371(4)
C9–N3	1.394(3)	C11–P1	1.814(3)
C17–P1	1.794(3)	C18–C19	1.375(4)
Li1–O1	1.929(5)	Li1–O2	1.946(5)
Li1–O1A	1.974(5)	Li1–N3A	2.076(5)
N3–Li1A	2.076(5)	N10–P1	1.613(2)
O1–P1	1.511(2)	O1–Li1A	1.974(5)
N3–C2–N10	129.2(2)	O1–P1–C11	108.1(1)
N3–C2–S1	113.7(2)	O1–P1–C17	109.6(1)
N10–C2–S1	117.1(2)	N10–P1–C11	109.1(1)
O1–Li1–O2	116.3(2)	N10–P1–C17	106.0(1)
O2–Li1–O1A	120.7(3)	C17–P1–C11	104.4(1)
O1–Li1–O1A	92.8(2)	P1–O1–Li1	140.6(2)
O1–Li1–N3A	123.3(3)	Li1–O1–Li1A	87.2(2)
O2–Li1–N3A	104.7(2)	C8–S1–C2	89.9(1)
O1A–Li1–N3A	98.4(2)	C9–N3–Li1A	125.2(2)
C2–N3–Li1A	121.2(2)	C2–N3–C9	111.3(2)
C2–N10–P1	118.7(2)	C9–C8–S1	109.5(2)
P1–O1–Li1A	112.0(2)	N3–C9–C8	115.5(3)
O1–P1–N10	118.7(1)		

The equimolar reaction of **2** with $Pb(NO_3)_2$ in THF, at room temperature and in presence of $NHEt_3Cl$ did not show the transformation of **2**. Nevertheless, after three months of storage at room temperature the solution contained some crystals which, after X-ray diffraction analysis, showed that they correspond to the tetrachlorodiphenylplumbate (IV) dianion bearing two molecules of protonated 2-aminobenzothiazole as counterions, compound **11**, Scheme 1. We can attribute the formation of **11** to the migration of phenyl groups from the phosphorus to the lead atom, the presence of NEt_3HCl (by-product in the synthesis of **1**) allowed the substitution of nitrate by chloride ions. There are no reports of similar transfer for lead, however a comparable phenyl migration in the reaction of $SbBr_2(C_6H_5)_2$ with $PtCl_2$ and *cis*-$[PtCl_2(P(C_6H_5)_3)_2]$ is proposed in order to explain the formation of *cis*-$[PtBr_2(Sb(C_6H_5)_3)_2]$, *trans*-$[PtBr(C_6H_5)(Sb(C_6H_5)_3)_2]$, *cis*-$[PtBr_2(P(C_6H_5)_3)(Sb(C_6H_5)_3)]$ and $[PtBr_3(Sb(C_6H_5)_3)]^-$ [32]. Reported anions such as $Cl_4(C_6H_5)_2Sn$(IV) and $Cl_4(C_6H_5)_2Sb$(IV) with one or two molecules of a protonated amine are isostructural with the new *bis*-phenyl plumbate. Jun et al. [33] reported the molecular structure of the complex $(C_6H_5)_2SbCl_4 \cdot 2,2'$-bipyridine having an hexacoordinated antimony atom with two phenyl groups in *anti* position, and explaining its formation from the hydrolysis of $(C_6H_5)_2SbCl_3 \cdot 2,2'$-bipyridine. Finally, Holmes et al. [34] found out that the hydrolysis of $(C_6H_5)_2SnCl_2 \cdot L$ (L = quinuclidine) produces the complex $[(C_6H_5)_2SnCl_4]^{-2}\ [LH]^{+1}{}_2$ through the formation of estanoxanes.

The reactions of the phosphates **7** and **8** with tin and germanium derivatives were attempted, but unfortunately no coordination compounds were observed.

3.1. NMR spectroscopy

Although ^1H, ^{13}C, ^{31}P and ^{77}Se NMR spectra clearly showed the phosphorus amides formation **2**–**8**, identification of the preferred tautomers and conformers remained to be carefully answered. The ^{15}N NMR data of compound **2** is shown in Scheme 2 and is compared with similar reported compounds. The value of the coupling constant

Table 6
Selected values of bond lengths (Å) and angles (°) for **11**

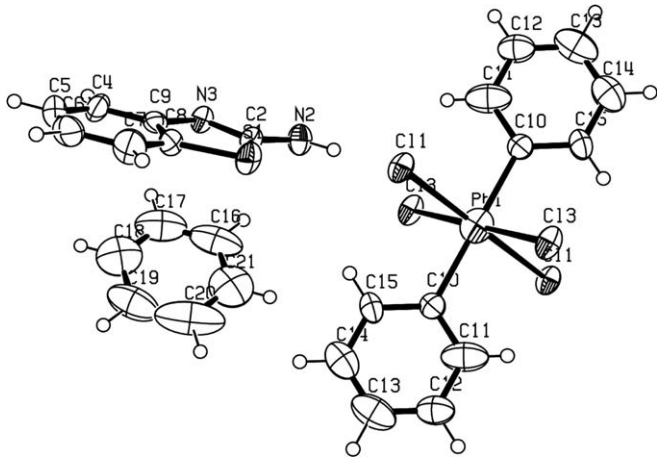

Pb1–Cl1	2.606(1)	Pb1–Cl1	2.606(1)
Pb1–Cl2	2.579(1)	Pb1–Cl2	2.579(1)
Pb1–C11	2.138(7)	Pb1–C11	2.138(7)
Cl1–Pb1–Cl2	88.92(5)	Cl1–Pb1–Cl2	91.08(5)
Cl1–Pb1–Cl2	91.08(5)	Cl1–Pb1–Cl2	88.92(5)
Cl2–Pb1–Cl2	180.00(4)	Cl1–Pb1–C11	90.3(2)
Cl1–Pb1–C11	89.6(2)	Cl2–Pb1–C11	89.6(2)
Cl2–Pb1–C11	90.4(2)	Cl1–Pb1–C11	89.7(2)
Cl1–Pb1–C11	90.3(2)	Cl2–Pb1–C11	90.4(2)
Cl2–Pb1–C11	89.6(2)	C11–Pb1–C11	179.99(4)
Cl1–Pb1–Cl1	180.00(4)		

$^{1}J(^{15}N–^{31}P)$ is characteristic of phosphoramides [35–37]. Comparison of these data with those of the starting 2-aminobenzimidazole **1** shows that the endocyclic nitrogen and C2 contribute with electronic density to the exocyclic nitrogen, in order to compensate the phosphorus electron withdrawing effect. An important difference in the values of ^{15}N of compound **2** with those of the diphenylphosphoramide derived from 2-imino-1,3-thiazolidine [38] was found, which indicates that the two molecules present different tautomers and conformers. The ^{77}Se data for compounds **6** and **8** confirmed the phosphorus oxidation. Data for compound **6** is similar with those of a $Ph_2P{=}Se$ amide derived from 2-imino-1,3-thiazolidine [38] depicted in Scheme 3. A different trend was found when the dimethyl amide derived from 2-imino-1,3-thiazolidine [3] is compared with compound **8**, the variation of their ^{77}Se chemical shifts is due to the different effect of P–N versus P–O bonds, Scheme 3.

Regarding the identification of the preferred tautomers in solution, the ^{13}C NMR analysis could give evidence by closely looking at C9 chemical shift for all the compounds, in solution compounds **1**–**3** and **9** presented for C9 a chemical shift (151.6–153.3) which is characteristic of a carbon atom vicinal to an sp^2 nitrogen bearing a lone pair, as is shown in tautomers depicted in Scheme 1 [39]. In contrast, compounds **7** and **8** show a typical C9 bound to an N–H group ($\delta = 137.2$–138.8) which indicates the preference of

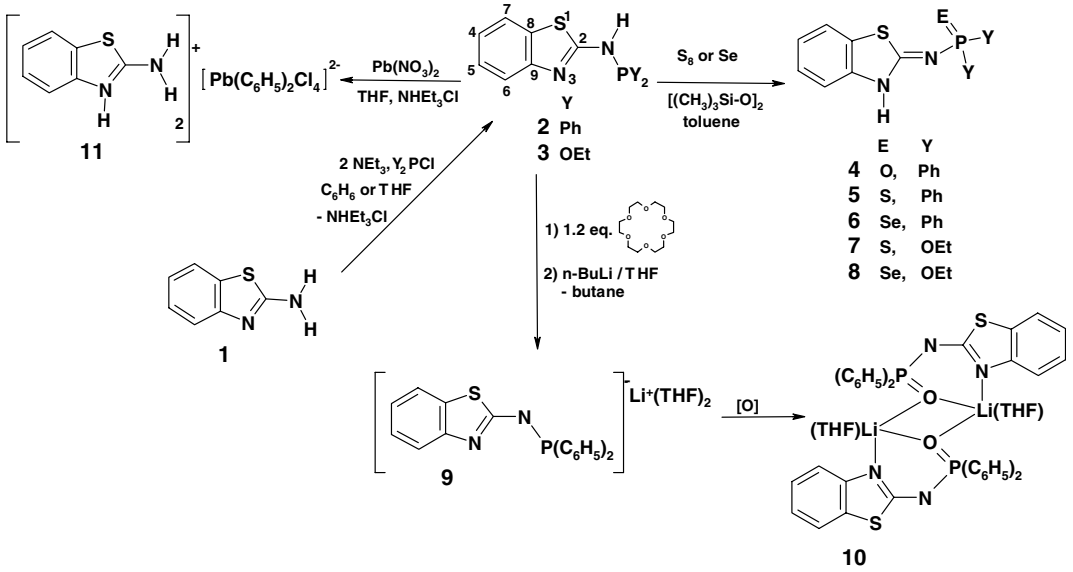

Scheme 1. Synthesis of compounds **2**–**10**.

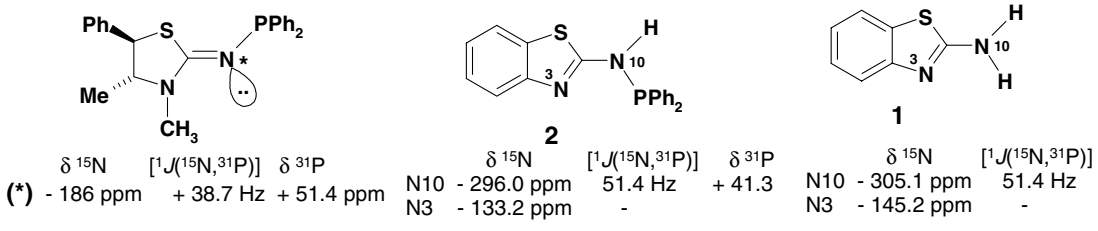

Scheme 2. ^{31}P and ^{15}N NMR data for **1**, **2** are compared with those of analogous compound [38].

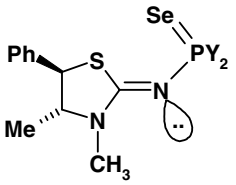

Y	δ ^{77}Se	[^{1}J(^{77}Se,^{31}P)]	δ ^{31}P
C_6H_5	- 217.9 ppm	723.4 Hz	+ 44.5 ppm
NMe_2	- 186.1 ppm	736.7 Hz	

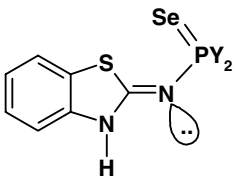

Y	δ ^{77}Se	[^{1}J(^{77}Se,^{31}P)]	δ ^{31}P
6 C_6H_5	- 203.0 ppm	689 Hz	+ 38.6 ppm
8 OEt_2	- 302.0 ppm	876 Hz	+ 68.5 ppm

Scheme 3. ^{31}P and ^{77}Se NMR data for **6** and **8** are compared with those of analogous compound [3].

the tautomer having protonated the endocyclic nitrogen. For compounds **4**–**6**, the chemical shift of C9 ($\delta = 144.0$–147.2) indicates a tautomeric equilibrium in solution, in fact it also agrees with the observation of NH protons signals at higher frequencies in ^{1}H NMR.

The configuration of the geometric isomers around the *exo* C=N bond [phosphorus atom in *cis* or *trans* position with respect to the endocyclic C–N (or C–S) bonds] was determined by the observation of *W* coupling constants $^{4}J(^{13}C–^{31}P)$ at C8 base of the sulfur, which indicate that P is on the same side of endocyclic nitrogen atom for compounds **2**, **3** and **9**. In contrast there is no visible phosphorus coupling with C8 for compounds **4**–**8** and therefore, it is proposed that these molecules present the conformation described in Scheme 1. However, an X-ray analysis of compound **2** showed the opposite conformation in solid state compared to the one found in solution.

NMR data gives evidence that the oxidation of the phosphorus atom changes the preferred tautomer of the molecule and therefore the electronic distribution in compounds **4**–**8**, Tables 1 and 2. It is quite interesting to observe some shielding effect at C8 resulting from the phosphorus oxidation which could be the consequence of O···S, S···S and Se···S electron donor acceptor interactions, Table 1. Oxidation also increases the coupling constants values ^{1}J and $^{2}J(^{13}C–^{31}P)$ of the $P(C_6H_5)_2$ groups; although a decreasing tendency in the order O < S < Se can be noticed for the coupling value $^{1}J(^{13}C_i–^{31}P)$ in **4**–**8**. The ^{1}H spectra of compounds **4**–**6** showed that the *ortho* protons of the phenyl group were shifted to higher frequencies with respect to **2**, indicating a proton interaction with the P-chalcogen, $\Delta\delta$ 0.29 (**4**); 0.39 (**5**), and 0.41 ppm (**6**).

^{7}Li NMR data of compound **9** indicates its ionic character and that the lithium atom is coordinated by THF molecules (δ ^{7}Li [+1.3; $\Delta\nu_{1/2} = 2.5$ Hz]). In addition, ^{13}C NMR confirmed the anionic character of the *exo*-nitrogen atom based on the shift at higher frequencies of the C2 signal.

The variation of N–H chemical shifts with the temperature ($\Delta\delta/\Delta T$) in a proton accepting solvent (THF-d_8) evidences the strength of intramolecular, intermolecular or with solvent N–H interactions. Values higher than 4×10^{-3} ppm/K usually correspond to solvated N–H and indicate weak intermolecular bonds, Table 2 [40]. Therefore, in compounds **2**, **4**–**8**, the values between 6.8 and 10×10^{-3} ppm/K indicating that they have weak hydrogen bonds in exchange with the solvent.

3.2. Crystal structures

Aminophosphine **2** crystallized from dried benzene at room temperature to give colorless crystals. The unit cell contains two molecules forming a dimer. The X-ray diffraction analysis showed that the diphenylphosphine group is on the same side of the sulfur atom, Fig. 1 and Table 3. The interatomic distance P···S 3.10 Å shorter than the sum of the van der Walls radii [$\sum r_{vdw}$ (P, S) = 3.65 Å] indicates a stabilizing contact. The phosphorus atom is almost in the molecular plane [torsional angles: S–C2–N_{exo}–P = 9.01°, N3–C2–N_{exo}–P = 171.13°]. The bond length N_{endo}–C2 [1.287(3) Å] indicates a localized double bond whereas the bond length C2–N_{exo} [1.347(3) Å] correspond to a delocalized bond, Table 4. The bond angles around N_{exo} (average 120.9(2)°) correspond to an sp^2 hybridization. The bond angles at phosphorus [N–P–C 101.1(1)°, C1–P–C2 103.6(1)°, N–P–C2 104.4(1)6°] denote 46% of sp^3 character and the P–N_{exo} bond length 1.689(2) Å is attributed to a delocalized P–N bond. The conformation of **2** favors six cooperative intermolecular hydrogen bonds, NH···N 2.14 and 2.22 Å and CH···C$^-$ 2.86, 2.84, 2.89 and 2.87 Å, Fig. 1. To our knowledge, this

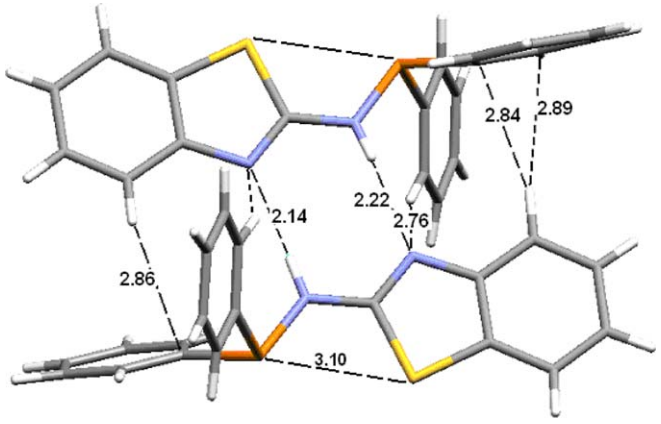

Fig. 1. Molecular structure of **2** showing six cooperative intermolecular hydrogen bonds.

is the first example of six hydrogen multiple bonds [41]. The crystalline cell of **2** shows a zig-zag polymeric arrangement.

Compound **7** crystallized from benzene, the X-ray analysis of the colorless monoclinic crystals shows the tautomer with the NH proton at the endocyclic nitrogen and the conjugate system C2═N–P═S, with endocyclic and exocyclic sulfur atoms almost coplanar and close to each other (3.13 Å); it is deduced that an S···S interaction occurs ($\sum r_{vdw}$ 3.60 Å), Fig. 2 and Table 4. The torsional angle S1–C2–N–P (1.31°) indicates that the phosphorus is in the molecular plane. The P–N bond length [1.633(3) Å], which falls between a P–N single bond (1.77 Å) and a P═N double bond (1.56 Å) indicates some delocalization, that is extended to bond C2–N3 [1.344(4) Å] and C2–N10 [1.312(4) Å]. Angles around phosphorus [S–P–N10 119.0(1)°, S–P–O16 113.9(1)°, S–P–O13 115.7(1)°, N–P–O16 103.8(1)°, O–P–O 99.8(1)°, N–P–O13 102.1(1)°] are characteristic of a distorted tetrahedral geometry.

The homodimerization of **7** can be seen in the unit cell through quadruple hydrogen bonds with an arrangement AADD–DDAA (A, acceptor site; D, donor site). This bonding situation generates three eight membered cycles

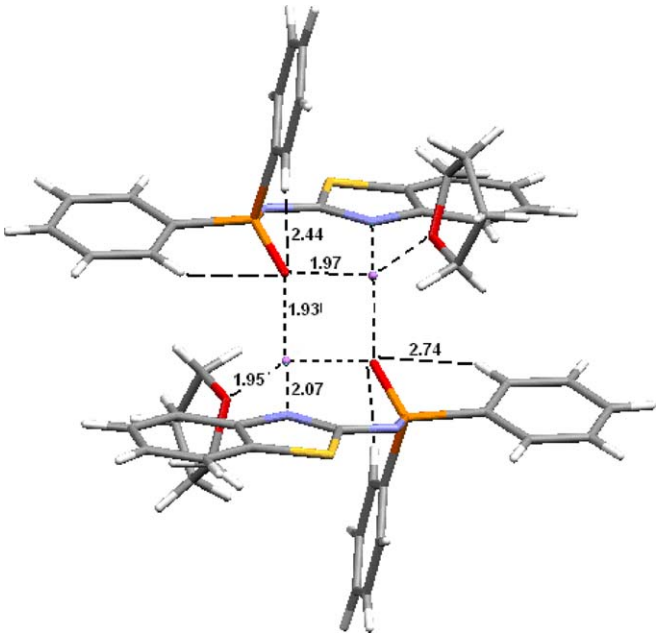

Fig. 4. X-ray structure of compound **10**.

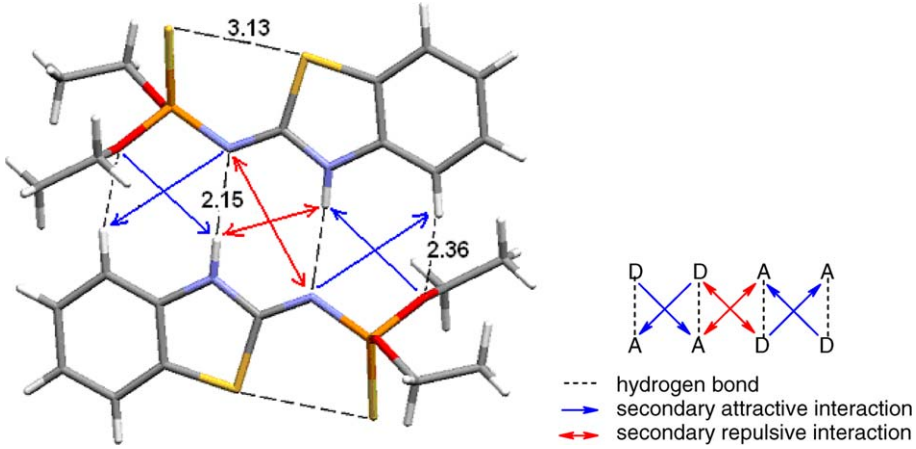

Fig. 2. Molecular structure of **7** showing quadruple hydrogen bonds, secondary repulsive and attractive interactions in AADD–DDAA arrangements.

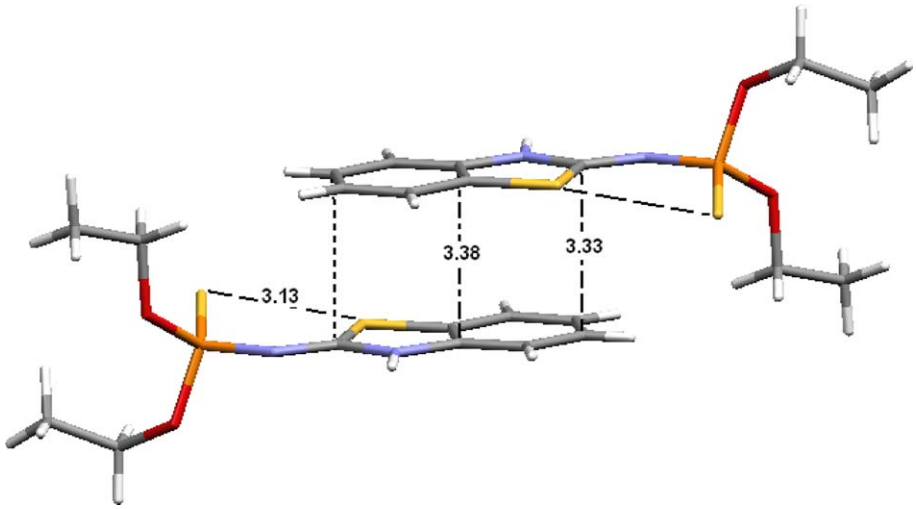

Fig. 3. Solid state structure of compound **7** showing π–π (3.33 and 3.38 Å) and S···S (3.13 Å) interactions.

by contacts NH···N$^-$ (2.152 Å) and H4···OP (2.36 Å), both shorter than the corresponding sum of the van der Waals radii ($\sum r_{vdw}(N, H) = 3.00$Å; $\sum r_{vdw}(O, H) = 2.95$ Å), Fig. 2. A π–π face to face interaction between the aromatic planes was observed (3.33 and 3.38 Å), Fig. 3.

As seen in Fig. 4 and Table 5, the crystal structure of **10** determined by X-ray diffraction shows a dimer containing an inversion center with O_{THF}–Li–Li–O_{THF} and N–Li–Li–N rotational angles of 180°. Each lithium atom is bound to three oxygen atoms and to the endocyclic nitrogen atom of one 2-aminobenzothiazole molecule. It is interesting to observe that in comparison to compound **4** where the preferred conformation in solution presents the P=O bond oriented *cis* to the S atom, in **10** the P=O group is *cis* to the endocyclic N. The bond lengths C2–N_{exo} [1.331(3) Å], C2–N_{endo} [1.326(3) Å], P–N_{exo} [1.613(2) Å] and P=O [1.511(2) Å] indicate an electronic delocalized system N–C2–N–P–O, Table 5. Torsional angles N–C2–N–P (10.8°), S–C2–N–P (169.2°) and C2–N–P–O (51.7°) showed that the P–O bond is out of the benzothiazole plane. The lengths N_{endo}–Li [2.08(5) Å] and Li···O [in average of 1.95 Å] are characteristic for covalent bonds. The Li–N–C2–N angle of 18.5° indicates that the lithium atom is slightly out of the benzothiazole plane. The

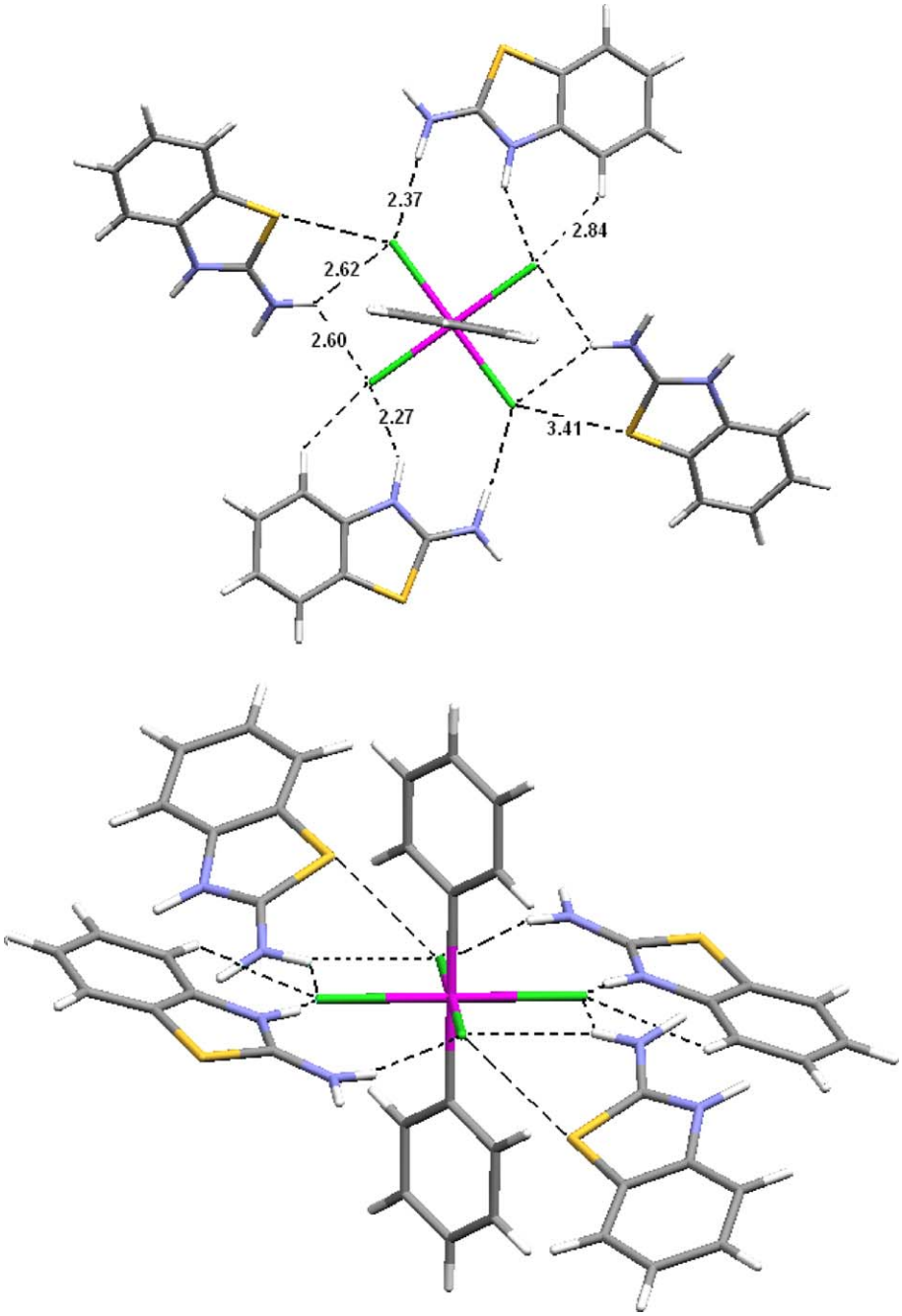

Fig. 5. Two views of the X-ray structure of compound **11**.

distance between the two lithium atoms is 2.69 and between the two P=O oxygen atoms is 2.82 Å. Each P=O oxygen atom has two short contacts with one *ortho* C–H of the P-phenyl group (2.74 and 2.44 Å), Fig. 4.

In compound **11** (Fig. 5 and Table 6), the metal atom is bound to two phenyl groups in *anti* position [Pb–C_{Ar} 2.138(7) Å; C_{Ar}–Pb–C_{Ar} 179.99(4)°] and to four coplanar chlorine atoms [Pb–Cl(1) 2.606(1) Å; Pb–Cl(2) 2.579(1) Å] [Cl(1)–Pb–Cl(1) = Cl(2)–Pb–Cl(2) = 180.0°], Table 6 and Fig. 5. In the cell four benzothiazolium cations interact by hydrogen bonds with the plumbate chlorine atoms, the distances of these multiple contacts are N2–H···Cl (2.37 Å), N3–H···Cl (2.27 Å) and S···Cl (3.41 Å) which are shorter than the corresponding sum of the van der Waals radii [$\sum r_{vdw}(H, Cl) = 2.90$–$3.35$ Å; $\sum r_{vdw}(S, Cl) = 3.70$ Å]. Two cations present three cooperative hydrogen bonds with two *cis* chlorine atoms (2.37, 2.27 and 2.84 Å) whereas the other two cations present only a bifurcate hydrogen bond with two *cis* chlorine atoms (2.6 Å). In addition, for each plumbate anion there are two chlorine–sulfur contacts of 3.41 Å, Fig. 5.

4. Summary

The 2-aminobenzothiazole phosphoramides are interesting polyfunctional and very reactive compounds, where preferred tautomers and conformers and hydrogen bonds were carefully established by multinuclear NMR.

We have found that phosphoramides are preferentially formed at the exocyclic nitrogen atom of the 2-aminobenzothiazole. In solution, compounds **2** and **3** have a preferred conformation with the P atom on the same side of the endocyclic nitrogen, and a preferred tautomer with the proton on the exocyclic nitrogen atom. Phosphorus oxidation changes the preferred tautomer and conformer to the one with a protonated endocyclic nitrogen.

In the solid state compound **2** presents a different conformer resulting from the extensive hydrogen bonds network which gives stabilized dimers through the cooperation of unusual six intermolecular hydrogen bonds and also forms the stabilizing S···P short contact of 3.11 Å, (sum of van der Walls radii 3.65 Å) where the P atom is in the plane of the heterocycle.

Compound **7** forms dimers through quadruple cooperative bonds two NH···N^- and two H4···O–P. The molecule presents a S···S interaction indicated by the geometry and the S···S distance (3.13 Å) which is smaller than the van der Waals radii (3.60 Å).

A lithiation of **2** furnishes **9** together with the dimeric lithium complex **10** as by product. The solid state structure of **10** presents a new conformation with the endocyclic nitrogen on the same side of the P=S bond. The reaction of **2** with $Pb(NO_3)_2$ did not afford the expected lead coordination compound but the diphenyl tetrachloro lead anion **11** resulting from phenyl and chloro migration to lead in very low yield. Compound **11** is remarkable regarding the structure of the hexacoordinated lead dianion unit and also by the protonated 2-aminobenzothiazole which establishes an interesting weak interactions network.

Acknowledgments

Z.G.-H and A.R.-O. thanks Conacyt for scholarships. Financial support by Conacyt (Grant 34714-E) and Cinvestav, Mexico is acknowledged.

Appendix A. Supplementary data

Crystallographic data of the structural analysis (excluding structure factors) have been deposited with the Cambridge Crystallographic Data Centre as supplementary publication numbers CCDC: 267771 for **2**, 267774 for **7**, 267773 for **10**, and 267772 for **11**. Copies of these data can be obtained, free of charge, from the director CCDC, 12 Union Road, Cambridge CB2 1EZ, UK, fax: +44 1223 336 033; e-mail: deposit@ccdc.cam.ac.uk or www:http://www.ccdc.cam.ac.uk. Supplementary data associated with this article can be found, in the online version, at doi:10.1016/j.poly.2005.11.018.

References

[1] A.R. Katritzky, C.W. ReesComprehensive Heterocyclic Chemistry, 6, Pergamon Press, New York; Toronto; Sydney; Paris, 1984, p. 250.
[2] G.W. Kabalka, Current Topics in the Chemistry of Boron, The Royal Society of Chemistry, Cambridge, 1994, p. 406.
[3] E.V. Bakhmutova, H. Nöth, R. Contreras, B. Wrackmeyer, Z. Anorg. Allg. Chem. 627 (2001) 1846.
[4] F.A. Cotton, W.H. Ilsey, Inorg. Chem. 20 (1981) 572.
[5] L. Sieroń, M. Bukowska-Strzyżewska, Acta Crystallogr., Sect. C 56 (2000) 19.
[6] D.R. Armstrong, S. Bennett, M.G. Davidson, R. Snaith, D. Stalke, D.S. Wright, J. Chem. Soc., Chem. Commun. (1992) 262.
[7] L. Antolini, A. Benedetti, A.C. Fabretti, A. Giusti, Inorg. Chem. 27 (1988) 2192.
[8] F. Téllez, Ph.D. thesis, Department of Chemistry-Cinvestav, Mexico, 2003.
[9] F. Téllez, A. Cruz, H. López-Sandoval, I. Ramos-García, R.E. Castillo-Sierra, B. Paz-Michel, H. Nöth, A. Flores-Parra, R. Contreras, Eur. J. Org. Chem. 20 (2004) 4203.
[10] F. Tellez, A. Flores-Parra, N. Barba-Behrens, R. Contreras, Polyhedron 23 (2004) 2481.
[11] J. Knizek, H. Nöth, A. Schlegel, Eur. J. Inorg. Chem. (2001) 181.
[12] J. Knizek, H. Nöth, J. Organomet. Chem. 168 (2000) 614.
[13] M. Niemeyer, P.P. Power, Inorg. Chem. 35 (1996) 7264.
[14] T. Chivers, M. Krahn, M. Parvez, G. Schatte, Chem. Commun. (2001) 1922.
[15] C. Kimblin, B.M. Bridgewater, T. Hascall, G. Parkin, J. Chem. Soc., Dalton Trans. (2000) 891.
[16] Y. Miyashita, Y. Yamada, K. Fujisawa, T. Cono, K. Kanamori, K. Okamoto, J. Chem. Soc., Dalton Trans. (2000) 981.
[17] K. Kitano, R. Tanaka, T. Kimura, T. Tsuda, S. Shimizu, H. Takagi, T. Nishioka, D. Shiomi, A. Ichimura, I. Kinoshita, K. Isobe, S. Ooi, J. Chem. Soc., Dalton Trans. (2000) 995.
[18] J.E. Huheey, E.A. Keiter, Inorganic Chemistry Principles of Structure and Reactivity, fourth ed., Harper Collins College, 1993, p. 292.
[19] G.A. Jeffrey (Ed.), An Introduction to Hydrogen Bonding, Oxford University Press, New York, 1997, p. 12.
[20] D.C. Sherrington, K.A. Taskinen, Chem. Soc. Rev. 30 (2001) 83.

[21] B. Gong, Y. Yan, H. Zeng, E. Skrzypczak-Jankunn, Y.W. Kim, J. Zhu, H. Ickes, J. Am. Chem. Soc. 121 (1999) 5607.
[22] F. Bernardi, Organic Sulfur Chemistry, Elsevier, 1985, p. 192.
[23] F.H. Allen, O. Kennard, D.G. Watson, L. Brammer, A.G. Orpen, R. Taylor, J. Chem. Soc., Perkin Trans. II (1987) S1.
[24] T.N.G. Row, R. Parthasarathy, J. Am. Chem. Soc. 103 (1981) 477.
[25] R.E. Rosenfield Jr., R. Parthasarathy, J.D. Dunitz, J. Am. Chem. Soc. 99 (1977) 4860.
[26] S. Oae, Organic Sulfur Chemistry, Structure and Mechanism, CRC-Press, Florida, 1991, p. 19.
[27] B.M. Goldstein, F. Takusagawa, H. Berman, P.C. Srivastava, R.K. Robins, J. Am. Chem. Soc. 105 (1983) 7416.
[28] F.T. Burling, B.M. Goldstein, J. Am. Chem. Soc. 114 (1992) 2313.
[29] J.C. Gálvez-Ruíz, C. Guadarrama-Pérez, H. Nöth, A. Flores-Parra, Eur. J. Inorg. Chem. (2004) 601.
[30] P.G. Cookson, A.G. Davies, N. Fazal. J. Organometal. Chem. 99 (1975) C31.
[31] H.G. Henning, U. Ladhoff, Zeitschrift fuer Chem. 6 (1966) 261.
[32] P. Sharma, A. Cabrera, M. Sharma, A. Alvarez, J.L. Arias, R.M. Gomez, S. Hernández, Z. Anorg. Allg. Chem. 626 (2000) 2330.
[33] M. Jun, M.J. Begley, D.B. Sowerby, I. Haiduc, Polyhedron 9 (1996) 3167.
[34] J. Vollani, R.O. Day, R.R. Holmes, Organometallics 3 (1984) 745.
[35] L.A. Fedorov, P. Savarino, G. Viskardi, A.I. Rebrov, E. Barni, Bull. Russ. Acad. Sci. 1 (1992) 3299.
[36] M. Raban, Chem. Commun. (1970) 1415.
[37] R. Contreras, J.M. Grevy, Z. García-Hernández, M. Güizado-Rodriguez, B. Wrackmeyer, Heteroatom. Chem. 12 (6) (2001) 542.
[38] E.V. Bakhmutova, A. Cruz, R. Ramírez-Trejo, R. Contreras, B. Wrackmeyer, Magn. Reson. Chem. 39 (2001) 739.
[39] A.E. Cisneros-Gómez, A. Ramos-Organillo, J. Hernández-Díaz, J. Nieto-Martínez, R. Contreras, S.E. Castillo-Blum, Heteroatom Chem. 11 (2000) 309.
[40] F.J. Martínez-Martínez, A. Ariza-Castolo, H. Tlahuext, M. Tlahuextl, R. Contreras, J. Chem. Soc., Perkin Trans. 2 (1993) 1481.
[41] C. Schmuck, W. Wienand, Angew. Chem., Int. Ed. 40 (2001) 4363.

are possible [1–6]. These are the nitro (Cu–NO_2) and (nitrito-*O*) via either nitrogen or oxygen binding, respectively [1–6]. As a bidentate ligand, NO_2^- can chelate or bridge via the two oxygens (nitrito-*O*,*O*′) [7–10], via one nitrogen and one oxygen or via a single oxygen atom [6,11]. The tridentate behavior of the nitrite ligand was also found in a few cases where the coordination mode is accomplished in two ways. In the first case, the NO_2^- is chelated to one metal through its two oxygen atoms and bridged to a second metal ion via the nitrogen atom [12]. In the second case, the two metal ions are bridged via one oxygen while the second oxygen binds to one of the two metal ions [13,14]. On the other hand, besides the ambi-monodentate nature of the NCS^- ion, the ligand was extensively used to synthesize bridged polynuclear copper(II) complexes with different dimensionality [15–20]. In bridged copper(II)–thiocyanato systems, two principal modes of coordination are exhibited namely end-to-end ($\mu_{N,S}$-NCS), and end-on binding modes via $\mu_{N,N}$-NCS and $\mu_{S,S}$-NCS. A few examples were reported in the bridging coordination modes $\gtrdot$NCS ($\mu_{N,N}$-NCS) [19] and $\gtrdot$SCN ($\mu_{S,S}$-NCS) [20]. The interaction of the thiocyanate group with Cu^{2+} in the end-to-end ($\mu_{N,S}$-NCS) coordination mode led to a variety of 1D singly and doubly bridged NCS-polynuclear species [15–18].

The stereochemistry adapted by the nitrito- and thiocyanato-copper complexes ranges between square pyramidal (SP) and trigonal bipyramidal (TBP); most of the complexes are known to adapt geometries that are intermediate between the two extremes [1,2,5,8,18]. However, tetragonally distorted octahedron geometry was also observed in a relatively large number of nitrito and thiocyanato copper (II) complexes such as in $[Cu(dpyam)_2(ONO)]^+$ [4],[1] $[Cu(TIMM)(NO_2)_2]$ [9],[1] $[Cu(NO_2)_2CuL]_n$ where L = *N*, *N*′-bis(2-methyl-2-aminopropyl)oxamide [11], and $[Cu_2(L)_2(\mu_{N,S}\text{-}NCS)_2(OClO_3)_2]$ (L = dien and dpt) [17].[1]

In this paper, we report the synthesis, properties and molecular structure of the monomeric nitrito-Cu(II) and the dinuclear doubly bridged thiocyanato-Cu(II) complexes derived from 3,3′-diamino-*N*-methyldipropylamine (Medpt) and diethylenetriamine (dien). Also, the study provides more structural data concerning the bridged thiocyanato-Cu(II) complexes in an attempt to shed the light on the structural factors that might affect the formation of a certain bonding coordination mode over the other.

2. Experimental

2.1. Materials and physical measurements

3,3′-Diamino-*N*-methyldipropylamine (Medpt) and diethylenetriamine (dien) were purchased from Aldrich Chemical Company and copper(II) perchlorate hexahydrate from Strem Chemical Company, USA. All other materials were reagent grade quality. Infrared spectra were recorded on JASCO FT/IR-480 plus spectrometer as KBr pellets. Electronic spectra were recorded using Agillent 8453 HP diode UV–Vis spectrophotometer. Elemental analyses were carried out by the Atlantic Microlaboratory, Norcross, GA, USA. The magnetic measurements were carried out in the "Servei de Magnetoquímica (Universitat de Barcelona)" on polycrystalline sample (40 mg) with a Quantum Design SQUID MPMSXL susceptometer in the temperature range 2–300 K and the magnetic field was 1 T.

Caution: Salts of perchlorate and their metal complexes are potentially explosive and should be handled with great care and in small quantities.

2.2. Synthesis of the complexes

2.2.1. [Cu(Medpt)(ONO)(H2O)]ClO4 (1)

Copper(II) perchlorate hexahydrate (0.93 g, 2.5 mmol) dissolved in 20 ml of methanol was added to 3,3′-diamino-*N*-methyldipropylamine (0.37 g, 2.5 mmol) in methanol (10 ml). To this solution, $NaNO_2$ (0.35 g, 5 mmol) dissolved in 50 ml of hot MeOH was added dropwise. The resulting blue solution was heated for 10 min on a steam bath, filtered while hot and then allowed to crystallize at room temperature. Upon standing at room temperature, the navy-blue crystals which separated out were collected by filtration, washed with ether, and air dried (overall yield: 0.70 g, 97%). Crystals suitable for X-ray analysis were obtained from dilute methanolic solution by slow crystallization. Characterization: *Anal*. Calc. for $C_7H_{21}ClCuN_4O_7$: C, 22.58; H, 5.69; N, 15.05. Found: C, 22.71; H, 5.65; N, 15.00%. Selected IR bands (KBr, cm^{-1}): ν(O–H) (H_2O) stretching, 3449 (mb); ν(O–N)(NO_2^-) 1439 (s), 1268 (s); ν(Cl–O)(ClO_4^-) centered at 1092 (vs).

2.2.2. [Cu(dien)(ONO)]ClO4 (2)

A similar procedure as that described above for **1** was followed, and the complex was separated as blue crystals (overall yield: 77%). Crystals suitable for X-ray analysis were obtained from the second batch upon crystallization at ambient temperature. Characterization: *Anal*. Calc. for $C_4H_{13}ClCuN_4O_6$: C, 15.39; H, 4.20; N, 17.95. Found: C, 15.28; H, 4.13; N, 18.01%. Selected IR bands (KBr, cm^{-1}): ν(O–N)(NO_2^-) 1472 (m), 1271 (s); ν(Cl–O)(ClO_4^-) at 1144 (vs), 1116 (vs), 1085 (vs).

2.2.3. [Cu2(Medpt)2(μN,S-NCS)2](ClO4)2 (3)

To a solution containing $Cu(ClO_4)_2 \cdot 6H_2O$ (0.375 g, 1.0 mmol) and 3,3′-diamino-*N*-methyldipropylamine (0.145 g, 1.0 mmol) in methanol (40 ml), NH_4NCS (0.085 g, 1 mmol) dissolved in MeOH (10 ml) was added drop by drop. The resulting blue solution was heated on a steam-bath for 5 min, filtered while hot and allowed to crystallize at room temperature. After a few minutes, small blue crystals were

[1] Ligand abbreviations: Medpt, 3,3′-diamino-*N*-methyldipropylmine; dpt, dipropylenetriamine; dien, diethylenetriamine; Et_2dien, *N*,*N*-diethyldiethylenetriamine; TPA, tris(2-pyridyl methyl)amine, dpyam, 2,2′-dipyridylamine; and TIMM, tris[2-(1-methyl)imidazolyl]methane.

obtained. These were collected by filtration, washed with ether and air dried (yield: 0.35 g, 96%). Crystals of X-ray quality were obtained from the first batch. Characterization: *Anal*. Calc. for $C_8H_{19}ClCuN_4O_4S$: C, 26.32; H, 5.23; N, 15.29. Found: C, 26.51; H, 5.35; N, 15.36%. Selected IR bands (KBr, cm^{-1}): ν(NCS), 2116 (vs); ν(Cl–O)-(ClO_4^-), 1092 (vs).

2.3. X-ray data collection and refinement for complexes 1–3

The X-ray single-crystal data were collected on a modified STOE four-circle diffractometer. Graphite-monochromatized Mo Kα radiation ($\lambda = 0.71069$ Å) with the ω-scan technique were used to collect the data sets. The accurate unit-cell parameters were determined from automatic centering of 36 reflections ($7.4° < \theta < 14.7°$) for **1**, 38 reflections ($10.3° < \theta < 15.5°$) for **2**, and 60 reflections ($12.1° < \theta < 16.4°$) for **3**, and refined by least-squares methods. The intensities were corrected for Lorentz-polarization effects, intensity decay (intensity drop of 4%, 6% and 7% for **1**–**3**, respectively) and for absorption using the DIFABS [21] computer program. The structures were solved by direct methods and refined by full-matrix least-squares methods on F^2, using the SHELXTL/PC V 5.03 [22] program package. All non-hydrogen atoms were refined anisotropically. In case of **1**, split occupancy of disordered oxygen atoms of ClO_4 counter ion: 0.687(10) and 0.313(10) were applied. The hydrogen atoms were assigned with isotropic displacement factors and included in the final refinement cycles on calculated positions, except for **1**, where nine distance restraints (2 O–H, 4 N–H, 3 H–H) were applied to fix the internal geometry of the water molecule and $–NH_2–$ groups of the Medpt ligand. Residual extremes in the final difference Fourier syntheses were observed in vicinity of metal atoms. Table 1 lists the crystallographic data for the three complexes. Selected bond parameters are given in Tables 2–4 for **1**–**3**, respectively.

3. Results and discussion

3.1. Crystal structure of the complexes

3.1.1. [Cu(Medpt)(ONO)(H_2O)]ClO_4 (1)

A perspective view together with the atom labeling scheme is given in Fig. 1 and selected bond parameters are given in Table 2. The structure consists of isolated $[Cu(Medpt)(ONO)(H_2O)]^+$ cations and perchlorate counter anions. The copper centers are pentacoordinated by the three N atoms of the Medpt, oxygen atom O(1) of nitrito group and oxygen atom O(3) of a water molecule. The

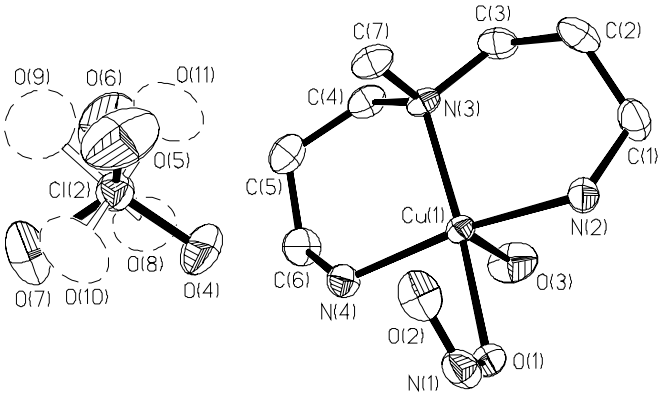

Fig. 1. Molecular geometry and atom labeling scheme of **1**.

Table 1
Crystal data and processing parameters of [Cu(Medpt)(ONO)(H_2O)]ClO_4 (**1**), [Cu(dien)(ONO)]ClO_4 (**2**) and [$Cu_2(\mu_{N,S}$-NCS)$_2$(Medpt)$_2$]$(ClO_4)_2$ (**3**)

Compound	1	2	3
Empirical formula	$C_7H_{21}ClCuN_4O_7$	$C_4H_{13}ClCuN_4O_6$	$C_{16}H_{38}Cl_2Cu_2N_8O_8S_2$
Formula mass	372.21	312.19	732.68
System	monoclinic	monoclinic	triclinic
Space group	$P2_1/c$	$C2/m$	$P\bar{1}$
a (Å)	7.899(3)	14.918(3)	14.111(3)
b (Å)	13.318(4)	8.632(2)	14.436(3)
c (Å)	14.191(5)	8.512(2)	14.608(3)
α (°)	90	90	82.72(3)
β (°)	96.75(3)	92.39(2)	77.90(3)
γ (°)	90	90	82.24(3)
V (Å^3)	1482.5(9)	1095.2(4)	2868.1(10)
Z	4	4	4
T (K)	293(2)	293(2)	100(2)
μ(Mo Kα) (mm^{-1})	1.688	2.259	1.869
D_{calc} (Mg/m^3)	1.668	1.893	1.697
Crystal size (mm)	$0.30 \times 0.16 \times 0.10$	$0.32 \times 0.26 \times 0.15$	$0.34 \times 0.26 \times 0.14$
θ Range (°)	2.89–27.00	3.56–25.96	2.50–25.50
Reflections collected	3898	1421	11 563
Independent reflections/R_{int}	3239/0.0250	1142/0.0433	10 560/0.0897
Parameters/restraints	240/9	85/0	689/0
Goodness-of-fit on F^2	1.109	1.111	1.228
R_1/wR_2 (all data)	0.0448/0.1235	0.0770/0.2752	0.0832/0.2849
Residual extrema (e/Å^3)	0.486/−0.399	1.057/−1.444	1.685/−1.474

Table 2
Selected bond lengths (Å) and angles (°) for **1**

Cu(1)–N(2)	1.975(3)	Cu(1)–N(4)	1.996(3)
Cu(1)–N(3)	2.052(3)	Cu(1)–O(1)	2.069(3)
Cu(1)–O(3)	2.297(3)	O(1)–N(1)	1.261(5)
N(1)–O(2)	1.213(5)	Cu(1)···O(2)	2.575(4)
Cu(1)···Cu(1A)	5.468(2)		
N(2)–Cu(1)–N(4)	168.08(13)	N(2)–Cu(1)–N(3)	95.53(13)
N(4)–Cu(1)–N(3)	94.07(13)	N(2)–Cu(1)–O(1)	84.62(13)
N(4)–Cu(1)–O(1)	84.68(13)	N(3)–Cu(1)–O(1)	169.74(11)
N(2)–Cu(1)–O(3)	95.3(2)	N(4)–Cu(1)–O(3)	90.5(2)
N(3)–Cu(1)–O(3)	96.65(13)	O(1)–Cu(1)–O(3)	93.55(14)
N(1)–O(1)–Cu(1)	108.8(2)	O(1)–N(1)–O(2)	114.2(3)

Symmetry code: (A) $-x, -y, 1-z$.

Table 3
Selected bond lengths (Å) and angles (°) for **2**

Cu(1)–N(2)	1.958(4)	Cu(1)–N(1)	2.000(4)
Cu(1)–N(2A)	2.000(4)	Cu(1)–O(1)	2.224(6)
Cu(1)–O(2)	2.430(8)	O(1)–N(4)	1.148(11)
N(4)–O(2)	1.218(11)	Cu(1)···O(1B)	2.670(6)
Cu(1)···Cu(1B)	4.1265(17)	Cu(1)···Cu(1C)	6.0481(17)
N(2)–Cu(1)–N(1)	84.23(10)	N(1)–Cu(1)–N(1A)	168.0(2)
N(1)–Cu(1)–O(1)	94.86(11)	N(2)–Cu(1)–O(1)	160.0(2)
N(2)–Cu(1)–O(2)	147.9(2)	N(1)–Cu(1)–O(2A)	95.77(11)
O(1)–Cu(1)–O(2)	52.1(2)	N(4)–O(1)–Cu(1)	100.0(5)
O(1)–N(4)–O(2)	120.2(8)	N(4)–O(2)–Cu(1)	87.7(5)

Symmetry code: (A) $x, -y, z$; (B) $1-x, y, 1-z$; (C) $1/2-x, 1/2+y, 1-z$.

coordination polyhedron may be described as an axially elongated square pyramid. The Cu(1)–O(1), Cu(1)–N(2), Cu(1)–N(3), Cu(1)–N(4) distances are 2.069(3), 1.975(3), 2.052(3) and 1.996(3) Å, respectively. The Cu(1)–O(3) distance is 2.297(3) Å and the Cu(1)···O(2) separation to non-coordinated oxygen atom of nitrito anion is 2.575(4) Å. The Cu···Cu separation is 5.468(2) Å. Hydrogen bonds of the types N–H···O and O–H···O (Table 5) form a 3D supramolecular network. In this case, the N(1)–O(1) distance [1.261(5) Å] of the nitrito group involving the stronger Cu(1)–O(1) interaction [2.069(3) Å] is longer than the N(1)–O(2) distance [1.213(5) Å] involving the very weak Cu(1)···O(2) [2.575(4) Å] interaction. Also, the Cu(1)–O(1)–N(1) angle [108.8(2)°] was found to be in the range reported for monodentate nitrite (pure monodentate nitrite angle Cu–O–NO is around 119.5°) [23], whereas the O(1)–N(1)–O(2) angle [114.2(3)°] is slightly smaller than 115.4° for the free nitrite ion [24].

3.1.2. *[Cu(dien)(ONO)]ClO$_4$ (**2**)*

A perspective view together with the atom labeling scheme is given in Fig. 2 and selected bond parameters are given in Table 3. The structure consists of [Cu(dien)(ONO)]$^+$ cations and perchlorate counter anions. Each copper atom forms bonds to the three N atoms of the dien ligand [Cu–N bonds from 1.958(4) to 2.000(4) Å], a short bond to oxygen atom O(1) [2.224(6) Å] and a longer bond [2.430(8) Å] to second oxygen atom O(2) of the nitrito group. The nitrito groups [N(4)–O(1) = 1.148(11) Å, N(4)–O(2) = 1.218(11) Å, O(1)–N(4)–O(2) = 120.2(8)°] act as μ-OO′ bridging ligands. Centrosymmetrically related pairs of [Cu(dien)(ONO)]$^+$ cations (Fig. 2) have Cu(1)···Cu(1B) and Cu(1)–O(1B) separations of 4.1265(17) and 2.670(6) Å, respectively, whereas the shortest inter-dimeric Cu···Cu separation is 6.0481(17) Å. Hydrogen bonds of type N–H···O are listed in Table 5. The O(1)–N(4)–O(2) angle is 120.2(8)° is larger than that found for the free nitrite ion [24], and the Cu(1)–O(1)–N(4) angle is 100.0(5)° which is in the range found for pure bidentate nitrite [93–100°] [25]. The O(1)–Cu(1)–O(2) bond angle of 52.1° agrees well with the values previously reported for the bite angle of the coordinated nitrite group reported in [Cu(dpyam)$_2$(ONO)]Y complexes (Y = ClO_4^-, NO_3^-, NO_2^-) [4a,23a]. Also, it is interesting to note that the bidentate nature of the nitrito group was established in the mononuclear analog diethylenetriamine-*N*,*N*′,*N*″-nitrito-O,O′nitrocopper(II) [10].

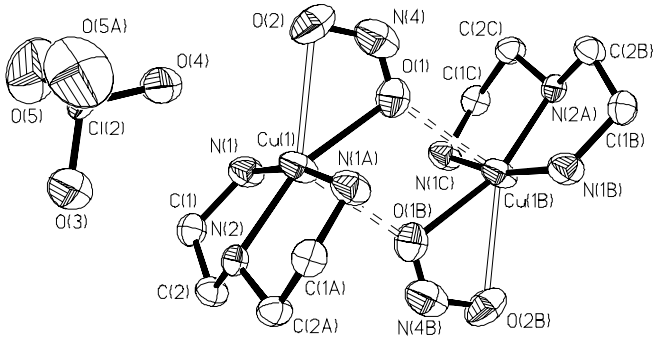

Fig. 2. ORTEP view (30% ellipsoids) with atom labeling scheme of **2**.

3.1.3. *[Cu$_2$(Medpt)$_2$($\mu_{N,S}$-NCS)$_2$](ClO$_4$)$_2$ (**3**)*

A perspective view together with the atom labeling scheme is given in Fig. 3(a)–(c) and selected bond parameters are given in Table 4. Each copper center is penta-coordinated by the three N atoms of the Medpt [Cu–N$_{(Medpt)}$ from 1.976(6) to 2.0786(6) Å], one N atom of NCS^- group in basal positions [Cu–N$_{(NCS)}$ bonds from 2.011(6) to 2.019(6) Å], and a sulfur atom from NCS^- ion in the apical position [Cu–S bonds from 2.698(2) to 2.735(2) Å]. The coordination polyhedra may be described as axially elongated square pyramids. The dinuclear subunits are established via the NCS groups which act as μ-NS bridging ligands. The structure consists of perchlorate counter anions and three crystallographically independent dinuclear [Cu$_2$(Medpt)$_2$(NCS)$_2$]$^{2+}$ cations. Two of the dinuclear units are located on inversion centers, one on a general position. The intradimeric Cu···Cu distances in these dinuclear units are 5.5132(15), 5.5157(16) and 5.4289(15) Å, and the shortest interdimeric Cu···Cu seperation is 6.1738(17) Å. The Cu$_2$(NCS)$_2$ rings are almost planar with mean "chair" angles of 8.4(3)°, 10.4(3)° and 15.4(4)°. The "chair" angle is defined as acute angle between plane formed by the two (NCS) bridges with (N–Cu–S) plane within a Cu$_2$(NCS)$_2$ ring. The deviations of the copper centers from their basal N$_4$ planes are 0.215(2), 0.216(2),

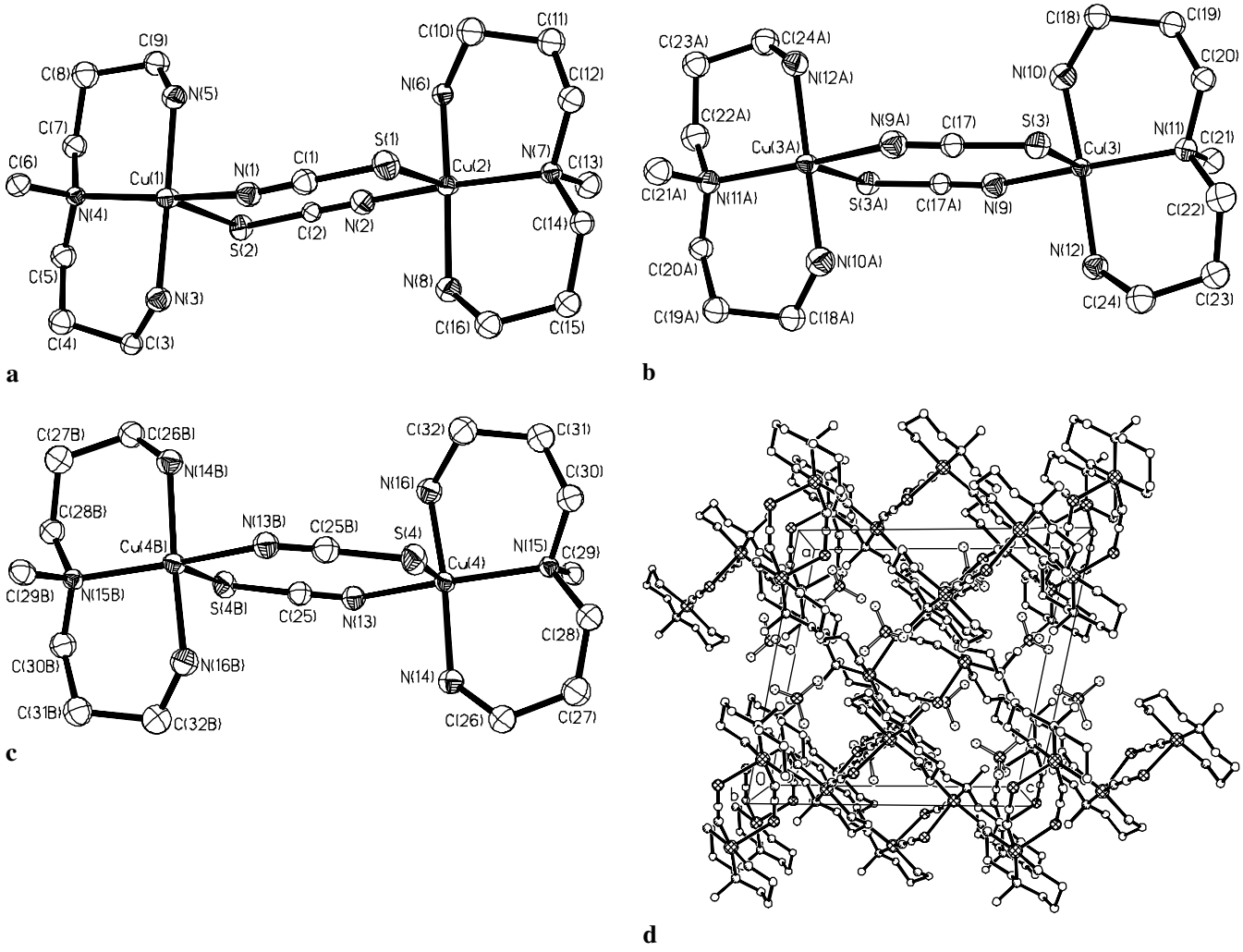

Fig. 3. (a)–(c) Molecular geometry with atom labeling scheme of the dinuclear $[Cu_2(Medpt)_2(\mu\text{-}NCS)_2]^{2+}$ subunits of **3**. (d) Packing view of **3**.

0.218(2) and 0.243(2) Å, respectively. Hydrogen bonds of type N–H···O (Table 5) form a 3D supramolecular network.

The same end-to-end bond fashion observed here in the doubly bridged thiocyanato-Cu(II)–Medpt complex **3** was observed with other Cu(II) complexes derived from linear tridentate amines such as dien, Et_2dien, and dpt [15].[1] The same type of bonding was also found in the azido complexes derived from Medpt and Et_2dien [15,26][1] but with dpt an end-on coordination mode was produced [27].

In the five-coordinate complexes, an intermediate structure may be found between the regular SP and the TBP geometries. The geometrical factor, τ which represents the degree of TBP distortion from ideal SP geometry ($\tau = 0$ for ideal SP and 1 for ideal TBP) [28] is used to obtain a quantitative picture for the degree of distortion in the complexes under investigation. The ratio between the two basal angles that would form the basal plane in the SP structure defines $\tau = (\theta - \phi)/60$. For the nitrito complexes **1** and **2** (see Figs. 1 and 2 for labeling) $\tau \approx 0.03$ and 0.13, respectively, whereas in **3** (Fig. 3 for labeling), the corresponding τ values are about 0.02, 0.01, 0.05 and 0.02 for Cu(1)–Cu(4), respectively. Aside from the relative strong distortion observed here in $[Cu(dien)(ONO)]^{2+}$ (**2**), these values still reveal the exclusive existence of the SP geometries in the three complexes.

3.2. Infrared spectra

The infrared spectrum of the nitrito complex **1** exhibits strong absorption bands at 1439 and 1268 cm^{-1} whereas **2** shows bands of medium intensities at 1472 and 1271 cm^{-1}, attributable to the stretching frequencies ν_{as}(O–N) and ν_s(O–N), respectively. The splitting between the two bands, $\Delta\nu(NO_2)$ (ν_{as}(O–N) − ν_s(O–N)) was used to distinguish between the various bridging modes of the coordinated NO_2^- group [29]. However, the observed $\Delta\nu(NO_2)$ values in these complexes (171 cm^{-1} for **1** and 201 cm^{-1} for **2**) did not provide a satisfactory conclusion concerning the coordination mode of the NO_2^- ligand [1,4,8,30]. This may result from the anisodentate nature of the NO_2^- group. The stretching frequency ν(Cl–O) of the perchlorate in complex **2** which occurs at 1116 cm^{-1} is split into three peaks indicating that the symmetry of

Table 4
Selected bond lengths (Å) and angles (°) for **3**

Cu(1)–N(5)	1.999(5)	Cu(1)–N(3)	2.018(5)
Cu(1)–N(1)	2.019(6)	Cu(1)–N(4)	2.101(5)
Cu(1)–S(2)	2.735(2)	Cu(2)–N(6)	1.993(5)
Cu(2)–N(2)	2.017(6)	Cu(2)–N(8)	2.048(5)
Cu(2)–N(7)	2.078(6)	Cu(2)–S(1)	2.730(2)
Cu(3)–N(10)	2.003(6)	Cu(3)–N(9)	2.011(6)
Cu(3)–N(12)	2.016(6)	Cu(3)–N(11)	2.118(5)
Cu(3)–S(3)	2.726(2)	Cu(4)–N(16)	1.976(6)
Cu(4)–N(14)	2.004(5)	Cu(4)–N(13)	2.017(5)
Cu(4)–N(15)	2.090(5)	Cu(4)–S(4)	2.698(2)
S(1)–C(1)	1.631(7)	C(1)–N(1)	1.168(9)
S(2)–C(2)	1.672(7)	C(2)–N(2)	1.139(9)
S(3)–C(17)	1.623(7)	C(17)–N(9A)	1.184(9)
S(4)–C(25B)	1.667(7)	C(25)–N(13)	1.155(9)
Cu(1)···Cu(2)	5.5157(16)	Cu(3)···Cu(3A)	5.5132(15)
Cu(4)···Cu(4B)	5.4289(15)	Cu(2)···Cu(3A)	6.1738(17)
N(5)–Cu(1)–N(3)	167.8(2)	N(5)–Cu(1)–N(1)	86.2(2)
N(3)–Cu(1)–N(1)	86.7(2)	N(5)–Cu(1)–N(4)	91.4(2)
N(3)–Cu(1)–N(4)	93.2(2)	N(1)–Cu(1)–N(4)	166.4(2)
N(5)–Cu(1)–S(2)	99.7(2)	N(3)–Cu(1)–S(2)	90.8(2)
N(1)–Cu(1)–S(2)	95.9(2)	N(4)–Cu(1)–S(2)	97.66(14)
N(6)–Cu(2)–N(2)	86.4(2)	N(6)–Cu(2)–N(8)	166.6(2)
N(2)–Cu(2)–N(8)	85.1(2)	N(6)–Cu(2)–N(7)	92.2(2)
N(2)–Cu(2)–N(7)	166.9(2)	N(8)–Cu(2)–N(7)	93.7(2)
N(6)–Cu(2)–S(1)	101.0(2)	N(2)–Cu(2)–S(1)	96.3(2)
N(8)–Cu(2)–S(1)	90.2(2)	N(7)–Cu(2)–S(1)	96.75(14)
N(10)–Cu(3)–N(9)	83.8(2)	N(10)–Cu(3)–N(12)	166.9(2)
N(9)–Cu(3)–N(12)	88.3(2)	N(10)–Cu(3)–N(11)	93.2(2)
N(9)–Cu(3)–N(11)	164.0(2)	N(12)–Cu(3)–N(11)	91.5(2)
N(10)–Cu(3)–S(3)	94.3(2)	N(9)–Cu(3)–S(3)	97.4(2)
N(12)–Cu(3)–S(3)	97.2(2)	N(11)–Cu(3)–S(3)	98.4(2)
N(16)–Cu(4)–N(14)	166.9(2)	N(16)–Cu(4)–N(13)	85.3(2)
N(14)–Cu(4)–N(13)	85.5(2)	N(16)–Cu(4)–N(15)	92.5(2)
N(14)–Cu(4)–N(15)	94.1(2)	N(13)–Cu(4)–N(15)	165.7(2)
N(16)–Cu(4)–S(4)	95.8(2)	N(14)–Cu(4)–S(4)	94.8(2)
N(13)–Cu(4)–S(4)	98.8(2)	N(15)–Cu(4)–S(4)	95.51(14)
C(1)–S(1)–Cu(2)	94.7(2)	N(1)–C(1)–S(1)	178.7(6)
C(1)–N(1)–Cu(1)	164.0(5)	C(2)–S(2)–Cu(1)	93.5(2)
N(2)–C(2)–S(2)	177.6(6)	C(2)–N(2)–Cu(2)	166.7(5)
C(17)–S(3)–Cu(3)	96.9(2)	N(9A)–C(17)–S(3)	177.9(6)
C(17A)–N(9)–Cu(3)	164.1(5)	C(25B)–S(4)–Cu(4)	93.6(2)
N(13)–C(25)–S(4B)	178.1(6)	C(25)–N(13)–Cu(4)	162.0(5)
C(3)–N(3)–Cu(1)	120.9(4)		

Symmetry codes: (A) $-x+1, -y+1, -z+1$; (B) $-x, -y, -z$.

Table 5
Hydrogen bond systems

Donor–H···A	[Symmetry of A]	D···A (Å)
Compound ***1***		
N(2)–H(8A)···O(1)	$[-x, -y, 1-z]$	3.110(5)
N(2)–H(8B)···O(2)	$[1-x, -y, 1-z]$	3.244(5)
N(4)–H(9A)···O(5)	$[-1+x, y, z]$	3.110(11)
N(4)–H(9B)···O(4)		3.259(7)
O(3)–H(10B)···O(7)	$[-1+x, 1/2-y, -1/2+z]$	2.919(10)
Compound ***2***		
N(1)–H(1A)···O(4)	$[1/2-x, 1/2+y, 1-z]$	3.336(6)
N(1)–H(1B)···O(5)	$[1/2+x, 1/2-y, z]$	3.150(10)
N(2)–H(2)···O(3)		3.148(9)
Compound ***3***		
N(3)–H(3C)···O(10)	$[1-x, 1-y, 1-z]$	3.203(8)
N(5)–H(5C)···O(3)	$[1+x, y, z]$	3.163(8)
N(6)–H(6D)···O(8)		3.125(8)
N(6)–H(6E)···O(13)	$[1+x, y, z]$	3.094(7)
N(8)–H(8C)···O(10)	$[1-x, 1-y, 1-z]$	3.293(8)
N(8)–H(8C)···O(11)	$[1-x, 1-y, 1-z]$	3.080(7)
N(8)–H(8D)···O(2)		3.010(7)
N(10)–H(10C)···O(11)		3.101(7)
N(10)–H(10D)···O(1)	$[1-x, 1-y, 1-z]$	3.131(8)
N(12)–H(12C)···O(1)		3.030(7)
N(12)–H(12D)···O(16)		3.198(7)
N(14)–H(14C)···O(7)	$[-1+x, y, z]$	2.961(7)
N(14)–H(14D)···O(14)		3.223(8)
N(16)–H(16C)···O(12)	$[x, -1+y, z]$	3.300(8)
N(16)–H(16D)···O(5)	$[1-x, -y, -z]$	3.027(7)
N(16)–H(16D)···O(7)	$[1-x, -y, -z]$	3.044(7)

D, donor; A, acceptor.

the perchlorate ion is lowered from T_d to C_{3v} which most likely may result from its location along the O(1B)–Cu(1)–O(4) axis [29].

The infrared spectrum of the doubly bridged end-to-end thiocyanato complex **3** shows a very strong absorption band at 2116 cm^{-1} attributable to the stretching frequency of $\nu(NCS^-)$. This band is located at a relatively higher position compared to that found in $[Cu_2(Et_2dien)_2(\mu_{N,S}\text{-}NCS)_2](ClO_4)_2$ [15] or in 1D polymeric bridged end-to-end thiocyanato complexes derived from *N*,*N*-dimethylaminoethanol and glycine ($\nu(NCS^-) = 2100\ cm^{-1}$) [31]. In 1D singly bridged thiocyanato complex derived from 1,4-diazacycloheptan, two bands were reported (2140 and 2088 cm^{-1}) [18a]. Also two strong bands were observed in the mono-coordinated thiocyanato complex $[Cu(TPA)(NCS)]ClO_4$ at 2092 and 2050 cm^{-1} [1]. Bridging thiocyanato groups are expected to exhibit two absorption bands above and below the 2100 cm^{-1} region due to the stretching frequency of S- and N-bonded thiocyanate group, respectively. Interestingly, we synthesized the doubly bridged thiocyanato complex $[Cu_2(dpt)_2(\mu_{N,S}\text{-}NCS)_2(ClO_4)_2]$ in which the coordination polyhedron around the Cu(II) ion is strongly elongated octahedral.[1] The IR of this complex exhibited two strong absorbed resolved bands at 2118 and 2076 cm^{-1}. The appearance of a single unresolved $\nu(NCS^-)$ IR band is not unusual but it has been observed in a number of $\mu_{N,S}$-NCS complexes [18c,32b]. Thus, it is obvious that stretching frequency of the thiocyanate group cannot be used to predict the bonding coordination mode in the thiocyanato-Cu(II) complexes. Most probably, this is, in part, due to the broadness of the stretching frequency band of the coordinated NCS^- group which may result in overlap of two or more vibrational modes and also to the ligand structural environment around the Cu(II) centers.

3.3. Visible spectra

The visible spectra of the nitrito and thiocyanato complexes were recorded in different solvents and the data are collected in Table 6. The solution spectra of $[Cu(Medpt)(ONO)(H_2O)]^+$, $[Cu(dien)_2(ONO)]^{2+}$ and $[Cu_2(Medpt)_2(\mu_{N,S}\text{-}NCS)_2]^{2+}$ display a single broad band between 580 and 640 nm range. These spectral features are consistent

Table 6
Visible spectral data {λ_{max}/nm (ε_{max}/$M^{-1}cm^{-1}$)} for [Cu(Medpt)(ONO)-(H_2O)]ClO_4 (**1**), [Cu(dien)(ONO)]ClO_4 (**2**) and [Cu_2(Medpt)$_2$($\mu_{N,S}$-NCS)$_2$](ClO_4)$_2$ (**3**) in different solvents

Solvent	1	2	3
H_2O	629 (146)	610 (154)	633 (208)
DMSO	612 (145)	596 (240)	637 (335)
CH_3NO_2	606 (188)	582 (201)	580 (266)
CH_3OH	600 (100)	590[a]	609[a]
CH_3CN	588 (188)	590 (239)	604 (286)

[a] Saturated solution.

with the five-coordinate geometry where the Cu(II) ion is adapting a distorted SP geometry. In general complexes with TBP geometry usually show a maximum at $\lambda >$ 800 nm with a higher energy shoulder [1,2,32]. This indicates that the solution spectrum of each complex ion is adequately explained by a d-d transition in Cu(II) ion in a distorted SP geometry with C_{4v} symmetry where the absorption maximum band observed in the visible region results from $^2B_1 \leftarrow {}^2E$ transition.

The spectra of the complexes and the position of λ_{max} show strong dependence on the nature of the solvent used with no sign to the appearance of a new band around 800 nm. This finding clearly rules out any stereochemical change around the central Cu(II) ion upon dissolution. The dissolution of the complexes was associated with color change which was also found to be temperature dependent. The absorption maxima of the complexes **1**–**3** were blue shifted by ca. 30–50 nm on going from H_2O or DMSO to CH_3CN or CH_3NO_2 without showing any specific trend (Table 6). These results could be explained by considering solvolysis of the complexes via the displacement of one of the coordinated ligands [15,33] and the presence of an equilibrium mixture between the dissolved complex and the solvolysis product at a given temperature. Most likely this process is taking place through water displacement in **1** [33], by replacement one of the coordinated oxygens of the nitrito group in **2** to form the mono-coordinated-nitrito species $[Cu(dien)(ONO)(solvent)]^+$ [10] or by displacement of one of the bridged thiocyanato ligands in **3** to form the bis(solvent) singly bridged species [Cu_2(Medpt)$_2$($\mu_{N,S}$-NCS)(solvent)$_2$]$^{3+}$ [15]. However, it is difficult to propose with certainty any nuclearity for the species in solution without measuring the electrical conductivity.

3.4. Magnetic measurements for [Cu_2(Medpt)$_2$($\mu_{N,S}$-NCS)$_2$](ClO_4)$_2$ (3)

The variable-temperature magnetic properties $\chi_M T$ (χ_M is the molar susceptibility for the two Cu^{2+} ions) versus T for **3** is illustrated in Fig. 4. In this complex, the $\chi_M T$ at 300 K is 0.87 cm^3 K mol^{-1}. This value which is similar to that expected for two uncoupled $S = 1/2$ spins ($g >$ 2.0), remains nearly constant upon cooling and decreases sharply in the low-temperature region, attaining a value of 0.55 cm^3 K mol^{-1} at 2 K. No maximum is observed in the plot of χ_M versus T. These features are characteristic

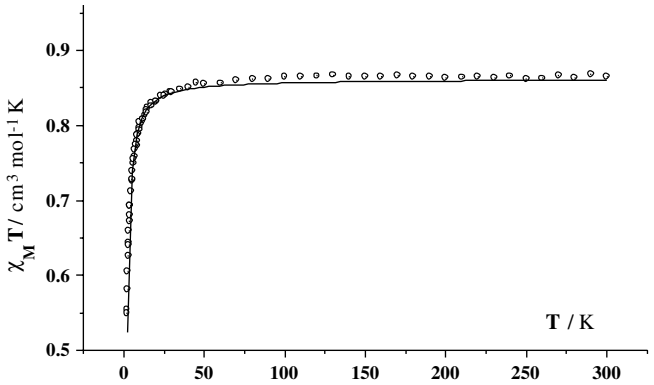

Fig. 4. Plot of $\chi_M T$ vs. T for [Cu_2(Medpt)$_2$(μ-NCS)$_2$](ClO_4)$_2$. The solid line has been generated from the best fit magnetic parameters (see text).

of week antiferromagnetic coupling between copper(II) ions. The experimental magnetic data have been fitted using the Bleaney–Bowers expression derived through the isotropic Hamiltonian $H = -JS_A \cdot S_B$, where J is the exchange coupling parameter and $S_A = S_B = 1/2$. Least-squares fitting of all experimental data leads to the following parameters: $J = -1.8(1)$ cm^{-1}, $g = 2.14(1)$ and $R = 7.5 \times 10^{-5}$ (R is the agreement coefficient and is defined as: $R = \sum[(\chi_M T)_{exp} - (\chi_M T)_{calcd}]^2 / \sum(\chi_M T)^2_{exp}$). The magnetic behavior of the complex under investigation was found to be very similar to that recently reported for the thiocyanato-bridged dimeric Cu(II) complex, [Cu_2(L)$_2$-($\mu_{N,S}$-NCS)$_2$] where L = *N*(3-aminopropyl)-salicylaldimine [34].

In conclusion, the results of X-ray structure determination for the complex [Cu_2(Medpt)$_2$($\mu_{N,S}$-NCS)$_2$](ClO_4)$_2$ are consistent with the dinuclear doubly-bridged thiocyanato groups. The copper centers in the complexes **1**–**3** are penta-coordinated with almost no significant (complexes **1** and **3**) to small distortion (complex **2**) from SP geometry. The same geometry was also confirmed in solution. The IR stretching frequencies $\nu(NO_2^-)$ or $\nu(NCS^-)$ reveal that we cannot always trust this technique to diagnose the bonding coordination mode in the nitrito or thiocyanato complexes.

Acknowledgements

S.S.M. acknowledges the summer research award (2005) and the financial support from the University of Louisiana at Lafayette (G 297), also thanks Dr. R.B. Braun. F.A.M. thanks Prof. Kratky and Prof. Belaj (University of Graz) for the use of the STOE four-circle diffractometer.

Appendix A. Supplementary data

Crystallographic data in CIF format have been deposited with the Cambridge Structural Database (CCDC-278095–CCDC-278097 for **1**–**3**, respectively). Copies of the data can be obtained free of charge, on application to CCDC, 12 Union Road, Cambridge CB2 IEZ, UK (fax: +44 1223 336 033 or e-mail: deposit@ccdc.cam.ac.uk).

Supplementary data associated with this article can be found, in the online version, at doi:10.1016/j.poly.2005.11.008.

References

[1] U. Mukhopadhyay, I. Bernal, S.S. Massoud, F.A. Mautner, Inorg. Chim. Acta 357 (2004) 3673.
[2] S.S. Massoud, F.A. Mautner, M. Abu-Youssef, N.M. Shuaib, Polyhedron 18 (1999) 2061.
[3] P. Gómez-Saiz, J. Garcia-Tojal, A. Media, B. Bonnadieu, L. Lezama, J.L. Pizarro, M.I. Arriortua, T. Rojo, Eur. J. Inorg. Chem. (2003) 518.
[4] (a) S. Youngme, N. Chaichit, N. Koonsaeng, Inorg. Chim. Acta 335 (2002) 36;
(b) S. Youngme, N. Chaichit, C. Pakawatchai, S. Booncoon, Polyhedron 21 (2002) 1279.
[5] R. Gupta, R. Mukherjee, Polyhedron 20 (2001) 2545.
[6] M.A. Hitchman, G.L. Rowbottom, Coord. Chem. Rev. 42 (1982) 55.
[7] (a) C. Diaz, J. Ribas, R. Costa, J. Tercero, M.S. El Fallah, X. Solans, M. Font-Bardía, Eur. J. Inorg. Chem. (2000) 675;
(b) S. Youngme, P. Phuengphai, N. Chaichit, Polyhedron 23 (2004) 1685.
[8] A. Camus, N. Marsich, A.M.M. Lanfredi, F. Uggozoli, C. Massera, Inorg. Chim. Acta 309 (2000) 1.
[9] R.T. Stibrany, J.A. Potenza, H.J. Schugar, Inorg. Chim. Acta 243 (1996) 33.
[10] A. Pajunen, S. Pajunen, Z. Kristallogr.-New Cryst. Struct. 213 (1998) 591.
[11] J.P. Costes, F. Dahan, J. Ruiz, J.P. Laurent, Inorg. Chim. Acta 239 (1995) 53.
[12] M. Nardelli, G. Pelizzi, Inorg. Chim. Acta 38 (1980) 15.
[13] J.-P. Costes, F. Dahan, J.-P. Laurent, M. Drillon, Inorg. Chim. Acta 294 (1999) 8.
[14] A. Gleyzes, A. Meyer, M.a. Hitchman, O. Khan, Inorg. Chem. 21 (1982) 2257.
[15] S.S. Massoud, F.A. Mautner, Inorg. Chim. Acta 358 (2005) 3334.
[16] (a) C. Diaz, J. Ribas, N. Sanz, X. Solans, M. Font-Bardía, Inorg. Chim. Acta 286 (1999) 169;
(b) J. Ribas, C. Diaz, X. Solans, M. Font-Bardía, Inorg. Chim. Acta 231 (1995) 229;
(c) P. Talukedr, A. Datta, S. Mitra, G. Rosair, M.S. El-Fallah, J. Ribas, J. Chem. Soc., Dalton Trans. (2004) 4161.
[17] (a) M. Cannas, G. Carta, G. Marongiu, J. Chem. Soc., Dalton Trans. (1974) 1972;
(b) M. Cannas, G. Carta, G. Marongiu, Gazz. Chim. Ital. 104 (1974) 581.
[18] (a) N.K. Karan, S. Mitra, T. Matsushita, V. Gramlich, G. Rosair, Inorg. Chim. Acta 332 (2002) 87;
(b) P. Gómez-Saiz, J. García-Tojal, F.J. Arnáiz, M.A. Maestro, L. Lezama, T. Rojo, Inorg. Chem. Commun. 6 (2003) 558;
(c) J.A.R. Navarro, M.A. Romero, J.M. Salas, M. Quirós, E.R.T. Tiekink, Inorg. Chem. 36 (1997) 4988;
(d) M.A.S. Goher, L.A. Al-Shatti, F.A. Mautner, Polyhedron 16 (1997) 889.
[19] (a) Z.-H. You, H.-L. Zhu, Z. Anorg. Allg. Chem. 630 (2004) 2754;
(b) A. Lorenz, D. Fenske, Z. Anorg. Allg. Chem. 627 (2001) 2232;
(c) M. Nardelli, J. Chem. Soc., Dalton Trans. (1975) 2357.
[20] C.V. Depree, U. Beckmann, K. Heslop, S. Brooker, J. Chem. Soc., Dalton Trans. (2003) 3071.
[21] N. Walker, D. Stuart, Acta Crystallogr., Sect. A 39 (1983) 158.
[22] SHELXTL 5.03 (PC-Version), Program library for the Solution and Molecular Graphics, Siemens Analytical Instruments Division, Madison, WI, 1995.
[23] (a) A. Walsh, B. Walsh, B. Murphy, B.J. Hathaway, Acta Crystallogr., Sect. B 37 (1981) 1512;
(b) G.B. Carpenter, Acta Crystallogr. 8 (1955) 852.
[24] M.G.B. Drew, D.M.L. Goodgame, M.A. Hitchman, D. Rogers, Proc. Chem. Soc. (1964) 363.
[25] (a) I.M. Procter, F.S. Stephens, J. Chem. Soc. A (1969) 1248;
(b) M.G.B. Drew, D. Rogers, Chem. Commun. (1965) 476.
[26] A. Escuer, M. Font-Bardía, S.S. Massoud, F.A. Mautner, E. Peñalba, X. Solans, R. Vicente, New J. Chem. 28 (2004) 681.
[27] P. Manikandan, R. Muthukumaran, K.R. Justin Thomas, B. Varghese, G.V.R. Chandramouli, P.T. Manoharan, Inorg. Chem. 40 (2001) 2378.
[28] (a) A.W. Addison, T.N. Rao, J. Reedijk, J. van Rijn, G.C. Verschoor, J. Chem. Soc., Dalton Trans. (1984) 1349;
(b) M. Duggan, N. Ray, B. Hathaway, G. Tomlinson, P. Brint, K. Pelin, J. Chem. Soc., Dalton Trans. (1980) 1342.
[29] K. Nakamoto, Infrared and Raman Spectra of Inorganic and Coordination Compounds, 4th ed., Wiley, New York, 1986, and Part B 5th ed., 1997.
[30] S.F. Stephens, J. Chem. Soc. A (1969) 2081.
[31] Y. Song, D.-R. Zhu, K.-L. Zhang, Y. Xu, C.-Y. Duan, X.-Z. You, Polyhedron 19 (2000) 1461.
[32] (a) B.J. Hathaway, in: G. Wilkinson, R.D. Gillard, J.A. McCleverty (Eds.), Comprehensive Coordination Chemistry, vol. 5, Pergamon Press, Oxford, 1987, p. 533;
(b) B.J. Hathaway, J. Chem. Soc., Dalton Trans. (1972) 1196.
[33] (a) C.-H. Kwak, J.-E. Jee, M. Pyo, J. Kim, R. van Eldik, Inorg. Chim. Acta 357 (2004) 2643;
(b) S.S. Massoud, F.A. Mautner, Inorg. Chem. Commun. 7 (2004) 559.
[34] S. Banerjee, M.G.B. Drew, C.-Z. Lu, J. Tercero, C. Diaz, A. Ghosh, Eur. J. Inorg. Chem. (2005) 2376.

Table 1
List of complexes

Complex	R
1 $[Mn_2(bipy)_2(\mu\text{-}O)(\mu\text{-}OOCR)_2(NO_3)(H_2O)](ClO_4)\cdot MeCN$	Ph
2 $[Mn_2(bipy)_2(\mu\text{-}O)(\mu\text{-}OOCR)_2(NO_3)(H_2O)](ClO_4)$	CH_2Cl
3 $[Mn_2(phen)_2(\mu\text{-}O)(\mu\text{-}OOCR)_2(NO_3)(H_2O)](ClO_4)$	CH_2Cl
4 $[Mn_2(bipy)_2(\mu\text{-}O)(\mu\text{-}OOCR)_2(H_2O)_2](ClO_4)_2$	CH_2NH_2
5 $[Mn_2(phen)_2(\mu\text{-}O)(\mu\text{-}OOCR)_2(H_2O)_2](ClO_4)_2$	CH_2NH_2
6 $[Mn_2(bipy)_2(\mu\text{-}O)(\mu\text{-}OOCR)_2(NO_3)(H_2O)](ClO_4)\cdot H_2O$	*p*-ClPh
7 $[Mn_2(phen)_2(\mu\text{-}O)(\mu\text{-}OOCR)_2(NO_3)(H_2O)](ClO_4)\cdot H_2O$	*p*-ClPh

Besides biological relevance, the study of magnetic exchange interactions through extended carboxylate bridging ligands is of major interest in the field of molecular magnetism [5,9]. In this context, sometimes the strong magnetic interactions between paramagnetic manganese centers and the search for the limiting distance for interaction between manganese centers has led magnetochemists to focus on binuclear and polynuclear manganese-complexes bridged by various carboxylate ligands (see Table 1).

2. Experimental

2.1. Materials

All chemicals and solvents were commercially available A.R. grade and were used without further purification.

2.2. Synthesis (*1*–*7*)

All complexes were prepared similarly by mixing and stirring an acetonitrile (10 mL) solution of benzoic or chloroacetic or *p*-chlorobenzoic acid or glycine (1.5 mmol), triethylamine (0.21 mL; 1.5 mmol) and 2,2′-bipyridyl or 1,10-phenanthroline (1.5 mmol) with an acetonitrile solution (10 mL) of $Mn(ClO_4)_2.6\,H_2O$ (0.547 g; 1.5 mmol). After a few minutes, an acetonitrile solution (25 mL) of ceric ammonium nitrate (1.1 g; 2.0 mmol) was added dropwise and the solution was stirred for 2 h at room temperature. The initial yellow color of the solution rapidly changed to brown. Some solids appeared during stirring which were separated by filtration and discarded. Solid $NaClO_4\cdot H_2O$ (0.56 g; 4.0 mmol) was added to the filtrate and the solution stirred briefly. The product separated as a black crystalline substance during slow evaporation of the solvent at room temperature. The solid was collected by filtration and washed with 1:1 ethanol–diethyl ether. Attempts to recrystallize this substance led only to decomposition upon dissolving in any solvent. Yields range from 70% to 80%.

Caution! Perchlorate salts are potentially explosive and should be used in small quantities with much care.

2.3. Physical measurements

Elemental analyses were performed using a Perkin–Elmer 2400II elemental analyzer. Electronic spectra were obtained using a JASCO 7850 spectrophotometer. For electrochemical and spectral measurements HPLC grade solvents were used. IR spectra were recorded on a JASCO FT/IR-460 spectrometer with samples prepared as KBr pellets. Electrochemical experiments were carried out using 'Echem' software supplied by PARC to control an EG&G PARC VersaStat II potentiostat with a three-electrode configuration consisting of a PARC glassy carbon working electrode, a Pt wire auxiliary electrode and a Ag/AgCl reference electrode. The supporting electrolyte was 0.1 mol dm^{-3} $[Et_4N][ClO_4]$ in acetonitrile or dimethylformamide solution. Data were collected under an atmosphere of dry nitrogen at room temperature. All electrochemical potentials are calibrated against a ferrocene/ferrocenium couple of 0.44 V under the same experimental conditions at the same temperature. The magnetic susceptibilities of complexes **1** and **2** were measured in the temperature range 2–300 K with a Quantum Design MPMS5S SQUID Magnetometer at a field strength of 1000 Oe. Diamagnetic corrections were estimated from Pascal Tables.

2.4. Crystallographic data collection and refinements for complex *2*

A black prismatic single crystal of $[Mn_2(bipy)_2(\mu\text{-}O)(\mu\text{-}OOCCH_2Cl)_2(NO_3)(H_2O)]$ (ClO_4) **2**, obtained by slow evaporation of a CH_3CN solution was used for the structure determination. The X-ray data were collected using a Bruker P4/CCD system with graphite monochromated Mo Kα radiation ($\lambda = 0.71073$ Å) and a sealed tube generator at −80 °C and are summarized in Table 2. A total of 21 385 reflections were measured of which 6193

Table 2
Summary of the X-ray crystal data for complex **2**

Empirical formula	$Mn_2C_{24}H_{22}N_5O_{13}Cl_3$
Formula weight	804.70
Crystal color, habit	green, prism
Crystal dimensions	$0.63\times0.14\times0.07$
Crystal system	monoclinic
a (Å)	10.6362(5)
b (Å)	15.3610(7)
c (Å)	19.1938(9)
α (°)	90.00
β (°)	105.1750(8)
γ (°)	90.00
V (Å^3)	3026.6(2)
Space group	$P2_1/n$ (#14)
Z value	4
μ(Mo Kα) (mm^{-1})	0.117
T_{max}, T_{min}	0.922, 0.525
F_{000}	1624.00
Index ranges	$-13\leqslant h\leqslant 13$, $-19\leqslant k\leqslant 19$, $-23\leqslant l\leqslant 23$
Data/restraints/parameters	6193/0/490
R_1; wR_2	0.033; 0.087
Maximum and minimum peak in difference map (e Å^{-3})	0.59; −0.41
Goodness-of-fit on F^2	1.03

$R_1 = \sum||F_o| - |F_c||/\sum|F_o|$, $wR_2 = [\sum(w(F_o^2 - F_c^2)^2)/\sum w(F_o^2)^2]^{1/2}$.
$w = 1/[\sigma^2(F_o^2) + (0.0449P)^2 + 1.7963P]$, $P = (\mathrm{Max}(F_o^2, 0) + 2F_c^2)/3$.

[$R_{int} = 0.032$] were independent. The structure was solved by direct methods [6] and expanded using Fourier techniques [7]. The non-hydrogen atoms were refined anisotropically. Hydrogen atoms were included in calculated positions but not refined. The structure was solved using SHELXL-97 [8] and was refined by full-matrix least-squares methods on F^2. The weighting scheme employed was $w = 1/\sigma^2(F_o^2) + (0.0449P)^2 + 1.7963P]$, $P = (\mathrm{Max}(F_o^2, 0) + 2F_c^2)/3$. The refinement converged with the residuals summarized in Table 2. Selected bond distances and angles are given in Table 4.

3. Results and discussion

3.1. Synthesis

The synthetic route involved in the formation of the binuclear complexes (**1**–**7**) is given in the Scheme 1. All the complexes have been isolated in good yield and their micro-analytical data (Table 3) confirm the composition given. The synthetic route used to synthesize the binuclear manganese(III) complexes involves direct oxidation of Mn(II) by ceric ammonium nitrate in the presence of bipy or phen and different carboxylate anions in the ratio of (bipy/phen):Mn(II):Ce(IV) = 1:1:1. Other research groups [9] have synthesized binuclear or polynuclear manganese complexes with the metal in various oxidation states using $KMnO_4$ as both oxidant as well as source of manganese ion. We, however, have synthesized all the complexes by oxidation of Mn(II) with ceric ammonium nitrate. The molar conductivities Λ_M for all the complexes except **4** and **5** are 120–160 Ω^{-1} cm^3 mol^{-1} [10] in acetonitrile and 65 and 90 Ω^{-1} cm^3 mol^{-1} [10] in dimethylformamide are consistent with the behavior of 1:1 electrolytes. Molar conductivities Λ_M for **4** and **5** are consistent with 1:2 electrolytes.

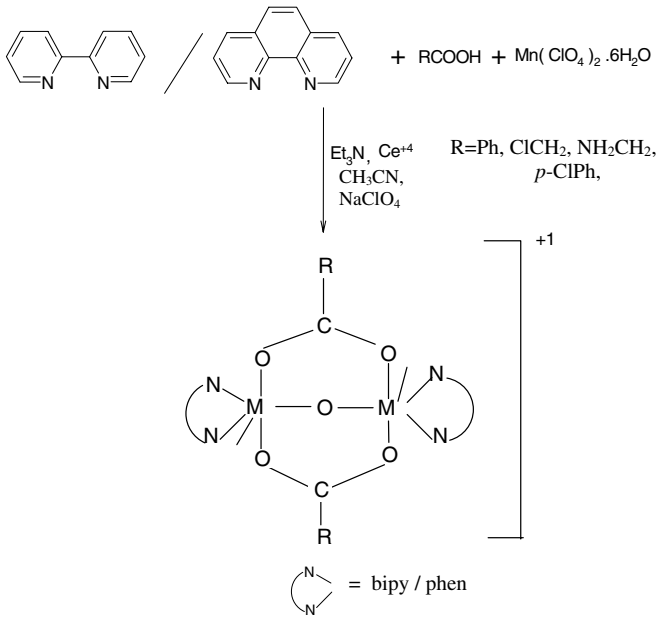

Scheme 1.

Table 3
Analytical data for complexes

Complex	Calc. (Found) (%)		
	C	H	N
1	47.97(48.01)	3.44(3.46)	9.32(9.35)
2	35.78(35.76)	2.73(2.75)	8.69(8.69)
3	39.41(39.42)	2.58(2.60)	8.21(8.19)
4	35.07(35.10)	3.41(3.43)	10.23(10.21)
5	38.66(38.68)	3.22(3.19)	9.66(9.65)
6	43.10(43.15)	2.95(2.98)	7.39(7.41)
7	45.85(45.82)	2.81(2.85)	7.03(7.01)

Table 4
Selected bond distances (Å) and bond angles (°) for **2**

Bond distances		*Bond angles*	
Mn(1)–O(1)	2.2012(16)	O(2)–Mn(2)–O(5)	99.85(7)
Mn(1)–O(3)	1.9580(16)	O(2)–Mn(2)–N(4)	90.83(7)
Mn(1)–O(5)	1.7875(14)	O(3)–Mn(1)–O(1)	89.55(7)
Mn(1)–O(9)	2.2090 (2)	O(3)–Mn(1)–O(5)	99.29(7)
Mn(1)–N(1)	2.0556(18)	O(3)–Mn(1)–N(2)	90.52(7)
Mn(1)–N(2)	2.0664(17)	O(4)–Mn(2)–O(2)	86.06(7)
Mn(2)–O(2)	1.9682(16)	O(5)–Mn(1)–O(1)	91.31(7)
Mn(2)–O(4)	2.1907(16)	O(5)–Mn(1)–N(1)	91.86(7)
Mn(2)–O(5)	1.7789(15)	O(5)–Mn(2)–N(3)	90.54(7)
Mn(2)–O(6)	2.2129(17)	O(6)–Mn(2)–O(5)	89.78(7)
Mn(2)–N(3)	2.0553(19)	N(1)–Mn(1)–O(9)	85.78(7)
Mn(2)–N(4)	2.0597(18)	N(2)–Mn(1)–O(1)	86.72(7)
Mn(1)–Mn(2)	3.1555(4)	N(2)–Mn(1)–N(1)	78.50(7)
		N(3)–Mn(2)–O(6)	89.77(7)
		N(4)–Mn(2)–N(3)	78.79(7)
		N(4)–Mn(2)–O(4)	87.85(7)
		Mn(1)–O(5)–Mn(2)	124.45(9)

3.2. Description of the crystal structure of 2

The ORTEP diagram and atom numbering scheme of the unsymmetrical binuclear manganese(III) complex **2** is

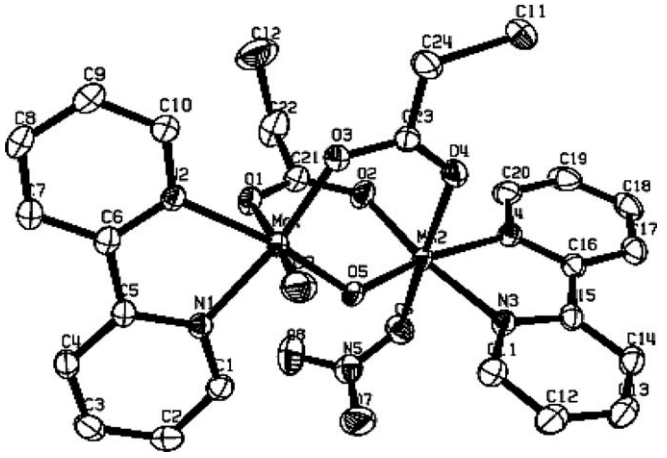

Fig. 1. ORTEP diagram for complex **2** [$Mn_2(bipy)_2(\mu\text{-}O)(\mu\text{-}OOCCH_2Cl)_2(NO_3)(H_2O)][ClO_4$] showing the atom labeling scheme and 50% probability ellipsoids for the non-hydrogen atoms. Hydrogen atoms and perchlorate ions have been excluded for clarity.

depicted in Fig. 1. The figure shows distorted manganese(III) atoms with the Mn–O_{oxo} bonds in the μ-*O* bridge being very little shorter (average 1.78 Å) than those of the μ-acetato bridges (average1.80 Å) of $[L_2Mn_2^{III}(\mu\text{-}O)(\mu\text{-}CH_3COO)_2](ClO_4)_2$ and $[L'_2Mn_2^{III}(\mu\text{-}O)(\mu\text{-}CH_3COO)_2](ClO_4)_2 \cdot H_2O$, where L and L′ are 1,4,7-triazacyclononane and *N*,*N*′,*N*″-trimethyl-1,4,7-triazacyclononane [12a]. On the other hand, that bond distance is much shorter than other μ-acetato bridges (average 2.05 Å) [14c]. The molecular cation consists of two hexacoordinated manganese(III) atoms bridged by a μ-oxide ion and two μ-chlorocarboxylate units. Each manganese atom is additionally ligated to the two N-atoms coming from a chelating bipyridyl. The sixth coordination position is occupied by NO_3^- ion in one case and by a water molecule in another. The manganese ions show a Jahn-Teller distortion as expected for high-spin d^4 manganese(III) ions in near octahedral geometry.

The Mn–O distances to each carboxylate oxygen are different. There are two types of Mn–O (carboxylate) distances, 1.9580/1.9682 Å and 2.2012/2.1907 Å, respectively, which was also found for other Mn_2(III) complexes such as $[Mn_2O(mpdp)(bipy)_2(H_2O)(MeCN)](ClO_4)_2$ (mpdp = *m*-phenylenedipropionate) [11]. The first two distances correspond to the bonds to oxygen atoms *trans* to the bipy ligand and the second pair of distances correspond to the bonds *trans* to the water molecule and nitrate ion, respectively. The average Mn–N (bipy) bond length (2.059 Å) is also very close to the average Mn–N (bipy) (2.069 Å) distance in the example above. The longer bonds, due to Jahn-Teller distortion along O_1–Mn_1–O_9 and O_4–Mn_2–O_6 (average 2.21 Å) are at the pseudo-axial positions and the shorter bonds are in pseudo-equatorial positions. The intramolecular Mn–Mn distance in the binuclear cation (3.155 Å) agrees well with those in the range 3.15–3.16 Å for known doubly carboxylato-bridged manganese(III) complexes [12,13]. The Mn–Mn distance in **2** is intermediate in length being longer than that of some similar types of compounds [14] and shorter than that in some other related compounds [15]. The bridging angle Mn–O–Mn is 124.45(9)° which is very close to those in some similar di-μ-carboxylato mono-μ-oxo Mn_2(III) complexes [12,13] and a little larger than that in the similar complex $[L_2Mn_4(III)(\mu\text{-}O)_2(\mu\text{-}CH_3COO)_4](ClO_4)_4 \cdot 3MeNO_2$ (L = α,α′-bis(bis(2-pyridylmethyl)-amino)-*m*-xylene) (118.5°) [15c]. A particularly noteworthy aspect of complex **2** is that the NO_3^- anion binds only to one manganese(III) atom while there is H_2O in the corresponding site on the other manganese atom. Comparative data for Mn–O–Mn angles and Mn–Mn distances are given in the Table 5 for similar types of compounds. The Mn(2) atom is 0.0178 Å below the basal plane defined by the four atoms O(2), O(5), N(3) and N(4) however, the Mn(1) atom is 0.0873 Å below the plane of O(1), O(5), O(9) and N(2). The dihedral angle between these two planes is 35.88°. The complex forms an infinite arrangement (Fig. 2) through two types of weak interaction. The O(6) and O(8) of the coordinated nitrate ion show close contact to H(22) of the coordinated H_2O. The other contact involves O(13) of ClO_4^- ion and H(21) of H_2O (Table 6) [16].

3.3. Infrared spectrum

All the complexes show two strong bands between 1630 and 1490 cm^{-1} in their infrared spectra attributable to carboxylate ν_a(CO) and ν_s(CO) vibrations, respectively. The difference between the asymmetric and symmetric stretching modes of the carboxylates of ca. 100 cm^{-1} can be attributed to the presence of bidentate bridging carboxylate ligands while the bands at ca. 615 and 620 cm^{-1} are due to δ(OCO) [17]. Two characteristic bands were observed at ca.

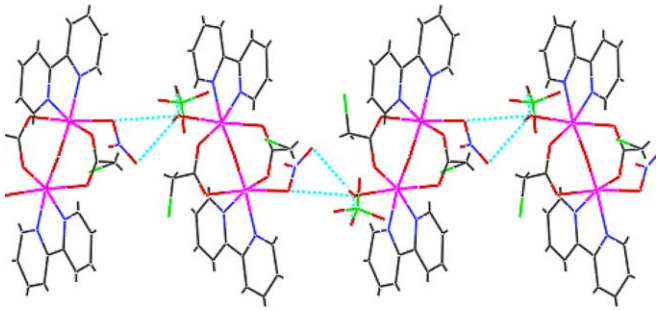

Fig. 2. Packing diagram for the complex $[Mn_2(bipy)_2(\mu\text{-}O)(\mu\text{-}OOCCH_2Cl)_2(NO_3)(H_2O)][ClO_4)$.

Table 5
Important bond distances (Å) angles (°) and magnetic parameters of some $[Mn_2^{III}(\mu\text{-}O)(\mu\text{-}O_2CR)_2]^{2+}$ complexes

Complex	*d*(Mn...Mn) (Å)	(∠Mn...O...Mn) (°)	*J* (cm^{-1})	Reference
$[Mn_2O(OAc)_2(Me_3TACN)_2]^{2+}$	3.153	120.9	9	[15a]
$[Mn_2O(OAc)_2\{HB(pz)_3\}_2]$	3.159	125.1	<−0.2	[14b]
$[Mn_2O(O_2CPh)_2(bipy)_2(N_3)_2]$	3.153	122.0	8.8	[13a]
$[Mn_2O(O_2CPh)_2(bipy)_2(OH)(NO_3)]$	3.141	124.1	1	[13b]
$[Mn_2O(OAc)_2(TMIP)_2]^{2+}$	3.164	124.4	−0.2 to −0.7	[13c]
$\{[Mn_2O(OAc)_2(bbpm)]^{2+}\}_2$	3.261	118.5	−0.4	[15c]
$[Mn_2O(mpdp)(bipy)_2(MeCN)(H_2O)]^{2+}$	3.139	122.9	−0.6	[11]
$[Mn_2O(OAC)_2(bipy)_2(H_2O)_2]^{2+}$	3.152	122.7	−3.4	[13a]
$[Mn_2O(OAC)_2(bipy)_2(Cl)_2]$	3.153	124.3	−4.1	[13a]
$[Mn_2(bipy)_2(\mu\text{-}O)(\mu\text{-}OOCPh)_2(NO_3)(H_2O)][ClO_4) \cdot MeCN$			0.43	[a]
$[Mn_2(bipy)_2(\mu\text{-}O)(\mu\text{-}OOCCH_2Cl)_2(NO_3)(H_2O)][ClO_4)$	3.155	124.4	−0.15	[a]

[a] This work.

Table 6
Intermolecular contacts of complex **2**

D–H ⋯ A	H ⋯ A (Å)	D ⋯ A (Å)	D–H ⋯ A (°)
O(9)–H(22)..O(6)[a]	2.44(3)	2.971(3)	134(3)
O(9)–H(22)..O(8)[b]	2.24(3)	2.935(3)	168(3)
O(9)–H(21)..O(13)[b]	2.12(3)	2.795(4)	159(3)

[a,b] Symmetry equivalent: [a]$1/2 - x, -1/2 + y, 1/2 - z$, [b]$1 - x, 1 - y, -z$.

1440 and 1305 cm^{-1} for all the complexes except **4** and **5**. These are attributable by comparison to the IR data of similar compounds [18] to unidentate, coordinated nitrate ion. In addition, the broad bands of uncoordinated perchlorates are noted near 1100 cm^{-1}. A broad peak centered at ca. 3450 cm^{-1} is observed for most of the complexes and is consistent with the presence of water. A strong band appearing at ca. 700 cm^{-1} is assigned to the Mn–O–Mn vibration by comparison to the spectra of some related compounds [18].

3.4. Electronic spectrum

The electronic spectra at 25 °C of all the μ-oxo and μ-carboxylato dimanganese(III) complexes (**1**–**7**) in acetonitrile except **2** have mostly similar features consisting of a band at ~625 nm, two bands of moderate intensity at ca. 510 and 470 nm and two more intense bands at 275–340 nm (Table 7). Similar types of electronic spectra have also been found for the dimanganese(III) complex $[Mn_2O(O_2CCH_3)_2(TACN)_2]^{+2}$ which displays at least four transitions at 495 nm ($\varepsilon = 324\ M^{-1}\ cm^{-1}$), 520 nm (250), 665 nm (95) and 910 nm (40) [19]. The low energy bands at ~625 nm could be assigned to d-d transitions by comparison with the spectrum of the related complex $[Mn_2O(O_2CCH_3)_2(bipy)_2]^{+2}$ [9d]. It is interesting to note that the two high intensity bands at ~510 and ~470 nm are also observed in spectra of complexes consisting of the $[Fe_2^{III}(\mu\text{-}O)(\mu\text{-}O_2CMe)_2]^{2+}$ core [20e] suggesting the presence of a similar core structure $[Mn_2^{III}(\mu\text{-}O)\ (\mu\text{-}O_2CR)_2]^{2+}$ in our complexes [20]. This is supported by the presence of bidentate bridging carboxylate bands at ~1630 and 1490 cm^{-1} and by a band at 730 cm^{-1} in the IR spectrum attributable to Mn–O–Mn vibration. The intense bands at ~280 and ~350 nm correspond to intra ligand transitions.

Table 7
Electronic spectral data for acetonitrile solutions

Complex	UV–vis [λ_{max} (nm)/ε ($M^{-1}\ cm^{-1}$)]
1	625(410), 510(615), 475(1020), 350(2045), 280(24555)
2[a]	630(295), 510(485), 460(625), 325(2425), 280(10000)
3	630(255), 510(410), 475(745), 360(1930), 280(12675)
4	625(255), 510(315), 460(570), 325(1580), 285(18225)
5	625(220), 510(465), 460(975), 360(2110), 280(11875)
6	630(315), 510(685), 460(1070), 325(3540), 285(12855)
7	625(265), 510(515), 480(790), 325(5645), 280(20645)

[a] In dimethylformamide solution.

3.5. Electrochemistry

The electron transfer properties of the mixed ligand complexes (**1**–**7**) were studied by the cyclic voltammetry and the differential pulse voltammetry (DPV) at a glassy carbon electrode. The electrochemical data are given in Table 8. All experiments were carried out at room temperature in acetonitrile or dimethylformamide solution using 0.1 mol dm^{-3} $[Et_4N][ClO_4]$ as a supporting electrolyte. The ligands, 2,2′-bipyridine(bipy) and 1,10-phenanthroline (phen), are electrochemically inactive from +1.5 to ~−1.4 V, but below −1.4 V all the complexes undergo two quasi-reversible reduction processes around −1.5 to −1.9 V versus Ag–AgCl at a glassy carbon electrode which are due to the reduction of the two ligands. On the other hand, at a Pt electrode, the reductive waves have been found to occur irreversibly. The reduction of bipy and phen in all the complexes can be represented according to Eqs. (1) and (2).

$$[Mn_2O(OOCR)_2(NO_3)(H_2O)(bipy)_2]^{1+} + e \rightleftharpoons [Mn_2O(OOCR)_2(NO_3)(H_2O)(bipy)(bipy^-)] \quad (1)$$

$$[Mn_2O(OOCR)_2(NO_3)(H_2O)(bipy)(bipy^-)] + e \rightleftharpoons [Mn_2O(OOCR)_2(NO_3)(H_2O)(bipy^-)_2]^- \quad (2)$$

Since each bipy or phen can accept two electrons in its lowest unoccupied molecular orbitals, one should expect to observe four such reduction steps in the series [21]. The observation of only two couples up to −2.0 V was the result

Table 8
Electrochemical data for acetonitrile solution

Complex	$E_{1/2}(Mn^{III}Mn^{IV}/Mn_2^{IV})$ [ΔE] (V) (all DPV)	$E_{1/2}(Mn_2^{III}/Mn^{III}Mn^{IV})$ [ΔE] (V)	$E_{1/2}(Mn_2^{III}/Mn^{III}Mn^{II})$ [ΔE] (V) (all irr)	$E_{1/2}(Mn^{III}Mn^{II}/Mn_2^{II})$ [ΔE] (V) (all DPV)
1[a]	1.09	0.43(0.09)[b]	−0.95	−1.29
2[a]		0.50(0.24)[b]	−0.81	
3	1.35	0.51(DPV)	−0.94	−1.36
4	1.01	0.38(DPV)	−0.81	−1.36
5	1.36	0.44(DPV)	−0.94	−1.40
6	1.07	0.44(0.07)[b]	−0.80	−1.34
7	1.25	0.45[c]	−0.87	−1.36

[*] $E_{1/2} = (E_{pa} + E_{pc})/2$ V, $\Delta E_p = E_{pa} - E_{pc}$ V, where E_{pa} and E_{pc} are anodic and cathodic peak potentials, respectively.
[a] In dimethylformamide solution.
[b] Quasi-reversible.
[c] Irreversible.

of limitations imposed by the cut-off potential of the supporting electrolyte in acetonitrile. The redox properties of all the complexes in a potential range +1.5 to −1.4 V consist of four single electron waves. The four different steps are probably due to two metal-centered one electron oxidative steps, $Mn_2^{III} \rightarrow Mn^{IV}Mn^{III} \rightarrow Mn_2^{IV}$, and two one electron reductive steps, $Mn_2^{III} \rightarrow Mn^{II}Mn^{III} \rightarrow Mn_2^{II}$ according to the Eqs. (3) and (4). These redox reactions are very similar to those reported for other (μ-oxo)(μ-carboxylato)Mn_2(III/III) complexes [12c,22].

$$[Mn_2^{III}O\ldots]^{+} \overset{E_1}{\underset{+e}{\overset{-e}{\rightleftharpoons}}} [Mn^{IV}Mn^{III}O\ldots]^{2+} \overset{E_2}{\underset{+e}{\overset{-e}{\rightleftharpoons}}} [Mn_2^{IV}O\ldots]^{3+} \tag{3}$$

$$[Mn_2^{III}O\ldots]^{+} \overset{E_3}{\underset{-e}{\overset{+e}{\rightleftharpoons}}} [Mn^{II}Mn^{III}O\ldots]^{0} \overset{E_4}{\underset{-e}{\overset{+e}{\rightleftharpoons}}} [Mn^{II}Mn^{II}O\ldots]^{-} \tag{4}$$

The single electron transfers proposed for the above couples have been confirmed by comparison of current height with the redox couple of a known complex $[Fe(bipy)_3]^{2+}$ under similar conditions. The cyclic voltammogram of **1** (Fig. 3) shows a quasi-reversible oxidation at $E^1_{1/2} = 0.43$ V ($\Delta E =$ 90 mV), probably due to $Mn_2^{III} \leftrightarrow Mn^{III}Mn^{IV}$. In addition, complex **1** shows a further three redox waves through DPV at +1.09, −0.95 and −1.29 V probably due to oxidation of $Mn^{IV}Mn^{III} \rightarrow Mn_2^{IV}$ and reductions of $Mn_2^{III} \rightarrow Mn^{II}Mn^{III} \rightarrow Mn_2^{II}$, respectively. By comparing the potential data of **6** ($E^2_{pa} = +1.07$ V, $E^1_{pa} = +0.44$ V, $E^3_{pc} = -0.80$ V and $E^4_{pc} = -1.34$ V) containing *p*-chloro benzoate as bridging ligand with the data for complex **1** having benzoate as bridging ligand, the electron-withdrawing group Cl can be seen to have little influence on oxidation potentials. However, there is a slightly more noticeable effect on reduction potentials by the Cl-group. Complex **7** involving *p*-chloro benzoate and phen as ligands also show four steps one electron transfer reactions. The voltammetric behaviour of complex **2** shows only two-electron transfer steps at potentials between +0.504 and −0.81 V that are assigned tentatively according to Eq. (5) by comparison to similar compounds mentioned in the literature [12a]. Surprisingly, the phen derivative of **2**, i.e., **3** exhibits four electron transfer processes according to Eqs. (3) and (4).

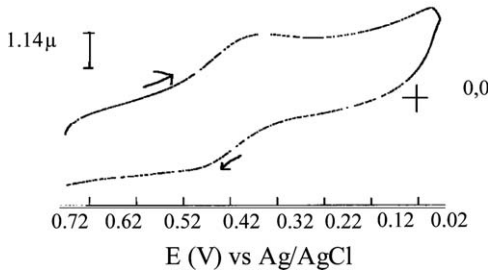

Fig. 3. Cyclic voltammogram of **1** in acetonitrile with 0.1 mol dm^{-1} $[Et_4N][ClO_4]$ as supporting electrolyte (working electrode; glassy-carbon; reference electrode; Ag/AgCl; scan rate 100 mV s^{-1}). (Only $Mn_2^{III}/Mn^{III}Mn^{IV}$ oxidation is shown.)

$$[Mn^{IV}Mn^{III}]^{+1} \overset{+e}{\underset{-e}{\rightleftharpoons}} Mn_2^{III} \overset{+e}{\underset{-e}{\rightleftharpoons}} [Mn^{II}Mn^{III}]^{-1} \tag{5}$$

Complexes **4** and **5**, the glycine-bridged complexes of bipy and phen, also show four electron transfer processes around the same potentials.

3.6. Magnetic properties

The room temperature magnetic moments of all the complexes lie within the range 2.1–2.8 BM and are lower than expected for uncoupled $S = 2$ ions. This suggests antiferromagnetic coupling [23] in the dimers as confirmed by the variable temperature susceptibility study. The results are similar to those reported for $[L_2Mn_4(III)(\mu\text{-}O)_2(\mu\text{-}CH_3COO)_4](ClO_4)_4.3MeNO_2$ (L = α,α′-bis(bis(2-pyridylmethyl)-amino)-*m*-xylene) [15c]. The cryomagnetic behavior of complex **1** is shown in Fig. 4 where the $\chi_M T$ value of 4.65 cm^3 mol^{-1} K at 300 K for this complex can be seen to be much lower than the calculated value of 5.99 cm^3 mol^{-1} K for two uncoupled spins ($S_1 = 2$, $S_2 = 2$) with $g = 2$. This value indicates that the local spin state of both the manganese centers is a quintet. With a decrease of temperature, $\chi_M T$ increases slowly to 4.95 cm^3 mol^{-1} K at 18 K and then decreases rapidly to 3.72 cm^3 mol^{-1} K at 2 K. The slight increase in $\chi_M T$ as the temperature decreases could arise from weak ferromagnetic interactions between the metal centers in **1**. The rapid decrease of $\chi_M T$ at low temperatures may be due to antiferromagnetic interdimer interactions. The susceptibility data were simulated with Eq. (6), which considers both the intramolecular and intermolecular interactions. Least-squares fittings of the susceptibility data with Eq. (6) converge with $J = 0.43$ cm^{-1}, $g = 1.75$, $zJ' = -0.12$ cm^{-1}, and $R = 2.15 \times 10^{-2}$

$$\chi_M = \frac{\chi_{M^D}}{1 - 2zJ'\chi_{1-D}/N\beta^2 g^2}, \tag{6}$$

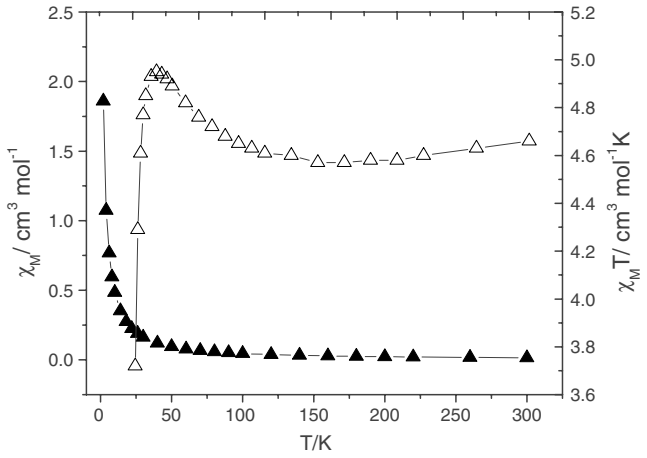

Fig. 4. Molar paramagnetic susceptibility (χ_M) and product of molar paramagnetic susceptibility and temperature ($\chi_M T$) vs. temperature curves for **1**.

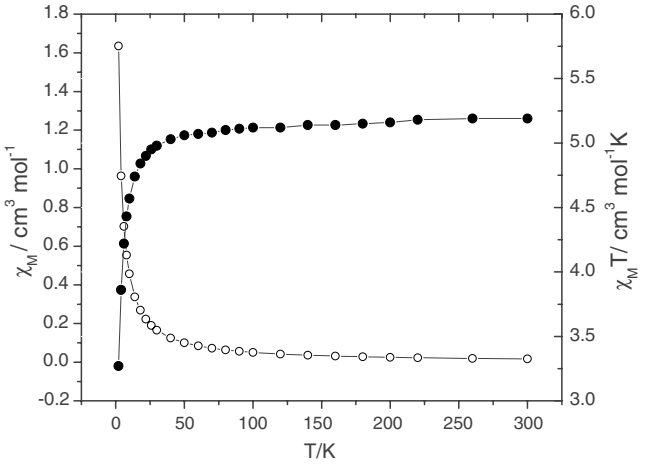

Fig. 5. Molar paramagnetic susceptibility (χ_M) and product of molar paramagnetic susceptibility and temperature ($\chi_M T$) vs. temperature curves for **2**.

where

$$\chi_{M^D} = \frac{N\beta^2 g^2}{kT}\frac{A}{B}$$

with $A = 2\exp(2x) + 10\exp(6x) + 28\exp(12x) + 60\exp(20x)$; $B = 1 + 3\exp(2x) + 5\exp(6x) + 7\exp(12x) + 9\exp(20x)$ and $x = 2J/kT$.

The variable-temperature (2–300 K) magnetic behavior of **2** is shown in Fig. 5, in χ_M versus T and $\chi_M T$ versus T plots. The $\chi_M T$ value of 5.19 $cm^3\ mol^{-1}$ K at 300 K for this complex is lower than the calculated value of 5.99 $cm^3\ mol^{-1}$ K for two uncoupled spins ($S_1 = 2$, $S_2 = 2$) with $g = 2$. With a decrease of temperatures, the $\chi_M T$ value decreases very slowly to 4.92 $cm^3\ mol^{-1}$ K at 22 K. On further lowering of temperatures, $\chi_M T$ decreases sharply to 3.26 $cm^3\ mol^{-1}$ K at 2 K. The trend of magnetic behavior indicates the existence of a weak antiferromagnetic interaction between the metal centers in **2**.

The susceptibility data were simulated with the theoretical expression [Eq. (7)] derived from the Heisenberg–Dirac–Van Vleck Hamiltonian ($\mathbf{H} = -2J\mathbf{S}_1 \cdot \mathbf{S}_2$) [23]. The global minimization takes place with $J = -0.15\ cm^{-1}$, $g = 1.85$; the agreement factor R defined as $[\sum\{(\chi_M T)_{obs} - (\chi_M T)_{calc}\}^2 / \sum(\chi_M T)^2_{obs}]$ being 1.68×10^{-2}

$$\chi_M = \frac{N\beta^2 g^2}{kT}\frac{A}{B}, \qquad (7)$$

where $A = 2\exp(2x) + 10\exp(6x) + 28\exp(12x) + 60\exp(20x)$; $B = 1 + 3\exp(2x) + 5\exp(6x) + 7\exp(12x) + 9\exp(20x)$ and $x = 2J/kT$.

So, for complexes **1** and **2**, the intradimer interactions are weak; ferromagnetic for **1** and antiferromagnetic for **2**. Similar trends in magnetic behavior for other complexes of $[Mn^{III}_2O(O_2CR_2)_2]^{2+}$ cores are reported [13b,24]. Christou et al. [11] have discussed the reason for variation between antiferromagnetic and ferromagnetic behavior as a result of changing the substituents in a series of $[Mn^{III}_2O(OAc)_2(bipy)_2X_2]$ [13a]. They observed a ferromagnetic interaction for X = azide but for chloride or water, the interaction is antiferromagnetic. They concluded that the substituent X influences the energy of the $d_{x^2-y^2}$ orbital. For a strong field ligand, the energy separation is high between the $d_{x^2-y^2}$ orbital and the orbitals of the carboxylate bridge and therefore, ferromagnetic interaction should be preferred. Experimentally, they found $J = +8.8\ cm^{-1}$ for N_3^- ion and $J = -4.1$ and $-3.4\ cm^{-1}$ for Cl^- and H_2O, respectively. In our case, we have observed $J = +0.43\ cm^{-1}$ for complex **1** and $J = -0.15\ cm^{-1}$ for complex **2** where both the terminal groups are H_2O and NO_3^-. The magneto-structural correlations here are compared with those of other Mn_2(III) systems in Table 5.

Acknowledgements

This study is supported by the UGC, CSIR and AICTE, India. We express our gratitude to Dr. Bob McDonald of the Department of Chemistry, University of Alberta, Canada, David O. Miller of the Department of Chemistry, Memorial University of Newfoundland, Canada for their assistance with the X-ray crystal structure and to Dr. Sasankashekhar Mohanta, Department of Chemistry, University of Calcutta for assistance with the magnetic measurements. We are also thankful to the DST-FIST program for providing FTIR and UV–vis Spectrophotometers.

Appendix A. Supplementary data

Crystallographic data for the structure have been deposited with the Cambridge Crystallographic Data, CCDC no. 277841. A copy of the data can be obtained free of charge on application to the CCDC, 12 Union Road, Cambridge CB2 1EZ, UK (fax: +44 1223 336033 or e-mail: deposit@ccdc.cam.ac.uk) or from the authors upon request. Supplementary data associated with this article can be found, in the online version, at doi:10.1016/j.poly.2005.11.022.

References

[1] N.A. Law, M.T. Caudle, V.L. Pecoraro, in: A.G. Sykes (Ed.), Advances in Inorganic Chemistry, vol. 46, Academic Press, London, 1998, p. 305.
[2] M.C.F. Yocum, V.L. Pecoraro, Curr. Opin. Chem. Biol. 3 (1999) 182.
[3] R. Manchanda, G.W. Brudvig, R.H. Crabtree, Coord. Chem. Rev. 1 (1995) 144.
[4] (a) M.J. Baldwin, V.L. Pecoraro, J. Am. Chem. Soc. 118 (1996) 11325;
(b) J.M. Carroll, J.R. Norton, J. Am. Chem. Soc. 114 (1992) 8744;
(c) G.C. Dismukes, Chem. Rev. 96 (1996) 2909;
(d) A.J. Wu, J.E.P. Hahn, V.L. Pecoraro, Chem. Rev. 104 (2004) 903.
[5] H. Miyasaka, R. Clerac, T. Ishii, H.-C. Chang, S. Kitagawa, M. Yamashita, J. Chem. Soc., Dalton Trans. (2002) 1528.
[6] SIR92: A. Altomore, M. Cascarano, C. Giacovazzo, A. Guagliardi, J. Appl. Crystallogr. 26 (1994) 343.
[7] P.T. Berskens, G. Admiraal, G. Beurskens, W.P. Bosman, R. de Gelder, R. Israel, J.M.M. Smits, The DIRDIF 94 program system, Technical Report of the Crystallography Laboratory, University of Nijmegen, The Netherlands, 1994.

[8] G.M. Sheldrick, SHELX97, 1997.
[9] (a) R. Manchanda, G.W. Brudvig, S. Gala, R.H. Crabtree, Inorg. Chem. 33 (1994) 5157;
(b) B. Albela, M. Corbella, J. Ribas, I. Castro, J. Sletten, H.S. Evans, Inorg. Chem. 37 (1998) 788;
(c) B.C. Dave, R.S. Czernuszewicz, Inorg. Chim. Acta 281 (1998) 25;
(d) S. Menage, J.J. Girerd, A. Gleizs, J. Chem. Soc., Chem Commun. (1988) 431.
[10] W.J. Geary, Coord. Chem. Rev. 7 (1971) 81.
[11] C. Canada-Vilalta, W.E. Streib, J.C. Huffman, T.A. O'Brien, E.R. Davidson, G. Christou, Inorg. Chem. 43 (2004) 101.
[12] (a) K. Wieghardt, U. Bossek, D. Ventur, J. Weiss, J. Chem. Soc., Chem Commun. (1985) 347;
(b) K. Wieghardt, U. Bossek, B. Nuber, J. Weiss, J. Bonvoisin, M. Corbella, S.E. Vitols, J.-J. Girerd, J. Am. Chem. Soc. 110 (1988) 7398;
(c) J.E. Sheats, R.S. Czernuszewicz, G.C. Dismukes, A.L. Rheingold, V. Petrouleas, J. Stubbe, W.H. Armstrong, R.H. Beer, S.J. Lippard, J. Am. Chem. Soc. 109 (1987) 1435.
[13] (a) J.B. Vincent, H.L. Tsai, A.G. Blackman, S. Wang, P.D.W. Boyd, K. Folting, J.C. Huffman, E.B. Lobkovsky, D.N. Hendrickson, G. Christou, J. Am. Chem. Soc. 115 (1993) 12353;
(b) R. Hotzelmann, K. Wieghardt, U. Floerke, H.-J. Haupt, D.C. Weatherburn, J. Bonvoisin, G. Blondin, J.-J. Girerd, J. Am. Chem. Soc. 114 (1992) 1681;
(c) F.J. Wu, D.M. Kurtz, K.S. Hagen, P.D. Nyman, P.G. Debrunner, V.A. Vankai, Inorg. Chem. 29 (1990) 5174.
[14] (a) H.S. Maslen, T.N. Waters, J. Chem. Soc., Chem Commun. (1973) 760;
(b) N. Torihara, M. Mikuriya, H. Okawa, S. Kida, Bull. Chem. Soc. Jpn. 53 (1971) 1610;
(c) M. Mikuriya, N. Torihara, H. Okawa, S. Kida, Bull. Chem. Soc. Jpn. 54 (1980) 1063.
[15] (a) J.A. Bonadies, M.J. Maroney, V.L. Pecoraro, Inorg. Chem. 28 (1989) 2044;
(b) J.A. Bonadies, M.L. Kirk, M.S. Lah, D.P. Kessissoglou, W.E. Hatfield, V.L. Pecoraro, Inorg. Chem. 28 (1989) 2037;
(c) Y. Gultneh, B. Ahvazi, A.R. Khan, R.J. Butcher, J.P. Tuchagues, Inorg. Chem. 34 (1995) 3633.
[16] G. Fernandez, M. Corbella, M. Alfonso, H.S. Evans, I. Castro, Inorg. Chem. 43 (2004) 6684.
[17] K. Nakamoto, Infrared and Raman Spectra of Inorganic and Coordination Compounds, 4th ed., Wiley Interscience, New York, 1986.
[18] (a) S.R. Cooper, M. Calvin, J. Am. Chem. Soc. 99 (1977) 6623;
(b) H. Visser, C.E. Dube, W.H. Armstrong, K. Sauer, V.K. Yachandra, J. Am. Chem. Soc. 124 (2002) 11008.
[19] K. Wieghardt, U. Bossek, B. Nuber, J. Weiss, J. Bonvoisin, M. Corbella, S.E. Vitols, J.-J. Girerd, J. Am. Chem. Soc. 110 (1988) 7398.
[20] (a) O. Horner, E.A. Mallart, M.-F. Charlot, L. Tchertanov, J. Guilhem, T.A. Mattioli, A. Boussac, J.-J. Girerd, Inorg. Chem. 38 (1999) 1222;
(b) R.C. Holz, T.E. Elgren, L.L. Pearce, J.H. Zhang, C.J. O'Connor, L. Que, Inorg. Chem. 32 (1993) 5844;
(c) A.L. Nivorozhkin, E.A. Mallart, P. Mialane, R. Davydov, J. Guilhem, M. Cesario, J.-P. Audihre, J.-J. Girerd, S. Styring, L. Schussler, J.-L. Seris, Inorg. Chem. 36 (1997) 846;
(d) L. Que Jr., A.E. True, Prog. Inorg. Chem. 38 (1990) 97;
(e) K. Wieghardt, K. Pohl, W. Gebert, Angew. Chem. Int. Ed. Engl. 22 (1983) 727.
[21] (a) A.A. Vlcek, Coord. Chem. Rev. 43 (1982) 39;
(b) J.L. Kahl, K.W. Hanck, K.J. Dettrmond, J. Phys. Chem. 82 (1978) 540.
[22] (a) N. Arulsamy, J. Glerup, A. Hazell, D.J. Hodgson, C.J. Mckenzie, H. Toftlund, Inorg. Chem. 33 (1994) 3023;
(b) Y. Gultneh, T.B. Yisgedu, Y.T. Tesema, R.J. Butcher, Inorg. Chem. 42 (2003) 1857.
[23] (a) C. O'Connor, Prog. Inorg. Chem. 29 (1979) 204;
(b) M.M. Morrison, D.T. Sawyer, J. Am. Chem. Soc. 99 (1977) 257;
(c) P.M. Plaksin, R.C. Stoufer, M. Mathew, G.J. Palenik, J. Am. Chem. Soc. 94 (1972) 2121.
[24] (a) M. Corbella, R. Costa, J. Ribas, P.H. Fries, J.M. Latour, L. Ohrstrom, X. Solans, V. Rodriguez, Inorg. Chem. 35 (1996) 1857;
(b) D.N. Hendrickson, G. Christou, E.A. Schmitt, E. Libby, J.S. Bashkin, S. Wang, H.L. Tsai, J.B. Vincent, P.D.W. Boyd, J. Am. Chem. Soc. 114 (1992) 2455;
(c) R.H. Beer, W.B. Tolman, S.G. Bott, S.J. Lippard, Inorg. Chem. 30 (1991) 2082.

complexes of VO_2^+ have been obtained using the N,N,O-donor monoanionic deprotonated *N*-(aroyl)-*N*′-(picolinylidene)hydrazines [8–10].

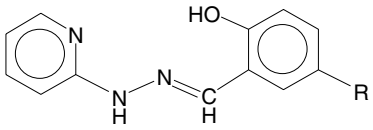

Hphsal (R = H)
HphsalOMe (R = OCH_3)
HphsalCl (R = Cl)
HphsalBr (R = Br)
HphsalNO_2 (R = NO_2)

In this work, we have explored the synthetic chemistry using [VO(acac)$_2$] and a similar Schiff base system *N*-(2-pyridyl)-*N*′-(5-R-salicylidene)hydrazines (HphsalR) which in the deprotonated state (phsalR^-) can coordinate a metal ion via the pyridine-N, the imine-N and the phenolate-O atoms. However, under aerobic and non-protic reaction conditions ternary complexes of oxovanadium(IV) have been isolated instead of dioxovanadium(V) complexes as observed before [8–10]. In the following account, we have described the syntheses and the physical properties of these ternary complexes having the general formula [VO(phsalR)(acac)]. The solid state molecular structures and self-assembly patterns of two representative complexes have been investigated by X-ray crystallography.

2. Experimental

2.1. Materials

The Schiff bases were prepared in 70–80% yield by condensation reactions of 2-hydrazinopyridine with the corresponding 5-substituted salicylaldehyde in methanolic media. Bis(acetylacetonato)oxovanadium(IV) was prepared by following a reported procedure [11]. All other chemicals and solvents used in this work were of analytical grade available commercially and were used without further purification.

2.2. Physical measurements

Microanalytical (C, H, N) data were obtained with a Thermo Finnigon Flash EA1112 series elemental analyzer. Infrared spectra were collected by using KBr pellets on a Jasco-5300 FT-IR spectrophotometer. A Shimadzu 3101-PC UV/vis/NIR spectrophotometer was used to record the electronic spectra. EPR spectra were recorded on a Jeol JES-FA200 spectrometer. Solution electrical conductivities were measured with a Digisun DI-909 conductivity meter. A Sherwood Scientific balance was used for magnetic susceptibility measurements. Diamagnetic corrections calculated from Pascal's constants [12] were used to obtain the molar paramagnetic susceptibilities.

2.3. Synthesis of [VO(phsal)(acac)] (1)

An acetonitrile solution (10 ml) of Hphsal (81 mg, 0.38 mmol) was added to an acetonitrile solution (25 ml) of [VO(acac)$_2$] (100 mg, 0.38 mmol). The mixture was heated on a water bath for 15–20 min. The resulting dark brown solution was kept in air at room temperature. Dark brown crystalline material separated in about 1–2 h was collected by filtration, washed with acetonitrile and finally dried in air. Yield, 65 mg (45%).

The other four complexes [VO(phsalOMe)(acac)] (**2**), [VO(phsalCl)(acac)] (**3**), [VO(phsalBr)(acac)] (**4**) and [VO(phsalNO_2)(acac)] (**5**) reported in this work were synthesized from acetonitrile media using one mole equivalent each of [VO(acac)$_2$] and the corresponding Schiff base in 30–48% yields by following similar procedures as described above.

2.4. X-ray crystallography

Single crystals of both [VO(phsal)(acac)] (**1**) and [VO(phsalCl)(acac)] (**3**) were collected directly from the products precipitated in the synthetic reaction mixtures. In each case, unit cell parameters and the intensity data were obtained on a Bruker–Nonius SMART APEX CCD single crystal diffractometer, equipped with a graphite monochromator and a Mo Kα fine-focus sealed tube ($\lambda = 0.71073$ Å) operated at 2.0 kW. The detector was placed at a distance of 6.0 cm from the crystal. Data were collected at 298 K with a scan width of 0.3° in ω and an exposure time of 15 s/frame. The SMART software was used for data acquisition and the SAINT-PLUS software was used for data extraction [13]. The absorption corrections were performed with the help of SADABS program [14]. The struc-

Table 1
Crystallographic data for [VO(phsal)(acac)] (**1**) and [VO(phsalCl)(acac)] (**3**)

Complex	**1**	**3**
Chemical formula	$VC_{17}H_{17}N_3O_4$	$VC_{17}H_{16}N_3O_4Cl$
Formula weight	378.28	412.72
Crystal system	monoclinic	monoclinic
Space group	$P2_1/c$	$P2_1/c$
a (Å)	8.3504(15)	9.1819(10)
b (Å)	16.434(3)	15.9499(17)
c (Å)	12.2006(18)	12.3903(13)
β (°)	97.86(2)	91.221(2)
V (Å^3)	1658.5(5)	1814.2(3)
Z	4	4
ρ (g cm^{-3})	1.515	1.511
μ (mm^{-1})	0.626	0.722
Reflections collected	19001	14668
Reflections unique	3978	3569
Reflections [$I \geqslant 2\sigma(I)$]	3395	3121
R_1, wR_2 [$I \geqslant 2\sigma(I)$]	0.0626, 0.1427	0.0498, 0.1198
R_1, wR_2 [all data]	0.0737, 0.1487	0.0575, 0.1242
Goodness-of-fit on F^2	1.209	1.095
Largest difference peak and hole (e Å^{-3})	0.826, −0.201	0.449, −0.219

tures were solved by direct methods and refined on F^2 by full-matrix least-squares procedures. Both complexes crystallize in the space groups $P2_1/c$. All non-hydrogen atoms were refined using anisotropic thermal parameters. The hydrogen atoms were included in the structure factor calculations at idealized positions by using a riding model but not refined. The SHELX-97 programs [15] were used for structure solution and refinement. The ORTEX6a [16] and PLATON [17] packages were used for molecular graphics. Selected crystallographic data for both **1** and **3** are listed in Table 1.

3. Results and discussion

3.1. Synthesis and some properties

All the complexes were synthesized from acetonitrile media by reacting $[VO(acac)_2]$ and HphsalR in 1:1 mole ratio. The elemental analysis data are consistent with the general molecular formula [VO(phsalR)(acac)] (Table 2). Unlike our previous observations [8–10] there is no oxidation of the metal ion in the present reactions. Only one acetylacetonate of $[VO(acac)_2]$ has been replaced by $phsalR^-$ and the ternary complexes are formed. The complexes are insoluble in common organic solvents except dimethylsulphoxide and dimethylformamide. In solutions, they are electrically non-conducting. The room temperature (298 K) magnetic moments of the complexes in the solid state are in the range 1.68–1.92 μ_B (Table 2). These values are consistent with an $S = 1/2$ ground state expected for the metal ion in mononuclear oxovanadium(IV) species.

3.2. Spectroscopic properties

Infrared spectra of the complexes display a strong band in the range 1622–1634 cm^{-1}. The origin of this band is most probably the C=N stretch of the tridentate Schiff base ligand [4–8]. A broad band centred at ~3400 cm^{-1} is attributed to the N–H stretch of the hydrazine fragment of the ligand. Two medium to strong bands observed in the ranges 1512–1553 and 1582–1601 cm^{-1} are most likely due to the coupled C---C and C---O stretches of the acetylacetonate moiety [18]. In all the spectra, the V=O stretch appears as a strong band within 928–949 cm^{-1} (Table 2). These values are consistent with the V=O stretching frequencies reported for distorted octahedral oxovanadium(IV) species [19,20].

The dimethylsulfoxide solutions of the complexes have been used to record the electronic spectra. The main features of all the spectra are quite similar. A representative spectrum is shown in Fig. 1 and the spectral data are given in Table 3. There are two major absorptions within the ranges 510–420 and 383–340 nm in the visible region. These are attributed to the ligand-to-metal charge transfer transitions (LMCT). The high energy absorption (275–262 nm) is most likely due to a transition involving ligand orbitals only. The complexes **1**–**3** show an additional weak absorption in the range 643–720 nm due to d–d transition [19–21]. For complexes **4** and **5** this absorption is probably obscured by the tail of the following LMCT band.

The EPR spectra of the complexes have been collected using powdered samples as well as dimethylsulfoxide solutions. At room temperature (298 K) the powdered samples

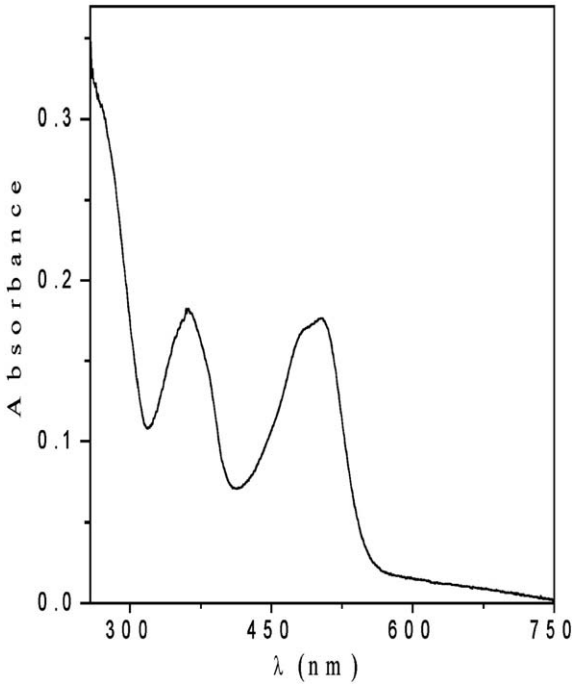

Fig. 1. Electronic spectrum of [VO(phsal)(acac)] (**1**) in dimethylsulphoxide solution.

Table 2
Elemental analysis, magnetic susceptibility[a] and infrared[b] spectroscopic data

Complex	Found (Calc.) (%)			μ_{eff} (μ_B)	$\nu_{V=O}$ (cm^{-1})
	C	H	N		
[VO(phsal)(acac)] (**1**)	53.85 (53.98)	4.42 (4.53)	10.98 (11.11)	1.78	928
[VO(phsalOMe)(acac)] (**2**)	52.73 (52.95)	4.73 (4.69)	10.14 (10.29)	1.72	943
[VO(phsalCl)(acac)] (**3**)	49.22 (49.47)	4.05 (3.91)	9.89 (10.18)	1.82	945
[VO(phsalBr)(acac)] (**4**)	44.39 (44.66)	3.38 (3.53)	8.97 (9.19)	1.68	949
[VO(phsalNO_2)(acac)] (**5**)	47.98 (48.24)	3.75 (3.81)	13.15 (13.24)	1.92	937

[a] At 298 K.
[b] In KBr disk.

Table 3
Electronic[a] and EPR[b] spectroscopic data

Complex	λ_{max} (nm) ($10^{-3} \times \varepsilon$ (M^{-1} cm^{-1}))	$g_{\parallel}$ ($A_{\parallel}$ (G))	$g_{\perp}$ ($A_{\perp}$ (G))
[VO(phsal)(acac)] (**1**)	670[c] (0.09), 503 (1.8), 480[c] (1.7), 362 (1.8), 275[c] (2.9)	1.95 (178)	1.99 (66)
[VO(phsalOMe)(acac)] (**2**)	720 (0.03), 510 (1.9), 489[c] (1.8), 383 (2.1), 267 (3.4)	1.95 (179)	1.99 (65)
[VO(phsalCl)(acac)] (**3**)	643 (0.03), 420 (0.7), 340 (0.9), 275[c] (1.3)	1.93 (198)	1.99 (73)
[VO(phsalBr)(acac)] (**4**)	510 (2.4), 488[c] (2.2), 370 (1.8), 265[c] (5.9)	1.95 (178)	1.98 (73)
[VO(phsalNO_2)(acac)] (**5**)	500 (5.2), 485[c] (5.1), 356 (7.6), 262[c] (5.5)	1.95 (178)	1.99 (67)

[a] In dimethylsulfoxide solution.
[b] In frozen (123 K) dimethylsulfoxide solution.
[c] Shoulder.

of **1** and **5** display an isotropic signal at $g = 1.98$ and 2.0, respectively. Interestingly the powdered samples of complexes **2**–**4** at 298 K display well resolved axial spectra with ^{51}V ($I = 7/2$) hyperfine structure having $g_{\parallel} \sim 1.94$ ($A_{\parallel} \sim 178$ G) and $g_{\perp} \sim 1.98$ ($A_{\perp} \sim 60$ G). Lowering of temperature to 123 K makes the signals more sharp for **2**–**4**. In the case of **1**, a similar well resolved axial spectrum is observed at 123 K instead of the isotropic signal observed at room temperature. On the other hand, for **5** the hyperfine structure due to the metal centre is reasonably resolved for the $g_{\parallel}$ component and partially resolved for the $g_{\perp}$ component at 123 K. The observation of the isotropic signal for **1** and **5** at room temperature could be due to several factors such as spin–spin interaction, exchange interactions, spin–lattice relaxation and dynamic Jahn–Teller effect. Considering that the metal ion is coordinatively saturated in all the complex molecules (**1**–**5**) which differ only by the substituent on the tridentate ligand and the observation of the resolved spectrum at low temperature, it appears that one of the last two factors or both are responsible for the different behavior of **1** and **5**. The spectra of the complexes in frozen (123 K) dimethylsulfoxide solutions are grossly identical and very similar with the powder phase spectra observed at 298 and 123 K for **2**–**4** and at 123 K for **1**. The frozen solution spectral parameters are listed in Table 3 and a representative spectrum is shown in Fig. 2. The $g_{\parallel} < g_{\perp}$ and $A_{\parallel} > A_{\perp}$ relationships for all the complexes are consistent with an axially compressed octahedral geometry around the vanadium(IV) centre with the unpaired electron in the d_{xy} orbital [22,23].

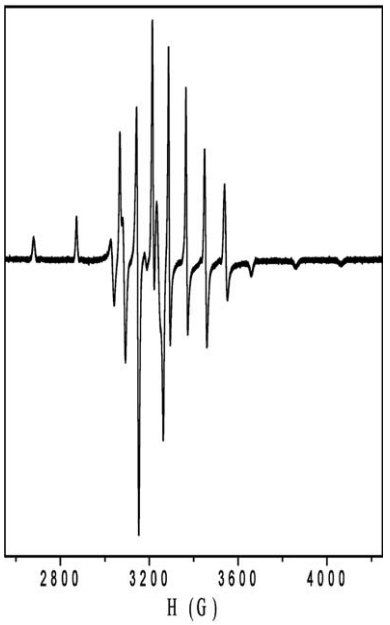

Fig. 2. EPR spectrum of [VO(phsalCl)(acac)] (**3**) in frozen (123 K) dimethylsulfoxide solution ($\sim 10^{-3}$ M).

3.3. Molecular structures of [VO(phsal)(acac)] (1) and [VO(phsalCl)(acac)] (3)

The molecular structures of **1** and **3** are depicted in Figs. 3 and 4, respectively. Bond parameters associated with the metal ions in both complexes are listed in Table 4. In each complex molecule, the metal centre is in a distorted octahedral N_2O_4 coordination sphere assembled by the pyridine-N, the imine-N and the phenolate-O donor phsalR^- (R = H or Cl), the O,O-donor acetylacetonate ($acac^-$) and the oxo group. The meridionally spaning tridentate ligand and one of the two O-atoms of $acac^-$ form a N_2O_2 square plane around the metal centre. The remaining two axial sites are occupied by the oxo group and the second O-atom of $acac^-$. The chelate bite angles are unexceptional and comparable in **1** and **3**. The V–N(pyridine), the V–N(imine) and the V=O bond lengths are very similar in both structures. However, the V–O(phenolate) bond length

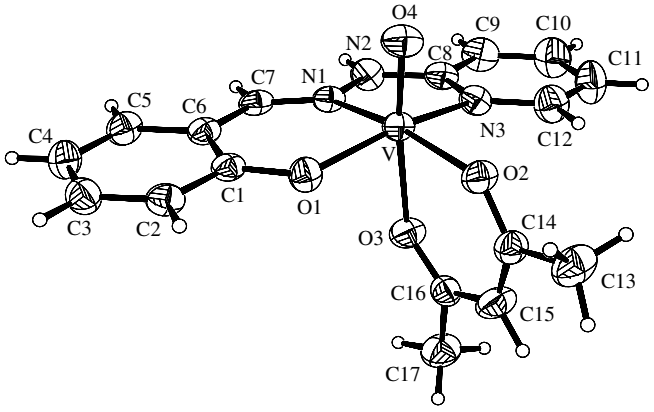

Fig. 3. Molecular structure of [VO(phsal)(acac)] (**1**) with the atom labeling scheme. All non-hydrogen atoms are represented by their 40% probability thermal ellipsoids.

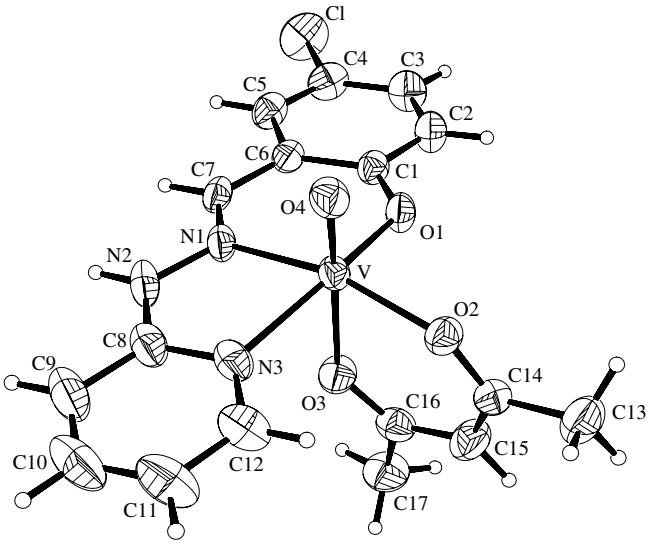

Fig. 4. Molecular structure of [VO(phsalCl)(acac)] (**3**) with the atom labeling scheme. All non-hydrogen atoms are represented by their 40% probability thermal ellipsoids.

Table 4
Selected bond lengths and angles for [VO(phsal)(acac)] (**1**) and [VO(phsalCl)(acac)] (**3**)

	1	**3**
Bond lengths (Å)		
V–N(1)	2.066(2)	2.066(2)
V–N(3)	2.121(2)	2.119(2)
V–O(1)	1.935(2)	1.9485(18)
V–O(2)	1.9837(18)	1.9787(18)
V–O(3)	2.182(2)	2.1769(19)
V–O(4)	1.6147(19)	1.6113(18)
Bond angles (°)		
N(1)–V–O(1)	88.72(8)	88.96(8)
N(1)–V–O(2)	165.96(8)	164.22(8)
N(1)–V–O(3)	83.52(8)	81.65(8)
N(1)–V–O(4)	99.05(9)	100.04(9)
N(1)–V–N(3)	76.57(9)	76.66(9)
N(3)–V–O(1)	158.55(8)	159.95(8)
N(3)–V–O(2)	97.02(9)	96.44(9)
N(3)–V–O(3)	78.40(8)	80.51(8)
N(3)–V–O(4)	96.30(10)	95.20(9)
O(1)–V–O(2)	93.70(8)	93.82(8)
O(1)–V–O(3)	84.57(8)	83.67(8)
O(1)–V–O(4)	101.44(10)	101.09(10)
O(2)–V–O(3)	82.94(8)	83.22(7)
O(2)–V–O(4)	94.03(9)	94.67(9)
O(3)–V–O(4)	173.47(10)	174.94(9)

is slightly longer in **3** than that in **1**. This difference is possibly due to the electron withdrawing effect of the Cl-atom at the *para* position of the phenolate-O in **3**. Not surprisingly the two V–O bond lengths associated with the $acac^-$ ligand are different in both complexes. The V–O bond which is *trans* to the oxo group is significantly longer than the V–O bond which is *cis* to the oxo group (Table 4). The *cis* and *trans* V–O bond lengths observed in **1** and **3** are comparable with those reported for oxovanadium(IV) species containing $acac^-$ as ligand in the same orientation [19,24]. In general, all the metal to coordinating atom bond lengths in both **1** and **3** are within the ranges reported for octahedral vanadium(IV) species containing the same coordinating atoms [19,20,22–24].

3.4. Intermolecular hydrogen bonding and self-assembly

The type of complex molecules described in this work contain two major functionalities which can participate in intermolecular hydrogen bond interactions. These are the N–H group of the hydrazine fragment of the tridentate ligand and the metal coordinated oxo group. It may be noted that the acidity of the N–H proton increases significantly in aroyl- or arylhydrazine based Schiff bases when the adjacent imine-N is coordinated to a metal ion [25]. A similar situation is expected in the present series of complexes also. The vanadium(IV/V) bound oxo group is fairly strong basic centre and is known to participate in intermolecular weak C–H···O interactions [10,24]. Thus, it is anticipated that the self-assembly of the molecules of both **1** and **3** in the crystal lattice will be guided by reasonably strong intermolecular N–H···O=V hydrogen bond interactions. Indeed this interaction is observed in both the structures. The N2···O4 distance and the N2–H···O4 angle are 2.909(3) Å and 177.4° for **1** and 2.980(3) Å and 175.6° for **3**. In each case, self-assembly of the complex molecules via these intermolecular N–H···O=V hydrogen bond interactions leads to one-dimensional supramolecular structure in the crystal lattice (Fig. 5). There are no significant short contacts and hence no additional non-covalent

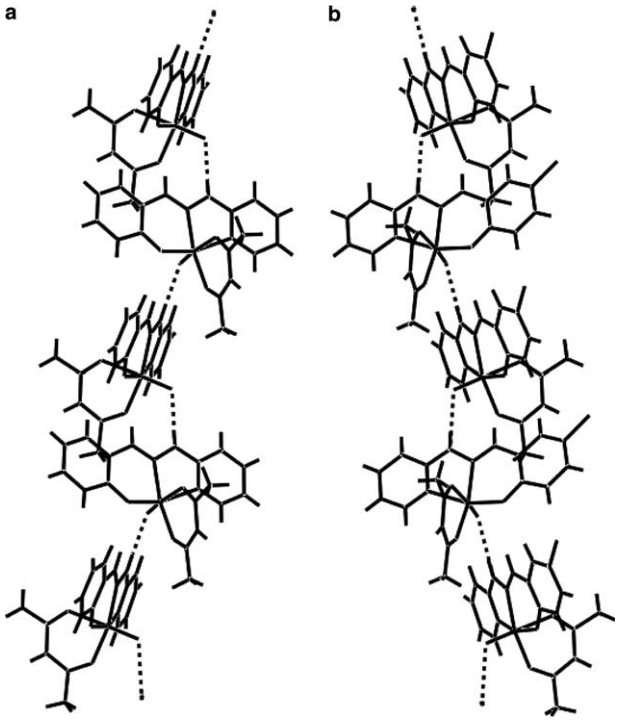

Fig. 5. One-dimensional ordering of (a) [VO(phsal)(acac)] (**1**) and (b) [VO(phsalCl)(acac)] (**3**) in the crystal lattice.

interactions between the parallel one-dimensional structures.

4. Conclusion

The synthesis and physical properties of a new series of oxovanadium(IV) ternary complexes are described. The general formula of these complexes is [VO(phsalR)(acac)] where Hacac and HphsalR represent the bidentate acetylacetone and the tridentate Schiff base *N*-(2-pyridyl)-*N*′-(5-R-salicylidene)hydrazine, respectively. The identities of the complexes have been established by microanalytical, magnetic, spectroscopic and X-ray crystallographic methods. The complexes display ligand-field and ligand-to-metal charge transfer bands in the electronic spectra. The EPR spectra of the complexes are characteristic of an axially compressed d^1_{xy} configuration. The crystal structures show that the meridional pyridine-N, imine-N and phenolate-O donor phsalR$^-$, the O,O-donor acac$^-$ and the oxo group form a distorted N_2O_4 octahedron around the metal centre. In the crystal lattice, the complex molecules are self-organized to one-dimensional supramolecular structure via intermolecular N–H···O=V hydrogen bond interaction.

5. Supplementary material

Crystallographic data for [VO(phsal)(acac)] (**1**) and [VO(phsalCl)(acac)] (**3**) have been deposited with the Cambridge Crystallographic Data Centre (deposition numbers are CCDC 286182 and 286183 for **1** and **3**, respectively). Copies of this information may be obtained from The Director, CCDC, 12 Union Road, Cambridge, CB2 1EZ, UK, fax: +44 1233 336 033; email: deposit@ccdc.cam.ac.uk; or the web: http://www.ccdc.cam.ac.uk.

Acknowledgements

Financial assistance for this work was provided by the Council of Scientific and Industrial Research (CSIR), New Delhi (Grant No. 01(1880)/03/EMR-II). Ms. A. Sarkar thanks the CSIR for a research fellowship. X-ray crystallographic studies were performed at the National Single Crystal Diffractometer Facility, School of Chemistry, University of Hyderabad (funded by the Department of Science and Technology, New Delhi). We thank the University Grants Commission, New Delhi for the facilities provided under the UPE and CAS programs.

References

[1] M.D. Chasteen (Ed.), Vanadium in Biological Systems, Kluwer, Dordrecht, 1990.
[2] D. Rehder, Coord. Chem. Rev. 182 (1999) 297.
[3] K.A. Jørgensen, Chem. Rev. 89 (1989) 435.
[4] A. Kumar Jr., S.K. Das, A. Kumar, J. Catal. 166 (1997) 108.
[5] M.R. Maurya, Coord. Chem. Rev. 237 (2003) 163.
[6] N.R. Sangeetha, V. Kavita, S. Wocadlo, A.K. Powell, S. Pal, J. Coord. Chem. 51 (2000) 55.
[7] N.R. Sangeetha, S. Pal, Bull. Chem. Soc. Jpn. 73 (2000) 357.
[8] S.N. Pal, S. Pal, J. Chem. Crystallogr. 30 (2000) 329.
[9] S.N. Pal, S. Pal, Acta Crystallogr., Sect. C 57 (2001) 141.
[10] S.N. Pal, K.R. Rahika, S. Pal, Z. Anorg. Allg. Chem. 627 (2001) 1631.
[11] R.A. Rowe, M.M. Jones, Inorg. Synth. 5 (1957) 113.
[12] W.E. Hatfield, in: E.A. Boudreaux, L.N. Mulay (Eds.), Theory and Applications of Molecular Paramagnetism, Wiley, New York, 1976, p. 491.
[13] SMART version 5.630 and SAINT-PLUS version 6.45, Bruker–Nonius Analytical X-ray Systems Inc., Madison, WI, USA, 2003.
[14] G.M. Sheldrick, SADABS, Empirical Absorption Correction Program, University of Göttingen, Göttingen, Germany, 1997.
[15] G.M. Sheldrick, SHELX-97, Structure Determination Software, University of Göttingen, Göttingen, Germany, 1997.
[16] P. McArdle, J. Appl. Crystallogr. 28 (1995) 65.
[17] A.L. Spek, PLATON A Multipurpose Crystallographic Tool, Utrecht University, Utrecht, The Netherlands, 2002.
[18] K. Nakamoto, in: Infrared and Raman Spectra of Inorganic and Coordination Compounds, Wiley, New York, 1986, p. 259.
[19] X. Li, M.S. Lah, V.L. Pecoraro, Inorg. Chem. 27 (1988) 4657.
[20] J.A. Bonadies, C.J. Carrano, J. Am. Chem. Soc. 108 (1986) 4088.
[21] C.J. Ballhausen, H.B. Gray, Inorg. Chem. 1 (1962) 111.
[22] P. Basu, S. Pal, A. Chakravorty, J. Chem. Soc., Dalton Trans. (1991) 3217.
[23] J. Chakravarty, S. Dutta, A. Dey, A. Chakravorty, J. Chem. Soc., Dalton Trans. (1994) 557.
[24] S.P. Anthony, L. Srikanth, T.P. Radhakrishnan, Mol. Cryst. Liq. Cryst. 381 (2002) 133.
[25] S.N. Pal, S. Pal, J. Chem. Soc., Dalton Trans. (2002) 2102.

In the framework of synthetic studies of cyclopentadienyl iron sulfur complexes, we have studied the reactions of the iron sulfides $(\mu\text{-}S_x)[CpFe(CO)_2]_2$ with a variety of nucleophiles such as acid chlorides, sulfonyl chlorides and chloroformates. These reactions give the sulfur containing complexes, thiocarboxylates ($CpFe(CO)_2SCOR$) [22–24], thiosulfonates ($CpFe(CO)_2SSO_2R$) [25] and thiocarbonates ($CpFe(CO)_2SCO_2R$) [26]. We hereby report the synthesis of dithiocarbonate complexes of iron by the reaction of the iron sulfides, $(\mu\text{-}S_x)[CpFe(CO)_2]_2$, with aryl chlorothionoformates.

2. Results and discussion

2.1. Synthesis and characterization

The reaction of $(\mu\text{-}S_x)[CpFe(CO)_2]_2$ with various aryl chlorothionoformates proceeds smoothly to give the corresponding dithiocarbonate complexes $CpFe(CO)_2SC(S)OAr$ (**1**) as shown in Eq. (1). The iron chloride, $CpFe(CO)_2Cl$ is obtained as a by-product of this reaction and can be separated from the products **1** by column chromatography.

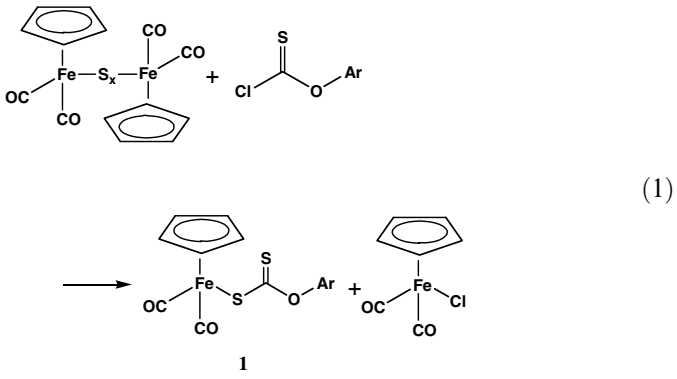

(1)

1

Ar = Ph (**a**), 4-C_6H_4Cl (**b**), 4-C_6H_4F (**c**), C_6F_5 (**d**), 4-$C_6H_4CH_3$ (**e**)

The new organoiron S-bonded dithiocarbonates (**1**) are stable solids and are also stable in solution. Structural features of **1** were identified on the basis of IR and ^1H NMR spectroscopy as well as by elemental analysis. The IR spectra of **1** in the carbonyl stretching region show two bands due to the terminal carbonyl groups in the ranges 2044–2049 and 1998–2006 cm^{-1}. These bands are higher than those reported for the corresponding thiocarboxylates $CpFe(CO)_2SCOR$ (2027–2060, 1984–1998 cm^{-1}) [22–24] and are similar to those of thiocarbonate complexes $CpFe(CO)_2SCO_2R$ (2044–2045 and 1997–1999 cm^{-1}) [26], suggesting that the mono- and di-thiocarbonate ligands have similar basicity. In the ^1H NMR spectra of **1**, the peak for the Cp-protons is found in the range 5.05–5.10 ppm. This chemical shift range is similar to that observed for the thiocarboxylate (4.98–5.13 ppm) [22–24] and thiocarbonate (4.98–5.12 ppm) analogues [26]. These results suggest a similar electron density around the iron center in all of these complexes.

When a THF solution containing $CpFe(CO)_2SCSOAr$ (**1**) was irradiated by UV-light for short time (ca. 30 min), the chelate complexes $CpFe(CO)(\kappa^2S,S\text{-}S_2COAr)$ (**2**) were obtained in high yields (Eq. (2)).

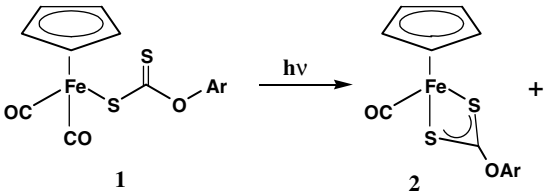

1 **2** (2)

Compounds **2** were characterized by IR, ^1H NMR spectroscopy and elemental analysis. The IR spectrum of each of complexes **2** in the carbonyl stretching region exhibits a singlet band in the range 1953–1961 cm^{-1} for the terminal carbonyl group coordinated to the iron center. This range is comparable to those found for iron complexes containing one CO-group such as $CpFe(CO)(EPh_3)SCOR$ (1950–1970 cm^{-1}). ^1H NMR spectra of **2** in $CDCl_3$ show singlet peak in the range 4.63–4.69 ppm for the cyclopentadienyl protons. This peak has lower chemical shift compared to the corresponding peak of the starting dicarbonyl complexes **1**. This shift may attributed to the higher electron-density around the Fe-atom in **2** compared to that in **1**. Comparing this peak to that of $CpFe(CO)(EPh_3)SCOR$, it is obvious that these values are comparable to each other.

2.2. Crystal structure

The structure of $CpFe(CO)_2SC(S)O\text{-}4\text{-}C_6H_4Cl$ (**1b**) was determined by single-crystal X-ray analysis and is shown in Fig. 1. Selected bond lengths and angles are shown in Table 1. The relevant bond parameters are listed in Table 2. As expected, the analysis proved that the dithiocarbonate ligand is bonded to the iron in a monodentate fashion through one sulfur atom with an Fe–S bond distance of 2.2765(5) Å. This distance is longer than the corresponding Fe–S distance in $CpFe(CO)_2SCO_2Et$ (2.2675(10) Å) and in $CpFe(CO)_2SCO\text{-}2\text{-}C_6H_4NO_2$ (2.266(1) Å) The Cp ligand is bound to the metal in an η^5-fashion with Fe–C bond distances comparable to those observed for Cp–iron complexes. The Fe–C (of carbonyl ligands) bond distances of 1.7745(19) and 1.7810(17) Å are in the normal range for $CpFe(CO)_2X$ complexes [24,26–28]. The Fe–S1–C8 angle is 113.50°.

3. Experimental

3.1. General

All reactions were carried out under an inert atmosphere of nitrogen using standard Schlenk line techniques. Solvents were dried by standard methods and were distilled under nitrogen prior to use. The complexes $(\mu\text{-}S_x)[CpFe(CO)_2]_2$ ($x = 2$, 3) were prepared by published method [29]. The reagents: aryl-chlorothionoformates,

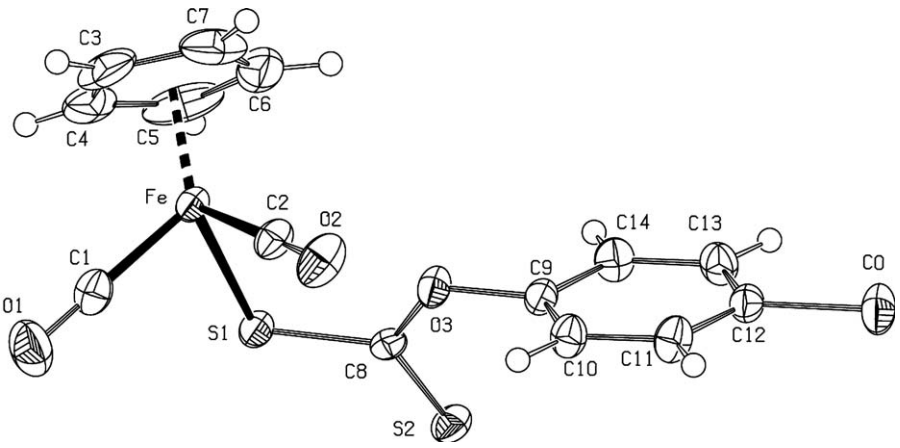

Fig. 1. ORTEP drawing of $CpFe(CO)_2SC(S)O\text{-}4\text{-}C_6H_4Cl$ (**1b**).

Table 1
Selected bond length (Å) and angles (°) of $CpFe(CO)_2SC(S)O\text{-}4\text{-}C_6H_4Cl$ (**1b**)

Fe–S1	2.2765(5)	C8–S1–Fe	113.50(5)
Fe–C1	1.77745(19)	C1–Fe–S1	89.25(6)
Fe–C2	1.7810(17)	C2–Fe–S1	94.92(5)
Fe–C3	2.0785(19)	C2–Fe–C1	92.24(9)
Fe–C4	2.1003(19)	C8–O3–C9	120.75(12)
Fe–C5	2.110(2)	O3–C8–S2	124.53(11)
Fe–C6	2.089(2)	O3–C8–S1	114.36(11)
Fe–C7	2.0818(19)	S1–C8–S2	121.10(9)
S1–C8	1.7095(16)		
S2–C8	1.6541(15)		
C1–O1	1.139(2)		
C2–O2	1.139(2)		
C3–O3	1.3553(18)		
C9–O3	1.4036(18)		

Table 2
Selected crystal data and refinement parameters for $CpFe(CO)_2SC(S)O\text{-}4\text{-}C_6H_4Cl$ (**1b**)

Empirical formula	$C_{14}H_9ClFeO_3S_2$
Formula weight	380.63
Crystal size (mm)	$0.13 \times 0.10 \times 0.08$
Crystal system	monoclinic
Space group	$P2_1/c$
Unit cell dimensions	
a (Å)	11.4680 (10)
b (Å)	9.7400 (10)
c (Å)	13.678 (10)
α (°)	90.00
β (°)	103.21(5)
γ (°)	90.00
V (Å^3)	1487.4 (2)
Z	4
Index ranges	$-16 \leqslant h \leqslant 9$, $0 \leqslant k \leqslant 13$, $0 \leqslant l \leqslant 19$
Number of total reflections	4334
Number of unique reflections ($>2\sigma(I)$)	3711
D_{calc} (Mg m^{-3})	1.855
Radiation type	Mo Kα
μ (mm^{-1})	1.478
λ (Å)	0.71069
θ Range (°)	1.82–30.05
$R[F^2 > 2\sigma(F^2)]$	0.0280
$\omega R(F^2)$[a]	0.0765

[a] $\omega = 1/[\sigma^2(F_o^2) + (0.0426P)^2]$, where $P = (F_o^2 + 2F_c^2)/3$.

$[CpFe(CO)_2]_2$, and sulfur were obtained from Acros and were used as received.

Nuclear magnetic resonance (NMR) spectra were recorded on a Bruker 200 MHz spectrometer. Chemical shifts are in ppm relative to TMS at 0 ppm. Infrared (IR) spectra were recorded on a Nicolat Nexus FT-IR spectrometer using NaCl solvent cells. Elemental analyses were done in Laboratoire d'Analyse Elémentaire, Université de Montréal, Montréal, Que., Canada. Melting points were reported on an electrothermal melting point apparatus and are uncorrected. The photolytic reactions were carried out in a medium pressure mercury lamp (150 W) with a quartz immersion cell.

3.2. General procedure for the preparation of $CpFe(CO)_2SC(S)OAr$ (*1*)

To a solution of $(\mu\text{-}S_x)[CpFe(CO)_2]_2$ (0.50 mmol) in diethylether (100 mL), aryl chlorothionoformate (0.55 mmol) was added and the resulting mixture was stirred overnight at room temperature. The volatiles were removed under reduced pressure and the resulting solid was redissolved in a minimum amount of CH_2Cl_2 and transferred to a silica gel column made up in hexane. The column was first eluted with hexane to remove any unreacted aryl chlorothionoformates. Then, it was eluted with hexane/dichloromethane solution (1:1 v:v ratio) to give a red-orange band which was collected and identified as $CpFe(CO)_2SC(S)OAr$, followed by a red band which was also collected and identified as $CpFe(CO)_2Cl$. The $CpFe(CO)_2SC(S)OAr$ (**1**) were recrystallized from dichloromethane/hexane.

3.2.1. $CpFe(CO)_2SC(S)OC_6H_5$ (*1a*)

Yield, 79%; m.p. 132–133 °C. *Anal.* Required for $C_{14}H_{10}FeO_3S_2$: C, 48.57; H, 2.91; S, 18.53. Found: C, 47.78; H, 2.65; S, 18.03%. IR (CH_2Cl_2, cm^{-1}): 2045s,

1998s ν(C≡O). ^{1}H NMR ($CDCl_3$, δ, ppm): 5.05 (s, 5H, C_5H_5), 7.07 (m, 3H, C_6H_5), 7.31 (m, 2H, C_6H_5).

*3.2.2. $CpFe(CO)_2SC(S)O$-4-C_6H_4Cl (**1b**)*

Yield, 87%; m.p. 134–136 °C. *Anal.* Required for $C_{14}H_9ClFeO_3S_2$: C, 44.18; H, 2.38; S, 16.58. Found: C, 44.10; H, 2.23; S, 15.98%. IR (CH_2Cl_2, cm^{-1}): 2046s, 1999s ν(C≡O). ^{1}H NMR ($CDCl_3$, δ, ppm): 5.05 (s, 5H, C_5H_5), 6.95 (d, 2H, C_6H_4), 7.32 (d, 2H, C_6H_4).

*3.2.3. $CpFe(CO)_2SC(S)O$-4-C_6H_4F (**1c**)*

Yield, 86%; m.p. 128–129 °C. *Anal.* Required for $C_{14}H_9FFeO_3S_2$: C, 46.17; H, 2.49; S, 17.61. Found: C, 45.88; H, 2.28; S, 17.01%. IR (CH_2Cl_2, cm^{-1}): 2046s, 2000s ν(C≡O). ^{1}H NMR ($CDCl_3$, δ, ppm): 5.09 (s, 5H, C_5H_5), 7.00 (d, 2H, C_6H_4), 7.40 (d, 2H, C_6H_4).

*3.2.4. $CpFe(CO)_2SC(S)OC_6F_5$ (**1d**)*

Yield, 90%; m.p. 115–116 °C. *Anal.* Required for $C_{14}H_5F_5FeO_3S_2$: C, 38.55; H, 1.16; S, 14.70. Found: C, 38.22; H, 0.99; S, 14.13%. IR (CH_2Cl_2, cm^{-1}): 2049s, 2006s ν(C≡O). ^{1}H NMR ($CDCl_3$, δ, ppm): 5.10 (s, H's, C_5H_5).

*3.2.5. $CpFe(CO)_2SC(S)O$-4-C_6H_4Me (**1e**)*

Yield, 85%; m.p. 138–140 °C. *Anal.* Required for $C_{15}H_{12}FeO_3S_2$: C, 50.01; H, 3.24; S, 17.58. Found: C, 49.79; H, 3.36; S, 17.58%. IR (CH_2Cl_2, cm^{-1}): 2044s, 2000s ν(C≡O). ^{1}H NMR ($CDCl_3$, δ, ppm): 2.31 (s, 3H, CH_3), 5.05 (s, 5H, C_5H_5), 6.91 (d, 2H, C_6H_4), 7.22 (d, 2H, C_6H_4).

*3.3. General procedure for the preparation of $CpFe(CO)(\kappa^2S,S$-$SC(S)OAr)$ (**2**)*

A THF solution (30 mL) of $CpFe(CO)_2SC(S)OAr$ (0.25 mmol) was irradiated under a stream of N_2 for 30 min. The products were separated by column chromatography. The column was eluted with (2:1 v:v ratio) CH_2Cl_2/hexane to separate the products which were recrystallized from dichloromethane/hexane.

*3.3.1. $CpFe(CO)(\kappa^2S,S$-$SC(S)OC_6H_5)$ (**2a**)*

Yield, 80%; m.p. 89–91 °C. *Anal.* Required for $C_{13}H_{10}FeO_2S_2$: C, 49.07; H, 3.17; S, 20.16. Found: C, 48.51; H, 3.11; S, 19.77%. IR (CH_2Cl_2, cm^{-1}): 1954s ν(C≡O). ^{1}H NMR ($CDCl_3$, δ, ppm): 4.65 (s, 5H, C_5H_5), 7.41 (m, 5H, C_6H_5).

*3.3.2. $CpFe(CO)(\kappa^2S,S$-$SC(S)O$-4-$C_6H_4Cl)$ (**2b**)*

Yield, 82%; m.p. 102–103 °C. *Anal.* Required for $C_{13}H_9ClFeO_2S_2$: C, 44.28; H, 2.57; S, 18.19. Found: C, 44.01; H, 2.54; S, 17.50%. IR (CH_2Cl_2, cm^{-1}): 1956s ν(C≡O). ^{1}H NMR ($CDCl_3$, δ, ppm): 4.66 (s, 5H, C_5H_5), 7.09 (d, 2H, C_6H_4), 7.37 (d, 2H, C_6H_4).

*3.3.3. $CpFe(CO)(\kappa^2S,S$-$SC(S)O$-4-$C_6H_4F)$ (**2c**)*

Yield, 68%; m.p. 92–93 °C. *Anal.* Required for $C_{13}H_9FFeO_2S_2$: C, 46.44; H, 2.70; S, 19.08. Found: C, 46.12; H, 2.29; S, 18.56%. IR (CH_2Cl_2, cm^{-1}): 1956s ν(C≡O). ^{1}H NMR ($CDCl_3$, δ, ppm): 4.67 (s, 5H, C_5H_5), 7.19 (d, 2H, C_6H_4), 7.40 (d, 2H, C_6H_4).

*3.3.4. $CpFe(CO)(\kappa^2S,S$-$SC(S)OC_6F_5)$ (**2d**)*

Yield, 87%; m.p. 78–79 °C. *Anal.* Calc. for $C_{13}H_5F_5FeO_2S_2$: C, 38.25; H, 1.23; S, 15.71. Found: C, 37.90; H, 1.11; S, 15.07%. IR (CH_2Cl_2, cm^{-1}): 1961s ν(C≡O). ^{1}H NMR ($CDCl_3$, δ, ppm): 4.69 (s, H's, C_5H_5).

*3.3.5. $CpFe(CO)(\kappa^2S,S$-$SC(S)O$-4-$C_6H_4Me)$ (**2e**)*

Yield, 75%; m.p. 95–96 °C. *Anal.* Required for $C_{14}H_{12}FeO_2S_2$: C, 50.61; H, 3.64; S, 19.30. Found: C, 50.31; H, 3.78; S, 19.50%. IR (CH_2Cl_2, cm^{-1}): 1953s ν(C≡O). ^{1}H NMR ($CDCl_3$, δ, ppm): 2.33 (s, 3H, CH_3), 4.63 (s, 5H, C_5H_5); 6.97 (d, 2H, C_6H_4), 7.17 (d, 2H, C_6H_4).

3.4. X-ray structure analysis

Crystals suitable for X-ray diffraction of **1b** were obtained from CH_2Cl_2/hexane mixture. The data were collected on a KappaCCD diffractometer with graphite monochromated Mo Kα radiation at 175 K. The crystallographic data are shown in Table 2. The cell parameters were determined from 4335 reflections collected in the range $1.82 \leqslant \theta \leqslant 30.05°$. There were 4334 independent reflections with 3711 observed reflections ($>2\sigma(I)$). The structure was solved by direct method using SHELXS-97 [30] and DIFMAP synthesis using SHELXTL-96 [31].

4. Supplementary data

Crystallographic data for the structural analysis have been deposited with the Cambridge Crystallographic Data Centre, CCDC No. 277850 for compound **1b**. Copies of this information may be obtained free of charge from The Director, CCDC, 12 Union Road, Cambridge, CB2 1EZ, UK (fax: +44 1233 336 033; e-mail: deposit@ccdc.cam.ac.uk or www:http://www.ccdc.cam.ac.uk).

Acknowledgments

The financial support (Grant No. 31/2002) from the Deanship of Scientific Research, Jordan University of Science and Technology is greatfully acknowledged. We thank Prof. Richard Welter (University of Strasburg, France) for determining the X-ray structure.

References

[1] R. Eisenberg, Prog. Inorg. Chem. 12 (1970) 295.
[2] D. Coucouvanis, Prog. Inorg. Chem. 26 (1979) 301.
[3] D. Coucouvanis, Prog. Inorg. Chem. 11 (1970) 233.
[4] J.F. Fackler, A.R. Hendrickson, R.L. Martin, N.M. Rhode, Inorg. Chem. 14 (1975) 1894.
[5] J.F. Fackler, A.R. Hendrickson, R.L. Martin, N.M. Rhode, Inorg. Chem. 13 (1974) 1433.

[6] R. Pastorek, Z. Travnicek, J. Marck, D. Dastych, Z. Sindelar, Polyhedron 19 (2000) 1713.
[7] G. Exatchos, S.D. Robinson, J.W. Steed, Polyhdron 19 (2000) 1511.
[8] A. Shaver, B.-S. Lum, P. Bird, K. Arnold, Inorg. Chem. 28 (1989) 1900.
[9] A. Shaver, M. El-khateeb, A.-M. Lebius, Inorg. Chem. 40 (2001) 5288.
[10] A. Shaver, M. El-khateeb, A.-M. Lebius, Inorg. Chem. 38 (1999) 6913.
[11] A. Shaver, P.-Y. Plouffe, P. Bird, E. Livingstone, Inorg. Chem. 29 (1990) 826.
[12] L.B. Reventos, A.G. Alonso, J. Organomet. Chem. 309 (1986) 179.
[13] A.M. Bond, Coord. Chem. Rev. 54 (1984) 23.
[14] E. Roman, D. Catheline, D. Astruc, J. Organomet. Chem. 236 (1982) 229.
[15] C. O'Connor, J.D. Gilbert, G. Wilkinson, J. Chem. Soc. A (1969) 84.
[16] A. Coto, M.J. Terorio, M.C. Puerta, P. Valerga, Organometallics 17 (1998) 4392.
[17] F.A. Cotton, J.A. McCleverty, Inorg. Chem. 3 (1964) 1398.
[18] M. Moran, I. Cuadrado, J.R. Masaguer, J. Losada, C. Foces-Foces, F.H. Cano, Inorg. Chim. Acta 143 (1988) 59.
[19] M. Moran, I. Cuadrado, C. Munoz-Reja, J.R. Masaguer, J. Losada, J. Chem. Soc., Dalton Trans. (1988) 149.
[20] M. Moran, I. Cuadrado, J.R. Masaguer, J. Losada, J. Organomet. Chem. 352 (1987) 255.
[21] R. Bruce, G. Knox, J. Organomet. Chem. 6 (1966) 67.
[22] M.A. El-Hinnawi, A. Ajlouni, J. Organomet. Chem. 332 (1987) 321.
[23] M.A. El-Hinnawi, A. Ajlouni, J.S. Abu-Nasser, A.K. Powell, H. Wahrenkamp, J. Organomet. Chem. 359 (1989) 79.
[24] M.A. El-Hinnawi, M. El-khateeb, I. Jibril, S.T. Abu-Orabi, Synt. React. Org. Met. Org. Chem. 19 (1989) 109.
[25] M. El-khateeb, T. Obidate, Polyhedron 20 (2001) 2393.
[26] M. El-khateeb, K.J. Asali, A. Lataifeh, Polyhedron 22 (2003) 3105.
[27] M. El-khateeb, A. Younes, J. Organomet. Chem. 664 (2002) 228.
[28] M. El-khateeb, Inorg. Chim. Acta 357 (2004) 4341.
[29] M.A. El-Hinnawi, A.A. Aruffo, B.D. Santarsiero, D.R. McAlister, V. Shomaker, Inorg. Chem. 22 (1983) 1585.
[30] G.M. Sheldrick, SHELXS-97, Program for the Solution of Crystal Structures, University of Göttingen, Germany, 1997.
[31] G.M. Sheldrick, SHELXL-96, Program for the Refinement of Crystal Structures, University of Göttingen, Germany, 1996.

Despite these considerations, recent results have shown that oxygen ligands such as tri-*n*-octyl phosphine oxide prefer to bind to actinides rather than to lanthanides in suitable anionic extraction media [9]. In addition, diamides such as malonamides [10] and their derivatives [11], and ligands containing both phosphine oxide and amide functionalities such as CMPO molecules (CMPO = carbamoyl methyl phosphine oxide molecules of formula R^1R^2PO–CH_2–CO–NR^3R^4) [12] are henceforth targeted for carrying out both the co-extraction of the trivalent f-elements from the aqueous wastes and their subsequent separation. In this context, it is of interest to isolate and compare the structural parameters of analogous complexes of trivalent actinide and lanthanide ions with O=P and O=C donor ligands, with the aim to get further insight into the nature of the metal–oxygen bonds. Following previous work on the complexation of MI_3 (M = La, Ce, Nd) and $[UI_3(py)_4]$ with triphenylphosphine oxide [13], we focused our attention on the coordination of the simplest neutral *N*,*N*-dialkylamide, e.g. dimethylformamide (dmf), to these metal iodides. While dmf complexes of trivalent lanthanides [14–19] and uranium in high oxidation states are well documented [2,3], no uranium(III) compound with carbonyl-containing ligands has been reported so far. Here, we present the syntheses and crystal structures of dimethylformamide adducts of uranium(III) and lanthanide(III) iodides.

2. Results and discussion

2.1. Synthesis of the complexes

Evaporation of a dmf solution of LnI_3 (Ln = La, Ce, Nd) and trituration of the residue with diethyl ether or pentane afforded a pale yellow or white powder of the neodymium or cerium compounds, respectively, and a sticky white lanthanum product. Difficulties were encountered for isolating the complexes with a well-defined number of coordinated dmf molecules. Despite prolonged drying under vacuum, elemental analyses of the $[LnI_3(dmf)_n]$ complexes gave values of *n* close to 4 and 5 for Ln = Nd or Ce, respectively, and varying from 3 to 6 for Ln = La.

Dissolving $[UI_3(py)_4]$ in dmf gave a clear solution, the dark red colour of which was characteristic of an uranium(III) species. The latter was stable for days at room temperature but oxidation occurred upon heating at 110 °C, as shown by the rapid colour change from red to yellow and the formation of pale green crystals of $[U(dmf)_9]I_4$ [3a] after slow diffusion of diethyl ether into the dmf solution. The formation of $[U(dmf)_9]I_4$ may result from a disproportionation reaction of the thermally instable $[U(dmf)_9]I_3$ with concomitant formation of reactive low-valent species immediately oxidized by the solvent into unidentified species. Attempts to isolate the uranium(III) complex $[UI_3(dmf)_n]$ at room temperature gave an untractable dark red oil which was characterized only by its IR and ^{1}H NMR spectra.

The ^{1}H NMR spectra of the $[MI_3(dmf)_n]$ complexes (M = Ce, Nd, U) in acetonitrile-d_3 exhibit paramagnetic dmf signals with chemical shifts depending on the value of *n*. The strong absorptions in the 1644–1652 cm^{-1} region of the IR spectra are assigned to the stretching ν(C–O) frequencies (1675 cm^{-1} for the free ligand). In particular, the ν(C–O) band of the uranium complex (1644 cm^{-1}) is very close to that reported for the uranium(IV) derivative $[UI_4(dmf)_6]$ (1643 cm^{-1}) [3a].

2.2. Crystal structures of the complexes

Dark red crystals of $[U(dmf)_9]I_3$ suitable for X-ray diffraction analysis were obtained upon slow diffusion of diethyl ether into a dmf solution of $[UI_3(py)_4]$. In parallel, and although some $[Ln(dmf)_n]X_3$ complexes have already been crystallographically characterized [14–19], those with X = I have been prepared in order to compare the structures of analogous cationic compounds of closely sized 4f and 5f-elements with the same counterion. While crystallization of the $[Ln(dmf)_n]X_3$ complexes with weakly coordinating X anions was reported to be difficult [16], large colourless (La, Ce) and light pink (Nd) crystals were deposited in a few days from solutions of LnI_3 in a mixture of dmf and diethyl ether.

The two complexes $[Ln(dmf)_8]I_3$ (Ln = Ce (**1**), Nd (**2**)) are isomorphous; a view of the cation of **1** is represented in Fig. 1 and selected bond lengths and angles are given in Table 1. The metal centre, located on a binary axis, is eight-coordinate, surrounded by the oxygen atoms of eight monodentate dmf molecules, in a distorted square antiprismatic configuration. The two square faces of the antiprism, defined by the O(1), O(2), O(3′), O(4′) and O(1′), O(2′), O(3), O(4) atoms, are planar with the same maximum

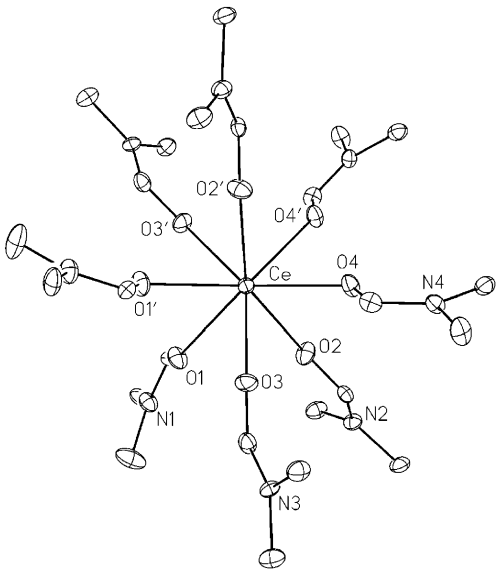

Fig. 1. View of the cation $[Ce(dmf)_8]^{3+}$ with displacement ellipsoids drawn at the 30% probability level. Hydrogen atoms are omitted for clarity. Symmetry code: $' = -x, y, 0.5 - z$.

Table 1
Selected bond lengths (Å) in complexes **1**–**5**

	$[Ce(dmf)_8]I_3$ (**1**)		$[Nd(dmf)_8]I_3$ (**2**)
M–O(1)	2.498(6)		2.469(2)
M–O(2)	2.455(5)		2.420(2)
M–O(3)	2.455(6)		2.423(2)
M–O(4)	2.479(5)		2.433(2)
⟨M–O⟩	2.472(18)		2.44(2)
	$[La(dmf)_9]I_3$ (**3**)	$[Ce(dmf)_9]I_3$ (**4**)	$[U(dmf)_9]I_3$ (**5**)
M(1)–O(1)	2.513(7)	2.499(8)	2.521(9)
M(1)–O(2)	2.509(5)	2.474(8)	2.499(9)
M(1)–O(3)	2.554(5)	2.534(8)	2.546(9)
M(1)–O(4)	2.597(5)	2.579(7)	2.575(8)
M(1)–O(5)	2.515(5)	2.488(8)	2.508(9)
M(1)–O(6)	2.506(5)	2.491(7)	2.509(8)
M(1)–O(7)	2.465(5)	2.449(8)	2.448(9)
M(1)–O(8)	2.523(5)	2.489(7)	2.515(8)
M(1)–O(9)	2.575(5)	2.560(8)	2.562(9)
M(2)–O(10)	2.546(9)	2.518(14)	2.540(13)
M(2)–O(11)	2.543(6)	2.520(9)	2.544(10)
M(2)–O(12)	2.498(9)	2.467(13)	2.479(12)
M(2)–O(13)	2.541(8)	2.518(10)	2.530(13)
M(2)–O(14)	2.469(5)	2.442(8)	2.444(9)
M(2)–O(15)	2.529(8)	2.480(12)	2.512(12)
M(2)–O(16)	2.534(8)	2.500(11)	2.525(12)
M(2)–O(17)	2.491(6)	2.461(9)	2.481(9)
M(2)–O(18)	2.623(6)	2.616(10)	2.628(11)
⟨M–O⟩	2.53(4)	2.50(4)	2.52(4)

deviation (due to the imposed symmetry) of 0.113(3) and 0.124(1) Å for **1** and **2**, respectively; these two bases are almost parallel with dihedral angles of 0.19(6)° (**1**) and 0.51(2)° (**2**). The geometry of the $[Ln(dmf)_8]^{3+}$ cation is quite identical to that found in the compounds $[Ce(dmf)_8]_2[WS_4]_3 \cdot H_2O$ [15], $\{[Ln(dmf)_8][Cu_6(CN)_9] \cdot 2dmf\}_\infty$ (Ln = Eu, Gd, Er) [14], $[Me_2NH_2][Gd(dmf)_8]_2[ClO_4]_4$ [16], $\{[Nd(dmf)_8][W_4Ag_5S_{16}]\}_\infty$ [18] and $[Ln(dmf)_8[ClO_4]_3$ (Ln = Gd, Tb) [16]. The average Ce–O and Nd–O bond lengths of 2.47(2) and 2.44(2) Å are similar to those measured in the aforementioned cerium and neodymium complexes [2.471 and 2.43 Å], and in the compound $\{[Nd(def)_8]_2[W_8Ag_{10}S_{32}]\}_\infty$ (def = diethylformamide) [2.42 (3) Å] [18,19].

Crystals of $[Ce(dmf)_9]I_3$ (**4**) were obtained in similar conditions from another batch of crystallization and were found to be isomorphous with those of the lanthanum and uranium analogues, **3** and **5**. Complex **5** provides, after $[U(MeCN)_9]I_3$ [20] and some compounds resulting from coordination of MX_3 (X = I, OSO_2CF_3) with polydentate nitrogen ligands [21], a new example of a uranium(III) trication. To the best of our knowledge, **5** is the first uranium(III) compound with coordinated O=C groups to have been isolated and crystallographically characterized. Aliphatic and aromatic ketones were found to be reductively coupled by U(III) species [22]. A view of one of the two independent and quite identical cations of **5** is shown in Fig. 2 and selected bond distances and angles are listed in Table 1, together with those of the lanthanum and cerium counterparts.

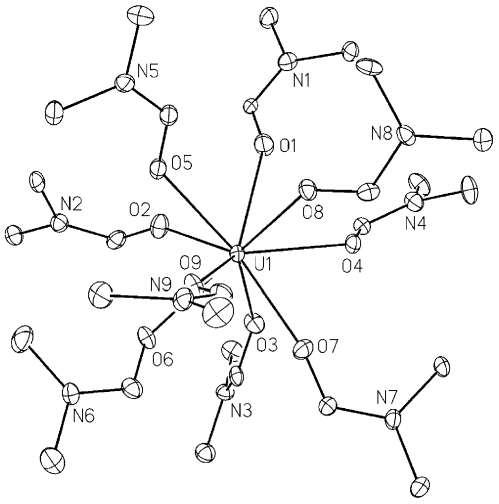

Fig. 2. View of one of the two independent cations $[U(dmf)_9]^{3+}$ with displacement ellipsoids drawn at the 20% probability level. Hydrogen atoms are omitted for clarity.

The metal atoms of **3**–**5** accommodate nine monodentate dmf ligands which form a slightly distorted monocapped square antiprism of oxygen atoms. The square faces are defined by the O(1,2,3,4) and O(5,6,7,8) atoms in the first cation and O(10,11,12,13) and O(14,15,16,17) atoms in the second, with atoms O(9) and O(18), respectively, in capping position of these second planes. The four atoms in each face are coplanar with a maximum deviation of 0.111(3) Å in **3**, 0.079(4) Å in **4** and 0.087(5) Å in **5**; the two mean planes in the two cations are almost parallel with dihedral angles of 2.8(3)° and 3.32(11)° in **3**, 2.5(5)° and 3.5(2)° in **4**, and 2.1(5)° and 3.8(2)° in **5**. The M(1)–O(9) and M(2)–O(18) axes are nearly perpendicular to the square faces, the angles with the normal to the proximal plane being 3.4° and 2.7° in **3**, 3.0° and 2.8° in **4**, and 3.4° and 2° in **5**. In the first independent cation of **3**–**5**, with the exception of the M(1)–O(4) distance of 2.597(5) Å in **3**, 2.579(7) Å in **4**, and 2.575(8) Å in **5**, the distances between M(1) and the capping O(9) atom of 2.575(5) Å in **3**, 2.560(8) Å in **4**, and 2.562(9) Å in **5** are longer than the distances between M(1) and the oxygen atoms of the square antiprism, which average 2.52(4), 2.50(4), and 2.52(3) Å for M = La, Ce and U, respectively. In the second independent cation, the M(2)–O(18) distances corresponding to the dmf ligand in capping position are the longest with values of 2.623(6) Å in **3**, 2.616(10) Å in **4**, and 2.628 (11) Å in **5**. The geometrical parameters of the $[La(dmf)_9]^{3+}$ cation are very similar to those found in $\{[La(dmf)_9]_2[Cu_{12}(CN)_{18}] \cdot 2dmf\}_\infty$ [14]. The trication $[U(dmf)_9]^{3+}$ adopts the same monocapped square antiprismatic configuration as the tetracation $[U(dmf)_9]^{4+}$ [3a]; the average distance between the uranium and oxygen atoms defining the square antiprism and that corresponding to the dmf ligands in capping position are longer in the uranium(III) complex, by ca. 0.13 and 0.14 Å, respectively. This difference reflects the variation in the radii of

the U^{3+} and U^{4+} ions and the distinct electronic charge of the complexes.

It is interesting to note that among the 4f series only the larger La^{3+} and Ce^{3+} ions can accommodate nine dmf ligands, whereas the other smaller lanthanide ions (Nd^{3+}, Eu^{3+}, Gd^{3+}, Tb^{3+}, Er^{3+}) give invariably the eight-coordinate solvate $[Ln(dmf)_8]^{3+}$. The U^{3+} ion, with an ionic radius intermediate between those of La^{3+} and Ce^{3+} [23], is also found in nine-coordination. The crystal structures of **3–5** confirm, after EXAFS studies of lanthanide perchlorates in dmf solution, that the nine-coordinate $[Ln(dmf)_9]^{3+}$ can exist in this solvent, particularly for Ln = La and Ce, while the eight-coordinate solvates were found to be present as the main species in dmf throughout the Ln(III) series [24]. These results would indicate that for the larger metals (La, U), $[M(dmf)_9]I_3$ predominates as the most easily crystallized complex, masking the isolation of the $[M(dmf)_8]I_3$ derivative.

Evidence for the more covalent character of the actinide–ligand versus lanthanide–ligand bonding was searched in the variations of bond distances in analogous An(III) and Ln(III) compounds [21,25,26]. A plot of the average M–O distances against the ionic radii of the metals in the eight- and nine-coordinate $[Ln(dmf)_n]^{3+}$ species (Ln = Yb, Gd, Nd, Ce and $n = 8$; M = La, Ce, U and $n = 9$) and also the nine-coordinate cation $[U(dmf)_9]^{4+}$ (Fig. 3) shows a quite perfect linear relationship, revealing that the M–dmf interactions in both trivalent and tetravalent 4f and 5f species are rather similar in nature. A similar observation was made with the complexes $[MX_2(OPPh_3)_4]X$ (M = Ce, U and $X = OSO_2CF_3$; M = Nd, Ce, La, U and X = I) where the variation of the M–O bond lengths of both the anionic and neutral ligands only reflected the differences between the radii of the M^{3+} ions [13]. This trend in the M–O distances whereas the U–N bond lengths of mono- and polyaromatic nitrogen ligands are systematically smaller than the corresponding Ln–N distances in analogous complexes demonstrates the presence of a larger contribution of covalency in the An–N bond.

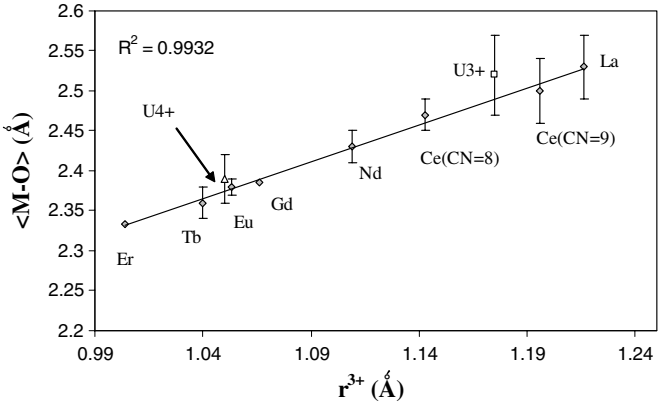

Fig. 3. Mean M–O distances as a function of the metal ionic radii in the $[Ln(dmf)_8]^{3+}$ (Ln = Er, Tb, Eu, Gd, Nd, Ce), $[M(dmf)_9]^{3+}$ (M = La, Ce, U) and $[U(dmf)_9]^{4+}$ cations. Standard deviations are indicated as vertical bars. The R^2 value corresponds to the line drawn for the sole Ln^{3+} ions.

3. Conclusion

Isolation of $[U(dmf)_9]I_3$, the first uranium(III) compound with carbonyl-containing ligands, demonstrates that uranium(III) species are stable at room temperature in dmf solution. The crystal structures of $[M(dmf)_9]I_3$ (M = La, Ce, U) confirm that the larger 4f and 5f trivalent ions can exist as nine-coordinate solvates in dmf solution. Comparison of the crystal structures of the $[M(dmf)_n]I_3$ compounds (M = Ce, Nd and $n = 8$; M = La, Ce, U and $n = 9$) and $[U(dmf)_9]I_4$ shows the difference between the average M–O distances to reflect the variation in the ionic radii of the metals, denoting that the nature of the M–O bonding is similar in these series of 4f and 5f compounds.

4. Experimental

4.1. General

All reactions were carried out under argon (<5 ppm oxygen or water) using standard Schlenk-vessel and vacuum-line techniques or in a glove box. Solvents (diethyl ether and acetonitrile) were dried over NaH and distilled immediately before use. Dimethylformamide (Aldrich) was stored over 3 Å molecular sieves and distilled immediately before use. Deuterated acetonitrile (Eurisotop) was dried over KH. $[UI_3(py)_4]$ was prepared as previously reported [27] and LnI_3 (Ln = La, Ce, Nd) (Aldrich) were used as received. ^{1}H NMR spectra were recorded on a Bruker DPX 200 instrument and referenced internally using the residual protio solvent resonances relative to tetramethylsilane (δ 0). IR spectra were recorded under nitrogen flush on a Perkin–Elmer FT-IR 1725X spectrometer, using nujol mulls of samples between KBr windows. The ultra-sound bath is a Branson 1510 apparatus (80 W, 40 kHz). Elemental analyses were performed by Analytische Laboratorien at Lindlar (Germany).

4.2. Syntheses

4.2.1. $[CeI_3(dmf)_5]$

A flask was charged with CeI_3 (79.5 mg, 0.15 mmol) and freshly distilled dmf (5 mL). The mixture was stirred for a few minutes until the solution was clear and the solvent was evaporated off. After drying under vacuum for 12 h at 25 °C, the white pasty powder was triturated in pentane (15 mL) and, after filtration, further dried for 15 h at room temperature, affording a white powder of $[CeI_3(dmf)_5]$ (135.3 mg, 80%).

^{1}H NMR (acetonitrile-d_3, 23 °C): 15.92 (1H, s, $w_{1/2}$ = 35 Hz, CH), 4.73 (3H, s, CH_3), 4.54 (3H, s, CH_3). IR ν/cm^{-1} 1645vs (CO). *Anal.* Calc. for $C_{15}H_{35}CeI_3N_5O_5$: C, 20.69; H, 4.04; N, 8.10. Found: C, 20.33; H, 3.98; N, 7.90%.

4.2.2. $[NdI_3(dmf)_n]$ (n = 4 and 4.5)

(a) A flask was charged with NdI_3 (136 mg, 0.259 mmol) and freshly distilled dmf (5 mL). The mixture was stirred at room temperature until a clear yellow-orange solution was obtained. Concentration to ca. 3 mL and addition of diethyl ether (ca. 10 mL) induced precipitation of a pale pink powder which was then washed with diethyl ether (2 × 5 mL). Drying under vacuum for 1 h at ca. 55 °C induce melting of the powder. The sticky residue was powdered by trituration in pentane (10 mL) and dried for 12 h at room temperature. The elemental analyses were in agreement with the formula $[NdI_3(dmf)_4]$ (169.4 mg, 80%).

^{1}H NMR (acetonitrile-d_3, 23 °C): 19.22 (1H, s, $w_{1/2}$ = 45 Hz, CH), 6.04 (3H, s, CH_3), 5.94 (3H, s, CH_3). IR ν/cm^{-1} 1650vs (CO). *Anal.* Calc. for $C_{12}H_{28}I_3N_4NdO_4$: C, 17.63; H, 3.45; N, 6.85. Found: C, 17.45; H, 3.31; N, 6.74%.

(b) A second experiment was carried out with NdI_3 (235 mg, 0.259 mmol) and freshly distilled dmf (5 mL). After complete dissolving, the solution was evaporated to dryness. The yellow residue melted when heated to ca. 50 °C, and was triturated and washed with pentane (10 mL). The yellow powder was dried under vacuum for 1 h at 65 °C (melting) and kept under dynamic vacuum for 15 h at room temperature. The elemental analyses were in agreement with the formula $[NdI_3(dmf)_{4.5}]$ (355 mg, 93%).

^{1}H NMR (acetonitrile-d_3, 23 °C): 17.09 (1H, s, $w_{1/2}$ = 30 Hz, CH), 5.35 (3H, s, CH_3), 5.20 (3H, s, CH_3). IR ν/cm^{-1} 1652vs (CO). *Anal.* Calc. for $C_{13.5}H_{31.5}I_3N_{4.5}NdO_{4.5}$: C, 18.42; H, 3.74; N, 7.43. Found: C, 18.77; H, 3.75; N, 7.44%.

4.2.3. $[LaI_3(dmf)_n]$ (n = 3 or 6)

(a) A flask was charged with LaI_3 (199 mg, 0.38 mmol) and freshly distilled dmf (5 mL). After heating at 70 °C for 1 h, the solution was evaporated to dryness and the residue dried under vacuum for 15 h, affording a white sticky residue. After addition of pentane (10 mL), the flask was immersed in the ultrasound bath for 30 min. Filtration and drying under vacuum for 2 h at room temperature afforded a white paste of $[LaI_3(dmf)_3]$ (276 mg, 97%).

^{1}H NMR (acetonitrile-d_3, 23 °C): 8.13 (1H, s, CH), 3.15 (3H, s, CH_3), 2.98 (3H, s, CH_3). IR ν/cm^{-1} 1644vs (CO). *Anal.* Calc. for $C_9H_{21}I_3LaN_3O_3$: C, 14.63; H, 2.86; N, 5.69. Found: C, 14.53; H, 2.96; N, 5.72%.

(b) An NMR tube was charged with LaI_3 (30 mg, 0.057 mmol) and freshly distilled dmf (1.5 mL). After heating at 110 °C for 3 h, diethyl ether (2 mL) was condensed under vacuum onto the colourless solution, inducing precipitation of a white powder. Filtration and drying under vacuum for 1 h at 60 °C then 12 h at room temperature afforded $[LaI_3(dmf)_6]$ as a white sticky powder (54 mg, 98%).

^{1}H NMR (acetonitrile-d_3, 23 °C): 8.14 (1H, s, CH), 3.13 (3H, s, CH_3), 2.94 (3H, s, CH_3). *Anal.* Calc. for $C_{18}H_{42}I_3LaN_6O_6$: C, 22.56; H, 4.42; N, 8.77. Found: C, 22.50; H, 4.35; N, 8.79%.

4.2.4. $[UI_3(dmf)_n]$

Dissolving $[UI_3(py)_4]$ in dmf led to a dark red solution. Evaporation of the solvent or attempts to precipitate the compound by concentration of the solution and addition of pentane or diethyl ether afforded a dark-red oil which was dried under vacuum for 12 h at room temperature.

^{1}H NMR (acetonitrile-d_3, 23 °C): 14.89 (1H, s, $w_{1/2}$ = 85 Hz, CH), 1.98 (3H, s, overlapped with solvent signal, CH_3), 1.86 (3H, s, CH_3). IR ν/cm^{-1} 1644vs (CO). The dark-red solution turned yellow by heating at 110 °C for 30 min; slow diffusion of diethyl ether into the solution induced the deposit of pale green crystals of $[U(dmf)_9]I_4$ in a few days.

4.3. Crystallography

Large well-shaped blocks, light pink (Nd), colourless (La, Ce) or dark red (U), were obtained in a few days at room temperature, by slow diffusion of diethyl ether into a dmf solution of LnI_3 or $[UI_3(py)_4]$. The data were collected at 100(2) K on a Nonius Kappa-CCD area detector diffractometer[1] using graphite-monochromated Mo Kα radiation (λ = 0.71073 Å). The crystals were introduced in glass capillaries with a protecting "Paratone-N" oil (Hampton Research) coating and quickly cooled in the nitrogen flow since all the crystals were found to melt in the oil within a few minutes. The data were processed with DENZO-SMN [28]. The structures were solved by direct methods with SHELXS-97 and subsequent Fourier-difference synthesis and refined by full-matrix least-squares on F^2 with SHELXL-97 [29]. Absorption effects were corrected empirically with the program DELABS from PLATON [30]. All non-hydrogen atoms were refined with anisotropic displacement parameters, with restraints for some unstable atoms in compounds **3**–**5**. Hydrogen atoms were introduced at calculated positions and were treated as riding atoms with a displacement parameter equal to 1.2 (CH) or 1.5 (CH_3) times that of the parent atom. Crystal data and refinement details are given in Table 2. The molecular plots were drawn with SHELXTL [31].

5. Supplementary material

Crystallographic data for the structures reported in this paper have been deposited with the Cambridge Crystallographic Data Center, CCDC 287215–287219 for **1**–**5**, respectively. Copies of this information may be obtained free of charge from The Director, CCDC, 12 Union Road, Cambridge, CB2 1EZ, UK on request (fax: +44 1223 336033; e-mail: deposit@ccdc.cam.ac.uk or www: http://www.ccdc.cam.ac.uk).

[1] Kappa-CCD Software, Nonius BV, Delft, The Netherlands, 1998.

Table 2
Crystal data and structure refinement details

	$[Ce(dmf)_8]I_3$ (**1**)	$[Nd(dmf)_8]I_3$ (**2**)	$[La(dmf)_9]I_3$ (**3**)	$[Ce(dmf)_9]I_3$ (**4**)	$[U(dmf)_9]I_3$ (**5**)
Chemical formula	$C_{24}H_{56}CeI_3N_8O_8$	$C_{24}H_{56}I_3N_8NdO_8$	$C_{27}H_{63}I_3LaN_9O_9$	$C_{27}H_{63}CeI_3N_9O_9$	$C_{27}H_{63}I_3N_9O_9U$
Crystal size (mm)	$0.14 \times 0.12 \times 0.10$	$0.16 \times 0.12 \times 0.08$	$0.28 \times 0.25 \times 0.16$	$0.18 \times 0.16 \times 0.10$	$0.30 \times 0.25 \times 0.20$
Colour	colourless	light pink	colourless	colourless	dark red
M (g mol^{-1})	1105.59	1109.71	1177.47	1178.68	1276.59
Crystal system	monoclinic	monoclinic	triclinic	triclinic	triclinic
Space group	$C2/c$	$C2/c$	$P\bar{1}$	$P\bar{1}$	$P\bar{1}$
a (Å)	22.9517(16)	22.7362(8)	12.7799(3)	12.8334(4)	12.8024(5)
b (Å)	16.0021(10)	15.9488(7)	16.8558(7)	16.8153(6)	16.8301(7)
c (Å)	11.6602(9)	11.6552(4)	21.6778(8)	21.6192(9)	21.6347(10)
α (°)	90	90	92.422(2)	92.547(2)	92.564(2)
β (°)	100.042(5)	100.025(3)	90.925(2)	90.854(2)	90.728(2)
γ (°)	90	90	95.188(2)	95.153(2)	95.240(3)
V (Å^3)	4216.9(5)	4161.8(3)	4645.5(3)	4641.1(3)	4636.8(3)
Z	4	4	4	4	4
ρ_{calcd} (g cm^{-3})	1.741	1.771	1.684	1.687	1.829
μ (Mo Kα) (mm^{-1})	3.322	3.519	2.963	3.026	5.548
$F(000)$	2148	2156	2304	2308	2444
Reflections collected	14144	13971	31630	149839	30537
Independent reflections	3980	3766	16131	17346	15914
Observed reflections [$I > 2\sigma(I)$]	2790	3366	13637	15534	12657
R_{int}	0.120	0.050	0.042	0.065	0.062
Parameters	208	208	883	883	883
R_1	0.054	0.025	0.052	0.069	0.069
wR_2	0.105	0.062	0.122	0.166	0.164
S	1.069	1.075	1.171	1.089	1.079
$\Delta\rho_{min}$ (e Å^{-3})	−0.86	−0.55	−0.78	−0.92	−1.55
$\Delta\rho_{max}$ (e Å^{-3})	0.66	0.56	1.33	1.28	1.43

References

[1] (a) V.K. Manchanda, P.N. Pathak, Sep. Purif. Technol. 35 (2004) 85;
(b) V.K. Manchanda, P.N. Pathak, A.K. Rao, Solvent Extr. Ion Exc. 22 (2004) 353;
(c) E.A. Mowafy, H.F. Aly, Solvent Extr. Ion Exc. 19 (2001) 629;
(d) V.K. Manchanda, P.B. Ruikar, S. Sriram, M.S. Nagar, P.N. Pathak, K.K. Gupta, R.K. Singh, R.R. Chitnis, P.S. Dhami, A. Ramanujam, Nucl. Technol. 134 (2001) 231.

[2] (a) T.R. Varga, A.C. Benyei, Z. Fazekas, H. Tomyasu, Y. Ikeda, Inorg. Chim. Acta 342 (2003) 291;
(b) S.Y. Kim, H. Tomiyasu, Y. Ikeda, J. Nucl. Sci. Technol. 39 (2002) 160;
(c) P. Thuéry, N. Keller, M. Lance, J.D. Vigner, M. Nierlich, Acta Crystallogr., Sect. C 51 (1995) 1526;
(d) A. Navaza, M.G. Iroulart, M. Nierlich, M. Lance, J. Vigner, Acta Crystallogr., Sect. C 49 (1993) 1767.

[3] (a) J.-C. Berthet, M. Nierlich, M. Ephritikhine, Inorg. Chem. 44 (2005) 1142;
(b) K.W. Bagnall, F. Benetollo, G. Bombieri, Polyhedron 11 (1992) 1765;
(c) P. Charpin, M. Lance, M. Nierlich, D. Vigner, H. Marquet-Hellis, Acta Crystallogr., Sect. C 44 (1988) 257.

[4] (a) J.-Y. Niu, M.-L. Wei, J.-P. Wang, D.-B. Dang, Eur. J. Inorg. Chem. (2004) 160;
(b) B. Yan, S.X. Wang, Z.D. Chen, J. Coord. Chem. 55 (2002) 573;
(c) H. Wang, Q. Xu, P. Quian, J. Tong, Z. Cao, Polyhedron 15 (1996) 4155.

[5] C. Musikas, Inorg. Chim. Acta 140 (1987) 197.

[6] M.P. Jansen, A.H. Bond, J. Am. Chem. Soc. 124 (2002) 9870, and references therein.

[7] (a) K.L. Nash, Solvent Extr. Ion Exc. 11 (1993) 729;
(b) K.L. Nash, in: K.A. GschneidnerJr., L. Eyring, G.R. Choppin, G.H. Lander (Eds.), Handbook on the Physics and Chemistry of Rare Earths, Lanthanides/Actinides: Chemistry, vol. 18, Elsevier Science, Amsterdam, 1994.

[8] (a) C. Madic, M.J. Hudson, J.O. Liljenzin, J.P. Glatz, R. Nannicini, A. Facchini, Z. Kolarik, R. Odoj, European Report EUR 19149 EN, Luxembourg, 2000.;
(b) Proceedings of the Fifth International Information Exchange Meeting on Actinides and Fission Products Partitioning and Transmutation, Mol, Belgium, 25–27 Nov. 1998, NEA/OECD Report, NEA/OECD, Paris, 1999.

[9] G. Suresh, M.S. Murali, J.N. Mathur, Radiochim. Acta 91 (2003) 127.

[10] (a) W. Liu, X. Li, Y. Wen, M. Tan, Dalton Trans. (2004) 640;
(b) S. Kannan, K.V. Chetty, V. Venugopal, M.G.B. Drew, Dalton Trans. (2004) 3604;
(c) L. Rao, P. Zanonato, P. Di Bernardo, A. Bismondo, J. Chem. Soc., Dalton Trans. (2001) 1939;
(d) C. Den Auwer, M.C. Charbonnel, M.G.B. Drew, M. Grigoriev, M.J. Hudson, P.B. Iveson, C. Madic, M. Nierlich, M.T. Presson, R. Revel, M.L. Russell, P. Thuéry, Inorg. Chem. 39 (2000) 1487;
(e) G.Y.S. Chan, M.G.B. Drew, M.J. Hudson, P.B. Iveson, J.O. Liljenzin, M. Skalberg, L. Spjuth, C. Madic, J. Chem. Soc., Dalton Trans. (1997) 649.

[11] (a) S. Nave, G. Modolo, C. Madic, F. Testard, Solvent Extr. Ion Exc. 22 (2004) 527;
(b) T. Yaita, A.W. Herlinger, P. Thiyagarajan, M.P. Jensen, Solvent Extr. Ion Exc. 22 (2004) 553;
(c) G.J. Lumetta, B.M. Rapko, B.P. Hay, P.A. Garza, J.E. Hutchison, R.D. Gilbertson, Solvent Extr. Ion Exc. 21 (2003) 29.

[12] (a) V. Rudzevitch, D. Schollmeyer, D. Braekers, J.F. Desreux, R. Diss, G. Wipff, V. Bohmer, J. Org. Chem. 70 (2005) 6027;
(b) K. Nakashima, F. Kubota, T. Maruyama, M. Goto, Ind. Eng. Chem. Res. 44 (2005) 4368;
(c) M.M. Reisona-Garcia, W. Verboom, D.N. Reinhoudt, F. Brisach, F. Arnaud-Neu, K. Liger, Solvent Extr. Ion Exc. 23 (2005) 425;
(d) S. Belair, C. Lamouroux, M. Tabarant, A. Labet, C. Mariet, P. Dannus, Solvent Extr. Ion Exc. 22 (2004) 791;

(e) K. Nakashima, F. Kubota, T. Maruyama, M. Goto, Anal. Sci. 19 (2003) 1097;
(f) M.W. Peters, E.J. Werner, M.J. Scott, Inorg. Chem. 41 (2002) 1707.
[13] J.-C. Berthet, M. Nierlich, M. Ephritikhine, Polyhedron 22 (2003) 3475.
[14] S. Liu, C.E. Plecnik, E.A. Meyer, S.G. Shore, Inorg. Chem. 44 (2005) 282.
[15] S. Jobic, S. Poirier-Coutansais, M. Evain, R. Brec, Mater. Res. Bull. 36 (2001) 2637.
[16] J.M. Harrowfield, B.W. Skelton, A.H. White, F.R. Wilner, Inorg. Chim. Acta 357 (2004) 2358.
[17] S. Liu, E.A. Meyers, S.G. Shore, Angew. Chem., Int. Ed. 41 (2002) 3609.
[18] Q. Huang, X. Wu, Q. Wang, T. Sheng, J. Liu, Angew. Chem., Int. Ed. 35 (1996) 868.
[19] L. Chen, X.-T. Wu, X.-C. Gao, W.-J. Zhang, P. Lin, J. Chem. Soc., Dalton Trans. (1999) 4303.
[20] (a) A.E. Enriquez, J.H. Matonic, B.L. Scott, M.P. Neu, Chem. Commun. (2003) 1892;
(b) A.E. Enriquez, B.L. Scott, M.P. Neu, Inorg. Chem. 44 (2005) 7403.
[21] (a) L. Karmazin, M. Mazzanti, J. Pécaut, Inorg. Chem. 42 (2003) 5900;
(b) J.-C. Berthet, Y. Miquel, P.B. Iveson, M. Nierlich, P. Thuéry, C. Madic, M. Ephritikhine, J. Chem. Soc., Dalton Trans. (2002) 3265;
(c) R. Wietzke, M. Mazzanti, J.-M. Latour, J. Pécaut, J. Chem. Soc., Dalton Trans. (2000) 4167.
[22] (a) M. Ephritikhine, O. Maury, C. Villiers, M. Lance, M. Nierlich, J. Chem. Soc., Dalton Trans. (1998) 3021;
(b) C. Villiers, M. Ephritikhine, Angew. Chem., Int. Ed. Engl. 36 (1997) 2380;
(c) A. Domingos, N. Marques, A. Pires de Matos, I. Santos, M. Silva, Organometallics 13 (1994) 654.
[23] R.D. Shannon, Acta Crystallogr., Sect. A 32 (1976) 751.
[24] S.-I Ishiguro, Y. Umebayashi, K. Kato, R. Takahashi, K. Ozutsumi, J. Chem. Soc., Faraday Trans. 94 (1998) 3607.
[25] (a) J.-C. Berthet, Y. Miquel, M. Nierlich, C. Madic, M. Ephritikhine, Dalton Trans. (2005) 369;
(b) J.-C. Berthet, C. Rivière, Y. Miquel, M. Nierlich, C. Madic, M. Ephritikhine, Eur. J. Inorg. Chem. (2002) 1439;
(c) C. Rivière, M. Nierlich, M. Ephritikhine, C. Madic, Inorg. Chem. 40 (2001) 4428.
[26] (a) L. Karmazin, M. Mazzanti, J.-P. Bezombes, C. Gateau, J. Pécaut, Inorg. Chem. 43 (2004) 5147;
(b) M. Mazzanti, R. Wietzke, J. Pécaut, J.-M. Latour, P. Maldivi, M. Remy, Inorg. Chem. 41 (2002) 2389;
(c) R. Wietzke, M. Mazzanti, J.-M. Latour, J. Pécaut, J. Chem. Soc., Dalton Trans. (1998) 4087.
[27] L.R. Avens, S.G. Bott, D.L. Clark, A.P. Sattelberger, J.G. Watkin, B.D. Zwick, Inorg. Chem. 33 (1994) 2248.
[28] Z. Otwinowski, W. Minor, Methods Enzymol. 276 (1997) 307.
[29] G.M. Sheldrick, SHELXS-97 and SHELXL-97, University of Göttingen, Germany, 1997.
[30] A.L. Spek, PLATON, University of Utrecht, The Netherlands, 2000.
[31] G.M. Sheldrick, SHELXTL, University of Göttingen, Germany, distributed by Bruker-AXS, Madison, WI, 1999.

Available online at www.sciencedirect.com
SCIENCE DIRECT®
Polyhedron 25 (2006) 1873
POLYHEDRON
www.elsevier.com/locate/poly

Corrigendum

Corrigendum to "Tris(imidazolyl) cadmium and zinc complexes: structural and spectroscopic characterization of M–OH_2 motifs" [Polyhedron 23 (2004) 405–412]

Janis K. Voo, Christopher D. Incarvito, Glenn P.A. Yap, Arnold L. Rheingold, Charles G. Riordan *

Department of Chemistry and Biochemistry, University of Delaware, Newark, DE 19716, USA

Available online 27 January 2006

During the refinement of the crystallographic data of **5**, the nitrogen of the N–CH_3 was inadvertently labeled as a carbon atom. This error has been corrected and the data subsequently refined. The conclusions drawn have not changed. The corrected CIF file has been deposited in the Cambridge Crystallographic Database. Additional changes resulting from the corrected refinement are as follows:

p. 408: Zn–OH_2 distance of **5** is 2.030(2) Å.
p. 409: O1···O2 distance is 2.808(3) Å in **5**.

Fig. 1. Correctly labeled structure of **5**.

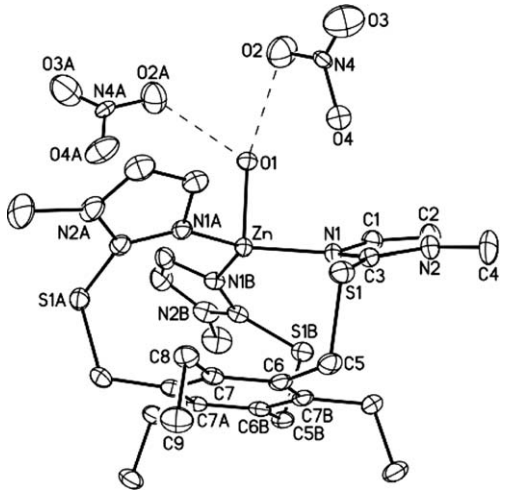

Table 1
Crystallographic data for **5**

Entries for **5**CH_3CN:	
Empirical formula	$C_{29}H_{41}N_9O_7S_3Zn$
μ(Mo, Kα) (cm^{-1})	9.28
$R(F)$, $R_w(F)$	0.0445, 0.0778
Goodness-of-fit on F^2	1.025

Table 2
Selected distances (Å) and angles (°) for complex **5**

Bond lengths	
Zn–N1	1.984(2)
Zn–O1	2.030(2)
O1···O2	2.808(2)
Bond angles	
N1–Zn–N2	119.11(2)
N1–Zn–O1	95.47(5)

DOI of original article: 10.1016/j.poly.2003.11.006.
* Corresponding author.
E-mail address: riordan@udel.edu (C.G. Riordan).

0277-5387/$ - see front matter © 2006 Elsevier Ltd. All rights reserved.
doi:10.1016/j.poly.2006.01.001

Our synthetic approach starts by focusing on the construction of new topological frameworks using flexible ligands by adjusting the lengths and flexibility, such as 1,2-bis(1,2,4-triazol-1-yl)ethane [9], 1,2-bis(benzotriazol-1-yl)ethane [10] and 1,4-bis(1,2,4-triazol-1-ylmethyl)-benzene [2e,11] due to their different conformations [12]. In order to investigate the influence of the flexibility of the ligand molecule, the counter anion and solvent system on the architecture of coordination polymers, we report in this paper the self-assembly reactions of the flexible ligand 1,2-bis(1,2,4-triazol-1-yl)ethane (bte) and cobalt(II) salts with different anions NO_3^-, NCO^- and NCS^-, and the structural characterization of five cobalt(II) coordination polymers, $\{[Co(bte)_2(H_2O)_2](NO_3)_2\}_n$ (**1**), $\{[Co(bte)(H_2O)_2(NCO)_2](H_2O)_2\}_n$ (**2**), $\{[Co(bte)_2(NCO)_2](H_2O)\}_n$ (**3**), $[Co(bte)_2(NCS)_2]_n$ (**4**) and $\{[Co(bte)(H_2O)_2(NCS)_2][Co(bte)_2(NCS)_2]\}_n$ (**5**). A conformational analysis of the ligand molecules in these complexes is also presented.

2. Experimental

2.1. General procedures

The flexible ligand 1,2-bis(1,2,4-triazol-1-yl)ethane was synthesized according to the literature method [12a]. All other reagents and solvents employed were commercially available and used as received without further purification. The C, H, N microanalyses were carried out with a Perkin–Elmer 240C analyser. IR spectra were obtained for KBr pellets on a Nicolet 170SX FT-IR spectrophotometer in the 4000–400 cm^{-1} region. Thermogravimetric data were collected on a Thermal Analyst 2100 TA Instrument and a SDT 2960 Simutaneous TGA-DTA Instrument in flowing dinitrogen at a heating rate 10 °C/min.

2.2. Preparation of the complexes

2.2.1. $\{[Co(bte)_2(H_2O)_2](NO_3)_2\}_n$ (**1**)

A methanolic solution (20 ml) of bte (0.164 g, 1.0 mmol) was added to an aqueous solution (20 ml) of $Co(NO_3)_2 \cdot 6H_2O$ (0.291 g, 1.0 mmol) with stirring. The pink single crystals 1 were obtained after the mixture was allowed to stand at room temperature for a month. Yield: 82%. *Anal*. Calc. for $C_{12}H_{20}CoN_{14}O_8$: C, 26.33; H, 3.68; N, 35.83. Found: C, 26.21; H, 3.52; N, 35.71%. IR data (cm^{-1}): 3372m, 3117m, 3040w, 1640w, 1531m, 1385vs, 1331 vs, 1285m, 1219w, 1138m, 1026m, 992w, 880w, 830w, 656s.

2.2.2. $\{[Co(bte)(H_2O)_2(NCO)_2](H_2O)_2\}_n$ (**2**)

A 20 ml DMF/H_2O (1:1, v/v) solution of $Co(NO_3)_2 \cdot 6H_2O$ (0.291 g, 1.0 mmol) and KNCO (0.162 g, 2.0 mmol) was added to one side of a "H-shape" tube, and 20 ml DMF/H_2O solution (1:1, v/v) of bte (0.164 g, 1.0 mmol) was added to the another side of the "H-shape" tube. After about two months, pale red crystals of **2** suitable for X-ray analysis were

Table 1
Crystallographic data for the five complexes

	1	**2**	**3**	**4**	**5**
Formula	$C_{12}H_{20}CoN_{14}O_8$	$C_8H_{16}CoN_8O_6$	$C_{14}H_{18}CoN_{14}O_3$	$C_{14}H_{16}CoN_{14}S_2$	$C_{22}H_{28}Co_2N_{22}O_2S_4$
Molecular weight	547.35	379.22	489.35	503.46	878.76
Crystal size (mm)	$0.30 \times 0.21 \times 0.05$	$0.80 \times 0.51 \times 0.22$	$0.41 \times 0.30 \times 0.12$	$0.50 \times 0.19 \times 0.11$	$0.50 \times 0.41 \times 0.20$
Temperature (K)	193.15	193.15	193.15	193.15	193.15
Crystal system	monoclinic	triclinic	monoclinic	monoclinic	triclinic
Space group	$P2_1/c$	$P\bar{1}$	$C2/m$	$P2_1/m$	$P\bar{1}$
a (Å)	8.640(2)	6.438(4)	9.904(6)	7.942(2)	7.786(2)
b (Å)	12.298(3)	7.229(4)	14.944(9)	14.143(3)	8.297(3)
c (Å)	10.246(2)	9.310(6)	7.425(5)	10.064(2)	14.740(5)
α (°)	90	110.77(2)	90	90	86.53(1)
β (°)	100.90(3)	99.22(2)	110.08(1)	98.26(3)	76.46(1)
γ (°)	90	99.84(2)	90	90	80.05(1)
V ($Å^3$)	1069.0(4)	387.6(4)	1032.2(11)	1118.6(4)	911.6(5)
Z	2	1	2	2	1
$F(000)$	562	195	522	514	448
D_{calc} (g cm^{-3})	1.700	1.625	1.575	1.495	1.601
μ (mm^{-1})	0.878	1.152	0.882	0.987	1.197
Reflections collected	7102	3707	4027	7395	7092
Unique reflections	2370	1710	1217	2503	3956
Parameters	168	122	83	151	246
Goodness-of-fit	1.095	1.033	1.077	1.023	1.082
$R_1[I > 2(\sigma I)]$	0.0665	0.0308	0.0350	0.0558	0.0304
wR_2 (all data)	0.1051	0.0861	0.0833	0.1279	0.0722

obtained. Yield: 46%. *Anal*. Calc. for $C_8H_{16}CoN_8O_6$: C, 25.33; H, 4.25; N, 29.56. Found: C, 25.24; H, 4.31; N, 29.48%. IR data (cm^{-1}): 3484m, 3133m, 2924m, 2855w, 2184vs, 1524s, 1439w, 1385m, 1319w, 1285m, 1211w, 1134s, 1015m, 988m, 891w, 675m, 644m, 625w, 509w.

2.2.3. $\{[Co(bte)_2(NCO)_2](H_2O)_2\}_n$ (3)

A DMF solution (10 ml) of bte (0.164 g, 1.0 mmol) was added to a DMF solution (10 ml) of $Co(NO_3)_2 \cdot 6H_2O$ (0.146 g, 0.5 mmol) and KNCO (0.081 g, 1.0 mmol) with stirring. Red crystals of **3** suitable for X-ray analysis were obtained after the mixture was allowed to stand for several days. Yield: 78%. *Anal*. Calc. for $C_{14}H_{18}CoN_{14}O_3$: C, 34.36; H, 3.71; N, 40.08. Found: C, 33.43; H, 3.75; N, 38.92%. IR data (cm^{-1}): 3482m, 3132m, 2170vs, 1525s, 1440m, 1384w, 1286m, 1209w, 1133s, 1014m, 987m, 893w, 676m, 645m, 626w, 510w.

2.2.4. $[Co(bte)_2(NCS)_2]_n$ (4)

The synthetic procedure was similar to the synthesis of **3**, except that KNCS was used instead of KNCO. Yield: 75%. *Anal*. Calc. for $C_{14}H_{16}CoN_{14}S_2$: C, 33.40; H, 3.20; N, 38.96. Found: C, 33.24; H, 3.14; N, 38.81%. IR data (cm^{-1}): 3476w, 3117w, 2076vs, 1524s, 1439m, 1385w, 1350w, 1285m, 1211w, 1130s, 1069w, 1011m, 992m, 895w, 791w, 677m, 660w, 529w.

2.2.5. $\{[Co(bte)(H_2O)_2(NCS)_2]\ [Co(bte)_2(NCS)_2]\}_n$ (5)

A 20 ml DMF/H_2O (1:1, v/v) solution of $Co(NO_3)_2 \cdot 6H_2O$ (0.291 g, 1.0 mmol) and KSCN (0.194 g, 2.0 mmol) was added to one side of a "H-shape" tube, and 20 ml DMF/H_2O solution (1:1, v/v) of bte (0.328 g, 2.0 mmol) was added to the another side of the "H-shape" tube. Pink crystals of **5** suitable for X-ray analysis were obtained after one month. Yield: 45%. *Anal*. Calc. for $C_{22}H_{28}Co_2N_{22}O_2S_4$: C, 30.07; H, 3.21; N, 35.07. Found: C, 30.11; H, 3.15; N, 34.92%. IR data (cm^{-1}): 3360m, 3125m, 2963w, 2074vs, 2064vs, 1524s, 1447w, 1435w, 1385m, 1350w, 1289s, 1211m, 1134s, 1069w, 1022m, 992m, 903m, 864w, 791w, 675s, 644m, 517w.

2.3. X-ray crystallography

All data collections were performed at a temperature of 193 K on a Rigaku Mercury CCD diffractometer with the ω-scan technique. The structures were solved by direct methods and refined with the full-matrix least-squares technique using the SHELXS-97 and SHELXL-97 programs [13]. Anisotropic thermal parameters were assigned to all non-hydrogen atoms. The hydrogen atoms of bte ligands were generated geometrically. The hydrogen atoms of water molecules except the hydrogen atoms of disordered water molecules of **3** were located from difference maps. The crystallographic data and experimental details for the structural analyses are listed in Table 1. The selected bond lengths and angles are listed in Table 2.

Table 2
Selected bond lengths (Å) and angles (°) for the five complexes[a]

1	
Co(1)–O(1)	2.078(3)
Co(1)–N(6)^{i}	2.136(3)
Co(1)–N(3)	2.165(3)
N(3)–Co(1)–N(6)^{i}	89.8(1)
O(1)–Co(1)–N(6)^{i}	89.7(1)
O(1)–Co(1)–N(3)	88.4(1)
2	
Co(1)–N(3)	2.170(2)
Co(1)–O(2)	2.136(2)
Co(1)–N(4)	2.084(2)
N(3)–Co(1)–N(4)	89.42(7)
O(2)–Co(1)–N(4)	88.70(7)
O(2)–Co(1)–N(3)	87.62(6)
3	
Co(1)–N(3)	2.170(2)
Co(1)–N(4)	2.110(2)
N(3)–Co(1)–N(3)^{i}	93.93(9)
N(3)–Co(1)–N(4)	89.33(7)
N(3)–Co(1)–N(3)^{ii}	86.07(9)
4	
Co(1)–N(3)	2.124(3)
Co(1)–N(7)	2.144(4)
Co(1)–N(6)^{ii}	2.172(3)
Co(1)–N(8)	2.161(4)
N(3)–Co(1)–N(3)^{i}	94.3(1)
N(3)–Co(1)–N(6)^{iii}	85.7(1)
N(7)–Co(1)–N(8)	175.7(1)
N(3)–Co(1)–N(8)	89.1(1)
N(8)–Co(1)–N(6)^{ii}	88.8(1)
N(3)–Co(1)–N(6)^{ii}	177.9(1)
N(6)^{ii}–Co(1)–N(6)^{iii}	94.2(1)
N(3)–Co(1)–N(7)	93.8(1)
N(7)–Co(1)–N(6)^{ii}	88.3(1)
5	
Co(1)–N(3)	2.182(1)
Co(1)–O(1)	2.100(1)
Co(2)–N(10)	2.130(2)
Co(1)–N(4)	2.102(2)
Co(2)–N(7)	2.137(2)
Co(2)–N(11)	2.120(2)
N(4)–Co(1)–N(3)	90.07(6)
O(1)–Co(1)–N(4)	86.88(6)
N(11)–Co(2)–N(7)	90.85(6)
O(1)–Co(1)–N(3)	91.07(5)
N(10)–Co(2)–N(7)	93.30(6)
N(11)–Co(2)–N(10)	89.27(6)

[a] Symmetry codes for **1**: (i) $x, -y-0.5, z-0.5$; for **3**: (i) $x, -y, z$; (ii) $-x, y, -z$; for **4**: (i) $x, -y+0.5, z$; (ii) $x+1, -y+0.5, z$; (iii) $x+1, y, z$.

3. Results and discussion

3.1. Preparation of the complexes, IR and thermogravimetric analyses

During the preparation of the Co/bte complexes, the direct reaction of bte with cobalt nitrate in MeOH/H_2O solution produced **1**. As NCO^- and NCS^- not only can act as counter anions to sustain charge neutral but also have various coordination modes, they can provide the suitable "building block" for assembling novel coordination polymers. We want to introduce these anionic ligands into the $Co(NO_3)_2 \cdot 6H_2O$/bte reaction mixture as co-ligands in order to prepare some novel bte/Co complexes.

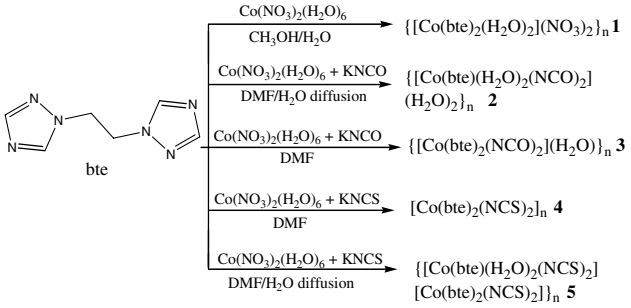

We found that the solvent systems and reaction methods (the direct reaction and the slow diffusion method) play a key role in the assembly of novel coordination polymers. Direct mixing of $Co(NO_3)_2 \cdot 6H_2O$, NCO^- or NCS^- and bte in MeOH/H_2O solution resulted in poor crystalline solids. The direct reaction of $Co(NO_3)_2 \cdot 6H_2O$, bte and NCO^- or NCS^- with different Co/bte stoichiometry (Co/bte = 1:2, 1:1.5, 1:1) in different solvent systems (DMF, DMF/H_2O) produces the similar double-stranded chain complexes **3** and **4**. When $Co(NO_3)_2 \cdot 6H_2O$, NCO^- or NCS^- react with bte in 1:2:1, 1:2:2 or 1:2:1.5 ratios in DMF/H_2O solution through the slow diffusion method the single chain complex **2** with $Co:NCO^-:bte = 1:2:1$ and the both single chain and double-stranded chain complex **5** with $Co:NCS^-:bte = 1:2:1.5$ are produced.

The very strong absorption at 1385 cm^{-1} in **1** is attributed to free nitrate anion. The very strong absorption bands at 2184 cm^{-1} in **2** and 2170 cm^{-1} in **3** are attributed to N-bonded NCO^- anions. The very strong absorption band in **4** at 2076 cm^{-1} is assigned to the N-bonded NCS^- anion. The very strong C≡N stretching vibrations of NCS^- ions at 2074 and 2064 cm^{-1} in **5** show two different coordination environment N-bonded NCS^- anions, which is confirmed by the crystal structure of **5** that contains both single- and double-stranded chains. The IR spectra determination show that the triazole ring breathing vibrations in complexes **1**, **2**, **3**, **4** and **5** are 1531, 1524, 1525, 1524 and 1524 cm^{-1}, respectively. The strong absorption bands at 1273 cm^{-1} assigned to the triazole ring stretching vibration for the free bte ligand are also present in the spectra of the complexes, these absorption band being shifted to 1285, 1285, 1286, 1285 and 1289 cm^{-1} in complexes **1**, **2**, **3**, **4** and **5**, respectively.

To study the stability of the five polymers, thermogravimetric analyses were performed (see supporting material). Thermal analysis of **1** shows that the coordinated water molecules were lost in a continuous fashion (obsd., 6.3%; calcd., 6.6%) from 120 to 190 °C, the next weight loss is about 58.6% from 190 to 303 °C, which is tentatively assigned to the loss of two bte molecules (obsd., 58.6%; calcd., 60.0%). Thermal analysis of **2** shows that the water molecules were lost from 30 to 120 °C (obsd., 18.2%; calcd., 19.0%). The weight of **2** rapidly decreased from 174 to 235 °C by 39.1%, and then the weight slowly decreased from 235 to 307 °C by 13.9%. Thermal analysis of **3** shows that lattice water molecules (obsd., 2.9%; calcd., 3.7%) were lost from 50 to 110 °C. Polymer **4** is stable up to 182 °C. The 31.6% weight loss of **3** and 33.5% weight loss of **4** occurred rapidly from 180 to 250 °C for **3** and from 182 to 262 °C for **4**, which can tentatively be assigned to one bte ligand (Calcd. 33.5% for **3** and 32.6% for **4**). Then 12.8% of the weight of **3** and 38.9% of the weight of **4** were lost from 250 to 303 °C for **3** and from 300 to 370 °C for **4**, respectively. Above this point, the weight of the samples slowly decreased. The coordinated water molecules of **5** were lost (obsd., 4.1%; calcd., 4.1%) from 150 to 193 °C. The 17.5% weight loss of **5**, occurring from 193 to 270 °C, is tentatively assigned to one bte ligand (calcd., 18.7%). Then the 42.1% weight loss from 310 to 370 °C may be assigned to two bte molecules (calcd., 37.4%) and part of NCS^-.

3.2. Crystal structures

The structure of **1** is isomorphous with those of the Cd and Zn derivatives $\{[Cd(bte)_2(H_2O)_2](NO_3)_2\}_n$ [9a] and $\{[Zn(bte)_2(H_2O)_2](NO_3)_2\}_n$ [9f]. The known bte complexes are presented in Table 3 for understanding the similarity/differences among them. As shown in Fig. 1(a), the cobalt(II) atom in **1** is in a distorted octahedral arrangement with two water molecules in *trans* positions (Co(1)–O(1) 2.078(3) Å) and four triazole nitrogen atoms in a basal plane (Co(1)–N(3) 2.165(3) Å, Co(1)–N(6)^i 2.136(3) Å) (Table 2). Each bte ligand connects two cobalt(II) atoms to form a two-dimensional (4,4) network containing square $Co_4(bte)_4$ units (Fig. 1(b)). The two-dimensional network structure consists of puckered rhombus grids with dimensions of 8.0 × 8.0 Å. The basic grid of the two-dimensional network is puckered [14,9a,9f] (Fig. 1(c)), which is different from that observed in previous grid-like

Table 3
The structures and space groups of the known bte complexes

Complex	Space group	Structure	Reference
$\{[Co(bte)_2(H_2O)_2](NO_3)_2\}_n$ (**1**)	$P2_1/c$	isomorphous with undulating 2D (4,4) network	this work
$\{[Cd(bte)_2(H_2O)_2](NO_3)_2\}_n$	$P2_1/c$		[9a]
$\{[Zn(bte)_2(H_2O)_2](NO_3)_2\}_n$	$P2_1/c$		[9f]
$\{[Co(bte)(H_2O)_2(NCO)_2](H_2O)_2\}_n$ (**2**)	$P\bar{1}$	1D single chain	this work
$\{[Co(bte)_2(NCO)_2](H_2O)\}_n$ (**3**)	$C2/m$	similar double-stranded chain	this work
$[Co(bte)_2(NCS)_2]_n$ (**4**)	$P2_1/m$		this work
$\{[Cd(bte)_2(H_2O)_2](H_2O)_2(ClO_4)_2\}_n$	$P\bar{1}$		[9a]
$\{[Co(bte)_2(NCS)_2][Co(bte)(H_2O)(NCS)_2]\}_n$ (**5**)	$P\bar{1}$	isomorphous containing both single chain and double-stranded chain	this work
$\{[Mn(bte)_2(NCS)_2][Mn(bte)(H_2O)(NCS)_2]\}_n$	$P\bar{1}$		[9b]
$[Mn(bte)_2(dca)_2]_n$	$P2_1$/n	isomorphous with double-stranded chain	[9b]
$[Zn(bte)_2(dca)_2]_n$	$P2_1$/n		[9c]
$[Zn(bte)(N_3)_2]_n$	$P\bar{1}$	1D chain	[9d]
$\{[Cd(bte)_3](NO_3)_2\}_n$	$R3$	3D α-polonium cubic network	[9a]
$\{[Cd(bte)(NO_2)_2]\}_n$	$P2_1/c$	2D rhombic network	[9a]
$[Cd(bte)(NCS)_2]_n$	$P\bar{1}$	2D rhombic network	[9a]
$[Cu(dien)(bte)](ClO_4)_2$	$P1$	1D chain	[9e]
$[Cu(en)_2(bte)](ClO_4)_2$	$P1$	1D chain	[9e]

structures where the basic grids are usually coplanar or quasi-coplanar [15]. The puckered shape of the basic grid in **1** is understandable because the bte ligands exhibit the *gauche* conformation in **1**. There are hydrogen bond interactions between hydrogen atoms of coordinated water molecules and oxygen atoms of nitrate anions [O(1)···O(3) $(-x+1,-y,-z+1)$ 2.735(4) Å, O(1)···O(2) $(-x+1,y-1/2,-z+1/2)$ 2.990(4) Å, O(1)···O(4) $(-x+1,y-1/2,-z+1/2)$ 2.910(4) Å].

The crystal structure of **2** consists of single chains. The cobalt(II) atom in **2** is in a distorted octahedral arrangement with two water molecules in *trans* positions (Co(1)–O(2) 2.136(2) Å), and two triazole nitrogen atoms (Co(1)–N(3) 2.170(2) Å) and two cyanate nitrogen atoms (Co(1)–N(4) 2.084(2) Å) (Table 2) in a basal plane (Fig. 2(a)). The bte ligand exhibits the *anti* conformation in **2**. Each bridging bte ligand links two Co(II) atoms to form a single chain. The Co···Co separation across the bridging bte is 12.138 Å. The coordinated water molecules act as a hydrogen bond donor, forming hydrogen bonds with the lattice water molecules [O(2)···O(3) $(-x,-y+1,-z+1)$ 2.739 Å, O(2)···O(3) $(x,y-1,z)$ 2.790 Å]. The lattice water molecules also act as a hydrogen bond donor, forming hydrogen bonds with the oxygen atom of the cyanate and the uncoordinated nitrogen atom in the 2-positions of the triazole rings in the neighboring one-dimensional chain [O(3)···O(1) $(x+1,y+1,z)$ 2.727 Å, O(3)···N(2) $(-x,-y+1,-z)$ 2.845 Å]. The three-dimensional network forms via these hydrogen bond interactions (Fig. 2(b)).

The structure of **3** is completely different from the structure of **2** although **2** and **3** are both constructed by cobalt(II), bte ligand and NCO^- anion. **3** forms a double-stranded chain structure whilst **2** exhibits a single chain structure. The key factor governing the structural topologies of these polymers is the Co/bte molar ratio (Co/bte = 1:1 in **2** and Co/bte = 1:2 in **3**).

3 and **4** have similar double-stranded chain structures and will be discussed together. The difference between **3** and **4** is that the lattice water is located at the voids for **3** but not for **4**. The cobalt(II) atom is in a distorted octahedral arrangement with two nitrogen atoms from two NCO^- anions in **3** (Fig. 3) and two NCS^- anions in **4** (Fig. 4) in *trans* positions and four triazole nitrogen atoms in a basal plane, which is similar to the coordination geometry of the cobalt(II) atoms in **1**, except two coordination water molecules in **1** are replaced by two coordination NCO^- anions or NCS^- anions in **3** and **4**, respectively. The four Co–$N_{triazole}$ bond lengths are all 2.170(2) Å in **3** and the two pairs of Co–$N_{triazole}$ bond lengths in **4** are 2.124(3) and 2.172(3) Å (Table 2). The two Co–$N_{cyanate}$ bond lengths in **3** are both 2.110(2) Å and the two Co–$N_{thiocyanate}$ bond lengths in **4** are 2.144(4) and 2.161(4) Å. **3**, **4** and **1** have the same Co/bte molar ratio (Co/bte = 1/2). The different structures in **1**, **3** and **4** show that the supramolecular topologies are highly influenced by the counter anions.

The bte ligands exhibit the *gauche* conformation in **3** and **4**. Two strands of bte ligands are wrapped around each other and are held together by Co(II) atoms, forming a double-stranded chain. Many double-stranded chain complexes have been reported recently [3a,7b,9a,9b,9c,14,16]. This structure is similar to other double-stranded chain structures containing the bte ligand, such as $\{[Cd(bte)_2(H_2O)_2](H_2O)_2(ClO_4)_2\}_n$ (**9a**), $[Mn(bte)_2(dca)_2]_n$ (dca = dicyanamide, **9b**) and $[Cd(bte)_2(dca)_2]_n$ (**9c**), which were reported by us recently. Each chain consists of 18-membered rings and a rhombic network with a size of 6.5×5.6 Å in **3** and **4** is formed. The

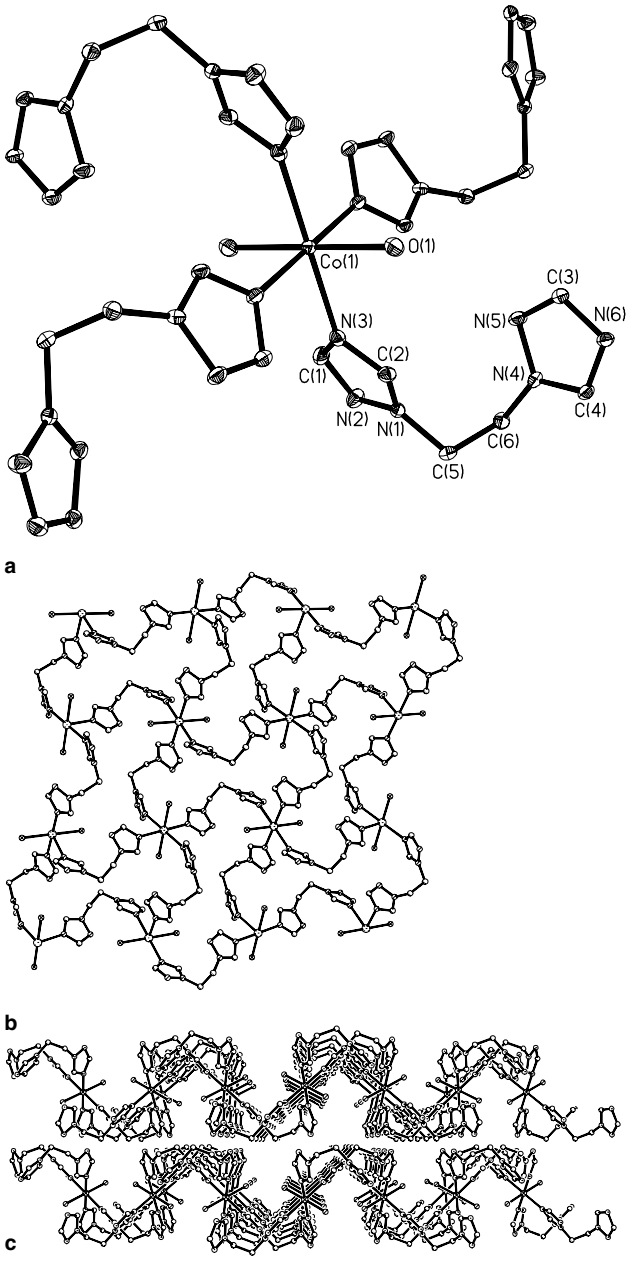

Fig. 1. (a) ORTEP drawing of the coordination environment of the cobalt(II) atom in **1**. (b) Viewing the 2D (4,4) network in **1** along the *a* direction. (c) Viewing the tightly packed structure in **1** along the *c* direction, only two layers are shown for clarity.

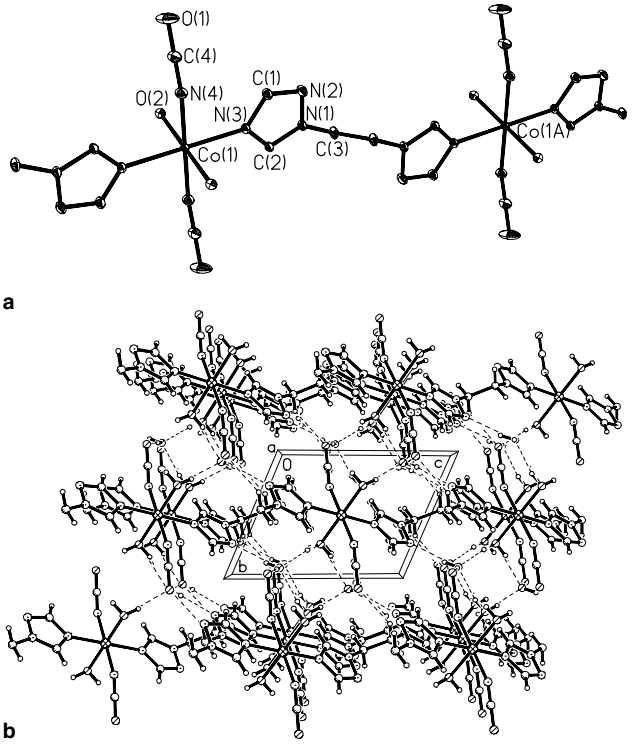

Fig. 2. (a) The coordination environment around the cobalt(II) center with 30% thermal ellipsoids in **2**. (b) The cell packing of **2** viewed along the *a* direction.

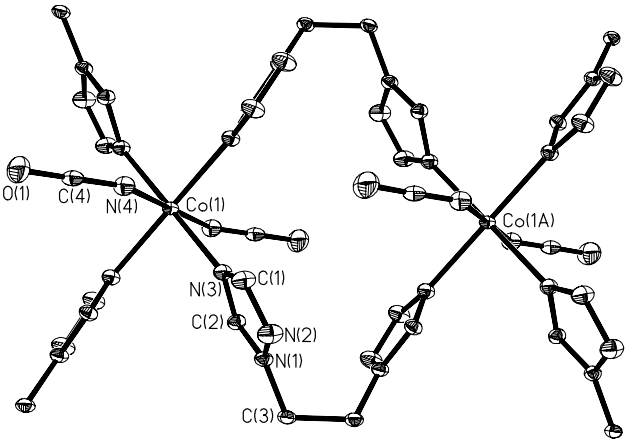

Fig. 3. The coordination environment around the cobalt(II) center with 30% thermal ellipsoids in **3**.

Co···Co separations across the bridging bte ligand are 7.425 and 7.942 Å in **3** and **4**, respectively.

The structure of **5** and $\{[Mn(bte)(H_2O)_2(NCS)_2]\text{-}[Mn(bte)_2(NCS)_2]\}_n$ (**9b**) are isomorphous, which is very interesting and can be regarded as a combination of two motifs (single chain + double-stranded chain). It is interesting to note that bte ligands adopt both the *gauche* and *anti* conformations in one compound.

As shown in Fig. 5(a), the single chain in **5** is very similar to that of **2**. The coordination environment of the cobalt (II) atom in **5** (Co(1)–N(3) 2.182(1) Å, Co(1)–N(4) 2.102(2) Å, Co(1)–O(1) 2.100(1) Å) (Table 2) is also similar to that of the cobalt(II) atom in **2**. The difference is only two NCS^- anions in **5** and two NCO^- anions in **2**. The bridging bte ligand links two cobalt(II) atoms forming the single chain. The Co···Co separation across the bridging bte in the single chain (12.320 Å) is similar to that in **2** (12.138 Å).

As depicted in Fig. 5(b), the double-stranded chain in **5** is very similar to that of **4** and **3**. The coordination environment of the cobalt (II) atom in **5** (Co(2)–N(7)

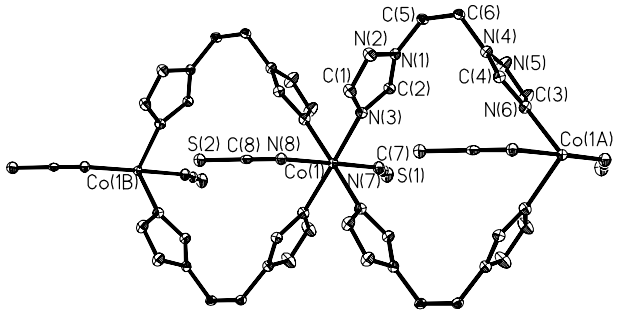

Fig. 4. The coordination environment around the cobalt(II) center with 30% thermal ellipsoids in **4**.

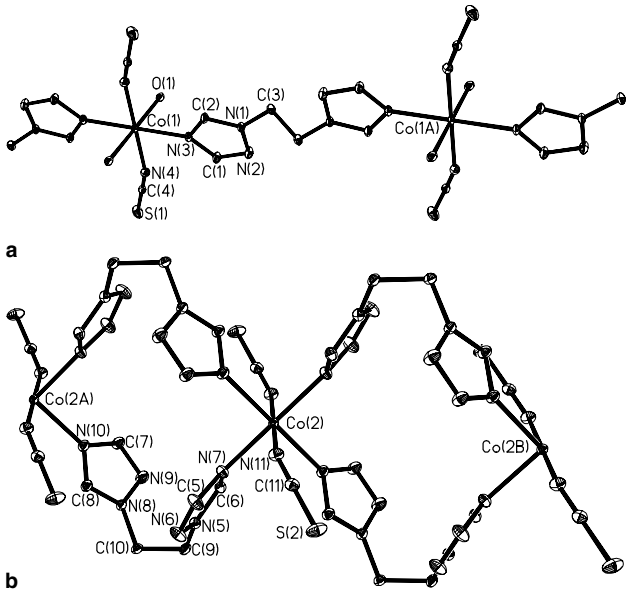

Fig. 5. The coordination environment around the cobalt(II) center with 30% thermal ellipsoids in **5**. (a) The single chain. (b) The double-stranded chain.

2.137(2) Å, Co(2)–N(10) 2.130(2) Å, Co(2)–N(11) 2.120(2) Å) (Table 2) is the same as that of the cobalt(II) atom in **4**. The Co···Co separation across the bridging bte ligand is equal to the *a* axis translation, 7.786 Å.

The most interesting structural feature of **5** is that there are two different structural motifs in one compound. Coordination polymers that have different topologies and/or chemical composition are relatively few at present [2,4a,4c,9b,17]. There are uncoordinated nitrogen atoms at the 2-position of the triazole rings of both the *gauche* and *anti* conformation bte molecules. A two-dimensional hydrogen bond network is formed by the hydrogen bond interactions between the oxygen atoms O(1) of coordinated water and the uncoordinated N(2) atoms at the 2-position of trazole rings of the *anti* conformation bte ligand of the neighboring 1D chains [O(1)···N(2)($-x, -y, -z+1$), 2.882 Å] (Fig. 6(a)). Hydrogen bond interactions also occur between the oxygen atoms O(1) of the single chains and uncoordinated nitrogen atoms N(6) at the 2-position of triazole rings of the *gauche* conformation bte ligand of the neighboring double-strand chains [O(1)···N(6) ($-x+1, -y, -z$), 2.791 Å]. The single chains and double-stranded chains in **5** stack alternately along the *c* axis via the hydrogen bond interactions and form the three-dimensional hydrogen bonding network (Fig. 6(b)).

3.3. Conformational analysis

In order to understand the influence of the flexibility of the bte ligand on the topologies of the motifs, the conformation of bte, N···N distance between two donor atoms of bte, Co···Co separation through bte, the torsion angles (°) $N_{triazole}$–$(C–C)_{ethane}$–$N_{triazole}$, $(N–N)_{triazole}$–$(C–C)_{ethane}$ and $(C–N)_{triazole}$–$(C–C)_{ethane}$ in free bte and the five cobalt(II) complexes are listed in Table 4. There are three motifs (2D (4,4) network, single chain and double-stranded chain) in the five complexes: 2D (4,4) network (**1**), single chain (**2**), double-stranded chain (**3** and **4**), and a combination of two motifs (single chain + double-stranded chain) (**5**). The bte ligands act in the *anti* conformation in **2**, part of **5** and free bte molecules, and act in the *gauche* conformation in **1**, **3**, **4** and part of **5**.

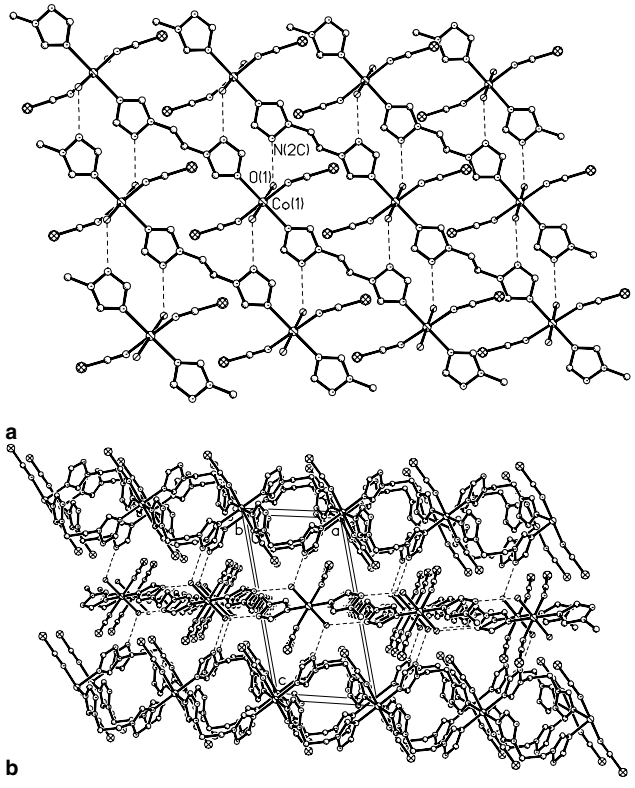

Fig. 6. (a) View of the hydrogen-bonding interaction between single chains in **5**. (b) The cell packing of **5** viewed along the *b* direction.

Table 4
The conformation of bte, N···N distance between two donor atoms of bte (Å), Co···Co separation through bte (Å), the torsion angles (°) $N_{triazole}$–$(C–C)_{ethane}$–$N_{triazole}$, $(N–N)_{triazole}$–$(C–C)_{ethane}$ and $(C–N)_{triazole}$–$(C–C)_{ethane}$ in bte and the five cobalt(II) complexes

	bte Conformation	N···N distance	Co···Co separation	Dihedral angle of two triazole rings	Torsion angle		
					$N_{triazole}$–$(C–C)_{ethane}$–$N_{triazole}$	$(N–N)_{triazole}$–$(C–C)_{ethane}$	$(C–N)_{triazole}$–$(C–C)_{ethane}$
Bte	*anti*	7.890		0.0	180.0	77.61(16)	−100.74(16)
1	*gauche*	5.619	8.003	32.7(2)	68.3(4)	88.7(4), −89.1(4)	−86.4(4), 91.3(4)
2	*anti*	7.969	12.138	0.0	180.0	65.7(2)	−116.5(2)
3	*gauche*	4.884	7.425	56.69(7)	48.8(3)	−61.5(4)	116.9(3)
4	*gauche*	5.314	7.942	66.29(9)	62.1(3)	67.3(4), 56.0(4)	−112.9(3), −126.0(3)
5							
A	*anti*	8.080	12.320	0.0	180.0	−49.3(3)	139.2(2)
B	*gauche*	5.204	7.786	65.35(6)	57.5(2)	63.2(2), −50.9(2)	−117.7(2), 127.75(19)

The transition from double-stranded chain (**3**, **4**, part of **5**), 2D (4,4) network (**1**), to single chain (**2** and part of **5**) corresponds to the change of the character of the bte molecules from angular (the *gauche* conformation in **3**, **4**, part of **5** and **1**) to more linear (the *anti* conformation in **2**, part of **5** and free bte). In consequence, the Co···Co separations through the *gauche* conformation bte molecules (7.425 Å in **3**, 7.942 Å in **4**, 7.786 Å in part of **5** and 8.003 Å in **1**) are about 4.1–4.9 Å shorter than the Co···Co separations through the *anti* conformation bte molecules (12.138 Å in **2** and 12.320 Å in part of **5**). The N···N distances between two donor atoms of the *gauche* conformation bte molecules (4.884 Å in **3**, 5.314 Å in **4**, 5.204 Å in part of **5** and 5.619 Å in **1**) are about 2.3–3.2 Å shorter than the corresponding N···N distances of the *anti* conformation bte molecules (7.969 Å in **2**, 8.080 Å in part of **5**, 7.890 Å in free bte).

The torsion angles $N_{triazole}$–$(C–C)_{ethane}$–$N_{triazole}$ and dihedral angles show great differences between the *gauche* and *anti* conformations of bte. The torsion angles and dihedral angles of the *anti* conformation bte are 180.0° and 0.0°, respectively, in **2**, part of **5** and free bte. The torsion angles of the *gauche* conformation bte show slight differences, which range from 48.8(3)° in **3** to 68.3(4)° in part of **5** in the four complexes, but the dihedral angles of the *gauche* conformation bte show large differences, which range from 32.7(2)° in **1**, to 56.69(7)° in **3**, 65.35(6)° in part of **5** and 66.29(9)° in **4**. There are also great differences of the torsion angles $(N–N)_{triazole}$–$(C–C)_{ethane}$ and $(C–N)_{triazole}$–$(C–C)_{ethane}$ between the *gauche* conformation bte molecules (in **1**, **3**, **4** and part of **5**) and in the *anti* conformation bte molecules (in **2**, part of **5** and free bte molecule) (Table 3). All these data indicate that the change of the spacer conformations and the relative orientations of the triazole rings are responsible for the N···N distances and Co···Co distances. The rotational freedom of the triazole rings and the conformational flexibility of the spacers (bte) result in the variety of topologies of the five cobalt complexes.

4. Conclusion

In spite of the similarity of the building blocks used, the products display a variety of topologies. There are three motifs (2D (4,4) network, single chain and double-stranded chain) in the five complexes: 2D (4,4) network (**1**), single chain (**2**), double-stranded chain (**3** and **4**), and a combination of two motifs (single chain + double-stranded chain) (**5**). The variety of the observed structural motifs confirms that rationalization of the resulting topologies is still difficult. Many factors play a role in the formation of the final product: (i) the effects of counter anions (NO_3^- in **1**, NCO^- in **2** and **3**, NCS^- in **4** and **5**); (ii) the conformation of the bte ligand (the *gauche* conformation in **1**, **3**, **4**, the *anti* conformation in **2**, both the *gauche* and *anti* conformations in **5**); (iii) the Co/bte molar ratio (1:2 in **1**, **3**, **4**; 1:1 in **2** and 1:1.5 in **5**); (iv) solvent system (**2** and **5** in DMF/H_2O, **3** and **4** in DMF). This work demonstrates the feasibility of achieving various polymeric frameworks by self-assembly of the flexible bis(triazole) ligand and metal salts and may provide useful information for crystal engineering.

Acknowledgements

This work was supported by the Natural Science Foundation of the University of Jiangsu Province (No. 03KJB150118), Funds of Key Laboratory of Organic Synthesis of Jiangsu Province, and the Funds of Civil Aviation University of China (No. 04-CAUC-26S), P.R. China.

Appendix A. Supplementary data

Crystallographic data for the structural analyses have been deposited with the Cambridge Crystallographic Data Centre, with CCDC reference numbers CCDC-209245

for **1**, CCDC-221762 for **2**, CCDC-209246 for **3**, CCDC-221763 for **4**, CCDC-221764 for **5**. These data can be obtained free of charge via www.ccdc.can.ac.uk/conts/retrieving.html (or from the Cambridge Crystallographic Data Center, 12 Union Road, Cambridge CB2 1EZ, UK; fax: +44 1223 336 033; or deposit@ccdc.cam.ac.uk). The TGA curves of the five complexes and XRD of complexes **1**, **3**, **4** and **5** are also provided. Supplementary data associated with this article can be found, in the online version, at doi:10.1016/j.poly.2005.07.042.

References

[1] (a) S.R. Batten, R. Robson, Angew. Chem. Int. Ed. 37 (1998) 1460;
(b) O.M. Yaghi, H. Li, C. Davis, D. Richardson, T.L. Groy, Acc. Chem. Res. 31 (1998) 474;
(c) S.S.Y. Chui, S.M.F. Lo, J.P.H. Chartmant, A.G. Orpen, I.D. Williams, Science 283 (1999) 1148;
(d) L.M. Zheng, T. Whitfield, X. Wang, A.J. Jacobson, Angew. Chem. Int. Ed. 39 (2000) 4528;
(e) M.J. Zaworotko, Chem. Commun. (2001) 1;
(f) J.P. Zhang, S.L. Zheng, X.C. Huang, X.M. Chen, Angew. Chem. Int. Ed. 43 (2004) 206;
(g) X.H. Bu, M.L. Tong, H.C. Chang, S. Kitagawa, S.R. Batten, Angew. Chem. Int. Ed. 43 (2004) 192;
(h) S. Kitagawa, R. Kitaura, S.I. Noro, Angew. Chem. Int. Ed. 43 (2004) 2334.

[2] (a) B. Moulton, M.J. Zaworotko, Chem. Rev. 101 (2001) 1629;
(b) B.F. Hoskins, R. Robson, D.A. Slizys, Angew. Chem., Int. Ed. Engl. 36 (1997) 2336;
(c) L. Carlucci, G. Ciani, D.M. Proserpio, Chem. Commun. (2004) 380;
(d) L. Carlucci, G. Ciani, D.M. Proserpio, L. Spadacini, CrystEngComm 6 (2004) 2–96;
(e) B.L. Li, Y.F. Peng, B.Z. Li, Y. Zhang, Chem. Commun. (2005) 2333.

[3] (a) Q.T.L. Hennigar, D.C. Macquarrie, P. Losier, R.D. Rogers, M.J. Zaworotko, Angew. Chem. Int. Ed. 36 (1997) 972;
(b) L. Carlucci, G. Ciani, D.M. Proserpio, S. Rizzato, Chem. Commun. (2000) 1319;
(c) M. Fujita, Y.J. Kwon, M. Miyazawa, K. Ogura, J. Chem. Soc., Chem. Commun. (1994) 1977.

[4] (a) L. Carlucci, G. Ciani, M. Moret, D.M. Proserpio, S. Rizzato, Angew. Chem. Int. Ed. 39 (2000) 1506;
(b) M.T. Bujaci, X. Wang, S. Li, C. Zheng, Inorg. Chim. Acta 333 (2002) 152;
(c) M.L. Tong, Y.M. Wu, J. Ru, X.M. Chen, H.C. Cheng, S. Kitagawa, Inorg. Chem. 41 (2002) 4846.

[5] (a) A.M. Schuitema, M. Engelen, I.A. Koval, S. Gorter, W.L. Driessen, J. Reedijk, Inorg. Chim. Acta 324 (2001) 57;
(b) K. Flinzner, A.F. Stassen, A.M. Mills, A.L. Spek, J.G. Haasnoot, J. Reedijk, Eur. J. Inorg. Chem. (2003) 671.

[6] (a) Effendy, F. Marchetti, C. Pettinari, R. Pettinari, B.W. Skelton, A.H. White, Inorg. Chem. 42 (2003) 112;
(b) L.F. Tang, Z.H. Wang, J.F. Chai, W.L. Jia, Y.M. Xu, J.T. Wang, Polyhedron 19 (2000) 1949.

[7] (a) G.A.V. Albada, R.C. Guijt, J.G. Haasnoot, M. Lutz, A.L. Spek, J. Reedijk, Eur. J. Inorg. Chem. (2000) 121;
(b) Q.H. Zhao, H.F. Li, X.F. Wang, Z.D. Chen, New J. Chem. 26 (2002) 1709.

[8] (a) B.F. Hoskins, R. Robson, D.A. Slizys, J. Am. Chem. Soc. 119 (1997) 2952;
(b) B.F. Hoskins, R. Robson, D.A. Slizys, Angew. Chem., Int. Ed. Engl. 36 (1997) 2336.

[9] (a) B.L. Li, X. Zhu, J.H. Zhou, Y.F. Peng, Y. Zhang, Polyhedron 23 (2004) 3133;
(b) J.H. Zhou, X. Zhu, Y.N. Zhang, Y. Zhang, B.L. Li, Inorg. Chem. Commun. 7 (2004) 949;
(c) B.L. Li, B.Z. Li, X. Zhu, L.M. Zhu, Y. Zhang, Acta Crystallogr., Sect. C 59 (2003) m350;
(d) X. Zhu, B.Z. Li, J.H. Zhou, B.L. Li, Y. Zhang, Acta Crystallogr., Sect. C 60 (2004) m191;
(e) B.L. Li, Z. Xu, Z.B. Cao, L.M. Zhu, K.B. Yu, Transition Met. Chem. 24 (1999) 622;
(f) B.L. Li, X. Zhu, J.H. Zhou, Y. Zhang, J. Coord. Chem. 58 (2005) 271.

[10] J.H. Zhou, Y.F. Peng, Y.P. Zhang, B.L. Li, Y. Zhang, Inorg. Chem. Commun. 7 (2004) 1181.

[11] B.Z. Li, Y.F. Peng, Y.P. Zhang, B.L. Li, Y. Zhang, Acta Crystallogr., Sect. C 60 (2004) m560.

[12] (a) B.Z. Li, X. Zhu, B.L. Li, Y. Zhang, J. Mol. Struct. 691 (2004) 159;
(b) B.Z. Li, J.H. Zhou, B.L. Li, Y. Zhang, J. Mol. Struct. 707 (2004) 187;
(c) Y.F. Peng, B.Z. Li, J.H. Zhou, B.L. Li, Y. Zhang, Chin. J. Struct. Chem. 23 (2004) 985.

[13] G.M. Sheldrick, SHELXS-97 and SHELXL-97, University of Göttingen, Germany, 1997.

[14] J.H. Luo, M.C. Hong, R.H. Wang, D.Q. Yuan, R. Cao, L. Han, Y.Q. Xu, Z.Z. Lin, Eur. J. Inorg. Chem. (2003) 3623.

[15] (a) K. Biradha, M. Fujita, J. Chem. Soc., Dalton Trans. (2000) 3805;
(b) K. Biradha, M. Fujita, Chem. Commun. (2001) 15;
(c) K. Biradha, Y. Hongo, M. Fujita, Angew. Chem. Int. Ed. 39 (2000) 3843;
(d) F. Wiesbrock, H. Schmidbaur, J. Chem. Soc., Dalton Trans. (2002) 3201;
(e) M.J. Plater, M.R.St.J. Foreman, T. Gelbrich, S.J. Coles, M.B. Hursthouse, J. Chem. Soc., Dalton Trans. (2000) 3065.

[16] (a) M.L. Hernández, M.G. Barandika, M.K. Urtiaga, R. Cortés, L. Lezama, M.I. Arriotua, T. Rojo, J. Chem. Soc., Dalton Trans. (1999) 1401;
(b) O.S. Jung, S.H. Park, D.C. Kim, K.M. Lin, Inorg. Chem. 37 (1998) 610.

[17] (a) K.W. Kim, M.G. Kanatzidis, J. Am. Chem. Soc. 114 (1992) 4878;
(b) D. Hagrman, R.P. Hammond, R. Haushalter, J. Zubieta, Chem. Mater. 10 (1998) 2091;
(c) M.B. Zaman, M.D. Smith, H.C. zur Loye, Chem. Commun. (2001) 2256;
(d) S.R. Batten, Curr. Opin. Solid State Mater. Sci. 5 (2001) 107;
(e) P. Ayyappan, O.R. Evans, W. Lin, Inorg. Chem. 41 (2002) 3328.

with the phosphorus functional groups exhibit higher selectivity in complexation and sufficient thermodynamic stability [18,19].

The ligand 1,4,8,11-tetraazacyclotetradecane-1,8-bis-(methylphosphonic acid) (H_4dipon, H_4L), belongs to a group of cyclam (cyclam = 1,4,8,11-tetraazacyclotetradecane) derivatives, which forms stable complexes with a wide range of metal ions [20–23]. Copper(II) forms H_4dipon with two isomeric [Cu(H_2L)] complexes (Fig. 1) [23]. In the pentacoordinated *pc*-[Cu(H_2L)] complex (complex **A**), five donor atoms of the ligand (four macrocycle nitrogen atoms and one oxygen atom of a phosphonate moiety) coordinate the copper(II) ion, while all six donor atoms (four nitrogen atoms and one oxygen atom of each phosphonate group) bind the copper(II) ion in the hexacoordinated *trans-O,O*-[Cu(H_2L)] complex (*hx*-[Cu(H_2L)]; complex **B**) forming axially elongated octahedral structure. The *pc*-[Cu(H_2L)] complex is prepared by mixing aqueous solutions of H_4dipon and copper(II) ion, with rapid complex formation, while the *hx*-[Cu(H_2L)] complex is formed by refluxing an aqueous solution of the *pc*-[Cu(H_2L)] complex for several hours [23]. The isomerization reaction can be accelerated by the presence of ammonia [23].

Nowadays separation methods, mainly high-performance liquid chromatography (HPLC) and capillary electrophoresis (CE), are often used for separation and determination of inorganic complex species and isomers [24]. Diogenes et al. have monitored the synthesis of the ruthenium(III) cyclam complex by reversed-phase HPLC [25,26] to control the progress of its synthesis with identification of the *cis* and *trans* ruthenium(III) cyclam isomers formed during the reaction. Similarly, the characterization and kinetic studies of *cis* and *trans* ruthenium(III) cyclen (1,4,7,10-tetraazacyclododecane) complexes in aqueous solution were performed using cyclic voltammetry [27].

On the contrary, electromigration, mainly using CE methods, was successfully applied to the study of the kinetic and thermodynamic behaviour of metal complexes. The kinetic behaviour of complexes of four lanthanide ions, Sm^{3+}, Dy^{3+}, Yb^{3+} and Lu^{3+}, with the tetraazamacrocyclic chelating ligand 1,4,7,10-tetraazacyclododecane-1,4,7,10-tetraacetic acid (H_4dota) was investigated by means of CE and stability constants and second-order rate formation constants of the complexes formed were determined [28]. Stability constants of H_4dota complexes with Y^{3+} and Ho^{3+} were determined using isotachophoresis [29]. It was also demonstrated that the CE method is a powerful probe of the stereochemical changes accompanying photoinitiated racemization and ligand substitution of optically active chromium(III) complexes with diimines (2,2′-bipyridine or 1,10-phenanthroline) in aqueous solution [30–32]. CE was proposed as an exceptional tool for the separation of enantiomers of metal complexes. Harris et al. have shown the possibility to apply various buffer additives that may help to separate chiral complexes of transition metal ions by means of CE [32]. The CE method was also employed in speciation studies. Gaspar and Buglyo applied CE for the separation and determination of chromium(III) complex species [33]. One of us studied iridium(IV) [34] and rhodium(III) [35] speciation in hydrochloric acid by CE and UV/Vis spectrophotometry. Aleksenko et al. demonstrated the feasibility of CE to distinguish the rhodium(III) complex species which occur in solutions of different acidity [36]. Recently, it was demonstrated that CE is suitable for reaction kinetic study of the oxidation of the thiocyanate anion by hydrogen peroxide and the reaction mechanism was proposed from such experimental data [37].

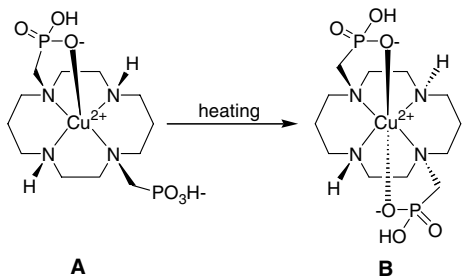

Fig. 1. Reaction scheme of isomerization of *pc*-$[Cu(L)]^{2-}$ (A) to *hx*-$[Cu(L)]^{2-}$ (B) (adapted from [23]).

This paper demonstrates the possibility of CE for separation of copper(II) complexes of 1,4,8,11-tetraazacyclotetradecane-1,8-bis(methylphosphonic acid) which would enable the reaction extent between copper(II) and the ligand to be followed. The CE procedure could be applied for kinetic study of the mechanism of the isomerization reaction of *pc*-[Cu(H_2L)] (A) into *hx*-[Cu(H_2L)] (B) (Fig. 1).

2. Experimental

All solutions were prepared in three times distilled water obtained from a quartz distillation apparatus (Heraeus, Germany). Stock copper(II) solution was prepared from $CuCl_2 \cdot 2H_2O$ (Pliva-Lachema, Czech Republic) and standardized by chelatometric titration. The ligand H_4dipon was synthesized according to the published procedure [20] and its stock solution was prepared from a weighed amount of $H_4L \cdot 4H_2O$. Disodium tetraborate decahydrate, boric acid, sodium phosphate dodecahydrate (Pliva-Lachema, Czech Republic) and *N*-tris(hydroxymethyl)methyl-2-aminoethanesulfonic acid (TAPS, Aldrich, USA) used in the electrophoretic study as the background electrolyte salts were of analytical grade purity. Other commonly used chemicals (Pliva-Lachema, Czech Republic) were of analytical grade purity.

CE experiments were carried out on the Agilent CE instrument (Agilent, USA) equipped with LC 3D Systems software running on ChemStation of the same company. The fused silica capillary column (Watrex, Czech Republic) was 47.5 cm long (the effective length to detector was 39 cm) with 75 μm inner diameter. UV/Vis detection was performed on-column for each compound separately at

three different wavelengths selective for the separated species: 220 nm (H_4dipon), 280 nm (*hx*-[Cu(H_2L)]) and 319 nm (*pc*-[Cu(H_2L)]). A new capillary column was rinsed by 0.1 M NaOH solution for 10 min at 40 °C, then 5 min flushed by deionized water and 10 min by the appropriate buffer solution prior to use. All solutions used in the CE system were filtered through 0.45 μm Spartan®-3 filters (Schleicher & Schull, Germany) prior to use and degassed in an ultrasonic bath (Branson, USA) for 10 min. The separation capillary was washed daily for 5 min with deionized water prior to and after use. Between each analysis, the capillary was washed for 2 min by the background electrolyte solution. Working conditions were: 50 mbar cathodic pressure injection for 5 s, capillary temperature 25 °C, applied voltage 15 kV (separation of isomers and ligand) and 20 kV (kinetic isomerization study). Mesityloxide (0.1% v/v solution) utilized as a marker of the electroosmotic flow was supplied by Fluka (Switzerland). The other conditions are specified in Section 4.

The isomerization reaction *pc*-[Cu(H_2L)] into *hx*-[Cu(H_2L)] (Fig. 1) was performed at two temperatures 80 ± 0.5 and 90 ± 0.5 °C. A stock solution of 0.3 mM *pc*-[Cu(H_2L)] (made from the solid sample of *pc*-[Cu(H_2L)]·5H_2O [23]; pH 4.56) was divided into set of sealed glass ampoules. This set was heated in a drying oven at constant temperature. The ampoules were sampled from the drying oven in a certain time interval and the reaction was stopped by cooling the ampoules to the laboratory temperature; the isomerization reaction does not proceed at ambient temperature [23]. Then the content of ampoules was analyzed by means of CE.

3. Theory

In general, the isomerization reactions proceed as one-step reaction (Reaction A) or multiple-step reaction (Reaction B). In the first case, the rate of the reaction can be expressed by Eq. (1):

$$[^{pc}\mathrm{CuL}] \xrightarrow{k} [^{hx}\mathrm{CuL}] \tag{A}$$

$$-\frac{\mathrm{d}[^{pc}\mathrm{CuL}]}{\mathrm{d}t} = \frac{\mathrm{d}[^{hx}\mathrm{CuL}]}{\mathrm{d}t} = k \times [^{pc}\mathrm{CuL}] \tag{1}$$

where $[^{pc}\mathrm{CuL}]$ and $[^{hx}\mathrm{CuL}]$ are concentrations of the pentacoordinated and hexacoordinated complexes, respectively, at time t and k represents a rate constant of the isomerization reaction. Using mass balance law (Eq. (2), c_{CuL} is the analytical – total concentration of copper(II) complexes)

$$c_{\mathrm{CuL}} = [^{pc}\mathrm{CuL}] + [^{hx}\mathrm{CuL}] \tag{2}$$

Eq. (1) can be written in an integral form as Eqs. (3) and (4):

$$[^{pc}\mathrm{CuL}] = [^{pc}\mathrm{CuL}]_0 \mathrm{e}^{-k\times t} \tag{3}$$

$$[^{hx}\mathrm{CuL}] = [^{hx}\mathrm{CuL}]_0 + [^{pc}\mathrm{CuL}]_0(1 - \mathrm{e}^{-k\times t}) \tag{4}$$

where $[^{pc}\mathrm{CuL}]_0$ is initial concentration of the pentacoordinated complex and $[^{hx}\mathrm{CuL}]_0$ is initial concentration of the hexacoordinated complex at the beginning of reaction ($t = 0$).

A general linear calibration function of concentration for analytical signal response (represented mostly by corrected and uncorrected peak area and/or a height of symmetric Gaussian peak) is defined by

$$S = a \times c_{\mathrm{CuL}} \tag{5}$$

where the parameter is the slope of the calibration straight line.

For copper(II) isomeric species the following expressions are valid:

$$S_{\mathrm{pc}} = a_{\mathrm{pc}}[^{pc}\mathrm{CuL}] \tag{6a}$$

$$S_{\mathrm{hx}} = a_{\mathrm{hx}}[^{hx}\mathrm{CuL}] \tag{6b}$$

where S_{pc} and S_{hx} are values of the analytical signal belonging to *pc*-$[\mathrm{Cu(L)}]^{2-}$ and *hx*-$[\mathrm{Cu(L)}]^{2-}$ species, respectively. Analogously the concentrations can be expressed by:

$$[^{pc}\mathrm{CuL}] = \frac{S_{\mathrm{pc}}}{a_{\mathrm{pc}}} \tag{7a}$$

$$[^{pc}\mathrm{CuL}]_0 = \frac{S^0_{\mathrm{pc}}}{a_{\mathrm{pc}}} \tag{7b}$$

$$[^{hx}\mathrm{CuL}] = \frac{S_{\mathrm{hx}}}{a_{\mathrm{hx}}} \tag{8a}$$

$$[^{hx}\mathrm{CuL}]_0 = \frac{S^0_{\mathrm{hx}}}{a_{\mathrm{hx}}} \tag{8b}$$

Considering a non-zero concentration of the product of the isomerization reaction at the beginning of the reaction, the substitution in Eqs. (3) and (4) by Eqs. (7) and (8) gives Eqs. (9) and (10):

$$S_{\mathrm{pc}} = S^0_{\mathrm{pc}} \times \mathrm{e}^{-k\times t} \tag{9}$$

$$S_{\mathrm{hx}} = S^0_{\mathrm{hx}} + S^0_{\mathrm{pc}} \times \frac{a_{\mathrm{hx}}}{a_{\mathrm{pc}}}(1 - \mathrm{e}^{-k\times t}) \tag{10}$$

Eq. (9) can be transformed into a logarithmic form

$$\ln(S_{\mathrm{pc}}) = \ln(S^0_{\mathrm{pc}}) - k \times t \tag{11}$$

From the assumption of a simple one-step reaction (Reaction A) it is clear, that the rate constants k evaluated from the experimental data using Eqs. (9) and (10) should be the same in both cases.

In contradiction, if a two-step mechanism is supposed (Reaction B)

$$[^{pc}\mathrm{CuL}] \xrightarrow{k_1} \quad \text{Intermediate} \xrightarrow{k_2} [^{hx}\mathrm{CuL}] \tag{B}$$

the reaction rates are defined by Eqs. (12)–(14) (k_1 and k_2 are the corresponding rate constants):

$$-\frac{\mathrm{d}[^{pc}\mathrm{CuL}]}{\mathrm{d}t} = k_1 \times [^{pc}\mathrm{CuL}] \tag{12}$$

$$-\frac{\mathrm{d}[\mathrm{Intermediate}]}{\mathrm{d}t} = k_2 \times [\mathrm{Intermediate}] - k_1 \times [^{pc}\mathrm{CuL}] \tag{13}$$

$$\frac{d[^{hx}CuL]}{dt} = k_2 \times [\text{Intermediate}] \quad (14)$$

After integration, one obtains Eqs. (15)–(17):

$$[^{pc}CuL] = [^{pc}CuL]_0 e^{-k_1 \times t} \quad (15)$$

$$[\text{Intermediate}] = [^{pc}CuL]_0 \times \frac{k_1}{k_2 - k_1}(e^{-k_1 \times t} - e^{-k_2 \times t}) \quad (16)$$

$$[^{hx}CuL] = [^{hx}CuL]_0 + [^{pc}CuL]_0 \times \left\{1 + \frac{1}{k_1 - k_2}(k_2 \times e^{-k_1 \times t} - k_1 \times e^{-k_2 \times t})\right\} \quad (17)$$

Using Eqs. (7) and (8), Eqs. (15) and (17) can be transformed to Eqs. (18) and (19):

$$S_{pc} = S^0_{pc} \times e^{-k_1 \times t} \quad (18)$$

$$S_{hx} = S^0_{hx} + S^0_{pc} \times \frac{a_{hx}}{a_{pc}} \times \left\{1 + \frac{1}{k_1 - k_2}(k_2 \times e^{-k_1 \times t} - k_1 \times e^{-k_2 \times t})\right\} \quad (19)$$

The time when the concentration of the **Intermediate** is maximal is given by

$$t_{max} = \frac{\ln\left(\frac{k_1}{k_2}\right)}{k_1 - k_2} \quad (20)$$

and after substitution into Eq. (16) and simplification, one obtains

$$\frac{[\text{Intermediate}]}{[^{pc}CuL]_0} = \left(\frac{k_2}{k_1}\right)^{\frac{k_2}{k_1 - k_2}} \quad (21)$$

Analyzing Eq. (21), two limiting cases can occur. If the rate-determining step (rds) of the reaction is the first step (i.e., $k_2 \gg k_1$), the concentration of the **Intermediate** will be negligible and the **Intermediate** will not be detectable. In the opposite case, when both steps proceed with a comparable rate ($k_2 \approx k_1$) and/or the rds is the second step ($k_2 \ll k_1$), the **Intermediate** may be detected in solution. It can be noted that Eqs. (3) and (15) are formally the same in both reaction mechanisms and, therefore, the determination of the rate constant of the starting complex decay is independent on an assumption of the reaction mechanism.

The magnitude of activation energy E_a can be calculated from the temperature dependence of the rate constant as

$$\ln(k) = \ln(A) - \frac{E_a}{RT} \quad (22)$$

where the activation parameters (activation enthalpy $\Delta H^{\neq}$ and entropy $\Delta S^{\neq}$) are calculated according to Eyring's theory [38–40]

$$\ln\left(\frac{k}{T}\right) = \ln\left(\frac{k_B}{h}\right) + \frac{\Delta S^{\neq}}{R} - \frac{\Delta H^{\neq}}{RT} \quad (23)$$

where R is the universal gas constant, T is the thermodynamic temperature, k_B is Boltzman's constant and h is Planck's constant.

4. Results and discussion

4.1. Development of the CE method for a separation of the isomeric complexes and the free ligand

The spectra of *pc*-[Cu(H_2L)], *hx*-[Cu(H_2L)] and H_4L species in aqueous solutions were recorded in order to select optimal wavelengths for spectrophotometric detection. Both isomers have different absorption maxima (319 and 280 nm) as described in the literature [23] and, therefore, three wavelengths (220, 280 and 319 nm) were selected for their simultaneous detection during the separation process in order to have the highest sensitivity of analysis. The species behave as acids and, therefore, the distribution diagrams showing all protonated forms for all three species were calculated (the protonation constants for H_4dipon and stability constants for its complexes were taken from the literature [20,23]) in order to find optimal pH values for the separation. The results are given in Fig. 2.

The pH of the background electrolyte solution was then selected to keep the charge of the species to be separated as high as possible in order to shorten the time of analysis (see distribution diagrams in Fig. 2) and this is possible at pH higher than 8. The optimal separation of a mixture of *pc*-$[Cu(L)]^{2-}$, *hx*-$[Cu(L)]^{2-}$ and $(H_2L)^{2-}$ was reached in 75 mM disodium tetraborate aqueous solution (pH 9.5) and it is presented in Fig. 3.

According to the basic theory of electromigration process [41], it can be supposed that both *pc*-$[Cu(L)]^{2-}$ and *hx*-$[Cu(L)]^{2-}$ species having the same charge and molecular weight should have the same molar mobility and/or conductivity. As was demonstrated in a real experiment (Fig. 3), the separation of a mixture of both isomers and the ligand is possible, however, the resolution of a *hx*-$[Cu(L])^{2-}$ and $(H_2L)^{2-}$ species is lower than that of *pc*-$[Cu(L)]^{2-}$ and *hx*-$[Cu(L)]^{2-}$ species (see Table 1). This can be explained either by a different solvation of the analysed complex species or by their interaction with borate/boric acid. Taking into account the knowledge of the structure of the species in the solid state and that the structures remain unchanged in aqueous solution [20,23], it can be expected that *hx*-$[Cu(L)]^{2-}$ and $(H_2L)^{2-}$ species have structure close to a sphere in aqueous solution. Therefore, their hydrodynamic radii are also of the same magnitude but the compounds have different molecular weights. In contrast, the *pc*-$[Cu(L)]^{2-}$ complex species having one non-bonding phosphonate group has a different shape in comparison with the former species. It probably would lead to a higher hydrodynamic radius due to a higher molecular volume and, certainly, to a different solvation of the complex. Further, it was observed that higher concentration of tetraborate in solution improved the resolution of the separation of *pc*-$[Cu(L)]^{2-}$ and *hx*-$[Cu(L)]^{2-}$ species. It means that borate/boric acid interacts differently with each of the isomeric species. This effect cannot be explained by an increase of the ionic strength of the solution because it was not observed in the presence of other compounds

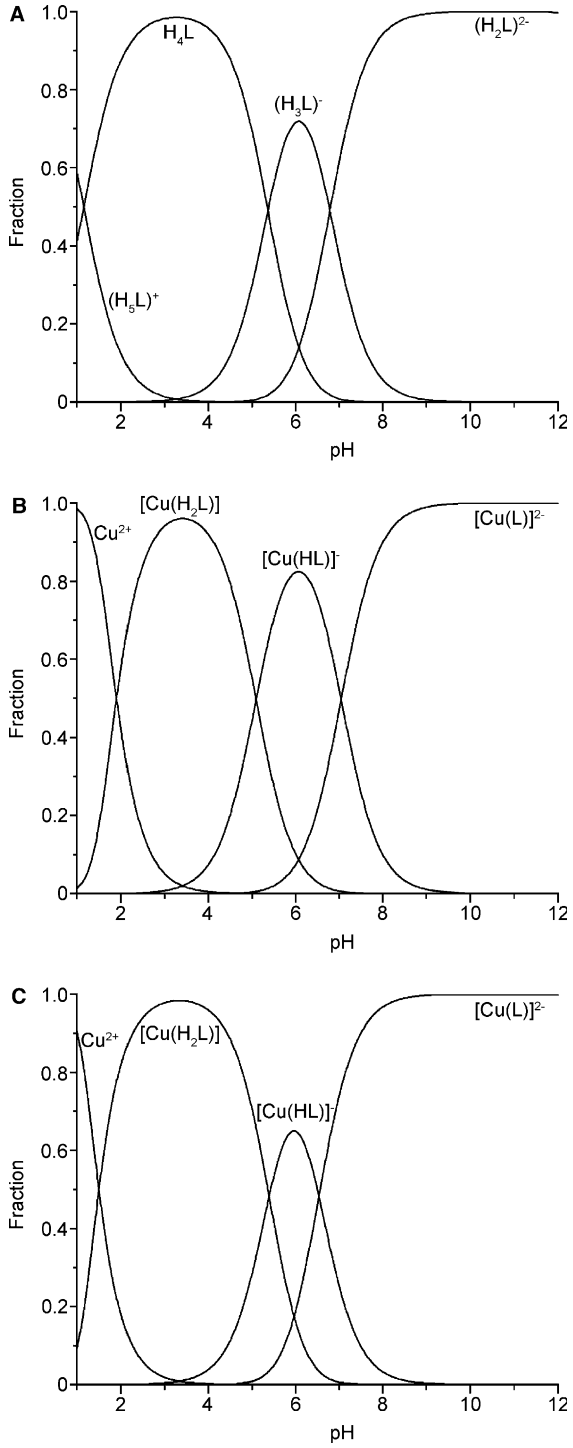

Fig. 2. Distribution diagrams for the $H^+ - H_4L$ (A), $H^+ - Cu^{2+} - H_4L$ (formation of *pc*-$[Cu(L)]^{2-}$ complex) (B) and $H^+ - Cu^{2+} - H_4L$ (formation of *hx*-$[Cu(L)]^{2-}$ complex) (C) systems in aqueous solutions ($c_L = c_{Cu} = 0.1$ mM).

(e.g., TAPS) used as a background electrolyte. A similar phenomenon has been also observed in case of CE separation of organophosphonates [42] and/or α- and β-naphthols [43] in tetraborate background electrolyte solution with the assumption that the complex/ester is formed. Another explanation can be the formation of hydrogen bonds between boric acid/borate and free phosphonate

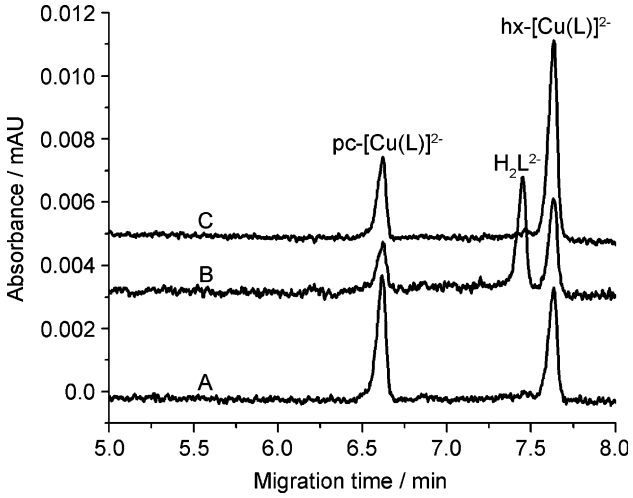

Fig. 3. CE separation of species under optimal experimental conditions (see text) for the aqueous solution mixture containing 98.7 μM *pc*-$[Cu(L)]^{2-}$, 145.5 μM *hx*-$[Cu(L)]^{2-}$ and 300.3 μM $(H_2L)^{2-}$. Detection wavelengths: (A) 319 nm, (B) 220 nm and (C) 280 nm.

Table 1
Effective mobilities, limit of detection (LOD) and quantification (LOQ) of analyzed species in aqueous solutions under optimal experimental conditions (75 mM sodium borate buffer, pH 9.5)

Parameter	*pc*-$[Cu(L)]^{2-}$	*hx*-$[Cu(L)]^{2-}$	$(H_2L)^{2-}$
$\log\beta$	25.40[a]	26.50[a]	26.41[b]
Effective mobility μ_{eff} ($cm^2\,kV^{-1}\,min^{-1}$)	-17.57 ± 0.09	-19.18 ± 0.08	-19.3 ± 0.3
LOD (μM)	6.4	6.1	19.6
LOQ (μM)	28	26	56

[a] For equilibria $Cu^{2+} + L^{4-} = [Cu(L)]^{2-}$, taken from Ref. [23].
[b] $\log\beta_2$ for equilibrium $2H^+ + L^{4-} = (H_2L)^{2-}$, taken from Ref. [20].

groups which is more pronounced for *pc*-$[Cu(L)]^{2-}$ than for *hx*-$[Cu(L)]^{2-}$ species. The separation of $(H_2L)^{2-}$ and *hx*-$[Cu(L)]^{2-}$ species is improved under more extreme experimental conditions (higher pH and tetraborate concentration of the background electrolyte solution) but such conditions could not be applied because of a worse reproducibility of the parameters used for quantification due to overheating of the capillary compared to that used under the working conditions specified in Section 2.

The reproducibility of experimental results such as peak height and area (analytical signal) was tested for a set of model samples of each species in the concentration range 0.05–0.4 mM and for detection wavelengths 220, 280 and 319 nm. These data were used for the construction of a calibration curve plot (figures are not shown). The squared correlation coefficients (R^2) of the calibration plots were typically about 0.999. If fluctuations of migration time of analyte, t_M, occur (this effect is reflected in a variation of the electroosmotic flow, EOF, between two consequent runs), then the correction of the peak area (peak area over the migration time, S_{pc}/t_M) leads to more precise results. Limits of detection (LOD) and quantification (LOQ) were estimated as the signal corresponding to three and ten times of the SD of the noise. The values of LOD's and

LOQ's are summarized in Table 1 and they are comparable with those estimated for spectrophotometric [44] and kinetic [45] copper(II) determination.

4.2. CE study of the isomerization reaction of *pc*-[Cu(H$_2$L)] → *hx*-[Cu(H$_2$L)]

CE analysis was applied in order to follow the extent of the isomerization reaction taking place in the aqueous solution at high temperature (Fig. 4). Since we would like to shorten analysis in batch analysis of aqueous solution where only two isomeric species are present, the formerly proposed method was modified (pH 9.0, separation voltage 20 kV). As can be seen from Figs. 3 and 4, the time of analysis was shortened from 8 to 6 min. The peak area divided by migration time was selected as a quantitative parameter in order to eliminate the fluctuation of migration times of the separated complex species. This new dependent variable is proportional to the concentration of the species and, therefore, can be used for a calculation of the abundance of the complex species as a function of time. An example of a time course of the isomerization reaction is shown in Fig. 5.

The rate constant of the first reaction step is independent of the knowledge of the correct chemical model as shown in Section 3 and, therefore, the time dependence of reactant concentration can be used for calculation of this rate constant. Fig. 6 presents the dependence according to Eq. (11) from which the rate constant can be estimated. Very close values of rate constants $k = (2.45 \pm 0.06) \times 10^{-3}$ and $(2.42 \pm 0.06) \times 10^{-3}$ min^{-1} were obtained from the dependence of the corrected and uncorrected peak areas versus time, respectively, for the temperature 90 °C (Table 2). The rate constant $k = (2.5 \pm 0.3) \times 10^{-3}$ min^{-1} and the ratio $a_{hx}/a_{pc} = 0.89 \pm 0.04$ with SD of the fit $\sigma_Y = 3.26$ were obtained by general least-squares fitting according to Eq. (10) through experimental data in order to verify the consistency of both methods. A good agreement between obtained values of rate constants and the ratio a_{hx}/a_{pc} compared to value 0.877 obtained independently from slopes of calibration curves was achieved. Analogously,

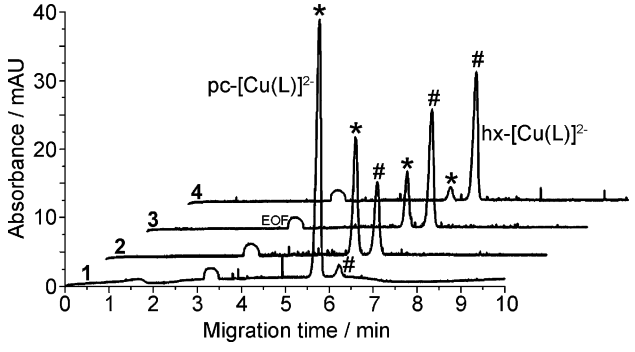

Fig. 4. Course of isomerization of *pc*-[Cu(L)]$^{2-}$ (*) to *hx*-[Cu(L)]$^{2-}$ (#) taking place in aqueous solution (pH 4.56) and at temperature 80 °C monitored by CE (detection wavelength 220 nm): (1) 35 min, (2) 310 min (5 h 10 min), (3) 606 min (10 h 6 min) and (4) 1261 min (21 h 1 min).

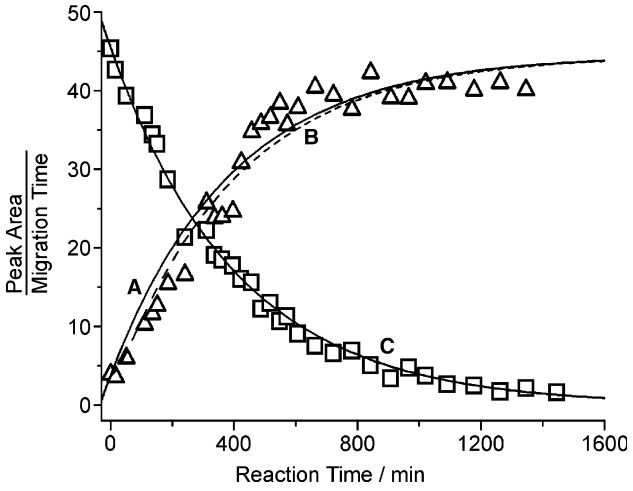

Fig. 5. Distribution of copper(II) complex species in aqueous solution as a function of time at temperature 90 °C: *pc*-[Cu(L)]$^{2-}$ (□) and *hx*-[Cu(L)]$^{2-}$ (Δ). (A) Curve simulated for the one-step reaction according to Eq. (10); (B) curve simulated for the two-step reaction according to Eq. (19); (C) decay of reactant (*pc*-[Cu(L)]$^{2-}$) with time; the curve was simulated accordingly to Eq. (9) (or Eq. (18), respectively).

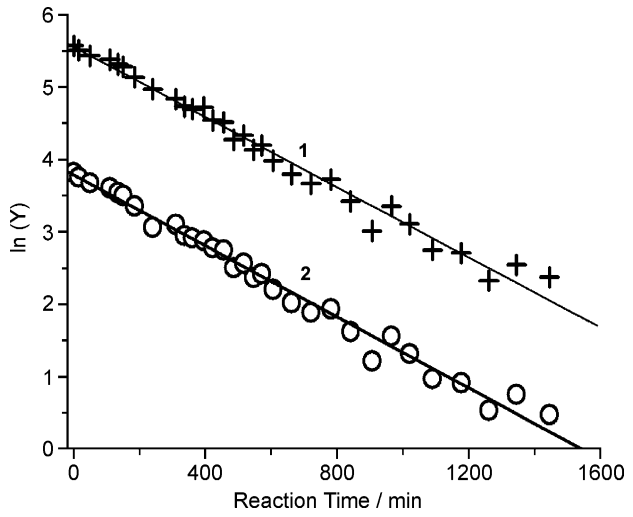

Fig. 6. Transformed time dependence of isomerization for the *pc*-[Cu(L)]$^{2-}$ complex accordingly to Eq. (11). Other experimental conditions are the same as in Fig. 5. Functions used: (1) $Y =$ (peak area) and (2) $Y =$ (peak area/migration time).

Table 2
The rate constants and activation parameters of the isomerization reaction *pc*-[Cu(L)]$^{2-}$ → *hx*-[Cu(L)]$^{2-}$

Parameters	Values
k_1 (80 °C)	$(1.37 \pm 0.07) \times 10^{-3}$ min^{-1}[a] $(1.23 \pm 0.09) \times 10^{-3}$ min^{-1}[b]
k_1 (90 °C)	$(2.42 \pm 0.06) \times 10^{-3}$ min^{-1}[a] $(2.45 \pm 0.06) \times 10^{-3}$ min^{-1}[b]
E_a	72 ± 8 kJ mol^{-1}[b]
$\Delta H^{\neq}$	69 ± 8 kJ mol^{-1}[b]
$\Delta S^{\neq}$	-106 ± 23 J K^{-1} mol^{-1}[b]

[a] Value from uncorrected values of ln(S_{pc}).
[b] Value from corrected values of ln(S_{pc}/t_M).

the corresponding rate constants k were estimated for the temperature 80 °C (Table 2). The activation parameters can be calculated according to Eqs. (22) and (23) and the estimated values are given in Table 2. The estimates of the error of activation parameters were calculated according to relationships published elsewhere [40].

The other question is the number of steps in the isomerization reaction (compare Reactions A and B). If there is only the one-step reaction, Eqs. (9) and (10) should give the same rate constants from the experimental data as discussed in the previous section. In the other case, the isomerization reaction is a multistep process. This can be resolved if the time traces of *hx*-$[Cu(L)]^{2-}$ concentration is simulated using the rate constant k (or k_1, respectively) evaluated from decay of *pc*-$[Cu(L)]^{2-}$. Below, we will consider that the reaction proceeds in two steps. As the other intermediate species were not detected, we can deduce that the rate of the first step is slower than the rate of the second step ($k_1 \ll k_2$). This means that the first step is the rds. Eq. (21) can be written in the logarithmic form as

$$\log\left(\frac{[\text{Intermediate}]}{[^{pc}\text{CuL}]_0}\right) = \frac{k_2}{k_1 - k_2} \times \log\left(\frac{k_2}{k_1}\right) \tag{24}$$

In the case $k_2 \gg k_1$, it can be simplified as

$$\log\left(\frac{[\text{Intermediate}]}{[^{pc}\text{CuL}]_0}\right) = \frac{k_2}{k_1 - k_2} \times \log\left(\frac{k_2}{k_1}\right) \approx -\log\left(\frac{k_2}{k_1}\right) \tag{25}$$

We consider a limit of quantification for **Intermediate** equal to 0.03 mM analogously to the other copper(II) complex species (Table 1) and the initial reactant concentration 0.3 mM. Then, after substitution into Eq. (24), one obtains $k_2 \geqslant 10k_1$ under the given experimental conditions. We used this initial estimate for the general least-squares fitting with Eq. (19) through experimental data and the following parameters $k_1 = (2.5 \pm 0.5) \times 10^{-3}\ \text{min}^{-1}$, $k_2 = (40 \pm 50) \times 10^{-3}\ \text{min}^{-1}$ and the ratio $a_{hx}/a_{pc} = 0.89 \pm 0.04$ with $\sigma_Y = 3.13$ were obtained. As it can be seen in Fig. 5, the difference between both models is not so dramatic. As it was pointed out elsewhere [46,47], the ability to distinguish among different chemical models is possible if some special mathematical procedure, e.g., Laplace transformation [46,47], can be applied. In our case using Ockham's razor theorem, the most probable mechanism will be the simpler mechanism (A).

In our previous work [23], the following mechanism (Reaction C):

$$\begin{aligned} &^{pc}\text{CuL}^{2-} + \text{NH}_3 \overset{K_{\text{NH}_3}}{\rightleftarrows} \text{CuL}(\text{NH}_3)^{2-}(\text{Intermediate}) \\ &\text{CuL}(\text{NH}_3)^{2-}(\text{Intermediate}) \overset{k_{\text{NH}_3}}{\rightarrow} {}^{hx}\text{CuL}^{2-} + \text{NH}_3 \end{aligned} \tag{C}$$

for the isomerization reaction taking place in the presence of ammonia was proposed and the corresponding relationship for kinetic law was derived

$$k_{obs} = \frac{k_{\text{NH}_3} K_{\text{NH}_3}[\text{NH}_3]}{1 + K_{\text{NH}_3}[\text{NH}_3]} \tag{26}$$

If $K_{\text{NH}_3}[\text{NH}_3] \ll 1$, then Eq. (26) can be simplified as

$$k_{obs} \approx k_{\text{NH}_3} K_{\text{NH}_3}[\text{NH}_3] = k^{is}_{\text{NH}_3}[\text{NH}_3] \tag{27}$$

Analogously we can propose the mechanism of the isomerization reaction:

$$\begin{aligned} &^{pc}\text{Cu}(\text{H}_2\text{L}) + \text{H}_2\text{O} \overset{K_{\text{H}_2\text{O}}}{\rightleftarrows} \text{Cu}(\text{H}_2\text{L})(\text{H}_2\text{O})(\text{Intermediate}) \\ &\text{Cu}(\text{H}_2\text{L})(\text{H}_2\text{O})(\text{Intermediate}) \overset{k_{\text{H}_2\text{O}}}{\rightarrow} {}^{hx}\text{Cu}(\text{H}_2\text{L}) + \text{H}_2\text{O} \end{aligned} \tag{D}$$

and the relationship is defined as

$$k_{obs} = \frac{k_{\text{H}_2\text{O}} K_{\text{H}_2\text{O}}[\text{H}_2\text{O}]}{1 + K_{\text{H}_2\text{O}}[\text{H}_2\text{O}]} \tag{28}$$

Again considering $[\text{H}_2\text{O}] \approx$ constant during the experiment and $K_{\text{H}_2\text{O}}[\text{H}_2\text{O}] \ll 1$, then Eq. (28) is simplified as

$$k_{obs} \approx k_{\text{H}_2\text{O}} K_{\text{H}_2\text{O}}[\text{H}_2\text{O}] = k^{is}_{\text{H}_2\text{O}}[\text{H}_2\text{O}] \tag{29}$$

and $k^{is}(\text{H}_2\text{O})$ can be calculated if we know the water concentration. Comparing the rate constants $k^{is}(\text{H}_2\text{O}) = 3.80 \times 10^{-7}\ \text{M}^{-1}\ \text{s}^{-1}$, $k^{is}(\text{NH}_3) = 7.61 \times 10^{-5}\ \text{M}^{-1}\ \text{s}^{-1}$ and $k^{is}(\text{H}_2\text{O}) = 7.67 \times 10^{-7}\ \text{M}^{-1}\ \text{s}^{-1}$, $k^{is}(\text{NH}_3) = 18.8 \times 10^{-5}\ \text{M}^{-1}\ \text{s}^{-1}$ for temperatures 80 and 90 °C, respectively, it can be seen that the values are two orders of magnitude different (the ratio $k^{is}(\text{NH}_3)/k^{is}(\text{H}_2\text{O})$ is equal to 200 and 246 for both the temperatures, respectively). This high difference of the rate of the isomerization reaction in both media favours the reaction pathway in ammonia more than in water and the results are in a good agreement with those published elsewhere [23]. In addition, this phenomena can be ascribed to various experimental conditions, mainly pH (H_2O: 4.56 versus NH_3: alkaline) while the species of different composition are present in solution ($[\text{Cu}(\text{H}_2\text{L})]$ versus $[\text{Cu}(\text{L})]^{2-}$). The values of activation parameters for the reaction in pure water ($E_a = 72 \pm 8\ \text{kJ mol}^{-1}$, $\Delta H^{\#} = 69 \pm 8\ \text{kJ mol}^{-1}$, $\Delta S^{\#} = -106 \pm 23\ \text{J K}^{-1}\ \text{mol}^{-1}$) can be compared with corresponding values found for isomerization of *pc*-$[Cu(L)]^{2-}$ complex species catalyzed by ammonia [23] ($E_a = 97 \pm 3\ \text{kJ mol}^{-1}$, $\Delta H^{\#} = 94 \pm 3\ \text{kJ mol}^{-1}$, $\Delta S^{\#} = 52 \pm 9\ \text{J K}^{-1}\ \text{mol}^{-1}$) [23]. The negative value of $\Delta S^{\neq}$ demonstrates that the overall reaction (Reaction D) has very probably a bimolecular character. Water molecule(s) as a weaker ligand stabilizes a transition state of the complex species less effectively than ammonia (two Cu–N bonds must be splitted during the isomerization process). In addition, ammonia is a good solvent as well and, therefore, the mechanism in the presence of ammonia is different because of solvent effects (e.g., orientation of solvent molecules around charged atom(s) and/or atoms with a developing charge, hydrogen bonds, etc.) [23,38–40]. The solvent effects can change the value of $\Delta S^{\neq}$ even if the molecularity of the reaction is the same (e.g., Reactions C and D) [38,39]. So, the fully deprotonated complex *pc*-$[Cu(L)]^{2-}$ is highly second-sphere solvated in ammonia

solution. Such solvation changes dramatically the reactivity of the copper(II) complex and it is reflected in the positive sign of the entropy of activation $\Delta S^{\neq}$ in Reaction C [23]. A less effective solvation is supposed in water with the diprotonated species.

5. Conclusions

The electrophoretic behaviour of copper(II) complexes with a recently synthesized macrocyclic ligand H_4dipon was studied as a function of pH and composition of background electrolyte solution. The optimum experimental conditions (composition, concentration and pH of background electrolyte, applied voltage, etc.) were used for the separation and determination of two isomeric complex species. The values of effective mobilities of the free ligand $(H_2L)^{2-}$ species and both copper(II) complexes, *pc*-$[Cu(L)]^{2-}$ and *hx*-$[Cu(L)]^{2-}$, in aqueous solution were estimated and explanation of a principle responsible for their separation was proposed. The knowledge of the electrophoretic behaviour of H_4dipon and its copper(II) complexes can be used to check the extent of the reaction between radioactive copper(II) and bifunctional chelating ligands and purity of prepared bifunctional chelates [12,48–55]. Introduction of chromophore or fluorophore into the structure of the ligand molecule would increase the sensitivity of the method and then the procedure can be applied for the determination of the content of labile copper in biological fluids as a consequence of copper metabolism diseases (e.g., Wilson disease [56]) or copper intoxication. The strategy is in progress in our laboratories.

The CE method was successfully applied to study the mechanism of the isomerization of the pentacoordinated copper(II) complex in aqueous solution. It was proved that the *pc*-$[Cu(L)]^{2-}$ complex species isomerizes into the *hx*-$[Cu(L)]^{2-}$ complex via a simple reaction process (Reaction A or D). The first reaction step is the rate-determining step while rate constant(s) of other reaction step(s) is/are at least 10 times faster coming from the fact that no intermediate was detected.

Acknowledgements

This work was supported by the Grant Agency of the Czech Republic (Grant No. 203/03/168), and EU-sponsored projects (NoE network DiMI and EMIL as well as COST D18 Action). We thank M. Malíková for help with the kinetic experiments.

References

[1] L.F. Lindoy, Adv. Inorg. Chem. 45 (1998) 75.
[2] K.P. Wainwright, Coord. Chem. Rev. 166 (1997) 35.
[3] S.F. Lincoln, Coord. Chem. Rev. 166 (1997) 255.
[4] M. Meyer, V. Dahaoui-Gindrey, C. Lecomte, R. Guilard, Coord. Chem. Rev. 178–180 (1998) 1313.
[5] R.D. Hancock, H. Maumela, A.S. de Sousa, Coord. Chem. Rev. 148 (1996) 315.
[6] A.E. Martell, R.D. Hancock, Metal Complexes in Aqueous Solutions, Plenum Press, New York, 1996.
[7] D. Parker, in: J.-M. Lehn (Ed.), Comprehensive Supramolecular Chemistry, vol. 10, Pergamon Press, Oxford, 1996, p. 487.
[8] S. Aime, M. Botta, M. Fasano, E. Terreno, Chem. Soc. Rev. 27 (1998) 19.
[9] P. Caravan, J.J. Ellison, T.J. McMurry, R.B. Laufer, Chem. Rev. 99 (1999) 2293.
[10] S. Aime, M. Botta, M. Fasano, E. Terreno, Acc. Chem. Res. 32 (1999) 941.
[11] M. Botta, Eur. J. Inorg. Chem. (2000) 399.
[12] C.J. Anderson, M.J. Welch, Chem. Rev. 99 (1999) 2219.
[13] W.A. Volkert, T.J. Hoffmann, Chem. Rev. 99 (1999) 2269.
[14] D.E. Reichert, J.S. Lewis, C.J. Anderson, Coord. Chem. Rev. 184 (1999) 3.
[15] R. Hancock, in: A.F. Williams, C. Floriani, A.E. Merbach (Eds.), Perspectives in Coordination Chemistry, Verlag Helv. Chim. Acta, Basel (1992) 129.
[16] J. Ren, A.D. Sherry, Inorg. Chim. Acta 246 (1996) 331.
[17] J. Huskens, A.D. Sherry, J. Am. Chem. Soc. 118 (1996) 4396.
[18] I. Lukeš, J. Kotek, P. Vojtíšek, P. Hermann, Coord. Chem. Rev. 216–217 (2001) 287.
[19] F.I. Belskii, Yu.M. Polikarpov, M.I. Kabachnik, Usp. Khim. 61 (1992) 415.
[20] J. Kotek, P. Vojtíšek, I. Císařová, P. Hermann, P. Jurečka, J. Rohovec, I. Lukeš, Collect. Czech. Chem. Commun. 65 (2000) 1289.
[21] J. Kotek, I. Císařová, P. Hermann, I. Lukeš, J. Rohovec, Inorg. Chim. Acta 317 (2001) 324.
[22] J. Kotek, P. Vojtíšek, I. Císařová, P. Hermann, I. Lukeš, Collect. Czech. Chem. Commun. 66 (2001) 363.
[23] J. Kotek, P. Lubal, P. Hermann, I. Císařová, I. Lukeš, T. Godula, I. Svobodová, P. Táborský, J. Havel, Chem. Eur. J. 9 (2003) 233.
[24] A.R. Timerbaev, A. Kung, B.K. Kepler, J. Chromatogr. A 945 (2002) 25.
[25] I.C.N. Diogenes, J.R. de Sousa, I.S. Moreira, Chromatographia 50 (1999) 105.
[26] I.C.N. Diogenes, J.R. de Sousa, I.S. Moreira, Chromatographia 51 (2000) 122.
[27] K.Q. Ferreira, A.M. Lucchesi, Z.N. da Rocha, R.S. da Silva, Inorg. Chim. Acta 328 (2002) 147.
[28] X.F. Zhu, S.Z. Lever, Electrophoresis 23 (2002) 1348.
[29] M. Koudelková, H. Vinšová, V. Jedináková-Křížová, J. Chromatogr. A 990 (2003) 311.
[30] C.M. Shelton, K.E. Seaver, J.F. Wheeler, N.A.P. Kane-Maguire, Inorg. Chem. 36 (1997) 1532.
[31] O.V. Mytykh, S.E. Martin, J.F. Wheeler, N.A.P. Kane-Maguire, Inorg. Chim. Acta 311 (2000) 143.
[32] J.E. Harris, N. Desai, K.E. Seaver, R.T. Watson, N.A.P. Kane-Maguire, J.F. Wheeler, J. Chromatogr. A 919 (2001) 427.
[33] A. Gaspar, P. Buglyo, Chromatographia 51 (2000) S143.
[34] J.M. Sanchez, V. Salvado, J. Havel, J. Chromatogr. 834 (1999) 329.
[35] J.M. Sanchez, V. Salvado, J. Havel, Talanta 56 (2002) 1061.
[36] S.S. Aleksenko, A.P. Gumenyuk, S.P. Mushtakova, A.R. Timerbaev, Fresenius J. Anal. Chem. 370 (2001) 865.
[37] A.A. Christy, P.K. Egeberg, Talanta 51 (2000) 1049.
[38] R.G. Wilkins, Kinetics and Mechanism of Reactions of Transition Metal Complexes, VCH, Weinheim, 1991.
[39] R.W. Hay, Reaction Mechanisms of Metal Complexes, Horwood Publishing, Chichester, 2000.
[40] L. Treindl, Chemická kinetika (in Slovak), SPN, Bratislava, 1990.
[41] V. Jokl, J. Chromatogr. 13 (1964) 451.
[42] W.H. Robbins, B.W. Wright, J. Chromatogr. A 680 (1994) 667.
[43] A.L. Revilla, J. Havel, P. Jandik, J. Chromatogr. A 745 (1996) 225.
[44] I. Svobodová, P. Lubal, P. Hermann, J. Kotek, J. Havel, J. Inclusion Phenomena Macrocycl. Chem. 49 (2004) 11.
[45] I. Svobodová, P. Lubal, P. Hermann, J. Kotek, J. Havel, Microchim. Acta 148 (2004) 21.

[46] S. Vajda, H. Rabitz, J. Phys. Chem. 92 (1988) 701.
[47] S. Vajda, H. Rabitz, J. Phys. Chem. 98 (1994) 5265.
[48] I. Novak-Hofer, P.A. Schubiger, Eur. J. Nucl. Med. 29 (2002) 821.
[49] S.V. Smith, J. Inorg. Biochem. 98 (2004) 1874.
[50] C.A. Boswell, P. McQuade, G.R. Weisman, E.H. Wong, C.J. Anderson, Nucl. Med. Biol. 32 (2005) 29.
[51] J.S. Lewis, A. Srinivasan, M.A. Schmidt, C.J. Anderson, Nucl. Med. Biol. 26 (1999) 268.
[52] J.S. Lewis, M.R. Lewis, A. Srinivasan, M.A. Schmidt, J. Wang, C.J. Anderson, J. Med. Chem. 42 (1999) 1341.
[53] L.A. Bass, M. Wang, M.J. Welch, C.J. Anderson, Bioconjugate Chem. 11 (2000) 527.
[54] X. Sun, M. Wuest, G.R. Weisman, E.H. Wong, D.P. Reed, C.A. Boswell, R. Motekaitis, A.E. Martell, M.J. Welch, C.J. Anderson, J. Med. Chem. 45 (2002) 469.
[55] X. Sun, M. Wuest, Z. Kovacs, A.D. Sherry, R. Motekaitis, Z. Wang, A.E. Martell, M.J. Welch, C.J. Anderson, J. Biol. Inorg. Chem. 8 (2003) 217.
[56] P. Karlson, W. Gerok, W. Gross, Pathobiochemie (Pathobiochemistry), Academia, Prague, 1987.

2. Experimental

2.1. Materials

All of used chemicals were reagent grade. Salicylaldehyde and aniline were used after distillation under reduced pressure. Ethylenediamine and cyclohexylamine were distilled before use. The other reagents were used without further purification. 5-Phenylazo salicylaldehyde was synthesized as described in the literature [20].

2.2. Physical measurements and methods

Infrared (FT-IR) spectra were recorded using KBr discs on a Bruker Tensor 27 instrument. ^{1}H NMR spectra were taken on a Bruker Spectrospin Avance 400 MHz ultrashield spectrometer. The electronic spectra in the 200–600 nm range were obtained on a Shimadzu UV-265 FW spectrophotometer and quartz cells of light pass length 1.00 cm, using solutions with the concentration of 1×10^{-5} in DMF. CHN elemental analyses were performed using a Heraeus CHN-O RAPID elemental analyzer. Melting points were taken using an electrothermal IA 9100 apparatus in open capillary tubes. Cyclic voltammograms were recorded using an AMEL instrument Model 2053 as potentiostat connected with AMEL Model 568 as function generator. All solutions were deoxygenated by passing a stream of argon into the solution for at least 10 min before recording the voltammogram. All potentials reported herein were measured at room temperature and referenced to the saturated Ag/AgCl electrode with ferrocene as an internal standard. A glassy carbon disc with a diameter of 3 mm was used as the working electrode and a platinum wire was used as counter electrode. Before each experiment the working electrode was polished with alumina and rinsed thoroughly with distilled water and acetone. The electrolytic medium consisted of 0.1 M $LiClO_4$ in DMF. Under these conditions the ferrocenium–ferrocene couple shows a peak separation of 89 mV. A Pentium IV computer with a 1200 MHz processor, 256 MB of RAM and the HYPERCHEM package version 7 [21] were used for quantum chemical calculations.

2.3. Synthesis of Schiff-base ligands

Schiff-base ligands were prepared in a similar manner according to the literature [22] as the following procedure: To a stirring solution of 2 mmol of appropriate aldehyde in ethanol was added a solution of 1 mmol diamine in ethanol dropwise and then refluxed for 2 h. The precipitated Schiff-base was filtered and recrystallized from hot ethanol giving *N*,*N*′-bis(5-X-salicylidene)-1,2-ethylenediamine, where X is H and N_2ph (diazophenyl) that will abbreviated here as H_2L^1 and H_2L^2, respectively. Some analytical and physical data of the ligands are summarized as follows.

2.3.1. Salen ($C_{16}H_{16}N_2O_2$) (H_2L^1)

Yellow crystals, yield 78% (0.4186 g); m.p.: 168 °C. ^{1}H NMR ($CDCl_3$): δ 13.22 (br s, 2H, OH), 8.35 (s, 2H, H_e), 8.29 (m, 2H, H_b), 7.22 (dd, 2H, H_d), 6.94 (d, 2H, H_a), 6.85 (m, 2H, H_c), 3.94 (s, 4H, $H_{f,g}$). FT-IR(KBr, cm^{-1}): 3300–3400 (m, OH), 2900 (aliphatic CH), 1645 (s, imine C═N), 1200 (phenolic CO).

2.3.2. Bis(5-phenyl azo)salen ($C_{28}H_{24}N_6O_2$) (H_2L^2)

Orange crystals, yield 92% (0.8768 g); m.p.: 229 °C. ^{1}H NMR ($CDCl_3$): δ 13.79 (br s, 2H, OH), 8.52 (s, 2H, H_e), 7.97 (dd, 2H, H_b), 7.92 (d, 2H, H_d), 7.84–7.87 (m, 4H, $H_{i,m}$), 7.42–7.52 (m, 6H, $H_{j,k,l}$), 7.07 (d, 2H, H_a), 4.04 (s, 4H, $H_{f,g}$). FT-IR(KBr, cm^{-1}): 3300–3400 (m, OH), 1635 (s, imine C═N), 1185 (phenolic CO).

2.4. Synthesis of the complexes

The complexes shown in Scheme 1 were synthesized as follows.

1 mmol of Co (II) acetate tetrahydrate, 1 mmol of the appropriate Schiff-base ligand, 2 mmol of axial amine and 4 mmol of $LiClO_4$ were added to 100 ml of ethanol. The obtained solution turned red rapidly upon the formation of $Co^{(II)}$(salen) complex. Then air was bubbled through the reaction mixture for oxidizing the $Co^{(II)}$(salen) and the mixture stirred and refluxed for 2 h. Then air bubbling and stirring was continued for 24 h. After which the obtained brown material was washed and recrystallized from appropriate solvent systems.

2.4.1. Preparation of [CoL^1(cyclohexylamine)$_2$]ClO_4

The complex was recrystallized from hot ethanol, yielding brown crystals. Yield 96.5% (0.6012 g). *Anal*. Calc. for $CoC_{28}H_{40}N_4O_6Cl$: C, 54.0; H, 6.5; N, 9.0. Found: C, 53.3; H, 6.4; N, 8.8%; m.p.: 199.2 °C. ^{1}H NMR (CD_3CN): δ 8.17

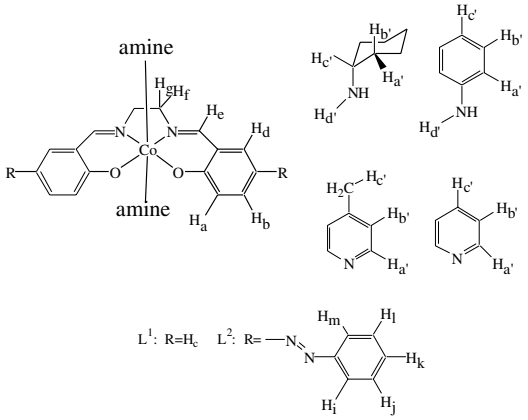

H_2L^1 (salen) complexes: amine= pyridine, picoline, aniline, cyclohexylamine

H_2L^2 (bis(5-phenylazo)salen) complex: amine= pyridine

Scheme 1. A schematic representation of the studied complexes.

(s, 2H, H_e), 7.34 (dd, 2H, H_d), 7.24 (m, 2H, H_b), 7.10 (d, 2H, H_a), 6.53 (q, 2H, H_c), 3.39 (s, 4H, $H_{f,g}$), 2.82 (br d, 4H, $H_{d'}$), 2.21 (br m, 2H, $H_{c'}$), {1.37 (m, 10H) and 0.85 (m, 10H): $H_{a'}$ and $H_{b'}$}. FT-IR(KBr, cm^{-1}): 3295.69 and 3245.86 (m, NH), 1629 (s, C=N), 1090 (br s, ClO_4^-).

2.4.2. Preparation of $[CoL^1(aniline)_2]ClO_4$

The complex was recrystallized from acetonitrile/ethanol (1:2 v/v) yielding brown crystals. Yield 98.2% (0.5999 g). *Anal.* Calc. for $CoC_{28}H_{28}N_4O_6Cl$: C, 55.1; H, 4.6; N, 9.2. Found: C, 54.3; H, 4.8; N, 8.9%; m.p.: 228.6 °C. ^1H NMR (CD_3CN): δ 7.92 (s, 2H, H_e), 7.32 (m, 2H, H_d), 7.16 (dd, 4H, $H_{a'}$), 7.06 (m, 2H, H_b), 6.90–6.94 (m, 4H, $H_{a,c'}$), 6.54–6.61 (m, 6H, $H_{c,b'}$), 4.52 (br s, 4H, $H_{d'}$), 3.80 (s, 4H, $H_{f,g}$). FT-IR(KBr, cm^{-1}): 3234 and 3145 (m, NH), 1631 (s, C=N), 1208 (phenolic CO), 1099 (br s, ClO_4^-).

2.4.3. Preparation of $[CoL^1(4\text{-picoline})_2]ClO_4$

The complex was recrystallized from acetonitrile/ethanol (1:2 v/v) yielding brown crystals. Yield 93.2% (0.5694 g). *Anal.* Calc. for $CoC_{28}H_{28}N_4O_6Cl$: C, 55.1; H, 4.6; N, 9.17. Found: C, 54.1; H, 4.7; N, 9.0%; m.p.: 249.1 °C. ^1H NMR(CD_3CN): δ 8.39 (s, 2H, H_e), 7.89 (d, 4H, $H_{a'}$), 7.21–7.34 (m, 8H, $H_{b,d,b'}$), 7.10 (d, 2H, H_a), 6.52 (m, 2H, H_c), 4.12 (s, 4H, $H_{f,g}$), 2.27 (s, 6H, $H_{c'}$). FT-IR(KBr, cm^{-1}): 1626 (s, C=N), 1210 (phenolic CO), 1097 (br s, ClO_4^-).

2.4.4. Preparation of $[CoL^1(pyridine)_2]ClO_4$

The complex was recrystallized from acetonitrile/ethanol (1:2 v/v) yielding brown crystals. Yield 94.0% (0.5479 g). *Anal.* Calc. for $CoC_{26}H_{24}N_4O_6Cl$: C, 53.6; H, 4.2; N, 9.6. Found: C, 53.4; H, 4.2; N, 9.5%; m.p.: 282.5 °C. ^1H NMR (CD_3CN): δ 8.42 (s, 2H, H_e), 7.89 (d, 4H, $H_{a'}$), 7.86 (m, 2H, H_b), 7.22–7.42 (m, 8H, $H_{d,b',c'}$), 7.12 (d, 2H, H_a), 6.52 (m, 2H, H_c), 4.14 (s, 4H, $H_{f,g}$). FT-IR(KBr, cm^{-1}): 1626 (s, C=N), 1210 (phenolic CO), 1093 (br s, ClO_4^-).

2.4.5. Preparation of $[CoL^2(pyridine)_2]ClO_4$

The complex was recrystallized from acetonitrile/ethanol (1:2 v/v) yielding brown crystals. Yield 90.0% (0.7120 g). *Anal.* Calc. for $CoC_{38}H_{32}N_8O_6Cl$: C, 57.7; H, 4.1; N, 14.2. Found: C, 57.0; H, 4.4; N, 13.8%; m.p.: 265.1 °C. ^1H NMR (CD_3CN): δ 8.66 (s, 2H, H_e), 8.14 (dd, 4H, $H_{a'}$), 8.06 (d, 2H, H_d), 7.87–7.94 (m, 4H, $H_{b,c'}$), 7.75–7.78 (m, 4H, $H_{i,m}$), 7.55 (m, 4H, $H_{b'}$), 7.44–7.5 (m, 6H, $H_{j,k,l}$), 7.32 (d, 2H, H_a), 4.25 (s, 4H, $H_{f,g}$). FT-IR(KBr, cm^{-1}): 1628 (s, C=N), 1117 (br s, ClO_4^-).

2.5. X-ray crystallography

The red plate like single crystals of the complex $[CoL^1(aniline)_2]ClO_4$ obtained by slow evaporation of solvent from acetonitrile/ethanol (1:1 v/v) solution of the complex at room temperature.

All the measurements were performed using graphite monochromatized Mo Kα radiation (0.71069 Å) at 95 K: $C_{28}H_{28}ClCoN_4O_6$, M_r 610.92, monoclinic, space group $P2_1/c$, $a = 11.422(3)$ Å, $b = 16.219(5)$ Å, $c = 14.216(4)$ Å, $\beta = 101.77(2)°$, $V = 2578.2(13)$ Å^3, $Z = 4$, $D_{calc} = 1.574$ g/cm^3, absorption coefficient $\mu = 0.822\ mm^{-1}$. Due to the large organic ligand, the linear absorption coefficient (μ) is only $0.822\ mm^{-1}$ and the crystal used was small (max diameter $r = 0.28$ mm), so the product of $\mu \times r$ is only 0.23 and the absorption correction was not carried out. The other crystal data and structure refinement information are as follows: crystal size: $0.28 \times 0.18 \times 0.12$(mm), $F(000)$: 1264, diffractometer: Stoe, radiation source: fine-focus sealed tube, scan type: ω scans, standard reflections: 3 for every 100 reflections, intensity decay: 1.4%, θ range for data collection: 2.51–26.00 (°), index ranges: $-14 \leqslant h \leqslant 13$, $-1 \leqslant k \leqslant 20$, $-1 \leqslant l \leqslant 17$, reflections collected/unique: 6080/5061, significant unique reflections: 4047 with $I > 2\sigma(I)$, R(int)/R(sigma): 0.0319/0.0635, completeness to $\Theta = 26.0°$: 99.8%, refinement method: full-matrix least-squares on F^2, data/parameters/restraints: 5061/371/2, goodness-of-fit on F^2: 1.063, final R indices [$I > 2(I)$]: $R_1 = 0.0452$, $wR_2 = 0.0925$, R indices (all data): $R_1 = 0.0647$, $wR_2 = 0.1029$, extinction expression: none, weighting scheme: $w = 1/[\sigma^2(F_o^2) + (aP)^2 + bP]$, where $P = (F_o^2 + 2F_c^2)/3$, weighting scheme parameters a, b: 0.0242, 2.0103, largest Δ/σ in last cycle: 0.001, largest difference peak and hole (e/Å^3): 0.401 and −0.318, structure solution program: SHELXS-97 (Sheldrick, 1990), structure refinement program: SHELXL-97 (Sheldrick, 1997).

3. Results and discussion

3.1. Crystal structure

The molecular and crystal structure of the $[Co(salen)(aniline)_2]ClO_4$ are shown in Figs. 1 and 2, respectively. Some selected bond angles and lengths are listed in Table 1. The complex is composed of the $[Co(salen)(aniline)_2]^+$ cation complex and the anion ClO_4^-. Cobalt (III) center is coordinated by two phenolate oxygens, two imine nitrogens of the salen ligand and by the two nitrogen atoms of aniline groups, which occupy the axial positions of a distorted octahedral coordination geometry. The two axial ligands are approximately normal to the salen plane. The axial bond angle N(3)–Co–N(4) is 175.92(10)° which is comparable with those of corresponding angles in similar Co(III) complexes [14,15,19]. The salen ligand has a planar coordination geometry and the Co atom lies in the best plane through the atoms O(1), O(2), N(1) and N(2) (max dev. 0.006 (11) Å). The Co–O (1.894(2), 1.911(2) Å) and Co–N_{imine} (1.895(3), 1.892(2) Å) bond lengths are in good agreement with those of similar complexes [14,15,19]. Every N(4) of ion complex is hydrogen bonded to two phenolate oxygen atoms of other symmetrically related ion complex (Table 2 and

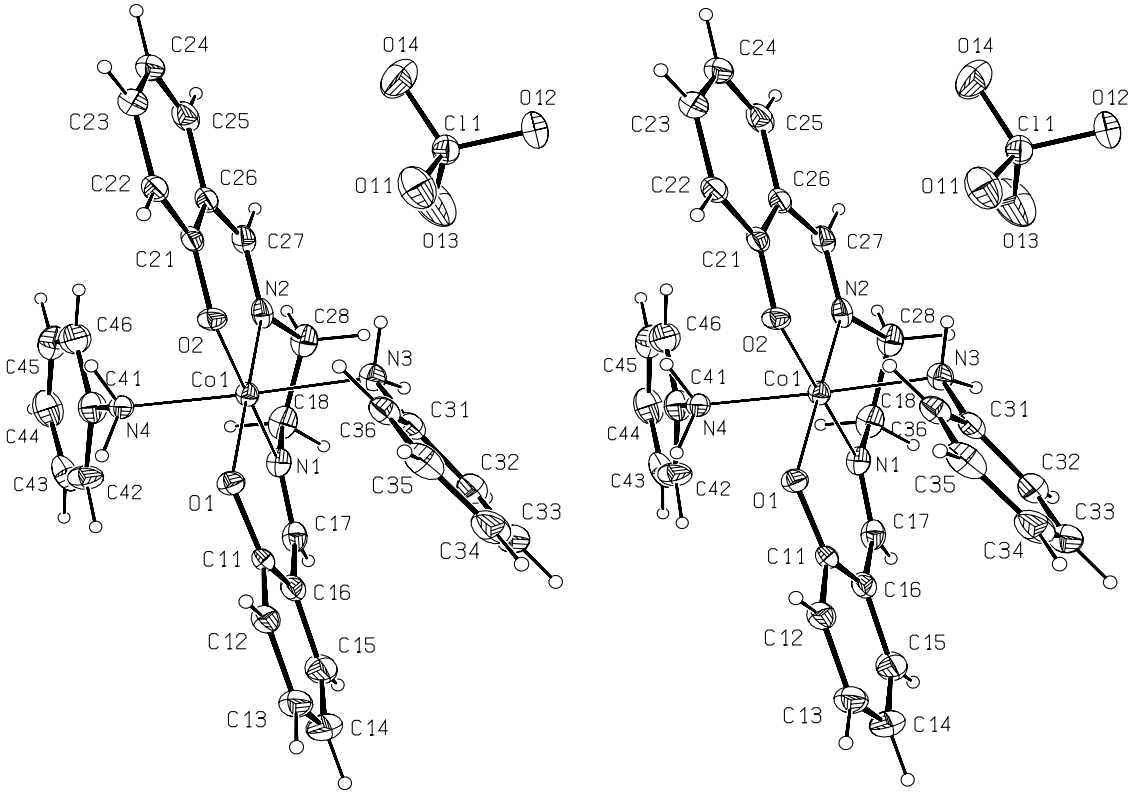

Fig. 1. Stereoscopic ORTEP plot of $[CoL^1(aniline)_2]ClO_4$, showing the atomic numbering scheme. The probability ellipsoids are drawn at the 50% probability level.

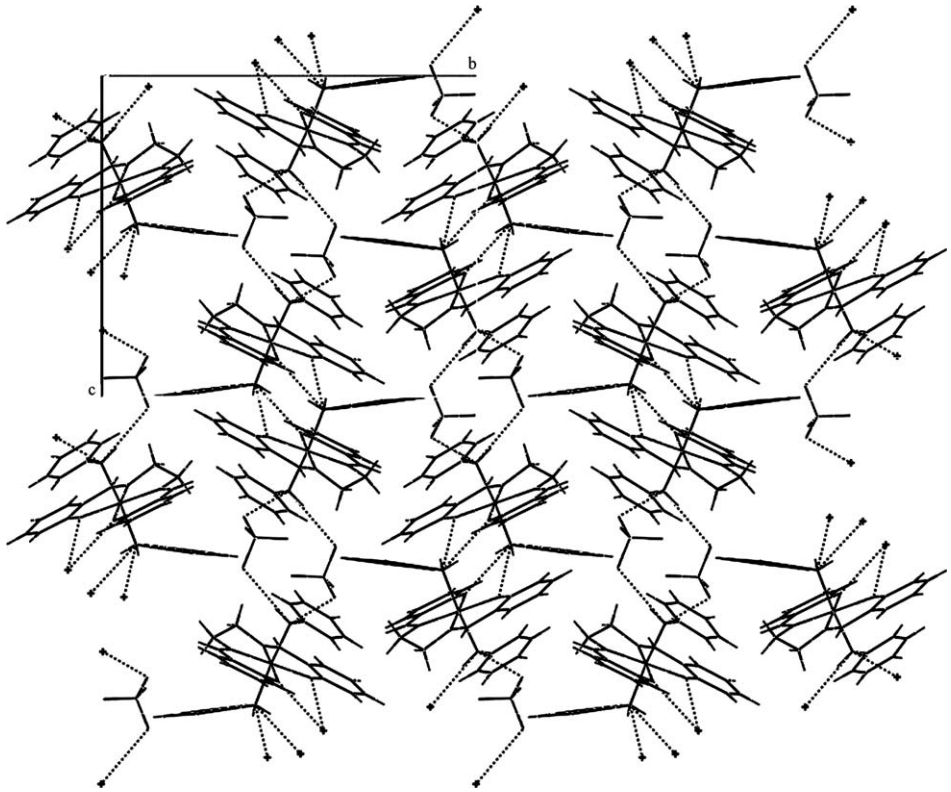

Fig. 2. *bc*-Plane of $[CoL^1(aniline)_2]ClO_4$, viewed along the *a*-axis. Hydrogen bonds are shown as dashed lines.

Table 1
Selected bond lengths (Å), bond angles (°) and torsion angles (°) for $[CoL^1(aniline)_2]ClO_4$

Bond lengths (Å)	
Co(1)–O(1)	1.894(2)
Co(1)–O(2)	1.911(2)
Co(1)–N(1)	1.895(3)
Co(1)–N(2)	1.892(2)
Co(1)–N(3)	2.006(2)
Co(1)–N(4)	2.002(2)
O(1)–C(11)	1.322(3)
C(16)–C(17)	1.434(4)
C(17)–N(1)	1.289(4)
N(1)–C(18)	1.477(4)
C(18)–C(28)	1.500(5)
O(2)–C(21)	1.320(3)
C(26)–C(27)	1.427(4)
C(27)–N(2)	1.290(4)
N(2)–C(28)	1.466(4)
N(3)–C(31)	1.455(4)
N(4)–C(41)	1.432(4)
Bond angles (°) and torsion angles (°)	
N(2)–Co(1)–O(1)	178.91(10)
N(1)–Co(1)–O(2)	179.26(9)
N(4)–Co(1)–N(3)	175.92(10)
C(11)–O(1)–Co(1)	125.25(18)
C(17)–N(1)–C(18)	119.5(3)
C(17)–N(1)–Co(1)	126.6(2)
C(18)–N(1)–Co(1)	113.81(19)
C(21)–O(2)–Co(1)	125.82(18)
C(27)–N(2)–C(28)	119.9(2)
C(27)–N(2)–Co(1)	126.5(2)
C(28)–N(2)–Co(1)	113.37(19)
C(31)–N(3)–Co(1)	118.37(18)
C(41)–N(4)–Co(1)	123.48(19)
N(2)–Co(1)–N(1)	85.01(11)
O(2)–Co(1)–O(1)	86.67(8)
O(1)–Co(1)–N(1)	93.95(9)
O(2)–Co(1)–N(2)	94.37(10)
N(1)–Co(1)–N(3)	91.60(10)
N(2)–Co(1)–N(3)	87.97(10)
O(1)–Co(1)–N(3)	92.39(9)
O(2)–Co(1)–N(3)	88.77(10)
N(1)–Co(1)–N(4)	92.39(10)
N(2)–Co(1)–N(4)	93.23(10)
O(1)–Co(1)–N(4)	86.49(9)
O(2)–Co(1)–N(4)	87.25(9)
N(1)–C(18)–C(28)–N(2)	−37.4(3)
N(2)–Co(1)–O(2)–C(21)	11.3(2)
N(1)–Co(1)–O(1)–C(11)	17.5(2)
O(1)–Co(1)–N(3)–C(31)	−4.6(2)
O(1)–Co(1)–N(4)–C(41)	−135.5(2)

Fig. 2), so that two ion complexes are linked to each other by four hydrogen bonds to form a dimerized ion complex. Every N(3), also, connects to two perchlorate ions by hydrogen bonds. One of the perchlorate oxygens is hydrogen bonded to one of the N(3) of the other dimerized ion complex, so that, the dimerized ion complexes are linked together via ClO_4^- bridging group and form a ribbon along the *c*-axis. The ribbons in *bc*-plane have short contacts by the distances of less than the max sum of atomic van der walls radii.

Table 2
Hydrogen bonds for $[CoL^1(aniline)_2]ClO_4$ (Å, °)

D–H···A	*d*(D–H)	*d*(H···A)	*d*(D···A)	∠(DHA)
N(3)–H···O(11)	0.92	2.25	3.160(4)	167.9
N(3)–H′···O(12)[a]	0.92	2.25	3.161(3)	173.4
N(4)–H···O(1)[b]	0.92	2.16	2.898(3)	136.7
N(4)–H′···O(2)[b]	0.92	2.22	3.032(3)	146.9

Symmetry transformations used to generate equivalent atoms: [a] $1-x$, $1-y$, $1-z$; [b] $1-x$, $1-y$, $-z$.

3.2. Spectral characterization of the ligands and complexes

The IR and ^1H NMR are in accord with the proposed structures. The FT-IR spectra of all complexes, compared with those of the corresponding ligands, indicate that the ν(C=N) band at 1631–1626 cm^{-1} is shifted to lower energy by 14–19 cm^{-1} for salen complexes, but 7 cm^{-1} in the case of azosalen complex, indicating that the ligands are coordinated to the metal ions through the nitrogen atoms of the azomethine groups. On the other hand, the OH proton signals in ^1H NMR spectra of free ligands (13.2 and 13.79 ppm for H_2salen and H_2azosalen, respectively) disappears in the case of complexes indicating that the OH group has been deporotonated and bonded to metal ions as oxygen anion, therefore, the presence of one perchlorate counter ion for each ion-complex of Co(III) can be expected. The appearance of a broad strong band in the IR spectra of the complexes in 1090–1118 cm^{-1} is assigned to perchlorate stretching vibrations, which are typical of non-coordinating perchlorate [24].

Comparing the ^1H NMR spectra of the free ligands and complexes, the imine proton resonances of the ligands (8.35 and 8.52 ppm for H_2L^1 and H_2L^2, respectively) are shifted to lower fields (8.39, 8.42 and 8.66 ppm) in the case of $[CoL^1(4\text{-picoline})_2]ClO_4$, $[CoL^1(pyridine)_2]ClO_4$ and $[CoL^2(pyridine)_2]ClO_4$, respectively, and are shifted to high-field (7.92 and 8.14 ppm) in the case of $[CoL^1(aniline)_2]ClO_4$ and $[CoL^1(cyclohexylamine)_2]ClO_4$, respectively.

Table 3 shows the electronic absorption data for ligands and complexes. The electronic absorption spectrum (>280 nm) of free salen ligand consists of an intense band centered at 316.6 nm attributable to $\pi \rightarrow \pi^*$ transitions associated with azomethine chromophore [25]. Since such a band is seen for reduced imines too, it seems that the charge transfer from phenolate oxygens to phenyl rings

Table 3
Electronic absorption data for ligands and complexes in DMF solution

Compound	λ (nm)				
H_2L^1	273.8			316.6	
H_2L^2	268.6			367.2	428 (sh)
$[CoL^1(cyclohexylamine)_2]ClO_4$	268.2	300 (sh)		390.6	420 (sh)
$[CoL^1(aniline)_2]ClO_4$	267.6	300 (sh)	328 (sh)	392.2	420 (sh)
$[CoL^1(4\text{-picoline})_2]ClO_4$	268.2	300 (sh)	330 (sh)	392.6	420 (sh)
$[CoL^1(pyridine)_2]ClO_4$	268.0	300 (sh)		390.0	420 (sh)
$[CoL^2(pyridine)_2]ClO_4$	267.4	300 (sh)		398.2	440 (sh)

are may be involved in this band appearance too [26]. The similar azomethine $\pi \rightarrow \pi^*$ transitions take place at 367 nm in the case of azosalen ligand. A new band, as a shoulder, with a maximum at 428 nm appears in the UV–Vis spectrum of azosalen in contrast to salen, which is attributable to azophenyl substitute. There is some other intense band in high-energy region (about 270 nm) of the spectra of the free ligands which are related to $\pi \rightarrow \pi^*$ transitions of phenyl rings [19].

The Co(III) complexes of these ligands exhibit absorption bands that are red shifted approximately. Complexation of this ligands with Co(III) with different axial ligands does not affect the energy of the phenyl rings $\pi \rightarrow \pi^*$ transitions, whereas the azomethine $\pi \rightarrow \pi^*$ transitions in complexes show red shift about 70 nm in salen complexes and 30 nm in azosalen complex. These $\pi \rightarrow \pi^*$ azomethine transition bands, show a shoulder at 420 nm in salen complexes and at 440 nm in azosalen complex. Fig. 3 compares the electronic spectra for complexes and free ligands.

These shoulders in salen complexes spectra are attributable to metal–ligand charge transfer transitions (MLCT) ($d \rightarrow \pi^*$) transitions [14,19], while in azosalen complexes the shoulder can be attributed to $\pi \rightarrow \pi^*$ intraligand charge transfer with a small contribution of MLCT. These assignments of shoulders are supported by electronic structure calculation employing Zindo/S semiempirical Hamiltonian with π–π overlap weighting factor of 0.585 for structures optimized by Zindo/1 method [27–34]. The selected main atomic orbitals contributions to HOMO and LUMO of the complexes are shown in Table 4.

Azosalen spectrum bands show red shift in comparison to salen spectra due to the extended conjugated system in azosalen complexes. Different axially coordinated ligands have no effect on the energies of the electronic transitions.

3.3. Electrochemical studies

By scanning in the negative direction initiated at 0.0 mV, the first and second reduction waves correspond to Co(III) → Co(II) and Co(II) → Co(I) processes appear in the range of (−586)–(−247) and (−1107)–(−1037) mV, respectively (Table 5). The peak separation between the related cathodic and anodic waves indicate a quasireversible and reversible redox reactions for Co(III)/Co(II) (min $\Delta E_p = 302$ mV) and Co(II)/Co(I) (max $\Delta E_p = 86$ mV) systems, respectively. The quasireversible redox reaction can be due to the structural changes say by elongation of axial bond lengths or losing of axial amine ligands because of the addition of one electron to $(d_{z^2})^*$ orbital [19]. The redox peak heights increase by increasing of scan rate. Multiple scans result in nearly superposable cyclic voltammograms, i.e., the three oxidation states of cobalt involved are markedly stable.

For the cathodic process of the Co(III) → Co(II), the observed peak potentials are strongly depend on donor strength of the appropriate axial ligands, since the electron affinity of the Co(III) complexes, decreases by

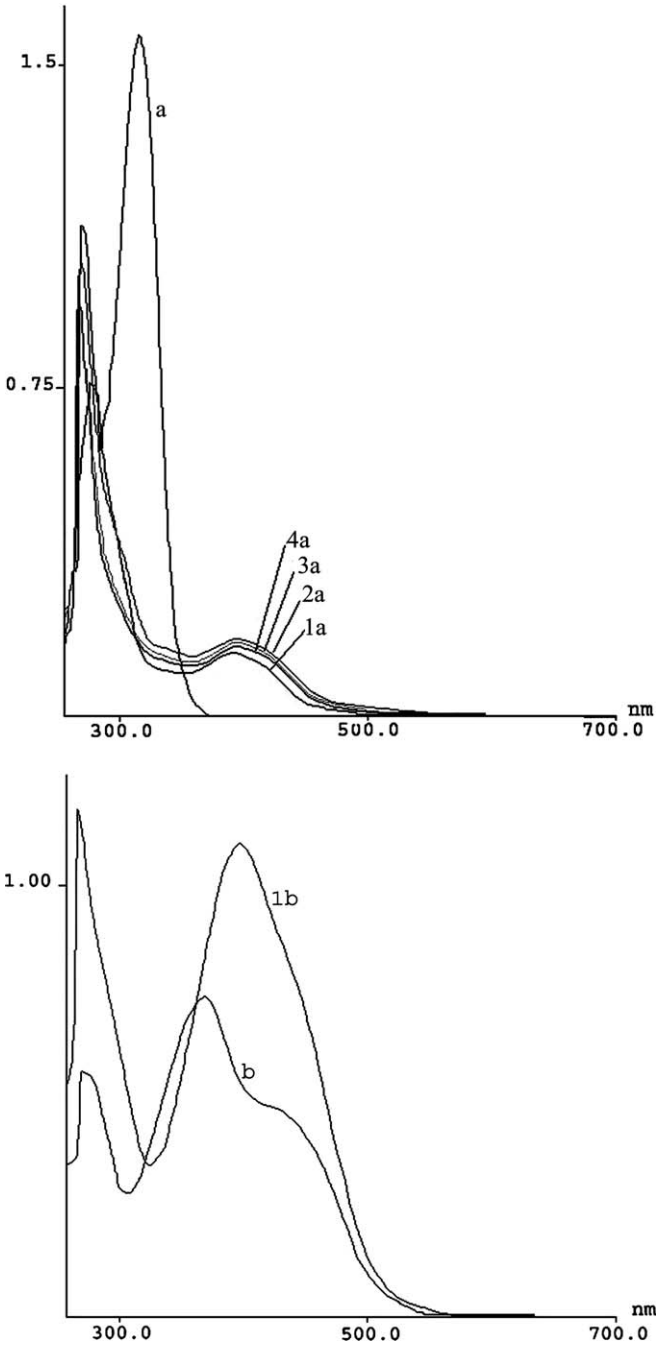

Fig. 3. The UV/Vis spectra of the ligands and complexes: H_2L^1 (a), $[CoL^1(cyclohexylamine)_2]ClO_4$ (1a), $[CoL^1(aniline)_2]ClO_4$ (2a), $[CoL^1(4\text{-picoline})_2]ClO_4$ (3a), $[CoL^1(pyridine)_2]ClO_4$ (4a), H_2L^2 (b) and $[CoL^2(pyridine)_2]ClO_4$ (1b).

increasing pK_a of the axial lewis base. The more negative cathodic potentials for Co(III) → Co(II) process are seen in the order of cyclohexylamine > 4-picoline > pyridine > aniline, that correlates with the pK_a values order (Table 5). Fig. 4 shows the cyclic voltamogram of $[CoL^1(cyclohexylamine)_2]ClO_4$.

Existing of a 5-phenylazo substitution on equatorial salen Schiff-base ligand, which acts as a good electron withdrawing group, causes a more electron affinity on cobalt

Table 4
The selected main atomic orbitals contributions to the HOMO and LUMO molecular orbitals of complexes

Complex	MO	E (eV)	Symmetry[a]	Contribution of AO to MO[b]					
				Co	C_{imine} (average)	N_{imine} (average)	$C_{phenolic}$ (average)	$O_{phenolic}$ (average)	N_{ax} (average)
$[CoL^1(cyclohexylamine)_2]+$	HOMO	−0.39034	π	0.02598	0.00247	0.03896	0.07473	0.07657	0.00109
	LUMO	−0.13475	π	0.00575	0.29903	0.09717	0.05460	0.01048	0.00035
$[CoL^1(aniline)_2]+$	HOMO	−0.38778	π	0.02304	0.00265	0.02859	0.04696	0.10592	0.00086
	LUMO	−0.13589	π	0.00574	0.20332	0.09629	0.05517	0.01052	0.00041
$[CoL^1(4\text{-picoline})_2]+$	HOMO	−0.38185	π	0.05220	0.00075	0.03886	0.06401	0.10796	0.00068
	LUMO	−0.12131	π	0.00357	0.19811	0.09713	0.05351	0.01108	0.00058
$[CoL^1(pyridine)_2]+$	HOMO	−0.38498	π	0.04997	0.00078	0.03829	0.06624	0.10403	0.00039
	LUMO	−0.12442	π	0.00312	0.19963	0.09672	0.05263	0.01060	0.00159
$[CoL^2(pyridine)_2]+$	HOMO	−0.36773	π	0.00995	0.00178	0.01214	0.03813	0.04218	0.00094
	LUMO	−0.12343	π	0.00545	0.20040	0.09768	0.04764	0.01084	0.00119

[a] Since the molecular plane acts as a nodal plane, the symmetry of the orbital is π.
[b] Calculated as the sum of the squared coefficient of the 2s, $2p_x$, $2p_y$ and $2p_z$ orbitals of C, N and O atoms and $3d_{z^2}$, $3d_{xz}$, $3d_{yz}$, $3d_{x^2-y^2}$, $3d_{xy}$, 4s, $4p_x$, $4p_y$ and $4p_z$ of Co atom in the linear combination that defines the MO.

Table 5
Cyclic voltammetry data (mV) for complexes in DMF solutions (scan rate 100 mV/s)[a]

Complex	E_{pc}(III → II)	E_{pa}(II → III)	ΔE_p(III ↔ II)	E_{pc}(II → I)	E_{pa}(I → II)	ΔE_p(II ↔ I)	$E_{1/2}$(II ↔ I)	pK_a (axial amine)[b]
$[CoL^1(cyclohexylamine)_2]ClO_4$	−586	27	613	−1107	−1040	67	−1073	10.64
$[CoL^1(aniline)_2]ClO_4$	−305	35	340	−1029	−1107	78	−1068	4.60
$[CoL^1(4\text{-picoline})_2]ClO_4$	−327	24	351	−1105	−1043	62	−1074	6.00
$[CoL^1(pyridine)_2]ClO_4$	−319	16	335	−1107	−1029	78	−1068	5.17
$[CoL^2(pyridine)_2]ClO_4$	−247	55	302	−1037	−951	86	−994	5.17

[a] The ferrocenium–ferrocene couple shows a peak separation of 89 mV under the experimental conditions.
[b] The pK_a values (in aqueous solution) of the used axial amines are reported from Ref. [23].

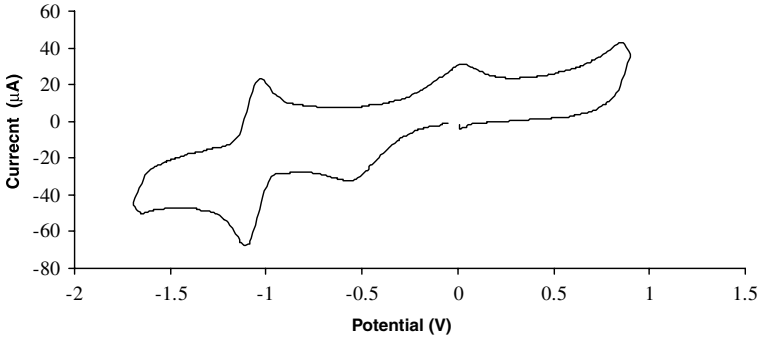

Fig. 4. Cyclic voltammogram of $[CoL^1(cyclohexylamine)_2]ClO_4$.

center and so a less negative cathodic peak for $[CoL^2(pyridine)_2]ClO_4$ complex in contrast with $[CoL^1(pyridine)_2]ClO_4$.

4. Supplementary material

Crystallographic data for the structural analysis have been deposited with the Cambridge Crystallographic Data Centre, CCDC No. 255047. Copies of this information may be obtained free of charge from The Director, CCDC, 12 Union Road, Cambridge, CB2 1EZ, UK (fax: +44 1223 336033; e-mail: deposit@ccdc.cam.ac.uk or http://www.ccdc.cam.ac.uk). Supplementary data associated with this article can be found, in the online version, at doi:10.1016/j.poly.2005.12.001.

Acknowledgments

We are grateful to Tabriz University Research Council for the financial support of this research. Also authors

are to thank prof. Dr. F. Belaj for X-ray structure determinations.

References

[1] E.C. Niederhoffer, J.H. Timmons, A.E. Martell, Chem. Rev. 84 (1984) 137.
[2] S. Yamada, Coord. Chem. Rev. 191 (1999) 537.
[3] N.J. Henson, P.J. Hay, A. Redondo, Inorg. Chem. 38 (1999) 1618.
[4] A.E. Martell, D.T. Sawyer, Oxygen Complexes and Oxygen Activation by Transition Metals, Plenum Press, New York, 1988.
[5] C. Bianchini, R.W. Zoeliner, Adv. Inorg. Chem. 44 (1997) 263.
[6] T. Nagata, K. Yorozu, T. Yamada, T. Mukaiyama, Angew. Chem. Int. Ed. Engl. 34 (1995) 2145.
[7] E.N. Jacobsen, W. Zhang, M.L. Guler, J. Am. Chem. Soc. 113 (1991) 6703.
[8] G.L. Estiu, A.H. Jubert, G. Costamagna, J. Vargas, Inorg. Chem. 35 (1996) 263.
[9] P.K. Mascharak, Coord. Chem. Rev. 225 (2002) 201.
[10] J.G. Muller, L.A. Kayser, S.J. Paikoff, V. Duarte, N. Tang, R.J. Perez, S.E. Rokita, C.J. Burrows, Coord. Chem. Rev. 185–186 (1999) 761.
[11] D.P. Kessissoglou, Coord. Chem. Rev. 185–186 (1999) 837.
[12] J.W. Pyrz, A.L. Roe, L.J. Stern, L. Que, J. Am. Chem. Soc. 107 (1985) 614.
[13] V.E. Kaasjager, L. Puglisi, E. Bouwman, W.L. Driessen, J. Reedijk, Inorg. Chim. Acta 310 (2000) 183.
[14] M. Amirnasr, K.J. Shenk, A. Gorji, R. Vafazadeh, Polyhedron 20 (2001) 695.
[15] Y. Zhang, W. Ruan, X. Zhao, H. Wang, Z. Zho, Polyhedron 22 (2003) 1535.
[16] M.M. Aly, J. Coord. Chem. 43 (1998) 89.
[17] R. Cini, S.J. Moore, L.G. Marzilli, Inorg. Chem. 37 (1998) 6890.
[18] S.M. Polson, R. Cini, C. Pifferi, L.G. Marzilli, Inorg. Chem. 36 (1997) 314.
[19] A. Bottcher, T. Takeuchi, K.I. Hardcastle, T.J. Meade, H.B. Gray, Inorg. Chem. 36 (1997) 2498.
[20] A.A. Khandar, Z. Rezvani, Polyhedron 18 (1998) 129.
[21] HYPERCHEM for windows, Release version 7.
[22] A.A. Khandar, K. Nejati, Polyhedron 19 (2000) 607.
[23] J.A. Dean, Handbook of Organic Chemistry, Mc Graw-Hill, 1987.
[24] A.A. Khandar, S.A. Hosseini-Yazdi, Polyhedron 22 (2003) 1481.
[25] S.D. Bella, I. Fragala, I. Ledoux, M.A. Diaz-Garcia, T.J. Marks, J. Am. Chem. Soc. 119 (1997) 9550.
[26] R. Klement, F. Stock, H. Elias, H. Paulus, M. Valko, M. Mazur, Polyhedron 18 (1999) 3617.
[27] W.P. Anderson, T.R. Cundari, R.S. Drago, M.C. Zerner, Inorg. Chem. 29 (1990) 1.
[28] D.R. Kains, M.A. Ratner, T.J. Marks, Chem. Mater. 3 (1991) 19.
[29] W.P. Anderson, T.R. Cundari, M.C. Zerner, Int. Quantum Chem. 39 (1991) 31.
[30] R.A. Metcalf, A.B.P. Lever, Inorg. Chem. 36 (1997) 4762.
[31] K.K. Stavrev, M.C. Zerner, T.J. Meyer, J. Am. Chem. Soc. 117 (1995) 8684.
[32] K.K. Stavrev, M.C. Zerner, Chem. Phys. Lett. 233 (1995) 179.
[33] K.K. Stavrev, M.C. Zerner, Theor. Chim. Acta 3 (1996) 141.
[34] K.K. Stavrev, M.C. Zerner, J. Chem. Phys. 102 (1995) 34.

$B_{16}H_{20}$ or the intractable $\{B_8H_{10}\}_x$ species observed by Schaeffer [5].

2. Results and discussion

2.1. The reaction between $[B_9H_{14}]^-$ and BCl_3

In the earlier studies [1,2] of the reaction between $[NMe_4][B_9H_{14}]$ and BCl_3, the reaction was represented as follows:

$$2[Me_4N][B_9H_{14}] + 2BCl_3 \rightarrow B_{10}H_{14} + 1/n(B_8H_{10})_n + 2[Me_4N][BCl_3H] + H_2 \quad (1)$$

Although the previous studies give no details of the unidentified product, it is possible that the relative complexity of the ^{11}B NMR spectrum of this material led to the initial postulation of a polymeric structure. This suggestion was reminiscent of a study of the thermal decomposition of B_8H_{12} that gave $B_{16}H_{20}$, and an intractable orange material, formulated as polymeric $\{B_8H_{10}\}_x$ [5]. It turns out, however, that this material is very different in nature to the proposed $1/n(B_8H_{10})_n$ material produced in this work, which is soluble in common polar solvents.

In view of the results described herein, we believe that the overall reaction is better represented by the following equation:

$$2[Me_4N][B_9H_{14}] + 2BCl_3 \rightarrow B_{10}H_{14} + [Me_4N][B_9H_{11}Cl_3] + [Me_4N][BCl_3H] + H_2 \quad (2)$$

This reaction is undoubtedly initiated by the removal of H^- from $[B_9H_{14}]^-$ to form $[HBCl_3]^-$ and the reactive, unsaturated intermediate B_9H_{13}. In order for $B_{10}H_{14}$ to be formed, effectively a $\{BH\}$ unit has to be added to B_9H_{13}. We believe that this could be accomplished through the initial combination of two $\{B_9H_{13}\}$ units to give $(B_9H_{13})_2$, most likely through hydrogen bridges in a manner analogous to two $\{BH_3\}$ units forming B_2H_6. In this case, however, the proposed $(B_9H_{13})_2$ dimer is unstable and dissociates to give $B_{10}H_{14}$, H_2, and B_8H_{10}. Insertion of $[HBCl_3]^-$ into B_8H_{10} would produce $[B_9H_{11}Cl_3]^-$.

The reaction of $[Me_4N][B_9H_{14}]$ with BCl_3 in the absence of solvent was carried out as previously reported [2]. After removal of the volatile products ($B_{10}H_{14}$ and H_2), the non-volatile residue is partially soluble in polar solvents such as THF, Glyme, MeCN, or 1,2-dichloroethane. In the current study, the non-volatile residue was extracted with THF, leaving behind $[Me_4N][HBCl_3]$ formed in the reaction.

Single crystals of the extract were obtained by solvent diffusion of hexane into a THF solution at −30 °C. This method affords two distinct crystal habits: small colorless blocks, **1A**, and large colorless needles, **1B**. Crystals **1B**, extremely prevalent and highly sensitive to solvent loss, have THF incorporated into their lattice, while less common crystals **1A** contain no solvent molecules. Molecular structures were obtained from X-ray diffraction analyses of both crystals and crystallographic data for both structures are given in Table 1.

The structures of all of the chlorinated anions presented here are numbered according to the system shown in Chart 1, and are presented in the same orientation, so as to facilitate comparison with each other, and with the structure of the parent $[B_9H_{14}]^-$ anion [6–8]. This arrangement corresponds to the ground state of the $[B_9H_{14}]^-$ anion, as recently calculated by Hofmann and Schleyer [9]. In each case B(4) is shown as the distinct "prow" atom associated with two geminal bridging H atoms, $\{BH(\mu\text{-}H)_2\}$. The ground state is calculated to possess a $\{3\times\ \mu\text{-H}, 2\times\ endo\}$ arrangement of its five "inner sphere" hydrogen atoms [10].

Single crystal analysis of **1A** reveals that it exists primarily as $[Me_4N][arachno\text{-}B_9H_{11}\text{-}6,7,8\text{-}Cl_3]$[1]. The molecular structure of the anion is shown in Fig. 1(a). Selected bond lengths and interbond angles for the $[arachno\text{-}B_9H_{11}\text{-}6,7,8\text{-}Cl_3]^-$ anion are given in Table 2.

Only a very small number of other examples of halogen-substituted analogues of *arachno*-nonaborate anions have been reported previously. The preparation and structure of $[Me_4N][arachno\text{-}B_9H_{12}\text{-}4,8,Br_2]$ was included as part of a large analysis of known *arachno*-nonaborane structures [8], and a conference report of sequential bromination and iodination of *arachno*-$[B_9H_{14}]^-$ exists in which the production a number of substituted isomers was mentioned [11].

Because the structure and substitution pattern in structures **1A** and **1B** of both systems is similar, only the structure of $[arachno\text{-}B_9H_{11}\text{-}6,7,8\text{-}Cl_3]^-$ derived from crystalline **1A** is discussed in detail here, since it is much less afflicted by problems of disorder. The occupancies of chlorine atoms Cl(1), Cl(2), and Cl(3) at the B(6), B(7), and B(8) positions were allowed to vary during refinement. The final occupancies obtained were: Cl(1) 0.95, Cl(2) 0.80, and Cl(3) 0.97. The remaining fractional occupancy at each of the B(6), B(7), and B(8) vertices was assigned as *exo*-hydrogen atoms, so as to retain an overall total stoichiometry value of 14 substituent atoms per cluster, as in the parent $[B_9H_{14}]^-$.

The anion derived from crystal **1A** is the chlorinated analog of the $[B_9H_{14}]^-$. Its basic structure is very similar to the structure of the $[B_9H_{14}]^-$ anion [6–8]. The structure of $[B_9H_{14}]^-$ has been obtained at room temperature [6] and at low temperature [7,8]. They are in good agreement with each other with the exception that the low temperature structures have a bridging hydrogen between boron atoms B(7) and B(8), while the room temperature structure has an *endo*-terminal hydrogen on B(7). In the present case

[1] Following conventional IUPAC numbering whereby the positions of the Cl substituents are accorded the lowest possible number affords the following: The anions in structures **1A** and **1B** would be represented as $[arachno\text{-}B_9H_{11}\text{-}4,5,6,\text{-}Cl_3]^-$, and anion **2** would be numbered $[arachno\text{-}B_9H_{13}\text{-}4\text{-}Cl]^-$.

Table 1
Crystallographic data for **1A**, **1B**, and **2**

	1A	1B	2
Empirical formula	$C_4H_{23.27}B_9Cl_{2.73}N$	$C_{16}H_{65.05}B_{18}Cl_{2.95}N_2O_2$	$C_4H_{25}B_9ClN$
Formula weight (amu)	279.57	616.91	219.99
Crystal system	triclinic	monoclinic	monoclinic
Space group	$P\bar{1}$ (no. 2)	$P2_1/n$ (no. 14)	$P2_1/c$ (no. 14)
a (Å)	7.642(2)	12.047(2)	9.729(3)
b (Å)	9.660(2)	16.336(3)	10.682(3)
c (Å)	10.771(2)	19.711(4)	14.000(5)
α (°)	89.37(3)		
β (°)	86.72(3)	93.29(3)	96.91(3)
γ (°)	81.89(3)		
V (Å^3)	786.0(2)	3872.7(12)	1444.5(8)
Z	2	4	4
ρ_{calc} (g cm^{-3})	1.181	1.058	1.012
T (°C)	−60(2)	−60(2)	−60(2)
Radiation (λ, Å)	Mo Kα (0.71073)	Mo Kα (0.71073)	Mo Kα (0.71073)
μ (mm^{-1})	0.506	0.253	0.227
R_1[a] [$I > 2\sigma(I)$]	0.0412	0.0686	0.0369
wR_2[b] (all data)	0.1221	0.1895	0.1077

[a] $R_1 = \sum\|F_o| - |F_c|/|F_o\|$.
[b] $wR_2 = \{\sum w(F_o^2 - F_c^2)^2/w(F_o^2)^2\}^{1/2}$.

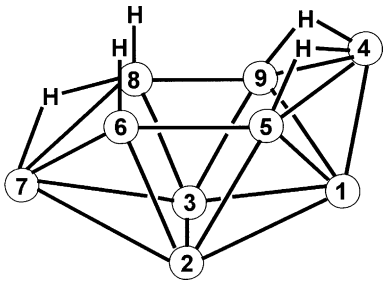

Chart 1. Ground state structure and numbering scheme for *arachno*-$[B_9H_{14}]^-$.

of **1A** the hydrogen in question appears closer to the (less commonly observed) terminal type located on B(7), although it does appear to have some semi-bridging character between B(7) and B(8). Relevant distances: B(7)–H(7) = 1.09(4) Å, and B(8)–H(7) = 1.63(4) Å. Distances between B(6)–Cl(1) and B(8)–Cl(3) are 1.835(3) Å and 1.837(2) Å, respectively, while the B(7)–Cl(2) separation appears anomalously short, at 1.792(3) Å. This may be explained by the disorder in the crystal, resulting in an approximately 20% contribution of *exo*-polyhedral bonding at B(7) to hydrogen.

Single crystal X-ray diffraction analyses of **1B** revealed an empirical composition of approximately $[(CH_3)_4N][B_9H_{12.5}Cl_{1.5}]\cdot$ THF. The disorder present may be better described as co-crystallization of a number of chlorononaborate anions in crystalline **1B**. The crystals were extremely solvent-sensitive, and rapidly lost solvent when removed from an atmosphere of THF vapor. This problem was circumvented by doubly coating the crystals in epoxy

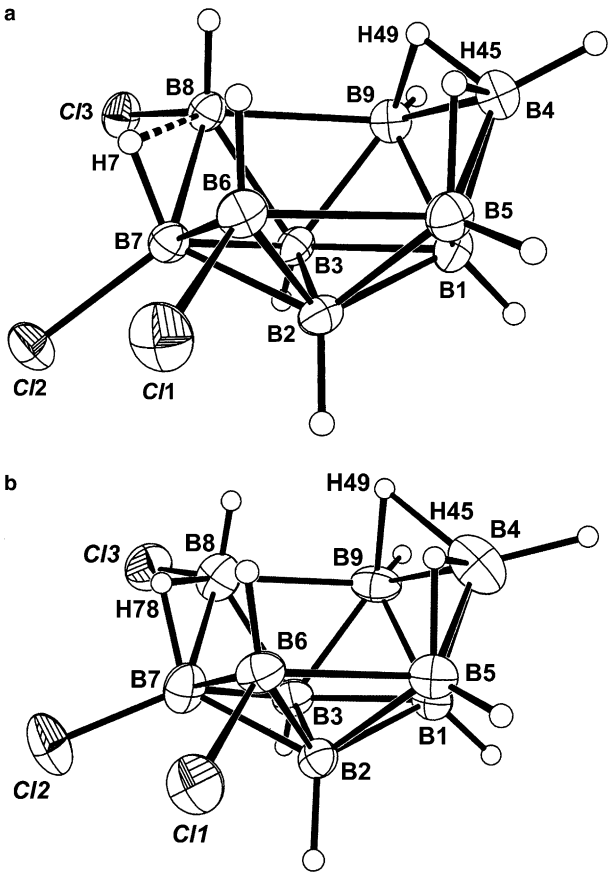

Fig. 1. (a) Plot of the [*arachno*-6,7,8-$B_9H_{11}Cl_3$]$^-$ anion derived from crystalline **1A**. Non-hydrogen atoms are shown as ellipsoids at the 25% probability level. H atoms are shown with arbitrary radius. (b) Plot of the [*arachno*-6,7,8-$B_9H_{11}Cl_3$]$^-$ anion derived from crystalline **1B**.

resin. There are two independent B_9 frameworks in the asymmetric unit and there is a wide variation in the occupancies of the chlorine atom positions. One of the anions is shown in Fig. 1(b). The anion shows the typical {3× μ-H, 2× *endo*} arrangement of inner sphere hydrogens observed in the majority of anions of this type [8]. Chlorine and *exo*-hydrogen occupancies were allowed to vary at the B(6), B(7) , and B(8) vertices, such that the anion retained an overall stoichiometry of 14 hydrogen and chlorine atoms per cluster. One vertex in each B_9 framework was assumed to be occupied by 100% chlorine, but the occupancy over the three positions, B(6), B(7) and B(8) varied widely. Specifically, final Cl occupancy values obtained from the refinement at the other positions were Cl(1) 0.305(7) and Cl(2) 0.326(6), with the other independent anion giving the following values Cl(2A) 0.069(6) and Cl(3A) 0.256(7). The average empirical formula of both anions in the structure was $[B_9H_{12.52}Cl_{1.48}]^-$. From difference maps and thermal parameters there is no evidence for chlorine occupying positions on other boron atoms. Information regarding the results of the X-ray study of crystalline **1B** is provided in the Supporting Information.

The $^{11}B\{^1H\}$ spectrum obtained from a single large crystal of **1B** is shown in Fig. 2. This spectrum is essentially

Table 2
Selected bond lengths and interbond angles in the [*arachno*-B_9H_{11}-6,7,8-Cl_3]$^-$ anion derived from structure **1A**

Bond lengths (Å)			
B(1)–B(4)	1.708(4)	B(4)–H(45)	1.18(3)
B(1)–B(9)	1.763(4)	B(4)–H(49)	1.15(3)
B(1)–B(5)	1.767(4)	B(5)–B(6)	1.980(4)
B(1)–B(2)	1.797(4)	B(5)–H(45)	1.25(3)
B(1)–B(3)	1.799(3)	B(5)–H(5)	1.05(3)
B(1)–H(1)	1.06(3)	B(6)–Cl(1)	1.835(3)
B(2)–B(5)	1.729(4)	B(6)–B(7)	1.884(3)
B(2)–B(6)	1.746(3)	B(6)–H(6)	1.06(3)
B(2)–B(7)	1.746(3)	B(7)–Cl(2)	1.792(3)
B(2)–B(3)	1.793(3)	B(7)–B(8)	1.875(3)
B(2)–H(2)	1.06(3)	B(7)–H(7)	1.09(4)
B(3)–B(9)	1.736(4)	B(8)–Cl(3)	1.837(2)
B(3)–B(8)	1.756(3)	B(8)–B(9)	2.032(4)
B(3)–B(7)	1.759(3)	B(8)–H(7)	1.63(4)
B(3)–H(3)	1.07(2)	B(8)–H(8)	1.04(3)
B(4)–B(9)	1.780(4)	B(9)–H(49)	1.29(3)
B(4)–B(5)	1.793(4)	B(9)–H(9)	1.06(3)
B(4)–H(4)	1.10(3)		
Selected angles (°)			
B(1)–B(4)–H(45)	102(1)	B(2)–B(7)–H(7)	128(2)
B(9)–B(4)–H(45)	118(1)	B(3)–B(7)–H(7)	115(2)
B(5)–B(4)–H(45)	44(1)	Cl(2)–B(7)–H(7)	107(2)
H(4)–B(4)–H(45)	108(2)	B(8)–B(7)–H(7)	60(2)
B(1)–B(4)–H(49)	103(1)	B(6)–B(7)–H(7)	80(2)
B(9)–B(4)–H(49)	46(1)	B(3)–B(8)–Cl(3)	111.0(2)
B(5)–B(4)–H(49)	118(1)	B(3)–B(8)–B(7)	57.8 (1)
H(4)–B(4)–H(49)	111(2)	Cl(3)–B(8)–B(7)	116.3(2)
H(45)–B(4)–H(49)	95(2)	B(3)–B(8)–B(9)	54.0(1)
B(2)–B(5)–H(45)	123(1)	Cl(3)–B(8)–B(9)	121.4(2)
B(1)–B(5)–H(45)	96(1)	B(7)–B(8)–B(9)	100.9(2)
B(4)–B(5)–H(45)	41(1)	B(3)–B(8)–H(7)	91(1)
B(6)–B(5)–H(45)	93(1)	Cl(3)–B(8)–H(7)	118(1)
H(45)–B(5)–H(5)	108(2)	B(7)–B(8)–H(7)	35 (1)
B(2)–B(6)–Cl(1)	111.8(2)	B(9)–B(8)–H(7)	119(1)
Cl(1)–B(6)–B(7)	117.7(2)	B(3)–B(8)–H(8)	136(1)
Cl(1)–B(6)–B(5)	119.3(2)	Cl(3)–B(8)–H(8)	110(1)
B(2)–B(6)–H(6)	137(2)	B(7)–B(8)–H(8)	114(1)
Cl(1)–B(6)–H(6)	110(2)	B(9)–B(8)–H(8)	92(1)
B(7)–B(6)–H(6)	111(2)	H(7)–B(8)–H(8)	82(2)
B(5)–B(6)–H(6)	95(1)	B(3)–B(9)–H(49)	123(1)
B(2)–B(7)–Cl(2)	119.0(2)	B(1)–B(9)–H(49)	95(1)
B(3)–B(7)–Cl(2)	118.7(2)	B(4)–B(9)–H(49)	40(1)
Cl(2)–B(7)–B(8)	120.2(2)	B(8)–B(9)–H(49)	94(1)
Cl(2)–B(7)–B(6)	121.9(2)	H(49)–B(9)–H(9)	112(2)
B(8)–B(7)–B(6)	113.2(2)		

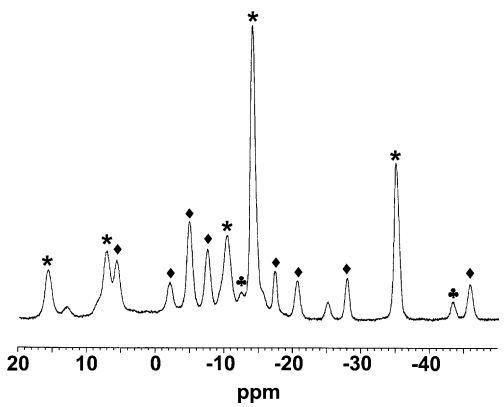

Fig. 2. $^{11}B\{^1H\}$ spectrum of a single large crystal of **1B**.

identical to that obtained from the extracted product prior to crystallization. Attempts to further purify the material by crystallization or thin layer chromatography also invariably yielded material that gave a spectrum with this essential complex appearance.

$^{11}B\{^1H\}$–$^{11}B\{^1H\}$ COSY spectroscopy was used to identify three distinct sets of resonances in the 2-dimensional spectrum. The $^{11}B\{^1H\}$–$^{11}B\{^1H\}$ COSY spectrum is available as Supporting Information. These sets of related resonances are identified by different labels (∗, ♦, and ♣) in Fig. 2.

Relative peak intensities indicate that the species corresponding to those peaks labeled ∗ is the most abundant species in the co-crystallized mixture. Further studies have been performed that show this species to be the *arachno*-monochlorononaborate $[Me_4N][B_9H_{13}Cl]$. Detailed NMR and structural information for this species is presented below. The second most prevalent species in the mixture is associated with the peaks labeled ♦. Although only 8 distinct resonances are observed for this species, it is likely that a ninth signal associated with it is coincident with another peak in the spectrum. For an *arachno*-nonaborate anion to display 9 resonances, it must have no effective symmetry in solution, so it appears reasonable to assign these resonances to a di-substituted species in solution in which the chlorine atoms are not related by an effective mirror plane. This suggests a species such as [*arachno*-B_9H_{12}-6,7-Cl_2]$^-$. Given that the NMR spectra of the initially-extracted mixture and of the very prevalent disordered crystals **1B** are essentially identical and the extreme difficulty in isolating appreciable quantities of crystals **1A** from the mixture, it then seems reasonable to suggest that the peaks of low relative intensity labeled ♣ may be attributable to the trisubstituted cluster [*arachno*-$B_9H_{11}Cl_3$]$^-$. We were fortunate enough to isolate crystals **1A** for X-ray study, but unfortunately they could not be isolated in sufficient quantity for further analyses. Furthermore, crystals **1A** also suffered from disorder, albeit much less so than **1B**.

Despite attempts to completely separate the individual anions in the co-crystallizing mixture by chromatographic methods, this has not proven possible. Given the propensity of the anions to co-exist in the solid state, with differently-substituted anions adopting equivalent positions in the crystal lattice, it is perhaps not surprising that they might also have extremely similar polarities and behavior in solution.

While we were unable to completely separate the co-crystallizing nonaborates, electrospray mass spectrometry was performed in negative ion mode on a sample of the co-crystallized species. Envelopes centered at *m*/*z* 214.076 ($[B_9H_{11}Cl_3]^-$, calculated: 214.745 amu); 180.122 $[B_9H_{12}Cl_2]^-$, calculated: 180.300 amu); and 146.2 ($[B_9H_{13}Cl]^-$, calculated: 145.855 amu) were observed, consistent with the presence of all three species in the crystalline material.

The production of a number of chloro-species in this reaction suggests that the actual process of cluster

expansion may be rather more complex than the simple representation in Eq. (2). Interestingly, BCl_3 (and the subsequently-produced intermediate $[HBCl_3]^-$) each initially have 3 chlorine atoms associated with a single boron atom. There is no evidence for more than one chlorine atom at any vertex in any of the products, suggesting that B–Cl cleavage and formation are central to the cluster formation processes. It is presumably as result of this chlorine-scrambling process that some significant fraction of the Cl atoms are lost from the clusters, possibly in the form of HCl or some chloroboranes such as BH_2Cl or $BHCl_2$, which could easily form a relatively stable adduct with a basic solvent such as THF. The ^{11}B NMR spectrum of the product mixture does not appear to change over prolonged periods of time, indicating that, once formed, the products are stable to positional rearrangement of their chlorine substituents.

2.2. Preparation and characterization of $[Me_4N][B_9H_{13}Cl]$

Due to the relative complexity of the above reaction, and the problems of disorder and co-crystallization suffered by the multiply-chlorinated products, an alternate, cleaner route to these types of species was investigated. In so doing, we were able to obtain a pure compound and alleviate the difficulties encountered above. Rather than starting from the *arachno*-$[B_9H_{14}]^-$ cluster, it was decided to begin with the known species *nido*-$[B_9H_{12}]^-$, (in the form of $[Me_4N][B_9H_{12}]$) which can be prepared by relatively simple literature methods [12]. In this case, rather than hydride abstraction by Lewis acid species, anhydrous HCl was used, which cleanly adds to the *nido*-cluster according to:

$$\textit{nido}\text{-}[B_9H_{12}]^- + HCl \rightarrow \textit{arachno}\text{-}[B_9H_{13}Cl]^- \quad (3)$$

The reaction is carried out in the absence of solvent, and produces only a single product, $[Me_4N][B_9H_{13}Cl]$. This salt has been characterized by ^{11}B, $^{11}B\{^1H\}$, and $^1H\{^{11}B\}$ NMR spectroscopy as well as by a single crystal X-ray study. X-ray data for **2** are contained in Table 1. The structure of the [*arachno*-B_9H_{13}-8-Cl]$^-$ anion is shown in Fig. 3. The structure is numbered according to the scheme shown in Chart 1[1]. Table 3 contains selected bond distances and angles within the anion. The anion is again isostructural with [*arachno*-$B_9H_{14}]^-$, with effective substitution of the *exo*-H atom on B(8) for Cl. The five inner-sphere H atoms are again disposed in a {3× μ-H, 2× *endo*} arrangement about the open face, with H atoms bridging the B(4)–B(5), B(4)–B(9), and B(6)–B(7) connectivities. The B(8)–Cl distance is typical, at 1.873(2) Å.

The $^{11}B\{^1H\}$ and ^{11}B NMR spectra of $[Me_4N][B_9H_{13}Cl]$ are shown in Fig. 4(a) and (b), respectively.

The $^{11}B\{^1H\}$ spectrum features 5 signals of relative intensities 1:1:1:4:2. These peaks clearly correspond to the peaks labeled ∗ in the $^{11}B\{^1H\}$ spectrum of the co-crystallized species (Fig. 2), above. That these 5 peaks are common to the co-crystallized material and the pure

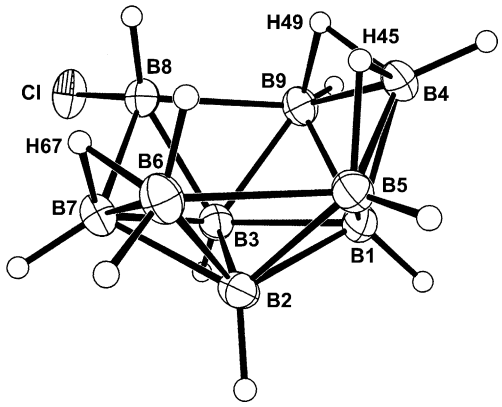

Fig. 3. Plot of the [*arachno*-8-$B_9H_{13}Cl]^-$ anion. Non-hydrogen atoms are shown as ellipsoids at the 25% probability level. H atoms are shown with arbitrary radius.

Table 3
Selected bond lengths and interbond angles in the [*arachno*-B_9H_{13}-8-Cl]$^-$ anion

Bond lengths (Å)			
Cl–B(8)	1.873(2)	B(4)–H(4)	1.05(2)
B(1)–B(4)	1.712(3)	B(4)–H(45)	1.18(2)
B(1)–B(5)	1.765(3)	B(4)–H(49)	1.27(2)
B(1)–B(3)	1.783(2)	B(5)–B(6)	1.969(3)
B(1)–B(9)	1.792(3)	B(5)–H(5)	1.09(2)
B(1)–B(2)	1.800(3)	B(5)–H(45)	1.35(2)
B(1)–H(1)	1.09(2)	B(6)–B(7)	1.885(3)
B(3)–B(8)	1.722(3)	B(6)–H(61)	1.14(2)
B(3)–B(9)	1.737(3)	B(6)–H(62)	1.08(2)
B(3)–B(7)	1.739(2)	B(6)–H(67)	1.31(2)
B(3)–B(2)	1.774(3)	B(7)–B(8)	1.860(3)
B(3)–H(3)	1.08(2)	B(7)–H(7)	1.07(2)
B(2)–B(5)	1.749(3)	B(7)–H(67)	1.21(2)
B(2)–B(6)	1.768(3)	B(8)–B(9)	1.908(3)
B(2)–B(7)	1.791(3)	B(8)–H(8)	1.06(2)
B(2)–H(2)	1.05(2)	B(9)–H(49)	1.26(2)
B(4)–B(5)	1.796(3)	B(9)–H(9)	1.08(2)
B(4)–B(9)	1.814(3)		
Selected angles (°)			
B(1)–B(4)–H(45)	107(1)	B(7)–B(6)–H(67)	40(1)
B(5)–B(4)–H(45)	47(1)	B(5)–B(6)–H(67)	121(1)
B(9)–B(4)–H(45)	119(1)	H(61)–B(6)–H(67)	113(1)
H(4)–B(4)–H(45)	111(1)	H(62)–B(6)–H(67)	90(1)
B(1)–B(4)–H(49)	102(1)	B(3)–B(7)–H(67)	128 (1)
B(5)–B(4)–H(49)	119(1)	B(2)–B(7)–H(67)	99(1)
B(9)–B(4)–H(49)	44(1)	B(8)–B(7)–H(67)	93(1)
H(4)–B(4)–H(49)	112(1)	B(6)–B(7)–H(67)	44(1)
H(45)–B(4)–H(49)	95(1)	H(7)–B(7)–H(67)	109(1)
B(2)–B(5)–H(45)	127(1)	B(3)–B(8)–B(7)	58.0(1)
B(1)–B(5)–H(45)	96(1)	B(3)–B(8)–H(8)	139(1)
B(4)–B(5)–H(45)	41(1)	B(3)–B(8)–Cl	111.5(1)
B(6)–B(5)–H(45)	97(1)	B(7)–B(8)–Cl	118.2(1)
H(5)–B(5)–H(45)	105(1)	Cl–B(8)–B(9)	117.1(1)
B(2)–B(6)–H(61)	109(1)	Cl–B(8)–H(8)	109(1)
B(7)–B(6)–H(61)	112(1)	B(9)–B(8)–H(8)	100(1)
B(5)–B(6)–H(61)	126(1)	B(3)–B(9)–H(49)	124 (1)
B(2)–B(6)–H(62)	132 (1)	B(1)–B(9)–H(49)	98(1)
B(7)–B(6)–H(62)	123(1)	B(4)–B(9)–H(49)	44(1)
B(5)–B(6)–H(62)	81(1)	B(8)–B(9)–H(49)	92(1)
H(61)–B(6)–H(62)	112(1)	H(49)–B(9)–H(9)	107(1)
B(2)–B(6)–H(67)	97(1)		

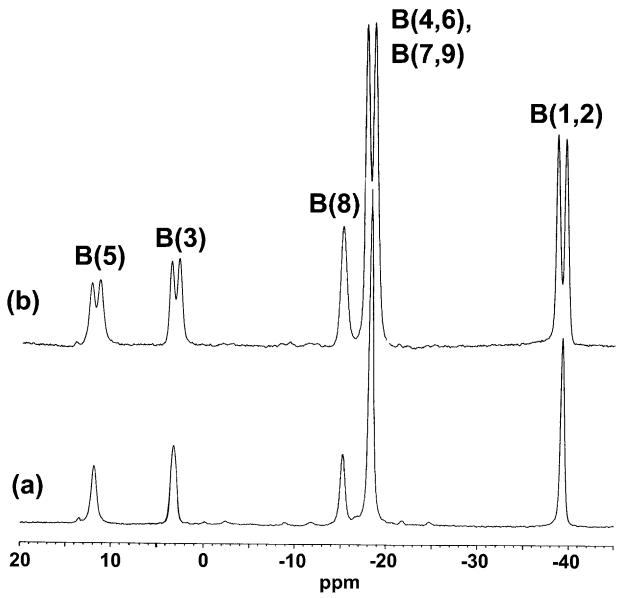

Fig. 4. (a) $^{11}B\{^1H\}$ spectrum; and (b) ^{11}B spectrum of $[Me_4N][arachno\text{-}8\text{-}B_9H_{13}Cl]$.

mono-chloro species is further clear evidence for co-crystallization of different chlorine-substituted analogs, rather than for any type of dynamic rearrangement process in solution after the clusters have been formed. The peak at −15.22 ppm is the only singlet in the ^{11}B spectrum, and so is assigned to the chlorine-bearing atom B(8). A 2-dimensional $^{11}B\{^1H\}$–$^{11}B\{^1H\}$ COSY experiment was also carried out for this compound, and afforded the assignment of all resonances in the spectrum. The $^{11}B\{^1H\}$–$^{11}B\{^1H\}$ COSY spectrum is available as Supporting Information. The peak of relative intensity 4 at −18.34 ppm in the $^{11}B\{^1H\}$ spectrum results from an accidental overlap of the B(4,6) and B(7,9) resonances. In addition to a signal for the tetramethylammonium ion, the $^1H\{^{11}B\}$ spectrum displays 6 signals of relative intensities 1:1:2:2:2:5, consistent with the effective C_s symmetry resulting from the fluxionality of the five inner sphere H atoms on the NMR timescale at ambient temperature.

Since the earliest structural studies on *arachno*-$\{B_9\}$ clusters [6], there has been some debate as to the exact nature and arrangement of the inner sphere hydrogen atoms associated with these clusters [10]. The earliest reported structure of the $[B_9H_{14}]^-$ anion was derived from a room temperature study of $Cs[B_9H_{14}]$, and showed a {2× μ-H, 3× *endo*} arrangement of its five inner-sphere H atoms [6]. This arrangement was accepted for many years as representing the most stable arrangement of bridging and *endo*-hydrogens in $[B_9H_{14}]^-$. More recently, the structure of $Cs[B_9H_{14}]$ was redetermined at low temperature [7], and an X-ray study of $K[B_9H_{14}]$ at 143 K has also been reported in recent years [8]. These two structures both indicate a {3× μ-H, 2× *endo*} arrangement of the inner sphere hydrogens. A detailed analysis of all known *arachno*-$\{B_9\}$ structures would appear to support the assertion that the {3× μ-H, 2× *endo*} arrangement represents the ground state of this structural type [8]. Of the three structures presented here, **1B** and **2** clearly display a {3× μ-H, 2× *endo*} arrangement, while the anion in structure **1A** has a structure closer to the {2× μ-H, 3× *endo*} type. However, the inner sphere hydrogen associated with B(7) in this structure is not symmetrically disposed above the open face of the cluster. It is closer to B(8) than to B(6), thus displaying at least some degree of bridging character. The original structure of $Cs[B_9H_{14}]$ was carried out at ambient temperature [6], and its {2× μ-H, 3× *endo*} structure is calculated to lie only 2.3 kcal/mol higher than the ground state [9].

3. Conclusion

The previously unidentified product of the reaction with BCl_3 and *arachno*-$[B_9H_{14}]^-$ was shown to consist of a mixture of multiply-chlorinated *arachno*-B_9 structures that crystallized in disordered fashions. This product had previously been thought to be polymeric in nature, perhaps as a result of the complex appearance of its ^{11}B NMR spectrum. Adoption of an alternate synthetic route that yielded the pure compound $[Me_4N][B_9H_{13}Cl]$ (**2**) in quantitative yield from $[Me_4N][B_9H_{12}]$ helped solve this problem. In addition to an X-ray structural analysis, a full spectral characterization of the monochloro compound was performed, which afforded understanding of the complicated spectral data of the mixture. This illustrates the need to explore alternative synthetic methodologies and their ability to help solve otherwise intractable problems of characterization.

Additionally, the central finding of this work that the initially-suspected polymeric species is actually a mixture of salts is very interesting, as it raises questions as to the nature of many boron hydride species previously proposed to have polymeric structures [3]. With the advent of more modern and improved methods of characterization, it is possible that at least some of these suspected polymeric species may indeed yet be found to possess discrete monomeric structures.

4. Experimental

4.1. General information

All materials were handled by standard vacuum line and inert atmosphere techniques [13]. $K[B_9H_{14}]$ was prepared from $B_{10}H_{14}$ by a published procedure [14]. $[Me_4N][B_9H_{12}]$ was prepared from $B_{10}H_{14}$ via $[(C_2H_5)_2S]_2B_{10}H_{12}$ using the literature procedure [12]. $B_{10}H_{14}$ was triply sublimed under vacuum prior to use. BCl_3 (Matheson) was fractionated through a −95 °C trap prior to use. HCl was purified by passing it through a trap held at −112 °C. Tetramethylammonium chloride was thoroughly dried under vacuum before use. All solvents were dried and distilled into vacuum storage bulbs prior to use.

4.2. NMR spectroscopy

^{11}B and ^{1}H NMR spectra were recorded on either a Brüker AM-250 or DRX-500 spectrometer operating at 80.2 and 250.1 MHz, or 160.4 and 500.0 MHz, respectively.

4.3. Mass spectrometry

All experiments were performed on a Micromass ESI-Tof™ II (Micromass, Wythenshawe, UK) mass spectrometer equipped with an orthogonal electrospray source (Z-spray) operated in negative ion mode. Sodium iodide was used for mass calibration for a calibration range of m/z 100–2000. Samples were prepared in a solution containing acidified methanol and infused into the electrospray source at a rate of 5–10 μL min^{-1}. Optimal ESI conditions were: capillary voltage 3000 V, source temperature 110 °C, and a cone voltage of 55 V. The ESI gas was nitrogen. Data were acquired in continuum mode until acceptable averaged data were obtained.

4.4. Preparation of $[Me_4N][B_9H_{14}]$

$K[B_9H_{14}]$ (0.395 g 2.62 mmol) and $[Me_4N]Cl$ (0.287 g, 2.62 mmol) were placed in a 100 mL flask fitted with a Solv-Seal adapter. The flask was evacuated and glyme (25 mL) was condensed into the system. The mixture was warmed to room temperature and stirred for one hour during which time a white precipitate formed. Filtration followed by removal of the solvent under vacuum afforded an approximately quantitative yield of $[Me_4N][B_9H_{14}]$.

4.5. Reaction of $[Me_4N][B_9H_{14}]$ with BCl_3

To $[Me_4N][B_9H_{14}]$ (2.62 mmol) was added BCl_3 by condensation of vapor, 2.62 mmol (measured manometrically) at −196 °C. The mixture was allowed to return to room temperature and was stirred vigorously for 3 h. The color of the mixture changed from pale yellow to orange-yellow, and small crystals of $B_{10}H_{14}$ were observed on the walls of the flask. The flask was cooled to −196 °C and H_2 gas (0.9 mmol) was removed. The $B_{10}H_{14}$ product was removed by vacuum sublimation (alternatively, it can be removed by extraction with Et_2O). Extraction of the remaining solid using polar solvents such as THF, glyme, or CH_3CN separates the chlorinated nonaborate salts (0.34 g, 45% yield if pure $[Me_4N][B_9H_{11}Cl_3]$) from the insoluble $[Me_4N][BCl_3H]$. The product was recrystallized by solvent diffusion of hexanes into a THF solution at −30 °C.

NMR data (THF-d_8). All peaks apparent doublets, except where noted. δ ppm (J_{BH}, Hz) 17.54 (146), 14.5 (140), 8.99 (146), 7.46 (146), −0.26 (148), −3.6 (d, 140), −5.76 (141), −8.61 (s), −12.46 (141), −15.53 (139), −18.80 (131), −23.16 (153), −26.13 (137), −33.35 (144), −41.73 (145), −44.10 (145).

IR (KBr pellet, cm^{-1}): 3048 (m), 2972 (w), 2937 (w), 2529 (vs), 1483 (s), 1225 (m, sh), 1197 (m), 1157 (w), 1075 (m), 1011 (w), 948 (s), 795 (m), 712 (m).

4.6. Preparation of $[Me_4N][B_9H_{13}Cl]$

$[Me_4N][B_9H_{12}]$ (0.1687 g, 0.919 mmol) was placed in a Solv-Seal flask fitted to a vacuum extractor, and the apparatus evacuated. HCl (0.921 mmol) was condensed into the reaction flask at −196 °C, and allowed to warm to −78 °C. Stirring was continued until the bath warmed to room temperature, then the volatiles were pumped away. The solid residue was washed with toluene (20 mL). A fresh receiver flask was fitted to the extractor and CH_2Cl_2 (25 mL) was condensed in at −196 °C, the mixture allowed to come to room temperature, and then filtered, and the colorless residue washed with CH_2Cl_2. The very pale yellow extract was reduced to dryness in vacuo to afford an off-white microcrystalline solid, $[Me_4N][B_9H_{13}Cl]$, in essentially quantitative yield.

NMR data (CD_3CN). ^{11}B: δ ppm (J_{BH}, Hz) 11.90 (1B, d, 146 Hz), 3.22 (1B, d, 134 Hz), −15.22 (1B, s, B(8)), −18.34, (4B, d, 139 Hz), −39.28 (2B, d, 143 Hz).

^{1}H: δ ppm 3.28, (12B, $(CH_3)_4N^+$), −1.13 (5H, μ- and *endo*-H).

$^{1}H\{^{11}B\}$: (CD_2Cl_2) δ ppm 3.74 (1H), 3.28 (12H, $(CH_3)_4N^+$), 3.01 (1H), 1.99 (2H), 1.53 (2H), 0.27 (2H), −1.13 (5H, μ- and *endo*-H).

IR (KBr pellet, cm^{-1}): 3033 (m), 2937 (w), 2910 (w), 2522 (vs), 1484 (s), 1417 (m), 1194 (m), 1154 (w), 1075 (m), 1055 (m, sh), 1011 (m), 975 (m), 948 (s), 769 (w), 726(w), 652 (m).

Colorless needle crystals of diffraction-quality were grown by solvent diffusion of hexane into a CH_2Cl_2 solution at −30 °C.

4.7. X-ray crystal structure determinations

Crystals were mounted on glass fibers using epoxy resin. Solvent-containing crystals were doubly coated with epoxy resin to prevent solvent loss. The crystallographic data for all structures were collected at −60 °C on an Enraf-Nonius CAD4 diffractometer with graphite-monochromated Mo Kα radiation. Unit cell parameters were obtained by a least squares refinement of the angular settings from 25 reflections, well distributed in reciprocal space and lying in a 2θ range of 24–30°. Intensity data were collected in the ω–2θ scan mode. All reflection data were corrected for Lorentz and polarization effects.

The structures were solved by direct methods and refined using SHELXTL (difference electron density calculations, full least-squares refinements) [15]. Additional calculations were performed using WINGX [16] and PLATON [17]. The partial Cl/H occupancies in structure **1B** were calculated using the SHELXL option "PART", with the fol-

lowing results for fractions of Cl: Cl(1) 0.305(7); Cl(2) 0.326(6); Cl(2A) 0.069(6); Cl(3A) 0.256(7). Chlorine occupancies of 0.8 or greater could not be treated this way. All non-hydrogen atoms were refined anisotropically. Hydrogen atoms in the anions were refined isotropically. Hydrogen atoms in the Me_4N^+ cations and THF molecules were calculated and their thermal and positional parameters were fixed during refinement. Crystallographic data for structures **1A**, **1B**, and **2** are provided in Table 1. Structure **1B** contains 1 THF solvent molecule per formula, and 2 crystallographically independent formulae per asymmetric unit, so the unit cell contains a total of 8 formulae.

Acknowledgments

We thank Professor S.G. Shore for generous access to analytical resources.

Appendix A. Supporting information available

Further details of the crystal structure determinations **1A**, **1B**, and **2** can be obtained from the Fachinformationszentrum Karlsruhe, 76344 Eggenstein-Leopoldshafen, Germany (fax: +49 7247 808 666; e-mail: crysdata @fiz.karslruhe.de) on quoting the depository numbers CSD-391332, CSD-391333, and CSD-391334, respectively. $^{11}B\{^1H\}$–$^{11}B\{^1H\}$(COSY) spectra are also available for each of the compounds discussed. Supplementary data associated with this article can be found, in the online version, at doi:10.1016/j.poly.2005.12.002.

References

[1] J.B. Leach, M.A. Toft, F.L. Himpsl, S.G. Shore, J. Am. Chem. Soc. 103 (1981) 988.
[2] M.A. Toft, J.B. Leach, F.A. Himpsl, S.G. Shore, Inorg. Chem. 21 (1982) 1952.
[3] A. Stock, Hydrides of Boron and Silicon, Cornell University Press, Ithaca, NY, 1933.
[4] W.N. Lipscomb, Inorg. Chem. 19 (1980) 1415.
[5] J. Rathke, R. Schaeffer, Inorg. Chem. 13 (1974) 3008.
[6] (a) N.N. Greenwood, H.J. Gysling, J.A. McGinnety, J.D. Owen, J. Chem. Soc., Chem. Commun. (1970) 505;
(b) N.N. Greenwood, J.A. McGinnety, J.D. Owen, J. Chem. Soc., Dalton Trans. (1972) 986.
[7] Huffman, J.D. Report 82210, Molecular Structure Center, Indiana University, Department of Chemistry, 1982. Cited (Ref. 10) in T.D. Getman, J.A. Krause, P.M. Niedenzu, S.G. Shore, Inorg. Chem. 28 (1989) 1507.
[8] J. Bould, R. Greatrex, J.D. Kennedy, D.L. Ormsby, M.G.S. Londesborough, K.L.F. Callaghan, M. Thornton-Pett, T.R. Spalding, S.J. Teat, W. Clegg, H. Fang, N.P. Rath, L. Barton, J. Am. Chem. Soc. 124 (2002) 7429.
[9] M. Hofmann, P.v.R. Schleyer, Inorg. Chem. 38 (1999) 652.
[10] Inner sphere refers to *endo*- and bridging-H atoms in single polyhedral borane fragments, as defined by W.N. Lipscomb, Boron Hydrides, W.A. Benjamin, New York, 1963, p. 53.
[11] B. Brellochs, in: Abstracts, Tenth International Conference on Boron Chemistry, Durham, UK, July 1999; Paper PA-13.
[12] B.M. Graybill, J.K. Ruff, M.F. Hawthorne, J. Am. Chem. Soc. 83 (1961) 2669.
[13] D.F. Shriver, M.A. Drezdzon, The Manipulation of Air Sensitive Compounds, second ed., Wiley, New York, 1986.
[14] P.J. Dolan, D.F. Gaines, D.C. Moody, C.K. Nelson, R. Schaeffer, Inorg. Synth. 26 (1989) 1.
[15] G.M. Sheldrick, SHELXTL-97: A Structure Solution and Refinement Program, University of Göttingen, Göttingen, Germany, 1997.
[16] L.J. Farrugia, J. Appl. Cryst. 32 (1999) 837.
[17] A.L. Spek, Acta Cryst. A 46 (1990) C34.

(20 mmol). The solution was stirred in a water bath at 90 °C for 8 h. The mixture (pH 3.5) was filtered and evaporated to about 20 ml. The colorless crystals obtained after standing for two days were collected and washed with 50% ethanol and 95% ethanol. Yield: 4.7 g (58%). *Anal.* Calc. for $C_{24}H_{50}Mo_4N_4Na_6O_{46}$: C, 17.4; H, 3.1; N, 3.4. Found: C, 17.4; H, 2.8; N, 3.3%. IR (KBr): ν(COOH) 1735_w; ν_{as}(C=O) 1652_{vs}; ν_s(C=O) 1446_m, 1383_{vs}, 1340_s; ν(Mo=O) 920_{vs}, 885_b; ν_{as}(MoO_bMo) 779_{vs}; ν_s(MoO_bMo) 685_m. ^{1}H NMR δ_H (500 MHz, D_2O, ppm): 4.137 (s). ^{13}C NMR δ_C (D_2O, ppm): 180.2, 179.0 and 177.8 $(CO_2)_\beta$, 65.5 (CH_2).

2.2. Preparation of $(NH_4)_{3n}[Mo_2O_5H(nta)_2]_n \cdot 4nH_2O$ (2)

Ammonium heptamolybdate (5 mmol) and nitrilotriacetic acid (35 mmol) were added to dilute ammonia (5 M, 40 ml). The solution (pH 4.0) was stirred until the color changed into light green and then it was evaporated to 20 ml. The colorless crystals obtained after standing overnight were collected and washed by 50% ethanol and 95% ethanol. Yield: 8.4 g (62%). *Anal.* Calc. for $C_{12}H_{33}Mo_2N_5O_{21}$: C, 18.6; H, 4.3; N, 9.0. Found: C, 18.2; H, 4.0; N, 8.0%. IR (KBr): ν(COOH) 1719_w; ν_{as}(C=O) 1639_{vs}; ν_s(C=O) 1448_s, 1399_{vs}, 1312_w; ν(Mo=O) 929_{vs}, 914_{vs}; ν_{as}(MoO_bMo) 883_s; ν_s(MoO_bMo) 690_m. ^{1}H NMR δ_H (500 MHz, D_2O, ppm): 3.976 (s). ^{13}C NMR δ_C (D_2O, ppm): 179.0 $(CO_2)_\beta$, 65.7 (CH_2).

Crystals of suitable quality for the subsequent X-ray diffraction studies were obtained as transparent prisms or rhombohedral blocks by slow evaporation of the related solution for one week at room temperature. The resulting crystals were sealed in a capillary to prevent loss of water molecules.

2.3. Transformation of 1–3 and 4

To the solution of $Na_{6n}\{[Mo_2O_5(ntaH)_2][(nta)_2Mo_2O_5]\}_n \cdot 12nH_2O$ (**1**) (pH 3.5), an appropriate amount of hydrochloric acid was added and the pH was adjusted to 2.5. The solution was then filtered and evaporated slowly. The crystals formed were collected and washed. The structural analysis shows the product as $Na_2[Mo_2O_5(Hnta)_2]$ (**3**). *Anal.* Calc. for $C_{12}H_{14}Mo_2N_2Na_2O_{17}$: C, 20.7; H, 2.0; N, 4.0. Found: C, 20.0; H, 2.4; N, 3.8%. IR (KBr): ν(COOH) 1750_s, ν_{as}(C=O) 1673_{vs}, 1600_v; ν_s(C=O) 1428_m, 1401_s, 1339_s, 1318_s; ν(Mo=O) 982_m, 947_s, 912_{vs}, 883_s; ν_{as}(MoO_bMo) 785_{vs}; ν_s(MoO_bMo) 695_m. ^{1}H NMR δ_H (500 MHz, D_2O, ppm): 4.119 (s). ^{13}C NMR δ_C (D_2O, ppm): 174.8 $(CO_2)_\beta$, 62.5 (CH_2).

In another experiment, sodium hydroxide was added and the pH was adjusted to 7.0. The solution was evaporated slowly. The crystals formed were collected and washed. The structural analysis shows the product as $Na_3[MoO_3(nta)] \cdot 4H_2O$ (**4**). *Anal.* Calc. for $C_6H_{14}MoNNa_3O_{13}$: C, 15.2; H, 3.0; N, 3.0. Found: C, 15.1; H, 2.8; N, 2.9%. IR (KBr): ν_{as}(C=O) 1644_s, 1602_{vs}; ν_s(C=O) 1439_m, 1409_s; ν(Mo=O) 939_{ms}, 897_s, 857_{vs}. ^{1}H NMR δ_H (500 MHz, D_2O, ppm): 3.982 (s). ^{13}C NMR δ_C (D_2O, ppm): 178.1 $(CO_2)_\beta$, 64.6 (CH_2).

2.4. Physical measurements

Infrared spectra were recorded as Nujol mulls between KBr plates using a Nicolet 360 FT-IR spectrometer. Elemental analyses were performed using EA 1110 elemental analyzers. ^{1}H NMR and ^{13}C NMR spectra were recorded on a Varian UNITY 500 NMR spectrometer with D_2O using DSS (sodium 2,2-dimethyl-2-silapentane-5-sulfonate) as internal reference.

2.5. X-ray data collection, structure solution and refinement

Crystallographic data for the nitrilotriacetato molybdates of **1**–**4** are summarized in Table 1. Diffraction data were collected on Bruker Smart CCD diffractometer with graphite monochromated Mo Kα ($\lambda = 0.71073$ Å) radiation at 296 K. Empirical absorption corrections were applied using the SADABS program [20]. The structures were primarily solved by the WINGX program [21] and refined by full-matrix least-squares procedures with anisotropic thermal parameters for all of the non-hydrogen atoms with SHELXL-97 [22]. Hydrogen atoms were located from the difference Fourier map and refined isotropically.

3. Results and discussion

3.1. Synthesis

Nitrilotriacetic acid is able to provide tetradentate chelation and different protonated forms, which might be expected to produce various types of anion complexes with molybdenum(VI). Previous potentiometric, spectrophotometric and enthalpimetric titrations in the molybdate (VI)–nitrilotriacetate system have been proceeded in the pH range 1.0–9.0 in solution [15]. The formation of the products may be represented by the general equation

$$p[MoO_4]^{2-} + q\text{nta}^{3-} + r\text{H}^+ \rightleftharpoons [\text{complex}]^{(2p+3q-r)-}$$

The major species are proposed to have Mo:nta:H ratios of 1:1:2, 1:1:3, 1:1:4, 2:2:7, 2:2:8, 2:1:5 and 2:1:6 in solution, depending mainly on the pH [15]. In our experiment, only the 1:1:2, 2:2:6, 2:2:7 and 2:2:8 species of nitrilotriacetato molybdates are separated in the acidic, weak acidic and neutral aqueous media. The transformation and the isolation of nitrilotriacetate complexes in different protonated forms have proven that 1:1 and 2:2 ratios (Mo:nta) of nitrilotriacetato molybdates are the major species. The 2:1 species is unfavorable due to the competitive formation of homopolyacid.

In an acidic solutions of pH 2.0–3.0, nitrilotriacetic acid can react with a Mo(VI) complex to form the protonated anion $[Mo_2O_5(Hnta)]^{2-}$, while in neutral solutions of pH 5.0–7.0, mononuclear $[MoO_3(nta)]^{3-}$ is formed. The adduct of protonated and deprotonated species

Table 1
Crystallographic data for $Na_{6n}\{[Mo_2O_5(ntaH)_2][(nta)_2Mo_2O_5]\}_n \cdot 12nH_2O$ (**1**), $(NH_4)_{3n}[Mo_2O_5H(nta)_2]_n \cdot 4nH_2O$ (**2**), $Na_2[Mo_2O_5(Hnta)_2]$ (**3**) and $Na_3[MoO_3(nta)] \cdot 4H_2O$ (**4**)

Complex	**1**	**2**	**3**	**4**
Empirical formula	$C_{24}H_{50}Mo_4N_4Na_6O_{46}$	$C_{12}H_{33}Mo_2N_5O_{21}$	$C_{12}H_{14}Mo_2N_2Na_2O_{17}$	$C_6H_{14}MoNNa_3O_{13}$
Formula weight	1652.38	775.31	696.11	473.09
Crystal system/space group	triclinic, $P\bar{1}$	triclinic, $P\bar{1}$	orthorhombic, *Pbca*	triclinic, $P\bar{1}$
a (Å)	10.0630(6)	6.7850(4)	13.0373(9)	8.0291(5)
b (Å)	11.6450(7)	9.6462(5)	11.2693(8)	9.4837(6)
c (Å)	12.9230(8)	10.0768(6)	14.257(1)	10.1010(6)
α (°)	80.381(1)	85.571(1)		84.267(1)
β (°)	85.258(1)	82.124(1)		87.065(1)
γ (°)	66.936(1)	82.994(1)		77.779(1)
V (Å^3)	1373.5(1)	647.19(6)	2094.7(3)	747.60(8)
Z	1	1	4	2
F(000)	824	392	1368	472
D_c (g cm^{-3})	1.998	1.989	2.207	2.102
μ (mm^{-1})	1.061	1.072	1.331	1.035
Crystal size (mm^3)	$0.12 \times 0.10 \times 0.05$	$0.16 \times 0.13 \times 0.06$	$0.15 \times 0.10 \times 0.10$	$0.18 \times 0.12 \times 0.10$
θ Range (°)	1.60–28.34	2.04–26.00	2.78–28.39	2.03–28.47
Radiation (λ/Å)	Mo Kα (0.7107)			
T (K)	296 (2)			
GOF on F^2	0.895	1.083	1.200	1.027
R_1 [$I > 2\sigma(I)$]	0.0463	0.0367	0.0767	0.0506
wR_2 [$I > 2\sigma(I)$]	0.0706	0.0934	0.1403	0.1383
R_1 (all data)	0.0718	0.0389	0.1103	0.0552
wR_2 (all data)	0.0760	0.0947	0.1534	0.1421
Maximum and minimum transmission $\Delta\rho$ (e Å^3)	0.788 and −0.562	0.677 and −0.794	1.040 and −1.673	1.932 and −1.341

$Na_{6n}\{[Mo_2O_5(ntaH)_2][(nta)_2Mo_2O_5]\}_n \cdot 12nH_2O$ (**1**) and hydrogen nitrilotriacetato molybdate $(NH_4)_{3n}[Mo_2O_5H(nta)_2]_n \cdot 4nH_2O$ (**2**) were isolated in weak acidic solutions of pH 3.5–4.0. The later represents an intermediate between protonated $[Mo_2O_5(Hnta)_2]^{2-}$ and deprotonated $[Mo_2O_5(nta)_2]^{4-}$ molybdenum (VI)–nitrilotriacetate complexes. In compound **1**, the two uncoordinated β-carboxyl groups of nitrilotriacetate in one dimer are protonated, while those in the other are deprotonated. This is supported by a downshift of the *v*(COOH) vibration from 1750 in **3** to 1735 cm^{-1} in **1**. Transformations between **1**, **3** and **4** can be accomplished by adjusting the pH. The pH values in the reactions are controlled easily by hydrochloric acid or sodium hydroxide as shown in Scheme 1. The transformations of monomeric and dimeric nitrilotriacetato molybdate (VI) are different from that described previously, in which only the monomeric species is considered in the precursor of a NiMo/SiO_2 hydrotreating catalyst [23].

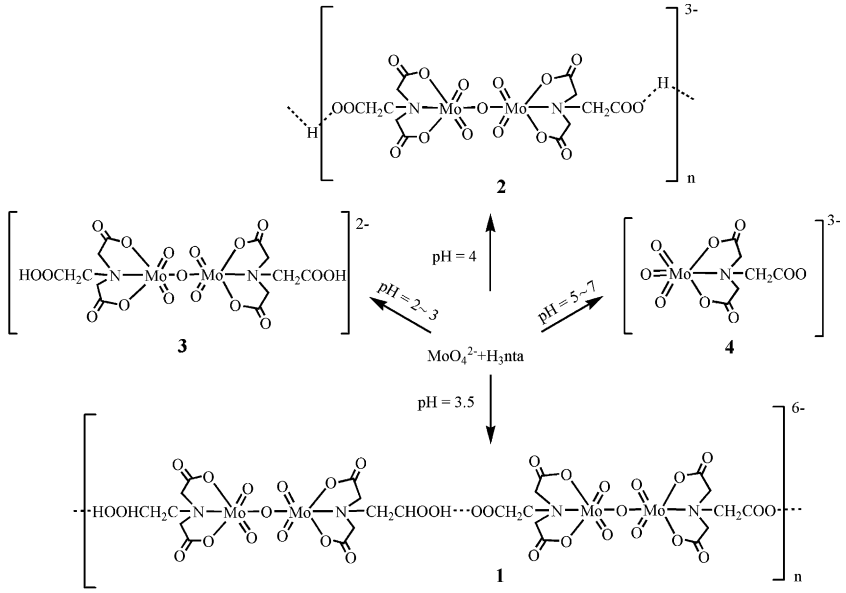

Scheme 1. Synthesis and transformation of nitrilotriacetato molybdates (VI).

3.2. Structure descriptions of complexes **1** and **2**

Complex **1** consists of a molybdenum–nitrilotriacetate adduct in a 2:2 stoichiometric ratio. The perspective view of the anion is presented in Fig. 1. Each molybdenum atom is octahedrally surrounded by two terminal oxygen atoms, one bridging oxygen atom and a tridentate nitrilotriacetate ligand, which binds through two β-carboxyl oxygen atoms and one nitrogen atom. The non-coordinated β-carboxyl oxygen O15 is protonated. This is supported by the relatively long C16–O15 bond, 1.307(9) Å, as compared with C16–O16, 1.214(9) Å. However, the non-coordinated carboxyl groups of the other do not show a distinct difference. The two neighboring carboxylate oxygen atoms are linked by a strong hydrogen bond [O5···H–O15 2.481(3) Å], generating a one-dimensional coordination polymer through the aggregation of fully protonated species $[Mo_2O_5(Hnta)_2]^{2-}$ and deprotonated units $[Mo_2O_5(nta)_2]^{4-}$.

Fig. 2 shows a perspective view of the anion in complex **2**. The crystal structure comprises ammonium cations, hydrogen oxo-μ-bis[*trans*-nitrilotriacetato-*cis*-dioxomolybdate] anions and lattice water molecules. The dimeric anion consists of MoO_2(Hnta) and MoO_2(nta) units bridged by an oxygen linkage [Mo–O–Mo = 180.00(3)°]. The two oxo atoms are *cis* to each other in the coordination octahedron. The two *cis*-dioxo groups are in a *trans*-configuration, which is the same as that found in tripotassium oxo-μ-bis[*trans*-nitrilotriacetato-*cis*-dioxotungstate] $K_3[W_2O_5H(nta)_2]\cdot 2H_2O$ [W–O–W = 161.9(7)°] [24]. The other three sites are occupied by the nta entity. Adjacent $Mo_2O_5H(nta)_2$ units are linked into an infinite zigzag chain through the acidic hydrogen [O6···H···O6b = 2.486(3) Å]. The space between the chains is occupied by the ammonium cations and the lattice water molecules.

The anion structures of compounds **3** and **4** are similar to the previous reported structures [11–14]. Evidently, the uncoordinated β-carboxyl groups in complex **3** are fully protonated, this is not only showed by the visibility of hydrogen atoms in difference maps, but also by the difference between the C–O distances of the terminal carboxylates, as well as from the consideration of charge balance. The conclusion of full deprotonation of the monomer **4** can be drawn from the observed carbon–oxygen bond distances of carboxyl groups that are equivalent [1.259(5), 1.251(5) Å] (see Figs. 3 and 4).

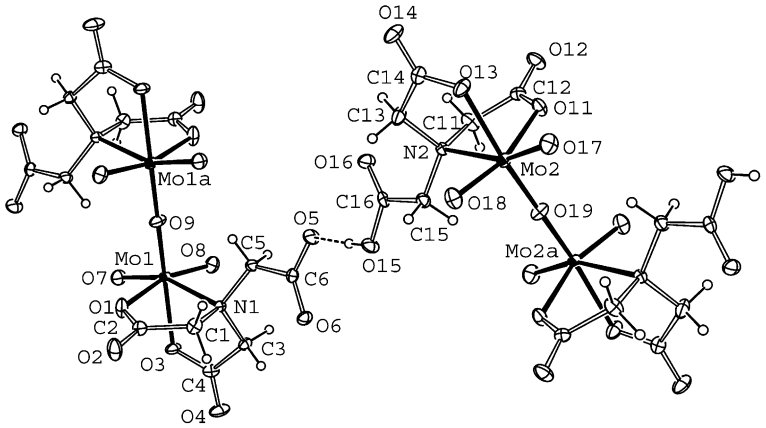

Fig. 1. ORTEP plot of the anion in $Na_{6n}\{[Mo_2O_5(ntaH)_2][(nta)_2Mo_2O_5]\}_n\cdot 12nH_2O$ (**1**) at the 30% probability level.

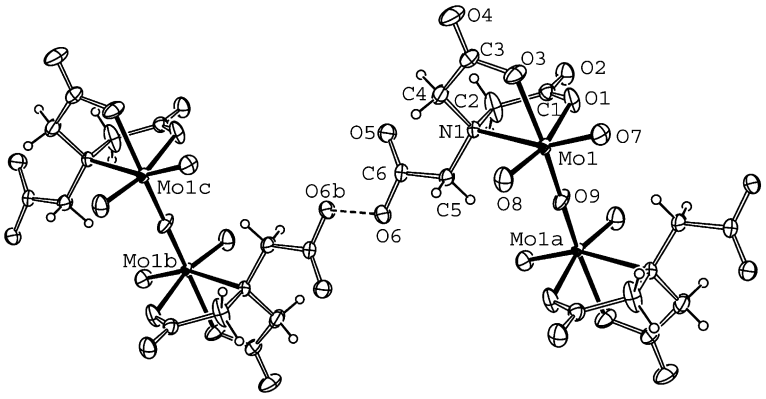

Fig. 2. ORTEP plot of the anion in $(NH_4)_{3n}[Mo_2O_5H(nta)_2]_n\cdot 4nH_2O$ (**2**) at the 30% probability level.

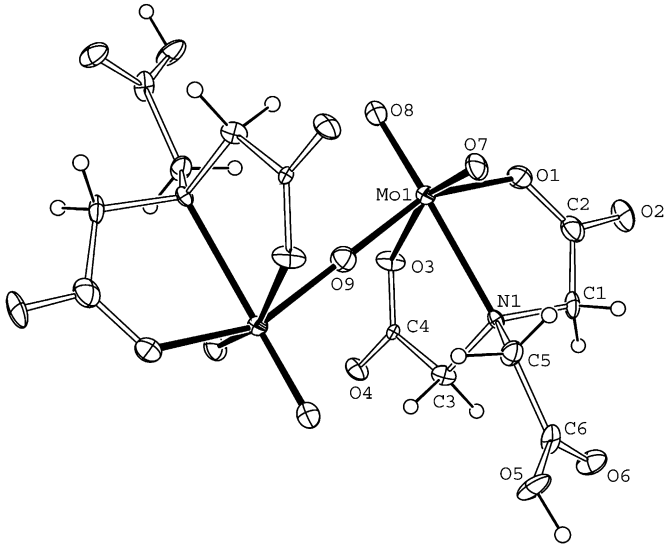

Fig. 3. ORTEP plot of the anion in $Na_2[Mo_2O_5(Hnta)_2]$ (**3**) at the 30% probability level.

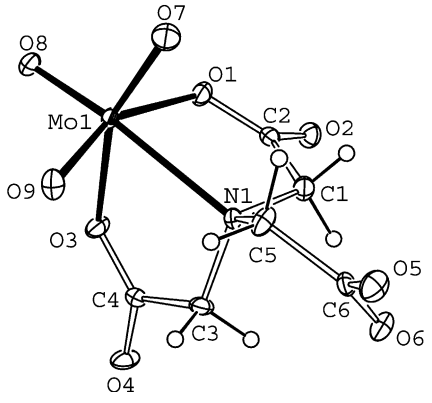

Fig. 4. ORTEP plot of the anion in $Na_3[MoO_3(nta)]\cdot 4H_2O$ (**4**) at the 30% probability level.

As shown in Table 2, the Mo–O distances in nitrilotriacetato molybdates vary systematically. The Mo=O bond lengths lie in the range 1.694–1.737 Å, indicating that they are double bonds. The observed O=Mo=O angles of 106.6(3), 106.1(3), 106.4(2), 105.8(2), 106.7(2), 104.9(2) and 105.8(1)° in compounds **1**–**4** are consistent with the large repulsion between oxo groups with short bonds to the metal atom. The bridging distances Mo–O_b–Mo are 1.8846(6), 1.8774(7), 1.8714(7) and 1.8724(3) Å. The Mo–N bonds are similar in all four structures, being in the range 2.37–2.46 Å.

3.3. IR spectroscopy

The infrared spectra of complexes **1**–**4** show strong and sharp absorption bands for the carboxylate groups of the coordinated nitrilotriacetate. Asymmetric stretching vibrations $\nu_{as}(COO^-)$ appear between 1673 and 1600 cm^{-1}. The corresponding symmetric stretches $\nu_s(COO^-)$ appear between 1448 and 1318 cm^{-1}. Compound **3** gives a typical band of a non-bonded and undissociated carboxylic acid group at 1750 cm^{-1}. The weak absorption bands at 1735 and 1719 cm^{-1} for compounds **1** and **2** indicate strong H-bonds between the free carboxylic acid and carboxyl groups. All of the carboxyl absorptions are shifted to lower frequencies with respect to those of the free nitrilotriacetic acid due to the influence of hydrogen bonds and counterions. These observations are in accord with the formation of a chelate ring and the bridging mode of the nitrilotriacetate ligand. Loss of the proton in compounds **1** and **2** and the absence of a oxo-bridge group in compound **4** reduce the number of bands and displace them to lower frequencies. In the region between 982 and 857 cm^{-1}, these complexes show several bands that result from the presence of *cis*-dioxo cores in two different environments. The low frequency symmetric MoO_2 stretching may be explained by intramolecular hydrogen bonding and the coordination of a sodium or ammonium cation. The strong IR band only observed for the dimers around 700 cm^{-1} may be attributed to the Mo–O_b–Mo bridges. The absence of IR bands between 1740–1700 cm^{-1} and 790–775 cm^{-1} indicate full deprotonation of β-carboxyl group in compound **4** [25].

3.4. Solution NMR spectroscopy

The solution ^{13}C NMR spectra of complexes **1**–**4** were measured in D_2O. The ^{13}C NMR spectra of **1** and **2** in Fig. 5 show two sets of resonances, which can be attributed to the nitrilotriacetate ligands in the molybdenum

Table 2
Comparisons of the Mo–O and Mo–N distances (Å) in the complexes of nitrilotriacetato molybdates (VI)

Compound	Mo–O_t	Mo–O_b	Mo–O_{c1}	Mo–O_{c2}	Mo–N	Ref.
$K_3[MoO_3(nta)]\cdot H_2O$	1.737(5)		2.176(4)	2.245(3)	2.388(5)	[11]
$Na_2[Mo_2O_5(Hnta)_2]\cdot 8H_2O$	1.695(6)	1.880(1)	2.069(5)	2.134(5)	2.410(6)	[12]
$(pyH)_2[Mo_2O_5(Hnta)_2]$	1.695(3)	1.870(3)	2.071(3)	2.145(3)	2.413(3)	[13]
$[(n\text{-}C_4H_9)N]_2[Mo_2O_5(Hnta)_2]\cdot H_2O$	1.702(7)	1.854(7)	2.077(7)	2.144(6)	2.457(7)	[14]
$Na_2[Mo_2O_5(Hnta)_2]$	1.703(5)	1.8846(6)	2.029(5)	2.187(5)	2.394(6)	
$Na_{6n}\{[Mo_2O_5(ntaH)_2][(nta)_2Mo_2O_5]\}_n\cdot 12nH_2O$	1.697(6)	1.8774(7)	2.083(5)	2.110(5)	2.436(6)	
	1.698(5)	1.8714(7)	2.074(5)	2.115(5)	2.377(6)	this work
$(NH_4)_{3n}[Mo_2O_5H(nta)_2]_n\cdot 4nH_2O$	1.695(3)	1.8724(3)	2.059(3)	2.162(3)	2.405(3)	
$Na_3[MoO_3(nta)]\cdot 4H_2O$	1.728(3)		2.186(3)	2.214(3)	2.395(3)	
Average (Å)	1.706	1.873	2.092	2.162	2.408	

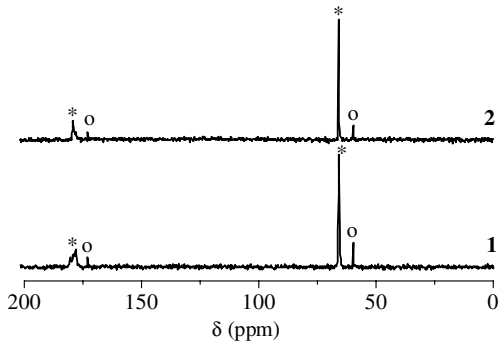

Fig. 5. ^{13}C NMR spectra of the complexes: (bottom) $Na_{6n}\{[Mo_2O_5(ntaH)_2][(nta)_2Mo_2O_5]\}_n \cdot 12nH_2O$ (**1**); (top) $(NH_4)_{3n}[Mo_2O_5H(nta)_2]_n \cdot 4nH_2O$ (**2**). The symbol '∗' indicates resonance signals of the coordinated ligand, '○' of the free ligand.

complexes and the decomposed free nitrilotriacetate [Na_2Hnta: ^{13}C NMR δ_C (D_2O) 171.3 $(CO_2)_\beta$, 58.1 (CH_2)]. Complex **1** shows one resonance in the high-field region (65.5 ppm) for the methylene groups of the nitrilotriacetate ligands. The resonances at 180.2, 179.0 and 177.8 ppm in the lower-field region can be assigned to the β-carboxylate carbons coordinated to the Mo(VI) central ion. The ^{13}C NMR spectra of **2**–**4** resemble one another. Large downfield shifts of the β-carboxylate ($\Delta\delta$ 7.7, 4.4, 6.8) and methylene ($\Delta\delta$ 7.6, 3.5, 6.5) carbons compared with the free nitrilotriacetate are observed for **2**–**4**, respectively. The downfield shifts of the β-carboxylate and CH_2 groups are in agreement with those in earlier studies [16,26]. The ^1H NMR spectra of all four complexes show one wide peak for the methylene protons, which may arise from the similar magnetic environment in solution. The similarities of the NMR spectra of the isolated Mo(VI) complexes suggest that the coordination mode of the nitrilotriacetate ligand is similar not only in the solid state but also in solution. The very strong hydrogen bonds in **1** and **2** may be related to the downshift of the β-carboxyl group from 177.8 to 179.0 ppm.

Acknowledgements

We thank the Ministry of Science and Technology (001CB108906 and 2005CB221408) and the National Science Foundation of China (20571061, 20021002 and 20423002) for their generous financial support.

Appendix A. Supplementary data

Crystallographic data are available from the CCDC, 12 Union Road, Cambridge CB2 1EZ, UK on request, quoting the Deposition Nos. 271976–271979 for compounds **1**–**4**. Supplementary data associated with this article can be found, in the online version, at doi:10.1016/j.poly.2005.12.017.

References

[1] K. Wieghart, U. Quilitzsch, J. Weiss, B. Nuber, Inorg. Chem. 19 (1980) 2514.
[2] K. Okamoto, J. Hidaka, M. Fukagawa, K. Kanamori, Acta Crystallogr., Sect. C 48 (1992) 1025.
[3] Q.Z. Zhang, C.Z. Lu, W.B. Yang, S.M. Chen, Y.Q. Yu, X. He, Y. Yan, J.H. Liu, X.J. Xu, C.K. Xia, L.J. Chen, X.Y. Wu, Polyhedron 23 (2004) 1975.
[4] M. Sokolov, H. Imoto, T. Saito, Inorg. Chem. Commun. 3 (2000) 96.
[5] H.G. Visser, W. Purcell, S.S. Basson, Polyhedron 18 (1999) 2795.
[6] G. Novitchi, J.P. Costes, V. Ciornea, S. Shova, I. Filippova, Y.A. Simonov, A. Gulea, Eur. J. Inorg. Chem. (2005) 929.
[7] S.L. Heath, A.K. Powell, H.L. Utting, M. Helliwell, J. Chem. Soc., Dalton Trans. (1992) 305.
[8] H.G. Visser, W. Purcell, S.S. Basson, Polyhedron 20 (2001) 185.
[9] N.R. Lien, M.A. Timmons, G.J.H. Belkin, J.R. Holst, M.L. Janzen, R. Kanthasamy, W.J. Lin, A. Mubayi, M.I. Perring, L.M. Rupert, A. Saha, N.J. Schoenfeldt, A.N. Sokolov, J.R. Telford, Inorg. Chim. Acta 358 (2005) 1284.
[10] X.Q. Lu, J.J. Jiang, C.L. Chen, B.S. Kang, C.Y. Su, Inorg. Chem. 44 (2005) 4515.
[11] R.J. Butcher, B.R. Penfold, Cryst. Mol. Struct. 6 (1976) 13.
[12] C.B. Knobler, W.T. Robinson, C.J. Wilkins, A.J. Wilson, Acta Crystallogr., Sect. C 39 (1983) 443.
[13] K. Matsumoto, Y. Marutani, S. Ooi, Bull. Chem. Soc. Jpn. 57 (1984) 2671.
[14] S.C. Liu, L.D. Ma, D. McGowty, J. Zubieta, Polyhedron 9 (1990) 1541.
[15] J.J. Cruywagen, J.B.B. Heyns, E.A. Rohwer, J. Chem. Soc., Dalton Trans. (1994) 45.
[16] K.F. Miller, R.A.D. Wentworth, Inorg. Chem. 17 (1978) 2679.
[17] S. Funahashi, Y. Kato, M. Nakayama, M. Thanaka, Inorg. Chem. 20 (1981) 1752.
[18] S.I. Chan, R.J. Kula, D.T. Sawyer, J. Am. Chem. Soc. 86 (1964) 377.
[19] K. Majlesi, K. Zare, F. Teimouri, J. Chem. Eng. Data 48 (2003) 680.
[20] SADABS, University of Göttingen, Germany, 1997.
[21] L.J. Farrugia, J. Appl. Crystallogr. 32 (1999) 837.
[22] G.M. Sheldrick, SHELXL-97 and SHELXS-97, University of Göttingen, Göttingen, Germany, 1997.
[23] L. Medici, R. Prins, J. Catal. 163 (1996) 28.
[24] Z.H. Zhou, S.Y. Hou, Z.J. Ma, H.L. Wan, K.R. Tsai, S.W. Ng, Inorg. Chem. Commun. 5 (2002) 388.
[25] N. Kazuo, Infrared and Raman Spectra of Inorganic and Coordination Compounds, Wiley, New York, 1997, pp. 59–62; 168–169.
[26] M.A. Freeman, F.A. Schultz, C.N. Reilley, Inorg. Chem. 21 (1982) 567.

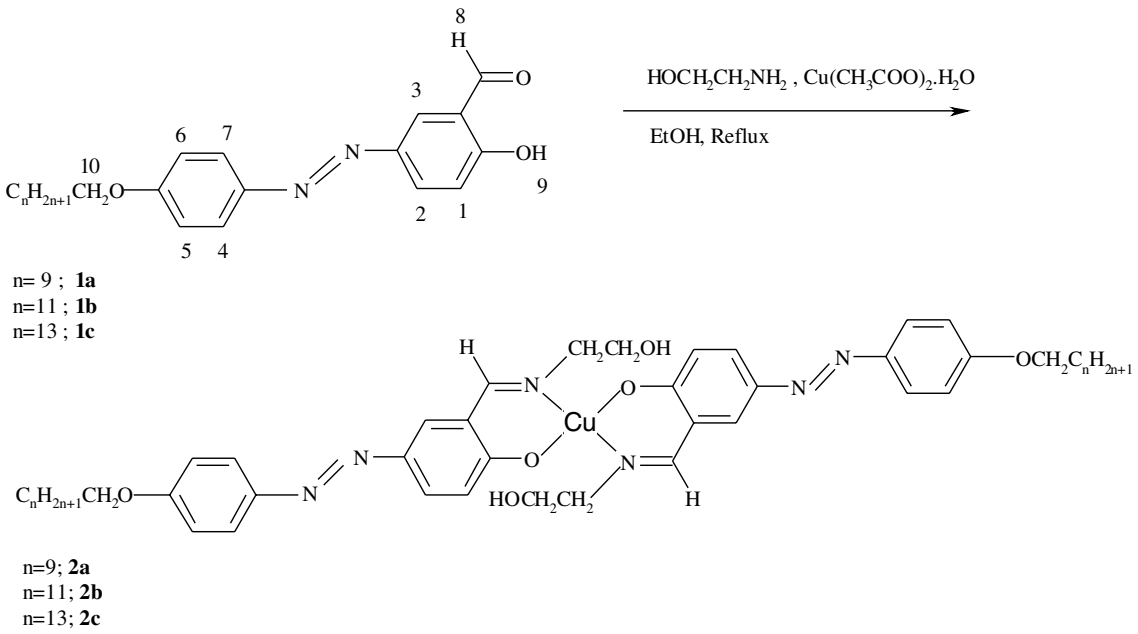

Scheme 1. Synthetic route to the copper complexes.

2.2. Physical measurements

Elemental (C, H and N) analyses were carried out on a Perkin–Elmer automatic equipment model 240B. Electron impact (70 eV) mass spectra were recorded on a Finnegan-mat GC–MS–DS spectrometer model 8430. Infrared spectra were taken with a FT-IR Bruker, vector 22 spectrometer using KBr pellets in the 400–4000 cm^{-1} range. The DSC thermograms of the compounds were obtained on a Mettler–Toledo DSC 822e module, which was calibrated with indium metal ($T = 156.6 \pm 0.3$, $\Delta H = 28.45 \pm 0.6$ J g^{-1}). Samples of 2–5 mg in the solid form were placed in aluminum pans (40 μl) with a pierced lid, and heated or cooled at a scan rate of 10 °C min^{-1} under a nitrogen flow. TGA was carried out on a Mettler–Toledo TGA 851e at a heating rate of 10 °C min^{-1} under a nitrogen atmosphere. The optical observations were made with a Zeiss polarizing microscope equipped with a Linkam THMSG 600 heating and cooling stage and a Linkam THMS 93 programmable temperature-controller. ^{1}H NMR spectra were obtained on a Bruker FT-NMR AC-400 (400 MHz) spectrometer with deutrated chloroform as the solvent. All chemical shifts are reported in δ(ppm) relative to tetramethylsilane as an internal standard.

2.3. Materials

All homologue materials were prepared similarly.

2.3.1. 5-(4-Decyloxyphenylazo) salicylaldehyde (*1a*)

This compound was prepared as described in the literature [20]. Yellow, yield 80%, m.p. 126 °C. MS *m/z* (relative intensity): 355.4 (M+1, 15), 354.3 (M, 40), 241.2 (M−$C_{10}H_{21}$, 25), 121.0 (M−$C_{10}H_{21}OC_6H_4N_2$, 100). *Anal.* Calc. for $C_{23}H_{30}N_2O_3$: C, 71.16; H, 7.39; N, 7.90. Found: C, 70.71; H, 7.12; N, 7.54%. ^{1}H NMR (400 MHz, $CDCl_3$) δ 11.27 (s, H-8), 10.02 (s, H-9), 8.18 (d, *J* 3.2 Hz, H-3), 8.14 (dd, *J* 3.1, 8.4 Hz, H-2), 7.91 (dd, *J* 3.1, 8.2 Hz, H-4, H-7), 7.10 (d, *J* 8.7, H-1), 7.01 (dd, *J* 3.6, 8.3 Hz, H-5,H-6), 4.05 (t, *J* 7.1 Hz, H-10), 1.81–1.00 (15H, alkyl chain).

2.3.2. 5-(4-Dodecyloxyphenylazo) salicylaldehyde (*1b*)

Yellow, yield 80%, m.p. 123 °C. MS *m/z* (relative intensity): 411.6 (M+1, 15), 410.6 (M, 45), 242.5 (M−$C_{12}H_{25}$, 25), 121.6 (M−$C_{12}H_{25}OC_6H_4N_2$, 100). *Anal.* Calc. for $C_{25}H_{34}N_2O_3$: C, 73.15; H, 8.35; N, 6.83. Found: C, 72.73; H, 8.14; N, 6.47%. ^{1}H NMR (400 MHz, $CDCl_3$) δ 11.26 (s, H-9), 10.02 (s, H-8), 8.15 (d, *J* 2.8 Hz, H-3), 8.13 (dd, *J* 2.9, 8.2 Hz, H-2), 7.89 (dd, *J* 3.0, 7.9 Hz, H-4, H-7), 7.11 (d, *J* 8.1 Hz, H-1), 7.01 (dd, *J* 3.2, 7.9 Hz, H-5, H-6), 4.04 (t, *J* 6.7 Hz, H-10), 1.84–0.87 (23H, alkyl chain).

2.3.3. 5-(4-Tetradecyloxyphenylazo) salicylaldehyde (*1c*)

Yellow, yield 80%, m.p. 123 °C. MS *m/z* (relative intensity): 411.6 (M+1, 15), 410.6 (M, 45), 242.5 (M−$C_{14}H_{29}$, 25), 121.6 (M−$C_{12}H_{25}OC_6H_4N_2$, 100). *Anal.* Calc. for $C_{27}H_{38}N_2O_3$: C, 73.15; H, 8.35; N, 6.83. Found: C, 72.73; H, 8.14; N, 6.47. ^{1}H NMR (400 MHz, $CDCl_3$) δ 11.26 (s, H-9), 10.02 (s, H-8), 8.15 (d, *J* 2.8 Hz, H-3), 8.13 (dd, *J* 2.9, 8.2 Hz, H-2), 7.89 (dd, *J* 3.0, 7.9 Hz, H-4, H-7), 7.11 (d, *J* 8.1 Hz, H-1), 7.01 (dd, *J* 3.2, 7.9 Hz, H-5, H-6), 4.04 (t, *J* 6.7 Hz, H-10), 1.84–0.87 (23H, alkyl chain).

2.3.4. Syntheses of the copper complexes

The copper complexes were prepared in similar manners using a method described elsewhere [21]. Thus, an alcoholic solution containing 10 mmol of ethanolamine was added to a solution of 5-alkoxyphenylazo salicylaldehyde (10 mmol)

in 50 ml of boiling absolute ethanol. Then 10 mmol sodium acetate in 10 ml water was added to the above reaction system. Finally 50 ml boiling ethanol solution containing 10 mmol $Cu(CH_3COO)_2 \cdot H_2O$ was added. The reaction mixture was kept boiling for 25 min. Crystals precipitated from the solution and recrystallization was performed from ethanol/chloroform (1:1 v/v) solution. The copper complexes were obtained as brown micro crystals. The micro crystals were filtered off, washed with absolute ethanol and then recrystallized from ethanol–chloroform (1:3 v/v).

Complex ***2a****:* Brown, yield 80%. *Anal.* Calc. for $C_{50}H_{68}N_6O_6Cu$: C, 65.83; H, 7.46; N, 9.22. Found: C, 65.4; H, 7.2; N, 9.2%.

Complex ***2b****:* Brown, yield 85%. *Anal.* Calc. for $C_{54}H_{76}N_6O_6Cu$: C, 66.98; H, 7.86; N, 8.68. Found: C, 66.6; H, 7.4; N, 8.2%.

Complex ***2c****:* Brown, yield 75%. *Anal.* Calc. for $C_{58}H_{84}N_6O_6Cu$: C, 68.00; H, 8.21; N, 8.21. Found: C, 67.6; H, 7.9; N, 8.0%.

3. Results and discussion

3.1. Synthesis

5-(4-Alkoxyphenylazo) salicylaldehyde homologues (**1a**–**c**; see Scheme 1) were synthesized in a three-step process, in which the hydroxy group in 4-nitrophenol is first replaced by an alkoxy chain followed by reduction of the nitro group to an amine. In the third step, salicylaldehyde was coupled with the diazonium chloride obtained from the 4-alkoxyaniline. **1a**–**c** were purified by repeated crystallization from ethanol to give a single spot on thin layer chromatography, and characterized by IR, ^{1}H NMR, mass spectroscopy and elemental analyses. The copper complexes were obtained in good yield and purity, and were characterized by C, H, N elemental analyses and IR spectroscopy. These copper compounds are all paramagnetic and their ^{1}H NMR spectra display only broad alkoxy signals. All other proton signals close to the paramagnetic copper centers are unobserved. The elemental analyses and spectroscopic data for the new compounds gave satisfactory results. Some physical and characterization data for 5-(4-alkoxyphenylazo) salicylaldehyde homologues and the copper complexes are given in the experimental section and selected IR data are tabulated in Table 1. The IR spectral frequencies of the synthesized compounds were obtained using KBr pellets as described in the experimental section. In the compounds **1a**–**c**, the hydroxyl group was observed at 3190 cm^{-1} because the intramolecular hydrogen bonding between OH and the formyl group in compound **1** leads to a decrease of the stretching frequency of OH, and the carbonyl group was observed at 1666 cm^{-1}. In the IR spectra of the copper complexes (**2a**–**c**), the phenolic OH group disappeared and a free lateral OH group was observed as a broad peak centered at 3320 cm^{-1} [21]. In addition, the C=N group was observed at 1620 cm^{-1}. It is well recognized that the C=N stretching frequency in bidentate salicylidenic schiff base ligands with N-alkyl structures appears in the 1635–1640 cm^{-1} region [14–17,22], so the appearance of C=N at 1622 cm^{-1} (at a lower wavenumber than the free schiff base ligands) in the copper complexes demonstrates that C=N has been formed by a [1 + 1] condensation reaction and that it is coordinated to the copper center. On the other hand, the lack of a phenolic OH group in the copper complexes indicates that the OH group has been deprotonated and is coordinated to the metal ion as $-O^-$. Reduction of the double bond character of the C=N bond, which is caused by the coordination of nitrogen into the metal center, is in agreement with results obtained from other similar complexes, described previously [14–17,22]. Based on these observations and the elemental analyses results we conclude that the Schiff-base ligands are coordinated to metal atoms as bidentate (N–O) ligands in a 2:1 ratio.

On the basis of the literature data for copper complexes with a similar coordination environment, the OH group is free of coordination [21] and is not bonded to the metal center. This fact may be related to the strong John–Teller effect in d^9 Cu^{+2}, which avoids the coordination of OH to the metal center. Therefore, it is suggested that the Cu(II) centres have square planar or nearly square planar coordination according to the common stereochemistry of this kind of compound [8,23].

3.2. Mesomorphism

The mesomorphic properties of 5-(4-^{n}alkoxyphenylazo) salicylaldehyde homologues (**1a**–**c**) and the Cu(II) complexes have been studied by polarizing optical microscopy observations using a heating–cooling stage and the phase transition temperature and enthalpy were obtained by differential scanning calorimetry (DSC). Phase transition temperatures along with the corresponding enthalpy values for the copper complexes are summarized in Table 2. The aldehyde homologues (**1a**–**c**) did not show any liquid crystalline character. These compounds clearly melted and transformed

Table 1
Selected IR data for the Schiff base ligands and metal complexes

Compound	ν (cm^{-1})					
	O–H	C–H (aromatic)	C–H (aliphatic)	C=N	C–O (etheric)	C=O
1(**a**–**c**)	3185–90(br, m)	3069–71(m)	2950–2850(s)		1241	1665–6(s)
2(**a**–**c**)	3220–40(br, m)	3050–60(m)	2955, 2860(s)	1621–3(s)	1255–86(s)	

s, strong; m, medium; br, broad.

Table 2
Transition temperatures and enthalpy changes of the copper(II) complexes

Compound	Transition[a]	T[b] (°C)	ΔH[b] (kJ mol^{-1})
2a	Cr_1–Cr_2	56.1	1.61
	Cr_2–Cr_3	167.0	1.59
	Cr_3–SmC	204.3	53.43
	SmC–I(dec)[c]	240.3	5.27
2b	Cr_1–Cr_2	173.6	9.58
	Cr_2–SmC	193.8	51.10
	SmC–I(dec)	235.1	3.54
2c	Cr_1–Cr_2	107.4	1.67
	Cr_2–Cr_3	171.3	17.06
	Cr_3–SmC	191.4	49.08
	SmC–I(dec)	230.9	13.41

[a] Cr, crystal; SmC, smectic C; I, isotropic liquid.
[b] Data obtained from first DSC cycle. Temperature data are at peak onset.
[c] dec: decomposition occurred immediately at clearing point.

into isotropic liquids and no mesophase was observed on the heating or cooling cycle from optical observations. The melting points of the ligands decrease with increasing n value (alkyl chain length, see Scheme 1).

All the copper complexes reported in this work exhibit liquid crystalline behavior. Fig. 1(**2a**–**2c**) shows the DSC curves of the copper complexes. The thermal behaviors of the complexes were similar as it is apparent from the DSC curves; therefore we describe here the behavior of compound **2a** as a representative example. The first heating cycle exhibits four endothermic transitions at 56.1, 167.0, 204.3 and 240.3 °C with ΔH values of 1.61, 1.59, 532.43 and 5.27 kJ mol^{-1}, respectively. The first two transitions correspond to the transition of a crystal phase to another crystal phase and cannot be observed optically. The third peak corresponds to the transition of a crystal phase to a mesophase. The mesophase was examined by optical observation. A highly viscous mesophase with a typical Schlieren texture [24] was observed for all copper complexes under POM. The fourth peak, having a relatively small ΔH value, corresponds to the transition of the mesophase to an isotropic liquid. This process can also be observed optically. A relatively larger clearing enthalpy for the mesophase-to-isotropic transition was observed at higher temperatures (203–240 °C) indicating that the mesophases were highly ordered. Results from DSC and POM therefore suggest the presence of a SmC mesophase. A microscopic picture from the SmC mesophase for complex **2a** is illustrated in Fig. 2.

Continued heating after the clearing point causes a considerable amount of decomposition immediately after isotropization, which has been detected by exothermic peaks in the DSC trace and optical observations. The subsequent cooling and heating processes do not give reproducible

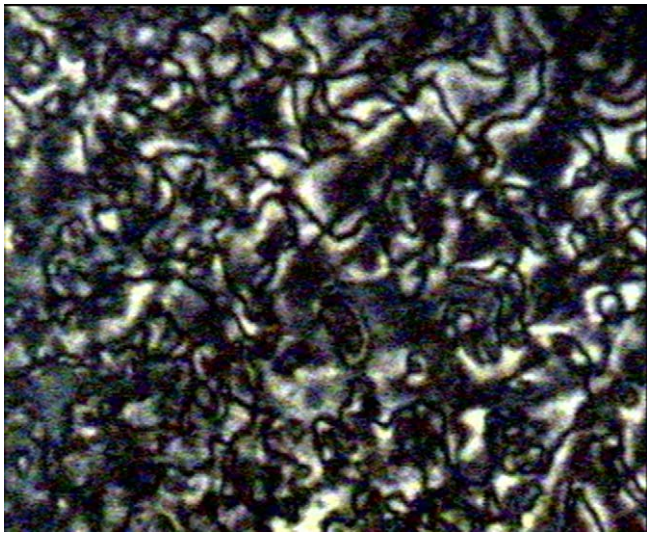

Fig. 2. Optical texture observed for **2a** through crossed polarizers at 210 °C.

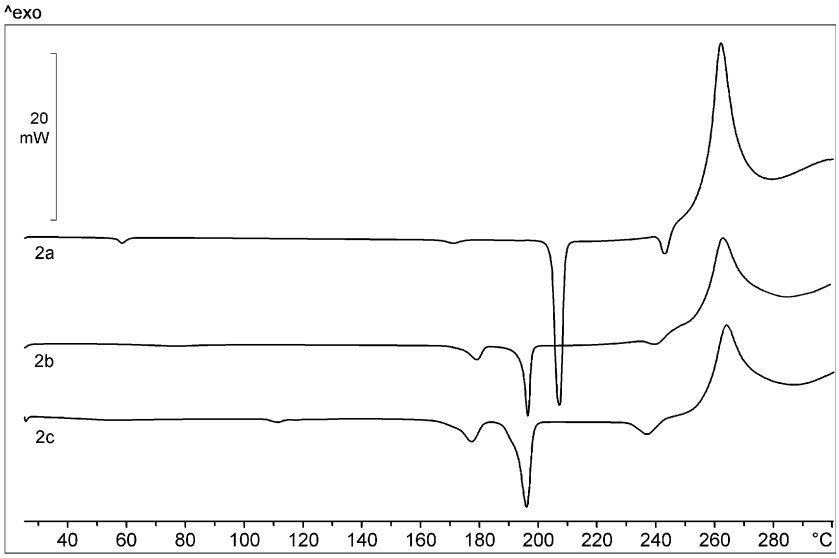

Fig. 1. DSC thermograms of the copper complexes.

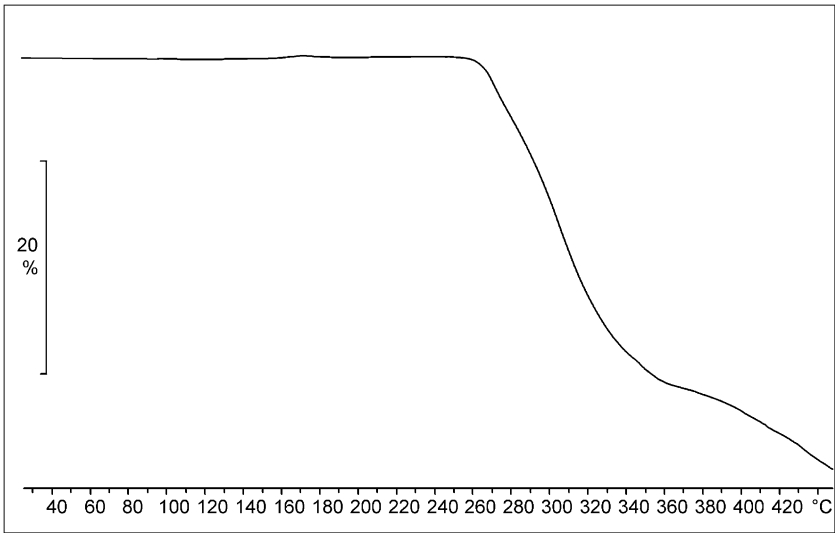

Fig. 3. TGA curve of **2a**.

results because thermal decomposition occurs during the first heating cycle. All the other members of this series of compounds also exhibit thermal decomposition behavior. Therefore, in Table 1, phase transition temperatures of the copper complexes are reported from the first heating cycle of the DSC thermogram. In general, melting temperatures of these copper compounds decrease slightly by increasing the alkyl chain length. The variation of clearing temperatures with increasing chain length has similar trends. In the first heating scan if the temperature increase is within the clearing point, in the first cooling stage the transition of isotropic liquid to mesophase is observed at 241 °C and the mesophase starts to crystallize at 224 °C, as detected by DSC and confirmed by POM, but after the clearing point the sample is decomposed and in the first cooling cycle no transitions was observed.

To understand the thermal decomposition process, the copper compounds were examined by thermogravimetric analysis (TGA). The TGA thermogram of the copper compounds at a heating rate of 10 °C/min shows that decomposition begins at 260 °C, which is near the temperature of clearing to the isotropic liquid. All the copper compounds have similar TGA thermograms. Fig. 3 shows the TGA thermogram of **2a** as a representative example.

The copper complexes reported in this work are the first example of metallomesogens based on two ring salicylidenic schiff base ligand system with an azo moiety and a polar OH on the ligands (N–CH_2CH_2OH). Recently some mesogenic copper complexes which have a similar structure to that of the title complex of this work have been reported. We have recently reported the investigation of liquid crystalline properties of bis[5-((4-^{n}alkoxyphenyl)azo)-*N*-(^{n}alkyl)-salicylaldiminato]copper(II) complex homologues [15]; metallomesogens based on two ring salicylidenic schiff base ligand with an azo moiety and an alkyl group on the ligands (N-alkyl). These complexes exhibited monotropic nematic (thermodynamically unstable) liquid crystalline character. Furthermore, Hoshino [25], Cruso [26], Marcos [27] and Barbera [28] have reported the nematic liquid crystalline properties of bis[4-((4-alkoxy)benzoyloxy)-salicylaldimine-*N*-alkyl]copper(II) complexes, but the complexes with an OH lateral group reported in this work exhibit a high order enantiotropic (thermodynamically stable) SmC phase. The comparison of mesogenic behavior of N-alkyl complexes with N–CH_2CH_2OH complexes demonstrates the role of the OH group on the mesogenic character. We can conclude that the presence of the OH group on the ligands considerably improves the liquid crystalline behavior from monotropic nematic to enantiotropic SmC phase in this type of metallomesogenic systems. This fact may be related to the attractive intermolecular interactions between HO···Cu and /or HO···HO.

4. Conclusion

In this work we have prepared copper complexes derived from 5-((4-^{n}alkoxyphenyl)azo)-*N*-(ethanol)-salicylaldimine homologues as the first example of azo-containing metallomesogens with a lateral OH group. In summary, the study outlined above has shown that all complexes exhibit an enantiotropic smectic C mesophase. Melting and clearing temperatures of the complexes slightly decrease with increasing alkoxy chain length. The mesomorphism can be greatly improved by introducing the lateral OH group close to the central core in this type of copper-containing metallomesogenic system.

Acknowledgement

Financial support from Azarbaijan University of Tarbiat Moallem research council is greatly appreciated.

References

[1] A.M. Giroud, Coord. Chem. Rev. 180 (1998) 1485.
[2] R. Ziessel, Coord. Chem. Rev. 216 (2001) 195.

[3] K. Binnemans, C. Görller-Warland, Chem. Rev. 102 (2002) 2303.
[4] R.W. Date, E.F. Iglesias, K.E. Rowe, J.M. Elliott, D.W. Bruce, J. Chem. Soc., Dalton Trans. (2003) 1914.
[5] R. Gimenez, D.P. Lydon, J.L. Serrano, Curr. Opin. Solid State Mater. Sci. 6 (2002) 527.
[6] N. Hoshino, Coord. Chem. Rev. 174 (1998) 77.
[7] R. Paschke, D. Balkow, E. Sinn, Inorg. Chem. 41 (2002) 1949.
[8] A.B. Blake, J.R. Chipperfield, W. Hussain, R. Paschke, E. Sinn, Inorg. Chem. 34 (1995) 1125.
[9] L. Laésker, T. Fischer, S.R. Marder, W.E. Torruellas, M. Blanchard-Desce, V. Ricci, G.I. Stegeman, S. Gilmour, J.L. Bredas, J. Li, G.U. Bublitz, S.G. Boxer, Science 276 (1997) 1233.
[10] W.M. Gibson, P.J. Shannon, S.T. San, B.J. Swetlin, Nature 351 (1991) 49.
[11] I. Aiello, M. Ghedini, M. La Deda, D. Pucci, O. Francescangeli, Eur. J. Inorg. Chem. (1999) 1367.
[12] I. Aiello, M. Ghedini, F. Neve, D. Pucci, Chem. Mater. 9 (1997) 2107.
[13] P.K. Sudhadevi Antharjanam, V. Ajay Mallia, S. Das, Chem. Mater. 14 (2002) 2687.
[14] A.A. Khandar, Z. Rezvani, Polyhedron 18 (1998) 129.
[15] Z. Rezvani, L. Rahimi Ahar, K. Nejati, S.M. Seyedahmadian, Acta Chim. Slov. 51 (2004) 675.
[16] Z. Rezvani, A.R. Abbasi, K. Nejati, S.M. Seyedahmadian, Polyhedron 24 (2005) 1467.
[17] K. Nejati, Z. Rezvani, New J. Chem. 27 (2003) 1665.
[18] R.V. Deun, K. Binnemans, J. Alloys Comp. 303–304 (2000) 146.
[19] E.C. HorningOrganic Syntheses, collective vol. III, Wiley, New York, 1955, p. 130.
[20] A.A. Khandar, Z. Rezvani, K. Nejati, A.I. Yanovsky, J.M. Martinez, Acta Chim. Slov. 49 (2002) 733.
[21] L. Chen, H. Xu, X. Yu, Y. Zhu, C. Yang, J. Polym. Sci. A 34 (1996) 721.
[22] M. Lee, Y.S. Yoo, M.G. Chol, Macromolecules 32 (1999) 2777.
[23] R. Paschke, S. Liebsch, C. Tschierske, M.A. Oakley, E. Sinn, Inorg. Chem. 42 (2003) 8230.
[24] I. Dierking, Textures of Liquid Crystals, Wiley-VCH, Weinheim, 2003.
[25] N. Hoshino, R. Hayakawa, T. Shiboya, Y. Matsunaga, Inorg. Chem. 29 (1990) 5129.
[26] (a) U. Caruso, A. Roviello, A. Sirigu, Liq. Cryst. 7 (1990) 421;
(b) U. Caruso, A. Roviello, A. Sirigu, Liq. Cryst. 7 (1990) 431;
(c) U. Caruso, A. Roviello, A. Sirigu, Liq. Cryst. 10 (1991) 85.
[27] (a) M. Maros, P. Romero, J.L. Serrano, J. Chem. Soc., Chem. Commun. (1989) 1641;
(b) M. Maros, P. Romero, J.L. Serrano, J. Barbara, A.M. Levelut, Liq. Cryst. 7 (1990) 421.
[28] J. Barbara, A.M. Levelut, M. Maros, P. Romero, J.L. Serrano, Liq. Cryst. 10 (1991) 119.

with respect to 2 M Na_2WO_4 for ^{183}W and 85% H_3AsO_4 for ^{75}As. Crystals of **1** were dissolved in 0.2 M NaCl for ^{183}W and ^{75}As NMR. In order to obtain sufficient concentration for ^{183}W NMR, compound of **3** was converted to the lithium salt by treatment with a Li^+-form cation-exchange resin.

2.2. Preparation of compounds

2.2.1. $Na_{12}[Na_2As_2W_{18}U_2O_{72}]\cdot 35H_2O$ (1)

Glacial acetic acid (3.5 mL) was added to a solution of $Na_2WO_4\cdot 2H_2O$ (14.85 g, 45 mmol) and $Na_2HAsO_4\cdot 7H_2O$ (1.1.58 g, 55 mmol) in 50 mL H_2O, and then the resulting solution was added in small portions to a solution of $UO_2(OAc)_2\cdot 2H_2O$ (2.25 g, 5.30 mmol) in 50 mL H_2O and refluxed for 2 h. Addition of solid NaCl (15 g) to the filtrate led to a yellow crystalline powder, which was recrystallized in 0.2 M NaCl solution. Yellow crystals were obtained at 5 °C after 10 days. Yield 11.2 g (74.2%) Elemental analysis for $Na_{12}[Na_2As_2W_{18}U_2O_{72}]\cdot 35H_2O$: Na, 5.33; As, 2.48; W, 54.79; U, 7.88; H_2O, 10.43. Found: Na, 5.20; As, 2.24; W, 54.45; U, 7.50; H_2O, 10.00%.

2.2.2. $(NH_4)_{13}[NH_4As_2W_{18}U_2O_{72}]\cdot 17H_2O$ (2)

Complex **1** was prepared in solution as described above, and then ammonium chloride (20 g) instead of sodium chloride was added to the solution with stirring. A yellow-green solid formed immediately which was filtered off, redissolved in the least amount of hot water and twice precipitated by ammonium chloride (10 g). The resulting yellow-green solid was recrystallized in warm water. Crystals suitable for structure determination were obtained overnight. Yield 11.0 g (78%).

Elemental analysis for $(NH_4)_{13}[NH_4As_2W_{18}U_2O_{72}]\cdot 17H_2O$: As, 2.65; W, 58.61; U, 8.43; NH_3+H_2O, 9.88. Found: As, 2.18; W, 57.55; U, 7.95; NH_3+H_2O, 9.45%.

2.2.3. $K_{13}[KAs_2W_{18}U_2O_{72}]\cdot 10H_2O$ (3)

$K_{13}[KAs_2W_{18}U_2O_{72}]\cdot 10H_2O$ (**3**) was prepared according to a procedure similar to that for **2**. Instead of ammonium chloride, potassium chloride (20 and 10 g) was added. Yield 12.5 g (86%).

Elemental analysis for $K_{13}[KAs_2W_{18}U_2O_{72}]\cdot 10H_2O$: K, 9.39; As, 2.57; W, 56.75; U, 8.14; H_2O, 3.40. Found: K, 8.65; As, 2.28; W, 56.00; U, 7.72; H_2O, 3.20%.

2.3. Single crystal X-ray diffraction analysis

A pale yellow plate of $(NH_4)_{13}[NH_4As_2W_{18}U_2O_{72}]\cdot 17H_2O$ with dimensions $0.40\times 0.35\times 0.1$ mm^3 which crystallizes in the monoclinic space group $P2_1/m$ with $a=12.488(2)$ Å, $b=20.248(4)$ Å, $c=17.579(5)$ Å, $\beta=101.43°$, $V=4364.5(13)$ Å^3 and $Z=2$ was used for crystallographic analysis. The data were collected at 120(2) K on a Brucker SMART 1000 CCD single crystal diffractometer with graphite-monochoromated Mo Kα radiation ($\lambda=0.71073$ Å). A total of 12760 independent reflections ($2\theta_{max}=60.14°$ and $R_{int}=0.1046$) were recorded, of which 6881 reflections were considered [$I>2\sigma(I)$]. The final cycle of refinement converged at $R=0.0639$ and $R_w=0.1396$ [$I>2\sigma(I)$].

Crystallographic data and structure refinement parameters are listed in Table 1. Routine Lorentz and polarization corrections were applied and an absorption correction was performed using the SADABS program [10]. The structure was refined with SHELXL-97 [11] by full-matrix least squares on F^2. Selected bond lengths and bonds angles of **2** are given in Table 2.

Table 1
Crystallographic data[a] for **2**

Formula weight	5646.06
Temperature (K)	120(2)
Wavelength (Å)	0.71073
Crystal system	Monoclinic
Space group	$P2_1/m$
a (Å)	12.448 (2)
b (Å)	20.284(4)
c (Å)	17.579(3)
β (°)	101.430(4)
Volume (Å^3)	43640.5(13)
Z	2
Density (calc) (Mg/m^3)	4.296
Absorption coefficient (mm^{-1})	28.185
Final R indices [$I>2\sigma(I)$]	$R_1=0.0639$; $wR_2=0.1396$
Largest difference peak and hole (e Å^{-3})	7.158 and −3.326

[a] $R_1=\sum||F_o|-|F_c||/\sum F_o|$, $wR_2=[\sum[w(F_o^2-F_c^2)_2]/\sum[w(F_o^2)_2]]^{1/2}$.

Table 2
Selected bond distances (Å) and angles (°) for **2**

1.839(12)	W1–$O2_d$(U)
1.807(13)	W2–$O8_d$(U)
1.809(13)	W8–$O33_d$(U)
1.801(14)	W7–$O28_d$(U)
1.749(13)	W3–$O12_d$(NH_4)
1.740(14)	W6–$O21_d$(NH_4)
2.352(11)	U1–$O8_d$
2.331(11)	U1–$O2_d$
2.357(14)	U1–$O28_d$
2.352(12)	U1–$O33_d$
2.523(12)	U1–$O6_c$
1.785(12)	U1–O42(Oa)
1.741(11)	U1–O41(Ia)
2.909(15)	N1–$O12_d$
2.835(18)	N1–$O21_d$
2.903(16)	N1–O41(Ia)
3.302(3)	N1–O24(AsO_4)
113.0(5)	W1–$O2_d$–U1
113.4(5)	W2–$O8_d$–U1
144.6(6)	W8–$O33_d$–U1
144.3(7)	W7–$O28_d$–U1
78.6(4)	$O33_d$–U1–$O28_d$
124.0(4)	$O2_d$–U1-$O8_d$
62.1(4)	$O2_d$–U1–$O6_c$
62.4(4)	$O8_d$–U1–$O6_c$

3. Results and discussion

3.1. Syntheses and stabilities

When the pH of the WO_4^{2-} and $HAsO_4^{2-}$ solution is adjusted to 7–7.5 by glacial acetic acid, it seems that A-$AsW_9O_{34}^{9-}$ is formed [12]. This solution reacts with Cd^{2+}, Co^{2+}, Mn^{2+}, Zn^{2+} to form $[As_2W_{18}M_4(H_2O)_2O_{68}]^{10-}$ in high yield with a 1–2 h reflux [13]. But due to size and space restrictions, the solution reacts with the trans dioxouranium(VI) ion (UO_2^{2+}) to form $[Na_2As_2W_{18}U_2O_{72}]^{12-}$ (**1**). The anion **1** is formed in solution in the presence of excess Na^+, with addition of the ammonium or potassium ion a yellow-green solid is immediately formed. With addition of the ammonium or potassium ion, **1** is converted to **2** or **3**, and with elimination of the potassium ion and addition of sodium ion (addition of $NaClO_4$), **3** is convert to **1**. The sodium salt in the presence of excess Na^+, and the ammonium and potassium salts are stable in aqueous solution pH 5.5–7. These complexes are unstable in acidic media, we observed that when a solution of **1**, **2** or **3** (1.0 g in 10 mL H_2O) is passed through a strongly acidic ion exchange (Dowex-50W-X8) column, the main product is the Dawson anion, $[As_2W_{18}O_{68}]^{6-}$, which is isolated as $H_6[As_2W_{18}O_{68}]$. The IR spectrum of this compound (972(s), 912(s), 868(s), 745(vs)) is the same as A-α-$H_6[As_2W_{18}O_{68}]$ [14]. This observation confirms that the $AsW_9O_{34}^{9-}$ units in the complexes are the A-isomer (see below).

3.2. IR and Raman spectroscopy

The infrared spectra of **2** and **3** are similar, but that of **1** is slightly different those of **2** and **3** (Fig. 1). IR and Raman spectra of **1** (Fig. 2) are not similar, therefore it confirms that **1** has a centrosymmetric structure.

3.3. NMR spectroscopy

The ^{75}As NMR spectrum of **1** shows one peak at 690.20 ppm and the ^{183}W NMR of **1** shows five peaks with an intensity ratio of 2:2:2:1:2 at −91.18, −115.34, −146.15, −177.27, −199.45, respectively (Fig. 3). These are consistent with the C_i structure. The results of the elemental analysis, the single-line ^{75}As and ^{31}P NMR and five-line ^{183}W NMR pattern of both of compounds show that**1** and $[Na_2P_2W_{18}U_2O_{72}]^{12-}$ are isostructural [8a]. Therefore, the structure of **1** consists of two A-α-$AsW_9O_{34}^{9-}$ that sandwich two uranyl and two sodium ions, leading to a structure of C_i symmetry. In the filling of the sandwich, the UO_2^{2+} and Na^+ ions occupy opposite corners of a rectangular array. In order to obtain a solution of **3** that was concentrated enough for ^{183}W NMR spectroscopy it was necessary to convert the potassium salt by the use of a lithium form of cation exchange resin. The ^{183}W NMR spectrum of the lithium salt of **3** shows eight peaks with an approximate intensity ratio of (2 + 1):2:2:(2 + 2):2:1:2:2

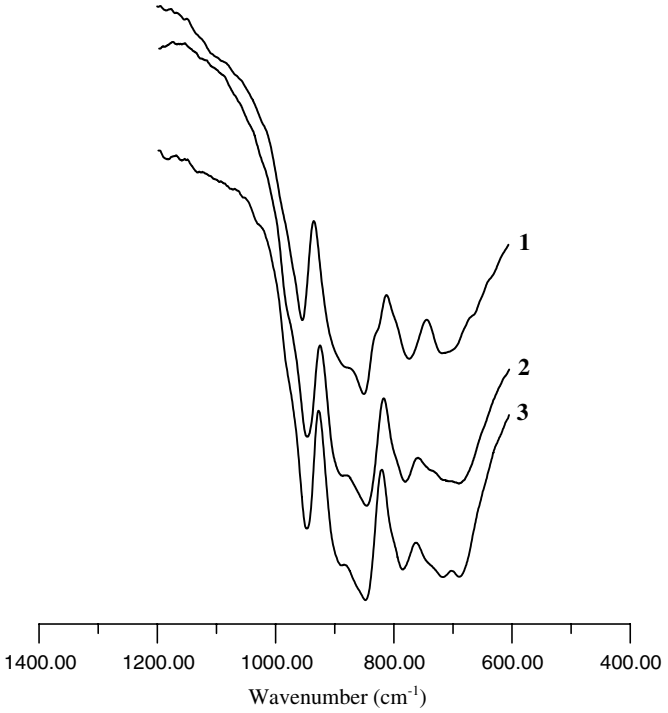

Fig. 1. IR spectra of **1**–**3**.

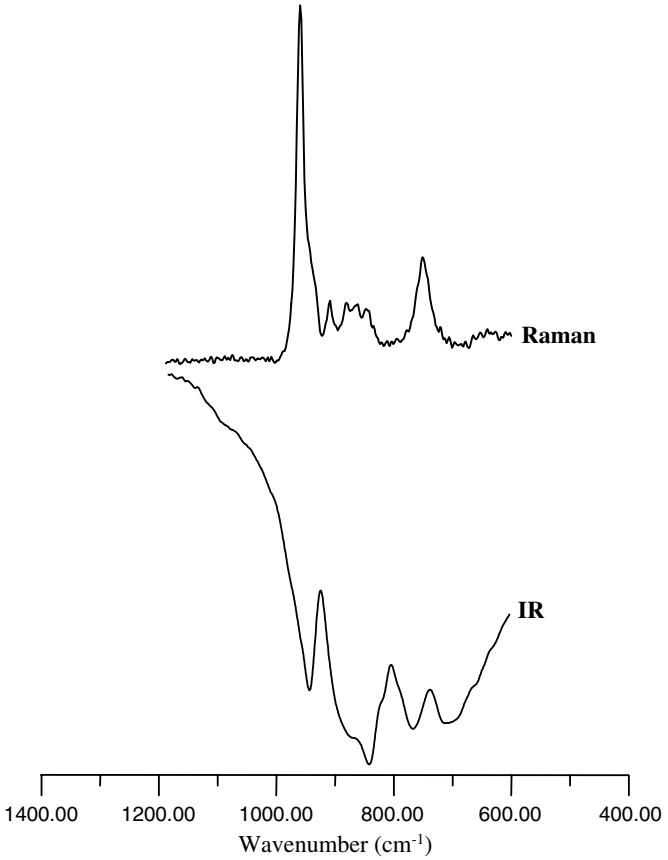

Fig. 2. IR and Raman spectra of **1**.

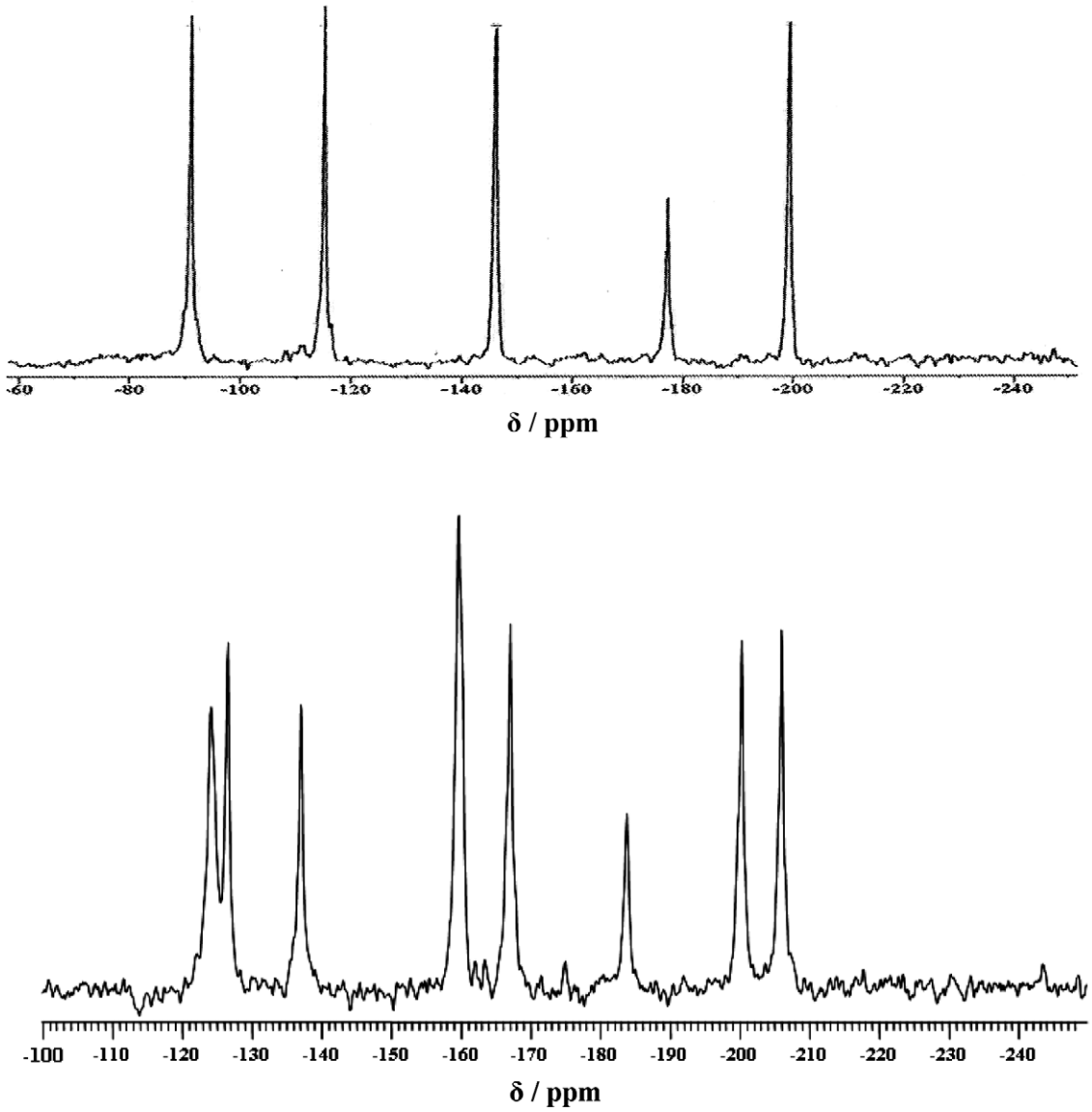

Fig. 3. ^{183}W NMR spectrum of **1** (top) and ^{183}W NMR spectrum of the lithium salt of **3** (bottom).

at −121, −127, −137, −160, −167, −184, −200, −206, respectively, (Fig. 3). The ^{183}W NMR pattern of the lithium salt shows that the anion has an approximate C_s structure. The anion structure in solution (lithium salt) and crystal (ammonium and potassium salt) is the same (see below). Therefore, due to their size, lithium ions cannot replace potassium ions in the anion hole.

3.4. X-ray single crystal structure analysis

Single crystal analysis has been carried out on **2**, which is isostructural with **3**. Since it is not possible on the basis of electron density to discriminate between water molecules and ammonium cations in the structures, the identity of the species occupying the equatorial lacunary site in the structure of anion **2** is not completely certain. Similar features were observed in the structures of the ammonium and potassium salts of the tungstophosphate complex and in the last case the atom could be modelled as a potassium ion [8a]. It therefore seems probable that the sandwiched "atom" is an ammonium ion in both phosphate and arsenate structures. The structure of **2** (Fig. 4) consist of two A-α-$AsW_9O_{34}^{9-}$ anions that sandwich unsymmetrically two uranyl and one ammonium ion. This arrangement leads to a structure with idealized C_s symmetry. The quasi-pentagonal-bipyramidal coordination demands of the uranium atoms means that the two $AsW_9O_{34}^{9-}$ groups are not equivalent; each uranium forms three U–O bonds to one $AsW_9O_{34}^{9-}$ moiety but only two such bonds to the other. Each uranium atom forms two equatorial bonds to the terminal oxygens (O_d) of an edge-shared pair of WO_6 octahedra of one

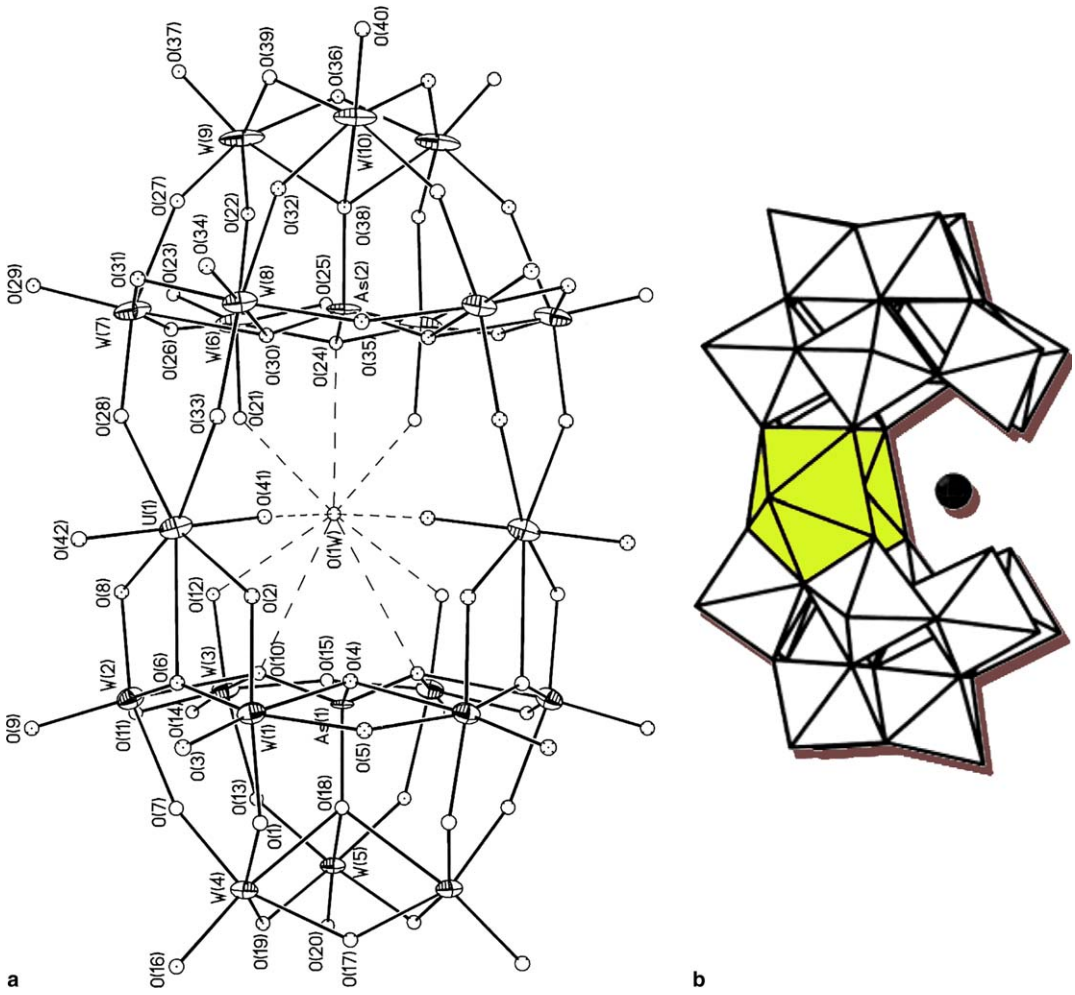

Fig. 4. (a) Thermal ellipsoid plot of **2**. (b) Polyhedral representations of **2**. The presumed ammonium cation (see text) is indicated by the black sphere.

$AsW_9O_{34}^{9-}$ and three bonds to terminal and bridging oxygen (O_c) of a corner-shared pair of octahedra of the other $AsW_9O_{34}^{9-}$ (Table 2). Oxo oxygens of the uranyl ion form the axial bonds of each pentagonal-bipyramid of the uranium atoms. The ammonium ion, Fig. 3, is surrounded by seven oxygens each within hydrogen bonding distances; two axial uranyl oxygens, four uncoordinated oxygens of $AsW_9O_{34}^{9-}$ units and one AsO_4 oxygen (see above).

4. Conclusion

The first examples of sandwich type polytungstate complexes incorporating As^V as a heteroatom and a seven-coordinate (pentagonal-bipyramidal) uranium atom have been synthesized by the facile "self-assembly" reaction of arsenate, tungstate and uranyl ions in a stoichiometric ratio. The anions' structures are controlled by the size of the counteractions, a C_i structure anion with a sodium ion and a C_s structure anion with ammonium or potassium ions are isolated. The anions are unstable in strongly acidic media and are converted to a $H_6As_2W_{18}O_{62}$ Dawson type polyoxometalate.

Acknowledgment

We thank Dr. Nebebech Belai, Department of Chemistry, Georgetown University, for critical recording of ^{183}W NMR spectra.

Appendix A. Supplementary data

Crystallographic data (CIF file) for the structural analysis has been deposited with the Fachinformationszentium Karlsruhe (FIZ), CSD-number 415521. E-mail: crysdata @FIZ-Karsruhe.de. Supplementary data associated with this article can be found, in the online version, at doi:10.1016/j.poly.2005.12.019.

References

[1] M.T. Pope, Heteropoly and Isopoly Oxometalates, Springer-Verlag, New York, 1983.
[2] M.T. Pope, in: G. Wilkinson, R.D. Gillard, J.A. McCleverty (Eds.), Comprehensive Coordination Chemistry, vol. 3, Pergamon Press, 1987, p. 1023.
[3] M.T. Pope, A. Müller, Angew. Chem., Int. Ed. 30 (1991) 34.

[4] M.T. Pope, A. Müller (Eds.), Polyoxometalates. From Platonic Solids to Anti-Retroviral Activity, Kluwer Academic Publishers, Dordrecht, The Netherlands, 1994.
[5] C.L. Hill (Ed.), Chem. Rev. 98 (1998) (special edition on polyoxometalates).
[6] M.T. Pope, A. Müller (Eds.), Polyoxometalate Chemistry: From Topology via Self-assembly to Applications, Kluwer Academic Publishers, Dordrecht, 2001.
[7] M.S. Milyukova, M.N. Litvina, B.F. Myasoedov, Radiochemistry (Engl. Transl.) 25 (1983) 665;
M.S. Milyukova, D.A. Malikov, E.V. Kuzovkina, B.F. Myasoedov, J. Radioanal. Nucl. Chem. 104 (1986) 81;
N.P. Molochinikova, V.Y. Frenkel, B.F. Myasoedov, J. Radioanal. Nucl. Chem. 121 (1988) 409;
N.Y. Kremlyakova, A.P. Novikov, B.F. Myasoedov, N.V. Katargin, J. Radioanal. Nucl. Chem. 145 (1990) 183;
D.A. Malikov, M.S. Milyukova, E.V. Kuzovkina, B.F. Myasoedov, Radiokhimiya 34 (1992) 131;
D.A. Malikov, M.S. Milyukova, B.F. Myasoedov, Radiokhimiya 35 (1993) 105.
[8] (a) K.-C. Kim, M.T. Pope, J. Am. Chem. Soc. 121 (1999) 8512;
(b) K.-C. Kim, M.T. Pope, J. Chem. Soc., Dalton Trans. (2001) 986;
(c) K.-C. Kim, A. Gaunt, M.T. Pope, J. Cluster Sci. 13 (2002) 423.
[9] K. Wassermann, M.T. Pope, M. Salmen, J.N. Dann, H.-J. Lunk, J. Solid State Chem. 149 (2000) 378.
[10] G.M. Sheldrick, in: SADABS v. 2.01, Bruker/Siemens Area Detector Absorption Correction Program, Brucker AXS, Madison, WI, 1998.
[11] G.M. Sheldrick, SHELEX v. 5.10, Structure Determination Software Suit, Brucker AXS, Madison, WI, 1998.
[12] L.H. Bi, R.D. Huang, J. Peng, E.B. Wang, Y.H. Wang, C.W. Hu, J. Chem. Soc., Dalton Trans. (2001) 121;
M.H. Alizadeh, H. Eshtiagh-Hosseini, R. Khoshnavazi, J. Mol. Struct. 688 (2004) 33.
[13] H.T. Evans, C. Tourné, G. Tourné, T.J.R. Weakley, J. Chem. Soc., Dalton Trans. (1986) 2699;
R. Khoshnavazi, Ph.D. Thesis, Ferdowsi University, Mashhad, Iran, 2003.
[14] R. Contant, R. Thouvenot, Inorg. Chim. Acta 212 (1993) 41.

Table 1
T_c as a function of solvent, S, for $V[TCNE]_x \cdot ySy$ prepared from $V(C_6H_6)_2$ and $V(CO)_6$

V-source	Solvent (S)	T_{on} (K)	Ref.
$V(C_6H_6)_2$	CH_2Cl_2	~350	[b]
$V(C_6H_6)_2$	THF	215	[16a]
$V(C_6H_6)_2$	MeCN	138	[16b][a]
$V(CO)_6$	None (CVD)	370	[12a]
$V(CO)_6$	CH_2Cl_2	387	this work
$V(CO)_6$	PhMe	390	this work
$V(CO)_6$	$PhCF_3$	396	this work
$V(CO)_6$	hexane, C_6H_{14}	388	this work

[a] 5 K.
[b] Extrapolated from 150 Oe data presented in Ref. [11b].

The interpretation of T_c is problematic, as it is determined from low-field magnetization, $M(T)$, measurements taken on warming a sample toward the expected magnetic transition temperature. An abrupt drop of $M(T)$ was observed above ~350 K [12]; however, its value did not recover upon cooling, suggesting an irreversible structural transformation (which rapidly degrades the magnetic properties) occurs at almost the same temperature as the magnetic transition (vide infra). Therefore, to evaluate the T_c of the materials, the temperature dependence of the saturated magnetization, $M_s(T)$, was fit to the Bloch $T^{3/2}$ law [12], and T_cs were ~400 K.

Due to the lack of data on the influence other non-coordinating solvents have on T_c of the $V[TCNE]_x$ magnets, alternative solvents were studied with the objective of extending the ferrimagnetic behavior to higher temperatures, which is important for a practical applications. It is possible that different solvent molecules trapped in the $V[TCNE]_x$ structure may strengthen (or weaken) the $V[TCNE]_x$ network (for instance, via short contacts) stabilizing it against thermal degradation. Alternative solvents might also reduce the occlusion of impurities arising from the decomposition of $V(CO)_6$ in CH_2Cl_2. Hence, the effect of several non-coordinating solvents including toluene (PhMe), trifluoromethylbenzene ($PhCF_3$), and hexane, were studied. $PhCF_3$ was particularly intriguing as it has a dielectric constant (9.2) comparable to CH_2Cl_2 (8.9) [17]. Herein, we report the solvent dependence of the magnetic properties of $V[TCNE]_x \cdot ySy$ in the vicinity of magneto-structural transition temperature (see Table 1).

2. Experimental

All manipulations were performed under an inert nitrogen atmosphere (<1 ppm O_2 and <1 ppm H_2O) using standard Schlenk techniques and Vacuum Atmospheres DriLab gloveboxes. Methylene chloride (CH_2Cl_2), PhMe, and hexanes were sparged with nitrogen and passed over two columns of activated alumina prior to use to remove traces of oxygen and water [18]. Trifluoromethylbenzene ($PhCF_3$) was purified by distillation from phosphorous pentoxide under a nitrogen atmosphere. Hexacarbonylvanadium(0), $V(CO)_6$, was prepared by oxidizing tetraethylammonium hexacarbonylvanadium(−1) with phosphoric acid and purified by vacuum sublimation (25 °C, 0.1 Torr) [19]. Tetracyanoethylene (TCNE) was purchased from Acros and purified by vacuum sublimation from activated carbon (80 °C, 0.1 Torr).

2.1. $V[TCNE]_x \cdot ySy$ ($x \sim 2$, $y \sim 0.5$)

All materials were prepared with the desired solvent using a nominally identical procedure exemplified by the following reaction performed in $PhCF_3$. A yellow solution of $V(CO)_6$ (44.7 mg, 0.204 mmol) dissolved in ~5 mL of $PhCF_3$ was added dropwise to a stirred suspension of 2 equiv. TCNE (52.3 mg, 0.408 mmol) in ~10 mL $PhCF_3$. The mixture immediately became black and CO evolved. The mixture was allowed to stir for 12 h. (As the reaction is rapid, the amount of time reaction is stirred does not have a significant impact on the yield or magnetic properties of the product, and was variable between samples.) The black precipitate was collected by suction filtration and dried under vacuum. Yield: 68.5 mg (88%) of $V(TCNE)_2 \cdot 0.5PhCF_3$. IR (KBr, cm^{-1}): 2190, 2151, 2089 (1324, only observed in samples prepared from $PhCF_3$). Elemental *Anal.* Calc. C, 48.97; H, 0.66; N, 29.47. Found: C, 48.59; H, 0.73; N, 29.22%. Thermogravimetric analysis shows broad nearly featureless decomposition above 50 °C.

2.2. Properties characterization

The thermal properties were studied on a TA Instruments Model 2050 thermogravimetric analyzer (TGA) equipped with a TA-MS Fison triple filter quadrupole mass spectrometer, to identify gaseous products with masses less than 300 amu. This instrument was located in a Vacuum Atmospheres DriLab under nitrogen to protect air and moisture sensitive samples. Samples were placed in an aluminum pan and heated at 20 °C/min under a continuous 10-mL/min nitrogen flow. A TA Instruments Model 2910 differential scanning calorimeter was used to carry out DSC experiments. Samples were loaded into an aluminum pan with a lid and hermetically sealed with a special press inside the box. The samples were loaded into the instrument and DSC experiments were performed under nitrogen gas flow.

The 5–300 K magnetic susceptibility was determined on a Quantum Design MPMS-5XL 5 T SQUID (sensitivity $= 10^{-8}$ emu or 10^{-12} emu/Oe at 1 T) as previously described [20]. In addition to correcting for the diamagnetic contribution from the sample holder, core diamagnetic corrections based on summing Pascal's constants were used. Infrared spectra (400–4000 cm^{-1}; with 1 cm^{-1} resolution) were obtained on a Bruker Tensor 37 FT IR-40 spectrophotometer as KBr pellets. Elemental analyses were performed by Complete Analysis Laboratories Inc. of Parsippany, NJ.

3. Results and discussion

Solutions of $V(CO)_6$ in CH_2Cl_2 were observed to gradually decompose over time. The initially bright yellow solutions became green or brown in color after about 15–30 min, and after 24 h a fine black precipitate formed leaving a nearly colorless supernatant. The IR spectrum of the precipitate was featureless between 400 and 4000 cm^{-1} indicating the loss of all CO, and that the material does not contain vanadium oxides or hydroxides (from perhaps reaction with trace amounts of O_2 or H_2O). The material may be a chloride, possibly formed via a chlorine radical intermediate. This decomposition is not unprecedented, as $V(CO)_5PPh_3$ was reported to be unstable in the presence of CH_2Cl_2 or toluene [21]. The identity of the decomposition product or the mechanisms of its formation have not been fully investigated, to our knowledge. No solutions showing visible signs of decomposition were used to prepare the magnetic materials in this study.

Due to the small sample-to-sample variations observed in the physical properties of the materials, a survey of the effects that altering various synthetic protocols have on these properties was undertaken in order to determine if the variations were caused by inadvertent slight variation in the synthetic methods. It was generally found that the volume of solvent used for the reaction should be as small as is practical. It is surprising to note that incomplete dissolution of the TCNE is not detrimental to the reaction. As a result of this observation, all of the materials were prepared from TCNE slurries, as TCNE is only moderately soluble in CH_2Cl_2 and PhMe, slightly soluble in $PhCF_3$, and essentially insoluble in hexane. The use of large volumes of CH_2Cl_2 to completely dissolve the TCNE typically resulted in slightly reduced magnetic ordering temperature. The order of combination of the reagents is, however, critical, and the $V(CO)_6$ solutions must be added dropwise to the TCNE solutions or slurries (although the rate of addition is not important). The amount of time that the reaction mixture is allowed to stand after combination of the reagents (1 min to 48 h) had no affect on the magnetic properties of the materials although several hours were generally allowed to ensure that all of the TCNE had dissolved and reacted in order to prevent the inclusion of unreacted TCNE into the products collected, which was monitored by IR spectroscopy.

The zero-field cooled (ZFC) magnetization of $V[TCNE]_x \cdot ySS$ synthesized from PhMe, $PhCF_3$, hexanes, and CH_2Cl_2 is nearly temperature independent below 300 K, showing a ~10% decrease from 300 to 5 K. In this region, the $M(T)$ is reproducible and the variation between samples is not solvent dependent. Above 300 K the $M(T)$ gradually decreases with different rates for different solvents (Fig. 1) suggesting a magnetic transition. We define the onset temperature, T_{on}, as a temperature at which the magnetization is an order of magnitude greater than its paramagnetic limit of 0.05 emuOe/mol {at 400 K and 5 Oe external field {assuming only paramagnetic contribution from $S = 3/2$ V^{II} and two $S = 1/2$ $[TCNE]^{\bullet -}$}. Using this criterion, T_{on} was determined to be 387, 388, 390, and 396 K for $V[TCNE]_x \cdot ySS$ synthesized in CH_2Cl_2, hexanes, PhMe, and $PhCF_3$, respectively. The T_{on} for the materials prepared from CH_2Cl_2, hexanes, and PhMe are not significantly different given that the observed T_{on} values for $V[TCNE]_x \cdot ySS$ vary slightly between samples (due to extreme air sensitivity), and the similarity of $M(T)$ curve shapes when approaching the transition. This suggests that solvent has a minimal effect on T_{on}. In addition, there is no correlation between the stability of $V(CO)_6$ in a solvent and the ordering temperature of the material prepared from that solvent.

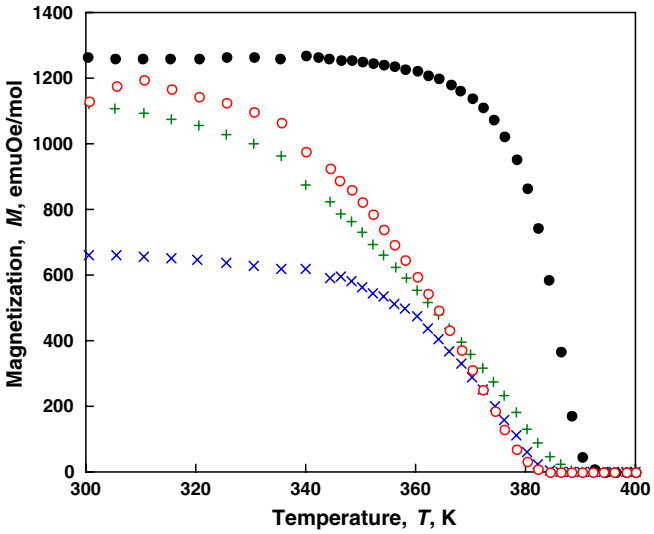

Fig. 1. $M(T)$ for $V[TCNE]_x \cdot ySS$ [S = CH_2Cl_2 (○) $PhCF_3$ (●), hexane (×), and PhMe (+)] in an applied field of 5 Oe.

We believe that the sample-to-sample variations are primarily a result of the extreme air sensitivity of $V[TCNE]_x$ and that slight amounts of oxidation occasionally contaminate the materials as they are being loaded into instruments for analysis, in spite of rigorous precautions taken to prevent as much oxidation as possible.

The reaction of $V(CO)_6$ and TCNE in CH_2Cl_2, hexanes, PhMe, and $PhCF_3$ form an immediate black precipitate, with IR spectra characteristic of $[TCNE]^{\bullet -}$ bonded to V^{II} (Fig. 2), i.e., ν_{CN} absorptions at 2150 and 2188 cm^{-1}, as well as two poorly resolved shoulders at ~2000 and ~2210 cm^{-1}. The position and peak intensity (with respect to the 2150 cm^{-1} band) of a broad feature at ~2090 ± 10 cm^{-1} is solvent dependent. However, no distinct correlation between its position and T_{on} was identified. We also observed similar variations in the ν_{CN} absorptions of $V[TCNE]_x \cdot ySS$ from different batches synthesized using the CH_2Cl_2 solvent with similar T_{on}'s. Earlier we tentatively assigned the 2150 and broad 2100 cm^{-1} bands to ν_{CN} of *trans*-μ-$[TCNE]^{\bullet -}$ and μ_4-$[TCNE]^{\bullet -}$ bonded to V, respectively [12a]. The relative insensitivity of the high frequency bands positions to solvent substitution most probably implies that the non-coordinating solvents do not change the effective electron

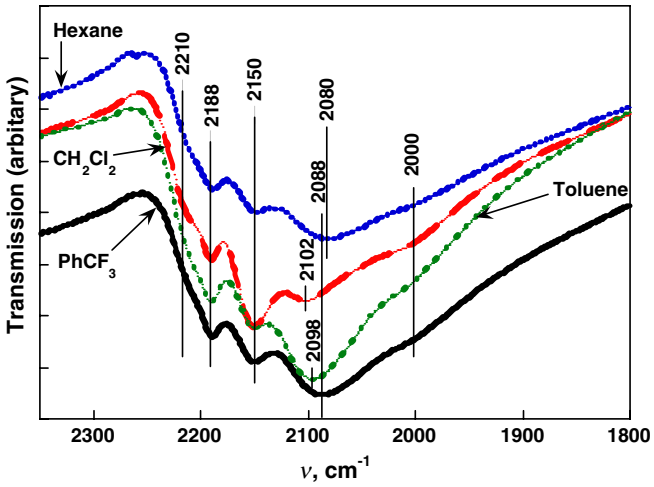

Fig. 2. ν_{CN} region of the IR spectra for $V[TCNE]_x \cdot ySS$ [S = CH_2Cl_2 (- - -) $PhCF_3$ (−), hexane (●●●), and PhMe (---)].

transfer between $[TCNE]^-$ and V, and therefore, do not affect T_{on}. The slight variations in numbers and structure of the μ_4-$[TCNE]^{\bullet -}$ are assumed to be related to the quantitatively non-reproducible intrinsic disorder in these amorphous materials regardless of the solvent from which the material was prepared. The degree of disorder is more sensitive to synthetic conditions, but much less (if any) to the solvent substitution.

However, the T_{on} for the $PhCF_3$-prepared sample is significantly higher. The drop in $M(T)$ with increasing temperature is very abrupt suggesting that the material preserves its structure to higher temperatures (Fig. 3). The DSC traces for $V[TCNE]_x \cdot ySS$ synthesized from CH_2Cl_2 and $PhCF_3$ reveals that the irreversible exothermic process associated with structural rearrangement and/or degradation in the prepared material prepared from CH_2Cl_2 starts ~13 K prior to that in the material prepared from $PhCF_3$ (Fig. 3). The enthalpy change, ΔH, of 129 kJ/mol for the $PhCF_3$-made

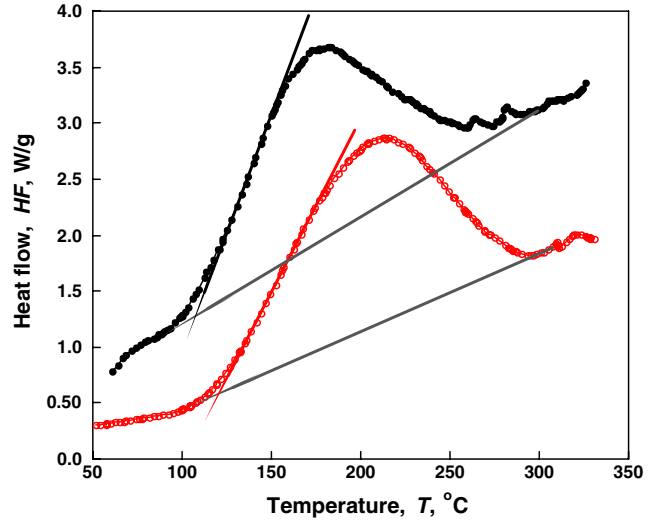

Fig. 3. DSC traces in the $50 \leqslant T \leqslant 325$ K region for $V[TCNE]_x \cdot ySS$ synthesized from CH_2Cl_2 (●), and $PhCF_3$ (○). Analysis was performed assuming a linear background between 100 and 300 K.

material is more than twice the 56 kJ/mol for the material made in CH_2Cl_2, This suggests that it is more robust against thermal degradation. The reason(s) of this effect are not entirely clear, but is under investigation. Hence, a new solvent has been identified that enables the preparation of a more thermally stable organic-based magnet.

Acknowledgments

The continued partial support by the Department of Energy Division of Materials Science (Grant No. DE-FG03-93ER45504) and Army Research Office (Grant No. DAAD19-01-1-0562) is appreciated.

References

[1] J.S. Miller, J.C. Calabrese, A.J. Epstein, R.W. Bigelow, J.H. Zhang, W.M. Reiff, J. Chem. Soc. Chem. Commun. (1986) 1026.
[2] J.S. Miller, J.C. Calabrese, H. Rommelmann, S. Chittipeddi, J.H. Zhang, W.M. Reiff, A.J. Epstein, J. Am. Chem. Soc. 109 (1987) 769.
[3] Recent conference proceedings: P. Day, A.E. Underhill, Phil. Trans. R. Soc. Lond. (A) 357 (1999).
[4] O. Kahn (Ed.), Proceedings of the 6th International Conference on Molecule-based Materials. Mol. Cryst., Liq. Cryst. 1999, vol. 334/335.
[5] K. Itoh, J.S. Miller, T. Takui (Eds.), Proceedings of the Conference on Molecular-Based Magnets. Mol. Cryst., Liq. Cryst., 1997, vol. 305/306.
[6] G. Christou (Ed.), Proceedings of the Conference on Molecule-based Magnets. Polyhedron 2001, vol. 20.
[7] Recent reviews: V.I. Ovcharenko, R.Z. Sagdeev, Russ. Chem. Rev. 68 (1999) 345.
[8] M. Kinoshita, Phil. Trans. R. Soc. Lond. (A) 357 (1999) 2855.
[9] J.S. Miller, A.J. Epstein, Chem. Commun. (1998) 1319.
[10] J.S. Miller, A.J. Epstein, Chem. Eng. News 73 (40) (1995) 30.
[11] (a) J.M. Manriquez, G.T. Yee, R.S. McLean, A.J. Epstein, J.S. Miller, Science 252 (1991) 1415;
(b) J.S. Miller, G.T. Yee, J.M. Manriquez, A.J. Epstein, in: Proceedings of Nobel Symposium #NS-81 Conjugated Polymers and Related Materials: The Interconnection of Chemical and Electronic Structure, Oxford University Press, Oxford, 1993, p. 461;
(c) La Chim. La Ind. 74 (1992) 845;
(d) J. Zhang, P. Zhou, W.B. Brinckerhoff, A.J. Epstein, C. Vazquez, R.S. McLean, J.S. Miller, ACS Symp. Ser. 644 (1996) 311.
[12] (a) K.I. Pokhodnya, A.J. Epstein, J.S. Miller, Adv. Mater. 12 (2000) 410;
(b) K.I. Pokhodnya, D. Pejakovic, A.J. Epstein, J.S. Miller, Phys. Rev. B 63 (2001) 174408.
[13] D. Haskel, Z. Islam, J. Lang, C. Kmety, G. Stajer, K.I. Pokhodnya, A.J. Epstein, J.S. Miller, Phys. Rev. B 70 (2004) 054422.
[14] V.N. Prigodin, N.P. Raju, K.I. Pokhodnya, J.S. Miller, A.J. Epstein, Adv. Mater. 14 (2002) 1230.
[15] (a) S.A. Wolf, J. Supercond. 13 (2000) 195;
(b) G. Prinz, Science 282 (1998) 1660;
(c) H. Ohno, F. Matsukura, Solid State Commun. 117 (2001) 179.
[16] (a) P. Zhou, S.M. Long, J.S. Miller, A.J. Epstein, Phys. Lett. A 181 (1993) 71;
(b) P. Zhou, B. Morin, A.J. Epstein, J.S. Miller, Phys. Rev. B 48 (1993) 1325.
[17] D.R. Lide (Ed.), CRC Handbook of Chemistry and Physics, 85th ed., CRC Press, LLC, Boca Raton, FL, 2004–2005, pp. 6-153–6-175.
[18] A.B. Pangborn, M.A. Giardello, R.H. Grubbs, R.K. Rosen, F.J. Timmers, Organometallics 15 (1996) 1518.
[19] X. Liu, J.E. Ellis, T.D. Selby, P. Ghalsasi, J.S. Miller, Inorg. Synth. 34 (2004) 68.
[20] E.J. Brandon, D.K. Rittenberg, A.M. Arif, J.S. Miller, Inorg. Chem. 37 (1998) 3376.
[21] J.E. Ellis, R.A. Faltynek, G.L. Rochfort, R.E. Stevens, G.A. Zank, Inorg. Chem. 19 (1980) 1082.

2.1. Syntheses of complexes

2.1.1. Synthesis of $[Cu_2L_2Cl_2]$ (1), $[Cu_2L_2Br_2]$ (2), $[Cu_2L_2(NO_3)_2]$ (3) and $[Cu_4L_4(SO_4)_2]\cdot 3H_2O$ (7)

The ligand HL (1 mmol) was dissolved in 20 ml of hot ethanol and the appropriate copper(II) salt (1 mmol) in the same solvent was added to it. The solution was heated under reflux for 2 h and then evaporated to a small volume. After cooling at room temperature, the dark blue crystals formed were isolated and dried under vacuum.

2.1.2. Synthesis of $[Cu_2L_2(N_3)_2]$ (4) and $[Cu_2L_2(SCN)_2]$ (5)

To a 20 ml hot ethanolic solution of the ligand HL (1 mmol) was added copper(II) acetate (1 mmol) in hot methanol. The solution was heated under reflux. To the refluxing solution, sodium azide or potassium thiocyanate were added in portions in the same molar ratio and further refluxed for 2 h. After cooling at room temperature, the dark blue crystals formed were isolated and dried under vacuum.

2.1.3. Synthesis of $[Cu_2LCl_3]$ (6)

The ligand HL (1 mmol) was dissolved in 20 ml of hot ethanol and $CuCl_2\cdot 2H_2O$ (2 mmol) in the same solvent was added to it. The solution was heated under reflux for 2 h and then evaporated to a small volume. After cooling at room temperature, the dark blue crystals formed were isolated and dried under vacuum.

2.2. X-ray crystallography

Single crystals of compound **7** suitable for X-ray diffraction studies were grown from its solution in a mixture of methanol and chloroform (1:1) by slow evaporation at room temperature in air. A single crystal of dimension $0.40\times 0.35\times 0.30$ mm with $P\bar{1}$ symmetry was selected and mounted on a Bruker SMART APEX CCD diffractometer, equipped with a fine focus sealed tube X-ray source. The unit cell dimensions and intensity data were measured at 293 K. SMART software was used for data acquisition and SAINT software for data extraction [15]. Corrections for absorption were carried out by the SADABS method [16]. The whole structure was refined with SHELXL 97 [17] by the full-matrix least squares technique and the graphics tool was DIAMOND [18]. All non-hydrogen atoms were refined anisotropically, while the hydrogen atoms were treated with a mixture of independent and constrained refinements.

2.3. Physical methods

Elemental analyses were carried out using a Heraeus Elemental Analyzer at the Regional Sophisticated Instrumentation Center, CDRI, Lucknow, India. Molar conductance measurements of the complexes were carried out in DMF solvent on a Century CC-601 digital conductivity meter with a dip type cell and platinum electrode. Approximately 10^{-3} M solutions were used. Magnetic moment measurements were carried out in the polycrystalline state on a Vibrating Sample Magnetometer at 5 kOe field strength. Infrared spectra were recorded on a Shimadzu DR 8001 series FTIR instrument as KBr pellets for spectra run from 4000 to 400 cm^{-1}, and using polyethylene for the range 500–100 cm^{-1} in a Nicolet Magna 550 FTIR instrument. Solid-state reflectance spectra were recorded on Ocean Optics SD 2000 Fibre Optic Spectrometer.

3. Results and discussion

Di-2-pyridyl ketone *N*(4),*N*(4)-(butane-1,4-diyl) thiosemicarbazone (HL) interacts with copper(II) ions in the presence of anions, in the molar ratio 1:1:1 yielding complexes with the empirical formula [CuLX] where X = Cl, Br, NO_3, N_3, SCN. Analogously, the complexes $[Cu_2LCl_3]$ (**6**) and $[Cu_4L_4(SO_4)_2]$ (**7**) were obtained when the metal–ligand ratios were 2:1 and 1:1, respectively. Upon evaporation of the solvent, the complexes are precipitated as dark blue solids. These complexes are sparingly soluble in most non-polar solvents but soluble in DMF and DMSO giving non-conducting solutions [19]. Single crystals of the complex **7** suitable for X-ray diffraction were obtained by slow evaporation of its solution in a 1:1 mixture of methanol and chloroform in air at room temperature. The elemental analyses, molar conductance and magnetic susceptibility values are presented in Table 1. The magnetic susceptibility

Table 1
Colors, partial elemental analysis data, magnetic moments and molar conductivities of the Cu(II) complexes

Compound	Color	Composition % found (calc)			λ_M[a]	μ_{eff}[b] (B.M.)
		Carbon	Hydrogen	Nitrogen		
HL	yellow	62.10 (62.70)	5.56 (5.46)	22.43 (22.53)		
$[CuLCl]_2$ (**1**)	blue	47.16 (46.94)	4.02 (3.94)	16.65 (17.11)	32	1.24
$[CuLBr]_2$ (**2**)	blue	42.40 (42.34)	3.56 (3.55)	14.92 (15.43)	23	0.92
$[CuL(NO_3)]_2$ (**3**)	blue	43.48 (44.08)	3.77 (3.67)	18.88 (19.28)	22	1.61
$[CuLN_3]_2\cdot H_2O$ (**4**)	blue	45.37 (45.22)	3.86 (4.03)	26.94 (26.37)	25	1.69
$[CuL(NCS)]_2$ (**5**)	greenish yellow	46.94 (47.26)	3.81 (3.73)	19.42 (19.45)	30	1.27
$[Cu_2LCl_3]$ (**6**)	blue	35.75 (35.33)	3.07 (2.94)	12.27 (12.88)	27	2.03
$[Cu_2L_2SO_4]_2\cdot 3H_2O$ (**7**)	blue	43.80 (44.13)	4.30 (4.05)	15.60 (16.08)	15	1.54

[a] Molar conductivity, 10^{-3} M DMF at 298 K.
[b] Magnetic susceptibility per copper atom.

values per copper atom are found to be less than the spin only value, indicating an exchange interaction between the copper centres. All complexes are reported to be paramagnetic at room temperature.

3.1. Molecular and crystal structures of the complex $[Cu_4L_4(SO_4)_2]\cdot 3H_2O$

The structure of the tetranuclear complex $[Cu_4L_4(SO_4)_2]\cdot 3H_2O$ is illustrated in Fig. 1 and the structural refinement parameters are given in Table 2. Selected bond lengths and bond angles are given in Tables 3 and 4. The structure contains four units comprising of two identical Cu(1)L outer units and two identical Cu(2)L inner units. In other words, it can be regarded as a dimeric structure of binuclear $[Cu_2L_2SO_4]$ units. The atom numbering scheme of the bimetallic unit is given in Fig. 1. Each copper atom in the outer unit is coordinated by a pyridyl nitrogen, azomethine nitrogen and thiolate sulfur of the thiosemicarbazone moiety and an oxygen of the bridging sulfato group. In addition to these, there is an additional Cu1–S3 bridging interaction at an apical distance of 2.942 Å, which renders a distorted (4 + 1) square pyramidal geometry around the Cu1 atoms. The Cu–$N_{pyridyl}$ bonds are 0.0781 Å farther away than Cu–N_{imine} bonds, denoting the strength of the azomethine nitrogen coordination. The C(6)–N(3) bond length is slightly shorter than the corresponding bond distance of 1.308(4) Å in the free ligand, [13] indicating that there is no clear decrease in the double bond character on chelation. This can be attributed to the stabilization of the C–$N_{azomethine}$ bond in the copper(II) complexes due to the presence of an important metal-

Table 2
Crystal data and structural refinement parameters for the complex $[Cu_2L_2(SO_4)]_2\cdot 3H_2O$

Parameters	$[Cu_2L_2(SO_4)]_2\cdot 3H_2O$
Empirical formula	$C_{64}H_{70}Cu_4N_{20}O_{11}S_6$
Formula weight (M)	1741.96
Temperature (T) K	293(2)
Wavelength (Mo Kα) (Å)	0.71073
Crystal system	triclinic
Space group	$P\bar{1}$
Lattice constants	
a (Å)	11.225(6)
b (Å)	13.201(7)
c (Å)	14.558(7)
α (°)	68.112(7)
β (°)	67.786(7)
γ (°)	78.048(8)
Volume, V (Å^3)	1847.6(16)
Z	2
Calculated density (ρ) (Mg m^{-3})	1.614
Absorption coefficient, μ (mm^{-1})	1.382
F(000)	924
Crystal size (mm)	$0.40\times0.35\times0.30$
θ Range for data collection	1.60–27.46
Limiting Indices	$-13\leqslant h\leqslant 13$, $-16\leqslant k\leqslant 17$, $-18\leqslant l\leqslant 18$
Reflections collected	19 156
Unique reflections	7528 [$R_{int}=0.0201$]
Completeness to θ	27.46 89.2%
Absorption correction	multiscan
Max and min transmission	0.6818 and 0.6078
Refinement method	full-matrix least-squares on F^2
Data/restraints/parameters	7528/0/623
Goodness-of-fit on F^2	1.079
Final R indices [$I>\sigma 2(I)$]	$R_1=0.0335$, $wR_2=0.0897$
R indices (all data)	$R_1=0.0407$, $wR_2=0.0944$
Largest difference peak and hole (e Å^{-3})	0.471 and −0.438

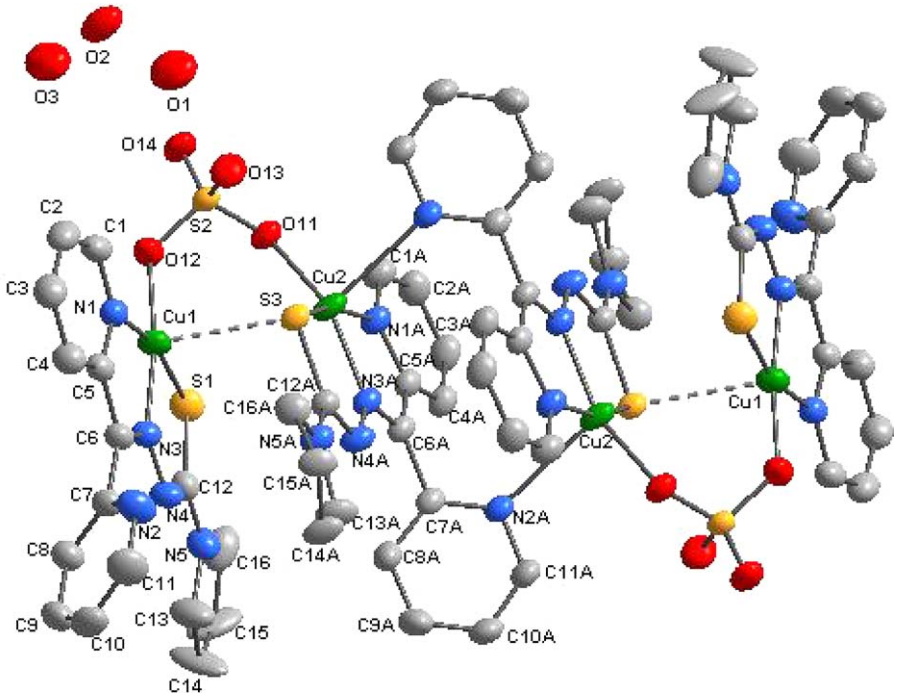

Fig. 1. Molecular structure of $[Cu_2L_2(SO_4)]_2\cdot 3H_2O$ with the atom numbering scheme. Hydrogen atoms are omitted for clarity.

Table 3
Selected bond lengths (Å) of HL and $[Cu_2L_2(SO_4)]_2 \cdot 3H_2O$

Bond length	HL	$[Cu_2L_2(SO_4)]_2 \cdot 3H_2O$
Cu(1)–S(1)		2.2771(12)
Cu(1)–O(12)		1.9322(15)
Cu(1)–N(1)		2.0274(18)
Cu(1)–N(3)		1.9493(17)
Cu(2)–S(3)		2.2871(12)
Cu(1)–S(3)		2.9417(15)
Cu(2)–O(11)		1.9386(13)
Cu(2)–N(1A)		2.0225(17)
Cu(2)–N(2A)		2.5958
Cu(2)–N(3A)		1.9534(15)
S(1)–C(12)	1.671(4)	1.745(2)
S(2)–O(11)		1.4967(13)
S(2)–O(12)		1.4886(14)
S(2)–O(13)		1.4449(15)
S(3)–C(12A)		1.7423(18)
N(3)–C(6)	1.308(4)	1.297(2)
N(3A)–C(6A)	1.308(4)	1.304(2)
N(3)–N(4)	1.371(4)	1.349(2)
N(3A)–N(4A)	1.371(4)	1.349(2)
N(4)–C(12)	1.386(4)	1.329(2)
N(4A)–C(12A)	1.386(4)	1.330(2)
N(5)–C(12)	1.349(5)	1.336(2)
N(5A)–C(12A)	1.349(5)	1.337(2)

Table 4
Selected bond angles (°) of HL and $[Cu_2L_2(SO_4)]_2 \cdot 3H_2O$

Bond angles	HL	$[Cu_2L_2(SO_4)]_2 \cdot 3H_2O$
S(1)–Cu(1)–O(12)		97.72(5)
S(1)–Cu(1)–N(1)		164.20(4)
S(1)–Cu(1)–N(3)		84.61(5)
O(12)–Cu(1)–N(1)		96.22(6)
O(12)–Cu(1)–N(3)		172.04(6)
N(1)–Cu(1)–N(3)		80.60(6)
S(3)–Cu(2)–O(11)		101.66(4)
S(3)–Cu(2)–N(1A)		164.61(4)
S(3)–Cu(2)–N(2A)		99.06
S(3)–Cu(2)–N(3A)		84.89(5)
O(11)–Cu(2)–N(1A)		93.63(5)
O(11)–Cu(2)–N(2A)		90.49
O(11)–Cu(2)–N(3A)		156.94(6)
N(1A)–Cu(2)–N(2A)		82.47
N(1A)–Cu(2)–N(3A)		80.27(6)
N(2A)–Cu(2)–N(3A)		110.48
N(3A)–Cu(2)–S(3)		84.89(5)
N(1A)–Cu(2)–S(3)		164.61(4)
N(4)–N(3)–C(6)	118.6(3)	119.13(14)
N(4A)–N(3A)–C(6A)	118.6(3)	119.09(14)
N(3)–N(4)–C(12)	118.7(3)	112.23(14)
N(3A)–N(4A)–C(12A)	118.7(3)	112.50(13)
N(5)–C(12)–N(4)	112.3(3)	114.88(16)
N(5A)–C(12A)–N(4A)	112.3(3)	114.19(14)
N(5)–C(12)–S(1)	123.2(3)	119.75(14)
N(5A)–C(12A)–S(3)	123.2(3)	119.91(13)

to-ligand π-back donation. The lengthening of the S(1)–C(12) bond from the corresponding bond distance in the free ligand of 1.671(4) Å can be attributed to the delocalization of the negative charge on the N(3)–N(4)–C(12) system which is generated as a result of N(4)H deprotonation on complexation. The bond angles also are in conformity with a distorted square pyramidal structure around the copper centres.

Each copper atom in the inner subunit is also pentacoordinate with the bonds Cu(2)–S(3), Cu(2)–O(11), Cu(2)–N(1A), Cu(2)–N(3A) and Cu(2)–N(2A) adapting a distorted square pyramidal geometry with N(2A) of the third ligand moiety at the apical site. The pyridyl nitrogen N(1A), the imino nitrogen N(3A), and the thiolate sulfur S(3) atom, together with O(11) of the sulfato group, constitute the basal plane. The bond lengths in the basal plane agree with those found in copper(II) complexes containing thiosemicarbazones which act as uninegative tridentate ligands [20]. The bond lengths and bond angles reveal a distorted square pyramidal geometry around Cu(2).

The unit cell-packing diagram of the complex viewed down the *a*-axis is given in Fig. 2. It can be observed that the molecules are packed in a two-dimensional manner parallel to the *bc*-plane. The adjacent tetrameric units are interconnected through hydrogen bonding interactions involving the oxygen atoms of the water molecules and the sulfato group. The assemblage of molecules in the respective manner in the unit cell is also assisted by the diverse π–π stacking, CH–π and ring–metal interactions as shown in Tables 5 and 6. The hydrogen bonding interactions are observed with donor–acceptor distances in the range 2.8048–3.5360 Å. The π–π interactions are rather weak, with 3.3457 Å being the minimum distance between the centroids. The π–π, CH–π, ring–metal and hydrogen bonding interactions stabilize the unit cell and point out the possibility for metalloaromaticity – a classic concept reviewed by Masui [21].

3.2. Electronic spectra

The electronic spectral data of the copper(II) complexes are given in Table 7. The UV–Vis spectra give much insight into the coordination geometry around the copper(II) ion. The broad band around 36 000 cm^{-1} can be attributed to the $\pi \rightarrow \pi^*$ transition (pyridyl ring and the imine function) of thiosemicarbazone moiety. The shift of the $\pi \rightarrow \pi^*$ bands to the longer wavelength region in the complexes is the result of the C=S bond being weakened and the conjugation system being enhanced on complexation [22]. The pyridyl and imine function $n \rightarrow \pi^*$ band, centered around 29 100 cm^{-1}, overlaps and undergoes a small blue shift to ca. 31 500 cm^{-1} on complexation indicating coordination via the pyridyl nitrogen with a reduction in intensity [23]. The ligand → metal CT bands are found at ~23 000–26 000 cm^{-1}. The band near 26 000 cm^{-1} in the complexes corresponds to S → Cu(II) ligand to metal charge transfer bands. This band is in accordance with previous studies of copper(II) complexes with a similar type of ligand [24,25]. The pyridyl nitrogen N → Cu(II) LMCT transitions are observed at ~23 000 cm^{-1}. The spectra of the complexes exhibit weak $d \rightarrow d$ bands centered around 16 000 cm^{-1} for compounds **5** and **7**. Such a feature is expected for square planar complexes [26]. For square planar complexes

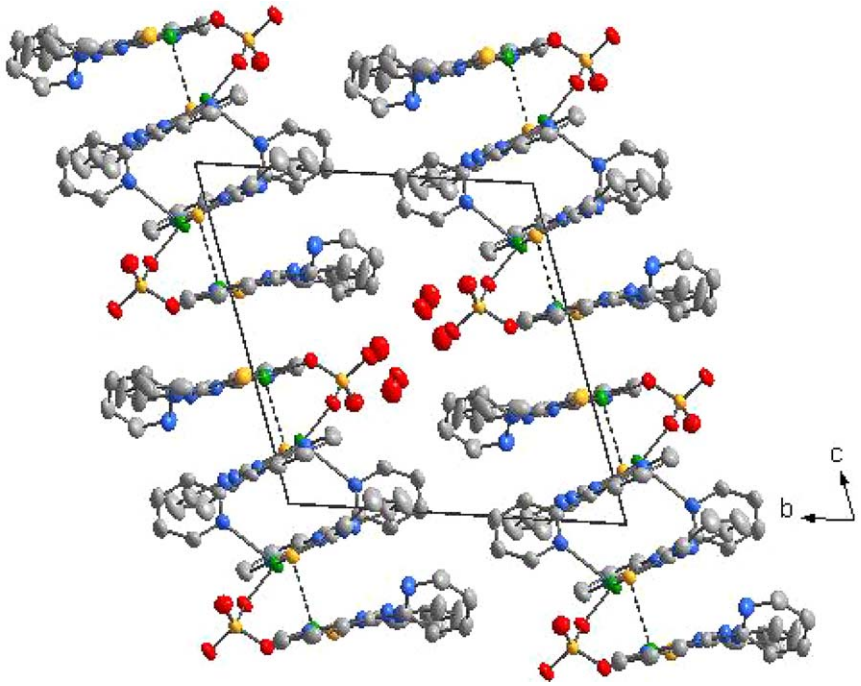

Fig. 2. Unit cell packing diagram of $[Cu_2L_2(SO_4)]_2 \cdot 3H_2O$ viewed down the '*a*' axis.

Table 5
H-bonding and π–π interaction parameters for $[Cu_2L_2(SO_4)]_2 \cdot 3H_2O$

H-bonding

Donor–H...A	D–H (Å)	H···A (Å)	D–A (Å)	D–H···A (°)
O(1)···H(101)···O(3)	0.69	2.19	2.8715	171
O(1)···H(11)···O(13)	0.87	1.94	2.8073	175
O(2)···H(200)···O(14)	0.73	2.10	2.8048	163
O(2)···H(201)···O(14)	0.75	2.24	2.9570	161
O(3)···H(300)···O(2)	0.75	2.09	2.8287	168
O(3)···H(301)···O(1)	0.64	2.17	2.7979	170
C(1A)···H(1A)···O(2)	0.95	2.56	3.4637	160
C(2)···H(2)···O(3)	0.93	2.45	3.3389	159
C(4)···H(4)···N(2)	0.95	2.49	3.1139	123
C(8A)···H(8A)···N(5)	0.94	2.62	3.5360	164
C(11A)···H(11A)···O(11)	0.95	2.59	3.1619	118
C(11A)···H(11A)···O(13)	0.95	2.59	3.5120	164

π–π interactions

Cg(I)-Res(I)···Cg(J)	Cg–Cg(Å)	α (°)	β (°)
Cg(3)-[1]···Cg(4)[a]	3.3457	14.65	16.19
Cg(3)-[1]···Cg(7)[a]	3.3703	15.37	13.24
Cg(4)-[1]···Cg(3)[a]	3.3457	14.65	1.54
Cg(4)-[1]···Cg(5)[a]	3.3637	14.37	5.31
Cg(4)-[1]···Cg(14)[b]	3.7415	5.18	26.63
Cg(5)-[1]···Cg(4)[a]	3.3637	14.37	16.16
Cg(5)-[1]···Cg(7)[a]	3.4142	15.00	15.45
Cg(7)-[1]···Cg(3)[a]	3.3703	15.37	05.64
Cg(7)-[1]···Cg(5)[a]	3.4142	15.00	10.82
Cg(7)-[1]···Cg(14)[b]	3.6512	04.10	24.76
Cg(8)-[1]···Cg(8)[b]	3.5172	0.00	19.10
Cg(14)-[1]···Cg(4)[b]	3.7415	05.18	29.40
Cg(14)-[1]···Cg(7)[b]	3.6512	04.10	26.32

Equivalent position codes
a = *x*, *y*, *z*
b = −*x*, −*y*, −*z*

Cg(3) = Cu(1), S(1), C(12), N(4)
Cg(4) = Cu(2), S(3), C(12A), N(4A)
Cg(5) = Cu(1), S(1), C(12), N(4), N(3)
Cg(7) = Cu(2), S(3), C(12A), N(4A), N(3A)
Cg(8) = Cu(2), N(1A), C(5A), C(6A), N(3A)
Cg(14) = N(1A), C(1A), C(2A), C(3A), C(4A), C(5A)

Table 6
CH–π and ring–metal interaction parameters of $[Cu_2L_2(SO_4)]_2 \cdot 3H_2O$

CH–π interactions			
X–H(I)···Cg(J)	H...Cg(Å)	X–H...Cg (°)	X–Cg (Å)
C(4A)–H(4A)···Cg(4)[b]	3.3153	80.05	3.2957
C(4A)–H(4A)···Cg(7)[b]	3.3660	76.58	3.2826
C(8A)–H(8A)···Cg(9)[b]	2.8918	140.20	3.6612
C(10A)–H(10A)···Cg(15)[c]	3.0467	151.69	3.8815
C(15A)–H(15B)···Cg(16)[d]	3.3162	159.61	4.1800
C(16A)–H(16A)···Cg(6)[a]	3.1225	136.23	3.8890

Equivalent position codes	Cg(4) = Cu(2), S(3), C(12A), N(4A)
a = *x*, *y*, *z*	Cg(6) = Cu(1), N(1), C(5), C(6), N(3)
b = −*x*, −*y*, −*z*	Cg(7) = Cu(2), S(3), C(12A), N(4A), N(3A)
c = *x*, −1 + *y*, *z*	Cg(9) = N(5), C(13), C(14), C(15), C(16)
d = 1−*x*, −*y*, −*z*	Cg(15) = N(2), C(7), C(8), C(9), C(10), C(11)
	Cg(16) = N(2A), C(7A), C(8A), C(9A), C(10A), C(11A)

Ring–metal interaction		
Cg(I) Res(I) Me(J)	Cg(I)–Me(J) (Å)	*β* (°)
Cg(3)-[1] → Cu(1)[e]	3.666	18.84
Cg(3)-[1] → Cu(2)[a]	3.884	38.81
Cg(4)-[1] → Cu(1)3[a]	3.346	30.69
Cg(5)-[1] → Cu(1)[e]	3.752	21.75
Cg(5)-[1] → Cu(2)[a]	3.975	41.57
Cg(7)-[1] → Cu(1)[a]	3.498	35.14

Equivalent position codes	Cg(3) = Cu(1), S(1), C(12), N(4)
a = *x*, *y*, *z*	Cg(4) = Cu(2), S(3), C(12A), N(4A)
e = −*x*, −*y*, 1 − *z*	Cg(5) = Cu(1), S(1), C(12), N(4), N(3)
	Cg(7) = Cu(2), S(3), C(12A), N(4A), N(3A)

with a $d_{x^2-y^2}$ ground state [27], three transitions are possible $d_{z^2} \leftarrow d_{x^2-y^2}$, $d_{xy} \leftarrow d_{x^2-y^2}$ and $d_{xz}, d_{yz} \leftarrow d_{x^2-y^2}$ ($^2A_{1g} \leftarrow {}^2B_{1g}$, $^2B_{2g} \leftarrow {}^2B_{1g}$ and $^2B_{2g} \leftarrow {}^2B_{1g}$). Since the four d orbitals lie very close together, each transition cannot be distinguished by their energy and hence it is very difficult to resolve the three bands into separate components.

3.3. Infrared spectra

A square pyramidal geometry can be assigned for **1**–**5** consisting of one of the pyridyl nitrogens, azomethine nitrogen, thiolate sulfur and the anion forming the basal plane, while the pyridyl nitrogen of the second ligand unit occupies the apical positions (Fig. 3) as reported by us before [25]. For compound **6** (Fig. 4), the terminal nature of the chlorine atoms indicates its structure to be similar to the copper(II) complex of a di-2-pyridyl ketone thiosemicarbazone prepared by Swearingen et al. [28]. Selected vibration bands of HL and its metal complexes are listed in Table 8. Since the compound contains a thioamide function, HL can exhibit thione–thiol tautomerism. The *ν*(S–H) band at ~2600 cm^{-1} is absent in the spectrum of the ligand, indicating that it exists as the thione tautomer in the solid state. This is further supported by a medium band at 3049 cm^{-1}, indicative of the *ν*(N–H) vibration. The absence of *ν*(NH) in the spectrum of the complexes provides strong evidence for the ligand coordination around Cu(II) ion in its deprotonated form. The vibrations *ν*(C=N) and *δ* (C=S) contribute substantially to the bands at 1582 and 808 cm^{-1}, respectively, in the ligand. The band corresponding to azomethine nitrogen, *ν*(C=N), shifts to higher energy on coordination due to the combination of *ν*(C=N) with the newly formed *ν*(N=C) bond which results

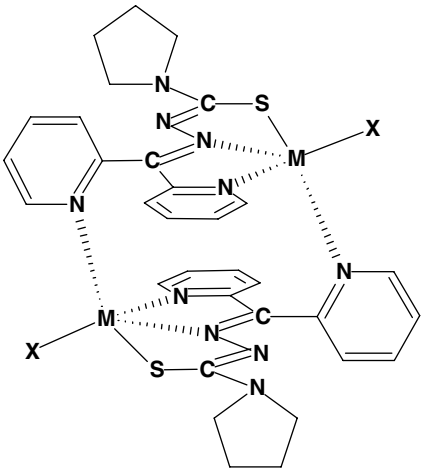

Fig. 3. Tentative structure of compounds **1**–**5**.

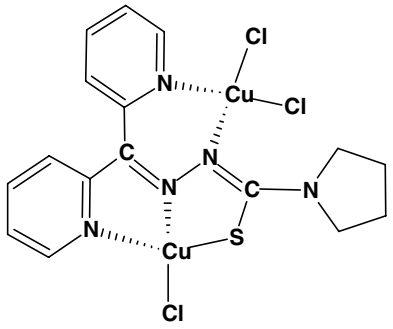

Fig. 4. Tentative structure of $[Cu_2LCl_3]$ (**6**).

Table 7
Solid state electronic spectral data (cm^{-1}) for the copper(II) complexes

Compound	d–d	CT	n → π*	π → π*
HL			30864, 29154 sh	36231 sh, 35087 sh
[CuLCl] (**1**)	17857, 13947 sh	27473, 23475 sh, 22573 sh	32154 s,	32679 sh
[CuLBr] (**2**)	17094 w, 14534 sh	25445 sh, 23310 s,b	32573 s, 31152 sh	34634 sh
[CuL(NO$_3$)] (**3**)	17793, 13263 sh	25445 sh, 23584 s,b	32467 s,b, 31446 sh	
[CuLN$_3$] · 1/2H$_2$O (**4**)	18050 sh, 14471 sh	25641sh, 22883 s,b,	32573 s,b	38167 m
[CuL(NCS)] (**5**)	16000 sh	25380 sh, 23041 s,b,	31446 s,b	
[Cu$_2$LCl$_3$] (**6**)	17730, 14347	26246 s, 22624 s,b	31250 s,	33112 sh
[Cu$_2$L$_2$SO$_4$]$_2$ · 3H$_2$O (**7**)	16025 sh	25125 sh, 23809 s,b	31645 sh, 31152 sh	

Table 8
Tentative assignments of the selected IR bands (cm^{-1}) of the copper(II) complexes

Compound	ν(N–H)	ν(C=N) + ν(N=C)	ν(C=S)	δ(C=S)	ν(Cu–N)	ν(Cu–S)	ν(Cu–X[a])
HL	3049 m	1582 s	1330 s	808 m			
[CuLCl] (**1**)		1593 s	1289 w	784 m	409 s	336 w	320 sh
[CuLBr] (**2**)		1594 s	1285 m	780 w	412 s	325 m	250 w
[CuL(NO_3)] (**3**)		1599 m	1278 m	789 m	411 s	328 m	445 m
[CuLN_3] · 1/2H_2O (**4**)		1592 s	1278 w	784 w	410 m	334 w	312 sh
[CuL(NCS)] (**5**)		1593 s	1295 m	787 w	419 m	325 m	318 sh
[Cu_2LCl_3] (**6**)		1599 m	1278 m	789 m	411 s	328 m	310 m
[$Cu_2L_2SO_4$]$_2$ · 3H_2O (**7**)		1593 s	1296 m	784 w	406 s	332 w	303 m

[a] X represents the anion Cl, Br, etc.

from the loss of the thioamide hydrogen from the thiosemicarbazone moiety [29–33]. The band at 808 cm^{-1} shifts to lower wavenumbers in all complexes and this can be assigned to the δ(C=S) vibration suggesting the change of bond order and strong electron-delocalization upon chelation [34]. Coordination of the pyridine nitrogen causes the out-of-the plane bending vibrational bands to shift from 600 cm^{-1} to higher frequencies by 12–20 cm^{-1} [20].

Compounds **1** and **6** showed sharp bands at 320 and 310 cm^{-1}, respectively, indicating terminally bonded rather than bridging chlorine ligands. A sharp band at 250 cm^{-1} due to ν(Cu–Br) vibrations is suggestive of terminally bonded bromine in **2**. The ratio of ν(Cu–Br)/ν(Cu–Cl) is 0.77, which is consistent with the usual values obtained for the first row transition metals. For the nitrato complex (**3**), medium bands are observed at 1384, 1285 and 1013 cm^{-1} corresponding to ν_4, ν_2 and ν_1, respectively, with a separation of 102 cm^{-1}, suggestive of terminally bonded monodentate nitrato groups [35]. The bands due to ν_3, ν_5 and ν_6 could not be assigned due to the richness of the spectrum. The ν(Cu–N) of the complex is found at 445 cm^{-1}. The spectrum of complex **4** showed a strong band at 2042 cm^{-1} due to the asymmetric $\nu(N_3)$ mode. The band associated with the symmetric $\nu(N_3)$ mode is located at 1369 cm^{-1}. The band at 312 cm^{-1} is assigned to the ν(Cu–N_{azide}) mode. We have obtained three bands for compound **5**, a strong sharp band at 2081 cm^{-1}, medium band at 787 cm^{-1} and a weak band at 480 cm^{-1} corresponding to ν(CN), ν(CS) and δ(NCS), respectively. The intensity and band position indicates the unidentate coordination of the thiocyanate through the nitrogen atom. The sulfato complex **7** exhibits four fundamental vibrations: 970 cm^{-1} due to ν_1, a medium band at 459 cm^{-1} due to ν_2, medium and weak bands at 1243, 1181 and 1112 cm^{-1} corresponding to ν_3, and medium and weak bands at 650, 615 and 575 cm^{-1} due to ν_4, which are assigned to the bidentately coordinated sulfato group [35].

3.4. EPR spectral investigations

EPR parameters found for the complexes in the polycrystalline state (293 K) and in DMF at 293 and 77 K are presented in Table 9. The spectra in the polycrystalline state gave much information about the coordination geometry around the copper(II) ion. The complexes **1** and **3** revealed rhombic features. The compounds **2**, **4**, **5** and **7**

Table 9
EPR spectral assignments of the copper(II) complexes

Compound	State	Temperature (K)	$g_\parallel$	g_1	$g_\perp$	g_2	g_3	g_{iso}
[CuLCl] (**1**)	polycrystalline	298		2.006		2.060	2.145	
	DMF	298						2.101
	DMF	77		2.176		2.058	1.980	
[CuLBr] (**2**)	polycrystalline	298	2.124		2.063			
	DMF	77	2.093		2.066			
[CuL(NO_3)] (**3**)	polycrystalline	298		2.040		2.070	2.180	
	DMF	298						2.110
	DMF	77		1.990		2.060	2.211	
[CuLN_3] · 1/2H_2O (**4**)	polycrystalline	298	2.084		2.036			
	DMF	298						2.076
	DMF	77	2.162		2.116			
[CuL(NCS)] (**5**)	polycrystalline	298	2.171		2.050			
	DMF	77	2.169		2.045			
Cu_2LCl_3 (**6**)	DMF	298						2.090
	DMF	77		2.020		2.061	2.789	
[$Cu_2L_2SO_4$]$_2$ · 3H_2O (**7**)	polycrystalline	298	2.151		2.060			
	DMF	298						2.080
	DMF	77	2.180		2.051			

showed an axial spectrum with well defined $g_{\|}$ and $g_{\perp}$ features. The variation in the g values indicates that the geometry of the compound is affected by the nature of the coordinating anions. The solution state EPR measurements in DMF at 298 K give isotropic spectra with well resolved hyperfine lines. The isotropic nature of the spectra is due to the tumbling motion of the molecules in DMF. The spectra of complexes showed clearly four well resolved hyperfine lines, which are due to the interaction of the electron spin with the copper nuclear spin (^{65}Cu, $I = 3/2$). The A_0 and g_0 values show variations indicating dissimilar bonding character of the complexes. The EPR spectra of compounds **1**, **3** and **6** in DMF at 77 K showed rhombic features with three g values g_1, g_2 and g_3. However the azido complex (**4**) shows an axial spectrum. The g values for complexes in the solid state at 298 K and in DMF at 77 K are close to each other, which perceives that the geometry around the copper(II) ion is unaffected on cooling the solution to liquid nitrogen temperature.

Acknowledgements

The authors are thankful to the Regional Sophisticated Instrumentation Centre, CDRI, Lucknow, India, for the elemental analysis. M.R.P. Kurup is thankful to the Department of Science and Technology, Government of India, New Delhi for financial assistance. The authors also acknowledge DST IRPHA for X-ray data collection.

Appendix A. Supplementary data

Crystallographic data for **7** has been deposited at the Cambridge Crystallographic Centre with CCDC No. 272580. These data can be obtained free of charge at www.ccdc.cam.ac.uk/conts/retrieving.html (or from the Cambridge Crystallographic Data Centre (CCDC), 12 Union Road, Cambridge CB2 1EZ, UK; fax: +44 0 1223 336033; e-mail: deposit@ccdc.cam.ac.uk). Supplementary data associated with this article can be found, in the online version, at doi:10.1016/j.poly.2005.12.023.

References

[1] G.Z. Bahur, Anorg. Allg. Chem. 268 (1952) 351.
[2] G.Z. Bahur, Anorg. Allg. Chem. 273 (1953) 351.
[3] G.Z. Bahur, E.Z. Schieitzer, Anorg. Allg. Chem. 278 (1955) 136.
[4] J.P. Scovill, D.L. Klayman, C.F. Franchino, J. Med. Chem. 25 (1982) 1261.
[5] P. Bindu, M.R.P. Kurup, T.R. Sathyakeerthy, Polyhedron 18 (1999) 321.
[6] B.S Garg, M.R.P. Kurup, S.K. Jain, Y.K. Bhoon, Transit. Met. Chem. 13 (1988) 309.
[7] A. Wada, Y. Fujibayshi, A. Yokoyamma, Arch. Biochem. Biophys. 310 (1994) 1.
[8] C.J. Mathias, M.J. Weich, M.E. Raichie, L.L. Lich, A.H. McGuire, K.R. Zinn, E. John, M.A. Green, J. Nucl. Med. 31 (1990) 351.
[9] J.L.J. Dearling, J.S. Lewis, D.W. McCarthy, M.J. Welch, P.J. Blower, J. Chem. Commun. (1988) 2531.
[10] J.L.J. Dearling, J.S. Lewis, G.E.D. Mullen, M.J. Welch, P.J. Blower, J. Biol. Inorg. Chem. 7 (2002) 249.
[11] A.W. Christopher, P.A.G. Yap, N.P. Raju, J.E. Greedan, R.J. Crutchley, Inorg. Chem. 38 (1999) 2548.
[12] H. Cheng, D. Chun-ying, F. Chen-jie, L. Yong-jiang, M. Qing-jin, J. Chem. Soc., Dalton Trans. (2000) 1207.
[13] A. Usman, I.A. Razak, S. Chantrapromma, H.K. Fun, V. Philip, A. Sreekanth, M.R.P. Kurup, Acta Crystallogr. 58 (2002) c652.
[14] J.P. Scovill, Phosphorous Sulfur Silicon 60 (1991) 25.
[15] Siemens, SMART and SAINT, Area Detector Control and Integration Software, Siemens Analytical X-ray Instrunments Inc., Madison, WI, USA, 1996.
[16] G.M. Sheldrik, SADABS, Program for Crystal Structure Refinement, University of Göttingen, Göttingen, Germany, 1993.
[17] G.M Sheldrick, SHELXS-97 Program for the Solution of Crystal Structures, University of Göttingen, Göttingen, Germany, 1997.
[18] K. Brandenburg, H. Putz, DIAMOND Version 3.0, Crystal Impact, GbR, Postfach 1251, D-53002 Bonn, Germany, 2004.
[19] W.J. Geary, Coord. Chem. Rev. 7 (1971) 81.
[20] A. Sreekanth, M.R.P. Kurup, Polyhedron 22 (2003) 3321.
[21] H. Masui, Coord. Chem. Rev. 957 (2001) 219.
[22] I.-X. Li, H.-A. Tang, Yi-Zhi Li, M. Wang, L.-F. Wang, C.-G. Xia, J. Inorg. Biochem. 78 (2000) 167.
[23] R.P. John, A. Sreekanth, M.R.P. Kurup, A. Usman, I.A. Razak, H.K. Fun, Spectrochim. Acta. 59A (2003) 1349.
[24] M.A. Ali, D.A. Chowdhary, M. Nazimuddin, Polyhedron 3 (1984) 595.
[25] V. Philip, V. Suni, M.R.P. Kurup, M. Nethaji, Polyhedron 24 (2005) 1133.
[26] R.P. John, A. Sreekanth, V. Rajakannan, T.A. Ajith, M.R.P. Kurup, Polyhedron 23 (2004) 2549.
[27] A.B.P. Lever, Inorganic Electronic Spectroscopy, 2nd ed., Elsevier, Amsterdam, 1984.
[28] J.K. Swearingen, W. Kaminsky, D.X. West, Transit. Met. Chem. 32 (2002) 7.
[29] M. Joseph, V. Suni, M.R.P. Kurup, M. Nethaji, A. Kishore, S.G. Bhat, Polyhedron 23 (2004) 3069.
[30] A. Ali, M.T.H. Tarafdar, J. Inorg .Nucl .Chem. 39 (1977) 1785.
[31] M.J.M. Campbell, Coord. Chem. Rev. 15 (1975) 279.
[32] B.S. Garg, M.R.P. Kurup, S.K. Jain, Y.K. Bhoon, Transit. Met. Chem. 13 (1988) 247.
[33] B.S. Garg, M.R.P. Kurup, S.K. Jain, Y.K. Bhoon, Transit. Met. Chem. 16 (1991) 111.
[34] R. Mayer, in: M. Jansen (Ed.), Organosulfur Chemistry, Interscience, Newyork, 1967, p. 219.
[35] K. Nakamoto, Infrared and Raman Spectra of Inorganic and Coordination Compounds, 4th ed., Wiley Interscience, New York, 1986.

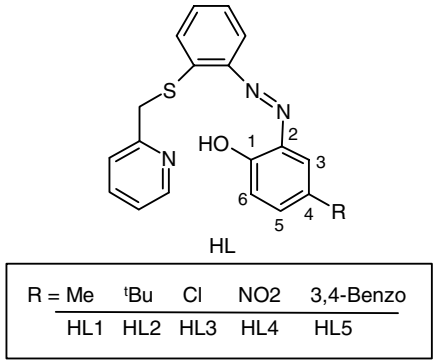

Scheme 1. The structures of the pyridylthioazophenols used as chelators.

this paper, we present an account of the *cis* and *trans* isomers of ruthenium (III) complexes of a series of tetradentate pyridylthioazophenolates (Scheme 1), and the role of the polarity of solvents in controlling the ratio of *cis* and *trans* isomers of the ruthenium (III) complexes. One of the complexes, *trans*-$[Ru(L1)Cl_2]$, has been subjected to single-crystal X-ray analysis to confirm the detailed structure, and the complex is found to be monomeric with the metal in an octahedral environment having the chlorines in mutually *trans* sites. It has been observed in our reactivity study that the two chlorines of the *cis*-isomers, but not of the *trans*-isomers, can be substituted successfully by bipyridine in the presence of $AgNO_3$. The resulting cationic ruthenium (III) complexes of the type $[Ru(L)(bipy)](PF_6)_2$ (bipy = 2,2′-bipyridine), bearing three heterocyclic N-donors in the coordination sphere of ruthenium (III) and obtained from the reaction of bipyridine with the *cis*-isomers using the $AgNO_3$ procedure, were characterized by elemental analyses, IR spectra, electrical conductivities and magnetic moment measurements.

2. Experimental

2.1. Materials

$RuCl_3 \cdot nH_2O$ was obtained from Arrora Matthey, Calcutta and was digested with concentrated HCl before use. The ligands were synthesized by the reported procedure [12]. Commercially available silica gel (60–120 mesh) from SRL was used for chromatographic separation. Purification of solvents for electrochemical and spectral work were carried out using appropriate drying agents [16]. Tetra-*n*-butylammonium perchlorate was prepared by the addition of sodium perchlorate to a hot solution of tetra-*n*-butylammoniumbromide (Aldrich). The products were recrystallised from aqueous ethanol and tested for the absence of bromide. All the reagents were obtained from commercial sources and used without further purification.

2.2. Physical measurements

IR spectra were measured on a JASCO FT-IR model 420 using KBr disks and UV–Vis spectra on a JASCO UV–Vis/NIR model V-570. Microanalyses were performed using a Perkin–Elmer 2400 CHN elemental analyzer. Molar conductances (Λ_M) were measured in a systronics conductivity meter 306 model using $\sim 10^{-3}$ M solutions in MeOH. Magnetic moments (μ, BM) were obtained from a vibrating sample magnetometer PAR 155 model. X-band EPR spectra were taken on a Brucker spectrometer with a variable temperature liquid nitrogen cryostat at NTHU, Hsinchu, Taiwan. The *g* values were measured at 77 K. Electrochemical measurements were made with a computer controlled EG&G PAR model 270 VERSTAT electrochemical instrument using platinum as the working electrode. All measurements were made at 298 K in dry DMF with $[Bu_4N]ClO_4$ as the supporting electrolyte with 50 mV S^{-1} scan rate. The experimental solutions were deoxygenated by bubbling with research grade dinitrogen. The reported potentials, referenced to the standard calomel electrode (SCE), were uncorrected for junction potential.

2.3. Synthesis of the Ru(III) complexes of the ligands (HL)

The preparation of the Ru(III) complexes follows a common procedure. To a methanolic/ethanolic solution (15 mL) of **1a** (0.335 g, 1.0 mmol), a ruthenium trichloride (1.0 mmol) solution in MeOH/EtOH was added dropwise and the resulting solution stirred for a period of 0.5 h at room temperature. The reddish brown solution was then evaporated in air and dissolved in a minimum volume of dichloromethane and chromatographed over a silica gel column prepared in CH_2Cl_2. Two brown colored bands were eluted by CH_2Cl_2–MeOH (95–5%) and CH_2Cl_2–MeOH (70–30%) successively to get the *trans* and *cis* isomers, respectively. The solvent of the eluents was removed using a rotary evaporator. The recrystallized products were obtained from MeCN–MeOH medium. They were then dried in vacuum. Total yield: 85–87%.

Other complexes were prepared under identical conditions; the yields varied in the range 55–70%. Here, the *cis*:*trans* ratio was ~3:1; but when CH_2Cl_2 was used as the solvent for preparation, the *cis*:*trans* ratio was the reverse to the above at ~1:3.

2.4. X-ray crystal structure analysis

Single crystals, suitable for X-ray work, of *trans*-$[Ru(L1)Cl_2]$ (**2a**) were grown by slow evaporation of a solution of the complex in methanol:toluene (1:2) at an ambient temperature of 293 K. Data were measured with Mo Kα radiation using the MARresearch Image Plate System. The crystal was positioned at 70 mm from the Image Plate. One hundred frames were measured at 2° intervals with a counting time of 2 min. Data analysis was carried out with the XDS program [17a] to provide 3450 independent reflections. The structure was solved using direct methods with the SHELX86 program [17b]. The hydrogen atoms bonded to carbon were included in geometric positions and given thermal parameters equivalent to 1.2 times those of the

atom to which they were attached. The structure was refined on F^2 using SHELXL [17c] to $R_1 = 0.0418$, $wR_2 = 0.0840$ for 2994 reflections with $I > 2\sigma(I)$.

3. Results and discussion

3.1. Syntheses

The ligands, having NSNO donor centres, act as tetradentate monobasic chelators on complexation with ruthenium (III). The mixture of ruthenium complexes (**1** and **2**) were obtained by their reaction with equimolar amounts of the chloro salts of the metals in MeOH/EtOH/CH_2Cl_2. On chromatographic separation, *trans*-dichloro and *cis*-dichloro ruthenium (III) complexes of pyridylthiazophenolates were eluted using 19:1 and 7:3 (v/v) DCM–MeOH mixtures, respectively. The reaction of the corresponding ligand and trichloro-ruthenium salts in methanol/ethanol at room temperature gave a *cis*:*trans* ratio of ~3:1, but in CH_2Cl_2 under the same conditions, the *cis*:*trans* ratio is reverse to the above and indeed it is almost ca. 1:3. On heating for 1 h in MeOH, the *trans* product is almost quantitatively converted to the *cis* isomer. It has been already observed under similar conditions, only *cis*-dichloro-iron (III) complexes have been obtained and not the isomeric mixtures having *cis* and *trans*-dichloro-iron (III) complexes of these ligands [12b]. Microanalytical data (Table 1) confirms the composition of the complexes. The conductivity measurement of the complexes **1** (*cis*) and **2** (*trans*) in methanolic solution suggest that both series of ruthenium (III) complexes exist as non-electrolytes. The magnetic moment studies exhibit that the complexes of both series (**1** and **2**) are one electron equivalent paramagnetic in nature and the magnetic moment values are in the range of 1.71–1.79 BM.

3.2. X-ray structure of trans-dichloro-2-(2-pyridylmethylthio)-phenylazo-(4-methyl)-phenolato-ruthenium (III) {[Ru^{III}(L1)Cl_2]} (**2a**)

The ORTEP view of **2a** is illustrated in Fig. 1 together with the numbering scheme. The crystallographic data, and the selected bond distances and angles are listed in Tables 2 and 3. In this monomeric complex, the metal ion centre is in a distorted octahedral environment, being bonded to four atoms of the ligand N(18), O(11), N(33) and S(26) in a equatorial plane together with two mutually *trans* chlorine atoms in axial positions. The two chlorine atoms are at same distance (2.362(3) and 2.369(3) Å) from the metal center, subtending an angle of 179.96(4)°. The

Table 1
Microanalytical data of the Ru(III) complexes

Compound	Observed (calculated)			μ (BM)	Conductance Λ_0 (mol^{-1} cm^{-1})
	C	H	N		
cis-[Ru(L1)Cl_2] (**1a**)	45.11 (45.05)	3.10 (3.16)	8.21 (8.30)	1.79	15
cis- [Ru(L2)Cl_2] (**1b**)	48.28 (48.17)	4.11 (4.01)	7.57 (7.66)	1.72	9
cis-[Ru(L3)Cl_2] (**1c**)	41.16 (41.25)	2.53 (2.47)	7.91 (7.97)	1.76	11
cis-[Ru(L4)Cl_2] (**1d**)	40.36 (40.22)	2.48 (2.42)	10.29 (10.43)	1.75	14
cis-[Ru(L5)Cl_2] (**1e**)	48.88 (48.70)	2.89 (2.95)	7.91 (7.75)	1.71	11
trans-[Ru(L1)Cl_2] (**2a**)	45.02 (45.05)	3.13 (3.16)	8.38 (8.30)	1.78	11
trans-[Ru(L2)Cl_2] (**2b**)	48.23 (48.17)	4.12 (4.01)	7.67 (7.66)	1.73	12
trans-[Ru(L3)Cl_2] (**2c**)	41.31 (41.25)	2.54 (2.47)	8.01 (7.97)	1.77	11
trans-[Ru(L4)Cl_2] (**2d**)	40.18 (40.22)	2.51 (2.42)	10.32 (10.43)	1.79	15
trans-[Ru(L5)Cl_2] (**2e**)	48.81 (48.70)	2.99 (2.95)	7.63 (7.75)	1.75	12
[Ru(L1)(bpy)] $(PF_6)_2$ (**3a**)	39.58 (39.50)	2.80 (2.72)	7.85 (7.94)	1.73	180
[Ru(L2)(bpy)] $(PF_6)_2$ (**3b**)	41.73 (41.60)	3.30 (3.25)	7.76 (7.58)	1.71	170
[Ru(L3)(bpy)] $(PF_6)_2$ (**3c**)	37.18 (37.27)	2.30 (2.33)	7.79 (7.76)	1.75	179
[Ru(L4)(bpy)] $(PF_6)_2$ (**3d**)	36.98 (36.84)	2.39 (2.30)	9.08 (9.21)	1.72	182
[Ru(L5)(bpy)] $(PF_6)_2$ (**3e**)	41.98 (41.87)	2.51 (2.62)	7.77 (7.63)	1.73	167

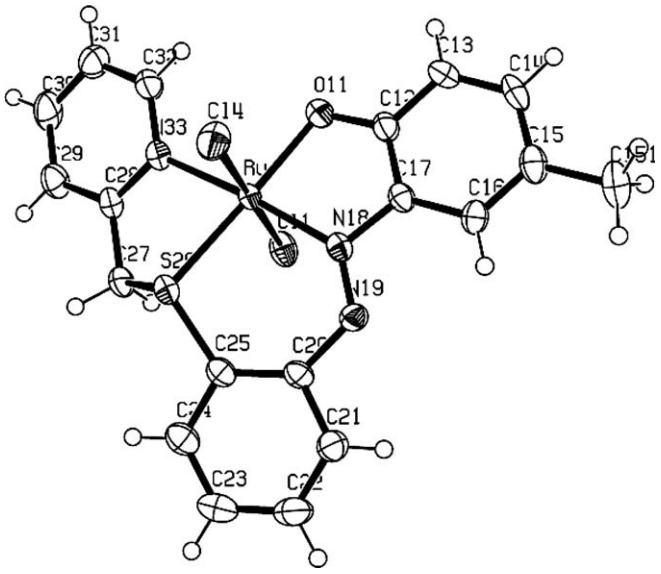

Fig. 1. An ORTEP view of *trans*-dichloro-[Ru(L1)Cl_2] (**2a**) with thermal ellipsoids at the 25% probability level and the atom numbering scheme.

Table 2
Crystallographic data of the complex **2a**

Empirical formula	$C_{19}H_{16}Cl_2N_3O$ SRu
Formula weight	506.38
Temperature (K)	293(2)
Wavelength (Å)	0.71073
Crystal system, space group	monoclinic, *P*21/*c*
Unit cell dimensions	
a (Å)	13.860(14)
b (Å)	11.082(13)
c (Å)	13.607(14)
β (°)	111.66(1)
Volume (Å^3)	1942 (4)
Z, Calculated density (g cm^{-3})	4, 1.732
Absorption coefficient (mm^{-1})	1.204
F(000)	1012
θ Range for data collection (°)	2.44–25.74
Goodness-of-fit on F^2	1.120
Final *R* indices [$I > 2\sigma(I)$ for 2994 reflections]	$R_1 = 0.0418$, $wR_2 = 0.0840$
R indices (all data)	$R_1 = 0.0535$, $wR_2 = 0.0881$

azo-N and pyridinic-N are mutually *trans* to each other (172.3(1)°), as are the phenolate-O and thioether-S atoms (175.9(1)°). The atoms in the equatorial plane are approximately coplanar with O(11) −0.11, N(18) 0.10, S(26) −0.10, N(33) 0.10 Å from the mean plane of these four donor atoms. The Ru atom is 0.03 Å from this plane. The thioether-S donor center behaves like a pyramidal μ_3-S type in that the angles subtended at this sulfur are 104.5(1)°, 96.3(1)° and 108.2(2)°. The six-membered ring forms a distorted envelope conformation with the metal 0.57 Å out of the plane formed by N(18), N(19), C(20), C(25) and S(26). The Ru–S(thioether) distance of 2.289 (2) Å is comparable with the average Ru–(μ_3-S) distance in the literature [18] and is very close to the values found in ruthenium (III) complexes of the type X[*trans*-$RuCl_4$(dmso–S)(imidazol)] (X = imidazol or Na for NAMI (2.296(1) Å) or NAMI-A (2.293(1) Å), respectively) which have interesting pharmacological properties in periclinical trials [19], but is longer than the Ru(II)–S distances, 2.353(3) Å [20] and Ru(III)–S (thiol) [21]. The N=N azo bond distance (1.288(5) Å) is longer than those found in the equivalent octahedral iron (III) (1.258 Å) and square planar copper (II) complexes (1.267 Å) of this ligand system but is comparable with the distance in the square pyramidal copper (II) complex (1.283 Å) of this ligand system[12]. The Ru(III)–pyridinic–N bond distance (1.980(4)) is longer that the bond length Ru(III–azo–N) (2.115(4)), as is usually found. There are no unusual intermolecular close contacts between molecules.

Table 3
Selected bond lengths (Å) and bond angles (°) of complex **2a**

Bond lengths (Å)			
Ru1–N18	1.980(4)	O11–C12	1.330(5)
Ru1–O11	2.008(3)	C17–N18	1.419(5)
Ru1–N33	2.115(4)	N18–N19	1.288(5)
Ru1–S26	2.289(2)	N19–C20	1.427(5)
Ru1–Cl1	2.369(3)	C25–S26	1.779(4)
Ru1–Cl4	2.362(3)	S26–C27	1.845(4)
C17–N18	1.419(5)		
Bond angles (°)			
N18–Ru1–O11	83.25(15)	N18–Ru1–N33	172.34(13)
O11–Ru1–N33	99.80(15)	N18–Ru1–S26	96.86(13)
O11–Ru1–S26	175.90(9)	N33–Ru1–S26	80.60(13)
Cl4–Ru1–Cl1	178.96(4)	O11–Ru1–Cl1	91.63(10)
N18–Ru1–Cl1	85.25(10)	S26–Ru1–Cl1	92.46(5)
N33–Ru1–Cl1	87.64(10)	O11–Ru1–Cl4	88.80(10)
N18–Ru1–Cl4	93.86(10)	S26–Ru1–Cl4	87.11(5)
N33–Ru1–Cl4	93.22(10)	C25–S26–Ru1	104.53(15)
C27–S26–Ru1	96.30(15)	N19 N18–Ru1	131.4(3)
C17–N18–Ru1	111.7(3)	C12–O11–Ru1	110.6(3)
C28–N33–Ru1	117.4(3)	C32–N33–Ru1	123.4(3)

3.3. Spectral properties

3.3.1. IR spectra

In the IR spectra of the complexes, the characteristic IR bands at ~3300 cm^{-1} for O–H of H bonded phenolic–OH [22] of the ligand systems are not observed. This indicates coordination of oxygen to the metal centre [23]. The $\nu_{N=N}$ mode of the *trans*-complexes is somewhat low in comparison to that found in the *cis*-Ru(III), Cu(II) and Fe(II) complexes. This band in the free ligand is 1495–1505 cm^{-1} and it is shifted to lower to wave numbers ($\Delta \sim 25$–35 cm^{-1}) in the complexes, suggesting coordination of the metal ions to the azo function [24]. The $\nu_{N=N}$ band is observed at 1460–1472 cm^{-1} for all the *trans*-complexes, but for the *cis*-isomers it is somewhat higher 1467–1480 cm^{-1}. In addition to this, ν_{C-S} (790 cm^{-1}) for the ligands shifts to ~750 cm^{-1} for the *trans* complexes and is about 760 cm^{-1} for the *cis* isomers. Deep brown colored [Ru(L)(bpy)]$(PF_6)_2$ derivatives of the *cis*-isomers show sharp absorption bands around 840 and 540 cm^{-1} assignable to $\nu_{(PF_6)}$, which are absent for *cis*-[Ru(L)Cl_2], and the conductivity studies in

MeOH are consistent with the presence of 1:2 electrolytes. Magnetic susceptibility data (Table 1) reveal spin-only values for all the complexes as the values are very close to one electron equivalent low spin complexes.

3.3.2. Electronic spectra

The electronic absorption spectra of all the complexes were recorded at room temperature in Table 4 using MeOH as the solvent. The spectra of the complexes exhibit a transition at lower than 400 nm corresponding to intramolecular $\pi \rightarrow \pi^*$ and $n \rightarrow \pi^*$ transitions [25]. The transitions in the range 400–500 nm are due to intra-ligand charge transfer transitions. The transition in the range of 630–672 nm which is absent in the free ligands, can be assigned to a $d(Ru) \rightarrow \pi^*$ transition (MLCT) where the π^* level has large azo character [26]. In general *cis*-dichlororuthenium (III) complexes (**1**) exhibit absorption in the lower energy region compared to the *trans* analogs **2**. Here, the $d(Ru) \rightarrow \pi^*$ transitions in **1** appear at lower energy compared to those in **2**, though the π-acceptor–donor pyridinic-N is *trans* to azo-N in **2** in the same plane and the azo-N in **1** *trans* to chlorine (comparing with the Fe(III) complexes where the chlorine atoms are in *cis* positions), and the *trans* isomers **2** possess more symmetry in comparison to the *cis* analogs **1**. The phenomenon is the opposite to that found with the ruthenium (II) system. The absorption due to the $d(Ru) \rightarrow \pi^*$ transition in the complexes **3**, where bipyridyl is present as a bidentate ligand in place of two chlorines in the coordination sphere of ruthenium (III), is in a slightly higher energy region than that of **1**. From this observation it may be mentioned that ruthenium (III), being a d^5 system, is not as good a π-donor as ruthenium (II) (d^6 system).

3.3.3. EPR spectra

EPR spectra of the *cis*-dichloro-$[Ru(L)Cl_2]$ complexes (**1**) have been recorded in DMF at 298 and 77 K. The data are tabulated in Table 4 and a representative spectra of **1a** is reported in Fig. 2. In the high field region, the complexes display one isotropic EPR signal at room temperature (298 K) and an anisotropic pattern EPR signal having three different g values ($g_x \neq g_y \neq g_z$) at liquid nitrogen temperature (77 K). The EPR spectra at low temperature (77 K) show three strong signals and some weak resonances due to the hyperfine interaction with the nuclei of ^{101}Ru ($I = 5/2$, natural abundance 16.8%) and ^{99}Ru ($I = 5/2$, natural abundance 12.81%). Of these three major resonances, two are lower and one is higher than the field (~3200 G). As a result, two g-values are higher and one g-value is lower than 2. From the spectra it is revealed that

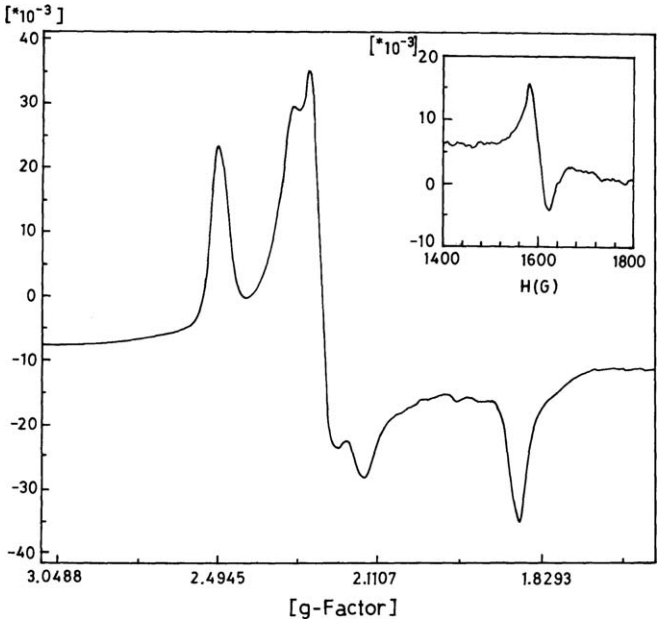

Fig. 2. EPR spectra of *cis*-dichloro $[Ru^{III}(L1)Cl_2]$ in DMF at 77 K ($g_1 = 2.481$, $g_2 = 2.184$ and $g_3 = 1.882$ at high field); in inset, display of one isotropic signal at low field.

Table 4
UV–Vis spectral, electrochemical and EPR data

Compound	λ nm (ε) (ε, $dm^3\ mol^{-1}\ cm^{-1}$)	Electrochemical data $E_{1/2}$, mV (ΔE_p, mV) [E_{pa}, mV; E_{pc}, mV]	EPR data		
			g_1	g_2	g_3
1a	664 (512), 476 (1702), 428 (2044)	152 (96) [200, 104]	2.481	2.184	1.882
1b	662 (499), 471 (1792), 426 (1967)	148 (114) [205, 91]	2.476	2.166	1.853
1c	668 (523), 482 (1821), 422 (1989)	181 (92) [227, 135]	2.474	2.193	1.882
1d	673 (501), 469 (1745), 429 (2089)	195 (104) [247, 143]	2.471	2.181	1.874
1e	672 (525), 477 (1859), 421 (2122)	167 (116) [225, 109]	2.465	2.177	1.888
2a	640 (531), 472 (1980), 442 (2070)	341 (150) [416, 266]			
2b	644 (524), 468 (1899), 450 (2097)	369 (178) [458, 280]			
2c	638 (539), 478 (2045), 444 (1992)	320.5 (165) [403, 238]			
2d	634 (519), 462 (1934), 438 (2065)	311.5 (171) [397, 226]			
2e	630 (534), 477 (2013), 434 (2099)	384 (184) [476, 292]			
3a	658 (660), 512 (2792), 480 (3114), 422 (3428)	267.5 (115) [325, 210]			
3b	652 (652), 506 (2751), 484 (3089), 420 (3398)	304.5 (127) [368, 241]			
3c	661 (677), 509 (2811), 480 (3142), 419 (3401)	275 (122) [336, 214]			
3d	653 (630), 510 (2769), 480 (3085), 424 (3379)	251 (102) [302, 200]			
3e	665 (672), 514 (2725), 480 (3170), 427 (3453)	299 (132) [365, 233]			

the t_g^5 configuration of the complexes **1** is a positive hole in the t_{2g} subshell as $g_\perp > g_\parallel$.

One weak isotropic band transition (Fig. 2, inset) corresponding to $\Delta M_s = 2$ at 77 K has been observed and it is centred around 1600 G, which is about half the field of the allowed $\Delta M_s = \pm 1$ transitions at around 3200 G. The spectra in this region show no splitting as here zero-field splitting is not possible. The results exhibit that the complexes are low-spin octahedral with one unpaired electron (low spin d^5 Ru^{III}, $S = 1/2$) [27–29].

3.4. Electrochemistry

The redox properties of the complexes were examined by cyclic voltammetry using a Pt-disk working electrode and a Pt-wire auxiliary electrode in dry DMF and in the presence of [*n*-Bu_4N]ClO_4 as supporting electrolyte. The potentials (Table 4 and Fig. 3) are expressed with reference to Ag|AgCl electrodes and all the complexes displayed a quasi-reversible voltammogram having $i_{pc}/i_{pa} \approx 1$. The influence of the geometrical isomerism of the complexes on the redox potential values is quite significant. The redox potential values for the *cis*-isomers are low in comparison to the corresponding trans-isomers. The ΔE_p is high in the *trans*-isomers compared to the *cis*-isomers, and it may be due to the greater stability of corresponding *trans*-dichloro-ruthenium (II) species over the *cis*-isomers. The ΔE_p values for the bipyridyl derivatives are comparable with those of the *cis* analogs. The influence of the substituents in the ligands is apparent from the data.

3.5. Reaction of [Ru(L)Cl_2] with bipyridyl to form [Ru(L)(bpy)$_2$](PF_6)$_2$

The *cis*-dichloro ruthenium (III) complexes **1** have been converted into a new series of ternary ruthenium (III) complexes **3**, having the general formula of [Ru(L)-$(bpy)_2$]$(PF_6)_2$, by the reaction with bipyridyl in the presence of $AgNO_3$. The conductivity measurements in MeOH support complexes **3** being 1:2 electrolytic.

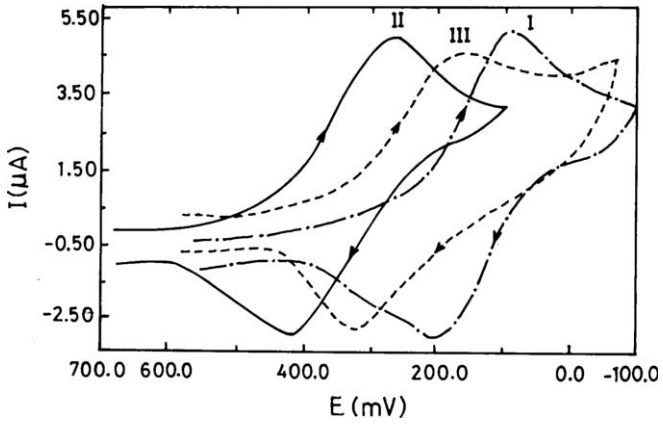

Fig. 3. Cyclic voltammogram of *cis*-[Ru(L1)Cl_2] (I), *trans*-[Ru(L1)Cl_2] (II) and [Ru(L1)(bipy)]$(PF_6)_2$ (III) in dry DMF, scan rate 50 mV S^{-1}.

The stretching band for $\nu_{(PF_6)}$ (around 840 cm^{-1} and 540 cm^{-1}) in the IR spectra confirms the presence of PF_6^- as the counter anion in the complexes **3**. All the complexes are one electron equivalent paramagnetic in nature which has been concluded from the magnetic moment measurement at room temperature. The electrochemical behavior of the *trans*-isomers is the same as that found for the *cis*-isomers with a difference only in the potential values.

4. Conclusion

The formation of *cis* and *trans* isomers of Ru(II) complexes of this series of ligands are dependent on the solvent used and the temperature. In relatively high polar solvents, formation of *cis* isomers is more favored whilst the yield of the *trans* isomers is greater than that of the *cis* analogs in less polar solvents. The X-ray crystal structure determination confirms the *trans*-dichloro type isomers. The structural data for the *cis*-dichloro type isomers could not be obtained, but the structure is likely to be similar to that found in recently published *cis*-dichloro-iron (III) complexes of this series of ligands and this is supported by spectroscopic data. In the case of the *cis* isomers, the donor atoms of the ligand are not in one plane, rather the pyridinic-N donor centre is located in an axial position, as is observed in the *cis*-dichloro-iron (III) complexes. However in the present work, in the *trans* isomers of the ruthenium (III) complexes, the donor sets of the pyridylthioazophenolate ligands are approximately planar, an arrangement which has not been observed in either the copper (II) or iron (III) complexes [12]. The redox potential values for the *cis*-isomers are low in comparison to the corresponding trans-isomers. The *cis* type isomers are reactive towards the bidentate bipyridyl ligand in the presence of $AgNO_3$ while, as might be expected, this is not true of the *trans* isomers.

Acknowledgements

Financial assistance from DST, New Delhi, is gratefully acknowledged. We thank EPSRC and the University of Reading for funds for the Image Plate System.

Appendix A. Supplementary data

Crystallographic data for the structural analyses have been deposited with the Cambridge Crystallographic Data Centre as CCDC No. 275390. Copies of this information are available on request, free of charge, from CCDC, 12 Union Road, Cambridge, CB2 1EZ, UK (fax: +44 1223 336 033; e-mail: deposit@ccdc.ac.uk or www: http://www.ccdc.cam.ac.uk). Supplementary data associated with this article can be found, in the online version, at doi:10.1016/j.poly.2005.12.020.

References

[1] M.J. Clarke, Coord. Chem. Rev. 236 (2003) 209.

[2] M.J. Clarke, Coord. Chem. Rev. 232 (2002) 69.
[3] M.J. Clarke, F. Zhu, D.R. Frasca, Chem. Rev. 99 (1999) 2511.
[4] G. Mestroni, E. Alessio, G. Sava, S. Pacor, M. Coluccia, in: B.K. Keppler (Ed.), Metal Complexes in Cancer Chemotherapy, VCH, Weinheim, 1993, p. 157.
[5] I. Turel, M. Pecanac, A. Golobic, E. Alessio, B. Serli, A. Bergamo, G. Sava, J. Inorg. Biochem. 98 (2004) 393, and references therein.
[6] A.H. Velders, A. Bergamo, E. Alessio, E. Zangrando, J.G. Haasnoot, C. Casarsa, M. Cocchietto, S. Zorzet, G. Sava, J. Med. Chem. 47 (2004) 1110, and references therein.
[7] A. Kung, T. Piper, R. Wissiack, E. Rosemberg, B.K. Keppler, J. Biol. Inorg. Chem. 6 (2001) 292.
[8] K.G. Lipponer, E. Vogel, B.K. Keppler, Met.-Based Drugs 3 (1996) 243.
[9] B.K. Keppler, New J. Chem. 14 (1990) 389.
[10] B.K. Keppler, M. Henn, U.M. Juhl, M.R. Berger, R. Niebl, F.E. Wagner, Prog. Clin. Biochem. Med. 10 (1989) 42.
[11] E. Iengo, G. Mestroni, S. Geremia, M. Calligaris, E. Alessio, J. Chem. Soc., Dalton Trans. (1999) 3361, and references therein.
[12] (a) P.K. Dhara, S. Pramanik, T.H. Lu, M.G.B. Drew, P. Chattopadhyay, Polyhedron 23 (2004) 2457;
(b) P.K. Dhara, S. Pramanik, T.H. Lu, P. Chattopadhyay, J. Coord. Chem. 58 (2005) 985.
[13] P.K. Dhara, B. Das, J.M. Lo, P. Chattopadhyay, Appl. Radiat. Isot. 62 (2005) 729.
[14] R.P. Happer, W. Roseboom, A.J. Pierik, S.P. Albracht, A. Bagley, Nature 385 (1997) 126.
[15] W. Kaim, B. Schwederski, Bioinorganic Chemistry: Inorganic Elements in the Chemistry of Life, Wiley, Chichester, 1994, and references therein.
[16] D.D. Perrin, W.L.F. Armarego, D.R. Perrin, Purification of Laboratory Chemicals, Pergamon Press, Oxford, UK, 1981.
[17] (a) W. Kabsch, J. Appl. Crystallogr. 21 (1988) 916;
(b) SHELX86:G.M Sheldrick, Acta Crystallogr., Sect. A 46 (1990) 467;
(c) G.M. Sheldrick, SHELXL: Program for Crystal Structure Refinement, University of Gottingen, Germany, 1993.
[18] S. Patra, B. Mondal, B. Sarkar, M. Niemeyer, G.K. Lahiri, Inorg. Chem. 42 (2003) 1322.
[19] (a) E. Alessio, G. Balducci, A. Lutman, G. Mestroni, M. Calligaris, W.M. Attia, Inorg. Chim. Acta 203 (1993) 205;
(b) G. Sava, I. Capozzi, K. Clericl, R. Gagliardi, E. Alessio, G. Mestroni, Clin. Exp. Metastasis (1998) 371.
[20] M. Calligaris, O. Carugo, Coord. Chem. Rev. 153 (1996) 83.
[21] A.M.W.C. Thompson, D.A. Bardwell, J.C. Jeffery, L.H. Rees, M.D. Ward, J. Chem. Soc., Dalton Trans (1997) 721.
[22] M.S. Masoud, A.M. Hindway, A.A. Soayed, Trans. Met. Chem. 16 (1991) 372.
[23] (a) P. Chattopadhyay, C. Sinha, Ind. J. Chem., Sect. A 34A (1995) 76;
(b) H.H. Freedman, J. Am. Chem. Soc. 63 (1961) 2900.
[24] S. Chattopadhyay, C. Sinha, S.B. Chowdhury, A. Chakravorty, J. Organomet. Chem. 427 (1992) 111.
[25] R.M. Silverstein, G.C. Bassler, T.C. Morrill, Spectrometric Identification of Organic Compounds, Wiley, New York, 1981.
[26] A.B.P. Lever, Inorganic Electronic Spectroscopy, Elsevier, Amsterdam, 1984.
[27] R.L. Dutta, A. Syamal, Elements of Magnetochemistry, 2nd ed., Affiliated East-West Press Pvt. Ltd. (EWP), New Delhi, 1993.
[28] G.K. Lahiri, S. Bhattacharya, B.K. Ghosh, A. Chakravorty, Inorg. Chem. 26 (1987) 4324.
[29] P.U. Jain, P. Munshi, M.G. Walawalkar, S.P. Rath, K.K. Rajak, G.K. Lahiri, Polyhedron 19 (2000) 801.

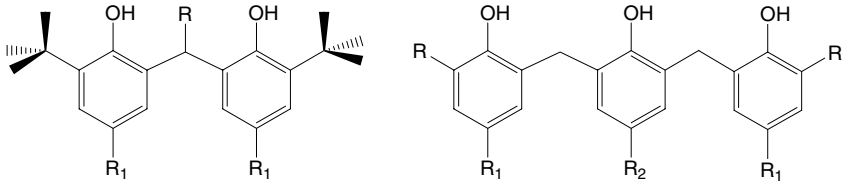

R = H, R_1 = Me (**A**)
R = Me, R_1 = ^{t}Bu (**B**)

R = R_1 = ^{t}Bu, R_2 = Me (**C**)
R = R_2 = ^{t}Bu, R_1 = Me (**D**)
R = R_1 = Me, R_2 = ^{t}Bu (**E**)

Scheme 1.

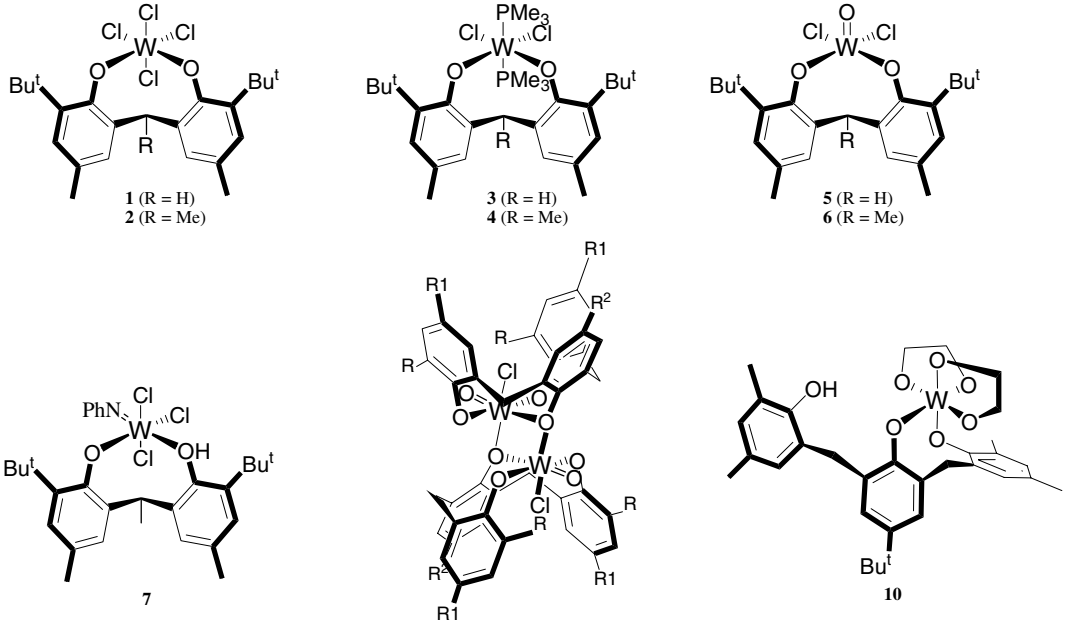

1 (R = H)
2 (R = Me)

3 (R = H)
4 (R = Me)

5 (R = H)
6 (R = Me)

7

R=R^1=Bu^t, R^2 = Me (**8**)
R=R^2=Bu^t, R^1 = Me (**9**)

Scheme 2.

ancillary chelate ligands. Such vanadyl species were found to be extremely active for the polymerisation of ethylene, when combined with dimethylaluminium chloride (DMAC) [9b]. Related niobium pro-catalysts were much less active under similar conditions [9c]. In an attempt to more fully understand the coordinating characteristics of these chelating aryloxides, we have extended our investigations to high valent tungsten, which is known to exhibit rich aryloxide chemistry [10]. Here, new tungsten(IV and VI) complexes incorporating linked aryloxide ligands derived from the triphenols **A** and **B**, and the trisphenols **C**, **D** and **E** are reported – see Schemes 1 and 2.

2. Results and discussion

2.1. Diphenolates

The starting material [WCl_6] has been used previously for the synthesis of aryloxides of tungsten(VI) [10a,10b]. The reaction of [WCl_6] and the biphenol ligands 2,2′-CHR[4,6-(Bu^t)$_2$C$_6$H$_2$OH]$_2$ (R = H (**A**), Me (**B**)) in either refluxing CCl_4 or toluene readily gives multi-gram quantities of [WCl_4{2,2′-CHR[4,6-(Bu^t)$_2$C$_6$H$_2$O]$_2$}] R = H (**1**), Me (**2**) as dark purple/black solids. Both **1** and **2** can be recrystallized from CH_2Cl_2 as dark purple needles and the structure of **1** was determined by a single crystal X-ray analysis. The tungsten centre (Fig. 1) is pseudo octahedral and resembles those found in the *cis*-aryloxide complexes [WCl_4(OC_6H_3-2,6-R_2)$_2$] (R = Ph, ^{i}Pr) [10a,10e]. The W–O bond lengths [1.848(3)–1.8621(4) Å] are typical [10], and the chelate bite angle is 92.52(15)°, with the 8-membered metallocyclic ring adopting the boat conformation. Selected bond lengths and angles are given in Table 1 and crystallographic data is presented in Table 3.

The reduction of **1** or **2** with sodium amalgam in toluene in the presence of PMe_3 gives red/brown prisms of the *cis*, *trans*-tungsten(IV) complexes [$WCl_2(PMe_3)_2${2,2′-CHR[4,6-(Bu^t)$_2$C$_6$H$_2$O]$_2$}] R = H (**3**), Me (**4**), respectively. For **4**, the ^{31}P NMR spectrum consists of a singlet at δ −8.8 ppm; ^{183}W satellites are present [J(P–W) = 222 Hz].

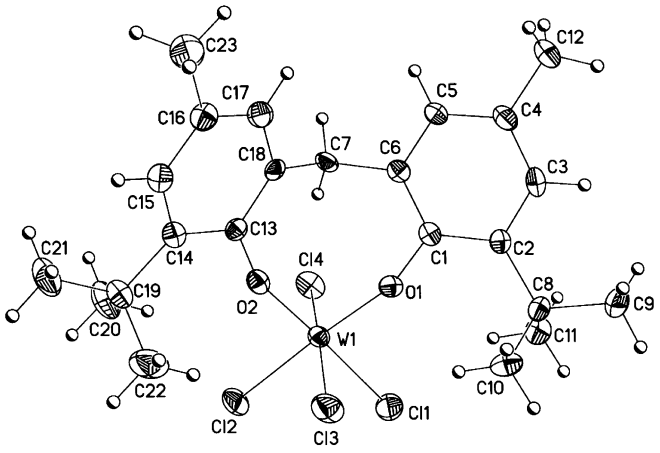

Fig. 1. ORTEP diagram of $[WCl_4\{2,2'\text{-}CH_2[4,6\text{-}(Bu^t)_2C_6H_2O]_2\}]$ (**1**). Ellipsoids are shown at 50% probability levels.

Table 1
Bond lengths (Å) and angles (°) for diphenolate complexes

	1	3	5
Bond lengths			
W(1)–O(1)	1.848(3)	1.933(2)	1.850(4)
W(1)–O(2)	1.862(4)		1.854(4)
W(1)–O(3)			1.678(4)
W(1)–Cl(1)	2.341(2)	2.4081(9)	2.319(2)
W(1)–Cl(2)	2.324(1)		2.322(2)
W(1)–Cl(3)	2.344(1)		
W(1)–Cl(4)	2.327(1)		
W(1)–P(1)		2.535(1)	
W(1)–P(2)		2.566(1)	
Bond angles			
O(1)–W(1)–O(2)	92.5(2)		89.6(2)
O(1)–W(1)–O(1A)		99.85(12)	
Cl(1)–W(1)–Cl(2)	176.9(1)		85.35(6)
Cl(1)–W(1)–Cl(1A)		82.61(5)	
P(1)–W(1)–P(2)		176.36(5)	

The molecular structure of **3** is shown in Fig. 2; selected bond lengths and angles are given in Table 1. The molecule has approximate octahedral geometry with *trans*-phosphines, but *cis*-chlorines that are coplanar with the dioxometallacycle. This arrangement contrasts with the *trans*, *trans*, *trans*-$WCl_2O_2P_2$ core observed for the related aryloxide complex $[WCl_2(OC_6H_3\text{-}2,6\text{-}Ph_2)_2(PMe_2Ph)_2]$ [10c], and reflects the geometrical constraints imposed by the chelating ligand. In **3**, there is evidence of a *trans*-phosphine influence: the mutually *trans*, formally chemically equivalent phosphines quite unexpectedly differ in bond lengths [2.535(1) and 2.556(1) Å], a phenomenon ascribed to competitive π-back bonding. The diphenolate binds symmetrically with equal W–O–C angles [133.7(2)°], a bite angle of 99.8(1)° and adopts the flattened boat conformation seen previously.

The reaction of an ethereal solution of $[WOCl_4]$ with the biphenols **A** and **B** forms $[WOCl_2\{2,2'\text{-}CHR[4,6\text{-}(Bu^t)_2\text{-}C_6H_2O]_2\}]$ R = H (**5**), Me (**6**) in good yields (55–60%). Crystals of **5** suitable for a single crystal X-ray determination were grown from a saturated hexane solution at 0 °C. The molecular structure is shown in Fig. 3; the geometrical parameters – see Table 1 (and spectroscopic data), are very similar to those reported by Takashima et al. for the same product obtained in refluxing THF and crystallised form hexane/toluene [5].

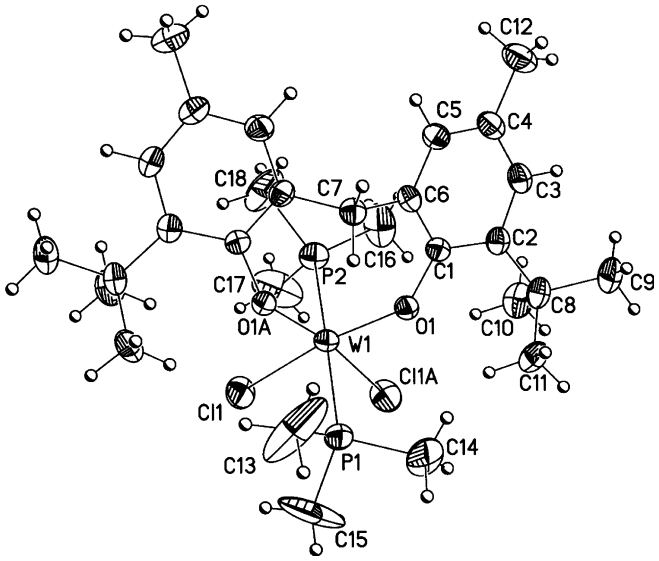

Fig. 2. ORTEP diagram of $[WCl_2(PMe_3)_2\{2,2'\text{-}CH_2[4,6\text{-}(Bu^t)_2C_6H_2O]_2\}]$ (**3**). Ellipsoids are shown at 50% probability levels.

A similar reaction of $[W(NPh)Cl_4(Et_2O)]$ with the biphenol $2,2'\text{-}CH_3CH[4,6\text{-}(Bu^t)_2C_6H_2OH]_2$ in diethyl ether at −78 °C leads to $[W(NPh)Cl_3\{(1,1'\text{-}O,OH)(2,2'\text{-}CH_3CH)\text{-}[4,6\text{-}(Bu^t)_2C_6H_2]_2\}]$ (**7**) in which the diphenol coordinates in a bidentate monoanionic form. Conformation of the monoanionic bonding is provided by IR spectra, where a band at 3492 cm^{-1} can be assigned as the stretch of the OH group. It is noteworthy that reaction of catechol with $[WOCl_4]$ has also been found to give a complex $[W(O)Cl(O_2C_6H_4)(O,OHC_6H_4)\cdot OEt_2]$ (see **F** below) containing a chelating monoanionic ligand [11].

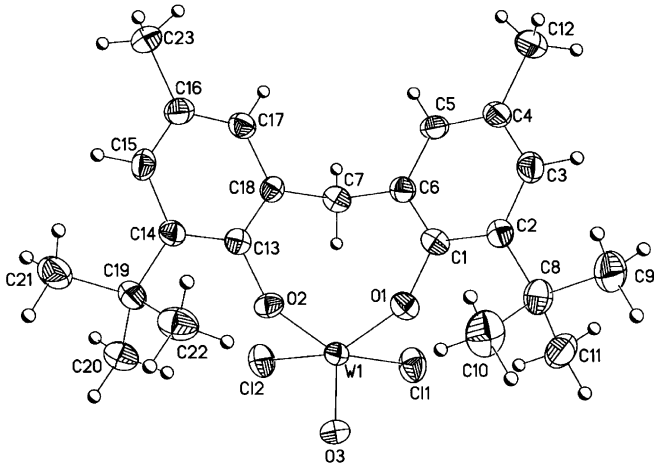

Fig. 3. ORTEP diagram of $[WOCl_2\{2,2'\text{-}CH_2[4,6\text{-}(Bu^t)_2C_6H_2O]_2\}]$ (**5**). Ellipsoids are shown at 50% probability levels.

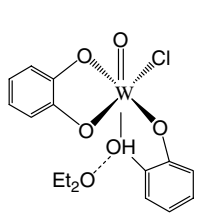

F

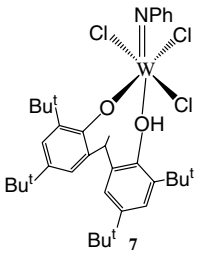

7

For 2,2′-methylenebis(6-*tert*-butyl-4-methylphenol), 2,2′-CH_2[4-Me,6-(Bu^t)$C_6H_2OH]_2$, it has previously been noted that the ^1H NMR resonances for the methylene bridge protons are sensitive to the changes in the metal coordination sphere [3a]. A similar situation is found in this work for both diphenols 2,2′-CHR[4,6-(Bu^t)$_2$-$C_6H_2OH]_2$) (R = H, Me), where dramatic changes in shifts are noted particularly for the CH proton of the bridge. For example, CH resonances for **1** and **5** (all recorded in $CDCl_3$) occur at δ 5.80, 3.99 and 4.11, 3.72, respectively.

2.2. Triphenolates

The interaction of $[WOCl_4]$ with the linear triphenol ligand $HOArCH_2Ar^1(OH)CH_2ArOH$ (Ar = 4,6-di-*t*-butylphenol; Ar^1 = 4-methylphenyl) **C**, in refluxing toluene yielded, on work-up, the complex $\{WOCl[OArCH_2Ar^1(O)CH_2ArO]\}_2$ (**8**), in good yield (ca. 55%). Crystals of **8**, suitable for a single crystal X-ray diffraction study, were obtained from a saturated acetonitrile solution on prolonged standing at ambient temperature. The molecular structure is shown in Fig. 4, with selected bond lengths and angles given in Table 2. The two pseudo octahedral tungsten centres are linked via asymmetric aryloxide bridges [W–O 2.053(5) and 2.207(5) Å], the bridges each derived from one of the *facially* bound triphenolate ligands, which adopts a *U* conformation. The W=O bond length [1.689(5) Å] is typical. The two halves of the molecule in **8** (space group *C*2/*c*, *Z* = 4) are related by an inversion site located at the centre of the W_2O_2 square. The core of the structure is reminiscent of that observed in a number of other tungsten(VI) oxo alkoxides – edge-shared bioctahedral structures featuring asymmetric alkoxide bridges, which are coplanar with terminal oxo ligands [10c].

Similar reaction of $[W(NPh)Cl_4(Et_2O)]$ with triphenol **D** 2,6-(3-*t*-butyl-5-methyl-2-hydroxybenzyl)-4-*t*-butylphenol, $HOAr^2CH_2Ar^3(OH)CH_2Ar^2OH$ (Ar^2 = 4-methyl-6-*t*-butylphenol; Ar^3 = 4-*t*-butylphenyl) afforded, on work-up, brown blocks of the hydrolysis product $\{WOCl[OAr^2CH_2Ar^3(O)CH_2Ar^2O]\}$ (**9**). Complex **9** can also be prepared directly from the reaction of $[WOCl_4]$ and **D**. The molecular

Table 2
Bond lengths (Å) and angles (°) for triphenolate complexes

	8	9	10
Bond lengths			
W(1)–O(1)	1.886(5)	1.890(3)	1.865(2)
W(1)–O(2)	2.207(5)	2.198(3)	1.951(2)
W(1)–O(3)	1.892(5)	1.883(3)	
W(1)–O(4)	1.689(5)	1.698(3)	1.910(2)
W(1)–O(5)			1.896(2)
W(1)–O(6)			1.914(2)
W(1)–O(7)			1.908(2)
W(1)–O(2A)	2.053(2)	2.074(3)	
W(1)–Cl(1)	2.335(2)	2.341(1)	2.319(2)
Bond angles			
W(1)–O(1)–W(1A)	113.9(2)	115.8(1)	
O(1)–W(1)–O(3)	162.6(2)	164.7(1)	
O(1)–W(1)–O(2)	86.1(2)	86.3(1)	85.65(8)
O(1)–W(1)–O(4)	96.5(2)	96.1(1)	85.84(8)
O(4)–W(1)–O(5)			79.13(9)

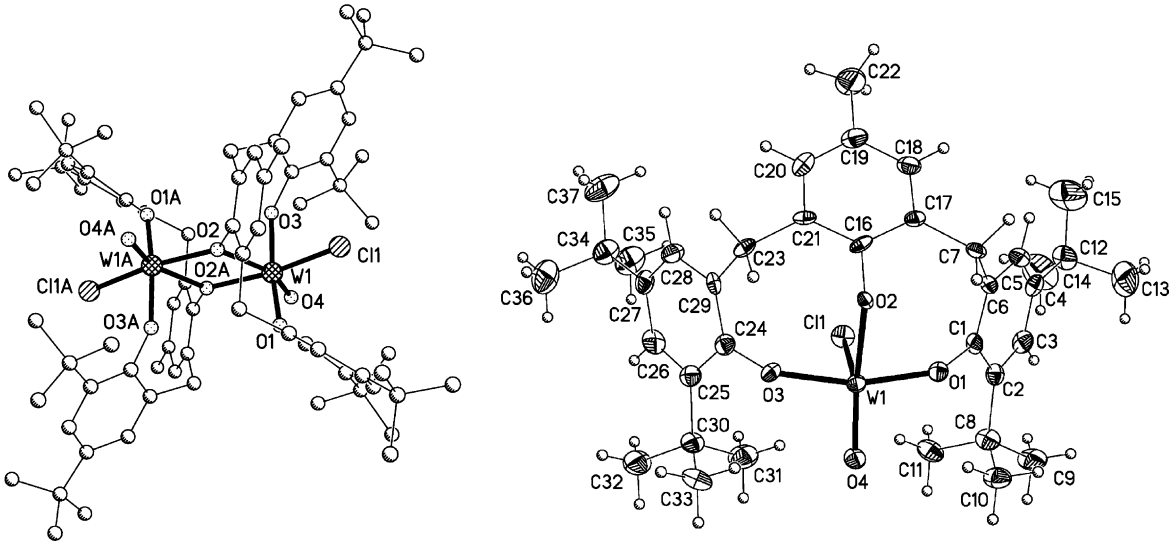

Fig. 4. (left) Structural diagram of the dimeric unit $\{WOCl[OArCH_2Ar^1(O)CH_2ArO]\}_2$ (**8**). Hydrogen atoms have been omitted for clarity; (right) ORTEP view of the asymmetric unit of **8**.

structure (Fig. 5) has the same dimeric form as isostructural **8**, while geometrical parameters are also similar (see Table 2 and Fig. 6).

The complex $[W(eg)_3]$ has recently been used as a precursor for tungsten aryloxide synthesis [5b,12]. Interaction of $[W(eg)_3]$ with triphenol **E** 2,6-bis(3,5-methyl-2-hydrox-

Table 3
Crystallographic data

Compound	**1**	**3**	**5**	**8**	**9**	**10**
Formula	$C_{23}H_{30}Cl_4O_2W$	$C_{29}H_{48}Cl_2P_2O_2W$	$C_{23}H_{30}Cl_2O_3W$	$C_{74}H_{98}Cl_2O_8W_2$	$C_{68}H_{86}Cl_2O_8W_2$	$C_{32}H_{40}O_7W$
Formula weight	664.12	745.36	609.22	1554.12	1469.97	720.49
Crystal system	monoclinic	orthorhombic	monoclinic	monoclinic	monoclinic	triclinic
Space group	$P2_1/c$	*Pnma*	$C2/c$	$C2/c$	$P2_1/c$	$P\bar{1}$
Unit cell dimensions						
a (Å)	9.6768(2)	16.4685(3)	29.7734(4)	24.8831(3)	16.6019(2)	11.3314(1)
b (Å)	27.0312(4)	16.5175(3)	10.9410(2)	10.8875(1)	20.2365(2)	11.8523(1)
c (Å)	9.6976(2)	12.1414(3)	19.1098(4)	29.2577(4)	19.3438(3)	12.2420(2)
α (°)	90	90	90	90	90	112.4766(6)
β (°)	100.4067(7)	90	128.6050(10)	98.5187(4)	105.0695(4)	94.7475(6)
γ (°)	90	90	90	90	90	91.4843(8)
V (Å^3)	2494.93(8)	3302.68(12)	4864.65	7838.89(16)	6275.34(14)	1511.07(3)
Z	4	4	8	4	4	2
Absorption coefficient, μ (mm^{-1})	5.076	3.779	4.989	3.048	3.802	3.868
Crystal size (mm)	$0.18\times0.07\times0.02$	$0.14\times0.12\times0.12$	$0.18\times0.04\times0.02$	$0.12\times0.10\times0.05$	$0.18\times0.12\times0.10$	$0.18\times0.16\times0.12$
θ_{max} (°)	27.49	27.47	27.51	20.39	28.73	29.15
Reflections measured	21582	22883	21422	25940	40691	17614
Unique reflections	5693	3906	5560	3847	16141	8073
Reflections with $F^2 > 2\sigma(F^2)$						
Transmission factors	0.607–0.904	0.575–0.644	0.4671–0.9068	0.801–0.940	0.5477–0.7023	0.573–0.637
R_{int}	0.0644	0.0609	0.0732	0.0715	0.0568	0.0350
Number of parameters	271	207	262	388	721	437
R[a] $[F^2 > 2\sigma(F^2)]$	0.0418	0.0291	0.0422	0.0369	0.0375	0.0251
R_w[b] (all data)	0.0557	0.0451	0.0685	0.0454	0.0606	0.0286
Goodness-of-fit[c] (S)	1.027	1.058	1.043	1.098	1.013	1.055
Largest difference peak and hole (e Å^{-3})	1.748 and −4.694	1.224 and −0.646	0.887 and −1.592	1.509 and −0.469	1.206 and −2.286	0.801 and −1.341

[a] Conventional $R = \sum||F_o| - |F_c||/\sum|F_o|$ for 'observed' reflections having $F^2 > 2\sigma(F^2)$.
[b] $R_w = [\sum w(F_o^2 - F_c^2)^2/\sum w(F_o^2)^2]^{1/2}$ for all data.
[c] $S = [\sum w(F_o^2 - F_c^2)^2/(\text{no. of unique reflections} - \text{no. of parameters})]^{1/2}$.

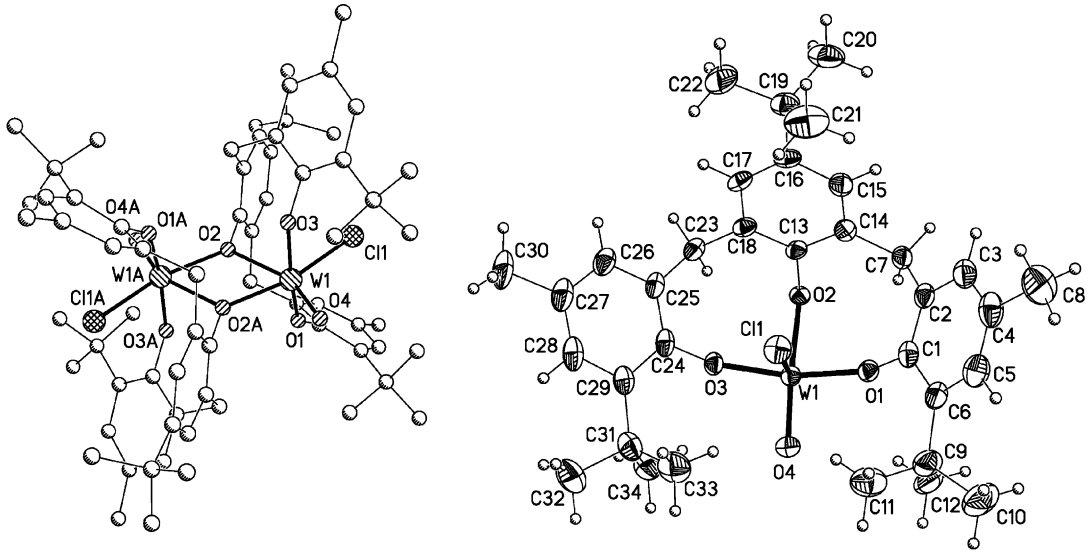

Fig. 5. ORTEP diagram of {WOCl[OAr^{2}CH$_2$Ar^3(O)CH$_2$Ar^{2}O]} (**9**). Ellipsoids are shown at 50% probability levels. Only half the molecule is shown for clarity.

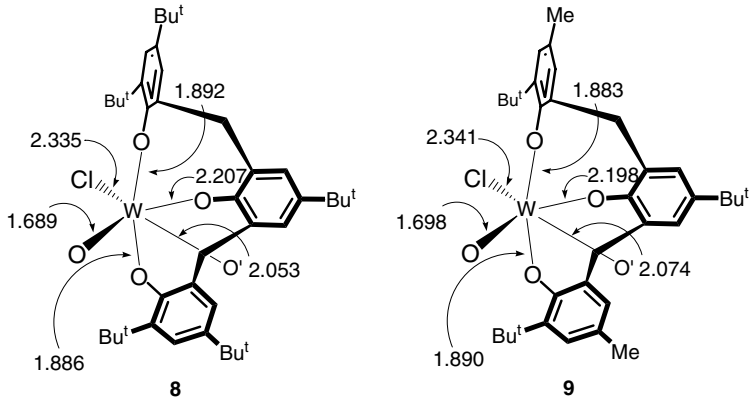

Fig. 6. Selected geometrical parameters associated with **8** and **9**.

ybenzyl)-4-*t*-butylphenol, $HOAr^4CH_2Ar^3(OH)CH_2Ar^4OH$ ($Ar^4 = 4,6$-di-methylphenol) in refluxing toluene afforded the orange complex $[W(eg)_2(OAr^4CH_2Ar^3(O)CH_2Ar^4OH)]$ (**10**) in good yield. Crystals suitable for an X-ray determination were grown from a saturated solution of acetonitrile at room temperature. The molecular structure is shown in Fig. 7. The tungsten centre is pseudo octahedral with coordination sites occupied by two chelating 1,2-ethanediolato ligands and a bidentate chelate ligand [bite angle = 85.65(8)°] derived from the triphenol **E** for which one of the phenolic groups remains unbound (pendant). The 8-membered metallocyclic ring adopting the boat conformation similar to that observed in the diphenolate complexes **1**, **3** and **5**, whilst the core geometry at tungsten resembles that reported for the diphenolate complexes $[W(eg)_2L]$ (L = 2,2′-methylenebis(6-methylphenolate) and 2,2′-methylenebis(6-isopropylphenolate) reported by Lehtonen and Sillanpää [12b].

In conclusion, the compounds described herein provide useful insight into the coordination environment afforded by the deprotonated forms of both bi- and tri-phenolate ligands. Further catalytic studies using these ligand systems will be published elsewhere.

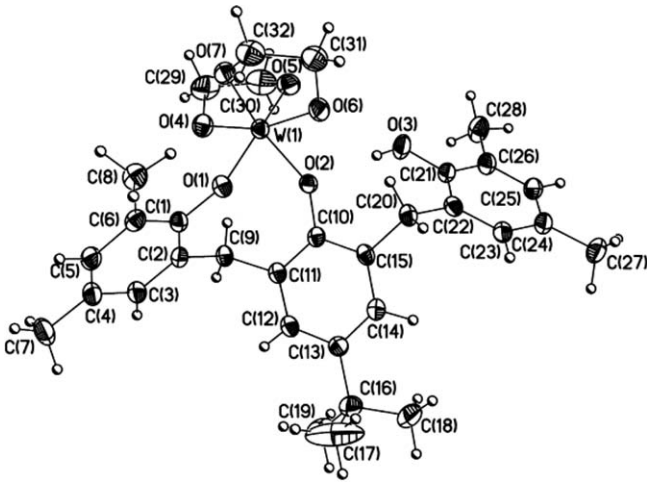

Fig. 7. Structural diagram of $[W(eg)_2(OAr^4CH_2Ar^3(O)CH_2Ar^4OH)]$ (**10**). Ellipsoids are shown at 50% probability levels.

3. Experimental

3.1. General

All manipulations were carried out under an atmosphere of nitrogen using standard Schlenk and cannula techniques or in a conventional nitrogen-filled glove-box. Solvents were refluxed over an appropriate drying agent, and distilled and degassed prior to use. Elemental analyses were performed by the microanalytical services of the Department of Chemistry at Durham and Medac Ltd. NMR spectra were recorded on a Varian VXR 400 S spectrometer at 399.9 MHz (^1H), and 161.9 MHz (^{31}P); chemical shifts are referenced to the residual protio impurity of the deuterated solvent; IR spectra (nujol mulls, CsI windows), Perkin–Elmer 577 and 457 grating spectrophotometers; $[WOCl_4]$, $[W(NPh)Cl_4(Et_2O)]$ and $[W(eg)_3]$ were prepared by literature methods [13–15]. Trimethylphosphine was prepared by the method of Wolfsberger and Schmidbaur [16]. The triphenol ligands **C**–**E** were prepared by the methods of Scott [7a]. All other chemicals were obtained commercially and used as received unless stated otherwise.

3.2. Preparation of $[WCl_4\{2,2'\text{-}CH_2\text{-}[4\text{-}Me,6\text{-}Bu^t\text{-}C_6H_2O]_2\}]$ (1)

$[WCl_6]$ (1.00 g, 2.52 mmol) and the diphenol **A** (0.93 g, 2.52 mmol) were combined in a dry-box. The system was then refluxed for 12 h in either CCl_4 or toluene (ca. 50 cm^3) to give a dark purple/black solid. This solid was washed with cold pentane (50 cm^3) and dried in vacuo. Yield: 1.24 g, 74%. Found: C, 42.1; H, 4.7%. $WCl_4O_2C_{23}H_{30}$ requires: C, 41.6; H, 4.6%. IR: 1599m, 1161w, 1140w, 1093bs, 1019bs, 917w, 871w, 865w, 799s. ^1H NMR ($CDCl_3$): δ 7.34 (d, 2H, $J_{HH} = 2.0$ Hz, aryl*H*), 7.25 (d, 2H, $J_{HH} = 1.5$ Hz, aryl*H*), 5.80 (d, 1H, $J_{HH} = 13.9$ Hz, CH_2), 3.99 (d, 1H, $J_{HH} = 13.9$ Hz, CH_2), 3.17 (s, 6H, CH_3), 1.57 (s, 18H, $(CH_3)_3C$).

3.3. Preparation of [WCl_4{2,2′-CH_3CH-[4,6-(Bu^t)$_2C_6H_2O$]$_2$}] (2)

[WCl_6] (3.39 g, 8.5 mmol) and the diphenol **B** (3.76 g, 8.6 mmol) were combined in a dry-box. The system was then refluxed for 12 h in either CCl_4 or toluene (ca. 50 cm^3) to give a dark purple/black solid. This solid was washed with cold pentane (50 cm^3) and dried in vacuo. Yield: 4.1 g, 62%. The compound can be crystallized from CH_2Cl_2 (−20 °C). Found: C, 46.9; H, 5.5%. $WCl_4O_2C_{30}H_{44}$ requires: C, 47.2; H, 5.8%. IR: 1583s, 1540w, 1363s, 1336w, 1261m, 1237m, 1200m, 1166s, 1157s, 1093s, 1022s, 927w, 908m, 885s, 875m, 800s, 769m, 759w, 749w, 723w, 684w, 657w, 628w, 565w, 444m, 357s, 318s, 308s. ^{1}H NMR ($CDCl_3$): δ 7.56 (d, 2H, J_{HH} = 2.0 Hz, aryl*H*), 7.37 (d, 2H, J_{HH} = 2.4 Hz, aryl*H*), 5.82 (q, 1H, J_{HH} = 6.8 Hz, C*H*), 1.57 (d, 3H, J_{HH} = 7.2 Hz, CH_3), 1.53 (s, 18H, (CH_3)$_3$C), 1.31 (s, 18H, (CH_3)$_3$C).

3.4. Preparation of [$WCl_2(PMe_3)_2${2,2′-CH_2-[4-Me,6-Bu^t-C_6H_2O]$_2$}] (3)

To a solution of **1** (1.00 g, 1.31 mmol) in toluene (40 cm^3) was added PMe_3 (0.31 cm^3, 3.0 mmol) and 0.2% sodium amalgam (0.09 g, 4.0 mmol). After stirring for 12 h, the suspension was filtered and the volatiles were removed in vacuo. The residue was dissolved in hexane (40 cm^3) and stored at 0 °C for 2 days to afford **3** as large red prisms. Yield: 0.47 g, 42%. Found: C, 46.3; H, 6.5%. $WCl_2P_2O_2C_{29}H_{48}$ requires: C, 46.7; H, 6.5%. IR: 1405m, 1286m, 1260s, 1229s, 1166m, 1120s, 1095bs, 1018bs, 953m, 918w, 900w, 861w, 848w, 831s, 796s, 737w, 722w, 567w.

3.5. Preparation of [$WCl_2(PMe_3)_2${2, 2′-CH_3CH-[4,6-(Bu^t)$_2C_6H_2O$]$_2$}] (4)

To a solution of **2** (2.00 g, 2.62 mmol) in toluene (ca. 50 cm^3) was added PMe_3 (0.6 cm^3, 5.3 mmol) and a 0.2% sodium amalgam (0.14 g Na, ca. 6 mmol). The mixture was stirred rapidly for 24 h, filtered and pumped dry in vacuo. Recrystallization from pentane at −20 °C gave a red crystalline solid. Yield: 1.45 g, 66%. Found: C, 50.8; H, 7.4%. $WCl_2P_2O_2C_{36}H_{62}$ requires: C, 51.2; H, 7.4%. IR: 1311s, 1284s, 1260s, 1236s, 1206s, 1186s, 1142s, 1122s, 1086s, 1023s, 952s, 913m, 872m, 853m, 828s, 812s, 773m, 741s, 728s, 670m, 647m, 633s, 600m, 550s. ^{31}P NMR ($CDCl_3$): δ −8.8 [s, with satellites $J_{(P-W)}$ 222 Hz].

3.6. Preparation of [$WOCl_2${2,2′-CH_2-[4-Me,6-Bu^t-C_6H_2O]$_2$}] (5)

To a solution of [$WOCl_4$] (1.00 g, 2.94 mmol) in diethyl ether (ca. 40 cm^3) at −78 °C was added the diphenol **A** (1.08 g, 2.94 mmol). After stirring the green solution at 25 °C (12 h), the volatiles were removed in vacuo and the solid residue was extracted with pentane. Filtration, reduction (to ca. 30 cm^3) and cooling (−20 °C) gave dark green cubes. Yield: 1.13 g, 63%. Found: C, 46.1; H, 5.2%. $WCl_2O_3C_{23}H_{30}$ requires: C, 45.3; H, 5.0%. IR: 1300w, 1261s, 1094bs, 1020bs, 986m, 941w, 930w, 800s, 722m. ^{1}H NMR ($CDCl_3$): δ 6.97 (d, 2H, $^4J_{HH}$ 2.0 Hz, aryl*H*), 6.95 (d, 2H, $^4J_{HH}$ 2.0 Hz, aryl*H*), 4.11 (d, 1H, $^2J_{HH}$ 16.1 Hz, CH_2), 3.72 (d, 1H, $^2J_{HH}$ 15.9 Hz, CH_2), 2.37 (s, 6H, 4-Me), 1.31 (s, 18H, (CH_3)$_3$C).

3.7. Preparation of [$WOCl_2${2,2′-CH_3CH-[4,6-(Bu^t)$_2C_6H_2O$]$_2$}] (6)

To a solution of [$WOCl_4$] (1.00 g, 2.94 mmol) in diethyl ether (ca. 40 cm^3) at −78 °C was added the diphenol **B** (1.29 g, 2.94 mmol). After stirring the green solution at 25 °C (12 h), the volatiles were removed in vacuo and the solid residue was extracted with pentane. Filtration, reduction (to ca. 30 cm^3) and cooling (−20 °C) gave dark green cubes. Yield: 1.14 g, 55%. Found: C, 54.1; H, 6.8%. $WCl_2O_3C_{35}H_{56}$ (pentane solvate) requires: C, 53.9; H, 7.2%. IR: 1589m, 1367s, 1261s, 1224s, 1200w, 1162w, 1109s, 1022s, 998s, 927m, 904w, 873s, 800s, 772m, 722w, 635w, 570w, 475w, 368m. ^{1}H NMR ($CDCl_3$): δ 7.16 (d, 2H, J_{HH} = 2.4 Hz, aryl*H*), 7.12 (d, 2H, J_{HH} = 2.0 Hz, aryl*H*), 3.76 (q, 1H, J_{HH} = 6.0 Hz, C*H*), 1.84 (d, 3H, J_{HH} = 6.4 Hz, CH_3), 1.31 (s, 18H, (CH_3)$_3$C), 1.21 (s, 18H, (CH_3)$_3$C).

3.8. Preparation of [$W(NPh)Cl_3${(1,1′-O,OH)-(2,2′-CH_3CH)[4,6-(Bu^t)$_2C_6H_2$]$_2$}] (7)

To a solution of [$W(NPh)Cl_4(Et_2O)$] (1.00 g, 2.0 mmol) in diethyl ether (ca. 40 cm^3) at −78 °C was added the diphenol **B** (0.9 g, 2.1 mmol). After stirring at 25 °C for 12 h, the volatiles were removed in vacuo and the residue was extracted with heptane. Concentration (to ca. 25 cm^3) and cooling (−20 °C) gave brown prisms. Yield: 0.69 g, 40%. Found: C, 49.9; H, 5.1; N, 1.7%; Calc. for $C_{36}H_{50}O_4NCl_3W$: C, 50.8; H, 5.9; N, 1.7%. IR: 3492m, 1595m, 1300m, 1260s, 1214s, 1170m, 1104s, 1027m, 924w, 882m, 864m, 804m, 761s, 726s, 681w. ^{1}H NMR ($CDCl_3$): δ 7.126 (m, 2H, aryl*H*), 7.47 (m, 2H, aryl*H*), 3.69 (q, 1H, J_{HH} 6.0 Hz, C*H*), 1.97 (d, 3H, J_{HH} 6.1 Hz, CH_3), 1.30 (s, 18H, (CH_3)$_3$C), 1.22 (s, 18H, (CH_3)$_3$C). O*H* obscurred.

3.9. Preparation of {$WOCl[OArCH_2Ar'(O)CH_2ArO]$}$_2$ Ar′ = 4-methylphenyl (8)

To a solution of [$WOCl_4$] (1.00 g, 2.94 mmol) in diethyl ether (ca. 40 cm^3) at −78 °C was added the triphenol **C** (1.60 g, 2.94 mmol). The system was refluxed for 12 h, volatiles were removed in vacuo, and the residue was extracted into warm MeCN (30 cm^3). Prolonged standing at ambient temperature (2–3 days), afforded purple needles of **8**. Yield: 0.98 g, 43%. Further crops can be obtained by concentration

of the mother-liquor. Total isolated yield 64%. Found: C, 60.8; H, 7.1%. Calc. for $C_{74}H_{104}O_8Cl_2W_2$: C, 61.6; H, 7.2%. IR: 1594w, 1359m, 1293w, 1261s, 1241w, 1218w, 1155m, 1095bs, 1019bs, 973s, 910w, 880w, 872w, 852m, 796s, 767m, 753w, 722w, 666w, 601w, 570m, 514w, 506w, 472w, 455w. ^{1}H NMR ($CDCl_3$): δ 7.27 (m, 8H, aryl*H*), 7.09 (s, 4H, aryl*H*), 5.07 (d, 4H, $^2J_{HH}$ 13.3 Hz, CH_2), 3.50 (d, 4H, $^2J_{HH}$ 13.3 Hz, CH_2), 2.27 (s, 6H, CH_3), 1.40 (s, 36H, C(CH_3)$_3$), 1.24 (s, 36H, C(CH_3)$_3$).

3.10. Preparation of {WOCl[OArCH$_2$Ar′(O)CH$_2$ArO]}$_2$ Ar′ = 4-tert-butylphenyl (9)

[W(NPh)Cl$_4$(Et$_2$O)] (1.00 g, 2.0 mmol) and triphenol **D** (1.01 g, 2.01 mmol) were refluxed in toluene (30 cm^3) for 12 h. On cooling, volatiles were removed in vacuo and the residue was extracted into hexane (30 cm^3). Cooling to −20 °C afforded brown blocks of **9** in 38% yield: 0.56 g. Alternatively, **9** can be prepared in ca. 60% yield using [WOCl$_4$] in the above procedure. Found: C, 54.8; H, 6.1%. Calc. for $C_{68}H_{86}O_8Cl_2W_2$: C, 55.6; H, 5.9%. IR: 1600w, 1293w, 1261s, 1206m, 1168m, 1096bs, 1019bs, 972m, 909w, 858m, 801s, 738m, 718m. ^{1}H NMR ($CDCl_3$): δ 7.21–7.24 (m, 4H, aryl*H*), 7.17 (s, 4H, aryl*H*), 7.10 (s, 4H, aryl*H*), 5.05 (d, 4H, $^2J_{HH}$ 13.4 Hz, CH_2), 3.52 (d, 4H, $^2J_{HH}$ 13.4 Hz, CH_2), 2.49 (s, 12H, CH_3), 1.42 (s, 36H, C(CH_3)$_3$), 1.19 (s, 18H, C(CH_3)$_3$).

3.11. Preparation of [W(eg)$_2$(OAr^{4}CH$_2$Ar^3(O)-CH$_2$Ar^{4}OH)] (10)

[W(eg)$_3$] (1.00 g, 2.75 mmol) and triphenol **E** (2.27 g, 5.49 mmol) were refluxed in toluene for 12 h. Volatiles were removed in vacuo and the residue was extracted into hot MeCN (40 cm^3). Prolonged standing at ambient temperature afforded **10** as orange needles. Yield: 1.08 g, 55%. Found: C, 52.9; H, 5.1%. Calc. for $C_{32}H_{40}O_7W$: C, 53.3; H, 5.6%. IR: 3367w, 1304m, 1248m, 1214s, 1146m, 1099w, 1049m, 1030s, 944w, 913s, 878m, 840m, 781w, 722m, 657s, 620s. ^{1}H NMR ($CDCl_3$): δ 7.11–7.58 (several m, 6H, aryl*H*), 5.91–6.01 (2× m, 4H, OCH_2), 5.53–5.74 (2× m, 4H, OCH_2), 4.29 (d, $^2J_{HH}$ 15.0 Hz, CH_2), 2.69 (s, 3H, CH_3), 2.32–2.58 (overlapping signals, 11H, 3x CH_3 + CH_2), 1.50 (s, 9H, C(CH_3)$_3$).

3.12. X-ray crystallography

Crystals were mounted on thin glass fibres using perfluoropolyether oil, which was frozen in situ by the cold nitrogen gas Cryostream flow. Data for compounds **1**, **3**, **5**, **8**, **9** and **10** were collected using an Enraf–Nonius Kappa CCD diffractometer using monochromated Mo Kα radiation ($\lambda = 0.71073$ Å). Data was collected to $\theta_{max} \geqslant 27.5°$ for all structures with the exception of **5** ($\theta_{max} = 20.4°$), due to lack of high-angle diffraction from the sample. Cell refinement and data reduction was performed using the HKL SCALEPACK and DENZO [16] and COLLECT [17] utilities. Absorption corrections were made based on ψ- and ω-scans using the SORTAV program [18]. Structures were solved using direct methods and refined on F^2 using the program SIR-92 [19] and then refined using SHELXTL-97 software [20]. Geometrical restraints were applied to improve refinement of PMe_3 ligands in compound **3**; all P–C bond distances have been restrained using a single common free variable, while C···C distances were treated similarly, in order to obtain idealized (tetrahedral) geometries for these moieties. All non-hydrogen atoms were refined anisotropically for all structures. Aromatic H-atoms were fixed based on idealised positions and their values of U_{iso} set to 1.5 times that of the carrier atom [21]. See Table 1 for further crystallographic information.

Acknowledgements

The University of East Anglia and Prof. V.C. Gibson (Imperial College) are thanked for financial support. We thank John Davies (Cambridge University) for help with crystal structure determinations.

Appendix A. Supplementary data

Atomic coordinates, bond lengths and angles, displacement parameters and hydrogen atom positions have been deposited with the Cambridge Crystallographic Data Centre, with deposition codes CCDC 290126 – 290131. Copies of this information may be obtained free of charge from The Director, CCDC, 12 Union Road, Cambridge, CB2 1EZ, UK, fax: +44 1223 366 033, e-mail: deposit@ccdc.ac.uk or on the web www: http://www.ccdc.cam.ac.uk. Supplementary data associated with this article can be found, in the online version, at doi:10.1016/j.poly.2005.12.008.

References

[1] (a) G.J.P. Britovsek, V.C. Gibson, D.F. Wass, Angew. Chem. Int. Ed. 38 (1999) 428;
(b) V.C. Gibson, S. Spitzmesser, Chem. Rev. 103 (2003) 283.
[2] P.J. Toscano, E.J. Schermerhorn, C. Dettelbacher, D. Macherone, J. Zubieta, J. Chem. Soc., Chem. Commun. (1991) 933.
[3] (a) C. Floriani, F. Corazza, W. Lesueur, A. Chiesi-Villa, C. Guastini, Angew. Chem., Int. Ed. Engl. 28 (1989) 66;
(b) J. Okuda, S. Fokken, H.-C. Kaug, W. Massa, Chem. Ber. 128 (1995) 221;
(c) F. Corazza, C. Floriani, A. Chiesi-Villa, C. Guastini, Inorg. Chem. 30 (1991) 145;
(d) M.H. Chisholm, J.-H. Huang, J.C. Huffman, W.E. Streib, D. Tiedtke, Polyhedron 16 (1997) 2941.
[4] (a) M.H. Chisholm, J.-H. Huang, J.C. Huffman, I.P. Parkin, Inorg. Chem. 36 (1997) 1642;
(b) D.R. Mulford, P.E. Fanwick, I.P. Rothwell, Polyhedron 19 (2000) 35.
[5] (a) Y. Takashima, Y. Nakalama, H. Yasuda, A. Harada, J. Organomet. Chem. 651 (2002) 114;
(b) A. Lehtonen, R. Sillanpää, Polyhedron 21 (2002) 1017.
[6] (a) B.-T. Ko, Y.-C. Chao, C.-C. Lin, J. Organomet. Chem. 598 (2000) 13;
(b) B.-T. Ko, C.-C. Wu, C.-C. Lin, Organometallics 19 (2000) 1864;

(c) I. Taden, H.-C. Kang, W. Massa, T.P. Spaniol, J. Okuda, Eur. J. Inorg. Chem. (2000) 441.
[7] (a) B.W.F. Gordon, M.J. Scott, Inorg. Chim. Acta 297 (2000) 206;
(b) H. Kawaguchi, T. Matsuo, Angew. Chem. Int. Ed. 41 (2002) 2792;
(c) T. Matsuo, H. Kawaguchi, Inorg. Chem. 41 (2002) 6090;
(d) W.O. Appiah, A.D. DeGreeff, G.L. Razidlo, S.J. Spessard, M. Pink, V.G. Young Jr., G.E. Hofmeister, Inorg. Chem. 41 (2002) 3656;
(e) T. Matsuo, H. Kawaguchi, M. Sakai, J. Chem. Soc., Dalton Trans. (2002) 2536;
(f) T. Matsuo, H. Kawaguchi, Organometallics 22 (2003) 5379;
(g) H. Kawaguchi, T. Matsuo, J. Organomet. Chem. 690 (2005) 5333.
[8] H. Kawaguchi, T. Matsuo, J. Organomet. Chem. 689 (2004) 4228.
[9] (a) C. Redshaw, Coord. Chem. Rev. 244 (2003) 45, and references therein;
(b) C. Redshaw, L. Warford, S.H. Dale, M.R.J. Elsegood, Chem. Commun. (2004);
(c) C. Redshaw, D.M. Homden, M.A. Rowan, M.R.J. Elsegood, Inorg. Chim. Acta 358 (2005) 4067.
[10] (a) See for example F. Quignard, M. Leconte, J.-M. Basset, J.J. Alexander, S.S. Shore, Inorg. Chem. 26 (1987) 4272;
(b) R.M. Kolodziej, R.R. Schrock, J.C. Dewan, Inorg. Chem. 28 (1989) 1243;
(c) J.L. Kerschner, P.E. Fanwick, I.P. Rothwell, J.C. Huffman, Inorg. Chem. 28 (1989) 780;
(d) W. Clegg, R.J. Errington, P. Kraxner, C. Redshaw, J. Chem. Soc., Dalton Trans. (1992) 1431;
(e) H. Yasuda, Y. Nakayama, K. Takei, A. Nakamura, Y. Kai, N. Kanehisa, J. Organomet. Chem. 473 (1994) 105.
[11] C. Persson, A. Oskarson, C. Andersson, Polyhedron 11 (1992) 2039.
[12] (a) A. Lehtonen, R. Sillanpää, Polyhedron 19 (2000) 2579;
(b) A. Lehtonen, R. Sillanpää, Polyhedron 22 (2003) 2755.
[13] V.C. Gibson, T.P. Kee, A. Shaw, Polyhedron 7 (1988) 579.
[14] S.F. Pedersen, R.R. Schrock, J. Am. Chem. Soc. 104 (1982) 7483.
[15] A. Lehtonen, R. Sillanpää, Polyhedron 13 (1994) 2519.
[16] W. Wolfsberger, H. Schmidbaur, Synth. React. Inorg. Met. Org. Chem 4 (1974) 149.
[17] Z. Otwinowski, W. Minor, HKL SCALEPACK, in: C.W. CarterJr., R.M. Sweet (Eds.), Macromolecular Crystallography, Part A, Methods in Enzymology, vol. 276, Academic Press, New York, 1997, p. 307.
[18] Nonius COLLECT, Nonius BV, Delft, The Netherlands.
[19] R.H. Blessing, SORTAV, Acta Cryst. A51 (1995) 33.
[20] A. Altamore, M.C. Burla, G. Camalli, G. Cascarano, C. Giacovazzo, A. Gualiardi, G. Polidori, J. Appl. Cryst. 27 (1994) 435.
[21] G.M. Shelderick, SHELXTL Version 6.10, Bruker AXS, Inc., Madison, Wisconsin, 1997.

of the higher field CD_2H quintet as the internal reference (δ 2.74 ppm, relative to $SiMe_4$). Time dependent visible (340–800 nm) and UV (220–320 nm) spectra and absorbance-time data generated from such data were recorded on a HP8453A diode array Vis/UV spectrophotometer thermostated to 25.0 ± 0.1 °C with use of a Lauda RM6 circulating water bath. Reported Vis/UV spectra for all compounds have been extrapolated to zero reaction time. Kinetic data were analysed by weighted non-linear regression on a Macintosh with the usual packages, or by importing the HP .kd files into Specfit® and carrying out Global Spectral Analysis (SVD data reduction) and subsequent fitting to either a single or double exponential integrated rate expression [14]. Carbon dioxide free Milli-Q® water was used for all physical measurements.

2.1. Synthesis and characterisation

$[Co(NH_3)_4(OCO_2)]NO_3 \cdot 0.5H_2O$ and $[Co(NH_3)_4(OCO_2)]Cl$ were prepared by two standard methods, the faster H_2O_2 oxidation procedure [15,16] being preferred over the aerial oxidation route [15,17]. $[Co(NH_3)_4(OCO_2)]_2SO_4 \cdot 3H_2O$ was made by the published procedure [10,18], as were *cis*-$[Co(NH_3)_4(OH_2)Cl]SO_4$ and *cis*-$[Co(NH_3)_4(OH_2)_2]_2(SO_4)_3 \cdot 3H_2O$ derived from it [15,18,19]. The carbonato sulfate was converted to the chloride by metathesis using the stoichiometric amount of $BaCl_2 \cdot 2H_2O$ to remove the sulfate and then crystallised by precipitation with methanol. *cis*-Diaqua sulfate was generated in situ from the carbonato sulfate with the required amount of H_2SO_4, and then treated with pyridine and $Na_2S_2O_6 \cdot 2H_2O$ to afford *cis*-$[Co(NH_3)_4(OH_2)OH]\ S_2O_6$ [20]. Much less pyridine (30 g) is required than that reported (85 g) for the synthesis on the same scale [20]. Dehydration of the latter product (130 °C, 3 h) yielded the *cis*-diol quantitatively [20]; the observed weight loss on dehydration was precisely that calculated. The resultant *cis–cis*-$[(NH_3)_4Co(OH)_2Co(NH_3)_4](S_2O_6)_2$ was converted to the chloride salt by trituration of a thin aqueous slurry with excess NH_4Cl, analogous to that described for the Cr(III) analogue [20]. The product was recrystallised from a saturated aqueous by addition of a fifth volume of saturated NH_4Cl and careful dilution with methanol. The product was collected, and washed with methanol and ether, and air dried.

2.1.1. *cis*-$[Co(NH_3)_4(OH_2)Cl]SO_4$

The crude material was recrystallised by adding sufficient conc. H_2SO_4 to a thick aqueous suspension of the crude sulfate salt to dissolve much of it, filtering rapidly, and then collecting the resultant crystals on cooling. The process was repeated to afford the pure sulfate. *Anal.* Calc. for $CoN_4H_{14}ClSO_5$: H, 5.30; N, 19.66; Cl, 12.27; S, 11.22. Found: H, 5.05; N, 19.99; Cl, 12.63; S, 11.29%.

2.1.2. *cis*-$[Co(NH_3)_4(OH_2)Cl]Cl_2$

cis-$[Co(NH_3)_4(OH_2)Cl]SO_4$ (10 g) was treated with conc. HCl (50 mL) at ambient temperature, and after stirring for 5 min was filtered, washed with ethanol and ether, and air dried. Two recrystallisations from a saturated aqueous solution by adding a third volume of conc. HCl and cooling yielded the pure chloride salt. *Anal.* Calc. for $CoN_4H_{14}Cl_3O$: H, 5.61; N, 22.29; Cl, 42.30. Found: H, 5.39; N, 22.04; Cl, 42.05%. Vis/UV spectrum (0.02 M $HClO_4$): 531 nm, ε(max) 57.5; 372 nm, ε(max) 49.0 $M^{-1}\,cm^{-1}$. ^1H NMR spectrum (D_2O, DCl): δ 4.30 (6H, *cis*-Cl, OH_2); δ 3.63 (3H, *trans*-OH_2); δ 3.20 ppm (3H, *trans*-Cl).

cis-$[Co(NH_3)_4(OH_2)Cl]S_2O_6 \cdot H_2O$ was obtained by adding aqueous $Na_2S_2O_6$ to a solution of the complex chloride. Crystals which formed on cooling overnight were washed with ice water, methanol and then ether and air dried. *Anal.* Calc. for $CoN_4H_{16}ClS_2O_8$: H, 4.50; N, 15.62; Cl, 9.88; S, 17.88. Found: H, 4.24; N, 15.63; Cl, 9.91; S, 17.50%.

2.1.3. *trans*-$[Co(NH_3)_5(OH_2)Cl]Cl_2$

trans-$[Co(NH_3)_5Cl_2]Cl_2 \cdot H_2O$ [18,21] (12.7 g, 50.5 mmol) was partly suspended/dissolved in a mixture of ice (150 g) and water (150 mL) acidified with a few drops of neat CF_3SO_3H or CF_3CO_2H while well-stirred in an ice bath. To this was added dropwise over 4–5 min an ice-cold suspension (yellow) of HgO (red; 10.9 g, 50.3 mmol, 1.0 equiv.) which had been well-stirred and cooled in ice (25 g)/water (10 mL) containing neat CF_3SO_3H (16 g, 107 mmol). The green salt gradually dissolved to yield a violet solution. Some unreacted green complex remained. The addition of a mixture of ice (25 g) and $HClO_4$ (70%; 25 mL) was added to ensure complete precipitation of the unreacted green substrate. The mixture was then filtered, and the residual green solid (<0.2 g) was washed with one bed volume of acetone (50 mL). The filtrate and washing was treated with ice (30 g)/conc. H_2SO_4 (20 mL), and acetone (75 mL) was added to the point of cloudiness. After further stirring on ice (ca. 3 min), the mixture was filtered to remove the precipitate of *cis*-$[Co(NH_3)_4(OH_2)Cl]SO_4$ (ca. 6 g) and washed with acetone (50 mL). The now lavender-grey filtrate was carefully diluted with acetone (ca. 125 mL) just to the point of permanent cloudiness. After 5 min stirring on ice and a then further addition of acetone (100 mL), the crystallisation of *trans*-$[Co(NH_3)_4(OH_2)Cl]SO_4$ was complete. It was removed by filtration, washed with acetone and ether, and air dried (5.1 g). A second crop (1.4 g) was obtained from the filtrate by diluting further with acetone (to 1 L total volume) and allowing to crystallise for 5 min.

The crude *trans* isomer was stirred in aqueous HCl (5 M) whence it transformed from a lavender grey to a fine grey-green Cl^- salt. It was filtered to remove the *cis* isomer which had selectively extracted. The extraction was repeated until the washings were virtually colorless and the residual solid had become a dull green. The purified *trans*-$[Co(NH_3)_4(OH_2)Cl]Cl_2$ was finally recrystallised from a minimum volume of ice water by filtering and quickly adding cold 5 M HCl. Shiny green-grey needles resulted, which were quickly collected, washed with methanol and

ether and air dried. *cis* Isomer is introduced if crystallisation is delayed. *Anal.* Calc. for $CoN_4H_{14}Cl_3O$: H, 5.65; N, 22.42; Cl, 42.55. Found: H, 5.64; N, 22.05; Cl, 41.68%. Vis/UV spectrum (0.02 M $HClO_4$): 593 nm, ε(max) 30.7; 470 nm, ε(max) 24.1; 367 nm, ε(max) 50.0; 530 nm, ε 20.4 $M^{-1}\,cm^{-1}$. ^1H NMR spectrum (D_2O, DCl): δ 4.36 ppm (6H, *cis*-Cl, OH_2).

An aqueous solution of the Cl^- salt yielded crystals of the SO_4^{2-} or $S_2O_6^{2-}$ using the appropriate precipitant (5 M H_2SO_4 or 5 M aqueous $Li_2S_2O_6$).

An alternative synthesis of the *trans*-aquachloro complex is via reaction of *trans*-$[Co(NH_3)_4Cl_2]Cl \cdot H_2O$ in neat triflic acid, as described for the bis(ethylenediamine) analogue [22]. The product mixture required fractionation of the sulfate salts, as described above.

2.1.4. *trans*-$[Co(NH_3)_4Cl_2]Cl \cdot H_2O$

This followed that described by Jørgensen, reaction of *cis*-$[Co(NH_3)_4(OH_2)_2]_2(SO_4)_3 \cdot 3H_2O$ in conc. H_2SO_4, followed by reaction with 37% HCl, all at ambient temperature [18,21]. By warming to 50–60 °C, the time scale of the synthesis can be reduced from 48 h to 30 min, and reduced further by using $[Co(NH_3)_4(OCO_2)]_2SO_4 \cdot 3H_2O$ directly rather than first converting it to the *cis*-diaqua complex using aqueous H_2SO_4. The grass-green product is reported to be the chloride salt, but it contains free sulfate and requires recrystallisation from H_2O/HCl to yield pure *trans*-$[Co(NH_3)_4Cl_2]Cl \cdot H_2O$. The perchlorate salt was obtained by metathesis in water using 5 M $HClO_4$ as precipitant. *Anal.* Calc. for $CoN_4H_{14}Cl_3O$: H, 5.61; N, 22.29; Cl, 42.30. Found: H, 5.38; N, 22.11; Cl, 42.13%. Vis/UV spectrum (0.02 M $HClO_4$): 634 nm, ε(max) 42.1; 538 nm, ε(min) 4.7; 467 nm, ε(max) 21.5; 377 nm, ε(max) 36.8; 370 nm, ε(max) 46.4 $M^{-1}\,cm^{-1}$. ^1H NMR spectra: DMF-d_7: δ 4.20 (12H, *cis*-Cl); D_2O, DCl: δ 4.06 ppm (12H, *cis*-Cl).

2.2. *cis*-$[Co(NH_3)_4Cl_2]ClO_4$

The following is a modification of Werner's procedure [1]. Concentrated HCl which had been saturated with HCl (g) at 0 °C was allowed to warm to ca. 15 °C and then 30 mL was added to *cis–cis*-$[(NH_3)_4Co(OH)_2Co(NH_3)_4]Cl_4$ (5.0 g) in a mortar and ground rapidly for ca. 40 s. The crystals that had quickly changed consistency and colour were filtered and the then chilled filtrate and ethanol washings (2 × 10 mL) were treated with cold $HClO_4$ (5 M; 1:1 70% mixed with ice). On scratching blue crystals deposited which were collected, washed with ethanol and ether and air dried. The original solid was extracted with small portions of ice water to give a red solution of the diaqua complex which contained a little of the *cis*-dichloro complex; this was again crystallised using 5 M $HClO_4$. The solid residue was crude blue *cis*-dichloro chloride which was extracted with sufficient ice water to dissolve it all, filtered, and treated with a fifth volume of cold $HClO_4$ (5 M). The three fractions of *cis*-$[Co(NH_3)_4Cl_2]ClO_4$ were combined and quickly recrystallised from water/$HClO_4$. Yield: 1.6 g (46%, based on diol). *Anal.* Calc. for $CoH_{12}N_4Cl_3O_4$: H, 4.07; N, 18.84; Cl, 35.76. Found: H, 4.34; N, 18.51; Cl, 35.32%. Vis/UV spectrum (0.02 M $HClO_4$): 594 nm, ε(sh) 54.2; 563 nm, ε(max) 57.1; 456 nm, ε(min) 9.5; 390 nm, ε(sh) 61.0 $M^{-1}\,cm^{-1}$. ^1H NMR spectrum: DMF-d_7: δ 4.25 (6H, *cis*-Cl); δ 2.74 (6H, *trans*-Cl); D_2O, DCl: δ 4.10 (6H, *cis*-Cl); δ 3.35 ppm (6H, *trans*-Cl).

trans-$[Co(NH_3)_4(NO_2)_2]Cl$ was synthesised as described [23]. It was recrystallised from a saturated aqueous solution by addition of a fifth volume of saturated NH_4Cl and careful dilution with methanol. The perchlorate salt was obtained by metathesis in water using $HClO_4$ as precipitant. Vis/UV spectrum (H_2O): λ(max) 441 and 347 nm. ^1H NMR spectrum (DMF-d_7): δ 3.82 (12H, *cis*-NO_2).

cis-$[Co(NH_3)_4(NO_2)_2]Cl$ was initially prepared as reported by aerial oxidation of Co(II) in the presence of excess NH_3 and NO_2^- [18]; the yield of pure material is poor. The high yield synthesis of *cis*-$[Co(NH_3)_4(NO_2)_2]NO_3$ has been reported [23]. We have made the Cl^- salt by warming *cis*-$[Co(NH_3)_4(OH_2)Cl]Cl_2$ with excess $NaNO_2$ (5 equiv.) after the addition of HCl to first generate the nitritochloro complex. The yellow product was reprecipitated from water with HCl, and then freed of a little *trans* isomer by extracting about 90% of the product with water and crystallising using HCl. This process was repeated to afford yellow needles of the pure *cis* salt. The perchlorate was obtained as described for the *trans* isomer. Vis/UV spectrum (H_2O): λ(max) 441 and 324 nm. ^1H NMR spectrum (DMF-d_7): δ 3.86 (6H, *cis*-NO_2); δ 3.60 ppm (6H, *trans*-NO_2).

An alternative synthesis, and one that gives cis isomer cleanly, is as follows. $[Co(NH_3)_4(OCO_2)]Cl$ in water was treated with sufficient H_2SO_4 to generate the *cis*-$[Co(NH_3)_4(OH_2)_2]^{3+}$ species, as described [20]. Addition of excess $NaNO_2$ (5 equiv.) was added, and the stirred mixture was allowed to stand 48 h to allow the nitrito species to isomerise to the nitro complex. Ethanol was added to precipitate the product, and the filtered material was recrystallised from hot water by addition of a fifth volume of saturated NH_4Cl and dilution with methanol. Fine yellow-orange crystals slowly deposited on cooling. Curiously, this material was much less soluble than the *cis*-dinitro chloride obtained as above, and proved to contain no chloride but rather anionic sulfate which had carried through from the H_2SO_4 plus carbonato chloride initial step.

cis-$[Co(NH_3)_4(NO_2)Cl]Cl$ was obtained by allowing a stirred, thin slurry of *cis*-$[Co(NH_3)_4(NO_2)_2]Cl$ in conc. HCl (1 g in 5 mL) to react for 18 h. The crude product was collected by filtration, washed with ethanol and ether, and air dried. This was extracted carefully with water to yield a claret solution and a green residue of the less soluble *trans*-$[Co(NH_3)_4Cl_2]Cl$. Addition of HCl precipitated the red-claret chloride salt which was recrystallised from water using HCl as precipitant to afford the Cl^- salt. Trituration of the Cl^- salt in a thin slurry with 70% $HClO_4$ removed Cl^- as HCl, and the filtered product was recrystallised from

water/$HClO_4$. ^1H NMR spectrum (DMF-d_7): δ 4.54 (6H, *cis*-NO_2, *cis*-Cl); δ 4.04 (3H, *cis*-Cl, *trans*-NO_2); δ 3.48 ppm (3H, *trans*-Cl).

trans-$[Co(NH_3)_4(NO_2)Cl]Cl$ was synthesised from *trans*-$[Co(NH_3)_4(NO_2)_2]Cl$ as described for the *cis* isomer above but allowing a 27 h reaction time. The *trans*-dinitro complex is not very soluble in HCl but cleanly transforms to the *trans*-nitrochloro product quantitatively, whereas the *cis* isomer partly dissolves in HCl and some loss of the second NO_2^- ligand occurs. The salmon pink *trans*-nitrochloro product was obtained as Cl^- and ClO_4^- salts. ^1H NMR spectrum (DMF-d_7): δ 3.70 ppm (12H, *cis*-NO_2, *cis*-Cl).

2.3. Kinetics of acid hydrolysis

Reactions were followed spectrophotometrically using a 8-cell compartment housed in an HP8453A diode array Vis/UV spectrophotometer and the in situ method described previously [24]. The solvent was 1.0, 0.1 or more usually 0.02 M $HClO_4$.

3. Results and discussion

3.1. Syntheses

trans-$[Co(NH_3)_4Cl_2]Cl \cdot H_2O$ was obtained by a modification of a published method [21]. It is much less soluble in water than the bis(ethylenediamine) analogue, and this is also true of methanol as solvent in which it is virtually insoluble. For the perchlorate salts, the water solubilities are reversed. The perchlorate counter ion does not precipitate the chloroaqua ions, and thus both *cis*- and *trans*-$[Co(NH_3)_4Cl_2]ClO_4$ are obtained free of the chloroaqua species which otherwise readily crystallise when Cl^-, SO_4^{2-} or $S_2O_6^{2-}$ are used as counterions.

Werner's classic *cis*-$[Co(NH_3)_4Cl_2]Cl$ complex was first synthesised by HCl cleavage of the *cis*-diol $[(NH_3)_4Co(\mu\text{-}OH)_2Co(NH_3)_4]Cl_4$ [1]. A 1:1 mixture of *cis*-$[Co(NH_3)_4Cl_2]Cl$ and *cis*-$[Co(NH_3)_4(OH_2)_2]Cl_3$ results. The HCl needs to be above the standard concentrated grade (11.7 M) or the yield of the dichloro complex from the bridge cleavage process is reduced. Treatment of *cis*-$[Co(NH_3)_4(NO_2)_2]Cl$ with concentrated HCl has been reported [18,25] as (rapidly) producing *cis*-$[Co(NH_3)_4Cl_2]Cl$, but in our hands it yielded (slowly) *cis*-$[Co(NH_3)_4(NO_2)Cl]Cl$, and on prolonged standing, *trans*-$[Co(NH_3)_4Cl_2]Cl$. Similarly, the *trans*-dinitro complex yielded *trans*-$[Co(NH_3)_4(NO_2)Cl]Cl$; these syntheses parallel the bis(ethylenediamine) chemistry [3]. Werner's alternative syntheses [3] of *cis*-$[Co(NH_3)_4Cl_2]Cl$ via reaction of $[Co(NH_3)_4(OCO_2)]Cl$ in aqueous or ethanolic HCl yielded only *cis*-$[Co(NH_3)_4(OH_2)Cl]Cl_2$ in our hands. Also, we found that the latter gives *trans*-$[Co(NH_3)_4Cl_2]Cl$ on prolonged reaction in HCl.

In hindsight, it is surprising that any of these syntheses for the *cis*-dichloro complex work, even the successful diol cleavage reaction! Werner envisaged the reaction as a simple *cis*-Co–O cleavage reaction, with such bond rupture occurring on the same Co centre. However, acid cleavage of the diol might have proceeded either way, as shown in Scheme 1.

However, we can confirm that no observable *cis*-$[Co(NH_3)_4(OH_2)Cl]Cl_2$ is produced in the diol cleavage reaction. Similarly, the acid cleavage reactions of the carbonato and dinitro complexes, each reported to yield the *cis*-$[Co(NH_3)_4Cl_2]Cl$ complex, might have expected to yield aqua complexes, given the known modes of bond cleavage revealed through tracer studies [4,26], Scheme 2.

In our hands, no *cis*-dichloro complex was formed.

We have found that neither *cis*- nor *trans*-$[Co(NH_3)_4(OH_2)Cl]^{2+}$ yield *cis*-$[Co(NH_3)_4Cl_2]^+$ on reaction with HCl under a variety of conditions, nor does evaporation of an aqueous solution of the *trans*-dichloro chloride, a strategy successful in the bis(ethylenediamine) system.

Finally, the anation of either *cis*-$[Co(NH_3)_4(OSMe_2)_2](ClO_4)_3$ using Et_4Cl in either DMSO or DMF failed to yield appreciable *cis*-dichloro isomer, yet in the corresponding bis(ethylenediamine) systems [27] the *cis*-dichloro complex is formed and is strongly stabilised by ion-pairing in such dipolar aprotic media.

cis-$[Co(NH_3)_4(OH_2)Cl]SO_4$ and *cis*-$[Co(NH_3)_4(OH_2)Cl]S_2O_6 \cdot H_2O$ were too insoluble to be generally useful, while the more soluble *cis*-$[Co(NH_3)_4(OH_2)Cl]Cl_2$ as prepared by various published routes was not pure (^1H NMR). Conversion to the sulfate and back to the chloride removed these impurities. The chloride and sulfate salts were anhydrous; hydrates have been reported [13].

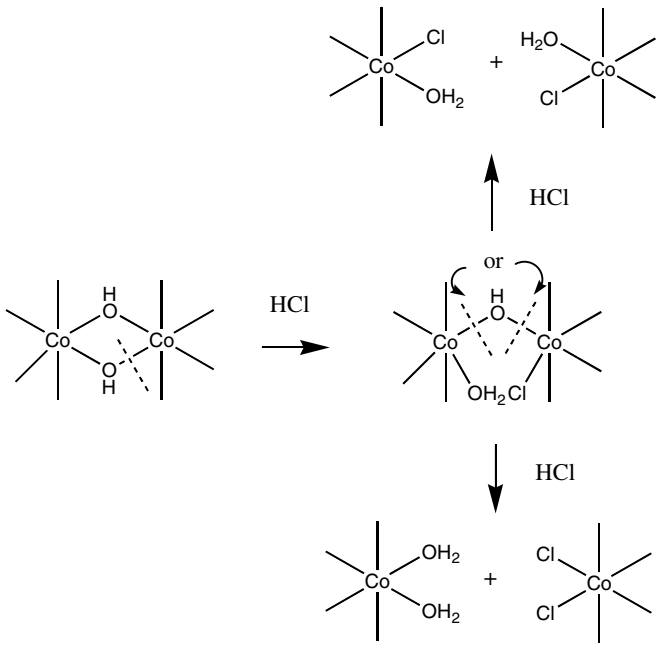

Scheme 1. Alternative modes of acid catalysed OH– bridge cleavage in the diol.

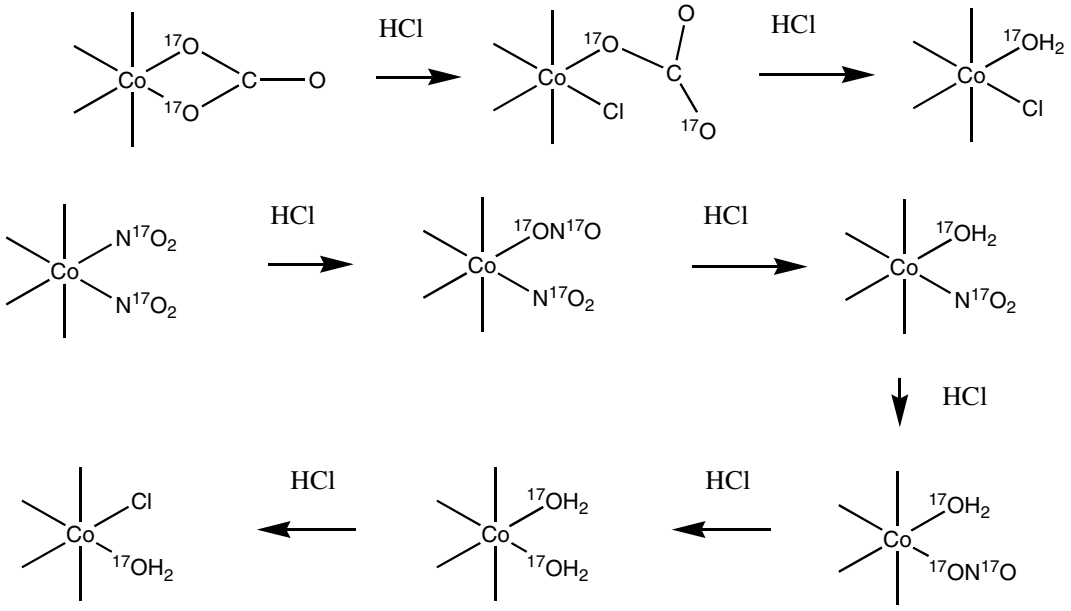

Scheme 2. Acid induced bond cleavage and rearrangement modes for carbonate and nitrite complexes of cobalt(III).

The *trans*-$[Co(NH_3)_4(OH_2)Cl]Cl_2$ complex is new. It was synthesised by Hg(II) induced aquation of *trans*-$[Co(NH_3)_4Cl_2]^+$, a method similar to that described for the bis(ethylenediamine) analogue [28]. It was also obtained [22] by reacting *trans*-$[Co(NH_3)_4Cl_2]Cl \cdot H_2O$ with triflic acid to yield $[Co(NH_3)_4(O_3SCF_3)Cl]CF_3SO_3$, which rapidly formed a *cis*-/*trans*-$[Co(NH_3)_4(OH_2)Cl]^{2+}$ mixture on hydrolysis, and this could be separated using the sulfate counter-ion. *cis*/*trans* Mixtures of salts of $[Co(NH_3)_4(OH_2)Cl]^{2+}$ proved virtually impossible to separate completely as the Cl^-, SO_4^{2-} or $S_2O_6^{2-}$ salts, due to the relatively rapid rate of trans to cis isomerisation and because, for SO_4^{2-} and $S_2O_6^{2-}$, the *trans* isomer is more soluble; the *cis* form then tends to co-crystallise. As the Cl^- salt, even small amounts of the *cis* form rendered the crystals grey, although they appeared homogeneous under the microscope. It could, however, be rendered completely free of it by successive extractions with small amounts of 1 M HCl until the extracts were a consistent pale violet colour. The residue was a dull green salt.

The four nitro complexes, of which *cis*- and *trans*-$[Co(NH_3)_4(NO_2)Cl]^+$ appear to be new, were reactants or products of the synthetic reactions described, and which did not proceed as reported. They are analogous to their bis(ethylenediamine) counterparts, and were characterised by their Vis/UV and ^1H NMR spectra; the characteristic difference between *cis* and *trans*-nitro species in the UV is noted.

3.2. Isomerisation of $[Co(NH_3)_4(OH_2)Cl]^{2+}$

The isomerisation of *trans*-$[Co(NH_3)_4(OH_2)Cl]^{2+}$ in dilute $HClO_4$ at 25 °C was followed in both the visible (340–700 nm) and UV (220–320, 270–300 nm) regions. In the visible region, two sharp isosbestic points were observed (589 nm, ε 30.7 $M^{-1}\,cm^{-1}$; and 473 nm, ε 23.8 $M^{-1}\,cm^{-1}$) and the absorbance changes were large (Fig. 1). Absorbance changes in the UV were much smaller (Figure 1S) because *cis*- and *trans*-$[Co(NH_3)_4(OH_2)Cl]^{2+}$ have very similar spectra throughout this region. Nonetheless, by working on the tail of the UV where the absorbance is low yet proportional absorbance changes are appreciable, and through raising the [Co] to take advantage of this, a sharp isosbestic point was observed at 284 nm (Figure 2S), and the absorbance-time data accurately fitted a single exponential ($k_{obsd} = 2.31 \times 10^{-3}\,s^{-1}$). The rate data obtained from the three spectral regions were in good agreement (Table 1), and k_{obsd} is not appreciably medium dependent (1.0, 0.1, 0.02 M $HClO_4$).

The *trans*/*cis* equilibrium, while it favours the *cis* side (88%), is not so far to that side that the rate could not be measured starting with the *cis* isomer. The spectral changes commencing with *cis* are small (Figure 3S) but sufficient to define the rate well (Table 1), and even the two isosbestic points (473 and 590 nm). The measured k_{obsd} should be the same since the sum of the forward and reverse rates are measured commencing with either isomer, and indeed this is born out by the results (Table 1).

Equilibrium $[Co(NH_3)_4(OH_2)Cl]^{2+}$ data are given in Table 2 and results are internally consistent for the four different starting materials. This result, $88 \pm 1\%$ *cis*, is not too different to that estimated by Linck's indirect method [10,13] ($90.5 \pm 1.0\%$ *cis*).

The ^1H NMR spectrum (Fig. 2) show the single line spectrum for the trans isomer in D_2O/DCl change into the 2:1:1 pattern expected for *cis*-$[Co(NH_3)_4(OH_2)Cl]^{2+}$, and confirm its presence at equilibrium to the extent of ca. 10%.

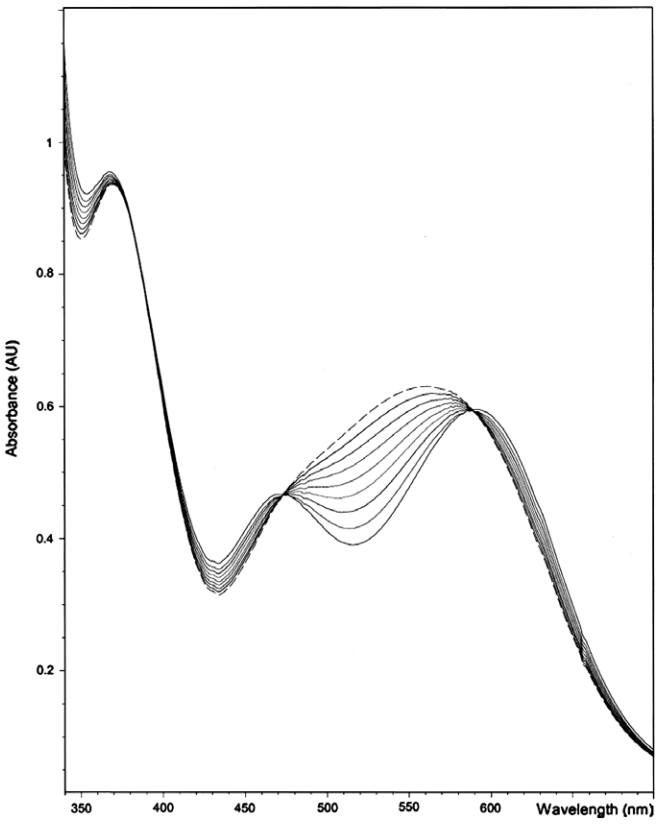

Fig. 1. Visible spectral changes for the isomerization of *trans*-$[Co(NH_3)_4(OH_2)Cl]^{2+}$ in H_2O/H^+, 25 °C.

Table 1
Rate data for the reversible isomerisation of *trans*-$[Co(NH_3)_4(OH_2)Cl]^{2+}$ in dilute $HClO_4$ at 25 °C

$[HClO_4]$ (M)	Region[c]	10^3k_2 (s^{-1})[a]
0.020	vis	2.31 (10)
	vis	2.32 (3)[b]
	UV	2.17 (6)
0.10	vis	2.36 (3)
1.0	vis	2.62 (9)

[a] $k_2 = k_{tc} + k_{ct}$; $k_{tc}/k_{ct} = 88/12$ (Table 2). The number of determinations is given in parenthesis.
[b] Reactant was *cis*-$[Co(NH_3)_4(OH_2)Cl]Cl_2$.
[c] Global analysis fits (refer text).

Table 2
Equilibrium data for the reversible isomerisation of *trans*-$[Co(NH_3)_4(OH_2)Cl]^{2+}$ in 0.020 M $HClO_4$ at 25 °C

Reactant	ε (530 nm) (M^{-1} cm^{-1})	%*cis*(equil)[a]
cis-$[(OH_2)Cl]SO_4$	53.0 (2)	88
cis-$[(OH_2)Cl]S_2O_6 \cdot H_2O$	52.8 (3)	87
cis-$[(OH_2)Cl]Cl_2$	53.7 (2)	90
trans-$[(OH_2)Cl]Cl_2$	53.5 (2)	89
trans-$[Cl_2]Cl \cdot H_2O$	53.0 (2)	88
cis-$[Cl_2]ClO_4$	52.6 (2)	87
Ave:	53.0 (13)	88 (13)

[a] Number of determination in parenthesis; results calculated from ε(530) for the *cis* isomer, 57.5, and ε(530) for the *trans* form, 20.4 M^{-1} cm^{-1}.

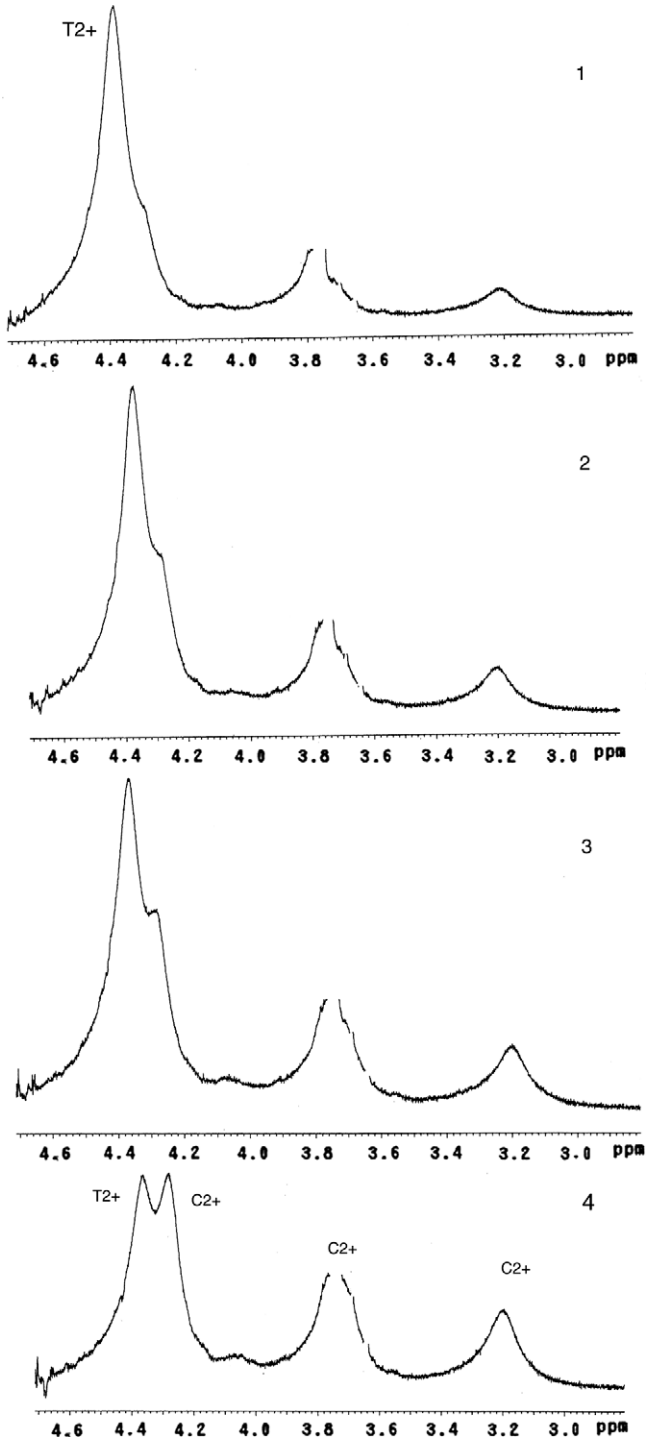

Fig. 2. ^1H NMR spectra (NH region) for the isomerization of *trans*-(T2+) to cis- (C2+) $[Co(NH_3)_4(OH_2)Cl]^{2+}$ in D_2O/D^+ at ca. 21 °C; times increase from 1 to 4.

3.3. Aquation of *cis*-$[Co(NH_3)_4Cl_2]^+$

The hydrolysis rate for the *cis* isomer has never been measured. It has been described as 'very fast' by Pearson et al. [8], and that the aquation was very rapid was implied by Werner [1,3] in his experimental descriptions of poor recovery through rapid recrystallisation from water. It is a myth. It hydrolyses at about the same rate as the *trans*

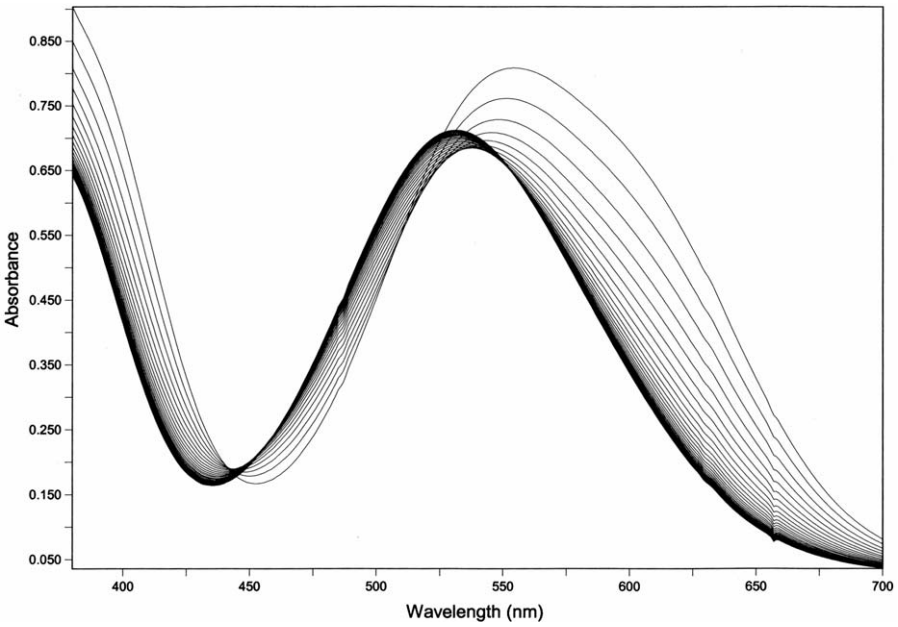

Fig. 3. Visible spectral changes for the hydrolysis of *cis*-$[Co(NH_3)_4Cl_2]^+$ in H_2O/H^+, 25 °C. The absorbance decreases with time at 600 nm.

isomer. The changes in visible spectra (340–700 nm; Fig. 3) with time hide the fact that there are two early sharp isosbestic points, one of which changes quickly with time (Fig. 4S. 440 nm, ε 13.0; 514 nm, ε 39.0 M^{-1} cm^{-1}). The first phase is loss of one Cl^- and the second is *cis*-/*trans*-$[Co(NH_3)_4(OH_2)Cl]^{2+}$ isomerisation. The final spectrum corresponds to a 88% *cis*/22% *trans* distribution (Table 2). The absorbance–time trace at 530 nm (Fig. 4) clearly indicates the biphasic behaviour, and in particular it shows that the second phase corresponds to *trans–cis* rather than *cis–trans* isomerisation, i.e., the initial hydrolysis reaction leads to not only both *cis*- and *trans*-$[Co(NH_3)_4(OH_2)Cl]^{2+}$ but an isomeric mixture which contains more *trans* isomer than does the equilibrium distribution.

The changes in the UV absorption spectra accompanying the hydrolysis of the *cis*-dichloro complex are relatively small (Figure 5S), but nonetheless sufficient to determine a rate constant for the hydrolysis. The data fitted a single exponential because in the region examined (280–320 nm) the absorbance changes for the secondary isomerisation process are much smaller, and negligible. The results (see below) bear this out – the visible and UV rate data agree.

The primary hydrolysis rate constant was determined by fitting the 589 nm data to a single exponential. The fits were good, since this wavelength is an isosbestic point for the secondary *trans*/*cis* isomerisation reaction. The 530 nm data (Fig. 4) were then fitted to two exponentials with the first exponential (k_1) fixed at the value determined from the 589 nm data. This yielded k_2 which is the aquachloro isomerisation rate, and the check on the correctness of the analysis is the reasonable agreement of this value and that determined independently for this reaction (Table 3; cf. Table 1).

It is evident that k_1 and k_2 are very similar in magnitude. Because of this, the global analysis of the visible absorption

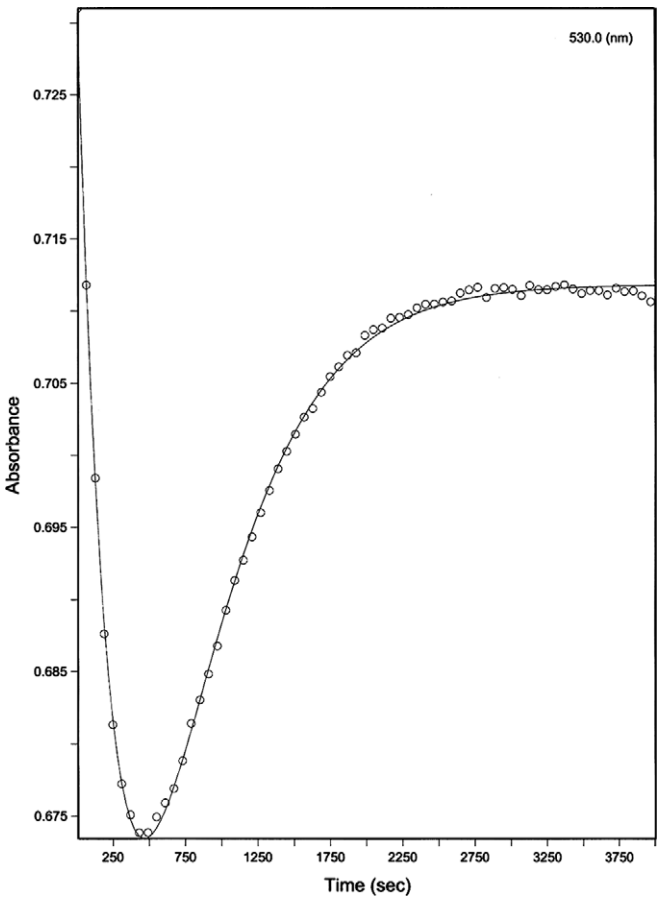

Fig. 4. Absorbance–time trace at 530 nm for the hydrolysis of *cis*-$[Co(NH_3)_4Cl_2]^{2+}$ in H_2O/H^+, 25 °C, illustrating the biphasic nature of the reaction.

spectral data (340–700 nm) involves a shallow minimum with considerable flexibility in the derived values for both k_1 and k_2 and the spectrum for the intermediate (kinetic)

Table 3
Rate data for the acid hydrolysis of *cis*-$[Co(NH_3)_4Cl_2]^+$ in 0.020 M $HClO_4$ at 25 °C

Region	10^3k_1 (s^{-1})	10^3k_1 (s^{-1}) (589 nm)[a]	10^3k_2 (s^{-1}) (530 nm)[b]
UV (260–300 nm)	2.12 (3)		
Vis		2.35 (9)[b]	2.47 (9)
		2.39[c]	2.46[c]
		2.33[c]	2.48[c]
		2.37[d]	2.31[d]

[a] Single exponential fit at one of the *cis*-/*trans*-$[Co(NH_3)_4(OH_2)Cl]^{2+}$ isomerisation isosbestic points.
[b] Double exponential fit, with k_1 fixed at the value determined at 589 nm for the same run.
[c] Global fit (340–700 nm) double exponential fit with no restriction on k_1 or k_2, for selected data sets (>95% reaction).
[d] Double exponential fit with k_2 fixed at the independently determined value.

$[Co(NH_3)_4(OH_2)Cl]^{2+}$ isomer distribution. This is a general problem when $k_1 \sim k_2$ [14]. However, fitting to a single wavelength data set such as the fall-rise seen at 530 nm gives much better defined parameters when the two rates are similar, provided the data cover a time period in excess of 95% reaction.

The steric course for the primary substitution reaction was determined as described previously [29] by fitting the ε, t data to Eq. (1) which applies to Scheme 3 as shown:

$$\varepsilon_{obsd} = \varepsilon_\infty + \{(\varepsilon_A - \varepsilon_C) + (k_1(\varepsilon_B - \varepsilon_C)/(k_2 - k_1))\} \times \exp(-k_1 t) - \{(k_1(\varepsilon_B - \varepsilon_C)/(k_2 - k_1))\} \times \exp(-k_2 t). \quad (1)$$

Here 'B' is the first formed *cis*-/*trans*-aquachloro mixture and 'C' is the equilibrium mixture. The initial *cis*/*trans* ratio is best defined from absorbance data at around 530 nm where the component spectra differ the most. We also carried out a multiwavelength version of this analysis by globally fitting (Specfit®) the 340–700 nm data to a A → B → C scheme fixing the values of k_1 (determined at 589 nm, Table 3) and k_2 (independently determined, Table 1), and determining the full spectrum of the intermediate isomer mixture (Fig. 5). Note that even though we are dealing with first order reactions, absolute times must be used to get the correct spectrum of the intermediate B. The intermediate spectrum was fitted to the spectra of its two components and yielded a 55% *cis*, 45% *trans* kinetic distribution; similarly, the final spectrum corresponded to 88% *cis*, 12% *trans*.

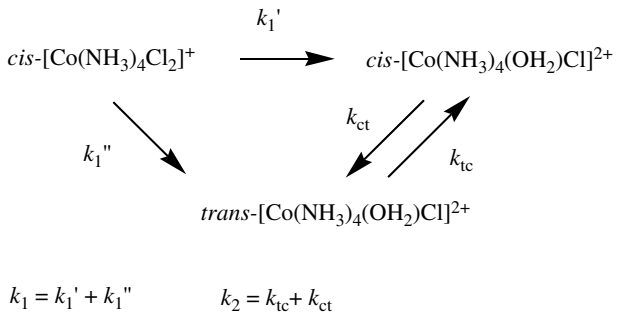

Scheme 3. The sequential hydrolysis reaction for *cis*-$[Co(NH_3)_4Cl_2]^+$.

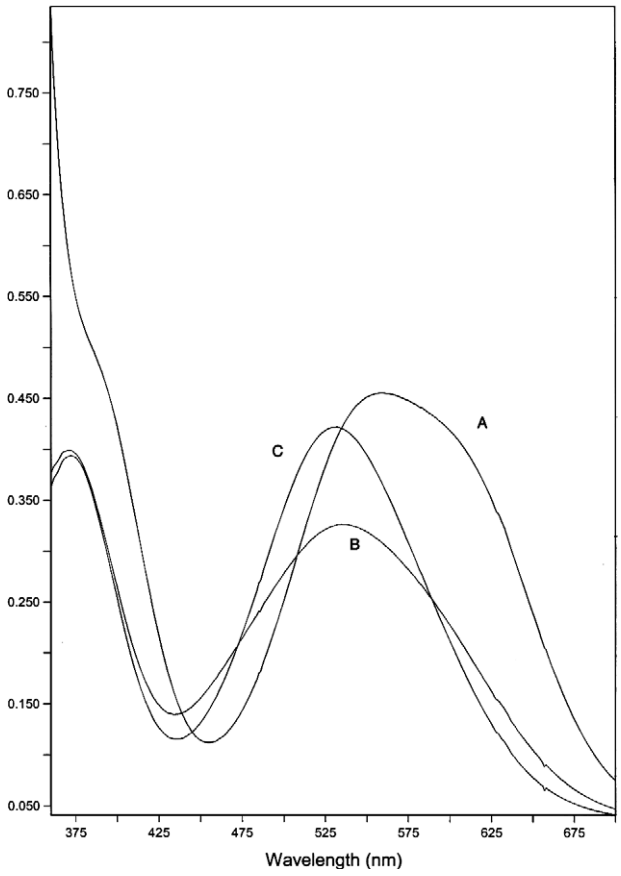

Fig. 5. Computed intermediate (B) and final (C) *cis*-/*trans*-$[Co(NH_3)_4(OH_2)Cl]^{2+}$ visible spectra, for the hydrolysis of *cis*-$[Co(NH_3)_4Cl_2]^+$ (A) in H_2O/H^+ at 25 °C. The vertical scale is absorbance, for an arbitrary [Co].

The 440 nm isosbestic point (ε 13.0; $\varepsilon(cis) = 11.0$, $\varepsilon(trans) = 19.3\ M^{-1}\ cm^{-1}$) is not very sensitive to the *trans*-/*cis*- product ratio but the 514 nm isosbestic is. The initial product distribution calculated from this (ε 39.0; $\varepsilon(cis) = 53.5$ and $\varepsilon(trans) = 19.7\ M^{-1}\ cm^{-1}$), while intrinsically less accurate, gives excellent agreement (57% *cis*). This shifts quite quickly with time, and it was important to define it using a number of scans collected within the first 40 s (10% reaction). After 2 min the isosbestic, still reasonably well defined, is at 516 nm (ε 40.5 $M^{-1}\ cm^{-1}$) and this corresponds to nearly 60% *cis* product. As the simulation shows (Table 4), for an initial 55% and final 88% *cis*, the 55% changes quickly in a system where k_1 and k_2 are very similar.

Fig. 6 shows the ^1H NMR spectra for the *cis*-dichloro complex hydrolysing in D_2O (pD 2, DCl) at ca. 21 °C. The *cis*- and *trans*-aquachloro ions grow in parallel, before ultimately the *trans* isomer decays back to the *cis*. The lowest field peak is *trans* (12H) and the next lowest is the major *cis* peak (6H), and from their areas the product distribution at 2–3 min reaction time is estimated as 60% *cis*, 40% *trans*, which is entirely in accord with the spectrophotometric determination.

Table 4
Changing product distribution with time for a consecutive reaction scheme for the *cis*-$[Co(NH_3)_4Cl_2]^+$ reactant and where $k_1 = 2.4 \times 10^{-3}\ s^{-1}$, $k_2 = 2.3 \times 10^{-3}\ s^{-1}$, and the initial and final *cis*-$[Co(NH_3)_4(OH_2)Cl]^{2+}$ product proportions are 55% and 88%

t	A	B	C	%*cis*
0	1.000	0.000	0.000	55.0
5	0.988	0.012	0.000	55.2
10	0.976	0.023	0.000	55.4
15	0.965	0.035	0.001	55.6
20	0.953	0.046	0.001	55.8
25	0.942	0.057	0.002	55.9
30	0.931	0.067	0.002	56.1
35	0.919	0.077	0.003	56.3
40	0.908	0.087	0.004	56.5
45	0.898	0.097	0.005	56.7
50	0.887	0.107	0.006	56.9
55	0.876	0.116	0.008	57.0
60	0.866	0.125	0.009	57.2
65	0.856	0.134	0.011	57.4
70	0.845	0.143	0.012	57.6
75	0.835	0.151	0.014	57.8
80	0.825	0.159	0.016	57.9
85	0.815	0.167	0.017	58.1
90	0.806	0.175	0.019	58.3
95	0.796	0.182	0.021	58.5
100	0.787	0.190	0.024	58.7
105	0.777	0.197	0.026	58.8
110	0.768	0.204	0.028	59.0
115	0.759	0.211	0.031	59.2
120	0.750	0.217	0.033	59.4
125	0.741	0.224	0.036	59.5
130	0.732	0.230	0.038	59.7
135	0.723	0.236	0.041	59.9
140	0.715	0.242	0.044	60.0
145	0.706	0.248	0.046	60.2
150	0.698	0.253	0.049	60.4
155	0.689	0.258	0.052	60.5
160	0.681	0.264	0.055	60.7
165	0.673	0.269	0.058	60.9
170	0.665	0.274	0.061	61.0
175	0.657	0.278	0.065	61.2
180	0.649	0.283	0.068	61.4

3.4. Aquation of *trans*-$[Co(NH_3)_4Cl_2]^+$

The UV absorption maximum at ca. 250 nm for the *trans*-dichloro ion [10] is associated with Co–Cl charge transfer absorption (ε ca. 15,000 $M^{-1}\ cm^{-1}$). It is roughly twice as intense and to lower energy than the corresponding absorption for the *trans*- and *cis*-monochloro ions (ca. 230 nm), and that, being associated with the Co–Cl charge transfer, is insensitive to the *cis* or *trans* stereochemistry. Thus the hydrolysis of the dichloro to monochloro ions involves a large absorption change in the UV region (Figure 6S) whereas the *trans*-/*cis*-isomerisation involves very little change. The latter change was sufficient, however, to easily determine the isomerisation rate spectrophotometrically (Table 1).

Although there is no isosbestic point for the isomerisation coincident with the isosbestic at 239 nm for the hydrolysis of *trans*-$[Co(NH_3)_4Cl_2]^+$ (the so-called triple isosbestic point), we have determined that the spectra for *cis*- and

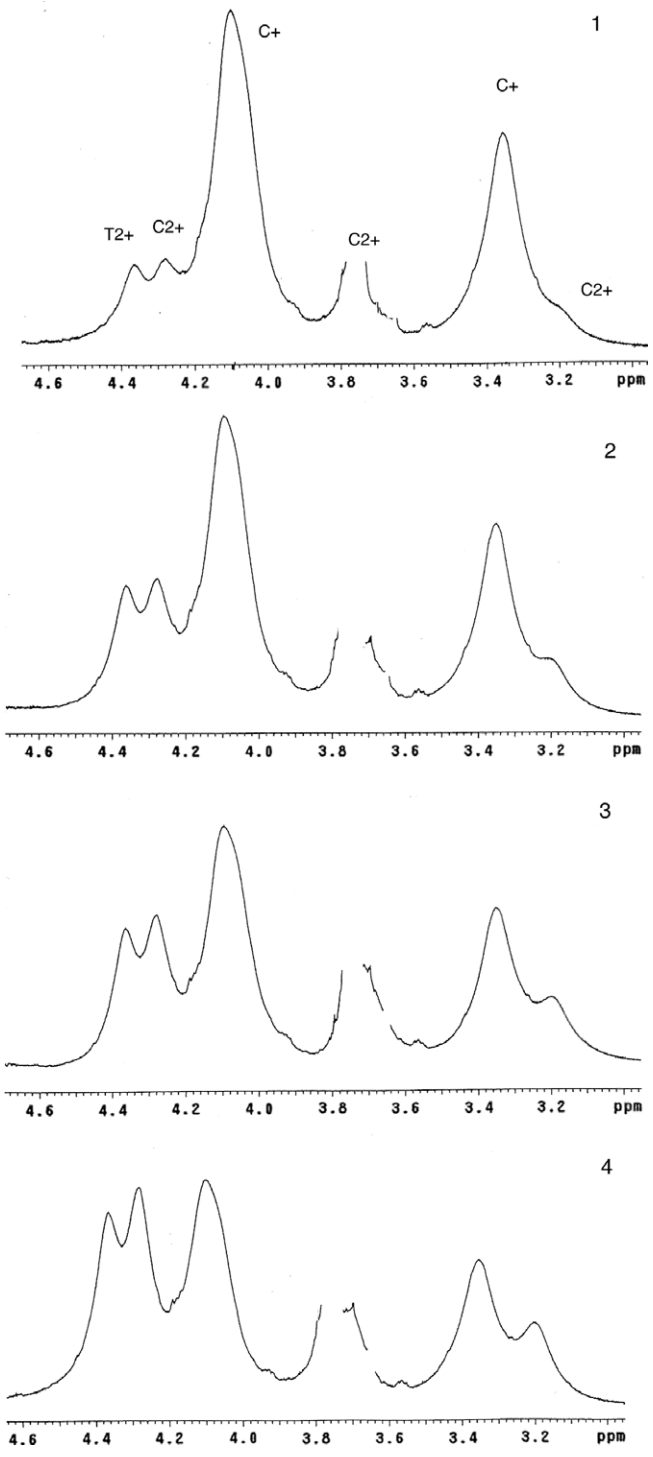

Fig. 6. ^1H NMR spectra (NH region) for the hydrolysis of *cis*-$[Co(NH_3)_4Cl_2]^+$ (C+) in D_2O/D^+ at ca. 21 °C; C2+ and T2+ denote the signals for *cis*- and *trans*-$[Co(NH_3)_4(OH_2)Cl]^{2+}$. Times increase, from 1 to 4.

trans-$[Co(NH_3)_4(OH_2)Cl]^{2+}$ are indeed very similar to each other and to the *trans*-$[Co(NH_3)_4Cl_2]^+$ ion in this region, and it confirms Linck's surmise [10] on this point, i.e., the persistence of the sharp isosbestic point at 239 nm for 10 $t_{1/2}$ of the primary reaction, despite the second step having essentially the same rate as the first step, the

primary aquation and secondary isomerisation reactions. Indeed, the small absorbance changes in the UV for the secondary reaction are the reason for the good single phase kinetics for the primary reaction as measured in the UV region at any wavelength. The rates obtained are all the same, and in particular the same as those determined from the UV data at 284 nm (Table 5), which is an isosbestic point for the *trans*-/*cis*-$[Co(NH_3)_4(OH_2)Cl]^{2+}$ isomerisation reaction (Figure 2S).

The reaction studied in the visible spectral region revealed four sharp isosbestic points: 353 nm, ε 43.4; 397 nm, ε 33.2; 467 nm, ε 21.5; 597 nm, ε 28.2 $M^{-1}\,cm^{-1}$ (Fig. 7). None were definitive of the steric course of substitution because the spectra of *cis*- and *trans*-$[Co(NH_3)_4(OH_2)Cl]^{2+}$ are very similar at each of these wavelengths (see Figs. 1 and 8).

Table 5
Rate data for the acid hydrolysis of *trans*-$[Co(NH_3)_4Cl_2]^+$ in 0.020 M $HClO_4$ at 25 °C

Region	$10^3 k_1$ (s^{-1})
UV	2.22 (12)[a]
Vis	2.22 (22)[b]
UV	2.23 (4)[c]

[a] Global analysis (UV: 220–320 nm) single exponential fit.
[b] Global analysis (Vis: 340–700 nm) double exponential fit, with k_2 fixed at $2.31 \times 10^{-3}\ s^{-1}$.
[c] Single exponential fit, for data collected at 284 nm, an isosbestic point for $[Co(NH_3)_4(OH_2)Cl]^{2+}$ isomerisation.

The data in the 340–700 nm visible range actually fit a single exponential quite well, but this is fortuitous, as discussed elsewhere [30]. The data were refitted to a double exponential, appropriate to a consecutive reaction scheme, with k_2 fixed at its known value $2.31 \times 10^{-3}\ s^{-1}$. The results for k_1 so obtained are presented in Table 5, and the value is in agreement with that determined in a more straightforward fashion from the UV data.

Quite remarkably, the hydrolysis rate for the *trans* isomer (k_1, $2.2 \times 10^{-3}\ s^{-1}$) is almost identical to that determined for the *cis* isomer ($2.4 \times 10^{-3}\ s^{-1}$), and also is essentially that for the subsequent isomerisation reaction ($2.3 \times 10^{-3}\ s^{-1}$).

The steric course of hydrolysis was determined as described above for the *cis* isomer – globally fitting the visible spectral data (340–700 nm) to a consecutive reaction scheme with the derived values for k_1 and k_2. The results are shown in Fig. 8. The average 530 nm result is $\varepsilon_B = 32.7\ M^{-1}\,cm^{-1}$ (22 determinations), which corresponds to 65% *trans* and 35% *cis* product. The error here is likely ±5%. Linck had estimated 45 ± 10% *trans* product by an indirect method [10,13].

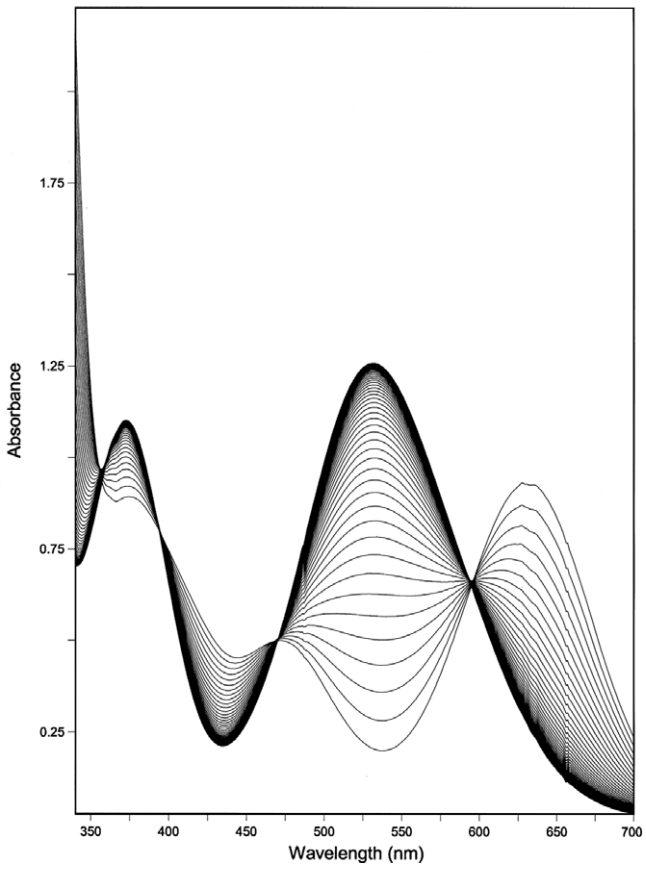

Fig. 7. Visible spectral changes for the hydrolysis of *trans*-$[Co(NH_3)_4Cl_2]^+$ in H_2O/H^+, 25 °C. The absorbance increases with time at 530 nm.

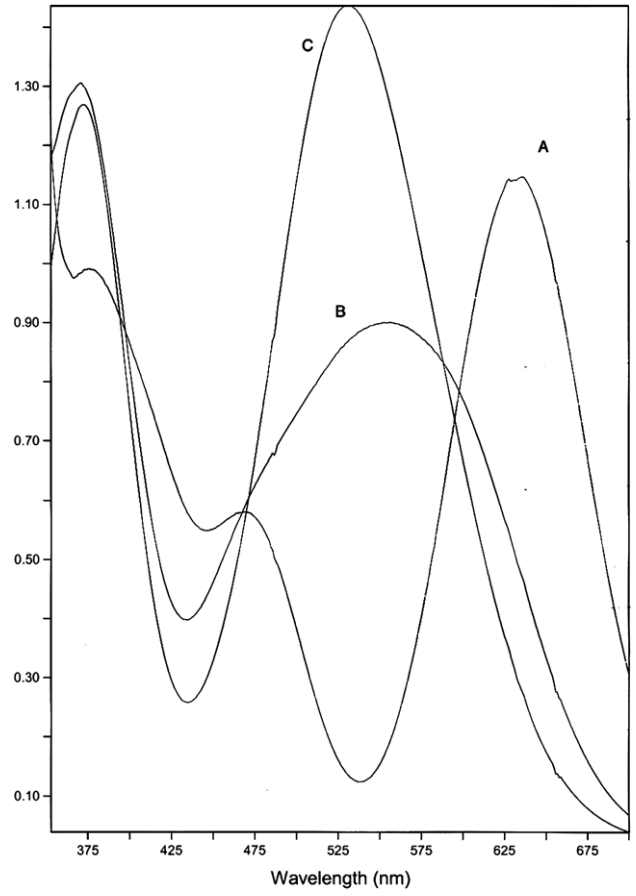

Fig. 8. Computed intermediate (B) and final (C) *cis*-/*trans*-$[Co(NH_3)_4(OH_2)Cl]^{2+}$ visible spectra, for the hydrolysis of *trans*-$[Co(NH_3)_4Cl_2]^+$ (A) in H_2O/H^+ at 25 °C. The vertical scale is absorbance, for an arbitrary [Co].

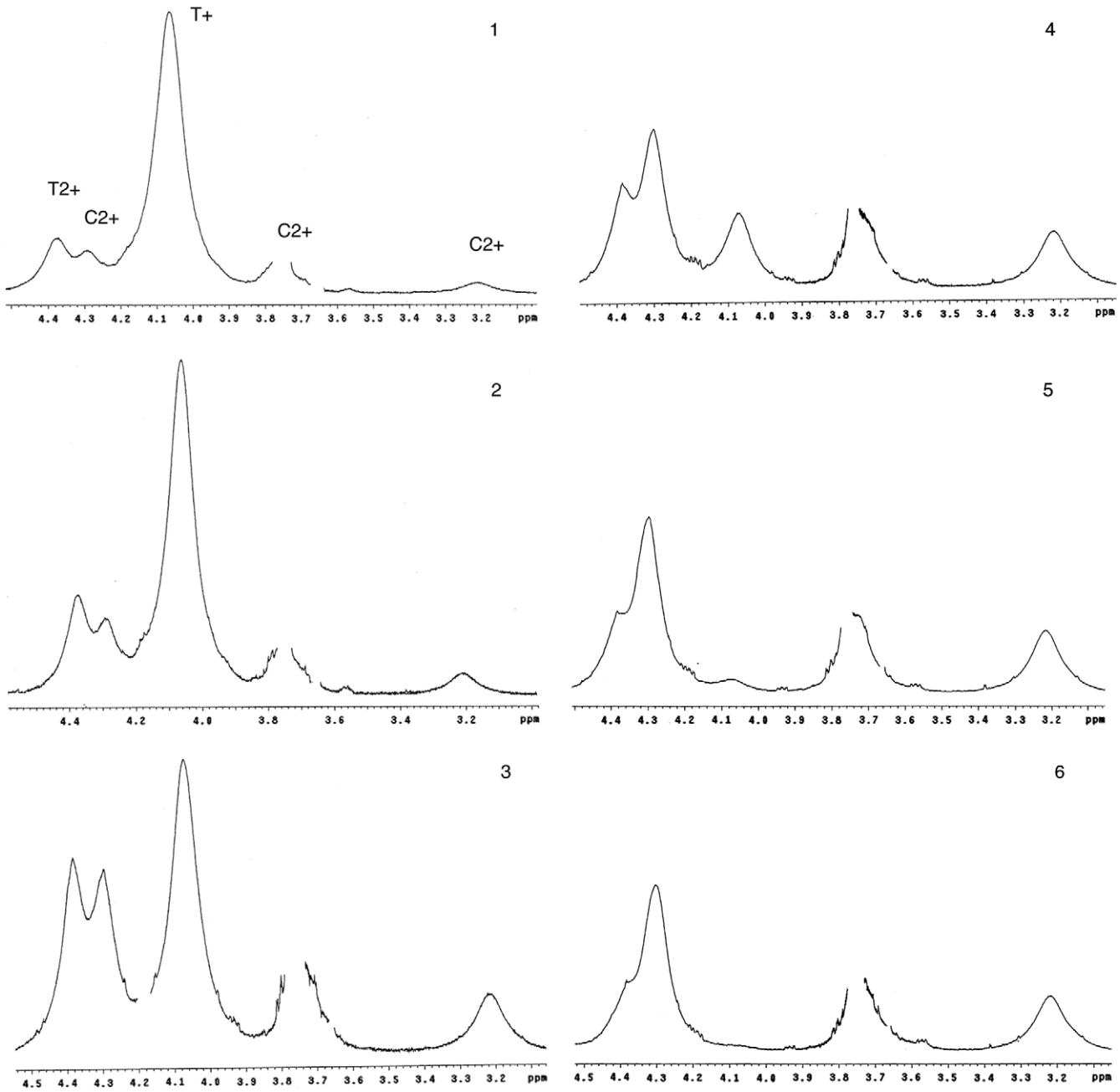

Fig. 9. ^{1}H NMR spectra (NH region) for the hydrolysis of *trans*-(T+) $[Co(NH_3)_4Cl_2]^+$ in D_2O/D^+ at ca. 21 °C; times increase from 1 to 6. C2+ and T2+ are *cis*- and *trans*-$[Co(NH_3)_4(OH_2)Cl]^{2+}$, respectively.

The ^{1}H NMR spectra for *trans*-$[Co(NH_3)_4Cl_2]^+$ reacting in D_2O/DCl are shown in Fig. 9. Compared to the corresponding changes for the *cis* isomer (Fig. 6), there is a little more *trans* product formed initially, estimated as 60% which is in good agreement with that determined spectrophotometrically.

4. Summary and conclusions

The *cis*- and *trans*-dichloro complexes hydrolyse at coincidentally the same rate. For the bis(ethylenediamine) analogues [7], the *cis* isomer is about sixfold more reactive than the *trans*, and both rates are between 10- and 50-fold smaller than the corresponding tetraammine rates; for the latter the *cis* isomer is about 10-fold more reactive than the *trans* isomer. The previous notion [8] that *cis*-$[Co(NH_3)_4Cl_2]^+$ hydrolyses extraordinarily rapidly is unfounded. Both isomers yield *cis*- and *trans*-$[Co(NH_3)_4(OH_2)Cl]^{2+}$ products directly, in different proportions, with the *trans* isomer showing more rearrangement (35% *cis* product; 65% rearrangement) than the *cis* form (55% *cis* product, 45% rearrangement). This also parallels the bis(ethylenediamine) chemistry, but there the extents of rearrangement are less (the *trans* reactant gives 74% *trans* product, the *cis* reactant gives 76% *cis* product; these numbers correspond to 26% and 24% rearrangement, respectively) [7]. The aquachloro

equilibrium isomer distributions in the two systems are also similar (en, 79% *cis*; NH_3, 88% *cis*).

The new stereochemical data for the tetraammine system again show that *cis* isomers are not universally retentive. It was once believed [4] the norm for the bis(ethylenediamine) complexes, but shown otherwise [6,29]. It thus seems unlikely that a study of the kinetics and stereochemistry of other $[Co(NH_3)_4AX]^{n+}$ complexes will uncover anything beyond what is described herein, notwithstanding the fact that the synthetic chemistry is not yet developed.

Acknowledgement

The author is grateful to Professor Hans Riesen for an accurate translation of sections of Werner's original Berichte paper.

Appendix A. Supplementary data

Figures 1S–6S, visible/UV spectral data. Supplementary data associated with this article can be found, in the online version, at doi:10.1016/j.poly.2005.12.015.

References

[1] A. Werner, Ber. Deut. Chem. Ges. 40 (1907) 4817.
[2] Werner Centennial, vol. 62, ACS, Washington, 1967.
[3] A. Werner, Ann 386 (1912) 1.
[4] F. Basolo, E.G. Pearson, Mechanisms of Inorganic Reactions, 2nd ed., Wiley, NY, 1967.
[5] M.L. Tobe, in: Advances in Inorganic and Bioinorganic Mechanisms, vol. 2, Academic Press, New York, 1983, p. 1.
[6] W.G. Jackson, A.M. Sargeson, in: P. deMayo (Ed.), Rearrangement in Coordination Complexes, vol. 2, Academic Press, New York, 1980, p. 273.
[7] W.G. Jackson, in: I. Bernal (Ed.), The Stereochemistry of the Bailar Inversion and Related Substitution Processes, vol. 1, Elsevier, 1986, p. 255.
[8] R.G. Pearson, R.C. Boston, F.J. Basolo, J. Phys. Chem. 59 (1955) 304.
[9] R. Tsuchida, Bull. Chem. Soc. Jpn. 11 (1936) 721.
[10] R.G. Linck, Inorg. Chem. 8 (1969) 1016.
[11] L.L. Borer, H.W. Erdman, C. Norris, J. Williams, J. Worrell, Inorganic Syntheses, vol. 31, Wiley, NY, 1997.
[12] G. Daffner, D.A. Palmer, H. Kelm, Inorg. Chim. Acta 61 (1982) 57.
[13] R.G. Linck, Inorg. Chem. 7 (1968) 2394.
[14] W.G. Jackson, A.F.M.M. Rahman, M.A. Wong, Inorg. Chim. Acta 357 (2004) 665.
[15] G.B. Kauffman, R.P. Pinnell, J.K. Crandall, W.L. Jolly, Inorganic Syntheses, vol. 6, McGraw-Hill, NY, 1960, p. 177.
[16] R.J. Angelici, 2nd ed.Synthesis and Technique in Inorganic Chemistry, University Science Books, CA, 1986, p. 16.
[17] G. Schlessinger, J.W. Simmons, G. Jabs, M.M. Chamberlain, Inorganic Syntheses, vol. 6, McGraw-Hill, 1960, p. 173.
[18] G. Brauer, in: Handbook of Preparative Inorganic Chemistry, vol. 2, Academic, NY, 1965, p. 1537.
[19] S.M. Jørgensen, Z. Anorg. Chem. 2 (1892) 296.
[20] J. Springborg, C.E. Schaffer, M.L. Wilson, J.M. Wharton, W.E. Hatfield, Inorganic Syntheses, vol. 18, Wiley, NY, 1978, p. 75.
[21] S.M. Jørgensen, Z. Anorg. Chem. 14 (1897) 404.
[22] P. Comba, N.J. Curtis, W.G. Jackson, A.M. Sargeson, Aust. J. Chem. 39 (1986) 1297.
[23] G.B. Kauffman, S.F. Abbott, S.E. Clark, J.M. Gibson, R.D. Meyers, Inorganic Syntheses, vol. 18, Wiley, NY, 1978, p. 69.
[24] W.G. Jackson, Inorg. Chem. 41 (2002) 7077.
[25] C. Duval, Comptes Rendus Hebd. Seances Acad. Sci. 182 (1926) 636.
[26] W.G. Jackson, Inorg. Chem. 26 (1987) 3857.
[27] W.R. Fitzgerald, A.J. Parker, D.W. Watts, J. Am. Chem. Soc. 90 (1968) 5744.
[28] W.G. Jackson, C.M. Begbie, Inorg. Synth. 21 (1982) 119.
[29] W.G. Jackson, A.M. Sargeson, Inorg. Chem. 17 (1978) 1348.
[30] W.G. Jackson, Int. J. Chem. Kinet. (submitted for publication).

and the colorless solution was stirred for 5 min at room temperature. A solution of 0.650 g (0.1 mmol) NaN_3 in 5 ml CH_3OH was then added, and the stirring was continued for an additional 20 min. Slow evaporation of the solvent at 0 °C, gave colorless crystals of the title compound (**1**) suitable for X-ray analysis. The crystals were collected by filtration, washed with cold acetonitrile, and dried under vacuum. The yield was 0.539 g, 77%. *Anal.* Calc. for $C_{38}H_{35}AgN_5P$: C, 65.14; H, 5.03; N, 9.99. Found: C, 63.83; H, 4.72; N, 10.15%. IR (KBr pellet, 400–4000 cm^{-1}) 1628 (C=N), 2010 (N_3). UV [chloroform; λ_{max} in nm ($\log\varepsilon$ in L mol^{-1} cm^{-1})]: 343 (3.04), 277 (4.90) ^1H NMR ($CDCl_3$) 3.87 (s, 4H, NCH_2CH_2N); 6.87, (dd, 2H, C=CH–C); 6.98 (d, 2H, –CH=C); 7.26–7.49 (m, 25H, 2PhC=C, ArH); 8.14 (d, 2H, 2CH=N).

2.3. Synthesis of [Ag(ca$_2$en)(PPh$_3$)SCN] (2)

This complex was prepared in a manner similar to that of (**1**) using KSCN (0.980 g, 0.1 mmol). The crystals were collected by filtration, washed with cold acetonitrile and dried under vacuum. The yield was 0.608 g, 85%. *Anal.* Calc. for $C_{39}H_{35}AgN_3PS$: C, 65.36; H, 4.92; N, 5.86. Found: C, 65.20; H, 5.00; N, 5.80%. IR (KBr pellet, 400–4000 cm^{-1}) 1627 (C=N), 2085 (SCN). UV [chloroform; λ_{max} in nm ($\log\varepsilon$ in L mol^{-1} cm^{-1})]: 276 (4.96) ^1H NMR ($CDCl_3$) 3.86 (s, 4H, NCH_2CH_2N); 6.91 (dd, 2H, C=CHC); 6.99 (d, 2H, –CH=C); 7.26–7.50 (m, 25H, 2PhC=C, ArH); 8.15 (d, 2H, 2CH=N).

2.4. X-ray crystallography

Suitable single crystals of [Ag(ca$_2$en)(PPh$_3$)(N$_3$)] (**1**) and [Ag(ca$_2$en)(PPh$_3$)(SCN)] (**2**), were obtained by evaporation of solvent at 0 °C. The crystals were found to shatter easily when attempts were made to cut them, so large, well formed crystals were used without cutting. Data were collected on an Oxford Diffraction Xcalibur2 diffractometer using graphite-monochromated Mo Kα radiation ($\alpha = 0.71069$ Å). The data were corrected for Lorentz and polarization effects, and corrections were applied for absorption and scaling using data redundancy (SADABS [16]). The structures were solved by direct methods (SHELXS-97 [17]) and refined by full-matrix least squares using F^2 (SHELXL-97 [17]). All non-hydrogen atoms were refined anisotropically, and all H atoms were treated as riders with isotropic U values constrained to 1.2 times the equivalent isotropic U values of their respective parent atoms.

3. Results and discussion

3.1. Synthesis

The *N*,*N*′-bis(*trans*-cinnamaldehyde)1,2-diaminoethane, ca$_2$en, ligand was prepared as reported elsewhere [18]. These colorless complexes are stable in air in the solid state for 20 weeks. The stability of these complexes in solution depends on the solvent used. While these complexes are stable in acetonitrile solution at room temperature for 10 days, they remain unchanged for 5 days in methanol but only two days in dicholoromethane at 0 °C.

3.2. Crystal structures of [Ag(ca$_2$en)(PPh$_3$)(N$_3$)] (1) and [Ag(ca$_2$en)(PPh$_3$)(SCN)] (2)

A summary of the key crystallographic information for the two complexes are listed in Table 1. The molecular structures and atom numbering schemes of (**1**) and (**2**) are presented in Figs. 1 and 2, respectively. Selected bond distances, bond angles and torsion angles are given in Table 2. The pseudohalides, N_3 and SCN, are known to coordinate to metal ions in both terminal and bridging modes [19–22], and they act as terminal ligands in complexes (**1**) and (**2**). While a tetrahedral geometry might be expected for a four coordinated silver(I) center, the coordination sphere around the silver atom in (**1**) and (**2**) is distorted by the restricting bite angle of the chelating ligand ca$_2$en. The N–Ag–N angles in (**1**) and (**2**) are only 73.86(7)° and 72.49(5)°, respectively. The coordination environment around the metal ion in each complex is

Table 1
Crystallographic and refinement data of Ag(ca$_2$en)(PPh$_3$)(N$_3$) (**1**) and Ag(ca$_2$en)(PPh$_3$)(SCN) (**2**)

Complex	**1**	**2**
Empirical formula	$C_{38}H_{35}AgN_5P$	$C_{39}H_{35}Ag\ N_3PS$
Formula weight	700.55	716.62
Crystal system space group	triclinic, $P\bar{1}$	triclinic, $P\bar{1}$
A (Å)	9.5408(10)	8.5868(3)
B (Å)	11.6048(11)	11.2702(3)
C (Å)	17.3660(15)	18.3670(6)
α (°)	97.045(8)	75.344(2)
β (°)	96.740(8)	84.042(3)
γ (°)	113.415(10)	88.638(3)
V (Å^3)	1721.7(3)	1710.34(9)
Z	2	2
ρ_{calc}	1.351	1.391
Crystal dimensions (mm)	$0.59 \times 0.43 \times 0.40$	$0.93 \times 0.74 \times 0.29$
μ (mm^{-1})	0.665	0.730
$F(000)$	720	736
θ Range for data collection (°)	4.79–25.00	5.09–27.50
Index range	$-11 \leqslant h \leqslant 11$, $-13 \leqslant k \leqslant 13$, $-20 \leqslant l \leqslant 20$	$-10 \leqslant h \leqslant 10$, $-14 \leqslant k \leqslant 14$, $-23 \leqslant l \leqslant 23$
Reflections collected, unique	6007	6942
Reflections collected, total	18014	27529
R_{int}	0.0165	0.0144
Maximum, minimum transmission	0.7767, 0.6656	0.8165, 0.6943
Parameters	406	411
Goodness-of-fit on F^2	1.078	1.112
Final R indices [$I > 2\sigma(I)$]	$R_1 = 0.0303$ $\omega R_2 = 0.0744$	$R_1 = 0.0273$ $\omega R_2 = 0.0668$
Final R indices (all data)	$R_1 = 0.0310$ $\omega R_2 = 0.0749$	$R_1 = 0.0281$ $\omega R_2 = 0.0673$
Weighting parameters [a, b]	0.0361, 2.1214	0.0304, 1.7947
Largest difference in peak and hole (e Å^{-3})	0.926 and −0.311	0.746 and −0.368

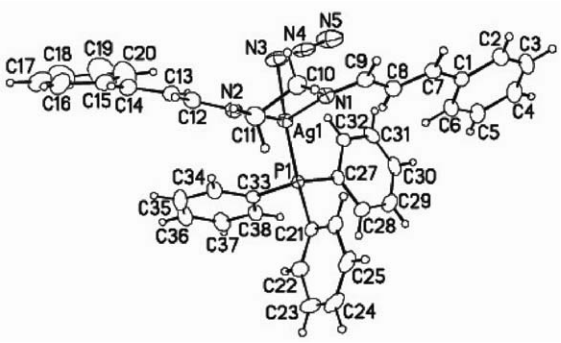

Fig. 1. The crystal structure of $[Ag(ca_2en)(PPh_3)(N_3)]$ (**1**).

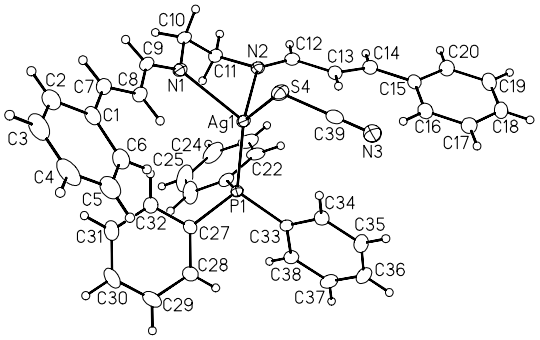

Fig. 2. The crystal structure of $[Ag(ca_2en)(PPh_3)(SCN)]$ (**2**).

pseudotetrahedral with large angular distortion, arising from the low intraligand N(1)–Ag(1)–N(2) chelate angle. This angle, fixed by the bite size of the ligand, is in the range found for ethylenediamine chelate compounds [76.3(6)°] [19]. The X–Ag(1)–P(1) angle is 118.33(6)° in (**1**) and 135.38(2)° in (**2**), being somewhat larger than the values for a tetrahedron. The dihedral angle between the best plane through the chelate ring and the plane defined by P(1)–Ag(1)–X, 85.05(8)° in (**1**) and 74.19(3)° in (**2**), are indicative of a deviation from idealized tetrahedral symmetry. The average Ag–N(ca_2en) distances of 2.365 in (**1**) and 2.390 Å in (**2**) are similar to those in the pseudotetrahedral (diimine) silver(I) complexes [22]. The Ag–N_3 bond length in (**1**) is 2.309(2) Å and that of Ag–S in (**2**) is 2.538(5) Å. The mode of coordination of the azide and thiocyanate anions to the transition metals is influenced by various factors such as the central metal and solvent polarity [20–22]. As expected, the SCN ligand is S-bonded in (**2**) due to the soft–soft interaction between Ag and S atoms. The terminal azido and thiocyanato ligands in these complexes are almost linear, with bond angles N–N–N, 177.33(3)° and S–C–N, 179.36(21)°. The geometries of the ca_2en ligand are as expected.

Table 2
Selected bond lengths, bond angles and torsion angles of $[Ag(ca_2en)(PPh_3)(N_3)]$ (**1**) and $[Ag(ca_2en)(PPh_3)(SCN)]$ (**2**)

	$[Ag(ca_2en)(PPh_3)(N_3)]$ (**1**)	$[Ag(ca_2en)(PPh_3)(SCN)]$ (**2**)
Bond length (Å)		
Ag(1)–N(1)	2.3859(19)	2.3916(15)
Ag(1)–N(2)	2.3446(19)	2.3885(17)
Ag(1)–X	2.309(2)	2.5380(5)
Ag(1)–P(1)	2.3825(7)	2.4126(4)
Bond angle (°)		
N(1)–Ag(1)–N(2)	73.86(7)	72.49(5)
N(1)–Ag(1)–X	100.62(8)	97.85(4)
N(2)–Ag(1)–X	99.68(7)	109.10(4)
N(1)–Ag(1)–P(1)	126.43(5)	118.45(4)
N(2)–Ag(1)–P(1)	127.71(5)	106.16(4)
X–Ag(1)–P(1)	118.33(6)	135.38(2)
Torsion angle (°)		
C(7)–C(8)–C(9)–N(1)	176.7(2)	175.65(17)
C(8)–C(9)–N(1)–C(10)	179.6(2)	−176.75(15)
C(9)–N(1)–C(10)–C(11)	−167.3(2)	−166.78(15)

3.3. Spectral characterization

The IR spectrum of the free ligand exhibits the characteristic band of an imine C=N, which appears at 1634 cm^{-1} [18]. This band is shifted to lower frequencies (~1627 cm^{-1}) in the IR spectra of the complexes due to the coordination of the imine nitrogen.

It is well known that silver(I) compounds are diamagnetic and colourless. Since no d–d transitions are expected for a d^{10} complex, the absorption bands are either of CT or intraligand character. The first MLCT band is clearly observed only for complex **1** at 343 nm, however this transition may have been obscured by the intraligand transitions in **2**. This is presumably due to the fact that the first MLCT band of complex **2** is blue shifted because of a better π-back bonding between Ag and SCN relative to N_3. An absorption band at about 277 nm, which can be assigned to the π–π^* transition of the coordinated ligand, is observed in the spectra of both complexes.

The ^{1}H NMR spectral data and peak assignments for (**1**) and (**2**) are presented in the experimental section. The proton resonances of the coordinated ca_2en are commonly observed in the spectra. The aromatic protons of the coordinated PPh_3 ligands overlap to some extent with those of the phenyl protons of ca_2en. Aside from the aromatic protons (C=C–Ph, PPh_3), which appear at about 7.24–7.49 ppm, the two imine protons (N=CH–) appear as a doublet at about 8.15 ppm. The four ethylenic protons appear as a doublet of doublets at about 6.87 ppm (C–CH=C) and a doublet at 6.97 ppm (C=HC–Ph). The downfield shift of the imine protons in the spectra of the complexes relative to the free ligand can be attributed to the deshielding effect resulting from the coordination of the ligand. The sharp singlet at about 3.87 ppm is assigned to the N–CH_2–CH_2–N protons of the chelate ring. The ^{1}H NMR data support the existence of Ag(I) in these pesudotetrahedral complexes. The appearance of a unique signal for each type of proton in CD_3CN solution indicates that the symmetry of the molecules is retained in solution and the ca_2en ligand is in its endo configuration as indicated in the structures.

4. Supplementary material

Crystallographic data (excluding structure factors) for the structures reported in this paper have been deposited with the Cambridge Crystallographic Center, CCDC Nos. 275388 for (**1**) and 275389 for (**2**). Copies of the data can be obtained free of charge on application to The Director, CCDC, 12 Union Road, Cambridge CB2 1EZ, UK, fax: +44 1223 336 033, e-mail: deposit@ccdc.cam.ac.uk or http:www.ccdc.cam.ac.uk.

Acknowledgments

The authors thank the Ministry of Education and Science (Spain) for support under Grant BQU2002-00554. M.A. and A.D.K. acknowledge the Isfahan University of Technology Research Council for partial support of this work.

References

[1] R. Mehrotra, R. Bohra, Metal Carboxylates, Academic Press, London, 1983.
[2] G. Xue, J. Dong, Y. Sun, Langmuir 10 (1994) 1477.
[3] S.J. Berners-Price, P.J. Sadler, Coord. Chem. Rev. 15 (1990) 1.
[4] S.J. Berners-Price, R.K. Johnson, C.K. Mirabelli, L.F. Faucette, F.L. McCabe, P.J. Sadler, Inorg. Chem. 26 (1987) 3383.
[5] S.J. Berners-Price, C. Brevard, P.J. Sadler, Inorg. Chem. 26 (1986) 3383.
[6] P.M. Henry, Adv. Organomet. Chem. 13 (1975) 363.
[7] H. Cohen, D. Meyerstein, Inorg. Chem. 25 (1986) 1505.
[8] S. Golldstein, G. Czapski, H. Cohen, D. Meyerstein, Inorg. Chem. 31 (1992) 5670.
[9] N. Navon, G. Golub, H. Cohen, D. Meyerstein, Organometallics 14 (1995) 5670.
[10] A. Cingolani, Effendy, F. Marchetti, C. Pettinari, B.W. Skelton, A.H. White, J. Chem. Soc., Dalton Trans. (1999) 4047.
[11] G.A. Bowmaker, Effendy, J.V. Hanna, P.C. Healy, J.C. Reid, C.E.F. Rickard, A.H. White, J. Chem. Soc., Dalton Trans. (2000) 753.
[12] Effendy, G.G. Lobbia, M. Pellei, C. Pettinari, C. Santini, B.W. Skelton, A.H. White, J. Chem. Soc., Dalton Trans. (2000) 2123.
[13] M.J. Hanon, C.L. Painting, N.W. Alock, Chem. Commun. (1999) 2023.
[14] P.K. Bowyer, K.A. Porter, A.D. Rae, A.C. Willis, S.B. Wild, Chem. Commun. (1998) 1153.
[15] M. Amirnasr, R. Welter, A.D. Khalaji, Acta Crystallogr. E61 (2005) m1452.
[16] G.M. Sheldrick, SADABS, program for correction of systematic errors in diffraction data, University of Göttingen, 2002.
[17] G.M. Sheldrick, SHELX97 [Includes SHELXS97, SHELXL97 and CIFTAB] – Programs for Crystal Structure Analysis (Release 97-2), Institüt für Anorganische Chemie der Universität, Göttingen, Germany, 1998.
[18] M. Amirnasr, K.J. Schenk, M. Salavati, A. Gorji, S. Dehghanpour, A. Taeb, A. Tajarrodi, J. Coord. Chem. 56 (2003) 231.
[19] G. Kickelbick, M. Amirnasr, A.D. Khalaji, S. Dehghanpour, Aust. J. Chem. 56 (2003) 323.
[20] L. Li, D. Liao, S. Liu, Z. Jiang, S. Yan, Inorg. Chem. Commun. 6 (2003) 225.
[21] P.S. Mukherjee, T.K. Maji, G. Mostafa, T. Mallah, N.R. Chaudhuri, Inorg. Chem. 39 (2000) 5147.
[22] T.G. Richmond, E.P. Kelson, A.M. Arif, J. Am. Chem. Soc. 110 (1988) 2334.

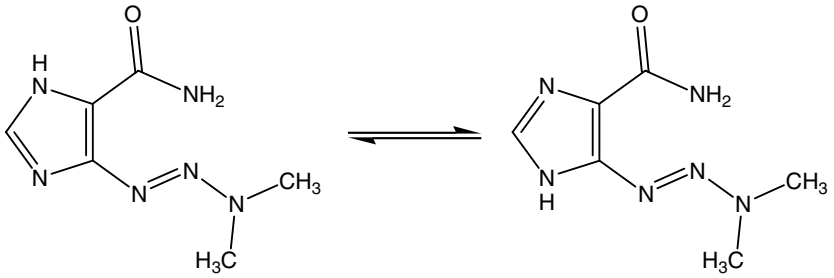

Fig. 1. Tautomeric forms of dacarbazine.

active against certain types of cancer and entered clinical studies [5,6]. In parallel, two gallium complexes: tris-(3-hydroxy-2-methyl-4*H*-pyran-4-onato)gallium(III) and tris(8-quinolinolato)gallium(III) (KP46, FFC11) have been evaluated in clinical studies to improve the bioavailability and increase the plasma concentration of orally administered gallium complexes in comparison with simple gallium salts [7–9].

The interaction between dacarbazine and metals has acquired clinical significance; in fact changes of reactivity, stability and transport properties can occur and increase the effectiveness of the compound. Several studies have been reported in the literature using different metals, like copper(II), iron(III), nickel(II), cobalt(II) and zinc(II), in order to synthesize and study dacarbazine complexes [10–12]. For example, both in vivo and in vitro studies of the anticancer activity of the dacarbazine-Fe(III) complex have shown that the iron(III) complex was more effective than dacarbazine itself: Multiplication of cells was inhibited and the tumor volume of BALB/c mice bearing sarcoma 180 was significantly reduced [11].

A powerful analytical tool for the characterization of metal complexes as well as to obtain information about molecular weight, charge and isotope distribution of molecules is electrospray ionization mass spectroscopy (ESI-MS). This method offers the advantage of consuming only a low sample amount (<μM) and permits the use of a variety of compatible solvent systems. ESI-MS is the softest desorption/ionization method and is therefore ideally suited to investigate the coordination behavior of transition metal complexes [13–15]. For example, ESI-MS was used to investigate both the coordination behavior of some heavy metal ions [e.g., mercury(II) and zinc(II)] towards thiacrown ether macrocycles [16] and also of Zn(II), Ag(II) and the hard alkali ions Li^+ and Na^+ towards ether and thioether-substituted ferrocenes [17]. Also, some metal complexes of ruthenium(II) with nitrogen-containing heterocyclic ligands [18] and the coordination of As(III), Sb(III), Cd(II), Hg(II), Tl(I), Pb(II) and Bi(III) towards polydentate ligands (e.g., glutathione) were characterized [19].

Dacarbazine with its seven donor atoms is expected to exhibit rich coordination chemistry. However, a crystallographic structure of the square-pyramidal dacarbazine–copper(II) complex, $[CuCl_2(dac)] \cdot 2CH_3OH$, showed that the ligand is bound bidentately through the oxygen of the carboxamide group and the nitrogen atom of the imidazole ring [10].

Herein, we report two approaches for characterization of metal complexes with dacarbazine: On the one hand, coordination compounds were isolated and characterized by classical analytical techniques. On the other hand, the complexes were allowed to form in situ and samples were characterized by ESI-MS.

2. Results and discussion

The complexation of dacarbazine was found to lead to promising tumor-inhibiting compounds [10–12]. Therefore, a series of transition metals was chosen: Representatives of groups VIII to X in the fourth period (Fe, Co, Ni) and for comparison purposes ruthenium as a member of the fifth period and VIIIth group were included in the studies. Also the influence of charge states and hardness of metal centers was taken into account: ions with oxidation states +2 (Ru, Co, Ni) and +3 (Fe) were evaluated for their binding properties towards dacarbazine.

cis-$[RuCl_2(dmso)_4]$, $CoCl_2$ and $NiCl_2$ were reacted with dacarbazine at a molar ratio of 1:2, while for the synthesis of the iron complex, comparable to previously published reports [11], a molar ratio of 1:1 ($FeCl_3$:dac) was chosen. The complexes were isolated by precipitation and analyzed by ^1H NMR and IR spectroscopy, elemental analysis and ESI-MS.

The NMR spectra of the products obtained from the paramagnetic ions Co(II), Ni(II) and Fe(III) were found to contain only rather broad peaks and it was not possible to assign the signals. Due to the large number of signals found in the spectrum of the Ru complex it is assumed that a compound of low symmetry was formed. Analysis of ^1H NMR spectra for all complexes made it evident that no uncoordinated dacarbazine was precipitated by the isolation process. However, NMR spectroscopy was found to be not suitable for the structural characterization of the obtained species. Only in the case of the Ni(II) complex (d^8) it can be concluded that the metal center does not have square planar geometry which would lead to diamagnetic properties.

The best fitting elemental analyses yielded: (i) a composition of Fe:dac:Cl = 1:1:3 with traces of solvent for the Fe

complex, (ii) $[RuCl_2(dac)_2(dmso)_2]\cdot H_2O$ for the reaction between *cis*-$[RuCl_2(dmso)_4]$ and dac, (iii) $[CoCl_2(dac)_2]$ impurified very probable with traces of $CoCl_2$ and methanol, as well as (iv) $[NiCl_2(dac)_2]$ containing the remaining unreacted $NiCl_2$ plus a trace of solvent. However, no structural information can be obtained. Note, the isolated Ru(II)-compound was found in a thermogravimetry experiment to be hygroscopic – one molecule of water was removed at 50 °C within 4 h and reincorporated at normal atmosphere within 1 h. This is in good accordance with the elemental analysis result.

Infrared spectroscopy results indicate that the amide-functionality might be involved into the coordination – a shift of the C=O-stretch vibration from 1655 cm^{-1} to 1635–1637 cm^{-1} was observed for all isolated complexes.

ESI-MS analysis in positive ion mode confirmed the proposed compositions of compounds based on elemental analysis data – the most abundant peaks for the Fe, Ru, Co and Ni complexes were assigned to $[FeCl(dac)_2]^+$, $[RuCl(dac)_2(dmso)]^+$, $[CoCl(dac)_2]^+$ and $[NiCl(dac)_2]^+$, respectively.

In order to investigate the influence of the incubation ratio, of the reaction time as well as of the isolation process, complexation studies by means of electrospray ionization mass spectrometry were performed. For this purpose, complexes of $FeCl_3$, *cis*-$[RuCl_2(dmso)_4]$, $CoCl_2$ and $NiCl_2$ with dacarbazine at both 1:1 and 1:2 ratios (metal:ligand) in methanol as solvent and at room temperature were prepared in situ and compared with the mass spectra of the isolated species. For the mass spectrometric study, the instrument was optimized in the positive ion mode on *m/z* 455.1 $[FeCl(dac)_2]^+$, 579.2 $[RuCl(dac)_2(dmso)]^+$, 458.1 $[CoCl(dac)_2]^+$ and 457.1 $[NiCl(dac)_2]^+$. In order to obtain comparable data, all mass spectra in the respective ion mode were recorded with the same parameter settings for each reaction.

3. The complexation of dacarbazine to iron(III)

With a sample taken from the incubation mixture with a molar ratio of 1:1 (Fe:dac) after 1 h of reaction the most intense peaks were found at *m/z* 455.0 ($[FeCl(dac)_2]^+$, 100%) and 387.1 ($[2dac+Na]^+$, 91%) (for assignment see Table 1). Giving the reaction 96 h to proceed, showed that only one major peak remained in the mass spectrum, at *m/z* 455.0 (see Fig. 2a). Increasing the dacarbazine content of the reaction mixture resulted in a spectrum with the peak at *m/z* 387.1 being the highest. Within 24 h of reaction again the signal assigned to $[FeCl(dac)_2]^+$, with Fe in the oxidation state 2+, was the most intense (see Fig. 2b), though $FeCl_3$ was used. Reduction is a common phenomenon during the electrospray process [20] and was also proven for other metals like Cu [21]. The mass spectra obtained from the isolated complex were relatively similar to that of the in situ-prepared ones after an incubation time of 24 h. In the negative ion mode spectra, the trichloroferrate(II)- and the tetrachloroferrate(III)-ions were identified beside a deprotonated species at *m/z* 453.2 $\{[FeCl(dac)_2-2H]^-\}$. No significant changes in the latter spectra were found over time.

Table 1
The theoretical *m/z* values for the highest peaks in positive mode mass spectra of the studied iron(III) complexes

m/z	Assignment
301.1	$[Fe(dac)(MeOH)_2-H]^+$
387.2	$[2dac+Na]^+$
425.9	$[Fe_2Cl_2(dac)(MeOH)_2-2H]^+$
455.1	$[Fe(dac)_2Cl]^+$
461.9	$[Fe_2Cl_3(dac)(MeOH)_2-H]^+$
486.0	$[FeCl(dac)_2(MeOH)-H]^+$
554.1	$[FeCl_2(dac)_2(MeOH)_2]^+$

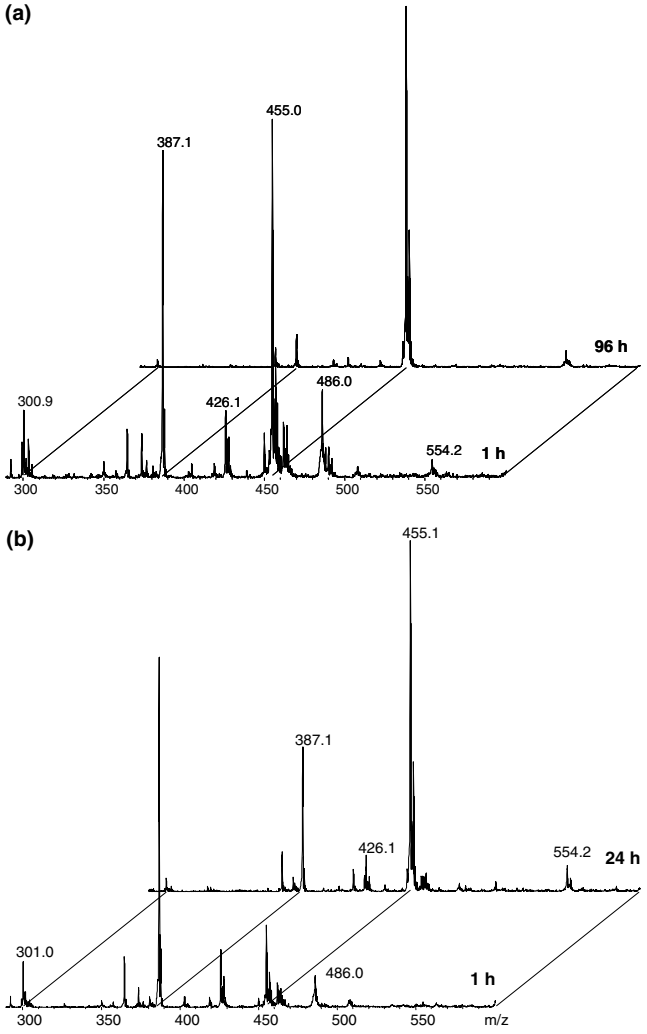

Fig. 2. Time resolved MS spectra of 1:1 (a) and 1:2 (b) incubation mixtures of $FeCl_3$ and dacarbazine.

Taking into account the information obtained by MS and elemental analysis leads to the conclusion that a species with the formula $[FeCl_2(dac)_2][FeCl_4]$ is formed if given an appropriate time period for the reaction. This is in contrast to the data published by Shukla and Pitre [11] who proposed as the reaction product of $FeCl_3$ with dacarbazine under the same conditions a species with the

formula [Fe^{III}(dac)]. The latter structure is quite implausible since no counterion was given in the publication and a threefold deprotonation of dacarbazine is not to be expected.

4. The complexation of dacarbazine to ruthenium(II)

Switching in the periodic table of elements from the 4th period into the 5th led us to compare the coordination behavior of iron with that of ruthenium.

The positive ESI-mass spectrum of the isolated Ru complex (Ru:dac = 1:2) yielded a peak at *m/z* 579.2 (100%) identified as $[RuCl(dac)_2(dmso)]^+$ and a further signal at 501.2 (15%) assignable to $[RuCl(dac)_2]^+$ (see Fig. 3a for comparison of the mass spectra of the isolated species and the in situ-prepared ones, for calculated *m/z*-values of the most important signals in the mass spectra see Table 2). The negative ion mode mass spectrum contained a main peak at *m/z* 136.0 ($[dac-H]^-$, 100%), and two less intense ones at *m/z* 499.0 and 579.1 identified as $[RuCl(dac)_2-2H]^-$ (42%) and $[RuCl(dac)_2(dmso)-2H]^-$ (31%), respectively. A peak at ca. *m/z* 530 (9%) might be a fragment ion after cleavage of the dacarbazine ligand, which could have been partly released from its metal-binding partner during the transfer from the liquid into the gaseous phase.

After 1 h of reaction of a *cis*-$[Ru(dmso)_4Cl_2]$ and dacarbazine mixture (1:1) the highest peak was found to be *m/z* 387.2 {$[2dac+Na]^+$}, changing within 48 h to 475.0 {$[RuCl(dac)(dmso)_2]^+$} (see Fig. 3b). Additionally, signals assigned to $[RuCl(dac)(dmso)_3]^+$ (95%), $[RuCl(dac)_2(dmso)]^+$ (82%), $[RuCl(dac)(dmso)_2(MeOH)_2-2H]^+$ (39%) and $[RuCl(dac)(dmso)]^+$ (17%) increased in abundance. Note that the oxidation states of the ruthenium centers in the $[RuCl(dac)(dmso)_2(MeOH)_2-2H]^+$- and $[RuCl_2(dac)(dmso)_3(MeOH)]^+$-ions are +4 and +3, respectively. These species might have been formed during the electrospray process (oxidation at the capillary tip) [22].

When freshly mixing two solutions of dacarbazine and the Ru-starting complex at a molar ratio of 2:1 (resembling the synthetic procedure), the mass spectrum in the positive ion mode showed as the highest peak a signal at *m/z* 387.2 (comparable to the 1:1 incubation) (see Fig. 3c). Additionally, less intense peaks (<5% relative intensity) were observed in the mass spectrum, having a rich isotope pattern. After 48 h the most intense signals were found to possess *m/z* 553.0 (100%) followed by 579.2 (48%), the latter having an increased relative intensity of 72% after a further 120 h of reaction.

Comparing the positive mode mass spectra of the isolated species with that of the in situ-prepared ones (reaction for 48 h) shows that the peak assigned to the Ru complex with one dacarbazine ligand is the highest one in the 1:1 incubation mixture, while in the other two mass spectra the peaks of compounds with two dacarbazine ligands significantly increase (see Fig. 3a). In the isolated species, the peak assigned to $[RuCl(dac)_2(dmso)]^+$ is nearly the exclusive one with a ruthenium isotope distribution.

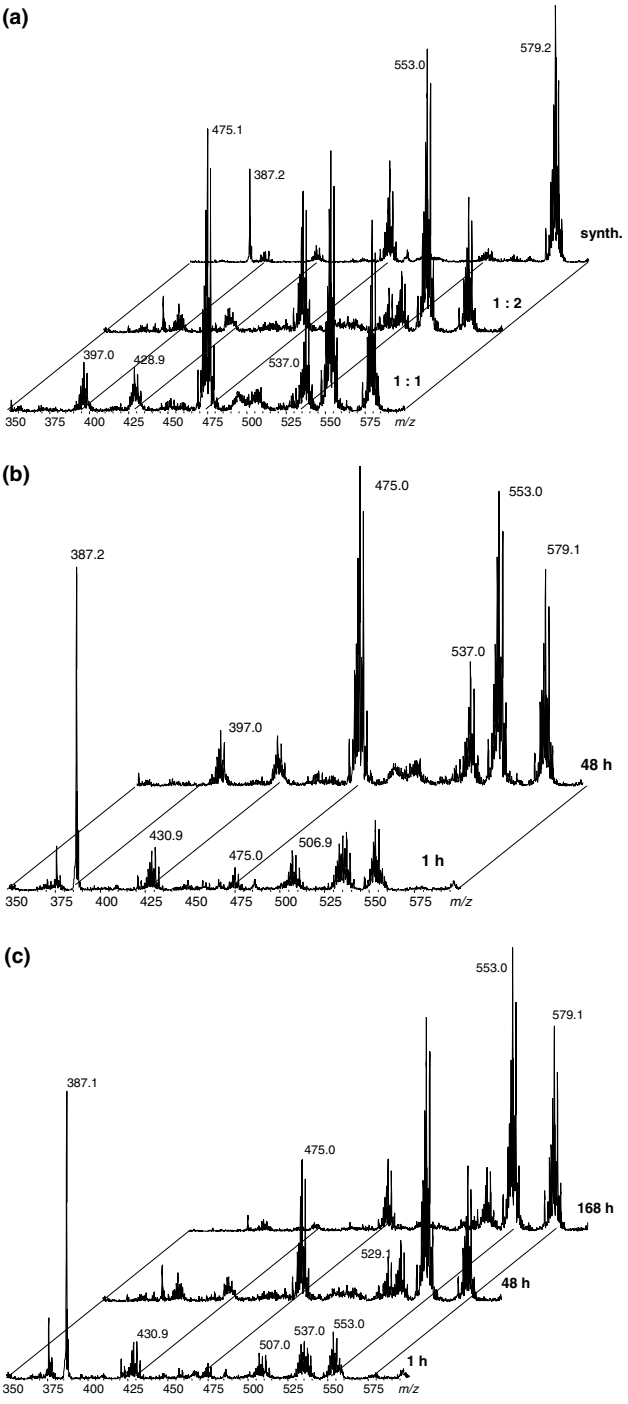

Fig. 3. (a) Comparison of in situ-synthesized Ru(II) complexes at incubation ratios of 1:1 and 1:2 (Ru:dac; after 48 h of incubation) with the synthesized complex and time resolved MS spectra of 1:1 (b) and 1:2 (c) incubation mixtures of *cis*-$RuCl_2(dmso)_4$ and dacarbazine.

In the negative ion mode mass spectra of all complexes, the peak at *m/z* 475.4 was found to have highest intensity, which correlates with calculated *m/z*-values for $[RuCl(dac)(dmso)-2H]^-$. Other signals could be assigned to $[RuCl(dac)_2(dmso)-2H]^-$ and $[RuCl_2(dac)(dmso)-H]^-$.

In contrast to the results obtained with iron(III) (data from MS experiments and elemental analysis indicates the formation of $[FeCl_2(dac)_2][FeCl_4]$), in the case of the

Table 2
The theoretical *m/z* values for the highest peaks in positive mode mass spectra of the studied ruthenium(II) complexes

m/z	Assignment
233.0	$[Ru(dac)_2]^{2+}$
387.2	$[2dac+Na]^+$
397.0	$[RuCl(dac)(dmso)]^+$
429.0	$[RuCl(dac)(dmso)(MeOH)]^+$
475.0	$[RuCl(dac)(dmso)_2]^+$
507.0	$[RuCl(dac)(dmso)_2(MeOH)]^+$
537.0	$[RuCl(dac)(dmso)_2(MeOH)_2-2H]^+$
553.0	$[RuCl(dac)(dmso)_3]^+$
579.1	$[RuCl(dac)_2(dmso)]^+$
607.0	$[RuCl(dac)(dmso)_3(MeOH)+Na-H]^+$
620.0	$[RuCl_2(dac)(dmso)_3(MeOH)]^+$
657.1	$[RuCl(dac)_2(dmso)_2]^+$

ruthenium complexes it is assumed that during the isolation process a species with the formula $[RuCl_2(dac)_2(dmso)_2]$ was obtained with the $[RuCl(dac)_2(dmso)]^+$-ion identified in the mass spectrum being probably a fragment of $[RuCl_2(dac)_2(dmso)_2]$. In general in mass spectrometric studies of synthesized (and characterized by other methods) Ru(II) and also of Ru(III) complexes, it has been recognized that these species frequently undergo fragmentation processes when transferred into the gaseous phase [23,24].

The isolation procedure might also have led to an enrichment of $[RuCl_2(dac)_2(dmso)_2]$ explaining the differences in the mass spectra (high abundance of ions assignable to ruthenium complexes with three dmso-ligands). Also it can be concluded that the reaction of dacarbazine with *cis*-$[RuCl_2(dmso)_4]$ proceeds rather slowly in comparison to other starting complexes (compare $CoCl_2$ and $NiCl_2$).

5. The complexation of dacarbazine to cobalt(II)

When incubating $CoCl_2$ and dacarbazine at a molar ratio of 1:2 and stirring for 2 h the coordination compound $[CoCl_2(dac)_2]$ was isolated by precipitation with diethylether. The elemental analysis showed that not only $[CoCl_2(dac)_2]$ but also unreacted $CoCl_2$ was precipitated during the isolation process.

Comparing the ESI mass spectra of the synthesized Co complex with that obtained after incubation of $CoCl_2$ with dacarbazine at molar ratios of 1:1 and 1:2 for 1 h at room temperature, which were also analyzed in both positive and negative ion modes, showed significant differences (see Fig. 4). While in all three mass spectra the most intense signal was found at *m/z* 458.0 and assigned to the $[CoCl(dac)_2]^+$-ion, the less abundant peaks varied significantly in regard in their abundance (for peak assignment see Table 3). For example, the peak at *m/z* 276.0 – the mono-dacarbazine complex – was much higher in the incubation mixtures than in the mass spectrum of the synthesized species. In contrast, signals derived from dacarbazine and higher adducts were more intense in the 1:2 sample and the isolated complex. Increasing the incubation time up to 24 h led only to minor changes in the mass spectra. The appearance of signals assignable to $[Co(dac)_2-NH(CH_3)_2-H]^+$ and $[Co(dac)_3-NH(CH_3)_2-3H]^+$ at *m/z* 377.1 and 577.1 (fragments of $[Co(dac)_2-H]^+$ and $[Co(dac)_3-H]^+$, respectively) indicates that the methylated amino group does not contribute to the coordination of the metal center to dacarbazine.

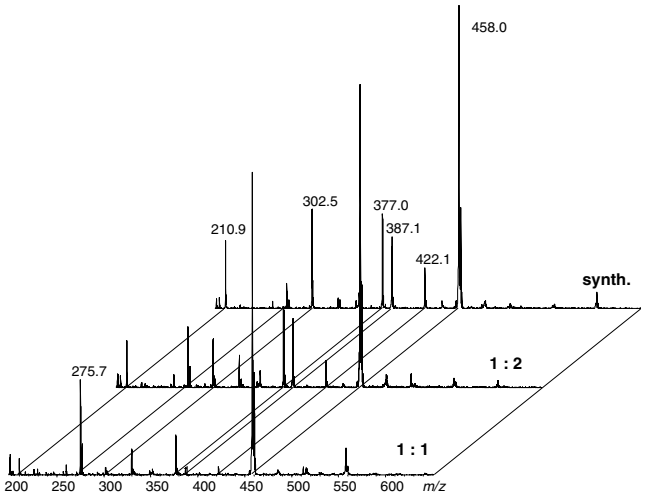

Fig. 4. Positive ion mode mass spectra for 1 h incubated $CoCl_2$–dacarbazine mixtures (1:1 and 1:2) and the isolated Co complex.

Table 3
The theoretical *m/z* values for the highest peaks in positive mode mass spectra of the studied cobalt(II) complexes

Positive ion mode (calculated) *m/z*	Assignment
211.6	$[Co(dac)_2]^{2+}$
276.0	$[CoCl(dac)]^+$
302.6	$[Co(dac)_3]^{2+}$
377.1	$[Co(dac)_2-NH(CH_3)_2-H]^+$
387.2	$[2dac+Na]^+$
422.1	$[Co(dac)_2-H]^+$
458.1	$[Co(dac)_2Cl]^+$
557.1	$[Co(dac)_3-NH(CH_3)_2-3H]^+$
604.2	$[Co(dac)_3-H]^+$

In the negative ion mode the species at *m/z* 163.8, 440.8 and 456.1 could be assigned to $[CoCl_3]^-$, a $[Co_2Cl_4(dac)-H]^-$ cluster and the $[CoCl(dac)_2-2H]^-$-anion, respectively. This might explain the rest of the unreacted $CoCl_2$ identified in the negative ion mode as the respective trichlorocobaltate(II) anion.

The data from elemental analysis and from mass spectrometric experiments led to the conclusion that the neutral complex $[CoCl_2(dac)_2]$ is the most favorable species to be formed between Co(II) and dacarbazine, independently of the molar ratio of incubation.

6. The complexation of dacarbazine to nickel(II)

Incubation of $NiCl_2$ with dacarbazine at a molar ratio of 1:2 yielded, after stirring for 2 h and precipitation with diethyl ether, $[NiCl_2(dac)_2]$ and a rest of unreacted $NiCl_2$. In the mass spectrum the main peak (100%) at *m/z* 457.2 was assigned to $[NiCl(dac)_2]^+$ (for assignment see Table 4).

Table 4
The theoretical *m/z* values for the highest peaks in positive mode mass spectra of the studied nickel(II) complexes

Positive ion mode (calculated) *m/z*	Assignment
211.1	$[Ni(dac)_2]^{2+}$
275.0	$[Ni(dac)Cl]^{+}$
302.1	$[Ni(dac)_3]^{2+}$
376.1	$[Ni(dac)_2-NH(CH_3)_2-H]^{+}$
387.2	$[2dac+Na]^{+}$
421.1	$[Ni(dac)_2-H]^{+}$
457.1	$[Ni(dac)_2Cl]^{+}$
515.1	$[Ni(dac)_3-2NH(CH_3)_2+H]^{+}$
556.1	$[Ni(dac)_3-NH(CH_3)_2-3H]^{+}$
603.2	$[Ni(dac)_3-H]^{+}$

Similar to the experiments with Co(II) the most abundant peaks were found to be $[NiCl(dac)_2]^{+}$ at *m/z* 457.1 and $[NiCl(dac)_2-2H]^{-}$ at *m/z* 455.1 in the positive and negative ion modes, respectively, for the isolated species and the 1:2 incubation mixture (Ni:dac) after an incubation period of 1 h, while in the 1:1 incubation mixture the peak at *m/z* 274.8 was the highest one $[NiCl(dac)]^{+}$ (see Fig. 5). After 24 h no significant changes in the mass spectra were found. Comparable to the cobalt complexes, in these experiments also fragment ions at *m/z* 376.1, 515.1 and 556.1 from the parent ions $[Ni(dac)_2-H]^{+}$ (*m/z* 421.1) or $[Ni(dac)_3-H]^{+}$ (*m/z* 603.2) were found which were assigned to $[Ni(dac)_2-NH(CH_3)_2-H]^{+}$, $[Ni(dac)_3-2NH(CH_3)_2+H]^{+}$ and $[Ni(dac)_3-NH(CH_3)_2-3H]^{+}$, respectively. Again, no involvement of the alkylated amino function in the binding was observed.

The negative ion mode spectrum of the isolated complex contained, beside the deprotonated species at *m/z* 455.3 $\{[NiCl(dac)_2-2H]^{-}\}$, a signal at *m/z* 311.4 $\{[NiCl_2(dac)]^{-}\}$ and another one at 164.4 ($[NiCl_3]^{-}$). In the 1:1 incubation mixture a cluster of two Ni ions with one dacarbazine ligand and chloride ions was the highest peak, accompanied by a $[NiCl_3]^{-}$ ion, while in the 1:2 reaction again the signal at *m/z* 455.3 was the most intense and the $[NiCl_3]^{-}$ ion was not detectable.

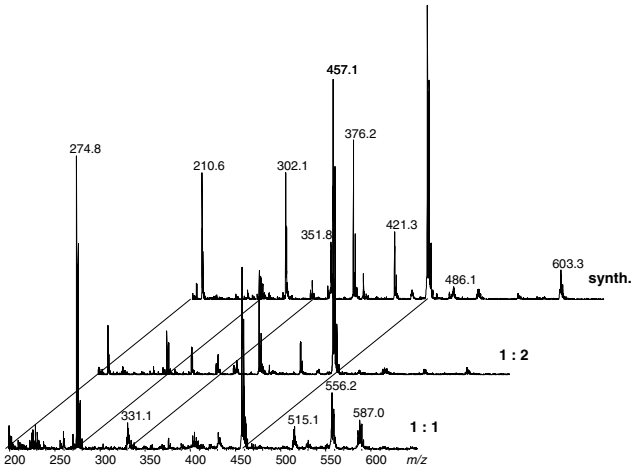

Fig. 5. Comparison of positive ion mass spectra for 1 h incubated $NiCl_2$–dacarbazine mixtures (1:1 and 1:2) and the isolated Ni complex.

In contrast to the Co complexes, it is assumed that $[NiCl_2(dac)_2]$ is the preferentially formed species only when incubating at a molar ratio of $NiCl_2$ to dacarbazine of 1:2, in the 1:1 incubation mixture the most intense signal was assigned to a [Ni(dac)]-type complex.

7. Conclusions

Dacarbazine and its metal complexes are of interest in antitumor chemotherapy. From the perspective of coordination chemists, attention is drawn to dacarbazine since it contains seven donor atoms representing potential coordination sites for transition metal ions. In order to study the coordination properties of this potential multidentate ligand, complexes with Fe, Ru, Ni and Co centers were synthesized and isolated or in situ characterized by electrospray ionization mass spectrometry.

It was found that Fe(III) forms, independently of the ratio between the iron salt and dacarbazine, at rather slow reaction kinetics exclusively a complex of the $[Fe(dac)_2]$ type. The also rather slow reaction between *cis*-$[Ru(dmso)_4Cl_2]$ with dacarbazine yields a mixture of [Ru(dac)] and $[Ru(dac)_2]$ type complexes. In contrast, the reactions with Ni(II) and Co(II) salts were observed to proceed much faster. While the reaction with Co(II) salts delivered only a $[Co(dac)_2]$ type complex, coordination compounds with Ni(II) were identified to be of [Ni(dac)] and $[Ni(dac)_2]$ types when being incubated at molar ratios Ni:dac of 1:1 or 1:2, respectively. Due to the paramagnetic character of most of the complexes no statement on the coordination geometry from NMR spectroscopy can be made. However, IR spectra elucidated the probable involvement of the amide functionality in the coordination process. This data were partly confirmed by MS data taking into account that the losses of $NH(CH_3)_2$ indicate that at least this nitrogen is not involved in the coordination processes.

8. Experimental

If necessary the reactions were carried out in dry solvents and under argon atmosphere. The NMR-spectra were recorded on a Bruker Avance DPX 400 instrument (Ultrashield™ Magnet) at 400.13 MHz (^{1}H).

Electrospray ionization mass spectra were recorded on a Bruker *esquire*$_{3000}$ ion trap mass spectrometer equipped with an orthogonal electrospray interface (Bruker Daltonics, Bremen, Germany). The Bruker Daltonics esquire 5.2 (Build 382) software bundle consisting of Bruker esquire Control 5.2 (Build 63.8) and Bruker Data Analysis 3.2 (Build 121) was used for acquiring spectra and data analysis, respectively. The samples were delivered at a flow rate of 4 μl/min using a syringe pump 74900 from Cole-Parmer Instrument Company (Vernon Hills, IL, USA) and N_2 was used as the drying (180 °C) and nebulizing gas (10 psi). The scan range was from 50 to 1200 *m/z*. The mass spectrometer was operated in both positive and negative ionization modes and the optimization was done to maximize the

Table 5
The operational MS parameters

Parameters	Fe	Ru	Co	Ni
HV capillary (V)	4500	2600	4500	3369
Dry gas flow (l min^{-1})	9	9	5	5
Skimmer 1 (V)	22.0	24.8	22.0	22.0
Skimmer 2 (V)	5.7	5.0	5.9	5.4
Octopole (V)	3.56	2.71	3.23	3.16
Trap drive	42.3	40.1	37.0	37.6

peak assignable to the most intense metal–dacarbazine adduct-signal in the positive ion mode (see Table 5 for measurement parameters). For MS studies, dacarbazine was incubated with the respective metal complexes at molar ratios of 1:1 and 2:1 by mixing methanol solutions yielding concentrations of about 0.1 mM. Measurements were done immediately after dissolution and repeated over a period of 4 days.

The thermogravimetric analyses were done on a Mettler Toledo TGA 850 and the elemental analyses by the Laboratory for Elemental Analysis of the Faculty of Chemistry, University of Vienna, with a Perkin–Elmer 2400 CHN Elemental Analyzer.

9. Syntheses of complexes

9.1. $FeCl_3 \cdot 6H_2O$

A solution of dacarbazine (50 mg, 0.27 mmol) in ethanol (6 mL) was added to a solution of $FeCl_3 \cdot 6H_2O$ (74 mg, 0.27 mmol) in ethanol (4 mL). The reaction mixture was refluxed for 2 h. Afterwards the solvent was removed and the dark solid was dried in vacuum (33.8 mg).

M.p. 178–180 °C. Elemental *Anal*. Calc. for $(C_{12}Cl_3FeH_{20}N_{12}O_2)_1(FeCl_3)_{1.15}(C_2H_5O)_{0.65}$: C, 21.50, H, 3.24, N, 22.62. Found: C, 21.45, H, 3.39, N, 22.54%. MS (ESI$^+$) m/z 489.9 $[Fe(dac)_2Cl_2]^+$.

9.2. *cis*-$RuCl_2(dmso)_4$

A solution of dacarbazine (200 mg, 1.1 mmol) in methanol (15 mL) was added to a solution of *cis*-$[RuCl_2(dmso)_4]$ (256 mg, 0.55 mmol) in methanol (15 mL). The reaction mixture was stirred for 4 h and diethyl ether (200 mL) was added. The solution was kept at 4 °C for 12 h and afterwards the precipitated product was isolated by filtration, washed with diethyl ether (3 × 20 mL), and dried in vacuum.

Yield: 265.3 mg (68%). M.p. 196–198 °C (decomp.). Elemental *Anal*. Calc. for $(C_{16}Cl_2H_{32}N_{12}O_4RuS_2)_1(H_2O)_1$: C, 27.04, H, 4.82, N, 23.65. Found: C, 26.89, H, 4.52, N, 23.76%. MS (ESI$^+$) m/z 579.3 $[Ru(dac)_2(dmso)Cl]^+$.

9.3. $CoCl_2 \cdot 6H_2O$

A solution of dacarbazine (50 mg, 0.27 mmol) in methanol (5 mL) was added to a solution of $CoCl_2 \cdot 6H_2O$ (33 mg, 0.14 mmol) in methanol (5 mL). The reaction mixture was stirred for 2 h and diethyl ether (50 mL) was added. Afterwards the precipitated product was isolated by filtration, washed with diethyl ether (3 × 10 mL), and dried in vacuum (38.1 mg).

M.p. 168–170 °C. Elemental *Anal*. Calc. for $(C_{12}Cl_2CoH_{20}N_{12}O_2)_1(CoCl_2)_{0.1}(CH_4O)_{0.4}$: C, 28.64, H, 4.19, N, 32.32. Found: C, 28.61, H, 4.20, N, 32.40%. MS (ESI$^+$) m/z 458.0 $[Co(dac)_2Cl]^+$.

9.4. $NiCl_2 \cdot 6H_2O$

A solution of dacarbazine (50 mg, 0.27 mmol) in methanol (5 mL) was added to a solution of $NiCl_2 \cdot 6H_2O$ (33 mg, 0.14 mmol) in methanol (5 mL). The reaction mixture was stirred for 2 h and diethyl ether (50 mL) was added. The solution was kept at 4 °C for 3 h and afterwards the precipitated product was isolated by filtration, washed with diethyl ether (3 × 10 mL), and dried in vacuum (39 mg).

M.p. 198–200 °C. Elemental *Anal*. Calc. for $(C_{12}Cl_2H_{20}N_{12}NiO_2)_1(NiCl_2)_{0.2}(CH_4O)_{0.5}(H_2O)_{0.4}$: C, 27.64, H, 4.23, N, 30.95. Found: C, 27.77, H, 4.29, N, 31.07%. MS (ESI$^+$) m/z 457.2 $[Ni(dac)_2Cl]^+$.

Acknowledgements

The authors gratefully thank Dr. Peter Unfried for the support with the thermogravimetric analyses.

References

[1] A.M.M. Eggermont, J.M. Kirkwood, Eur. J. Cancer 40 (2004) 1825.
[2] M. Spasova, E. Golovinski, Pharmacol. Ther. 27 (1985) 333.
[3] J.L. Skibba, D.D. Beal, G. Ramirez, G.T. Bryan, Cancer Res. 30 (1970) 147.
[4] B. Rosenberg, L. VanCamp, J.E. Trosko, V.H. Mansour, Nature (London) 222 (1969) 385.
[5] M. Galanski, V.B. Arion, M.A. Jakupec, B.K. Keppler, Curr. Pharm. Design 9 (2003) 2078.
[6] G. Sava, R. Gagliardi, A. Bergamo, E. Alessio, G. Mestroni, Anticancer Res. 19 (1999) 969.
[7] L.R. Bernstein, T. Tanner, C. Godfrey, B. Noll, Metal-Based Drugs 7 (2000) 33.
[8] P. Collery, J.L. Domingo, B.K. Keppler, Anticancer Res. 16 (1996) 687.
[9] M. Thiel, T. Schilling, D.C. Gey, R. Ziegler, P. Collery, B.K. Keppler, Contrib. Oncol. 54 (1999) 439.
[10] H.C. Freeman, N.D. Hutchinson, Acta Crystallogr., Sect. B 35 (1979) 2045.
[11] J. Shukla, K.S. Pitre, Ind. J. Physiol. Pharmacol. 42 (1998) 223.
[12] F. Zalaru, D. Ionescu, C. Zalaru, C. Parnau, Analele Universitatii Bucuresti, Chimie 10 (2001) 9.
[13] R.B. Cole, Electrospray Ionization Mass Spectrometry: Fundamentals, Instrumentation, and Applications, Wiley, New York, 1997.
[14] J.H. Gross, Mass Spectrometry, Springer, Berlin, 2004.
[15] K.J. Fisher, Prog. Inorg. Chem. 50 (2001) 343.
[16] S.M. Williams, J.S. Brodbelt, A.P. Marchand, D. Cal, K. Mlinaric-Majerski, Anal. Chem. 74 (2002) 4423.
[17] C.G. Hartinger, A.A. Nazarov, V. Chevchenko, V.B. Arion, M. Galanski, B.K. Keppler, J. Chem. Soc., Dalton Trans. (2003) 3098.

[18] M.G.O. Santana-Marques, F.M.L. Amado, A.J.F. Correia, M. Lucena, J. Madureira, B.J. Goodfellow, V. Felix, T.M. Santos, J. Mass Spectrom. 36 (2001) 529.
[19] N. Burford, M.D. Eelman, K. Groom, J. Inorg. Biochem. 99 (2005) 1992.
[20] M.C.B. Moraes, C.L.d. Lago, Quim. Nova 26 (2003) 556.
[21] H. Lavanant, H. Virelizier, Y. Hoppilliard, J. Am. Soc. Mass Spectrom. 9 (1998) 1217.
[22] A.T. Blades, M.G. Ikonomou, P. Kebarle, Anal. Chem. 63 (1991) 2109.
[23] M. Pongratz, P. Schluga, M.A. Jakupec, V.B. Arion, C.G. Hartinger, G. Allmaier, B.K. Keppler, J. Anal. Atom. Spectrom. 19 (2004) 46.
[24] R.E. Shepherd, J.M. Slocik, T.W. Stringfield, K.V. Somayajula, A.A. Amoscato, Inorg. Chim. Acta 357 (2004) 965.

pK_a caused by the changes of the electronic and steric properties of the co-ordinated ligands L.

2. Experimental

All reagents were Aldrich or Fluka products in the highest available purity and were used without any further treatment. Solvents were dried using standard techniques.

2.1. Physical measurements

Infrared spectra (4000–400 cm^{-1}, KBr disks) were recorded on a Perkin–Elmer Spectrum One spectrophotometer. NMR spectra (^1H, $^{31}P\{^1H\}$, $^{31}P\{^1H\}$ with inverse-gated decoupling) were obtained either on AC 200 or AVANCE 300 Bruker spectrometers in CD_3NO_2 at temperatures comprised between 298 and 243 K. ^1H NMR spectra are referred to internal tetramethylsilane, while ^{31}P NMR chemical shifts are reported with respect to 85% H_3PO_4. SwaN-MR and MestRe-C software packages were used to treat the NMR data [2]. The conductivity of 1×10^{-3} mol dm^{-3} solutions of the new complexes in DMF at 25° was measured with a Radiometer CDM 83 instrument. Elemental analyses (C, H, N) were performed by the microanalytical laboratory at the Department of Pharmaceutical Sciences, University of Padua.

2.2. Computational details

Computational geometry optimisation of the complexes was performed using the restricted DFT B3PW91 method with the CEP-121G basis set (CEP-31G on the Pt atom). Geometry convergence was accelerated using the GDIIS algorithm and a first refinement of the structures was obtained using the restricted semi-empirical PM3 method. Geometry optimisation of the free nitrogen-donor ligands was obtained with restricted DFT B3LYP/6-311+G** calculations [3]. All calculations were carried out with computers equipped with Intel Pentium 4 Northwood processors operating at 2.6 GHz frequency or IBM G4 operating at 1.25 GHz. Software used were GAUSSIAN-98 and SPARTAN-02 [4].

2.3. Preparation of the complexes

The $[PtCl(triphos)]^+$ species has already been reported as the chloride salt [5], but we preferred to isolate it as the perchlorate salt following the procedure described below [6].

To a warm (ca. 50 °C) solution of *cis*/*trans*-$PtCl_2(SMe_2)_2$ [7] (0.390 g, 1.0 mmol) in methanol (25 mL) a stoichiometric amount of solid triphos (0.534 g, 1.0 mmol) was added in successive small portions. After 10 min the reaction mixture was allowed to cool to room temperature and a solution of an excess of $LiClO_4$ (0.202 g, 1.5 mmol) in methanol (10 mL) was slowly added. The white solid complex $[PtCl(triphos)](ClO_4)$ which separated out of the solution was filtered off, washed with methanol and diethylether and dried under vacuum (yield >90%).

2.4. *[Pt(4-R-py)(triphos)](ClO$_4$)$_2$ ($\mathbf{1}^R$)* *{R = CN, COOH, COOMe, MeCO, H, Me, NH$_2$}* *[Pt(4-R-an)(triphos)](ClO$_4$)$_2$ ($\mathbf{2}^R$)* *{R = NO$_2$, CN, Cl, H, Me, MeO}*

The complexes $[Pt(4\text{-}R\text{-}py)(triphos)](ClO_4)_2$ ($\mathbf{1}^R$) and $[Pt(4\text{-}R\text{-}an)(triphos)](ClO_4)_2$ ($\mathbf{2}^R$) have been prepared by adding the stoichiometric amount of solid $AgClO_4$ to a solution of $[PtCl(triphos)](ClO_4)$ in nitromethane. In a typical preparation, 0.021 g (0.1 mmol) of $AgClO_4$ were added to a 5 mL solution of $[PtCl(triphos)](ClO_4)$ (0.086 g, 0.1 mmol) in CH_3NO_2. After 12 h under stirring the AgCl formed was filtered off and a slight excess (1.5:1) of the appropriate pyridine or aniline was added. The resulting solution was heated to about 50 °C for 2 h and then filtered if necessary. By slow addition of diethylether the product which separated out was filtered, washed twice with diethylether and dried under vacuum (yield >70% in all cases).[1]

Anal. Calc. for $C_{40}H_{37}Cl_2N_2O_8P_3Pt$ ($\mathbf{1}^{CN}$): C, 46.52; H, 3.61; N, 2.71. Found: C, 46.61; H, 3.62; N, 2.73%. *Anal.* Calc. for $C_{40}H_{38}Cl_2NO_{10}P_3Pt$ ($\mathbf{1}^{COOH}$): C, 45.68; H, 3.64; N, 1.33. Found: C, 45.59; H, 3.65; N, 1.32%. *Anal.* Calc. for $C_{41}H_{40}Cl_2NO_{10}P_3Pt$ ($\mathbf{1}^{COOMe}$): C, 46.21; H, 3.78; N, 1.31. Found: C, 46.09; H, 3.80; N, 1.29%. *Anal.* Calc. for $C_{41}H_{40}Cl_2NO_9P_3Pt$ ($\mathbf{1}^{MeCO}$): C, 46.91; H, 3.84; N, 1.33. Found: C, 46.81; H, 3.82; N, 1.34%. *Anal.* Calc. for $C_{39}H_{38}Cl_2NO_8P_3Pt$ ($\mathbf{1}^{H}$): C, 46.49; H, 3.80; N, 1.39. Found: C, 46.36; H, 3.78; N, 1.40%. *Anal.* Calc. for $C_{40}H_{40}Cl_2NO_8P_3Pt$ ($\mathbf{1}^{Me}$): C, 47.02; H, 3.95; N, 1.37. Found: C, 47.14; H, 3.97; N, 1.39%. *Anal.* Calc. for $C_{39}H_{39}Cl_2N_2O_8P_3Pt$ ($\mathbf{1}^{NH_2}$): C, 45.80; H, 3.84; N, 2.74. Found: C, 45.93; H, 3.85; N, 2.72%. *Anal.* Calc. for $C_{40}H_{39}Cl_2N_2O_{10}P_3Pt$ ($\mathbf{2}^{NO_2}$): C, 45.04; H, 3.69; N, 2.63. Found: C, 45.11; H, 3.70; N, 2.65%. *Anal.* Calc. for $C_{41}H_{39}Cl_2N_2O_8P_3Pt$ ($\mathbf{2}^{CN}$): C, 47.05; H, 3.76; N, 2.68. Found: C, 47.13; H, 3.74; N, 2.70%. *Anal.* Calc. for $C_{40}H_{39}Cl_3NO_8P_3Pt$ ($\mathbf{2}^{Cl}$): C, 45.49; H, 3.72; N, 1.33. Found: C, 45.60; H, 3.70; N, 1.34%. *Anal.* Calc. for $C_{40}H_{40}Cl_2NO_8P_3Pt$ ($\mathbf{2}^{H}$): C, 47.02; H, 3.95; N, 1.37. Found: C, 46.90; H, 3.93; N, 1.36%. *Anal.* Calc. for $C_{41}H_{42}Cl_2NO_8P_3Pt$ ($\mathbf{2}^{Me}$): C, 47.55; H, 4.09; N, 1.35. Found: C, 47.49; H, 4.11; N, 1.36%. *Anal.* Calc. for $C_{41}H_{42}Cl_2NO_9P_3Pt$ ($\mathbf{2}^{OMe}$): C, 46.82; H, 4.03; N, 1.33. Found: C, 46.90; H, 4.01; N, 1.34.

All the $\mathbf{1}^R$ and $\mathbf{2}^R$ complexes show the signals due to the triphos and the pyridine or the aniline ligands in the ^1H NMR and IR spectra. Some characteristic IR and ^1H NMR data are reported below:

[1] Safety note: perchlorate salts of metal complexes with organic ligands are potentially explosive; however, all the prepared compounds, in the experimental conditions described, appeared to be stable both in solution and in the solid state.

Table 1
^{31}P {^{1}H} NMR data for complexes **1**–**2** and pK_a values of the 4-substituted pyridines and anilines

Complex		^{31}P {^{1}H} NMR δ (J/Hz)	pK_a
$\mathbf{1}^{CN}$	$[Pt(4\text{-}CN\text{-}py)(triphos)]^{2+}$	82.5 (s, $^{1}J_{Pt-P1} = 2895$, P_1); 49.3 (s, $^{1}J_{Pt-P2} = 2382$, P_2)	1.90
$\mathbf{1}^{COOH}$	$[Pt(4\text{-}COOH\text{-}py)(triphos)]^{2+}$	82.7 (s, $^{1}J_{Pt-P1} = 2861$, P_1); 48.8 (s, $^{1}J_{Pt-P2} = 2390$, P_2)	3.26
$\mathbf{1}^{COOMe}$	$[Pt(4\text{-}COOMe\text{-}py)(triphos)]^{2+}$	82.8 (s, $^{1}J_{Pt-P1} = 2861$, P_1); 48.8 (s, $^{1}J_{Pt-P2} = 2390$, P_2)	3.26
$\mathbf{1}^{MeCO}$	$[Pt(4\text{-}MeCO\text{-}py)(triphos)]^{2+}$	82.6 (s, $^{1}J_{Pt-P1} = 2855$, P_1); 48.8 (s, $^{1}J_{Pt-P2} = 2392$, P_2)	3.51
$\mathbf{1}^{H}$	$[Pt(4\text{-}H\text{-}py)(triphos)]^{2+}$	82.4 (s, $^{1}J_{Pt-P1} = 2827$, P_1); 48.6 (s, $^{1}J_{Pt-P2} = 2404$, P_2)	5.17
$\mathbf{1}^{Me}$	$[Pt(4\text{-}Me\text{-}py)(triphos)]^{2+}$	82.8 (s, $^{1}J_{Pt-P1} = 2815$, P_1); 47.9 (s, $^{1}J_{Pt-P2} = 2406$, P_2)	6.03
$\mathbf{1}^{NH2}$	$[Pt(4\text{-}NH_2\text{-}py)(triphos)]^{2+}$	83.0 (s, $^{1}J_{Pt-P1} = 2768$, P_1); 46.7 (s, $^{1}J_{Pt-P2} = 2424$, P_2)	9.11
$\mathbf{2}^{NO_2}$	$[Pt(4\text{-}NO_2\text{-}an)(triphos)]^{2+}$	85.0 (s, $^{1}J_{Pt-P1} = 3292$, P_1); 48.4 (s, $^{1}J_{Pt-P2} = 2364$, P_2)	1.00
$\mathbf{2}^{CN}$	$[Pt(4\text{-}CN\text{-}an)(triphos)]^{2+}$	85.0 (s, $^{1}J_{Pt-P1} = 3255$, P_1); 48.4 (s, $^{1}J_{Pt-P2} = 2520$, P_2)	1.74
$\mathbf{2}^{Cl}$	$[Pt(4\text{-}Cl\text{-}an)(triphos)]^{2+}$	85.0 (s, $^{1}J_{Pt-P1} = 2949$, P_1); 48.1 (s, $^{1}J_{Pt-P2} = 2461$, P_2)	3.98
$\mathbf{2}^{H}$	$[Pt(4\text{-}H\text{-}an)(triphos)]^{2+}$	80.8 (s, $^{1}J_{Pt-P1} = 2806$, P_1); 48.2 (s, $^{1}J_{Pt-P2} = 2447$, P_2)	4.60
$\mathbf{2}^{Me}$	$[Pt(4\text{-}Me\text{-}an)(triphos)]^{2+}$	84.8 (s, $^{1}J_{Pt-P1} = 2918$, P_1); 47.8 (s, $^{1}J_{Pt-P2} = 2469$, P_2)	5.08
$\mathbf{2}^{MeO}$	$[Pt(4\text{-}MeO\text{-}an)(triphos)]^{2+}$	80.4 (s, $^{1}J_{Pt-P1} = 2780$, P_1); 47.9 (s, $^{1}J_{Pt-P2} = 2457$, P_2)	5.34

IR (cm^{-1}): $\mathbf{1}^{CN}$ 2237 w (ν_{CN}); $\mathbf{1}^{COOH}$ 1733 s (ν_{CO}); $\mathbf{1}^{COOMe}$ 1730 s (ν_{CO}); $\mathbf{1}^{MeCO}$ 1694 s (ν_{CO}); $\mathbf{1}^{NH_2}$ 3466 m, 3363 m (ν_{NH}); $\mathbf{2}^{CN}$ 2251 s, 2210 sh (ν_{CN}).

^{1}H NMR (ppm, 298 K): $\mathbf{1}^{COOMe}$ 3.93 (s, 3H, CH_3); $\mathbf{1}^{MeCO}$ 2.56 (s, 3H, CH_3); $\mathbf{1}^{Me}$ 2.36 (s, 3H, CH_3); $\mathbf{1}^{NH_2}$ (s, br, 2H, NH_2); $\mathbf{2}^{Me}$ 2.19 (s, 3H, CH_3); $\mathbf{2}^{OMe}$ 3.93 (s, 3H, CH_3).

^{31}P NMR chemical shifts and $^{1}J_{Pt-P}$ coupling constants are collected in Table 1. All the Λ_M values measured are comprised between 140 and 150 Ω^{-1} mol^{-1} cm^2, as expected for 2:1 electrolytes in DMF [8].

3. Results and discussion

3.1. Preparation of the complexes

The synthetic routes used for the preparation of the complexes $[PtCl(triphos)](ClO_4)$, $[Pt(4\text{-}R\text{-}py)(triphos)](ClO_4)_2$ ($\mathbf{1}^{R}$) and $[Pt(4\text{-}R\text{-}an)(triphos)](ClO_4)_2$ ($\mathbf{2}^{R}$) are outlined in Scheme 1 and the details are given in Section 2, so here only few comments are made. Although the isolation of the chloro-complex $[PtCl(triphos)]^{+}$ as chloride salt has already been reported [5], we have used an alternative method starting from the isomeric mixture of $PtCl_2(SMe_2)_2$, which we found very convenient for the synthesis of a wide variety of Pt(II) chloro-complexes with polydentate ligands [6]. Treatment of $[PtCl(triphos)](ClO_4)$ with silver perchlorate followed by the addition of the appropriate nitrogen-donor ligand afforded the desired $\mathbf{1}^{R}$ or $\mathbf{2}^{R}$ complex in pure form and in good yield. All the characterization data (IR, ^{1}H NMR, ^{31}P NMR, conductivity, elemental analyses) are in good agreement with the purposed formulations. Spectroscopic data of the $\mathbf{1}^{H}$ derivative have been also compared with those of the already known $[Pt(pyridine)(triphos)](CF_3SO_3)_2$ complex [9].

The pyridines and anilines, all *para*-substituted, were chosen to cover a wide range of basicity ($1.90 \leqslant pK_a$ pyridines $\leqslant 9.11$, $1.00 \leqslant pK_a$ anilines $\leqslant 5.34$). Moreover, the relationship between the basicity and the nucleophilic behaviour of some of the nitrogen-donor ligands considered has been already investigated and discussed in kinetic studies [10]. It is also known [11] that there is a linear relationship between the pK_a values and the proton affinity, PA (i.e., the enthalpy of a proton breaking-off in the gaseous phase) for the series of the considered pyridines and anilines, so the medium contribution to the pK_a determination is almost constant for both the types of nitrogen-donor ligands.

3.2. NMR and DFT studies

The ^{31}P {^{1}H} NMR spectra of all the $\mathbf{1}^{R}$ and $\mathbf{2}^{R}$ complexes consist of two sharp peaks, each with ^{195}Pt satellites. The J_{P1-P2} phosphorus–phosphorus couplings are unobservable for all the prepared complexes, but this is expected for square-planar triphos derivatives with all the phosphorus atoms co-ordinated to the same metal centre [9,12]. The ^{31}P NMR data of the $\mathbf{1}^{R}$ and $\mathbf{2}^{R}$ derivatives are reported in Table 1, together with the pK_a values [13] of the *para*-substituted pyridines and anilines.

There in no apparent regularity in the variation of the ^{31}P chemical shifts, while there are interesting trends for the coupling constants. For the *para*-substituted pyridines, a variation of pK_a in the range 1.90–9.11 leads to a linear variation of $^{1}J_{Pt-P1}$ (P_1 = phosphorus nucleus *trans* to N) from 2895 to 2768 Hz. The linear relationship $^{1}J_{Pt-P1} = 2918 \pm 4 - 16.9 \pm 0.9\ pK_a$ is followed, as shown in Fig. 1A. There is also a linear rise (42 Hz within the considered pK_a range) of the $^{1}J_{Pt-P2}$ couplings (P_2 = phosphorus nuclei *cis* to N) while the pK_a value increases (see Fig. 1B); the equation is $^{1}J_{Pt-P2} = 2371 \pm 1 + 5.8 \pm 0.2\ pK_a$. It is to be noted that the derivatives of 4-COOH-py and 4-COOMe-py, both having the same pK_a (3.26), give exactly the same *trans* and *cis* $^{1}J_{Pt-P}$ coupling constants.

The linear relationship between $^{1}J_{Pt-P1}$ and $^{1}J_{Pt-P2}$ coupling constants is given by the equation $^{1}J_{Pt-P1} = 9700 \pm 300 - 2.9 \pm 0.1\ ^{1}J_{Pt-P2}$. The variation of donor capability of the pyridines affects mostly the *trans* $^{1}J_{Pt-P}$ coupling constant, also considering that there are two *cis* phosphorus atoms and only one *trans* phosphorus atom.

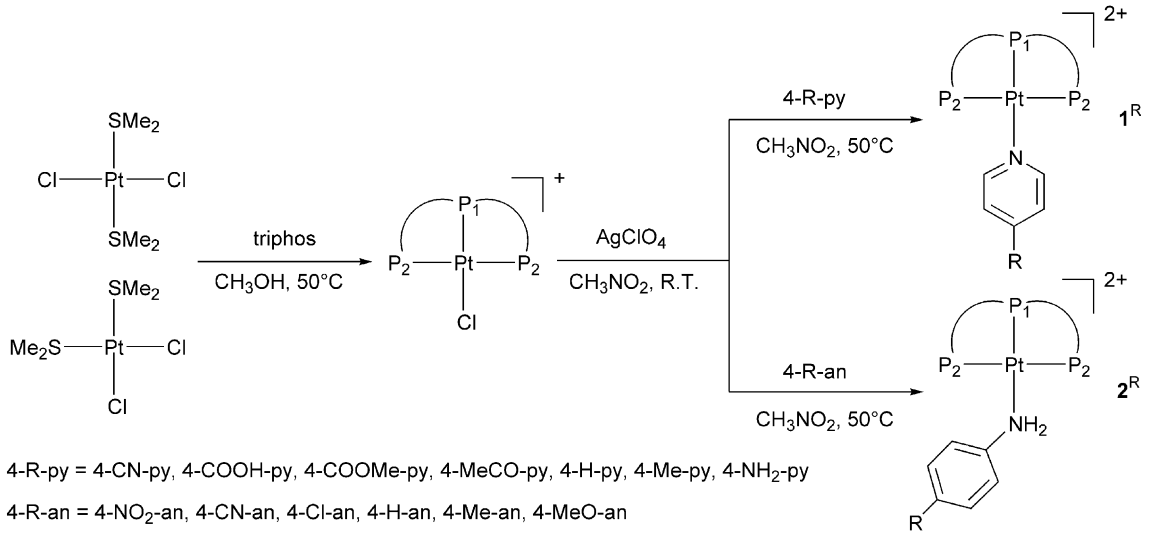

Scheme 1. Synthesis of $[PtCl(triphos)]^+$, $[Pt(4\text{-R-py})(triphos)]^{2+}$ ($\mathbf{1}^R$) and $[Pt(4\text{-R-an})(triphos)]^{2+}$ ($\mathbf{2}^R$) complexes.

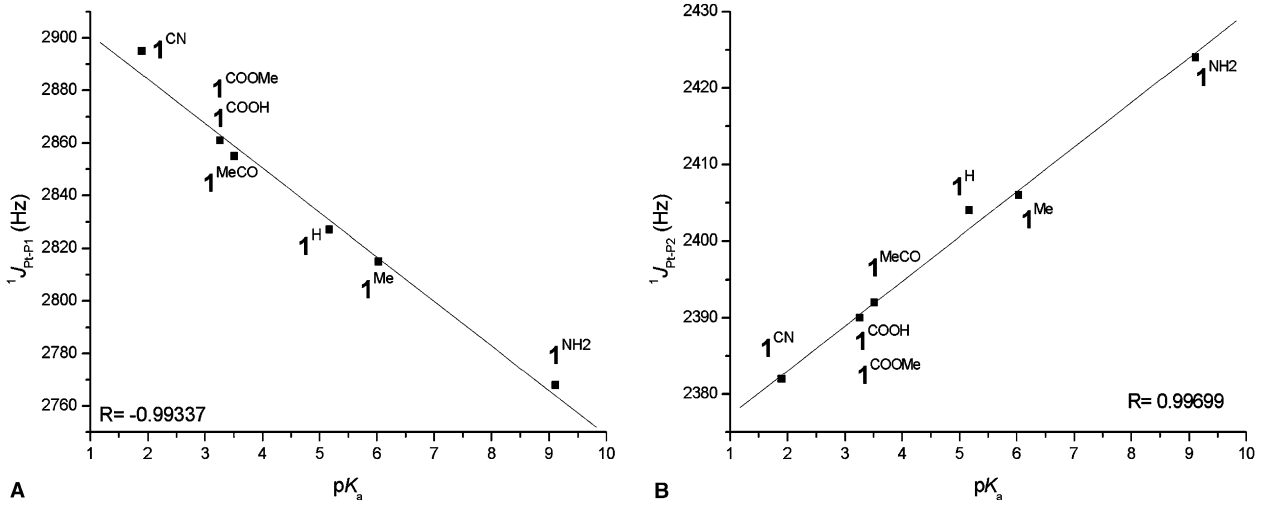

Fig. 1. Plot of $^1J_{Pt-P1}$ against pK_a (A) and of $^1J_{Pt-P2}$ against pK_a (B) for $\mathbf{1}^R$ complexes.

The use of 4-substituted pyridines allows to exclude steric effects due to the different R groups, so that the linear relationships between the pK_a and the $^1J_{Pt-P}$ values can be attributed only to electronic effects. It is generally assumed [1] that the magnitude of the $^1J_{Pt-P}$ coupling constant is dominated by the Fermi contact term, expressed by the following relation:

$$^1J_{Pt-P} \propto \frac{\gamma_{Pt}\gamma_P\alpha_{Pt}^2\alpha_P^2\left|\psi_{Pt(6s)}(0)\right|^2\left|\psi_{P(3s)}(0)\right|^2}{\Delta E}. \quad (1)$$

In the relation, γ_{Pt} and γ_P are the gyromagnetic ratios for the ^{195}Pt and ^{31}P isotopes, α_{Pt}^2 and α_P^2 represent the s-characters of the localized hybrid orbitals in a valence bond description, $|\psi_{Pt(6s)}(0)|^2$ and $|\psi_{P(3s)}(0)|^2$ are the electron densities of the s orbitals at nucleus, ΔE is an average singlet–triplet excitation energy. It is also assumed that the most important term for the variation of the magnitude of $^1J_{Pt-P}$ is α_{Pt}^2 so, following relation (1), the decrease of the *trans* $^1J_{Pt-P1}$ coupling constant with the increase of the pK_a represents primarily the change in 6s character of the hybrid orbital of platinum used in the bond with P_1. The increase of donor capability of the co-ordinated pyridine increase the Pt 6s character of the Pt–N bond at the expense of the *trans* Pt–P bond. The $^1J_{Pt-P2}$ trend suggests that the weakening of the Pt–P_1 bond strengthens the bonds between the metal centre and the other two phosphorus atoms in the *cis* positions.

Mather et al. have reported a correlation of the $^1J_{Pt-P}$ coupling constants with the Pt–P bond lengths in some trialkyl phosphine complexes of Pt(II) and Pt(IV) [14] and subsequent studies for Pt(0) complexes [15] have shown similar results, in which the shorter Pt–P distances are associated with larger values of $^1J_{Pt-P}$. We tried to correlate the $^1J_{Pt-P}$ coupling constants of the $\mathbf{1}^R$ complexes with the

bond lengths by optimising with DFT calculations the geometries of the derivatives of the pyridines with the greatest pK_a difference, the $[Pt(4\text{-CN-py})(triphos)]^{2+}$ ($\mathbf{1}^{CN}$) and $[Pt(4\text{-NH}_2\text{-py})(triphos)]^{2+}$ ($\mathbf{1}^{NH_2}$) cations. The difference in nucleophilicity between the two considered pyridines is well expressed by both the calculated dipolar moment μ (whose vector is oriented from the R group towards the pyridine-N atom) and the Mulliken charge on the pyridine-N atoms for the free species (see Table 2). Also the electrostatic potential surfaces on the pyridine-N atoms shown in Fig. 2 allow to understand the different nucleophilicity of the two pyridines.

The calculated r_{Pt-P1}, r_{Pt-P2} and r_{Pt-N} bond lengths for the $\mathbf{1}^{CN}$ and $\mathbf{1}^{NH_2}$ complexes are reported in Table 2; unfortunately, the differences between the corresponding bond lengths of the two derivatives are too small to be really significant, probably because of the relatively small difference of the $^1J_{Pt-P}$ couplings of the two complexes.

Also in the case of the complexes with the *para*-substituted anilines $\mathbf{2}^{R}$ a relationship between the pK_a values of the anilines and the $^1J_{Pt-P1}$ coupling constants of the $\mathbf{2}^{R}$ derivatives is observed (see Fig. 3), but this correlation is less linear in comparison with the one of the $\mathbf{1}^{R}$ derivatives. Moreover, for the $\mathbf{2}^{R}$ complexes there is an irregular trend of the $^1J_{Pt-P2}$ values against pK_a.

A possible explanation for the different behaviour of the $\mathbf{2}^{R}$ derivatives compared to $\mathbf{1}^{R}$ complexes is that steric effects due to the change of the 4-R group of the anilines cannot be completely excluded, as done in the case of the 4-substituted pyridines. In fact, by rotating the P_2–Pt–N–H dihedral angle in the optimised models of the $[Pt(4\text{-R-an})(triphos)]^{2+}$ cations, a steric interaction between the R group and the phenyl rings bonded to the P_2 atoms can be observed. If the steric hindrance between the phenyl rings bonded to the P_2 atoms and the aniline blocked the rotation around the Pt–N bond, two different rotamers at an energy minimum would be possible, with the phenyl ring bonded to the P_1 atom and the aryl group of the aniline in *Z* (*sin* rotamer) or *E* (*anti* rotamer) position, as shown in Fig. 4. The calculated energy difference between the two rotamers is quite small, about 5 kcal/mol.

As, on the contrary, the NMR spectra of the $\mathbf{2}^{R}$ derivatives show the signals of only one species in a temperature range between 298 and 243 K, there should be free rotation around the Pt–N bond. This means that the geometry in solution of the $\mathbf{2}^{R}$ derivatives in not affected only by the nucleophilicity of the aniline ligand, as observed for the $\mathbf{1}^{R}$ complexes, but also by the different bulk of the 4-R group. The sum of the electronic and the steric effects on the geometry of the $[Pt(4\text{-R-an})(triphos)]^{2+}$ cations

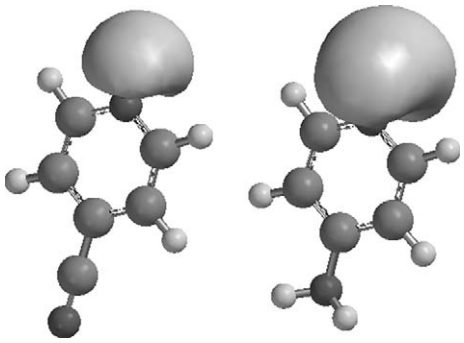

Fig. 2. Potential electrostatic surfaces on the pyridine-N atom for the 4-CN-py and 4-NH_2-py ligands.

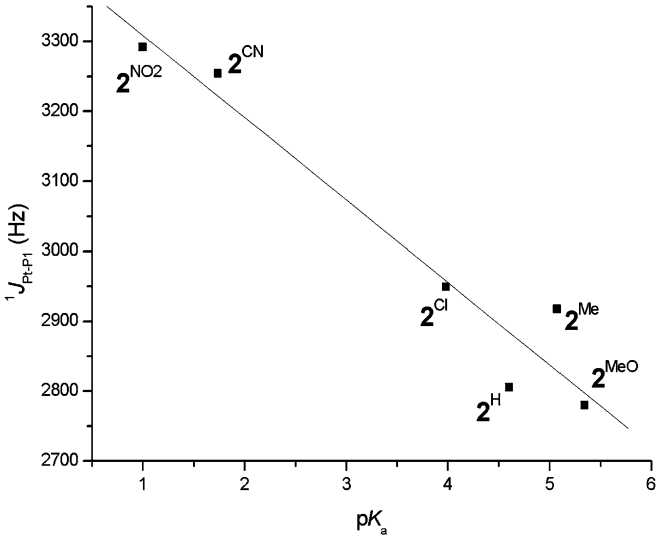

Fig. 3. Plot of $^1J_{Pt-P1}$ against pK_a for $\mathbf{2}^{R}$ complexes.

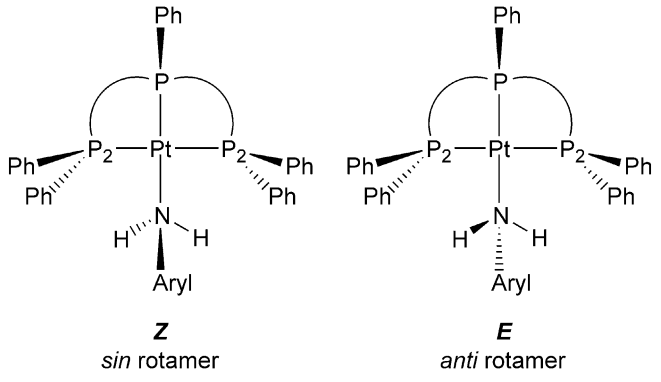

Fig. 4. Rotamers of the $[Pt(4\text{-R-an})(triphos)]^{2+}$ cations.

Table 2
Calculated r_{Pt-P} and r_{Pt-N} bond lengths for complexes $\mathbf{1}^{CN}$ and $\mathbf{1}^{NH_2}$, dipolar moment and Mulliken charge on the pyridine-N atom for the free ligands

Complex		r_{Pt-P1} (Å)	r_{Pt-P2} (Å)	r_{Pt-N} (Å)	Pyridine	μ (Debye)	N charge
$\mathbf{1}^{CN}$	$[Pt(4\text{-CN-py})(triphos)]^{2+}$	2.3258	2.4083	2.1070	4-CN-py	2.00	−0.060
$\mathbf{1}^{NH_2}$	$[Pt(4\text{-NH}_2\text{-py})(triphos)]^{2+}$	2.3270	2.4055	2.1023	4-NH_2-py	4.08	−0.112

explains the less linear correlation between the pK_a and the $^1J_{Pt-P1}$ values of these derivatives and the irregular trend of the $^1J_{Pt-P2}$ values.

4. Conclusions

In conclusion, the ^{31}P NMR spectroscopy of derivatives of the Pt(II)–triphos fragment allowed us to observe small changes of the electronic and steric properties of the co-ordinated ligands by measuring the $^1J_{Pt-P}$ coupling constants. Further investigations will be carried out in order to ascertain whether this approach could be an effective way for investigating and comparing other series of molecules with co-ordinating ability.

Acknowledgement

We thank the Ca' Foscari University of Venice for financial support (Ateneo fund 2004).

References

[1] (a) L.D. Quin, J.G. Verkade, Phosphorus-31 NMR Spectral Properties in Compound Characterization and Structural Analysis, Wiley–VCH, Weinheim, 1994;
(b) T.G. Appleton, M.A. Bennett, Inorg. Chem. 17 (1978) 738, and references therein;
(c) P.S. Pregosin, R.W. Kunz, ^{31}P and ^{13}C NMR of Transition Metal Phosphine Complexes, Springer, New York, 1979, and references therein.

[2] (a) G. Balacco, J. Chem. Inf. Comput. Sci. 34 (1994) 1235;
(b) J.C. Cobas Gómez, F.J. Sardina López, MestRe-C, Universidad de Santiago de Compostela, Spain.

[3] (a) P. Geerlings, F. De Proft, W. Langenaker, Chem. Rev. 103 (2003) 1793;
(b) A. Dedieu, Chem. Rev. 100 (2000) 543.

[4] (a) M.J. Frisch, G.W. Trucks, H.B. Schlegel, G.E. Scuseria, M.A. Robb, J.R. Cheeseman, V.G. Zakrzewski, J.A. Montgomery Jr., R.E. Stratmann, J.C. Burant, S. Dapprich, J.M. Millam, A.D. Daniels, K.N. Kudin, M.C. Strain, O. Farkas, J. Tomasi, V. Barone, M. Cossi, R. Cammi, B. Mennucci, C. Pomelli, C. Adamo, S. Clifford, J. Ochterski, G.A. Petersson, P.Y. Ayala, Q. Cui, K. Morokuma, D.K. Malick, A.D. Rabuck, K. Raghavachari, J.B. Foresman, J. Cioslowski, J.V. Ortiz, A.G. Baboul, B.B. Stefanov, G. Liu, A. Liashenko, P. Piskorz, I. Komaromi, R. Gomperts, R.L. Martin, D.J. Fox, T. Keith, M.A. Al-Laham, C.Y. Peng, A. Nanayakkara, M. Challacombe, P.M.W. Gill, B. Johnson, W. Chen, M.W. Wong, J.L. Andres, C. Gonzalez, M. Head-Gordon, E.S. Replogle, J.A. Pople, GAUSSIAN-98, Gaussian, Inc., Pittsburgh, PA, 1998, We thank Dr. A. Zambon for the use of his software package;
(b)Spartan'02, Wavefunction Inc., Irvine, CA, 2002.

[5] D.W. Dockter, P.E. Fanwick, C.P. Kubiak, J. Am. Chem. Soc. 118 (1996) 4846.

[6] (a) B. Pitteri, G. Annibale, M. Bortoluzzi, G. Marangoni, Transition Met. Chem. 30 (2005) 748;
(b) G. Annibale, B. Pitteri, Inorg. Synth. 34 (2004) 76.

[7] G.S. Hill, M.J. Rendina, R.J. Puddephatt, Inorg. Synth. 31 (1998) 149.

[8] W. Geary, Coord. Chem. Rev. 7 (1971) 81.

[9] G. Annibale, P. Bergamini, M. Cattabriga, Inorg. Chim. Acta 316 (2001) 25.

[10] (a) B. Pitteri, G. Marangoni, L. Cattalini, Dalton Trans. (1994) 3539;
(b) B. Pitteri, G. Marangoni, L. Cattalini, F. Visentin, V. Bertolasi, P. Gilli, Polyhedron 20 (2001) 869, and references therein.

[11] (a) R. Voets, J.P. Francois, J.M.L. Martin, J. Mullens, J. Yperman, L.C. Van Poucke, J. Comput. Chem. 4 (1989) 449;
(b) A.N. Pankratov, I.M. Uchaeva, S.Y. Doronin, R.K. Charnova, J. Serb. Chem. Soc. 66 (2001) 161.

[12] M. Karplus, J. Chem. Phys. 30 (1959) 11.

[13] D.D. Perrin, Dissociation Constants of Organic Bases in Aqueous Solution, Butterworths, London, 1965.

[14] G.G. Mather, A. Pidcock, G.J.N. Rapsey, J. Chem. Soc., Dalton Trans. (1973) 2095.

[15] R. Mason, D.W. Meek, Angew. Chem. 90 (1978) 195.

NBO analysis. The spin-allowed singlet–singlet electronic transitions of [Re(NO)Cl_2(PPh_3)(PPh_2py-P,N)] have been calculated with the time-dependent DFT method (TDDFT method), and the UV–Vis spectrum of the title complex has been discussed on this basis.

The calculations with the TDDFT method for open-shell organic, inorganic and organometallic molecules have supported the TDDFT method to be applicable for such systems giving good assignment of experimental spectra [24–27]. There are also several works performed with this method for 5d-metal (including rhenium complexes) in which good correlations between experimental and calculated results have been confirmed [28–34].

2. Experimental

2.1. General procedure

The reaction was carried out under argon atmosphere. All the reagents used to the synthesis of the complex are commercially available and were used without further purification. The [Re(NO)Cl_3(PPh_3)($OPPh_3$)] complex was prepared according to the literature method [17].

IR spectra were recorded on a Nicolet Magna 560 spectrophotometer in the spectral range 4000–400 cm^{-1} with the samples in the form of KBr pellets. Electronic spectra were measured on a spectrophotometer Lab Alliance UV–Vis 8500 in the range 900–200 nm in deoxygenated dichloromethane solution. Elemental analyses (C, H, N) were performed on a Perkin–Elmer CHN-2400 analyzer.

2.2. Preparation of [Re(NO)Cl_2(PPh_3)(PPh_2py-P,N)]

[Re(NO)Cl_3(PPh_3)($OPPh_3$)] (1 g, 1.15 mmol) and PPh_2py (0.3 g, 1.15 mmol) in chloroform (100 cm^3) were refluxed for 6 h. The volume was condensed to 20 cm^3 and dark orange microcrystalline solid was formed by an addition of 100 cm^3 of ethanol. The product was washed with cold ether, and dried in vacuo. The crystals suitable for X-ray investigation were obtained by recrystallization from $CHCl_3$–EtOH (yield 70%).

IR (KBr, cm^{-1}) 3063(m), 3049(w), 3055(w), 1683(vs), 1586(m) 1572(w), 1481(s), 1450(m), 1434(m), 1313(w), 1270(w), 1186(m) 1157(w), 1122(m), 1091(s), 1023(m), 998(w), 747(s), 726(w), 696(s), 617(w), 584(w), 532(sh), 522(s), 505(s), 433(m), 423(m).

Anal. Calc. for $C_{35}H_{29}Cl_2N_2OP_2Re$: C, 51.79; H, 3.48; N, 3.45. Found: C, 51.90; H, 3.55; N, 3.56%.

2.3. Crystal structures determination and refinement

The X-ray intensity data of [Re(NO)Cl_2(PPh_3)(PPh_2py-P,N)] were collected on a KM-4-CCD automatic diffractometer equipped with CCD detector and 37 s exposure time was used. The unit cell parameters were determined from least-squares refinement of the setting angles of 14 536 strongest reflections. Details concerning crystal data and refinement are given in Table 1. Lorentz, polarization and numerical absorption corrections [35] were applied. The structure was solved by means of the Patterson method and subsequently completed by the difference Fourier recycling. All the non-hydrogen atoms were refined anisotropically using full-matrix, least-squares technique. The hydrogen atoms of the phenyl rings were treated as "riding" on their parent carbon atoms [d(C–H) = 0.96 Å] and assigned isotropic temperature factors equal 1.2 times the value of equivalent temperature factor of the parent carbon atom. SHELXS 97 [36], SHELXL 97 [37] and SHELXTL [38] programs were used for all the calculations. Atomic scattering factors were those incorporated in the computer programs.

Table 1
Crystal data and structure refinement for [Re(NO)Cl_2(PPh_3)(PPh_2py-P,N)]

Empirical formula	$C_{35}H_{29}Cl_2N_2OP_2Re$
Formula weight	812.6
Temperature (K)	293(2)
Wavelength (Å)	0.71073
Crystal system	orthorhombic
Space group	$P2_12_12_1$
Unit cell dimensions	
a (Å)	11.3118(4)
b (Å)	15.3821(5)
c (Å)	18.8572(6)
Volume (Å^3)	3281.14(19)
Z	4
D_{calc} (Mg/m^3)	1.645
Absorption coefficient (mm^{-1})	3.995
F(000)	1600
Crystal size (mm)	0.29 × 0.27 × 0.22
θ Range for data collection (°)	3.20–25.13
Index ranges	$-13 \leqslant h \leqslant 13$, $-16 \leqslant k \leqslant 18$, $-22 \leqslant l \leqslant 22$
Reflections collected	35 191
Independent reflections [R_{int}]	5836 [0.0353]
Completeness to 2θ	99.6%
Maximum and minimum transmission	0.3254 and 0.0722
Data/restraints/parameters	5836/0/416
Goodness-of-fit on F^2	1.082
Final R indices [$I > 2\sigma(I)$]	$R_1 = 0.0177$, $wR_2 = 0.0370$
R indices (all data)	$R_1 = 0.0184$, $wR_2 = 0.0372$
Largest difference peak and hole (e Å^{-3})	0.831 and −0.694

2.4. Computational details

GAUSSIAN 03 program [39] was used in the calculations. The geometry optimization was carried out with the DFT method with the use of B3LYP functional [40,41]. The electronic spectrum was calculated with the TDDFT method [42]. The calculations were performed by using ECP basis set on the rhenium atom, the standard 6-31+G** basis for chlorine, oxygen and nitrogen, 6-31+G* for carbon and 6-31G basis for hydrogen atoms. The Xe core electrons of Re were replaced by an effective core potential and DZ quality Hay and Wadt Los Alamos ECP basis set (LANL2DZ) [43] was used for the valence electrons. Additional d function with exponent $\alpha = 0.3811$ and f function with exponent $\alpha = 2.033$ on the rhenium atom were added.

Natural bond orbital (NBO) calculations were performed with the NBO code [44] included in GAUSSIAN 03.

3. Results and discussion

3.1. Preparation

The complex $[Re(NO)Cl_2(PPh_3)(PPh_2py\text{-}P,N)]$ has been obtained in high yield in the reaction of $[Re(NO)Cl_3(PPh_3)(OPPh_3)]$ with diphenyl(2-pyridyl)phosphine in chloroform. Diphenyl(2-pyridyl)phosphine is a versatile ligand which can coordinate as a monodentate or chelating ligand depending on the requirements of the metal. In the title complex, P,N-coordination of the PPh_2py ligand is observed.

3.2. Crystal structure

The $[Re(NO)Cl_2(PPh_3)(PPh_2py\text{-}P,N)]$ complex crystallises in the orthorhombic space group $P2_12_12_1$ and its crystal structure is composed of the molecules located in general positions linked via weak intermolecular C(15)–H(15)···Cl(1) $(1/2 + x,\ 1/2 - y,\ -z + 2)$ hydrogen bonds [45,46]. Two intramolecular hydrogen bond linking C(12)–H(12)···Cl2(1) (D···A distance 3.291(5) Å and D–H···A angle 116.2°) and C(31)–H(31)···N(3) (D···A distance 3.337(12) Å and D–H···A angle 136.9°) provide additional stabilisation of the $[Re(NO)Cl_2(PPh_3)(PPh_2py\text{-}P,N)]$ molecule.

The structure of $[Re(NO)Cl_2(PPh_3)(PPh_2py\text{-}P,N)]$ has been modelled with the Cl(2), Cl(3) and NO ligands disordered over two sites using fractional occupancies equal 0.47 for Cl(3), N(2), O(2) atoms and 0.53 for Cl(2), N(3) and O(3). The rhenium atom is in a distorted octahedral environment with the triphenylphosphine molecule in *trans* geometry to the pyridine ring of the chelating ligand. Strong deviations of the rhenium coordination sphere from an ideal octahedron can be ascribed to the restricted bite angle of the four membered chelate ring. Fig. 1 shows a displacement ellipsoids plot of $[Re(NO)Cl_2(PPh_3)(PPh_2py\text{-}P,N)]$, and the selected bond lengths and angles of this compound are summarized in Table 2. The Re–NO and N–O bond lengths and the Re–N–O angles confirm the linear co-ordination of the distorted nitrosyl groups and they are compared with values previously found [1,14–23]. The Re–N_{py} of 2.187(3) Å is longer in comparison with the value obtained from the sum of the relevant covalent radii (2.08 Å) or average value of the Re–N_{py} distances (2.12 Å) in *mer*-$[ReX_3(py)_3]$ (X = Cl, Br) [47]. It can be attributed to the *trans* influence of the PPh_3 ligand. Similarly, the Re–Cl(1) bond length is considerable longer than Re–Cl(2) and Re–Cl(3) distances.

3.3. Infrared data and magnetochemical measurements

The IR spectrum of $[Re(NO)Cl_2(PPh_3)(PPh_2py\text{-}P,N)]$ exhibits strong band at 1683 cm^{-1} assignable to ν(NO).

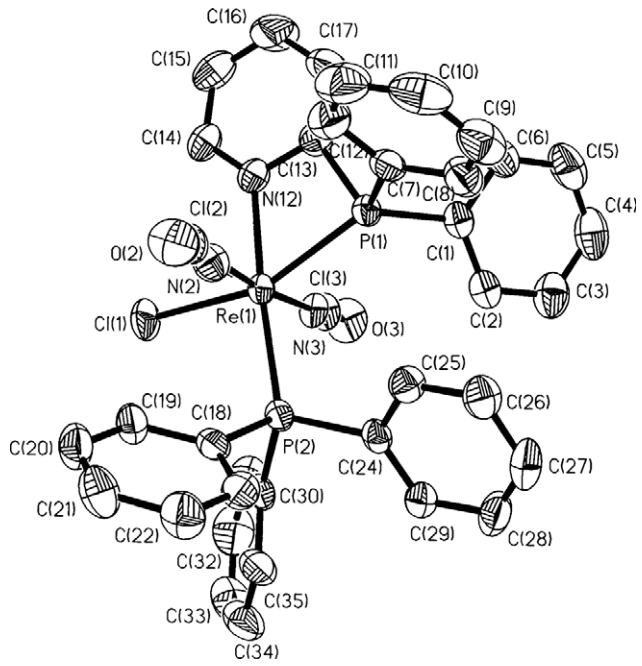

Fig. 1. Thermal ellipsoid plot of $[Re(NO)Cl_2(PPh_3)(PPh_2py\text{-}P,N)]$ showing the atom numbering scheme (50% probability ellipsoids).

The value of ν(NO) corresponds to linear NO range of Haymore and Ibers [ν(NO) above 1620–1610 cm^{-1} were assigned to linear M–N–O systems, while ν(NO) below 1610 cm^{-1} were assigned to bent M–N–O systems] [48]. The considerable lowering of the ν_{NO} of $[Re(NO)Cl_2(PPh_3)(PPh_2py\text{-}P,N)]$ in comparison with the starting $[Re(NO)Cl_3(PPh_3)(OPPh_3)]$ nitrosyl (1745 cm^{-1}) [17] is consistent with increase of electron number n in the $\{MNO\}^n$ unit. It results in an increased backdonation of electron density from the filled rhenium d orbitals into the π^* antibonding orbital of the NO group.

The characteristic bands of the C=C and C=N stretching modes are observed at 1586 and 1572 cm^{-1} [49].

3.4. Optimised geometry

The geometry of $[Re(NO)Cl_2(PPh_3)(PPh_2py\text{-}P,N)]$ was optimised in a singlet state by the DFT method with the B3LYP functional. The optimised geometric parameters are gathered in Table 2. The calculated bond lengths and angles are in agreement with the values based upon the X-ray crystal structure data, and the general trends observed in the experimental data are well reproduced in the calculations.

3.5. Charge distribution and spin densities

Table 3 presents the atomic charges from the natural population analysis (NPA) for $[Re(NO)Cl_2(PPh_3)(PPh_2py\text{-}P,N)]$. The calculated charge on the nitrogen atom of the nitrosyl group is positive, whereas the oxygen atom is negatively charged. The total charge on the NO group of the title complex is negative: −0.165. The calculated charge on the

Table 2
The experimental and optimized bond lengths (Å) and angles (°) for [Re(NO)Cl_2(PPh_3)(PPh_2py-P,N)]

	Experimental	Optimized		Experimental	Optimized
Bond lengths			*Bond angles*		
Re(1)–N(12)	2.187(3)	2.212	N(2)–Re(1)–N(3)	175.5(6)	
Re(1)–N(2)	1.786(16)	1.755	N(2)–Re(1)–N(12)	90.2(5)	95.18
Re(1)–N(3)	1.797(12)		N(3)–Re(1)–N(12)	88.6(4)	
Re(1)–Cl(1)	2.4509(7)	2.504	N(3)–Re(1)–Cl(2)	173.6(4)	
Re(1)–Cl(2)	2.362(3)		N(12)–Re(1)–Cl(2)	85.31(14)	
Re(1)–Cl(3)	2.368(3)	2.489	N(2)–Re(1)–Cl(3)	175.4(5)	176.06
Re(1)–P(1)	2.4104(8)	2.456	N(12)–Re(1)–Cl(3)	85.74(11)	82.91
Re(1)–P(2)	2.4112(9)	2.468	Cl(2)–Re(1)–Cl(3)	171.06(14)	
N(2)–O(2)	1.26(3)	1.192	N(2)–Re(1)–P(1)	88.7(4)	92.05
N(3)–O(3)	1.22(3)		N(3)–Re(1)–P(1)	66.39(7)	
			Cl(2)–Re(1)–P(1)	88.72(9)	
			Cl(3)–Re(1)–P(1)	87.74(8)	84.02
			N(2)–Re(1)–P(2)	89.6(5)	92.77
			N(3)–Re(1)–P(2)	91.3(4)	170.83
			N(12)–Re(1)–P(2)	175.40(7)	
			Cl(2)–Re(1)–P(2)	94.58(12)	
			Cl(3)–Re(1)–P(2)	94.34(9)	88.87
			P(1)–Re(1)–P(2)	109.01(3)	109.46
			N(2)–Re(1)–Cl(1)	92.2(4)	94.37
			N(3)–Re(1)–Cl(1)	92.1(4)	
			N(12)–Re(1)–Cl(1)	90.90(7)	89.79
			Cl(2)–Re(1)–Cl(1)	90.17(9)	
			Cl(3)–Re(1)–Cl(1)	89.92(8)	89.08
			P(1)–Re(1)–Cl(1)	157.28(3)	155.19
			P(2)–Re(1)–Cl(1)	93.70(3)	94.15
			O(3)–N(3)–Re(1)	177.0(11)	
			O(2)–N(2)–Re(1)	179.3(13)	178.33

Table 3
Atomic charges and spin densities of [Re(NO)Cl_2(PPh_3)(PPh_2py-P,N)]

Atom	Atomic charge
Re(1)	0.107
Cl(1)	−0.522
Cl(3)	−0.508
N(2)	0.167
O(2)	−0.332
P(1)	1.347
N(12)	−0.469
P(2)	1.409

rhenium atom of [Re(NO)Cl_2(PPh_3)(PPh_2py-P,N)] is far from the formal charge +1. It results from charge donation from the chloride ions and P-donor ligands. There are large positive charges on the P atoms, and the charges on the chloride ions are significantly smaller than −1. The charge on the pyridine nitrogen atom bonded with the rhenium is negative.

3.6. NBO analysis

Each natural bond orbital (NBO) σ_{AB} can be written in terms of two directed valence hybrids (NHOs) h_A and h_B on atoms A and B:

$$\sigma_{AB} = c_A h_A + c_B h_B$$

where c_A and c_B are polarization coefficients. Each valence bonding NBO must in turn be paired with a corresponding valence *anti*-bonding NBO:

$$\sigma^*_{AB} = c_B h_A - c_A h_B$$

to complete the span of the valence space. The Lewis-type (donor) NBOs are thereby complemented by the non-Lewis-type (acceptor) NBOs that are formally empty in an idealized Lewis picture. The interactions between 'filled' Lewis-type NBOs and 'empty' non-Lewis NBOs lead to loss of occupancy from the localized NBOs of the idealized Lewis structure into the empty non-Lewis orbitals, and they are referred to as 'delocalization' corrections to the zeroth-order natural Lewis structure. The stabilization energy ΔE_{ij} (kcal/mol) associated with delocalization is estimated by the second-order perturbative as:

$$\Delta E_{ij} = q_i(F(i,j)^2)/(\varepsilon_j - \varepsilon_i)$$

where q_i is the donor orbital occupancy, ε_i, ε_j are diagonal elements (orbital energies) and $F(i,j)$ is the off-diagonal NBO Fock or Kohn–Sham matrix element [50].

In the case of the [Re(NO)Cl_2(PPh_3)(PPh_2py-P,N)] complex, three natural bond orbitals were detected for the Re–N bond, and one orbital – for the N–O bond. The occupancies and hybridization of the calculated Re–N and N–O natural bond orbitals (NBOs) are given in Table 4. The Re–N bond orbital of σ-character is polarized towards the nitrogen atom and the s and d orbitals of Re take part in the bonding. The Re–N bond orbitals of π-character are insignificantly polarized toward the metal atom and only d-orbitals of Re are included into the

Table 4
The occupancies and hybridization of the calculated Re–N and N–O natural bond orbitals (NBOs) for [Re(NO)Cl_2(PPh_3)(PPh_2py-P,N)]

BD	Occupancy	Hybridization of NBO
Re–N	1.958 (0.385)	$0.499(sd^{2.63})_{Re} + 0.866(sp^{0.65})_N$
	1.964 (0.463)	$0.720(d)_{Re} + 0.694(p)_N$
	1.950 (0.453)	$0.738(d)_{Re} + 0.675(p)_N$
N–O	1.997 (0.015)	$0.673(sp^{1.81})_N + 0.740(sp^{2.35})_O$

BD denotes two-center bond.

bonding. The N–O bond orbital is slightly polarized towards the oxygen end. Table 5 presents the occupancies and atomic orbital compositions of the lone pairs (LP) orbitals detected on the oxygen atom of the nitrosyl group, as well as the character of the acceptor orbital and stabilization energies (ΔE_{ij}) for the corresponding donor–acceptor interactions. The oxygen atom of the nitrosyl ligand possesses three lone pair (LP) orbitals. The electron density from the LP orbitals described by p orbitals is strongly delocalized into π^*_{Re-N} orbitals (Table 5).

In the valence-bond treatment a linear bonding mode of the nitrosyl group may be represented by the following resonance forms [1]:

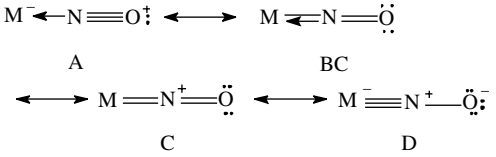

The results of the NBO analysis indicate that the resonance structure of D makes a significant contribution to the structure of the [Re(NO)Cl_2(PPh_3)(PPh_2py-P,N)] complex.

It is consistent with the charges on the nitrogen and oxygen atoms of the nitrosyl group and relatively low nitrosyl stretching frequency.

Table 5
The occupancies and atomic orbital compositions of the lone pairs (LP) detected on the oxygen atom of the nitrosyl group and the character of the acceptor orbital, as well as stabilization energies (ΔE_{ij}) for the corresponding donor–acceptor interactions

LP orbital	Occupancy of donor orbital	Acceptor orbital	ΔE_{ij} (kcal/mol)
$(sp^{0.42})_{O(2)}$	1.978	$0.866(sd^{2.63})_{Re} - 0.499(sp^{0.65})_N$	9.32
$(p)_{O(2)}$	1.634	$0.694(d)_{Re} - 0.720(p)_N$	10.59
		$0.675(d)_{Re} - 0.738(p)_N$	95.78
$(p)_{O(2)}$	1.607	$0.694(d)_{Re} - 0.720(p)_N$	80.45
		$0.675(d)_{Re} - 0.738(p)_N$	10.69

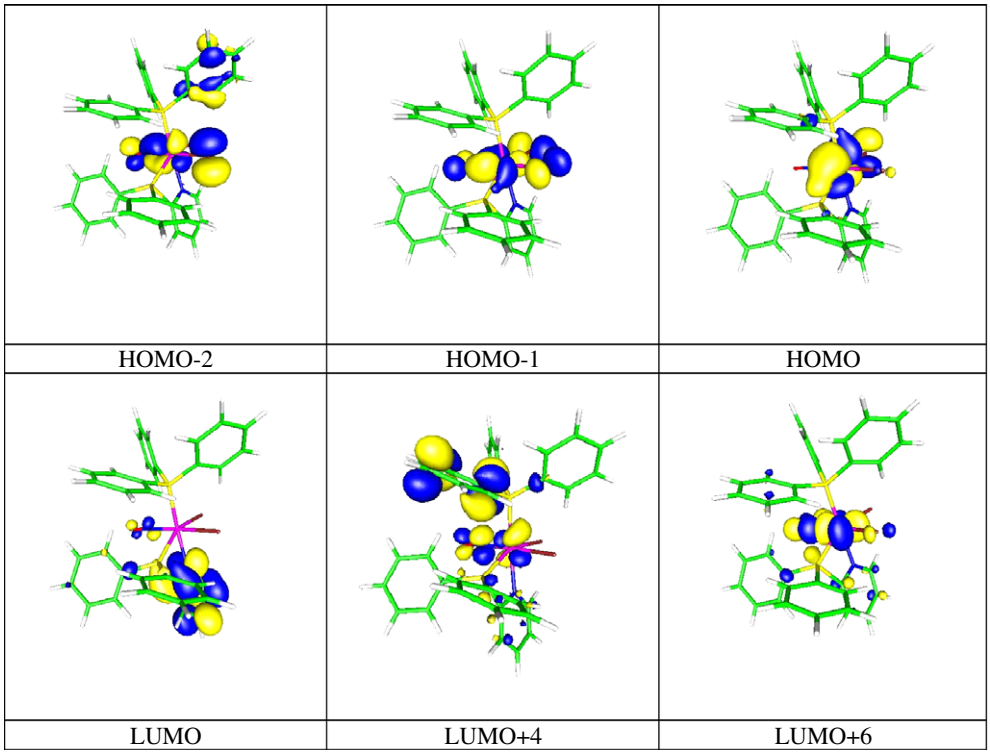

Fig. 2. The selected HOMO and LUMO orbitals of [Re(NO)Cl_2(PPh_3)(PPh_2py-P,N)]. Positive values of the orbital contour are represented in blue (0.04) and negative values – in yellow (−0.04). (For interpretation of the references to colour in this figure legend, the reader is referred to the web version of this article.)

3.7. Electronic structure

The bonding of NO to the rhenium center involves a synergic interaction between the nitrosyl ligand orbitals and the metal orbitals. The Re–NO bond consists of two components: (i) a donation of electron density from a σ-type orbital on NO onto the metal orbital; and (ii) a donation of electron density from the occupied metal d-orbitals into the π^* antibonding orbitals of NO ligand. The occupied d_{xy} and d_{xz} rhenium orbitals participate in the backdonation from the central ion to the nitrosyl ligand in the [Re(NO)-Cl_2(PPh_3)(PPh_2py-P,N)] complex. The π_{Re-NO} bonding interaction makes the largest contribution into the H − 2 and H − 1 orbitals. Some participation of π_{Re-NO} orbitals, however, is also seen in other occupied molecular orbitals of [Re(NO)Cl_2(PPh_3)(PPh_2py-P,N)] (Fig. 2).

The π^*_{Re-NO} orbitals are distributed among several lowest unoccupied molecular orbitals. Their contribution is visible in L + 3, L + 4, L + 5, L + 6, L + 7, L + 8 and L + 9. The HOMO orbital of [Re(NO)Cl_2(PPh_3)(PPh_2py-P,N)] is composed of the d_{yz} metal orbital and chlorine π orbitals in anti-bonding arrangement. The LUMO orbital is mainly localised on the phenyl and pyridine rings of PPh_2py ligand. The d_z^2 orbital of Re atom makes the largest contribution into L + 13, whereas L + 15 has $d_{x^2-y^2}$–σ_{Cl}–σ_P–σ_N character. The selected HOMO and LUMO orbitals of [Re(NO)Cl_2(PPh_3)(PPh_2py-P,N)] are depicted in Fig. 2. The following orientation of the axes has been used for

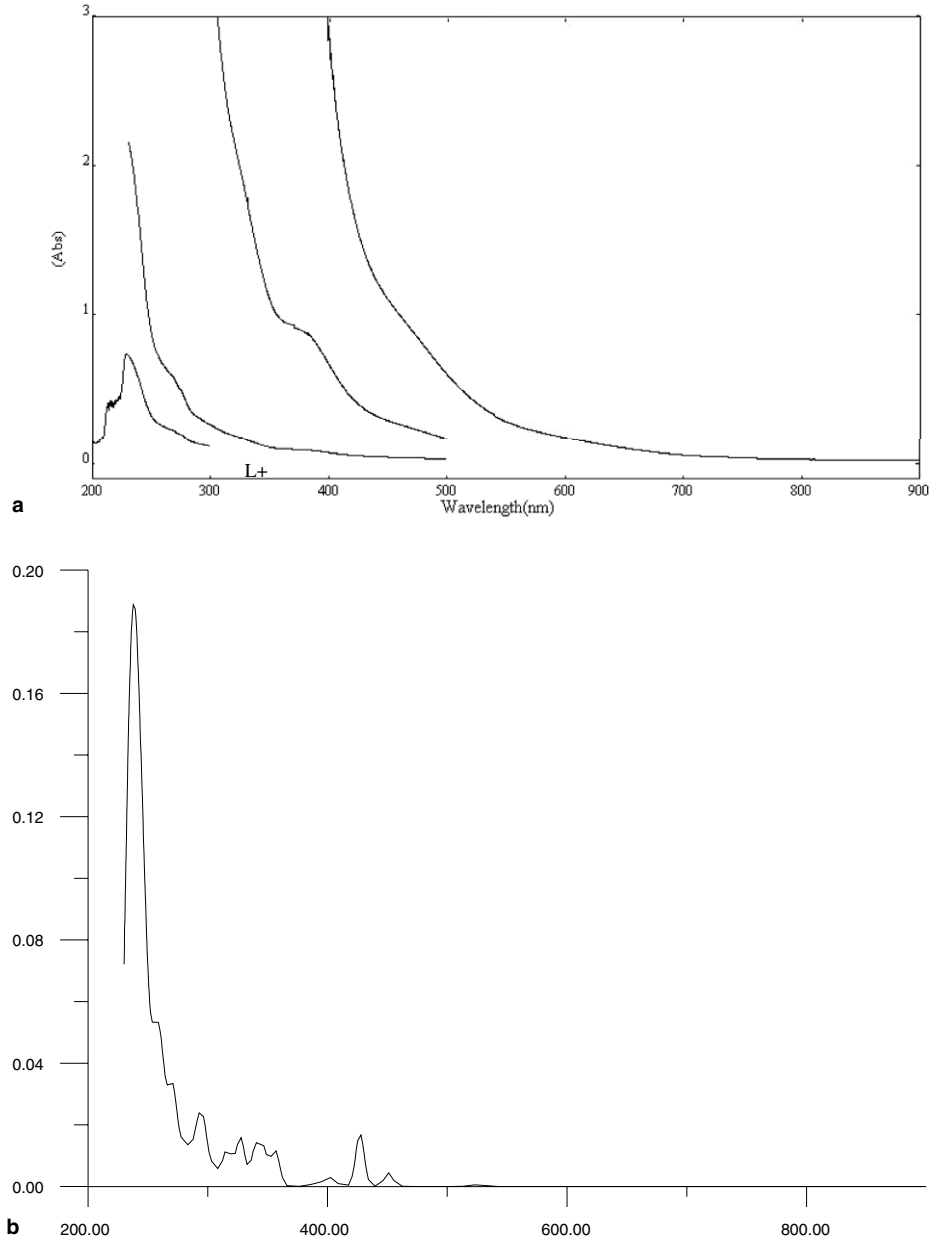

Fig. 3. The experimental (a) and calculated (b) electronic absorption spectrum of [Re(NO)Cl_2(PPh_3)(PPh_2py-P,N)].

determination of the MO characters: the z axis goes along Cl(1)–Re–P(1) linkage and y goes through the N(12)–Re–P(2) bonds.

3.8. Electronic spectra

The experimental and calculated electronic spectra of $[Re(NO)Cl_2(PPh_3)(PPh_2py\text{-}P,N)]$ are presented in Fig. 3. Each calculated transition in Fig. 3b was represented by a gaussian function with the height equal to the oscillator strength and width equal to 0.04.

Table 6 shows the spin-allowed singlet–singlet electronic transitions calculated with the TDDFT method for $[Re(NO)Cl_2(PPh_3)(PPh_2py\text{-}P,N)]$. For the high energy part of the spectrum (below 250 nm), only transitions with oscillator strengths larger than 0.010 are listed in Table 6.

A hundred electron transitions calculated by the TDDFT method do not comprise all the experimental

Table 6
The energy and molar absorption coefficients of experimental absorption bands and the electronic transitions calculated with the TDDFT method for $[Re(NO)Cl_2(PPh_3)(PPh_2py\text{-}P,N)]$

The most important orbital excitations	Character	λ (nm)	E (eV)	f	Experimental λ (nm) [E (eV)] ε
H → L	d → $\pi^*_{py/Ph}(PPh_2py)$	527.0	2.35	*0.0009*	570.0 (2.18) 80
H → L + 1	d → $\pi^*_{py/Ph}(PPh_2py)$	450.8	2.75	*0.0044*	380.0 (3.26) 1280
H → L + 2	d → $\pi^*_{Ph}(PPh_2py)$	427.0	2.90	*0.0171*	
H → L + 3	d → $\pi^*_{Ph}(PPh_2py)/\pi^*(NO)$	403.4	3.07	*0.0029*	
H → L + 6	d → $\pi^*(NO)$	393.4	3.15	*0.0013*	
H − 1 → L	d → $\pi^*_{py/Ph}(PPh_2py)$	388.3	3.19	*0.0006*	
H → L + 3	d → $\pi^*_{Ph}(PPh_2py)/\pi^*(NO)$	356.9	3.47	*0.0064*	335.0 (3.70) 2450
H → L + 4	d → $\pi^*_{Ph}(PPh_3)/\pi^*(NO)$				
H − 2 → L	d → $\pi^*_{py/Ph}(PPh_2py)$	355.1	3.49	*0.0057*	
H − 1 → L + 1	d → $\pi^*_{py/Ph}(PPh_2py)$	346.0	3.58	*0.0116*	
H → L + 4	d → $\pi^*_{Ph}(PPh_3)/\pi^*(NO)$	339.3	3.65	*0.0113*	
H → L + 8	d → $\pi^*_{Ph}(PPh_3)/\pi^*_{Ph}(PPh_2py)/\pi^*(NO)$				
H → L + 5	d → $\pi^*_{Ph}(PPh_3)/\pi^*(NO)$	329.7	3.76	*0.0020*	
H − 1 → L + 1	d → $\pi^*_{py/Ph}(PPh_2py)$	327.0	3.79	*0.0140*	
H − 1 → L + 2	d → $\pi^*_{Ph}(PPh_2py)$				
H − 2 → L + 1	d → $\pi^*_{py/Ph}(PPh_2py)$	318.1	3.90	*0.0031*	
H − 1 → L + 2	d → $\pi^*_{Ph}(PPh_2py)$	315.6	3.93	*0.0081*	
H → L + 9	d → $\pi^*_{Ph}(PPh_3)/\pi^*(NO)$	312.8	3.96	*0.0013*	
H − 2 → L + 2	d → $\pi^*_{Ph}(PPh_2py)$	306.7	4.04	*0.0018*	
H − 1 → L + 6	d → $\pi^*(NO)$	303.9	4.08	*0.0039*	
H − 1 → L + 3	d → $\pi^*_{Ph}(PPh_2py)/\pi^*(NO)$				
H → L + 10	d → $\pi^*_{Ph}(PPh_2py)$	296.3	4.18	*0.0110*	
H − 2 → L + 2					
H → L + 10	d → $\pi^*_{Ph}(PPh_2py)$	292.3	4.24	*0.0048*	
H − 4 → L + 1	$\pi_{Ph}(PPh_3)/\pi_{Cl} \rightarrow \pi^*_{py/Ph}(PPh_2py)$	291.1	4.26	*0.0074*	273.5 (4.53) 15800
H − 3 → L + 1					
H − 8 → L	$\pi_{Ph}(PPh_3)/\pi_{Ph}(PPh_2py)/\pi_{Cl} \rightarrow \pi^*_{py/Ph}(PPh_2py)$	280.2	4.42	*0.0069*	
H − 9 → L	$\pi_{Ph}(PPh_3)/\pi_{Ph}(PPh_2py)/\pi_{Cl} \rightarrow \pi^*_{py/Ph}(PPh_2py)$	271.0	4.58	*0.0126*	
H − 5 → L + 2	$\pi_{Ph}(PPh_3)/\pi_{Cl} \rightarrow \pi^*_{/Ph}(PPh_2py)$	261.8	4.74	*0.0093*	
H − 11 → L	$\pi_{Ph}(PPh_2py)/\pi_{Ph}(PPh_3) \rightarrow \pi^*_{py/Ph}(PPh_2py)$	259.4	4.78	*0.0135*	
H − 3 → L + 3	$\pi_{Ph}(PPh_3)/\pi_{Cl} \rightarrow \pi^*_{Ph}(PPh_2py)/\pi^*(NO)$				
H − 15 → L	$\pi_{Ph}(PPh_2py)/\pi_{Cl} \rightarrow \pi^*_{py/Ph}(PPh_2py)$	255.7	4.85	*0.0098*	
H − 3 → L + 5	$\pi_{Ph}(PPh_3)/\pi_{Cl} \rightarrow \pi^*_{Ph}(PPh_3)/\pi^*(NO)$	246.8	5.02	*0.0106*	230.6 (5.38) 47540
H − 3 → L + 5	$\pi_{Ph}(PPh_3)/\pi_{Cl} \rightarrow \pi^*_{Ph}(PPh_3)/\pi^*(NO)$	245.5	5.05	*0.0218*	
H − 3 → L + 6	$\pi_{Ph}(PPh_3)/\pi_{Cl} \rightarrow \pi^*(NO)$				
H − 16 → L	$\pi_{Ph}(PPh_2py)/\pi_{Cl} \rightarrow \pi^*_{Ph}(PPh_2py)$	244.4	5.07	*0.0196*	
H − 4 → L + 5	$\pi_{Ph}(PPh_3)/\pi_{Cl} \rightarrow \pi^*_{Ph}(PPh_3)/\pi^*(NO)$	242.2	5.12	*0.0125*	
H − 4 → L + 5	$\pi_{Ph}(PPh_3)/\pi_{Cl} \rightarrow \pi^*_{Ph}(PPh_3)/\pi^*(NO)$	241.3	5.14	*0.0100*	
H − 6 → L + 3	$\pi_{Ph}(PPh_3)/\pi_{Cl} \rightarrow \pi^*_{Ph}(PPh_2py)/\pi^*(NO)$				
H − 11 → L + 1	$\pi_{Ph}(PPh_2py)/\pi_{Ph}(PPh_3) \rightarrow \pi^*_{py/Ph}(PPh_2py)$	239.5	5.17	*0.0189*	
H − 5 → L + 4	$\pi_{Ph}(PPh_3)/\pi_{Cl} \rightarrow \pi^*_{Ph}(PPh_3)/\pi^*(NO)$	239.6	5.17	*0.0234*	
H − 7 → L + 5	$\pi_{Ph}(PPh_3)/\pi_{Cl} \rightarrow \pi^*_{Ph}(PPh_3)/\pi^*(NO)$	239.3	5.18	*0.0163*	
H − 13 → L + 1	$\pi_{Ph}(PPh_3)/\pi_{Ph}(PPh_2py)/\pi_{Cl} \rightarrow \pi^*_{py/Ph}(PPh_2py)$	238.6	5.20	*0.0101*	
H − 7 → L + 3	$\pi_{Ph}(PPh_3)\pi_{Cl} \rightarrow \pi^*_{Ph}(PPh_2py)/\pi^*(NO)$	237.2	5.23	*0.0125*	
H − 15 → L + 1	$\pi_{Ph}(PPh_2py)/\pi_{Cl} \rightarrow \pi^*_{py/Ph}(PPh_2py)$	236.1	5.25	*0.0154*	
H − 5 → L + 5	$\pi_{Ph}(PPh_3)/\pi_{Cl} \rightarrow \pi^*_{Ph}(PPh_3)/\pi^*(NO)$	235.8	5.26	*0.0177*	
H − 8 → L + 3	$\pi_{Ph}(PPh_3)/\pi_{Ph}(PPh_2py)/\pi_{Cl} \rightarrow \pi^*_{Ph}(PPh_2py)/\pi^*(NO)$	232.4	5.34	*0.0220*	
H − 6 → L + 5	$\pi_{Ph}(PPh_3)\pi_{Cl} \rightarrow \pi^*_{Ph}(PPh_3)/\pi^*(NO)$	231.7	5.35	*0.0154*	

absorption bands. The UV–Vis spectrum of $[Re(NO)Cl_2(PPh_3)(PPh_2py\text{-}P,N)]$ was calculated to 230 nm, so the shortest wavelength experimental band cannot be assigned completely to the calculated transitions. Some additional intraligand and interligand transitions are expected to be found at higher energies in the calculation for $[Re(NO)Cl_2(PPh_3)(PPh_2py\text{-}P,N)]$.

The assignment of the calculated transitions to the experimental bands is based on the criterion of the energy and oscillator strength of the calculated transitions. In the description of the electronic transitions only the main components of the molecular orbital are taken into consideration. The bonding π_{Re-NO} orbitals are described as d orbitals, and the antibonding π^*_{Re-NO} orbitals – as π^*_{NO}.

The absorption experimental bands at 570, 380 and 335 nm are attributed to MLCT transitions occurring from the rhenium center to the π-antibonding orbitals of the nitrosyl, triphenylphospine or diphenyl(2-pyridyl)phosphine ligands. Considering the values of oscillator strengths, we can noticed that the transitions of $d \rightarrow \pi^*_{NO}$ are significantly weaker in comparison with the transitions of $d \rightarrow \pi^*_{py/Ph}(PPh_2py)$ and $d \rightarrow \pi^*_{Ph}(PPh_3)$ character. It means that $d \rightarrow \pi^*_{NO}$ transitions do not contribute significantly to the overall shape of the bands at 380 and 335 nm. They are hidden under the more intense MLCT transitions from Re ion to the π-antibonding orbitals of the PPh_3 and PPh_2py. A similar trend has been supported previously for $\{ReNO\}^5$ nitrosyls [51–53].

The absorption bands at 273.5 and 230.6 nm are assigned to the calculated transitions of LLCT with large oscillator strengths. The intra- and interligand transitions occur from the chlorine and phosphine ligand to the π-antibonding orbitals of the nitrosyl, triphenylphospine or diphenyl(2-pyridyl)phosphine ligands.

4. Conclusions

A novel $\{ReNO\}^6$ complex – $[Re(NO)Cl_2(PPh_3)(PPh_2py\text{-}P,N)]$ has been prepared and structurally as well as spectroscopically characterized. X-ray studies confirm linear coordination of the nitrosyl group and P,N-coordination of the diphenyl(2-pyridyl)phosphine. The Re–N and N–O bond lengths and ν(NO) indicates a strong backdonation of electron density from the filled rhenium d orbitals into the π^* antibonding orbital of the NO group. These results are in good agreement with the DFT and NBO studies. The Re–N bond can be considered as a triple one, whereas the N–O is a single bond. The π_{Re-NO} molecular orbitals results from overlapping between the occupied d_{xy} and d_{xz} rhenium orbitals and π-antibonding orbitals of the nitrosyl ligand.

5. Supplementary data

Supplementary data for $C_{35}H_{29}Cl_2N_2OP_2Re$ are available free of charge at www.ccdc.cam.ac.uk/conts/retrieving.html [or from the Cambridge Crystallographic Data Centre, 12, Union Road, Cambridge CB2 1EZ, UK; fax: (internat.) +44 1223 336 033, e-mail: deposit@ccdc.cam.ac.uk] on request, quoting the deposition number 290236.

Acknowledgements

The GAUSSIAN 03 calculations were carried out in the Wrocław Centre for Networking and Supercomputing, WCSS, Wroc3aw, Poland. Crystallographic part was financed by funds allocated by the Ministry of Scientific Research and Information Technology to the Institute of General and Ecological Chemistry, Technical University of Łódź.

References

[1] G.B. Richter-Addo, P. Legzdins, Metal Nitrosyls, Oxford University Press, Oxford, 1992.
[2] J.A. McCleverty, Chem. Rev. 79 (1979) 53.
[3] J.N. Kukuškin, Reakcionnaja sposobnost koordinacjonnych soedinienij, Chimija, Leningrad, 1987.
[4] J.H. Enemark, R.D. Feltham, Coord. Chem Rev. 13 (1974) 339.
[5] K.G. Caulton, Coord. Chem Rev. 14 (1975) 317.
[6] F. Bottomley, Coord. Chem. Rev. 26 (1978) 7.
[7] K.K. Pandey, Coord. Chem. Rev. 51 (1983) 70.
[8] G. WilkinsonComprehensive Coordination Chemistry, vol. 2, Pergamon Press, Oxford, 1987, p. 100.
[9] G.B. Richter-Addo, P. Legzdins, J. Burstyn, Chem. Rev. 102 (2002) 857.
[10] T.W. Hayton, P. Legzdins, W.B. Sharp, Chem. Rev. 102 (2002) 935.
[11] J.A. McCleverty, Chem. Rev. 104 (2004) 403.
[12] W. Volkert, W.F. Goeckeler, G.J. Ehrhardt, A.R. Ketring, J. Nucl. Med 32 (1991) 174.
[13] E.A. Deutsch, K. Libson, J.L. Vanderheyden, Technetium and Rhenium in Chemistry and Nuclear Medicine, Raven Press, New York, 1990.
[14] J.O. Dzięgielewski, B. Machura, J. Marek, Polyhedron 15 (1996) 3713.
[15] J.O. Dzięgielewski, B. Machura, T.J. Bartczak, Polyhedron 15 (1996) 2813.
[16] T.J. Bartczak, W. Czurak, J.O. Dzięgielewski, B. Machura, Polish J. Chem. 72 (1998) 633.
[17] J.O. Dzięgielewski, B. Machura, T. Kupka, T.J. Bartczak, W. Czurak, Polish J. Chem. 72 (1998) 1009.
[18] J.O. Dzięgielewski, B. Machura, T.J. Bartczak, W. Czurak, J. Kusz, J. Warczewski, J. Coord. Chem. 48 (1999) 125.
[19] T.J. Bartczak, W. Czurak, J.O. Dzięgielewski, B. Machura, A. Jankowska, J. Kusz, J. Warczewski, Polyhedron 18 (1999) 2313.
[20] T.J. Bartczak, W. Czurak, J.O. Dzięgielewski, B. Machura, J. Kusz, J. Warczewski, Polish J. Chem. 74 (2000) 265.
[21] T.J. Bartczak, W. Czurak, J.O. Dzięgielewski, B. Machura, A. Jankowska, J. Kusz, J. Warczewski, J. Coord. Chem. 52 (2001) 361.
[22] B. Machura, J.O. Dzięgielewski, S. Michalik, T.J. Bartczak, R. Kruszynski, J. Kusz, Polyhedron 21 (2002) 2617.
[23] B. Machura, R. Kruszynski, M. Jaworska, Polyhedron 24 (2005) 419.
[24] S. Hirata, M. Head-Gordon, Chem. Phys. Lett. 302 (1999) 375.
[25] R. Andreu, J. Orduna, J. Garín, Tetrahedron 57 (2001) 1358.
[26] E. Brocławik, T. Borowski, Chem. Phys. Lett. 339 (2001) 433.
[27] M.J. Calhorda, M.G.B. Drew, V. Félix, L.P. Fonseca, C.A. Gamelas, S.S.M.C. Godinho, I.S. Gonçavles, E. Hunstock, J.P. Lopes, A.J. Parola, F. Pina, C.C. Romão, A.G. Santos, J. Organomet. Chem. 632 (2001) 94.
[28] M.C. Aragoni, M. Arca, T. Cassano, C. Denotti, F.A. Devillanova, F. Isaia, V. Lippolis, D. Natali, L. Niti, M. Sampietro, R. Tommasi, G. Verani, Inorg. Chem. Commun. 5 (2002) 869.

[29] P. Romaniello, F. Lelj, Chem. Phys. Lett. 372 (2003) 51.
[30] P. Norman, P. Cronstrand, J. Ericsson. Chem. Phys. 285 (2002) 207.
[31] J. Bossert, N.B. Amor, A. Strich, C. Daniel, Chem. Phys. Lett. 342 (2001) 617.
[32] C.E. Powell, M.P. Cifuentes, A.M. McDonagh, S.K. Hurst, N.T. Lucas, C.D. Delfs, R. Stranger, M.G. Humphrey, S. Houbrechts, I. Asselberghs, A. Persoons, D.C.R. Hockless, Inorg. Chim. Acta 352 (2003) 9.
[33] J.P. Morral, C.E. Powell, R. Stranger, M.P. Cifuentes, M.G. Humphrey, G.A. Heath, J. Organomet. Chem. 670 (2003) 248.
[34] P. Romaniello, F. Lelj, J. Mol. Struct. Theochem. 636 (2003) 23.
[35] STOE & Cie (1999). X-RED. Version 1.18. STOE & Cie GmbH, Darmstadt, Germany.
[36] G.M. Sheldrick, Acta Cryst. A46 (1990) 467.
[37] G.M. Sheldrick, SHELXL97. Program for the Solution and Refinement of Crystal Structures, University of Göttingen, Germany, 1997.
[38] G.M. Sheldrick, SHELXTL: Release 4.1 for Siemens Crystallographic Research Systems, 1990.
[39] M.J. Frisch, G.W. Trucks, H.B. Schlegel, G.E. Scuseria, M.A. Robb, J.R. Cheeseman, J.A. Montgomery Jr., T. Vreven, K.N. Kudin, J.C. Burant, J.M. Millam, S.S. Iyengar, J. Tomasi, V. Barone, B. Mennucci, M. Cossi, G. Scalmani, N. Rega, G.A. Petersson, H. Nakatsuji, M. Hada, M. Ehara, K. Toyota, R. Fukuda, J. Hasegawa, M. Ishida, T. Nakajima, Y. Honda, O. Kitao, H. Nakai, M. Klene, X. Li, J.E. Knox, H.P. Hratchian, J.B. Cross, C. Adamo, J. Jaramillo, R. Gomperts, R.E. Stratmann, O. Yazyev, A.J. Austin, R. Cammi, C. Pomelli, J.W. Ochterski, P.Y. Ayala, K. Morokuma, G.A. Voth, P. Salvador, J.J. Dannenberg, V.G. Zakrzewski, S. Dapprich, A.D. Daniels, M.C. Strain, O. Farkas, D.K. Malick, A.D. Rabuck, K. Raghavachari, J.B. Foresman, J.V. Ortiz, Q. Cui, A.G. Baboul, S. Clifford, J. Cioslowski, B.B. Stefanov, G. Liu, A. Liashenko, P. Piskorz, I. Komaromi, R.L. Martin, D.J. Fox, T. Keith, M.A. Al-Laham, C.Y. Peng, A. Nanayakkara, M. Challacombe, P.M.W. Gill, B. Johnson, W. Chen, M.W. Wong, C. Gonzalez, J.A. Pople, GAUSSIAN 03, Revision B.03, Gaussian Inc., Pittsburgh, PA, 2003.
[40] A.D. Becke, J. Chem. Phys. 98 (1993) 5648.
[41] C. Lee, W. Yang, R.G. Parr, Phys. Rev. B 37 (1988) 785.
[42] M.E. Casida, in: J.M. Seminario (Ed.), Recent Developments and Applications in Modern Density Functional Theory, Theoretical and Computational Chemistry, Vol. 4, Elsevier, Amsterdam, 1996.
[43] P.J. Hay, W.R. Wadt, J. Chem. Phys. 82 (1985) 299.
[44] E.D. Glendening, A.E. Reed, J.E. Carpenter, F. Weinhold, NBO, Version 3.1.
[45] G.A. Jeffrey, W. Saenger, Hydrogen Bonding in Biological Structures, Springer-Verlag, Berlin, 1994.
[46] G.R. Desiraju, T. Steiner, The Weak Hydrogen Bond in Structural Chemistry and Biology, Oxford University Press, 1999.
[47] B.J. Coe, S.J. Glenwright, Coord. Chem. Rev. 203 (2000) 5.
[48] B.L. Haymore, I.A. Ibers, Inorg. Chem. 14 (1975) 3060.
[49] K. Nakamoto, Infrared and Raman Spectra of Inorganic and Coordination Compounds, 4th ed., Wiley-Interscience, New York, 1986.
[50] A.E. Reed, L.A. Curtiss, F. Weinhold, Chem. Rev. 88 (1988) 899.
[51] B. Machura, Polyhedron 23 (2004) 2363.
[52] B. Machura, M. Jaworska, R. Kruszynski, Polyhedron 23 (2004) 2523.
[53] B. Machura, M. Jaworska, R. Kruszynski, Polyhedron 24 (2005) 267.

2. Results and discussion

New dirhodium(II) complexes: $[\mathbf{2}(HO_2CCF_3)_2]$ and $[\mathbf{3}(HO_2CEt)_2]\cdot HO_2CEt$ with orthometallated tris(*p*-methoxyphenyl)phosphine (PMP) were obtained by exchange of the acetato bridges in $[\mathbf{1}(HOAc)_2]$ by trifluoroacetato and propionato bridges, respectively (Scheme 1).

The reactions of adduct formation by [*cis*-Rh_2-(μ-$O_2CR)_2$(PMP-$C)_2$] with pyrazole or imidazole in $CHCl_3$ were followed by UV–Vis and NMR spectroscopies.

2.1. Molecular structures established with X-ray methods

Crystal data for complexes: $[\mathbf{2}(H_2O)(PrOH)]\cdot PrOH$, $[\mathbf{3}(HO_2CEt)_2]\cdot HO_2CEt$, $[\mathbf{2}(Hpz)_2]$ and $[\mathbf{3}(Hpz)_2]$ are given in Table 1. Tables 2–5 present selected bond lengths and angles. Molecular structures of these complexes are shown in Figs. 1–6.

2.1.1. Structure of $[\mathbf{3}(HO_2CEt)_2]\cdot HO_2CEt$

The compound $[\mathbf{3}(HO_2CEt)_2]\cdot HO_2CEt$ crystallizes in the triclinic crystal system, space group $P\bar{1}$. The unit cell consists of two independent sets (A and B) of enantiomers of $[\mathbf{3}(HO_2CEt)_2]\cdot HO_2CEt$.

Each molecule of $[\mathbf{3}(HO_2CEt)_2]\cdot HO_2CEt$ consists of a binuclear rhodium core bridged by two propionato groups and two PMP ligands in which orthometallation has occurred at one of the phenyl rings. The phosphine ligands are in the *cis* position with a H–T (head–tail) structure. The axial sites are occupied by two molecules of propanoic acid. There are only slight differences between the structures of molecules A and B.

The molecular structures of both molecules exhibit distorted octahedral coordination around the central atoms. This complex is in a distorted eclipsed conformation. Torsion angles O1A–Rh1A–Rh2A–O2A and O3A–Rh1A–Rh2A–O4A of the propionato bridges in molecule A are 19.1° and 18.0°, respectively; while for molecule B: torsion angles O1B–Rh1B–Rh2B–O2B and O3B–Rh1B–Rh2B–O4B are 16.1° and 17.2°, respectively. The Rh1A–Rh2A and Rh1B–Rh2B distances are 2.504(1) and 2.506(1) Å, respectively, and indicate a rather strong single bond between the two metal atoms. Distances for Rh – equatorial atoms in molecules A and B are similar. The bond lengths between the phosphorus atom and carbon atom of the metallated rings are slightly shorter than those between the phosphorus atoms and carbon atoms of non-metallated rings. The structure of $[\mathbf{3}(HO_2CEt)_2]\cdot HO_2CEt$

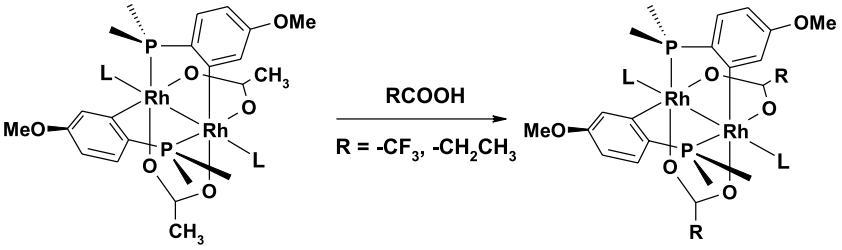

Scheme 1. Schematic representation of $[\mathbf{1}(L)_2]$ and carboxylato bridges exchange.

Table 1
Crystal data for $[\mathbf{2}(H_2O)(PrOH)]\cdot PrOH$, $[\mathbf{2}(Hpz)_2]$, $[\mathbf{3}(HO_2CEt)_2]\cdot HO_2CEt$ and $[\mathbf{3}(Hpz)_2]$

	$[\mathbf{2}(H_2O)(PrOH)]\cdot PrOH$	$[\mathbf{2}(Hpz)_2]$	$[\mathbf{3}(HO_2CEt)_2]\cdot HO_2CEt$	$[\mathbf{3}(Hpz)_2]$
Empirical formula	$C_{52}H_{58}F_6O_{13}P_2Rh_2$	$C_{52}H_{48}F_6N_4O_{10}P_2Rh_2$	$C_{57}H_{88}O_{16}P_2Rh_2$	$C_{54}H_{58}N_4O_{10}P_2Rh_2$
Formula weight	1272.74	1270.7	1276.9	1190.8
T (K)	100(2)	100(2)	100(2)	100(2)
Crystal system	triclinic	orthorhombic	triclinic	orthorhombic
Space group	$P1$ (no. 1)	$P2_12_12$ (no. 18)	$P\bar{1}$ (no. 2)	$Fdd2$ (no. 43)
a (Å)	12.398(2)	21.505(4)	13.944(3)	28.133(1)
b (Å)	13.000(3)	22.675(5)	17.685(4)	36.217(2)
c (Å)	17.463(3)	10.784(2)	24.527(5)	10.2954(4)
α (°)	80.33(3)		73.91(3)	
β (°)	74.64(3)		87.81(3)	
γ (°)	81.30(3)		79.01(3)	
V (Å^3)	2658.6(9)	5259(2)	5704(2)	10490.0(8)
Z	2	4	4	8
D_{calc} (Mg m^{-3})	1.590	1.605	1.487	1.058
μ (mm^{-1})	0.765	0.771	0.703	0.752
$F(000)$	1296	2568	2632	4880
Goodness-of-fit (F^2)	1.036	0.989	1.012	1.120
Final R_1/wR_2 indices ($I > 2\sigma_I$)	0.0433/0.1033	0.0578/0.0618	0.0813/0.1936	0.0282/0.0558

Table 2
Selected bond lengths (Å) and angles (°) for $[\mathbf{3}(HO_2CEt)_2]\cdot HO_2CEt$

	A	B
Bond lengths		
Rh1–Rh2	2.504(1)	2.506(1)
Rh1–P1	2.207(2)	2.200(2)
Rh1–O1	2.209(5)	2.210(5)
Rh1–O3	2.186(5)	2.166(5)
Rh1–C42	2.005(8)	2.018(7)
Rh1–O5	2.274(5)	2.278(5)
Rh2–P2	2.210(2)	2.208(2)
Rh2–O2	2.158(5)	2.173(5)
Rh2–O4	2.174(5)	2.186(5)
Rh2–C12	2.025(8)	2.006(8)
Rh2–O7	2.347(5)	2.334(5)
Bond angles		
P1–Rh1–Rh2	87.46(6)	88.02(6)
O1–Rh1–Rh2	83.9(1)	83.7(2)
O3–Rh1–Rh2	86.8(1)	87.2(2)
C42–Rh1–Rh2	96.8(2)	97.1(2)
O5–Rh1–Rh2	170.7(1)	170.0(2)
P2–Rh2–Rh1	87.63(6)	88.50(6)
O2–Rh2–Rh1	85.63(1)	87.2(1)
O4–Rh2–Rh1	83.4(1)	83.4(2)
C12–Rh2–Rh1	96.6(2)	96.6(2)
O7–Rh2–Rh1	168.9(2)	169.7(2)

Hydrogen bonds	A–H	H···B	A···B	∠AHB
O6A–H6A···O3A	0.84	1.77	2.609(8)	176
O8A–H8A···O2A	0.84	1.79	2.625(8)	175
O6B–H6B···O3B	0.84	1.75	2.585(8)	173
O8B–H8B···O2B	0.84	1.78	2.621(8)	174
O2C–H2C···O1A	0.84	1.86	2.686(8)	169
O1D–H1D···O1B	0.84	1.86	2.699(8)	172

is similar to the structure of $[cis\text{-}Rh_2(\mu\text{-}OAc)_2\{\mu\text{-}(C_6H_4)\text{-}PPh_2\}_2(HOAc)_2]$ [1].

The axial molecules of propanoic acid are rather weakly bound to the dirhodium core. The Rh1–O5 distances are 2.274(5) and 2.278(5) Å for A and B molecules respectively, Rh2–O7: 2.347(5) (A) and 2.334(5) Å (B). These distances are similar to the distances between the rhodium and axial oxygen atom found in complexes: $[cis\text{-}Rh_2(\mu\text{-}OAc)_2\{\mu\text{-}(C_6H_3\text{-}3\text{-}OMe)P(C_6H_4\text{-}3\text{-}OMe)_2\}_2(HOAc)(H_2O)]$ [21], $[cis\text{-}Rh_2(\mu\text{-}OAc)_2\{\mu\text{-}(C_6H_3\text{-}3\text{-}OMe)P(C_6H_4\text{-}3\text{-}OMe)_2\}_2(H_2O)_2]$ [23] and $[cis\text{-}Rh_2(\mu\text{-}OAc)_2\{\mu\text{-}(C_6H_4)PPh_2\}_2(HOAc)_2]$ [1]. The OH groups of axial molecules of HO_2CEt form strong hydrogen bonds with oxygen atoms (O3 and O2) of propionato bridges. Relatively strong asymmetry in coordinating axial molecules of propanoic acid ($d_{Rh1-O5} < d_{Rh2-O7}$) results probably because of the weak steric interaction of one axial HO_2CEt molecule with a crystallization molecule of propanoic acid, forming a hydrogen bond with the oxygen atom (O1) of the propionato bridge (EtC(O)OH···O1A and EtC(O)OH···O1B; Fig. 1.).

2.1.2. $[\mathbf{2}(H_2O)(PrOH)]\cdot PrOH$

The compound $[\mathbf{2}(H_2O)(PrOH)]\cdot PrOH$ crystallizes in the triclinic crystal system, space group $P\bar{1}$. The unit cell consists of two independent molecules of $[\mathbf{2}(H_2O)(PrOH)]\cdot PrOH$. Usually this kind of complex forms centrosymmetric unit cells (most frequently $P\bar{1}$ space group), like the complex $[\mathbf{3}(HO_2CEt)_2]\cdot HO_2CEt$ described above. The unit cell of the complex $[\mathbf{2}(H_2O)(PrOH)]\cdot PrOH$ contains two diastereoisomeric molecules A and B.

Table 3
Selected bond lengths (Å) and angles (°) for $[\mathbf{2}(H_2O)(PrOH)]\cdot PrOH$

	A	B
Bond lengths		
Rh1–Rh2	2.516(1)	2.519(1)
Rh1–P1	2.213(2)	2.216(2)
Rh1–O1	2.213(5)	2.204(5)
Rh1–O3	2.166(4)	2.177(4)
Rh1–C42	1.997(6)	1.989(7)
Rh1–O5	2.270(4)	2.313(4)
P1–C11	1.800(7)	1.788(7)
P1–C21	1.845(7)	1.839(7)
P1–C31	1.822(6)	1.826(7)
Rh2–P2	2.216(2)	2.222(2)
Rh2–O2	2.172(5)	2.177(5)
Rh2–O4	2.202(5)	2.199(4)
Rh2–C12	1.993(7)	1.980(6)
Rh2–O6	2.321(5)	2.391(5)
O6–C5	1.672(17)	1.464(9)
Bond angles		
P1–Rh1–Rh2	87.99(5)	87.44(6)
O1–Rh1–Rh2	83.7(1)	85.0(1)
O3–Rh1–Rh2	87.3(1)	87.8(1)
C42–Rh1–Rh2	97.8(2)	97.8(2)
O5–Rh1–Rh2	162.4(1)	164.1(1)
Rh1–P1–C11	113.1(2)	113.3(2)
Rh1–P1–C21	118.4(2)	119.0(2)
Rh1–P1–C31	110.5(2)	110.8(2)
P2–Rh2–Rh1	87.91(6)	87.89(6)
O2–Rh2–Rh1	87.0(1)	86.8(1)
O4–Rh2–Rh1	83.5(1)	82.4(1)
C12–Rh2–Rh1	97.6(2)	98.1(2)
O6–Rh2–Rh1	165.3(2)	163.4(1)
Rh2–O6–C5	115.5(5)	116.9(4)

Hydrogen bonds	A–H	H···B	A···B	∠AHB
O6A–H6A···O14B_1	0.90	2.04	2.921(7)	163
O5A–H5AA···O1C	1.00	1.90	2.875(6)	164
O5B–H5BA···O1C_2	0.86	2.21	2.854(6)	131
O5B–H5BA···O1B	0.86	2.42	2.989(6)	124
O5B–H5BB···O1D	0.86	2.08	2.786(6)	139
O6B–H6B···O14A_3	0.85	2.14	2.996(7)	180
O1C–H1C···O3A	0.84	2.13	2.882(7)	149
O1D–H1D···O3B	0.84	2.10	2.828(7)	144

Symmetry transformations used to generate equivalent atoms: none = $[x, y, z]$, _1 = $[x, y, z-1]$, _2 = $[x, y+1, z]$, _3 = $[x, y, z+1]$.

The molecular structure of $[\mathbf{2}(H_2O)(PrOH)]\cdot PrOH$ is similar to the structure of $[\mathbf{3}(HO_2CEt)_2]\cdot HO_2CEt$ and consists of a binuclear rhodium core bridged by two trifluoroacetato groups and two orthometallated phosphine ligands. The axial sites are occupied by molecules of water and 1-propanol.

The complex exhibits a distorted eclipsed conformation. The torsion angles of the trifluoroacetato bridges in molecule A, O1A–Rh1A–Rh2A–O2A and O3A–Rh1A–Rh2A–O4A, are 17.7° and 18.5°, respectively, for molecule B, O1B–Rh1B–Rh2B–O2B and O3B–Rh1B–Rh2B–O4B are −15.8° and −18.4°, respectively, and these values are

Table 4
Selected bond lengths (Å) and angles (°) for [**3**(Hpz)$_2$]

Bond lengths	
Rh1–Rh1_1	2.5290(4)
Rh1–P1	2.2049(8)
Rh1–O1	2.168(2)
Rh1–O2	2.177(2)
Rh1–C12	2.000(3)
Rh1–N1	2.250(2)
P1–C11_1	1.802(3)
P1–C21	1.830(3)
P1–C31	1.834(3)
N1–N2	1.356(3)
N2–C3	1.345(4)
C3–C4	1.380(4)
C4–C5	1.395(4)
C5–N1	1.331(4)
Bond angles	
P1–Rh1–Rh1_1	86.67(2)
O1–Rh1–Rh1_1	85.47(5)
O2–Rh1–Rh1_1	83.70(5)
C12–Rh1–Rh1_1	97.34(8)
N1–Rh1–Rh1_1	165.93(6)
Rh1–N1–N2	112.2(2)
N2–N1–C5	105.0(2)

Hydrogen bonds	A–H	H···B	A···B	∠AHB
N2–H2···O1	0.81	2.03	2.675(3)	137
N2–H2···O31_2	0.81	2.89	3.281(4)	112

Symmetry transformations used to generate equivalent atoms: none = [x, y, z], _1 = [$-x+1, -y, z$], _2 = [$x+1/4, -y+1/4, z-3/4$].

Table 5
Selected bond lengths (Å) and angles (°) for [**2**(Hpz)$_2$]

	A (_x = _1)	B (_x = _2)
Bond lengths		
Rh1–Rh1_x	2.5374(9)	2.5422(9)
Rh1–P1	2.216(1)	2.207(1)
Rh1–O1	2.227(3)	2.210(3)
Rh1–O2_x	2.165(3)	2.191(3)
Rh1–C12_x	2.010(4)	2.007(4)
Rh1–N1	2.252(4)	2.218(4)
N1–N2	1.359(5)	1.353(5)
N2–C3	1.339(6)	1.345(6)
C5–N1	1.341(6)	1.344(6)
Bond angles		
P1–Rh1–Rh1_x	87.17(4)	86.13(4)
O1–Rh1–Rh1_x	82.65(8)	83.85(9)
O2_x–Rh1–Rh1_x	85.64(9)	84.87(9)
C12_x–Rh1–Rh1_x	96.8(2)	97.0(1)
N1–Rh1–Rh1_x	165.1(1)	163.5(1)
Rh1–N1–N2	114.6(3)	114.7(3)

Hydrogen bonds	A–H	H···B	A···B	∠AHB
N2A–H2A···O2A	0.88	2.11	2.707(6)	125
N2A–H2A···O24B_1	0.88	2.38	3.025(6)	130
N2B–H2B···O2B	0.88	2.01	2.639(6)	127

Symmetry transformations used to generate equivalent atoms: none = [x, y, z], _1 = [$-x+1, -y+1, z$], _2 = [$-x, -y+1, z$].

similar to those found in [**3**(H_2O)(HO_2CEt)] · HO_2CEt. The Rh1A–Rh2A and Rh1B–Rh2B distances are 2.516(1) and 2.519(1) Å, respectively, and are longer than the Rh–Rh distances in [**3**(HO_2CEt)$_2$] · HO_2CEt. The Rh–P distances are also longer on comparing to those of [**3**(H_2O)(HO_2CEt)] · HO_2CEt.

The axial sites of the Rh–Rh core are occupied by molecules of water and 1-propanol. These molecules are rather weakly bound to the dirhodium core. The values of Rh–O^{PrOH} distances do not differ considerably from those found in other complexes described above.

The existence of two diastereoisomers, A and B, results mainly from different positions of the methoxy groups of the non-metallated phenyl rings, as shown in Fig. 3a. The torsion angles of the methoxy groups in the exo rings in molecule A are 12.8 (C63A–C64A–O64A–C76) and 0.5° (C33A–C34A–O34A–C73) and in molecule B, −179.0 (C63B–C64B–O64B–C86) and 3.0° (C33B–C34B–O34B–C83). In the endo rings, the torsion angles in molecule A are 179.0 (C53A–C54A–O54A–C75) and −15.6° (C23A–C24A–O24A–C72), and in molecule B, −2.2 (C53B–C54B–O54B–C85) and −3.5° (C23B–C24B–O24B–C82).

There are two crystallization molecules of 1-propanol in the unit cell. One molecule is bound to molecule A of [**2**(H_2O)(PrOH)] · PrOH via hydrogen bonds to the oxygen atom of the trifluoroacetato bridge (O1C–H1C···O3A) and to the axial water molecule (O5A–H5AA···O1C). The second molecule of 1-propanol is bound in the same way to molecule B. There are three intermolecular hydrogen bonds in the crystal. Two hydrogen bonds are formed between axial molecules of 1-propanol and oxygen atoms of the methoxy group of the metallated ring: O6A–H6A···O14B_1 and O6B–H6B···O14A_3 and third between the axial molecule of water and a crystallization molecule of 1-propanol: O5B–H5BA···O1C_2. This leads to the formation of a two-dimensional net.

2.1.3. [*3*(*Hpz*)$_2$]

The complex [**3**(Hpz)$_2$] crystallizes in the orthorhombic crystal system, space group *Fdd2*.

The molecular structure of [**3**(Hpz)$_2$] is similar to the structure of [**3**(HO_2CEt)$_2$] · HO_2CEt with the axial molecules of propanoic acid replaced with two molecules of pyrazole.

The main structural difference between [**3**(Hpz)$_2$] and [**3**(HO_2CEt)$_2$] · HO_2CEt results in the different space orientations of the $-CH_2CH_3$ groups of the propionato bridges, as shown in Fig. 5.

Coordination of pyrazole to the axial sites of the dirhodium core causes Rh–Rh bond lengthening: from 2.504(1) to 2.506(1) Å in [**3**(HO_2CEt)$_2$] · HO_2CEt to 2.5290(4) Å in [**3**(Hpz)$_2$]. This difference is smaller than that found in the acetic acid and pyridine adducts: [*cis*-Rh_2(μ-OAc)$_2$-{μ-(C_6H_4)PPh_2}$_2$($HOAc$)$_2$] and [*cis*-Rh_2(μ-OAc)$_2$-{μ-(C_6H_4)-PPh_2}$_2$(py)$_2$] [1] in which the Rh–Rh bond lengths are 2.508(1) and 2.556(2) Å, respectively, despite the similar donor properties of the pyrazole and pyridine ligands (proton affinities are 930 kJ/mol for pyridine and 894.1 kJ/mol for Hpz [24]). The bond lengths for the rhodium-equatorial ligands are approximately the same in [**3**(Hpz)$_2$] and [**3**(HO_2CEt)$_2$] · HO_2CEt. The O1–Rh1–Rh1_1–O1_1 tor-

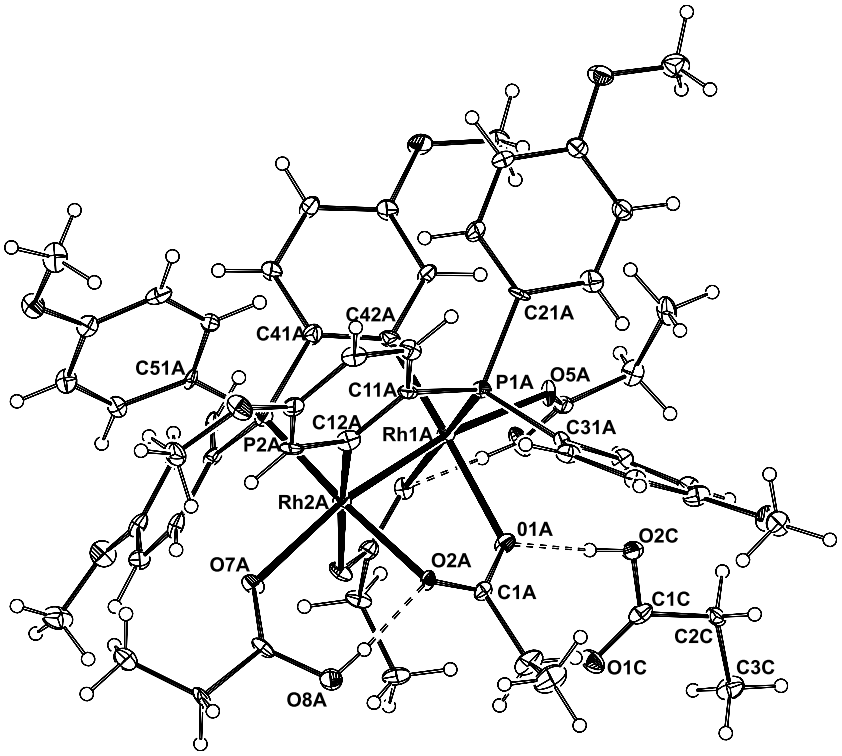

Fig. 1. Molecular structure of molecule A (an ORTEP view) of [**3**($HO_2CEt)_2$] · HO_2CEt with 25% thermal ellipsoids (the structure of molecule B is almost the same – with some exceptions discussed in the text).

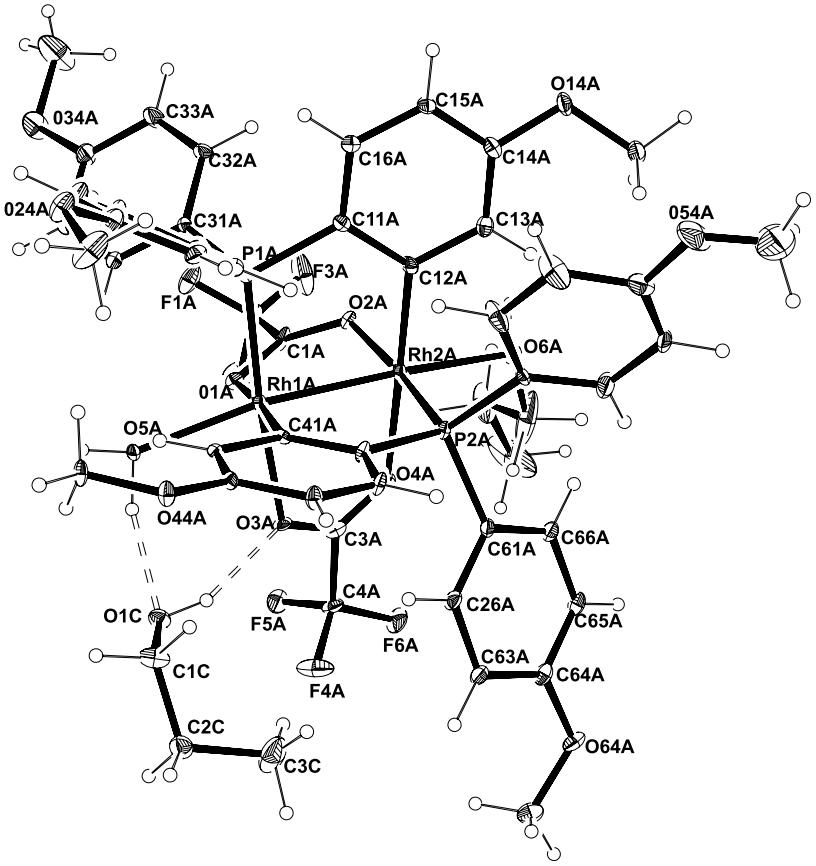

Fig. 2. Structure of molecule A of [**2**(H_2O)(PrOH)] · PrOH with 25% thermal ellipsoids (an ORTEP view).

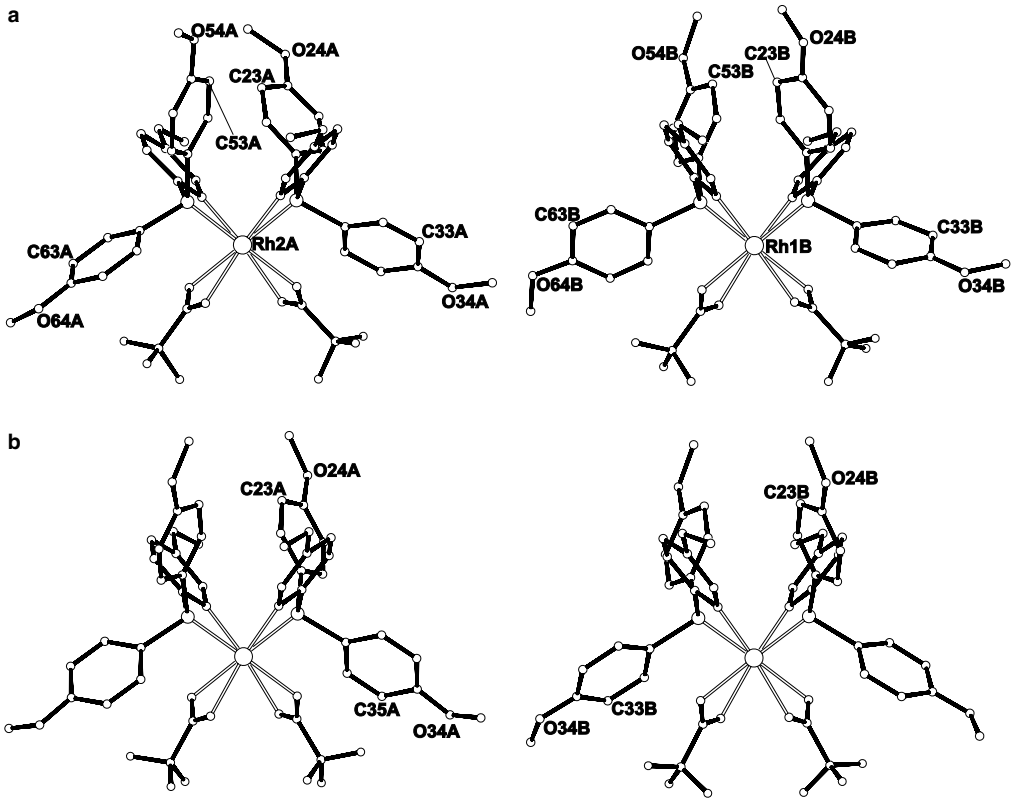

Fig. 3. View (PLATON) perpendicular to the Rh–Rh axis of diastereoisomers of [**2**(H_2O)(PrOH)] · PrOH (a) and [**2**($Hpz)_2$] (b). Hydrogen atoms and axial ligands are omitted for clarity.

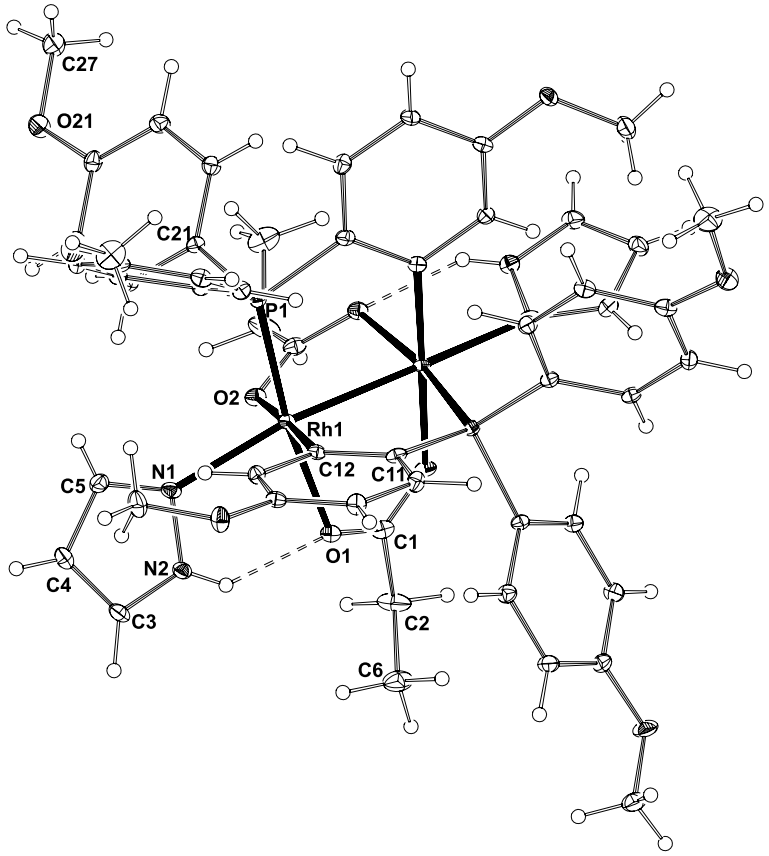

Fig. 4. ORTEP view of molecule A of [**3**($Hpz)_2$] with 25% thermal ellipsoids.

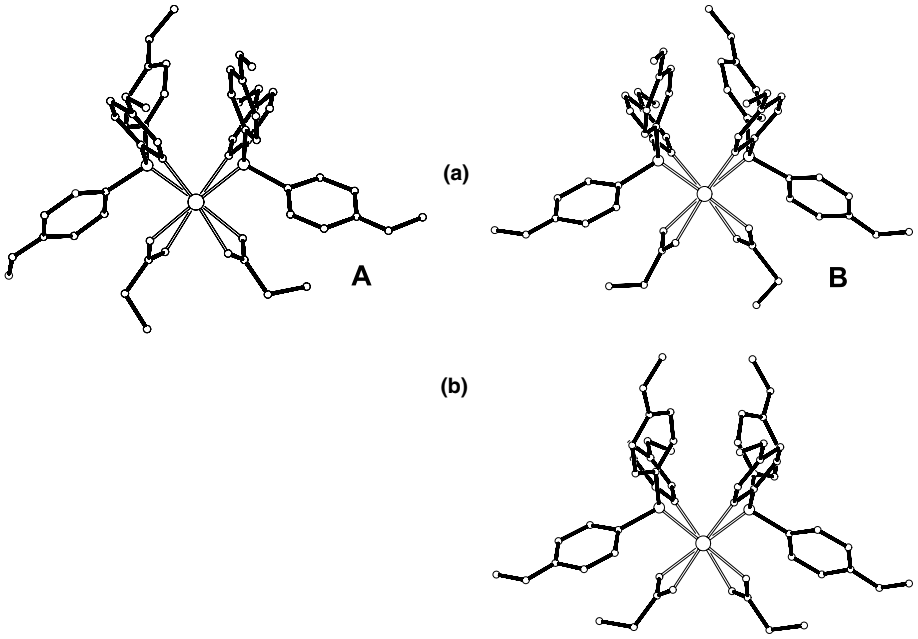

Fig. 5. View (PLATON) perpendicular to the Rh–Rh axis of diastereoisomers of $[\mathbf{3}(HO_2CEt)_2]\cdot HO_2CEt$ (a) and $[\mathbf{3}(Hpz)_2]$ (b). Hydrogen atoms and axial ligands are omitted for clarity.

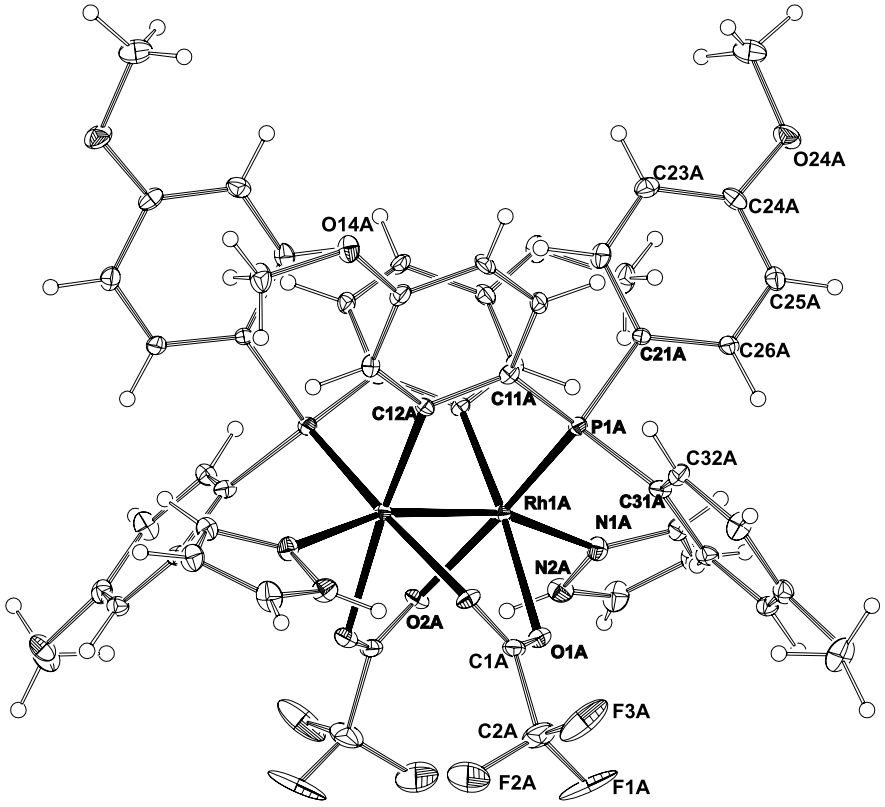

Fig. 6. ORTEP view of molecule A of $[\mathbf{2}(Hpz)_2]$ with 30% thermal ellipsoids.

sion angle in $[\mathbf{3}(Hpz)_2]$ is equal to 19.7° and is only slightly larger than the torsion angles in $[\mathbf{3}(HO_2CEt)_2]\cdot HO_2CEt$ (see Fig. 5).

The length of the rhodium – axial pyrazole ligand bond (Rh1–N1 = 2.250(2) Å) indicates a relatively strong bonding of pyrazole. The bonding of pyrazole is stronger than the bonding of propanoic acid (oxygen donor) in $[\mathbf{3}(HO_2CEt)_2]\cdot HO_2CEt$. The stronger coordination of the Hpz axial molecules in comparison with oxygen axial ligands leads to the increase in the Rh–Rh distance. The Rh1–N1 bond length is also shorter than the Rh–N bond length (2.281(9) Å) in the pyridine adducts [*cis*-Rh_2-

(μ-OAc)$_2${μ-(C$_6$H$_4$)PPh$_2$}$_2$(py)$_2$] [1] and [*cis*-Rh$_2$(μ-OOCCMe$_3$)$_2${μ-(C$_6$H$_4$)PMePh}$_2$(py)$_2$] [3]: 2.271(32) and 2.306(34) Å.

The molecule of pyrazole is almost planar; the deviations from the mean least-squares planes are very small. In contrast to the molecular structure of free pyrazole [25], which rather exhibits the betaine form, the carbon–carbon bond lengths indicate that the coordinated molecule of pyrazole is a neutral ligand. This is typical for most metal–pyrazole complexes (for example [NiCl$_2$(Hpz)$_4$] [26], [RhCl$_2$(Hpz)$_4$]Cl [27] and [RhCl$_2$(Hpz)$_4$][RhCl$_4$(Hpz)$_2$] [28]). The pyrazole molecule forms a hydrogen bond with the oxygen atom of the propionato bridge: N2–H2···O1. The H2 atom also forms a weak intermolecular hydrogen bond with the –OMe group of another complex molecule (N2A–H2A···O31_2).

2.1.4. [2(Hpz)$_2$]

The complex [**2**(Hpz)$_2$] crystallizes in the orthorhombic crystal system, space group *P*2(1)2(1)2. The unit cell consists of four molecules of [**2**(Hpz)$_2$]. There are two independent centrosymmetric molecules A and B in it. The structure of [**2**(Hpz)$_2$] is very similar to the structure of [**3**(Hpz)$_2$].

The torsion angles (molecule A: O1A–Rh1A–Rh1A_1–O2A = 22.3°, molecule B: O1B–Rh1B–Rh1B_2–O2B = −22.1°) show larger deviations from the eclipsed conformation than in [**2**(H$_2$O)(PrOH)] (Fig. 3). The Rh1A–Rh1A_1 and Rh1B–Rh1B_2 distances are 2.5374(9) and 2.5422(9) Å, respectively, and are longer than Rh–Rh distances in [**2**(H$_2$O)(PrOH)]. The lengths of the rhodium – axial pyrazole ligand bonds (Rh1A–N1A = 2.252(4), Rh1B–N1B = 2.218(4) Å) are similar to those in [**3**(Hpz)$_2$] (Rh1–N1 = 2.250(2) Å).

The pyrazole molecules form two intramolecular hydrogen bonds with oxygen atoms of trifluoroacetato bridges: N2A–H2A···O2A and N2B–H2B···O2B and one weak intermolecular hydrogen bond (N2A–H2A···O24B_1), leading to the formation of the two-dimensional structure.

In the complex [**2**(Hpz)$_2$], similarly as in [**2**(H$_2$O)(PrOH)], there are two diastereoisomeric molecules A and B in the unit cell. The differences in the diastereoisomeric molecules A and B (shown in the Fig. 3b) are, similarly as in [**2**(H$_2$O)(HO$_2$CEt)], caused by different orientations of the methoxy groups. For molecule A, the torsion angle C35A–C34A–O34A–C37 is −160.4° (exo) and C23A–C24A–O24A–C27 equals 2.1° (endo). In the case of molecule B, the torsion angle C33B–C34B–O34B–C67 is −10.9° (exo) and C23B–C24B–O24B–C57 is −5.2° (endo).

According to our best knowledge, crystals of [**2**(H$_2$O)(PrOH)] · PrOH and [**2**(Hpz)$_2$] are the first crystals grown in non-centrosymmetric space groups obtained from solutions of racemic mixtures of dirhodium(II) carboxylates with two molecules of metallated phosphines. Single crystals after dissolution give again a mixture of enantiomers.

2.2. Spectroscopic studies

2.2.1. Properties of [1(HOAc)$_2$], [2(HO$_2$CCF$_3$)$_2$] and [3(HO$_2$CEt)$_2$] · HO$_2$CEt

There are two bands in the electronic spectra of Rh$_2$(μ-O$_2$CR)$_4$ complexes in the visible region, which are assigned to the $\pi^*(Rh_2) \rightarrow \sigma^*(Rh_2)$ and $\pi^*(Rh_2) \rightarrow \sigma^*(Rh\text{–}O)$ transitions. The first band in the UV–Vis spectrum of [*cis*-Rh$_2$(μ-O$_2$CR)$_2$(μ-PMP-C)$_2$(HO$_2$CR)$_2$], corresponding to the $\pi^*(Rh_2) \rightarrow \sigma^*(Rh_2)$ transition [19], is observed at $\nu = 17\,990\ cm^{-1}$ ($\varepsilon = 308$) for [**3**(HO$_2$CEt)$_2$] · HO$_2$CEt, $\nu = 17\,860\ cm^{-1}$ ($\varepsilon = 362$) for [**1**(HOAc)$_2$] and $\nu = 17\,570\ cm^{-1}$ ($\varepsilon = 499$) for [**2**(HO$_2$CCF$_3$)$_2$] (Table 7). The second band is hidden under an intense P → Rh charge transfer transition. The energies of the $\pi^*(Rh_2) \rightarrow \sigma^*(Rh_2)$ transitions change in the following order: [**3**(HO$_2$CEt)$_2$] · HO$_2$CEt > [**1**(HOAc)$_2$] > [**2**(HO$_2$CCF$_3$)$_2$]. Thus they diminish with decreasing σ-donor properties of the appropriate acids (acid dissociation constants: $K_a(HO_2CEt) = 1.3 \times 10^{-5} < K_a(HOAc) = 1.8 \times 10^{-5} < K_a(HO_2CF_3) = 6.0 \times 10^{-1}$).

The chemical shifts in the $^{31}P\{^1H\}$ NMR spectra in $CDCl_3$ of the [*cis*-Rh$_2$(μ-O$_2$CR)$_2$(PMP-C)$_2$] complexes are 18.1 for [**3**(HO$_2$CEt)$_2$] · HO$_2$CEt, 17.4 for [**1**(HOAc)$_2$] and 14.1 ppm for [**2**(HO$_2$CCF$_3$)$_2$] (Table 6.) The signals in $^{31}P\{^1H\}$ NMR spectra are the AA′ part of an AA′XX′ or AA′MM′XX′ pattern, but they cannot be easily resolved due to broadening of the peaks. Thus the δ (^{31}P) values depend in the same manner on the acidity of carboxylic acids as the energy of $\pi^*(Rh_2) \rightarrow \sigma^*(Rh_2)$ transitions.

The ^{1}H NMR spectra of all the complexes are presented in Table 6. The chemical shifts of the methoxy substituents almost do not change with the change of the carboxylato bridges. Changes of chemical shifts and coupling constants of the aromatic protons also differ rather little in [**3**(HO$_2$CEt)$_2$] · HO$_2$CEt, [**1**(HOAc)$_2$] and [**2**(HO$_2$CCF$_3$)$_2$]. The only exception is the proton ($H^{3,m}$) of the metallated ring in the ortho position with respect to the Rh–C bond ([**3**(HO$_2$CEt)$_2$] · HO$_2$CEt: 6.41, [**1**(HOAc)$_2$]: 6.36, [**2**(HO$_2$CCF$_3$)$_2$]: 5.99 ppm). Thus these chemical shifts decrease with the increase of K_a of the carboxylic acid.

Generally there are two sets of signals (AA′MM′X type) for the protons of the non-metallated phenyl rings: A and B. A comparison of their chemical shifts (Table 6) with the analogous chemical shifts of the free phosphine (7.22 and 6.85 ppm [20]) suggests that A – type rings are most probably exo rings (in molecular structures established by X-ray methods: C31–C36 and C61–C66 rings) and B – type rings are in endo positions. On the same basis, the signals of OMe groups at 3.26 for [**3**(HO$_2$CEt)$_2$] · HO$_2$CEt, 3.28 for [**1**(HOAc)$_2$] and 3.30 ppm for [**2**(HO$_2$CCF$_3$)$_2$] can be assigned to metallated rings (for free PMP: δ(OMe) = 3.77 ppm).

2.2.2. Interactions of complexes with pyrazole and imidazole

The first band in the UV–Vis spectra of the dirhodium(II) complexes, assigned to the $\pi^*(Rh_2) \rightarrow \sigma^*(Rh_2)$ transition, is very sensitive to the nature of the axial ligand [22]. This is also true for dirhodium(II) carboxylates with

Table 6
NMR spectra of [**1**$(HOAc)_2$], [**2**$(HO_2CF_3)_2$] and [**3**$(HO_2CEt)_2]\cdot HO_2CEt$ complexes and their adducts with pyrazole: $[Rh_2] + x$Hpz (solvent: $CDCl_3$; chemical shifts (ppm); coupling constants (Hz))

x		[**1**$(HOAc)_2$]	[**3**$(HO_2CEt)_2]\cdot HO_2CEt$	[**2**$(HO_2CF_3)_2$]
0	$^{31}P\{^1H\}$	17.4	18.1	14.1
	^1H carboxylates	1.27 (s, 6H) bridges; 2.13 (s, 6H)	0.58 (t, 6H), ^3J(H–H) = 7.6, CH_3-bridges; 1.52 (q, 4H), CH_2-bridges; 1.17 (t, 6H), ^3J(H–H) = 7.5, CH_3; 2.39 (q, 4H), CH_2	
	OMe groups	3.77 (s, 6H); 3.73 (s, 6H); 3.28 (s, 6H)$^{(m)}$	3.75 (s, 6H); 3.73 (s, 6H); 3.26 (s, 6H)$^{(m)}$	3.77 (s, 6H); 3.75 (s, 6H); 3.30 (s, 6H)$^{(m)}$
	Aromatic protons	$H^{2,6\text{-A}}$: 7.55 (t, 4H) $^3J(H^{2,6}\text{–P}) \approx {}^3J(H^{2,6\text{-A}}\text{–}H^{3,5\text{-A}}) = 9.16$; $H^{3,5\text{-A}}$: 6.86 (d, 4H), $^3J(H^{2,6\text{-A}}\text{–}H^{3,5\text{-A}}) = 7.50$; $H^{2,6\text{-B}}$: 6.66 (t, 4H), $^3J(H^{2,6\text{-B}}\text{–P}) \approx {}^3J(H^{2,6\text{-B}}\text{–}H^{3,5\text{-B}}) = 9.14$; $H^{3,5\text{-B}}$: 6.56 (d, 4H), $^3J(H^{2,6\text{-B}}\text{–}H^{3,5\text{-B}}) = 7.25$; $H^{3,m}$: 6.36 (s*, 2H); $H^{5,m}$: 6.30 (d*, 2H); $H^{6,m}$: 6.49 (t, 2H), $^3J(H^{5,m}\text{–}H^{6,m.}) \approx {}^3J(H^{6,m}\text{–P}) = 8.7$	$H^{2,6\text{-A}}$: 7.54 (t, 4H) $^3J(H^{2,6}\text{–P}) \approx {}^3J(H^{2,6\text{-A}}\text{–}H^{3,5\text{-A}}) = 9.26$; $H^{3,5\text{-A}}$: 6.82 (dd, 4H), $^4J(H^{3,5\text{-A}}\text{–P}) = 1.33$, $^3J(H^{2,6\text{-A}}\text{–}H^{3,5\text{-A}}) = 8.64$; $H^{2,6\text{-B}}$: 6.71 (t, 4H), $^3J(H^{2,6\text{-B}}\text{–P}) \approx {}^3J(H^{2,6\text{-B}}\text{–}H^{3,5\text{-B}}) = 9.22$; $H^{3,5\text{-B}}$: 6.57 (dd, 4H), $^4J(H^{3,5\text{-B}}\text{–P}) = 1.54$, $^3J(H^{2,6\text{-B}}\text{–}H^{3,5\text{-B}}) = 8.00$; $H^{3,m}$: 6.41 (t, 2H), $^4J(H^{3,m}\text{–}H^{5,m}) \approx {}^4J(H^{3,m}\text{–P}) = 2.84$; $H^{5,m}$: 6.25 (dd, 2H) $^4J(H^{5,m}\text{–P}) \approx {}^4J(H^{5,m}\text{–}H^{3,m}) = 2.05$; $H^{6,m}$: 6.53 (t, 2H), $^3J(H^{5,m}\text{–}H^{6,m.}) \approx {}^3J(H^{6,m}\text{–P}) = 8.78$	$H^{2,6\text{-A}}$: 7.45 (t, 4H), $^3J(H^{2,6\text{-A}}\text{–P}) \approx {}^3J(H^{2,6\text{-A}}\text{–}H^{3,5\text{-A}}) = 9.4$; $H^{3,5\text{-A}}$: 6.86 (d, 4H), $^3J(H^{2,6\text{-A}}\text{–}H^{3,5\text{-A}}) = 7.6$; $H^{2,6\text{-B}}$: 6.71 (t, 4H), $^3J(H^{2,6\text{-B}}\text{–P}) \approx {}^3J(H^{2,6\text{-B}}\text{–}H^{3,5\text{-B}}) = 9.3$; $H^{3,5\text{-B}}$: 6.61 (d, 2H), $^3J(H^{2,6\text{-B}}\text{–}H^{3,5\text{-B}}) = 7.4$; $H^{3,m}$: 5.99 (s*, 2H); $H^{5,m}$: 6.38 (d*, 2H); $H^{6,m}$: 6.55 (t, 2H), $^3J(H^{5,m}\text{–}H^{6,m.}) \approx {}^3J(H^{6,m}\text{–P}) = 9.0$
1	$^{31}P\{^1H\}$	19.9	21.1	18
	^1H carboxylates	1.29 (s, 6H) bridges; 2.05 (s, 6H)	0.65 (t, 6H), ^3J(H–H) = 7.5, CH_3-bridges; 1.54 (m, 4H), CH_2-bridges; 1.11 (t, 6H), ^3J(H–H) = 7.5, CH_3; 2.32 (q, 4H), CH_2	
	OMe groups	3.77 (s, 6H); 3.73 (s, 6H); 3.09 (s, 6H)$^{(m)}$	3.75 (s, 6H); 3.73 (s, 6H); 3.01 (s, 6H)$^{(m)}$	3.75 (s, 12H); 3.18 (s, 6H)$^{(m)}$
	Hpz	6.36 (t) ^3J(H–H) = 2.15; 7.60 (d) ^3J(H–H) = 2.08	6.35 (s*); 7.59 (s*)	6.42 (t) ^3J(H–H) = 2.13; 7.62 (d) ^3J(H–H) = 2.06
	Aromatic protons	$H^{2,6\text{-A}}$: 7.58 (t, 4H) $^3J(H^{2,6}\text{–P}) \approx {}^3J(H^{2,6\text{-A}}\text{–}H^{3,5\text{-A}}) = 9.20$; $H^{3,5\text{-A}}$: 6.84 (dd, 4H), $^4J(H^{3,5\text{-A}}\text{–P}) = 1.30$, $^3J(H^{2,6\text{-A}}\text{–}H^{3,5\text{-A}}) = 8.67$; $H^{2,6\text{-B}}$ and $H^{3,5\text{-B}}$: 6.56–6.58; $H^{3,m}$: 5.90 (s*, 2H); $H^{5,m}$: 6.24 (dt, 2H) $^4J(H^{5,m}\text{–P}) \approx {}^4J(H^{5,m}\text{–}H^{3,m}) = 2.01$; $H^{6,m}$: 6.47 (t, 2H), $^3J(H^{5,m}\text{–}H^{6,m.}) \approx {}^3J(H^{6,m}\text{–P}) = 8.80$	$H^{2,6\text{-A}}$: 7.53 (t, 4H) $^3J(H^{2,6}\text{–P}) \approx {}^3J(H^{2,6\text{-A}}\text{–}H^{3,5\text{-A}}) = 9.19$; $H^{3,5\text{-A}}$: 6.80 (d, 4H) $^3J(H^{2,6\text{-A}}\text{–}H^{3,5\text{-A}}) = 7.55$; $H^{2,6\text{-B}}$ and $H^{3,5\text{-B}}$: 6.57–6.58; $H^{3,m}$: 5.73 (s*, 2H); $H^{5,m}$: 6.21 (dt, 2H) $^4J(H^{5,m}\text{–P}) \approx {}^4J(H^{5,m}\text{–}H^{3,m}) = 1.84$; $H^{6,m}$: 6.45 (t, 2H), $^3J(H^{5,m}\text{–}H^{6,m.}) \approx {}^3J(H^{6,m}\text{–P}) = 8.82$	$H^{2,6\text{-A}}$: 7.34 (t*, 4H) $^3J(H^{2,6}\text{–P}) \approx {}^3J(H^{2,6\text{-A}}\text{–}H^{3,5\text{-A}}) = 8.31$; $H^{3,5\text{-A}}$: 6.79 (d, 4H), $^4J(H^{3,5\text{-A}}\text{–P}) = 7.84$; $H^{2,6\text{-B}}$ and $H^{3,5\text{-B}}$: 6.59–6.62; $H^{3,m}$: 5.98 (s*, 2H); $H^{5,m}$: 6.32 (d*, 2H); $H^{6,m}$: 6.49 (t, 2H), $^3J(H^{5,m}\text{–}H^{6,m.}) \approx {}^3J(H^{6,m}\text{–P}) = 9.00$
2	$^{31}P\{^1H\}$	20.1	21.2	19.9
	^1H carboxylates	1.30 (s, 6H) bridges; 2.04 (s, 6H)	0.67 (t, 6H), ^3J(H–H) = 7.5, CH_3-bridges; 1.56 (m, 4H), CH_2- bridges; 1.14 (t, 6H), ^3J(H–H) = 7.5, CH_3; 2.38 (q, 4H), CH_2	
	OMe groups	3.77 (s, 6H); 3.73 (s, 6H); 3.08 (s*, 6H)$^{(m)}$	3.74 (s, 6H); 3.73 (s, 6H); 2.99 (s, 6H)$^{(m)}$	3.76 (s, 6H); 3.73 (s, 6H); 3.06 (s, 6H)$^{(m)}$
	Hpz	6.36 (t) ^3J(H–H) = 2.12; 7.60 (d) ^3J(H–H) = 2.08	6.35 (s*); 7.87 (s*)	6.37 (s*); 7.63 (s*)
	Aromatic protons	$H^{2,6\text{-A}}$: 7.58 (t, 4H) $^3J(H^{2,6}\text{–P}) \approx {}^3J(H^{2,6\text{-A}}\text{–}H^{3,5\text{-A}}) = 9.17$; $H^{3,5\text{-A}}$: 6.86 (dd, 4H), $^4J(H^{3,5\text{-A}}\text{–P}) = 1.27$, $^3J(H^{2,6\text{-A}}\text{–}H^{3,5\text{-A}}) = 8.71$; $H^{2,6\text{-B}}$ and $H^{3,5\text{-B}}$: 6.56–6.58; $H^{3,m}$: 5.88 (s*, 2H); $H^{5,m}$: 6.24 (dt, 2H) $^4J(H^{5,m}\text{–P}) \approx {}^4J(H^{5,m}\text{–}H^{3,m}) = 2.00$; $H^{6,m}$: 6.47 (t, 2H), $^3J(H^{5,m}\text{–}H^{6,m.}) \approx {}^3J(H^{6,m}\text{–P}) = 8.81$	$H^{2,6\text{-A}}$: 7.53 (t, 4H) $^3J(H^{2,6}\text{–P}) \approx {}^3J(H^{2,6\text{-A}}\text{–}H^{3,5\text{-A}}) = 9.39$; $H^{3,5\text{-A}}$: 6.80 (dd, 4H), $^4J(H^{3,5\text{-A}}\text{–P}) = 1.19$, $^3J(H^{2,6\text{-A}}\text{–}H^{3,5\text{-A}}) = 8.69$; $H^{2,6\text{-B}}$ and $H^{3,5\text{-B}}$: 6.51–6.60; $H^{3,m}$: 5.66 (t, 2H) $^4J(H^{3,m}\text{–}H^{5,m}) \approx {}^4J(H^{3,m}\text{–P}) = 2.56$; $H^{5,m}$: 6.21 (dt, 2H) $^4J(H^{5,m}\text{–P}) \approx {}^4J(H^{5,m}\text{–}H^{3,m}) = 2.00$; $H^{6,m}$: 6.46 (t, 2H), $^3J(H^{5,m}\text{–}H^{6,m.}) \approx {}^3J(H^{6,m}\text{–P}) = 8.84$	$H^{2,6\text{-A}}$: 7.30 (dd, 4H) $^3J(H^{2,6}\text{–P}) = 10.03$, $^3J(H^{2,6\text{-A}}\text{–}H^{3,5\text{-A}}) = 8.90$; $H^{3,5\text{-A}}$: 6.74 (dd, 4H), $^4J(H^{3,5\text{-A}}\text{–P}) = 1.46$, $^3J(H^{2,6\text{-A}}\text{–}H^{3,5\text{-A}}) = 8.73$; $H^{2,6\text{-B}}$ and $H^{3,5\text{-B}}$: 6.56–6.64; $H^{3,m}$: 5.97 (t, 2H) $^4J(H^{3,m}\text{–}H^{5,m}) \approx {}^4J(H^{3,m}\text{–P}) = 2.61$; $H^{5,m}$: 6.27 (dt, 2H) $^4J(H^{5,m}\text{–P}) \approx {}^4J(H^{5,m}\text{–}H^{3,m}) = 2.10$; $H^{6,m}$: 6.49 (dd, 2H), $^3J(H^{5,m}\text{–}H^{6,m.}) = 8.50$, $^3J(H^{6,m}\text{–P}) = 9.71$

Table 7
UV–Vis spectra of adducts with pyrazole and imidazole: $[Rh_2] + x$HPz (or HIm) (at room temperature; solvent: $CHCl_3$)

Ligand:	HPz	ν (cm^{-1}) (ε)	HIm	ν [cm^{-1}] (ε)
[**1**$(HOAc)_2$]	$x = 0$	$\nu_0 = 17860$ (362)	$x = 0$	$\nu_0 = 17860$ (362)
	$x = 1$	$\nu_1 = 18690$ (423)	$x = 1$	$\nu_0 = 18690$ (521)
	$x = 2$	$\nu_1 = 18660$-sh (317)	$x = 2$	$\nu_1 = 18730$ (505)
		$\nu_1 = 21010$ (461)		$\nu_1 = 20960$-sh (368)
	$x = 4$	$\nu_2 = 21050$ (628)	$x = 4$	$\nu_1 = 18730$ (459)
				$\nu_2 = 20960$ (439)
	$x = 7$	$\nu_2 = 21050$ (647)	$x = 9$	$\nu_2 = 18730$-sh (393)
				$\nu_2 = 20960$ (550)
[**2**$(HO_2CF_3)_2$]	$x = 0$	$\nu_0 = 17570$ (499)	$x = 0$	$\nu_0 = 17570$ (499)
	$x = 1$	$\nu_1 = 18730$ (657)	$x = 1$	$\nu_1 = 18690$ (811)
	$x = 2$	$\nu_1 = 18730$-sh (399)	$x = 2$	$\nu_1 = 18690$-sh (668)
		$\nu_1 = 20830$ (769)		$\nu_1 = 20660$ (777)
	$x = 4$	$\nu_1 = 20960$ (1024)	$x = 4$	$\nu_2 = 20960$ (1250)
	$x = 5.5$	$\nu_2 = 21010$ (1002)	$x = 7.5$	$\nu_2 = 20960$ (1327)
[**3**$(HO_2CEt)_2]\cdot HO_2CEt$	$x = 0$	$\nu_0 = 17990$ (308)	$x = 0$	$\nu_0 = 17990$ (308)
	$x = 1$	$\nu_1 = 19300$ (334)	$x = 1$	$\nu_1 = 18800$ (426)
	$x = 2$	$\nu_2 = 21010$ (408)	$x = 2$	$\nu_1 = 18800$ (424)
	$x = 4$	$\nu_2 = 21010$ (456)	$x = 4$	$\nu_1 = 18800$ (396)
	$x = 6$	$\nu_2 = 21010$ (470)	$x = 13$	$\nu_1 = 18800$-sh (283)
				$\nu_2 = 20580$ (344)

two molecules of orthometallated phosphines [19,20]. Reactions of [*cis*-$Rh_2(\mu\text{-}O_2CR)_2(\mu\text{-PMP-C})_2$] with pyrazole or imidazole in $CHCl_3$ were followed by UV–Vis spectroscopy.

Analysis of the UV–Vis spectra (Table 7, Figs. 7 and 8) indicates that formation of monoadducts of imidazole (or pyrazole) proceeds very easily. One can observe the formation of monoadducts at a complex:ligand molar ratio equal to 1:1. The completion of the formation of bis-adducts with pyrazole or imidazole only at high pyrazole(imidazole)/complex ratios suggests rather weak and labile interactions of these molecules with the investigated complexes and a strong trans effect of the Rh–Rh bond.

The reactivities of the complexes with imidazole change in the following order: [**3**$(HO_2CEt)_2]\cdot HO_2CEt <$ [**1**$(HOAc)_2] <$ [**2**$(HO_2CCF_3)_2$] and differences between these reactivities are easy to distinguish (Fig. 7). Only for the complex [**2**$(HO_2CCF_3)_2$] is complete formation of imidazole biadducts observed. The same order of reactivities of the complexes can also be deduced from spectra at molar ratios equal to 1:2. It agrees with the order of the dissociation constants of the carboxylic acids.

For complexes $Rh_2L^N_2$, $Rh_2L^NL^O$ and $Rh_2L^O_2$ (where Rh_2 are complexes [**1**], [**2**] or [**3**]; L^O = HOAc, HOPr, $HOOCCF_3$, H_2O; L^N = , Him) the differences between the energies of the $\pi^*(Rh_2) \rightarrow \sigma^*(Rh_2)$ transitions $\Delta\nu_1 = \nu_1(Rh_2L^NL^O) - \nu_0(Rh_2L^O_2)$ and $\Delta\nu_2 = \nu_2(Rh_2L^N_2) - \nu_0(Rh_2L^O_2)$ are for [**3**]: 810 and 2590 cm^{-1}, for [**1**]: 870 and 3100 cm^{-1} and for [**2**]: 1120 and 3390 cm^{-1}. It follows that the Rh–Rh bond in **2** is the most influenced by coordination of imidazole.

Imidazole and pyrazole σ-donor properties, established as PA (proton affinity), are equal to 942.8 kJ/mol for Him and 894.1 for Hpz [24]. Therefore imidazole is a better σ-donor and should coordinate more strongly as an axial ligand, whilst the presented data indicate that the reactivities of the investigated complexes with pyrazole are generally higher than those with imidazole.

The reactivities of the complexes with pyrazole (as concluded from Fig. 8) are different than with imidazole and change in the following order: [**1**$(HOAc)_2] \leqslant$ [**2**$(HO_2CCF_3)_2] <$ [**3**$(HO_2CEt)_2]\cdot HO_2CEt$, and are much less distinct.

The influence of the pyrazole axial ligand on the electronic structure of monoadducts of complexes [**1**], [**2**] and [**3**] is different to that of imidazole because the $\Delta\nu_1$ values change in the series [**1**] (830 cm^{-1}) < [**2**] (1160 cm^{-1}) < [**3**] (1310 cm^{-1}). However the influence of pyrazole in biadducts is analogous with that of imidazole. In this case $\Delta\nu_2$ values increase in the series: [**3**] (3020 cm^{-1}) < [**1**] (3190 cm^{-1}) < [**2**] (3440 cm^{-1}).

The interactions leading to formation of mono- and bisadducts of [*cis*-$Rh_2(\mu\text{-}O_2CR)_2(\mu\text{-PMP-C})_2$] with Hpz were also followed by ^1H and $^{31}P\{^1H\}$ NMR spectroscopy in $CDCl_3$ solutions (Table 6). Mixtures of [*cis*-$Rh_2(\mu\text{-}O_2CR)_2(\mu\text{-PMP-C})_2$] with Hpz at molar ratios of 1:1 and 1:2 were prepared in situ.

The $^{31}P\{^1H\}$NMR signals were shifted to lower fields for all complexes. The largest changes were observed for [**2**$(HO_2CCF_3)_2$]: $\Delta\delta_1 = 3.9$ and $\Delta\delta_2 = 5.8$ ppm, where $\Delta\delta_x$ is defined as the difference between the chemical shift of the phosphorus atom in a mixture of the complex and pyrazole and the chemical shift in the starting complex ($\Delta\delta_x = \delta_{[Rh_2]+x\text{Hpz}} - \delta_{[Rh_2]}$). The changes of chemical shifts for [**1**$(HOAc)_2$] ($\Delta\delta_1 = 2.5$, $\Delta\delta_2 = 2.7$ ppm) and [**3**$(HO_2CEt)_2]\cdot HO_2CEt$ ($\Delta\delta_1 = 1.9$, $\Delta\delta_2 = 2.9$ ppm) are much smaller. Significant broadening of signals in all spectra reveals the dynamic nature of these interactions.

Detailed analysis of the ^1H NMR spectra of [**3**$(HO_2CEt)_2]\cdot HO_2CEt$ and its mixtures with pyrazole reveals some interesting features. With increasing Hpz concentration,

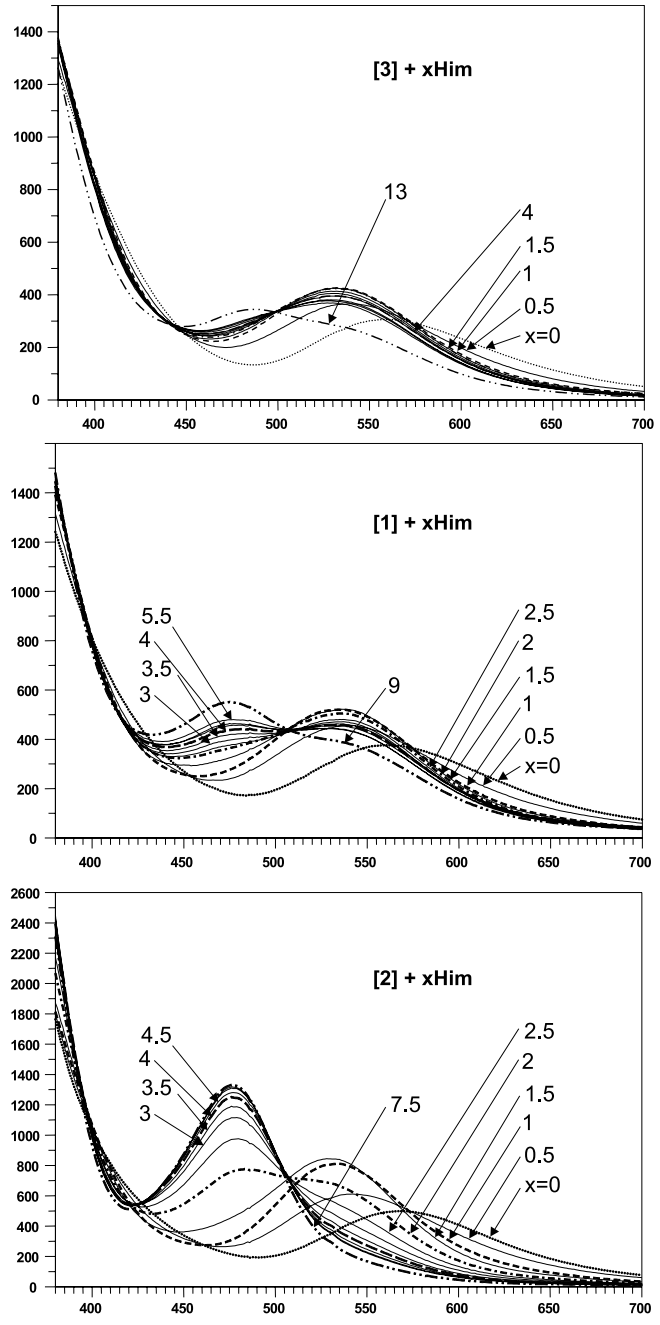

Fig. 7. UV–Vis spectra of mixtures of $[\mathbf{1}(HOAc)_2]$, $[\mathbf{2}(HO_2CCF_3)_2]$ and $[\mathbf{3}(HO_2CEt)_2]\cdot HO_2CEt$ complexes with imidazole (at room temperature; solvent: $CHCl_3$; X axis – λ (wavelengths) [nm], Y axis – ε (molar absorption coefficients) [$dm^3\,cm^{-1}\,mol^{-1}$]).

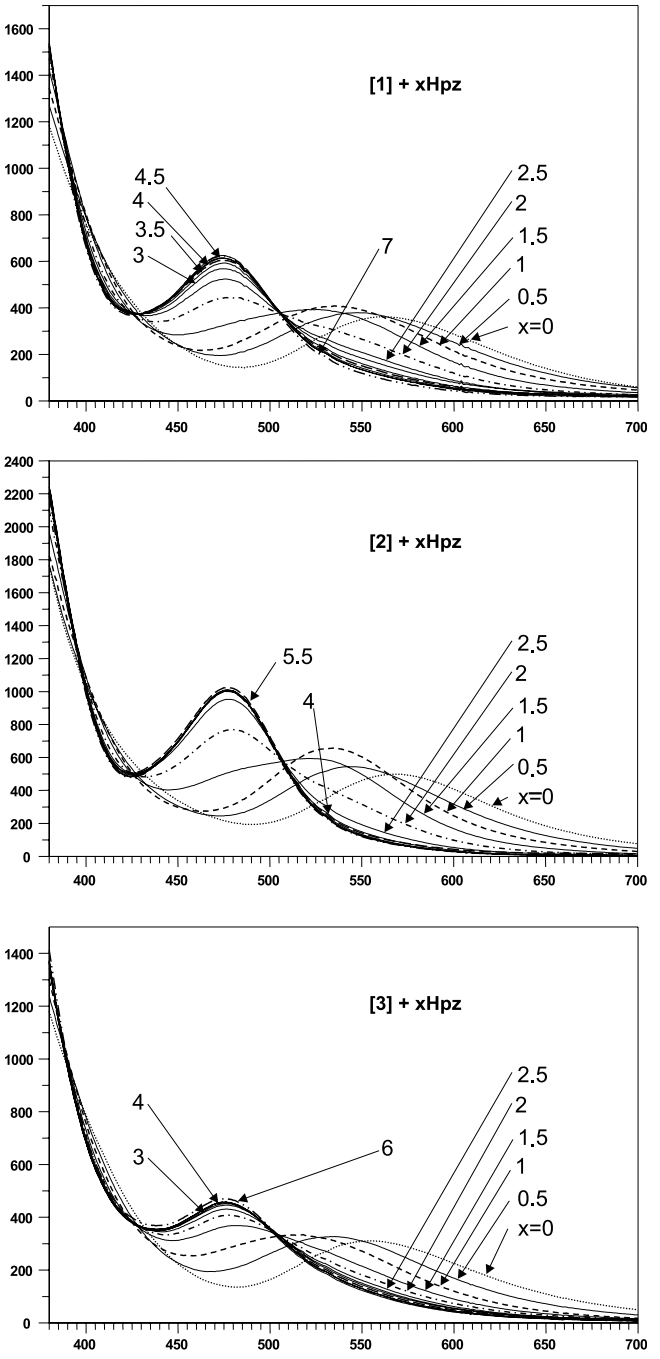

Fig. 8. UV–Vis spectra of mixtures of $[\mathbf{1}(HOAc)_2]$, $[\mathbf{2}(HO_2CCF_3)_2]$ and $[\mathbf{3}(HO_2CEt)_2]\cdot HO_2CEt$ complexes with pyrazole (at room temperature; solvent: $CHCl_3$; X axis – λ (wave lengths) [nm], Y axis – ε (molar absorption coefficients) [$dm^3\,cm^{-1}\,mol^{-1}$]).

the signals of the aromatic protons of the exo rings (A) remain almost unchanged. The signals of $H^{2,6}$ protons of endo (B) rings change their positions, lowering the difference between the chemical shifts of $H^{2,6}$ and $H^{3,5}$ almost to zero. The signals of protons of metallated rings are moved to higher fields. The largest changes are observed for $H^{3,m}$. The chemical shift of this proton changes from 6.41 to 5.66 ppm at a complex:Hpz ratio equal to 1:2. The signal of $H^{3,m}$ in $[\mathbf{1}(HOAc)_2]$ was less shifted (from 6.36 to 5.88 ppm), however in the case of $[\mathbf{2}(HO_2CCF_3)_2]$, the chemical shift of $H^{3,m}$ was changed very slightly (from 5.99 to 5.97 ppm). Thus the differences between the chemical shifts of $H^{3,m}$ in adducts with oxygen ligands and pyrazole adducts strongly depend on the acidity of the carboxylato bridging ligands.

Another interesting feature in these spectra is the signal of the $–CH_2–$ group in the propionato bridges. For the starting compound $[\mathbf{3}(HO_2CEt)_2]\cdot HO_2CEt$ one can observe a quartet for the CH_2 group at 1.17 ppm and a

triplet for the CH_3 group at 0.58 ppm (^3J(H–H) = 7.58 Hz). Owing to the coordination of the pyrazole these signals are shifted to lower fields and spectrum changes from an A_2X_3 type into an ABX_3 pattern. It indicates an unequivalency of the protons of the $–CH_2–$ group, caused by a slowing down of the rotation of the CH_3 groups. A similar, but much weaker, effect is observed in spectra of [**3**$(HO_2CEt)_2$] · HO_2CEt at lower temperatures.

3. Experimental

3.1. Procedures and materials

All solvents were deoxidized prior to use. UV–Vis spectra were measured on a Beckman DU 7500 spectrometer. ^1H NMR, $^{13}C\{^1H\}$ NMR and $^{31}P\{^1H\}$ NMR spectra were measured in $CDCl_3$ on a Bruker AMX 300 spectrometer with traces of $CHCl_3$ as an internal reference for ^1H ($\delta = 7.23$ ppm) and 85% H_3PO_4 in H_2O as an external standard for ^{31}P.

3.2. Syntheses

All operations were performed in dinitrogen or argon atmosphere using standard Schlenk techniques. [**1**$(HOAc)_2$] [21] was synthesized according to the literature methods.

3.2.1. [**2**$(HO_2CCF_3)_2$]

[**1**$(HOAc)_2$] (0.200 g) was dissolved in 3 cm^3 of CF_3COOH, heated to 50 °C and evaporated to dryness. The operation was repeated two times. The exchange of acetate bridges to trifluoroacetates occurred with 100% efficiency (proved by NMR spectra) after this procedure.

Crystals of [**2**(H_2O)(PrOH)] · PrOH suitable for X-ray structure determination were obtained by slow evaporation of a 1-propanol/water (5:1, v:v) solution of [**2**$(HO_2CF_3)_2$] in air.

3.2.2. [**3**$(HO_2CEt)_2$] · HO_2CEt

[**1**$(HOAc)_2$] (0.200 g) was dissolved in 3 cm^3 of HO_2CEt (propanoic acid), heated to 50 °C and evaporated to dryness. The operation was repeated two times. This procedure results in complete exchange (proved by NMR spectra) of acetate bridges to propionates. Crystals of [**3**$(HO_2CEt)_2$] · HO_2CEt suitable for X-ray structure determination were obtained by slow evaporation of a propanoic acid/acetone (1:1, v:v) solution of [**3**$(HO_2CEt)_2$] · HO_2CEt in air.

3.2.3. [**2**$(Hpz)_2$] and [**3**$(Hpz)_2$]

Spectroscopic studies were performed in situ.

Crystals of [**2**$(Hpz)_2$] suitable for crystallographic measurements were obtained by slow evaporation of a solution of [**2**$(HO_2CCF_3)_2$] in 1-propanol/water (5:1, v:v) with a large excess of pyrazole in air. The single crystals of [**3**$(Hpz)_2$] were prepared analogously from a mixture of water and ethanol (5:1, v:v).

3.3. X-ray structure determination

All measurements were made at 100(2) K on a Kuma KM4CCD κ-axis diffractometer with graphite-monochromated Mo Kα radiation ($\lambda = 0.71073$ Å). Crystallization procedures are given in Section 3.2. The crystallographic data, together with data collection and structure refinement details, are given in Table 1. All the data were corrected for Lorenz and polarization effects but absorption and extinction were not applied. Data reduction and analysis were carried out with the Kuma Diffraction programs [29,30]. The structures were solved by direct methods and refined by full-matrix least-squares methods on F^2 [31]. The refinement was performed using the SHELXL program [32]. Non-hydrogen atoms were refined with anisotropic thermal parameters. The positions of hydrogen atoms were found from ΔF syntheses or geometrically and refined in rigid groups with the heavy atoms connected to them. Pictures were prepared with PLATON [33,34] or ORTEP-3 [35] software.

Appendix A. Supplementary data

Anisotropic displacement parameters and hydrogen atom parameters has been also deposited with the Cambridge Crystallographic Data Center, 12 Union Road, Cambridge CB2 1EZ, UK: CCDC 238033 – [**2**(H_2O)-(PrOH)] · PrOH; CCDC 238034 – [**2**$(Hpz)_2$]; CCDC 238035 – [**3**$(HO_2CEt)_2$] · HO_2CEt; CCDC 238036 – [**3**$(Hpz)_2$]. Copies of the data may be obtained free of charge upon request from The Director, Cambridge Crystallographic Data Centre, fax: +44 1223 336 033, e-mail: deposit@ccdc.cam.ac.uk; web: http://www.csdc.cam.ac.uk. Supplementary data associated with this article can be found, in the online version, at doi:10.1016/j.poly.2005.12.018.

References

[1] A.R. Chakravarty, F.A. Cotton, D.A. Tocher, J.H. Tocher, Organometallics 4 (1985) 8.
[2] F.A. Cotton, F. Barceló, P. Lahuerta, R. Llusar, J. Payá, M.A. Úbeda, Inorg. Chem. 27 (1988) 1010.
[3] E.C. Tocher, D.A. Tocher, Inorg. Chim. Acta 157 (1989) 139.
[4] P. Lahuerta, J. Payá, E. Peris, M.A. Pellinghelli, A.J. Tiripicchio, Organomet. Chem. 373 (1989) C5.
[5] P. Lahuerta, J. Payá, X. Solans, M.A. Úbeda, Inorg. Chem. 31 (1992) 385.
[6] P. Lahuerta, J. Payá, E. Peris, A. Aguirre, S. García-Granda, F. Gomez-Beltrán, Inorg. Chim. Acta 192 (1992) 43.
[7] P. Lahuerta, E. Peris, Inorg. Chem. 31 (1992) 4547.
[8] P. Lahuerta, J. Payá, S. García-Granda, F. Gomez-Beltrán, A. Anillo, J. Organomet. Chem. 443 (1993) C14.
[9] M.V. Borrachero, F. Estevan, S. García-Granda, P. Lahuerta, J. Latorre, E. Peris, M. Sanau, J. Chem. Soc. Chem. Commun. 1864 (1993).
[10] A. Padwa, D.J. Austin, A.T. Price, M.A. Semones, M.P. Doyle, M.N. Protopopova, W.R. Winchester, A. Tran, J. Am. Chem. Soc. 115 (1993) 8669.
[11] S. García-Granda, P. Lahuerta, J. Latorre, M. Martinez, E. Peris, M. Sanau, M.A. Úbeda, J. Chem. Soc., Dalton Trans. 539 (1994).
[12] G. Gonzalez, P. Lahuerta, M. Martinez, E. Peris, M. Sanaú, J. Chem. Soc., Dalton Trans. 545 (1994).

[13] F. Estevan, P. Lahuerta, E. Peris, M.A. Úbeda, S. García-Granda, F. Gomez-Beltrán, E. Pérez-Carreno, G. Gonzalez, M. Martinez, Inorg. Chim. Acta 218 (1994) 198.
[14] A. Garcia-Bernabe, P. Lahuerta, M.A. Úbeda, S. García-Granda, P. Pertierra, Inorg. Chim. Acta 229 (1995) 203.
[15] F. Estevan, S. García-Granda, P. Lahuerta, J. Latorre, E. Peris, M. Sanaú, Inorg. Chim. Acta 229 (1995) 365.
[16] F. Estevan, P. Lahuerta, J. Pérez-Prieto, S.-E. Stiriba, M.A. Úbeda, Synlett 1121 (1995).
[17] F. Estevan, G. Gonzalez, P. Lahuerta, M. Martinez, E. Peris, R. Van Eldik, J. Chem. Soc. Dalton Trans. 1045 (1996).
[18] G. Gonzalez, M. Martinez, F. Estevan, A. Garcia-Bernabe, P. Lahuerta, E. Peris, M.A. Úbeda, M.R. Diaz, S. García-Granda, B. Tejerina, New J. Chem. 20 (1996) 83.
[19] F.P. Pruchnik, R. Starosta, P. Smolenski, E. Shestakova, P. Lahuerta, Organometallics 17 (1998) 3684.
[20] F.P. Pruchnik, R. Starosta, T. Lis, P. Lahuerta, J. Organomet. Chem. 568 (1998) 177.
[21] F.P. Pruchnik, R. Starosta, Z. Ciunik, A. Opolski, J. Wietrzyk, E. Wojdat, D. Dus, Can. J. Chem. 79 (2001) 868.
[22] F.A. Cotton, R.A. Walton, Multiple Bonds Between Metal Atoms, Clarendon Press, Oxford, 1993.
[23] F.P. Pruchnik, R. Starosta, Z. Ciunik, unpublished results.
[24] E.P. Hunter, S.G. Lias, in: P.J. Linstrom, W.G. Mallard (Eds.), Proton Affinity Evaluation, NIST Chemistry WebBook, NIST Standard Reference Database Number 69, July 2001, National Institute of Standards and Technology, Gaithersburg, MD, 20899. Available from: <http://webbook.nist.gov>.
[25] H.W.W. Enrlich, Acta Cryst. 13 (1960) 946.
[26] R.B. Helmholdt, W. Hinrichs, J. Reedijk, Acta Crystallogr., Sect. C 43 (1987) 226.
[27] R. Ma, Y.-L. Li, J.A. Muir, M.M. Muir, Acta Crystallogr., Sect. C 49 (1993) 89.
[28] F.P. Pruchnik, P. Jakimowicz, Z. Ciunik, J. Zakrzewska-Czerwinska, A. Opolski, J. Wietrzyk, E. Wojdat, Inorg. Chim. Acta 334 (2002) 59.
[29] KM4CCD data collection program Kuma Diffraction Ltd.; Wrocław, Poland, 1997.
[30] KM4RED data reductions program Kuma Diffraction Ltd.; Wrocław, Poland, 1997.
[31] G.M. Sheldrick, SHELXS-97 – A Program for Automatic Solution of Crystal Structures (Release 97-2), University of Goettingen, Germany, 1997.
[32] G.M. Sheldrick, SHELXL-97 – A Program for Automatic Solution of Crystal Structures (Release 97-2), University of Goettingen, Germany, 1997.
[33] A.L. Spek, Acta. Crystallogr. Sect. A 46 (1990) C34.
[34] A.L. Spek, PLATON – A Multipurpose Crystallographic Tool, Utrecht University, Utrecht, The Netherlands, 2002.
[35] L.J. Farrugia, J. Appl. Cryst. 30 (1997) 565, ORTEP-3 (for Win32 v. 1.076).

networks [3b,10]. Cyano-bridged compounds have been reported to exhibit interesting electrochemical, magnetooptical, and zeolite properties [3,11]. In particular, some cyano-bridged compounds exhibit spontaneous magnetization at significantly higher temperatures [3,11a] to act as a molecular magnet.

Using $[Fe(CN)_6]^{3-}$ as a starting material, in most cases, the expected ferricyanide containing compounds have been isolated. Although in a few cases the ferricyanide anion has been reported to be reduced to ferrocyanide by nickel(II) or copper(II) compounds derived from cyclic or tertiary amines [5f,7d,10b], the species that is responsible for the reduction and the factors that affect the reduction process have not been explored.

Recently, the crystal structures and magnetic properties of a few nickel(II) and copper(II) bis-*trans*-1,2-diaminocyclohexane–ferricyanide systems have been reported [7a,7e,7f]. During the course of our studies with the nickel(II) system, we have noted that depending upon the reaction conditions, either exclusively ferricyanide or ferrocyanide compounds or their mixtures are formed. The present study is concerned with the isolation of the ferrocyanide complex, $[Ni^{II}L_2]_2[Fe^{II}(CN)_6]\cdot 5H_2O$ (**1**; L = *trans*-1,2-diaminocyclohexane), involving ferricyanide as the reactant, as well as the crystal engineering and magnetic properties of **1**. It has been shown from spectrophotometric titration that *trans*-1,2-diaminocyclohexane is responsible for the reduction of $[Fe(CN)_6]^{3-}$ to $[Fe(CN)_6]^{4-}$.

2. Experimental

2.1. Materials and physical measurements

All the reagents and solvents were purchased from commercial sources and used as received. Elemental (C, H, and N) analyses were performed on a Perkin–Elmer 2400 II analyzer. IR spectra were recorded in the region 400–4000 cm^{-1} on a Bio-Rad FTS40 infrared spectrophotometer in KBr disks. UV–Vis spectra were obtained with a Hitachi U-3501 spectrophotometer. Variable-temperature (2–300 K) magnetic susceptibility measurements under fixed field strength of 1 T were carried out with a Quantum Design MPMS SQUID magnetometer. Diamagnetic corrections were estimated from Pascals constants.

2.2. Syntheses

2.2.1. $[Ni^{II}L_2]_2[Fe^{II}(CN)_6]\cdot 5H_2O$ (1)

Method A: An aqueous solution (20 mL) of potassium ferricyanide (0.11 g, 0.33 mmol) was dropwise added to a pink aqueous solution (70 mL) containing nickel(II) chloride hexahydrate (0.119 g, 0.5 mmol) and *trans*-1,2-diaminocyclohexane (0.114 g, 1 mmol). The color of the mixture changed to brown. After a few hours, a brown crystalline compound **2** was deposited and filtered off. The green filtrate was kept undisturbed for several hours, during which time green diffraction quality single crystals of **1** were deposited and then collected by filtration. Yield: 0.055 g (25%) and 0.065 g (30%) for **1** and **2**, respectively. Anal. Calc. for $C_{30}H_{68}N_{14}O_5Ni_2Fe$ (**1**): C, 41.03; H, 7.80; N, 22.33. Found: C, 41.18; H, 7.70; N, 22.44%. Anal. Calc. for $C_{48}H_{88}N_{24}O_2Ni_3Fe_2$ (**2**): C, 43.64; H, 6.71; N, 25.44. Found: C, 43.86; H, 6.52; N, 25.32%. IR (**1**; KBr/cm^{-1}): ν(water), 3413m; ν_{as}(NH), 3336m; ν_s(NH), 3270m; ν_{as}(CH), 2930m; ν_s(CH), 2860w; ν(CN), 2033vs; δ(NH), 1589m; δ(CH), 1450w. IR (**2**; KBr/cm^{-1}): ν(water), 3513m; ν_{as}(NH), 3339s; ν_s(NH), 3279s; ν_{as}(CH), 2929s; ν_s(CH), 2859w; ν(CN), 2116s; δ(NH), 1593s; δ(CH), 1449w.

Method B: To an aqueous solution (25 mL) containing nickel(II) chloride hexahydrate (0.119 g, 0.5 mmol) and *trans*-1,2-diaminocyclohexane (0.114 g, 1 mmol), was added dropwise an aqueous solution (10 mL) of potassium ferrocyanide trihydrate (0.106 g, 0.25 mmol). After stirring for 10 min, the mixture was filtered to remove any suspended particles and the green solution was kept at room temperature. After few hours, the green crystalline compound **1** that deposited was collected by filtration. Yield: 0.16 g (73%). The IR spectrum of this compound is identical with that of **1** obtained by method A. In addition, the elemental analyses of the product obtained by method B agreed well with the molecular formula $C_{30}H_{68}N_{14}O_5Ni_2Fe$.

2.3. Crystal structure determination

Pertinent crystallographic data of **1** are summarized in Table 1. Diffraction data were collected on a Siemens P4 diffractometer in the ω–2ϑ scan mode using graphite monochromated Mo K_α radiation, having $\lambda = 0.71073$ Å. The accurate unit cell was obtained by means of least-squares fittings of 25 centered reflections. The intensity data were corrected for Lorentz and polarization effects, and semiempirical absorption corrections were made from

Table 1
Crystallographic data for **1**

Empirical formula	$C_{30}H_{68}N_{14}O_5Ni_2Fe$
Formula weight	878.25
Crystal system	monoclinic
Space group	*C*2/*c*
a (Å)	16.0621(12)
b (Å)	30.516(2)
c (Å)	8.9595(6)
β (°)	109.269(1)
V (Å^3)	4145.5(5)
Z	4
T (K)	294(2)
λ (Mo K_α) (Å)	0.71073
D_{calc} (g cm^{-3})	1.407
F(000)	1872
μ (mm^{-1})	1.298
R_1[a]/wR_2[b] ($I > 2\sigma(I)$ data)	0.0738/0.1451
R_1[a]/wR_2[b] (all data)	0.0942/0.1526

[a] $R_1 = [\sum \|F_o| - |F_c\|/\sum |F_o|]$.

[b] $wR_2 = \left[\sum w(F_o^2 - F_c^2)^2/\sum w(F_o^2)^2\right]^{1/2}$.

ψ-scans. A total of 11 160 reflections were collected for **1** in the range $2\vartheta = 3.68$–$50°$ with $0 \leqslant h \leqslant 10$, $-12 \leqslant k \leqslant 12$, $-13 \leqslant l \leqslant 13$, of which 3674 independent reflections ($R_{int} = 0.0453$) were used for structure determinations. During the development of the structure, it became obvious that both the cyclohexyl rings were highly disordered. For one ring, the four carbon atoms C(4), C(6), C(7), and C(9) are disordered over two sites with occupancies of 0.5, while the other two carbon atoms C(5) and C(8) remain in common positions. In the case of the second ring, all the carbon atoms C(10) to C(15) are distributed over two sites with the same occupancies. All disorders were treated using fully restrained refinement (site occupancies, coordinates, cycles planarity). The H atoms were geometrically fixed and allowed to ride on the atom to which they are attached. The structure was solved by direct and Fourier methods and refined by full-matrix least-squares methods based on F^2 using the programs SHELXS-97 and SHELXL-97 [12a,12b]. All programs used in the structure refinement were incorporated in the WINGX package [12c]. The final least-squares refinements (R_1) based on $I > 2\sigma(I)$ converged to 0.0738.

3. Results and discussion

3.1. Synthesis

Using *trans*-1,2-diaminocyclohexane as the blocking ligand and ferricyanide as the linker, three bimetallic assemblies all having the same composition, $[Ni^{II}(diamine)_2]_3[Fe^{III}(CN)_6]_2 \cdot 2H_2O$, have been reported recently [7a,7e,7f]. These three types of 2D assemblies differ in terms of their chiralities. They have been prepared by reacting either a mixture of enantiometrically pure $[Ni(diamine)_3](ClO4)_2 \cdot H_2O$, $[Ni(H_2O)_6](ClO4)_2$, and $K_3[Fe(CN)_6]$ in 1:1:1 stoichiometry in acetonitrile–water or a mixture of *trans*-1,2-diaminocyclohexane, $NiCl_2 \cdot 6H_2O$, and $K_3[Fe(CN)_6]$ in the ratio 1:1:0.65 in methanol–water. In all cases, the product was isolated as a brown material after standing.

During the course of our study, we have observed that the ratio of the reactants has profound effect on the composition of the product isolated. For example, if an aqueous solution of $K_3[Fe(CN)_6]$ (0.65 equivalent) is added to an aqueous solution containing 1 equivalent of $NiCl_2 \cdot 6H_2O$ and 2 equivalents of *trans*-1,2-diaminocyclohexane, within a few hours a brown colored compound is deposited first and from the filtrate on standing for further several hours a green colored product is obtained. The brown product has been identified to have the composition $[Ni^{II}(diamine)_2]_3[Fe^{III}(CN)_6]_2 \cdot 2H_2O$ and its IR spectrum is consistent with the presence of a ferricyanide moiety. The composition of the green compound is $[Ni^{II}(diamine)_2]_2[Fe^{II}(CN)_6] \cdot 5H_2O$ and its IR spectrum indicates that it contains a ferrocyanide moiety. If 0.65 equivalent of $K_3[Fe(CN)_6]$ is added to a mixture of 3 equivalents of *trans*-1,2-diaminocyclohexane and 1 equivalent of $NiCl_2 \cdot 6H_2O$, no brown compound formation takes place and the green compound is isolated exclusively in about 60% yield. Keeping the amount of other reactants the same but using 4 equivalents of the diamine, again only the green compound is isolated but in a slightly reduced yield (55%). Change of solvent composition, e.g., acetonitrile–water or methanol–water does not have any significant effect on the nature of the products, provided the reactant ratios remain the same. On the other hand, the concentration of the reactants affect the course of the reaction. For example, with the earlier mentioned ratio when both the brown and green products were obtained, only the brown compound is isolated if the reaction is carried out in half of the total volume. Conversely, if the total volume is 2.5-fold increased, then only the green product is obtained after standing for about 2 days.

As already reported and verified by us, the reaction involving $NiCl_2 \cdot 6H_2O$, *trans*-1,2-diaminocyclohexane, and $K_3[Fe(CN)_6]$ in the ratio 1:1:0.65 produces the brown product exclusively, while changing the reactants ratio to 1:3:0.65 gives rise to the formation of only the green colored ferrocyanide compound. It thus appears that the reduction of $[Fe(CN)_6]^{3-}$ to $[Fe(CN)_6]^{4-}$ is carried out by the non-coordinated diamine present in the solution.

3.2. IR spectrum

The IR spectra of the compounds **1** and **2** are shown in Fig. 1. It may be noted that **1** exhibits a single CN stretching at 2033 cm^{-1}, whereas this band appears at 2116 cm^{-1} for **2**. It is known that $K_4[Fe(CN)_6]$ exhibits ν_{CN} at

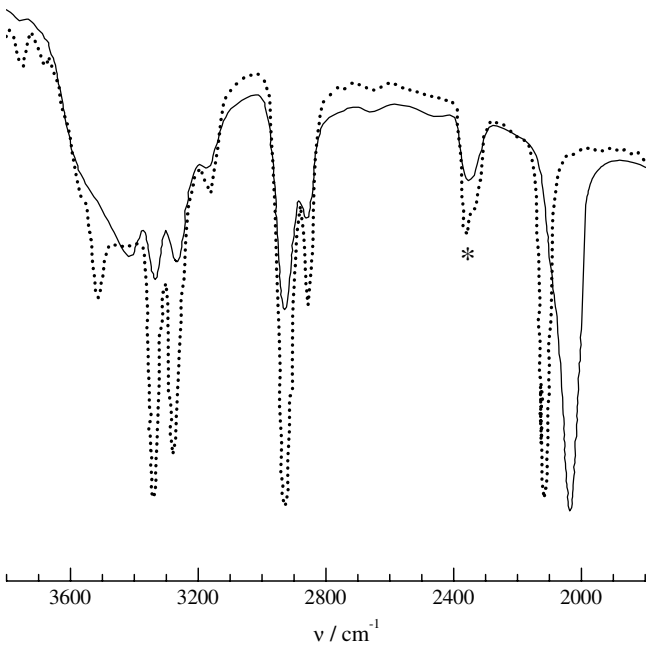

Fig. 1. A part of the IR spectra of **1** (solid lines) and **2** (dotted lines). The asterisk marked band indicates carbon dioxide vibration.

2044 cm^{-1}, while this band is observed at 2118 cm^{-1} for $K_3[Fe(CN)_6]$ [13]. Clearly, the green compound **1** contains a ferrocyanide unit, while the brown compound **2** contains a ferricyanide unit. Thus, the formation of **1** is accompanied by the reduction of the reactant ferricyanide. As will be seen, the structure of **1** contains both bridging and terminal cyanides. Generally, the stretching frequencies of terminal cyanides are observed at lower energies relative to those of bridging cyanides [13]. Therefore, **1** should have exhibited more than one CN vibrations. However, examples are known where for a similar situation only a single band has been observed [7f,9c]. Again, there are cases where more than one band have been observed for compounds with one type of cyano moiety [14].

3.3. Spectrophotometric titration

In order to verify that the reduction of $[Fe(CN)_6]^{3-}$ to $[Fe(CN)_6]^{4-}$ is accomplished by *trans*-1,2-diaminocyclohexane, a spectrophotometric titration of $K_3[Fe(CN)_6]$ has been carried out with the diamine. Fig. 2 shows the spectral changes for the solutions containing $[Fe(CN)_6]^{3-}$ and *trans*-1,2-diaminocyclohexane in the ratio of 1:0 to 1:4. It may be noted that the absorption maxima observed at 260, 302, 322, and 420 nm for $[Fe(CN)_6]^{3-}$ get depleted in intensity with the addition of *trans*-1,2-diaminocyclohexane in an increasing amount. When threefold or more amount of the diamine is added all the $[Fe(CN)_6]^{3-}$ bands practically vanish leaving a shoulder at 320 nm. The successive absorption curves pass through two isosbestic points at 285 and 350 nm. This clearly indicates that the redox reaction takes place smoothly. Further, as may be noted in Fig. 2, the position of the shoulder observed at 320 nm in the spectra of 1:3 or 1:4 ferricyanide–diamine solutions coincides with a similar absorption envelope observed for $[Fe(CN)_6]^{4-}$. Thus, it is clear that the formation of the green product takes place due to the reduction of $[Fe(CN)_6]^{3-}$ to $[Fe(CN)_6]^{4-}$ by the diamine.

3.4. Description of the Structure of *1*

An ORTEP view of **1**, demonstrating the coordination environment of the metal ions, is shown in Fig. 3, while the bridging pattern involved therein is illustrated in Fig. 4. The selected bond lengths and angles are summarized in Table 2. There are two crystallographically different nickel(II) centers (Ni(1) and Ni(2)), each of which is hexacoordinated. Two *trans* diequatorial 1,2-diaminocyclohexanes act as the blocking ligands for both the nickel(II) centers. For Ni(1), the remaining two coordination positions, which are *cis*, are occupied by the nitrile nitrogens of two different ferrocyanides, the *trans* cyanides of each link to two other Ni(1) centers resulting in one-dimensional chains that propagate along the crystallographic *c*-axis. Evidently, the *trans* cyanides of the hexacyanoferrate(II) bridge the *cis* positions of Ni(1) to result in these one-dimensional chains. In the case of Ni(2), the

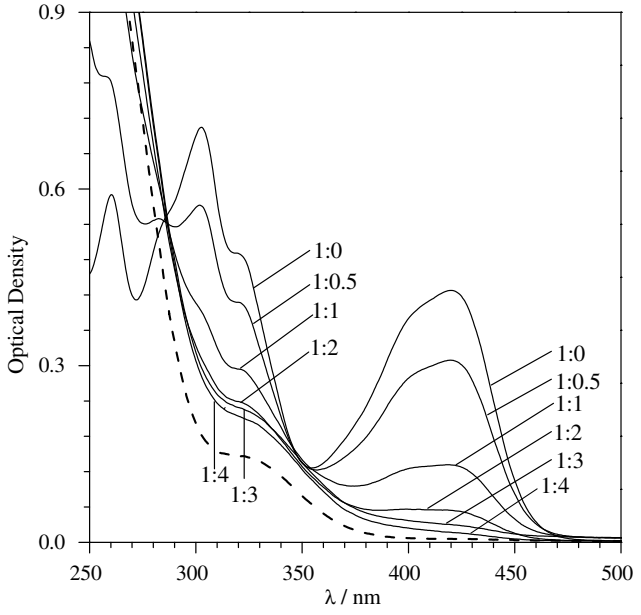

Fig. 2. Spectrophotometric titration of potassium ferricyanide (0.435 mM) with *trans*-1,2-diaminocyclohexane in water. The ferricyanide–diamine ratio has been indicated in the figure. The dashed lines are the absorption profile of an aqueous solution of potassium ferrocyanide (0.435 mM).

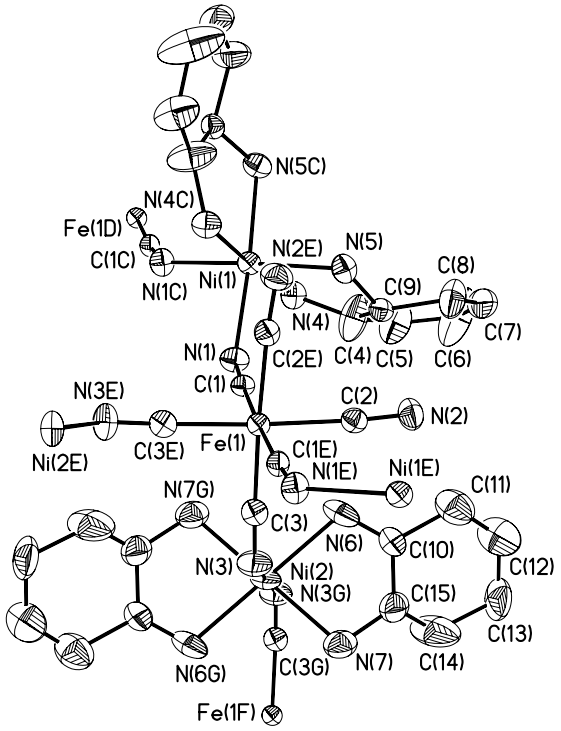

Fig. 3. ORTEP representation of $[Ni^{II}L_2]_2[Fe^{II}(CN)_6]\cdot 5H_2O$ (**1**) demonstrating the coordination environments of the iron(II) and two crystallographically different nickel(II) centers as well as the bridging pattern. Symmetry: C, $-x$, y, $2.5 - z$; D, x, y, $1 + z$; E, $-x$, y, $1.5 - z$; F, $0.5 + x$, $0.5 - y$, $0.5 + z$; G, $0.5 - x$, $0.5 - y$, $2 - z$.

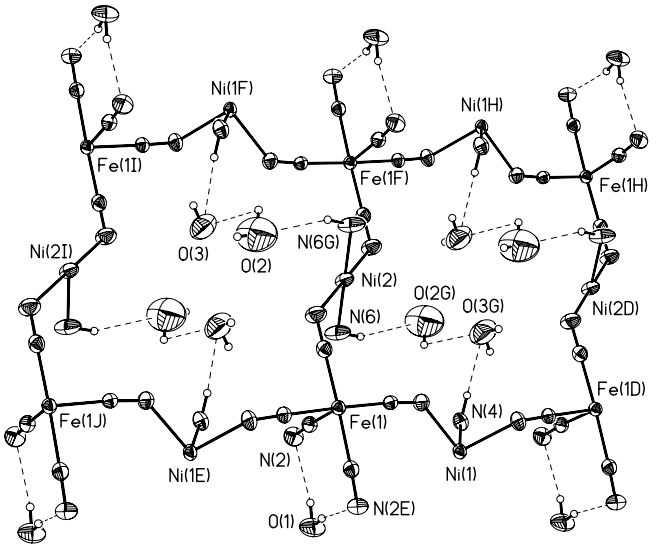

Fig. 4. A perspective view to demonstrate the grid-like bridging pattern of the cyanides as well as the hydrogen bonds between water and amine or non-coordinated cyanide nitrogens. The carbon atoms of the diamine and N(5) are omitted for clarity. Water hydrogens and the hydrogens that are involved in hydrogen bonds within the two-dimensional grids only are shown. Bridging of the *trans* cyanides to Ni(1) centers takes place along the crystallographic *c*-axis, while two *cis* cyanides coordinate to Ni(2) centers along the crystallographic *a*-axis. Symmetry: D–G, as in Fig. 3; H, $0.5 + x$, $0.5 - y$, $3 - z$; I, $0.5 - x$, $0.5 - y$, $1 - z$; J, x, y, $z - 1$.

Table 2
Selected bond lengths (Å) and angles (°) for **1**

Ni(1)–N(1)	2.159(4)	N(4)–Ni(1)–N(5C)	96.10(18)
Ni(1)–N(4)	2.090(4)	N(5)–Ni(1)–N(5C)	93.2(3)
Ni(1)–N(5)	2.123(4)		
Ni(2)–N(3)	2.179(5)	N(3)–Ni(2)–N(3G)	180
Ni(2)–N(6)	2.106(5)	N(6)–Ni(2)–N(6G)	180
Ni(2)–N(7)	2.089(5)	N(7)–Ni(2)–N(7G)	180
N(1)–Ni(1)–N(5C)	171.22(17)	N(3)–Ni(2)–N(6)	88.2(2)
N(4)–Ni(1)–N(4C)	176.4(3)	N(3)–Ni(2)–N(7)	91.2(2)
N(1)–Ni(1)–N(1C)	93.4(2)	N(3)–Ni(2)–N(6G)	91.8(2)
N(1)–Ni(1)–N(4C)	89.82(17)	N(3)–Ni(2)–N(7G)	88.8(2)
N(1)–Ni(1)–N(5)	87.36(18)	N(6)–Ni(2)–N(7)	81.6(2)
N(1)–Ni(1)–N(4)	92.65(18)	N(6)–Ni(2)–N(7G)	98.4(2)
N(4)–Ni(1)–N(5)	81.40(17)		

Symmetry: C, $-x$, y, $2.5 - z$; G, $0.5 - x$, $0.5 - y$, $2 - z$.

remaining two coordination positions are *trans* to each other and these are occupied by two cyanides of two different ferrocyanides, another *cis* cyanide of each then link to two other Ni(2) centers to result in a second type of one-dimensional chain that propagates along the crystallographic *a*-axis. The combination of these two types of one-dimensional chains generates a two-dimensional grid-like bridging network in compound **1**. The shortest metal···metal separations are: Ni(1)···Ni(1E) = 8.96 Å, Ni(1)···Ni(2) = 6.64 Å, and Ni(2)···Ni(2E) = 7.79 Å.

The coordination environment of both the nickel centers is a distorted octahedron. The Ni–N(cyanide) bond distances (Ni(1)–N(1) = 2.159(4) Å, Ni(2)–N(3) = 2.179 (5) Å) are slightly longer relative to the Ni–N(amine) distances (Ni(1)–N(4) = 2.090(4) Å, Ni(1)–N(5) = 2.123(4) Å, Ni(2)–N(6) = 2.106(5) Å, Ni(2)–N(7) = 2.089(5) Å). For the Ni(1) center, the *cisoid* and *transoid* angles lie in the range 81.40(17)–96.10(18)° and 171.22(17)–176.4(3)°, respectively. In contrast, for the Ni(2) center the *transoid* angles are 180° and the *cisoid* angles range from 81.6(2)° to 98.4(2)°. In the case of Ni(1), the average displacements of the nitrogen atoms forming the least-squares planes, N(1)N(1C)N(5)N(5C) and N(4)N(1C)N(5)N(4C), are 0.163 and 0.017 Å, respectively. The nickel(II) center, on the other hand, is exactly located in the first plane and only slightly displaced (0.029 Å) from the second plane. In case of the Ni(2) environment, the four donor nitrogens and the metal ion define exact planes. Evidently, the coordination environment of Ni(2) is less distorted from octahedral geometry.

The ferrocyanide moiety in **1** is almost free from distortion as evident from the facts that the *cisoid* (86.7(3)–92.0(2)°), *transoid* (177.3(2)–178.8(3)°) and Fe–C–N (175.6(5)–176.9(5)°) angles vary only to a small extent. The cyanide groups coordinate to the nickel(II) centers in a significantly bent way (Ni(1)–N(1)–C(1) = 133.2(4)°, Ni(2)–N(3)–C(3) = 126.0(4)°).

Among the three types of water molecules, two types, viz. $H_2O(2)$ and $H_2O(3)$, reside in the square blocks of the cyano-bridged assemblies by forming hydrogen bonds between each other and also with the amine nitrogens (Fig. 4). One water molecule, $H_2O(3)$, behaves as a bifurcated acceptor and interacts with H(21) and H(42F), which are bonded to O(2) and N(4F) (H(21)···O(3) = 2.457 Å, O(2)···O(3) = 2.736 Å, O(2)–H(21)···O(3) = 98.3°; H(42F)···O(3) = 2.534 Å, N(4F)···O(3) = 3.330 Å, N(4F)–H(42F)···O(3) = 147.8°), respectively. The second water molecule within the square blocks, $H_2O(2)$, in addition to being a donor to O(3), also acts as a single acceptor and makes hydrogen bond with H(63G) linked to N(6G) (H(63G)···O(2) = 2.534 Å, N(6G)···O(2) = 3.311 Å, N(6G)–H(63G)···O(2) = 145.0°).

The third water molecule, $H_2O(1)$, acts as a donor to two non-coordinated cyanides (Fig. 4; H(1)···N(2) = 2.086 Å, O(1)···N(2) = 2.965 Å, O(1)–H(1)···N(2) = 142.9°). The Fe(1)···N(2) and O(1)···N(2) distances (Fe(1)···N(2) = 3.079 Å, O(1)···N(2) = 2.965 Å) are very close and the internal angles (N(2)···Fe(1)···N(2E) = 83.4°, N(2)···O(1)···N(2E) = 87.4°, Fe(1)···N(2)···O(1) = 94.6°) in the Fe(1)N(2)O(1)N(2E) tetragon are deviated slightly from 90°. Thus, as the Fe(1)–C(2)–N(2) moiety is almost linear (175.6°), the donor and acceptor centers, along with the Fe–C–N moiety, form an approximate square. The dihedral angle between these hydrogen bonded squares with the cyanobridged square block, defined by the four iron(II) centers Fe(1), Fe(1F), Fe(1I), and Fe(1J) or Fe(1), Fe(1F), Fe(1H), and Fe(1D), is 97.1° indicating that the cyano-bridged and the hydrogen bonded squares are almost perpendicular; the later resides in the crystallographic *ab*-plane. Thus, the hydrogen bonded squares may be considered to be appended with the two-dimensional cyano-bridged grids.

As shown in Fig. 5, the two-dimensional cyano-bridged grids with the water molecules inside the square blocks are interlinked due to the intersheet hydrogen bonds between the hydrogens attached to one amine nitrogen (N(5L)) and the water molecule of the appended squares (H(53L)···O(1) = 2.314 Å, N(5L)···O(1) = 3.139 Å, N(5L)–H(53L)···O(1) = 152.3°). In Fig. 5, the two one-dimensional chains, ···Fe(1K)···Ni(1L)···Fe(1L)···Ni(1M)···Fe(1M)··· and ···Ni(1E)···Fe(1)···Ni(1)···Fe(1D)···Ni(1D)···, belong to two different two-dimensional cyano-bridged assemblies. An extended view down the crystallographic *c*-axis of the structure of **1** is shown in Fig. 6. The two-dimensional cyano-bridged grids look like waved sheets that are self-assembled into a three-dimensional network. Evidently, the grids are self-assembled into three dimensions due to the interlinking through the appended squares.

3.5. Magnetic properties

Variable-temperature (2–300 K) magnetic behavior of **1** is shown in Fig. 7 in the form of χ_M versus T and $\chi_M T$ versus T plots. The $\chi_M T$ value at 300 K is 2.35 $cm^3\,mol^{-1}\,K$. On lowering the temperature, the $\chi_M T$ values remain almost constant down to 20 K, and then decreases rapidly to 1.13 $cm^3\,mol^{-1}\,K$ at 2 K. The profile indicates that there may exist only a very weak antiferromagnetic interaction between the nickel(II) centers in **1**. As mentioned earlier, the paramagnetic centers in **1** are separated via five-atom bridges in two-dimensional cyano-bridged grids with the metal···metal separations of 6.64, 7.79, and 8.96 Å. Evidently, the extent of superexchange in this compound is expected to be very weak and the rapid decrease of $\chi_M T$ may be due to the single ion zero-field effect (ZFS) of the nickel(II) ions. Therefore, the susceptibility data have been simulated with the mononuclear model ($\mathbf{H} = D(\mathbf{S}_z^2 - 1/3\ S(S+1))$; Eq. (1)) that considers the zero-field effect of the nickel(II) ion

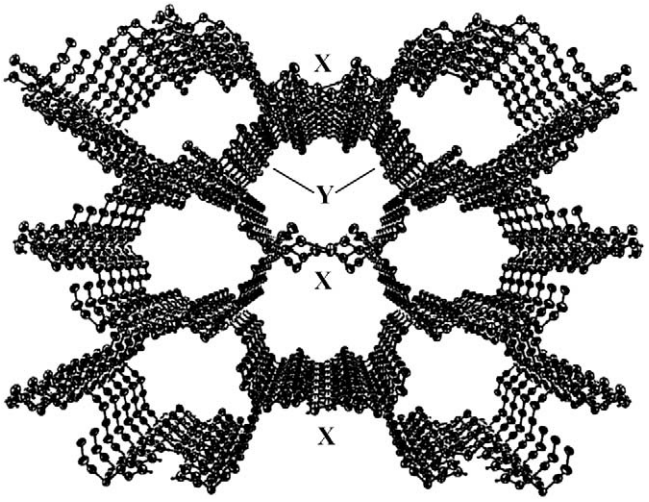

Fig. 6. A perspective view down the crystallographic *c*-axis to demonstrate the three dimensional structure that is generated due to the interlinking (region X; as in Fig. 5) of the waved sheets of the cyano-bridged grids (region Y). The carbon atoms, N(4), N(6), and N(7) of the diamines as well as O(2) and O(3) are omitted for clarity. Except the two hydrogens bonded to O(1) and one of the two hydrogens bonded to N(5), other hydrogen atoms are also omitted. Hydrogen bonds are shown by solid lines here.

$$\chi_M = \frac{4N\beta^2 g^2}{kT}\,\frac{e^{-D/kT}}{1+2e^{-D/kT}}. \qquad (1)$$

Least-squares fitting of the susceptibility data with Eq. (1) leads to $|D| = 1.9\ cm^{-1}$ and $g = 2.18$; the agreement factor (R) defined as $[\sum\{(\chi_M T)_{obs} - (\chi_M T)_{calc}\}^2 / \sum(\chi_M T)^2_{obs}]$ being 1.39×10^{-2}. The susceptibility data have been also simulated with the dinuclear model ($\mathbf{H} = -2J\mathbf{S_1}\cdot\mathbf{S_2} + D(\mathbf{S}_{1z}^2 + \mathbf{S}_{2z}^2)$) that considers superexchange as well

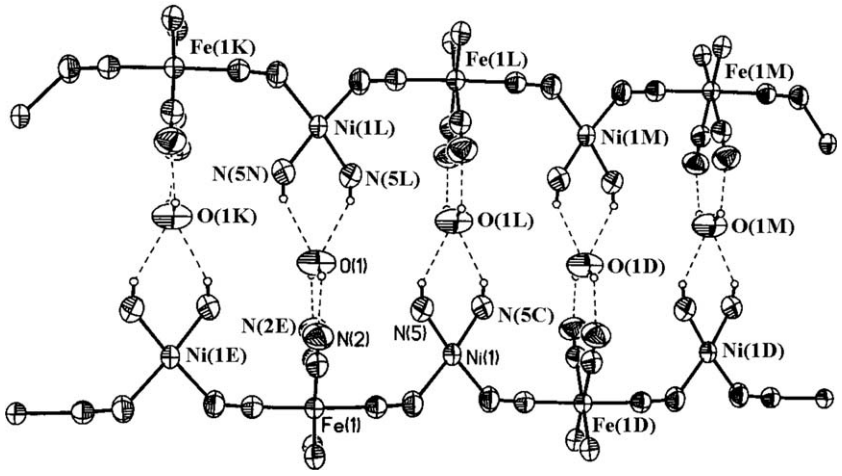

Fig. 5. A perspective view down the crystallographic *a*-axis to show the linking of two-dimensional sheets due to the hydrogen bonds between O(1) and the hydrogens of one amine nitrogen (N(5)). The Ni(2) center and the diamine coordinated to this metal ion, O(2), and O(3) atoms as well as the carbon and one nitrogen atoms of the diamine coordinated to Ni(1) center are omitted for clarity. Only those hydrogens participating in intersheet interactions are shown. Symmetry codes: D–G, as in Fig. 3; K, $-x, -y, 1-z$; L, $-x, -y, 2-z$; M, $-x, -y, 3-z$; N, $x, -y, z-0.5$.

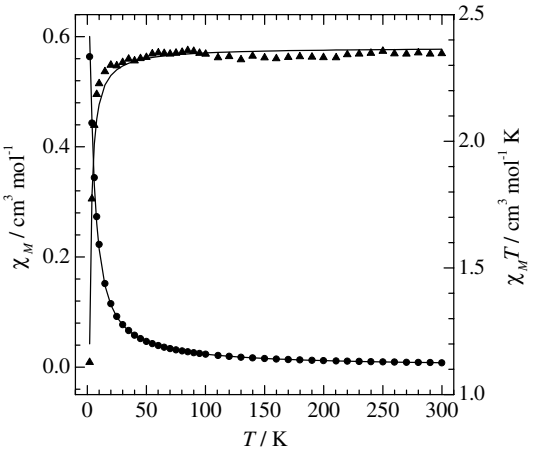

Fig. 7. Plots of χ_M (solid circles) and $\chi_M T$ (solid triangles) vs. T for **1**. Solid lines represent best least-squares fit of the experimental data with the theoretical equation (Eq. (1)) in the text).

as the single ion zero-field effect of nickel(II) [15]. The global minimization of the least-squares fittings (Fig. S1) takes place with $J = -0.3\ \mathrm{cm}^{-1}$, $g = 2.16$, and $|D| = 4.8\ \mathrm{cm}^{-1}$; the agreement factor ($R$), defined as $[\sum\{(\chi_M T)_{obs} - (\chi_M T)_{calc}\}^2 / \sum(\chi_M T)^2_{obs}]$, being 1.65×10^{-2}. On fixing the J value at zero, the simulation (Fig. S1) converges with $g = 2.15$, $|D| = 9.6\ \mathrm{cm}^{-1}$, and $R = 2.15 \times 10^{-2}$. Although the three simulations are almost superimposable, the rapid decrease of $\chi_M T$ at low temperatures are better defined in the mononuclear model as well as in the dinuclear model with imposed $J = 0$. However, the mononuclear model leads to more realistic estimate of the ZFS. From these simulations, it can be concluded that the superexchange interaction between the paramagnetic centers in **1** is negligible and the rapid decrease at low temperatures takes place due to the zero-field effect of the nickel(II) centers. It may be noted that the exchange interactions observed through the five-atom bridge, as in **1**, in the previously reported examples are only very weak ferromagnetic interactions [5d,10c]. Thus, the non-correlation between the paramagnetic centers in **1** is approximately consistent with the reported cases.

As mentioned earlier, three possible types of $[Ni^{II}(diamine)_2]_3[Fe^{III}(CN)_6]_2 \cdot 2H_2O$ (**2**) have been reported previously [7a,7e,7f]. All these three systems have similar two-dimensional structures. Magnetic properties of all these compounds are also similar and these exhibit ferromagnetic ordering at ca. 15 K.

Acknowledgements

Financial support from the Department of Science and Technology, Government of India (Grant SR/S1/IC-27/2002) and National Science Council, Taiwan (Grant NSC-93-2113-M-032-020) is gratefully acknowledged. S. M. is grateful to Prof. K. Nag for helpful discussion. M.N. thanks CSIR, Government of India for providing a fellowship.

Appendix A. Supporting informations

Crystallographic information for **1** and Fig. S1. Crystallographic data are available (CCDC No. 260216) from the Cambridge Crystallographic Data Center, 12 Union Road, Cambridge CB2 1EZ, UK (fax: +44 1223 336 033; e-mail: deposit@ccdc.cam.ac.uk). Supplementary data associated with this article can be found, in the online version, at doi:10.1016/j.poly.2005.12.024.

References

[1] (a) B.S. Thyagarajan, Chem. Rev. 58 (1958) 439;
(b) K.B. Wiberg, H. Maltz, M. Okano, Inorg. Chem. 7 (1968) 830;
(c) E.C. Gilbert, J. Phys. Chem. 35 (1931) 3631;
(d) R.C. Kapoor, O.P. Kachhwaha, B.P. Sinha, J. Phys. Chem. 73 (1969) 1627;
(e) E.P. Burrows, D.H. Rosenblatt, J. Org. Chem. 48 (1983) 992.
[2] (a) A.W. Adamson, E. Gonick, Inorg. Chem. 2 (1963) 129;
(b) D.G. Lambert, M.M. Jones, J. Am. Chem. Soc. 88 (1966) 4615;
(c) L. Meites, R.H. Schlossel, J. Phys. Chem. 67 (1963) 2397;
(d) P. Ertl, B. Unterladstaetter, K. Bayer, S.R. Mikkelsen, Anal. Chem. 72 (2000) 4949;
(e) Z. Bradić, P.C. Harrington, R.G. Wilkins, G. Yoneda, Biochemistry 19 (1980) 4149;
(f) E. Antonini, M. Brunori, J. Wyman, Biochemistry 4 (1965) 545;
(g) I.M. Kolthoff, A. Anastasi, J. Am. Chem. Soc. 80 (1958) 4248.
[3] (a) M. Verdaguer, A. Bleuzen, V. Marvaud, J. Vaissermann, M. Seuleiman, C. Desplanches, A. Scuiller, C. Train, R. Garde, G. Galley, C. Lomenech, I. Rosenman, P. Veillet, C. Cartier, F. Villain, Coord. Chem. Rev. 190–192 (1999) 1023;
(b) M. Ohba, H. Ōkawa, Coord. Chem. Rev. 198 (2000) 313.
[4] P.V. Bernhardt, B.P. Macpherson, M. Martinez, Inorg. Chem. 39 (2000) 5203.
[5] (a) C.P. Berlinguette, J.R. Galán-Mascarós, K.R. Dunbar, Inorg. Chem. 42 (2003) 3416;
(b) J.Y. Yang, M.P. Shores, J.J. Sokol, J.R. Long, Inorg. Chem. 42 (2003) 1403;
(c) R.J. Parker, L. Spiccia, S.R. Batten, J.D. Cashion, G.D. Fallon, Inorg. Chem. 40 (2001) 4696;
(d) G. Rogez, S. Parsons, C. Paulsen, V. Villar, T. Mallah, Inorg. Chem. 40 (2001) 3836;
(e) R.J. Parker, K.D. Lu, S.R. Batten, B. Moubaraki, K.S. Murray, L. Spiccia, J.D. Cashion, A.D. Rae, A.C. Willis, J. Chem. Soc., Dalton Trans. (2002) 3723;
(f) R.J. Parker, D.C.R. Hockless, B. Moubaraki, K.S. Murray, L. Spiccia, J. Chem. Soc., Chem. Commun. (1996) 2789.
[6] H. Oshio, H. Onodera, O. Tamada, H. Mizutani, T. Hikichi, T. Ito, Chem. Eur. J. 6 (2000) 2523.
[7] (a) F. Bellouard, M. Clemente-León, E. Coronado, J.R. Galán-Mascarós, C.J. Gómez-García, F. Romero, K.R. Dunbar, Eur. J. Inorg. Chem. (2002) 1603;
(b) E. Colacio, M. Ghazi, H. Stoeckli-Evans, F. Lloret, J.M. Moreno, C. Pérez, Inorg. Chem. 40 (2001) 4876;
(c) M.S.E. Fallah, J. Ribas, X. Solans, M. Font-Bardia, J. Chem. Soc., Dalton Trans. (2001) 247;
(d) E. Colacio, J.M. Domínguez-Vera, M. Ghazi, R. Kivekäs, J.M. Moreno, A. Pajunen, J. Chem. Soc., Dalton Trans. (2000) 505;
(e) E. Coronado, C. Giménez-Saiz, J.M. Martínez-Agudo, A. Nuez, F.M. Remero, H. Stoeckli-Evans, Polyhedron 22 (2003) 2435;
(f) E. Coronado, C. Giménez-Saiz, A. Nuez, F.M. Remero, E. Rusanov, H. Stoeckli-Evans, Inorg. Chem. 41 (2002) 4615.
[8] R. Lescouëzec, F. Lloret, M. Julve, J. Vaissermann, M. Verdaguer, R. Llusar, S. Uriel, Inorg. Chem. 40 (2001) 2065.
[9] (a) H. Miyasaka, H. Ieda, N. Matumoto, K.-i. Sugiura, M. Yamashita, Inorg. Chem. 42 (2003) 3509;

(b) N. Re, R. Crescenzi, C. Floriani, H. Miyasaka, N. Matsumoto, Inorg. Chem. 37 (1998) 2717;
(c) H. Miyasaka, N. Matsumoto, N. Re, E. Gallo, C. Floriani, Inorg. Chem. 36 (1997) 670;
(d) E. Colacio, J.M. Domínguez-Vera, F. Lloret, J.M. Moreno Sánchez, R. Kivekäs, A. Rodriguez, R. Sillanpää, Inorg. Chem. 42 (2003) 4209;
(e) H. Xiang, S. Gao, T.-B. Lu, R.L. Luck, Z.-W. Mao, X.-M. Chen, L.-N. Ji, New J. Chem. 25 (2001) 875;
(f) J.A. Smith, J.-R. Galán-Mascarós, R. Clérac, K.R. Dunbar, Chem. Commun. (2000) 1077.

[10] (a) S.-W. Zhang, D.-G. Fu, W.-Y. Sun, Z. Hu, K.-B. Yu, W.-X. Tang, Inorg. Chem. 39 (2000) 1142;
(b) T. Lu, H. Xiang, C. Su, P. Cheng, Z. Mao, L. Ji, New J. Chem. 25 (2001) 216;
(c) N. Fukita, M. Ohba, H. Ōkawa, K. Matsuda, H. Iwamura, Inorg. Chem. 37 (1998) 842.

[11] (a) S.M. Holmes, G.S. Girolami, J. Am. Chem. Soc. 121 (1999) 5593;
(b) S.-I. Ohkoshi, K. Hashimoto, J. Am. Chem. Soc. 121 (1999) 10591.

[12] (a) G.M. Sheldrick, SHELXS-97: A Program for Crystal Structure Solution, University of Göttingen, Göttingen, Germany, 1997;
(b) G.M. Sheldrick, SHELXL-97: A Program for Crystal Structure Refinement, University of Göttingen, Göttingen, Germany, 1997;
(c) WINGX-1.70.000: An integrated systems of windows programs, program for the solution, refinement, and analyses of single-crystal X-ray diffraction data: L.J. Farrugia, J. Appl. Crystallogr. 32 (1999) 837.

[13] K. Nakamoto, Infrared and Raman Spectra of Inorganic and Coordination Compounds, Wiley, New York, 1986.

[14] S.C. Davies, D.L. Hughes, R.L. Richards, J.R. Sanders, J. Chem. Soc., Dalton Trans. (2002) 1442.

[15] G. De Munno, M. Julve, F. Lloret, A. Derory, J. Chem. Soc., Dalton Trans. (1993) 1179.

cations to form stable complexes with general formula $[WM(RSn)_2(MW_9O_{34})_2]^{10-}$ where M = Co or Zn and R = CH_3, C_2H_5, *n*-C_4H_9.

The di-tin precursors α,ω-bis-(trichlorostannyl)alkanes with general formula $Cl_3Sn(CH_2)_nSnCl_3$ have previously been reported for the synthesis of organotin-oxo clusters [24]. In this paper, we report the use of $Cl_3Sn(CH_2)_4SnCl_3$ as a new polyoxometalate linker by reacting it with $[SiW_{11}O_{39}]^{8-}$ to connect two lacunary POMs and also to form linear oligomers from $[WZn(Zn(H_2O))_2(ZnW_9O_{34})_2]^{12-}$.

Although the nonaqueous synthesis of $[PhSnW_5O_{18}]^{3-}$ and $[PhGeW_5O_{18}]^{3-}$ from WO_4^{2-} and $PhMCl_3$ has been reported [25], we now show that reaction of $K_{10}[Ce(W_5O_{18})_2]$ and CH_3SnCl_3 yields $[CH_3W_5O_{18}]^{3-}$ in aqueous solution.

2. Experimental

The sodium salts of $[WM_3(H_2O)_2(MW_9O_{34})_2]^{12-}$ (M_5W_{19}) M = Co, Zn, $K_9[Ce^{III}(W_5O_{18})_2]\cdot nH_2O$ ($Ce(W_5)_2$) and $K_8[\alpha\text{-}SiW_{11}O_{39}]$ (SiW_{11}) were synthesized following published methods and identified by infrared spectroscopy and for Zn_5W_{19}, $Ce(W_5)_2$, and SiW_{11}, by ^{183}W NMR spectroscopy [17,18,26,27]. α,ω-Bis-(trichlorostannyl)butane ($Cl_3Sn(CH_2)_4SnCl_3$) was synthesized via α,ω-bis-(triphenylstannyl)butane [24,28]. Methyltintrichloride ($MeSnCl_3$), and butyltintrichloride ($BuSnCl_3$) (Aldrich) and ethyltintrichloride ($EtSnCl_3$) (Organometallics, Inc.) were used as supplied.

*$Cs_{10}[WZn(CH_3Sn)_2(ZnW_9O_{34})_2]\cdot 19.5H_2O$ (Cs_{10}**1**).* A solution of 5.0 g of $Na_{12}[WZn_3(H_2O)_2(ZnW_9O_{34})_2]\cdot nH_2O$ (0.9 mmol) in 10 mL water was heated to 80 °C and added to a solution of 0.43 g of CH_3SnCl_3 (1.8 mmol) in 10 mL of water. The resulting mixture was stirred at 80 °C for 30 min, 2.25 mL of 4 M CsCl solution was added and the mixture stored in the refrigerator overnight. The solid product was filtered off and recrystallized from 15 mL of hot (90–95 °C) water by adding 1 mL of 4 M CsCl solution. The fine crystals were filtered off and air-dried overnight. Yield: 4.6 g (77%). *Anal.* Calc. for $C_2H_{45}Cs_{10}O_{87.5}Sn_2W_{19}Zn_3$: C, 0.36; Cs, 19.8; Sn, 3.53; W, 51.9; Zn, 2.9. Found: C, 0.39; Cs, 20.4; Sn, 3.70; W, 56.1; Zn, 3.0%. IR (metal oxygen stretching region): 1203, 935, 880, 751, 658 cm^{-1}.

*$Cs_{10}[Co(CH_3Sn)_2(CoW_9O_{34})_2]\cdot 20H_2O$ (Cs_{10}**2**), $Cs_{10}[WZn(CH_3CH_2\ Sn)_2(ZnW_9O_{34})_2]\cdot 15H_2O$ (Cs_{10}**3**)* and *$Cs_{10}[WCo(CH_3CH_2Sn)_2(CoW_9O_{34})_2]\cdot 14H_2O$ (Cs_{10}**4**)* were prepared in a similar fashion.

*Cs_{10}**2***. Yield: 4.5 g (75%). *Anal.* Calc. for $C_2H_{46}Co_3Cs_{10}O_{88}W_{19}$: C, 0.36; Co, 2.63; Cs, 19.8; Sn, 3.54; W, 52.02. Found: C, 0.32; Co, 2.70; Cs, 19.6; Sn, 3.45; W, 54.8%. IR: 1203, 935, 885, 745, 660 cm^{-1}.

*Cs_{10}**3***. Yield: 3.9 g (65%). *Anal.* Calc. for $C_4H_{40}Cs_{10}O_{83}Sn_2W_{19}Zn_3$: C, 0.72; Cs, 19.9; Sn, 3.6; W, 52.4; Zn, 2.9. Found: C, 0.67; Cs, 19.6; Sn, 3.73; W, 52.9; Zn, 3.2%. IR: 1192, 933, 884, 750, 658, 539 cm^{-1}.

*Cs_{10}**4***. Yield: 3.6 g (60%). *Anal.* Calc. for $C_4H_{38}Co_3Cs_{10}O_{82}Sn_2W_{19}$: C, 0.72; Co, 2.7; Cs, 20.0; Sn, 3.6; W, 52.5. Found: C, 0.71; Co, 2.8; Cs, 20.3; Sn, 3.7; W, 55.1%. IR: 1190, 934, 883, 857, 751, 655, 538 cm^{-1}.

*$Cs_{10}[WZn(C_4H_9Sn)_2(ZnW_9O_{34})_2]\cdot 18H_2O$ (Cs_{10}**5**)* was prepared using the same procedure and quantity as above except that before and during the addition of the solution of $[WZn_3(H_2O)_2(ZnW_9O_{34})_2]^{12-}$ to the $C_4H_9SnCl_3$ the temperature was maintained at ca. 40 °C. After 5 min the temperature was slowly raised to 80 °C and kept there for 30 min. Yield: 3.0 g (50%). *Anal.* Calc. for $C_8H_{54}Cs_{10}O_{86}Sn_2W_{19}Zn_3$: C, 1.42; Cs, 19.6; Sn, 3.50; W, 51.5; Zn, 2.9. Found: C, 1.52; Cs, 19.4; Sn, 3.56; W, 51.9; Zn, 2.9%. IR: 1167, 1086, 936, 879, 752, 657, 600, 535 cm^{-1}

*$Cs_{10}[WCo(C_4H_9Sn)_2(CoW_9O_{34})_2]\cdot 17H_2O$ (Cs_{10}**6**)* was prepared using the same procedure used for **5**. Yield: 3.4 g (57%). *Anal.* Calc. for $C_8H_{52}Co_3Cs_{10}O_{85}Sn_2W_{19}$: C, 1.43; Co, 2.62; Cs, 19.7; Sn, 3.52; W, 51.8. Found: C, 1.45; Co, 2.71; Cs, 19.8; Sn, 3.63; W, 53.2%.

*$Cs_{10}[WCo(CH_3Sn)_2(ZnW_9O_{34})_2]\cdot 20H_2O$ (Cs_{10}**7**)*. To 20 mL of a warm solution (80 °C) of $Co(NO_3)_2\cdot 6H_2O$ (2.16 g, 9.1 mmol) was added 10 mL of a solution of $MeSn_2Zn_3W_{19}$ (10.5 g, 1.8 mmol). The solution changed color from pink to reddish brown and the resulting mixture was heated to near boiling for 2 h. The solution was then allowed to cool and passed through a cation exchange column (K^+) to remove excess unreacted cobalt. The eluate had a reddish green color. CsCl solution (4 M) was added to obtain a solid which was then recrystallized from the minimum amount of hot water (yield 6.5 g, 62%). *Anal.* Calc. for $C_2H_{46}CoCs_{10}O_{88}W_{19}Zn_2$: C, 0.36; Co, 0.88; Cs, 19.8; Sn, 3.53; W, 52.0. Found: C, 0.39; Co, 0.91, Cs, 20.2; Sn, 3.21; W 53.3%.

The isostructural but *achiral analogs* of **1**, **3** and **5**, $[(RSn)_2Zn_2(PW_9O_{34})_2]^{8-}$ (R = Me, Et, *n*-Bu) were also prepared for spectroscopic comparisons, see below and in Supplementary material.

*$K_{10}[SiW_{11}O_{39}Sn(CH_2)_4SnSiW_{11}O_{39}]\cdot H_2O$ (**8**)*. In 40 mL of DMF $Cl_3Sn(CH_2)_4SnCl_3$ (0.47 g, 0.93 mmol) and SiW_{11} (6 g, 1.9 mmol) were mixed and the slurry was heated at 100 °C overnight. The solution was filtered hot and 5 mL of a saturated solution of KCl was added first, followed by ethanol to yield a solid product which was recrystallized from the minimum of water. Yield: 5.4 g (90%).

Samples containing *$[(SnC_4H_8Sn)_{2n}\{WZn(ZnW_9O_{34})_2\}_n]^{10n-}$ (**9**)* were prepared as follows. A solution of $Cl_3SnC_4H_8SnCl_3$ (0.91 g, 1.8 mmol) in 40 mL of DMF was treated with solid Zn_5W_{19} (5 g, 0.9 mmol) and the slurry was heated at 100 °C overnight. After filtration to remove undissolved material, ethanol was added to precipitate 4.5 g (90%) of product.

2.1. Physical measurements

Infrared spectra were recorded in KBr pellets on a Spectrum One FT-IR spectrometer (Perkin–Elmer Instruments)

and electronic spectra on an Agilent 8453 UV–Vis spectrophotometer. Elemental analyses were performed by Schwarzkopf Microanalytical Lab Inc., Woodside, NY. and water content was determined by thermogravimetric analysis using a Q600 SDT DSC/TGA (TA Instruments, New Castle, Delaware). Cyclic voltammograms were recorded at room temperature on a BAS 100A instrument. A glassy carbon working electrode, platinum wire counter electrode, and Ag|AgCl reference electrode were used, and the measurements were carried out in sodium sulfate (pH 2 and 3), acetate/acetic acid (pH 4–6), and tris buffers (pH 7 and 8). All ^{183}W and ^{119}Sn NMR data were recorded on a Bruker AM-300WB spectrometer equipped with an Aspect 3000 computer or Tecmag DeSpect system. Proton NMR spectra were recorded on a Mercury 300 instrument with Varian VNMR software and carbon-13 spectra on an Oxford 500 MHz NMR with Varian Unity INOVA system. Resonance frequencies were 300.107 MHz for ^{1}H in 5 mm tubes, 125.68 MHz for ^{13}C in 5 mm tubes, 111.92 MHz for ^{119}Sn in 10 mm tubes, 12.505 MHz for ^{183}W NMR in 10 mm tubes. Chemical shifts are reported with respect to 2 M $NaWO_4$ (^{183}W) $(CH_3)_4Sn$ (^{119}Sn), and $(CH_3)_4Si$ (^{1}H, ^{13}C). Chemical shifts downfield of the references are reported as positive. All NMR measurements were made in 99.9% D_2O. For ^{183}W and ^{119}Sn, concentrations of 0.1–0.15 M were used. Cesium salts were treated with lithium perchlorate and subsequent removal of precipitated $CsClO_4$; potassium salts were soluble enough to require no ion exchange.

2.2. Crystal structure analysis

Crystals were grown from reaction mixtures as cesium, potassium, or sodium salts or as a combination of these cations. Structural analyses were performed on a Bruker-Siemens SMART CCD single-crystal diffractometer equipped with a Mo anode and graphite monochromator ($\lambda = 0.71073$ Å). The crystals were mounted on a glass fiber

Table 1
Crystallographic data for salts of anions **1**, **3**, **5**, and **7**

Anion	**1**	**3**	**5**	**7**
Formula	$K_6Na_3C_3O_{68}Sn_2W_{19}Zn_3 \cdot 17.6H_2O$	$K_8C_4O_{68}Sn_2W_{19}Zn_3 \cdot 24H_2O$	$Cs_{7.7}Na_2C_8O_{68}Sn_2W_{19}Zn_3 \cdot 20.5H_2O$	$Na_6C_2CoK_3O_{68}Sn_2W_{19}Zn_2 \cdot 21.5H_2O$
Molecular weight	5635.84	5759.48	6508.11	5631.46
Temperature (K)	173	173	173	173
System	triclinic	triclinic	triclinic	orthorhombic
Space group	$P\bar{1}$	$P\bar{1}$	$P\bar{1}$	*Pccn*
a (Å)	12.0986(10)	12.1982(9)	12.5246(14)	28.576(6)
b (Å)	12.2261(10)	12.3040(9)	13.2626(15)	13.180(3)
c (Å)	16.2203(14)	16.1433(12)	16.3125(18)	21.727(5)
α (°)	81.6780(10)	80.8950(10)	92.753(2)	90.00
β (°)	80.488(2)	81.4060(10)	102.025(2)	90.00
γ (°)	66.2770(10)	66.8730(10)	108.947(2)	90.00
V (Å^3)	2158.2(3)	2189.9(3)	2486.9(5)	8183(3)
Z	1	1	1	4
Density (calculated) (Mg m^{-3})	4.336	4.367	4.346	4.571
Absorption coefficient μ (mm^{-1})	26.998	26.697	25.958	28.260
Maximum and minimum transmission	0.073043 and 0.024308	0.086142 and 0.033751	0.046985 and 0.010283	0.053105 and 0.015459
$F(000)$	2446	2508	2798	9776
λ (Mo Kα)	0.71073	0.71073	0.71073	0.71073
θ Range (°)	1.28–28.32	1.28–28.26	1.64–28.00	1.43–28.34
h_{min}/h_{max}	$-15 \leqslant h \leqslant 15$	$-16 \leqslant h \leqslant 16$	$-16 \leqslant h \leqslant 16$	$-37 \leqslant$ h $\leqslant 37$
k_{min}/k_{max}	$-16 \leqslant k \leqslant 15$	$-16 \leqslant k \leqslant 16$	$-17 \leqslant k \leqslant 17$	$-17 \leqslant$ k $\leqslant 17$
l_{min}/l_{max}	$-21 \leqslant l \leqslant 21$	$-20 \leqslant$ l $\leqslant 21$	$-21 \leqslant l \leqslant 21$	$-28 \leqslant$ l $\leqslant 28$
Number of measured reflections	24334	24015	27212	88689
Number of unique reflections [R_{int}]	10172 [0.0610]	10137 [0.0419]	11451 [0.0626]	10068 [0.1499]
Number of refined parameters	335	336	348	332
Goodness-of-fit on F^2	1.078	1.093	1.037	1.082
Final R indices	$R_1 = 0.0587$,	$R_1 = 0.0627$,	$R_1 = 0.0539$,	$R_1 = 0.0577$,
[$I > 2\sigma(I)$]	$wR_2 = 0.1353$	$wR_2 = 0.1667$	$wR_2 = 0.1489$	$wR_2 = 0.1368$
R indices (all data)	$R_1 = 0.0818$,	$R_1 = 0.0715$,	$R_1 = 0.0680$,	$R_1 = 0.1012$,
	$wR_2 = 0.1496$	$wR_2 = 0.1739$	$wR_2 = 0.1532$	$wR_2 = 0.1562$

$R_1 = \sum \| F_o | - | F_c \| / \sum | F_o |$.
$wR_2 = [\sum [w(F_o^2 - F_c^2)^2] / \sum [w(F_o^2)^2]]^{1/2}$.

and placed in a nitrogen stream at 173 K and an approximate sphere of data was collected using ω-scans. Following routine Lorentz and polarization correction, an empirical absorption correction was based on measured intensities of equivalent reflections at different ϕ and ω values [29,30]. All structures were solved using direct methods and refined against $|F^2|$ over all independent reflections. SMART, SAINT, SHELX-97, and X-SEED software were used to solve and refine the data [31–33]. As is frequently seen in polyoxometalate crystals there is extensive disorder of the cations and water molecules. In order to determine the occupancy of the disordered atoms their atomic displacement parameters were first set to be comparable to the corresponding non disordered atoms and their occupancies were refined. Then the occupancy numbers were held fixed and their atomic displacement factors were refined.

3. Results and discussion

Crystallographic data for structures containing $[(RSn)_2ZnW(ZnW_9O_{34})_2]^{10-}$ (R = CH_3), C_2H_5, and *n*-C_4H_9, are summarized in Table 1. The polytungstate skeleton is identical to that reported by Tourné and Zonnevijlle and consists of two α-B-$[ZnW_9O_{34}]^{12-}$ lacunary derivatives sandwiching Zn, W, and Sn(R) atoms as shown for the butyl derivative in Fig. 1. Although each anion has only C_2 symmetry, the belt W and Zn atom sites are disordered with 50% occupancy as a consequence of the centrosymmetric space group.

Tungsten-183 NMR spectra (Fig. 2) are similar to that reported for $[\{(H_2O)Zn\}_2ZnW(ZnW_9O_{34})_2]^{12-}$ with ten lines of relative intensity 1:2:2:2:2:2:2:2:2:2. Tungsten-183 and Tin-119 NMR data are summarized in Table 2.

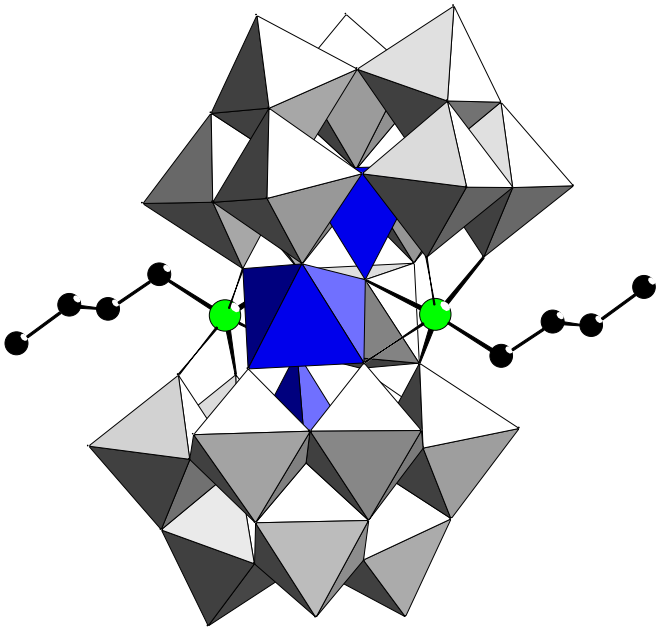

Fig. 1. Combination polyhedral and ball-and-stick representation of the structure of anion **5**.

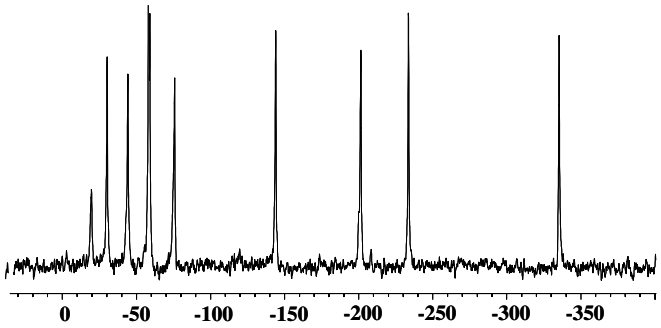

Fig. 2. Tungsten-183 NMR spectrum of anion **5**.

The proton NMR spectra of solutions of anions *3* and *5* reveal that the α-methylene protons are diastereotopic, see Fig. 3 and Table 3. We do not believe that this is a consequence of the chirality of the polyoxoanion structure for the following reasons: (1) the spectrum of the methyl derivative, **1**, is a singlet; (2) the spectra of *achiral* $[(RSn)_2Zn_2(PW_9O_{34})_2]^{8-}$ (R = Et, *n*-Bu) show similar splittings of the α-protons (Supplementary material). We tentatively suggest that the spectra result from restricted rotation about the Sn–C bond.

The well-known Keggin anion $[CoW_{12}O_{40}]^{6-}$ containing a tetrahedral cobalt(II) center within a rigid polytungstate shell is oxidizable to a stable cobalt(III) analog [34,35], a rare example of tetrahedral (high-spin) Co^{III}. Anions **2**, **4** and **6**, as well as the precursor Co_5W_{19} Tourné–Zonnevijlle species share a similar feature, although this does not seem to have been explored previously. Cyclic voltammograms of **2** and Co_5W_{19} (Fig. 4) show two reversible one-electron oxidations at pH 5–6. Solutions of the $Co^{II}Co^{III}$ and Co_2^{III} anions, both golden yellow, were easily generated by controlled potential electrolysis. In more acidic solutions the two one-electron waves coalesced into a single reversible two-electron feature, a consequence of the routinely-observed protonation effects in polyoxometalate electrochemistry [36]. The difference in oxidation potentials (ca. 300 mV, Table 4) between the two polyoxometalates is attributed to the anionic charge difference of 10– versus 12– [36].

3.1. Diplacement of cerium(III)

In earlier work we had shown that the pentatungstate anion in complexes such as $[Ce(W_5O_{18})_2]^{9-}$ had sufficient kinetic stability in aqueous solution to allow its transfer to other lanthanide polyoxometalates [37]. We have therefore considered the possibility of displacing the cerium atom by RSn^{3+} to generate $[RSnW_5O_{18}]^{3-}$. The only previously known examples of the latter structure, with phenyltin and phenylgermanium groups, were synthesized in non-aqueous solution from mononuclear tungstate [25].

In a preliminary investigation in aqueous solution $K_9[Ce(W_5O_{18})_2]\cdot nH_2O$ (3 g, 0.96 mmol) in 20 mL of water was added to one of $MeSnCl_3$ (0.46 g, 1.9 mmol) in 10 mL

Table 2
^{183}W and ^{119}Sn NMR data of zinc-containing anions

Anion	$\delta(^{119}Sn)$	$\delta(^{183}W)$
1	−509	−27.7(1), −31.5(2), −48.2(2), −61.1(2), −62.7(2), −82.2(2), −153.2(2), −208.0(2), −234.6(2), −335.4(2)
3	−521	−23.0(1), −32.2(2), −48.5(2), −59.4(2), −59.9(2), −79.7(2), −144.0(2), −201.6(2), −233.9(2), −334.5(2)
5	−548	−20.3(1), −30.9(2), −45.0(2), −58.9(2), −59.7(2), −76.4(2), −144.7(2), −201.6(2), −233.7(2), −335.5(2)
Zn_5W_{19}		+21.5(1), −19.7(2), −45.1(2), −87.9(2), −92.1(2), −97.4(2), −157.1(2), −190.5(2), −228.7(2), −307.5(2)

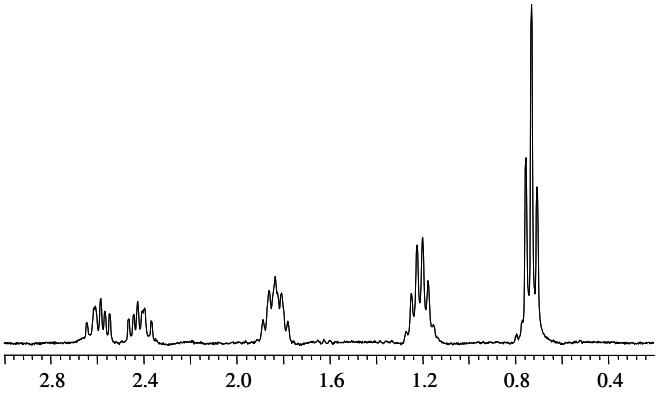

Fig. 3. Proton NMR spectrum of anion **5**, showing the diastereotopic α-methylene protons.

Table 3
^{1}H and ^{13}C chemical shifts

Anion	$\delta(^{1}H)$	$\delta(^{13}C)$
1	1.06 (s, 3H)	13.00
3	1.03 (t, 3H), 2.02 (m, 1H), 2.18 (m, 1H)	11.74, 31.69
5	0.32 (t, 3H), 0.79 (m, 2H), 1.42 (m, 2H), 2.02 (m, 1H), 2.18 (m, 1H)	13.01, 26.26, 28.86, 38.01

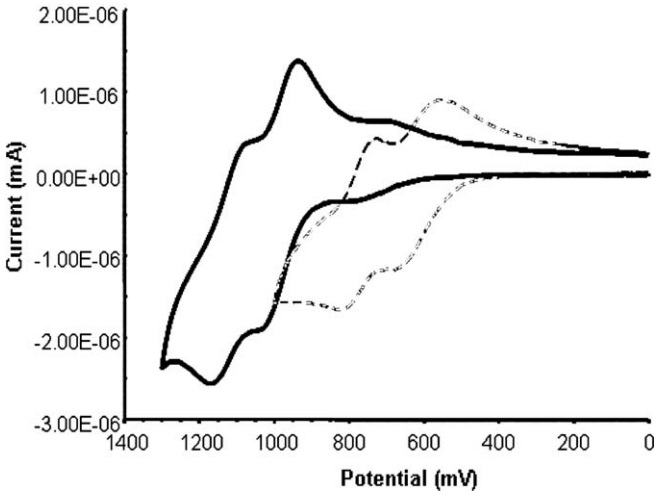

Fig. 4. Cyclic voltammograms of $[WCo_3(MeSn)_2(CoW_9O_{34})_2]^{10-}$ at pH 5 (solid line) and $[WCo_3(H_2O)_2(CoW_9O_{34})_2]^{12-}$ at pH 6 (broken line).

water, the pH of which had previously been adjusted to ca. 6. A white cloudy precipitate formed in about 5 min and the mixture was stirred for 1 h before filtration through a Millipore membrane (0.22 μm). The filtrate was concentrated to half volume by heating, and allowed to stand overnight. Orange block crystals (1 g). were separated manually and were confirmed to be the starting tungstocerate salt by X-ray analysis (and by NMR, see below). The pale yellow filtrate was treated with ethanol to yield a pale yellow solid (0.83 g, 28%). The product was characterized by IR (1414.9, 939.5, 839.7, 721.1, 579.6, 544.0, 418.7 cm^{-1}) and by ^{1}H and ^{183}W NMR spectroscopy, the results of which, δ(H) 1.36, $^{2}J_{H-Sn}$ 124 Hz; δ(W) −16.0 (1W), −20.3 (4W), are fully consistent with the formation of $[CH_3SnW_5O_{18}]^{3-}$. Prior to separation of crystals of the starting complex a ^{183}W NMR spectrum of the solution showed only signals for the product and for those of $[Ce(W_5O_{18})_2]^{9-}$ at +51.5 (1W) and +149.1 (4W) ppm.

Table 4
Voltammetric peak potentials for $Co^{II/III}$ processes[a]

Anion	E_{pa}	E_{pc}	$E_{pa} - E_{pc}$
$[WCo_3(H_2O)_2(CoW_9O_{34})_2]^{12-}$ (Co_5W_{19}), pH 6	659, 824	571, 738	88, 86
$[WCo_3(MeSn)_2(CoW_9O_{34})_2]^{10-}$ (**2**), pH 5	1021, 1163	923, 1067	98, 96

[a] mV vs. Ag|AgCl; sweep rate 100 mV s^{-1}.

3.2. Di-tin polyoxometalate linkers

The recent availability of (α,ω-bis(trichlorostannyl)alkanes, $Cl_3Sn(CH_2)_nSnCl_3$ [24], provides an opportunity to covalently link polyoxometalate units using the procedure described here. Two sets of initial experiments demonstrate the ease of this approach.

The dumbbell-shaped anion, $[SiW_{11}O_{39}Sn(CH_2)_4SnSiW_{11}O_{39}]^{10-}$, prepared in high yield as described in the experimental section, was identified by proton NMR which showed only two signals for the four sets of methylene protons, at 1.59 (with $^{2}J_{H-Sn} = 112$ Hz) and 2.15 ppm. Tungsten-183 and tin-119 NMR data are given in Table 5 with those of $[BuSnSiW_{11}O_{39}]^{5-}$ for comparison.

Preliminary light-scattering measurements[1] on aqueous solutions of the oligomers, $[(SnC_4H_8Sn)_{2n}\{WZn(ZnW_9O_{34})_2\}_n]^{10n-}$, described in the experimental section, indicate average *n*-values of about 4. Further synthetic and analytical work directed at longer chain-lengths is in progress and will be reported in due course.

[1] Measurements made by Dr. Guang Liu and Prof. Tianbo Liu.

Table 5
Sn and W NMR data for anion **8** and $[BuSnSiW_{11}O_{39}]^{5-}$

Anion	$\delta(^{119}Sn)$	$\delta(^{183}W)$
$[SiW_{11}Sn(CH_2)_4SnSiW_{11}]^{10-}$ (**8**)	−528	−67.2(2), −109.8(2), −137.2(2), −141.4(2) −152.0(1), −195.6(2)
$[BuSnSiW_{11}O_{39}]^{5-}$	−501	−94.8(2), −106.3(2), −126.2(2), −129.6(2)−134.7(1), −189.1(2)

4. Conclusions

The feasibility of incorporating organotin (and presumably organogermanium) groups into polyoxotungstates by displacement of transition metal centers from preformed heteropolyanions has been demonstrated. This opens new rational aqueous synthetic routes to organic derivatives of polyoxometalates. Coupling of polyoxometalate anions into "dimers" and oligomeric assemblies can be achieved through reaction with α,ω-bis-(trichlorostannyl)alkanes.

Acknowledgments

Acknowledgment is made to the Donors of the American Chemical Society Petroleum Research Fund for support of this research though Grant 39529-AC3. We thank Dr. Guang Liu and Professor Tianbo Liu (Lehigh University) for preliminary light-scattering measurements and advice.

Appendix A. Supplementary material

Synthesis and NMR spectra of $[(RSn)_2Zn_2(PW_9O_{34})_2]^{8-}$ anions. CIF files for all structure determinations have been deposited with the Cambridge Crystallographic Data Centre (288155–288158). Supplementary data associated with this article can be found, in the online version, at doi:10.1016/j.poly.2006.01.012.

References

[1] J. McCleverty, T.J. Meyer (Eds.), Comprehensive Coordination Chemistry II, A.G. Wedd (Ed.), vol. 4, Pergamon Press, Oxford, Chapters by M.T. Pope, pp. 635–678; C.L. Hill, pp. 679–759, 2004.
[2] J. Borrás-Almenar, E. Coronado, A. Müller, M.T. Pope (Eds.), NATO Science Series II: Mathematics, Physics and Chemistry, vol. 98, Kluwer Academic Publishers, Dordrecht, 2003.
[3] M.T. Pope, A. Müller (Eds.), Polyoxometalate Chemistry: From Topology via Self-Assembly to Applications, Kluwer Academic Publishers, Dordrecht, 2001, pp. 1–467.
[4] C.L. Hill (Ed.), Polyoxometalate issue, Chem. Rev. 98 (1998).
[5] W.H. Knoth, J. Am. Chem. Soc. 101 (1979) 759.
[6] F. Zonnevijlle, M.T. Pope, J. Am. Chem. Soc. 101 (1979) 2731.
[7] F. Xin, G.S. Chorghade, M.T. Pope, J. Am. Chem. Soc 109 (1987) 5134.
[8] F. Xin, M.T. Pope, Organometallics 13 (1994) 4881.
[9] F. Xin, M.T. Pope, G.J. Long, U. Russo, Inorg. Chem. 35 (1996) 1207.
[10] F. Xin, M.T. Pope, Inorg. Chem. 35 (1996) 5693.
[11] Q.H. Yang, H.C. Dai, J.F. Liu, Transit. Met. Chem. 23 (1998) 93.
[12] X.H. Wang, H.C. Dai, J.F. Liu, Polyhedron 18 (1999) 2293.
[13] X.H. Wang, J.F. Liu, J. Coord. Chem. 51 (2000) 73.
[14] G. Sazani, M.H. Dickman, M.T. Pope, Inorg. Chem. 39 (2000) 939.
[15] X. Wang, J. Liu, R. Zhang, B. Li, J. Liu, Main Group Metal Chem. 25 (2002) 535.
[16] G. Sazani, M.T. Pope, Dalton Trans. (2004) 1989.
[17] C.M. Tourné, G.F. Tourné, F. Zonnevijlle, J. Chem. Soc., Dalton Trans. (1991) 143.
[18] P.T. Witte, P.L. Alsters, W. Jary, R. Muellner, P. Poechlauer, D. Sloboda-Rozner, R. Neumann, Org. Process Res. Develop. 8 (2004) 524.
[19] R. Neumann, A.M. Khenkin, M. Dahan, Angew. Chem., Int. Ed. Engl. 34 (1995) 1587.
[20] R. Neumann, M. Gara, J. Am. Chem. Soc. 117 (1995) 5066.
[21] R. Neumann, A.M. Khenkin, Inorg. Chem. 34 (1995) 5753.
[22] R. Neumann, A.M. Khenkin, J. Mol. Catal. A 114 (1996) 169.
[23] R. Neumann, D. Juwiler, Tetrahedron 52 (1996) 8781.
[24] B. Zobel, A. Duthie, D. Dakternieks, E.R.T. Tiekink, Organometallics 20 (2001) 2820.
[25] B. Krebs, R. Klein, in: M.T. Pope, A. Müller (Eds.), Polyoxometalates: From Platonic Solids to Anti-retroviral Activity, Kluwer Academic Publishers, Dordrecht, The Netherlands, 1994, p. 41.
[26] A. Tézé, G. Hervé, Inorg. Synth. 27 (1990) 85.
[27] R.D. Peacock, T.J.R. Weakley, J. Chem. Soc. A (1971) 1836.
[28] Y. Azuma, M. Newcomb, Organometallics 3 (1984) 9.
[29] R. Blessing, Acta Crystallogr., Sect. A 51 (1995) 33.
[30] G.M. Sheldrick, SADABS Absorption Correction Method, University of Gottingen, Germany, 1996.
[31] G.M. Sheldrick, SAINT, 4.050, Siemens Analytical X-ray Instruments, Inc., Madison, WI, 1996.
[32] G.M. Sheldrick, SAINT, 4.050, Siemens Analytical X-ray Instruments, Inc., Madison, WI, 1997.
[33] L.J. Barbour, X-SEED, 1999.
[34] L.C.W. Baker, V.E. Simmons, J. Am. Chem. Soc. 81 (1959) 4744.
[35] V.E. Simmons, Ph.D. Thesis, Boston University, 1963 (Diss. Abstr. 24, 1391).
[36] M.T. Pope, G.M. Varga Jr., Inorg. Chem. 5 (1966) 1249.
[37] N. Belai, M. Sadakane, M.T. Pope, J. Am. Chem. Soc. 123 (2001) 2087.

fluorescence decay in aqueous solutions and that has been explained by the emission from non-interconverting rotamers which have different lifetimes due to different rates of intramolecular charge transfer [16].

DSC measurements on a L-tryptophanium hydrogen selenite powdered sample revealed the existence of a second-order transition at −82.5 °C.

We report here these DSC measurements and a thorough single-crystal X-ray diffraction study performed at room and low temperature to unravel the nature of the phase transition.

2. Experimental

2.1. Preparation of L-tryptophanium hydrogen selenite

A few drops of selenious acid were added to an aqueous solution of L-tryptophan. Within a few months transparent light brown crystals of prismatic shape grew from the solution.

2.2. Physical measurements

Single-crystal X-ray diffraction data for the title compound were collected both with a Mach3 diffractometer, equipped with a conventional detector at room temperature and another similar diffractometer equipped with an area detector at 80 K. The room temperature data were collected using ω–2θ scans and CuKα radiation ($\lambda = 1.5408$ Å). The unit cell parameters were determined by least-squares refinement of diffractometer angles ($21° < \theta < 37°$) for 25 automatically centered reflections.

The low temperature data were collected using φ and ω scans and Mo Kα radiation ($\lambda = 0.71073$ Å). The unit cell parameters were determined by least-squares refinement of diffractometer angles ($2.60° < \theta < 36.11°$) for 9018 automatically centered reflections.

For both temperatures the structure was solved by direct methods using SHELXS-97 [17] and refined anisotropically (non-H atoms) by full-matrix least-squares on F^2 using the SHELXL-97 program [17]. All the hydrogen atoms with the exception of that involved in the strong O1–H1···O3 hydrogen bond were allowed to ride on their parent atoms using SHELXL-97 defaults. H1 was freely refined with an isotropic displacement parameter multiple of the parent atom. The crystallographic details and selected interatomic distances and angles are given in Tables 1–4.

Thermal behaviour was studied using a power compensation differential scanning calorimeter DSC Pyris1, from Perkin–Elmer, equipped with a liquid nitrogen Cryofill

Table 2
Selected bond lengths (Å) and angles (°) at room and low temperatures

	293 K	80 K
Se–O5	1.625(3)	1.6342(14)
Se–O3	1.711(3)	1.7224(16)
Se–O4	1.765(3)	1.7637(16)
N1–C2	1.498(4)	1.497(3)
O5–Se–O3	103.52(14)	102.96(8)
O5–Se–O4	97.84(13)	97.28(7)
O3–Se–O4	97.82(15)	98.83(8)
O2–C1–O1	126.1(3)	126.09(18)
C5–C4–C3–C2	−102.5(4)	−100.6(2)
O1–C1–C2–N1	167.7(3)	167.11(17)
O2–C1–C2–N1	−15.5(4)	−15.8(3)
O2–C1–C2–C3	107.4(3)	107.1(2)
O1–C1–C2–C3	−69.5(3)	−70.0(2)
C4–C3–C2–N1	55.8(4)	55.2(2)
C4–C3–C2–C1	−65.8(4)	−66.3(2)

Table 1
Crystal data and structure refinement parameters

Temperature (K)	293(2)	80(2)
Empirical formula	$C_{11}H_{14}N_2O_5Se$	$C_{11}H_{14}N_2O_5Se$
Formula weight	333.20	333.20
Wavelength (Å)	1.5408	0.71073
Crystal system	orthorhombic	orthorhombic
Space group	$P2_12_12_1$	$P2_12_12_1$
a (Å)	5.4406(6)	5.3910(3)
b (Å)	8.2436(6)	8.2097(4)
c (Å)	27.539(3)	27.3216(14)
Volume (Å^3)	1235.1(2)	1209.21(11)
Z	4	4
Calculated density (g/cm^3)	1.792	1.830
Absorption coefficient (mm^{-1})	4.328	3.125
$F(000)$	672	672
Crystal size (mm^3)	$0.37 \times 0.24 \times 0.15$	$0.40 \times 0.40 \times 0.15$
θ Range for data collection (°)	3.21–72.16	1.49–30.56
Index ranges	$-6 < h < 6$, $-10 < k < 10$, $0 < l < 34$	$-7 < h < 7$, $-11 < k < 11$, $-21 < l < 38$
Reflections collected/unique (R_{int})	4955/2439 (0.0335)	8551/3640 (0.0247)
Completeness to $\theta = 72.16$	100%	99%
Data/restraints/parameters	2439/0/179	3640/0/177
Goodness-of-fit on F^2	1.111	1.036
Final R indices [$I > 2\sigma(I)$]	$R_1 = 0.0346$, $wR_2 = 0.0938$	$R_1 = 0.0250$, $wR_2 = 0.0583$
R indices (all data)	$R_1 = 0.0348$, $wR_2 = 0.0940$	$R_1 = 0.0273$, $wR_2 = 0.0619$
Largest difference in peak and hole (e Å^{-3})	0.846 and −1.271	0.490 and −0.383

Table 3
Hydrogen bond geometry (Å, °) at 293(2) K

	D–H	H···A	D···A	Angle	Acceptor site symmetry
O1–H1···O3	1.22(6)	1.27(6)	2.482(3)	172(5)	
O4–H4···O2	0.82	2.20	2.789(4)	128.9	$x-1, y, z$
O4–H4···O3	0.82	2.53	3.220(4)	143.0	$x-1, y, z$
N1–H1A···O3	0.89	2.26	2.981(4)	138.3	$-x, y+0.5, -z+1.5$
N1–H1A···O4	0.89	2.56	3.290(4)	140.0	$-x, y+0.5, -z+1.5$
N1–H1A···O2	0.89	2.68	3.367(4)	135.3	$-x+1, y+0.5, -z+1.5$
N1–H1B···O5	0.89	1.93	2.806(4)	168.1	$x+1, y+1, z$
N1–H1B···O4	0.89	2.55	3.128(4)	123.7	$x+1, y+1, z$
N1–H1C···O1	0.89	2.15	2.945(4)	149.1	$x+1, y, z$

Table 4
Hydrogen bond geometry (Å, °) at 80(2) K

	D–H	H···A	D···A	Angle	Acceptor site symmetry
O1–H1···O3	0.71(3)	1.82(3)	2.473(2)	154(3)	
O4–H4···O2	0.82	2.22	2.800(2)	127.5	$x-1, y, z$
O4–H4···O3	0.82	2.47	3.169(2)	143.8	$x-1, y, z$
N1–H1A···O3	0.89	2.28	2.980(3)	135.4	$-x, y+0.5, -z+1.5$
N1–H1A···O4	0.89	2.63	3.314(3)	134.8	$-x, y+0.5, -z+1.5$
N1–H1A···O2	0.89	2.55	3.278(2)	139.7	$-x+1, y+0.5, -z+1.5$
N1–H1B···O5	0.89	1.89	2.776(2)	172.5	$x+1, y+1, z$
N1–H1B···O4	0.89	2.54	3.070(2)	118.9	$x+1, y+1, z$
N1–H1C···O1	0.89	2.10	2.911(2)	150.7	$x+1, y, z$

cooling unit. Purge was performed with a helium flux (20 mL/min). The crystalline product was powdered to obtain the sample and aluminum pans recommended for non-volatile substances were used for the sample and for the reference. An empty pan was used as the reference. Temperature calibration was performed with cyclohexane (Merck, GC, $x > 99.7\%$) and cyclopentane (Merck, GC, $x > 99.7\%$) [18]. DSC cooling and heating curves were traced at 10, 20 and 50 °C min^{-1} scanning rates, in the temperature range $-170\ °C \leqslant T \leqslant 25\ °C$.

3. Results and discussion

3.1. Structural properties

Tryptophan molecules can be divided in two parts: the hydrophobic ring and the hydrophilic amino-carboxylate tail. In cationic form the tail is positively charged with both the amine and carboxylic group protonated. The indole ring is practically planar, the five-membered ring has an average torsion angle of 0.36(14)° [0.96(9)° at 80 K] and the six-membered ring has an average torsion angle of 1.1(2)° [0.83(2)° at 80 K]. The least-squares plane of the indole ring makes an angle of 51.51(15)° [50.66(10)° at 80 K] with the carboxylic plane.

The stereographic projection about C_α–C_β (C2–C3) shows that the cation adopts a staggered conformation with N1 *gauche* to C4 that is *gauche* to C1. This conformation has been named the G+ conformer, according to Cao and Fisher [19]. This latter study, using ab initio molecular orbital calculations with a non-aqueous self-consistent reaction field (SCRF), identified three possible conformers of the zwitterionic aminoacid. The dominant conformer was found to be the one with N1 *gauche* to C4 that is *trans* to C1, determined by comparison of the predicted fundamental vibrational frequencies and intensities with the experimental IR spectra.

In the title compound the conformation of the positively charged aminoacid molecules practically does not change with the lowering of the temperature, as seen by the value of the torsion angles: N1–C2–C3–C4, 55.8(4)° and C1–C2–C2–C4 −65.8(4)° at room temperature and 55.2(2)° and −66.3(2)°, respectively, at low temperature.

The differences between the structure at room and low temperature are found in the geometry of the carboxylic group. While the length of the C–O double bond does not change significantly with temperature [1.232(4) Å and 1.237(2) Å for 80 K], the single C–O bond elongates from 1.278(4) Å to 1.288(3) Å as the temperature decreases. This suggests that the hydrogen atom in this group is closer to O1 at lower temperatures.

The geometry of the anion does not change much with the temperature as seen in Table 2. The $HSeO_3^-$ is pyramidal with one short Se–O bond, one long and another of intermediate length [Se–O3, 1.711(3) Å (at 293 K), 1.7224(16) Å (at 80 K)].

There is a hydrogen atom (H1) strongly shared between the anion (O3) and the cation (O1), in a strong H-bond

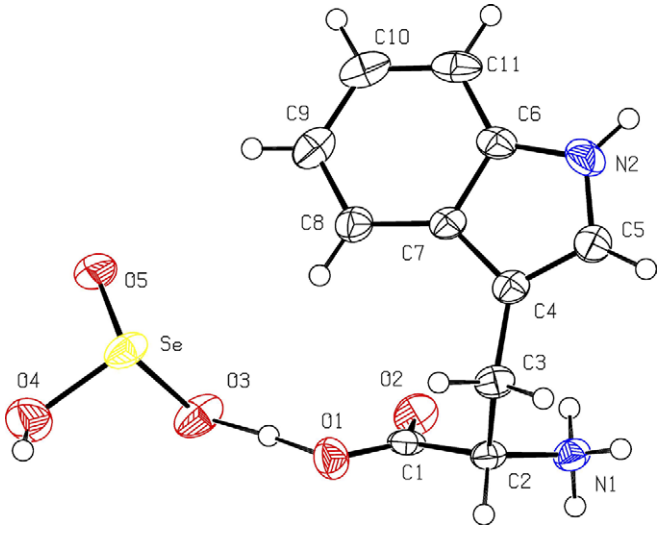

Fig. 1. ORTEPII plot of the title compound. Displacement ellipsoids are drawn at the 50% level.

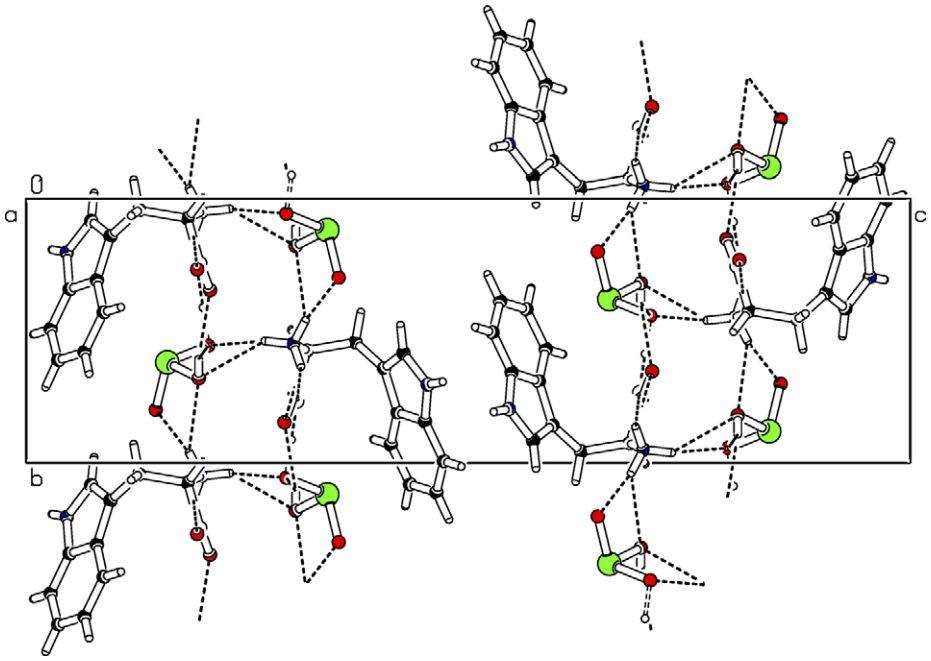

Fig. 2. Conventional hydrogen bond pattern viewed along the *a* axis.

(Fig. 1). The free refinement of this atom has shown that at room temperature H1 locates halfway between O1 and O3 as seen by the distances O1–H1 1.23(5) Å and O3–H1 1.26(5) Å. Difference electron density shows that the most likely explanation for such unusual O–H distances is that the proton is disordered between the O atoms. At low temperature O1–H1 decreases to 0.71(3) Å and O3–H1 increases to 1.82(3) Å, showing an ordering of the proton involved into an O1–H···O3 bond.

In the crystal, anions and cations assemble forming a vast 3-dimensional network of hydrogen bonds. The bond O4–H4···O3^{i} (i: $x-1,y,z$) links the selenite ions in chains along the *a*-axis. Also along the *a*-axis, the bond N1–H1C···O1^{ii} (ii: $x+1,y,z$) joins the cations in chains. Those chains are connected by other H-bonds between the anions and cations as described in Tables 3 and 4, where one can find bifurcated and trifurcated bonds.

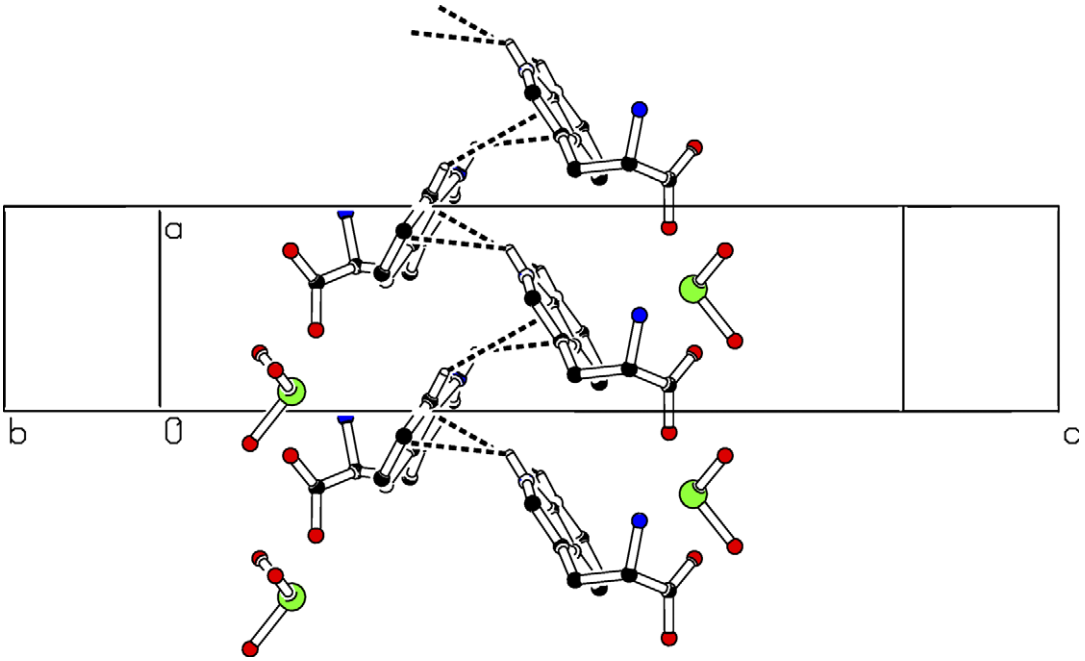

Fig. 3. X–H···π interactions shown as dashed lines. All hydrogen atoms not involved in these bonds were omitted for clarity.

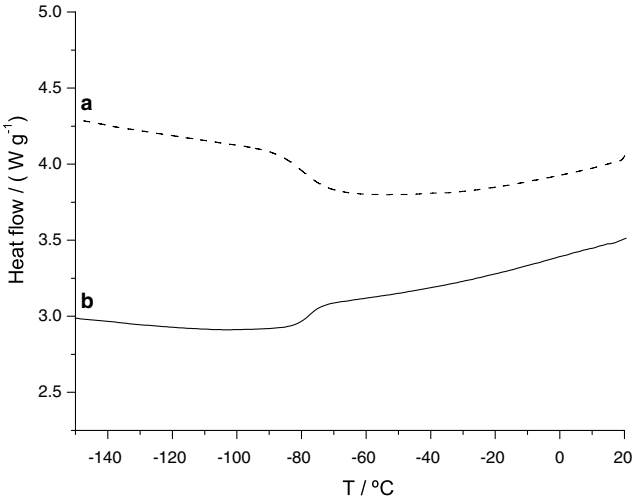

Fig. 4. Typical DSC L-tryptophanium hydrogen selenite (a) cooling curve and (b) heating curve, for the temperature range investigated.

Projecting the crystal packing down the *a*-axis one sees double layers of aminoacid tails and pyramidal anions strongly linked by hydrogen bonds (Fig. 2). Between those layers there are double layers of indole rings connected by N–H···π and C–H···π bonds, with the π electron system of the aromatic rings acting as the acceptor. The N2–H2 bond points towards the edge of the C6–C11 ring of a neighbouring molecule with the shared hydrogen situated above the centre ring. The H2-centroid distance is 2.681 Å, the interaction angle N2–H2···centroid is 127.83°, and the angle between the H2-centroid line and the ring perpendicular is 25.80°. This geometry is described as type III by Malone et al. [20]. The same geometry is seen in the intermolecular interaction, C11–H11···(N2–C6 centroid), with a slightly larger distance, 3.184 Å, and angle, 131.40°. Fig. 3 shows these intermolecular interactions joining the cations.

3.2. Thermal behaviour

The thermal behaviour of L-tryptophanium hydrogen selenite between $T = 25$ °C and $T = -170$ °C is illustrated in Fig. 4. For all scan rates investigated a second-order transition is observed on cooling. The behaviour is reversible on heating, with a transition temperature $T = -82.5$ °C. These observations are compatible with the existence of the hydrogen disorder at room temperature found in the X-ray experiments.

4. Conclusion

A new selenite compound has been synthesised and characterised by DSC and X-ray single crystal diffraction. The crystal structure of the L-tryptophanium hydrogen selenite has been solved at room and low temperature. An ordering of a hydrogen atom shared between the anion and the cation is seen and that is the probable cause of the DSC observed anomaly at −82.5 °C.

Acknowledgement

This work was supported by Fundação para a Ciência e a Tecnologia under project POCI/FIS/57876/2004.

Appendix A. Supplementary material

Crystallographic data for structural analysis have been deposited with the Cambridge Crystallographic Data Center, CCDC No. 284629 for the room temperature phase and 284630 for the low temperature phase. Copies of this information may be obtained free of charge on application to CCDC, 12 Union Road, Cambridge CB2 1EZ, UK (fax: +44 1223 336033; e-mail: deposit@ccdc.cam.ac.uk or http://www.ccdc.cam.ac.uk). Supplementary data associated with this article can be found, in the online version, at doi:10.1016/j.poly.2005.12.028.

References

[1] E. de Matos Gomes, A. Matos Beja, J.A. Paixão, L. Alte da Veiga, M. Ramos Silva, J. Martín-Gil, F.J. Martín-Gil, Z. Kristallogr. 210 (1995) 929.
[2] J.A. Paixão, M. Ramos Silva, A. Matos Beja, E. Matos Gomes, L. Alte da Veiga, J. Martín-Gil, F.J. Martín-Gil, Z. Kristallogr. 212 (1997) 51.
[3] J.A. Paixão, A. Matos Beja, M. Ramos Silva, E. Matos Gomes, L. Alte da Veiga, J. Martín-Gil, F.J. Martín-Gil, Acta Cryst. C 53 (1997) 1113.
[4] E. de Matos Gomes, E. Nogueira, I. Fernandes, M. Belsley, J.A. Paixão, A. Matos Beja, M. Ramos Silva, J. Martín-Gil, F. Martín-Gil, J.F. Mano, Acta Cryst. B 57 (2001) 828.
[5] R. Pepinsky, K. Vedam, Phys. Rev. 114 (1959) 1217.
[6] K. Vedam, Y. Okaya, R. Pepsinsky, Phys. Rev. 119 (1960) 1252.
[7] L.A. Shuvalov, N.R. Ivanov, T.K. Sitnik, Sov. Phys. – Crystallogr. 12 (1967) 315.
[8] Y. Makita, J. Phys. Soc. Jap. 20 (1965) 1567.
[9] L.A. Sannikov, N.R. Ivanov, T.K. Stinik, Sov. Phys. Crystallogr. 12 (1967) 315.
[10] V.V. Gladkii, V.A. Krikov, V.K. Magataev, L.A. Shuvalov, Sov. Phys. – Solid State 19 (1977) 167.
[11] M. Vijayan, Acta Cryst. B 24 (1968) 1237.
[12] O.R. Evans, W. Lin, Chem. Mater. 13 (2001) 3009.
[13] W. Lin, O.R. Evans, R.-G. Xiang, Z. Wang, J. Am. Chem. Soc. 120 (1998) 13272.
[14] A.P. Demchenko, Luminescence 17 (2002) 19.
[15] A.H.A. Clayton, W.H. Sawyer, Eur. Biophys. J. 31 (2002) 9.
[16] J.W. Pietrich, M.C. Chang, D.B. McDonald, G.R. Fleming, J. Am. Chem. Soc. 105 (1983) 3824.
[17] G.M. Sheldrick, SHELXS-97 and SHELXL-97, University of Gottingen, Germany, 1997.
[18] R. Sabbah, X.W. An, J.S. Chickos, M.L.P. Leitão, M.V. Roux, L.A. Torres, Thermochim. Acta 331 (1999) 93.
[19] X. Cao, G. Fischer, Phys. Chem. A 103 (1999) 9995.
[20] J.F. Malone, C.M. Murray, M.H. Charlton, R. Docherty, A.J. Lavery, J. Chem. Soc., Faraday Trans. 93 (1997) 3429.

unsaturated, or contain readily exchangeable ligands, such as water or other solvent components [5].

The use of amino acid-derived Schiff bases as model systems has been mainly justified by the participation of these ligands in similar biological compounds in key biological reactions [2–10]. The magnetic, electrochemical and spectroscopic studies of the synthetic systems provide important information about redox and spin states of the metal centre(s), the magnitude of the exchange interaction, and the coordination environment which has a profound influence on the functional properties of the complexes. These models also allow structure and the magnetic, electronic, and optical properties of the metal sites present in biological systems to be correlated [11–15].

In a recent paper on $Fe_2(\mu\text{-carboxylate})_2(L_2)_2$ complexes, where L is a Schiff base derived from an α-amino acid and salycilaldehyde, we postulated that the dimeric iron(III) complexes are hexacoordinated, the metal ion being surrounded by water molecules, the salicylidenimine ligand and bridging carboxylate groups [16]. In this work, we report the synthesis of mixed valence dinuclear iron(II,III) complexes of the type $[Fe_2L_2(H_2O)_4](NO_3)(H_2O)_3$, where L is a Schiff base derived from an α-amino acids (glycine or L-isoleucine) and 5-bromosalicylaldehyde (Fig. 1). We have characterised these complexes using different spectroscopic techniques, plus magnetic susceptibility, conductivity, and electrochemical measurements.

2. Experimental

The reagents 5-bromosalicylaldehyde, glycine (Gly) and L-isoleucine (Ile) were purchased from Merck (analytical grade) and were used without further purification.

The ligands were synthesised as described by Paredes et al. [16] (yields 73–85%). Both ligands synthesised by this method are solids and were isolated as potassium salts. They were characterised by elemental analysis, and FTIR, UV–Vis and ^{1}H NMR spectroscopic methods.

The mixed valence complexes were prepared as described by Casella et al. [17]. The ligand (1 mmol) was dissolved in methanol at room temperature, and 1 mmol of potassium hydroxide was added. Finally, $Fe(NO_3)_3 \cdot 9H_2O$ (1 mmol), was added directly to the solution. The reaction mixture was left for 5–6 h at room temperature with continuous stirring under nitrogen. The KNO_3 formed was filtered off and the solution was concentrated; the product was precipitated with *n*-hexane and was dried under vacuum. The complexes synthesised by this method are dark violet amorphous solids with molecular formulae $[Fe_2L_2(H_2O)_4](NO_3)(H_2O)_3$ (yields 60–70%). In general, the complexes are highly insoluble in most low-polarity organic solvents and, unfortunately, single crystals suitable for X-ray diffraction were not obtained.

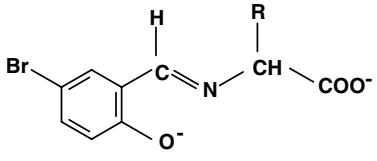

R = H, N-5-bromosalycylideneglycine
R = sec-Bu, N-5-bromosalicylideneisoleucine

Fig. 1. Structural formulae for Schiff base ligands (L^{2-}) derived from glycine, isoleucine and 5-bromosalicylaldehyde.

*$[Fe_2(BrSA\text{-}Gly)_2(H_2O)_4](NO_3)(H_2O)_3$ (**1**):* Yield: 73%. *Anal.* Calc. for $C_{18}H_{26}Br_2N_3O_{16}Fe_2$: C, 26.63; H, 3.23; N, 5.18; Fe, 13.76. Found: C, 25.81; H, 3.14; N, 5.31; Fe, 13.41%. Conductivity in DMF at 25 °C, $\Lambda = 64.5$ S cm^2 mol^{-1} L.

*$[Fe_2(BrSA\text{-}Ile)_2(H_2O)_4](NO_3)(H_2O)_3$ (**2**):* Yield: 76%. *Anal.* Calc. for $C_{26}H_{42}Br_2N_3O_{16}Fe_2$: C, 33.79; H, 4.58; N, 4.55; Fe, 12.08. Found: C, 34.71; H, 4.41; N, 4.67; Fe, 12.44%. Conductivity in DMF at 25 °C, $\Lambda = 64.0$ S cm^2 mol^{-1} L.

Microanalyses were performed with a Fisons elemental analyzer, model EA1108, and with a Shimadzu atomic absorption spectrophotometer, model AA-6200. The infrared spectra (KBr pellets) were recorded using a Bruker spectrophotometer, model AMX300. The Mössbauer spectra of these complexes, as fine powder samples, were obtained with a conventional spectrometer with constant acceleration. The source was 10 mCi ^{57}Co in a Pd matrix. The gamma ray detection was carried out with a Reutes–Stokes detector connected to an Ortec amplifying and selecting system. A 1024 channel Canberra multichannel analyser was used for the data acquisition. The Mössbauer spectra were recorded at 298 K in the absence of an external magnetic field. The reported isomer shift values are relative to sodium nitroprusside. Electrochemical studies were done with a PAR 173 potentiostat and PAR 175 programmer, equipped with a digital coulometer model 179. Polarographic measurements were done with a BAS CV27 cyclic voltammetry setup. Molar conductance was measured at 25 °C on a Radiometer conductimeter, model CDM-83 with a CDC-304 electrode. Cyclic voltammograms of the complexes were recorded in DMF with [TBA][PF_6] as supporting electrolyte in the potential range +1.3 to −1.8 V versus SCE. Ferrocenium was used as an internal reference. Electronic spectra were recorded on a Unicam II UV-Vis spectrophotometer. Variable temperature magnetic susceptibility data (5–300 K) were obtained with a CRYOGENICS Model S600 SQUID susceptometer–magnetometer, calibrated with Hg[$Co(SCN)_4$]. The diamagnetic corrections were calculated from Pascal's constants [18].

3. Results and discussion

The complexes can be considered as species with two six-coordinated iron centres, with the metal ions surrounded by water molecules, and the salicylaldimine ligand coordinated through the imine nitrogen and the phenolic oxygen, constituting a NO_5 donor set. Both metal ions are bridged by the carboxylate groups of the amino acids residues, Fig. 2.

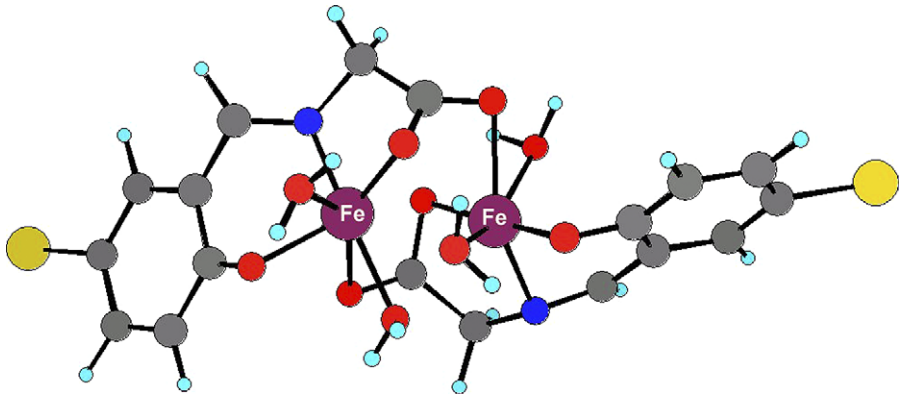

Fig. 2. Structures of dinuclear iron(II,III) complexes with Schiff bases derived from 5-bromosalicylaldehyde and α-amino acids (R = H, Sec-Bu).

3.1. Infrared and UV–Vis spectra

The mixed valence complexes show the same pattern for analogous vibrations. The vibration of the –C=N bond in the complexes is displaced towards lower energies, in comparison with the free ligand (15 cm^{-1} for (**1**) and 21 cm^{-1} for (**2**)). The $–C–O_{phenolic}$ group band is displaced to higher energies (~30 cm^{-1} in both complexes). Two strong bands at 1362–1372 and 1527–1529 cm^{-1}, associated with symmetric and asymmetric stretching absorptions of the carboxylate group, also show a decrease in energy in respect to the free ligand. The difference between these bands is correlated with the coordination mode of the carboxylate ligands. For the free ligands the differences between ν_a and ν_s ($\Delta\nu$) of the carboxylate groups are 224 and 230 cm^{-1} for the glycine and isoleucine Schiff base ligands, respectively. In the complexes, $\Delta\nu$ has a value of about 170 cm^{-1}, indicative of a bridging carboxylate group between the two metal atoms [19–21]. The spectra of the two complexes show a broad band at 3400 cm^{-1} due to coordinated water molecules. The single absorption at 1383 cm^{-1} is indicative of an ionic nitrate group [21].

In agreement with the infrared data and reported assignments for analogous diiron(III) complexes [16], it is possible to infer that each iron ion in these mixed valence complexes has a hexa-coordinated environment, in which the metal ion is coordinated to two water oxygens, a phenol oxygen, an imine nitrogen and two carboxylate oxygen atoms; the latter groups bridging both iron atoms (Fig. 2).

The electronic spectra of the complexes are strongly dominated by the electronic transitions due to the iron-salicylaldiminate cromophores. The charge transfer bands, from phenolate to the metal, are of intermediate intensity, appear near 450 nm, and are responsible for the red-purple colour of the complexes. These transitions can be assigned to a charge transfer from the pπ orbital of the phenolic oxygen to the dπ orbital of the iron centre [22,23].

3.2. Mössbauer spectroscopy

To assign the oxidation states of the iron centres in these dinuclear complexes, Mössbauer spectroscopy was used, since the isomer shift and the quadrupolar splitting can be related directly to populations of valence shell orbitals. Fig. 3 shows a representative spectrum and the fit of the data using least squares. The Mössbauer parameters obtained for the iron complexes are summarised in Table 1.

The Mössbauer spectra of both complexes exhibit two highly asymmetric quadrupole doublets. The integrated absorption intensities of the two spectral subcomponents show a 1:1 ratio, and therefore the relative amount of iron in both sites is the same.

For the first site of complex (**1**) the isomer shift (δ_1) is 0.51 mm s^{-1} and for complex (**2**) it is 0.56 mm s^{-1}. The quadrupolar splitting values (ΔE_{Q1}) are 0.91 mm s^{-1} for (**1**) and 0.96 mm s^{-1} for (**2**). These data correspond to high spin iron(III) ions ($S = 5/2$, $^6A_1$) [16,24–27]. For the second site, the chemical shifts (δ_2) are 1.40 mm s^{-1} for (**1**) and 1.41 mm s^{-1} for (**2**). The quadrupolar splitting (ΔE_{Q2}) is 2.68 mm s^{-1} for (**1**) and 2.65 mm s^{-1} for (**2**); these values correspond to high spin iron(II) ($S = 2$, $^5T_2$) [25–27].

On the other hand, complexes (**1**) and (**2**) have similar hyperfine parameters for site one. This allows us to assume that the coordination sphere and distortion of the octahedral geometry are the same for both complexes. The previous analysis can also be applied to the second site, since the hyperfine values for the two complexes are comparable. Furthermore, in these Fe(II,III) complexes, the iron(III) ion has a lower electronic density and a greater distortion of the octahedral geometry than in the analogous

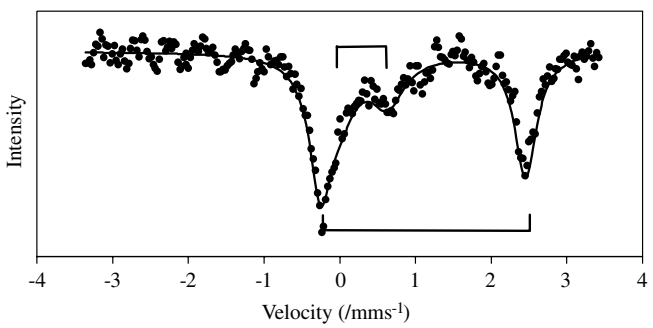

Fig. 3. Mössbauer spectrum for (**1**) at 300 K.

Table 1
Mössbauer parameters for dinuclear mixed valence complexes at 298 K

Complexes	I.S.[a] (mm s^{-1})		ΔE_Q[b] (mm s^{-1})		A_1/A_2[c]
	Site 1	Site 2	Site 1	Site 2	
(**1**)	0.51	1.39	0.91	2.67	1.05
(**2**)	0.56	1.41	0.96	2.65	1.32

The values of the chemical shifts are referred to sodium nitroprusside.
[a] Isomer shift.
[b] Quadrupolar splitting.
[c] Area ratio.

Fe(III,III) complexes ($\delta = 0.61$–0.66 mm s^{-1}, $\Delta E_Q = 0.70$–0.76 mm s^{-1}).

Lippard et al. have shown that high spin iron(II) dinuclear complexes with carboxylate bridges have a smaller isomer shift when the coordination number is lower [28]. For example, iron (II) sites with coordination number four tend to have a smaller isomer shift (1.0–1.1 mm s^{-1}) compared with those with coordination number six (1.3 mm s^{-1} approximately). The same authors also found that the carboxylate bridged diiron(II) species with a single N and variable number of O donor atoms present different isomer shifts. Iron(II) centres with a tetrahedral environment have an isomer shift of 1.04 mm s^{-1}. However diiron(II) complexes with an NO_4 environment in a square pyramidal geometry have an isomer shift of 1.12 mm s^{-1}, while in pentacoordinated complexes with a trigonal bipyramidal geometry the isomer shift is 1.19 mm s^{-1}. Finally, octahedral complexes with an NO_5 coordination sphere have an isomer shift of 1.35 mm s^{-1}. In our case, the Mössbauer data obtained for the two complexes show that the isomer shift for the iron(II) site is 1.40 mm s^{-1}, corroborating an octahedral arrangement for this type of iron centres. Consequently, it is correct to propose for complexes (**1**) and (**2**) a mixed valence (II,III) species with a pseudo-octahedral arrangement for each iron atom.

3.3. Cyclic voltammetry

The electrochemical behaviour of the dinuclear complexes was studied by cyclic voltammetry. The redox parameters are summarised in Table 2. The redox processes were observed at essentially identical potentials for complex (**1**) and complex (**2**). This result is indicative of a similar electronic environment for the metal ions in both complexes. Fig. 4 shows the voltammogram of mixed valence complex (**1**). In the first cycle (reduction sweep), only two redox processes are seen; the first peak at −0.51 V can be attributed to the Fe(II,III)/Fe(II,II) redox process and the second peak at −0.90 V, that involves more than one electron, may be assigned to the reduction of the Fe(II,II) species. In the oxidation sweep, it is possible to observe three processes: the first one at −1.00 V, can be assigned to the regeneration of the Fe(II,II) species; the second process at −0.53 V involves the formation of the Fe(II,III) species, and the third process at −0.18 V can be assigned to the formation of the Fe(III,III) species. In the second cycle a new reduction process at −0.18 V corresponding to the Fe(III,III)/Fe(II,III) reduction process is observed. In summary, in the first cycle it is possible to find only two reduction processes and three oxidation processes, while after this cycle, three reduction and three oxidation processes are detected, with half wave potentials at $E^1_{1/2} = -0.21$ V, $E^2_{1/2} = -0.48$ V and $E^3_{1/2} = -0.95$ V. Complex (**2**) shows a similar behaviour as complex (**1**), with half wave potentials at $E^1_{1/2} = -0.22$ V, $E^2_{1/2} = -0.50$ V and $E^3_{1/2} = -1.13$ V.

The redox processes are quasireversible and correspond to a diffusion-controlled process. It is important to remark that under the same experimental conditions, the cyclic voltammograms for the free ligands do not present any redox process, and therefore all the redox process observed can be attributed to the metal centres.

Previous work on the substituent effect on the electrochemical potentials was done for a series of [FeIII-(X–SA)$_2$trien]$^+$ complexes, (where SA = salicylaldehyde, trien = triethylamine, and X represents different substituents on the benzene ring, such as, H, NO_2, OCH_3, Br, Cl) [29,30]. The redox process in these complexes involves a one-electron transfer, which was assigned to the Fe(III)/Fe(II) reduction. The half wave potentials vary between −0.21 and −0.53 V versus SCE, depending on the substituent. For example, electron-donating groups such as OCH_3 make the metal centre more electron-rich thus hindering the reduction process. Electron-withdrawing groups, such as Cl, Br or NO_2, have an opposite effect on the reduction process [29–31].

A similar result is obtained for complexes (**1**) and (**2**) as seen in the second cycle; the bromine-substituted complexes have their redox processes at lower potentials than the analogous unsubstituted diiron(III) complexes. This difference may be attributed to the inductive effect of the bromine atom on the benzene ring. From the difference of the redox potentials, $E_2 - E_1 = (RT/F)\mathrm{Ln}K$, the conproportionation constant K at 293 K of the following reaction can be calculated.

$$Fe^{II}Fe^{II} + Fe^{III}Fe^{III} \rightarrow 2Fe^{II}Fe^{III}$$

Table 2
Electrochemical data for dinuclear mixed valence complexes[a]

Complexes	Redox wave	E_{pa}	E_{pc}	ΔE	$E_{1/2}$	i_{pa}/i_{pc}
(**1**)	I	−0.18	−0.24	0.04	−0.21	0.45
	II	−0.43	−0.53	0.10	−0.48	1.07
	III	−0.90	−1.00	0.10	−0.95	1.17
(**2**)	I	−0.20	−0.24	0.04	−0.22	0.63
	II	−0.44	−0.56	−0.12	−0.50	0.76
	III	−0.92	−1.24	0.32	−1.13	0.76

[a] Potential values are in volts and referred to SCE. E_{pa} and E_{pc} are the anodic and cathodic peak potentials respectively. $\Delta E = E_{pa} - E_{pc}$; $E_{1/2} = (E_{pa} + E_{pc})$.

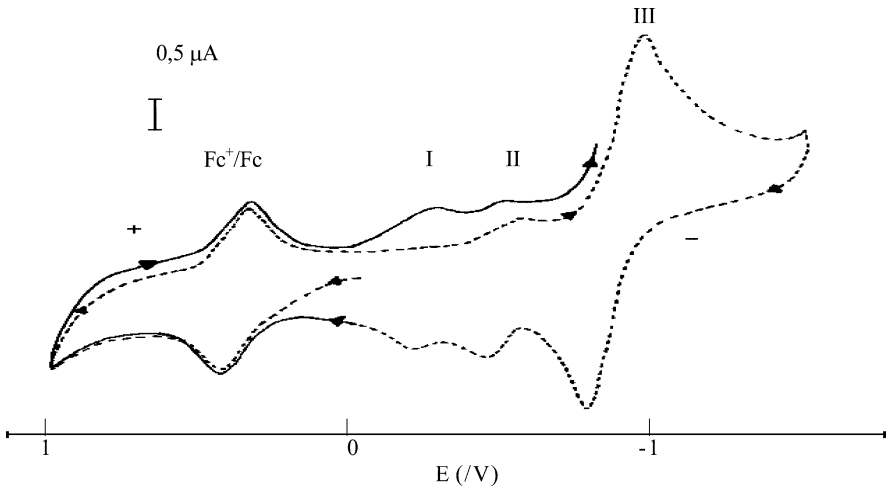

Fig. 4. Cyclic voltammogram of (**1**).

The K values obtained for the complexes were 3.7×10^4 and 5.4×10^4 for (**1**) and (**2**), respectively. These values are consistent with moderate electron coupling and charge delocalisation between the metal centres.

The degree of interaction between the two centres depends on the bridging ligand and on the nature of the metal. For example, a molybdenum complex with perfluorophthalate as bridging ligand presents a K value of 13. However, when the ligand is oxalate the K value is 5.4×10^4; the greater delocalisation is attributed to the shorter bridging group. On the other hand, when molybdenum is substituted by tungsten, in the oxalate complex, the K value is 1.3×10^{12}, that is, the extent of delocalisation is increased [32].

3.4. Magnetic susceptibilities

The magnetic susceptibilities of $[Fe_2(L_2(H_2O)_4](NO_3)\text{-}(H_2O)_3$ were recorded over the temperature range 5–300 K. The plot of the reciprocal molar susceptibility versus temperature for complex (**1**) is shown in Fig. 5, and corresponds to a Curie–Weiss behaviour. The glycine-derived Schiff base complex has an effective magnetic moment per molecule (μ_{eff}), which decreases from 6.82 μ_B at 300 K to 5.96 μ_B at 5 K. The trend is similar for (**2**), that is, μ_{eff} is 6.65 μ_B per molecule at 300 K and decreases to 5.96 μ_B at 5 K. For these complexes the μ_{eff} values at 300 K are lower than the expected spin-only value of 7.68 μ_B for the moment of two independent high spin iron(III) and iron(II) ions ($S = 5/2$, $S = 2$). The decrease of μ_{eff} at lower temperature indicates that the two iron centres are weakly antiferromagnetically coupled.

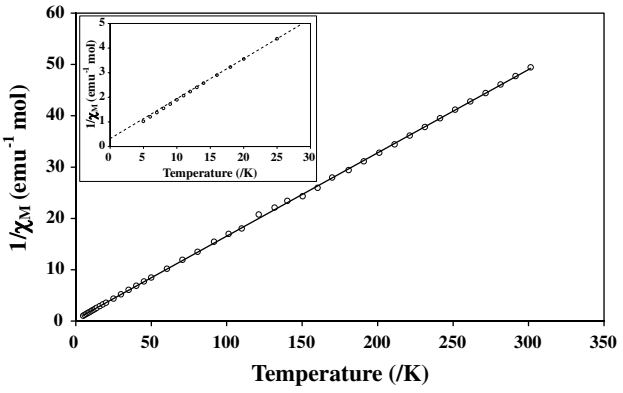

Fig. 5. Temperature dependence of the reciprocal molar susceptibility for (**1**).

The magnetic susceptibility of the mixed valence binuclear iron(II,III) complexes was analysed using the van Vleck equation, with a spin exchange Hamiltonian $\boldsymbol{H} = -2JS_1 \times S_2$, where $S_1 = 5/2$ and $S_2 = 2$. All the calculations were performed using a least-squares minimisation routine, where $\mathrm{SSQ} = \sum_i [(\chi_i^{obs} - \chi_i^{calc})/\chi_i^{obs}]^2$. The parameter $R = \mathrm{SSQ}/(n-p)$, where n is the number of experimental points and p is the number of parameters allowed to vary in the minimisation routine, is reported. The final magnetic parameters obtained for complexes (**1**) and (**2**) are $J = -0.17\ \mathrm{cm}^{-1}$, $g = 2.62$, $\theta = -2.50$ and $J = -\ 0.14\ \mathrm{cm}^{-1}$, $g = 2.53$ $\theta = -2.23$ K, respectively, indicating that the two iron ions are weakly antiferromagnetically coupled.

The results obtained for complexes (**1**) and (**2**), are comparable to those obtained for dinuclear iron(III) complexes with analogous ligands, in which the J values vary between -0.09 and $-0.21\ \mathrm{cm}^{-1}$ as reported in previous work, and as shown in Table 3 [16].

On the other hand, these values can be also compared with those reported for other carboxylate-bridged complexes, in which the magnetic properties of the diiron complexes depend significantly on metal–metal distances, as well as on the nature of the other bridging ligands [30]. Table 3 presents the J values for a series of different dinuclear iron complexes with carboxylates bridged. Nevertheless, according to these data, it is possible to infer that the weak antiferromagnetic coupling interaction exhibited by complexes (**1**) and (**2**) can be explained by a large distance

Table 3
Magnetic parameters for carboxylate-bridged iron complexes

Complexes	Distance Fe···Fe (Å)	J (cm^{-1})	Ref.
Fe^{II}–Fe^{III}			
(**1**)		−0.17	this work
(**2**)		−0.14	this work
$[Fe_2(salmp)_2]^-$ [a]	3.080	+8.6	[33]
$[Fe_2(O_2CCH_3)_2(TPA)_2]$ $(BPh_4)_2$ [b]	4.288	−1.0	[34]
$[Fe_2(bpmp)(\mu\text{-}O_2CC_2H5)_2]^+$ [c]	3.365	−2.5	[33]
$[Fe_2(\mu\text{-}OH)(\mu\text{-piv})_2](ClO_4)_2$ [d]	3.400	−12.9	[35]
Fe^{II}–Fe^{II}			
$[Fe_2(\mu\text{-XDK})(\mu\text{-}O_2CPh)$-$(ImH)_2(O_2CPh)(MeOH)]$ [e]	3.609	−0.51	[36]
$[Fe_2(\mu\text{-}O_2CAr)_2(O_2CAr)_2L_2]$ [f]	4.218	−0.90	[19]
$[Fe_2(O_2CH)_4(BIPhMe)_2]$ [g]	3.575	−0.16	[37]
$[Fe_2O(O_2CH)_4(BIPhMe)_2]$ [g]	3.211	−31.0	[37]
Fe^{III}–Fe^{III}			
$[Fe_2L_2(H_2O)_4](NO_3)(H_2O)_3$ [h]		−0.12	[16]
$[Fe_2L_2(H_2O)_4](NO_3)(H_2O)_3$ [h]		−0.12	[16]
$[Fe_2(O_2CCH_3)_2L_2](ClO_4)$ [i]	4.482	−1.5	[38]
$[Fe_2(OH)(OAc)_2(HBpz_3)_2]$ [j]	3.439	−17.0	[39]
$[Fe_2(\mu\text{-O})(\mu\text{-pivalate})_2](ClO_4)_2$ [d]	3.123	−111.0	[35]
$[Fe_2O(OAc)_2(HBpz_3)_2]$ [j]	3.145	−121.0	[39]

[a] salmp = bis(salicylidenamino)-2-methylphenolate.
[b] TPA = tris(2-pyridylmethyl)amine.
[c] bpmp = 2,6-bis[bis(pyridylmethyl)aminomethyl]-4-methylphenolate.
[d] piv = pivalic acid.
[e] KDX = Kemp's derived triacid.
[f] L = C_5H_5N.
[g] BIPhMe = 2,2′-bis-(1-methylimidazolyl)phenyl methoxymethane.
[h] L = salyciledeneamino acids.
[i] L = *N*,*N*′-dimethyl-*N*,*N*′-bis(2-pyridylmethyl ethane)-1,2-diamine.
[j] $HBpz_3$ = hydrotris(1-pyrazolyl)borato.

between both metal centres, and by the absence of a more efficient exchange pathway such as oxo, hydroxo or alkoxo bridges [16,19,33–39].

4. Conclusions

Two hexacoordinated mixed valence complexes, with an NO_5 coordination sphere, were obtained with Schiff base ligands derived from 5-bromosalicylaldehyde and glycine (**1**) or isoleucine (**2**). The FTIR data show that each ligand is coordinated to the metal centres through the imine nitrogen, phenolic oxygen and carboxylate groups, which also act as bridging ligands between both iron atoms. The remaining coordination positions are occupied by water molecules.

With Mössbauer spectroscopy it was possible to find two sites for the iron atoms. The isomer shifts and quadrupolar splittings for both sites correspond to high spin Fe(II) and Fe(III). The hyperfine values obtained for both complexes are comparable, and indicate that these complexes have a greater distortion than analogous Fe(III,III) complexes.

From cyclic voltammetry the presence of a mixed valence Fe(II,III) complex was confirmed. In the case of the studied bromine-substituted ligands, the complexes show lower values for all the redox potentials as compared to the complexes with unsubstituted ligands. This difference is attributed to the presence of the electron-withdrawing groups on the aromatic ring.

Magnetic susceptibility data for complexes (**1**) and (**2**) show that the two iron centres have a weak antiferromagnetic exchange coupling, which is principally attributed to three factors: (i) the strong distortion of the octahedral geometry, (ii) relatively large Fe-Fe distance and (iii) the absence of a more efficient exchange pathway. The J values obtained for both complexes are comparable to other dinuclear iron complexes with carboxylate bridges.

From the complete analyses done in this work, it is important to remark that when 5-bromosalicylaldehyde is used to form the Schiff base, a mixed valence species is obtained. Apparently the electronic effect of the bromine atom in the aromatic ring stabilises a mixed valence species.

Acknowledgement

Financial support for this work provided by FONDECYT 2960043, FONDAP 11980002 and PICS 922 Grants is gratefully acknowledged.

References

[1] A.L. Feig, S.J. Lippard, Chem. Rev. 94 (1994) 759.
[2] E.I. Solomon, T.C. Brunold, M.I. Davis, J.N. Kemsley, S.K. Lee, N. Lehnert, F. Neese, A.J. Skulan, Y.S. Yang, J. Zhou, Chem. Rev. 100 (2000) 235.
[3] B.J. Wallar, J.D. Lipscomb, Chem. Rev. 96 (1996) 2625.
[4] M. Merkx, D.A. Kopp, M.H. Sazinsky, J.L. Blazyk, J. Müller, S.J. Lippard, Angew. Chem., Int. Ed. Engl. 40 (2001) 2782.
[5] E.Y. Tshuva, S.J. Lippard, Chem. Rev. 104 (2004) 987.
[6] R.H. Holm, P. Kennepohl, E.I. Solomon, Chem. Rev. 96 (1996) 2239.
[7] E.I. Solomon, D.W. Randall, T. Glaser, Coord. Chem. Rev. 200–202 (2000) 595.
[8] S.J. Lippard, Angew.Chem., Int. Ed. Engl. 27 (1988) 344.
[9] F. Dianzhong, W. Bo, Trans. Met. Chem. 18 (1993) 101.
[10] R.E. Norman, S. Yan, G. Backes, J. Ling, S. O'Connor, J.H. Zhang, L. Que, J. Am. Chem. Soc. 112 (1990) 1554.
[11] W. Kwik, A.W.N. Tay, Tetrahedron 9 (1990) 1293.
[12] L. Canali, D.C. Sherrington, Chem. Soc. Rev. 28 (1999) 85.
[13] Y.Z. Voloshin, O.A. Varzatskii, E. Tkachenko, Y.A. Maletin, S.P. Degtyarov, D.I. Kochubey, Inorg. Chim. Acta 255 (1997) 255.
[14] (a) G. Blondin, J. Girerd, Chem. Rev. 90 (1990) 1359;
(b) D.M. Kurtz, Chem. Rev. 90 (1990) 585;
(c) J. Vincent, G. Olivier, B. Averill, Chem. Rev. 90 (1990) 1447;
(d) S. Lippard, Angew. Chem., Int. Ed. Engl. 27 (1988) 344.
[15] A. Nivorozhkin, P. Mialane, R. Davydov, J. Guilhem, J.J. Girerd, S. Styring, Inorg. Chem. 36 (1997) 846.
[16] V. Paredes-García, R.O. Latorre, E. Spodine, Polyhedron 23 (2004) 1869.
[17] L. Casella, M. Gullotti, A. Pintar, L. Messori, M. Györ, Inorg. Chem. 26 (1987) 1031.
[18] A. Earnshaw, Introduction to Magnetochemistry, Academic Press, London, 1968.
[19] D. Lee, S.J. Lippard, Inorg. Chem. 41 (2002) 2704.
[20] D. Sattari, E. Alipour, S.J. Shirani, Inorg. Biochem. 45 (1992) 115.
[21] K. Nakamoto, Infrared and Raman Spectra of Inorganic Coordination Compounds, Wiley, New York, 1986, pp. 232.

[22] K. Ramesh, R. Mukherjee, J. Chem. Soc., Dalton Trans. (1992) 83.
[23] D. Cook, D. Cummins, E.D. McKenzie, J. Chem. Soc., Dalton Trans. (1976) 1369.
[24] S. Herold, S.J. Lippard, Inorg. Chem. 36 (1997) 50.
[25] G. Long, Mössbauer Spectroscopy Applied to Inorganic Chemistry, Plenum Press, New York, 1984, p. 43.
[26] L. May, An Introduction to Mössbauer Spectroscopy, Plenum Press, New York, 1971.
[27] V.I. Gol'danskii, R.H. Herber, Chemical Applications of Mössbauer Spectroscopy, Academic Press, New York, 1968.
[28] S. Yoon, S.J. Lippard, J. Am. Chem. Soc. 127 (2005) 8386.
[29] A. Bettelheim, R. Paresh, O. Dozen, J. Electrochem. Soc. 129 (1982) 2247.
[30] K. Kadish, C.H. Su, J. Wilson, Inorg. Chem. 21 (1982) 2312.
[31] D. Lee, J.L. DuBois, B. Pierce, B. Hedman, K.O. Hodgson, M.P. Hendrich, S.J. Lippard, Inorg. Chem. 41 (2002) 3172.
[32] A.W. Bott, Curr. Separ. 16 (1997) 61.
[33] G. Peng, J. van Elp, H. Hang, L. Que Jr., W.H. Armstrong, S.P. Cramer, J. Am. Chem. Soc. 117 (1995) 2515.
[34] S. Ménage, Y. Zang, P. Hendrich, L. Que Jr., J. Am. Chem. Soc. 114 (1992) 7786.
[35] U. Bossek, H. Hummel, T. Weyhermüller, E. Bill, K. Wieghardt, Angew. Chem., Int. Ed. Eng. 34 (1995) 2642.
[36] (a) S. Herold, S.J. Lippard, J. Am. Chem. Soc. 119 (1997) 145;
(b) V. Grillo, R. Hanson, W.H. Trevor, L. Gaham, K. Murray, B. Molubaraki, J. Chem. Soc., Dalton Trans. (1997) 305.
[37] W.B. Tolman, S. Liu, J.G. Bensten, S.J. Lippard, J. Am. Chem. Soc. 113 (1991) 152.
[38] R. Hazell, K.B. Jensen, J. McKenzie, H. Toftlund, J. Chem. Soc., Dalton Trans. (1995) 707.
[39] W.H. Armstrong, A. Spool, G.C. Papaefthymiou, R.B. Frankel, S.J. Lippard, J. Am. Chem. Soc. 106 (1984) 3653.

addition, two silver complexes containing quinone ligand, which do not need redox stabilizing ligands, that are analogous to the title complexes have also been reported. In these cases, the Ag–O distances are long, 2.37–2.47 Å [9,14].

In light of these reports, and as part of our continuation of silver coordination chemistry investigation [15–19], we have endeavored to discover what catechol structures could be used to obtain stable, characterizable silver complexes and to better understand silver catechol reactivity. We now report that stable silver catechol complexes can be prepared but that the ability to obtain these complexes is limited to catechols having highly electron-withdrawing substituents (four halides, in these examples); yet they still require triphenylphosphine ligand stabilizers. The preparation and solid-state structures of these first stable silver catechol complexes, bis-triphenylphosphine-tetra-halocatechol silver, are described below.

2. Experimental

2.1. Preparation of $Ag(Br_4C_6(OH)O)(Ph_3P)_2$

Solution ligand exchange of the catechol with silver acetate was successfully utilized to isolate the title complex according to the following scheme:

$$Ag(O_2CCH_3)(Ph_3P)_2 + Br_4C_6(OH)_2 \rightarrow Ag(Br_4C_6(OH)O)(Ph_3P)_2 + HO_2CCH_3$$

To 134 mg of $Ag(O_2CCH_3)(Ph_3P)_2$ [20] was added 7 mL toluene and 88 mg tetra-bromocatechol, $Br_4C_6(OH)_2$ (Aldrich). A clear yellow solution resulted, which was layered with an equal volume of ether. Yellow crystals (0.12 g) grew overnight. DSC shows a single decomposition exotherm at 167 °C (the starting silver acetate phosphine complex shows this transition at 192 °C). For $C_{42}H_{31}O_2AgP_2Br_4$ elemental C, H (theory) C, H = 47.65 (47.70), 2.81 (2.93). The Raman spectrum is dominated by the triphenylphosphine ligand bands: primarily 998, 1025, and 1096 cm^{-1}. The silver tetra-bromo-catechol complex was submitted for NMR analysis to ascertain its molecular structure in solution (DMSO-d_6). While both the proton and P-31 spectra (supplementary data section) are suggestive of the proposed hydrogen-bonded dimer structure, long term C-13 analysis, due to inherent solution instability, is not.

2.2. Preparation of $Ag(Cl_4C_6(OH)O)(Ph_3P)_2$

Ag_2O as the deprotonating base for the catechol ligand, in place of acetate exchange from silver acetate, was also used to isolate the complex, according to the following scheme:

$$Ag_2O + 2Cl_4C_6(OH)_2 + 4Ph_3P \rightarrow 2Ag(Cl_4C_6(OH)O)(Ph_3P)_2 + H_2O$$

To 60 mg Ag_2O and 0.26 g Ph_3P in 5 mL toluene was added 128 mg tetra-chlorocatechol, $Cl_4C_6(OH)_2$ (Aldrich). Stirring at room temperature produced a nearly clear solution, which was colorless on filtration. A mixture of pink crystals in a slight oil remained after slow evaporation. The crystals (0.18 g) were removed after ether washing. DSC is completely similar to the bromine complex, an exotherm centered at 170 °C, preceded by a melting point endotherm at 155 °C. For $C_{42}H_{31}O_2AgP_2Cl_4$ elemental C, H (theory) C, H = 57.32 (57.34), 3.54 (3.53). The Raman spectrum is dominated by the triphenylphosphine ligand bands: primarily 998, 1025, and 1097 (1092 shoulder) cm^{-1}.

Differential scanning calorimetry (DSC) was obtained on a TAInstruments Model 910, heating at 10 °C/min under nitrogen flow (~50 mL/min).

Elemental analysis was obtained from Prevalere (8282 Halsey Road, Whitesboro, NY 13492).

Raman spectra were collected in micro mode with a JY Horiba LabRam, equipped with a CCD dectector, at 180 backscatter with a MSPlan 100× objective. The excitation wavelength was 785 nm with the laser power at approximately 300 mW, and the collection time was 100 s.

2.3. Single-crystal X-ray diffraction

Single-crystal structure determination by X-ray diffraction was performed on a Nonius KappaCCD [21] equipped with a normal focus, sealed-tube X-ray source. Data reductions were performed using DENZO-SMN [22]. The structures were solved and refined by using the SHELXTL [23]

Table 1
Selected bond distances and angles for $Ag(Br_4C_6(OH)O)(Ph_3P)_2$ and $Ag(Cl_4C_6(OH)O)(Ph_3P)_2$

	$Ag(Br_4C_6(OH)O)(Ph_3P)_2$	$Ag(Cl_4C_6(OH)O)(Ph_3P)_2$
Ag1–O2	2.390(3)	2.3575(19)
Ag1–P1	2.4626(12)	2.4201(7)
Ag1–P2	2.4333(11)	2.4565(8)
C39–X1	1.902(4)	1.733(3)
C40–X2	1.896(4)	1.736(3)
C41–X3	1.885(4)	1.731(3)
C42–X4	1.899(4)	1.730(3)
Ag1–X1	3.1864(6)	3.1838(9)
O1–Ag1–P2	123.789(127)	122.66(8)
O1–Ag1–P1	95.6274(127)	96.83(8)
P2–Ag1–P1	139.756(64)	139.53(5)

Table 2
Hydrogen bonds with H···A < r(Å) + 2.000 Å and A–DHA > 110°, where r is atomic radius, A is acceptor atom, D is donor atom and ∠DHA is donor–hydrogen–acceptor angle

D–H	d(D–H)	d(H···A)	∠DHA	d(D···A)	A
$Ag(Br_4C_6(OH)O)(Ph_3P)_2$					
O1–H1	0.820	1.900	142.82	2.601	O2 [$-x+2, -y, -z$]
O1–H1	0.820	2.314	112.90	2.739	O2
$Ag(Cl_4C_6(OH)O)(Ph_3P)_2$					
O1–H1	0.820	1.935	138.49	2.607	O2 [$-x+2, -y, -z$]
O1–H1	0.820	2.316	113.40	2.747	O2

Table 3
Details of crystal data, data collection and structure refinement for $Ag(Br_4C_6(OH)O)(Ph_3P)_2$ and $Ag(Cl_4C_6(OH)O)(Ph_3P)_2$

Parameters	$Ag(Br_4C_6(OH)O)(Ph_3P)_2$	$Ag(Cl_4C_6(OH)O)(Ph_3P)_2$
Crystal data		
Empirical formula	$C_{42}H_{31}AgBr_4O_2P_2$	$C_{42}H_{31}AgCl_4O_2P_2$
Formula weight	1057.12	879.28
Temperature (K)	293(2)	293(2)
Wavelength (Å)	0.71073	0.71073
Crystal system	triclinic	triclinic
Space group	$P\bar{1}$	$P\bar{1}$
Unit-cell dimensions		
a (Å)	12.3140(3)	12.3730(2)
b (Å)	12.8990(3)	12.7070(3)
c (Å)	13.5710(4)	13.4380(3)
α (°)	79.4320(10)	79.8220(11)
β (°)	69.3420(10)	68.9060(12)
γ (°)	81.6250(10)	81.7380(9)
Volume (Å^3)	1975.09(9)	1932.78(7)
Z	2	2
D_{calc} (Mg/m^3)	1.778	1.511
Absorption coefficient (mm^{-1})	4.673	0.917
$F(000)$	1032	888
Crystal size (mm^3)	$0.17 \times 0.12 \times 0.10$	$0.32 \times 0.17 \times 0.07$
Data collection		
Diffractometer	kappaCCD	kappaCCD
θ Range for data collection (°)	4.19–25.99	3.35–26.77
Scan width (°)	2	2
Exposure time (s/°)	600	200
Index ranges	$-14 \leqslant h \leqslant 15$, $-15 \leqslant k \leqslant 15$, $-16 \leqslant l \leqslant 16$	$-15 \leqslant h \leqslant 15$, $-16 \leqslant k \leqslant 16$, $-16 \leqslant l \leqslant 17$
Reflections collected	21 831	28 786
Independent reflections	7694	8159
R_{int}	0.0643	0.0798
Completeness to $\theta = 25.00°$	99.10%	99.20%
Absorption correction [24]	multiscan	multiscan
Refinement		
Data/restraints/parameters	7694/0/461	8159/0/461
Goodness-of-fit on F_2	0.98	0.965
Final R indices $[I > \sigma 2(I)]$, R_1	0.0395	0.0387
wR_2	0.0716	0.0808
R indices (all data), R_1	0.0829	0.0769
wR_2	0.0848	0.0949
Largest different peak and hole (e Å^{-3})	0.417 and −0.618	0.323 and −0.798

suite of programs. The hydrogen atoms were incorporated into idealized positions. Selected bond distances and angles are shown in Table 1, and hydrogen bonding distances in Table 2. Pertinent experimental details of crystal data, data collection, and structure refinement are summarized in Table 3.

3. Results and discussion

Our attempts to prepare silver complexes of various *ortho*-di-hydroxybenzenes under basic conditions rapidly resulted in metallic silver, regardless of the substituents. Using milder conditions, such as simple replacement of the acetate from water-soluble silver acetate, still resulted in rapid formation of metallic silver, again regardless of the derivative. The high reactivity of these catechols, coupled with the lack of silver catechol complexes reported in the literature, indicated that a different approach was clearly needed.

Organo-phosphines are known to act as good stabilizers of metal ions in unusual or unstable oxidation states [25,26]. Considering the high reactivity of Ag^+ with catechols, this ion might be thought of as a suitable candidate for stabilization with phosphine-based ligands. Two approaches were successful in the preparation of phosphine-stabilized silver catechol complexes, preparation of the complex from silver acetate or its Ph_3P derivative (acetic acid by-product), and silver oxide (water by-product):

$$Ag_2O + 4Ph_3P + 2catechol \rightarrow 2Ag(catechol)(Ph_3P)_2 + H_2O$$

$$[Ag(O_2CCH_3)]_2 + 4Ph_3P + 2catechol \rightarrow 2Ag(catechol)(Ph_3P)_2 + 2HO_2CCH_3$$

The triphenylphosphine complex of silver acetate, $Ag(O_2CCH_3)(Ph_3P)_2$, is well known whose structure has been reported [20]. Similar to the long-chain analog, C_{18} (stearate), $AgStearate(Ph_3P)_2$ [27], the acetate is chelated to the silver, and the two phosphines simply fill out the coordination sphere. For the catechol reactions, it was found that either the $Ag(O_2CCH_3)(Ph_3P)_2$ can be prepared separately, or it can be generated in situ.

Given that electron-rich catechols were found to be exceedingly reducing for Ag^+, even in the presence of the stabilizing ligand, highly electron-withdrawing groups were investigated as most likely to form stable silver catechol complexes. While these halogenated catechols do reduce silver acetate to metallic silver in the absence of the stabilizing ligand, in the presence of triphenylphosphine, however, rapidly cleared solutions were formed that slowly grew crystals suitable for X-ray structure analysis.

While the silver tetra-bromo-catechol complex was successfully obtained from silver acetate with triphenylphosphine as a stabilizing ligand, the tetra-chloro-catechol complex did not form suitable crystals under these reaction conditions. A second approach was taken to facilitate the complex formation and crystallization. In this case, we found that Ph_3P appears to partially "dissolve" Ag_2O, presumably a low molecular weight oligomer of $[Ph_3P–Ag–O]_x$, which should simply yield H_2O as a byproduct. Using this approach, well-formed crystals of the tetrachloro-catechol complex were obtained. This complex is seen to be completely structurally isomorphous with the bromine analog, Fig. 1, including the chelate function of the catechol via the O–Ag–Cl ring.

While normal Ag–O bonds between the silver and oxygen are observed in the $Ag(Br_4C_6(OH)O)(Ph_3P)_2$ and $Ag(Cl_4C_6(OH)O)(Ph_3P)_2$ complexes, 2.390(3) and 2.3575 (19) Å, two significant observations related to the Ag–O bonding can be made. First, unlike the normal catechol

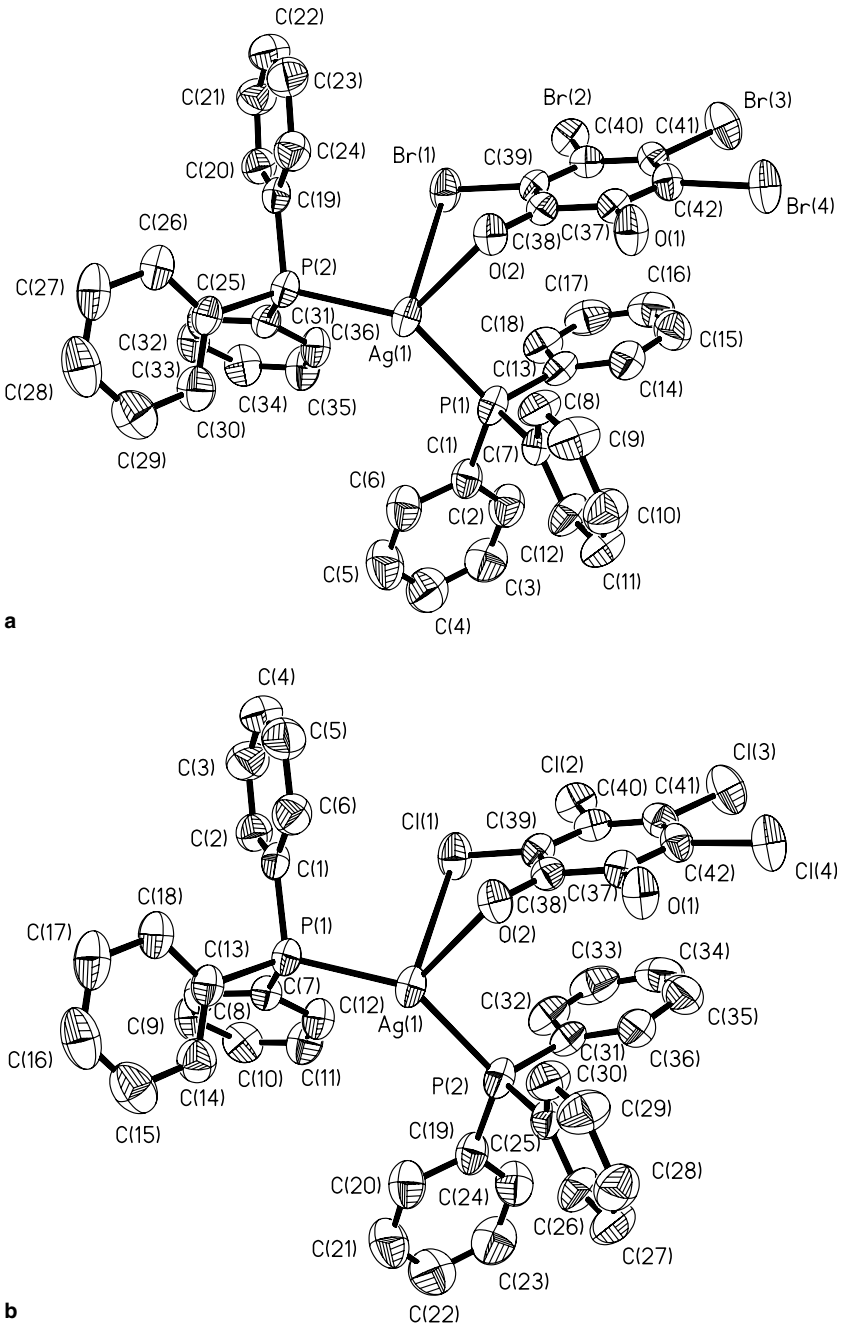

Fig. 1. ORTEP diagrams of: (a) $Ag(Br_4C_6(OH)O)(Ph_3P)_2$, and (b) $Ag(Cl_4C_6(OH)O)(Ph_3P)_2$ with 50% probability of thermal ellipsoids, showing atomic numbering schemes (hydrogen atoms omitted for clarity).

chelating functionality in which both oxygens are bound to the same metal ion, only one of the oxygens is bound to the silver. Second, similar to the silver–phenol complexes noted above, there is a significant Ag–X bond involving the halide ortho to the coordinated phenolic oxygen, Ag–Br = 3.1864(6) Å and Ag–Cl = 3.1838(9) Å. These are long Ag–X interactions compared to previously reported Ag–X–organic ligands (Ag–Br 2.7–3.0 Å [7–9], Ag–Cl 2.5–2.9 Å) [7,10,11]. The bond distances and crystallographically significant orientation makes it clear that the formation of an O–Ag–X chelated structure is more important than that of an O–Ag–O chelated structure.

An interesting unique feature of these structures is O–H···O hydrogen bonding interactions that result in crystal structure stabilization by formation of dimers as shown in Fig. 2. The available O(1)–H is bonded, about 2.60 Å, to the silver bound O(2) in the adjacent molecule.

In addition, when viewed in the solid-state crystal packing, Fig. 3, there are significant π–π interactions between aromatic rings of a phosphine phenyl group and the catechol. The stacking distance is about 3.41 Å, which is similar to that reported for other silver complexes [28].

Overall, the ability to prepare a stable silver catechol complex is limited to the highly electron-withdrawing

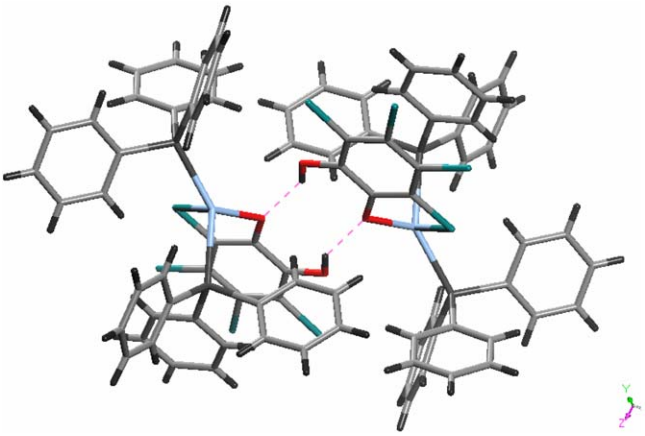

Fig. 2. Packing of $Ag(X_4C_6(OH)O)(Ph_3P)_2$ complexes in the unit cell showing hydrogen bonding associations between molecules forming a dimer in the solid-state lattice.

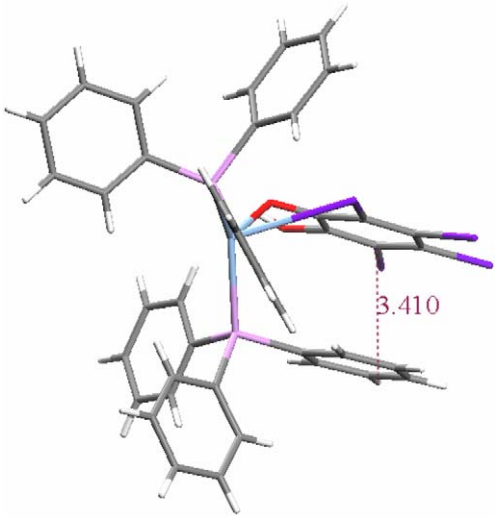

Fig. 3. Aromatic π–π interactions in $Ag(X_4C_6(OH)O)(Ph_3P)_2$.

tetra-halo-catechol in the presence of Ph_3P as a stabilizing ligand. All attempts to obtain silver catechol complexes having fewer halide groups on the catechol ligand, $BrH_3C_6(OH)_2$, $Br_2H_2C_6(OH)_2$, and $Br_3HC_6(OH)_2$, were unsuccessful, even using the triphenylphosphine stabilizing ligand.

4. Conclusions

The solid-state structures of the first verifiable silver complexes containing bound catechol ligands are reported. Only catechols containing highly electron-withdrawing groups, such as tetra-substituted catechols coupled with triphenylphosphine stabilizing ligands, can be used to obtain these complexes. Without these two key features, the silver is too readily reduced to the metal. In both complexes reported here, $Ag(Br_4C_6(OH)O)(Ph_3P)_2$ and $Ag(Cl_4C_6(OH)O)(Ph_3P)_2$, a single oxygen of the catechol is coordinated to the silver along with the *ortho*-halogen to form an O–Ag–X chelated structure. The second phenolic group is not involved with the coordination of the metal. Additional hydrogen bonding between the catechol groups provide for the formation of dimeric species in the solid state.

Acknowledgements

Helpful discussions with our colleagues at Eastman Kodak Company, P.J. Cowdery-Corvan, K. Chen-Ho, R. Ho, L. Olson, S. Chen, B. Stwertka (who also collected the Raman spectra), and W. Lenhart (also collected NMR spectra) are gratefully acknowledged. We also thank the reviewer for bringing Refs. [9] and [14] to our attention.

Appendix A. Supplementary data

Crystallographic data for this structure has been deposited with the Cambridge Crystallographic Data Centre as supplementary data numbers 273648 and 273649 for $Ag(Cl_4C_6(OH)O)(Ph_3P)_2$ and $Ag(Br_4C_6(OH)O)(Ph_3P)_2$, respectively. Copies of the data may be obtained free of charge upon request from The Director, Cambridge Crystallographic Data Centre, 12 Union Road, Cambridge CB2 1EZ, UK (fax: +44 1223 336033); e-mail: deposit @ccdc.cam.ac.uk; web: http://www.ccdc.cam.ac.uk. Supplementary data associated with this article can be found, in the online version, at doi:10.1016/j.poly.2006.01.009.

References

[1] M.C. Lea, A Manual of Photography: Intended as a Text Book for Beginners and a Book of Reference for Advanced Photographers, Benerman & Wilson, Philadelphia, 1868.
[2] B.V. Rao, Ind. J. Chem. A 25 (1986) 1071.
[3] A.A. Chernyavskaya, T.V. Koval'chik, N.V. Loginova, G.I. Polozov, O.I. Shadiro, Vestnik Belorusskogo Gosudarstvennogo Universiteta, Seriya 2: Khimiya, Biologiya, Geografiya 1 (2004) 20.
[4] N.V. Loginova, A.A. Chernyavskaya, G.I. Polozov, T.V. Koval'chuk, E.V. Bondarenko, N.P. Osipovich, A.A. Sheryakov, O.I. Shadyro, Polyhedron 24 (2005) 611.
[5] G. Smith, E.J. O'Reilly, B.J. Reynolds, C.H.L. Kennard, T.C.W. Mak, J. Organomet. Chem. 331 (1987) 275.
[6] G. Wulfsberg, D. Jackson, W. Ilsley, J. Gagliardi Jr., Z. Naturforsch. A 47 (1992) 75.
[7] T. Laube, A. Weidenhaupt, R. Hunziker, J. Am. Chem. Soc. 113 (1991) 2561.
[8] F. Charbonnier, R. Faure, H. Loiseleur, Acta Cryst. B 34 (1978) 3598.
[9] W. Frenzer, R. Wartchow, H. Bode, Z. Krist. 212 (1997) 237.
[10] T.D. Newbound, M.R. Colsman, M.M. Miller, G.P. Wulfsberg, O.P. Anderson, S.H. Strauss, J. Am. Chem. Soc. 111 (1989) 3762.
[11] D.M. VanSeggen, O.P. Anderson, S.H. Strauss, Inorg. Chem. 31 (1992) 2987.
[12] J. Powell, M. Horvath, A. Lough, J. Chem. Soc., Chem. Commun. (1993) 733.
[13] H.L. Zhu, X.J. Wang, F.J. Meng, X.Y. Liu, Acta Cryst. E 59 (9) (2003) m698.
[14] M.-L. Tong, X.-L. Yu, X.-M. Chen, Inorg. Chem. Commun. 3 (2000) 694.
[15] D.R. Whitcomb, M. Rajeswaran, J. Imag. Sci. Technol. 48 (2005) 381.
[16] S.J. Archibald, N.W. Alcock, D.H. Busch, D.R. Whitcomb, J. Clust. Sci. 11 (2000) 261.

[17] S.J. Archibald, D.H. Busch, N.W. Alcock, D.R. Whitcomb, Inorg. Chem. 38 (1999) 5571.
[18] D.R. Whitcomb, R.D. Rogers, J. Imag. Sci. Technol. 43 (1999) 504.
[19] B.P. Tolochko, S.V. Chernov, S.G. Nikitenko, D.R. Whitcomb, Nucl. Instr. Meth. Phys. Res. (A) 405 (1998) 428.
[20] S.W. Ng, A.H. Othman, Acta Cryst. C 53 (1997) 1396.
[21] Nonius, COLLECT, Nonius BV, Delft, The Netherlands, 1998.
[22] Z. Otwinowski, W. Minor, in: Methods in Enzymology, in: C.W. CarterJr., R.M. Sweets (Eds.), Macromolecular Crystallography, Part A, vol. 276, Academic Press, New York, 1997, pp. 307–326.
[23] SHELXTL: Structure Analysis Program, Version 6.10, Bruker-Nonius Analytical X-ray systems, Madison, WI, 2001.
[24] SORTAV (Multiscan Absorption correction) program is based on the method of Blessing: R.H. Blessing, Acta Cryst. A 51 (1995) 33.
[25] G. Booth, Adv. Inorg. Chem. Radiochem. 6 (1964) 1.
[26] H.J. Emeléus, A.G. Sharpe, 2nd ed., in: G.M. Kosolapoff, L. Maier (Eds.), Organic Phosphorus Compounds, vol. 1, Interscience, New York, 1972.
[27] D.R. Whitcomb, R.D. Rogers, J. Chem. Cryst. 26 (1996) 99.
[28] X.-L. Zhao, Q.-M. Wang, T.C.W. Mak, Inorg. Chem. 42 (2003) 7872.

was prepared and used as a catalyst precursor for epoxide ring opening [16]. This reaction makes use of bulky 2,6 substituents to create a pocket in a similar manner to the designer Lewis acid catalysts based on aluminium tris-phenoxo complexes [17]. For these reactions the influence of local coordination environment is important and this can be varied more easily by changing substituents on the aromatic ring of phenoxo ligands than it can with the alkoxo ligands in the complexes $[TiCl(OR)_3]$ which also have an extensive use in organic synthesis [18]. However, chloro-tris-phenoxo complexes containing *ortho*-phenyl ring substituents are not well known. $[TiCl(OC_6H_2Me_3\text{-}2,4,6)_3]$ has been prepared [19,20] and some bis-amine adducts formed [20]. $[TiCl\{OC_6H_3(CHMe_2)_2\text{-}2,6\}_3]$ has been briefly described [20,21] and the X-ray structure of $[TiCl\{OC_6H_3(CMe_3)_2\text{-}2,6\}_3]$ obtained [22]. We report here work that is based on identifying pockets in chloro-tris-phenoxo complexes of titanium(IV) and investigate how this site topology may be retained.

2. Results and discussion

We have found that the best method for preparing the chloro-tris-phenoxo complexes even when there is a relatively large *ortho*-substituent on the phenyl ring is to simply thermalise the phenol and $[TiCl_4]$ in toluene (Eq. (1)).

$$[TiCl_4] + 3ArOH \rightarrow [TiCl(OAr)_3] + 3HCl \quad (1)$$

$$\begin{aligned} OAr = {} & OC_6H_4CMe_3\text{-}4, \\ & OC_6H_3Me_2\text{-}2,4, \\ & OC_6H_2Me_3\text{-}2,4,6, \\ & OC_6H_3(CHMe_2)_2\text{-}2,6, \\ & OC_6H_3(CMe_3)_2\text{-}2,4, \\ & OC_6H_4Ph\text{-}2. \end{aligned}$$

Obtaining very high yields relies on reaching the reaction end-point and this can be easily determined by monitoring the HCl exhaust gas production using amine hydrochloride cloud formation. This has been found to be successful for the general preparation of mono and bis-phenoxo complexes of titanium [23,24].

To ascertain the features associated with a chloro-tris-phenoxo complex in which there are no *ortho*-substituents on the phenyl ring, the reaction of 4-*tert*-butylphenol and $[TiCl_4]$ in a 3:1 ratio was undertaken. The production of HCl gas was vigorous at first but the reaction took 35 h for the last traces of HCl to be expelled. After removing the solvent, a non-crystalline material was obtained which failed to crystallise. Analytical data and the NMR spectra showed that even after extended periods of drying in vacuo, the complex retained toluene solvate and was characterised as $[TiCl(OC_6H_4CMe_3\text{-}4)_3] \cdot 0.5C_7H_8$ (**1**). Both the ^1H NMR and $^{13}C\{^1H\}$ NMR spectra showed the toluene as well-defined resonances whereas the 4-*tert*-butylphenoxo ligand resonances were broad suggesting solution dynamics [24]. In particular, the *ipso*-carbon resonance occurred at δ 164.5 which is upfield of that found for the mono-phenoxo complex $[TiCl_3(OC_6H_4CMe_3\text{-}4)]$ (δ 169.7) [23] and the bis-phenoxide complex $[TiCl_2(OC_6H_4CMe_3\text{-}4)_2]$ (δ 166.3) and is likely to represent a decrease in the π-bonding from each phenoxo ligand when the number of these ligands increases [24].

When $[TiCl_4]$ was reacted with 2,4-dimethylphenol using the standard conditions, a crystalline solid analysing as $[TiCl(OC_6H_3Me_2\text{-}2,4)_3]$ was obtained for which an X-ray crystal structure determination showed the dimeric phenoxo bridged complex **2**. The coordination geometry about each Ti is that of a trigonal bipyramid consisting of two bridging phenoxides, two terminal phenoxides and a terminal chloro ligand (Fig. 1a). Bond lengths and angles are shown in Table 1. The Ti–O(3) bond length [1.757(1) Å] is similar to that found in the mono-phenoxo complex $[TiCl_3\{OC_6H_2(CMe_3)_2\text{-}2,6\text{-}Me\text{-}4\}]$ [Ti–O bond length 1.750(2) Å] for which a theoretical study shows π-donation of both oxygen atom lone pairs to titanium and some π-bonding between the oxygen and the phenyl ring π-system [24]. The Ti–O(3)–C(31) bond angle [171.4(1)°] in **2** is more 'linear' than that found in $[TiCl_3\{OC_6H_2(CMe_3)_2\text{-}2,6\text{-}Me\text{-}4\}]$ [163.1(1)°] for which theoretical studies show significant changes in energy (and thus decrease in O_π–Ti_d donation) occur only after the Ti–O–C bond angle moves below ca. 160°. The Ti–O(2) bond length in **2** [1.794(2) Å] is significantly longer than the Ti–O(3) bond length and the Ti–O(2)–C(21) bond angle decreases to 138.8(1)° reflecting the decreased π-donation from the oxygen of this ligand. The Ti–O(1) bond length of 1.927(1) Å and Ti–O(1)–C(11) bond angle of 126.1(1)° suggest that there is minimal π-donation to Ti with the bridging phenoxo ligand. The bond length of the terminal chloro ligand [2.269(1) Å] is appreciably longer than that observed for the two terminal chloro ligands in the bridging phenoxo complex $[\{TiCl_2(OC_6H_4CMe_3\text{-}4)(\mu\text{-}OC_6H_4CMe_3\text{-}4)_2\}_2]$ [2.2186(11) and 2.2256(11) Å] [24] as a result of the lessened need for Cl_p–Ti_d π-donation when there is a third phenoxo ligand present.

For chloro-tris-phenoxo complexes, the local environment of the terminal chloro ligand is of importance when development of a pocket is considered since it is this ligand and any replacement that will be affected by local steric influences. Inspection of **2** and the space-filled model (Fig. 1b) shows that the orientation of the phenyl rings in the solid state is such that the methyl substituents in the *ortho*-positions of the three phenoxo ligands associated with each of the titanium atoms point up towards the terminal chloro ligand and as such start to build a 'wall' around one side of the upper Ti(1)–Cl bond but do not create a significant pocket. In fact the phenyl rings attached to the adjacent Ti atom create more of a wall but are further away from the chloro ligand. In solution, the influences playing on the chloro ligand would appear to be different from the solid state since the NMR spectra of **2** in $CDCl_3$ solution do not reflect the dimeric structure shown by the X-ray analysis but point to the three phenoxides being

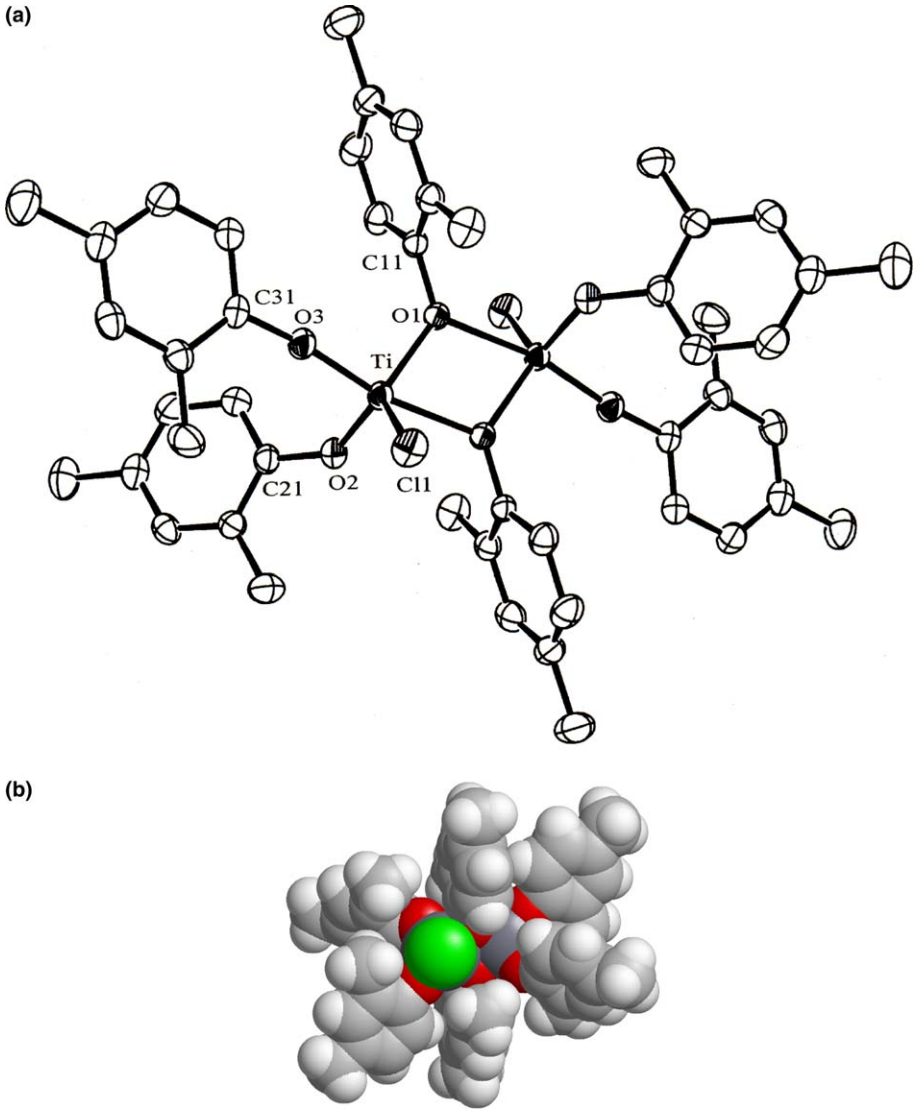

Fig. 1. (a) ORTEP diagram of [{TiCl($OC_6H_3Me_2$-2,4)$_2$(μ-$OC_6H_3Me_2$-2,4)}$_2$] (**2**) showing the molecular structure. Hydrogen atoms have been omitted for clarity. Only the major coordination site for Cl is shown. (b) Space-filling model looking down the Cl–Ti bond showing the position of the *o*-methyl groups on the Ti(1) phenoxo ligands and the phenoxo phenyl groups on Ti(2).

equivalent. The ^{1}H NMR spectrum shows a single set of sharp resonances for the *ortho* and *para*-methyls, a multiplet for the two *meta*-phenyl ring hydrogens and the $^{13}C\{^1H\}$ NMR spectrum a single set of resonances for the relevant phenoxide group carbons. The *ipso*-carbon resonance appears at δ 164.4 which is in a position similar to that found for **1** (δ 164.5). The absence of resonances for bridging and terminal ligands and the sharpened nature of the resonances suggest that solution dynamics are less important than for **1** so that the complex is likely to be monomeric in the NMR solvent and have a tetrahedral geometry in which the *ortho*-methyl groups all point up around the Ti–Cl bond. In comparison, the resonances of complex **1**, particularly those associated with the aromatic ring, were broad which may suggest monomer–dimer equilibria. We have found previously that [$TiCl_2(OAr)_2$] complexes without *ortho*-methyl substituents are dimeric in the solid state but are monomeric in solution. DFT calculations show that there is only a small dimerisation energy involved (-26.2 kJ mol^{-1}) [24].

Of fundamental importance in these systems is whether the structure of any pocket is maintained in the presence of other coordinating ligands. Addition of one or two equivalents of pyridine to **2** gave what appeared to be isomeric mixtures, which were difficult to distinguish by NMR spectroscopy. 4,4′-Dimethyl-2,2′-bipyridine (dmbipy) was used since isomeric mixtures can be more easily identified using this ligand [23,24]. Addition to **2** expanded the coordination number giving [TiCl($OC_6H_3Me_2$-2,4)$_3$(dmbipy)] (**3**) for which the NMR spectra showed one isomer. Based on a 2:1 ratio of phenoxo ligand resonances and a symmetrical dmbipy ligand shown by a singlet for the two methyl groups and a single set of resonances for the ring protons in the ^{1}H NMR spectrum and the required number of carbon resonances in the $^{13}C\{^1H\}$ NMR spectrum, dmbipy symmetric structure (a) rather than either of asymmetric

Table 1
Selected bond distances (Å) and angles (°) for [{TiCl($OC_6H_3Me_2$-2,4)$_2$-(μ-$OC_6H_3Me_2$-2,4)}$_2$] (**2**)

Ti–Cl(1)	2.269(1)
Ti–O(1)	1.927(1)
Ti–O(2)	1.794(2)
Ti–O(3)	1.757(1)
Ti–O(1)′	2.138(1)
Ti–O(1)–C(11)	126.1(1)
Ti–O(2)–C(21)	138.8(1)
Ti–O(3)–C(31)	171.4(1)
Ti–O(1)′–C(11)′	125.6(1)
Cl(1)–Ti–O(1)	121.21(7)
Cl(1)–Ti–O(2)	115.90(8)
Cl(1)–Ti–O(3)	96.86(5)
Cl(1)–Ti–O(1)′	89.75(4)
O(1)–Ti–O(1)′	71.76(6)
O(1)–Ti–O(2)	118.23(7)
O(1)–Ti–O(3)	95.89(6)
O(2)–Ti–O(1)′	87.41(6)
O(2)–Ti–O(3)	98.96(7)
O(3)–Ti–O(1)′	167.65(6)
Ti–O(1)–Ti′	108.24(6)

structures (b) and (c) is preferred. We have been unable to obtain suitable crystals to identify the absolute structure in the isomer but with one phenoxo ligand coordinating *trans*- to the chloro ligand the cavity structure about Cl is certainly destroyed.

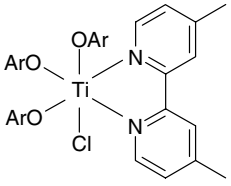

Symmetric structure (a)

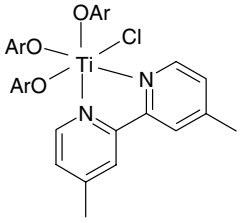

Asymmetric structure (b)

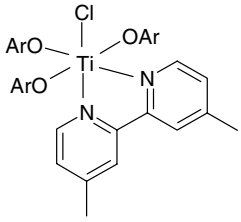

Asymmetric structure (c)

The structural features shown by the solid state structure of **2** indicate that one side of the titanium has become enclosed to some extent by the phenoxo ligand *ortho*-methyl groups so that the complex has the beginnings of a pocket with defined local structure. A more well-defined topology could arise if the complex were a tetrahedral monomer as suggested by the NMR spectra. However, analysis of the structure indicates that some rotation of the phenyl C–O bonds in the monomer or dimer forms may occur in solution taking the methyl groups away from the chloro ligand. Thus, 2,4,6-trimethylphenol and 2,6-di-*iso*-propylphenol were reacted with $TiCl_4$ using the standard conditions to form complexes in which phenoxo ligand C–O bond rotations are less likely to occur on account of the other *ortho*-position of the phenyl ring having a larger substituent than hydrogen. [TiCl($OC_6H_2Me_3$-2,4,6)$_3$] (**4**) [19] formed as a solid which, characterised by NMR spectroscopy, showed a single set of sharp resonances for the relevant hydrogens and carbons as found for complex **2** and with an *ipso*-carbon resonance in the $^{13}C\{^1H\}$ NMR spectrum at δ 163.9 suggesting a monomeric and thus tetrahedral complex. [TiCl{OC_6H_3-($CHMe_2$)$_2$-2,6}$_3$] (**5**) [20,21] was characterised by NMR spectral comparison with the product formed by thermalisation in benzene [21] as NMR analysis of the toluene reaction crude material indicated there was a significant amount of the phenol present as well as the *tetra*-phenoxide [Ti{$OC_6H_3(CHMe_2)_2$-2,6}$_4$] (identified by NMR spectral comparison with an independently prepared sample). Based on the single set of ligand resonances in the NMR spectra (in particular the *ipso*-carbon ^{13}C resonance at δ 163.1) **5** is also a tetrahedral monomer.

Of more importance than methyl or *iso*-propyl groups for pocket development are large *ortho*-substituents. The X-ray structures of [TiI{$OC_6H_3(CMe_3)_2$-2,6}$_3$] [22] and [TiCl($OC_6H_3Ph_2$-2,6)$_3$] [16] show cavity formation and would appear to be ideal molecules for cavity collapse studies. However, the former complex is difficult to prepare and the ligand for the latter is expensive. We therefore turned our attention to ligands that had a *tert*-butyl or phenyl substituent in only one of the phenoxide aryl ring *ortho*-positions. Reaction of 2,4-di-*tert*-butylphenol with [$TiCl_4$] under the standard conditions gave [TiCl{OC_6H_3-(CMe_3)$_2$-2,4}$_3$] (**6**) which could also be prepared in good yield by the reaction of 3 equivalents of $LiOC_6H_3$-(CMe_3)$_2$-2,4 with $TiCl_4$ dissolved in diethyl ether. The complex forms a crystalline mass that is analytically pure when the solvent is removed from the reaction mixture but may be recrystallised from petroleum spirit or diethyl ether. An X-ray crystal structure determination showed a distorted tetrahedron consisting of three terminal phenoxo ligands and a single terminal chloro ligand (Fig. 2a), the metal and chloro ligand lying along a threefold axis. Bond lengths and angle are shown in Table 2. The three identical Ti–O bond lengths [1.757(2) Å] are similar to the Ti–O(3) bond length in **2** which involves the most oxygen atom lone pair π-donation. The Ti–Cl bond length in **6** [2.240(2) Å] is slightly shorter than that observed in **2** [2.269(1) Å] resulting from the greater need for electron density at the metal with the lower coordination number. It is considerably shorter than the three terminal Ti–Cl bonds in [$TiCl_3${$OC_6H_2(CMe_3)_2$-2,6-Me-4}] [Ti–Cl bond length range 2.1822(8)–2.1945(9) Å] in which there is only one π-donating phenoxo ligand. In [$TiCl_4$] where each chloride must π-donate 2 electron pairs to attain an electron count of 16, the Ti–Cl bond lengths are 2.170(2) Å [25].

The Ti–O–C bond angles in **6** [158.8(2)°] are slightly smaller than those found in [$TiCl_3${$OC_6H_2(CMe_3)_2$-2,6-

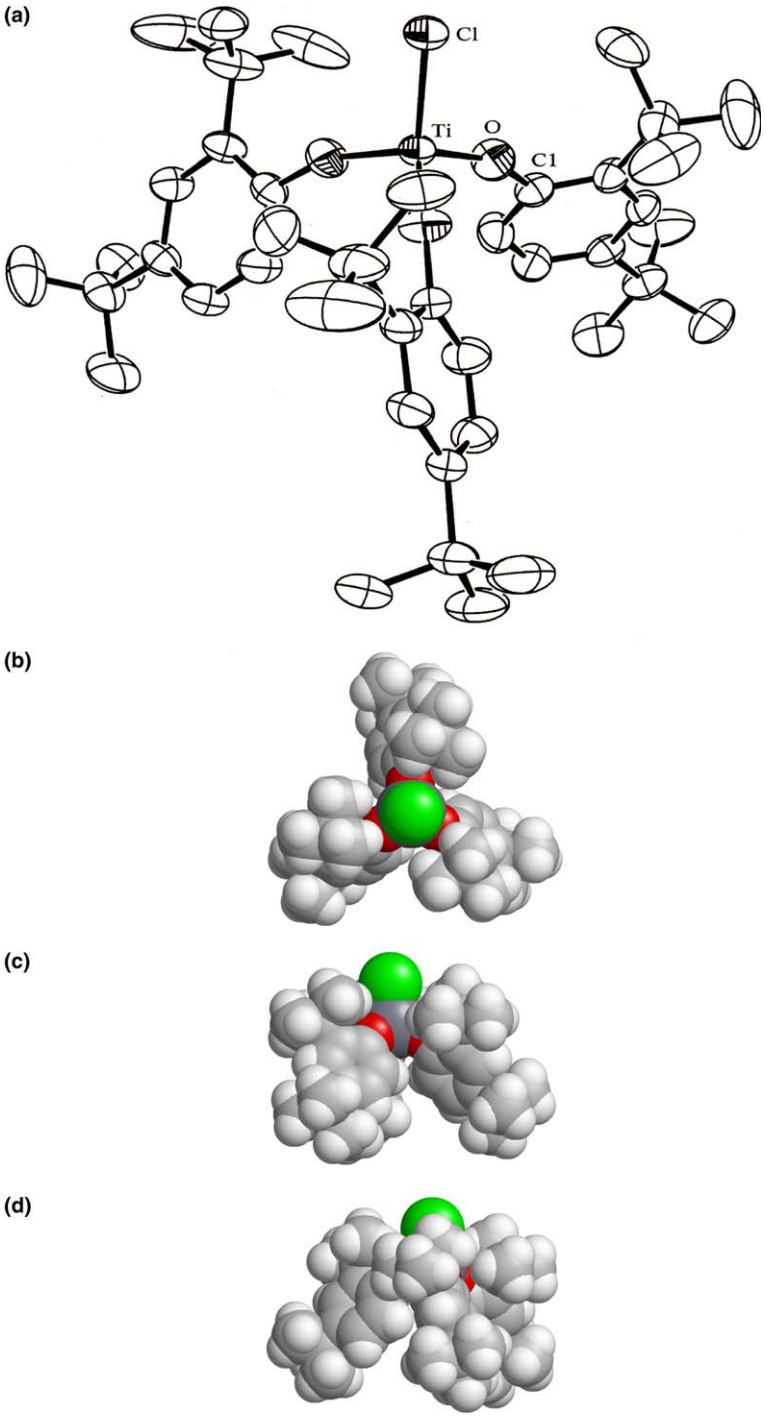

Fig. 2. (a) ORTEP diagram of $[TiCl\{OC_6H_3(CMe_3)_2\text{-}2,4\}_3]$ (**6**) showing the molecular structure. Hydrogen atoms are omitted for clarity. Only one of the disordered positions for the *tert*-butyl group is shown. (b) Space-filling model looking down the Cl–Ti bond showing the pocket arrangement about Cl. (c and d) Space-filling model, side-on view of the Ti–Cl bond showing the extent to which the *tert*-butyl group methyls cover the Cl atom.

Me-4}] [163.1(2)°] [23] and the Ti–O(3)–C(31) bond angle in complex **2** [171.4(1)°] but the angle in **6** is only a little less than the 160° for which theoretical studies with this type of ligand show a steep rise in energy when this value is reduced [23]. In $[TiI\{OC_6H_3(CMe_3)_2\text{-}2,6\}_3]$ where both phenyl ring *ortho*-positions have *tert*-butyl substituents the Ti–O–C bond angles range from 155.2(4)° to 158.2(4)° [22]. In **6** the O–Ti–O′ and O–Ti–Cl bond angles are 108.90(8)° and 110.03(8)°, respectively, hence the geometry does not deviate significantly from a tetrahedral arrangement. In $[TiI(OC_6H_3(CMe_3)_2\text{-}2,6)_3]$ the O–Ti–O bond angles range from 110.7(3)° to 114.9(3)° and the O–Ti–I bond angle range is 102.9(3)–108.6(3)° [22].

The phenyl rings in complex **6** orientate so that two of the methyl groups of the 2-*tert*-butyl group straddle the chloro ligand but lie slightly to the side of this ligand. The two closest methyl group carbon contacts with the chloro ligand are 3.13 and 3.11 Å which, taken with the

Table 2
Selected bond distances (Å) and angles (°) for [TiCl{$OC_6H_3(CMe_3)_2$-2,4}$_3$] (**6**)

Ti–Cl	2.240(2)
Ti–O(1)	1.757(2)
Ti–O(1)–C(1)	158.8(2)
Cl–Ti–O(1)	110.03(8)
O(1)–Ti–O(1)′	108.90(8)

Ti–O–C(1) bond angles [158.8(2)°], and the near ideal tetrahedral geometry, indicate that the 2-*tert*-butyl substituent exerts little steric pressure. However, it is more constrained than its counterpart in the 4-position of the phenyl ring which is seen to occupy two disordered sites. No such disorder was observed for the 2-substituent. It provides something of a steric shield about the chloro ligand and thus creates a pocket for this fourth coordination site as the space filled models show (Fig. 2b–d). Molecular models indicate that if the Ti–O–C bond angles are maintained in solution near the solid state value of ca. 159° then rotation about the phenyl ring C–O bond is difficult. However, since this angle can flatten with little energy consequence [23] rotation may be possible although the C–O π-bond would need to be broken in this process.

The 4-coordination of complex **6** can be broken by the addition of dmbipy but whereas the *ortho*-methyl complex **2** gave one product which NMR spectroscopy showed to have a symmetric structure, reaction with **6** gave a product analysing as [TiCl{$OC_6H_3(CMe_3)_2$-2,4}$_3$(dmbipy)] (**7**) but the NMR spectra showed three products (ratio ca. 72:21:7) based on the easily distinguished features of the dmbipy hydrogens in the ^{1}H NMR spectrum. The major product, however, had spectral characteristics similar to complex **3** [symmetric structure (a)]. Of the three possible structures only (c) has the potential for three *tert*-butyl groups to surround Cl. We have also looked at the possibility of coordinating only one extra ligand to **6** by adding 1 equivalent of pyridine or various aldehydes but these reactions give gummy substances that are hard to purify. However, the NMR spectra show mainly single resonances for the phenoxo ligands indicating the ligands are equivalent which offers the possibility of a 5-coordinate structure (see later).

The structural features shown by complex **6** suggest that the chloro ligand would sit in a more effective pocket if the 2-*tert*-butyl substituent of the phenoxo ligands were replaced by a 2-phenyl substituent which, although less sterically demanding than the former, would protrude further out. Reaction of 2-phenylphenol with [$TiCl_4$] under the standard conditions gave an oil which failed to solidify but was identified as [TiCl(OC_6H_4Ph-2)$_3$] (**8**) on the basis of its NMR spectra. In particular, the more easily identified ^{13}C{^{1}H} NMR spectrum showed a single set of resonances for each of the carbons of the ligand and the *ipso*-carbon resonance (δ 163.6) was in a similar position to the other chloro-tris-phenoxide complexes prepared.

Reaction of [$TiCl_4$] with 3 equivalents of $LiOC_6H_4$Ph-2 in diethyl ether gave [TiCl(OC_6H_4Ph-2)$_3$(diethyl ether)] (**9**) which had nearly identical NMR spectral characteristics in the aromatic region to those shown by complex **8** with the *ipso*-carbon at δ 163.2. Interestingly, when complex **8** was dissolved and refluxed in diethyl ether the NMR spectra of the reaction product indicated that no diethyl ether was incorporated. This is probably related to the retention of coordinated ether during the reaction with the titanium starting material [$TiCl_4$(diethylether)$_2$]. An X-ray crystal structure determination of **9** showed a distorted trigonal bipyramidal coordination geometry with the diethyl ether ligand bound in a *trans* position to the chloro ligand and the three phenoxide ligands forming the equatorial plane (Fig. 3a). Bond lengths and angle are shown in Table 3. The Ti–O bond lengths lie in the range 1.790(1)–1.794(1) Å and, together with the Ti–Cl bond length [2.3067(6) Å], are much longer than the corresponding bonds in [TiCl{$OC_6H_3(CMe_3)_2$-2,4}$_3$] (**6**) [Ti–O and Ti–Cl are 1.757(2) and 2.240(2) Å, respectively]. This is a result of **9** having a reduced π-loading [26] requirement compared to **8** with the addition of the 2-electon donor diethyl ether ligand. Consequently, the Ti–O–C bond angles of 152.3(1)°, 155.0(1)° and 157.1(1)° relax a little in comparison with those in **6** where Ti–O–C bond angle is 158.8(2)°. The phenoxide oxygen atoms push away from the chloro ligand [O(1)–Ti–Cl, 96.12(4)°; O(2)–Ti–Cl, 95.90(5)°] but the O–Ti–O bond angles are close to the ideal trigonal angle [the range is 117.88(6)–119.99(6)°]. The phenyl rings are rotated into the equatorial plane to remove interaction with the diethyl ether ligand and this takes the 2-phenyl substituent on each phenoxo ligand away from the chloro ligand and destroys any substantial cavity present if the substituents all lie upright. The space-filling model looking down the Cl–Ti bond (Fig. 3b) shows the cavity effect which is different from that observed in [TiCl($OC_6H_3Ph_2$-2,6)$_3$] [16] where the substituents form an open-ended groove (Fig. 3c). This results from a face-to-face orientation of two of the phenyl substituents and an end wall in which the substituent has moved aside slightly. The extent to which the phenyl groups cover the chloro ligand in **9** is much less than in [TiCl($OC_6H_3Ph_2$-2,6)$_3$] (compare Fig. 3d and e) being somewhat similar to that found in [TiCl{$OC_6H_3(CMe_3)_2$-2,4}$_3$] (**6**) (compare Fig. 3d with Fig. 2c).

The structural features shown by complexes **6** and **9** indicate that the local cavity geometry is easily effected by the addition of another ligand. We therefore looked at tying back one of the three phenoxo ligands with a nitrogen donor using the benzylamine ligand structure (d) to form complexes of structural type (e).

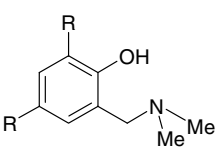

Structure (d) (R = CMe_3)

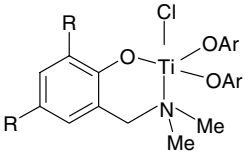

Structural type (e) (R = CMe_3)

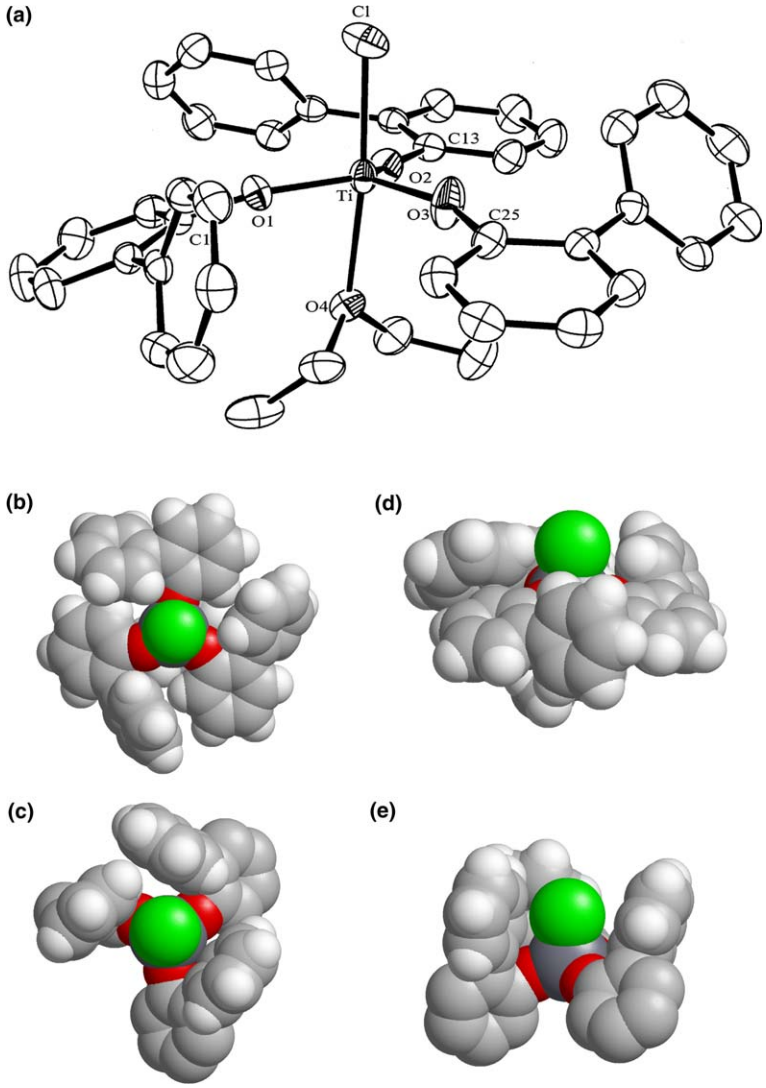

Fig. 3. (a) ORTEP diagram of [TiCl(OC_6H_4Ph-2)$_3$(diethyl ether)] (**9**) showing the molecular structure. Hydrogen atoms are omitted for clarity. Only the major site of the coordinated ether ligand is shown. (b) Space-filling model of **9** looking down the Cl–Ti bond showing the collapsed *o*-phenyl group arrangement about Cl. (c) Space-filling model of [TiCl($OC_6H_4Ph_2$-2,6)$_3$] [16] showing the upright *o*-phenyl groups and the resulting groove (the 6-phenyl groups and the phenoxo ligand Hs have been removed for clarity). (d) Space-filling model, side-on view of **9** showing the extent to which the *o*-phenyl groups cover Cl. (e) Space-filling model, side-on view of [TiCl($OC_6H_4Ph_2$-2,6)$_3$] [16] showing the molecular groove (the 6-phenyl groups and the phenoxo ligand Hs have been removed for clarity).

This approach is then expected to produce one rigid phenoxo ligand and two more that are less rigid if the isomer with Cl *trans* to N is formed, allowing the influences made on the cavity ligand to be varied. Preliminary results of this work indicate that reaction of [$TiCl_2$($OC_6H_4CMe_3$-4)$_2$] [24] with $LiOC_6H_2(CMe_3)_2$-2,4-(CH_2NMe_2)-6 gives a solid analysing as the complex [TiCl($OC_6H_4CMe_3$-4)$_2$-{$OC_6H_2(CMe_3)_2$-2,4-(CH_2NMe_2)-6}] but the NMR spectra show the complex is made up of two isomers. Similarly, reaction of [$TiCl_4$] with two equivalents of $LiOC_6H_3$-(CMe_3)$_2$-2,4 in diethyl ether followed by one equivalent of $LiOC_6H_2(CMe_3)_2$-2,4-(CH_2NMe_2)-6 gives a complex analysing as [TiCl{$OC_6H_4(CMe_3)_2$-2, 4}$_2$($OC_6H_2(CMe_3)_2$-2,4-(CH_2NMe_2)-6)] which was also shown by the NMR spectra to consist of two isomers. The complexes do not appear to crystallise from solution so the structural details of any cavity formed in any of the isomers cannot as yet be assessed. The only success we have had with forming a single isomer complex using this type of tie-back is from a reaction of [$TiCl_2$({$OC_6H_2(CMe_3)$-2-Me-4}$_2CH_2$-6)] [27] with one equivalent of $LiOC_6H_2(CMe_3)_2$-2,4-(CH_2NMe_2)-6 which gives a product analysing as [TiCl({$OC_6H_2(CMe_3)$-2-Me-4}$_2CH_2$-6) ($OC_6H_2(CMe_3)_2$-2,4-(CH_2NMe_2)-6)]. The NMR spectra indicate the presence of only one isomer but crystals have not yet been obtained to identify the overall geometry by X-ray crystallography.

In further pursuing a non-collapsible coordination geometry about titanium, we have looked at the coordination properties of the tripodal ligand type tris(2-hydroxyphenyl)benzylamine, ($HOArCH_2$)$_3$N) for which the methyl and *tert*-butyl substituted compounds (HOC_6H_2-Me_2-2,4-CH_2-6)$_3$N [structure (f), R = Me] and

Table 3
Selected bond distances (Å) and angles (°) for [TiCl(OC$_6$H$_4$Ph-2)$_3$(diethyl ether)] (**9**)

Ti–Cl	2.3067(6)
Ti–O(1)	1.791(1)
Ti–O(2)	1.794(1)
Ti–O(3)	1.790(1)
Ti–O(4)	2.312(3)
Ti–O(1)–C(1)	152.3(1)
Ti–O(2)–C(13)	155.0(1)
Ti–O(3)–C(25)	157.1(1)
Cl–Ti–O(1)	96.12(4)
Cl–Ti–O(2)	95.90(5)
Cl–Ti–O(3)	95.80(6)
Cl–Ti–O(4)	173.41(9)
O(1)–Ti–O(2)	118.95(6)
O(1)–Ti–O(3)	119.99(6)
O(1)–Ti–O(4)	79.72(9)
O(2)–Ti–O(3)	117.88(6)
O(2)–Ti–O(4)	81.83(9)
O(3)–Ti–O(4)	90.72(11)

[HOC$_6$H$_2$(CMe$_3$)$_2$-2,4-CH$_2$-6]$_3$N [structure (f), R = CMe$_3$], respectively, should give the "tied back" versions of complexes **2** and **6**.

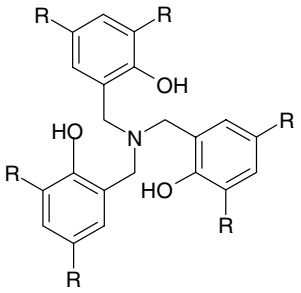

Structure (f) (R = Me, CMe$_3$)

Several alkoxo and phenoxo complexes of titanium containing these ligands have been reported [28–30]. In attempting to prepare chloro complexes, it was found that reactions of [TiCl$_4$] with either of these ligands in benzene in the presence of Et$_3$N gave mixtures which proved difficult to purify. This type of reaction is reported to give [TiCl{(OC$_6$H$_2$Me$_2$-2,4-CH$_2$-6)$_3$N}] in low yield but the complex has not been well characterised [31]. The complex was initially obtained via a circuitous route (Scheme 1).

We have noticed that when undried samples of (HOC$_6$H$_2$Me$_2$-2,4-CH$_2$-6)$_3$N, [(HOAr)$_3$N], are used in the reaction with [TiCl$_4$] and Et$_3$N, the oxo-bridged dimer [{N(ArO)$_3$}Ti–O–Ti{(OAr)$_3$N}]·1.5C$_6$H$_6$ (**10a**) is formed in good yield and this reacts with Me$_3$SiCl to give chloro complex **11**. There is an initial report of this dimer formed by the hydrolysis of [Ti(OCHMe$_2$){(OC$_6$H$_2$Me$_2$-2,4-CH$_2$-6)$_3$N}] in air [28] and the crystal structure of [{N(Ar′O)$_3$}Ti–O–Ti{(OAr′)$_3$N}]. [(OAr′)$_3$N = OC$_6$H$_2$-(CMe$_3$)$_2$-2,4-CH$_2$-6]$_3$N which is more resistant to hydrolysis has been obtained [30]. An X-ray crystal structure determination of the oxo-bridged dimer prepared in this work containing a pentane solvent molecule **10b** shows a distorted trigonal bipyramidal coordination geometry (Fig. 4) with bond lengths and angles (Table 4) which are similar to those found for the reported *tert*-butyl substituted analogue. The only significant difference between the two is the smaller Ti–O–Ti bond angle in **10b** [147.5(1)° cf. 155.5(1)°] which is apparently related to the smaller *ortho*-substituents providing less of a clash across the two sides of the molecule. In the *tert*-butyl substituted complex the *tert*-butyl groups are forced into close contact in the dimer with eight inter-titanium methyl–methyl contacts with C···C contacts shorter than the 4.0 Å sum of the van der Waals radii [30] but in **10b** there are no such close contacts.

[TiCl{(OC$_6$H$_2$Me$_2$-2,4-CH$_2$-6)$_3$N}] (**11**) was obtained more conveniently and in virtually quantitative yield by the reaction of the free ligand with [TiCl(OCHMe$_2$)$_3$] [18] prepared in diethyl ether from [TiCl$_4$] and 3 equivalents of [Ti(OCHMe$_2$)$_4$]. Complex **11** is not particularly soluble compared with the very soluble analogue [Ti(OCHMe$_2$){(OC$_6$H$_2$Me$_2$-2,4-CH$_2$-6)$_3$N}] [28]. The ^{1}H NMR spectrum shows a single set of resonances for the phenyl rings and the substituents while the benzylic CH protons form two very broad resonances. However, the ^{13}C{^{1}H}NMR spectrum shows only one CH$_2$ carbon resonance along with the other single set of carbon resonances. The *ipso*-carbon resonance appears at δ 160.2 which is upfield to that found for the non-tied-back analogue **2** (δ 164.4).

Addition of tris(3,5-di-*tert*-butyl-2-hydroxyphenyl)benzylamine to a diethyl ether solution of [TiCl(OCHMe$_2$)$_3$] gave the highly soluble complex [TiCl({OC$_6$H$_2$(CMe$_3$)$_2$-2,4-CH$_2$-6}$_3$N)]·diethyl ether (**12**) in virtually quantitative yield. The ^{1}H NMR spectrum showed a single set of resonances for the phenyl groups and the substituents and a well-defined AB spin system for the methylene protons. Although the structure has C_3-symmetry (see later for the X-ray structure) the methylene protons are non-equivalent due to the methylene carbon being pushed to one side in

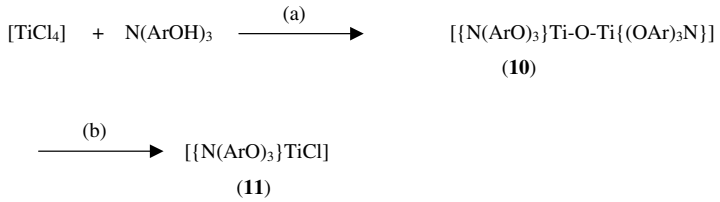

Scheme 1. (a) NEt$_3$ in benzene, reflux 14 h; (b) Me$_3$SiCl in toluene, stir 8 h.

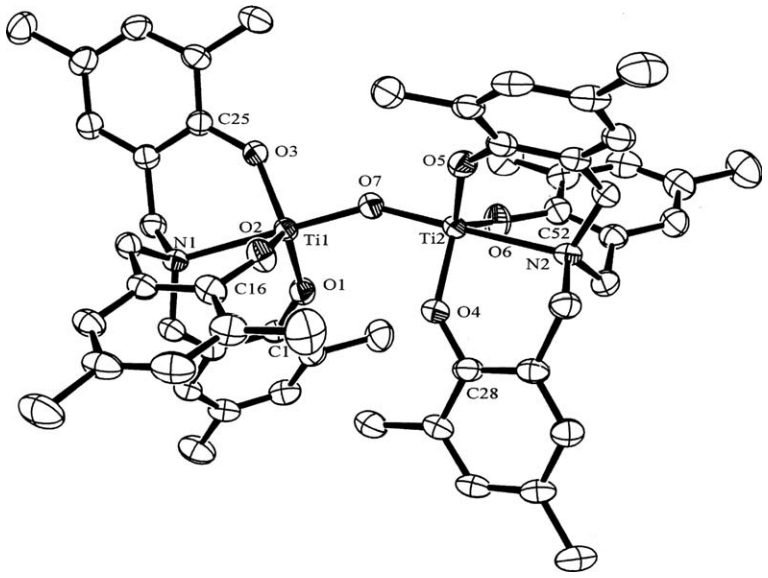

Fig. 4. ORTEP diagram of $[(Ti\{(OC_6H_2Me_2\text{-}2,4\text{-}CH_2\text{-}6)_3N\})_2O]\cdot n$-pentane (**10b**) showing the molecular structure. Hydrogen atoms are omitted for clarity. The *n*-pentane solvent molecule is not shown.

the six-membered ring. The AB system also indicates that rapid inversion of the structure does not occur on the NMR time scale [28]. In the $^{13}C\{^1H\}$ NMR spectrum there was a single set of resonances with the *ipso*-carbon resonances appearing at δ 160.8 which is similar to that found in methyl substituted complex **11** but lies upfield to the non-tied-back analogue 4-coordinate **6** (δ 164.4). An X-ray crystal structure of **12** showed a 5-coordinate distorted trigonal bipyramidal structure (Fig. 5a) in which the diethyl ether solvent molecule lies between the Ti complex molecules in the unit cell and is not coordinated. Bond lengths and angle are contained in Table 5.

The Ti–Cl bond [2.3074(7) Å] is similar to that found in the non-tied back trigonal bipyramidal $[TiCl(OC_6H_4Ph\text{-}2)_3\cdot(diethyl\ ether)]$ (**9**) [2.3067(6) Å] and both these bond lengths are longer than in tetrahedral $[TiCl\{OC_6H_3(CMe_3)_2 2,4\}_3]$ (**6**) [2.240(2) Å] which has a greater need for electron density at the metal. This electronic situation is further illustrated by the Ti–O bond lengths for the three molecules that are longer for the 5-coordinate complexes [ranges 1.809(2)–1.817(2) and 1.790(1)–1.794(1) Å for **12** and **9** cf. 1.756(2) Å for **6**]. In the trigonal bipyramidal complexes $[Ti(OCHMe_2)(\{OC_6H_2(CMe_3)_2\text{-}2,4\text{-}CH_2\text{-}6\}_3N)]$ [28] and $[Ti(OH)(\{OC_6H_2(CMe_3)_2\text{-}2,4\text{-}CH_2\text{-}6\}_3N)]$ [30] where there is an alkoxo or hydroxo ligand instead of Cl, the Ti–O bond lengths [ranges, respectively, 1.825(6)–1.866 Å and 1.783(2)–1.865(2) Å] are mostly longer than in **12** and **9** indicating that Cl is the poorer π-donor. This effect is also illustrated by comparison of the relative Ti–N bond lengths [2.216(2) Å in **12**; 2.334(5) and 2.364(2) Å, respectively, in the reported isopropoxo and hydroxo complexes] where the bond is shorter when N is trans to Cl. These features show there is a tightening of the Ti–O and Ti–N bonds when there is a less effective π-donor lying *trans* to the nitrogen atom.

In further comparisons of the relevant features of the coordination geometries for the complexes reported here, the O–Ti–Cl angles in the tied-back trigonal bipyramid (**12**) are similar to those in the non-tied-back trigonal bipyramid (**9**) [ranges 97.01(5)–97.18(5)° and 95.80(6)–96.12(4)°, respectively] as are the O–Ti–O bond angles [ranges 115.48(7)–120.72(7)° and 117.88(6)–119.99(6)°, respectively] showing that tying back has little effect on the trigonal bipyramidal geometry. However, for the tied-back trigonal bipyramidal geometry there is a significant effect for the Ti–O–C bond angles. In **12** the angles range from 143.5(2)° to 144.0(1)° whereas the angle widens in non-tied-back **9** [152.3(1)–157.1(1)°] (the complexes are expected to have similar electronic environments). In **6** where there is no tie-back constraint, the Ti–O–C bond angles are similar to those found for **9** [158.8(2)°]. There is obvious flexibility in this angle and this is even more pronounced in other complexes of this type of ligand. In the zwitterionic complex $[Zr\{(OC_6H_2Me_2\text{-}2,4\text{-}CH_2\text{-}6)_3NH\}_2]$ which has a low requirement for π-donation with six phenoxo ligands present and in which there is also room for a hydrogen atom on the inside of the cage at a non-agostic distance [2.688(3) Å], the angles range from 154(2)° to 160(2)° [32]. In $[W(O)(OCH_2CH_2OH)(\{OC_6H_2(CMe_3)_2\text{-}2,4\text{-}CH_2\text{-}6\}_3N)]$ where there is a similar low π-loading requirement for the phenoxo ligands the angles range from 126.0(2)–141.9(2)° [33]. For 1σ–2π donation from a phenoxo ligand, DFT calculations show there is a shallow minimum in the energy for the angle between about 160° and 180°, at 140° the energy is 20 kJ mol^{-1} and at 120° this energy rises to 60 kJ mol^{-1} [23].

Where the Ti–O–C bond angle is reduced it might be expected that the *tert*-butyl group would move away from the terminal Cl and create a wider but less well developed pocket about this ligand. However, inspection of the inter-

Table 4
Selected bond distances (Å) and angles (°) for [(Ti{($OC_6H_2Me_2$-2,4-CH_2-6)$_3$N})$_2$O] · *n*-pentane (**10b**)

Ti(1)–O(7)	1.8076(17)
Ti(1)–O(2)	1.8328(18)
Ti(1)–O(1)	1.8362(17)
Ti(1)–O(3)	1.8456(17)
Ti(1)–N(1)	2.379(2)
Ti(2)–O(7)	1.8219(17)
Ti(2)–O(5)	1.8304(18)
Ti(2)–O(4)	1.8348(18)
Ti(2)–O(6)	1.8387(19)
Ti(2)–N(2)	2.388(2)
O(1)–C(1)	1.357(3)
O(2)–C(16)	1.367(3)
O(3)–C(25)	1.355(3)
O(4)–C(28)	1.360(3)
O(5)–C(43)	1.360(3)
O(6)–C(52)	1.365(3)
O(7)–Ti(1)–O(2)	99.36(8)
O(7)–Ti(1)–O(1)	98.15(8)
O(2)–Ti(1)–O(1)	116.97(8)
O(7)–Ti(1)–O(3)	97.66(8)
O(2)–Ti(1)–O(3)	118.80(9)
O(1)–Ti(1)–O(3)	117.96(8)
O(7)–Ti(1)–N(1)	179.41(8)
O(2)–Ti(1)–N(1)	81.23(7)
O(1)–Ti(1)–N(1)	81.54(7)
O(3)–Ti(1)–N(1)	82.07(7)
O(7)–Ti(2)–O(5)	97.24(8)
O(7)–Ti(2)–O(4)	97.86(8)
O(5)–Ti(2)–O(4)	115.75(9)
O(7)–Ti(2)–O(6)	98.45(8)
O(5)–Ti(2)–O(6)	122.94(9)
O(4)–Ti(2)–O(6)	115.78(9)
O(7)–Ti(2)–N(2)	178.52(8)
O(5)–Ti(2)–N(2)	81.29(7)
O(4)–Ti(2)–N(2)	82.69(7)
O(6)–Ti(2)–N(2)	82.51(8)
C(1)–O(1)–Ti(1)	144.72(16)
C(16)–O(2)–Ti(1)	142.42(17)
C(25)–O(3)–Ti(1)	141.63(16)
C(28)–O(4)–Ti(2)	139.95(17)
C(43)–O(5)–Ti(2)	143.33(16)
C(52)–O(6)–Ti(2)	140.04(17)
Ti(1)–O(7)–Ti(2)	147.48(11)

atomic distances between the central *tert*-butyl group carbons and Cl in **6** and **12** shows that this effect is minimal on changing from the tetrahedral structure (C···Cl distance 4.87 Å) to the trigonal bipyramid (C···Cl distances 4.87, 4.91 and 4.93 Å). Noticeable in the two structures is that the titanium atom lies 0.60 Å above the plain made by the three phenoxide oxygen atoms in the tetrahedron but only 0.22 Å above them in the trigonal bipyramid. This is, of course, to be expected but it results in the chloro ligand lying 2.15 Å above the central carbon atoms of the three *tert*-butyl groups in the tetrahedron and 1.69, 1.78 and 1.85 Å in the trigonal bipyramid. The net effect is that when the methyl groups are taken into account, the trigonal bipyramidal structure creates a slightly better pocket about Cl than does the tetrahedron. The pocket structure in **12** is shown by the space-filling models in Fig. 5b and c.

Given the trigonal bipyramidal nature of complex **12** and the relevance of coordination expansion in the present studies, an excess of pyridine was added to the complex resulting in the formation of [(TiCl({$OC_6H_2(CMe_3)_2$-2,4-CH_2-6)$_3$N})(NC_5H_5)] (**13**). The ^{1}H NMR spectrum shows the methylene protons as a broadened singlet for this 6-coordinate compound compared with the AB quartet found for the 5-coordinate parent. The pyridine resonances in both the ^{1}H and ^{13}C{^{1}H} NMR spectra were very well-defined suggesting that fluxional processes are absent or are fast on the NMR timescale. Suitable crystals of the complex for X-ray crystallography have not yet been obtained but the structure is expected to be octahedral with the pyridine ligand coordinating *trans* to one of the phenoxo ligands. For this geometry the chloro ligand would still be surrounded by the *tert*-butyl groups but the pocket would be opened up on one side by the pyridine ligand. Recently, reported X-ray crystal structures show that this type of coordination geometry can be obtained from bidentate oxygen and nitrogen ligands [34].

3. Conclusion

The results of this work indicate that substituents in the *ortho*-position of the phenoxo ligand ring in tetrahedral chloro-tris-phenoxo complexes of titanium are positioned so as to create a coordination pocket or cavity about the chloro ligand. Where the substituent is a methyl group the effect is minimal but a *tert*-butyl substituent gives rise to a more substantial pocket. Coordination expansion can occur when a further donor ligand is available which removes this special environment. A phenyl substituent creates a better pocket but this can also be reduced in size when a further ligand binds creating a trigonal bipyramidal structure in which the pocket collapses somewhat. The collapse is due to the need to remove interactions of the phenoxo ligand phenyl ring with the ligand lying *trans* to the chloro ligand. Where an octahedral structure forms by filling two coordination sites, the possibility of isomers complicates the issue producing structures in which not all the *ortho*-substituents influence the chloro ligand. Where the collapse needs to be prevented, the tied-back ligand system gives rise to a trigonal bipyramidal structure of a more robust nature. A further ligand may coordinate leading to an octahedral structure which is expected to be more open on one side but it is obvious that the nature of this ligand is important given that diethyl ether does not coordinate but pyridine does. Overall it is apparent that *tert*-butyl groups in these complexes do not cover Cl completely forming what is best described as a steric pressure pocket [10d] whereas substituents that reach further outwards would form a more enclosed pocket or cavity. Given the availability of a wide variety of phenol ligands substituted in the *ortho*-position, the chloro-tris-phenoxo approach to the molecular engineering of coordination pockets should have future potential. By varying the size of the substituent,

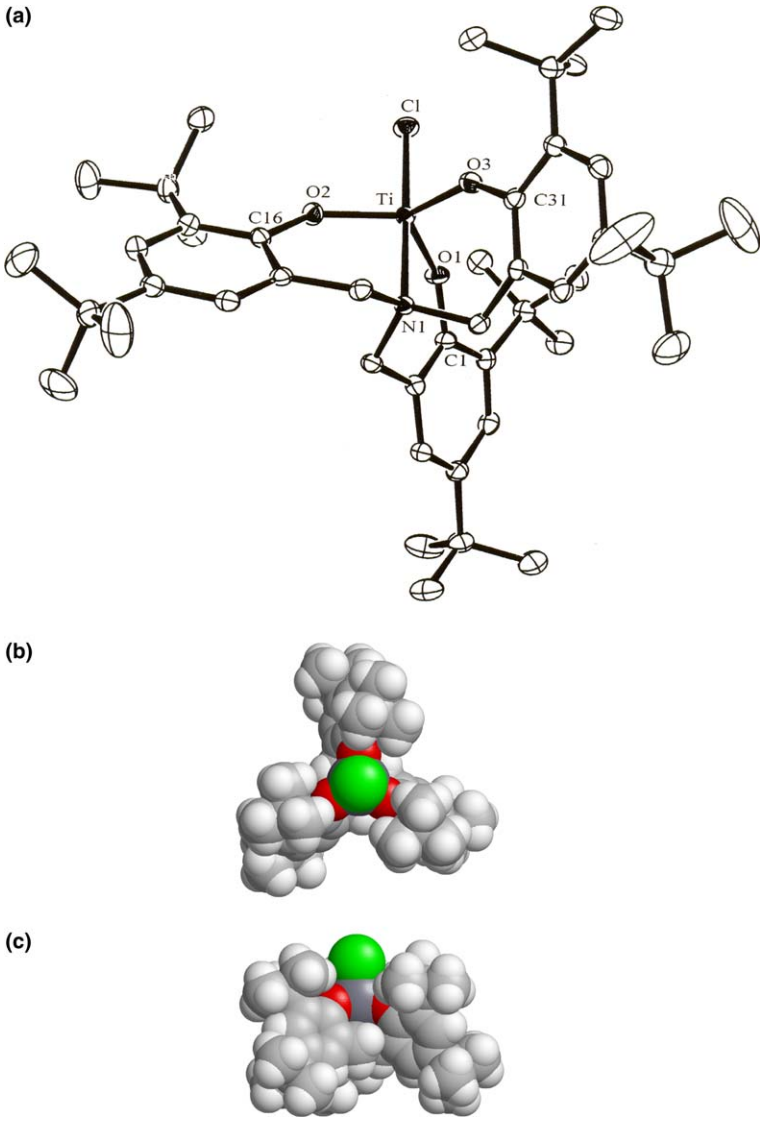

Fig. 5. (a) ORTEP diagram of $[TiCl(\{OC_6H_2(CMe_3)_2\text{-}2,4\text{-}CH_2\text{-}6\}_3N)]\cdot$ diethyl ether (**12**) showing the molecular structure. Hydrogen atoms have been removed for clarity. The diethyl ether solvent is not shown. (b) Space-filling model looking down the Cl–Ti bond showing the pocket arrangement about Cl. (c) Space-filling model, side-on view of the Ti–Cl bond showing the extent to which the *tert*-butyl group methyls cover the Cl atom.

collapsible through to non-collapsible complexes with different pocket characteristics may be realised.

4. Experimental

4.1. General methods and materials

All preparations and manipulations were carried out under dry oxygen-free nitrogen using standard bench-top techniques for air-sensitive substances. $[TiCl_4]$ and the phenols were used as received from commercial sources. 4,4′-Dimethyl-2,2′-bibyridyl (dmbipy) was dried under vacuum before use. Tris(2-hydroxy-4,6-di-*tert*-butylbenzyl)amine and tris(2-hydroxy-4,6-dimethylbenzyl)amine were prepared by the literature procedures [28]. Light petroleum (b.p. 40–60 °C) and toluene were distilled from sodium wire and dichloromethane from freshly ground CaH_2. ^1H and $^{13}C\{^1H\}$ NMR spectra were recorded at 400 and 100 MHz, respectively, on a Bruker AM400 spectrometer. $CDCl_3$ and CD_2Cl_2 were dried over, and distilled from, freshly ground CaH_2 and benzene-d_6 from sodium wire. C, H and N analyses were determined by Dr. A. Cunninghame and associates, University of Otago, New Zealand. The production of HCl gas in the thermalisation reactions was monitored by passing the exhaust gases from the nitrogen bubbler over *N*,*N*,*N*′,*N*′-tetramethylethylenediamine and observing the white cloud produced.

4.2. Synthesis

4.2.1. $[TiCl(OC_6H_4CMe_3)_3\text{-}4]\cdot 0.5C_7H_8$ (**1**)

4-*tert*-Butylphenol (4.75 g, 31.6 mmol) in toluene (40 cm^3) was added to $[TiCl_4]$ (2.0 g, 10.5 mmol) in toluene (40 cm^3) and the mixture was refluxed until no more HCl

Table 5
Selected bond distances (Å) and angles (°) for [TiCl({$OC_6H_2(CMe_3)_2$-2,4-CH_2-6}$_3$N)]·(OEt_2) (**12**)

Ti–O1	1.809(2)
Ti–O2	1.817(2)
Ti–O3	1.811(2)
Ti–N1	2.216(2)
Ti–Cl	2.3074(7)
O1–C1	1.363(3)
O2–C16	1.370(3)
O3–C31	1.367(3)
N1–C7	1.501(3)
N1–C22	1.495(3)
N1–C37	1.497(3)
O(1)–Ti–O(2)	119.29(7)
O(1)–Ti–O(3)	115.48(7)
O(3)–Ti–O(2)	120.72(7)
O(1)–Ti–N(1)	82.76(7)
O(2)–Ti–N(1)	82.66(7)
O(3)–Ti–N(1)	83.30(7)
O(1)–Ti–Cl(2)	97.10(5)
O(3)–Ti–Cl(2)	97.18(5)
O(2)–Ti–Cl(2)	97.01(5)
N(1)–Ti–Cl(2)	179.51(5)
C(1)–O(1)–Ti	143.54(15)
C(16)–O(2)–Ti	143.66(14)
C(31)–O(3)–Ti	143.97(14)

gas was produced (12 h). NMR spectroscopy at this stage confirmed that no 4-*tert*-butylphenol was present. The cooled solution was filtered, the solvent was removed and the residue held under vacuum for 2 h giving the complex as a deep-red flaky solid. Yield: 5.82 g, 97%. *Anal*. Calc. for $C_{33.5}H_{43}ClO_3Ti$: C, 69.73; H, 7.51. Found: C, 69.48; H, 7.58%. ^{1}H NMR: δ 1.27 (s, 27H, CMe_3), 2.40 [s, 1.5H, 0.5CH_3(toluene)], 7.11 (b, 12H, *o* and *m*-Hs), 7.22 and 7.30 (m, 2.5H, 0.5 aromatics (toluene). ^{13}C{^{1}H} NMR: δ 21.5 [Me(toluene)], 31.5 (CMe_3), 34.2 (C), 118.7 (b, *o*-C) 124.7 (toluene), 124.6 (b, *m*-C), 128.2 (toluene), 129.0 (toluene), 137.9 [*ipso*-C(toluene)], 145.8 (b, C), 164.6 (*ipso*-C).

4.2.2. [{TiCl($OC_6H_3Me_2$-2,4)$_2$(μ-$OC_6H_3Me_2$-2,4)}$_2$] (**2**)

2,4-Dimethylphenol (3.87 g, 31.7 mmol) in toluene (40 cm^3) was added to [$TiCl_4$] (2.0 g, 10.5 mmol) in toluene (40 cm^3) and the mixture was refluxed until no more HCl gas was produced (12 h). The cooled solution was filtered, the solvent was removed and the residue held under vacuum for 2 h giving a gum that formed the complex as a deep-red crystalline mass on standing overnight. Yield: 4.5 g, 96%. *Anal*. Calc. for $C_{24}H_{27}ClO_3Ti$: C, 64.51; H, 6.09. ^{1}H NMR: δ (s, 9H, Me), 2.20 (s, 9H, Me), 6.72–6.89 (m, 9H, *o* and *m*-Hs). ^{13}C{^{1}H} NMR: δ 16.6 (Me), 20.7 (Me), 119.5 (CH), 126.3 (C), 126.9 (CH), 131.0 (CH), 133.2 (C), 164.4 (*ipso*-C). Crystalline material was cut from the mass and used for the X-ray analysis.

4.2.3. [TiCl($OC_6H_3Me_2$-2,4)$_3$(dmbipy)] (**3**)

4,4′-Dimethyl-2,2′-bipyridine (0.4 g, 2.17 mmol) in CH_2Cl_2 (20 cm^3) was added to complex **2** (0.96 g, 2.15 mmol) in CH_2Cl_2 (20 cm^3) and the mixture was stirred for 1 h. The solution was filtered and the solvent removed to give the complex as an orange flaky solid. Yield: 1.30 g, 96%. *Anal*. Calc. for $C_{36}H_{39}ClN_2O_3Ti$: C, 68.52; H, 6.23, N, 4.44. Found: C, 67.80; H, 6.73, N, 4.68%. ^{1}H NMR: δ 1.67 (s, 3H, Me); 2.06 (s, 3H, Me); 2.24 (s, 6H, 2Me); 2.34 (s, 6H, 2Me); 2.40 (s, 6H, 2Me); 6.25 [d, ^3J(HH) 8.1, 1H, *o*-H]; 6.46 [dd, ^3J(HH) 8.1, ^4J(HH) 1.6, 1H, *m*-H]; 6.58 [d, ^4J(HH) 1.6, 1H, *m*-H]; 6.83 [dd, ^3J(HH) 8.1, ^4J(HH) 1.5, 2H, *m*-Hs]; 6.91 [d, ^4J(HH) 1.5, 2H, *m*-Hs]; 7.20 [d, ^3J(HH) 5.5, 2H, *m*-H dmbipy]; 7.38 [d, ^3J(HH) 8.1, 2H, *o*-Hs]; 7.81 [bd, 2H, *m*-Hs dmbipy]; 8.95 [d, ^3J(HH) 5.5, 2H, *o*-Hs dmbipy]. ^{13}C{^{1}H} NMR: δ 16.1 (1Me); 17.1 (2Me); 20.4 (1Me); 20.7 (2Me); 21.5 (2Me, dmbipy); 118.5 (1CH); 120.1 (2CH); 122.2 (*m*-CH, dmbipy); 126.3 (2C); 126.4 (1*m*-CH); 126.6 (2*m*-CHs, dmbipy); 127.0 (2*m*-CHs); 128.7 (1C); 128.9 (1C); 130.1 (2C); 130.3 (1*m*-CH); 130.7 (2*m*-CHs); 149.0 (2*o*-CHs, dmbipy); 150.7 (2Cs, dmbipy); 151.7 (2Cs, dmbipy); 162.7 (1 *ipso*-C); 163.51 (2 *ipso*-Cs).

4.2.4. [TiCl($OC_6H_2Me_3$-2,4,6)$_3$] (**4**)

2,4,6-Trimethylphenol (4.31 g, 31.7 mmol) in toluene (40 cm^3) was added to [$TiCl_4$] (2.0 g, 10.5 mmol) in toluene (40 cm^3) and the mixture was refluxed until no more HCl gas was produced (15.5 h). The cooled solution was filtered from a small amount of solid, the solvent was removed and the residue held under vacuum for 2 h giving a gum which formed the complex as a deep-red crystalline mass on standing overnight. Yield: 4.5 g, 87%. *Anal*. Calc. for $C_{27}H_{33}ClO_3Ti$: C, 66.33; H, 6.80. Found: C, 65.88; H, 6.70%. ^{1}H NMR: δ 2.19 (s, 9H, Me), 2.26 (bs, 18H, Me), 6.72 (bs, 6H, *m*-Hs). ^{13}C{^{1}H} NMR: δ 16.9 (*o*-Me), 20.6 (*p*-Me), 126.7 (*o*-C), 128.6 (CH), 132.4 (*p*-C), 163.9 (*ipso*-C).

4.2.5. [TiCl{$OC_6H_3(CHMe_2)_2$-2,6}$_3$] (**5**)

2,6-Di-*iso*-propylphenol (3.0 g, 16.8 mmol) in toluene (30 cm^3) was added to [$TiCl_4$] (1.0 g, 5.27 mmol) in toluene (30 cm^3) and the mixture was refluxed until no more HCl gas was produced (19.5 h). The cooled solution was filtered and the solvent removed giving an orange solid. NMR spectroscopy at this stage indicated the presence of unreacted phenol and two coordination products. The crude material was dissolved in toluene (50 cm^3), the volume reduced to ca. 30 cm^3 and the solution stood at −20 °C, giving the complex as a non-crystalline orange solid containing several large crystals of [Ti{$OC_6H_3(CHMe_2)_2$-2,6}$_4$] which were manually removed from the product. Yield: 1.30 g, 40%. *Anal*. Calc. for $C_{36}H_{51}ClO_3Ti$: C, 70.29; H, 8.36. Found: C, 70.78; H, 8.88%. ^{1}H NMR: δ 1.13 [d, ^3J(HH) 6.9, 36H, CMe_2], 3.42 [sept, ^3J(HH) 6.9, CH], 6.91 (t, 3H, *p*-Hs), 7.03 (m, 6H, *m*-Hs). ^{13}C{^{1}H} NMR: δ 23.2 (Me), 27.5 (CH), 123.0 (*m*-C), 123.8 (*p*-C), 137.4 (*o*-C), 163.1 (*ipso*-C). The NMR spectra are identical to that found for the complex prepared in refluxing benzene [20,21].

*4.2.6. [TiCl{$OC_6H_3(CMe_3)_2$-2,4}$_3$] (**6**)*

Method A: 2,4-Di-*tert*-butylphenol (9.8 g, 47.5 mmol) in toluene (60 cm^3) was added to [$TiCl_4$] (3.0 g, 15.8 mmol) in toluene (50 cm^3) and the mixture was refluxed until no more HCl gas was produced (14.5 h). After refluxing for a further 2 h, the cooled solution was filtered and the solvent removed giving a crystalline orange-red solid. Crude yield: 11.0 g, 99%. This material has a slight red tinge and NMR spectroscopy indicated the presence of a small amount of unreacted phenol (ca. 3–5%) but it was sufficiently pure for further use. The solid was washed with petroleum spirit (40 cm^3) giving the complex as an orange crystalline solid. Yield: 9.21 g, 83%. (Further complex can be obtained by cooling the petroleum spirit washings.) *Anal*. Calc. for $C_{42}H_{63}ClO_3Ti$: C, 72.13; H, 9.08. Found: C, 71.96; H, 9.26%. ^{1}H NMR: δ 1.29 (s, 27H, CMe_3), 1.46 (s, 27H, CMe_3), 7.10 (s, 6H, *o* and *m*-Hs), 7.29 [d, ^4J(HH) 1.3, 3H, *m*-H). $^{13}C\{^1H\}$ NMR: δ 30.3 (Me), 31.6 (Me), 34.6 (C), 35.1 (C), 122.7 (CH), 123.4 (CH), 124.0 (CH), 135.6 (C), 146.3 (C), 163.2 (*ipso*-C). On a larger scale, a reaction between 26.15 g of 2,4-di-*tert*-butylphenol (0.127 mol) and 8 g of [$TiCl_4$] (0.0422 mol) in 120 cm^3 of toluene produced 28.5 g (97%) of the crude product after refluxing for 21 h.

Method B: *n*-Butyl lithium (9.8 cm^3 of a 1.6 mol L^{-1} solution, 15.8 mmol) in hexane was added dropwise to a solution of 2,4-di-*tert*-butylphenol (3.26 g, 15.8 mmol) in diethyl ether (50 cm^3) cooled to −30°C and the solution was stirred with the cooling bath removed for 2 h. [$TiCl_4$] (1.0 g, 5.27 mmol) was added to a flask which was then cooled to −78 °C and diethyl ether (50 cm^3) was added. The solution was heated until all the yellow solid dissolved and then recooled to −78 °C and the lithium phenoxide solution added via a cannula. The cooling bath was removed and the solution stirred for 20 h, filtered and the solvent removed to give the crude complex as an orange crystalline solid (yield: 3.08 g) which was dissolved in diethyl ether (50 cm^3). The solution was filtered and the volume reduced to ca. 25 cm^3 giving the complex as yellow-orange crystals on standing. Yield: 1.24 g, 34%. *Anal*. Calc. for $C_{42}H_{63}ClO_3Ti$: C, 72.13; H, 9.08. Found: C, 72.14; H, 8.72%. The complex has identical NMR spectra to the sample prepared under method A. A single crystal from the mass was used for the X-ray analysis.

4.2.7. [TiCl{$OC_6H_3(CMe_3)_2$-2,4}$_3$(dmbipy)] (7)

4,4′-Dimethyl-2,2′-bipyridine (0.267 g, 1.45 mmol) in CH_2Cl_2 (20 cm^3) was added to complex **6** (1.014 g, 1.45 mmol) in CH_2Cl_2 (20 cm^3) and the mixture was stirred for 2 h. The solution was filtered and the solvent removed to give the complex as an orange flaky solid. Yield: 1.28 g, 99%. *Anal*. Calc. for $C_{54}H_{75}ClN_2O_3Ti$: C, 73.40; H, 5.56, N, 3.17. Found: C, 73.04; H, 5.76, N, 3.09%. The NMR spectra are very complicated due to the presence of isomers. Only the ^{1}H NMR of the distinguishable major isomer is reported: δ 1.28 (s, 18H, $2CMe_3$); 1.31 (s, 9H, CMe_3); 1.37 (s, 18H, $2CMe_3$); 1.51 (s, 9H, CMe_3); 2.31 (s, 6H, 2Me dmbipy); 6.96 [dd, ^3J(HH) 8.2, ^4J(HH) 2.4, 2H, *m*-Hs]; 6.98 (obscured dd, 1H, *m*-H); 7.09 [d, ^3J(HH) 5.6, 2H, *m*-Hs dmbipy]; 7.11 [d, ^3J(HH) 8.4, ^4J(HH) 2.3, 1H, *m*-H]; 7.23 [d, ^4J(HH) 2.4, 2H, *m*-Hs]; 7.29 [d, J(HH) 2.3, 1H, *m*-H]; 7.55 [bd, ^3J(HH) 8.2, 2H, *o*-Hs]; 7.91 (s, 2H, *m*-Hs dmbipy); 8.93 [d, ^3J(HH) 5.6, 2H, *o*-Hs dmbipy]. Easily distinguishable *ortho*-hydrogen resonances for the other isomers are at δ 8.79 and 8.53.

*4.2.8. [TiCl(OC_6H_4Ph-2)$_3$] (**8**)*

2-Hydroxybiphenyl (8.1 g, 47.6 mmol) in dichloromethane (50 cm^3) was added to [$TiCl_4$] (3.0 g, 15.8 mmol) in dichloromethane (50 cm^3) and the mixture was refluxed until no more HCl gas was produced (30 h). The cooled solution was filtered, the solvent was removed giving a dark red gum which failed to solidify on extended pumping. The complex was identified on the basis of NMR spectral characteristics that were similar to complex **9**. ^{1}H NMR: δ 6.58 [d, ^3J(HH) 7.4, 3H, *o*-H], 7.01 [t, ^3J(HH) 7.4, 3H, *p*-H], 7.07 [t, ^3J(HH) 7.4, 3H, *m*-H], 7.12–7.18 [m, 9H, *m* and *p*-Hs(phenyl substituent)], 7.20 [dd, ^3J(HH) 7.4, ^4J(HH) 1.4, 3H, *m*-H], 7.32 [d, ^3J(HH) 7.4, 6H, *o*-Hs(phenyl substituent)]. $^{13}C\{^1H\}$ NMR: δ 120.4 (CH), 124.0 (CH), 127.3 (CH), 128.2 (CH), 128.3 (CH), 129.2 (CH), 130.0 (CH), 130.6 (C), 137.3 (C), 163.6 (*ipso*-C).

*4.2.9. [TiCl(OC_6H_4Ph-2)$_3$(diethyl ether)] (**9**)*

n-Butyl lithium (15.3 cm^3 of a 1.6 mol L^{-1} solution, 24.4 mmol) in hexane was added dropwise to a solution of 2-hydroxybiphenyl (4.15 g, 24.4 mmol) in diethyl ether (80 cm^3) cooled to −30°C and the solution was stirred with the cooling bath removed for 2 h. [$TiCl_4$] (1.54 g, 8.1 mmol) was added to a flask which was then cooled to −78 °C and diethyl ether (80 cm^3) was added. The solution was heated until all the yellow solid dissolved and after cooling to room temperature, it was added via a cannula to the suspension of the lithium phenoxide cooled to −78 °C. The cooling bath was removed and the solution stirred for 20 h, filtered and the remaining solid washed with diethyl ether until it was no longer coloured orange. The combined filtrate and washings were kept hot while the volume was reduced to approximately half and on standing the complex formed as large ruby-red crystals. Yield: 1.8 g, 51%. *Anal*. Calc. for $C_{40}H_{37}ClO_4Ti$: C, 72.24; H, 5.61. Found: C, 71.91; H, 5.48%. ^{1}H NMR: δ 1.13 [t, ^3J(HH) 7.0, 6H, Me], 3.45 [q, ^3J(HH) 7.0, 4H, CH_2], 6.62 (d, 3H, aromatic-H), 6.99 (t, 3H, aromatic-H), 7.05 (t, 3H, aromatic-H), 7.09–7.20 (m, 12H, aromatic-Hs), 7.32 (d, 6H, aromatic-Hs). $^{13}C\{^1H\}$ NMR: δ 15.0 (Me), 66.0 (CH_2), 120.5 (CH), 123.6 (CH), 127.2 (CH), 128.2 (CH), 129.2 (CH), 130.0 (CH), 130.3 (C), 137.5 (*o*-C),163.2 (*ipso*-C). A single crystal from the mass was used for the X-ray analysis.

*4.2.10. [(Ti{($OC_6H_2Me_2$-2,4-CH_2-6)$_3$N})$_2$O] · 1.5C_6H_6 (**10a**)*

Undried tris(2-hydroxy-4,6-dimethylbenzyl)amine (1.77 g, 4.22 mmol) in benzene (40 cm^3) was added dropwise to

a stirred solution of [$TiCl_4$] (0.8 g, 4.28 mmol) in benzene (40 cm^3) and triethylamine (1.8 cm^3, 12.74 mmol) was added dropwise. The mixture was refluxed for 14 h, the cooled solution filtered and the solvent removed to give the complex as yellow crystalline solid which was washed with chilled diethyl ether (30 cm^3). Yield: 2.0 g, 100%. *Anal.* Calc. for $C_{54}H_{60}N_2O_7Ti_2 \cdot 1.5C_6H_6$: C, 71.25; H, 6.55; N, 2.64. Found: C, 71.39; H, 6.76; N, 2.90%. ^{1}H NMR: δ (C_6D_6) 2.15 (s, 9H, Me), 2.38 (s, 9H, Me), 2.8 (b, 3H, CH), 3.8 (b, 3H, CH), 6.54 (bs, 3H, *m*-CH), 6.73 (bs, 3H, *m*-CH), 7.28 (benzene). ^{13}C{^{1}H} NMR: δ 16.1 (Me), 20.7 (Me), 58.8 (CH_2),124.3 (C), 125.0 (C), 128.5 (CH), 129.3 (C), 131.0 (CH), 160.8 (*ipso*-C). A single crystal obtained from the mass produced on recrystallisation from *n*-pentane was used for the X-ray analysis [complex **10b**].

4.2.11. [TiCl{($OC_6H_2Me_2$-2,4-CH_2-6)$_3$N}] (**11**)

Method A: Chlorotrimethylsilane (2 cm^3, 1.34 mmol) was added via a syringe to [(Ti{($OC_6H_2Me_2$-2,4-CH_2-6)$_3$N})$_2$O] (0.6 g, 0.67 mmol) in toluene (30 cm^3) and the mixture was stirred for 8 h. The solution was filtered and the orange precipitate dried under vacuum. Yield: 0.49 g, 73%. *Anal.* Calc. for $C_{27}H_{30}ClNO_3Ti$: C, 64.87; H, 6.05, N, 2.80. Found: C, 64.82; H, 6.32; N, 2.97%. ^{1}H NMR (the complex is only slightly soluble in $CDCl_3$): δ 2.22 (s, 9H, Me), 2.25 (s, 9H, Me), 2.9 (b, 3H, CH), 3.9 (b, 3H, CH), 6.73 (bs, 3H, *m*-H), 6.88 (bs, 3H, *m*-H). ^{13}C{^{1}H} NMR: δ 15.8 (Me), 20.7 (Me), 58.5 (CH_2), 122.8 (C), 124.4 (C), 127.2 (CH), 131.1 (CH), 131.3 (C), 160.2 (*ipso*-C).

Method B: [$TiCl_4$] (0.29 g, 1.52 mmol) was cooled to −78 °C and diethyl ether (40 cm^3) was added. The solution was heated to dissolve the yellow solid, cooled to room temperature and added dropwise to [$Ti(OCHMe_2)_4$] (1.30 g, 4.57 mmol) in diethyl ether (30 cm^3). The mixture was stirred for 30 min [$TiCl(OCHMe_2)_3$] equivalent: (1.59 g, 6.08 mmol) and dry tris(2-hydroxy-4,6-dimethylbenzyl)amine (2.55 g, 6.08 mmol) in diethyl ether (40 cm^3) added dropwise. The mixture was stirred for 2 h and the orange precipitate filtered off and dried under vacuum. Yield: 2.92 g, 96%. *Anal.* Calc. for $C_{27}H_{30}ClNO_3Ti$: C, 64.87; H, 6.05, N, 2.80. Found: C, 65.31; H, 6.41; N, 2.81%. The complex had similar NMR spectra to the sample prepared under method A.

4.2.12. [TiCl({$OC_6H_2(CMe_3)_2$-2,4-CH_2-6}$_3$N)] · diethyl ether (**12**)

[$TiCl_4$] (0.234 g, 1.23 mmol) was cooled to −78 °C and diethyl ether (40 cm^3) was added. The solution was heated to dissolve the yellow solid, cooled to room temperature and added dropwise to [$Ti(OCHMe_2)_4$] (1.05 g, 3.69 mmol) in diethyl ether (30 cm^3). The mixture was stirred for 30 min ([$TiCl(OCHMe_2)_3$] equivalent: 1.286 g, 4.95 mmol) and dry tris(2-hydroxy-4,6-di-*tert*-butylbenzyl)amine (3.33 g, 4.96 mmol) in diethyl ether (40 cm^3) added dropwise. The mixture was stirred for 2 h, the solution filtered and the solvent removed to give an orange crystalline solid. Yield: 2.92 g, 96%. *Anal.* Calc. for $C_{45}H_{66}ClNO_3Ti$ (i.e., [{$N(ArO)_3$}TiCl]): C, 71.81; H, 8.84, N, 1.86. Found: C, 72.99; H, 8.76; N, 2.01%. The solid was dissolved in diethyl ether (120 cm^3) and the solvent kept hot and removed in vacuo until crystallisation could no longer be prevented. On standing, well formed orange crystals were formed. Further crystalline product was obtained by repeating this process. *Anal.* Calc. for $C_{49}H_{76}ClNO_4Ti$: C, 71.21; H, 9.27; N, 1.70. Found: C, 71.45; H, 9.36; N, 1.69%. ^{1}H NMR: δ 1.26 (t, 6H, diethyl ether),1.34 (s, 27H, CMe_3), 1.52 (s, 27H, CMe_3), 3.18 [d, ^2J(AB) 13.9, 3H, CH], 3.53 [d, ^2J(AB) 13.9, 3H, CH], 7.09 [d, ^3J(HH) 2.1, 3H, *m*-H], 7.31 [d, ^3J(HH) 2.1, 3H, *m*-H]. ^{13}C{^{1}H} NMR: δ 15.3 (Me, diethyl ether), 29.6 (CMe_3), 31.6 (CMe_3), 34.5 (C), 34.9 (C), 58.7 (CH_2), 65.8 (CH_2,diethyl ether), 123.3 (*o*-C), 123.5 (*m*-CH), 124.0 (*m*-CH), 135.7 (*p*-C), 144.3 (*o*-C), 160.8 (*ipso*-C). A single crystal from the mass was used for the X-ray analysis.

4.2.13. [TiCl{($OC_6H_2(CMe_3)_2$-2,4-CH_2-6)$_3$N}(NC_5H_5)] (**13**)

Pyridine (0.2 g, 2.5 mmol) in diethyl ether (10 cm^3) was added dropwise from a syringe to a rapidly stirred solution of complex **12** (0.373 g, 0.45 mmol) in diethyl ether and the mixture was stirred for 2 h. The solution was filtered and the brown microcrystalline solid dried in vacuo. Yield: 0.364 g, 97%. *Anal.* Calc. for $C_{50}H_{71}ClN_2O_3Ti$: C, 72.23; H, 8.61; N, 3.44. Found: C, 72.70; H, 9.27; N, 3.66%. ^{1}H NMR (CD_2Cl_2): δ 1.99 (t, 6H, Me), 1.32 (s, 27H, CMe_3), 1.49 (s, 27H, CMe_3), 3.47 (q, 4H, CH_2), 3.64 (bs, 6H, CH_2), 7.09 [d, ^3J(*HH*) 2.2, 3H, *m*-H], 7.31 [d, ^3J(*HH*) 2.2, 3H, *m*-H], 7.31–7.35 (obsm, 2H, *m*-H_{py}), 7.73 (td, ^3J(*HH*) 7.7, 1H, (*p*-H_{py})), 8.63 (bs, 2H, *o*-H_{py}). ^{13}C{^{1}H} NMR: δ 15.5 ($Me_{diethyl\ ether}$), 29.7 (CMe_3), 31.7 (CMe_3), 34.8 (C), 35.2(C), 59.0 (CH_2), 66.1 ($CH_{2diethyl\ ether}$), 123.9 (CH), 123.95 (*o*-C), 124.2 (*m*-CH_{py}), 135.8 (*p*-C), 136.4 (*p*-CH_{py}),144.8 (*o*-C), 150.1 (*o*-CH_{py}), 161.1 (*ipso*-C).

4.3. X-ray crystallography

Crystallographic and refinement data are given in Table 6. Data collected, with graphite monchromated Mo Kα X-radiation, were measured on a Siemens SMART CCD area detector diffractometer with the omega scan method. The data were corrected for Lorentz and polarisation effects and for absorption by the multi-scan method [35]. The structures were solved by direct methods [36] and refined by full-matrix least-squares methods [37] on F^2. Hydrogen atoms were placed in calculated positions and were refined with a riding model ($U_{iso} = 0.08$). Diagrams were prepared by ORTEP [38] and RASTOP [39]. Selected bond distances and angles are listed in Tables 1–5. Complex **2** is dimeric lying across a centre of symmetry. Some disorder was noted for the Cl (with a site occupancy ratio of ca. 90:10) and also for the H atoms in the Me group in the 4 positions of both terminal phenoxo ligands. The occupancies of these latter were fixed at 0.5. In **6** the *tert*-butyl group in the para

Table 6
Crystallographic data and structural information

Compound	**2**	**6**	**9**	**10b**	**12**
Molecular formula	$C_{24}H_{27}ClO_3Ti$	$C_{42}H_{63}ClO_3Ti$	$C_{40}H_{37}ClO_4Ti$	$C_{39}H_{72}N_2O_7Ti_2$	$C_{40}H_{37}ClNO_4Ti$
M_r	446.81	699.27	665.05	1016.99	826.46
T (K)	150(2)	293(2)	150(2)	150(2)	189(2)
Crystal size (mm)	$0.40 \times 0.30 \times 01.6$	$0.22 \times 0.24 \times 0.38$	$0.50 \times 0.40 \times 0.40$	$0.42 \times 0.30 \times 0.22$	$0.38 \times 0.18 \times 0.18$
Crystal system	monoclinic	hexagonal	monoclinic	triclinic	monoclinic
Space group	$P2_1/c$	$R\bar{3}$	$P2_1/n$	$P\bar{1}$	$P2_1/n$
a (Å)	10.9316(1)	16.680(2)	13.1474(2)	12.3309(2)	15.0358(3)
b (Å)	25.7193(1)	16.680(2)	17.3038(2)	12.9833(2)	15.8104(2)
c (Å)	8.0853(1)	27.248(5)	15.3222(2)	20.0930(2)	20.6045(4)
α (°)	90.0	90.0	90.0	84.258(1)	90.0
β (°)	93.882(1)	90.0	94.725(1)	72.168(1)	92.630(1)
γ (°)	90.0	120.0	90.0	66.649(1)	90.0
V (Å^3)	2267.99(4)	6565.3(16)	3473.95(8)	2810.61(7)	4892.98(15)
Z	4	6	4	2	4
D_{calc} (mg cm^{-3})	1.309	1.061	1.272	1.202	1.122
μ (mm^{-1})	0.516	0.289	0.363	0.335	0.270
F (000)	936	2268	1392	1080	1792
θ Range for data collection (°)	1.58–23.32	1.60–25.00	1.78–26.30	1.06–25.35	1.62 to 26.43
Reflections collected	10347	11450	19986	24227	28138
Unique reflections (R_{int})	3267 (0.0172)	2582 (0.0242)	7008 (0.0193)	10220 (0.0252)	10004 (0.0440)
Reflections with [$I > 2\sigma(I)$]	2983	2203	5712	8045	7179
Refined parameters	275	173	443	647	526
Completeness to $\theta = x°$ (%)	23.32, 99.8	25.0, 100.0	26.30, 99.3	25.35, 99.2	26.43, 99.3
Absorption correction T_{max}, T_{min}	0.922, 0.820	0.939, 0.898	0.869, 0.839	0.930, 0.872	0.953, 0.905
Goodness-of-fit (all data)	1.045	1.124	1.056	1.051	1.051
Final R indices [$I > 2\sigma(I)$] (R_1,wR_2)	0.0303, 0.0824	0.0613, 0.1895	0.0357, 0.0891	0.0451, 0.1143	0.0496, 0.1035
R indices (all data) (R_1, wR_2)	0.0338, 0.0843	0.0699, 0.1961	0.0492, 0.0974	0.0632, 0.1287	0.0833, 0.1204
Maximum, minimum $\Delta\rho$ (e Å^{-3})	0.396, −0.374	0.658, −0.576	0.240, −0.373	0.511, −0.437	0.533, −0.419

position is disordered (ratio ca. 80:20) and in **9** two sites (ratio 65:35) have been distinguished for the co-ordinated ether molecule. Solvent of crystallisation was present in **10b** (*n*-pentane) and **12** (ether).

5. Supplementary data

CCDC 281293–281297 contains the supplementary crystallographic data for this paper. These data can be obtained free of charge from The Cambridge Crystallographic Data Centre via www.ccdc.cam.ac.uk/datarequest/cif.

References

[1] N. Kitajima, W.B. Tolman, Prog. Inorg. Chem. (1995) 419.
[2] S.R. Colinson, D.A. Fenton, Coord. Chem. Rev. 148 (1996) 19.
[3] G. Parkin, Chem. Rev. 104 (2004) 702.
[4] B. Kersting, Z. Anorg. Allg. Chem. 630 (2004) 765.
[5] A.R. van Doorn, M. Bos, S. Harkema, J. van Eerden, W. Verboom, D.N. Reinhoudt, J. Org. Chem. 56 (1991) 2371.
[6] V. van Axel-Castelli, A. Dalla-Cort, L. Mandolini, D.N. Reinhoudt, L. Schiaffino, Chem. Eur. J. 6 (2000) 1193.
[7] V. van Axel-Castelli, A. Dalla-Cort, L. Mandolini, V. Pinto, D.N. Reinhoudt, F. Ribaudo, C. Sanna, L. Schiaffino, B.H.M. Snellinkruel, Supramol. Chem. 14 (2002) 211.
[8] R.R. Conry, G. Ji, A.A. Tipton, Inorg. Chem. 38 (1999) 906.
[9] B.S. Hammes, D. Ramos-Maldonado, G.P.A. Yap, L. Liable-Sands, A.L. Rheingold, V.G. Young Jr., A.S. Borovik, Inorg. Chem. 36 (1997) 3210.
[10] (a) For recent work related to reduction of ammonia see: D.V. Yandulov, R.R. Schrock, Can. J. Chem. 83 (2005) 341;
(b) D.V. Yandulov, R.R. Schrock, Inorg. Chem. 44 (2005) 1103;
(c) V. Ritleng, D.V. Yandulov, W.W. Weare, R.R. Schrock, A.S. Hock, W.M. Davis, J. Am. Chem. Soc. 126 (2004) 6150;
(d) For general work related to this ligand type see: R.R. Schrock, Acc. Chem. Res. 30 (1997) 9.
[11] (a) For titanium see: J.C. Peters, A.R. Johnson, A.L. Odom, P.W. Wanandi, W.M. Davis, C.C. Cummins, J. Am. Chem. Soc. 118 (1996) 10175;
(b) For molybdenum see: A.R. Johnson, P.W. Wanandi, C.C. Cummins, Organometallics 13 (1994) 2907;
(c) E.L. Sceats, J.S. Figueroa, C.C. Cummins, M.M. Loening, P. van der Wel, R.G. Griffen, Polyhedron 23 (2004) 2751;
(d) W. Zhang, S. Kraft, J.S. Moore, Chem. Commun. (2003) 832;
(e) T. Agapie, P.L. Diaconescu, C.C. Cummins, J. Am. Chem. Soc. 124 (2002) 2412;
(f) A. Fuerstner, C. Mathes, C.W. Lehmann, Chem. Eur. J. 7 (2001) 5299;
(g) J.B. Greco, J.C. Peters, T.A. Baker, W.M. Davis, C.C. Cummins, G. Wu, J. Am. Chem. Soc. 123 (2001) 5003;
(h) A. Fuerstner, C. Mathes, C.W. Lehmann, J. Am. Chem. Soc. 121 (1999) 9453.
[12] D.C. Bradley, I.M. Thomas, J. Chem. Soc. (1960) 3857.
[13] T. Tanaka, T. Onoue, K. Kamei, K. Murakami, C. Iwata, J. Chem. Soc., Chem. Commun. (1990) 906.
[14] H. Ohno, K. Hiramatsu, T. Tanaka, Tetrahedron Lett. 45 (2004) 75.
[15] D. Seebach, L. Widler, Helv. Chim. Acta 65 (1982) 1972.
[16] A. Sato, A. Hattori, K. Ishihara, S. Saito, H. Yamamoto, Chem. Lett. 32 (2003) 1006.
[17] S. Saito, H. Yammoto, Chem. Commun. (1997) 1585.
[18] R. Imwinkelreid, D. Seebach, Org. Synth. 67 (1989) 180.
[19] A. Shah, A. Singh, R.C. Mehotra, Polyhedron 5 (1986) 1285.
[20] A. Shah, A. Singh, R.C. Mehotra, Indian J. Chem. A 32 (1993) 632.
[21] H. Noeth, M. Schmidt, Organometallics 14 (1995) 4601.
[22] S.L. Latesky, J. Keddington, A.K. McMullen, I.P. Rothwell, Inorg. Chem. 24 (1985) 995.

[23] A.J. Nielson, P. Schwerdtfeger, J.M. Waters, J. Chem. Soc., Dalton Trans. (2000) 529.
[24] A.J. Nielson, C. Shen, P. Schwerdtfeger, J.M. Waters, Eur. J. Inorg. Chem. (2005) 1343.
[25] Y. Morino, H. Uehara, J. Chem. Phys. 45 (1966) 4543.
[26] Y.E. Chao, P.M. Rodgers, D.E. Wigley, S.J. Alexander, A.L. Reingold, J. Am. Chem. Soc. 113 (1991) 6326.
[27] (a) P.J. Toscano, E.J. Shermerhorn, E. Barren, S. Liu, J. Zubieta, J. Coord. Chem. (1998) 169;
(b) M.H. Chisholm, J.-H. Huang, J.C. Huffman, W.E. Streib, D. Tiedtke, Polyhedron 43 (1997) 2941;
(c) C. Floriani, F. Corazza, W. Lesueur, A. Chiesi-Villa, C. Guastini, Angew. Chem. 101 (1989) 93.
[28] M. Kol, M. Shamis, I. Goldberg, Z. Goldschmidt, S. Alfi, E. Hayut-Salant, Inorg. Chem. Commun. 4 (2001) 177.
[29] (a) Y. Kim, J.G. Verkade, Organometallics 21 (2002) 2395;
(b) W. Wang, M. Fujiki, K. Nomura, Macromol. Rapid Commun. 25 (2004) 504.
[30] V. Ugrinova, G.A. Ellis, S.N. Brown, Chem. Commun. (2004) 468.
[31] L. Michalczyk, S. de Gala, J.W. Bruno, Organometallics 20 (2001) 5547.
[32] (a) M.G. Davidson, C.H. Doherty, A.L. Johnson, M.F. Mahon, Chem. Commun. (2003) 1832;
(b) A.J. Nielson, C. Shen, J.M. Waters, Acta Crystallogr., Sect. C 59 (2003) m494.
[33] A. Lehtonen, R. Sillanpaeae, Organometallics 24 (2005) 2795.
[34] K.C. Fortner, J.B. Bigi, S.N. Brown, Inorg. Chem. 44 (2005) 2803.
[35] R.H. Blessing, Acta Crystallogr., Sect. A 51 (1995) 33.
[36] G.M. Sheldrick, Acta Crystallogr., Sect. A 46 (1990) 467.
[37] G.M. Sheldrick, Program for the Refinement of Crystal Structures, University of Göttingen, Göttingen, Germany, 1997.
[38] L.J. Farrugua, ORTEP-3 for Windows, Version 1.06, University of Glasgow, Scotland, UK.
[39] H.J. Bernstein, C. Duque, G. Grossman, M. Molinaro, A. Mueller, N. Salame, R. Sayle, P. Valadon, RASTOP, version 2.1 – September 14 (P. Valadon, P.O. Box 13014, La Jolla, CA 928064, USA), 2004.

compounds [7,8] as precursors of heterocyclic molecules [9–11], including *N*-arylpyrazole derivatives have been studied by some of us owing to their wide applications in the pharmaceutical and agrochemical industries [12–14].

On the other hand, pyrazolyl and pyrazolyl-derived ligands can form relevant coordination compounds with different metal ions. Copper complexes have been extensively studied, especially dinuclear and polynuclear species, as mimics of the proteins hemocyanin and tyrosinase [15] or as compounds with interesting catalytic and magnetic properties [16–18]. In most of these complexes, copper ions are linked by *N*,*N*′-bridging pyrazolato anions, or coordinated by one nitrogen atom of the pyrazole ring [19]. However, recently an unusual coordination mode of this type of ligand was described, where nitrogen atoms of the pyrazole rings are not bound to copper, but involved in strong intramolecular hydrogen bonds [20]. Additionally, pyrazolone derivatives have interesting spectroscopic and structural properties owing to its keto-enol tautomerism [21]. Recently, some Schiff bases derived from 3-methyl-1-(4′-methylphenyl)-2-pyrazolin-5-one and aromatic amines were prepared and had their molecular structures determined. These ligands can exist in three tautomeric forms: keto-imine, imine-ol, and keto-amine, although the keto-amine form is predominant in the solid state [22]. Their corresponding mononuclear copper(II) complexes were also prepared and characterized by spectroscopic techniques, indicating a tetragonal geometry around the copper(II) ion, N,O coordinated.

Herein, we report a new method for preparing 4-(5-hydroxy-4-pyrazolylimino)-2-pyrazolin-5-one (**3**), from 2-pyrazolin-4,5-dione (**1**), in an one-step diazo-transfer process (see Scheme 1), and its corresponding crystal structure, that showed a near-linear intramolecular H-bonding. Further, since this compound shows different coordinating groups its binding ability towards copper(II) ions was investigated. A dark red complex **4** was obtained by reaction of **3** with copper(II) ions at stoichiometric ratio, in ethanol/water solution, at pH 4–5 adjusted with HCl. Compound **4** has been characterized as a neutral 1:1 species, [**3**:$CuCl_2$], involving tautomeric forms, by ESI-MS, ESI-MS/MS, IR, UV/Vis and EPR spectra, in addition to conductivity and elemental analysis. The deprotonation of **4**, in which the copper(II) ion is coordinated to ligand **3** solely by oxygen atoms, was monitored by UV/Vis, and a corresponding pK_a value was determined.

2. Experimental

2.1. Reagents and techniques

Melting points were determined on a Fisher–Johns apparatus and are uncorrected. Column chromatography was performed on silica gel 60 (Merck 70–230 mesh). Infrared spectra were recorded on Perkin–Elmer 1420 and BOMEM 3.0 instruments in the range 4000–400 cm^{-1}, in KBr pellets. NMR spectra were recorded with a Varian Unity Plus 300 spectrometer, operating at 300 MHz (^1H) and 75 MHz (^{13}C), with tetramethylsilane as the internal standard. Elemental analyses were performed at *Central Analítica* of the Instituto de Química-USP, using a Perkin–Elmer 2400 CHN Elemental Analyzer. Electronic spectra were recorded on an Olis modernized-Aminco DW 2000 instrument, using a thermostated cell compartment, and standard 1.00 cm quartz cells. The pH of the solutions was monitored using a Digimed DMPH-2 instrument, coupled to a combined pH electrode either from Ingold or Radiometer. Appropriate buffer solutions were used to calibrate the instrument. Conductivity experiments of 1 mmol dm^{-3} aqueous solutions were carried out on a Digimed DM-31 instrument, using a 10.0-mmol dm^{-3} KCl solution as standard (specific conductivity = 1412.0 μS cm^{-1} for aqueous solution, or 0.141 μS cm^{-1} for organic solutions, both at 298 K) [23]. EPR spectra were recorded

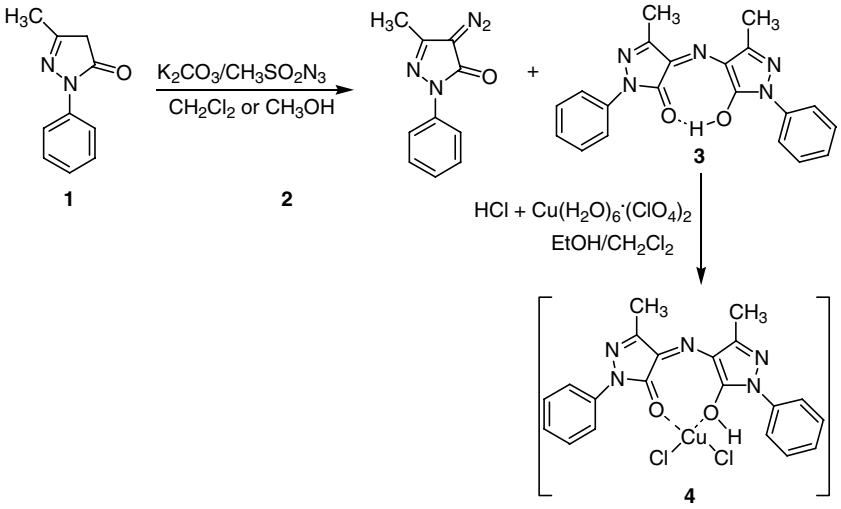

Scheme 1. Synthetic route used for obtaining compounds **2**–**4**.

on a Bruker EMX instrument, operating at X-band frequency, using standard Wilmad quartz tubes, at 77 K. DPPH (α,α′-diphenyl-β-picrylhydrazyl) was used as frequency calibrant ($g = 2.0036$) with samples in frozen CH_3CN:water (8:1, v/v) solutions, at 77 K. Usual conditions used in these measurements were 2.83×10^4 receiver gain, and 15G modulation amplitude. ESI mass and tandem mass spectrometric measurements were made using a Micromass (Manchester – UK) QTof instrument of ESI-QqTof configuration with 7.000 mass resolution in the TOF mass analyzer. The following typical operating conditions were used: 3 kV capillary voltage, 40 V cone voltage and dessolvation gas temperature of 100 °C. Tandem ESI-MS/MS spectra were collected after 15–20 eV collision induced dissociation (CID) of mass-selected ions with argon. Mass-selection was performed by Q1 using a unitary *m/z* window, and collisions were performed in the rf-only quadrupole collision cell, followed by mass analysis of product ions by the high-resolution orthogonal-reflectron Tof analyzer.

2.2. Synthetic procedures

2.2.1. 2-Diazo-3-methyl-1-phenyl-5-pyrazolone (2) and 2,4-dihydro-4-[(5-hydroxy-3-methyl-1-phenyl-1H-pyrazol-4-yl)imino]-5-methyl-2-phenyl-3H-pyrazol-3-one (3)

To a stirred suspension of potassium carbonate (2.5 mmol) in anhydrous dichloromethane (or methanol) (5 mL) under nitrogen at room temperature, was added a solution of **1** (1.0 mmol) in anhydrous dichloromethane (or methanol) (4 mL). After stirring the ice-cooled mixture for 0.5 h, a solution of mesyl azide (1.4 mmol) in dichloromethane (or methanol) (1 mL) was added dropwise. The reaction mixture was then stirred for other 3 h at room temperature, and the solvent was removed under vacuum to leave a red oily residue, which was separated by column chromatography on silica gel, using 40% dichloromethane in hexane as eluent to give **2** and **3**.

Compound **2**. ^{1}H NMR ($CDCl_3$) δ: 2.39 (s, Me), 7.20 (tt, 1H, *J* 1.2 and 7.5 Hz, H–Ar), 7.37–7.43 (m, 2H, H–Ar), 7.87–7.91 (m, 2H, H–Ar) . ^{13}C NMR ($CDCl_3$) δ: 13.9 (CH_3), 66.4 (C=N_2), 119.1(C-2′), 125.1 (C-4′), 128.7 (C-3′), 138.4 (C-1′), 141.8 (C-4), 163.0 (C=O). IR (KBr, cm^{-1}) $\nu_{C=O}$ 1681; ν_{N-N} 2133. EIMS (*m/z*) 200 [M^+, 100%]. UV/Vis (CH_2Cl_2, nm) λ_{max}: 251 ($\varepsilon_1 = 5.3 \times 10^4$), and 332 ($\varepsilon_2 = 2.3 \times 10^3$).

Compound **3**. M.p. 183–184 °C (lit. 183 °C). Elemental *Anal*. Calc. for $C_{20}H_{17}N_5O_2 \cdot 3H_2O$: C, 58.10; H, 5.61; N, 16.94. Found: C, 57.20; H, 5.04; N, 17.14%; ^{1}H NMR ($CDCl_3$) δ: 2.37 (s, 2Me), 7.30 (tt, 2H, *J* 1.2 and 7.5 Hz, H–Ar), 7.43–7.49 (m, 4H, H–Ar), 7.89–7.93 (m, 4H, H–Ar), 17.97 (s, 1H, OH). ^{13}C NMR ($CDCl_3$) δ: 11.8 (CH_3), 120.5 (C2′), 125.7 (C4), 126.7 (C4′), 128.8 (C3′), 137.4 (C1′), 152.1 (C3), 154.3 (C5). IR (KBr, cm^{-1}) $\nu_{C=O}$, 1729; ν_{OH} 2922, 2852. EIMS (*m/z*) 359 [M^+, 88%]. UV/Vis (CH_2Cl_2) λ_{max}/nm (ε/mol^{-1} dm^3 cm^{-1}): 250 ($\varepsilon_3 = 3.2 \times 10^3$), 359 ($\varepsilon_2 = 1.4 \times 10^3$) and 460 ($\varepsilon_1 = 1.3 \times 10^3$); UV/Vis ($CH_3CN$) λ_{max}/nm (ε/mol^{-1} dm^3 cm^{-1}): 204 (4.9×10^4), 240 (3.2×10^4), 368 (1.3×10^4) and 445 (2.6×10^4).

2.2.2. Preparation of the copper(II) complex (4)

A solution of $Cu(ClO_4)_2 \cdot 6H_2O$ (0.150 g, 0.4 mmol) in H_2O (0.5 mL) was added at room temperature and under stirring to a solution of **3** (0.165 g, 0.4 mmol) in ethanol (10 mL). The apparent pH of the reaction mixture was adjusted to 4–5 by dropwise addition of aqueous HCl solution (~1 M). After stirring for 6 h, tiny brownish-red crystals were collected, washed with cold ethanol and ether, and dried under reduced pressure over P_2O_5 to yield 0.122 g (60%) of the complex **4**.

Elemental *Anal*. Calc. for $[C_{20}H_{18}N_5O_2CuCl_2]$: C, 48.54; H, 3.67; N, 14.15; Cu, 12.84; Cl, 14.33. Found: C, 48.28/48.62; H, 3.34/3.59; N, 13.74/14.60; Cu, 11.88; Cl, 13.80%. $\Lambda_M = 21$ S cm^2 mol^{-1} in water solution, 17 S cm^2 mol^{-1} in CH_3OH, and 0 S cm^2 mol^{-1} in CH_2Cl_2. IR (KBr, cm^{-1}): ν_{OH}, 3432 (m); $\nu_{C_{sp3}-H}$, 3065 (w); $\nu_{C_{sp2}-C}$ 2924 (w); $\delta_{C_{sp2}-C}$, 995–775; $\nu_{C=O}$, 1614 (s); $\nu_{C=N}$, 1596 (m); ν_{C-N}, 1532 (w). UV/Vis (CH_3CN) λ_{max}/nm (ε/mol^{-1} dm^3 cm^{-1}): 203 (8.9×10^4), 255 (8.8×10^4), 348 (3.0×10^4) and 540 (2.4×10^4).

2.3. X-ray crystallography data collection and processing

Room temperature data were collected on a Bruker SMART area CCD diffractometer whilst low temperature date were collected on a Enraf Nonius KappaCCD diffractometer at the UK's EPSRC X-ray crystallographic service, based at the University of Southampton. The structure was solved by direct methods with SHELXS-97 and refined using SHELXL-97 [24] in the triclinic spacegroup $P\bar{1}$. Two dimers were present in each asymmetric unit to give **4** in the unit cell. The data completeness for the low temperature data set was somewhat lower than that of the room temperature set, as shown in Table 1, so discussion will concentrate on the room temperature data, although no major differences were discernable between the two results. All H atoms were located from difference maps and then treated as riding atoms, with C–H distances of 0.96 Å (methyl) or 0.93 Å (aromatic) and U_{iso}(H) values of $1.5U_{eq}$(methyl) or $1.2U_{eq}$(aromatic). The exceptions were the hydrogen atoms bridging two oxygen atoms, H11 and H31, which were allowed to refine freely. Conformational and H-bonding analysis was performed using PLATON [25].

3. Results and discussion

3.1. Compounds 2 and 3

Our synthetic route to **2**–**4** is shown in Scheme 1. Pyrazolone **1** on reaction with mesyl azide or tosyl azide in the presence of a base at room temperature furnished the diazo-pyrazolone **2** and the bis-pyrazole **3**. The diazo transfer reaction was attempted under a variety of conditions (Table 2), but most of the experimental conditions

Table 1
Crystal data and structure refinement data for 4-(5-hydroxy-4-pyrazolylimino)-2-pyrazolin-5-one (**3**) at room temperature and at 120 K

	292 K data	120 K data
Formula	$C_{40}H_{34}N_{10}O_4$	$C_{40}H_{34}N_{10}O_4$
Formula weight	718.77	718.77
Wavelength (Å)	0.71073	0.71073
Crystal system, space group	triclinic, $P\bar{1}$	triclinic, $P\bar{1}$
Unit cell dimensions		
A (Å)	9.7844(13)	9.6488(5)
B (Å)	9.9517(12)	9.8123(6)
C (Å)	18.630(2)	18.4526(13)
α (°)	80.677(3)	81.091(2)
β (°)	84.281(3)	83.933(2)
γ (°)	88.120(3	87.039(5)
Volume (Å^3)	1780.9(4)	1715.18(18)
Z, Calculated density (Mg/m^3)	2, 1.337	2
Absorption coefficient (mm^{-1})	0.091	0.094
F(000)	752	752
Crystal size (mm)	$0.50 \times 0.14 \times 0.07$	$0.15 \times 0.10 \times 0.04$
θ Range for data collection (°)	2.07–32.61	3.30–27.46
Index ranges	$-14 \leqslant h \leqslant 13$, $-15 \leqslant k \leqslant 11$, $-28 \leqslant l \leqslant 27$	$-12 \leqslant h \leqslant 12$, $-12 \leqslant k \leqslant 12$, $-23 \leqslant l \leqslant 23$
Reflections collected/unique [R_{int}]	16661/12168 [0.0392]	20717/7307 [0.1437]
Completeness to θ (%)	27.50, 98.4	27.46, 92.8
Absorption correction	semi-empirical from equivalents	empirical
T_{max} and T_{min}	0.9281 and 0.7723	1.00855 and 0.99083
Data/restraints/parameters	12166/0/499	7307/0/499
Refinement method	full-matrix least-squares on F^2	full-matrix least-squares on F^2
Goodness-of-fit on F^2	0.855	0.885
Final R indices [$I > 2\sigma(I)$]	$R_1 = 0.0703$, $wR_2 = 0.1178$	$R_1 = 0.0697$, $wR_2 = 0.1099$
R indices (all data)	$R_1 = 0.2748$, $wR_2 = 0.1577$	$R_1 = 0.2593$, $wR_2 = 0.1570$
Largest peak and hole (e/Å^3)	0.199 and −0.190	0.270 and −0.281

Table 2
Conditions used for the preparation of **2** and **3** by a diazo-transfer process: (**1**) + RN_3 + Base → (**2**) + (**3**)

Entry	**1** (mmol)	RN_3 (mmol)	Base	Solvent	Diazo **2** (%)	**3** (%)
1	1	MsN_3/0.9	Et_3N	CH_2Cl_2	81	2
2	1	MsN_3/2.0	Et_3N	CH_2Cl_2	80	1
3	2	MsN_3/1.0	Et_3N	CH_2Cl_2	83	
4	1.0	MsN_3/1.0	DMAP	CH_2Cl_2	72	2
5	1.0	TsN_3/1.0	Et_3N	CH_2Cl_2	63	
6	1.0	TsN_3/1.0	DMAP	CH_2Cl_2	68	1
7	1.0	MsN_3/1.0	K_2CO_3	CH_2Cl_2	86	
8	1.0	MsN_3/1.4	K_2CO_3	MeOH		55

provided the diazo-pyrazolone **2** in moderate to good yield (entries 1–7) with only traces of **3**. However, when the diazo transfer reaction was performed in methanol, only **3** was isolated in moderate yield (entry 8). Several other conditions were tested but led mostly to **2**. Mesyl azide appears to be a more convenient reagent than tosyl azide for **3** (entries 1–7).

A different preparation of **3** was published by Hansel in 1976 [26], following a much earlier article in 1887 [27]. Hansel's synthesis employed **5** and 2-pyrazolin-4,5-dione (**6**) [28]. However, as only the m.p. of **3** was given, we present herein selected spectral details for **3** as well as its crystal structure.

Compounds **2** and **3** were characterized by IR, ^{1}H, ^{13}C NMR spectroscopies and ESI mass spectrometry. In the IR spectrum of **2**, the N=N absorption appears at 2133 cm^{-1} and the C=O stretch at 1682 cm^{-1} [29]. IR spectrum of **3** shows a reactively weak C=O absorption band at 1729 cm^{-1}, a cluster of bands between 2970 and 2850 cm^{-1}, with maxima at 2922 and 2851 cm^{-1}, the most intense bands in the spectrum, and a broad weak absorption band centered at 3400 cm^{-1}. The NMR spectrum of **3** indicates one set of chemical shifts for the two halves of the molecule. Of some significance is the δ^1H (OH) value in $CDCl_3$ solution at −50 °C of 17.95 ppm.

Usually, direct diazo transfers alpha to carbonyl are performed via reaction of sulfonyl azides on enolates [30,31]. Without success, we attempted to convert diazo-pyrazolone **2**–**3** under different reaction conditions. Therefore, we conclude that **3** must be formed from a different precursor. We speculate (Scheme 2) that **3** is produced by a second attack of the pyrazolone carbanion (**I**) on the intermediate (**II**). Participation of intermediate (**II**) in other side reactions has already been reported [32].

3.2. Crystallographic data for *3*

Fig. 1 shows the numbering scheme and atom arrangements for **3**. As shown by the selected data in Table 3, the two independent molecules exhibit only subtle differences in bond angles and lengths. Each molecule exhibits extensive delocalization and overall the molecule exhibits a structure almost midway between the two canonical

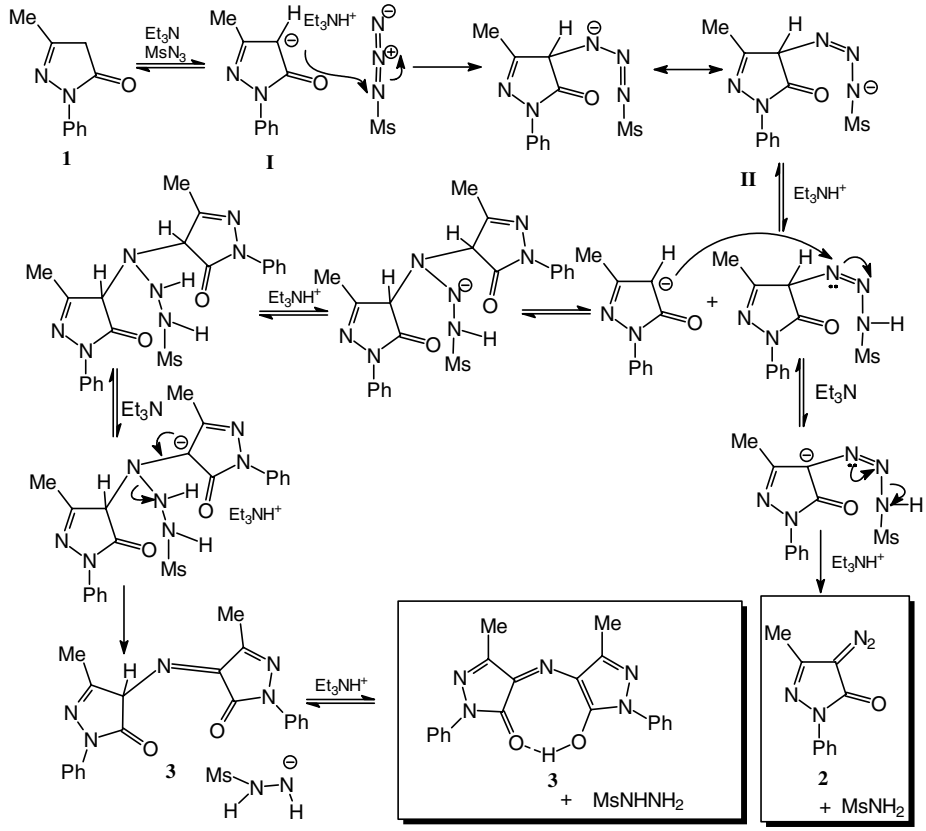

Scheme 2. Proposed mechanism for formation of **3**.

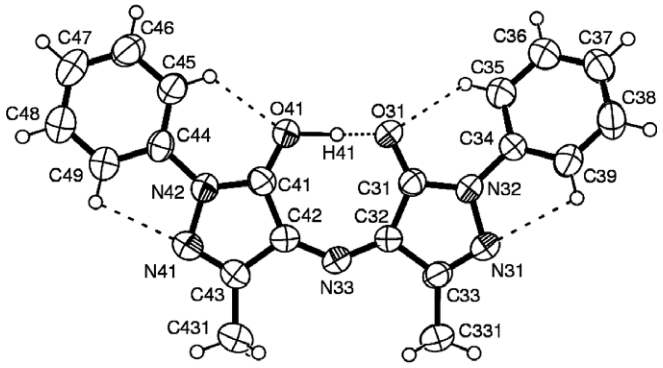

Fig. 1. Atom arrangements and the numbering scheme for the two independent molecules of **3**; probability ellipsoids are dawn at the 30% level. Intramolecular hydrogen bonds are shown as dotted lines.

forms IIIA and IIIB, Scheme 3, with a very strong, near linear O–H–O hydrogen bond closing a 8-membered central ring (see values in Table 3). This situation is similar to those found in several 3-aryl-pentane-2,4-diones, in which the 6-membered rings in the enol tautomers are remarkably symmetrical and with O---O distances of ca. 2.4–2.5 Å [33]. The C–O bond lengths in the two independent molecules of **3** are in the region 1.271(3)–1.290(3) Å – values between those expected for single and double bonds. Neither of the two molecules has a plane of symmetry in the solid state, but as shown by the single set of chemical

Table 3
Selected bond lengths (Å), and angles (°) for **3** (room temperature data)

C(11)–O(11)	1.290(3)	C(31)–O(31)	1.279(3)
C(11)–N(12)	1.344(3)	C(31)–N(32)	1.349(3)
C(11)–C(12)	1.435(3)	C(31)–C(32)	1.441(3)
C(12)–N(13)	1.330(3)	C(32)–N(33)	1.319(3)
C(12)–C(13)	1.440(3)	C(32)–C(33)	1.442(4)
C(13)–N(11)	1.304(3)	C(33)–N(31)	1.304(3)
C(13)–C(13)	1.490(3)	C(33)–C(331)	1.493(3)
N(11)–N(12)	1.407(3)	N(31)–N(32)	1.418(3)
N(12)–C(14)	1.432(3)	N(32)–C(34)	1.425(3)
N(13)–C(22)	1.316(3)	N(33)–C(42)	1.327(3)
C(21)–O(21)	1.274(3)	C(41)–O(41)	1.271(3)
C(21)–N(22)	1.348(3)	C(41)–N(42)	1.347(3)
C(21)–C(22)	1.449(3)	C(41)–C(42)	1.452(3)
C(22)–C(23)	1.441(4)	C(42)–C(43)	1.439(4)
C(23)–N(21)	1.298(3)	C(43)–N(41)	1.302(3)
N(21)–N(22)	1.423(3)	N(41)–N(42)	1.419(3)
N(22)–C(24)	1.433(3)		
O(11)–C(11)–C(12)	131.9(3)	O(31)–C(31)–C(32)	131.4(3)
N(13)–C(12)–C(11)	134.7(2)	N(33)–C(32)–C(31)	135.4(3)
C(22)–N(13)–C(12)	133.9(2)	C(32)–N(33)–C(42)	134.6(2)
O(21)–C(21)–C(22)	130.7(3)	O(41)–C(41)–C(42)	131.1(3)
N(13)–C(22)–C(21)	135.5(3)	N(33)–C(42)–C(41)	134.8(3)
O(11)–H(21)	1.28(4)	O(31)–H(41)	1.23(4)
O(21)–H(21)	1.15(4)	O(41)–H(41)	1.20(4)
O(11)–H(21)–O(21)	170(4)	O(31)–H(41)–O(41)	175(3)
C(11)–O(11)–H(21)	112.9(16)	C(31)–O(31)–H(41)	114.4(15)
C(21)–O(21)–H(21)	115.4(18)	C(41)–O(41)–H(41)	115.4(15)

shift values for the atoms in the diazole rings in each of the ^{1}H and ^{13}C NMR spectra, in solution the molecule is symmetrical.

Further intramolecular C–H···O and C–H···N hydrogen bonds (Fig. 1) provide extra rigidity to the structure of **3**. Intermolecular interactions involve both the C16-H16···O11^{i} hydrogen bond, which forms a dimer centred on (0.5, 0.5, 0.5) with motif $R_4^2(10)$, Fig. 2, (symmetry operation: *i*: $-x+1$, $-y+1$, $-z+1$) and $\pi\cdots\pi$ interactions which lead to a "chain" of molecules along [1 0 0] as seen in Fig. 3. These involve the rings defined by N41–N42–C41–C42–C43 and C24–C25–C26–C27–C28–C29. There are also $\pi\cdots\pi$ interactions between the two molecules of the asymmetric unit.

Finally, the IR spectrum of **3** in KBr discs exhibits only a medium intensity band in the carbonyl region, at 1728 cm^{-1}.

3.3. Copper complex *4*

The complex **4** was obtained by the 1:1 reaction of **3** with copper(II) perchlorate hexahydrate in ethanol/aqueous HCl at pH 4–5, as tiny red-brown crystals. While in Scheme 1, complex **4** is drawn as a localized structure, it is considered much more likely to exist as a tautomeric compound, as shown in Scheme 3. Since suitable crystals for X-ray structure determination could not be grown, different spectroscopic techniques have been employed to characterize this complex. Confirmation of the presence of copper in the complex **4** came both from ESI-MS(/MS) data and from UV/Vis and EPR spectra.

The ESI mass spectrum of an acetonitrile solution of **4** reveals a cluster of four major isotopologue ions of *m*/*z* 463, 464, 465, and 466 with abundance ratios of

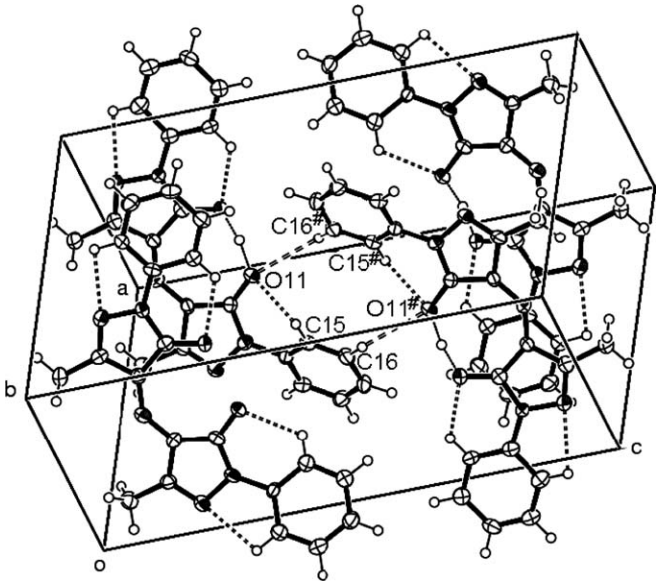

Fig. 2. Intra- and inter-molecular hydrogen bonds, shown as dotted lines, within the unit cell of **3** showing formation of a dimer. Geometric parameters are included as Supplementary Material.

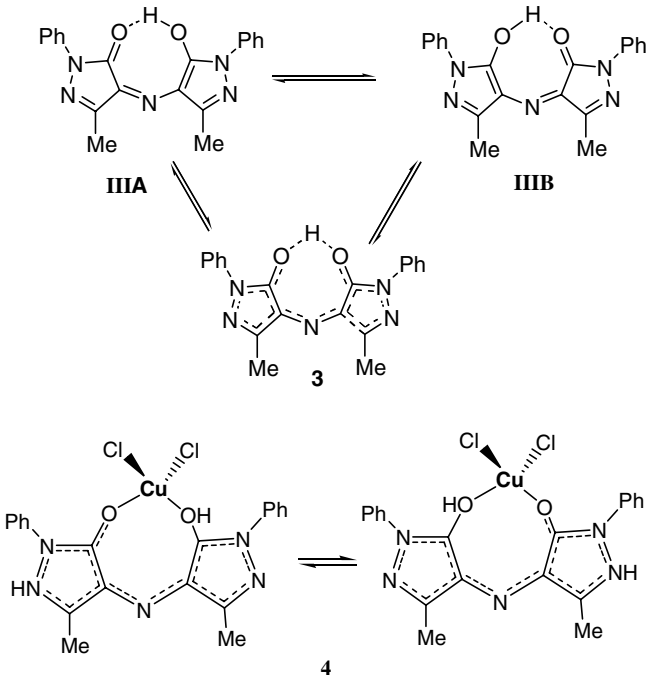

Scheme 3. Structures of **3** and **4**.

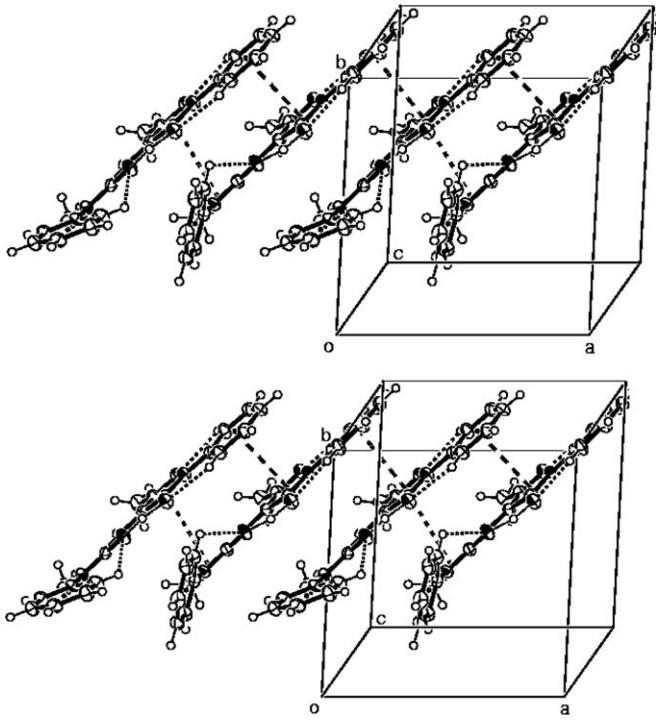

Fig. 3. π–π Interactions in **3**, forming a "chain" of molecules along [1 0 0].

1:0.26:0.48:0.12 that is expected for a mono-nuclear Cu species of formula $[C_{22}H_{20}N_6O_2Cu]^{+}$, i.e., ion **4A** (Scheme 4), a chloride free Cu(I) complex coordinated to a single acetonitrile ligand. Collision-induced dissociation of the ^{63}Cu-isotopologue ion of *m*/*z* 463 shows that **4A** dissociates mainly by the loss of acetonitrile to form **4B** of *m*/*z* 422, and subsequently by the loss of a neutral species of

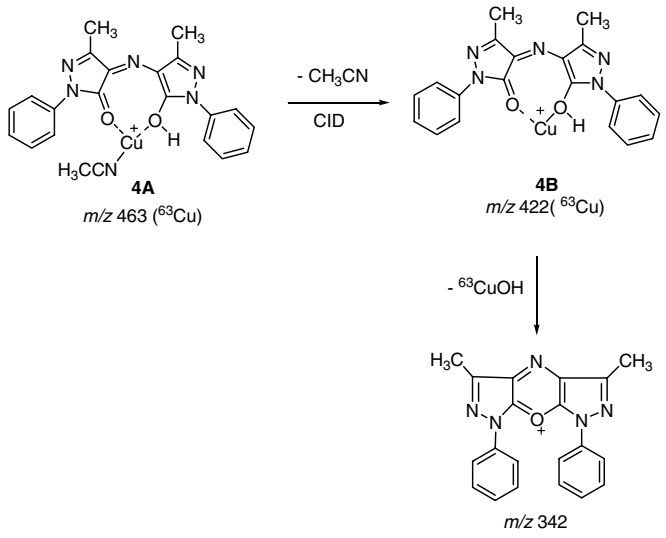

Scheme 4. Dissociation patterns for the singly charged ions of m/z 463 from ESI-MS/MS of **4**.

80 Da, ^{63}CuOH, to form the fragment ion of m/z 342 ion. This last fragmentation provides evidence for Cu–O coordination in **4**.

Conductivity measurements of solutions of **4** in CH_3OH and in CH_2Cl_2, at 298 K, indicate a non-electrolyte. Measurements in water are unexpected low, probably due to the very low solubility of this complex in aqueous solution. In the IR spectrum in KBr pellets, fail to observe strong bands near 1090 and 625 cm^{-1} suggests the absence of non-coordinated perchlorate ions. The addition of HCl to the reaction mixture during the synthesis of **4** clearly favored the involvement of Cl^- rather than ClO_4^- in the isolated complex. The C, H, N elemental analyses of solid **4** gave C, 48.28/48.62; H, 3.34/3.59; N, 13.74/14.60; Cu, 11.88; Cl, 13.80%, which is in excellent agreement with those expected for the complex, $[LCuCl_2]$, which requires C, 48.54; H, 3.67; N, 14.15; Cu, 12.84; Cl, 14.33%.

Other evidence that copper(II) ion binds to ligand **3** via oxygen atoms comes from the shift of the medium intensity band found at 1726 cm^{-1} in **3** to a much more intense band at 1614 cm^{-1} in **4**. Furthermore, the ν(C=N) bands at 1599 cm^{-1} for **3** and 1596 cm^{-1} for **4** suggest that Cu is not coordinated to the imine nitrogens. The bands at around 3074–2920 cm^{-1}, for both **3** and **4**, are assigned to $\nu(C_{sp3}–H)$ and $\nu(C_{sp2}–H)$, whereas the corresponding bending modes are observed in the 995–755 cm^{-1} range.

Analogously, a copper(II) complex with a new pyrazole-based ligand, $Na[Cu(bdmpb)_2(OOCCH_3)H_2O]$, where Hbdmpb = 1,3-bis(3,5-dimethylpyrazol-1-yl)-2-butanoic acid, has been recently prepared, and its crystal structure determined by X-ray analysis indicated that the nitrogen atoms of the pyrazole rings do not coordinate to the metal center. Instead, these nitrogen atoms are involved in strong intramolecular hydrogen bonds, and the copper ion is coordinated by four nearly coplanar oxygen atoms [20]. In this complex, as well as in our complex **4** there are methyl substituents that provide some steric hindrance around the nitrogen atoms in the pyrazole moiety.

Electronic spectra of **3** and **4** (Fig. 4) were obtained in CH_3CN solution. The absorption bands for the ligand **3** were observed at 204, 240, 368 and 445 nm (see Section 2). Analogous bands were observed for complex **4**; however, the maximum of the characteristic d–d band ($T_{2g} \leftarrow E_g$) for **4** is probably hidden under the dominant and overlapping LMCT transition band, at 540 nm. On the other hand, spectral changes in aqueous solution of **4** at different pHs were also verified, by appropriate addition of either HCl or NaOH solutions (0.1 mol dm^{-3}). The LMCT transition band for **4**, detected at 540 nm at pH $\geqslant$ 5.5, shift to the maximum absorption corresponding to free ligand transition at 445 nm, in more acidic medium (Fig. 5A), with an isosbestic point at 475 nm. A concomitant variation of the solution color was observed, from yellow to purple. A plot of pH versus log $[(A - A_{min})/(A_{max} - A)]$,

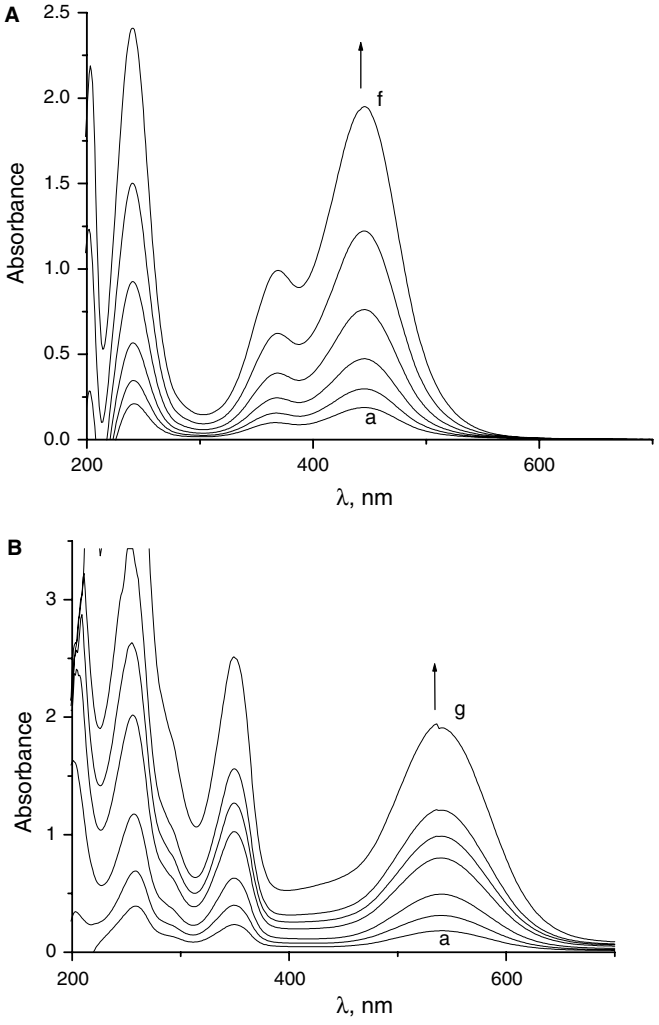

Fig. 4. Electronic spectra of: (A) compound **3** and (B) complex **4** in CH_3CN solution. For spectra in (A) a: 0.62×10^{-6}, b: 1.0×10^{-5}, c: 1.7×10^{-5}, d: 0.29×10^{-4}, e: 0.48×10^{-4}, f: 0.80×10^{-4} mol dm^{-3}. For spectra in (B) a: 4.0×10^{-5}, b: 0.81×10^{-5}, c: 0.16×10^{-4}, d: 0.32×10^{-4}, e: 0.46×10^{-4}, f: 0.65×10^{-4}, g: 1.3×10^{-4} mol dm^{-3}.

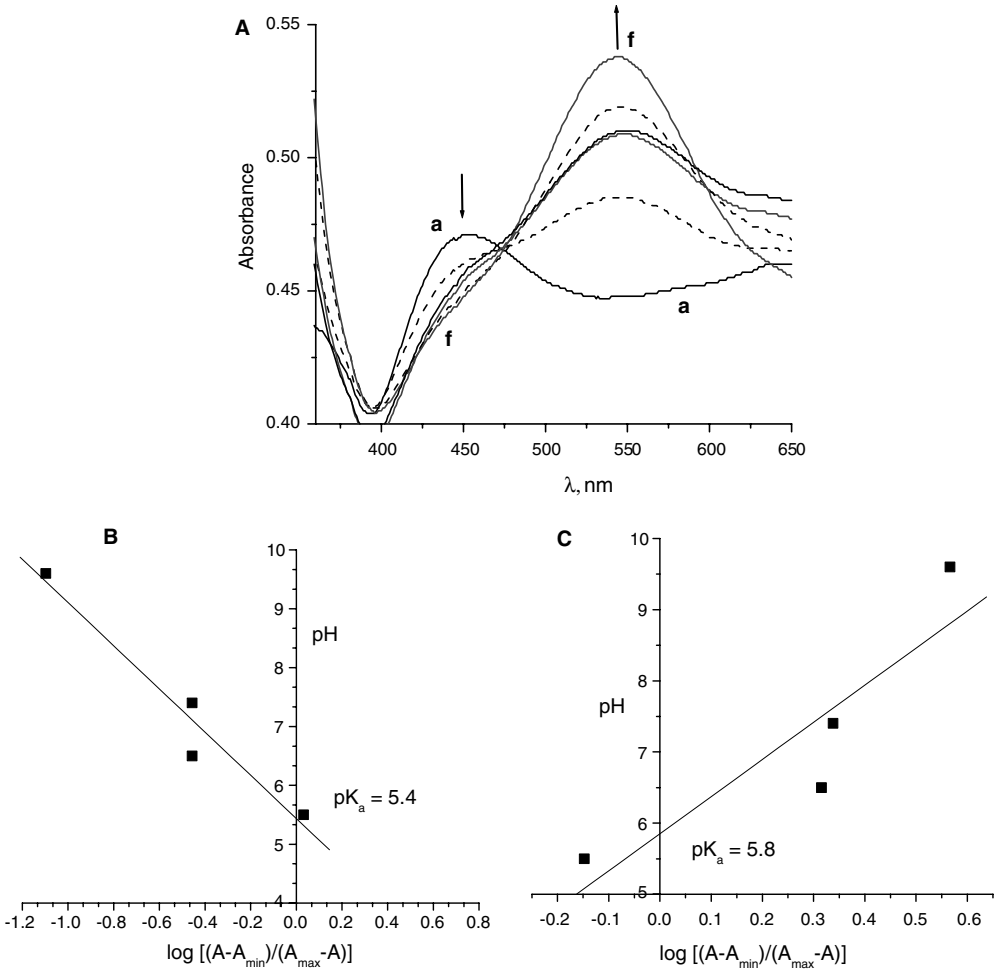

Fig. 5. (A) UV/Vis spectra of the complex **4** (20 μmol dm^{-3}), in water, at different pH values (a–f): (a) 3.0; (b) 5.5; (c) 6.5; (d) 7.3; (e) 9.6; (f) 10.5. (B) Plot of pH versus log $[(A - A_{min})/(A_{max} - A)]$, at $\lambda = 440$ nm. (C) Plot of pH versus log $[(A - A_{min})/(A_{max} - A)]$, at $\lambda = 540$ nm.

where A = absorbance of the band at $\lambda = 440$ nm (Fig. 5B) or at $\lambda = 540$ nm (Fig. 5C), led to the calculation of a p$K_a = (5.6 \pm 0.2)$ as expressed simplistically below:

$$[LCu]^{2+} + OH^- \leftrightharpoons [LH_{-1})Cu]^+ + H_2O \quad K_a$$

Similar equilibria have been recently observed with isatin-Schiff base copper(II) compounds, and for these complexes different tautomers were isolated, depending on the ligand [34]. On the other hand, the acid dissociation constants determined for acylpyrazolone derivatives indicated a pK_a around 4 [35].

The EPR spectrum of **4** (Fig. 6) in frozen CH_3CN:water solution (8:1, v:v) shows a characteristic profile of an axial environment around the copper(II) center, with $g_\parallel > g_\perp$. The EPR parameters were determined as $A_\parallel = 140.9 \times 10^{-4}$ cm^{-1}, $g_\parallel = 2.389$, $A_\perp = 12.7$ G and $g_\perp = 2.077$. The empirical ratio $g_\parallel/A_\parallel$ has been used to evaluate tetrahedral distortions in tetragonal structures of Cu(II) compounds, where a $g_\parallel/A_\parallel$ value close to 100 cm indicates a roughly square planar or tetragonal structure around the copper(II) ion, and values between 170 and 250 cm are indicative of a

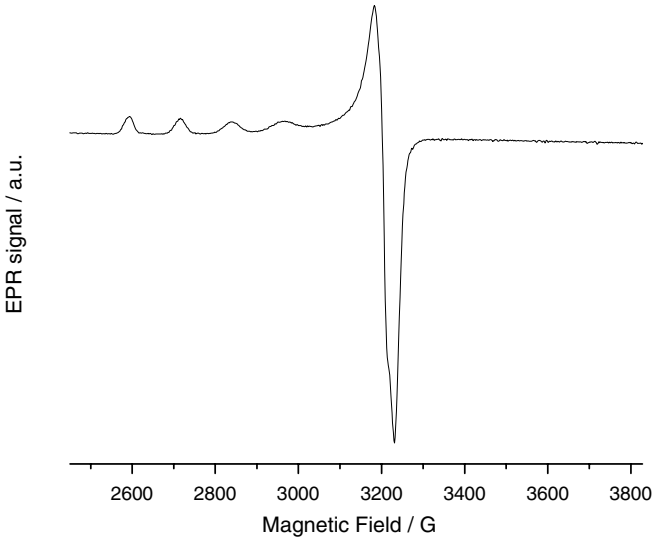

Fig. 6. EPR spectrum of the copper(II) complex **4** (0.5 mmol dm^{-3}), in CH_3CN:H_2O (8:1, v:v), at 77 K. Conditions: 2.83×10^4, receiver gain; 15 G, modulation amplitude; 20.48 s, time constant; 8 scans.

distorted tetrahedral copper(II) symmetry [36]. Based on these data, **4** exhibits a geometry closely to a distorted tetrahedron from the $g_{\|}/A_{\|}$ value of 169 cm. Evidence for substitution of chloride ligands by the CH_3CN solvent was obtained by inspection of EPR spectra. Duplication of copper hyperfine structure, $g_{\|} = 2.375$ and 2.343, with corresponding $A_{\|} = 149$ and 163×10^{-4} cm^{-1}, respectively, was observed at apparent pH $\geqslant 7$ (data not shown). Furthermore, evidence of a gradual reduction of Cu(II) to Cu(I) (an EPR silent ion) was detected at higher pH values, with consequent decreases in the intensity of the EPR signal, estimated by double integration of the bands, and concomitant oxidation of the ligand, similarly to what occurs during the ESI-MS/MS experiment (see Scheme 4). Reduction to provide the stable $[Cu^{I}(CH_3CN)_4]^{+}$ ion is a strong possibility [37].

4. Conclusions

A new route to 4-(5-hydroxy-4-pyrazolylimino)-2-pyrazolin-5-one, **3**, is reported, via an one-pot diazo transfer reaction of pyrazolin-5-one (**1**). The structure of **3** has been determined by X-ray crystallography and by NMR. Both in solution and in the solid state, **3** exhibits extensive delocalization with a very strong near-linear, near-symmetrical O–H–O hydrogen bond closing the central 8-membered ring. In the ^1H NMR spectrum in $CDCl_3$ solution the δ^1H (OH) value is 17.95 ppm. A mononuclear copper complex **4** was obtained on reaction of **3** with copper(II) ions in ethanol/water/HCl (pH 4–5) and structurally characterized as the complex $[LCuCl_2]$, via elemental analysis, FT-IR, UV/Vis, EPR, ESI-MS, and ESI-MS/MS spectra. IR spectra provided strong evidence for coordination of Cu(II) to ligand **3** via the C–O groups, replacing the bridging H atom. EPR data indicated a distorted tetrahedral environment to copper(II) ion. The pK_a value of **4**, determined by UV/Vis spectroscopy, was calculated to be (5.6 ± 0.2).

Acknowledgements

This work was supported by the Brazilian agencies CNPq, FAPESP and FAPERJ. Fellowships granted to GC (FAPESP), ABT (CNPq-PIBIC), HMM (CNPq-PIBIC), and to AMCF, VFF, MNE and JLW (CNPq) are gratefully acknowledged. The authors thank the EPSRC X-ray Crystallographic Service, at the University of Southampton, GB, for the low temperature data collection, and the University of Aberdeen for funding the SMART CCD diffractometer.

Appendix A. Supplementary material

Supplementary data are available from the CCDC, 12 Union Road, Cambridge, CB2 1EZ, UK, fax: +44 1223 366 033, e-mail: deposit@ccdc.ac.uk or on the web www: http://www.ccdc.cam.ac.uk on request, quoting the Deposition Nos. 266268 (for room temperature data) and 266269 (for data at 120 K). Supplementary data associated with this article can be found, in the online version, at doi:10.1016/j.poly.2006.01.002.

References

[1] A. Gürsoy, M.S. Demirayak, G. Çapan, K. Erol, K. Vural, Eur. J. Med. Chem. 35 (2000) 359.
[2] E.A.M. Badawey, I.M. El-Ashmawey, Eur. J. Med. Chem. 33 (1998) 349.
[3] J.B. Jiang, D.P. Hesson, B.A. Dusak, D.L. Dexter, G.J. Kang, E. Hamel, J. Med. Chem. 33 (1990) 1721.
[4] K. Anzai, M. Furuse, A. Yoshida, A. Matsuyama, T. Moritake, K. Tsuboi, N. Ikota, J. Radiat. Res. 45 (2004) 319.
[5] X. Qi, Y. Okuma, T. Hosoi, Y. Nombra, J. Pharmacol. Exp. Therap. 311 (2004) 388.
[6] S. Abe, K. Kirima, K. Tsuchiya, M. Okamoto, T. Hasegawa, H. Houchi, M. Yoshizumi, T. Tamaki, Chem. Pharm. Bull. 52 (2004) 186.
[7] V.F. Ferreira, L.O.R. Pereira, M.C.B.V. de Souza, A.C. Cunha, Quim. Nova 24 (2001) 540.
[8] R.D. Rianelli, M.C.B.V. de Souza, V.F. Ferreira, Synth. Commun. 34 (2004) 951.
[9] L.O.R. Pereira, A.C. Cunha, V.F. Ferreira, M.C.B.V. de Souza, R.O.P. Souza, J. Braz. Chem. Soc. 13 (2002) 368.
[10] A.C. Cunha, L.O.R. Pereira, R.O.P. Souza, M.C.B.V. de Souza, V.F. Ferreira, Nucleos. Nucleot. Nucl. 20 (2001) 1555.
[11] (a) A.C. Cunha, L.O.R. Pereira, R.O.P. Souza, M.C.B.V. de Souza, V.F. Ferreira, Synth. Commun. 40 (2000) 3215;
(b) G.A. Romeiro, L.O.R. Pereira, M.C.B.V. de Souza, V.F. Ferreira, A.C. Cunha, Tetrahedron Lett. 38 (1997) 5103.
[12] J.T. Gupton, S.C. Clough, R.B. Miller, B.K. Norwood, C.R. Hickenboth, I.B. Chertudi, S.R. Cutro, S.A. Petrich, F.A. Hicks, D.R. Wilkinson, J.A. Sikorski, Tetrahedron 58 (2002) 5467.
[13] A.A. Bekhit, T. Abdel-Aziem, Bioorg. Med. Chem. 12 (2004) 1935.
[14] D. Kumar, S.P. Singh, Heterocycles 63 (2004) 145.
[15] S. Trofimenko, Chem. Rev. 93 (1993) 943.
[16] (a) X. Liu, M.P. de Miranda, E.J.L. McInnes, C.A. Kilner, M.A. Halcrow, J. Chem. Soc., Dalton Trans. (2004) 59;
(b) E. Kavlakoglu, A. Elmali, Y. Elerman, I. Svoboda, Polyhedron 21 (2002) 1539.
[17] (a) M. Zareba, K. Drabent, Z. Ciunik, S. Wolowiec, Inorg. Chem. Commun. 7 (2004) 82;
(b) W.L. Driessen, L. Chang, C. Finazzo, S. Gorter, D. Rehorst, J. Reedijk, M. Lutz, A.L. Spek, Inorg. Chim. Acta 350 (2003) 25.
[18] (a) S. Sharma, N. Barooah, J.B. Baruah, J. Mol. Catal. A: Chem. 229 (2005) 171;
(b) A.M. Schuitema, P.G. Aubel, I.A. Koval, M. Engelen, W.L. Driessen, J. Reedijk, M. Lutz, A.L. Spek, Inorg. Chim. Acta 355 (2003) 374.
[19] T.N. Ronson, H. Adams, M.D. Ward, Inorg. Chim. Acta 358 (2005) 1943.
[20] B. Kozlevcar, A. Golobic, P. Gamez, I.A. Koval, W.L. Driessen, J. Reedjik, Inorg. Chim. Acta 358 (2005) 1135.
[21] Y. Akama, A. Tong, N. Matsumoto, T. Ikeda, S. Tanaka, Vib. Spectrosc. 13 (1996) 113.
[22] R.N. Jadeja, J.R. Shah, E. Suresh, P. Paul, Polyhedron 23 (2004) 2465.
[23] W.J. Geary, Coord. Chem. Rev. 7 (1971) 81.
[24] G.M. Sheldrick, SHELXS97 and SHELXL97, University of Göttingen, Germany, 1997.
[25] A.L. Spek, J. Appl. Cryst. 36 (2003) 7.
[26] W. Hansel, Justus Liebigs Ann. Chem. (1976) 1380.
[27] L. Knorr, Justus Liebigs Ann. Chem. 238 (1887) 137, 190.
[28] M.F. El-Zohry, M.I. Younes, S.A. Metwally, Synthesis (1984) 972.
[29] A. Padwa, A.D. Woolhouse, J.J. Blounts, J. Org. Chem. 48 (1983) 1069.

[30] E.F.V. Scriven, Chem. Rev. 88 (1988) 297.
[31] (a) G. L'Abbé, Chem. Rev. 69 (1969) 345;
(b) D.S. Breslow, M.F. Sloan, N.R. Newburg, W.B. Renfrow, J. Am. Chem. Soc. 91 (1969) 2273;
(c) J.B. Hendrickson, W.A. Wolf, J. Org. Chem. 33 (1968) 3610.
[32] R. Boeckman, Org. Synth. 73 (1995) 134.
[33] (a) J. Emsley, L.Y.Y. Ma, S.C. Nyburg, A.W. Parkins, J. Mol. Struct. 240 (1990) 59;
(b) J. Emsley, L.Y.Y. Ma, S.A. Karaulov, M. Motevalli, M.B. Hursthouse, J. Mol. Struct. 216 (1990) 143;
(c) J. Emsley, L.Y.Y. Ma, P.A. Bates, M.B. Hursthouse, J. Mol. Struct. 178 (1988) 297;
(d) J. Emsley, L.Y.Y. Ma, P.A. Bates, M. Motevalli, M.B. Hursthouse, J. Chem. Soc, Perkin Trans. 2 (1989) 527.
[34] (a) G. Cerchiaro, P.L. Saboya, A.M.D.C. Ferreira, D.M. Tomazela, M.N. Eberlin, Transit. Met. Chem. 29 (2004) 495;
(b) G. Cerchiaro, G.A. Micke, M.F.M. Tavares, A.M.D.C. Ferreira, J. Mol. Catal. A: Chem. 221 (2004) 29.
[35] S. Umetani, Y. Kawase, Q.T.H. Le, M. Matsui, J. Chem. Soc., Dalton Trans. (2000) 2787.
[36] (a) W.A. Alves, R.H.A. Santos, A. Paduan-Filho, C.C. Becerra, A.C. Borin, A.M.D.C. Ferreira, Inorg. Chim. Acta 357 (2004) 2269;
(b) A. Neves, A. Anjos, A.J. Bortoluzzi, B. Szpoganicz, E.W. Schwingel, A.S. Mangrich, Inorg. Chim. Acta 356 (2003) 41;
(c) J. Muller, D. Schübl, C. Maichle-Mössmer, J. Strähle, U. Weser, J. Inorg. Biochem. 75 (1999) 63;
(d) J. Muller, K. Felix, C. Maichle, E. Lengfelder, J. Strähle, U. Weser, Inorg. Chim. Acta 233 (1995) 11.
[37] (a) P. Hemmerich, C. Sigwart, Experientia 19 (1963) 488;
(b) A.M.D.C. Ferreira, M.R. Ciriolo, L. Marcocci, G. Rotilio, Biochem. J. 292 (1993) 673.

affect the ability of the platinum drug to block replication and transcription.

A series of DNA adducts with 1,2-diaminocyclohexane-Pt, 1,4-diaminocyclohexane-Pt, homopiperazine-Pt complexes have been reported by us previously [28–30]. In a continuous effort to investigate any correlation between anticancer activity and the DNA adduct profile, which may contribute to the understanding mechanism of action of such platinum-based anticancer agents, that are structurally and functionally distinct form cisplatin prompted us to report here the synthesis and characterization of a series of homopiperazine Pt(II) mono and diadducts with DNA bases and nucleosides along with the crystal structure of one of these complexes, [Pt^{II}(homopiperazine)-(9-ethylguanine)$_2$]$(NO_3)_2$.

2. Experimental

2.1. Chemicals

K_2PtCl_4 was purchased from Johnson Mathey (Seabrook, NH). Silver nitrate was purchased from Alfa Aesar (Ward Hill, MA). Homopiperazine (hmp), adenine (Ade), 9-ethylguanine (9-EtGua), 7-methylguanine (7-MeGua), cytosine (Cyt), 1-methylcytosine, (1-MeCyt), cytidine (Cytd), methylene chloride, and acetone were purchased from Aldrich Chemical Co. (Milwaukee, WI). Silver sulfate, silver nitrate, HCl, nitric acid, *N*,*N*-dimethylformamide (DMF), and potassium iodide (KI) were purchased from Fisher Scientific Co. (Houston, TX).

2.2. Physical measurements

Elemental analysis of the complexes was performed by Robertson Laboratories Inc. (Madison, NJ). ^1H, ^{13}C, and ^{195}Pt NMR spectra were recorded for complexes in solution with D_2O and DCl using a 300-MHz spectrometer. Shifts in the ^{195}Pt spectra were measured relative to an external standard of 0.2 M Na_2PtCl_6 in D_2O at 0.00 ppm.

2.3. Synthesis of platinum complexes

2.3.1. Preparation of [Pt^{II}(hmp)(Ade)Cl]NO_3 (**1**)

[Pt^{II}(hmp)Cl_2] was synthesized as described previously [28]. [Pt^{II}(hmp)Cl_2] was (1.00 g, 2.73 mmol) dissolved in 150 mL of *N*,*N*-dimethylformamide, and to this solution $AgNO_3$ (0.46 g, 2.73 mmol) was added. The reaction mixture was then continuously stirred in the dark for 24 h. The AgCl precipitate was filtered off, using celite as a filter. To the filtrate [Pt^{II}(hmp)(H_2O)Cl]NO_3, Ade (0.36 g, 2.73 mmol) was added. The reaction mixture was then stirred for 36 h at 45 °C. A pale yellow solution was obtained, concentrated to 10 mL under reduced pressure, and excess acetone was added. A pale yellow product [Pt^{II}(hmp)(Ade)Cl]NO_3 was obtained, filtered, washed with CH_2Cl_2, and acetone. The final product was dried in vacuo.

The same procedure was adopted for the preparation of complexes **3**, **5**, **7**, **9** and **11** using the corresponding bases.

2.3.2. Preparation of [Pt^{II}(hmp)(Ade)$_2$]$(NO_3)_2$ (**2**)

[Pt^{II}(hmp)Cl_2] (1.00 g, 2.73 mmol) was dissolved in 200 mL of dimethylformamide, and $AgNO_3$ (0.91 g, 5.46 mmol) was added to this solution. The reaction mixture was protected from light and stirred for 5 days at 45 °C. AgCl was filtered off, using celite as filter. To the filtrate [Pt^{II}(hmp)(H_2O)$_2$]$(NO_3)_2$, Ade (0.73 g, 5.46 mmol) was added, and the reaction mixture was then stirred continuously for 96 h. The pale yellow solution formed was filtered through celite, concentrated to 10 mL under reduced pressure, and precipitated with acetone. The product [Pt^{II}(hmp)(Ade)$_2$]$(NO_3)_2$ was filtered, washed with CH_2Cl_2 and acetone, and dried in vacuo.

The same procedure was adopted for the synthesis of complexes **4**, **6**, **8**, **10**, and **12**.

2.4. Crystallographic measurements

Each single crystal was glued to a glass fiber and mounted on a Bruker Smart 1000 diffractometer equipped with a CCD area detector. Graphite monochromated Mo Kα radiation ($\lambda = 0.71073$ Å) in the $\omega - 2\theta$ scanning mode was used. The data were collected at room temperature and corrected for Lorentz and polarization effects. An absorption correction was applied using the program SADABS. No decay of the crystal was detected during the data collection. Heavy atoms in the compounds were located using Patterson methods. The structures were solved using direct methods using SHELXTL software package and refined by full matrix least-square techniques on F^2. Hydrogen atoms were included in calculated positions and refined using riding model. All thermal ellipsoid are drawn at the 50% probability level (see Table 1).

3. Results and discussion

3.1. Chemistry

The synthesis of platinum(II) complexes is shown in Scheme 1. [Pt(hmp)Cl_2] was used as a precursor for both [Pt^{II}(hmp)(X)Cl]NO_3 and [Pt^{II}(hmp)X_2]$(NO_3)_2$ type of complexes. The reaction of [Pt^{II}(hmp)Cl_2] with 1 equiv. of $AgNO_3$ in DMF yielded [Pt^{II}(hmp)(H_2O)Cl]NO_3 (reaction A). The reaction of [Pt^{II}(hmp)(H_2O)Cl]NO_3 with 1 equiv. of the desired nucleobase in DMF produced [Pt^{II}(hmp)-(X)Cl]NO_3 type of complexes (reaction B). The reaction of [Pt^{II}(hmp)Cl_2] with 2 equiv. of $AgNO_3$ and the corresponding nucleobase produced [Pt^{II}(hmp)X_2]$(NO_3)_2$ type of complexes (reactions C and D).

3.2. Characterization of complexes

Structures of the platinum complexes are shown in Fig. 1. Elemental analysis showed a good correlation

Table 1
Crystal data and structure refinement for [Pt^{II}(homopiperazine)-(9-ethylguanine)$_2$]$(NO_3)_2$

Empirical formula	$C_{19}H_{28}N_{14}O_8Pt$
Formula weight	775.64
Temperature (K)	298(2)
Wavelength (Å)	0.71073
Crystal system	monoclinic
Space group	$P2(1)/c$
Unit cell dimensions	
a (Å)	11.389(2)
b (Å)	18.890(3)
b (Å)	13.314(3)
α (°)	90
β (°)	104.379(3)
γ (°)	90
Volume (Å)^3	2774.7(9)
Z	4
D_{calc} (Mg/m^3)	1.857
Absorption coefficient (mm^{-1})	5.128
$F(000)$	1528
Crystal size (mm)	$0.3 \times 0.18 \times 0.1$
Range for data collection (°)	1.91–24.76
Limiting indices	$-13 < h < 13$, $-22 < k < 22$, $-15 < l < 15$
Reflections collected	19365
Independent reflections (R_{int})	4738 (0.2170)
Completeness to θ	24.76°, 99.7%
Absorption correction	multiscan
Maximum and minimum transmission	1.000000 and 0.477532
Refinement method	full-matrix least-squares on F^2
Data/restraints/parameters	4738/0/379
Goodness-of-fit on F^2	1.034
Final R indices [$I > 2\sigma(I)$]	$R_1 = 0.0663$, $wR_2 = 0.1635$
R indices (all data)	$R_1 = 0.1572$, $wR_2 = 0.2147$
Largest difference in peak and hole (e Å^{-3})	2.042 and −1.207

between the theoretical and actual values. These values are displayed in Table 2.

Infrared spectroscopy was used to identify the functional groups of the ligands in compounds. A broad band between 3300 and 3100 cm^{-1} confirmed the N–H stretching vibrations in the spectra. The intense bands between 1690 and 1600 cm^{-1} for hmp and 1380 and 1200 cm^{-1} for nucleobase complexes were attributed to ν_{as}(C–O) and ν_s(C–O) vibration, respectively. Pt–N and Pt–Cl stretching frequencies gave rise to peaks around 580 and 360 cm^{-1}, respectively.

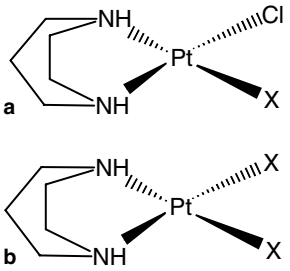

Fig. 1. (a) Structure of [Pt^{II}(hmp)XCl]NO_3, (b) Structure of [Pt^{II}(hmp)X_2]-$(NO_3)_2$ (where hmp = homopiperazine and X = adenine, 9-ethylguanine, 7-methylguaninine, cytosine, 1-methylcytosine, or cytidine).

All complexes were further characterized by ^{1}H, ^{13}C, and ^{195}Pt NMR spectroscopic techniques. The ^{1}H, ^{13}C, and ^{195}Pt NMR spectroscopic data given were most informative with respect to the structure of the complexes (Table 3). The peaks corresponding to homopiperazine were observed between 1.76–1.77 and 2.89–2.92 ppm. In complexes **1** and **2**, C_8H- and C_2H-proton resonance peaks of adenine were shifted downfield as compared with those of the free ligand. The shift of C_8H protons to the range of 0.08–0.30 ppm, as compared with that of C_2H protons to the ranged, 0.05–0.20 ppm, suggests that the site of coordination to the Pt metal ion is N7. The downfield shift of C_8–H proton to the range of 0.19–0.20 ppm observed for 9-ethylguanine complexes **3** and **4** and 0.46–0.51 ppm for 7-methylguanine complexes **5** and **6** complex supports the coordination of N7 or N9 with the metal ion. In cytosine, 1-methyl cytosine, and cytidine complexes (**7**–**12**), the two doublets corresponding to the C_5H protons exhibited a smaller shift than did the C_6H protons, which supports coordination through the N3 atom of the ligands. All of the peaks due to the ribose ring in cytidine complexes **11** and **12** were not shifted substantially; therefore,

Monoadducts

$$[Pt^{II}(hmp)Cl_2] + AgNO_3 \rightarrow [Pt^{II}(hmp)(H_2O)Cl]NO_3 + AgCl \quad (A)$$

$$[Pt^{II}(hmp)(NO_3)Cl] + X \rightarrow [Pt^{II}(hmp)(X)Cl]NO_3 + H_2O \quad (B)$$

Diadducts

$$[Pt^{II}(hmp)Cl_2] + 2AgNO_3 \rightarrow [Pt^{II}(hmp)(H_2O)_2](NO_3)_2 + 2AgCl \quad (C)$$

$$[Pt^{II}(hmp)(H_2O)_2](NO_3)_2 + 2X \rightarrow [Pt^{II}(hmp)X_2](NO_3)_2 + 2H_2O \quad (D)$$

X = adenine, 9-ethylguanine, 7-methylguanine, cytosine, 1-methylcytosine, or cytidine

Scheme 1.

Table 2
Elemental analysis of $[Pt^{II}(hmp)XCl]NO_3$ and $[Pt^{II}(hmp)X_2](NO_3)_2$ type complexes

Complex number	Complex name	Observed (calculated)			
		C	H	N	%Yield
1	$[Pt^{II}(hmp)(Ade)Cl]NO_3$	22.93 (22.77)	3.34 (3.22)	21.00 (21.25)	64
2	$[Pt^{II}(hmp)(Ade)_2](NO_3)_2$	26.30 (26.16)	3.55 (3.05)	28.40 (28.48)	98
3	$[Pt^{II}(hmp)(9\text{-}EtGua)Cl]NO_3$	25.16 (25.19)	3.52 (3.67)	19.89 (19.59)	66
4	$[Pt^{II}(hmp)(9\text{-}EtGua)_2](NO_3)_2$	31.67 (31.88)	3.79 (4.19)	25.67 (25.45)	77
5	$[Pt^{II}(hmp)(7\text{-}MeGua)Cl]NO_3$	23.79 (23.67)	3.51 (3.40)	11.40 (11.47)	80
6	$[Pt^{II}(hmp)(7\text{-}MeGua)_2](NO_3)_2$	27.49 (27.23)	3.52 (3.47)	26.34 (26.16)	90
7	$[Pt^{II}(hmp)(Cyt)Cl]NO_3$	21.70 (21.42)	3.62 (3.57)	16.39 (16.66)	65
8	$[Pt^{II}(hmp)(Cyt)_2](NO_3)_2$	24.05 (24.30)	3.38 (3.43)	21.71 (21.80)	85
9	$[Pt^{II}(hmp)(1\text{-}MeCyt)Cl]NO_3$	23.35 (23.20)	3.64 (3.68)	16.34 (16.25)	67
10	$[Pt^{II}(hmp)(1\text{-}MeCyt)_2](NO_3)_2$	26.89 (26.90)	4.07 (3.98)	20.85 (20.92)	80
11	$[Pt^{II}(hmp)(Cytd)Cl]NO_3$	26.68 (26.43)	4.31 (3.93)	13.37 (13.21)	88
12	$[Pt^{II}(hmp)(Cytd)_2](NO_3)_2$	30.58 (30.49)	4.28 (4.19)	15.25 (15.46)	98

hmp, homopiperazine; Ade, adenine; 9-EtGua, 9-ethylguanine; 7-MeGua, 7-methyguanine; Cyt, cytosine; 1-MeCyt, 1-methylcytosine; Cytd, cytidine.

coordination through the ribose ring for complexes **11** and **12** is excluded.

The proton-decoupled ^{13}C NMR spectra of purine and pyrimidine bases were obtained from the Integrated Spectral Data Base System for Organic Compounds (SDBS). In complexes **1** and **2** shifts of 1.19, 1.82, and 4.00 ppm were observed at C_4, C_5, and C_8, respectively, as compared with adenine free ligand. In complexes **3** and **4**, shifts of 1.6 ppm at C_4, 2.32 ppm at C_5, and 3.26 ppm at C_8 were observed as compared with 9-EtGua. The identical shifts

Table 3
^1H, ^{13}C, and ^{195}Pt NMR spectroscopic data for $[Pt^{II}(hmp)XCl]NO_3$ and $[Pt^{II}(hmp)X_2](NO_3)_2$ type complexes

Complex number	Complex name	^1H				^{13}C							^{195}Pt
		C2	C8	CH_2	CH_3	C2	C4	C5	C6	C8	CH_2	CH_3	
	Adenine	8.07	8.09			152.39	154.68	118.59	150.61	141.30			
1	$Pt^{II}(hmp)(Ade)Cl]NO_3$	8.35	8.39			152.76	155.87	116.77	149.58	145.43			−2701
2	$[Pt^{II}(hmp)(Ade)_2](NO_3)_2$	8.15	8.17			152.50	149.76	115.93	148.73	142.52			−2746
	9-Ethylguanine		7.85	4.08	1.42	154.31	157.73	117.47	151.82	137.86	38.56	16.20	
3	$[Pt^{II}(hmp)(9\text{-}EtGua)Cl]NO_3$		8.04	4.07	1.36	155.13	156.21	115.08	150.84	141.17	39.95	15.67	−2514
4	$[Pt^{II}(hmp)(9\text{-}EtGua)_2](NO_3)_2$		8.00	3.97	1.26	155.42	158.22	114.49	150.93	141.16	40.20	14.48	−2641
	7-Methylguanine		8.56		3.03	154.91	155.13	108.51	149.77	139.15		35.58	
5	$[Pt^{II}(hmp)(7\text{-}MeGua)Cl]NO_3$		8.05[a]		3.40	151.75[a]	153.01	109.84	147.14	144.15		34.90	−2536[a]
6	$[Pt^{II}(hmp)(7\text{-}MeGua)_2](NO_3)_2$		8.10[a]		3.58	152.40[a]	153.82	109.88	149.41	144.26		35.40	−2706[a]
		C_6H	C_5H	C_3H		C2	C4	C5	C6	CH_3			
	Cytosine	5.97	7.49			159.91	168.95	95.79	144.05				
7	$[Pt^{II}(hmp)(Cyt)Cl]NO_3$	6.05	7.45			156.47	166.56	94.68	143.87				−2605
8	$[Pt^{II}(hmp)(Cyt)_2](NO_3)_2$	6.08	7.50			157.40	166.48	94.87	144.14				−2749
	1-Methylcytosine	5.61	7.55	3.17		159.32	166.87	95.61	147.98	37.82			
9	$[Pt^{II}(hmp)(1\text{-}MeCyt)Cl]NO_3$	6.15	7.62	3.41		156.84	168.25	96.13	150.12	40.29			−2591
10	$[Pt^{II}(hmp)(1\text{-}MeCyt)_2](NO_3)_2$	5.95	7.53	3.39		156.69	166.18	94.88	148.89	38.43			−2820
	Cytidine	6.03	7.84			158.25	166.86	96.92	142.43				
11	$[Pt^{II}(hmp)(Cytd)Cl]NO_3$	6.04	7.87			155.23	165.28	95.79	142.06				−2992
12	$[Pt^{II}(hmp)(Cytd)_2](NO_3)_2$	6.09	7.83			155.29	165.24	95.77	142.20				−2830

[a] DCI.

in adenine complexes **1** and **2** and in (N9-substituted) 9-ethylguanine complexes **3** and **4** support the notion that N7 serves as a binding site. In complexes **5** and **6** the C_2, C_6, and C_8 carbons showed 2.5, 2.63, and 5.11 ppm shifts as compared with the 7-methylguanine suggesting that coordination site is N9 and not N7 because of the methyl substituent. X-ray diffraction and NMR studies of the complexes formed between platinum and N9- and N7-alkylated purines, N1-alkylated pyrimidines, nucleosides, and nucleotides have been used to elucidate the platinum binding sites. The preferred binding site is N7 for adenine and 9-ethylguanine and N9 for 7-methylguanine purine complexes, respectively, and N3 for pyrimidine complexes [31–35]. NH_2 is apparently not involved in coordination since there was only a negligible shift in NH_2 protons in DMF-d_7. This is further supported by the results of ^{195}Pt NMR spectroscopy.

In the ^{195}Pt NMR spectra, the Pt(II) complexes **1**, **3**, **5**, **7**, **9**, and **11** showed a signal in the range of −2514 to −2605 ppm for monoadducts and a signal in the range of −2641 to −2830 ppm for diadducts **2**, **4**, **6**, **8**, **10**, and **12**. Such chemical shifts are typical for square-planar Pt(II) complexes that contain three nitrogen and one chlorine donor for monoadducts and four nitrogen donors for diadducts, respectively. Fig. 1 shows the proposed structure of such complexes.

3.3. X-ray crystal structures

Fig. 2 shows a perspective view of the crystal structure of [Pt^{II}(homopiperazine)(9-ethylguanine)$_2$](NO$_3$)$_2$ along with its atom labeling. The selected bond lengths and bond angles are given in Table 4. The platinum atom was found to have a distorted square planar geometry due to a longer bite distance in the chelating ligand, hmp. The distortion is indicated by the contraction of the N_{11}–Pt_1–N_{12} angle in the hmp region to 77.2(7)° and contraction of the N_{4A}–Pt_1–N_{4B} angle in the 9-ethylguanine region to 89.2(6)°, similar to the N_1–Pt_1–N_2 and N_2–Pt_1–N_1 angles of 76.8(3)°, and 77.8(8)° as observed in [Pt(hmp)Cl$_2$] and [Pt(1-methylhomopiperazine)(methylmalonato)] · 2H$_2$O, respectively [28,36]. However, the same bond angle in the cisplatin adducts is about 90°, as reported previously for complexes *cis*-[(NH$_3$)$_2$Pt(9-ethylguanine)$_2$]SO$_4$ · 4H$_2$O (93.2°) [37], *cis*-[(NH$_3$)$_2$Pt(9-ethylguanine)$_2$][Pt(CN)$_4$] · 3H$_2$O (87.8°) [37], [Pt(NH$_3$)$_2$(9-ethylguanine)(1-methylcytosine)](ClO$_4$)$_2$ · nH$_2$O (90.0°) [33], and *cis*-[Pt(NH$_3$)$_2$(9-methyladenine)(9-ethylguanine)](NO$_3$)$_2$ (88.9°) [32]. The contraction of the bond angle is compensated for by expansion of the N_{11}–Pt_1–N_{4B} and N_{12}–Pt_1–N_{4A} bond angles to 97.6(6)° and 96.1(6)°, respectively. Homopiperazine forms a 5-membered chelate ring with the platinum atom.

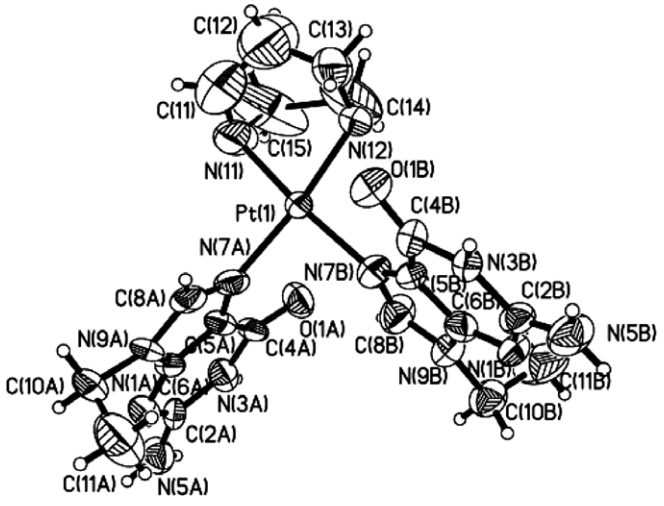

Fig. 2. ORTEP representation of the structure of [Pt^{II}(homopiperazine)(9-ethylguanine)$_2$](NO$_3$)$_2$.

Table 4
Selected bond lengths (Å) and angles (°) for [Pt^{II}(homopiperazine)-(9-ethylguanine)$_2$](NO$_3$)$_2$

Pt(1)–N(11)	2.030(15)
Pt(1)–N(12)	2.043(17)
Pt(1)–N(4A)	2.046(14)
Pt(1)–N(4B)	2.069(14)
N(11)–Pt(1)–N(12)	77.2(7)
N(11)–Pt(1)–N(4A)	173.0(6)
N(12)–Pt(1)–N(4A)	96.1(6)
N(11)–Pt(1)–N(4B)	97.6(6)
N(12)–Pt(1)–N(4B)	172.8(9)
N(4A)–Pt(1)–N(4B)	89.2(6)
C(5A)–N(4A)–Pt(1)	126.0(12)
C(2A)–N(4A)–Pt(1)	126.1(12)
C(14)–N(12)–Pt(1)	108(2)
C(13)–N(12)–Pt(1)	106(2)
C(11)–N(11)–Pt(1)	112.2(15)
C(15)–N(11)–Pt(1)	106.4(14)
C(2B)–N(4B)–Pt(1)	129.3(12)
C(5B)–N(4B)–Pt(1)	119.8(13)

Because of the unsymmetrical nature of the hmp ligand d(GpG) can coordinate in two ways with H8 atoms of the nucleobases disposed towards the two carbon chain of the hmp or toward the three carbon chain. Interconversions between two isomers cannot takes place with out breaking and reforming of coordinate Pt–N bonds [10]. The rotation about Pt–N7 (G) bond is restricted by the conformationally rigid nature of the hmp ligand. Therefore [Pt(hmp)d(GpG) adducts adopt any of the noninterconverting six geometries, two head-to-head and four head-to-tail [10]. In the crystal structure the two 9-ethylguanine ligands are oriented in such a way that the exocyclic oxygen atoms are on the opposite side of the platinum coordination plane in a head to tail fashion as shown in Fig. 2 [37]. The two 9-ethylguanine ligands are thus related by a pseudo C_2 axis. Rigorous C_2 symmetry for the molecule is not possible owing to the asymmetry in the homopiperazine ligand. The average angles for C(13)–N(12)–Pt(1) and C(15)–N(11)–Pt(1) are 106.2(2)° and 106.4(14)°, respectively, which are similar to those for [PtII(methylhomopiperazine)(methylmalonato)] · 2H$_2$O, and [Pt(hmp)Cl$_2$] and closer to the values seen in 1,2-DACH-platinum complexes

[30,40–44]. All Pt–N bond lengths were in the ranges normally observed for mono- or diadducts. The average Pt–N bond lengths of 2.047(15) Å [23] in the complexes are within the range normally observed for cisplatin-nucleobase adducts [38,33,37]. For example, the average bond length is 2.03(3) Å in [Pt^{IV}(*trans*-1*R*,2*R*-diaminocyclohexane)*trans*-(acetate)$_2$$Cl_2$], 2.038 Å in [Pt(*trans*-*R*,*R*-DACH-(*N*-Me-IDA))Cl]Cl, 2.06 Å in [Pt(*trans*-D,L-DACH)Cl_4], 2.04 Å in [Pt(*trans*-D,L-DACH(9-methylguanine)$_2$$Cl_2$]-$(NO_3)_2 \cdot 11H_2O$, 2.03 Å in [Pt(*cis*-1*R*,2*R*-DACH)*trans*-(Cl_2)(CBDCA)] · 1/2 MeOH, 2.01(1) Å in Pt–N(7) in *cis*-[$Pt(NH_3)_2$GC]$(ClO_4)_2$, 2.04(1) Å in [$Pt(NH_3)_2$(1-MeC)-(9-EtG)]$^{2+}$, and 2.006(8) Å in *cis*-[$(NH_3)_2$Pt(9-MA-N7)-(9-EtG-N7)]$NO_3 \cdot 1.5H_2O$ [29,31,33,39,42–44]. A stereoscopic view of the molecular packing of the crystals structures is shown in Fig. 3. The molecules in the crystal are held together by a system of hydrogen bonds between the amine hydrogen atom of one molecule and the carbonyl oxygen atom of the 9-ethylguanine. Homopiperazine and 9-ethylguanine ligands are attached to the platinum atom in a square planar configuration. The platinum and four attached nitrogen atoms are all within 0.08(1) Å of the least-squares plane defined by those five atoms. The planes of the 9-ethylguanine ligands lie at an 81.76° angle with respect to each other. Generally, all hydrogen bonds are formed through the interaction of the NH group on the 9-ethylguanine and homopiperazine with the nitrate or NH groups within or with other molecules. For example, N5A···N2B (3.220 Å) and N5A···N2B (3.220 Å) result from the intermolecular hydrogen bonds involving two 9-ethylguanine molecules related by symmetry. Similarly, the hydrogen bonds N11···O1B (3.263 Å) and N12···O10B (2.928 Å) are established through the interaction of the NH of homopiperazine with either a nitrate group or a 9-ethylguanine oxygen from a second molecule. The most abundant hydrogen bonds are those between the nitrate molecules that together generate an intricate network of intermolecular hydrogen bonds. The nitrate ions appear either in a bridged configuration via two oxygen atoms (O11A···N5B [2.871 Å] and O12A···N5A [3.166 Å]), in a simple hydrogen bond via one oxygen (N1B···O11B [2.866 Å]).

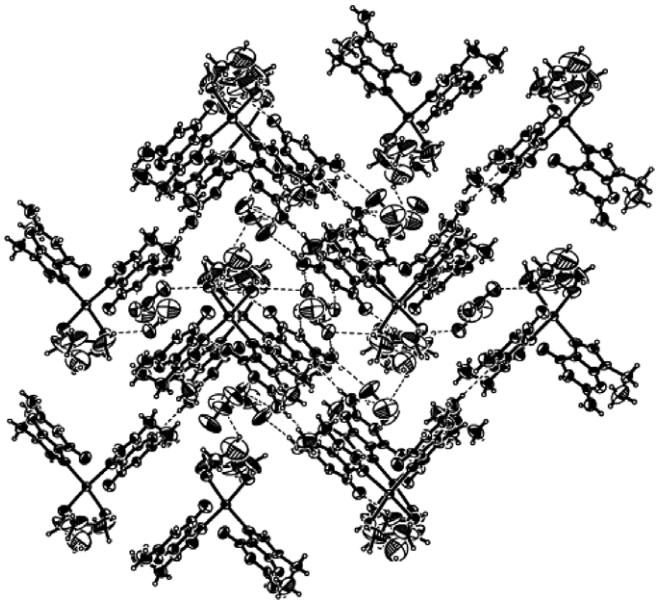

Fig. 3. A view of the molecular packing of [Pt^{II}(homopiperazine)-(9-ethylguanine)$_2$]$(NO_3)_2$.

4. Conclusions

A series of homopiperazine-Pt(II) mono adducts and diadducts formed with nucleobases and nucleosides, respectively, were synthesized and characterized by elemental analysis and NMR spectroscopic techniques. The crystal structure of [Pt^{II}(homopiperazine)(9-EtGua)$_2$]$(NO_3)_2$ was determined by X-ray crystallography.

Acknowledgement

This work was supported in part by Grant C-0976 from The Robert Welch Foundation.

Appendix A. Supporting information available

Supplementary data in CIF format are available from CCDC, 12 Union Road, Cambridge, CB2 1EZ, UK, fax: +44 1223 366 033, e-mail: deposit@ccdc.ac.uk or on the web www: http://www.ccdc.cam.ac.uk, on request, quoting the Deposition No. 276452. Supplementary data associated with this article can be found, in the online version, at doi:10.1016/j.poly.2006.01.003.

References

[1] J.G. Colloins, N.J. Wheate, J. Inorg. Biochem. 98 (2004) 1578.
[2] N. Farrell, L.R. Kelland, in: N.P. Farrell (Ed.), Platinum Based Drugs in Cancer Chemotherapy, Humana Press, Totowa, NJ, 2000, p. 321.
[3] N. Farrell, in: Interaction of Metal Ions with Nucleotides, Nucleic Acids, and their Constituents, vol. 32, Marcel Dekker, Basel, 1996, p. 603.
[4] L.S. Hollis, in: Platinum and Other Metal Coordination Compounds in Cancer Chemotherapy, Plenum, New York, 1991, p. 115.
[5] L.S. Hollis, W.I. Sundquist, N.J. Burstyn, W.J. Heiger-Bernays, S.F. Bellon, K.J. Ahmed, A.R. Anderson, E.W. Stern, S.J. Lippard, Cancer Res. 51 (1991) 1866.
[6] L.S. Hollis, A.R. Amundson, E.W. Stern, J. Med. Chem. 32 (1989) 128.
[7] E.R. Jemmison, S.J. Lippard, Chem. Rev. 99 (1999) 2467.
[8] N.P. Johnson, J.L. Butour, G. Villani, F.L. Wimmer, M. Defais, V. Pierson, V. Brabec, Prog. Clin. Biochem. Med. 10 (1989) 1.
[9] V. Brabec, J. Kasparkova, Drug Resist. Updates 5 (2002) 147.
[10] T.W. Hambley, E.C.H. Ling, B.A. Messerle, Inorg. Chem. 35 (1996) 4663.
[11] A.L. Pinto, S.J. Lippard, Biochem. Biophys. Acta 780 (1985) 167.
[12] J.L. van der Veer, J.J. Reedijk, J. Chem. Brit. 24 (1988) 775.
[13] N. Sheibani, M.M. Jennerwein, A. Eastman, Biochemistry 28 (1989) 3120.
[14] A. Eastman, Biochemistry 22 (1983) 3927.

[15] A.M.J. Fichtinger-Schepman, P.H.M. Lohman, J. Reedijk, Nucleic Acids Res. 10 (1982) 5345.
[16] A.M.J. Fichtinger-Schepman, J.L. van der Veer, J.H.J. den Hartog, P.H.M. Lohman, J. Reedijk, Biochemistry 24 (1985) 707.
[17] A. Eastman, Biochemistry 24 (1985) 5027.
[18] A. Eastman, Biochemistry 25 (1986) 3912.
[19] J.C. Jones, W. Zhen, E. Reed, R.J. Parker, A. Sancer, V.A. Bohr, J. Biol. Chem. 266 (1991) 7101.
[20] W. Zhen, C.J. Link Jr., P.M. O'Connor, E. Reed, R. Parker, S.B. Howell, V.A. Bohr, Mol. Cell Biol. 12 (1992) 3689.
[21] Y. Corda, C. Job, M.F. Anin, M. Leng, D. Job, Biochemistry 32 (1993) 8582.
[22] N. Sheibani, M.M. Jennerwein, A. Eastman, Biochemistry 28 (1989) 3120.
[23] A.L. Pinto, L.J. Naser, J.M. Essigmann, S.J. Lippard, J. Am. Chem. Soc. 108 (1986) 7405.
[24] E.C.H. Ling, G.W. Allen, T.W. Hambley, J. Am. Chem. Soc. 116 (1994) 2673.
[25] T.W. Hambley, E.C.H. Ling, V.P. Munk, M.S. Davis, J. Biol. Inorg. Chem. 6 (2001) 534.
[26] F. Reeder, J. Kozelka, J.C. Chottard, Inorg. Chem. 35 (1996) 1413.
[27] J. Zhang, X. Wang, C. Tu, J. Lin, J. Ding, L. Lin, Z. Wang, C. He, C. Yan, X. You, Z. Guo, J. Med. Chem. 46 (2003) 3502.
[28] M.S. Ali, K.H. Whitmire, T. Toyomasu, Z.H. Siddik, A.R. Khokhar, J. Inorg. Biochem. 77 (1999) 231.
[29] M.S. Ali, A.R. Khokhar, J. Inorg. Biochem. 96 (2003) 452.
[30] M.S. Ali, S.R. Ali-Khan, H. Ojima, I.Y. Guzman, K.H. Whitmire, Z.H. Siddik, A.R. Khokhar, J. Inorg. Biochem. 99 (2005) 795.
[31] R. Faggiani, C.J.L. Lock, B. Lippert, J. Am. Chem. Soc. 102 (1980) 5418.
[32] G. Schröder, J. Kozalka, M. Sabat, M. Fouchet, R. Beyerle-Pfnür, B. Lippert, Inorg. Chem. 35 (1996) 1647.
[33] R. Faggiani, B. Lippert, C.L.J. Lock, R.A. Speranzini, Inorg. Chem. 21 (1982) 3216.
[34] G. Schröder, M. Sabat, I. Baxter, J. Kozelka, B. Lippert, Inorg. Chem. 36 (1997) 490.
[35] S.E. Sherman, S.J. Lippard, Chem. Rev. 87 (1987) 1153.
[36] V.P. Munk, R.R. Fenton, T.W. Hambley, Polyhedron 18 (1999) 1034.
[37] H. Schröllhorn, G. Raudaschl-Sieber, G. Müller, U. Thewalt, B. Lippert, J. Am. Chem. Soc. 107 (1985) 5932.
[38] J. Reedijik, Inorg. Chim. Acta 198 (1992) 873.
[39] A. Erxleben, S. Metzger, J.F. Britten, C.J.L. Lock, A. Albinati, B. Lippert, Inorg. Chim. Acta 339 (2002) 461.
[40] S.R. Ali Khan, S. Haung, S. Shamsuddin, S. Inutsuka, K.H. Whitmire, Z.H. Siddik, A.R. Khokhar, Bioorg. Inorg. Med. Chem. 8 (2000) 515.
[41] A.R. Khokhar, Q. Xu, S. Al-Baker, Inorg. Chim. Acta 194 (1992) 243.
[42] Q. Xu, A.R. Khokhar, J. Inorg. Biochem. 48 (1992) 217.
[43] A.R. Khokhar, Q. Xu, S. Al-Baker, J. Inorg. Biochem. 52 (1993) 51.
[44] S. Shamsuddin, J.W. Van Hal, J.L. Stark, K.H. Whitmire, Z.H. Siddik, A.R. Khokhar, Inorg. Chem. 36 (1997) 5969.

but other bulk properties like magnetic susceptibility may depend both on the molecular structure as well as on the solid state packing of the molecular entities.

In this work we present the structural and magnetic study of a group of dinuclear copper(II) macrocycles $[Cu_2L]^{2+}$, obtained with different counteranions, and where LH_2 is the ligand derived from the condensation of 2,6-diformyl-4-methylphenol and 1,3-diamino-2-propanol with different counteranions. The influence of the counteranion on the solid state molecular structure and the crystal lattice which define the bulk magnetic properties will be discussed. We present also an example of a butterfly distortion in on of the macrocycles, which takes place along the axis joining both copper centres, and which is assumed to produce a decrease in the value of the magnetic exchange coupling. There are examples in the literature of some μ-hydroxo dinuclear copper(II) complexes presenting a similar distortion, but along the line joining both hydroxo oxygens in which a decrease of the magnetic exchange coupling is also observed [13].

2. Experimental

2.1. Physical measurements

The diffuse reflectance UV–Vis spectra were recorded using a Perkin–Elmer Lambda 20 UV–Vis spectrophotometer equipped with a Labsphere RSA-PE-20 diffuse reflectance accessory. Magnesium oxide was used as reference and the spectra were recorded in the range of 1.0 and 6.0 eV at room temperature. Reflectance measurements were converted to absorption spectra using the Kubelka-Munk function F(R8).

Solution spectra were obtained with a UV–Vis spectrometer, Unicam UV3. Infrared spectra were recorded in KBr pellets using a Bruker Vector 22 FTIR instrument in the range 250–4000 cm^{-1}.

The magnetic susceptibility measurements were carried out on polycrystalline samples at CEPEDEQ, University of Chile with a Cryogenics Susceptometer-Magnetometer SQUID S-600, and at the Servei de Magnetoquímica of the Universitat de Barcelona and University of Rennes-1 with a Quantum Design SQUID MPMS XL.

2.2. Preparations

All reagents and solvents from commercial sources were used without further purification. The macrocyclic copper(II) complexes **1**–**3** were synthesised by the template method. A general synthetic procedure was used to obtain these complexes. In 20 mL of methanol, 2 mmol of 2,6-diformyl-4-methylphenol and 2 mmol of the corresponding copper(II) salts ($CuCl_2 \cdot 2H_2O$, $Cu(acetate)_2 \cdot H_2O$,

Table 1
Crystal and structure refinement data

Identification code	(**1**) $[Cu_2LCl_2] \cdot 2H_2O$	(**2**) $[Cu_2L(\mu_2\text{-ac})]$ (ac) $[Cu_2L(\mu\text{-ac})_2(H_2O)_2] \cdot 6H_2O$	(**3**) $[Cu_2L(H_2O)_2] \cdot 2SO_4H \cdot 2H_2O$
Empirical formula	$C_{24}H_{30}Cl_2Cu_2N_4O_6$	$C_{56}H_{80}Cu_4N_8O_{24}$	$C_{24}H_{36}Cu_2N_4O_{16}S_2$
Formula weight	668.50	1503.44	827.77
T (K)	296(2)	295(2)	297(2)
Wavelength (Å)	0.71073	0.71073	0.71073
Crystal system	triclinic	orthorhombic	triclinic
Space group	$P\bar{1}$ (#2)	*Pnma* (#62)	$P\bar{1}$ (#2)
a (Å)	7.7223(16)	15.1671(11)	7.727(5)
b (Å)	9.3901(19)	27.4366(19)	8.663(4)
c (Å)	10.167(2)	15.9786(11)	11.753(4)
α (°)	73.377(3)	90	82.199(6)
β (°)	85.768(4)	90	85.519(10)
γ (°)	65.766(3)	90	75.830(11)
V ($Å^3$)	643.4(2)	6649.2(8)	754.8(7)
Z	1	4	1
D_c (g cm^{-3})	1.725	1.502	1.817
μ (mm^{-1})	1.909	1.345	1.632
F(000)	342	3120	426
Crystal size (mm^3)	$0.30 \times 0.20 \times 0.02$	$0.42 \times 0.30 \times 0.20$	$0.50 \times 0.13 \times 0.08$
θ Range (°)	2.09–25.00	1.85–24.99	1.75–25.00
Index ranges	$-9 \leqslant h \leqslant 9$, $-11 \leqslant k \leqslant 11$, $-12 \leqslant l \leqslant 12$	$-17 \leqslant h \leqslant 18$, $-32 \leqslant k \leqslant 32$, $-18 \leqslant l \leqslant 18$	$-9 \leqslant h \leqslant 9$, $-10 \leqslant k \leqslant 10$, $0 \leqslant l \leqslant 13$
Data			
$N_{collected}$	4032	32776	4987
$N_{indep.}$, R_{int}	2246, 0.053	5974, 0.071	2616, 0.078
$N_{Obs.}$ [$I > 2\sigma(I)$]	1743	4549	2006
Number of independent reflections per parameters	12.1	12.1	11.3
Goodness-of-fit on F^2	1.099	1.116	0.944
R indices [$I > 2\sigma(I)$]	$R_1 = 0.0626$, $wR_2 = 0.1675$	$R_1 = 0.0629$, $wR_2 = 0.2017$	$R_1 = 0.0634$, $wR_2 = 0.1787$
R indices (all data)	$R_1 = 0.0794$, $wR_2 = 0.1753$	$R_1 = 0.0838$, $wR_2 = 0.2172$	$R_1 = 0.0792$, $wR_2 = 0.1883$
Largest peak and hole (e $Å^{-3}$)	1.26, −0.69	0.95, −0.71	0.65, −0.77

$CuSO_4 \cdot 5H_2O$) were dissolved in methanol under nitrogen atmosphere. The green solution was refluxed for 2–3 h giving a green precipitate. Then 2 mmol of 1,3-diaminopropanol and 1 mL of triethylortoformiate were added to the reaction. The reaction mixture was refluxed for 8 h obtaining a green solution and a precipitate. The solid was filtered off and washed with small amounts of methanol. In the cases when no solid was obtained, a small amount of diethyl ether was added to induce the precipitation. All the complexes were dried under vacuum at 110 °C for 3 h. The microcrystalline solids were recrystallised from methanol.

$[Cu_2LCl_2] \cdot 2H_2O$ (**1**): yield: 24.3%. *Anal*. Calc. for $C_{24}H_{30}N_4O_6Cu_2Cl_2$: C, 43.12; H, 4.52; N, 8.38, Cu, 19.01. Found: C, 41.98; H, 4.41; N, 8.51, Cu, 18.92%. {$[Cu_2L(\mu_2\text{-acetate})]$(acetate) (**2a**) $[Cu_2L(acetate)_2(H_2O)_2]$

Table 2
Selected bond lengths (Å) and angles (°)

*(**1**)*			
Cu(1)–N(2)#1	1.957(5)	Cu(1)–O(1)#1	1.976(4)
Cu(1)–O(1)	1.959(4)	Cu(1)–Cl(1)	2.529(2)
Cu(1)–N(1)	1.965(6)		
N(2)#1–Cu(1)–O(1)	161.5(2)	N(1)–Cu(1)–O(1)#1	165.5(2)
N(2)#1–Cu(1)–N(1)	96.5(2)	N(2)#1–Cu(1)–Cl(1)	95.85(18)
O(1)–Cu(1)–N(1)	92.4(2)	O(1)–Cu(1)–Cl(1)	99.18(15)
N(2)#1–Cu(1)–O(1)#1	91.6(2)	N(1)–Cu(1)–Cl(1)	96.7(2)
O(1)–Cu(1)–O(1)#1	76.61(19)	O(1)#1–Cu(1)–Cl(1)	94.40(15)
*(**2a**)*			
Cu(1a)–O(1a)#3	1.967(4)	Cu(1a)–O(1a)	1.982(4)
Cu(1a)–N(1a)	1.974(4)	Cu(1a)–O(1W)	2.377(6)
Cu(1a)–N(2a)#3	1.975(4)	Cu(1a)–O(2a)	2.623(6)
O(1a)#3–Cu(1a)–N(1a)	169.28(17)	N(2a)#3–Cu(1a)–O(1W)	88.6(2)
O(1a)#3–Cu(1a)–N(2a)#3	93.19(16)	O(1a)–Cu(1a)–O(1W)	93.3(2)
N(1a)–Cu(1a)–N(2a)#3	96.93(19)	O(1a)#3–Cu(1a)–O(2a)	93.47(18)
O(1a)#3–Cu(1a)–O(1a)	77.15(16)	N(1a)–Cu(1a)–O(2a)	83.94(19)
N(1a)–Cu(1a)–O(1a)	92.63(17)	N(2a)#3–Cu(1a)–O(2a)	85.0(2)
N(2a)#3–Cu(1a)–O(1a)	170.24(17)	O(1a)–Cu(1a)–O(2a)	94.09(18)
O(1a)#3–Cu(1a)–O(1W)	93.5(2)	O(1W)–Cu(1a)–O(2a)	170.8(2)
N(1a)–Cu(1a)–O(1W)	90.3(2)		
*(**2b**)*			
Cu(1b)–N(1b)#2	1.961(4)	Cu(2b)–N(2b)	1.959(4)
Cu(1b)–N(1b)	1.961(4)	Cu(2b)–N(2b)#2	1.959(4)
Cu(1b)–O(1b)	1.963(3)	Cu(2b)–O(1b)#2	1.973(3)
Cu(1b)–O(1b)#2	1.963(3)	Cu(2b)–O(1b)	1.973(3)
Cu(1b)–O(2b)	2.225(5)	Cu(2b)–O(3b)	2.223(5)
N(1b)#2–Cu(1b)–N(1b)	96.7(2)	N(2b)–Cu(2b)–N(2b)#2	96.2(3)
N(1b)#2–Cu(1b)–O(1b)	165.02(17)	N(2b)–Cu(2b)–O(1b)#2	161.83(17)
N(1b)–Cu(1b)–O(1b)	91.77(15)	N(2b)#2–Cu(2b)–O(1b)#2	91.38(16)
N(1b)#2–Cu(1b)–O(1b)#2	91.77(15)	N(2b)–Cu(2b)–O(1b)	91.38(16)
N(1b)–Cu(1b)–O(1b)#2	165.02(17)	N(2b)#2–Cu(2b)–O(1b)	161.83(17)
O(1b)–Cu(1b)–O(1b)#2	77.5(2)	O(1b)#2–Cu(2b)–O(1b)	77.0(2)
N(1b)#2–Cu(1b)–O(2b)	101.66(15)	N(2b)–Cu(2b)–O(3b)	103.11(16)
N(1b)–Cu(1b)–O(2b)	101.66(15)	N(2b)#2–Cu(2b)–O(3b)	103.11(16)
O(1b)–Cu(1b)–O(2b)	88.62(15)	O(1b)#2–Cu(2b)–O(3b)	91.18(15)
O(1b)#2–Cu(1b)–O(2b)	88.62(15)	O(1b)–Cu(2b)–O(3b)	91.18(15)
*(**3**)*			
Cu(1)–N(2)#1	1.935(5)	Cu(1)–N(1)	1.960(5)
Cu(1)–O(1)#1	1.959(3)	Cu(1)–O(1W)	2.271(5)
Cu(1)–O(1)	1.961(4)		
N(2)#1–Cu(1)–O(1)#1	92.76(17)	O(1)–Cu(1)–N(1)	92.41(17)
N(2)#1–Cu(1)–O(1)	167.04(18)	N(2)#1–Cu(1)–O(1W)	92.3(2)
O(1)#1–Cu(1)–O(1)	75.93(16)	O(1)#1–Cu(1)–O(1W)	99.03(18)
N(2)#1–Cu(1)–N(1)	97.4 (2)	O(1)–Cu(1)–O(1W)	95.7(2)
O(1)#1–Cu(1)–N(1)	164.21(18)	N(1)–Cu(1)–O(1W)	92.6(2)

Symmetry transformations used to generate equivalent atoms throughout this work: (#1) $1-x, -y, 1-z$; (#2) $x, 1.5-y, z$; (#3) $1-x, 1-y, 1-z$; (#4) $1-x, -y, 2-z$; (#5) $x, 1+y, -1+z$; (#6) $-1+x, 1+y, -1+z$; (#7) $x, y, 1+z$; (#8) $-0.5+x, y, 0.5-z$; #9 $0.5+x, y, 0.5-z$; (#10) $0.5+x, y, 1.5-z$; (#11) $0.5-x, 1-y, 0.5+z$; (#12) $1-x, -y, -z$; (#13) $-1+x, -y, -z$; (#14) $1-x, -1-y, 1-z$; (#15) $2-x, -1-y, 1-z$; (#16) $-0.5+x, y, 1.5-z$.

(**2b**)}·$6H_2O$: yield: 45.3%. *Anal*. Calc. for $C_{56}H_{80}N_8O_{24}Cu_4$: C, 44.74; H, 5.36; N, 7.45, Cu, 16.91. Found: C, 45.83; H, 5.28; N, 7.63, Cu, 16.86%. $[Cu_2L(H_2O)_2]$-$2(SO_4H)\cdot 2H_2O$ (**3**): yield: 54%. *Anal*. Calc. for $C_{24}H_{36}N_4O_{16}Cu_2S_2$: C, 34.82; H, 4.38; N, 6.77, S, 7.75; Cu, 15.35. Found: C, 33.89; H, 4.28; N, 6.96, S, 7.96; Cu, 15.60%. The protonation of the sulfate anions is obviously due to the deprotonation of the phenolic groups during the complex formation reaction.

2.3. X-ray structure determination

Crystals of $[Cu_2LCl_2]\cdot 2H_2O$ (**1**); {$[Cu_2L(acetate)_2(H_2O)_2]$ $[Cu_2L(\mu_2\text{-acetate})]$}$(acetate)\cdot 6H_2O$ (**2a**,**2b**) and $[Cu_2L(H_2O)_2](SO_4H)_2\cdot 2H_2O$ (**3**) were glued with epoxy-resin on the tip of a capillary glass, and then mounted on a SMART-APEX Bruker diffraction system. Preliminary X-ray examination of the samples showed poor crystal quality, but cell determination was possible. A complete data set was measured for each compound [14], using 10 s by frame and 0.3° rotation between them. Reciprocal space exploration using RLATT [15] showed a main crystal plus secondary components for the complete series. The main component data was isolated and data reduction (SAINTPLUS [16]) and structure solution and refinement (SHELXTL [17]) was performed. Empirical absorption corrections were applied using SADABS [18]. Structures **2** and **3** present one of the amine-alcohol oxygen atoms disordered in two half-occupied positions (O13x and O13y in **2**, O12X and O12Y in **3**). Besides, in compound **2** there are a number of interstitial water molecules occupying depleted sites and whose occupations were refined and held constant in the last stages of refinement. Complex **3**, in turn presents a counterion with a severe rotational disorder. This was modelled using three partially occupied SO_4H moieties rotated around the sulphur centre and adding up to one complete sulphate unit.

In all cases hydrogen atoms attached to carbon were located at idealised positions. Some efforts were made in order to adequately find the position of those H atoms relevant for the H-bonding description. As a result, all those in structure **1** as well as a few (those pertaining to aqua molecules) in **2** and **3** could be trustfully inferred from a combined analysis of the Difference Fourier and the environment of potential acceptors for H-bonding. The resulting atoms were refined with metric restraints (O–H, 0.85(1) Å; H...H, 1.40(2) Å) and a riding isotropic displacement parameter. The remaining OHs could not be confidentially located and were accordingly disregarded from the model. Integrated information for all three

Table 3
H-bonding interactions and short contacts ascribable to H-bonding (O...O < 3.1 Å)

Compound	D	H	A	D–H (Å)	H...A (Å)	D...A (Å)	∠(DHA) (°)
1	O12	H12	Cl1#4	0.85(6)	2.20(6)	3.042(7)	170(8)
	O1W	H1Wa	Cl1#5	0.84(6)	2.34(6)	3.082(9)	146(8)
	O1W	H1Wb	O12#6	0.84(6)	2.51(6)	3.220(14)	142(11)
2	O1W	H1Wa	O2W	0.85(6)	2.35(6)	3.087(14)	144(6)
	O1W	H1Wb	O3a#3	0.85(6)	1.94(6)	2.643(10)	139(8)
	O2a		O12a			2.64	
	O12b		O2c#7			2.68	
	O13x		O3c#8			2.49	
	O2W		O12a#9			2.87	
	O2W		O6W			3.02	
	O2W		O7W			3.03	
	O3W		O3b#10			2.84	
	O3W		O12b			2.80	
	O4W		O3a			2.75	
	O4W		O5W#3			2.87	
	O4W		O6W#11			2.52	
	O4W		O7W#3			2.85	
	O5W		O2b#10			2.80	
	O5W		O13y			2.77	
	O7W		O13x			2.82	
	O7W		O2c			2.77	
	O8W		O12a#9			3.01	
3[a]	O1W	H1Wa	O2b	0.85(5)	2.06(5)	2.744(4)	137(4)
	O1W	H1Wb	O2W	0.85(4)	2.19(4)	2.865(8)	136(4)
	O12x		O2W#12			2.78	
	O12x		(SO_4)#12			(2.6–2.8)	
	O12y		O2W#13			3.00	
	O12y		(SO_4)#13			(2.7–2.8)	

See Table 2 for symmetry codes and Figs. 1–3 for atoms labelling.
[a] O...O contacts involving the disordered SO_4 groups reported as a range.

Table 4
π...π contacts

Compound	Group 1	Group 2	ipa (°)	ipd (Å)	ccd (Å)	sa (°)
1	C1 → C6	[C1 → C6]#14	0	3.47(1)	3.75(1)	22.3(1)
	C1 → C6	[C1 → C6]#15	0	3.43(1)	4.10(1)	33.2(1)
2	C1a → C6a	C1b → C6b	4.5(1)		3.68(1)	20(2)
	C1a → C6a	[C1b → C6b]#16	9.6(1)		4.37(1)	39(2)
3	C1 → C6	[C1 → C6]#15	0	3.55(1)	4.03(1)	28.3(1)
	C1 → C6	[C1 → C6]#14	0	3.39(1)	3.82(1)	27.5(1)

See Table 2 for symmetry codes and Figs. 1–3 for atoms labelling.
Column coding: ipa, interplanar angle; ipd, interplanar distance; ccd, centre-to-centre distance; sa, slippage angle [31].

structures (**1**–**3**), are presented in Table 1 (data collection, crystallographic and refinement details), Table 2 (selected bond length and angles), Table 3 (hydrogen bonds and short O...O contacts) and Table 4 (π...π interactions).

3. Results and discussion

3.1. Description of structures

3.1.1. $[Cu_2LCl_2]\cdot 2H_2O$ (**1**)

Fig. 1 presents a molecular drawing with the atom numbering for **1**, selected bond distances and angles are given in Table 2. The molecular structure corresponds to a binuclear copper(II) species with a Cu_2O_2 plane, which presents an inversion centre. Each copper atom shows a square pyramidal geometry, where the basal plane is formed by two nitrogen atoms from the macrocyclic ligand and two oxygen atoms, which are shared by both metallic atoms (Cu1–N1, 1.965(6) Å; Cu1–N2#1, 1.957(5) Å; Cu1–O1, 1.959(4) Å; Cu1–O1#1, 1.976(4) Å). The best mean plane through these atoms presents a maximum deviation of 0.040(1) Å for O1#1. The axial chloride ligand is 2.529(2) Å from this mean plane, and the copper(II) atom is shifted in the same direction in 0.22 (1) Å.

The macrocyclic ligand is made up of two parallel, almost planar halves, respectively, defined by O1, O12, N1, N2, C1–C9 and their corresponding centrosymmetric counterparts. These two groups are planar within a mean deviation of 0.03 and a maximum departure of 0.095(1) Å for O1 (O1#1), and displaced 0.66(1) Å from one another. The non-planar part is to be found in the C10–C12 group, with C1 1 presenting the most significant deviation, 0.29 (1) Å. The two centrosymmetric chloride atoms lay at 2.33(1) Å from their respective planes, while each copper(II) atom is shifted by 0.11(1) Å.

The fact that all those hydrogen atoms intervening in H-bonding could be located allowed a neat description of the H-bonding scheme. The main interactions are presented in Table 3: the one defined by the alcoholic hydrogen (H12) defines chains of (H-bonded) dimers running along the crystallographic *a*-axis, while those mediated by the hydration water ones H1Wa and H1Wb join these chains into 2D structures parallel to (0 1 0). Finally, the protruding phenyl groups in the L ligands fit into the open spaces left in neighbouring arrays, in such a way as to have the aromatic rings (forced by symmetry to be strictly parallel to each other) at a π–π interacting distances from one another. The details are presented in Table 4.

3.1.2. $\{[Cu_2L(acetate)_2(H_2O)_2]$ (**2a**) $[Cu_2L(\mu_2\text{-acetate})](acetate)$ (**2b**)$\}\cdot 6H_2O$

The crystalline structure of the acetate macrocyclic complex consists of two molecular forms, **2a** and **2b**. One of the complex molecules **2a** corresponds to a planar species with a Cu_2O_2 plane which presents an inversion centre (Fig. 2a), similar to the one observed for **1**. The geometry around each copper(II) centre can be described as highly distorted octahedral. The basal plane is similar to the one described for **1**, with copper–nitrogen and copper–oxygen distances being Cu1a–N2a#3, 1.975(4) Å; Cu1a–N1a, 1.974(4) Å Cu1a–O1a#3, 1.967(4) Å; Cu1a–O1a, 1.982(4) Å. The axial ligands are a water molecule (Cu1a–O1W, 2.377(6) Å) and a monodentate acetate ion (Cu1a–O2a, 2.623(6) Å), coordinated to each metal centre in a *trans* arrangement relative to the basal plane and subtending a O1W–Cu1a–O2a angle of 170.8(2)°. The fact that the acetate oxygen atom lays at a semi-coordinating distance from the metal centre allows an

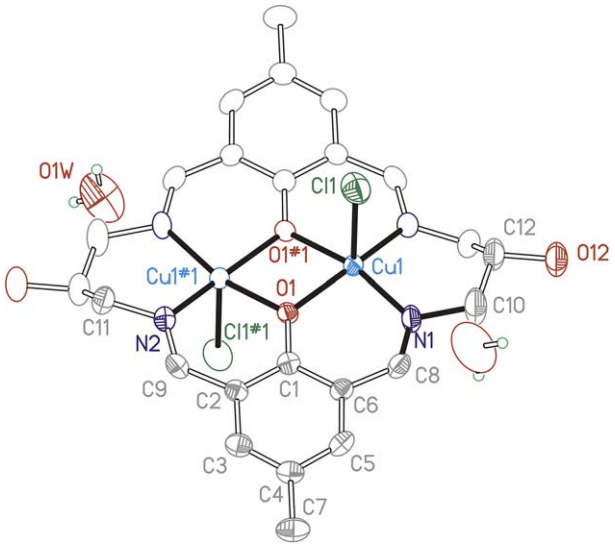

Fig. 1. Molecular diagram of **1**, with the independent and symmetry related parts, respectively, drawn as full and open displacement ellipsoids (40% probability level). In full solid bonds the copper coordination polyhedra. For symmetry codes, see Table 2 footnote.

alternative description of the environment around copper as being square-base pyramidal, with the aqua ligand occupying the apex.

As in the case of **1**, the macrocyclic ligand is composed of two planar sheets defined by O1a, N1a, N2a, C1a > C9a (and their centrosymmetric counterparts) parallel to each other at 0.30 Å from each other. Deviations from planarity of the individual halves are smaller than those found in **1** (with a maximum of 0.047 Å for O1a and a mean of 0.017 Å) as it is the shift between both planar moieties. The copper centres are "sandwiched" by these sheets, an lay at from 0.117(1) Å the nearest one.

The OH groups of the amine fragments of the planar macrocyclic complex **2** are axial and rest in a *trans* position with respect to the plane of the ligand. However, for complex **1** these same atoms are equatorial. A different ordering was reported from X-ray data by Tandon et al. [19], where a 4:1 equatorial to axial position of the hydroxo group of the diaminopropanol fragment of the macrocycle is mentioned.

The second binuclear copper(II) complex molecule **2b** (Fig. 2b) presents a folded macrocyclic ligand with a butterfly distortion [20]. Table 2 presents selected bond distances and angles. The acetate ligand bridges the copper(II) centres in a *syn–syn* mode, with two almost identical copper oxygen distances (Cu1b–O2b, 2.225(5) Å and Cu2b–O3b, 2.223(5) Å). This axial distance and the metal ligand atom distances are slightly shorter for the folded binuclear complex molecule, as compared to the planar one. A second acetate acts as counterion and balances

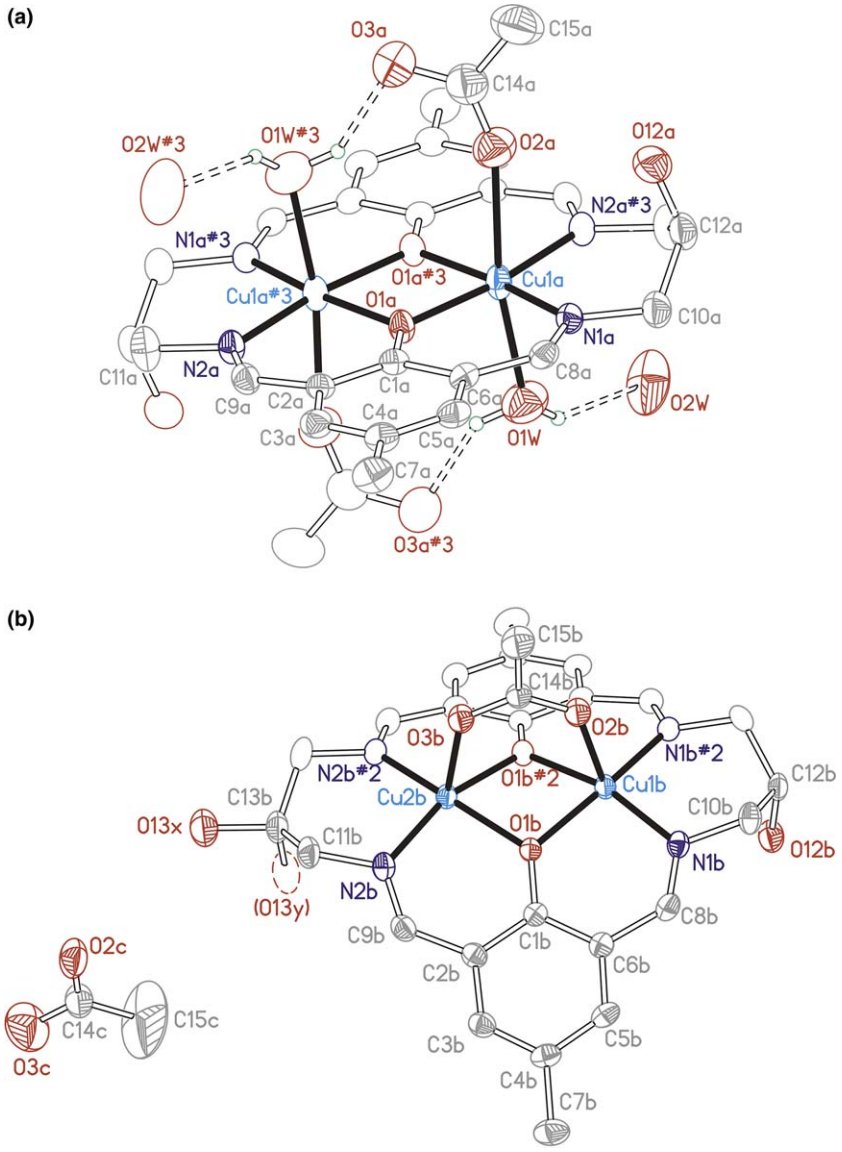

Fig. 2. Molecular diagram of **2**, with the independent and symmetry related parts, respectively, drawn as full and open displacement ellipsoids (40% probability level). In full solid bonds the copper coordination polyhedra. Disordered hydration water molecules not drawn, for clarity. For symmetry codes see Table 2 footnote. (a) Moiety **2a** $[Cu_2L(ac)_2(H_2O)_2]$: note the intramolecular H-bond connecting the aqua and the acetate groups. (b) Moiety **2b** $[Cu_2L(\mu_2\text{-ac})](ac)$: both positions for the split amine-alcohol oxygen shown, one of them in broken lines.

the charge of the complex species. The bond distances of copper oxygen and copper nitrogen atoms from the first coordination sphere are Cu1b–O1b, 1.963(3) Å and Cu1b–N1b, 1.961(4) Å.

The molecule possesses a crystallographic mirror plane containing the two copper atoms, the bridging acetate skeleton and the hydroxo groups of the diamine fragment of the macrocyclic ligand. This plane bisects the macrocycle, whose two planar halves (O1b, N1b, N2b, C1b > C9b, maximum deviation of 0.128(1) Å for O1b with a mean of 0.043(1) Å) are now far from parallel but define a dihedral angle of 46.9(1)°. Due to the intrinsic symmetry of the macrocycle, the molecule presents a non-crystallographic mirror plane, orthogonal to the former, which bisects the group along C7b, C4b, C1b, C14b, C15b, C7ba, C4ba, C1ba.

The crystal lattice presents six water molecules per molecule, disordered over several positions. The two unrelated dinuclear units organise as independent sets of columns, those containing Cu1a running along the *a*-axis, the remaining ones along *c*. These non-intersecting linear arrays define some kind of a 3D fabric, where the interleaving voids are filled by the free acetate anions as well as the disordered water molecules which act as connectors, via H bonding to the Os, OHs and water molecules in the columns. The existence of a large quantity of potentially good donors and acceptors for this type of interaction ensures a complex H-bonding scheme. Unfortunately, an accurate description of the H-bonding network was rendered impossible because of low data quality, which prevented finding many of the hydrogen atoms involved. An exception to this was the case of the aqua hydrogens, in particular H1Wb, the one making a strong intermolecular H-bond to the free O3c of the semi-coordinated acetate (Fig. 2b). The columns crossover is accomplished in such a way as to have the benzyl groups from the orthogonal, non-intersecting columns almost aligned along the *a* direction, with interplanar angles, centre to centre distances and slippage angles in the range 4–11°, 3.68(1)–4.37(1) Å and 20–40°, respectively. (For details see Table 4.) Thus the structure appears as stabilised by a large and varied quantity of non-bonding interactions.

3.1.3. $[Cu_2L(H_2O)_2](SO_4H)_2 \cdot 2H_2O$ (3)

Fig. 3 presents the molecular structure and atom numbering scheme for **3** and Table 2 presents selected bond distances and angles. For complex **3** the first coordination sphere of the copper atoms is square-base pyramidal, with the basal plane defined by the macrocycle (Cu1–N1, 1.960(5) Å; Cu1–N2#1, 1.935(5) Å; Cu1–O1, 1.961(4) Å; Cu1–O1#1, 1.959(3) Å) and the fifth position corresponding to the axial water ligand. This copper oxygen distance is 2.271(5) Å, being the shortest axial distance in the series of reported complexes. The least-square plane in the macrocyclic ligand is defined by N1–N2–O6–C1–C2–C3–C4–C5–C6–C7–C8–C9–C10 and the mean deviation of the atoms from this plane is 0.032 Å.

The crystalline structure presents isolated SO_4H counteranions, showing highly disordered oxygen atoms. These SO_4H groups form a chain along the *a*-axis. The existence of hydrogen bonds and van der Waals interactions, suggested by close contacts, stabilises the packing of the diaminopropanol fragment via hydrogen bonds.

Although the binuclear macrocyclic complex was prepared by the template reaction of 4-methyl-2,6-diformylphenol with 1,3-diamine-2-propanol in the presence of cupric sulphate, the counterions resulted to be two SO_4H species. The presence of two monovalent anions is evident by the experimental value of the percentage of the sulphur found for the complex, and X-ray diffraction data.

Again here the lack of precise information on some hydrogens, in addition to the severe disordered SO_4H counterions, turned the H-bonding description a rather speculative task, mainly based on the otherwise unexplainable short O...O contacts. Thus the counterion seems to serve as a double H-bonding bridge between neighbouring units, by accepting both an aqua (H1wa) and a diaminopropanol hydrogen. These interactions lead to the formation of H-bonded chains running along the *c*-axis, which present the benzyl group outwards, ready for a π–π interaction. This is achieved by the partial overlap of neighbouring chains when stacking along *a*. The resulting interaction is very similar to the ones already described (Table 4).

4. Spectral data

4.1. Infrared spectra

Selected IR data are presented in Table 5. All complexes show the same spectral pattern and the main differences

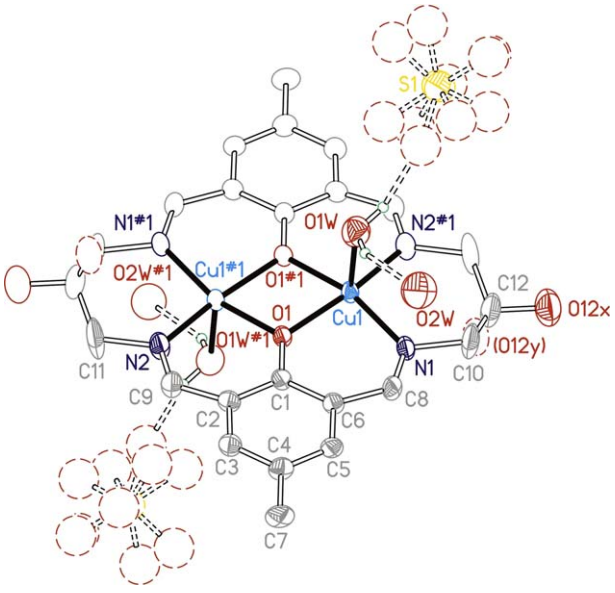

Fig. 3. Molecular diagram of **3**, with the independent and symmetry related parts, respectively, drawn as full and open displacement ellipsoids (40% probability level). In full solid bonds the copper coordination polyhedra. The disordered SO_4H counterions drawn as broken ellipsoids. Both depleted positions for the amine-alcohol oxygen shown, one of them in broken lines. For symmetry codes, see Table 2 footnote.

arise from absorptions due to the counteranions. Complex {**2a**,**2b**} shows stretching bands for the acetate ions at 1566 and 1408 cm^{-1}, corresponding to the asymmetric and symmetric absorptions of the carboxylate group, respectively. This allows to infer that the group is in its ionic form and also bridging the two metal atoms [21], in accordance to the structural data. Complex **3**, shows bands at 1113, 847 and 618 cm^{-1}; indicating the presence of the SO_4H species [21,22].

The complexes show the $\nu_{(C=N)}$ stretching bands in the range 1636–1639 cm^{-1} [23], and the $\nu_{C=C/C=N}$ ones between 1547 and 1568 cm^{-1}. The metal–ligand vibration zone shows three bands in all cases, one at 400 cm^{-1} assignable to the Cu–O stretching, and the remaining two at 350 and 370 cm^{-1} to the symmetric and asymmetric Cu–N vibrations [21].

4.2. Electronic spectra

All three reflectance spectra show a similar pattern, with strong electronic absorptions at 270, 390 and 420 nm attributed to the π–π^* ligand transitions [23]. The bands found at 352–363 nm are attributable to the phenolate-to-copper(II) charge-transfer band [2,5,24]. Much weaker, less defined absorption bands are found at lower energy (610–667 nm) associated to a d–d transitions [19].

Solution electronic spectra were recorded in methanol, and a similar pattern as for the reflectance spectra was obtained. All three copper(II) complexes show a very weak d–d transition band between 610–670 nm, indicative of a square pyramidal geometry [25–27]. Thus, it is possible to infer that the observed geometry of the binuclear copper(II) complexes in the solid state is maintained in solution.

5. Magnetic studies

Magnetic susceptibility measurements at variable temperature were performed for complexes **1**–**3**, in the temperature range 2–300 K. For compounds **1** and **3** measurements at different fields were also recorded. The results are summarised in Table 6, and presented as χ_M versus T plots in Figs. 4a and b (complexes **1** and **2**) and as χ'_M versus T plot in Fig. 4c (complex **3**). χ'_M corresponds to the molar magnetic susceptibility corrected by TIP.

The variable temperature–magnetic susceptibility data at 10 kOe for complex **1** were fitted with the Bleaney–Bowers equation, using the isotropic exchange Hamiltonian ($H = -2JS_1 \cdot S_2$) for the two interacting $S = 1/2$ centres [28]:

$$\chi_M(J,g,\rho,\theta) = \frac{2Ng^2\beta^2}{k(T-\theta)(3+e^{-2J/kT})}(1-\rho) + \frac{Ng^2\beta^2\rho}{4KT} + \mathrm{TIP} \quad (1)$$

where ρ is the fraction of paramagnetic impurity and θ corresponds to interdimer interactions.

The best fit to Eq. (1) gave $g = 2.175$, $2J = -1015$ cm^{-1}, $\rho = 0.025$, and $\theta = -5.0$ K ($10^3R = 5.9$). R is defined as $R = \left[\sum(\chi_{obs}-\chi_{calc})^2/\sum\chi^2_{obs}\right]^{1/2}$. A TIP value of 6×10^{-4} emu mol^{-1} was used. Complex **1** presents a stronger antiferromagnetic behaviour as compared to the analogue $[Cu_2(UPM)Cl_2]\cdot 6H_2O$ ($2J = -722$ cm^{-1}), where $UPMH_2$ is the macrocyclic ligand formed by the condensation of 4-methyl-2,6-diformylphenol with 1,3-diaminepropane [29]. This ligand lacks the secondary alcohol group present in LH_2, and the reported complex presents slightly different

Table 5
Infrared vibrations for the copper(II) macrocyclic complexes (wavenumber in cm^{-1})

Complex	$\nu_{C=N}$	$\nu_{C=C/C=N}$	ν_{C-O} phenolic	ν_{C-H} aliphatic	δ_{C-H} iminic	δ chelate ring	ν_{Cu-N}	ν_{Cu-O}
1	1636 (s)	1568 (s)	1241 (m)	1436 (s)	821 (m)	500 (w)	376–356 (w)	465 (w)
2	1637 (s)	1566 (s)	1241 (m)	1437 (s)	822 (m)	500 (w)	378–351 (w)	478 (w)
3	1639 (s)	1547 (s)	[a]	1437 (s)	821 (m)	512 (w)	377–354 (w)	447 (w)

s, strong; m, medium; w, weak.
[a] The ν_{C-O} band is overlapped by the SO_4H ion absorptions.

Table 6
Comparative crystallographic and magnetic data for the binuclear copper(II) macrocyclic complexes

Compound	Axial ligand	Cu–Cu distance	Axial distance	Cu–O–Cu angle	Deviation of Cu[a]	$-2J$
$[Cu_2LCl_2]\cdot 2H_2O$	Cl	3.088	2.529	103.37	0.223	1015
$[Cu_2L(\mu\text{-}CH_3COO)]CH_3COO$	O^1	3.026	2.224 2.225	100.46		306
$[Cu_2L(CH_3COO)_2(H_2O)_2]$	O^2 O^3	3.087	2.624 2.376	102.86	0.109	921
$[Cu_2L(H_2O)_2]\cdot 2SO_4H\cdot 2H_2O$	O^3	3.091	2.271	104.08	0.042	
$[Cu_2L(H_2O)_2(NO_3)_2]$	O^4 O^3	3.097	2.586 2.429	102.05	0.033	631

Distance in Å, $2J$ in cm^{-1}.
[a] From ligand atoms plane N_2O_2 basal plane.

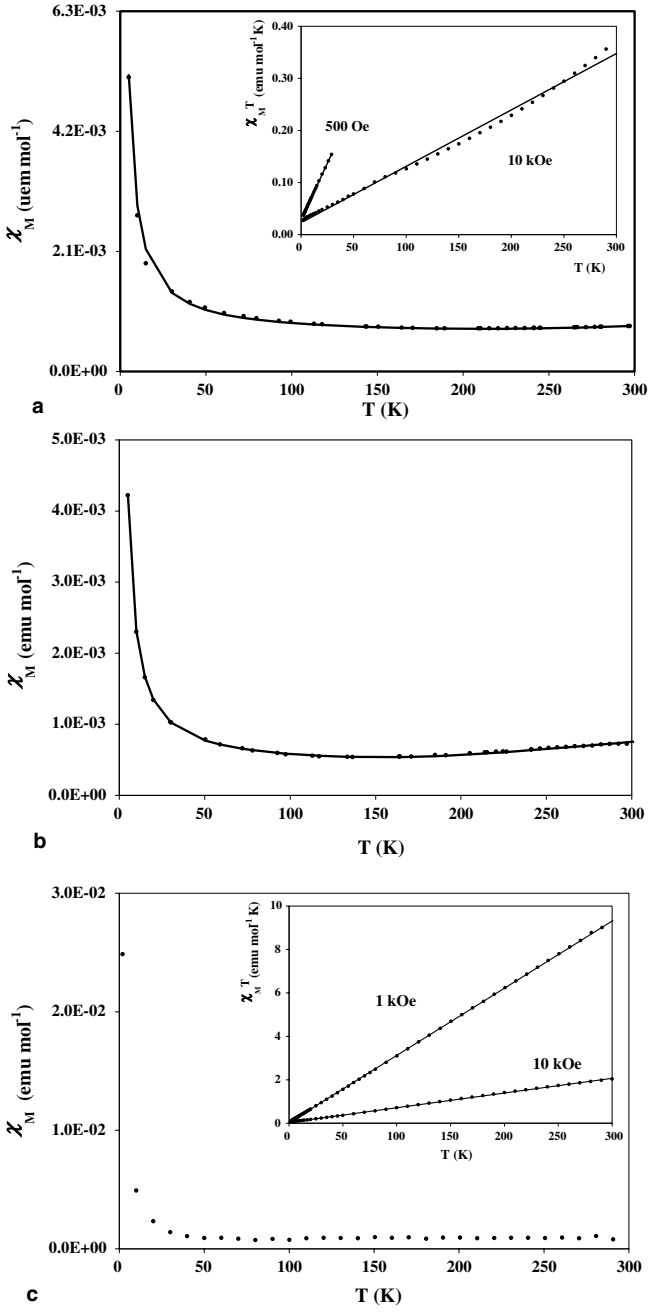

Fig. 4. Plots of χ_M vs. temperature for: (a) **1**; (b) **2a** and **2b**; (c) **3**. In (a) the solid line was calculated from Eq. (1), and in (b) the solid line was calculated from Eq. (2). In (c) $\chi'_M = (\chi_M - \text{TIP})$. Inset in (a) and (c) show a plot of $\chi_M \cdot T$ vs. T at different fields.

geometrical parameters: a copper–copper separation of 3.133 Å and a phenoxo bridge of 104.5°, as compared to 3.088 Å (Cu–Cu) and 103.34° (Cu–O–Cu) for **1**.

The magnetic data at 10 kOe for complex {**2a**,**2b**} was fitted with a modified Bleaney–Bowers equation, assuming that each binuclear macrocyclic copper(II) complex is characterised by a particular magnetic exchange constant, related to their different connectivities and distortions of the first coordination sphere. A TIP value of 3.8×10^{-4} emu mol^{-1} was considered for the fit of the data.

$$\chi^T_{MCu} = (\chi^1_M + \chi^2_M)(1-\rho) + \frac{N(g_1+g_2)^2\beta^2\rho}{4KT} + \text{TIP} \qquad (2)$$

For complex {**2a**,**2b**} the best fit to Eq. (2) gave $g_1 = 2.20$, $g_2 = 2.22$, $2J_1 = -306\ \text{cm}^{-1}$, $2J_2 = -921\ \text{cm}^{-1}$, $\rho = 0.021$, and $\theta = -15$ K ($10^2R = 1.2$).

Dihydroxo bridged dimers with butterfly distortions have been shown to present lower $2J$ parameters, than the completely planar systems [13]. In the reported dinuclear complexes the distortion occurs through the axis along both hydroxo oxygen atoms. This distortion produces a decrease in the overlap of the $d_{x^2-y^2}$ magnetic orbitals of the copper centres with the corresponding orbitals of the bridging phenoxo oxygen atoms, thus decreasing the antiferromagnetic interaction. This phenomenon has been explained theoretically by Kahn et al. [9]. In complex **2b** the distortion is induced by the μ-acetate coordination, along the axis through the copper centres. Therefore the intramolecular magnetic coupling in the non-planar $Cu_2O_{2(phenoxo)}$ system of complex **2b** should be described by the lower $2J$ value of $-306\ \text{cm}^{-1}$ and that of **2a** by the $2J$ value of $-921\ \text{cm}^{-1}$. The obtained parameters for **1** and **2a** are indicative of a strong antiferromagnetic coupling between the metal ions, which is commonly observed for this type of phenoxo bridged dicopper(II) complexes [5].

Complex **3** presents a high value for the measured susceptibility at 300 K. The inset of Fig. 4c shows the magnetic behaviour of this compound, which is assumed to correspond to temperature independent paramagnetism (TIP). The observed effect can not be attributed to paramagnetic impurities, since in such case the effect would have shown a behaviour independent of the applied field. However the observed phenomenon is shown to be dependent upon the magnitude of the applied field. The obtained TIP value from the $\chi_M T$ versus T plot is 308×10^{-4} emu mol^{-1} (1 kOe) and 68×10^{-4} emu mol^{-1} (10 kOe). From the corrected experimental susceptibility data, effective magnetic moments lower than the expected value for one unpaired electron (1.73 BM) per metal centre were obtained. It is important to remark that the Bleaney–Bowers equation was not used to fit the corrected susceptibility data for complex **3**, since this equation can fit the experimental data with different values for $2J$ and ρ parameters for extremely antiferromagnetic systems such as **3**.

Even though complex **3** and the reported $[Cu_2L(H_2O)_2](NO_3)_2$ [30] have similar pentacoordinated metal centres, with water molecules as axial ligands, the first is strongly antiferromagnetic with temperature independent paramagnetism, while the second has a pure intramolecular antiferromagnetic phenomenon with $2J = -631\ \text{cm}^{-1}$. The obtained magnetic data for **3**, together with aforementioned $2J$ value reported for the nitrate macrocyclic complex [30], clearly indicate that the lattice effects can play an important role on the magnitude of the magnetic exchange phenomenon.

A previous study of a family of compounds [29] with macrocyclic copper(II) complexes, derived from the

condensation of 4-methyl-2,6-diformylphenol with 1,3-diaminepropane and with different halogen axial ligands (Cl, Br, I) reports a trend of the intramolecular magnetic coupling with the nature of the coordinated halogen. Since the bulk geometry of the macrocycle is dependent on the nature of the halogen, it is not possible to infer that just the electronegativity of the axial ligand is responsible for the different magnetic behaviour. On the other hand, Tandon et al. [19] have also reported a rather high TIP value for a similar complex $[Cu_2L]$ with $Cu_2Cl_4^{2-}$ as counteranion.

We show in the present work that the nature of the counterion can play different roles, i.e., affecting the overall geometry of the macrocycle and acting, in some cases, as axial ligands. A dramatic example is observed in the acetate complex **2b** where the macrocycle is folded due to the presence of a bridging acetate anion. Therefore it is interesting to point out that the electronic and packing effects associated with the different anions can affect the bulk magnetic properties of the macrocyclic dinuclear copper(II) complexes.

6. Conclusions

While all the reported complexes can be described as pentacoordinated species with a square pyramidal geometry; the coordinated axial ligand depends on the nature of the counteranion of the used copper salt. The monodentate binding mode of the axial ligand generates planar macrocyclic complexes, while the *syn–syn* bridging mode of the acetate anion permits the formation of a folded macrocyclic moiety.

All the crystalline structures show the existence of a lattice with a great number of non-bonding interactions, such as hydrogen bonding and π–π stacking. All these interactions are due exclusively to the macrocyclic ligands, the solvate molecules and the different counteranions and not to the crystallisation conditions.

In the case of the planar species, the strongest antiferromagnetic exchange was observed for complex **3**, where the bisulphate anion is outside the first coordination sphere. The participation of the counteranion as axial ligand (compounds **1**, **2a**) produces a decrease in the antiferromagnetic exchange due to electronic interactions. Finally, dramatic distortions of the macrocycle are observed for compound **2b**, where the acetate anion is bridging the two metal centres and therefore the smallest $2J$ value is associated with this structure.

The reported binuclear complexes permit to asses that the existence of different bonding interactions of the anions, as those observed in the obtained crystalline structures, influence the bulk magnetic properties of the solid samples. Therefore counteranions should be considered relevant parameters for modulating magnetic properties.

Acknowledgements

Authors thank financial support from FONDAP (Grant 11980002) and ECOS-CONICYT (Grant C02E01). Fundación Andes is acknowledged for partially financing the purchase of the SMART-APEX Bruker diffraction system. We thank Prof. Jaime Llanos from Universidad Católica del Norte, Chile for recording the reflectance spectra. Authors thank Professors Joan Ribas and Dr. M. Salah El Fallah from Universitat de Barcelona, Spain, for important discussions and for magnetic measurements.

Appendix A. Supplementary data

Crystallographic data for **1**–**3** in the CIF format have been deposited with the Cambridge Crystallographic Data Centre, CCDC, 12 Union Road, Cambridge CB2 1EZ, UK. On request quote numbers 286700, 286701 and 286702. We provide comments for the structural refinement process. Packing of complexes **1**–**3** together with overlapping diagram of **2b** are available. Supplementary data associated with this article can be found, in the online version, at doi:10.1016/j.poly.2006.01.008.

References

[1] V. Fusi, A. Llobet, J. Mahia, M. Micheloni, P. Paoli, X. Ribas, P. Rossi, Eur. J. Inorg. Chem. 987 (2002).
[2] M. Thirumavalavan, P. Akilan, M. Kandaswamy, K. Chinnakali, G.S. Kumar, H.K. Fun, Inorg. Chem. 42 (2003) 3308.
[3] E. Ruiz, P. Alemany, S. Alvarez, J. Cano, Inorg. Chem. 36 (1997) 3683.
[4] E. Ruiz, S. Alvarez, P. Alemany, Chem. Commun. 2767 (1998).
[5] L.K. Thompson, S.K. Mandal, S.S. Tandon, J.N. Bridson, M.K. Park, Inorg. Chem 35 (1996) 3117.
[6] A.S. Borovik, Comm. Inorg. Chem. 23 (2002) 45.
[7] D. Braga, J. Chem. Soc., Dalton Trans. (2000) 3705.
[8] R. Robson, J. Chem. Soc., Dalton Trans. (2000) 3735.
[9] M.F. Charlot, O. Kahn, S. Jeannin, Y. Jeannin, Inorg. Chem. 19 (1980) 1410.
[10] H. Okawa, H. Furutachi, D.E. Fenton, Coord. Chem. Rev. 174 (1998) 51.
[11] E. Berti, A. Caneschi, C. Daiguebonne, P. Dapporto, M. Formica, V. Fusi, L. Giorgi, A. Gerri, M. Micheloni, P. Paoli, R. Pontellini, P. Rossi, Inorg. Chem. 42 (2003) 348.
[12] H. Grover, T.L. Kelly, L.K. Thompson, L. Zhao, Z. Xu, T.S.M. Abedin, D.O. Muller, A.E. Goeta, C. Wilson, J.A.K. Howard, Inorg. Chem. 43 (2004) 4278.
[13] S. Youngme, G.A. van Albada, O. Roubeau, Ch. Pakawatchai, N. Chaichit, J. Reedijk, Inorg. Chim. Acta 342 (2003) 48.
[14] SMART NT V5.625 Bruker AXS Inc., Madison, WI, USA.
[15] RLATT V3.0 Bruker AXS Inc. Madison, WI, USA.
[16] SAINTPLUS V6.22 Bruker AXS Inc., Madison, WI, USA.
[17] G.M. Sheldrick, SHELXTL NT/2000 Version 6.10., Bruker AXS Inc., Madison, WI, USA, 2000.
[18] SADABS V2.05 Bruker AXS Inc. Madison, WI, USA.
[19] S.S. Tandon, L.K. Thompson, J.N. Bridson, V. McKee, A. Downars, J. Inorg. Chem. 31 (1992) 4635.
[20] B. Dutta, P. Bag, U. Flörke, K. Nag, Inorg. Chem. 44 (2005) 147.
[21] K. Nakamoto, Infrared and Raman spectra of inorganic and Coordination Compounds, John Wiley & Sons, New York, USA, 1986.
[22] G. Socrates, Infrared Characteristic Groups frequencies, John Wiley & Sons, Great Britain, 1980.
[23] A. Aguiari, E. Bullita, U. Casellato, P. Guerriero, P.A. Vigato, Inorg. Chim. Acta 202 (1992) 157.

[24] B. Dutta, P. Bag, B. Adhikary, U. Flörke, K. Nag, J. Org. Chem. 69 (2004) 5419.
[25] R. Kannappan, R. Mahalakshmy, T.M. Rajendiran, R. Venkatesan, S. Rao, Proc. Indian Acad. Sci. (Chem. Sci.). 115 (2003) 1.
[26] S. Korupoju, N. Mangayarkarasi, S. Ameerunisha, E. Valente, P. Zacharias, J. Chem. Soc., Dalton Trans. (2000) 2845.
[27] C.R.K. Rao, P.S. Zacharias, Polyhedron 16 (1997) 1209.
[28] O. Kahn, Molecular Magnetism, Wiley-VCH Inc., USA, 1993.
[29] S.K. Mandal, L.K. Thompson, M.J. Newlands, E.J. Gabe, K. Nag, Inorg. Chem. 29 (1990) 1324.
[30] E. Spodine, Y. Moreno, M.T. Garland, O. Pena, R. Baggio, Inorg. Chim. Acta 309 (2000) 57.
[31] C. Janiak, J. Chem. Soc. Dalton Trans. (2000) 3885.

uranium(III) trichlorides. Adjusting of water concentration enabled precipitation of three different compounds with formulas: $UCl_3 \cdot 2H_2O \cdot 2CH_3CN$, $UCl_3 \cdot 6H_2O$ and $UCl_3 \cdot 7H_2O$. The synthesis of these compounds is described and their crystal structures have been determined by single crystal X-ray measurements. The structures of hydrated uranium trichlorides are discussed and compared with analogues lanthanide compounds. We have not been able to prove the existence of $UCl_3 \cdot 5H_2O \cdot CH_3CN$ compound reported in Ref. [3].

Table 1
Compositions of the mother solutions used for the synthesis of the uranium trichloride hydrates

Compound	UCl_4 (g)	Methylcyanide (ml)	Propionic acid (ml)	Water (ml)
$UCl_3 \cdot 2H_2O \cdot 2CH_3CN$	1.15	25	0.47	0.25
$UCl_3 \cdot 6H_2O$	1.15	25	0.47	0.625
$3UCl_3 \cdot 7H_2O$	1.15	23	1.15	0.72

2. Experimental

2.1. Synthesis

For the synthesis of the single crystals three different solutions consisting of appropriate amounts of uranium tetrachloride, methylcyanide, propionic acid and water were prepared. The detailed compositions of the solutions are summarized in Table 1. The solutions were left standing for 24 h and afterward filtrated. Subsequently, 5 ml of the appropriate mother solution was placed together with 0.3 ml of a 2.4% liquid zinc amalgam in a glass ampoule, ~15 cm long and about 0.8 cm in diameter. The solutions were degassed by evaporation for 2–5 min in vacuum.

Table 2
Experimental data of the uranium(III) hydrates

Crystal data	$UCl_3 \cdot 2H_2O \cdot 2CH_3CN$	$UCl_3 \cdot 6H_2O$	$UCl_3 \cdot 7H_2O$
Formula weight	462.52	452.48	470.49
Crystal system	triclinic	monoclinic	triclinic
Space group	$P\bar{1}$	$P2/n$	$P\bar{1}$
a (Å)	7.153(3)	9.732(3)	7.932(2)
b (Å)	8.639(4)	6.592(3)	8.242(2)
c (Å)	10.541(4)	8.065(3)	9.220(2)
α (°)	108.85(4)		70.48(3)
β (°)	105.05(4)	93.56(3)	73.16(3)
γ (°)	93.57(4)		81.54(3)
V (Å^3)	587.6(4)	516.4(3)	542.9(2)
Z	2	2	2
μ (mm^{-1})	14.461	16.474	15.682
D_{calc} (g/cm^3)	2.614	2.910	2.878
Crystal size (mm^3)	$0.1 \times 0.13 \times 0.03$	$0.2 \times 0.2 \times 0.1$	$0.02 \times 0.04 \times 0.02$
Crystal form	needle	plate	needle
Data collection			
Diffractometer		Kuma KM4 automatic diffractometer	
Monochromator		graphite	
Radiation type		Mo Kα	
Temperature (K)		100(2)	
θ Range (°)	2.99–37.39	3.19–37.42	3.45–38.39
Index range	$-12 \leqslant h \leqslant 12$, $-14 \leqslant k \leqslant 13$, $-17 \leqslant l \leqslant 17$	$-16 \leqslant h \leqslant 11$, $-11 \leqslant k \leqslant 11$, $-13 \leqslant l \leqslant 13$	$-13 \leqslant h \leqslant 13$, $-14 \leqslant k \leqslant 13$, $-15 \leqslant l \leqslant 15$
Absorption correction	analytical from crystal shape	analytical from crystal shape	analytical from crystal shape
T_{min}/T_{max}	0.212/0.572	0.094/0.195	0.367/0.688
Number of measured reflections	11076	8074	11619
Number of independent reflections	5303	2469	5232
Number of observed reflections	4686	2318	4218
R_{int}	0.0715	0.0681	0.0455
$\Delta\rho_{min}/\Delta\rho_{max}$ (e Å^{-3})	−4.85/6.17	−4.30/2.94	−1.83/1.86
Refinement			
Refinement on	F^2	F^2	F^2
Data/restraints/parameters	5303/4/124	2469/6/71	5232/14/142
$R(F_o > 4\sigma(F_o))$	0.0385	0.0295	0.0346
R (all data)	0.0462	0.0324	0.0552
wR^2	0.0904	0.0725	0.0421
Goodness-of-fit	1.003	1.041	1.028
Weighting parameters a	0.0587	0.0446	0.006
Weighting parameters b	0	0.6385	0
$w = 1/[(\sigma^2/(F_o)^2) + (aP)^2 + bP]$		$P = (\max(F_o^2, 0) + 2F_c^2)/3$	

Table 3
Atomic coordinates and equivalent or isotropic thermal parameters (Å^2) in $UCl_3 \cdot 2H_2O \cdot 2CH_3CN$ crystal

Atom	x	y	z	U_{eq}/U_{iso}
U	0.62132(2)	0.77541(2)	0.54335(2)	0.00728(5)
Cl1	0.3606(2)	1.0048(2)	0.6163(2)	0.0096(2)
Cl2	0.7249(2)	0.7532(2)	0.8088(2)	0.0159(2)
Cl3	0.2789(2)	0.5576(1)	0.5201(2)	0.0133(2)
O1	0.4689(7)	0.6217(5)	0.2902(4)	0.0233(9)
O2	0.9508(5)	0.7714(5)	0.5070(5)	0.0166(7)
N1	0.8589(7)	1.0541(6)	0.7073(5)	0.0163(8)
C1	0.9622(7)	1.1763(6)	0.7695(5)	0.0153(8)
C2	1.0919(10)	1.3345(8)	0.8490(7)	0.0254(12)
N2	1.3583(10)	0.7013(7)	1.0489(6)	0.0280(11)
C3	1.3126(8)	0.7752(7)	0.9747(6)	0.0184(9)
C4	1.2558(9)	0.8670(8)	0.8826(6)	0.0223(10)
H1	0.436(13)	0.662(11)	0.224(7)	0.028
H2	0.421(13)	0.519(3)	0.263(10)	0.028
H3	1.040(9)	0.857(6)	0.554(8)	0.020
H4	1.012(11)	0.688(6)	0.494(9)	0.020
H2A	1.2074	1.334	0.819	0.033
H2B	1.129	1.350	0.947	0.033
H2C	1.025	1.423	0.833	0.033
H4A	1.293	0.984	0.935	0.029
H4B	1.116	0.842	0.840	0.029
H4C	1.320	0.837	0.811	0.029

Subsequently, the ampoules with the degassed solutions were sealed under nitrogen and left standing motionless for 24 h at the room temperature. The accomplished slow reduction process yields good quality crystals of two new uranium(III) compounds of the formulas $UCl_3 \cdot 2H_2O \cdot 2CH_3CN$ and $UCl_3 \cdot 6H_2O$. In the case of $UCl_3 \cdot 7H_2O$, such reduction process did not lead to the precipitation of the compound but resulted in the formation of a separate uranium(III) oily-phase, only. In order to force the crystallization of the heptahydrate, the solution has been shaken for a few minutes with liquid zinc amalgam, which resulted in the immediate formation of a very fine crystalline precipitate. The crystals obtained in this way were of poor quality, but after leaving them in the mother solution for 1–2 days, some single crystals suitable for X-ray measurements could be selected from the coarse crystalline powder.

During the reduction process the colour of the solutions changes from olive-green to dark reddish-brown. The $UCl_3 \cdot 2H_2O \cdot 2CH_3CN$, $UCl_3 \cdot 6H_2O$ and $UCl_3 \cdot 7H_2O$ compounds crystallize as deep dark reddish needles, purple plates and greyish ink blue needles, respectively. The ampoules with the precipitated crystals were opened in an

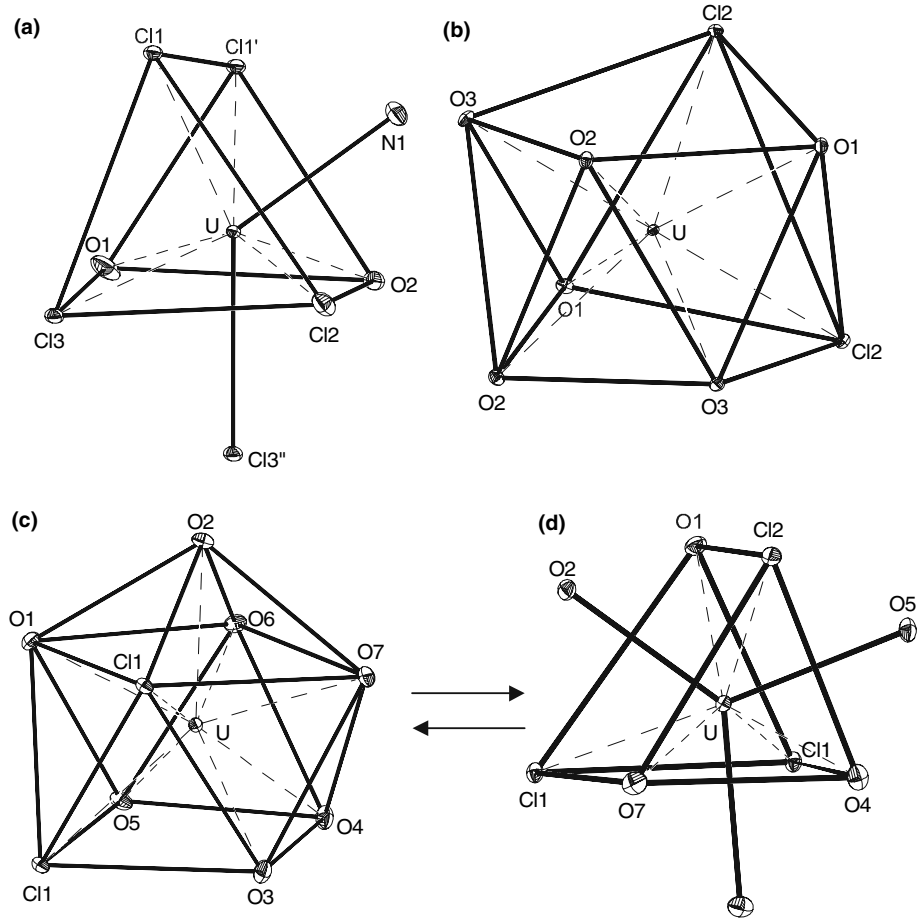

Fig. 1. The co-ordination geometry of the U^{3+} ion in $UCl_3 \cdot 2H_2O \cdot 2CH_3CN$-bicapped trigonal prism: (a) $UCl_3 \cdot 6H_2O$ – distorted square antiprism; (b) $UCl_3 \cdot 7H_2O$; (c) capped square antiprism; (d) tricapped trigonal prism.

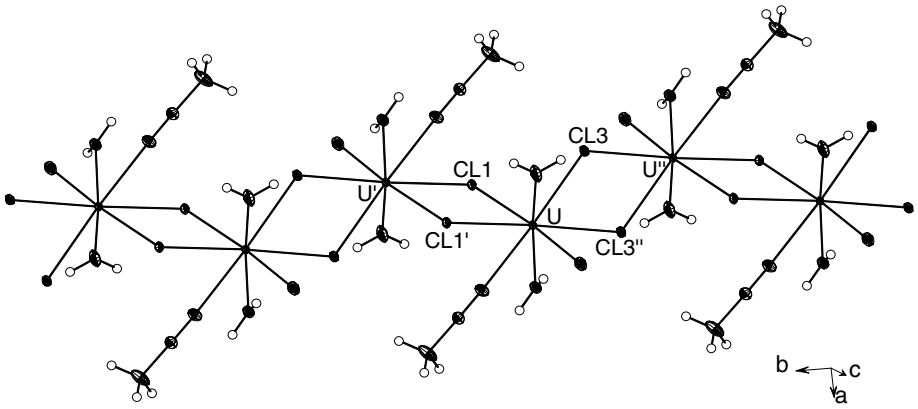

Fig. 2. The fragment of $[UCl_3 \cdot 2H_2O \cdot CH_3CN]_n$ polymeric chain viewed along [1 0 0] direction. See Table 4 for symmetry codes.

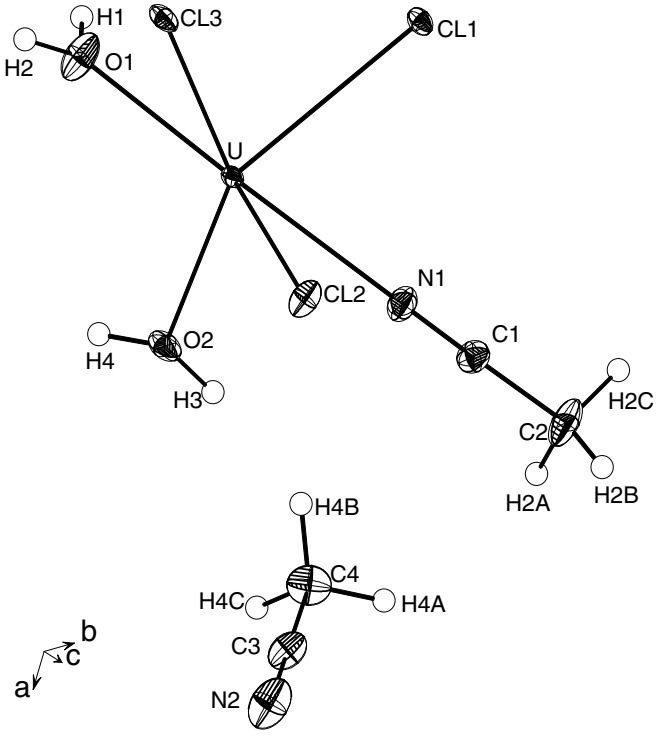

Fig. 3. The molecular structure of the asymmetric unit in the $[UCl_3 \cdot 2H_2O \cdot CH_3CN]_n \cdot [CH_3CN]_n$ polymeric chain. Displacement ellipsoids are shown at 50% probability level. The hydrogen atoms are shown as a small circle of arbitrary radii.

inert gas glove-box, drained off from the solvent and immediately immersed in a dry paraffin oil. Since uranium trichloride hydrates are moisture sensitive and they decompose very quickly in the contact with air, they were protected during X-ray measurements by a cold nitrogen gas stream.

2.2. Crystallographic experimental details

The crystallographic measurements of the uranium hydrates were performed on a Kuma KM4CCD diffractometer using graphite-monochromatized Mo Kα radiation. The data were collected at 100 K using in all cases the Cryosystem cooler. The conditions for the data collections as well as the used parameters of the structure refinements are summarized in Table 2.

The structure of the $UCl_3(H_2O)_2(CH_3CN)_2$ was solved by the heavy-atom method, using the SHELXS-97 program [12] and was refined by a full-matrix least-squares technique using the SHELXL-97 program [13] with anisotropic thermal parameters for non-H atoms.

The initial values of the co-ordinates of all non-H atoms for $UCl_3(H_2O)_6$ and $UCl_3(H_2O)_7$ were taken from the data reported for $AmCl_3(H_2O)_6$ [11] and $CeCl_3(H_2O)_7$ [14], respectively. The H-atoms were found from difference-Fourier maps and the C–H and O–H distances were constrained to 0.96 and 0.86 Å, respectively. All figures presented in the paper were prepared by using the XP program [15].

3. Results and discussion

The reduction of UCl_4 solutions in methylcyanide, with specific amounts of water and propionic acid, enabled the isolation of the three different uranium trichloride hydrates. From solutions containing 25 ml of methylcyanide, 1.15 g of UCl_4, 0.47 ml of propionic acid and 1–1.5% of water crystallizes $UCl_3 \cdot 2H_2O \cdot 2CH_3CN$. An increase of the water content to 2% results in the precipitation of a mixture of $UCl_3 \cdot 2H_2O \cdot 2CH_3CN$ and $UCl_3 \cdot 6H_2O$ crystals. Pure $UCl_3 \cdot 6H_2O$ crystals have been obtained from a solution containing 2.5% of water. An increase of the water content above this value leads to the formation of a separate uranium(III) oily-phase. The $UCl_3 \cdot 7H_2O$ crystals may be obtained from methylcyanide solution with a 2.5–5% water content, providing that the uranium tetrachloride and propionic acid concentrations have been also increased.

We have noticed differences in resistance of these hydrates against hydrolysis and oxidation processes. It was observed, that the quality of $UCl_3 \cdot 2H_2O \cdot 2CH_3CN$ as well as of $UCl_3 \cdot 6H_2O$ crystals, left in the mother solution in sealed glass ampoules filled with nitrogen, degraded

Table 4
Principal interatomic distances (Å), bond angles (°) and torsion angles (°) in the U^{3+} hydrate crystals[a]

Distance (Å)		Angle (°)			Torsion angle (°)
$UCl_3 \cdot 2H_2O \cdot 2CH_3CN$					
U–Cl1	2.867(2)	Cl1–U–Cl2	91.88(5)	Cl2–U–Cl1–U^{i}	146.99(4)
U–Cl2	2.775(2)	Cl1–U–Cl3	78.01(5)	Cl3–U–Cl1–U^{ii}	−133.90(5)
U–Cl3	2.901(2)	Cl1–U–$Cl1^{i}$	74.84(5)	$Cl3^{ii}$–U–Cl1–U^{i}	−142.06(7)
U–$Cl1^{i}$	2.932(2)	Cl1–U–$Cl3^{ii}$	150.81(3)	$Cl1^{i}$–U–Cl3–U^{ii}	123.73(5)
U–$Cl3^{ii}$	2.914(2)	Cl2–U–Cl3	79.76(6)	O1–U–Cl3–U^{ii}	75.59(13)
U–O1	2.468(4)	U–Cl1–U^{i}	105.16(5)		
U–O2	2.485(4)	U–Cl3–U^{ii}	106.91(5)		
U–N1	2.636(5)	Cl1–U–O1	103.95(13)		
N1–C1	1.137(6)	Cl2–U–O2	97.68(12)		
C1–C2	1.459(7)	O1–U–O2	89.8(2)		
N2–C3	1.158(8)	Cl1–U–N1	76.27(11)		
C3–C4	1.439(8)	C1–N1–U	175.1(4)		
		U^{ii}–U–U^{i}	137.22(2)		
$UCl_3 \cdot 6H_2O$					
U–Cl2	2.856(2)	$Cl2^{iii}$–U–Cl2	84.71(5)		
U–O1	2.518(3)	O1–U–O2	138.12(9)		
U–O2	2.491(3)	O2–U–O3	74.74(10)		
U–O3	2.509(3)	O3–U–O1	120.55(10)		
		$O1^{iii}$–U–O2	69.79(9)		
		$O2^{iii}$–U–O3	69.41(10)		
		$O3^{iii}$–U–O1	73.12(10)		
$UCl_3 \cdot 7H_2O$					
U–Cl1	2.927(2)	Cl1–U–$Cl1^{iv}$	74.18(4)	O1–U–Cl1–U^{iv}	−84.45(7)
U–$Cl1^{iv}$	2.905(2)	U–Cl1–U^{iv}	105.82(4)	O2–U–Cl1–U^{iv}	−47.01(8)
U–O1	2.543(3)	Cl1–U–O1	71.23(6)	O3–U–Cl1–U^{iv}	78.53(7)
U–O2	2.542(3)	Cl1–U–O2	128.77(6)	O4–U–Cl1–U^{iv}	137.18(7)
U–O3	2.579(3)	Cl1–U–O3	68.65(6)	O5–U–Cl1–U^{iv}	−164.12(7)
U–O4	2.536(3)	Cl1–U–O4	107.44(7)	O6–U–Cl1–U^{iv}	−140.68(9)
U–O5	2.560(3)	Cl1–U–O5	68.70(6)	O7–U–Cl1–U^{iv}	59.78(11)
U–O6	2.526(3)	Cl1–U–O6	133.95(7)		
U–O7	2.529(2)				

[a] Symmetry codes: (i) $-x+1, -y+2, -z+1$; (ii) $-x+1, -y+1, -z+1$; (iii) $-x+1/2, y, -z+1/2$; (iv) $-x, -y, -z+2$.

after about 48 h, and they usually decomposed within next 2–5 days, whereas the $UCl_3 \cdot 7H_2O$ crystals were relatively stable and could be kept in the mother solution for a few weeks.

The $UCl_3 \cdot 7H_2O$ and $UCl_3 \cdot 2H_2O \cdot 2CH_3CN$ crystals separated from solution and sealed under nitrogen in a glass tube were relatively stable and could be stored below 5 °C for a few months and a few weeks, respectively. In contrast to these, the $UCl_3 \cdot 6H_2O$ crystals underwent oxidation to green uranium(IV) products very easily and could not have been stored. Absorption spectra of $UCl_3 \cdot 6H_2O$ (not presented here) indicate that in the presence of air the compound initially attaches one water molecule forming $UCl_3 \cdot 7H_2O$ and afterward undergoes fast decomposition and oxidation.

3.1. Uranium trichloride bis(methylcyanide) dihydrate

Uranium trichloride bis(methylcyanide) dihydrate crystallizes with a structure that is, to our knowledge, unknown so far. The compound with the same formula and similar main features of the structure was reported only for the gadolinium(III) [16]. However, the authors have found gadolinium atoms in five slightly different positions.

The final atomic data of $UCl_3 \cdot 2H_2O \cdot 2CH_3CN$ are summarized in Table 3. The central U^{3+} ion is eight-coordinated by five chlorine anions, two water and one methylcyanide molecules, which are forming a distorted bicapped trigonal prism (see Fig. 1(a)).

The characteristic feature of this structure is the link of the uranium atoms through the two common edges of the Cl1 and Cl3 chlorine atoms into an infinite zigzag chain in the [0 1 0] direction. In Fig. 2, one may notice two planes, formed by the Cl1–U–$Cl1^{i}$–U^{i} [1] and Cl3–U–$Cl3^{ii}$–U^{ii} atoms, respectively. The angle between their normals is equal to 45.45(4)°. The torsion angle $Cl1^{i}$–U–Cl3–U^{ii} is equal to 123.73(5)° and the angle between the three neighboring uranium atoms (U^{i}–U–U^{ii}) amounts to 137.22(2)°.

The asymmetric unit is presented in Fig. 3. The U–Cl1 and U–Cl3 distances are equal to 2.867(2) and 2.901(2) Å, respectively. However, the distances between the uranium ion and bridging $Cl1^{i}$ and $Cl3^{ii}$ ions (Fig. 2) are somewhat larger and amount to 2.932(2) and 2.914(2) Å, respectively. The interatomic distances as well as the angles and torsion angles are presented in Table 4.

[1] Symmetry codes as in Table 4.

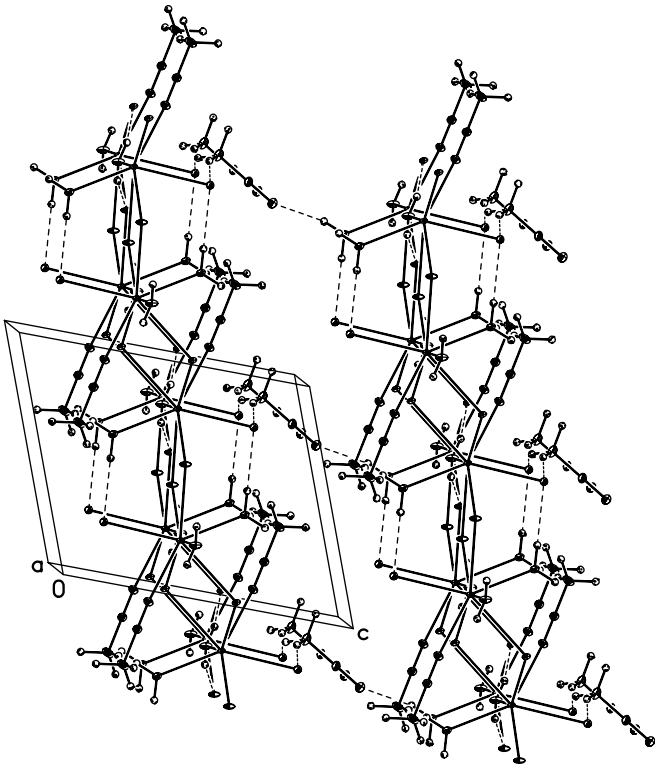

Fig. 4. The packing diagram of the $[UCl_3 \cdot 2H_2O \cdot CH_3CN]_n \cdot [CH_3CN]_n$ polymeric chains. The hydrogen bonds are shown as the dashed lines.

Although all crystals described in this paper, have been prepared from the methylcyanide solutions, molecules of this solvent are present only in the structure of $UCl_3 \cdot 2H_2O \cdot 2CH_3CN$ crystals. One of the two CH_3CN molecules is coordinated through the N atom to the uranium atom, while the second molecule is located between the main chains and link them through the hydrogen bonds – see Fig. 4.

The distances between the donor, acceptor and hydrogen atoms as well as the angles between them are listed in Table 5.

The polymeric structure has been reported for a number of uranium(III) compounds [7,17,18]. A comparison of the interatomic distances for selected uranium(III) chlorocomplexes with a polymeric structure is presented in Table 6. The U–Cl as well as the U···U distances in $UCl_3 \cdot 2H_2O \cdot 2CH_3CN$ are very similar to those in Rb_2UCl_5 and K_2UCl_5, but significantly shorter than those determined for $CsUCl_4 \cdot 3H_2O$. For the last compound the distances are among the longest of those found for the uranium(III) complex chlorides, comparable to distances observed for UCl_3 [19].

3.2. Uranium trichloride hexahydrate

We have not discerned any substantive qualitative differences between the crystal structures of uranium and americium trichloride hexahydrates [11] as well as their lanthanide analogues [10]. The found atomic coordinates for $UCl_3(H_2O)_6$ are summarized in Table 7.

Table 5
Geometry of the proposed hydrogen bonds[a]

D–H···A	d(H···A) (Å)	d(D···A) (Å)	Angle D–H···A (°)
$UCl_3 \cdot 2H_2O \cdot 2CNCH_3$			
O1–H2···Cl2^{ii}	2.30(2)	3.163(5)	177(9)
O1–H1···N2^{v}	1.93(2)	2.779(7)	167(9)
O2–H3···Cl1^{vi}	2.37(4)	3.161(4)	153(7)
O2–H4···Cl3^{vi}	2.28(4)	3.078(4)	155(7)
C4–H4B···Cl2	2.76	3.675(7)	159
$UCl_3 \cdot 6H_2O$			
O1–H1···Cl1^{vii}	2.39(2)	3.226(3)	164(7)
O1–H2···Cl2^{viii}	2.31(2)	3.161(3)	171(6)
O2–H3···Cl1^{ix}	2.35(2)	3.200(3)	170(7)
O2–H4···Cl2^{x}	2.28(2)	3.131(3)	173(10)
O3–H5···Cl1	2.34(2)	3.170(3)	161(7)
O3–H6···Cl2^{xi}	2.31(2)	3.147(3)	165(6)
$UCl_3 \cdot 7H_2O$			
O1–H1···Cl2^{xii}	2.32(2)	3.143(3)	161(3)
O1–H2···Cl2^{vii}	2.21(2)	3.043(3)	164(4)
O2–H3···Cl3^{xiii}	2.39(2)	3.200(3)	158(4)
O2–H4···Cl2^{ii}	2.36(2)	3.145(3)	152(4)
O3–H5···Cl3^{xiv}	2.33(2)	3.159(3)	161(4)
O3–H6···O1^{iv}	2.00(2)	2.863(4)	175(4)
O4–H7···O3^{xv}	2.19(2)	3.035(4)	169(4)
O4–H8···Cl3^{ii}	2.53(2)	3.339(3)	157(4)
O4–H8···Cl1^{xv}	2.94(4)	3.375(3)	114(3)
O5–H9···Cl3^{vii}	2.43(2)	3.258(3)	161(4)
O5–H10···Cl2	2.48(2)	3.303(3)	161(3)
O6–H11···Cl3	2.30(2)	3.129(3)	161(3)
O6–H12···Cl2	2.34(2)	3.171(3)	162(4)
O7–H13···Cl2^{ii}	2.69(2)	3.427(3)	145(4)
O7–H13···Cl1^{x}	2.88(4)	3.309(3)	113(3)
O7–H14···Cl3^{xiv}	2.44(2)	3.260(3)	160(3)

[a] Symmetry codes: (i) $-x+1, -y+2, -z+1$; (ii) $-x+1, -y+1, -z+1$; (iii) $-x+1/2, y, -z+1/2$; (iv) $-x, -y, -z+2$; (v) $x-1, y, z-1$; (vi) $x+1, y, z$; (vii) $-x+1, -y, -z+1$; (viii) $x+1/2, -y, z+1/2$; (ix) $-x+1, -y+1, -z$; (x) $x, y+1, z$; (xi) $x+1/2, -y, z-1/2$; (xii) $x-1, y, z$; (xiii) $-x, -y+1, -z+1$; (xiv) $x, y, z+1$; (xv) $-x+1, -y, -z+2$.

Table 6
Comparison of interatomic distances (Å) for selected uranium(III) chlorocomplexes with a polymeric structure

	Rb_2UCl_5 [18]	K_2UCl_5 [17]	$CsUCl_4 \cdot 3H_2O$ [7]	$UCl_3 \cdot 2H_2O \cdot 2CH_3CN$ [a]
d(U–Cl)	2.774–2.805	2.775–2.823	2.894–2.990	2.775(2)
d(U–Cl) [b]	2.880–2.886	2.839–2.888	3.067	2.867(2)–2.932(2)
d(U–O)			2.521–2.571	2.468(4)–2.485(4)
d(U···U)	4.651	4.550	4.886	4.606(2)

[a] This paper.
[b] The bridging chlorine atoms.

The basic unit of the crystal structure are Cl^- anions and $[UCl_2(H_2O)_6]^+$ cations (Fig. 5). The U atom is eight-coordinated by the six water molecules and two chlorine atoms. The characteristic feature of this structure is the existence of hydrogen bonds, which link the uranium eight-coordinated polyhedra, forming a three-dimensional network.

The Cl1 atoms, which are located in gaps of the three-dimensional network, are octahedrally coordinated by the

Table 7
Atomic coordinates and equivalent or isotropic thermal parameters (Å^2) for $UCl_3 \cdot 6H_2O$ crystals

Atom	x	y	z	U_{eq}/U_{izo}
U	0.25	0.14410(2)	0.25	0.00727(5)
Cl1	0.75	0.3776(2)	0.25	0.0118(2)
Cl2	0.05292(9)	−0.1760(2)	0.2590(2)	0.0117(2)
O1	0.2821(3)	0.0425(4)	0.5509(4)	0.0136(5)
O2	0.1443(3)	0.4276(4)	0.0825(4)	0.0131(4)
O3	0.4444(3)	0.3000(5)	0.1043(4)	0.0138(5)
H1	0.260(8)	−0.074(5)	0.589(9)	0.03(2)
H2	0.350(5)	0.089(10)	0.613(7)	0.02(2)
H3	0.179(7)	0.467(11)	−0.007(5)	0.03(2)
H4	0.126(11)	0.541(8)	0.13(2)	0.07(3)
H5	0.519(5)	0.349(10)	0.150(11)	0.04(3)
H6	0.457(6)	0.268(10)	0.003(3)	0.02(2)

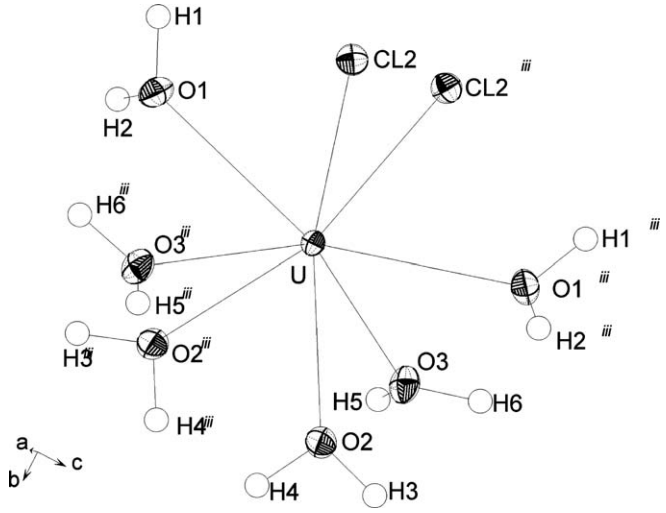

Fig. 5. The co-ordination of the U^{3+} in $UCl_2(H_2O)_6^+$ ion and labelling of the atoms.

water molecules through six hydrogen bonds (Fig. 6). It is worth noting that the same water molecules, which are hydrogen bonded to the Cl1 atoms, are also connected with the Cl2 by other hydrogen bonds. The packing diagram with the interatomic hydrogen bonds is shown in Fig. 7. The determined interatomic distances as well as bond angles are shown in Table 4, while the distances between donor, acceptor and hydrogen atoms as well as the appropriate angles are listed in Table 5.

The geometry around the eight-coordinated U^{3+} ion, which is located on the twofold axis, may be seen as a very distorted square antiprism, the bases of which are rhombuses folded along the shorter diagonal (see Fig. 1(b)).

A comparison of interatomic distances for $UCl_3 \cdot 6H_2O$ and selected chloro-complexes with a monomeric structure is presented in Table 8. The structure of $NH_4UCl_4 \cdot 4H_2O$ [8] is similar to that of uranium trichloride hexahydrate. As a consequence of this also the U–Cl as well as the U···U distances are for $UCl_3 \cdot 6H_2O$ close to those of $NH_4UCl_4 \cdot 4H_2O$. In Cs_2NaUCl_6 the U–Cl bonds are shorter, while the distance between two nearest uranium

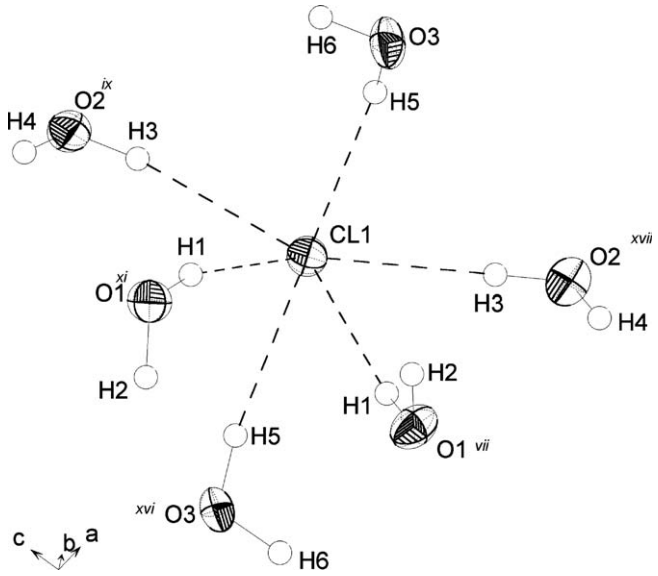

Fig. 6. The octahedral coordination sphere of the chloride anion in the $[UCl_2(H_2O)_6]Cl$ structure. The dashed line shows the hydrogen bond between chloride ions and water molecules. [Added symmetry codes are: (*xvi*) $3/2 - x$, y, $1/2 - z$; (*xvii*) $1/2 + x$, $-y + 1$, $1/2 + z$].

ions is considerably longer as compared with the hydrated monomeric forms.

3.3. Uranium trichloride heptahydrate

As has been mentioned above, $UCl_3 \cdot 7H_2O$ crystals suitable for X-ray measurements were obtained by recrystalization. Unfortunately, all of them turned out to be the penetration twins. Similarly, very small crystals, which could be found in the precipitate before submitting it to the recrystalization process, were also twinned. Therefore, the crystals for the crystal date collection were cut from larger ones.

Similarly, as in the case of the described above hexahydrate, we have not found any qualitative differences between the structure of uranium trichloride heptahydrate and its lanthanide analogue [9]. The atomic coordinates for $UCl_3(H_2O)_7$ are summarized in Table 9.

The uranium trichloride heptahydrate crystals are built up from separate $[U_2Cl_2(H_2O)_{14}]^{4+}$ and Cl^- ions. The characteristic feature of this structure are centrosymmetric dimers, formed by two U^{3+} ions connected by the (Cl1) bridging chlorine atoms. The shortest distance between uranium ions is equal to 4.652(2) Å, and remains in the range observed for other chloro-complexes with a polymeric structure – see Table 6.

The U^{3+} central metal ion is coordinated by two chloride anions and seven water molecules, forming a nine-coordinated dodecahedron. For the ML_9 type complexes the coordination polyhedron may be characterized as related to a D_{3h} tricapped trigonal prism or C_{4v} monocapped square antiprism, the first being energetically favorable [21].

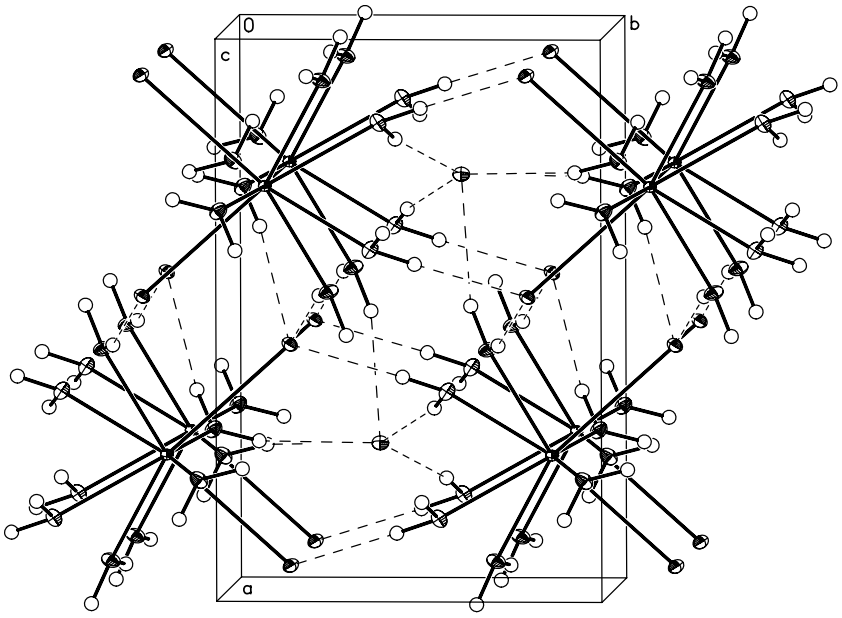

Fig. 7. The packing diagram of the $UCl_3 \cdot 6H_2O$. Dashed lines show the O–H···Cl hydrogen bonds in the crystal structure.

Table 8
Comparison of interatomic distances (Å) in selected crystals of uranium(III) chloro-complexes with a monomeric structure

	Cs_2NaUCl_6 [20]	$NH_4UCl_4 \cdot 4H_2O$ [8]	$UCl_3 \cdot 6H_2O$[a]
d(U–Cl)	2.734	2.845–2.847	2.856(2)
d(U–O)		2.510–2.568	2.491(3)–2.518(3)
d(U···U)	7.732	6.681	6.412(2)

[a] This paper.

Table 9
Atomic coordinates and equivalent or isotropic thermal parameters ($Å^2$) in $UCl_3 \cdot 7H_2O$

Atom	*x*	*y*	*z*	U_{eq}/U_{izo}
U	0.21713(2)	0.18477(2)	0.82487(2)	0.00681(3)
Cl1	0.14644(11)	−0.17952(10)	0.98556(9)	0.0091(2)
Cl2	0.78919(11)	0.22317(10)	0.46432(10)	0.0118(2)
Cl3	0.34315(11)	0.38783(10)	0.21278(10)	0.0126(2)
O1	0.0718(3)	0.0813(3)	0.6619(3)	0.0126(5)
O2	0.0304(3)	0.4223(3)	0.6750(3)	0.0115(5)
O3	0.2308(3)	0.0931(3)	1.1176(3)	0.0140(5)
O4	0.5207(3)	0.2266(3)	0.8414(3)	0.0142(5)
O5	0.4510(3)	−0.0101(3)	0.6961(3)	0.0119(5)
O6	0.3863(3)	0.3515(3)	0.5492(3)	0.0123(5)
O7	0.2209(4)	0.4605(3)	0.8871(3)	0.0149(5)
H1	0.015(4)	0.136(4)	0.592(3)	0.015
H2	0.132(4)	0.003(3)	0.623(4)	0.015
H3	−0.068(3)	0.454(5)	0.731(4)	0.014
H4	0.072(5)	0.517(3)	0.607(4)	0.014
H5	0.271(5)	0.153(5)	1.160(4)	0.017
H6	0.141(3)	0.044(5)	1.188(4)	0.017
H7	0.600(4)	0.144(3)	0.840(5)	0.017
H8	0.577(5)	0.307(4)	0.844(5)	0.017
H9	0.486(5)	−0.113(2)	0.742(4)	0.014
H10	0.549(3)	0.027(5)	0.631(4)	0.014
H11	0.349(5)	0.353(5)	0.470(3)	0.015
H12	0.4982(9)	0.332(5)	0.537(5)	0.015
H13	0.187(5)	0.560(2)	0.832(4)	0.018
H14	0.263(5)	0.467(5)	0.961(3)	0.018

The coordination geometry of the $[La_2Cl_2(H_2O)_{14}]^{4+}$ ion was described by Bakakin et al. [9] as a highly disordered capped square antiprism. Similarly, Paterson et al. [22] described the dodecahedron observed for $CeCl_3 \cdot 7H_2O$ as an almost ideal capped square antiprism. The structure of $CeCl_3 \cdot 7H_2O$ was solved in the triclinic system in the space group $P1$, but it is essentially the same as that obtained in the space group $P\bar{1}$ for $LaCl_3 \cdot 7H_2O$ or $UCl_3 \cdot 7H_2O$.

The two polytopal forms, possible for uranium trichloride heptahydrate, are presented in Fig. 1(c) and (d). Since the D_{3h} form was found for most of ML_9 complexes as well as for boron and metal M_9 clusters [21], one may assume, that the coordination geometry of U^{3+} in $UCl_3 \cdot 7H_2O$ complex should be characterized as related to the tricapped trigonal prism (D_{3h}), rather than to a square antiprism.

In the $UCl_3 \cdot 7H_2O$ network the chloride anions are located in the gaps between the $[U_2Cl_2(H_2O)_{14}]^{4+}$ cations. The structure is held together by O–H···Cl hydrogen bonds. Furthermore, an intermolecular hydrogen bond is located inside the cation, between the oxygen atoms (O3–H6···O1^{iv}),[2] with the O3···O1^{iv} distance equal to 2.863(4) Å. In Table 4 interatomic distances as well as angles and torsion angles are shown, while the distances between the donor, acceptor and hydrogen atoms as well as the appropriate angles, are summarized in Table 5. The structure of the $[U_2Cl_2(H_2O)_{14}]^{4+}$ ion and the packing diagram of the ions in the unit cell are shown in Figs. 8 and 9, respectively.

For uranium trichloride heptahydrate the mean U–Cl and U–O distances are equal to 2.916 and 2.545 Å, respectively, and are somewhat longer as compared to those of

[2] Symmetry codes as in Table 5.

uranium trichloride hexahydrate and uranium trichloride bis(methylcyanide) dihydrate. Since $UCl_3 \cdot 7H_2O$ is the first dimeric uranium(III) hydrate with a known crystal structure, we could not perform for this type of compounds a comparison of the U–Cl or U–O distances. It is worth noting, that uranium(III) is, besides praseodymium(III) the only f-electron ion for which crystal structure has been determined both for hexa- and heptahydrated trichlorides [23,24]. Hence, one may compare the interatomic distances between hexa- and heptahydrates, as well as between the

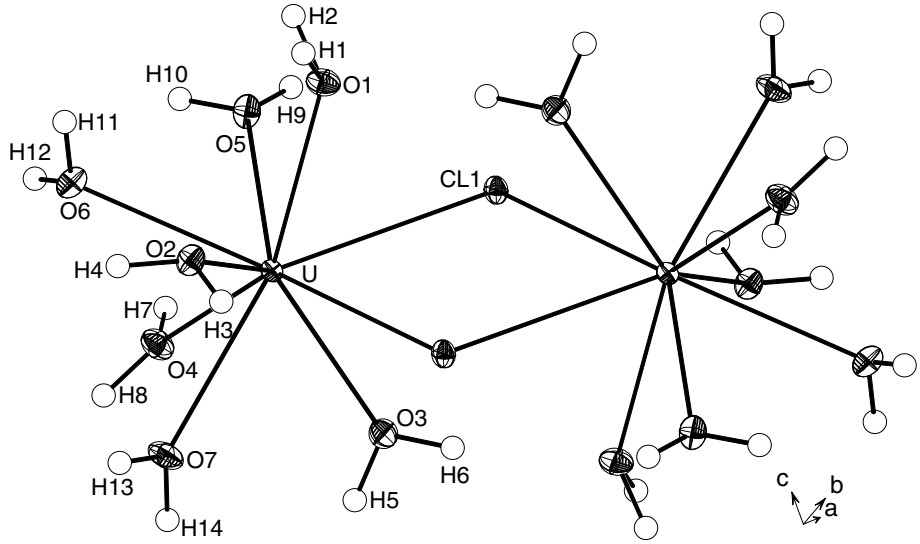

Fig. 8. The molecular structure of the $[U_2Cl_2(H_2O)_{14}]^{4+}$ cation. Displacement ellipsoids are shown at 50% probability. The hydrogen atoms are shown as a small circle of arbitrary radii.

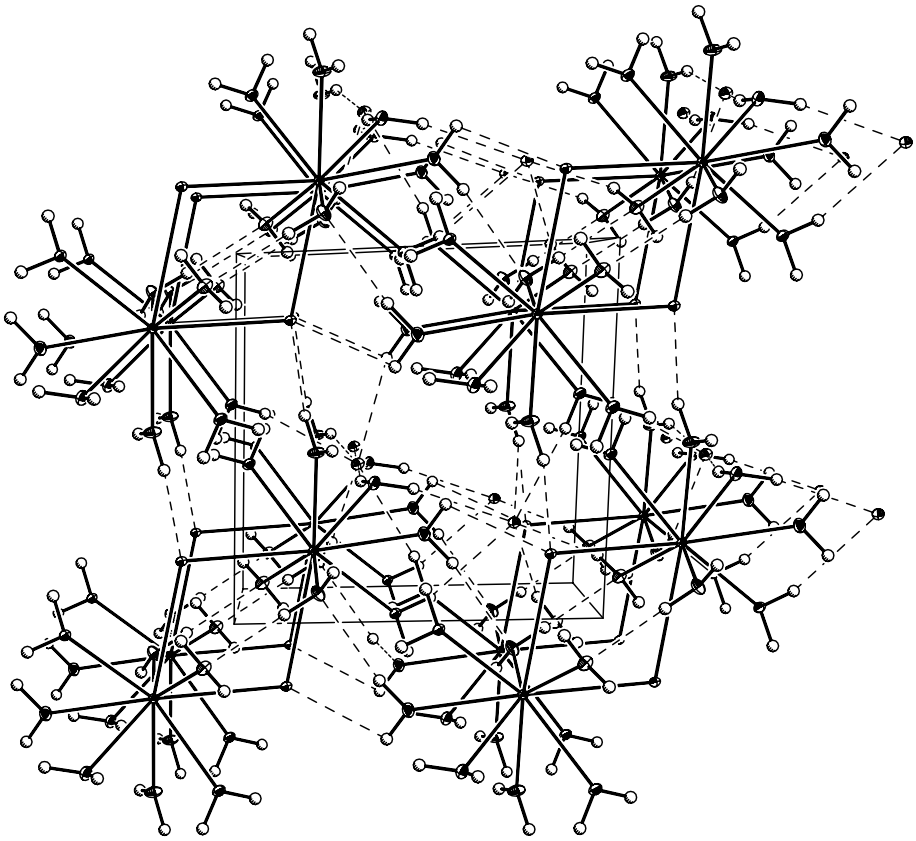

Fig. 9. The crystal packing diagram of the $UCl_3 \cdot 7H_2O$. The dashed lines show O–H···Cl and O–H···O hydrogen bonds.

Table 10
The mean interatomic distances (Å) in the praseodymium and uranium trichloride hydrates

	$PrCl_3 \cdot 6H_2O$ [23]	$PrCl_3 \cdot 7H_2O$ [24]	$UCl_3 \cdot 6H_2O$[a]	$UCl_3 \cdot 7H_2O$[a]
M–Cl	2.833	2.910	2.856	2.916
M–O	2.472	2.518	2.506	2.545

[a] This paper.

actinide and lanthanide analogues. The mean M–Cl and M–O distances in lanthanide and actinide complexes are summarized in Table 10. As one may notice, for the uranium as well as for the praseodymium hexahydrated trichlorides, the M–O and M–Cl distances are shorter than for the heptahydrates. For praseodymium the differences of the M–O and M–Cl distances between the hexa- and heptahydrates amounts to 1.9% and 2.7%, while for uranium this changes are considerably smaller and are equal to 1.6% and 2.1%, respectively. For the hexa- as well as for the heptahydrates, both M–O and M–Cl distances are, as expected, larger for the uranium(III) than for praseodymium(III) compounds, what reflects the increase in the ionic radius of the M^{3+} metal ion (ionic radius: U^{3+} −116.5 pm, Pr^{3+} −108 pm).

4. Supplementary materials

Supplementary data are available from The Director, ICSD, FIZ Karlsruhe, Hermann-von-Helmholtz-Platz 1, 76344 Eggenstein-Leopoldshafen, Germany, by quoting the deposition numbers: 415442-$UCl_3 \cdot 6H_2O$, 415443-$UCl_3 \cdot 7H_2O$, 415444-$UCl_3 \cdot 2H_2O \cdot 2CH_3CN$ (fax: +49 7247 808 132; e-mail: crysdate@fiz-karlsruhe.de or http://www.fiz-karlsruhe.de).

References

[1] J. Drożdżyński, Chemistry of tervalent uranium, in: A.J. Freeman, C. Keller (Eds.), Handbook on the Physics and Chemistry of the Actinides, vol. 6, Nord Holland, 1991, pp. 281–336 (Chapter 5).
[2] J. Drożdżyński, Inorg. Chim. Acta 109 (1985) 79.
[3] E. Zych, J. Drożdżyński, Inorg. Chim. Acta. 115 (1986) 219.
[4] M. Karbowiak, J. Drożdżyński, J. Less-Common Met. 132 (1987) 69.
[5] M. Karbowiak, J. Drożdżyński, J. Alloys. Compd. 190 (1993) 291.
[6] R. Barnard, J.I. Bullock, B.J. Gellatly, L.F. Larkworthy, J. Chem. Soc., Dalton 18 (1972) 1932.
[7] K. Krämer, G. Meyer, M. Karbowiak, J. Drożdżyński, J. Less-Common Met. 175 (1995) 342.
[8] M. Karbowiak, J. Drożdżyński, J. Janczak, Polyhedron 15 (1996) 241.
[9] V.V. Bakakin, R.F. Klevtsova, L.P. Solov'eva, Zh. Strukt. Khim. 15 (1974) 820.
[10] A. Habenschuss, H.F. Spedding, Cryst. Struct. Commun. 9 (1980) 71.
[11] J.H. Burns, J.R. Peterson, Inorg. Chem. 10 (1971) 147.
[12] G.M. Sheldrick, SHELXS-97. Program for the Solution of the Crystal Structures, University of Göttingen, Germany, 1997.
[13] G.M. Sheldrick, SHELXL-97. Program for the Refinement of the Crystal Structures, University of Göttingen, Germany, 1997.
[14] W. Levason, M. Webster, Acta. Cryst. E 58 (2002) 76.
[15] XP – Interactive Molecular Graphics – ver. 5.1. Bruker Analytical X-ray Systems, 1998.
[16] M.D. Rudd, N.W. Alcock, G.R. Willey, Inorg. Chim. Acta 353 (2003) 276.
[17] L. Keller, A. Furrer, P. Fischer, P. Allenspach, K. Kramer, H.U. Guedel, A. Doenni, T. Suzuki, Phys. Rev. B 51 (1995) 2881.
[18] K. Kramer, H.U. Guedel, G. Meyer, T. Heuer, N.M. Edelstein, B. Jung, L. Keller, P. Fischer, E. Zych, J. Drożdżyński, Z. Anorg. Allg. Chem. 620 (1994) 1339.
[19] J.C. Taylor, P.W. Wilson, Acta Cryst. B 30 (1974) 2803.
[20] Z. Mazurak, J. Drożdżyński, J. Hanuza, J. Mol. Struct. 174 (1988) 321.
[21] L.J. Guggenberger, E.L. Muetterties, J. Am. Chem. Soc. 98 (1976) 7221.
[22] J.E. Peterson, E.I. Onstott, Acta. Cryst. B 35 (1979) 805.
[23] B.J. Chen, D. Xu, L. Li, J. Wu, G. Xu, Acta. Cryst. C 47 (1991) 1074.
[24] A. Habenschuss, F.H. Spedding, Cryst. Struct. Commun. 7 (1978) 535.

of semi-coordinate bonds between adjacent dimers. The discussion of exchange pathways in these studies have focused on the through-bond intradimer and intrachain/stack interactions. Unfortunately, the discussion of the role of the close halogen–halogen (2H) contacts within these dimer structures has generally been ignored [7]. However, recently two neutron scattering studies in $A_2Cu_2Cl_6$ salts have shown that the 2H pathways are stronger than the intrachain/stack interactions [8]. Since this is true in chloride salts, it is expected that the 2H pathway will play an even more significant role in bromide salts.

This was observed to be the case in our recent study of the $(morpholinium)_2Cu_2Cl_{6-x}Br_x$ salts [9]. Here, semi-coordination of the morpholinium group to the copper ion results in the formation of isolated, essentially planar dimers. The morpholinium groups play an additional role; hydrogen bonding adjacent dimers together, forcing relatively short (3.92–4.07 Å) halide···halide contacts between dimers. In this way, magnetic exchange pathways between dimers are developed, defining in this manner, alternating AFM chains. Analysis of the magnetic susceptibility data showed that the magnitude of the larger exchange constants in the chain increased essentially linearly, and rapidly, as the fraction of bromide in the dimer increased. It was argued that this exchange constant represented the 2H pathway.

In this paper, we extend the above investigation by examining the structural and magnetic behavior in the $(BIPY)Cu_2Cl_{6-x}Br_x$ compounds, where BIPY denotes the 4,4′-bipyridinium cation. The previous studies of the chloro and bromo end members of these compounds showed extremely strong magnetic coupling [10]. These compounds assume the extended stack structure with bridging halides forming semi-coordinate bonds with the dimer directly above or below. N–H···X hydrogen bonds force very short X···X contacts between dimers, that can also produce effective magnetic exchange pathways. Thus, based on the assumption that the exchange coupling through the semi-coordinate bonds is weak, the compounds are expected to behave as alternating AFM chains, based on the through-bond intradimer coupling and the through-space halide–halide contact. In this study, the structural and magnetic properties of both the $(BIPY)Cu_2Cl_6$ and $(BIPY)Cu_2Br_6$ end members are reinvestigated and the properties of a series of mixed $(BIPY)Cu_2Cl_xBr_{6-x}$ compounds are reported.

2. Experimental

2.1. Synthesis

The compounds were grown from acidic aqueous solutions. The pH of these solutions is critical, since at very low pH, a dark brown precipitate is formed (presumably $(BIPY)CuX_4$), while at higher pH values, a green insoluble material is formed (presumably $CuX_2(bipy)$, bipy = 4,4′-bipyridine).

2.1.1. (4,4′-Bipyridinium)Cu_2Cl_6, (BIPY)Cu_2Cl_6 (**1**)

4,4′-Bipyridinium hydrochloride (0.457 g, 2 mmol) and copper chloride dihydrate (0.689 g, 4 mmol) were added to a mixture of 20 mL of 4 M hydrochloric acid, and 8 mL water. The red, pleochroic, nearly opaque crystals were collected after several days of evaporation, and allowed to dry (490 mg, 34% yield).

2.1.2. (4,4′-Bipyridinium)Cu_2Br_6, (BIPY)Cu_2Br_6 (**11**)

4,4′-Bipyridinium hydrobromide (0.636 g, 2 mmol) and copper bromide (0.893 g, 4 mmol) were added to a mixture of 15 mL of 4 M hydrobromic acid, and 28 mL water. The dark red, pleochroic, crystals were collected after several days of evaporation and allowed to dry (554 mg, 36% yield).

2.1.3. (4,4′-Bipyridinium)$Cu_2Cl_{6-x}Br_x$, (BIPY)$Cu_2Cl_{6-x}Br_x$ (**2**–**10**)

The compounds were synthesized by combining various ratios of 4,4′-bipyridinium hydrochloride/4,4′-bipyridinium hydrobromide (2 mmol total) salts and $CuCl_2\cdot 2H_2O/CuBr_2$ (4 mmol total). This was added to a mixture of the appropriate ratio of 4 M hydrochloric/hydrobromic acid (20 mL total). Water was slowly added to this solution until the brown precipitate dissolved (7–12 mL). The acidic solution was allowed to stir for 10 min. The red, pleochroic crystals were collected after several days of evaporation, and allowed to dry. Typical yields were 155–304 mg (21–34%).

2.2. Crystallography

Crystals were attached to a glass fiber using glue. Datasets were collected at 293(2) K, either using a Bruker/Siemens SMART 1K instrument or a Syntex $P2_1$ diffractometer upgraded to Bruker P4 specifications (Mo Kα radiation, $\lambda = 0.71073$ Å). Data obtained with the SMART system were measured using omega scans of 0.3° per frame for 30 s, and a half sphere of data were collected. The first 50 frames were recollected at the end of data collection to monitor for decay. Cell parameters were retrieved using SMART [11] software and refined using SAINT-PLUS [12] on all observed reflections. Data reduction and correction for Lp and decay were performed using the SAINT-PLUS software. Absorption corrections were applied using SADABS [13]. For the Syntex system, lattice dimensions were obtained from 25 accurately centered high angle reflections [14]. Data were corrected for absorption utilizing ψ-scan data assuming an ellipsoidal shaped crystal. The structures were solved by direct methods and refined by least squares method on F^2 using the SHELXTL program package [15]. No decomposition was observed during data collection. Structure refinements were straightforward in all cases and no disorder was observed. Further details are provided in the Supporting Information.

Crystallographic data on the mixed salts were collected on samples from nine different preparations (compounds

Table 1
Composition data using X-ray diffraction techniques compared to analytical methods (Desert Analytics)

	X-ray		Chemical analysis	
	Cl	Br	Cl	Br
$(BIPY)Cu_2Cl_6$ (**1**)	6	0	6.09	<0.01
$(BIPY)Cu_2Cl_{5.62}Br_{0.38}$ (**2**)	5.62	0.38	5.65	0.82
$(BIPY)Cu_2Cl_{5.32}Br_{0.68}$[a] (**3**)	5.32	0.68		
$(BIPY)Cu_2Cl_{4.48}Br_{1.53}$[a] (**4**)	4.48	1.52		
$(BIPY)Cu_2Cl_{4.28}Br_{1.72}$[a] (**5**)	4.28	1.72		
$(BIPY)Cu_2Cl_{2.87}Br_{3.13}$[a] (**6**)	2.87	3.13		
$(BIPY)Cu_2Cl_{2.26}Br_{3.74}$[a] (**7**)	2.26	3.74		
$(BIPY)Cu_2Cl_{1.60}Br_{4.40}$ (**8**)	1.610	4.40	1.47	4.30
$(BIPY)Cu_2Cl_{1.18}Br_{4.82}$ (**9**)	1.18	4.82	0.97	4.98
$(BIPY)Cu_2Cl_{0.32}Br_{5.68}$[a] (**10**)	0.32	5.68		
$(BIPY)Cu_2Br_6$ (**11**)	0	6	0.04	5.95

[a] Composition measurements were not made.

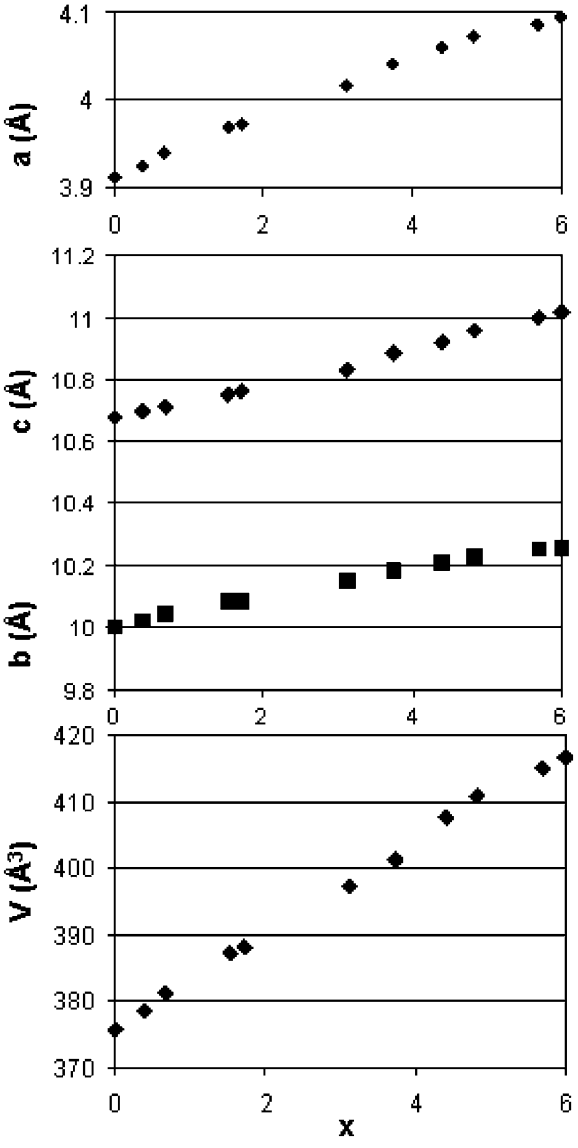

Fig. 1. Lattice constants and cell volume as a function of total bromine in $(BIPY)Cu_2Cl_{6-x}Br_x$ salts.

2–**10**, Table 1). The site occupancies for the three unique halide ion sites were refined independently, with the constraint that the site occupancies for each site should add to unity. The total site occupancy values obtained agreed well with the chemical analyses of the samples (Table 1). The fractions of Cl and Br found from the refinements correlates well with the unit cell constants and the unit cell volumes, as seen in Fig. 1. Consistent results were obtained between two refinement procedures: the first where the Cl and Br were constrained to be in the same location for each site; the second where the Cl and Br atoms were allowed to have different coordinates. Since the former process defines a unique average X···X distance for correlation with the magnetic data, it is those results that are reported here. Refinement information is available in the Supplementary Data.

2.3. Magnetic measurements

The susceptibility studies were done on crushed single crystals of samples **1**, **2**, **5**, **7**–**9** and **11** using a Quantum Design MPMS-XL SQUID Magnetometer. The magnetization of each sample was first determined at 1.8 K in fields between 0 and 5 T. The magnetization was linear with field up to at least 1 T for each compound. No hysteresis was detected for any of the compounds. For the determination of the molar magnetic susceptibility, χ_M, the magnetic moment of the compound in a field of 1000 Oe (0.1 T) was determined as a function of temperature between 1.8 and 325 K. Corrections for the small diamagnetic contribution of the sample holder were applied. Corrections to the molar susceptibility have been made for the temperature independent magnetization of the Cu(II) ion (60×10^{-6} emu/mol) and the diamagnetic contribution as calculated from Pascal's constants

3. Structure description

All of the $(BIPY)Cu_2X_6$ salts are isomorphous, containing planar $BIPY^{2+}$ dications linked to centrosymmetric pseudo-planar $Cu_2X_6^{2-}$ dimers through bifurcated N–H···X hydrogen bonds. The $Cu_2X_6^{2-}$ species are assembled into stacks via semi-coordinate Cu···X synthons, as shown in Fig. 2 for $(BIPY)Cu_2Cl_6$. This forces a distorted octahedral geometry around each Cu^{2+} ion. In addition, the N–H···X bonds (light lines in Fig. 3) link the stacks of $Cu_2X_6^{2-}$ dimers. In this manner, a two-dimensional structural network consisting of hydrogen bonded stacks is formed. These networks are tied together into the overall three-dimensional structure via a series of weaker C–H···X interactions (dotted lines in Fig. 3). As a consequence of these interactions between these structural networks, short X2···X2 contacts (heavy dashed lines in Fig. 3) are formed between dimers in adjacent layers.

Within the stacks of dimers, systematic changes in bond lengths occur as chloride ions are replaced by bromide ions. As seen in Fig. 4, the mean Cu–X distances increase nearly

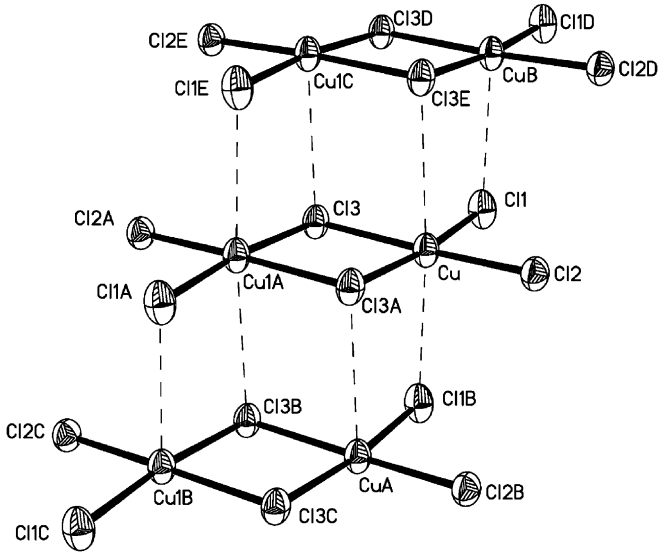

Fig. 2. Illustration of the stacking of dimers found in the (BIPY)Cu_2X_6 salts. The semi-coordinated bonds linking the dimers are shown as dashed lines.

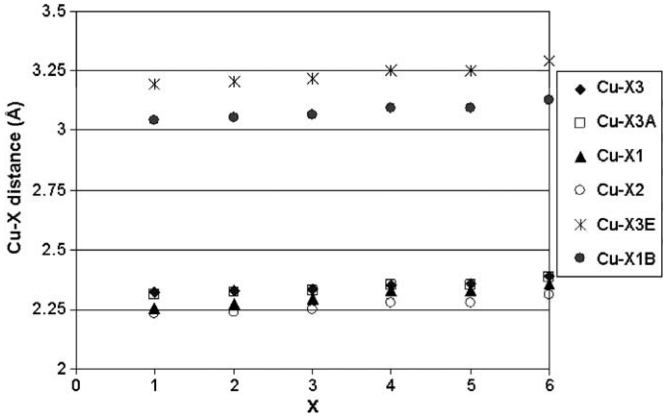

Fig. 4. Plot of Cu–X distances as a function of bromide ion content. Refer to Fig. 2 for label identification.

linearly with an increase of ~0.13 Å for the normal in-plane Cu–X bonds and ~0.16 Å for the semi-coordinate bonds. The bridging Cu–X bonds are significantly longer than the terminal bonds, as anticipated. In addition, it is seen that, for the terminal bonds, the mean Cu–X1 distances are ~0.02 Å longer than the mean Cu–X2 bond distances for the pure end members, and up to 0.05 Å longer for the mixed salts. The shortening of the Cu–X2 distances is a consequence of the electrostatic repulsion induced by the short X2···X2 contacts between layers. More significantly, it is also observed (Fig. 5) that the occupancy of the three independent halide ion sites is non-statistical for the mixed halide salts, with the X1 site preferentially occupied by the bromide ions. Again, this is anticipated based on electrostatic arguments.

As noted above, the weaker C–H···X interactions between layers force short, nearly linear X2···X2 contacts

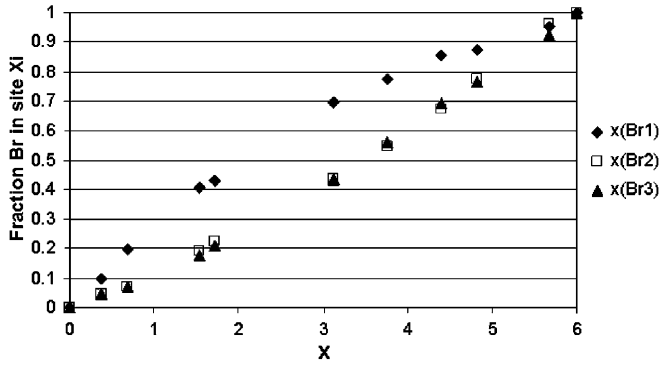

Fig. 5. Plot of the fractional occupancy of each halide ion site as a function of total Br content.

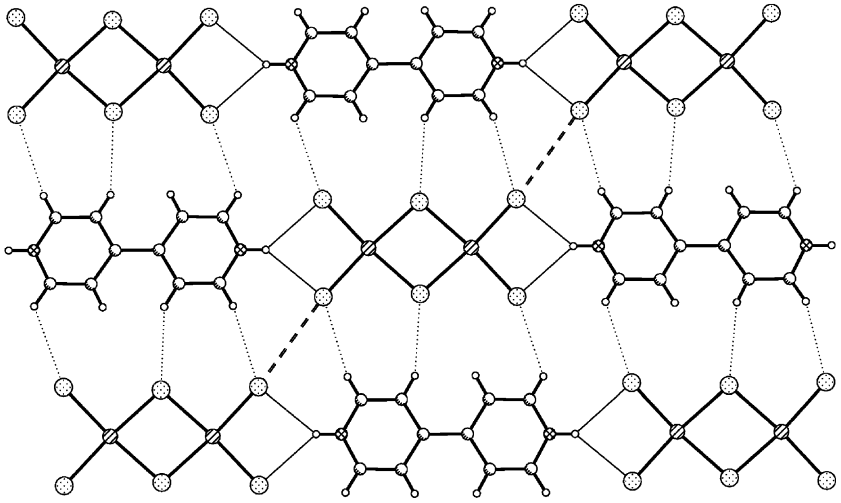

Fig. 3. Illustration of the hydrogen bonding network in the (BIPY)Cu_2X_6 salts. The view is perpendicular to the plane of the dimeric species. The N–H···X hydrogen bonds are shown as light solid lines, while the C–H···X interactions are shown as dotted lines. The resulting short X2···X2 contacts are shown as dashed lines.

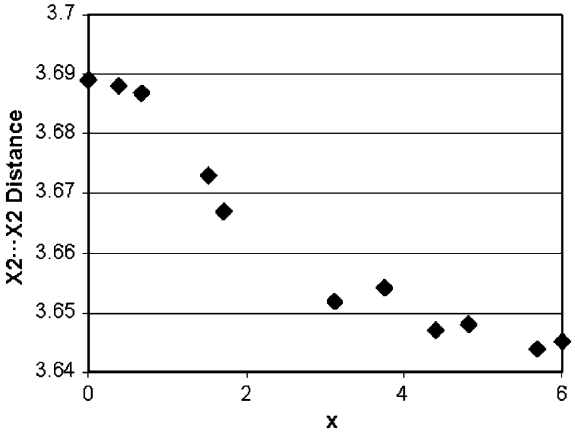

Fig. 6. Plot of the X2···X2 distance as a function of the total Br content.

between dimers in adjacent layers. These contacts will be crucial in the interpretation of the magnetic properties, thus the analysis of their structural properties is important. In the pure chloride salt, the contact distance (3.690 Å) is slightly larger than the sum of the Cl^- radii (3.6 Å), but in the bromide salt, the observed distance (3.645 Å) is substantially less than the sum of the Br^- radii (3.9 Å). Surprisingly, it is also noted that the contact distance for the bromide salt is less than that in the chloride salt. This is due to presence of the C–H···X interactions between the layers, which hold adjacent $Cu_2X_6^{2-}$ anions and $BIPY^{2+}$ cations in juxtaposition and keeps the Cu–X2···X2 contact interactions essentially linear. Given the increase in radii of ~0.15 Å when Cl^- is replaced by Br^-, it can be calculated that the X2···X2 distance must decrease by ~0.05 Å in order to retain the linear geometry. This is in good agreement with the observed decrease of 0.045 Å.

Another consequence of the non-random distribution for the halide ions is that the X2···X2 contact distance between the dimers varies non-linearly as the chloride ions are replaced by bromide ions, as shown in Fig. 6. Since the Br^- ions avoid the X2 site as their initial inclusion occurs, the primary type of contact will be of the Cl···Cl type in this composition regime. This means that the hydrogen bonding can more readily force the dimers closer together. For $x > 0.5$, the Br^- ions must now start to occupy the X2 site, so the contraction of the X2···X2 distance is much less.

4. Magnetic properties

As described above, the structures of both the chloride and bromide salts contain isolated $(BIPY)Cu_2X_6$ molecules that form stacks of $Cu_2X_6^{2-}$ dimers tied together by 4,4′-bipyridinium cations. Three possible exchange pathways exist: the intradimer pathway, J_d; the intrastack pathways via the semi-coordinate Cu···X bonds, J_{id}; and the 2H X···X contacts J_{2H}. Given the short X···X distances between dimers, it is expected that the 2H pathways will have relatively large AFM exchange couplings, even in the salts with high chloride content. In contrast, the intrastack interactions, which involve parallel planar arrangement of the magnetic orbitals, are expected to be relatively weak since the magnetic orbitals lie in the plane of the dimer. Thus, the significant exchange pathways are expected to be the intradimer coupling, J_d, and the 2H coupling between dimers, J_{2H}. These link the dimers together into magnetic chains with alternating exchange pathways containing J_d and J_{2H}. Given the structural characteristics discussed above, the magnetic behavior of both salts was modeled as alternating antiferromagnetic chains (AAFM) with exchange constants J_1 and J_2, characterized by the Hamiltonian $H = -2J_1\Sigma[s_i \cdot s_{i+1} + \alpha s_{i+1} \cdot s_{i+2}]$ with $0 < \alpha < 1$ and $J_2 = \alpha J_1$. The high temperature series expansion previously reported was used in the data analysis [16].

4.1. Magnetic properties of the pure compounds

Both the chloride and bromide salts exhibit dominant antiferromagnetic behavior as demonstrated by the continuously decreasing value of $\chi_M T$ versus T as the temperature is decreased. The results are in agreement with the experimental values reported earlier [10], with χ (max) occurring

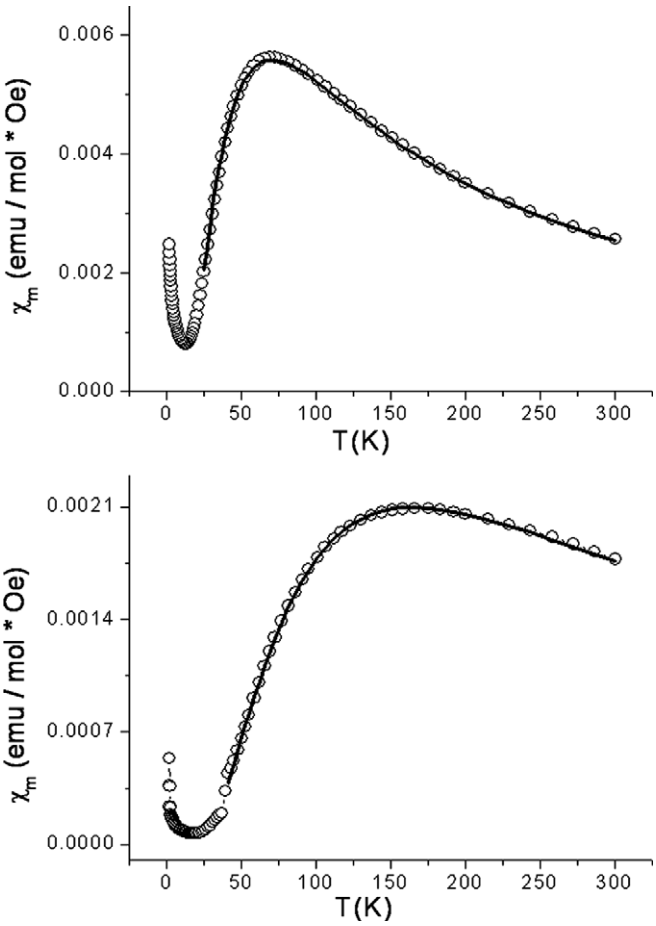

Fig. 7. Plot of χ_M vs. T for $(BIPY)Cu_2Cl_6$ (top) and $(BIPY)Cu_2Cl_5Br$ (bottom). Solid lines are calculated fits to the AAFM model with parameters given in text.

Table 2
Site occupancies, mean X···X distances and magnetic parameters

Sample	1	2	3	4	5	6	7	8	9	10	11
R_1	0.0252	0.0347	0.0208	0.0259	0.0322	0.0241	0.0285	0.0266	0.0441	0.0388	0.0389
x(Br)	0	0.38	0.68	1.53	1.72	3.13	3.76	4.40	4.82	5.68	6
x(Br1)	0	0.096	0.196	0.406	0.429	0.695	0.774	0.857	0.872	0.951	6
x(Br2)	0	0.049	0.072	0.191	0.226	0.435	0.547	0.671	0.774	0.963	6
x(Br3)	0	0.047	0.071	0.179	0.211	0.434	0.560	0.690	0.765	0.926	6
Cu–X3 (Å)	2.320	2.326	2.334	2.353	2.356	2.389	2.408	2.421	2.431	2.445	2.450
Cu–X3A (Å)	2.313	2.321	2.329	2.349	2.352	2.384	2.407	2.417	2.427	2.443	2.448
Cu–X1 (Å)	2.254	2.272	2.296	2.328	2.328	2.359	2.368	2.376	2.378	2.385	2.387
Cu–X2 (Å)	2.232	2.240	2.249	2.275	2.278	2.310	2.327	2.342	2.352	2.366	2.368
Cu···X3B (Å)	3.193	3.204	3.219	3.250	3.252	3.291	3.313	3.328	3.338	3.341	3.354
Cu···X1D (Å)	3.039	3.053	3.065	3.093	3.094	3.124	3.145	3.161	3.175	3.189	3.193
Cu–X3–CuA (°)	96.48	96.42	96.16	95.77	95.70	95.47	95.52	95.64	95.85	95.96	96.16
X2···X2B (Å)	3.689	3.688	3.687	3.673	3.667	3.652	3.654	3.646	3.645	3.644	3.645
Cu–X2···X2B (°)	172.98	173.10	172.87	172.81	172.85	172.46	172.34	172.15	172.13	171.93	171.88
J_1/k (K)	−57.2(6)	−60.00(7)			−78.0(4)		−104.0(3)	−131.2(7)	−137.9(9)		−162(2)
J_2/k (K)	−27(4)	−27.0(4)			−43(2)		−60(1)	−76.0(7)	−69(3)		−93(5)
Paramagnetic defects (%)	0.04	0.60			0.45		0.70	0.50	1.5		0.45

at substantially higher temperature for the bromide salt than the chloride salt. Data were fit with high temperature series expansions for χ_{AAFM} with a correction for the paramagnetic 'impurity' that is observed at very low temperatures, according to the equation $\chi_{dimer} = 2(1-f)\chi_{AAFM} + 2f(C/T)$, where f is the mole fraction impurity and C is the Curie constant for a spin 1/2 species. As with many other copper halide systems, the paramagnetic impurity is assumed to be intrinsic, due to defects in the crystal, rather than due to the presence of an impurity compound. The resulting fits are shown in Fig. 7 and the parameters given in Table 2. For the chloride salt, it is found that $J_1/k = -52.6(2)$ K and $J_2/k = -27(4)$ K, while the bromide salt has $J_1/k = -162(2)$ K and $J_2/k = -93(5)$ K. The fact that the exchange coupling in the bromide salt is substantially stronger than in the chloride analog, despite the isomorphous structures, is consistent with the previous report, with the general trend observed in isostructural copper halide dimers [6d], and with the observation in the diammonium layer perovskite system that the Br···Br exchange pathway is considerably stronger than the Cl···Cl pathway.

4.2. Magnetic properties of the $(BIPY)Cu_2Cl_{6-x}Br_x$ salts $(0 > x > 6)$

All these compounds assume the triclinic structure with a non-statistical distribution of halide ions. Qualitatively, the magnetic behavior of these salts is similar to that of the pure compounds, with the temperature at which χ_{max} occurs increasing monotonically as the fraction of bromide ion in the salts increased. Since the distribution of halide ions is disordered (although not completely random), these systems are, in principle, examples of spin 1/2 system random chains with dimerization ($\chi \sim T^{-\gamma}$, with γ varying continuously). However, for this to be observed, the width of the distribution of exchange parameters must be greater than twice the value of the average exchange coupling [17]. This is not the case here. Thus, the data were analyzed in the same manner as the pure salts, modeled as an AAFM chain with a relatively small paramagnetic impurity. The results are summarized in Table 2 and in Fig. 8. It is seen that J_1/k increases nearly linearly with the bromide content, to a maximum value near −163 K.

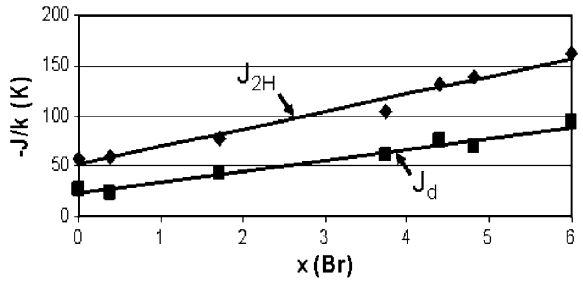

Fig. 8. Plot of the exchange constants for the alternating AFM chains. Solid lines are guides to the eye only.

5. Discussion

Although three possible exchange pathways can be identified from the structural analyses in these compounds, the analyses of the magnetic data clearly indicate that only two of these pathways contribute substantially to the magnetic behavior. Based on the arguments presented in the previous section, only two pathways will be considered here; the intradimer coupling, J_d, and the halide···halide coupling, J_{2H}. Unfortunately, the thermodynamic measurement of the magnetic susceptibility does not allow a definitive assignment correlation between the magnetic exchange parameters, J_1 and J_2, and the structural pathways, J_d and J_{2H}. Nevertheless, qualitative arguments can be made as to the appropriate assignment.

Structurally, it is observed that the Cu–X···X contacts are essentially linear, in contrast to other dimer systems where the effect of the 2H exchange pathways have been investigated [8]. This linear geometry is similar to that observed in the (diammonium)CuX_4 salts, where very strong AFM exchange is observed for X···X distances similar to those reported here [1–3]. In the latter, the AFM exchange arises through overlap of b_{1g}^* orbitals. It is known from EPR experiments that ~50% of the magnetic electron density in these orbitals is delocalized into the ligand p_σ orbitals. A similar delocalization into the p_σ orbitals of the terminal halide ions is anticipated in the pseudo-planar dimeric species. Thus, extremely strong AFM coupling is anticipated via the 2H pathways in these compounds.

It has been observed in studies of the 2H exchange in the diammonium layer perovskite salts, and in salts containing the distorted tetrahedral CuX_4^{2-} anions, that the 2H exchange coupling is typically 5–7 times larger for bromide salts than the corresponding chloride salts when the X···X distances are the same [1–3]. Table 2 shows that the X···X distances decrease slightly when the chloride ligand is replaced by bromide. Thus, for the (BIPY)$Cu_2Cl_{6-x}Br_x$ salts with substantial percentage Br, the larger exchange constant, J_1, is clearly associated with J_{2H}.

For the (BIPY)Cu_2Cl_6 salt the observed value of J_2 is consistent with the intradimer coupling observed in the spin liquid dimer system in $KCuCl_3$ [8b]. Thus, it is likely that for the pure chloride salt, that the intradimer coupling is associated with J_2 and the exchange in the 2H pathway is given by J_1. Thus, the association of exchange pathways with exchange parameters is as shown in Fig. 8.

In summary, this study has further elucidated the crucial role of the 2H exchange pathways in the determination of the magnetic behavior of copper halide dimers. The specific contribution of this study is the conclusion that the 2H pathway can become the dominant exchange pathway in the bromide dimers. Thus, discussions of the interpretation of the magnetic behavior of copper halide dimer systems must take this pathway into consideration.

Acknowledgments

Work supported in part by ACS-PRF 34779-AC5. The SQUID Magnetometer at Clark University was purchased with funds from the NSF(DMR-0314773) and from the Kreske Foundation.

Appendix A. Supplementary data

Crystallographic data for the mixed halide structures reported here have been deposited with the Cambridge Crystallographic Data Center as Supplementary Publication Nos. CCDC-282099 through CCDC-282108. Copies of this information may be obtained free of charge from: The Director, CCDC, 12 Union Road, Cambridge, CB2 1EZ, UK (fax: +44 1223 336 033; e-mail: deposit@ccdc.cam.ac.uk or www.ccdc.cam.ac.uk). Supplementary data associated with this article can be found, in the online version, at doi:10.1016/j.poly.2006.01.005.

References

[1] K. Halvorson, R.D. Willett, Acta Crystallogr. C44 (1988) 2071.
[2] (a) L.O. Snively, G. Tuthill, J.E. Drumheller, Phys. Rev. B 24 (1981) 5349;
(b) R. Block, L. Jansen, Phys. Rev. B 26 (1982) 148;
(c) P. Straatman, R. Block, L. Jansen, Phys. Rev. B 29 (1984) 1415.
[3] P. Straatman, R. Block, L. Jenson, Phys. Rev. B 29 (1984) 1415.
[4] (a) A.S. Albrecht, C.P. Landee, Z. Slanic, M.M. Turnbull, Mol. Cryst. Liq. Cryst. 305 (1997) 333;
(b) M.M. Turnbull, A.S. Albrecht, G.B. Jameson, C.P. Landee, Mol. Cryst. Liq. Cryst. 335 (1999) 245;
(c) T. Matsumoto, Y. Miyazaki, A.S. Albrecht, C.P. Landee, M.M. Turnbull, M. Sorai, J. Phys. Chem. B 104 (2000) 9993.
[5] (a) B.R. Patyal, B. Scott, R.D. Willett, Phys. Rev. B 41 (1990) 1657;
(b) B.C. Watson, V.N. Kotov, M.W. Meisel, D.W. Hall, G.E. Granoth, W.T. Montfrooij, S.E. Nagler, D.A. Jensen, R. Backov, M.A. Petruska, G.E. Fanucci, D.R. Talham, Phys. Rev. Lett. 86 (2001) 5168;
(c) C.P. Landee, M.M. Turnbull, C. Galeriu, J. Giantsidis, F.M. Woodward, Phys. Rev. B, Rapid Commun. 63 (2001) 100402R;
(d) M.M. Turnbull, C. Galeriu, J. Giantsidis, C.P. Landee, Mol. Cryst. Liq. Cryst. 376 (2002) 469;
(e) R.D. Willett, C. Galeriu, C.P. Landee, M.M. Turnbull, B. Twamley, Inorg. Chem. 43 (2004) 3804.
[6] (a) R.D. Willett, Inorg. Chem. 25 (1986) 1918;
(b) R.D. Willett, T. Grigereit, K.E. Halvorson, B. Scott, Proc. Indian Acad. Sci. 98 (1987) 147;
(c) B. Scott, R.D. Willett, J. Appl. Phys. 61 (1987) 3289;
(d) B. Scott, R.D. Willett, Inorg. Chim. Acta 141 (1988) 193;
(e) T. Grigereit, J.E. Drumheller, B. Scott, G. Pon, R.D. Willett, J. Magn. Magn. Mater. 104-107 (1992) 1.
[7] (a) H. Manaka, I. Yamada, K. Yamaguchi, J. Phys. Soc. Jpn. 63 (1997) 564;
(b) H. Manaka, I. Yamada, M. Hagiwara, M. Tokunaga, Phys. Rev. B 63 (2001) 144428;
(c) H. Manaka, I. Yamada, Z. Honda, H. Katori, K. Katsumata, J. Phys. Soc. Jpn. 67 (1998) 3913;
(d) H. Manaka, I. Yamada, N.V. Musunikow, T. Goto, J. Phys. Soc. Jpn. 69 (2001) 675;
(e) H. Manaka, I. Yamada, H. Katori, Phys. Rev. B 63 (2001) 104408.

[8] (a) M.B. Stone, I. Zaliznyak, D.H. Reich, C. Broholm, Phys. Rev. B 64 (2001) 144405;
(b) N. Cavadini, G. Heigold, W. Henggelert, A. Furrer, H.-U. Güdel, J. Phys.: Condens. Matter 12 (2000) 5463.
[9] R.T. Butcher, R.D. Willett, C.P. Landee, B. Twamley, Polyhedron (in press).
[10] (a) C. Näther, I. Jeß, M. Bolte, Acta Crystallogr. E57 (2001) m78;
(b) J. Mroziski, M. Bukowska-Strzyewska, J. Mol. Struct. 65 (1980) 277;
(c) A. Tosik, M. Bukowska-Strzyewska, J. Mroziski, J. Coord. Chem. 21 (1990) 253.
[11] Bruker, SMART Version 5.626, Bruker AXS Inc., Madison, WI, USA, 1996.
[12] Bruker, SAINT-PLUS Version 6.22, Bruker AXS Inc., Madison, WI, USA, 1996.
[13] Bruker, SADABS Version 2.03, Bruker AXS Inc., Madison, WI, USA, 1996.
[14] Bruker, SHELXTL (including XPREP, XCIF, XL, XP, XS). Version 6.10, Bruker AXS Inc., Madison, WI, USA, 2001.
[15] XSCANS, Version 2.00, Siemen Analytical X-ray Instrument Inc., Madison, WI, USA, 1993.
[16] J.W. Hall, W.E. Marsh, R.R. Weller, W.E. Hatfield, Inorg. Chem. 20 (1981) 1033.
[17] S. Todo, K. Kato, H. Takayama, in: D.P. Landau, H.-B. Schüttler (Eds.), Computer Simulation Studies in Condensed Matter Physics XI, Springer, Heidelberg, Berlin, 1998.

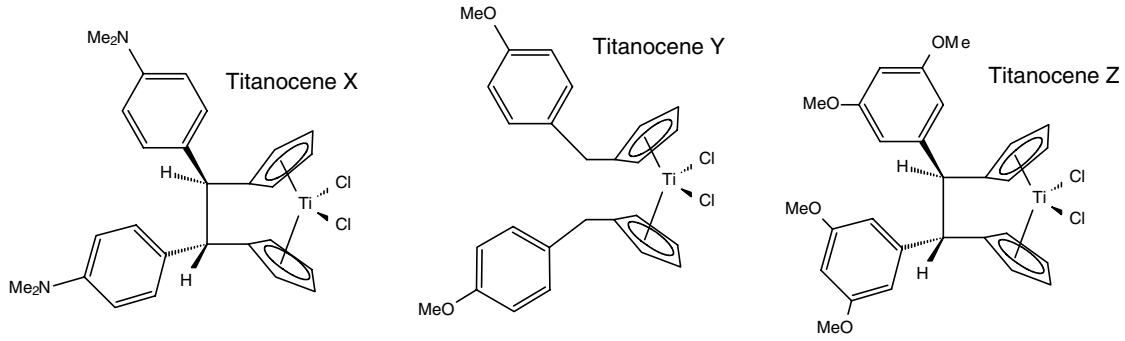

Fig. 1. Structure of Titanocene **X**, **Y** and **Z**.

substituted titanocenes as possible anti-cancer drugs using substituted benzyl lithium, benzyl substituted fulvenes and titanium tetrachloride, resulting in the formation of unbridged diarylmethyl substituted titanocenes. The optimised synthesis, underlined by quantum chemical calculations, and first results of very promising in vitro studies will be shown.

2. Experimental

2.1. General conditions

Titanium tetrachloride (1.0 M solution in toluene) and *tert*-butyl lithium (1.7 M solution in cyclohexane) were obtained commercially from Aldrich Chemical Co. THF was dried over Na and benzophenone and it was freshly distilled and collected under an atmosphere of argon prior to use. Manipulations of air and moisture sensitive compounds were done using standard Schlenk techniques, under an argon atmosphere. NMR spectra were measured on either a Varian 300 or a 500 MHz spectrometer. Chemical shifts are reported in ppm and are referenced to TMS. IR spectra were recorded on a Perkin–Elmer Paragon 1000 FT-IR Spectrometer employing a KBr disk. UV–Vis spectra were recorded on a Unicam UV4 Spectrometer.

2.2. Synthesis

6-(*p*-*N*,*N*-Dimethylanilinyl)fulvene (**3a**), 6-*p*-(methoxyphenyl)fulvene (**3b**) and 3,5-dimethoxyphenyl fulvene (**3c**) were synthesised according to the already published procedures [21,23].

2.3. Bis-[di-(p-N,N-dimethylaminophenyl)-methylcyclopentadienyl] titanium (IV) dichloride, $\{\eta^5\text{-}C_5H_4\text{–}CH\text{–}[C_6H_4\text{–}N(CH_3)_2]_2\}_2TiCl_2$ (*5a*)

To a Schlenk flask with 1.00 g (5.18 mmol) of 4-bromo-*N*,*N*-dimethylaniline (**1a**), 20 ml of THF was added until a transparent solution was formed, while stirring. The solution was cooled down to −78 °C for 15 min and 3.30 ml (5.57 mmol) of *tert*-butyl lithium was added. The solution was warmed up to 0 °C for 20 min, resulting in the formation of the yellow lithium intermediate (**2a**).

In a second Schlenk flask, 1.00 g (5.07 mmol) of 6-(*p*-*N*,*N*-dimethylanilinyl)fulvene (**3a**) was dissolved in 25 ml of THF and the resultant red solution was added via a *cannula* at −78 °C to the Schlenk flask containing the lithiated intermediate (**2a**). The reaction mixture was allowed to warm up to room temperature and left stirring for 40 min. Afterwards, 2.53 ml (2.53 mmol) of titanium tetrachloride was added at room temperature and the mixture was refluxed for 24 h. The solvent was removed under vacuum, resulting in a dark brown precipitate. This precipitate was dissolved in dichloromethane and filtered through celite to remove the LiCl, followed by two gravity filtrations. The solvent was removed under reduced pressure forming a shiny black solid (**5a**), which was washed with 150 ml of pentane and then dried in vacuo (2.05 g, 2.82 mmol, 55.1% yield).

^{1}H NMR (δ ppm $CDCl_3$, 300 MHz): 6.95 [d, 8H, *J* 8.68 Hz, $C_6H_4N(CH_3)_2$]; 6.74 [d, 8H, *J* 7.53 Hz, $C_6H_4N(CH_3)_2$]; 5.92–5.56 [m, 8H, C_5H_4]; 5.52 [s, 2H, C_5H_4–C*H*–($C_6H_4N(CH_3)_2$)$_2$]; 2.92 [s, 24H, $C_6H_4N(CH_3)_2$].

^{13}C NMR (δ ppm $CDCl_3$, 125 MHz): 148.2, 141.5, 133.2, 129.69, 129.68, 120.44, 113.4 [C_5H_4 and C_6H_4]; 50.3 [$C_6H_4N(CH_3)_2$]; 41.3 [Cp–*C*H–($C_6H_4N(CH_3)_2$)$_2$].

IR absorptions (cm^{-1} KBr): 3100, 3085, 2920, 2852, 1593, 1488, 1478, 1440, 1345, 1163, 1128, 802, 548, 527.

Anal. Calc. for $C_{44}H_{50}N_4Cl_2Ti$: Theory: C, 70.25; H, 6.94; N, 7.45; Cl, 4.71. Found: C, 70.00; H, 6.90; N, 7.40; Cl, 4.71%.

UV–Vis (CH_2Cl_2/ε:[cm^2/mol]): λ 230 nm (ε 22 770), λ 402 nm (ε 2020), λ 509 nm (ε 210), λ_{max} 521 nm (weak).

2.4. Bis-[di-(p-methoxyphenyl)methylcyclopentadienyl] titanium (IV) dichloride, $\{\eta^5\text{-}C_5H_4\text{–}CH\text{–}[C_6H_4\text{–}O\text{–}CH_3]_2\}_2TiCl_2$ (*5b*)

To a Schlenk flask with 1.5 ml (5.43 μmol) of 4-bromoanisole (**1b**), 20 ml of THF was added until a transparent solution was formed, while stirring at room temperature. The solution was cooled down to −78 °C for 15 min and 5.3 ml (85.7 μmol) of *tert*-butyl lithium was added. The

solution was allowed to warm up to 0 °C for 20 min, resulting in the formation of the yellow lithium intermediate (**2b**).

In a second Schlenk flask, 1.00 g (5.43 mmol) of *p*-(methoxyphenyl)fulvene (**3b**) was dissolved in 25 ml of THF and the resultant red solution was added via a *cannula* at −78 °C to the Schlenk flask containing the lithiated intermediate. The reaction mixture was then allowed to warm up to room temperature and left for stirring for 40 min. Titanium tetrachloride (2.7 ml, 2.715 mmol) was added afterwards in situ at room temperature and the mixture was refluxed for 24 h. Subsequently, the solvent was removed under vacuum, resulting in the formation of a dark brown to black precipitate. This precipitate was dissolved in dichloromethane and filtered through celite to remove the LiCl, followed by two gravity filtrations. The solvent was removed under reduced pressure forming a shiny black solid (**5b**), which was washed with pentane and then dried in vacuo (3.83 g, 5.45 mmol, 43.5% yield).

^{1}H NMR (δ ppm $CDCl_3$, 300 MHz): 6.96 [d, 8H, *J* 8.68 Hz, $C_6H_4OCH_3$]; 6.74 [d, 8H, *J* 7.53 Hz, $C_6H_4OCH_3$]; 5.92–5.56 [m, 8H, C_5H_4]; 5.52 [s, 2H, C_5H_4–C*H*–$(C_6H_4OCH_3)_2$]; 2.92 [s, 12H, $C_6H_4OCH_3$].

^{13}C NMR (δ ppm $CDCl_3$, 125 MHz): 158.5, 141.5, 135.9, 130.13, 130.12, 120.3, 114.0 [C_5H_4 and C_6H_4]; 55.4 [$C_6H_4OCH_3$]; 50.7 [Cp–*C*H–$(C_6H_4OCH_3)_2$].

IR absorptions (cm^{-1} KBr): 3100, 3085, 2929, 2832, 1606, 1502, 1461, 1301, 1176, 1108, 1033, 827, 771, 527.

Anal. Calc. for $C_{40}H_{38}O_4Cl_2Ti$: Theory: C, 68.50; H, 5.46; Cl, 10.11. Found: C, 68.34; H, 5.46; Cl, 10.09%.

UV–Vis (CH_2Cl_2/ε:[cm^2/mol]): λ 268 nm (ε 21 000), λ 393 nm (ε 1070) λ 404 nm (ε 1120), λ 509 nm (ε 210), λ_{max} 523 nm (weak).

2.5. Bis-[di-(3,5-dimethoxyphenyl)methylcyclopentadienyl] titanium (IV) dichloride, {η^5-C_5H_4–CH–[C_6H_4–$(OCH_3)_2$]$_2$}$_2$$TiCl_2$ (5c)

To a Schlenk flask with 1.32 g (4.66 mmol) of 1-bromo-3,5-dimethoxybenzene (**1c**), 20 ml of THF was added until a transparent solution was formed, while stirring at room temperature. The solution was cooled down to −78 °C for 15 min and 3.02 ml (5.13 mmol) of *tert*-butyl lithium was added. The solution was allowed to warm up to 0 °C for 20 min, resulting in the formation of the yellow lithium intermediate (**2c**).

In a second Schlenk flask, 0.92 g (4.66 mmol) of 3,5-dimethoxyphenylfulvene (**3c**) was dissolved in THF, and the resultant red solution was added via a *cannula* at −78 °C to the Schlenk flask containing the lithiated intermediate. The reaction mixture was then allowed to warm up to room temperature and left stirring for 40 min. Titanium tetrachloride (2.33 ml, 2.33 mmol) was added afterwards in situ at room temperature and the mixture was refluxed for 24 h. Subsequently, the solvent was removed under vacuum, resulting in the formation of a dark green oil that was dissolved in dichloromethane and filtered through celite to remove the LiCl. The black filtrate was filtered additionally twice by gravity filtration. The solvent was removed under reduced pressure forming a shiny black solid (**5c**), which was washed with 20 ml of pentane and then dried in vacuo (3.33 g, 4.05 mmol, 43.5% yield).

^{1}H NMR (δ ppm $CDCl_3$, 300 MHz): 7.18 [t, 4H, *J* 2.24 Hz, $C_6H_3(OCH_3)_2$]; 6.61 [dd, 4H, J_1 6.61 Hz, J_2 2.23 Hz, $C_6H_3(OCH_3)_2$]; 6.49 [dd, 4H, J_1 6.61 Hz, J_2 2.42 Hz, $C_6H_3(OCH_3)_2$]; 6.53 [d, 4H, *J* 2.23 Hz, C_5H_4–CH–$(C_6H_3(OCH_3)_2)$]; 6.52 [d, 4H, *J* 2.23 Hz, C_5H_4–CH–$(C_6H_3(OCH_3)_2)$]; 5.29 [s, 2H, C_5H_4–C*H*–$(C_6H_3(OCH_3)_2)$]; 3.72 [m, 24H, $C_6H_3(OCH_3)_2$].

^{13}C NMR (δ ppm $CDCl_3$, 500 MHz): 161.1, 160.7, 129.9, 122.9, 109.9, 109.6, 106.0, 100.2, 99.6 [C_5H_4 and C_6H_3]; 56.33, 56.26 [$C_6H_3(OCH_3)_2$]; 33.9 [Cp–*C*H–$(C_6H_3(OCH_3)_2)_2$]. (The rotation of the 3,5-dimethoxyphenyl group is hindered.)

IR absorptions (cm^{-1} KBr): 2931, 2832, 1606, 1509, 1461, 1425, 1299, 1174, 1108, 1031, 831.

Anal. Calc. for $C_{44}H_{46}O_8Cl_2Ti$: Theory: C, 64.32; H, 5.64; Cl, 8.62. Found: C, 64.14; H, 5.60; Cl, 8.57%.

UV–Vis (CH_2Cl_2/ε:[cm^2/mol]): λ 275 nm (ε 79 830), λ 378 nm (ε 17 830), λ 525 nm (ε 3820), λ 580 nm (weak), λ_{max} 685 nm (weak).

3. Results and discussion

3.1. Synthesis

Fulvenes **3a**, **3b**, and **3c** were synthesised by reacting the corresponding benzaldehyde with freshly distilled cyclopentadiene in the presence of pyrrolidine as a base [21,23] and their structures are shown in Fig. 2.

The use of aryl lithium species for asymmetric addition in the synthesis of other metallocenes has been previously published [28–31]. This time, the method is used as a straightforward approach for the synthesis of diarylmethyl substituted metallocenes, as seen with titanocenes **5a**–**c** (Fig. 3).

The first step of the reaction consists of a bromine–lithium exchange, in which the use of *tert*-butyl lithium resulted in the formation of the functionalised lithium intermediates **2a**–**c**, obtaining better yields and no side-reactions in comparison to *n*-butyl lithium. Side-reactions were also avoided by cooling down the reaction to −78 °C during the addition of *tert*-butyl lithium and subsequent warming up to 0 °C.

This step was followed by the nucleophilic addition of the lithiated intermediate to the double bond of the fulvenes **3a**, **3b** or **3c** at −78 °C. Then, the reaction mixture was allowed to warm up to room temperature and it resulted in the formation of the appropriate substituted lithium cyclopentadienyl intermediates, **4a**–**c**. After stirring the reaction mixture for 40 min, two molar equivalents of **4a, 4b** or **4c** underwent a transmetallation reaction when reacted with one molar equivalent of $TiCl_4$ in THF under reflux for 24 h, to give the appropriate unbridged

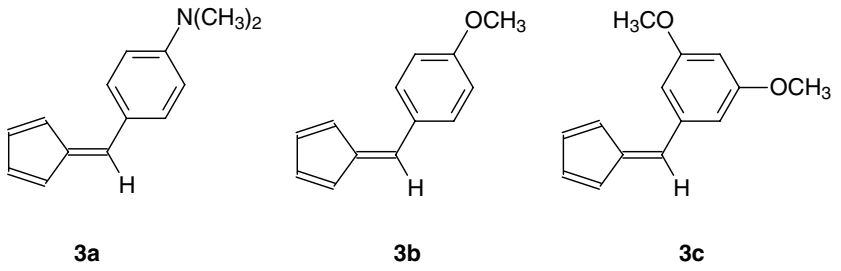

3a **3b** **3c**

Fig. 2. Structure of fulvenes **3a**–**c**.

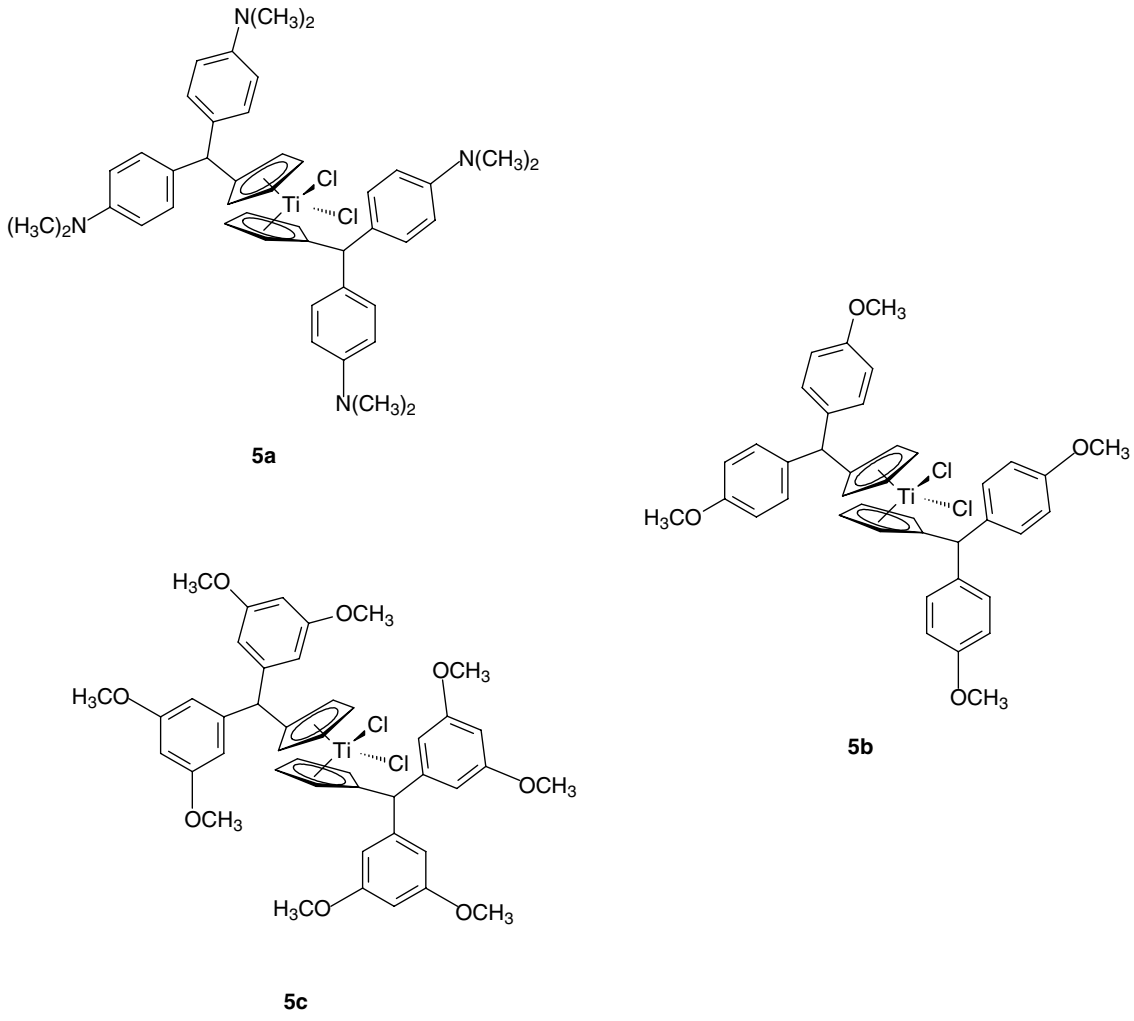

5a **5b** **5c**

Fig. 3. Structure of Titanocenes **5a**–**c**.

substituted titanocenes, **5a**–**c**. The compounds obtained are shiny dark red to dark brown solids (Scheme 1).

3.2. Structural discussion

Despite our attempts to crystallise these three titanocenes, only one crystal structure for **5a** was obtained. Unfortunately, this crystal structure was not publishable. Nevertheless, the principal molecular structure of **5a** could be proven and even the pyramidal carbons 6 and 6′ could be observed (see Scheme 2), as the single methylic protons were sitting on their respective carbons.

In order to overcome the problem of missing crystal structures, density functional theory (DFT) calculations were carried out for titanocenes **5a** and **5b** at the B3LYP level using the 6-31G** basis set. Selected bond lengths of the optimised structures of these titanocenes are listed in Table 1 (for atom numbering, see Scheme 2). The molecular structures of **5a** and **5b** are presented in Fig. 4.

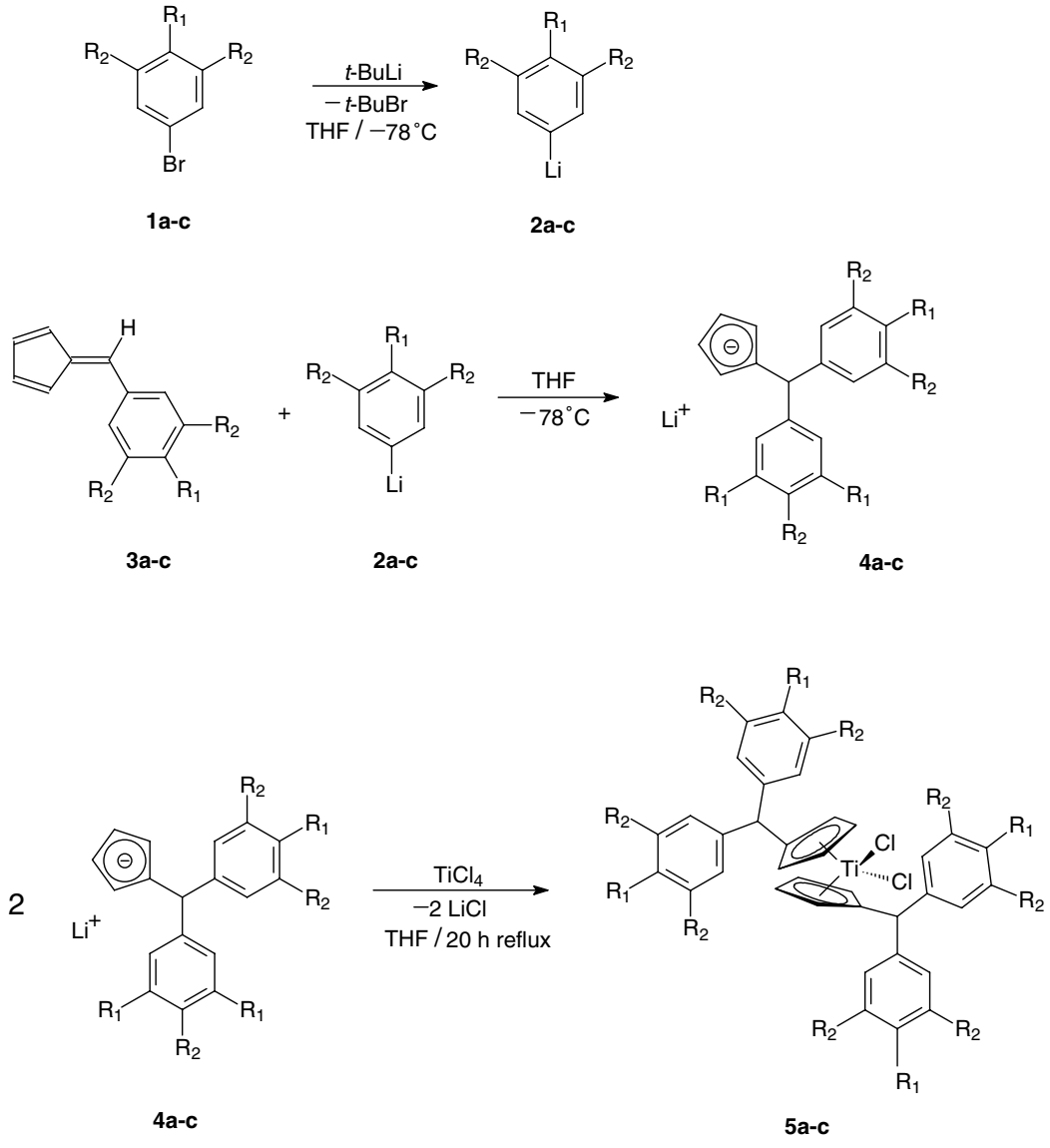

	1-5a	1-5b	1-5c
R_1	-$N(CH_3)_2$	-OCH_3	H
R_2	H	H	-OCH_3

Scheme 1. Synthesis of Titanocenes **5a**–**c**.

The length of the bond between the metal centre and the cyclopentadienyl carbons is similar for both titanocene structures. They vary between 237.9–249.9 pm for **5a** and 238.1–250.3 pm for **5b** with slightly different values for the different Cp rings. The same applies for the carbon–carbon bonds of the cyclopentadienyl rings with bond lengths between 141.0–141.9 pm for **5a** and 141.0–143.6 pm for **5b**. These values suggest that the titanocenes have a plane of symmetry bisecting the Cl–Ti–Cl plane and the calculated structures exhibit C_2 symmetry.

The bond length between the methylic carbon centre and the carbon centre of the Cp group is similar for both titanocenes within the range of 152.3–152.4 pm and the same occurs for the methylic carbon–aryl bond (153.0–153.7 pm).

The steric impediment of the aryls attached to the methylic carbons causes a lengthening of the bond, in order to relieve the resultant steric strain. The bond length between the methylic carbons is in both cases too large to suggest any bridge formation, 424.3 pm for **5a** and 432.7 pm for **5b**. As well the titanium–chlorine bond lengths are almost identical in both cases.

The Cl–Ti–Cl angle was calculated for **5a** to be 94.4° and 96.9° for **5b**. For **5a**, the angle formed by the bonds

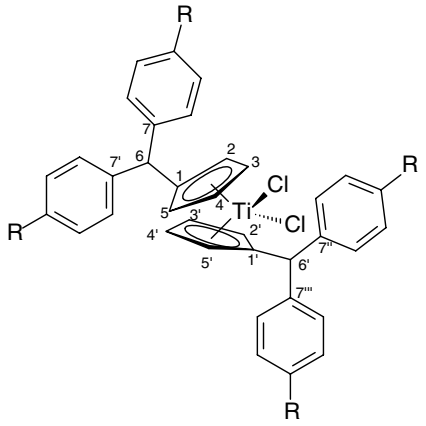

	5a	5b
R	-N(CH$_3$)$_2$	-OCH$_3$

Scheme 2. Numbering scheme for structural discussion of titanocenes **5a** and **5b**.

Table 1
Selected bond lengths from the DFT-calculated structures of complexes **5a** and **5b**

	DFT structure	
	Bond length (pm) **5a**	Bond length (pm) **5b**
Ti–C(1)	249.9	250.3
Ti–C(2)	242.4	244.7
Ti–C(3)	239.5	238.1
Ti–C(4)	237.9	240.1
Ti–C(5)	244.7	242.5
Ti–C(1′)	247.6	247.3
Ti–C(2′)	246.5	246.6
Ti–C(3′)	240.6	240.8
Ti–C(4′)	239.8	239.9
Ti–C(5′)	238.9	238.6
C(1)–C(2)	143.3	141.5
C(2)–C(3)	141.1	142.0
C(3)–C(4)	141.6	141.5
C(4)–C(5)	141.9	141.2
C(5)–C(1)	141.6	143.4
C(1′)–C(2′)	141.6	141.6
C(2′)–C(3′)	141.9	141.9
C(3′)–C(4′)	141.4	141.4
C(4′)–C(5′)	141.0	141.0
C(5)–C(1′)	141.3	143.4
C(1)–C(6)	152.4	152.4
C(1′)–C(6′)	152.3	152.4
C(6)–C(6′)	432.7	424.3
C(6)–C(7)	153.5	153.4
C(6)–C(7′)	153.0	153.6
C(6′)–C(7″)	153.5	153.0
C(6′)–C(7‴)	153.5	153.7
Ti–Cl(1)	237.5	237.2
Ti–Cl(2)	236.0	235.7

between C(6), C(7) and C(7′) is 112.7°, and the angle formed between C(6′), C(7″) and C(7‴) is 111.4°. The corresponding calculated values for **5b** are 111.9° and 111.4°. The angle between C(1) or C(1′), the correspondent methylic atom, and C(7) or C(7‴), respectively, is smaller than the one formed by C(1) or C(1′), the correspondent methylic atom, and C(7′) or (C7″), respectively, by approximately 10° in both **5a** and **5b**, due to the steric impediment.

3.3. Cytotoxicity studies

The in vitro cytotoxicity of compounds **5a–c** was determined by MTT-based assays involving a 48 h drug exposure period, followed by 24 h of recovery time [32]. The compounds were tested for their activity on pig kidney carcinoma (LLC-PK) cells and the results are shown in Fig. 5. Compound **5a**, which contains dimethyl amino groups, has an IC_{50} value of 3.8×10^{-5} M, showing a higher cytotoxicity than its *ansa* and mono-benzyl substituted analogues. The *ansa* analogue of **5a**, compound Titanocene **X**, has an IC_{50} value of 4.5×10^{-4} M and the mono-benzyl substituted analogue has an IC_{50} value of 1.2×10^{-4} M. Compound **5b**, which contains *p*-methoxy groups, shows an IC_{50} value of 4.5×10^{-5} M, very similar to the value obtained for by the mono-benzyl substituted analogue Titanocene **Y**, that showed the most significant IC_{50} value of 2.1×10^{-5} M up to now. Compound **5c**, which we expected to have an increased aqueous solubility and consequently increased cytotoxicity due to the higher number of methoxy groups, has an IC_{50} value of 7.8×10^{-5} M, which shows a slight decrease in magnitude in comparison to **5a** and **5b**. It must also be noted that the cytotoxic action of **5a**, **5b** and **5c** differs from the mono-benzyl substituted analogue Titanocene **Y**: at lower concentrations the compounds show a less effective cell death induction than Titanocene **Y**.

The best compound in this series, titanocene **5a**, has an over 10-fold decrease in magnitude in terms of IC_{50} values when compared to the unsubstituted titanocene dichloride. Compared to the value for *cis*-platin, the IC_{50} value for these titanocenes shows an increase of approximately 6.4 in the order of magnitude when tested on the LLC-PK cell line.

Titanocenes **5a–c** presented in this paper do not have stereocentres and therefore stereoisomers do not exist, unlike their *ansa* analogues. But for **5c**, the rotation of the 3,5-dimethoxyphenyl groups was found to be hindered, which explains the NMR-spectroscopic results. In terms of in vivo and in vitro cell testing, this is advantageous. Previously, the presence of unseparated stereoisomers means that the issue of whether the compounds' cytotoxicities are related to specific isomers was not addressed. This is not of concern in the achiral bis-benzyl-substituted titanocenes **5a–c**.

4. Conclusions and outlook

The carbolithiation of 6-arylfulvenes with aryl lithium species followed by transmetallation offers a general way into the synthesis of achiral diarylmethyl substituted metallocenes. In the case of methoxy or dimethylamino substituents and titanium(IV) as the central metal, these

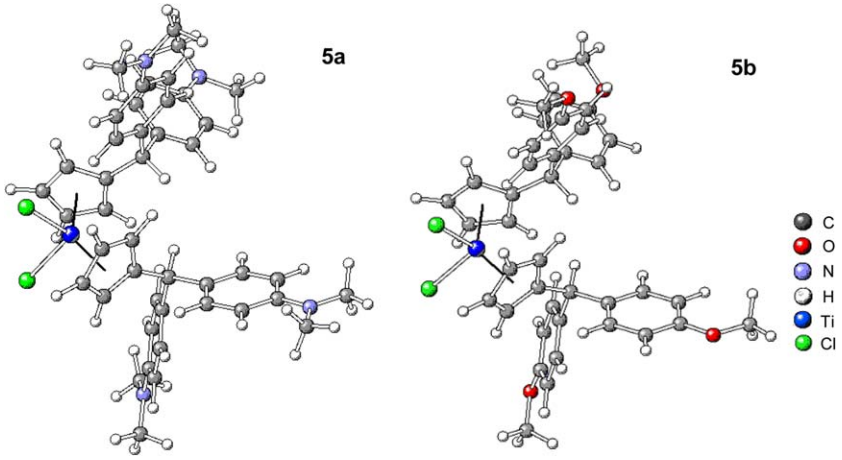

Fig. 4. DFT calculated structures of **5a** and **5b**.

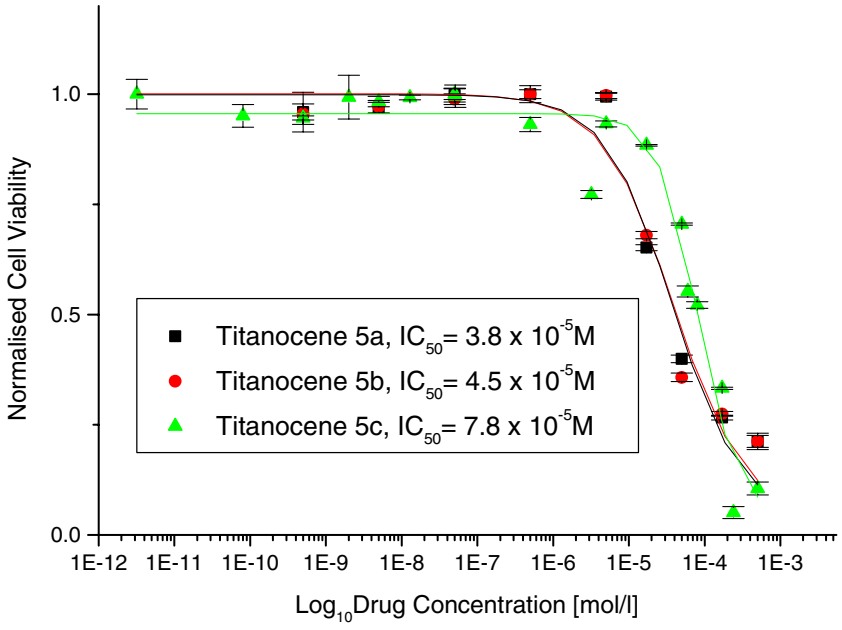

Fig. 5. MTT-based cytotoxicity curves show the effect of compounds **5a–c** on pig kidney carcinoma (LLC-PK) cells.

compounds exhibit significant cytotoxicity against kidney cancer cells with IC_{50} values in the 10^{-5} M region, which makes them already promising anti-cancer drugs. Nevertheless, it is intended to employ this carbolithiation method for future synthesis of titanocenes exhibiting cytotoxicities in the single digit μM region.

Acknowledgements

The authors thank Science Foundation Ireland (SFI) for funding through grant (04/BRG/C0682). In addition, funding from the Higher Education Authority (HEA) and the Centre for Synthesis and Chemical Biology (CSCB) through the HEA PRTLI cycle 3 as well as COST D20 (WG 0001) was provided. The authors also thank Dr. W.M. Gallagher of the Department of Pharmacology, Conway Institute of Biomolecular and Biomedical Research, UCD, for the use of tissue culture facilities for the cell testing experiments and for his advice on the subject.

Appendix A. Supplementary data

Supplementary data associated with this article can be found, in the online version, at doi:10.1016/j.poly.2006.01.007.

References

[1] A. Gelasco, S.J. Lippard, Top. Biol. Inorg. Chem. 1 (1999) 1.
[2] E.R. Jamieson, S.J. Lippard, Chem. Rev. 99 (1999) 2467.
[3] N. Farrell, Y. Qu, J.D. Roberts, Top. Biol. Inorg. Chem. 1 (1999) 99.

[4] P. Köpf-Maier, H. Köpf, Chem. Rev. 87 (1987) 1137.
[5] P. Köpf-Maier, H. Köpf, Struct. Bonding 70 (1988) 105.
[6] G. Lummen, H. Sperling, H. Luboldt, T. Otto, H. Rubben, Cancer Chemother. Pharmacol. 42 (1998) 415.
[7] N. Kröger, U.R. Kleeberg, K. Mross, L. Edler, G. Saß, D.K. Hossfeld, Onkologie 23 (2000) 60.
[8] G. Mokdsi, M.M. Harding, Metal-Based Drugs 5 (1998) 207.
[9] O.R. Allen, L. Croll, A.L. Gott, R.J. Knox, P.C. McGowan, Organometallics 23 (2004) 288.
[10] R.J. Boyles, M.C. Baird, B.G. Campling, N. Jain, J. Inorg. Biochem. 84 (2001) 159.
[11] P.W. Causey, M.C. Baird, Organometallics 23 (2004) 4486.
[12] R. Meyer, S. Brink, C.E.J. van Rensburg, G.K. Joone, H. Görls, S. Lotz, J. Organomet. Chem. 690 (2005) 117.
[13] R. Teuber, G. Linti, M. Tacke, J. Organomet. Chem. 545–546 (1997) 105.
[14] F. Hartl, L. Cuffe, J.P. Dunne, S. Fox, T. Mahabiersing, M. Tacke, J. Mol. Structure 559 (2001) 331.
[15] M. Tacke, J.P. Dunne, S. Fox, G. Linti, R. Teuber, J. Mol. Structure 570 (2001) 197.
[16] S. Fox, J.P. Dunne, R. Dronskowski, D. Schmitz, M. Tacke, Eur. J. Inorg. Chem. (2002) 3039.
[17] J.J. Eisch, S. Xian, F.A. Owuor, Organometallics 17 (1998) 5219.
[18] J.J. Eisch, F.A. Owuor, S. Xian, Organometallics 18 (1999) 1583.
[19] K.M. Kane, P.J. Shapiro, A. Vij, R. Cubbon, A.L. Rheingold, Organometallics 16 (1997) 4571.
[20] S. Fox, J.P. Dunne, M. Tacke, J.F. Gallagher, Inorg. Chim. Acta 357 (2004) 225.
[21] M. Tacke, L.T. Allen, L.P. Cuffe, W.M. Gallagher, Y. Lou, O. Mendoza, H. Müller-Bunz, F.-J.K. Rehmann, N. Sweeney, J. Organomet. Chem. 689 (2004) 2242.
[22] F.-J.K. Rehmann, L.P. Cuffe, O. Mendoza, D.K. Rai, N. Sweeney, K. Strohfeldt, W.M. Gallagher, M. Tacke, Appl. Organomet. Chem. 19 (2005) 293.
[23] M. Tacke, L.P. Cuffe, W.M. Gallagher, Y. Lou, O. Mendoza, H. Müller-Bunz, F.-J.K. Rehmann, N. Sweeney, J. Inorg. Biochem. 98 (2004) 1987.
[24] F.-J.K. Rehmann, A.J. Rous, O. Mendoza, N.J. Sweeney, K. Strohfeldt, W.M. Gallagher, M. Tacke, Polyhedron 24 (2005) 1250.
[25] N. Sweeney, O. Mendoza, H. Müller-Bunz, C. Pampillón, F.-J.K. Rehmann, K. Strohfeldt, M. Tacke, J. Organomet.Chem. 690 (2005) 4537.
[26] G. Kelter, N. Sweeney, K. Strohfeldt, H.-H. Fiebig, M. Tacke, Anticancer Drugs 16 (2005) 1091.
[27] O. Oberschmidt, A.-R. Hanauske, F.-J.K. Rehmann, K. Strohfeldt, N. Sweeney, M. Tacke, Anticancer Drugs 16 (2005) 1071.
[28] T. Suzuka, M. Ogasawara, T. Hayashi, J. Org. Chem 67 (2002) 3355.
[29] Y. Qian, J. Huang, J. Yang, A.S.C. Chan, W. Chen, X. Chen, G. Li, X. Jin, Q. Yang, J. Organomet.Chem. 547 (1997) 263.
[30] M. Horacek, P. Stepnicka, S. Gentil, K. Fejfarova, J. Kubista, N. Pirio, P. Meunier, F. Gallou, L.A. Paquette, K. Mach, J. Organomet.Chem 656 (2002) 81.
[31] S. Knuppel, C. Wang, G. Kehr, R. Fröhlich, G. Erker, J.Organomet.Chem 690 (2005) 14.
[32] T. Mosmann, J. Immunol. Methods 65 (1983) 55.

ligands [8,12], and only one tantalum complex has been structurally documented that contains an η^2-trimethylhydrazido(1−) ligand [10]. We are interested in the development of new metalorganic film growth precursors for TaN, and also seek to understand the mechanistic paths by which simple tantalum precursors are converted to TaN films in a CVD process. Within this context, we describe the synthesis and structural characterization of a series of niobium and tantalum complexes that are obtained upon treatment of the metal pentachlorides with 1,1-dialkylhydrazine derivatives. Depending upon the nature of the alkyl groups and the presence or absence of tetramethylethylenediamine (TMEDA), cationic complexes of the formula $[M(NNR_2)Cl_2(NH_2NR_2)(TMEDA)]^+Cl^-$ and $[M(NN(CH_2)_5)Cl_2(NH_2N(CH_2)_5)_2]^+Cl^-$ were obtained. These complexes were structurally characterized and possess several hydrazido ligand coordination modes.

2. Results and discussion

2.1. Treatment of niobium and tantalum pentachloride with 1,1-dialkyl-2-trimethylsilylhydrazines and TMEDA

Dichloromethane solutions of metal pentachloride/TMEDA (1 equivalent each) and 1,1-dialkyl-2-trimethylsilylhydrazine (2 equivalents, alkyl = CH_3, $0.5C_5H_{10}$) were mixed at −78 °C, allowed to warm to ambient temperature, and then stirred for 18 h. Workup entailed removal of the volatile components under reduced pressure to eliminate the chlorotrimethylsilane product, followed by fractional crystallization from concentrated dichloromethane solutions. In this way, $[Nb(NNMe_2)Cl_2(NH_2NMe_2)(TMEDA)]Cl \cdot CH_2Cl_2$ (**1**, 30%), $[Ta(NNMe_2)Cl_2(NH_2NMe_2)(TMEDA)]Cl \cdot CH_2Cl_2$ (**2**, 27%), $[Nb(NN(CH_2)_5)Cl_2(NH_2N(CH_2)_5)(TMEDA)]Cl \cdot CH_2Cl_2$ (**3**, 13%), and $[Ta(NN(CH_2)_5)Cl_2(NH_2N(CH_2)_5)(TMEDA)]Cl \cdot CH_2Cl_2$ (**4**, 23%) were isolated as yellow crystalline solids (Eq. (1)). The crude products revealed mixtures of **1**–**4** with either 1,1-dimethylhydrazinium chloride (**1**, **2**) or 1-ammoniumpiperidine chloride (**3**, **4**). There were no other products observed in the ^1H NMR spectra of the crude reaction mixtures, suggesting very clean reactions. Yields of the crude product mixtures, including the hydrazinium salts, were 95–98%. The solubility characteristics of **1**–**4** were similar to those of the hydrazinium chloride salts, but selective crystallization of **1**–**4** from dichloromethane could be achieved after most of the slightly less soluble hydrazinium salts had precipitated. However, the yields of crystalline **1**–**4** were low because of the stringent control required to achieve selective crystallization. The formulations of **1**–**4** were based upon spectral and analytical data, as well as X-ray crystal structure determinations. Complexes **1**–**4** are cationic monomers in the solid state with a chloride counterion. One equivalent of dichloromethane solvate per metal center was present in the crystals of **1**–**4**. The ^1H and $^{13}C\{^1H\}$ NMR data for **1**–**4** are uniquely consistent with retention of the solid state structures in solution. For example, all of the methyl groups in **1** and **2** exist in different chemical environments, and eight methyl signals were observed in the $^{13}C\{^1H\}$ spectra. The $^{13}C\{^1H\}$ NMR spectra of **3** and **4** reveal resonances for 16 carbon atoms, which is consistent with the solid state structures. The ^1H and $^{13}C\{^1H\}$ NMR spectra for **1**–**4** also show the expected resonances for the dichloromethane solvate.

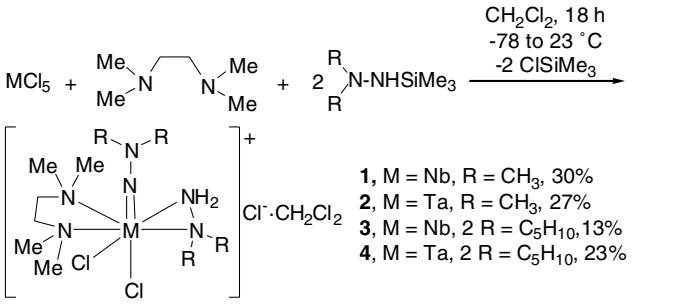

(1)

2.2. Treatment of niobium and tantalum pentachloride with 1-trimethylsilylaminopiperidine and 1-aminopiperidine

Experience gained from the syntheses of **1**–**4**, which showed that one equivalent of the neutral 1,1-dialkylhydrazine coordinates to the metal center to saturate the coordination sphere, suggested that stable complexes might be obtained without TMEDA if an additional equivalent of the 1,1-dialkylhydrazine was added to the reaction mixture. Accordingly, treatment of the metal pentachlorides with 1-trimethylsilylaminopiperidine (2 equivalents) and 1-aminopiperidine (1 equivalent) in dichloromethane at −78 °C, followed by stirring for 18 h at room temperature, afforded $[Nb(NN(CH_2)_5)Cl_2(NH_2N(CH_2)_5)_2]Cl \cdot [(CH_2Cl_2)(C_6H_{14})_{0.5}]$ (**5**, 61%) and $[Ta(NN(CH_2)_5)Cl_2(NH_2N(CH_2)_5)_2]Cl \cdot [(CH_2Cl_2)(C_6H_{14})_{0.5}]$ (**6**, 26%) as yellow crystalline solids (Eq. (2)). In **5** and **6**, two neutral 1-aminopiperidine ligands coordinate to the metal centers, which again leads to cationic complexes by elimination of a chloride ion from the inner coordination sphere. Like **1**–**4**, **5** and **6** were obtained as mixtures with the 1-ammoniumpiperidine salts. Accordingly, careful fractional crystallization was required to obtain pure materials, and reported yields are moderate to low. Structural assignments for **5** and **6** were based upon spectral and analytical data. An X-ray crystal structure determination was also performed for **5**. A low precision X-ray crystal structure analysis was performed on **6**, which confirmed a structure very similar to that of **5**. Complexes **5** and **6** both crystallize with one equivalent of dichloromethane and one-half equivalent of hexane in the asymmetric unit. The ^1H and $^{13}C\{^1H\}$ NMR spectra of **5** and **6** were consistent with the solid state structures. In **5** and **6**, there is a mirror plane that passes through the MCl_2 atoms, which makes the η^2-aminopiperidine ligands identical by symmetry. However, the five carbon atoms within each η^2-aminopiperidine ligand reside in different chemical environments, provided that exchange between the two faces of the piperidine fragment is slow on the NMR timescale. The ^1H

and $^{13}C\{^1H\}$ NMR spectra of **5** and **6** revealed sharp resonances for the 10 carbon atom sites, demonstrating that the exchange process for the η^2-aminopiperidine ligands is slow.

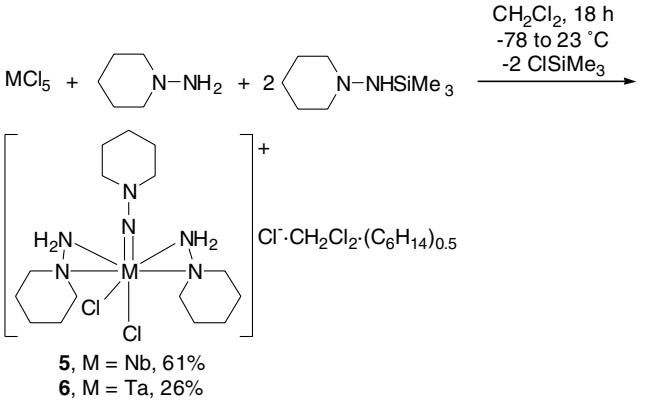

(2)

2.3. X-ray crystal structures of 1–5

X-ray crystal structures of **1**–**5** were determined to establish the geometry about the metal centers and the bonding modes of the hydrazine-derived ligands. Experimental crystallographic data are summarized in Table 1, selected bond distances and angles are given in Tables 2–6, and perspective views of **1**–**5** are presented in Figs. 1–5. Figs. 6 and 7 show intermolecular hydrogen bonding interactions that are present in **1** and **5**.

Complexes **1**–**4** adopt similar molecular structures, with monomeric formulations and approximate pentagonal bipyramidal geometry about each metal center. The axial sites contain one terminal, linear NNR_2 ligand and one chloride ion. The equatorial sites contain one chloride ion, one η^2-hydrazine ligand, and one η^2-TMEDA ligand. The $-NH_2$ fragments of the η^2-hydrazine ligands are situated *syn* to one of the TMEDA dimethylamino groups, apparently for steric reasons. The equatorial chloro ligand resides between one of the TMEDA dimethylamino groups and the $-NR_2$ fragment of the η^2-hydrazine ligands. The metal coordination sphere has an overall positive charge, and there is a chloride ion that serves to balance this charge. Each complex also crystallizes with one dichloromethane molecule per metal center. Since the niobium(V) and tantalum(V) ions are the same size ($r(Nb(V)) = 0.64$ Å, $r(Ta(V)) = 0.64$ Å for six-coordinate complexes [13]), the bond lengths of **1**–**4** can be directly compared. For the NNR_2 ligands, the metal–nitrogen bond lengths range from 1.773 to 1.785 Å, the nitrogen–nitrogen distances are between 1.32 and 1.36 Å, and the metal–nitrogen–nitrogen angles lie between 171.5° and 172.3°. The metal–nitrogen bond lengths associated with the neutral hydrazine ligands range between 2.179 and 2.190 Å for

Table 2
Selected bond lengths (Å) and angles (°) for **1**

Nb–N(1)	2.374(3)
Nb–N(2)	2.369(3)
Nb–N(3)	2.187(3)
Nb–N(4)	2.221(3)
Nb–N(5)	1.776(3)
Nb–Cl(1)	2.4681(8)
Nb–Cl(2)	2.5505(9)
N(3)–N(4)	1.437(3)
N(5)–N(6)	1.317(4)
Nb–N(5)–N(6)	171.8(3)
Cl(1)–Nb–Cl(2)	86.67(3)
Cl(1)–Nb–N(1)	82.34(7)
Cl(1)–Nb–N(2)	156.62(8)
Cl(1)–Nb–N(4)	82.31(7)
Cl(1)–Nb–N(5)	93.79(9)
Cl(2)–Nb–N(1)	89.65(8)
Cl(2)–Nb–N(2)	83.82(8)
Cl(2)–Nb–N(4)	89.39(8)
Cl(2)–Nb–N(5)	179.20(10)
N(1)–Nb–N(2)	76.30(10)
N(1)–Nb–N(4)	164.65(10)
N(1)–Nb–N(5)	89.77(11)
N(2)–Nb–N(4)	118.80(10)
N(2)–Nb–N(5)	95.51(12)

Table 1
Crystal data and data collection parameters for **1**–**5**

Compound	**1**	**2**	**3**	**4**	**5**
Empirical formula	$C_{11}H_{32}Cl_5N_6Nb$	$C_{11}H_{32}Cl_5N_6Ta$	$C_{17}H_{40}Cl_5N_6Nb$	$C_{17}H_{40}Cl_5N_6Ta$	$C_{34}H_{77}Cl_8N_{12}Nb_2$
Formula weight	518.59	606.63	598.71	686.75	1123.50
Space group	$P2_1/c$	$P2_1/c$	$P2_1/n$	$P2_1/n$	$P2_12_12$
a (Å)	8.7598(7)	8.7602(8)	12.3920(13)	12.388(8)	16.644(13)
b (Å)	14.0554(11)	14.0692(14)	12.2934(14)	12.350(8)	25.64(2)
c (Å)	18.9378(14)	18.9540(19)	18.635(2)	18.646(12)	12.224(8)
β (°)	98.118(2)	97.975(2)	103.767(2)	103.891(11)	
V (Å^3)	2308.2(3)	2313.5(4)	2757.2(5)	2769(3)	5217(7)
Z	4	4	4	4	4
T (K)	298	298	298	298	298
λ (Å)	0.71073	0.71073	0.71073	0.71073	0.71073
D_{calc} (g cm^{-3})	1.492	1.742	1.442	1.647	1.430
μ (mm^{-1})	1.106	5.335	0.937	4.467	0.886
$R(F)$ (%)	4.04	2.54	3.66	2.29	3.81
$R_w(F)$ (%)	11.22	6.07	9.73	5.97	8.80

$R(F) = \sum||F_o| - |F_c||/\sum|F_o|$, $R_w(F)^2 = [\sum w(F_o^2 - F_c^2)^2/\sum w(F_o^2)^2]^{1/2}$ for $I > 2\sigma(I)$.

Table 3
Selected bond lengths (Å) and angles (°) for **2**

Ta–N(1)	1.773(3)
Ta–N(3)	2.346(3)
Ta–N(4)	2.356(3)
Ta–N(5)	2.219(3)
Ta–N(6)	2.179(3)
Ta–Cl(1)	2.451(1)
Ta–Cl(2)	2.528(1)
N(1)–N(2)	1.328(5)
N(5)–N(6)	1.440(4)
Ta–N(1)–N(2)	172.3(3)
Cl(1)–Ta–Cl(2)	86.38(4)
Cl(2)–Ta–N(1)	178.78(11)
Cl(2)–Ta–N(3)	83.86(9)
Cl(2)–Ta–N(4)	89.50(10)
Cl(2)–Ta–N(5)	88.76(9)
Cl(2)–Ta–N(6)	86.14(9)
Cl(1)–Ta–N(1)	94.75(10)
Cl(1)–Ta–N(3)	156.20(10)
Cl(1)–Ta–N(4)	82.07(9)
Cl(1)–Ta–N(5)	82.25(8)
Cl(1)–Ta–N(6)	120.06(8)
N(1)–Ta–N(3)	94.92(13)
N(1)–Ta–N(4)	90.18(15)
N(1)–Ta–N(5)	91.87(14)
N(1)–Ta–N(6)	93.70(13)

Table 4
Selected bond lengths (Å) and angles (°) for **3**

Nb–N(1)	2.190(2)
Nb–N(2)	2.210(2)
Nb–N(3)	1.780(2)
Nb–N(5)	2.380(3)
Nb–N(6)	2.390(2)
Nb–Cl(1)	2.5360(8)
Nb–Cl(2)	2.4652(8)
N(1)–N(2)	1.432(3)
N(3)–N(4)	1.338(3)
Nb–N(3)–N(4)	172.2(2)
Cl(1)–Nb–Cl(2)	88.48(3)
Cl(1)–Nb–N(1)	84.93(6)
Cl(1)–Nb–N(2)	89.88(6)
Cl(1)–Nb–N(3)	175.19(8)
Cl(1)–Nb–N(5)	83.83(7)
Cl(1)–Nb–N(6)	86.62(8)
Cl(2)–Nb–N(1)	119.40(6)
Cl(2)–Nb–N(2)	81.97(6)
Cl(2)–Nb–N(3)	95.43(8)
Cl(2)–Nb–N(5)	156.58(6)
Cl(2)–Nb–N(6)	81.06(7)
N(1)–Nb–N(2)	37.99(8)
N(1)–Nb–N(3)	95.53(9)
N(1)–Nb–N(5)	81.98(8)
N(1)–Nb–N(6)	157.55(9)
N(3)–Nb–N(2)	93.43(10)
N(3)–Nb–N(5)	91.48(10)
N(3)–Nb–N(6)	91.22(10)

the M–NH_2 linkage and 2.210 and 2.221 Å for the M–NR_2 fragment. The nitrogen–nitrogen bond distances within the neutral hydrazine ligands lie between 1.43 and 1.45 Å. The metal–nitrogen bond lengths associated with the TMEDA ligand range from 2.346 to 2.390 Å, and average 2.368 Å.

Table 5
Selected bond lengths (Å) and angles (°) for **4**

Ta–N(1)	2.190(2)
Ta–N(2)	2.211(3)
Ta–N(3)	1.785(3)
Ta–N(5)	2.364(3)
Ta–N(6)	2.367(3)
Ta–Cl(1)	2.521(2)
Ta–Cl(2)	2.452(1)
N(1)–N(2)	1.448(3)
N(3)–N(4)	1.355(3)
Ta–N(3)–N(4)	171.5(2)
Cl(1)–Ta–Cl(2)	87.86(4)
Cl(1)–Ta–N(1)	84.73(7)
Cl(1)–Ta–N(2)	89.77(7)
Cl(1)–Ta–N(3)	174.72(9)
Cl(1)–Ta–N(5)	83.71(7)
Cl(1)–Ta–N(6)	86.31(8)
Cl(2)–Ta–N(1)	119.59(8)
Cl(2)–Ta–N(2)	81.83(8)
Cl(2)–Ta–N(3)	96.45(8)
Cl(2)–Ta–N(5)	156.34(7)
Cl(2)–Ta–N(6)	80.80(9)
N(1)–Ta–N(2)	38.42(8)
N(1)–Ta–N(3)	95.72(10)
N(1)–Ta–N(5)	81.66(9)
N(1)–Ta–N(6)	157.29(10)
N(2)–Ta–N(3)	93.85(11)
N(2)–Ta–N(5)	120.08(10)
N(2)–Ta–N(6)	162.32(9)
N(3)–Ta–N(5)	91.14(11)
N(3)–Ta–N(6)	91.37(11)
N(5)–Ta–N(6)	76.64(11)

The metal–chlorine distances for the chlorine atoms that are *cis* to the NNR_2 ligand range between 2.451 and 2.468 Å, while the related values for the chlorine atoms that are *trans* to the NNR_2 ligand lie between 2.521 and 2.550 Å. The latter bond lengths are longer than the former due to the strong *trans*-influence of the NNR_2 ligand.

The molecular structure of **5** is broadly similar to those of **1**–**4**. The cationic fragment in **5** is monomeric with approximate pentagonal bipyramidal geometry about the niobium center. The axial sites contain one terminal, linear NNR_2 ligand and one chloride ion. The equatorial sites contain one chloride ion and two η^2-aminopiperidine ligands. The –NH_2 fragments are *syn* to each other within the equatorial plane, which places the equatorial chloride ion in between the two piperidine groups. The imidopiperidine group has a niobium–nitrogen bond distance of 1.763(4) Å, a nitrogen–nitrogen bond length of 1.347(5) Å, and a niobium–nitrogen–nitrogen angle of 172.4(3)°. These values are within experimental uncertainty of those observed for **1**–**4**. The η^2-aminopiperidine ligands have niobium–nitrogen bond lengths of 2.184(4) and 2.188(4) Å for the –NH_2 fragments and 2.246(4) and 2.258(4) Å for the piperidine moieties. The asymmetry within the metal–nitrogen bond lengths for the η^2-aminopiperidine ligands in **5** (0.062–0.070 Å) is larger than the related values in **1**–**4** (0.021–0.040 Å), possibly due to the

Table 6
Selected bond lengths (Å) and angles (°) for **5**

Nb(1)–N(1)	1.763(4)
Nb(1)–N(3)	2.246(4)
Nb(1)–N(4)	2.184(4)
Nb(1)–N(5)	2.258(4)
Nb(1)–N(6)	2.188(4)
Nb(1)–Cl(1)	2.580(2)
Nb(1)–Cl(2)	2.416(2)
N(1)–N(2)	1.347(5)
N(3)–N(4)	1.457(5)
Nb(1)–N(1)–N(2)	172.4(3)
Cl(1)–Nb(1)–Cl(2)	88.05(5)
Cl(1)–Nb(1)–N(1)	174.49(13)
Cl(1)–Nb(1)–N(3)	88.88(11)
Cl(1)–Nb(1)–N(4)	83.55(11)
Cl(1)–Nb(1)–N(5)	88.77(11)
Cl(1)–Nb(1)–N(6)	82.01(11)
Cl(2)–Nb(1)–N(1)	97.41(13)
Cl(2)–Nb(1)–N(3)	92.49(12)
Cl(2)–Nb(1)–N(4)	129.99(11)
Cl(2)–Nb(1)–N(5)	94.63(10)
Cl(2)–Nb(1)–N(6)	131.61(11)
N(1)–Nb(1)–N(3)	90.13(15)
N(1)–Nb(1)–N(4)	92.31(15)
N(1)–Nb(1)–N(5)	91.47(15)
N(1)–Nb(1)–N(6)	94.83(15)
N(3)–Nb(1)–N(4)	38.36(14)
N(3)–Nb(1)–N(5)	172.44(15)
N(3)–Nb(1)–N(6)	134.18(15)
N(4)–Nb(1)–N(5)	134.15(15)
N(4)–Nb(1)–N(6)	95.86(15)
N(5)–Nb(1)–N(6)	38.30(12)

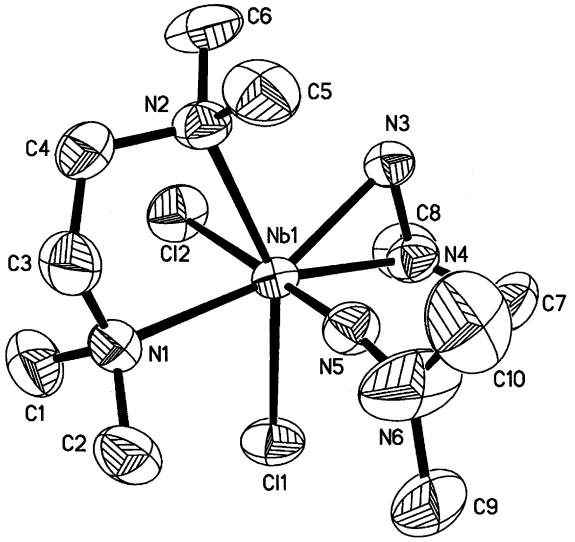

Fig. 1. Perspective view of $[Nb(NNMe_2)Cl_2(NH_2NMe_2)(TMEDA)]$-$Cl \cdot CH_2Cl_2$ (**1**) with probability ellipsoids at the 50% level.

steric effects of accommodating two bulky equatorial η^2-aminopiperidine ligands in the former. The nitrogen–nitrogen bond lengths within the η^2-aminopiperidine ligands are 1.457(5) and 1.460(5) Å. The niobium–chlorine distances for the chlorine atom that is *cis* to the NNR_2 ligand is 2.416(2) Å, while the related values for the chlorine atom that is *trans* to the NNR_2 ligand is 2.580(2) Å.

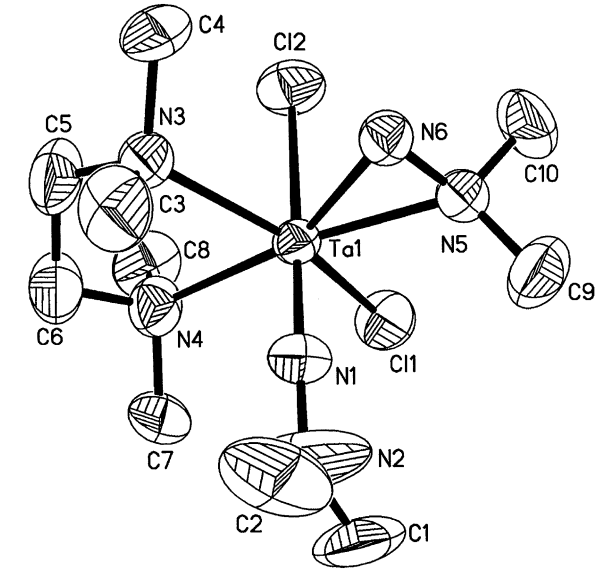

Fig. 2. Perspective view of $[Ta(NNMe_2)Cl_2(NH_2NMe_2)(TMEDA)]$-$Cl \cdot CH_2Cl_2$ (**2**) with probability ellipsoids at the 50% level.

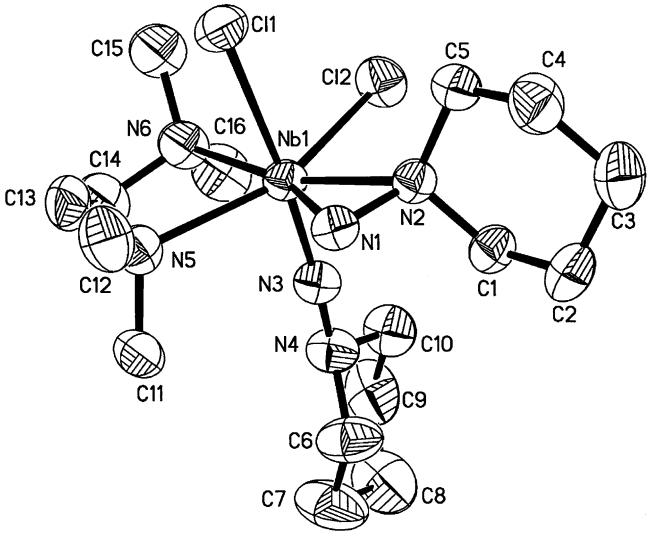

Fig. 3. Perspective view of $[Nb(NN(CH_2)_5)Cl_2(NH_2N(CH_2)_5)(TMEDA)]$-$Cl \cdot CH_2Cl_2$ (**3**) with probability ellipsoids at the 50% level.

Complexes **1**–**5** exhibit interesting crystal structures that contain hydrogen bonds between the hydrogen atoms of the coordinated neutral η^2-dimethylhydrazine and η^2-aminopiperidine ligands and the chloride counterions. In **1**–**4**, the nitrogen-bound hydrogen atoms of neutral η^2-hydrazine ligands of two adjacent cationic molecules form hydrogen bonds to two chloride counterions. This hydrogen bond network leads to an eight-membered $H_4N_2Cl_2$ ring, as depicted in Fig. 6 for **1**. In **1**–**4**, the nitrogen–chloride ion distances for the atoms involved in hydrogen bonding are separated by 3.11–3.23 Å. The hydrogen atom positions in **1** were calculated, resulting in nitrogen–hydrogen distances of 0.9 Å, hydrogen–chlorine distances of 2.25 and 2.37 Å,

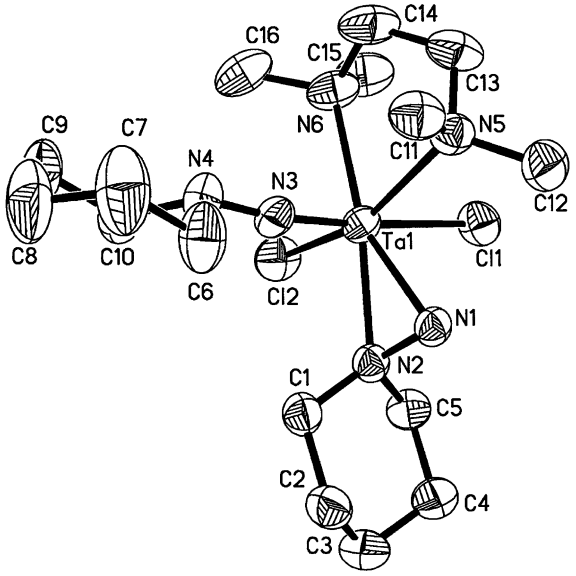

Fig. 4. Perspective view of $[Ta(NN(CH_2)_5)Cl_2(NH_2N(CH_2)_5)(TMEDA)]Cl \cdot CH_2Cl_2$ (**4**) with probability ellipsoids at the 50% level.

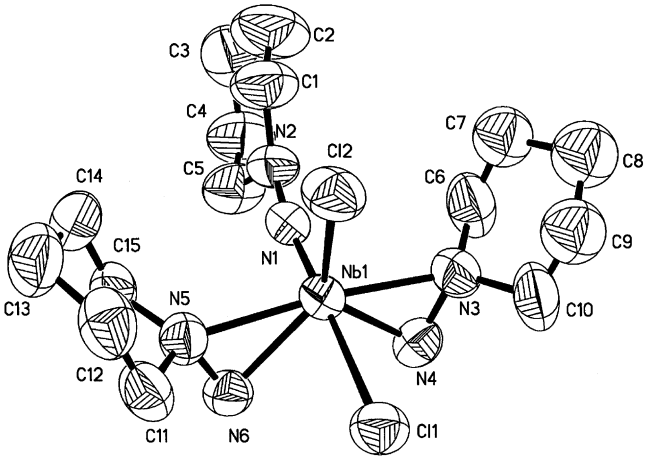

Fig. 5. Perspective view of $[Nb(NN(CH_2)_5)Cl_2(NH_2N(CH_2)_5)_2]Cl \cdot [(CH_2Cl_2)(C_6H_{14})_{0.5}]$ (**5**) with probability ellipsoids at the 50% level.

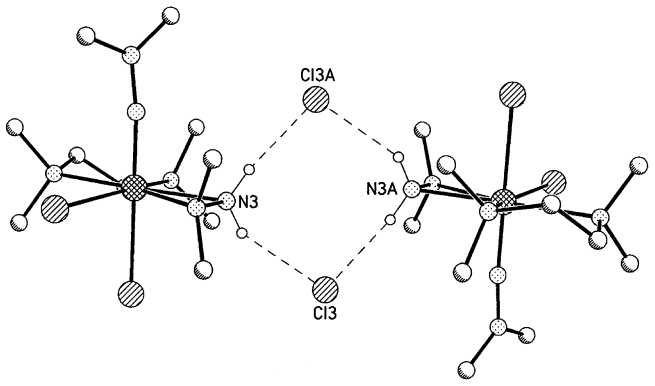

Fig. 6. View emphasizing the $H_4N_2Cl_2$ hydrogen bond network in $[Nb(NNMe_2)Cl_2(NH_2NMe_2)(TMEDA)]Cl \cdot CH_2Cl_2$ (**1**).

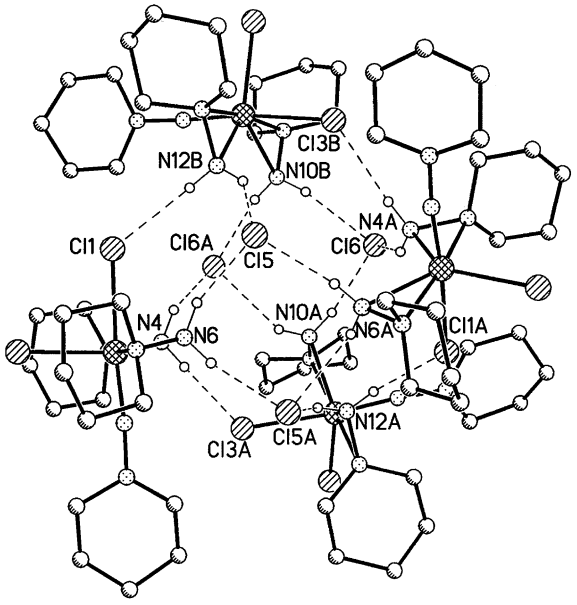

Fig. 7. Hydrogen bond network in the unit cell of $[Nb(NN(CH_2)_5)Cl_2(NH_2N(CH_2)_5)_2]Cl \cdot [(CH_2Cl_2)(C_6H_{14})_{0.5}]$ (**5**).

and nitrogen–hydrogen–chlorine angles of 146° and 171°. There were no hydrogen bonds to the chlorine atoms of the dichloromethane solvate molecules. In **5**, the hydrogen bonding network is more complicated due to the presence of two neutral η^2-aminopiperidine ligands. As depicted in Fig. 7, there is an eight-membered $H_4N_2Cl_2$ ring similar to those observed in **1**–**4** that incorporates the four nitrogen-bound hydrogen atoms of the η^2-aminopiperidine ligands on two adjacent cationic molecules and two chloride counterions. The nitrogen–chloride ion distances for the atoms involved in the eight-membered ring are separated by 3.11–3.22 Å. The hydrogen atoms were placed in calculated positions with nitrogen–hydrogen distances of 0.90 Å, which afforded hydrogen–chlorine distances of 2.22 and 2.45 Å, and nitrogen–hydrogen–chlorine angles of 144° and 169°. One of the other η^2-aminopiperidine ligand hydrogen atoms on each metal center is engaged in hydrogen bonding to one of the chloride ions of the eight-membered $H_4N_2Cl_2$ ring, with nitrogen–chlorine distances of 3.15 Å, hydrogen–chlorine distances of 2.41 and 2.42 Å, and nitrogen–hydrogen–chlorine angles of 138° and 140°. Finally, the remaining η^2-aminopiperidine ligand hydrogen atom forms a hydrogen bond to the niobium-bound chloride ion that is *trans* to the NNR_2 ligand, and possesses a nitrogen–chlorine distances of 3.32 and 3.36 Å, hydrogen–chlorine distance of 2.45 and 2.47 Å, and nitrogen–hydrogen–chlorine angles of 164° and 169°.

2.4. Discussion

A significant aspect of the work described herein is the synthesis and structural documentation of **1**–**6**. There are very few crystallographically characterized niobium and tantalum complexes that contain hydrazine-derived

ligands. The complexes $(C_5H_4Me)_2NbCl(NNMe_2)$ (Nb–N 1.794(2) Å, N–N 1.340(3) Å, Nb–N–N 178.8(2)°) [8a], $CpNbCl_2(NNMe_2)(P(OMe)_3)$ (Nb–N 1.789(2) Å, N–N 1.338(2) Å, Nb–N–N 170.4(2)°) [8b], and $Cp_2Nb_2Cl_2(NNMe_2)_2$ (Nb–N 1.67(2) Å, N–N 1.38(2) Å, Nb–N–N 168.7(17)°) [8b] contain terminal dimethylhydrazido(2−) ligands. The complex $Cp_2Nb_2Cl_2(NNMe_2)_2$ also contains a μ:η^1,η^2-dimethylhydrazido(2−) ligand (Nb–N 1.88(1), 2.15(2), 2.28(1) Å; N–N 1.39(2) Å, Nb–N–N 127.9(10)°) [8b]. The complex $[NHEt_3]$- $[TaCl_4(NNC_9H_{18})_2]$ contains two linear 1-imido-2,2,6,6-tetramethylpiperidine ligands (Ta–N 1.865(7), 1.882(6) Å; N–N 1.283(9), 1.259(8) Å, Ta–N–N 176.4(5)°, 176.5(5)°) [12]. Complex $[Ta(S_2CNEt_2)_3(NMeNMe_2)]Br$ contains an η^2-1,1,2-trimethylhydrazido(1−) ligand [10], with tantalum–nitrogen distances of 1.932(12) and 2.209(16) Å and a nitrogen–nitrogen distance of 1.389(22) Å. Complexes **1**–**5** contain linear NNR_2 ligands with structural parameters that are very similar to previously reported neutral complexes containing similar ligands. Complexes **1**–**5** are the first niobium and tantalum complexes that contain neutral 1,1-dialkylhydrazine ligands. NMR studies for **1**–**5** in DMSO show that the η^2-hydrazine ligands exchange very slowly with the strong donor ligand DMSO at ambient temperature, and are thus strongly bound ligands. The complex $[NHEt_3][TaCl_4(NNC_9H_{18})_2]$ has longer tantalum–nitrogen bond lengths than those of **1**–**5** by about 0.1 Å, and also has nitrogen–nitrogen bond lengths that are about 0.05 Å shorter than those of **1**–**5**. The authors of this work suggested that this complex contains isodiazene ligands, rather than hydrazido(2−) ligands [12]. As outlined in Chart 1, isodiazene ligands are formally neutral donor ligands and contain a formal nitrogen–nitrogen double bond. In complexes containing isodiazene ligands, the metal–nitrogen bond lengths are longer and the nitrogen–nitrogen bond lengths are shorter compared to complexes containing hydrazido(2−) ligands. In **1**–**5**, the metal–nitrogen bond distances range from 1.76 to 1.79 Å, which is slightly shorter to about the same as in several of the neutral niobium cyclopentadienyl complexes described above. We have reported the structural characterization of a series of niobium and tantalum alkylimido complexes [14], and found metal–nitrogen bond lengths between 1.73 and 1.77 Å. The values in **1**–**5** are about the same to slightly longer than those of the alkylimido complexes. The nitrogen–nitrogen distances in the NNR_2 ligands of **1**–**5** were between 1.32 and 1.36 Å, while the corresponding values for the neutral hydrazine donor ligands in **1**–**5** ranged from 1.43 to 1.45 Å. The bond lengths in the latter ligands can be considered as a typical value for a nitrogen–nitrogen single bond. The combination of slightly longer metal–nitrogen bond lengths and short nitrogen–nitrogen bond lengths in **1**–**5** suggest at least some isodiazene character to the NNR_2 linkages.

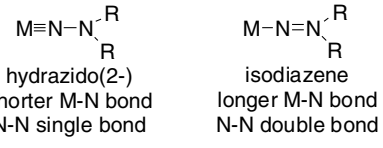

Chart 1. Hydrazido(2−) and isodiazene ligands.

Notably, since isodiazene ligands are formally neutral, the metal centers in complexes containing such ligands are formally reduced compared to complexes containing hydrazido(2−) ligands. A recent theoretical study has examined the bonding between metal ions and hydrazido(2−) ligands, and concluded that NNR_2 ligands have approximate charges of 1- in complexes of group 6 metals [15]. Accordingly, these ligands lead to a reduction in the formal oxidation state of the metal. We propose that the lower group 4 and 5 metal nitride film growth temperatures observed with hydrazine derivatives as coreactants, compared to similar film growth employing ammonia as the coreactant, are related to the formal reduction of the metal centers by isodiazene-like ligand intermediates that are formed in the film growth process. Complexes **1**–**5** represent models for the types of intermediates that could be formed in a film growth process from tantalum pentachloride and 1,1-dialkylhydrazines.

One of the goals of our work was to prepare new volatile complexes that might be employed as molecular precursors for the low temperature growth of TaN films. However, the cationic nature of **1**–**5** afforded essentially non-volatile complexes, which are not useful in film growth procedures employing conventional thermal precursor delivery. Attempts to replace the chloride ligands in **1**–**5** by salt metathesis reactions with lithium dimethylamide or potassium 3,5-di-*tert*-butylpyrazolate led to complex mixtures of products. Thus, **1**–**5** do not appear to be useful reagents for the preparation of niobium and tantalum complexes containing NNR_2 ligands. By contrast, complexes of the formula $M(NR)Cl_3py_2$ (M = Nb, Ta; R = alkyl; py = pyridine) are versatile starting materials for the synthesis of a range of niobium and tantalum imido complexes [16].

3. Experimental

3.1. General considerations

All manipulations were performed under an inert atmosphere of argon using either glovebox or Schlenk line techniques. Hexane was distilled from P_2O_5 and dichloromethane was distilled from calcium hydride. Niobium pentachloride, tantalum pentachloride, 1,1-dimethylhydrazine, 1-aminopiperidine, TMEDA, and chlorotrimethylsilane were purchased from Aldrich Chemical Company and were used as received. 1,1-Dimethyl-2-trimethylsilylhydrazine [17] and 1-trimethylsilyl-1-aminopiperidine [18] were prepared according to the literature procedures. ^1H and $^{13}C\{^1H\}$ NMR were obtained at 400, 300, 100, or 75 MHz in dichloromethane-d_2 or dimethylsulfoxide-d_6 as indicated. Infrared spectra were obtained using Nujol as the medium.

Elemental analyses were performed by Midwest Microlab, Indianapolis, Indiana. In spite of multiple submissions and addition of V_2O_5, satisfactory analyses could not be obtained for **1**, **2**, **5**, and **6**. Melting points were obtained on a Haake-Buchler HBI digital melting point apparatus and are uncorrected.

3.2. Preparation of *[Nb(NNMe$_2$)Cl$_2$(NH$_2$NMe$_2$)(TMEDA)]Cl · CH$_2$Cl$_2$ (**1**)*

A 100-mL Schlenk flask was charged with tantalum pentachloride (0.380 g, 1.06 mmol), dichloromethane (20 mL), and TMEDA (0.123 g, 1.06 mmol). The resultant mixture was stirred at ambient temperature for 0.5 h. The solution was then cooled to −78 °C, and was treated with a solution of 1,1-dimethyl-2-trimethylsilylhydrazine (0.281 g, 2.12 mmol) in dichloromethane (15 mL). The reaction mixture was allowed to warm to room temperature and was stirred for 18 h. The volatile components were removed under reduced pressure to afford a light orange powder. This powder was extracted with dichloromethane (25 mL) to afford an orange solution and a white precipitate. The dichloromethane extract was filtered through a 2-cm pad of Celite on a coarse glass frit to afford an orange-yellow solution. Storage of this solution at −20 °C for 24 h afforded **1** as yellow crystals (0.174 g, 27%): mp (dec) 139 °C; IR (Nujol, cm^{-1}) 3166 (w), 1582 (s), 1562 (w), 1283 (m), 1238 (w), 1204 (w), 1127 (m), 1075 (w), 1039 (w), 1000 (m), 944 (s), 893 (s), 844 (w); ^{1}H NMR (dichloromethane-d_2, 22 °C, δ) 11.55 (broad s, 1H, N*H*H′), 6.10 (broad s, 1H, NH*H*′), 3.44 (s, 3H, CH_3), 3.40 (s, 3H, CH_3), 3.29 (s, 3H, CH_3), 3.16 (s, 3H, CH_3), 3.10 (s, 6H, 2 CH_3), 2.97 (s, 3H, CH_3), 2.96 (s, 3H, CH_3), 2.4–2.9 (m, 4H, CH_2 of TMEDA); ^{13}C{^{1}H} NMR (dimethylsulfoxide-d_6, 22 °C, ppm) 58.79 (s, *C*H$_2$ of TMEDA), 58.14 (s, *C*H$_2$ of TMEDA), 54.97 (s, *C*H$_3$), 54.73 (s, *C*H$_3$), 54.60 (s, *C*H$_3$), 53.97 (s, *C*H$_3$), 52.38 (s, *C*H$_3$), 50.89 (s, *C*H$_3$), 49.38 (s, *C*H$_3$), 43.29 (s, *C*H$_3$).

Anal. Calc. for $C_{11}H_{32}Cl_5N_6Ta$: C, 21.78; H, 5.32; N, 13.85. Found: C, 24.60; H, 5.73; N, 12.57%.

3.3. Preparation of *[Ta(NNMe$_2$)Cl$_2$(NH$_2$NMe$_2$)(TMEDA)]Cl · CH$_2$Cl$_2$ (**2**)*

In a fashion similar to the preparation of **1**, treatment of niobium pentachloride (0.380 g, 1.41 mmol) with TMEDA (0.163 g, 1.40 mmol) and 1,1-dimethyl-2-trimethylsilylhydrazine (0.372 g, 2.81 mmol) afforded **2** as yellow crystals (0.262 g, 30%): mp (dec) 161 °C; IR (Nujol, cm^{-1}) 3168 (w), 1583 (s), 1565 (m), 1284 (m), 1231 (w), 1194 (w), 1120 (s), 1075 (m), 1041 (w), 1005 (s), 951 (s), 887 (s), 847 (w); ^{1}H NMR (dichloromethane-d_2, 22 °C, δ) 11.18 (d, 1H, $J = 7.8$ Hz, N*H*H′), 6.72 (d, 1H, $J = 7.8$ Hz, NH*H*′), 3.58 (s, 3H, CH_3), 3.48 (s, 3H, CH_3), 3.38 (s, 3H, CH_3), 3.27 (s, 3H, CH_3), 3.06 (s, 3H, CH_3), 3.03 (s, 6H, 2 CH_3), 2.96 (s, 3H, CH_3), 2.88 (m, 2H, CH_2 of TMEDA), 2.55 (m, 2H, CH_2 of TMEDA); ^{13}C{^{1}H} NMR (dimethylsulfoxide-d_6, 22 °C, ppm) 58.78 (s, *C*H$_2$ of TMEDA), 58.08 (s, *C*H$_2$ of TMEDA), 56.65 (s, *C*H$_3$), 54.97 (s, *C*H$_3$), 54.42 (s, *C*H$_3$), 52.46 (s, *C*H$_3$), 51.23 (s, *C*H$_3$), 49.26 (s, *C*H$_3$), 45.28 (s, *C*H$_3$), 42.24 (s, *C*H$_3$).

Anal. Calc. for $C_{11}H_{32}Cl_5N_6Nb$: C, 25.48; H, 6.22; N, 16.21. Found: C, 24.10; H, 5.80; N, 15.90%.

3.4. Preparation of *[Nb(NN(CH$_2$)$_5$)Cl$_2$(NH$_2$N(CH$_2$)$_5$)(TMEDA)]Cl · CH$_2$ Cl$_2$ (**3**)*

In a fashion similar to the preparation of **1**, treatment of niobium pentachloride (0.380 g, 1.41 mmol) with TMEDA (0.123 g, 1.06 mmol) and 1-trimethylsilyl-1-aminopiperidine (0.485 g, 2.81 mmol) afforded **3** as yellow crystals (0.168 g, 23%): mp (dec) 166 °C; IR (Nujol, cm^{-1}) 3190 (w), 3152 (w), 1575 (s), 1557 (w), 1539 (w), 1505 (w), 1353 (w), 1336 (w), 1317 (w), 1283 (m), 1271 (m), 1231 (s), 1204 (w), 1185 (w), 1178 (m), 1122 (m), 1078 (m), 1050 (s), 1006 (m), 998 (m), 986 (w), 968 (m), 951 (s), 907 (w), 890 (w), 872 (s), 865 (m), 853 (w), 846 (w), 811 (s), 778 (m), 762 (m), 702 (m), 671 (m), 661 (w); ^{1}H NMR (dimethylsulfoxide-d_6, 22 °C, δ) 9.32 (broad s, 1H, N*H*H′), 7.66 (s, 1H, NH*H*′), 3.12 (s, 3H, CH_3 of TMEDA), 3.01 (s, 3H, CH_3 of TMEDA), 2.75 (s, 3H, CH_3 of TMEDA), 2.74 (s, 3H, *C*H$_3$ of TMEDA), 1.2–3.7 (many multiplets, 24H, 2 $C_5H_{10}N$ + CH_2 of TMEDA); ^{13}C{^{1}H} NMR (dimethylsulfoxide-d_6, 22 °C, ppm) 58.80 (s, *C*H$_2$ of TMEDA), 58.33 (s, *C*H$_2$ of TMEDA), 57.40 (s, *C*H$_3$), 54.97 (s, *C*H$_3$), 54.52 (s, *C*H$_3$), 54.05 (s, *C*H$_3$), 52.70 (s, 2 N*C*H$_2$), 52.54 (s, N*C*H$_2$), 50.91 (s, N*C*H$_2$), 24.62 (s, 2 *C*H$_2$), 24.10 (s, *C*H$_2$), 23.28 (s, *C*H$_2$), 22.47 (s, *C*H$_2$), 22.04 (s, *C*H$_2$).

Anal. Calc. for $C_{17}H_{40}Cl_5N_6Nb$: C, 34.10; H, 6.73; N, 14.04. Found: C, 34.55; H, 6.78; N, 14.09%.

3.5. Preparation of *[Ta (NN(CH$_2$)$_5$)Cl$_2$(NH$_2$N(CH$_2$)$_5$)(TMEDA)]Cl · CH$_2$Cl$_2$ (**4**)*

In a fashion similar to the preparation of **1**, treatment of tantalum pentachloride (0.380 g, 1.41 mmol) with TMEDA (0.163 g, 1.40 mmol) and 1-trimethylsilyl-1-aminopiperidine (0.485 g, 2.81 mmol) afforded **4** as yellow crystals (0.109 g, 13%): mp (dec) 157 °C; IR (Nujol, cm^{-1}) 3208 (w), 3157 (w), 1578 (s), 1353 (w), 1338 (w), 1319 (w), 1283 (w), 1271 (w), 1223 (s), 1200 (w), 1172 (m), 1122 (m), 1081 (m), 1052 (m), 1044 (m), 1009 (w), 1001 (w), 974 (w), 954 (m), 905 (w), 891 (w), 871 (s), 848 (w), 810 (s), 775 (m), 764 (m), 701 (m), 673 (w), 660 (m); ^{1}H NMR (dimethylsulfoxide-d_6, 22 °C, δ) 9.50 (broad s, 1H, N*H*H′), 7.72 (broad s, 1H, NH*H*′), 3.22 (s, 3H, CH_3 of TMEDA), 3.13 (s, 3H, CH_3 of TMEDA), 2.85 (s, 3H, CH_3 of TMEDA), 2.83 (s, 3H, CH_3 of TMEDA), 1.2–3.7 (many multiplets, 24H, 2 $C_5H_{10}N$ + CH_2 of TMEDA); ^{13}C{^{1}H} NMR (dimethylsulfoxide-d_6, 22 °C, ppm) 58.79 (s, *C*H$_2$ of TMEDA), 58.28 (s, *C*H$_2$ of TMEDA), 57.39 (s, *C*H$_3$), 56.27 (s, *C*H$_3$), 54.97 (s, *C*H$_3$), 54.80 (s, *C*H$_3$), 54.64 (s, 2 N*C*H$_2$), 52.61 (s, N*C*H$_2$), 51.22 (s, N*C*H$_2$), 25.04 (s, *C*H$_2$), 23.91 (s, *C*H$_2$), 23.52 (s, *C*H$_2$), 23.05 (s, *C*H$_2$), 22.80 (s, *C*H$_2$), 21.87 (s, *C*H$_2$).

Anal. Calc. for $C_{17}H_{40}Cl_5N_6Ta$: C, 29.73; H, 5.87; N, 12.24. Found: C, 29.80; H, 5.83; N, 12.22%.

3.6. Preparation of $[Nb(NN(CH_2)_5)Cl_2(NH_2N(CH_2)_5)_2]Cl \cdot [(CH_2Cl_2)(C_6H_{14})_{0.5}]$ (5)

In a fashion similar to the preparation of **1**, treatment of niobium pentachloride (0.380 g, 1.41 mmol) with 1-aminopiperidine (0.141 g, 1.41 mmol) and 1-trimethylsilyl-1-aminopiperidine (0.485 g, 2.81 mmol) afforded **5** as yellow crystals after crystallization from dichloromethane/hexane at −20 °C (0.537 g, 61%): mp (dec) 121 °C; IR (Nujol, cm^{-1}) 3176 (w), 3152 (w), 1578 (s), 1549 (w), 1229 (s), 1124 (w), 1078 (w), 1031 (m), 1016 (w), 965 (m), 935 (w), 917 (w), 892 (w), 872 (m), 850 (w), 819 (w), 767 (m); ^{1}H NMR (dimethylsulfoxide-d_6, 22 °C, δ) 6.46 (broad s, 4H, N*HH′*), 2.8–3.4 (overlapping m, 12H, NCH_2), 1.1–2.1 (overlapping m, 18H, CH_2); ^{13}C{^{1}H} NMR (dichloromethane-d_2, 22 °C, ppm) 55.02 (s, 2 overlapping N*C*H_2), 54.33 (s, N*C*H_2), 53.84 (s, N*C*H_2), 25.18 (s, *C*H_2CH'_2CH''_2 of η^2-aminopiperidine ligand), 24.78 (s, CH_2*C*H'_2CH''_2 of η^2-aminopiperidine ligand), 25.51 (s, CH_2CH'_2*C*H''_2 of η^2-aminopiperidine ligand), 23.16 (s, *C*H_2CH'_2CH''_2 of imidopiperidine ligand), 22.99 (s, CH_2*C*H'_2CH''_2 of imidopiperidine ligand), 22.68 (s, CH_2CH'_2*C*H''_2 of imidopiperidine ligand).

Anal. Calc. for $C_{19}H_{43}Cl_5N_6Nb$: C, 36.47; H, 6.93; N, 13.43. Found: C, 35.21; H, 6.19; N, 14.12%.

3.7. Preparation of $[Ta(NN(CH_2)_5)Cl_2(NH_2N(CH_2)_5)_2]Cl \cdot [(CH_2Cl_2)(C_6H_{14})_{0.5}]$ (6)

In a fashion similar to the preparation of **1**, treatment of tantalum pentachloride (0.380 g, 1.06 mmol) with 1-aminopiperidine (0.106 g, 1.06 mmol) and 1-trimethylsilyl-1-aminopiperidine (0.366 g, 2.12 mmol) afforded **6** as yellow crystals after crystallization from dichloromethane/hexane at −20 °C (0.197 g, 26%): mp (dec) 143 °C; IR (Nujol, cm^{-1}) 3192 (w), 3145 (w), 1580 (s), 1575 (s), 1558 (w), 1237 (m), 1181 (w), 1155 (m), 1129 (w), 1109 (w), 1030 (m), 961 (s), 912 (w), 877 (s), 850 (m), 819 (m), 769 (s), 754 (w), 700 (w); ^{1}H NMR (dimethylsulfoxide-d_6, 22 °C, δ) 5.95 (broad s, 4H, N*HH′*), 2.8–3.6 (overlapping m, 12H, N*C*H_2), 1.1–2.1 (overlapping m, 18H, CH_2); ^{13}C{^{1}H} NMR (dichloromethane-d_2, 22 °C, ppm) 56.43 (s, N*C*H_2), 56.40 (s, N*C*H_2), 55.91 (s, N*C*H_2), 55.02 (s, 2 N*C*H_2), 25.11 (s, *C*H_2CH'_2CH''_2 of η^2-aminopiperidine ligand), 24.72 (s, CH_2*C*H'_2CH''_2 of η^2-aminopiperidine ligand), 25.60 (s, CH_2CH'_2*C*H''_2 of η^2-aminopiperidine ligand), 22.81 (s, *C*H_2CH'_2CH''_2 of imidopiperidine ligand), 22.07 (s, CH_2*C*H'_2CH''_2 of imidopiperidine ligand), 21.95 (s, CH_2CH'_2*C*H''_2 of imidopiperidine ligand).

Anal. Calc. for $C_{19}H_{43}Cl_5N_6Ta$: C, 31.97; H, 6.07; N 11.77. Found: C, 30.15; H, 5.63; N, 12.30%.

3.8. X-ray crystallographic structure determinations for 1–6

Crystalline samples of **1**–**6** were air-sensitive and were mounted in sealed thin walled capillaries under a nitrogen atmosphere for X-ray data collection. All datasets were collected at room temperature on a Bruker P4/CCD diffractometer equipped with Mo Kα radiation. For each collection, a full sphere of data was collected at 10 s/frame with 0.2° between each frame. The frame data were integrated with the manufacturer's SMART and SAINT software [19]. Absorption corrections were applied with Sheldrick's SADABS program [19] and the structures were solved and refined using the programs of SHELXL-97 [20]. All hydrogen atoms were placed in calculated positions.

Complex **1** crystallized as irregular yellow fragments. The asymmetric unit contains one complex cation, one chloride ion, and one dichloromethane solvate.

Complex **2** crystallized as yellow rods. The asymmetric unit contains one complex cation, one chloride ion, and one dichloromethane solvate. The dichloromethane molecule was disordered and was described with two partial carbon positions. This complex is isostructural with **2**.

Complex **3** crystallized as yellow triangles. The asymmetric unit contains one complex cation, one chloride ion, and one dichloromethane solvate molecule.

Complex **4** crystallized as yellow diamonds. The asymmetric unit contains one complex cation, one chloride ion, and one dichloromethane solvate molecule. This complex is isostructural with **3**.

Complex **5** crystallized as yellow irregular fragments. There are two niobium cationic complexes, two chloride ions, one dichloromethane molecule, and one-half hexane solvate in the asymmetric unit. The hexane was badly disordered on a twofold axis and was accounted for by using Spek's SQUEEZE program [21]. The organic portion of the ligands was also disordered and described by partial isotropic atoms. A network of hydrogen bonds exists between the amine hydrogen atoms and the chloride ions.

Complex **6** was isostructural with **5**. Its composition was clear but extensive disorder produced non-positive definite thermal parameters and unreasonable chemical parameters. Cell constants for **6** are $a = 16.827(1)$ Å, $b = 25.630(2)$ Å, $c = 12.189(1)$ Å, $\alpha = \beta = \gamma = 90°$ $V = 5257(1)$ Å^3, space group $P2_12_12$.

Acknowledgments

We are grateful to the US National Science Foundation (Grant No. CHE-0314615) for support of this research.

Appendix A. Supplementary material

Crystallographic data for the structural analyses have been deposited with the Cambridge Crystallographic Data Centre, quoting No. 288727 for **1**, No. 288728 for **2**, No. 288729 for **3**, No. 288730 for **4**, and No. 288731 for **5**. Copies of this information may be obtained free of charge from The Director, CCDC, 12 Union Road, Cambridge CB2 1EZ, UK (fax: +44 1233 336 033; e-mail: deposit@ccdc.cam.ac.uk or www: http://www.ccdc.cam.ac.uk). Supplementary data associated with this article can be

found, in the online version at doi:10.1016/j.poly.2006.01.010.

References

[1] (a) Selected overviews: B. Roberts, A. Harrus, R.L. Jackson, Solid State Technol. 38 (1995) 69;
(b) S.P. Murarka, R.J. Gutmann, A.E. Kaloyeros, W.A. Lanford, Thin Solid Films 236 (1993) 257.

[2] S.-Q. Wang, MRS Bull. 19 (1994) 30.

[3] C.H. Winter, Aldrichim. Acta 33 (2000) 3.

[4] T. Oku, E. Kawakami, M. Uekubo, K. Takahiro, S. Yamaguchi, M. Murakami, Appl. Surf. Sci. 99 (1996) 265.

[5] (a) C.H. Winter, K.C. Jayaratne, J.W. Proscia, Mater. Res. Soc. Symp. Proc. 327 (1994) 103;
(b) J.T. Scheper, P.J. McKarns, T.S. Lewkebandara, C.H. Winter, Solid-State Electron. 2 (1999) 149.

[6] (a) For leading references, see: M. Juppo, M. Ritala, M. Leskelä, J. Electrochem. Soc. 147 (2000) 3377;
(b) M. Leskelä, M. Ritala, J. Phys. IV 9 (1999) 837;
(c) X. Liu, J.R. Babcock, M.A. Lane, J.A. Belot, A.W. Ott, M. Metz, C.R. Kannewurf, R.P.H. Chang, T.J. Marks, Chem. Vapor Depos. 7 (1) (2001) 25;
(d) C. Amato-Wierda, D.A. Wierda, J. Mater. Res. 15 (2000) 2424.

[7] For a review article on organoimido complexes of transition metals, see: D.E. Wigley, Prog. Inorg. Chem. 42 (1994) 239.

[8] (a) M.L.H. Green, J.T. James, A.N. Chernega, J. Chem. Soc., Dalton Trans. (1997) 1719;
(b) M.L.H. Green, J.T. James, J.F. Saunders, J. Souter, J. Chem. Soc., Dalton Trans. (1997) 1281.

[9] J. Bultitude, L.F. Larkworthy, D.C. Povey, G.W. Smith, J.R. Dilworth, G.J. Leigh, Chem. Commun. (1986) 1748.

[10] F.P. O'Flaherty, R.A. Henderson, D.L. Hughes, J. Chem. Soc., Dalton Trans. (1990) 1087.

[11] J.R. Dilworth, R.A. Henderson, P. Dahlstrom, T. Nicholson, J.A. Zubieta, J. Chem. Soc., Dalton Trans. (1987) 529.

[12] A.A. Danopoulos, R.S. Hay-Motherwell, G. Wilkinson, T.K.N. Sweet, M.B. Hursthouse, Polyhedron 16 (1997) 1081.

[13] Ionic radii for six-coordinate complexes were taken from: N.N. Greenwood, A. Earnshaw, Chemistry of the Elements, 2nd ed., Butterwood-Heinemann, Oxford, 1997, p. 949.

[14] K.C. Jayaratne, G.P.A. Yap, B.S. Haggerty, A.L. Rheingold, C.H. Winter, Inorg. Chem. 35 (1996) 4910.

[15] S. Kahlal, J.-Y. Saillard, J.-R. Hamon, C. Manzur, D. Carrillo, J. Chem. Soc., Dalton Trans. (1998) 1229.

[16] (a) H.-T. Chiu, S.-H. Chuang, C.-E. Tsai, G.-H. Lee, S.-M. Peng, Polyhedron 17 (1998) 2187;
(b) J. Sundermeyer, J. Putterlik, M. Foth, J.S. Field, N. Ramesar, Chem. Ber. 127 (1994) 1201;
(c) H.-T. Chiu, J.-C. Lin, S.-H. Chuang, G.-H. Lee, S.-M. Peng, J. Chin. Chem. Soc. 45 (1999) 355.

[17] U. Wannagat, H. Friedrich, Monatsh. Chem. 97 (1966) 976.

[18] A. Meller, M. Armbrecht, Chem. Ber. 119 (1986) 1.

[19] SMART, SAINT, SADABS are collection and processing programs distributed by the manufacturer, Bruker AXS, Inc., Madison, WI, USA.

[20] G. Sheldrick, SHELX-97, University of Göttingen, Göttingen, Germany, 1997.

[21] (a) A.L. Spek, PLATON, Utrecht University, The Netherlands, 2003;
(b) A.L. Spek, J. Appl. Crystallogr. 36 (2003) 7.

Here we describe the syntheses of the compounds $(Bu_4N)_2[Ni(R\text{-}SO_2N{=}CS_2)_2]$ (R = CH_3CH_2 (**1**), 4-IC_6H_4 (**2**), 2,5-$Cl_2C_6H_3$ (**3**)), which were characterized by IR, UV–Vis, ^1H NMR, ^{13}C NMR and by single crystal X-ray diffraction.

2. Experimental

2.1. Methods and materials

The solvents were purchased from Merck and used without further purification, except in the preparation of potassium *N*-2,5-dichlorophenyldithiocarbimate where DMF was dried over molecular sieves 4A. The ethanesulfonyl chloride, 4-iodobenzenesulphonyl chloride, 2,5-dichlorobenzenesulphonyl chloride and nickel(II) chloride hexahydrate were purchased from Aldrich. Carbon disulfide, potassium hydroxide and tetrabutylammonium bromide were purchased from Vetec, Merck and Carlo Erba, respectively. The ethane, 4-iodobenzene and 2,5-dichlorobenzene sulfonamides were prepared from the corresponding sulfonyl chlorides according to the methodology applied for the syntheses of similar compounds [10]. Melting points (m.p.) were determined with a Mettler FPS equipment. The IR spectra were recorded with a Perkin–Elmer 283 B infrared spectrophotometer using CsI pellets. The UV–Vis spectra were recorded with a Varian Cary 50 Conc spectrophotometer using a quartz cell of 1 cm path length in acetonitrile. The ^1H (300 MHz) and ^{13}C (75 MHz) NMR spectra were recorded with a Varian Mercury 300 spectrophotometer in D_2O for the dithiocarbimate potassium salts, $CDCl_3$ for compound **1** and DMSO-d_6 for compounds **2** and **3**. Microanalyses of C, H and N were obtained from a Perkin–Elmer 2400 CHN Elemental Analyzer. Nickel was analyzed by atomic absorption on a Hitachi Z-8200 Atomic Absorption Spectrophotometer.

2.2. Syntheses

2.2.1. Dithiocarbimate potassium salts

The *N*-ethanesulfonyldithiocarbimate and *N*-4-iodobenzenesulfonyldithiocarbimate potassium salts were prepared according to the methodology applied for the syntheses of similar compounds [11,12]: Carbon disulfide (0.02 mol) and potassium hydroxide (0.01 mol) were added to a solution of the corresponding sulfonamide (0.02 mol) in DMF (20 mL). The mixture was stirred at room temperature for 2 h previous to the addition of a second portion of potassium hydroxide (0.01 mol). After stirring for further 1 h, the yellow solid formed was filtered, washed with DMF, ethanol and ethyl acetate and dried under reduced pressure yielding the *N*-R-sulfonyldithiocarbimates (ca. 80% based on the sulfonamide). These salts were recrystallized in ethanol:water 1:1 mixture.

A variation of this methodology was used in the preparation of the potassium *N*-2,5-dichlorophenyldithiocarbimate: A slight excess of carbon disulfide (0.026 mol) was employed, the solution was more concentrated using 12 mL DMF only, previously dried over molecular sieves 4A and the reaction mixture temperature was kept between 4 and 8 °C. After 3 h of reaction, 10 mL of ice cold ethanol was added, the mixture was stirred for further 50 min and the temperature was allowed to rise up to room temperature. The yellowish solid was separated by filtration, washed with ethanol and ethyl acetate, dried under reduced pressure and used without further purification (ca. 63% based on the sulfonamide).

2.2.1.1. Potassium N-ethanesulfonyldithiocarbimate. IR (most important bands) (cm^{-1}): 3444 and 1630 (water), 1300 (νCN), 1251 (νSO_{2ass}), 1111 (νSO_{2sym}), 962 (νCS_{2ass}). ^1H NMR (δ), *J* (Hz): 1.19 (t, 3H, $J = 13.8$ Hz, CH_3), 3.41 (q, 2H, $J = 13.8$ Hz, CH_2). ^{13}C NMR (δ): 223.86 ($N{=}CS_2$), 45.43 (CH_2), 7.59 (CH_3).

2.2.1.2. Potassium N-4-iodophenylsulfonyldithiocarbimate. IR (most important bands) (cm^{-1}): 3435 and 1637 (water), 1280 (νCN), 1255 (νSO_{2ass}), 1134 (νSO_{2sym}), 971 (νCS_{2ass}). ^1H NMR (δ), *J* (Hz): 7.94 (d, $J = 8.4$, 2H), 7.58 (d, $J = 8.4$, 2H). ^{13}C NMR (δ): 225.62 ($N{=}CS_2$), 142.01 (C1), 128.84 (C2, C6), 138.31 (C3, C5), 98.65 (C4).

2.2.1.3. Potassium N-2,5-dichlorophenylsulfonyldithiocarbimate. IR (most important bands) (cm^{-1}): 3421 and 1621 (water), 1269 (νCN), 1246 (νSO_{2ass}), 1119 (νSO_{2sym}), 977 (νCS_{2ass}). ^1H NMR (δ), *J* (Hz): 7.31–7.34 (m, 2H), 7.83–7.82 (m, 2H). ^{13}C NMR (δ): 224.07 ($N{=}CS_2$), 141.25 (C1), 129.14 (C2), 132.43 (C3), 132.59 (C4), 132.20 (C5), 130.78 (C6).

2.2.2. Nickel complexes

A solution of nickel(II) chloride hexahydrate (1.0 mmol) and tetrabutylammonium bromide (2.0 mmol) in methanol (10 mL) was added to a solution of the appropriate potassium dithiocarbimate salt (2.0 mmol) in methanol:water 1:1 (10 mL) and the mixture was stirred for 1 h at room temperature. The green solid produced was filtered, washed with distilled water and dried under reduced pressure for one day, yielding $(Bu_4N)_2[Ni(C_2H_5SO_2N{=}CS_2)_2]$, $(Bu_4N)_2$-$Ni(IC_6H_4SO_2N{=}CS_2)_2]$ and $(Bu_4N)_2[Ni(2,5\text{-}Cl_2C_6H_4$-$SO_2N{=}CS_2)_2]$ (ca. 80%, based on nickel(II) chloride hexahydrate). Dark green crystals suitable for X-ray structure analyses were obtained by slow evaporation of their solutions in methanol: water (3:1) at room temperature.

*2.2.2.1. Tetrabutylammonium bis(ethanesulphonyldithiocarbimato)nickelate(II) (**1**).* Elemental *Anal.* Calc.: C, 50.15; H, 9.08; N, 6.16; Ni, 6.45. Found: C, 49.64; H, 9.00; N, 6.18; Ni, 6.50%. M.p. (°C): 129–132 (with decomposition). IR (most important bands) (cm^{-1}): 1399 (νCN), 1264 (νSO_{2ass}), 1117 (νSO_{2sym}), 939 (νCS_{2ass}), 394 (νNiS). UV–Vis [λ (nm), ε(L mol^{-1} cm^{-1})]: 233 (44 375) ($\pi \rightarrow \pi^*$ (NCS) + $\pi \rightarrow \pi^*$ (SCS)), 328 (37 188) ($n \rightarrow \pi^*$ (S)), 415 (7734) (CT), 618 (20) ($d \rightarrow d$). ^1H NMR (dithiocarbimate

anion signals) (δ), J (Hz): 3.12 (q, $J = 7.5$, 4H), 1.30 (t, $J = 7.2$, 6H). ^{13}C NMR (dithiocarbimate anion signals) (δ): 209.32 (N=CS_2), 47.83 (CH_2SO_2), 8.52 (CH_3).

*2.2.2.2. Tetrabutylammonium bis(4-iodophenylsulphonyldithiocarbimato)nickelate(II) (**2**).* Elemental *Anal.* Calc.: C, 43.92; H, 6.41; N, 4.45; Ni, 4.67. Found: C, 43.88; H, 6.43; N, 4.33; Ni, 4.73%. M.p. (°C): 173–175 (with decomposition). IR (most important bands) (cm^{-1}): 1382 (νCN), 1286 (νSO_{2ass}), 1141 (νSO_{2sym}), 940 (νCS_{2ass}), 386 (νNiS). UV–Vis [λ (nm), ε (L mol^{-1} cm^{-1})]: 235 (30659) ($\pi \rightarrow \pi^*$ (NCS)), 260 (29401) ($\pi \rightarrow \pi^*$ (SCS)), 347 (11165) ($n \rightarrow \pi^*$ (S)), 429 (5635) (CT), 604 (93) ($d \rightarrow d$). ^{1}H NMR (dithiocarbimate anion signals) (δ), J (Hz): 7.95–7.92 (m, 4H, H2, H6), 7.75–7.73 (m, 4H, H3, H5). ^{13}C NMR (dithiocarbimate anion signals) (δ): 210.38 (N=CS_2), 141.64 (C1), 135.37 (C3, C5), 127.52 (C2, C6), 96.64 (C4).

*2.2.2.3. Tetrabutylammonium bis(2,5-dichlorophenylsulphonyldithiocarbimato)nickelate(II) (**3**).* Elemental *Anal.* Calc.: C, 48.29; H, 6.87; N, 4.90; Ni, 5.13. Found: C, 48.44; H, 6.81; N, 4.59; Ni, 5.33%. M.p. (°C): 186–189 (with decomposition). IR (most important bands) (cm^{-1}): 1382 (νCN), 1294 (νSO_{2ass}), 1141, 1131 (νSO_{2sym}), 944 (νCS_{2ass}), 390 (νNiS). UV–Vis [λ (nm), ε (L mol^{-1} cm^{-1})]: 226 (60632) ($\pi \rightarrow \pi^*$ (NCS) + $\pi \rightarrow \pi^*$ (SCS)), 327 (30473) ($n \rightarrow \pi^*$ (S)), 413 (7619) (CT), 616 (22) ($d \rightarrow d$). ^{1}H NMR (dithiocarbimate anion signals) (δ), J (Hz): 8.13–8.11 (m, 6H, H3, H4 and H6). ^{13}C NMR (dithiocarbimate anion signals) (δ): 210.59 (N=CS_2), 141.37 (C1), 130.71 (C4), 130.49 (C3), 129.91 (C6), 129.11 (C5), 128.71 (C2).

All spectra (IR and NMR) showed the expected signals for the tetrabutylammonium cation. The integration curves in the ^{1}H NMR spectra were consistent with the 2:1 cation:complex anions.

2.3. X-ray diffraction experiments

The low temperature X-ray diffraction data collections for all crystals (φ scans and ω scans with κ offsets) were performed on an Enraf-Nonius Kappa-CCD diffractometer (95 mm CCD camera on κ-goniostat) using graphite monochromatic Mo Kα radiation (0.71073 Å). Data collections were made using the COLLECT program [13] up to 50° in 2θ with a redundancy of four. The final unit cell parameters were based on all reflections. The temperature was

Table 1
Crystal data, data collection and refinement details for complexes **1**–**3**

Compound	**1**	**2**	**3**
Empirical formula	$C_{38}H_{82}N_4O_4S_6Ni$	$C_{46}H_{80}I_2N_4O_4S_6Ni$	$C_{46}H_{78}Cl_4N_4O_4S_6Ni$
Formula weight	910.17	1258.01	1143.99
Crystal system	monoclinic	monoclinic	triclinic
Space group	$P2_1/n$	$P2_1/c$	$P\bar{1}$
a (Å)	9.1120(1)	18.0774(2)	10.205(1)
b (Å)	22.4841(4)	12.6570(2)	10.246(1)
c (Å)	12.2161(2)	23.9715(3)	14.504(2)
α (°)	90°	90°	105.041(6)
β (°)	92.787(1)	94.964(1)	107.019(5)
γ (°)	90°	90°	94.167(6)
V (Å^3)	2499.81(7)	5464.2(1)	1382.1(3)
Z	2	4	1
Crystal size (mm)	$0.40 \times 0.20 \times 0.18$	$0.25 \times 0.14 \times 0.12$	$0.18 \times 0.14 \times 0.05$
ρ_{calc} (mg m^{-3})	1.209	1.529	1.374
μ(Mo Kα) (mm^{-1})	0.677	1.758	0.815
Minimum/maximum transmission	0.8337/0.9105	0.676/0.7253	0.8552/0.9583
Temperature (K)	150(2)	110(2)	150(2)
θ Range (°)	3.00–27.48	2.95–27.48	2.94–26.12
Index range	$-11 \leqslant h \leqslant 11$, $-28 \leqslant k \leqslant 29$, $-15 \leqslant l \leqslant 15$	$-23 \leqslant h \leqslant 23$, $-16 \leqslant k \leqslant 16$, $-31 \leqslant l \leqslant 31$	$-12 \leqslant h \leqslant 12$, $-12 \leqslant k \leqslant 12$, $-16 \leqslant l \leqslant 17$
Reflection collected	43479	85945	9916
Number of unique reflections [R_{int}]	5728 [0.0583]	12537 [0.0700]	5072 [0.0687]
Number of observed reflection, $I > 2\sigma(I)$	4667	9668	3444
Number of parameters refined	246	576	299
R[a], R_w[b] [$I > 2\sigma(I)$]	0.0351, 0.0888	0.0368; 0.0792	0.0583, 0.1594
R[a], R_w[b] [all data]	0.0496, 0.0951	0.0580, 0.0878	0.0950, 0.1985
S[c]	1.098	1.039	1.001
RMS peak (e Å^{-3})	0.335	0.606	0.499

[a] $R = \sum \| F_o| - |F_c| \| / \sum |F_o|$.

[b] $R_w = [\sum w(|F_o^2| - |F_c^2|)^2 / \sum w|F_o^2|^2]^{1/2}$; $w = 1/\sigma^2(|F_o^2|)$.

[c] $S = [\sum w(F_o^2 - F_c^2)^2/(N_{obs} - N_{param})]^{1/2}$.

controlled using an Oxford Cryosystem low temperature device. Integration and scaling of the reflections, correction for Lorentz and polarization effects were performed with the HKL Denzo-Scalepack system of programs [14]. Multi-scan absorption corrections were applied [15].

The structures were solved by direct methods with SHELXS-97 [16]. The models were refined by full-matrix least squares on F^2 using SHELXL-97 [17]. All the hydrogen atoms were stereochemically positioned and refined with the riding model. Hydrogen atoms of the CH and CH_2 groups were set isotropic with a thermal parameter 20% greater than the equivalent isotropic displacement parameter of the atom to which each one was bonded. This percentage was set to 50% for the hydrogen atoms of the CH_3 group. Data collections and experimental details for the compounds are summarized in Table 1. The programs SHELXL-97 [17] and ORTEP-3 [18] were used within WINGX [19] to prepare materials for publication.

3. Results and discussion

The potassium dithiocarbimates are soluble in water and insoluble in most organic solvents. To the best of our knowledge the spectroscopic data for these salts are not published elsewhere. The *N*-ethanesulfonyldithiocarbimate and *N*-4-iodobenzenesulfonyldithiocarbimate potassium salts were prepared (Scheme 1) by reaction of the corresponding sulfonamides, carbon disulfide (1 equiv.) and potassium hydroxide (2 equiv.) in DMF at room temperature. Attempts to prepare the potassium *N*-2,5-dichlorophenylsulfonyldithiocarbimate using the same conditions failed, yielding a white solid with a strong sulfurous odor. As described in the experimental section, it was necessary to use a dry solvent, low temperature and a more concentrated medium. The recrystallization of this salt was not possible and instead of the formation of the expected yellow crystals a white solid was produced. It is important to note that, although the other ditiocarbimates seem to be more stable, a white solid is also obtained from the aqueous solutions of potassium *N*-4-iodophenylsulfonyldithiocarbimate after some weeks at room temperature. When kept in the solid state at ambient temperature, these potassium salts were also converted in white solids after several months. The composition of these solids was not investigated yet.

On the other hand, the compounds **1**–**3** are stable at the ambient conditions. They were obtained (Scheme 1) by the reaction of the appropriate potassium *N*-R-sulfonyldithiocarbimate ($RSO_2N{=}CS_2K_2$) with nickel(II) chloride hexahydrate in methanol/water and are considerably soluble in most of organic solvents and insoluble in water. However, compounds **2** and **3** are much less soluble in chloroform than compound **1**. Thus, their NMR spectra were obtained in dimethylsulfoxide-d_6.

The electronic spectra of the nickel complexes in acetonitrile showed four or five bands. The band V (ca. 615 nm) appeared in the same region of the d–d transition of the spectra of $(Bu_4N)_2[Ni(CH_3SO_2N{=}CS_2)_2]$ and $(Bu_4N)_2$-$[Ni(4\text{-}CH_3C_6H_4SO_2N{=}CSO_2)_2]$ [1,2]. The band around 420 nm was assigned to the charge transfer transition. These bands are also observed in the spectra of many other diamagnetic planar nickel(II) complexes that contain the NiS_4^{2-} chromophore [20]. The other bands were assigned to the internal transitions of the ligands [1,2].

In the IR spectra of the potassium dithiocarbimates a prominent band is observed at ca. 3430 cm^{-1}. This band, associated to the one observed in the 1630 cm^{-1} region, indicates that these compounds are hydrated. It is known that some potassium dithiocarbimates crystallize with n lattice water molecules (*n* usually varying from 1 to 2) [12,21], which explains the observation of these bands. In the region of 1300–1245 cm^{-1} in the spectra of the dithiocarbimate potassium salts, two very intense bands were observed. The lower wavenumber band was assigned to the νSO_2 and the band of higher wavenumber was assigned to the νCN. Although these wavenumbers are rather low for a formal C=N band, possible hydrogen bonding with lattice water molecules might contribute to this effect. The SO_2 group neighbor to the nitrogen atom also explains the low values observed. This band is shifted to ca. 1385 cm^{-1} in the spectra of the complexes, which is explained both by the fact that the complexes are not hydrated and by the increased importance of the canonical form (c) upon complexation (Scheme 2). This band is observed at ca. 1440 cm^{-1} in the spectra of neutral complexes of general formula $[Ni(Ph_3P)_2(RSO_2N{=}CS_2)]$ where R = 2-$CH_3C_6H_4$, 4-$CH_3C_6H_4$ and 4-BrC_6H_4 [22].

The $\nu_{ass}CS_2$ were observed at higher frequencies in the spectra of the potassium dithiocarbimates (ca. 975 cm^{-1}) than in the spectra of the complexes (ca. 940 cm^{-1}). The shifts are also consistent with complexation by the sulfur atoms of the dithiocarbimate groups. The spectra of the complexes also show the expected medium/strong band in the 300–400 cm^{-1} range assigned to the NiS vibrations.

All the NMR spectra showed the expected signals for the tetrabutylammonium cation. The NMR spectra were typical for diamagnetic species and the integration curves on the ^1H NMR spectra were consistent with a

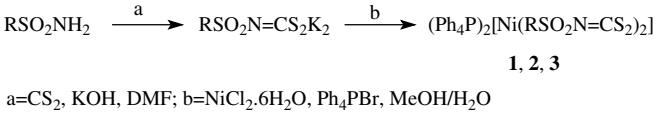

Scheme 1.

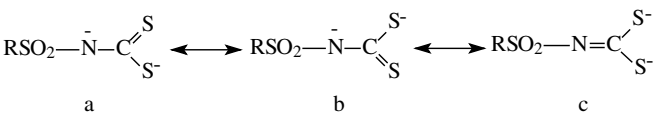

Scheme 2.

2:1 proportion between the tetrabutylammonium cation and the complex anions. In the ^{13}C NMR spectra of the complexes the signal due to the carbon of the dithiocarbimate moiety (N=CS_2, ca. 210 δ) is shifted upfield when compared to the correspondent signal in the potassium dithiocarbimates spectra (ca. 225 δ) as observed with analogous compounds [3]. In the neutral complexes [$Ni(Ph_3P)_2$-(RSO_2N=CS_2)] this signal is observed at (ca. 197 δ) [22].

Single crystal X-ray diffraction data confirmed that the compounds **1**–**3** are constituted by two tetrabutylammonium cations and one complex anion. The crystal structure shows that the nickel atom is coordinated by four sulfur atoms of two R-sulfonyldithiocarbimate ligands, in a distorted square-planar configuration. With the exception of

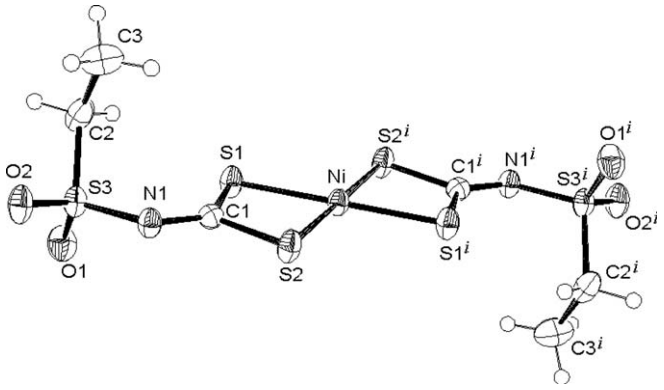

Fig. 1. ORTEP-3 drawing of the anion of compound **1**, showing displacement ellipsoids at 50% probability level. Symmetry code (i) $-x$, $-y$, $-z$.

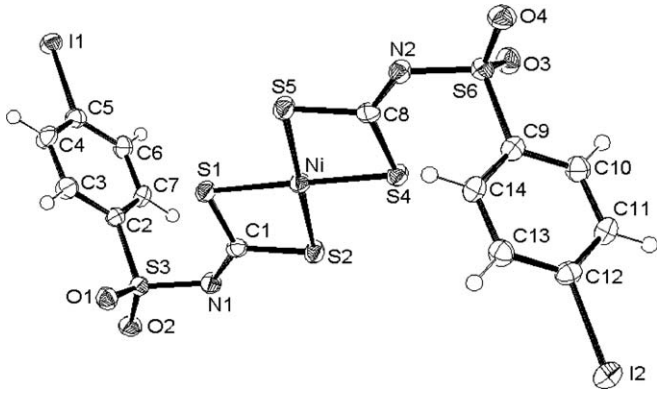

Fig. 2. ORTEP-3 drawing of the anion of compound **2**, showing displacement ellipsoids at 50% probability level.

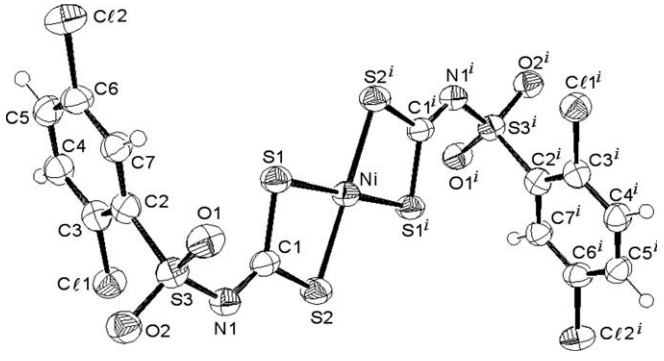

Fig. 3. ORTEP-3 drawing of the anion of compound **3**, showing displacement ellipsoids at 50% probability level. Symmetry code (i) $-x$, $-y$, $-z$.

Table 2
Selected bond lengths (Å) for **1**–**3** anion complex

	1	**2**	**3**	**2**	
Bond lengths				*Bond lengths*	
Ni–S1	2.1989(4)	2.2002(7)	2.192(1)	Ni–S4	2.2009(7)
Ni–S2	2.1966(4)	2.2141(7)	2.203(1)	Ni–S5	2.2133(7)
C1–S1	1.733(2)	1.738(3)	1.751(5)	C8–S4	1.738(3)
C1–S2	1.734(2)	1.734(3)	1.740(4)	C8–S5	1.739(3)
C1–N1	1.309(2)	1.315(3)	1.300(6)	C8–N2	1.313(3)
N1–S3	1.614(1)	1.625(2)	1.612(4)	N2–S6	1.623(2)
O1–S3	1.442(1)	1.440(2)	1.440(3)	O3–S6	1.445(2)
O2–S3	1.444(1)	1.448(2)	1.439(4)	O4–S6	1.444(2)
C2–S3	1.776(2)	1.778(3)	1.791(5)	C9–S6	1.778(3)

Table 3
Selected angles (°) for **1**–**3** anion complex

	1	**2**	**3**	**2**	
Bond angles				*Bond angles*	
				S1–Ni–S4	179.01(3)
S1–Ni–S2	79.08(2)	78.95(3)	79.09(4)	S1–Ni–S5	101.03(3)
S1^i–Ni–S2	100.92(2)		100.91(4)	S2–Ni–S4	101.10(3)
C1–S1–Ni	86.57(6)	86.62(9)	87.2(2)	C1–S4–Ni	86.85(9)
C1–S2–Ni	86.61(6)	86.28(9)	87.1(2)	C1–S5–Ni	86.41(9)
S1–C1–S2	107.63(9)	107.8(1)	106.6(3)	S(4)–C(8)–S(5)	107.6(2)
S1–C1–N1	131.9(1)	130.5(2)	131.0(3)	S(4)–C(8)–N(2)	130.9(2)
S2–C1–N1	120.4(1)	121.7(2)	122.4(4)	S(5)–C(8)–N(2)	121.6(2)
O1–S3–O2	116.26(8)	117.2(1)	116.5(2)	O3–S6–O4	116.7(1)
O1–S3–N1	111.97(8)	112.4(1)	112.5(2)	O3–S6–N2	112.4(1)
O2–S3–N1	105.14(7)	105.1(1)	106.2(2)	O4–S6–N2	105.6(1)
O1–S3–C2	107.02(9)	108.2(1)	106.1(2)	O3–S6–C9	107.5(1)
O2–S3–C2	106.82(9)	105.3(1)	106.2(2)	O4–S6–C9	106.3(1)
N1–S3–C2	109.41(9)	108.2(1)	109.1(2)	N2–S6–C9	107.8(1)
S3–N1–C1	124.4(1)	121.3(2)	120.4(3)	S6–N2–C8	121.4(2)

(i) $-x$, $-y$, $-z$.

Table 4
Tetrabutylammonium diedral angles

Compound	Atoms	Angle (°)
1	C4–C5–C6–C7	175.8(2)
	C8–C9–C10–C11	−177.3(2)
	C12–C13–C14–C15	166.6(2)
	C16–C17–C18–C19	179.7(2)
2	C15–C16–C17–C18	−176.2(2)
	C19–C20–C21–C22	175.5(2)
	C23–C24–C25–C26	179.2(2)
	C27–C28–C29–C30	−57.4(3)
	C31–C32–C33–C34	−174.0(2)
	C35–C36–C37–C38	−177.4(2)
	C39–C40–C41–C42	−165.1(2)
	C43–C44–C45–C46	−175.5(2)
3	C8–C9–C10–C11	177.3(4)
	C12–C13–C14–C15	60.9(6)
	C16–C17–C18–C19	56.9(6)
	C20–C21–C22–C23	174.7(4)

the compound **2**, in the other complexes the metal ion lies on an inversion center.

The crystal structure of the anions of the compounds **1**, **2** and **3** are illustrated in Figs. 1–3, respectively. The square planar geometry around the nickel atom, differently from the tetrahedral zinc complexes with similar ligands [23], indicate that the dithiocarbimates anions are strong field ligands enough to affect the spin pairing necessary for stabilization of the square planar arrangement.

Selected bond lengths and angles are listed in Tables 2 and 3. In all complexes the CS bond lengths, of the $N{=}CS_2$ fragments, are nearly equal and are slightly shorter than typical C–S single bond length (ca. 1.81 Å) due to partial π-delocalization in the S–C–S group. Similar behavior is observed for others nickel complexes of dithiocarbimates [3,22].

Both, the spectroscopic data and the X-ray experiments showed that the C–N bond lengths have a double bond character. However, the CN bonds in these anionic complexes are longer than in the neutral complexes $[Ni(PPh_3)_2(RSO_2N{=}CS_2)]$ [22]. This fact is probably due to a major negative charge on the Ni atom in the anionic complexes **1**–**3** in comparison to the neutral complexes. These data are consistent with the spectroscopic experiments results, which indicate the increase of importance of the canonical form (c) (Scheme 2) from the free ligands to the neutral complexes with similar ligands [22], passing through the anionic complexes.

The S1–C1–N1 angles of 131.9(2)°, 130.5(2)° and 131.0(3)° in the compounds **1**–**3**, respectively, are significantly greater than S2–C1–N1 [120.4(1)° in **1**, 121.7(2)° in **2** and 122.4(4)° in **3**] due to the repulsive interaction

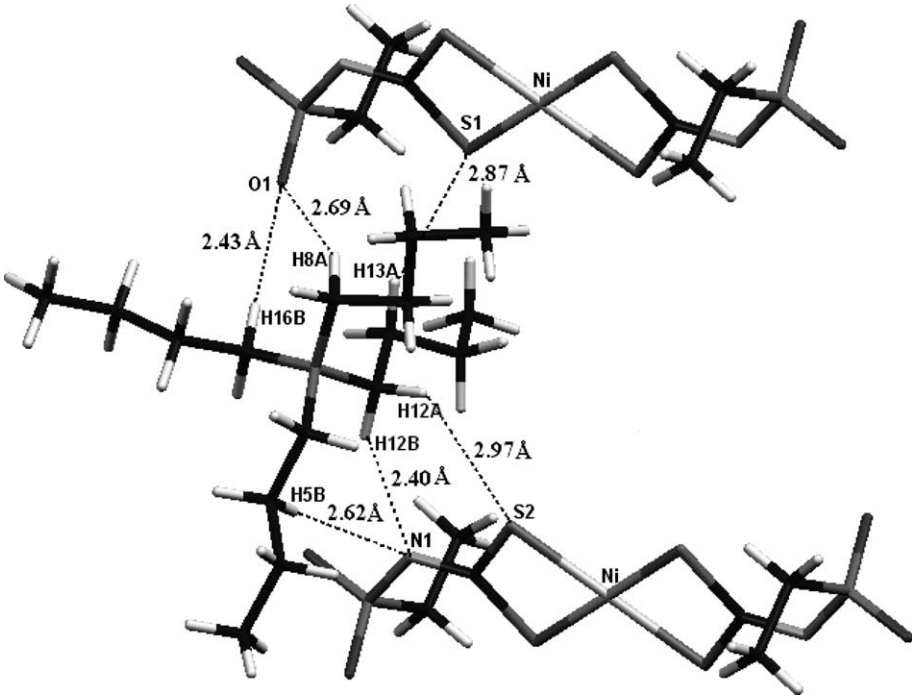

Fig. 4. Weak attractive C_{sp3}–H···O, C_{sp3}–H···N and C_{sp3}–H···S interactions between the cation and the complex anions in the crystal packing of the compound **1**.

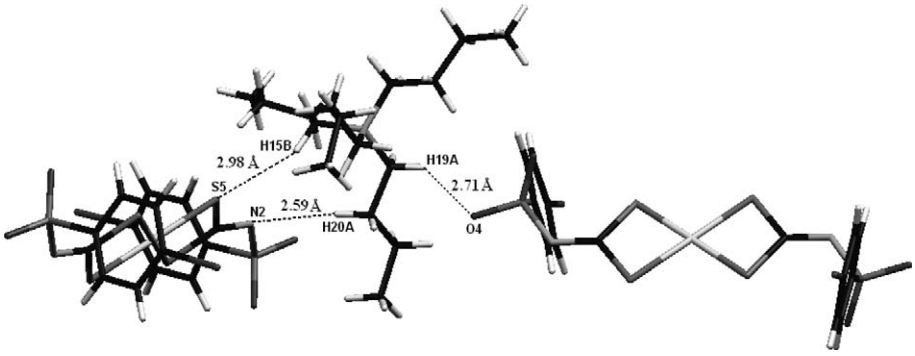

Fig. 5. Weak attractive C_{sp3}–H···O, C_{sp3}–H···N and C_{sp3}–H···S interactions between the cation and the complex anions in the crystal packing of the compound **2.**

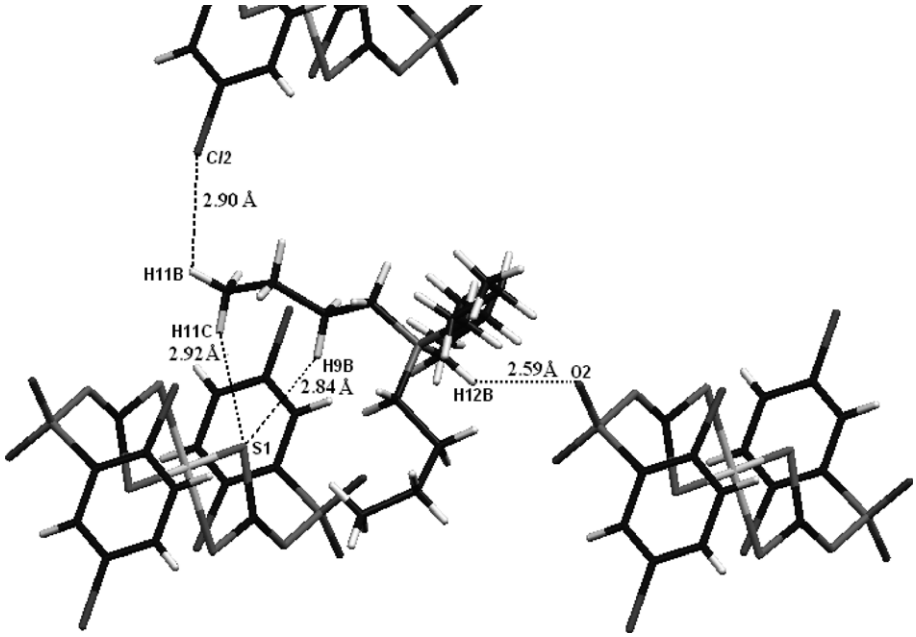

Fig. 6. Weak attractive C_{sp3}–H···O, C_{sp3}–H···S and C_{sp3}–H···Cl interactions between the cation and the complex anions in the crystal packing of the compound **3**.

between the SO_2R group and the S1 atom, which are in *cis* position in relation to the C1–N1 bond. This steric effect between the R-sulfonyl group and the S1 sulfur atom is greater than the repulsion between the lone-pair of the nitrogen N1 and sulfur S2 leading to an increase on the S1–C1–N1 bond angle.

The bond lengths and angles of the tetrabutylammonium cations are in agreement with expected values. However, the dihedral angles of some carbonic chains of the cations deviated from 180° due to the repulsive interaction between hydrogen atoms from neighbor carbonic chains (Table 4). Moreover, in the crystal packing are observed weak attractive C_{sp3}–H···X (X = O, N and/or S and Cl) interactions between the cation and the complex anions with donor–acceptor distances ranged from 3267(2) to 3911(4) Å (Figs. 4–6).

Therefore the competition between attractive and repulsive interactions may affect the conformation of the carbonic chains of the tetrabutylammonium cations.

4. Conclusion

Three new tetra-*n*-butylammonium salts of nickel(II) dithiocarbimates complexes were prepared and characterized by elemental analyses, UV–Vis, IR, ^{1}H NMR and ^{13}C NMR and by single crystal X-ray diffraction techniques.

In the IR spectra the wavenumbers of the *ν*CN are smaller for the ligands than for the compounds **1**–**3**. The NMR spectra show that the carbon atom of the dithiocarbimate moiety are more shielded in the complexes than in the parent ligands. The crystallographic data show that the CN bond are shorter in the complexes than in similar ligands [12]. The same tendency is observed when the data for the compounds **1**–**3** are compared with the data for neutral complexes of general formula $[Ni(PPh_3)_2(RSO_2N{=}CS_2)]$ [22]. Thus, the chemical shifts of the signal for the carbon atom of the $N{=}CS_2$ fragment is observed at lower field in the ^{13}C NMR spectra of compounds **1**–**3** if compared to these neutral complexes. The CN bonds are longer in the anionic complexes and the correspondent *ν*CN bands appear at lower wavenumbers in the IR spectra of **1**–**3** if compared to the neutral complexes [22]. These data pointed to an increase of the contribution of the canonical form (c) to the resonance hybrid from the ligands to the anionic complexes and from anionic complexes to analogous neutral complexes (Scheme 2).

Acknowledgement

This work has been supported by FAPEMIG (Grant CEX 1123/90 and CEX 200/02), FINEP, CNPq and CAPES (Brazil).

Appendix A. Supplementary data

Crystallographic data for the structural analysis have been deposited with the Cambridge Crystallographic Data Centre, CCDC Nos. 281872, 281871 and 281873 for the **1**, **2** and **3**, respectively. Copies of this information may be obtained free of charge from The Director, CCDC, 12 Union Road, Cambridge, CB2 1EZ, UK, fax: +44 1223 366 033, e-mail: deposit@ccdc.ac.uk or on the web www: http://www.ccdc.cam.ac.uk. Supplementary data associated with this article can be found, in the online version, at doi:10.1016/j.poly.2005.11.035.

References

[1] M.R.L. Oliveira, V.M. De Bellis, N.G. Fernandes, Struct. Chem. 8 (3) (1997) 205.
[2] M.R.L. Oliveira, J.E.J.C. Graúdo, V.M. De Bellis, N.L. Speziali, Struct. Chem. 10 (1) (1999) 41.
[3] M.R.L. Oliveira, R. Diniz, V.M. De Bellis, N.G. Fernandes, Polyhedron 22 (2003) 1561.
[4] H.U. Hummel, U.Z. Korn, Naturforsch 44 (B) (1989) 29.
[5] M.J. Cox, E.R.T. Tienkink, Z. Kristallogr. 214 (1999) 630.
[6] D. Coucouvanis, Prog. Inorg. Chem. 11 (1969) 233.
[7] G. Faraglia, D. Fregona, S. Sitran, L. Giovagnini, C. Marzano, F. Baccichetti, U. Casellato, R. Graziani, J. Inorg. Biochem. 83 (2001) 31.
[8] A. Mastrolorenzo, A. Scozzafava, C.T. Supuran, Eur. J. Pharm. Sci. 11 (2000) 99.
[9] Z. Brzozowsky, F. Sączewsky, M. Gdaniec, Eur. J. Med. Chem. 37 (2002) 285.
[10] A.I. Vogel, A Textbook of Practical Organic Chemistry Including Qualitative Organic Analysis, 3rd ed., Longmans, London, 1956, p. 543.
[11] K. Hartke, Arch. Pharm. 299 (1966) 174.
[12] H.U. Hummel, U. Korn, Z. Naturforsch. 44B (1989) 24.
[13] Enraf-Nonius, COLLECT, Nonius BV, Delft, The Netherlands, 1997–2000.
[14] Z. Otwinowski, W. Minor, in: C.W. CarterJr., R.M. Sweet (Eds.), Methods in Enzymology, vol. 276, Academic Press, New York, 1997, p. 307.
[15] R.H. Blessing, Acta Crystallogr. A51 (1995) 33.
[16] G.M. Sheldrick, SHELXS-97 Program for Crystal Structure Resolution, Univ. of Göttingen, Göttingen, Germany, 1997.
[17] G.M. Sheldrick, SHELXL-97 Program for Crystal Structure Refinement, Univ. of Göttingen, Göttingen, Germany, 1997.
[18] L.J. Farrugia, J. Appl. Crystallogr. 30 (1997) 565.
[19] L.J. Farrugia, J. Appl. Crystallogr. 32 (1999) 837.
[20] C.A. Tsipis, I.J. Meleziadis, D.P. Kessissoglou, G.A. Katsoulos, Inorg. Chim. Acta 90 (1984) L19.
[21] K. Hartke, J.M. Bickert, S.A. Warda, Z. Naturforsch. 52B (1997) 735.
[22] M.R.L. Oliveira, H.P. Vieira, G.J. Perpétuo, J. Janczak, V.M. De Bellis, Polyhedron 21 (2002) 2243.
[23] G.J. Perpétuo, M.R.L. Oliveira, J. Janczak, H.P. Vieira, F.F. Amaral, V.M. De Bellis, Polyhedron 22 (2003) 3355.

of metal ions from solution and the activations of small molecules gave impetus to this endeavour [2–27]. The synthesis of organic substrates that preferentially interact with particular metal ions is of fundamental importance to many areas of chemistry [28–32]. For example, condensation between carbonyl and amine has played an important role in the development of synthetic macrocyclic ligands [33–43]. Usually such syntheses are carried out in the presence of a suitable metal ion, which serves to direct the steric course of the reaction preferentially towards cyclic rather than oligomeric or polymeric products.

The coordination geometry and properties of most transition metal complexes with 14-membered hexaaza macrocyclic ligands containing amine have been studied [1–43]. However, most of them contained tetraaza macrocyclic ligands, and 14-membered macrocyclic ligands containing six nitrogen atoms with a phenylene group's macrocyclic framework have not been reported yet. We have been interested in the synthesis of various types of polyaza macrocyclic complexes containing amino alkyl groups from in situ one-pot template synthesis (IOPTS). Metal template condensation reactions often provide selective routes towards products that are not obtainable in the absence of metal ions. Especially, template reactions involving formaldehyde and amines facilitate the preparation of saturated polyaza multidentate macrocyclic and macropolycyclic complexes. Metal template condensation reactions involving amines and formaldehyde have been employed in the preparation of various saturated polyaza macrocyclic complexes [1–43].

In this paper, we report the synthesis, characterization and properties of the new nickel(II) complexes of dibenzo-1,3,5,8,10,12-hexaazacyclotetradecane, [Ni(Bzo_2[14]aneN$_6$)]-(ClO_4)$_2$ (**1**); 3,10-dimethyl-, [Ni(Me_2Bzo_2[14]aneN$_6$)](ClO_4)$_2$ (**2**); 3,10-diethyl-, [Ni(Et_2Bzo_2[14]aneN$_6$)](ClO_4)$_2$ (**3**); 3,10-dibutyl-, [Ni(Bu_2Bzo_2[14]aneN$_6$)](ClO_4)$_2$ (**4**); 3,10-dibenzyl-, dibenzo-1,3,5,8,10,12-hexaazacyclotetradecane [Ni((benzyl)$_2$-Bzo_2[14]aneN$_6$)](ClO_4)$_2$ (**5**); [Ni(Bzo_2[14]aneN$_6$)](PF_6)$_2$ (**6**); [Ni(Me_2Bzo_2[14]aneN$_6$)](PF_6)$_2$ (**7**); [Ni(Et_2Bzo_2[14]aneN$_6$)]-(PF_6)$_2$ (**8**); [Ni(Bu_2Bzo_2[14]aneN$_6$)](PF_6)$_2$ (**9**); [Ni((benzyl)$_2$$Bzo_2$[14]aneN$_6$)]($PF_6$)$_2$ (**10**); [Ni(Bzo_2[14]aneN$_6$)Cl_2] (**11**); [Ni(Me_2Bzo_2[14]aneN$_6$)Cl_2] (**12**); [Ni(Et_2Bzo_2[14]-aneN$_6$)Cl_2] (**13**); [Ni(Bu_2Bzo_2[14]aneN$_6$)Cl_2] (**14**); [Ni((benzyl)$_2$$Bzo_2$[14]aneN$_6$)$Cl_2$] (**15**); [Ni($Bzo_2$[14]aneN$_6$)(NCS)$_2$] (**16**); [Ni($Me_2Bzo_2$[14]aneN$_6$)(NCS)$_2$] (**17**); [Ni($Et_2Bzo_2$-[14]aneN$_6$)(NCS)$_2$] (**18**); [Ni($Bu_2Bzo_2$[14]aneN$_6$)(NCS)$_2$] (**19**) and [Ni((benzyl)$_2$$Bzo_2$[14]aneN$_6$)(NCS)$_2$] (**20**) are given in Schemes 1 and 2.

2. Experimental

2.1. Materials and measurements

Safety note. Caution! Perchlorate salts of metal complexes are potentially explosive and due care must be employed when handling them. In particular, such compounds should never be heating as solids. All chemicals and solvents used in the syntheses were of reagent grade and were used without further purification. For the spectroscopic measurements, water was distilled and organic solvents were purified according to the literature method [44]. For electrochemical experiments, high-purity acetonitrile was obtained from Aldrich Chemical Co. and dried over 4 Å molecular sieves. Electronic absorption spectra were obtained with a Shimadzu UV–Vis scanning

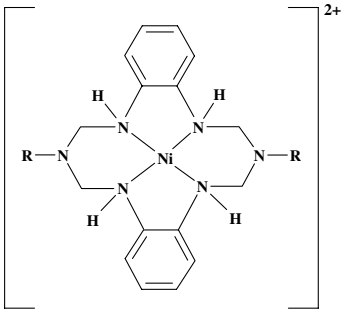

R	Complex	Number
H	[Ni(H_2Bzo[14]aneN$_6$)](ClO_4)$_2$	1
Me	[Ni(Me_2Bzo[14]aneN$_6$)](ClO_4)$_2$	2
Et	[Ni(Et_2Bzo[14]aneN$_6$)](ClO_4)$_2$	3
Bu	[Ni(Bu_2Bzo[14]aneN$_6$)](ClO_4)$_2$	4
Benzyl	[Ni((Benzyl)$_2$Bzo[14]aneN$_6$)](ClO_4)$_2$	5
H	[Ni(H_2Bzo[14]aneN$_6$)](PF_6)$_2$	6
Me	[Ni(Me_2Bzo[14]aneN$_6$)](PF_6)$_2$	7
Et	[Ni(Et_2Bzo[14]aneN$_6$)](PF_6)$_2$	8
Bu	[Ni(Bu_2Bzo[14]aneN$_6$)](PF_6)$_2$	9
Benzyl	[Ni((Benzyl)$_2$Bzo[14]aneN6](PF_6)$_2$	10

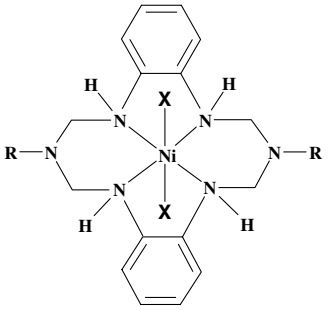

R	X	Complex	Number
H	Cl	[Ni(H_2Bzo[14]aneN$_6$$Cl_2$]	11
Me	Cl	[Ni(Me_2Bzo[14]aneN$_6$$Cl_2$]	12
Et	Cl	[Ni(Et_2Bzo[14]aneN$_6$$Cl_2$]	13
Bu	Cl	[Ni(Bu_2Bzo[14]aneN$_6$$Cl_2$]	14
Benzyl	Cl	[Ni((Benzyl)$_2$Bzo[14]aneN$_6$$Cl_2$]	15
H	NCS	[Ni(H_2Bzo[14]aneN6](NCS)$_2$]	16
Me	NCS	[Ni(Me_2Bzo[14]aneN$_6$(NCS)$_2$]	17
Et	NCS	[Ni(Et_2Bzo[14]aneN$_6$(NCS)$_2$]	18
Bu	NCS	[Ni(Bu_2Bzo[14]aneN$_6$(NCS)$_2$]	19
Benzyl	NCS	[Ni((Benzyl)$_2$Bzo[14]aneN$_6$(NCS)$_2$]	20

Scheme 1.

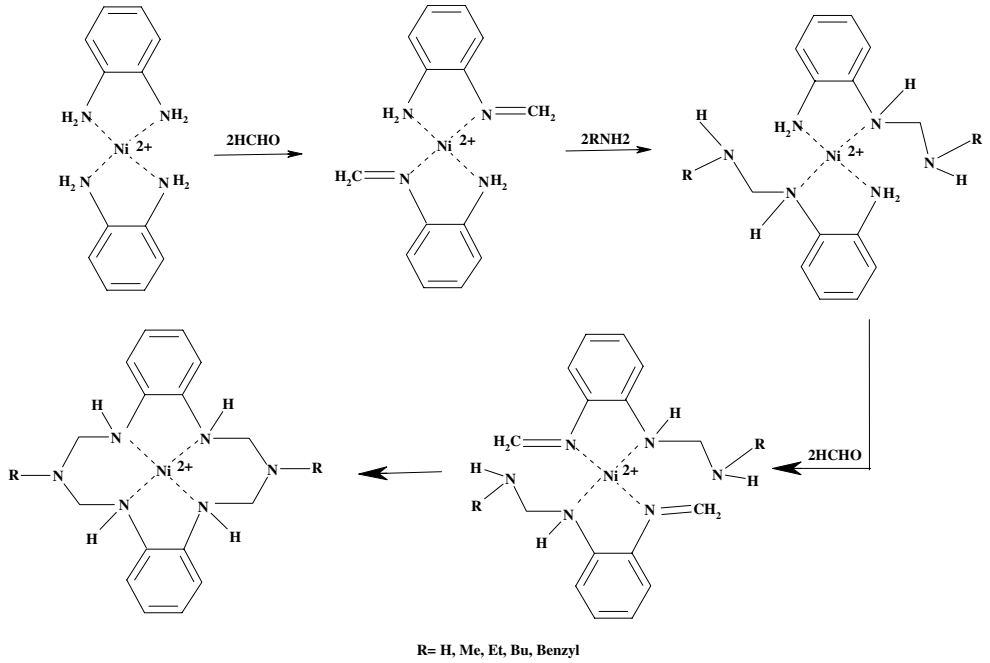

Scheme 2.

spectrophotometer (Model 2101 PC), FTIR spectra with a Shimadzu Varian 4300 spectrophotometer, NMR spectra with a Varian Mercury 300 NMR spectrometer, and conductance measurements with a Metrohm Herisau conductometer E 518. The elemental analysis (carbon, hydrogen and nitrogen) of the complexes was obtained from Carlo ERBA Model EA 1108 analyzer. Magnetic moments were calculated from magnetic susceptibility data obtained by using a Johnson Matthey MK-1 magnetic susceptibility balance. The electrochemical data was obtained in acetonitrile with 0.1 M $(n\text{-Bu})_4NClO_4$ as supporting electrolyte. The working electrode was a platinum disk, the auxiliary electrode was a coiled platinum wire and the reference electrode was $Ag|AgClO_4$ (0.1 M in CH_3CN), which showed +0.24 V versus SCE. Atomic absorption spectra (AAS) were recorded on a Perkin–Elmer 4100-1319 spectrophotometer. FAB mass spectra were recorded on a Kratos MS50TC spectrometer.

2.2. Preparation of $[Ni(H_2Bzo_2[14]aneN_6)](ClO_4)_2$ (1)

To a stirred methanol solution (100 ml) of $Ni(ClO_4)_2 \cdot 6H_20$ (15.38 g, 42.07 mmol) was slowly added 1,2-phenylenediamine (9.11 g, 84.20 mmol), 36% formaldehyde (15 ml) and 25% ammonia (6.30 ml, 84.20 mmol). The mixture was heated at reflux for 24 h until a dark solution resulted. The solution was cooled to room temperature and filtered to remove nickel hydroxide. The deep yellow crystals were filtered, washed with methanol, and air-dried. The crystals were recrystallized from hot water. (Yield: ~46%; FAB mass (m/z): 456 ($[M - ClO_4]^+$)). *Anal.* Calc. for **1**: Ni, 10.56; C, 34.56; H, 3.99; N, 15.12. Found: Ni, 10.41; C, 34.40, H, 3.81; N, 15.24%.

2.3. Preparation of $[Ni(Me_2Bzo_2[14]aneN_6)](ClO_4)_2$ (2)

This compound was prepared by a method similar to that for the preparation of $[Ni(H_2Bzo_2[14]aneN_6)](ClO_4)_2$ except that methylamine (84.20 mmol, 10.47 ml) was used instead of ammonia. (Yield: ~54%; FAB mass (m/z): 484 ($[M - ClO_4]^+$)). *Anal.* Calc. for **2**: Ni, 10.05; C, 37.01; H, 4.49; N, 14.39. Found: Ni, 9.92; C, 36.88; H, 4.38; N, 14.55%.

2.4. Preparation of $[Ni(Et_2Bzo_2[14]aneN_6)](ClO_4)_2$ (3)

This complex was prepared by a method similar to that for $[Ni(H_2Bzo_2[14]aneN_6)](ClO_4)_2$ except that 50% ethylamine (8.72 ml, 84.20 mmol) was used instead of ammonia. (Yield: ~57%; FAB mass (m/z): 513 ($[M - ClO_4]^+$)). *Anal.* Calc. for **3**: Ni, 9.59; C, 39.24; H, 4.94; N, 13.73. Found: Ni, 9.47, C, 39.08; H, 4.81; N, 13.84%.

2.5. Preparation of $[Ni(Bu_2Bzo_2[14]aneN_6)](ClO_4)_2$ (4)

This complex was prepared by a method similar to that for $[Ni(H_2Bzo_2[14]aneN_6)](ClO_4)_2$ except that *iso*-butylamine (8.36 ml, 84.20 mmol) was used instead of ammonia. (Yield: ~44%; FAB mass (m/z): 568 ($[M - ClO_4]^+$)). *Anal.* Calc. for **4**: Ni, 8.79; C, 43.14; H, 5.73; N, 12.58. Found: Ni, 8.66; C, 43.02; H, 5.60; N, 12.65%.

2.6. Preparation of $[Ni((benzyl)_2Bzo_2[14]aneN_6)](ClO_4)_2$ (5)

This complex was prepared by a method similar to that for $[Ni(H_2Bzo_2[14]aneN_6)](ClO_4)_2$ except that benzylamine

(9.20 ml, 84.20 mol) was used instead of ammonia. (Yield: ~41%; FAB mass (*m*/*z*): 638 ($[M - ClO_4]^+$)). *Anal*. Calc. for **5**: Ni, 7.97; C, 48.94; H, 4.66; N, 11.42. Found: Ni, 7.81; C, 48.81; H, 4.53; N, 11.55%.

2.7. Preparation of $[Ni(R_2Bzo_2[14]aneN_6)](PF_6)_2$ (6–10)

To an acetonitrile (50 ml) suspension of $[Ni(R_2Bzo_2[14]aneN_6)](ClO_4)_2$ (0.50 g) was added excess NH_4PF_6, and white precipitates of NH_4ClO_4 were formed. NH_4ClO_4 was filtered off and the filtrate was concentrated to 25 ml. Water (25 ml) was added to the solution, and the mixture was kept in the refrigerator. The yellow precipitates were filtered, washed with a 6:1 mixture of water and acetonitrile, and dried in vacuum. (**6**, FAB mass (*m*/*z*): 502 ($[M - PF_6]^+$)). *Anal*. Calc. Ni, 9.07; C, 29.70; H, 3.43; N, 12.99. Found: Ni, 8.94; C, 29.58; H, 3.32; N, 13.04%. (**7**, FAB mass (*m*/*z*): 530 ($[M - PF_6]^+$)). *Anal*. Calc. Ni, 8.70; C, 32.02; H, 3.88; N, 12.45. Found: Ni, 8.57; C, 31.90; H, 3.75; N, 12.56%. (**8**, FAB mass (*m*/*z*): 558 ($[M - PF_6]^+$)). *Anal*. Calc. Ni, 8.35; C, 34.16; H, 4.30; N, 11.95. Found: Ni, 8.22; C, 34.02; H, 4.18; N, 12.06%. (**9**, FAB mass (*m*/*z*): 614 ($[M - PF_6]^+$)). *Anal*. Calc. Ni, 7.73; C, 37.97; H, 5.04; N, 11.07. Found: Ni, 7.60; C, 37.85; H, 4.91; N, 11.13%. (**10,** FAB mass (*m*/*z*): 682 ($[M - PF_6]^+$)). *Anal*. Calc. Ni, 7.10; C, 43.56; H, 4.14; N, 10.16. Found: Ni, 6.94; C, 43.44; H, 4.03; N, 10.24%.

2.8. Preparation of $[Ni(R_2Bzo_2[14]aneN_6Cl_2)]$ (11–15)

To a stirred methanol solution (100 ml) of $NiCl_2 \cdot 6H_2O$ (10.00 g, 42.07 mmol) were slowly added 1,2-phenylenediamine (9.11 g, 84.20 mmol), 36% formaldehyde (15 ml) and 25% ammonia (6.3 ml, 84.20 mmol). The mixture was heated at reflux for 24 h until a dark solution resulted. The solution was cooled to room temperature and filtered to remove nickel hydroxide. The dark brown crystals were filtered, washed with methanol and air-dried. The crystals were recrystallized from hot water. *Anal*. Calc. for **11**: Ni, 13.72; C, 30.18; H, 5.18; N, 19.64. Found: Ni, 13.58; C, 30.08; H, 5.10; N, 19.73%. *Anal*. Calc. for **12**: Ni, 12.87; C, 47.40; H, 5.75; N, 18.43. Found: Ni, 12.76; C, 47.29; H, 5.62; N, 18.56%. *Anal*. Calc. for **13**: Ni, 12.13; C, 49.62; H, 6.25; N, 17.36. Found: Ni, 12.01; C, 49.48; H, 6.18; N, 17.45%. *Anal*. Calc. for **14**: Ni, 10.87; C, 53.36; H, 7.09; N, 15.56. Found: Ni, 10.75; C, 53.22; H, 6.91; N, 15.64%. *Anal*. Calc. for **15**: Ni, 9.65; C, 56.24; H, 5.63; N, 13.82. Found: Ni, 9.54; C, 26.10; H, 5.48; N, 13.95%.

2.9. Preparation of $[Ni(R_2Bzo_2[14]aneN_6)(NCS)_2]$ (16–20)

To a saturated hot aqueous solution of the perchlorate salt of the appropriate "$[Ni(R_2Bzo_2[14]aneN_6)](ClO_4)_2$ (R = H, Me, Et, Bu, Benzyl)" was added excess KSCN dissolved in a minimum amount of hot water. The solution was allowed to stand at room temperature, and then the deep pink precipitate formed was filtered, washed with a 1:2 mixture of water and methanol, and dried in a vacuum. *Anal*. Calc. for **16**: Ni, 12.40; C, 45.68; H, 4.69; N, 23.68. Found: Ni, 12.29; C, 45.55; H, 4.56; N, 23.75%. *Anal*. Calc. for **17**: Ni, 11.71; C, 47.92; H, 5.23; N, 22.35. Found: Ni, 11.59; C, 47.80; H, 5.11; N, 22.46%. *Anal*. Calc. for **18**: Ni, 11.09; C, 49.92; H, 5.71; N, 21.17. Found: Ni, 10.91; C, 49.80; H, 5.58; N, 21.26%. *Anal*. Calc. for **19**: Ni, 10.03; C, 53.34; H, 6.54; N, 19.14. Found: Ni, 9.92; C, 53.21; H, 6.41; N, 19.23%. *Anal*. Calc. for **20**: Ni, 8.98; C, 58.81; H, 5.24; N, 17.15. Found: Ni, 8.83; C, 58.70; H, 5.12; N, 17.23%.

2.10. Preparation of $[Ni(Bzo_2[10]aneN_4)](ClO_4)_2$ (21)

To a stirred methanol solution (100 ml) of $Ni(ClO_4)_2 \cdot 6H_20$ (15.38 g, 42.07 mmol) were slowly added 1,2-phenylenediamine (9.11 g, 84.20 mmol) and 36% formaldehyde (30 ml). The mixture was heated at reflux for 24 h until a dark yellow solution resulted. The solution was cooled to room temperature and filtered to remove nickel hydroxide. The dark yellow crystals were filtered, washed with methanol and air-dried. The crystals were recrystallized from hot water. (Yield: ~58%; FAB mass (*m*/*z*): 398 ($[M - PF_6]^+$)). *Anal*. Calc. for **21**: Ni, 11.78; C, 33.77; H, 3.24; N, 11.25. Found: Ni, 11.61; C, 33.58, H, 3.16; N, 11.37%.

2.11. Preparation of $[Ni((Allyl)_2Bzo_2[14]aneN_6)](ClO_4)_2$ (22)

This compound was prepared by a method similar to that for the preparation of $[Ni(H_2Bzo_2[14]aneN_6)](ClO_4)_2$ except that allylamine "3-amino-1-propene" (84.20 mmol, 4.81 g) was used instead of ammonia. (Yield: ~54%; FAB mass (*m*/*z*): 568 ($[M - PF_6]^+$)). *Anal*. Calc. for **23**: Ni, 8.78; C, 39.54; H, 5.13; N, 16.77. Found: Ni, 8.57; C, 39.38; H, 5.01; N, 16.83%.

3. Results and discussion

In situ one-pot template synthesis (IOPTS) of 1,2-phenylenediamine with formaldehyde, in the presence of the nickel(II) ion, was expected to produce of the mononuclear 14-membered hexaaza macrocycle complex "$[Ni(R_2Bzo_2[14]aneN_6)]^{2+}$". It was observed that the product obtained from the reactions was largely affected by the molar ratio of the reactants. The mononuclear hexaaza complex "$[Ni(R_2Bzo_2[14]aneN_6)](ClO_4)_2$ (**1**–**5**)" was readily prepared as the main product by the reaction of the nickel(II) ion, 1,2-phenylenediamine, CH_2O and amine in a 1:2:4:2 molar ratio. The crude product often contained a small amount of the 10-membered tetraaza macrocyclic nickel(II) complex (**21**) as a by-product (Section 2.10). However, the mononuclear complex could be readily isolated by fractional recrystallization of the product from ca. 0.05 M $HClO_4$ aqueous solutions.

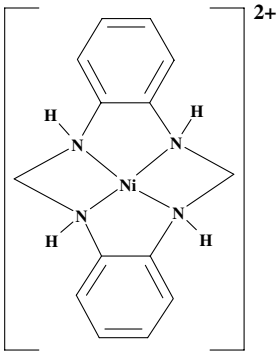

21

The deep yellow complexes "$[Ni(R_2Bzo_2[14]aneN_6)](ClO_4)_2$ (**1**–**5**) and $[Ni(R_2Bzo_2[14]aneN_6)](PF_6)_2$ (**6**–**10**)" readily dissolve in polar solvents such as H_2O, CH_3CN, CH_3NO_2 and Me_2SO_2. However, PF_6^- salts of the complexes readily dissolve in nitromethane and water. The nickel(II) complexes are extremely stable in the solid state and in solution and are relatively stable against ligand dissociation even in highly acidic solutions. $[Ni(R_2[14]aneN_6)]^{2+}$ react with excess KSCN in aqueous solution to form tetragonal complexes $[Ni(R_2[14]aneN_6)(NCS)_2]$, whose IR spectra (Table 1) show that the nitrogen atoms of the NCS^- ligands are coordinated to the Ni(II) ion [45].

The molecular formulae of the complexes "$[Ni(R_2Bzo_2[14]aneN_6)](ClO_4)_2$, $[Ni(R_2Bzo_2[14]aneN_6)](PF_6)_2$, $[Ni(R_2Bzo_2[14]aneN_6)Cl_2]$ and $[Ni(R_2Bzo_2[14]aneN_6)(NCS)_2]$" have been assigned on the basis of the results of their elemental analyses and the molecular ion peaks in the mass spectra. All mass spectra showed molecular ion peaks for the 1:1 metal-to-ligand stoichiometry with no further peaks above them. A preliminary identification of the metal complexes was made on the basis of their IR spectra, which exhibited no bands characteristic of free primary amine, thus supporting the proposed macrocyclic skeleton (Scheme 1).

The IR spectra of all the complexes (Table 1) showed a single sharp absorption around $\sim$3230 cm^{-1} which may possibly arise from a secondary amine, ν_{N-H}, although its position has been found to be lower by 40–60 cm^{-1} than the analogous metal-free hexaaza ligands [46]. This suggests that the secondary amine nitrogens take part in coordination to the metal ions, which has been further confirmed by the appearance of bands in the 320–365 cm^{-1} region in all the complexes, corresponding to ν_{M-N} vibrations. A much higher ν_{N-H} value (3235 cm^{-1}) for $[Ni\{(CH_3)_2Bzo_2[14]aneN_6\}](ClO_4)_2$ than that (3220 cm^{-1}) for $[Ni\{(CH_3)_2[14]aneN_6\}](ClO_4)_2$ [57], indicates that the Ni–N interaction in **2** is much stronger than in the $[Ni\{(CH_3)_2[14]aneN_6\}](ClO_4)_2$ complex. The absorption bands in the 2850–3050 and 1400–1450 cm^{-1} regions observed in the complexes may reasonably correspond to CH stretching and CH bending vibrational modes. However, a medium intensity band at 280–290 cm^{-1} may unambiguously be assigned to the M–Cl stretching mode in complexes **11**–**15**.

The molar conductance values of **1**–**10** ($\sim$240 Ω^{-1} mol^{-1} cm^2), measured in water, correspond to 1:2 electrolytes.

Table 1
Spectral and conductance data for 14-membered hexaaza macrocyclic nickel(II) complexes

Complex	IR (cm^{-1})	Electronic spectra, λ_{max} (nm (ε, M^{-1} cm^{-1}))					Λ_M[a] (Ω^{-1} cm^2 M^{-1})	μ_{eff} (MB)
		$MeNO_2$	MeCN	H_2O	In 3.0 M NaCl aqueous solution	DMSO		
$[Ni(H_2Bzo_2[14]aneN_6)](ClO_4)_2$	ν_{N-H} 3240	441 (56)	450 (39)	454 (51)	447 (53)		250	−0.08
$[Ni((CH_3)_2Bzo_2[14]aneN_6)](ClO_4)_2$	ν_{N-H} 3235	441 (55)	451 (40)	455 (52)	447 (54)		248	−0.09
$[Ni(Et_2Bzo_2[14]aneN_6)](ClO_4)_2$	ν_{N-H} 3232	442 (56)	452 (40)	456 (52)	448 (53)		240	−0.09
$[Ni(Bu_2Bzo_2[14]aneN_6)](ClO_4)_2$	ν_{N-H} 3225	442 (67)	452 (39)	457 (67)	449 (53)		236	−0.10
$[Ni((Allyl)_2Bzo_2[14]aneN_6)](ClO_4)_2$	ν_{N-H} 3227	443(67)	452 (39)	458 (67)	450 (54)		230	−0.11
$[Ni((benzyl)_2Bzo_2[14]aneN_6)](ClO_4)_2$	ν_{N-H} 3245	440 (56)	449 (39)	453 (52)	445 (53)		234	−0.12
$[Ni(H_2Bzo_2[14]aneN_6)](PF_6)_2$	ν_{N-H} 3239	442 (57)	451 (36)	453 (50)	446 (54)		258	−0.10
$[Ni((CH_3)_2Bzo_2[14]aneN_6)](PF_6)_2$	ν_{N-H} 3235	441 (55)	450 (35)	456 (51)	446 (52)		256	−0.11
$[Ni(Et_2Bzo_2[14]aneN_6)](PF_6)_2$	ν_{N-H} 3232	443 (56)	453 (35)	456 (52)	447 (53)		248	−0.12
$[Ni(Bu_2Bzo_2[14]aneN_6)](PF_6)_2$	ν_{N-H} 3226	443 (67)	453 (36)	457 (67)	450 (52)		245	−0.12
$[Ni((benzyl)_2Bzo_2[14]aneN_6)](PF_6)_2$	ν_{N-H} 3243	441 (57)	450 (35)	454 (52)	446 (54)		237	−0.13
$[Ni(H_2Bzo_2[14]aneN_6)Cl_2]$	ν_{N-H} 3255					506	18	2.82
$[Ni((CH_3)_2Bzo_2[14]aneN_6)Cl_2]$	ν_{N-H} 3253					506	15	2.83
$[Ni(Et_2Bzo_2[14]aneN_6)Cl_2]$	ν_{N-H} 3250					507	14	2.84
$[Ni(Bu_2Bzo_2[14]aneN_6)Cl_2]$	ν_{N-H} 3245					508	12	2.82
$[Ni((benzyl)_2Bzo_2[14]aneN_6)Cl_2]$	ν_{N-H} 3248					504	10	2.83
$[Ni(H_2Bzo_2[14]aneN_6)(NCS)_2]$	ν_{N-H} 3258; $\nu_{C=N}$ 2052; $\nu_{C=S}$ 785					497	16	2.83
$[Ni((CH_3)_2Bzo_2[14]aneN_6)(NCS)_2]$	ν_{N-H} 3256; $\nu_{C=N}$ 2052; $\nu_{C=S}$ 784					496	13	2.84
$[Ni(Et_2Bzo_2[14]aneN_6)(NCS)_2]$	ν_{N-H} 3255; $\nu_{C=N}$ 2049; $\nu_{C=S}$ 784					496	12	2.82
$[Ni(Bu_2Bzo_2[14]aneN_6)(NCS)_2]$	ν_{N-H} 3257; $\nu_{C=N}$ 2047; $\nu_{C=S}$ 783					495	10	2.83
$[Ni((benzyl)_2Bzo_2[14]aneN_6)(NCS)_2]$	ν_{N-H} 3261; $\nu_{C=N}$ 2050; $\nu_{C=S}$ 787					490	9	2.82

[a] In DMSO solution.

The observed low molar conductivities recorded (**10**–**20**) in DMSO indicate that these are non-electrolytes in nature. The overall geometries of all macrocycles have been deduced on the basis of the observed values of the magnetic moments and the band positions in the electronic spectra. The magnetic moments (−0.08 to −0.13 μ_B) of the nickel(II) complexes (**1**–**10**) measured in the solid state correspond to a square-planar coordination geometry of the complexes. The diamagnetic nature of the Ni(II) complex **7** has allowed its characterization by NMR spectrometry. ^{1}H NMR spectra of the Ni(II) complexes of **6**–**10** exhibit very broad peaks in D_2O, CH_3CN-d_3 and Me_2SO-d_6, but sharp resolvable peaks in CH_3NO_2-d_3. This indicates that a considerable amount of the paramagnetic octahedral species $[Ni(R_2Bzo_2[14]aneN_6)(Solvent)_2]^{2+}$ exists in the donating solvents, where as the Ni(II) complexes of "$R_2Bzo_2[14]aneN_6$" exist primarily as diamagnetic square-planar species in CH_3NO_2-d_3. The ^{1}H NMR spectra of the nickel complex "$[Ni\{((CH_3)_2Bzo_2[14]aneN_6)\}](PF_6)_2$" gave a singlet at 1.67 ppm corresponding to CH_3 (6H) protons. However, the ^{1}H NMR spectra of the complexes "$[Ni(R_2Bzo_2[14]aneN_6)](PF_6)_2$" showed a multiplet in the region 7.51–7.70 ppm, corresponding to the phenyl ring protons (8H). The ^{1}H NMR spectra of all the complexes showed a broad signal at 8.23–8.41 ppm and can be assigned to secondary amine protons (4H). A singlet for the complexes at 3.08–3.16 ppm corresponds to CH_2 (8H) protons adjacent to nitrogen. However, the spectra of all the complexes do not show any signal corresponding to free primary amine protons.

Nickel(II) complexes with the 14-membered hexaaza macrocyclic ligand "$R_2Bzo_2[14]aneN_6$" exist in aqueous solution as an equilibrium mixture of a yellow, square-planar, diamagnetic, low spin species and a blue, octahedral, paramagnetic, high-spin species. Solutions of hexaaza macrocyclic nickel(II) complexes in coordinating solvents (such as water, acetonitrile, etc.) show an absorption maximum at 450 nm, characteristic for square-planar yellow species, and at 350 and 500 nm, characteristic for blue octahedral species. Table 1 shows that the molar absorption coefficient of the ligand field transition band for complexes measured in water or acetonitrile is smaller than that in nitromethane, a non-coordinating solvent. These results are quite similar to those reported for other related polyaza macrocyclic complexes, indicating that the complex dissolves in water or acetonitrile to produce an equilibrium mixture of square-planar $[Ni\{R_2Bzo_2[14]aneN_6]^{2+}$ and octahedral *trans*-$[Ni(R_2Bzo_2$-$[14]aneN_6)(solvent)_2]^{2+}$; (solvent = H_2O or MeCN) [47–51]. Generally, the ligand structure, nature of the solvent and concentration of added electrolyte affect the equilibrium. The molar absorption coefficient of the ligand field transition band for $[Ni(R_2Bzo_2[14]aneN_6)]^{2+}$, measured in 3.0 M NaCl aqueous solutions, is somewhat higher than that in pure water (Table 1). A similar result was also observed in solutions containing NaBr, $NaNO_3$, or $NaClO_4$. This corresponds to the generally observed trend that neutral salts such as NaCl, dissolved in water from their hydrate, reduce the effective concentration of free water and thus increase the concentration of square-planar species [52,53]. The electronic spectra (Table 1) of the Ni(II) complexes are comparable to other square-planar tetraaza macrocyclic nickel(II) complexes, indicating that the hexaaza ligands of this study do not differ significantly from the tetraaza ligands with respect to the ligand field strength [1–43].

The absorption spectra of $[Ni((Allyl)_2Bzo_2[14]aneN_6)](ClO_4)_2$ and $[Ni(Bu_2Bzo_2[14]aneN_6)](ClO_4)_2$ were recorded and the results are given in Table 1 along with the spectral properties of analogous complexes. For aqueous solutions of the $[Ni(R_2Bzo_2[14]aneN_6)]^{2+}$ complexes, the ε value at $\lambda_{max} = 441$ nm increases from 56 to 67 $M^{-1}\,cm^{-1}$ as the alkyl chain length increases from methyl to butyl groups. Moreover, contrary to $[Ni(R_2Bzo_2[14]aneN_6)]^{2+}$ (R = H, Me, Et, Benzyl), both the $[Ni(Bu_2Bzo_2[14]aneN_6)]^{2+}$ and $[Ni((Allyl)_2Bzo_2[14]aneN_6)]^{2+}$ complexes exhibit the same ε value ($\varepsilon = 67\ M^{-1}\,cm^{-1}$) in nitromethane and water. This is probably due to the presence of butyl/propylene groups on the macrocyclic skeleton, which can exert a mechanical resistance towards the axial coordination and hence both $[Ni((Allyl)_2Bzo_2[14]aneN_6)]^{2+}$ and $[Ni(Bu_2Bzo_2[14]aneN_6)]^{2+}$ complexes seem to exist in the deep yellow, square-planar form in water and nitromethane. So it can be assumed that in aqueous solution $[Ni(Bu_2Bzo_2[14]aneN_6)]^{2+}$ and $[Ni((Allyl)_2Bzo_2[14]aneN_6)]^{2+}$ exist in the square-planar form and the propenyl/propyl groups of these complexes provide steric hindrance to the incoming water molecules for coordination [54,55]. The molecular models showed that the propylene group of $[Ni(Bu_2Bzo_2[14]aneN_6)]^{2+}$ and $[Ni((Allyl)_2Bzo_2[14]aneN_6)]^{2+}$ can block the axial positions for water molecules easily by tending towards the metal center (Scheme 3).

The 14-membered hexaaza macrocyclic nickel(II) complexes undergo intense color changes due to deprotonation of the macrocyclic ligand in the presence of amine bases such as pyridine and Et_3N. Similar N–H deprotonations have been observed with other metal complexes containing N–H linkages. For the nickel(II) complexes, Et_3N is sufficiently basic to facilitate formation of the molecular complexes. For preparation of the deprotonation form of $[Ni(Me_2Bzo_2[14]aneN_6)](ClO_4)_2$, Et_3N (0.5 cm^3) was added

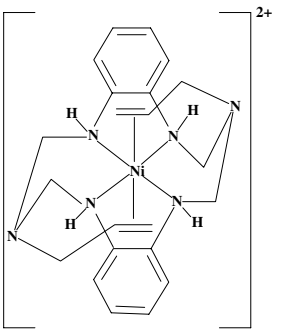

Scheme 3.

to a deaerated solution of 200 mg of $[Ni(Me_2Bzo_2[14]aneN_6)](ClO_4)_2$ in 15 cm^3 of MeCN. The shiny-brown product, which began precipitating within minutes, was filtered after 0.5 h under a N_2 atmosphere, washed with anhydrous EtOH, and dried in a vacuum. IR. (KBr, cm^{-1}): 3214 (ν_{N-H}). $[Ni(C_{18}H_{24}N_6)]$ (**23**): Calc.: Ni, 15.18; C, 56.30; H, 6.16; N, 22.08. Found: Ni, 15.32; C, 56.43; H, 6.31; N, 21.94%. The N–H stretching frequency of this compound, $[Ni(C_{18}H_{24}N_6)]$, 3214 cm^{-1}, is reduced significantly from its dicationic precursor, $[Ni(Me_2Bzo_2[14]aneN_6)](ClO_4)_2$, 3235 cm^{-1}.

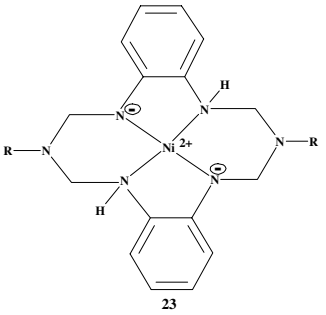

23

Table 2
Cyclic voltammetric data for Ni(II) complexes with 16-membered hexaaza macrocycles[a,b]

Complexes	Oxidation potential (V), $[Ni(polyaza)]^{2+}/[Ni(polyaza)]^{3+}$	Reduction potential (V) $[Ni(polyaza)]^{2+}/[Ni(polyaza)]^{+}$	Ref.
$[Ni(H_2Bzo_2[14]aneN_6)](ClO_4)_2$	1.06	−1.50	this work
$[Ni((CH_3)_2Bzo_2[14]aneN_6)](ClO_4)_2$	1.07	−1.47	this work
$[Ni(Et_2Bzo_2[14]aneN_6)](ClO_4)_2$	1.07	−1.47	this work
$[Ni(Bu_2Bzo_2[14]aneN_6)](ClO_4)_2$	1.09	−1.45	this work
$[Ni((Allyl)_2Bzo_2[14]aneN_6)](ClO_4)_2$	1.10	−1.41	this work
$[Ni((benzyl)_2Bzo_2[14]aneN_6)](ClO_4)_2$	1.05	−1.52	this work
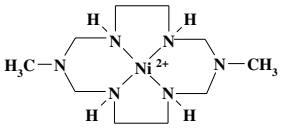	+0.93	−1.55	[57]
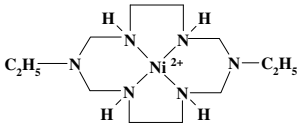	+0.90	−1.47	[57]
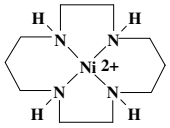	+0.91	−1.46	[56,58]
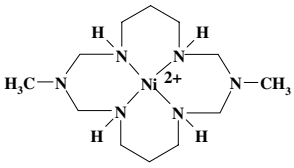	+0.94	−1.57	[19]
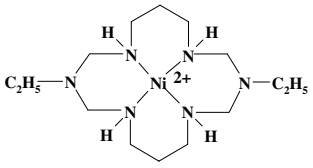	+0.93	−1.47	[19]
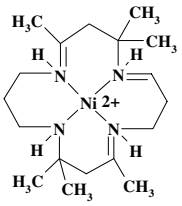	1.30	−1.30	[56,59]

[a] Measured in acetonitrile solutions; 0.1 M $(n\text{-}Bu)_4NClO_4$; vs. SCE.
[b] Redox potential of this work and Ref. [56] were measured against a $Ag|Ag^+$ (0.1 M) reference electrode and converted to the values measured against the SCE by adding +0.24 V.

Cyclic voltammetry data are summarized in Table 2. Table 2 shows that the oxidation and reduction potentials of the Ni(II) complexes of **1**–**5** do not differ significantly from other [14]aneN$_4$ complexes. This suggests that macrocycles **1**–**5** have Lewis basicities and hole size similar to the [14]aneN$_4$ ligand in spite of the structural differences. A pronounced shift in oxidation state stability occurs when there is a change in the macrocyclic ring size. An increase in ring size promotes the ease of formation of Ni(I), while rendering the oxidation to Ni(III) more difficult. The difference between the $[(Ni[14]aneN_4)]^{2+}$ and $[Ni((CH_3)_6[16]1,4,12\text{-trieneN}_4)]^{2+}$ complexes is 0.3 V. Busch and co-workers suggested that this difference is primarily due to deviations from the ideal metal-donor atom distances accompanying the redox changes [56]. This concept of optimum fit between the coordinated metal ion and the "hole size" provided by the macrocyclic ligand is also in accord with theoretical conclusions and electronic spectral studies. The more common effect of ligand unsaturation also favors the formation of the lower valent states of the complexes and causes the Ni(II) to Ni(III) process to occur at higher energy. The effect of the Bzo function on the reduction reactions of the nickel macrocycles is very pronounced and the structures containing this moiety form the stable complexes in lower valence states under the influence of relatively mild potentials.

References

[1] N.F. Curtis, Coord. Chem. Rev. 3 (1968) 3.
[2] M. Shakir, S.P. Varkey, O.S.M. Nasman, Polyhedron 14 (1995) 1283.
[3] V. Goedken, S. Peng, J. Chem. Soc., Chem. Commun. (1973) 62.
[4] D.E. Fenton, P.A. Vigato, Chem. Soc. Rev. 17 (1988) 69.
[5] B.Z. Shan, X.Z. Yu, H.K. Fun, K. Sivakumar, Acta Crystallogr., Sect. C 52 (1996) 3035.
[6] M. Shakir, A.K. Mohamed, S.P. Varkey, Z.A. Siddiqi, Trans. Metal Chem. 21 (1996) 162.
[7] R.W. Hay, J.A. Crayston, T.J. Cromie, P. Lightfoot, D.C.L. Dealwis, Polyhedron 16 (1997) 3557.
[8] R.W. Hay, A. Dandy, P. Lightfoot, Y.D. Lampeka, Polyhedron 16 (1997) 2777.
[9] R.W. Hay, T.J. Cromie, P. Lightfoot, Trans. Metal Chem. 22 (1997) 510.
[10] A. Deblas, G. Desantis, L. Fabbrizzi, M. Licchelli, A.M.M. Lanfredi, P. Morosini, P. Pallavicini, F. Ugozzoli, J. Chem. Soc., Dalton Trans. (1993) 1411.
[11] N. Sardone, M. Licchelli, Acta Crystallogr., Sect. C 52 (1996) 2713.
[12] R.M. Izatt, J.J. Christensen, Synthetic Multidentate Macrocyclic Compounds, Academic Press, New York, 1987.
[13] S.V. Rosokha, Y.D. Lampeka, J. Chem. Soc., Chem. Commun. (1991) 1077.
[14] M.P. Suh, S. Kim, Inorg. Chem. 32 (1993) 3562.
[15] M.P. Suh, W. Shin, H. Kim, C. Koo, Inorg. Chem. 26 (1987) 1846.
[16] L. Fabbrizzi, M. Licchelli, A.M.M. Lanfredi, O. Vassalli, F. Ugozzoli, Inorg. Chem. 35 (1996) 1582.
[17] D. Anastasi, N.F. Curtis, O.P. Gladkikh, T.J.C. Goode, D.C. Weatherburn, Aust. J. Chem. 51 (1998) 673.
[18] H. Bang, E.J. Lee, E.Y. Lee, J. Suh, M.P. Suh, Inorg. Chim. Acta 308 (2000) 150.
[19] M. Salavati-Niasari, H. Najafian, Polyhedron 22 (2003) 2633.
[20] M. Salavati-Niasari, M. Rezai-Adaryani, Polyhedron 23 (2004) 1325.
[21] M. Salavati-Niasari, Polyhedron 24 (2005) 1405.
[22] M. Salavati-Niasari, A. Amiri, Trans. Met. Chem. 30 (2005) 720.
[23] M. Salavati-Niasari, M. Rezai-Adaryani, S. Hydarzadeh, Trans. Met. Chem. 30 (2005) 445.
[24] M. Salavati-Niasari, Inorg. Chem. Commun. 8 (2005) 174.
[25] M. Salavati-Niasari, Inorg. Chem. Commun. 7 (2004) 963.
[26] M. Salavati-Niasari, Inorg. Chem. Commun. 7 (2004) 698.
[27] M. Salavati-Niasari, F. Davar, Inorg. Chem. Commun. 9 (2005) 175.
[28] S.-G. Kang, K. Ryu, S.-K. Jung, J. Kim, Inorg. Chim. Acta 293 (1999) 140.
[29] M. Shakir, S.P. Varkey, Polyhedron 14 (1995) 1117.
[30] M.P. Suh, I.S. Kim, B.Y. Shim, D. Hong, T.-S. Yoon, Inorg. Chem. 35 (1996) 3595.
[31] M. Salavati-Niasari, Chem. Lett. 34 (2005) 1444.
[32] M. Salavati-Niasari, Chem. Lett. 34 (2005) 244.
[33] H.-Z. Kou, S. Gao, B.-Q. Ma, D.-Z. Liao, Chem. Commun. (2000) 713.
[34] T.-B. Lu, H. Xiang, R.L. Luck, L. Jiang, Z.-W. Mao, L.-N. Ji, New J. Chem. 26 (2002) 969.
[35] M. Salavati-Niasari, A. Amiri, J. Mol. Catal. A 235 (2005) 114.
[36] M. Salavati-Niasari, H. Najafian, J. Chem. Res. 9 (2003) 586.
[37] S.V. Rosokha, Y.D. Lampeka, I.M. Maloshtan, J. Chem. Soc., Dalton Trans. (1993) 631.
[38] M. Salavati-Niasari, J. Mol. Catal. A 217 (2004) 87.
[39] M. Salavati-Niasari, J. Mol. Catal. A 229 (2005) 159.
[40] M. Salavati-Niasari, J. Mol. Catal. A 245 (2005) 192.
[41] S. Kang, S. Jung, J. Kweon, M. Kim, Polyhedron 12 (1993) 353.
[42] R.W. Hay, J.M. Armstrong, M.M. Hassan, Trans. Metal Chem. 17 (1992) 270.
[43] F. Abba, G. De Santis, L. Fabbrizzi, M. Licchelli, A.M.M. Lanfredi, P. Pallavicini, A. Poggi, F. Ugozzoli, Inorg. Chem. 33 (1994) 1366.
[44] D.D. Perrin, W.L.F. Armarego, D.R. Perrin, Purification of Laboratory Chemicals, 2nd ed., Pergamon Press, Headington Hill Hall, Oxford, London, England, 1980.
[45] K. Nakamoto, Infrared and Raman Spectra of Inorganic and Coordination Compounds, 3rd ed., Wiley, New York, 1978, p. 270.
[46] D.H. Cook, D.E. Fenton, Inorg. Chim. Acta 25 (1977) L95.
[47] R.W. Hay, B. Jeragh, G. Ferguson, B. Kaiter, B.L. Rule, J. Chem. Soc., Dalton Trans. (1982) 1531.
[48] R.W. Hay, D.P. Piplani, J. Chem. Soc., Dalton Trans. (1977) 1956.
[49] L. Fabbrizzi, Inorg. Chem. 18 (1977) 438.
[50] A. Anichini, F. Fabbrizzi, F. Paoletti, Inorg. Chem. Acta 24 (1977) L21.
[51] M.P. Suh, B.Y. Shim, T.-S. Yoon, Inorg. Chem. 33 (1994) 5509.
[52] S.-J. Kim, J.-S. Choi, S.-G. Kang, C.-S. Kim, M.P. Suh, Bull. Korean Chem. Soc. 16 (1995) 217.
[53] L. Fabbrizzi, A.M.M. Lanfredi, P. Pallavicini, A. Perotti, A. Taglietti, F. Ugozzoli, J. Chem. Soc., Dalton Trans. (1991) 3263.
[54] M. Ciampolini, L. Fabbrizzi, M. Licchelli, A. Perotti, F. Pezzini, A. Poggi, Inorg. Chem. 25 (1986) 4131.
[55] K.V. Gobi, Koichi Tokuda, T. Ohsaka, Electrochim. Acta 43 (1998) 1013.
[56] F.V. Lovecchio, E.S. Gore, D.H. Busch, J. Am. Chem. Soc. 96 (1974) 3109.
[57] M.P. Suh, S.-G. Kang, Inorg. Chem. 27 (1988) 2544.
[58] E.K. Barefield, Inorg. Chem. 11 (1972) 2273.
[59] E.K. Barefield, D.H. Busch, Inorg. Chem. 10 (1971) 108.

high nuclearity structure. The product we have obtained from the reaction is a new tetranuclear copper(II) complex $[Cu_4L_2(3\text{-ppz})_2]$ (**1**) which crystallizes in the hexahydrate form ($\mathbf{1}\cdot 6H_2O$). The crystal structure shows the presence of a discrete decanuclear water aggregate anchored onto two tetranuclear host units through hydrogen bonding interactions. Herein, we present the synthesis, crystal structure, magnetic properties of the complex along with the supramolecular structure of the water assembly. Stabilization of water aggregates of a larger size in metalloorganic hosts is of current interest to unravel their properties in restricted confinements as observed in crystal lattices and biological systems [8–14]. A detailed theoretical study of the variable-temperature magnetic susceptibility data of **1** shows the antiferromagnetic nature of the spin coupling in the complex.

2. Experimental

2.1. Materials

All reagents and chemicals were procured from commercial sources and used without further purification. The Schiff base *N*,*N*′-(2-hydroxypropane-1,3-diyl)bis(salicylaldimine) (H_3L) and 3-phenylpyrazole were prepared following literature methods [15,16]. The precursor complex $[Cu_2LBr]$ was prepared from the reaction of H_3L and $CuBr_2\cdot H_2O$ using a method that is similar to the one used for an analogous complex with a related Schiff base [15].

2.2. Measurements

The elemental analyses were done using a Heraeus CHN-O Rapid instrument. The electronic and infrared spectral data were obtained from Perkin–Elmer Lambda 35 UV–Vis and Bruker Equinox 55 spectrophotometers, respectively. Variable temperature magnetic susceptibility data in the temperature range 300–17 K were obtained for the polycrystalline sample using George Associates Inc. Lewis-coil-force magnetometer system (Berkeley, CA), equipped with a closed cycle cryostat (Air Products) and a Cahn balance. $Hg[Co(NCS)_4]$ was used as a standard. Experimental susceptibility data were corrected for diamagnetic contributions [$\chi_{dia} = -521.7\times10^{-6}\ cm^3\ M^{-1}$] [17]. The magnetic moments at various temperatures were calculated in μ_B units [$\mu_B = 9.274\times10^{-24}\ J\ T^{-1}$]. TGA analysis was done on a Mettler Toledo Star thermal analyzer.

2.3. Synthesis

$[Cu_2LBr]$ (0.4 g, 0.8 mmol) in MeCN (10 ml) was reacted with a methanol (10 ml) solution of 3-phenylpyrazole (0.12 g, 0.8 mmol) under refluxing conditions for 1 h. The solution was cooled to an ambient temperature and a green solid thus obtained was isolated, washed with a mixture of methanol and diethyl ether (1:1 v/v), and dried in vacuo over P_4O_{10} [Yield: 0.36 g (~78%)]. *Anal.* Calc. for $C_{52}H_{44}Cu_4N_8O_6$ (**1**): C, 55.21; H, 3.92; N, 9.91. Found: C, 55.09; H, 3.95; N, 9.75%. IR (KBr disc): 3415br, 1628s, 1601s, 1534m, 1464m, 1449s, 1396m, 1318m, 1195m, 1149w, 1132m, 1072w, 1042w, 981w, 860w, 759s, 694m cm^{-1} [s, strong; m, medium; w, weak; br, broad]. Electronic spectral data in MeOH [λ_{max}, nm (ε, $M^{-1}\ cm^{-1}$)]: 620 (340), 367 (19 100). Magnetic moment per molecule (μ_{eff}): 3.33 μ_B at 300 K; 0.56 μ_B at 17 K.

2.4. X-ray crystallography

Single crystals of $\mathbf{1}\cdot 6H_2O$ were obtained on slow evaporation of an aqueous methanol solution of the complex. A crystal of approximate size $0.25\times0.2\times0.14\ mm^3$ was mounted on a glass fiber with epoxy cement. The X-ray diffraction data were measured in frames with increasing ω (width of 0.3° per frame) at a scan speed of 8 s per frame using a Bruker SMART APEX CCD diffractometer, equipped with a fine focus sealed tube X-ray source. The SMART software was used for data acquisition and the SAINT software for data extraction [18]. Empirical absorption corrections were made on the intensity data [19]. The structure was solved by the heavy atom method and refined by full-matrix least-squares using the SHELX system of programs [20]. All non-hydrogen atoms of the complex except the positionally disordered solvent water molecule were refined anisotropically. All the hydrogen atoms belonging to the complex were generated, assigned isotropic thermal parameters and refined using the riding model. One water oxygen atom was found to be positionally disordered to

Table 1
Selected crystallographic data for $[Cu_4L_2(3\text{-ppz})_2]\cdot 6H_2O$ ($\mathbf{1}\cdot 6H_2O$)

	$\mathbf{1}\cdot 6H_2O$
Empirical formula	$C_{52}H_{56}Cu_4N_8O_{12}$
Formula mass	1239.21
Temperature (K)	293(2)
Wavelength (Å)	0.71073
Crystal system	triclinic
Space group	$P\bar{1}$
a (Å)	12.609(3)
b (Å)	12.719(3)
c (Å)	18.171(4)
α (°)	81.429(4)
β (°)	77.644(4)
γ (°)	66.691(4)
Unit cell volume (Å^3)	2607.5(11)
Z	2
D_{calc} (g cm^{-3})	1.578
μ(Mo) (mm^{-1})	1.680
Reflections collected	10 223
Independent reflections	6038
Restraints/parameters	0/684
R_{int}	0.1033
R (observed data) [R (all data)]	0.0562 [0.1153]
R_w (observed data) [R_w (all data)]	0.1167 [0.1417]
Weight factor $w = 1/[\sigma_2(F_o^2) + (AP)^2 + BP]$	$A = 0.0633$, $B = 1.1454$

two sites that were refined as O(11) and O(11A) with site occupancy values of 0.6 and 0.4, respectively. The structure refinement gave a goodness-of-fit (GoF) value of 0.896. Selected crystallographic data are given in Table 1. The perspective view of the complex was obtained by ORTEP [21].

3. Results and discussion

3.1. Synthetic and general aspects

Dicopper(II) complexes of trianionic pentadentate Schiff base ligands have been studied for magneto-structural correlations that show a counter-complimentary spin coupling effect in the $\{Cu_2(\mu\text{-alkoxo})(\mu\text{-carboxylato})\}$ core [15,22–27]. The $\{Cu_2L\}$ unit has also been used in designing tricopper(II) complexes as models for multicopper oxidases, in the synthesis of high nuclearity clusters and for designing supramolecular host structures stabilizing different types of water clusters based on the carboxylate ligand used [6,7,28–31]. In the present work, we have attempted to synthesize a complex having a $\{Cu_2L\}$ unit using 3-phenylpyrazole as a linker to form either a binuclear complex with a $\{Cu_2(\mu\text{-alkoxo})(\mu\text{-pyrazolato})\}$ core or a higher nuclearity complex. The reaction of $[Cu_2LBr]$ with 3-ppz is found to form a discrete tetracopper(II) species $[Cu_4L_2(3\text{-ppz})_2]$ (**1**) in good yield (Scheme 1). The complex has been characterized from analytical and spectral methods, and by X-ray crystallography. It exhibits a d–d band at 620 nm in MeOH in its electronic spectrum. The complex shows antiferromagnetic behavior due to spin–spin coupling through alkoxo and pyrazolato bridges giving magnetic moment values of 3.33 and 0.56 μ_B at 300 and 17 K, respectively (Fig. 1). The magnetic behavior is similar to those of antiferromagnetically coupled dicopper(II) complexes having a $\{Cu_2(\mu\text{-alkoxo})(\mu\text{-carboxylato})\}$ core [15,22–27]. Thermogravimetric studies of $\mathbf{1}\cdot 6H_2O$ show loss of water (~8% weight loss) in the temperature range 30–140 °C followed by further weight loss due to 3-ppz and Schiff base decomposition. The gradual weight loss is observed till 250 °C, possibly due to the loss of 3-phenylpyrazole along with the water aggregate, thus, making it difficult for an accurate estimate of the water loss.

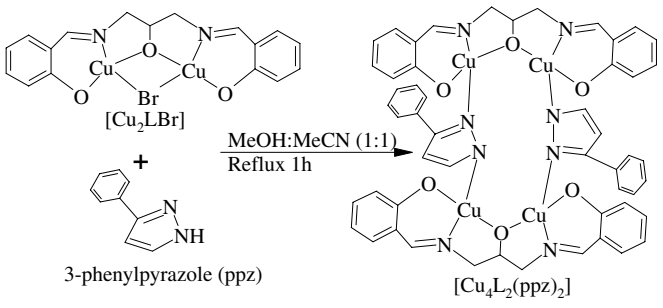

Scheme 1. The synthetic methodology for the tetranuclear copper(II) complex $[Cu_4L_2(3\text{-ppz})_2]$ (**1**).

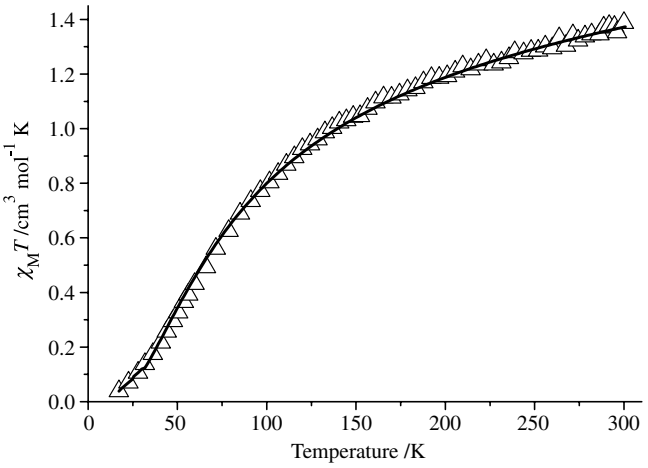

Fig. 1. $\chi_M T$ vs. T plot for the complex $[Cu_4L_2(3\text{-ppz})_2]$ (**1**) with the theoretical fit to the experimental data shown by the solid line.

3.2. Crystal structure

The complex with six solvent water molecules crystallizes in the centrosymmetric triclinic space group $P\bar{1}$ with a Z value of 2. Selected bond distances and angles are given in Table 2. The ORTEP diagram of the complex is shown

Table 2
Selected bond distances (Å) and angles (°) for $[Cu_4L_2(3\text{-ppz})_2]\cdot 6H_2O$ ($\mathbf{1}\cdot 6H_2O$)

Cu(1)···Cu(2)	3.472(1)	Cu(1)–O(5)–Cu(3)	96.49(14)
Cu(1)···Cu(3)	3.261(1)	Cu(1)–O(5)–Cu(4)	105.34(15)
Cu(1)···Cu(4)	3.457(1)	Cu(3)–O(5)–Cu(4)	120.70(18)
Cu(2)···Cu(3)	3.492(1)	Cu(2)–O(2)–Cu(3)	106.03(15)
Cu(3)···Cu(4)	3.457(1)	Cu(1)– N(5)–N(6)	120.9(3)
Cu(1)–O(1)	1.937(4)	Cu(2)–N(8)–N(7)	126.7(3)
Cu(1)–N(1)	1.941(5)	Cu(3)– N(7)–N(8)	119.1(3)
Cu(1)–N(5)	1.959(4)	Cu(4)– N(6)–N(5)	124.1(3)
Cu(1)–O(2)	2.019(4)	O(1)–Cu(1)–O(2)	175.15(16)
Cu(1)–O(5)	2.360(4)	O(1)–Cu(1)–O(5)	98.14(16)
Cu(2)–O(3)	1.909(4)	O(2)–Cu(1)–O(5)	83.89(14)
Cu(2)–N(2)	1.931(5)	O(1)–Cu(1)–N(1)	92.11(19)
Cu(2)–N(8)	1.945(5)	O(1)–Cu(1)–N(5)	90.00(19)
Cu(2)–O(2)	1.986(3)	O(2)–Cu(1)–N(1)	83.08(17)
Cu(3)–O(4)	1.927(4)	O(2)–Cu(1)–N(5)	94.49(17)
Cu(3)–N(3)	1.953(4)	O(5)–Cu(1)–N(1)	107.20(16)
Cu(3)–N(7)	1.975(4)	O(5)–Cu(1)–N(5)	87.63(16)
Cu(3)–O(5)	2.000(4)	N(1)–Cu(1)–N(5)	164.55(19)
Cu(3)–O(2)	2.375(4)	O(2)–Cu(2)–O(3)	175.88(17)
Cu(4)–O(6)	1.890(4)	O(2)–Cu(2)–N(2)	84.17(17)
Cu(4)–N(4)	1.935(5)	O(2)–Cu(2)–N(8)	93.07(17)
Cu(4)–N(6)	1.941(5)	O(3)–Cu(2)–N(2)	92.33(18)
Cu(4)–O(5)	1.978(4)	O(3)–Cu(2)–N(8)	90.54(17)
N(5)–N(6)	1.361(6)	N(2)–Cu(2)–N(8)	175.7(2)
N(7)–N(8)	1.361(6)	O(2)–Cu(3)–O(4)	96.82(15)
Cu(1)–O(2)–Cu(2)	120.14(18)	O(2)–Cu(3)–O(5)	83.92(15)
Cu(1)–O(2)–Cu(3)	95.47(14)	O(4)–Cu(3)–O(5)	174.63(16)
O(2)–Cu(3)–N(3)	106.41(16)	O(5)–Cu(4)–O(6)	173.91(18)
O(2)–Cu(3)–N(7)	87.61(15)	O(5)–Cu(4)–N(4)	84.14(17)
O(4)–Cu(3)–N(3)	91.64(18)	O(5)–Cu(4)–N(6)	94.05(17)
O(4)–Cu(3)–N(7)	91.37(18)	O(6)–Cu(4)–N(4)	91.99(19)
O(5)–Cu(3)–N(3)	83.06(17)	O(6)–Cu(4)–N(6)	89.70(19)
O(5)–Cu(3)–N(7)	93.97(17)	N(4)–Cu(4)–N(6)	177.8(2)
N(3)–Cu(3)–N(7)	165.19(18)		

in Fig. 2. The structure consists of a tetranuclear copper(II) complex in which two dimeric $\{Cu_2L\}$ units are covalently linked by two mono-anionic 3-phenylpyrazole ligands. The trianionic Schiff base shows a pentadentate mode of coordination, providing the alkoxo-bridge. The coordination geometries at the copper centers are shown in Fig. 3. The Cu(1) and Cu(3) atoms have five-coordinate square-pyramidal geometry in which the nitrogen, alkoxo and phenoxo oxygen atoms are in the basal plane. The alkoxo oxygen atom belonging to the Schiff base displays the μ_3-mode of bonding with two equatorial bonds and one significantly long axial Cu–O bond. The Cu(2) and Cu(4) atoms have four-coordinate planar geometry. The four copper basal planes in the structure are not coplanar. The dihedral angle between the Cu(1) and Cu(2) planes is ~70° and the same for the Cu(3) and Cu(4) planes is ~68°. The alkoxo oxygen atoms are not planar due to the μ_3-bonding mode. The Cu···Cu distances are in the range 3.261(1)–3.492(1) Å. The Cu(1)···Cu(3) distance in the unit having axial–equatorial bridging alkoxo oxygen atoms is 3.261(1) Å. The Cu(1)–O(2)–Cu(2) and Cu(3)–O(5)–Cu(4) angles of ~120° are expected to give moderately strong antiferromagnetic spin-coupling involving two $\{d_{x^2-y^2}\}^1$ orbitals of the metal centers. In contrast, the other Cu–O–Cu angles of ~95° should promote ferromagnetism. However, magnetic interactions involving these super-exchange pathways are expected to be negligible as the $d_{x^2-y^2}$ and d_{z^2} orbitals of the metal centers are orthogonal to each other and the axial Cu–O bond is significantly longer than the equatorial ones.

The tetranuclear complex is involved in hydrogen bonding interactions with the lattice water molecules to form a supramolecular octanuclear copper(II) species in which two tetranuclear units are non-covalently linked by a decanuclear water cluster (Table 3 and Fig. 4). Besides, each complex is hydrogen bonded to an isolated lattice water molecule. The decanuclear water cluster is formed by hydrogen bonding interactions of two dimeric water aggregates with a cyclic hexameric water cluster that is anchored on two tetranuclear complexes involving four water molecules and four phenoxo oxygen atoms. Interestingly, the

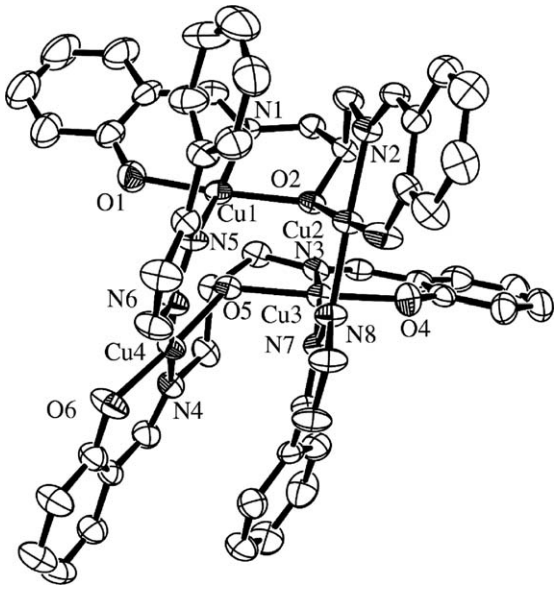

Fig. 2. An ORTEP view of the tetranuclear copper(II) complex showing the atom labelling scheme for the metal and hetero atoms, with thermal ellipsoids at the 50% probability level. The axial Cu(1)–O(5) and Cu(3)–O(2) bonds are not shown for clarity.

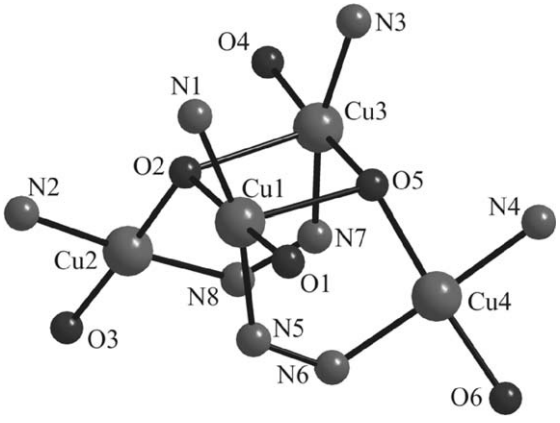

Fig. 3. A perspective view of the tetranuclear core in $[Cu_4L_2(3\text{-ppz})_2] \cdot 6H_2O$ showing the coordination geometry at the copper(II) centers.

Table 3
Selected hydrogen bonding distances (Å), angles (°) and torsional angles (°) in $[Cu_4L_2(3\text{-ppz})_2] \cdot 6H_2O$ (**1** · $6H_2O$)[a]

O(1)···O(7)	2.875(11)	O(8)···O(7)···O(9)#1	149.5(6)
O(4)···O(12)	2.880(7)	O(8)···O(9)···O(10)	74.3(6)
O(6)···O(8)	2.772(12)	O(9)···O(10)···O(11)	143.3(6)
O(7)···O(8)	2.964(17)	O(7)···O(8)···O(9)···O(7)#1	−23.1(7)
O(8)···O(9)	2.382(19)	O(1)···O(7)···O(9)#1···O(8)#1	92.8(7)
O(9)···O(10)	2.744(19)	O(1)···O(7)···O(8)···O(9)	−95.5(6)
O(10)···O(11)	2.778(17)	O(6)···O(8)···O(7)···O(1)	39.6(6)
O(1)···O(7)···O(8)	109.7(4)	O(6)···O(8)···O(9)···O(7)#1	−129.5(8)
O(1)···O(7)···O(9)#1	94.6(5)	O(6)···O(8)···O(7)···O(9)#1	−179.5(9)
O(6)···O(8)···O(7)	103.4(5)	O(8)···O(7)···O(9)#1···O(8)#1	−51(1)
O(6)···O(8)···O(9)	134.3(7)	O(9)···O(8)···O(7)···O(9)#1	45(1)
O(7)···O(8)···O(9)	87.6(6)	O(8)···O(9)···O(10)···O(11)	−97(1)
O(8)···O(9)···O(7)#1	113.1(7)		

#1: $-x+1, -y+1, -z$.

[a] For the positionally disordered water oxygen atom, hydrogen bonding parameters are given only for O(11) with a higher site occupancy.

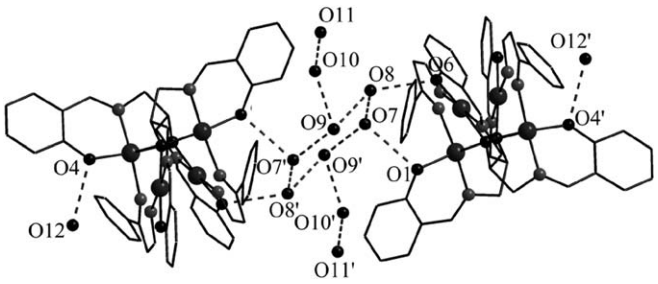

Fig. 4. A view of the discrete decanuclear water cluster anchored onto two tetracopper(II) units.

hexameric water aggregate resembles cyclohexane in its chair conformation. This rare and high-energy form of the cyclic hexameric structure is previously known in liquid helium droplets, organic supramolecular hosts and metal-organic framework structures [11,13,31]. The av. O···O···O angle of ~116.7° in the cyclic structure compares well to the value of 116.5° observed for water hexamers in organic hosts, but differ from the angle of 109.3° in hexagonal ice [13,32]. This could be due to the steric constraints imposed by the synthetic host. The O···O distances do, however, compare well with the corresponding distance of 2.759 Å reported for hexagonal ice (I_h) at −90 °C [33]. The important hydrogen bonding parameters are given in Table 3.

3.3. Magnetic properties

The temperature dependence of the magnetic susceptibility of the tetranuclear copper(II) complex is shown as a $\chi_M T$ versus T plot in Fig. 1. The $\chi_M T$ value decreases gradually in the beginning from 300 K and then rapidly, as the temperature is decreased below 150 K. The magnetic behavior shows that an antiferromagnetic interaction is predominant in the system. The structure of the {Cu_4} core shows that the Cu(1) and Cu(3) atoms are five-coordinate with a square-pyramidal geometry in which the nitrogen and phenoxo oxygen atoms are in the basal plane. The alkoxo oxygen atom belonging to the Schiff base displays the μ_3-mode of bonding with two short equatorial and one axially elongated Cu–O bond. The Cu(2) and Cu(4) atoms have a four-coordinated planar structure. The four basal planes in the structure are not coplanar giving dihedral angles of ~70°. The alkoxo oxygen atoms are not planar due to the μ_3-bonding mode. There are no bridging ligand atoms between Cu(2) and Cu(4) atoms and hence there is no exchange pathway between these two sites. Besides, the long Cu···Cu distances in the range 3.261(1)–3.492(1) Å precludes any direct bonding between the metal centers. Hence, the exchange constant for the magnetic interaction between Cu(2) and Cu(4) sites is zero. The Cu(1)···Cu(3) distance in the {$Cu_2(\mu\text{-}OR)_2$} unit is 3.261(1) Å. The presence of two axial–equatorial bridging alkoxo oxygen atoms in this unit is likely to make the exchange interaction (J_3) different from the other units. There exists only five exchange constants between the four magnetic Cu(II) ions in the complex. The symmetry of the molecule further reduces them to three unique exchange constants (Fig. 5). The Cu–O–Cu bond angles involving the pathway with exchange constant J_1 is 120.18° and that involving J_2 is 106.03°. This suggests that the interactions J_1 and J_2 are both expected to be antiferromagnetic [34]. The Cu(1)–O(2)–Cu(3) and Cu(1)–O(5)–Cu(3) bond angles for the pathway involving J_3 are 95.47° and 96.49° suggesting that this exchange interaction could be ferromagnetic [35]. The 3-phenylpyrazole ligands that act as linkers of the two binuclear units are unlikely to play any significant role in the magnetic exchange processes involving the copper(II) centers. The bond angles and bond lengths suggest that $|J_1| > |J_2| > |J_3|$. Based on the structural data, the magnetic interactions in the system are modelled using the Hamiltonian

$$\hat{H} = -J_1(\hat{S}_1\hat{S}_2 + \hat{S}_3\hat{S}_4) - J_2(\hat{S}_1\hat{S}_4 + \hat{S}_2\hat{S}_3) - J_3(\hat{S}_1\hat{S}_3) + g\mu_B H\sum_i \hat{S}_i^z - zJ'\langle S_{tot}^z\rangle\sum_i \hat{S}_i^z \quad (1)$$

where the positive and negative sign of J corresponds to ferromagnetic and antiferromagnetic interactions, respectively, and z is the number of nearest neighboring molecules. All the spin operators ($\hat{S}$s) correspond to spin-1/2 objects. The last term in the Hamiltonian takes into account intermolecular interactions in the system within the mean field approximation with $|J'| \ll \{|J_1|, |J_2|, |J_3|\}$ due to the large separation of the tetranuclear complexes from each other in the presence of the diamagnetic water cluster. Using the above model we can compute the square of the magnetization, $M^2(T)$, as a function of temperature

$$M^2(T) = \frac{\sum_S \sum_{M_s=-S}^{S} M_S^2 \exp(-E(S,M_S)/k_B T)}{\sum_S \sum_{M_s=-S}^{S} \exp(-E(S,M_S)/k_B T)} \quad (2)$$

where the eigenvalues $E(S, M_s)$ of $\hat{H}$ are given by $E(S, M_s) = E_o(S, M_s) + M_s(g\beta H - zJ'\langle S_z\rangle)$, $E_o(S, M_s)$ being the eigenvalues of the exchange Hamiltonian in the absence of an external magnetic field and intermolecular interactions. The temperature dependent magnetic susceptibility, $\chi_M(T)$ is then given by

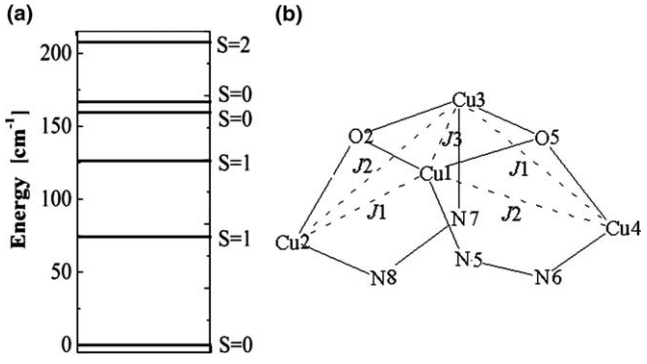

Fig. 5. (a) Energy levels of the {Cu_4} cluster from solving the Hamiltonian in Eq. (1) for the best-fit exchange constants. (b) The spin–spin coupling scheme in the complex.

$$\chi_M(T) = g^2M^2(T)/[T - zJ'M^2(T)] \quad (3)$$

where g is the gyromagnetic ratio. To account for trace concentrations of paramagnetic impurities present in the analytically pure sample, an additional Curie-like contribution to the magnetic susceptibility has been assumed and the total magnetic susceptibility is given by

$$\chi_{tot}(T) = \chi_M(T) + C/T \quad (4)$$

where C is the Curie constant. The error in the fit (R) is calculated from the expression,

$$R = \sum_i [(\chi_{obs}(T_i) - \chi_{cal}(T_i))^2/\chi_{obs}(T_i)^2] \quad (5)$$

where $\chi_{obs}(T_i)$ and $\chi_{cal}(T_i)$ are the observed and calculated magnetic susceptibilities at temperature T_i, respectively.

The magnetic data for the complex are fitted using the model Hamiltonian. The best fit gives J_1, J_2 and J_3 values as $-86.3\ cm^{-1}$, $-47.32\ cm^{-1}$ and $11.13\ cm^{-1}$, respectively. The intermolecular interaction (J') is weak and antiferromagnetic in nature, giving a value of $-0.765\ cm^{-1}$. The g value used for the theoretical fitting of the magnetic data are 2.02. The Curie constant obtained from the fit corresponds to an impurity concentration of 0.03 free-spins per tetranuclear unit. The error (R) of the fit is 1.7×10^{-4}. The energy levels of the copper cluster are shown in Fig. 5. The ground state is a low-spin singlet with a triplet state lying above because of the dominant antiferromagnetic interactions present in the system. The singlet triplet gap is $74.2\ cm^{-1}$ and the quintet state is $207.6\ cm^{-1}$ above the singlet ground state.

4. Conclusions

A new tetranuclear copper(II) complex showing a covalent linkage of two dicopper(II) units by two 3-phenylpyrazole ligands has been prepared and structurally characterized. The crystal structure shows the presence of a discrete decameric water aggregate that is formed from two dimeric and one cyclic hexameric water unit and the water assembly is stabilized by the host structure through hydrogen bonding interactions involving the phenoxo oxygen atoms of the Schiff base. The important role of the copper(II) complex containing a multidentate Schiff base as the host structure is observed in the stabilization of a large size water aggregate. The results are of significance considering the presence of hexameric water clusters in bulk water. The theoretical fitting of the magnetic data shows the presence of two dominant antiferromagnetic and one minor ferromagnetic exchange pathway, leading to the singlet magnetic ground state of the pseudo-linear tetranuclear copper(II) complex.

Acknowledgments

We thank the Department of Science and Technology, Government of India, for the CCD facility and financial support (grant SP/S1/F-01/2000). We thank the Convener, Bioinformatics Centre of our Institute, for the database search.

Appendix A. Supplementary data

Crystallographic data for $\mathbf{1} \cdot 6H_2O$ in the CIF format have been deposited with the Cambridge Crystallographic Data Center, CCDC No. 280462. Copies of this information may be obtained free of charge from The Director, CCDC, 12 Union Road, Cambridge, CB2 1EZ, UK (fax: +44 1223 366 033; e-mail: deposit@ccdc.ac.uk or http://www.ccdc.cam.ac.uk). Supplementary data associated with this article can be found, in the online version, at doi:10.1016/j.poly.2005.12.025.

References

[1] (a) R.E.P. Winpenny, Adv. Inorg. Chem. 52 (2001) 1;
(b) V.G. Makhankova, O.Y. Vassilyeva, V.N. Kokozay, B.W. Skelton, J. Reedijk, G.A. Vanalbada, L. Sorace, D. Gatteschi, New J. Chem. 25 (2001) 685;
(c) K.S. Murray, Adv. Inorg. Chem. 43 (1995) 261.
[2] (a) S.J. Lippard, J.M. Berg, Principles of Bioinorganic Chemistry, University Science Books, Mill Valley, CA, 1994;
(b) W. Kaim, B. Schwerderski, Bioinorganic Chemistry: Inorganic Elements in the Chemistry of Life, Wiley, Chichester, 1994;
(c) A. Messerschmidt (Ed.), Multi-Copper Oxidases, World Scientific, Singapore, 1997;
(d) R.H. Holm, P. Kennepohl, E.I. Solomon, Chem. Rev. 96 (1996) 2239;
(e) E.I. Solomon, U.M. Sundaram, T.E. Machonkin, Chem. Rev. 96 (1996) 2563;
(f) A. Messerschmidt, Struct. Bond. (Berlin) 90 (1998) 37.
[3] (a) H. Oshio, Y. Saito, T. Ito, Angew. Chem., Int. Ed. Engl. 36 (1997) 2673;
(b) J. Sletten, A. Sørensen, M. Julve, Y. Journaux, Inorg. Chem. 29 (1990) 5054;
(c) R. Wegner, M. Gottschaldt, H. Görls, E.-G. Jäger, D. Klemm, Chem. Eur. J. 7 (2001) 2143;
(d) X. Shi-tan, R. Nukada, M. Mikuriya, Y. Nakano, J. Chem. Soc., Dalton Trans. (1999) 2415.
[4] (a) L. Merz, W. Hasse, J. Chem. Soc., Dalton Trans. (1978) 1594;
(b) R. Mergehenn, L. Merz, W. Hasse, J. Chem. Soc., Dalton Trans. (1980) 1703;
(c) L. Walz, H. Paulus, W. Hasse, J. Chem. Soc., Dalton Trans. (1983) 657;
(d) H. Astheimer, F. Nepveu, L. Walz, W. Hasse, J. Chem. Soc., Dalton Trans. (1985) 315.
[5] D. Gatteschi, R. Sessoli, Angew. Chem., Int. Ed. 42 (2003) 268.
[6] A. Mukherjee, M. Nethaji, A.R. Chakravarty, Angew. Chem., Int. Ed. 43 (2004) 87.
[7] A. Mukherjee, R. Raghunathan, M.K. Saha, M. Nethaji, S. Ramasesha, A.R. Chakravarty, Chem. Eur. J. 11 (2005) 3087.
[8] (a) A. Mukherjee, M.K. Saha, M. Nethaji, A.R. Chakravarty, Chem. Commun. (2004) 716;
(b) A. Mukherjee, M.K. Saha, M. Nethaji, A.R. Chakravarty, New J. Chem. 29 (2005) 596.
[9] (a) B. Sreenivasulu, J.J. Vittal, Angew. Chem., Int. Ed. 43 (2004) 5769;
(b) L.E. Cheruzel, M.S. Pometun, M.R. Cecil, M.S. Mashuta, R.J. Wittebort, R.M. Buchanan, Angew. Chem., Int. Ed. 42 (2003) 5452.
[10] (a) J.N. Moorthy, R. Natarajan, P. Venugopalan, Angew. Chem., Int. Ed. 41 (2002) 3417;
(b) J.M. Ugalde, I. Alkorta, J. Elguero, Angew. Chem., Int. Ed. 39 (2000) 717.

[11] (a) S.K. Ghosh, P.K. Bharadwaj, Inorg. Chem. 43 (2004) 5180;
(b) S.K. Ghosh, P.K. Bharadwaj, Inorg. Chem. 42 (2003) 8250;
(c) S. Neogi, G. Savitha, P.K. Bharadwaj, Inorg. Chem. 43 (2004) 3771;
(d) S.K. Ghosh, P.K. Bharadwaj, Inorg. Chem. 43 (2004) 6887;
(e) S. Neogi, P.K. Bharadwaj, Inorg. Chem. 44 (2005) 816;
(f) S.K. Ghosh, J. Ribas, M.S. El Fallah, P.K. Bharadwaj, Inorg. Chem. 44 (2005) 3856.
[12] R. Ludwig, Angew. Chem., Int. Ed. 40 (2001) 1808.
[13] R. Custelcean, C. Afloroaei, M. Vlassa, M. Polverejan, Angew. Chem., Int. Ed. 39 (2000) 3094.
[14] (a) F.N. Keutsch, J.D. Cruzan, R.J. Saykally, Chem. Rev. 103 (2003) 2533;
(b) F.N. Keutsch, R.J. Saykally, Proc. Natl. Acad. Sci. USA 98 (2001) 10533;
(c) K. Liu, J.D. Cruzan, R.J. Saykally, Science 271 (1996) 929;
(d) K. Liu, M.G. Brown, C. Carter, R.J. Saykally, J.K. Gregory, D.C. Clary, Nature 381 (1996) 501;
(e) L.J. Barbour, G.W. Orr, J.L. Atwood, Nature 393 (1998) 671;
(f) M. Matsumoto, S. Saito, I. Ohmine, Nature 416 (2002) 409.
[15] W. Mazurek, K.J. Berry, K.S. Murray, M.J. O'Connor, M.R. Snow, A.G. Wedd, Inorg. Chem. 21 (1982) 3071.
[16] S. Trofimenko, J.C. Calabrese, J.S. Thompson, Inorg. Chem. 26 (1987) 1507.
[17] O. Kahn, Molecular Magnetism, VCH, Weinheim, 1993.
[18] Bruker SMART and SAINT, Version 6.22a, Bruker AXS Inc., Madison, WI, USA, 1999.
[19] G.M. Sheldrick, SADABS Version 2, Multi-Scan Absorption Correction Program, University of Göttingen, Göttingen, Germany, 2001.
[20] G.M. Sheldrick, SHELX-97, Programs for Crystal Structure Solution and Refinement, University of Göttingen, Göttingen, Germany, 1997.
[21] M.N. Burnett, C.K. Johnson, ORTEP-III; Report ORNL-6895, Oak Ridge National Laboratory, Oak Ridge, TN, 1996.
[22] (a) M. Mikurriya, K. Minowa, R. Nukada, Bull. Chem. Soc. Jpn. 75 (2002) 2595;
(b) K. Geetha, M. Nethaji, N.Y. Vasanthacharya, A.R. Chakravarty, J. Coord. Chem. 47 (1999) 77;
(c) T. Kawata, M. Yamanaka, S. Ohba, Y. Nishida, M. Nagamatsu, T. Tokii, M. Kato, O.W. Steward, Bull. Chem. Soc. Jpn. 65 (1992) 2739.
[23] T. Kawata, S. Ohba, Y. Nishida, T. Tokii, Acta Crystallogr. 49C (1993) 2070.
[24] (a) Y. Nishida, S. Kida, J. Chem. Soc., Dalton Trans. (1986) 2633;
(b) Y. Nishida, M. Takeuchi, K. Takahashi, S. Kida, Chem. Lett. (1985) 631;
(c) Y. Nishida, M. Takeuchi, K. Takahashi, S. Kida, Chem. Lett. (1983) 1815.
[25] P.J. Hey, J.C. Thibeault, R.H. Hoffmann, J. Am. Chem. Soc. 97 (1975) 4884.
[26] W. Mazurek, B.J. Kennedy, K.S. Murray, M.J. O'Connor, J.R. Rodgers, M.R. Snow, A.G. Wedd, P.R. Zwack, Inorg. Chem. 24 (1985) 3258.
[27] W.M. Davis, D. Busch, Acta Crystallogr. 43C (1987) 639.
[28] A. Mukherjee, I. Rudra, S.G. Naik, S. Ramasesha, M. Nethaji, A.R. Chakravarty, Inorg. Chem. 42 (2003) 5660.
[29] S. Gupta, A. Mukherjee, M. Nethaji, A.R. Chakravarty, Polyhedron 23 (2004) 643.
[30] (a) K. Geetha, M. Nethaji, A.R. Chakravarty, Inorg. Chem. 36 (1997) 6134;
(b) A. Mukherjee, I. Rudra, M. Nethaji, S. Ramasesha, A.R. Chakravarty, Inorg. Chem. 42 (2003) 463.
[31] K. Nauta, R.E. Miller, Science 287 (2000) 293.
[32] A.H. Narten, W.E. Thiessen, L. Blum, Science 217 (1982) 1033.
[33] D. Eisenberg, W. Kauzmann, The Structure and Properties of Water, Oxford University Press, Oxford, 1969.
[34] S.K. Pati, S. Ramasesha, D. Sen, in: J. Miller, M. Drillon (Eds.), Magnetoscience – From Molecules to Materials (IV), Wiley-VCH, Germany, 2003, p. 119.
[35] A.R. Edmonds, Angular Momentum in Quantum Mechanics, Princeton University Press, Princeton, NJ, 1957.

oxygen-sensitive, therefore an inert gas atmosphere was a requisite. Referring to labile gold trialkoxysilanethiolates, which were stable only in the presence of additional triphenylphosphine ligand [8], we expected that in the present case chelating heterocyclic N-donor bases like 2,2′-bipyridine may transform **1** not only to the more stable but also to less reactive manganese silanethiolate species.

Ligands containing the 2,2′-bipyridine fragment have found widespread use – recently they have been regarded as ideal for synthesizing complexes which exhibit a high luminescence quantum yield [9] and are being considered as promising candidates for non-linear optics [10]. So far, only three manganese(II) complexes with S-donor (albeit not thiolate) and heterocyclic chelating N-donor ligands simultaneously bonded to the same metal centre [11–13] have been described. Heteroleptic manganese(II) silanethiolate with chelating tetramethylethylenediamine as an additional ligand-[$Mn(SSiPh_3)_2$(tmeda)] has also been reported [14].

For our purposes 2,2′-bipyridine (bipy), 1,10-phenanthroline (phen) and 2,9-dimethyl-1,10-phenanthroline (neocuproine, neo) have been selected. The present paper reports our findings concerning the preparation, structure and properties of manganese silanethiolate complexes incorporating these ligands.

2. Experimental

2.1. Materials

Solvents and reagents were dried according to common procedures, degassed and distilled prior to use. Bis(tri-*tert*-butoxysilanethiolato)tetra(methanol)manganese(II) complex (**1**) was prepared as described elsewhere [7] using standard Schlenk techniques, vacuum line and inert gas atmosphere. Other chemicals were obtained from commercial sources and used as received. 1,10-Phenanthroline (phen) and 2,2-bipyridine (bipy) were purchased from POCh (Poland) and 2,9-dimethyl-1,10-phenanthroline (neo) from Aldrich Chemical.

2.2. Synthesis of complexes

Solutions of **1** [7] in methanol were mixed at room temperature under argon atmosphere with equimolar amounts of the ligand L (L = bipy, phen, neo) also dissolved in methanol. The products precipitated almost immediately as very fine microcrystals – orange [$Mn\{SSi(OBu^t)_3\}_2$(bipy)] (**2**), canary yellow [$Mn\{SSi(OBu^t)_3\}_2$(phen)] (**3**) and pale yellow [$Mn\{SSi(OBu^t)_3\}_2$(neo)] (**4**). They were collected, filtered off, washed with methanol and finally recrystallized from hot methanol.

Complex ***2****:* Yield 96%, *Anal*. Calc. for $C_{34}H_{62}O_6N_2S_2Si_2Mn$ ($M_r = 770.12$) C, 53.03; S, 8.33, H, 8.11; N, 3.64. Found: C, 52.88; S, 8.28; H, 8.12; N, 3.51%. M.p. 255–259 °C (dec.); t, dec_{max} 265 °C. IR (KBr pellet, cm^{-1}): *ν*(C–O) 1189; *ν*(Si–O) 1041, 1021, 957; *ν*(Si–S) 692, 648, 558.

Complex ***3****:* Yield 88%, *Anal*. Calc. for $C_{36}H_{62}O_6N_2S_2Si_2Mn$ ($M_r = 794.14$) C, 54.45; S, 8.07; H, 7.87; N, 3.53. Found: C, 54.39; S, 7.84; H, 8.29; N, 3.57%. M.p. 298–301 °C (dec.); t, dec_{max} 349 °C. IR (KBr pellet, cm^{-1}): *ν*(C–O) 1190; *ν*(Si–O) 1052, 1024, 946; *ν*(Si–S) 689, 652, 550.

Complex ***4****:* Yield 87%, *Anal*. Calc. for $C_{38}H_{66}O_6N_2S_2Si_2Mn$ ($M_r = 822.19$) C, 55.51; S, 7.80; H, 8.09; N, 3.41. Found: C, 55.41; S, 7.72; H, 8.17; N, 3.51%. M.p. 334–338 °C (dec.); t, dec_{max} 355 °C. IR (KBr pellet, cm^{-1}): *ν*(C–O) 1190; *ν*(Si–O) 1040, 1009; *ν*(Si–S) 683, 654, 552.

Monocrystals of the compounds containing bipyridine and phenanthroline ligands of quality sufficient for X-ray measurements were obtained by dissolution of complexes **2** and **3** in methanol and slow crystallization at 5 °C. This simple procedure gave well-shaped crystals of complex **2**. Unexpectedly, when **3** was analogously recrystallized, the monocrystals of [$Mn\{SSi(OBu^t)_3\}_2$(phen)(MeOH)] (**3a**) were obtained. These were not stable and quickly became opaque (in a few minutes at RT and visibly faster when reduced pressure was applied) and then transformed to a yellowish powder of **3**. When, instead of MeOH, EtOH was used only microcrystalline **3** deposited. Attempts to prepare monocrystals of **4** (poorly soluble in MeOH) were unsuccessful.

3. Physical measurements

3.1. Elemental analysis

Elemental analysis of **2**–**4** for carbon, hydrogen, nitrogen and sulfur were performed using an automatic Elementary Analyser model EA 1108 (Carlo Erba Instruments, Italy).

3.2. Spectrometric measurements

IR spectra were recorded on a FTIR Mattson Genesis II Gold, externally controlled by WinFirst software. Spectra were registered in the solid state (KBr pellet) and in solution (CCl_4, KBr cuvette, 0.248 mm) in the range 4000–400 cm^{-1}.

UV spectra were recorded with Unicam UV300 spectrometer, externally controlled by Vision32 software. Methanol and quartz cuvettes were used.

3.3. Mass spectroscopy

MS spectra were recorded using LC Agilent 1100 Series chromatograph coupled with two-channel pump, automatic sampler, DAD detector, thermostat and MS detector with APCI (*atmospheric pressure chemical ionization*) and ES (*electrospray*) modes. Measurements were carried out at 30 °C with injection volume −20 μl, flow rate −0.5 ml/min and analysis time 3 min. A solution of acetic acid in methanol (0.1%) was used as the eluent. MS detection

resulted from either the ES or APCI ionization method. The positive ion mode was applied and fragmentation was performed with 20, 70 as well as 200 eV.

3.4. Thermal analysis

Thermal stability was determined with a Pyris 1 thermal analyzer (Perkin–Elmer). Measurements were made for samples of about 3–8 mg in the 50–500 °C range with 20 °C/min heating rate under an inert gas atmosphere (N_2). Differential scanning calorimetry measurements were performed with a DSC 7 (Perkin–Elmer). Samples of ca. 5 mg, encapsulated in aluminum containers, were melted and recrystallized at 20 °C/min rate under an inert gas atmosphere (N_2).

3.5. Crystal structure determination

Single crystals of **2** and **3a** were mounted on quartz capillaries using frozen epoxy resin. Experimental intensity data were collected at $T = 100(2)$ K on a KM4 diffractometer, goniometer equipped with a Sapphire 2 CCD detector (Oxford Diffraction) with monochromated Mo Kα radiation ($\lambda = 0.71073$ Å) at a crystal-detector distance of 50 mm. In both cases, data were collected in series of 152 frames at $\varphi = 0°$, 90°, 180° and 270°; ω scan with an increment of 0.75° and exposure time of 80 and 60 s per frame for **2** and **3a**, respectively. The unit cell dimensions, additional crystallographic data and refinement results for both complexes are given in Table 1.

The structures were solved by direct methods and refined by least-squares calculation in anisotropic approximation for non-hydrogen atoms. In these structures H atoms were added at idealized positions and refined using the riding model, except the H atom from the hydroxyl group of the methanol molecule in **3a** which was revealed from a difference electron-density map.

Data collection and editing, as well as refinement of unit cell parameters, was performed using CrysAlis 1.171 CCD (Oxford Diffraction, 2004). The structure solution and refinement (by full-matrix least-squares against F^2) were performed with the WINGX program package (ver.1.70.00, 2005) [15,16]. Selected bond lengths and angles for crystal structures of **2** and **3a** are listed in Tables 2 and 3.

4. Results and discussion

All manganese thiolates so far obtained have been found to be sensitive towards oxidation. This property may hamper significantly any potential applications. It also concerns silanethiolates. Since **1** was found to be labile and reactive towards oxygen its transformation into a more stable and less reactive manganese silanethiolate was considered. As it was previously mentioned we supposed that the exchange of the weakly bonded methanol into another, more strongly coordinating ligand could improve the stability

Table 1
Selected crystal data for [Mn{SSi(OBu^t)$_3$}$_2$(bipy)] (**2**) and [Mn{SSi(OBu^t)$_3$}$_2$(phen)(MeOH)] (**3a**)

	2	**3a**
Empirical formula	$C_{34}H_{62}O_6N_2S_2Si_2Mn$	$C_{37}H_{66}O_7N_2S_2Si_2Mn$
Formula weight (g mol^{-1})	770.12	826.18
Crystal system	monoclinic	monoclinic
Space group	$C2/c$	$P2_1/c$
Crystal shape/colour	plate/orange	block/yellow
Crystal size (mm)	$0.16 \times 0.11 \times 0.04$	$0.5 \times 0.4 \times 0.3$
Unit cell dimensions		
a (Å)	16.811(6)	10.090(1)
b (Å)	9.574(2)	25.299(1)
c (Å)	25.920(5)	18.714(2)
β (°)	98.45(4)	103.50(1)
V (Å^{-3})	4126.5(19)	4645.0(4)
Z	4	4
D_{calc} (g cm^{-3})	1.24	1.181
Temperature (K)	100(2)	100(2)
μ [Mo Kα] (mm^{-1})	0.52	0.468
θ Range	2.52–30	2.66–30
Range of h, k and l	$-23 < h < 23$; $-13 < k < 13$; $-36 < l < 29$	$-14 < h < 14$; $-35 < k < 30$; $-26 < l < 26$
F(000)	1652	1772
R_{int}	0.0472	0.0359
N (reflections total)	6037	13460
N (reflections observed)	5747	12323
Criterion of significance	$I > 2\sigma(I)$	$I > 2\sigma(I)$
N (parameters)	244	483
Weighting scheme	$w = 1/[s^2F_o^2 + (0.0140 \cdot P)^2 + 16.4580 \cdot P$; $P = (F_o^2 + 2F_c^2)/3$	$w = 1/[s^2F_o^2 + (0.0418 \cdot P)^2 + 4.6874 \cdot P$; $P = (F_o^2 + 2F_c^2)/3$
S (goodness-of-fit) on F^2	1.190	1.091
R_1, $w_2(F^2 > 2\sigma(F^2))$	0.0573, 0.1158	0.0483, 0.1082
$\Delta\rho_{max}$, $\Delta\rho_{min}$ (e/A^3)	1.140, −0.675	0.565, −0.306
Absorption correction	numerical	none

Table 2
Selected bond lengths (Å) and angles (°) for complex **2**

Mn1–N1	2.310(2)	N1–Mn1–N1	70.08(10)	O3–Si1–O2	104.53(9)
Mn1–O1	2.4648(15)	N1–Mn1–O1	90.20(6)	O3–Si1–O1	104.05(8)
Mn1–S1	2.4979(9)	O1–Mn1–O1′	173.24(7)	O2–Si1–O1	112.05(9)
S1–Si1	2.070(1)	N1–Mn1–S1′	160.19(5)	O3–Si1–S1	116.07(7)
Si1–O3	1.6325(17)	N1–Mn1–S1	93.74(6)	O2–Si1–S1	116.39(7)
Si1–O2	1.6316(17)	O1–Mn1–S1′	103.02(5)	O1–Si1–S1	103.26(7)
Si1–O1	1.6679(16)	O1–Mn1–S1	72.68(5)		
O1–C10	1.470(2)	N1–Mn1–S1	93.74(6)		
O2–C20	1.442(3)	S1–Mn1–S1′	104.19(4)		
O3–C30	1.441(3)	Si1–S1–Mn1	85.26(4)		

Symmetry code: $-x, y, -z + 3/2$.

Table 3
Selected bond lengths (Å) and angles (°) for complex **3a**

Mn1–O8	2.2099(12)	O8–C9–H9A	109.5	S2–Mn1–S1	110.594(16)
Mn1–N2	2.2515(13)	O8–Mn1–N2	86.42(5)	Mn1–O8–H8	105.5(19)
Mn1–N1	2.2721(14)	O8–Mn1–N1	159.60(5)	Si1–S1–Mn1	115.80(2)
Mn1–S2	2.4377(5)	N2–Mn1–N1	73.36(5)	Si2–S2–Mn1	97.08(2)
Mn1–S1	2.4788(5)	O8–Mn1–S2	99.09(3)	O5–Si1–S1	113.83(5)
O1–Si2	1.6499(12)	N2–Mn1–S2	146.51(4)	O6–Si1–S1	114.56(5)
O2–Si2	1.6381(13)	N1–Mn1–S2	96.49(4)	O4–Si1–S1	108.76(5)
O3–Si2	1.6355(13)	O8–Mn1–S1	96.03(3)	O3–Si2–S2	115.93(5)
S1–Si1	2.0605(6)	N2–Mn1–S1	101.52(4)	O2–Si2–S2	113.93(5)
S2–Si2	2.0708(6)	N1–Mn1–S1	90.69(4)	O1–Si2–S2	105.45(5)
O8–H8···O4	2.690(3)				

of the complex. Since manganese is regarded as an *a* class metal, N-donor ligands, especially strongly bonding chelating heterocyclic bases, seemed to be the most promising. We have selected 2,2′-bipyridine and, to exclude any possibility of twisting around the central C–C axis and thus coordination to two different metallic centres (a very rare case [17,18]) we have also used 1,10-phenanthroline. To see the influence (if any) of imposed steric hindrance we have also selected 2,9-dimethyl-1,10-phenanthroline.

Indeed, an equimolar amount of phenanthroline, bipyridine or neocuproine added to the solution of [Mn{SSi(OBu^t)$_3$}$_2$(MeOH)$_4$] (**1**) in methanol resulted in almost immediate formation of solid microcrystalline (as checked by XRD) products with a very good yield. Despite the similarities between all three ligands, the results of their reaction with **1** were, however, not always the same. With bipyridine and neocuproine stable products **2** and **4** were obtained, respectively. The stability of the product formed in the reaction of **1** with phenanthroline varied but finally we managed to obtain stable **3** and unstable **3a**, depending on the conditions used (Scheme 1). Then it became obvious that in the case of the phenanthroline containing complex we deal with two different products which may be quite easily converted into each other.

Elemental analysis of compounds **2**–**4** suggested a Mn{SSi(OBu^t)$_3$}$_2$(N–N) composition, where N–N represents the chelating ligand. FTIR spectra recorded in the solid state confirmed the presence of a silanethiolate substituent (e.g., strong bands at 1050–1000 cm^{-1} typical for Si–O and C–O vibrations) as well as bands typical for heterocyclic bases (C=C and C=N at around 1600–1550 cm^{-1}

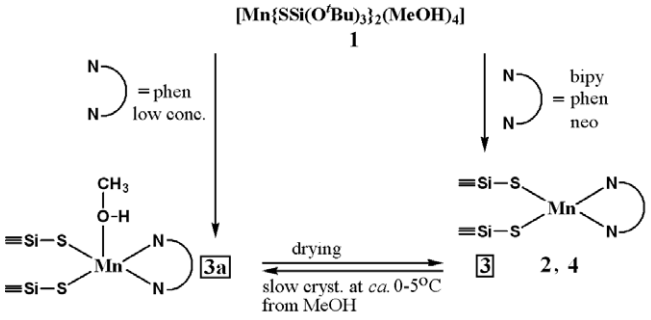

Scheme 1.

and vibrations for bipyridine systems below 1000 cm^{-1}). For **4** also a band at 1450 cm^{-1}, characteristic for an asymmetric distortional vibration of the methyl group attached to an aromatic ring, can be noticed. For **3**, a Raman spectrum was also recorded.

Electronic spectra have also been examined. None of the complexes exhibited absorptions in the visible range. In the ultraviolet region **2**, **3** and **4** absorb at 204–215 nm, which is associated with σ(Si–S)) $\rightarrow \sigma^*$(Si–S) transitions in silanethiolate ligands [19]. Two absorption maxima at around 230 and 270 nm are caused by typical n $\rightarrow \pi^*$ transitions for heterocyclic compounds.

The mass spectra were similar in all cases and confirmed the composition of Mn{SSi(OBu^t)$_3$}$_2$(N–N). Although the parent ion could not be seen, the spectra allowed a hypothesis to be put forward concerning the main fragmentation pattern through elimination of OBu^t and Si–OBu^t

fragments from the tri-*tert*-butoxysilanethiolate substituent. Ions comprising a chelate ligand molecule (e.g., for **3**: *m/z* 296 $[(phen)MnSSi]^{\bullet+}$, 268 $[(phen)MnS]^{\bullet+}$, 236 $[(phen)Mn]^{\bullet+}$, 181 $[phen]^{\bullet+}$ and 155 $[C_{10}H_6N_2]^{\bullet+}$) can be easily traced in the lower mass part of the spectrum.

Compounds **2**–**4** are very stable in spite of being based on Mn(II). Thus the main goal of our work has been achieved. They may be stored in normal laboratory atmosphere without taking any precautions – after six months no signs of change were noticeable, even with additional irradiation with an UV lamp (40 W, 254 nm) for 5 h. All three compounds melt with decomposition which was confirmed using differential scanning calorimetry measurements. Thermogravimetric analysis indicated that the most stable complexes are those containing phenanthroline and neocuproine, which decompose to gaseous products with a maximum rate at 349 and 355 °C respectively.

IR spectra recorded in CCl_4 solution for **3** and **3a** differed. Bands at ca. 3500 cm^{-1}, characteristic for free ν(OH) can be seen for **3a**. Crystals of **3a** exposed to air became opaque after a few minutes so we anticipated the presence of MeOH (the reaction solvent) within the crystal structure. Compound **3a** required storage under inert gas atmosphere at temperatures near 0 °C. Any attempts to dry it, e.g., in a stream of argon, resulted in facile lost of methanol and formation of **3**.

The role of MeOH remained unknown until the structure was solved, and methanol was found in **3a** as a third type of ligand bonded to manganese. The outline of the reaction can be therefore summarized as shown in Scheme 1. One should note that the graphical representations of the products do not represent their structures.

Crystal and molecular structures have been determined for compounds **2** and **3a**. The structures are presented in Figs. 1 and 2. Selected bond lengths and angles are given in Tables 2 and 3. Both complexes represent quite uncommon structures, mainly because of the set of ligands bonded to manganese.

Looking at the structure of **2**, one can predict the reason of its stability. Complexation of Mn by three chelating ligands should visibly enhance the stability of the complex, however some favorable conditions must be met to reveal chelating properties of tri-*tert*-butoxysilanethiolato ligand. We know that the $(Bu^tO)_3SiS$ group can act as chelate [20,21] but it is not very usual situation. Comparison between **2** and any similar compound is difficult because related manganese complexes (or complexes for any other metal) have not yet been described, the closest one being bis(2-pyridinethiolato)(2,2′-bipyridine)-bis(tetrahydrofuran) europium with an $EuN_4O_2S_2$ kernel and eight-coordination at Eu [22]. Bond lengths and angles in **2** are unexceptional and similar to those in other silanethiolates. The only difference that can be seen between these bonds (and appropriate angles) relate to those which are or are not engaged in the formation of chelate rings.

Even more interesting is the structure of **3a**. Two thiolate ligands, a chelate nitrogen-donor ligand and a methanol molecule bonded to Mn form a structure which has no parallels among other complexes. When the structure of **3a** is compared to the structure of **2** some differences can be

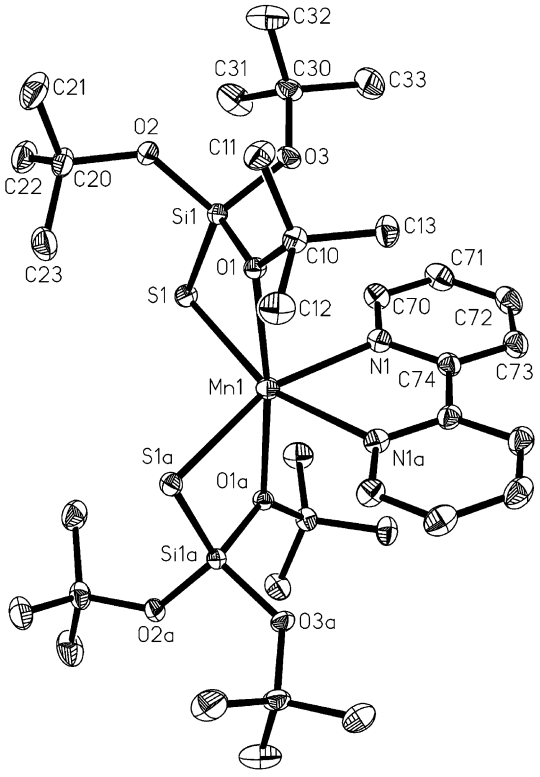

Fig. 1. Crystal and molecular structure of $[Mn\{SSi(OBu^t)_3\}_2(bipy)]$ (**2**). Hydrogen atoms are omitted for clarity. Thermal ellipsoids, 50%.

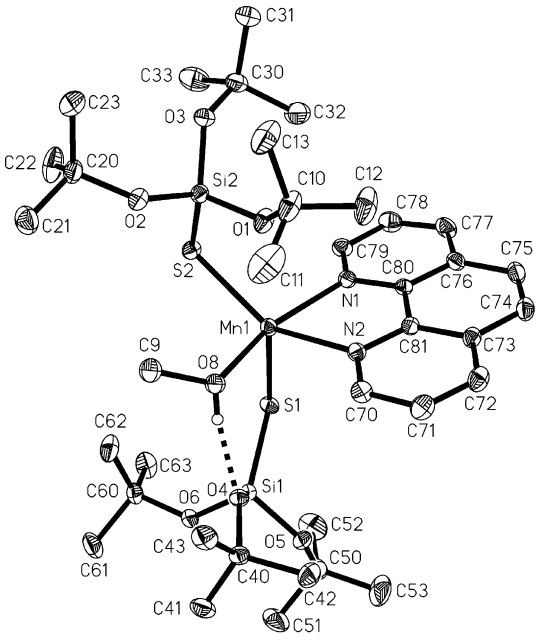

Fig. 2. Crystal and molecular structure of $[Mn\{SSi(OBu^t)_3\}_2(phen)\text{-}MeOH]$ (**3a**). Hydrogen atoms (except OH) are omitted for clarity. The O8–H···O4 hydrogen bond is shown as a broken line. Thermal ellipsoids, 50%.

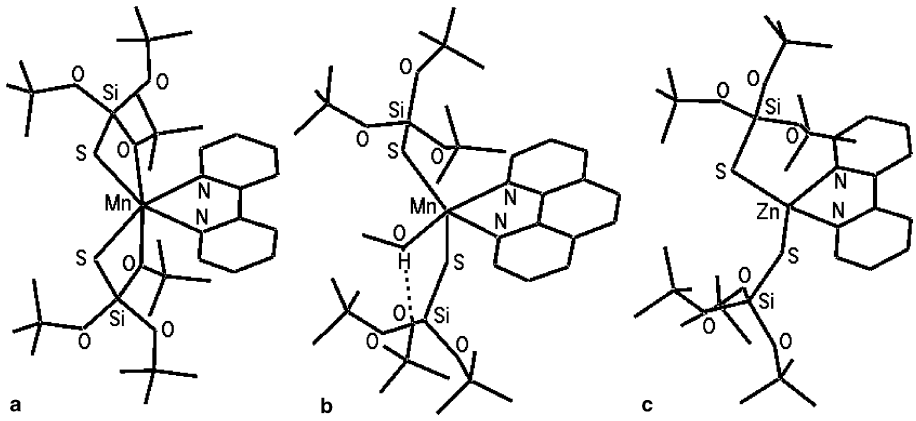

Fig. 3. (a) $[Mn\{SSi(OBu^t)_3\}_2(bipy)]$ $MnN_2O_2S_2$ (**2**); (b) $[Mn\{SSi(OBu^t)_3\}_2(phen)(MeOH)]$ MnN_2OS_2 (**3a**); (c) $[Zn\{SSi(OBu^t)_3\}_2(bipy)]$ MnN_2S_2 [21].

immediately noticed – the non-chelating nature of the silanethiolate ligand in **3a** and penta-coordination at Mn. Furthermore, there is a hydrogen bond between the O4 atom from one tri-*tert*-butoxysilanethiolate ligands and O8 from methanol (O4···O8 distance of 2.690 Å). Undoubtedly, the hydrogen bond should strengthen the complex and it may be the sole reason of sufficient stability of complex **3a**. Si–S bonds in **2** and **3a** are virtually the same and can be regarded as rather short. We also note the difference in Mn–O distances: $Mn–O_{SiOBu}$ 2.465 Å (part of the chelate ring in **2**) and $Mn–O_{MeOH}$ 2.210 Å (not restricted in **3a**), with Mn–O distances usually in the range 2.100–2.200 Å.

Are the structures of **3** and **4** similar to that of **2**? All three compounds show remarkable stability and their nitrogen-donor ligands are similar. However, we know only the structure of **3a**, not **3** and in the case of **4**, really hardly dissolving in all common solvents, we did not manage to obtain crystals suitable for diffraction measurement and the monometallic nature of the complex is not fully confirmed. All gathered data suggest that in **3** and **4** two silanethiolate ligands and a heterocyclic base coordinate to the same metal centre giving a monometallic species. We need to mention here the very stable zinc complex $[Zn\{SSi(OBu^t)_3\}_2(bipy)]$ [21], with tetra-coordinated Zn (ZnN_2S_2 kernel) lacking any secondary Zn–O interactions. Compared to complexes **2** and **3a**, it provides yet another, although closely related, structure type (Fig. 3).

It remains unknown how the silanethiolate ligands coordinate in **3** and **4**. Are they chelating as in **2** (CN = 6) or, according to greater steric hindrance introduced with neocuproine in **4**, only bonded through sulfur (CN = 4) as in the Zn silanethiolate (Fig. 3)? Of course a case with only one chelating silanethiolate ligand (CN = 5, as in **3a**) should be also considered.

Three silanethiolates of manganese(II) described in the present paper – in contrast to many other manganese(II) thiolates – are stable under normal conditions so that we can deliberate on their potential applications.

On the other hand, the preparation of labile **3a**, where methanol, thiolate ligands and heterocyclic base are bonded to the same metal centre, approaches the long studied problem of a complex of which the kernel should mimic the active centre $[ZnCys_2His(ROH)]$ of alcohol dehydrogenase [23–25]. So far, it has been impossible to prepare such a zinc compound where all four donor atoms (N, O, S, S) are provided by four independent ligands. Now, it seems that we can look for a very similar Mn-based complex starting with $[Mn\{SSi(OBu^t)_3\}_2(MeOH)_4]$ **1** as a substrate. Related work is now in progress.

Appendix A. Supplementary data

Crystallographic data for the structures have been deposited with the Cambridge Crystallographic Data Centre. Copies of the data can be obtained free of charge on application to The Director, CCDC, 12 Union Road, Cambridge CB2 1EZ, on full quoting the journal citation and deposition nos. CCDC 290752 (**2**), CCDC 290753 (**3a**). Supplementary data associated with this article can be found, in the online version, at doi:10.1016/j.poly.2005.12.030.

References

[1] G. Willkinson (Ed.), Comprehensive Coordination Chemistry, vol. 2, Pergamon Press, Oxford, 1987.
[2] B.T. Langeland, D.L. Morris, J.S. McKinley-McKee, Comp. Biochem. Phys. B 123 (1999) 155.
[3] R.I. Lindstad, P. Koll, J.S. McKinley-McKee, Eur. J. Biochem. 330 (1998) 479.
[4] M.K. Corbierre, R.B. Lennox, Chem. Mater. 17 (2005) 5691.
[5] T. Nguyen, A. Panda, M.M. Olmstead, A.F. Richards, M. Stender, M. Brynda, P.P. Power, J. Am. Chem. Soc. 127 (2005) 8545, and references cited therein.
[6] A. Kropidłowska, B. Becker, Chem. Listy 98 (2004) 786.
[7] A. Kropidłowska, J. Chojnacki, B. Becker, Inorg. Chem. Commun., doi:10.1016/j.inoche.2005.12.017.
[8] J. Chojnacki, B. Becker, A. Konitz, W. Wojnowski, Z. Anorg. Allg. Chem. 626 (2000) 2173.
[9] V. Balzani, A. Juris, M. Venturi, S. Campagna, S. Serroni, Chem. Rev. 96 (1996) 759.
[10] N.J. Long, Angew. Chem., Int. Ed. 34 (1995) 21.
[11] T.E. Kokina, L.A. Glinskaya, R.F. Klevtsova, P.P. Semyannikov, S.V. Trubin, S.V. Larionov, Zh. Nieorg. Khim. 48 (2003) 913.

[12] V.N. Kirichenko, L.A. Glinskaya, R.F. Klevtsova, T.G. Leonova, S.V. Larionov, Zh. Strukt. Khim. 35 (1994) 106.
[13] J.A. Castro, J. Romero, J.A. Garcia-Vazquez, A. Castineiras, A. Sousa, J. Zubieta, Polyhedron 14 (1995) 2841.
[14] T. Komuro, H. Kawaguchi, K. Tatsumi, Inorg. Chem. 41 (2002) 5083.
[15] L.J. Farrugia, J. Appl. Cryst. 32 (1999) 837.
[16] SHELX97 (SHELX97, SHELX97, CIFTAB) – Programs for Crystal Structure Analysis (Release 97–2). G.M. Sheldrick, Institüt für Anorganische Chemie der Universität, Tammanstrasse 4, D-3400 Göttingen, Germany, 1998.
[17] B.S. Creaven, C. Long, R.A. Howie, G.P. McQuillan, J. Low, Inorg. Chim. Acta 157 (1989) 151.
[18] R. Uson, J. Fornies, M. Tomas, F. Martinez, J.M. Casas, C. Fortuno, Inorg. Chim. Acta 235 (1995) 51.
[19] A. Herman, B. Dręczewski, J. Organomet. Chem. 339 (1988) 41.
[20] B. Becker, K. Radacki, A. Konitz, W. Wojnowski, Z. Anorg. Allg. Chem. 621 (1995) 904.
[21] B. Becker, K. Radacki, W. Wojnowski, J. Organomet. Chem. 521 (1996) 39.
[22] M. Berardini, J. Brennan, Inorg. Chem. 34 (1995) 6179.
[23] B. Miller, A. Schneider, M. Tesmer, H. Vahrenkamp, Inorg. Chem. 38 (1999) 1900.
[24] G. Parkin, Chem. Commun. (2000) 1971.
[25] J. Seebacher, M. Shu, H. Vahrenkamp, Chem. Commun. (2001) 1026.

2.2. Physical measurements

C, H and N elemental analyses were carried out using a Heraeus Carlo Erba 1108 elemental analyzer. The IR spectra were obtained on a Jasco 5300 FT-IR spectrophotometer. Electronic spectra were recorded on a Shimadzu UV-240 spectrophotometer. NMR spectra were recorded by using a Bruker DPX 300 NMR spectrometer.

Single crystals of cyclopalladate **1** were grown by slow diffusion of a dichloromethane solution of **1** into *n*-hexane. A suitable single crystal was carefully selected under a polarizing microscope and glued to a thin glass fiber with cyanoacrylate adhesive. A single crystal structure determination by X-ray diffraction was performed on a Siemens Smart-CCD diffractometer equipped with a normal focus, 2.4 kW sealed tube X-ray source (Mo Kα radiation, $\lambda = 0.71073$ Å) operating at 50 kV and 40 mA. The structure was solved by direct methods using SHELXS-86 [36,37] and difference Fourier syntheses. An empirical absorption correction based on symmetry equivalent reflections was applied for the compounds using the SADABS [38] program. All the hydrogen positions for both compounds were initially located in the difference Fourier maps, and for the final refinement, the hydrogen atoms were placed geometrically and held in the riding mode. The last cycles of refinement included atomic positions for all the atoms, anisotropic thermal parameters for all non-hydrogen atoms and isotropic thermal parameters for all the hydrogen atoms. Full-matrix-least-squares structure refinement against $|F^2|$ was carried out using the SHELXTL-PLUS [39] package of programs.

2.3. Synthesis of [PdL(Pic)] (1)

An orange-yellow ethanolic solution (10 mL) of H_2L, (0.03 g, 0.114 mmol) was slowly added to a brown solution of $Na_2[PdCl_4]$ (0.04 g, 0.136 mmol) in ethanol (10 mL). Immediately the colour of the mixture changed to deep red and the mixture was stirred for 2 h at room temperature. A solution of 4-picoline (0.02 g, 0.21 mmol) in benzene (5 mL) was added drop-wise to the above mixture. The mixture was further stirred for 0.5 h at room temperature and the colour changed to reddish pink. The solvent was removed by evaporation and the residue was thoroughly washed with water, ethanol and diethyl ether. The solid mass was dried and dissolved in dichloromethane. The solution was chromatographed on silica gel (60–120 mesh size). Initially an orange yellow band of H_2L was eluted by a mixture of petroleum ether and benzene (1:1, v/v) followed by a pink band of compound **1**, which was eluted by pure benzene. Red microcrystals of compound **1** were collected by the removal of solvent and finally dried in vacuo. (Yield: 0.025 g, 0.0544 mmol, 47.5%). *Anal.* Calc. for $C_{23}H_{19}N_3OPd$: C, 60.04; H, 4.13; N, 9.13. Found: C, 60.40; H, 4.22; N, 8.91%. $R_f = 0.3$; MP: 234 °C (decomp.). IR (KBr; ν/cm^{-1}): 1442 (N=N), 1190 (C–O). UV/Vis (CH_2Cl_2), λ/nm ($\varepsilon/dm^3\ mol^{-1}\ cm^{-1}$): 540(9500), 467(9200), 438(7800), 346(7900), 291 ^{sh}(16 000), 280(17 600). ^1H NMR in $CDCl_3$ (ppm): 2.25 (s, 3H, 5′-Me), 2.42 (s, 3H, 4-Pic), 6.7–8.8 (other aromatic protons). $^{13}C\{^1H\}$ NMR in $CDCl_3$ (ppm): 158.16 (C8), 156.95, 152.44, 150.75, 150.23, 138.70, 137.52, 134.15, 132.99, 130.39, 128.51, 126.15, 125.99, 124.55, 123.47, 122.93, 111.87, 21.27, 19.99.

Caution: *Benzene is a highly hazardous chemical. This should be handled with great care.*

3. Results and discussion

3.1. Synthesis and spectral properties

At room temperature 1-(2′-hydroxy-5′-methylphenylazo)-naphthalene (H_2L) reacts with disodium tetrachloropalladate in ethanol medium and slowly produces an insoluble mass which readily reacts with the neutral Lewis base 4-picoline and yields a soluble pink coloured monomeric cyclometallate [PdL(Pic)] (Scheme 1). The observed elemental analytical data (experimental section) of the compound is consistent with its proposed composition.

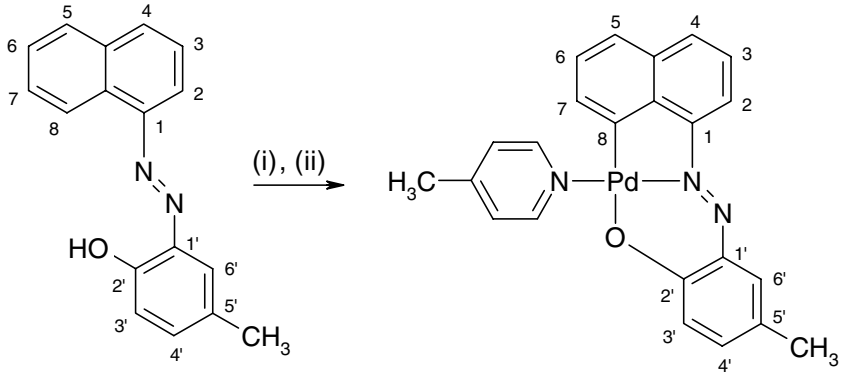

1

Scheme 1. (i) $Na_2[PdCl_4]$ (1 equivalent), EtOH, room temperature, 2 h; (ii) 4-picoline (2 equivalents), benzene, 30 min.

The IR absorption band of the phenolic group of HL at 3053 cm^{-1} indicates strong intra-molecular hydrogen bonding and it disappears on the formation of compound **1**. The IR spectrum of compound **1** shows absorptions at 1442 and 1190 cm^{-1} which are attributable to N=N (azo) [40,41] and the palladium(II) bound phenolato (C–O) [42,43] groups, respectively.

The cyclopalladate **1** is soluble in common organic solvents. The electronic spectrum of **1** shows strong absorptions in the visible region. These transitions are assigned to metal to ligand MLCT [d(Pd) → π (azo)] bands. The bands observed in the high-energy region with a high molar extinction coefficient arise from an intra-ligand charge transfer transition. The absorption in the ultraviolet region may be attributed to the usual n → π*, π → π* transitions occurring within the ligand orbitals [44].

The ^{1}H NMR signal at 12.97 ppm for the phenolic group of free HL disappears on complex formation. The methyl groups attached to the phenyl and picoline rings in **1** appear as singlets at 2.25 [42] and 2.42 ppm [42,45], respectively. The signals for the aromatic protons appear as a complex pattern in the region 6.7–8.8 ppm with the correct integration ratio. The $^{13}C\{^{1}H\}$ NMR spectrum of **1** shows a signal for the palladated C(8) of the naphthyl group at 158.16 ppm, which is in agreement with the reported values of chemical shifts for palladated carbons in the literature [32]. The signals for the methyl group of 4-picoline and 5′-methyl in **1** appear at 21.27 and 19.99 ppm, respectively.

3.2. X-ray structure of [PdL(Pic)] (1)

The molecular geometry of the cyclopalladate **1** along with the atomic numbering scheme is shown in Fig. 1. Significant crystal data and data collection parameters for **1** are listed in Table 1. Selected bond lengths and bond angles for **1** are given in Table 2.

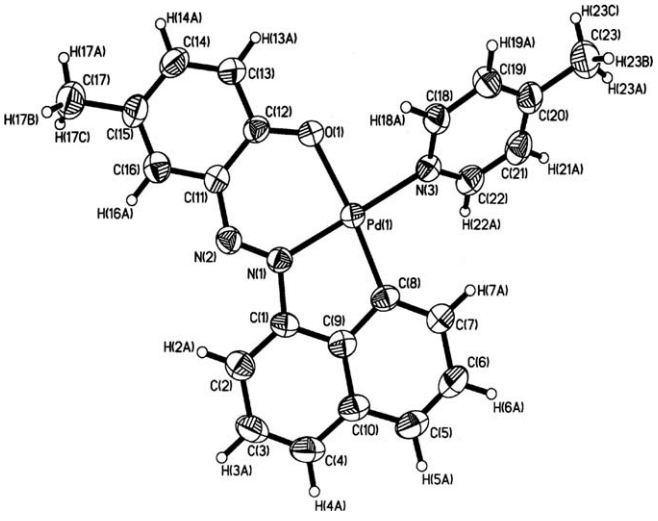

Fig. 1. Molecular structure of [Pd(L)(Pic)], **1**.

Table 1
Crystal data and structure refinement for [PdL(Pic)] (**1**)

Empirical formula	$C_{23}H_{19}N_3OPd$
Formula weight	459.81
Temperature (K)	293(2)
Wavelength (Å)	0.71073
Crystal system	monoclinic
Space group	$P2_1/c$
Unit cell dimensions	
a (Å)	14.48010(10)
b (Å)	7.7345(2)
c (Å)	17.5364(4)
α (°)	90
β (°)	105.2080(10)
γ (°)	90
Volume (Å^3)/Z	1895.23(7)/4
Density (calculated) (Mg/m^3)	1.611
Absorption coefficient (mm^{-1})	0.998
$F(000)$	928
Crystal size (mm)	$0.35 \times 0.14 \times 0.14$
θ Range for data collection (°)	1.46 to 23.27
Limiting indices	$-12 \leqslant h \leqslant 16$, $-8 \leqslant k \leqslant 8$, $-19 \leqslant l \leqslant 17$
Reflections collected	7480
Independent reflections	2727 ($R_{int} = 0.0289$)
Maximum and minimum transmission	1.000000 and 0.756626
Refinement method	Full-matrix-least-squares on F^2
Data/restraints/parameters	2727/0/254
Goodness-of-fit on F^2	1.171
Final R indices [$I > 2\sigma(I)$]	$R_1 = 0.0330$, $wR_2 = 0.0908$
R indices (all data)	$R_1 = 0.0454$, $wR_2 = 0.0969$
Extinction coefficient	0.0130(8)
Largest difference in peak and hole (e Å^{-3})	0.622 and −0.540

Table 2
Selected bond lengths (Å) and angles (°) for [PdL(Pic)] (**1**)

Bond lengths	(Å)	*Bond lengths*	(Å)
Pd(1)–N(1)	1.976(4)	Pd(1)–C(8)	1.987(4)
Pd(1)–O(1)	2.062(3)	Pd(1)–N(3)	2.068(4)
C(1)–N(1)	1.430(5)	N(2)–C(11)	1.377(5)
N(1)–N(2)	1.271(5)	C(12)–O(1)	1.290(4)
Bond angles	(°)	*Bond angles*	(°)
N(1)–Pd(1)–C(8)	83.1(2)	N(1)–Pd(1)–O(1)	91.12(12)
C(8)–Pd(1)–O(1)	173.96(13)	N(1)–Pd(1)–N(3)	177.36(12)
C(8)–Pd(1)–N(3)	97.3(2)	O(1)–Pd(1)–N(3)	88.39(12)

The palladium(II) center is bonded to C8 (the *peri* position of the 1-azonaphthyl fagment), N1 of the diazo group, O1 of the phenolato function and N(3) of the picoline ligand. Therefore 1-(2′-hydroxy-5′-methylphenylazo)naphthalene binds palladium(II) as a dianionic terdentate [C, N, O] ligand.

The tetra-coordination around palladium is essentially planar and coplanar with the *peri* palladated naphthyl ring, but in a distorted square-planar geometry. The maximum deviation is represented by the 'bite' angle C(8)–Pd(1)–N(3) of 97.3(2)°. This type of deviation is observed for cyclopalladates [46]. The Pd–C8 bond length of 1.987(4) Å is in agreement with the reported palladium(II)–C8(naphthyl) bond length of 1.971(5) Å [31].

The shortening of the C(11)–N(2) bond, 1.377(5) Å, with respect to the C(1)–N(1) bond, 1.430(5) Å, reveals the presence of more π-electron density in the six membered diazapalladacycle than that present in the five membered azapalladacycle.

4. Conclusion

At room temperature 1-(2′-hydroxy-5′-methylphenylazo)naphthalene undergoes a cyclopalladation reaction with disodium tetrachloropalladate in ethanol and behaves as a dianionic terdentate [C, N, O] ligand. Palladium–carbon bond formation occurs at the C8 (*peri*-) position exclusively in contrast to the reported palladation of 1-phenylazonaphthalene which occurs at the C2 (*ortho*-) position. Thus the presence of the 2′-hydroxy group as an additional donor in the ligand frame influences the exclusive *peri*-palladation of the naphthyl group of 1-(2′-hydroxy-5′-methylphenylazo) naphthalene. The cyclopalladate has been isolated as a picoline adduct in the pure form and has been characterized by spectral and X-ray diffraction methods.

Acknowledgements

The financial support (SR/S1/IC-10/2003) from DST, Government of India, is gratefully acknowledged. One of us (P.D.) thanks CSIR (India) for the award of a senior fellowship. We also thank UGC for granting a Special Assistance Programme to our Department.

Appendix A. Supplementary data

Crystallographic data for structural analysis of **1** has been deposited at the Cambridge Crystallographic Data Centre, CCDC, No. 281701. Copies of this information can be obtained free of charge from The Director, CCDC, 12, Union Road, Cambridge CB2 1EZ, UK (fax: +44 1223 336033; e-mail: deposit@ccdc.cam.ac.uk or http://www.ccdc.cam.ac.uk). Supplementary data associated with this article can be found, in the online version, at doi:10.1016/j.poly.2005.12.029.

References

[1] J. Dupont, C.S. Consorti, J. Spencer, Chem. Rev. 105 (2005) 2527.
[2] I. Omae, Coordin. Chem. Rev. 248 (2004) 995.
[3] A.D. Ryabov, R. van Eldik, G. Le Borgne, M. Pfeffer, Organometallics 12 (1993) 1386.
[4] M. Pfeffer, J.P. Sutter, M.A. Rottvel, A. de Cian, J. Fischer, Tetrahedron 48 (1992) 2427.
[5] M. Pfeffer, Recl. Trav. Chim. Pays-Bas 109 (1990) 567.
[6] A.D. Ryabov, Synthesis (1985) 233.
[7] I.P. Beletskaya, A.V. Cheprakov, J. Organomet. Chem. 689 (2004) 4055.
[8] M. Albrecht, B.M. Cocks, A.L. Spek, G. van Koten, J. Organomet. Chem. 624 (2001) 271.
[9] J. Dupont, M. Pfeffer, J. Spencer, Eur. J. Inorg. Chem. (2001) 1917.
[10] C. Schlenk, A.W. Kleij, H. Frey, G. van Koten, Angew. Chem. Int. Ed. 39 (2000) 3445.
[11] D. Morales-Morules, R. Redon, C. Yung, C.M. Jensen, Chem. Commun. (2000) 1619.
[12] R.B. Bedford, S.M. Draper, P.N. Scully, S.L. Welch, New J. Chem. 24 (2000) 745.
[13] A.S. Gruber, D. Zim, G. Ebeling, A.L. Monteiro, J. Dupont, Org. Lett. 2 (2000) 1287.
[14] D.E. Bergbreiter, P.L. Osburn, Y.S. Liu, J. Am. Chem. Soc. 121 (1999) 9531.
[15] F. Miyazaki, K. Yamaguchi, M. Shibasaki, Tetrahedron Lett. 40 (1999) 7379.
[16] M. Ohff, A. Ohff, D. Milstein, Chem. Commun. (1999) 357.
[17] H. Weissman, D. Milstein, Chem. Commun. (1999) 1901.
[18] R.A.M. Abbenhuis, J. Boersma, G. van Koten, J. Org. Chem. 63 (1998) 4282.
[19] M. Ghedini, I. Aiello, M. La Deda, A. Grisolia, Chem. Commun. (2003) 2198.
[20] I. Aiello, M. Ghedini, M. La Deda, J. Lumin. 96 (2002) 249.
[21] F. Neve, A. Crispini, C. Depietro, S. Campagna, Organometallics 21 (2002) 3511.
[22] I. Aiello, D. Dattilo, M. Ghedini, A. Golemme, J. Am. Chem. Soc. 123 (2001) 5598.
[23] I. Aiello, D. Dattilo, M. Ghedini, A. Bruno, R. Termine, A. Golemme, Adv. Mater. 14 (2002) 1233.
[24] M.J. Baena, J. Buey, P. Espinet, C.E. García-Prieto, J. Organomet. Chem. 690 (2005) 998.
[25] L. Díez, P. Espinet, J.A. Miguel, M. Paz Rodríguez-Medina, J. Organomet. Chem. 690 (2005) 261.
[26] B.B. Eran, D. Singer, K. Praefcke, Eur. J. Inorg. Chem. (2001) 111.
[27] T. Hegmann, J. Kain, S. Diele, B. Schubert, H. Bögel, C. Tschierske, J. Mater. Chem. 13 (2003) 991.
[28] R.W. Date, E.F. Iglesias, K.E. Rowe, J.M. Elliot, D.W. Bruce, J. Chem. Soc., Dalton Trans. (2003) 1914.
[29] M. Ghedini, D. Pucci, A. Crispini, I. Aiello, F. Barigelletti, A. Gessi, O. Francescangeli, Appl. Organometal. Chem. 13 (1999) 565.
[30] A.D. Ryabov, Chem. Rev. 90 (1990) 403.
[31] L. Kind, A.J. Klaus, P. Rys, V. Gramlich, Helv. Chim. Acta 81 (1998) 307.
[32] A.J. Klaus, P. Rys, Helv. Chim. Acta 64 (1981) 1453.
[33] K. Gehrig, A.J. Klaus, P. Rys, Helv. Chim. Acta 67 (1984) 113.
[34] M. Hugentobler, A.J. Klaus, H. Mettler, P. Rys, G. Wehrle, Helv. Chim. Acta 65 (1982) 1202.
[35] B.S. Furniss, A.J. Hannaford, V. Rogers, P.W.G. Smith, A.R. Tatchell (Eds.), Vogel's Text Book of Practical Organic Chemistry, fourth ed., ELBS and Longman Group Ltd., London, 1978.
[36] G.M. Sheldick, SHELXS-86 Program for Crystal Structure Determination, University of Göttingen, Göttingen, Germany, 1986.
[37] Acta Crystallogr. 35 (1990) 467.
[38] G.M. Sheldick, SADABS Siemens Area Detector Absorption Correction Program, University of Göttingen, Göttingen, Germany, 1994.
[39] G.M. Sheldick, SHELXS-93 Program for Crystal Structure Solution and Refinement, University of Göttingen, Göttingen, Germany, 1993.
[40] J. Albert, A. González, J. Granell, R. Moragas, X. Solans, M. Font-Bardía, J. Chem. Soc., Dalton Trans. (1998) 1781.
[41] J. Albert, A. González, J. Granell, R. Moragas, C. Puerta, P. Valerga, Organometallics 16 (1997) 3775.
[42] A.K. Mahapatra, D. Bandyopadhyay, P. Bandyopadhyay, A. Chakravorty, Inorg. Chem. 25 (1986) 2214.
[43] A.K. Mahapatra, D. Bandyopadhyay, P. Bandyopadhyay, A. Chakravorty, J. Chem. Soc., Chem. Commun. (1984) 999.
[44] S. Dutta, S. Peng, S. Bhattacharya, J. Chem. Soc., Dalton Trans. (2000) 4623.
[45] R. Bhawmick, P. Bandyopadhyay, Trans. Met. Chem. 20 (1995) 415.
[46] A. Fernández, D. Vazquez-García, J.J. Fernández, M. López-Torres, A. Suárez, S. Castro- Juiz, J.M. Vila, New J. Chem. 26 (2002) 398.

(**2**) with infinite 1D chain structures, and their magnetic properties have been investigated based on the simple tetranuclear model.

2. Experimental

2.1. Materials and synthesis

3-Carboxylsalicylidene was prepared by the literature method [20], 1-(2-hydroxybenzamido)-2-(amino) ethane was prepared by the literature method [13], the ligand H_4L and the copper precursor ($K_2CuL \cdot 1.5H_2O$) were prepared by the literature method [21]. Other chemicals were of reagent grade and obtained commercially without further purification.

2.1.1. Synthesis of the complex *1*

A methanol solution (100 mL) of $K_2CuL \cdot 1.5H_2O$ (0.25 g, 0.5 mmol) was gently poured into a methanol solution (100 mL) of Mn(II) acetate tetrahydrate (0.12 g, 0.5 mmol) at ambient temperature. The resulting solution was allowed to stand for several days. The poor light red crystals that formed were collected by filtration and dried in air. Yield based on [$CuLMn \cdot CuLMn(CH_3OH)(H_2O)$]: 90%. The crystals were only soluble in dimethyl sulfoxide (DMSO). Therefore, the single crystals suitable for X-ray analysis were grown by a slow diffusion method using a test-tube. 5 mL $Mn(OAC)_2 \cdot 4H_2O$ aqueous solution (5 mmol L^{1-}), 10 mL ethanol–water solution (3:1 V/V) and 5 mL $K_2CuL \cdot 1.5H_2O$ methanol solution (5 mmol L^{1-}) were carefully added in order to a 30 mL test-tube, and then the top of the tube was sealed. The light red single crystals of **1** were formed at the upper interface in one month. Calc. for $C_{36.5}H_{35}Cu_2Mn_2N_4O_{13}$: Cu, 13.04; Mn, 11.27; C, 44.98; H, 3.62; N, 5.75. Found: Cu, 12.75; Mn, 11.01; C, 44.82; H, 3.42; N, 5.58%. $\nu_{C=O}$ (amido moiety) at 1647 cm^{-1}.

2.1.2. Synthesis of the complex *2*

The compound **2** was prepared similarly to **1**. The yield based on [$CuLCo \cdot CuLCo\ (H_2O)_2] \cdot H_2O$: 93% Calc. for $C_{34}H_{30}Cu_2Co_2N_4O_{13}$: Cu, 13.40; Co, 12.43; C, 43.09; H, 3.19; N, 5.91. Found: Cu, 13.28; Co, 12.56; C, 43.22; H, 3.09; N, 5.80%. $\nu_{C=O}$ (amido moiety) at 1653 cm^{-1}.

2.2. Physical measurements

Elemental analyses for carbon, hydrogen and nitrogen were carried out on a Perkin–Elmer 2400II analyzer. The metal contents were determined by EDTA titration. The infrared spectra were recorded on an Avatar-360 spectrometer using KBr pellets in the range of 400–4000 cm^{-1}. UV–Vis spectra were recoded in DMSO (DMSO = dimethyl sulfoxide) with a UV-550 spectrometer in the range of 200–800 nm. The temperature-dependent magnetic susceptibilities in the temperature range of 5–300 K under a constant external magnetic field of 10 kG were measured with a MPMS-7 SQUID magnetometer.

2.3. Crystallographic studies

The single crystals used for data collection of the complexes **1** ($0.17 \times 0.13 \times 0.05$ mm^3) and **2** ($0.281 \times 0.125 \times 0.098$ mm^3) were selected and mounted on a Bruker Smart APEX diffractometer with a CCD detector using graphite monochromated Mo Kα radiation ($\lambda = 0.71073$ Å). Data were collected by the ω scan mode at 293(2) K to a θ_{max} of 25.00° with a total of 9790 reflections collected including 6568 independent reflections ($R_{int} = 0.0881$) for complex **1** and to a θ_{max} of 26.41° with a total 10403 reflections collected including 7113 independent reflections ($R_{int} = 0.0524$) for complex **2**. A summary of the crystallographic data is given in Table 1. Lorentz and polarization factors were made for the intensity data and absorption corrections were performed using the SADABS program [22]. The crystal structures were solved using the SHELXTL program and refined using full matrix least squares [23]. The positions of the hydrogen atoms were calculated theoretically and included in the final cycles of refinement in a riding model along with the attached carbons. For **1**, the uncoordinated CH_3OH and CH_3CH_2OH molecules appear to be disordered and their occupied factors are 0.5. Selected bond distances and angles are given in Table 2.

3. Results and discussion

3.1. Description of the crystal structures

The crystal structures were determined by single-crystal X-ray diffraction analyses. Their crystallographic data are summarized in Table 1. Selected bond distances and angles are shown in Tables 2 and 3. As their molecular structures are similar to each other, only the structure of **1** is described in detail. Each dissymmetrical unit of complex **1** consists of

Table 1
Crystal data and structure refinement for the two polymers

	Polymer **1**	Polymer **2**
Empirical formula	$C_{36.5}H_{35}Cu_2Mn_2N_4O_{13}$	$C_{34}H_{30}Cu_2Co_2N_4O_{13}$
Formula weight	974.646	947.56
Crystal system	triclinic	triclinic
Space group	$P\bar{1}$	$P\bar{1}$
a (Å)	9.917(2)	10.578(2)
b (Å)	13.974(3)	11.724(2)
c (Å)	14.346(3)	15.049(3)
α (°)	86.199(3)	85.213(3)
β (°)	85.122(4)	75.219(3)
γ (°)	73.936(4)	82.444(3)
V (Å^3)	1901.7(7)	1787.1(6)
Z	2	2
D_{calc} (g cm^{-1})	1.727	1.761
λ (Mo Kα) (Å)	0.71073	0.71073
μ (Mo Kα) (mm^{-1})	1.827	2.159
T (K)	293(2)	293(2)
$R_1[I > 2\sigma(I)]$	0.0681	0.0404
wR_2	0.1373	0.0982

$w^{-1} = [\sigma^2(F_o^2) + (0.1325P)^2 + (0.2304P)]$, $p = [(F_o^2) + 2F_c^2]/3$ for **1**.
$w^{-1} = [\sigma^2(F_o^2) + (0.0579P)^2 + (0.0000P)]$, $p = [(F_o^2) + 2F_c^2]/3$ for **2**.

Table 2
Selected bond lengths (Å) and angles (deg) for polymer **1**

Bond length			
Cu1–O1	1.933(5)	Cu2–O6	1.941(5)
Cu1–O2	1.885(5)	Cu2–O7	1.891(6)
Cu1–N1	1.916(7)	Cu2–N3	1.897(7)
Cu1–N2	1.899(7)	Cu2–N4	1.910(7)
Mn1–O1	2.173(5)	Mn2–O6	2.234(6)
Mn1–O2	2.138(6)	Mn2–O7	2.157(6)
Mn1–O3	2.090(6)	Mn2–O8	2.113(6)
Mn1–O8	2.428(5)	Mn2–O1w	2.199(6)
Mn1–O9	2.178(6)	Mn2–O11	2.254(6)
Mn1–O5#1	2.114(6)	Mn2–O10#2	2.139(6)
Bond angles			
N2–Cu1–N1	85.7(3)	N3–Cu2–N4	86.1(3)
N2–Cu1–O2	96.8(3)	N3–Cu2–O6	93.6(3)
N1–Cu1–O1	94.5(3)	N4–Cu2–O7	95.9(3)
O1–Cu1–O2	83.5(2)	O7–Cu2–O6	85.4(3)
O3–Mn1–O1	81.0(2)	O6–Mn2–O8	80.6(2)
O3–Mn1–O2	153.2(2)	O6–Mn2–O1w	170.2(2)
O3–Mn1–O8	82.7(2)	O6–Mn2–O7	72.6(2)
O1–Mn1–O2	72.3(2)	O7–Mn2–O1w	112.9(2)
O1–Mn1–O8	153.8(2)	O7–Mn2–O8	153.0(2)
O2–Mn1–O8	123.0(2)	O1w–Mn2–O8	93.1(2)
O9–Mn1–O5#1	140.3(2)	O10#2–Mn2–O11	176.2(2)
Cu1–O1–Mn1	99.8(2)	Cu2–O6–Mn2	97.6(2)
Cu1–O2–Mn1	102.6(2)	Cu2–O7–Mn2	101.8(2)

#1 $-x-1, -y+2, -z+1$; #2 $-x-1, -y+3, -z$.

Table 3
Selected bond lengths (Å) and angles (°) for polymer **2**

Bond length			
Cu1–N1	1.906(3)	Cu2–N3	1.904(3)
Cu1–N2	1.902(3)	Cu2–N4	1.909(3)
Cu1–O1	1.931(2)	Cu2–O5	1.937(2)
Cu1–O2	1.897(2)	Cu2–O6	1.873(2)
Co1–O1	2.072(2)	Co2–O5	2.042(2)
Co1–O2	2.126(2)	Co2–O6	2.090(2)
Co1–O3	2.055(2)	Co2–O7	2.030(2)
Co1–O9#1	2.026(2)	Co2–O3	2.183(2)
Co1–Ow1	2.180(2)	Co2–O4	2.156(2)
Co1–Ow2	2.118(2)	Co2–O10#2	2.062(2)
Bond angles			
N2–Cu1–O2	96.6(1)	N3–Cu2–N4	86.8(1)
N2–Cu1–N1	86.0 (1)	N3–Cu2–O5	92.7(1)
O1–Cu1–O2	85.7(9)	N4–Cu2–O6	96.8(1)
N1–Cu1–O1	92.8(1)	O5–Cu2–O6	84.6(9)
O3–Co1–O1	86.7(8)	O3–Co2–O7	85.7(9)
O3–Co1–O2	163.3(8)	O3–Co2–O5	151.1(9)
O3–Co1–Ow2	89.5(8)	O3–Co2–O6	109.9(9)
O1–Co1–O2	76.7(8)	O4–Co2–O10#2	155.0(2)
O1–Co1–Ow2	168.3(1)	O7–Co2–O5	86.9(9)
O2–Co1–Ow2	106.5(9)	O7–Co2–O6	163.4(9)
O9#1–Co1–Ow1	175.9(9)	O5–Co2–O6	76.7(9)
Cu1–O1–Co1	98.33(9)	Cu2–O5–Co2	98.90(10)
Cu1–O2–Co1	97.58(9)	Cu2–O6–Co2	99.34(11)

#1 $-x+2, -y, -z+1$; #2 $-x+2, -y+1, -z$.

a dissymmetrical tetranuclear unit, a disordered methanol molecule and a disordered ethanol molecule (Fig. 1). The tetranuclear unit comprises two different neutral binuclear moieties Cu1Mn1L (Cu1Mn1L = **A**) and Cu2Mn2(H_2O)-(CH_3OH)L (Cu2Mn2 (H_2O)(CH_3OH)L = **B**), which are united together by the carboxylic group (O8C34O9) of **B** with a Mn1···Mn2 distance of 4.133 Å. The dihedral angle of the **A** and **B** moieties is 85.5°.

In moiety **A**, Cu1 has a square planar coordination geometry with N_2O_2 (N1, N2, O1, O2) donor atoms. The Cu–$N2_{(amido)}$ (1.899(7) Å) distance is considerably shorter than that of Cu–$N1_{Schiff}$ (1.916(7) Å). Both Cu–N and Cu–O distances are similar to the literature [3,12,13]. The Mn1 ions are coordinated by two bridged phenoxo atoms (O1, O2), one carboxylic oxygen atom (O3) from the **A** moiety, two carboxylic oxygen atoms (O8, O9) from the **B** moiety and one amido oxygen atom (O5#1) from the **A** moiety (**A**$^{\#}$) of an adjacent unit to form an octahedral coordination configuration, as shown in Figs. 1 and 2a. The Cu1 and Mn1 ions are bridged together by two

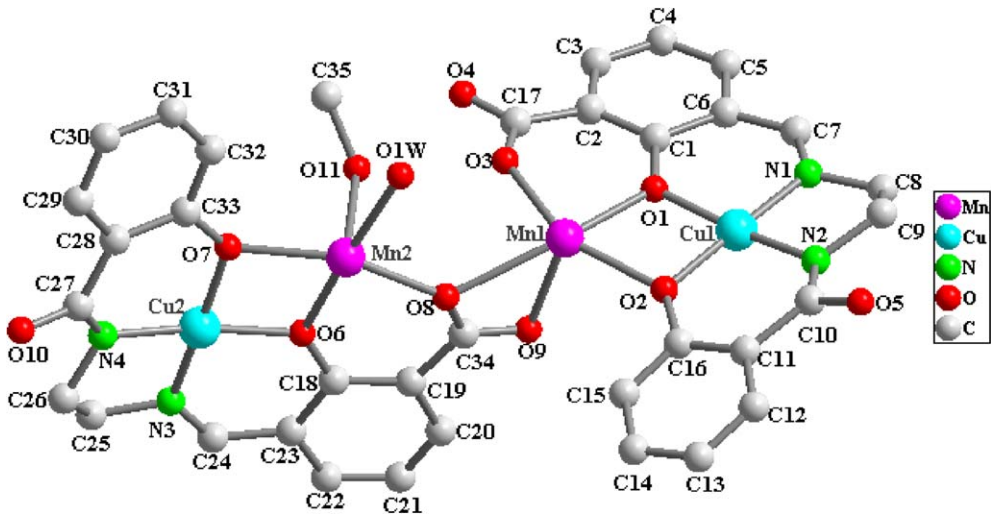

Fig. 1. Thee tetranuclear dissymmetrical unit of complex **1**, the hydrogen atoms, a disordered methanol molecule and a disordered ethanol molecule are omitted for clarity.

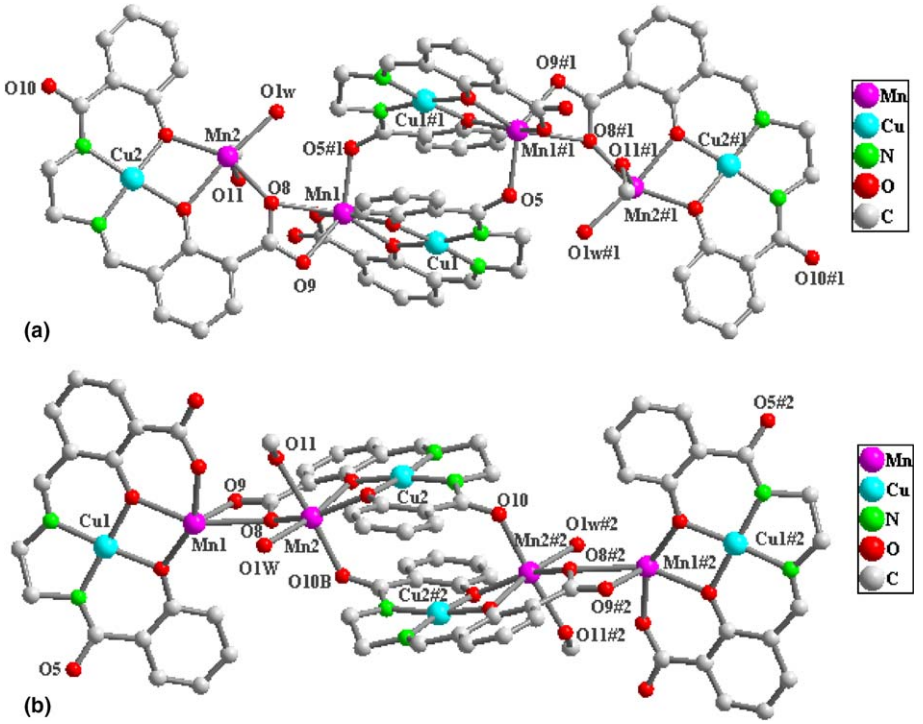

Fig. 2. (a) The tetranuclear cycle constructed by Cu1Mn1(H_2O)(CH_3OH)L moieties of two adjacent units and selected atom labelling scheme. (b) The tetranuclear cycle constructed by Cu2Mn2L moieties of two adjacent units and selected atom labelling scheme.

phenoxo atoms (O1, O2) with Cu1–O1 = 1.933(5) Å, O1–Mn1 = 2.173(5) Å, Cu1–O2 = 1.885(5) Å, O2–Mn1 = 2.138(6) Å, Cu1–O1–Mn1 = 99.8(2)°, Cu1–O2–Mn1 = 102.6(2)°; the Cu1···Mn1 distance is 3.145(2) Å. From Fig. 2a, we can also find that **A** and $\mathbf{A}^{\#}$ of the adjacent unit are bridged together through Mn1–O5#1and Mn1#1–O5 (2.114(6)?) to form a novel cyclic cylindrical tetranuclear structure (**AA**). From bond angles, the hexacoordinated Mn1 has four almost coplanar bonds Mn1–O3, Mn1–O1, Mn1–O2, Mn1–O8 with O3–Mn1–O1 = 81.0(2)°, O1–Mn1–O2 = 72.3(2)°, O2–Mn1–O8 = 123.0 (2)°, O8–Mn1–O3 = 82.7(2)°, O2–Mn1–O3 = 153.2(2)°, O1–Mn1–O8 = 153.8(2)° and two axial bonds Mn1–O5#1, Mn1–O9 with O9–Mn1–O5#1 = 140.3(2)°. Therefore, the Mn1 ions are located in a distorted octahedral configuration.

The structure of the **B** moiety is similar to that of **A** except as follows: (1) the Cu–$N4_{(adiom)}$ distance is considerably longer than that of Cu–$N3_{(Schiff)}$. (2) Although Mn2 is still a distorted octahedral coordination configuration, the coordination atoms are very different from Mn1. Mn2 ion is coordinated by two bridged phenoxo atoms (O6, O7), one carboxylic oxygen atom (O8), one oxygen atom (O1w) from a water molecule, one oxygen atom (O11) from a methanol molecule and an amido oxygen atom (O10#2) from the B moiety ($\mathbf{B}^{\#}$) of another adjacent unit, as shown in Figs. 1 and 2b. (3) The carboxylic group (O8C34O9) in moiety **B** acts as a bridge to coordinate to the Mn1 atom in the **A** moiety, as shown in Figs. 1 and 2. Similar to **A**, a cyclic cylindrical tetranuclear structure (**BB**) is also formed by the coordination bonds Mn2#2–O10 and Mn2–O10#2 (Fig. 2b). (4) The bond lengths and angles in the **B** moiety are slightly different from that of **A**, as shown in Table 2.

From the above discussion, the dissymmetrical tetranuclear unit forms two different tetranuclear cycles (**AA** and **BB**) through the coordination bonds Mn1–O5#1, Mn1#1–O5, Mn2#2–O10 and Mn2–O10#2. These dissymmetrical tetranuclear units are united together by these

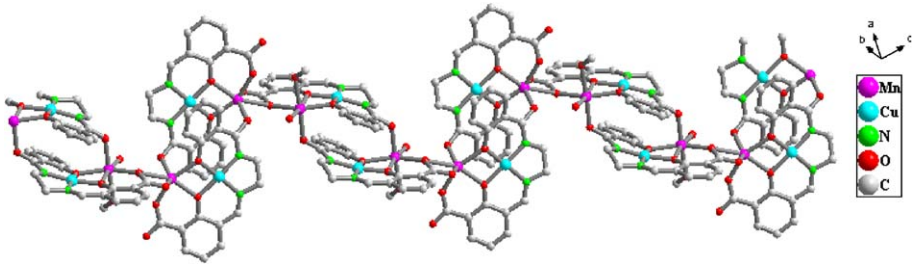

Fig. 3. Space filling representation of complex **1** showing the 1D chain.

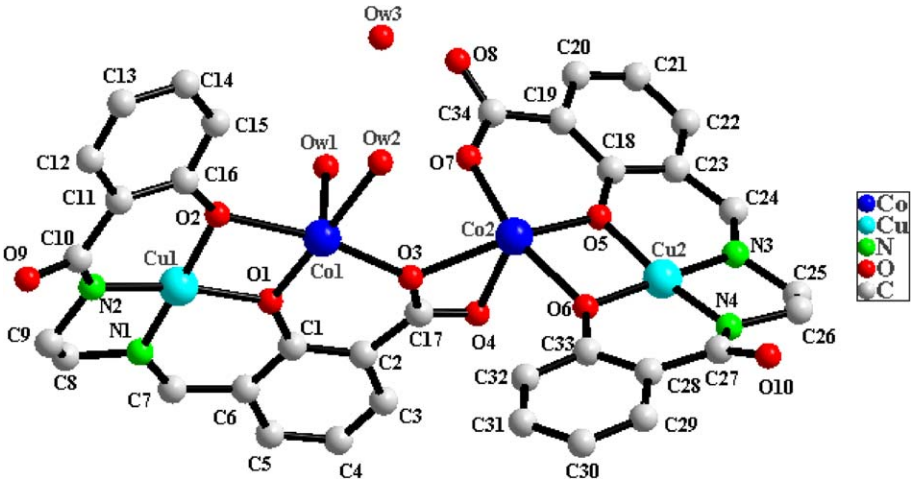

Fig. 4. The tetranuclear dissymmetrical unit of complex **2**, the hydrogen atoms are omitted for clarity.

coordination bonds between amido oxygen atoms and Mn^{II} ions to form a novel ...(**AA**)(**BB**)(**AA**)(**BB**)(**AA**)(**BB**)... 1D chain, as shown in Fig. 3. No hydrogen bonds are shown in the interchains (Fig. 3).

The structure of **2** is very similar to that of **1** except as follow: (1) Each dissymmetrical unit of **2** consists of a dissymmetrical tetranuclear unit and a solvent water molecule. (2) Two water molecules (O1w, O2w) coordinate to the same Co^{II} ion (Co1 ion) in the dissymmetrical tetranuclear unit. In a word, complex **2** not only has no methanol and ethanol solvent molecules, but also has no coordinated methanol molecule, as shown in Fig. 4.

3.2. Spectroscopic characterization

IR spectra of the ligand H_4L exhibits an intense absorption band assignable to the $\nu_{C=O}$ vibration of the amido moiety at 1638 cm^{-1} [24]; the band shifts to higher frequency by 6, 9 and 15 cm^{-1} in the IR spectra of $K_2CuL \cdot 1.5H_2O$, compound **1** and compound **2**, respectively. Owing to the conjugation of C=N group on the aromatic ring, the $\nu_{C=N}$ band of H_4L occurs at 1590 cm^{-1}. The band is shifted to higher frequency by 5, 8 and 7 cm^{-1} in the IR spectra of the $K_2CuL \cdot 1.5H_2O$, **1** and **2**, respectively. The COO^- asymmetrical vibration bands of **1** (or **2**), $\nu_{as(coo)}$, exhibits two intense absorption bands at 1578 cm^{-1} (or 1570 cm^{-1}) and 1538 cm^{-1} (or 1533 cm^{-1}), which may be attributed to $\nu_{as(coo)}$ bands of the monodentate and bidentate coordinated carboxyl groups, while the two intense absorption bands at 1395 cm^{-1} (or 1398 cm^{-1}) and 1428 cm^{-1} (or 1437 cm^{-1}) may be assigned to $\nu_{s(coo)}$, the symmetrical vibration bands of monodentate and bidentate coordinated carboxyl groups.

The d–d bands of $K_2CuL \cdot 1.5H_2O$ exhibit a very broad peak around 520 nm, which is consistent with the d–d bands of the Cu^{II} ion in a nearly square planar geometry. The electronic spectra of **1** show a broad band in the same region with a maximum absorption at 520 nm, a fact which indicates that the planarity of $[CuN_2O_2]$ in **1** is the same as that of $K_2CuL \cdot 1.5H_2O$. The d–d bands of Mn^{II}, due to spin-forbidden transitions, are all too weak to be observed or are overlapped by the d–d bands of Cu^{II}. The electronic spectra of **2** show a broad band in the region with a maximum absorption at 500 nm. Such a blue shift of the d–d band may be attributed to the d–d transitions of the Co^{II} ion in an octahedral field.

3.3. Magnetic properties

The variable temperature magnetic susceptibility data for a crystalline sample of the complexes **1** and **2** were measured on a MPMS-7 SQUID magnetometer over the temperature range of 5–300 K. The plots of μ_{eff} (where μ_{eff} is the effective magnetic moment) and χ_M versus T are shown in Fig. 5 (**1**) and Fig. 6 (**2**). For complex **1**, at 300 K, μ_{eff} is equal to 8.65 BM, a value a little lower than the expected one for two non-interacting $S = 5/2$ Mn^{II} centers and two $S = 1/2$ Cu^{II} centers (8.72 BM). For complex **2**, at 300 K, μ_{eff} is equal to 6.29 BM, a value slightly larger than that expected for two non-interacting $S = 3/2$ Co^{II} centers

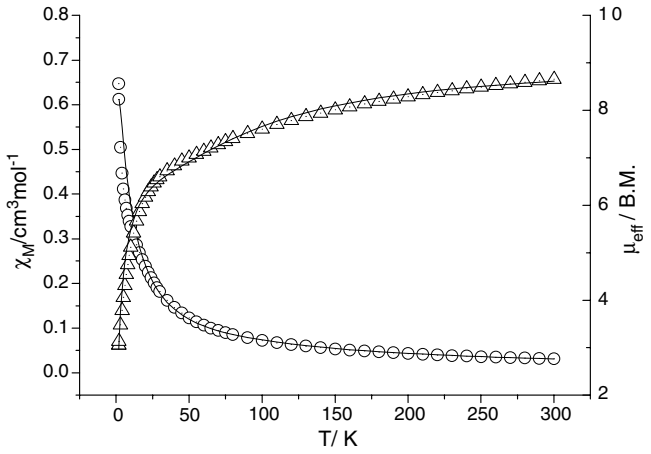

Fig. 5. The plots of μ_{eff} and x_M vs. T for complex **1**.

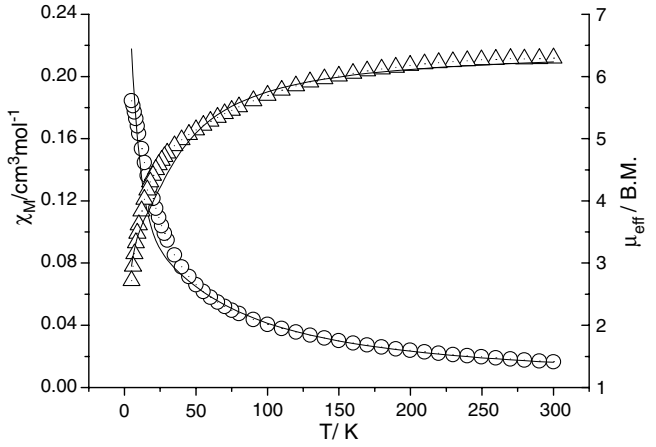

Fig. 6. The plots of μ_{eff} and x_M vs. T for complex **2**.

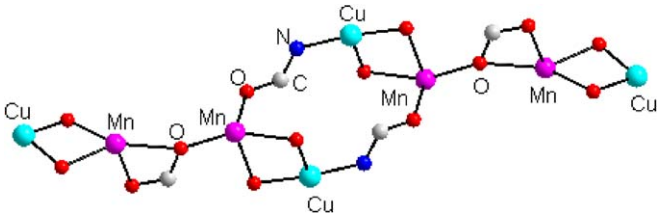

Scheme 1.

and two $S = 1/2$ Cu^{II} centers (6.0 BM). On decreasing the temperature, the μ_{eff} value decreases gradually to the value of 6.29 BM at 22 K for **1** and 4.41 BM at 20 K for **2**; then decreases sharply with the temperature being further lowered and approaches a minimum at around 5 K with $\mu_{eff} = 4.06$ BM for **1** and $\mu_{eff} = 2.95$ BM for **2**.

There are at least three kinds of magnetic interactions for the present systems, namely, (i) Cu^{II}–M^{II} through the phenoxo bridge, (ii) $Cu^{II}1M^{II}1$–$M^{II}2Cu^{II}2$ through the carboxylate oxygen bridge, and (iii) $Cu^{II}A$–M^{II} through the amido bridge, as shown in Scheme 1. These magnetic interactions compete to produce the magnetic properties of these complexes. It is difficult to find an appropriate model for this complicated situation and the difference of the bond angles between Cu1–O1–Mn1(99.8(2)°) and Cu2–O6–Mn2 (97.6(2)°) and between Cu1–O2–Mn1(102.6(2)°) and Cu2–O7–Mn2 (101.8(2)°) are small. As a preliminary treatment, we take these systems as isolated linear tetranuclear complexes with only (i) $Cu^{II}1$–$M^{II}1$ (or $Cu^{II}2$–$M^{II}2$) through the phenoxo bridge and (ii) $Cu^{II}1M^{II}1$–$M^{II}2Cu^{II}2$ through the carboxylate oxygen bridge, and take (iii) M^{II}–$Cu^{II}A$ (or $M^{II}A$–Cu^{II}) through the amido bridge into account in the θ value to deal with the magnetic interactions of the linear tetranuclear complexes. The magnetic analysis was then carried out by Eq. (1) for complex **1** and Eq. (2) for complex **2** derived from this model [25,26], previously reported, as shown in the following:

$$\mathrm{Cu}\overset{J}{-}\mathrm{Mn}\overset{j}{-}\mathrm{Mn}\overset{J}{-}\mathrm{Cu}, \quad X_M = \frac{Ng^2\beta^2}{K(T-\theta)}\frac{A}{B}, \tag{1}$$

where $A = 28 + 60\exp(4j/KT) + 10\exp(-3j/KT) + 2\exp(-5j/KT) + 420\exp(3J/KT) + 392\exp(6J/KT)$, $B = 7 + 9\exp(4j/KT) + 5\exp(-3j/KT) + 3\exp(-5j/KT) + \exp(-6j/KT) + 70\exp(3J/KT) + 49\exp(6J/KT)$.

$$\mathrm{Cu}\overset{J}{-}\mathrm{Co}\overset{j}{-}\mathrm{Co}\overset{J}{-}\mathrm{Cu}, \quad X_M = \frac{Ng^2\beta^2}{3K(T-\theta)}\frac{A}{B}, \tag{2}$$

where $A = 184\exp[(6J+4j)/KT] + 84\exp(6J/KT) + 30\exp[(6J-3j)/KT] + 6\exp[(6J-5j)/KT] + 168\exp[(4J+2j)/KT] + 60\exp[(4J-j)/KT] + 12\exp[(4J-3j)/KT] + 30\exp[(2J+j)/KT] + 6\exp[(2J-2j)/KT]$, $B = 9\exp[(6J+4j)/KT] + 7\exp(6J/KT) + 5\exp[(6J-3j)/KT] + 3\exp[(6J-5j)/KT] + \exp[(6J-6j)/KT] + 14\exp[(4J+2j)/KT] + 10\exp[(4J-j)/KT] + 6\exp[(4J-3j)/KT] + 5\exp[(2J+j)/KT] + 3\exp[(2J-j)/KT] + \exp[(2J-2j)/KT]$, J corresponds to the exchange integral between the M ion and the Cu ion, j stands for the exchange integral between two $Cu^{II}M^{II}$ units through carboxylic oxygen bridges. The best-fit parameters are $J = -41.6\ \mathrm{cm}^{-1}$, $g = 2.10$, $j = -0.12\ \mathrm{cm}^{-1}$, $\theta = -7.0$ K for **1** and $J = -25.1\ \mathrm{cm}^{-1}$, $g = 2.15$, $j = -1.12\ \mathrm{cm}^{-1}$, $\theta = -4.1$ K for **2**. The agreement factor $R = \sum(\chi_{obsd} - \chi_{cacld})^2/\sum\chi^2_{obsd}$ is equal to 5.76×10^{-3} for **1** and 9.52×10^{-3} for **2**, which corresponds to a reasonable agreement as can be seen in Figs. 5 and 6. The negative J and j values suggest that the magnetic interactions between the M^{II} and Cu^{II} ions through the phenoxo bridge, and between two $Cu^{II}M^{II}$ units through a carboxylic oxygen bridge are all antiferromagnetic, the $\theta < 0$ value indicates that the magnetic interaction between linear tetranuclear units is also antiferromagnetic.

The magnetic susceptibility data of complex **1** was well reproduced over the entire temperature range, while that of complex **2** was limited to the 50–300 K range. The interpretation of the magnetic properties of complex **2** is difficult due to the unquenched orbital momentum of the Co^{II} ion. The isotropic Heisenberg exchange model is not strictly applicable to octahedral Co^{II} complexes because of the strong spin–orbit coupling of the $^4T_{1g}$ ground term. Moreover, at low temperatures the states arising from the $^4T_{1g}$ term are split into two Kramer doublets by zero-field splitting, and the Heisenberg model may fail. Anyway, a reasonable fit could be performed in the higher temperature regions, neglecting the zero-field splitting.

4. Conclusion

The "bridging ligand complex" $K_2CuL \cdot 1.5H_2O$ plays a very important role during the construction of two heterometallic coordination polymers. Through the self-assembly method, two chain coordination polymers with carboxylate and amido bridges have been obtained. Complexes **1** and **2** do not dissolved in common organic and inorganic solvents, therefore, we employed the slow diffusion method in a test-tube to obtain the single crystals of the two compounds. Their magnetic properties were preliminary investigated by treating these systems as isolated linear tetranuclear systems.

5. Supporting material

CCDC-282749 and CCDC-282750 contain the supplementary crystallographic data for this paper. These data can be obtained, free of charge, from the Cambridge Crystallographic Data Centre, 12 Union Road, Cambridge CB2 1EZ, UK; fax: (internat.) +44 1223 336 033; e-mail: deposit@ccdc.cam.ac.uk.

Acknowledgments

The authors thank to the Technology Chamber of Henan Province (0311020800) and the Education Chamber of Henan Province (2002150003) for financial support.

References

[1] (a) O. Kahn, Adv. Inorg. Chem. 43 (1996) 179;
(b) O. Kahn, Struct. Bonding (Berlin) 68 (1987) 89.
[2] (a) O. Kahn, Molecular Magnetism, VCH, New York, 1993;
(b) S.J. Gruber, C.M. Harris, E. Sinn, J. Inorg. Nucl. Chem. 30 (1986) 1805;
(c) N.B. O' Brien, T.O. Maier, I.C. Paul, R.S. Drago, J. Am. Chem. Soc. 95 (1973) 6640;
(d) H. Ojima, K. Nonoyama, Coord. Chem. Rev. 92 (1988) 85;
(e) A. Escuer, R. Vicente, J. Ribas, R. Costa, X. Solans, Inorg. Chem. 31 (1992) 2627.
[3] (a) H.O. Stumpf, L. Ouahab, Yu. Pei, P. Bergerat, O. Kahn, J. Am. Chem. Soc. 116 (1994) 3866;
(b) M. Ohba, N. Maruono, H. Okawa, T. Enoki, J. Latour, M. J. Am. Chem. Soc. 116 (1994) 11566;
(c) H. Miyasaka, N. Matsumoto, H. Okawa, N. Re, E. Gallo, C. Floriani, J. Am. Chem. Soc. 118 (1996) 981;
(d) M.l. Kahn, M. Verelst, P. Lecante, C. Mathonière, O. Kahn, Eur. J. Inorg. Chem. 527 (1999);
(e) O. Kahn, J. Larionova, J.V. Yakhmi, Chem. Eur. J. 5 (1999) 3443;
(f) M.L. Kahn, P. Lecante, M. Verelst, C. Mathonière, O. Kahn, Chem. Mater. 12 (2000) 3073;
(g) A. Fragoso, M.L. Kahn, A. Castineiras, J.P. Sutter, O. Kahn, R. Cao, Chem. Commun. 1547 (2000);
(h) S.Q. Zang, R.J. Tao, Q.L. Wang, N.H. Hu, Y.X. Cheng, J.Y. Niu, D.Z. Liao, Inorg. Chem 42 (2003) 761;
(i) R.J. Tao, S.Q. Zang, Q.L. Wang, N.H. Hu, Y.X. Cheng, J.Y. Niu, D.Z. Liao, Inorg. Chim. Acta 353 (2003) 325.
[4] H.Z. Kou, J.K. Tang, D.Z. Liao, S. Gao, P. Cheng, Z.H. Jiang, S.-P. Yan, G.L. Wang, C. Benoît, J.P. Tuchagues, Inorg. Chem. 40 (2001) 4839.
[5] H.Z. Kou, S. Gao, B.Q. Ma, D.Z. Liao, Chem. Commun. 713 (2000).
[6] H.Z. Kou, W.M. Bu, S. Gao, D.Z. Liao, Z.H. Jiang, S.P. Yan, Y.G. Fan, G.L. Wang, J. Chem. Soc., Dalton Trans. 2996 (2000).
[7] J. Larionova, S.A. Chavan, J.V. Yakhmi, F. Gulbrandsen, J. Sletten, C. Sourisseau, O. Kahn, Inorg. Chem. 36 (1997) 6374.
[8] M.G.F. Vaz, L.M.M. Pinheiro, H.O. Stumpf, A.F.C. Alcântara, S. Golhen, L. Ouahab, O. Cador, C. Mathonière, O. Kahn, Chem. Eur. J. 5 (1999) 1486.
[9] O. Kahn, J. Larionova, J.V. Yakhmi, Chem. Eur. J. 5 (1999) 3443.
[10] (a) Y. Journaux, O. Kahn, J. Zarembowitch, J. Galy, J. Jaud, J. Am. Chem. Soc. 105 (1983) 7585;
(b) O. Kahn, J. Galy, Y. Journaux, I. Moregenstern-Badarau, J. Am. Chem. Soc. 104 (1982) 2165;
(c) I. Moregenstern-Badarau, M. Rerat, O. Kahn, J. Jaud, J. Galy, J. Inorg. Chem. 21 (1982) 3050;
(d) M. Ohba, H. Tamaki, N. Matsumoto, H. Okawa, Inorg. Chem. 32 (1993) 5385.
[11] J.P. Costes, F. Dahan, B. Donnadieu, M.J.R. Douton, M.I.F. Garcia, A. Bousseksou, J.P. Tuchagues, Inorg. Chem. 43 (2004) 2736.
[12] S. Osa, Y. Sunatsuki, Y. Yamamoto, M. Nakamura, T. Shimamoto, N. Matsumoto, N. Re, Inorg. Chem. 42 (2003) 5507.
[13] T. Kido, Y. Ikuta, Y. Sunatsuki, Y. Ogawa, N. Matsumoto, Inorg. Chem. 42 (2003) 398.
[14] T. Kido, S. Nagasato, Y. Sunatsaki, N. Matsumoto, Chem. Commun. 2113 (2000).
[15] S. Osa, T. Kido, N. Matsumoto, N. Re, A. Pochaba, J. Mrozinski, J. Am. Chem. Soc. 126 (2004) 420.
[16] J.P. Costes, J.M. Clemente-Juan, F. Dahan, J. Milon, Inorg. Chem. 43 (2004) 8200.
[17] W.L. Liu, Z. Yang, C.S. Lu, C.L. Ni, D.B. Dang, Y.Z. Li, Q. Meng, J. Inorg. Chem. Comm. 7 (2004) 434.
[18] B.H. Ye, M.L. Tong, X.M. Chen, Coord. Chem. Rev. 249 (2005) 545.
[19] Y. Xu, L. Han, Z.Z. Lin, C.P. Liu, D.Q. Yuan, Y.F. Zhou, M.C. Hong, Eur. J. Inorg. Chem. 4457 (2004).
[20] C.A. Buehler, B.C. Bass, R.B. Darling, M.B. Lubs, J. Am. Chem. Soc. 62 (1940) 890.
[21] R.J. Tao, F.A. Li, S.Q. Zang, Y.X. Cheng, J.Y. Niu, Science in China 36 (1) (2006) 47.
[22] R.H. Blessing, Acta Crystallogr., Sect. A 51 (1995) 33.
[23] G.M. Sheldrick, SHELXTL, Version 5.1, Bruker Analytical X-ray Systems, Inc., Madison, WI, 1997.
[24] K. Nakamoto, Infrared and Raman Spectra of Inorganic, Coordination Compounds, fifth ed., Wiley, New York, 1997, Part B.
[25] C. Rancurel, D.B. Leznoff, J.P. Sutter, P. Guionneau, D. Chasseau, J. Kliava, O. Kohn, Inorg. Chem. 39 (2000) 1602.
[26] L.Y. Wang, B. Zhao, C.X. Zhang, D.Z. Liao, Z.H. Jiang, S.P. Yan, Inorg. Chem. 42 (2003) 5804.

reported to our best knowledge. In this article, we have obtained two heteroleptic cyclometallated Rh(III) complexes. Both the photophysical and electrochemical properties of the two complexes have been thoroughly examined to probe the bonding information of their coordination chemistry.

2. Experimental

2.1. Instrumentation

Recording of NMR, IR, mass and absorption spectra have been detailed elsewhere [13]. Low temperature (77 K) emission spectra were obtained with a SLM 8000™ spectrofluorometer (SLM Instrument, Inc.) compact with photo-multiplier tubes which were used as detectors. An Xe–Hg lamp was utilized as the excitation source. Emission photoselection measurements of these complexes under study were obtained with the same instrument as the emission spectra, augmented with two additional sheets of polarizer placed in both the paths of the exciting light and emitting light. The luminescence lifetime was determined by a LN 3000 nitrogen laser with 337.1 nm pulses triggered and integrated by a SRS Model SR250 Gated Integrator (Standford Research Systems, Inc.) and Boxcar Average Module. Cyclic voltammetry (CV) and normal pulse voltammetry (NPV) experiments were carried out using a BAS-100B electrochemical analyzer (Bioanalytical Systems, Inc.) equipped with a three-electrode cell system. All experiments were conducted out under a N_2 atmosphere. A Pt working electrode (BAS Model MF-2103, 1.6 mm dia.), a Pt wire auxiliary electrode and a saturated calomel reference electrode (SCE) were used for voltammetric measurements. The ferrocenium/ferrocence redox couple was used as an internal standard, $E_{1/2}$ ($Fc^{+/0}$) = 0.40 V versus SCE. An H-type cell with a porous glass frit was used for controlled potential electrolysis (CPE) experiments using a Pt plate for the working and auxiliary electrodes.

2.2. Reagents

$RhCl_3 \cdot 3H_2O$ (Merck), 2,2′-bipyridine, 2-benzoylpyridine and 1,10-phenanthroline (Aldrich) were used as received. K[Rh(phen)Cl_4] was prepared according to the published procedure [14]. Me_2SO (Uvasol, Merck) was dried for spectroscopy. Et_4NClO_4 (TEAP), used as a base electrolyte, was obtained from Showa Chemical Co. and further purified by three recrystallizations from distilled H_2O. Laboratory grade solvents were used unless otherwise specified.

2.3. Synthesis

2.3.1. *[Rh(Hbzpy)(bzpy)Cl$_2$]*

[Rh(Hbzpy)(bzpy)Cl_2] was prepared according to the published procedure [12]. The orange-yellow product was characterized by its ^{1}H NMR spectrum which was consistent with the literature data [12].

2.3.2. *cis-[Rh(bzpy)(bipy)Cl$_2$] · 0.5H$_2$O (**1**)*

An intimate mixture of [Rh(Hbzpy)(bzpy)Cl_2] (0.324 g, 0.60 mmol) and bipy (0.562 g, 3.6 mmol) was placed in a ceramic boat (10 cm and 1.3 cm in length and width, respectively) and heated in an oven at 160 °C for 15 h. After cooling, the resulting reaction mixture was stirred for 2 h with 40 ml of methanol and then filtered. The precipitate was washed repeatedly with methanol and then dried under vacuum. 0.118 g (38%) of yellow crystalline product (**1**) was obtained. IR (cm^{-1}): ν(C=O) 1674; ν(Rh–Cl) 343, 324. δ_H(dmso-d_6) 9.19 (1H, d, $J = 5.6$ Hz, $H_{b'6}$) (b′ = bipy), 8.82 (1H, d, $J = 8.4$ Hz, $H_{b'3}$), 8.79–8.69 (3H, m, $H_{b6} + H_{b'6'} + H_{b3}$) (b = bzpy), 8.34 (1H, t, $J = 7.6$ Hz, $H_{b'4}$), 8.31 (1H, t, $H_{b'4'}$), 8.25 (1H, t, $J = 7.6$ Hz, H_{b5}), 8.15 (1H, d, $J = 7.6$ Hz, $H_{b'3'}$), 7.95 (1H, d, $J = 8.0$ Hz, $H_{b6'}$), 7.89–7.85 (2H, m, $H_{b'5} + H_{b'5'}$), 7.68 (1H, t, $J = 6.8$ Hz, H_{b4}), 7.66 (1H, d, $J = 7.6$, 1.2 Hz, $H_{b3'}$), 7.41 (1H, td, $J = 7.6$, 1.6 Hz, $H_{b5'}$), 7.25 (1H, t, $J = 7.2$ Hz, $H_{b4'}$), δ(dmso-d_6) 187.39 (CO), 163.75, 163.50, 157.37, 157.14, 154.54, 154.31, 153.29, 148.68, 140.77, 140.31, 139.84, 139.53, 129.65, 127.08, 126.93, 126.82, 126.27, 125.09, 123.86, 123.56, 123.47. *Anal.* Calc. for $C_{22}H_{17}N_3O_{1.5}Cl_2Rh$: C, 50.70; H, 3.29; N, 8.06; Cl, 13.60. Found: C, 50.62; H, 3.38; N, 8.17; Cl, 13.72%.

2.3.3. *cis-[Rh(bzpy)(phen)Cl$_2$] · 0.5H$_2$O (**2**)*

An intimate mixture of K[Rh(phen)Cl_4] (0.464 g, 1.0 mmole) and Hbzpy (0.660 g, 3.6 mmole) was placed in a ceramic boat (10 and 1.3 cm in length and width, respectively) and heated in an oven at 210 °C for 15 h. After cooling, the resulting reaction mixture was stirred overnight with 50 ml of methanol/H_2O (1:1, v/v) solution and then filtered. The yellow-brown filtrate was evaporated to dryness, followed by washing with dichloromethane. A deep yellow-green precipitate was obtained and washed repeatedly with acetone. After drying under vacuum, 0.169 g (31%) of yellow-green crystalline product (**2**) was obtained. IR (cm^{-1}): ν(C=O) 1666; ν(Rh–Cl) 342, 325. δ_H(dmso-d_6) 9.97 (1H, d, $J = 5.6$ Hz, H_{b6}) (b = bzpy), 9.55 (1H, d, $J = 4.8$ Hz, H_{p2}) (p = phen), 9.00 (1H, d, $J = 8.0$ Hz, H_{p4}), 8.92 (1H, d, $J = 8.0$ Hz, H_{p5}), 8.44–8.29 (5H, m, $H_{b3} + H_{b4} + H_{p7} + H_{p8} + H_{p9}$), 8.16 (1H, dd, $J = 8.0$, 2.8 Hz, H_{p3}); 7.99–7.88 (2H, m, $H_{b5} + H_{p6}$), 7.67 (1H, d, $J = 7.6$ Hz, $H_{b6'}$), 6.94 (1H, t, $J = 7.2$ Hz, $H_{b5'}$), 6.67 (1H, t, $J = 7.2$ Hz, $H_{b4'}$), 5.86 (1H, d, $J = 8.0$ Hz, $H_{b3'}$), δ_C(dmso-d_6) 189.55 (CO), 156.44, 155.29, 154.99, 152.27, 151.13, 146.55, 140.30, 138.86, 138.76, 138.34, 137.91, 133.66, 130.90, 130.77, 129.21, 128.29, 127.86, 127.69, 126.93, 126.24, 126.13, 125.98, 124.02. *Anal.* Calc. for $C_{24}H_{17}N_3O_{1.5}Cl_2Rh$: C, 52.87; H, 3.14; N, 7.71; Cl, 13.01. Found: C, 52.76; H, 3.21; N, 7.84; Cl, 13.15%.

3. Results and discussion

3.1. Synthesis and assessment of structure

First [Rh(Hbzpy)(bzpy)Cl_2] was prepared according to published procedures [12] at this laboratory. Complex **1** was then prepared by heating the intimate mixture of [Rh(Hbzpy)(bzpy)Cl_2] and bipy in an oven at 160 °C for 15 h. Elimination of Hbzpy had been ascribed to the cleavage of the rather weak Rh–O bond, which led to a loss of stabilization due to the chelate effect [12]. Replacement of Hbzpy by phen under the same conditions, however, generated a mixture of at least two isomers, which we were unable to separate. The synthesis of complex **2** was accomplished by heating an intimate mixture of K[Rh(phen)Cl_4] and Hbzpy in an oven at 210 °C for 15 h. Attempts to get complex **1** by the latter procedure failed since a mixture of isomers was obtained again. The synthetic studies of the two different routes in connection with the stereochemistry of complexes **1** and **2** remain unknown to the authors to date.

The base peaks in the mass spectra of complexes **1** and **2** are *m*/*z* 512 and 536, corresponding to the molecular mass of *cis*-[Rh(bzpy)(bipy)Cl_2] and *cis*-[Rh(bzpy)(phen)Cl_2], respectively. The infrared spectra of the two complexes exhibit the ν(C=O) stretching bands in the vicinity of 1666 cm^{-1}. On the basis that the ν(C=O) stretching bands of complexes **1** and **2**, as well as the free Hbzpy ligand (ca. 1668 cm^{-1}), are almost the same, it is evident that the chelated bzpy ligand forms a six-member *N*,*C* metallacycle, not a five-member *N*,*O* metallacycle. The stereochemistry of the $RhCl_2$ moiety in these complexes has been determined by IR data. Both complexes show two ν(Rh–Cl) bands near 342 and 324 cm^{-1}, indicating that the two chlorides are *cis* to each other [15].

The proton peaks in the ^{1}H NMR spectrum of each complex show sixteen chemically different protons. From the ^{13}C spectra, complexes **1** and **2** exhibit 22 and 24 carbons, respectively. In addition, the ^{13}C DEPT of complexes **1** and **2** exhibit six and eight non-protonated carbon peaks, respectively. As a further confirmation of the double bond character of the C=O bond in the N,O ligands, δ_{CO} falls close to 200 ppm [8]. On the basis that δ_{CO} of complexes **1** and **2** relative to free Hbzpy ($\delta_{CO} = 193.5$ ppm) are almost the same, the NMR data are inconsistent with *N*,*O*-coordination of 2-benzoylpyridine. Due to the IR and NMR data, complexes **1** and **2** are consistent with the *N*,*C*-coordination of 2-benzoylpyridine. There are two possible isomers for [Rh(bzpy)(NN)Cl_2] (NN = bipy or phen) deduced from the hetero-bischelated complexes as displayed below.

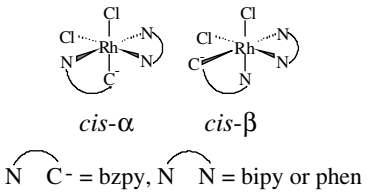

In the *cis*-α conformation, $H_{b3'}$ of the phenyl moiety of the bzpy ligand is located above (or below) the pyridine of the bipy/phen ligand (see Fig. 1). For complex **1**, the resonance position of $H_{b3'}$, $\delta = 7.66$, is somewhat deshielded compared to that of $H_{b4'}$, $\delta = 7.25$, as presented in Section 2. This is therefore inconsistent with the NMR chemical shift data since this hydrogen would indeed be more shielded due to the π-electron ring current of pyridine. In the *cis*-β isomer, however, H_{b6} of the pyridyl moiety of the bzpy ligand is located below the plane of the pyridine of the bipy/phen ligand, which exhibit significant upfield shifts as expected due to the shielding effect of the ring current. For complex **1**, the resonance position of H_{b6}, $\delta = 8.79$, is more shielded compared to $H_{b'6}$ in the plane of the pyridine of the bipy ligand, $\delta = 9.19$, as expected by the shielding effect of the ring current. Therefore, the NMR chemical shift data of complex **1** are consistent with

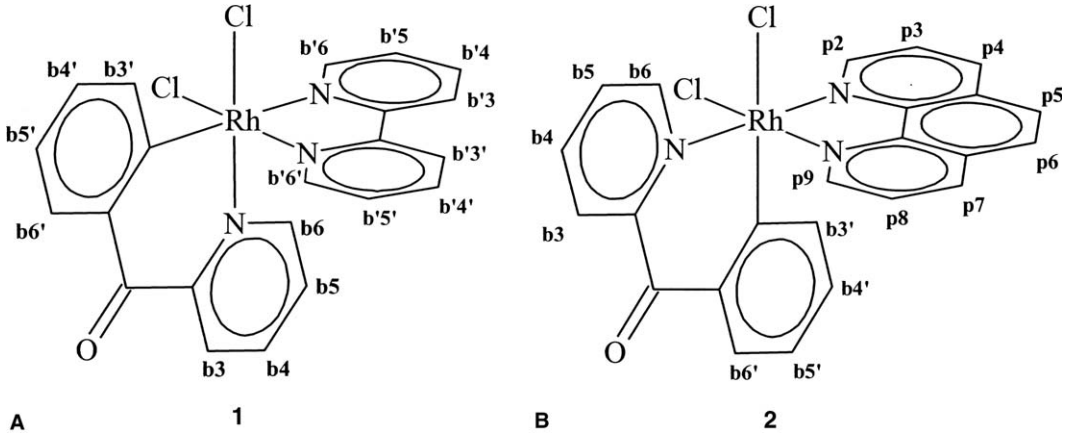

Fig. 1. The proposed structures of *cis*-[Rh(bzpy)LCl_2]: (A) *cis* β-[Rh(bzpy)(bipy)Cl_2] (**1**); (B) *cis* α-[Rh(bzpy)(phen)Cl_2] (**2**).

the *cis*-β structure as illustrated in Fig. 1. The conformer of complex **1** is further evidenced by the NOESY experiment, available in the supplementary material. $H_{b'6}$ (b′ = bipy) is spatially correlated with H_{b6} of pyridine in bzpy as demonstrated in the same figure.

For complex **2**, the chemical shift of $H_{b3'}$, $\delta = 5.86$, more upfield than that of $H_{b6'}$, $\delta = 7.67$, is due to the anisotropic effect resulting from the inductive ring current of the pyridyl ring. $H_{b3'}$ is located just above (or below) the pyridine of the phen ligand, and hence corresponds to the relative location of protons in space for the *cis*-α structure as illustrated in Fig. 1. The appearance of the chemical shift of $H_{b'6}$ for complex **1**, $\delta = 9.19$, more upfield than that of H_{p2} for complex **2**, $\delta = 9.55$, is due to the π-donor ability of the metallated phenyl ring, which is located *trans* to $H_{b'6}$, as demonstrated in the same figure.

Further assignments of the ^{1}H NMR spectra for complexes **1** and **2** have been done through ^{1}H COSY NMR experiments, available in the supplementary material.

3.2. Absorption spectra

The free Hbzpy ligand exhibits one intense ($\varepsilon \sim 10^4\ cm^{-1}\ M^{-1}$) absorption at about $3.78 \times 10^4\ cm^{-1}$, arising from the spin-allowed π–π* transition. The weaker ($\varepsilon \sim 10^2\ cm^{-1}\ M^{-1}$) absorption band observed at about $2.84 \times 10^4\ cm^{-1}$ is assigned as the carbonyl n–π* transition on the basis that the energy of this absorption peak exhibits a hypsochromic shift when the solvent polarity is increased [7]. The room temperature absorption spectra for complexes **1** and **2** are presented in Fig. 2A. Both shows an intense ($\varepsilon \sim 10^4\ cm^{-1}\ M^{-1}$) absorption in the 3.1–$3.9 \times 10^4\ cm^{-1}$ region which most likely arise from a spin-allowed π–π* absorption of the coordinated ligands [7,16]. Each complex also exhibits an intermediate ($\varepsilon \sim 10^3\ cm^{-1}\ M^{-1}$) absorption in the 3.0–$2.7 \times 10^4\ cm^{-1}$ region. According to the absorption spectra of the related free ligands [7,16] and *cis*-$[Rh(dpk)_2Cl_2]^+$ (dpk = di-2-pyridyl ketone) [17], this absorption can be assigned as a carbonyl n–π* band [18], which was not observed for *cis*-$[Rh(bipy)_2Cl_2]^+$ and *cis*-$[Rh(phen)_2Cl_2]^+$ [19]. It is noted that the absorption band profile extended to lower energy (below $2.6 \times 10^4\ cm^{-1}$), which was not observed for the related ligands either. This might be the tail of the carbonyl n–π* band in combination with a rather weak dd* absorption.

The excitation polarization spectrum of complex **1** is shown in Fig. 2B. The excitation polarization spectrum of complex **2** is very similar to that of complex **1**. The symmetry of each complex is lower than C_{2V} and hence only a singly symmetric species is considered in the analysis of the electronic spectrum. In other words, the polarization limits pertaining to planar oscillators will not be pertinent here. The calculated limits are 0.5 and −0.33 [20], resulting from the combination of a linear absorption and a linear emission oscillator. The polarizations in the π–π* region of the two complexes are quite similar, showing little structure having minima (−10% for complex **1**; −14% for complex **2**) in the polarization spectra. These data also reveal that the absorption and emission are both linear oscillators [20]. Deviation of the polarization from −0.33 may be explained by the existence of other states having similar energies in the region [21].

The slightly structured shape and increased value for the excitation polarization spectrum in the $3.3–2.5 \times 10^4\ cm^{-1}$ region suggest that there may be more than one absorption mode involved in this region, consistent with the carbonyl n–π* transitions assignment. The polarization spectra increase sharply to about 0.20 in the lowest energy wavelength region (below $25 \times 10^4\ cm^{-1}$) for both complexes. The magnitude that approaches the limit value 0.5 is expected for a linear absorber-linear emitter case [20]. Therefore, involvement other transitions is implied and one could reasonably conclude that the dd* absorption is buried in this low-energy region. Therefore, the carbonyl n–π* transition must be involved and in which all spin-forbidden dd* transitions were likely buried, similar to that of *cis*-$[Rh(dpk)_2Cl_2]^+$ [17].

3.3. Luminescence properties

Hbzpy shows a structural emission with a single vibrational progression of $1650\ cm^{-1}$, assigned as an n–π* transition [22]. The emission spectra recorded in ethanol/

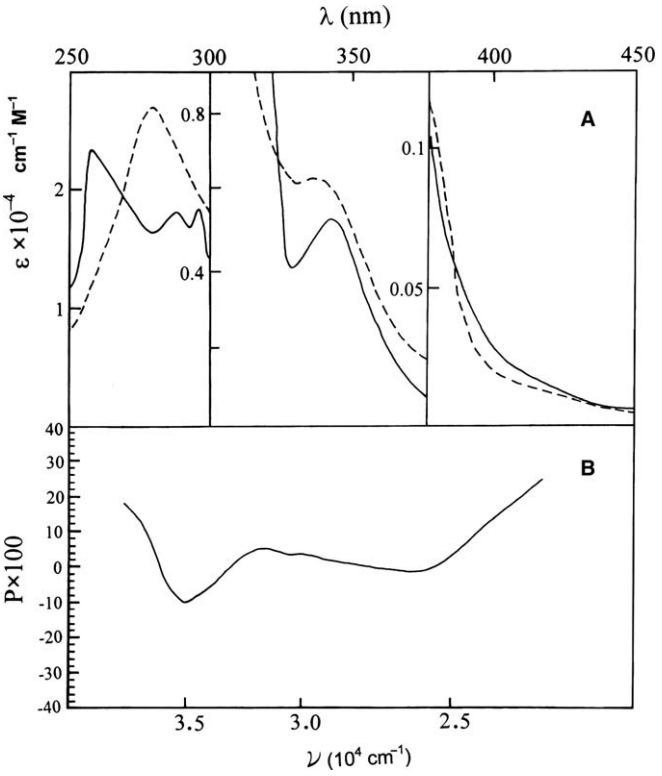

Fig. 2. Absorption and excitation polarization spectra: (A) absorption spectra (room temperature): *cis* β-$[Rh(bzpy)(bipy)Cl_2]$ (**1**) (——); *cis* α-$[Rh(bzpy)(phen)Cl_2]$ (**2**) (– –). (B) excitation polarization spectrum of *cis* β-$[Rh(bzpy)(bipy)Cl_2]$ (**1**) (77 K, 689 nm emission).

methanol (9:1, v/v) at 77 K of complexes **1** and **2** are presented in Fig. 3. No emission behavior is observed at room temperature. Contained in Table 1 are the luminescent data of these complexes. The red emissions ($1.2–1.7 \times 10^4$ cm^{-1}) recorded for complexes **1** and **2** are broad (with around 2.2×10^3 cm^{-1} in half-width) and both are symmetric and structureless, as seen in Fig. 3. The lifetimes measured at the emission maximum are respectively 58 and 60 μs for complexes **1** and **2** (see Table 1). The energy of the emission peak is unaffected by changing the solvent from ethanol/methanol to DMSO. In comparison with the band shape, lifetime and peak position studies performed on the cyclometallated Rh(III) complexes [3], the emission types of complexes **1** and **2** have excluded the possibilities of ^{3}MLCT, ^{3}SBLCT or $^3\pi\pi^*$ emissions and hence are classified as a dd* phosphorescence [17,23].

The emission polarization spectra of both complexes, excited at 313 and 365 nm, are flat with a vanished slope. This observation indicates that the combination of absorber and emitter(s) gives the same polarization across the emission band. Therefore, it is reasonable to conclude that there is no other emission buried in the observed emission band. In other words, both complexes show a band of single emissions rather than multiple ones.

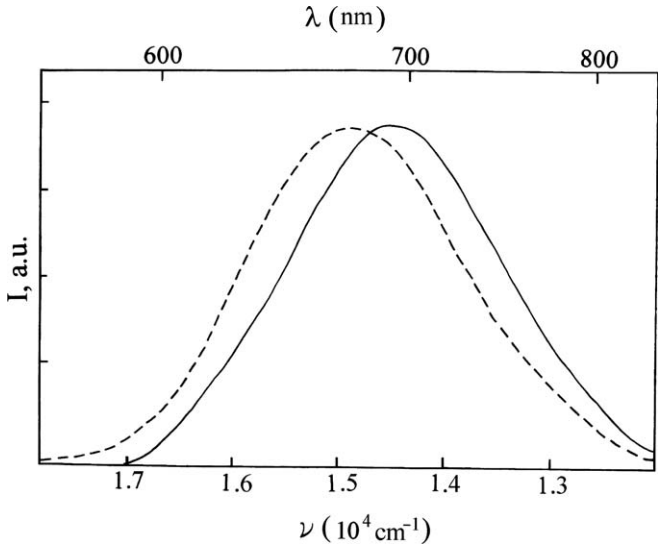

Fig. 3. Emission spectra of *cis* β-[Rh(bzpy)(bipy)Cl_2] (**1**) (——) and *cis* α-[Rh(bzpy)(phen)Cl_2] (**2**) (––) (77 K, 313 nm excitation).

Table 1
Phosphorescence data and lifetime (τ) for Rh(III) complexes at 77 K

Complex	Phosphorescence[a]	
	ν_{max} ($\times 10^4$ cm^{-1})	τ_p (μs)
1	1.45	58
2	1.49	60
cis-[Rh(bipy)$_2$$Cl_2$]$^+$	1.42[b]	47[b]
cis-[Rh(phen)$_2$$Cl_2$]$^+$	1.41[b]	41[b]

[a] In EtOH/MeOH (9:1).
[b] Ref. [16].

No emission could be detected from [Rh(Hbzpy)(bzpy)Cl_2] [12], but emission could be obtained from *cis*-[Rh(bzpy)(NN)Cl_2] (NN = bipy/phen). On one hand, it might be possible that the emission is occurring but is beyond the detection limits of our equipment [24]. On the other hand, it is possible that the phenyl ring of chelated Hbzpy can undergo rotation and then facilitate the non-radiative energy loss in this complex [25]. The bipyridyl-like ligands are more rigid than the *N*,*O*-coordinated Hbzpy ligand. When the N,O ligand (Hbzpy) is substituted by bipy/phen (a more rigid ligand), the emission could be observed. The latter reason at least is therefore supported by our results.

The metallated phenyl ring of bzpy is a weaker π-acceptor and a stronger-donor compared to bipy or phen. A strong-donor can move the metal d*(e_g) orbitals to a higher energy, but a strong π-acceptor can lead to the lowering of the metal d(t_{2g}) orbitals. Therefore, the dd* emission of complexes **1** and **2** were observed at a higher energy than that of *cis*-[Rh(bipy)$_2$$Cl_2$]$^+$ and *cis*-[Rh(phen)$_2$$Cl_2$]$^+$ (see Table 1) [16]. It is examined that the degree of raising of the metal d*(e_g) orbitals for complexes **1** and **2** is more than the degree of lowering of the metal d(t_{2g}) orbitals for *cis*-[Rh(bipy)$_2$$Cl_2$]$^+$ and *cis*-[Rh(phen)$_2$$Cl_2$]$^+$, which results in the higher energy gap of the ^{3}d–d* excited state for complexes **1** and **2**. In other word, bzpy exhibits a higher ligand field strength compared with that of bipy or phen.

3.4. Electrochemical properties

Electrochemical studies were conducted in 0.10 M TEAP/DMSO solutions containing the corresponding Rh(III) complexes. Cyclic voltammetric data such as the peak potentials are collected in Table 2. No oxidation wave was observed when the potential was scanned from 0.0 to +2.0 V.

3.4.1. Electrochemistry of complexes *1* and *2*

The cyclic voltammograms of complexes **1** and **2** have similar patterns, showing two reduction waves, c_I and c_{II} (see Table 2), and no corresponding oxidation wave appeared upon scan reversal with respect to c_I. The number

Table 2
Cyclic voltammetric reduction potentials for Rh(III) complexes[a]

Complex	ν (V/s)	$(E_{pc})_I$	$(E_{pc})_{II}$
1	0.1	−1.19	−1.64
	2.0	−1.24	−1.67
2	0.1	−1.16	−1.65
	2.0	−1.22	−1.69
cis-[Rh(bipy)$_2$$Cl_2$]$^+$	0.1	−0.84[b]	−1.46[b]
cis-[Rh(phen)$_2$$Cl_2$]$^+$	0.1	−0.85[c]	−1.46[c]

[a] Results for 1.2 mM samples in 0.10 M TEAP/DMSO solutions at a Pt electrode. E_{pc} in V vs. SCE.
[b] Ref. [31].
[c] Ref. [32].

of electrons transferred at the wave c_I, estimated from controlled-potential electrolysis experiments at −1.20 and −1.15 V $(E_{pc})_I$, were found to be 1.80 and 1.85 for complexes **1** and **2**, respectively, indicating that wave c_I for both complexes involved essentially a two-electron charge transfer process. An oxidation wave due to oxidation of the chloride ion was also observed at 1.07 V in the voltammograms obtained for the solutions after the electrolysis. For each complex, the ratio of the peak current of the chloride ion to that of wave c_I is close to one, indicating that two chlorides had been eliminated from the complex after electrolysis at wave c_I. It has also been reported that electrochemical reduction of halide-coordinated complexes will generate products via dissociation of halide(s) [26–30]. As stated earlier, the emission of the two complexes is confirmed to be a dd* transition. The two-electron transfer reduction (wave c_I) results in higher electron density on the metal and, hence, destabilizes these complexes. This can rationalize the transfer of two electrons, in which the chemical reaction involves the loss of two chloride ions, and lead to the irreversible process at wave c_I.

The more negative values of $(E_{pc})_I$ obtained for complexes **1** and **2** compared to those reported for *cis*-$[Rh(bipy)_2Cl_2]^+$ and *cis*-$[Rh(phen)_2Cl_2]^+$, as shown in Table 2, may be ascribed to the higher electron densities on the metal. This is well understood based on the nature of the negatively charged bzpy ligand, which is a better σ-donor but a poorer π-acceptor (vide supra). On the whole, reductions of the neutral species are more demanding than those for the cationic complexes.

Normal pulse voltammograms (NPV) were also recorded for the two complexes. Similar to the cyclic voltammograms, the NPV also exhibited reduction waves c_I and c_{II} for each complex. It was found that the ratio of the limiting current of waves c_I and c_{II} is 2:1. Furthermore, the ratio of the peak current of wave c_I to that of wave c_{II} is also close to two at relatively high scan rates. Because wave c_I is a two-electron charge transfer process, this result suggests that wave c_{II} is possibly a one-electron charge transfer process. When phenol was added into the solutions as the proton donor, no significant changes were observed for wave c_I in the cyclic voltammograms of the complexes, suggesting that wave c_I is due to the reduction at the metal-localized orbitals. On the other hand, the addition of phenol resulted in an evident potential shift and peak current increased for wave c_{II}. Based on the influence of phenol, the reduction at wave c_{II} can be assigned to be localized at the carbonyl π* orbital of bzpy. The same result was observed for the pik-coordinated or dpk-coordinated complexes of rhodium(III) [13,17].

4. Conclusions

In this study, two heteroleptic cyclometallated Rh(III) complexes, *cis*-$[Rh(bzpy)(bipy)Cl_2]$ (**1**) and *cis*-$[Rh(bzpy)(phen)Cl_2]$ (**2**), have been synthesized and characterized. The anionic bzpy ligand is *N*,*C* coordinated to Rh(III) based on IR and NMR data. Through analysis of NMR chemical shifts, structures of complexes **1** and **2** are consistent with *cis*-β and *cis*-α conformers, respectively. Each complex shows high intensity bands in the UV region, assigned as spin-allowed π–π* transitions. The medium-intensity absorption band profile in the lower energy region can be explained by convolution of carbonyl n–π* and d–d* transitions. At 77 K, each complex shows a broad, symmetric and structureless red emission with microsecond lifetime, assigned as dd* phosphorescence. The electrochemical data also provide evidence in support of the assigned dd* emissions of the two complexes. The first two-electron reduction process occurs at the metal and is coupled with the elimination of two chlorides. Through examination of the influence of phenol on the reduction potentials, the redox orbital involved in the second reduction is assigned as the π* orbital localized at the carbonyl fragment of bzpy.

5. Supplementary material

2D NMR for complexes **1** and **2** are available from the author on request. Copies of the data can be obtained free of charge on application to The Director, CCDC, 12 Union Road, Cambridge CB2 1EZ, UK, fax: +44 1223 336033, e-mail: deposit@ccdc.cam.ac.uk or http:www.ccdc.cam.ac.uk.

Acknowledgement

Financial support from the National Science Council of the Republic of China is acknowledged.

References

[1] (a) S. Sprouse, K.A. King, P.J. Spellane, R.J. Watts, J. Am. Chem. Soc. 106 (1984) 6647;
(b) K.A. King, P.J. Spellane, R.J. Watts, J. Am. Chem. Soc. 107 (1985) 1431;
(c) M.G. Colombo, T.C. Brunold, T. Riedener, H.U. Güdel, M. Förtsch, H.-B. Bürgi, Inorg. Chem. 33 (1994) 545.
[2] (a) P. Didier, I. Ortmans, A.K.-D. Mesmaeker, R.J. Watts, Inorg. Chem. 32 (1993) 5239;
(b) I. Ortmans, P. Didier, A.K.-D. Mesmaeker, Inorg. Chem. 34 (1995) 3695;
(c) G. Calogero, G. Giuffrida, S. Serroni, V. Ricevuto, S. Campagna, Inorg. Chem. 34 (1995) 541;
(d) F. Neve, A. Crispini, S. Campagna, S. Serroni, Inorg. Chem. 38 (1999) 2250;
(e) K.K.-W. Lo, C.-K. Chung, T.K.-M. Lee, L.-H. Lui, K.H.-K. Tsang, N. Zhu, Inorg. Chem. 42 (2003) 6886.
[3] (a) M. Maestri, D. Sandrini, V. Balzani, U. Maeder, A.V. Zelewsky, Inorg. Chem. 26 (1987) 1323;
(b) D. Sandrini, M. Maestri, V. Balzani, U. Maeder, A.V. Zelewsky, Inorg. Chem. 27 (1988) 2640.
[4] (a) D. Kovala-Demertzi, A. Michaelides, A. Aubry, Inorg. Chim. Acta 194 (1992) 189;
(b) C. Pettinari, F. Accorroni, A. Cingolani, F. Marchetti, A. Cassetta, L. Barba, J. Organomet. Chem. 566 (1998) 187.
[5] I.S. Ahuja, C.L. Yadava, Indian J. Chem., Sect. A 27 (1988) 169.

[6] (a) D. Rehder, K. Ihmels, Inorg. Chim. Acta 76 (1983) L313;
(b) M.A.M. Abu-Youssef, A. Escuer, D. Gatteschi, M.A.S. Goher, F.A. Mautner, R. Vicente, Inorg. Chem. 38 (1999) 5716.
[7] M. Plytzanopoulos, G. Pneumatikakis, N. Hadjiliadis, D. Katakis, J. Inorg. Nucl. Chem. 39 (1977) 965.
[8] (a) M.A.S. Goher, T.C.W. Mak, Inorg. Chim. Acta 99 (1985) 223;
(b) T.C.W. Mak, M.A.S. Goher, Inorg. Chim. Acta 115 (1986) 17;
(c) M.A.S. Goher, R.-J. Wang, T.C.W. Mak, J. Crystallogr. Spectrosc. Res. 20 (1990) 265;
(d) F.A. Mautner, M.A.S. Goher, A.E.H. Abdou, Polyhedron 12 (1993) 2815;
(e) M.A.S. Goher, A.E.H. Abdou, W.-H. Yip, T.C.W. Mak, Polyhedron 12 (1993) 2981;
(f) G. Bellachioma, G. Cardaci, V. Gramlich, A. Macchioni, M. Valentini, C. Zuccaccia, Organometallics 17 (1998) 5025;
(g) C. Sudbrake, H. Vahrenkamp, Inorg. Chim. Acta 318 (2001) 23;
(h) D.L. Reger, J.R. Gardinier, M.D. Smith, P.J. Pellechia, Inorg. Chem. 42 (2003) 482;
(i) C.J. Milios, T.C. Stamatatos, P. Kyritsis, A. Terzis, C.P. Raptopoulou, R. Vicente, A. Escuer, S.P. Perlepes, Eur. J. Inorg. Chem. (2004) 2885.
[9] P.J. Steel, G.B. Caygill, J. Organomet. Chem. 327 (1987) 101.
[10] (a) Y. Fuchita, K. Hiraki, Y. Kage, Bull. Chem. Soc. Jpn. 55 (1982) 955;
(b) I. Aiello, A. Crispini, M. Ghedini, M.L. Deda, F. Barigelletti, Inorg. Chim. Acta 308 (2000) 121.
[11] Y. Fuchita, H. Ieda, Y. Tsunemune, J. Kinoshita-Nagaoka, H. Kawano, J. Chem. Soc., Dalton Trans. (1998) 791.
[12] D.J. de Geest, P.J. Steel, Aust. J. Chem. 48 (1995) 1573.
[13] (a) J.R. Lee, Y.R. Liou, W.L. Huang, Inorg. Chim. Acta 319 (2001) 83;
(b) J.R. Lee, H.Y. Huang, W.L. Huang, Inorg. Chim. Acta 323 (2001) 105.
[14] J.R. Lee, J.W. Luang, W.L. Huang, J. Chin. Chem. Soc. 50 (2003) 227.
[15] (a) R.D. Gillard, B.T. Heaton, J. Chem. Soc. A (1969) 451;
(b) N. Kazuo, Infrared and Raman Spectra of Inorganic and Coordination Compounds, 3rd ed., Wiley, New York, 1978, pp. 317–324.
[16] M.K. DeArmond, J.E. Hillis, J. Chem. Phys. 54 (1971) 2247.
[17] W.L. Huang, J.R. Lee, S.Y. Shi, C.Y. Tsai, Transition Met. Chem. 28 (2003) 381.
[18] J.D. Ortego, M.J. Seymour, Polyhedron 1 (1982) 21.
[19] (a) E.D. McKenzie, R.A. Plowman, J. Inorg. Nucl. Chem. 32 (1970) 199;
(b) M. Nishizawa, T.M. Suzuki, S. Sprouse, R.J. Watts, P.C. Ford, Inorg. Chem. 23 (1984) 1837.
[20] M.K. DeArmond, W.L. Huang, C.M. Carlin, Inorg. Chem. 18 (1979) 3388.
[21] T. Ohno, S. Kato, Bull. Chem. Soc. Jpn. 47 (1974) 2953.
[22] (a) G. Favaro, J. Chem. Soc. Perkin II (1976) 869;
(b) K.J. Latas, R.K. Power, A.M. Nishimura, Chem. Phys. Lett. 65 (1979) 272.
[23] W.L. Huang, D.P. Segers, M.K. DeArmond, J. Phys. Chem. 85 (1981) 2080.
[24] R.A. Krause, K. Krause, Inorg. Chem. 19 (1980) 2600.
[25] R.A. Krause, K. Krause, Inorg. Chem. 23 (1984) 2195.
[26] U. Kolle, M. Grutzel, Angew. Chem., Int. Ed. Engl. 26 (1987) 567.
[27] P.R. Sharp, K.G. Frank, Inorg. Chem. 24 (1985) 1808.
[28] J.R. Bradbury, F.A. Schultz, Inorg. Chem. 25 (1986) 4408.
[29] M. Ladwig, W. Kaim, J. Organomet. Chem. 419 (1991) 233.
[30] W. Bruns, W. Kaim, M. Ladwig, B. Olbrich-Deussner, T. Roth, B. Schwederski, in: A.J.L. Pombeiro, J.A. McCleverty (Eds.), Molecular Electrochemistry of Inorganic, Bioinorganic and Organometallic Compounds, Kluwer Academic Publishers, 1993, p. 255.
[31] G. Kew, K. DeArmond, K. Hanck, J. Phys. Chem. 78 (1974) 727.
[32] G. Kew, K. Hanck, M.K. DeArmond, J. Phys. Chem. 79 (1975) 1828.

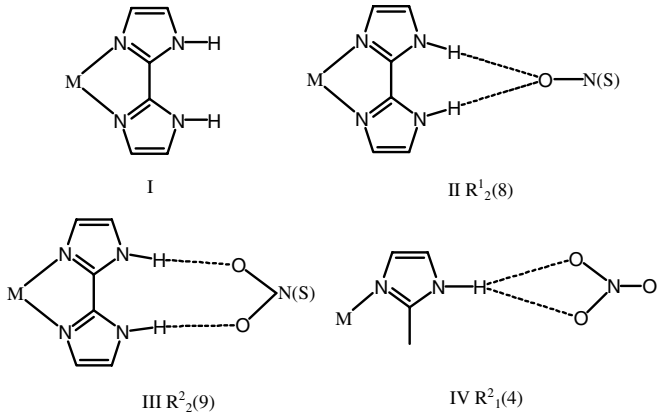

Scheme 1. Three supramolecular synthons (II–IV) formed by M(H_2biim) (I) and SO_4^{2-}(NO_3^-).

elemental analyzer. IR spectra were recorded on a Magna 750 FT-IR spectrometer photometer as KBr pellets in the 4000–400 cm^{-1}. Fluorescent spectra were measured with a PE LS55 fluorescent analytical instrument.

2.1. Synthesis of $[Zn(H_2biim)_3]SO_4$ (1)

A mixture of $ZnSO_4 \cdot 7H_2O$ (0.144 g, 0.5 mmol) and H_2biim (0.134 g, 1 mmol) in H_2O (16 ml) was heated at 160 °C for three days under autogenous pressure. Colorless single crystals were isolated after the reaction solution was cooled gradually. Yield: 35%. *Anal*. Calc. for $C_{18}H_{18}N_{12}O_4SZn$: C, 38.34; H, 3.22; N, 29.81. Found: C, 38.39; H, 3.28; N, 29.61%. IR (KBr; cm^{-1}): 3450m, 3153m, 3123m, 3069m, 3001m, 2900m, 2815m, 2782m, 2739m, 2686m, 2651m, 1630w, 1544m, 1426m, 1406w, 1384w, 1331w, 1312w, 1148s, 1131s, 1115s, 1106s, 1050s, 988s, 891w, 773m, 759s, 691s, 624m, 617m.

2.2. Synthesis of $[Cu(H_2biim)_2(H_2O)]SO_4 \cdot 3H_2O$ (2)

A mixture of $CuSO_4 \cdot 5H_2O$ (0.063 g, 0.25 mmol) and H_2biim (0.067 g, 0.5 mmol) in H_2O (16 ml) was heated at 160 °C for about five days under autogenous pressure. The resulting mixture was filtered off after the reaction solution was cooled down gradually. The filtrate was left in air to evaporate the solvent, and crystals were obtained after one week. The product was collected by filtration, washed with ethanol and dried in air. Yield: 34%. *Anal*. Calc. for $C_{12}H_{20}CuN_8O_8S$: C, 25.56; H, 3.58; N, 19.88. Found: C, 25.73; H, 3.65; N, 19.99%. IR (KBr; cm^{-1}): 3436m, 3121m, 2994m, 2916m, 1628w, 1524s, 1429m, 1384w, 1324m, 1179s, 1134s, 1107s, 1002w, 851w, 802w, 758m, 681m, 617m.

2.3. Synthesis of $[Cd(H_2biim)_2(NO_3)(H_2O)]_4(NO_3)_4$ (3)

A suspension of H_2biim (0.143 g, 1 mmol) in water (20 ml) was added slowly to $Cd(NO_3)_2 \cdot 4H_2O$ (0.308 g, 1 mmol) dissolved in water (20 ml), with stirring. The mixture was stirred at 80 °C for 30 min. The resulting solution was filtered. The filtrate was left in air to evaporate and crystals were obtained after a few days. Colorless crystals were collected by filtration, washed with water and dried under vacuum. Yield: 42%. *Anal*. Calc. for $C_{48}H_{56}Cd_4N_{40}O_{28}$: C, 27.57; H, 2.70; N, 26.80. Found: C, 27.59; H, 2.81; N, 26.77%. IR (KBr; cm^{-1}): 3245m, 3204m, 3144m, 3122m, 3076m, 3001m, 2898m, 2807m, 1632w, 1547m, 1524m, 1384s, 1218w, 1172w, 1105s, 1094s, 988w, 940m, 888w, 832w, 762m, 748m, 689w, 669m.

2.4. Synthesis of $[Zn(H_2biim)_2(H_2O)](NO_3)_2$ (4)

A suspension of H_2biim (0.268 g, 2 mmol) in water (30 ml) was added slowly to $Zn(NO_3)_2 \cdot 6H_2O$ (0.297 g, 1 mmol) dissolved in water (20 ml), with stirring. The mixture was stirred at 353 K for 30 min. The resulting solution was filtered. The filtrate was left in air to evaporate and crystals were obtained after a few days. Colorless crystals were collected by filtration, washed with water and dried under vacuum. Yield: 75%. *Anal*. Calc. for $C_{12}H_{14}N_{10}O_7Zn$: C, 30.30; H, 2.97; N, 29.45. Found: C, 30.45; H, 3.05; N, 29.40%. IR (KBr; cm^{-1}): 3251m, 3153s, 3128s, 3048m, 3005m, 2936w, 2767w, 1646w, 1624w, 1529s, 1513w, 1426m, 1384s, 1312s, 1176s, 1130s, 1105s, 1048w, 997w, 936w, 833w, 769s, 753s, 716w, 683s.

2.5. X-ray single-crystal determination

Suitable single crystals of complexes **1**–**4** were mounted on a Siemens Smart CCD diffractometer equipped with graphite-monochromated Mo Kα radiation ($\lambda = 0.71073$ Å) at 298 K. All absorption corrections were performed using the SADABS program. All structures were solved by direct methods and refined by full-matrix least-squares fitting on F^2 by SHELXTL-97 [6]. All non-hydrogen atoms were refined with anisotropic thermal parameters. Hydrogen atoms were located at geometrically calculated positions and treated by a mixture of independent and constrained refinement. Crystallographic data and structural refinements for compounds **1**–**4** are summarized in Table 1. Selected bond distances and angles are listed in Table 2.

3. Results and discussions

3.1. $[Zn(H_2biim)_3]SO_4$ (1)

The asymmetric unit of **1** consists of half of $[Zn(H_2biim)_3]^{2+}$ and SO_4^{2-}. The structure of the cation is shown in Fig. 1. It has crystallographic C_2 symmetry with the twofold rotation axis going through Zn^{2+} and the middle of the C8–C8′ bond. The coordination geometry of the zinc(II) center can be described as a distorted $[ZnN_6]$ octahedron with the six nitrogen atoms from the chelating H_2biim ligands. A comparable example is $[Zn(H_2biim)_2]_2$-(μ-H_2biim) [8] reported by Krebs et al. wherein Zn^{2+} is

Table 1
Crystallographic data for compounds **1**–**4**

	1	**2**	**3**	**4**
Formula	$C_{18}H_{18}N_{12}O_4SZn$	$C_{12}H_{20}CuN_8O_8S$	$C_{48}H_{56}Cd_4N_{40}O_{28}$	$C_{12}H_{14}N_{10}O_7Zn$
M	563.87	499.96	2090.93	475.70
Crystal system	tetragonal	orthorhombic	triclinic	monoclinic
Space group	$I4_1$	$Fdd2$	$P\bar{1}$	$C2/c$
a (Å)	12.8314(10)	24.8426(16)	8.938(3)	19.868(2)
B (Å)	12.8314(10)	25.7409(12)	13.814(4)	6.8617(8)
c (Å)	14.2702(15)	11.9597(5)	14.907(4)	14.2880(16)
α (°)	90	90	79.568(6)	90
β (°)	90	90	87.096(7)	114.227(2)
γ (°)	90	90	89.161(7)	90
V (Å^3)	2349.5(4)	7647.9(7)	1807.7(10)	1776.3(3)
Z	4	16	1	4
D_{calc} (g/cm$_3$)	1.594	1.737	1.921	1.779
μ (cm^{-1})	1.188	1.314	1.272	2.775
$F(000)$	1152	4112	1040	1128
Crystal size	$0.22\times0.12\times0.08$	$0.40\times0.35\times0.20$	$0.20\times0.15\times0.15$	$0.34\times0.14\times0.06$
Data/restraint/parameters	1368/1/164	4038/1/271	10725/3/1076	1473/0/137
Reflections collected	4972	14464	14037	2579
Independent reflections	1368	4038	10725	1404
Goodness-of-fit	1.032	1.087	1.066	1.268
$R_1[I>2\sigma(I)]$	0.0773	0.0246	0.0434	0.0466
$wR_2[I>2\sigma(I)]$	0.1431	0.0618	0.0969	0.1088
R_1 (all data)	0.1247	0.0250	0.0464	0.0617
wR_2 (all data)	0.1630	0.0620	0.1000	0.1165
Residuals (e Å^{-3})	0.274, −0.288	0.459, −0.321	2.732, −0.882	0.079, −0.088

Table 2
Selected bond lengths (Å) and angles (°) for **1**–**4**

Complex ***1***					
Zn–N(1)	2.16(1)	Zn–N(3)	2.22(1)	Zn–N(5)	2.20(1)
N(1)#1–Zn–N(1)	97.9(6)	N(1)#1–Zn–N(5)	160.5(4)	N(5)–Zn–N(3)#1	87.6(4)
N(1)–Zn–N(5)	94.9(4)	N(5)–Zn–N(5)#1	76.9(6)	N(3)–Zn–N(3)#1	166.8(6)
N(1)#1–Zn–N(3)	94.3(5)	N(1)–Zn–N(3)	76.9(4)	N(5)–Zn–N(3)	102.9(5)
Complex ***2***					
Cu–N(5)	2.006(2)	Cu–N(1)	2.009(2)	Cu–O(1)	2.198(1)
Cu–N(3)	2.014(2)	Cu–N(7)	2.015(2)	N(7)–Cu–O(1)	91.78(7)
N(5)–Cu–N(1)	95.98(9)	N(5)–Cu–N(3)	152.37(7)	N(5)–Cu–O(1)	103.11(8)
N(1)–Cu–N(3)	82.32(8)	N(5)–Cu–N(7)	82.73(7)	N(3)–Cu–O(1)	104.38(7)
N(1)–Cu–N(7)	178.6(1)	N(3)–Cu–N(7)	99.12(9)	N(1)–Cu–O(1)	87.87(8)
Complex ***3***					
Cd(1)–O(11)	2.364(5)	Cd(1)–N(13)	2.312(7)	Cd(1)–N(17)	2.326(6)
Cd(1)–N(11)	2.310(6)	Cd(1)–N(15)	2.279(6)	O(14)–Cd(1)	2.355(6)
N(15)–Cd(1)–N(11)	110.0(2)	N(15)–Cd(1)–N(13)	176.0(2)	N(11)–Cd(1)–N(13)	73.9(2)
N(15)–Cd(1)–N(17)	75.0(2)	N(11)–Cd(1)–N(17)	171.1(2)	N(13)–Cd(1)–N(17)	101.0(2)
N(15)–Cd(1)–O(14)	90.1(2)	N(11)–Cd(1)–O(14)	83.4(2)	N(13)–Cd(1)–O(14)	89.5(2)
N(17)–Cd(1)–O(14)	89.2(2)	N(15)–Cd(1)–O(11)	100.7(2)	N(11)–Cd(1)–O(11)	78.7(2)
N(13)–Cd(1)–O(11)	80.7(2)	N(17)–Cd(1)–O(11)	108.0(2)	O(14)–Cd(1)–O(11)	161.4(2)
Complex ***4***					
Zn(1)–O(1)	2.029(4)	Zn(1)–N(1)	2.055(3)	Zn(1)–N(3)	2.148(3)
O(1)–Zn(1)–N(1)	110.99(8)	O(1)–Zn(1)–N(3)	93.74(7)	N(1)–Zn(1)–N(3)	81.6(1)
N(1)–Zn(1)–N(1)#1	138.0(2)	N(1)–Zn(1)–N(3)#1	95.7(1)	N(3)#1–Zn(1)–N(3)	172.5(2)

Symmetry code: **1**: #1: $-x+1$, $-y+2$, z; **4**: #1: $-x$, y, $-z+1/2$.

five-coordinated. The Zn–N distances [Zn–N1, 2.16(1); –N3, 2.22(1); –N5, 2.20(1) Å] are similar to those of the reported Zn–H_2biim complexes (Zn–N, 2.030–2.240 Å) [7,8]. The bond angles around Zn^{2+} deviate appreciably from the ideal octahedral values with the maximum deviations being, as expected, due to the chelating 'bite' of H_2biim. The N–Zn–N bite angles (av. 76.9°) are slightly smaller than in the known Zn–H_2biim complexes (78.2–80.0°) [4d,8].

Each sulfate anion interacts with the surrounding three $[Zn(H_2biim)_3]^{2+}$ units via six hydrogen bonds, as shown in Fig. 1 (type III, Scheme 1), with the N···O separations

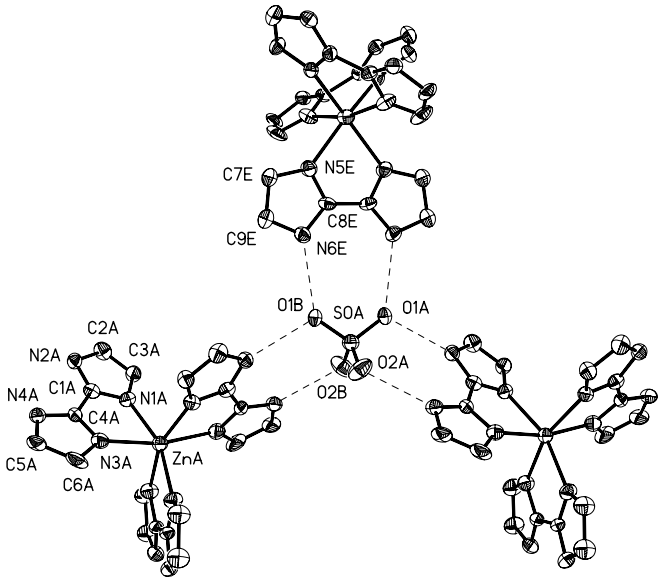

Fig. 1. Hydrogen bonds between $[Zn(H_2biim)_3]^{2+}$ and SO_4^{2-}.

ranging from 2.70(2) to 2.77(2) Å. Each cation is correspondingly linked to three sulfate anions (Fig. 2) to form a supramolecular framework structure as depicted in Fig. 1S in the supplementary material.

3.2. $[Cu(H_2biim)_2(H_2O)]SO_4 \cdot 3H_2O$ (2)

The asymmetric unit of **2** consists of $[Cu(H_2biim)_2(H_2O)]^{2+}$, one SO_4^{2-} and three lattice water molecules. The coordination environment around Cu^{2+} can be described as a distorted square pyramidal geometry (Fig. 3). Four nitrogen atoms of two chelating H_2biim ligands form the basal plane of the pyramid, and the metal is displaced by 0.189 Å from this plane towards the apical ligand, where the apical position is occupied by one water molecule. The Cu–N distances [Cu–N1 = 2.009(2) Å, Cu–N3 = 2.014(2) Å, Cu–N5 = 2.006(2) Å, Cu–N7 = 2.015(2) Å] are shorter than the apical Cu–O distance [2.198(1) Å]. These distances and those of the biimidazole ligand lie in the range observed for biimidazole-Cu complexes retrieved from the CSD [7]. The N–Cu–N bite angles (av. 82.32(8)°) are found in the upper limit of the range registered in the CSD so far (range: N–Cu–N: 78.6–81.6°) [7]. The chelating H_2biim ligands are almost planar, with dihedral angles of 4.6° and 0.7°.

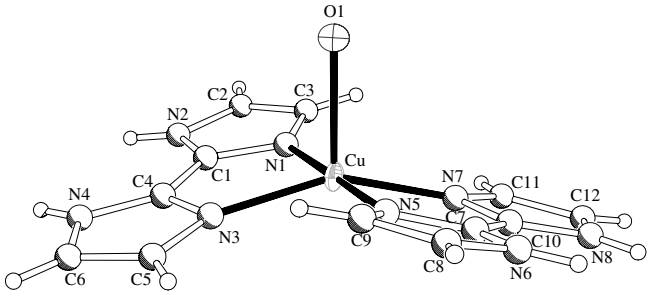

Fig. 3. ORTEP drawing of $[Cu(H_2biim)_2(H_2O)]^{+}$.

Unlike in the case of compound **1**, the hydrogen bond donors of **2** ($[Cu(H_2biim)_2(H_2O)]^{2+}$) have two *trans* H_2biim groups that are nearly coplanar. As a consequence, a hydrogen bonded dimeric structure (Fig. 4) through type II hydrogen bonds (Scheme 1) has been observed for **2** instead of the 3D framework found in **1**. The N···O distances range from 2.762(3) to 3.272(3) Å. It is interesting that the three lattice water molecules that are linked together by hydrogen bonds (2.743–2.780 Å) generate a hexanuclear water cluster through a twofold rotation axis. The water hexamer has an unprecedented open structure consisting of a cyclic water tetramer rather than the cage structure with an energy minimum [9]. The hexameric cluster is stabilized by hydrogen bonding to the sulfate (O1w···O3, 2.716; O1w···O5, 2.778 Å) forming the sulfate-

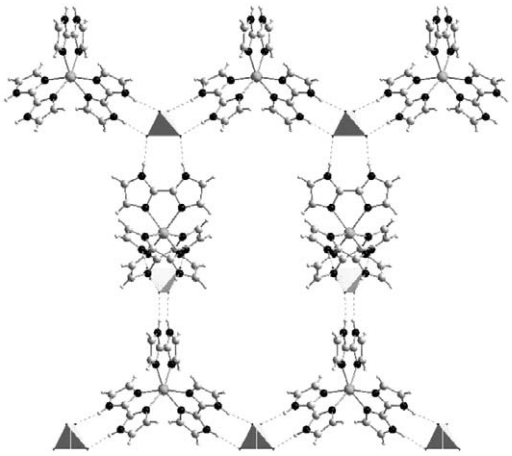

Fig. 2. Extended hydrogen bond network of **1**.

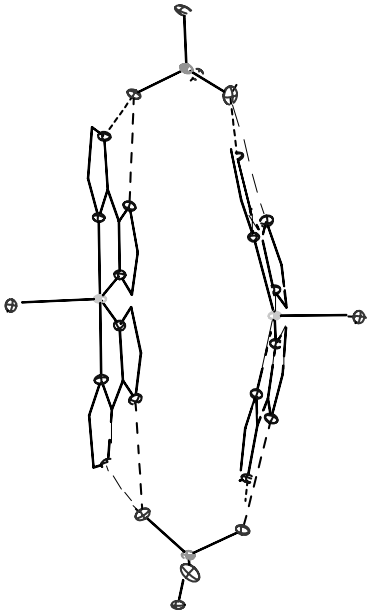

Fig. 4. Hydrogen bonded dimeric structure of $[Cu(H_2biim)_2(H_2O)]SO_4$.

assisted sheet (Fig. 5). There are extensive hydrogen bonds between sulfate and water molecules of coordination and lattice origin, which leads to the formation of the framework structure of **2** (Fig. 6).

3.3. *[Cd(H$_2$biim)(NO$_3$)(H$_2$O)]$_4$(NO$_3$)$_4$ (**3**)*

The molecule of **3** consists of four independent $[Cd(H_2biim)(NO_3)(H_2O)]^+$ cations and four nitrate anions. The bond lengths and angles in the four cations are similar to each other and thus only one set of the selected bond distances and angles are given in Table 2. The cadmium atom has a [CdO2N4] octahedral coordination environment with the four nitrogen atoms from the two H_2biim ligands in equatorial positions and the two oxygen donor atoms from nitrate and water molecules in apical sites (Fig. 7). The Cd–N distances range from 2.279(6) to 2.326(6) Å, slightly shorter than the Cd–O distances (2.364(5), 2.355(6) Å). The N–Cd–N bite angles are 73.9(2)° and 75.0(2)°, smaller than those observed for **1** and **2** as expected for longer Cd–N distances. The two rings of each H_2biim ligand are slightly twisted with dihedral angles of 3.2° and 6.4°.

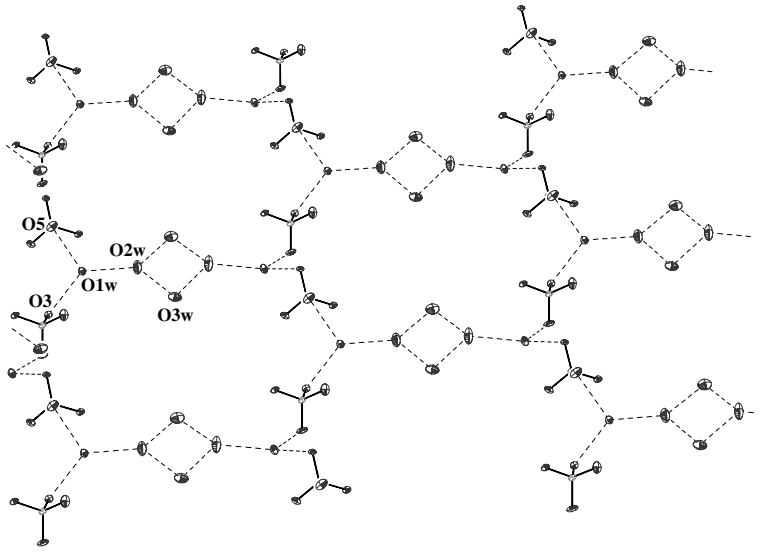

Fig. 5. Sulfate-assisted sheet of the water hexamer.

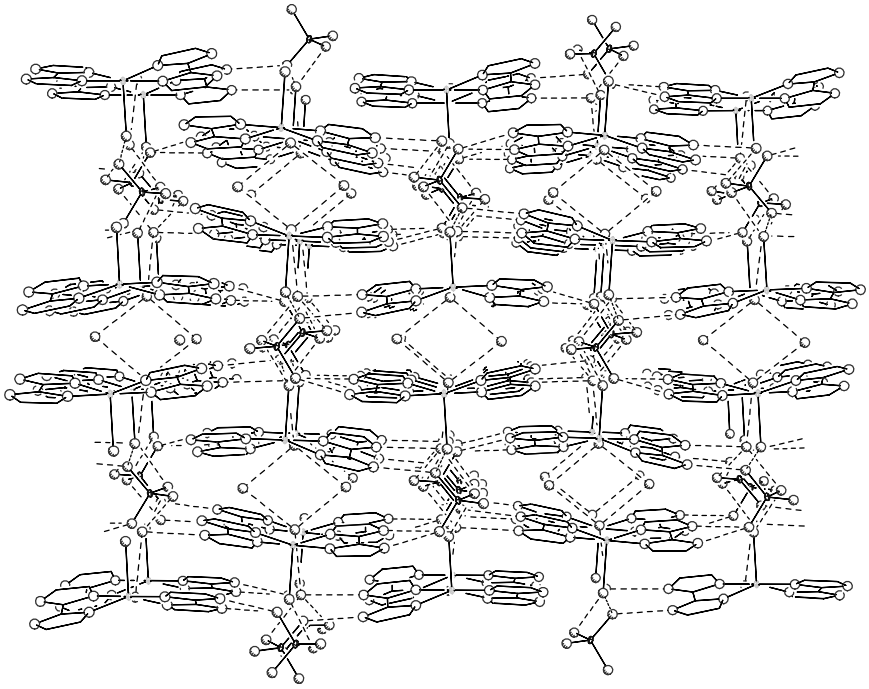

Fig. 6. Supramolecular framework structure of **2**.

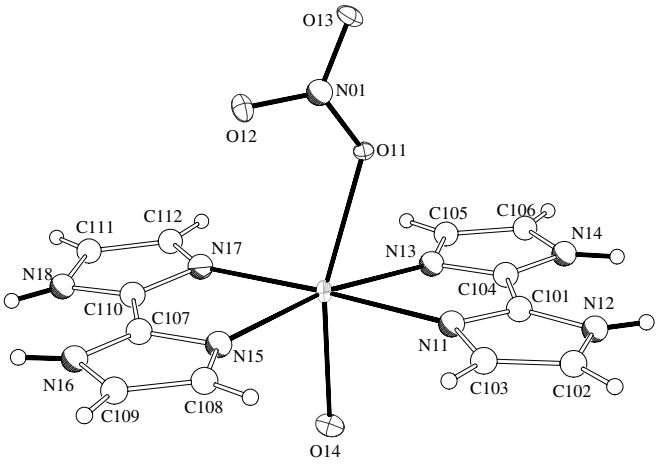

Fig. 7. Molecular structure of one independent $[Cd(H_2biim)_2(H_2O)(NO_3)]^+$.

Although the hydrogen bond donors (cationic H_2biim metal complexes) of **2** and **3** have a similar geometry of donor atoms, the different geometry of the counter-anions leads to their distinct hydrogen bonded structures. Fig. 8 shows the hydrogen bonds between $[Cd(H_2biim)_2(NO_3)(H_2O)]^+$ and nitrate. There are two types of hydrogen bonds ($R_2^1(8)$ and $R_2^2(9)$) that link the cations and counter-anions into a one-dimensional structure. The N···O separations range from 2.829(9) to 3.017(8) Å. The hydrogen bonds (2.749–3.121 Å) between the free nitrate and the apical oxygen donor atoms are responsible for the two-dimensional structure (see Fig. 9). The further hydrogen bonds (2.730–3.070 Å) between the coordinated nitrate and water molecules interconnect the layers into the network structure as illustrated in Fig. 10.

3.4. $[Zn(H_2biim)_2(H_2O)](NO_3)_2$ (**4**)

Complex **4** consists of two $[Zn(H_2biim)_2(H_2O)]_{1/2}$ and two nitrate anions. $[Zn(H_2biim)_2(H_2O)]^{2+}$ shown in Fig. 11 has C_2 symmetry with the twofold rotation axis going through the Zn^{2+} ion and apical oxygen donor atom. The coordination environment around the Zn^{2+} ion can be described as a distorted square pyramidal geometry. The four nitrogen atoms of the two chelating H_2biim ligands form the basal plane of the pyramid (mean plane: 0.2994 Å) [Zn1–N1 = 2.055(5) Å, Zn1–N3 = 2.154(5) Å]. The Zn–O distances are slightly different (Zn1–O1 = 2.032(8) Å). These values and those in the H_2biim ligands are comparable with those registered for biimidazole-Zn complexes in the CSD [Zn–N, 2.030–2.240 Å]. The bite angles [N1–Zn1–N3 = 81.8(2)°] lie in the upper limit of the range registered in the CSD so far (range: 76.9–81.6°).

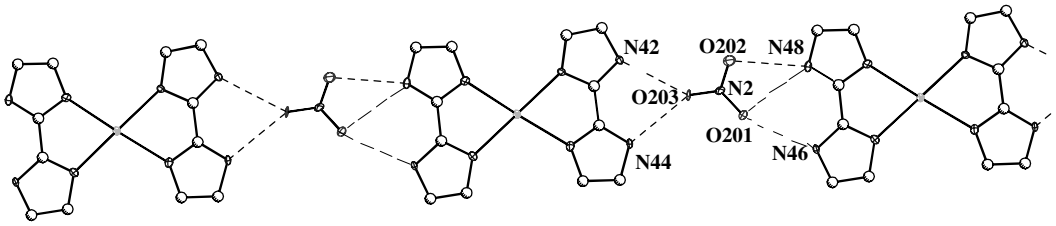

Fig. 8. Hydrogen bonded ribbon structure of $[Cd(H_2biim)_2(H_2O)(NO_3)]NO_3$.

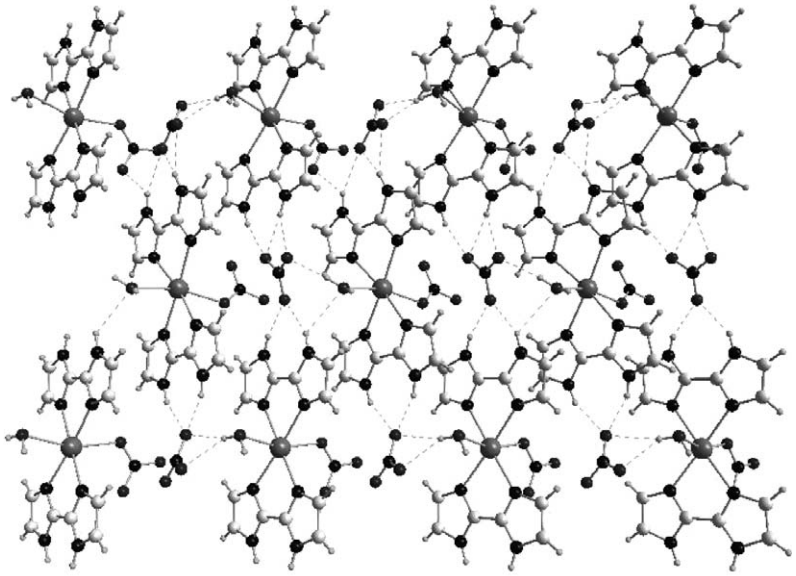

Fig. 9. Two dimensional structure of **3**.

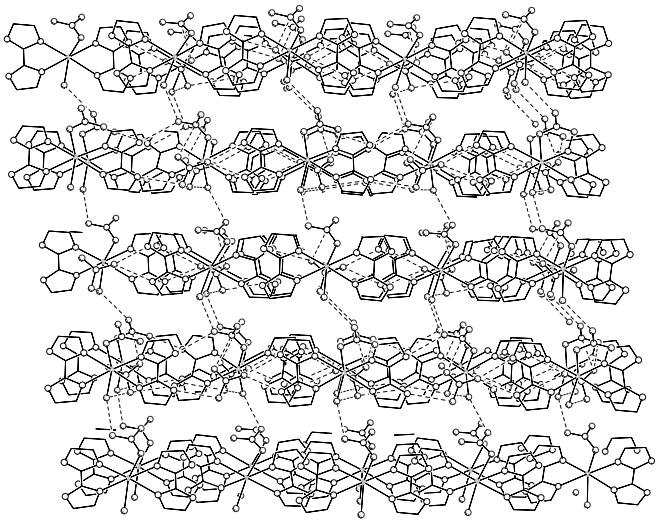

Fig. 10. Network structure of **3**.

Although the hydrogen bond donor $[Zn(H_2biim)_2(H_2O)]^{2+}$ of **4** has two *trans* H_2biim groups, as in the case of **3**, the hydrogen bonding patterns between the donors and acceptors are quite different. In compound **4**, the acceptors are hydrogen bonded to the only one donor via Type II ($R_2^1(8)$) hydrogen bonds to form a discrete structure. This may be attributed to the two non-coplanar H_2biim groups in **4** with the dihedral angle of 32°. The N···O separations range from 2.801(8) to 2.815(8) Å. Additional hydrogen bonds between nitrate and the apical oxygen atoms (O···O, 2.719(7) and 3.079(7) Å) account for the formation of an infinite tape structure with a pitch of 12.29 Å running along the *c* axis (Fig. 11). A single hydrogen bond between H_2biim and nitrate (N···O, 3.168(8) Å) interconnect the tapes into a three-dimensional architecture as shown in Fig. 2S in the supplementary material.

3.5. Fluorescent properties

The emission and excitation spectra of H_2biim and compounds **1**–**4** in the solid state at room temperature are shown in Fig. 3S in the supplementary material. Compounds **1**, **3** and **4** have the same ligands and thus a comparison of the fluorescence spectra of H_2biim, **1**, **3** and **4** are suggestive of the emission origin and influence of metal coordination. H_2biim exhibits a broad photoluminescence emission at 334 nm ($\lambda_{ex} = 431$ nm) similar to that of Me_2biim ($\lambda_{em} = 330$ nm, $\lambda_{ex} = 305$). [9] The single emission maximum at 425 nm ($\lambda_{ex} = 350$ nm) in **1** with three chelating H_2biim is similar to those in free H_2biim. Compounds **3** and **4** with the two chelating H_2biim ligands exhibit very similar fluorescence spectra [422 and 485 nm ($\lambda_{ex} = 350$ nm) for **3**, and 426 and 470 nm ($\lambda_{ex} = 340$ nm) for **4**], that are independent of the metal center and the axial coordination. It is obvious that the axial coordination makes significant influence on the photoluminescence.

4. Conclusion

A systematic study of the hydrogen bonded system constructed by cationic M–H_2biim fragments as donors and inorganic counter-anions (sulfate, nitrate) as acceptors has been established. The M–H_2biim moieties can serve as effective hydrogen bonding donors to construct supramolecular structures via strong hydrogen bonding with inorganic counter-anions. Three types of supramolecular synthons (Type II ($R_2^1(8)$), III ($R_2^2(9)$), IV ($R_1^2(4)$)) have been observed. Those with six peripheral donor atoms such as $[Zn(H_2biim)_3]^{2+}$ in **1** can form a 3D hydrogen bonded framework with spherical inorganic counter-anions such as SO_4^{2-}. The cationic donors with *trans* H_2biim groups can form discrete, dimeric and 1D hydrogen bonded structures depending on the shapes of the counter-anions and the coplanarity of the two H_2biim groups. The coplanar arrangement of the H_2biim groups favors the 1D hydrogen bonded structure. These hydrogen bonded structures may allow the presence of unusual water clusters as observed in **2**.

Acknowledgements

This work was supported by the National Science Foundation of China (Grant No. 20473092) and the "One Hundred Talents Program" of the Chinese Academy of Science.

Appendix A. Supplementary data

The luminescence spectra and the packing diagrams of complexes **1** and **4**. CCDC 242516, 243695, 242519 and 242517 corresponding to complexes **1**–**4** contain the supplementary crystallographic data for this paper. These data

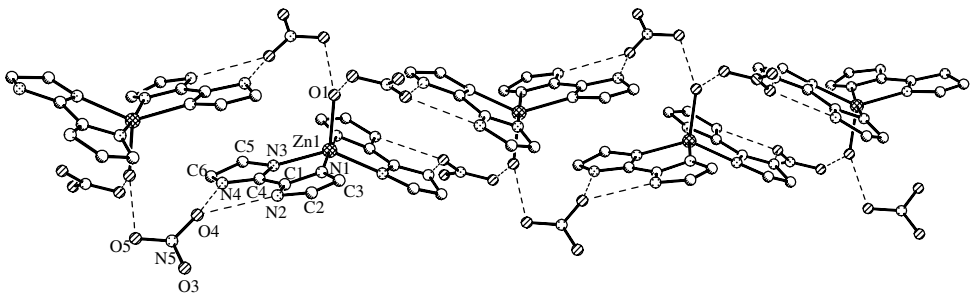

Fig. 11. One-dimensional tape structure of **4**.

can be obtained free of charge via www.ccdc.cam.ac.uk/conts/retrieving.html (or from the CCDC, 12 Union Road, Cambridge CB2 1EZ, UK; fax: +44 1223 336 033; e-mail: deposit@ccdc.cam.ac.uk). Supplementary data associated with this article can be found, in the online version, at doi:10.1016/j.poly.2005.12.031.

References

[1] (a) J.M. Lehn, Angew. Chem., Int. Ed. Engl. 29 (1990) 1304;
(b) J.R. Fredericks, A.D. Hamilton, in: J.L. Atwood, J.E.D. Davies, D.D. MacNicol, F. Vogtle (Eds.), Comprehensive Supramolecular Chemistry, Pergamon Press, Oxford, 1996, p. 565;
(c) V.R. Pedireddi, W. Jones, A.P. Chorlton, R. Docherty, Chem. Commun. (1996) 997;
(d) L.J. Prins, J. Huskens, F. de Jong, P. Timmerman, D.N. Reinhoudt, Nature 398 (1999) 498;
(e) P. Lightfoot, A. Snedden, J. Chem. Soc., Dalton Trans. (1999) 3549.

[2] (a) M.M. Chowdhry, D.M.P. Mingos, A.J.P. White, D.J. Williams, Chem. Commun. (1996) 899;
(b) M. Tadokoro, H. Kanno, T. Kitajima, H. Shimada-Umemoto, N. Nakanishi, K. Isobe, K. Nakasuji, Proc. Natl. Acad. Sci. USA 99 (2002) 4950;
(c) M. Tadokoro, T. Shiomi, K. Isobe, K. Nakasuji, Inorg. Chem. 40 (2001) 5476;
(d) L. Öhrström, K. Larsson, S. Borg, S.T. Norberg, Chem. Eur. J. 7 (2001) 4805.

[3] (a) D. Braga, J. Chem. Soc., Dalton Trans. (2000) 3705;
(b) A.D. Burrows, Struc. Bond 108 (2004) 55;
(c) I. Dance, in: G.R. Desiraju (Ed.), Supermolecular Inorganic Chemistry, The Crystal as Supermolecular Entity, Wiley, New York, 1996, p. 145 (Chapter 5);
(d) O.M. Yaghi, Nature 423 (2003) 707.

[4] (a) M. Tadokoro, K. Isobe, H. Uekusa, Y. Ohashi, J. Toyoda, K. Tashiro, K. Nakasuji, Angew. Chem., Int. Ed. 38 (1999) 95;
(b) M. Tadokoro, K. Nakasuji, Coord. Chem. Rev. 198 (2000) 205;
(c) R. Atencio, M. Chacón, T. González, A. Briceño, G. Agrifoglio, A. Sierraalta, J. Chem. Soc., Dalton Trans. (2004) 505;
(d) R. Atencio, K. Ramirez, J.A. Reyes, T. González, P. Silva, Inorg. Chim. Acta 358 (2005) 520;
(e) S. Fortin, A.L. Beauchamp, Inorg. Chem. 40 (2001) 105;
(f) B.-H. Ye, B.-B. Ding, Y.-Q. Weng, X.-M. Chen, Inorg. Chem. 43 (2004) 6866;
(g) B.-H. Ye, B.-B. Ding, Y.-Q. Weng, X.-M. Chen, Cryst. Growth Des. 5 (2005) 801.

[5] R.P. Thummel, V. Goulle, B. Chen, J. Org. Chem. 54 (1989) 3057.

[6] G.M. Shelderic, SHELXL-97, University of Gottingen, Germany, 1997.

[7] The Cambridge Structural Data Base: F.H. Allen, Acta Crystallogr., Sect. B 58 (2002) 380.

[8] C. Kirchner, B. Krebs, Inorg. Chem. 26 (1987) 3569.

[9] (a) J.M. Ugalde, I. Alkorta, J. Elguero, Angew. Chem., Int. Ed. 39 (2000) 717;
(b) K. Kim, K.D. Jordan, T.S. Zwier, J. Am. Chem. Soc. 116 (1994) 11568;
(c) K. Liu, M.G. Brown, C. Carter, R.J. Saykally, J.K. Gregory, D.C. Clary, Nature 381 (1996) 501.

the coordination around the metal centre is approximately octahedral.

The molecular heterometallic iron-containing trinuclear carboxylates $[Fe_2MO(RCOO)_6(L)_3]$, where M is a bivalent 3d transition metal, attract special attention due to being able to provide an opportunity to study many spin-coupling interactions in the system with the same configuration [18]. A considerable number of such complexes containing either heterometallic $[Fe_2MnO]^{6+}$ [18,19], $[Fe_2CoO]^{6+}$ [20,21], $[Fe_2NiO]^{6+}$ [18,22], $[Fe_2ZnO]^{6+}$ [23,24] or homometallic mixed-valence $[Fe_2FeO]^{6+}$ [4,25–34] cores, has been investigated by various methods.

All of the above-mentioned complexes contain iron (III) and bivalent 3d metals: Mn, Fe, Co, Ni, Zn. The difference in the atomic radii of iron and the other 3d elements is negligible. For example, the atomic radius of high-spin iron (III) is equal to 0.65 Å, while the atomic radii for 3d bivalent elements Mn(II), Fe(II), Co(II), Ni(II) range from 0.75 to 0.80 Å. This difference does not essentially influence the stability of the trinuclear $[Fe_2MO]$ core. A survey of the CCDC [35] revealed that in neutral complexes which include a $\{Fe_2^{III}Fe^{II}O\}$ core, the average Fe···Fe separation is equal to 3.280(2) Å (Fe–O(μ_3) 1.875(3) Å, Fe–O_{carb} 2.040(3) Å). In ionic compounds with a $\{Fe_3^{III}O\}$ core, the corresponding distances adopt the values 3.290(2), 1.890(2) and 2.025 Å, respectively. These values suggest a skeleton of the molecular structure with a symmetry close to D_{3h}.

Previously reported was the preparation and the study of complexes containing the $[Fe_2MgO]^{6+}$ core [22]. In the compound $[Fe_2MgO(CCl_3COO)_6(Py)_3]\cdot CH_3C_6H_5$, one iron atom occupies a special position on the mirror plane, while the other iron and the magnesium atom of the Fe_2MgO core occupy the known general position with equal probability (50%). This arrangement occurs in spite of a different mode of interaction of the coordination environment with the d(Fe) and s(Mg) metals. The rather different ionic radii of Fe(III) 0.65 Å and Mg(II) 0.72 Å conserved a practically equilateral triangle of the three metal atoms. The geometric rather than the electronic factor, probably, avoid any dramatic rearrangements in the trinuclear cluster.

The present study describes the results obtained with the alkaline-earth elements Ca (ionic radius 1.00 Å), Sr (1.18 Å) and Ba (1.35 Å) and the way to synthesize new iron-containing molecular μ_3-oxo clusters.

2. Experimental

2.1. General

The carbon and hydrogen content was determined by standard micro-methods. Atomic absorption spectroscopy was used to determine the Fe(III), Ca(II), Sr(II) and Ba(II) content.

IR spectra of polycrystalline samples were recorded as oil mulls on a Specord M-75 spectrophotometer.

TG studies were performed on a Paulik–Paulik–Erdey derivatograph in air, with Al_2O_3 as the standard calibration. DTG – 1/5; DTA – 1/10; TG – 100/100. T_{max} = 1000 °C for **1** and **3**, and 500 °C for **2**.

Magnetic measurements of **1** and **3** were performed using the Gouy method in the temperature range 110.0–293.0 K. The temperature of the sample was determined with ±1.5 K accuracy using the Cu–Constantan thermocouple. The variable temperature susceptibility of **2** was measured with an Oxford Instruments Vibrating Sample Magnetometer (VSM) working between 0 and 12 T and in the 1.5–350.0 K temperature range. Diamagnetic Pascal's constants were used to correct the magnetic values [36].

The Mossbauer spectrum for **1** was acquired using a constant acceleration system with a symmetrical waveform. A ^{57}Co (1.0 MBq) source in a Rh matrix was used, but the isomer shift refers to α-Fe.

2.2. Synthesis

Most of the precursors, except $Ca(CCl_3COO)_2\cdot 4H_2O$, $Sr(CCl_3COO)_2\cdot 4H_2O$ and $Ba(CCl_3COO)_2\cdot 4H_2O$, which were synthesized by the reaction between $CaCO_3$, $SrCO_3$or $BaCO_3$ with trichloroacetic acid, were commercially obtained and used without any further purification.

All the products are air stable and also soluble in common organic solvents such as MeOH, EtOH, THF, CH_3CN and DMSO. Single crystals suitable for X-ray crystallography for **1** and **3** were obtained by slow evaporation of their THF solutions, at room temperature.

2.2.1. Synthesis of $[Fe_2CaO(CCl_3COO)_6(THF)_4]\cdot THF$ (**1**)

A mixture of $Fe(NO_3)_3\cdot 9H_2O$ (0.808 g, 2.00 mmol) and $Ca(CCl_3COO)_2\cdot 4H_2O$ (1.748 g, 4.00 mmol) in 30 ml of methanol was heated on a water bath (~70 °C) with permanent stirring until dryness. The solid product was extracted with three small portions (10 ml) of THF. After 2 days a light red microcrystalline material precipitated from the THF solution, which was filtered off, washed with hexane and finally dried in air. Yield: 65% (on iron basis). *Anal.* Calc. for $C_{32}H_{40}Cl_{18}O_{18}CaFe_2$: C, 25.58; H, 2.68; Fe, 7.43; Ca, 2.67. Found: C, 25.27; H, 2.54; Fe, 7.32; Ca, 2.48%. IR data (oil mulls, cm^{-1}): 3650 m, 3470 mb, 1700 m, 1673 msh, 1645 s, 1593 s, 1590 m, 1380 s, 1340 s, 1010 w, 940 w, 832 s, 826 s, 748 sh, 720 m, 675 m, 670 s, 469 m, 440 m.

2.2.2. Synthesis of $[Fe_2SrO(CCl_3COO)_6(THF)_6]\cdot 0.5THF\cdot 0.5H_2O$ (**2**)

The light red coloured complex **2** was synthesized identically to **1**, but using $Sr(CCl_3COO)_2\cdot 4H_2O$ instead of $Ca(CCl_3COO)_2\cdot 4H_2O$. Yield: ~ 52% (on iron basis). *Anal.* Calc. for $C_{38}H_{53}Cl_{18}O_{20}Fe_2Sr$: C, 27.37; H, 3.20; Fe, 6.70; Sr, 5.25. Found: C, 27.11; H, 3.17; Fe, 6.31; Sr, 5.01%. IR data (oil mulls, cm^{-1}): 3650 m, 3540 mb, 3180 wb, 1690 s,

1675 ssh, 1660 s, 1380 s, 1340 ssh, 1030 w, 1015 w, 950 w, 910 w, 830 ssh, 820 s, 740 s, 730 msh, 690 msh, 675 s, 460 m, 430 w.

2.2.3. Synthesis of $[Fe_2BaO(CCl_3COO)_6(THF)_6]\cdot 0.5THF\cdot 0.5H_2O$ (3)

A mixture of $Fe(NO_3)_3\cdot 9H_2O$ (0.808 g, 2.00 mmol) and $Ba(CCl_3COO)_2\cdot 4H_2O$ (2.136 g, 4.00 mmol) in 50 ml of methanol was heated on a water bath (~70 °C) with stirring for 3 h. The solution was filtered to remove insoluble $Ba(NO_3)_2$ and evaporated at room temperature. The solid product was dissolved in 50 ml THF. After 1 week, as a result of very slow evaporation, a dark red crystalline material was filtered off, washed with hexane and air dried. It is necessary to mention that using this procedure crystals up to ~0.5 cm^3 were obtained. Yield: ~83% (on iron basis). *Anal*. Calc. for $C_{38}H_{53}Cl_{18}O_{20}BaFe_2$: C, 26.58; H, 3.11; Fe, 6.50; Ba, 8.00. Found: C, 25.88; H, 2.91; Fe, 6.60; Ba, 7.68%. IR data (oil mulls, cm^{-1}): 3460 mb, 1675 s, 1630 s, 1380 s, 1340s, 1120 vw, 1020 m, 940 w, 890 vw, 860 sh, 832 s, 820 s, 720 m, 690 m, 670 s, 465 m, 445 w.

2.3. Crystallographic data

The structural parameters together with details of data collection and refinement for compounds **1** and **3** are given in Table 1.

The X-ray intensity data for **1** were collected at 150 K on a Nonius Kappa CCD diffractometer equipped with graphite monochromated Mo Kα radiation using ω rotation with a sample-to-detector distance of 40 mm. Unit cell parameters were obtained and refined using the whole data set. Frames were integrated and corrected for Lorenz and polarization effects using DENZO [37]. The scaling, as well as the global refinement of the crystal parameters, was performed by SCALEPACK [38]. Reflections, which were partly measured on previous and subsequent frames, were used to scale these frames on each other. The absorption correction for **1** and **3** were introduced by a semi-empirical method based on symmetry equivalent reflections [37].

Data collection for **3** was performed on a KUMA KM-4 CCD diffractometer equipped with graphite monochromated Mo Kα radiation at 100 K. The unit cell determination and data integration were carried out using the CrysAlis package of Oxford Diffraction [39]. Intensity data were corrected for Lorentz and polarization effects. The mean value of 0.693 for $|E^2-1|$ suggested a non-centrosymmetric space group, but taking into consideration the R_{int} 0.071 value for the Laue group $4/m$ and systematic absences, the structure settlement with SHELXS-97 [40] was initially envisaged by using the $P4_2/nmc$ space group. The $M_3O(COO)_6$ core was easily recognized on the Fourier map though further calculations of the ΔF maps did not allow a better value of R than 0.12 to be obtained. In subsequent attempts, the structure was successfully solved via SHELXL-97 [40] using a twinning approach by introducing the instruction TWIN 0 1 0 1 0 0 0 0 $\bar{1}$. The fractional contributions of the two twin domains in structure **3** are in a 1:1 ratio. Refinement of the structures revealed that THF (coordinated to Fe) in compound **1**, one of the two THF

Table 1
Summary of crystal data for **1** and **3**

Compound	**1**	**3**
Empirical formula	$C_{32}H_{40}CaCl_{18}Fe_2O_{18}$	$C_{38}H_{53}BaCl_{18}Fe_2O_{20}$
M	1502.52	1716.94
T (K)	150	100
λ (Å)	0.71073	0.71073
Space group	*Pbcn*	$P4_2/n$
a (Å)	17.1653(2)	16.0020(7)
b (Å)	19.3427(3)	16.0020(7)
c (Å)	17.5660(3)	27.0470(12)
V (Å^3)	5832.32(15)	6925.6(5)
Z	4	4
ρ_{calc} (Mg/m^3)	1.711	1.647
μ_{Mo} (mm^{-1})	1.471	1.730
$F(000)$	3016	3420
Crystal size (mm)	$0.20\times0.20\times0.15$	$0.50\times0.40\times0.325$
θ Range (°)	2.32 to 25.35	2.84 to 24.97
Index ranges	$-20\leqslant h\leqslant 20$, $-23\leqslant k\leqslant 23$, $-21\leqslant l\leqslant 21$	$-19\leqslant h\leqslant 16$, $-18\leqslant k\leqslant 19$, $-32\leqslant l\leqslant 32$
Number of measured reflections	10148	48089
Number of unique reflections (R_{int})	5342 (0.0206)	6110 (0.0453)
Number of refined parameters	351	371
Maximum and minimum transmission	0.894 and 0.801	0.306 and 0.255
Goodness-of-fit for F^2	1.029	1.086
R[a]	0.0388	0.0738
wR[b]	0.0933	0.0860
$\Delta\rho_{max}$ and $\Delta\rho_{min}$ (e Å^3)	0.662 and −0.728	1.310 and −0.831

[a] $R=\sum\|F_o|-|F_c\|/\sum|F_o|$.
[b] $wR=[\sum w(|F_o^2|-|F_c^2|)^2/\sum w|F_o^2|^2]^{1/2}$.

(coordinated to Ba), as well as solvated THF molecules in **3** occupy two positions each with 50% probability. Only one of the three asymmetrical $-CCl_3$ groups was found to be disordered into two resolute positions, in both complexes **1** and **3**.

3. Results and discussion

To date, various heterotrinuclear complexes with chloro containing acetic acids have been synthesized and structurally characterized [19,20,22,23]. Most of these complexes were synthesized through a step concerning treatment of basic acetates of d-elements with the corresponding acids in aqueous solutions. It is worth mentioning that complexes **1**–**3** were prepared by a self-assembly reaction of $Fe(NO_3)_3 \cdot 9H_2O$ with trichloroacetates of alkaline earth metals in methanol.

3.1. Molecular structures of *1* and *3*

The X-ray study revealed that the compounds **1** and **3**, containing Ca and, respectively, Ba, belong to molecular complexes with THF solvated molecules placed in the external coordination sphere. It has to be mentioned that compound **3** includes solvated water molecules too. As in the case of the complex $[Fe_2MnO(CHCl_2COO)_6(THF)_2 \cdot H_2O]$ [19], the character of distribution of the metal cations in the various M_3–μ_3-O cores was unambiguously demonstrated. It appeared possible even in the case of an essential difference in the values of ionic radii of the metals used, M^{2+} (Ca, Ba) and Fe^{3+}. This difference produced the formation of an isosceles triangle of C_2 symmetry (Fig. 1a and b), with the lateral equivalent distances Ca···Fe 3.750(1) Å for **1** (Ba···Fe 4.177(1) Å for **3**) and the basal distance Fe···Fe 3.229(2) Å for **1** and 3.201(1) Å for **3**. The data show that this difference in the length of the sides of the triangle could be dictated by the stability of the molecular core, $[M_3O(R–COO)_6]$. The character of the bridges forming this core was not essentially changed in comparison with the classic μ_3-oxo-iron complexes. The stability of the trinuclear core is dictated by the μ_3-bridge oxygen atom O^{2-} and by six carboxylate anions joint in a *syn–syn* mode along the sides of the triangle. Although the general architecture of the core remains the same, the locations in the first coordination sphere of the metal differ essentially.

3.1.1. Compound $[Fe_2CaO(CCl_3COO)_6(THF)_4] \cdot THF$ (*1*)

Fig. 1a presents the molecular trinuclear complex structure. The geometric characteristics of the coordination core (Table 2) denoted by iron(III) metals in compound **1** do not differ essentially from those reported in [35]. The coordination number of Fe(1) atoms equals 6, and represent a weakly distorted octahedron. Four oxygen atoms of four carboxylic groups occupy the equatorial plane with Fe–O distances ranging from 1.996(2) to 2.065(2) Å. The coordination is completed by oxygen atom O(1) and oxygen atom O(9) of THF molecules at the distances of 1.827(1) Å and, respectively, 2.155(2) Å. Atom Fe(1) is out of the plane of the four carboxyl oxygen atoms in the direction of the μ_3-oxygen at a distance of 0.286(2) Å.

The Ca^{2+} local arrangement differs essentially from the surrounds of the Fe(1) atom: the coordination number of calcium is 7; the coordination sphere includes four carboxylic oxygen atoms at distances in the range 2.336(2)–

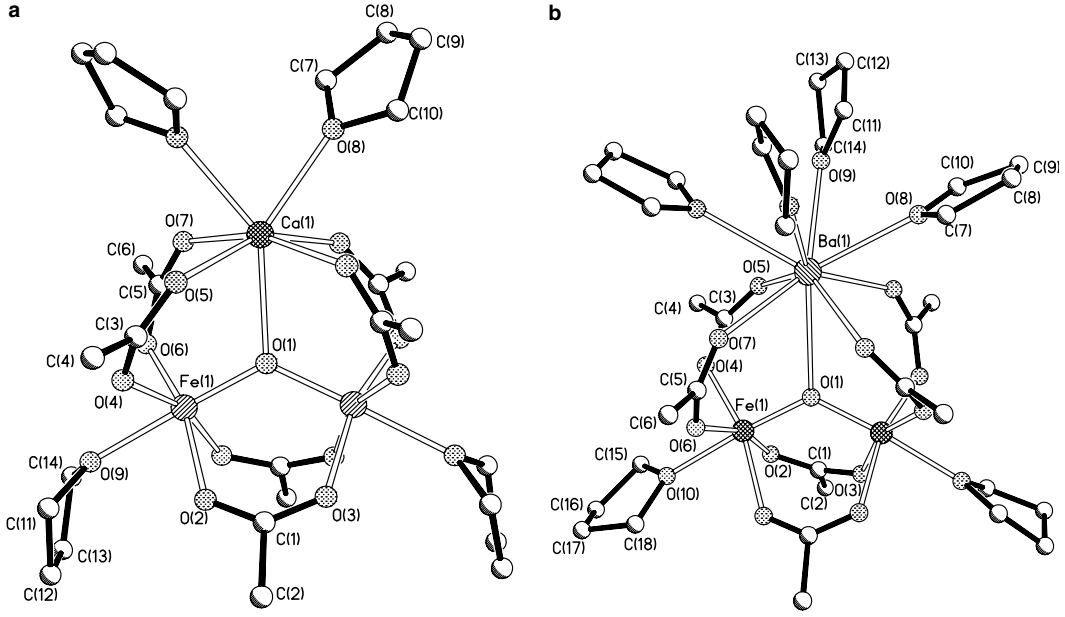

Fig. 1. Structures of the molecular complexes: (a) $[Fe_2CaO(CCl_3COO)_6(THF)_4]$ (**1**); (b) $[Fe_2BaO(CCl_3COO)_6(THF)_6]$ (**3**). Chlorine atoms are omitted for clarity.

Table 2
Interatomic distances (Å) in coordination polyhedra of Ca, Ba and Fe in **1** and **3**

Compound **1**		Compound **3**	
Ca(1)–O(1)	2.530(3)	Ba(1)–O(1)	3.000(7)
Ca(1)–O(5)	2.353(2) × 2	Ba(1)–O(5)	2.697(6) × 2
Ca(1)–O(7)	2.336(2) × 2	Ba(1)–O(7)	2.688(7) × 2
Ca(1)–O(8)	2.424(2) × 2	Ba(1)–O(8)	2.850(7) × 2
		Ba(1)–O(9)	2.803(7) × 2
Fe(1)–O(1)	1.827(1)	Fe(1)–O(1)	1.816(3)
Fe(1)–O(2)	2.065(2)	Fe(1)–O(2)	2.078(6)
Fe(1)–O(3)$^{(1)}$	2.060(2)	Fe(1)–O(3)$^{(2)}$	2.065(6)
Fe(1)–O(4)	1.996(2)	Fe(1)–O(4)	1.997(7)
Fe(1)–O(6)	2.003(2)	Fe(1)–O(6)	1.993(6)
Fe(1)–O(9)	2.155(2)	Fe(1)–O(10)	2.178(6)

Symmetry transformations: (1) $-x, y, -z + 0.5$; (2) $-x + 0.5, -y + 0.75, z$.

2.353(2) Å, two oxygen atoms of THF ligands (Ca(1)–O(8) 2.424(2) Å) and μ_3-O at 2.530(3) Å. The difference in the M–O(1) distances (Ca–O and Fe–O) is 0.703(2) Å, which exceeds the difference in the ionic radii of Ca^{2+} (1.00 Å) and Fe^{3+} (0.65 Å). The Ca atom deviates by 0.443 Å from the plane of the four oxygen atoms in the direction of the neutral ligands. Concluding, the main result of the X-ray study is related to reliable information about the magnetic moiety that includes two iron(III) atoms interacting via Fe–O–Fe and two *syn–syn* carboxylic groups bridges.

The X-ray study of the compounds $[Fe_2SrO(CCl_3COO)_6(THF)_6]\cdot 0.5H_2O\cdot 0.5THF$ (**2**) and $[Fe_2BaO(CCl_3COO)_6(THF)_6]\cdot 0.5H_2O\cdot 0.5THF$ (**3**) has shown that they are isostructural. In the following, as an example, is described in detail the structure of **3**, for which a complete X-ray single crystal investigation was carried out.

The main distinction between compound **3** and compound **1** consists of a different coordination geometry for the s elements. There is a 9-coordination number for Ba^{2+} and its environment includes four THF ligands (Fig. 1b). The Ba atom deviates considerably, at 1.003(6) Å, from the plane of four coordinated oxygen atoms of carboxylate groups towards neutral ligands. The coordination polyhedron of Fe^{3+} is similar to that observed in **1**. The deviation of the Fe(1) atom from the main plane of four carboxylate oxygen atoms was found to be 0.304(7) Å in the direction of O(1) oxygen.

The crystal packing for both **1** and **3** compounds was derived from the arrangement of the corresponding neutral complexes $[Fe_2CaO(CCl_3COO)_6(THF)_4]$ and $[Fe_2BaO(CCl_3COO)_6(THF)_6]$ according to the Cl···Cl intermolecular contacts, which adopt the shortest values of 3.566 Å for **1** and 3.522 Å for **3**. All other intermolecular separations are not smaller than the sum of Van der Waals radii. The disordered solvate THF and water molecules are accommodated within the free space formed by the packing of the bulky trinuclear complexes (Figs. 2 and 3). These spaces represent closed cavities formed by staggered two-dimensional layers in structure **1** (Fig. 2) and the channels propagated along the *c*-crystallographic axes in structure **3** (Fig. 3).

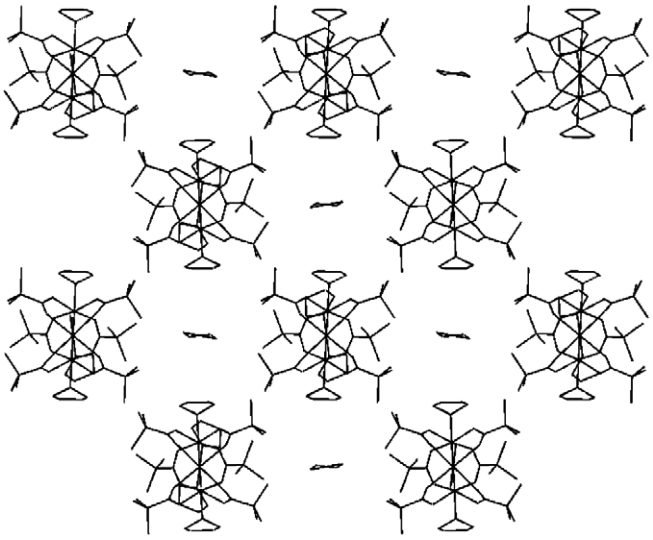

Fig. 2. Structure of the 2D layer in **1**.

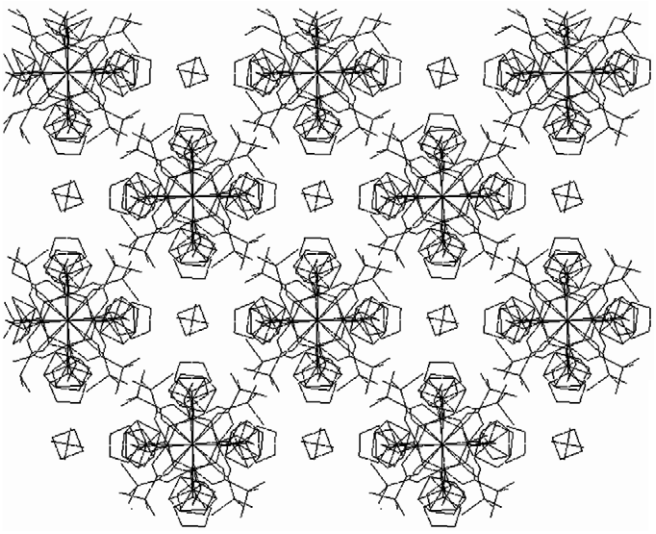

Fig. 3. Projection of the crystal structure **3** along the *c*-axis.

3.2. Infrared spectra

The solid state IR spectra of complexes **1**–**3** indicate the presence of carboxylate, THF and $\{Fe_2MO\}$ groups. The characteristic vibration frequencies for THF groups appear at ~3450–3600 and 2800–3000 cm^{-1}. The IR data for compounds **1**–**3** show a single pair of carboxylate stretching vibrations at 1645 and 1380 cm^{-1} for **1**, 1670 and 1380 cm^{-1} for **2** and 1675 and 1380 cm^{-1} for **3** assigned to ν_{as}(COO) and ν_s(COO), respectively, suggesting the existence of only one type of carboxylate group in their crystal structures. These bands are shifted to lower energy by 45–75 cm^{-1} relative to the trinuclear basic acetates [4] due to the replacement of the CH_3 radical by the much more powerfully electron-accepting CCl_3 moieties which weaken the $M–O_{carb}$ force constant.

In Table 3, some band assignments for (COO), (CCl), (CH) and (CC) groups for μ_3-oxo heterotrinuclear clusters

Table 3
Some band assignments of IR spectra of μ_3-oxo heterotrinuclear clusters $[Fe_2M(Ca, Sr, Ba)O(CCl_3COO)_6(THF)_n]\cdot mSolv$

$Ca(TCA)_2$[a]	$\{Fe_2CaO\}$	$Sr(TCA)_2$[a]	$\{Fe_2SrO\}$	$Ba(TCA)_2$[a]	$\{Fe_2BaO\}$	Assignments
1649 vs	1645 s	1660 s	1670 s	1670 s	1675 s	ν_{as}(COO)
1596 vs	1593 s		1660 s		1630 s	
1372 s	1380 s	1373 s	1380 s	1379 s	1380 s	ν_s(COO)
				1370 s		
947 w	940 w	942 w	950 w	940 w	940 w	ν(CC)
	832 s		830 ssh		832 s	ν_{as}(C–Cl); A″
	826 s		820 s		820 s	ν_{as}(C–Cl); A′
	720 m		730 msh		720 m	δ(COO)
	675 m		690 msh		690 m	$\nu_{as}(Fe_2MO)$; A_1
	670 s		675 s		670 s	ρ(OCO)
	460 m		460 m		465 m	$\nu_{as}(Fe_2MO)$; B_2
	440 m		430 w		445 w	ν_s(C–Cl)

$CCl_3COO \equiv$ TCA; s – strong; v – very; m – medium; w – weak; sh – shoulder; ν – stretching.
[a] Data from [42].

according to [41,42] are given. It is worth mentioning that the band corresponding to $\nu_{as}(Fe_3O) = 595\ cm^{-1}$ from homotrinuclear basic acetates is missing in IR spectra of compounds **1**–**3**. This band is replaced by another two bands at ~690–675 cm^{-1}, corresponding to $\nu_{as}(Fe_2MO)$ (A_1), and at 465–460 cm^{-1}, corresponding to $\nu_{as}(Fe_2MO)$ (B_2) according to [4]. Cannon and co-workers [43–45] have examined the Fe_2M–O vibration modes and such bands have been found for a number of $[Fe_2M^{II}(\mu_3\text{-}O)(RCOO)_6(L)_3]$ complexes. Such behaviour was expected because of symmetry lowering of the complexes from D_{3h} to C_{2v} [4,46].

3.3. TG study

A specific feature of the investigated complexes is related to their low temperature stability. Already at temperatures higher than 50–70 °C *exo* and *endo* effects accompanied by weight loss have been registered.

On TG and DTG curves of the investigated compounds, it is possible to notice that the basic processes of decomposition finishes in the range 300–360 °C.

The first endothermic stage of decomposition corresponds to removal of solvent molecules (THF, or THF and H_2O) and some quantity of intrasphere THF (1.5 for **1**, and 0.5 for **2** and **3**).

It is very probably the removal of intrasphere molecules of THF is accompanied by reorganisation of the cluster in such a way to assure all coordination places of the s-metal ion by changing the *syn–syn* mode of coordination of the carboxylic ligands to a cyclo-bridged one [8,9].

The subsequent second process for all three clusters is characterised by several superpositioned processes: removal of coordinated molecules of THF, decomposition of trichloroacetic acid anions and reorganisation of the complexes with the formation of the final product, Fe_2MO_4, with a small quantity of impurities.

3.4. Mössbauer spectrum

The Mössbauer spectrum of compound **1** at room temperature presents only one doublet with slightly asymmetric lines (Fig. 4). The value of the isomer shift parameter δ_{Fe} is 0.46 mm/s and that of the quadrupole splitting parameter ΔE_Q is 1.11 mm/s. These parameters indicate the presence of iron(III) in a high spin state ($S = 5/2$). There are rather insignificant changes in δ_{Fe} and ΔE_Q values related to the substitution of one trivalent Fe^{3+} cation [47] by a bivalent Ca^{2+}.

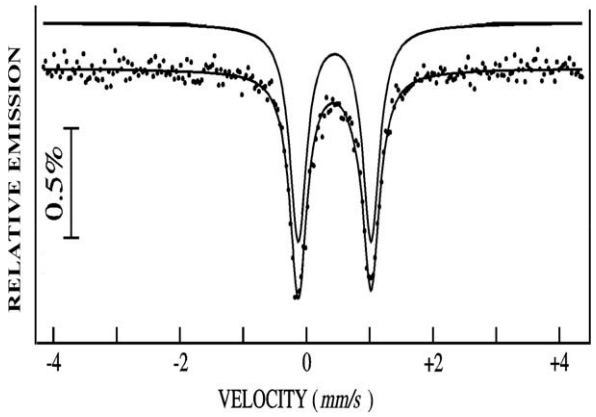

Fig. 4. Fe^{57} Mössbauer spectrum of **1** at room temperature; the solid line is the least-squares fit; isomer shifts are referred to α-iron at room temperature.

3.5. Magnetic properties

The magnetic properties of compounds **1**–**3** have been measured in different ranges of temperatures: 300–110 K for **1** and **3**, and 300–2.9 K for **2**. All three substances are characterized by a gradual reduction of the $\chi_M T$ value with the lowering of temperature, thus indicating an antiferromagnetic interaction between the iron (III) ions. It is evident that ions of s-metals do not contribute to the magnetic exchange. In order to describe the magnetic properties of the investigated complexes the following spin–spin interaction Hamiltonian was used [36]:

$$\mathbf{H}_{exch} = -2\mathbf{J}_{12}\mathbf{S}_1 \cdot \mathbf{S}_2. \quad (1)$$

The energy levels of Hamiltonian (1) are given by the following expression:

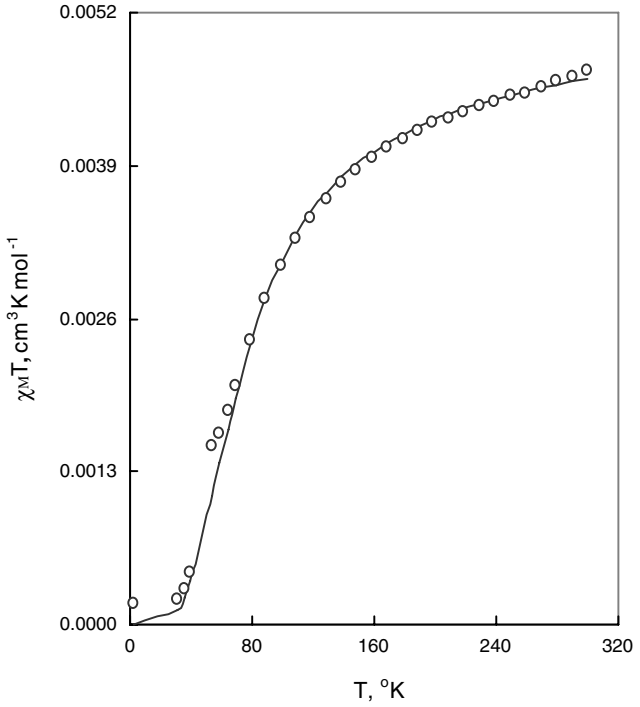

Fig. 5. Temperature dependence of the magnetic susceptibility of **2**, plotted as $\chi_M T$ vs. T; the solid line is the least-squares fit.

$$E(S') = -J_{12}[S'(S'+1) - S_1(S_1+1) - S_2(S_2+1)], \qquad (2)$$

where S' is the total spin of the system. $S' = (S_1 + S_2), (S_1 + S_2 - 1), \ldots |S_1 - S_2|$; $S_1 = S_2$ is the iron(III) ion spin, equal to 5/2. For the investigated systems the values of S' are: 5, 4, 3, 2, 1, 0. The expression for molar magnetic susceptibility χ_M could be presented as

$$\chi_M = \frac{3g^2}{4T} \frac{[55\exp(30x) + 30\exp(20x) + 14\exp(12x) + 5\exp(6x) + \exp(2x)]}{[11\exp(30x) + 9\exp(20x) + 7\exp(12x) + 5\exp(6x) + 3\exp(2x) + 1]}, \qquad (3)$$

where g is the Lande factor of splitting, $x = J_{12}/(kT)$.

Using the fitting program MAGMUN [48], the parameters of magnetic exchange J_{12} have been determined, giving the following values: $J_{12} = J_{Fe-Fe} = -58.9 \pm 0.5\ cm^{-1}$ for **1**; $-75.4 \pm 0.8\ cm^{-1}$ for **2**; $-60.4 \pm 0.4\ cm^{-1}$ for **3**; g is equal to 2.0 for **1** and **3**, and 2.14 for **2** (see Fig. 5).

From the acquired data, it is obvious that the absolute value of the magnetic exchange parameter J_{12} changes from complex to complex. At the same time it is useful to note that the values of the parameter of exchange between iron (III) ions in the discussed trinuclear clusters are significantly larger in their absolute values compared to similar homonuclear carboxylates of iron (III) [16,36,49], but they are practically the same for heteronuclear acetates with $\{Fe_2MO\}$ cores, where M is a 3d-element [18]. From the comparison of L(Fe–Fe) and $|J_{Fe-Fe}|$ values for **1** and **3**, one can see that they have a certain mutual correlation. The fact that the value $|J_{Fe-Fe}|$ for **2** is considerably different from those of **1** and **3** probably is the result of the different temperature ranges in which the susceptibility curves have been measured and the different values of the fitted g factor.

4. Conclusions

Three new μ_3-oxo heterotrinuclear iron and s-metal containing carboxylates of the composition $[Fe_2M(Ca, Sr, Ba)O(RCOO)_6(L)_n]$, where R = CCl_3, L = tetrahydrofuran (THF), have been synthesized.

For the first time the possibility to obtain a trinuclear core $[Fe_2MO(R–COO)_6]$ with M differing in both electronic property (Fe – alkaline-earth metals) and dimension (Fe/Ba, Fe/Sr, Fe/Ca) was demonstrated. The positions of paramagnetic and diamagnetic centres in the core of the trinuclear molecule have been assigned unambiguously. This allows an analysis of the magnetic interactions in the Fe–Fe fragment where the iron atoms are connected by two different bridges.

The absolute value of the antiferromagnetic interaction between iron(III) ions (magnetic exchange parameter $-58.9 \pm 0.5\ cm^{-1}$ for **1**, $-75.4 \pm 0.8\ cm^{-1}$ for **2**, $-60.4 \pm 0.4\ cm^{-1}$ for **3**) is higher than the analogous parameter in homo-iron carboxylates, but they are practically the same for heteronuclear acetates with $\{Fe_2MO\}$ cores, where M is a 3d-element.

5. Supplementary material

Crystallographic data (excluding structure factors) for **1** and **3** have been deposited with the Cambridge Crystallographic Data Centre as a supplementary publication, CCDC reference number 247520 for **1** and 247519 for **3**. Copies of the data can be obtained, free of charge, on application to CCDC, 12 Union Road, Cambridge CB2 1EZ, UK [fax: +44 1223 336 033 or e-mail: deposit@ccdc.cam.ac.uk].

Acknowledgements

The research described in this publication was made possible in part by Award No. BGP III #MOB-2-3058-CS-03 of the Moldovan Research and Development Association (MRDA) and the US Civilian Research & Development Foundation (CRDF) and by INTAS-00565 Grant. V. Mereacre thanks also the Alexander von Humboldt Foundation for financial support.

References

[1] P. Norlund, B.-M. Sjoberg, H. Eklund, Nature (London) 345 (1990) 593.

[2] S. Sheriff, W.A. Hendrickson, J.L. Smith, J. Mol. Biol. 197 (1987) 273.
[3] A. Rosenzwieg, P. Norlund, C.A. Frederick, S.J. Lippard, Nature (London) 366 (1993) 537.
[4] R.D. Cannon, R.P. White, Prog. Inorg. Chem. 36 (1988) 195.
[5] S.J. Lippard, Angew. Chem., Int. Ed. Engl. 27 (1988) 344.
[6] T. Sato, M. Katada, K. Endo, M. Nakada, H. Sano, J. Radioanal. Nucl. Chem. 173 (1993) 107.
[7] M. Yoshida, T. Nakamoto, S. Kwata, M. Katada, H. Sano, Hyperfine Interact. 84 (1994) 589.
[8] Y.M. Shulga, O.S. Roshchupkina, G.I. Dzhardimalieva, I.V. Chernushevich, A.F. Dodonov, Y.V. Baldokhin, P.Y. Kolotyrkin, A.S. Rozenberg, A.D. Pomogailo, Russ. Chem. Bull. 42 (1993) 1661.
[9] Y.M. Shulga, I.V. Chernushevich, G.I. Dzhardimalieva, O.S. Roshchupkina, A.F. Dodonov, A.D. Pomogailo, Russ. Chem. Bull. 43 (1994) 983.
[10] M. Högbom, P. Nordlund, FEBS Lett. 567 (2004) 179.
[11] K.S. Gavrilenko, A. Vertes, G. Vanko, L.F. Kiss, A.W. Addison, T. Weyhermüller, V.V. Pavlishchuk, Eur. J. Inorg. Chem. (2002) 3347.
[12] K.I. Turta, A.O. Solonenco, I.I. Bulgak, F.K. Jovmir, M. Rosenberg, P. Stelmaszyk, G. Filoti, J. Radioanal. Nucl. Chem. (Ar.) 190 (1995) 347.
[13] N.V. Gerbeleu, A.S. Batsanov, G.A. Timko, Y.T. Struchkov, K.M. Indrichan, G.A. Popovich, Proc. Acad. Scien. USSR (Dokl. Akad. Nauk. SSSR) 293 (1987) 364.
[14] A.B. Blake, E. Sinn, A. Yavari, K.S. Murray, B. Moubaraki, J. Chem. Soc., Dalton Trans. (1998) 45.
[15] R.C. Mehrota, R. Bohra, Metal Carboxylates, Academic Press, London, 1983.
[16] B.S. Tsukerblat, M.I. Belinsky, Magnetochemistry and radiospectroscopy of exchange clusters, Shtiintsa, Eishinev, Moldova (1983) 280 (in Russian).
[17] L. Meesuk, R.P. White, B. Templeton, U.A. Jayasooriya, R.D. Cannon, Inorg. Chem. 29 (1990) 2389.
[18] A.B. Blake, A. Yavari, W.E. Hatfield, C.N. Sethulekshmi, J. Chem. Soc., Dalton Trans. (1985) 2509.
[19] S. Shova, D. Prodius, V. Mereacre, Yu.A. Simonov, J. Lipkowski, K. Turta, Inorg. Chem. Commun. 7 (2004) 292.
[20] Z.-M. Wang, X.-F. Yu, Chin. J. Struct. Chem. 9 (1990) 14.
[21] T.K. Jovmir, K.I. Turta, S.G. Shova, Yu.A. Simonov, M. Gdaniec, I.I. Bulhac, I.G. Kadel'nic, G. Filoti, Russ. J. Struct. Chem. 40 (1999) 1155 (in Russian).
[22] S. Shova, V. Mereacre, M. Gdaniec, Yu.A. Simonov, T. Jovmir, D. Prodius, K. Turta, Russ. J. Inorg. Chem. 48 (2003) 72.
[23] C. Turta, S. Shova, D. Prodius, V. Mereacre, M. Gdaniec, Yu. Simonov, J. Lipkowski, Inorg. Chim. Acta 357 (2004) 4396.
[24] B. Singh, J.R. Long, F.F. de Biani, D. Gatteschi, P. Stavropoulos, J. Am. Chem. Soc. 119 (1997) 7030.
[25] V.I. Ponomarev, O.S. Filipenco, L.O. Atovmian, S.A. Bobcova, K.I. Turta, Proc. Acad. Sci. USSR (Dokl. AN SSSR) 262 (1982) 346 (in Russian).
[26] I.N. Ivleve, S.B. Echmaev, R.A. Stukan, K.I. Turta, S.A. Bobkova, M.E. Veksel'man, Russ. J. Inorg. Chem. 6 (1982) 1479 (in English).
[27] V.I. Ponomarev, O.S. Filipenco, L.O. Atovmian, S.A. Bobcova, K.I. Turta, Russ. J. Coord. Chem. 13 (1987) 1097 (in Russian).
[28] S.M. Oh, D.N. Hendrickson, K.L. Hassett, R.E. Davis, J. Am. Chem. Soc. 106 (1984) 7984.
[29] S.M. Oh, D.N. Hendrickson, K.L. Hassett, R.E. Davis, J. Am. Chem. Soc. 107 (1985) 8009.
[30] C. Wilson, B.B. Iversen, J. Overgaard, F.K. Larsen, G. Wu, S.P. Palii, G.A. Timco, N.V. Gerbeleu, J. Am. Chem. Soc. 122 (2000) 46, 11370.
[31] R.H. Laye, F.K. Larsen, J. Overgaard, C.A. Muryn, E.J. McInnes, E. Rentschler, V. Sanchez, S.J. Teat, H.U. Guedel, O. Waldmann, G.A. Timco, R.E.P. Winpenny, Chem. Commun. 9 (2005) 1125.
[32] T. Sato, F. Ambe, K. Endo, M. Katada, H. Maeda, T. Nakamoto, H. Sano, J. Am. Chem. Soc. 118 (1996) 14, 3450.
[33] C. Stadler, J. Daub, J. Kohler, R.W. Saalfrank, V. Coropceanu, V. Schunemann, C. Ober, A.X. Trautwein, S.F. Parker, M. Poyraz, T. Inomata, R.D. Cannon, J. Chem. Soc., Dalton Trans. 22 (2001) 3373.
[34] K. Prassides, Mixed Valence Systems: Applications in Chemistry and Biology, Kluwer, Dordrecht, 1991.
[35] F.H. Alen, Acta Crystallogr., Sect. B 58 (2002) 380.
[36] O. Kahn, Molecular Magnetism, VCH Publishers Inc., New York, USA, 1993, p. 225.
[37] Z. Otwinowski, W. Minor, in: C.W. Carter, R.M. Sweet (Eds.), Methods in Enzymology, vol. 276, Academic Press, London, 1996, p. 307.
[38] R.H. Blessing, Acta Crystallogr., Sect. A 51 (1995) 33.
[39] CrysAlis RED, Oxford Diffraction Ltd.,Version 1.170.32, 2003.
[40] G.M. Sheldrick, SHELXL-97, University of Göttingen, Göttingen, Germany, 1997.
[41] A.V.R. Warrier, R.S. Krishnam, Spectrochim. Acta A 27 (1971) 1243.
[42] J.A. Faniran, K.S. Patel, M.A. Mesubi, Spectrochim. Acta A 31 (1974) 117.
[43] M.K. Johnson, D.B. Powell, R.D. Cannon, Spectrochim. Acta A 37 (1981) 993.
[44] L. Montri, R.D. Cannon, Spectrochim. Acta A 41 (1985) 643.
[45] L. Meesuk, U.A. Jayasooriya, R.D. Cannon, Spectrochim. Acta A 43 (1987) 687.
[46] K.I. Turta, T.A. Spatari, V. Vrajmashu, Russ. J. Coord. Chem. 25 (1999) 835 (in Russian).
[47] K. Turta, S. Shova, T. Spatari, M. Mazus, T. Malinowsky, Russ. J. Struct. Chem. 35 (1994) 112.
[48] Z. Xu, K. He, L.K. Thompson, O. Waldmann, MAGMUN. Available from: <http://zhiqiangxu.tripod.com>.
[49] Yu.V. Rakitin, V.T. Kalinnikov, The modern magnetochemistry. S.-Petersburg. "Nauka" (1994) 272.

are markedly influenced by the steric demand of the substituents on the pendant silicon atom as well as by the alkyl chain length of the carbosilyl groups bonded to skeletal silicon backbone. As a part of this ongoing research, it has been our endeavor to understand structural features of new disilaalkanes which can be utilized as precursors in the synthesis of a variety of silicon polymers. We report herein the synthesis and characterization of some hitherto unknown asymmetrically substituted disilaalkanes $Ph_3SiCH_2CH_2SiRR'_2$ [R = Me, R′ = Cl (**1**); R = Ph, R′ = Cl (**2**); R = R′ = Cl (**3**), Ph (**4**), OEt (**5**), H (**6**)]. The crystal structures of **1** and **4** reveal the presence of C–H···Cl and/or C–H···π interactions which afford 3-D supramolecular assemblies.

2. Results and discussion

2.1. Synthesis and spectral studies

As evident from Scheme 1, the hydrosilylation reaction between equimolar quantities of triphenylsilane and dichloromethyl/dichlorophenyl/trichlorovinylsilane in the presence of Karstedt's catalyst (10^{-5} mol of Pt/mol of silane) affords the corresponding disilaalkanes, $Ph_3SiCH_2CH_2SiRR'_2$ [R = Me, R′ = Cl (**1**); R = Ph, R′ = Cl (**2**); R = R′ = Cl (**3**)] along with minor amounts of 1,1,1,4,4,4-hexaphenyl-1,4-disilabutane (**4**; yield: 4.4–8.8%) in each case. The isolation of these disilaalkanes as analytically pure products from the mixture has been accomplished by taking advantage of the preferential solubility of **1**–**3** in *n*-hexane. By analogy with the literature precedence [13], the formation of **4** in these reactions is believed to arise from a ligand-exchange phenomenon involving vinyl/H groups in the precursors under Pt-catalyzed conditions (Eq. (1)). The resulting triphenylvinylsilane subsequently undergoes hydrosilylation with triphenylsilane to yield compound **4**

$$Ph_3SiH + CH_2{=}CHSiRCl_2 \rightleftarrows CH_2{=}CHSiPh_3 + HSiRCl_2 \quad (1)$$

On the other hand, the reaction between triphenylsilane and triethoxyvinylsilane under similar conditions proceeds regioselectively to yield the disilaalkane **5** as the exclusive product, which upon subsequent treatment with lithium aluminum hydride affords **6** with a SiH_3 end group.

The disilaalkanes obtained herein are white solids or a viscous liquid (for **2**) and are soluble in common organic solvents such as dichloromethane, chloroform, toluene, THF etc. The identity of these compounds has been established by IR as well as ^1H, $^{13}C\{^1H\}$ and $^{29}Si\{^1H\}$ NMR spectroscopy. ^1H NMR spectra of **1**–**3**, **5** and **6** reveal two distinct multiplets in the region δ 1.58–0.73 due to methylene groups. The 2D-TOCSY spectra confirm these spectral features to arise from both geminal and vicinal coupling of non-equivalent CH_2 protons. For **4**, a singlet at δ1.43 for the methylene protons is in accord with the symmetrical structure and is supported by a single $^{29}Si\{^1H\}$ NMR resonance at δ −8.5 due to Ph_3Si groups. $^{29}Si\{^1H\}$ NMR spectra of all other silaalkanes display an additional singlet at the chemical shift values which are characteristic of the functionally substituted silicon moieties (see Section 3).

2.2. X-ray crystal structures

Single crystals suitable for X-ray structure analysis were obtained upon cooling the solution of the compounds in dichloromethane (for **1**) and dichloromethane/toluene (80:20) (for **4**). The molecular structure of **1**, along with atomic labelling scheme, is shown in Fig. 1, while the crystal data and selected bond lengths and angles are listed in Tables 1 and 2, respectively. The molecule adopts a *trans*-planar conformation of the Si–C–C–Si unit (torsional angle −178.4(1)°), similar to related symmetrically substituted 1,4-disilabutanes known earlier [5,8,9]. However, the Si–C–C angles subtended by the methylene groups [117.0(1)°;

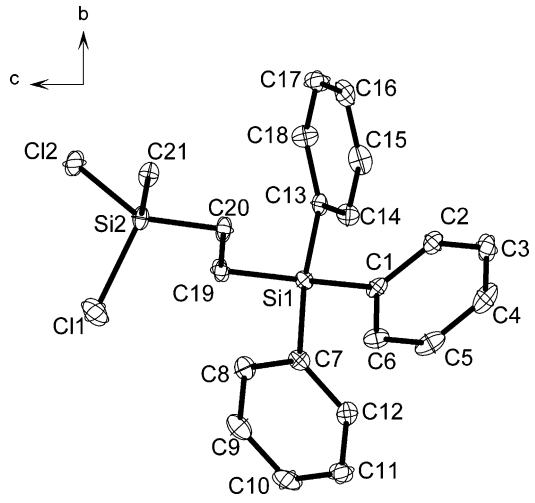

Fig. 1. ORTEP view of **1**. Thermal ellipsoids are shown at 50% probability. Hydrogen atoms are omitted for clarity.

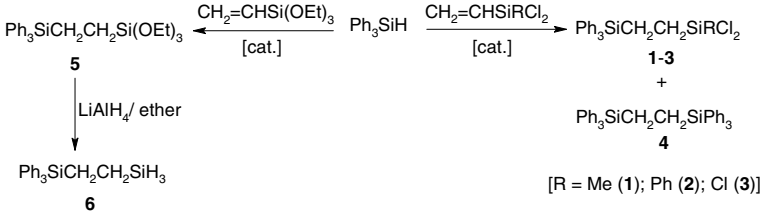

Scheme 1.

Table 1
Crystal data and structure refinement parameters for **1** and **4**

	1	**4**
Empirical formula	$C_{21}H_{22}Cl_2Si_2$	$C_{38}H_{34}Si_2$
M_r	401.47	546.83
T (K)	100(2)	100(2)
λ (Å)	0.71073	0.71073
Crystal system	monoclinic	triclinic
Space group	$P2_1/c$	$P\bar{1}$
a (Å)	7.6677(9)	7.8468(9)
b (Å)	11.5230(13)	9.4743(10)
c (Å)	23.061(3)	21.464(2)
α (°)	90	96.460(2)
β (°)	91.200(1)	93.190(2)
γ (°)	90	111.239(2)
V (Å^3)	2037.1(4)	1469.9(3)
Z	4	2
Crystal size (mm)	$0.201 \times 0.195 \times 0.130$	$0.319 \times 0.108 \times 0.098$
ρ_{calc} (Mg m^{-3})	1.309	1.236
μ (mm^{-1})	0.438	0.147
$Refl_{collected/unique}$	14926/3793	13836/5131
R_{int}	0.1050	0.0380
R_1/wR_2 ($I > 2\sigma(I)$)	0.0389/0.1030	0.0916/0.2472
R_1/wR_2 (all data)	0.0426/0.1054	0.1032/0.2498

$R_1 = (\sum||F_o| - |F_c||/\sum|F_o|)$, $wR_2 = \sum w(F_o^2 - F_c^2)^2 / \sum[(F_o^2)^2]^{1/2}$, $s = [\sum w(F_o^2 - F_c^2)^2/n - p)]^{1/2}$.

Table 2
Selected bond lengths (Å) and angles (°) for **1**

Bond lengths			
Si2–Cl1	2.049(8)	Si2–Cl2	2.044(7)
C19–C20	1.531(3)	Si1–C19	1.899(2)
Si2–C20	1.865(2)	Si2–C21	1.861(1)
Bond angles			
C20–C19–Si1	117.0(1)	C19–C20–Si2	116.7(1)
C21–Si2–C20	114.9(9)	Cl2–Si2–Cl1	105.4(3)
C20–Si2–Cl2	108.6(7)	C20–Si2–Cl1	109.6(7)
C21–Si2–Cl2	109.3(7)	C21–Si2–Cl1	108.3(7)
Dihedral angles			
Si1–C19–C20–Si2	−178.4(1)	C21–Si2–C20–C19	−174.4(1)
Cl1–Si2–C20–C19	−52.1(1)	Cl2–Si2–C20–C19	62.6(1)
C13–Si1–C7–C8	66.1(1)	C13–Si1–C1–C2	2.4(1)
C7–Si1–C1–C6	64.2(1)	C7–Si1–C13–C14	21.1(1)
C1–Si1–C13–C18	81.2(1)	C1–Si1–C7–C12	4.4(2)

116.7(1)°] are found to be the largest known so far, as might be expected in a sterically congested system. The influence of the bulky Ph_3Si group is also reminiscent in the observed Si1–C19 bond length, 1.899(2) Å, which lies at the upper end of the normal range accepted for the Si–C bond (1.86–1.91 Å) [14]. In addition, a large deviation from a tetrahedral geometry around the Si2 atom is discernible from a considerable reduction of Cl1–Si2–Cl2 [105.4(3)°] and a concomitant increase of C21–Si2–C20 [114.9(9)°] angles. The observed deformation in the Cl–Si–Cl angle is in contrast to those found in the solid state structures of related compounds such as $Cl_3SiCH_2CH_2SiCl_3$ [107.1(3)–108.5(3)°] [8] and H_2SiCl_2 [109.0(1)°], but is close to that of the adduct $[(H_3C)_2O \cdot H_2SiCl_2]_2$ [104.7(1)°] [15] in which the silicon atom adopts a hexacoordinate structure. A consequence of this structural deformation also results in significant deviation of the Cl1–Si2–C20–C19 moiety from an ideal gauche conformation (torsion angle, −52.1(1)°). The triphenylsilyl fragment in the molecule adopts a propeller-shape conformation [16,17] in order to relieve the steric strain due to interactions between the *ortho*-hydrogen atoms of the adjacent phenyl groups. A qualitative interpretation of the extent of propeller-twist distortion is obtained by an examination of the dihedral angles C_{ipso}–Si–C'_{ipso}–C'_{ortho} subtended between the phenyl rings. The mean distortion of these dihedral angles has been found to be 39.9° in comparison to the idealized value of 30° expected in the absence of an *ortho–ortho* interaction between the phenyl groups [17]. A detailed analysis of the X-ray structure of **1** reveals the existence of weak hydrogen bonding involving C–H···Cl [18] and C–H···π [19] interactions, leading to a 3-D supramolecular network. A perspective view of the self assembly is shown in Fig. 2. Noticeably, the Cl(2) atom is involved in a bifurcated C–H···Cl interaction involving CH (arene) and CH_2 (methylene) hydrogens of the two neighboring molecules, while Cl(1) atom is intramolecularly associated with H19A of the methylene group. The crystallographic numbering scheme represents the corresponding parameters as follows [H10–Cl2 = 3.12 Å, C10–Cl2 = 3.99 Å, C10–H10–Cl2 = 158.3°; H20B–Cl2 = 3.07 Å, C20–Cl2 = 3.90 Å, C20–H20B–Cl2 = 143.2°, H19A–Cl1 = 3.12 Å, C19–Cl1 = 3.58 Å, C19–H19A–Cl1 = 111.3°]. In addition, one of the arene hydrogens, H16, is involved in an intermolecular CH···π interaction with a H16–centroid distance of 3.05 Å, the corresponding C16–centroid distance being 3.84 Å and the associated C16–H16–centroid angle 144.2°. The 2-D structure thus formed along the *bc* plane self assembles into a 3-D network by intermolecular C–H···Cl and C–H···π interactions, with the Cl1 atom involved in bifurcated H-bonding. The metric parameters involved are H19A–Cl1 = 3.06 Å; C19–Cl1 = 3.97 Å, C19–H19A–Cl1 = 156.9°; H21C–centroid = 3.05 Å, C21C–centroid = 3.69 Å, C21C–H21C–centroid angle = 125.6°. The overall structure adopts stacked layers along the crystallographic *a* axis.

The molecular structure of **4** comprises two independent molecules in the unit cell, of which only one is shown in Fig. 3. The crystal data are summarized in Table 1 and selected bond lengths and angles are listed in Table 3. Each molecule lies on a crystallographic inversion centre and adopts a *trans*-planar conformation of the Si–C–C–Si unit with nearly identical metrical parameters [Si1–C19 1.881(5) Å, Si2–C38 1.879(4) Å, C19–C19 1.538(9) Å, C38–C38 1.537(8) Å, C19–C19–Si1 116.5(4)°, C38–C38–Si2 117.0(4)°]. However, there are subtle structural differences in the relative orientations of various phenyl rings with respect to the C–Si–C_{ipso} plane, as evident from the dihedral angles C–Si–C_{ipso}–C_{ortho} (Table 3), the largest observed deviation being 3.9°. These results are in conformity with the superposition plot shown in Fig. 4. The Ph_3Si fragments in each molecule also exhibit propeller twist distortion with a mean value of the dihedral angles

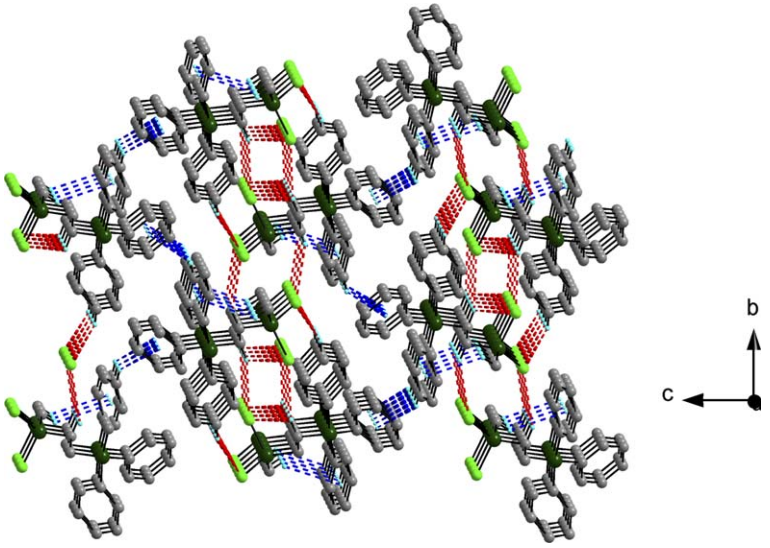

Fig. 2. 3-D supramolecular assembly of **1** showing hydrogen bonding interactions: C–H···Cl (red dotted lines) and C–H···π (blue dotted lines). The hydrogen atoms not involved in hydrogen bonding are omitted for clarity. Color code: Si, dark green; C, grey; H, cyan; Cl, green. (For interpretation of the references to color in this figure legend, the reader is referred to the web version of this article.)

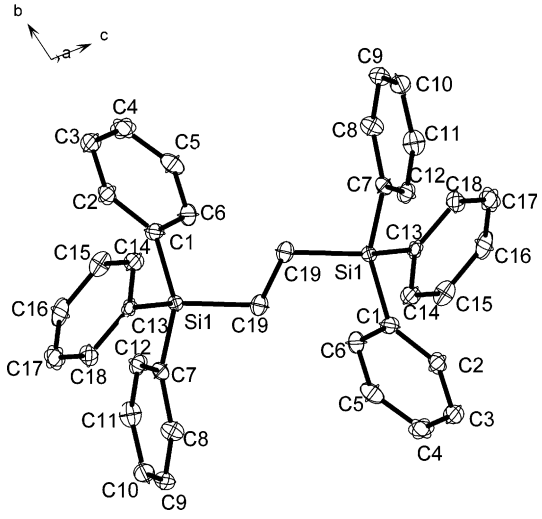

Fig. 3. ORTEP view of **4** (one independent molecule). Thermal ellipsoids are shown at 50% probability. Hydrogen atoms are omitted for clarity.

Table 3
Selected bond lengths (Å) and angles (°) for **4**

Bond lengths			
Si1–C19	1.881(5)	Si2–C38	1.879(4)
C19–C19	1.538(9)	C38–C38	1.537(8)
Bond angles			
C19–C19–Si1	116.5(4)	C38–C38–Si2	117.0(4)
Dihedral angles			
C19–Si1–C13–C18	118.8(4)	C38–Si2–C26–C31	120.6(3)
C19–Si1–C1–C6	−48.8(4)	C38–Si2–C20–C25	−44.9(4)
C19–Si1–C7–C12	118.4(4)	C38–Si2–C32–C33	120.3(4)
C13–Si1–C7–C8	59.0(4)	C13–Si1–C1–C2	6.4(5)
C7–Si1–C1–C6	66.2(4)	C7–Si1–C13–C18	3.0(4)
C1–Si1–C13–C14	60.5(4)	C1–Si1–C7–C12	−0.8(4)
C26–Si2–C32–C37	62.6(4)	C26–Si2–C20–C21	13.1(4)
C20–Si2–C26–C27	61.1(4)	C20–Si2–C32–C33	0.3(4)
C32–Si2–C20–C25	72.3(4)	C32–Si2–C26–C31	2.7(4)

Symmetry codes: (i) $2-x, -y, 1-z$; (ii) $-x, 1-y, -z$.

C_{ipso}–Si–C'_{ipso}–C'_{ortho} of 32.6° for the Si1 molecule and 35.3° for the Si2 molecule. In addition, extensive CH···π interactions between the arene rings have been observed which results in the formation of a 3-D supramolecular assembly (Fig. 5). A view along the crystallographic *a* axis reveals that one of the asymmetric molecules, designated with the Si1 atom, involves H5 and H11 atoms for CH···π interactions with the adjacent arene molecules. Similar characteristic CH···π interactions are also evident for the Si2 molecule, involving H24 and H34 atoms [H5–centroid = 2.83 Å, C5–centroid = 3.56 Å, C5–H5–centroid angle = 134.5°; H11–centroid = 2.89 Å, C11–centroid = 3.53 Å, C11–H11–centroid angle = 125.9°; H24–centroid = 2.83 Å, C24–centroid = 3.61 Å, C24–H24–centroid angle = 139.5°; H34–centroid = 3.04 Å, C34–centroid = 3.69 Å, C34–H34–centroid angle = 127.6°]. The Si2 mole-

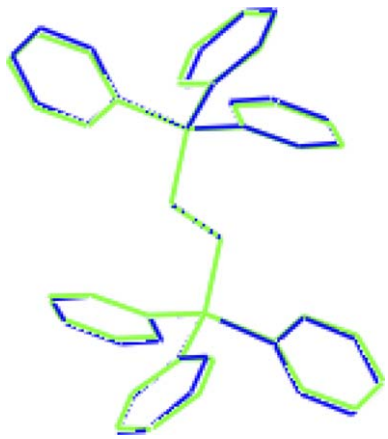

Fig. 4. Superposition plot of **4**.

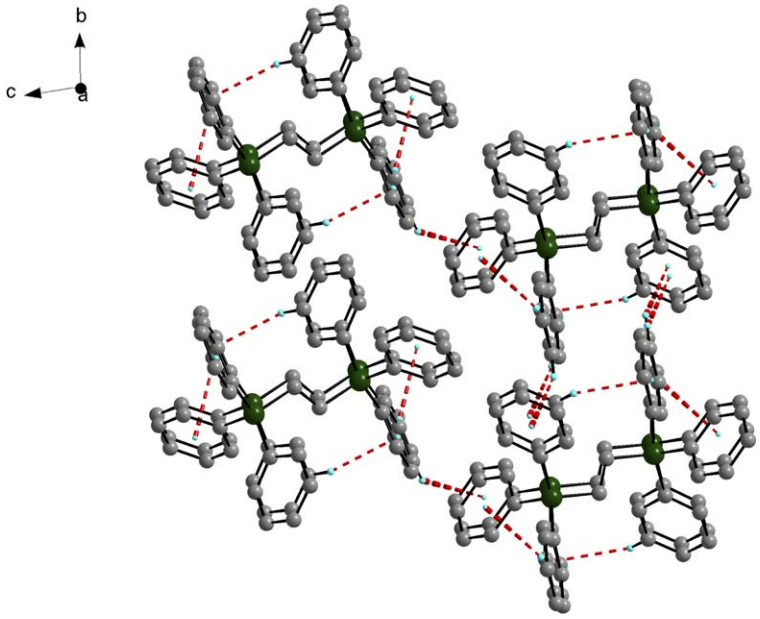

Fig. 5. 3-D view of **4** showing C–H···π interactions (red dotted lines). The hydrogen atoms not involved in hydrogen bonding are omitted for clarity. (For interpretation of the references to color in this figure legend, the reader is referred to the web version of this article.)

cules are associated along the *bc* plane via a C35–H35···π interaction with a H35–centroid distance of 2.58 Å and C35–H35–centroid angle of 157.4°, while Si1 molecules are devoid of such interactions. The two asymmetric molecules are interconnected via a CH···π interaction involving the H10 atom of one molecule with the arene moiety of the other [H10–centroid = 2.95 Å, C10–centroid = 3.78 Å, C10–H10–centroid angle = 146.3°].

In conclusion, the disilaalkanes **1**–**6** have been synthesized by the hydrosilylation reaction between triphenylsilane and the corresponding vinylsilanes in the presence of Karstedt's catalyst. The formation of **4** in these reactions has been rationalized by invoking a redistribution of the vinyl and H groups in the precursors under the catalyzed conditions. The molecular structures of **1** and **4** reveal a considerable increase in the Si–C bond lengths and Si–C–C bond angles in order to relieve the steric strain imposed by the bulky triphenylsilyl group. The formation of a 3-D supramolecular assembly in these structures is mediated through extensive C–H···Cl (for **1**) and C–H···π interactions. To our knowledge, there is no such precedence of supramolecular aggregation in the family of disilaalkanes. The implications of these structural characteristics on the electronic properties of the resulting polysilanes derived from the disilaalkane precursors are currently under investigation.

3. Experimental

3.1. General comments

All operations were carried out using standard schlenk line techniques under dry nitrogen atmosphere. Solvents were freshly distilled under inert atmosphere over P_2O_5 (dichloromethane and *n*-hexane) or sodium benzophenone (toluene) before use. Glassware were dried in an oven at 100–120 °C and further flame dried under vacuum prior to use. Dichloromethylvinylsilane, trichlorovinylsilane and triethoxyvinylsilane (Aldrich) were freshly distilled before use. Karstedt's catalyst (platinum(0)-1,3-divinyl-1,1,3,3-tetramethyldisiloxane complex), triphenylsilane (Aldrich) were used as received. Dichlorophenylvinylsilane was prepared by the literature method [20].

Infrared spectra were obtained as thin films on KBr pellets on a Nicolet FT-IR (Protégé) spectrophotometer. ^{1}H, $^{13}C\{^{1}H\}$ and $^{29}Si\{^{1}H\}$ NMR spectra were recorded in $CDCl_3$ on a Bruker spectrospin DPX 300 MHz instrument at frequency 300, 75.5, 59.6 MHz, respectively, and chemical shifts are quoted relative to Me_4Si. 2-D TOCSY (Total Correlation Spectroscopy) experiments using the standard pulse sequence were carried out in $CDCl_3$. The mixing time used for these experiments were 4 and 80 ms. A total of 32 scans containing 1 K data points were accumulated for 512 experiments with a delay time of 2 s. Elemental analysis (C, H and N) was performed on a Perkin–Elmer model 2400 CHN elemental analyzer.

3.2. Synthesis of disilaalkanes *1*–*6*

Dichloromethyl/dichlorophenyl/trichlorovinylsilane (16.19 mmol) was added dropwise to a melt of triphenylsilane (15.61 mmol) containing a catalytic amount of Karstedt's reagent (10^{-5} mol of Pt/mol of silane) at 50 °C. No induction period was observed during the complete addition. The reaction mixture was heated at 75 °C for 12 h. The contents were cooled and *n*-hexane (50 ml) was added to afford 1,1,1,4,4,4-hexaphenyl-1,4-disilabutane (**4**) as a white solid, which was filtered and dried under vacuum.

The filtrates obtained from these reactions were concentrated under vacuum to yield the corresponding disilaalkanes **1**–**3**.

*3.2.1. $Ph_3SiCH_2CH_2SiMeCl_2$ (**1**)*

Yield: (4.72 g, 75.4%), m.p. 94–95 °C. *Anal.* Calc. for $C_{21}H_{22}Cl_2Si_2$: C, 62.84; H, 5.48. Found: C, 62.75; H, 5.34%. ^{1}H NMR 7.57–7.13 (m, 15H, *Ph*), 1.43–1.37 (m, 2H, CH_2SiMeCl$_2$), 1.10–1.04 (m, 2H, Ph$_3$SiCH_2), 0.78 (s, 3H, *Me*). ^{13}C{^{1}H} NMR 135.93, 135.60, 129.68, 128.03 (Si–*Ph*), 14.69 (*C*H$_2$SiMeCl$_2$), 4.38 (Si–*Me* + Ph$_3$Si*C*H$_2$). ^{29}Si{^{1}H} NMR −8.38 (Ph$_3$*Si*), 32.68 (*Si*MeCl$_2$).

*3.2.2. $Ph_3SiCH_2CH_2SiPhCl_2$ (**2**)*

Yield: (5.84 g, 80.8%), viscous liquid. *Anal.* Calc. for $C_{26}H_{24}Cl_2Si_2$: C, 67.38; H, 5.18. Found: C, 67.23; H, 5.12%. ^{1}H NMR 7.63–7.28 (m, 20H, *Ph*), 1.43–1.38 (m, 2H, CH_2SiPhCl$_2$), 1.32–1.29 (m, 2H, Ph$_3$SiCH_2). ^{13}C{^{1}H} NMR 138.22, 133.94, 133.81, 131.94, 129.46, 128.62, 128.10 (Si–*Ph*), 13.82 (*C*H$_2$SiPhCl$_2$), 4.56 (Ph$_3$Si*C*H$_2$). ^{29}Si{^{1}H} NMR −8.53 (Ph$_3$*Si*), 20.41 *Si*PhCl$_2$).

*3.2.3. $Ph_3SiCH_2CH_2SiCl_3$ (**3**)*

Yield: (4.28 g, 65.0%), m.p. 135–137 °C. *Anal.* Calc. for $C_{20}H_{19}Cl_3Si_2$: C, 56.93; H, 4.50. Found: C, 56.72; H, 4.39%. ^{1}H NMR 7.65–7.38 (m, 15H, *Ph*), 1.58–1.51 (m, 2H, CH_2SiCl$_3$), 1.46–1.39 (m, 2H, Ph$_3$SiCH_2). ^{13}C{^{1}H} NMR 136.78, 135.54, 129.83, 128.12 (Si–*Ph*), 17.87 (*C*H$_2$SiCl$_3$), 4.61 (Ph$_3$Si*C*H$_2$). ^{29}Si{^{1}H} NMR −8.68 (Ph$_3$*Si*), 12.40 (*Si*Cl$_3$).

*3.2.4. $Ph_3SiCH_2CH_2SiPh_3$ (**4**)*

Yield: (4.4–8.8%), m.p. 195–196 °C. *Anal.* Calc. for $C_{38}H_{34}Si_2$: C, 83.51; H, 6.22. Found: C, 83.32; H, 6.15%. ^{1}H NMR 7.47–7.30 (m, 30H, *Ph*), 1.43 (s, 4H, CH_2). ^{13}C{^{1}H} NMR 135.73, 134.85, 129.41, 127.85 (Si–*Ph*), 5.64 (*C*H$_2$). ^{29}Si{^{1}H} NMR −8.50 (Ph$_3$*Si*).

*3.2.5. $Ph_3SiCH_2CH_2Si(OEt)_3$ (**5**)*

The title compound was prepared using triphenylsilane (3.67 g, 14.09 mmol) and triethoxyvinylsilane (2.70 g, 3.0 ml, 14.23 mmol) by following a similar procedure as described above. Compound **5** was obtained as a low melting solid. Yield: (4.69 g, 73.2%), m.p. 46–48 °C. *Anal.* Calc. for $C_{26}H_{34}Si_2O_3$: C, 69.33; H, 7.55. Found: C, 69.10; H, 7.43%. ^{1}H NMR 7.47–7.27 (m, 15H, *Ph*), 3.74–3.63 (q, 6H, CH_2(Et), $^3J_{HH} = 6.88$ Hz), 1.36–1.30 (m, 2H, Ph$_3$SiCH_2), 1.12 (t, 9H, CH_3(Et), $^3J_{HH} = 6.93$ Hz), 0.66–0.60 (m, 2H, CH_2Si(OEt)$_3$). ^{13}C{^{1}H} NMR 135.66, 134.90, 129.34, 127.79 (Si–*Ph*), 58.38 (*C*H$_2$(Et)), 18.27 (*C*H$_3$(Et)), 4.31 (Ph$_3$Si*C*H$_2$), 2.83 (*C*H$_2$Si(OEt)$_3$). ^{29}Si{^{1}H} NMR −8.30 (Ph$_3$*Si*), −44.92 (*Si*(OEt)$_3$).

*3.2.6. $Ph_3SiCH_2CH_2SiH_3$ (**6**)*

A solution of **5** (3.84 g, 7.74 mmol) in diethylether was added dropwise to a dispersion of $LiAlH_4$ (0.45 g, 11.84 mmol) in same solvent at 0 °C. The reaction mixture was gently refluxed for 5–6 h. Thereafter, the contents were treated with 1 N HCl, then the ether layer was extracted and dried over anhydrous Na_2SO_4. The solvent was removed under vacuum to afford **6** as a white solid. Yield: (1.52 g, 61.7%), m.p. 95–96 °C. *Anal.* Calc. for $C_{20}H_{22}Si_2$: C, 75.47; H, 6.91. Found: C, 75.21; H, 6.68%. ^{1}H NMR 7.53–7.34 (m, 15H, *Ph*), 3.50 (t, 3H, Si*H*, $^3J_{HH} = 3.63$ Hz), 1.45–1.39 (m, 2H, Ph$_3$SiCH_2), 0.86–0.79 (m, 2H, CH_2SiH$_3$). ^{13}C{^{1}H} NMR 136.36, 135.63, 129.47, 127.87 (Si–*Ph*), 9.00 (Ph$_3$Si*C*H$_2$), −0.60 (*C*H$_2$SiH$_3$). ^{29}Si{^{1}H} NMR −8.95 (Ph$_3$*Si*), −55.6 (*Si*H$_3$).

3.3. X-ray crystallography

The suitable crystals of **1** and **4** were mounted lengthways with the largest dimension in sealed capillaries and were used for data collection. The intensity data were collected on a Bruker SMART APEX diffractometer equipped with a molybdenum sealed tube and a highly orientated graphite monochromator. The structures were solved by direct methods and refined using the SHELXTL package [21,22]. Non-hydrogen atoms were refined anisotropically by the full-matrix least square method while the hydrogen atoms were constrained by a rigid model. All calculations were done on an IBM compatible PC using SMART [23], SAINT [24] and SADABS [25]. Details of crystallographic data are given in Table 1.

Acknowledgements

The authors are grateful to CSIR (India) for financial support and SRF to A.J.

Appendix A. Supplementary material

Crystallographic data for the structural analysis have been deposited with the Cambridge Crystallographic Data Center, CCDC Nos. 260286 for **1**, 260285 for **4**. Copies of this information may be obtained free of charge from The Director, CCDC, 12 Union Road, Cambridge, CB2 1EZ, UK (fax: +44 1233 336033; e-mail: deposit@ccdc.cam.ac.uk or www: http://www.ccdc.cam.uk). Supplementary data associated with this article can be found, in the online version, at doi:10.1016/j.poly.2006.01.021.

References

[1] (a) N.W. Mitzel, H. Schmidbaur, D.W.H. Rankin, B.A. Smart, M. Hofmann, P.v.R. Schleyer, Inorg. Chem. 36 (1997) 4360;
(b) N.W. Mitzel, P. Bissinger, J. Riede, K.-H. Dreihäupl, H. Schmidbaur, Organometallics 12 (1993) 413;
(c) N.W. Mitzel, M. Hofmann, K. Angermaier, A. Schier, P.v.R. Schleyer, H. Schmidbaur, Inorg. Chem. 34 (1995) 4840.
[2] J.-P. Majoral, A.-M. Caminade, Chem. Rev. 99 (1999) 845, and references cited therein.
[3] (a) R.J.P. Corriu, M. Enders, S. Huille, J.E. Moreau, Chem. Mater. 6 (1994) 15;
(b) P. Roux, J.-P. Pillot, M. Birot, J. Dunoguès, P. Lapouyade, J. Organometal. Chem. 499 (1995) 199;
(c) R.M. Shaltout, J.Y. Corey, Organometallics 15 (1996) 2866.

[4] A. Almenningen, H.M. Seip, R. Seip, Acta Chem. Scand. 24 (1970) 1697.
[5] N.W. Mitzel, B.A. Smart, A.J. Blake, H.E. Robertson, D.W.H. Rankin, J. Phys. Chem. 100 (1996) 9339.
[6] T. Fjeldberg, R. Seip, M.F. Lappert, A.J. Thorne, J. Mol. Struct. 99 (1983) 295.
[7] C. Glidewell, D. Liles, J. Organometal. Chem. 234 (1982) 15.
[8] N.W. Mitzel, J. Riede, H. Schmidbaur, Acta Crystallogr. Sect. C 53 (1997) 1335.
[9] N.W. Mitzel, J. Riede, H. Schmidbaur, Acta Crystallogr. Sect. C 52 (1996) 980.
[10] Y.E. Ovchinnikov, V.E. Shklover, Y.T. Struchkov, Y.P. Polyakov, L.E. Guselnikov, Acta Crystallogr. Sect. C 41 (1985) 1055.
[11] R. Tacke, R. Niedner, J. Frohnecke, L. Ernst, W.S. Sheldrick, Justus Liebigs Ann. Chem. (1980) 1859.
[12] (a) R. Shankar, A. Saxena, A.S. Brar, J. Organometal. Chem. 628 (2001) 262;
(b) R. Shankar, A. Saxena, A.S. Brar, J. Organometal. Chem. 650 (2002) 223;
(c) R. Shankar, A. Joshi, Macromolecules 38 (2005) 4176.
[13] J.L. Speier, Adv. Organometal. Chem. 17 (1979) 407.
[14] W.S. Sheldrick, in: S. Patai, Z. Rapport (Eds.), The Chemistry of Organosilicon Compounds, Wiley, Chichester, 1989, p. 245 (Part 1).
[15] K. Vojinovic, U. Losehand, N.W. Mitzel, J. Chem.Soc., Dalton Trans. (2004) 2578.
[16] K. Mislow, Acc. Chem. Res. 9 (1976) 26.
[17] J.B. Lambert, C.L. Stern, Y. Zhao, W.C. Tse, C.E. Shawl, K.T. Lentz, L. Kania, J. Organometal. Chem. 568 (1998) 21.
[18] G.R. Desiraju, T. Steiner, in: The Weak Hydrogen Bond in Structural Chemistry and Biology, Oxford University Press, Oxford, 1999, p. 215.
[19] (a) J.A.R.P. Sarma, G.R. Desiraju, Acc. Chem. Res. 19 (1986) 222;
(b) M. Nishio, M. Hirota, Y. Umezawa, in: The CH···π Interaction. Evidence, Nature and Consequences, Wiley-VCH, New York, 1998.
[20] R. Corriu, G.J. Royo, J. Organometal. Chem. 14 (1968) 291.
[21] G.M. Sheldrick, Acta Crystallogr. Sect. C 46 (1990) 467.
[22] G.M. Sheldrick, SHELXTL-NT2000, version 6.12, reference Manual, University of Göttingen, Germany.
[23] SMART (Ver 5.624). Software for data collection on a CCD Detector system, Bruker X-ray Analytical Instruments, Madison, WI, 1995.
[24] SAINT+ (Ver 5.6). Software for data reduction on a CCD Detector system, Bruker X-ray Analytical Instruments, Madison, WI, 1995.
[25] G.M. Sheldrick, SADBAS (Ver 2.03). Bruker X-ray Analytical Instruments, Madison, WI, 1999.

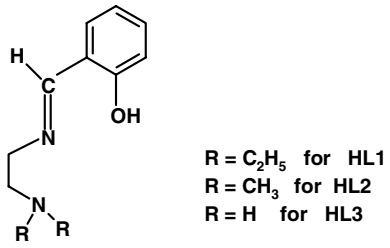

Scheme 1.

certainly influence the structural diversity of metal assembled complexes. Recently, we have reported a structurally characterized tetranuclear copper (II) azido complex containing salen (salenH$_2$ = *N*,*N*′-bis-(salicylidehyde)-ethylenediimine) as co-ligand [10]. An end-on azido group and a monophenoxo group from salen bridged four copper (II) centers to form a tetranuclear moiety. On changing the co-ligand salen to a tridentate Schiff base viz. HL3 (Scheme 1), the copper (II) azido system afforded a dinuclear moiety where copper (II) ions are bridged by two end-on azido groups [11]. In fact structurally characterized metal azido systems containing Schiff base co-ligands were not so well documented before our reports [12,13].

We now report our investigation on the synthesis, characterization and the crystal structure analysis of two copper (II) azido systems in which 1-(*N*-salicylideneimine)-2-(*N*,*N*-diethyl)-aminoethane (HL1) and 1-(*N*-salicylideneimine)-2-(*N*,*N*-dimethyl)-aminoethane (HL2) are two different tridentate Schiff base ligands acting as co-ligand. Interestingly, while a monomeric complex [Cu(L1)(N$_3$)] (**1**) is obtained in case of HL1, HL2 afforded a polymeric ID chain, [Cu(L2)(N$_3$)]$_n$ (**2**), containing end-to-end azido bridges. The present work constitutes a part of our continuing study on metal-azido complexes of tridentate Schiff base ligands based on substituted ethylenediamines.

2. Experimental

2.1. General

All chemicals and solvents used during the synthesis were of AR grade and used as received. Elemental analyses (CHN) were performed using a Perkin–Elmer 240 elemental analyzer. IR spectra were recorded on a Nicolate Magna IR 750 Series II FT-IR spectrophotometer. The instruments used for other measurements were reported earlier [10].

2.1.1. Synthesis of the complex [Cu(Ll)(N$_3$)] (*1*)

A methanolic solution (20 ml) of *N*,*N*-diethyl-ethylenediamine (1 mmol, 0.106 g) was added to a methanolic solution (20 ml) of salicylaldehyde (1 mmol, 0.122 g). The reaction mixture was then stirred for 30 min. To this copper (II) nitrate trihydrate (1 mmol, 0.241 g) dissolved in methanol was added and was stirred for 10 min. Finally, 5 ml aqueous solution of NaN_3 (2 mmol, 0.130 g) was added drop-wise to the mixture with continuous stirring and the resulting solution was then filtered. The green filtrate was then kept in air. From the green solution black crystals were formed within few days. They were then collected by filtration and dried in a desiccator. A suitable crystal was selected for X-ray crystallographic analysis. (Yield ca. 60%). *Anal.* Calc. for $C_{13}H_{19}CuN_5O$: C, 48.0; H, 5.8; N, 21.5. Found: C, 48.2; H, 5.9; N, 22.0%. IR (KBr): $\nu_{as}(N_3)$, 2020 cm^{-1}; $\nu_s(N_3)$, 1320 and 1340 cm^{-1}; $\delta(N_3)$, 610 cm^{-1}; ν(C=N), 1630 cm^{-1}, $\mu_{eff} = 1.83$ BM.

2.1.2. Synthesis of the complex [Cu(L2)(μ-1, 3-N$_3$)]$_n$ (*2*)

This complex was prepared by refluxing a methanolic solution (20 ml) of *N*,*N*-dimethyl-ethylenediamine (1 mmol, 0.088 g) and a methanolic solution (20 ml) of salicylaldehyde (1 mmol, 0.122 g) for 1 h and evaporated on a water-bath until the volume reduced is to ca. 10 ml to obtain a viscous liquid which was added to the methanolic solution (10 ml) of copper (II) nitrate trihydrate (1 mmol, 0.241 g). The resulting mixture was refluxed for 15 min. To it, an aqueous solution of NaN_3 (2 mmol, 0.130 g) was added drop-wise with continuous stirring and the resulting solution was filtered. Black single crystals suitable for structure determination were obtained by slow evaporation of the resulting green solution in the air. (Yield ca. 67%). *Anal.* Calc. for $C_{11}H_{15}CuN_5O$: C, 44.5; H, 5.0; N, 23.6. Found: C, 45.2; H, 5.8; N, 23.7%. IR (KBr): $\nu_{as}(N_3)$, 2030 cm^{-1}; $\nu_s(N_3)$, 1330 and 1345 cm^{-1}; $\delta(N_3)$, 620 cm^{-1}; ν(C=N), 1640 cm^{-1}.

Caution! Although our samples never exploded during handling, metal azido complexes are potentially explosive: only a small amount of material should be prepared and it should be handled with care.

2.2. X-ray crystallography

The crystal data, intensity data collection and refinement details of (**1**) and (**2**) are given in Table 1. A chip of black single crystal of complex (**1**) and a rectangular block single crystal of complex (**2**) were selected for collecting X-ray data. All measurements were made on a Rigaku AFC7 diffractometer using graphite monochromated Mo Kα radiation ($\lambda = 0.71070$ Å) equipped with a Rigaku Mercury CCD detector. The unit cell parameters and orientation matrix were determined by least square refinements. Of the 24126 and 82332 reflections that were collected, 3533 ($R_{int} = 0.022$) and 6561 ($R_{int} = 0.040$) were unique for complex (**1**) and (**2**), respectively. The collected intensity data were corrected for Lorentz and polarization effects and an empirical absorption correction was also employed. Data were collected and processed using CrystalClear (Rigaku) program [14]. The structures were solved by direct methods (SIR 97) [15] and expanded using Fourier techniques. The non-hydrogen atoms were refined anisotropically. Hydrogen atoms were refined isotropically for complex (**1**) while they were refined using the riding model for complex (**2**). All calculations were carried out using the CrystalStructure [16], CRYSTALS [17] and PLATON [18].

Table 1
Crystal data for complex **1** and **2**

	Complex	
	1	**2**
Empirical formula	$C_{13}H_{19}CuN_5O$	$C_{11}H_{15}CuN_5O$
Formula weight	324.87	296.82
Crystal system	monoclinic	orthorhombic
Space group	$P2_1/c$	$Pbca$
a (Å)	6.6922(4)	14.5628(4)
b (Å)	13.0373(5)	18.5282(4)
c (Å)	17.1312(8)	19.2649(5)
α (°)	90	90
β (°)	97.1846(7)	90
γ (°)	90	90
V (Å)^3	1482.93(13)	5198.1(2)
R_{int}	0.02	0.04
Z	4	16
μ (cm^{-1})	14.76	16.77
T (K)	296	296
ρ_{calc} (gm cm^{-3})	1.455	1.517
θ_{max} (°)	27.47	27.48
Crystal size (mm)	$0.40 \times 0.35 \times 0.20$	$0.75 \times 0.30 \times 0.25$
$F(000)$	676.00	2448.00
Reflections measured	24126	82332
Unique reflections	3533	6561
$R_1[I > 2\sigma(I)]$	0.032	0.037
$wR_2[I > 2\sigma(I)]$	0.088	0.098

$R_1 = \sum\|F_o| - |F_c\|/\sum|F_o|$.
$wR_2 = [\sum w(|F_o| - |F_c|)^2]/\sum[w(F_o^2)]^{1/2}$.

3. Results and discussion

3.1. Synthesis and spectroscopic studies

Elemental analyses of the complexes convincingly demonstrate that (**1**) and (**2**) can be formulated as [Cu(L1)(N_3)] and [Cu(L2)(N_3)], respectively. IR spectral measurements of (**1**) and (**2**) show a strong band in the range 1630–1630 attributable due to the azomethine group [19]. The ν_{as} band for azide group appears around 2020 and 2030 cm^{-1} for complex (**1**) and (**2**), respectively. Similar characteristic bands for azides have been observed in a number of mononuclear and azido bridged polynuclear complexes [5,10,11]. The electronic spectra of the complex (**1**) and (**2**) have been measured in methanolic solution. A relatively weak band appears at around 610 nm for both the complexes can be assigned as d–d transition while a broad intense band centered at around 365 nm for (**1**) and (**2**) attributable due to the ligand metal charge transfer.

3.2. Description of structures

3.2.1. [Cu(Ll)(N_3)] (1)

The principal structural features of complex (**1**) are given in Fig. 1. The structure consists of discrete molecules of [(CuLl)(N_3)]. The copper ion occupies the central position of a regular square planar arrangement. Out of its four coordination sites three positions are occupied by the tridentate Schiff base through two nitrogen (amino and imino) atoms and while other one is occupied by de-protonated phenoxo group. The remaining fourth coordination is satisfied by an azido ligand. The Cu–N bond lengths are found to be Cu(1)–N(1) = 1.935(2); Cu(1)–N(2) = 2.063(2); Cu(1)–N(3) = 1.946(2) Å while the Cu(1)–O(1) bond length is 1.888(2) Å. The azide group, which acts as a monodentate ligand is slightly asymmetric [N(3)–N(4) = 1.184(3) and N(4)–N(5) = 1.141(3) Å] and linear within the experimental error [N(5)–N(4)–N(3) = 175.6(2)]. The other bond lengths and angles are gathered in Table 2. The distance between the central Cu(1) ion and the unused terminal N atom of the azide ligand of the symmetry related moieties are found to be ca. 5.735 Å. The bond lengths and bond angles determined from X-ray measurements are in agreement with the other similar reported systems. The structure of the complex (**1**), however, differs from the other X-ray crystallographically investigated copper (II) azide complexes containing terminal azido ligand [20]. In most of the cases the coordination geometry around copper ions are either pseudo octahedral or distorted trigonal bipyramidal while square planar is not so common. The present complex acquires a square planar environment around the copper ion probably due to the presence of two ethyl groups attached to the N atom in 1,1 position of the ethylenediamine backbone of Schiff base ligand.

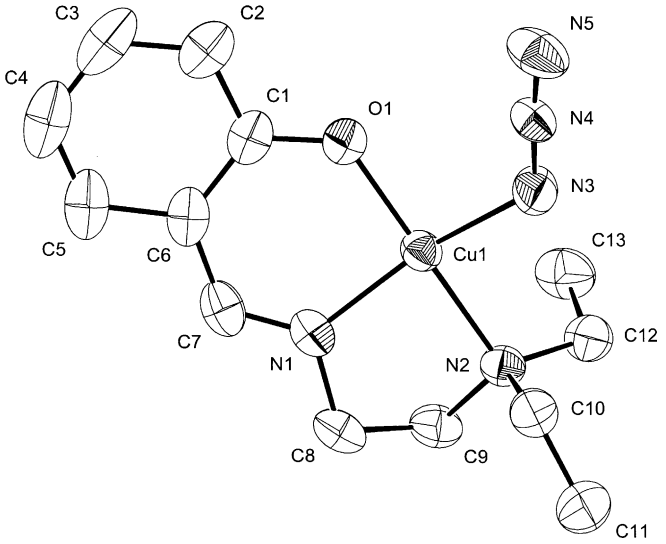

Fig. 1. ORTEP diagram of complex **1** showing atom numbering scheme.

3.2.2. [(CuL2)(μ-1,3-N_3)]$_n$ (2)

The structure determination reveals that the neutral [Cu(L2)(N_3)] units in complex (**2**) are connected by the single (μ-1,3-azido ligands) to form an infinite 1D polymeric chain. The tridentate NNO donor Schiff base ligand acts as a chelating ligand. An ORTEP [21] drawing of the chain with atom labeling scheme is shown in Fig. 2. The copper (II) ion in complex (**2**) is pentacoordinated. Of them two nitrogen atoms and one oxygen atom of the Schiff base ligand and one nitrogen atom of the bridging azido ligand define the basal plane around the copper (II) ion in this

Table 2
Selected bond lengths (Å) and angles (°) for (**1**) and (**2**)

Complex (**1**)	
Cu(1)–O(1) 1.888(2)	O(1)–Cu(1)–N(1) 94.05(8)
Cu(1)–N(1) 1.935(2)	N(1)–Cu(1)–N(3) 164.74(9)
Cu(1)–N(2) 2.063(2)	O(1)–Cu(1)–N(2) 169.72(7)
Cu(1)–N(3) 1.946(2)	N(2)–Cu(1)–N(3) 90.75(8)
N(3)–N(4) 1.184(3)	N(4)–N(3)–Cu(1) 124.4(2)
N(4)–N(5) 1.141(3)	O(1)–Cu(1)–N(3) 92.97(8)
	N(1)–Cu(1)–N(2) 84.67(8)
	N(5)–N(4)–N(3) 175.6(2)
Complex (**2**)	
Molecule 1	Molecule 2
Cu(1)–O(1) 1.901(3)	Cu(2)–O(2) 1.907(3)
Cu(1)–N(1) 1.955(3)	Cu(2)–N(6) 1.948(3)
Cu(1)–N(2) 2.071(3)	Cu(2)–N(7) 2.072(3)
Cu(1)–N(3) 1.980(3)	Cu(2)–N(8) 1.970(3)
Cu(1)–N(10) 2.473(4)	Cu(2)–N(5^{i}) 2.457(4)
N(3)–N(4) 1.188(5)	N(8)–N(9) 1.181(5)
N(4)–N(5) 1.151(5)	N(9)–N(10) 1.158(5)
O(1)–Cu(1)–N(1) 93.5(1)	O(2)–Cu(2)–N(6) 92.8(1)
O(1)–Cu(1)–N(2) 175.4(1)	O(2)–Cu(2)–N(7) 174.3(1)
O(1)–Cu(1)–N(3) 92.1(1)	O(2)–Cu(2)–N(8) 92.1(1)
N(1)–Cu(1)–N(2) 83.5(1)	N(6)–Cu(2)–N(7) 84.0(1)
N(1)–Cu(1)–N(3) 161.2(1)	N(6)–Cu(2)–N(8) 164.9(2)
N(2)–Cu(1)–N(3) 89.8(1)	N(7)–Cu(2)–N(8) 89.9(1)
O(1)–Cu(1)–N(10) 93.06(13)	O(2)–Cu(2)–N(5^{i}) 94.08(12)
N(1)–Cu(1)–N(10) 95.96(13)	N(6)–Cu(2)–N(5^{i}) 91.34(12)
N(2)–Cu(1)–N(10) 90.68(12)	N(7)–Cu(2)–N(5^{i}) 90.72(12)
N(3)–Cu(1)–N(10) 101.69(16)	N(8)–Cu(2)–N(5^{i}) 102.52(15)
N(4)–N(3)–Cu(1) 125.2(3)	N(9)–N(8)–Cu(2) 123.9(3)
N(5)–N(4)–N(3) 177.2(4)	N(10)–N(9)–N(8) 178.0(4)
N(4)–N(5)–Cu(2^{ii}) 116.3(3)	Cu(1)–N(10)–N(9) 122.3(3)

Symmetry codes (i) = $3/2 - x$, $1/2 + y$, z; (ii) = $3/2 - x$, $-1/2 + y$, z.

complex. A nitrogen atom of azido ligand from the symmetry related unit (symmetry operation $3/2 - x$, $1/2 + y$, z) occupies the remaining fifth position of the coordinated polyhedra. Azido ligand bridges Cu(1) with Cu(2) through basal-apical linkage in this complex. The bond lengths and bond angles of complex (**2**) is given in Table 2. The Cu-azido-Cu chains are propagated along the crystallographic *b*-axis while chains are stacked one upon another along crystallographic *c*-axis (Fig. 3). No appreciable inter-chain interaction is apparent from the crystallographic study. The trigonality index $\tau(=(\phi_1 - \phi_2)/60$, where ϕ_1, ϕ_2 are the two largest L–M–L angles of the coordination sphere) has been calculated for the pentagonal copper sites [22]. The τ values are found to be 0.24 and 0.16 for Cu1 and Cu2, respectively, confirming the square pyramidal character of both sites ($\tau = 0$ infers a perfect square pyramid, and a $\tau = 1$ a perfect trigonal bipyramid). The apical Cu–N bond lengths are little longer than usual [Cu(1)–N(10) = 2.473(4) and Cu(2)–N(5^{i}) = 2.457(4)]. The other bond distances and angles are close to the expected values. The intra-chain Cu–Cu distance is found to be 5.318(3) Å. Jiang et al. have reported a μ-1,3-azido complex containing the same co-ligand as that in complex (**2**), but structurally they are different [23]. Therefore, present complex can be considered as a polymorph of the former one.

3.3. Magnetic properties of [Cu(Ll)(N_3)] (**1**) and [(CuL2)(μ-1,3-N_3)]$_n$ (**2**)

The temperature dependence of the molar magnetic susceptibility, χ_M, for complex (**2**) in the 4–300 K temperature range was measured with a superconducting quantum interference device (SQUID) magnetometer, under magnetic fields of 20 kG and is shown in Fig. 4. The χ_M value of 5.5×10^{-3} cm^3 mol^{-1} at 300 K for complex (**2**) is slightly higher than the value expected for an isolated magnetically uncoupled copper (II) ion ($\chi_M = 1.25 \times 10^{-3}$ cm^3 mol^{-1} for

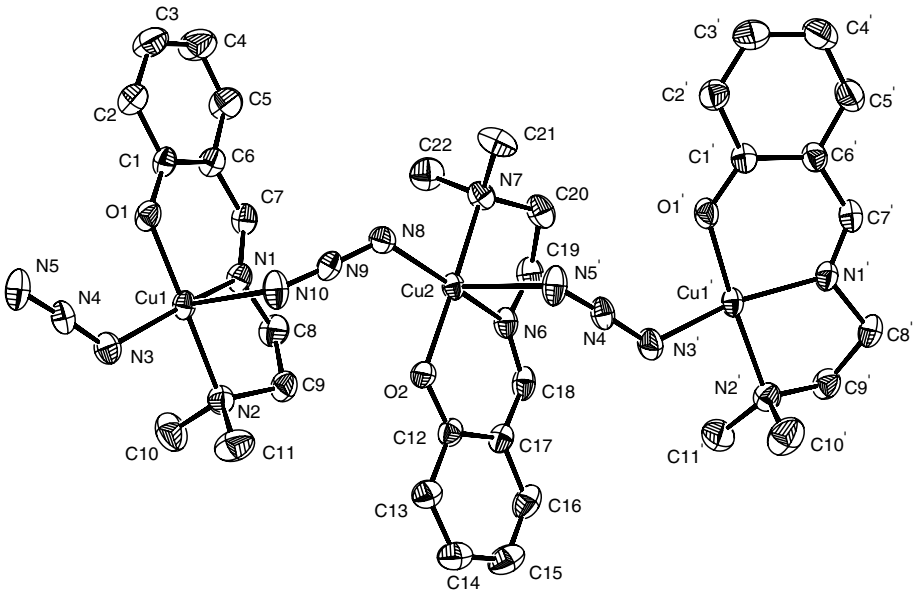

Fig. 2. ORTEP diagram of complex **2** showing part of the 1D infinite chain with atom numbering scheme. Symmetry code for primed atoms is $3/2 - x$, $1/2 + y$, z.

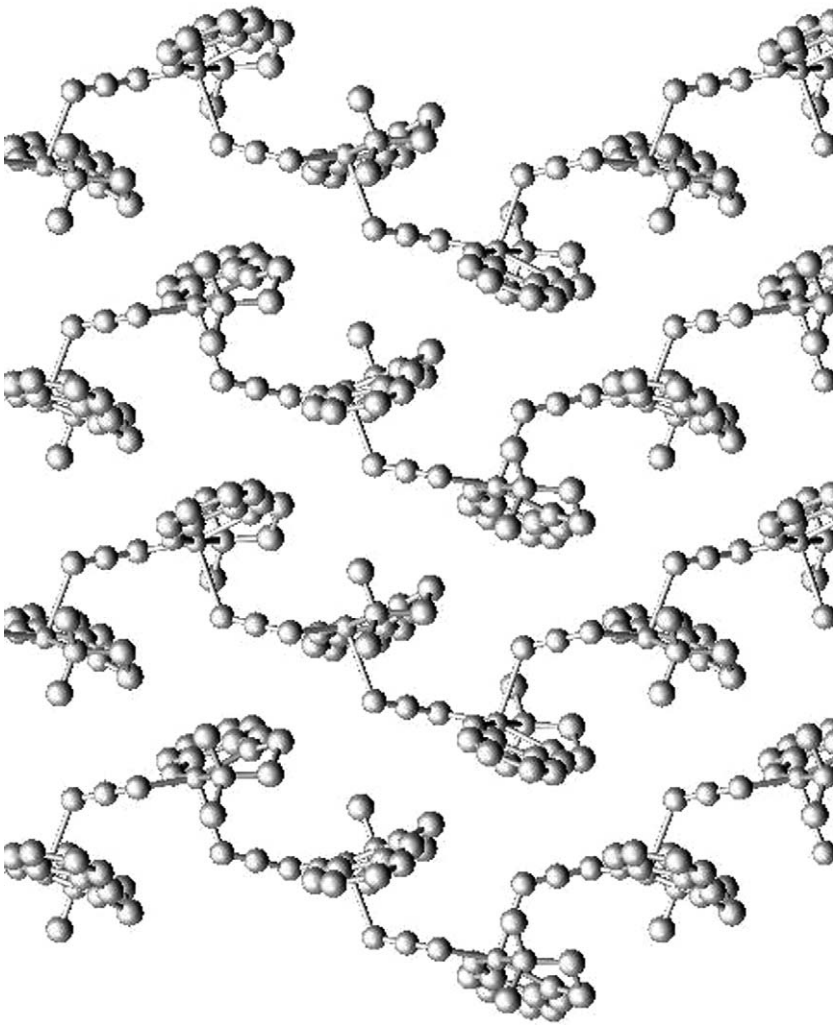

Fig. 3. Diagram showing stacking of 1D chains of complex **2**.

$g = 2.0$). Upon cooling the χ_M value for complex (**2**) increases gradually with temperature until ca. 125 K, and then rapidly, reaching a maximum of 3.7×10^{-2} cm^3 mol^{-1} at ca. 22 K. The typical folded-knee shaped χ_M versus T curve indicates a bulk antiferromagnetic interaction is operative in the complex (**2**). The $\chi_M T$ value for complex (**1**) is equal to 0.37 ± 0.01 cm^3 mol^{-1} K over the whole temperature range (4–300 K), confirming the paramagnetic nature of this mononuclear species.

In order to explain the magnetic properties of complex (**2**), a simplest case of isotropic infinite chain model that is provided by an array of equally spaced copper (II) ions bridged through μ-1,3-azido ligands with $S = 1/2$ local spins has been considered. The spin Hamiltonian of such a system considering isotropic interaction between nearest neighbour ions is

$$H = -J \sum_{i=1}^{n-1} S_{A_i} \cdot S_{A_{i+1}} \quad (1)$$

where summation runs over the n site of the chain. For the condition $n \to \infty$ no analytical method is available so as to determine the energies of low-lying states and magnetic susceptibility. Nevertheless, the problem can be dealt with numerical solution of the Hamiltonian by considering ring chains of increasing size and extrapolating for the case

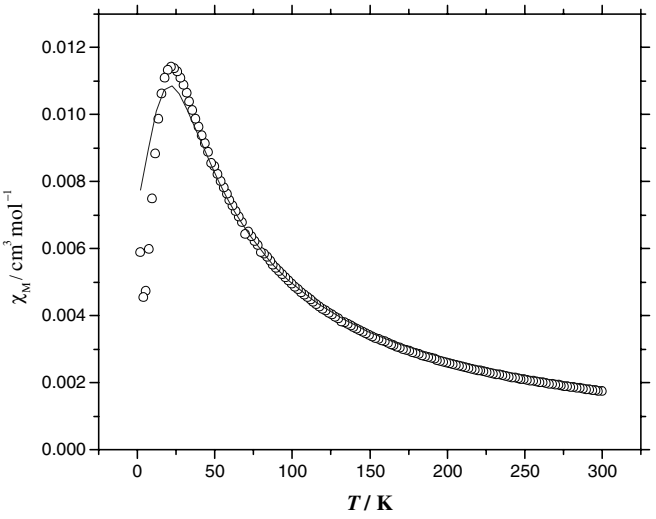

Fig. 4. χ_M vs. T(Δ) plot for complex **2**. Solid lines represent the best fit of the data with the model described in the text.

where n becomes infinite. The ring structure permits the limiting condition as follows [24,25]:

$$S_{A_{i+n}} = S_{A_i} \quad \text{for any } n \tag{2}$$

Finally, a numerical expression can be used to fit magnetic susceptibility data are given by [26]:

$$\chi_M = \frac{Ng^2\beta^2}{kT}\,\frac{0.25 + 0.074975x + 0.075235x^2}{1.0 + 0.9931x + 0.172135x^2 + 0.757825x^3} \tag{3}$$

where

$$x = |J|/kT \tag{4}$$

Fitting of the magnetic susceptibility data considering the Eq. (3) yielded the parameter values $J = -22.5(\pm 0.2)\ \mathrm{cm}^{-1}$, $g = 2.2(\pm 0.01)$, with an agreement factor $R = 7.2 \times 10^{-6}$. Fig. 4 shows the result of this fit.

4. Conclusions

It is evident from the above discussion that we have successfully isolated a series of copper (II) azido complexes with diverse structural motifs using NNO donor Schiff bases. Copper azido complexes with these types of Schiff bases are not so well documented in the literature. In an earlier attempt we were successful in isolating rather a rare variety of asymmetric double μ-1,1-azido copper (II) dimer using a tridentate Schiff base HL3 as co-ligand where ethylenediamine substructure of the Schiff base has no substitution [11]. The present study shows that by introducing the simple substitutions in the amine nitrogen of the diamine from which Schiff base is derived structural diversity can be achieved. The copper-azido complex containing Schiff base HL3 gives a double μ-1,1-azido bridged dimeric moiety while Schiff base HL2 gives a 1D polymeric chain bridged through a single μ-1,3-azido group. On the other hand, a mononuclear species having only terminal azido group is formed with co-ligand HL1. Magnetic measurement shows while complex (**2**) is showing bulk antiferromagnetism, complex (**1**) is a paramagnet. This type of studies certainly has relevance in designing newer molecular architecture for synthesizing novel molecular materials.

Acknowledgements

We thank reviewers for their valuable comments. The work was financially supported by the University Grants Commission, New Delhi, by a grant (F.12-9/2002(SR-I)) to SK. We are grateful to SAIF, CDRI, Lucknow for elemental analyses (on chargeable basis).

Appendix A. Supplementary data

Supplementary data are available from The Director, CCDC, 12 Union Road, Cambridge, CB2 1EZ, UK (fax: +44-1223-336033; e-mail: deposit@ccdc.cam.ac.uk or www: http://www.ccdc.cam.ac.uk) on request, quoting the deposition number CCDC 269113 for complex **1** and 269112 for complex **2**. Supplementary data associated with this article can be found, in the online version, at doi:10.1016/j.poly.2006.01.011.

References

[1] R.D. Willet, D. Gatteschi, O. Kahn (Eds.), Magneto-Structural Correlations in Exchange Coupled Systems, NATO ASI Series, Reidel, Dordrecht, 1985.
[2] O. Kahn, Molecular Magnetism, VCH, New York, 1993, p. 145.
[3] M.M. Turnbull, T. Sugimoto, L.K. Thompson (Eds.), Molecular Based Magnetic Materials: Theory, Techniques and Applications, ACS Symposium Series, no. 644, ACS, Washington, 1996.
[4] A. Caneschi, D. Gatteschi, L. Pardi, R. Sessoli, Clusters, chains and layered molecules: The chemists way to magnetic materials, in: A.F. Williams (Ed.), Perspectives in Coordination Chemistry, VCH, Weinheim, 1992.
[5] J. Ribas, A. Escuer, M. Monfort, R. Vicente, R. Cortes, L. Lezama, T. Rojo, Coord. Chem. Rev. 193 (1999) 1027, and references therein.
[6] (a) P.N.W. Baxter, J.-M. Lehn, G. Baum, D. Fenske, Eur. J. Chem. 5 (1999) 102;
(b) A.J. Balke, N.R. Champness, P. Hubberstey, W.S. Li, M.A. Withersby, M. Schorder, Coord. Chem. Rev. 183 (1999) 117.
[7] (a) O. Khan, Adv. Inorg. Chem. 43 (1995) 179;
(b) H. Okawa, H. Furatachi, D.E. Fenton, Coord. Chem. Rev. 174 (1998) 51.
[8] R. Robson, Aust. J. Chem. 23 (1970) 2217.
[9] (a) J. Ribas, M. Monfort, X. Solans, M. Drillon, Inorg. Chem. 33 (1994) 742;
(b) Z.E. Serna, L. Lezama, M.K. Urtiaga, M.I. Arriortua, M.G.B. Barandika, R. Cortés, T. Rojo, Angew. Chem., Int. Ed. 39 (2000) 344;
(c) M.A. Halcrow, J.S. Sun, J.C. Huffman, G. Christou, Inorg. Chem. 35 (1995) 4167;
(d) G.S. Papaefstathiou, S.P. Perlepes, A. Escuer, R. Vicente, M. Font-Barida, X. Solans, Angew. Chem., Int. Ed. 40 (2001) 884.
[10] S. Koner, S. Saha, K. Okamato, J.-P. Tuchagues, Inorg. Chem. 42 (2003) 4668.
[11] S. Koner, S. Saha, T. Mallah, K. Okamato, Inorg. Chem. 43 (2004) 840.
[12] (a) P.S. Mukherjee, S. Dalai, G. Mostafa, T.H. Lu, E. Rentschler, N. Ray Chaudhuri, New J. Chem. 25 (2001) 1203;
(b) P.S. Mukherjee, T.K. Maji, A. Escuer, R. Vicente, J. Ribas, G. Rosair, F.A. Maunter, N.R. Chaudhuri, Eur. J. Inorg. Chem. (2002) 943.
[13] (a) P.S. Mukherjee, S. Dalai, E. Zangrando, F. Lloret, N. Ray Chaudhuri, Chem. Commun. (2001) 1444;
(b) C.R Chaudhury, K. Dey, R. Karmaker, C.-D. Wu, C.-Z. Lu, M.S.E. Fallah, S. Mitra, New J. Chem. 27 (2003) 1360.
[14] (a) CrystalClear: CrystalClear Software User's Guide, Molecular Structure Corporation, 1999;
(b) J.W. Plugrath, Acta Cryst. D 55 (1999) 1718.
[15] SIR97: A. Altomare, M. Burla, M. Camalli, G. Cascarano, C. Giacovazzo, A. Guagliardi, A. Moliterni, G. Polidori, R. Spagna, J. Appl. Cryst. 32 (1999) 115.
[16] Crystal Structure 3.5.1: Crystal Structure Analysis Package, Rigaku and Rigaku/MSC (2000-2003). 9009 New Trails Dr. The Woodlands, TX 77381 USA.
[17] CRYSTALS issue 10: D.J. Watkin, C.K. Prout, J.R. Carruthers, P.W. Betteridge, Chemical Crystallography Laboratory, Oxford, UK, 1996.
[18] A.L. Spek, J. Appl. Cryst. 36 (2003) 7.

[19] K. Nakamoto, Infrared and Raman Spectra of Inorganic and Coordination Compounds, fourth ed., Wiley, New York, 1986, p. 290.
[20] (a) F.A. Maunter, M.A.S. Goher, Polyhedron 15 (1996) 5;
(b) F.A. Maunter, M.A.S. Goher, Polyhedron 12 (1993) 2823;
(c) F.A. Maunter, M.A.S. Goher, A.E.H. Abdou, Polyhedron 12 (1993) 2815.
[21] C.K. Johnson, ORTEP, Report ORNL-5138, Oak Ridge National Laboratory, Oak Ridge, TN, 1976.
[22] (a) B.J. Hathaway, Struct. Bond. 14 (1973) 49;
(b) A.W. Addison, T. Nageswara, J. Reedijk, J. van Rijn, G.C. Verchoor, J. Chem. Soc., Dalton Trans. (1984) 1349.
[23] Y.-B. Jiang, H.-Z. Kou, R.-J. Wang, A.-L. Cui, Eur. J. Inorg. Chem. (2004) 4608.
[24] J.C. Bonner, M.E. Fisher, Phys. Rev. A 135 (1964) 640.
[25] R.L. Orbach, Phys. Rev. 112 (1958) 309.
[26] W.E. Estes, D.P. Gavel, W.E. Hatfield, D. Hodgson, Inorg. Chem. 17 (1978) 1415.

(bpy) and 1,10-phenanthroline (phen) and have isolated several new phases in such organic–inorganic metal-phosphate systems. In the present study, two novel examples of the chelating didentate amines-phosphate system, $[Cu_2(bpy)_2(\mu,\eta^2\text{-}HPO_4)(\mu,\eta^1\text{-}H_2PO_4)(\mu,\eta^2\text{-}H_2PO_4)]_n$ (**1**) and $[Cu_4(phen)_4(\mu_3,\eta^2\text{-}HPO_4)_2(\mu,\eta^2\text{-}H_2PO_4)_2(H_2PO_4)_2]\cdot(H_2O)_4$ (**2**) are reported, and their structural, spectroscopic and magnetic properties are discussed.

2. Experimental

All reagents were commercial grade materials and were used without further purification. Elemental analyses (C, H and N) were performed by the Microanalytical Service of Science and Technological Research Equipment Centre, Chulalongkorn University on a Perkin–Elmer PE2400 CHNS/O analyzer. IR spectra were recorded on a Perkin–Elmer spectrum One FT-IR spectrophotometer as KBr disc in the 4000–450 cm^{-1} spectral range. Solid-state (diffuse reflectance) electronic spectra were measured as polycrystalline samples on a Perkin–Elmer Lambda2S spectrophotometer, within the range 8000–18 000 cm^{-1}. The X-band powder EPR spectra were obtained on polycrystalline samples at room temperature and 77 K with a JEOL RE2X electron spin resonance spectrometer with DPPH ($g = 2.0036$) as a reference. Magnetic susceptibility measurements were carried out using a Quantum design MPMS-5S SQUID magnetometer (measurements carried out at 1000 G). Data were corrected for magnetization of the sample holder and for diamagnetic contributions, which were estimated from the Pascal constants.

2.1. Synthesis of the compounds

2.1.1. Synthesis of $[Cu_2(bpy)_2(\mu,\eta^2\text{-}HPO_4)(\mu,\eta^1\text{-}H_2PO_4)(\mu,\eta^2\text{-}H_2PO_4)]_n$ (1)

A solution of bpy (0.16 g, 1.0 mmol) in dimethyl sulfoxide (5 ml) was slowly added to a solution of $Cu(NO_3)_2\cdot 3H_2O$ (0.24 g, 1.0 mmol) in dimethyl sulfoxide (10 ml) after which a solution of KH_2PO_4 (0.27 g, 2.0 mmol) in water (5 ml) was added resulting blue green solution. Bluish-green crystals of **1** were deposited after two weeks, which were collected by filtration. Yield: 60%. *Anal*. Calc. for $C_{20}H_{21}Cu_2N_4O_{12}P_3$: C, 32.93; H, 2.90; N, 7.67. Found: C, 32.71; H, 2.91; N, 7.46%.

2.1.2. Synthesis of $[Cu_4(phen)_4(\mu_3,\eta^2\text{-}HPO_4)_2(\mu,\eta^2\text{-}H_2PO_4)_2(H_2PO_4)_2](H_2O)_4$ (2)

The complex **2** was prepared by adding an aqueous solution (10 ml) of $Cu(NO_3)_2\cdot 3H_2O$ (0.24 g, 1.0 mmol) to a solution of phen (0.18 g, 1.0 mmol) in methanol (15 ml) after which an aqueous solution (5 ml) of KH_2PO_4 (0.27 g, 2.0 mmol) was added. The blue-green solution was slowly evaporated at room temperature. Green crystals of **2** were collected from the solution by filtration after several days. Yield: 65%. *Anal*. Calc. for $C_{48}H_{50}Cu_4N_8O_{28}P_6$: C, 35.43; H, 3.09; N, 6.89. Found: C, 36.38; H, 3.12; N, 6.92%.

2.2. Crystallography

The X-ray single-crystal data for compounds **1** and **2** were collected at 293 K on a 1 K Bruker SMART CCD area detector diffractometer using graphite monochromated Mo Kα radiation ($\lambda = 0.71073$ Å) at a detector distance of 4.5 cm and swing angle of −35°. A hemisphere of the reciprocal space was covered by combination of three sets of exposures; each set had a different ϕ angle (0°, 88°, and 180°) and each exposure of 40 s covered 0.3° in ω. Data reduction and cell refinements were performed using the program SAINT [9]. An empirical absorption correction by using the SADABS [10] program was applied, which resulted in transmission coefficients ranging from 0.708 to 1.000 for compound **1** and 0.737 to 1.000 for compound **2**. The structures were solved by direct methods and refined by full-matrix least-squares method on $(F_{obs})^2$ with anisotropic thermal parameters for all non-hydrogen atoms using the SHELXTL-PC v 6.12 software package [11]. All hydrogen atoms were located geometrically and refined isotropically except two hydrogen atoms of dihydrogenphosphate group in compound **1**. The molecular graphics were created by using the SHELXTL-PC [11] package. The crystal and refinement details for compounds **1** and **2** are listed in Table 1. Selected bond lengths and angles are given in Tables 2 and 3.

3. Results and discussion

3.1. Crystal structure of $[Cu_2(bpy)_2(\mu,\eta^2\text{-}HPO_4)(\mu,\eta^1\text{-}H_2PO_4)(\mu,\eta^2\text{-}H_2PO_4)]_n$ (1)

The structure showing several repeat units is depicted in Fig. 1 together with the numbering scheme. Selected bond distances and angles are listed in Table 2. The structure consists polymeric chains of $[Cu_2(bpy)_2(\mu,\eta^2\text{-}HPO_4)(\mu,\eta^1\text{-}H_2PO_4)(\mu,\eta^2\text{-}H_2PO_4)]$ bridged by $\mu,\eta^2\text{-}HPO_4$, $\mu,\eta^1\text{-}H_2PO_4$ and $\mu,\eta^2\text{-}H_2PO_4$ groups with different coordination modes. Two nearest Cu(II) ions are doubly-bridged by $\mu,\eta^2\text{-}HPO_4$ and $\mu,\eta^1\text{-}H_2PO_4$ ligands, and singly-bridged by a $\mu,\eta^2\text{-}H_2PO_4$ ligand to another copper(II) ion, providing a chain of distorted square-pyramidal geometries for CuN_2O_2O' chromophores with τ values of 0.03 for Cu(1) and 0.30 for Cu(2) (The τ value describes the relative amount of trigonality; $\tau = 0$ for square pyramid and $\tau = 1$ for trigonal bipyramidal [12]). Hence, the Cu(II) ions are alternatively doubly-bridged and singly-bridged along the polymeric chain. The dihydrogenphosphato ligands exhibit different coordination modes. One is in a O–P–O-bridging mode with an *antisyn–syn* configuration and the other is in a monoatomic-O-bridging mode, while the hydrogenphosphato ligand is in a O–P–O-bridging mode with a *syn–syn* configuration. The $\mu,\eta^2\text{-}HPO_4$ ligand joins two copper(II) ions in an equatorial–equatorial configuration, while the $\mu,\eta^1\text{-}H_2PO_4$ and $\mu,\eta^2\text{-}H_2PO_4$ ligands join in an axial–equatorial configuration. The Cu···Cu separation are 3.322(1) and 5.283(1) Å for a double bridge and a single bridge, respectively.

Table 1
Crystal and refinement data for complexes **1** and **2**

Complex	**1**	**2**
Chemical formula	$[Cu_2(bpy)_2(\mu\text{-}HPO_4)(\mu\text{-}H_2PO_4)(\mu\text{-}H_2PO_4)]_n$	$[Cu_4(phen)_4(\mu_3\text{-}HPO_4)_2(\mu\text{-}H_2PO_4)_2(H_2PO_4)_2](H_2O)_4$
Chemical formula weight	729.4	1626.98
Temperature (K)	293(2)	293(2)
Crystal system	monoclinic	triclinic
Space group	*Cc*	$P\bar{1}$
a (Å)	12.8704(10)	10.2271(9)
b (Å)	11.1575(8)	10.4060(9)
c (Å)	17.4207(13)	15.0672(13)
α (°)	90	91.4740(10)
β (°)	91.0990(10)	92.3310(10)
γ (°)	90	116.2210(10)
V (Å^3)	2501.2(3)	1435.6(2)
Z	4	1
D_{calc} (g cm^{-3})	1.937	1.882
Absorption coefficient (mm^{-1})	1.967	1.730
F(000)	1472	824
Crystal size (mm)	$0.286 \times 0.168 \times 0.112$	$0.152 \times 0.127 \times 0.097$
θ Range (°)	2.34–28.28	1.4–28.3
Number of reflection collected	10724	12711
Number of unique reflections [R_{int}]	5659 [0.016]	6648 [0.023]
T_{max} and T_{min}	1.000, 0.708	1.000, 0.737
Data/restraints/parameter	5659/2/454	6648/0/524
Goodness-of-fit	1.008	1.039
Final *R* indices	$R_1 = 0.0238$	$R_1 = 0.0391$
$[I > 2\sigma(I)]$	$wR_2 = 0.0575$	$wR_2 = 0.0942$
R indices (all data)	$R_1 = 0.0254$	$R_1 = 0.0499$
	$wR_2 = 0.0583$	$wR_2 = 0.0998$
Largest difference peak and hole (e Å^{-3})	0.351, −0.259	0.640, −0.342

$R = \sum\|F_o| - |F_c\|/\sum|F_o\|$, $R_w = [\sum w\{|F_o| - |F_c|\}^2/w|F_o|^2]^{1/2}$.

Table 2
Selected bond lengths (Å) and angles (°) with e.s.d. in parentheses of compound **1**

Bond lengths (Å)			
Cu(1)–O(2)	1.914(1)	Cu(1)–O(5)	1.986(1)
Cu(1)–N(2)	2.010(2)	Cu(1)–N(1)	2.027(2)
Cu(1)–O(9)	2.203(1)	Cu(2)–O(1)	1.929(1)
Cu(2)–O(10)	1.931(1)	Cu(2)–N(4)	2.001(2)
Cu(2)–N(3)	2.011(1)	Cu(2)–O(5)	2.420(1)
Cu(1)–Cu(2)	3.322(1)	Cu(1)A–Cu2	5.283(1)
Bond angles (°)			
O(2)–Cu(1)–O(5)	93.4(1)	O(2)–Cu(1)–N(2)	164.1(1)
O(5)–Cu(1)–N(2)	92.1(1)	O(2)–Cu(1)–N(1)	91.2(1)
O(5)–Cu(1)–N(1)	166.0(1)	N(2)–Cu(1)–N(1)	80.3(1)
O(2)–Cu(1)–O(9)	99.5(1)	O(5)–Cu(1)–O(9)	95.2(1)
N(2)–Cu(1)–O(9)	94.8(1)	N(1)–Cu(1)–O(9)	97.1(1)
O(1)–Cu(2)–O(10)	94.5(1)	O(1)–Cu(2)–N(4)	174.2(1)
O(10)–Cu(2)–N(4)	89.6(1)	O(1)–Cu(2)–N(3)	94.3(1)
O(10)–Cu(2)–N(3)	156.3(1)	N(4)–Cu(2)–N(3)	80.3(1)
O(1)–Cu(2)–O(5)	91.7(1)	O(10)–Cu(2)–O(5)	100.5(1)
N(4)–Cu(2)–O(5)	91.6(1)	N(3)–Cu(2)–O(5)	101.2(1)

Hydrogen bonds	D–H	H···A	D···A	D–H···A
O(8)–H(23)···O(9)	0.71(4)	1.87(3)	2.553(1)	159(2)
O(12)–H(25)···O(1)	0.89(1)	1.77(1)	2.636(1)	165(2)
O(6)–H(22)···O(4) [$x - 1/2$, $y - 1/2$, z]	0.69(3)	1.83(1)	2.514(1)	169(1)
O(3)–H(21)···O(7)	0.67(3)	2.02(3)	2.683(1)	167(1)

Symmetry code: A = $x + 1/2$, $y - 1/2$, z.

Both copper ions have a planar square base with a CuN_2O_2 chromophore consisting of two oxygen atoms of bridging HPO_4^{2-} and $H_2PO_4^-$ groups with Cu–O distances vary from 1.914(1) to 1.986(1) Å and two nitrogen atoms of a bpy ligand with Cu–N distances vary from 2.001(2) to 2.027(2) Å. An oxygen atom of the O–P–O-bridged and monoatomic-bridged dihydrogenphosphato ligands for Cu(1) and Cu(2), respectively completes the five-coordination of a square-pyramidal geometry with Cu(1)–O(9) distance of 2.203(1) Å and Cu(2)–O(5) distance of 2.420(1) Å. The four basal atoms show a small tetrahedral distortion with a dihedral angle of 18.5° and 21.9° formed between the CuO_2 and the CuN_2 planes, while the copper atoms are displaced by 0.23 and 0.21 Å from the basal planes toward the O(9) and O(5) atoms, respectively. Details of the hydrogen bondings are also listed in Table 2.

3.2. Crystal structure of $[Cu_4(phen)_4(\mu_3,\eta^2\text{-}HPO_4)_2(\mu,\eta^2\text{-}H_2PO_4)_2(H_2PO_4)_2](H_2O)_4$ (**2**)

A thermal ellipsoid plot of the structure is depicted in Fig. 2 with selected bond distances and angles given in Table 3. The crystal structure consists of a centrosymmetric tetranuclear $[Cu_4(phen)_4(\mu_3,\eta^2\text{-}HPO_4)_2(\mu,\eta^2\text{-}H_2PO_4)_2$-

Table 3
Selected bond lengths (Å) and angles (°) with e.s.d. in parentheses of compound **2**

Bond lengths (Å)			
Cu(1)–O(5)	1.923(1)	Cu(1)–O(9)	1.949(1)
Cu(1)–N(1)	2.021(2)	Cu(1)–N(2)	2.031(2)
Cu(1)–O(1)	2.217(1)	Cu(2)–O(10)	1.937(1)
Cu(2)–O(6)	1.949(1)	Cu(2)–N(3)	2.010(2)
Cu(2)–N(4)	2.027(2)	Cu(2)–O(6A)	2.247(1)
Cu(2)–Cu(2)A	3.162(1)	Cu(1)–Cu(2)	5.060(1)
Bond angles (°)			
O(5)–Cu(1)–O(9)	97.2(1)	O(5)–Cu(1)–N(1)	162.9(1)
O(9)–Cu(1)–N(1)	87.7(1)	O(5)–Cu(1)–N(2)	89.9(1)
O(9)–Cu(1)–N(2)	161.1(1)	N(1)–Cu(1)–N(2)	80.8(1)
O(5)–Cu(1)–O(1)	97.9(1)	O(9)–Cu(1)–O(1)	103.3(1)
N(1)–Cu(1)–O(1)	96.9(1)	N(2)–Cu(1)–O(1)	93.0(1)
O(10)–Cu(2)–O(6)	96.0(1)	O(10)–Cu(2)–N(3)	90.1(1)
O(6)–Cu(2)–N(3)	172.6(1)	O(10)–Cu(2)–N(4)	165.0(1)
O(6)–Cu(2)–N(4)	91.7(1)	N(4)–Cu(2)–N(3)	81.4(1)
O(10)–Cu(2)–O(6A)	96.3(1)	O(6)–Cu(2)–O(6A)	82.4(1)
N(3)–Cu(2)–O(6A)	101.2(1)	N(4)–Cu(2)–O(6A)	97.4(1)

Hydrogen bonds	D–H	H-···A	D···A	D–H–A
O(3)–H(25)···O(1) [−x, −y, −z + 1]	0.75(3)	1.89(1)	2.627	166(1)
O(14)–H(17)···O(2) [x + 1, y + 1, z]	0.71(1)	2.22(3)	2.928	172(3)
O(15)–H(18)···O(2) [−x, −y, −z + 1]	0.67(4)	2.32(1)	2.948	156(4)[a]
O(15)–H(18)···O(3) [−x, −y, −z + 1]	0.67(4)	2.48(4)	2.977	132(1)[a]
O(11)–H(19)···O(15)	0.73(4)	1.84(3)	2.560	168(1)
O(4)–H(16)···O(7)	0.90(3)	1.72(1)	2.606	167(1)
O(8)–H(21)···O(14) [x − 1, y − 1, z]	0.65(1)	2.04(4)	2.687	174(1)
O(15)–H(24)···O(2) [x + 1, y, z]	0.81(4)	1.94(3)	2.757	179(1)
O(14)–H(23)···O(11) [x, y + 1, z]	0.76(1)	2.26(1)	2.974	158(1)
O(12)–H(26)···O(7)	0.60(1)	1.99(3)	2.590	175(3)

Symmetry code: A = −x, −y, −z.

$(H_2PO_4)_2$] unit and four molecules of lattice water. The four copper ions of the tetranuclear identity are linked through a double hydrogenphosphate bridge in an equatorial–equatorial and a double dihydrogenphosphate bridge in an equatorial–axial configuration with a double terminal dihydrogenphosphate group. The Cu···Cu distances varying from 3.162(1) to 5.060(1) Å. The tetranuclear unit has an inversion centre located between the Cu(2) and Cu(2)A atoms. The geometry around the copper atom is square pyramidal, having a CuN_2O_2O' chromophore and with τ values of 0.03 for Cu(1)and 0.13 for Cu(2), respectively. The basal plane consists of two oxygen atoms from each bridging dihydrogenphosphato and hydrogenphosphato group, with Cu–O distances vary from 1.923(1) to 1.949(1) Å and of phen ligand coordinated almost symmetrically through two nitrogen atoms, with Cu–N distances vary from 2.010(2) to 2.031(2) Å. The fifth (axial) coordination site is occupied by an oxygen atom of a non-bridging monodentate dihydrogenphosphato group at a distance of 2.217(1) Å for the terminal chromophore and an oxygen atom of the bridging hydrogenphosphato group at a Cu–O distance of 2.247(1) Å for the inner chromophores. The square bases are essentially planar with only a small tetrahedral twist (dihedral angles between the CuN_2 and CuO_2 planes are 22.6° and 13.1°). The Cu atom lies 0.27 and −0.14 Å above these planes towards O(1) and O(6A), respectively.

Consequently, the Cu(2) and Cu(2A) ions are doubly bridged by a monoatomic-bridged μ_3,η^2-HPO_4 anion in an equatorial–axial configuration. Both hydrogenphosphate ligands exhibit a unique tridentate anion displaying a dual nature, i.e., triatomic-O–P–O and monoatomic-O bridges. Details of the hydrogen bondings are also listed in Table 3.

For both compounds several moderate to strong intermoleculrar H bonds are observed; these are not further discussed.

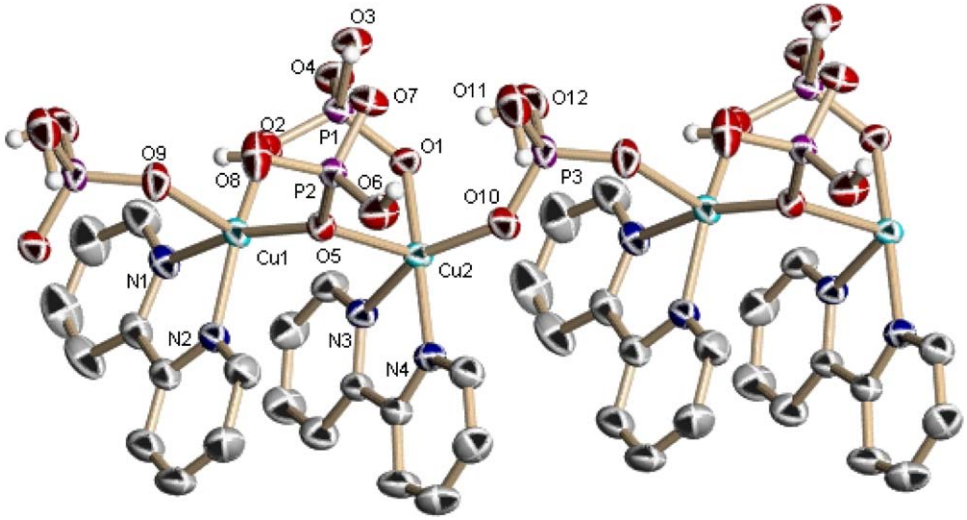

Fig. 1. Thermal ellipsoid plot (50% probability) of two units of [Cu_2(bpy)$_2$(μ,η^2-HPO_4)(μ,η^1-H_2PO_4)(μ,η^2-H_2PO_4)]$_n$ (**1**). The hydrogen atoms of pyridine ring are omitted for clarity.

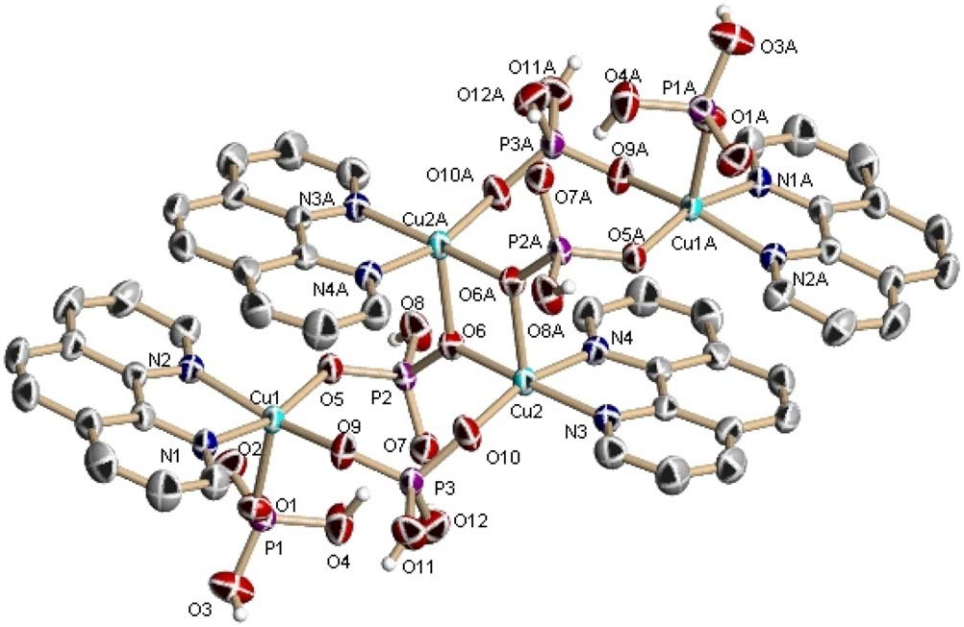

Fig. 2. Thermal ellipsoid plot (50% probability) plot of $[Cu_4(phen)_4(\mu_3,\eta^2\text{-}HPO_4)_2(\mu,\eta^2H_2PO_4)_2(H_2PO_4)_2](H_2O)_4$ (**2**). Atoms with an "A" are generated by an inversion centre and hydrogen atoms of pyridine ring are omitted for clarity.

3.3. Structure comparisons

The polymeric structure of complex **1** is comparable to those of earlier reported complexes with chelate didentate amine-phosphate system, $\{[Cu_3(dpyam)_3(\mu_3,\eta^3\text{-}HPO_4)(\mu_3,\eta^4\text{-}PO_4)(H_2O)](PF_6)\cdot 3H_2O\}_n$ (**3**) [13], $[Cu(dpyam)(\mu,\eta^3\text{-}HPO_4)]_n$ (**4**) [14] and $[Cu(phen)(\mu\text{-}HPO_4)(H_2O)_2]$ (**5**) [15] (see Table 4) all having a polymeric structure with bridging polyvalent hydrogenphosphate groups. The Cu atoms of **3** are bridged unsymmetrically through mixed 3M,3L (where M = metal and L = ligand) hydrogenphosphate and 3M,4L phosphate coordination modes. The bridging HPO_4^{2-} and PO_4^{3-} groups join copper(II) ions in an equatorial–equatorial and axial– equatorial configurations between two distorted square-pyramidal chromophores and two different geometry chromophores. The copper(II) ions in compound **4** are bridged by tridentate hydrogenphosphato ligands giving a 2M,3L coordination mode with the HPO_4 bridge linking Cu(II) ions in an equatorial–equatorial and axial–equatorial configurations. While those of compound **5** are bridged by didentate hydrogenphosphato ligands, giving a 2M,2L coordination mode, joining two copper(II) ions in an axial–axial configuration. However, compound **1** is also comparable to the $[Cu(dpyam)(\mu,\eta^2\text{-}H_2PO_4)(H_2PO_4)]_2$ (**6**) complex containing the monovalent dihydrogenphosphate group [14], Cu(II) ions being doubly bridged by two didentate dihydrogenphosphato anions with the 2M,2L coordination mode. The bridging oxoanion ligand joins two copper(II) ions in an equatorial–equatorial configuration (see Table 4).

The square-pyramidal CuN_2O_2O' chromophore of complex **2** corresponds to the copper environments of the known tetranuclear structures; $[Cu_4(dpyam)_4(\mu_4,\eta^3\text{-}HPO_4)_2(\mu\text{-}Cl)_2](Cl)_2\cdot 6H_2O$ (**7**) [16], $[Cu_4(dpyam)_4(\mu_4,\eta^3\text{-}HPO_4)_2(\mu\text{-}Br)_2](Br)_2\cdot 6H_2O$ (**8**) [16] and $[Cu_4(dpyam)_4(\mu_3,\eta^3\text{-}HPO_4)_2(NO_3)_2(H_2O)_2](NO_3)_2\cdot 2H_2O$ (**9**) [17] (see Table 5). Complexes **7** and **8** involve two pairs of five-coordinated copper(II) ions bridged by two tetrahedral, tridentate hydrogenphosphato groups in each molecules. All copper (II) ions are linked to each other via double-bridged HPO_4^{2-} groups in an equatorial–equatorial configuration giving a 4M,3L coordination mode. While four copper ions of complex **9**, are linked through a double hydrogenphosphate bridge, they give a 3M,3L coordination mode. Each chromophore is linked to another Cu(II) via a HPO_4^{2-} group in an equatorial–equatorial configuration between square pyramidal chromophores and in an axial–equatorial configuration between different geometry chromophores.

3.4. Spectroscopic properties

The electronic diffuse reflectance spectra of **1** and **2** show a broad band at 14000 and 14410 cm^{-1}, respectively. This observed single broad peak is consistent with the square pyramidal stereochemistry and assigned to be d_{z^2}, d_{xy}, d_{xz}, $d_{yz} \rightarrow d_{x^2-y^2}$ transition [18].

The infrared spectrum of complex **1** displays the characteristic bands of δ(P–O–(H)) in-plane deformation, ν_{as}(P–O), ν_s(P–O), δ(P–O–(H)) out-of-plane deformation and δ(O–P–O) at about 1317 and 1247; 1158–1024; 977; 878 cm^{-1}; and 527 and 487 cm^{-1}, respectively, which corresponds to those reported in the literature [19–22]. The IR spectrum of complex **2** shows bands at about 1320 and 1259; 1156–1065; 975 cm^{-1}; and 852 cm^{-1} characteristic

Table 4
Structural and magnetic data of complex **1** and relevant complexes

Complex[a]	Chromophore	Coordination geometry[b]	τ	Mode of $H_xPO_4^{(3-x)-}$[c]	Bridging configuration[d]	J value (cm^{-1})	Reference
Polynuclear							
$[Cu_2(bpy)_2(\mu,\eta^2\text{-}HPO_4)(\mu,\eta^1\text{-}H_2PO_4)\ (\mu,\eta^2\text{-}H_2PO_4)]_n$ (**1**)	CuN_2O_2O'	dist. sp	0.03, 0.30	2M,2L; 2M,1L	eq–eq, ax–eq	−5.3	this work
$\{[Cu_3(dpyam)_3(\mu_3,\eta^3\text{-}HPO_4)(\mu_3,\eta^4\text{-}PO_4)(H_2O)](PF_6)\cdot 3H_2O\}_n$ (**3**)	CuN_2O_2O', CuN_2O_3	dist. sp, tbp	0.17, 0.13, 0.57	3M,3L; 3M,4L	eq–eq, ax–eq	−4.98	[12]
$[Cu(dpyam)(\mu,\eta^3\text{-}HPO_4)]_n$ (**4**)	CuN_2O_2O'	dist. sp	0.12	2M,3L	eq–eq, ax–eq	−26.20(2)	[13]
$[Cu(phen)(\mu,\eta^2\text{-}HPO_4)(H_2O)_2]_n$ (**5**)	$CuN_2O_2O_2'$	dist. oct.		2M,2L	ax–ax	−5.86	[14]
Dinuclear							
$[Cu(dpyam)(\mu,\eta^2\text{-}H_2PO_4)(H_2PO_4)]_2$ (**6**)	CuN_2O_2O'	dist. sp	0.12	1M,1L; 2M,2L	eq–eq	−2.85(1)	[13]

[a] *Abbreviation*: dpyam, di-2-pyridylamine; bpy, 2,2′-bipyridine; phen = 1,10-phenanthroine.
[b] dist. oct., distorted octahedral; dist. sp, distorted square pyramidal; tbp, trigonal bipyramidal.
[c] M, metal; L, ligand.
[d] ax, axial; eq, equatorial configuration.

Table 5
Structural and magnetic data of complex **2** and relevant complexes

Complex[a]	Chromophore	Coordination geometry[b]	τ[c]	Mode of $H_xPO_4^{(3-x)-}$[d]	Bridging configuration[e]	J value (cm^{-1})	Reference
Tetranuclear							
$[Cu_4(phen)_4(\mu_3,\eta^2\text{-}HPO_4)_2(\mu,\eta^2\text{-}H_2PO_4)_2\ (H_2PO_4)_2]\cdot 2H_2O$ (**2**)	CuN_2O_2O'	dist. sp	0.031[1], 0.132[2]	1M,1L; 2M,2L; 3M,2L	eq–eq, ax–eq	0.12, −1.32, 0.10	this work
$[Cu_4(dpyam)_4(\mu_4,\eta^3\text{-}HPO_4)_2(\mu\text{-}Cl)_2](Cl)_2\cdot 6H_2O$ (**7**)	CuN_2O_2O'	dist. sp	0.020–0.053	4M,3L	eq–eq	22(2), −79(1), 46(4)	[15]
$[Cu_4(dpyam)_4(\mu_4,\eta^3\text{-}HPO_4)_2(\mu\text{-}Br)_2](Br)_2\cdot 6H_2O$ (**8**)	CuN_2O_2O'	dist. sp	0.001–0.071	4M,3L	eq–eq	33(1), −83(1), 12(3)	[15]
$[Cu_4(dpyam)_4(\mu_3,\eta^3\text{-}HPO_4)_2(NO_3)_2(H_2O)_2](NO_3)_2\cdot 2H_2O$ (**9**)	CuN_2O_2O'	dist. sp, intermediate	0.321[1], 0.492[2]	3M,3L	eq–eq, ax–eq	−10.3(1), −5.3(2)	[16]

[a] *Abbreviation*: phen, 1,10-phenanthroine; dpyam, di-2-pyridylamine.
[b] dist. oct., distorted octahedral; dist. sp, distorted square pyramidal; tbp, trigonal bipyramidal.
[c] 1, Cu(1) chromophore ; 2, Cu(2) chromophore.
[d] M, metal; L, ligand.
[e] ax, axial; eq, equatorial configuration.

of δ(P–O–(H)) in-plane deformation, ν_{as}(P–O), ν_s(P–O) and δ(P–O–(H)) out-of-plane deformation, respectively. The δ(O–P–O) vibrations are found at 531 and 524 cm^{-1} [23,24].

3.5. EPR and magnetic properties

The EPR spectrum of the powdered compounds reveals at room temperature and at 77 K an axial signal with $g_\perp = 2.09$ and an unresolved $g_\parallel = 2.28$ for compound **1** and $g_\perp = 2.04$ and an unresolved $g_\parallel = 2.26$ for compound **2**. The signals are consistent with the $d_{x^2-y^2}$ ground state and the planar based geometry [18]. No triplet signal has been observed.

The magnetic susceptibility of a powdered sample of compound **1** was measured from 5 to 350 K. The magnetic properties of the compound are depicted in Fig. 3 in the form of a plot of $\chi_m T$ versus T. At 350 K the $\chi_m T$ value is 0.83 $cm^3\,mol^{-1}$ K, slightly higher from that expected for two uncoupled Cu(II) centres ($\chi_m T = 0.75\ cm^3\ mol^{-1}$ K, with $g = 2$). With decreasing temperature the $\chi_m T$ value remains constant until at about 20 K, where it starts to decrease until 0.46 $cm^3\,mol^{-1}$ K at 5 K. This behaviour agrees with a weak antiferromagnetic interaction.

The chain-like structure can be considered as formed by dinuclear units bridged by hydrogenphosphato anions. The Cu–Cu distance between the copper dinuclear units bridged by the hydrogenphosphato anion is 5.28 Å and is large enough to consider these dinuclear units as being independent and any interaction between these dinuclear units as intermolecular.

The theoretical expression for the magnetic susceptibility for two interacting $S = 1/2$ centres, which is based on the general Hamiltonian [25] is: $H_{ex} = -JS_1S_2$, in which the exchange parameter J, is negative for antiferromagnetic and positive for ferromagnetic interaction. The magnetic data were fitted to the equation given in the literature for dinuclear copper compounds [25]: $\chi_m = 2Ng^2\beta^2[kT - 2zJ'/(3 + \exp(-J/kT)]^{-1}[3 + \exp(-J/kT)]^{-1}) \cdot (1 - p) + (Ng^2\beta^2/2kT) \cdot p + \mathrm{TIP}$, in which N, g, β, k and T have their usual meanings [25]. The parameter p denotes the fraction of paramagnetic impurity in the sample and zJ' the interaction between the neighbouring dinuclear units.

The best fit, depicted in Fig. 3 as a solid line, was obtained (fixing the TIP, temperature independent paramagnetism, to $140 \times 10^{-6}\ cm^3\,mol^{-1}$ K) for $J = -5.3\ cm^{-1}$, $g = 2.05$, $zJ' = 0.28\ cm^{-1}$, $p = 0$. As the two copper centres are in a square pyramidal (SP) geometry, their magnetic orbital is the $d_{x^2-y^2}$. One of the hydrogenphosphato anions is bridging the two centres through two of its oxygen atoms, which are coordinated to the metals in the basal plane. This path allows a weak antiferromagnetic interaction to occur between the coppers. The magnitude of the interaction is explained by the fact that the two basal planes of the copper atoms are almost parallel to each other and thus their overlap will be small. The other hydrogenphosphato anion bridges the two centres through a non-magnetic orbital of one of the coppers (d_{z^2}), and any type of interaction will be weak and thus masked by the major one. The zJ' value points to a weak interdimer ferromagnetic interaction. If $z = 2$, as it is a 1-D polymer, then $J' = 0.14$.

The distance between the coppers and the fact that one of the orbitals involved in the overlapping is non-magnetic, account for the weakness of the interaction. The ferromagnetic character of the interaction is evidenced by the perpendicularity of the d_{z^2} and the $d_{x^2-y^2}$ orbitals involved in this bridge. An "overall" antiferromagnetic behaviour determined by the intradimer interaction is observed for compound **1**.

The magnetic susceptibility of a powdered sample of compound **2** was measured from 5 to 200 K. The magnetic properties of the bulk compound are depicted in Fig. 4 in the form of a plot of $\chi_m T$ versus T and χ_m versus T.

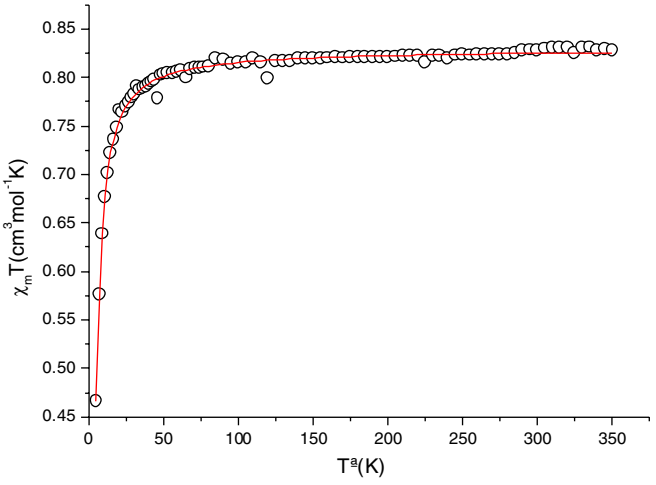

Fig. 3. A plot of the temperature dependence of $\chi_m T$ vs. T for compound **1**. The solid line represents the calculated curve for the parameters $J = -5.3\ cm^{-1}$, $g = 2.05$, $zJ' = 0.28\ cm^{-1}$ (see text).

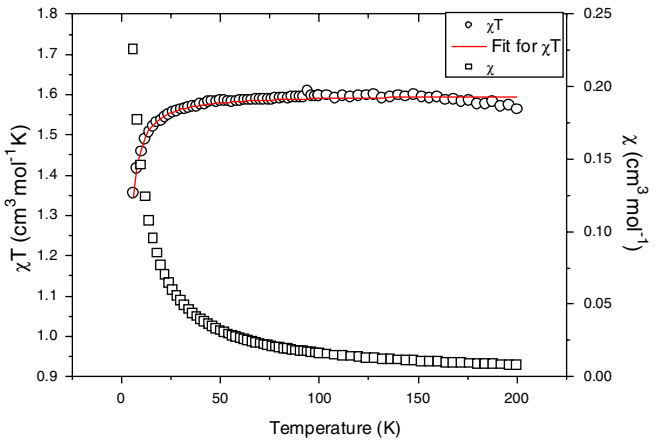

Fig. 4. The χ_m vs. T (□) and $\chi_m T$ vs. T (○) plots for compound **2**. The solid line represents the calculated curve for the parameters given in the text.

At 200 K the $\chi_m T$ value is 1.58 $cm^3\ mol^{-1}\ K$, which corresponds to the value for four uncoupled Cu(II) centres ($\chi_m T = 1.5\ cm^3\ mol^{-1}\ K$, with $g = 2$). With lowering temperature the $\chi_m T$ value remains constant until at about 16 K, where it starts to decrease to 1.35 $cm^3\ mol^{-1}\ K$ at 5 K. This behaviour agrees with an overall weak antiferromagnetic interaction.

For a tetranuclear compound with the present topology (see Scheme 1), the following Hamiltonian can be used [15,26,27].

$$\begin{aligned} H = &-2\cdot J_1(\mathbf{S}_2\mathbf{S}_{2a}) - 2\cdot J_2(\mathbf{S}_2\mathbf{S}_1 + \mathbf{S}_{2a}\mathbf{S}_{1a}) \\ &- 2\cdot J_3(\mathbf{S}_2\mathbf{S}_{1a} + \mathbf{S}_{2a}\mathbf{S}_1) - 2\cdot J_4(\mathbf{S}_{1a}\mathbf{S}_1) \end{aligned}$$

Considering the energy levels and the spin quantum numbers as follows:

$$\begin{aligned}
&S_1 = 2, \quad E_1 = -J_1 - J_2/2 - J_3 - J_4/2 \\
&S_2 = 1, \quad E_2 = -J_1 - J_2/2 + J_3 - J_4/2 \\
&S_3 = 1, \quad E_3 = (J_2 + J_4)/2 + [(J_2 - J_4)^2 + (J_3 - J_1)^2]^{1/2} \\
&S_4 = 1, \quad E_4 = (J_2 + J_4)/2 - [(J_2 - J_4)^2 + (J_3 - J_1)^2]^{1/2} \\
&S_5 = 0, \quad E_5 = J_1 + J_3 + (J_2 + J_4)/2 + [4(J_1^2 + J_3^2) + J_2^2 + J_4^2 - 2J_1(J_2 + 2J_3 + J_4) - 2J_2(J_3 - J_4) - 2J_3J_4]^{1/2} \\
&S_6 = 0, \quad E_6 = J_1 + J_3 + (J_2 + J_4)/2 - [4(J_1^2 + J_3^2) + J_2^2 + J_4^2 - 2J_1(J_2 + 2J_3 + J_4) - 2J_2(J_3 - J_4) - 2J_3J_4]^{1/2}
\end{aligned}$$

Then the expression for the magnetic susceptibility per tetranuclear unit is described by:

$$\begin{aligned} \chi_M = &(N_A g^2\beta^2/k_B T)[10\exp(-E_1/K_B T) + 2\exp(-E_2/K_B T) \\ &+ 2\exp(-E_3/K_B T) + 2\exp(-E_4/K_B T)] \\ &/[5\exp(-E_1/K_B T) + 3\exp(-E_2/K_B T) \\ &+ 3\exp(-E_3/K_B T) + 3\exp(-E_4/K_B T) \\ &+ \exp(-E_5/K_B T) + \exp(-E_6/K_B T)] + \mathrm{TIP} \end{aligned}$$

The values of N, g, β, k and T have their usual meanings and the TIP was fixed to $60\times10^{-6}\ cm^3\ mol^{-1}\ K$ per copper atom [25]. An impurity factor (p) was considered to account for any paramagnetic impurity. When fixing $J_4 = 0$, the best set of parameters were obtained as: $g = 2.06$, $J_1 = 0.12\ cm^{-1}$, $J_2 = -1.32\ cm^{-1}$, $J_3 = 0.1\ cm^{-1}$ and $p = 0.001$.

The values obtained indicate that the overall magnetic behaviour is dominated by the interaction parameter J_2. The lack of a clear path for any interaction to occur can justify the weakness of the coupling constants. The parameter J_1, the coupling constant between the two central copper centres (see Scheme 1), is weak ferromagnetic. Both metal centres have SP geometry, thus both have the $d_{x^2-y^2}$ as their magnetic orbital. In each case the path to communicate implies the magnetic orbital of one metal centre ($d_{x^2-y^2}$) with a non-magnetic orbital of the other copper (d_{z^2}), hindering the interaction. The low electronic-paramagnetic density of the d_{z^2} and its perpendicularity with respect to the $d_{x^2-y^2}$ makes the small value for J_1 reasonable. A negative value for the interaction parameter J_2 is obtained, pointing at a weak antiferromagnetic interaction between the central and the external coppers ($Cu_1\cdots Cu_2$, 5.06 Å). This is in agreement with the relative positions of the magnetic orbitals of the metal centres. With respect to the previous constant, in this case both orbitals implied are magnetic, and a much stronger interaction could be expected. The long distance between the coppers, created by the anion (5.06 Å), can account for the weakness of the interaction [12]. The parameter J_3, like J_1, is ferromagnetic. The μ-O-hydrogenphosphato anion bridges Cu1 and Cu2a (J_3) with a hydrogenphosphato-O,O mode. The interaction occurs between two perpendicular orbitals in which one of them is non-magnetic, explaining both sign and intensity of the interaction. Moreover, the long distance between the coppers, due to the hydrogenphosphato-O,O bridge mode, makes the interaction almost negligible. In previous cases, the distortion of the copper geometry and the subsequent diminish of the electron delocalization, was pointed as a plausible explanation of the weak interaction [12,16]. In the present case the compound's fairly regular SP geometry of the copper discards this possibility. The long distances between coppers created by the hydrogenphosphato-O,O-bridge mode or the involvement of a non-magnetic orbital in the communication path, must account for this weak bulk magnetic interaction.

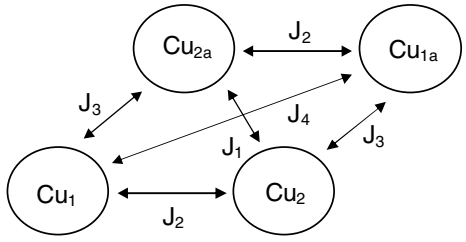

Scheme 1. Scheme of the magnetic interactions in the tetranuclear compound **2**.

4. Conclusions

The crystal structure determination of the two new hydrogenphosphate-bridged Cu(II) compounds, a dinuclear compound bridged by hydrogenphosphate molecules to form a polynuclear identity **1** and a tetranuclear compound **2**. In all cases the Cu–Cu distances are fairly large and the magnetic interaction must occur via the hydrogenphosphate molecules.

As can be seen from Table 4, which shows a number of compounds related to compound **1**, the magnetic interaction in these compounds is in general weakly antiferromagnetic.

In Table 5 a number of compounds are shown which are related to compound 2 and as can be seen from these the magnetic interaction is rather complicated and varies from a weak antiferromagnetic to a weak ferromagnetic interaction.

Acknowledgements

The authors thank the Thailand Research Fund (TRF: Agreement Number RTA 4880008) for a research grant and also gratefully acknowledge the Higher Education Development Project: Postgraduate Education and Research Program in Chemistry, funded by the Royal Thai Government, for support. The work described in the present paper has been supported by the Leiden University Study group WFMO (Werkgroep Fundamenteel MaterialenOnderzoek).

Appendix A. Supplementary data

Crystallographic data for the structures in this paper have been deposited with the Cambridge Crystallographic Data Centre as supplementary publication CCDC Nos. 292489 and 292488 for structures **1** and **2**, respectively. Copies of the data can be obtained free of charge from The Director, CCDC, 12 Union Road, Cambridge CB2 1EZ, UK (fax: +44-1223-336033; e-mail: deposit@ccdc.cam.ac.uk, http://www.ccdc.cam.ac.uk). Supplementary data associated with this article can be found, in the online version, at doi:10.1016/j.poly.2006.01.014.

References

[1] C.R. Kagan, D.B. Mitzi, C.D. Dimitrakopoulos, Science 286 (1999) 945.
[2] (a) O.M. Yaghi, H. Li, C. Davis, D. Richardson, T.L. Groy, Acc. Chem. Res. 31 (1998) 474;
(b) S.R. Batten, R. Robson, Angew. Chem., Int. Ed. 37 (1998) 1460.
[3] (a) C.T. Kressge, M.E. Leonowicz, W.J. Roth, J.C. Vartuni, J.S. Beck, Nature 359 (1992) 710;
(b) X.-Y. Huang, J. Li, H.-X. Fu, J. Am. Chem. Soc. 122 (2000) 8789.
[4] D.E.W. Vaughan, in: R.P. Townsend (Ed.), Properties and Applications of Zeolites, The Chemical Society, London, 1979.
[5] C.T. Kressge, M.E. Leonowicz, W.J. Roth, J.C. Vartuli, J.S. Beck, Nature 365 (1993) 499.
[6] (a) P. Feng, X. Bu, G.D. Stucky, Nature 388 (1997) 735;
(b) A.K. Cheetham, G. Ferey, T. Loiseau, Angew. Chem., Int. Ed. 38 (1999) 3268;
(c) S.N. Natarajan, C.N.R. Rao, Angew. Chem., Int. Ed. 38 (1999) 3480.
[7] S. Mann, Nature 365 (1993) 499.
[8] (a) P.J. Hagrman, D. Hagrman, J. Zubieta, Angew. Chem., Int. Ed. 38 (1999) 2638;
(b) D.J. Chesnut, K. Hagrman, P.J. Zapf, R.P. Hammond, R. LaDuca, R.C. Haushalter, J. Zubieta, Coord, Chem. Rev. 190–192 (1999) 737;
(c) T. Chirayil, P.Y. Zavalij, M.S. Whittingham, Chem. Mater. 10 (1998) 2629.
[9] Siemens, SAINT, 1996, Version4 Software Reference Manual, Siemens Analytical X-Ray Systems, Inc., Madison, WI, USA, 1996.
[10] G.M. Sheldrick, SADABS, Program for Empirical Absorption correction of Area Dectector University of Göttingen, University of Göttingen, Göttingen, Germany, 1996.
[11] Siemens, SHELXTL. 1997, Version 6.12 Reference Manual, Siemens Analytical X-Ray Systems, Inc., Madison, WI, USA, 1997.
[12] A.W. Addison, T.N. Rao, J. Reedijk, J. van Rijn, G.C. Verschoor, J. Chem. Soc. Dalton Trans. (1984) 1349.
[13] S. Youngme, P. Phuengphai, C. Pakawatchai, G.A. van Albada, J. Reedijk, Inorg. Chim. Acta 358 (2005) 2125.
[14] S. Youngme, P. Phuengphai, N. Chaichit, C. Pakawatchai, G.A. van Albada, O. Roubeau, J. Reedijk, Inorg. Chim. Acta 357 (2004) 3603.
[15] S. Youngme, P. Phuengphai, C. Pakawatchai, G.A. van Albada, S. Tanase, I. Mutikainen, U. Turpeinen, J. Reedijk, Inorg. Chem. Commun. 8 (2005) 335.
[16] S. Youngme, P. Phuengphai, N. Chaichit, G.A. van Albada, O. Roubeau, J. Reedijk, Inorg. Chim. Acta 358 (2005) 2262.
[17] S. Youngme, P. Phuengphai, N. Chaichit, G.A. van Albada, O. Roubeau, J. Reedijk, Inorg. Chim. Acta 358 (2005) 849.
[18] B.J. Hathaway, in: G. Wilkinson, R.D. Gill, J.A. McCleverty (Eds.), Comprehensive Coordination Chemistry, vol. 5, Pergamon Press, Oxford, 1987.
[19] A.M. Krogh Andersen, P. Norby, J.C. Hanson, T. Vogt, Inorg. Chem. 37 (1998) 876.
[20] M. Roca, P. Amoros, J. Cano, M.D. Marcos, J. Alamo, A. Beltran-Porter, D. Beltran-Porter, Inorg. Chem. 37 (1998) 3167.
[21] Z. Bircsak, W.T.A. Harrison, Inorg. Chem. 37 (1998) 3204.
[22] C.-H. Lin, S.-L. Wang, Inorg. Chem. 40 (2001) 2918.
[23] Y. Zhang, R.C. Haushalter, J. Zubieta, Inorg. Chim. Acta 260 (1997) 105.
[24] A.C. Chapman, L.E. Thirlwell, Spectrochim. Acta 20 (1964) 937.
[25] O. Kahn, Molecular Magnetism, VCH, Weinheim, Germany, 1993.
[26] B. Chiari, O. Piovesana, T. Tarantelli, P.F. Zanazzi, Inorg. Chem. 32 (1993) 4834.
[27] A.N. Papadopoulos, V. Tangoulis, C.P. Raptopoulou, A. Terzis, D.M. Kessissoglou, Inorg. Chem. 35 (1996) 559.

complex **1** became Ni(tpp-*N*-O) (**2**) [12]. However, until now there has been no X-ray structural data available for the diamagnetic and bridged metal [M(III)] porphyrin complexes with an oxygen atom being inserted between one metal–N unit and with a coordination number (CN) above 4 (i.e., with CN $\geqq$ 5).

In order to investigate the range of metal ions that can be inserted into H_2(tpp-*N*-O), we present the results upon replacing Ni(II) with Tl(III) in Ni(tpp-*N*-O) (**2**) forming a new complex Tl(tpp-*N*-O)(OAc) (**3**). This replacement increases the coordination number (CN) from four for **2** to six for Tl(tpp-*N*-O)(OAc) (**3**). The presence of acetate ligands in **3** plays a potential role in increasing the coordination number.

In order to figure out the structural features of oxygen and nitrogen inserted into the Tl–N bond, we also describe the synthesis and X-ray structural investigation on the metallation of 21-(4-*tert*-butyl-benzensulfonamido)-5,10,15,20-tetraphenylporphyrin [N-*p*-$HNSO_2C_6H_4{}^t$Bu-Htpp (**4**)], leading to the mononuclear complex *cis*-acetato-N-*p*-*tert*-butylbenzensulfonylimido-*meso*-tetraphenylporphyrinato-thallium(III) Tl(N-*p*-$NSO_2C_6H_4{}^t$Bu-tpp)(OAc) (**5**). Because of the large size of Tl^{3+} (r_{ion} = 1.025 Å) [13] the relative position of acetate and the 4-*tert*-butylbenzensulfonyl (^{t}BuBS) group coordinated to the Tl atom might lead to a *cis* configuration in **5** [5,8,9]. Prompted by earlier studies on the acetato exchange of Tl(tpp)(OAc) and Tl(N-NTs-tpp)-(OAc) in CD_2Cl_2(NTs = tosylimido) [8,14,15], we investigated a similar intermolecular acetato exchange for **3** and **5** in CD_2Cl_2 by ^{1}H and ^{13}C dynamic NMR methods. Thallium shows rich coupling patterns to the nuclei of the porphyrin core and to the porphyrin substituents and axial ligands. Many long-range Tl–C and Tl–H couplings to the porphyrin substituents and to the axial ligands are observed [16,17]. Moreover, there is no precedence in the literature that the magnitude of two- and three-bond thallium–carbon spin–spin coupling constants between the Tl atom and the OAc^- group of **3** and **5** depends on the electronegative substituents X (i.e., X = O in **3** and N in **5**) attached to the thallium atom. Thus, the electronegative dependence of spin–spin coupling constants $^nJ(Tl-{}^{13}C)$ (n = 2, 3) for the OAc^- ligand of **3** and **5** will be studied for the first time in the chemistry of thallium porphyrins. The compound **3** is the first thallium porphyrin complex with a Tl–O–N(Por) linkage and **5** represents the fourth thallium complex with a Tl–N(R)–N(Por) linkage reported in the literature [5,8,9].

2. Experimental

2.1. Tl(tpp-*N*-O)(OAc) (3)

A mixture of H_2(tpp-*N*-O) (0.063 g, 0.1 mmol) in CH_2Cl_2 (20 cm^3) and $Tl(OAc)_3$ (0.08 g, 0.2 mmol) in MeOH (10 cm^3) was refluxed for 3 h (Scheme 1) [12]. After concentrating, the residue was redissolved in CH_2Cl_2, dried with anhydrous Na_2SO_4, and filtered. The filtrate was concentrated and recrystallized from CH_2Cl_2–MeOH [1:2 (v/v)] yielding the blue solid of **3** (0.062 g, 7×10^{-2} mmol, 70%). Compound **3** was dissolved in toluene to crystallize out as blue crystals for single-crystal X-ray analysis. ^{1}H NMR (599.95 MHz, $CDCl_3$, 20 °C): δ 9.18 [dd, 2H, H_β

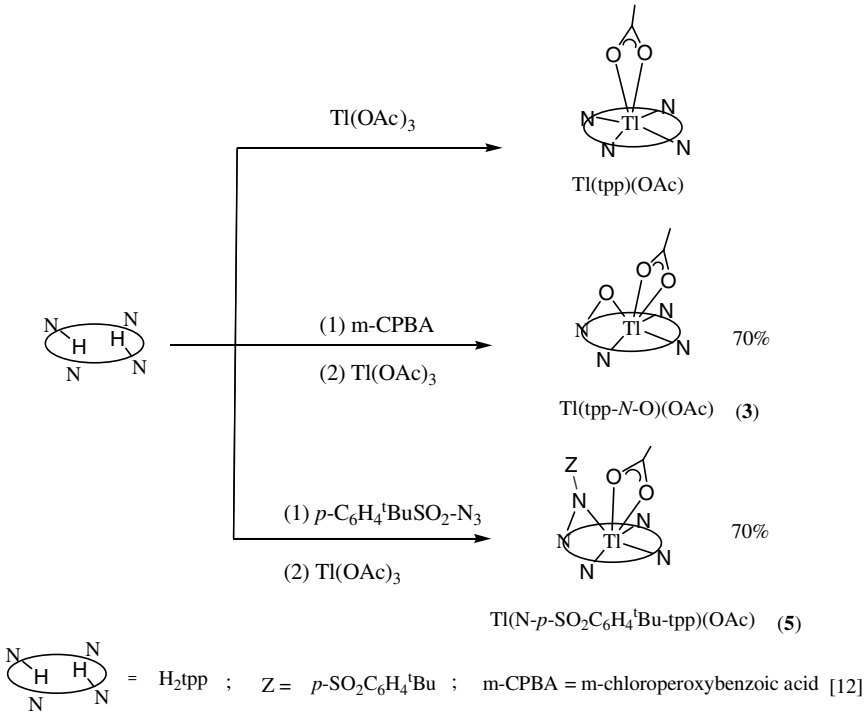

Scheme 1.

(2, 13), ^4J(Tl–H) = 13 Hz and ^3J(H–H) = 4.8 Hz], H_β (a, b) represents the 2 equiv. β-pyrrole protons attached to carbons a and b, respectively; 8.93 [dd, 2H, H_β (3, 12), ^4J(Tl–H) = 20 Hz and ^3J(H–H) = 4.8 Hz]; 8.79 [d, 2H, H_β (7, 8), ^4J(Tl–H) = 79 Hz]; 6.65 [s, 2H, H_β (17, 18)]; 8.45 [d, 2H, *o*-H (26, 28), ^3J(H–H) = 4.4 Hz], *o*-H represents *ortho* phenyl protons; 8.07 [s, 2H, *o*-H (22, 32)]; 7.72–7.81(m, 12H) for *meta* and *para* phenyl protons (*m*-, *p*-H); 0.54 (s, 3H, OAc). FAB MS, *m*/*z* (assignment, rel. intensity): 154 ($[NBA + H]^+$, 100), 614 ($[H_2tpp]^+$, 36.31), 630 ($[H_2tpp\text{-}N\text{-}O]^+$, 40.13), 631 ($[H_2tpp\text{-}N\text{-}O + H]^+$, 42.67), 833 ($[Tl(tpp\text{-}N\text{-}O)]^+$, 64.31), UV/Vis spectrum, λ/nm [$\varepsilon \times 10^{-3}$ ($M^{-1}\,cm^{-1}$)] in CH_2Cl_2: 333.2 (17.1), 477.2 (173.0), 584.4 (9.1), 626.0 (10.9).

2.2. Tl(N-*p*-$NSO_2C_6H_4{}^t$Bu-tpp)(OAc) (5)

A mixture of $Tl(OAc)_3$ (0.05 g, 1.31×10^{-4} mol) in MeOH (20 cm^3) and N-*p*-$HNSO_2C_6H_4{}^t$Bu-Htpp (0.05 g, 6.06×10^{-5} mol) in CH_2Cl_2 (50 cm^3) was refluxed for 3 h (Scheme 1) [9]. After concentrating, the residue was dissolved in CH_2Cl_2, dried with anhydrous Na_2SO_4, and filtered. The filtrate was concentrated and recrystallized from CH_2Cl_2–MeOH [1:3 (v/v)] yielding the bluish-purple solid of **5** (0.046 g, 4.23×10^{-5} mol, 70%) which was again dissolved in CH_2Cl_2 and layered with MeOH to get purple crystals for single crystal X-ray analysis. ^{1}H NMR (299.95 MHz, CD_2Cl_2, 20 °C): δ 9.05 [dd, 2H, H_β (10, 19), ^4J(Tl–H) = 17.1 Hz and ^3J(H–H) = 4.8 Hz]; 8.92 [dd, 2H, H_β (9, 20), ^4J(Tl–H) = 10.4 Hz and ^3J(H–H) = 4.8 Hz]; 8.69 [d, 2H, H_β (4, 5), ^4J(Tl–H) = 76.5 Hz]; 8.38 [d, 2H, ^3J(H–H) = 7 Hz] and 8.10 [d, 2H, ^3J(H–H) = 7 Hz] for *ortho* protons; 7.85–7.76 (m, 12H, for *meta* and *para* protons); 7.07 [d, 2H, ^{t}BuBS-$H_{3,5}$ or H (49, 51), ^3J(H–H) = 8 Hz]; 6.94 [s, 2H, H_β (14, 15)], 6.09 [d, 2H, ^{t}BuBS-$H_{2,6}$ or H (48, 52), ^3J(H–H) = 8 Hz]; 1.15 (s, 9H, *t*-butyl protons); 0.62 (s, 3H, OAc). ESI–MS, *m*/*z* (assignment, rel. intensity): 1087 ($[Tl(N\text{-}p\text{-}NSO_2C_6H_4{}^t$Bu-tpp)(OAc)$]^+$, 12.26), 1086 ($[Tl(N\text{-}p\text{-}NSO_2C_6H_4{}^t$Bu-tpp)(OAc)-H$]^+$, 16.34), 1030 ($[Tl(N\text{-}p\text{-}NSO_2C_6H_4{}^t$Bu-tpp) + 2 H$]^+$, 100), 1028 ($[Tl(N\text{-}p\text{-}NSO_2C_6H_4{}^t$Bu-tpp$)]^+$, 74.18). UV/Vis spectrum, λ/nm [$\varepsilon \times 10^{-3}$ ($M^{-1}\,cm^{-1}$)] in CH_2Cl_2: 332 (23.0), 446 (354), 555 (8.4), 609 (19.1).

2.3. Spectroscopy

Proton and ^{13}C NMR spectra were recorded at 299.95 (or 599.95) and 75.43 (or 150.87) MHz, respectively, on Varian VXR-300 (or Varian Unity Inova-600) spectrometers locked on deuterated solvent, and referenced to the solvent peak. Proton NMR is relative to CD_2Cl_2 or $CDCl_3$ at $\delta = 5.30$ or 7.24 and ^{13}C NMR to the center line of CD_2Cl_2 or $CDCl_3$ at $\delta = 53.6$ or 77.0. HMQC (heteronuclear multiple quantum coherence) was used to correlate protons and carbon through one-bond coupling and HMBC (heteronuclear multiple bond coherence) for two- and three-bond proton–carbon coupling. Nuclear Overhauser effect (NOE) difference spectroscopy was employed to determine the ^{1}H–^{1}H proximity through space over a distance of up to about 4 Å.

Positive ion mode ESI mass spectra were acquired at room temperature on a ThermoFinnigan LCQ Advantage mass spectrometer. The positive-ion fast atom bombardment mass spectrum (FAB MS) was obtained in a nitrobenzyl alcohol (NBA) matrix using a JEOL JMS-SX/SX 102A mass spectrometer. UV/Vis spectra were recorded at 20 °C on a HITACHI U-3210 spectrophotometer.

2.4. Crystallography

Table 1 presents the crystal data as well as other information for **3** and **5**. Measurements for **3** were taken on a Nonius Kappa CCD diffractometer using monochromatized Mo Kα radiation ($\lambda = 0.71073$ Å) at a temperature of 100(1) K. Measurements for **5** were taken on a Bruker AXS SMART-1000 diffractometer using monochromatized Mo Kα radiation ($\lambda = 0.71073$ Å) at a temperature of 100(2) K. Muti-scan absorption corrections were made for **3** and empirical absorption corrections were made for **5**. The structures were solved by direct methods (SHELXL-97) [18] and refined by the full-matrix least-squares method. The OAc group within **3** is disordered with an occupancy factor of 0.6 for O(2)O(3)C(45)C(46) and 0.4 for O(2′)O(3′)C(45′)C(46′). These four atoms (i.e., O(2), O(3), C(45) and C(46)) were refined with isotropic displacement parameters. All non-hydrogen atoms, except the

Table 1
Crystal data for $\mathbf{3} \cdot CH_2Cl_2$ and **5**

Empirical formula	$C_{47}H_{33}Cl_2N_4O_3Tl$ ($\mathbf{3} \cdot CH_2Cl_2$)	$C_{56}H_{44}N_5O_4STl$ (**5**)
Formula weight	977.04	1087.39
Space group	$P\bar{1}$	$P2_1/n$
Crystal system	triclinic	monoclinic
a (Å)	10.3685(4)	12.9290(8)
b (Å)	12.2132(4)	24.4703(15)
c (Å)	17.4671(6)	14.9484(9)
α (°)	71.214(2)	90
β (°)	77.251(2)	102.981(1)
γ (°)	69.573(2)	90
V (Å^3)	1947.72(12)	4608.5(5)
Z	2	4
F(000)	964	2176
D_{calcd} (g cm^{-3})	1.666	1.567
μ(Mo Kα) (mm^{-1})	4.333	3.605
S	1.088	0.959
Crystal size (mm^3)	$0.20 \times 0.08 \times 0.08$	$0.50 \times 0.41 \times 0.12$
$2\theta_{max}$ (°)	55.0	56.68
T (K)	100(1)	100(2)
Number of reflections measured	8846	11415
Number of reflections observed	7605	9395 ($I > 2\sigma(I)$)
R_1[a]	0.0426	0.0300
wR_2[b]	0.0987	0.0699

[a] $R_1 = [\sum\|F_o| - |F_c\|/\sum|F_o|]$.
[b] $wR_2 = \{\sum[w(F_o^2 - F_c^2)^2]/\sum[w(F_o^2)^2]\}^{1/2}$.

Table 2
Selected bond distances (Å) and bond angles (°) for compounds **3** · CH_2Cl_2 and **5**

3 · CH_2Cl_2			
Bond lengths			
Tl–O(2)	2.357(9)	Tl–O(3)	2.348(8)
Bond angles			
O(2)–Tl–O(3)	55.2(4)	O(1)–Tl–N(3)	83.85(14)
O(2)–Tl–N(1)	92.6(3)	O(3)–Tl–N(1)	147.7(3)
O(2)–Tl–N(2)	100.0(3)	O(3)–Tl–N(2)	98.8(3)
O(2)–Tl–N(3)	145.9(3)	O(3)–Tl–N(3)	90.8(2)
O(2)–Tl–O(1)	103.1 (2)	O(3)–Tl–O(1)	101.0(2)
N(1)–Tl–O(1)	87.51(14)	O(3)–C(45)–O(2)	121.9(9)
N(1)–Tl–N(2)	83.41(16)	Tl–O(1)–N(4)	106.2(3)
N(3)–Tl–N(2)	81.53(16)		
5			
Bond lengths			
Tl(1)–O(1)	2.337(2)	Tl(1)–O(2)	2.350(2)
Bond angles			
O(1)–Tl(1)–O(2)	55.85(7)	O(2)–Tl(1)–N(1)	93.26(8)
O(1)–Tl(1)–N(1)	148.99(8)	O(2)–Tl(1)–N(2)	94.16(9)
O(1)–Tl(1)–N(2)	100.86(9)	O(2)–Tl(1)–N(3)	145.97(8)
O(1)–Tl(1)–N(3)	91.97(8)	O(2)–Tl(1)–N(5)	111.79(9)
O(1)–Tl(1)–N(5)	102.91(8)	Tl(1)–O(1)–C(45)	91.60(18)
Tl(1)–N(5)–S(1)	133.96(14)	Tl(1)–O(2)–C(45)	91.01(18)
Tl(1)–N(5)–N(4)	109.36(17)	O(1)–C(45)–O(2)	121.5(3)
N(5)–Tl(1)–N(1)	85.08(9)	N(5)–Tl(1)–N(3)	83.80(9)

above four atoms, were refined with anisotropic thermal parameters, whereas all hydrogen atoms were placed in calculated positions and refined with a riding model. Table 2 lists selected bond distances and bond angles for complexes **3** and **5**.

3. Results and discussion

3.1. Molecular structures of 3 and 5

The X-ray molecules are depicted in Fig. 1a for the complex Tl(tpp-*N*-O)(OAc) (**3**) and in Fig. 1b for Tl(N-*p*-$NSO_2C_6H_4{}^t$Bu-tpp)(OAc)**5**. The complex **3** co-recrystallizes with 1 equiv. of CH_2Cl_2 solvent molecule in the triclinic space group $P\bar{1}$, and complex **5** recrystallizes in the monoclinic space group $P2_1/n$. In both **3** and **5**, it is obvious that the oxygen and $NSO_2C_6H_4{}^t$Bu moieties have been inserted into the Tl–N bond of acetato(*meso*-tetraphenylporphyrinato)thallium(III) Tl(tpp)(OAc) (see Scheme 1) [15].

The metal–ligand bond distances and the bond angles are summarized in Table 2. The bond distance (Å) are Tl–O(2) = 2.357(9), Tl–O(3) = 2.348(8) and Tl–O(1) = 2.126(4) and the mean Tl–N(*p*) = 2.264(4) for **3**; for **5** the values are Tl(1)–O(1) = 2.337(2) and Tl(1)–O(2) = 2.350(2) and the mean Tl(1)–N(*p*) = 2.241(2). Since the acetate of **3** was disordered, data reported involving O(2) and O(3) refer to the acetate at the higher occupancy factor of 0.6.

The geometry around Tl^{3+} is described as a distorted square-based pyramid in which the apical site is occupied

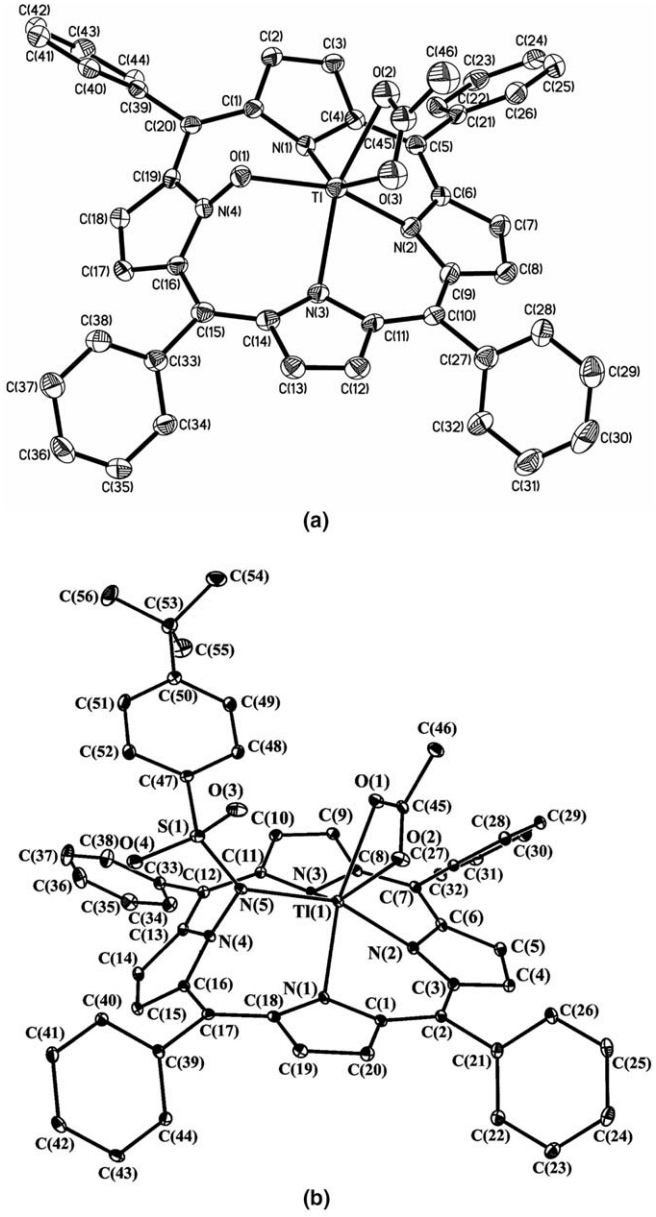

Fig. 1. Molecular configuration and atom labelling scheme for (a) Tl(tpp-*N*-O)(OAc) (**3**), (b) Tl(N-*p*-$SO_2C_6H_4{}^t$Bu-tpp)(OAc) (**5**), with ellipsoids drawn at 50% probability for **3** and at 30% probability for **5**. Hydrogen atoms for all compounds are omitted for clarity.

by a bidentate chelating OAc^- group for **3** and **5**. Fig. 2 shows the actual porphyrin skeleton of **3** and **5**. The pyrrole nitrogens N(4) (in **3** and **5**) are no longer bonded to the thallium as indicated by their longer internuclear distances, 2.831(4) Å for N(4)···Tl (in **3**) and 2.899(2) Å for N(4)···Tl(1) (in **5**). The plane of three strongly bound pyrrole nitrogen atoms (i.e., N(1)–N(3) for **3** and **5**) is adopted as a reference plane 3*N*. It is noted that the ionic radius increases from 0.63 Å for Ni^{2+} to 1.025 Å for Tl^{3+} [1,13]. Because of the larger size of Tl^{3+}, Tl and O(1) lie 1.11 and 1.34 Å, respectively, above the 3*N* plane in **3**, compared to 1.15 Å for Tl(1) and 1.30 Å for N(5) in **5** (cf. 0.05 Å for Ni(II) in Ni(OEP-*N*-O)) (Fig. 2) [1].

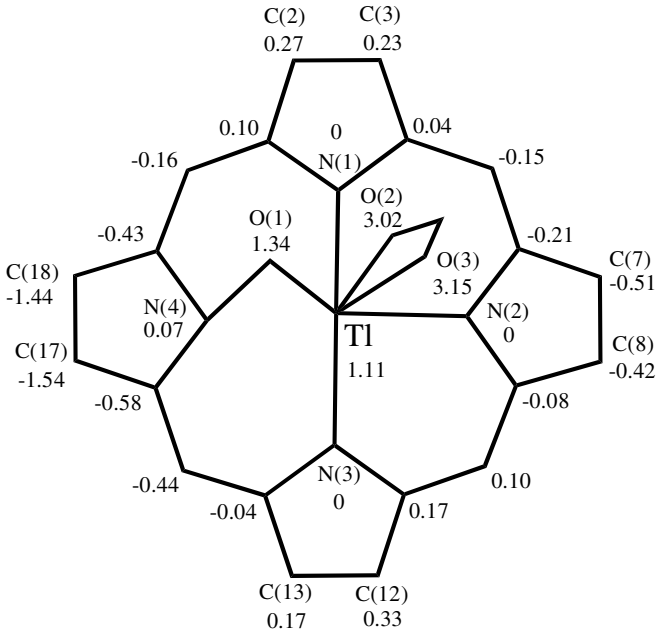

(a) Tl(tpp-*N*-O)(OAc) **3**

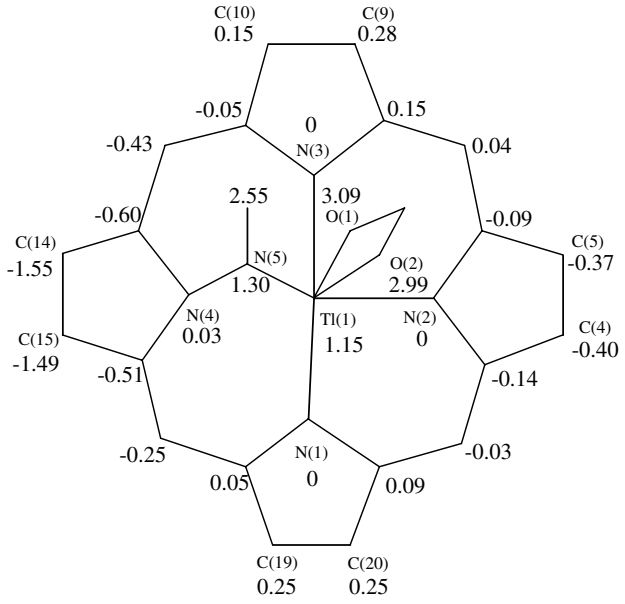

(b) Tl(N-*p*-$NSO_2C_6H_4{}^t$Bu-tpp)(OAc) **5**

Fig. 2. Diagram of the porphyrinato core ($C_{20}N_4$, M, O, ^{t}BuBS and OAc^-) of (a) **3** · CH_2Cl_2 and (b) **5**. The values represent the displacements (in angstroms) of the atoms from the mean 3*N* plane (i.e., N(1)–N(3) for **3** · CH_2Cl_2 and **5**).

The porphyrin macrocycle is indeed distorted because of the presence of the oxygen [O(1)] and the $NSO_2C_6H_4{}^t$Bu group in **3** and **5**, respectively (Fig. 2). Thus, N(4) in the **3** and **5** pyrrole rings bearing the oxygen and the $NSO_2C_6H_4{}^t$Bu group is deviated most from the 3*N* plane and oriented separately with a dihedral angle of 47.3° and of 46.7°, whereas small angles of 7.0°, 13.1° and 9.0° occur with N(1), N(2) and N(3) pyrroles for compound **3** and 6.8°, 10.8° and 7.9° with N(1), N(2) and N(3) pyrroles for compound **5**. The dihedral angles between the mean plane of the skeleton (3*N*) and the plane of the phenyl group are 49.8° [C(24)], 53.1° [C(30)], 44.7° [C(36)] and 44.0° [C(42)] for **3** and the corresponding angles are 49.4°, 57.4°, 45.0° and 53.1° for **5**.

Table 3
Comparison of distances (Å) and bond angles (°) in **3** and **5** with oxygen and nitrogen units (X) inserted between one Tl–N unit

Parameters	X = O (**3**)	Parameters	X = $NSO_2C_6H_4{}^t$Bu (**5**)
3		**5**	
O(1)–Tl	2.126(4)	Tl(1)–N(5)	2.128(2)
N(1)–Tl	2.306(4)	Tl(1)–N(1)	2.320(2)
N(2)–Tl	2.150(4)	Tl(1)–N(2)	2.153(2)
N(3)–Tl	2.335(4)	Tl(1)–N(3)	2.364(2)
N(4)···Tl	2.831(4)	Tl(1)···N(4)	2.899(2)
N(4)–O(1)	1.369(5)	N(4)–N(5)	1.386(3)
O(1)–Tl–N(2)	155.45(16)	N(5)–Tl(1)–N(2)	151.74(9)
N(1)–Tl–N(3)	121.28(15)	N(3)–Tl(1)–N(1)	118.84(8)

Table 3 contains some comparative data. The N(4)–O(1) distance of 1.369(5) Å in **3** is comparable to that in Ni(OEP-*N*-O) [1.363(6) Å] [1]. The *trans* O(1)–Tl–N(2) and N(1)–Tl–N(3) angles [155.45(16)° and 121.28(15)°] in **3** and the corresponding N(5)–Tl(1)–N(2) and N(1)–Tl(1)–N(3) angles [151.74(9)° and 118.84(8)°] in **5** indicate that both complexes are severely distorted from linearity.

In compound **3**, such a large deviation from planarity for the N(4) pyrrole is also reflected by observing a 19–22 ppm upfield shift of the C_β (C17, C18) at 112.9 ppm compared to 135.2 ppm for C_β (C2, C13), 133.7 ppm for C_β (C3, C12) and 131.8 ppm for C_β (C7, C8). In compound **5**, a similar deviation is also found for the N(4) pyrrole by observing a 16–21 ppm upfield shift of the C_β (C14, C15) at 115.7 ppm compared to 136.4 for C_β (C10, C19), 133.7 ppm for C_β (C9, C20) and 132.2 ppm for C_β (C4, C5). Similarly, the non-planarity of the porphyrins causing upfield shifts of C_β resonances were also observed with a magnitude of 16–21 ppm for Tl(N-NTs-tpp)(OAc) [8].

3.2. ^1H and ^{13}C NMR for **3** and **5** in CD_2Cl_2 and $CDCl_3$

Complexes **3** and **5** were characterized by ^{1}H (Fig. 3) and ^{13}C NMR analysis. In solution, the molecules have effective C_s symmetry with a mirror plane running through the N(2)–Tl–O(1)–N(4) unit for **3** and the N(2)–Tl(1)–N(4)–N(5) unit for **5**. There are four distinct β-pyrrole protons H_β, four β-pyrrole carbons C_β, four α-pyrrole carbons C_α, two different *meso* carbons C_{meso} and two phenyl-C_1 carbons for both the complexes.

The NMR study of **3** showed four different types of Tl–H coupling constants for H_β in CD_2Cl_2 at 20 °C (Fig. 3a). The doublet at 8.70 ppm is assigned as H_β (7, 8) with ^4J(Tl–H) = 78 Hz and the singlet at 6.64 ppm is due to H_β (17, 18). The doublet of a doublets at 9.18 ppm is due to H_β (2, 13) with ^4J(Tl–H) = 14 Hz and ^3J(H–H) = 4.2 Hz and the doublet of a doublets at 8.93 ppm is due to H_β

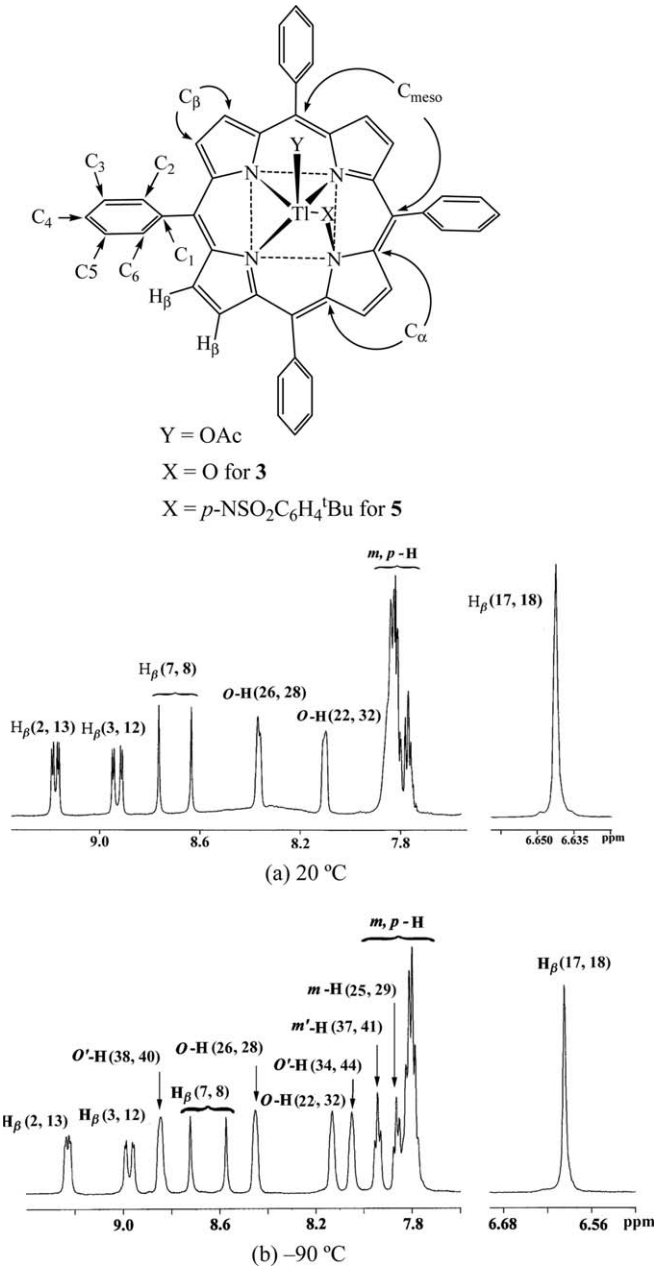

Fig. 3. ^{1}H NMR spectra for Tl(tpp-*N*-O)(OAc) at 599.95 MHz in CD_2Cl_2 showing four different β-pyrrole protons H_β and phenyl protons (*o*-H, *m*, *p*-H): (a) 20 °C; (b) −90 °C.

(3, 12) with ^4J(Tl–H) = 20 Hz and ^3J(H–H) = 4.2 Hz. Likewise, there were also four different types of Tl–^{13}C coupling constants for C_β **3** in $CDCl_3$ at 20 °C. The doublet at 131.8 ppm is due to C_β (C7, C8) with ^3J(Tl–^{13}C) = 156 Hz and the singlet at 133.7 ppm is due to C_β (C3, C12). The doublet at 135.2 ppm is due to C_β (C2, C13) with ^3J(Tl–^{13}C) = 44 Hz and the doublet at 112.9 ppm is due to C_β (C17, C18) with ^4J(Tl–^{13}C) = 80 Hz.

The NMR study of **5** showed four different types of Tl–H coupling constants for H_β in CD_2Cl_2 at 20 °C. The doublet at 8.69 ppm is assigned as H_β (4, 5) with ^4J(Tl–H) = 76.5 Hz and the singlet at 6.94 ppm is due to H_β (14, 15). The doublet of a doublets at 9.05 ppm is due to H_β (10, 19) with ^4J(Tl–H) = 17.1 Hz and ^3J(H–H) = 4.8 Hz and the doublet of a doublets at 8.92 ppm is due to H_β (9, 20) with ^4J(Tl–H) = 10.4 Hz and ^3J(H–H) = 4.8 Hz. Likewise, there were also four different types of Tl–^{13}C coupling constants for C_β **5** in CD_2Cl_2 at 20 °C. The doublet at 132.2 ppm is due to C_β (C4, C5) with ^3J(Tl–^{13}C) = 165 Hz and the doublet at 136.4 ppm is due to C_β (C10, C19) with ^3J(Tl–^{13}C) = 37 Hz. The singlet at 133.7 ppm supposedly due to C_β (C9, C20) with ^3J(Tl–^{13}C) is not observed and the doublet at 115.7 ppm is due to C_β (C14, C15) with ^4J(Tl–^{13}C) = 78 Hz. The ^{1}H NMR spectra reveal that the aromatic protons of the ^{t}BuBS group appear as a doublet at 6.94 (^{t}BuBS-$H_{3,5}$) and a doublet at 6.09 ppm (^{t}BuBS-$H_{2,6}$) for **5**. Due to the porphyrin ring current effect, all $NSO_2C_6H_4{}^t$Bu and acetato protons are shifted upfield compared to their counterparts in free $NSO_2C_6H_4{}^t$Bu and OAc^-. The above ring current effect indicates that both the $NSO_2C_6H_4{}^t$Bu and acetate ligands are bonded to Tl in **5** in the solution phase. The $NSO_2C_6H_4{}^t$Bu bonding argument is further confirmed by the result that the ^{t}BuBS–C_1 (i.e., C(47)) peak in **5** was observed at 137.6 ppm with ^3J(Tl–C) = 46 Hz. X-ray diffraction analysis unambiguously confirms that **5** is a bidentate complex in the solid phase.

Fig. 3 depicts representative ^{1}H spectra for **3** in CD_2Cl_2 at 20 and −90 °C. At 20 °C, the rotation of the phenyl group along the C_1–C_{meso} [C(5)–C(21) or C(10)–C(27)] bond is intermediately slow [19]. This intermediately slow rotation is supported by the two broad singlets at 8.36 and 8.10 ppm for the *ortho* protons *o*-H (26, 28) and *o*-H (22, 32), respectively. Moreover, the rotation of the phenyl group along the C(15)–C(33) [or C(20)–C(39)] bond is at the intermediate exchange region [21]. In this intermediate exchange region, the signals are broadened beyond detection. Hence, no signals of *o*′-H (34, 44) and *o*′-H (38, 40) have been found at 20 °C (Fig. 3a). At −90 °C, this rotation is extremely slow. Hence, the rate of intramolecular exchange of the *ortho* protons for **3** in CD_2Cl_2 is also extremely slow. The singlet at 8.85 ppm is assigned to *ortho* protons *o*′-H (38, 40) (Fig. 3b). The other singlet at 8.05 ppm is due to *ortho* protons *o*′-H (34, 44). Likewise, the singlet at 8.45 ppm is due to the *ortho* protons *o*-H (26, 28) and singlet at 8.13 ppm is due to the *ortho* protons *o*′-H (22, 32) (Fig. 3b). In a similar way, the *meta* and *para* protons appearing as multiplet (7.76–7.84 ppm) at 20 °C (Fig. 3a) changed to 7.94 [t, *m*′-H (37, 41)], 7.86 [t, *m*-H (25, 29)], 7.82 [m, *m*′-H (35, 43)], 7.81 [m, *p*′-H (36, 42)] and 7.80 [m, *m*-H (23, 31) and *p*-H (24, 30)] ppm at −90 °C (Fig. 3b). The interpretation of these data was confirmed by NOE difference spectroscopy for **3** in CD_2Cl_2 at 20 and −90 °C.

In a similar fashion, the rotation for the phenyl group of **5** in CD_2Cl_2 at 20 °C along the C(2)–C(21) [or C(7)–C(27)] bond is slow and that rotation along C(12)–C(33) [or C(17)–C(39)] is at the intermediate region. Hence, the ^{1}H resonances for the *ortho* protons of **5** were observed with two sets of doublets: one doublet at 8.38 ppm is assigned

to *ortho* protons *o*-H (26, 28) with ^3J(H–H) = 7 Hz and the other doublet at 8.10 ppm is due to *ortho* protons *o*-H (22, 32) with ^3J(H–H) = 7 Hz. Moreover, no signals of *o*′-H (38, 40) and *o*′-H (34, 44) of **5** have been detected at 20 °C.

3.3. Dynamic NMR of 3 and 5 in CD_2Cl_2

Upon cooling of a 0.02 M CD_2Cl_2 solution of **3**, the methyl proton signal of OAc^-, being a single peak at 20 °C ($\delta = 0.45$ ppm), first broadened (coalescence temperature $T_c = -89$ °C) and then split into two peaks with a separation of 12 Hz at $\delta = 0.35$ ppm at −100 °C. As the exchange of OAc^- within **3** is reversible, the results at 599.95 MHz confirm the separation as a coupling of ^4J (Tl–H) rather than a chemical shift difference. The most likely cause of loss of coupling is due to the reversible dissociation of acetate with a small dissociation constant.

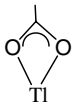

3

$$\xrightarrow[\rightleftharpoons]{CD_2Cl_2} \text{Tl(tpp-}N\text{-O)}^+ + OAc^- \qquad (1)$$

Such a scenario would lead to the change in the chemical shift with temperature and no detectable free OAc^- and Tl(tpp-*N*-O)$^+$ at low temperature, but would lead to the loss of coupling between acetate and thallium at higher temperature [20]. The chemical shift in the high-temperature limit is the average of the two species (i.e., Tl(tpp-*N*-O)(OAc) and OAc^-) in Eq. (1) weighted by their concentration. The free energy of activation $\Delta G^{\ddagger}_{184} = 39.3$ kJ/mol is therefore determined for the intermolecular exchange of OAc^- in **3**. The free energy of activation at the coalescence temperature T_c for a similar OAc^- exchange of **5** in CD_2Cl_2 is determined to be $\Delta G^{\ddagger}_{208} = 44.1$ kJ/mol. At 20 °C, intermolecular exchange of the OAc^- group for **3** is rapid as indicated by the appearance of singlet signals due to carbonyl carbons at 175.8 ppm and methyl carbons at 18.9 ppm. At −100 °C, the rate of intermolecular exchange of OAc^- for **3** in CD_2Cl_2 is slow. Hence, at this temperature, the methyl and carbonyl carbons of OAc^- are observed at δ 18.5 ppm [with ^3J(Tl–C) = 135 Hz] and 176.0 ppm [with ^2J(Tl–C) = 156 Hz] as doublets, respectively. These ^{13}C resonances are quite close to that of **5** in which the two corresponding carbons were observed in CD_2Cl_2 at δ 18.6 ppm [with ^3J(Tl–C) = 221 Hz] and 176.4 ppm [with ^2J(Tl–C) = 205 Hz] as doublets at −90 °C, but with different $^{2,3}J$(Tl–C) coupling constants. The bulky ^{t}Bu group in **5** increases the free energy of activation for the intermolecular OAc^- exchange in CD_2Cl_2 from $\Delta G^{\ddagger}_{171} = 36.0$ kJ/mol for Tl(N-NTs-tpp)(OAc) to $\Delta G^{\ddagger}_{208} = 44.1$ kJ/mol for **5** [8].

3.4. O(1) and N(5) atoms connected to α-thallium

The effect of a different electronegative atom O(1) [or N(5)] attached to the thallium(III) in **3** (or **5**) on ^2J(Tl–C) and ^3J(Tl–C) of the OAc^- ligand was studied. The importance of the thallium carbon coupling comes mainly from the Karplus-type dependence of ^3J(Tl–C) on the torsion angle $\Phi_{Tl\alpha-C\delta}(Tl_\alpha–O_\beta–C_\gamma–{}^{13}C_\delta)$ [21–23]. Hence, the complexity of the ^3J(Tl–C) coupling is primarily due to the angular dependence on Φ and also due to the substituent effects arising from the nature, position and orientation. The substituents (X) bonded to the coupled Tl_α thallium induces an additional angular dependence on the torsion angle $\Psi_{X-C\gamma}(X–Tl_\alpha–O_\beta–C_\gamma)$. Experimentally, the dependence of the ^3J(Tl–C) coupling on the torsion angles Φ, Ψ and electronegativity (χ) for **3** and **5** is shown in Table 4. Analytically, the effect upon ^nJ(Tl–C) ($n = 2, 3$) of a substituent X (X = O, N) attached to a thallium atom is defined by the difference Δ^nJ(Tl–C, X) = ^nJ(Tl–C, X)–^nJ(Tl–C, P), where ^nJ(Tl–C, X) and ^nJ(Tl–C, P) are the ^nJ(Tl–C) coupling for the X-monosubstituted Tl(tpp)(OAc) and for the parent molecule of Tl(tpp)(OAc), respectively [21]. In Table 4, the coupling constants from our study and the published ones for thallium porphyrin derivatives are provided for a comparison of the experimental Δ^nJ(Tl–C, X) values [5,8,14]. A maximum positive contribution to ^3J(Tl–C) is expected in the *transoid* arrangement ($\Phi = 180°$ and $\Psi = 180°$). The absolute values of Φ and Ψ are observed to be approximately constant around 180° and 80.1 6.8° for complexes **3**, **5** and their homologue, respectively (Table 4), therefore the magnitude of ^3J(Tl–C) in the system X–Tl_α–O_β–C_γ–$^{13}C_\delta$ shows a strong dependence on the electronegativity (χ) of the substituent X. A large negative value of Δ^3J(Tl–C, O) = −145 Hz is observed for **3** while a small negative values of Δ^3J(Tl–C, N) = −57 ± 3 Hz are assessed for **5**, **6** and **7** (Table 4) [5,8]. Likewise, the magnitude of the geminal thallium–carbon coupling constant, ^2J(Tl–C), for the OAc^- of **3** and **5** in the system X–Tl_α–O_β–$^{13}C_\gamma$ depends on the electronegativity (χ) of X (Table 4). Experimentally, a large negative value of Δ^2J(Tl–C, O) = −79 Hz is observed for **3** while a small negative value of Δ^2J(Tl–C, N) = −28 ± 3 Hz is calculated for **5**, **6** and **7** (Table 4) [5,8]. Owing to the magnitude of Δ^nJ(Tl–C, X) ($n = 2, 3$) increasing with increasing electronegativity of X, the smaller electronegativity of N(5)–$SO_2C_6H_4{}^t$Bu (with χ [N(5) = 2.98]) for **5** than the O(1) atom (with χ [O(1) = 3.44]) for **3** [24,25] results in the magnitude of $|\Delta^3J$(Tl–C, N)| = 59 Hz in **5** being smaller than that of $|\Delta^3J$(Tl–C, O)| = 145 Hz in **3** (Table 4). In a similar case, the absolute value of $|\Delta^2J$(Tl–C, N)| = 30 Hz in **5** is smaller than that of $|\Delta^2J$(Tl–C, O)| = 79 Hz in **3** (Table 4).

4. Conclusions

We have investigated two new diamagnetic and mononuclear thallium(III) porphyrin complexes **3** and **5** and their X-ray structures are established. NOE difference spectroscopies, HMQC and HMBC were employed for the unambiguous assignment of the ^{1}H and ^{13}C NMR resonances of **3** and **5** in $CDCl_3$ at 20 °C and in CD_2Cl_2 at 20 and −90 °C. In brief, the electronegativity (χ) of the X atom attached to the α-thallium nucleus correlates to the

Table 4
Effect of α-oxygen and nitrogen substituents on ^{n}J(Tl–C) ($n = 2, 3$) for the OAc^{-} group of Tl(tpp-*N*-O)(OAc), **3**, **5** and thallium porphyrin complexes in CD_2Cl_2 at low temperature[a]

Compounds	OAc		OAc		Φ (°)[c]	Ψ (°)[d]	χ (Ξ)[e]
	CH_3 ^{3}J(Tl–C)	$\Delta^{3}J$(Tl–C, X) (Hz)[b]	CO ^{2}J(Tl–C)	$\Delta^{2}J$(Tl–C, X) (Hz)[b]			
Tl(tpp)(OAc)[14] (−90 °C)	280		235				
Tl(tpp-*N*-O)(OAc) (**3**) (−100 °C)	135	−145	156	−79	−178.9	82.9	3.44
Tl(N-*p*-$NSO_2C_6H_4{}^{t}$Bu-tpp)(OAc) (**5**) (−90 °C)	221	−59	205	−30	−175.2	73.3	2.98
Tl(N-NTs-tpp)(OAc)[8] (**6**) (−110 °C)	220	−60	205	−30	178.5	−86.2	2.98
Tl(N-*p*-$NCOC_6H_4NO_2$-tpp)(OAc)[5] (**7**) (in THF-d_8, −110 °C)	227	−53	211	−24	176.6	78.1	2.89

[a] Measured in CD_2Cl_2 unless specified.
[b] $\Delta^{n}J$(Tl–C, X) = ^{n}J(Tl–C, X)–^{n}J(Tl–C, P) ($n = 2$, 3 and X = O, N), where ^{n}J(Tl–C, X) and ^{n}J(Tl–C, P) are the ^{n}J(Tl–C) coupling for the X-mono-substituted Tl(tpp)(OAc) and for the parent molecule of Tl(tpp)(OAc).
[c] The torsion angle $\Phi(Tl_\alpha–O_\beta–C_\gamma–{}^{13}C_\delta)$ is the dihedral angle between coupled atoms Tl_α and C_δ.
[d] The torsion angle $\psi(X–Tl_\alpha–O_\beta–{}^{13}C_\gamma)$ is the dihedral angle between C_γ and electronegative X.
[e] Pauling scale value calculated by electronegativity equalisation, where Ξ = O for **3**, N–^{t}BuBs for **5**, N–NTs for **6** and $NCOC_6H_4NO_2$ for **7** [24].

magnitude of the $\Delta^{2,3}J$ (Tl–C, X) coupling for the Tl(O_2CCH_3) fragment in the thallium porphyrin system. The two compounds, despite the different electronic and steric properties for O(1) in **3**, and for the *N*-imido-benzensulfonyl group in **5**, the structural deformations occurring in the tetrapyrrole macrocycles are similar.

Acknowledgement

The financial support from the National Science Council of the ROC under Grant NSC 93-2113-M-005-015 is gratefully acknowledged.

Appendix A. Supplementary data

Fig. S1 shows the ^{1}H NMR spectrum of **5** in CD_2Cl_2 at 20 °C. Figs. S2 and S3 show the HMQC and HMBC spectra of **3** in CD_2Cl_2 at 20 °C. CCDC 288278 (for **3**) and CCDC 261305 (for **5**) contain the supplementary crystallographic data for this paper. Copies of this information may be obtained free of charge from The Director, CCDC, 12 Union Road, Cambridge, CB2 1EZ, UK on request (fax: +44 1223 336 033; e-mail deposit@ccdc.cam.ac.uk or www: http://www.ccdc.cam.ac.uk). Supplementary data associated with this article can be found, in the online version, at doi:10.1016/j.poly.2006.01.020.

References

[1] A.L. Balch, Y.W. Chan, M.M. Olmstead, J. Am. Chem. Soc. 107 (1985) 6510.
[2] Y.I. Li, C.S. Chang, J.Y. Tung, C.H. Tsai, J.H. Chen, F.L. Liao, S.L. Wang, Polyhedron 19 (2000) 413.
[3] C.H. Chen, Y.Y. Lee, B.C. Liau, S. Elango, J.H. Chen, H.Y. Hsieh, F.L. Liao, S.L. Wang, L.P. Hwang, J. Chem. Soc., Dalton Trans. (2002) 3001.
[4] F.A. Yang, J.H. Chen, H.Y. Hsieh, S. Elango, L.P. Hwang, Inorg. Chem. 42 (2003) 4603.
[5] C.S. Chang, C.H. Chen, Y.I. Li, B.C. Liau, B.T. Ko, S. Elango, J.H. Chen, L.P. Hwang, Inorg. Chem. 40 (2001) 2905.
[6] H.J. Callot, B. Chevrier, R. Weiss, J. Am. Chem. Soc. 100 (1978) 4733.
[7] J.P. Mahy, P. Battioni, D. Mansuy, J. Am. Chem. Soc. 108 (1986) 1079.
[8] J.Y. Tung, J.I. Jang, C.C. Lin, J.H. Chen, L.P. Hwang, Inorg. Chem. 39 (2000) 1106.
[9] W.Z. Shil, K.Y. Cho, C.W. Cheng, J.H. Chen, S.S. Wang, F.L. Liao, J.Y. Tung, H.Y. Hsieh, S. Elango, Polyhedron (2006) in press.
[10] M.M. Olmstead, R.J. Cheng, A.L. Balch, Inorg. Chem. 21 (1982) 4143.
[11] A.L. Balch, Y.W. Chan, M.M. Olmstead, M.W. Renner, J. Am. Chem. Soc. 107 (1985) 2393.
[12] (a) H. Tsurumaki, Y. Watanabe, I. Morishima, Inorg. Chem. 33 (1994) 4186;
(b) L.E. Andrews, R. Bonnett, R.J. Ridge, E.H. Appelman, J. Chem. Soc., Perkin Trans. 1 (1983) 103.
[13] J.E. Huheey, E.A. Keiter, R.L. Keiter, Inorganic Chemistry, 4th ed., Harper Collins College Publishers, New York, 1993, pp. 117, 292.
[14] J.C. Chen, H.S. Jang, J.H. Chen, L.P. Hwang, Polyhedron 10 (1991) 2069.
[15] S.C. Suen, W.B. Lee, F.E. Hong, T.T. Jong, J.H. Chen, L.P. Hwang, Polyhedron 11 (1992) 3025.
[16] K.M. Kadish, K.M. Smith, R. Guilard, The Porphyrin Handbook, vol. 5, Academic Press, London, 2000, pp. 45–46.
[17] A.G. Coutsolelos, D. Daphnomili, Inorg. Chem. 36 (1997) 4614.
[18] G.M. Sheldrick, SHELXL-97, Program for the Refinement of Crystal Structure from Diffraction Data, University of Gottingen, Germany, 1997.
[19] R.S. Drago, Physical Methods for Chemists, 2nd ed., Saunder College Publishing, New York, 1992, pp. 290–295.
[20] J.P. Jenson, E.L. Muetterties, in: L.M. Jackman, F.A. Cotton (Eds.), Dynamic Nuclear Magnetic Resonance Spectroscopy, Academic press, New York, 1975, pp. 299–304.
[21] J.S. Fabian, J. Guilleme, E. Diez, J. Mol. Struct. (Theochem.) 426 (1998) 117.
[22] M. Morvai, T. Nagy, A. Kocsis, L.F. Szabo, B. Podanyi, Magn. Reson. Chem. 98 (2000) 343.
[23] R.H. Contreras, J.E. Peralta, Prog. Nucl. Magn. Reson. 37 (2000) 321.
[24] H. Liu, Q. Wang, L. Liu, J. Chem. Educ. 69 (1992) 783.
[25] S.G. Bratsch, J. Chem. Educ. 62 (1985) 101.

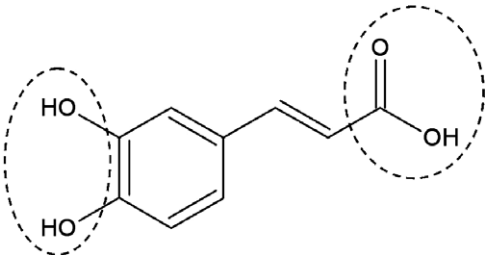

Fig. 1. Structure of caffeic acid with its two complexing sites in competition.

H^+–Al^{3+}–caffeic acid system has already been reported in the literature. Notably, Adams et al. [15] reported the equilibrium constants of complexation of various species such as $AlHL^+$, AlL^0, $Al(OH)L^-$, AlL_2^{3-}, $Al(OH)L_2^{4-}$ and AlL_3^{6-}, where L is the fully deprotonated ligand. These results were obtained from potentiometric titrations (25 °C, 0.10 M KCl) and allow the metal speciation versus pH. On the other hand, Sikora and McBride [16] have found a 1:1 complex by UV–Vis spectroscopy for this same system; however, the electronic absorption spectrum of the complex was not reported. The main aim of this work is to obtain a spectral characterization of the different species formed during the complexation of Al(III) by caffeic acid. This mechanism was followed by both UV–Vis absorption and synchronous fluorescence spectroscopic techniques combined with chemometric methods in order to determinate the stoichiometry and to estimate the stability constants of the different complexes at pH 5 and 6.5. However, in a first step of our study, we have applied these methods to the determination of the first acidity constants of caffeic acid and have compared the results with those found in the literature.

2. Experimental

2.1. Materials and methods

Sample of caffeic acid (*trans*-3-(3′,4′-dihydroxyphenyl)propenoic acid) was obtained commercially from Sigma. Al^{3+} stock solutions were prepared from aluminium chloride $AlCl_3 \cdot 6\,H_2O$. For all working solutions, sodium chloride has been added to give a constant ionic strength of 0.10 M. The molar ratio method [17] has allowed the determination of the complexes composition in solution from UV–Vis or fluorescence spectra. In this method, the electronic spectra of solutions containing a constant concentration of caffeic acid in water (5×10^{-5} M for UV–Vis and 2×10^{-5} M for fluorescence measurements) and variable concentration of $AlCl_3$ were recorded. The titrations were effected by incremental additions of aluminium chloride and additions of NaOH to keep a constant pH. A Minipuls II (Gibson) peristaltic pump was used to circulate solution from the thermostated titration cell (25 °C) to the flow cell (Hellma) for both absorption and fluorescence measurements. Due to the dilution of the ligand solution, all the electronic spectra were corrected before exploitation.

2.2. Instrumentation

UV–Vis spectra were run on a double-beam spectrophotometer (Cary 100-Varian) using cells of 1 cm path length. Fluorescence spectra were recorded using a Fluoromax-3 (Jobin-Yvon) spectrofluorimeter with slits width of 5 nm. Three-dimensional spectra were acquired to obtain excitation–emission matrix (EEM) plots, the excitation wavelengths are plotted on the *y*-axis and the emission wavelengths are plotted on the *x*-axis, the third dimension represents the relative intensity.

2.3. Chemometrics methods

The different pK_a and the formation constants of the Al(III) complexes with caffeic acid were estimated by using a multivariate data analysis program for modelling and fitting equilibrium titration 3D data sets obtained from experimental measurements. The UV–Vis absorption and fluorescence spectra were refined using the SPECFIT software (version 3.0.32) [18]. The set of spectra obtained at variable pH or variable Al(III) concentration were treated by evolving factor analysis (EFA) [19] in order to determine the number of different species in the system and the pure spectrum of each species. The SPECFIT software has also been used to estimate the apparent stability constants (β) of the complexes and the standard deviation (σ) of each value.

3. Results and discussion

3.1. Acidobasic properties of caffeic acid

Fig. 2A shows the absorption spectra of caffeic acid in aqueous solution at different pH (from 2 to 10). UV–Vis spectra clearly present two isosbestic points at 291 and 320 nm within the studied pH region, reflecting the successive presence of two acid–base equilibriums. The first one corresponds to an equilibrium between the fully protonated H_3CA and singly-deprotonated H_2CA^- forms (with a deprotonation of the COOH group). The second one relates to the deprotonation of a hydroxyl group of the catechol (H_2CA^-/HCA^{2-} equilibrium). Oxidation processes of the molecule for high pH values (>9) prevent the observation of the third equilibrium corresponding with a complete deprotonation of the hydroxyl functions to give the CA^{3-} species. The set of spectra treated by evolving factor analysis (EFA) has allowed the determination of the pure absorption spectrum of each form of caffeic acid (Fig. 2B). The acidic form presents a spectrum characterized by a double band located at 320 and 295 nm and absorption under 250 nm. The deprotonation of the carboxylic function leads to a hypsochromic shift of the double band to 309 and 284 nm. A bathochromic shift is then observed with the first deprotonation of the catechol group

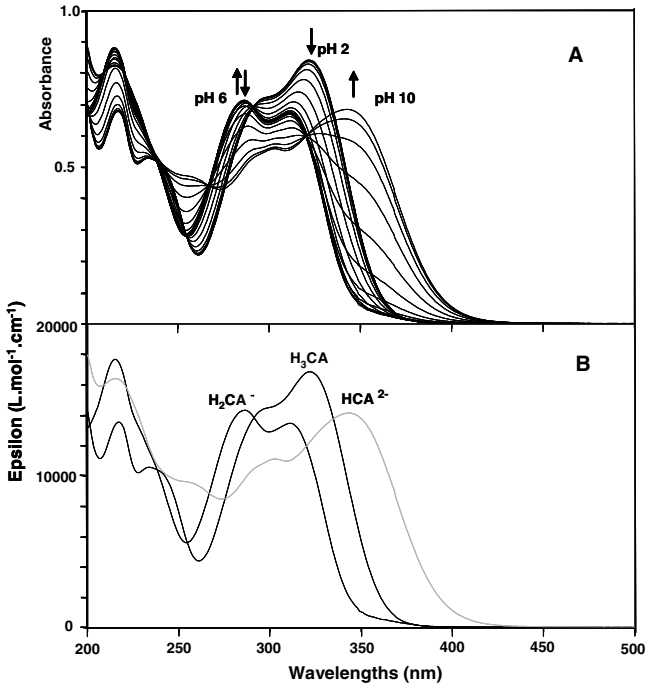

Fig. 2. Variation of the UV–Vis spectra of caffeic acid with the pH in the range 2–10 (A) and absorption spectra of the pure species (B).

(341 and 298 nm). The same experiments have been carried out using synchronous fluorescence spectroscopy with a constant wavelength difference between excitation and emission of 112 nm. The evolution of fluorescence spectra with the pH are illustrated in Fig. 3A. In a same way, the pure synchronous fluorescence spectra of the three forms of caffeic acid have been determined using the SPECFIT program and are reported in Fig. 3B. The fluorescence spectrum of caffeic acid presents a low intensity ($<4\times10^4$ cps) compared with the other spectra, and is characterized by a large band with a maximum for $\lambda_{ex}=322$ nm. Caffeate fluorescence spectrum is more intense and presents a maximum for $\lambda_{ex}=313$ nm. The second deprotonation leads to a large enhancement of the emission intensity (40 times more important than caffeic acid) and gives rise to a band located at $\lambda_{ex}=375$ nm.

From absorption and emission spectra sets, the two first acidity constants were calculated and refined with the SPECFIT program. The estimated values of the dissociation constants with their uncertainties are shown in Table 1, along with the values obtained by potentiometric titrations and reported in the literature. Satisfactory agreement of protonation constants obtained from UV–Vis experiments with those found in the literature was reached. However,

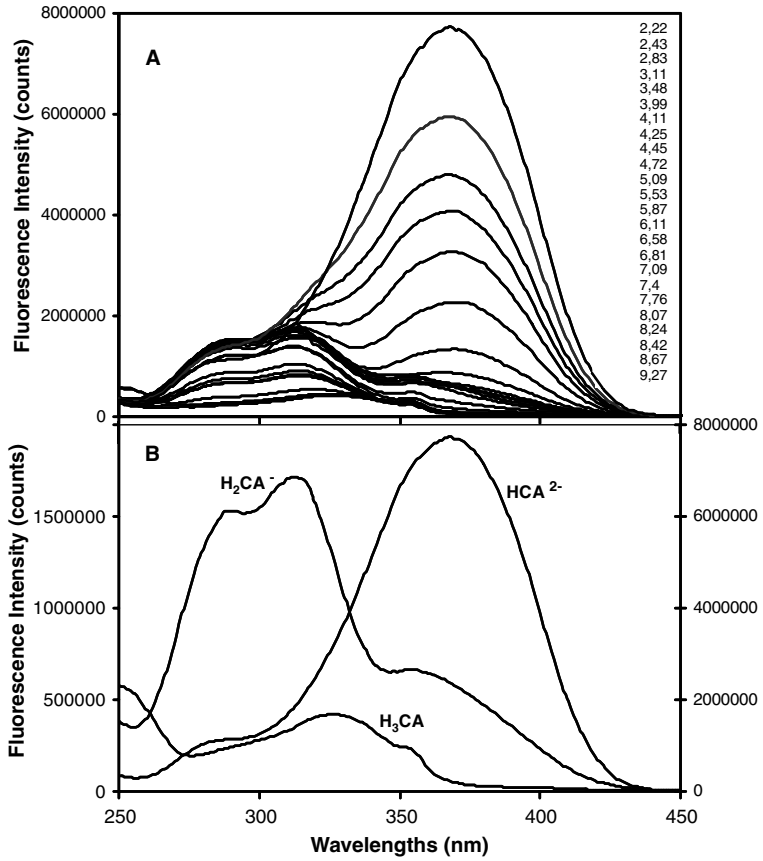

Fig. 3. Variation of the synchronous fluorescence spectra (offset: 112 nm) of caffeic acid with the pH (A) and synchronous fluorescence spectra of the pure species (B) the left scale is relative to H_3CA and H_2CA^- forms whereas the right scale is relative to the bi-deprotonated form.

Table 1
Acidity constants estimated in this work by both UV–Vis and synchronous fluorescence spectroscopies and comparison with values obtained by potentiometric or spectroscopic measurements with various ionic strength

	This work		Literature			
	UV–Vis	Fluo	(a)	(b)	(c)	(d)
pK_a (–COOH)	4.47 ± 0.6	4.22 ± 0.02	4.38	4.37	4.41	4.45
pK_a (–O_4H)	8.59 ± 0.04	8.28 ± 0.01	8.67	8.55	8.72	8.66
pK_a (–O_3H)			12.6	12.5		11.8

(a) Adams et al., 0.10 M KCl [15]; (b) Kiss et al., 0.20 M KCl [20]; (c) Linder and Voyé, 0.10 M NaCl [21]; and (d) Lamy et al., 0.10 $NaClO_4$ [22].

the values obtained from synchronous fluorescence spectroscopy are slightly lower than those obtained from UV–Vis measurements. This observation may be explained by the fact that the value obtained reflects the acido-basic properties of the excited state involved in the emission process.

3.2. Complexation of Al(III) by caffeic acid

The complexation of Al(III) by caffeic acid was investigated at pH 5 and 6.5 under constant ionic strength of 0.1. The pH was chosen in the range where no precipitation of metal hydroxide takes place, and for values close to the pH generally found in the soils. At pH 5, the solution is mixture of caffeic acid (26%) and caffeate (74%), whereas at pH 6.5 caffeate ion (H_2CA^-) is the only species present in the solution.

It should be noticed that, in spite of the use of a system ensuring the circulation of the solution, the acid caffeic molecule undergoes a photodegradation under the action of the excitation beam of fluorescence. This phenomenon is particularly visible on the EEM recorded on a caffeic solution at pH 6.5 (Fig. 4(1)). The broad signal A made up of two fluorescence bands at 281/419 nm and 310/419 nm ($\lambda_{ex}/\lambda_{em}$) is characteristic of caffeic acid, whereas the signal noted B at 383/471 nm corresponds to a photo-product. However, the appearance of this photo-product is not instantaneous (several hours were necessary to record fluorescence EEM) and this last is not highlighted on the emission spectrum when a caffeic acid solution freshly prepared is excited at 383 nm. To complete the assignment of the fluorescence EEM, one can observed the first and second-order Raman bands of water (bands C and D, respectively). A fluorescence EEM of the 3,4-dimethoxycinnamic acid (Fig. 4(2)) does not present the signal B. In this case, the substitution of the hydroxyls of the catechol moiety by –OCH_3 functions prevents the deprotonation of the catechol and so a photo-oxidation of the molecule. Fig. 4(3) presents the fluorescence EEM of a caffeic acid solution (pH 6.5) in the presence of Al(III) for a molar ratio of 1. A new intense signal appears at 338/508 nm corresponding to the formation of the complexed species whereas the signal A is less intense than this observed in Fig. 4(1) but still present. In opposition the photo-product has totally disappeared of the EEM, that

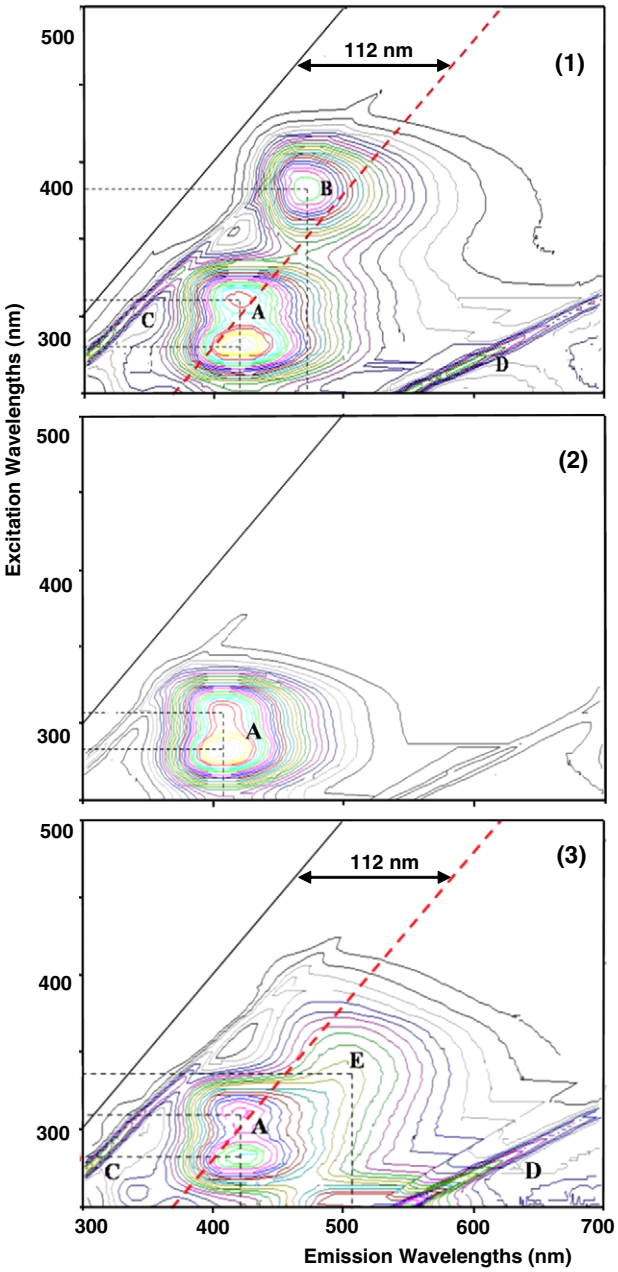

Fig. 4. 3D fluorescence excitation–emission matrix (EEM) plots are shown for caffeic acid at pH 6.5 (1), 3-4-dimethoxycinnamic acid (2) and the Al–caffeic acid system with a molar ratio of 1 (3).

reinforces the assumption of a chelation of Al(III) on the catechol group combined with a complete deprotonation of the hydroxyl functions [13,15]. One can observe in Fig. 4 that an offset of 112 nm between the excitation and emission wavelengths is well adapted to observe simultaneously the evolution of the fluorescence signal of both free and complexed forms of caffeic acid upon complexation.

3.2.1. Complexation at pH 5

Fig. 5A illustrates the evolution of the UV–Vis spectra of the caffeic acid–Al(III) system at pH 5 for different [Al(III)]/[Caf] molar ratios from 0 to 25. The intensity of

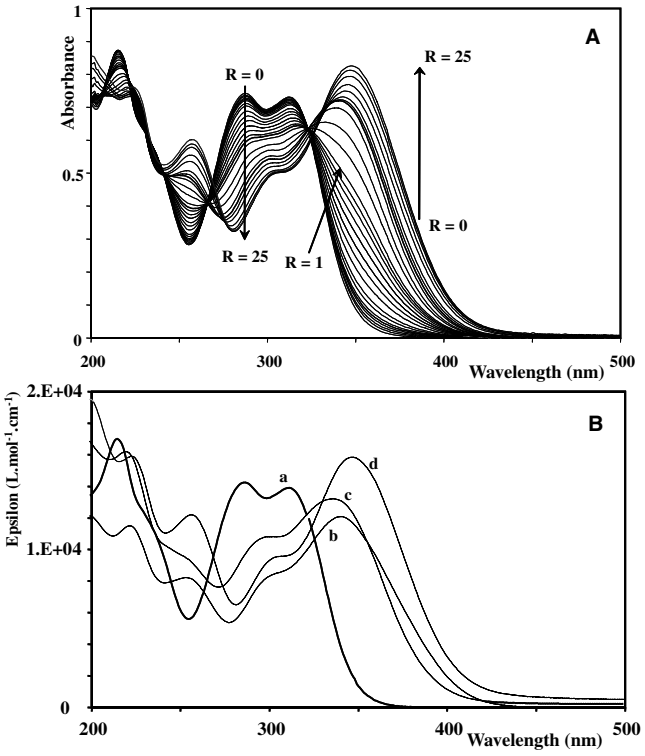

Fig. 5. UV–Vis absorption spectra of caffeic acid in absence and in presence of $AlCl_3$. [Al(III)]/[CA] molar ratio vary from 0 to 25, in aqueous solution at pH 5 (A). Absorption spectra of pure species (B): caffeic acid (a), complex 1:2 (b), complex 1:1 (c) and complex 2:1 (d).

the double band characteristic of the caffeic acid decreases with the amount of $AlCl_3$ added, whereas a new band appears in the higher wavelengths range. The maximum of this band moves towards the high wavelengths with the increase of the molar ratio. The absence of a single isosbestic point shows that several complexed species are formed simultaneously and/or successively during the complexation process. Using the molar ratio method, the curves of absorbance variations versus [Al(III)]/[Caf] molar ratio plotted at 348 nm (λ_{max} of complexed form) and 285 nm (λ_{max} of free form) allow us to observe the formation of five species of stoichiometry (Al:AC) 1:6, 1:3, 1:2, 1:1 and 2:1. Our previous works, as well as the results found in the literature [13,15,16], show that the chelation of aluminium takes place at the level of the catechol site with a complete deprotonation of the hydroxyl groups. Under these conditions, the formation of the complex 1:6 would be obtained with the coordination to an aluminium ion of three dimers of caffeic acid. From the UV–Vis spectra set, the determination of the number of different absorbing species was estimated by the EFA method. With this method, only three complexed forms could be detected and the absorption spectra of the corresponding pure species are represented in Fig. 5B (spectra b, c and d). This result suggests that among the five complexes obtained with the molar ratios method, two of them are minority species, which either present very weak concentrations, or are present in the mixture only at the beginning of the dosage. To determine the stoichiometry of the three major complexes and to estimate their stability constants, a numerical treatment of the UV–Vis spectra has been carried out implicating the different possible models. The model best-fitting the experimental data involves the complexes of stoichiometry 1:2 ($\lambda_{max} = 340$ nm, spectrum b), 1:1 ($\lambda_{max} = 335$ nm, spectrum c) and 2:1 ($\lambda_{max} = 347$ nm, spectrum d). The spectrum a (Fig. 5B) corresponds to the sum of the absorbance of H_3CA and H_2CA^- forms. The apparent stability constants of the three major complexes are reported in Table 2. This result comes from the following reaction between aluminium and the ligand (L) both protonated and mono-deprotonated:

$$aAl + bL \leftrightarrow Al_aL_b$$

with the corresponding apparent stability constant:

$$\beta = \frac{[Al_aL_b]}{[Al]^a[L]^b}.$$

It can be concluded, that the complexes of stoichiometry 1:6 and 1:3 are present at very low concentration in the solution only for very low amount of $AlCl_3$ added.

The complexation of aluminium (III) by caffeic acid at pH 5 has been also followed by fluorescence emission spectroscopy ($\lambda_{exc} = 320$ nm) and by synchronous fluorescence spectroscopy (offset of 112 nm). Only the results obtained by this last technique will be presented in details. The synchronous fluorescence spectra of caffeic acid at pH 5 with different amounts of $AlCl_3$ are reported in Fig. 6A. As already observed in UV–Vis spectroscopy, no distinct isoemissive point is detected, indicating the simultaneous formation of several complexes. The chemometric methods applied to the data set have allowed the determination of

Table 2
Stability constants estimated from different spectroscopic methods for the main complexes of the Al(III)–caffeic acid system at pH 5 and 6.5 in aqueous solution

	Stoichiometry	1:6	1:3	1:2	1:1	2:1
	Formulae	$[AlCaf_6]^{9-}$	$[AlCaf_3]^{6-}$	$[AlCaf_2]^{3-}$	[AlCaf]	$[Al2Caf]^{3+}$
pH 5	UV–Vis			8.4 ± 0.3	5.6 ± 0.1	9.3 ± 0.1
	fluo ($\lambda_{ex} = 320$ nm)			8.97 ± 0.07	5.04 ± 0.02	8.95 ± 0.08
	fluo synchronous			8.64 ± 0.07	4.83 ± 0.02	8.85 ± 0.07
pH 6.5	UV–Vis		12.9 ± 0.1	8.6 ± 0.2		
	fluo ($\lambda_{ex} = 320$ nm)		13.40 ± 0.08	8.96 ± 0.04		
	fluo synchronous		13.41 ± 0.09	8.6 ± 0.1		

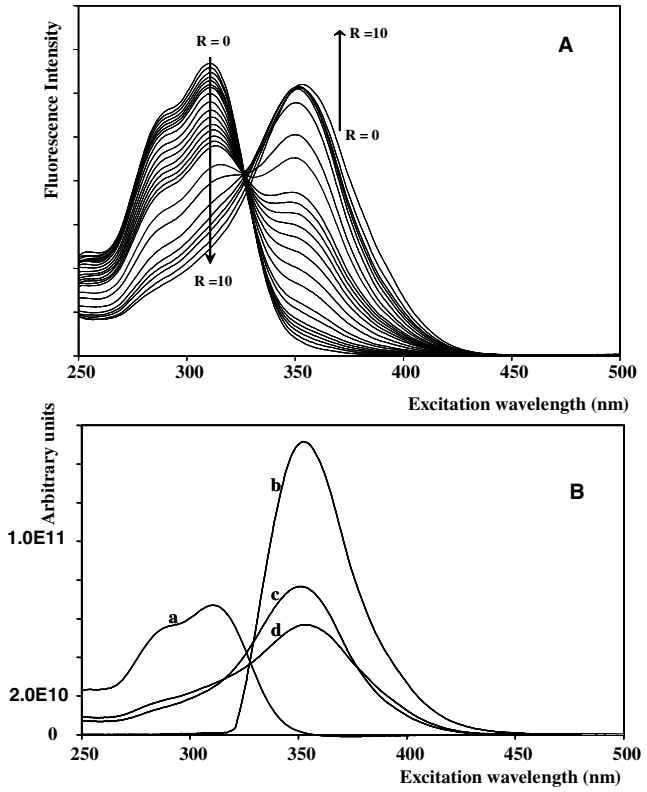

Fig. 6. Synchronous fluorescence spectra of caffeic acid in absence and in presence of $AlCl_3$. [Al(III)]/[CA] molar ratio vary from 0 to 10, in aqueous solution at pH 5 (A). Synchronous fluorescence spectra of pure species (B): caffeic acid (a), complex 1:2 (b), complex 1:1 (c) and complex 2:1 (d).

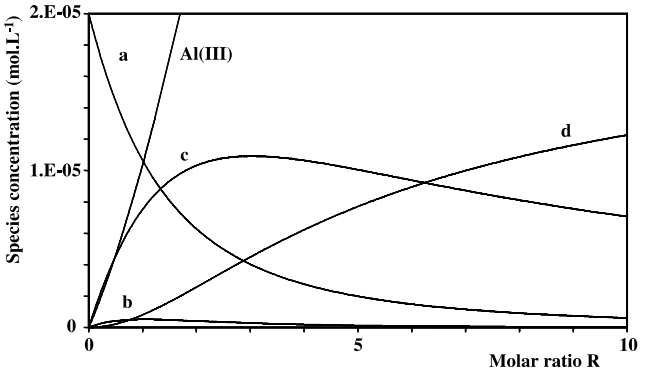

Fig. 7. Distribution curves of the concentration of aluminium complexes with caffeic acid at pH 5 as a function of the [Al(III)]/[CA] molar ratio. Caffeic acid (a), complex 1:2 (b), complex 1:1 (c) and complex 2:1 (d).

four pure species, whose spectra are presented in Fig. 6B. The spectrum a is relative to caffeic acid, and spectra b, c and d can be assigned to the complexes of stoichiometry 1:2, 1:1 and 2:1, respectively. One can notice that the maximum of the three synchronous fluorescence spectra of complexes are very close. In the same way as the results obtained by UV–Vis spectroscopy, the 1:6 and 1:3 species were highlighted by the molar ratios method, but not by the EFA method. The stability constants obtained from fluorescence measurements, reported in Table 2, stand comparison with those estimated from UV–Vis measurements. However, on can notice that the value of the 1:2 complex stability constant is calculated slightly higher with the fluorescence techniques than with the absorption technique; while the situation is reversed for the 1:1 and 2:1 complexes. The concentration variations of the free and complexed ligands versus quantity of aluminium added (molar ratios) is illustrated in Fig. 7. Both absorption and fluorescence measurements lead to obtaining the same variations. The curves show that the 1:2 and 1:1 complexes are simultaneously formed from the beginning of the aluminium addition, however, the 1:1 species is largely predominant (curve c). The formation of very weak amounts of the 1:2 complex observed on this curve, suggests that the 1:3 and 1:6 species must present concentrations even weaker and consequently explains why they were not easily detected. This result is consistent with this obtained by Sikora and McBride that found only the 1:1 species between pH 3.8 and 4.5 [16]. The 2:1 complex starts to be formed for molar ratios higher than 0.1. This fact indicates that the second complexation site, in this case the carboxylic function, is implied in the coordination of aluminium relatively quickly, whereas less than 10% of the catechol sites are occupied. That shows that, even if the carboxylic and carboxylate functions have less affinity than the catechol group with respect to Al(III), these two sites have rather close chelating powers, at pH 5. Simultaneous coordination of metal ions to both the carboxylic and catechol sites has been already observed for the binding of caffeic acid to various divalent metal [23].

3.2.2. Complexation at pH 6.5

At pH 6.5, the precipitation of aluminium hydroxide prevents obtaining high concentrations of Al(III) in solution. In this study, we limited ourselves to a molar ratio value of 2, in order to not observe a continuous background on the electronic spectra, as illustrated in the two last spectra (not included in the calculations) that show the $Al(OH)_3$ precipitation. At pH 6.5, the follow-up of dosage by spectroscopy shows a very different evolution of the data sets with the addition of aluminium compared to the results obtained at pH 5. The UV–Vis spectra obtained for different molar ratios (Fig. 8A) show the formation of several complexes insofar as no isosbectic point is observed. The molar ratio method applied to the spectral data allows the determination of three species of stoichiometry 1:6, 1:3 and 1:2. Once again, the complex 1:6 is a minority species and was not detected by EFA method. The spectra of the complexes 1:3 and 1:2 are presented in Fig. 8B (spectrum b and c, respectively). The same conclusions can be drawn from the data obtained by synchronous fluorescence spectroscopy (Fig. 9A), where only the complexes 1:3 and 1:2 are highlighted (Fig. 9B) by the chemometric methods. The stability constants of the two found complexes are reported in Table 2 for the different techniques. One can observe slight differences between the values of the constants according to the spectroscopic

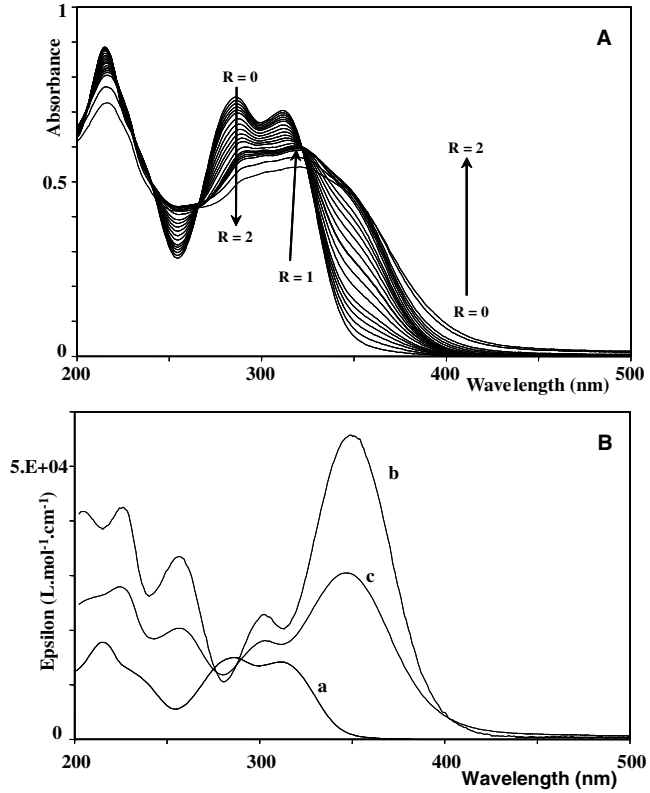

Fig. 8. UV–Vis absorption spectra of caffeic acid in absence and in presence of $AlCl_3$. [Al(III)]/[CA] molar ratio vary from 0 to 2, in aqueous solution at pH 6.5 (A). Absorption spectra of free species (B): caffeic acid (a), complex 1:3 (b) and complex 1:2 (c).

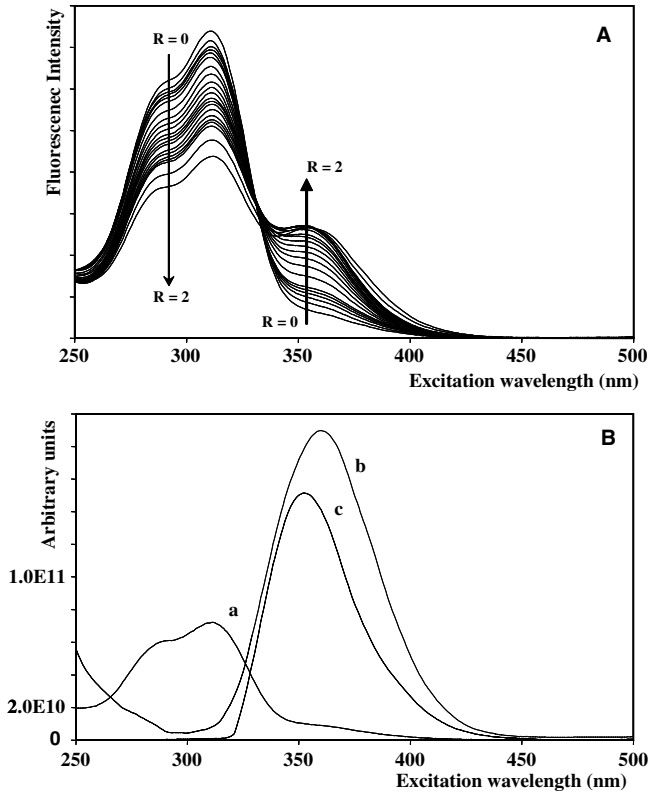

Fig. 9. Synchronous fluorescence spectra of caffeic acid in absence and in presence of $AlCl_3$. [Al(III)]/[CA] molar ratio vary from 0 to 2, in aqueous solution at pH 6.5 (A). Synchronous fluorescence spectra of free species (B): caffeic acid (a), complex 1:3 (b) and complex 1:2 (c).

technique used, but the magnitude order is preserved. It should be noted that, for the 1:2 complex which is common to the experiments at pH 5 and 6.5, the EFA method leads to the obtaining of the same electronic spectra of this species at both pH. As the concentration evolution of the various species according to the molar ratio shows it (Fig. 10), the two chelates are formed simultaneously and in the same proportions. For a molar ratio of 3, one observes neither the formation of the complex 1:1, nor that of the complex 2:1; thus even for large quantity of added metal, only one complexation site is involved. It is obvious that the chelating power of the ligand towards Al(III) increases with pH. On the one hand, complexes of higher stoichiometry are obtained at pH 6.5 than at pH 5 and, on the other hand, the formation of the 1:2 complex slightly increases with the pH.

If this study has allowed the spectroscopic characterization, both in absorption and fluorescence, of the 1:3, 1:2, 1:1 and 2:1 complexes of Al(III) with caffeic acid, it did not permit the determination of the protonation state of these complexes. Indeed, for instance, only one spectrum could be highlighted by the spectroscopic techniques for the 1:1 complex, whereas Adams et al. reported, for this one, the existence of three possible species: $AlHL^+$, AlL^0 and $Al(OH)L^-$ with different stability constants. These three species must present very close electronic spectra

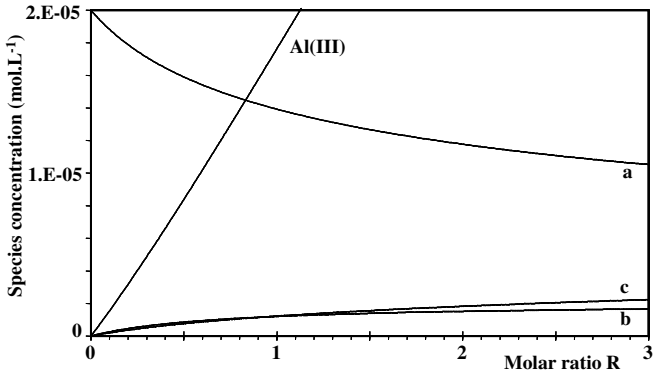

Fig. 10. Distribution curves of the concentration of aluminium complexes with caffeic acid at pH 6.5 as a function of the [Al(III)]/[CA] molar ratio. Caffeic acid (a), complex 1:3 (b) and complex 1:2 (c).

which it is impossible to distinguish by spectral decomposition. Thus, the conditional equilibrium constant calculated in this study for the 1:1 complex is not directly comparable with those obtained by potentiometric methods.

The presence of the CH=CH–COOH function on the 1-2-dihydroxybenzene seems not very affected the chelation ability of the catechol function. Indeed, the stability constants which one can calculate starting from the results of Adams et al. (16.25) [15] or Sikora and McBride (15.06)

[16] for the AlL^0 complex of caffeic acid are very close to that obtained for the pyrocatechol (16.20) [24]. Thus, this chemical function has an effect definitely weaker than the nitro group, which significantly decreases the complexing capacity of catechol, since the AlL^0 complex obtained with nitrocatechol presents a stability constant of 13.80 [25].

The iron(II)–caffeic acid system studied by absorption spectroscopy leads to the formation of a 1:1 complex presenting an equilibrium constant of 8.12 [26]. The comparison of this value with that calculated in this study for the Al 1:1 complex (average: 5.15) shows that caffeic acid presents a greater chelating power towards Fe(II) than Al(III).

4. Conclusion

The aqueous solution chemistry of Al(III)–caffeic acid system has been examined using both UV–Vis and synchronous fluorescence spectroscopic techniques. The experiments show that, at pH 5, the 1:1 complex largely predominates in solution, however, the protonation of this complex could be given neither by absorption spectroscopy nor by fluorescence spectroscopy. It is interesting to note that small amounts of metal ions are necessary to obtain a binuclear complex, where the two sites in competition are involved. At pH 6.5, only one site, the catecholate group, coordinates to Al(III) leading to the formation of 1:2 and 1:3 complexes. This study confirms ours previous results concerning the competition of carboxylic and catechol functions to complex aluminium ions. It is patent that the catechol group presents a chelating capacity higher than that of the carboxylic or carboxylate functions with respect to Al(III). This complexing capacity increases, as one could expect it, with the pH. The polyphenolic functions omnipresent in the humic substances have a considerable role in the retention of metal traces in the soil and are in favourable competition with respect to the more acid groups in the coordination of aluminium. It is obvious that in the natural environments, the metal/potential complexing sites ratios are very weak and very largely lower than the ratios used in this study, therefore, only the species formed for small added amounts of Al(III) are of interest within this framework.

References

[1] S. Hiradate, N.U. Yamaguchi, J. Inorg. Biochem. 97 (2003) 26.
[2] S.J.M. Holmström, P.A.W. Van Hees, U.S. Lundström, Geoderma 127 (2005) 280.
[3] P. Zhou, H. Yan, B. Gu, Chemosphere 58 (2005) 1327.
[4] E. Tipping, C. Rey-Castro, S.E. Bryan, J. Hamilton-Taylor, Geochim. Cosmochim. Acta 66 (2002) 3211.
[5] K.M. Elkins, D.J. Nelson, Coord. Chem. Rev. 228 (2002) 205.
[6] P.A.W. Van Hees, E. Tipping, U.S. Lundström, Sci. Total Environ. 278 (2001) 215.
[7] D.S. Smith, J.R. Kramer, Anal. Chim. Acta 416 (2000) 211.
[8] P. Blaser, A. Heim, J. Luster, Environ. Int. 25 (1999) 285.
[9] S.H. Sutheimer, S.E. Cabaniss, Geochim. Cosmochim. Acta 61 (1997) 1.
[10] J.B. Harborne, Biochemistry of Phenolic Compounds, Academic Press, New York, 1964.
[11] F.J. Stevensson, Humus Chemistry: Genesis, Composition, Reaction, Wiley, New York, 1982.
[12] R.A. Olsen, J.C. Brown, J.H. Bennet, D. Blume, J. Plant. Nutr. 5 (1982) 433.
[13] J.P. Cornard, C. Lapouge, J. Phys. Chem. A 108 (2004) 4470.
[14] L. Boilet, J.P. Cornard, C. Lapouge, J. Phys. Chem. A 109 (2005) 1952.
[15] M.L. Adams, B. O'Sullivan, A. Downard, K.J. Powell, J. Chem. Eng. Data 47 (2002) 289.
[16] F.J. Sikora, M.B. McBride, Soil Sci. Soc. Am. J. 54 (1990) 78.
[17] J.H. Yoe, L. Jones, Ind. Eng. Chem. Anal. 16 (1944) 11.
[18] Specfit Global Analysis System, Spectrum software Associates, Marlborough, MA, USA.
[19] H. Gampp, M. Maeder, C.J. Meyer, A. Zuberbühler, Talanta 33 (1986) 943.
[20] T. Kiss, G. Navy, M. Pécsi, Polyhedron 8 (1989) 2345.
[21] P.W. Linder, A. Voyé, Polyhedron 6 (1987) 53.
[22] I. Lamy, M. Seywert, M. Cromer, J.P. Scharff, Anal. Chim. Acta 176 (1985) 201.
[23] S. Cocks, P.W. Linder, A. Voyé, J. Coord. Chem. 25 (1992) 211.
[24] T. Kiss, K. Atkari, M. Jezowska-Bojczuk, P. Decock, J. Coord. Chem. 29 (1993) 81.
[25] S. Giroux, S. Aury, P. Rubini, S. Parant, J.R. Desmurs, M. Dury, Polyhedron 23 (2004) 2393.
[26] M. Andjelkovic, J.V. Camp, B. De Meulenaer, G. Depaemelaere, C. Socaciu, M. Verloo, R. Verhe, Food Chem. (in press).

spectrophotometer using KBr discs in the range of 4000–400 cm^{-1}. Electronic spectra were recorded on a Systronics 119 UV–Vis spectrophotometer using methanol as solvent. Elemental analyses were performed with a Vario EL III Elementar analyzer. Room temperature EPR spectra were recorded using an E-112 Varian model instrument. Cyclic voltammetric experiments were carried out using BAS CV-27 electrochemical analyzer with a glassy carbon working electrode. A platinum wire and silver–silverchloride electrode were used as counter- and reference electrodes, respectively. Melting points were recorded with a Lab India apparatus.

2.3. Crystallography

Single crystals of [Ru(dipic)$(PPh_3)_2$Cl] suitable for X-ray diffraction studies were obtained from slow evaporation of a solution of the complex in benzene/ethanol mixture. Intensity data were collected on a Nonius MACH 3 four circle diffractometer equipped with graphite monochromated Mo Kα radiation ($\lambda = 0.7107$ Å). The structure was solved by the direct method. All non-hydrogen atoms were refined anisotropically by full-matrix least-squares, with a ridging model for the hydrogen atoms, using the SHELXTL/PC package [30].

2.4. Synthesis of [Ru(dipic)$(EPh_3)_2X$] (X = Cl, Br; E = P, As)

All the new ruthenium(III) complexes were prepared by the following general procedure. A benzene (20 ml) solution of [$RuX_3(EPh_3)_3$] (where E = P, As; X = Cl, Br) (0.1 mmol) was added to a refluxing solution of dipicolinic acid (0.1 mmol) in ethanol (20 ml). The mixture was heated under reflux for 6 h. The solution was filtered while hot, reduced to half of its volume and left for slow evaporation. The crystalline product that separated out was filtered off, washed with ethanol and dried under vacuum. The product was recrystallized from benzene/ethanol mixture.

[Ru(dipic)$(PPh_3)_2$Cl] (**1**) was prepared from [$RuCl_3(PPh_3)_3$] (0.0994 g, 0.1 mmol) and dipicolinic acid (0.018 g, 0.1 mmol) as reddish brown crystals. Yield: 75%. *Anal*. Calc. for $RuC_{43}H_{33}NO_4ClP_2$: C, 62.51; H, 4.02; N, 1.69. Found: C, 62.04; H, 4.51; N, 1.74%. IR: 1659, 1352, 1431, 1091, 697 cm^{-1}. UV: λ_{max}: 268(4236), 405(9219) nm(dm^3/mol/l); m.p. >230 °C.

[Ru(dipic)$(AsPh_3)_2$Cl] (**2**) was prepared from [$RuCl_3(AsPh_3)_3$] (0.112 g, 0.1 mmol) and dipicolinic acid (0.018 g, 0.1 mmol) as shining red crystals. Yield: 80%. *Anal*. Calc. for $RuC_{43}H_{33}NO_4ClAs_2$: C, 56.44; H, 3.63; N, 1.53. Found: C, 56.17; H, 3.82; N, 1.60%. IR: 1671, 1344, 1434, 1077, 692 cm^{-1}. UV: λ_{max}: 268(4767), 315(6296), 530(964) nm(dm^3/mol/l); m.p. >290 °C.

[Ru(dipic)$(AsPh_3)_2$Br] (**3**) was prepared from [$RuBr_3(AsPh_3)_3$] (0.125 g, 0.1 mmol) and dipicolinic acid (0.018 g, 0.1 mmol) as brown crystals. Yield: 85%. *Anal*. Calc. for $RuC_{43}H_{33}NO_4BrAs_2$: C, 59.32; H, 3.82; N, 1.60. Found: C, 59.27; H, 3.94; N, 1.58%. IR: 1673, 1350, 1434, 1077, 692 cm^{-1}. UV: λ_{max}: 268(4706), 315(5652), 416(10 184), 534(590) nm(dm^3/mol/l); m.p. >270 °C.

[Ru(dipic)$(PPh_3)_2$Br] (**4**) was prepared from [$RuBr_3(PPh_3)_2$(MeOH)] (0.0897 g, 0.1 mmol) and dipicolinic acid (0.018 g, 0.1 mmol) as orange brown crystals. Yield: 75%. *Anal*. Calc. for $RuC_{43}H_{33}NO_4BrP_2$: C, 53.82; H, 3.46; N, 1.45. Found: C, 53.79; H, 3.63; N, 1.39%. IR: 1666, 1347, 1440, 1080, 690 cm^{-1}. UV: λ_{max}: 268(4344), 416(9180) nm(dm^3/mol/l); m.p. >240 °C.

2.5. Catalytic oxidation

To a solution of the alcohol (1 mmol) in CH_2Cl_2 (20 ml), *N*-methyl morpholine-*N*-oxide (3 mmol) and ruthenium complex (0.01 mmol) were added. The solution was heated under reflux for 3 h. The mixture was evaporated to dryness and extracted with petroleum ether (60–80 °C). The combined petroleum ether mixture was filtered and evaporated to give the corresponding aldehyde, which was then quantified as its 2,4-dinitrophenyl hydrazone derivative [31].

3. Results and discussion

New hexa-coordinated Ru(III) complexes of the type [Ru(dipic)$(EPh_3)_2$X] have been prepared by reacting 2,6-pyridine dicarboxylic acid (dipicolinic acid, H_2dipic) with [$RuCl_3(PPh_3)_3$], [$RuCl_3(AsPh_3)_3$], [$RuBr_3(AsPh_3)_3$] and [$RuBr_3(PPh_3)_2$(MeOH)] in a 1:1 mole ratio. The ligand replaces one EPh_3 and two X atoms, (E = As or P; X = Cl or Br), from the starting complex to yield [Ru(dipic)-$(EPh_3)_2$X] (Scheme 1). Dipicolinic acid acts as a dibasic tridentate ligand in all the complexes. The analytical data conform to the stoichiometry of the ruthenium(III) complexes as [Ru(dipic)$(EPh_3)_2$X].

3.1. Infrared spectroscopy

The IR spectrum of the free ligand (H_2dipic) shows a strong band around 1700 cm^{-1} assignable to ν(C=O) of COOH moiety [7]. In all the complexes, the band due to $\nu_{as}(COO^-)$ was observed in the region 1675–1610 cm^{-1} and that due to $\nu_s(COO^-)$ in the region 1352–1344 cm^{-1}. A large difference of 327–307 cm^{-1} between ν_{as} and ν_s vibrations indicates a monodentate coordination of the carboxylic group in all the complexes [32]. A broad band observed in the region 3340–2500 cm^{-1} region due to ν(O–H) of the carboxyl group in the free ligand disappeared in all the complexes indicating the deprotonation and subsequent coordination through oxygen donor atom. The absence of any peak around 1700 cm^{-1} reveals that both COOH groups are involved in coordination. All the characteristic peaks due to PPh_3/$AsPh_3$ were observed in the usual regions [31].

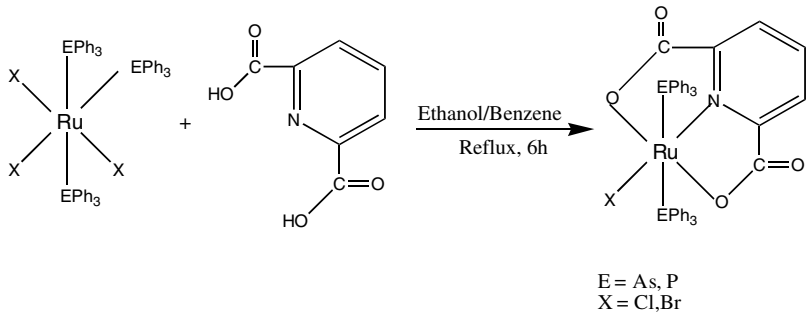

Scheme 1.

3.2. EPR spectroscopy

The EPR spectra of the powdered samples were recorded at room temperature at X-band frequencies. The nature of the spectra revealed the absence of any hyperfine splitting due to interaction with any other nuclei present in the complexes. Complexes **1** and **4** showed two lines with two different '*g*' values ($g_x = g_y \neq g_z$) indicating magnetic anisotropy and suggestive of tetragonal distortion in octahedral geometry [33]. However, complexes **2** and **3** showed three lines with three different '*g*' values ($g_x \neq g_y \neq g_z$) indicating rhombic distortion [34]. The '*g*' values are in the range 2.12–2.21. The nature of spectra obtained is in good agreement with that of the previously reported Ru(III) complexes [35]. A representative case is depicted in Fig. 1.

3.3. Electrochemistry

The redox behavior of the complexes was studied using cyclic voltammetry at a glassy carbon working electrode at a scan rate of 100 mV s^{-1}. $[NBu_4]BF_4$ (0.1 M) was used as supporting electrolyte in acetonitrile solution of 0.001 M of complex. The cyclic voltammetric data are given in Table 1 and a representative cyclic voltammogram is displayed in Fig. 2. The $E_{1/2}$ of the oxidation process was in the range from 0.71 to 0.79 V and reduction process was in the range from −0.73 to −0.80 V. The oxidation and reduction waves

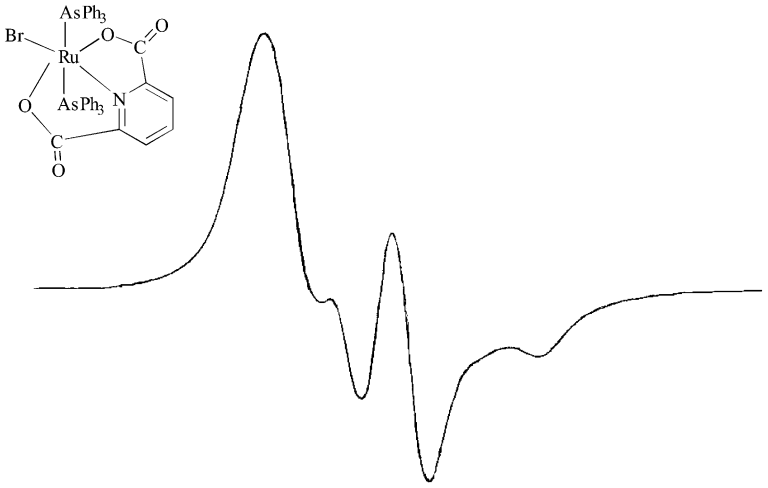

Fig. 1. EPR spectrum of **3**.

Table 1
Cyclic voltammetric data[a] of new Ru(III) complexes

Complex	Ru(III)–Ru(IV)				Ru(III)–Ru(II)			
	E_{pc} (V)	E_{pa} (V)	E_f (V)	ΔE_p (mV)	E_{pc} (V)	E_{pa} (V)	E_f (V)	ΔE_p (mV)
1	0.60	0.84	0.72	236	−0.87	−0.72	−0.79	152
2	0.65	0.77	0.71	120	−0.84	−0.62	−0.73	224
3	0.72	0.84	0.78	127	−0.87	−0.73	−0.80	141
4	0.69	0.88	0.79	192	−0.84	−0.71	−0.78	137

[a] Supporting electrolyte: $[NBu_4]ClO_4$ (0.05 M); complex concentration: 0.01 M; scan rate: 100 mV s^{-1}; all the potentials are referenced to Ag/AgCl.

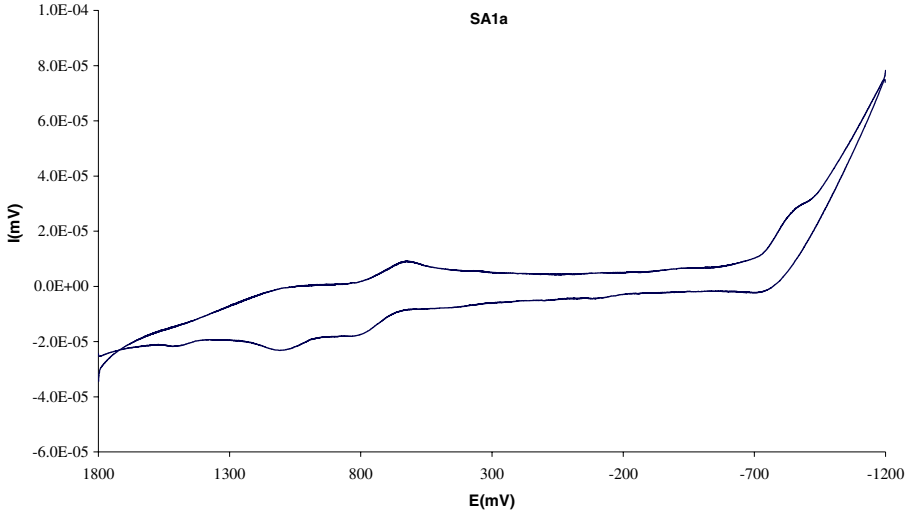

Fig. 2. Cyclic voltammogram of **1**.

are due to the metal centered Ru(III) → Ru(IV) and Ru(III) → Ru(II) processes, respectively. Any redox behavior of the ligand in the range 0.71 to −0.80 V is ruled out because dipicolinic acid showed quasi-reversible and irreversible processes only around −1.58 V in its complexes [36]. Moreover, potential difference between the two successive oxidation processes is ≈1.5 V which agrees well with the average potential difference between the redox processes of the ruthenium center ($Ru^{II/III}$–$Ru^{III/IV}$) (≈1.0–1.5 V) observed for other mononuclear complexes [37]. All the complexes exhibit quasi-reversible oxidative couples with peak to peak separations (ΔE_p) of 120–236 mV [38]. Replacement of PPh_3 by $AsPh_3$ showed no much variation in the redox potential. It has been observed from the electrochemical data that the present ligand system is ideally suitable for stabilizing the higher oxidation state of the ruthenium ion [39–41].

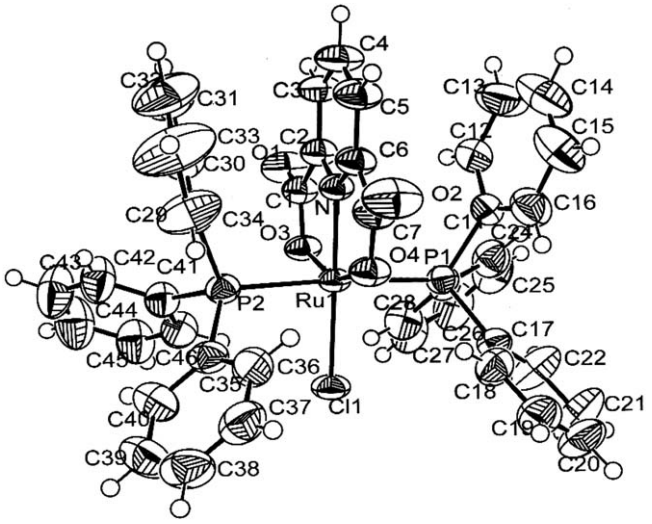

Fig. 3. ORTEP diagram [Ru(dipic)(PPh_3)$_2$Cl] (**1**).

3.4. Crystal structure of [Ru(dipic)(PPh_3)$_2$Cl]

The ORTEP diagram of [Ru(dipic)(PPh_3)$_2$Cl] is shown in Fig. 3. The crystal data and refinement parameters are summarized in Table 2. Selected bond lengths and bond

Table 2
Crystal data and structure refinement parameters for [Ru(dipic)(PPh_3)$_2$Cl]

Empirical formula	$C_{43}H_{33}ClNO_4P_2Ru$
Formula weight	826.16
Temperature (K)	293(2)
Wavelength (Å)	0.71073
Crystal system, space group	monoclinic, *C*2/*c*
Unit cell dimensions	
a (Å)	34.882(14)
b (Å)	9.998(4)
c (Å)	29.132(12)
α (°)	90
β (°)	121.32(3)
γ (°)	90
Volume (Å^3)	8679(6)
Z, calculated density (Mg/m^3)	8, 1.265
Absorption coefficient (mm^{-1})	0.535
F(000)	3368
Crystal size (mm)	0.22 × 0.19 × 0.14
θ Range for data collection (°)	2.15–24.98
Limiting indices	$0 \leqslant h \leqslant 41$, $-1 \leqslant k \leqslant 11$, $-34 \leqslant l \leqslant 29$
Reflections collected/unique (R_{int})	8653/7584 (0.0171)
Completeness to θ = 24.98 (%)	99.4
Absorption correction	ψ-scan
Maximum and minimum transmission	0.9998 and 0.9647
Refinement method	full-matrix least-squares on F^2
Data/restraints/parameters	7584/0/469
Goodness-of-fit on F^2	1.057
Final *R* indices [$I > 2\sigma(I)$]	$R_1 = 0.0327$, $wR_2 = 0.0913$
R indices (all data)	$R_1 = 0.0517$, $wR_2 = 0.1055$
Largest difference in peak and hole (e A^{-3})	0.530 and −0.603

angles are given in Table 3. The N(1)–Ru(1)–Cl(1) bond angle is 178.95(9)° showing that Cl atom lies *trans* to ring nitrogen. The bite angles around Ru(III) are N(1)–Ru(1)–O(4) = 77.42(10)°; N(1)–Ru(1)–O(3) = 77.28(9)°; O(4)–Ru(1)–Cl(1) = 103.60(7)° and O(3)–Ru(1)–Cl(1) = 101.70(6)°, summing up the in-plane angle to be exactly 360°. This shows the high planarity of the Cl and O, N, O donor atoms of dipicolinic acid. This is further supported by the other *cis* angles mentioned in Table 3. Thus, the acid occupies the equatorial plane around the Ru(III) octahedron, along with Cl. The bond angle P(1)–Ru(1)–P(2) = 175.62(3)° shows that the two PPh_3 groups are trans to each other occupying the axial positions. The two Ru–P bonds are slightly bent away from the dipicolinic acid towards the Cl atom which is evident from the P(1)–Ru(1)–Cl(1) bond angle is 88.84° which is smaller than P(1)–Ru(1)–N(1) = 91.41° and P(2)–Ru(1)–N(1) = 92.51° [42]. The Ru–P, Ru–O, Ru–N and Ru–Cl bond lengths found in the complex agree well with that reported for similar ruthenium complexes [3,7,43,44].

3.5. Catalytic activity

The oxidation of benzyl alcohol and cinnamyl alcohol to benzaldehyde and cinnamaldehyde was carried out with the new ruthenium(III) complexes as catalysts in the presence of *N*-methyl morpholine-*N*-oxide as co-oxidant in CH_2Cl_2. After 3 h of reflux the aldehydes formed were quantified as their 2,4-dinitrophenyl hydrazone derivatives [25]. The results obtained are given in Table 4. In cinnamyl alcohol, only the alcoholic group gets oxidized selectively without affecting the double bond. The relatively higher yield of cinnamaldehyde when compared to benzaldehyde is due to the fact that α-CH unit of cinnamyl alcohol is more acidic than benzyl alcohol [45]. The replacement of PPh_3 by $AsPh_3$ group in the complexes did not result in much. On comparing the catalytic activity of these complexes with that of the other reported ruthenium(III) complexes, it is found that theses complexes exhibit comparatively lower activity [31,46]. This may be due to the stronger chelation of the ligand which may hinder the formation of catalytically active species.

Table 3
Selected bond lengths (Å) and bond angles (°) for [Ru(dipic)(PPh_3)$_2$Cl]

Bond lengths	
Ru(1)–Cl(1)	2.3340(12)
Ru(1)–O(4)	2.050(2)
Ru(1)–N(1)	1.996(3)
Ru(1)–P(1)	2.3945(12)
Ru(1)–O(3)	2.053(2)
Ru(1)–P(2)	2.4052(12)
Bond angles	
N(1)–Ru(1)–O(4)	77.42(10)
O(3)–Ru(1)–P(1)	90.81(8)
N(1)–Ru(1)–O(3)	77.28(9)
Cl(1)–Ru(1)–P(1)	88.84(3)
O(4)–Ru(1)–O(3)	154.70(8)
N(1)–Ru(1)–P(2)	92.57(8)
N(1)–Ru(1)–Cl(1)	178.95(9)
O(4)–Ru(1)–P(2)	89.36(8)
O(4)–Ru(1)–Cl(1)	103.60(7)
O(3)–Ru(1)–P(2)	91.85(8)
O(3)–Ru(1)–Cl(1)	101.70(6)
Cl(1)–Ru(1)–P(2)	87.22(3)
N(1)–Ru(1)–P(1)	91.41(8)
P(1)–Ru(1)–P(2)	175.62(3)
O(4)–Ru(1)–P(1)	89.72(8)

Table 4
Catalytic activity of new Ru(III) complexes

Complex	Substrate	Yield[a] (%)	Turnover number[b]
1	benzyl alcohol	56	57
	cinnamyl alcohol	60	59
2	benzyl alcohol	36	37
	cinnamyl alcohol	60	59
3	benzyl alcohol	30	30
	cinnamyl alcohol	67	66
4	benzyl alcohol	39	40
	cinnamyl alcohol	62	61

[a] Yield based on substrate.
[b] Moles of product per mole of catalyst.

4. Conclusion

Dipicolinic acid can coordinate to the metal in a number of fashions. In spite of this variable ligating ability, it acts as tridentate dibasic chelating ligand forming only mononuclear complex irrespective of the metal-to-ligand ratio.

Acknowledgement

UGC-CSIR, New Delhi, India, is acknowledged for their financial assistance.

Appendix A. Supplementary data

Crystallographic data for [Ru(dipic)(PPh_3)$_2$Cl] (**1**) have been deposited with the Cambridge Crystallographic Data Centre, CCDC No. 288561. Copies of this information may be obtained free of charge from the Director, CCDC, 12, Union Road, Cambridge, CB2 1EZ, UK (fax: +44 1223 336033; e-mail: deposit@ccdc.cam.ac.uk or http://www.ccdc.cam.ac.uk). Supplementary data associated with this article can be found, in the online version, at doi:10.1016/j.poly.2006.01.023.

References

[1] M.P. Garcia, A.M. Lopez, M.A. Esteruelas, F.J. Lahoz, L.A. Oro, J. Chem. Soc., Dalton Trans. (1990) 3465.
[2] B.K. Panda, S. Sengupta, A. Chakravorty, Eur. J. Inorg. Chem. 178 (2004).
[3] S.A. Serron, C.M. Haar, S.P. Nolan, L. Brammer, Organometallics 16 (1997) 5120.
[4] I. del Rio, G.V. Koten, Tet. Lett. 40 (1999) 1401.

[5] W.K. Wong, X.P. Chen, J.P. Guo, Y.G. Chi, W.X. Pan, W.Y. Wong, J. Chem. Soc., Dalton Trans. 1139 (2002).
[6] T. Naota, H. Takaya, S.-I. Murahashi, Chem. Rev. 98 (1998) 2599.
[7] P. Sengupta, S. Ghosh, T.C.W. Mak, Polyhedron 20 (2001) 975.
[8] S.K. Sengupta, S.K. Sahni, R.N. Kapoor, Polyhedron 2 (1983) 317.
[9] B.R. Cameron, M.C. Darkes, I.R. Baird, R.T. Skerlj, Z.L. Santucci, S.P. Fricker, Inorg. Chem. 42 (2003) 4102.
[10] R. Karvembu, K. Natarajan, Synth. React. Inorg. Met-Org. Chem. 31 (2001) 743.
[11] X.Y. Zhou, N.M. Kostic, Inorg. Chem. 27 (1988) 4402.
[12] A.M. Herring, L. Henling, J.A. Labinger, J.E. Bercaw, Inorg. Chem. 30 (1991) 851.
[13] M.G.B. Drew, G.W.A. Fowles, R.W. Matthews, R.A. Walton, J. Am. Chem. Soc. 91 (1969) 7769.
[14] W. Furst, P. Gouzerth, Y. Jeannin, J. Coord. Chem. 8 (1979) 237.
[15] G. Nardin, L. Randaccio, R.P. Bonomo, E. Rizzaretti, J. Chem. Soc., Dalton Trans. (1980) 369.
[16] I. Morimoto, S. Tanaka, Anal. Chem. 35 (1963) 1234.
[17] Y. Kanay, Analyst 115 (1990) 809.
[18] R.L. Every, O.L. Riggs Jr., Mater Prot. 3 (1964) 46.
[19] C.G. Pope, E. Matijeric, R.C. Patel, J. Coll. Inter. Sci. 80 (1981) 847.
[20] G.F. Bailey, S. Karp, T.E. Sacks, J. Bacteriol. 89 (1965) 984.
[21] B. Setlow, P. Setlow, Appl. Environ. Microbial. 59 (1993) 640.
[22] L.D. Waterbury, C. Serrato, G.R. Martinez, Proc. West. Pharm. Soc. 32 (1989) 9.
[23] P. Laine, A. Gourdon, J.P. Launay, Inorg. Chem. 34 (1995) 5129.
[24] J.T. Groves, I.O. Kady, Inorg. Chem. 32 (1993) 3868.
[25] A.I. Vogel, Textbook of Practical Organic Chemistry, 5th ed., Longman, London, 1989.
[26] J. Chatt, G.J. Leigh, D.M.P. Mingos, R.J. Parke, J. Chem. Soc. A 2636 (1968).
[27] R.K. Poddar, I.P. Khullar, U. Agarwala, J. Inorg. Nucl. Chem. Lett. 10 (1974) 221.
[28] K. Natarajan, R.K. Poddar, U. Agarwala, J. Inorg. Nucl. Chem. Lett. 39 (1977) 431.
[29] T.A. Stephenson, G. Wilkinson, J. Inorg. Nucl. Chem. 28 (1966) 945.
[30] A.L. Spek, J. Appl. Crystallogr. 36 (2003) 7.
[31] R. Karvembu, C. Jayabalakrishnan, K. Natarajan, Trans. Met. Chem. 27 (2002) 574.
[32] A.C.G. Baro, E.E. Castellano, O.E. Piro, B.S.P. Costa, Polyhedron 24 (2005) 49.
[33] G. Harris, Theoret. Chim. Acta (Berl.) 5 (1966) 379.
[34] M.M.T. Khan, D. Srinivas, R.I. Kureshy, N.H. Khan, Inorg. Chem. 29 (1990) 2320.
[35] O.K. Medhi, U. Agarwala, Inorg. Chem. 19 (1980) 1381.
[36] M. Chatterjee, M. Maji, S. Ghosh, T.C.W. Mak, J. Chem. Soc., Dalton Trans. (1998) 3641.
[37] S. Chakraborty, M.G. Walawalkar, G.K. Lahiri, J. Chem. Soc., Dalton Trans. (2000) 2875.
[38] J. Heinze, Angew. Chem., Int. Ed. Engl. 23 (1984) 831.
[39] R. Prabhakaran, A. Geetha, M. Thilagavathi, R. Karvembu, V. Krishnan, H. Bertagnoli, K. Natarajan, J. Inorg. Biochem. 98 (2004) 2131.
[40] T.D. Thangadurai, K. Natarajan, Trans. Met. Chem. 25 (2000) 347.
[41] R. Prabhakaran, V. Krishnan, K. Pasumpon, D. Sukanya, E. Vendel, C. Jayabalakrishnan, H. Bertagnoli, Appl. Org. Met. Chem. 20 (2006) 203.
[42] J.-H. Ding, L.-S. Li, Y.-C Dong, Q.-F. Zhang, Z. Kristal NCS (2005) 220.
[43] S.M. Couchman, J.M.D. Vera, J.C. Jeffery, C.A. Mckee, S. Nevitt, M. Pohlman, C.M. White, M.D. Ward, Polyhedron 17 (1998) 3541.
[44] D. Ooyama, M. Sato, Anal. Sci. 19 (2003) 39.
[45] R. Ramesh, Inorg. Chem. Commun. 7 (2004) 274.
[46] C. Jayabalakrishnana, R. Karvembu, K. Natarajan, Synth. React. Inorg. Met-Org. Chem. 32 (2002) 1101.

metal cations and therefore the biological activities of its metal complexes should be significantly altered. The most salient feature of these isomorphous crystal structures is that the individual ionic subunits self-assemble via π–π stacking and extensive intermolecular hydrogen bonding, resulting in a 3D supramolecular architecture.

2. Experimental

2.1. Materials

High purity 5-nitrosalicylic acid, anhydrous magnesium chloride, zinc sulfate heptahydrate, cobalt sulfate heptahydrate and nickel chloride hexahydrate were purchased from Acros (USA) and used without further purification.

2.2. Physical measurement

Elemental analyses (C, H and N) were performed on a Perkin–Elmer 2400 analyzer. Thermal analysis (TG-DTA) was carried out using a TGA7 Perkin–Elmer thermal analyzer under N_2. The ^1H NMR spectra were recorded with Bruker AC 200 P (200 MHz) spectrometer; the chemical shifts are expressed in terms of ppm. The IR spectra were recorded with Bruker Vector 22 spectrometer.

2.3. Preparation of the complexes

2.3.1. $[Mg(H_2O)_5(5\text{-nsa})]^+(5\text{-nsa})^- \cdot H_2O$ (1)

Sodium 5-nitrosalicylate was prepared by neutralizing 5-nitrosalicylic acid (0.915 g, 5 mmol) with 5 ml of 1 M NaOH. To this solution was added anhydrous $MgCl_2$ (0.238 g, 2.5 mmol) in 3 ml of water. After a few days **1** was filtered, crystallized in water and dried over calcium chloride. Yield: 0.620 g (64%). *Anal.* Calc. for $C_{14}H_{20}N_2O_{16}Mg$ (**1**): C, 33.85; H, 4.07; N, 5.64. Found: C, 33.60; H, 3.96; N, 5.55%. Thermal study (TG-DTA) reveals a weight loss of 20.5% (Calc. 21.7%) at 75–230 °C, corresponding approximately to loss of six crystalline water molecules (both crystallization and coordination water). IR (neat, cm^{-1}): 3423(m), 1624(m), 1590(s), 1475(s), 1450(s), 1386(m), 1332(s), 1150(s), 1074(m), 926(m), 842(m), 808(m), 751(m), 698(s), 639(m).

2.3.2. $[Zn(H_2O)_5(5\text{-nsa})]^+(5\text{-nsa})^- \cdot H_2O$ (2)

Sodium 5-nitrosalicylate was prepared by neutralizing 5-nitrosalicylic acid (0.915 g, 5 mmol) with 5 ml of 1 M NaOH. To this solution was added $ZnSO_4 \cdot 7H_2O$ (0.720 g, 2.5 mmol) in 3 ml of water. After a few days **2** was filtered, crystallized in water and dried over calcium chloride. Yield: 1.076 g (80%). *Anal.* Calc. for $C_{14}H_{20}N_2O_{16}Zn$ (**2**): C, 31.27; H, 3.76; N, 5.21. Found: C, 31.16; H, 3.99; N, 5.25%. Thermal study (TG-DTA) reveals a weight loss of 19.7% (Calc. 20.1%) at 55–160 °C, corresponding to loss of six crystalline water molecules (both crystallization and coordination water). ^1H NMR (D_2O, 200 MHz) δ: 8.62 (d, $J = 2.6$ Hz, 1H, H-6), 8.24 (dd, $J = 9.3$, 2.6 Hz, 1H, H-4), 6.99 (d, $J = 9.3$ Hz, 1H, H-3). IR (neat, cm^{-1}): 3407(m), 1623(m), 1588(s), 1503(m), 1475(s), 1447(s), 1386(s), 1333(s), 1287(s), 1151(s), 1074(m), 926(m), 888(m), 844(m), 807(m), 750(m), 710(m), 640(m).

2.3.3. $[Co(H_2O)_5(5\text{-nsa})]^+(5\text{-nsa})^- \cdot H_2O$ (3)

Sodium 5-nitrosalicylate was prepared by neutralizing 5-nitrosalicylic acid (0.915 g, 5 mmol) with 5 ml of 1 M NaOH. To this solution was added $CoSO_4 \cdot 7H_2O$ (0.702 g, 2.5 mmol) in 3 ml of water. After a few days **3** was filtered, crystallized in water and dried over calcium chloride. Yield: 0.888 g (67%). *Anal.* Calc. for $C_{14}H_{20}N_2O_{16}Co$ (**3**): C, 31.65; H, 3.80; N, 5.27. Found: C, 31.46; H, 3.91; N, 5.16%. Thermal study (TG-DTA) reveals a weight loss of 20.2% (Calc. 20.3%) at 75–165 °C, corresponding to loss of six crystalline water molecules (both crystallization and coordination water). IR (neat, cm^{-1}): 3403(m), 1624(m), 1589(s), 1503(m), 1475(s), 1448(s), 1386(m), 1332(s), 1288(s), 1150(s), 1073(m), 926(m), 895(m), 843(m), 808(m), 750(m), 710(m), 698(m), 640(m).

2.3.4. $[Ni(H_2O)_5(5\text{-nsa})]^+(5\text{-nsa})^- \cdot H_2O$ (4)

Sodium 5-nitrosalicylate was prepared by neutralizing 5-nitrosalicylic acid (0.915 g, 5 mmol) with 5 ml of 1 M NaOH. To this solution was added $NiCl_2 \cdot 6H_2O$ (0.594 g, 2.5 mmol) in 3 ml of water. After a few days **4** was filtered, crystallized in water and dried over calcium chloride. Yield: 0.887 g (67%). *Anal.* Calc. for $C_{14}H_{20}N_2O_{16}Ni$ (**4**): C, 31.66; H, 3.80; N, 5.27. Found: C, 31.44; H, 3.75; N, 5.14%. Thermal study (TG-DTA) reveals a weight loss of 20.1% (Calc. 20.3%) at 70–190 °C, corresponding to loss of six crystalline water molecules (both crystallization and coordination water). IR (neat, cm^{-1}): 3406(m), 1624(m), 1589(s), 1503(m), 1475(s), 1448(s), 1386(s), 1332(s), 1287(s), 1151(s), 1074(m), 927(m), 890(m), 844(m), 809(m), 750(m), 710(s), 697(s), 640(m).

2.4. X-ray diffraction study

Diffraction data were collected on a Bruker-SMART three axis diffractometer equipped with a SMART 1000 CCD area detector using graphite monochromated Mo Kα X-radiation (wavelength $\lambda = 0.71073$ Å) at 100.0(1) K. The low temperature was reached by an evaporated liquid nitrogen stream over the crystal, provided by the Oxford Cryosystem device. Data collection and processing were carried out using Bruker SMART programs [3] and empirical absorption correction was applied using SADABS computer program [3]. The structure was solved by direct methods SIR97 [4], and refined by full-matrix least-squares based on F using CRYSTALS software [5]. All non-hydrogen atoms were anisotropically refined. The hydrogen atoms were located in difference Fourier maps. H atoms were refined isotropically with $U_{iso} = 1.20\ U_{eq}$

where U_{eq} is the equivalent isotropic atomic displacement parameter of the attached atom. The crystal parameters, data collection and the refinement details of compounds **1**, **2**, **3** and **4** are reported in Table 1.

3. Results and discussion

The structure determinations show that all these complexes are isomorphous and crystallize in *Pna2₁* orthorhombic space group. The asymmetric unit can be represented by the general formula: $[M_1(H_2O)_5(5\text{-nsa})]^+(5\text{-nsa})^- \cdot H_2O$ where M_1 = magnesium, zinc, cobalt or nickel. Since complexes **1**–**4** are isomorphous, no notable differences were observed between their structural parameters. For that reason, only the details of the X-ray structure of Ni(II) complex (**4**), arbitrarily chosen, were reported and discussed in the present paper. The canonical drawing and the CAMERON [6] molecular structure of the Ni(II) complex (**4**) are represented in Figs. 1 and 2, respectively, with the atom numbering system used in Table 2, which lists the most relevant bond distances and angles.

The structure of $[Ni(H_2O)_5(5\text{-nsa})]^+(5\text{-nsa})^- \cdot H_2O$ (**4**) consists of one $[Ni(H_2O)_5(5\text{-nsa})]^+$ cation, one $(5\text{-nsa})^-$ serves as a counter-anion and one water molecule exists as solvate molecule. The cation is a monomeric complex in which Ni(II) is coordinated to five aqua ligands and the carboxylato O(36)-atom from the 5-nitrosalicylato ligand, forming a slightly distorted octahedron. The *cis* angles around the Ni center vary between 86.13(6)° and 94.32(7)° while the *trans* angles vary from 173.22(6)° to 176.29(7)°. The Ni–O(36) distance [2.026(2) Å] is notably shorter than those for Ni–O(10), Ni–O(11), Ni–O(12), Ni–O(13), Ni–O(14), [2.040(2), 2.095(2), 2.086(2), 2.067(2), 2.043(2) Å, respectively]. These bonds are probably quite dependent on the H-bonding system, which is very important in this structure. The presence of six water molecules leads to a very extensive and complicated H-bonding network. All the aqua ligands and the solvate water molecule form strong H-bonds between themselves, with the carboxylato O-atoms, the nitro O-atoms and the phenoxo O-atoms. A list of the most probable atoms involved in H-bonds with their related angles is given in Table 3. Fig. 3 shows the H-bonding association in the asymmetric unit. The H-bonds are extended in all directions

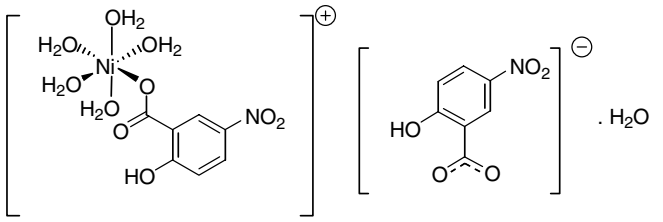

Fig. 1. Canonical representation of $[Ni(H_2O)_5(5\text{-nsa})]^+(5\text{-nsa})^- \cdot H_2O$ (**4**).

Table 1
Crystal data and structure refinement parameters for $C_{14}H_{20}N_2O_{16}M_1$ (M_1 = Mg, Zn, Co or Ni)

Compound	**1**	**2**	**3**	**4**
Empirical formula	$C_{14}H_{20}N_2O_{16}Mg$	$C_{14}H_{20}N_2O_{16}Zn$	$C_{14}H_{20}N_2O_{16}Co$	$C_{14}H_{20}N_2O_{16}Ni$
Molecular weight	496.62	537.70	531.25	531.03
Color	ocher	yellow	salmon pink	greenish
Crystal system	orthorhombic	orthorhombic	orthorhombic	orthorhombic
Space group	*Pna2₁*	*Pna2₁*	*Pna2₁*	*Pna2₁*
a (Å)	18.081(5)	18.085(5)	18.081(5)	17.996(5)
b (Å)	15.736(5)	15.720(5)	15.736(5)	15.688(5)
c (Å)	7.151(5)	7.137(5)	7.151(5)	7.142(5)
α (°)	90	90	90	90
β (°)	90	90	90	90
γ (°)	90	90	90	90
V (Å^3)	2034 (2)	2029 (2)	2034 (2)	2016 (2)
Z	4	4	4	4
Calculated density (g cm^{-3})	1.621	1.760	1.734	1.749
Absorption coefficient (mm^{-1})	0.176	1.300	0.932	1.052
F(000)	1032	1104	1092	1096
Crystal size (mm^3)	$0.17 \times 0.22 \times 0.27$	$0.18 \times 0.22 \times 0.25$	$0.17 \times 0.22 \times 0.28$	$0.16 \times 0.20 \times 0.25$
θ Ranges (°)	1.72–29.96	1.72–29.72	1.72–29.96	1.72–29.98
h/*k*/*l*	0,25/0,21/−9,10	0,25/0,21/−9,9	0,24/0,21/−9,9	0,25/0,22/−10,9
T (K)	100	100	100	100
Number of reflections collected	14381	14293	14628	14586
Number of independent reflections	5126	5129	5149	4839
Number of reflections used $\geqslant 3\sigma(I)$	3927	4502	3829	3155
Parameters	299	300	299	300
R [*F*]	0.0285	0.0218	0.0228	0.0210
wR [*F*]	0.0335	0.0237	0.0247	0.0221
Goodness-of-fit on *F*	1.0731	1.1184	1.1265	1.1448
Residual density (e Å^{-3})	−0.24; 0.30	−0.34; 0.44	−0.50; 0.31	−0.49; 0.50
Refine ls shift/su.max	0.0006	0.0014	0.0005	0.0013

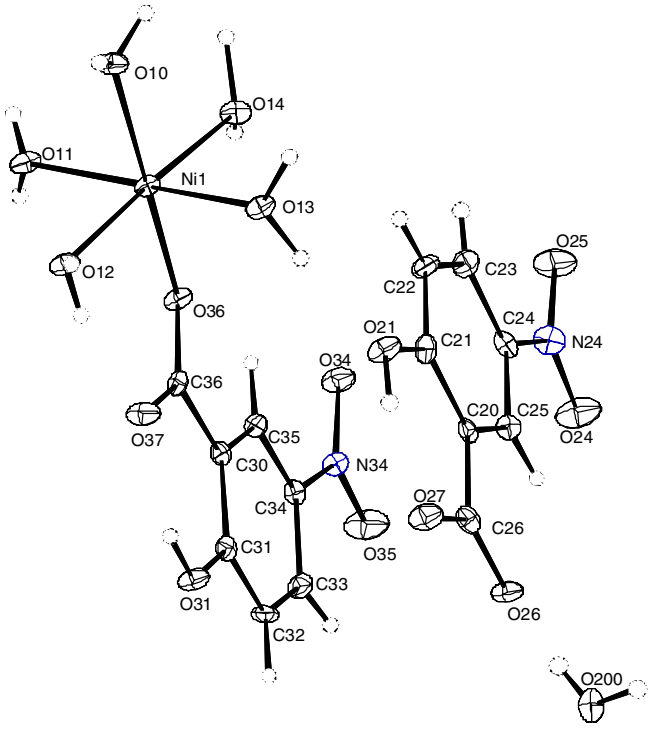

Fig. 2. Labeled CAMERON diagram of $[Ni(H_2O)_5(5\text{-nsa})]^+(5\text{-nsa})^- \cdot H_2O$ (**4**). Ellipsoids are drawn at 50% probability level.

forming a H-bonded 3D network, as illustrated in Fig. 4. The crystal cohesion is thus ensured by fourteen hydrogen bonds per asymmetric unit: three intramolecular, two intermolecular intra-asymmetric unit and nine intermolecular inter-asymmetric unit (Figs. 3 and 4).

In both aromatic units, the 5-nitro group is roughly coplanar with the adjacent phenyl ring [torsion angle C(23)–C(24)–N(24)–O(24): 174.13° (non-ligating aromatic moiety); torsion angle C(33)–C(34)–N(34)–O(34): 174.36° (metal-bonded aromatic moiety)]. However, a notable dissymmetry was observed between the N–O lengths of each

Table 2
Selected bond distances (Å) and bond angles (°) for $[Ni(H_2O)_5(5\text{-nsa})]^+(5\text{-nsa})^- \cdot H_2O$ (**4**)

Bond lengths			
Ni–O(14)	2.043(2)	Ni–O(11)	2.095(2)
Ni–O(12)	2.086(2)	Ni–O(13)	2.067(2)
Ni–O(10)	2.040(2)	Ni–O(36)	2.026(2)
Non-ligating aromatic moiety		Metal-bonded aromatic moiety	
O(21)–C(21)	1.343(2)	O(31)–C(31)	1.342(3)
O(24)–N(24)	1.228(3)	O(34)–N(34)	1.241(3)
O(25)–N(24)	1.241(3)	O(35)–N(34)	1.221(3)
O(26)–C(26)	1.256(3)	O(36)–C(36)	1.252(3)
O(27)–C(26)	1.274(3)	O(37)–C(36)	1.277(3)
C(20)–C(21)	1.420(3)	C(30)–C(31)	1.412(3)
C(21)–C(22)	1.396(3)	C(31)–C(32)	1.410(3)
C(22)–C(23)	1.385(3)	C(32)–C(33)	1.376(3)
C(23)–C(24)	1.392(3)	C(33)–C(34)	1.392(3)
C(24)–C(25)	1.381(3)	C(34)–C(35)	1.390(3)
C(25)–C(20)	1.396(3)	C(35)–C(30)	1.396(3)
C(20)–C(26)	1.493(3)	C(30)–C(36)	1.505(3)
C(24)–N(24)	1.446(3)	C(34)–N(34)	1.460(3)
Bond angles			
O(14)–Ni–O(12)	176.29(7)	O(14)–Ni–O(13)	89.02(8)
O(11)–Ni–O(13)	175.43(7)	O(12)–Ni–O(13)	87.51(7)
O(10)–Ni–O(36)	173.22(6)	O(10)–Ni–O(13)	90.80(7)
O(14)–Ni–O(10)	89.17(7)	O(14)–Ni–O(36)	86.36(7)
O(12)–Ni–O(10)	92.20(7)	O(12)–Ni–O(36)	92.57(7)
O(14)–Ni–O(11)	94.32(7)	O(11)–Ni–O(36)	89.12(7)
O(12)–Ni–O(11)	89.21(8)	O(13)–Ni–O(36)	94.21(7)
O(10)–Ni–O(11)	86.13(6)	Ni–O(36)–C(36)	127.8(2)

Table 3
H-bond donor/acceptor scheme (Å, °) for $[Ni(H_2O)_5(5\text{-nsa})]^+(5\text{-nsa})^- \cdot H_2O$ (**4**)

D–H···A	*d*(D–H)	*D*(H···A)	∠(DHA)
O(21)–H(21)···O(27)	0.8723(2)	1.649(2)	156.33(7)
O(31)–H(31)···O(37)	0.8227(2)	1.744(2)	155.89(7)
O(12)–H(122)···O(37)	0.8322(2)	1.811(2)	162.64(8)
O(13)–H(132)···O(21)	0.8682(2)	1.939(2)	175.16(8)
O(200)–H(201)···O(26)	0.8045(2)	1.969(2)	159.09(6)
O(13)–H(131)···O(200)^{i}	0.8852(4)	1.860(3)	176.04(8)
O(10)–H(102)···O(26)^{i}	0.9007(4)	1.930(2)	175.46(6)
O(11)–H(111)···O(31)^{i}	0.7232(2)	2.167(2)	172.27(6)
O(14)–H(141)···O(27)^{i}	0.9227(2)	1.755(2)	169.98(7)
O(10)–H(101)···O(200)^{ii}	0.8459(2)	1.841(2)	176.99(8)
O(12)–H(121)···O(26)^{ii}	0.8245(2)	2.027(2)	165.28(7)
O(200)–H(202)···O(12)^{iii}	0.8276(4)	2.128(3)	140.03(7)
O(14)–H(142)···O(25)^{iv}	0.8621(3)	1.958(2)	163.39(7)
O(11)–H(112)···O(34)^{iv}	0.8852(3)	2.299(3)	161.54(7)

Symmetry codes: i, $x-1/2$, $-y+3/2$, z; ii, $-x+3/2$, $y+1/2$, $z+1/2$; iii, $x+1/2$, $-y+3/2$, $z-1$; iv, $-x+1$, $-y+1$, $z+1/2$.

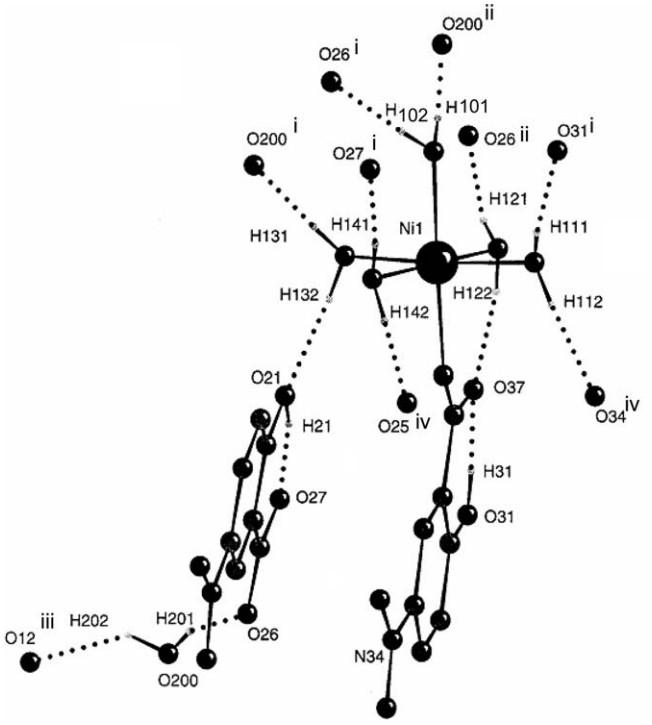

Fig. 3. Labeled diagram of $[Ni(H_2O)_5(5\text{-nsa})]^+(5\text{-nsa})^- \cdot H_2O$ (**4**) showing the H-bonding associations as broken lines [Symmetry codes: i, $x-1/2$, $-y+3/2$, z; ii, $-x+3/2$, $y+1/2$, $z+1/2$; iii, $x+1/2$, $-y+3/2$, $z-1$; iv, $-x+1$, $-y+1$, $z+1/2$.].

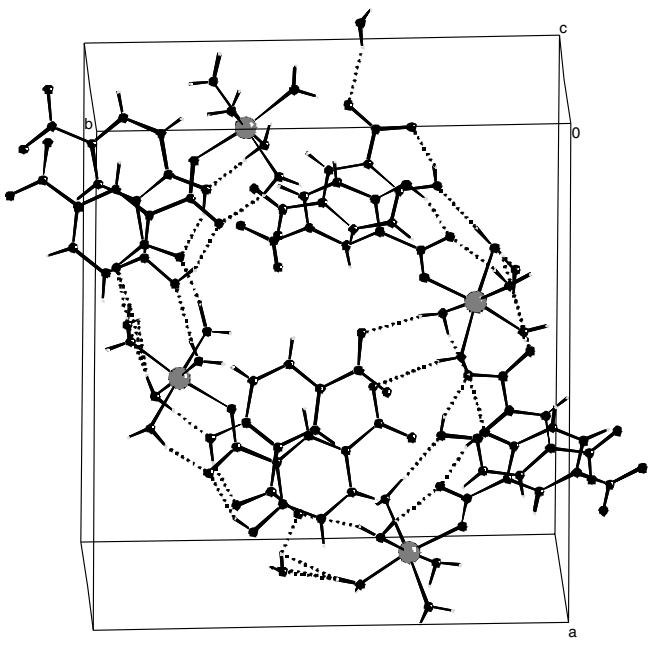

Fig. 4. Perspective diagram of packing of $[Ni(H_2O)_5(5\text{-nsa})]^+(5\text{-nsa})^- \cdot H_2O$ (**4**) in the unit cell showing the extensive 3D H-bonded network (dashed lines). Ni centers are symbolized by large gray tone circles.

aromatic moiety [N(24)–O(24): 1.228(3) Å, N(24)–O(25): 1.241(3) Å; N(34)–O(34): 1.241(3) Å, N(34)–O(35): 1.221(3) Å]. This can be rationalized by invoking that O(25) and O(34) are both implicated in intermolecular hydrogen bonds [with H(142) and H(112), respectively], Fig. 3. Similarly, the carboxylate group of each aromatic unit is essentially coplanar with the adjacent phenyl ring [torsion angle C(21)–C(20)–C(26)–O(26): 178.48° (non-ligating aromatic moiety); torsion angle C(31)–C(30)–C(36)–O(36): 176.95° (metal-bonded aromatic moiety)] with a marked dissymmetry between the C–O lengths [C(26)–O(26): 1.256(3) Å, C(26)–O(27): 1.274(3) Å; C(36)–O(37): 1.277(3) Å, C(36)–O(36): 1.252(3) Å]. This dissymmetry is typical of asymmetrically-bonded (unidentate) carboxylato ligands, and is seen in the crystal structure of a variety of (salicylato) metal complexes [2e,2f]. Another salient geometrical feature of this structure is that the non-ligating 5-nsa moiety [C(20) to C(25) plane, denoted P(1)] and the metal-bonded one [C(30) to C(35) plane, denoted P(2)] are pairwise linked by π–π stacking interactions (Figs. 5 and 6). Remarkably, this stacking implicates a *syn*-facial arrangement of the aromatic nuclei (superimposition of the same faces); in sharp contrast, Smith and co-workers have observed an *anti*-facial arrangement of the π-bonded 5-nsa ligands (superimposition of the opposite faces) in the proton-transfer compounds with a variety of Lewis bases [7]. The dihedral angle between mean planes P(1) and P(2) is 5.86(6)°. The two 5-nsa rings have a centroid separation *Cg*P(1)…*Cg*P(2) of 3.847 Å and a mean interplanar spacing of 3.400 Å [orthogonal projection of *Cg*P(2) on P(1)] corresponding to a ring-centroid offset of 1.800 Å (Table 4). Although this offset is quite large, a notable π-overlapping exists between the two aromatic nuclei (Fig. 5). On the other hand, the metal-bonded nucleus is slightly rotated counterclockwise around C(32)–C(35) axis (by ca. 1°) relatively to the non-ligating nucleus plane, as highlighted in Fig. 6. Besides the anchoring of the metal-bonded cationic moiety to the non-ligating anionic counterpart through π–π interaction, these are connected by two types of intermolecular hydrogen bonds: seven inter-asymmetric unit bonds [$O(26)^{i}$…H(102)–O(10)–Ni, $O(26)^{ii}$···H(121)–O(12)–Ni, $O(200)^{ii}$···H(101)–O(10)–Ni, $O(200)^{i}$···H(131)–O(13)–Ni, H(202)···$O(12)^{iii}$–Ni, $O(27)^{i}$···H(141)–O(14)–Ni, $O(25)^{iv}$···H(142)–O(14)–Ni] and one intra-asymmetric unit bond [O(21)···H(132)–O(13)–Ni] (Fig. 3).

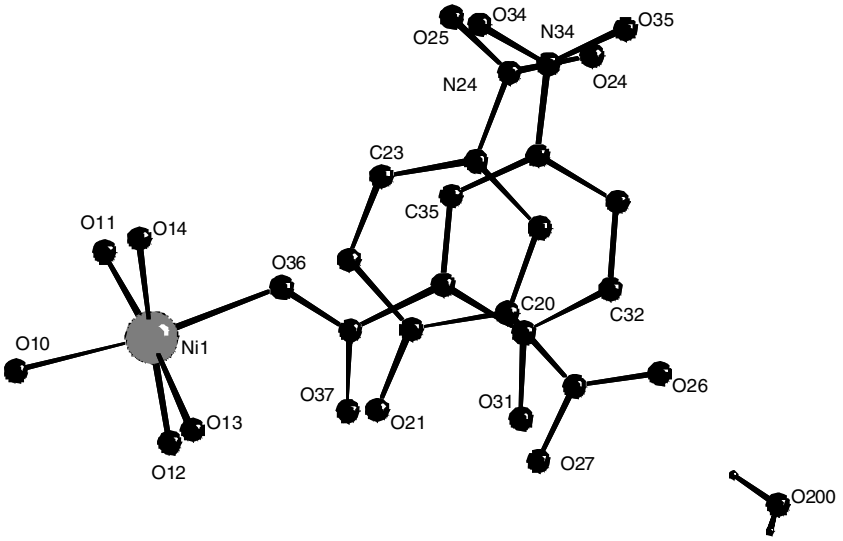

Fig. 5. Perspective diagram of $[Ni(H_2O)_5(5\text{-nsa})]^+(5\text{-nsa})^- \cdot H_2O$ (**4**) with labeled heteroatoms and some representative carbon atoms concentrating on the π–π stack viewed perpendicularly to the plane of the non-ligating aromatic nucleus.

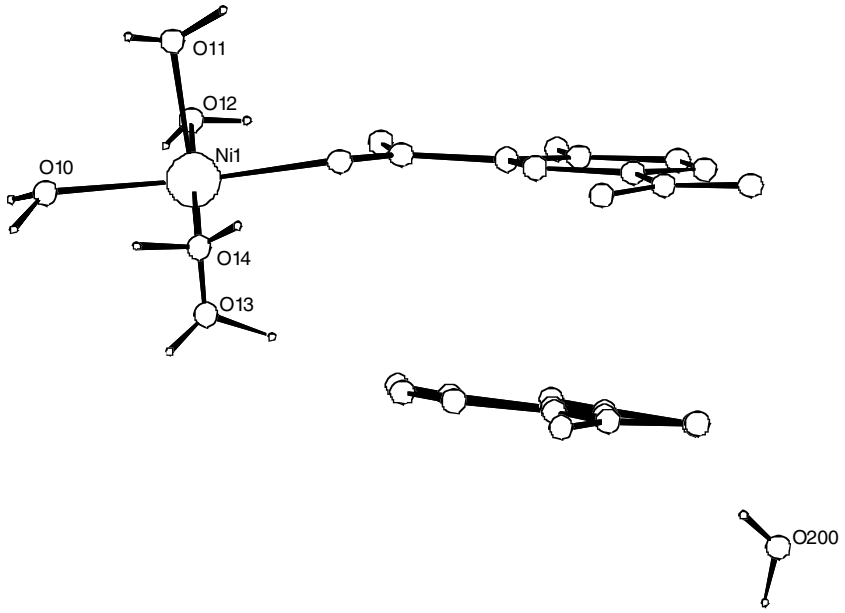

Fig. 6. Perspective diagram of $[Ni(H_2O)_5(5\text{-nsa})]^+(5\text{-nsa})^- \cdot H_2O$ (**4**) focusing on the edges of the π–π stacked aromatic nuclei viewed in the plane of the non-ligating nucleus.

Table 4
Structural details of the π-stacking interactions in $[Ni(H_2O)_5(5\text{-nsa})]^+(5\text{-nsa})^- \cdot H_2O$ (**4**)

Distance from C(35) to P(1) (Å)	3.261(3)	Dihedral angle between P(1) and P(2) (°)	5.86(6)
Distance from C(30) to P(1) (Å)	3.300(3)	Ring-centroid separation (Å)	3.847
Distance from C(34) to P(1) (Å)	3.368(3)	Mean interplanar spacing[a] (Å)	3.400
Distance from C(31) to P(1) (Å)	3.428(3)	Ring-centroid offset (Å)	1.800
Distance from C(33) to P(1) (Å)	3.545(3)		
Distance from C(32) to P(1) (Å)	3.547(3)		

[a] Orthogonal projection of the metal-bonded nucleus centroid on the non-ligating nucleus plane.

4. Conclusion

We have shown that the individual ionic subunits of the 5-nsa complexes with Mg(II), Zn(II), Co(II) and Ni(II) self-assemble via π–π stacking and extensive hydrogen bonding involving water molecules, leading to a 3D supramolecular architecture. The propensity for the 5-nsa ligand to be paired via π–π stacking interaction, already reported by Smith and co-workers [7], is noteworthy. In sharp contrast, the isomorphous 4-nsa complexes of Zn(II), Co(II) and Ni(II) reported par Ulkü and co-workers [2e], regioisomers of complexes **2**, **3** and **4**, respectively, consist of centrosymmetric monomers with the metal atom occupying the two inversion centers at $0,0,0$ and $0,1/2,1/2$ of a monoclinic unit cell. This work is being continued in two directions. First, the biological activities of complexes **1**–**4** are currently under evaluation in connection with the elaboration of potent (salicylato) metal complexes-based drugs. Secondly, the original metallo-organic framework of these complexes consisting of cationic/anionic aromatic moieties linked together through π-stacking and hydrogen bonding might be of peculiar interest in the design of functional materials. For instance, the π–π stacking interactions have been utilized in several research areas such as molecular conductors [8] and electronics [9]. In other respects, since the five shortest separations between Ni centers in **4** are 6.78, 7.14, 9.25, 10.66 and 11.76 Å, long-range magnetic interactions are expected, which could be exploited to elaborate molecular-based magnetic materials [10].

5. Supplementary data

Crystallographic data for the structures reported in this paper have been deposited with the Cambridge Crystallographic Data Center as supplementary publication Nos. CCDC 286184 (**3**) – CCDC 286185 (**1**) – CCDC 28186 (**4**) – CCDC 28187 (**2**). Copies of this information can be obtained free of charge from The Director, CCDC, 12, Union Road, Cambridge CB2 1EZ, UK (fax: +44 1223 336033; e-mail: deposit@ccdc.cam.ac.uk or http://www.ccdc.cam.ac.uk).

Acknowledgements

This paper is dedicated to Professor John R.J. Sorenson (University of Arkansas, USA). Financial support of Université Paris XI, CNRS and Ecole Centrale Paris is gratefully acknowledged. The authors thank Mrs. S. Mairesse-Lebrun for performing elemental analyses and Mr. M. Sghaier for performing DTA analyses.

References

[1] (a) J.R.J. Sorenson, J. Med. Chem. 19 (1976) 135;
(b) J.R.J. Sorenson, Prog. Med. Chem. 15 (1978) 211.

[2] (a) M.N. Tahir, D. Ulkü, E.M. Movsumov, Acta Cryst. C52 (1996) 593;
(b) M.N. Tahir, D. Ulkü, E.M. Móvsümov, Acta Cryst. C52 (1996) 2436;
(c) M. Devereux, M. Curran, M. McCann, Rev.M.T. Casey, Polyhedron 15 (1996) 2029;
(d) X.S. Tan, W.X. Tang, J. Chen, P.J. Zheng, Polyhedron 15 (1996) 2087;
(e) M.N. Tahir, D. Ulkü, E.M. Movsumov, T. Hökelek, Acta Cryst. C53 (1997) 176;
(f) G. Morgant, B. Viossat, J.-C. Daran, M. Roch-Arveiller, J.-P. Giroud, D. Nguyen-Huy, J.R.J. Sorenson, J. Inorg. Biochem. 70 (1998) 137;
(g) N.J. Brownless, D.A. Edwards, M.F. Mahon, Inorg. Chim. Acta 287 (1999) 89;
(h) G. Morgant, D. Nguyen Huy, J.-C. Daran, B. Viossat, X. Labouze, M. Roch-Arveiller, F.T. Greenaway, W. Cordes, J.R.J. Sorenson, J. Inorg. Biochem. 81 (2000) 11;
(i) A. Marzotto, D.A. Clemente, T. Gerola, G. Valle, Polyhedron 20 (2001) 1079;
(j) B. Viossat, G. Morgant, J.R.J. Sorenson, M. Roch-Arveiller, J.-C. Daran, F.T. Greenaway, D. Nguyen Huy, Ann. Pharm. Fr. 60 (2002) 102;
(k) P. Lemoine, B. Viossat, G. Morgant, F.T. Greenaway, A. Tomas, D. Nguyen Huy, J.R.J. Sorenson, J. Inorg. Biochem. 89 (2002) 18;
(l) B. Viossat, J.-C. Daran, G. Savouret, G. Morgant, F.T. Greenaway, D. Nguyen Huy, V.A. Pham-Tran, J.R.J. Sorenson, J. Inorg. Biochem. 96 (2003) 375;
(m) H. Icbudak, H. Olmez, O.Z. Yesilel, F. Arslan, P. Naumov, G. Jovanovski, A.R. Ibrahim, A. Usman, H.-K. Fun, S. Chantrapromma, S.W. Ng, J. Mol. Struct. 657 (2003) 255;
(n) P. Lemoine, B. Viossat, D. Nguyen-Huy, A. Tomas, G. Morgant, F.T. Greenaway, J.R.J. Sorenson, J. Inorg. Biochem. 98 (2004) 1734;
(o) J. Abdelhak, S. Namouchi Cherni, T. Jouini, Z. Kristallogr. 220 (2005) 183.

[3] ASTRO (5.00), SAINT (5.007), SADABS (5.007). Data Collection and Processing Software for the SMART System (5.054). Siemens (BRUKER-AXS) Analytical X-ray Instruments Inc., Madison, WI, 1998.

[4] A. Altomare, M.C. Burla, M. Camalli, G.L. Cascarano, G. Giacovazzo, A. Guagliardi, A. Grazia, G. Moliterni, G. Polidori, R. Spagna, SIR97 – a program for automatic solution of crystal structures by direct methods, J. Appl. Crystallogr. 32 (1999) 115.

[5] D.J. Watkin, C.K. Prout, J.R. Carruthers, P.W. Betteridge, R.I. Prout, CRYSTALS Issue 11, Chemical Crystallography Laboratory, University of Oxford, UK, 2001.

[6] D.J. Watkin, C.K. Prout, L.J. Pearce, CAMERON, Chemical Crystallography Laboratory, University of Oxford, UK, 1996.

[7] (a) G. Smith, A.W. Hartono, U.D. Wermuth, P.C. Healy, J.M. White, A.D. Rae, Aust. J. Chem. 58 (2005) 47;
(b) G. Smith, U.D. Wermuth, J.M. White, Acta Cryst. C61 (2005) 464.

[8] (a) R. Kato, Chem. Rev. 104 (2004) 5319;
(b) R.P. Shibaeva, E.B. Yagubskii, Chem. Rev. 104 (2004) 5347;
(c) T. Inabe, H. Tajima, Chem. Rev. 104 (2004) 5505.

[9] C.P. Collier, E.W. Wong, M. Belohradsky, F.M. Raymo, J.F. Stoddart, P.J. Kuekes, R.S. Williams, J.R. Heath, Science 285 (1999) 391.

[10] O. Kahn, Molecular Magnetism, VCH, New York, 1993.

L = ethanol and 2-amimopyrimidine (abbreviated as ampym)), $[Mn(dca)_2(C_2H_5OH)_2]_n$ (**1**) and $[Mn(dca)_2(ampym)_2]_n$ (**2**), together with spectroscopic and magnetic observations.

2. Experimental

2.1. Synthesis of the compounds

All chemicals were purchased from commercial sources and used as received.

$Mn(dca)_2(C_2H_5OH)_2]_n$ (**1**): 0.5 mmol $MnCl_2$ in ethanol and 1.0 mmol sodium dicyanamide in ethanol plus a small amount of water were carefully mixed together and filtered to remove any solid particles. Colourless crystals were obtained by diffusion into ether. When crystals are taken out of the solvent mixture and remain in open air, solvent is lost rapidly within a few hours to form $Mn(dca)_2$, which was confirmed by elemental analysis and infrared spectroscopy (vide infra). Such a decomposition in open air was also observed earlier in the literature for other related $Mn(dca)_2$ compounds [5c]. For IR and X-ray measurement freshly prepared crystals were used.

$[Mn(dca)_2(ampym)_2]_n$ (**2**): 0.5 mmol $Mn(CF_3SO_3)_2$ and 1 mmol ampym were each dissolved in an ethanol/water (1:1) mixture and warmed up until about 50 °C. To this solution, an aqueous solution of 1 mmol sodium dicyanamide was added dropwise. The white solution was filtered and left to evaporate at room temperature. White-yellowish crystals were obtained in a few days. (yield 48%); *Anal.* Calc. for $C_{12}H_{12}N_{12}Mn$: C, 38.0; H, 3.2; N, 44.3. Found: C, 37.9; H, 3.1; N, 44.3%.

2.2. Physical techniques

C, H, N determinations were performed on a Perkin Elmer 2400 Series II analyzer.

FTIR spectra were obtained on a Perkin Elmer Paragon 1000 FTIR spectrophotometer equipped with a Golden Gate ATR device, using the reflectance technique (4000–300 cm^{-1}, res. 4 cm^{-1}). X-band EPR spectra were recorded on polycrystalline samples at RT at 77 K with a Jeol RE2X electron spin resonance spectrometer using DPPH ($g = 2.0036$) as a standard. Magnetic susceptibility measurement (5–300 K) were carried out using a Quantum Design MPMS-5S SQUID magnetometer (measurements carried out at 0.1 T). Data were corrected for magnetisation of the sample holder and for diamagnetic contributions, which were estimated from Pascal constants.

2.3. Crystallography

Freshly prepared crystals suitable for structure determination were mounted on Lindemann-glass capillaries and transferred into the cold nitrogen stream of a Nonius KappaCCD diffractometer on rotating anode (Mo Kα radiation, graphite monochromator, $\lambda = 0.71073$). The intensity data were corrected for Lorentz and polarisation effects, for absorption and extinction. The structures were solved by direct methods. The programs COLLECT [6a], SHELXS-97 [6b], SHELXL-97 [6c] were used for data reduction, structure solution and structure refinement, respectively. All non-hydrogen atoms were refined anisotropically. All H atoms were introduced in calculated positions and refined with fixed geometry with respect to their carrier atoms. Crystallographic data of the compounds are listed in Table 1.

3. Results and discussion

3.1. Structures

3.1.1. Crystal structure of $[Mn(dca)_2(C_2H_5OH)_2]_n$ (1)

A plot showing the numbering scheme is given in Fig. 1 and selected bond distances and angles are given in Table 2. The structure of **1** contains 1D linear chains with double-bridged $\mu_{1,5}$-bridging dca molecules. The geometry of the Mn ion is octahedral and the octahedron is formed by four

Table 1
Crystallographic data

	Compound **1**	Compound **2**
Compound	$C_8H_{12}MnN_6O_2$	$C_{12}H_{12}MnN_{12}$
Molecular weight	279.18	379.28
Crystal system	monoclinic	orthorhombic
Temperature (K)	173(2)	173(2)
Space group	*C2/m*	*Cccm*
a (Å)	12.500(3)	13.964(3)
b (Å)	7.5059(15)	16.187(3)
c (Å)	7.1511(14)	7.5800(15)
β (°)	112.69(3)	90.0
V (Å^3)	619.0(2)	1713.3(6)
Z	2	4
D_{calc} (g cm^{-3})	1.498	1.470
μ (cm^{-1})	1.067	0.794
F(000)	286	772
Crystal size (mm)	0.30 × 0.01 × 0.01	0.40 × 0.20 × 0.20
Reflection collection	4440	8770
Independent reflection (R_{int})	774(0.0883)	1051(0.0491)
Number of reflection parameters	47	71
R_1 [$(I) > 2\sigma(I)$]	0.0513	0.0278
$wR(F^2)$	0.1356	0.0731
S	1.048	1.089
$\Delta\rho_{min}$, $\Delta\rho_{max}$	−1.449, 0.608	−0.567, 0.255

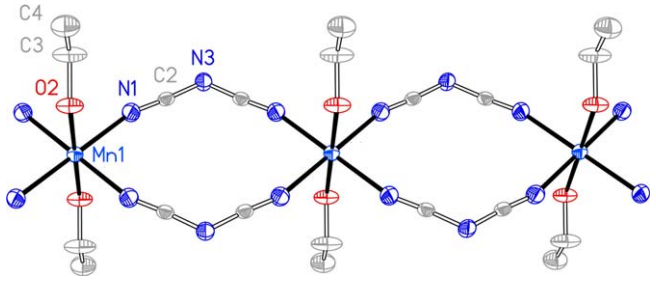

Fig. 1. Atomic displacement plot (50% probability) of structure $[Mn(dca)_2(C_2H_5OH)_2]_n$ (**1**). H atoms are omitted for clarity.

Table 2
Selected bond lengths (Å) and angles (°) for $[Mn(dca)_2(C_2H_5OH)_2]_n$ (**1**)

Mn(1)–O(2)	2.216(3)	Mn(1)–N(1)	2.217(2)
Mn(1)–Mn(1)A	7.506(3)		
O(2)–Mn(1)–N(1)	89.12(8)	O(2)–Mn(1)–N(1)A	90.88(8)
N(1)–Mn(1)–N(1)B	88.52(13)	N(1)A–Mn(1)–N(1)B	91.48(13)

Relevant hydrogen bonds:

	D–H	H···A	D···A	D–H···A
N3–H31···O2 [−1/2 + x, −1/2 + y, z]	0.88	2.10	2.855(6)	143

$A = -x + 1, -y + 1, -z + 1$, $B = -x + 1, y, -z + 1$.

nitrogen atoms of four different dca molecules with a Mn–N distance of 2.217(2) Å and two oxygen atoms of two *trans*-ethanol molecules with a Mn–O distance of 2.216(3) Å. The Mn–Mn distance is 7.506. A hydrogen-bonding network is formed by the hydrogen atom of the nitrile nitrogen atom of the bridging dca molecule to an oxygen atom of a neighbouring ethanol molecule with a N3···O2 distance of 2.855(6) Å. Further details of the hydrogen bonding are listed in Table 2. This compound **1** can be considered as an isomer of the compound $\{[Mn(dca)_2(C_2H_5OH)_2]\ ((CH_3)_2CO)\}_n$ [5c]; however, this last compound does form a sheet like structure and, due to the fact that an acetone molecule is present in the lattice, has a different hydrogen bond structure.

3.1.2. Crystal structure of $[Mn(dca)_2(ampym)_2]_n$ (2)

A plot showing the numbering scheme is given in Fig. 2 and selected bond distances and angles are given in Table 3.

The structure of **2** contains 1D linear chains with double-bridged $\mu_{1,5}$-bridging dca molecules. The geometry of the Mn ion is octahedral and the octahedron is formed by four nitrogen atoms of four different dca anions with a Mn–N distance of 2.2193(13) Å and two nitrogen atoms of two *trans*-ampym molecules with a Mn–N distance of 2.3191(18) Å. The Mn–Mn distance is 7.580 Å. A hydrogen-bonding network is formed by the hydrogen atom of an amino nitrogen atom of the ampym ligand to a nitrile nitrogen atom of a neighbouring dca molecule with a N···N distance of 3.303(3) Å. The crystal lattice is further stabilised by an H-bonding system (Watson-Crick type) between the amino nitrogen N7 and the uncoordinated pyrimidine nitrogen atom N3 of a neighbouring ampym ligand (N3···N7 3.085(3) Å). A similar H-bonding pattern was reported earlier for compounds containing ampym as a ligand [7]. Furthermore some weak intramolecular H-bonds occur, and more details are given in Table 2.

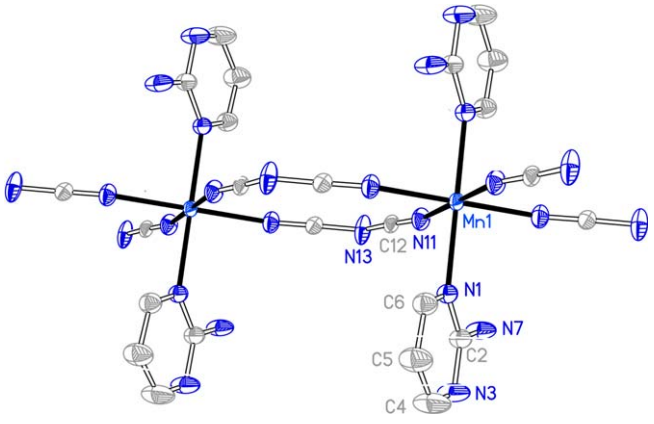

Fig. 2. Atomic displacement plot (50% probability) of structure $[Mn(dca)_2(ampym)_2]_n$ (**2**). H atoms are omitted for clarity.

3.2. Infrared spectra

Both compounds exhibit a strong absorption in the 2370–2150 cm^{-1} region corresponding to the modes of vibration of dca anion. These bands are characteristic of the $\nu_{s(C-N)} + \nu_{as(C-N)}$ and $\nu_{(C\equiv N)}$ vibrations, for which the first band is diagnostic for the metal binding mode [8]. In compound **1**, the bands are observed at 2290, 2248 and 2178 cm^{-1} for a freshly prepared sample. After staying in open air for a short time compound **1** decomposes into $Mn(dca)_2$ and IR vibration are observed at 2363, 2338, 2294, 2258 and 2188 cm^{-1}, which compare to observations made in the literature [5c]. Compound **2** exhibits IR bands similar as compound **1** at 2305, 2245 and 2172 cm^{-1}. The observed IR bands are in agreement with the literature for coordinated dca and ampym ligands [8].

3.3. Magnetic properties

Due to the decomposition of compound **1** (see Section 2), only from compound **2** an EPR spectrum and magnetic susceptibility measurements could be obtained. The EPR spectrum of compound **2**, measured as a polycrystalline powder at RT, shows an isotropic very broad signal centred at $g = 2.01$, in accordance to observations in the literature [5f].

The magnetic susceptibility of a powdered sample **2** was measured from 5 to 300 K. The temperature dependence of $\chi_M T$ versus T is shown in Fig. 3. The $\chi_M T$ value at 300 K is 4.266 $cm^3\ K\ mol^{-1}$, a value which is closed to the value expected for one isolated manganese(II) ion of spin $S = 5/2$ ($\chi_M T = 4.375\ cm^3\ K mol^{-1}$), with g equal to 2. This value stays almost constant till about 50 K, from which it slowly decreases to 2.734 $cm^3\ K\ mol^{-1}$ at 5 K. The behaviour is indicative for a weak antiferromagnetic coupling between Mn(II) ions. The variable temperature magnetic susceptibility data follow the Curie-Weiss law with $\Theta = -2.9$ K and $C = 4.309\ cm^3\ K\ mol^{-1}$.

Table 3
Selected bond lengths (Å) and angles (°) for $[Mn(dca)_2(ampym)_2]_n$ (**2**)

Mn(1)–N(1)	2.3191(18)	Mn(1)–N(11)	2.2193(13)
Mn(1)–Mn(1)A	7.580(3)		
N(11)–Mn(1)–N(11)B	87.31(7)	N(11)–Mn(1)–N(11)C	92.69(7)
N(11)A–Mn(1)–N(1)A	91.50(5)	N(11)–Mn(1)–N(1)A	88.50(5)

Relevant hydrogen bonds:

	D–H	H···A	D···A	D–H···A
N3–H3A···N7 [$-x$, $-1-y$, z]	0.88	2.21	3.085(3)	180
N7–H7A···N3 [$-x$, $-1-y$, z]	0.88	2.21	3.085(3)	178
N7–H7B···N13 [$-x$, y, $1/2-z$]	0.88	2.60	3.303(3)	138

$A = -x+1/2, -y+1/2, -z+1$; $B = -x+1/2, -y+1/2, z$; $C = x, y, -z+1$.

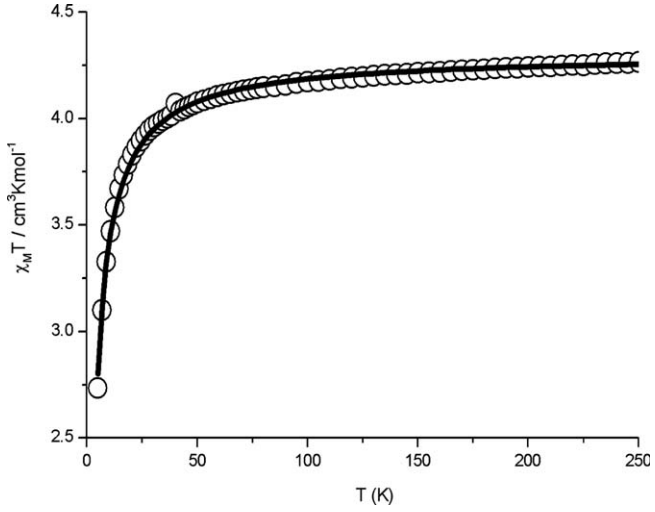

Fig. 3. A plot of the temperature dependence of χ_M. T vs. T for compound **2**. The solid line represents the calculated curve for $g = 2.00$ and $J = -0.22\ cm^{-1}$ (see text).

The magnetic susceptibility can be described using the 1D antiferromagnetic chain model for classical $S = 5/2$ spins derived by Fischer from the Heisenberg model [9], with the Hamiltonian used: $H = -J\sum S_i S_{i+1}$, where J is the magnetic exchange coupling between two adjacent paramagnetic metal ions. The best fit parameters obtained were $J = -0.22\ cm^{-1}$, $g = 2.00$ with $R = 1.2 \times 10^{-4}$ (see solid line in Fig. 3). The large Mn–Mn distance agrees with the weak magnetic exchange.

4. Conclusions

Two new polymeric Mn(II) compounds with doubly bridged $\mu_{1,5}$-dca molecules which forms an 1D array. The magnetic interaction of compound (**2**) is very weakly antiferromagnetic. In Table 4 a number of related relevant compounds together with their magnetic properties are presented. As can be seen from this table in all compounds the antiferromagnetic interaction is very weak, clearly due to the fact that the Mn–Mn distance is large (about 7.5 Å) and no serious overlap of the magnetic metal orbitals can take place via the dca ligands. The same kind of weak interaction ($J < 1\ cm^{-1}$) is also observed for a number of polymeric dca-bridged Cu(II) compounds [8c].

5. Supplementary material

Crystallographic data (excluding structure factors) for the structure reported in this paper have been deposited with the Cambridge Crystallographic Data Centre as supplementary publication nos. CCDC-284104 and 284105, for compounds **1** and **2**, respectively. Copies of this information can be obtained free of charge from The Director, CCDC, 12, Union Road, Cambridge CB2 1EZ, UK (fax:

Table 4
Magnetic results of relevant Mn(II) polymeric bis-dca-bridged compounds

Compound[a]	Mn–Mn distance (Å)	Θ (K)	J (cm^{-1})	Ref.
$[Mn(dca)_2(pdz)_2]_n$	7.432	[b]	−0.75(1)	[5f]
$[Mn(dca)_2(py)_2]_n$	7.5212(3)	−2.4	−0.12	[5b,5c]
$[Mn(dca)_2(CH_3OH)_2]_n$	7.481(1)	−2.0	−0.12	[5c]
$[Mn(dca)_2(DMF)_2]_n$	7.4907(4)	−2.1	−0.12	[5c]
$\{[Mn(dca)_2(H_2O)_2]\cdot 2\ Me_4pyz\}_n$	7.713	−1.35	−0.08	[5g]
$[Mn(dca)_2(pyr)_2]_n$	7.538	−2.5	−0.8	[5e]
$[Mn(dca)_2(2,4'\text{-bpy})_2]_n$	7.525	−1.96	[b]	[5a]
$\{[Mn(dca)_2(NITpPy)_2](NITpPyr)\}_n$	7.368	−0.7	[b]	[5d]
$[Mn(dca)_2(pic)_2]_n$	7.457(1)	[b]	−0.33	[3e]
$[Mn(dca)_2(1\text{-Mebta})_2]_n$	7.468	[b]	−0.15	[5h]
$[Mn(dca)_2(ampym)_2]_n$	7.580(3)	−2.9	−0.22	this work

[a] pdz, pyridazine; py, pyridine; Me_4pyz, tetramethylpyrazine; pyr, 2-pyrrolidone; 2,4′-bpy, 2,4′-bipyridine; NITpPyr, 2-(4-pyridil)-4,4,5,5-tetramethylimidazoline-1-oxyl-3-oxide; pic, 4-picoline; 1-Mebta, 1-methylbenzotriazole.
[b] Not given.

+44 1223 336033; e-mail: deposit@ccdc.cam.ac.uk or http://www.ccdc.cam.ac.uk).

Acknowledgement

The work described in the present paper has been supported by the Leiden University Study group WFMO (Werkgroep Fundamenteel MaterialenOnderzoek) and the Council for Chemical Sciences of the Netherlands Organisation for Scientific Research (CW-NWO). Part of the work has been supported financially by the Graduate Research School Combination "Catalysis".

References

[1] (a) J. Kohout, L. Jäger, M. Hvastijová, J. Kožíšek, J. Coord. Chem. 51 (2000) 169, and references cited therein;
(b) J.S. Miller, J.L. Manson, Acc. Chem. Res. 34 (2001) 563;
(c) S.R. Batten, K.S. Murray, Coord. Chem. Rev. 246 (2003) 103, and references cited therein.

[2] (a) U. Geiser, A.M. Kini, H.H. Wang, M.A. Beno, J.M. Williams, Acta Cryst. C47 (1991) 190;
(b) H. Yamochi, T. Nakamura, T. Komatsu, N. Matsukawa, T. Inoue, G. Saito, T. Mori, M. Kusunoki, K. Sakaguchi, Solid State Commun. 82 (1992) 101.

[3] (a) S. Konar, S. Dalai, P.S. Mukherjee, M.G.B. Drew, J. Ribas, N.R. Chaudhuri, Inorg. Chim. Acta 358 (2005) 957, and references cited therein;
(b) G.-Y. Hsu, C.-W. Chen, S.-C. Cheng, S.-H. Lin, H.-H. Wei, C.-J. Lee, Polyhedron 24 (2005) 487;
(c) H.-L. Sun, S. Gao, B.-Q. Ma, G. Su, S.R. Batten, Cryst. Growth Design 5 (2005) 268, and references cited therein;
(d) M. Du, X.-J. Zao, S.R. Batten, J. Ribas, Cryst. Growth Design 5 (2005) 901, and references cited therein;
(e) D. Ghoshal, A.K. Ghosh, J. Ribas, E. Zangrando, G. Mostafa, T.K. Maji, N.R. Chaudhuri, Cryst. Growth Design 5 (2005) 941, and references cited therein;
(f) G.A. van Albada, I. Mutikainen, U. Turpeinen, J. Reedijk, Acta Cryst. E57 (2001) m421;
(g) H. Kooijman, A.L. Spek, G.A. van Albada, J. Reedijk, Acta Cryst. C58 (2002) m124;
(h) A. Mohamadou, G.A. van Albada, H. Kooijman, B. Wieczorek, A.L. Spek, J. Reedijk, New J. Chem. 27 (2003) 983;
(i) G.A. van Albada, I. Mutikainen, U. Turpeinen, J. Reedijk, Acta Cryst. E59 (2003) m889;
(j) H. Kooijman, A.L. Spek, G.A. van Albada, P. Gamez, J. Reedijk, Acta Cryst. C60 (2004) m51.

[4] (a) J. Mroziński, J. Kohout, M. Hvastijová, Polish J. Chem. 71 (1997) 883;
(b) A. Escuer, F.A. Mautner, N. Sanz, R. Vincente, Inorg. Chem. 39 (2000) 1668.

[5] (a) C.-M. Liu, D.-Q. Zhang, D.-B. Zhu, X. Jin, Trans. Met. Chem. 28 (2003) 336;
(b) J.L. Manson, A.M. Arif, C.D. Incarvito, L.M. Liable-Sands, A.L. Rheingold, J.S. Miller, J. Solid State Chem. 145 (1999) 369;
(c) S.R. Batten, P. Jensen, C.J. Kepert, M. Kurmoo, B. Moubaraki, K.S. Murray, D.J. Price, J. Chem. Soc., Dalton Trans. 2987 (1999);
(d) I. Dasna, S. Golhen, L. Ouahab, O. Pena, J. Guillevic, M. Fettouhi, J. Chem. Soc., Dalton Trans. 129 (2000);
(e) B.-W. Sun, S. Gao, B.-Q. Ma, Z.-M. Wang, Inorg. Chem. Commun. 4 (2001) 72;
(f) A. Escuer, F.A. Mautner, N. Sanz, R. Vicente, Inorg. Chim. Acta 340 (2002) 163;
(g) A.M. Kutasi, S.R. Batten, A.R. Harris, B. Moubaraki, K.S. Murray, Aust. J. Chem. 55 (2002) 311;
(h) L.F. Jones, L. O'Dea, D.A. Offermann, P. Jensen, B. Moubaraki, K.S. Murray, Polyhedron 25 (2006) 360.

[6] (a) Nonius, COLLECT, Nonius BV, Delft, The Netherlands, 2002;
(b) G.M. Sheldrick, SHELXS97 Program for Crystal Structure Determination, University of Göttingen, Germany, 1997;
(c) G.M. Sheldrick, SHELXL-97-2 Program for Crystal Structure Refinement, University of Göttingen, Germany, 1997.

[7] (a) G.A. van Albada, M.E. Quiroz-Castro, I. Mutikainen, U. Turpeinen, J. Reedijk, Inorg. Chim. Acta 298 (2000) 221;
(b) G.A. van Albada, W.J.J. Smeets, A.L. Spek, J. Reedijk, J. Chem. Cryst. 30 (2000) 11;
(c) G.A. van Albada, I. Mutikainen, U. Turpeinen, J. Reedijk, Polyhedron 23 (2004) 993.

[8] (a) S. Martín, M.G. Barandika, J.I. Ruiz de Larramendi, R. Cortés, M. Font-Bardia, L. Lezama, Z.E. Serna, X. Solans, T. Rojo, Inorg. Chem. 40 (2001) 3687;
(b) J.-H. Luo, M.-C. Hong, R. Cao, Y.-C. Liang, Y.-J. Zhao, R.-H. Wang, J.-B. Weng, Polyhedron 21 (2002) 893;
(c) J. Carranza, J. Sletten, F. Lloret, M. Julve, Inorg. Chim. Acta 357 (2004) 3304.

[9] (a) M.E. Fischer, Am. J. Phys. 32 (1964) 343;
(b) O. Kahn, Molecular Magnetism, VCH Publishers, New York, 1993, p. 258.

group [2]. The azide ion usually bridges the metal centers in end-on, end-to-end or a combination of both modes to yield dinuclear, tetranuclear, cubane, 1-D, 2-D and 3-D compounds [3–11]. Focusing on Cu(II) systems, both type of bridges can be either symmetrical or unsymmetrical due to active Jahn–Teller effects on the metal centre which make the structures even more versatile [12]. The magnetic exchange via the azide bridge can be ferro- or antiferromagnetic depending upon the bridging mode and bonding parameters. For example, when the azido ligand bridges two Cu(II) ions in an end-on, basal–basal manner, the nature of the exchange coupling changes from ferromagnetic to antiferromagnetic when the Cu–N–Cu angle is around 108° [13]. On the other hand, for basal–apical coordination, no such theoretical calculation has been reported. The literature data for this bridging mode are limited and the J values with regard to Cu–N–Cu angles are so dispersed that no meaningful correlation can be done [14–27]. Therefore, new complexes need to be prepared with this kind of coordination to be able to draw clearer magneto-structural conclusions. A tridentate blocking ligand and one azide ion should be an ideal combination to produce such complexes. Recently, we have found that a group of mononegative N,N,O donor tridentate Schiff base ligands indeed yielded double EO azido bridged basal–apical dimers in all cases [28]. Interestingly, it was found that very subtle differences in the H-bonding network and structural parameters could be responsible for drastic changes in the magnetic behavior of such complexes.

In order to introduce variation in such complexes, we intend to use neutral N,N,N donor tridentate Schiff base blocking ligands. As in the case of NNO donor ligands [28], we want to keep one of the primary amine groups of the diamine free to allow it to form H-bonds. In this paper, we describe a very easy and convenient method to synthesize four new complexes of the general formula $CuL(N_3)(ClO_4)$, where L^1–L^4 are four different monocondensed, tridentate N,N,N donor Schiff base ligands (Scheme 1), their crystal structures and magnetic properties.

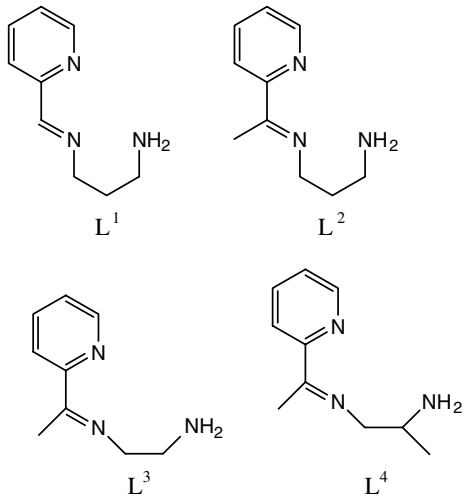

Scheme 1.

2. Experimental

All chemicals were of reagent grade, purchased from commercial sources and used without further purification.

Caution!!! All the complexes contain azide and perchlorate groups and are potentially explosive. Only a small amount of the material should be prepared and it should be handled with care.

2.1. Preparations

2.1.1. Synthesis of the ligands N^1-pyridin-2-yl-methylene-propane-1,3-diamine (L^1), N^1-(1-pyridin-2-yl-ethylidene) propane-1,3-diamine (L^2), N^1-(1-pyridin-2-yl-ethylidene) ethane-1,2-diamine (L^3) and N^1-(1-pyridin-2-yl-ethylidene) propane- 1,2-diamine (L^4)

All four tridentate Schiff base ligands L^1, L^2, L^3 and L^4 were synthesized in a similar way by refluxing the respective diamine (10 mmol) with pyridine-2-carboxaldehyde or 2-acetyl pyridine (10 mmol) in methanol solution (20 ml) for ca. 3 h. The ligands were not isolated. The methanolic solutions were used for the syntheses of the complexes.

L^1 and L^2 were synthesized by refluxing 1,3-propanediamine (10 mmol, 0.84 cm^3) with pyridine-2-carboxaldehyde (10 mmol, 0.98 cm^3) and 2-acetylpyridine (10 mmol, 1.2 cm^3), respectively. L^3 and L^4 were synthesized by refluxing 1,2-ethanediamine (10 mmol, 0.67 cm^3) and 1,2-propanediamine (10 mmol, 0.76 cm^3), respectively, with 2-acetylpyridine (10 mmol, 1.2 cm^3).

2.1.2. Synthesis of complexes $[(CuL^1N_3)_2](ClO_4)_2$ (**1**), $[(CuL^2N_3)_2](ClO_4)_2$ (**2**), $[CuL^3(N_3)(ClO_4)]_n$ (**3**) and $[CuL^4(\mu\text{-}1,1\text{-}N_3)(\mu\text{-}1,3\text{-}N_3)(ClO_4)]_n$ (**4**)

To prepare complexes **1**, **2**, **3** and **4**, a methanol solution (20 ml) of copper(II) perchlorate hexahydrate (10 mmol, 3.7 g) was added to the ligand solution (10 mmol) of HL^1, HL^2, HL^3 and HL^4, respectively, and refluxed for 1 h. A solution of NaN_3 (10 mmol, 0.37 g) in methanol was then added to it with constant stirring. For complex **1** a deep blue precipitate separated out immediately and was collected by filtration. Diffraction quality single crystals were obtained after a few days by slow evaporation of a dark green acetonitrile solution of the compound in open atmosphere. In the case of complex **2**, there was no immediate separation of a compound. Crystalline compounds started to separate after ca. 2 h and were collected by filtration after ca. 5 h. Single crystals suitable for X-ray diffraction were obtained from the filtrate by slow evaporation in a refrigerator. For both complexes **3** and **4**, deep blue solids separated out immediately after addition of azide and were separated by filtration. Deep blue parallelepiped-shaped single crystals of **3** suitable for X-ray diffraction were obtained from a CH_3CN solution of the compound by slow evaporation in air. For complex **4** deep

Table 1
Crystal data and refinement details of complexes **1**, **2**, **3** and **4**

Compound	**1**	**2**	**3**	**4**
Formula	$C_{18}H_{26}N_{12}O_8Cl_2Cu_2$	$C_{20}H_{30}N_{12}O_8Cl_2Cu_2$	$C_9H_{13}N_6O_4ClCu$	$C_{20}H_{30}N_{12}O_8Cl_2Cu_2$
Formula weight	736.51	764.56	368.25	764.56
T (K)	293	293	293	293
Space group	$C2/c$	$P\bar{1}$	$P21/n$	$C2/c$
Crystal system	monoclinic	triclinic	monoclinic	monoclinic
a (Å)	19.64(2)	8.686(9)	13.148(14)	41.45(4)
b (Å)	8.995(9)	10.442(12)	7.336(10)	10.602(12)
c (Å)	16.855(17)	17.063(19)	15.079(17)	15.442(17)
α (°)	90	84.442(10)	90	90
β (°)	104.158(10)	88.003(10)	100.852(10)	111.139(10)
γ (°)	90	80.067(10)	90	90
V (Å^3)	2887(5)	1517(3)	1428(3)	6329(12)
Z	4	2	4	8
D_{calc} (g/cm^3)	1.695	1.674	1.713	1.605
μ (mm^{-1})	1.7	1.6	1.7	1.6
F(000)	1496	780	748	3120
Total reflections	5533	9665	6737	10737
Unique reflections	2614	5347	2665	5227
Observed data ([$I > 2\sigma(I)$])	2322	4251	2450	3632
Number of parameters refined	191	400	192	387
R_{int}	0.032	0.033	0.037	0.085
R indices [$I > 2\sigma(I)$]	$R_1 = 0.0557$, $wR_2 = 0.1347$	$R_1 = 0.0523$, $wR_2 = 0.1226$	$R_1 = 0.0451$, $wR_2 = 0.1315$	$R_1 = 0.1120$, $wR_2 = 0.2010$

blue parallelepiped-shaped single crystals suitable for X-ray diffraction were grown in a CH_3CN solution of the compound by a slow diffusion of ether in a sealed tube.

Complex **1**: (Yield: 5.30 g, 72%). *Anal.* Calc. for $C_{18}H_{26}N_{12}O_8Cl_2Cu_2$ (736.50): C, 29.32; H, 3.56; N, 22.82. Found: C, 29.4; H, 3.3; N, 22.2%. λ_{max} (nm) [ε_{max} (dm^3 mol^{-1} cm^{-1})] (acetonitrile) 603 (294).

Complex **2**: (Yield: 5.33 g, 69.8%). *Anal.* Calc. for $C_{20}H_{30}N_{12}O_8Cl_2Cu_2$ (764.56): C, 31.39; H, 3.92; N, 21.97. Found: C, 31.5; H, 4.0; N, 21.9%. λ_{max} (nm) [ε_{max} (dm^3 mol^{-1} cm^{-1})] (acetonitrile) 600 (101).

Complex **3**: (Yield: 2.31 g, 63%). *Anal.* Calc. for $C_9H_{13}N_6O_4ClCu$ (368.25): C, 29.33; H, 3.53; N, 22.81. Found: C, 29.4; H, 3.6; N, 22.9%. λ_{max} (nm) [ε_{max} (dm^3 mol^{-1} cm^{-1})] (acetonitrile) 587 (282).

Complex **4**: (Yield: 5.81 g, 76%). *Anal.* Calc. for $C_{20}H_{30}N_{12}O_8Cl_2Cu_2$ (764.56): C, 31.39; H, 3.92; N, 21.97. Found: C, 31.6; H, 3.8; N, 22.1%. λ_{max} (nm) [ε_{max} (dm^3 mol^{-1} cm^{-1})] (acetonitrile) 606 (138).

2.2. Physical measurements

Elemental analysis (carbon, hydrogen and nitrogen) was performed using a Perkin–Elmer 240C elemental analyzer. IR spectra in KBr (4500–500 cm^{-1}) were recorded using a Perkin–Elmer RXI FT-IR spectrophotometer. Electronic spectra in acetonitrile (1200–350 nm) were recorded in a Hitachi U-3501 spectrophotometer. The magnetic measurements were carried out in the "Servei de Magnetoquimica (Universitat de Barcelona)" on polycrystalline samples (20 mg) with a Quantum Design SQUID MPMSXL susceptometer in the temperature range of 2–300 K and the magnetic field was 1 T. Magnetization measurements were made in the same SQUID at 2 K. EPR spectra were recorded on powder samples at X-band frequency with a Bruker 300E automatic spectrometer, varying the temperature between 4 and 300 K.

2.3. X-ray crystallography

Data for all four crystals were measured with Mo Kα radiation using the MAR research Image Plate System. The crystals were positioned at 70 mm from the Image Plate. 100 frames were measured at 2° intervals with a counting time of 2 min. Data analysis was carried out with the XDS program [29]. The structures were solved using direct methods with the SHELX-86 program [30]. Non-hydrogen atoms were refined with anisotropic thermal parameters. The hydrogen atoms were included in geometric positions and given thermal parameters equivalent to 1.2 times those of the atom to which they were attached. Empirical absorption corrections were carried out using DIFABS [31]. The structures were refined on F^2 using SHELXL [32]. A summary of the crystallographic data are given in Table 1. The poor quality of the crystals of **4** gave rise to misshapen large spots in the diffraction pattern which in turn led to high R values. The crystallographic illustrations were prepared using ORTEP-3 [33].

3. Results and discussion

3.1. Syntheses

All four Schiff base ligands and their complexes were synthesized in a very facile and essentially identical way. The respective diamine and the carbonyl compound were

mixed in a 1:1 stoichiometric ratio in methanol and refluxed. The methanolic solution of the Schiff base ligand thus prepared was added to a methanolic solution of copper perchlorate, refluxed for 1 h and then a stoichiometric amount of sodium azide was added when the desired complexes were separated. It is to be noted that there is a possibility that the diamines may undergo condensation at both ends to produce a tetradentate di-Schiff base. We, therefore, repeated the syntheses several times and found that as long as the stoichiometry of the diamine and carbonyl compound are strictly maintain as 1:1, no compound other than that of monocondensed tridentate ligand is separated. If the amount of carbonyl compound is increased, however, a compound of the tetradentate ligands starts to separate together with the desired complex. A similar approach was adopted earlier for the syntheses of mononuclear Zn(II) and Ni(II) complexes of N_3-donor tridentate Schiff base ligands [34].

The four tridentate Schiff base blocking ligands are very similar; all the complexes have the same general formula $CuL(N_3)(ClO_4)$, yet the bridging topologies are drastically different. The complexes of the ligands L^1 and L^2 are double azido bridged dimers, that of L^3 is a 1-D chain bridged by perchlorate ions and the complex of L^4 is a 1-D chain with alternate single EO and EE azido bridges. Two 1-D chains of complex **3** are linked by H-bonds, which play all important roles in magnetic interactions. The structure of the complex of L^4 is very interesting as the occurrence of alternate single EO and EE bridges between two metal ions is very rare. To our knowledge, only two such compounds have been reported to date and the magnetic interactions mediated by the bridges in the two complexes are opposite to each other [25,26].

3.2. IR and electronic spectra

The most important aspects concerning the infrared spectra of the four compounds **1**, **2**, **3** and **4** deal with the possibility of characterizing the different coordination modes for the azido ligand to a transition metal, which is usually detected by the intense IR band due to $\nu_{as}(N_3)$ that occurs above 2000 cm^{-1}. In general, it appears above 2055 cm^{-1} for the bridging azide and below 2055 cm^{-1} for the terminal ion [13a]. In the same way, the presence of the $\nu_s(N_3)$ vibration mode in the region of 1360–1280 cm^{-1} is related to the existence of the terminal or end-on bridging azide, not appearing for the end-to-end bridging mode [35].

The two complexes **1** and **2** show only a single absorption band, consistent with the presence of only one type of azide ion in the structures. However, all of them appear at lower frequencies viz. 2044 and 2047 cm^{-1}, respectively, than usually expected for μ_2-1,1-azide bridging and this may be attributed to the highly asymmetrical nature of the azide bridges in the present complexes (vide structure description). For compound **3**, the $\nu_{as}(N_3)$ stretching vibration of the azido group appears at 2054 cm^{-1} and the band at 1320 cm^{-1} is attributed to the $\nu_s(N_3)$ vibration mode corresponding to the presence of terminal azido ligand as confirmed by the crystal structure for the compound **3**. Complex **4** shows a strong absorption band at 2062 cm^{-1}. Although the compound contains two types of azide bridges the appearance of single peak can be attributed to the very weak coordination mode of the EE bridge and asymmetric nature of the EO bridge.

All four complexes show two bands above 3000 cm^{-1} at 3309 and 3263 cm^{-1} for complex **1**, 3322 and 3263 cm^{-1} for complex **2**, 3310 and 3246 cm^{-1} for complex **3** and 3285 and 3127 $cm^{-1}$for complex **4**. These bands can be attributed to the ν_{NH_2} frequency. The band corresponding to the azomethine (C=N) group is distinct in all the four complexes; it occurs at 1599, 1593, 1583 and 1596 cm^{-1} for complexes **1**, **2**, **3** and **4**, respectively. Concerning the ClO_4^- anions, the ν_3 mode at 1098, 1088 and 1095 cm^{-1} for **1**, **2** and **4**, respectively, is somewhat broadened but the ν_4 band at 620, 619 and 621 cm^{-1}, respectively, is devoid of any splitting and are consistent with the IR-active normal modes for T_d symmetry suggesting that these anions are not coordinated to the copper atoms as substantiated by the crystal structures. The splitting of the band at 1092 cm^{-1} for **3** is indicative of coordinated perchlorate ions.

The electronic spectra of **1**, **2** and **4** in acetonitrile solution display a single absorption band 603, 600 and 606 nm, respectively. The positions of these bands are consistent with the observed square-pyramidal geometry around the copper centers [36]. The octahedral nature of complex **3** is evident by the appearance of a single broad peak at 587 nm, a position somewhat lower than the square-pyramidal geometry [37].

3.3. Description of the structures

3.3.1. Complexes $[(CuL^1N_3)_2](ClO_4)_2$ (1) and $[(CuL^2N_3)_2](ClO_4)_2$ (2)

The structure determination reveals that both complexes **1** and **2** consist of a discrete, centrosymmetric dinuclear complex cation $[(CuLN_3)_2]^{2+}$ and two non-coordinated perchlorate anions. In complex **2** there are two independent centrosymmetric dimers (A and B) with equivalent geometry. A view of the complex species is given in Fig. 1 for complex **1** (complex **2** has very similar molecular structure: Figure S1 for dimer A, Supporting Information). Selected bond lengths and angles for **1** and **2** are summarized in Tables 2 and 3, respectively. In the dimers of both complexes **1** and **2**, two distorted square-pyramidal copper(II) centers are bridged by the two centrosymmetrically related azide ions in asymmetric, basal–apical, end-on fashion leading to relatively small Cu···Cu distances (3.285(3) Å for **1**). Within the dimeric units each of the two trigonally distorted square-pyramidal copper(II) centers is coordinated equatorially by three ligating nitrogen atoms, N(1), N(2) and N(3), of the corresponding tridentate Schiff base ligand and a nitrogen atom, N(11), of one of the bridging

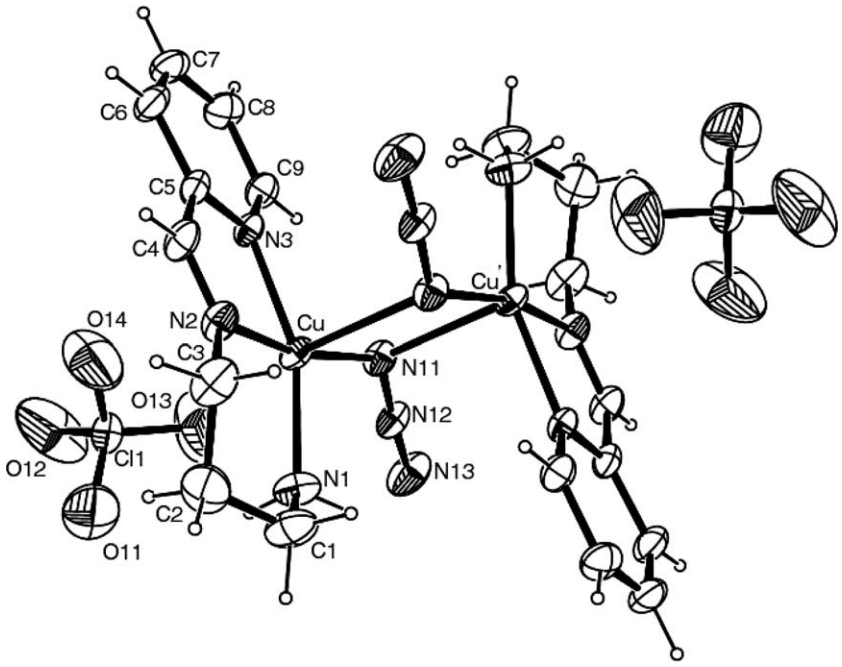

Fig. 1. ORTEP-3 view of complex **1** (30% thermal ellipsoids). Atoms marked with a prime are transformed by symmetry element $3/2 - x$, $3/2 - y$, $2 - z$.

Table 2
Selected bond lengths (Å) and angles (°) for complexes **1** and **3**

	1	**3**
Cu–N1	1.994(6)	2.013(4)
Cu–N2	2.003(4)	1.957(4)
Cu–N3	2.030(4)	2.020(5)
Cu–N11	1.988(4)	1.955(5)
Cu–N11\$1′	2.409(5)	
Cu–O11		2.430(5)
Cu–O13*		2.633(5)
N1–Cu–N2	93.2(2)	83.6(1)
N2–Cu–N3	80.6(2)	79.9(1)
N1–Cu–N3	159.4(2)	163.6(1)
N1–Cu–N11	96.5(2)	98.7(2)
N1–Cu–N11\$1′	104.3(2)	
N2–Cu–N11	167.7(2)	174.4(1)
N2–Cu–N11\$1′	86.5(2)	
N3–Cu–N11	92.7(2)	97.7(2)
N3–Cu–N11\$1′	94.9(1)	
N11–Cu–N11\$1′	83.8(2)	
Cu–N11–Cu\$1′	96.2(2)	
O11–Cu–N1		89.8(2)
O11–Cu–N2		96.6(2)
O11–Cu–N3		91.9(1)
O11–Cu–N11		88.6(2)
O13*–Cu–N1		87.9(1)
O13*–Cu–N2		83.6(1)
O13*–Cu–N3		90.5(1)
O13*–Cu–N11		91.3(1)
O11–Cu–O13*		177.6(2)

Symmetry elements \$1′: $3/2 - x$, $3/2 - y$, $2 - z$ for complex **1**.
'*' denotes different asymmetric unit along the *b*-axis for complex **3**.

azides; this comprises the basal plane. A second nitrogen atom, N(11)′, from the centrosymmetrically related bridging azide coordinates axially at a rather long distance furnishing an elongated square-pyramidal $(4 + 1)$ geometry for each copper(II) center in the two complexes.

In the two crystallographically independent dimers of **2** there are minor variations in their bond lengths and bond angles. The intradimeric Cu···Cu distances are 3.244(3) and 3.335(3) Å in A and B, respectively. The axial Cu–N distances, 2.318(5) and 2.477(5) Å and bridging Cu–N–Cu angles, 97.5(2)° and 83.8(2)°, respectively, for dimer A and B are considerably different. As usual for a square-pyramid structure, the copper atom for each model is slightly pulled out of the mean squares plane towards the apical donor atom at a distance 0.085(1) Å, 0.194(1) Å and 0.015(1) Å in **1**, A and B of **2**, respectively. The addition parameter (τ) for complex **1** is 0.14; but these values are 0.33 and 0.01 for dimer A and B, respectively, for complex **2** indicating that the distortion towards trigonal-bipyramidal geometry is more pronounced for dimer A [38]. The six-membered chelate ring within each dimer incorporating the trimethylene fragment from the starting diamine assumes a twist-boat conformation with puckering parameters [39] $q = 0.515(7)$, 0.535(6) and 0.520(6) Å, $\phi = 14.4(16)°$, 4.1(2)° and 12.5(9)° and $\theta = 154.1(7)°$, 159.3(5)° and 142.1(6)°, respectively, in complex **1** and in dimer A and B of complex **2**.

The bridging Cu_2N_2 network is exactly planar as dictated by symmetry. Due to formation of basal–apical μ_2-1,1-N_3 bridging, the bridging Cu–N bond lengths are significantly different ($\Delta d = 0.58$, 0.33 and 0.49 for complex **1** and for A and B of **2**, respectively). The bridging N_3^- anions are quasi-linear; the N–N–N angles are 175.9(5)° for **1** and 177.5(6)° and 175.2(5)° for A and B of **2**, respectively.

The two crystal structures exhibit different hydrogen bonding patterns (Table 4). Perchlorate ions play a

Table 3
Selected bond lengths (Å) and angles (°) for complexes **2** and **4**

	2	4
Cu1–N1	2.016(5)	2.009(9)
Cu1–N2	1.986(5)	1.982(8)
Cu1–N3	2.011(4)	2.053(9)
Cu1–N11	1.986(5)	2.342(9)
Cu1–N11$1′	2.318(5)	
Cu1–N21		1.969(11)
Cu2–N4	1.992(4)	2.012(10)
Cu2–N5	2.016(4)	1.981(9)
Cu2–N6	2.014(4)	2.031(10)
Cu2–N21	1.982(5)	
Cu2–N21$1′	2.477(5)	
Cu2–N11		1.983(9)
Cu2–N23$1′		2.643(15)
N1–Cu1–N2	94.0(2)	82.2(3)
N2–Cu1–N3	80.7(1)	79.7(3)
N1–Cu1–N3	152.8(2)	161.1(4)
N1–Cu1–N11	92.9(2)	92.7(3)
N1–Cu1–N11$1′	100.3(2)	
N2–Cu1–N11	172.6(2)	94.8(3)
N2–Cu1–N11$1′	93.9(1)	
N3–Cu1–N11	94.3(1)	94.2(3)
N3–Cu1–N11$1′	106.7(1)	
N11–Cu1–N11$1′	82.5(2)	
Cu1–N11–Cu1$1′	97.5(2)	
N1–Cu1–N21		100.3(4)
N2–Cu1–N21		165.4(4)
N3–Cu1–N21		95.9(4)
N4–Cu2–N5	96.7(2)	83.5(4)
N5–Cu2–N6	80.3(2)	79.5(4)
N4–Cu2–N6	165.3(2)	163.0(4)
N4–Cu2–N21	94.6(2)	
N4–Cu2–N21$1′	96.3(2)	
N5–Cu2–N21	164.8(2)	
N5–Cu2–N21$1′	84.8(1)	
N6–Cu2–N21	91.3(2)	
N6–Cu2–N21$1′	97.7(2)	
N21–Cu2–N21$1′	83.8(2)	
Cu2–N21–Cu2$1′	96.2(2)	
N4–Cu2–N11		95.5(4)
N5–Cu2–N11		175.9(4)
N6–Cu2–N11		101.5(4)
N4–Cu2–N23$1′		94.4(2)
N5–Cu2–N23$1′		84.6(2)
N6–Cu2–N23$1′		85.6(2)
Cu1–N11–Cu2		131.6(4)
N11–Cu2–N23$1′		91.5(3)

Symmetry elements $1′: $1 - x$, $1 - y$, $1 - z$ for Cu1 and $-x$, $2 - y$, $-z$ for Cu2 of complex **2** and x, $-y$, $-1/2 + z$ for complex **4**.

significant role in the hydrogen bonding network. Both H(1a) and H(1b) of **1** and dimer A of **2** are involved in strong N–H···O hydrogen bonding with the perchlorate oxygen atoms giving a one-dimensional supramolecular entity. The one-dimensional structure for complex **1** is shown in Fig. 2. Dimer B of **2** does not form any such H-bonded one-dimensional structure.

3.3.2. Complex $[CuL^3(N_3)(ClO_4)]_n$ (3)

The structure of complex **3** consists of a quasi-one-dimensional infinite chain system with the repeating unit $[CuL^3N_3]^+$ bridged by perchlorate anions. The perspective view with the atom labelling scheme of the monomeric unit of $[CuL^3(N_3)(ClO_4)]_n$ is shown in Fig. 3. A view of the extended chain and the supramolecular hydrogen-bonded array of complex **3** is displayed in Fig. 4. Selected bond lengths and angles are summarized in Table 2. The copper atom is six-coordinated, being bonded to three ligating nitrogen atoms N(1), N(2) and N(3) from the tridentate Schiff base ligand L^3, another nitrogen N(11) of the terminal azide anion in the base plane and two oxygen atoms O(10) and O(13)* from two different perchlorate ions in the two apical positions. Thus, the six coordinated copper(II) center in this complex assumes a tetragonally distorted octahedron. In the complex reported here the two Cu–O distances with the perchlorate oxygen atoms are distinguishable and the bond Cu–O(10) is 2.430(5) Å whereas Cu–O(13)* is 2.633(5) Å, which may be considered as "semicoordinated" as proposed by Hathaway [40]. The azide ion is nearly linear with a N(11)–N(12)–N(13) angle of 176.0(4)°. The N–N distances within the azide ion are not equal [N(11)–N(12) = 1.198(5) Å and N(12)–N(13) = 1.151(5) Å] and the difference between them is 0.047 Å. The copper–copper repeating distance is 7.336 Å along the chain.

The pyridine ring can be considered as practically planar and the five membered chelate ring Cu–N(1)–C(1)–C(2)–N(2) has an envelope conformation on C(1) with puckering parameters [39] $q_2 = 0.418(4)$ Å and $\phi_2 = 107.2(4)°$.

An interesting feature of this complex is the joining of two neighbouring Cu-containing chain fragments via hydrogen bonds (Table 4, Fig. 4). There are two available hydrogen atoms [H(1a) and H(1b)] for hydrogen bond formation, both of which are involved in strong hydrogen bonding with the symmetry related units. H(1b) is engaged in bifurcated hydrogen bond formation with the coordinating nitrogen N(11′) of the pendant azide ion and O(11′) of the perchlorate anion from same crystallographically related unit $(2 - x, -y, -z)$. But H(1a) is involved in N–H···N hydrogen bond formation with the terminal nitrogen N(13′) of the pendant azide ion from another crystallographically related unit $(2 - x, 1 - y, -z)$. The shortest copper–copper distance between the two H-bonded chains is 5.170 Å. It is to be noted here that although there are several examples where a perchlorate ion bridges Cu^{II} centres to form one-dimensional chains [41], only one other complex has been reported to date in which a perchlorate ion bridges the Cu(II) centres in spite of the presence of a versatile bridging azide ion as a monodentate ligand [14]. In that structure, however, the linking of neighbouring chains by H-bonding, which plays a very important role in the magnetism of **3** (see magnetic studies), has not been observed.

3.3.3. Complex $[CuL^4(\mu\text{-}1,1\text{-}N_3)(\mu\text{-}1,3\text{-}N_3)(ClO_4)]_n$ (4)

An ORTEP drawing of the one-dimensional complex $[CuL^4(N_3)(ClO_4)]_n$, with the atom labelling scheme, is shown in Fig. 5. Selected bond lengths and angles are

Table 4
Hydrogen bonding distances (Å) and angles (°) for the complexes **1**, **2**, **3** and **4**

Compound	D–H···A	D–H	D···A	H···A	∠D–H···A
1	N1–H1a···O13	0.900	3.324(11)	2.791	119
	N1–H1b···O11^{i}	0.899	3.288(11)	2.540	141
2	N1–H1a···O13	0.899	3.170(8)	2.588	123
	N1–H1b···O12^{j}	0.899	3.103(7)	2.306	147
	N4–H4a···O24^{k}	0.901	3.233(10)	2.576	130
3	N1–H1a···N13^{l}	0.901	3.103(6)	2.301	148
	N1–H1b···O11^{m}	0.900	3.166(7)	2.487	132
	N1–H1b···N11^{m}	0.900	3.275(6)	2.488	146
4	N1–H1a···O12	0.901	3.10(2)	2.24	160
	N1–H1b···O21	0.900	3.38(2)	2.50	166
	N4–H4a···O21^{n}	0.898	3.28(2)	2.38	175
	N4–H4b···N21	0.901	3.082(15)	2.217	161

Symmetry elements: (i) $3/2 - x$, $5/2 - y$, $2 - z$; (j) $-x$, $1 - y$, $1 - z$; (k) $-1 - x$, $3 - y$, $-z$; (l) $2 - x$, $1 - y$, $-z$; (m) $2 - x$, $-y$, $-z$; (n) x, $-y$, $-1/2 + z$.

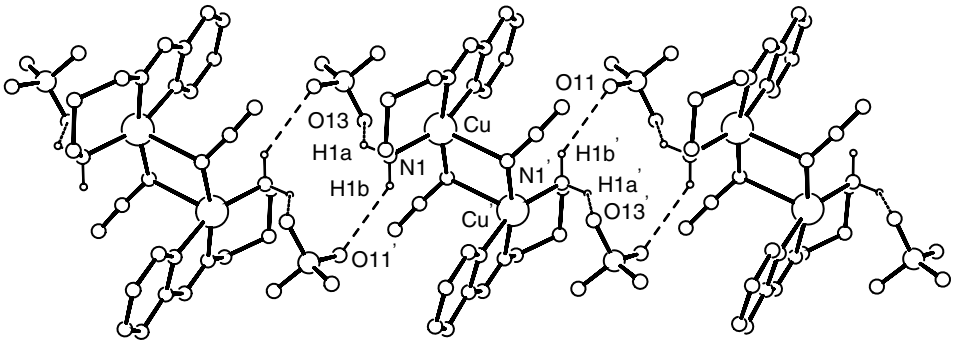

Fig. 2. Scheme of the packing (one-dimensional) in complex **1**. The intermolecular hydrogen bonds are shown as dashed lines. Atoms marked with a prime are transformed by symmetry element $3/2 - x$, $3/2 - y$, $2 - z$.

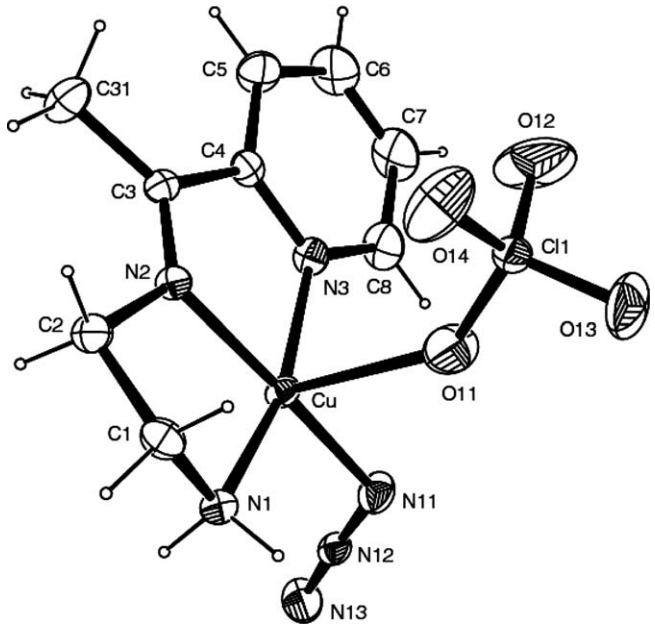

Fig. 3. ORTEP-3 view of monomeric $[CuL^{3}N_{3}(ClO_{4})]_{n}$ (**3**) with the atom numbering scheme.

summarized in Table 3. The structure determination reveals that the copper atoms are bridged singly and alternately by end-on and end-to-end azido ligands with the occurrence of a 1-D polymeric infinite chain. Two independent copper atoms Cu(1) and Cu(2), having different environments, possess distorted square-pyramidal geometries. Each copper center is linked to one neighboring copper center by an azide in an end-on fashion and another copper atom through end-to-end fashion to form the 1-D alternate chain. Cu(1) is coordinated equatorially by three ligating nitrogen atoms, N(1), N(2) and N(3), of the tridentate Schiff base ligand L^{4} and a nitrogen atom, N(21), of the end-to-end bridged azido ligand; this defines the basal plane. The apical position is occupied by one nitrogen atom N(11) of the end-on bridged azido ligand. Similarly for Cu(2), the three coordinating nitrogen atoms N(4), N(5) and N(6) of the tridentate Schiff base and one nitrogen atom N(11) of the end-on bridged azido ligand comprises the basal plane and here the apical position is occupied by the nitrogen atom N(23)′ of the another end-to-end bridged azido ligand from a crystallographically related unit. Thus, both EO and EE bridges assume an

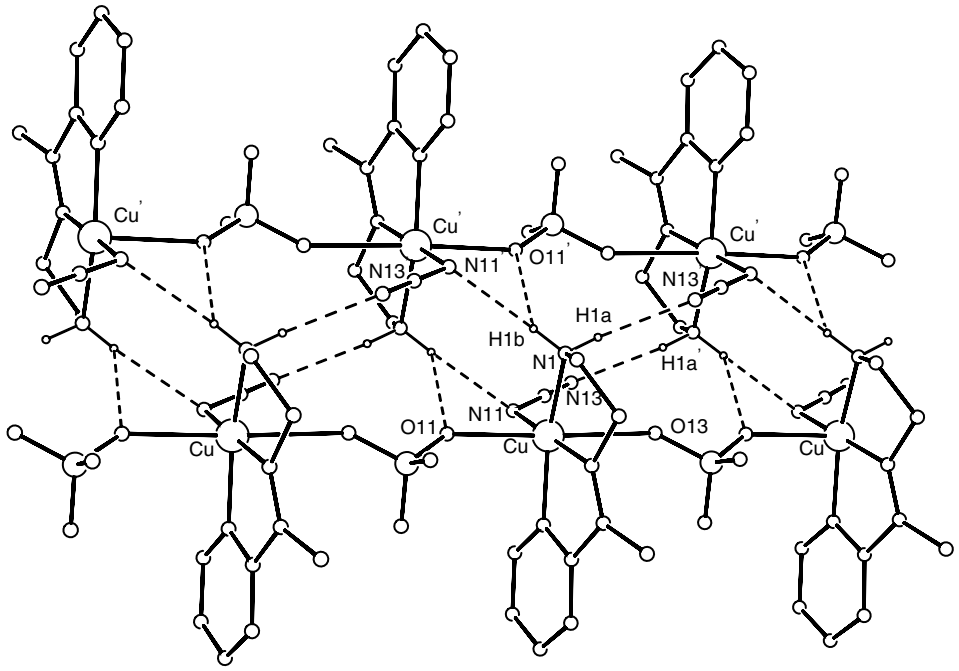

Fig. 4. Extended chain structure and two-dimensional array of $[CuL^3N_3(ClO_4)]_n$ (**3**) formed by an intermolecular hydrogen bonding network.

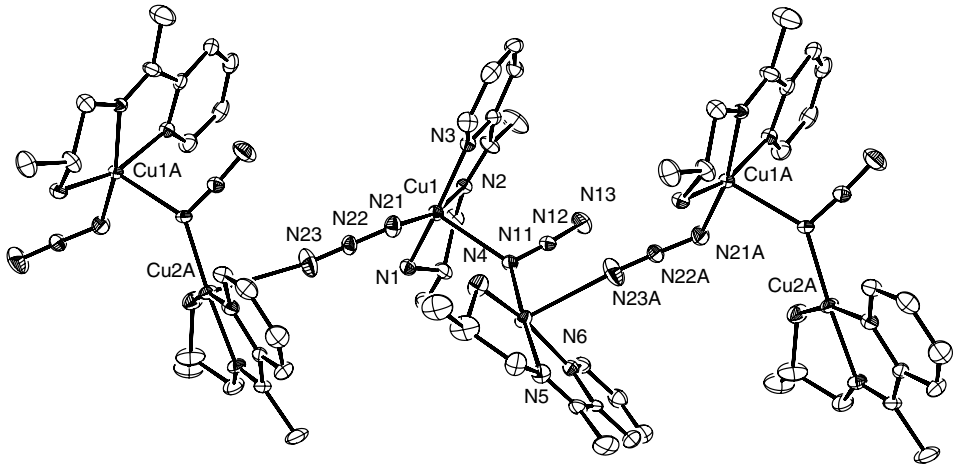

Fig. 5. ORTEP-3 diagram of $[CuL^4(\mu\text{-}1,1\text{-}N_3)(\mu\text{-}1,3\text{-}N_3)(ClO_4)]_n$ (**4**) with the atom labelling scheme, showing 30% probability thermal ellipsoids for all non-hydrogen atoms.

asymmetric apical–basal disposition between neighboring Cu(II) ions; i.e., the same azido bridge resides on the apical position of one copper but in the basal plane of the neighboring copper, with the apical Cu–N distance being significantly longer than the basal one; specially the distance Cu(2)–N(23) (2.643 Å) is very long and should be considered as semicoordinated. If it is not considered as a bond, compound **4** would be a very unusual singly EO azide bridged dimer (as substantiated by magnetic properties) with the two copper atoms having different coordination spheres – Cu(1) is five-coordinate square-pyramidal while Cu(2) is four-coordinate square planar. The Cu(1)–N(11)–Cu(2) bond angle for the end-on azido bridging mode is 131.6(4)° which is the highest among the EO bridging azides with Cu(II) reported to date. The angles of other two known singly EO bridged azides in similar alternating EE and EO bridged structures are 130.0° [25] and 116.6° [26].

The τ values are 0.07 and 0.22 for Cu(1) and Cu(2), respectively [38]. Deviation of the Cu(1) and Cu(2) atoms from the mean plane towards the apical donor atom is about 0.188(1) and 0.029(2) Å, respectively. The bridging N_3^- anions for both end-on and end-to-end modes are quasi-linear; the N–N–N angles are 176.0(11)° and 177.7(12)° for end-on and end-to-end bridging, respectively. The intrachain Cu···Cu distance is 3.947(3) and 6.372 Å in the end-on and end-to-end bridges, respectively. The five-membered chelate ring [Cu(1)–N(1)–C(1)–C(2)–N(2)] connected with Cu(1) assumes a half-chair conformation twisted on N(1)···C(1) whereas a similar type chelate ring formed by the same diamine with Cu(2), [Cu(2)–

N(4)–C(9)–C(10)–N(5)], is envelope on C(9) with puckering parameters [39] $q_2 = 0.432(11)$ and 0.381(13) Å, $\phi = 237.9(12)°$ and 67.7(16)°, respectively.

In this one-dimensional polymeric chain, different asymmetric units are also linked by strong hydrogen bonds via perchlorate ions (Table 4). There are four available hydrogen atoms [H(1a), H(1b), H(4a) and H(4b)] for hydrogen bond formation in each asymmetric unit. H(1a) and H(1b) of the nitrogen N(1) coordinated with Cu(1) are involved in strong N–H···O hydrogen bond formation with the oxygen atoms O(12) and O(21), respectively, from two different perchlorate ions. H(4b) of N(4) coordinated with Cu(2) forms a strong N–H···N hydrogen bond with N(21) of the end-to-end bridging azide. H(4a) of the similar nitrogen forms an intramolecular hydrogen bond between the different units via O(21)′ of the symmetry related perchlorate ions.

3.4. Magnetic properties

Variable temperature (2–300 K) magnetic susceptibility data were collected for microcrystalline samples of compounds 1–4. The agreement factor R is defined as $R = \sum_i[(\chi_M T)_{obsd} - (\chi_M T)_{calcd}]^2/\sum_i[(\chi_M T)_{obsd}]$. The temperature-independent paramagnetism (TIP) was taken as 60×10^{-6} cm^3 mol^{-1} K, for each copper(II) atom in all cases.

3.4.1. Complex *1*

A $\chi_M T$ versus T plot (χ_M is the molar susceptibility for two Cu^{II} ions) for complex **1** is shown in Fig. 6 top. The value of $\chi_M T$ for **1** at 300 K is 0.83 cm^3 mol^{-1} K, which is as expected for two magnetically quasi-isolated spin doublets ($g > 2.00$). The $\chi_M T$ values decrease very slowly and then abruptly at low temperatures, reaching a value of 0.083 cm^3 mol^{-1} K at 2 K. In Fig. 6 top (inset), the χ_M versus T plot is shown. The plot displays the occurrence of a maximum at 10 K in χ_M, which is a signature of antiferromagnetic coupling. At 3.7 K, an increase in the χ_M values appears due to the presence of a small amount of paramagnetic impurity, as pointed in the study of the EPR spectra at low temperatures. So the fit of the experimental data was performed until 10 K, and the possible interactions through the dinuclear entities, that are important at low temperatures, are not evaluated. The Bleaney–Bowers formula for a dinuclear $S = 1/2$ system was used [1d,42] The Hamiltonian employed is $H = -JS_1S_2$. The best-fit parameters were: $J = -12.18 \pm 0.09$ cm^{-1}, $g = 2.12 \pm 0.00$ and $R = 4 \times 10^{-5}$. The field dependence of magnetization at 2 K is displayed in Fig. 6 bottom. The reduced molar magnetization tends to $0.3N\mu_B$ when the field approaches 5 T. The value of the molar magnetization at 5 T is far from the expected value for two isolated copper(II) complexes, indicating a global antiferromagnetic coupling. The powder EPR spectra from 298 to 4 K show the typical pattern for a square-pyramidal geometry, $g_\parallel = 2.22$ and $g_\perp = 2.07$ ($g_{av} = 2.12$).

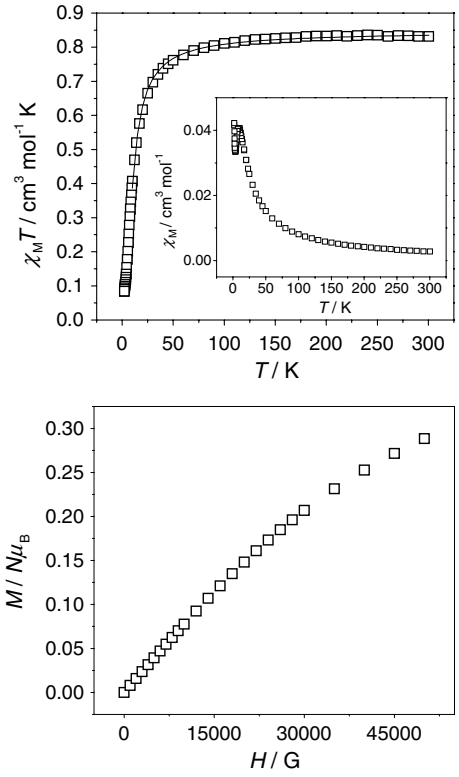

Fig. 6. Top: A plot of χ_M (inset) and $\chi_M T$ vs. T for complex **1**. The solid lines represented the best fit and the square the experimental date. Bottom: A plot of $M/N\mu_B$ vs. H at 2 K.

3.4.2. Complex *2*

The $\chi_M T$ and χ_M (inset) versus T plots (χ_M is the molar magnetic susceptibility for 2 Cu^{II} ions) are shown in Fig. 7. The value of $\chi_M T$ at 300 K is 0.79 cm^{3}mol^{-1} K, which is as expected for two magnetically quasi-isolated spin doublets ($g > 2.00$). The $\chi_M T$ values decrease very slowly and then abruptly at low temperatures, reaching a value of 0.026 cm^3 mol^{-1} K at 2 K. No maximum was found in the χ_M versus T plot. The global feature is characteristic of weak antiferromagnetic coupling. According to the structural data, there are two crystallographically independent dimers, A and B, with different values on their geometrical parameters (see structure description of complex **2**). Focusing in the inter-dimer interactions, isomer A forms a supramolecular structure in which the dinuclear entities are linked by strong hydrogen bonds resulting in a one-dimensional system whereas isomer B is a one-dimensional system formed by quasi-isolated dinuclear entities linked only by van der Waals forces. Taking into account these features, the intra-dinuclear magnetic coupling through the azide ligand and the possible interactions through the dinuclear entities in the two dimers must be different. So the possible interactions were evaluate in a global J value by the Bleaney–Bowers formula for a dinuclear $S = 1/2$ system. The Hamiltonian employed is $H = -JS_1S_2$. The best-fit parameters were: $J = -4.43 \pm 0.1$ cm^{-1}, $g = 2.07 \pm 0.00$ and $R = 1.8 \times 10^{-4}$. The reduced

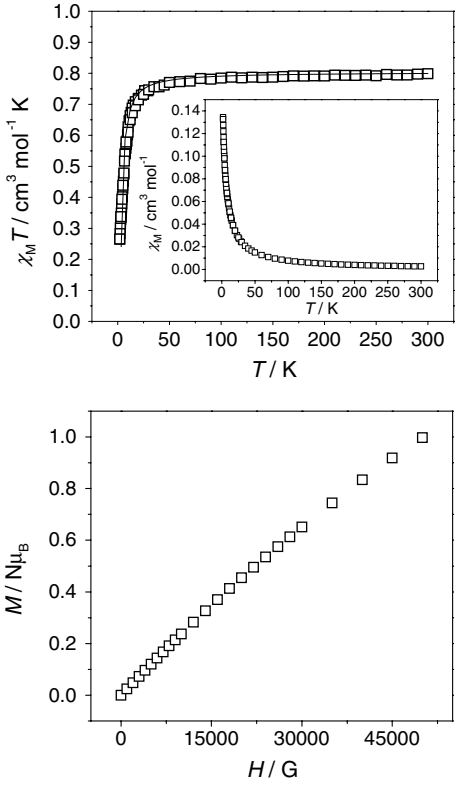

Fig. 7. Top: A plot of χ_M (inset) and $\chi_M T$ vs. T for complex **2**. The solid lines represented the best fit and the square the experimental date. Bottom: A plot of $M/N\mu_B$ vs. H at 2 K.

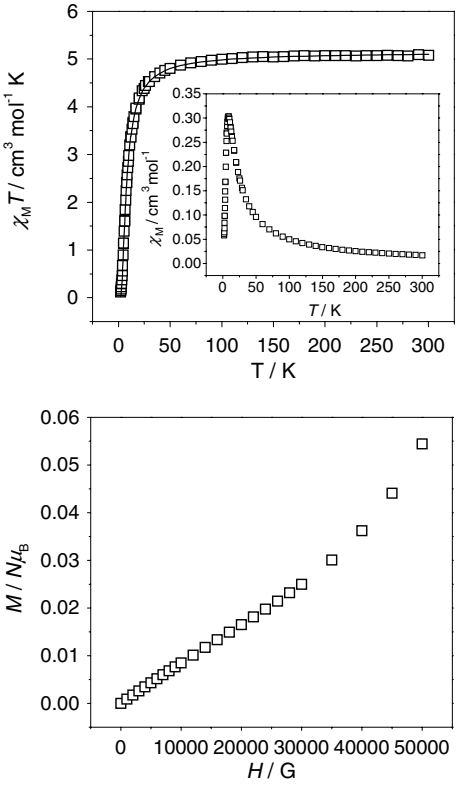

Fig. 8. Top: A plot of χ_M (inset) and $\chi_M T$ vs. T for complex **3**. The solid lines represented the best fit and the square the experimental date. Bottom: A plot of $M/N\mu_B$ vs. H at 2 K.

molar magnetization tends to $1N\beta$ when the field reaches 5 T (Fig. 7 bottom) clearly indicating that the global coupling is less antiferromagnetic than that for complex **1**. The EPR spectra show a broad band centered at 2.6 and a shoulder at 2.1.

3.4.3. Complex *3*

The $\chi_M T$ and χ_M (inset) versus T plots (χ_M is the molar magnetic susceptibility for 12 Cu^{II} ions) are shown in Fig. 8 top. The value of $\chi_M T$ at 300 K is 5.10 $cm^3\ mol^{-1}$ K, which is as expected for 12 magnetically quasi-isolated spin doublets ($g > 2.00$). The $\chi_M T$ values decrease very slowly and then abruptly at low temperatures reaching a value of 0.02 $cm^3\ mol^{-1}$ K at 2 K. The χ_M versus T plot displays the occurrence of a maximum at 9 K, which is a signature of an overall antiferromagnetic coupling. The structure of complex **3**, as can be seen from the crystal structure, consists of a double one-dimensional chain derived from mononuclear units linked by hydrogen bonds that involve perchlorate ions and azide groups (Fig. 4). The perchlorate anion acts as a pseudo-bridge between two copper(II) ions through two of their oxygen atoms, O11 and O13, giving a 1-D supramolecular structure. The distance from the oxygen O13 of the pseudo-coordinated perchlorate anion and the Cu (II) ion is 2.633 Å. Taking into account this large distance and the small efficient transmission of the magnetic interaction of the perchlorate ion we could consider these interactions as nil.

Each of these mononuclear entities is bridged to two other mononuclear entities of the neighboring chain by four hydrogen bonds (2 + 2) giving the double chain structure (Scheme 2). Each $[CuL^3N_3]$ mononuclear entity is bridged, asymmetrically, to two other mononuclear units of the neighboring chain. In both cases the bridge occurs through a pair of equivalent hydrogen bonds. The first pair involved the N1 atom (from L^3) of one monomer and the N11 (from the N_3) of a neighboring monomer and vice-versa. The second pair of hydrogen bonds takes place between the N1 atom (from L^3) of one monomer and the N13 (from the N_3), respectively, of the corresponding monomers.

From the magnetic point of view we considered the structure as an alternating zig-zag chain (Scheme 2). To fit the experimental data we have assumed a chain of 12 copper(II) atoms, which should describe the behavior of the infinite chain. The fit to the experimental data were performed according to the following Hamiltonian:

$$H = -J_1(S_1S_2 + S_3S_4 + S_4S_5 + S_5S_6 + S_7S_8 + S_9S_{10} + S_{11}S_{12}) - J_2(S_2S_3 + S_4S_5 + S_6S_7 + S_8S_9 + S_{10}S_{11}).$$

The free parameters were J_1, J_2 and g (average). The fit made by the irreducible tensor operator formalism (ITO), using the CLUMAG program [43], gave the following results: $J_1 = -9.69 \pm 0.03\ cm^{-1}$, $J_2 = 1.00 \pm 0.01\ cm^{-1}$, $g = 2.12 \pm 0.05$ and $R = 5.3 \times 10^{-5}$. Each J value involved the two

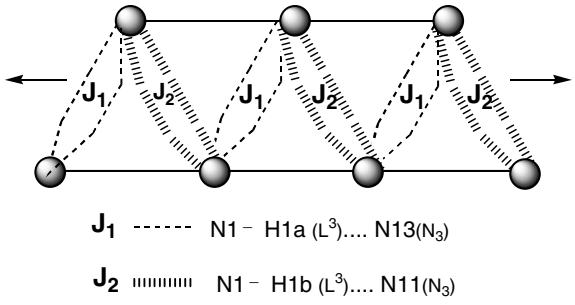

Scheme 2.

kinds of equivalent hydrogen bonds (see Scheme 2). We could not conclude the assignment of each J value for each different magnetic interaction through the two kinds of hydrogen bonds. The field dependence of magnetization at 2 K is displayed in Fig. 8 bottom. The reduced molar magnetization tends to 0.06 $N\mu_B$ when the field approaches 5 T. The value of the molar magnetization at 5 T is far from the expected value for one isolated copper(II) complex, indicating a global antiferromagnetic coupling.

The powder EPR spectra from 298 to 4 K show the typical pattern for a square-pyramidal geometry, $g_{\parallel} = 2.21$ and $g_{\perp} = 2.06$ ($g_{av} = 2.11$).

3.4.4. Complex 4

The structure determination reveals that the copper atoms are bridged singly and alternately by end-on and end-to-end azido ligands with the occurrence of a 1-D polymeric infinite chain. Only intramolecular hydrogen bonds are present in the structure. The susceptibility measurements (for 2 copper atoms) are shown in Fig. 9 (top).

The $\chi_M T$ value at 300 K is 0.84 $cm^3\ mol^{-1}\ K$, which is as expected for two magnetically quasi-isolated spin doublets ($g > 2.00$). Upon cooling, $\chi_M T$ slightly increases when the temperature is lowered, after 35 K increases quickly and reaches a value of 1.04 $cm^3\ mol^{-1}\ K$ at 2 K. This behavior indicates an overall ferromagnetic interaction between the Cu(II) ions within the chain. The χ_M values increase monotonically when the temperature decreases (Fig. 9 top inset). The presence of two kinds of bridges (1,1-N_3) and (1,3-N_3) is consistent with the presence of two different exchange-coupling parameters. The fit of the magnetic data have been carried out with the CLUMAG program [43], with the same conditions as for complex **3**. The best-fit parameters obtained with this computing program are $J_1 = 1.91\ cm^{-1}$, $J_2 = -0.38 \times 10^{-2}\ cm^{-1}$, $g = 2.12$ and $R = 6.1 \times 10^{-6}$. Since the EE bridging moiety has three atoms between the metal ions, the distances Cu1···Cu2 (6.372 Å) and Cu2···N23 (2.643 Å) are longer, we assign J_1 and J_2 to the EO and EE bridges, respectively. Considering the low J_2 value as practically nil, a fit using the Bleaney–Bowers formula for a dinuclear $S = 1/2$ system was used [1d,42]. The Hamiltonian employed is $H = -JS_1S_2$. The best-fit parameters were $J = 1.91 \pm 0.01\ cm^{-1}$, $g = 2.12 \pm 0.00$ and $R = 5.6 \times 10^{-6}$ (Fig. 9 top). Therefore, from the magnetic point of view we can conclude that complex **4** is a ferromagnetic dinuclear complex. The reduced magnetization value (Fig. 9, bottom) at 5 T clearly tends to $2N\mu_B$, the expected value for two isolated (or ferromagnetically coupled) copper(II) ions. The shape of the curve formed by the experimental points does not follow the Brillouin formula, but the tendency to reach the value of $2N\mu_B$ is more pronounced which is the typical signature of ferromagnetic coupling. To our knowledge, only two compounds consisting of 1-D chains in which the copper atoms with square-pyramidal geometry are alternately bridged containing single end-to-end (EE) and single end-to-on (EO) azido ligands, both adopting a basal–apical disposition, are found in the literature (**5** [25], **6** [26]). In complex **6**, the interchain interactions are ferromagnetic, compounds **5** is just the opposite, while in complex **4** the interaction through the EO azide bridge is ferromagnetic and through the EE azide bridge is negligible (Table 5). The powder EPR spectra show a signal centered at 2.11.

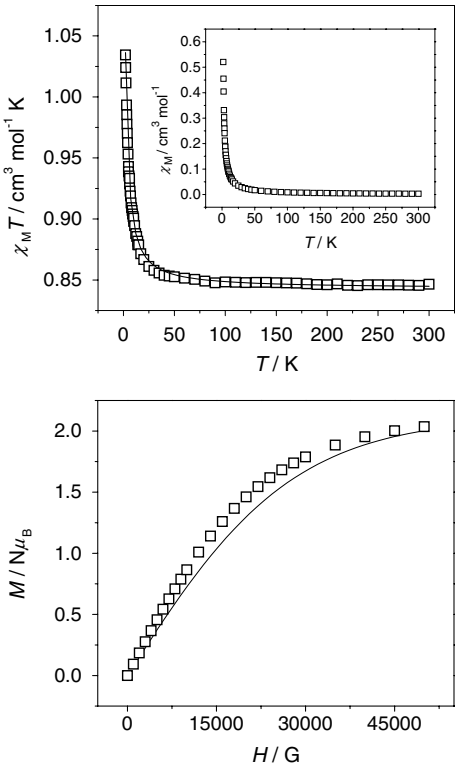

Fig. 9. Top: A plot of χ_M (inset) and $\chi_M T$ vs. T for complex **4**. The solid lines represented the best fit and the square the experimental date. Bottom: A plot of $M/N\mu_B$ vs. H at 2 K. The solid line represents the simulation of the Brillouin function for two copper(II) ions with $g = 2.12$.

3.4.5. Discussion

In complexes **1**, **2** and **4** (considering it from the magnetic point of view as dinuclear species), the copper(II) ions are in square-pyramidal geometries with an axially elongated bond length, and the end-on azido group bridges the copper centers in a basal–apical fashion. The magnetic orbital describing the single electron in the two copper

Table 5
Structural and magnetic parameters for alternating 1-D compounds, containing single end-to-end and single end-to-on azido ligands

Compound	$\tau^{(a)}$		EE			EO				J values	
	Cu1	Cu2	Cu–Cu (Å)	Cu–azido-basal (Å)	Cu–azido-apical (Å)	Cu–N–Cu (°)	Cu–Cu (Å)	Cu–azido-basal (Å)	Cu–azido-apical (Å)	J_{EE} (cm^{-1})	J_{EO} (cm^{-1})
4 (this work)	0.07	0.22	6.372	1.964	2.643	131.61	3.974	1.983	2.342	0	1.91
5 (Ref. [4a])	0.10	0.02	5.629	2.013	2.295	129.98	3.883	2.007	2.276	−2.69	−11.55
6 (Ref. [4b])	0.10	0.21	5.590	1.971	2.355	116.60	3.691	1.992	2.341	0.45	14.1

atoms are mainly of a $d_{x^2-y^2}$ orbital lying in the basal plane of the copper atoms and have only small contribution on the axis perpendicular to the basal plane. The consequence is the good delocalization of the electron density of one copper(II) towards the bridging azido, while the delocalization is poor in the second copper atom because the azide occupies an axial position of it, with a longer distance, and so an extremely weak interaction should be expected, as observed experimentally. In these kinds of complexes (azide bridged acting in basal–apical fashion), the variations in the J parameter are small and consequently, it is difficult to establish clear trends connecting theoretical parameters to variation in J. Theoretical calculations demonstrate that J can be antiferromagnetic or ferromagnetic depending mainly on the Cu–N_3–Cu angle when the azido bridge is in a basal–basal position [13]. This reasoning is not valid when the azido bridges are in basal–apical coordination, although too many papers devoted to this kind of coupling try to relate this angle with the J parameter. Looking in the literature for: (a) structural and magnetic data for both single and double asymmetric EO azide bridges in copper (II) complexes [13a,17,19,21,25–28], and (b) copper (II) species with single EE bridges [11,25,26,44,45], it would be difficult to establish clear trends connecting structural parameters to variation in J. This difficulty is due to: (a) the small values of J coupling for the basal–apical fashion of the azide ligand and (b) the dispersion of these J values with regard to several geometrical parameters.

4. Conclusion

Four Cu^{II} complexes having very similar, singly condensed tridentate blocking ligands and having both azide and perchlorate as anions have been synthesized in a very facile way. The bridging topologies of the complexes are drastically different with a small change in the blocking ligands. Complexes **1** and **2** are double azido bridged dimers, **3** is a 1-D chain, bridged by perchlorate ions and **4** is best described as a 1-D chain with alternate single EO and EE azido bridges. However, from the magnetic point of view **4** is a dinuclear complex since interaction through the EE bridge is practically nil due to a very long Cu···N distance (axial bond). Complexes **1** and **2** are antiferromagnetically coupled as is usual for this kind of complex. The EO bridge in complex **4** shows a ferromagnetic interaction. Comparison of Cu–N–Cu bond angles of **4** and two other reported compounds clearly indicates that the accidental orthogonality for this kind of bridging mode does not depend upon this angle as the compound having lowest and highest angles (**4** and **6**) are ferromagnetic while the other with an intermediate angle (**5**) is antiferromagnetic. The magnetic interaction in compound **3** is mediated solely through H-bonds. It is well known that hydrogen bonds play an important role in the transmission of magnetic interactions. For many years, hydrogen bonds have been reported to propagate essentially antiferromagnetic interactions between metal centers, but presently, the number of ferromagnetically coupled hydrogen-bonded systems is growing. Magnetism of complex **3** is interesting in that of two kinds of H-bonds are present in it, one transmits antiferromagnetic while the other ferromagnetic interactions.

Acknowledgements

This work was supported by CSIR, India (Fellowship for S.C. Sanction No. 9/28(614)/2003-EMR-I). We thank the Spanish government (Grant BQU2003-00539) and EPSRC, the University of Reading for funds for the image plate system.

Appendix A. Supplementary data

ORTEP diagram for compound **2**. Crystallgraphic data for the analysis have been deposited with the Cambridge Crystallographic Data Centre, CCDC Nos. 276332 (complex **1**), 276333 (complex **2**), 276334 (complex **3**) and 276335 (complex **4**). Copies of this information may be obtained free of charge from CCDC, 12 Union Road, Cambridge CB2 1EZ, UK (fax: +44 1223 336 033; e-mail: deposit@ccdc.cam.ac.uk or www: http://www.ccdc.cam.ac.uk). Supplementary data associated with this article can be found, in the online version, at doi:10.1016/j.poly.2006.01.024.

References

[1] (a) D. Gatteschi, A. Caneschi, L. Pardi, R. Sessoli, Science 265 (1994) 1054;
(b) A.L. Barra, A. Caneschi, A. Cornia, F.F. Biani, D. Gatteschi, C. Sangregorio, R. Sessoli, L. Sorace, J. Am. Chem. Soc. 121 (1999) 5302;
(c) J.S. Miller, M. Drillon (Eds.), Magnetism: Molecules to Materials II; Molecule-Based Magnets, Wiley–VCH, Weinheim, 2001;
(d) O. Kahn, Molecular Magnetism, VCH, New York, 1993.

[2] J. Ribas, A. Escuer, M. Monfort, R. Vicente, R. Corte's, L. Lezama, T. Rojo, Coord. Chem. Rev. 193–195 (1999) 1027, and references therein.
[3] E.-Q. Gao, S.-Q. Bai, Y.-F. Yue, Z.-M. Wang, C.-H. Yan, Inorg. Chem. 42 (2003) 3642.
[4] (a) R. Cortés, M. Drillon, X. Solans, L. Lezama, T. Rojo, Inorg. Chem. 36 (1997) 677;
(b) M. Abu-Youssef, A. Escuer, D. Gatteschi, M.A.S. Goher, F.A. Mautner, R. Vicente, Inorg. Chem. 38 (1999) 5716.
[5] (a) M. Abu-Youssef, A. Escuer, M.A.S. Goher, F.A. Mautner, R. Vicente, Eur. J. Inorg. Chem. (1999) 687;
(b) M. Villanueva, J.L. Mesa, M.K. Urtiaga, R. Corte's, L. Lezama, M.I. Arriortua, T. Rojo, Eur. J. Inorg. Chem. (2001) 1581.
[6] (a) A. Escuer, J. Cano, M.A.S. Goher, Y. Journaux, F. Lloret, F.A. Mautner, R. Vicente, Inorg. Chem. 39 (2000) 4688;
(b) E.-Q. Gao, S.-Q. Bai, Z.-M. Wang, C.-H. Yan, J. Am. Chem. Soc. 125 (2003) 4984.
[7] (a) M. Abu-Youssef, A. Escuer, M.A.S. Goher, F.A. Mautner, G. Reiss, R. Vicente, Angew. Chem., Int. Ed. 39 (2000) 1624;
(b) M. Abu-Youssef, M. Drillon, A. Escuer, M.A.S. Goher, F.A. Mautner, R. Vicente, Inorg. Chem. 39 (2000) 5022.
[8] (a) J. Ribas, M. Monfort, I. Resino, X. Solans, P. Rabu, F. Maingot, M. Drillon, Angew. Chem., Int. Ed. Engl. 35 (1996) 2520;
(b) A. Escuer, R. Vicente, M.S.El. Fallah, M.A.S. Goher, F.A. Mautner, Inorg. Chem. 37 (1998) 4466.
[9] (a) J. Ribas, M. Monfort, C. Diaz, C. Bastos, C. Mer, X. Solans, Inorg. Chem. 34 (1995) 4986;
(b) A. Escuer, R. Vicente, J. Ribas, M.S.El. Fallah, X. Solans, M. Font-Bardia, Inorg. Chem. 33 (1994) 1842;
(c) J. Ribas, M. Monfort, B.K. Ghosh, R. Cortes, X. Solans, M. Font-Bardia, Inorg. Chem. 35 (1996) 864.
[10] C.S. Hong, Y. Do, Angew. Chem., Int. Ed. 38 (1999) 193.
[11] (a) T.K. Maji, P.S. Mukherjee, G. Mostafa, T. Mallah, J.C. Boquera, N.R. Chaudhuri, Chem. Commun. (2001) 1012;
(b) P.S. Mukherjee, T.P. Maji, A. Escuer, R. Vicente, J. Ribas, G. Rosair, F. Mautner, N.R. Chaudhuri, Eur. J. Inorg. Chem. (2002) 943;
(c) P.S. Mukherjee, S. Dalai, G. Mostafa, T.-H. Lu, E. Rentschler, N.R. Chaudhuri, New J. Chem. 25 (2001) 1203.
[12] S. Sikorav, I. Bkouche-Waksman, O. Kahn, Inorg. Chem. 23 (1984) 490.
[13] (a) S.S. Tandon, L.K. Thompson, M.E. Manuel, J.N. Bridson, Inorg. Chem. 33 (1994) 5555;
(b) E. Ruiz, J. Cano, S. Alvarez, P. Alemany, J. Am. Chem. Soc. 120 (1998) 11122.
[14] P. Manikandar, R. Muthukumaran, K.R.J. Thomas, B. Varghese, C.V.R. Chandramouli, P.T. Manoharan, Inorg. Chem. 40 (2001) 2378.
[15] L. Li, Z. Jiang, D. Liao, S. Yan, G. Wang, Q. Zhao, Transition Met. Chem. (London) 25 (2000) 630.
[16] H.-Y. Shen, W.M. Bu, E.-Q. Gao, D.Z. Liao, Z.H. Jiang, S.P. Yan, G.L. Wang, Inorg. Chem. 39 (2000) 396.
[17] (a) G. de Munno, M.G. Lombardi, M. Julve, F. Lloret, J. Faus, Inorg. Chim. Acta 282 (1998) 82;
(b) Z. Shen, J.L. Zhou, Z. Yu, Y. Zhang, J.F. Bai, C.M. Che, H.K. Fun, J.J. Vittal, X.Z. You, J. Chem. Soc., Dalton Trans. (1999) 3393.
[18] K. Matsumoto, S. Ooi, K. Nakatsuka, W. Mori, S. Suzuki, A. Nakahara, Y. Nakao, J. Chem. Soc., Dalton Trans. (1985) 2095.
[19] (a) R. Cortés, K.K. Urtiaga, L. Lezama, J.I.R. Larramendi, M.I. Arriortua, T. Rojo, J. Chem. Soc., Dalton Trans. (1993) 3685;
(b) Y.S. You, C.S. Hong, K.M. Kim, Polyhedron 24 (2005) 249.
[20] L. Li, D. Liao, Z. Jiang, S. Yan, Polyhedron 20 (2001) 681.
[21] J.P. Costes, F. Dahan, J. Ruiz, J.P. Laurent, Inorg. Chim. Acta 239 (1995) 53.
[22] A. Escuer, M. Font-Bardía, E. Peñalba, X. Solans, R. Vicente, Polyhedron 18 (1998) 211.
[23] T.K. Maji, P.S. Mukherjee, S. Koner, G. Mostafa, J.P. Tuchagues, N.R. Chaudhuri, Inorg. Chim. Acta 314 (2001) 111.
[24] S. Koner, S. Saha, T. Mallah, K.I. Okamoto, Inorg. Chem. 43 (2004) 840.
[25] P.S. Mukherjee, T.K. Maji, G. Mostafa, T. Mallah, N.R. Chaudhuri, Inorg. Chem. 39 (2000) 5147.
[26] E.-Q. Gao, S.-Q. Bai, C.-F. Wang, Y.-F. Yue, C.-H. Yan, Inorg. Chem. 42 (2003) 8456.
[27] X.J. Lin, Z. Shen, Y. Song, H.J. Xu, Y.Z. Li, X.Z. You, Inorg. Chim. Acta 358 (2005) 1963.
[28] (a) M.S. Ray, A. Ghosh, R. Bhattacharya, G. Mukhopadhyay, M.G.B. Drew, J. Ribas, Dalton Trans. (2004) 252;
(b) M.S. Ray, A. Ghosh, S. Chaudhuri, M.G.B. Drew, J. Ribas, Eur. J. Inorg. Chem. (2004) 3110.
[29] W. Kabsch, J. Appl. Crystallogr. 21 (1988) 916.
[30] G.M. Sheldrick SHELX-86, Acta Crystallogr., Sect. A 46 (1990) 467.
[31] N. Walker, D. Stuart, Acta Crystallogr., Sect. A 39 (1983) 158.
[32] G.M. Sheldrick, SHELXL-93: Program for Crystal Structure Refinement, University of Göttingen, Göttingen, Germany, 1993.
[33] M.N. Burnett, C.K. Johnson, ORTEP-3: Oak Ridge Thermal Ellipsoid Plot Program for Crystal Structure Illustrations, Report ORNL-6895, Oak Ridge National Laboratory, Oak Ridge, TN, USA, 1996.
[34] (a) S. Gourbatsis, S.P. Perlepes, I.S. Butler, N. Hadjiliadis, Polyhedron 18 (1999) 2369;
(b) C.-M. Liu, R.-G. Xiong, J.-L. Zuo, X.-Z. You, X.-Y. Huang, Polyhedron 15 (1996) 2051;
(c) S. Banerjee, J. Gangopadhyay, C.-Z. Lu, J.-T. Chen, A. Ghosh, Eur. J. Inorg. Chem. (2004) 2533.
[35] F.A. Mautner, S. Hanna, R. Cortes, L. Lezama, M.G. Barandika, T. Rojo, Inorg. Chem. 38 (1999) 4647.
[36] B.J. Hathaway, A.A.G. Tomlinson, Coord. Chem. Rev. 5 (1970) 1.
[37] R. Shukla, S. Mondal, P.K. Bharadwaj, Polyhedron 11 (1992) 1837.
[38] A.W. Addison, T.N. Rao, J. Reedijk, J. van Rijn, G.C. Verschoor, J. Chem. Soc., Dalton Trans. (1984) 1349.
[39] (a) D. Cremer, J.A. Pople, J. Am. Chem. Soc. 97 (1975) 1354;
(b) J.C.A. Boyens, J. Cryst. Mol. Struct. 8 (1978) 31.
[40] B.J. Hathaway, Struct. Bond. (Berlin) 57 (1984) 55.
[41] (a) J. Foley, D. Kennefick, D. Phelan, S. Tyagi, B. Hathaway, J. Chem. Soc., Dalton Trans. (1983) 2333;
(b) T.-H. Lu, S.-C. Lin, H. Aneetha, K. Panneerselvam, C.-S. Chung, J. Chem. Soc., Dalton Trans. (1999) 3385;
(c) A. Escuer, M. Font-Bardia, E. Penalba, X. Solans, R. Vicente, Inorg. Chim. Acta 286 (1999) 189;
(d) G.A. Lawrance, M. Rossignoli, B.W. Skelton, A.H. White, Aust. J. Chem. 40 (1987) 1441;
(e) P.V. Bernhardt, E.J. Hayes, Inorg. Chem. 42 (2003) 1371;
(f) M.-H. Choi, B.J. Kim, I.-C. Kim, S.-H. Kim, Y. Kim, J.M. Harrowfield, M.-K. Lee, M. Mocerino, E. Rukmini, B.W. Skelton, A.H. White, J. Chem. Soc., Dalton Trans. (2001) 707;
(g) S. Autzen, H.-G. Kortz, R. Boese, H. de Groot, R. Sustmann, Eur. J. Inorg. Chem (2003) 1401;
(h) T.H. Fawcett, S.M. Rudich, B.H. Toby, R.A. Lalancette, J.A. Potenza, H.J. Schugar, Inorg. Chem. 19 (1980) 940;
(i) C.-H. Kwak, J. Jeong, J. Kim, Inorg. Chem. Commun. 4 (2001) 264;
(j) P.V. Bernhardt, P.C. Sharpe, Inorg. Chem. 39 (2000) 4123.
[42] B. Bleaney, K.D. Bowers, Proc. R. Soc. Lond., Ser. A 214 (1952) 45.
[43] D. Gatteschi, L. Pardi, Gazz. Chim. Ital. 123 (1993) 231.
[44] (a) Z. Shen, J.L. Zuo, S. Gao, Y. Song, C.M. Che, H.K. Fun, X.Z. You, Angew. Chem., Int. Ed. 39 (2000) 3633;
(b) G.D. Munno, M.G. Lombardi, P. Paoli, F. Lloret, M. Julve, Inorg. Chim. Acta 282 (1998) 252;
(c) M.A.S. Goher, A. Escuer, F.A. Mautner, N.A. Al-Salem, Polyhedron 20 (2001) 2971.
[45] (a) S. Dalai, P.S. Mukherjee, M.G.B. Drew, T.H. Lu, N.R. Chaudhuri, Inorg. Chim. Acta 335 (2002) 85;
(b) A. Escuer, M. Font-bardía, E. Peñalva, X. Solans, R. Vicente, Inorg. Chim. Acta 298 (2000) 195.

have higher activity [3,11,23] or/and prolonged action as compared to the free ligand [21].

The present paper is part of this systematic study and it is dedicated to complex formation between copper(II) and 1-[2-[2-hydroxy-3-(propylamino)propoxy]phenyl]-3-phenyl-1-propanone, propafenone. The latter is an effective antiarrythmic agent with a moderate β-blocking activity and an acceptable side effect profile for the acute and long-term treatment of supraventricular arrythmias. From a chemical point of view it represents an aminoalcohol and therefore it is of interest to compare its behaviour as a ligand with that of another group of aminoalcohol medications – that of the β-blockers, which easily form stable complexes with copper(II) [16–22]. Some of these complexes exhibit even better pharmacological effects in comparison with the non-coordinated free drugs that offer good perspectives for their clinical application [3,11,21,22].

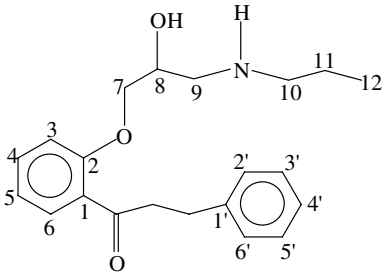

Propafenone, HPr

The aminoalcohol chain in propafenone is linked to the phenyl ring through an oxygen atom as in the β-blockers and thus one might expect to find similar coordination ability of these ligands. We have already discussed the role of the oxygen for the chemical and biological properties of other aminoalcohol drugs such as effortil, clenbuterol, salbutamol and sotalol [1,2,14,22]. On the other hand the presence of bulky substituents in the aromatic ring of propafenone could create steric hindrance and decrease to some extent the complexation with copper. Therefore, a comparison between the coordination ability of propafenone and the other aminoalcohol drugs mentioned above seems to be of interest.

We have found that, like many other aminoalcohols, propafenone forms mono- and binuclear complexes, depending mainly on the molar metal-to-ligand ratio in the reaction system. Due to the relatively lower solubility of the ligand in water, we used methanol as a reaction medium for the synthesis of the complexes. In alkaline methanolic solution and with an excess of the ligand ($M{:}HPr \cdot HCl \leqslant 1{:}10$; $HPr \cdot HCl{:}NaOH \leqslant 1{:}2$) the violet mononuclear complex **1** was obtained, in which copper(II) is coordinated via the NH and the deprotonated OH groups of the ligand, forming a stable five-membered chelate ring. With comparable amounts of the reagents ($M{:}HPr \cdot HCl$ from 1:2 to 2:1) and the same alkalinity ($HPr \cdot HCl{:}NaOH \leqslant 1{:}2$) the green binuclear complex **2** was formed with participation of the same donor groups of the ligand.

2. Experimental

2.1. Materials and synthesis

Propafenone was obtained from Sigma, Germany as the hydrochloric salt, $HPr \cdot HCl$ and was used without further purification. The metal salt $CuCl_2 \cdot 2H_2O$ and NaOH were supplied by Riedel E. de Haën AG and MeOH from Fluka. All reagents and solvents used were of analytical grade.

The mononuclear complex **1** was obtained at room temperature when 1.00 cm^3 0.025 M solution of $CuCl_2 \cdot 2H_2O$ (0.0426 g $CuCl_2 \cdot 2H_2O$ in 10.0 cm^3 MeOH) was added to 10.00 cm^3 0.025 M of the ligand in the same solvent (0.0945 g $Pr \cdot HCl$ in 10.0 cm^3 MeOH). Dropwise addition of 5.0 cm^3 0.10 M NaOH (0.0800 g NaOH in 20.0 cm^3 MeOH) to the reaction solution resulted in a violet coloration. From this solution violet crystals precipitated after 5 days. The crystals were filtered, washed with methanol, recrystallized from EtOH and dried over P_2O_5 (yield ca. 35%). *Anal.* Calc. for $CuPr_2$: C, 67.76; H, 7.04; N, 3.76; Cu, 8.54. Found: C, 67.24; H, 6.86; N, 3.92; Cu, 8.45%. M.p.: 146 °C.

The binuclear complex **2** was synthesized at ambient temperature when 10.00 cm^3 0.025 M solution of $Pr \cdot HCl$ (0.0945 g $Pr \cdot HCl$ in 10.0 cm^3 MeOH) was mixed with 10.00 cm^3 0.025 M solution of $CuCl_2 \cdot 2H_2O$ (0.0426 g $CuCl_2 \cdot 2H_2O$ in 10.0 cm^3 MeOH). The dropwise addition of 5.0 cm^3 0.10 M NaOH (0.0800 g NaOH in 20.0 cm^3 MeOH) resulted in the formation of a green precipitate, that was filtered, washed with MeOH and dried over P_2O_5 (yield ca. 60%). *Anal.* Calc. for $Cu_2Pr_2Cl_2$: C, 57.40; H, 5.96; N, 3.19; Cl, 8.07; Cu, 14.46. Found: C, 57.31; H, 5.91; N, 3.28; Cl, 8.26; Cu, 14.06%. M.p.: 158 °C. Unfortunately, we were not able to obtain crystals of proper size and quality in order to perform a direct X-ray single crystal structure determination of complex **2**.

2.2. Instrumentation and analysis

Electronic spectra were obtained on a Specord UV–Vis (Carl-Zeiss, Jena) instrument. IR spectra were recorded in the range 4000–400 cm^{-1} on a Specord-75 IR spectrometer, and in the range 500–75 cm^{-1} on a Bruker 113 V instrument in polyethylene. Thermogravimetric analyses were performed using a Perkin–Elmer TGS-2 instrument. The EPR spectra in the X-band were obtained with an ERS 220/Q instrument, using Mn/ZnS standard. Magnetic measurements were carried out under a helium atmosphere on a SQUID magnetometer with a sensitivity of $\sim 2 \times 10^{-5}$ emu. The magnetic susceptibility was measured with an increment of 2 K over the whole temperature range 2–300 K and the validity of the Curie–Weiss law was estimated using the correlation coefficient, with values higher than 0.9900. Elemental analyses were performed

according to classical methods: C, H were determined as CO_2 and H_2O, N through the Dumas' method, chlorine by titration with $Hg(NO_3)_2$ after wet digestion of the sample. Copper was determined by atomic absorption after wet digestion of the sample. The NMR spectra were recorded in $CDCl_3$ solutions on a JEOL EX-400 instrument (^{13}C at 100 MHz, ^{1}H at 400 MHz) and on a Varian 300 (^{13}C at 75 MHz, ^{1}H at 300 MHz).

For the structure determination of **1**, a transparent needle shaped pink crystal was mounted on a SIEMENS SMART X-ray diffractometer with a 1 K CCD area detector. Data were collected at room temperature using graphite-monochromatized Mo Kα radiation ($\lambda = 0.71073$ Å). A hemisphere of data (1271 frames at 5 cm detector distance) was collected using a narrow-frame method with scan widths of 0.30° in ω and an exposure time of 30 s/frame. The first 50 frames were measured again at the end of the data collection to monitor instrument and crystal stability. The data were integrated using the Siemens SAINT program [23]. The program SADABS was used for the absorption correction [24]. The structure was solved by direct methods and refined by full-matrix least-squares techniques with the SHELX97 software package [25]. All non-hydrogen atoms have been located and assigned directly from the Fourier maps. The hydrogen atoms have been introduced as riding models and their thermal parameters refined isotropically [25]. The main crystallographic details are summarized in Table 1.

Table 1
Crystal data and structure refinement for $CuPr_2$ (**1**)

Complex **1**	
Empirical formula	$C_{16.80}H_{17.60}Cu_{0.40}N_{0.80}O_{2.40}$
Formula weight	294.39
Temperature (K)	293(2)
Wavelength (Å)	0.71073
Crystal system, space group	monoclinic, $P2_1/c$ (#14)
Unit cell dimensions	
a (Å)	4.7106(9)
b (Å)	12.507(2)
c (Å)	31.979(6)
α (°)	90
β (°)	92.858(4)
γ (°)	90
Volume (Å^3), Z	1881.7(6), 5
Calculated density (g cm^{-3})	1.338
$F(000)$	794
Crystal size (mm)	$0.44 \times 0.09 \times 0.06$
θ Range for data collection (°)	1.28–22.50
Limiting indices	$-5 \leqslant h \leqslant 5$, $-13 \leqslant k \leqslant 13$, $-34 \leqslant l \leqslant 34$
Reflections collected/unique	11 218/2439
Refinement method	full-matrix least-squares on F^2
Data/parameters	2439/239
Goodness-of-fit on F^2	1.424
Final R indices [$I > 2\sigma(I)$][a,b]	$R_1 = 0.1080$, $wR_2 = 0.2681$
R indices (all data)	$R_1 = 0.1111$, $wR_2 = 0.2709$

[a] $R_1 = \sum||F_o| - |F_c|/\sum|F_o|$ (based on reflections with $I > 2\sigma(I)$).

[b] $wR_2 = \left[\sum w(|F_o| - |F_c|)^2/\sum w|F_o|2\right]^{1/2}$; $w = 1/[\sigma^2(F_o^2) + (0.0533P)^2 + 28.15P]$; $P = [\max(F_o^2, 0) + 2F_c^2]/3$ (all data).

3. Results and discussion

3.1. Mononuclear $CuPr_2$ complex *1*

3.1.1. X-ray data and crystal structure

The asymmetric unit of the title compound consists of one copper atom and one propafenone molecule (Fig. 1). The copper atoms are located on inversion centers occupying one special (2*a*: 0, 0, 0) position while all other atoms occupy general (4*e*: *x*, *y*, *z*) positions. Each copper atom is coordinated by two propafenone molecules acting as bidentate ligands through O1 and N1 (Fig. 2). All five atoms of the resulting CuO_2N_2 unit lie in the same plane with Cu—O1 and Cu—N1 distances of 1.900(6) and 2.024(7) Å, respectively, and a O1—Cu—N1 angle of 86.9(3)° (Table 2). Hence, the copper coordination could be described as a plain squared one (Fig. 2). All C—O, C—N and C—C distances and angles in the propafenone molecule are well within the corresponding limits.

The $CuPr_2$ complexes are packed on top of each other forming slabs that run parallel to the *a*-axis (Fig. 3). The shortest intermolecular O···H distances are of order of 2.4 Å (O3···H11 = 2.35 Å, O2···H14 = 2.39 Å and O2···H10 = 2.45 Å) indicating the presence of only a small number of weak hydrogen bonds. No solvent molecules have been detected in the structure.

3.1.2. Electronic and IR spectra

The electronic spectrum of the mononuclear complex **1** in methanol shows one broad asymmetric absorption band at 520 nm ($\varepsilon \approx 100$ l mol^{-1} cm^{-1}), and a shoulder at 650 nm, due to the d–d transition in the distorted octahedral structure of the Cu(II) complex, where copper is bound with nitrogen and oxygen donor atoms.

The IR spectrum of the ligand shows two bands at 3295 and 3160 cm^{-1} assigned to the stretching vibrations of the NH and OH groups, respectively, engaged in the formation of H-bonds, as follows from the absorbance in the 2800–

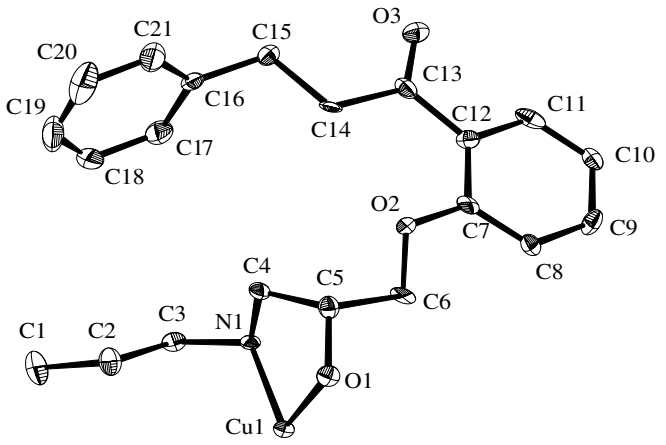

Fig. 1. Asymmetric unit, 50% thermal ellipsoids and labelling scheme in complex **1**.

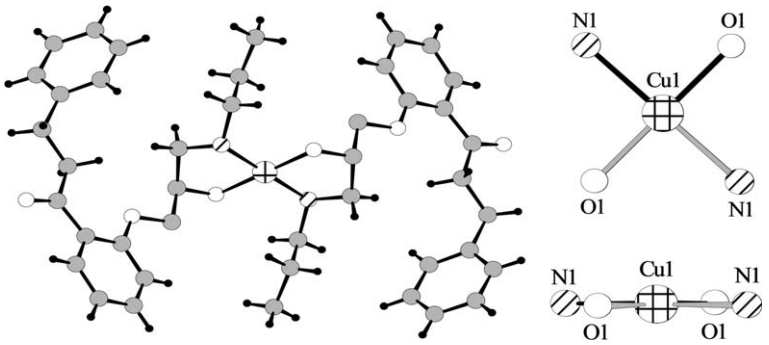

Fig. 2. Cu coordination in complex **1**. Copper, nitrogen, oxygen, carbon and hydrogen atoms are shown as cross-hatched, hatched, open, filled and black circles, respectively.

Table 2
Selected bond lengths (Å) and bond angles (°) in the mononuclear complex **1**

Cu(1)—O(1)#1	1.900(6)
Cu(1)—O(1)	1.900(6)
Cu(1)—N(1)#1	2.024(7)
Cu(1)—N(1)	2.024(7)
O(1)#1—Cu(1)—O(1)	180.0(5)
O(1)#1—Cu(1)—N(1)#1	86.9(3)
O(1)—Cu(1)—N(1)#1	93.1(3)
O(1)#1—Cu(1)—N(1)	93.1(3)
O(1)—Cu(1)—N(1)	86.9(3)
N(1)#1—Cu(1)—N(1)	180.0(5)

Symmetry transformations used to generate equivalent atoms: (#1) $-x, -y, -z$; (#2) $-x+1, -y, -z$.

2300 cm^{-1} range. The coordination of the ligand with Cu(II) and the formation of **1** lead to disappearance of the ν(OH) stretching vibration as a result of deprotonation of the hydroxyl group and to a shift of the ν(NH) to the 3000–2800 cm^{-1} range, where the bands due to $\nu(Ar_{C-H})$ of the aromatic ring are also present. At the same time two new bands are observed in the far IR-spectrum at 600 and 430 cm^{-1}, assigned to the stretching vibrations of ν(Cu—N) and ν(Cu—O) in the complex [26].

3.1.3. EPR data

The X-band EPR spectrum of complex **1** in a methanolic solution frozen at 113 K presents an anisotropic signal with $g_{\|} = 2.212$, $A_{\|} = 170$ G and an unresolved perpendicular component. Qualitatively, these parameters and the relation $g_{\|} > g_{\perp}$ indicate that the unpaired d-electron is located mainly on the $d_{x^2-y^2}$-orbital and a considerable axial deformation is realized, leading practically to a square-planar complex. The same spectra also exhibit an unresolved SHSF from ^{14}N in the perpendicular magnetic field, due to the coordination of the NH-function to copper. A solid sample of complex **1** at the same temperature (113 K) shows a broad signal for a magnetically concentrated sample of a paramagnetic copper(II) complex.

These experimental EPR data are in a good accordance with those for other similar copper(II) complexes [1,22].

3.1.4. Magnetochemical data

The magnetochemical studies of the mononuclear complex **1** in the temperature range 2–290 K revealed that the magnetic susceptibility χ decreases with increasing temperature, which is indicative of the paramagnetic character of the complex. The Curie–Weiss law is followed in the whole

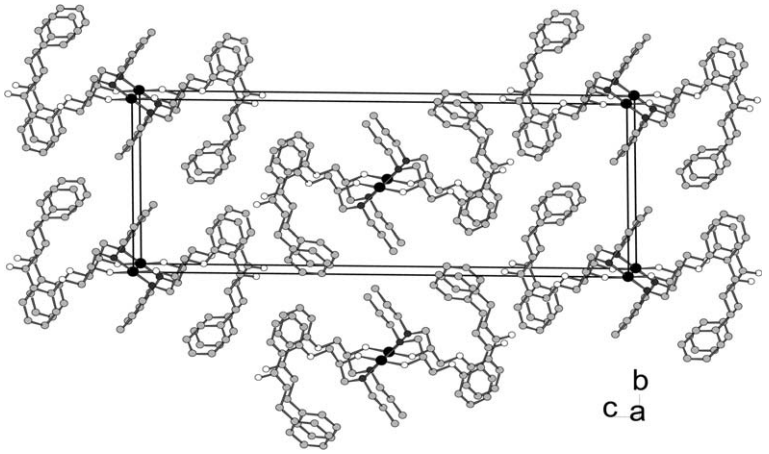

Fig. 3. Unit cell and 3D packing in complex **1**.

temperature range studied with a correlation coefficient of 0.9943. The effective magnetic moment determined with a value of the Weiss constant $\theta = -16$ was $\mu_{eff} = 1.70\mu_{eff}/\mu_B$.

The fulfillment of the Curie–Weiss law indicates that the Cu^{2+}-ions are in an octahedral crystal field, as μ_{eff} does not depend on the temperature. The experimentally found magnetic moment is lower than the theoretical one, which for a crystal field of 10 000 cm^{-1} is about $2.01\mu_{eff}/\mu_B$ [27]. The smaller value of the experimental magnetic moment is probably due to a weak intermolecular antiferromagnetic exchange interaction between the copper centers. This assumption is in accordance with the X-ray data showing a distance of 4.711 Å between the copper ions in axial positions along the *a*-axis.

3.1.5. Thermogravimetric data

The thermogravimetric (TG) study confirmed the elemental analysis, the IR and X-ray data that there is no solvent included in the isolated mononuclear species **1**.

3.2. Binuclear $Cu_2Pr_2Cl_2$ complex **2**

3.2.1. Electronic and IR spectra

The UV–Vis spectra of the complex **2** in methanol show two absorption bands: a broad band of low intensity at 710 nm ($\varepsilon \approx 40$ l mol^{-1} cm^{-1}) assigned to a d–d transition in the near square-planar copper(II) structure, and a second, more intense one at 385 nm ($\varepsilon \approx 1330$ l mol^{-1} cm^{-1}), that is typical for copper(II) polynuclear complexes with oxygen bridges of the type Cu—O—Cu. This band has been attributed to a charge-transfer transition O → Cu, which explains its higher intensity [28,29].

The IR spectra of **2** show that the *v*(NH) band is shifted 110 cm^{-1} to lower frequency, in comparison with the same band in the free ligand, while *v*(OH) is absent, indicating that the ligand is coordinated again through its NH group and deprotonated OH function. This conclusion is supported also by the appearance of new bands in the far IR-spectrum at 590, 415 and 270 cm^{-1} ascribed to the stretching vibrations *v*(Cu—N), *v*(Cu—O) and *v*(Cu–Cl), respectively [26].

3.2.2. NMR spectra

Additional information about the coordination mode of the ligand in **2** was obtained by a comparison between the NMR spectra of the free ligand and complex **2**. In the ^{13}C spectrum of **2** the signals for C_7, C_8, C_9, C_{10}, $C_{11}$and C_{12} (at 70.40, 64.79, 49.73, 48.80, 18.71 and 10.97 ppm, respectively) disappeared, due to the strong influence of the adjacent paramagnetic copper(II) centers, bonded to O^- and NH functions. At the same time the intensities of the signals for the other C-atoms remained practically unchanged. Analogous results were revealed also by the ^1H NMR spectra of the ligand and complex **2**. Here again a strong decrease in the intensities down to a complete disappearance was observed for the proton signals of the NH- and OH-groups (9.05 and 5.94 ppm) and for those bonded with the carbon atoms C_7, C_8, C_9, C_{10}, C_{11} and C_{12} (at 4.12, 4.27, 3.08, 2.72, 1.64 and 0.04 ppm, respectively), while the intensities for the protons at the other C-atoms were practically unchanged. Such effects have been already observed with another copper(II) complex with an aminoalcohol drug [1,16,30].

These results confirmed again the coordination sites of the ligand in the complexes formed with copper(II).

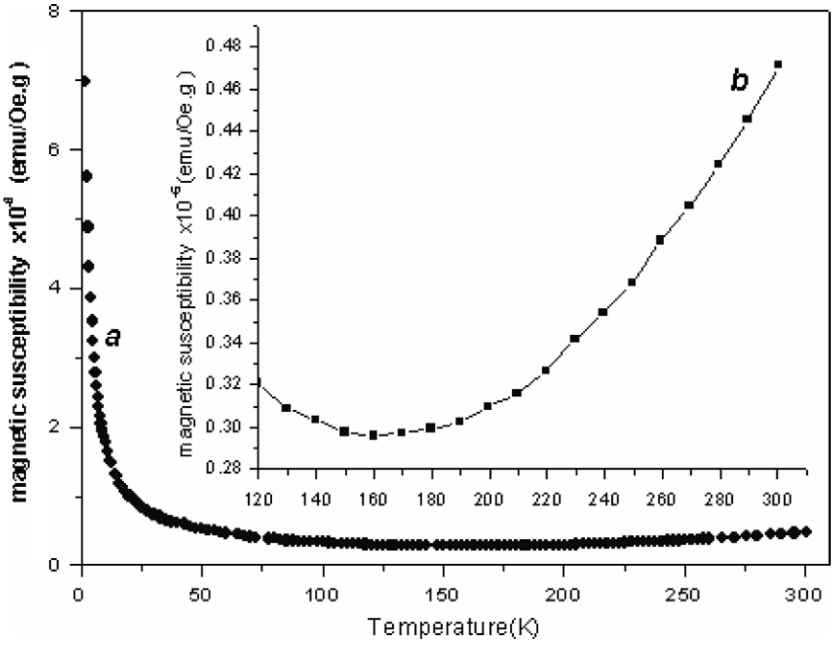

Fig. 4. Magnetic susceptibility vs. *T* for the binuclear complex **2**, measured at 1kOe applied field: (a) in the range 2–300 K; (b) in the range 120–300 K, χ_g being shown in a different scale.

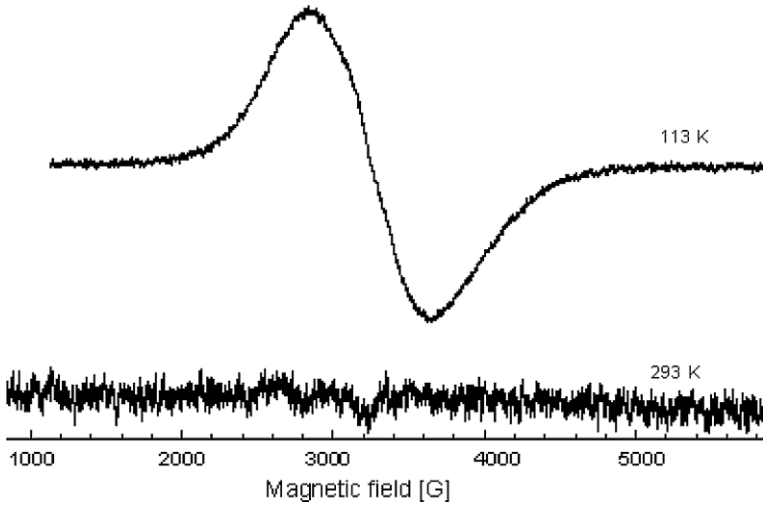

Fig. 5. The X-band EPR-spectra of the methanolic green solution of complex **2**.

3.2.3. Magnetochemical and EPR data

The temperature dependence of the specific magnetic susceptibility χ_g is given in Fig. 4a. In the range 2–150 K the complex shows a typical paramagnetic character. At temperatures above 150 K, χ_g begins to increase (Fig. 4b). The Curie–Weiss law is not followed in the whole temperature range (2–300 K). This complicated behaviour of χ_g could be considered as a result of superposition of the data for two different components. The first is a paramagnetic one, present as a monomeric impurity. The second component is an antiferromagnetic one, formed as a result of an intramolecular indirect exchange interaction between the copper(II) centers. An analogous course of the χ_g/T plot is also observed for other copper(II) complexes, described in the literature [31–35].

According to the theory [36,37] for complexes with closely located copper centers, the χ versus T plot must have a different course and is expected to pass through a maximum. In the present system such a maximum was not yet reached in the temperature range studied.

Similar effect must be also expected for the EPR spectra, measured at low and high temperatures. Fig. 5 shows the EPR spectra of the complex at 113 and 293 K in solution. Analogous spectra were obtained also with a solid state sample. At low temperatures the typical broad signal for paramagnetic Cu(II) has been observed. At higher temperatures the increased antiferromagnetic interaction leads to the complete quenching of the signal.

3.2.4. Thermogravimetric (TG) data

The TG study showed that, as in **1**, there are no solvent molecules included in the structure.

4. Conclusion

Propafenone forms two complexes with copper(II) – the mononuclear $CuPr_2$ (**1**) and the binuclear $Cu_2Pr_2Cl_2$ (**2**). In both cases the drug acts as a bidentate ligand through its NH- and deprotonated OH-functions. In **1** only two ligands are coordinated around copper(II), while in **2**, each one of the two metal centers are bound by one nitrogen, by one terminal chlorine and by two deprotonated OH-groups from two different propafenone molecules, forming oxygen bridges between the metal centers in the $Cu_2Pr_2Cl_2$ chromophore. No solvent molecules have been detected in the crystal structures of **1** and **2**. The relatively short distance between the two metal centers in **2**, linked by the oxygen bridges, leads to the appearance of a measurable antiferromagnetism.

5. Supplementary information

Full crystallographic details have been deposited in cif-format with the Cambridge Crystallographic Data Centre, CCDC 279128 for **1**. Copies of this information could be obtained free of charge from the Director, CCDC, 12 Union Road, Cambridge, CB2 1EZ, UK (fax: +44 1223 336 033, email: deposit@ccdc.cam.ac.uk, web: http://www.ccdc.cam.ac.uk/conts/retrieving/html).

Acknowledgements

The authors greatly acknowledge the financial support provided by the National Research Fund of Bulgaria. They also thank Dr. V. Skumryev from the Universitat Autonoma de Barcelona, Spain, for checking some of the magnetochemical data.

References

[1] P.R. Bontchev, I.N. Pantcheva, Transit. Met. Chem. 27 (2002) 1.
[2] P.R. Bontchev, B.B. Ivanova, R.P. Bontchev, D.R. Mehandjiev, D.S. Ivanov, Polyhedron 19 (2000) 1843.
[3] P.R. Bontchev, Ch. Nachev, B. Evtimova, N.D. Yordanov, E. Zhecheva, D. Mehandjiev, in: Proceedings of the 12th International Conference on Coordination Chemistry, Smolenice, Slovakia, 1989, p. 47.

[4] P.R. Bontchev, B.B. Ivanova, R.P. Bontchev, D. Mehandjiev, Polyhedron 20 (2001) 231.
[5] M.J. Kendrick, M.T. May, M.J. Plishka, K.D. Robinson, Metals in Biological Systems, Ellis Horwood, New York, 1992.
[6] J.J.R.F. da Silva, R.J.P. Williams, The Biological Chemistry of the Elements, 2nd ed., Clarendon Press, Oxford, 1993.
[7] M. Apostolova, P.R. Bontchev, Ch. Nachev, I. Sirakova, Jpn. J. Med. Sci. Biol. 45 (1992) 185.
[8] M. Apostolova, P.R. Bontchev, Ch. Nachev, I. Sirakova, J. Chromat. (Biomed. Appl.) 620 (1993) 191.
[9] M. Apostolova, P.R. Bontchev, Ch. Nachev, I. Sirakova, Compt. Rend. Bulg. Acad. Sci. 46 (1993) 75.
[10] M. Apostolova, Ch. Nachev, M. Koleva, P.R. Bontchev, I. Kehaiov, Talanta 46 (1998) 325.
[11] Ch. Nachev, P.R. Bontchev, B. Evtimova, D. Ivanov, J. Clin. Pharmacol. 28 (1988) 923.
[12] P.R. Bontchev, G. Gochev, B. Evtimova, H. Kadum, Ch. Nachev, J. Inorg. Biochem. 46 (1992) 23.
[13] P.R. Bontchev, H. Kadum, G. Gochev, B. Evtimova, J. Maciček, Ch. Nachev, Polyhedron 11 (1992) 1973.
[14] P.R. Bontchev, B.B. Ivanova, D.R. Mehandjiev, Bulg. Chem. Commun. 35 (2003) 21.
[15] P.R. Bontchev, D.R. Mehandjiev, B.B. Ivanova, R.P. Bontchev, Transit. Met. Chem. 28 (2003) 745.
[16] P.R. Bontchev, I.N. Pantcheva, T. Todorov, D.R. Mehandjiev, N. Savov, J. Inorg. Biochem. 83 (2001) 25.
[17] P.R. Bontchev, B.B. Ivanova, R.P. Bontchev, D.R. Mehandjiev, J. Coord. Chem. 54 (2001) 25.
[18] P.R. Bontchev, I.N. Pantcheva, G. Gochev, D.R. Mehandjiev, D.S. Ivanov, Transit. Met. Chem. 25 (2000) 196.
[19] P.R. Bontchev, I.N. Pantcheva, B. Ivanova, D.R. Mehandjiev, Bulg. Chem. Commun. 31 (1999) 59.
[20] P.R. Bontchev, H. Kadum, B. Evtimova, Ch. Nachev, E. Zhecheva, D.R. Mehandjiev, D. Ivanov, J. Inorg. Biochem. 48 (1992) 153.
[21] P.R. Bontchev, I.N. Pantcheva, R.P. Bontchev, D.S. Ivanov, N.D. Danchev, BioMetals 15 (2002) 78.
[22] V.T. Getova, P.R. Bontchev, D.R. Mehandjiev, V. Skumryev, P.R. Bontchev, Polyhedron 24 (2005) 1983.
[23] Siemens Analytical X-ray Instruments; SAINT, Version 4.05, Madison, WI, 1995.
[24] G.M. Sheldrick, SADABS, v. 2.10. Program for Empirical Absorption Correction of Area Detector Data, University of Göttingen, Göttingen, Germany, 2003.
[25] G.M. Sheldrick, SHELX97 (Includes SHELXS97, SHELXL97, CIFTAB) – Programs for Crystal Structure Analysis (Release 97-2). Institüt für Anorganische Chemie der Universität, Tammanstrasse 4, D-3400 Göttingen, Germany, 1998.
[26] K. Nakamoto, Infrared and Raman Spectra of Inorganic and Coordination Compounds, 5th ed., Wiley, New York, Toronto, 1997.
[27] A. Earnshaw, Introduction to Magnetochemistry, Academic Press, London, New York, 1968.
[28] G.A. van Albada, M.T. Lakin, N. Veldman, A.L. Spek, J. Reedijk, Inorg. Chem. 34 (1995) 4910.
[29] G.A. van Albada, W.J.J. Smeets, A.L. Spek, J. Reedijk, Inorg. Chim. Acta 260 (1997) 151.
[30] W. Holzer, Molecules 6 (2001) 796.
[31] Y. Nishida, S. Kida, J. Inorg. Nucl. Chem. 38 (1976) 451.
[32] R. Mergehenn, L. Merz, W. Haase, J. Chem. Soc., Dalton Trans. 9 (1980) 1703.
[33] N.F. Curtis, F.W.B. Einstein, K.R. Morgan, A.C. Willis, Inorg. Chem. 24 (1985) 2026.
[34] S. Wang, S.J. Trepanier, J.C. Zheng, Z. Pang, M.J. Wagner, Inorg. Chem. 31 (1992) 2118.
[35] T. Lindgren, R. Sillanpää, K. Rissanen, L.K. Thompson, C.J. O'Connor, G.A. VanAlbada, J. Reedijk, Inorg. Chim. Acta 171 (1990) 95.
[36] O. Kahn, Molecular Magnetism, Wiley, Chichester, UK, 1994.
[37] E.A. Boudreaux, L.N. Mulay, Theory and Applications of Molecular Paramagnetism, Wiley, New York, 1976.

2. Experimental

2.1. Materials

The starting compound tetramethyldiamidophosphoric acid chloride was prepared according to [14] and isolated via double distillation on b_8 106–107 °C [15] and *p-tert*-butylcalix[4]arene was synthesized according to procedure reported [16].

All solvents used, $NaClO_4 \cdot H_2O$ and $NaAuClO_4 \cdot 2H_2O$ were purchased from Fluka AG and Aldrich. The solvents were dried before use by standard procedures.

2.2. Analytical and physicochemical measurements

Elemental analyses for C, H, N were performed by Dr. H. Eder from the Microchemical Laboratory of the University of Geneva, of P – according to the method described in [17], of Cl in the Laboratory of Elemental Analysis of the Department of Chemistry, University of Sofia, Bulgaria.

The atomic absorption analysis (AAA) for Na and Au was performed on a Perkin–Elmer 1100 B spectrometer. The IR spectra were recorded on a FT-IR spectrometer "IFS 113v Bruker" (KBr and CsI pellets), ^1H, $^{13}C\{^1H\}$-DEPT-135, $^{31}P\{^1H\}$ NMR spectra were recorded (solvent $CDCl_3$) on a "Bruker Biospin Avance 400". Chemical shifts (δ) are expressed in ppm from $(CH_3)_4Si$; J values are in Hertz. In the NMR spectra, the Ar notation defines the aromatic nuclei of the calixarene backbone, considering the phenol oxygen as the main substituent to which the *ipso*, *ortho*, *meta* and *para* position refer. A DEPT spectrum was used to distinguish resonances belonging to tertiary or quaternary carbons.

The ES-MS spectra were obtained on a Finnigan SSQ 710C spectrometer using 10^{-5}–10^{-4} M solutions in methanol, capillary temperature 200 °C and acceleration potential 4.5 kV. In the case of the ligand, the liquid phase was $CH_3OH/H_2O/HCOOH$ 50/50/1 (by volume) and in the case of the complexes – CH_3OH. The FAB-MS spectra were obtained on a Fision VG Autospect instrument employing 3-nitrobenzyl alcohol as a matrix.

2.3. Synthesis of L

A solution of tetramethyldiamidophosphoric acid chloride (3.46 g, 20.3 mmol) in toluene (20 cm^3) was added dropwise to a refluxed fine suspension of the sodium derivative of *p-tert*-butylcalix[4]arene in toluene. The latter was prepared by addition of sodium (0.47 g, 20.3 mmol) to a solution of *p-tert*-butylcalix[4]arene (2.92 g, 4.5 mmol), methanol (50 cm^3) and toluene (150 cm^3), followed by remove of methanol by distillation. The suspension thus obtained was refluxed with stirring under a nitrogen atmosphere for 60 h. After cooling the reaction system it was washed repeatedly with water until a negative reaction for chloride ions was obtained, followed by drying over Na_2SO_4 and evaporation of the solvent. The yield of the crude product was 3.83 g (72%). The latter was recrystallized from DMSO; m.p. 305–310 °C with decomposition ($R_f = 0.57$, C_6H_{12}:$CHCl_3$:CH_3COOH 7:3:1 v/v). Calc. for $C_{52}H_{78}N_4O_6P_2$ (917.16): C, 68.10; H, 8.57; N, 6.11; P, 6.75. Found: C, 67.96; H, 8.60; N, 6.00; P, 6.67. IR (KBr disc, cm^{-1}): ν(P=O) 1242 cm^{-1}, ν(P–O–Ph) 1186(s), δ(P–N–CH_3) 1306, ν(Ar–OH) 3538.

2.4. Synthesis of [NaL]$AuCl_4 \cdot 4H_2O$ (1)

An ethanolic solution of L (0.020 g, 0.0218 mmol in 1.5 ml) and $NaAuCl_4 \cdot 2H_2O$ (0.0079 g, 0.0218 mmol in 1 ml) were mixed with constant stirring at ambient temperature, resulting in the formation of a yellow precipitate. The latter was centrifugated, washed repeatedly with ethanol and dried under high vacuum over P_4O_{10} for 4 h. Yield: 0.0274 g (95.47%). Calc. for $C_{52}H_{84}N_2O_9P_2Cl_4AuNa$ (1332.9): C, 46.86; H, 6.35; Cl, 10.64; Au, 14.78; Na, 1.72. Found: C, 46.55; H, 6.51; Cl, 9.05; Au, 15.06; Na, 1.75%. IR (KBr and CsI pellet, cm^{-1}) ν(P=O) 1200 (s), ν(P–O–Ph) 1169(s), ν(P–N–CH_3) 999 (s), ν(Ar–OH) 3561(s), $AuCl_4^-$ vibrations [18]: $\nu_1 = 361$, $\nu_2 = 140$, $\nu_4 \sim 324$ (sh).

2.5. Synthesis of [Na_2L_2](ClO_4)$_2 \cdot 4CH_3OH$ (2)

Methanolic solutions of L (0.020 g, 0.0218 mmol in 1 ml) and $NaClO_4 \cdot H_2O$ (0.0031 g, 0.0218 mmol in 1 ml) were mixed and stirred for 1 week at ambient temperature, resulting in the formation of a colourless precipitate of $[Na_2L_2](ClO_4)_2 \cdot 4CH_3OH$.

2.6. X-ray crystallography for L and [Na_2L_2](ClO_4)$_2 \cdot 4CH_3OH$ (2)

Basic crystallographic data for the free ligand and the complex, data collection and structural refinement are listed in Table 1.

Single crystals of the ligand L suitable for X-ray diffraction were obtained from DMSO solution of the compound by slow evaporation of the solvent. Diffraction data were collected at 143 K on a mar345 Imaging Plate. Data reduction was performed with marHKL release 1.9.1 [19]. The structure solution was determined with ab initio direct methods [20]. The structure was refined using the full-matrix least-squares on F^2 with all non-H atoms anisotropically defined. H atoms were placed at calculated positions using the «riding model» with $U_{iso} = a \times U_{eq}(X)$ [where a is 1.5 for CH_3 and OH groups and 1.2 for others, while X is the parent atom]. Structure refinement, molecular graphics and geometrical calculation have been carried with the SHELXTL software package, release 5.1 [21].

Colourless transparent single crystals of $[Na_2L_2](ClO_4)_2 \cdot 4CH_3OH$ were obtained from a methanolic solution of the compound by slow evaporation of the solvent.

Table 1
Crystal data for the free ligand L and the complex $[Na_2L_2](ClO_4)_2 \cdot 4CH_3OH$ (**2**)

Compound	Ligand L	Complex $[Na_2L_2](ClO_4)_2 \cdot 4CH_3OH$ (**2**)
Empirical formula	$C_{52}H_{78}N_4O_6P_2$	$C_{108}H_{172}Cl_2N_8Na_2O_{24}P_4$
Formula weight	917.12	2207.30
Temperature (K)	143(2)	140(2)
Wavelength (Å)	0.71070	0.71070
Crystal system	triclinic	triclinic
Space group	$P\bar{1}$	$P\bar{1}$
Unit cell dimensions		
a (Å)	12.879(3)	12.830(5)
b (Å)	12.918(3)	16.523(11)
c (Å)	16.261(3)	17.620(12)
α (°)	97.35(3)	99.45(6)
β (°)	96.74(3)	108.40(5)
γ (°)	90.52(3)	111.66(5)
Volume (Å^3)	2663.8(9)	3123(3)
Z	2	1
Density (calculated) (Mg/m^3)	1.143	1.174
Absorption coefficient (mm^{-1})	0.131	0.177
F(000)	992	1184
Crystal size (mm^3)	$0.23 \times 0.20 \times 0.15$	$0.18 \times 0.17 \times 0.13$
Θ range for data collection (°)	1.59–24.46	2.52–27.61
Index ranges	$-14 \leqslant h \leqslant 14$, $-14 \leqslant k \leqslant 15$, $-16 \leqslant l \leqslant 18$	$-14 \leqslant h \leqslant 15$, $-21 \leqslant k \leqslant 21$, $-22 \leqslant l \leqslant 22$
Reflections collected	12729	26074
Independent reflections [R_{int}]	7102 [0.0414]	13351 [0.1190]
Completeness to theta = 24.46° (27.61°)	80.6%	92.0%
Absorption correction	none	semi-empirical from equivalents (MULABS)
Refinement method	full-matrix least-squares on F^2	full-matrix least-squares on F^2
Data/restraints/parameters	7102/0/578	13351/10/667
Goodness-of-fit on F^2	0.921	0.810
Final R indices [$I > 2\sigma(I)$]	$R_1 = 0.0560$, $wR_2 = 0.1453$	$R_1 = 0.0957$, $wR_2 = 0.2381$
R indices (all data)	$R_1 = 0.1011$, $wR_2 = 0.1658$	$R_1 = 0.2557$, $wR_2 = 0.3188$
Largest differential peak and hole (e Å^{-3})	0.456 and −0.220	1.091 and −0.507

These crystals are stable only in the presence of CH_3OH. If they are dried, a sharp increase of the lattice defects appears leading to a quick collapse of the crystal lattice. This phenomenon has been observed for other compounds as well, where the solvent is fundamental for retainment of the crystal lattice [9]. For this reason the intensity data were collected from crystals sealed in a quartz capillary in the presence of the solvent.

Data collection was performed on a mar345 IPDS diffractometer system by using graphite-monochromated Mo Kα (0.71070 Å) radiation at 140(2) K. Data reduction was performed by CrysAlis RED, release 1.7.0 [22]. A semiempirical absorption correction [23] was applied to the raw data set. Structure solution, refinement and molecular graphics were performed by using the SHELXTL release 5.1 [21] software package. The structure was solved by direct methods and successive interpretation of the difference Fourier maps, followed by full-matrix least-squares refinement (against F^2). All atoms were refined anisotropically. The contribution of the hydrogen atoms, at their calculated positions, was included in the refinement using a riding model (except the hydrogen belonging to the bridging methanol). Some geometrical restraints (card DFIX) have been employed for the coordinating ClO_4^- anion. Crystallographic data are in cif format.

3. Results and discussion

3.1. Synthesis and structural characterization of L

The ligand was prepared in 72% yield by refluxing the sodium derivative of *p-tert*-butylcalix[4]arene and tetramethyldiamidophosphoric acid chloride in toluene.

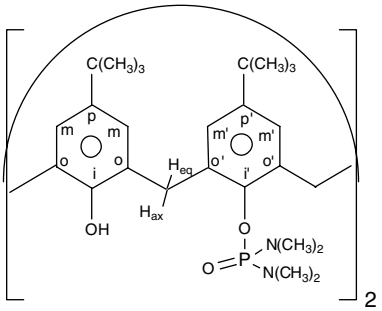

L

3.1.1. Crystal structure of the ligand

The orientation of the four aromatic rings, which lie below the reference plane passing through the four CH_2 bridging groups, determine the well known flattened cone conformation of the molecule (Fig. 1).

Above the reference plane a top hydrophilic part of the molecule is formed by the hydroxyl groups and the phosphoamide groups. Compound L has an elliptic conformation testified by the following geometric parameters:

(a) The angles between the aromatic rings of the calix[4]-arene are:
[A^C = 9.92°; B^D = 80.41°; A^B = 84.23°; B^C = 88.33°; C^D = 83.46°; A^D = 88.89°], where [A(C1, C2, C3, C4, C5, C6); B(C8, C9, C10, C11, C12, C13); C(C15, C16, C17, C18, C19, C20); D(C22, C23, C24, C25, C26, C27)].
The two opposite rings (A^C = 9.92°) are almost parallel while the other two (B^D = 80.41°) are almost perpendicular.

(b) The distances between the opposite *t*-butyl groups are: [C29...C37 = 6.199(6) Å; C33...C41 = 11.967(7) Å]. The steric orientation of the four *t*Bu groups is different due to free rotation around C–*t*Bu, which is conformationally advantageous.

Parameters dealing with the two P atoms are in good agreement with the presence of double bonds between P1 and O5 [1.457(3) Å] and P2 and O6 [1.451(3) Å] whereas all the other bond lengths refer to single ones [P–O_{av} = 1.623(2) Å, P–N_{av} = 1.624(3) Å]. Both P=O groups are oriented in opposite directions.

The geometry around the two P atoms is, as expected, tetrahedral, showing some distortions [O5–P1–N1 = 116.3(2)°, N1–P1–O1 = 98.1(2)°, O6–P2–N4 = 115.9(2)°, N4–P2–O3 = 98.4(1)°]. O5 and O6 interact only weakly with –$N(Me)_2$ or –CH_2-groups [O5···H48B = 2.48 Å, O5···H7A = 2.49 Å, O5···H45B = 2.69 Å; O6···H21A = 2.46 Å, O6···H49B = 2.54 Å, O6···H51B = 2.63 Å].

The torsion angles [C2–C1–O1–P1 = 98.08°; C16–C15–O3–P2 = 99.17°] show almost one and the same orientation of the P=O groups towards the aromatic part of the molecule. This fact explains the presence of only one $\nu_{P=O}$ band in the IR spectrum.

The molecular structure is stabilized by the formation of two strong intramolecular H-bonds: O2···O1 and O4···O3 (Table 2). The 3D packing of the molecules is stabilized by intermolecular hydrogen bonds of C–H···O type and C–H···π(Ph) interactions (Table 2, Fig. 2).

In the unit cells two calixarene molecules are present (Fig. 3a), arranged head to tail.

3.1.2. Structure of L in solution

The NMR and ES-MS data obtained (Tables 3–5) show the existence of the cone structure of the ligand in solution as well. The ^{1}H NMR data (Table 3) correspond to the structure of the cone symmetrical 1,3-esterificated *p-tert*-butylcalix[4]arene and not to 1,2-esterification, as the ^{1}H NMR spectrum shows only signals for one kind of Ar–CH_2–Ar protons present. The resonances of these protons are two doublets with equal $^2J_{HH}$ of 13.8 Hz. An additional evidence of the molecule symmetry is the fact that only two kinds of Ar–*H* protons are present. The resonance signals for two kinds of $(CH_3)_3C$ were registered too: one for the non-esterificated unit and the second for the esterificated one. The first one is observed at a stronger field (δ 0.83 ppm) and the second at δ 1.34 ppm. Moreover, the

Table 2
H-bond lengths in the ligand L

D	H	A	D–H	H...A	D...A	D–H...A	Symmetry codes
O2	H2	O1	0.84	2.12	2.936(3)	163.1	
O4	H4	O3	0.84	2.15	2.979(3)	168.2	
C48	H48B	O5	0.98	2.48	2.979(6)	111.1	
C7	H7A	O5	0.99	2.49	3.177(4)	126.2	
C45	H45B	O5	0.98	2.69	3.141(5)	108.7	
C21	H21A	O6	0.99	2.46	3.178(4)	129.2	
C49	H49B	O6	0.98	2.54	3.024(6)	110.1	
C51	H51B	O6	0.98	2.63	3.100(5)	109.9	
C51	H51A	C9	0.98	2.85	3.756(2)	154.6	$-x, -y, -z$
C52	H52C	C13	0.98	2.89	3.580(1)	128.1	$-x, -y, -z$
C45	H45A	C23	0.98	2.78	3.740(1)	166.4	$1-x, -y, -z$
C46	H46C	C27	0.98	2.86	3.686(2)	142.5	$1-x, -y, -z$
C48	H48C	C5	0.98	2.84		133.7	$1-x, 1-y, -z$

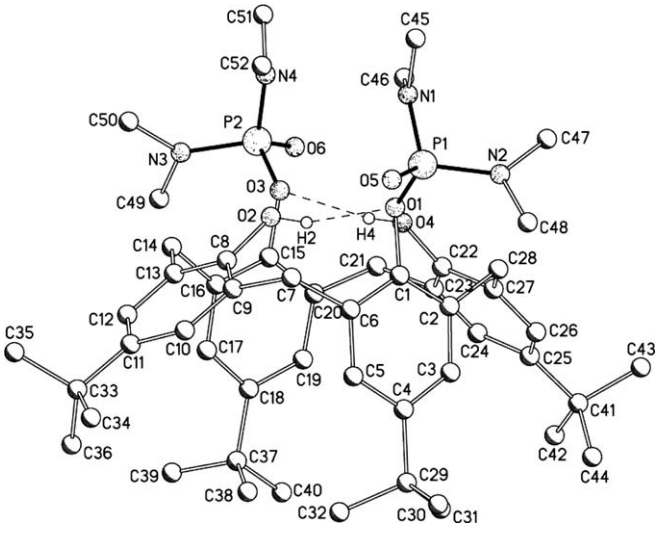

Fig. 1. Crystal structure of the ligand L.

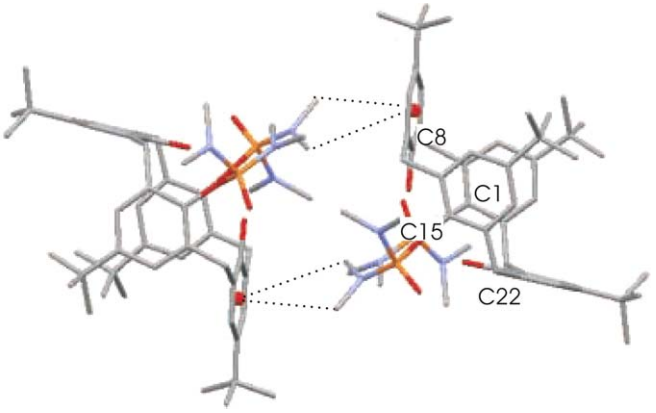

Fig. 2. Non-classical π-H bonds realized in the ligand L.

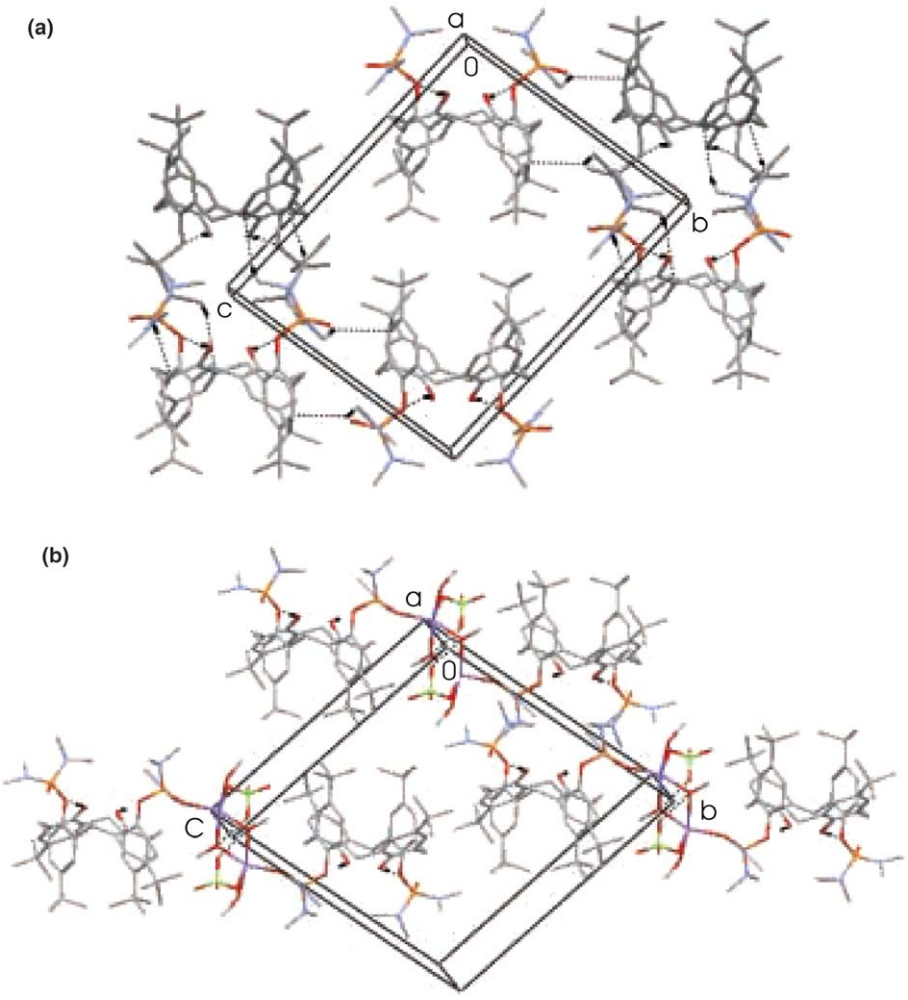

Fig. 3. Packing in the unit cell in the ligand L (a) and in the complex **2** (b).

presence of two distinct and quite separate singlets for aromatic protons (at δ 7.12 and 6.63) and for the *tert*-butyl groups ($CH_3)_3$C– (at δ 1.34 and 0.83) indicates again on the cone conformation of the ligand in solution. The resonance signals of the CH_3 groups of the amide $(CH_3)_2$N protons were registered at δ 2.82 (d) with a typical $^3J_{P,H}$ coupling constant of 9.8 Hz which corresponds to the resonance in hexamethylphosphortriamide $^3J_{P,H} = 9.5$ Hz

Table 3
^{1}H and ^{31}P{^{1}H} NMR data of 5,11,17,23-tetra-*tert*-butyl-25,27-dihydroxy-26,28-bis[(tetramethyldiamidophosphinyl)oxy]calix[4]arene (L) and its complex with $NaAuCl_4$ (**1**): solvent $CDCl_3$ δ in ppm, J in Hz

Compound	Ar–H_b	Ar–H_a	H–ax	H–eq	P–N(CH_3)$_2$	Ar–OH	C(CH_3)$_3$	^{31}P{^{1}H} NMR according to 85% H_3PO_4
L	7.12 (s)	6.63 (s)	4.37 (d) (13.7)	3.40 (d) (14.16)	2.82 (d) (9.8)	5.24 (s)	0.83 (s) 1.34 (s)	16.62 (s)
[NaL](AuCl$_4$) · 4H$_2$O	7.14 (s)	6.67 (s)	4.34 (d) (13.8)	3.38 (d) (13.8)	2.79 (d) (9.8)	5.23 (s)	0.84 (s) 1.33 (s)	16.84 (s)

Table 4
^{13}C NMR data of 5,11,17,23-tetra-*tert*-butyl-25,27-dihydroxy-26,28-bis[(tetramethyldiamidophosphinyl)oxy]calix[4]arene (L) and its complex with $NaAuCl_4$ (**1**): solvent $CDCl_3$, δ in ppm, J in Hz

Compound	Ar–$C(i)$–OH	Ar–$C(i')$–OR	Ar–$C(o,o')$	Ar–$C(p,p')$	Ar–$C(m,m')$	(O)P[N(CH_3)$_2$]$_2$	C(CH$_3$)$_3$	Ar–CH_2–Ar	C(CH_3)$_3$
L	150.2 (s)	147.1 (s)	142.7 (s) 142.5 (s)	128.8 (s) 131.3 (s)	125.9 (s) 125.2 (s)	37.0 (s) 36.9 (s)	33.9 (s) 33.7 (s)	32.1 (s)	31.7 (s) 30.9 (s)
[NaL](AuCl$_4$) · 4H$_2$O	150.0 (s)	147.6 (s)	142.9 (s) 142.7 (s)	128.6 (s) 131.2 (s)	126.0 (s) 125.4 (s)	37.0 (s) 36.9 (s)	34.0 (s) 33.8 (s)	32.0 (s)	31.7 (s) 30.8 (s)

Table 5
Molecular peaks and main fragments observed in ES-MS and FAB-MS (in italics) spectra (positive modes) for L and its complexes $[NaL](AuCl_4)\cdot 4H_2O$ (**1**) and $[Na_2L_2](ClO_4)_2\cdot 4CH_3OH$ (**2**)

Compound	M.W.	Species	Registered *m/z*	Calc. *m/z*
$C_{52}H_{78}N_4O_6P_2$ – L	917.16	$(L + CH_3CN + CH_3COOH + 2H_2O + 2H)^{2+}$	528.8	528.2
		$(L + H)^+$	917.3	918.2
		$(L + CH_3COOH + H)^+$	977.3	978.2
		$(L + CH_3CN + CH_3COOH + CH_3OH + H)^+$	1051.3	1051.3
$[NaL](AuCl_4)\cdot 4H_2O$ (**1**)	1332.97	$(2L + 3Na + 3H_2O + 3CH_3OH)^{3+}$	685.3	684.5
		$(L + H)^+$	917.3	918.5
		$(L - H)^+$	*917.9*	916.5
		$(L + Na)^+$	939.3	940.2
		$(L + Na)^+$	*939.9*	*939.2*
$[Na_2L_2](ClO_4)_2\cdot 4CH_3OH$ (**2**)	2207.3	$(L + Na + H + 3CH_3OH)^{2+}$	519.3	518.6
		$(L + Na)^+$	940.4	940.2
		$(L + H)^+$	917.8	918.2

[24]. Also only singlets are observed for the aromatic carbon atoms in the $^{13}C\{^1H\}$ spectrum in $CDCl_3$ (Table 4) and the $^{13}C\{^1H\}$ NMR shows only one absorption for the bridging methylene carbon at 32.1 ppm.

The only resonance signal for the $^{31}P\{^1H\}$ NMR is a singlet, whilst that of ^{31}P NMR is septet at the same shift.

3.2. Synthesis and characterization of the complex $[NaL]^+[AuCl_4]^-\cdot 4H_2O$ (*1*)

The elemental analysis data for complex **1** indicates the formation of the complex salt $[NaL]^+[AuCl_4]^-\cdot 4H_2O$. The IR data available are also in agreement with this supposition as in the range 500–150 cm^{-1} region three bands due to $AuCl_4^-$ vibrations are observed (see Section 2).

Comparing the IR spectral data for the free ligand and the complex in the range 4000–400 cm^{-1}, a significant shift of the P=O valent vibration is observed – from 1242 to 1200 cm^{-1} thus indicating coordination of the P=O groups via the O atom. This supposition was supported by $^{31}P\{^1H\}$ NMR data – in the $^{31}P\{^1H\}$ NMR spectrum of complex **1** a shift from 16.62 to 16.84 ppm is seen (Table 3).

All the resonances of complex **1** in the ^1H , $^{13}C\{^1H\}$ and DEPT-135 NMR spectra (see Tables 3 and 4) also show the cone conformation of the ligand.

Both ES-MS and FAB spectral data confirm the formation of the complex salt (Table 5). The corresponding spectra display peaks due to $[L + Na]^+$, $[L]^+$ and $[L + H]^+$ species.

The presence of four H_2O molecules was proved by TG analysis. In the temperature range 50–200 °C a mass loss of 5.5% is observed, the calculated one being 5.4%.

3.3. Crystal structure for $[Na_2L_2](ClO_4)_2\cdot 4CH_3OH$ (*2*)

The X-ray structure of complex **2** is shown in Fig. 4. It is evident that the whole molecule lies over an inversion centre and comprises of 2 calix[4]arene ligands, $2Na^+$, $2(ClO_4)^-$ and $4CH_3OH$. Each of the calix[4]arene ligands participate in the complex, bonded to Na^+ only by one of the P=O groups. It should be noted that both Na^+ cations are placed outside of the ligand cavities. As in free L, the modified calix[4]arenes show an elliptic conformation. The asymmetric unit contains a calix[4]arene molecule coordinated to Na^+ via a P=O group. At the same time, each cation is coordinated to one ClO_4^- (Na^+ is directly bonded to one oxygen of the perchlorate), one terminal and two bridging CH_3OH molecules.

The geometric parameters of the ligand in complex **2** are as follows:

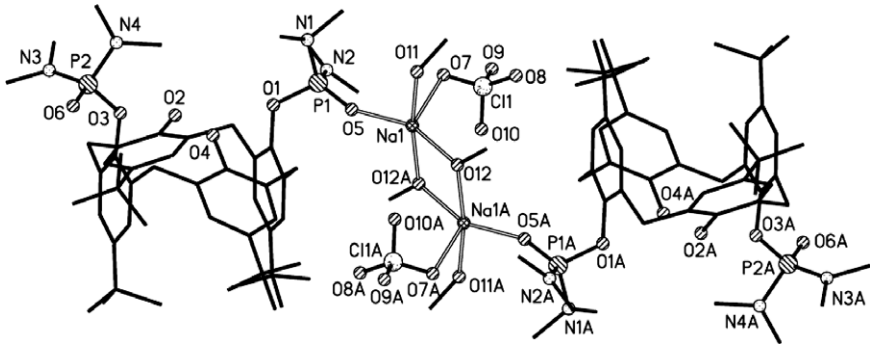

Fig. 4. Crystal structure of complex **2**.

Table 6
H-bond lengths in complex **2**

D	H	A	D–H	H···A	D···A	D–H···A	Symmetric codes
O2	H2	O3	0.84	2.16	2.987(6)	166.2	
O4	H4	O1	0.84	2.38	3.204(6)	166.3	
O11	H11	O6	0.84	1.93	2.707(7)	152.8	$-1-x, -1-y, -z$
C47	H47A	O3	0.98	2.62	3.404(4)	137.3	$-x, -1-y, -z$
C45	H45A	C9	0.98	2.78	3.67(3)	151.4	$-x, -1-y, -z$

(a) The dihedral angles are:
[A^C = 3.72°; B^D = 74.57°; A^B = 88.72°; B^C = 86.40°; C^D = 85.65°; A^D = 82.20°], where [A(C1, C2, C3, C4, C5, C6); B(C8, C9, C10, C11, C12, C13); C(C15, C16, C17, C18, C19, C20); D(C22, C23, C24, C25, C26, C27)].
(b) The torsion angles:
C2–C1–O1–P1 = 80.98° (at the coordinated P═O group)C16–C15–O3–P2 = 104.20°.

There are two complex molecules in the unit cell (Fig. 3b) arranged head to tail and exhibiting a cone conformation of the ligand.

The geometrical parameters of both P atoms are in good agreement with those found for the free ligand L. In the complex a number of inter and intramolecular hydrogen bonds are formed (Table 6).

The formation of intramolecular hydrogen bonds of the type O–H···O is realized within the ligand moiety, though, due to the coordination of Na^+ via the P═O group, the hydrogen bond distances are different. Two intramolecular H-bonds exist in the complex: in the ligand part [O2···O3 (at P-uncoordinated) = 2.987 Å and O4···O1 (at P-coordinated) = 3.204 Å]. In addition there is one intermolecular H-bond: O6–O11 = 2.708 Å (between the oxygen of the uncoordinated P═O group of the ligand and a terminal CH_3OH of the neighboring complex moiety). It was impossible to find the position of the OH hydrogen atom. In spite of that, it is evident that there is a strong hydrogen bond between the O12···O10 (ClO_4) atoms, because the O12···O10 distance is 2.740 Å. The 3D packing of the complex moiety is stabilized by C–H···π(Ph) interactions, similarly to that in the structure of L (Table 6).

*3.4. Comparison between the structure of the ligand L and complex **2***

Both compounds crystallize in the $P\bar{1}$ space group. The coordination seems to play a negligible influence on the general features of the ligand conformation and structure. In fact the lattice parameter *a*, which depends mainly on the steric interactions between calixarenes, does not change significantly in both structures; while the length of the *c* axis, which depends mainly on the size of the ions housed in the intermolecular cavity, shows a small but significant increase passing from the free ligand to the complex $[Na_2L_2](ClO_4)_2 \cdot 4CH_3OH$ (Fig. 3a and b). The bond distances and angles within the calix[4]arene moiety are comparable in both compounds. The molecular geometry characteristics of complex **2** are only slightly different, as it was mentioned above.

4. Conclusion

A new ligand, containing two functional groups, phosphine oxide and tertiary amide, on the same arm has been synthesized. The Na^+ coordination does not induce a serious conformation change in the ligand part of the complex. The complexation is realized outside the ligand cavity. The presence of phenyl rings leads to the formation of a series of C–H···π(Ph) interactions, which together with hydrogen bonds stabilize the 3D packing of both structures.

5. Supplementary Data

Crystallographic data for the structural analyses have been deposited with the Cambridge Crystallographic Data Centre, CCDC reference numbers 282678 and 282679. Copies of this information may be obtained free of charge from CCDC, 12 Union Road, Cambridge, CB2 1EZ, UK (fax: +44 1223 336033; e-mail: deposit@ccdc.cam.ac.uk or www: http://www.ccdc.cam.ac.uk).

Acknowledgments

The authors thank Prof. Dr. Sci. T. Spassov from the Department of Chemistry, Sofia University for running the TG analysis. This work was supported through a grant from the Swiss National Science Foundation (Project SCOPES 7BUPJ062293.00/1).

References

[1] C.D. Gutsche, Calixarenes, Monographs in Supramolecular Chemistry, Royal Society of Chemistry, Cambridge, 1989.
[2] M.-J. Schwing-Weill, M.A. McKervey, J. Vicens, V. Bohmer (Eds.), Calixarenes: A Versatile Class of Macrocyclic Compounds, Kluwer, Dordrecht, 1991.
[3] F. Arnaud-New, E.M. Collins, M. Deasy, G. Ferguson, S.J. Harris, B. Kaitner, A.J. Lough, M.A. McKervey, E. Margues, B.L. Ruhl, M.J. Schwing-Weill, E.M. Seward, J. Am. Chem. Soc. 111 (1989) 8681.
[4] A. Cadogan, D. Diamond, M.R. Smyth, G. Svehla, M.A. McKervey, E.M. Seward, S.J. Harris, Analyst 115 (1990) 1207.
[5] M. Telting-Diaz, M.R. Smyth, D. Diamond, E.M. Seward, G. Svehla, M.A. McKervey, Anal. Proc. 26 (1989) 29.
[6] M.R. Yaftian, M. Burgard, A. El Bachiri, D. Matt, C. Wieser, C.B. Dielman, J. Inclusion Phenom. Mol. Recogn. Chem. 29 (1997) 137.
[7] M.R. Yaftian, M. Burgard, A. El Bachiri, D. Matt, C. Wieser, C.B. Dielman, J. Inclusion Phenom. Mol. Recogn. Chem. 27 (1997) 127.
[8] F. Arnaud-Neu, J.K. Browne, D. Byrne, D.J. Marrs, M.A. McKervey, P. O'Hagan, M.J. Schwing-Weill, A. Walker, Chem. Eur. J. 5 (1) (1999) 175.
[9] A. Arduini, E. Ghidini, A. Pochini, R. Ungaro, G.D. Andreetti, G. Calestani, F. Ugozzoli, J. Inclusion Phenom. 6 (1988) 119.
[10] S.K. Chang, S.K. Kwon, I. Cho, Chem. Lett. (1987) 947.
[11] L. le Saulnier, S. Varbanov, R. Scopelliti, M. Elhabiri, J.-C.G. Bunzli, J. Chem. Soc., Dalton Trans. (1999) 3919.
[12] V. Videva, A.-S. Chauvin, S. Varbanov, C. Baux, R. Scopelliti, M. Mitewa, J.-C.G. Bunzli, Eur. J. Inorg. Chem. (2004) 2173.

[13] V. Videva, A.-S. Chauvin, S. Varbanov, M. Mitewa, Ann. Sofia Univ. 98–99 (2006) (in press).
[14] P. Lester, US 2,678,335, CA 49 (1955) 6300 g.
[15] H. Tolkmith, J. Am. Chem. Soc. 75 (1953) 5270.
[16] C.D. Gutsche, M. Iqbal, Organic Syntheses, Collective Volume 8, John Wiley & Sons, Inc., New York, 1993, pp. 75–77.
[17] S.G. Varbanov, E.D. Ruseva, N.N. Nikolov, Bulg. Chem. Commun. 26 (1) (1999) 91.
[18] K. Nakamoto, Infrared and Raman Spectra of Inorganic and Coordination Compounds, Part A, 5th ed., Wiley Interscience, New York, 1997, p. 207.
[19] Z. Otwinowski, W. Minor, in: C.W. CarterJr., R.M. Sweet (Eds.), Methods in Enzymology, Macromolecular Crystallography Part A, vol. 276, Academic Press, 1997, pp. 307–326.
[20] G.M. Sheldrick, Acta Crystallogr. A46 (1990) 467.
[21] G.M. Sheldrick, University of Göttingen, Germany, Bruker AXS, Inc., Madison, WI, 1997.
[22] Oxford Diffraction Ltd, 68 Milton Park, Abingdon, UK, 2003.
[23] R.H. Blessing, Acta Crystallogr., Sect. A 51 (1995) 33.
[24] Tabellen zur Strukturauf klärung organischer Verbindungen mit spektroskopischen Methoden, Springer-Verlag, Berlin Heidelberg, NY, 1981, Pretsch Clerc Seibl Simon.

easy oxidation of copper(I) to copper(II) has retarded the progress of research on copper(I) compounds considerably.

Very few two-coordinated copper(I) complexes comprising simple unidentate nitrogen donor ligands without any steric bulk are represented in the literature. The structurally characterized ones are even rarer primarily due to the relative instability of two-coordinated copper(I) compounds [6–10]. Different strategies have been employed to overcome the challenge of stabilizing cuprous ions. Sorrell et al. observed that two-coordinate linear copper(I) complexes with sterically hindered heterocyclic ligands having increased orbital overlap between the ligating atoms and copper(I) are inert toward reaction with CO and less reactive with O_2 in aprotic solvents [6]. However, in protic solvents, these complexes react rapidly and irreversibly with dioxygen to form Cu^{2+}. Sanyal et al. also observed a similar phenomenon in a two-coordinate linear complex of copper(I) with the imidazole ligand [7]. On the other hand, Le Clainche et al. emphasized the importance of preorganization of the metal binding site provided by the calix[4]-arene platform and an increased orbital overlap between the imidazole-nitrogen atom and copper(I) as the key features for the inertness of copper(I) ions toward dioxygen in the solid state as well as in coordinating or protic solvents [8]. However, the analogous pyridine-based complex is extremely sensitive to air and undergoes auto-oxidation within seconds [8]. Recently, we have demonstrated a simple model system with a unidentate ligand that allows more geometrical freedom as well as exceptional inertness toward dioxygen [10]. The unusual stability was attributed to the electronic factors provided by the 4-aminophthalimide moiety of the ligand framework and the perchlorate counteranion moieties [10]. In this study, we now establish that the extraordinary stabilization of the copper(I) complexes is provided by the electron deficient 4-aminophthalimide moiety of the ligand framework and the perchlorate counteranion by presenting a new ligand system $\mathbf{L^2}$ and its copper(I) complex $\mathbf{Cu(L^2)_2}$. This new copper(I) complex, which has been characterized by X-ray crystallography, is also highly resistant towards oxidation in the solid state and is stable in air even in potentially coordinating or protic solvents. However, the present complex, in which the metal center is more separated from the 4-aminophthalimide moieties, exhibits lesser stability than $\mathbf{Cu(L^1)_2}$. Thus, the electronic factor provided by an electron-deficient 4-aminophthalimide moiety is indeed one of the key features for the stabilization of cuprous ions. The single crystal structure of both the ligand systems, $\mathbf{L^1}$ and $\mathbf{L^2}$, are also described in this report.

2. Experimental

2.1. Materials and methods

The solvents used in this study, dioxane, tetrahydrofuran and acetonitrile were rigorously purified following standard procedure [11]. 4-Aminophthalimide (TCI (Japan)) was recrystallized twice from ethanol for spectroscopic measurements but used as received for synthesis. All other reagents are commercially available and used as received. Column chromatography was performed using Brockman I activated neutral aluminium oxide (150 mesh). Thin-layer chromatography (TLC) analysis was performed using Merck F254 aluminium oxide-60 and viewed by UV light. IR spectra were recorded on a Jasco FT-IR/5300 spectrometer as KBr pellets. NMR spectra were recorded on a Bruker AVANCE 400 MHz spectrometer at ambient temperature and were referenced to the internal ^1H and ^{13}C solvent peaks. EPR spectra were recorded on a Jeol JES-FA200 spectrometer. Solution electrical conductivities were measured with a Digisun DI-909 conductivity meter. *Caution:* The copper complexes contain perchlorate ions, which can detonate explosively and without warning. Although we have encountered no incidents with the reported compounds, all due precautions should be taken.

2.2. Synthesis of 2-(4′-aminophthalimidomethyl)pyridine ($\boldsymbol{L^1}$)

4-Aminophthalimide (0.5 g, 3.09 mmol) and 2-aminomethylpyridine (0.38 mL, 3.7 mmol) were placed in a 25-mL pear-shaped flask fitted with a water condenser and potassium hydroxide guard tube. The reaction mixture was heated at 65 °C with constant stirring for 6 h. The sticky material thus formed was purified by column chromatography on neutral alumina using chloroform as an eluent to obtain the desired product that was further recrystallized from chloroform/hexane to yield a yellow crystalline solid. Single crystals suitable for X-ray crystallography were grown by the slow evaporation of the chloroform solution over a period of several days. Yield: 0.7 g, 90%.

CHN *Anal*. Calc. for $C_{14}H_{11}N_3O_2$: C, 66.4; H, 4.35; N, 16.6. Found: C, 65.8; H, 4.24; N, 16.4%. IR (KBr, cm^{-1}): 3422, 3312, 1769, 1696, 1618; ^1H NMR ($CDCl_3$, 25 °C): δ (ppm) = 4.45 (s, 2H), 4.96 (s, 2H), 6.79 (dd, 1H), 6.99 (d, 1H), 7.14 (m, 2H), 7.56–7.60 (m, 2H), 8.51 (d, 1H); ^{13}C NMR ($CDCl_3$, 25 °C): δ (ppm) = 168.84, 168.51, 155.72, 153.46, 148.96, 137.20, 134.68, 12 5.33, 122.57, 121.46, 119.14, 117.71, 108.38, 42.43.

2.3. Synthesis of 2-(4′-aminophthalimidoethyl)pyridine ($\boldsymbol{L^2}$)

4-Aminophthalimide (0.5 g, 3.09 mmol) and 2-aminoethylpyridine (0.44 mL, 3.7 mmol) were placed in a 25-mL pear-shaped flask fitted with a water condenser and potassium hydroxide guard tube. The reaction mixture was heated at 80 °C with constant stirring for 6 h. Initially a clear solution was formed which then solidified into a thick mass, which was triturated and washed with hexane. Recrystallization from chloroform/hexane yielded the desired product as a yellow crystalline solid. Single crystals suitable for X-ray crystallography were grown by the slow evaporation of the chloroform solution over a period of several days. Yield: 0.76 g, 92%.

CHN *Anal. Calc.* for $C_{15}H_{13}N_3O_2$: C, 67.42; H, 4.87; N, 15.73. Found: C, 67.1; H, 4.78; N, 15.55%. IR (KBr, cm^{-1}): 3401, 3350, 1755, 1696, 1615; ^1H NMR ($CDCl_3$, 25 °C): δ (ppm) = 3.15 (t, 2H), 4.04 (t, 2H), 4.33 (s, 2H), 6.79 (dd, 1H), 6.99 (d, 1H), 7.14–7.18 (m, 2H), 7.56–7.60 (m, 2H), 8.51 (d, 1H); ^{13}C NMR ($CDCl_3$, 25 °C): δ (ppm) = 168.89, 168.63, 158.0, 153.44, 148.77, 137.07, 134.51, 125.0, 123.58, 121.89, 119.0, 117.46, 108.11, 37.43, 36.48.

2.4. Synthesis of $[Cu(L^2)_2]ClO_4$ ($Cu(L^2)_2$)

To a solution of L^2 (4 mmol) in 1:1 methanol–acetonitrile (50 mL), $Cu(ClO_4)_2 \cdot 6H_2O$ (1 mmol) dissolved in methanol (20 mL) was added drop-wise and the resulting solution was stirred for 24 h at room temperature and filtered. The filtrate was subsequently stored for slow evaporation to afford brown colored crystals suitable for X-ray crystallography. Conductivity measurements of both the complexes reveal the 1:1 cation:anion ratio. Both the complexes are EPR silent.

$Cu(L^2)_2$: Yield: 65%; IR (KBr, cm^{-1}): 3437, 3360, 1752, 1689, 1609, 1076; ^1H NMR (CD_3CN, 25 °C): δ (ppm) = 3.12 (t, 2H), 3.92 (t, 2H), 5.12 (bs, 2H), 6.85 (dd, 1H), 6.94 (d, 1H), 7.34–7.39 (m, 2H), 7.48 (d, 1H), 7.82 (m, 1H), 8.48 (b, 1H).

2.5. Collection and reduction of X-ray data

A tiny single crystal was mounted on the tip of a glass fiber and then mounted on the goniometer. The X-ray data for L^1, L^2 and $Cu(L^2)_2$ were collected on a Bruker CCD X-ray diffraction system with graphite-monochromatized Mo Kα radiation ($\lambda = 0.71073$ Å) controlled by a Pentium-based PC running the SMART software package [12]. The raw data frames were integrated by the SAINTPLUS program package [12]. Empirical absorption corrections were applied with the SADABS program [12] and the space group was determined by examining systematic absences and confirmed by the successful solution and refinement of the structure. The structures were solved by direct methods for L^1 and L^2; by Patterson methods for $Cu(L^2)_2$ and refined by full matrix least-squares and difference Fourier techniques with SHELXTL [12]. Multipurpose crystallographic tools, PLATON [13], ORTEP-3 [14] and MERCURY [15] were used for molecular graphics. Hydrogen atoms attached to amine nitrogen atoms were introduced as found on the Fourier difference maps and refined with the restraint N–H = 0.87 Å and a displacement parameter equal to 1.5 times that of the parent atom. All other hydrogen atoms were introduced geometrically and refined using a riding model with a displacement parameter equal to 1.2 (CH, CH_2) times that of the parent atom. All non-hydrogen atoms were refined anisotropically. The high proportion of weak reflections for $Cu(L^2)_2$ is due to the not very good quality of the crystal. In fact, during the refinement process, a disorder of position was observed for the terminal oxygen atom of the perchlorate anion that was split over two distinct sites with an occupancy factor of 0.5 each.

2.6. Steady-state absorption and emission spectroscopy

The UV–Vis absorption spectra were recorded using a Shimadzu spectrophotometer (UV-3101PC). Steady-state emission spectra were recorded with a Spex spectrofluorimeter (Fluoromax-3). All spectra were corrected for instrumental response. The fluorescence quantum yield of the samples was determined relative to that of 4-aminophthalimide ($\phi_f = 0.7$ in tetrahydrofuran) [16].

2.7. Cyclic voltammetry

A CH-Instruments model 620A electrochemical analyzer was used for cyclic voltammetric experiments with acetonitrile solutions of the systems containing $[Bu_4N]ClO_4$ as supporting electrolyte. The three-electrode measurements were carried out at room temperature under nitrogen atmosphere with a platinum disk working electrode, a platinum wire auxiliary electrode and a saturated calomel reference electrode. The potentials reported are uncorrected for junction contributions.

3. Results and discussion

3.1. Synthesis

The syntheses of the ligands L^1 and L^2 are straightforward and high yielding. The reaction of 4-aminophthalimide with neat 2-aminomethylpyridine or 2-aminoethylpyridine at 65 or 80 °C yielded L^1 or L^2 respectively (Scheme 1). The copper(I) complex, $Cu(L^2)_2$, was prepared by reacting L^2 with $Cu(ClO_4)_2 \cdot 6H_2O$ in 1:1 methanol–acetonitrile at room temperature for 24 h. One novel aspect about the synthesis of these complexes is that neither the use of any external reducing agent nor that of the relatively unstable copper(I) salt is needed. The relative stability of copper(I) and copper(II) in solution depend very strongly on the nature of the anions and the ligands present and vary considerably with solvent or nature of the neighboring atoms [10]. When the reaction was carried out with 1:2 metal–ligand molar ratio, the yield of the desired complex reduces substantially, suggesting that the ligand systems L^1 or L^2 acts as a reducing agent for Cu^{2+} [10]. It should be noted here that when the corresponding NO_3^- salt was used, neither the Cu^{2+} nor the Cu^+ complex could be isolated. Thus, the ClO_4^- anion also plays an important role in the stabilization Cu^+. In recent years, hydrothermal/solvothermal reactions under pressure have been used as a synthetic strategy to reduce various metal ions, including copper. Thus, the simultaneous reduction of copper(II) and formation of a two-coordinate copper(I) complex has significant implication with a synthetic viewpoint.

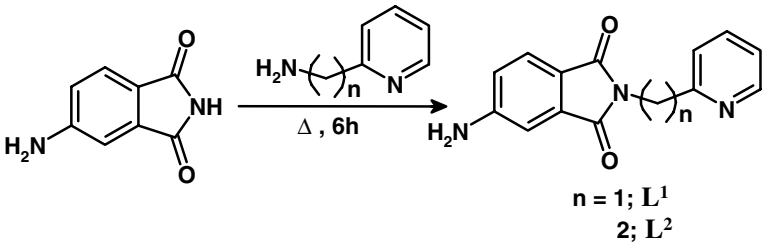

Scheme 1.

3.2. Absorption and fluorescence properties

The absorption and fluorescence spectra of $\mathbf{L^1}$, $\mathbf{L^2}$ and $\mathbf{Cu(L^2)_2}$ are characterized by broad bands, typical of the transition to the intramolecular charge-transfer state of the fluorophore moiety. A typical plot in acetonitrile (AN) is shown in Fig. 1. The 4-aminophthalimide moiety in these systems gives rise to a charge transfer transition in the UV–Vis region due to the push-pull effect of the electron-donating amino and the electron-withdrawing carbonyl groups of the fluorophore. Both the absorption and the fluorescence spectra are red-shifted (9–10 nm in absorption and 14–22 nm in the fluorescence) relative to the parent fluorophore. Apart from the spectral shift, the photophysical behavior of these systems are similar to that of the parent fluorophore, 4-aminophthalimide. These systems exhibit high fluorescence quantum yield ($\phi_f \sim 0.8$ in AN). The fluorescence quantum yield of the complexes is found to be slightly lower ($\phi_f \sim 0.6$ in AN) than that of their respective ligand systems, which could be due to the interaction of the fluorophore with the metal center. The photophysical data of the present systems in acetonitrile are listed in Table 1.

Table 1
Absorption and fluorescence[a] properties of 4-aminophthalimide (**AP**), $\mathbf{L^1}$, $\mathbf{L^2}$, $\mathbf{Cu(L^1)_2}$ and $\mathbf{Cu(L^2)_2}$ in acetonitrile (AN)

Compounds	λ_{max}^{abs} (nm)[b]	λ_{max}^{flu} (nm)[b]	ϕ_f[c]
AP	357	458	0.63
$\mathbf{L^1}$	366	472	0.78
$\mathbf{L^2}$	366	474	0.75
$\mathbf{Cu(L^1)_2}$	367	480	0.53
$\mathbf{Cu(L^2)_2}$	367	477	0.58

[a] $\lambda_{exc} = 360$ nm.
[b] ±2 nm.
[c] ±10%.

3.3. Structural studies. Crystal structure of L^1 and L^2

Slow evaporation of the chloroform solution of $\mathbf{L^1}$ and $\mathbf{L^2}$ yielded yellow crystals, suitable for X-ray diffraction studies. An ORTEP view with the atom numbering scheme is given in Fig. 2(a) and (b), respectively. Compounds $\mathbf{L^1}$ and $\mathbf{L^2}$ bearing a *fluorophore–spacer–receptor* architecture differ only in one methylene unit that separates the 4-aminophthalimide and pyridine moieties. However, a large difference exists in their crystallization space groups. While $\mathbf{L^1}$ crystallizes in the non-centrosymmetric orthorhombic space group *Fdd*2, $\mathbf{L^2}$ crystallizes in the monoclinic space group *C*2/*c* (Table 2). In both the compounds, the packing is determined by the intermolecular N–H···O and N–H···N hydrogen bonds involving the amino nitrogen atom, the carbonyl oxygen atom and the pyridine nitrogen atom. However, the network of the packed molecules in these systems is largely different (Fig. 3). Moreover, the molecules are more closely packed in $\mathbf{L^1}$ as compared to $\mathbf{L^2}$. This difference in the packing of the molecules is also reflected by the bending of the plane of the pyridine ring with respect to the phthalimide ring in these compounds. The dihedral angle between the planes defined by phthalimido and pyridyl rings in $\mathbf{L^1}$ and $\mathbf{L^2}$ is 85.79(23)° and 39.33(6)°, respectively.

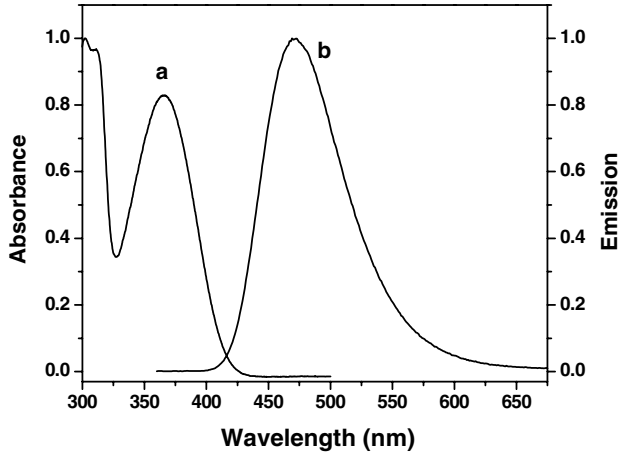

Fig. 1. Absorption (a) and fluorescence (b) spectra of $\mathbf{L^2}$ in acetonitrile.

3.4. Crystal structure of $Cu(L^2)_2$

The crystal structure of $[Cu(L^2)_2]ClO_4$ ($\mathbf{Cu(L^2)_2}$) shows a mononuclear complex in which copper is coordinated to the pyridine nitrogen atom of each ligand unit. The crystallographic parameters and data are collected in Table 2 and the molecular structure is shown in Fig. 2(c). The copper atom is situated on a two-fold axis and the geometry of the cationic portion is a linear L–Cu^I–L moiety with Cu1–N1 = Cu1–N1A = 1.89 Å. The Cu–N bond length is very similar to that previously reported for two-coordinate copper(I) complexes with nitrogen donor ligands [6–8]. A strong intermolecular N–H···O hydrogen bond between

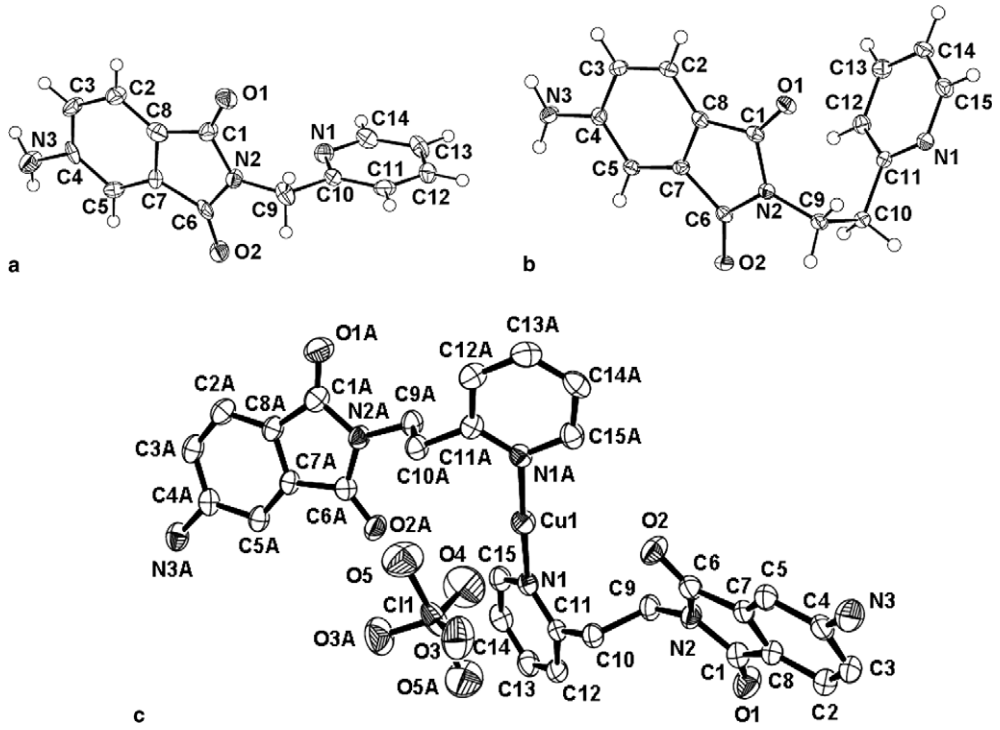

Fig. 2. Ortep diagram of (a) $\mathbf{L^1}$ with atoms represented by thermal ellipsoid at the 50% probability level; selected atom distances (Å): C1–O1 = 1.207(9), C6–O2 = 1.204(9), C4–N3 = 1.374(9), (b) $\mathbf{L^2}$ with atoms represented by thermal ellipsoid at the 50% probability level; selected atom distances (Å): C1–O1 = 1.213(2), C6–O2 = 1.216(2), C4–N3 = 1.362(2), (c) $\mathbf{Cu(L^2)_2}$ with atoms represented by thermal ellipsoid at the 20% probability level; two occupancy sites for the disordered perchlorate oxygen atom are displayed; hydrogen atoms are not shown for clarity; selected atom distances (Å) and bond angles (°): Cu1–N1 = Cu1–N1A = 1.891(4), C1–O1 = 1.215(7), C6–O2 = 1.199(6), C4–N3 = 1.378(8), ∠N1–Cu1–N1A = 176.85(25)°.

Table 2
Crystallographic data for compounds $\mathbf{L^1}$, $\mathbf{L^2}$ and the copper(I) complex $\mathbf{Cu(L^2)_2}$

	$\mathbf{L^1}$	$\mathbf{L^2}$	$\mathbf{Cu(L^2)_2}$
Formula	$C_{14}H_{11}N_3O_2$	$C_{15}H_{13}N_3O_2$	$C_{30}H_{26}ClCuN_6O_8$
Formula weight	253.26	267.28	697.56
Crystal system	orthorhombic	monoclinic	monoclinic
Space group	*Fdd*2	*C*2/*c*	*C*2/*c*
a (Å)	48.067 (16)	26.312 (4)	24.761 (2)
b (Å)	7.504 (3)	5.2500 (8)	7.5815 (7)
c (Å)	13.292 (4)	21.028 (3)	16.3684 (15)
α (°)	90	90	90
β (°)	90	116.08 (2)	102.915 (2)
γ (°)	90	90	90
V (Å^3)	4795 (3)	2609.0 (7)	2995.0 (5)
Z	16	8	4
F(000)	2112	1120	1432
ρ_{calcd} (g cm^{-3})	1.403	1.361	1.547
μ (mm^{-1})	0.097	0.093	0.881
Temperature (K)	100	100	293
Crystal size	0.48 × 0.05 × 0.02	0.48 × 0.29 × 0.15	0.24 × 0.15 × 0.05
Color, habit	yellow, block	yellow, thin plates	brown, thin plates
Absorption correction	multi-scan	multi-scan	multi-scan
T_{min}, T_{max}	0.798, 0.998	0.862, 0.986	0.792, 0.957
Total number of reflections	12726	14482	18730
Number of unique reflections	1492	3130	3616
Number of observed reflections[a]	1245	2510	1430
θ_{max} (°)	28.17	28.25	28.27
Number of parameters	178	189	220
R indices[b]: *R*, R_w	0.0970, 0.2279	0.0544, 0.1237	0.0854, 0.1947
Goodness-of-fit	1.288	1.075	1.027
$\Delta\rho_{max}$, $\Delta\rho_{min}$ (e/Å^3)	0.616, −0.318	0.425, −0.217	0.407, −0.189

[a] $[I > 2\sigma(I)]$.
[b] Refinement on F^2.

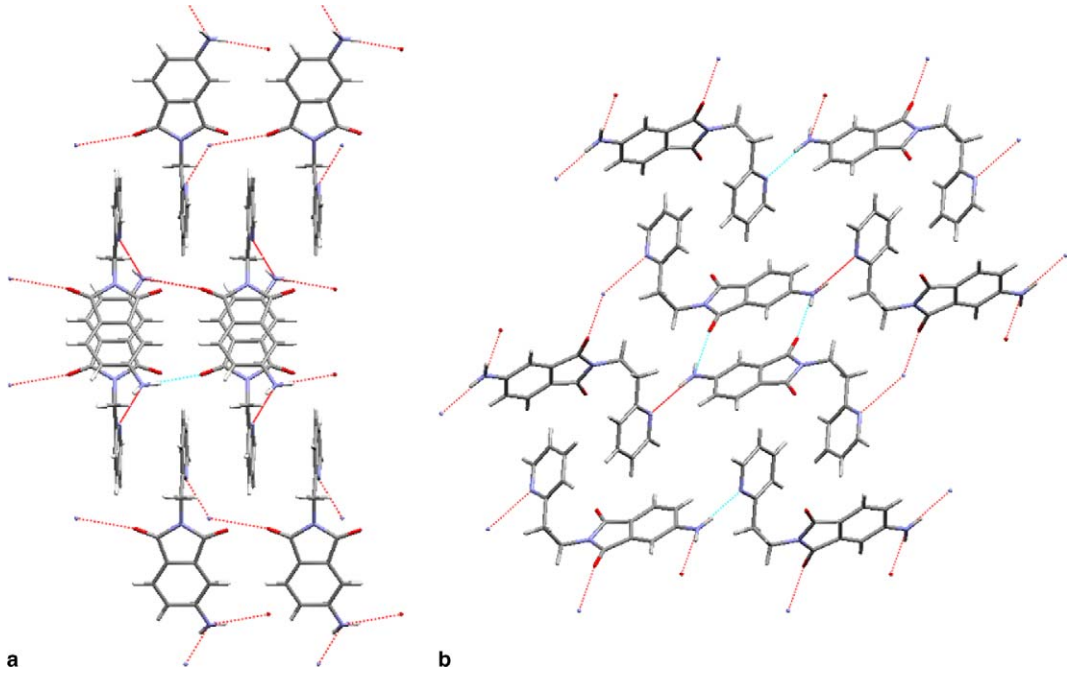

Fig. 3. Packing diagram along the y-axis illustrating the intermolecular hydrogen bonding shown as dashed lines for (a) $\mathbf{L^1}$: d(N3–H3A···N1[$-x$, $-y$, z]) = 3.034 Å, ∠N3–H3A···N1[$-x$, $-y$, z] = 158.95°; d(N3–H3B···O1[$-x$, $-y+1/2$, $z+1/2$]) = 3.026 Å, ∠N3–H3B···O1[$-x$, $-y+1/2$, $z+1/2$] = 152.45° and (b) $\mathbf{L^2}$: d(N3–H3A···N1[x, $-y+1$, $z-1/2$]) = 3.020 Å, ∠N3–H3A···N1[x, $-y+1$, $z-1/2$] = 167.89°; d(N3–H3B···O2[$-x$, $-y$, $-z$]) = 3.044 Å, ∠N3–H3B···O2[$-x$, $-y$, $-z$] = 155.71°.

the amino nitrogen atom and the imide oxygen atom of a neighboring molecule, forming a two-dimensional network, is observable in the complex (Fig. 4). The dihedral angle between the planes defined by the pyridyl and phthalimido rings is 22.49(15)°. Comparison with $\mathbf{L^2}$ indicates that the twisting of the pyridyl ring with respect to the phthalimido ring is significantly reduced upon coordination. The relatively large bending in $\mathbf{Cu(L^1)_2}$ (61.8(16)°) [10] brings O2 and O2A in close contact with the copper ion (Cu1···O2 = Cu1···O2A = 3.03 Å and ∠O2···Cu1···O2A = 180°), reflecting a weak electronic interaction between Cu^I and one of the imide oxygen atoms of the ligand unit. On the other hand, $\mathbf{Cu(L^2)_2}$ experiences a very weak interaction from the imide oxygen atom (Cu1···O2 = Cu1···O2A = 4.0 Å).

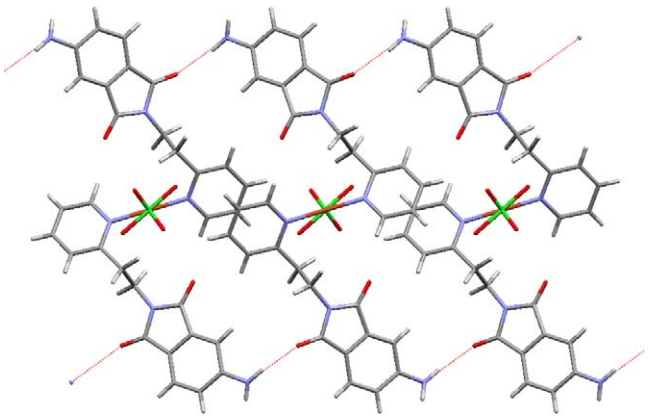

Fig. 4. View of $\mathbf{Cu(L^2)_2}$ along the y-axis illustrating the intermolecular hydrogen bonding, shown as dashed lines, leading to a 2-D network: d(N3–H3A···O1[x, $-y+1$, $z+1/2$]) = 2.965 Å and ∠N3–H3A···O1[x, $-y+1$, $z+1/2$] = 172.75°.

Upon careful inspection, a weak $Cu^I\cdots O$ interaction between Cu^+ and oxygen atoms of the ClO_4^- anion was also observed (Cu1···O4 = 2.707 Å). It should be noted that the ClO_4^- anion is disordered and that there are errors in the oxygen positions. However, the interacting oxygen atom is situated on a 2-fold axis and that leads to a T-shaped structure. The T-shaped molecular units are stacked over one another to form a linear network (Fig. 5). Weak Cu···O interactions of about 3 Å are found in copper-containing enzymes [17]. Although such additional or multiple weak interactions [18] with an oxygen atom of the ClO_4^- anion are known for linear L–M–L complexes [19], the resulting T-shaped geometry leading to a linear network illustrates the novelty of this complex.

3.5. Stability and redox properties

$\mathbf{Cu(L^2)_2}$ exhibits indefinite stability in the solid state. Oxidation of Cu^+ to Cu^{2+} in polar or coordinating solvents such as acetonitrile or even in protic solvents such as methanol was not observed even when kept in the open air for several months. Although the linear geometry is known to disfavor O_2 and CO interaction under certain conditions, two-coordinate copper(I) complexes with sterically unhindered monodentate ligands undergo rapid auto-oxidation in air, especially in protic solvents [6–8]. Thus, the stability of the complex towards oxidation is remarkable and quite interesting.

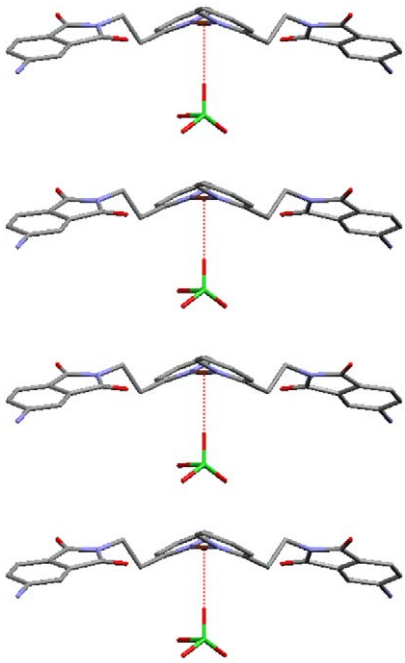

Fig. 5. View of $\mathbf{Cu(L^2)_2}$ along the z-axis showing the close contact of copper with one of the oxygen atoms of the ClO_4^- counter-anion, forming a T-shaped molecule and leading to a linear network: Cu1···O4 = 2.707(8) Å, ∠O4···Cu1···N1 = ∠O4···Cu1···N1A = 91.58(12)°.

Cyclic voltammetry studies of the ligands $\mathbf{L^1}$, $\mathbf{L^2}$ and their copper(I) complexes, $\mathbf{Cu(L^1)_2}$ and $\mathbf{Cu(L^2)_2}$ in acetonitrile reveal an irreversible oxidation with very high current associated with the oxidation property of the electron-deficient 4-aminophthalimide of the ligand framework (Fig. 6). The measured potentials range between 1.58 and 1.44 V (vs Fc/Fc^+ in CH_3CN/0.1 M $[Bu_4N]ClO_4$). The absence of an oxidation wave for the Cu(I)/Cu(II) couple [20,21] indicates significant stabilization of the monovalent oxidation state. The extraordinary stabilization of the Cu(I) state in these complexes is achieved by its weak interactions with the imide and perchlorate oxygen atoms which put the Cu^+ ion in an octahedral hole. This is further substantiated by the fact that $\mathbf{Cu(L^2)_2}$, the metal center of which is more separated from the 4-aminophthalimide moiety, exhibits a lesser stability compared to $\mathbf{Cu(L^1)_2}$. Moreover, copper(II) complexes have a tendency to form four-coordinate and in some cases five-coordinate complexes in solution, typically via coordination of a solvent molecule as the fifth ligand. Steric and/or electronic shielding provided by the 4-aminophthalimide moiety is also likely to disfavor the formation of the Cu(II) oxidation state. Therefore, this exceptional inertness is attributable to the highly favorable electronic factors provided by the 4-aminophthalimide and the perchlorate moieties.

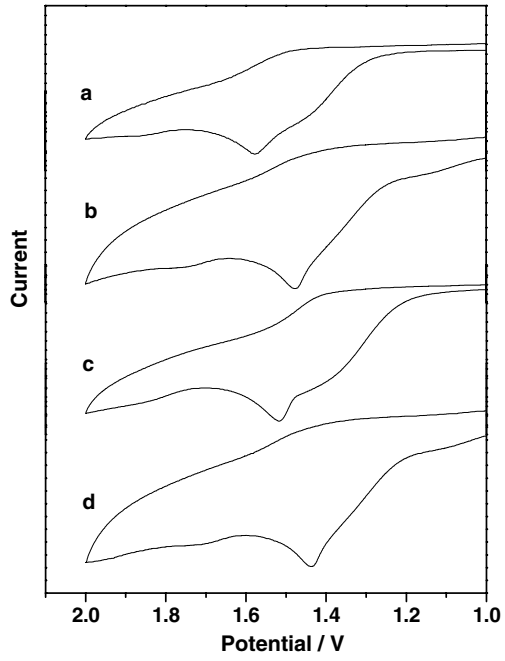

Fig. 6. Cyclovoltammogram for $\mathbf{L^1}$ (a), $\mathbf{Cu(L^1)_2}$ (b), $\mathbf{L^2}$ (c) and $\mathbf{Cu(L^2)_2}$ (d) in acetonitrile with 0.1 M $[Bu_4N]ClO_4$ as supporting electrolyte (potential plotted against the Fc/Fc^+ couple).

4. Conclusions

In conclusion, we have synthesized a new fluorescent ligand $\mathbf{L^2}$ and its two-coordinate copper(I) complex, $\mathbf{Cu(L^2)_2}$, having a linear geometry and resistance to oxidation even in a protic aerated medium. The single crystal structures of $\mathbf{L^2}$ and a previously reported ligand $\mathbf{L^1}$ are also presented. The new copper(I) complex $\mathbf{Cu(L^2)_2}$, in which the metal center is more separated from the 4-aminophthalimide moiety, exhibits lesser stability than the copper(I) complex of $\mathbf{L^1}$, $\mathbf{Cu(L^1)_2}$, suggesting the importance of the electronic environment around the metal binding site in controlling the Cu(I)-oxidation reactivity. The judicious choice of the ligand system and the counter-anion forms an essential condition in the formation of stable two-coordinate complexes of copper(I). This complex is a second example of its kind with a potential for the development of copper(I) chemistry. Furthermore, the spectroscopic properties associated with these complexes may be utilized to monitor the reactivity of copper(I) with various other molecules.

5. Supplementary data

CCDC-278525–278527 contain the supplementary crystallographic data for this paper. These data can be obtained free of charge from CCDC, 12 Union Road, Cambridge, CB2 1EZ, UK, fax: +44 1223 366 033, e-mail: deposit@ccdc.ac.uk or on the web www: www.ccdc.cam.ac.uk/data_request/cif.

Acknowledgements

The authors thank Prof. S. Pal for his help and suggestions in solving the crystal structure of the compounds. Financial support for this work is provided by the Council

of Scientific and Industrial Research (CSIR) and the Department of Science and Technology (DST), Government of India. S.B. thanks CSIR for a Fellowship. The National Single Crystal Diffractometer Facility (funded by the DST), School of Chemistry, University of Hyderabad, India and the UPE Program of the University Grants Commission (UGC) are gratefully acknowledged.

References

[1] D.R. McMillin, K.M. McNett, Chem. Rev. 98 (1998) 1201.
[2] N. Armaroli, Chem. Soc. Rev. 30 (2001) 113.
[3] R.H. Holm, P. Kennepohl, E.I. Solomon, Chem. Rev. 96 (1996) 2239.
[4] W. Kaim, J. Rall, Angew. Chem., Int. Ed. Engl. 35 (1996) 43.
[5] T.N. Sorell, M.R. Malachowski, Inorg. Chem. 22 (1983) 1883.
[6] T.N. Sorell, D.L. Jameson, J. Am. Chem. Soc. 105 (1983) 6013.
[7] I. Sanyal, K.D. Karlin, R.W. Strange, N.J. Blackburn, J. Am. Chem. Soc. 115 (1993) 11259.
[8] L. Le Clainche, M. Giorgi, O. Reinaud, Eur. J. Inorg. Chem. (2000) 1931.
[9] H.-C. Liang, E. Kim, C.D. Incarvito, A.L. Rheingold, K.D. Karlin, Inorg. Chem. 41 (2002) 2209.
[10] S. Banthia, A. Samanta, Inorg. Chem. 43 (2004) 6890.
[11] D.D. Perrin, W.L.F. Armarego, D.R. Perrin, Purification of Laboratory Chemicals, Pergamon Press, New York, 1980.
[12] SMART, SAINTPLUS, SHELXTL, SADABS, Bruker AXS, Inc., Madison, WI, 2003.
[13] A.L. Spek, PLATON, Utrecht University, Utrecht, The Netherlands, 1998.
[14] L.J. Farrugia, J. Appl. Cryst. 30 (1997) 565.
[15] MERCURY 1.2.1, CCDC, UK, 2004.
[16] S. Banthia, A. Samanta, J. Phys. Chem. B 106 (2002) 5572.
[17] W. Kaim, B. Schwederski, Bioinorganic Chemistry, Wiley, Chichester, UK, 1994.
[18] M. Albrecht, K. Hubler, S. Zalis, W. Kaim, Inorg. Chem. 39 (2000) 4731.
[19] M. Munukata, S. Kitagawa, H. Shimono, H. Masuda, Inorg. Chim. Acta 168 (1989) 217.
[20] M.K. Eggleston, D.R. McMillin, K.S. Koenig, A.J. Pallenberg, Inorg. Chem. 36 (1997) 172.
[21] M.T. Miller, P.K. Gantzel, T.B. Karpishin, Inorg. Chem. 38 (1999) 3414.

such as monodentate, bridging bidentate and as monoatomic bridge, either alone (one oxygen atom connect two metal ions) or with an additional bridging (the second oxygen atom acts as monodentate) [4]. In particular, in the coordination polymers obtained from $Zn(OAc)_2 \cdot 2H_2O$ with NN spacers the acetate ion has shown several of its structural arrays: (a) monodentate in the complex $[Zn(OAc)_2(4,4'\text{-dps})]_n$ (4,4′-dps = 4,4′-dipyridylsufide) [5] with the cation Zn(II) as node, (b) bidentate and bridging bidentate modes in the complex $[Zn(OAc)_2(4,4'\text{-bpy})]_n$ (4,4′-bpy = 4,4′-bipyridine) that it includes the neutral binuclear $\{Zn(OAc)_2\}_2$ core [6], (c) bidentate, bridging and monoatomic with additional bridging configurations in the complex $[Zn_2(OAc)_4(4,4'\text{-bpy})]_n$ [7] with $\{Zn(OAc)_2\}$ dimeric units as nodes and (d) bridging and monoatomic with additional bridging modes in the heptanuclear derivatives $[Zn_7(\mu_4\text{-}O)_2(OAc)_{10}(bpe)]_n$ (bpe = 1,2-bis (4-pyridyl)ethane) and $[Zn_7(\mu_4\text{-}O)_2(OAc)_{10}(dpds)]_n$ (dpds = 4,4′-dipyridyldisulfide) [8] with the oxo-acetate core $\{Zn_7(\mu_4\text{-}O)_2(OAc)_{10}\}$. These results show that the species that reach the highest nuclearity are the metal-organic frameworks $[Zn_7(\mu_4\text{-}O)_2(OAc)_{10}(NN)]_n$. which involves the flexible NN spacers bpe and dpds. The main characteristic of these two Zn_7 compounds is in the presence of two assembled tetrahedral oxo groups $\{Z_4(\mu_4\text{-}O)\}$ [9], which together with the ten bridging acetates interconnect the seven zinc ions. These oxoacetate products, obtained by reacting zinc acetate with the plastic NN spacers in a 7:1 ratio, form one-dimensional coordination polymeric chains. On the other hand, the results also show that by using non-flexible NN ligands in reactions with zinc acetate have lead exclusively to the synthesis of low nuclearity Zn(II) systems. In other words, the rigid linkers 4,4′-bpy and 4,4′-dps lead to coordination polymers with metal-to-ligand ratio of 1:1 ($[Zn(OAc)_2(NN)]_n$ (NN = 4,4′-bpy; 4,4′-dps)) [5,6] and 2:1 ($[Zn_2(OAc)_4(4,4'\text{-bpy})]_n$) [7]. Other carboxylate systems containing the $\{Zn_7(\mu_4\text{-}O)_2(carboxylate)_{10}\}$ core have been reported, but they are formulated as the discrete acetate-based clusters $[Zn_7(\mu_4\text{-}O)_2(OAc)_{10}(L_2)]$ (L = pyridine [10], 1-methylimidazole [11], pyrazine [12]) and the 2,6-difluorobenzoate-based clusters $[Zn_7(\mu_4\text{-}O)_2(2,6\text{-difluorobenzoate})_{10}(L_2)]$ (L = THF, MeCN) [13].

Considering the above overview we decided to study how the increase of the length of the linker ligands affect to the nuclearity and the overall framework of polymeric structures. In this regard, herein we report on our finding when zinc acetate reacts with the NN spacers 1,4-bis(3-pyridyl)-2,3-diaza-1,3-butadiene (3pdb) [14] and 1,4-bis(4-pyridyl)-2,3-diaza-1,3-butadiene (4pdb) [15] (Scheme 1), which would appear at this moment as the longest employed in this type of systems. These *N*,*N*′ bidentate azine ligands have been used to generate coordination polymers with several metal centres (Co^{II}, Cd^{II}, Ni^{II}, Ag^{I}, Mn^{II}, Pb^{II}, Cu^{II}) containing diverse counterions (NO_3^-, SCN^-, I^-, saccharinate, α-thenoyltrifluoroacetonate) [14–16] where carboxylates are not included. Besides, the conjugated 3pdb and 4pdb ligands have demonstrated to be rigid connectors like

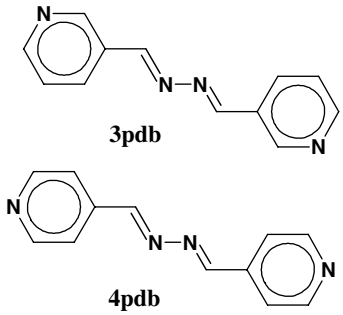

Scheme 1.

4,4′-bpy and 4,4′-dps, but longer than them due to the introduction of the spacer portion –CH=N–N=CH– between two pyridyl groups. Apparently, this could justify that the longer ligands 3pdb and 4pdb show a different behaviour from that of 4,4′-bpy and 4,4′-dps; they are able to carry out self-assembly reactions with zinc acetate to produce very easily under mild conditions the high nuclearity coordination polymers $[Zn_7(\mu_4\text{-}O)_2(OAc)_{10}(3pdb)]_n$ (**1**) and $[Zn_7(\mu_4\text{-}O)_2(OAc)_{10}(4pdb)]_n$ (**2**).

2. Experimental

All solvents were purchased from commercial sources and used without further purification. The compound $Zn(OAc)_2 \cdot 2H_2O$ was obtained from Merck. The 3pdb [14] and 4pdb [15] ligands were prepared following the literature procedures. The coordination polymers $[Zn_7(\mu_4\text{-}O)_2(OAc)_{10}(3pdb)]_n$ and $[Zn_7(\mu_4\text{-}O)_2(OAc)_{10}(4pdb)]_n$ were prepared in a similar manner from the reaction of $Zn(OAc)_2 \cdot 2H_2O$ with the appropriate bidentate Schiff-base ligand in a 7:1 metal-to-ligand ratio. A typical preparation is described below.

Synthesis of $[Zn_7(\mu_4\text{-}O)_2(OAc)_{10}(3pdb)]_n$ (**1**). The ligand 3pdb (4.0 mg, 0.019 mmol) was dissolved in MeCN (1.0 cm^3). A methanolic solution (2.0 cm^3) of $Zn(OAc)_2 \cdot 2H_2O$ (29.2 mg, 0.133 mmol) was then added and the mixture stirred for 1 min. The solution was warmed with gentle heating (60 °C) for 3 h. The crystalline solid formed was washed firstly with MeOH (3×3.0 cm^3) and then with diethyl ether (2×3.0 cm^3). The well formed yellow crystals were dried on the air (9.0 mg, 36.6% yield). *Anal.* Calc. for $C_{32}H_{40}N_4O_{22}Zn_7$: C, 29.79; H, 3.12; N, 4.34. Found: C, 29.87; H, 3.25; N, 4.16%. IR (KBr disc, cm^{-1}): 3433 (br), 1595 (s), 1430 (s), 1028 (m), 674 (m). For $[Zn_7(\mu_4\text{-}O)_2(OAc)_{10}(4pdb)]_n$ (**2**): (22.4% yield). *Anal.* Calc. for $C_{32}H_{40}N_4O_{22}Zn_7$: C, 29.79; H, 3.12; N, 4.34. Found: C, 29.63; H, 3.30; N, 4.22%. IR (KBr disc, cm^{-1}): 3440 (br), 1603 (s), 1429 (s), 1025 (m), 678 (m).

3. Instruments

IR spectra were recorded as KBr pellets on a Bruker Model IFS-55 FTIR instrument. The C, H and N contents of the compounds were determined on a Fisons-Carlo Erba EA 1108 microanalizer (CEPEDEQ Universidad de Chile).

4. Crystallography

The pertinent crystal and structure refinement are summarized in Table 1 and Table 2 lists the selected bond lengths and angles for compounds **1** and **2**. The yellow crystals measured approximately $0.22 \times 0.16 \times 0.10\ mm^3$ (**1**) and $0.40 \times 0.32 \times 0.18\ mm^3$ (**2**), respectively. Data were collected on a Bruker AXS SMART APEX CCD diffractometer with SMART [17] as the driving software; data integration was performed using SAINT [18] and a semi-empirical absorption correction applied. The structure was solved by direct methods and difference Fourier, and refined by least squares on F^2 with anisotropic displacement parameters for non-H atoms. All the hydrogen atoms were defined by the stereochemistry and accordingly placed at their calculated positions and allowed to ride onto their host carbons (C–H_{arom}, 0.95 Å; C–H_{methyl}, 0.95 Å) both in coordinates as well as thermal parameters (U_{iso} values were set to $1.2U_{eq}$ for aryl H and $1.5U_{eq}$ for methyl H). All calculations to solve the structures, refine the models proposed and obtain derived results were carried out with the computer programs SHELXTL [19] and local programs. Full use of the CCDC package was also made for searching in the CSD database [20].

Table 1
Crystal data and structure refinement for **1** and **2**

	Compound **1**	Compound **2**
Empirical formula	$C_{32}H_{40}N_4O_{22}Zn_7$	$C_{32}H_{40}N_4O_{22}Zn_7$
Formula weight	1290.27	1290.27
Temperature (K)	293(2)	273(2)
Wavelength (Å)	0.71073	0.71073
Crystal system	monoclinic	orthorhombic
Space group	*C*2/*m*	*Pnnm*
a (Å)	15.469(2)	14.3832(14)
b (Å)	13.268(2)	12.1848(12)
c (Å)	12.1198(19)	13.1534(13)
α (°)	90	90
β (°)	112.063(3)	90
γ (°)	90	90
V (Å^3)	2305.4(6)	2305.2(4)
Z	2	2
D_c (g cm^{-3})	1.859	1.859
μ (mm^{-1})	3.661	3.662
F(000)	1292	1292
Θ range (°)	1.81–27.90	2.10–27.98
Index ranges	$-20 \leqslant h \leqslant 20$, $-17 \leqslant k \leqslant 16$, $-15 \leqslant l \leqslant 15$	$-18 \leqslant h \leqslant 18$, $-15 \leqslant k \leqslant 15$, $-17 \leqslant l \leqslant 17$
Reflections collected	9507	18 618
Independent reflections [R_{int}]	2694 [0.0343]	2777 [0.0418]
Absorption correction	multi-scan	multi-scan
Maximum and minimum transmission	0.72 and 0.50	0.55 and 0.30
Data/parameters	2694/170	2777/170
Goodness-of-fit on F^2	1.068	1.038
Final *R* indices [$I > 2\sigma(I)$]	$R_1 = 0.0517$, $wR_2 = 0.1208$	$R_1 = 0.0578$, $wR_2 = 0.1491$
R indices (all data)	$R_1 = 0.0693$, $wR_2 = 0.1288$	$R_1 = 0.0766$, $wR_2 = 0.1620$
Largest differential peak and hole (e Å^{-3})	0.933 and −0.922	1.148 and −1.412

Table 2
Selected bond lengths (Å) and angles (°) for **1** and **2**

Bond lengths /bond angles	Compound **1**	Compound **2**
Zn(1)–O(1)	1.968(4)	1.959(4)
Zn(1)–O(2C)	2.161(3)	2.164(3)
Zn(2)–O(1)	1.915(2)	1.918(2)
Zn(2)–O(2A)	1.943(4)	1.945(4)
Zn(2)–O(1C)#1	1.948(3)	1.947(4)
Zn(2)–O(1B)	1.974(4)	1.978(4)
Zn(3)–O(1)	1.960(4)	1.971(4)
Zn(3)–O(1A)	2.048(3)	2.046(4)
Zn(3)–N(3)	2.070(5)	
Zn(3)–N(4)		2.069(5)
Zn(3)–O(2C)	2.468(3)	2.419(3)
Zn(1)...Zn(3)	3.0016(8)	2.9727(8)
O(1)–Zn(1)–O(2C)	81.75(11)	81.70(13)
O(2C)–Zn(1)–O(2C)#2	82.49(17)	81.8(2)
O(1)–Zn(2)–O(2A)	113.74(16)	113.56(16)
O(1)–Zn(2)–O(1C)#1	119.46(15)	119.63(15)
O(2A)–Zn(2)–O(1C)#1	104.90(18)	104.8(2)
O(1)–Zn(2)–O(1B)	108.64(15)	108.52(17)
O(2A)–Zn(2)–O(1B)	103.65(18)	102.31(19)
O(1C)#1–Zn(2)–O(1B)	105.03(17)	106.50(18)
O(1)–Zn(3)–O(1A)	103.19(12)	102.20(13)
O(1)–Zn(3)–O(1A)#2	103.19(12)	102.20(13)
O(1A)–Zn(3)–O(1A)#2	94.3(2)	93.8(3)
O(1)–Zn(3)–N(3)	155.88(17)	
O(1A)–Zn(3)–N(3)	93.07(13)	
O(1A)#3–Zn(3)–N(3)	93.07(13)	
O(1)–Zn(3)–N(4)		157.8(2)
O(1A)–Zn(3)–N(4)		92.88(15)
O(1A)#3–Zn(3)–N(4)		92.88(15)
O(1A)–Zn(3)–O(2C)#2	97.60(14)	97.26(16)
O(2C)–Zn(3)–O(2C)#2	70.52(14)	71.66(17)
Zn(2)–O(1)–Zn(2)#2	113.30(19)	113.5(2)
Zn(2)–O(1)–Zn(1)	109.66(12)	109.72(12)
Zn(2)–O(1)–Zn(3)	111.84(12)	112.24(12)
Zn(3)–O(1)–Zn(1)	99.67(16)	98.31(19)

Symmetry transformations used to generate equivalent atoms.
For **1**: #1 $-x, -y, -z$; #2 $x, -y, z$.
For **2**: #1 $-x, -y, -z$; #2 $x, y, -z$.

5. Results and discussion

The coordination polymers **1** and **2** were isolated from a MeOH–MeCN solution by treatment of $Zn(O_2CMe)_2 \cdot 2H_2O$ with the bis-pyridyl Shiff-base ligands 3pdb and 4pdb in a molar ratio 7:1 (metal-to-ligand) under gentle conditions (60 °C). Both compounds are stable in air and insoluble in common organic solvents. The IR spectra for **1** and **2** are very similar in the region characteristic of the acetate anions [4] showing the bands for ν_{asym}(COO) [1595 cm^{-1} (**1**); 1603 cm^{-1} (**2**)], ν_{sym}(COO) [1430 cm^{-1} (**1**); 1429 cm^{-1} (**2**)] and δ(OCO) [674 cm^{-1} (**1**); 677 cm^{-1} (**2**)]. For acetate derivatives the difference between ν_{asym}(COO) and ν_{sym}(COO) ($\Delta\nu$) in comparison with the ionic species has been used as a criteria for establishing its bonding mode [4,21]. In particular, the bands are shifted to higher frequencies with respect to that of the sodium acetate and they present a $\Delta\nu$ value of 165 cm^{-1} for **1** and 159 cm^{-1} for **2**, which is very close to that of the NaOAc of 159 cm^{-1}. This behaviour would indicate that

the acetate ions are bonded to the zinc atoms in a bridging mode which agree with the X-ray results discussed below.

The molecular diagrams of **1** and **2** are shown in Fig. 1(a) and (b), respectively, while in Table 1 the crystal and refinement data are presented. These compounds join the few ones already reported in the literature [8,10–12] containing the very tightly bound $\{Zn_7(\mu_4\text{-}O)_2(OAc)_{10}\}$ core. In both structures the unsaturated heptanuclear units act as nodes connected by the bridging 3pdb and 4pdb ligands to form chains. The Zn–N bond distances (2.070(5) and 2.069(5) Å, respectively) are slightly shorter than those observed in the related Zn(II) complexes, the non-polymeric compounds $[Zn(4pdb)_2(MeOH)_2(H_2O)_2](ClO_4)_2 \cdot 4pdb \cdot 1.72MeOH \cdot 1.28H_2O$ (2.120(2) Å) [22] and $[Zn(4pdb)_2(H_2O)_4](ClO_4)_2$ (2.131(3) Å) [23]. The N···N separation between the pyridyl nitrogen atoms in **1** (10.65(1) Å) and **2** (11.45(1) Å) are notably longer than the terminal N···N separations of 4,4′-dps (7.40(1) Å) and 4,4′-bpy (7.17(1) Å) found, e.g., in the 1:1 metal-to-ligand ratio complexes $[Zn(OAc)_2(4,4'\text{-dps})]_n$ [5] and $[Zn(OAc)_2(4,4'\text{-bpy})]_n$ [6], respectively.

Each seven nuclear core in **1** and **2** reveals a central Zn1 laying on a symmetry centre, two Zn3 atoms on a mirror plane which halves the hole group and four Zn2 atoms at general positions, thus accounting for the seven Zn sites per formula. Two oxo groups, also laying on the mirror plane are fourfold linked to four different zinc cations, acting as quadruple bridges. The remaining intercationic cohesion is implemented by six bidentate acetates (four of them generated by a single unit (A) in a general position and two by a second one (B) in a special position, halved by the mirror plane) in addition to four tridentate acetates, generated by single moiety (C) also in a general position. Completing the assemblage, there are two organic spacer molecules bonded to the Zn3 providing two nitrogens to the overall bonding scheme. The final result is Zn1 and Zn3 being

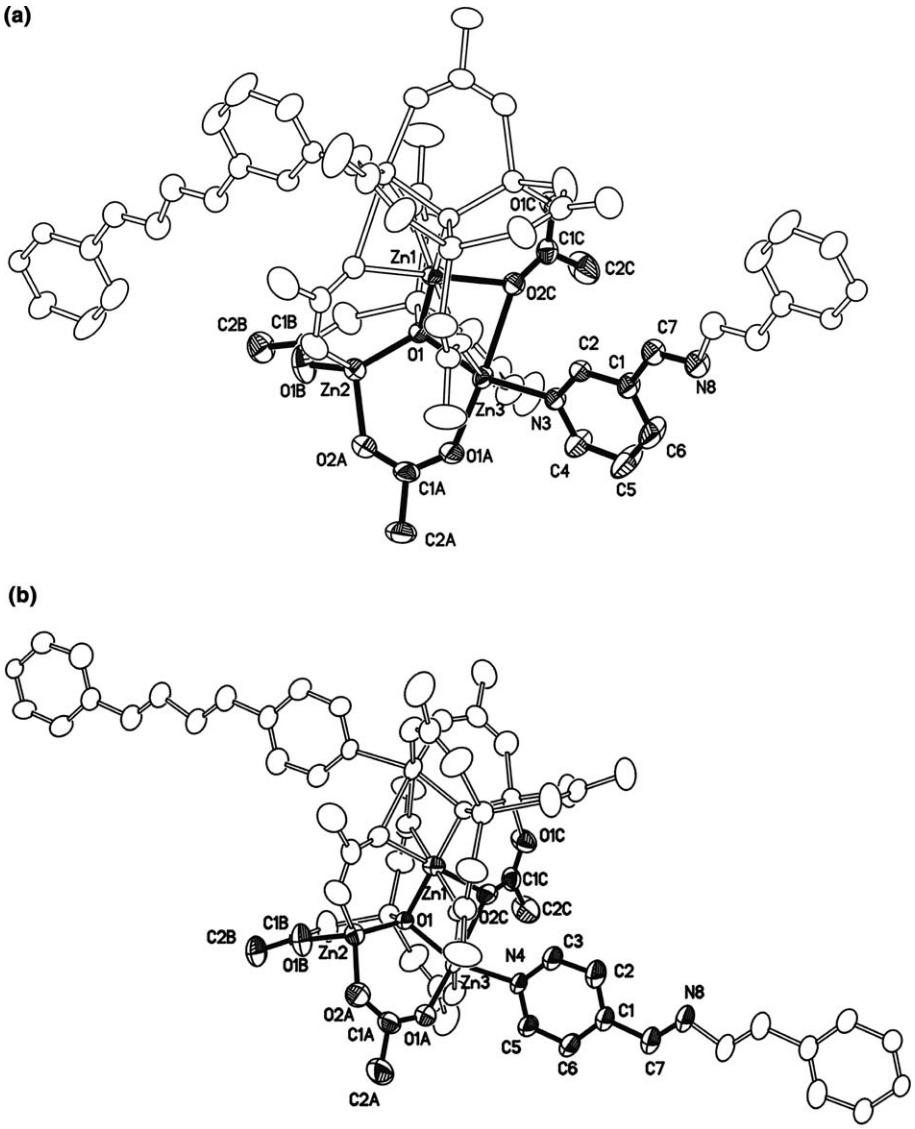

Fig. 1. (a) Molecular diagram of **1** and (b) molecular diagram of **2**. In both cases showing the independent part of the structure in full 40% thermal ellipsoids, and symmetry related atoms as open ellipsoids joined by open bonds.

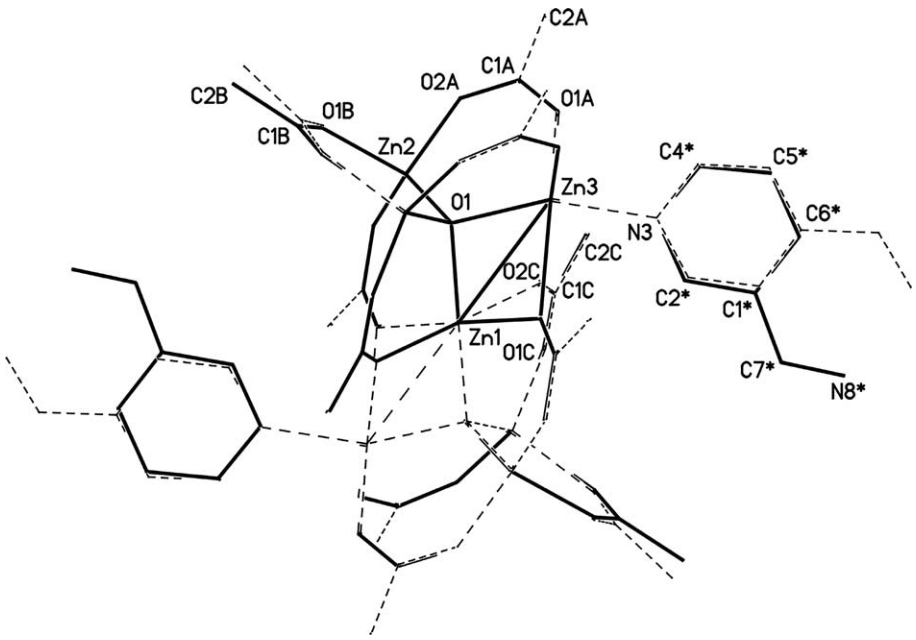

Fig. 2. Least squares fitting of the (enlarged) $\{Zn_7(\mu_4\text{-}O)_2(OAc)_{10}(NN)\}$ cores in **1** and **2**. Labelling corresponds to atoms in **1**. Starred atoms not included in the calculations.

octahedrally coordinated while Zn2 displays a tetrahedral environment, in due balance with the 34 bonds provided by the ligands. The Zn3 octahedron appears as highly distorted with four rather normal bonds (those to the pyridyl nitrogen, one oxo group and two oxygens from two bridging acetates, in a 1.960(4)–2.070(5) Å range) and two apical, loosely bonded, symmetry related oxygens from the tridentate acetates ($Zn\text{–}O_{apical}$: $2 \times 2.468(3)$ Å in **1**, $2 \times 2.419(3)$ Å in **2**). These latter weak Zn···O interactions are present in all the previously reported species containing the $\{Zn_7(\mu_4\text{-}O)_2(OAc)_{10}\}$ core [8,10–12], and are decidedly shorter than the sum of the van der Waals radii (2.9 Å) [24].

Table 2 presents a detailed survey of distances and angles around the metal centres. Inspection of the values therein confirms that in all cases the geometry around the cations is rather irregular in consonance with the stringent restraints imposed by chelation. In spite of this, the whole unit is very robust, and little prone to further distortions. This can be assessed by comparison of the present two $\{Zn_7(\mu_4\text{-}O)_2(OAc)_{10}\}$ moieties, even though that they appear surrounded by different environments and bound to dissimilar ligands, they look strikingly similar. In particular, the least squares fitting of the 41 atoms in the enlarged cores (two coordinated N atoms included) in **1** and **2** gave a r.m.s. deviation for the matched atoms as low as 0.09 Å (see Fig. 2). Being the cores identical, the main reason for the structural differences between **1** and **2** (viz., crystal system, space group, etc.) resides in the coordination mode of the bridging *N*,*N*′-bipyridyl ligands. When the coordinating nitrogens are in positions 4,4′ the coordination is "straighter", and the resulting chain less twisted than in the case of 3,3′. Fig. 3(a) and (b) show this in detail as well as the consequences of this has on the piling mode of the chains. The very twisted ones in **1** can superpose parallel to each other but with a shift along the chain direction, (parallel to the *a*-axis, Fig. 3(a)) of half a link, so as to have the very thin diazine ligands[1] superimposed to the bulky $\{Zn_7(\mu_4\text{-}O)_2(OAc)_{10}\}$ nodes of the neighbouring chains. In the case of **2**, this can only be achieved through a right angle disposition of the 1D arrays, with chains at level 0 running in one direction and those at level 0.5 at right angles (Fig. 3(b)).

The interaction between chains are very weak, with just one C–H···O contact per structure (Table 3). These interactions link chains at different heights (Fig. 3(a) and (b)), in an alternating way so as to determine a very weakly bound 3D network. These two at first sight quite dissimilar types of chain disposition in **1** and **2**, are however much alike in that they seek the opposition of peaks in one layer with troughs in the next, promoting a good fit between layers. This is a very different approach to the packing modes found in the remaining two polymeric structures already reported $[Zn_7(\mu_4\text{-}O)_2(OAc)_{10}(NN)]_n$ (NN = 1,2-bis(4-pyridyl)ethane, 4,4′-dipyridyldisulfide) [8], where "planes" of adjacent chains are simply superimposed to each other by means of a unit cell translation, with the result that peaks oppose with peaks and troughs oppose with troughs. The difference in packing efficiency is apparent: both **1** and **2** surprisingly achieve the same density, D_c: 1.859 g/cm^3, significantly larger than 1.65 and 1.72 g/cm^3 for the other two, in spite of a formula weight some 3% smaller. The reasons for this compactness preference are not clear, since the spacers 1,2-bis(4-pyridyl)ethane and 4,4′-dipyridyldisulfide

[1] The 3pdb and 4pdb ligands are halved by crystallographic symmetry centres, for what they show a strictly planar structure.

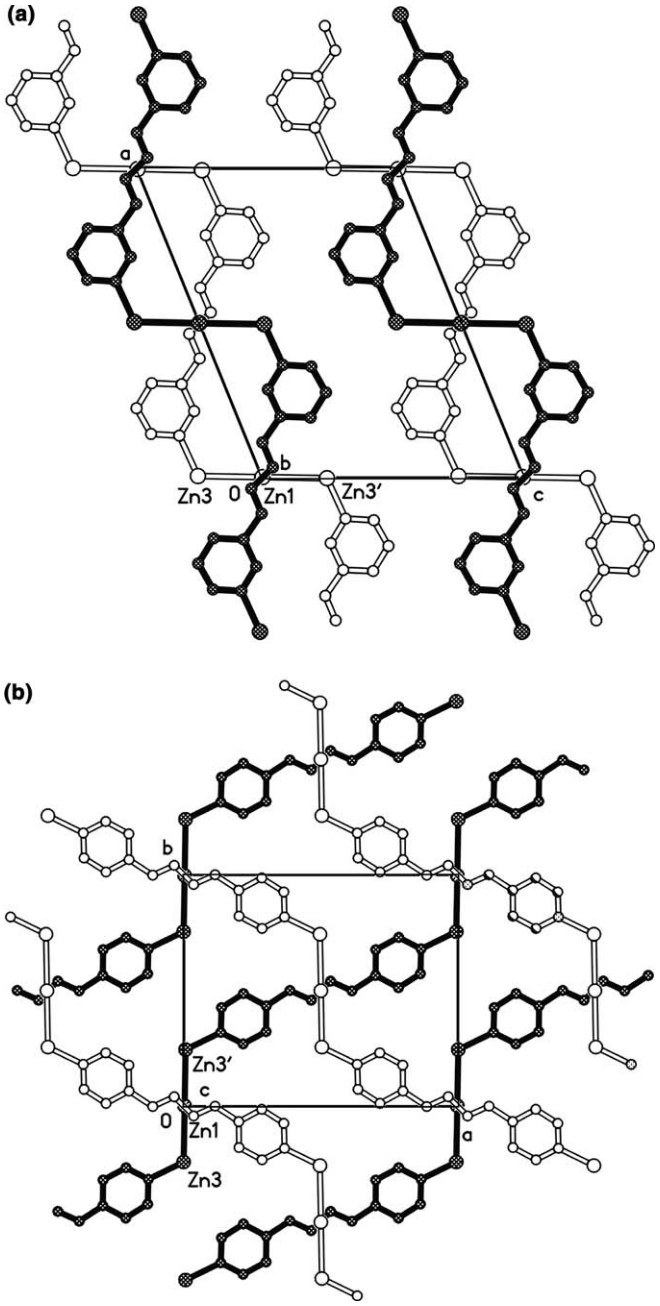

Fig. 3. (a) Packing diagram of **1**, drawn down the *b*-axis. (b) Packing diagram of **2**, drawn down the *c*-axis. The two figures show in heavy lining, chains at height $y = 0$, in light lining, those at $y = 0.50$. The bulky $\{Zn_7(\mu_4\text{-}O)_2(OAc)_{10}\}$ groups have been schematized by their Zn3–Zn1–Zn3′ nuclei, for clarity.

are in principle more flexible than 3pdb and 4pdb, the ones in **1** and **2**, and accordingly potentially able to adapt a variety of conformations and prone to avoid undesirable steric collisions. Additional structural information on related polymers will be needed to clarify the subject, as well as to assess which is the leading parameter deciding the formation of the Zn_7 nuclei under very similar synthetic conditions. So far, the trend seems to be that those ligands promoting a very weak interaction between potentially adjacent Zn_7 groups (very long bridging spacers) favour the formation and stability of these nuclei. On the other hand, when shorter spacers are used, instead (4,4′-bpy, 4,4′-dps) much simpler Zn nuclei are stabilized.

Table 3
Weak interchain contacts (Å, °)

Structure	Contact	C—H	H···O	C···O	∠C–H···O
1	C2A–H2AB···O2A#3	0.96	2.53	3.470(9)	166
2	C2A–H2AB···O1C#4	0.96	2.58	3.532(8)	174

Symmetry codes. #3: $-1/2 - x$, $-1/2 - y$, $1 - z$; #4: $-1/2 + x$, $1/2 - y$, $-1/2 + z$.

6. Conclusion

This research gives evidence that the thin, rigid and long ligands 1,4-bis(3-pyridyl)-2,3-diaza-1,3-butadiene (3pdb) and 1,4-bis(4-pyridyl)-2,3-diaza-1,3-butadiene (4pdb) are able to join the bulky heptanuclear $\{Zn_7(\mu_4\text{-}O)_2(OAc)_{10}\}$ fragments through their terminal 3- and 4-pyridyl nitrogen donor atoms. Indeed, the results show that divergent *N*,*N*′-bipyridyl spacers could form coordination polymers with zinc carboxylates nodes of significant high nuclearities, under the requirement that they be long enough to avoid steric repulsions. On the other hand, the characteristic rigid planar structure of the ligands like 3pdb and 4pdb could be a factor to be considered that would permit an efficient piling producing a high density packing scheme, such as the observed in the compounds **1** and **2**, in contrast with the low density of the polymers with the flexible 4,4′-bpy and 4,4′-dps linkers.

Acknowledgements

We are grateful to the Universidad de La Frontera for financial support (Proyecto DIUFRO 120416), CONICYT-FONDAP (project 11980002) for the purchase of a CCD detector and the Spanish Research Council (CSIC) for provision of a free-of-charge license to the CSD system.

Appendix A. Supplementary data

Crystallographic data (excluding structure factors) have been deposited with the Cambridge Crystallographic Data Centre as supplementary publication CCDC Nos. 280714 and 280715. Copies of the data can be obtained free of charge on application to CCDC, 12 Union Road, Cambridge CB2 1EZ, UK (fax: +44 1223 336 033; e-mail: deposit@ccdc.cam.ac.uk). Supplementary data associated with this article can be found, in the online version, at doi:10.1016/j.poly.2006.01.015.

References

[1] A. Erxleben, Coord. Chem. Rev. 246 (2003) 203.
[2] N. Lalioti, C.P. Raptopoulou, A. Terzis, A.E. Aliev, I.P. Gerothanassis, E. Manessi-Zoupa, S.P. Perlepes, Angew. Chem. Int. Ed. 40 (2001) 3211.
[3] G. Guilera, J.W. Steed, Chem. Commun. (1999) 1563.

[4] G.B. Deacon, R.J. Phillips, Coord. Chem. Rev. 33 (1980) 227.
[5] S. Muthu, Z. Ni, J.J. Vittal, Inorg. Chim. Acta 358 (2005) 595.
[6] B. Conerney, P. Jensen, P.E. Kruger, B. Moubaraki, K.S. Murray, Cryst. Eng. Commun. 5 (2003) 454.
[7] T.-W. Lee, J.P.-K. Lau, W.-T. Wong, Polyhedron 23 (2004) 999.
[8] M.T. Ng, T.C. Deivaraj, J.J. Vittal, Inorg. Chim. Acta 348 (2003) 173.
[9] (a) F.A Cotton, L.M. Daniels, L.R. Falvello, J.H. Matonic, C.A. Murillo, X. Wang, H. Zhou, Inorg. Chim. Acta 266 (1997) 91;
(b) J. Tao, M.-L. Tong, J.-X. Shi, X.-M. Chen, S.W. Ng, Chem. Commun. (2000) 2043;
(c) H.K. Chae, M. Eddaoudi, J. Kim, S.I. Hauck, J.F. Hartwig, M. O'Keeffe, O.M. Yaghi, J. Am. Chem. Soc. 123 (2001) 11482.
[10] D. Attanasio, G. Dessy, V. Fares, J. Chem. Soc., Dalton Trans. (1979) 28.
[11] N. Lalioti, C.P. Raptopoulou, A. Terzis, A.E. Aliev, S.P. Perlepes, I.P. Gerothanassis, E. Manessi-Zoupa, Chem. Commun. (1998) 1513.
[12] A. Waheed, R.A. Jones, J. McCarty, X. Yang, J. Chem. Soc., Dalton Trans. (2004) 3840.
[13] D.J. Darensbourg, J.R. Wildeson, J.C. Yarbrough, Inorg. Chem. 41 (2002) 973.
[14] Y.-B. Dong, M.D. Smith, R.C. Layland, H.-C. zur Loye, Chem. Mater. 12 (2000) 1156.
[15] D.M. Ciurtin, Y.-B. Dong, M.D. Smith, T. Barclay, H.-C. zur Loye, Inorg. Chem. 40 (2001) 2825.
[16] (a) H. Davis, L. Peterson Jr., A.M. Goforth, M.D. Smith, P. Zhang, H.-C. zur Loye, J. Chem. Crystallogr. 34 (2004) 299;
(b) Y.-B. Dong, M.D. Smith, H.-C. zur Loye, J. Solid State Chem. 155 (2000) 143;
(c) Y.-B. Dong, M.D. Smith, H.-C. zur Loye, Inorg. Chem. 39 (2000) 4927;
(d) S. Kallil, L. Peterson Jr., A.M. Goforth, T.J. Hansen, M.D. Smith, H.-C. zur Loye, J. Chem. Crystallogr. 35 (2005) 405;
(e) L. Shen, Inorg. Chem. Commun. 6 (2003) 1133;
(f) Y.-J. Shi, L.-H. Li, Y.-Z. Li, Y. Xu, X.-T. Chen, Z. Xue, X.-Z. You, Inorg. Chem. Commun. 5 (2002) 1090;
(g) Y.-J. Shi, Y.-Z. Li, W.-J. Tong, X.-T. Chen, X.-Z. You, Acta Crystallogr. E58 (2002) m293;
(h) W.J. Perkins, T. Maxwell, A.M. Goforth, M.D. Smith, L. Peterson Jr., H.-C. zur Loye, Acta Crystallogr. E61 (2005) m2047.
[17] Bruker, SMART-NT V5.624. Data Collection Software, Siemens Analytical X-ray Instruments Inc., Madison, WI, USA, 2001.
[18] Bruker, SAINT-NT V6.02a. Data Reduction Software, Siemens Analytical X-ray Instruments Inc., Madison, WI, USA, 2000.
[19] Bruker, SHELXTL version 6.10, Bruker AXS Inc., Madison, WI, USA, 2000.
[20] F.H. Allen, Acta Crystallogr. B 58 (2002) 380.
[21] H.-L. Hu, M.-C. Suen, C.-W. Yeh, J.-D. Chen, Polyhedron 24 (2005) 1497.
[22] R. Shoshnik, H. Elengoz, I. Goldberg, Acta Crystallogr. C61 (2005) m187.
[23] E. Tirosh, R. Maman, I. Goldberg, Acta Crystallogr. E61 (2005) m751.
[24] A. Bondi, J. Phys. Chem. 68 (1964) 441.

Electrochemical measurement was performed (acetonitrile solution) on a CH 620A electrochemical analyzer using a platinum electrode. Tetraethylammonium perchlorate (TEAP) [9] was used as a supporting electrolyte and the potentials are referenced to the standard calomel electrode (SCE) without junction correction. Magnetic measurement was carried out on a polycrystalline sample with a Quantum Design MPMS XL SQUID susceptometer operating at a magnetic field of 0.1 T between 2 and 300 K. The diamagnetic corrections were evaluated from Pascal's constants. Elemental analysis (C, H, N) was performed on a Perkin–Elmer 2400 Series II elemental analyzer.

2.3. Synthesis of the complex

$[Ni_2(L)(HL)(\mu_{1,1}\text{-}N_3)_2]ClO_4$ (**1**). To a methanolic solution (10 mL) of nickel(II) perchlorate hexahydrate (0.183 g, 0.5 mmol) was added HL (0.168 g, 0.5 mmol) and sodium azide (0.046 g, 0.7 mmol). The resulting pale blue solution was stirred for 0.5 h at room temperature. Slow evaporation of the solution yielded the pale blue crystalline product. Yield: 0.140 g (70%). *Anal.* Calc. for $C_{42}H_{45}N_{12}ClO_6Ni_2$: C, 52.1; H, 4.7; N, 17.4. Found: C, 51.6; H, 4.7; N, 17.6%. UV–Vis (λ_{max}/nm (ε/M^{-1} cm^{-1}) CH_3CN solution): 388 (sh, 322); 590 (31); 987 (54). IR (KBr, cm^{-1}): ν(OH) 3320; $\nu(N_3^-)$ 2085, 2070; (νClO_4^-) 1120, 620. $E_{1/2}$ (Ni^{III}/Ni^{II} couple): 0.47 V (ΔE_p, 50 mV).

2.4. Crystallographic studies

Suitable crystals of complex **1** were grown by slow evaporation of the methanolic solution. The X-ray intensity data were measured at 293 K on Bruker AXS SMART APEX CCD diffractometer (Mo Kα, $\lambda = 0.71073$ Å). The detector was placed at a distance of 6.03 cm from the crystal. A total of 606 frames were collected with a scan width of 0.3° in different settings of φ. The data were reduced in SAINTPLUS [10] and empirical absorption correction was applied using the SADABS package [10]. Nickel atoms were located by direct methods and the rest of the non-hydrogen atoms emerged from successive Fourier synthesis. The structures were solved by the direct method using the program SHELXS-97 [11] and were refined by the full matrix least-square procedure on F^2. All non-hydrogen atoms were refined anisotropically. The hydrogen atoms of the methyl groups (C(20), C(21), C(41) and C(42)) were included in calculated positions. All other hydrogen atoms of the complex were directly located in difference Fourier maps. Calculations were performed using the SHELXTL V5.03 [12] program package. The molecular structure plot was drawn using ORTEP [13]. Relevant crystal data are given in Table 1.

Table 1
Crystallographic data

	1
Formula	$C_{42}H_{45}N_{12}ClO_6Ni_2$
Formula weight	966.77
Crystal system	monoclinic
Space group	$P2_1/n$
a (Å)	16.209(3)
b (Å)	12.792(3)
c (Å)	21.629(4)
β (°)	95.94
V (Å^3)	4460.3(15)
Z	4
D_{calc} (g cm^{-3})	1.440
μ (Mo Kα) (mm^{-1})	0.965
θ (°)	1.85–26.37
Measured reflections	24430
Unique reflections/R_{int})	9033/0.0266
Temperature (K)	293(2)
R_1,[a] wR_2[b] [$I > 2\sigma(I)$]	0.0362, 0.0948
GOF on F^2	1.031

[a] $R_1 = \sum|F_o| - |F_c|/\sum|F_o|$.
[b] $wR_2 = [\sum w(F_o^2 - F_c^2)^2/\sum w(F_o^2)^2]^{1/2}$.

3. Results and discussion

The tetradentate tripodal ligand of the general formula HL has been used in this present work and it has been synthesised by the reported procedure [8].

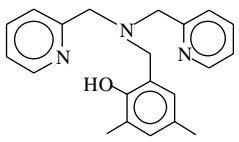

HL

The stoichiometric reaction of $[Ni(H_2O)_6](ClO_4)_2$ with HL in the presence of an excess of sodium azide furnished the pale blue colored complex of the formula $[Ni_2(L)(HL)(\mu_{1,1}\text{-}N_3)_2]ClO_4$, **1**, in good yield.

The perchlorate stretches occur near 600 and 1100 cm^{-1} and the hydrogen bonded phenolic OH appears as a broad peak near 3250 cm^{-1} [14]. The azide stretches appear as a doublet at 2085 and 2070 cm^{-1}.

The solution of the complex exhibits relatively weak peaks at about 580 and 980 nm. These two broad peaks are presumably assigned as $^3A_2 \rightarrow {}^3T_2$ and $^3A_2 \rightarrow {}^3T_1$ transitions, respectively. On the other hand, a shoulder is observed near 400 nm and this absorption is due to phenolate $\rightarrow Ni^{II}$ LMCT origin [15].

The cyclic voltammogram was recorded in acetonitrile solution at a scan rate of 50 mV/s and displays a quasireversible couple near 0.5 V. This is probably due to $Ni^{II} \rightarrow Ni^{III}$ oxidation [16].

3.1. Crystal structure

The crystal structure of $[Ni_2(L)(HL)(\mu_{1,1}\text{-}N_3)_2]ClO_4$ (**1**) has been determined. The ORTEP diagram of the cationic part is shown in Fig. 1. Selected bond distances and angles are given in Table 2. In the compound, three nitrogen atoms of the tetradentate ligand assume a *fac* configuration and the phenolic oxygen is coordinated equatorially.

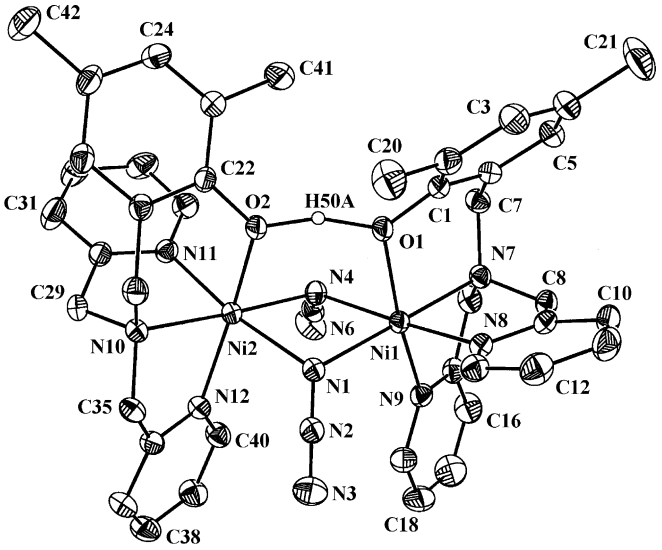

Fig. 1. Perspective view and atom-labelling scheme of the cationic part of $[Ni_2(L)(HL)(\mu_{1,1}\text{-}N_3)_2]ClO_4$ (**1**).

Table 2
Selected bond distances (Å) and angles (°) for **1**

Bond distances			
Ni(1)–O(1)	2.047(2)	Ni(2)–O(2)	2.0316(14)
Ni(1)–N(1)	2.122(2)	Ni(2)–N(1)	2.171(2)
Ni(1)–N(4)	2.158(2)	Ni(2)–N(4)	2.114(2)
Ni(1)–N(7)	2.112(2)	Ni(2)–N(10)	2.119(2)
Ni(1)–N(8)	2.075(2)	Ni(2)–N(11)	2.079(2)
Ni(1)–N(9)	2.112(2)	Ni(2)–N(12)	2.084(2)
Ni....Ni	3.240(6)		
Bond angles			
N(1)–Ni(1)–N(4)	79.61(7)	N(1)–Ni(2)–N(4)	79.49(7)
N(1)–Ni(1)–N(7)	175.89(7)	N(1)–Ni(2)–N(10)	100.78(7)
N(1)–Ni(1)–N(8)	95.09(7)	N(1)–Ni(2)–N(11)	174.09(7)
N(1)–Ni(1)–N(9)	101.57(7)	N(1)–Ni(2)–N(12)	87.60(7)
N(1)–Ni(1)–O(1)	90.55(6)	N(1)–Ni(2)–O(2)	86.48(7)
N(4)–Ni(1)–N(7)	104.50(7)	N(4)–Ni(2)–N(10)	179.62(7)
N(4)–Ni(1)–N(8)	172.18(7)	N(4)–Ni(2)–N(11)	97.99(7)
N(4)–Ni(1)–N(9)	88.33(7)	N(4)–Ni(2)–N(12)	101.38(7)
N(4)–Ni(1)–O(1)	85.73(7)	N(4)–Ni(2)–O(2)	90.26(7)
N(7)–Ni(1)–N(8)	80.83(7)	N(10)–Ni(2)–N(11)	81.71(7)
N(7)–Ni(1)–N(9)	78.65(7)	N(10)–Ni(2)–N(12)	78.91(7)
N(7)–Ni(1)–O(1)	89.86(6)	N(10)–Ni(2)–O(2)	89.49(6)
N(8)–Ni(1)–N(9)	98.43(7)	N(11)–Ni(2)–N(12)	98.16(7)
N(8)–Ni(1)–O(1)	88.59(7)	N(11)–Ni(2)–O(2)	88.20(7)
N(9)–Ni(1)–O(1)	165.33(7)	N(12)–Ni(2)–O(2)	165.76(7)
Ni(1)–N(1)–Ni(2)	97.97(8)	Ni(1)–N(4)–Ni(2)	98.63(8)

The nickel units are linked by a bridging azide ion forming a double end-on asymmetric bridged dimeric complex. The geometry around each nickel ion is distorted octahedron. In the NiN_5O environment, the equatorial plane is formed by three nitrogen atoms and one oxygen atom, and the nickel atom is shifted by ~0.065 Å towards the axial pyridine nitrogen atom. The remaining position is occupied by the bridging azide nitrogen atom of the other unit. The Ni–N bond distances are usual [6a] and span the range 2.075–2.171 Å. The N–N–N angle of the azide ion is ~179° and the N–N bond lengths are ~1.15 and 1.2 Å, respectively. In the dimer the Ni···Ni bond separation is 3.240(6) Å and the Ni–N–Ni angle is ~98°.

Recently, we have reported [17] an end-on double azido-bridged copper(II) complex with the same ligand in which both the phenolic oxygen atoms bind in the protonated form and are coordinated axially *trans* to each other. In the present case, the two phenolic groups are disposed equatorially in a *cis* configuration and one of them binds in the protonated form. These two *cis* phenolic groups are linked by an O–H···O hydrogen bond [O···O, 2.369(4) Å]. However the Ni–O bond distances, Ni(1)–O(1), 2.047(2) Å and Ni(2)–O(2), 2.0316(14) Å and O–H bond lengths, O(1)–H(50A), 1.171(5) Å and O(1)···H(50A), 1.230(6) Å, strongly support extensive charge delocalisation between the two phenolic oxygen atoms via the hydrogen atom. From this point of view it is assumed that besides the double end-on azido-bridge the complex is also linked by an $[O_{phenol}\text{–}H\cdots O_{phenoxide}]^-$ moiety.

3.2. Magnetic studies

The variable temperature magnetic susceptibility measurement was carried out in the temperature range of 2–300 K. The experimental $\chi_M T$ value is 2.8 $cm^3\,mol^{-1}$ K at 300 K [characteristic feature for a Ni^{II} ion with $g > 2.00$]. This value increases to 3.6 $cm^3\,mol^{-1}$K at 25 K. After passing through the maximum, the $\chi_M T$ value decreases abruptly to 2.4 $cm^3\,mol^{-1}$ K at 2 K. The shape of the curve is typical of intramolecular ferromagnetic coupling with the presence of either zero-field splitting (D parameter) and/or an intermolecular antiferromagnetic interaction (J'). Both D and J' are strongly correlated and show same results at low temperature. Thus it is not possible to separate them in any attempt to fit the experimental data [18]. So two different approaches have been used to fit the experimental data: the first one was full diagonalisation formalism introducing the single-ion D parameter employing, thus, the spin Hamiltonian $H = -JS_1S_1 + D[S_z^2 - 1/3S(S+1)] + g\beta HS_z$ and the second one using the molecular field approximation, with the intermolecular J' parameter, according to the method given by Kahn with the Hamiltonian, $H = -JS_1S_1 + g\beta HS_z - z'J'\langle S_z^2\rangle S_z$ [19]. In both the approaches, the best J values were obtained by minimizing the function $R = \sum(\chi_M^{calc} - \chi_M^{obs})^2/\sum(\chi_M^{obs})^2$. By using the molecular field approach (neglecting the D parameter), the best-fit parameters obtained were as follows: $J = 12.26\ cm^{-1}$, $J' = -0.42\ cm^{-1}$, $g = 2.31$ and $R = 2.9 \times 10^{-4}$ (Fig. 2). By using the full diagonalisation method introducing the D parameter (Fig. 3), the best-fit was obtained with the following parameters: $J = 10.65\ cm^{-1}$, $D = 6.5\ cm^{-1}$, $g = 2.30$ and $R = 2.3 \times 10^{-3}$.

The magnitude of both the J values are in good agreement. The D value is consistent with those typical for nickel(II) complexes [20]. The reduced magnetisation has been performed at 2 K and the plot of the reduced magnetisation versus H is shown in Fig. 4. The curve of

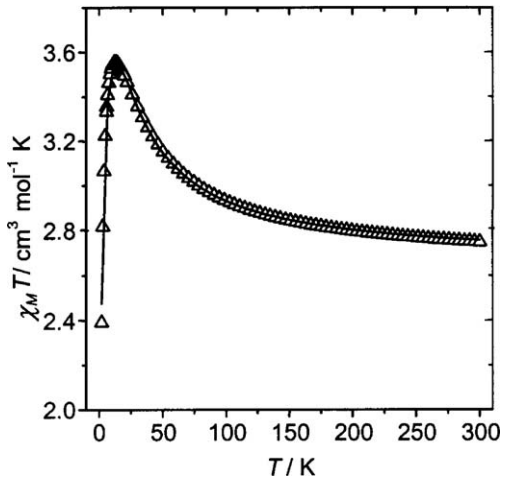

Fig. 2. Plot of $\chi_M T$ vs. T for complex **1**, solid line represents the best-fit assuming intermolecular interaction (J').

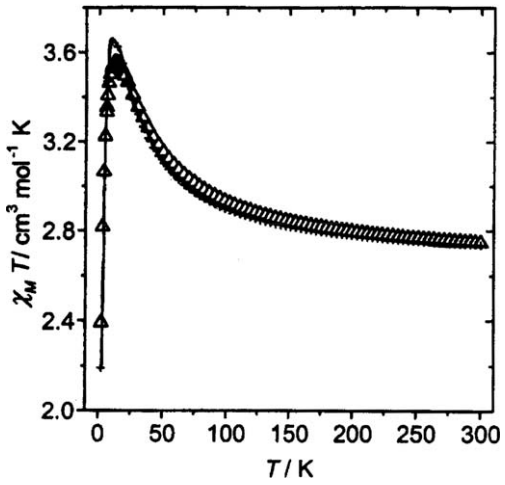

Fig. 3. Plot of $\chi_M T$ vs. T for complex **1**. Solid state indicates the fit considering the D parameter.

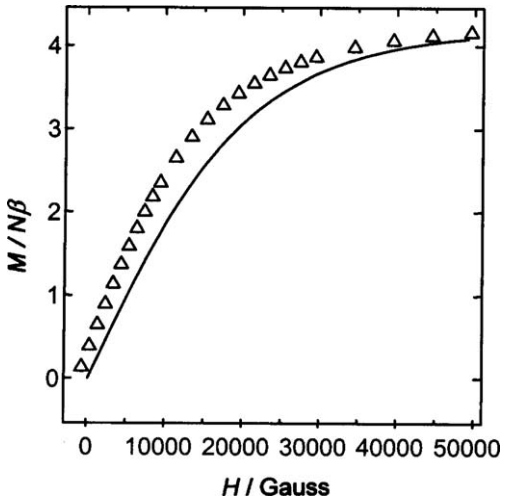

Fig. 4. Plot of the reduced magnetization (M/Nβ) vs. H at 2 K for **1**.

the reduced magnetisation is useful to know whether D or J' is predominant. The shape of the curve is Brillouin-like for $S = 2$ and $g = 2.2$, with the experimental points lying above the theoretical ones. This feature is indicative of a dominant ferromagnetic coupling.

End-on and end-to-end azido bridged nickel(II) complexes exhibit ferromagnetic and antiferromagnetic interactions, respectively [21]. It has been observed that in the case of end-on azido bridged binuclear nickel(II) complexes the J values fall in the range 20–40 cm^{-1} for a Ni–N–Ni angle close to 101–104° [22]. However in the present case the Ni–N–Ni angles are comparatively lower. These geometrical features may explain the low J value.

4. Conclusion

We have prepared and characterised a binuclear complex of the formula $[Ni_2(L)(HL)(\mu_{1,1}\text{-}N_3)_2]ClO_4$ (**1**) incorporating a N_3O-coordinating tripodal ligand. In the complex the two phenoxide oxygen atoms are linked by an O–H···O hydrogen bond. The variable temperature magnetic moment confirmed the ferromagnetic behavior. Further research aimed at the synthesis of polynuclear nickel(II) complexes involving both a bridging ligand and hydrogen bonding using different polydentate ligands along with the study of their solid and solution state is currently in progress.

Acknowledgements

Financial supports from the Council of Scientific and Industrial Research, New Delhi, India and from the Department of Science and Technology, New Delhi, India are gratefully acknowledged. We are also thankful to DST for the data collection on the CCD facility setup (Indian Institute of Science, Bangalore, India) under the IRHPA-DST program. Joan Ribas acknowledges the financial support from the Spanish Government (Grant BQU2000/0791).

Appendix A. Supplementary data

Crystallographic data for the structural analysis have been deposited with the Cambridge Crystallographic Data Centre with CCDC number 273626. Supplementary data associated with this article can be found, in the online version, at doi:10.1016/j.poly.2006.01.029.

References

[1] (a) A. Escuer, R. Vicente, J. Ribas, M.S. El Fallah, X. Solans, M. Font-Bardía, Inorg. Chem. 32 (1993) 3727;
(b) M. Monfort, I. Resino, J. Ribas, X. Solans, M. Font-Bardía, New J. Chem. 25 (2001) 1577.
[2] (a) M.-F. Charlot, O. Kahn, M. Chaillet, C. Larrieu, J. Am. Chem. Soc. 108 (1986) 2574;
(b) L.K. Thompson, S.S. Tandon, M.E. Manuel, Inorg. Chem. 34 (1995) 2356.

[3] E. Ruiz, J. Cano, S. Alvarez, P. Alemany, J. Am. Chem. Soc. 120 (1998) 11122.
[4] S. Sarkar, A. Datta, A. Mondal, D. Chopra, J. Ribas, K.K. Rajak, S.M. Sairam, S.K. Pati, J. Phys. Chem. B 110 (2006) 12.
[5] (a) R.J. Butcher, C.J. O'Connor, E. Sinn, Inorg. Chem. 21 (1982) 616; (b) S. Sikorav, I. Bkouche-Waksman, O. Kahn, Inorg. Chem. 23 (1984) 490; (c) R. Vicente, A. Escuer, J. Ribas, M.S. El Fallah, X. Solans, M. Font-Bardía, Inorg. Chem. 32 (1993) 1920; (d) M.G. Barandika, R. Cortés, L. Lezama, M.K. Urtiaga, M.I. Arriortua, T.G. Rojo, J. Chem. Soc., Dalton Trans. (1999) 2971.
[6] (a) M. Monfort, I. Resino, J. Ribas, H. Stoeckli-Evans, Angew. Chem., Int. Ed. Engl. 39 (2000) 191; (b) M. Monfort, I. Resino, M.S. El Fallah, J. Ribas, X. Solans, M. Font-Bardía, H. Stoeckli-Evans, Chem. Eur. J. 7 (2001) 280; (c) S. Martin, M.G. Barandika, L. Lezama, J.L. Pizzaro, Z.E. Serna, J.I.R. de Larramendi, M.I. Arriortua, T. Rojo, R. Cortes, Inorg. Chem. 40 (2001) 4109; (d) A. Escuer, R. Vicente, F.A. Mautner, M.A.S. Goher, M.A.M. Abu-Youssef, Chem. Commun. (2002) 64.
[7] (a) S. Deoghoria, S. Sain, M. Soler, W.T. Wong, G. Christou, S.K. Bera, S.K. Chandra, Polyhedron 22 (2003) 257; (b) S.K. Dey, N. Mondal, M.S. El Fallah, R. Vicente, A. Escuer, X. Solans, M. Font-Bardía, T. Matsushita, V. Gramlich, S. Mitra, Inorg. Chem. 43 (2004) 2427.
[8] R. Kannappan, R. Mahalakshmy, T.M. Rajendiram, R. Venkatesan, P. Sambasiva Rao, Proc. Indian Acad. Sci. (Chem. Sci.) 115 (2003) 1.
[9] G.K. Lahiri, S. Bhattacharya, B.K. Ghosh, A. Chakravorty, Inorg. Chem. 26 (1987) 4324.
[10] SMART, SAINT, SADABS, XPREP, SHELXTL; Bruker AXS Inc.: Madison. WI, 1998.
[11] G.M. Sheldrick, Acta Crystallogr. Sect. A 46 (1990) 467.
[12] G.M. Sheldrick, SHELXTL, Version 5.03, Siemens Analytical Instruments Inc., Madison, WI, 1994.
[13] C.K. Johnson, ORTEP; Report ORNL-5138, Oak Ridge National Laboratory, Oak Ridge, TN, 1976.
[14] S. Torelli, C. Belle, I. Gautier-Luneau, J.L. Pierre, E. Saint-Aman, J.M. Latour, L. Le Pape, D. Luneau, Inorg. Chem. 39 (2000) 3526.
[15] E. Berti, A. Caneschi, C. Daiguebonne, P. Dapporto, M. Formica, V. Fusi, L. Giorgi, A. Guerri, M. Micheloni, P. Paoli, R. Pontellini, P. Rossi, Inorg. Chem. 42 (2003) 348.
[16] K. Pramanik, S. Karmakar, S.B. Choudhury, A. Chakravorty, Inorg. Chem. 36 (1997) 3562.
[17] S. Sarkar, A. Mondal, J. Ribas, M.G.B. Drew, K. Pramanik, K.K. Rajak, Eur. J. Inorg. Chem. (2004) 4633.
[18] A.P. Ginsberg, R.L. Martin, R.W. Brookes, R.C. Sherwood, Inorg. Chem. 11 (1972) 2884.
[19] O. Kahn, Molecular Magnetism, VCH, New York, 1993.
[20] R. Boca, Coord. Chem. Rev. 248 (2004) 757.
[21] C.S. Hong, J. Koo, S.-K. Son, Y.S. Lee, Y.-S. Kim, Y. Do, Chem. Eur. J. 7 (2001) 4243.
[22] J. Ribas, A. Escuer, M. Monfort, R. Vicente, R. Cortes, L. Lezama, T. Rojo, Chem. Rev. 193–195 (1999) 1027.

fluorescent whereas complexes with pyridyltriazine and pyrazinyltriazine ligands exhibit weak fluorescence in solution.

2. Results and discussion

2.1. Synthesis and characterisation

The heterocyclic ligands used in the present work are 5,6-diphenyl-3-(2-pyridyl)-1,2,4-triazine (L^1) (**1**), 5,6-diphenyl-3-(pyrazin-2-yl)-1,2,4-triazine (L^2) (**2**) and triazolopyridine (L^3) (**3**) (general abbreviation L). The ligands L^1 and L^2 were synthesized as in the reported procedure [6,7]. The reported syntheses of the triazolo ligand L^3 includes the reaction of 2-picolinic acid (or its acid chloride/ester) with 2-hydrazinopyridine [8] and the oxidative cyclization of the 2-pyridylhydrazone of pyridine-2-aldehyde [9]. We have found that L^3 is also formed in good yield (70%) via the reactions of Scheme 1 in which the cyclization step involves loss of ammonia from the intermediate amidrazone.

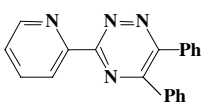

L^1
1

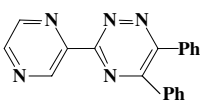

L^2
2

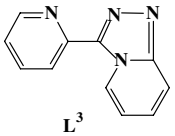

L^3
3

Upon reaction of $Re^I(CO)_5Cl$ with L^1 in boiling benzene in the molar ratio 1:1.1, the red colored $Re^I(CO)_3Cl(L^1)$ was obtained in good yield. The complex $Re^I(CO)_3Cl(L^2)$ was prepared similarly. In the case of L^3, the reaction was carried out in a boiling 5:1 benzene–acetonitile mixture and the complex $Re^I(CO)_3Cl(L^3)$ is bright yellow in color.

The complexes show C≡O stretches in the frequency range 1870–2030 cm^{-1}. In addition to bands in the UV region, the complexes (in dichloromethane) display a band of moderate intensity in the visible region near 440 nm (Table 1). This band is tentatively assigned to a $\pi(Re)$–$\pi^*(L)$ MLCT excitation. The solutions are also fluorescent, the peak lying near 675 nm in the case of the L^1 and L^2 complexes and near 590 nm in the case of the L^3 complex. Relevant data are collected in Table 1. Excitation spectral studies have demonstrated that the fluorescence is associated with the above noted MLCT band. A representative case is shown in Fig. 1.

The fluorescence is believed to originate from the ^{3}MLCT state. It is interesting to note that whereas $Re^I(CO)_3Cl(L^1)$ and $Re^I(CO)_3Cl(L^2)$ are weakly fluorescent with quantum yields (Φ) near 6×10^{-4} (Table 1), the $Re^I(CO)_3Cl(L^3)$ complex is much more strongly fluorescent with $\Phi = 0.036$. This can be attributed to the presence of the quinoid structure in L^3. Indeed it is nearly as fluorescent as $Ru(bpy)_3^{2+}$ ($\Phi = 0.042$) [10]. We note that the $Re^I(CO)_3Cl(bpy)$ complex is only weakly fluorescent ($\Phi = 0.0031$ (295 K)) [11]. Further studies on the photophysical properties of the present complexes are in progress and in this context we record that $Re^I(CO)_3$ complexes are of current interest in terms of their potential photophysical properties [5,12] (e.g. photosensitizers for photochemical reactions). The complexes display well-resolved ^{1}H NMR spectra in $CDCl_3$ solution. The $Re^I(CO)_3Cl(L)$ complexes are electroactive in acetonitrile solution, exhibiting an irreversible one-electron oxidative response near 1.4 V versus SCE which is assigned to the Re^{II}/Re^I couple. Representative voltammograms are shown in Fig. 2. The acidity, i.e., electron withdrawing ability order of the ligands is $L^2 > L^1 > L^3$ [13]. The observed electrochemical pattern of the $Re^I(CO)_3Cl(L)$ species is qualitatively similar with the ligand acidity and the anodic peak potentials order is $Re^I(CO)_3Cl(L^2) > Re^I(CO)_3Cl(L^1) > Re^I(CO)_3Cl(L^3)$.

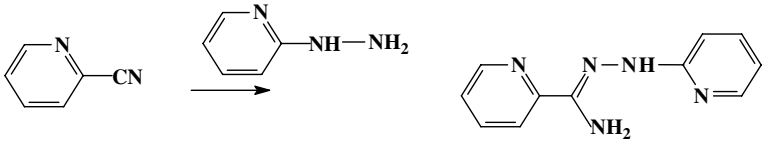

amidrazone

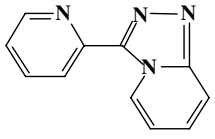

L^3
3

Scheme 1.

Table 1
Electronic, emission spectral data and quantum yields (Φ_x) in CH_2Cl_2 solution for $[Re(CO)_3Cl(L)]$ at 298 K

Compound	UV–Vis data λ_{max} (nm) (ε, $M^{-1}\,cm^{-1}$)	λ_{em}[a] (nm)	Φ_x
$[Re(CO)_3Cl(L^1)]$	262(13650), 293(11300), 433(3100)	679	5.6×10^{-4}
$[Re(CO)_3Cl(L^2)]$	231(12200), 310(9100), 451(3300)	671	5.5×10^{-4}
$[Re(CO)_3Cl(L^3)]$	261(6450), 293(5150), 350(1850), 440(1350)	592	0.036

[a] Excitation at the absorption peak in the region of 433–451 nm.

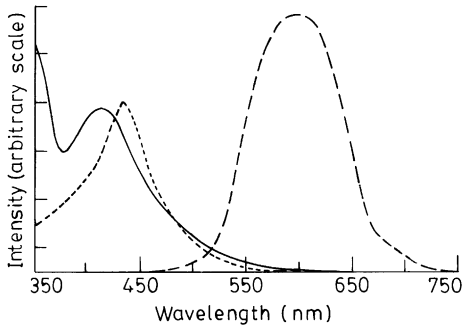

Fig. 1. (a) Absorption (—), (b) fluorescence (---) and (c) excitation (···) spectra of $[Re(CO)_3Cl(L^3)]$ in 2.3×10^{-4} M CH_2Cl_2 solution at 298 K.

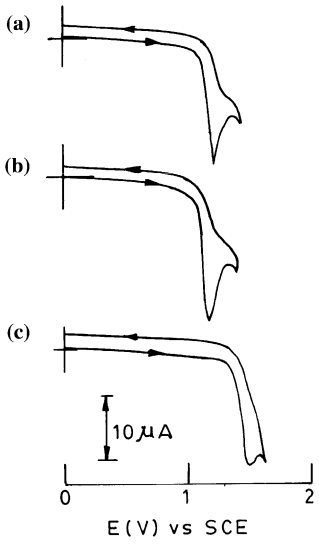

Fig. 2. Cyclic voltammograms of $\approx10^{-3}$ mol dm^{-3} solutions of (a) $[Re(CO)_3Cl(L^3)]$, (b) $[Re(CO)_3Cl(L^1)]$ and (c) $[Re(CO)_3Cl(L^2)]$ in acetonitrile solution (scan rate 50 mV s^{-1}, working electrode, platinum; reference electrode, SCE).

2.2. Structure

The X-ray structures of $Re(CO)_3Cl(L^1)$ and $Re(CO)_3Cl(L^3)$ have been accurately determined. Molecular views are shown in Figs. 3 and 4 and selected bond parameters are listed in Table 2. In the distorted octahedral ReC_3N_2Cl coordination sphere the three carbon monoxide ligands are facially disposed to maximize Re—CO back-bonding.

In $Re^I(CO)_3Cl(L^1)$ the chelate ring is satisfactorily planar with a mean deviation of 0.03 Å. The dihedral angles

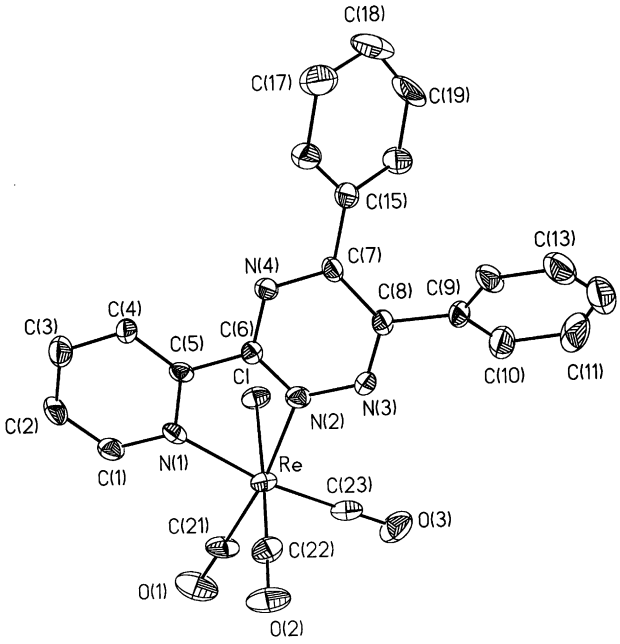

Fig. 3. Molecular view and atom labelling scheme for $[Re(CO)_3Cl(L^1)]$.

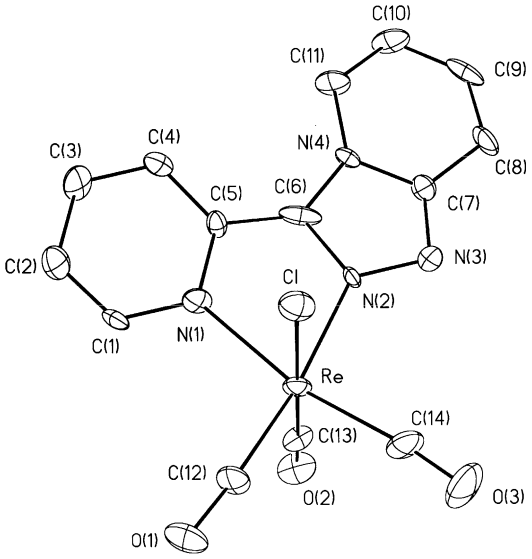

Fig. 4. Molecular view and atom labelling scheme for $[Re(CO)_3Cl(L^3)]$.

of the two pendant phenyl rings with the triazine ring are 38.3° (C9–C14) and 40.7° (C15–C20). The triazine and the pyridine rings are not quite coplanar, the dihedral angle between them being 6.3°.

Table 2
Selected bond distances (Å), angles (°) and their estimated standard deviations for $[Re(CO)_3\ Cl(L^1)]$ and $[Re(CO)_3Cl(L^3)]$

	$[Re(CO)_3Cl(L^1)]$	$[Re(CO)_3Cl(L^3)]$
Bond distances		
Re—N1	2.145(9)	2.18(2)
Re—N2	2.154(9)	2.136(13)
Re—Cl	2.484(3)	2.501(5)
Re—C[a]	1.900(13)	1.92(2)
C6—N2	1.324(13)	1.36(6)
N2—N3	1.367(11)	1.39(2)
C13—O2		1.06(2)
C22—O2	1.21(2)	
C12—O1		1.18(3)
C21—O1	1.157(14)	
C14—O3		1.11(3)
C23—O3	1.15(2)	
C5—N1	1.384(13)	1.36(2)
C5—C6	1.453(12)	1.41(3)
Bond angles		
Cl—Re—N2	82.4(3)	85.0(4)
Cl—Re—C12		91.5(8)
Cl—Re—C21	94.5(4)	
Cl—Re—C13		178.4(5)
Cl—Re—C22	177.5(4)	
N1—Re—Cl	81.6(2)	82.6(4)
N1—Re—N2	74.7(3)	73.7(5)
N1—Re—C12		99.0(8)
N1—Re—C21	96.9(5)	
N1—Re—C13		96.6(7)
N1—Re—C22	96.0(4)	
N1—Re—C14		167.7(8)
N1—Re—C23	170.8(4)	
Cl—Re—C14		92.6(7)
Cl—Re—C23	93.7(3)	
N2—Re—C12		172.3(8)
N2—Re—C21	171.4(4)	
N2—Re—C13		93.5(7)
N2—Re—C22	96.5(5)	
N2—Re—C14		94.8(7)
N2—Re—C23	96.8(4)	

[a] Average value of Re—C bonds.

In $Re^I(CO)_3Cl(L^3)$ the mean deviation of the chelate ring is again 0.03 Å. The ligand L^3 is only approximately planar (mean deviation 0.06 Å). This happens because the otherwise highly planar pyridine ring (incorporating C5) and the bicyclic triazolo fragment are not quite coplanar, there being a dihedral angle of 7.4° between them. The average Re—N, Re—C and Re—Cl lengths in the present complexes are closely like those reported [14] in $Re^I(CO)_3$ complexes having a ReC_3N_2Cl coordination sphere.

3. Experimental

3.1. Materials

The ligands L^1 and L^2 were prepared by the method [6,7]. The commercially available chemicals utilized in the present work were of analytical grade and in most cases these were used as obtained. The utilized chemicals and their sources are as follows: 2-hydrazinopyridine, pentacarbonylchlororhenium(I) from Aldrich (USA); acetic acid from Merk (India); phosphorus pentoxide (P_4O_{10}) from S.D Fine Chem. Ltd. (India). The purification and dying of dichloromethane and acetonitrile for synthesis as well as for electrochemical and spectral work were done using standard procedures [15].

3.2. Physical measurements

Electronic and IR spectra were recorded with a Shimadzu UV-1601PC spectrophotometer and a Nicolet Magna IR series II spectrometer, respectively. ^1H NMR spectra were obtained using a Bruker 300 MHz FT NMR spectrometer. The numbering scheme used for ^1H NMR is the same as in the crystallography. Spin–spin structures are abbreviated as: s, singlet; d, doublet; t, triplet; m, multiplet. Microanalyses (C, H, N) were performed using a Perkin–Elmer 240 C elemental analyzer. The electrochemical measurements were performed at a platinum electrode under nitrogen atmosphere in dichloromethane solution by using a model 620A electrochemical analyzer of CHI Instruments. The supporting electrolyte was tetraethylammonium perchlorate and potentials are referenced to the saturated calomel electrode (SCE).

3.3. Preparation of ligand (L^3)

2-Cyanopyridine (500 mg, 4.76 mmol) and 2-hydrazinopyridine (520 mg, 4.76 mmol) were mixed in a small amount of ethanol. After stirring overnight at room temperature, the crystals of 2-pyridine carboxamidrazone could be filtered off. The product was washed with diethyl ether and dried in the air. The solid obtained (~820 mg) was added to a mixture of acetic acid and acetic anhydride (1:1) at 0 °C and the solution was then brought to room temperature and stirred for 2 h. The solution was then concentrated under reduced pressure and the resulting oil was heated at 130 °C for 1 h. The solid obtained was purified by repeated crystallization from di-isopropyl ether. Yield: 660 mg (70%).

3.4. Synthesis of $Re^I(CO)_3Cl(L)$

The three complexes were prepared by the same general procedure and details are given for one.

3.4.1. $Re^I(CO)_3Cl(L^3)$

L^3 (30 mg, 0.153 mmol) was added to a hot solution of $Re(CO)_5Cl$ (50 mg, 0.138 mmol) in 40 mL benzene (better in a benzene–acetonitrile mixture 5:1). On subsequent heating to reflux for 1 h the solution color changed from light yellow to bright yellow. The solvent was then evaporated under reduced pressure and the residue was washed thoroughly with hexane for the removal of excess ligand. It was dried, and then recrystallized from a dichloromethane/hexane mixture affording a crystalline

product which was dried in vacuo over fused calcium chloride. Yield: 56 mg (81%). *Anal.* Calc. for $C_{14}H_8ClN_4O_3Re$: C, 33.50; H, 1.61; N, 11.20. Found: C, 33.42; H, 1.55; N, 11.20%. IR (cm^{-1}, KBr pellet): 1896, 2021 (C≡O). ^1H NMR ($CDCl_3$, δ, J/Hz): 9.11 (d, 1H, H(1), J 5.22), 7.81 (t, 1H, H(2), J 6.99), 8.40 (t, 1H, H(3), J 7.77), 8.81 (d, 1H, H(4)), 9.31 (d, 1H, H(8), J 6.75), 7.77 (t, 1H, H(9), J 7.47), 7.46 (t, 1H, H(10), J 6.78), 8.19 (d, 1H, H(11), $J = 8.82$). $E_{pa}(Re^{II}/Re^{I}$ couple): 1.37 V.

3.4.2. $Re(CO)_3Cl(L^1)$

$Re(CO)_5Cl$ (50 mg, 0.138 mmol) and L^1 (44 mg, 0.142 mmol) were employed. Yield: 66 mg (78%). *Anal.* Calc. for $C_{23}H_{14}ClN_4O_3Re$: C, 44.84; H, 2.29; N, 9.09. Found: C, 44.80; H, 2.25; N, 9.10%. IR (cm^{-1}, KBr pellet): 1902, 1936, 2017 (C≡O). ^1H NMR ($CDCl_3$, δ, J/Hz): 9.10 (d, 1H, H(1), J 5.62), 8.77 (t, 1H, H(2), J 7.65), 8.18 (t, 1H, H(3), J 7.77), 7.96 (d, 1H, H(4), J 7.92), 7.99–7.41 (aromatic multiplet). $E_{pa}(Re^{II}/Re^{I}$ couple): 1.43 V.

3.4.3. $Re(CO)_3Cl(L^2)$

$Re(CO)_5Cl$ (50 mg, 0.138 mmol) and L^2 (33 mg, 0.142 mmol) were used. Yield: 68 mg (80%). *Anal.* Calc. for $C_{22}H_{13}ClN_5O_3Re$: C, 42.82; H, 2.12; N, 11.35%. Found: C, 42.75; H, 2.15; N, 11.30%. IR (cm^{-1}, KBr pellet): 1881, 1906, 2021 (C≡O). ^1H NMR ($CDCl_3$, δ, J/Hz): 8.98 (d, 1H, H(1), J 5.03), 9.04 (d, 1H, H(2), J 4.99), 9.94 (s, 1H, H(3)), 7.75–7.43 (aromatic multiplet) E_{pa}-$(Re^{II}/Re^{I}$ couple): 1.48 V.

3.5. X-ray structure determination

Single crystals of $Re(CO)_3Cl(L^1)$ ($0.25 \times 0.25 \times 0.20$ mm^3) and $Re(CO)_3Cl(L^3)$ ($0.30 \times 0.25 \times 0.20$ mm^3) were grown by slow diffusion of hexane into dichloromethane solutions at room temperature. Cell parameters were determined by a least-squares fit of 30 machine-centred reflections ($2\theta = 14$–$28°$). Data were collected by the ω-scan technique on a Siemens R3m/V four-circle diffractometer with graphite-monochromated Mo Kα radiation ($\lambda =$ 0.71073 Å). Two check reflections measured after every 198 reflections showed no significant intensity reduction in any case. All data were corrected for Lorentz polarisation effects and an empirical absorption correction [16] was done on the basis of an azimuthal scan of six reflections for the crystals.

The metal atom was located from Patterson maps and the rest of the non-hydrogen atoms emerged from successive Fourier syntheses. The structures were refined by full matrix least-squares procedures. All non-hydrogen atoms were refined anisotropically. The hydrogen atoms of $Re(CO)_3Cl(L^1)$ and $Re(CO)_3Cl(L^3)$ were located and refined isotropically. Calculations were performed using the SHELXTL, Version 5.03 [17] program package. Significant crystal data are listed in Table 3.

Table 3
Crystal data for $Re(CO)_3Cl(L^1)$ and $Re(CO)_3Cl(L^3)$

Complex	$Re(CO)_3Cl(L^1)$	$Re(CO)_3Cl(L^3)$
Empirical formula	$C_{23}H_{14}ClN_4O_3Re$	$C_{14}H_8ClN_4O_3Re$
Formula weight	616.03	501.89
Crystal system	monoclinic	orthorhombic
Space group	$C2/c$	$P2_12_12_1$
a (Å)	31.182(6)	7.2400(6)
b (Å)	7.656(2)	11.2220(6)
c (Å)	23.165(5)	19.0980(9)
α (°)		
β (°)	127.21(3)	
γ (°)		
V (Å^3)	4404(2)	1551.7(2)
Z	8	4
μ (Mo Kα) (mm^{-1})	5.672	8.018
D_{calc} (g cm^{-1})	1.858	2.140
Total reflections	3368	1567
Independent reflections (R_{int})	3368(0.0000)	1567(0.0000)
R_1[a], wR_2[b] [$I > 2\sigma(I)$]	0.0597, 0.1552	0.0618, 0.1549

[a] $R_1 = \sum\|F_o\| - \|F_c\| / \sum\|F_o\|$.
[b] $wR_2 = [\sum w(F_o^2 - F_c^2)^2 / \sum w(F_o^2)^2]^{1/2}$.

3.5.1. Determination of quantum yield (Φ)

Quantum yields were determined by comparing with a $Ru(bpy)_3^{2+}$ standard [10] ($\Phi_s = 0.042$) measured in aqueous solution. The relevant formula is given in the following equation:

$$\Phi_x = [\Phi_s(A_s XI_x)/A_x XI_s](\eta_x/\eta_s)^2 \quad (1)$$

Here x and s subscripts refer to the experimental sample and standard, respectively, A is the absorbance (set near 0.1 in a 1 cm cell) at the absorption peak (436 nm in the case of the standard), I is the area under the emission spectrum and η is the refractive index of the solvent used in the standard solution – water in this case.

4. Conclusion

Complexes of the type $Re^I(CO)_3Cl(L)$, incorporating a facial ReC_3N_2Cl coordination sphere, have been synthesized and characterized including structure determination of the L^1 and L^3 complexes.

The complexes are electroactive in acetonitrile solution (irreversible oxidation, 1.4 V) and display fluorescence in the visible region near 675 nm in the case of $Re^I(CO)_3Cl(L^1)$ and $Re^I(CO)_3Cl(L^2)$, and near 592 nm in the case of $Re^I(CO)_3Cl(L^3)$. The quantum yield of the L^3 complex, 0.036, is comparable to that of $Ru(bpy)_3^{2+}$.

Acknowledgements

We are thankful to Professor Animesh Chakravorty for providing facilities and valuable suggestions. We are thankful to the Department of Science and Technology, the Council of Scientific and Industrial Research, New Delhi, India, for financial support.

Appendix A. Supplementary material

Crystallographic data for the structure analysis have been deposited with the Cambridge Crystallographic Data Centre, CCDC nos. 289840 and 289841 corresponding to $Re(CO)_3Cl(L^1)$ and $Re(CO)_3Cl(L^3)$, respectively. Copies of this information may be obtained free of charge from The Director, CCDC, 12 Union Road, Cambridge CB2 1EZ, UK (fax: +44 1223 336033; email: deposit@ccdc.cam.ac.uk or www: http://www.ccdc.cam.ac.uk). Supplementary data associated with this article can be found, in the online version, at doi:10.1016/j.poly.2006.01.028.

References

[1] A. Juris, V. Balzani, F. Barigelletti, S. Campagna, P. Belser, A. Von Zelewsky, Coord. Chem. Rev. 84 (1988) 85.
[2] V. Balzani, A. Juris, M. Ventura, S. Champagne, S. Serroni, Chem. Rev. 96 (1996) 759.
[3] D.J. Stuffkens, A. Vlcek Jr., Coord. Chem. Rev. 177 (1998) 127.
[4] A. Vogler, H. Kunkely, Coord. Chem. Rev. 200–202 (2000) 991.
[5] D.R. Striplin, G.A. Crosby, Coord. Chem. Rev. 211 (2001) 163.
[6] F.H. Case, J. Org. Chem. 30 (1965) 931.
[7] F.H. Case, J. Heterocycl. Chem. 5 (1968) 223.
[8] K.T. Potts, H.R. Burton, J. Org. Chem. 31 (1966) 251.
[9] R.N. Butler, S.M. Johnston, J. Chem. Soc., Chem. Commun. (1981) 376.
[10] D.P. Rillema, D.G. Taghdiri, D.S. Jone, L.A. Worl, T.J. Mayer, H.A. Levy, C.D. Keller, Inorg. Chem. 26 (1987) 578.
[11] L.A. Worl, R. Duesing, P. Chen, L.D. Ciana, T.J. Mayer, J. Chem. Soc., Dalton Trans. (1991) 849.
[12] (a) A.D. Guerzo, S. Leroy, F. Fages, R.H. Schmehl, Inorg. Chem. 41 (2002) 359;
(b) K.K. Lo, W. Hui, D.C. Ng, K. Cheung, Inorg. Chem. 41 (2002) 40;
(c) S. Sun, D.T. Tran, O.S. Odongo, A.J. Lees, Inorg. Chem. 41 (2002) 132.
[13] R.T. Morrison, R.N. Boyd, Organic Chemistry, 4th ed., Allyn & Bacon, Boston, 1983.
[14] (a) B.K. Panda, S. Sengupta, A. Chakravorty, J. Organomet. Chem. 689 (2004) 1780;
(b) E.P. Civitello, P.S. Dragovich, T.B. Karpishin, S.G. Novick, G. Bierach, J.F. O'Connel, T.D. Westmoreland, Inorg. Chem. 32 (1993) 237.
[15] (a) G.K. Lahiri, S. Bhattacharya, B.K. Ghosh, A. Chakravorty, Inorg. Chem. 26 (1987) 4324;
(b) D.T. Sawyer, J.L. Roberts Jr., Experimental Electrochemistry for Chemists, Wiley, New York, 1974, p. 167.
[16] A.C.T. North, D.C. Phillips, F.A. Mathews, Acta Crystallogr. Sect. A 24 (1968) 351.
[17] G.M. Sheldrick, SHELXTL, Version 5.03, Siemens Analytical X-ray System Madison, WI, 1994.

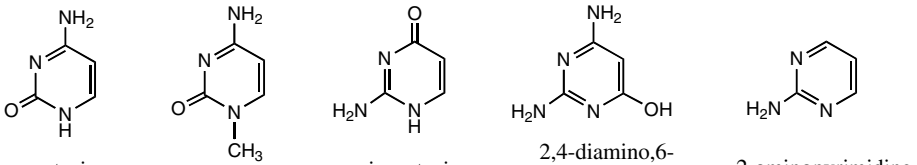

1 2 3 4 5

Scheme 1.

as well as stereospecific interligand interactions [10,11]. Thus, in the present work we decided to explore the effect of changing the adjacent groups of the potential bonding nitrogen atom in several pyrimidine derivatives.

Differences and similarities of the pyrimidine ligands presented in this paper are drawn in Scheme 1. In the cytosine and isocytosine ligands there exist a similar moiety, H_2N–C═N–C═O, with a nitrogen sterically hindered by the two flanking amino and carbonyl groups, but its relative position inside the pyrimidine ring is able to discriminate between N(1) or N(3) binding to the metal ion. Two opposite effects should be considered: intramolecular hydrogen bond interactions [NH_2(ligand)···O(binary complex)] that facilitate the stabilisation of the complexes and the presence of stereo-electronic effects [C═O(ligand)···O(binary complex)] that disturb their formation. The resulting interaction with the ligand should be that which presents a maximum of attractive interactions between the copper(II)–N-salicylideneserinato moiety and the ligand (hydrogen bonds) and a minimum of repulsive interactions (stereo-electronic effects). On the other hand, although there are several ternary complexes with 2-aminopyridines which present an additional H-bond interaction [1,7,8], the 2-aminopyrimidine ligand has been chosen for comparison with a structure free of negative stereo-electronic effects.

The nitrogen atom N(3) has been established as the predominant metal binding site of the natural nucleobase cytosine [11–15], 1-methylcytosine [16,17] and the non-natural isomer isocytosine [18,19], a moiety of the biopterine ligand. However, monodentate exocyclic oxygen coordination have been also reported in Mn(II) [20] and Ni(II) [21,22] compounds. In addition, crystallographic studies of the related ligand 2-pyridone (2-hydroxypyridine) show three modes for metal coordination in mono-nucleating complexes: interaction via the exocyclic O-atom, interaction via the endocyclic N-atom and through a double interaction via both O and N atoms [23].

As a continuation of our work on the preparation and characterization of ternary copper(II) N-salicylideneaminoacidato Schiff base complexes, in this paper, we present five new crystal structures in order to evaluate the effects mentioned above: [Cu(sal-ser)(cytosine)] · $2H_2O$ (**1**), [Cu(sal-ser)-(1-methylcytosine)] · $1.25H_2O$ (**2**), [Cu(sal-ser)(isocytosine)]· $1.25H_2O$ (**3**), [Cu(sal-ser)(2,4-diamino-6-hydroxypyrimidine)] · $2H_2O$ (**4**) and [Cu(sal-ser)(2-aminopyrimidine) (H_2O)] · H_2O (**5**).

2. Experimental

2.1. General remarks

Elemental analyses of the complexes were carried out using a Carlo Erba Analyser Model 1106. The infrared spectra (KBr pellets) were recorded on a PE 683 with a PE 1600 infrared data station. The visible absorption spectra were recorded in DMSO solutions on a PE 552 spectrophotometer. Thermogravimetric data in the range from 30 to 700 °C were obtained (heating rate 5 °C/min) on a PE TGA-2 thermobalance. Magnetic susceptibility measurements (at 298 K) were carried out on polycrystalline samples with a Manics DSM8 pendulum-type magnetometer equipped with a helium continuous-flow cryostat and a Bruker BE15 electromagnet. The magnetic field was ca. 1.5 T. Diamagnetic corrections were estimated from Pascal's constants. The ESR spectra were recorded at X-band frequencies with a Bruker ES200 spectrometer at 298 K.

2.2. Materials

Salicylaldehyde, L-serine, cytosine, 1-methylcytosine, isocytosine, 2,4-diamino-6-hydroxipyrimidine (6-aminoisocytosine), 2-aminopyrimidine and copper(II) acetate monohydrate were obtained from Aldrich and used without further purification. The [Cu(sal-L-ser)H_2O] · H_2O starting complex was obtained as indicated in reference [8].

2.3. Syntheses

The complexes were synthesised by treatment of [Cu(sal-L-ser)H_2O] · H_2O with the pyrimidine ligand in water, EtOH/H_2O or MeOH/H_2O. In all cases, the synthetic procedure has been difficult because of the appearance of a polymeric blue precipitate of variable composition which must be carefully filtered off to obtain transparent solutions where, slowly, appear a few dark green crystals over another sticky polymeric material. Sometimes its is very difficult to isolate completely these crystals and the use of few drops of ethanol or methanol permit the isolation of them in a pure form, but the yield is reduced to a considerable extent.

2.3.1. [Cu(sal-ser)(cytosine)] · $2H_2O$ (**1**)

Cytosine (0.11 g, 1 mmol) was added to a warm solution (60 °C) of 1 mmol (0.30 g) of [Cu(sal-L-ser)H_2O] · H_2O in

25 mL of 2:1 water/ethanol mixture. The dark green solution was stirred at 60 °C for 2 h until a blue precipitate of variable composition was obtained and separated by filtration. A few dark green crystals appeared in the mother solution after several days of evaporation of the solvent in air. Yield: 10%. Due to the poor yield and reproducibility and stability of this complex, the 1-methylcytosine derivative was also synthesised. TG: The complex exhibits a mass decrease (found 8.6; calcd. 8.6%) between 115 and 150 °C corresponding to the loss of two water molecules per formula unit. *Anal*. Calc. for $C_{14}H_{18}N_4O_7Cu$ (417.9): C, 40.23; H, 4.31; N, 13.41. Found: C, 40.23; H, 4.27; N, 13.31%. IR (KBr disk, cm^{-1}): $\nu = 3395$ (s), 3190 [s, $\nu_s(NH_2)$ and $\nu_a(NH_2)$], 1643 [sh, ν(C=N)], 1605 [s, ν_a(COO)], 1525 (m), 1449 (s), 1360 [s, ν_s(COO)], 1303 (m), 744 (w), 757 (m), 438 [w, ν(Cu–N)], 332 [m, ν(Cu–O)]. UV–Vis (DMSO): nm (ε): 662 (144), 366 (1.3×10^4), 268 (3.5×10^4). Λ_M (Ω^{-1} cm^2 $mol^{-1}/10^{-3}$ M in DMSO, 24 °C) = 1.8.

2.3.2. [Cu(sal-ser)(1-methylcytosine)] · 1.25H_2O (2)

Prepared as described for **1** although [1-methylcytosine (0.12 g, 1 mmol) in H_2O (10 mL) was added to the starting complex [Cu(sal-L-ser)H_2O] · H_2O in 10 mL of 2:1 water/ethanol warm solution]. Yield: 15%. TG: The complex exhibits a mass decrease (found 5.4; calcd. 5.5%) between 130 and 160 °C corresponding to the loss of 1.25 water molecules per formula unit. *Anal*. Calc. for $C_{15}H_{18.5}N_4O_{6.25}Cu$ (418.4): C, 43.06; H, 4.42; N, 13.39. Found: C, 42.99; H, 4.38; N, 13.15%. IR (KBr disk, cm^{-1}): $\nu = 3376$ (s), 3173 (s), 3157 [s, $\nu_s(NH_2)$ and $\nu_a(NH_2)$], 1663 [sh, ν(C=N)], 1607 [sh, ν_a(COO)], 1535 (m), 1469 (m), 1448 (s), 1344 [s, ν_s(COO)], 1308 (s), 764 (m), 450 [w, ν(Cu–N)], 347 [w, ν(Cu–O)]. UV–Vis (DMSO): nm (ε): 655 (118), 369 (6.8×10^3), 270 (2.2×10^4). Λ_M (Ω^{-1} cm^2 $mol^{-1}/10^{-3}$ M in DMSO, 24 °C) = 2.5.

2.3.3. [Cu(sal-ser)(isocytosine)] · 1.25H_2O (3)

[Cu(sal-L-ser)H_2O] · H_2O (0.30 g, 1 mmol) in 1:1 water/methanol mixture (20 mL) was added to a warm water solution (10 mL, 60 °C) of isocytosine (0.11 g, 1 mmol). The dark green solution was stirred at 60 °C for 1 h. The obtained precipitate was separated by filtration. Dark green crystals appeared after several days from a solution of the obtained solid in 1:1 water/methanol. Yield: 18%. TG: The complex exhibits a mass decrease (found 5.5; calcd. 5.5%) between 160 and 190 °C corresponding to the loss of 1.25 water molecules per formula unit. *Anal*. Calc. for $C_{14}H_{16.5}N_4O_{6.25}Cu$ (404.3): C, 41.58; H, 4.08; N, 13.86. Found: C, 41.60; H, 4.09; N, 13.81%. IR (KBr disk, cm^{-1}): $\nu = 3385$ (s), 3351 [s, $\nu_s(NH_2)$ and $\nu_a(NH_2)$], 1661 [s, ν(C=N)], 1575 [sh, ν_a(COO)], 1533 (m), 1476 (m), 1356 [s, ν_s(COO)], 1307 (s), 770 (m), 446 [w, ν(Cu–N)], 349 [w, ν(Cu–O)]. UV–Vis (DMSO): nm (ε): 657 (111), 370 (6.6×10^3), 272 (1.8×10^4). Λ_M (Ω^{-1} cm^2 $mol^{-1}/10^{-3}$ M in DMSO, 24 °C) = 1.6.

2.3.4. [Cu(sal-ser)(2,4-diamino-6-hydroxypyrimidine)] · 2H_2O (4)

Prepared as described for **1** although in this case [Cu(sal-L-ser)H_2O] · H_2O (0.30 g, 1 mmol) in 1:1 water/ethanol mixture (40 mL) was added to a warm 1:1 water/ethanol solution (10 mL, 60 °C) of 2,4-diamino-6-hydroxy pyrimidine (0.12 g, 1 mmol). Yield: 20%. TG: The complex exhibits a mass decrease (found 8.3; calcd. 8.3%) between 70 and 160 °C corresponding to the loss of two water molecules per formula unit. *Anal*. Calc. for $C_{14}H_{19}N_5O_7Cu$ (432.9): C, 38.84; H, 4.39; N, 16.18. Found: C, 38.93; H, 4.39; N, 16.33%. IR (KBr disk, cm^{-1}): $\nu = 3477$ (s), 3338 [s, $\nu_s(NH_2)$ and $\nu_a(NH_2)$], 1645 [s, ν(C=N)], 1617 [s, ν_a(COO)], 1545 (m), 1460 (m), 1452 (s), 1348 [s, ν_s(COO)], 1293 (s), 745 (w), 763 (m), 770 (m), 465 [w, ν(Cu–N)], 326 (w), 348 [w, ν(Cu–O)]. UV–Vis (DMSO): nm (ε): 662 (115), 369 (7.7×10^3), 269 (3.2×10^4). Λ_M (Ω^{-1} cm^2 $mol^{-1}/10^{-3}$ M in DMSO, 24 °C) = 1.3.

2.3.5. [Cu(sal-ser)(2-aminopyrimidine)(H_2O)] · H_2O (5)

Prepared as described for **1** although 2-hydroxipyrimidine (0.38 g, 4 mmol) was added to a warm 1:1 water/ethanol solution (40 mL, 60 °C) of [Cu(sal-L-ser)H_2O] · H_2O (0.30 g, 1 mmol). Yield: 10%. TG: The complex exhibits a mass decrease (found 5.5; calcd. 5.0%) between 130 and 150 °C corresponding to the loss of one water molecule per formula unit. *Anal*. Calc. for $C_{14}H_{16}N_4O_5Cu$ (383.9): C, 43.80; H, 4.17; N, 14.60. Found: C, 43.80; H, 4.19; N, 14.68%. IR (KBr disk, cm^{-1}): $\nu = 3521$ (s), 3423 (s), 3310 [s, $\nu_s(NH_2)$ and $\nu_a(NH_2)$], 1661 [s, ν(C=N)], 1600 [s, ν_a(COO)], 1587 (s), 1566 (s), 1539 (m), 1494 (s), 1449 (s), 1356 [s, ν_s(COO)], 1309 (s), 804 (sh), 796 (s), 766 (s), 422 (w), 401 [w, ν(Cu–N)], 354 [w, ν(Cu–O)]. UV–Vis (DMSO): nm (ε): 660 (112), 365 (8.7×10^3), 268 (2.3×10^4). Λ_M (Ω^{-1} cm^2 $mol^{-1}/10^{-3}$ M in DMSO, 24 °C) = 2.0.

2.4. X-ray crystallography

X-ray data for single crystals of **1**–**5** were collected with an Enraf-Nonius CAD4 diffractometer using monochromatic Mo Kα radiation ($\lambda = 0.71069$ Å). The cell parameters were determined from least-squares refinement against a set of reflections randomly searched. Data were collected at room temperature using ω–2θ scans. Lorentz-polarisation, decay and ψ-scan empirical absorption [24] corrections were applied using the WinGX program [25] for **1** and **3** and the MolEN package [26] for **2**, **4** and **5**. The structures were solved by direct methods and refined by a full-matrix, least squares method using the SHELX-97 programs [27]. Non-H atoms were anisotropically refined. H atoms were positioned in calculated positions, except those in water molecules, which were located in Fourier difference maps. In **3**, **4** and **5** a global isotropic vibration parameter was refined for all hydrogens while in **1** and **2** the isotropic thermal vibrations of these atoms were fixed to 1.2–1.5 times the U_{iso} of the bonded atom. Crystal

Table 1
Crystal data and structure refinement for complexes **1**–**5**

Compound	**1**	**2**	**3**	**4**	**5**
Empirical formula	$C_{14}H_{18}CuN_4O_7$	$C_{15}H_{18}CuN_4O_6$	$C_{14}H_{14}CuN_4O_5$	$C_{14}H_{19}CuN_5O_7$	$C_{14}H_{16}CuN_4O_5$
Formula weight	417.86	413.87	381.83	432.88	383.85
T (K)	293(2)	293(2)	293(2)	294(2)	293(2)
Crystal system	monoclinic	monoclinic	triclinic	monoclinic	monoclinic
Space group	$P2_1/c$	$C2/c$	$P\bar{1}$	$P2_1/n$	$P2_1/n$
a (Å)	8.751(1)	28.979(14)	8.780(1)	7.981(1)	6.255(2)
b (Å)	19.738(3)	11.303(3)	9.344(1)	12.187(2)	9.566(4)
c (Å)	9.822(1)	11.027(2)	9.913(1)	17.628(2)	25.375(9)
α (°)	90.00	90.00	107.74(1)	90.00	90.00
β (°)	97.95(1)	110.81(2)	105.10(1)	94.748(8)	91.04(3)
γ (°)	90.00	90.00	95.56(1)	90.00	90.00
V (Å^3)	1680.3(8)	3376(2)	733.98(14)	1708.7(4)	1518.1(10)
Z	4	8	2	4	4
μ(Mo Kα) (cm^{-1})	13.47	13.36	15.23	13.29	14.73
Number of reflections measured	5303	5365	4667	5517	5286
Number of unique reflections (R_{int})	5042 (0.1008)	5120 (0.0649)	4437 (0.0150)	5186 (0.0307)	2673 (0.0507)
Final R_1, wR_2 [$I > 2\sigma(I)$]	0.0516, 0.0985	0.0635, 0.1471	0.0417, 0.1005	0.0563, 0.1391	0.0308, 0.0826
R indices (all data)	0.2587, 0.1343	0.2607, 0.1858	0.0908, 0.1154	0.1425, 0.1642	0.0424, 0.0872
Largest difference peak and hole (e Å^{-3})	0.654 and −0.875	0.611 and −0.858	0.622, −0.373	1.369 and −1.814	0.426 and −0.500

parameters, data collection details and results of the refinements are summarized in Table 1.

3. Results and discussion

Although a number of structural studies have been performed on Cu(II)–salicylideneserinato [Cu(sal-ser)] ternary compounds with different substituted pyridines [28–33], no systematic studies are known with ligands able to stabilize the Cu(sal-ser) moiety with additional weak interactions. In order to explore the main factors working on the formation and stabilization of copper salicylideneserinato ternary complexes we have checked several pyrimidine ligands that are potentially able to form additional hydrogen bond interactions, namely cytosine, 1-methylcytosine, isocytosine, 2,4-diamino-6-hydroxypyrimidine and 2-aminopyrimidine. In the cytosine derivative compounds with two flanking groups, amino and carbonyl substituents [O=C–N(3)=C–NH_2], specific repulsive interactions with exocyclic oxygens of the ligand can also exert their influence on the relative orientation of the pyrimidine plane or even decide the specific ring donor atom to the metal cation.

Reaction between the binary [Cu(sal-L-ser)H_2O]·H_2O complex and the corresponding pyrimidine ligand, has permitted the isolation of five new ternary complexes in the form of suitable monocrystals for X-ray diffraction studies. Crystal parameters, data collection details and results of the refinements are summarised in Table 1.

3.1. Structures of complexes *1*–*5*

Complexes **1** and **2** have a slightly distorted square planar geometry, with the four coordination sites occupied by the tridentate N-salicylideneserinato group [N(9), O(16) and O(7)] and the heterocyclic nitrogen N(3) of the pyrimidine ligand (Figs. 1 and 2). As observed in other cytosine

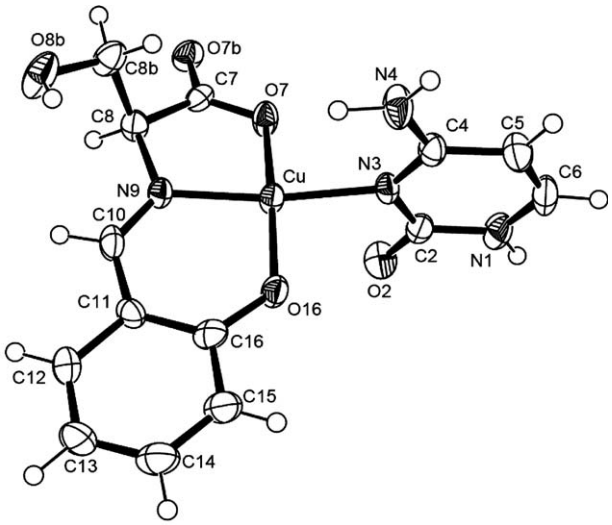

Fig. 1a. ORTEP of [Cu(sal-ser)(cytosine)]·$2H_2O$ (**1**).

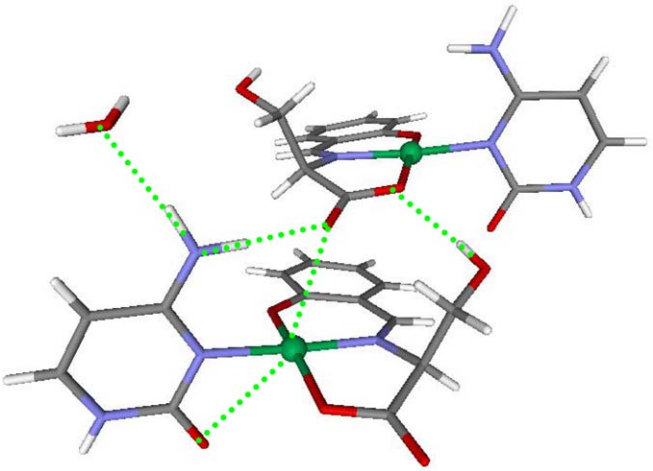

Fig. 1b. Additional interactions observed in complex **1**: [Cu···O(7b)($COO^{\#}$): 2.818 Å; O(8b)–H···O(7)($COO^{\#}$): 2.763 Å; N(4)–H···O(7b)($COO^{\#}$): 2.829 Å; N(4)–H···O(W): 2.909 Å].

compounds [34], an additional weak interaction between copper(II) and the C=O group is observed in both complexes [Cu–O(2): 2.856 Å for **1** and 2.731 Å for **2**].

Complexes **3** and **4** present a similar basal coordination with the isocytosine moiety bonded via N(1) in complex **3** while complex **4** interacts through the exocyclic oxygen O(4). Additional weaker axial interactions on Cu(II) are: Cu–N(2):2.656 Å for **3** and Cu–O(16): 2.627 Å for **4** which allows the association of dimeric complex units (Figs. 3 and 4).

Complex **5** has a square pyramidal geometry with the oxygen atom of one water molecule occupying the fifth axial position (Fig. 5). Copper(II) environment distances are shown in Table 2.

A slight distortion in the square planar environment of Cu(II) in all cases is indicated by the observed bond angles, which vary from 82.38 to 95.87 °C. The distance of N–C(CH_2OH) is shorter than the usual C–N single bond and the values of C=N are in good agreement with the values of Schiff bases Type I described by Ueki et al. [35]. Selected bond distances and angles are given in Table 3.

Additional intramolecular interactions between the ligand and the Cu(sal-ser) moiety are not observed in cytosine complexes **1** and **2** in which the pyrimidine base, coordinated through N(3) to the copper atom, is nearly perpendicular to the Schiff base plane. In the case of a coplanar disposition, a repulsive interaction between O(phenol) and O(C=O) necessarily occurs and can force

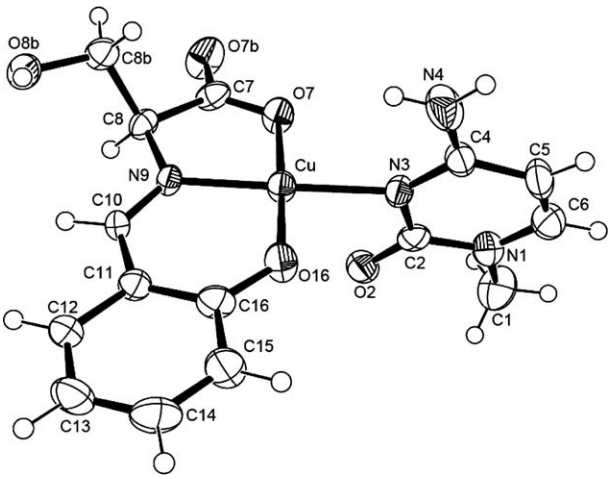

Fig. 2a. ORTEP of [Cu(sal-ser)(1-methylcytosine)] 1.25H_2O (**2**).

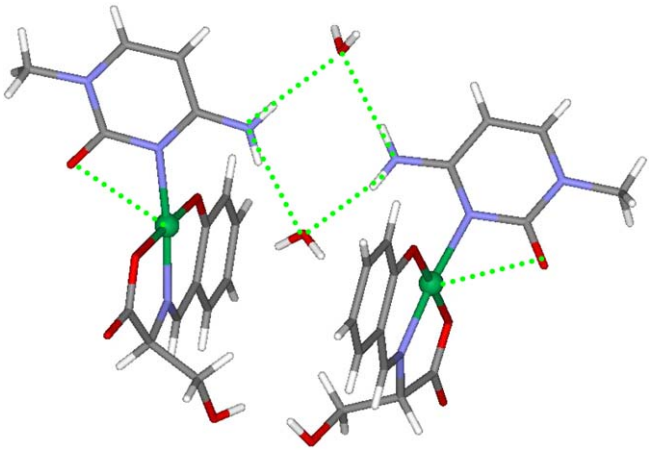

Fig. 2b. Additional interactions observed in complex **2**: [N(4)–H···O(W1): 2.895 Å; N(4)–H···O(W2): 2.844 Å].

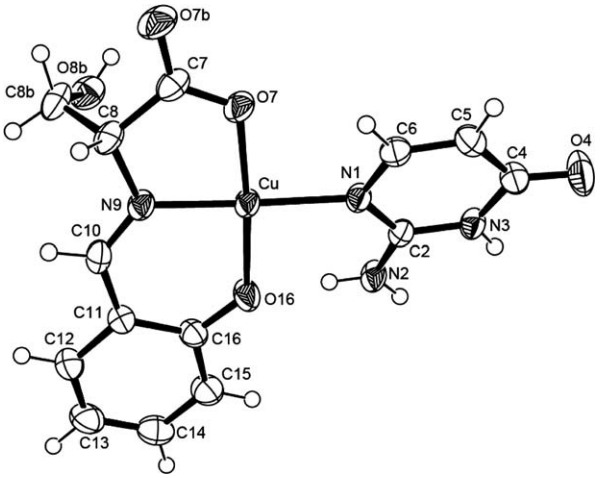

Fig. 3a. ORTEP of [Cu(sal-ser)(isocytosine)] · 1.25H_2O (**3**).

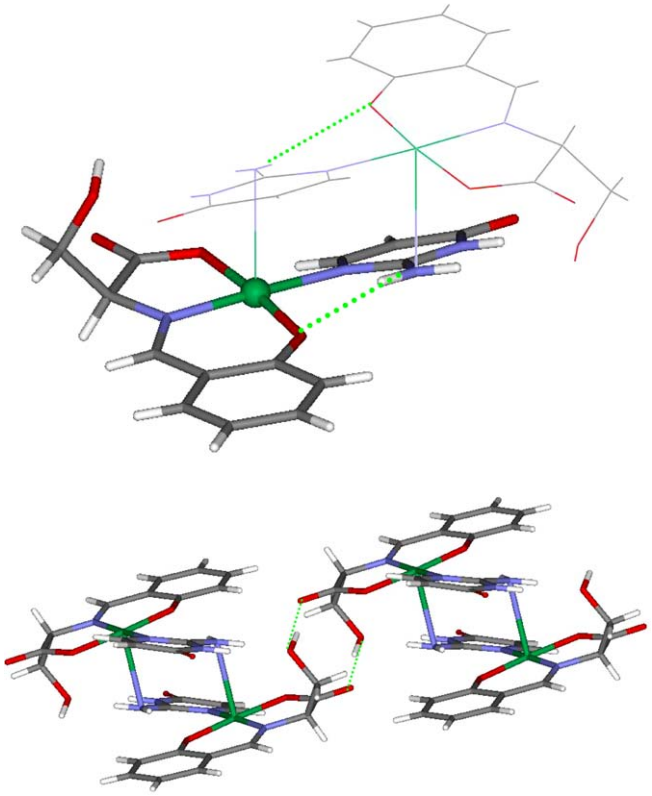

Fig. 3b. Additional interactions observed in complex **3**: [O(8b)–H···O(7b)($COO^{\#}$): 2.684 Å; O(8b)–$H^{\#}$···O(7b)(COO): 2.684 Å].

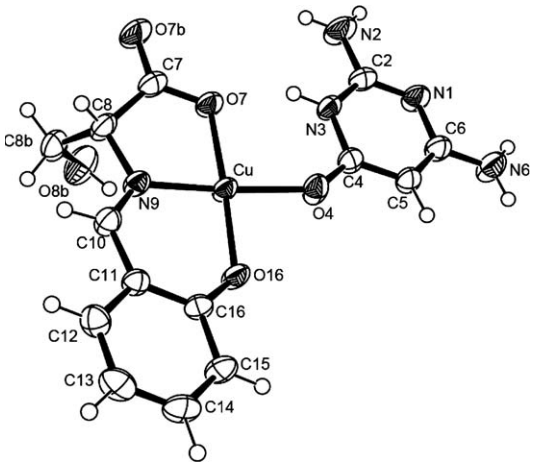

Fig. 4a. ORTEP of [Cu(sal-ser)(2,4-diamino-6-hydroxypyrimidine)]·$2H_2O$ (**4**).

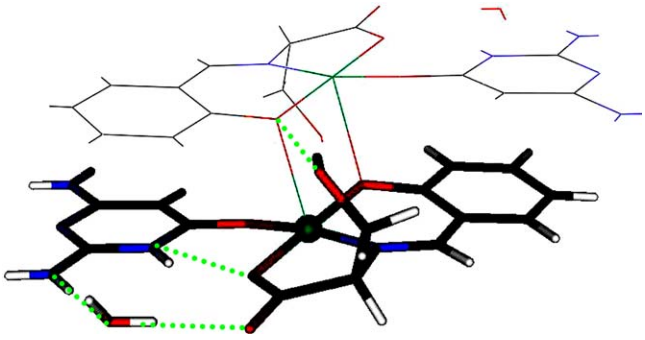

Fig. 4b. Additional interactions observed in complex **4**: [O(8b)–H···O(16)$^{\#}$: 2.852 Å; N(2)–H···O(W): 2.776 Å; O(W)–H···O(7b)(COO): 2.766 Å].

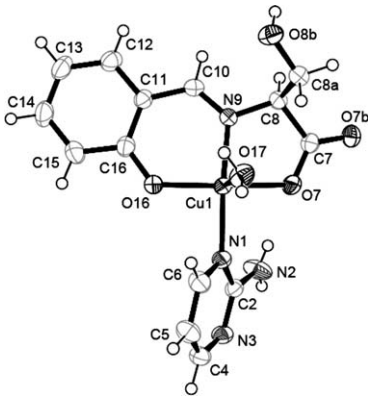

Fig. 5a. ORTEP of [Cu(sal-ser)(2-aminopyrimidine)(H_2O)] (**5**).

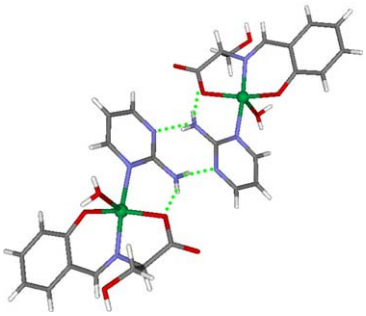

Fig. 5b. Additional interactions observed in complex **5**: [N(2)–H···N(3)$^{\#}$: 3.093 Å; N(2)–H$^{\#}$ ···N(3): 3.093 Å].

the pyrimidine plane towards the orthogonal orientation to avoid steric hinderance. Contrarily to that reported in rhodium(II)–cytosine studies [11] these are two specific cases in which the cytosine ligand is bound through the sterically hindered N(3) to the metal atom without the participation of O(C=O) and N(amino) substituents in intramolecular hydrogen bonds. In the case of complex **3**, the isocytosine ligand is coplanar and is coordinated to Cu(II) through N(1), probably due to the effective and strong additional intramolecular interaction between the amino group of the pyrimidine ligand and the O(phenol) [N(2)–H···O(16): 2.631(3) Å] which is not possible in the cytosine analogs where the ligand is bound to the metal via N(3). Several structural studies [10] on interligand interactions affecting specific metal bonding to nucleobases and quantum chemical studies [36] about rotation of N(3) metallated cytosines have been described.

Surprisingly, monodentate coordination via O(4) of the 2,4-diamino-6-hydroxypyrimidine ligand with both [H_2N–C–N(1)–C–NH_2] and [O–C–N(3)–C–NH_2] moieties, is obtained in the coplanar complex **4** which permits the

Table 2
Comparison between selected bonds relating to the coordination sphere of the complexes

Compound	Cu Schiff base			Pyrimidine base	Cu–OW
	Cu–N(9)	Cu–O(16)	Cu–O(7)		
Binary complex [8]	1.924(8)	1.913(6)	1.957(7)		2.006(7)
Cytosine complexes					
1	1.935(5)	1.899(3)	1.965(3)	Cu–N(3) = 2.000(3)	
2	1.926(4)	1.888(3)	1.950(3)	Cu–N(3) = 2.013(4)	
Isocytosine complexes					
3	1.946(2)	1.893(2)	1.936(1_8)	Cu–N(1) = 2.047(2)	
4	1.917(3)	1.921(2)	1.960(2)	Cu–O(4) = 1.943(2)	
2-Aminopyrimidine complex					
5	1.932(2)	1.911(2)	1.990(2)	Cu–N(1) = 2.029(2)	2.379(2)

Table 3
Selected bond lengths (Å) and angles (°) for complexes **1**–**5**

*[Cu(N-salicylideneserinato)cytosine] (**1**)*			
Cu–O(16)	1.899(3)	Cu–N(9)	1.935(3)
Cu–O(7)	1.965(3)	Cu–N(3)	2.000(3)
O(16)–Cu–N(9)	94.65(13)	O(16)–Cu–O(7)	170.79(13)
N(9)–Cu–O(7)	83.45(13)	N(9)–Cu–N(3)	171.93(14)
N(3)–Cu–O(16)	90.88(13)	O(7)–Cu–N(3)	92.00(13)
C(10)–N(9)–Cu	126.2(3)	C(8)–N(9)–Cu	112.6(2)
C(7)–O(7)–Cu	115.8(3)	C(16)–O(16)–Cu	125.6(3)
C(4)–N(3)–Cu	126.9(3)	C(2)–N(3)–Cu	111.6(3)
*[Cu(N-salicylideneserinato)(1-methylcytosine)] (**2**)*			
Cu–O(16)	1.888(3)	Cu–N(9)	1.926(4)
Cu–O(7)	1.950(3)	Cu–N(3)	2.013(4)
O(16)–Cu–N(9)	94.36(16)	O(16)–Cu–O(7)	177.81(16)
N(9)–Cu–O(7)	83.50(16)	N(9)–Cu–N(3)	173.39(17)
N(3)–Cu–O(16)	91.25(16)	O(7)–Cu–N(3)	90.86(16)
C(10)–N(9)–Cu	125.9(3)	C(8)–N(9)–Cu	114.6(3)
C(7)–O(7)–Cu	116.8(3)	C(16)–O(16)–Cu	126.8(3)
C(4)–N(3)–Cu	131.8(4)	C(2)–N(3)–Cu	107.7(3)
*[Cu(N-salicylideneserinato)isocytosine] (**3**)*			
Cu–O(16)	1.893(2)	Cu–N(9)	1.946(2)
Cu–O(7)	1.9364(18)	Cu–N(3)	2.047(2)
O(16)–Cu–N(9)	91.47(9)	O(16)–Cu–O(7)	175.14(8)
N(9)–Cu–O(7)	83.78(9)	N(9)–Cu–N(3)	173.13(8)
N(3)–Cu–O(16)	93.08(8)	O(7)–Cu–N(1)	91.56(8)
C(10)–N(9)–Cu	127.41(18)	C(8)–N(9)–Cu	113.67(17)
C(7)–O(7)–Cu	116.74(18)	C(16)–O(16)–Cu	129.56(17)
C(2)–N(1)–Cu	127.11(17)	C(6)–N(1)–Cu	118.07(16)
*[Cu(N-salicylideneserinato)(2,6-diamino-4-hydroxypyrimidine)] (**4**)*			
Cu–O(16)	1.921(2)	Cu–N(9)	1.917(3)
Cu–O(7)	1.960(2)	Cu–O(4)	1.943(2)
O(16)–Cu–N(9)	93.41(11)	O(16)–Cu–O(7)	176.91(10)
N(9)–Cu–O(7)	83.85(10)	N(9)–Cu–O(4)	170.72(11)
O(4)–Cu–O(16)	87.05(10)	O(7)–Cu–O(4)	95.87(10)
C(10)–N(9)–Cu	125.6(2)	C(8)–N(9)–Cu	114.3(2)
C(7)–O(7)–Cu	115.2(2)	C(16)–O(16)–Cu	124.9(2)
*[Cu(N-salicylideneserinato)(2-aminopyrimidine)(H_2O)] (**5**)*			
Cu–O(16)	1.911(2)	Cu–N(9)	1.932(2)
Cu–O(7)	1.9899(19)	Cu–N(1)	2.029(2)
Cu–O(W)	2.379(2)		
O(16)–Cu–N(9)	93.50(9)	O(16)–Cu–O(7)	164.12(9)
N(9)–Cu–O(7)	82.37(8)	N(9)–Cu–N(1)	174.65(8)
N(1)–Cu–O(16)	90.28(9)	O(7)–Cu–N(1)	92.98(9)
O(16)–Cu–O(W)	101.72(9)	N(9)–Cu–O(W)	90.94(9)
O(7)–Cu–O(W)	93.70(8)	N(1)–Cu–O(W)	92.00(9)
C(10)–N(9)–Cu	127.41(18)	C(8)–N(9)–Cu	114.34(17)
C(7)–O(7)–Cu	115.87(16)	C(16)–O(16)–Cu	126.82(18)
C(2)–N(1)–Cu	124.01(18)	C(6)–N(1)–Cu	118.95(17)

adjacent heterocyclic nitrogen to participate in an additional intramolecular hydrogen bond interaction [N(3)–H···O(7): 2.821 Å] that stabilizes the structure. As indicated previously, in order to avoid steric constraints about the metal center, cytosine can binds to the metal ion via the exocyclic O(2) atom [20,21,37–40].

In the case of complex **5**, the aminopyrimidine ligand rotates to permit the optimal and typical intramolecular interaction between the amino group and the carboxylate oxygen atom [N(2)–H···O(7): 2.920 Å] [8].

Intermolecular interactions involving crystallisation water molecules and interactions between complex units stabilize the crystal packing in all the complexes (see Figs. 1–5).

3.2. Infrared and electronic spectra

The IR spectra of the complexes were recorded down to the region around 400 cm^{-1} and compared with those of the free ligand. Tentative band assignments (cm^{-1}) for the cytosine derivatives have been published previously [14,15,18–20]. For 2,4-diamino-6-hydroxypyrimidine and 2-aminopyrimidine tentative assignments have been made by analogy with those of cytosine. In all the complexes several peaks are observed between 3500 and 3200 cm^{-1} which are related to the stretching vibrations $\nu_{as}(NH_2)$ and $\nu_s(NH_2)$. The strong band appearing between 1660 and 1630 cm^{-1} is assignable to ν(CN) [41] and the peaks located in the ranges 1620–1570 and 1390–1350 cm^{-1} are attributed to ν_{as}(COO) and ν_s(COO), respectively [42]. The separation between the two bands is consistent with a monodentate coordination of the carboxylate group. Other bands in the range 1500–1100 cm^{-1} are related to ν(Phe) ring and ν(OPhe). Finally, the peaks appearing between 460–420 and 380–320 cm^{-1} are attributed to ν(Cu–N) and ν(Cu–O).

The d–d transition spectra of the complexes in DMSO show a broad band between 655 and 662 nm that is suggestive of approximate square pyramidal geometry about Cu(II) in solution. The π–π^* bands corresponding to the pyrimidine ligand appear in the 370–268 nm range. For these compounds, the Λ_M (10^{-3} M) values in DMSO at 20 °C imply the presence of non-electrolyte type species [43].

3.3. ESR spectra and magnetic properties

The effective magnetic moments $\mu_{eff} = 1.93$ (**2**), 1.77 MB (**3**), 1.80 MB (**4**) and 1.98 MB (**5**) at room temperature are normal for magnetically diluted d^9 systems. The X-band ESR spectra of a polycrystalline powder of the complexes recorded at 298 K show axial symmetry with values of $g_\parallel = 2.21$ and $g_\perp = 2.06$ (**2**), $g_\parallel = 2.24$ and $g_\perp = 2.07$ (**3**), $g_\parallel = 2.13$ and $g_\perp = 2.05$ (**4**) and $g_\parallel = 2.20$ and $g_\perp = 2.09$ (**5**). Simulated spectra obtained by using the WINEPR program gave good agreement with the experimental g values. These spectra are consistent with square planar or square pyramidal geometry. The results are in agreement with the symmetry of Cu(II) derived from the X-ray structure determination. Unfortunately, the values for complex **1** were not obtained owing to difficulties in preparing enough pure crystalline sample and the highest instability of this complex compared to compound **2**.

4. Conclusion

In this study, we have synthesized and structurally characterized five new Schiff base ternary Cu(sal-ser) complexes with different pyrimidine (cytosine or isocytosine derivatives) ligands and explored the effect of changing the adjacent

groups of the potential binding heterocyclic atom. The presence of an intramolecular hydrogen bond and specific interligand repulsive interactions seem to be important factors, playing a crucial role on the stability of the complexes and the relative orientation of the pyrimidine plane or even deciding the particular donor atom to the copper(II) ion.

As a consequence of repulsive O(C=O)···O(Phe) interactions, the approximate orthogonal disposition is obtained allowing an additional weak attractive interaction Cu···O(C=O) in the cytosine derivatives (**1** and **2**).

For the isocytosine complex **3**, the chosen metal binding site N(1) and a coplanar disposition allow the additional hydrogen bond interaction NH(amino)···O(Phe). In complex **4**, the aminoisocytosine ligand binds to the metal ion through the oxygen atom in a monodentate way which permits the additional [N(3)H···O(COO)] interaction. Finally, in the case of complex **5**, the additional hydrogen bond [N(amino)···O(carboxylate) = 2.92Å] implies rotation of the 2-amino pyrimidine plane with respect to the Schiff base plane.

Acknowledgments

We are grateful to Spanish CICYT (BQ2002-02546) for financial support and to COST D20 (WG 0006) Project.

Appendix A. Supplementary data

CCDC-286127–286131 contains the supplementary crystallographic data for this paper. These data can be obtained free of charge at www.ccdc.cam.ac.uk [or from the Cambridge Crystallographic Data Centre, 12, Union Road, Cambridge CB2 1EZ, UK; fax: (internat.) +44 1223 336 033; e-mail: deposit@ccdc.cam.ac.uk]. Supplementary data associated with this article can be found, in the online version, at doi:10.1016/j.poly.2006.01.032.

References

[1] A. García-Raso, J.J. Fiol, A. López-Zafra, J.A. Castro, A. Cabrero, I. Mata, E. Molins, Polyhedron 22 (2003) 403, and references therein.
[2] J.B. Longenecker, E.E. Snell, J. Am. Chem. Soc. 79 (1956) 142.
[3] E.E. Snell, A. Braunstein, E.S. Severin, V.M. Torchinsky, Pyridoxal Catalysis: Enzymes and Model Systems, Interscience, New York, 1968.
[4] G.M. Mockler, R.J. Butcher, O. McKern, M. Sheil, J. Inorg. Biochem. 74 (1999) 238.
[5] J. Sivy, V. Kettmann, J. Krätsmár-Smogrovic, O. Svajlenová, C. Friebel, G. Plesch, Z. Anorg. Allg. Chem. 583 (1990) 55.
[6] A. García-Raso, J.J. Fiol, F. Bádenas, F. Muñoz, Polyhedron 20 (2001) 2609.
[7] A. García-Raso, J.J. Fiol, F. Bádenas, E. Lago, E. Molins, Polyhedron 20 (2001) 2877.
[8] A. García-Raso, J.J. Fiol, A. López-Zafra, A. Cabrero, I. Mata, E. Molins, Polyhedron 18 (1999) 871.
[9] V. Kettmann, E. Fresova, M. Blahova, J. Kratsmar-Smogrovic, Acta Crystallogr., Sect. C 49 (1993) 1932.
[10] M.A. Salam, K. Aoki, Inorg. Chim. Acta 311 (2000) 15.
[11] K. Aoki, M.A. Salam, Inorg. Chim. Acta 316 (2001) 50.
[12] G. De Munno, M. Medaglia, D. Armentano, J. Anastassopoulou, T. Theophanides, J. Chem. Soc., Dalton Trans. (2000) 1625.
[13] M.C. Capllonch, A. García-Raso, A. Terrón, M.C. Apella, E. Espinosa, E. Molins, J. Inorg. Biochem. 85 (2001) 173.
[14] G. De Munno, S. Mauro, T. Pizzino, D. Viterbo, J. Chem. Soc., Dalton Trans. (1993) 1113.
[15] A. Panfil, A. Terrón, J.J. Fiol, Polyhedron 13 (1994) 2513, and references therein.
[16] S. Cosar, M.B.L. Janik, M. Flock, E. Freisinger, E. Farkas, B. Lippert, J. Chem. Soc., Dalton Trans. (1999) 2329.
[17] P.T. Selvi, M. Murali, M. Palaniandavar, M. Kockerling, G. Henkel, Inorg. Chim. Acta 340 (2002) 139.
[18] A. García-Raso, J.J. Fiol, B. Adrover, V. Moreno, E. Molins, I. Mata, J. Chem. Soc., Dalton Trans. (1998) 1031.
[19] A. García-Raso, J.J. Fiol, B. Adrover, A. Caubet, E. Espinosa, I. Mata, E. Molins, Polyhedron 21 (2002) 1197.
[20] K. Aoki, J. Chem. Soc., Chem. Commun. (1976) 748.
[21] G. Cervantes, J.J. Fiol, A. Terrón, V. Moreno, J.R. Alabart, M. Aguiló, M. Gómez, X. Solans, Inorg. Chem. 29 (1990) 5168.
[22] J.J. Fiol, A. García-Raso, A. Terrón, I. Mata, E. Molins, Inorg. Chim. Acta 262 (1997) 85.
[23] J.M. Rawson, R.E.P. Winpenny, Coord. Chem. Rev. 139 (1995) 313.
[24] A.C.T. North, D.C. Phillips, F.S. Mathews, Acta Crystallogr., Sect. A 24 (1968) 351.
[25] L.J. Farrugia, J. Appl. Crystallogr. 32 (1999) 837.
[26] C.K. Fair, MolEN: An Interactive Intelligent System for Crystal Structure Analysis, Enraf Nonius, Delft, The Netherlands, 1990.
[27] G.M. Sheldrick, SHELX-97: Programs for Crystal Structure Analysis Release (97-2), University of Göttingen, Göttingen, Germany, 1997.
[28] S.A. Warda, Acta Crystallogr., Sect. C 53 (1997) 1010.
[29] S.A. Warda, Acta Crystallogr., Sect. C 53 (1997) 1184.
[30] S.A. Warda, Acta Crystallogr., Sect. C 54 (1998) 187.
[31] S.A. Warda, Acta Crystallogr., Sect. C 54 (1998) 1236.
[32] S.A. Warda, Acta Crystallogr., Sect. C 54 (1998) 768.
[33] S.A. Warda, Acta Crystallogr., Sect. C 54 (1998) 1754.
[34] D.J. Szalda, L.G. Marzilli, T.J. Kistenmacher, Inorg. Chem. 14 (1975) 2076.
[35] T. Ueki, T. Ashida, V. Sasada, K. Kakudo, Acta Crystallogr., Sect. B 25 (1969) 328.
[36] J.E. Sponer, F. Glahé, J. Leszczynski, B. Lippert, J. Sponer, J. Phys. Chem. B 105 (2001) 12171.
[37] K. Ogawa, M. Kumihashi, K. Tomita, S. Shirotake, Acta Crystallogr., Sect. B 36 (1980) 1793.
[38] K. Saito, R. Terashima, T. Sakaki, K. Tomita, Biochem. Biophys. Res. Commun. 61 (1974) 83.
[39] T.J. Kistenmacher, T. Szalda, L.G. Marzilli, Acta Crystallogr., Sect. B 31 (1975) 2416.
[40] O. Renn, H. Preut, B. Lippert, Inorg. Chim. Acta 188 (1991) 133.
[41] M.S. Palacios, E. Medina, F.G. Manrique, M.T.P. Gambardella, R.H.A. Santos, M.L. Rodriguez, J.M. Dance, Polyhedron 8 (1989) 2131.
[42] K. Nakamoto, Infrared and Raman Spectra of Inorganic and Coordination Compounds, Wiley, New York, 1978.
[43] W.J. Geary, Coord. Chem. Rev. 7 (1971) 81.

The ammine ligand in $[(\eta^5\text{-}C_5H_5)Ru(PPh_3)(CN^tBu)(NH_3)]PF_6$ had proved to be resistant to replacement by carbonylation and to deprotonation [9].

There are very comprehensive nomenclature systems for the unique identification of isomeric transition metal compounds but they have proved very cumbersome for routine application [10,11]. We have opted for the simple approach related to that used by organic practitioners. The stereochemical descriptors used for organometallic compounds are a modification of the Cahn–Ingold–Prelog rules and treat the cyclopentadienyl group as a single atom of atomic weight 60 for prioritization [12,13]. The structural diagrams in this paper are drawn to normally show the metal chirality denoted as $\mathbf{S}_{Ru}$ for convenience ($Cp > PPh_3 > NH_2R > CN^tBu$) but unless explicitly stated the starting materials and products represented are racemic. One of the spectroscopic probes used throughout this work is that of diamagnetic anisotropy; protons held over an aromatic ring system will normally be shielded (δ decreases) in ^1H NMR spectra while protons held over a triple bond will be deshielded (δ increases). The effect is usually observable at distances up to 4 Å and drops off rapidly although measurable effects up to 14 Å have been observed in polyaromatic systems [14,15].

2. Results and discussion

Treatment of $[(\eta^5\text{-}C_5H_5)Ru(PPh_3)(CN^tBu)(Cl)]$ (**1**) with a halide abstractor in the presence of cyclohexylamine produced yellow crystalline $[(\eta^5\text{-}C_5H_5)Ru(PPh_3)(CN^tBu)(NH_2C_6H_{11})]PF_6$ (**2**). The halide abstraction system could be either thallium hexafluorophosphate in dichloromethane or the methanolic potassium hexafluorophosphate–thallium (I) carbonate mixture used previously to prepare ammine complexes [9]. The first system gave a 97% yield compared with 38% for the latter indicating some degree of competition between methanol and the amine for the solvento cationic intermediate in that synthetic route. The main features of spectroscopic interest are the differentiation of the diastereotopic NH protons by 1.21 ppm in the ^1H NMR spectrum and weak bands at 3311, 3270, and 1587 cm^{-1} in the infrared spectrum due to the amine ligand. Encouraged by the degree of chemical shift difference which suggested that one of the amine protons is oriented into the region near the phenyl rings of the triphenylphosphine ligand and hence shielded, implying strongly preferred conformations and a useful spectroscopic probe, we decided to prepare a family of cations containing *C*-chiral amines in order to investigate diastereomeric resolution. The chiral amines used were of at least 98% e.e. and the diastereomeric excesses reported below have not been recalculated; given the integration errors for routine ^1H NMR spectroscopy the diastereomeric excesses reported probably underestimate the true selectivities.

Reaction of **1** with thallium hexafluorophosphate in dichloromethane and *S*(−)-α-methylbenzylamine, *R*(−)-1-cyclohexylethylamine, or (±)-1-(1-naphthyl)ethylamine gave the salts $[(\eta^5\text{-}C_5H_5)Ru(PPh_3)(CN^tBu)(NH_2CH\{Me\}Ph)]PF_6$ (**3**), $[(\eta^5\text{-}C_5H_5)Ru(PPh_3)(CN^tBu)(NH_2CH\{Me\}Cy)]PF_6$ (**4**), and $[(\eta^5\text{-}C_5H_5)Ru(PPh_3)(CN^tBu)(NH_2CH\{Me\}Np)]PF_6$ (**5**), respectively. Initial crystallization of **3** from dichloromethane–diethyl ether (1:3) at −78 °C gave fine yellow crystals, which proved to be predominantly the $\mathbf{R}_{Ru}\mathbf{S}_C$ diasteromer (**3RS**) in 74% diastereomeric excess. Concentration of the filtrate and crystallization at −25 °C gave a second set of yellow crystals, which proved to be predominantly the $\mathbf{S}_{Ru}\mathbf{S}_C$ diastereomer (**3SS**) in 98% d.e. The infrared spectrum of **3** contains four bands due to ν(NH) at 3325, 3308, 3284, and 3265 cm^{-1} confirming the presence of two diastereomers with the bands at 3325 and 3284 cm^{-1}being due to the more soluble diastereomer **3SS**. While the definitive assignment of absolute structure for the two diastereomeric salts was made by single crystal X-ray crystallography our initial assignment was made by consideration of the ^1H NMR spectra of the enriched diastereomers. The spectrum of the least soluble compound **3RS** has a cyclopentadienyl singlet resonance at δ 4.30 and a doublet at δ 1.11 for the α-methyl group whereas the more soluble compound **3SS** has these resonances at δ 4.72 and δ 1.29, respectively. The diastereomers **3RR** and **3SR** were also prepared, from *R*(+)-α-methylbenzylamine to ensure complementarity and reciprocity and this pair were used for the X-ray single crystallographic studies (Scheme 1).

Davies has demonstrated the use of α-methyl group shielding by the aromatic ring current of triphenylphosphine to distinguish stereoisomers of the metal acyls $[(\eta^5\text{-}C_5H_5)Fe(PPh_3)(CO)(COCH(Me)R)]$; in $\mathbf{S}_{Fe}\mathbf{S}_C/\mathbf{R}_{Fe}\mathbf{R}_C$ diastereomers the group resonates between δ 0.00 and δ 0.50 whereas in the $\mathbf{S}_{Fe}\mathbf{R}_C/\mathbf{R}_{Fe}\mathbf{S}_C$ diastereomers the resonance is found between δ 0.8 and δ 1.30 [16]. Fig. 1 illustrates the relative relationships between the ruthenium and iron compounds; note that the priority rules reverse the metal centre descriptors on changing from an amine group to an acyl group.

The single crystal X-ray structures of **3SR** and **3RR** (vide infra) confirm the basic conformations shown in Fig. 2 and support the additional assumption that the phenyl ring of the amine ligand shields the cyclopentadienyl protons in **3SR** and **3RS**. Our criterion is that the diastereomer with the highest ^1H NMR chemical shifts for both the cyclopentadienyl and α-methyl groups is the **RR** or **SS** diastereomer while that with the lowest values for both chemical shifts is the **RS** or **SR** isomer in the isonitrile series. Davies has published extensively on the conformational preferences of the alkyl groups in the iron acyl complexes [17]; we have not performed similar modeling studies but the close spectroscopic similarities suggest that qualitatively the structures indicated are correct, in particular that the methine hydrogen points in towards the isonitrile or carbonyl group.

While the described preparation of **3** yields an overall racemic product in that equal amounts of **3RS** and **3SS** are produced from **2** and *S*(−)-α-methylbenzylamine

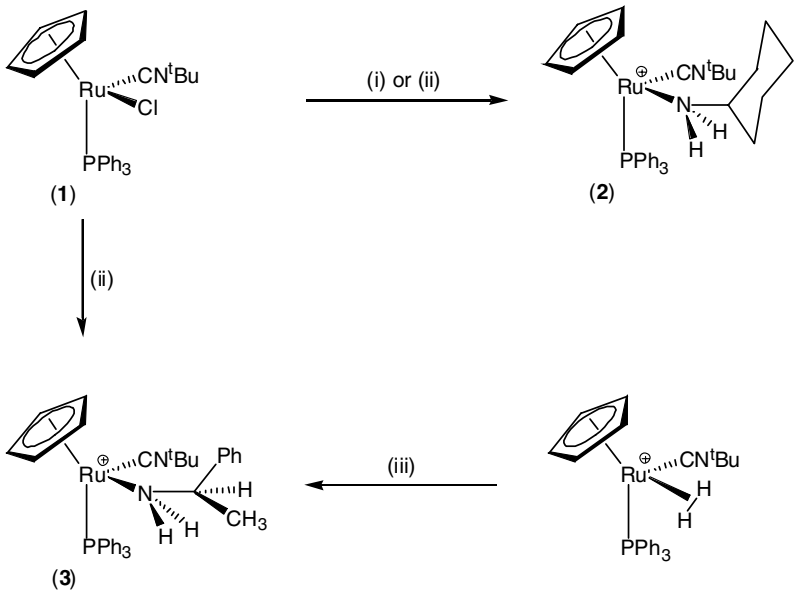

(i) KPF_6, Tl_2CO_3, MeOH, amine, 60°C (ii) $TlPF_6$, amine, CH_2Cl_2, RT (iii) amine, CH_2Cl_2

Scheme 1. Synthetic routes to **2** and **3**.

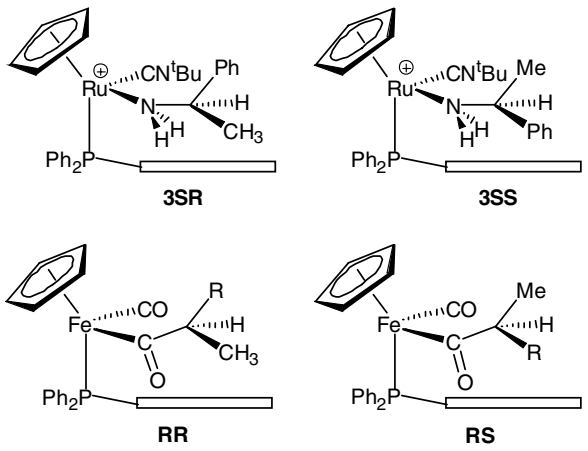

Fig. 1. Relationship of chirality descriptors to structure.

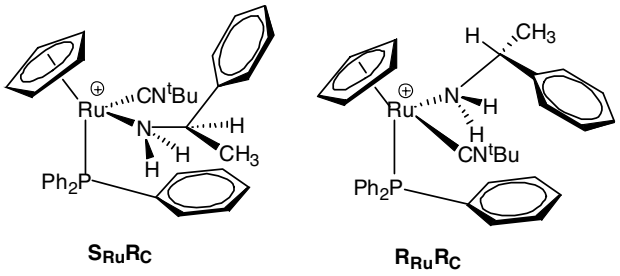

Fig. 2. Idealized solution conformation of **3SR** and **3RR**.

thermodynamically, this was not necessarily anticipated. A kinetic experiment was therefore carried out by monitoring the formation of **3SS** and **3RS** from the reaction of the molecular hydrogen cation $[(\eta^5\text{-}C_5H_5)Ru(PPh_3)(CN^tBu)(\eta^2\text{-}H_2)]PF_6$ [18] with *S*(−)-α-methylbenzylamine in deuterodichloromethane by ^1H NMR spectroscopy at room temperature. Addition of 0.3 equivalents of the amine immediately generated only **3SS** and the further addition of 0.7 equivalents of amine subsequently generated **3RS** within 10 min; the final ratio of diastereomers was 50:50 and remained unchanged after 1 h at room temperature. Under the ambient conditions the Lewis acid fragment $[(\eta^5\text{-}C_5H_5)Ru(PPh_3)(CN^tBu)]^+$ formed initially does not racemise and despite a kinetic preference for **3SS** the lack of racemization prevents diastereomeric induction. Under these conditions there is no interconversion of **3SR** and **3SS** as evidenced both by this experiment and from monitoring enriched samples over a period of days. Further, the single crystals used for the X-ray structural determinations of **3RR** and **3SR**, respectively were each dissolved in CD_2Cl_2 at 22 °C and ^1H NMR spectra of the solutions were immediately obtained; in each case the appropriate single diastereomer was the only observed species and the other diastereomers, **3SR** and **3RR**, respectively, were not observed after several hours.

There has been a considerable history of investigating the ease of racemization of chiral at metal compounds [4–8] with the general conclusion that such centres are often not stereochemically rigid; we conclude that in this case the rate of racemization is much less than the rate of complexation and that none of the ligands attached to ruthenium in the final products reversibly dissociate (Scheme 2).

The salt $[(\eta^5\text{-}C_5H_5)Ru(PPh_3)(CN^tBu)(NH_2CH\{Me\}\text{-}Cy)]PF_6$ (**4**) was also enriched on initial crystallization to produce **4SR** as the least soluble diastereomeric salt in 61% d.e. and the more soluble isomer **4RR** in 79% d.e.

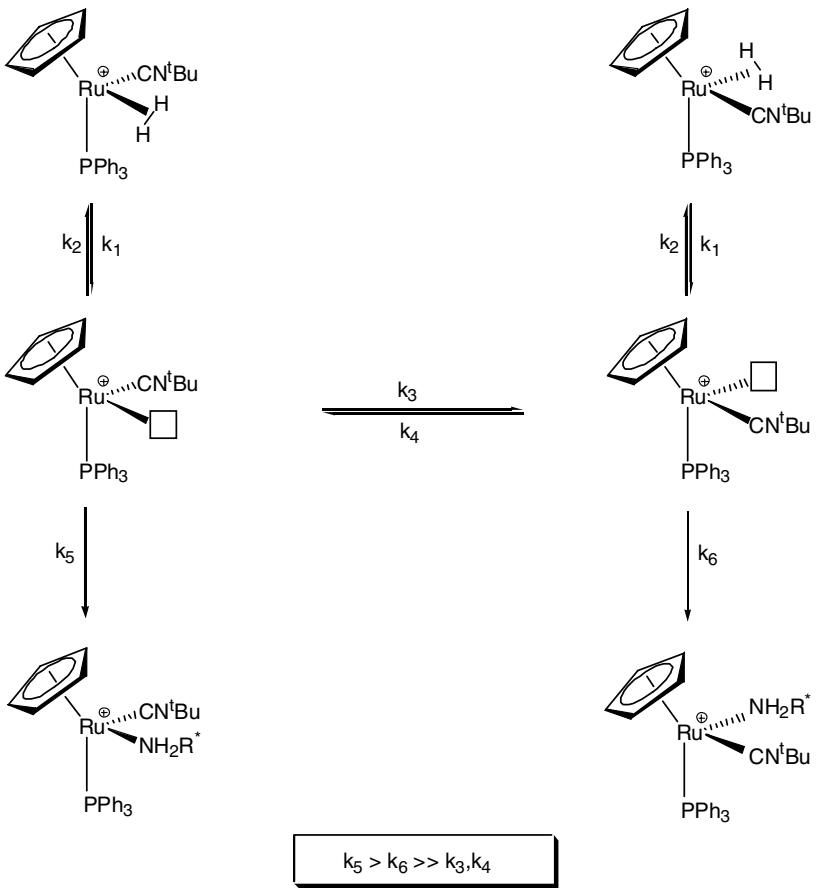

Scheme 2. Curtin–Hammett scheme for the interconversion of **3**.

Similarly a single crystallization of $[(\eta^5\text{-}C_5H_5)Ru(PPh_3)(CN^tBu)(NH_2CH\{Me\}Np)]PF_6$ (**5**) gave the **RS/SR** product in 73% d.e. and the more soluble **RR/SS** product in 56% d.e. A further recrystallization of the **RS/SR** product increased the diastereomeric excess up to 91%; both products in this case being racemic because racemic (±)-1-(1-naphthyl)ethylamine was used. In contrast to the large difference in ^{1}H NMR chemical shift, (0.43 ppm), for the cyclopentadienyl resonances of **3RS** and **3SS** these resonances differ by 0.001 ppm for the diastereomers of **4** suggesting that the aromatic ring of the amine in **3** can shield these protons. In the case of **5** which also contains an aromatic group in the amine ligand the separation is 0.54 ppm for the diastereomers.

Further diastereomeric enrichment of **3** and **5** was carried out to establish the principle and usually a maximum of three crystallizations was sufficient to give products of ca. 98.5% d.e. for **3** and **5**. Enrichment of **4** was not explored fully because the spectroscopic parameters of **4** made accurate quantitation problematic beyond the 90% d.e. level.

The reaction of $[(\eta^5\text{-}C_5H_5)Ru(PPh_3)(CO)Cl]$ (**6**) with thallium hexafluorophosphate and *S*(−)-α-methylbenzylamine in dichloromethane produced a very low yield (3%) of yellow crystals of $[(\eta^5\text{-}C_5H_5)Ru(PPh_3)(CO)(NH_2CH\{Me\}Ph)]PF_6$ (**7**). The two diastereomeric salts were again partially separable with the $\mathbf{R_{Ru}S_C}$ product (**7RS**) being the least soluble. The assignment of $\mathbf{R_{Ru}}$ stereochemistry in this diastereomeric salt was made by comparing the cyclopentadienyl resonances in the ^{1}H NMR spectra at δ 5.13 and 4.57 with the lower chemical shift being assigned to **7RS** and the higher to **7SS**; this reflects the pattern found for the diastereomers of **3** and **5** induced by the orientation of the aromatic substituent on the amine ligand. The small quantity of **7SS** obtained after the initial crystallization which gave a sample of **7RS** in 42% d.e. combined with the low chemical yield, prevented the full assignment of the ^{1}H NMR spectrum and means that we have used a single parameter in this case.

Decomplexation of the bound amine from diastereomerically enriched samples of **3**, **4**, or **7** should produce enantiomerically enriched samples of the metal moieties. A variety of procedures was explored using $[(\eta^5\text{-}C_5H_5)Ru(PPh_3)(CN^tBu)(NH_2C_6H_{11})]PF_6$ (**2**) as a model compound. Reaction of **2** with carbon monoxide (5 atm., 294 K, 120 h.) in dichloromethane, with iodomethane or tetraethylammonium fluoride or tetraethylammonium cyanide in dichloromethane, with methanolic sodium methoxide, with sodium iodide or sodium azide in acetone, with lithium triethylborohydride in THF (all at 294 K, 1–48 h), or with 2-methyl-1-butanethiol in refluxing methanol gave in each case high recovery (>80%) of

2 and no other tractable products. Treatment of **2** with excess sodium iodide and excess trimethylamine-*N*-oxide in methanol under reflux generated [(η^5-C_5H_5)-Ru(PPh_3)(CN^tBu)(I)] (**8**) in moderate yield together with recovered **2**. Since this reaction probably proceeds by the generation of iodine and its subsequent reaction with **2** we proceeded to react **2** with iodomethane in refluxing 1,2-dichloroethane or by photolysis of a solution in dichloromethane containing iodine. Careful optimization of these reactions suggested initial conditions for the attempted decomplexation of **3**, the chiral metal centre target. Samples of **3RS** (90% d.e.) and **3SS** (96% d.e.) were converted via the iodomethane route into **8** in 98% and 82% isolated yield, respectively. A sample of **3RS** of the same purity was also converted via the photolysis route in 54% isolated yield.

The samples of **8** obtained were assayed for enantiomeric purity by two methods; reaction with *S*(−)-α-methylbenzylamine to regenerate **3RS** and **3SS** and by a ^{1}H NMR spectroscopic method. Addition of *R*(−)-2,2,2-trifluoro-1-(9-anthryl)ethanol (*R*(−)-TFAE) to racemic **8** causes doubling of the cyclopentadienyl and *tert*-butyl resonances with the optimum separation (300 MHz: 5.7 and 3.6 Hz, respectively) occurring on addition of 1.2 equivalents of TFAE. Both methods confirmed that the samples of **8** obtained on decomplexation from **3RS** and **3SS** were racemic (±2%). The high chemical stability of **3** and the nature of the forcing conditions required to produce **8** demonstrates that our resolution strategy was unsuccessful.

The reaction of a secondary amine ligand could potentially generate an additional chiral centre and [(η^5-C_5H_5)-Ru(PPh_3)(CN^tBu)(Cl)] (**1**) was reacted with diethylamine and $TlPF_6$ in dichloromethane to confirm that a secondary amine could ligate to the ruthenium centre. The orange-yellow crystals of [(η^5-C_5H_5)Ru(PPh_3)(CN^tBu)($NHEt_2$)]PF_6 (**9**) were moderately air-sensitive and showed a single band at 3269 cm^{-1} (ν_{NH}) in the infrared spectrum in contrast to the two bands seen for a primary amine containing cation. The ^{1}H and ^{13}C{^{1}H} NMR spectra of **9** demonstrated that the ethyl groups of the diethylamine ligand were diastereotopic as expected. *S*(−)-*N*-methyl-1-phenylethylamine reacted similarly to yield yellow crystalline [(η^5-C_5H_5)-Ru(PPh_3)(CN^tBu)(NH(Me)CH{Me}Ph)]PF_6 (**10**) as a mixture of four diastereomers in the ratio 9.6%:38.5%:3.9%:48.0% while concentration of the initial mother-liquor and crystallization produced the same diastereomers in the ratio 21.7%:52.2%:8.7%:17.4%. While these precise ratios reflect the degree of crystallization achieved they also indicate the relative stability of the nitrogen chiral centres, these being freely selectable under the reaction conditions unlike the ruthenium and carbon chiralities, one of which is not racemisable under the conditions and the other of which is set. Analysis of the ^{1}H NMR spectra of these mixtures using the criteria established above for the relative disposition of the metal and carbon chiralities suggests the assignments $\mathbf{S_{Ru}S_NS_C}$:$\mathbf{S_{Ru}R_NS_C}$:$\mathbf{R_{Ru}R_NS_C}$:$\mathbf{R_{Ru}S_NS_C}$ for the diastereomers (Table 1). In particular the cyclopentadienyl group and α-methyl resonances reflect the neighbouring phenyl ring induced shieldings. The *N*-methyl group shieldings also reflect the existence of two diastereomers with these groups pointing towards the isonitrile unsaturation (deshielded) and two with these groups pointing away (shielded).

Calculation of the total quantities of each diastereomer *isolated* reveals the overall ratio is 12.3%:41.4%:4.9%:41.4%; fortuitously the quantity of **10RSS** and **10SRS** material is similar and demonstrates that the metal centre prefers to induce opposite chirality at the nitrogen centre. While the *isolated* material does not represent 100% of the theoretical yield it is clear that a preference of at least 4:1 is present. Fig. 3 below shows all four diastereomers.

The conformations shown are those that can be reasonably predicted based upon the structures of the diastereomeric salts of **3RR** and **3SR** analyzed earlier by ^{1}H NMR spectroscopy and confirmed by X-ray single crystal structure determination. It is clear that the *N*-methyl group would prefer to be external (**SRS**,**RSS**) rather than internal (**RRS**,**SSS**) on steric grounds.

Table 1
Comparison of chemical shifts for the diastereomers of **3** and **10**

Assignments	3RS	3SS	10RSS	10RRS	10SRS	10SSS
C*Ph*	7.25	6.97	7.05	6.65	6.80	6.15
C_5H_5	4.29	4.72	4.64	4.74	4.81	4.83
C*H*Me	3.35	3.34	3.63	3.73	3.88	3.78
N*H*	3.69, 1.87	3.49, 2.13	2.05	obscured	2.51	1.85
NH*Me*			2.29	2.53	2.23	2.46
CH*Me*	1.11	1.30	1.34	1.40	1.55	1.50
C*Me*$_3$	1.30	1.25	1.25	1.18	1.30	1.26

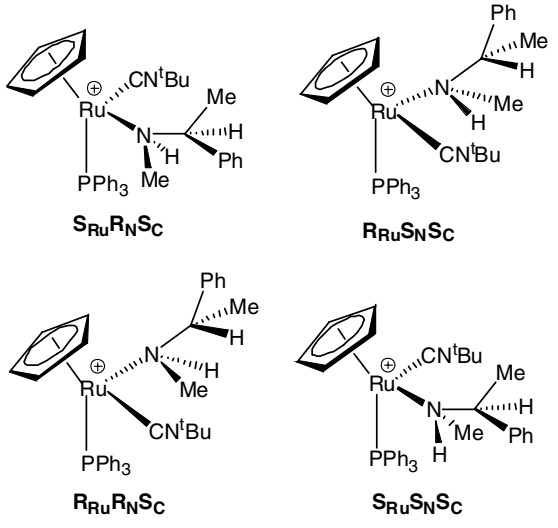

Fig. 3. The diastereomers of **10** derived from *S*(−)-*N*-methyl-1-phenylethylamine.

An alternative method to produce a ruthenium complex resolved at the metal centre which could be taken on further in asymmetric chemistry would involve the preparation of $[(\eta^5\text{-}C_5H_5)Ru(PPh_3)(CNZ)(Cl)]$, where Z contains a chiral element. Combining our experience of the amine chemistry and the utility of the ring shielding effect as a spectroscopic probe we decided to use *S*(−)-α-methylbenzylisonitrile (*S*(−)-Ph(Me)CHNC) as a ligand. A sample of *S*(−)-α-methylbenzylamine was determined to be >99.6% e.e by ^{1}H NMR spectroscopy using *R*(−)-TFAE as a chiral auxiliary [19]. Conversion of this amine to the isonitrile was achieved in 50% yield by a phase transfer Hofmann carbylamine procedure; polarimetry and subsequent reactions indicate that the optical purity was retained in the product.

Reaction of $[(\eta^5\text{-}C_5H_5)Ru(PPh_3)_2(Cl)]$ with *S*(−)-α-methylbenzylisonitrile in hot toluene gave a bright orange powder after chromatography in 45% yield. Characterization of this material showed it to be a racemic mixture of the diastereomeric salts $[(\eta^5\text{-}C_5H_5)Ru(PPh_3)(CNCH(Me)Ph)(Cl)]$ (**11SS**,**11RS**). The solid and solution infrared spectra of the product contained bands at 2102 and 2104 cm^{-1} assignable to *ν*(CN), while the mass spectrum contained the parent ion and then subsequent losses of the chloro group and the isonitrile group. It proved possible with considerable effort to enrich a sample to 30% d.e. by crystallization from toluene–hexane mixtures in order to assign the individual ^{1}H NMR parameters to each diastereomer. The ^{1}H NMR spectroscopic signals of the C*H*Me (*δ* 4.87 and 4.70) and CH*Me* (*δ* 1.29 and 1.39) groups were baseline resolved in the diastereomer mixture and could be used quantitatively. The remoteness of the chiral centre in **11** in comparison to the amine complexes such as **3** did not permit complete confidence in an absolute assignment because the linear isonitrile functionality removes the α-methyl group away from the ring current of the triphenylphosphine aromatic rings, but after looking at the solid state structures of **12**, we assign the signals at *δ* 4.87 and 1.29 to **11SS**.

The mixture (**11SS**,**11RS**) was converted into the ammine salts $[(\eta^5\text{-}C_5H_5)Ru(PPh_3)(CNCH(Me)Ph)(NH_3)]PF_6$ (**12SS**,**12RS**) by means of ammonium hexafluorophosphate and thallium carbonate in hot methanol with a view to improving the separation of the diastereomeric centres by crystallization. It should be noted that the ruthenium chirality descriptors reverse when the chloro ligand is replaced by the ammine ligand. Thus, assuming retention at the metal centre, **11SS** produces **12RS** and **11RS** produces **12SS**. The yellow crystalline product obtained in 47% yield proved to an equimolar mixture of the diastereomeric salts. All attempts to effect partial resolution failed and indeed single crystals of **12** proved to contain both diastereomeric centres. In particular the single crystal used for the X-ray single crystal structure determination was later dissolved in CD_2Cl_2 and confirmed this point and that the equimolar mixture was perfectly configurationally stable in solution.

3. X-ray crystal structures

The X-ray single crystal structure of **2** was determined at 223 K; many crystals of **2** were examined under a polarizing microscope and found to be twinned but a few single crystals were located and examined. The crystal used for the data collection was of an acceptable quality for the intended purpose. The crystal specimens of **3RR** and **3SR** were of very high optical quality and highly faceted; it would be possible to resolve a mixed sample by triage, picking the diastereomers apart under a microscope. Both structures were determined at 233 K (Table 2).

The crystal of **2** contained molecules with the *R*-configuration at ruthenium and the absolute structure parameter of 0.31(8) reflects the correct choice for the single chiral centre. Analysis of a second crystal revealed that it only contained molecules with an *S*-configuration at ruthenium (Rogers *η* 1.11(12)), thus the bulk sample is probably best described as a racemic conglomerate. The unit cell also contained one molecule of dichloromethane per cation. Racemic twin refinement was attempted on the data obtained for the first crystal and did not significantly improve the refinement; the nature of the sample did not suggest that further exploration was necessary or required.

The overall geometry of the cation is pseudo octahedral as expected with the cyclohexyl group in a chair conformation with the proton on C(41) pointing in towards the isonitrile ligand (Fig. 4). One of the amine protons points towards the centre of a phenyl ring while the other is oriented away as anticipated providing the origin of the chemical shift differentiation in the ^{1}H NMR spectrum. The ruthenium–nitrogen bond length of 2.172(8) Å compares with 2.190(5), 2.216(2) and 2.174(8) Å for

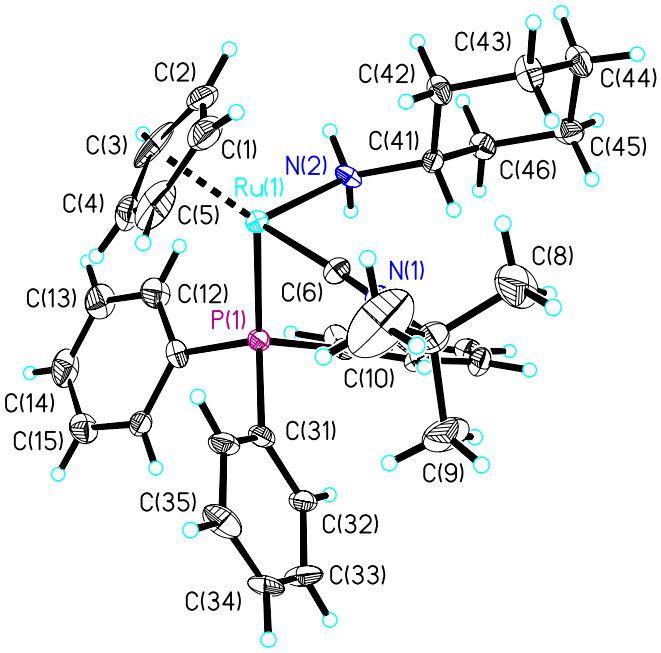

Fig. 4. The cation present in **2** showing 25% probability ellipsoids.

Table 2
Crystallographic data collection parameters for **2**, **3SR**, **3RR**, and (**12RS**,**12SS**)

Identification code	**2** · CH_2Cl_2	**3SR**	**3RR**	(**12RS**,**12SS**)
Empirical formula	$C_{35}H_{44}Cl_2F_6N_2P_2Ru$	$C_{36}H_{40}F_6N_2P_2Ru$	$C_{36}H_{40}F_6N_2P_2Ru$	$C_{32}H_{32}F_6N_2P_2Ru$
Formula weight	840.63	777.71	777.71	721.61
Temperature (K)	223(2)	233(2)	233(2)	233(2)
Wavelength (Å)	0.71073	0.71073	0.71073	0.71073
Crystal system	monoclinic	monoclinic	monoclinic	monoclinic
Space group	$P2_1$	$P2_1$	$P2_1$	$P2_1$
Unit cell dimensions				
a (Å)	11.048(3)	10.083(2)	9.444(2)	9.902(4)
b (Å)	16.983(3)	18.628(3)	18.932(3)	17.934(8)
c (Å)	11.204(2)	10.704(2)	11.022(2)	18.283(9)
α (°)	90	90	90	90
β (°)	114.04(2)	117.68(2)	115.13(1)	92.63(4)
γ (°)	90	90	90	90
Volume (Å^3)	1919.9(8)	1780.4(6)	1784.1(6)	3243(3)
Z	2	2	2	4
Density (calculated) (Mg/m^3)	1.454	1.451	1.448	1.478
Absorption coefficient (mm^{-1})	0.687	0.589	0.588	0.641
F(000)	860	796	796	1464
Crystal size (mm^3)	$0.35 \times 0.25 \times 0.25$	$0.40 \times 0.35 \times 0.30$	$0.55 \times 0.40 \times 0.25$	$0.45 \times 0.20 \times 0.14$
Θ range for data collection (°)	1.99–27.50	2.28–31.07	2.04–31.07	2.27–25.09
Index ranges	$-1 \leqslant h \leqslant 14$, $-22 \leqslant k \leqslant 1$, $-14 \leqslant l \leqslant 13$	$-2 \leqslant h \leqslant 13$, $0 \leqslant k \leqslant 27$, $-15 \leqslant l \leqslant 14$	$-2 \leqslant h \leqslant 13$, $0 \leqslant k \leqslant 27$, $-16 \leqslant l \leqslant 15$	$0 \leqslant h \leqslant 11$, $-1 \leqslant k \leqslant 21$, $-21 \leqslant l \leqslant 21$
Reflections collected	5598	7316	7368	6726
Independent reflections [R_{int}]	4865 [0.0356]	5859 [0.0209]	5835 [0.0276]	6342 [0.0499]
Completeness to θ_{max} (%)	99.2	99.8	99.4	99.3
Refinement method	full-matrix least-squares on F^2	full-matrix least-squares on F^2	full-matrix least-squares on F^2	full-matrix least-squares on F^2
Data/restraints/parameters	4864/1/433	5859/18/424	5835/34/460	6342/1/776
Goodness-of-fit on F^2	1.096	1.024	1.085	1.022
Final R indices [$I > 2\sigma(I)$]	$R_1 = 0.0712$, $wR_2 = 0.1755$	$R_1 = 0.0330$, $wR_2 = 0.0755$	$R_1 = 0.0333$, $wR_2 = 0.0867$	$R_1 = 0.0544$, $wR_2 = 0.1111$
R indices (all data)	$R_1 = 0.0988$, $wR_2 = 0.1905$	$R_1 = 0.0425$, $wR_2 = 0.0808$	$R_1 = 0.0398$, $wR_2 = 0.0918$	$R_1 = 0.0945$, $wR_2 = 0.1290$
Absolute structure parameter	0.31(8)	0.00(3)	−0.01(3)	0.03(6)
Largest differential peak and hole (e Å^{-3})	1.703 and −0.640	0.554 and −0.453	0.561 and −0.614	0.529 and −0.377

$[(\eta^5\text{-}C_5H_5)Ru(PPh_3)_2(NH_2CH_2Ph)]BF_4$ [20], $[(\eta^5\text{-}C_5H_5)Ru(PPh_3)(P\{OMe\}_3)(NH_2CMe_3)]SO_3CF_3$ [21], and $[(\eta^5\text{-}C_5H_5)Ru(Cy_2PCH_2CH_2PCy_2)(NH_2C_8H_{17})]SO_3CF_3$ [22], respectively.

The structures of **3SR** (Fig. 5) and **3RR** (Fig. 6) have the same gross geometry as that found in **2**, and are both absolute structure determinations with parameter values of −0.01(3) and 0.00(3), respectively. The ruthenium–nitrogen bond lengths are 2.168(3) and 2.184(3) Å, respectively, and there are other small metric differences at the ruthenium centre (Table 3). These differences for the diastereomeric cations are likely to be due to steric factors such as the disposition of the benzyl group. The most striking structural difference between **3RR** and **3SR** is the position of the α-methyl group caused by the preference of the benzyl hydrogen atom to point inwards towards the isonitrile group in both diastereomers. The proximity of the α-methyl group in **3SR** to the aromatic rings of the triphenylphosphine ligand and of the α-phenyl group to the cyclopentadienyl ring hydrogens supports the earlier ^{1}H NMR spectroscopic analysis where both these interactions produce shielding relative to **3RR**. The differentiation of the two NH resonances in the ^{1}H NMR spectrum of each diastereomeric salt can also be seen to be a consequence of shielding from aromatic rings. It is implicit in this analysis that the solid state structures and solution structures for each diastereomeric cation are similar; given that rotation around the Ru(1)–N(1) bond and about the N(1)–C(8) bond is likely to be restricted in both diastereomers this is a reasonable outcome.

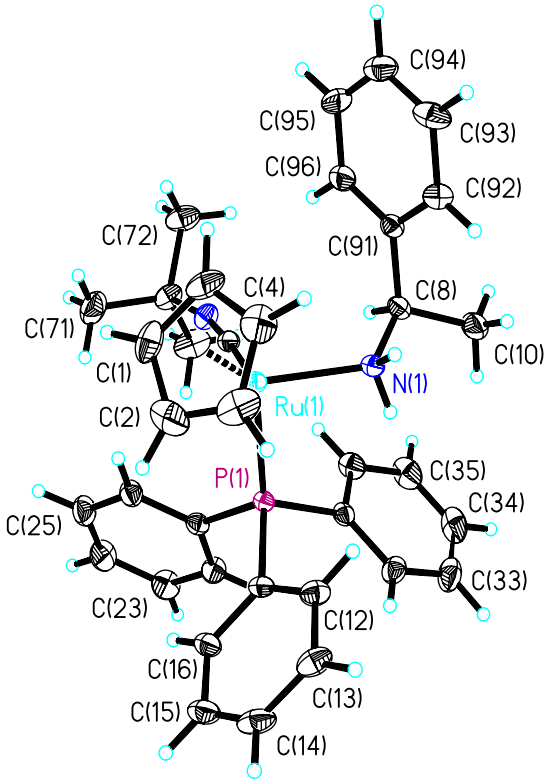

Fig. 5. The cation present in **3SR** showing 25% probability ellipsoids.

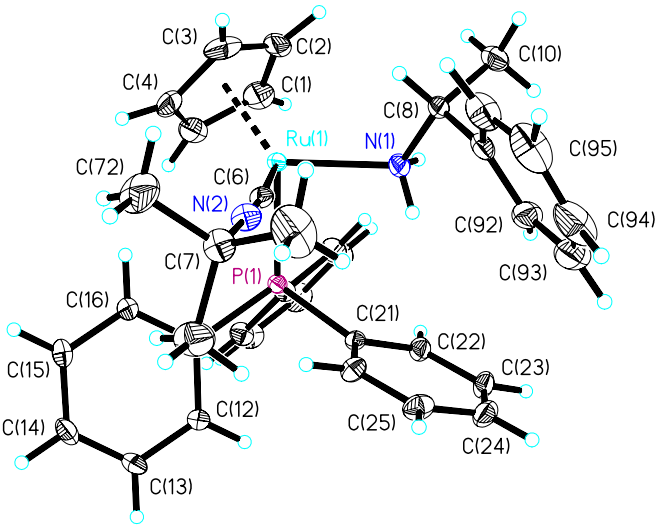

Fig. 6. The cation present in **3RR** showing 25% probability ellipsoids.

Table 3
Selected bond lengths (Å) and bond angles (°) for **3RR** and **3SR**

	3SR	3RR
Ru(1)–P(1)	2.2948(10)	2.2964(10)
Ru(1)–N(1)	2.184(3)	2.168(3)
Ru(1)–C(6)	1.936(3)	1.946(4)
P(1)–Ru(1)–N(1)	89.71(9)	90.53(9)
P(1)–Ru(1)–C(6)	89.16(10)	88.79(10)
N(1)–Ru(1)–C(6)	95.65(13)	90.10(15)
Ru(1)–N(1)–C(8)	121.6(2)	118.1(2)
Ru(1)–C(6)–N(2)	171.9(3)	175.2(4)
C(6)–N(2)–C(7)	169.0(4)	176.5(2)

The X-ray single crystal structure of **12** was carried out at 233 K and the crystal contained both diastereomers of the cation in the unit cell, permitting both a relative and an absolute structure determination. The outcome is that the isonitrile ligand was confirmed to be of *S*-configuration. Visual comparison of the two diastereomeric cations suggests why the **12RS** (Fig. 7) and **12SS** (Fig. 8) compounds are difficult to fractionally separate and do co-crystallize; the volumes and molecular shapes are very similar in that only the disposition of the α-methyl group perturbs the near mirror symmetry in the unit cell (see Table 4).

4. Conclusions

Diastereomers containing only two chiral centres can be designated as *p*-(RR or SS) or *n*-(RS or SR) [23,24]. The most soluble diastereomeric salts in dichloromethane are the *p*-forms of **3**, **4**, **5**, and **7**; possibly this relationship will also hold if small modifications are made to these generic molecules (e.g., change of cyclopentadienyl group, use of PR_2Ph in place of PPh_3, ring *para*-substitution at phenyl rings of phosphine or amine). The use of ring shielding effects in ^{1}H NMR spectroscopy has proved a useful tool in determining diastereomer ratio and relative assignment

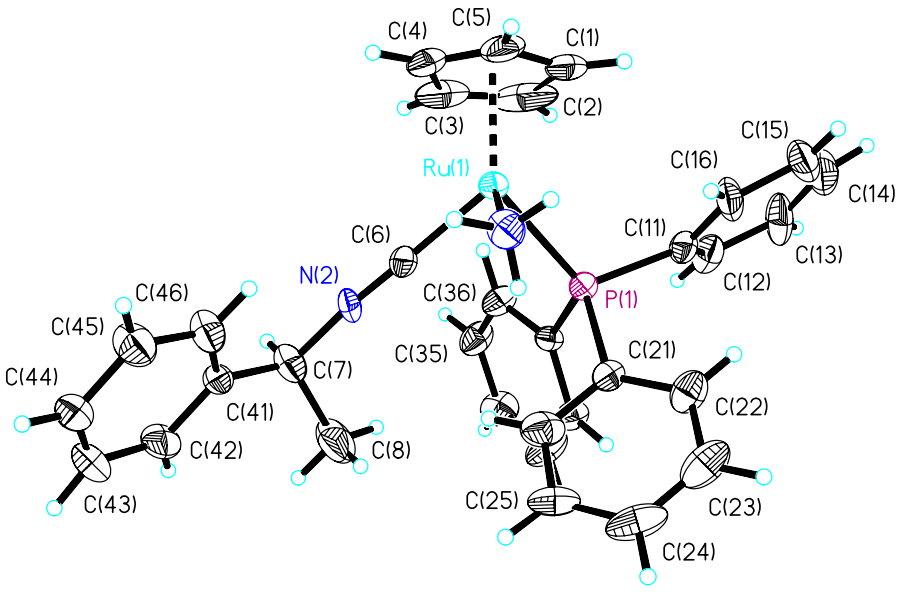

Fig. 7. The cation present in **12RS** showing 25% probability ellipsoids.

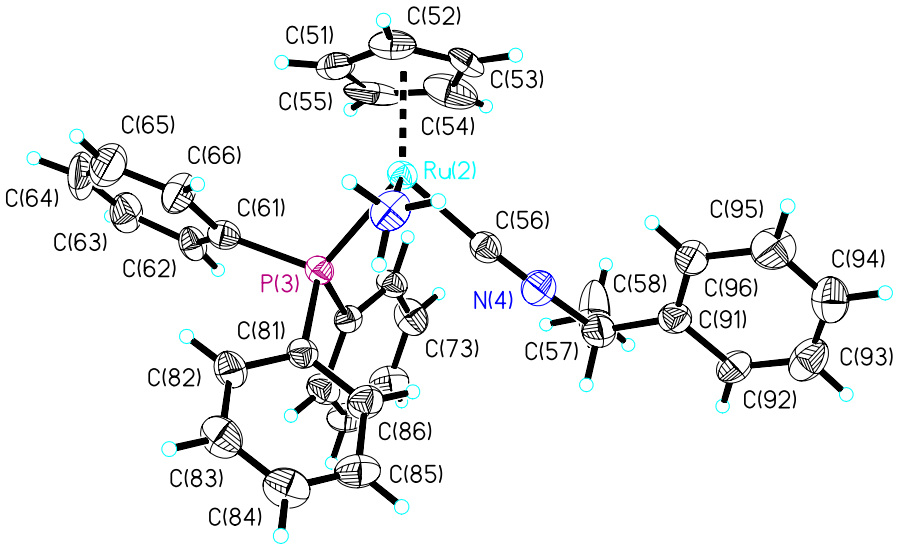

Fig. 8. The cation present in **12SS** showing 25% probability ellipsoids.

Table 4
Selected bond lengths (Å) and bond angles (°) for **12RS** and **12RR**

	12RS		**12RR**
Ru(1)–P(1)	2.301(3)	Ru(2)–P(3)	2.298(3)
Ru(1)–N(1)	2.153(9)	Ru(2)–N(3)	2.182(9)
Ru(1)–C(6)	1.917(14)	Ru(2)–C(56)	1.913(15)
C(6)–N(2)	1.156(15)	C(56)–N(4)	1.175(17)
P(1)–Ru(1)–N(1)	91.5(3)	P(3)–Ru(1)–N(3)	91.5(3)
P(1)–Ru(1)–C(6)	88.6(3)	P(3)–Ru(2)–C(56)	88.4(4)
N(1)–Ru(1)–C(6)	91.4(4)	N(3)–Ru(2)–C(56)	89.7(5)
Ru(1)–C(6)–N(2)	177.7(11)	Ru(2)–C(56)–N(4)	176.6(12)
C(6)–N(2)–C(7)	174.6(12)	C(56)–N(4)–C(57)	165.5(15)

for this family of compounds and extends the work of Davies on cyclopentadienyliron compounds. The crystallographic work illustrates some of the variations possible when one or more chiral centres are present. For example **2** crystallized as a racemic conglomerate where each single crystal is itself homochiral but the bulk sample is racemic, **3** can be crystallized to yield single crystals of each of the four diastereomers, while **12** generated by using a homochiral ligand produces single crystals containing both possible diastereomers.

All of the cationic compounds in this work are configurationally stable in solution at room temperature for periods in excess of one week. In particular the single crystal actually used for each structural measurement was redissolved and monitored by ^{1}H NMR spectroscopy within minutes of solution and then periodically. The solution spectra exactly mirrored the composition determined in the crystal. The nature of the ligands used in this study

and the strong metal–ligand bonding undoubtedly prevents epimerization which has been found to be a major problem elsewhere [6–8]. Indeed the bond strengths in compounds such as **2** and **3** prevented our ultimate aim of producing resolved at ruthenium materials for subsequent asymmetric synthesis.

5. Experimental

5.1. General comments

All reactions and preparations were carried out using conventional Schlenk tube techniques and all solvents were degassed prior to use. Chromatographic work-ups were performed with columns made up of Grade IV neutral alumina prepared with petroleum ether (40–60 °C). Cyclohexylamine and diethylamine were dried over barium oxide and distilled before use. *R*(+)- and *S*(−)-α-methylbenzylamine (99.6% e.e.) were supplied by Seal Sands Chemicals Ltd. The amines *R*(−)-α-cyclohexylethylamine (98% e.e.) and (±)-1-(1-naphthyl)ethylamine from Aldrich were used as supplied. *S*(−)-*N*-methyl-1-phenylethylamine (98% e.e.) was supplied by Fluka Chemika. *R*(−)-2,2,2-trifluoro-1-(9-anthryl)ethanol (99.5% e.e., Aldrich) was dried under reduced pressure at 70 °C overnight. Photolysis reactions were performed using a P.W. Allen A409 medium pressure mercury lamp (313, 366 nm). Infrared spectra were recorded on a Perkin–Elmer 1710 FT-IR instrument calibrated against polystyrene film and only significant absorption bands are reported. Optical rotation measurements were made on an Optical Activity Ltd. AA–100 polarimeter. Nuclear magnetic resonance spectra were recorded on Bruker AC300 (300.13 MHz, ^{1}H NMR; 75.47 MHz, ^{13}C; 121.49 MHz, ^{31}P) and Avance 400 (400.13 MHz, ^{1}H NMR; 100.61 MHz, ^{13}C; 161.98 MHz, ^{31}P) spectrometers. All ^{1}H and ^{13}C NMR chemical shifts are expressed in ppm relative to $SiMe_4$ (0.0 ppm) and ^{31}P shifts relative to $P(OPh)_3$ (126.5 ppm). All spectra were measured at room temperature and homonuclear decoupling and DEPT spectra were obtained when appropriate. Elemental analyses were obtained by Butterworth Laboratories, London. Mass spectral analyses were performed by Fast Atom Bombardment (FAB) on a Kratos Concept S1 Spectrometer. Crystal structure data were collected on a Siemens R3m/V Diffractometer at 233 K for $[(\eta^5\text{-}C_5H_5)Ru(PPh_3)(CN^tBu)(NH_2Cy)]PF_6$ (**2**), ($S_{Ru}R_C$)- and ($R_{Ru}R_C$)-$[(\eta^5\text{-}C_5H_5)Ru(PPh_3)(CN^tBu)(NH_2CHMePh)]PF_6$ (**3SR**) and (**3RR**), and at 293 K for $[(\eta^5\text{-}C_5H_5)Ru(PPh_3)(CNCH(Me)Ph)(NH_3)]PF_6$ (**12**). The starting compounds $[(\eta^5\text{-}C_5H_5)Ru(PPh_3)(CN^tBu)Cl]$ (**1**) [25,26], $[(\eta^5\text{-}C_5H_5)Ru(PPh_3)(CO)Cl]$ (**6**) [27], and $[(\eta^5\text{-}C_5H_5)Ru(PPh_3)(CN^tBu)I]$ (**8**) [28] were prepared by the published literature procedures.

The optical purity of the *R*(+)- and *S*(−)-α-methylbenzylamines was checked by ^{1}H NMR spectroscopy using *R*(−)-2,2,2-trifluoro-1-(9-anthryl)ethanol [19]. The optical purity of the *R*(−)-α-cyclohexylethylamine and *S*(−)-*N*-methyl-1-phenylethylamine was not verified.

5.2. Preparation of *S*(−)-α-methylbenzylisonitrile {*S*(−)-CNCHMePh}

The published procedure for the synthesis of *tert*-butylisonitrile was adapted [29,30]. A two-neck round-bottomed flask (500 ml) equipped with a magnetic stirrer bar, a reflux condenser, and a pressure equalising dropping funnel was charged with sodium hydroxide (24 g, 0.6 mol). Stirring was commenced and deionized water (3 × 30 ml) was added in portions to maintain smooth stirring. The funnel was charged with a mixture of *S*(−)-α-methylbenzylamine (20 ml, 0.158 mol), chloroform (15 ml, 0.188 mol) and benzyltriethylammonium chloride (0.4 g, 1.75 mmol) in dichloromethane (30 ml). The mixture was added dropwise to the stirred, warm solution (at ca. 45 °C) over a 30-min period. The reaction mixture began to reflux slowly 10 min after initiation of the addition and subsided within 2 h; stirring was continued for an additional hour. The reaction mixture was diluted with ice and deionized water (1:1, 150 ml), and the organic layer (pale yellow) was separated and retained. The colourless aqueous layer was extracted with dichloromethane (2 × 30 ml), and the combined extracts were successively washed with deionized water (20 ml), aqueous sodium chloride solution (5% w/w, 20 ml), and dried over excess anhydrous magnesium sulphate for 1 h.

The drying agent was removed by filtration, washed with dry dichloromethane (10 ml), and the pale yellow combined filtrate and washings were distilled at ca. 65 °C using a Vigreux column (1.5 cm × 10 cm) to remove the solvent (dichloromethane).

The remaining yellow solution was placed under nitrogen, and distilled under reduced pressure to remove final traces of dichloromethane, unreacted chloroform (at 25 °C, 13 mmHg), and any excess *S*(−)-α-methylbenzylamine (34–39 °C, 3 mmHg). Finally, the fraction which distilled at 29–30 °C (0.01 mmHg) was collected as a colourless oil. Yield 11.0 ml (50%).

IR (neat): ν_{max} 2140vs cm^{-1} (CN). ^{1}H NMR ($CDCl_3$): δ 7.29–7.42 (m, 5H, Ph), 4.81 (q{1:1:1}t, 1H, ^{3}J(HH) 7 Hz and ^{2}J(NH) 2 Hz, C*H*MeN), 1.67 (d{1:1:1}t, 3H, ^{3}J(HH) 7 Hz and ^{3}J(NH) 2 Hz, CH*Me*N) ppm. ^{13}C{^{1}H} NMR ($CDCl_3$): δ 156.6 (t, *J*(CN) 4.5 Hz, *C*N), 138.6 (s, C_{ipso}, Ph), 128.9 (s, C_{ortho}, Ph), 128.3 (s, C_{para}, Ph), 125.4 (s, C_{meta}, Ph), 53.8 ({1:1:1}t, ^{1}J(NC) 6 Hz, N*C*HPh), 25.1 (s, CH*Me*). Optical rotation $[\alpha]_{589}$ −30.5° (21°C, neat *d* 0.97 g cm^{-1}).

{Lit. [31] IR: ν_{max} 2141 (CN), 759, 698 cm^{-1}; ^{1}H NMR: δ 7.20 (m, 5H, Ph), 4.70 (m, 1H, C*H*MeN), 1.60 (d, 3H, CH*Me*N) ppm. ^{13}C{^{1}H} NMR (proton coupled): δ 157.0 (t, *J*(CN) 4.3 Hz, *C*N), 53.8 (dt, N*C*HPh), 25.0 (q, CH*Me*) ppm. Lit. [32,33] IR: ν_{max} 3000, 2950, 2160 (CN), 1600, 1500, 770, 700 cm^{-1}; ^{1}H NMR (CCl_4): δ 7.35 (s, 5H, Ph), 4.83 (q{1:1:1}t, 1H, ^{3}J(HH) 7 Hz and ^{2}J(NH) 2 Hz, C*H*MeN, 1.68 (d{1:1:1}t, 3H, ^{3}J(HH) 7 Hz and ^{3}J(NH) 2 Hz, CH*Me*N; Optical rotation [33,34] $[\alpha]_{589}$ −30° (20 °C, neat)}.

*5.2.1. [(η^5-C_5H_5)Ru(PPh_3)(CN^tBu)(NH_2Cy)]PF_6 (**2**)*

A Schlenk tube was charged with a solution of **1** (1.00 g, 1.83 mmol) in dichloromethane (40 ml), thallium hexafluorophosphate (1.60 g, 4.58 mmol), and a magnetic stirrer bar. The orange solution was stirred in the dark under nitrogen at room temperature for 1 h to give a tomato-orange suspension. Excess cyclohexylamine (2 ml, 17.48 mmol) was added and the solution was stirred in the dark at room temperature overnight. Filtration, evaporation of the filtrate under reduced pressure, and crystallization of the yellow residue from dichloromethane and diethylether (1:3, 40 ml) at −30 °C for 2 days afforded bright yellow crystals of **2**. Yield 1.34 g (97%). (Calc. for $C_{34}H_{42}F_6N_2P_2Ru \cdot CH_2Cl_2$: C, 50.00; H, 5.28; N, 3.33. Found: C, 49.93; H, 5.33; N, 3.30%). IR (Nujol): ν_{max} 3311w, 3270w, 1587vw (NH), 2121m (CN), and 842s cm^{-1} (PF_6). ^1H NMR (CD_2Cl_2): δ 7.2–7.5 (m, 15H, PPh_3), 4.74 (s, 5H, C_5H_5), 3.20 (br.t, 1H, $^{2,3}J$(HH) 11 Hz, NH), 1.99 (br.d, 1H, ^2J(HH) 12 Hz, NH), 0.7–1.90 (m, 11H, Cy), 1.25 (s, 9H, C*Me*$_3$) ppm. $^{13}C\{^1H\}$ NMR (CD_2Cl_2): δ 134.20 (d, C_{ipso}, PPh_3), 133.77 (d, ^2J(PC) 11 Hz, C_{ortho}), 131.05 (s, C_{para}), 129.14 (d, ^3J(PC) 10 Hz, C_{meta}), 81.94 (s, C_5H_5), 59.29 (s, C_1, Cy), 58.00 (s, *C*Me$_3$), 35.82 (s, C_2, Cy), 33.13 (s, C_3, Cy), 30.73 (s, C*Me*$_3$), 25.49 (s, C_4 and C_5, Cy), 25.29 (s, C_6, Cy) ppm. $^{31}P\{^1H\}$ NMR (CD_2Cl_2): δ 59.91 (s, PPh_3), −145.40 (septet, ^1J(PF) 712 Hz, PF_6) ppm. MS (FAB): 611 $[M - PF_6]^+$(50%), 512(100), 429(41).

*5.2.2. ($S_{Ru}R_C$)-[(η^5-C_5H_5)Ru(PPh_3)(CN^tBu)-($NH_2CHMePh$)]PF_6 (**3SR**)*

A solution of **1** (0.23 g, 0.42 mmol) in dichloromethane (30 ml) was treated with thallium hexafluorophosphate (0.42 g, 1.20 mmol) and excess *R*(+)-α-methylbenzylamine (0.8 ml, 6.21 mmol). This yellow-orange solution was stirred in the dark at room temperature for 24 h. After filtration and solvent removal from the filtrate under reduced pressure, fine yellow crystals were obtained by crystallizing the residue at −30 °C from dichloromethane and diethylether (1:3, 20 ml) overnight. Yield 0.19 g (58%) 80% d.e. (Calc. for $C_{36}H_{40}F_6N_2P_2Ru.CH_2Cl_2$: C, 51.51; H, 4.91; N, 3.25. Found: C, 50.93; H, 4.82; N, 3.39%.) IR (Nujol): ν_{max} 3307w, 3264w, 1580vw (NH), 2115m (CN), 1712w (Ph overtone), and 840s cm^{-1} (PF_6). ^1H NMR (CD_2Cl_2): δ 7.25–7.51 (m, 15H, PPh_3), 7.21–7.25 (m, 5H, Ph), 4.30 (s, 5H, C_5H_5), 3.71 (br.t, 1H, $^{2,3}J$(HH) 11 Hz, NH), 3.35 (m, 1H, NC*H*Me), 1.88 (br.d, 1H, ^2J(HH) 11 Hz, NH), 1.30 (s, 9H, C*Me*$_3$), 1.11 (d, 3H, ^3J(HH) 7 Hz, Me) ppm. $^{13}C\{^1H\}$ NMR (CD_2Cl_2): δ 134.09 (d, C_{ipso}, PPh_3), 133.78 (d, ^2J(PC) 11 Hz, C_{ortho}), 131.11 (s, C_{para}), 129.26 (d, ^3J(PC) 10 Hz, C_{meta}), 128.86 (s, C_{para}, Ph), 127.42 (s, C_{meta}, Ph), 81.71 (s, C_5H_5), 61.76 (s, N*C*HPh), 30.82 (s, C*Me*$_3$), 25.34 (s, CH*Me*) ppm. $^{31}P\{^1H\}$ NMR (CD_2Cl_2): δ 60.04 (s, PPh_3), −145.30 (septet, ^1J(PF) 712 Hz, PF_6) ppm. MS (FAB): 633 $[M - PF_6]^+$(21%), 512(100), 429(54).

*5.2.3. ($R_{Ru}R_C$)-[(η^5-C_5H_5)Ru(PPh_3)(CN^tBu)-($NH_2CHMePh$)]PF_6 (**3RR**)*

The mother-liquor from the crystallization procedure above was reduced in volume (to ca. 10 ml) under reduced pressure, and was left to crystallize out at −80 °C for 2 days, producing yellow crystals which were isolated by filtration. Yield 0.07 g (21%) 98% d.e.

IR (Nujol): ν_{max} 3325w, 3284w, 1591w (NH), 2126s (CN), 1712w (Ph overtone) and 840s cm^{-1} (PF_6). ^1H NMR (CD_2Cl_2): δ 7.23–7.45 (m, 15H, P*Ph*$_3$), 6.96–6.98 (m, 5H, Ph), 4.72 (s, 5H, C_5H_5), 3.49 (br.t, 1H, $^{2,3}J$(HH) 10 Hz, NH), 3.35 (m, 1H, NC*H*Me), 2.12 (br.d, 1H, ^2J(HH) 10 Hz, NH), 1.29 (d, 3H, ^3J(HH) 7 Hz, Me), 1.25 (s, 9H, C*Me*$_3$) ppm. $^{13}C\{^1H\}$ NMR (CD_2Cl_2): δ 134.11 (d, C_{ipso}, PPh_3), 133.63 (d, ^2J(PC) 11 Hz, C_{ortho}), 130.98 (s, C_{para}), 129.17 (d, ^3J(PC) 8 Hz, C_{meta}), 128.23 (s, C_{para}, Ph), 126.21 (s, C_{meta}, Ph), 81.81 (s, C_5H_5), 61.65 (s, N*C*HPh), 30.65 (s, C*Me*$_3$), 22.63 (s, CH*Me*) ppm. $^{31}P\{^1H\}$ NMR (CD_2Cl_2): δ 59.08 (s, PPh_3) ppm.

*5.2.4. ($R_{Ru}S_C$)-[(η^5-C_5H_5)Ru(PPh_3)(CN^tBu)-($NH_2CHMePh$)]PF_6 (**3RS**)*

To a solution of **1** (0.16 g, 0.29 mmol) in dichloromethane (30 ml) was added thallium hexafluorophosphate (0.4 g, 1.15 mmol) and excess *S*(−)-α-methylbenzylamine (0.8 ml, 6.21 mmol). This yellow/orange solution was stirred overnight in the dark, at room temperature. After solvent removal under reduced pressure, fine yellow crystals were obtained by crystallising the residue at −80 °C from dichloromethane and diethylether (1:3, 20 ml) overnight. Yield 0.13 g (57%) 74% d.e.

*5.2.5. ($S_{Ru}S_C$)-[(η^5-C_5H_5)Ru(PPh_3)(CN^tBu)-($NH_2CHMePh$)]PF_6 (**3SS**)*

The mother-liquor from above was concentrated to low volume (to ca. 10 ml) under reduced pressure, and was left to crystallize out in the dark at −30 °C for 7 h, from which yellow crystals were isolated. Yield 0.05 g (22%) 98% d.e.

*5.2.6. ($S_{Ru}R_C$)-[(η^5-C_5H_5)Ru(PPh_3)(CN^tBu)-($NH_2CHMeCy$)]PF_6 (**4SR**)*

To a solution of **1** (0.21 g, 0.384 mmol) in dichloromethane (30 ml) was added thallium (I) hexafluorophosphate (0.40 g, 1.15 mmol) and excess *R*(−)-1-cyclohexylethylamine (1.0 ml, 6.81 mmol). This orange solution was stirred at room temperature in the dark under nitrogen for 67 h. After solvent removal under reduced pressure, fine yellow crystals were obtained by crystallising the yellow residue at −30 °C from dichloromethane and diethylether (1:3, 40 ml) overnight. Yield 0.13 g (43%) 61% d.e. (Calc. for $C_{36}H_{46}F_6N_2P_2Ru \cdot CH_2Cl_2$: C, 51.16; H, 5.57; N, 3.22. Found: C, 52.98; H, 5.57; N, 3.45%.) IR (Nujol): ν_{max} 3312m, 3275w, 1584w (NH), 2116s (CN), 1721br.w (Ph overtone) and 843vs cm^{-1} (PF_6). ^1H NMR (CD_2Cl_2): δ 7.28–7.50 (m, 15H, PPh_3), 4.744 (s, 5H, C_5H_5), 3.15 (br.dd, 1H, $^{2,3}J$(HH) 12, 6 Hz, NH), 2.09 (qd, 1H, $^{3,3}J$(HH) 6, 4 Hz, NC*H*Me), 1.24 (s, 9H, C*Me*$_3$), 0.70 (d, 3H, ^3J(HH)

7 Hz, Me), 0.7–0.98, 1.05–1.45 and 1.65–1.74 (m, 11H, $^{2,3,3}J$(HH) 12, 12, 4 Hz, Cy) ppm. $^{13}C\{^1H\}$ NMR (CD_2Cl_2): δ 133.77 (d, ^1J(PC) 44 Hz, C_{ipso}, P*Ph*$_3$), 133.71 (d, ^2J(PC) 11 Hz, C_{ortho}, PPh_3), 131.10 (s, C_{para}, PPh_3), 129.24 (d, ^3J(PC) 9 Hz, C_{meta}, PPh_3), 81.88 (s, C_5H_5), 60.99 (s, N*C*HCy), 42.59 (s, C_1, Cy), 30.66 (s, C*Me*$_3$), 26.84 (s, C_2, Cy), 26.71 (s, C_3, Cy), 26.34 (s, C_4 and C_5, Cy), 25.49 (s, C_6, Cy), 17.02 (s, CH*Me*) ppm. $^{31}P\{^1H\}$ NMR (CD_2Cl_2): δ 59.57 (s, PPh_3) ppm. MS (FAB): 639 $[M - PF_6]^+$(20%), 512(100), 429(31).

5.2.7. ($R_{Ru}R_C$)-[(η^5-C_5H_5)Ru(PPh_3)(CN^tBu)-($NH_2CHMeCy$)]PF_6 (**4RR**)

The mother-liquor from above was concentrated to low volume (ca. 10 ml) under reduced pressure, and was then left to crystallize out in the dark at −30 °C overnight, from which yellow crystals were isolated. Yield 0.11 g (37%) 79% d.e.

IR (Nujol): ν_{max} 3315w, 3274w, 1585w (NH), 2121m (CN), 1725br.w (Ph overtone) and 843s cm^{-1} (PF_6). ^1H NMR (CD_2Cl_2): δ 7.28–7.51 (m, 15H, PPh_3), 4.745 (s, 5H, C_5H_5), 2.95 (br.t, 1H, $^{2,3}J$(HH) 11 Hz, NH), 2.00 (m, 1H, NC*H*Me), 1.26 (s, 9H, C*Me*$_3$), 0.99 (d, 3H, ^3J(HH) 7 Hz, Me), 0.52–0.70, 1.0–1.3 and 1.60–1.83 (m, 11H, $^{2,3,3}J$(HH) 11, 11, 4 Hz, Cy) ppm. $^{13}C\{^1H\}$ NMR (CD_2Cl_2): δ 134.02 (d, ^1J(PC) 44 Hz, C_{ipso}, PPh_3), 133.83 (d, ^2J(PC) 11 Hz, C_{ortho}, PPh_3), 131.12 (s, C_{para}, PPh_3), 129.22 (d, ^3J(PC) 10 Hz, C_{meta}, PPh_3), 81.95 (s, C_5H_5), 61.35 (s, N*C*HCy), 45.22 (s, C_1, Cy), 30.74 (s, C*Me*$_3$), 29.61 (s, C_2, Cy), 27.04 (s, C_3, Cy), 26.50 (s, C_4 and C_5, Cy), 25.91 (s, C_6, Cy), 16.24 (s, CH*Me*) ppm. $^{31}P\{^1H\}$ NMR (CD_2Cl_2): δ 59.68 (s, PPh_3) ppm.

5.2.8. ($R_{Ru}S_C$,$S_{Ru}R_C$)-[(η^5-C_5H_5)Ru(PPh_3)(CN^tBu)-(NH_2CHMe{1-$C_{10}H_7$}$)]PF_6$ (**5RS,5SR**)

An orange solution of **1** (0.20 g, 0.366 mmol) and thallium (I) hexafluorophosphate (0.40 g, 1.15 mmol) in dichloromethane (30 ml) was stirred for 90 min to give a tomato-orange solution. Excess (±)-1-(1-naphthyl)ethylamine (1.0 ml, 6.21 mmol) was added. The mixture was stirred at room temperature in the dark under nitrogen for 52 h to give a bright yellow solution. After solvent removal under reduced pressure, the yellow treacly solid was washed with diethylether (2 × 15 ml). Extraction with dichloromethane (2 × 15 ml), filtration, and concentration under reduced pressure (ca. 10 ml) gave a yellow solution. Addition of diethylether (30 ml) afforded fine yellow crystals on storing at −30 °C under nitrogen overnight. Yield 0.05 g (17%) 73% d.e.

IR (Nujol): ν_{max} 3303w, 3271vw, 1587vw (NH), 2108m (CN) and 843vs cm^{-1} (PF_6). ^1H NMR (CD_2Cl_2): δ 7.93–7.97 (m, 2H, Np), 7.88 (d, 1H, ^3J(HH) 8 Hz, Np), 7.24–7.63 (m, 19H, Np and PPh_3), 4.35 (m, 1H, NC*H*Me), 4.23 (s, 5H, C_5H_5), 3.68 (br.t, 1H, $^{2,3}J$(HH) 11 Hz, NH), 2.15 (br.d, 1H, ^2J(HH) 11 Hz, NH), 1.29 (d, 3H, ^3J(HH) 7 Hz, Me), 1.23 (s, 9H, C*Me*$_3$) ppm. $^{13}C\{^1H\}$ NMR (CD_2Cl_2): δ 138.97 (s, C_{ipso}, Np), 134.18 and 130.82 (s, 2× $C_{bridging}$, Np), 133.66 (d, ^1J(PC) 45 Hz, C_{ipso}, PPh_3), 133.71 (d, ^2J(PC) 11 Hz, C_{ortho}, PPh_3), 131.19 (s, C_{para}, PPh_3), 129.67, 128.96, 126.81, 126.34, 126.09, 123.19, and 122.57 (s, 7× C_{aryl}, Np), 129.32 (d, ^3J(PC) 10 Hz, C_{meta}, PPh_3), 81.50 (s, C_5H_5), 58.34 (s, N*C*HNp), 30.68 (s, C*Me*$_3$), 25.53 (s, CH*Me*) ppm. $^{31}P\{^1H\}$ NMR (CD_2Cl_2): δ 59.46 (s, PPh_3) ppm.

5.2.9. ($R_{Ru}R_C$,$S_{Ru}S_C$)-[(η^5-C_5H_5)Ru(PPh_3)(CN^tBu)-(NH_2CHMe{1-$C_{10}H_7$}$)]PF_6$ (**5RR,5SS**)

The mother-liquor from above was reduced in volume (ca. 10 ml) under reduced pressure, and was then left to crystallize out in the dark at −30 °C for 46 h, from which yellow crystals were isolated. Yield 0.07 g (23%) 56% d.e. of the least soluble (**5RS,5SR**). (Calc. for $C_{40}H_{42}F_6N_2P_2Ru \cdot 0.5CH_2Cl_2$: C, 55.90; H, 4.98; N, 3.22. Found: C, 56.29; H, 4.75; N, 3.40%.) IR (Nujol): ν_{max} 3314w, 3257w, 1587w (NH), 2108m (CN) and 841s cm^{-1} (PF_6). ^1H NMR (CD_2Cl_2): δ 7.70 (m, 2H, Np), 7.20–7.59 (m, 19H, Np and PPh_3), 7.40 (t, 1H, ^3J(HH) 7 Hz, Np), 4.35 (m, 1H, NC*H*Me), 4.77 (s, 5H, C_5H_5), 3.84 (br.t, 1H, $^{2,3}J$(HH) 11 Hz, NH), 3.05 (br.d, 1H, ^2J(HH) 11 Hz, NH), 1.42 (d, 3H, ^3J(HH) 7 Hz, Me), 1.21 (s, 9H, C*Me*$_3$) ppm. $^{13}C\{^1H\}$ NMR (CD_2Cl_2): δ ~133.58 (d, ^2J(PC) 11 Hz, C_{ortho}, PPh_3), ~133.37 (d, ^1J(PC) 45 Hz, C_{ipso}, PPh_3), ~129.13 (d, ^3J(PC) 10 Hz, C_{meta}, PPh_3), 128.30, 126.65, 126.25, 122.25, and 121.90 (s, C_{aryl}, Np), 81.81 (s, C_5H_5), 56.93 (s, N*C*HNp), 30.78 (s, C*Me*$_3$), 22.95 (s, CH*Me*) ppm. $^{31}P\{^1H\}$ NMR (CD_2Cl_2): δ 59.57 (s, PPh_3) ppm. MS (FAB): 682 $[M - PF_6]^+$(34%), 511(100), 428(44).

5.2.10. ($R_{Ru}S_C$)-[(η^5-C_5H_5)Ru(PPh_3)(CO)-($NH_2CHMePh$)]PF_6 (**7RS**)

To a yellow-brown solution of **6** (0.50 g, 1.02 mmol) in dichloromethane (30 ml) was added thallium hexafluorophosphate (0.81 g, 2.33 mmol) and *S*(−)-α-methylbenzylamine (1 ml, 7.76 mmol). The brown mixture was stirred under nitrogen at 45–50 °C for 17.5 h (overnight) to give a cream brown suspension. Filtration, washing the off-white residue with dichloromethane (3 × 5 ml) gave a brown filtrate. After solvent removal under reduced pressure, the brown residue was extracted with diethylether (5 × 10 ml) and filtered to give a yellow solution. This was placed onto an alumina column (2 × 15 cm), the excess amine was eluted with light petroleum ether (60 ml) and the pale yellow product band was eluted with dichloromethane (60 ml) to give a pale yellow solution. After solvent removal under reduced pressure, a mustard yellow powder was obtained by crystallising the residual oil from diethylether (10 ml) at −80 °C for 54 h. Yield 0.04 g (5%) 42% d.e. (Calc. for $C_{32}H_{31}F_6NOP_2Ru$: C, 53.19; H, 4.32; N, 1.94. Found: C, 53.30; H, 4.60; N, 1.75%.) IR (Nujol): ν_{max} 3306w, 3267w, 1587vw (NH), 1950sh.w, 1941m (CO) and 843s cm^{-1} (PF_6). ^1H NMR (CD_2Cl_2/$CDCl_3$): δ 7.55–7.60 and 7.34–7.40 (m, 15H, PPh_3), 7.26 (m, 5H, Ph), 4.57 (s, 5H, C_5H_5), 4.26 (br.t, 1H, $^{2,3}J$(HH) 11 Hz, NH), 3.26 (br.sextet {br.m}, 1H,

^3J(HH) 7 Hz, NC*H*Me), 1.95 (br.d, 1H, ^2J(HH) 11 Hz, NH), 1.09 (d, 3H, ^3J(HH) 7 Hz, CH*Me*) ppm. $^{13}C\{^1H\}$ NMR ($CD_2Cl_2/CDCl_3$): δ 203.92 (d, ^2J(PC) 19 Hz, CO), 134.34 (d, C_{ipso}, PPh_3), 133.95 (d, ^2J(PC) 11 Hz, C_{ortho}, PPh_3), 132.11 (s, C_{para}, P*Ph*$_3$), 129.92 (d, ^3J(PC) 10 Hz, C_{meta}, PPh_3), 129.54 (s, C_{ortho}, Ph), 129.12 (s, C_{para}, Ph), 128.12 (s, C_{meta}, Ph), 86.39 (s, C_5H_5), 64.19 (s, N*C*HPh), 25.59 (s, CH*Me*) ppm. $^{31}P\{^1H\}$ NMR ($CD_2Cl_2/CDCl_3$): δ 55.58 (s, PPh_3) ppm. MS (FAB): 578 $[M - PF_6]^+$(37%), 457(63), 429(100).

5.2.11. ($S_{Ru}S_C$)-[(η^5-C_5H_5)Ru(PPh_3)(CN^tBu)-($NH_2CHMePh$)]PF_6 (**7SS**)

The partial data was obtained from the spectra obtained from the sample of (**7RS**) above.

^1H NMR ($CD_2Cl_2/CDCl_3$): δ 7.40–7.52 and 7.27–7.34 (m, 15H, P*Ph*$_3$), 6.95 (m, 5H, Ph), 5.13 (s, 5H, C_5H_5), 1.39 (d, 3H, ^3J(HH) 7 Hz, CH*Me*) ppm. $^{13}C\{^1H\}$ NMR ($CD_2Cl_2/CDCl_3$): δ 142.67 (s, C_{ipso}, PPh_3), 133.85 (d, ^2J(PC) 11 Hz, C_{ortho}, PPh_3), 131.56 (s, C_{para}, PPh_3), 129.38 (d, ^3J(PC) 10 Hz, C_{meta}, PPh_3), 127.03 (s, C_{meta}, Ph), 86.71 (s, C_5H_5), 64.06 (s, N*C*HPh), 23.17 (s, CH*Me*) ppm. $^{31}P\{^1H\}$ NMR ($CD_2Cl_2/CDCl_3$): δ 54.25 (s, PPh_3) ppm.

5.2.12. [(η^5-C_5H_5)Ru(PPh_3)(CN^tBu)($NHEt_2$)]PF_6 (**9**)

A Schlenk tube was charged with a solution of **1** (0.20 g, 0.37 mmol) in dichloromethane (30 ml), thallium hexafluorophosphate (0.19 g, 0.54 mmol), and a magnetic stirrer bar. The orange solution was stirred in the dark under nitrogen at room temperature for 1 h to give a tomato-orange suspension. Excess diethylamine (0.4 ml, 3.87 mmol) was added and the solution was stirred in the dark at room temperature overnight. Filtration, evaporation of the filtrate under reduced pressure, and crystallization of the yellow residue from dichloromethane and diethylether (1:3, 20 ml) at −30 °C afforded orange-yellow crystals of **9**. Yield 0.16 g (60%).

IR (Nujol): ν_{max} 3269w, 1613vw (NH), 2129m, 2062sh.w (CN), and 841s cm^{-1} (PF_6). ^1H NMR (CD_2Cl_2): δ 7.26–7.49 (m, 15H, PPh_3), 4.78 (s, 5H, C_5H_5), 2.78 (m, 2H, $^{2,3}J$(HH) 7 Hz, CH_2CH_3), 2.67 (m, 2H, $^{2,3}J$(HH) 7 Hz, CH_2CH_3), 1.68 (br.s, 1H, NH), 1.20 (s, 9H, C*Me*$_3$), 1.08 (t, 3H, $^{2,3}J$(HH) 7 Hz, CH_2CH_3), 0.44 (t, 3H, $^{2,3}J$(HH) 7 Hz, CH_2 CH_3) ppm. $^{13}C\{^1H\}$ NMR (CD_2Cl_2): δ 133.88 (d, C_{ipso}, PPh_3), 133.37 (d, ^2J(PC) 11 Hz, C_{ortho}), 131.32 (s, C_{para}), 129.52 (d, ^3J(PC) 10 Hz, C_{meta}), 82.08 (s, C_5H_5), 58.45 (s, *C*Me$_3$), 56.13, 51.54 (2s, CH_2), 30.45 (s, C*Me*$_3$), 14.67, 14.08 (2s, CH_3) ppm. $^{31}P\{^1H\}$ NMR (CD_2Cl_2): δ 58.3 (s, PPh_3), −145.40 (septet, ^1J(*P*F) 712 Hz, PF_6) ppm. MS (FAB): 585 $[M - PF_6]^+$(15%), 512(100), 454(9), 429(37).

5.2.13. [(η^5-C_5H_5)Ru(PPh_3)(CN^tBu)(NH(*Me*)-*CHMePh*)]PF_6 (**10**)

A solution of **1** (0.20 g, 0.37 mmol) in dichloromethane (30 ml) was treated with thallium hexafluorophosphate (0.20 g, 0.57 mmol) and excess *S*(−)-*N*-methyl-1-phenylethylamine (0.25 ml, 1.72 mmol). This yellow-orange solution was stirred in the dark at room temperature for 24 h. After filtration and solvent removal from the filtrate under reduced pressure, fine yellow crystals were obtained by crystallizing the residue at −30 °C from dichloromethane and diethylether (1:3, 15 ml) overnight. Yield 0.18 g (62%). IR (Nujol): ν_{max} 3263w, 1585vw (NH), 2122s (CN), and 841br.s cm^{-1} (PF_6). MS (FAB): 647 $[M - PF_6]^+$(11%), 511(100), 454(11), 429(38).

The ^1H NMR spectrum of the crystals revealed four diastereomers were present; integration of the cyclopentadienyl ligand singlets produced a ratio of 5:20:2:25 for **SSS**:**SRS**:**RRS**:**RSS**. Concentration of the mother-liquor above to ca. 7 ml and cooling to −25 °C gave yellow crystals, yield 0.05 g. (17%), whose spectrum showed the diastereomer ratio to be 5:12:2:4.

10RSS: ^1H NMR (CD_2Cl_2): δ 7.33–7.54 (m, 15H, PPh_3), 7.05 (m, 5H, Ph), 4.64 (s, 5H, C_5H_5), 3.63 (quintet, 1H, ^3J(HH) 7 Hz, NHC*H*), 2.29 (d, 3H, ^3J(HH) 6 Hz, NHCH_3), 2.05 (br.q, 1H, ^3J(HH) 6 Hz, NH), 1.34 (d, 3H, ^3J(HH) 6 Hz, CHCH_3), 1.25 (s, 9H, Bu) ppm. $^{13}C\{^1H\}$ NMR (CD_2Cl_2): δ 139.68 (s, C_{ipso}, Ph), 133.40 (d, J(PC) 44 Hz, C_{ipso}, PPh_3), 133.39 (d, ^2J(PC) 11 Hz, C_{ortho}, PPh_3), 131.39 (s, C_{para}, PPh_3), 129.61 (d, ^3J(PC) 10 Hz, C_{meta}, PPh_3), 129.08 (s, C_{ortho}, Ph), 128.97 (s, C_{para}, Ph), 127.85 (s, C_{meta}, Ph), 82.18 (s, C_5H_5), 68.08 (s, N*C*HPh), 58.57 (s, *C*Me$_3$), 45.70 (s, NHCH_3), 30.48 (s, C*Me*$_3$), 23.99 (s, CH*Me*) ppm. $^{31}P\{^1H\}$ NMR (CD_2Cl_2): δ 58.3 (s, PPh_3) ppm.

10SRS: ^1H NMR (CD_2Cl_2): δ 7.32–7.51 (m, 15H, PPh_3), 6.80 (m, 5H, Ph), 4.81 (s, 5H, C_5H_5), 3.88 (qd, 1H, ^3J(HH) 7 Hz, ^4J(PH) 1.8 Hz, NHC*H*), 2.51 (br.s, 1H, N*H*CH$_3$), 2.23 (d, 3H, ^3J(HH) 6 Hz, NHCH_3), 1.55 (d, 3H, ^3J(HH) 7 Hz, CHCH_3), 1.30 (s, 9H, Bu) ppm. $^{13}C\{^1H\}$ NMR (CD_2Cl_2): δ 139.41 (s, C_{ipso}, Ph), 133.52 (d, J(PC) 44 Hz, C_{ipso}, PPh_3), 133.56 (d, ^2J(PC) 10 Hz, C_{ortho}, PPh_3), 131.39 (s, C_{para}, PPh_3), 129.62 (d, ^3J(PC) 9 Hz, C_{meta}, PPh_3), 129.64 (s, C_{ortho}, Ph), 127.82 (s, C_{para} + C_{meta}, Ph), 82.44 (s, C_5H_5), 65.73 (s, N*C*HPh), 58.62 (s, *C*Me$_3$), 41.35 (s, NHCH_3), 30.75 (s, C*Me*$_3$), 24.80 (s, CH*Me*) ppm. $^{31}P\{^1H\}$ NMR (CD_2Cl_2): δ 58.1 (s, PPh_3) ppm.

10SSS: ^1H NMR (CD_2Cl_2): δ 6.15 (m, 5H, Ph), 4.83 (s, 5H, C_5H_5), 3.78 (q, 1H, ^3J(HH) 7 Hz, NHC*H*), 2.51 (br.s, 1H, N*H*CH$_3$), 2.46 (d, 3H, ^3J(HH) 6 Hz, NHCH_3), 1.85 (br.s, 1H, *NH*CH$_3$), 1.50 (d, 3H, ^3J(HH) 7 Hz, CHCH_3), 1.26 (s, 9H, Bu) ppm. $^{13}C\{^1H\}$ NMR (CD_2Cl_2): δ 82.30 (s, C_5H_5), 60.79 (s, *C*Me$_3$), 47.18 (s, NHCH_3), 30.64 (s, C*Me*$_3$), 14.75 (s, CH*Me*) ppm. $^{31}P\{^1H\}$ NMR (CD_2Cl_2): δ 55.7 (s, PPh_3) ppm.

10RRS: ^1H NMR (CD_2Cl_2): δ 6.65 (m, 5H, Ph), 4.74 (s, 5H, C_5H_5), 3.73 (qd, 1H, ^3J(HH) 7 Hz, ^4J(PH) 1.8 Hz, NHC*H*), 2.53 (d, 3H, ^3J(HH) 6 Hz, NHCH_3), 1.40 (d, 3H, ^3J(HH) 7 Hz, CHCH_3), 1.18 (s, 9H, Bu) ppm. $^{13}C\{^1H\}$ NMR (CD_2Cl_2): δ 81.65 (s, C_5H_5), 41.05 (s, NHCH_3), 30.36 (s, C*Me*$_3$), 20.80 (s, CH*Me*) ppm.

*5.2.14. ($R_{Ru}S_C$,$R_{Ru}S_C$)-[(η^5-C_5H_5)Ru(PPh_3)-(CNCHMePh)Cl] (**11RS,11SS**)*

A suspension of **1** (0.70 g, 0.964 mmol) and excess (*S*)-α-methylbenzylisonitrile (0.5 ml, 3.58 mmol) in toluene (30 ml) was stirred and heated under reflux at 100 °C under nitrogen for 24 h. The cooled orange solution was reduced in volume (to ca. 10 ml) under reduced pressure and put onto an alumina column (1.5 × 20 cm.). PPh_3 was eluted with toluene (20 ml) and the orange product band eluted with dichloromethane (30 ml) and ultimately acetone (10 ml) to give an orange solution. Solvent removal under reduced pressure gave a frothy orange solid. Wash with petroleum ether (b.p. 40–60 °C, 2 × 10 ml) followed by drying under reduced pressure afforded a bright orange powder. Yield 0.26 g (45%) [**11SS**:**11RS** 49:51].

Recrystallization of a small sample (0.15 g) from toluene and hexane (1:3, 20 ml) at −30 °C for 16 h afforded an oily orange solid after filtration and solvent removal under reduced pressure. Yield 0.02 g [**11SS**:**11RS** 65:35].

IR (Nujol): ν_{max} 2104, 2102s cm^{-1} (CN). MS (FAB): 595 $[M]^+$(38%), 560(85), 429(93).

11SS: ^{1}H NMR ($CDCl_3$): δ 7.41–7.54 and 7.22–7.33 (m, 15H, PPh_3), 7.10–7.13 and 7.03–7.06 (m, 5H, Ph), 4.87 (q, 1H, ^3J(HH) 7 Hz, C*H*Me), 4.55 (s, 5H, C_5H_5), 1.39 (d, 3H, ^3J(HH) 7 Hz, CH*Me*) ppm. $^{13}C\{^1H\}$ NMR ($CDCl_3$): δ 136.65 (d, ^1J(PC) 44 Hz, C_{ipso}, P*Ph*$_3$), 133.71 (d, ^2J(PC) 11 Hz, C_{ortho}, P*Ph*$_3$), 129.41 (s, C_{para}, PPh_3), 128.65 (s, C_{para}, Ph), 127.82 (d, ^3J(PC) 11 Hz, C_{meta}, PPh_3), 125.37 (s, C_{meta}, Ph), 81.66 (s, C_5H_5), 56.20 (s, N*C*HPh), 25.01 (s, CH*Me*) ppm.

11RS: ^{1}H NMR ($CDCl_3$): δ 7.41–7.54 and 7.22–7.33 (m, 15H, P*Ph*$_3$), 7.10–7.13 and 7.03–7.06 (m, 5H, Ph), 4.70 (q, 1H, ^3J(HH) 7 Hz, C*H*Me), 4.53 (s, 5H, C_5H_5), 1.29 (d, 3H, ^3J(HH) 7 Hz, CH*Me*) ppm. $^{13}C\{^1H\}$ NMR ($CDCl_3$): δ 136.47 (d, ^1J(PC) 44 Hz, C_{ipso}, PPh_3), 133.71 (d, ^2J(PC) 11 Hz, C_{ortho}, PPh_3), 129.41 (s, C_{para}, PPh_3), 128.65 (s, C_{para}, Ph), 127.82 (d, ^3J(PC) 11 Hz, C_{meta}, PPh_3), 125.37 (s, C_{meta}, Ph), 81.66 (s, C_5H_5), 56.09 (s, N*C*HPh), 25.01 (s, CH*Me*) ppm.

*5.2.15. ($R_{Ru}S_C$,$R_{Ru}S_C$)-[(η^5-C_5H_5)Ru(PPh_3)-(CNCHMePh)(NH_3)]PF_6 (**12RS,12SS**)*

A mixture of (**11RS**,**11SS**) (0.21 g, 0.353 mmol), ammonium hexafluorophosphate (0.25 g, 1.54 mmol), and thallium (I) carbonate (0.50 g, 1.07 mmol) in methanol (40 ml) was stirred at 60 °C for 22 h. Removal of the solvent under reduced pressure and crystallization of the residue from dichloromethane–diethylether (1:3, 40 ml) at −30 °C afforded yellow crystals of (**12RS**,**12SS**). Total yield 0.12 g (47%) [racemate]. (Calc for $C_{32}H_{32}F_6N_2P_2Ru \cdot 3CH_2Cl_2$: C, 43.06; H, 3.92; N, 2.87. Found: C, 43.56; H, 3.63; N, 3.13%.) IR (Nujol): ν_{max} 3370m, 3296w, 1622w (NH), 2119br.s (CN) and 838br.vs cm^{-1} (PF_6). ^{1}H NMR ($(CD_3)_2CO$): δ 7.36–7.58 (m, 30H, P*Ph*$_3$), 7.25–7.36 and 7.11–7.14 (m, 10H, Ph), 5.21 (q, 1H, ^3J(HH) 7 Hz, C*H*Me) and 5.19 (q, 1H, ^3J(HH) 7 Hz, C*H*Me), 4.88 (s, 10H, C_5H_5), 2.60 (br, 6H, NH_3), 1.52 (d, 3H, ^3J(HH) 7 Hz, CH*Me*), 1.43 (d, 3H, ^3J(HH) 7 Hz, CH*Me*) ppm. $^{13}C\{^1H\}$ NMR ($(CD_3)_2CO$): δ 135.41 (d, ^1J(PC) 45 Hz, C_{ipso}, PPh_3), 134.29 (d, ^2J(PC) 11 Hz, C_{ortho}, PPh_3), 131.29 (s, C_{para}, PPh_3), 129.58 (d, ^3J(PC) 10 Hz, C_{meta}, PPh_3), 128.88 (s, C_{ortho}, PPh_3), 126.48 (s, C_{para}, Ph), 126.36 (s, C_{meta}, Ph), 82.52 (s, C_5H_5), 57.38 (s, N*C*HPh), 25.22 (s, CH*Me*), 25.09 (s, CH*Me*) ppm. $^{31}P\{^1H\}$ NMR (CD_2Cl_2): δ 58.47 (s, PPh_3) and 58.17 (s, PPh_3) ppm. MS (FAB): 577 $[M - PF_6]^+$(24%), 560(100), 429(53).

5.3. Decomplexation of amine ligands

*5.3.1. [(η^5-C_5H_5)Ru(PPh_3)(CN^tBu)(NH_2Cy)]PF_6 (**2**)*

Method A. Complex **2** (0.10 g, 0.13 mmol), trimethylamine *N*-oxide dehydrate (0.05 g, 0.45 mmol), and sodium iodide (0.08 g, 0.53 mmol) were placed in a Fischer–Porter bottle and suspended in methanol (30 ml). After heating and stirring at 85 °C for 48 h the solvent was removed under reduced pressure. Extraction with dichloromethane (30 ml) gave an orange-red solution which was washed with water (3 × 10 ml). The dichloromethane layer was dried with anhydrous magnesium sulphate, filtered and the solvent removed. The orange foam (0.09 g) was identified as a mixture (70:30) of **8** and unreacted **2** by ^{1}H NMR and infrared spectroscopies.

Method B. A Fischer–Porter bottle was charged with **2** (0.20 g, 0.27 mmol), iodomethane (2 ml, 32 mmol), and 1,2-dichloroethane (30 ml). Heating and stirring for 22 h at 120 °C gave a dark red solution. Cooling, removal of solvent, and washing the residue with petroleum ether (2 × 5 ml) then water (3 × 5 ml) gave a red solid which was dried under reduced pressure and identified as **8** (0.16 g, 95%) by ^{1}H NMR and infrared spectroscopies.

Method C. A stirred solution of **2** (0.10 g, 0.13 mmol) and iodine (0.10 g, 0.39 mmol) in dichloromethane was photolyzed for 24 h at room temperature. The product solution was washed with sodium thiosulfate solution (10%, 3 × 20 ml), the separated organic layer was washed with water (3 × 20 ml), then dried with granular calcium chloride. Removal of the solvent under reduced pressure gave **8** (0.08 g, 95%).

*5.3.2. ($S_{Ru}S_C$)-[(η^5-C_5H_5)Ru(PPh_3)(CN^tBu)-($NH_2CHMePh$)]PF_6 (**3SS**)*

A sample of **3RS** (96% d.e.) was treated under Method B above. The isolated **8** was recrystallized from dichloromethane and petroleum ether. Analysis of the ^{1}H NMR spectra obtained in the absence and presence of *R*(−)-TFAE (1.05 equiv) showed the product to be a racemic mixture of **8R** and **8S**.

*5.3.3. ($R_{Ru}S_C$)-[(η^5-C_5H_5)Ru(PPh_3)(CN^tBu)-($NH_2CHMePh$)]PF_6 (**3RS**)*

A sample of **3RS** (90% d.e.) was treated under Method B above. The isolated **8** was treated with thallium hexafluorophosphate and excess *S*(−)-*N*-methyl-1-phenylethylamine using the procedures described earlier. The crude product

before crystallization was shown by ^{1}H NMR spectroscopy to be a racemic mixture of **3RS** and **3SS**.

A sample of **3RS** (90% d.e.) was treated under Method C above. The product **8** was analyzed by the ^{1}H NMR–TFAE method and by conversion back to **3**. Both methods revealed the original sample of **8** to be racemic.

5.4. X-ray crystallography

The crystals of **2**, **3SR**, **3RR**, and **12** were grown by slow layer diffusion of diethyl ether into dichloromethane solutions. Suitable crystal specimens were mounted on a glass fibre with epoxy resin and cooled on the goniometer head by means of nitrogen gas. Precession photographs and intensity data were collected on a Siemens R3m/V diffractometer using graphite monochromatized Mo Kα X-rays. Cell dimensions were obtained from 25 to 50 centred reflections with 2θ values from 20° to 32°. Intensity data were collected using a 2θ–θ scan technique. The intensities of three reflections measured periodically showed a decrease of less than 1% over the data collection for all four datasets. An empirical absorption correction was applied using azimuthal scan data for twelve selected reflections. The structures were solved by standard heavy atom routines and refined by full-matrix least-squares methods. All non-hydrogen atoms were given anisotropic temperature factors. Hydrogen atoms were placed in the models at calculated positions and allowed to ride on their respective carbon atoms. The hexafluorophosphate anions were rotationally disordered in both **3SR** and **3RR** and were modeled by simple partial occupancy methods. Table 2 contains the collection and solution parameters for all four determinations.

Acknowledgements

We thank the E.P.S.R.C. for a studentship (D.M.W.) and Johnson-Matthey Chemicals Ltd. for a generous loan of ruthenium trichloride. Dr. N.M. Boag (Salford) is thanked for stimulating discussions and we acknowledge the use of the E.P.S.R.C. Chemical Database Service at Daresbury [35].

Appendix A. Supplementary data

The supplementary crystallographic data for this paper are contained in the deposition files CCDC-277650 (**2**), CCDC-277651 (**3SR**), CCDC-277652 (**3RR**), and CCDC-277653 (**12**). These data can be obtained free of charge via ccdc.cam.ac.uk/data_request/cif, by emailing data_request@ccdc.cam.ac.uk, or by contacting The Cambridge Crystallographic Data Centre, 12 Union Road, Cambridge, CB2 1EZ, UK: fax +44 1223 336033. Supplementary data associated with this article can be found, in the online version, at doi:10.1016/j.poly.2006.01.016.

References

[1] A. Werner, Chem. Ber. 44 (1911) 1887.
[2] H. Brunner, Angew. Chem., Int. Ed. Engl. 8 (1969) 382.
[3] R. Dabard, A. Meyer, G. Jaouen, C.R. Seances, Acad. Sci., Ser. C C286 (1969) 201.
[4] H. Brunner, Angew. Chem., Int. Ed. Engl 38 (1999) 1194.
[5] H. Brunner, Eur. J. Inorg. Chem. (2001) 905.
[6] J.W. Faller, J. Parr, A.R. Lavoie, New J. Chem. 27 (2003) 899.
[7] H. Brunner, T. Zwack, Organometallics 19 (2000) 2423.
[8] M. Pfeffer, Organometallics 19 (2000) 2427.
[9] F.M. Conroy-Lewis, S.J. Simpson, J. Organomet. Chem. 396 (1990) 83.
[10] A. von Zelewsky, Stereochemistry of Coordination Compounds, Wiley, Chichester, 1995.
[11] G.J. Leigh, Nomenclature of Inorganic Chemistry, Blackwell, Oxford, 1990.
[12] K. Stanley, M.C. Baird, J. Am. Chem. Soc. 97 (1975) 6598.
[13] T.E. Sloan, Top. Stereochem. 12 (1981) 1.
[14] N.H. Martin, N.W. Allen III, K.D. Moore, L. Vo, J. Mol. Struct. (Theochem) 454 (1998) 161.
[15] Y.H. Lai, Z.L. Zhou, J. Org. Chem. 62 (1997) 925.
[16] S.G. Davies, I.M. Dordor, J.C. Walker, P. Warner, Tetrahedron Lett. 25 (1984) 2709.
[17] B.K. Blackburn, S.G. Davies, M. Whittaker, in: I. Bernal (Ed.), Stereochemistry of Organometallic and Inorganic Compounds, vol. 3, Elsevier, Amsterdam, 1989, and references therein.
[18] F.M. Conroy-Lewis, S.J. Simpson, J. Chem. Soc., Chem. Commun. (1986) 506.
[19] E. Francotte, R.W. Lang, T. Winkler, Chirality 3 (1991) 177.
[20] J.A. Cabeza, I. del Rio, M. Elena-Navarro, S. Garcia-Granda, Acta Crystallogr., Sect. E: Struct. Rep. Online 57 (2001) m162.
[21] F.L. Joslin, M.P. Johnson, J.T. Mague, D.M. Roundhill, Organometallics 10 (1991) 41.
[22] F.L. Joslin, M.P. Johnson, J.T. Mague, D.M. Roundhill, Organometallics 10 (1991) 2781.
[23] J. Jacques, A. Collet, S.H. Wilen, Enantiomers, Racemates, and Resolutions, Krieger, Malabar, 1981, pp. 251–252.
[24] I. Ugi, Z. Naturforsch. 20B (1965) 405.
[25] M.I. Bruce, R.C. Wallis, Aust. J. Chem. 34 (1981) 209.
[26] F.M. Conroy-Lewis, Ph.D. Thesis, University of Salford, 1987.
[27] S.G. Davies, S.J. Simpson, J. Chem. Soc., Dalton Trans. (1984) 993.
[28] F.M. Conroy-Lewis, A.D. Redhouse, S.J. Simpson, J. Organomet. Chem. 366 (1989) 357.
[29] G.W. Gokel, R.P. Widera, W.P. Weber, Org. Synth. 55 (1976) 96.
[30] G.W. Gokel, R.P. Widera, W.P. Weber, Org. Synth. Coll. Vol. 6 (1988) 232.
[31] K. Gollnick, S. Koegler, D. Maurer, J. Org. Chem. 57 (1992) 229.
[32] S. Terashima, K. Takashima, T. Sato, S. Yamada, Chem. Pharm. Bull 21 (1973) 1135.
[33] S. Yamada, K. Takashima, T. Sato, S. Terashima, J. Chem. Soc. D (1969) 811.
[34] D. Seebach, G. Adam, T. Gees, M. Schiess, W. Weigand, Chem. Ber. 121 (1988) 507.
[35] The United Kingdom Chemical Database Service, D.A. Fletcher, R.F. McMeeking, D. Parkin, J. Chem. Inf. Comput. Sci. 36 (1996) 746.

an infinite 1D coordination polymer. The anion-encapsulated 3D cages, induced by the anion-templating assembly, are $[[[Cu_4(\mu\text{-}OMe)_4(\mu\text{-}btp)_4(BF_4)_2(MeCN)_2] \supset (BF_4)](BF_4)]$-$[[[Cu_4(\mu\text{-}OMe)_4(\mu\text{-}btp)_4(BF_4)(MeOH)(MeCN)_2] \supset (BF_4)]$-$(BF_4)_2]$ (**2**) and $[[Cu_4(\mu\text{-}OMe)_4(\mu\text{-}btp)_4(ClO_4)_2(MeCN)_2] \supset (ClO_4)](ClO_4) \cdot 2H_2O$ (**3**). A 1D infinite coordination polymer of $[[Cu_2(\mu\text{-}OMe)_2(\mu\text{-}OTf)_2(btp)_2](H_2O)]_n$ (**4**) was also isolated.

2. Experimental

2.1. Material and instrumentation

Infrared spectra were recorded on Nicolet AVATAR 360 FT-IR instrument as KBr plates. Elemental analysis (C, H, N) were performed with Element Analysis system EA 1112 CE Instruments by the Korea Basic Science Institute. 2,6-Bis(*N*1-1,2,4-triazolyl)pyridine (btp) was prepared according to the literature [9]. All other materials were used as received without further purification.

2.2. Synthesis

2.2.1. $[Cu_2(OAc)_4(btp)_2] \cdot 2MeOH$ (**1**)

To a methanol solution (100 mL) containing $Cu(OAc)_2 \cdot H_2O$ (1.917 g, 9.6 mmol) was added a solution of btp (1.023 g, 4.8 mmol) in a mixture of MeOH (100 mL) and CH_2Cl_2 (20 mL). After stirring for 24 h, the solution was concentrated to ca. half of its original volume. The green microcrystalline product was collected by filtration and dried in air (1.92 g, 96%). *Anal*. Calc. for $C_{28}H_{32}Cu_2N_{14}O_{10}$ (851.76): C, 39.48; H, 3.79; N, 23.02. Found: C, 39.35; H, 3.70; N, 23.39%. IR (KBr, *v*): 1632(s), 1607(s), 1515(m), 1478(s), 1426(s), 1277(m), 1211(m), 1138(m), 1064(w), 980(m), 810(m), 778(w), 681(m), 644(w) cm^{-1}.

2.2.2. $[[[Cu_4(\mu\text{-}OMe)_4(\mu\text{-}btp)_4(BF_4)_2(MeCN)_2] \supset (BF_4)](BF_4)][[[Cu_4(\mu\text{-}OMe)_4(\mu\text{-}btp)_4(BF_4)(MeOH)(MeCN)_2] \supset (BF_4)](BF_4)_2]$ (**2**)

A mixture of **1** (0.248 g, 0.3 mmol) in acetonitrile (50 mL) and CH_3OH (50 mL) was added dropwise to a methanol solution (100 mL) of $Cu(BF_4)_2 \cdot 6H_2O$ (0.140 g, 0.6 mmol) over 24 h. This solution was concentrated to ca. a quarter of its original volume. Carefully covered with *n*-pentane, X-ray suitable single crystals **2** were obtained at low temperature (0.142 g, 28%). *Anal*. Calc. for $C_{89}H_{105}B_8Cu_8F_{32}N_{60}O_9$ (3362.13): C, 31.79; H, 3.15; N, 25.00. Found: C, 32.01; H, 2.86; N, 24.74%. IR (KBr, *v*): 1614(s), 1533(s), 1487(s), 1373(m), 1286(s), 1224(s), 1147(s), 1072(s), 983(s), 891(m), 808(s), 781(m), 671(m), 521(w) cm^{-1}.

2.2.3. $[[Cu_4(\mu\text{-}OMe)_4(\mu\text{-}btp)_4(ClO_4)_2(MeCN)_2] \supset (ClO_4)](ClO_4) \cdot 2H_2O$ (**3**)

The procedure is similar with that of **2** using $Cu(ClO_4)_2 \cdot 6H_2O$ (0.222 g, 0.6 mmol) instead of $Cu(BF_4)_2 \cdot 6H_2O$ (0.133 g, 25%). *Anal*. Calc. for $C_{44}H_{46}Cl_4Cu_4N_{30}O_{20}$ (1711.02, vacuum-dried sample): C, 30.89; H, 2.71; N, 24.56. Found: C, 30.61; H, 2.90; N, 24.17%. IR (KBr, *v*): 1613(s), 1530(s), 1480(s), 1371(m), 1283(s), 1222(s), 1146(s), 1120(s), 1174(s), 1077(s), 981(s), 890(m), 807(s), 780(m), 670(m), 636(w), 539(w) cm^{-1}.

2.2.4. $[[Cu_2(\mu\text{-}OMe)_2(\mu\text{-}OTf)_2(btp)_2](H_2O)]_n$ (**4**)

The procedure is similar with that of **2** using $Cu(OTf)_2$ (0.217 g, 0.6 mmol) in place of $Cu(BF_4)_2 \cdot H_2O$ (0.184 g, 37%). *Anal*. Calc. for $C_{22}H_{20}Cu_2F_6N_{14}O_9S_2$ (929.72): C, 28.42; H, 2.16; N, 21.09. Found: C, 28.40; H, 2.62; N, 20.85%. IR (KBr, *v*): 1612(m), 1533(s), 1482(s), 1291(s), 1250(s), 1224(s), 1166(m), 1143(m), 1074(m), 1030(s), 980(m), 894(w), 808(m), 780(m), 671(m), 637(s), 562(w), 517(w) 410(m) cm^{-1}.

2.3. Crystal structure and determination

X-ray diffraction measurements were performed on a Bruker SMART diffractometer equipped with a CCD area detector with graphite-monochromated Mo Kα radiation ($\lambda = 0.71073$ Å) at 233(2) K for **1** and **4**. The reflections were successfully indexed by an automated indexing routine built in the SMART program [10]. The structures of complexes **1** and **4** were solved by direct methods and refined by full-matrix least-squares calculations on F^2 with SHELX-97 [11]. All non-hydrogen atoms were refined anisotropically and hydrogen atoms were located in the calculated positions using the riding model. The diffraction data for complex **2** and **3** were collected on a Nonius Kappa-CCD diffractometer using Mo Kα radiation ($\lambda = 0.71073$ Å) at 150(1) K. The CCD data were integrated and scaled using the DENZO-SMN software package [12]. The structures were solved by SIR-92 and refined by using SHELXTL/PC V6.12 [13]. All hydrogen atoms were located in calculated positions using the riding model. Crystallographical data and refinement details for **1**–**4** are listed in Table 1.

3. Results and discussion

3.1. Synthesis of complexes

The btp ligand reacted with two equivalents of $Cu(OAc)_2 \cdot H_2O$ to afford the SBU precursor **1**. In the IR spectrum of **1** the characteristic bands of the acetate groups appear at 1632 and 1426 cm^{-1}, which means that the acetate ligands bridge two copper ions to lead to a paddle wheel type copper acetate ($Cu_2(OAc)_4$). In accordance with elemental analysis, **1** possesses two btp ligands and two methanol molecules per $Cu_2(OAc)_4$ unit. Btp acts as a unidentate ligand in **1**, though it has a strong tendency [9,14] to bridge metal ions for polymeric architectures. Even when 1:1 and 1:2 ligand to metal ion ratios were employed only **1** was isolated. In the reaction of **1** with CuX_2 salts ($X = [BF_4]^-$, $[ClO_4]^-$ and $[OTf]^-$), a novel $[Cu_2(OMe)_2]^{2+}$ SBU appears where each copper center is bridged by two methoxide ligand in the μ-mode. As the solvothermal reaction

Table 1
Crystal data and refinement data for **1**, **2**, **3** and **4**

	1	**2**	**3**	**4**
Empirical formula	$C_{28}H_{32}Cu_2N_{14}O_{10}$	$C_{89}H_{105}B_8Cu_8F_{32}N_{60}O_9$	$C_{44}H_{48}Cl_4Cu_4N_{30}O_{24}$	$C_{22}H_{20}Cu_2F_6N_{14}O_9S_2$
Molecular mass	851.76	3362.13	1777.08	929.72
Temperature (K)	233(2)	150(1)	150(2)	233(2)
Crystal system	triclinic	orthorhombic	orthorhombic	orthorhombic
Space group	$P\bar{1}$	*Pnma*	*Cmcm*	*Pbcn*
a (Å)	7.9917(1)	33.0386(4)	18.4800(5)	9.209(2)
b (Å)	8.7885(1)	24.4895(3)	16.5320(7)	21.472(5)
c (Å)	13.2799(2)	37.1741(4)	25.3520(1)	33.808(7)
α (°)	76.075(2)			
β (°)	78.464(2)			
γ (°)	87.669(2)			
V (Å^3)	886.99(2)	30077.5(6)	7745.3(5)	6685(3)
Z, ρ_{calcd} (Mg m^{-3})	1	8	4	8
μ (Mo Kα) (mm^{-1})	1.274	1.215	1.308	1.504
θ Range (°)	1.61–25.53	2.55–26.02	2.59–24.99	1.90–25.54
F(000)	436	13528	3592	3728
Crystal size (mm)	$0.24 \times 0.18 \times 0.12$	$0.20 \times 0.12 \times 0.08$	$0.30 \times 0.27 \times 0.16$	$0.60 \times 0.20 \times 0.20$
Goodness-of-fit	1.023	1.011	1.749	1.365
R_1 [$I > 2\sigma(I)$]	0.0425	0.0949	0.1220	0.0916
R_1 (all data)	0.0567	0.1669	0.1453	0.1119

[15] of copper acetate in methanol afforded copper methoxide, the acetate ligands of **1** play an important role in fabricating methoxide-bridged dicopper SBUs on the grounds that the admixture of CuX_2 salts ($X = [BF_4]^-$ and $[ClO_4]^-$) with just btp ligands instead of **1** does not afford $[Cu_2(OMe)_2]^{2+}$ modules but gives 1D coordination polymers of $[Cu(btp)_2X_2]_n$ in which the copper ions are doubly bridged by btp ligands and the anions occupy the axial sites of the metal centers [16]. The cage **2** was prepared by the reaction of **1** with $Cu(BF_4)_2 \cdot 6H_2O$ in a mixture of MeOH and MeCN at room temperature. Similarly **1** also reacted with $Cu(ClO_4)_2 \cdot 6H_2O$ to afford 3D cage (**3**). Slow evaporation of the reaction mixture afforded blue-green crystals of **2** and **3**, which lost their crystallinity out of the mother liquor. The infrared spectra of **2** show a very strong vibration absorption band of the $[BF_4]^-$ anion (1072 cm^{-1}). The absorption bands of the $[ClO_4]^-$ anion appear at 1077 cm^{-1} in **3**. Meanwhile, the reaction of **1** with $Cu(OTf)_2$ led to the 1D coordination polymer of **4**. The presence of the triflate anion is indicated by infrared absorptions around 1030, 1250 and 1291 cm^{-1}. In all cases of **2**, **3** and **4**, the absorption bands corresponding to acetate ligands vanish.

3.2. Structural properties

A single crystal X-ray analysis of **1** revealed that four acetate ligands bridge copper centers in a μ-mode leading to a paddle wheel type copper acetate. Two btp ligands acting as a unidentate ligands bind the axial sites of the copper centers through the 4-positioned nitrogen atoms in its triazole unit, with a Cu1–N1 distance of 2.167(3) Å (see Fig. 1).

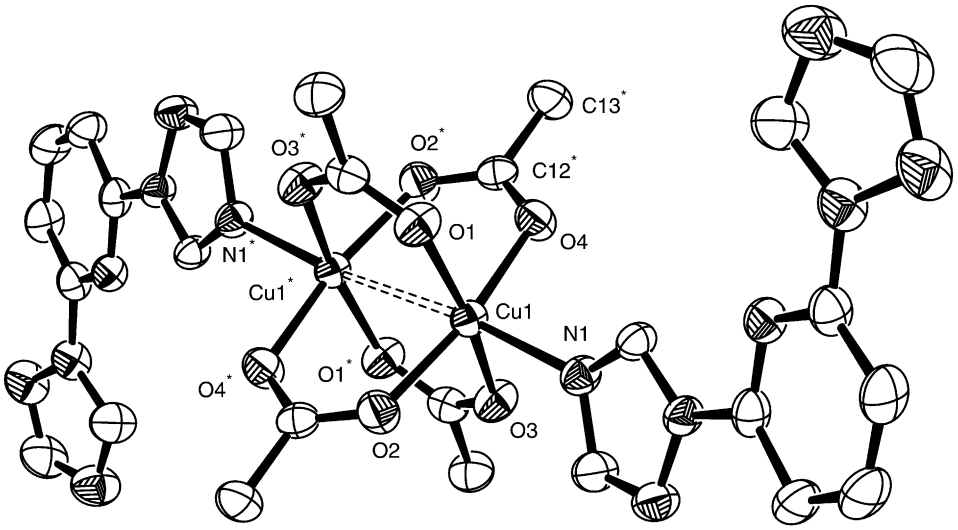

Fig. 1. Ortep drawing of **1** with 50% ellipsoid level. H atoms and MeOH molecules are omitted for clarity. Symmetry code: (*) $-x+1, -y+1, -z+2$.

An inversion center lies on the midpoint of the copper centers (Cu1 and Cu1*). Thus, **1** is centrosymmetric. The distance of Cu1–Cu1* is 2.6452(8) Å and the angle of N1–Cu1–Cu1a is 173.84(7)° and is nearly linear. Selected bond lengths and bond angles of **1** are listed in Table 2.

In the cage **2** there exist four crystallographically independent cages which are classified into two types. Each cage is represented by **2A** and **2B** which are intrinsically induced by anion-templating self-assembly with $[Cu_2(OMe)_2(btp)_2]$ units (see Fig. 2). Counter ions are often

Table 2
Selective bond lengths (Å) and bond angles (°) for **1**

Compound ***1***			
Cu1–Cu1*	2.6452(8)	Cu1–O2	1.975(2)
Cu1–N1	2.167(3)	Cu1–O3	1.962(2)
Cu1–O1	1.960(2)	Cu1–O4	1.979(2)
N1–Cu1–Cu1*	173.84(7)	O3–Cu1–N1	93.15(1)
O1–Cu1–N1	98.84(1)	O4–Cu1–N1	100.27(1)
O2–Cu1–N1	91.88(1)		

Symmetry code: (*) $= -x+1; -y+1; -z+2$.

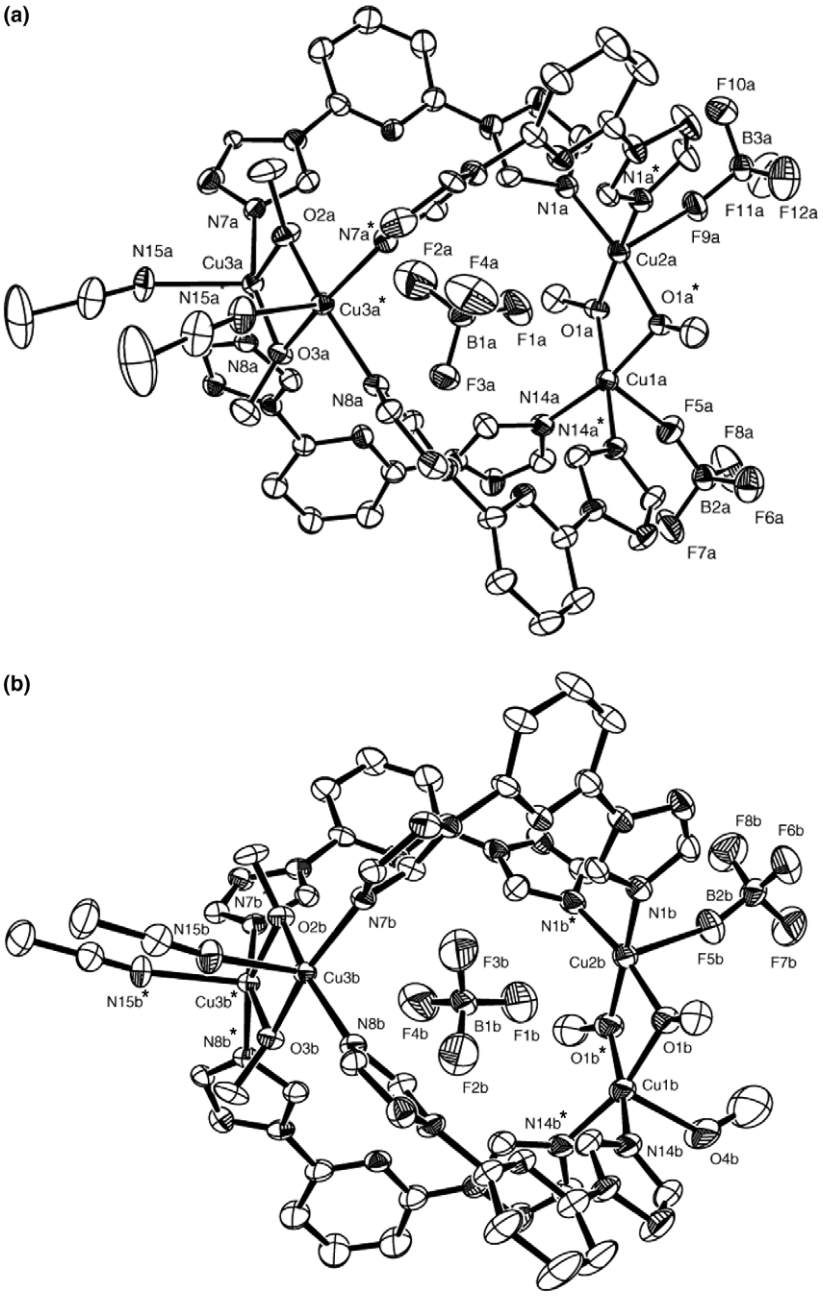

Fig. 2. The 3D cage structure of **2A** (top) and **2B** (bottom) showing that the $[BF_4]^-$ anion is encapsulated in each cavity. Displacement ellipsoids are drawn at the 30% probability level. H atoms and uncoordinated $[BF_4]^-$ anions are omitted for clarity. Symmetry code: (*) $-x+1, -y+1, -z+2$.

able to exert a templating effect in forming 3D cages in which the central void encapsulates the anions [6]. In addition to the orthogonal arrangement of Cu···Cu axes, the bending of Cu_2O planes along the O···O hinge causes btp arms to get close enough to interconnect two $[Cu_2(OMe)_2]^{2+}$ SBUs, which affords tetracupric 3D cages. Each copper center has square pyramidal geometry in common. The equatorial planes comprise two oxygen atoms of methoxide ligands and two nitrogen atoms of btp ligands. Solvent molecules and counter anions occupy the apical sites to complete the environment of the copper centers. Four btp ligands interconnect the dicopper modules through 4-positioned nitrogen atoms of the triazole rings. Since each edge-shared plane is bent down towards the void, the Cu···Cu separation (2.8848(2)–2.9640(2) Å) is much shorter than that of the average value of 3.0(1) Å found in methoxide bridged copper complexes [15]. While methoxide groups bridging the copper centers (Cu1a and Cu2a in **2A**, Cu1b and Cu2b in **2B**) incline in the direction of the cavity, the other methoxide groups pin towards the apical direction of the copper centers (Cu3a and Cu3a* in **2A** and Cu3b and Cu3b* in **2B**). The different behaviors of the methoxide ligands discriminate the copper centers to exert an influence on selective coordination of apical ligands. The apical sites of Cu1a, Cu2a, Cu1b and Cu2b are less hindered than those of Cu3a and Cu3b on account of small dihedral angles of the CuO_2 planes (for **2A**, $\Delta Cu1aO_2$ and $\Delta Cu2aO_2$ (148.7°); for **2B**, $\Delta Cu1bO_2$ and $\Delta Cu2bO_2$ (158.6°)). Thus, two large $[BF_4]^-$ anions prefer the less hindered copper centers of Cu1a and Cu2a in **2A**. In another crystallographically independent cage of **2B** one MeOH molecule and one $[BF_4]^-$ anion locate in the axial sites of Cu1b and Cu2b, respectively. The MeOH molecule binds Cu1b with a Cu–O–C angle of 129.5(1)°, which means that MeOH has an effective volume comparable to the $[BF_4]^-$ anion (Fig. 2, bottom). On the other hand, owing to the crowded environment around Cu3a and Cu3b the only linear MeCN molecules can protrude towards the copper centers to complete the square pyramidal geometry. In **2A** the angle of Cu3a–N–C is 164.9(9)°. In **2B** the Cu3b–N–C angle is 166.7(7)°. Each cage captures one $[BF_4]^-$ anion in its cavity. Similar to the $[BF_4]^-$ anion, the $[ClO_4]^-$ anion can also play a role in forming another 3D cage (**3**) which is structurally similar to **2A**. The apical sites of the Cu centers are occupied with two $[ClO_4]^-$ anions and two MeCN molecules. A $[ClO_4]^-$ anion locates in the cavity of **3** instead of the $[BF_4]^-$ anion. Two $[ClO_4]^-$ anions lie on the less hindered axial sites of Cu1 rather than those of Cu2, owing to the small dihedral angles (149.5°) of the $Cu1O_2$ planes. The selected bond lengths and angles of **2** and **3** are listed in Table 3.

As depicted in Fig. 3, **4** turns to be a sinusoidal 1D infinite coordination polymer, since the large $[OTf]^-$ anion is not able to template a 3D cage structure. The components of **4** are much like **2** and **3** in that btp ligands connect $[Cu_2(OMe)_2]^{2+}$ SBUs with a 1:1 molar ratio of metal to ligand. The $[Cu_2(OMe)_2]^{2+}$ SBUs are doubly bridged by btp ligands in a zigzag pattern. The dihedral angle of CuO_2 planes along the O···O hinge is 179.2°. The Cu···Cu distance of 2.9517(1) Å is comparable with 2.9385(2) Å of the linear 1D coordination polymer of $[Cu(OMe)_2]_n$ [15]. Since the methoxide groups lie coplanar with the Cu_2O_2 plane, the axial sites of the copper centers are bared to better coordinate $[OTf]^-$ than $[BF_4]^-$ and $[ClO_4]^-$ anions [17]. Above and below the Cu_2O_2 plane two $[OTf]^-$ anions are located to bridge copper centers in a μ-mode. The distances of Cu centers and oxygen atoms (O1, O2, O4, and O5) of $[OTf]^-$ anions are much shorter that the sum of the van der Waals radii [18]. All equatorial Cu–X (X = N or O) distances remain in the range 1.90–2.00 Å while axial Cu–O distances fall in the range 2.49–2.67 Å, as expected for Jahn-Teller distorted copper(II) systems. This means the local coordination environment around the copper centers

Table 3
Selective bond lengths (Å) and bond angles (°) for **2** and **3**

Compound ***2***			
Cu1a–O1a	1.912(5)	Cu3a–O2a	1.916(4)
Cu1a–N14a	1.986(6)	Cu3a–O3a	1.934(4)
Cu1a–F5a	2.550(8)	Cu3a–N7a	1.997(5)
Cu1A···Cu2a	2.8848(2)	Cu3a–N8a	2.015(6)
Cu2a–O1a	1.920(5)	Cu3a–N15a	2.268(6)
Cu2a–N1a	1.977(6)	Cu3a···Cu3a*	2.9640(2)
Cu2a–F9a	2.572(8)		
O1a–Cu1a–O1a*	77.4(3)	O2a–Cu3a–N7a	92.9(2)
O1a–Cu1a–N14a	95.7(2)	O2a–Cu3a–N8a	163.1(3)
O1a–Cu1a–N14a*	169.0(2)	O2a–Cu3a–N15a	102.6(3)
N14a–Cu1a–N14a*	89.7(4)	O3a–Cu3a–N7a	162.1(2)
O1a–Cu2a–O1a*	76.9(3)	O3a–Cu3a–N8a	91.9(2)
O1a–Cu2a–N1a	96.3(2)	O3a–Cu3a–N15a	100.2(3)
O1a–Cu2a–N1a*	170.8(2)	N7a–Cu3a–N8a	91.6(2)
N1a–Cu2a–N1a*	89.7(4)	N7a–Cu3a–N15a	97.1(3)
O2a–Cu3a–O3a	79.1(2)	N8a–Cu3a–N15a	93.1(3)
Cu1b–O1b	1.927(7)	Cu3b–O2b	1.938(4)
Cu1b–N14b	1.998(8)	Cu3b–O3b	1.926(4)
Cu1b–O4b	2.251(9)	Cu3b–N7b	2.009(6)
Cu1b···Cu2b	2.9351(2)	Cu3b–N8b	2.017(6)
Cu2b–O1b	1.903(7)	Cu3b–N15b	2.231(6)
Cu2b–N1b	1.994(7)	Cu3b···Cu3b*	2.9629(2)
Cu2b–F5b	2.440(7)		
O1b–Cu1b–O1b*	75.9(4)	N1b–Cu2b–N1b*	90.3(4)
O1b–Cu1b–O4b	98.2(3)	O2b–Cu3b–O3b	79.9(2)
O1b–Cu1b–N14b	95.5(3)	O2b–Cu3b–N7b	92.4(2)
O1b–Cu1b–N14b*	165.4(3)	O2b–Cu3b–N8b	161.2(3)
N14b–Cu1b–N14b*	90.2(4)	O3b–Cu3b–N7b	162.8(2)
O1b–Cu2b–O1b*	77.0(4)	O3b–Cu3b–N8b	91.8(2)
O1b–Cu2b–N1b	95.8(3)	N7b–Cu3b–N8b	90.9(2)
O1b–Cu2b–N1b*	170.0(3)		
Compound ***3***			
Cu1–O1	1.895(9)	Cu2–N7	2.010(7)
Cu1–N1	1.982(1)	Cu2–N8	2.258(1)
Cu1···Cu1a	2.938(4)	Cu2···Cu2a	2.966(3)
Cu2–O2	1.930(6)		
O1–Cu1–O1a	73.1(7)	O2–Cu2–O2a	79.6(4)
O1–Cu1–N1	97.3(5)	O2–Cu2–N7	91.3(3)
O1–Cu1–N1b	167.5(4)	O2–Cu2–N7c	161.2(3)
N1–Cu1–N1b	91.0(6)	N7–Cu2–N7c	92.6(4)

Symmetry code: (*) = $-x+1$; $-y+1$; $-z+2$.
Symmetry code: (a) $-x$, y, $-z+1/2$; (b) x, y, $-z+1/2$; (c) $-x$, y, z.

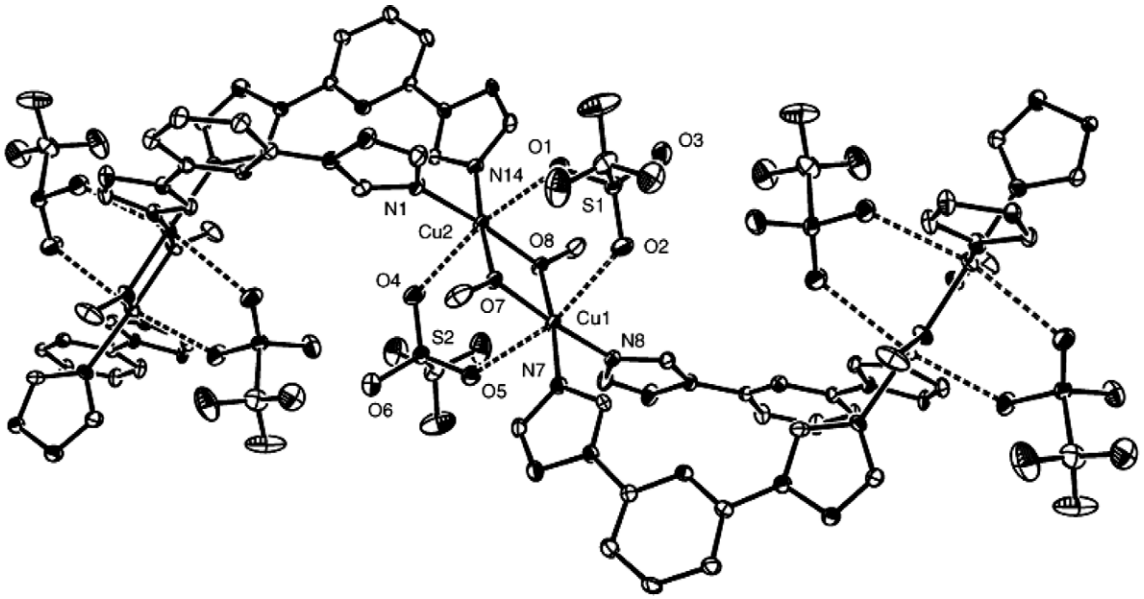

Fig. 3. 1D coordination polymer of **4** showing that planar $[Cu_2(OMe)_2]^{2+}$ SBUs are doubly bridged by btp ligands and triflate anions. Displacement ellipsoids are drawn at the 30% probability level. H atoms and H_2O molecules are omitted for clarity.

Table 4
Selective bond lengths (Å) and bond angles (°) for **4**

*Compound **4***			
Cu1–O7	1.908(4)	Cu1···Cu2	2.9517(1)
Cu1–O8	1.921(4)	Cu2–O7	1.923(4)
Cu1–N7	2.005(5)	Cu2–O8	1.913(4)
Cu1–N8	1.993(5)	Cu2–N14	2.008(5)
Cu1···O2	2.668(5)	Cu2···O1	2.488(5)
Cu1···O5	2.544(5)	Cu2···O4	2.624(5)
O7–Cu1–O8	79.33(2)	O7–Cu2–N1	93.62(2)
O7–Cu1–N7	96.54(2)	O7–Cu2–N14	174.66(2)
O7–Cu1–N8	171.82(2)	O8–Cu2–O7	79.17(2)
O8–Cu1–N7	174.21(2)	O8–Cu2–N1	172.6(2)
O8–Cu1–N8	92.51(2)	O8–Cu2–N14	96.65(2)
N7–Cu1–N8	91.6(2)	N1–Cu2–N14	90.6(2)

adopts an axially elongated octahedral geometry. Selected bond lengths and bond angles of **4** are listed in Table 4.

Acknowledgments

The authors acknowledge the financial support of the Korea Science and Engineering Foundation (Grant No. RO1-2001-00053) and Dr. A.J. Lough (University of Toronto) for X-ray structure analysis of **2** and **3**.

Appendix A. Supplementary data

CCDC-225480 (for **1**), CCDC-225481 (for **2**), CCDC-225482 (for **3**) and CCDC-225483 (for **4**) contains the supplementary crystallographic data for this paper. These data can be obtained free of charge from the Director, CCDC, 12 Union Road, Cambridge, CB2 1EZ, UK (fax: +44 1223 336 033; e-mail: deposit@ccdc.cam.ac.uk or www.ccdc.cam.ac.uk/conts/retrieving.html). Supplementary data associated with this article can be found, in the online version, at doi:10.1016/j.poly.2006.01.030.

References

[1] (a) J.-M. Lehn, Supramolecular Chemistry, VCH, Weinheim, 1996;
(b) J.W. Steed, J.L. Atwood, Supramolecular Chemistry, Wiley, Chichester, 2000.
[2] F. Hof, J. Rebek Jr., Proc. Natl. Acad. Sci. USA 99 (2002) 4775.
[3] (a) S. Leinger, B. Olenyuk, P.J. Stang, Chem. Rev. 100 (2000) 853;
(b) L.R. MacGillivray, J.L. Atwood, Angew. Chem. Int. Ed. 38 (1999) 1018;
(c) S. Mann, G. Huttner, L. Zsolnai, K. Heinze, Angew. Chem., Int. Ed. Engl. 35 (1996) 2808;
(d) F. Fochi, P. Jacopozzi, E. Wegelius, K. Rissanen, P. Cozzini, E. Marastoni, E. Fisicaro, P. Manini, R. Fokkens, E. Dalcanale, J. Am. Chem. Soc. 123 (2001) 7539;
(e) S.-S. Sun, A.J. Lees, Chem. Commun. (2001) 103.
[4] (a) L.J. Barbour, G. William, J.L. Atwood, Nature 393 (1998) 671;
(b) W.Y. Sun, T. Kusukawa, M. Fujita, J. Am. Chem. Soc. 124 (2002) 11570;
(c) M. Fujita, K. Umemoto, M. Yoshizawa, N. Fujita, T. Kusukawa, K. Biradha, Chem. Commun. (2001) 509, and reference therein;
(d) J. Rebek Jr., Acc. Chem. Res. 32 (1999) 278.
[5] (a) D. Fiedler, D.H. Leung, R.G. Bergman, K.N. Raymond, Acc. Chem. Res. 38 (2005) 351;
(b) L.O. Abouderbala, W.J. Belcher, M.G. Boutelle, P.J. Cragg, J.W. Steed, D.R. Turner, K.J. Wallace, Proc. Natl. Acad. Sci. USA 99 (2002) 5001;
(c) V. Balzani, A. Credi, F.M. Raymo, J.F. Stoddart, Angew. Chem. Int. Ed. 39 (2000) 3348.
[6] (a) R. Vilar, Angew. Chem. Int. Ed. 42 (2003) 1460;
(b) P.A. Gale, Coord. Chem. Rev. 213 (2001) 79;
(c) P.A. Gale, Coord. Chem. Rev. 199 (2000) 181;
(d) P.D. Beer, P.A. Gale, Angew. Chem. Int. Ed. 40 (2001) 487;
(e) D. Rais, D.M.P. Mingos, R. Vilar, A.J.P. White, D.J. Williams, J. Organomet. Chem. 652 (2002) 87.

[7] (a) B. Hasenknopf, J.-M. Lehn, G. Baum, B. Kneisel, D. Fenske, Angew. Chem., Int. Ed. Engl. 35 (1996) 1838;
(b) B. Hasenknopf, J.-M. Lehn, N. Boumediene, A. Dupont-Gervais, A.V. Dorsselaer, B. Kneisel, D. Fenske, J. Am. Chem. Soc. 119 (1997) 10956;
(c) R.L. Paul, Z.R. Bell, J.C. Jeffery, J.A. McCleverty, M.D. Ward, Proc. Natl. Acad. Sci. USA 99 (2002) 4883;
(d) D.A. McMorran, P.J. Steel, Angew. Chem. Int. Ed. 37 (1998) 3295;
(e) C.-Y. Su, Y.-P. Cai, C.-L. Chen, H.-X. Zhang, B.-S. Kang, J. Chem. Soc., Dalton Trans. (2001) 359;
(f) P.J. Steel, C.J. Sumby, Chem. Commun. (2002) 322.
[8] (a) M. Eddaoudi, D.B. Moler, H.L. Li, B. Chen, T. Reineke, M. O'Keeffe, O.M. Yaghi, Acc. Chem. Res. 34 (2001) 319;
(b) M. O'Keeffe, M. Eddaoudi, H.L. Li, T. Reineke, O.M. Yaghi, J. Solid State Chem. 152 (2000) 3.
[9] Y. Kim, S.-J. Kim, A.J. Lough, Polyhedron 20 (2001) 3073.
[10] SMART Area-Detector Software Package, Bruker AXS, Inc., Madison, WI, 1995.
[11] G.M. Sheldrick, SHELX-97: A Program for Structure Determination, University of Göttingen, Göttingen, Germany, 1997.
[12] Nonius Kappa-CCD Server Software, Nonius B.V. Delft, The Netherlands, 1997.
[13] G.M. Sheldrick, SHELXTL/PC Version 6.12 for Windows NT, Bruker AXS, Inc., Madison, WI, USA, 2001.
[14] J.Y. Ryu, J.Y. Lee, J.S. Seo, C. Kim, Y. Kim, Appl. Organometal. Chem. 17 (2003) 805.
[15] K.J. Nelson, I.A. Guzei, G.S. Lund, R.W. McGraff, Polyhedron 21 (2002) 2017.
[16] S.-G. Yoo, J.Y. Ryu, J.Y. Lee, C. Kim, S.-J. Kim, Y. Kim, J. Chem. Soc., Dalton Trans. (2003) 1454.
[17] G.A. Lawrance, Chem. Rev. 86 (1986) 17.
[18] A. Bondi, J. Phys. Chem. 68 (1964) 441.

and $[Zn(bpp)(SO_4)\cdot CH_3OH]_n$, form the subject of this report.

2. Experimental

2.1. General procedures

The IR spectra were recorded on a Jasco FT/IR-460 plus spectrometer. Elemental analyses were obtained from a PE 2400 series II CHNS/O analyzer, Perkin–Elmer CHN-2400 analyzer and Heraeus VaruoEL analyzer. Thermogravimetric analyses (TGA) were obtained on a DuPon TGA 2050. Differential scanning calorimetry (DSC) measurements were carried on a Dupon DSC Q-10.

2.2. Starting materials

The reagents $Zn(O_2CCH_3)_2\cdot 6H_2O$, $ZnSiF_6\cdot 6H_2O$, $ZnSO_4\cdot 6H_2O$, and bpp (bpp = 1,3-bis(4-pyridyl)propane) were purchased from Aldrich Chemical Co. and used as received.

2.3. Preparation of $[Zn_7(O_2CCH_3)_{10}(\mu_4\text{-}O)_2(bpp)\cdot 4H_2O]_n$ (1)

Bpp (0.20 g, 1.0 mmol) in 10 mL CH_3OH was layered onto a solution of $Zn(O_2CCH_3)_2\cdot 6H_2O$ (1.3 g, 7.0 mmol) in 5 mL H_2O. The resultant solution was allowed to slowly diffuse for several weeks to give colorless crystals. The crystals were collected, washed by methanol and dried in vacuum. Yield: 0.91 g (68%). *Anal.* Calc. for $C_{33}H_{52}N_2O_{26}Zn_7$: C, 29.35; H, 3.88; N, 2.07. Found: C, 29.43; H, 3.70; N, 1.92%. IR (KBr disk): 3418(br), 2951(s), 1618(m), 1586(m), 1433(m), 1393(m), 1336(m), 1223(s), 1071(m), 1030(m), 932(m), 856(m), 821(m), 809(s), 675(m), 619(m), 517(m).

2.4. Preparation of $[Zn(SiF_6)(bpp)_2\cdot 4H_2O\cdot 2CH_3OH]_n$ (2)

Prepared as described as for **1**. Yield: 0.66 g (78%). *Anal.* Calc. for $C_{28}H_{44}F_6N_4O_6SiZn$: C, 45.44; H, 5.99; N, 7.57. Found: C, 45.41; H, 5.88; N, 7.72%. IR (KBr disk): 3418(br), 3037(m), 2859(m), 2493(m), 1949(m), 1621(m), 1558(m), 1505(m), 1456(m), 1416(m), 1357(m), 1221(m), 1071(m), 1031(m), 991(m), 857(m), 619(s), 603(m), 575(s), 506(s).

2.5. Preparation of $[Zn(bpp)(SO_4)\cdot CH_3OH]_n$ (3)

Prepared as described as for **1**. Yield: 0.32 g (83%). *Anal.* Calc. for $C_{14}H_{18}N_2O_5SZn$, C, 42.92; H, 4.63; N, 7.15%. Found: C,42.84; H, 4.42; N, 7.06%. FT-IR (cm^{-1}) (KBr disk): 3386(br), 3050(m), 2950(m), 1978(m), 1619(m), 1558(m), 1508(m), 1434(m), 1226(m), 1118(m), 1006(m), 948(m), 860(m), 802(m), 651(s), 620(m), 520(s), 489(s).

3. X-ray crystallography

The diffraction data of **1**–**3** were collected on a Siemens CCD diffractometer which was equipped with graphite-monochromated Mo Kα ($\lambda_\alpha = 0.71073$ Å) radiation [12]. Data reduction was carried by standard methods with the use of well-established computational procedures [13].

A crystal of **1** suitable for X-ray crystallography was mounted on the top of a glass fiber with epoxy cement. The hemisphere data collection method was used to scan the data points at $4.62 \leqslant 2\theta \leqslant 50.00°$. The structure factors were obtained after Lorentz and polarization corrections. The positions of the heavier atoms, including the Zn atom, were located by the direct method. The remaining atoms were found in a series of alternating difference Fourier maps and least-square refinements. The final residuals of the refinement were $R_1 = 0.0541$ and $wR_2 = 0.1512$ for **1**. The X-ray crystallographic procedures for **2** and **3** were similar to those for **1**. Basic information pertaining to crystal parameters and structure refinement is summarized in Table 1.

4. Results and discussion

4.1. Syntheses and spectroscopic studies

The complexes, $[Zn_7(O_2CCH_3)_{10}(\mu_4\text{-}O)_2(bpp)\cdot 4H_2O]_n$ (**1**), $[Zn(SiF_6)(bpp)_2\cdot 4H_2O\cdot 2CH_3OH]_n$ (**2**), and $[Zn(bpp)(SO_4)\cdot CH_3OH]_n$ (**3**), were prepared by layering solutions of bpp (bpp = 1, 3-bis(4-pyridyl)propane) in CH_3OH with solutions of $Zn(O_2CCH_3)_2\cdot 6H_2O$, $ZnSiF_6\cdot 6H_2O$ and $ZnSO_4\cdot 6H_2O$, respectively, in H_2O. The IR spectra of complexes **1**–**3** show characteristic C–N and C–C vibrational frequencies for the bpp ligands.

4.2. Structure of $[Zn_7(O_2CCH_3)_{10}(\mu_4\text{-}O)_2(bpp)\cdot 4H_2O]_n$ (1)

The structure of complex **1** was solved in the space group *Pccn*. Selected bond distances and angles are listed in Table 2. Fig. 1(a) shows a perspective view of the heptanuclear building block. Complex **1** forms 1-D chains which consists of bent bpp ligands bridging two $\{Zn_7(O_2CCH_3)_{10}(\mu_4\text{-}O_2)\}$ clusters (Zn(2)–N = 2.040(7) Å). The overall Zn_7 framework involves two $\{Zn_4O\}$ tetrahedrons joined at Zn(1), Fig. 1(b). The Zn(1) atom occupies an inversion center and adopts a slightly distorted octahedral coordination geometry with the O–Zn–O bond angles only deviating slightly from 90° or 180°. The heptanuclear cluster of **1** closely resembles the related polymeric structures of $[Zn_7(O_2CCH_3)_{10}(\mu_4\text{-}O)_2(bpe)]$ (bpe = 1,2-bis (4-pyridyl)ethane) [14a], $[Zn_7(O_2CCH_3)_{10}(\mu_4\text{-}O)_2(dpds)]$ (dpds = 4,4′-dipyridyldisulfide) [14a] and the discrete cluster $[Zn_7(O_2CCH_3)_{10}(\mu_4\text{-}O)_2(Pz)_2]$ (Pz = pyrazine) [14b]. In all these complexes, the coordination geometry of the Zn atoms coordinated by the nitrogen atoms of the ligands may be described as a [4+2] geometry with two long Zn–O bonds, and in the absence of these two weak Zn–O

Table 1
Crystal data for compounds **1**–**3**

Compound	**1**	**2**	**3**
Formula	$C_{33}H_{52}N_2O_{26}Zn_7$	$C_{28}H_{44}F_6N_4O_6SiZn$	$C_{14}H_{18}N_2O_5SZn$
Formula weight	1350.36	740.13	391.73
Crystal system	orthorhombic	orthorhombic	orthorhombic
Space group	*Pccn*	*Imm2*	*Pbca*
a (Å)	22.247(2)	7.7795(8)	9.5232(16)
b (Å)	11.9196(12)	12.4312(13)	15.846(3)
c (Å)	20.1679(19)	18.1072(19)	22.369(4)
V (Å^3)	5348.1(9)	1751.1(3)	3375.5(10)
Z	4	2	8
d_{calc} (g/cm^3)	1.677	1.404	1.542
$F(000)$	2728	772	1616
μ(Mo Kα) (mm^{-1})	3.165	0.811	1.604
Range (2θ) for data collection (°)	$3.88 \leqslant 2\theta \leqslant 55.08$	$3.98 \leqslant 2\theta \leqslant 55.02$	$5.14 \leqslant 2\theta \leqslant 56.08$
Temperature (°C)	25	25	25
Limiting indices	$-28 \leqslant h \leqslant 28$, $-3 \leqslant k \leqslant 15$, $-21 \leqslant l \leqslant 23$	$-10 \leqslant h \leqslant 8$, $-16 \leqslant k \leqslant 14$, $-23 \leqslant l \leqslant 23$	$-12 \leqslant h \leqslant 12$, $-21 \leqslant k \leqslant 15$, $-8 \leqslant l \leqslant 29$
Reflections collected	18 516	5527	12 937
Independent reflections [R_{int}]	5062 [0.0307]	2227 [0.0390]	4109 [0.0417]
Data/restraints/parameters	5062/0/306	2227/1/124	4109/0/264
Quality-of-fit indicator[c]	1.003	1.044	1.094
Final R indices [$I > 2\sigma(I)$][a,b]	$R_1 = 0.0541$, $wR_2 = 0.1336$	$R_1 = 0.0554$, $wR_2 = 0.1549$	$R_1 = 0.0507$, $wR_2 = 0.1169$
R indices (all data)	$R_1 = 0.1512$, $wR_2 = 0.1467$	$R_1 = 0.0722$, $wR_2 = 0.1732$	$R_1 = 0.0779$, $wR_2 = 0.1272$
Largest difference in peak and hole (e Å^{-3})	0.854 and −0.935	1.223 and −0.705	1.082 and −0.308

[a] $R_1 = \sum||F_o| - |F_c||/\sum|F_o|$.
[b] $wR_2 = [\sum w(F_o^2 - F_c^2)^2/\sum w(F_o^2)^2]^{1/2}$. $w = 1/[\sigma^2(F_o^2) + (ap)^2 + (bp)]$, $p = [\max(F_o^2 \text{ or } 0) + 2(F_c^2)]/3$. $a = 0.362$, $b = 0.0000$ for **1**; $a = 0.1057$, $b = 2.5556$ for **2**; $a = 0.0226$, $b = 8.8780$ for **3**.
[c] Quality-of-fit $= [\sum w(|F_o^2| - |F_c^2|)^2/[N_{observed} - N_{parameters}]]^{1/2}$.

Table 2
Selected bond distances (Å) and angles (°) for **1**

Distances			
Zn(1)–O(10)	2.150(6)	Zn(1)–O(11)	1.963(5)
Zn(1)–O(8)	2.191(5)	Zn(2)–O(2)	2.007(6)
Zn(2)–O(11)	1.954(6)	Zn(2)–O(4)	2.050(7)
Zn(2)–N	2.040(7)	Zn(3)–O(11)	1.906(6)
Zn(2)–O(8A)	2.488(6)	Zn(3)–O(9)	1.932(7)
Zn(3)–O(1)	1.932(7)	Zn(4)–O(3)	1.925(7)
Zn(3)–O(6)	1.964(8)	Zn(4)–O(5)	1.961(8)
Zn(4)–O(11)	1.927(5)	Zn(4)–O(7)	1.961(6)
Angles			
O(11A)–zn(1)–O(11)	180.0(4)	O(11A) −zn(1)–O(10)	82.4 (2)
O(11)–Zn(1)–O(10)	97.6(2)	O(10)–Zn(1)–O(10A)	180.0(3)
O(8)–Zn(1)–O(8A)	180.0(3)	O(11)–Zn(1)–O(8)	97.8(2)
O(11A)–Zn(1)–O(8)	82.2(2)	O(10A)–Zn(1)–O(8)	96.0(2)
O(10)–Zn(1)–O(8)	84.0(2)	O(11)–Zn(2)–O(2)	104.2(3)
O(11)–Zn(2)–N	155.7(3)	O(2)–Zn(2)–N	93.3(3)
O(11)–Zn(2)–O(4)	103.2(2)	O(2)–Zn(2)–O(4)	95.4(3)
N–Zn(2)–O(4)	91.5(3)	O(11)–Zn(2)–O(8A)	74.9(2)
O(2)–Zn(2)–O(8A)	96.6(2)	N–Zn(2)–O(8A)	86.6(3)
O(4)–Zn(2)–O(8A)	168.0(2)	O(11)–Zn(3)–O(9)	118.7(3)
O(11)–Zn(3)–O(1)	112.2(3)	O(11)–Zn(3)–O(6)	109.4(3)
O(1)–Zn(3)–O(9)	104.9(3)	O(9)–Zn(3)–O(6)	101.7(4)
O(1)–Zn(3)–O(6)	109.3(3)	O(3)–Zn(4)–O(5)	106.3(3)
O(3)–Zn(4)–O(11)	113.2(3)	O(3)–Zn(4)–O(7)	104.3(3)
O(11)–Zn(4)–O(5)	109.6(3)	O(5)–Zn(4)–O(7)	101.8(3)
O(11)–Zn(4)–O(7)	120.3(3)		

Symmetry transformations used to generate equivalent atoms: A: $-x + 1$, $-y + 1$, $-z$.

interactions, the coordination geometry at these Zn atoms can be described as a highly distorted tetrahedral geometry [14a]. It is noted that the distances of the two longer bonds in $[Zn_7(O_2CCH_3)_{10}(\mu_4\text{-}O)_2(bpe)]$ are 2.341(4) and 2.539(4) Å, and those in $[Zn_7(O_2CCH_3)_{10}(\mu_4\text{-}O)_2(dpds)]$ are from 2.420(11) to 2.584 Å [14a], which are significantly different from the two long Zn–O distances, Zn(2)–O(8A) = 2.488(7) and Zn(2)–O(10A) = 2.512(6) Å, in **1**, most probably due to the different nature of the spacer ligands. These distances are also significantly different from those in the discrete cluster $[Zn_7(O_2CCH_3)_{10}(\mu_4\text{-}O)_2(Pz)_2]$, which are 2.508 and 2.735 Å [14b]. These distances are all far less than the sum of the van der Waals radii of the Zn and O atoms, which is 2.9 Å. Both Zn(3) and Zn(4) atoms are bonded to four oxygen atoms to form the distorted-tetrahedral coordination geometry.

The heptanuclear building blocks are linked by the bpp ligands to form a zig-zag polymeric structure, Fig. 1(c). For comparison, it is noted that by changing the backbone of the dipyridyl ligand from –CH_2–CH_2– [14] to –CH_2–CH_2–CH_2–, the structure of the 1-D polymeric complex varies from quasi-linear to zig-zag chain, which is similar to that of the complex $[Zn_7(O_2CCH_3)_{10}(\mu_4\text{-}O)_2(dpds)]$ (dpds = 4,4′-dipyridyldisulfide) containing the dpds ligand with the –S–S– backbone [14a]. While the ligand identity plays an important role in determining the structural type, no significant difference in the Zn–N bond distances is found for these complexes.

4.3. Structure of $[Zn(SiF_6)(bpp)_2 \cdot 4H_2O \cdot 2CH_3OH]_n$ (**2**)

Colorless crystals of complex **2** conform to the space group *Imm2*. Selected bond distances and angles are listed

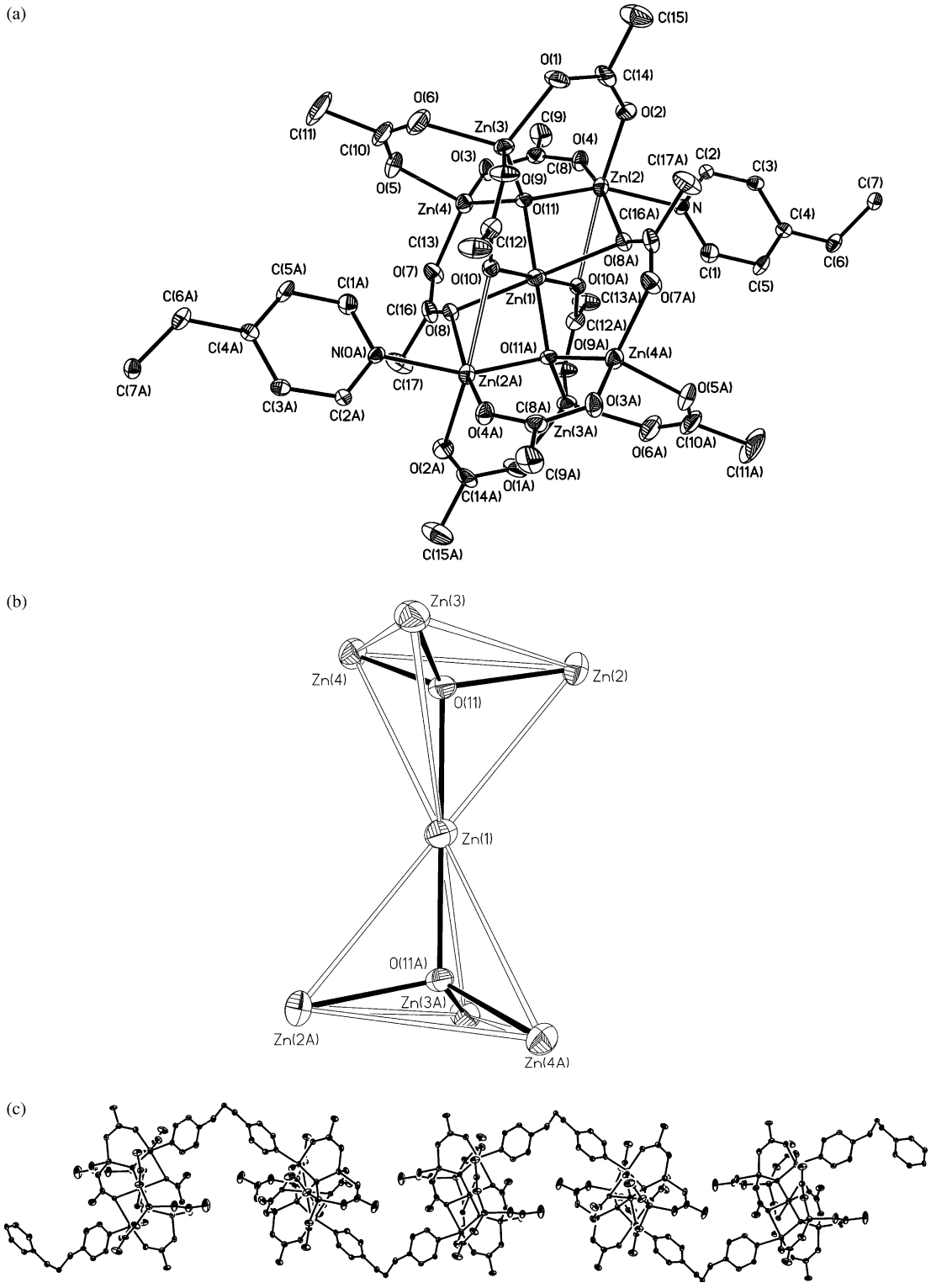

Fig. 1. (a) ORTEP drawing of the local coordination of Zn in **1**. Ellipsoids are scaled to enclose 20% of the electron density. (b) ORTEP drawing shows the tetrahedron of $\{Zn_4O\}$ in $\{Zn_7(O_2CCH_3)_{10}O_2\}$. (c) The polymeric zig-zag chain of **1**.

in Table 3. Fig. 2 shows an ORTEP diagram about the Zn metal center. It is seen that the Zn atom is bonded to four pyridyl nitrogen atoms (Zn–N = 2.145(2)–2.170(2) Å) in the equatorial plane. The dihedral angle of the two *trans* pyridyl rings that are coordinated to the Zn atom is 0.1°. Each bpp ligand acts as a bidentate ligand and exhibits a typical twisted conformation, with dihedral angles between the planes of two pyridyl rings

Table 3
Selected bond distances (Å) and angles (°) for **2** and **3**

Complex ***2***			
Zn–N(1)	2.145(2)	Zn–N(2)	2.170(2)
Zn–F(2)	2.135(1)		
N(2A)–Zn–N(2)	92.4(4)	F(2)–Zn–N(1)	90.6(1)
N(2)–Zn–N(1)	179.7(3)	N(1A)–Zn–N(1)	91.8(3)
N(2)–Zn–F(2)	89.3(1)	F(2A)–Zn–F(2)	178.2(4)
N(2)–Zn–N(1A)	87.9(1)		
Complex ***3***			
Zn–O(2A)	1.956(3)	Zn–O(1)	1.965(2)
Zn–N(2)	2.015(3)	Zn–N(1B)	2.015(3)
O(2A)–Zn–O(1)	96.9(1)	O(2A)–Zn–N(2)	108.1(1)
O(1)–Zn–N(2)	112.9(1)	O(2A)–Zn–N(1B)	106.8(1)
O(1)–Zn(1)–N(1B)	111.0(1)	N(2)–Zn–N(1B)	118.5(1)

Symmetry transformations used to generate equivalent atoms: A: $-x+1$, $-y+1$, z for **2**; A: $x+1/2$, $-y+3/2$, $-z+1$; B: $-x+1/2$, $-y+1$, $z-1/2$ for **3**.

of 78.5° and 78.7°. The Zn atom is also bonded to two hexafluorosilicate ligands through the fluorine atoms (Zn–F = 2.1352(14) Å, F–Zn–F = 178.2(4)° in the axial position to complete the distorted octahedral coordination geometry. The octahedron contains a crystallographic C_4 axis passing through the two bonded F atoms and the Zn center. Along the *b* axis, adjacent Zn atoms are linked to each other through the pyridyl nitrogen atoms to form double-stranded chains involving 24-membered rings (Fig. 3, top), while along the *a* axis, adjacent Zn atoms are linked to each other through the fluoride atoms from hexafluorosilicate to form linear chains (Fig. 3, middle). A view looking down the *c* axis shows that the molecules of **2** form a 2-D grid involving double-stranded chains linked by the SiF_6^{2-} anions (Fig. 3, bottom). The rectangular cavities, each with an area of 7.780×12.431 Å^2, are occupied by the solvent molecule. The water and methanol molecules are interlinked through OH–F (O–F = 2.828 Å) and OH–O (O–O = 1.910, 2.465 and 2.550 Å) interactions in the cavities. For comparison, it is noted that complex **2** is similar to the 3-D rectangular network $[Cu(SiF_6)(4,4'\text{-bipyridine})_2]_n$ that was based on the square grid of $[Cu(4,4'\text{-bipyridine})_2]_n$ and pillars of SiF_6^{2-} anions [15].

4.4. Structure of $[Zn(bpp)(SO_4)\cdot CH_3OH]_n$ (3)

The structure of complex **3** was solved in the space group *Pbca* and each asymmetric unit of **3** contains one Zn atom, one bpp group, a sulfate molecule and one included methanol. Selected bond distances and angles are listed in Table 3. Fig. 4(a) shows an ORTEP diagram about the Zn metal center. The Zn atom is bonded to two pyridyl rings through the nitrogen atoms (Zn–N = 2.015(3) Å, N–Zn–N = 118.52(11)°, with a dihedral angle of 145.8° between the two pyridyl rings. The Zn atom is also bonded to two oxygen atoms from two sulfate ligands (Zn–O = 1.956(3)–1.965(2) Å, O–Zn–O = 96.93(11)° to complete the distorted tetrahedral geometry.

Along the *b* axis, adjacent Zn atoms are linked to each other through the bpp ligands to form helical chains, Fig. 4(b), which are interlinked by the μ_2-SO_4^{2-} anions to form a 3-D porous structure, where the open channels are occupied by the methanol molecules, Fig. 4(c). The longer Zn–Zn distance, separated by bridging bpp ligands, is 12.184 Å, while the shorter Zn–Zn distance, separated by the SO_4^{2-} anions, is 5.184 Å. Each bpp ligand acts as a bidentate ligand and exhibits a typical twisted conformation, with a dihedral angle of 141.3° between the pyridyl rings. In the helical chain, each pitch contains two zinc metals and two bpp ligands and the Zn–Zn separation distance is 22.396 Å. The methanol molecules are interlinked through CH–O (O–H = 2.318 Å, ∠C–H–O = 173.2°) interactions, while the sulfate groups are also interlinked through CH–O (O–H = 2.492–2.503 Å, ∠C–H–O = 150.9–152.1°) hydrogen bondings.

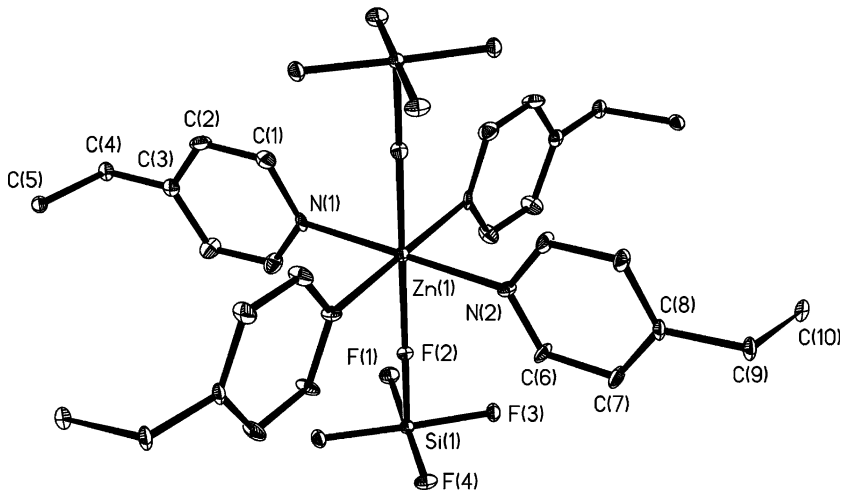

Fig. 2. An ORTEP drawing of the local coordination of Zn(II) in **2**. Ellipsoids are scaled to enclose 20% of the electron density.

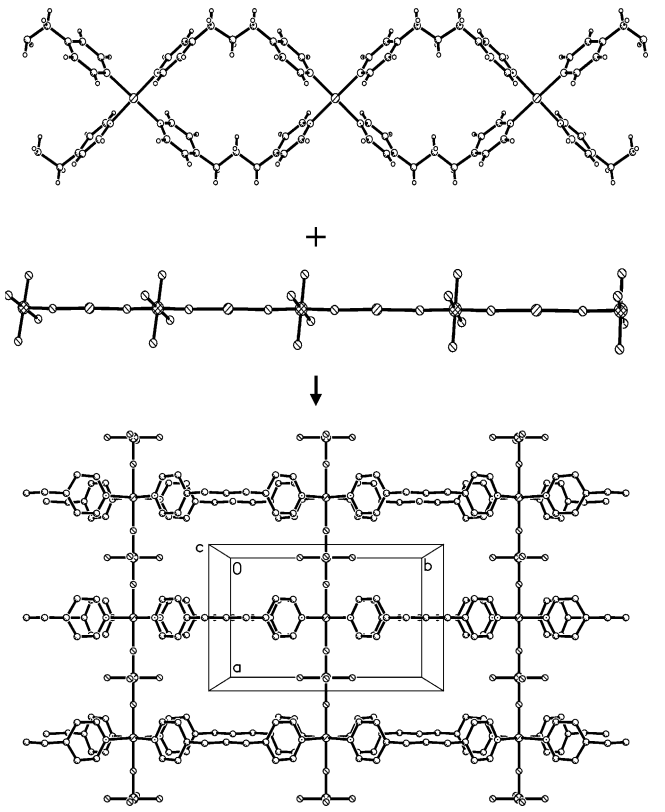

Fig. 3. ORTEP drawings for **2**, showing the double-stranded chain involving bpp ligands, top, linear chain involving anions, middle, and the two dimensional structure, bottom.

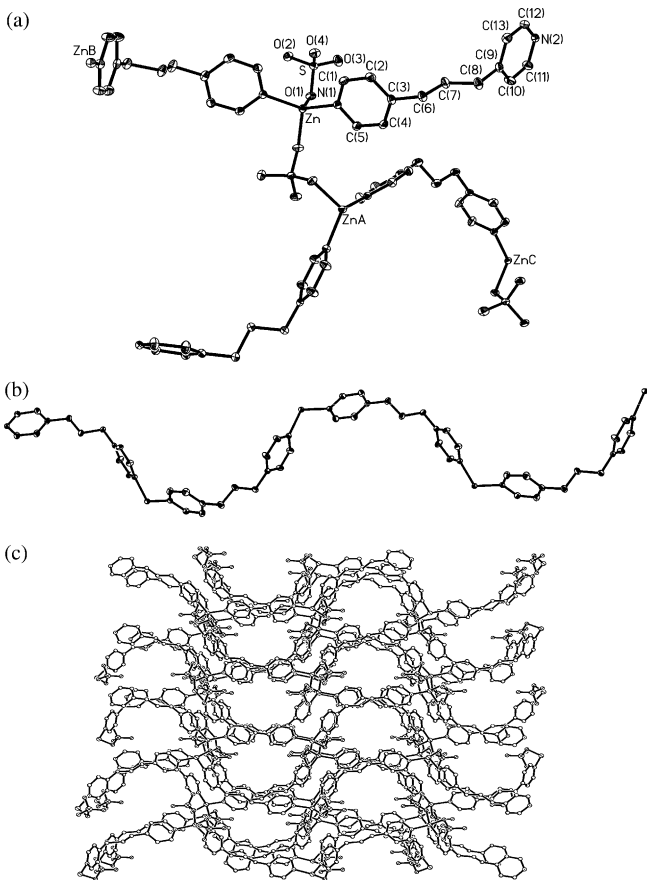

Fig. 4. (a) ORTEP drawing showing the coordination geometry of zinc metal center for **3**. Ellipsoids are scaled to enclose 20% of the electron density. (b) Along the *b* axis, adjacent Zn atoms are linked by bpp to form a helical chain, viewing down the *b* axis. (c) The 3-D porous structure of **3**, viewing down the *c* axis.

4.5. Conformation of the bpp ligand

All the bpp ligands in complexes **2** and **3** adopt the *gauche, gauche*-conformation. While the C–C–C–C dihedral angles of the bpp ligands in **2** are all 180°, those in **3** are 171.2° and 173.9°. Noticeably, the bpp ligand in complex **1** adopts the *anti*, *anti*-conformation with a dihedral angle of 65.0 °.

4.6. Thermogravimetric analyses

Complexes **1**–**3** are very stable in air at ambient temperature and almost insoluble in common solvents such as water, alcohol, acetonitrile, chloroform, methanol and acetone. Thermal gravimetric analyses (TGA) were carried out to examine their thermal stability. The samples of **1**–**3** were heated from 50 to 800 °C in air at 1 atm pressure with a heating rate of 10 °C min^{-1}. The TGA curve shows that **1** is stable up to 56 °C. A total weight loss of 5.1% occurred in the temperature range 56–156 °C, presumably due to the removal of the guest water molecules per formula unit (calculated 5.3%), and a sharp weight loss occurred in the temperature range 210–297 °C, consistent with the removal of bpp ligands and decomposition of the polymeric chain. On further heating, another weight loss between 380 and 430 °C was observed, corresponding to the decomposition of the $\{Zn_7(O_2CCH_3)_{10}(\mu_4\text{-}O)_2\}$ cluster. The results of **2** showed that **2** is stable up to 116 °C with the first weight loss of 15.3% in the range 116–200 °C, corresponding to the loss of the two methanol and four water guest molecules per formula (calculated 15.6%). In the temperature range of 200–443 °C, complex **2** underwent complicated multiple weight loss steps, with the total weight loss corresponding to loss of the two bpp ligands (observed 45.1%, calculated 44.9%). The thermal decomposition behavior of **3** is quite different from that of compound **2**, showing that the first weight loss (8.1%) occurs from 80 to 180 °C which corresponds to the loss of the methanol guest molecules (calculated 8.2%). On further heating, another weight loss between 180 and 320 °C was observed, corresponding to the loss of the bpp ligand (observed 50.9%, calculated 50.7%). Their T_m values have been measured by using differential scanning calorimetry (DSC), and they are 187, 239 and 226 °C for complexes **1**–**3**, respectively. The 2-D and 3-D Zn(II) polymeric complexes show higher T_m values than the 1-D complex.

5. Conclusions

The synthesis and structures of three complexes $[Zn_7(O_2CCH_3)_{10}(\mu_4\text{-}O)_2(bpp)\cdot 4H_2O]_n$ (**1**), $[Zn(SiF_6)$-

$(bpp)_2 \cdot 4H_2O \cdot 2CH_3OH]_n$ (**2**) and $[Zn(bpp)(SO_4) \cdot H_3OH]_n$ (**3**) have been successfully accomplished. In complex **1**, the CH_3COO^- anions coordinate to the Zn(II) metal centers to form heptanuclear clusters which are bridged by the bpp ligands to form 1-D zig-zag chains. In complex **2**, the double-strained chains of octahedral Zn(II) cations containing bpp ligands are bridged by the octahedral SiF_6^{2-} anions through two *trans* F atoms to form 2-D grids, while in complex **3**, the single-strained helical chain of tetrahedral Zn(II) cations containing bpp ligands are bridged by the tetrahedral μ_2-SO_4^{2-} anion to form a 3-D porous structure. The structures of these complexes are in marked contrast to that found in $Zn(NO_3)_2(bpp)$ [9a], where the monodentate NO_3^- anions coordinate to the Zn(II) metal center in a zig-zag chain to complete the tetrahedral coordination geometry. The role of anions in controlling network formation has been noted in several cases [16,17]. The anions thus show significant influence on the supramolecular structures of Zn(II) complexes containing bpp ligands, presumably due to the various types of coordination abilities and geometries of the anions.

Acknowledgements

We thank the Nanya Institute of Technology and the National Science Council of the Republic of China for support.

Appendix A. Supplementary data

Crystallographic data (CIF files) for the structures **1**–**3** have been deposited with the Cambridge Crystallographic Data Centre, CCDC Nos. 245068–245070. Copies of this information may be obtained free of charge from The Director, CCDC, 12 Union Road, Cambridge, CB2 1EZ, UK (fax: +44 1223 336 033; e-mail: deposit@ccdc.cam.ac.uk or www: http://www.ccdc.cam.ac.uk). Supplementary data associated with this article can be found, in the online version, at doi:10.1016/j.poly.2006.01.031.

References

[1] (a) O.M. Yaghi, H. Li, J. Am. Chem. Soc. 117 (1995) 10401;
(b) O.M. Yaghi, H. Li, T.L. Groy, J. Am. Chem. Soc. 118 (1996) 9096;
(c) P.J. Hagrman, D. Hagrman, J. Zubieta, Angew. Chem. Int. Ed. 38 (1999) 2638;
(d) A. Mayr, L.F. Mao, Inorg. Chem. 37 (1998) 5776;
(e) C. Janiak, Dalton Trans. (2003) 2781;
(f) S.L. James, Chem. Soc. Rev. 32 (2003) 276.

[2] (a) L.F. Mao, A. Mayr, Inorg. Chem. 35 (1996) 3183;
(b) H.J. Choi, M.P. Suh, J. Am. Chem. Soc. 120 (1998) 10622;
(c) A.J. Blake, N.R. Champness, P. Hubberstey, W.-S. Li, M.A. Withersby, M. Schrokder, Coord. Chem. Rev. 183 (1999) 117;
(d) S. Batten, R. Robson, Angew. Chem. Int. Ed. 37 (1998) 1460;
(e) S. Kitagawa, R. Kitaura, S.-I. Noro, Angew. Chem. Int. Ed. 116 (2004) 2388.

[3] (a) O.M. Yaghi, G. Li, H. Li, Nature 378 (1995) 703;
(b) P. Losier, M.J. Zaworotko, Angew. Chem., Int. Ed. Engl. 35 (1996) 2779;
(c) K.N. Power, T.L. Hennigar, M.J. Zaworotko, Chem. Commun. (1998) 595;
(d) M. Fujita, H. Oka, K. Yamaguchi, K. Ogura, Nature 378 (1995) 469;
(e) S.-L. Zheng, X.-M. Chen, Aust. J. Chem. 57 (2004) 703.

[4] (a) M. Fujita, Y.J. Kwon, O. Sasaki, K. Yamaguchi, K. Ogura, J. Am. Chem. Soc. 117 (1995) 7287;
(b) R.A. Heintz, H. Zhao, X. Ouyang, G. Grandinetti, J. Cowen, K.R. Dunbar, Inorg. Chem. 38 (1999) 144;
(c) A. Mayr, J. Guo, Inorg. Chem. 38 (1999) 921;
(d) C.V.K. Sharma, G.A. Broker, J.G. Huddleston, J.W. Baldwin, R.M. Metzger, R.D. Rogers, J. Am. Chem. Soc. 121 (1999) 1137;
(e) D. Maspoch, D. Ruiz-Molina, J. Veciana, J. Mater. Chem. 14 (2004) 2713.

[5] (a) M. Fujita, Y.J. Kwon, S. Washizu, K. Ogura, J. Am. Chem. Soc. 116 (1994) 1151;
(b) W. Lin, O.R. Evans, R.-G. Xiong, Z. Wang, J. Am. Chem. Soc. 120 (1998) 13272;
(c) G.B. Garder, D. Venkataraman, J.S. Moore, S. Lee, Nature 374 (1995) 792;
(d) S.R. Batten, K.S. Murray, Coord. Chem. Rev. 246 (2003) 103.

[6] (a) K. Inoue, T. Hayamizu, H. Iwamura, D. Hashizume, Y. Ohashi, J. Am. Chem. Soc. 118 (1996) 1803;
(b) H. Tamaki, Z.J. Zhong, N. Matsumoto, S. Kida, M. Koikawa, N. Achiwa, Y. Hashimoto, H. Okawa, J. Am. Chem. Soc. 114 (1992) 6974;
(c) G.B. Garder, Y.-H. Kiang, S. Lee, A. Asgaonkar, D. Venkataraman, J. Am. Chem. Soc. 118 (1996) 6946;
(d) O. Kahn, Y. Pei, M. Verdguer, J.P. Renard, J. Sletten, J. Am. Chem. Soc. 110 (1998) 782.

[7] (a) M. Eddaoudi, S.R. Batten, R. Robson, Angew. Chem., Int. Ed. 37 (1998) 1460;
(b) D.B. Moler, H. Li, B. Chen, T.M. Reineke, M. O'Keeffe, O.M. Yaghi, Acc. Chem. Res. 34 (2001) 319;
(c) B. Moulton, M.J. Zaworotko, J. Chem. Res. 101 (2001) 1629;
(d) K. Kim, Chem. Soc. Rev. 31 (2002) 96;
(e) O.R. Evans, W. Lin, Acc. Chem. Res. 35 (2002) 511.

[8] (a) M.-L. Tong, Y.-M. Wu, J. Ru, X.-M. Chen, H.-C. Chang, S. Kitagawa, Inorg. Chem. 41 (2002) 4846;
(b) E.-Q. Gao, Z.-M. Wang, C.-S. Liao, C.-H. Yan, New J. Chem. 26 (2002) 1096;
(c) M.J. Plater, M.R.St.J. Foremen, T. Gelbrich, S.J. Coles, M.B. Hurathouse, J. Chem. Soc., Dalton Trans. (2000) 3065;
(d) T. Soma, T. Iwamoto, Acta Crystallogr., Sect. c 53 (1997) 1819;
(e) L. Carlucci, G. Ciani, M. Moret, D.M. Proserpio, S. Rizzato, Angew. Chem. Int. Ed. 39 (2000) 1506;
(f) R.L.L. Duca Jr., R. Ratkoski, R.S. Ragig Jr., J. Zubieta, Inorg. Chem. Commun. 4 (2001) 621.

[9] (a) M.-C. Suen, Y.-T. Wu, G.-C. Dong, J.-D. Chen, T.-C. Keng, J.-C. Wang, J. Chin. Chem. Soc. 49 (2002) 331;
(b) Y.-B. Dong, M.D. Smith, R.C. Layland, H.-C. zur Loye, Inorg. Chem. 38 (1999) 5027;
(c) M.J. Plater, M.R.St.J. Foreman, A.M.Z. Slawin, Inorg. Chim. Acta 303 (2000) 132;
(d) W.J. Belcher, C.A. Longstaff, M.R. Neckening, J.W. Steed, Chem. Commun. (2002) 1602;
(e) L. Carlucci, G. Ciani, D.W.V. Gudenberg, D.M. Proserpio, Inorg. Chem. 36 (1997) 3812;
(f) L. Pan, E.B. Woodlock, X. Wang, K.-C. Lam, A.L. Rheingold, Chem. Commun. (2001) 1762;
(g) S.R. Batten, J.C. Jeffery, M.D. Ward, Inorg. Chim. Acta 292 (1999) 231.

[10] (a) M.J. Plater, M.R.St. J. Foreman, T. Gelbrich, M.B. Hursthouse, Inorg. Chim. Acta 318 (2001) 171;
(b) T. Bujaci, X. Wang, S. Li, C. Zheng, Inorg. Chim. Acta 333 (2002) 152;

(c) F.M. Tabellion, S.R. Seidel, A.M. Arif, P.J. Stang, Angew. Chem. Int. Ed. 40 (2001) 1529;
(d) X.-Y. Yu, M. Maekawa, T. Morita, H.-C. Chang, S. Kitagawa, G.-X. Jin, Bull. Chem. Soc. Jpn. 75 (2002) 267.

[11] (a) F.M. Tabellion, S.R. Seidel, A.M. Arif, P.J. Stang, J. Am. Chem. Soc. 123 (2001) 11982;
(b) C.V.K. Sharma, R.J. Diaz, A.J. Hessheimer, A. Clearfield, Cryst. Eng. 3 (2000) 201;
(c) M.J. Plater, M.R.St. J. Foreman, J.M.S. Skakle, Cryst. Eng. 4 (2001) 293;
(d) S.R. Seidel, F.M. Tabellion, A.M. Arif, P.J. Stang, Israel J. Chem. 41 (2001) 149;
(e) M.J. Plater, M.R.St. J. Foreman, T. Gelbrich, M.B. Hursthouse, J. Chem. Soc., Dalton Trans. (2000) 1995.

[12] SMART/SAINT/ASTRO, Release 4.03, Siemens Energy Automation, Inc., Madison, WI, USA, 1995.

[13] G.M. Sheldrick, SHELXTL PLUS, Release 4.1, Siemens Analytical X-ray Instruments Inc., Karlsruhe, Germany, 1991.

[14] (a) M.T. Ng, T.C. Deivaraj, J.J. Vittal, Inorg. Chim. Acta 348 (2003) 173;
(b) A. Waheed, R.A. Jones, J. McCarty, X. Yang, J. Chem. Soc., Dalton Trans. (2004) 3840.

[15] S.I. Noro, S. Kitagawa, M. Kondo, K. Seki, Angew. Chem. Int. Ed. 39 (2000) 2081.

[16] (a) H.-P. Wu, C. Janiak, G. Rheinwald, H. Lang, J. Chem. Soc., Dalton Trans. (1999) 183;
(b) M.A. Withersby, A.J. Blake, N.R. Champness, P. Hubberstey, W.-S. Li, M. Schröder, Angew. Chem., Int. Ed. Engl. 36 (1997) 2327;
(c) C. Janiak, L. Uehlin, H.-P. Wu, P. Klüfers, H. Piotrowski, T.G. Scharmann, J. Chem. Soc., Dalton Trans. (1999) 3121;
(d) D.-L. Long, R.J. Hill, A.J. Blake, N.R. Champness, P. Hubberstey, C. Wilson, M. Schröder, Chem. Eur. J. 11 (2005) 1384.

[17] (a) L.P. Harding, J.C. Jeffery, T. Riis-Johannessen, C.R. Rice, Z. Zeng, J. Chem. Soc., Dalton Trans. (2001) 2396;
(b) N. Schultheiss, D.R. Powell, E. Bosch, Inorg. Chem. 42 (2003) 8886;
(c) L.P. Harding, J.C. Jeffery, T. Riis-Johannessen, C.R. Rice, Z. Zeng, Chem. Commun. (2004) 654;
(d) S. Sailaja, M.V. Rajasekharan, Inorg. Chem. 42 (2003) 5675, and references therein.

2. Experimental

2.1. Materials and measurements

α-Naphthylamine and β-naphthylamine were purchased from Thomas Baker & Co. Pyridine-2-carboxaldehyde was purchased from Lancaster Ltd., England. Alkyl halides (MeI, EtI) were Merck reagents. The organic solvents were purified and dried by standard methods [24]. α/β-Naphthyl-(2-pyridylmethylene)amine were synthesized by equimolar condensation of pyridine 2-carboxaldehyde and naphthylamine in ethanol following the reported procedure [13]. 1-Alkyl-2-(naphthylazo)imidazoles were prepared by the published procedure [22]. All other chemicals used were of A.R. quality and were used as received.

UV–Vis spectra were recorded using JASCO UV–VIS–NIR V-570 spectrophotometer and infrared spectra were obtained from a JASCO FTIR-420 instrument. Microanalyses were collected from a Perkin–Elmer 2400 CHN elemental analyser. ^{1}H NMR spectra were recorded on a Brucker 300 MHz FT-NMR. Solution electrical conductivity was measured in a Systronics 305 digital conductivity meter. Luminescence property was measured using a Perkin–Elmer LS 55 fluorescence spectrophotometer at room temperature (298 K) and low temperature (77 K) in MeCN solution using a 1 cm path length quartz cell.

The fluorescence quantum yield of the Schiff bases (NaiPy) and their zinc-azido complexes was determined using Coumarin-120 laser dye as a reference with a known ϕ_R of 0.63 in MeCN. The complex and the reference dye were excited at 340 nm, maintaining nearly equal absorbance (~0.1), and the emission spectra were recorded from 350 to 600 nm. The area of the emission spectrum was integrated using the software available in the instrument and the quantum yield is calculated according to the following equation:

$$\phi_S/\phi_R = [A_S/A_R] \times [(\mathrm{Abs})_R/(\mathrm{Abs})_S] \times [\eta_S^2/\eta_R^2]$$

Here, ϕ_S and ϕ_R are the fluorescence quantum yields of the sample and reference, respectively. A_S and A_R are the areas under the fluorescence spectra of the sample and the reference respectively, $(\mathrm{Abs})_S$ and $(\mathrm{Abs})_R$ are the respective optical densities of the sample and the reference solution at the wavelength of excitation, and η_S and η_R are the values of refractive index for the respective solvents used for the sample and reference.

2.1.1. Synthesis of bis-azido-(α-naphthyl-(2-pyridylmethylene)amine)zinc(II)Zn(α-NaiPy)(N_3)$_2$] (5)

α-Naphthyl-(2-pyridylmethylene)amine (0.25 g, 1.08 mmol) in MeOH (10 cc) was added dropwise to a methanolic solution (10 cc) of $Zn(OAc)_2 \cdot 2H_2O$ (0.1 g, 0.46 mmol) at room temperature and stirred for 30 min. To the yellow solution NaN_3 (0.065 g, 1.00 mmol) was added and stirred for an additional 2 h. The deep brown solution was filtered and allowed to evaporate slowly in air. Orange-yellow crystals were deposited on the wall of the beaker. These were then filtered and washed with water followed by cold methanol–water (1:1, V/V). The crystals were then dried in a $CaCl_2$ desiccator. The yield was 0.12 g (68%).

Microanalytical and different spectral data are given as follows. *Anal.* Calc. for $C_{16}H_{12}N_8Zn$ (**5**): C, 50.35; H, 3.15; N, 29.37. Found: C, 50.27; H, 3.08; N, 29.50%. UV–Vis spectral data in MeCN λ_{max}(nm) (10^{-3} ε ($dm^3\,mol^{-1}\,cm^{-1}$)), for [Zn(α-NaiPy)(N_3)$_2$]$_2$ 344 (8850), 296 (8350), 269 (11,370). ^{1}H NMR ($CDCl_3$), δ, ppm (*J*, Hz): 8.16 (3H, d, 7.0 Hz), 8.19 (4, 5H, t, 8.0 Hz), 8.45 (6H, d, 8.0 Hz), 8.90 (7H, s), 8.10 (9H, d, 7.0 Hz), 8.00 (10, 11H, m), 7.75 (12H, m), 7.55 (13, 14H, m), 7.95 (15H, d, 7.0). [Zn(β-NaiPy)(N_3)$_2$]$_2$ was prepared similarly in 68% yield. *Anal.* Calc. for $C_{16}H_{12}N_8Zn$ (**6**): C, 50.35; H, 3.15; N, 29.37. Found: C, 50.25; H, 3.18; N, 29.47%. UV–Vis spectral data in MeCN λ_{max}(nm) (10^{-3} ε ($dm^3\,mol^{-1}\,cm^{-1}$)), 334 (7780), 300 (6850), 270 (10.980). ^{1}H NMR ($CDCl_3$), δ, ppm (*J*, Hz): 8.15 (3H, d, 7.0 Hz), 8.18 (4, 5H, t, 8.0 Hz), 8.43 (6H, d, 8.0 Hz), 8.92 (7H, s), 7.91 (8H, s), 8.04 (10H, d, 7.0), 8.00 (11H, m), 7.74 (12H, m), 7.56 (13, 14H, m), 7.63 (15H, d, 7.0).

2.1.2. Synthesis of [Zn(1-ethyl-2-(naphthyl-β-azo)-imidazole)$_2$(N_3)$_2$], [Zn(β-NaiEt)$_2$(N_3)$_2$] (8b)

1-Ethyl-2-(naphthyl-β-azo)imidazole (0.25 g, 1.00 mmol) in MeOH (10 cc) was added dropwise to a methanolic solution (10 cc) of $Zn(OAc)_2 \cdot 2H_2O$ (0.11 g, 0.50 mmol) at room temperature and stirred for 1/2 h. To the orange-red solution NaN_3 (0.065 g, 1.00 mmol) was added and stirred for a further 2 h. The volume of solution was reduced to half of its original volume by slow evaporation in air. It was then filtered and allowed to evaporate slowly. Red crystalline compounds were deposited on the beaker and filtered. The bright crystalline product was then recrystallized by diffusion of a CH_2Cl_2 solution into hexane. The yield was 0.18 g, 55%.

Other compounds were prepared following identical procedures and isolated in yields of 54–65%. Microanalytical data are as follows: *Anal.* Calc. for Zn(α-NaiMe)$_2$(N_3)$_2$ (**7a**) $C_{28}H_{24}N_{14}Zn$: C, 54.08; H, 3.86; N, 31.55. Found: C, 54.00; H, 3.90; N, 31.48%. UV–Vis spectral data in MeCN λ_{max}(nm) (10^{-3} ε ($dm^3\,mol^{-1}\,cm^{-1}$)), for [Zn(α-NaiMe)$_2$-(N_3)$_2$] 420 (450), 345 (7900), 290 (12000), 245 (7860). ^{1}H NMR ($CDCl_3$), δ, ppm (*J*, Hz): 7.40 (4H, b), 7.33 (5H, b), 8.40 (9H, d, 7.0 Hz), 7.75 (10H, t, 7.0 Hz), 7.44 (11H, m), 7.08 (12H, m), 7.08 (13H, m), 7.11 (14H, m), 7.00 (15H, d, 7.0 Hz), 4.10 (1Me, s). *Anal.* Calc. Zn-(α-NaiEt)$_2$(N_3)$_2$ (**7b**) $C_{30}H_{28}N_{14}Zn$: C, 55.44; H, 4.31; N, 30.19. Found: C, 55.53; H, 4.27; N, 30.14%. UV–Vis spectral data in MeCN λ_{max}(nm) (10^{-3} ε ($dm^3\,mol^{-1}\,cm^{-1}$)), for [Zn(α-NaiEt)$_2$(N_3)$_2$] 414 (600), 348 (7590), 295 (12480), 245 (8600). ^{1}H NMR ($CDCl_3$), δ, ppm (*J*, Hz): 7.44 (4H, b), 7.38 (5H, b), 8.41 (9H, d, 7.0 Hz), 7.73 (10H, t, 7.0 Hz), 7.44 (11H, m), 7.11 (12H, m), 7.11 (13H, m), 7.14 (14H, m), 7.05 (15H, d, 7.0 Hz), 4.40 (1–CH_2–, q, 12.0 Hz), 1.48 (CH_3, t, 7.0 Hz). *Anal.* Calc. Zn(β-NaiMe)$_2$(N_3)$_2$ (**8a**) $C_{28}H_{24}N_{14}Zn$: C, 54.08; H, 3.86;

N, 31.55. Found: C, 54.03; H, 3.81; N, 31.50%. UV–Vis spectral data in MeCN λ_{max}(nm) (10^{-3} ε ($dm^3\,mol^{-1}\,cm^{-1}$)), for $[Zn(\beta\text{-NaiMe})_2(N_3)_2]_2$ 422 (760), 358 (8890), 300 (12,680), 250 (8880). ^1H NMR ($CDCl_3$), δ, ppm (J, Hz): 7.40 (4H, b), 7.30 (5H, b), 8.05 (8H, sb), 7.70 (10H, t, 7.0 Hz), 7.45 (11H, m), 7.26 (12H, m), 7.26 (13H, m), 7.33 (14H, m), 7.15 (15H, d, 7.0 Hz), 3.98 (1Me, s). *Anal.* Calc. $Zn(\beta\text{-NaiEt})_2(N_3)_2$ (**8b**) $C_{30}H_{28}N_{14}Zn$: C, 55.44; H, 4.31; N, 30.19. Found: C, 55.50; H, 4.37; N, 30.26%. UV–Vis spectral data in MeCN λ_{max}(nm) (10^{-3} ε ($dm^3\,mol^{-1}\,cm^{-1}$)), for $[Zn(\beta\text{-NaiEt})_2(N_3)_2]$ 420 (850), 345 (9500), 295 (11,600), 245 (9450). ^1H NMR ($CDCl_3$), δ, ppm (J, Hz): 7.44 (4H, b), 7.38 (5H, b), 8.01 (8H, sb), 7.73 (10H, t, 7.0 Hz), 7.48 (11H, m), 7.28 (12H, m), 7.28 (13H, m), 7.34 (14H, m), 7.20 (15H, d, 7.0 Hz), 4.40 (1–CH_2–, q, 12.0 Hz), 1.48 (CH_3, t, 7.0 Hz) (where s, singlet; sb, singlet broad; t, triplet; m, multiplet; d, doublet).

2.2. Crystallographic data collection and refinement

The data of $[Zn(\beta\text{-NaiPy})(N_3)_2]_2$ (**6**) (crystal size: $0.30 \times 0.20 \times 0.20$ mm) were collected on an Enraf-Nonius CAD-4 diffractometer (Mo Kα radiation, $\lambda = 0.70930$ Å). A crystal suitable for X-ray analysis of $[Zn(\beta\text{-NaiEt})_2(N_3)_2]$ (**8b**) (crystal size: $0.40 \times 0.30 \times 0.25$ mm) was mounted in a fine focus sealed tube in a CCD Area detector with graphite monochromated Mo Kα radiation ($\lambda = 0.71073$ Å). Data were collected at 293 (2) K for both the crystals. Unit cell parameters were determined from least-squares refinement of setting angles within the 2θ range 3.8–56.14° for **6** and 4.58–49.86° for **8b**. A summary of the crystallographic data and structure refinement parameters are given in Table 1. Unique data of **6** are 2655 ($R_{int} = 0.000$) and out of 9111 collected data 3443 are unique ($R_{int} = 0.068$) for **8b** ($I > 2\sigma(I)$) recorded using the ω-scan technique. Data were corrected for Lorentz polarization effects and for linear decay. A semi-empirical absorption correction based on ψ-scans was applied. The structure **6** was solved by direct methods using a Nonius MACH3 data collection, refinement and reduction process. The structure of **8b** was solved by direct methods using the Bruker SMART data collection and refinement technique following the Bruker SHELXTL and XPREP reduction process [26]. All non-hydrogen atoms were refined anisotropically. The hydrogen atoms were fixed geometrically and refined using the riding model. In the final difference Fourier map the residual maxima and minima were 0.226 and −0.269 e $Å^{-3}$ for **6** and 0.493 and −0.180 e $Å^{-3}$ for **8b**. All calculations were carried out using SHELXL-97 [27], ORTEP-32 [28] and PLATON-99 [29] programs.

Table 1
Summarized crystallographic data for (**6**) and (**8b**)

Compound	$[Zn(\beta\text{-NaiPy})(N_3)\text{-}(1,1\text{-}N_3)]_2$ (**6**)	$[Zn(\beta\text{-NaiEt})_2\text{-}(N_3)_2]$ (**8b**)
Empirical formula	$C_{32}H_{24}N_{16}Zn_2$	$C_{30}\,H_{28}\,N_{14}Zn$
Formula weight	763.45	650.04
Temperature (K)	293(2)	293(2)
Crystal system	monoclinic	monoclinic
Space group	$P2_1/n$	$C2/c$
Crystal size (mm)	$0.30 \times 0.20 \times 0.20$	$0.40 \times 0.30 \times 0.25$
Unit cell dimensions		
a (Å)	9.9990(5)	19.134(2)
b (Å)	14.6640(10)	14.3310(16)
c (Å)	11.3450(5)	13.4479(15)
β (°)	99.583(4)	122.737(2)
V ($Å^3$)	1640.25(16)	3101.9(6)
Z	4	4
hkl	$0 \leqslant h \leqslant 11$, $0 \leqslant k \leqslant 17$, $-13 \leqslant l \leqslant 13$	$-25 \leqslant h \leqslant 24$, $-18 \leqslant k \leqslant 12$, $-17 \leqslant l \leqslant 17$
λ (Å)	0.70930	0.71073
μ (Mo Kα) (mm^{-1})	1.514	0.838
ρ_{calc} ($mg\,m^{-3}$)	1.546	1.392
Refinement parameters	274	204
Total data	2655	9111
Unique data (R_{int})	2655 (0.000)	3443 (0.068)
R[a] [$I > 2\sigma(I)$]	0.0248	0.0426
wR_2[b]	0.0618	0.0879
Goodness-of-fit[c]	1.107	0.744

[a] $R = \sum|F_o - F_c|/\sum F_o$.

[b] $wR = [\sum w(F_o^2 - F_c^2)/\sum wF_o^4]^{1/2}$, $w = 1/[\sigma^2(F_o^2) + (0.0352P)^2 + 0.3755P]$ where $P = (F_o^2 + 2F_c^2)/3$ for **6**, $w = 1/[\sigma^2(F_o^2) + (0.0465P)^2 + 0.0000P]$ where $P = (F_o^2 + 2F_c^2)/3$ for **8b**.

[c] Goodness-of-fit is defined as $[w(F_o - F_c)/(n_o - n_v)]^{1/2}$ where n_o and n_v denote the number of data and variables, respectively.

3. Results and discussion

3.1. The synthesis and formulation

α/β-Naphthyl-(2-pyridylmethylene)amine, (α-NaiPy (**1**), β-NaiPy (**2**)) and 1-alkyl-2-(naphthyl-α/β-azo)imidazoles (α-NaiMe (**3a**), α-NaiEt (**3b**); β-NaiMe (**4a**), β-NaiEt (**4b**)) are used in this work

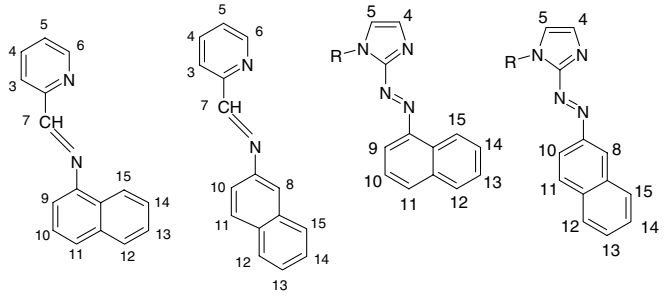

The complexes were synthesized by reacting methanolic solutions of the ligands and $Zn(OAc)_2$ in equimolar quantities followed by the addition of two equivalents of NaN_3 to the same reaction mixture. The solution was then filtered and evaporated slowly in air. Orange-red crystals of $[Zn(\mathbf{3}\text{ or }\mathbf{4})_2(N_3)_2]$ (**7** or **8**) were filtered in good yield while $[Zn(\mathbf{1}\text{ or }\mathbf{2})(N_3)_2]_2$ (**5** or **6**) are orange-yellow. Microanalytical data support the composition of the complexes. Interestingly, an increase in the Schiff base (NaiPy, **1** or **2**): Zn(II) molar ratio > 3:1 proportion could prepare complexes of the

same composition as have been obtained from the 1:1 molar ratio of ligand:Zn(II) in the presence of 2 equiv. of NaN_3. Molar conductance measurements suggest that the compounds are non-conducting in acetonitrile.

3.2. Molecular structures

3.2.1. [Zn(β-NaiPy)(N$_3$)$_2$]$_2$ (6)

The crystal structure is shown in Fig. 1 and metric parameters are listed in Table 2. The structure shows an azido bridged ZnN_5 coordination sphere, which includes the coordination from a chelated ligand, two end-on bridged azido-N and one terminal azido-N. The ligand serves as a diimine (—N=C—C=N—) chelator in which one N is pyridine-N and second one is an exocyclic imine, —C=N—, group. The chelate plane constituting from Zn, N(1), C(5), C(6), N(2) is planar (deviation < 0.02 Å). The pendant β-naphthyl makes a dihedral angle of 18.59(8)° with the chelate plane. The chelate angle, N(1)–Zn–N(2), is 77.68(7)° and is deviated from a regular pentagonal angle. The end-on bridge angle N(3)–Zn–N(3)* is 78.71(8)° (*symmetry: $-x, 1-y, 1-z$). The angles around Zn do not fit exactly indicate a regular square pyramidal geometry; rather the terminal N_3 is inclined to one of the bridged end-on N_3 groups. The imine —C=N— distance is 1.270(3) Å; the Zn–N(pyrdine) [Zn–N(1), 2.0870(18) Å] and Zn–N(naphthylimine) [Zn–N(2), 2.2027(17) Å] bond distances are not equivalent and show better interaction with the pyridine nitrogen than the imine-N. An intermolecular hydrogen bond is observed between the bridged azide-N and pyridine C–H: C(2)–H(2)–N(5), distances are C(2)–H(2), 0.95; H(2)–N(5), 2.72(3), C(2)–N(5), 3.564(4) Å and angle ∠C–H–N, 172.0(2)° (symmetry: $1-x, 1-y, 1-z$). This implies a hydrogen bonded dimer of azido bridged motif. A packing view shows hydrogen bonding and π–π interactions between proximately disposed naphthyl groups (Fig. 2). A significant C–H–π interaction, C(11)–H(11)–Cg(3): H–Cg(3), 3.351 Å and ∠C–H–Cg(3), 80.79° forms a π-polymer. Besides, the π–π interaction [Cg(2)–Cg(5), 3.934 Å; Cg(3)–Cg(5), 3.667 Å; Cg(3)–Cg(4), 3.580 Å, where Cg(2): Zn(1), N(1), N(2), C(5), C(6); Cg(3): N(1), C(1), C(2), C(3), C(4), C(5); Cg(4): C(7), C(8), C(9), C(10), C(15), C(16); Cg(5): C(10), C(11), C(12), C(13), C(14), C(15). Symmetry: $1/2+x, 3/2-y, -1/2+z$] enhances the strength of the non-covalent interaction.

Table 2
Selected bond distances (Å) and angles (°) for [Zn(β-NaiPy)(N$_3$)(1,1-N$_3$)]$_2$ (**6**)

Bond distance (Å)		Bond angle (°)	
Zn(1)–N(1)	2.0870(18)	N(6)–Zn(1)–N(3)[a]	117.77(9)
Zn(1)–N(2)	2.2027(17)	N(6)–Zn(1)–N(1)	117.86(8)
Zn(1)–N(3)	2.1904(18)	N(3)[a]–Zn(1)–N(1)	124.31(8)
Zn(1)–N(3)[a]	2.0465(19)	N(6)–Zn(1)–N(3)	95.50(8)
Zn(1)–N(6)	1.973(2)	N(3)–Zn(1)–N(3)[a]	78.71(8)
N(3)–N(4)	1.206(3)	N(3)–Zn(1)–N(1)	93.67(7)
N(4)–N(5)	1.138(3)	N(6)–Zn(1)–N(2)	100.76(7)
N(6)–N(7)	1.187(3)	N(2)–Zn(1)–N(3)[a]	94.63(7)
N(7)–N(8)	1.150(3)	N(1)–Zn(1)–N(2)	77.68(7)
		N(3)–Zn(1)–N(2)	163.69(7)
		Zn(1)–N(3)–Zn(1)[a]	101.29(8)
		N(3)–N(4)–N(5)	178.1(3)
		N(6)–N(7)–N(8)	175.8(3)

[a] Symmetry: $-x, 1-y, 1-z$.

3.2.2. [Zn(β-NaiEt)$_2$(N$_3$)$_2$] (8b)

The molecular structure of Zn(β-NaiEt)$_2$(N$_3$)$_2$ (**8b**) is shown in Fig. 3 and bond parameters are given in

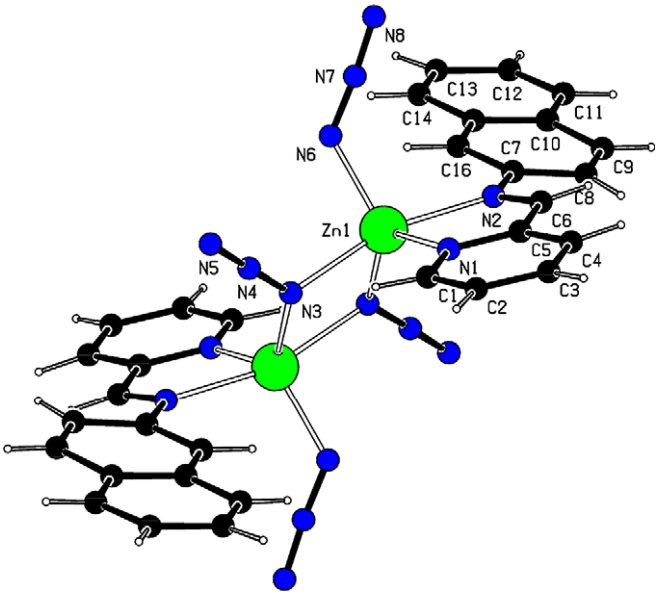

Fig. 1. Molecular structure of [Zn(β-NaiPy)(N$_3$)$_2$]$_2$ (**6**).

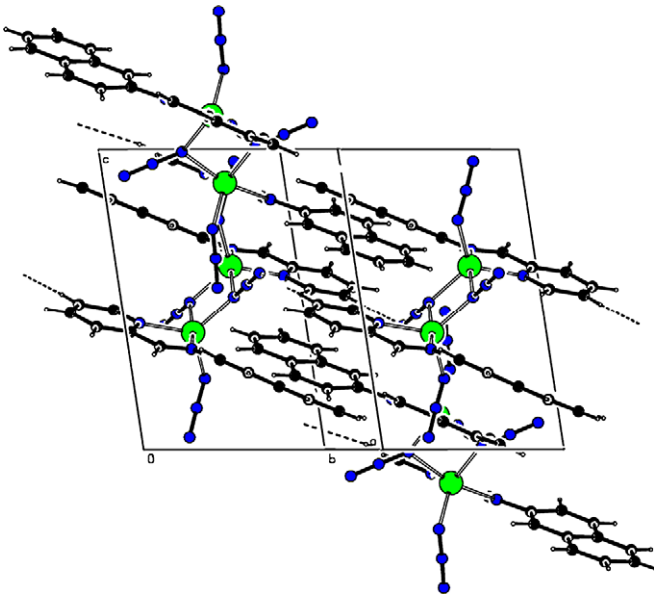

Fig. 2. Packing view along the *b*-axis of **6** showing intermolecular hydrogen bonding.

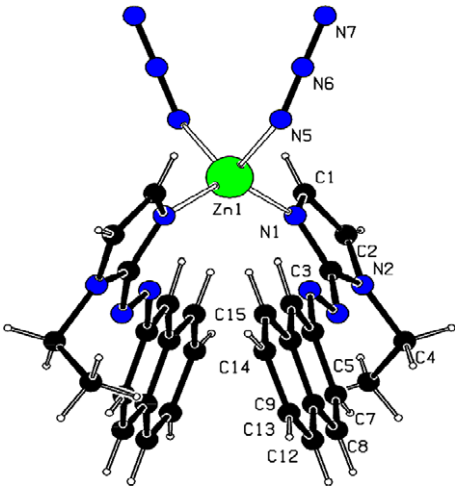

Fig. 3. X-ray structure of $[Zn(\beta\text{-NaiEt})_2(N_3)_2]$ (**8b**).

Table 3
Selected bond distances (Å) and angles (°) for $[Zn(\beta\text{-NaiEt})(N_3)_2]$ (**8b**)

Bond distance (Å)		Bond angle (°)	
Zn(1)–N(1)	2.016(2)	N(1)–Zn–N(5)	113.50(11)
Zn(1)–N(5)	1.993(3)	N(1)–Zn(1)–N(5)[a]	95.11(11)
Zn(1)–N(1)[a]	2.016(2)	N(5)–Zn(1)–N(5)[a]	104.71(19)
Zn(1)–N(5)[a]	1.993(3)	N(1)–Zn(1)–N(1)[a]	132.93(15)
N(5)–N(6)	1.176(3)	N(1)[a]–Zn(1)–N(5)[a]	113.50(11)
N(6)–N(7)	1.161(4)	C(3)–N(1)–Zn(1)	128.14(19)
N(3)–N(4)	1.267(3)	C(1)–N(1)–Zn(1)	126.0(2)
C(3)–N(3)	1.393(4)	N(6)–N(5)–Zn(1)	131.5(2)
C(6)–N(4)	1.420(3)	N(1)[a]–Zn(1)–N(5)	95.11(11)

[a] Symmetry: $1-x, y, 3/2-z$.

Table 3. The structure shows a distorted tetrahedral structure with ZnN_4 coordination. In the coordination zone two azide groups act as monodenate donors and the two β-NaiEt also act as monodentate imidazole-N donor ligands. Azoimidazoles act as both bidentate chelators, N(azo) and N(imidazole), [20,21] as well as monodentate imidazole-N donor ligands [15,16,30,31]. The distortion from a regular tetrahedral geometry is reflected from the metric parameters: Zn–N(imidazole) (Zn(1)–N(1)), 2.016(2) Å is longer than Zn–N(azide) (Zn(1)–N(5)), 1.993(3) Å. The N=N distance is 1.267(3) Å which is closer to the free ligand data [23]. The bond angles, which are extended by N(imidazole) and N(azide) with Zn(II) and are equal to 95.11(11)° (N(5)–Zn(1)–N(1)*, *symmetry: $1-x, y, 3/2-z$) and 113.50(11)° (N(5)–Zn(1)–N(1)), are away from the tetrahedral angle. The maximum deviation is observed for ∠N(1)–Zn(1)–N(1)*, 132.93 (15)° (*symmetry: $1-x, y, 3/2-z$). This may be due to large steric crowding provided by two pendant azonaphthyl groups. Additionally, the imidazole and β-naphthyl are inclined at an angle of 13.57(18)°.

The packing view of this structure (Fig. 4) shows two intermolecular hydrogen bondings: C(2)–H(2)–N(7) (C–H, 0.93 Å; H(2)–N(7), 2.566(8) Å, C(2)–N(7), 3.407(4) Å; ∠C–H–N, 150.61°) and C(4)–H(4a)–N(3) (C(4)–H(4a), 0.97 Å; H(4a)–N(3), 2.523(1) Å, C(4)–N(3), 2.940(4) Å; ∠C–H–N, 105.83° (symmetry: $1-x, 1-y, 1-z$)) which make a hydrogen bonded dimer with a 16 membered ring. Two C–H–π interactions (C(5)–H(5b)–Cg(2), 3.349(6) Å; C(11)–H(11)–Cg(1), 2.863(2) Å; symmetry: $1-x, y, 3/2-z$, where Cg(1) and Cg(2) refer to imidazole and β-naphthyl rings) and a π–π interaction between imidazole and β-naphthyl rings (distance 4.022 Å; symmetry: $3/2-x, 3/2-y, 2-z$) enhance the rigidity of the structure.

3.3. Spectral characterization

The vibration bands are assigned by comparing to the free ligand data [13,32]. The $\nu_{asym}(N_3)$ appears as a sharp strong single band at 2070–2080 cm^{-1} for **5** and **6** [33] while doublets are found at 2095–2098 and 2063–2075 cm^{-1} for **7** and **8** [34]. In **5** and **6** N_3^- serves as only a terminal donor while in **7** and **8** both end-on bridging and terminal bonds are present. The N=N and C=N vibrations are observed at 1420–1430 and 1590–1600 cm^{-1}, respectively, for **7** and **8**. The complexes **5** and **6** exhibit a very strong vibration at 1590–1605 cm^{-1} and support the presence of ν(C=N) which is red shifted by 15 cm^{-1} compared to the free ligand value (1620 cm^{-1}).

The electronic spectra in MeCN solution of $[Zn(NaiPy)(N_3)(\mu\text{-}1,1\text{-}N_3)]$ (**5**, **6**) show intense absorptions in the UV region at ca. 350 nm and ca. 300 nm ($\varepsilon \sim 10^4$ M^{-1} cm^{-1}). These transitions may be assigned to intraligand charge transfer (n–π^* and π–π^*) transitions. Naphthylazo complexes are intense orange by virtue of the —N=N— function while Schiff bases are yellow. $[Zn(NaiR)_2(N_3)_2]$ (**7** and **8**) exhibits intense transitions in the UV region which correspond to intraligand charge transfer transitions along with a weak absorption ($\varepsilon \sim 400$–900 M^{-1} cm^{-1}) at the longer wavelength (414–422 nm) region. The longer wavelength weak transition may be assigned to the $d^{10}(Zn) \rightarrow \pi^*$(azoimine) transition. The spectra of the complexes were taken in three different solvents: MeCN, $CHCl_3$ and DMF. However, the complexes do not exhibit any significant solvatochromism.

The ^1H NMR spectra are recorded in $CDCl_3$ solution. Data are given in Section 2. The assignment has been made on the basis of spin–spin interactions, and on comparing with free ligand values [13a]. In the complexes **5** and **6**, the proton signals of the coordinated ligand α/β-naphthyl-(2-pyridylmethylene)amine are shifted to downfield by 0.1–0.2 ppm compared to the free ligand value. The most downfield singlet is assigned to —HC=N— (7H) (8.90–8.92 ppm). Pyridyl protons (3H–6H) appear at 8.2–8.5 ppm and naphthyl protons (8H–15H) exhibit resonances at the upperfield side, 8.1–7.6 ppm. In $Zn(NaiR)_2(N_3)_2$ (**7** and **8**) the imidazole protons (4-, 5H) show signals at 7.3–7.4 ppm, which are 0.3–0.4 ppm downfield shifted, while the naphthyl protons are insignificantly shifted compared to the free ligand data [24]. This, in fact, supports the structural aspect of these complexes as depicted in Fig. 3.

The photoluminescence properties of pyridyl-2-(naphthylmethylene)amines and their Zn(II)-complexes (**5**

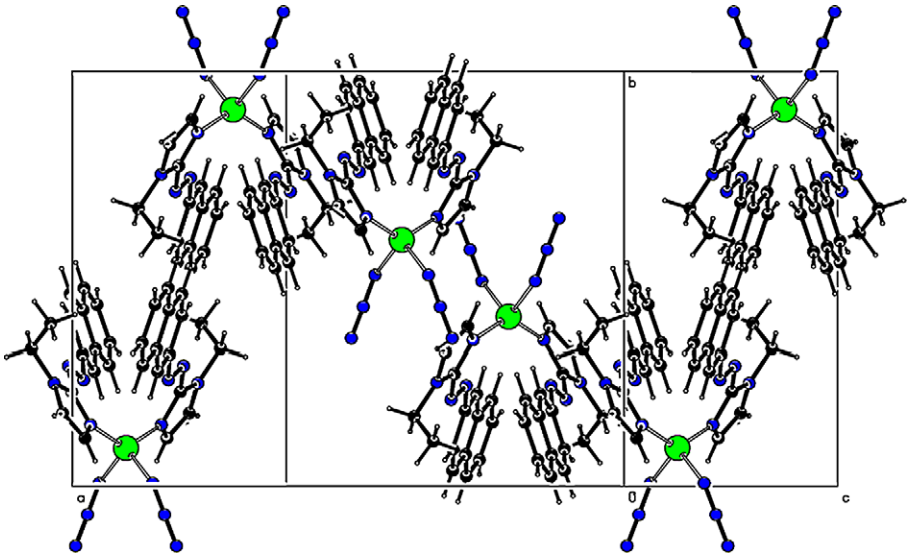

Fig. 4. Packing view in the unit cell of **8b** showing hydrogen bonding and π–π interactions.

and **6**) were studied at room temperature (298 K) and 77 K (Fig. 5). Naphthylazoimidazoles (NaiR) and their Zn(II)-compounds do not exhibit emission phenomena. The Schiff bases exhibit photoluminescence with emissions at 431 and 406 nm for α-NaiPy and β-NaiPy, respectively, at 298 K upon excitation at 340 nm. Under low temperature conditions (77 K) these compounds show emissions at 455 nm for α-NaiPy and 448 nm for β-NaiPy.

No emission originating from metal-centred or MLCT/LMCT excited states are expected for the Zn(II) complexes, since the Zn(II) ion is difficult to oxidize or reduce due to its d^{10} configuration. Thus, the emission observed in the complexes is tentatively assigned to the (π–π^*) intraligand fluorescence. It is interesting that the Zn(II) complexes show higher intensity than that of the free ligand values. This is supported from their calculated quantum yield (Table 4) with reference to coumarin-120. It has been reported that the metal ions can enhance or quench the fluorescence emission of pyridine containing compounds [35–37]. In the absence of metal ions the fluorescence of the ligand is probably quenched by the occurrence of a photoinduced electron transfer (PET) process due to the presence of a lone pair of nitrogen atoms. Such a PET process is prevented by the complexation of L with metal ions; thus the fluorescence intensity may be greatly enhanced by the coordination of Zn(II). The chelation of the ligands to Zn(II) increases the rigidity of the ligands and thus reduces the loss of energy by thermal vibrational decay. At low

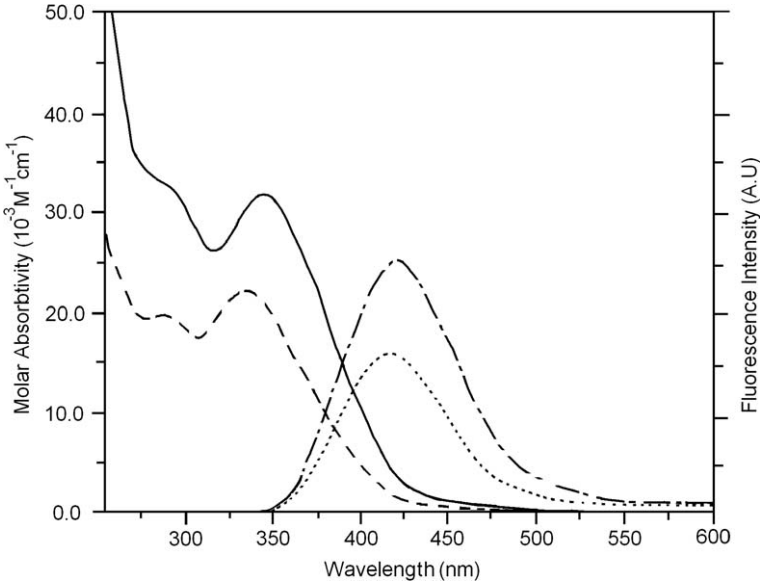

Fig. 5. Electronic spectra of **5** (——), α-NaiPy (-----) and emission spectrum of **5** (— · — · —) and α-NaiPy (– – –) in MeCN at 298 K.

Table 4
Absorption (main band), emission spectral data and quantum yield[a]

Compound	Abs (λ_{max})	Emission (λ_{max})	Quantum yield (ϕ)
α-NaiPy	342	431	0.0018
β-NaiPy	340	406	0.0008
$[Zn(\alpha\text{-NaiPy})(N_3)(1,1\text{-}N_3)]_2$ (**5**)	344	426	0.0165
$[Zn(\beta\text{-NaiPy})(N_3)(1,1\text{-}N_3)]_2$ (**6**)	324	398	0.0044

[a] Solvent: MeCN, excitation at 340 nm, reference compound is coumarine-120, $\phi_R = 0.63$ in MeCN.

temperature (77 K) the complexes show a bright greenish-blue emission and have been red shifted by 40–50 nm from the emission in solution at 298 K. This is probably caused by intermolecular interactions in the frozen conditions that effectively decreases the energy gap.

4. Conclusion

Diimine (—N=C—C=N—) and azoimine (—N=N—C=N—) are isoelectronic functions. α/β-Naphthyl-(2-pyridylmethylene)amine (α/β-NaiPy) belongs to the diimine family and 1-alkyl-2-(naphthyl-α/β-azo)imidazoles (α/β-NaiR) belongs to the azoimine family. Zinc(II)-azide complexes of these two molecules are described. α/β-NaiPy forms an azido bridged complex while α/β-NaiR gives monodenate Zn-N_3 bonding. Additionally a structural study reveals that α/β-NaiPy acts as a chelating ligand and α/β-NaiR serve as a monodentate imidazole-N donor system. Photoluminescence studies prove that $Zn(\alpha/\beta\text{-NaiR})_2(N_3)_2$ complexes are photo-inactive while $[Zn(\alpha/\beta\text{-NaiPy})(N_3)\text{-}(\mu\text{-}1,1\text{-}N_3)]_2$ complexes are photo-active.

5. Supplementary material

Crystallographic data for the structural analysis have been deposited with the Cambridge Crystallographic data centre, CCDC No. 290239 for $[Zn(\beta\text{-NaiPy})(N_3)_2]_2$ (**6**) and 288382 for $[Zn(\beta\text{-NaiEt})_2(N_3)_2]$ (**8b**). Copies of this information may be obtained free of charge from the Director, CCDC, 12 Union Road, Cambridge, CB2 1EZ, UK, fax: +44 1233 336 033; email: deposit@ccdc.cam.ac.uk; or the web: http://www.ccdc.cam.ac.uk.

Acknowledgements

Financial support from the All India Council of Technical Education (AICTE) and Department of Science and Technology, New Delhi are gratefully acknowledged. We thank the Single Crystal X-Ray Diffraction Facility Centre, Indian Institute of Technology, Bombay, India for X-ray data collection. We also thank Dr. G. Mostafa, Department of Physics, Jadavpur University for his help regarding the structure solution.

References

[1] (a) S. Ernst, W. Kaim, J. Am. Chem. Soc. 108 (1986) 3578;
(b) E.C. Constable, Adv. Inorg. Chem. Radiochem. 30 (1986) 69;
(c) L.A. Summers, Adv. Heterocycle Chem. 35 (1984) 281.
[2] K.E. Erkkila, D.T. Odam, J.K. Barton, Chem. Rev. 99 (1999) 2777.
[3] C. Kaes, A. Katz, M.W. Hosseini, Chem. Rev. 100 (2000) 3553.
[4] F.A. Cotton, G. Wilkinson, C.A. Murillo, M. Bochmann, Advanced Inorganic Chemistry, 6th ed., Wiley, New York, 1999.
[5] J.M. Lehn, Supramolecular Chemistry, VCH, Weinheim, 1995.
[6] K. Kalyansundaram, Coord. Chem. Rev. 46 (1982) 159.
[7] B.K. Ghosh, A. Chakravorty, Coord. Chem. Rev. 95 (1989) 239.
[8] (a) R.-Q. Fan, D.-S. Zhu, Y. Mu, G.-H. Li, Y.-L. Yang, Q. Su, S.-H. Feng, Eur. J. Inorg. Chem. (2004) 4891;
(b) Y.L. Pui, K.K. Cheung, J. Chem. Soc., Dalton Trans. (2000) 3658.
[9] Y. Wang, X.-M. Ouyang, Y.-Z. Li, W.-Y. Sun, Bull. Chem. Soc. Jpn. 76 (2003) 1403.
[10] H.-F. Zhu, L. Li, T. Okamura, W. Zhao, W.-Y. Sun, N. Ueyama, Bull. Chem. Soc. Jpn. 76 (2003) 761.
[11] E.C. Constable, Coord. Chem. Rev. 93 (1989) 205.
[12] (a) M. Menon, A. Pramanik, N. Bag, A. Chakravorty, Inorg. Chem. 33 (1994) 403;
(b) M. Menon, A. Pramanik, A. Chakravorty, Inorg. Chem. 34 (1995) 3310;
(c) S. Chowdhury, A.K. Deb, S. Goswami, Polyhedron 13 (1994) 1063.
[13] (a) J. Dinda, C. Sinha, Trans. Met. Chem. 28 (2003) 864;
(b) J. Zhang, W. Li, W. Bu, L. Wu, L. Ye, G. Yang, Inorg. Chim. Acta 358 (2005) 964;
(c) L.G. Nickolacheva, C.M. Vogels, R.A. Stefan, H.A. Warwish, S.J. Duffy, R.J. Ireland, A. Decken, R.H. Hudson, S.A. Westcott, Can. J. Chem. 81 (2003) 269;
(d) M. Boiocchi, G. Colucci, M. Licchelli, E. Monzani, D. Sacchi, Chem. Commun. (2003) 2906.
[14] S. Goswami, A.R. Chakravarty, A. Chakravorty, Inorg. Chem. 20 (1981) 2246.
[15] B.G. Chand, U.S. Ray, J. Cheng, T.-H. Lu, C. Sinha, Polyhedron 22 (2003) 1213.
[16] B.G. Chand, U.S. Ray, G. Mostafa, T.-H. Lu, C. Sinha, J. Coord. Chem. 57 (2004) 627.
[17] B.G. Chand, G. Mostafa, T.-H. Lu, L.R. Falvello, C. Sinha, Polyhedron 22 (2003) 3161.
[18] B.G. Chand, U.S. Ray, G. Mostafa, T.-H. Lu, C. Sinha, Polyhedron 23 (2004) 1669.
[19] B.G. Chand, U.S. Ray, P.K. Santra, G. Mostafa, T.-H. Lu, C. Sinha, Polyhedron 22 (2003) 1205.
[20] T.K. Misra, D. Das, C. Sinha, P.K. Ghosh, C.K. Pal, Inorg. Chem. 37 (1998) 1672.
[21] S. Pal, D. Das, C. Sinha, C.H.L. Kennard, Inorg. Chim. Acta 313 (2001) 21.
[22] P. Byabartta, P.K. Santra, T.K. Misra, C. Sinha, C.H.L. Kennard, Polyhedron 20 (2001) 905.
[23] J. Dinda, K. Bag, C. Sinha, G. Mostafa, T.-H. Lu, Polyhedron 22 (2003) 1367.
[24] J. Dinda, Sk. Jasimuddin, G. Mostafa, C.-H. Hung, C. Sinha, Polyhedron 23 (2004) 493.
[25] J. Reedijk, in: G. Wilkinson, R.D. Gillard, J.A. MeCleverty (Eds.), Comprehensive Coordination Chemistry, vol. 2, Pergamon Press, Oxford, 1987.
[26] G.M. Sheldrick, SHELXS-97, Program for the Solution of Crystal Structure, University of Gottingen, Germany, 1997.
[27] G.M. Sheldrick, SHELXL 97, Program for the Refinement of Crystal Structure, University of Gottingen, Germany, 1997.
[28] L.J. Farrugia, J. Appl. Crystallogr. 30 (1997) 565.
[29] A.L. Spek, PLATON, Molecular Geometry Program, University of Utrecht, The Netherlands, 1999.

[30] D. Banerjee, U.S. Ray, S. Chantrapromma, H.-K. Fun, J.-N. Lin, T.-H. Lu, C. Sinha, Polyhedron 24 (2005) 1071.
[31] T. Mathur, U.S. Ray, B.N. Baruri, C. Sinha, J. Coord. Chem. 58 (2005) 399.
[32] T.K. Misra, Ph.D. thesis, Burdwan University, Burdwan, 1999.
[33] U.S. Ray, D. Banerjee, G. Mostafa, T.-H. Lu, C. Sinha, New J. Chem. 28 (2004) 1432.
[34] U.S. Ray, B.G. Chand, G. Mostafa, J. Chang, T.-H. Lu, C. Sinha, Polyhedron 22 (2003) 2587.
[35] M. Prabhakar, P.S. Zacharias, S.K. Das, Inorg. Chem. 44 (2005) 2585.
[36] H.F. Zhu, L. Li, T. Okamura, W. Zhao, W.Y. Skn, N. Ueyama, Bull. Chem. Soc. Jpn. 76 (2003) 761.
[37] X.H. Be, H. Liu, M. Du, K.M.C. Wong, V.W.W.W. Yam, Inorg. Chim. Acta 333 (2002) 32.

arrays [2,3]. A wide variety of donor groups can be readily attached to the cyclotriphosphazene platform via nucleophilic substitution reactions at the phosphorus with primary and secondary amine, alcohol and phenol groups that incorporate appropriate donor atoms such as nitrogen or phosphorus. Previously, it has been shown that pyrazolyl substituted cyclotriphosphazenes are particularly versatile multimodal ligands which bind to metals via both the ring nitrogen atoms of the cyclophosphazene and the pyridinic nitrogen atom of the pyrazolyl rings [4]. More recently we have reported [5] that the reaction of hexakis(2-pyridyloxy)cyclotriphosphazene (L) and the related hexakis(4-methyl-2-pyridyloxy)cyclotriphosphazene (MeL) both form a diverse range of complexes with copper(II) halides which exhibit both κ^3N and κ^5N coordination modes, including $[(CuCl_2)_2(MeL)]$, which contains two copper(II) ions bound to the cyclotriphosphazene ring nitrogen atoms. The ligand L also forms a cationic dimeric copper(II) complex $[(CuLCl)_2(CuCl_2)]^{2+}$, which contains two octahedral κ^5N-CuCl centres linked by a $CuCl_2$ moiety [6]. A key feature of the design of L is the incorporation of the flexible pyridyloxy pendant arms which facilitate binding of the metal ion to the less basic phosphazene ring nitrogen atoms. In this paper, we extend our work with copper(II) halides to examine the structures of the products formed when the divalent halides of cobalt, nickel and zinc react with L and MeL and report that some new structural types are found. As for the copper(II) halides, cobalt and nickel form five-coordinate κ^3N complexes, e.g., $[CoLCl_2]$, but in the case of nickel a six-coordinate κ^4N complex $[NiLCl_2]$ is also obtained. The dimetallic cobalt complexes of the empirical formula $[(CoX_2)_2L]$ (X = Cl or Br) are in fact zwitterions with the formulation $[(CoLX)CoX_3]$. Only one of the cobalt(II) ions bound to a phosphazene ring nitrogen in a six-coordinate κ^5N environment with the other bound to a single pyridyloxy nitrogen. In contrast, the dimetallic zinc complex contains one metal ion in a five-coordinate κ^3N environment and the other in a tetrahedral κ^2N site.

2. Experimental

2.1. Materials and instrumentation

All manipulations were carried out under nitrogen using standard Schlenk techniques. Analytical grade solvents were purchased from standard chemical suppliers and with the exception of tetrahydrofuran (THF), which was distilled from sodium/benzophenone, were used without further purification. Hydrated metal halides were dehydrated at 110 °C prior to use except for $ZnCl_2$ which was used from a freshly opened container. The ligands (L and MeL) and $[Ag(CH_3CN)_4]PF_6$ were prepared by the literature methods [5,7,8]. Mass spectra were obtained using a Varian VG70-250S double-focussing magnetic sector spectrometer by the method of liquid secondary ion mass spectroscopy (LSIMS) using *m*-nitrobenzyl alcohol as the matrix or by the electrospray technique (ESMS) from MeCN solutions using a micromass ZMD spectrometer. Listed peaks correspond to the most abundant isotopomer; assignments were made by a comparison of observed and simulated spectra. Microanalyses were performed by the Campbell Microanalytical Laboratory, University of Otago.

2.2. Preparation of the complexes

2.2.1. *[CoLCl$_2$] (**1**)*

To a stirred suspension of anhydrous $CoCl_2$ (9.3 mg, 0.071 mmol) in CH_2Cl_2 (20 mL), L (50 mg, 0.071 mmol) was added and the mixture was stirred overnight at room temperature. The solvent was removed under vacuum affording a pale blue residue which was filtered, dissolved in hot CH_3CN which on cooling yielded purple/blue crystals of **1** (49 mg, 83%). *Anal.* Calc. for $C_{30}H_{24}Cl_2CoN_9O_6P_3$: C, 43.48; H, 2.92; N, 15.22. Found: C, 43.45; H, 2.80; N, 15.69%. *m*/*z* (LSIMS): 793 $[CoLCl]^+$.

2.2.2. *[CoLBr$_2$] (**2**)*

Using the same procedure as for **1** but with $CoBr_2$ (15.6 mg, 0.071 mmo1), purple/blue crystals of **2** (40 mg, 61%) were obtained. *Anal.* Calc. for $C_{30}H_{24}Br_2CoN_9O_6P_3$: C, 39.24; H, 2.63; N, 13.73. Found: C, 39.50; H, 2.40; N, 13.54%. *m*/*z* (LSIMS): 839 $[CoLBr]^+$.

2.2.3. *[Co(MeL)Cl$_2$] · 1.5CH$_2$Cl$_2$ (**3** · 1.5CH$_2$Cl$_2$)*

A mixture of $CoCl_2$ (8.3 mg, 0.064 mmol) and MeL (50 mg, 0.064 mmol) in CH_2Cl_2 (20 mL) was stirred at room temperature overnight. The resulting solution was filtered and reduced in volume to ca. 5 mL. *t*-Butylmethyl ether was added and slow evaporation of the solution yielded small, violet blue crystals of $\mathbf{3} \cdot 1.5CH_2Cl_2$ (38 mg, 57%). *Anal.* Calc. for $C_{36}H_{36}Cl_2CoN_9O_6P_3 \cdot 1.5CH_2Cl_2$: C, 43.27; H, 3.78; N, 12.11. Found: C, 43.34; H, 3.80; N, 12.33%. *m*/*z* (LSIMS): 877 $[Co(MeL)Cl]^+$.

2.2.4. *[Co(MeL)Br$_2$] · 1.5CH$_2$Cl$_2$ (**4** · 1.5CH$_2$Cl$_2$)*

Following the same procedure as described for compound **3** but using $CoBr_2$ (14 mg, 0.064) yielded **4**.l.5CH_2Cl_2 (40 mg, 55%). *Anal.* Calc. for $C_{36}H_{36}Br_2CoN_9O_6P_3 \cdot 1.5CH_2Cl_2$: C, 39.87; H, 3.48; N, 11.16. Found: C, 39.69; H, 3.19; N, 11.16%. *m*/*z* (LSIMS): 923 $[Co(MeL)Br]^+$. Crystals suitable for X-ray diffraction were grown from *t*-butylmethylether/CH_2Cl_2.

2.2.5. *[(CoLCl)CoCl$_3$] · 0.5CH$_2$Cl$_2$ (**5** · 0.5CH$_2$Cl$_2$)*

To a stirred suspension of $CoCl_2$ (30 mg, 0.231 mmol) in THF (20 mL), L (50 mg, 0.071 mmol) was added and the reaction heated at reflux for 24 h. The reaction mixture was filtered and the solvent removed under vacuum. The residue was dissolved in CH_3CN, taken to dryness and extracted with CH_2Cl_2 (this intermediary CH_3CN dissolution improved the CH_2Cl_2 extraction). The CH_2Cl_2 solution was filtered and after *t*-butylmethylether was added

slow evaporation yielded blue crystals of $\mathbf{5}\cdot 0.5CH_2Cl_2$ (25 mg, 37%). *Anal.* Calc. for $C_{30}H_{24}Cl_4Co_2N_9O_6P_3\cdot 0.5CH_2Cl_2$: C, 36.57; H, 2.52; N, 12.59. Found: C, 36.60; H, 2.35; N, 12.62%. *m/z* (LSIMS): 959 $[Co_2LCl_3]^+$, 793 $[CoLCl]^+$. Crystals of $\mathbf{5}\cdot 2CH_3CN$ suitable for X-ray diffraction were grown from a CH_3CN/diethylether solution at −20 °C.

2.2.6. *[(CoLBr)CoBr$_3$] (**6**)*

A mixture of $CoBr_2$ (125 mg, 0.571 mmol) and L (100 mg, 0.143 mmol) in $CHCl_3$ (25 mL) was stirred at reflux temperature for ca. 18 h. and the reaction worked-up as described for **5**. Evaporation of the CH_2Cl_2 solution yielded blue crystals of **6** (110 mg, 68%). *Anal.* Calc. for $C_{30}H_{24}Br_4Co_2N_9O_6P_3$: C, 31.69; H, 2.13; N, 11.09. Found: C, 31.67; H, 1.71; N, 11.00%. *m/z* (LSIMS): 1058 $[Co_2LBr_3]^+$, 839 $[CoLBr]^+$. Evaporation from CH_2Cl_2 yielded crystals of $\mathbf{6}\cdot 3CH_2Cl_2$ suitable for X-ray diffraction which readily lost solvent.

2.2.7. *[{Co(MeL)Cl}CoCl$_3$]·0.5CH$_2$Cl$_2$ (**7**·0.5CH$_2$Cl$_2$)*

A mixture of $CoCl_2$ (16.6 mg, 0.128 mmol) and MeL (50 mg, 0.064 mmol) in CH_2Cl_2 (20 mL) was stirred at room temperature overnight. The solution was filtered, concentrated, *t*-butylmethylether added and cooled to −20 °C to afford blue crystals of $\mathbf{7}\cdot 0.5CH_2Cl_2$ (55 mg, 79%). *Anal.* Calc. for $C_{36}H_{36}Cl_4Co_2N_9O_6P_3\cdot 0.5CH_2Cl_2$: C, 40.38; H, 3.43; N, 11.61. Found: C, 40.41; H, 3.41; N, 11.65%. *m/z* (LSIMS): 877 $[Co(MeL)Cl]^+$. Slow evaporation of the *t*-butylmethylether/CH_2Cl_2 solution yielded crystals suitable for X-ray diffraction.

2.2.8. *[{Co(MeL)Br}CoBr$_3$]·CH$_2$Cl$_2$ (**8**·CH$_2$Cl$_2$)*

The same procedure as described for **7** was used but using $CoBr_2$ (28 mg, 0.128 mmol). Slow evaporation of the *t*-butylmethylether/CH_2Cl_2 solution yielded blue crystals of $\mathbf{8}\cdot CH_2Cl_2$ (37 mg, 44%). *Anal.* Calc. for $C_{36}H_{36}Br_4Co_2N_9O_6P_3\cdot CH_2Cl_2$: C, 34.03; H, 2.93; N, 9.65. Found: C, 34.21; H, 2.64; N, 9.67%.

2.2.9. *[CoLCl]PF$_6$·CH$_2$Cl$_2$ (**9**·CH$_2$Cl$_2$)*

Following the same procedure as for **1** but after stirring overnight $[Ag(CH_3CN)_4]PF_6$ (15 mg, 0.071 mmol) was added and the reaction stirred in the absence of light for an additional 1 h. The reaction mixture was filtered, the filtrate volume reduced to ca. 5 mL and hexane (2–3 mL) was added. Slow evaporation of this solution yielded pale-purple crystals of $\mathbf{9}\cdot CH_2Cl_2$ (47 mg, 64%). *Anal.* Calc. for $C_{30}H_{24}ClCoF_6N_9O_6P_4\cdot CH_2Cl_2$: C, 36.37; H, 2.56; N, 12.31. Found: C, 36.41; H, 2.48; N, 12.11%.

2.2.10. *[CoLBr]PF$_6$·CH$_2$Cl$_2$ (**10**·CH$_2$Cl$_2$)*

Following the same method described for **9** but using $CoBr_2$ (15.6 mg, 0.071 mmol) yielded pale-purple crystals of $\mathbf{10}\cdot CH_2Cl_2$ (61 mg, 80%). *Anal.* Calc. for $C_{30}H_{24}BrCoF_6N_9O_6P_4\cdot CH_2Cl_2$: C, 34.86; H, 2.45; N, 11.80. Found: C, 34.83; H, 2.23; N, 11.66%. *m/z* (LSIMS): 839 $[CoLBr]^+$.

2.2.11. *[NiLCl$_2$] (**11**)*

A mixture of L (100 mg, 0.143 mmol) and $NiCl_2$ (18.5 mg, 0.143 mmol) in CH_2Cl_2 (25 mL) was stirred for 5 days at room temperature. The reaction mixture was filtered and the volume of the filtrate reduced to ca. 8 mL. After a small volume of hexane was added to the solution, slow evaporation afforded light-green crystals of **11** (92 mg, 78%). *Anal.* Calc. for $C_{30}H_{24}Cl_2N_9NiO_6P_3$: C, 43.46; H, 2.92; N, 15.20 Found: C, 42.97; H, 2.82; N, 14.92%. *m/z* (LSIMS): 792 $[NiLCl]^+$. Diffusion of pentane into CH_2Cl_2 or $CHCl_3$ solutions of **11** resulted in the crystallisation of the red isomer, **12**.

2.2.12. *[NiLCl]PF$_6$ (**13**)*

A mixture of L (100 mg, 0.143 mmol) and $NiCl_2$ (18.5 mg, 0.143 mmol) in CH_2Cl_2 (25 mL) was allowed to stir over 5 days. $[Ag(CH_3CN)_4]PF_6$ (30 mg, 0.143 mmol) was added and the mixture stirred in the absence of light for a further 1 h. The reaction mixture was filtered, the filtrate reduced to ca. 5 mL and hexane (2–3 mL) was added, to yield pale green crystals of **13**. *Anal.* Calc. for $C_{30}H_{24}ClF_6N_9NiO_6P_4$: C, 38.39; H, 2.58; N, 13.43. Found: 38.00, 2.94, 13.19%. *m/z* (LSIMS): 792 $[NiLCl]^+$.

2.2.13. *[(ZnCl$_2$)$_2$L] (**14**)*

A mixture $ZnCl_2$ (39 mg, 0.286 mmol) and L (100 mg, 0.143 mmol) in CH_2Cl_2 (25 mL) was stirred overnight. The reaction mixture was filtered and the volume of the filtrate reduced (ca. 8 mL). After a small volume of hexane was added to the solution slow evaporation yielded colourless crystals of **14** (123 mg, 88%). *Anal.* Calc. for $C_{30}H_{24}Cl_4N_9O_6P_3Zn_2$: C, 37.07; H, 2.49; N, 12.97. Found: C, 37.20; H, 2.49; N, 12.77. ^{31}P NMR (CD_2Cl_2): δ 5.5 ppm. *m/z* (LSIMS): 798 $[ZnLCI]^+$. Slow diffusion of hexane into a 1,2-dichloroethane solution of **14** yielded crystals suitable for X-ray diffraction.

2.3. Crystallography

The X-ray data was collected on a Siemens P4 four circle diffractometer, using a Siemens SMART 1K CCD area detector. The crystals were mounted in an inert oil, transferred into the cold gas stream of the detector and irradiated with graphite monochromated Mo Kα ($\lambda =$ 0.71073 Å) X-rays. The data were collected by the SMART program and processed with SAINT to apply Lorentz and polarisation corrections to the diffraction spots (integrated 3 dimensionally). Crystal data are given in Table 1. The structures were solved by direct methods and refined using the SHELXTL program [9]. Hydrogen atoms were calculated at ideal positions. Complexes **4**, **7**, and **14** contained disordered solvent which could not be modelled satisfactorily. The contributions in each case were removed using PLATON/SQUEEZE [10]. Complex **4**: 29 electrons per cell corresponding to approximately 0.33 CH_2Cl_2 (disordered around the position 1, 0.5, 0.5) was removed and 266 Å^3

Table 1
Crystal and refinement data for the complexes

Compound	**4** · $0.17CH_2Cl_2$	**5** · $2CH_3CN$	**6** · $3CH_2Cl_2$	**7** · $2CH_2Cl_2$	**10** · $2CH_2Cl_2$
Molecular formula	$C_{36.17}H_{36.33}Br_2Cl_{0.33}CoN_9O_6P_3$	$C_{34}H_{30}Cl_4Co_2N_{11}O_6P_3$	$C_{33}H_{30}Br_4Cl_6CoN_9O_6P_3$	$C_{38}H_{40}Cl_8Co_2N_9O_6P_3$	$C_{32}H_{28}BrCl_4CoF_6N_9O_6P_4$
M	1016.43	1041.26	1391.77	1383.02	1153.15
T (K)	293(2)	150(2)	203(2)	200(2)	163(2)
Crystal System	triclinic	triclinic	triclinic	monoclinic	orthorhombic
Space group	$P\bar{1}$	$P\bar{1}$	$P\bar{1}$	$P2(1)/n$	$Pna2(1)$
a (Å)	10.794(7)	11.7266(6)	13.0237(3)	19.1746(4)	27.148(10)
b (Å)	11.132(7)	14.0516(7)	14.6433(3)	13.9006(3)	14.750(5)
c (Å)	21.881(14)	14.1553(8)	15.7900(3)	19.8557(3)	10.922(4)
α (°)	92.826(8)	79.919(1)	115.978(1)		
β (°)	102.100(8)	67.906(1)	113.546(1)	107.167(1)	
γ (°)	114.624(8)	83.044(1)	91.533(1)		
V (Å^3)	2309(3)	2123.92(19)	2406.16(9)	5056.53(17)	4373(3)
Z	2	2	2	4	4
μ(Mo Kα) (mm^{-1})	2.275	1.204	4.496	1.227	1.777
ρ_{calc} (g cm^{-3})	1.461	1.628	1.921	1.816	1.751
$2\theta_{max}$ (°)	53.22	53.00	52.74	54.48	52.72
Number of unique reflections	9297	8538	9631	10913	8527
Data/restraints/parameters	9297/0/520	8538/0/541	9631/22/589	10931/0/541	8527/1/568
Final R indices [$I > 2\sigma(I)$]	$R_1 = 0.0260$; $wR_2 = 0.0731$	$R_1 = 0.0750$; $wR_2 = 0.1414$	$R_1 = 0.0641$; $wR_2 = 0.1546$	$R_1 = 0.0710$; $wR_2 = 0.1803$	$R_1 = 0.0314$; $wR_2 = 0.0722$
R indices (all data)	$R_1 = 0.0302$; $wR_2 = 0.0744$	$R_1 = 0.1710$; $wR_2 = 0.1788$	$R_1 = 0.1117$; $wR_2 = 0.1889$	$R_1 = 0.1131$; $wR_2 = 0.2011$	$R_1 = 0.0397$; $wR_2 = 0.0739$
Goodness-of-fit on F^2	1.083	1.053	0.960	1.024	1.021

	11 · CH_2Cl_2	**12** · $CHCl_3$	**13** · $2CH_2Cl_2$	**14** · $1.4CH_2ClCH_2Cl$
Molecular formula	$C_{31}H_{26}Cl_4N_9NiO_6P_3$	$C_{32}H_{25}Cl_5N_9NiO_6P_3$	$C_{32}H_{28}Cl_5F_6N_9NiO_6P_3$	$C_{32.8}H_{29.6}Cl_{6.8}N_9O_6P_3Zn_2$
M	914.03	1067.84	1108.47	1110.56
T (K)	168(2)	163(2)	293(2)	203(2)
Crystal system	triclinic	monoclinic	orthorhombic	orthorhombic
Space group	$P\bar{1}$	$C2/c$	$Pna2(1)$	$Pbca$
a (Å)	9.587(3)	15.342(8)	27.1276(1)	19.7586(3)
b (Å)	12.220(3)	29.866(19)	14.7449(2)	15.0435(1)
c (Å)	16.798(5)	9.272(5)	10.8542(1)	32.4780(5)
α (°)	99.491(4)			
β (°)	90.420(4)	94.642(8)		
γ (°)	103.708(4)			
V (Å^3)	1883.5(9)	4234(4)	4341.61(7)	9653.7(2)
Z	2	4	4	8
μ(Mo Kα) (mm^{-1})	0.983	1.132	0.983	1.518
ρ_{calc} (g cm^{-3})	1.612	1.675	1.696	1.528
$2\theta_{max}$ (°)	52.84	52.88	55.04	52.14
Number of unique reflections	7577	4318	9135	9245
Data/restraints/parameters	7577/0/487	4318/0/268	9135/13/570	9245/0/523
Final R indices [$I > 2\sigma(I)$]	$R_1 = 0.0321$; $wR_2 = 0.0769$	$R_1 = 0.0678$; $wR_2 = 0.1539$	$R_1 = 0.0400$; $wR_2 = 0.1002$	$R_1 = 0.0473$; $wR_2 = 0.1185$
R indices (all data)	$R = 0.0480$; $wR_2 = 0.0831$	$R_1 = 0.1226$; $wR_2 = 0.1737$	$R_1 = 0.0521$; $wR_2 = 0.1118$	$R_1 = 0.0599$; $wR_2 = 0.1252$
Goodness-of-fit on F^2	1.006	0.924	0.957	1.086

was left by the void. The reported formula is **1** · $0.17CH_2Cl_2$. Complex **7**: 339 electrons per cell corresponding to 2 · CH_2Cl_2 molecules (disordered over several positions and orientations) were removed and 937 Å^3 was left by the void. The reported formula is **7** · $2CH_2Cl_2$. Complex **14**: 163 electrons per cell corresponding to 3.2 $C_2H_4Cl_2$ molecules were removed and 1789 Å^3 was left by the void. Another molecule of $C_2H_4Cl_2$ per formula unit is present and was refined in the model. The reported formula is **14** · $1.4C_2H_4Cl_2$.

3. Results and discussion

3.1. Syntheses of compounds

The reactions between L or MeL and CoX_2 (X = Cl or Br) are shown in Scheme 1. Allowing CoX_2 suspended in a solution of L or MeL in CH_2Cl_2 in equimolar amounts to stir at room temperature affords the 1:1 complexes **1**–**4**. From the reactions between an excess of CoX_2 and L or MeL, the dimetallic compounds **5**–**8** were

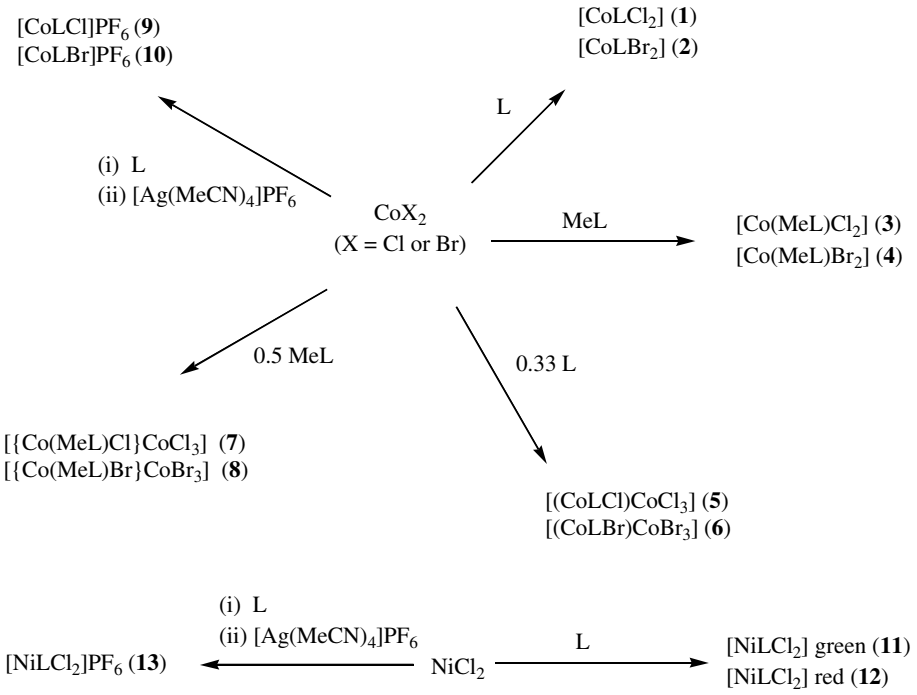

Scheme 1. The reactions of L and MeL with cobalt(II) and nickel(II) halides.

obtained which contain both four- and six-coordinate cobalt(II) centres. Following the treatment of the 1:1 adducts in situ with $[Ag(MeCN)_4]PF_6$, the monocationic CoX adducts were isolated as hexafluorophosphate salts (**9** and **10**).

The reaction between 3 equiv. of $NiCl_2$ and **L** also produces a 1:1 adduct. Green and red crystalline forms of $[NiLCl_2]$ (**11** and **12**) were obtained under different crystallisation conditions, in which the nickel(II) centres are six- and five-coordinate, respectively. Treatment of the monoadduct in situ with $[Ag(MeCN)_4]PF_6$ produces the six-coordinate $[NiLCl]PF_6$ (**13**). We were only able to isolate 1:1 adducts of L using $NiCl_2$. From the reaction between $ZnCl_2$ and L we isolated the dimetallic adduct, $[(ZnCl_2)_2L]$ (**14**), which contains both four- and five-coordinate zinc(II) centres. In all cases the positive ion mass spectra (LSIMS) of the complexes exhibit significant peaks assignable to $[MLX]^+$ ions although the dimetallic cobalt complexes of L also show weak peaks corresponding to $[Co_2LX_3]^+$ (X = Cl or Br) ions.

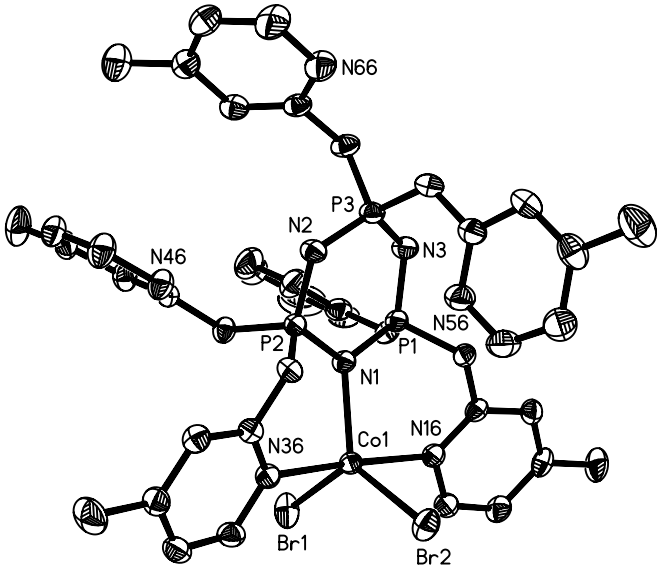

Fig. 1. View of the complex $[Co(MeL)Br_2]$ (**4**). Ellipsoids are drawn at the 50% probability level.

3.2. Description of structures

3.2.1. The five-coordinate complexes $[Co(MeL)Br_2]$ (**4**) and $[NiLCl_2]$ (**12**)

The $[Co(MeL)Br_2]$ (**4**) complex (Fig. 1) is a neutral species containing a five-coordinate 'CoN_3Br_2' centre. The ligand MeL coordinates in a κ^3N non-geminal *cisoid* manner (Scheme 2a) through phosphazene ring nitrogen N(1) and the nitrogen atoms N(16) and N(36) from two pyridyloxy arms. The geometry around the cobalt is distorted trigonal bipyramidal ($\tau = 0.83$[1]) with the axial bonds being defined as Co–N(16) and Co–N(36). Selected bond lengths and bond angles are given in Table 2. The overall structure is similar to that observed for $[CuLCl_2]$ although **4** is considerably less distorted from trigonal bipyramidal geometry

[1] The structural index, τ, is used to define the geometry of five coordinate systems and equals 1 for a perfect trigonal bipyramid and 0 for a perfect square pyramid Ref. [11].

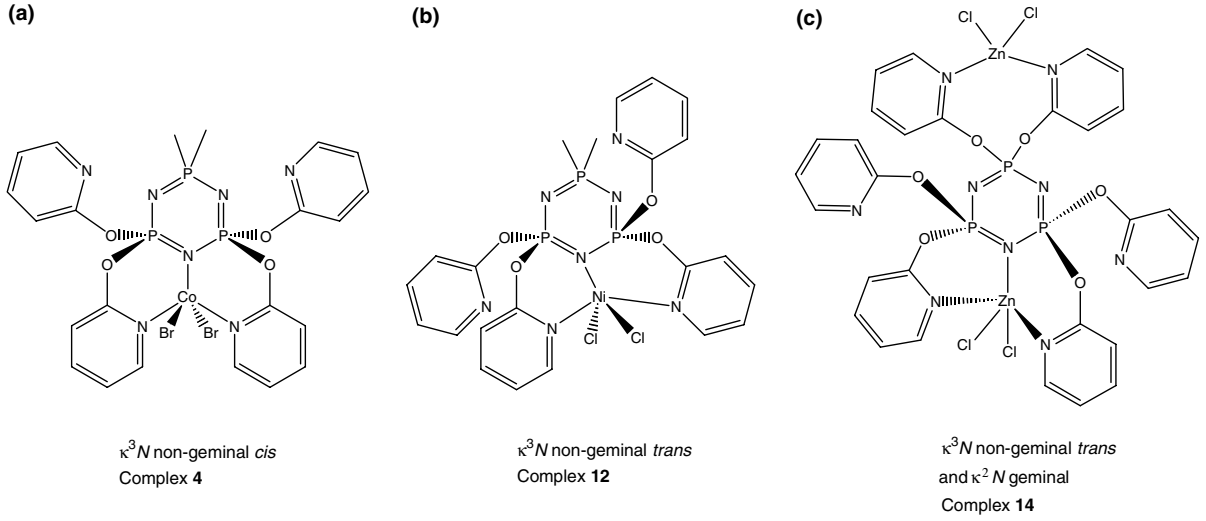

Scheme 2. Structural types: complexes **4**, **12** and **14**. Some parts have been omitted for clarity.

Table 2
Selected bond lengths (Å) and bond angles (°) for complexes **4**, **12** and **14**

*[Co(MeL)Br$_2$] · 0.17CH$_2$Cl$_2$ (**4** · 0.17CH$_2$Cl$_2$)*			
Co(1)–N(1)	2.0895(19)	Co(1)–Br(1)	2.4414(13)
Co(1)–N(16)	2.243(2)	Co(1)–Br(2)	2.4505(13)
Co(1)–N(36)	2.243(2)		
P(1)–N(1)	1.6263(18)	P(1)–N(3)	1.5733(18)
P(2)–N(1)	1.6277(17)	P(2)–N(2)	1.5757(17)
	1.5918(19)	P(3)–N(3)	1.5942(18)
N(16)–Cu(1)–N(36)	174.97(6)	Br(1)–Cu(1)–Br(2)	125.37(2)
N(1)–Cu(1)–N(36)	91.55(6)	N(1)–Cu(1)–N(16)	90.94(6)
*[NiLCl$_2$] · 2CH$_2$Cl$_2$ (**12** · 2CH$_2$Cl$_2$)*			
Ni(1)–N(1)	2.023(6)	Ni(1)–Cl(1)	2.3136(17)
Ni(1)–N(16)	2.160(4)		
P(1)–N(1)	1.608(3)	P(1)–N(2)	1.549(5)
P(2)–N(2)	1.581(4)		
N(16)–Ni(1)–N(16A)	178.3(2)	Cl(1)–Ni(1)–Cl(1A)	131.32(9)
N(1)–Ni(1)–N(16)	90.87(11)		90.87(11)
*[(ZnCl$_2$)$_2$L] · 1.4CH$_2$ClCH$_2$Cl (**14** · 1.4CH$_2$ClCH$_2$Cl)*			
Zn(1)–N(1)	2.089(3)	Zn(1)–Cl(1)	2.2360(11)
Zn(1)–N(16)	2.328(3)	Zn(1)–Cl(2)	2.2447(11)
Zn(1)–N(46)	2.349(3)		
Zn(2)–N(56)	2.057(4)	Zn(2)–Cl(3)	2.2046(15)
Zn(2)–N(66)	2.057(3)	Zn(2)–Cl(4)	2.2133(13)
P(1)–N(1)	1.603(3)	P(1)–N(3)	1.563(3)
P(2)–N(1)	1.612(3)	P(2)–N(2)	1.565(3)
P(3)–N(2)	1.571(3)	P(3)–N(3)	1.562(3)
N(16)–Zn(1)–N(46)	172.17(10)	Cl(1)–Zn(1)–Cl(2)	118.42(5)
N(1)–Zn(1)–N(46)	85.69(10)	N(1)–Zn(1)–N(16)	86.75(11)
N(56)–Zn(2)–N(66)	118.17(12)	Cl(3)–Zn(2)–Cl(4)	113.75(7)
N(66)–Zn(2)–Cl(3)	105.78(10)	N(56)–Zn(2)–Cl(4)	103.55(10)

($\tau = 0.47$ in [CuLCl$_2$]) [5]. The contact between the metal and the phosphazene ring, Co–N(1), is much closer in **4** [2.0897(19) cf. 2.264(2) Å] and this bond is significantly shorter than the axial Co–N bonds [both 2.243(2) Å], whereas in [CuLCl$_2$] the converse is true. The angles within the cobalt(II) coordination sphere are unremarkable. The phosphazene ring in **4** is more distorted from planarity than in [CuLCl$_2$]: the distances of N(1) and N(2) above and below the plane described by the remaining atoms in the ring are approximately 0.164 and 0.189 Å (cf. 0.068 and 0.096). P–N–P and N–P–N angles in the ring are typical for cyclophosphazenes but the P(1)–N(1) and P(2)–N(1) bonds [1.6261(18) and 1.6277(17) Å] which flank the coordinated ring nitrogen are longer than the remaining P–N bonds [1.5724(18)–1.5944(18) Å]. This feature has been observed on other cyclic phosphazene complexes that contain a coordinated ring nitrogen [4,5].

Complex **12**, the red NiCl$_2$ adduct of L (Fig. 2 and Table 2), has a similar five-coordinate structure to **4** but

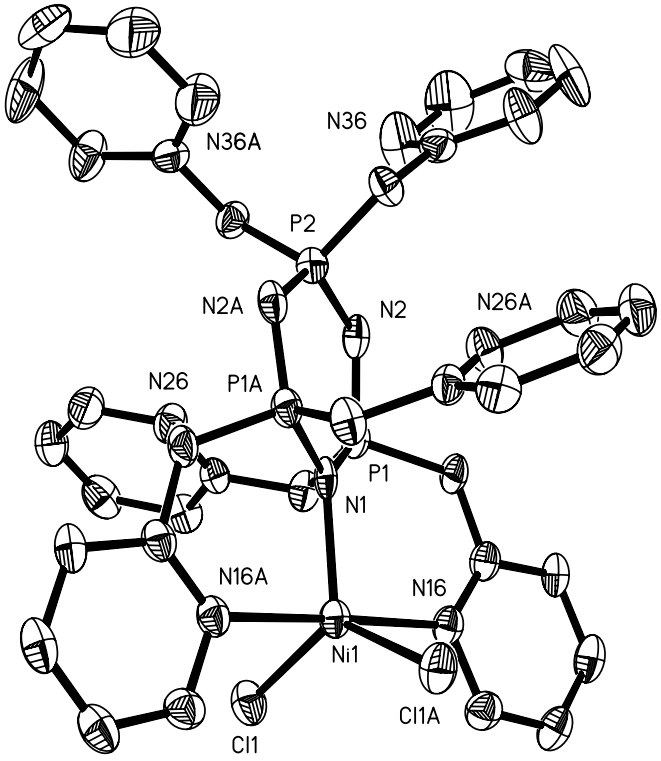

Fig. 2. View of the complex [NiLCl$_2$] (**12**). Ellipsoids are drawn at the 50% probability level.

in this case the ligand coordinates in a κ^3N non-geminal *transoid* manner (Scheme 2b). The geometry about the nickel(II) ion in $[NiLCl_2]$ is also approximately trigonal bipyramidal although it is more distorted than **4** ($\tau = 0.78$). The nickel(II) ion makes a short contact of 2.023(6) Å with N(1) in the phosphazene ring and longer contacts of 2.160(4) Å with the symmetry related axial pyridyl nitrogen atoms. The nickel centre lies directly in the plane described by N(1), P(1), P(1A) and P(2). N(2) and its symmetry equivalent lie approximately 0.137 Å above and below this plane. Other distortions in the phosphazene ring are apparent in the P–N bond lengths and as with **4**, the flanking P–N(1) bond lengths are the longest [1.608(3) Å]. The P(1)–N(2) and P(1A)–N(2A) distances are considerably shorter [1.549(5) Å] and the final pair, P(2)–N(2) and P(2)–N(2A), have an intermediate value of 1.581(4) Å.

3.2.2. The dimetallic complexes *[(CoLCl)$CoCl_3$] (**5**), [(CoLBr)$CoBr_3$] (**6**), [{Co(MeL)Cl}$CoCl_3$] · (**7**) and [($ZnCl_2$)$_2$L] (**14**)*

The dimetallic cobalt(II) complexes **5**, **6** and **7**, have the same basic structure in which the ligands (L or MeL) bridge two Co(II) ions (Fig. 3). The ligands coordinate in both the tetrapodal κ^5N binding mode, using four pendant pyridyloxy arms and a phosphazene ring nitrogen, and in a monodentate κ^1N binding mode, using one pyridyloxy arm. The complexes contain both six-coordinate 'CoN_5X' and four-coordinate '$CoNX_3$' centres making them neutral and zwitterionic (Scheme 3a). Selected bond lengths and angles are given in Table 3. The geometry at the six-coordinate centres is elongated rhombic octahedral, similar to that previously observed in the $[CuLCl]^+$ monocation [5]. The complexes contain a pair of long axial bonds, Co–N(16) and Co–N(46) which range between 2.327(4) and

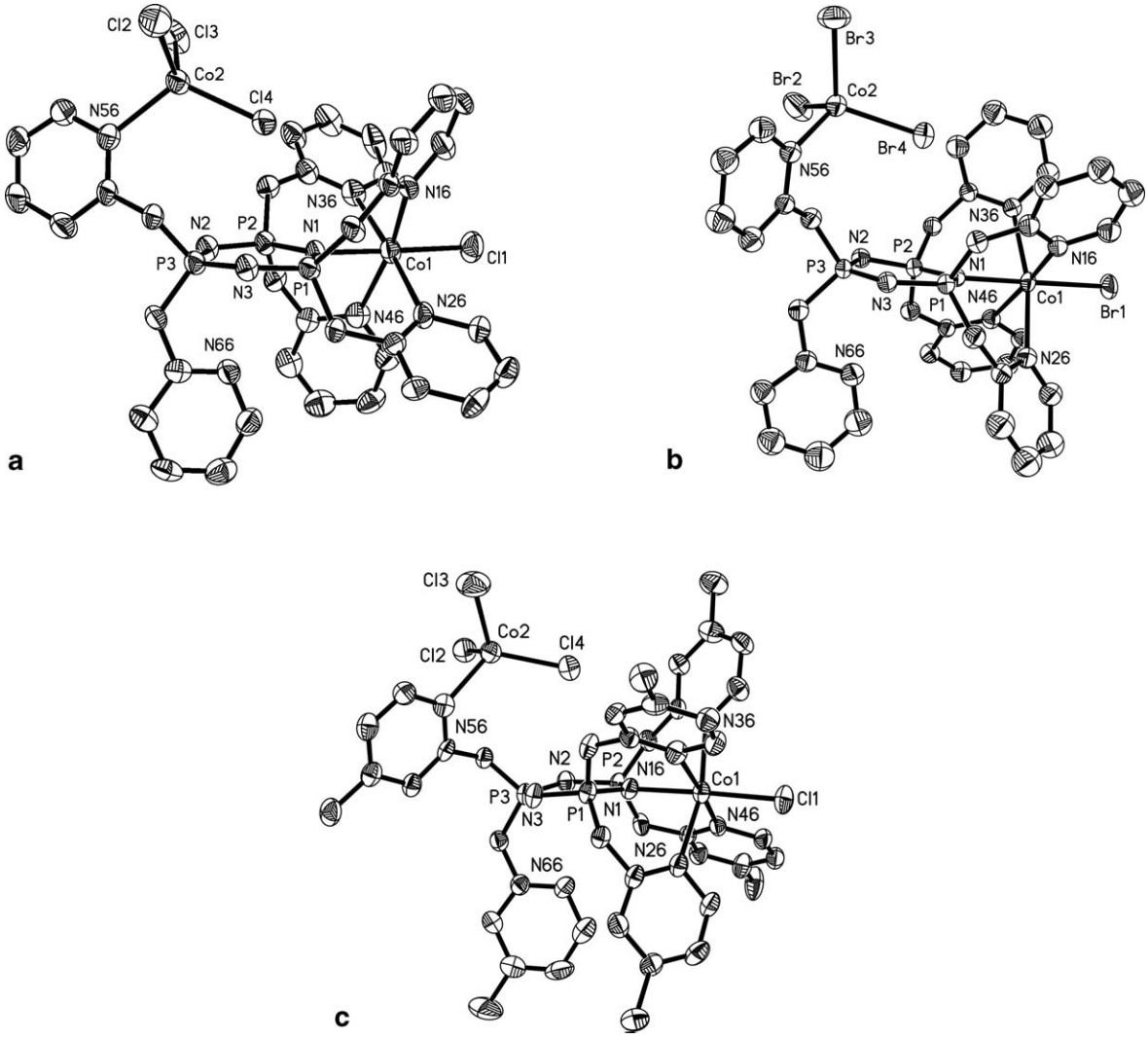

Fig. 3. View of the complexes: (a) [(CoLCl)$CoCl_3$] (**5**); (b) [(CoLBr)$CoBr_3$] (**6**); (c) [{Co(MeL)Cl}$CoCl_3$] (**7**). Ellipsoids are drawn at the 50% probability level.

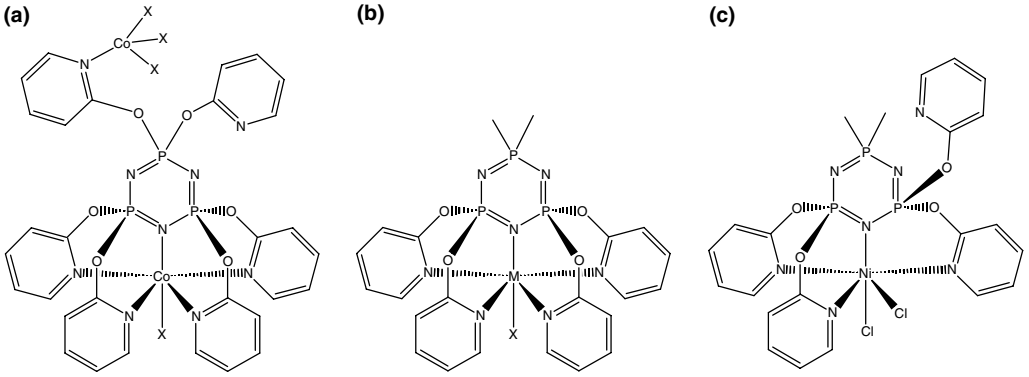

Scheme 3. Structural types: complexes **5**, **6**, **7**, **10**, **11** and **13**. Some parts have been omitted for clarity.

Table 3
Bond lengths (Å) and bond angles (°) for dimetallic cobalt species **5**, **6** and **7**

Complex	[(CoLCl)$CoCl_3$]·$2CH_3CN$ (**5**·$2CH_3CN$)	[(CoLBr)$CoBr_3$]·$3CH_2Cl_2$ (**6**·$3CH_2Cl_2$)	[{Co(MeL)Cl}$CoCl_3$]·$2CH_2Cl_2$ (**7**·$2CH_2Cl_2$)
	X = Cl	X = Br	X = Cl
Co(1)–N(1)	2.032(5)	2.034(5)	2.035(4)
Co(1)–N(16)	2.381(6)	2.341(5)	2.382(4)
Co(1)–N(26)	2.191(6)	2.189(6)	2.190(4)
Co(1)–N(36)	2.197(6)	2.192(6)	2.198(4)
Co(1)–N(46)	2.375(5)	2.402(5)	2.327(4)
Co(1)–X(1)	2.281(2)	2.4492(11)	2.2893(14)
Co(2)–N(56)	2.102(6)	2.071(6)	2.093(5)
Co(2)–X(2)	2.261(2)	2.3768(14)	2.2606(17)
Co(2)–X(3)	2.249(2)	2.4010(13)	2.2576(18)
Co(2)–X(4)	2.236(2)	2.3626(12)	2.2317(16)
P(1)–N(1)	1.592(5)	1.581(5)	1.589(4)
P(2)–N(1)	1.597(5)	1.586(5)	1.583(4)
P(2)–N(2)	1.558(5)	1.542(5)	1.565(4)
P(3)–N(2)	1.577(5)	1.572(5)	1.571(4)
P(1)–N(3)	1.552(6)	1.552(5)	1.555(4)
P(3)–N(3)	1.581(5)	1.583(5)	1.583(4)
N(16)–Co(1)–N(46)	175.5(2)	172.39(19)	175.15(14)
N(26)–Co(1)–N(36)	164.9(2)	166.7(2)	166.04(16)
N(1)–Co(1)–X(1)	178.86(16)	177.24(14)	177.05(12)
N(56)–Co(1)–X(2)	106.18(6)	109.50(16)	98.67(13)
N(56)–Co(1)–X(3)	101.06(16)	102.03(15)	103.81(13)
N(56)–Co(1)–X(4)	117.12(17)	111.77(16)	115.57(13)

2.402(5) Å and a pair of shorter equatorial Co–N(py) bonds, Co–N(26) and Co–N(36) that range between 2.189(6) and 2.198(4) Å. The pyridyl rings that give rise to the axial bonds are approximately coplanar (the mean planes are twisted by approximately between 2.2° (**8**), 6.4° (**5**) and 11.2° (**6**) to one another) whereas the mean planes of the equatorial pyridyl rings are twisted to one another by approximately 73°, 69° and 70°. In each case the shortest metal to ligand contact at ~2.035(4) Å in the six-coordinate centre is between the cobalt and the phosphazene ring nitrogen N(1).

A close examination of the '$CoNX_3$' centres points to an interaction of the halogen atoms with the π-electron density on pyridyl rings 1 or 3 (Scheme 4). These compressed tetrahedral centres in **5**, **6** and **7** are more distorted than similar '$CoNCl_3$' and '$CoNBr_3$' centres reported in the literature [12–15]. The Co–N(56) distances are approximately 0.2–0.5 Å longer than the corresponding bonds in the related structures and the tetrahedral angles are more varied. Particularly affected is the angle N(56)–Co(1)–X(4) which varies between 111.77(16)° and 117.12(17)°. The persistent orientation of the '$CoNX_3$' fragment in this manner is significant since it is independent of the ligand, the nature

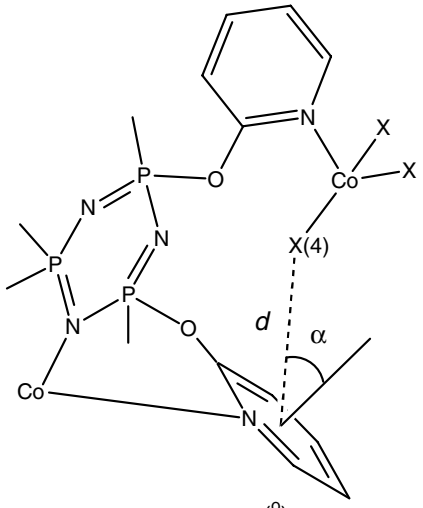

	α (°)	d (Å)
[(CoLCl)$CoCl_3$] (**5**)	32	3.774
[(CoLBr)$CoBr_3$] (**6**)	20	3.744
[{Co(MeL)Cl}$CoCl_3$] (**7**)	38	3.928

Scheme 4. Interaction of halogen atoms with pyridyloxy rings for complexes **5**, **6** and **7**.

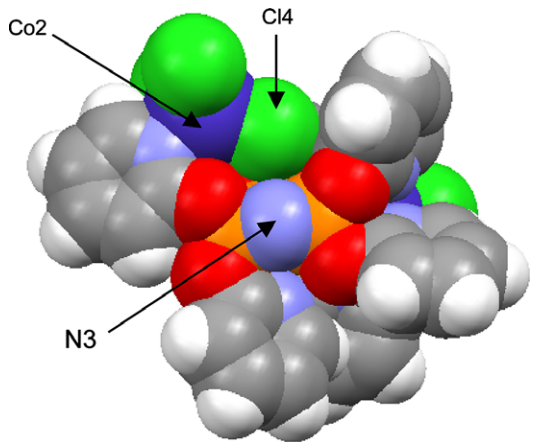

Fig. 4. Space filling diagram of $[(CoLCl)CoCl_3]$ (**5**) showing the interaction of a Cl with a pendant pyridyloxy ring.

of the anion and the different unit cell types. The zwitterions have an overall compact shape (Fig. 4) because of this interaction with the pyridyl rings 1 or 3. The influence of halogen–π interactions on crystal packing has been recognised before (e.g., Refs. [16–18]) and the geometrical parameters for complexes **5**–**7** relevant to the recent treatment by Swierczynski et al. [19] are given in Scheme 4. In each case the distance (*d*) of X(4) from the closest pyridyl ring centroid is below 4 Å (being in the range 3.744–3.928 Å) and the angle (α) between the vector along the aryl ring centroid-halogen centre and the perpendicular vector originating in the aryl centre is between 20° and 38°.

In contrast, the dimetallic zinc complex $[(ZnCl_2)_2L]$ (**14**) (Fig. 5 and Table 2), contains two $ZnCl_2$ units in both five- and four-coordinate geometry, bridged by L. Here L acts in κ^2N geminal bidentate and κ^3N non-geminal *transoid* coordination modes (Scheme 2c). The five-coordinate centre is comparable to that in the five-coordinate nickel complex $[NiLCl_2]$ (**12**). The geometry is distorted trigonal bipyramidal ($\tau = 0.82$) with the axial bonds being to the pyridyloxy nitrogen atoms N(16) and N(46). As in **12**, the equatorial bond length, Zn(1)–N(1) at 2.089(3) Å, is considerably shorter than the axial Zn–N bonds [2.328(3) and 2.349(3) Å]. The four coordinate '$ZnCl_2$' centre is approximately tetrahedral and similar to that observed for $[Zn(py)_2Cl_2]$ (py = pyridine) [20] although the Zn–N distances in this complex are shorter [2.046(5) and 2.052(6) Å]. The phosphazene ring plane in **14** is essentially undistorted. The atoms N(1) and N(3) lie 0.0813 and 0.0675 Å, respectively, above and below the plane described by the other atoms in the ring and are the biggest deviations. Within the ring, as in the other five-coordinate complexes, $[Co(MeL)Br_2]$ (**4**) and $[NiLCl_2]$ (**12**), the P–N(1) bonds flanking the metal binding site are the longest [1.612(3) and 1.603(3) Å] with the remaining P–N bonds ranging between 1.563(3) and 1.571(3) Å.

3.2.3. The six-coordinate complexes $[CoLBr]PF_6$ (**10**), $[NiLCl_2]$ (**11**) and $[NiLCl]PF_6$ (**13**)

The cationic cobalt complex $[CoLBr]PF_6$ (**10**) (Fig. 6 and Table 4) contains a distorted rhombic 'CoN_5Br' coordination sphere derived from the tetrapodal κ^5N binding mode of L (Scheme 3b) which is essentially the same as that found in the dimetallic complex **6** although the bond to the phosphazene ring nitrogen atom, Co–N(1), is longer than the corresponding bond in **6** [2.064(2) cf. 2.025(8) Å]. The two longest Co–N bonds involve the nitrogen atoms from two of the bound pyridyloxy rings. The structure of $[NiLCl]PF_6$ (**13**) (Fig. 7 and Table 4) is essentially the same as that of (**10**) and, in fact, crystals of **10** · $2CH_2Cl_2$, **13** · $2CH_2Cl_2$ and $[CuLCl]PF_6 \cdot 2CH_2Cl_2$ [5] are all isomorphous belonging to the space group $Pna2_1$.

The green complex $[NiLCl_2]$ (**11**) (Fig. 8 and Table 4) contains a six-coordinate 'NiN_4Cl_2' coordination sphere which is best described as distorted octahedral. The ligand acts as a tripodal κ^4N donor forming two short bonds to

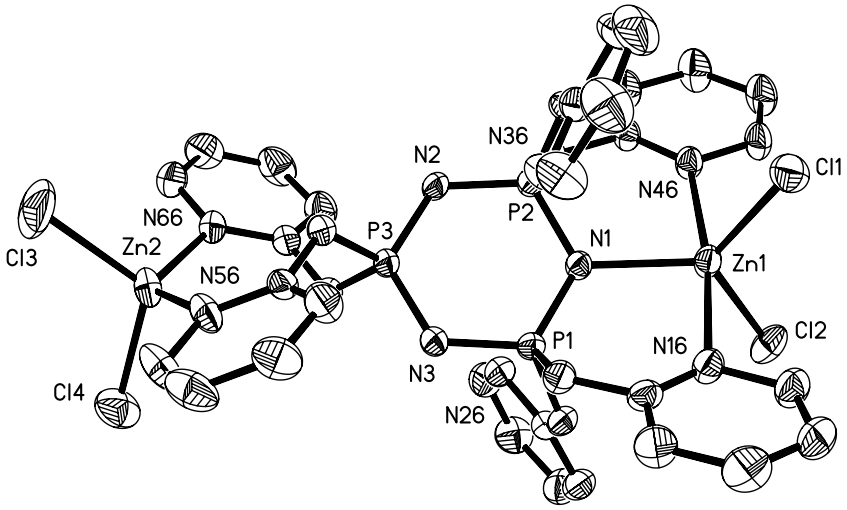

Fig. 5. View of the complex $[(ZnCl_2)_2L]$ (**14**). Ellipsoids are drawn at the 40% probability level.

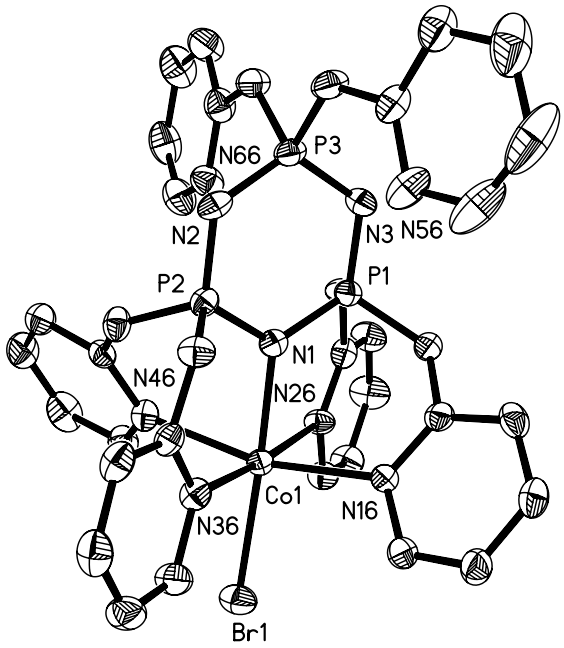

Fig. 6. View of the complex $[CoLBr]PF_6$ (**10**). Ellipsoids are drawn at the 50% probability level.

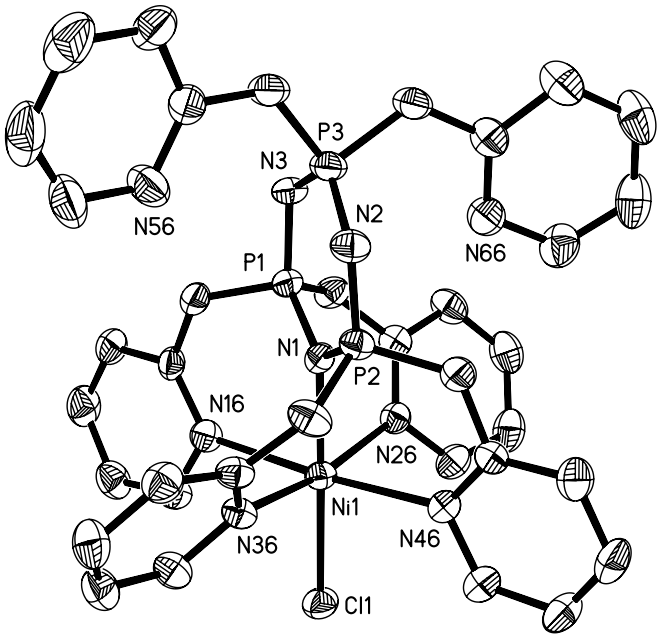

Fig. 7. View of the complex $[NiLCl]PF_6$ (**13**). Ellipsoids are drawn at the 50% probability level.

Table 4
Bond lengths (Å) and bond angles (°) for six coordinate complexes **10**, **11** and **13**

Complex	$[CoLBr]PF_6 \cdot 2CH_2Cl_2$ ($\mathbf{10} \cdot 2CH_2Cl_2$)	$[NiLCl_2] \cdot CH_2Cl_2$ ($\mathbf{11} \cdot CH_2Cl_2$)	$[NiLCl]PF_6 \cdot 2CH_2Cl_2$ ($\mathbf{13} \cdot 2CH_2Cl_2$)
	M = Co, X = Br	M = Ni, X = Cl	M = Ni, X = Cl
M(1)–N(1)	2.064(2)	2.1075(18)	2.027(3)
M(1)–N(16)	2.208(3)	2.221(2)	2.326(4)
M(1)–N(26)	2.347(3)		2.176(4)
M(1)–N(36)	2.397(3)	2.180(2)	2.157(4)
M(1)–N(46)	2.219(3)	2.3652(19)	2.311(4)
M(1)–X(1)	2.4562(9)	2.3860(8)	2.3118(10)
P(1)–N(1)	1.589(3)	1.6057(18)	1.590(3)
P(2)–N(1)	1.591(3)	1.5950(18)	1.591(3)
P(2)–N(2)	1.562(3)	1.5709(19)	1.561(4)
P(3)–N(2)	1.587(3)	1.587(2)	1.593(4)
P(1)–N(3)	1.568(3)	1.571(2)	1.559(3)
P(3)–N(3)	1.586(3)	1.588(2)	1.590(4)
N(16)–M(1)–N(46)	165.58(9)	167.71(7)	175.54(13)
N(26)–M(1)–N(36)	174.14(9)		168.74(13)
N(1)–M(1)–X(1)	177.33(7)	166.64(5)	179.38(10)
N(36)–M(1)–X(2)		177.00(6)	

the nickel through N(1) and N(36) which are *cis* [2.1705(18) and 2.180(2) Å, respectively] and two longer bonds through N(16) and N(46) which are *trans* [2.221(2) and 2.3652(16) Å, respectively]. As a result of L acting as a pentadentate in **13** there is a closer contact between the nickel (II) ion [2.027(3) Å] and the phosphazene ring nitrogen N(1) than in **11**. Also the nickel(II) ion lies closer to the mean plane of the phosphazene ring (approximately 0.0678 from the plane, cf. 0.4576 Å in **11**).

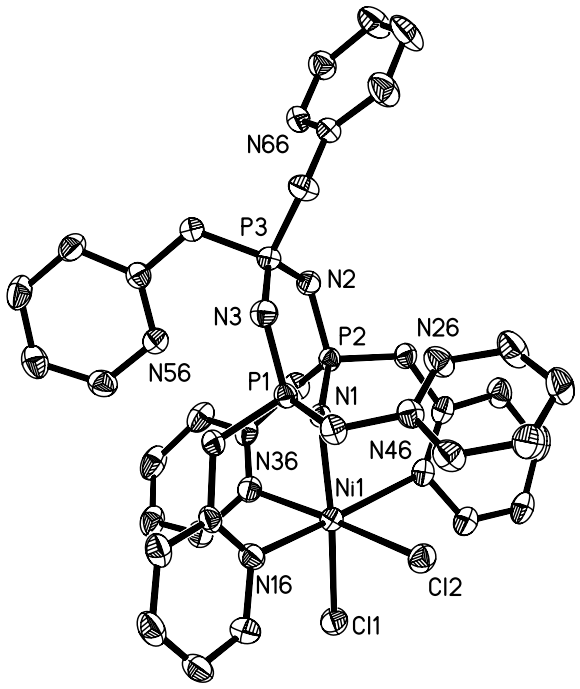

Fig. 8. View of the complex $[NiLCl_2]$ (**11**). Ellipsoids are drawn at the 50% probability level.

4. Conclusions

This report, along with our earlier work [3,5,6], clearly demonstrates that the design of the ligands L and MeL makes them particularly effective multimodal ligands capable of binding one or two metal atoms in a variety of coordination modes, ranging from κ^1N to κ^5N, depend-

Table 5
X-ray structural parameters of the four- and five-coordination centres for the L and MeL complexes

Compound	Binding mode[a]	τ[b]	M–N(phosphazene)/Å	M–N(pyridyloxy)/Å
$[Co(MeL)Br_2]$ (**4**)	κ^3N non-gem *cis*	0.83	2.0895(19)	2.243(2), 2.243(2)
$[NiLCl_2]$ (**12**)	κ^3N non-gem *trans*	0.78	2.023(6)	2.160(4)
$[(ZnCl_2)_2L]$ (**14**)	κ^3N non-gem *trans*	0.82	2.089(3)	2.328(3), 2.349(3)
$[CuLCl_2]$[a]	κ^3N non-gem *cis*	0.47	2.264(2)	2.061(3), 2.058(3)
$[(CuCl_2)_2(MeL)]$[a]	κ^3N non-gem *cis*	0.57	2.214(3)	2.056(3), 2.084(3)
$[NiLCl_2]$ (**11**)	κ^4N tripodal		2.1075(18)	2.180(2)–2.3652(19)
$[(CoLCl)CoCl_3]$ (**5**)	κ^5N tetrapodal		2.032(5)	2.191(6)–2.381(6)
$[(CoLBr)CoBr_3]$ (**6**)	κ^5N tetrapodal		2.034(5)	2.189(6)–2.402(5)
$[\{Co(MeL)Cl\}CoCl_3]$ (**7**)	κ^5N tetrapodal		2.035(4)	2.190(4)–2.382(4)
$[CoLBr]PF_6$ (**10**)	κ^5N tetrapodal		2.064(2)	2.208(3)–2.397(3)
$[NiLCl]PF_6$ (**13**)	κ^5N tetrapodal		2.027(3)	2.157(4)–2.326(4)
$[CuLCl]PF_6$[a]	κ^5N tetrapodal		1.993(3)	2.140(3)–2.482(3)
$[(CuLCl)_2(CuCl_2)][Cu_2Cl_6]$[b]	κ^5N tetrapodal		1.988(2)	2.090(3)–2.559(3)

[a] From Ref. [5].
[b] From Ref. [6].

ing on the number of pyridyloxy pendant arms are involved. Monodentate κ^1N binding using a pyridyloxy nitrogen atom, as exhibited in the tetrahedral sites in the dimetallic complexes $[(CoLX)CoX_3]$ (X = Cl or Br) (**5** and **6**) and $[\{Co(MeL)Cl\}CoCl_3]$ (**7**), do not involve the phosphazene ring nitrogen atom as a donor. However, this binding mode does allow the linking of two cyclophosphazene platforms into a dimer, viz., $[(CuLCl)_2(CuCl_2)]^{2+}$ [6]. Bidentate κ^2N binding is seen in the tetrahedral site in the dimetallic complex, $[(ZnCl_2)_2L]$ (**14**), and again the phosphazene nitrogen atoms do not bind to the metal. In contrast, in the silver(I) complexes, $\{[AgL]^+\}_\infty$ and $\{[Ag(MeL)]^+\}_\infty$, a different κ^2N binding mode is observed with one nitrogen donor coming from the phosphazene ring and the other from a pendant pyridyloxy nitrogen hence affording supramolecular cationic columns [3]. Complexes with five-coordinate sites all have the ligand binding in a κ^3N fashion via the nitrogen atoms from two non-geminal pyridyloxy pendant arms and a nitrogen atom in the phosphazene ring, e.g., in $[Co(MeL)Br_2]$ (**4**), the red isomer of $[NiLCl_2]$ (**12**), the five-coordinate site in $[(ZnCl_2)_2L]$ (**14**), $[CuLCl_2]$ and both copper sites in $[\{CuCl_2\}_2MeL]$ [5]. In the majority of the six-coordinate sites, the ligand binds via the κ^5N mode using nitrogen atoms from four pendant pyridyloxy arms and a phosphazene ring nitrogen, e.g., in $[CoLBr]PF_6$ (**10**), $[NiLCl]PF_6$ (**13**) the six-coordinate sites in the dimetallic complexes **5**, **6** and **7** and in $[CuLCl]PF_6$ [5]. The exception to this in found in the green isomer of $[NiLCl_2]$ (**11**) which has the nickel bound to L via a κ^4N mode using only three of the pendant pyridyloxy nitrogen donors.

In the compounds of L and MeL reported in this study and in our earlier papers [3,5,6], the cyclophosphazene platform does not deviate significantly from planarity which is in marked contrast to what is observed for complexes of hexakis(3,5-dimethylpyrazolyl)cyclotriphosphazene, $N_3P_3(3,5\text{-}Me_2Pz)_6$, and related ligands [4,21]. Another major difference is that for each of the κ^3N, κ^4N and κ^5N complexes of L and MeL with the divalent metal ions with the exception of κ^3N copper complexes (which are significantly distorted from trigonal bipyramidal), the phosphazene nitrogen metal bond is shorter than the pendant pyridyloxy nitrogen metal bonds (Table 5) whereas a reversal of these bond lengths is seen when the pyrazolyl is the pendant arm [4,21] For example, L and $N_3P_3(3,5\text{-}Me_2Pz)_6$ form dimetallic complexes with zinc(II) with the same stoichiometry, i.e., $[(ZnCl_2)_2L]$ (**14**) and $[(ZnCl_2)_2\{N_3P_3(3,5\text{-}Me_2Pz)_6\}]$ [21], which contain the metal in both κ^2N four-and κ^3N five-coordinate sites. However, to accommodate the steric demands of $N_3P_3(3,5\text{-}Me_2Pz)_6$ the cyclophosphazene ring puckers markedly towards the zinc atom in the five-coordinate site, the displacement of the phosphazene nitrogen bound to the zinc being 0.490 Å from the plane defined the other ring atoms. As mentioned in Section 3.2.2, the phosphazene ring is essentially undistorted in **14**. The phosphazene nitrogen bond distance in **14** is 2.089(3) Å [cf. 2.328(3) and 2.349(3) Å for the other Zn–N bonds] whereas in the analogous $N_3P_3(3,5\text{-}Me_2Pz)_6$ complex it is longer at 2.332(6) Å [cf. 2.200(6) and 2.141(6) Å]. The marked differences observed between the L and MeL complexes and the pyrazolyl complexes can be ascribed to the presence of the phenoxy hinge linking the pyridyloxy pendant arms to the phosphazene ring, hence allowing the formation of six-membered chelate rings rather than the more strained five-membered rings in the latter systems.

Acknowledgements

We acknowledge financial support, including postdoctoral fellowships (to C.V.D. and C.A.O.), from the Massey University Research Fund and the RSNZ Marsden Fund (MAU208). We thank Dr. A.K. Burrell, Dr. A. Derwahl and Professor G.B. Jameson for valued crystallographic advice and the Otsuka Chemical Co. Ltd. for a gift of cyclotriphosphazene.

Appendix A. Supplementary material

Crystallographic data for the structural analysis has been deposited with the Cambridge Crystallographic Data Centre, CCDC Nos. CCDC 293045–293053. Copies of this information may be obtained free of charge from: The Director, CCDC, 12 Union Road, Cambridge, CB2 1EZ, UK (fax: +44 1223 336 033; e-mail: deposit@ccdc.cam.ac.uk or www: http://www.ccdc.cam.ac.uk). Supplementary data associated with this article can be found, in the online version, at doi:10.1016/j.poly.2006.02.001.

References

[1] M. Gleria, R. De Jaeger (Eds.), Applicative Aspects of Cyclophosphazenes, Nova Science Publishers, Inc., New York, 2004.
[2] P.I. Richards, A. Steiner, Inorg. Chem. 43 (2004) 2810.
[3] E.W. Ainscough, A.M. Brodie, C.V. Depree, G.B. Jameson, C.A. Otter, Inorg. Chem. 44 (2005) 7325.
[4] V. Chandrasekhar, S. Nagendran, Chem. Soc. Rev. 30 (2001) 193, and references therein.
[5] E.W. Ainscough, A.M. Brodie, C.V. Depree, B. Moubaraki, K.S. Murray, C.A. Otter, Dalton Trans. (2005) 3337.
[6] E.W. Ainscough, A.M. Brodie, C.V. Depree, J. Chem. Soc., Dalton Trans. (1999) 4123.
[7] Y. Cho, H. Baek, Y.S. Sohn, Macromolecules 32 (1999) 2167.
[8] G.J. Kubas, Inorg. Synth. 28 (1990) 68.
[9] G.M. Sheldrick, SHELXL Suite of Programs for Crystal Structure Analysis, Institüt für Anorganische Chemie der Universität, Tammanstrasse 4, Göttingen, Germany, 1998.
[10] P. van der Sluis, A.L. Spek, Acta Crystallogr., Sect. A 46 (1990) 194.
[11] A.W. Addison, T.N. Rao, J. Reedijk, J. Van Rijn, G.C. Verschoor, J. Chem. Soc., Dalton Trans. (1984) 1349.
[12] M. Bloy, M. Kretschmann, S. Scholz, M. Teichert, U. Diefenbach, Z. Anorg. Allg. Chem. 626 (2000) 1946.
[13] G.J.E. Davidson, S.J. Loeb, N.A. Parekh, J.A. Wisner, J. Chem. Soc., Dalton Trans. (2001) 3135.
[14] V. Divjakovic, V.M. Leovac, B. Ribar, G. Argay, A. Kalman, Acta Crystallogr., Sect. B 38 (1982) 1738.
[15] H. Xu, J. Li, Z. Wu, J. Zou, Z. Xu, X. You, Polyhedron 12 (1993) 2261.
[16] M.D. Prasanna, T.N. Guru Row, Cryst. Eng. 3 (2000) 135.
[17] R. Bishop, M.L. Scudder, D.C. Craig, A.N.M.M. Rahman, S.F. Alshahteet, Mol. Cryst. Liq. Cryst. 440 (2005) 173.
[18] B. Nagaraj, T. Narasimhamurthy, H.S. Yathirajan, P. Nagaraja, R.S. Narasegowda, R.S. Rathore, Acta Crystallogr., Sect. C 61 (2005) o177.
[19] D. Swierczynski, R. Lubradzki, G. Dolognos, J. Lipowski, H.-J. Schneider, Eur. J. Org. Chem. (2005) 1172.
[20] W.L. Steffen, G.J. Palenik, Acta Crystallogr., Sect. B 32 (1976) 298.
[21] Y. Byun, D. Min, J. Do, H. Yun, Y. Do, Inorg. Chem. 35 (1996) 3981.

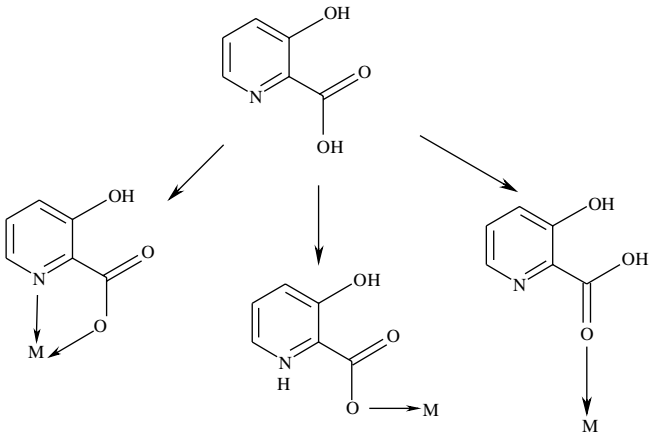

Scheme 1. The most usual coordination modes of 3-hydroxypicolinic acid in 12th group metal complexes.

bridging ligand as found in the structure of $[Cu(pic)_2]\cdot 2H_2O$ [4] and $[Mn(pic)(N_3)(H_2O)]_n$ [10]. In the structure of $[Mn(pic)(picH)Cl]_2$ was established the co-existence of both neutral and *N*,*O*-bidentate forms, as in Hg(pic)(picH). Another example of a *N*,*O*,*O*-tridentate chelating bridge ligand is found in $[Mn(pic)(N_3)(H_2O)]_n$, but interestingly even a *N*,*O*,*O*,*O*′-tetradentate coordination mode of binding of picH is observed in $[Cu(pic)Cl]_n$ [9]. The cadmium ion is well known for making coordination polymers by catenation, in contrast, for instance, to zinc of the group 12 elements. Catenation is achieved by cadmium's ability to form polymers with extended coordination numbers (usually six in the form of a distorted octahedron or seven in the form of a pentagonal bipyramid) and simultaneously pyridinecarboxylic acids, by suitable positions of the donor atoms, uphold two or more cadmium ions. Various solvent molecules can be accommodated in the coordination sphere as well.

Table 1 lists the major structural features of Cd complexes with mono pyridinecarboxylic acids and with benzoic acid for comparison.

The benzoic acid, acting as ligand, appears in Cd complexes as an anionic *O*,*O*′-bidentate ligand forming a four-membered chelate ring (bite distance angle around 55°) [11]. Three such mononuclear complexes are known (Table 1) indicating Cd coordination between trigonal prismatic and octahedral, such as in the case of diaquabis(*p*-chlorobenzoato)cadmium(II) [11] and diaquabis(*p*-nitrobenzoato)cadmium(II) [11], while in the structure of aquabis(*p*-chlorobenzoato)bis(pyridine)cadmium(II) [11] the cadmium coordination number is seven in the form of a pentagonal bipyramid. The additional ligand molecules, such as water or pyridine, occupy the remaining cadmium coordination sites. The Cd–O (carboxylato) bond distances are rather different in these complexes, varying from 2.255(2) Å to 2.502(2) Å [both in the structure of diaquabis(*p*-nitrobenzoato)cadmium(II)]. It is obvious that one carboxylato oxygen atom participates in bond formation with cadmium poorly. The water oxygen atom is bonded to cadmium in the range 2.213(2)–2.254(3) Å.

The structural survey reveals that in Cd complexes the most usual ligation of picolinic acid is the *N*,*O*-chelate mode for picolinic acid [12] (in compound NELNIB one picolinic acid is bonded as a neutral ligand and another as a picolinato anionic ligand, but in the same *N*,*O*-chelate coordination mode) [12], or *N*,*O*,*O*′-bridging between two (REXJAF) [13] or three cadmium ions (REXHUX) [14]. In the structure of $Cd(pic)_2$ [15] *N*,*O*,*O*′-bridging between two Cd(II) ions is achieved, too.

In the structures of Cd complexes with nicotinic acid the *O*,*O*′-chelate mode is observed (ZOZKII) [16], (HIBSBUG) [17], while simultaneously polymerization occurs through pyridine N-atoms [17] and/or Br^- bridge anions [16]. The complex of the formula $[Cd(SCN)_2(HL^1)_2]\cdot HL^1$ (HL^1 = nicotinic acid) is an example with an uncoordinated carboxylic group which forms head-to-head double intermolecular hydrogen bonds [17]. In the structures with isonicotinic acid [17,18] three complexes are found (QIFMIB, KEJBOQ and KEJHIQ) in the form of three-dimensional wave-like networks (QIFMIB) [17] or polymeric diamondoid structures (KEJBOQ and KEJHIQ) [19].

As a part of our wider interest in coordination chemistry of the metals of 12th group of elements with molecules of biological interest, we synthesized the titled cadmium(II) complexes with 3-hydroxypicolinic acid, identified them by chemical analysis, characterized the species that exist in solution as well as in the solid state to get some more information on how to control Zn, Cd, Hg homeostasis.

2. Experimental

2.1. Materials and physical measurements

3-hydroxypicolinic acid, cadmium(II) chloride and cadmium(II) bromide tetrahydrate were used as received from Aldrich without further purification. CHN analyses were performed in the Analytical Services Laboratories of the Institute Ruđer Bošković. The IR spectra were obtained from KBr pellets in the range 4000–450 cm^{-1} with a Bruker Equinox 55 spectrometer.

The one- and two-dimensional homo- and heteronuclear ^1H and ^{13}C NMR spectra were recorded with a Bruker AV 600 spectrometer, operating at 600.133 MHz for the ^1H nucleus and 150.917 MHz for the ^{13}C nucleus. Samples were measured from DMF-d7 solutions at 22 °C (295 K) in 5 mm NMR tubes. Chemical shifts, in ppm, are referred to TMS as internal standard. FID resolution in ^1H NMR and ^{13}C NMR spectra was 0.29 Hz and 0.54 Hz per point, respectively. The following measurement techniques were used: standard ^1H, ^{13}C gated proton decoupling, APT, COSY, HMQC and HMBC. The 2D NMR spectra, were measured in pulsed field gradient mode (*z*-gradient).

The thermal measurements were performed using a simultaneous TGA-DTA analyser (*TA Instruments*, SDT Model 2960). The samples were placed in small aluminium oxide sample pans. The TGA and DTA curves were obtained by placing samples of about 10 mg in mass, in

Table 1
A survey of the main structural features of cadmium complexes with benzoic and mono pyridinecarboxylic acids (2-pyridinecarboxylic, 3-pyridinecarboxylic and 4-pyridinecarboxylic acids)

Structure	Cd coordination	Bond length (Å)	Refcode	Reference
Diaquabis(*p*-chlorobenzoato)cadmium(II)	Between trigonal prism and octahedral; Cd on a twofold axis	Cd–O1 2.267(2) Cd–O2 2.464(2) Cd–Ow 2.215(2)	BUYVUM10	[11]
Diaquabis(*p*-nitrobenzoato)-cadmium(II)	Between trigonal prism and octahedral; Cd on a twofold axis	Cd–O1 2.255(2) Cd–O2 2.502(2) Cd–Ow 2.213(2)	BUYVUM10	[11]
Aquabis(*p*-chlorobenzoato)-bis(pyridine)cadmium(II)	Pentagonal bipyramid; Cd and Ow on a twofold axis	Cd–O1 2.408(2) Cd–O2 2.428(2) Cd–Ow 2.254(3) Cd–N 2.346(2)	BUYVUM10	[11]
Di-μ-chloro-bis[(2-pyridinecarboxylato-*N*,*O*) (2-pyridinecarboxylic acid-*N*,*O*)cadmium(II)] ethanol solvate	Distorted ocathedral coordination	Cd1–Cl1 2.588(1) Cd1–Cl2 2.608(1) Cd1–O1 2.313(3) Cd1–O3 2.332(3) Cd1–N1 2.326(4) Cd1–N8 2.309(4)	NELNIB	[12]
catena-(μ_2-thiocyanato)(μ_3-picolinato)-cadmium(II)	Distorted octahedral	Cd1–O1 2.293(3) Cd1–N2 2.275(4) Cd1–O1′ 2.355(3) Cd1–N1 2.315(4) Cd1–S1′ 2.594(2) Cd1–O2′ 2.453(3)	REXJAF	[13]
catena-(μ_2-azido)(μ_3-picolinato)-cadmium(II)	Distorted octahedral	Cd1–N11 2.258(7) Cd1–O1′ 2.459(5) Cd1–O1 2.327(5) Cd1–N1 2.356(6) Cd1–N11′ 2.335(6) Cd1–O2′ 2.247(5)	REXHUX	[14]
Cadmium(II) picolinate	Distorted octahedral	Cd–N1 2.35(1) Cd–O2 2.35(2) Cd–N2 2.34(2) Cd–O4 2.36(2) Cd–O2′ 2.23(2) Cd–O3′ 2.25(1)		[15]
Poly[μ-(nicotinato-*O*,*O*′:*N*)-μ-bromo-monoaquacadmium]	Distorted octahedral coordination	Cd–Br 2.6678(9) Cd–Br′ 2.7804(8) Cd–O1 2.348(3) Cd–O2 2.331(3) Cd–O3 2.373(3) Cd–N″ 2.272(3)	ZOZKII	[16]
$[Cd(SCN)_2(HL^1)_2]\cdot HL^1$ (HL^1 = nicotinic acid)	Two structurally different Cd atoms coordinated octahedrally and lying on an inversion centre	Cd1–N2 2.294(3) Cd1–$N3_{(from\ acid)}$ 2.381(3) Cd1–S1 2.709(2) Cd2–N1 2.311(3) Cd2–$N4_{(from\ acid)}$ 2.358(3) Cd2–S2 2.738(2)		[17]
Poly[aquacadmium-bis(μ-nicotinato-κ*N*:κ*O*, κ*O*′]	Distorted pentagonal bipyramidal	Cd–O1 2.276(2) Cd–O3 2.251(2) Cd–O2 2.639(2) Cd–O4 2.879(2) Cd–Ow 2.378(2) Cd–N1′ 2.353(2) Cd–N2″ 2.307(3)	HIBSUG	[17]
catena-[(μ_2-thiocyanato)-aqua-(isonicotinato)cadmium(II)]	Distorted octahedral	Cd1–Ow1 2.288(3) Cd1–N1′ 2.289(4) Cd1–N2 2.346(3) Cd1–O1′ 2.381(3)	QIFMIB	[17]

(*continued on next page*)

Table 1 (*continued*)

Structure	Cd coordination	Bond length (Å)	Refcode	Reference
catena[bis(μ_2-isonicotinato-*N*,*O*,*O*′)-ethanolcadmium(II)] ethanol solvate	Distorted pentagonal bipyramidal	Cd1–O2′ 2.448(3) Cd1–S1 2.588(1) Cd1–O2 2.664(4) Cd1–O4 2.279(5) Cd1–N8 2.343(5) Cd1–O11$_{(\text{from EtOH})}$ 2.327(4) Cd1–O14 2.442(4) Cd1–O16 2.384(4) Cd1–N20 2.366(5)	KEJBOQ	[18]
catena[aqua-bis(μ_2-isonicotinato-*N*,*O*,*O*′) cadmium(II)] pyrazine solvate	Distorted pentagonal bipyramidal	Cd1–O2 2.573(2) Cd1–O4 2.306(2) Cd1–N8 2.318(2) Cd1–O11 2.465(2) Cd1–O13 2.355(2) Cd1–N17 2.396(3) Cd1–O20$_{(\text{from } H_2O)}$ 2.334(3)	KEJHIQ	[18]

open sample pans, with a heating rate of 5 °C/min and argon (purity above 99.996%) pouring at a flow rate of 50 ml/min. The SDT was calibrated with indium.

2.2. [CdCl(OH-pic)(OH-picH)(H_2O)]$_2$ (**1**)

A solution of 3-hydroxypicolinic acid (0.25 g, 1.8 mmol) in 20 mL of water was added dropwise to a solution of cadmium(II) chloride (0.165 g, 0.9 mmol) in 15 mL water. Yellowish needles started to crystallize upon mixing but the reaction mixture was left to stand for a few days to complete the crystallization. The crystals were filtered off, washed with cold water and dried. Yield: 0.31 g (77.8%). *Anal*. Calc. for $C_{12}H_{11}CdClN_2O_7$ (443.097): C, 32.53; H, 2.50; N, 6.32. Found: C, 32.74; H, 2.64; N, 6.50%.

2.3. [CdBr(OH-pic)(OH-picH)(H_2O)]$_2$ (**2**)

A solution of 3-hydroxypicolinic acid (0.25 g, 1.8 mmol) in 20 mL of water was added dropwise to a solution of cadmium(II) bromide tetrahydrate (0.31 g, 0.9 mmol) in 25 mL water. Yellowish needles started to crystallize upon mixing but the reaction mixture left to stand for a few days to complete the crystallization. The crystals were filtered off, washed with cold water and dried. Yield: 0.35 g (79.5%). *Anal*. Calc. for $C_{12}H_{11}CdBrN_2O_7$ (487.548): C, 29.56; H, 2.27; N, 5.74. Found: C, 29.57; H, 2.35; N, 5.88%.

2.4. X-ray crystallographic structure determination of **1** and **2**

The general and crystal data and summary of intensity data collection and structure refinement for compounds **1** and **2** are given in Table 2.

The data collection for both structures was carried out on Xcalibur four-circle κ geometry single-crystal diffractometer with Xcalibur Sapphire 3 CCD detector by applying the CrysAlis Software system, Version 171.23 [20]. Seven sets containing 1047 data collection frames were collected (four sets with 0.75° scan width and three sets with 1.00° scan width) at a crystal-detector distance of 60 mm with an exposure time of 20 s and ω scan type for both structures.

The Lorentz-polarization effect was corrected and intensity data reduced by the CrysAlis RED application of the CrysAlis Software system, Version 171.23 [20]. The diffraction data were corrected for absorption by the optimization of a built 3-D shape model against the diffraction data.

The coordinates of the heavy atoms were determined by direct methods with the SHELXS program [21]. The coordinates and anisotropic thermal displacement parameters for all non-hydrogen atoms were refined by the least-squares methods based on F^2 using the SHELXL97 program [22]. The coordinates of the hydrogen atoms belonging to the oxygen or nitrogen atoms were found by the examination of electron-density Fourier maps at the final stages of refinement and refined freely [the bond distance range is from 0.75(3) Å for O1–H1O to 0.89(4) Å for O4–H4O].

The other hydrogen atoms, which belong to pyridine carbon atoms were generated at ideal geometrical positions [Csp^2–H 0.93 Å, $U_{iso}(H) = 1.2\ U_{eq}(C)$] and refined applying the riding model. The molecular graphics were obtained using the PLATON98 program [23].

3. Results and discussion

3.1. Preparation

The interaction between cadmium(II) halides and 3-hydroxypicolinic acid in aqueous solution afforded yellowish needle crystals of complexes **1** and **2**. Both complexes have the same general formula [CdX(OH-pic)(OH-picH)-(H_2O)]$_2$, X = Cl$^-$, Br$^-$. They are air-stable substances and very soluble in methanol, *N*,*N*-dimethylformamide (DMF) and dimethylsulfoxide (DMSO). The NMR measurements in a DMSO solution of the prepared complexes

Table 2
General and crystal data and summary of intensity data collection and structure refinement for the compounds **1** and **2**

Compound	**1**	**2**
Formula of the dimer	$C_{24}H_{22}Cd_2Cl_2N_4O_{14}$	$C_{24}H_{22}Cd_2Br_2N_4O_{14}$
M_r	886.18	975.08
Colour and habit	colourless, needle-like prism	colourless, needle-like prism
Crystal system, space group	monoclinic, $P2_1/c$	monoclinic, $P2_1/c$
Crystal dimensions (mm^3)	$0.48 \times 0.39 \times 0.10$	$0.48 \times 0.33 \times 0.07$
Temperature (K)	296	296
Unit cell parameters		
a (Å)	9.0596(10)	9.1591(6)
b (Å)	15.9048(15)	16.0432(9)
c (Å)	10.0898(8)	10.0257(6)
β (°)	95.000(8)	95.360(5)
V ($Å^3$)	1448.3(2)	1466.7
Z	2	2
D_{calc} ($g\,cm^{-3}$)	2.032	2.208
μ (mm^{-1})	1.732	4.252
$F(000)$	872	944
θ Range for data collection (°)	4–30	4–27
h, k, l Range	−12:12; −22:22; −14:14	−11:11; −20:20; −12:12
Diffractometer	Xcalibur κ geometry with CCD detector	
Scan type	ω	ω
Number of measured reflections	21 488	18 651
Number of independent reflections (R_{int})	4168 (0.062)	3189 (0.1217)
Number of refined parameters	228	228
Number of observed reflections, $I \geqslant 2\sigma(I)$	3645	2885
Range of transmission factors minimum and maximum[a]	0.455, 0.841	0.345, 0.802
R[b], wR[c] [$I \geqslant 2\sigma(I)$]	0.0320, 0.0792	0.048, 0.1261
R, wR [all data]	0.0413, 0.0751	0.0535, 0.1207
g_1, g_2 in w[d]	0.0441, 0.3305	0.0720, 1.2792
Goodness of fit on F^2, S[e]	1.08	1.09
Maximum, minimum electron density ($e\,Å^{-3}$)	−0.74, 1.25	−1.602, 1.219
Maximum Δ/σ	<0.001	0.001
Extinction coefficient	none	none

[a] Crystal face indices, distances from centroid (mm): 0 −8 13 0.11143; 1 9 13 0.09219; −1 −22 −1 0.09542; 1 22 1 0.04940; 12 1 −5 0.19320; −12 3 5 0.23770 for compound **1** and 0 7 7 0.0608; 0 −7 −7 0.0747; 0 6 −8 0.3558; 0 −6 8 0.3109; −2 7 7 0.4827; 2 −7 −7 0.4860 for compound **2**. Absorption correction type: numerical for both compounds **1** and **2**.

[b] $R = \sum\|F_o| - |F_c\|/\sum|F_o|$.

[c] $wR = [\sum(F_o^2 - F_c^2)^2/\sum w(F_o^2)^2]^{1/2}$.

[d] $w = 1/[\sigma^2(F_o^2) + [(g_1P)^2 + g_2P]$ where $P = (F_o^2 + 2F_c^2)/3$.

[e] $S = \sum[w(F_o^2 - F_c^2)^2/(N_{obs} - N_{param})]^{1/2}$.

showed that they are not stable in DMSO. This conclusion was drawn from the fact that there are no significant changes in the ^1H and ^{13}C NMR chemical shifts of the dissolved compounds in comparison with those of the free ligand. By contrast in DMF solution $Cd(OH\text{-}pic)_2$ is identified as the only existing compound (vide infra).

3.2. Infrared and NMR spectra

The room temperature IR spectral data of the crystalline OH-picH and its cadmium(II) complexes **1** and **2** were analyzed and their tentative assignments were based on those found in the literature [19,24–28]. From the analysis of the IR spectral data the isostructural nature of **1** and **2** was recognized and this has been approved by the results of the X-ray structure determinations. From the observed absorption bands, which were assigned as asymmetric and symmetric modes of vibration of the carboxylic group i.e., from the shifting of these absorption bands relatively to IR data of free OH-picH, one can conclude that OH-picH acts as a chelate *N*,*O*-ligand. There are two bands at 1390 cm^{-1} and 1300 cm^{-1} for **1** and 1370 cm^{-1} and 1300 cm^{-1} for **2** suggesting two different modes of binding of the COO-group. Shifting of ν_s(COO) to lower wavenumbers compared to the free ligand (1322 cm^{-1}) is indicative of a unidentate mode of binding of the carboxylic group. Moreover, the presence of two bands which correspond to a ν(C–N) stretching vibration is also indicative of two modes of binding OH-picH to the cadmium(II) ion. In the spectrum of the free acid (OH-picH) in the high frequency region where hydrogen bonding is found of the type O–H···O involving the carboxylic acid group, a very broad band centred around 3440 cm^{-1} is observed, whilst hydrogen bonding of the type O–H···N is supported by the presence of broad medium strong bands near 2600 cm^{-1} and 2000 cm^{-1}. In the IR spectra of the complexes **1** and **2** the very broad absorption band of medium intensity centered at 3246 cm^{-1} for **1** and 3244 cm^{-1} for **2**, as well as

bands around 2600 cm^{-1} and 2000 cm^{-1}, are indicative of hydrogen bonding in the structures of **1** and **2**, respectively.

The assignment of NMR spectra of the free ligand (OH-picH) and its cadmium(II) complexes **1** and **2** are shown in Table 3. The enumeration of the atoms is consistent with IUPAC nomenclature and it is shown in Scheme 2.

Table 3
^{1}H and ^{13}C NMR chemical shifts (δ/ppm)[a] and cadmium induced chemical shifts ($\Delta\delta$/ppm)[b], H–H coupling constants ($^{n}J_{HH}$/Hz)[c] and C–H coupling constants ($^{n}J_{CH}$/Hz) of 3-hydroxy picolinic acid and DMF solutions of **1** and **2**

Molecule	OH-picH	DMF solution of **1**	DMF solution of **2**
Atom			
H-2,3			
Δ	13.000 (2)	not observed	not observed
$\Delta\delta$			
H-4			
Δ	7.839 (1)	7.658 (1)	7.665 (1)
$^{3}J_{HH}$	8.56 (d)	8.46 (d)	8.20 (d)
$\Delta\delta$		−0.192	−0.185
H-5			
Δ	7.862 (1)	7.724 (1)	7.734 (1)
$^{3}J_{HH}$	8.56; 4.52 (dd)	8.49; 4.67 (dd)	8.37; 4.72 (dd)
$\Delta\delta$		−0.131	−0.121
H-6			
Δ	8.332 (1)	8.218 (1)	8.223 (1)
$^{3}J_{HH}$	4.62 (d)	4.64 (d)	4.62 (d)
$\Delta\delta$		−0.112	−0.107
C-2			
Δ	130.32	132.32	132.07
$\Delta\delta$		2.00	1.75
C-3			
Δ	160.49	160.25	160.05
$\Delta\delta$		−0.24	−0.44
C-4			
Δ	130.93	129.33	129.35
J_{CH}	168.53	165.81 (d)	166.41 (d)
$\Delta\delta$		−1.60	−1.58
C-5			
Δ	130.09	129.86	129.84
J_{CH}	169.71	167.47 (d)	167.96 (d)
$\Delta\delta$		−0.23	−0.25
C-6			
Δ	135.36	137.34	137.42
J_{CH}	190.86	185.94 (d)	185.60 (d)
$\Delta\delta$		1.98	2.06
COOH			
Δ	167.49	169.40	169.28
$\Delta\delta$		1.91	1.79

[a] Recorded in DMF-d_7 solutions. Referred to TMS. Number of protons in brackets.

[b] Cadmium induced chemical shifts ($\Delta\delta$/ppm) are obtained by substracting the chemical shifts of the parent compound (OH-picH) from the chemical shifts of the Cd-complex. Sign (+) denotes deshielding effect, while (−) denotes shielding effect of cadmium.

[c] *n* denotes the number of bonds between nuclei in spin–spin coupling; (s) singlet, (d) doublet.

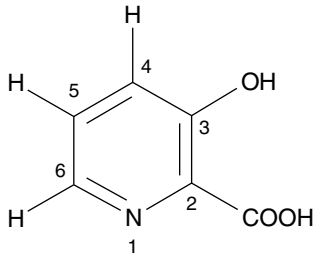

Scheme 2. Enumeration of the atoms in 3-hydroxypicolinic acid.

Since **1** and **2** dissociate in DMSO, NMR measurements were performed in DMF solution. The ^{1}H and ^{13}C NMR spectra are very simple suggesting that $Cd(OH\text{-}pic)_2$ exists in DMF solution.

NMR spectra of DMF solutions of **1** and **2** are very similar. Cadmium induced ^{1}H and ^{13}C NMR shifts are defined as the difference of proton or carbon chemical shifts in the complexes and the free ligand molecule.

The ^{1}H NMR spectra revealed the largest complexation shift ($\Delta\delta$) for the H-4 proton in both complexes. This proton is far off from the cadmium atom that has a shielding effect on this proton. Complexation with cadmium induces shielding effects for all H-atoms (−0.107 to −0.192 ppm) of the ligand molecule. The signal of the hydroxyl group, due to large broadening, was not observed.

In the ^{13}C NMR spectra the greatest change upon complexation with cadmium was observed for the chemical shift of C-6. Deshielding effects were observed for C-2, C-6 and the carboxylic carbon (1.75–2.06 ppm) and shielding effects for C-3, C-4 and C-5 (−0.23 to −1.60 ppm). It has to be mentioned that all signals were broadened.

From both ^{1}H and ^{13}C NMR experiments it seems that cadmium complexes of OH-picH in DMF solution exist only in the symmetrical form. The cadmium ion has an influence on all proton and carbon atoms of the ligand molecule.

NMR data demonstrate that both hydrogen and carbon atoms are sensitive to cadmium binding even if they are not near and thus long-range shifts may be useful for the complexation monitoring. Long-range complexation shifts are the consequence of conformational changes and an extensive network of both intramolecular and intermolecular hydrogen bonds, which in turn induces a subtle electron redistribution throughout the molecule.

*3.2.1. Structural description of **1** and **2***

ORTEP views of the molecular structures of compounds **1** and **2** are depicted in Fig. 1, and their crystal structures in Fig. 2. The selected molecular geometry is listed in Table 4 along with the hydrogen bond geometry in Table 5.

Complexes **1** and **2** are isostructural. The molecular structures of the complexes comprise centrosymmetrical dimers containing the two Cd(II) ions with distorted octahedral coordination geometries. The coordination environment contains two Cl atoms, one water molecule

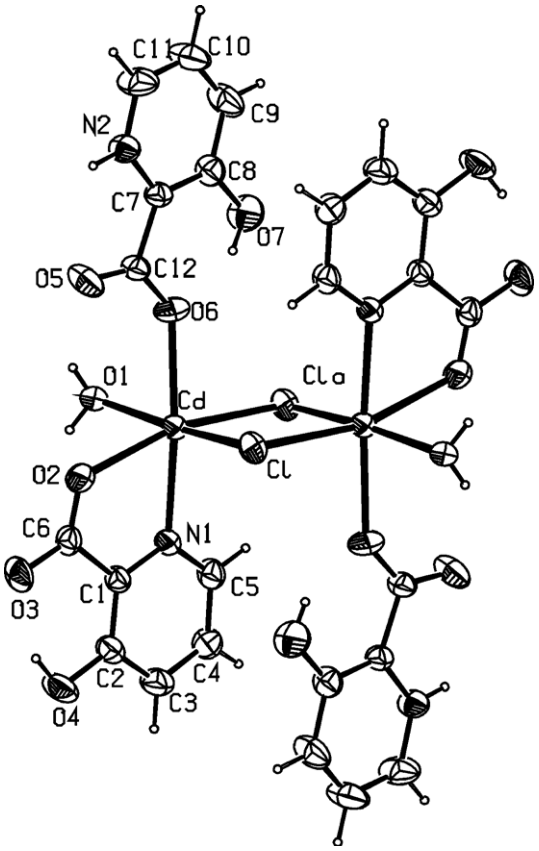

Fig. 1. ORTEP drawing of di-μ-chloro-[aqua-(3-hydroxypyridine-2-carboxylato-*N*,*O*)(3-hydroxypyridinium-2-carboxylato-*O*)cadmium(II)] (**1**) with the atomic numbering scheme of the asymmetric unit. The thermal ellipsoids are drawn at the 50% probability level at 293 K. The bromo derivative (**2**) is isostructural.

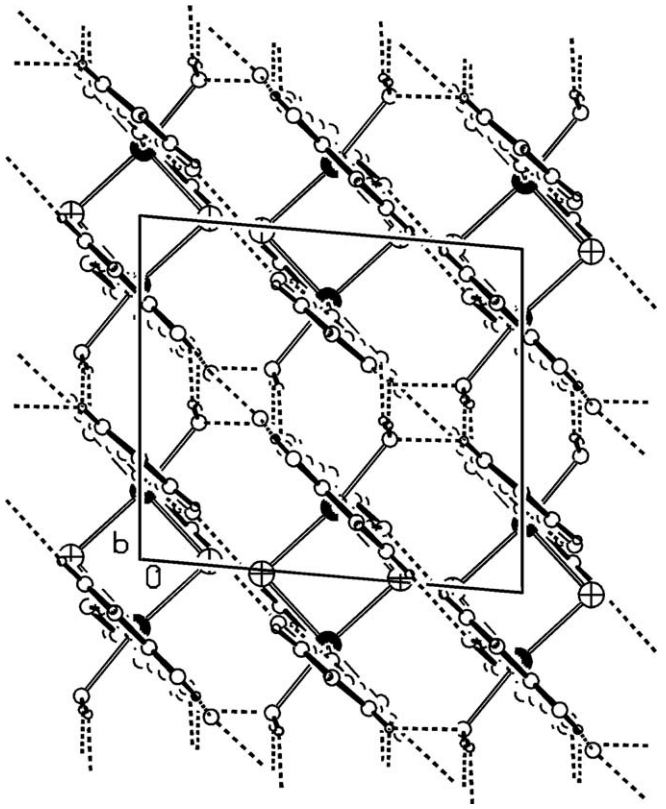

Fig. 2. Crystal structure of di-μ-chloro-[aqua-(3-hydroxypyridine-2-carboxylato-*N*,*O*)(3-hydroxypyridinium-2-carboxylato-*O*)cadmium(II)] (**1**) in *ac* projection. Hydrogen bonds are indicated by dashed lines.

Table 4
Selected bond distances (Å) and angles (°)

	1	**2**
Bond distances		
Cd–X	2.6056(7)	2.7418(6)
Cd–X^i	2.6231(7)	2.7488(5)
Cd–O1	2.3045(19)	2.307(4)
Cd–O2	2.3440(17)	2.340(3)
Cd–O6	2.3144(18)	2.324(3)
Cd–N1	2.3280(18)	2.334(4)
Bond angles		
X–Cd–O1	170.36(5)	170.85(10)
X–Cd–O2	91.03(4)	90.41(8)
X–Cd–O6	92.71(5)	93.00(9)
X–Cd–N1	96.03(5)	94.70(8)
X–Cd–X^i	89.59(2)	91.232(17)
O1–Cd–O2	84.14(6)	84.76(13)
O1–Cd–O6	81.07(7)	81.34(14)
O1–Cd–N1	90.35(7)	91.09(13)
X^i–Cd–O1	97.29(5)	95.50(10)
O2–Cd–O6	109.28(6)	109.38(12)
O2–Cd–N1	71.35(6)	71.09(12)
X^i–Cd–O2	164.47(5)	164.50(8)
O6–Cd–N1	171.23(7)	172.29(13)
X^i–Cd–O6	86.18(5)	85.92(10)
X^i–Cd–N1	93.15(5)	93.41(9)

X = Cl$^-$ (**1**) and Br$^-$ (**2**); $i = -x, -y, 1 - z$.

and two OH-pic ligands, one bonded to the Cd(II) ion in a monodentate mode through the carboxylate O atom and the other in the bidentate *N*,*O*-chelated mode forming a five-membered chelate ring. The hydroxyl group does not take part in the coordination. There has been no example of OH-participation in the metal coordination sphere in complexes with OH-picolinic acid up until now. The charge balance of the molecular formulas of the complexes requires one OH-pic ligand to be in a neutral form (that is the ligand acting monodentately) and the other acting as a *N*,*O*-chelate is an anion formed by the deprotonation of the carboxylic group. The proton transfer from the carboxylic group to the pyridine N-atom, revealing its zwitterionic form, realizes the neutral form of one of the ligands. The example of a Cd complex with the two same ligands, but coordinated as picH acid and the pic$^-$ anion is di-μ-chloro-bis[(2-pyridinecarboxylato-*N*,*O*)(2-pyridinecarboxylic acid-*N*,*O*)cadmium(II)] ethanol solvate (NELNIB) [12], but tautomerization from the carboxylic oxygen to the pyridine nitrogen atom is not observed due to the participation of the N-atom in coordination. There are two examples of 3-OH-pic coordination in the zwitterionic form in the vanadium complex aqua-bis(3-hydroxypyridine-2-carboxylato)-oxo-vanadium hydrate [29] and in the structure of *catena*-(μ_2-3-hydroxypicolinato)-aqua-bis(3-hydroxypicolinato)europium(III) hydrate [30].

Table 5
Hydrogen bond geometry (Å, °)

D–H···A	D–H	H···A	D···A	∠DHA	Symmetry code
Compound ***1***					
O1–H1O···O2	0.75(3)	2.01(3)	2.738(2)	164(4)	$1-x, -y, 1-z$
N2–H2N···O5	0.86(3)	2.28(3)	2.673(3)	108(3)	
N2–H2N···O3	0.86(3)	1.95(3)	2.766(3)	159(3)	$1-x, -/2+y, 1/2-z$
O1–H2O···O5	0.78(5)	1.93(4)	2.695(3)	167(4)	$1-x, -y, 1-z$
O4–H4O···O3	0.89(4)	1.76(5)	2.562(3)	150(4)	
O7–H7O···O6	0.81(5)	1.82(4)	2.581(3)	155(4)	
C4–H4···O7	0.93	2.50	3.242(3)	137	$-x, 1/2+y, 3/2-z$
C11–H11···O1	0.93	2.35	3.160(4)	146	$x, -1/2-y, -1/2+z$
Compound ***2***					
O1–H1O···O2	0.80(5)	1.96(5)	2.734(6)	163(6)	$1-x, -y, 1-z$
N2–H2N···O5	0.92(6)	2.36(6)	2.677(7)	100(5)	
N2–H2N···O3	0.92(6)	1.86(6)	2.759(6)	167(6)	$1-x, -/2+y, 1/2-z$
O1–H2O···O5	0.84(8)	1.87(8)	2.695(6)	167(8)	$1-x, -y, 1-z$
O4–H4O···O3	0.94(10)	1.69(11)	2.567(6)	153(9)	
O7–H7O···O6	0.74(8)	2.02(7)	2.588(7)	133(7)	

The coordination environment contains two halogen atoms [Cd–Cl 2.6056(7) Å; Cd–Cl^{i} 2.6231(7) Å; $i = -x, -y, 1-z$; Cd–Br 2.7418(6) Å; Cd–Br^{i} 2.7488(5) Å in **1** and **2**, respectively], one water molecule [Cd–O1 2.305(2) and 2.307(4) Å in **1** and **2**, respectively] and two OH-pic ligands, one bonded to the Cd(II) ion in a monodentate mode through the carboxylate O atom [Cd–O2 2.344(2) and 2.340(3) Å in **1** and **2**, respectively] and the other in the bidentate *N*,*O*-chelated mode forming a five-membered chelate ring [Cd–N1 2.328(2) and 2.334(4) Å; Cd–O6 2.314(2) and 2.324(3) Å in **1** and **2**, respectively]. The participation of Cl atoms in the Cd coordination sphere is found in dimeric di-μ-chloro-bis[(2-pyridinecarboxylato-*N*,*O*)(2-pyridinecarboxylic acid-*N*,*O*)cadmium(II)]ethanol solvate (NELNIB) [12], with similar bond distance values (2.588(1) and 2.608(1) Å) as in our complex. In the structure of poly-[μ-(nicotinato-*O*,*O*′:*N*)-μ-bromo-monoaquacadmium] [13] the Cd–Br distances are 2.6678(9) and 2.7804(8) Å, comparable with our Cd–Br bond distance values.

The bond distances Cd–O_w are in agreement with those found in the structures of other Cd complexes with pyridinecarboxylic acids (see Table 1). The bond distances Cd–O_w in the structures of Cd complexes with pyridinecarboxylic acids vary in the range 2.288(3) Å in $Cd(SCN)_2(HL^1)_2]\cdot HL^1$, ($HL^1$ = nicotinic acid) [17] to 2.378(2) Å in poly-[aquacadmium-bis(μ-nicotinato-κ*N*:κ*O*, κ*O*′] [17], being longer than in the Cd-benzoato complexes, in general. The bond distances Cd–O(solvate) are usually shorter than those with oxygen atoms from acids since the later oxygen atoms usually act as bridging atoms. The bond range for Cd–N(pyridine) distances is 2.272(3) Å in poly[μ-(nicotinato-*O*,*O*′:*N*)-μ-bromo-monoaquacadmium] (octahedral coordination) [18] to 2.396(3) Å in catena[aqua-bis(μ_2-isonicotinato-*N*,*O*,*O*′) cadmium(II)] pyrazine solvate (pentagonal bipyramid coordination) [18]. The Cd–O (from protonated or non-protonated acids) bond distances vary to a greater extent than Cd-(pyridine) distances, being in the range 2.247(5) Å in *catena*-(μ_2-azido)(μ_3-picolinato)-cadmium(II) (distorted octahedral coordination) [14] to 2.879(2) Å in poly[aquacadmium-bis(μ-nicotinato-κ*N*:κ*O*, κ*O*′] (distorted pentagonal bipyramidal coordination) [17]. The later complex is of particular interest since the nicotinato ligand acts as a bridging ligand only through the N-atom, while the carboxylato groups are coordinated only to one Cd(II) ion with one Cd–O bond considerably longer than the other. A similar trend is observed in the monomeric diaquabis(*p*-nitrobenzoato)cadmium(II) [11] (2.255(2) vs. 2.502(2) Å).

Angles indicating the largest distortion from the ideal octahedral geometry, O2–Cd–N1 amounting to 71.4(1) and 71.1(1)° in **1** and **2**, respectively, are the bite angles of the five-membered chelate rings with the donor atoms O2 and N1.

The dihedral angles between the least squares calculated planes through the atoms of the two pyridine rings are 4.5(1)° and 4.6(2)° in **1** and **2**, respectively. The measures of carboxylic (and carboxylato) group distortion from coplanarity with the pyridine rings to which they are attached, are the dihedral angles of 5.4(1)° and 4.6(2)° in **1** and 5.2(3)° and 5.1(3)° in **2**, calculated for the chelating bonded ligand and for the zwitterionic ligand, respectively. This coplanarity is preserved by intramolecular hydrogen bond formation of the type O–H···O between carboxylic (carboxylato) and hydroxyl groups (see Table 5) and it is an indicator of the stereochemical rigidity of the ligands themselves and their ability to accommodate to the cadmium coordination sphere.

There are three intramolecular hydrogen bonds, two of the type O–H···O (formed by the hydroxyl groups and one of the carboxylato oxygens) and one of the type N–H···O (in the zwitterionic picH ligand). The intramolecular O–H···O bond in the anionic pic^- ligand is shorter [O4···O3 2.562(3) and 2.567(6) Å, in **1** and **2**, respectively] than the O–H···O bond in the zwitterionic picH ligand [O7···O6 2.581(3) and 2.588(7) Å, in **1** and **2**, respectively] since in the later the proton acceptor is the O6 atom which

is also a donor atom. The N···O distance in the zwitterionic ligand is 2.673(3) Å in **1** and 2.677(7) Å in **2**, both being longer than O–H···O bonds.

Intermolecular hydrogen bonds of the type O–H···O are formed between water molecules and the carboxylato oxygen atoms (O···O distances are 2.738(2) and 2.734(6) Å in **1** and **2**, respectively) (Table 5).

3.3. Thermal analysis (TGA-DTA)

Samples of the complexes **1** and **2** were heated from room temperature up to 500 °C. Thermal decomposition of the complexes is shown in Figs. 3 and 4. A similar shape of both DTA and TGA curves can be seen in Figs. 3 and 4. This thermal behaviour is in good correlation with their isostructurality established by X-ray structure analysis. In addition, the determined bond distances in the complexes can be incorporated into the explanation of their thermal behaviour. Compounds **1** and **2** are thermally stable up to 150 °C. Above this temperature, a water molecule is eliminated in one stage in the temperature range 150–200 °C. The minimum of the endothermic peak is at a lower temperature (214.0 °C) for **2** and at a higher temperature for **1** (228.0 °C) and in good agreement with a stronger Cd–O1 bond in **1** (2.304 Å) and a weaker bond in **2** (2.307 Å). A further step of the thermal decomposition, which takes place in the temperature range 200–270 °C, is characterized by the release of two OH-pic ligands. The products are thermally stable up to 300 °C. The thermal degradation continues through an

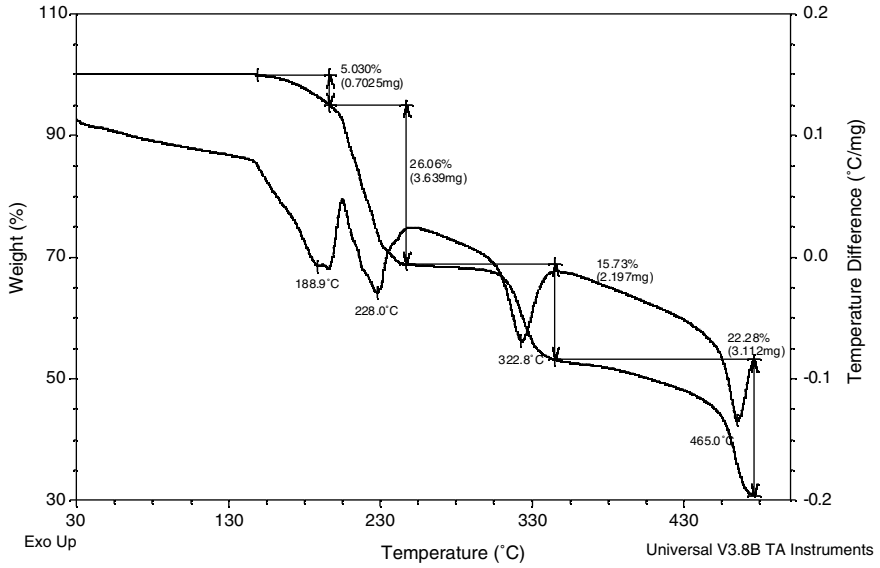

Fig. 3. DTA/TGA curves of **1**.

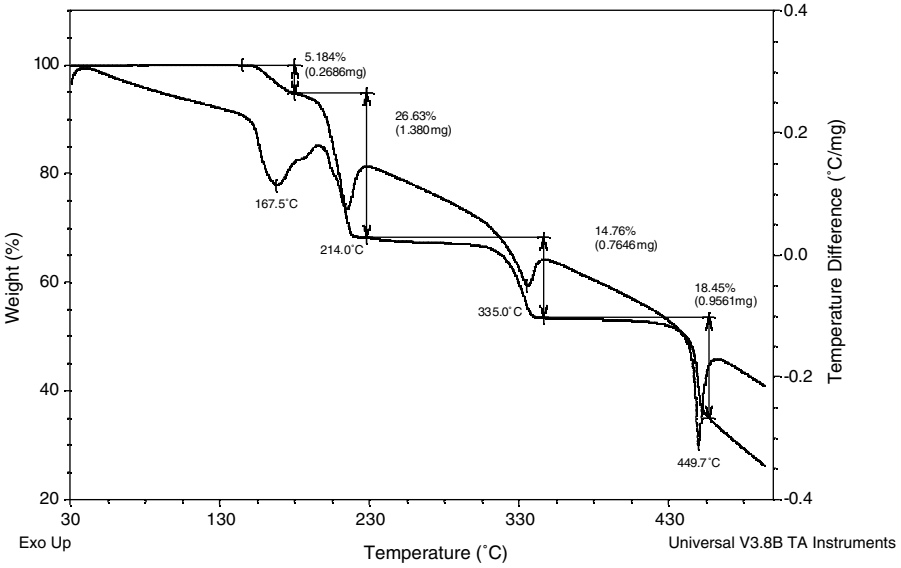

Fig. 4. DTA/TGA curves of **2**.

additional two steps. The first one happens in the temperature range 300–420 °C and the second one in the range 420–470 °C. Based on the mass loss results, we suppose that in the first step the elimination of one OH-pic ligand per complex takes place (endothermic effect on the DTA curves) at 322.8 and 335.0 °C, for **1** and **2**, respectively. The rest of the complexes partially degrade in the final stage in which the remainder of the ligand decomposes through an endothermic processes at 465.0 and 449.7 °C. The higher value of the temperature of the endothermic peak in **2** (in the second-to-last step) indicates the important role of the stronger Cd–N1 bond. During the last step, a lower temperature of the endothermic peak in **2** is observed, which refers to a weaker bond in **2** complex than in **1** complex.

4. Conclusions

Cadmium(II) chloride and bromide react almost instantaneously with 3-hydroxypicolinic acid in water solution giving isostructural dinuclear complexes of the general formula $[CdX(OH\text{-}pic)(OH\text{-}picH)(H_2O)]_2$; $X = Cl^-$, Br^-, which has been established by X-ray structural analysis and also supported by thermal analysis. These compounds are not stable in solutions and NMR spectral analysis revealed the presence of cadmium(II) 3-hydroxypicolinate as the only cadmium(II) compound in solution. Although the synthesis conditions permit the formation of $Cd(OHpic)_2$, apparently the packing forces in the solid state yield the title complexes.

Acknowledgements

The Ministry of Science and Technology of the Republic of Croatia, Zagreb (grants Nos. 0119633, 0098033 and 0192007) supported this work.

Appendix A. Supplementary material

CCDC 276100 and 276101 contain the supplementary crystallographic data for this paper. These data can be obtained free of charge at www.ccdc.cam.ac.uk/conts/retrieving.html [or from the Cambridge Crystallographic Data Centre (CCDC), 12 Union Road, Cambridge CB2 1EZ, UK; fax: +44(0)1223-336033; e-mail: deposit@ccdc.cam.ac.uk]. A structure factors table is available from the authors. Supplementary data associated with this article can be found, in the online version, at doi:10.1016/j.poly.2006.02.010.

References

[1] D. Matković-Čalogović, G. Pavlović, Z. Popović, Ž. Soldin, 20th European Crystallographic Meeting, Krakow, Poland, Book of Abstract 2001, p. 116.
[2] M.A.S. Goher, A.E. Abdon, W.-H. Yip, T.C.W. Mak, Polyhedron 12 (1993) 1879.
[3] P.J.-P. Deloume, R. Faure, H. Loiseleur, Acta Cryst. B 33 (1977) 2709.
[4] A. Takenaka, N. Utsumi, T. Yamamoto, I. Nita, Nippon Kagaku Zsashi 91 (1970) 928.
[5] G.W.A. Fowels, R.A. Matthews, R.A. Walton, J. Chem. Soc. (A) (1968) 1108.
[6] P.J.-P. Deloume, H. Loiseleur, G. Thomas, Acta Cryst. B 29 (1973) 668.
[7] S.C. Chang, J.K.H. Ma, J.S. Wang, N.C. Li, J. Coord. Chem. 2 (1972) 31.
[8] A. Kleinstein, G.A. Webb, J. Inorg. Nucl. Chem. 33 (1971) 405.
[9] M.A.S. Goher, M.A.M. Abu-Youssef, F.A. Mautner, A. Popitsch, Polyhedron 12 (1993) 1751.
[10] M.A.S. Goher, M.A.M. Abu-Youssef, F.A. Mautner, A. Popitsch, H.P. Fritzer, F.A. Mautner, Monatsh. Chem. 125 (1994) 833.
[11] P.F. Rodesiler, E.A.H. Griffith, N.G. Charles, E.L. Amma, Acta Cryst. C 41 (1985) 673.
[12] M. Odoko, N. Isomoto, N. Oakbe, Acta Cryst. E 57 (2001) m371.
[13] C. Zhang, D. Xu, Y. Xu, X. Huang, Acta Cryst. C 52 (1996) 591.
[14] G. Yang, H.-G. Zhu, B.-H. Liang, X.-M. Chen, J. Chem. Soc., Dalton Trans. (2001) 580.
[15] W. Clegg, J.T. Cressey, A. McCamley, B.P. Straughan, Acta Cryst. C 51 (1995) 234.
[16] O.R. Evans, Z. Wang, R.-G. Xiong, M. Foxman, W. Lin, Inorg. Chem. 38 (1999) 2969.
[17] F.A. Mautner, M.A. Abu-Youssef, M.A.S. Goher, Polyhedron 16 (1997) 235.
[18] P.J.-P. Deloume, H. Loiseleur, Acta Cryst. B 30 (1974) 607.
[19] V.L. Constantino, L.F.C. de Oliviera, P.S. Santos, H.E. Toma, Trans. Met. Chem. 19 (1994) 103.
[20] Oxford Diffraction. Oxford Diffraction Ltd., Xcalibur CCD system, CrysAlis Software system, Version 171.23, 2004.
[21] G.M. Sheldrick, Acta Cryst. A 46 (1990) 467.
[22] G.M. Sheldrick, SHELXL97, Program for the Refinement of Crystal Structures, University of Göttingen, Germany, 1997.
[23] A.L. Spek, Acta Cryst. A 46 (1990) 34.
[24] S.M.O. Quintal, H.I.S. Nogueira, V. Felix, M.G.B. Drew, New J. Chem. 24 (2000) 511.
[25] S. Gatto, T.I.A. Gerber, G. Bandoli, J. Perils, J.G.H. du Preez, Inorg. Chim. Acta 269 (1998) 235.
[26] A. Shaver, J.B. Ng, D.A. Hall, B.S. Lum, B.I. Posner, Inorg. Chem. 32 (1993) 3109.
[27] S.M.O. Quintal, H.I.S. Nogueira, H.M. Carapuça, V. Félix, M.G.B. Drew, J. Chem. Soc., Dalton Trans. (2001) 3169.
[28] P. Koczoń, Cz. Dobrowolski, W. Lewandowski, A.P. Mazurek, J. Mol. Struct. 655 (2003) 89.
[29] S. Yano, M. Nakai, F. Sekiguchi, M. Obata, M. Kato, M. Shiro, I. Kinoshita, M. Mikurya, H. Sakurai, C. Orvig, Chem. Lett. (2002) 916.
[30] P.C.R. Soares-Santos, H.I.S. Noguiera, V. Felix, M.G.B. Drew, R.A. Sa Ferreira, L.D. Carlos, T. Trinidade, Chem. Mater. 15 (2003) 100.

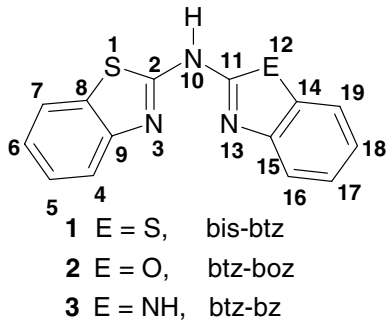

Scheme 1. Benzothiazole derived ligands.

posses versatile chemical, structural and tautomeric behavior, that upon coordination to metal ions, may give rise to different structures. Our aim was to study the effect of the heteroatoms (nitrogen, oxygen or sulfur) in their coordination mode; as to investigate the participation of the metal ions, in the formation of six-membered rings with alternating sp^2 carbon and nitrogen atoms in an aromatic pentacyclic system [30]. Therefore, herein we report the synthesis and characterization of coordination compounds **4**–**16** of these benzothiazole ligands **1**–**3** with Co^{2+}, Ni^{2+}, Zn^{2+} and Hg^{2+} ions (Scheme 2), which may form supramolecular arrangements by interaction of the heteroatoms, hydrogen bonds or π stacking. Compounds **4** and **5** have been described in a patent [34] but their structural study was not reported.

2. Experimental

2.1. Materials

All chemicals were reagent grade: methanol (J.T. Baker), 2-aminobenzothiazole (Aldrich); $Co(OAc)_2 \cdot 4H_2O$, $Ni(OAc)_2 \cdot 4H_2O$, $Zn(OAc)_2 \cdot H_2O$ and $Hg(OAc)_2$ (J.T. Baker), were used without further purification. Compounds **1**–**3** were synthesized according to the reported methods by Merchán et al. [35,36].

2.2. Physical measurements

A FT IR spectrometer (Perkin–Elmer 1600) was used for obtaining IR spectra of solid samples in KBr pellets (4000–400 cm^{-1}). UV–Vis–NIR spectra (diffuse reflectance, 40 000–4000 cm^{-1}) were recorded on a Cary-5E (Varian) spectrometer. Elemental analyses were carried out with a Fisons EA 1180 analyzer. The MS spectra were obtained by DIP (Direct Insertion Probe) at 20 eV in an HP 5989 spectrometer.

2.3. Crystallography

Crystal data and information about the data collection and structure refinement details are given in Table 1. X-ray diffraction studies were performed with KAPPA-CCD area detector and CAD4-Enraf-Nonius. The crystal structures were determined and refined with the SHELXTL [*x*, *y*] system. Hydrogen atoms of compounds **6**, **7**, **9** and **12** were systematically placed on idealized positions and refined with a riding model. For compounds **14** and **15** all aromatic hydrogen atoms were found on the difference-Fourier maps and refined with free coordinates and fixed isotropic thermal parameters [37].

2.4. Syntheses of complexes: general procedure

All compounds were synthesized following the same procedure as described for compound **4**. Compounds **5**–**13** from a 2:1 molar ratio (ligand:metal) and **14**–**16** employing an equimolar ratio.

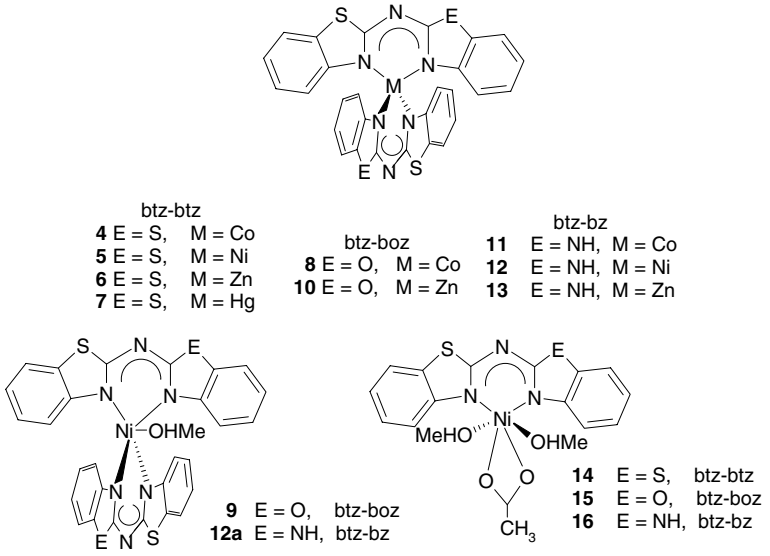

Scheme 2. Obtained coordination compounds from ligands **1**–**3**.

Table 1
Crystal data

Compound	**4**	**6**	**7**	**9**	**12**	**14**	**15**
Formula	$C_{58}H_{38}N_{12}OS_9Co_2$	$C_{58}H_{38}N_{12}OS_9Zn_2$	$C_{30}H_{22}N_6OS_5Hg$	$C_{29}H_{20}N_6O_3S_2Ni$	$C_{28}H_{18}N_8NiS_2$	$C_{18}H_{19}N_3O_4S_2Ni$	$C_{18}H_{19}N_3O_5SNi$
Formula weight	1325.49	1338.37	843.46	623.34	589.33	464.19	448.13
Crystal size (mm)	$0.40\times0.25\times0.20$	$0.30\times0.25\times0.18$	$0.25\times0.15\times0.05$	$0.50\times0.25\times0.20$	$0.20\times0.10\times0.10$	$0.55\times0.30\times0.05$	$0.30\times0.10\times0.10$
Color	orange	pale yellow	pale yellow	red	red	green	green
Crystal system	monoclinic	monoclinic	monoclinic	triclinic	triclinic	monoclinic	triclinic
Space group	$P2_1/n$	P_12_1/n_1	P_12_1/c_1	$P\bar{1}$	$P\bar{1}$	C_12/c_1	$P\bar{1}$
a (Å)	21.7074(3)	21.7556(4)	15.167(1)	8.599(3)	10.3504(2)	31.6471(4)	9.749(3)
b (Å)	11.2747(2)	11.2937(3)	12.328(1)	11.788(6)	13.7626(2)	7.2485(1)	9.917(3)
c (Å)	25.6315(4)	25.5796(5)	16.819(1)	14.139(7)	19.5850(4)	20.7356(3)	10.849(2)
α (°)	90.0	90.0	90.0	82.997(2)	76.770(1)	90.0	82.673(16)
β (°)	112.391(1)	112.546(1)	102.2(1)	72.755(2)	84.843(1)	121.445(1)	74.118(15)
γ (°)	90.0	90.0	90.0	86.741(2)	89.732(1)	90.0	73.44(2)
V (Å^3)	5800.2(2)	5804.6(2)	3074.1675(2)	1358.4(11)	2704.45(9)	4058.07(10)	965.6(15)
Z	4	4	4	2	4	8	2
D_{calc}	1.518	1.531	1.822	1.524	1.447	1.52	1.541
Temperature (K)	293(2)	293(2)	298	293(2)	293(2)	293(2)	293(2)
θ (°)	3.47–27.49	3.449–27.58	3.492–27.515	3.04–29.98	3.45–27.87	3.41–27.88	2.59–26.96
Reflections collected	24036	20915	27901	12341	22935	29847	2822
Independent reflections (R_{int}, %)	13254 (0.0694)	13179 (0.033)	5738 (0.04)	7842 (0.0462)	12746 (0.0621)	4800 (0.0497)	2667 (0.0093)
Reflections observed	6577	5844	2451	4129	6115	3635	2664
S = goodness-of-fit	1.018	1.024	0.9065	1.024	0.973	1.023	1.111
Final R_1 factor gt	0.0562	0.0525	0.0635	0.0744	0.0494	0.0337	0.0368
Final wR_2 factor	0.1251	0.0504	0.0733	0.1843	0.0914	0.0781	0.0985
Diffractometer	KAPPA-CCD	KAPPA-CCD	KAPPA-CCD	KAPPA-CCD	KAPPA-CCD	KAPPA-CCD	CAD4

$R_{int}=\frac{\sum|F_o^2-\langle F_o^2\rangle|}{\sum F_o^2}$, $R_1=\frac{\sum||F_o|-|F_c||}{\sum|F_o|}$, $wR_2=\sqrt{\frac{\sum w(F_o^2-F_c^2)^2}{\sum w(F_o^2)^2}}$, $S=\sqrt{\frac{\sum w(F_o^2-F_c^2)^2}{m-n}}$.

2.4.1. *[Co(bis-btz)$_2$] · DMSO (**4**)*

Bis-btz (284 mg, 1 mmol) was dissolved in hot methanol (30 mL), and a solution of $Co(OAc)_2\cdot4H_2O$ (125 mg, 0.5 mmol) in hot methanol (5 mL) was added. An orange precipitate was obtained by evaporation of the solvent, which was filtered and recrystallized in DMSO, the orange crystals were suitable for X-ray diffraction studies. Yield: 203 mg (65%). Dec. at 380 °C. *Anal.* Calc. for $C_{28}H_{16}N_6S_4Co$: C, 53.92; H, 2.58; N; 13.48. Found: C, 53.86; H, 2.61; N, 13.42%. $\mu_{eff}=4.79$ BM. MS: m/z 623(72) $[M]^+$.

2.4.2. *[Ni(bis-btz)$_2$] (**5**)*

The previous procedure was repeated using $Ni(OAc)_2\cdot4H_2O$ (125 mg, 0.5 mmol) and bis-btz (284 mg, 1 mmol), yielding a dark red microcrystalline powder. Yield: 153 mg (49%). Dec. at 320 °C. . *Anal.* Calc. for $C_{28}H_{16}N_6S_4Ni$: C, 53.94; H, 2.58; N, 13.48. Found: C, 54.02; H, 2.59; N, 13.49%. $\mu_{eff}=2.99$ BM. MS: m/z 623(56) $[M]^+$.

2.4.3. *[Zn(bis-btz)$_2$] · 0.5DMSO (**6**)*

$Zn(OAc)_2\cdot H_2O$ (100 mg, 0.5 mmol) was reacted with bis-btz (284 mg, 1 mmol). A pale yellow powder was isolated which was recrystallized from hot DMSO. The crystals were suitable for X-ray diffraction. Yield: 194 mg (62%). Dec. at 310 °C. *Anal.* Calc. for $C_{29}H_{19}N_6O_{0.5}S_{4.5}Zn$: C, 52.05; H, 2.86; N, 12.56. Found: C, 51.45; H, 2.76; N, 12.23%. MS: m/z 628(98) $[M]^+$.

2.4.4. *[Hg(bis-btz)$_2$] · DMSO (**7**)*

The previous procedure was repeated using $Hg(OAc)_2$ (160 mg, 0.5 mmol) and bis-btz (284 mg, 1 mmol). A pale yellow powder was filtered off and recrystallized from hot DMSO. Yield: 238 mg (63%). Dec. at 260 °C. *Anal.* Calc. for $C_{30}H_{22}N_6O_1S_5Hg$: C, 42.72; H, 2.63; N, 9.96. Found: C, 42.68; H, 2.42; N, 10.16%. MS: m/z 283(100) $[C_{14}H_9N_3S_2]^+$.

2.4.5. *[Co(btz-boz)$_2$] (**8**)*

The same procedure was repeated using $Co(OAc)_2\cdot4H_2O$ (125 mg, 0.5 mmol) and btz-boz (267 mg, 1 mmol), yielding a microcrystalline orange powder. Yield: 156 mg (52%). Dec. at 375 °C. *Anal.* Calc. for $C_{28}H_{16}N_6S_2O_2Co$: C, 56.85; H, 2.72; N, 14.20. Found: C, 56.77; H, 2.66; N, 14.02%. $\mu_{eff}=5.11$ BM. MS: m/z 591(100) $[M]^+$.

2.4.6. *[Ni(btz-boz)$_2$(MeOH)] (**9**)*

$Ni(OAc)_2\cdot4H_2O$ (125 mg, 0.5 mmol) was reacted with btz-boz (267 mg, 1 mmol). A dark red powder was isolated and recrystallized from hot DMSO. An X-ray diffraction study was carried out for the obtained crystals. Yield: 144 mg (48%); m.p. 322–326 °C. *Anal.* Calc. for $C_{29}H_{20}N_6S_2O_3Ni$: C, 55.88; H, 3.23; N, 13.48. Found: C, 55.92; H, 2.61; N, 13.67%. $\mu_{eff}=2.99$ BM. MS: m/z 591(100) $[M]^+$.

2.4.7. *[Zn(btz-boz)$_2$] · 0.5DMSO (**10**)*

$Zn(OAc)_2\cdot H_2O$ (100 mg, 0.5 mmol) was reacted with btz-boz (267 mg, 1 mmol), it was recrystallized from hot DMSO, yielding a microcrystalline pale yellow powder. Yield: 203 mg (68%). Dec. at 300 °C. *Anal.* Calc. for $C_{29}H_{19}N_6S_{2.5}O_{2.5}Zn$: C, 54.67; H, 3.01; N, 13.20. Found: C, 54.33; H, 2.98; N, 12.90%. MS: m/z 593(100) $[M]^+$.

2.4.8. *[Co(btz-bz)$_2$] · MeOH (**11**)*

The previous procedure was repeated using $Co(OAc)_2\cdot4H_2O$ (125 mg, 0.5 mmol) and btz-bz (267 mg, 1 mmol).

An orange powder was filtered off and washed in methanol. Yield: 153 mg (49%). Dec. at 350 °C. *Anal*. Calc. for $C_{29}H_{22}N_8O_1S_2Co$: C, 55.86; H, 3.17; N, 18.74. Found: C, 56.03; H, 3.57; N, 18.03%. $\mu_{eff} = 4.49$ BM. MS: *m*/*z* 589(100) $[M]^+$.

*2.4.9. [Ni(btz-bz)$_2$(MeOH)] (**12a**)*

$Ni(OAc)_2 \cdot 4H_2O$ (125 mg, 0.5 mmol) was reacted with btz-bz (267 mg, 1 mmol). A dark red powder was obtained. Yield: 97 mg (31%). Dec. at 390°. IR(KBr), *v* (cm^{-1}): 3435.5 (OH). *Anal*. Calc. for $C_{29}H_{20}N_8O_1S_2Ni$: C, 56.06; H, 3.57; N, 18.03. Found: C, 56.25; H, 3.15; N, 18.46%. $\mu_{eff} = 3.05$ BM. MS: *m*/*z* 589(100) $[M]^+$. The red crystalline powder was recrystallized from methanol, by standing at r.t. for 2 months, it gave crystals suitable for single X-ray diffraction. During crystallization the MeOH molecule was lost giving compound [Ni(btz-bz)$_2$] (**12**), which was characterized by X-ray diffraction analysis.

*2.4.10. [Zn(btz-bz)$_2$] (**13**)*

A solution of $Zn(OAc)_2 \cdot H_2O$ (100 mg, 0.5 mmol) was added to btz-bz (267 mg, 1 mmol). The product of the reaction was isolated and filtered. A pale yellow powder was obtained. Yield: 150 mg (50%). Dec. at 310 °C. *Anal*. Calc. for $C_{28}H_{18}N_8S_2Zn$: C, 56.43; H, 3.04; N, 18.80%. Found: C, 56.29; H, 3.30; N, 18.80%. MS: *m*/*z* 594(10) $[M]^+$.

The coordination compounds **14**–**16** were synthesized following the same procedure, as described for compound **14** using an equimolar ratio ligand to metal.

*2.4.11. [Ni(bis-btz)(OAc)(MeOH)$_2$] (**14**)*

Bis-btz (284 mg, 1 mmol) was dissolved in hot methanol (30 mL) and a solution of $Ni(OAc)_2 \cdot 4H_2O$ (249 mg, 1 mmol) in hot methanol (5 mL) was added. Green crystals were obtained by partial evaporation of the solvent and isolated by filtration. Yield: 195 mg (42%). Dec. at 370 °C. *Anal*. Calc. for: $C_{18}H_{19}N_3O_4S_2Ni$: C, 46.57; H, 4.12; N, 9.05. Found: C, 46.53; H, 4.11; N, 8.97%. MS: *m*/*z* 464(90) $[M]^+$.

*2.4.12. [Ni(btz-boz)(OAc)(MeOH)$_2$] (**15**)*

The previous procedure was repeated using $Ni(OAc)_2 \cdot 4H_2O$ (249 mg, 1 mmol) and btz-boz (267 mg, 1 mmol). After two weeks, green crystals suitable for X-ray diffraction were obtained by slow evaporation at r.t. Yield: 204 mg (46%). *Anal*. Calc. for $C_{18}H_{19}N_3O_5SNi$: C, 48.25; H, 4.27; N, 9.38. Found: C, 48.26; H, 4.20; N, 9.48%. The obtained compound was not suitable for mass spectrometry, it decomposed without melting.

*2.4.13. [Ni(btz-bz)(OAc)(MeOH)$_2$] (**16**)*

Complex **16** was synthesized with an analogous procedure to **14**. A solution of $Ni(OAc)_2 \cdot 4H_2O$ (249 mg, 1 mmol) in methanol was added to a solution of btz-bz (267 mg, 1 mmol). A green powder was obtained by slow evaporation of the solvent. Yield: 145 g (32%). *Anal*. Calc. for $C_{18}H_{19}N_4O_4S_1Ni$: C 48.46; H, 4.29; N, 12.56. Found: C, 47.95; H, 4.47; N, 12.47%. The obtained compound was not suitable for mass spectrometry, it decomposed without melting.

3. Results and discussion

Ligands **1**–**3** were reacted with cobalt(II), nickel(II) and zinc(II) acetates; ligand **1** was also reacted with mercury(II) acetate; in all coordination compounds the N–H group was deprotonated, as was deduced from the neutral character of the compounds. Cobalt(II) compounds **4**, **8**, **11** presented an orange color, while zinc(II) **6**, **10**, **13** and mercury(II) **7** complexes were characterized as pale yellow microcrystalline powders, regardless of the ligand used in the reaction synthesis. While for nickel(II), red compounds were isolated when two ligands are coordinated to the metal center **5**, **9**, **12**, **12a**; when only one ligand is present, green complexes **14**–**16** were obtained.

3.1. Mass spectrometry

The analyses by mass spectrometry at 20 eV for compounds **4**–**6**, **8** and **10**–**13**, showed the molecular ion peaks. This behavior confirms that both ligands are strongly attached to the metal(II) ion, surrounding the metal atom and preventing further reactions that could lead to fragmentation. Whereas for mercury(II) **7**, the molecular ion peak was not observed indicating weaker coordination bonds, only the main peak at *m*/*z* 283 due to the ligand $[C_{14}H_8N_3S_2]^+$ was identified. In compound **9**, the methanol molecule was lost and the peak at 590 corresponds to the nickel(II) bonded to two ligands. The molecular ion for compound [Ni(bis-btz)(OAc)(MeOH)$_2$] (**14**) is observed together with another at *m*/*z* 622 which corresponds to two ligand molecules attached to the metal ion due to intermolecular rearrangements. Compounds [Ni(btz-boz)-(OAc)(MeOH)$_2$] (**15**) and [Ni(btz-bz)(OAc)(MeOH)$_2$] (**16**) decomposed without melting and their mass spectra were not recorded.

3.2. Infrared spectroscopy

The symmetric ligand bis-btz **1**, exhibits two IR bands assigned to the *v*(C=N) at 1560 and 1542 cm^{-1}, which are shifted ($\Delta \cong 100$ cm^{-1}) upon coordination to the metal ions **4**–**7** to 1479–1462 and 1451–1444 cm^{-1}, respectively. Whereas for the non-symmetric ligands, btz-boz and btz-bz and their corresponding coordination compounds **8**–**13**, different *v*(C=N) bands corresponding to the thiazole, oxazole or benzimidazole rings were observed (Table 2), which shifted upon coordination. In all cases a strong bonding of the nitrogen atoms to the metal ions is shown. The *v*(C=N) bands in complexes **14**–**16** are in the expected regions.

3.3. Electronic spectra

*3.3.1. Cobalt(II) compounds **4**, **8** and **11***

The orange [Co(bis-btz)$_2$] (**4**), [Co(btz-boz)$_2$] (**8**) and [Co(btz-bz)$_2$] (**11**) compounds, have a magnetic moment

Table 2
IR spectroscopic data (cm^{-1}) for compounds **1**–**16**

		ν(C=N)
1	bis-btz	1460, 1542
2	btz-boz	1577, 1536(br)
3	btz-bz	1629, 1597
4	$[Co(bis\text{-}btz)_2]\cdot DMSO$	1462, 1444
5	$[Ni(bis\text{-}btz)_2]$	1462, 1439
6	$[Zn(bis\text{-}btz)_2]\cdot 0.5DMSO$	1479, 1450
7	$[Hg(bis\text{-}btz)_2]\cdot DMSO$	1473, 1451
8	$[Co(btz\text{-}boz)_2]$	1531, 1477, 1464, 1442
9	$[Ni(btz\text{-}boz)_2(MeOH)]$	1529, 1476, 1464, 1442
10	$[Zn(btz\text{-}boz)_2]\cdot 0.5DMSO$	1536, 1479, 1466, 1453
11	$[Co(btz\text{-}bz)_2]\cdot MeOH$	1533, 1483, 1452(br)
12a	$[Ni(btz\text{-}bz)_2(MeOH)]$	1534, 1482, 1452(br)
13	$[Zn(btz\text{-}bz)_2]$	1533, 1484, 1453(br)
14	$[Ni(bis\text{-}btz)(OAc)(MeOH)_2]$	1546, 1474, 1446(br)
15	$[Ni(btz\text{-}boz)(OAc)(MeOH)_2]$	1549, 1490, 1450(br)
16	$[Ni(btz\text{-}bz)(OAc)(MeOH)_2]$	1549, 1491, 1450(br)

characteristic of a cobalt(II) ion, $\mu_{eff} = 4.79$, 5.11 and 4.49 BM, respectively.

The diffuse reflectance spectra of these tetrahedral compounds are unusual with two CT broad absorption bands in the 28 000–22 500 cm^{-1} region which are extended up to the visible region. The $\nu_3\ {}^4T_1(P) \leftarrow {}^4A_2(F)$ transition is observed as a well defined a shoulder at 20 250, 20 768 and 21 818 cm^{-1}, for **4**, **8** and **11** respectively; while a multicomponent band in the NIR assigned to $\nu_2\ {}^4T_1(P) \leftarrow {}^4A_2(F)$, at 9456, 9775 and 9534 cm^{-1} respectively, Table 3. Their electronic spectra show the influence of the high electronic density from the planar conjugated ligands, when coordinated to the cobalt(II) ion, forming a six-membered chelate ring. The electronic delocalization in the system, which is extended to the metal ion, would also explain the shifting of the transitions ν_2 and ν_3 to higher energy giving rise to the orange color of the complexes. It is observed that when changing the heteroatom in the 12 position, S in **1** (bis-btz), O in **2** (btz-boz) and N in **3** (btz-bz), the electronic transitions are shifted respectively, indicating stronger ligand fields. This is consistent with their mass spectra and IR, which are in agreement with a strong bonding from the ligands towards the metal ions.

3.3.2. Nickel(II) compounds 5, 9 and 12a

The electronic spectrum of the crystalline complex $[Ni(bis\text{-}btz)_2]$ (**5**) is rather similar to the already discussed tetrahedral cobalt(II) compounds, with two CT broad absorption bands extended up to the visible region (32 500–20 000 cm^{-1}) and transitions at 18 900 and 8009 cm^{-1} assigned to $\nu_3\ {}^3T_1(P) \leftarrow {}^3T_1(F)$ and $\nu_2\ {}^3A_2(F) \leftarrow {}^3T_1(F)$ for a nickel(II) ion in a distorted tetrahedral geometry [38,39].

Compounds $[Ni(btz\text{-}boz)_2(MeOH)]$ (**9**) and $[Ni(btz\text{-}bz)_2(MeOH)]$ (**12a**) showed the corresponding bands for a pentacoordinated nickel(II) in a square pyramidal geometry with absorption bands centered at 20 000, 16 500, 10 826, 9730 and 8190 cm^{-1} for compound **9**, whereas for **12a** are at 20 720, 16 413, 10 600, 9325 and 7250 cm^{-1}. They also present two charge transfer bands in the 30 400–24 000 cm^{-1} region (Table 3).

3.3.3. Nickel(II) compounds 14–16

The reflectance spectra of the green nickel(II) complexes, $[Ni(bis\text{-}btz)(OAc)(MeOH)_2]$ (**14**), $[Ni(btz\text{-}boz)(OAc)(MeOH)_2]$ (**15**) and $[Ni(btz\text{-}bz)(OAc)(MeOH)_2]$ (**16**) showed three absorption bands (Table 3), which may be assigned to a distorted octahedral geometry, as observed in previously reported thiabendazol nickel(II) bis- and tris-chelates [28]; with transitions $\nu_1\ {}^3T_{2g}(F) \leftarrow {}^3A_{2g}(F)$, $\nu_2\ {}^3T_{1g}(F) \leftarrow {}^3A_{2g}(F)$ and $\nu_3\ {}^3T_{1g}(P) \leftarrow {}^3A_{2g}(F)$ in the regions 9300–9800, 14 828–14 964 and 23 252–25 000 cm^{-1}, respectively. Additionally,

Table 3
UV–Vis–NIR electronic spectra data (cm^{-1}) for compounds **1**–**16**

Ligands		
1	bis-btz	27 250
2	btz-boz	25 300
3	btz-bz	27 431
Cobalt(II) compounds		
4	$[Co(bis\text{-}btz)_2]\cdot DMSO$	28 000, 24 038, 20 250(ν_3), 9456(ν_2)
8	$[Co(btz\text{-}boz)_2]$	28 000, 25 100, 20 768(ν_3), 9775(ν_2)
11	$[Co(btz\text{-}bz)_2]\cdot MeOH$	28 800, 25 328, 21 818(ν_3), 9534(ν_2)
Nickel(II) compounds		
5	$[Ni(bis\text{-}btz)_2]$	29 820, 25 300, 18 900, 8009
9	$[Ni(btz\text{-}boz)_2(MeOH)]$	30 400, 24 088, 20 000[a], 16 500[b], 10 826[c], 9730[d], 8190[e]
12a	$[Ni(btz\text{-}bz)_2(MeOH)]$	31 410, 25 470, 20 720[a], 16 413[b], 10 600[c], 9325[d], 7250[e]
14	$[Ni(bis\text{-}btz)(OAc)(MeOH)_2]$	26 190(br), 23 252(ν_3), 14 964(ν_2), 9299(ν_1)
15	$[Ni(btz\text{-}boz)(OAc)(MeOH)_2]$	31 500, 27 838, 24 378(ν_3), 14 958(ν_2), 9797(ν_1)
16	$[Ni(btz\text{-}bz)(OAc)(MeOH)_2]$	29 700, 27 500, 25 000(ν_3), 14 828(ν_2), 9655(ν_1)
Zinc(II) and mercury(II) compounds		
6	$[Zn(bis\text{-}btz)_2]\cdot 0.5DMSO$	26 000
10	$[Zn(btz\text{-}boz)_2]\cdot 0.5DMSO$	27 150
13	$[Zn(btz\text{-}bz)_2]$	27 390
7	$[Hg(bis\text{-}btz)_2]\cdot DMSO$	28 500, 26 000, 24 900

[a–e] Electronic transitions: ${}^3E(P)$, ${}^3A_2$, ${}^3E$; ${}^3A_2$; ${}^3B_2$; ${}^3E$.

the spectra presented two broad charge transfer bands in the 31 500–26 000 cm^{-1} region.

3.3.4. Zinc(II) 6, 10, 13 and mercury(II) 7 compounds

For [Zn(bis-btz)$_2$] (**6**), [Zn (btz-boz)$_2$] (**10**) and [Zn(btz-bz)$_2$] (**13**), the broad absorptions at 26 000, 27 150 and 27 390 cm^{-1} are associated to charge transfer ligand to metal bands, whereas for [Hg(bis-btz)$_2$] (**7**), three well defined charge transfer bands at 28 500, 26 000 and 24 900 were observed, Table 3.

3.4. X-ray structure determination

3.4.1. Tetrahedral compounds 4, 6, 7 and 12

X-ray diffraction analyses for the bis-btz isostructural compounds **4**, **6**, **7** and the btz-bz complex **12** show a metal

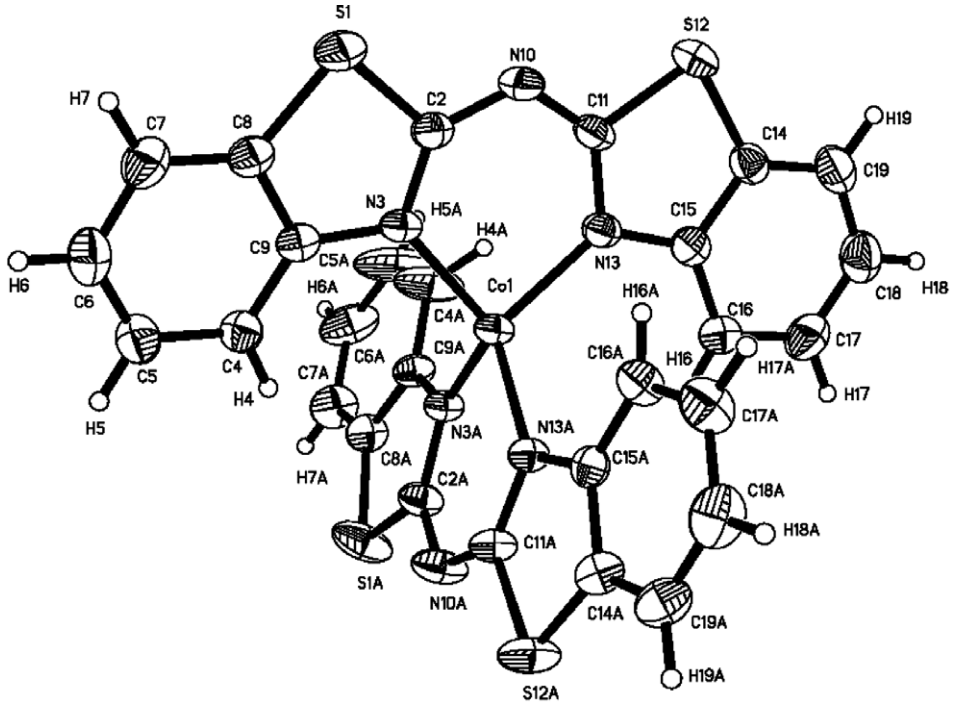

Fig. 1. ORTEP view of [Co(bis-btz)$_2$] · DMSO (**4**) with thermal ellipsoids for non-H atoms at the 30% probability level.

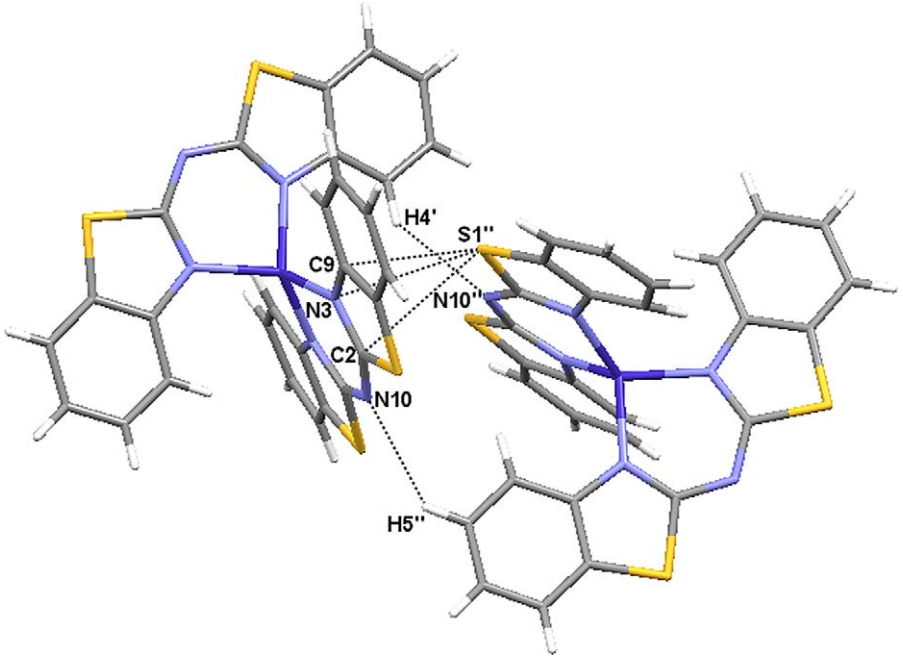

Fig. 2. View of compound **6** showing the sulfur π allylic interaction with C2–N3–C9 atoms with distances S1···C2 3.44 Å, S1···N3 3.32 Å and S1···C9 3.37 Å, and two N···H bonds N10···H5‴ 2.71Å and N10″···H4′ 2.64 Å.

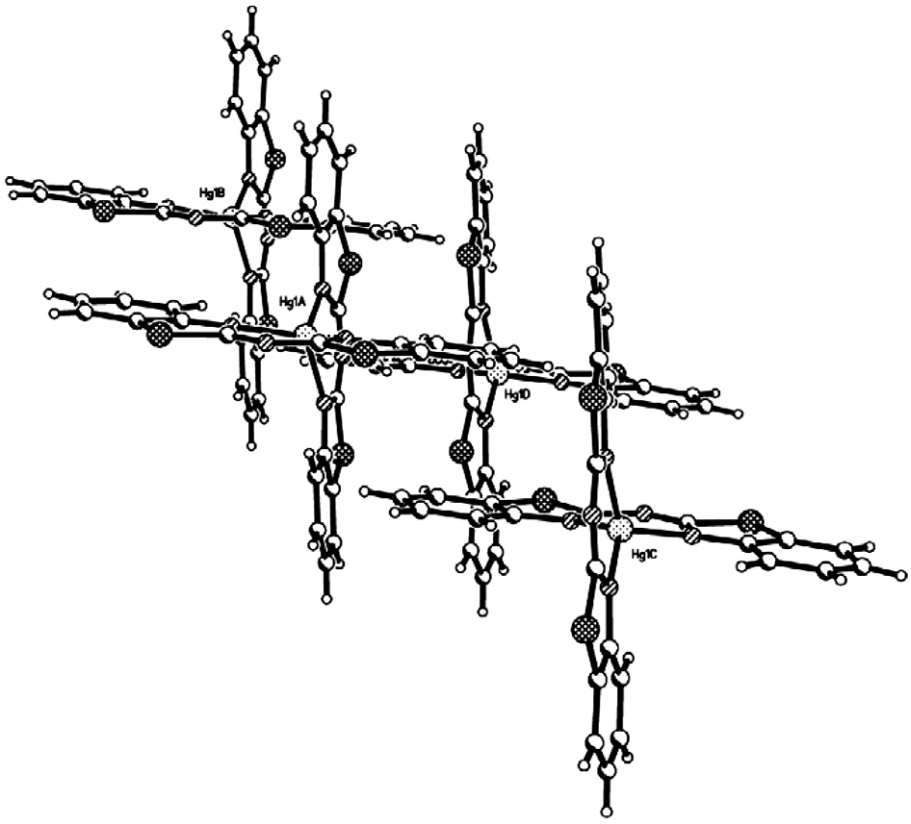

Fig. 3. Crystal packing in compound $[Hg(bis\text{-}btz)_2] \cdot DMSO$ (**7**).

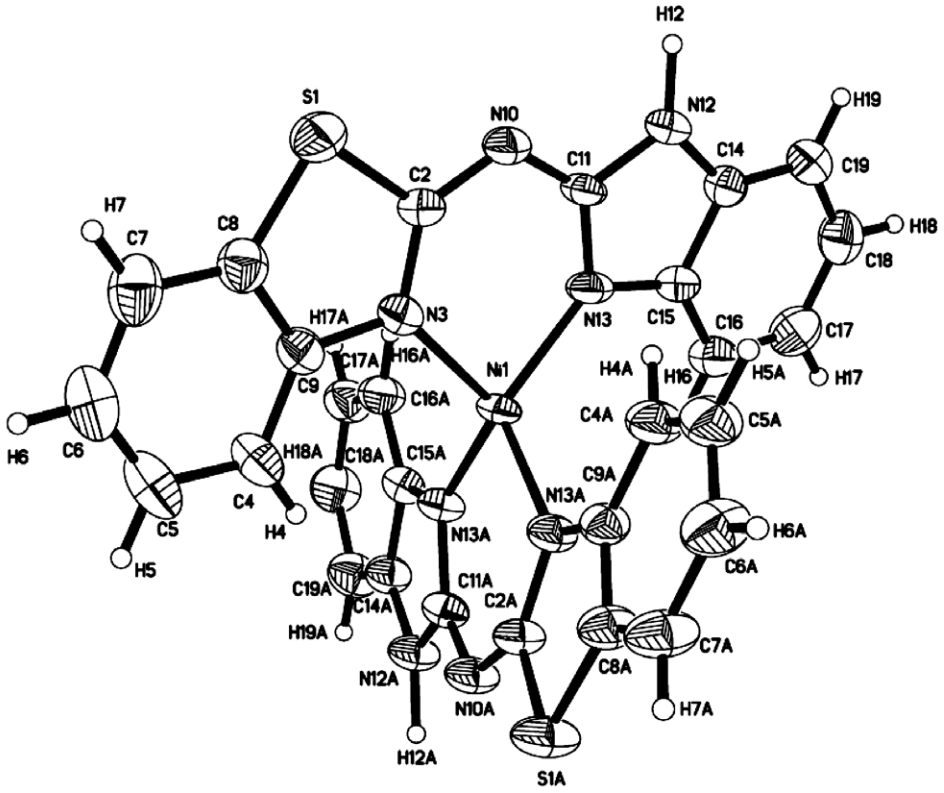

Fig. 4. ORTEP view of the crystal structure of the $[Ni(btz\text{-}bz)_2]$ (**12**) showing the 30% probability thermal ellipsoid.

atom with two deprotonated ligands chelating through the nitrogen atoms N3 and N13, in a distorted tetrahedral geometry, Figs. 1–5.

In these compounds the N–metal(II) bond lengths are very similar and relatively short (Table 4), **4** Co–N ca. 1.98 Å, **6** Zn–N ca. 1.99 Å, **7** Hg–N ca. 2.2 Å and **12** Ni–N 1.97 Å. In addition, the C–N bond lengths of the central six-membered rings have similar values in between double and single bonds of sp^2 C and N atoms (ca. 1.33 Å) indicating an electronic delocalized π-system where the metal(II) ion participates in the system, as deduced from the electronic spectra for the cobalt(II) **4**, **8**, **11** and nickel(II) **5** compounds. The short bond lengths M–N are in agreement with the observation of their molecular ion peaks in mass spectra.

The two ligands are in a perpendicular arrangement, with an angle between the planes close to 90°. The bite

Table 4
Selected bond lengths (Å) and angles (°) for compounds **4**, **6**, **7** and **12**

	4	**6**	**7**	**12**
M1–N3	1.979(3)	1.988(4)	2.24(1)	1.989(3)
M1–N13	1.978(3)	1.993(4)	2.17(1)	1.950(3)
M1–N3A	1.987(3)	1.996(4)	2.20(1)	1.983(3)
M1–N13A	1.984(3)	1.986(4)	2.20(1)	1.957(3)
N3–C2	1.326(5)	1.328(6)	1.32(2)	1.334(4)
N10–C11	1.320(5)	1.327(7)	1.30(2)	1.353(4)
N10–C2	1.342(5)	1.334(7)	1.35(2)	1.355(4)
C11–N13	1.350(5)	1.333(6)	1.36(2)	1.346(4)
S12–C11	1.755(4)	1.754(5)	1.77(1)	
N3–M1–N13	92.5(1)	93.1(2)	84.8(4)	92.4(1)
N3A–M1–N13A	92.8(1)	93.1(2)	85.1(5)	92.0(1)
N13–M1–N3A	120.7(1)	116.8(2)	123.4(5)	120.8(1)
N13–M1–N13A	117.1(1)	117.4(2)	129.7(4)	123.8(1)
N3–M1–N3A	117.6(1)	117.2(2)	125.7(4)	107.3(1)

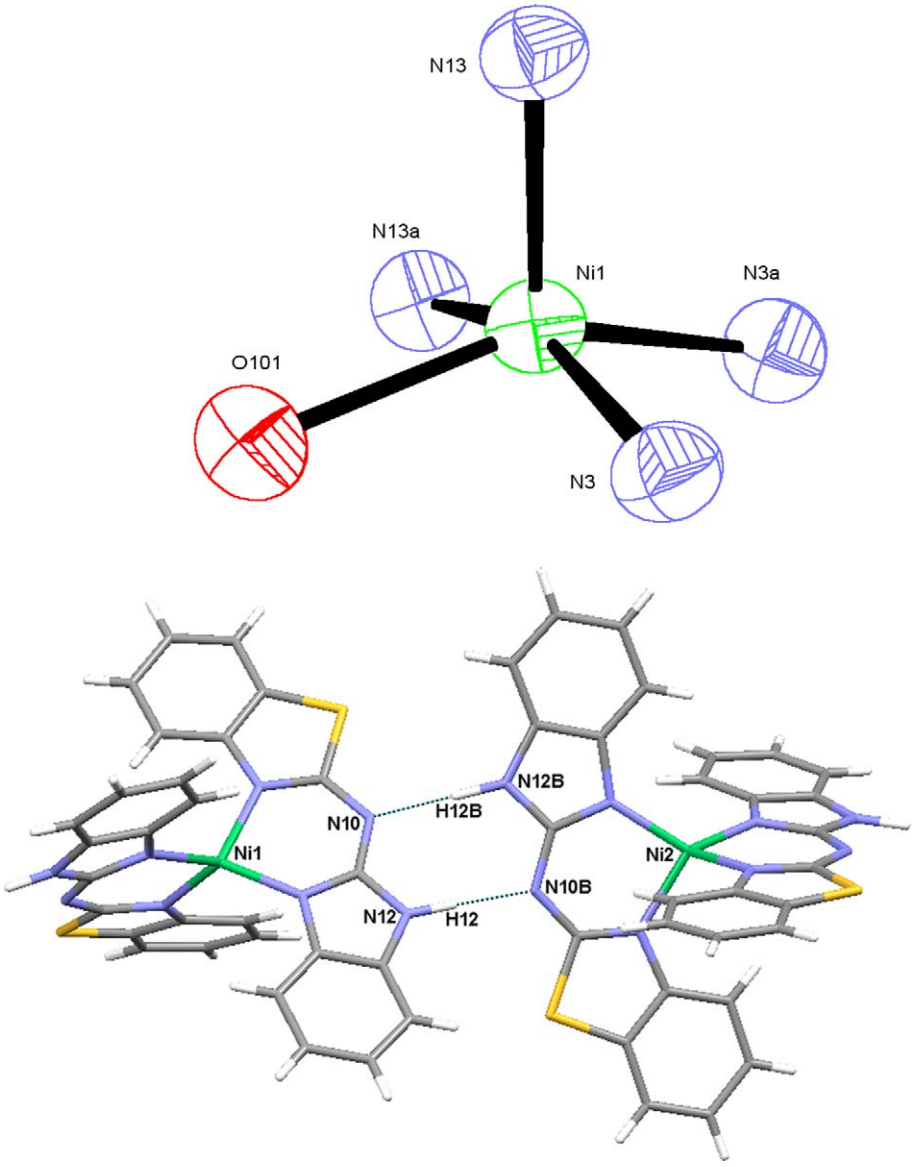

Fig. 5. Hydrogen bonds in compound **12**.

angles of the ligands are ca. 92° in compounds **4** and **12**, ca. 93° in **6** and while for **7** is 85°, due to its larger ionic radii. Coordination to the metal atoms gives rise to a quasi-planar pentacyclic arrangement for the aromatic rings, some distortion of the ligand is observed, in the cobalt(II) compound **4** the torsion angle M1–N3–C9–C4 is 12°, while in zinc(II) **6** is 14°, in the mercury(II) **7** is 5° and for **12** there is no distortion.

In compound **6** two molecules are associated through two N···H hydrogen bonds and one sulfur atom has an intermolecular π allylic interaction with three atoms [C2–N3–C9] as is shown in Fig. 2.

The crystal packing for compound **7** is shown in Fig. 3. In compound **12**, hydrogen bonding between N10 and N13, 2.926 Å (176.64°) gives rise to a dimeric arrangement, Fig. 5.

3.4.2. Square-based pyramidal geometry, compound *9*

The nickel(II) compound **9** is pentacoordinated in a square pyramidal geometry, which is consistent with its observed electronic spectrum, with two btz-boz ligands and a methanol molecule, Fig. 6. This complex has a structural angular parameter τ value of 0.14, where $\tau = (\beta - \alpha)/60$; $\alpha = 151.94$ and $\beta = 160.15$, indicating a square pyramidal geometry with a small trigonal component [40]. The bond lengths between the nickel(II) ion and the nitrogen atoms are in the range of 2 Å, Table 5. The apical position is occupied by N13 of the boz ring, Fig. 6. The Ni–O1 bond length [2.107(3) Å] is in the range expected for oxygen–nickel(II) bonds. Similar values of the bond lengths in the central ring between N3–C2 1.324(5), N10–C2 1.345(5), C11–N10 1.320(5) indicate the delocalization of the π system. A supramolecular arrangement is formed by hydrogen bonding of the imino nitrogen N10 with the oxygen atom of the coordinated methanol N10···H1–O1 1.951 Å, Fig. 6.

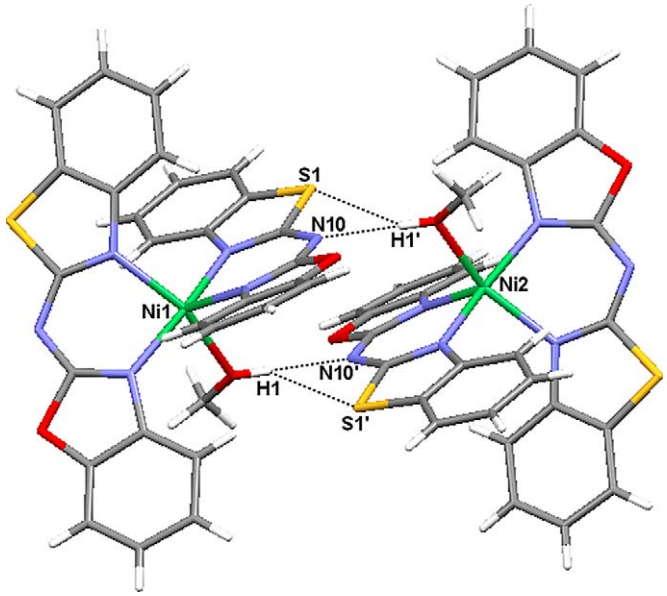

Fig. 6. Dimeric association by short hydrogen bonding between N10···H1′ 2.726, N10′···H1 1.951 and S1′···H1 2.944 Å, in compound **9**. The upper inset represents the square-based pyramidal geometry of nickel atom **9**.

Table 5
Selected bond lengths (Å) and angles (°) for **9**, **14** and **15**

	9	14	15
M1–N3	2.038(3)	2.032(2)	2.043(4)
M1–N13	1.988(3)	2.019(2)	2.011(3)
M1–N3A	2.043(4)		
M1–N13A	2.011(4)		
M1–O1	2.107(3)	2.072(2)	2.111(3)
M1–O2		2.139(2)	2.090(3)
M1–O3		2.091(1)	2.191(2)
M1–O4		2.147(1)	2.061(3)
N3–C2	1.324(5)	1.326(3)	1.321(4)
N13–C11	1.334(5)	1.324(3)	1.322(4)
N10–C2	1.345(5)	1.347(3)	1.341(4)
N10–C11	1.320(5)	1.346(3)	1.322(5)
N3–M1–N13	88.1(1)	88.32(7)	88.8(1)
N3A–M1–N13A	86.0(2)		
O1–M1–O2		176.81(7)	171.9(1)
O3–M1–O4		61.98(6)	61.1(1)
N13A–M1–N3	160.1(1)		
N3A–M1–N13	109.5(2)		
N3A–M1–N3	92.8(1)		

3.4.3. Octahedral compounds *14* and *15*

The nickel(II) compounds **14** and **15** have a similar distorted octahedral geometry, with one ligand molecule bonded to the metal ion forming a pentacyclic frame, a bidentate acetate group, and two *trans*-methanol molecules completing the hexacoordination (Figs. 7–10).

The compounds have two slightly different nickel(II)-nitrogen bond lengths, Ni–N3 2.032(2) and Ni–N13 2.019(2) for **14** and 2.043(4) and 2.011(3) Å for **15**, which are longer that those observed in the bis-chelate tetrahedral compound **12** [Ni–N3 1.989(3) Å and Ni–N13 1.950(3) Å]. In both compounds, the *trans* methanol molecules are perpendicular to the main plane and in the range of 2.10 Å, as those of the bidentate chelating carboxylates, Table 5.

The main difference between both compounds is that the conformation of the bis-btz ligand in **14** is folded in a butterfly shape, the torsional angle between the two halves of the pentacyclic system is 127°, whereas in **15** the btz-boz ligand is planar, Fig. 8. The explanation for this difference is that in **15** there is a double intermolecular π-interaction between C2 and C11 of two molecules (3.318 Å), this dimer is reinforced by two cooperative intermolecular hydrogen bonding of the coordinated methanol and the imine nitrogen, O1–H1···N10′ (2.101 Å), Fig. 9. In addition, the dimers form a mono dimensional polymer by two O2–H2···O3′ hydrogen bonds (2.018 Å). Whereas in **14** there is a 2D arrangement formed by intermolecular interactions: a π-interaction of O–CH proton with C15 (2.892 Å) and two hydrogen bonds, O1–H1···N10′ (1.920 Å) and O2–H2···O4″ (1.990 Å), Fig. 10.

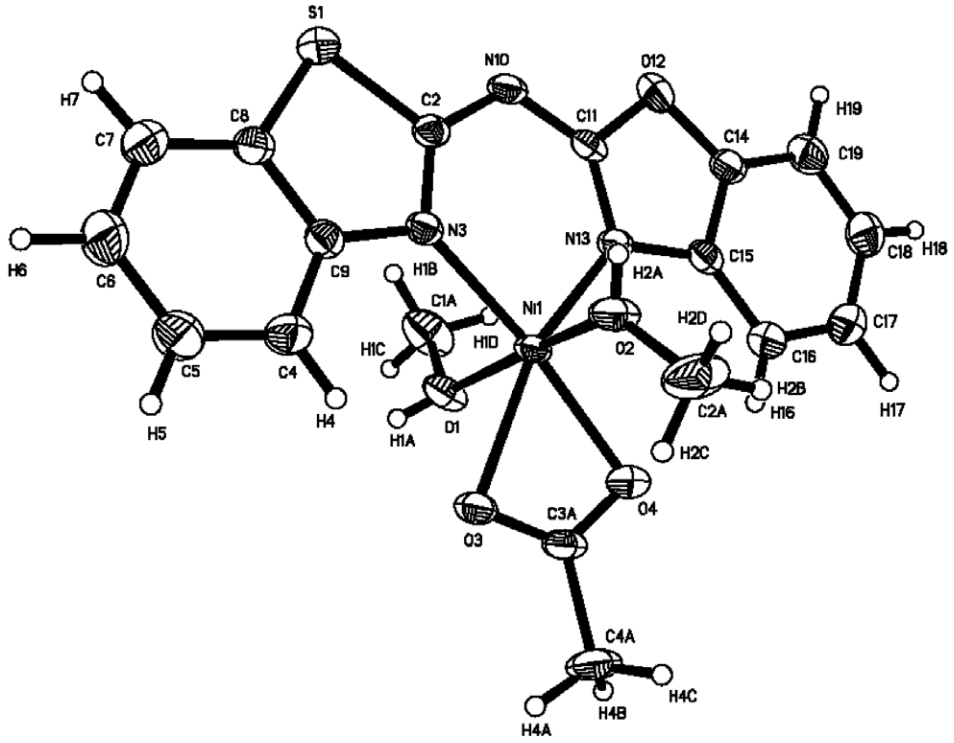

Fig. 7. ORTEP drawing of the molecular structure of **15**. Thermal ellipsoids are drawn on the 30% probability level.

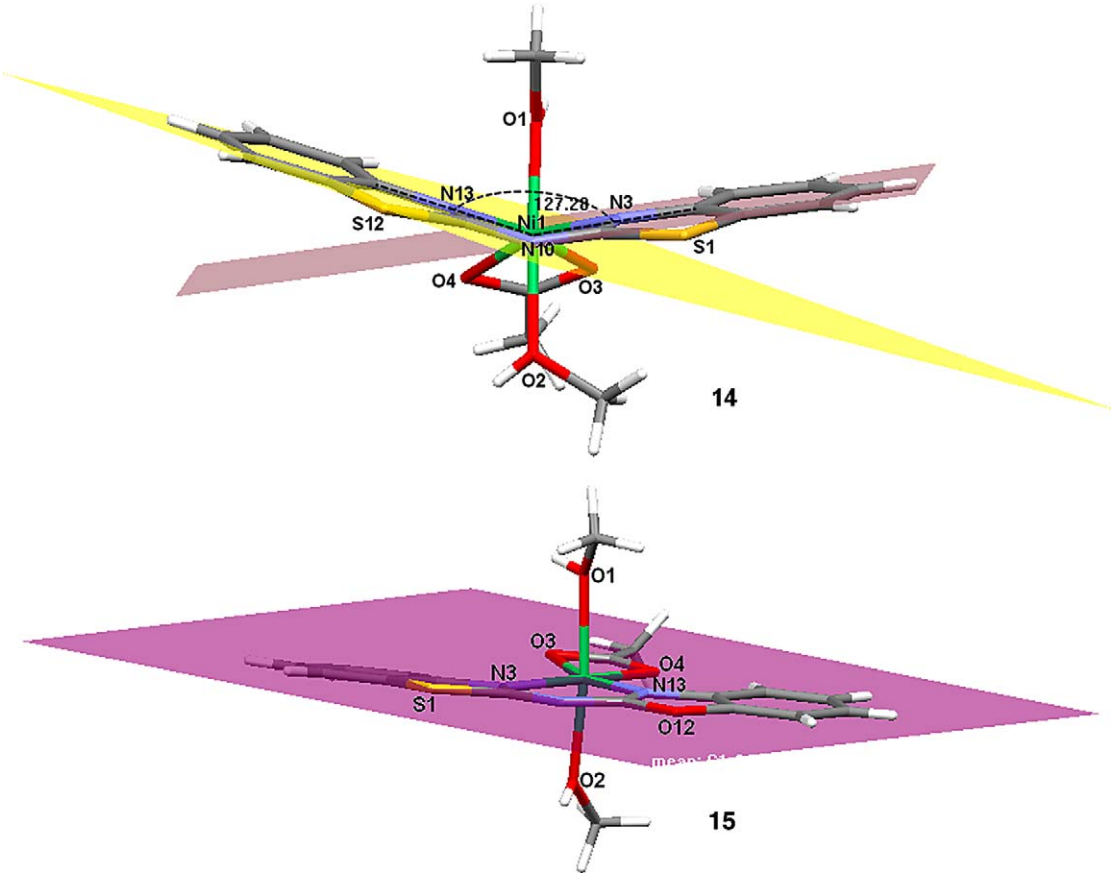

Fig. 8. Butterfly shape of the bis-btz ligand in **14** hydrogen atoms are omitted for clarity and a view of compound **15** showing the plane depicted by the pentacyclic framework.

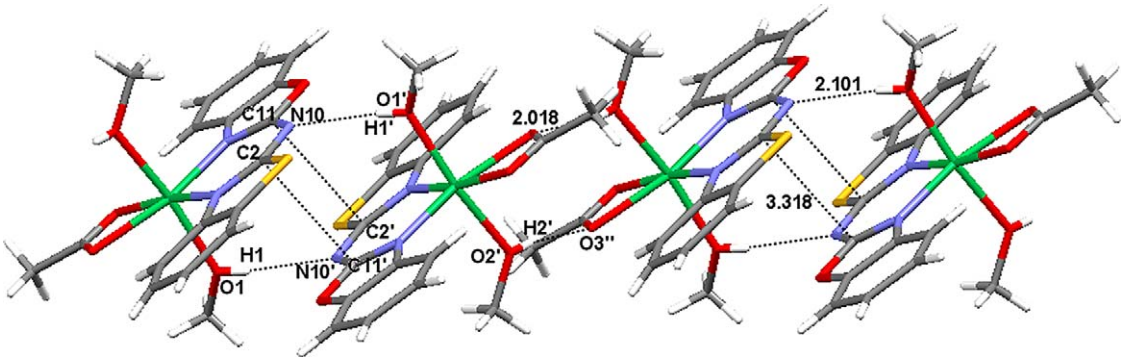

Fig. 9. Mono dimensional arrangement in compound **15** due to intermolecular hydrogen bonds between O1–H1···N10′ and O2′–H2′···O3″ and π-interactions between C2···C11″ and C11···C2′.

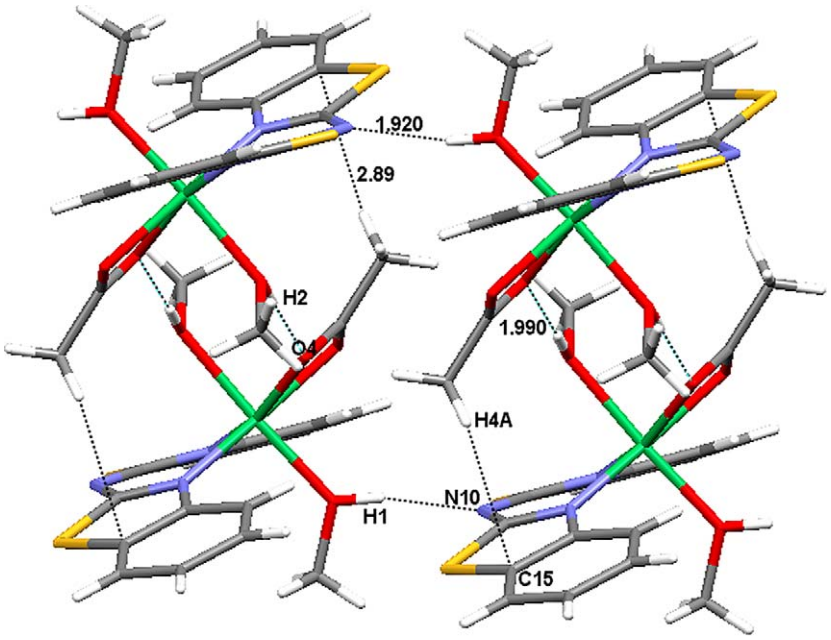

Fig. 10. Two dimensional polymer in compound **14** is formed by π and hydrogen bonds cooperative interactions.

4. Summary

We have obtained a series of interesting compounds that have in common a six-membered ring, by inclusion of a metal(II) ion in a planar delocalized system, formed by alternating sp^2 carbon and nitrogen atoms, integrated in a pentacyclic aromatic framework. Nitrogens N3 and N13 atoms were the binding sites with the metal ions, the nature of the heteroatom (S, O, N) in 12 position, did not affected the coordination behavior of the ligand. The orange cobalt(II) compounds, showed the participation of the metal ions in the electronic delocalization.

In the tetrahedral compounds, with exception of the mercury compound **7**, the two large polycyclic systems surround the metal ion, protecting it and allowing to observe the molecular ions in their mass spectra.

In the studied compounds, supramolecular arrangements were formed by intermolecular hydrogen bonds with the iminic nitrogen N10 and by π-interactions. In the octahedral nickel(II) compounds, with coordinated acetate and methanol molecules, the oxygen atoms participated into stabilizing 1D and 2D network systems, via intermolecular hydrogen bonds.

Acknowledgements

F.T. and A. P.-H. thank Conacyt for Ph.D. scholarship and F.T. thanks DGPA-UNAM for postdoctoral scholarship. Financial support by Conacyt (Gant 34714-E) and Cinvestav is acknowledged.

Appendix A. Supplementary material

Crystallographic data have been deposited with the Cambridge Crystallographic Data Centre CCDC Nos. 257701 (**4**), 257702 (**6**), 257703 (**7**), 257988 (**9**), 280064 (**12**), 257705 (**14**) and 257704 (**15**). Copies of this information may be

obtained free of charge from The Director, CCDC Data Centre, 12 Union Road, Cambridge, CB2 1EZ, UK (fax: +44 1223 336033; e-mail: deposit@ccdc.cam.ac.uk). Supplementary data associated with this article can be found, in the online version, at doi:10.1016/j.poly.2006.03.003.

References

[1] C. Ramalingan, S. Balasubramanian, S. Kabilan, M. Vasudevan, Eur. J. Med. Chem. 39 (2004) 527.
[2] G.T. Zitouni, S. Demirayak, A. Özdemir, Z.A. Kaplancikli, M.T. Yildiz, Eur. J. Med. Chem. 39 (2003) 267.
[3] P.L. López-Tudanca, L. Labeaga, A. Innerárity, L. Alonso-Cires, I. Tapia, R. Mosquera, A. Orjales, Bioorg. Med. Chem. 11 (2003) 2709.
[4] Y. Kasura, S. Nishino, M. Ohno, K. Sakane, Y. Matsumoto, Ch. Morinanga, H. Ishikawa, H. Tagasugi, J. Med. Chem. 42 (1999) 2920.
[5] P. Jimonet, J. Med. Chem. 42 (1999) 2828.
[6] Y. Tanabe, A. Hawai, Y. Yoshida, M. Ogura, H. Okamura, Heterocycles 45 (1997) 11579.
[7] R.C. Schnur, A.F.J. Fliri, S. Kajiji, V.A. Pollack, J. Med. Chem. 34 (1991) 914.
[8] E. Koyama, G. Yang, S. Tsuzuki, K. Hiratani, Eur. J. Org. Chem. (2002) 1996.
[9] K.-Y. Ho, W.-Y. Yu, K. Cheung, C.-M. Che, J. Chem. Soc., Dalton Trans. (1999) 1581.
[10] M.M. Bishop, A.H.W. Lee, L.F. Lindoy, P. Turner, Polyhedron 22 (2003) 735.
[11] M.M. Bishop, L.F. Lindoy, B.W. Skelton, A. White, Supramol. Chem. 13 (2001) 293.
[12] A. Decken, R.A. Gossage, J. Inorg. Biochem. 99 (2005) 664.
[13] D.E. Lynch, H.L. Duckhouse, Acta Crystallogr., Sect. C: Cryst. Struct. Commun. 57 (2001) 1036.
[14] L. Sieron, M. Bukowska-Strzyzewska, Acta Crystallogr., Sect. C: Cryst. Struct. Commun. 56 (2000) 19.
[15] K. Davarski, J. Macicek, L. Konovalov, J. Coord. Chem. 38 (1996) 123.
[16] E.S. Raper, R.E. Oughtred, I.W. Nowell, L.A. March, Acta Crystallogr., Sect. B: Cryst. Struct. Chem. 38 (1982) 2044.
[17] C. Avendaño, J. Elguero, F. Florencio, J. Aparicio, Inorg. Chim. Acta 174 (1990) 169.
[18] F.A. Cotton, L.M. Daniels, G.T. Jordan, C.A. Murillo, Polyhedron 17 (1998) 589.
[19] F. Téllez-Bárcenas, Ph.D. Thesis, Cinvestav, Chemistry Department, México, 2004.
[20] F. Téllez, A. Flores-Parra, N. Barba-Behrens, R. Contreras, Polyhedron 23 (2004) 2481.
[21] F.J. Yoe-Reyes, S. Bernès, N. Barba-Behrens, Acta Crystallogr. E61 (2005) M875.
[22] R.M. Hernández-García, N. Barba-Behrens, R. Salcedo, G. Höjer, Theochem. J. Mol. Spectrosc. 603 (2003) 55.
[23] S.E. Castillo-Blum, N. Barba-Behrens, Coord. Chem. Rev. 196 (2000) 3.
[24] A.E. Ceniceros-Gómez, N. Barba-Behrens, S. Bernès, H. Nöth, S.E. Castillo-Blum, Inorg. Chim. Acta 304 (2000) 230.
[25] A.E. Ceniceros-Gómez, N. Barba-Behrens, E. Quiróz-Castro, S. Bernès, H. Nöth, S.E. Castillo-Blum, Polyhedron 19 (2000) 1821.
[26] E. Quiróz-Castro, S. Bernès, N. Barba-Behrens, R. Tapia-Benavides, R. Contreras, H. Nöth, Polyhedron 19 (2000) 1479.
[27] M.P. Fialon, E. García-Baéz, N. Andrade-López, G. Osorio-Monreal, G. Canseco-Melchor, I. Velázquez-Montes, N. Barba-Behrens, R. Contreras, Heteroatom. Chem. 10 (1999) 577.
[28] J.M. Grevy, F. Téllez, S. Bernès, H. Nöth, R. Contreras, N. Barba-Behrens, Inorg. Chim. Acta 339 (2002) 532.
[29] M.P. Fialon, N. Andrade-López, N. Barba-Behrens, R. Contreras, Heteroatom. Chem. 9 (1998) 637.
[30] N. Andrade-López, A. Vázquez-Olmos, A. Ariza-Castolo, H. Tlahuext, N. Barba-Behrens, R. Contreras, Heteroatom. Chem. 8 (1997) 397.
[31] N. Barba-Behrens, A. Vázquez-Olmos, S.E. Castillo-Blum, R.M. Hernández, S. Meza-Höjer, G. Höjer, R. Vicente, A. Escuer, Transition Met. Chem. 21 (1996) 31.
[32] F. Téllez, A. Cruz, H. López-Sandoval, I. Ramos-García, M. Gayosso, R.N. Castillo-Sierra, B. Paz-Michel, H. Nöth, A. Flores-Parra, R. Contreras, Eur. J. Org. Chem. (2004) 4203.
[33] N. Andrade-López, R. Cartas-Rosado, E. García-Baéz, R. Contreras, H. Tlahuext, Heteroatom. Chem. 9 (1998) 399.
[34] U. Lehmann, P. Sutter, B. Schmidhalter, J.-L. Bury, EP Patent 1599878, 2004.
[35] F.L. Merchán, J. Garín, E. Meléndez, D. Ortiz, T. Tejero, Synthesis (1987) 368.
[36] F.L. Merchán, J. Garín, E. Meléndez, T. Tejero, Synthesis (1982) 1066.
[37] G.M. Sheldrick, SHELX-97: Program for X-ray Crystal Structure Solution and Refinement, University of Göttingen, Germany, 1997.
[38] A.B.P. Lever, Inorganic Electronic Spectroscopy, 2nd ed., Elsevier, The Netherlands, 1984.
[39] W.E. Smith, Spectrochim. Acta 38A (1982) 1063.
[40] A.W. Addison, T.N. Rao, J. Reedijk, J. Van Rijn, G.C. Verschoor, J. Chem. Soc., Dalton Trans. 00 (1984) 1349.

chemical and oxotransfer properties of oxomolybdenum complexes [13,17]. One of our previous studies [13a] on the Mo^{VI} complexes provided the first instance of using thiosemicarbazone-type ONS donor ligands in the modeling of molybdenum-binding site of the molybdenum cofactor (contains a mononuclear molybdenum atom coordinated to the sulfur atoms of a pterin derivative named molybdopterin) and showed for the first time that the steric factor is not absolutely essential to prevent the (μ-oxo)Mo^{V} dimer formation.

In this contribution we report the synthesis and structural characterization of some diamine/diimine-bridged dinuclear oxomolybdenum(VI) complexes of the type $[(MoO_2L)_2(\mu\text{-N–N})]$ (**2**–**5**) as well as their precursor complex $[MoO_2L(C_2H_5OH)]$ (**1**) where L^{2-} is the dianion of a tridentate ONO donor ligand and N–N is a neutral *exo*-bidentate ligand. Again, oxo abstraction from the dimolybdenum(VI,VI)-dioxo complex (**2**) using PPh_3 has been successfully used to obtain the corresponding dimolybdenum(IV,IV)-oxo species (**2a**) which is quite stable in the solid state and is hitherto unreported. An account of the chemistry of all the oxomolybdenum complexes, synthesized in this study, is presented here with special references to their formation, structure, and spectral and electrochemical properties.

2. Results and discussion

2.1. Synthesis

The complex **1**, $[MoO_2L(C_2H_5OH)]$ was prepared by refluxing an ethanol solution of the ligand H_2L and $MoO_2(acac)_2$ in equimolar quantities for 3 h. The Schiff base ligand H_2L was prepared by condensing 2-hydroxybenzoylhydrazine and 2-hydroxybenzaldehyde in 1:1 molar proportion at room temperature by stirring in alcohol for 2–3 h. Compounds **2**–**5** are synthesized by refluxing an ethanol solution of **1**, $[MoO_2L(C_2H_5OH)]$ and the appropriate spacer in 2:1 molar ratios for 4 h. All the compounds are sparingly soluble in alcohol, CH_3CN, $CHCl_3$, and CH_2Cl_2 but fairly soluble in DMF and DMSO. The compounds are air and heat stable, non-conducting in DMF solution and are diamagnetic as expected for a species with d^0 Mo(VI) center.

2.2. Spectral characteristics

The spectral data of all the complexes are summarized in Table 1. IR spectrum of the ligand exhibits prominent bands at 3075 and 1660 cm^{-1} assigned to ν(NH) and ν(C=O) modes [13c,13d,18–21], respectively. Characteristic strong bands in the spectra of both the complexes and the ligands are located at 3390 and 3195 cm^{-1} due to O–H stretching modes of the ligand, [13c,13d,18–21]. Conspicuous high intensity bands located in the 1600–1610 cm^{-1} region in the spectra of both the ligand and these are due to ν(C=N) bands [13b,13c,13d,20,21]. All the complexes exhibit two new bands in the 920–893 cm^{-1} region which are assigned to the symmetric and the antisymmetric ν(Mo=O) vibrations of the *cis*-dioxo molybdenum(VI) moiety [13].

Table 1
Characteristics IR[a] bands (cm^{-1}) and electronic spectral[b] data [nm ($dm^3\ mol^{-1}\ cm^{-1}$)] for the complexes

Complex	ν(Mo=O)	λ_{max} (ε)
$MoO_2L(C_2H_5OH)$ (**1**)	912, 900	405 (6393); 310 (22768)
$[(MoO_2L)_2(\mu\text{-}4,4'\text{-bpy})]$ (**2**)	918, 896	402 (9439); 315 (25123)
$[(MoO_2L)_2(\mu\text{-bpe})]\cdot 0.5C_2H_5OH$ (**3**)	914, 898	407 (8963); 312 (24685)
$[(MoO_2L)_2(\mu\text{-bpa})]$ (**4**)	916, 894	401 (11309); 314 (28323)
$[(MoO_2L)_2(\mu\text{-ppda})]$ (**5**)	914, 898	410 (10801); 315 (34070)
$[(MoOL)_2(\mu\text{-}4,4'\text{-bpy})]$ (**2a**)	945	603 (148); 431 (930); 329 (1872)

[a] In KBr pellet.
[b] In DMF.

Electronic spectra (Table 1) of all the complexes **1**–**5** in DMF exhibit two intense absorption bands in the 410–400, and the 320–310 nm region, which are assignable to L → Mo LMCT and intraligand transitions, respectively [13].

The ^1H NMR (DMSO d_6) data of the free ligand and its monomeric and dimeric oxomolybdem(VI) complexes are given in the experimental section. The spectrum of the free ligand exhibits two different OH (phenolic) resonances at two different positions (12.02 and 11.76 ppm), one CH proton signal at 8.68 ppm, one NH proton response at 11.18 ppm and aromatic proton bands at 7.90–6.90 ppm, respectively [13c,13d,21]. The signals for one OH proton and the NH proton are found to disappear in the spectra of the monomeric **1** and all the dimeric MoO_2L **2**–**5** complexes and only one OH proton signal is located at 11.38 ppm. These changes imply that the ligand coordinates to the MoO_2^{2+}-core in the enolate form.

2.3. Cyclic voltammetry

Results of cyclic voltammetric studies of all the complexes are given in Table 2. The CV trace of the complex **1** displays two irreversible reductive responses [13] within the potential window −0.9 to −1.4 V. These are assigned to the Mo(VI)/Mo(V) and the Mo(V)/Mo(IV) processes [13,22,23], respectively. The ligand is found to be redox inactive within this potential window. The dinuclear complexes **2**–**5** exhibit three successive irreversible one-electron reductions within the potential window −0.60 to −2.0 V versus SCE in acetonitrile which are assigned to

Table 2
Cyclic voltammetric results[a] for mononuclear and dinuclear oxomolybdenum(VI) complexes (**1**–**5**) at 298 K

Complex	E_{pc} (V)
1	−0.92, −1.35
2	−0.67, −1.52, −1.94
3	−0.71, −1.51, −1.73
4	−0.65, −1.28, − 1.69
5	−0.66, −1.44, −2.0

[a] Solvent, CH_3CN; working electrode, glassy carbon; reference electrode, SCE; supporting electrolyte, 0.1 M TEAP; scan rate, 50 mV s^{-1}.

Mo^{VI}–Mo^{VI}/Mo^{V}–Mo^{VI} and Mo^{V}–Mo^{VI}/Mo^{V}–Mo^{V} processes [24] and the ligand (bridging)-centered reduction, respectively. The presence of strong and hard (N,O) donor points in the Schiff base ligand tend to stabilize the molybdenum center in the higher oxidation state.

2.4. Description of crystal structure

2.4.1. $[MoO_2L(C_2H_5OH)]$ (1)

The molecular structure and the atom-numbering scheme for the complex **1** are shown in Fig. 1 and the bond parameters are given in Table 3. The mononuclear complex **1** has a distorted octahedral geometry with one nitrogen atom and five oxygen atoms. Three atoms, O(1), N(1) and O(2) (from the tridentate ligand), and one terminal oxo atom, O(3), occupy the meridional plane. The Mo(1) atom lies 0.253 Å out from this plane in the direction of the other terminal oxygen atom O(4). Both O(4) and O(6), the latter from the coordinated ethanol molecule, occupy the axial positions forming an O(4)–Mo–O(6) angle of 170.15(14)° which indicate the distorted octahedral nature of the donor environment around the Mo(VI) center. The MoO_2 moiety has a *cis* configuration with conventional [13c,13d,25] average values for the Mo–O(3)/O(4) distance (1.698(3) Å), and O(3)–Mo–O(4) bond angle (106.03(16)°), which is close to the energy minimum value estimated from MO theory [26]. The Mo–O(6) bond *trans* to the terminal oxygen atom O(4) is significantly longer [2.356(4) Å] compared to the length of other molybdenum oxygen bonds (enolate) Mo–O(2) distance (1.917(3) Å) and (phenolate) Mo–O(1) distance [2.021(3) Å], indicating that the ethanol molecule is weakly coordinated to the metal center and can behave as a substrate-binding site. This expectation is realized in the formation of the binuclear complexes **2**–**5** which are formed by the replacement of the weakly coordinated C_2H_5OH molecule by the nitrogen atom of one-half of the N–N bridging ligands.

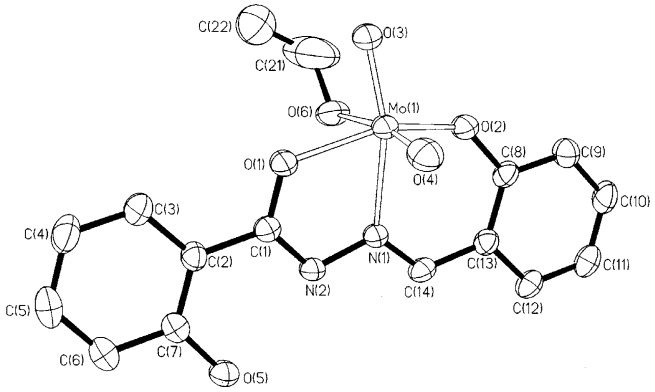

Fig. 1. An ORTEP plot and atom-numbering scheme of $[MoO_2L(C_2H_5OH)]$ (**1**) hydrogen atoms are omitted for clarity.

Table 3
Selected bond distances (Å) and angles (°) for $[MoO_2L(C_2H_5OH)]$ (**1**)

Bond distances			
Mo(1)–O(3)	1.696(3)	Mo(1)–O(4)	1.699(3)
Mo(1)–O(2)	1.917(3)	Mo(1)–O(1)	2.021(3)
Mo(1)–N(1)	2.234(3)	Mo(1)–O(6)	2.356(4)
Bond angles			
O(3)–Mo(1)–O(4)	106.03(16)	O(3)–Mo(1)–O(2)	102.57(13)
O(4)–Mo(1)–O(2)	99.88(15)	O(3)–Mo(1)–O(1)	97.11(12)
O(4)–Mo(1)–O(1)	96.76(15)	O(2)–Mo(1)–O(1)	149.48(13)
O(3)–Mo(1)–N(1)	158.44(14)	O(4)–Mo(1)–N(1)	93.84(13)
O(2)–Mo(1)–N(1)	81.68(11)	O(1)–Mo(1)–N(1)	71.80(11)
O(3)–Mo(1)–O(6)	83.22(15)	O(4)–Mo(1)–O(6)	170.15(14)
O(2)–Mo(1)–O(6)	80.99(15)	O(1)–Mo(1)–O(6)	78.42(15)

The estimated standard deviations are shown in parentheses.

2.4.2. $[(MoO_2L)_2(\mu\text{-}4,4'\text{-bpy})]$ (2)

The orange dimeric complex $[(MoO_2L)_2(\mu\text{-}4,4'\text{-bpy})]$ (**2**) crystallized in the triclinic space group $P\bar{1}$ and two halves of the dimeric complex **2** are not crystallographically equivalent but they posses closely matching structural dimensions. Therefore, structure of one of the halves will be representing the structure of the other half of the dimeric molecule quite closely. Molecular structure and the atom labelling scheme of complex **2** is illustrated in Fig. 2 and all metric data are collected in Table 4. Structure of one-half of the complex involving the Mo(1) acceptor center is described in details.

The two oxo-oxygen atoms of one $Mo(1)O_2^{2+}$ moiety, ONO donor atoms of the ligand H_2L and one nitrogen atom of the bridging 4,4′-bipy molecule complete the distorted octahedral coordination around the metal center Mo(1) in a $MoO_2L \cdot 0.5$ 4,4′-bipy unit. The ligand binds the metal in it's enolate form and behaves in a dianionic tridentate manner, the three donor points O(2), N(1), O(1) occupying a meridonial plane [27,28] and forming one five-membered and another six-membered chelate ring around one $Mo(1)O_2^{2+}$ center with bite angles of 71.36(14)° and 81.06(15)° in case of Mo(1). Similar bite angle of 71.90(15)° and 81.34(15)° are also generated at Mo(2). Least-square calculations shows the molybdenum

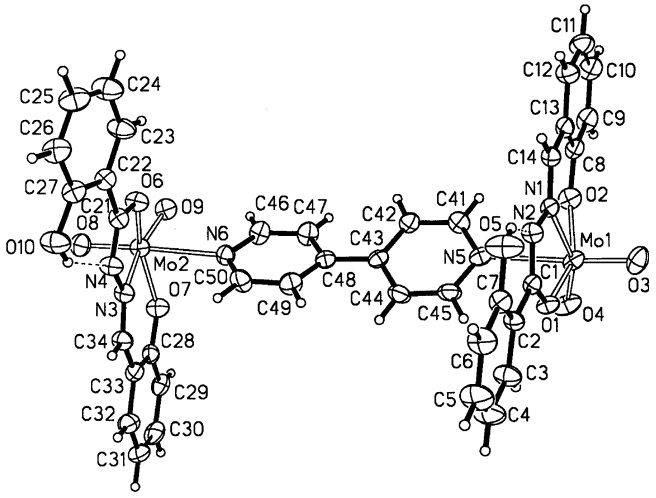

Fig. 2. An ORTEP plot and atom-numbering scheme of $[(MoO_2L)_2(\mu\text{-}4,4'\text{-bpy})]$ (**2**) hydrogen atoms are omitted for clarity.

Table 4
Selected bond distances (Å) and angles (°) for $[(MoO_2L)_2(\mu\text{-}4,4'\text{-bpy})]$ (**2**)

Bond distances			
Mo(1)–O(3)	1.688(4)	Mo(1)–O(4)	1.699(4)
Mo(1)–O(2)	1.919(4)	Mo(1)–O(1)	2.012(3)
Mo(1)–N(1)	2.247(4)	Mo(1)–N(5)	2.477(5)
Mo(2)–O(9)	1.684(4)	Mo(2)–O(8)	1.691(4)
Mo(2)–O(7)	1.919(4)	Mo(2)–O(6)	2.012(4)
Mo(2)–N(3)	2.242(4)	Mo(2)–N(6)	2.501(5)
Bond angles			
O(3)–Mo(1)–O(4)	105.9(2)	O(3)–Mo(1)–O(2)	99.41(19)
O(4)–Mo(1)–O(2)	105.08(17)	O(3)–Mo(1)–O(1)	98.03(17)
O(4)–Mo(1)–O(1)	95.27(17)	O(2)–Mo(1)–O(1)	148.30(15)
O(3)–Mo(1)–N(1)	94.39(19)	O(4)–Mo(1)–N(1)	157.27(19)
O(2)–Mo(1)–N(1)	81.06(15)	O(1)–Mo(1)–N(1)	71.36(14)
O(3)–Mo(1)–N(5)	171.18(17)	O(4)–Mo(1)–N(5)	80.44(19)
O(2)–Mo(1)–N(5)	81.12(16)	O(1)–Mo(1)–N(5)	78.56(15)
N(1)–Mo(1)–N(5)	78.94(15)		
O(9)–Mo(2)–O(8)	104.6(2)	O(9)–Mo(2)–O(7)	104.14(17)
O(8)–Mo(2)–O(7)	101.77(19)	O(9)–Mo(2)–O(6)	96.22(17)
O(8)–Mo(2)–O(6)	96.92(18)	O(7)–Mo(2)–O(6)	147.70(16)
O(9)–Mo(2)–N(3)	160.98(19)	O(8)–Mo(2)–N(3)	91.82(18)
O(7)–Mo(2)–N(3)	81.34(15)	O(6)–Mo(2)–N(3)	71.90(15)
O(9)–Mo(2)-N(6)	82.03(18)	O(8)–Mo(2)–N(6)	172.82(17)
O(7)–Mo(2)–N(6)	78.97(17)	O(6)–Mo(2)–N(6)	79.36(16)
N(3)–Mo(2)–N(6)	81.20(16)		

The estimated standard deviations are shown in parentheses.

atom Mo(1) to be 0.311 Å above the basal plane defined by [O(2) N(1) O(1) O(4)], the other oxo-oxygen O(3) occupying an apical position in the coordination sphere of Mo(1) and this deviation of the Mo(1) atom from the basal plane towards the apical oxo-oxygen atom O(3) is also apparent from the angles subtended at the Mo center. The other apical position in the coordination octahedron of Mo(1) is occupied by the nitrogen atom N(5) of one-half of the 4,4′-bipy group. The Mo(1)–N(5) bond [2.477(5)] Å is much longer than the other Mo(1)–N(1) bond [2.247(4)] Å and indicates that the bipyridine nitrogen is weakly bonded to the MoO_2^{2+}-core pointing to the possibility of further ligand exchange reaction at this point.

2.4.3. $[(MoO_2L)_2(\mu\text{-bpe})]\cdot 0.5C_2H_5OH$ (**3**)

The molecular structure and atom-labeling scheme for complex **3** are shown in Fig. 3. Selected bond distances and angles are collected in Table 5. The dinuclear complex crystallizes in the triclinic space group $P\bar{1}$ with the molecule sitting across a crystallographic center of inversion. Accordingly, the two equivalent halves of the molecule have a *trans* disposition with respect to the double bond [C(20)═C(20A)] at the center. An ethanol moiety was found to be disordered about another center of symmetry and was modeled with partial occupancy, giving an overall stoichiometry of $[(MoO_2L)_2(\mu\text{-bpe})]\cdot 0.5C_2H_5OH$.

The coordination environment around the Mo(VI) center is octahedral and highly distorted. As is the case in compounds **2** and **5**, the ligand H_2L is dianionic and tridentate, with its meridionally situated donor sites O(2), N(1), and O(1) lying in the equatorial plane along with the oxo oxygen O(4). The bond distances about Mo(1) reveal the

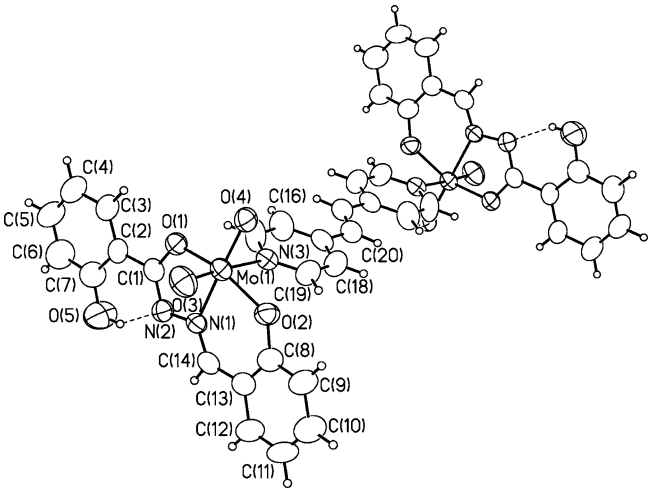

Fig. 3. Thermal ellipsoid plot of one molecule of $[(MoO_2L)_2(\mu\text{-bpe})]$ (**3**) showing the atom naming scheme. Non-hydrogen atoms are represented by their 50% probability ellipsoids.

Table 5
Selected bond distances (Å) and angles (°) for $[(MoO_2L)_2(\mu\text{-bpe})]\cdot 0.5\text{-}C_2H_5OH$ (**3**) and $[(MoO_2L)_2(\mu\text{-ppda})]$ (**5**)

	Complex **3**	Complex **5**
Bond distances		
Mo(1)–O(3)	1.681(5)	1.693 (4)
Mo(1)–O(4)	1.692(4)	1.708(4)
Mo(1)–O(2)	1.922(4)	1.911(5)
Mo(1)–O(1)	2.001(4)	1.994(4)
Mo(1)–N(1)	2.249(5)	2.273(5)
Mo(1)–N(3)	2.461(5)	2.470(5)
Bond angles		
O(3)–Mo(1)–O(4)	105.2(2)	106.5(2)
O(3)–Mo(1)–O(2)	99.6(2)	100.9(2)
O(4)–Mo(1)–O(2)	103.79(18)	102.7(2)
O(3)–Mo(1)–O(1)	95.7(2)	96.5(2)
O(4)–Mo(1)–O(1)	97.04(17)	98.24(19)
O(2)–Mo(1)–O(1)	149.79(18)	147.60(18)
O(3)–Mo(1)–N(1)	94.3(2)	93.4(2)
O(4)–Mo(1)–N(1)	158.45(19)	158.7(2)
O(2)–Mo(1)–N(1)	81.48(17)	80.33(19)
O(1)–Mo(1)–N(1)	71.49(17)	71.47(18)
O(3)–Mo(1)–N(3)	172.11(18)	170.4(2)
O(4)–Mo(1)–N(3)	82.18(18)	82.85(19)
O(2)–Mo(1)–N(3)	81.05(17)	78.63(18)
O(1)–Mo(1)–N(3)	80.37(16)	79.76(18)
N(1)–Mo(1)–N(3)	77.99(16)	77.08(18)

Estimated standard deviations are shown in parentheses.

magnitude of the distortions, as can be seen in Table 5. The Mo–O distances range from 1.681(5) Å for the oxo ligand O(3), located in an axial position, to 2.001(4) Å for the enolate oxygen O(1). The Mo(1)–O(2) (phenolate) distance is slightly shorter at 1.922(4) Å. The second axial position is occupied by a nitrogen atom of the bridging bpe ligand, which is significantly farther from the Mo center than are the other five ligated atoms. Mo(1)–N(3), at 2.461(5) Å, is undoubtedly the weakest of the six Mo–L bonds and consequently the most susceptible to ligand exchange. The *trans* angles in the equatorial plane

[O(1)–Mo(1)–O(2), 149.79(18)°; O(4)–Mo(1)–N(1), 158.45(19)°] indicate that the central Mo is not in the equatorial plane; it lies 0.312(2) Å out of the plane, toward the distal oxo ligand O(3). The chelate bite angles for the five- and six-membered rings have values within the expected ranges [O(1)–Mo(1)–N(1), 71.49(17)°; O(2)–Mo(1)–N(1), 81.48(17)°].

The extended structure of **3** can be viewed as having a basic bilayer motif in which layers formed by the tridentate ligand L are separated by bpe spacers. Fig. 3 shows the pattern formed by four complete molecules. The distance between the planes of the phenyl groups of two adjacent molecules (related to each other by a center of symmetry) is 3.67(4) Å. Fig. 3 displays a detail of the intermolecular interactions. Three half-molecules are shown in the figure. The phenyl ring labeled C2A...C7A is related to the basic unit (no letters appended to the atom names) by the center of symmetry at (0.5, 0.0, 0.5); this is the 3.67(4) Å interaction.

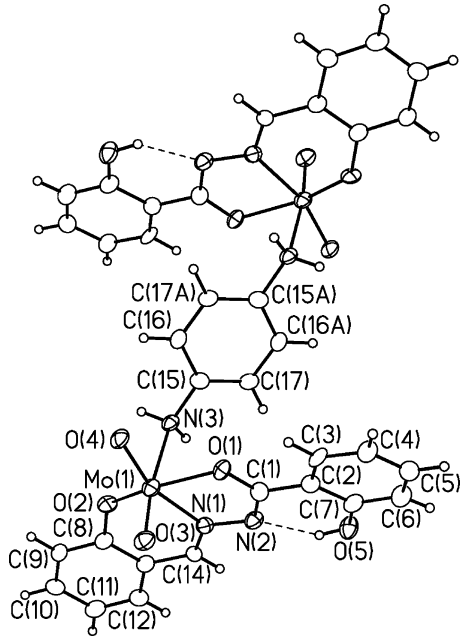

Fig. 4. Thermal ellipsoid plot of one molecule of $[(MoO_2L)_2(\mu\text{-ppda})]$ (**5**) showing the atom labeling scheme. Non-hydrogen atoms are represented by their 50% probability ellipsoids.

2.4.4. $[(MoO_2L)_2(\mu\text{-ppda})]$ (**5**)

The dinuclear molecule $[(MoO_2L)_2(\mu\text{-ppda})]$ (**5**) (where ppda = *p*-phenylenediamine) sits astride a crystallographic inversion center in space group *Pbca*, with the symmetry element lying in the middle of the ppda ligand. Fig. 4 shows one complete molecule, and selected bond distances and angles are collected in Table 5. The ligand, as found in complex **5**, is the result of enolisation followed by deprotonation to give a planar, dianionic, tridentate moiety with a meridional disposition. The donor points O(1) (enolate), N(1) (azomethine), and O(2) (phenolate) occupy the equatorial plane [27,28] along with oxo oxygen atom O(4). The highly distorted octahedral coordination environment about Mo is completed at the axial positions by oxo ligand O(3) and the amine nitrogen atom N(3) of ppda. As with compound **3**, the Mo–L bond distances are bounded at the short end by the Mo=O bonds of ca. 1.7 Å (Table 6) and at the long end by a weak interaction to the amine nitrogen atom of the organic spacer [Mo(1)–N(3) = 2.470(5) Å]. The latter suggests that the Mo(1)–N(3) bond is a possible target for ligand exchange. The *trans* angles in the equatorial plane, O(2)–Mo(1)–O(1) [147.60(18)°] and O(4)–Mo(1)–N(1) [158.7(2)°], deviate significantly from linearity, as the Mo(VI) center is shifted out of the basal plane towards the apical oxo-oxygen atom O(3). The distance of Mo(1) from the plane of O(1), N(1), O(2), and O(4) is 0.338(2) Å.

Table 6
Crystal and refinement data for complexes **1**, **2**, **3** and **5**

Compound	**1**	**2**	**3** · $0.5C_2H_5OH$	**5**
Chemical formula	$C_{16}H_{16}MoN_2O_6$	$C_{38}H_{28}Mo_2N_6O_{10}$	$C_{41}H_{33}Mo_2N_6O_{10.5}$	$C_{34}H_{28}Mo_2N_6O_{10}$
F_w	428.3	920.5	969.61	872.5
Crystal system	triclinic	triclinic	triclinic	orthorhombic
Space group	$P\bar{1}$	$P\bar{1}$	$P\bar{1}$	*Pbca*
a (Å)	7.6414(5)	7.9276(11)	8.168(2)	17.707(4)
b (Å)	10.2738(7)	12.0583(17)	10.427(3)	9.605(19)
c (Å)	11.5162(8)	19.860(3)	13.535(4)	18.614(4)
α (°)	88.4840(10)	74.422(3)	108.495(6)	90.00
β (°)	84.140(2)	88.444(3)	95.532(6)	90.00
γ (°)	74.6960(10)	81.333(3)	108.605(7)	90.00
V (Å^3)	867.48(10)	1807.7(4)	1010.7(5)	3165.7(12)
Z	2	2	1	4
D_{calc} (g cm^{-3})	1.640	1.691	1.593	1.831
F(000)	432	924	489	1752
μ(Mo Kα) (mm^{-1})	0.790	0.763	0.688	0.900
θ_{max} (°)	26	28	30.64	25
Collected reflections	5314	12475	8260	15868
Independent reflections	3392	8606	5825	2771
$R_1[I > 2\sigma(I)]$	0.0410	0.0555	0.0646	0.0617
wR_2[all data]	0.1143	0.1414	0.1812	0.1246

Due to enolisation of the ligand, the C(1)–O(1) bond assumes single bond character, but the bond length of 1.307(8) Å lies between the lengths of C–O single and C=O double bonds and reflects a certain degree of electron delocalisation in the coordinated ligand [22,23]. The adjacent C(1)–N(2) bond length of 1.313(8) Å is closer to the usual C=N distance than to the normal C–N distance. The N(1)–N(2) bond distance of 1.375(7) Å reveals its predominantly single bond character. All of the above facts are consistent with enolisation of the hydrazone ligand and subsequent coordination to the MoO_2^{2+} core in the enolate form, with concomitant delocalisation along the ligand backbone [22,23]. The bite angles of the ligand in complex **5** are 71.47(18)° for O(1)–Mo(1)–N(1) and 80.33(19)° for O(2)–Mo(1)–N(1), typical values for five- and six-membered chelate rings, respectively.

3. Reactivity of the complex 2 [$(MoO_2L)_2(\mu$-4,4′-bpy)]

3.1. Oxo transfer to substrate: Isolation of dimolybdenum(IV,IV)-oxo complex (2a)

The dimolybdenum(IV,IV)-oxo complex (**2a**) was synthesized by a common method reported previously [13,17]. Formation of this complex illustrates the oxo transfer ability of the precursor dioxodimolybdenum(VI) complex, **2** [5,6,12–14]. This Mo(IV)–Mo(IV) dimer is quite rare. To the best of our knowledge, no diimine- and diamine-bridged dinuclear oxomolybdenum(IV) complex has been reported previously.

This Mo^{IV} dimer is air stable in the solid state and is found to be much stable in solution than the previously reported [13c,13d] Mo^{IV} monomers in similar type ligand environment. However, the compound is not sufficiently stable to get them recrystallized from acetonitrile or any other solvent and are slowly transformed to the parent yellow Mo(VI)–Mo(VI) dimer after 3–4 days. We failed to isolate good single crystals of Mo(IV)–Mo(IV) dimer by this process or from the actual reaction medium. Like the corresponding Mo(VI)–Mo(VI) dimers this Mo(IV)–Mo(IV) dimer is also sparingly soluble in solvents like CH_2Cl_2, $CHCl_3$ and CH_3CN, but are highly soluble in DMF and DMSO. This complex is a non-electrolyte and diamagnetic at room temperature [13].

Some spectral (IR and UV–Vis) characteristics of the compound **2a** are listed in Table 1. As in the case of the dinuclear MoO_2^{2+} complexes, IR spectral features of this MoO(IV) complex clearly reveals coordination from the deprotonated phenolic and enolic oxygens and the azomethine nitrogen. This complex exhibits a single strong, sharp band in the 960–940 cm^{-1} region, representing the $\nu(Mo{=}O)_t$ [13] mode.

Electronic spectra of the dimeric Mo(IV)-oxo compound is recorded in dry DMF solution, and the complex is found to display (Table 1) several absorption maxima in the 310–620 nm region and a new band of moderate intensity in the low energy 600–620 nm region. Absorption in this region is a characteristic feature of the $[MoO]^{2+}$ core [13,29,30].

4. Experimental

4.1. Materials

$[MoO_2(acac)_2]$ was prepared as described in the literature [31]. Reagent grade solvents were dried and distilled prior to use. All other chemicals were reagent grade, available commercially and used as received. Tetraethylammonium perchlorate (TEAP) used for electrochemical work was prepared as reported in the literature [32].

4.2. Physical measurements

Elemental analyses were performed on a Perkin–Elmer 240 C, H, N analyser. IR spectra were recorded on a Perkin–Elmer 783 spectrometer. ^1H NMR spectra were recorded with a Bruker AVANCE DPX 300 MHz spectrometer using $SiMe_4$ as internal standard. Electronic spectra were recorded on a Shimadzu UV/Vis recording spectrophotometer. Magnetic susceptibility was measured with a PAR model 155 vibrating sample magnetometer with Hg $[Co(SCN)_4]$ as calibrant. Electrochemical data were collected using an EG&G PARC electrochemical analysis system (model 250/5/0) and using a PC-controlled EG&G/PARC-VERSASTAT2 potentiostat at 298 K under a dry nitrogen. Cyclic voltammetry experiments were carried out with platinum working electrode, platinum auxiliary electrode and SCE as reference electrode and TEAP as supporting electrolyte.

4.3. Synthesis of ligand (H_2L)

The ligand, 2-hydroxybenzoylhydrazone of 2-hydroxybenzoylhydrazine (H_2L) was prepared [21] by reacting 2-hydroxybenzoylhydrazine (7.5 g, 49.34 mmol) and 2-hydroxybenzaldehyde (6.1 g, 50.00 mmol) in stirring ethanol (25 ml) for 2 h. The resulting yellowish-white compound was filtered, washed thrice with ethanol and dried over fused $CaCl_2$; m.p. 170 °C. Yield 70%. *Anal.* Calc. for $C_{14}H_{12}N_2O_3$: C, 65.62; H, 4.72; N, 10.94. Found: C, 65.36; H, 4.59; N, 11.06%. ^1H NMR (DMSO d_6, δ): 7.91–6.91 (m, 8H, C_6H_4), 8.68 (s, 1H, CH), 11.18 (s, 1H, NH), 11.76 (s, 1H, OH), 12.02 (s, 1H, OH),

4.4. Synthesis of [$MoO_2L(C_2H_5OH)$] (1)

0.28 g (1.09 mmol) of H_2L was dissolved in 30 mL ethanol by refluxing on a water bath and 0.33 g (1.01 mmol) of solid $MoO_2(acac)_2$ was added to the ligand solution and the mixture was refluxed for 3 h and filtered. Slow evaporation of the orange filtrate over 5 days produced orange-red crystals. Yield 75%. *Anal.* Calc. for $C_{16}H_{16}N_2O_6Mo$: C, 44.83; H, 3.76; N, 6.53. Found: C, 44.45; H, 3.51; N,

6.51%. ^{1}H NMR (DMSO d_6, δ): 7.82–6.97 (m, 8H, C_6H_4), 9.12 (s, 1H, CH), 11.39 (s, 1H, OH).

4.5. Synthesis of $[(MoO_2L)_2(\mu\text{-}4,4'\text{-bpy})]$ (2)

To a clear orange solution (obtained by refluxing) **1** (0.22 g, 0.51 mmol) in ethanol (50 mL) alcoholic solution of 4,4′-bpy (0.08 g, 0.51 mmol) was added and the mixture was allowed to reflux for 2 h. The yellowish turbid solution was filtered through qualitative filter paper. On standing for 12–14 h at room temperature, the yellow filtrate deposited orange crystals. The crystals were thoroughly washed with alcohol and dried over fused $CaCl_2$ and a suitable single crystal was selected for X-ray crystal structure analysis. Yield 79%. *Anal*. Calc. for $C_{38}H_{28}N_6O_{10}Mo_2$: C, 49.54; H, 3.06; N, 9.12. Found: C, 49.57; H, 2.94; N, 9.27%. ^{1}H NMR (DMSO d_6, δ): 8.73–6.96 (m, 16H, C_6H_4, $C_{10}H_8N_2$), 9.12 (s, 1H, CH), 11.39 (s, 1H, OH).

4.6. Synthesis of $[(MoO_2L)_2(\mu\text{-}4,4'\text{-bpe})]\cdot 0.5C_2H_5OH$ (3)

This compound was prepared using same procedure as in the case of compound **2** using *trans*-1,2-bis(4-pyridyl) ethene (bpe) in place of 4,4′-bipy as the bridging ligand. Yield 80%. *Anal*. Calc. for $C_{41}H_{33}N_6O_{10.5}Mo_2$: C, 50.74; H, 3.43; N, 8.66. Found C, 50.51; H, 3.52; N, 8.67%. ^{1}H NMR (DMSO d_6, δ): 8.60–6.96 (m, 16H, C_6H_4, $C_{12}H_{10}N_2$), 9.12 (s, 1H, CH), 11.39 (s, 1H, OH).

4.7. Synthesis of $[(MoO_2L)_2(\mu\text{-}4,4'\text{-bpa})]$ (4)

This compound was prepared using same procedure used in the case of compound **2** taking *trans*-1,2-bis(4-pyridyl) (bpa) ethane as the bridging ligand. Yield 80%. *Anal*. Calc. for $C_{42}H_{36}N_6O_{11}Mo_2$: C, 50.77; H, 3.65; N, 8.46. Found: C, 50.61; H, 3.75; N, 8.59%. ^{1}H NMR (DMSO d_6, δ): 8.55–6.95 (m, 16H, C_6H_4, $C_{12}H_{12}N_2$), 9.10 (s, 1H, CH), 11.24 (s, 1H, OH).

4.8. Synthesis of $[(MoO_2L)_2(\mu\text{-}4,4'\text{-ppda})]$ (5)

This compound was prepared using same procedure used in the case of compound **2** using *p*-phenylenediamine (ppda) as the bridging ligand. Yield 78%. *Anal*. Calc. for $C_{34}H_{28}N_6O_{10}Mo_2$: C, 46.76; H, 3.23; N, 9.62. Found: C, 47.20; H, 3.25; N, 9.65%. ^{1}H NMR (DMSO d_6, δ): 7.81–6.35 {m, 12H, C_6H_4, $C_6H_4(NH_2)_2$}, 9.12 (s, 1H, CH), 11.39 (s, 1H, OH), 4.28 (s, 2H, NH_2).

4.9. Synthesis of $[(MoOL)_2(\mu\text{-}4,4'\text{-bpy})]$ (2a)

This compound was prepared using same procedure as our previous works [13]. To a refluxing solution of 0.22 g (0.24 mmol) of $[(MoO_2L)_2(\mu\text{-}4,4'\text{-bpy})]$ (**2**) in 25 mL of degassed acetonitrile 0.197 g (0.75 mmol) of PPh_3 in 5 mL of acetonitrile is added. The orange solution turned reddish brown and a reddish brown compound separated within 1 h was collected by rapid filtration of the hot mixture, washed well with hot acetonitrile and dried in vacuo; yield 65%. *Anal*. Calc. for $C_{38}H_{28}N_6O_9Mo_2$: C, 50.41; H, 3.12; N, 9.29. Found: C, 50.77; H, 3.04; N, 9.13%.

4.10. Crystal structure determination

Suitable single crystals of **1** ($0.34\times0.32\times0.24$ mm), **2** ($0.23\times0.28\times0.19$ mm), **3**, ($0.18\times0.17\times0.08$ mm^3) and **5** ($0.10\times0.10\times0.15$ mm) were chosen for X-ray diffraction studies. Crystal data and other parameters for Complexes **1**, **2**, **3**, and **5** are given in Table 6. Intensity data for **1**, **2** and **3** were collected at room temperature and for **5** at 100 K, on Bruker Smart CCD diffractometers using graphite-monochromated Mo Kα radiation ($\lambda = 0.71073$ Å). The intensities were corrected for absorption effects using SADABS [33]. The structures were solved by direct methods. All non-hydrogen atoms were refined anisotropically by full-matrix least squares, with a riding model for the hydrogen atoms, using the SHELXTL package [34].

5. Concluding remarks

A few diamine/diimine-bridged dimolybdenum(VI) complexes of the type $[(MoO_2L)_2(\mu\text{-N–N})]$ (**2–5**) are obtained from their mononuclear precursor $[MoO_2L(C_2H_5OH)]$ (**1**) involving a dianionic tridentate ONO donor ligand. Three such dinuclear Mo(VI)–Mo(VI) complexes are structurally characterized by X-ray crystallography. One corresponding Mo(IV)–Mo(IV) complex **2a** is prepared by utilizing the oxo-transfer (to substrate) capacity of the corresponding Mo(VI)–Mo(VI) dinuclear species to the substrate triphenylphosphine.

6. Supplementary data

The view of the extended crystal structure and the details of the packing for the complex $[(MoO_2L)_2(\mu\text{-bpe})]$ (**3**) are reported as Supporting Information (Fig. 3a and b). Crystallographic data have been deposited with the CCDC. Copies of this information may be obtained free of charge from the director, CCDC, 12, Union Road, Cambridge, CB2 1EZ, UK [fax(internet.): +44 1223/336 033; e-mail: deposit@ccdc.ac.uk or on the web www: http://www.ccdc.cam.ac.uk quoting the deposition number CCDC 244288 (complex **1**), 244289 (complex **2**), 244290 (complex **3**) and 244291 (complex **5**).

Acknowledgments

Financial support from the Spanish Ministry of Science and Technology (Grant BQU2002-00554) and the European Regional Development Fund is gratefully acknowledged by L.R.F. and M.T. Valuable assistance from Drs. Rosa Llusar and Tatiana Soler is also appreciated.

R.D. thanks Dr. S.K. Chattopadhyay, Bengal Engineering College (Deemed University) for fruitful discussion.

References

[1] F.A. Cotton, G. Wilkinson, C.A. Murillo, M. Bochmann, Advanced Inorganic Chemistry, 6th ed., John Wiley & Sons, Inc., 1999, p. 725 and references cited therein.
[2] V.C. Gibson, C. Redshaw, G.L.P. Walker, W. Clegg, M.R.J. Elsegood, J. Organomet. Chem. 689 (2004) 332.
[3] J.A. MaCleverty, M.D. Ward, Acc. Chem. Res. 31 (1998) 842.
[4] (a) P.J. Zapf, R.C. Haushalter, J. Zubieta, Chem. Commun. (1997) 321;
(b) P.J. Zapf, R.C. Haushalter, J. Zubieta, Chem. Mater. 7 (1997) 2019;
(c) P.J. Zapf, R.L. LaDuca, R.S. Rarig, K.M. Johnson III, J. Zubieta, Inorg. Chem. 37 (1998) 3411;
(d) P.J. Zapf, C.J. Warren, R.C. Haushalter, J. Zubieta, Chem. Commun. (1997) 1543;
(e) D. Hagram, C. Zubieta, D.J. Rose, R.C. Haushalter, J. Zubieta, Angew. Chem., Int. Ed. 36 (1997) 795.
[5] C.J. Doonan, D.A. Slizys, C.J. Young, J. Am. Chem. Soc. 121 (1999) 6430.
[6] (a) R.H. Holm, J.M. Berg, Pure Appl. Chem. 56 (1984) 1645;
(b) J.M. Berg, R.H. Holm, J. Am. Chem. Soc. 107 (1985) 917;
(c) J.M. Berg, R.H. Holm, J. Am. Chem. Soc. 107 (1985) 925;
(d) R.H. Holm, J.M. Berg, Acc. Chem. Res. 19 (1986) 363;
(e) E.W. Harlen, J.M. Berg, R.H. Holm, J. Am. Chem. Soc. 108 (1986) 6992;
(f) J.P. Caradonna, E.W. Harlen, R.H. Holm, J. Am. Chem. Soc. 108 (1986) 7856;
(g) J.P. Caradonna, P.R. Reddy, R.H. Holm, J. Am. Chem. Soc. 110 (1988) 2139;
(h) J.A. Craig, R.H. Holm, J. Am. Chem. Soc. 111 (1989) 2111.
[7] (a) S.F. Gheller, B.E. Schultz, M.J. Scott, R.H. Holm, J. Am. Chem. Soc. 114 (1992) 6934;
(b) B.E. Schultz, S.F. Gheller, M.C. Muetterties, M.J. Scott, R.H. Holm, J. Am. Chem. Soc. 115 (1993) 2714.
[8] (a) S.A. Roberts, C.G. Young, W.E. Cleland, R.B. Ortega, J.H. Enemark, Inorg. Chem. 27 (1988) 3044;
(b) S.A. Roberts, C.G. Young, C.A. Kipke, W.E. Cleland Jr., K. Yamanouchi, M.D. Carducci, J.H. Enemark, Inorg. Chem. 29 (1990) 3650.
[9] S.K. Das, P.K. Chaudhury, D. Biswas, S. Sarkar, J. Am. Chem. Soc. 116 (1994) 9061.
[10] N. Yoshinaga, N. Ueyama, T. Okamura, A. Nakamura, Chem. Lett. (1990) 1655.
[11] H. Arzoumanian, R. Lopez, G. Agrifoglio, Inorg. Chem. 33 (1994) 3177.
[12] (a) L.J. Laughlin, C.G. Young, Inorg. Chem. 35 (1996) 1050;
(b) C.G. Young, L.J. Laughlin, S. Colmanet, S.D.B. Scrofani, Inorg. Chem. 35 (1996) 5368.
[13] (a) S. Purohit, A.P. Koley, L.S. Prasad, P.T. Manoharan, S. Ghosh, Inorg. Chem. 28 (1989) 3735;
(b) A. Rana, R. Dinda, P. Sengupta, L.R. Falvello, S. Ghosh, Polyhedron 21 (2002) 1023;
(c) R. Dinda, P. Sengupta, S. Ghosh, H.M. Figge, W.S. Sheldrick, J. Chem. Soc., Dalton Trans. (2002) 4434;
(d) R. Dinda, P. Sengupta, S. Ghosh, W.S. Sheldrick, Eur. J. Inorg. Chem. (2003) 363.
[14] C.G. Young, in: B. Meunier (Ed.), Biomimetic Oxidations Catalyzed by Transition Metal Complexes, Imperial College Press, London, 2000, p. 415 (Chapter 9).
[15] P.D. Smith, A.J. Millar, C.G. Young, A. Ghosh, P. Basu, J. Am. Chem. Soc. 122 (2000) 9298.
[16] V.N. Nemykin, J. Laskin, P. Basu, J. Am. Chem. Soc. 126 (2004) 8604.
[17] (a) S. Ghosh, S. Purohit, Ind. J. Chem. 26A (1987) 131;
(b) S. Purohit, S. Ghosh, J. Chem. Res. (S) (1988) 158;
(c) S. Purohit, A.P. Koley, S. Ghosh, Polyhedron 9 (1990) 881;
(d) A. Rana, R. Dinda, S. Ghosh, A.J. Blake, Polyhedron 22 (2003) 3075.
[18] W. Kemp, Organic Spectroscopy, Macmillan Hampshire, 1987, p. 62.
[19] K. Nakamoto, Infrared and Raman Spectra of Inorganic and Coordination Compounds, Wiley, New York, 1986, p. 241.
[20] S. Ghosh, T.K. Bandyopadhyay, P.K. Ray, M.S. Mitra, J. Inorg. Biochem. 20 (1984) 79.
[21] R. Dinda, P. Sengupta, T.C.W. Mak, S. Ghosh, Inorg. Chem. 41 (2002) 1684.
[22] J. Topich, Inorg. Chem. 20 (1981) 3704.
[23] N.S. Rao, D.D. Mishra, R.C. Maurya, N.N. Rao, Bull. Chem. Soc. Jpn. 68 (1995) 1589.
[24] A.S. Attia, S.F. El-Mashtoly, M.F. El-Shahat, Polyhedron 22 (2003) 895.
[25] N. Ueyama, H. Oku, M. Kondo, T. Okamura, N. Yoshinaga, A. Nakamura, Inorg. Chem. 35 (1995) 643.
[26] K. Tatsumi, R. Hoffmann, Inorg. Chem. 19 (1980) 2656.
[27] J.A. Craig, E.W. Harlan, Inorg. Chem. 28 (1989) 2082.
[28] R. Hahn, U. Kusthardt, W. Scherer, Inorg. Chm. Acta 210 (1993) 177.
[29] I.W. Boyd, J.T. Spence, Inorg. Chem. 21 (1982) 1602.
[30] B.B. Kaul, J.H. Enemark, S.L. Merbs, J.T. Spence, J. Am. Chem. Soc. 107 (1985) 2885.
[31] G.J.J. Chen, J.W. McDonald, W.E. Newton, Inorg. Chem. 15 (1976) 2612.
[32] D.T. Sawyer, J.L. Roberts, Experimental Electrochemistry for Chemists, Wiley, New York, 1974, p. 212.
[33] G.M. Sheldrick, SADABS, Program for Empirical Absorption Correction of Area Detector Data, University of Göttingen, Göttingen, Germany, 1996.
[34] G.M. Sheldrick, SHELXTL 5.10, Structure Determination Software Package, Bruker Analytical X-ray Systems, Madison, WI, 1998.

2. Experimental

2.1. Materials and methods

Cadmium acetate, mercury acetate, tmeda (*N*,*N*,*N*′,*N*′-tetramethylethylenediamine), tri-*n*-octylphosphineoxide (TOPO) and hexadecylamine (HDA) were obtained from commercial sources and were used without further purification. $HgCl_2 \cdot$ tmeda was prepared by refluxing $HgCl_2$ and excess tmeda in dichloromethane under an inert atmosphere for 2 h. Bis(2-dimethylaminoethyl)diselenide was prepared according to the literature method [25]. Solvents were dried and distilled before use under a nitrogen atmosphere. HPLC grade toluene was used in all experiments involved with a capping agent and pyridine was used in pyrolysis experiments for optical studies. Melting points were determined in capillary tubes and are uncorrected. Elemental analyses were carried out by the Analytical Chemistry Division of B.A.R.C. ^{1}H and $^{13}C\{^1H\}$ NMR spectra were recorded on a Bruker DPX-300 NMR spectrometer operating at 300 and 75.47 MHz, respectively. Chemical shifts are relative to the internal chloroform peak at δ 7.26 for ^{1}H and δ 77.0 for $^{13}C\{^1H\}$. UV–Vis absorption spectra were recorded on a Chemito Spectrascan UV 2600 double beam UV–Vis spectrophotometer. Fluorescence spectra were recorded using a Hitachi F-4010 spectrofluorometer. Time-resolved fluorescence measurements were carried out using a diode laser based time-correlated-single-photon-counting (TCSPC) spectrometer. In the present investigation, a 408 nm diode laser (1 MHz) was used as the excitation source and a TBX4 detection module coupled with a special Hamamatsu PMT was used for fluorescence detection. The instrument response function was ~230 ps at the FWHM. IR spectra were recorded on a Bomem MB-102 FT-IR spectrometer. Thermogravimetric analyses (TGA) were carried out on a Mettler TA–3000 instrument, which was calibrated with $CaC_2O_4 \cdot H_2O$. TG curve was recorded at a heating rate of 10 °C min^{-1} under a flow of nitrogen. X-ray powder diffraction data were collected on a Philips X-ray diffractometer (Model PW 1729) using Cu Kα radiation. A JEOL-2000FX transmission electron microscope operating at accelerating voltages up to 200 kV was used for TEM studies. The samples for TEM and SAED were prepared by placing a drop of a dilute solution of nanoparticles in acetone or pyridine on a carbon coated copper grid. EDAX was performed using a JEOL JSM-T330A instrument.

2.2. Synthesis of complexes

2.2.1. $[Cd(SeCH_2CH_2NMe_2)_2]$

A dichloromethane suspension (20 cm^3) of $Cd(OAc)_2 \cdot 2H_2O$ (664 mg, 2.49 mmol) was added to a freshly prepared methanolic solution of $NaSeCH_2CH_2NMe_2$ [prepared from $(Me_2NCH_2CH_2Se)_2$ (757 mg, 2.51 mmol) and $NaBH_4$ (193 mg, 5.10 mmol)] with continuous stirring at room temperature. After 3 h the colorless solution was dried in vacuo and the oily residue was washed with hexane and dried again in vacuo. The residue was extracted with CH_2Cl_2 (3×10 cm^3), filtered to remove NaOAc and the filtrate was evaporated under reduced pressure to give a white solid, which was recrystallized from dichloromethane-ethylacetate mixture. Yield: 702 mg (68%). mp 93–95 °C. *Anal.* Calc. for $C_8H_{20}N_2CdSe_2$: C, 23.2; H, 4.8; N, 6.8. Found: C, 23.0; H, 4.9; N, 6.6%. ^{1}H NMR (in $CDCl_3$) δ: 2.28 (s, NMe_2); 2.56 (br, $SeCH_2$); 2.74 (br, NCH_2). $^{13}C\{^1H\}$ NMR (in $CDCl_3$) δ: 15.5 (s, $SeCH_2$); 45.8 (s, NMe_2); 62.9 (s, NCH_2). The NMR spectra (^{1}H) in some samples showed additional peaks of low intensity (<5%) which may be attributed to $[Cd_3(OAc)_2(SeCH_2CH_2NMe_2)_4]$. The microanalysis of the latter (Calc. for $C_{20}H_{46}Cd_3N_4O_4Se_4$: C, 22.6; H, 4.3; N, 5.3%) is not significantly different from the bis derivative.

2.2.2. $[Cd_3(OAc)_2(SeCH_2CH_2NMe_2)_4]$

To a dichloromethane solution (5 cm^3) of $[Cd(SeCH_2CH_2NMe_2)_2]$ (187 mg, 0.45 mmol), a methanolic solution (5 cm^3) of $Cd(OAc)_2 \cdot 2H_2O$ (59 mg, 0.22 mmol) was added and the whole was heated at 40 °C with stirring for 2 h. The solvents were evaporated under vacuum and the residue was extracted with dichloromethane (5 cm$^3 \times 4$) and filtered through a fine filter. The filtrate was concentrated under vacuum to give a colorless powder (230 mg, 96%), mp 170 °C (dec. turns red). ν_{max}/cm^{-1} 1560 (C=O). ^{1}H NMR (in $CDCl_3$) δ: 2.05 (s, O_2CMe); 2.33 (s, NMe_2); 2.63 (br, $SeCH_2$); 2.82 (br, NCH_2). $^{13}C\{^1H\}$ NMR (in $CDCl_3$) δ: 16.4 (s, $SeCH_2$, ^1J(Se–C) = 57 Hz); 21.6 (s, O_2CMe); 45.5 (s, NMe_2); 62.0 (s, NCH_2); 179.4 (s, C=O).

2.2.3. Attempted preparation of $[Hg(SeCH_2CH_2NMe_2)_2]$

A dichloromethane solution (20 cm^3) of $HgCl_2 \cdot$ tmeda (201 mg, 0.51 mmol) was added to a freshly prepared methanolic solution of $NaSeCH_2CH_2NMe_2$ [prepared from $(Me_2NCH_2CH_2Se)_2$ (159 mg, 0.53 mmol) and $NaBH_4$ (44 mg, 1.16 mmol)] with continuous stirring at room temperature. After 3 h, a black precipitate settled down. The supernatant was decanted and the black precipitate was washed with hexane, acetone in sequence and then with water, acetone and dried in vacuo. Found: C, 1.8; H, 0.2; N, <0.2%. XRD pattern of this black powder was well in agreement with the pattern for cubic HgSe (JCPDS File No.73-1668). Similar results were obtained when $Hg(OAc)_2$ was used in place of $[HgCl_2 \cdot$ tmeda].

2.3. Synthesis of CdSe nanoparticles

2.3.1. Pyrolysis of $[Cd(SeCH_2CH_2NMe_2)_2]$ in HDA–TOPO mixture

In a three necked flask fitted with a thermometer, a continuously stirred mixture of HDA (2.39 g) and TOPO (185 mg) was degassed at 120 °C under argon atmosphere for 1 h. The temperature was slowly raised to 187 °C and stabilised at this temperature. To this, a solution of $[Cd(SeCH_2CH_2NMe_2)_2]$ (140 mg, 0.34 mmol) in a mixture

of dichloromethane (2 cm^3), toluene (2 cm^3) and TOPO (200 mg) was injected rapidly. The temperature dropped to 160 °C and was slowly raised to and maintained at 185 °C. Fractions were collected at 4 min (***fraction 1***) and 6 min (***fraction 2***) in vials containing methanol (5 cm^3). The hot solution at the end of 30 min (***fraction 3***) was cooled down to 70 °C and methanol was added to precipitate red nanoparticles. The red floculate was given a thorough washing with methanol followed by centrifuging and drying under vacuum.

Under similar conditions, a larger quantity of $[Cd(SeCH_2CH_2NMe_2)_2]$ (414 mg, 1.00 mmol) was pyrolysed in a mixture of HDA (7.09 g) and TOPO (1.00 g) and the reaction was quenched after 20 min (***fraction 4***) by adding methanol.

2.3.2. Pyrolysis of $[Cd(SeCH_2CH_2NMe_2)_2]$ in a furnace

Pyrolysis of $[Cd(SeCH_2CH_2NMe_2)_2]$ was carried out in a furnace under different conditions. In each experiment a weighed quantity (~80 mg) of the complex was dispersed in a small quartz boat by using dichloromethane and was subjected to pyrolysis. In one experiment the boat containing the complex was rapidly introduced into a preheated (180 °C) furnace and was kept at this temperature for 1 h under flowing nitrogen whereupon a yellowish-orange coat of CdSe (***fraction 5***: Found: C, 6.3; H, 1.8; N, 2.8%) was formed. In other experiments the furnace temperature was raised from room temperature to 200 °C in 5 min and the samples were heated at this temperature for 1 h either under flowing N_2 (***fraction 6***: Found: C, 6.9; H, 1.2; N, 1.6%) or under vacuum (***fraction 7***: Found: C, 5.6; H, 1.0; N, 1.6%), leading to the formation of a dark red CdSe coat. For optical measurements, small quantities of ***fractions 5–6*** were immediately dissolved in pyridine.

Table 1
Crystallographic and refinement data for $[Cd_3(OAc)_2(SeCH_2CH_2NMe_2)_4]$

Chemical formula	$C_{20}H_{46}Cd_3N_4O_4Se_4$
Formula weight	1059.65
Crystal size (mm^3)	$0.2 \times 0.2 \times 0.1$
Wavelength (Å)	0.71069
Crystal system	monoclinic
Space group	C_2/c
Unit cell dimensions	
a (Å)	24.700 (5)
b (Å)	13.309 (3)
c (Å)	11.575 (3)
β (°)	115.38 (4)
V ($Å^3$)	3437.8 (14)
D_{calc} ($g\,cm^{-1}$)	2.047
Z	4
μ (mm^{-1})	6.012
$F(000)$	2024
θ Range for data collection (°)	2.33–25.00
Limiting indices	$0 \leqslant h \leqslant 29$; $0 \leqslant k \leqslant 15$; $-13 \leqslant l \leqslant 12$
Reflections collected/unique (R_{int})	3245/3034 (0.0559)
Absorption correction	ψ scan
Data/restraints/parameters	3034/128/193
Final R_1 [$I > 2\sigma(I)$], ωR_2	0.0579, 0.1586
R_1, ωR_2 (all data)	0.1277, 0.1895
Largest difference in peak and hole (e $Å^{-3}$)	1.002 and −0.774

2.4. Crystallography

X-ray data of a colorless crystal of $[Cd_3(OAc)_2(SeCH_2CH_2NMe_2)_4]$ were collected at room temperature on an Enraf-Nonius CAD-4 diffractometer using graphite monochromated Mo Kα radiation ($\lambda = 0.71069$ Å) and employing the ω–2θ scan technique. The unit cell parameters (Table 1) were determined from 25 reflections measured by a random search routine. The intensity data were corrected for Lorentz, polarization and absorption effects (ψ scans). The structure was solved by direct methods using the SIR-92 program. The structure was completed by successive Fourier synthesis and refined using the SHELXL-97 program. The non-hydrogen atoms were refined with anisotropic thermal parameters. Hydrogen atoms could not be located reliably through difference Fourier maps due to disorder of the carbon atoms and hence were ignored.

3. Results and discussion

3.1. Synthesis and spectroscopy

Reaction of $Cd(OAc)_2 \cdot 2H_2O$ with $NaSeCH_2CH_2NMe_2$, prepared by the reduction of $(Me_2NCH_2CH_2Se)_2$ with $NaBH_4$ in methanol, gave a colorless homoleptic selenolate complex $[Cd(SeCH_2CH_2NMe_2)_2]$ (Eq. (1)). The freshly prepared complex is soluble in CH_2Cl_2, $CHCl_3$, benzene, toluene and methanol, but solubility decreases with aging, finally leading to a poorly soluble product. The NCH_2 and $SeCH_2$ proton resonances in the ^1H NMR spectrum appeared as broadened triplets which were shielded from the corresponding resonances for $(Me_2NCH_2CH_2Se)_2$. Several attempts to recrystallize the product from a mixture of solvents (CH_2Cl_2–hexane, CH_2Cl_2–MeCOOEt) gave either a colorless powder or flakes from which in some cases a few cubic crystals were separated which were identified by X-ray crystallography as a trinuclear cadmium complex, $[Cd_3(OAc)_2(SeCH_2CH_2NMe_2)_4]$. The latter complex, however, can readily be prepared by a redistribution reaction between $Cd(OAc)_2 \cdot 2H_2O$ and the bis complex, $[Cd(SeCH_2CH_2NMe_2)_2]$. Attempts to prepare the mercury complex, $[Hg(SeCH_2CH_2NMe_2)_2]$ using reaction route 1 led to excessive decomposition with the formation of cubic HgSe at room temperature.

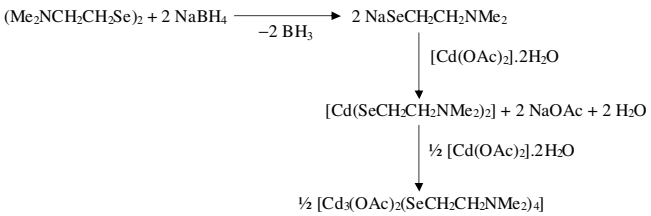

(1)

3.2. Crystal structure of $[Cd_3(OAc)_2(SeCH_2CH_2NMe_2)_4]$

The molecular structure of $[Cd_3(OAc)_2(SeCH_2CH_2NMe_2)_4]$, established unambiguously by X-ray diffraction analysis, is shown in Fig. 1 and selected interatomic parameters are listed in Table 2. The molecule has a twofold rotation axis passing through the central cadmium atom and hence half the molecule forms the crystallographic asymmetric unit. The $Me_2NCH_2CH_2Se$ fragments in the molecule are disordered and act in a chelating bridging fashion. The two terminal cadmium atoms adopt a skew trapezoidal planar geometry in which the basal plane is defined by two O and two Se atoms. The two remaining positions are occupied by the N atoms which are almost linear (∠N(1)–Cd(1)–N(2) 178.2 (3)°). The acetate ligand is asymmetrically chelated with two slightly different Cd–O distances, whereas the two C–O distances are essentially similar. The two Cd–Se distances differ marginally.

The coordination around the central cadmium is defined by four selenium bridges and adopts a pyrimidalized configuration with various angles varying between the ideal values of tetrahedral (109°) and square plane (90°). The two Cd–Se bonds are shorter than the other two. All the Cd–Se [28,29], Cd–N [28,30] and Cd–O [31] distances are well in agreement with values reported in other complexes.

Table 2
Selected bond lengths (Å) and angles (°) for $[Cd_3(OAc)_2(SeCH_2CH_2NMe_2)_4]$

Cd(1)–O(1)	2.311 (9)	Cd(2)–Se(1)	2.538 (3)
Cd(1)–O(2)	2.395 (9)	Cd(2)–Se(1′)	2.729 (3)
Cd(1)–Se(1)	2.724 (3)	Cd(2)–Se(2)	2.726 (3)
Cd(1)–Se(1′)	2.732 (3)	Cd(2)–Se(2′)	2.618 (3)
Cd(1)–Se(2)	2.800 (3)	Se(1)–C(6)	1.96 (2)
Cd(1)–Se(2′)	2.652 (2)	Se(1′)–C(10′)	2.03 (3)
Cd(1)–N(1)	2.413 (9)	Se(2)–C(10)	1.91 (3)
Cd(1)–N(2)	2.437 (12)	Se(2′)–C(6′)	2.06 (3)
O(1)–Cd(1)–O(2)	54.4 (3)	O(1)–Cd(1)–Se(2)	151.5 (3)
O(1)–Cd(1)–N(1)	93.5 (4)	O(2)–Cd(1)–Se(2)	101.5 (2)
O(2)–Cd(1)–N(1)	90.9 (3)	N(1)–Cd(1)–Se(2)	102.7 (2)
O(1)–Cd(1)–N(2)	88.0 (4)	N(2)–Cd(1)–Se(2)	76.3 (3)
O(2)–Cd(1)–N(2)	90.7 (4)	Se(1)–Cd(1)–Se(2)	96.14 (9)
N(1)–Cd(1)–N(2)	178.2 (3)	Se(1)–Cd(2)–Se(2)	102.61 (9)
O(1)–Cd(1)–Se(1)	109.3 (3)	Se(1′)–Cd(2)–Se(2′)	99.51 (8)
O(2)–Cd(1)–Se(1)	162.1 (2)	Cd(1)–Se(1)–Cd(2)	82.74 (9)
N(1)–Cd(1)–Se(1)	82.1 (2)	Cd(1)–Se(1′)–Cd(2)	79.20 (7)
N(2)–Cd(1)–Se(1)	96.4 (3)	Cd(1)–Se(2)–Cd(2)	78.07 (7)

3.3. Thermal studies

The TG curve (Fig. 2) of $[Cd(SeCH_2CH_2NMe_2)_2]$ showed that the complex decomposed in a single step at 155 °C to CdSe as inferred from the weight loss (Found: weight loss 52.6%; calcd. weight loss 53.8%).

Pyrolysis of $[Cd(SeCH_2CH_2NMe_2)_2]$ was carried out under different conditions, either in HDA/TOPO mixture or in a furnace. Pyrolysis of $[Cd(SeCH_2CH_2NMe_2)_2]$ in a furnace gave either cubic (***fractions 5*** and ***6***) or hexagonal (***fraction 7***) CdSe nanoparticles (from XRD, see later) which were formed under a flowing inert gas or vacuum, respectively. The microanalyses data of ***fractions 5–7*** suggest that the CdSe may be capped by the amine residues evolved on pyrolysis of the complex.

Pyrolysis of $[Cd(SeCH_2CH_2NMe_2)_2]$ in a HDA/TOPO mixture gave HDA capped CdSe nanoparticles. The IR

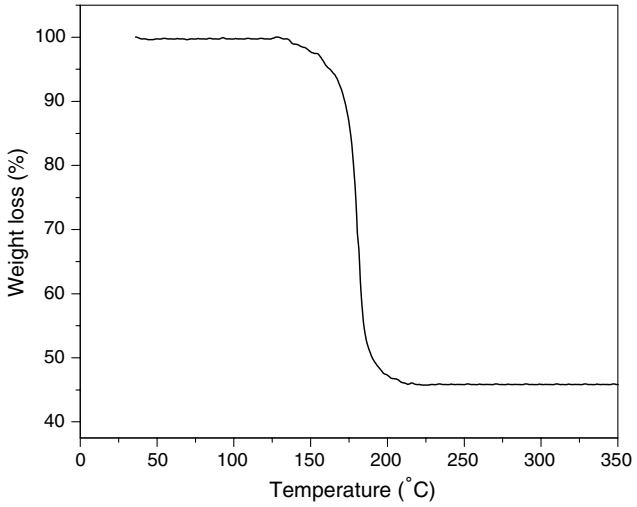

Fig. 2. TG curve of $[Cd(SeCH_2CH_2NMe_2)_2]$.

spectra of ***fractions 1–4*** (Fig. 3) displayed a shift of ν(N–H) to lower wavenumbers compared to that of free HDA (for free HDA ν(N–H) = 3333 cm^{-1}), indicating coordination of HDA. The $^{31}P\{^1H\}$ NMR chemical shifts for

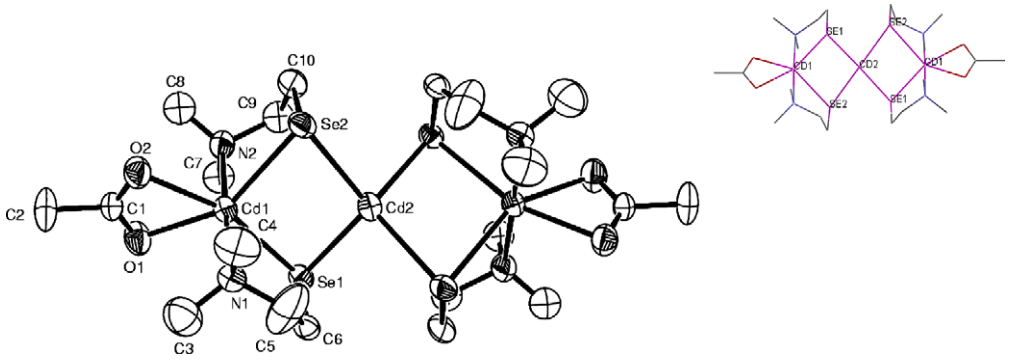

Fig. 1. ORTEP of $[Cd_3(OAc)_2(SeCH_2CH_2NMe_2)_4]$ with the atomic numbering scheme. Inset shows skeletal atoms.

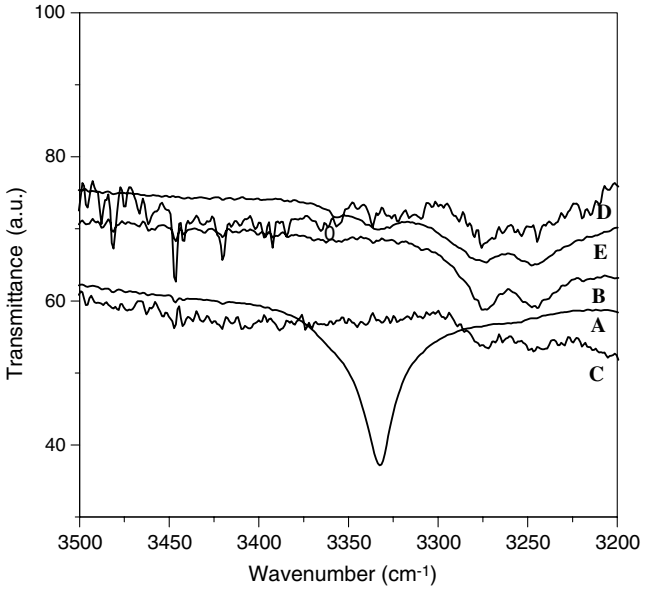

Fig. 3. IR spectra of **A**: free HAD, **B**: ***fraction 1***, **C**: ***fraction 2***, **D**: ***fraction 3*** and **E**: ***fraction 4***.

fraction 4 (δ 44.0 ppm) and free TOPO (δ 43.5 ppm) are comparable suggesting the absence of TOPO capping of CdSe nanoparticles.

3.4. Powder X-ray diffraction

XRD patterns (Fig. 4) of CdSe prepared by pyrolysis of $[Cd(SeCH_2CH_2NMe_2)_2]$ under different conditions showed broad peaks which are typical for particles in the nano regime. The particle sizes estimated from Scherrer's formula come out to be 12, 6, 4, 9 and 8.3 nm for ***fractions 3***, ***4***, ***5***, ***6*** and *7*, respectively. The pattern can be assigned to the cubic phase of CdSe in the case of ***fractions 5*** and ***6*** and the hexagonal phase of CdSe in the case of ***fraction 7*** (Table 3). In the case of ***fraction 7***, we have used X-ray peak fitting software to confirm whether the first peak is a single peak or the overlap of three peaks and it is fitted into three peaks, which coincides with the hexagonal phase of CdSe. Assignment of the hexagonal phase of CdSe to ***fraction 7*** is further confirmed by its SAED pattern.

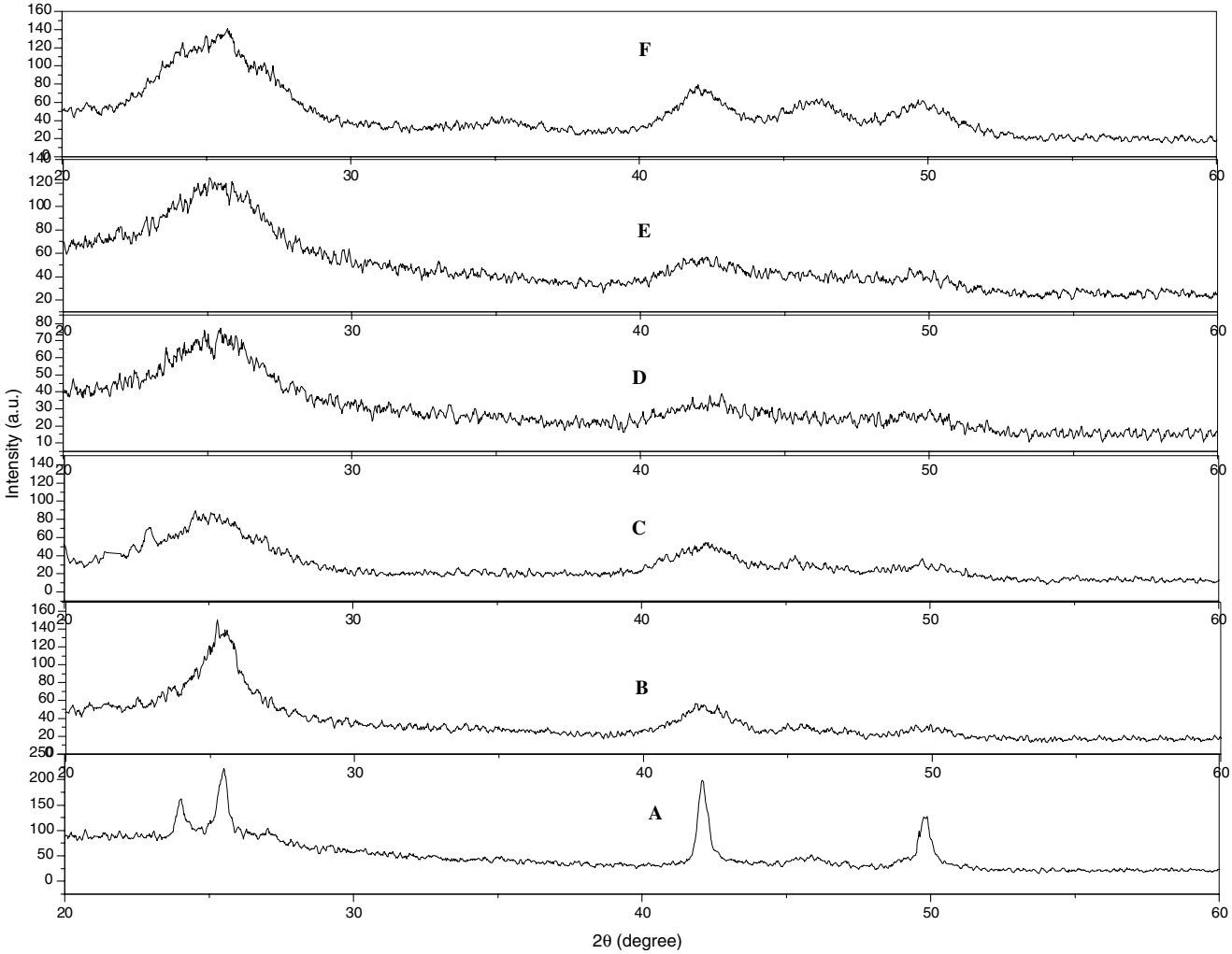

Fig. 4. XRD pattern of **A**: bulk CdSe obtained at 400 °C, **B**: ***fraction 3***, **C**: ***fraction 4***, **D**: ***fraction 5***, **E**: ***fraction 6*** and **F**: ***fraction 7***.

Table 3
XRD data of CdSe nanoparticles prepared by different routes and the particle sizes of different fractions

Fraction	XRD data				Size calculated from Brus expression (nm)	Size calculated from Scherrer's formula (nm)	Size obtained from TEM (nm)
	d (Å)			Lattice parameter (Å)			
1					5		
2					6.4		
3	3.49	2.15	1.83	6.046	12.2	12	
4	3.55	2.16	1.83	6.149	7.9	6	7.5
5	3.47	2.14	1.83	6.011	4.8	4	
6	3.54	2.15	1.83	6.131	6.7	9	
7	3.66	2.14	3.27	4.274, 6.958	6.5	8.3	21[c]
CdSe (cubic)[a]	3.51	2.15	1.83	6.077			
CdSe (hexagonal)[b]	3.72	2.15	3.29	4.299, 7.010			

[a] JCPDS File No. 80-0021 (International Centre for Diffraction data – 1998).
[b] JCPDS File No. 08-0459 (International Centre for Diffraction data – 1998).
[c] TEM of the sample was recorded after one month and therefore ripening might have taken place and hence a larger size compared to the one estimated from the XRD pattern.

3.5. Electron microscopy

The selected area electron diffraction (SAED) patterns of ***fractions 4*** and *7* (Fig. 5) revealed the formation of crystalline CdSe. Clear diffraction rings corresponding to the lattice planes (111), (220) and (311) in the SAED pattern of the ***fraction 4*** were attributed to cubic CdSe. The SAED pattern of ***fraction*** *7* has been interpreted in terms of the hexagonal phase of CdSe with diffraction rings corresponding to the lattice planes (100), (101), (102), (110), (103), (112), (202) and (203). The phases determined from the SAED and XRD patterns were in agreement with each other. The TEM images of ***fraction 4*** (Fig. 6) and ***fraction*** *7* (Fig. 7) shows the particles are spherical in shape. The average diameters of particles of ***fraction 4*** and ***fraction*** *7*, estimated from TEM images, are $7.5 \pm 4\%$ and $21 \pm 8\%$ nm, respectively. In the case of ***fraction 4***, the particle size obtained from the TEM image is closer to that of the particle size calculated from the XRD pattern using Scherrer's formula. EDX spectra of ***fractions 3***, ***4***, ***6*** and *7* exhibited peaks for Cd and Se, which were in 1:1 ratios.

3.6. Optical properties

CdSe nanoparticles, prepared by pyrolysis of $[Cd(SeCH_2CH_2NMe_2)_2]$ in a furnace, displayed absorption maxima at 423 (***fraction 5***), 538, 580 (***fraction 6***) and 455 nm (***fraction*** *7*) (Fig. 8). The excitation spectrum of ***fraction*** *7* at room temperature showed a broad exciton peak at 400 nm, whereas a broad maximum at 499 nm was observed in the emission spectrum (Fig. 8).

Absorption, excitation and emission spectra of HDA capped CdSe nanoparticles, prepared by pyrolysis of $[Cd(SeCH_2CH_2NMe_2)_2]$ in HDA/TOPO mixture are given in Figs. 9–11. Absorption spectra (Fig. 9) of HDA capped CdSe nanoparticles displayed a typical band edge absorption with an exciton band and the spectra are well in agreement with those reported earlier [17,19,32]. ***Fractions 1–4*** showed exciton maxima at 490, 549, 625 and 582 nm,

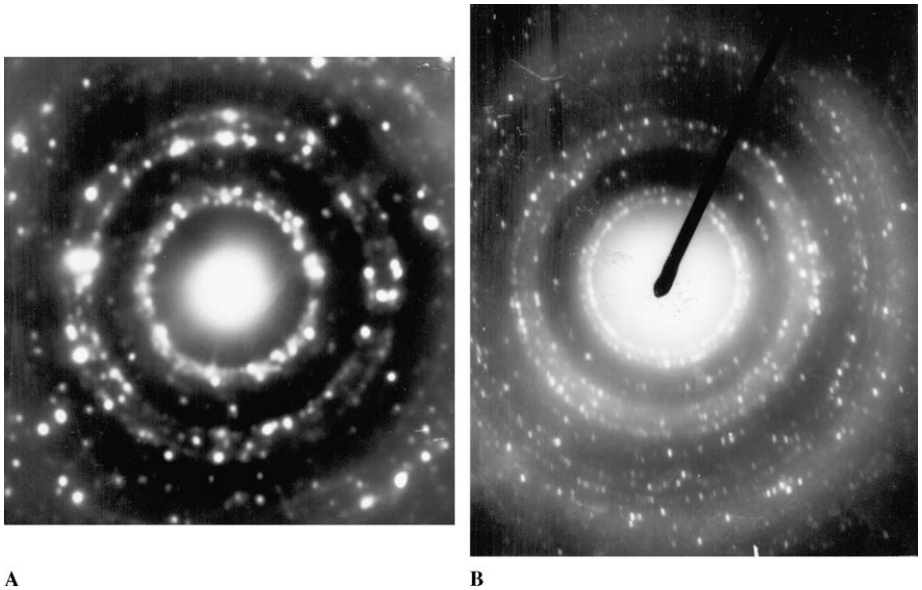

A B

Fig. 5. SAED pattern CdSe nanoparticles of **A**: ***fraction 4*** and **B**: ***fraction*** *7*.

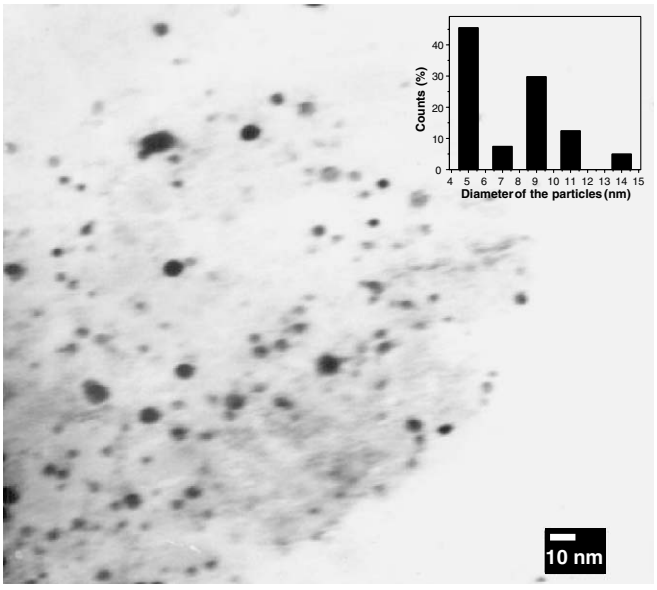

Fig. 6. TEM picture of capped CdSe nanoparticles of ***fraction 4***. Inset shows particle size distribution.

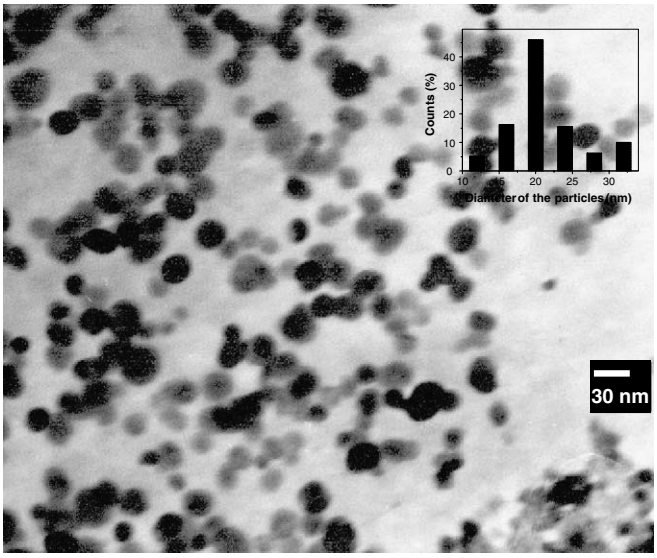

Fig. 7. TEM picture of CdSe nanoparticles of ***fraction 7***. Inset shows particle size distribution.

respectively, which are blue shifted with respect to bulk CdSe ($\lambda_{onset} = 713$ nm), confirming the quantum confinement effect of the particles. The absorption maximum of the fractions collected at different time intervals showed a red shift with increasing time, which is in accordance with earlier reports [33]. The excitation spectra (Fig. 10) for each fraction are found to have maxima at 494, 549 and 625 nm, respectively, at room temperature. These excitation maxima coincide well with the absorption band edges of the three ***fractions 1–3*** at 490, 547 and 625 nm, respectively. The emission spectra (Fig. 11) displayed two peaks each in ***fractions 1*** (518, 640 nm) and ***2*** (573 and 719 nm) corresponding to band edge and trap state emissions [34–36].

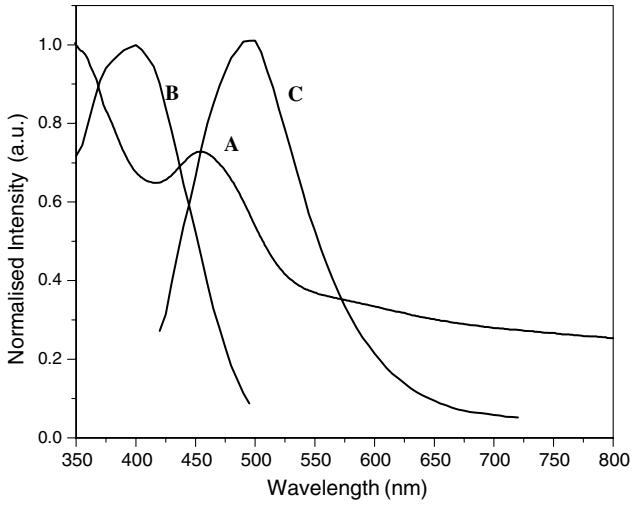

Fig. 8. **A**: Absorption spectrum, **B**: excitation spectrum and **C**: emission spectrum of CdSe nanoparticles of ***fraction 7***.

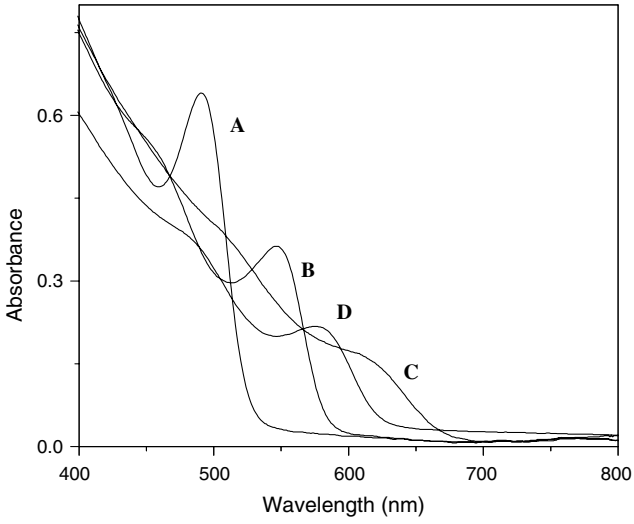

Fig. 9. Absorption spectra of HDA capped CdSe nanoparticles **A**: ***fraction 1***, **B**: ***fraction 2***, **C**: ***fraction 3*** and **D**: ***fraction 4***.

The spectra showed narrow band edge emission peaks in these fractions, implying that the particle size distribution is narrow as the width of the emission peaks depend on the size distribution of the particles [19]. The ***fractions 3*** and ***4***, however, showed only a broad and a narrow peak corresponding to band edge emissions at 637 and 605 nm, respectively, implying a slightly broad and narrow distribution of the particles in these fractions. The particle sizes estimated using Brus's expression [37] for the ***fractions 1–4*** are 5, 6.4, 12.2 and 7.9 nm, respectively, and compare well with the size estimated employing Scherrer's formula (Table 3).

To understand the charge carrier dynamics, we have carried out time-resolved luminescence measurements (Fig. 12) of ***fractions 1*** and ***3***. For all the samples, excitation was carried out at 408 nm. For ***fraction 1***, lifetimes for both the band edge and trap state components were taken while

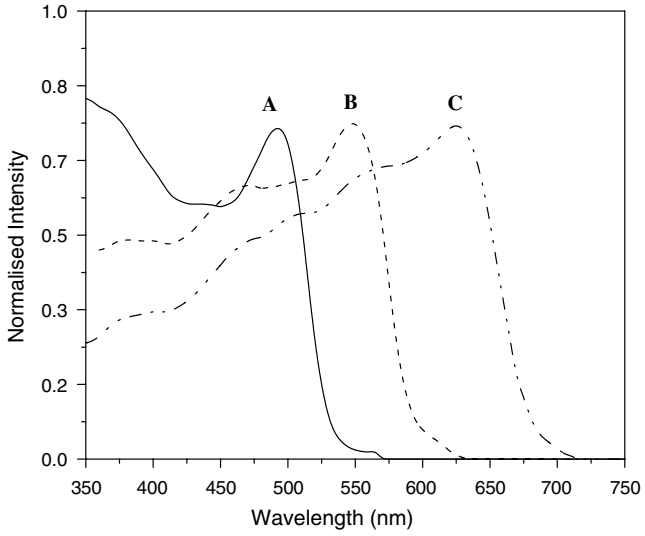

Fig. 10. Excitation spectra of HDA capped CdSe nanoparticles **A**: ***fraction 1***, **B**: ***fraction 2*** and **C**: ***fraction 3***.

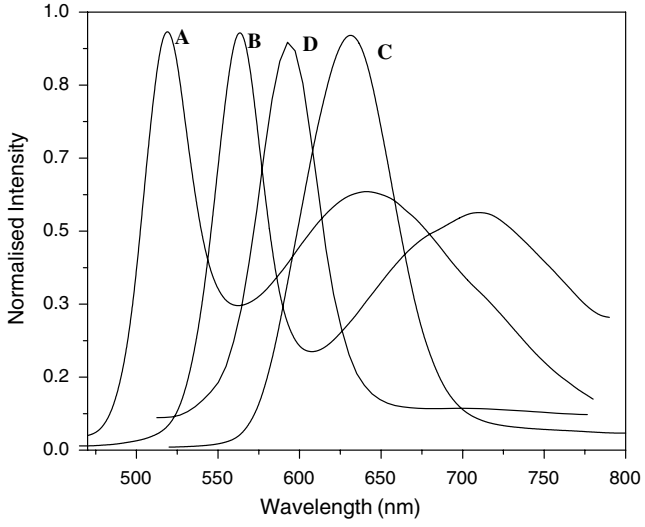

Fig. 11. Emission spectra of HDA capped CdSe nanoparticles **A**: ***fraction 1***, **B**: ***fraction 2***, **C**: ***fraction 3*** and **D**: ***fraction 4***.

for ***fraction 3***, the band edge component was studied. A multi-exponential function has been used to fit the data for a reasonable fit in all the cases. Three different decay times for each band edge [0.5 (68%), 8.3 (24%), 61.5 (8%) ns] and trap state components [1.8 (29%), 12.3 (36%), 73.7 (35%) ns] for ***fraction 1*** were observed. Similarly three decay times [2.9 (45%), 12.5 (46%) and 49.1 (9%) ns] for the band edge emission for ***fraction 3*** were identified. The multi-exponential character of the decay, even when photoluminescence shows well resolved lines, can be attributed to the overlap of various contributions arising from different particles [38]. The decay times of band edge and trap state emission of ***fraction 1*** shows that the former component is faster than the latter. The decay times of the band edge component of ***fraction 1*** is also faster than that of ***fraction 3***, showing size dependence of life times and is in agreement with the reported data [32].

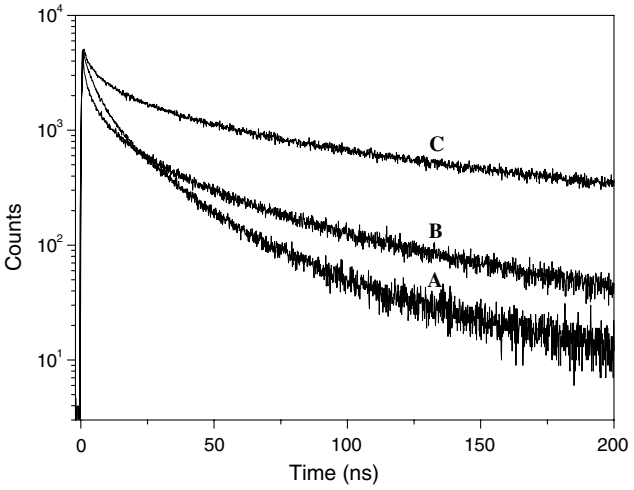

Fig. 12. Lifetime measurements of **A**: band edge component of ***fraction 3***, **B**: band edge component of ***fraction 1*** and **C**: trap state component of ***fraction 1***.

4. Conclusion

The single source precursor $[Cd(SeCH_2CH_2NMe_2)_2]$, prepared conveniently, has been employed for the synthesis of CdSe nanoparticles. The size and phase (cubic and hexagonal) of these particles is conveniently controlled by varying the pyrolysis conditions. Both absorption and emission bands of these nanoparticles showed size dependence and were blue shifted with decreasing particle size. The band edge and trap state showed three different decay times.

5. Supplementary materials

CCDC-277552 contains the supplementary crystallographic data for this paper. These data can be obtained free of charge at www.ccdc.cam.ac.uk/conts/retrieving.html or from the Cambridge Crystallographic Data Centre, 12 Union Road, Cambridge CB2 1EZ, UK [fax: (internat.) +44 1223 336 033; e-mail: deposit@ccdc.cam.ac.uk].

Acknowledgements

We thank Drs. T. Mukherjee and S.K. Kulshreshtha for encouragement of this work. We are also grateful to Dr. M. Sudarsanan, Head, Analytical Chemistry Division for providing microanalyses of the complexes and Dr. G. Ramakrishna for helpful discussions.

References

[1] T. Trindade, P. O'Brien, N.L. Pickett, Chem. Mater. 13 (2001) 3843.
[2] M. Nirmal, L. Brus, Acc. Chem. Res. 32 (1999) 407.
[3] T.S. Ahmadi, Z.L. Wang, T.C. Green, A. Henglein, M.A. Elsayed, Science 272 (1996) 1924.
[4] W. Huynch, X.G. Peng, A.P. Alivisatos, Adv. Mater. 11 (1999) 923.
[5] L.H. Qu, Z.A. Peng, X.G. Peng, Nano Lett. 1 (2001) 331.

[6] (a) W.C.W. Chan, S. Nie, Science 281 (1998) 2016;
(b) D.R. Larson, W.R. Zipfel, R.W. Williams, S.W. Clark, M.P. Bruchez, F.W. Wise, W.W. Webb, Science 300 (2003) 1434;
(c) M. Green, Angew. Chem., Int. Ed. 43 (2004) 4129.
[7] J.W. Jlot, H.J. Geuze, J. Cell. Biol. 90 (1981) 533.
[8] X.G. Peng, L. Manna, W.D. Yang, J. Wickham, E. Scher, A. Kadavanich, A.P. Alivisatos, Nature 404 (2000) 59.
[9] J.T. Hu, L.S. Li, W.D. Yang, L. Manna, L.W. Wang, A.P. Alivisatos, Science 292 (2001) 2060.
[10] L.S. Li, J. Hu, W. Yang, A.P. Alivisatos, Nano Lett. 1 (2001) 349.
[11] P.S. Nair, K.P. Fritz, G.D. Sckoles, Chem. Commun. (2004) 2084.
[12] M.S. Gudiksen, J. Wang, C.M. Lieber, J. Phys. Chem. B 106 (2002) 4036.
[13] X.C. Jiang, B. Mayers, T. Herricks, Y.N. Xia, Adv. Mater. 15 (2003) 1740.
[14] C. Ma, Y. Ding, D. Moore, X. Wang, Z.L. Wang, J. Am. Chem. Soc. 126 (2004) 708.
[15] L. Manna, E.C. Scher, A.P. Alivisatos, J. Am. Chem. Soc. 122 (2000) 12700.
[16] M. Green, P. O'Brien, Chem. Commun. (1999) 2235.
[17] C.B. Murray, D.J. Norris, M.G. Bawendi, J. Am. Chem. Soc. 115 (1993) 8706.
[18] M. Grätzel, Nature 338 (1989) 540.
[19] M.A. Malik, P. O'Brien, Adv. Mater. Opt. Electron. 3 (1994) 171.
[20] P. Reiss, J. Bleuse, A. Pron, Nano Lett. 2 (2002) 781.
[21] (a) D.J. Crouch, P. O'Brien, M.A. Malik, P.J. Skabara, S.P. Wright, Chem. Commun. (2003) 1454;
(b) M.A. Malik, N. Revaprasadu, P. O'Brien, Chem. Mater. 13 (2001) 913.
[22] UK Gautam, M. Rajamathi, F. Meldrum, P. Morgan, R. Seshadri, Chem. Commun. (2001) 629.
[23] M.L. Steigerwald, A.P. Alivisatos, J.M. Gibson, T.D. Harris, R. Kortan, A.J. Muller, A.M. Thayer, T.M. Duncan, D.C. Douglass, L.E. Brus, J. Am. Chem. Soc. 110 (1988) 3046.
[24] D.E. Fenton, in: J.A. McCleverty, T.J. Meyer (Eds.), Comprehensive Coordination Chemistry–II, vol. 6, Pergamon Press, Oxford, 2004 p. 1253.
[25] S. Dey, V.K. Jain, S. Chaudhury, A. Knoedler, F. Lissner, W. Kaim, J. Chem. Soc., Dalton Trans. (2001) 723.
[26] (a) S. Dey, V.K. Jain, A. Knoedler, W. Kaim, S. Zalis, Eur. J. Inorg. Chem. (2001) 2965;
(b) S. Dey, V.K. Jain, A. Knoedler, W. Kaim, S. Zalis, Inorg. Chem. 41 (2002) 2864;
(c) S. Dey, V.K. Jain, A. Knoedler, W. Kaim, Indian J. Chem. A 42 (2003) 2339.
[27] S. Dey, V.K. Jain, S. Chaudhury, A. Knoedler, W. Kaim, Polyhedron 22 (2003) 489.
[28] Y. Cheng, T.J. Emge, J.G. Brennan, Inorg. Chem. 33 (1994) 3711.
[29] M.T. Ng, P.A.W. Dean, J.J. Vittal, J. Chem. Soc., Dalton Trans. (2004) 2890.
[30] M.D. Nyman, M.J. Hampden Smith, E.N. Duesler, Inorg. Chem. 36 (1997) 2218.
[31] R.S. Honkonen, P.D. Ellis, J. Am. Chem. Soc. 106 (1984) 5488.
[32] D.M. Mittleman, R.W. Schoenlein, J.J. Shiang, V.L. Colvin, A.P. Alivisatos, C.W. Shank, Phys. Rev. B 49 (1994) 14435.
[33] (a) S.D. Bunge, K.M. Krueger, T.J. Boyle, M.A. Rodriguez, T.J. Headley, V.L. Colvin, J. Mater. Chem. 13 (2003) 1705;
(b) H. Nakamura, Y. Yamaguchi, M. Miyazaki, H. Maeda, M. Uehara, P. Mulvaney, Chem. Commun. (2002) 2844.
[34] (a) A. Hasselbarth, A. Eychmuller, H. Weller, Chem. Phys. Lett. 203 (1993) 271;
(b) M.G. Bawendi, P.J. Carroll, W.L. Wilson, L.E. Brus, J. Chem. Phys. 96 (1992) 946.
[35] (a) R. Jaeger-Waldau, N. Stuecheli, M. Braun, M. Luse Steiner, E. Bucher, R. Tenne, H. Flaisher, W. Kerfin, R. Braun, W. Koschel, J. Appl. Phys. 64 (1988) 2601;
(b) J.Y. Lin, D. Baum, Q. Zhu, A. Honig, H.X. Jiang, J. Lumin. 45 (1990) 251.
[36] M. Nirmal, C.B. Murray, M.G. Bawendi, Phys. Rev. B 50 (1994) 2293.
[37] J.Z. Zhang, J. Phys. Chem. B 104 (2000) 7239.
[38] P. Lefebvre, H. Mathieu, J. Allegre, T. Richard, A. Combettes-Roos, M. Pauthe, W. Granier, Semicond. Sci. Technol. 12 (1997) 958.

Table 1
Crystal data for Os,Os-**3a**, Ru,Os-**3a**, **3b**, **3c**, **3f**, Ru,Os-**3h** and Ru,Ru-**3h**

Compound	Os,Os-**3a**	Ru,Os-**3a**	**3b**	**3c**	**3f**	Ru,Os-**3h**	Ru,Ru-**3h**
Empirical formula	$C_{47}H_{32}O_{11}Os_3P_2Ru$	$C_{47}H_{32}O_{11}Os_3P_2Ru \cdot CH_2Cl_2$	$C_{47}H_{32}As_2O_{11}Os_3Ru$	$C_{47}H_{32}O_{11}Os_3RuSb_2 \cdot 1/4C_6H_{14}$	$C_{47}H_{56}O_{11}Os_3P_2Ru \cdot C_6H_{14}$	$C_{17}H_{20}O_{11}Os_3P_2Ru$	$C_{17}H_{20}O_{11}Os_3P_2Ru$
Formula weight	1506.34	1591.26	1594.24	1709.44	1616.70	1133.94	1133.94
Temperature (K)	295(2)	223(2)	293(2)	293(2)	293(2)	223(2)	223(2)
Crystal system	triclinic	triclinic	triclinic	triclinic	monoclinic	monoclinic	monoclinic
Space group	$P\bar{1}$	$P\bar{1}$	$P\bar{1}$	$P\bar{1}$	$P2_1/m$	$P2_1/n$	$P2_1/n$
a (Å)	11.6739(1)	12.8424(9)	11.9089(1)	9.5595(2)	10.0594(4)	9.3405(2)	11.3605(2)
b (Å)	13.0787(2)	13.7712(10)	13.6400(1)	13.9882(2)	20.3820(7)	16.8965(5)	17.256
c (Å)	17.7705(1)	17.4424(12)	14.9247(2)	20.4536(3)	14.6764(5)	17.6967(5)	14.0633(2)
α (°)	73.390(1)	73.519(2)	96.581(1)	82.950(1)	90	90	90
β (°)	71.690(1)	70.141(2)	103.390(1)	78.418(1)	106.334(1)	99.821(1)	105.159(1)
γ (°)	66.283(1)	65.718(2)	94.928(1)	74.074(1)	90	90	90
Volume (Å^3)	2318.28(4)	2607.1(3)	2326.93(4)	2569.89(8)	2887.66(18)	2751.99(13)	2660.95(6)
Z	2	2	2	2	2	4	4
ρ_c (g cm^{-3})	2.158	2.027	2.275	2.209	1.859	2.737	2.831
μ(Mo Kα) (mm^{-1})	8.642	7.790	9.953	8.764	6.945	14.510	15.006
F(000)	1408	1492	1480	1577	1556	2048	2048
Crystal size (mm^3)	$0.10 \times 0.05 \times 0.04$	$0.16 \times 0.12 \times 0.10$	$0.40 \times 0.40 \times 0.28$	$0.113 \times 0.113 \times 0.092$	$0.22 \times 0.18 \times 0.06$	$0.24 \times 0.22 \times 0.11$	$0.26 \times 0.24 \times 0.12$
θ Range (°)	2.03–29.33	2.23–26.37	2.19–29.33	1.52–29.41	2.00–29.32	2.32–29.37	2.06–29.32
Reflections collected	19382	36070	18810	19370	18971	17672	17682
Independent reflections [R_{int}]	11085 [0.0621]	10645 [0.0470]	11014 [0.0223]	12167 [0.0321]	7327 [0.0380]	6850 [0.0400]	6650 [0.0377]
Maximum and minimum transmission	0.724 and 0.479	0.510 and 0.369	0.154 and 0.074	0.527 and 0.421	0.604 and 0.357	0.264 and 0.144	0.264 and 0.131
Data/restraints/parameters	11085/4/584	10645/34/649	11014/4/584	12167/55/458	7327/183/302	6850/0/316	6650/6/313
Goodness-of-fit on F^2	1.032	1.122	1.224	1.040	1.111	1.088	1.102
Final R indices [$I > 2\sigma(I)$]	$R_1 = 0.0686$ $wR_2 = 0.1133$	$R_1 = 0.0480$ $wR_2 = 0.1179$	$R_1 = 0.0368$ $wR_2 = 0.0900$	$R_1 = 0.0480$ $wR_2 = 0.1003$	$R1 = 0.0485$ $wR_2 = 0.1111$	$R_1 = 0.0346$ $wR_2 = 0.0778$	$R_1 = 0.0335$ $wR_2 = 0.0771$
R indices (all data)	$R_1 = 0.1507$ $wR_2 = 0.1450$	$R_1 = 0.0593$ $wR_2 = 0.1237$	$R_1 = 0.0445$ $wR_2 = 0.0958$	$R_1 = 0.0884$ $wR_2 = 0.1194$	$R_1 = 0.0762$ $wR_2 = 0.1257$	$R_1 = 0.0470$ $wR_2 = 0.0834$	$R_1 = 0.0420$ $wR_2 = 0.0806$
Largest differential peak and hole (e Å^{-3})	1.701 and −2.150	2.055 and −1.304	2.477 and −1.555	1.609 and −1.755	1.339 and −1.651	1.329 and −2.445	1.978 and −2.142

2.2. Preparation of $RuOs_3(\mu\text{-}H)_2(CO)_{11}(PMe_3)_2$

The previously reported procedure was employed, except that an excess of PMe_3 was used, which upon chromatographic separation afforded two isomers initially as separate bands.

$RuOs_3(\mu\text{-}H)_2(CO)_{11}(PMe_3)_2$, Ru,Os-**3h**, yield = 38%; ν_{CO}/cm^{-1} (hexane) 2076m, 2050mw, 2042vs, 2012s, 2001s, 1992mw, 1970mw, 1755mw, br. MS: 1133.5 (M^+). *Anal.* Calc. for $C_{17}H_{20}O_{11}Os_3P_2Ru \cdot CH_2Cl_2$: C, 17.73; H, 1.82. Found: C, 17.61; H, 1.93%.

$RuOs_3(\mu\text{-}H)_2(CO)_{11}(PMe_3)_2$, Ru,Ru-**3h**, yield = 35%; ν_{CO}/cm^{-1} (hexane) 2082m, 2050s, 2025vs, 2005s, 1984m, 1978m, 1943mw. MS: 1133.5 (M^+).

2.3. Crystal structure determinations

Crystals were mounted on quartz fibres. X-ray data were collected on a Bruker AXS APEX system, using Mo Kα radiation, with the SMART suite of programs [3]. Data were processed and corrected for Lorentz and polarisation effects with SAINT [4], and for absorption effects with SADABS [5]. Structural solution and refinement were carried out with the SHELXTL suite of programs [6]. Atomic coordinates are given in the Supporting Information; crystal and refinement data are listed in Table 1.

The structures were solved by direct or Patterson methods to locate the heavy atoms, followed by difference maps for the light, non-hydrogen atoms. Organic hydrogen atoms were placed in calculated positions and refined with a riding model. The metal hydrides were either located by low angle difference maps (Ru,Os-**3a**,**3h**) or placed by potential energy calculations with the program XHYDEX [7]. The hydrides were given fixed isotropic thermal parameters and the M–H distance fixed at 1.84 Å. With the exception of those mentioned below involving disordered parts, all non-hydrogen atoms were given anisotropic thermal parameters in the final model. Refinements were on $\sum[w(F_o^2 - F_c^2)^2]$.

With the exception of Ru,Ru-**3h**, all the clusters exhibited disorder of the metal core. Each disordered site was modelled with a partial osmium and ruthenium, given identical anisotropic thermal parameters and positions, with sum of the occupancies of ruthenium over all sites restrained to 1.0. The Ru/Os disorder was modelled over two sites and (except for Os,Os-**3a**) these were the vertices attached to the group 15 atoms. There was also disorder of phenyl over cyclohexyl rings over two sites in **3f**, and of one of the phenyl rings in **3c** over two orientations, which were modelled with fixed occupancies and the same isotropic thermal parameters for atoms at the same corresponding site. Appropriate restraints were also applied. Solvent molecules were found in Ru,Os-**3a**, **3c** and **3f**, and they were also disordered and modelled accordingly with restraints as appropriate.

3. Results and discussion

3.1. Solid state structures

The single crystal X-ray structures of seven disubstituted derivatives have been determined, which are those for the ligands EPh_3 (E = P, As, Sb), PCy_2Ph, and PMe_3. As may be expected, the number of structural types is more diverse than for the monosubstituted derivatives; the six clusters may be classified into four structural types A–D. The ORTEP plots for Os,Os-**3a**, **3b**, Ru,Os-**3h** and Ru,Ru-**3h**, illustrating the four structural types, are shown in Figs. 1–4, respectively. For PPh_3,

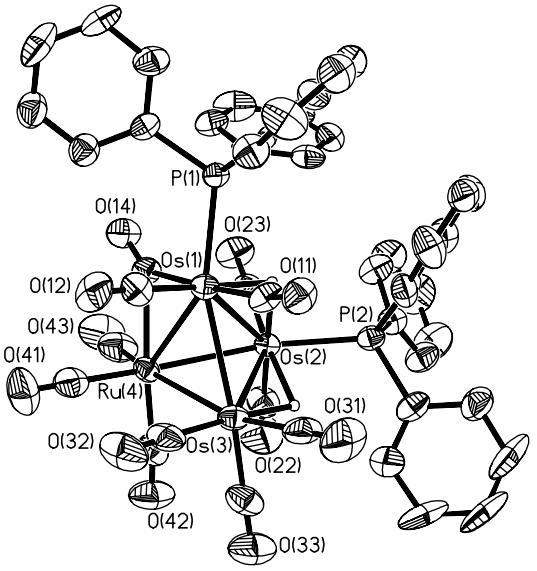

Fig. 1. ORTEP diagram of Os,Os-**3a** (50% thermal ellipsoids) with organic hydrogens omitted.

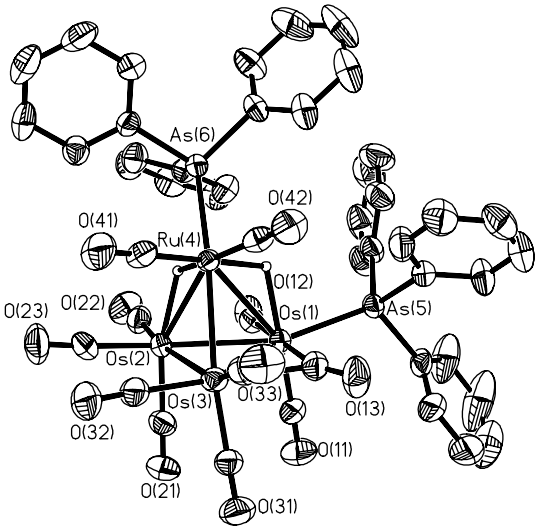

Fig. 2. ORTEP diagram of **3b** (50% thermal ellipsoids) with organic hydrogens omitted.

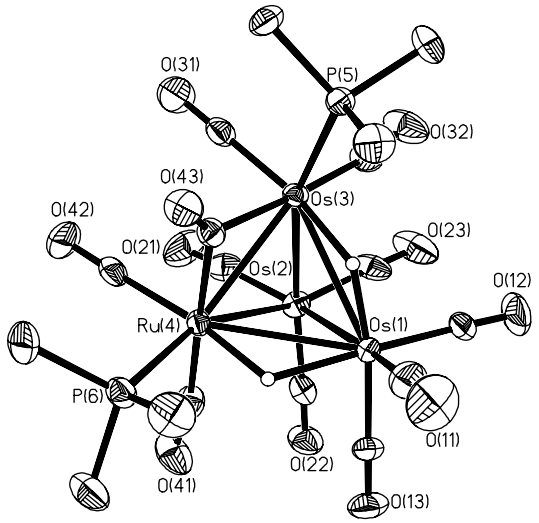

Fig. 3. ORTEP diagrams of Ru,Os-**3h**. Thermal ellipsoids are drawn at the 50% probability level; organic hydrogens are omitted.

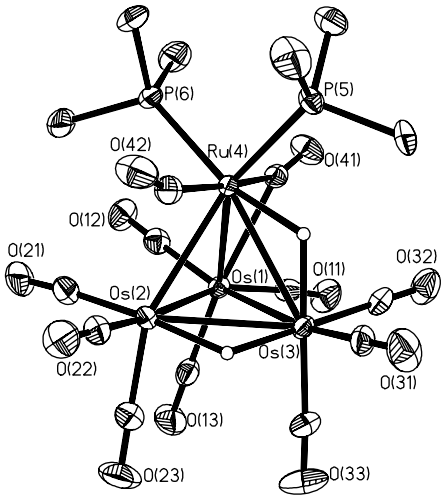

Fig. 4. ORTEP diagrams of Ru,Ru-**3h**. Thermal ellipsoids are drawn at the 50% probability level; organic hydrogens are omitted.

the disorder in the structure of Os,Os-**3a** has been modelled such that in 2/3 (refined value) of the molecules both the phosphine ligands are on different Os vertices, while the other 1/3 has one of the phosphine ligands on the Ru vertex; they correspond to structural types A and B, respectively. For PMe_3, two isomeric forms were available as crystals, one of which had both the phosphine ligands substituted at the same Ru vertex (Ru,Ru-**3h**). With the exception of Ru,Ru-**3h**, the solid-state structures of the others exhibit disorder of the Ru/Os vertices. There appears to be some trend to the disorder for, with the exception of Os,Os-**3a**, the Ru/Os disorder is over the

Table 2
Common atomic numbering scheme and selected bond parameters for Os,Os-**3a**, Ru,Os-**3a**, **3b**, **3c**, **3f**, Ru,Os-**3h** and Ru,Ru-**3h**

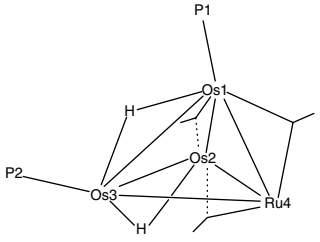

A

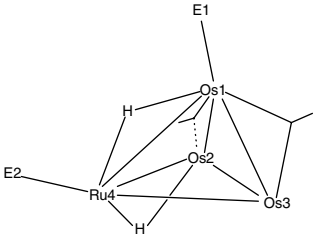

B (E = P, As, Sb)

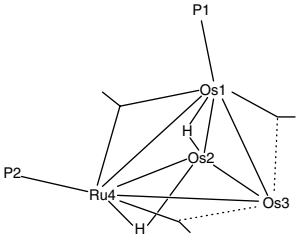

C

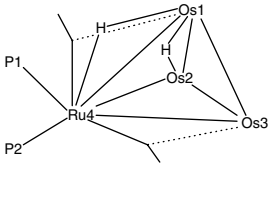

D

Compound:	Os,Os-**3a**	Ru,Os-**3a**	**3b**	**3c**	**3f**	Ru,Os-**3h**	Ru,Ru-**3h**
Structural type:	A	B	B	B	C	C	D
Bond parameter							
Os(1)–Os(2)	2.8489(8)	2.8547(6)	2.8437(4)	2.8223(6)	2.9991(5)	2.9729(4)	2.9172(3)
Os(1)–Os(3)	2.9813(9)	2.7751(5)	2.8055(4)	2.7940(5)	2.8271(5)	2.8531(4)	2.8197(3)
Os(2)–Os(3)	2.9455(8)	2.7975(5)	2.8087(4)	2.8110(5)	2.7914(7)	2.8001(4)	2.8007(3)
Os(1)–Ru(4)	2.8117(9)	2.9850(7)	3.0028(5)	2.9823(7)	2.8271(5)	2.7809(5)	2.9755(5)
Os(2)–Ru(4)	2.8006(10)	2.9423(7)	2.9401(5)	2.9399(7)	2.9991(5)	2.9637(4)	2.8912(5)
Os(3)–Ru(4)	2.8041(10)	2.7854(7)	2.7786(5)	2.7808(7)	2.8271(5)	2.7918(4)	2.8370(5)
Os(1)–E(1)	2.388(3)	2.366(2)	2.4803(7)	2.6176(7)	2.134(8)	2.3645(17)	2.3434(17)
Ru(4)–E(2)	2.356(4)	2.367(2)	2.4892(7)	2.621[c]	2.134(8)	2.3468(18)	2.3355(17)
∠E(1)Os(1)Os(2)[b]	161.90(9)	164.44(6)	155.39(2)	155.60(2)	114.86(5)	110.88(4)	145.25(5)
∠E(1)Os(1)Os(3)[b]	134.16(8)	132.28(6)	141.28(2)	139.73(2)	158.10(5)	161.57(4)	103.81(5)
∠E(1)Os(1)Ru(4)[b]	113.18(9)	114.58(6)	115.228(19)	113.41(2)	137.47(5)	130.80(5)	142.05(5)
∠E(2)Ru(4)Os(1)[a]	118.99(9)	118.74(6)	114.82(2)	112.27[c]	137.47(5)	134.51(5)	162.51(5)
∠E(2)Ru(4)Os(2)[a]	110.38(9)	107.37(6)	109.01(2)	110.90[c]	114.86(5)	111.77(5)	108.29(5)
∠E(2)Ru(4)Os(3)[a]	168.47(9)	165.60(6)	167.54(2)	167.99[c]	158.10(5)	157.83(5)	105.47(5)

[a] For Os,Os-**3a**, Ru(4) and Os(3) should be interchanged.
[b] For Ru,Ru-**3h**, Os(1) and Ru(4) should be interchanged.
[c] These are the mean values for the two disordered sites.

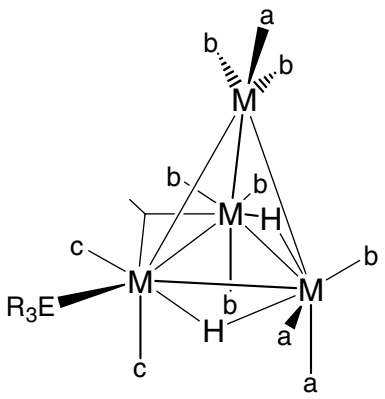

Fig. 5. Possible substitution sites for a second ER_3 ligand in a monosubstituted derivative. Position of the bridging carbonyl is arbitrary.

two vertices carrying the group 15 ligands. Furthermore, for those with the EPh_3 (E = P, As, Sb) ligands, viz., **3a**–**c**, the degree of disorder is similar (an approximate 1:3 ratio).

Table 2 shows the selected bond parameters for the six structurally characterised disubstituted derivatives. Besides the two bridging hydrides, which share a common vertex, there are at least two bridging or semi-bridging carbonyls as well. Five of the clusters have a group 15 ligand on a Ru and an Os vertex. As already pointed out for the monosubstituted derivatives, there is an electronic preference for substitution at a Ru vertex; the reason for generally only one substitution at a vertex is probably steric since disubstitution at the same vertex is observed only for the ligand with the smallest cone angle

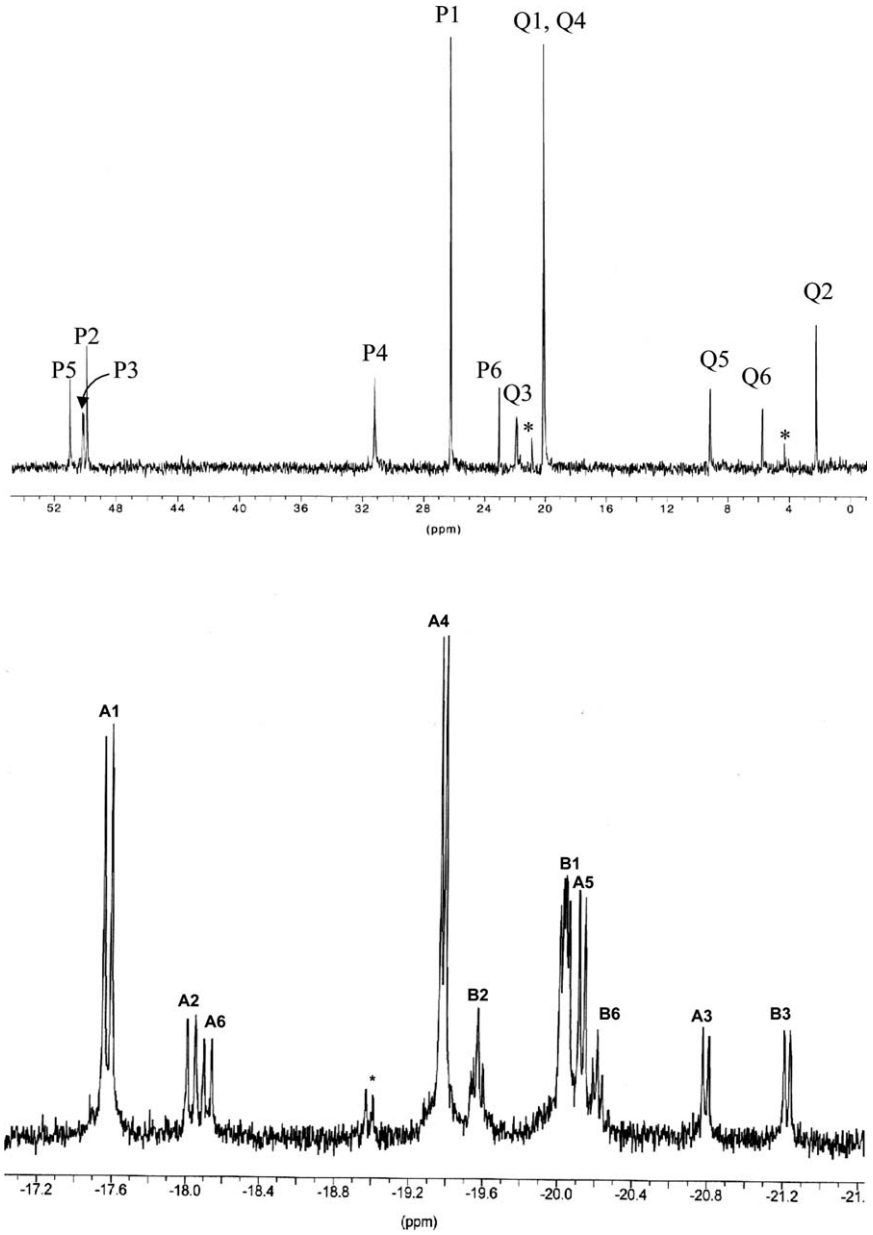

Fig. 6. $^{31}P\{^1H\}$ (top) and ^1H (bottom) NMR spectra ($CDCl_3$, 300 K) of **3a**. Resonances marked (*) have not been assigned.

(PMe_3). Similarly, without exception, both hydrides share a common vertex.

All the structures also exhibit at least two bridging or semi-bridging carbonyls. This probably is a consequence of the greater electron density imparted to the cluster core by the strong σ donating group 15 ligands; bridging carbonyls are better π-acceptors than terminal CO ligands [8]. Furthermore, most of the structures contain a $RuOs_2$ face that is bridged by two hydrides and one carbonyl ligand.

There are four pairs of compounds for which the crystal structures of both mono- and disubstituted derivatives have been obtained. These are for the ligands PPh_3 (Os-**2a**, Os-**2a**, Os,Os-**3a** and Ru,Os-**3a**), $AsPh_3$ (**2b** and **3b**), $SbPh_3$ (**2c** and **3c**) and PCy_2Ph (**2f** and **3f**). The disubstituted derivatives may be regarded as being derived from the corresponding monosubstituted derivatives by substitution of a carbonyl ligand by the second ER_3 ligand. Surprisingly, it seems that the positions substituted are those that are in closer proximity to the first ER_3 ligand (positions 'a' in Fig. 5), rather than those for which the ligand would have pointed away from it (positions 'b'). Thus the site of the substitution of the second ER_3 ligand is dictated by electronic rather than steric factors. This point is further reinforced by substitution at position 'c' for the sterically small PMe_3 ligand, (i.e., double ligand substitution at the Ru vertex). This is unlike the case for $M_3(CO)_{10}L_2$ clusters where the two L ligands occupy equatorial sites on adjacent metal centres and are oriented away from each other [9].

As in the case of the monosubstituted derivatives, the similarity of the Ru and Os atomic radii predisposes the $RuOs_3$ clusters to positional disorder. For five of the disubstituted structures, the disorder merely interchanges the ER_3-substituted vertices in the cluster and thus does not

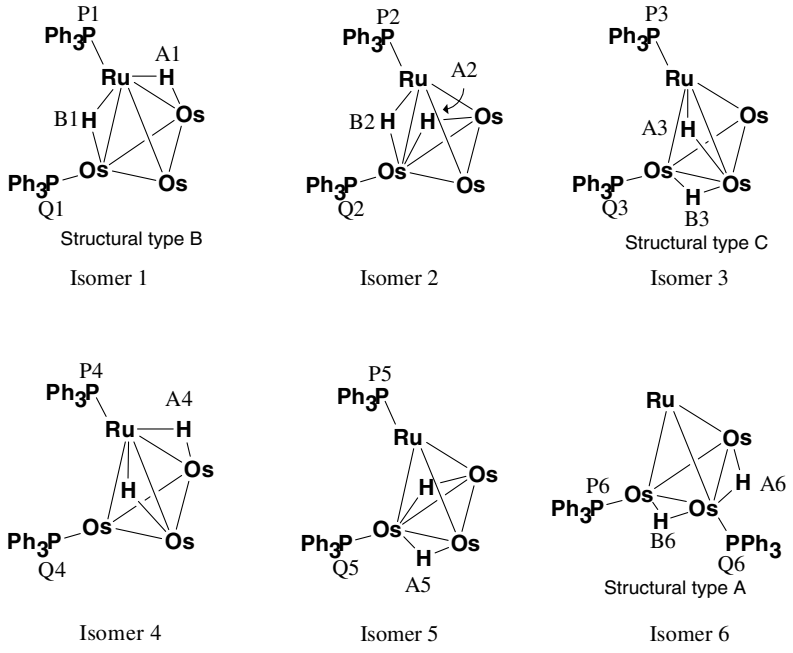

Fig. 7. Proposed structures and tentative NMR assignments for the six isomers of **3a**. Structural types corresponding approximately to the solid-state structures are also indicated.

Table 3
^1H NMR assignments for **3a**–**h**

Cluster	δ_H (relative amount)					
	Isomer 1	Isomer 2	Isomer 3	Isomer 4	Isomer 5	Isomer 6
3a	−17.58; −20.04 (1.00)[a]	−18.03; −19.57 (0.27)	−20.79; −21.22 (0.19)	−19.38 (0.23)	−20.13 (0.20)	−18.12; −20.19 (0.10)
3b	−17.61; −19.95 (1.00)	−18.10; −19.42 (0.15)	−20.44; −21.09 (0.13)	−19.29 (0.07)	−20.00 (0.05)	−18.21; −20.20 (0.05)
3c	−17.95; −20.59 (1.00)	−18.60; −19.95 (0.20)	−20.35; −21.25 (0.24)	−19.50 (0.15)	−20.27 (0.05)	not identified
3d[b]			−21.69; −22.27 (1.00)	−20.03 (0.09)	−20.86 (0.19)	
3f			−20.91; −21.48			
Ru,Os-**3h**			−21.58; −22.32 (1.0)	−19.83 (0.40)	−20.61 (0.20)	

Relative amounts are obtained by integration of NMR resonances with respect to isomer 1 (major isomer); for those with two resonances the value given is the mean and for those with one resonance it is halved.

[a] From integration of $^{31}P\{^1H\}$ resonances.

[b] From a sample that has been allowed to stand for ~2 months.

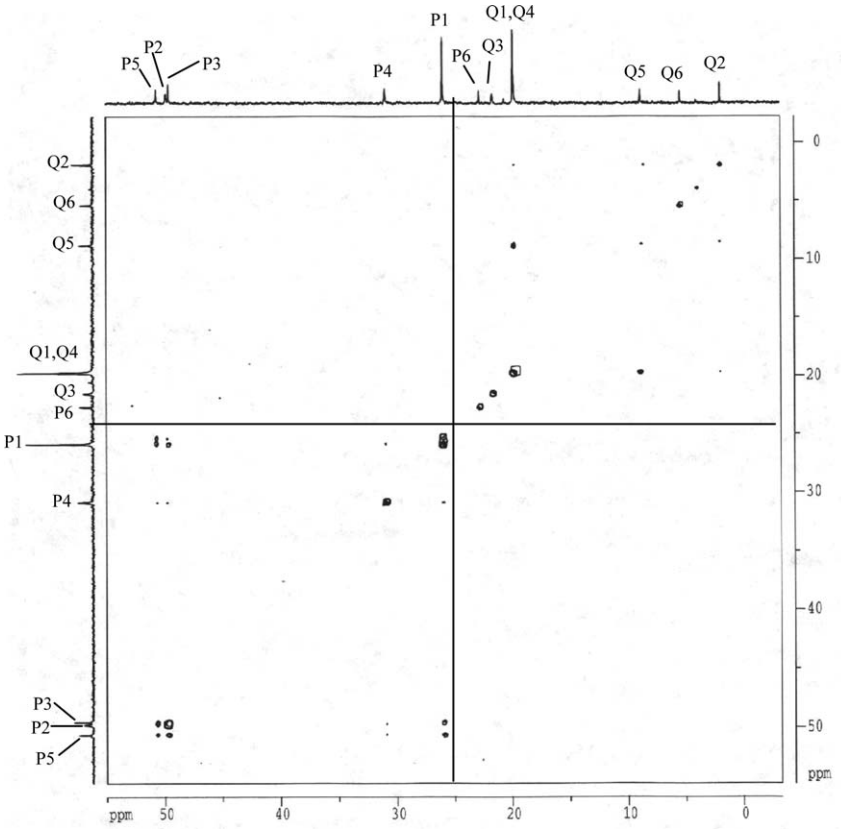

Fig. 8. ^{31}P EXSY spectrum ($CDCl_3$, 300 K) of **3a**.

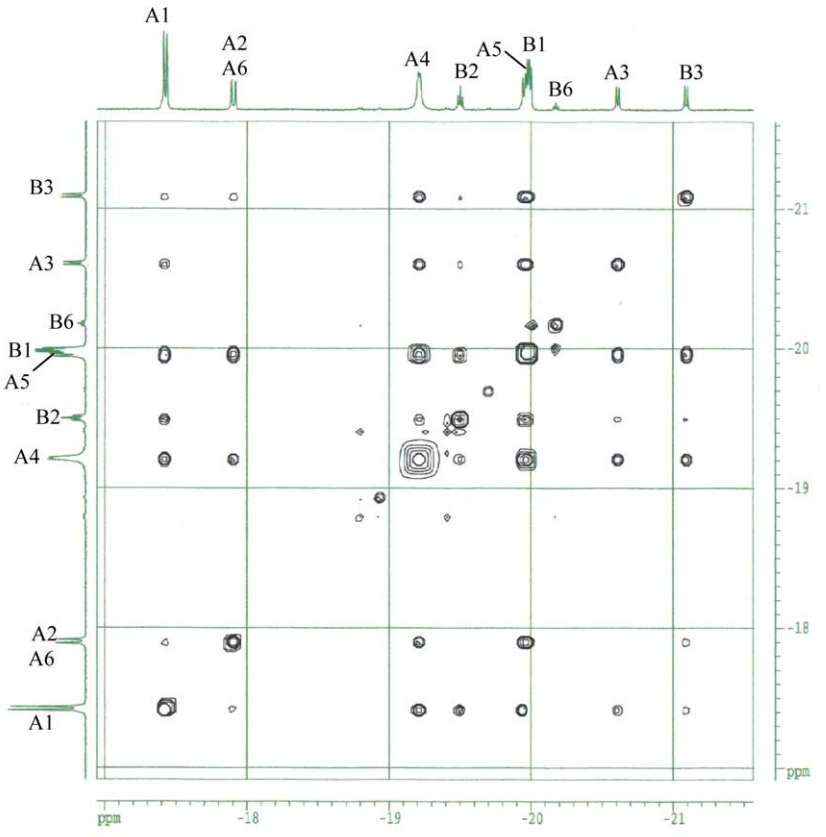

Fig. 9. ^{1}H EXSY spectrum ($CDCl_3$, 300 K, $\tau_m = 0.5$ s) of **3a**.

necessarily suggest different isomers. For Os,Os-**3a**, however, the modelled disorder implies a minor isomer of structural type B, i.e., Os,Os-**3a**. Evidence for the existence of many of these minor isomers in solution comes from the ^{1}H and ^{31}P NMR spectra, and is discussed presently.

3.2. Solution structures

The solution spectra suggest that there is more than one isomer in solution. For instance, the $^{31}P\{^{1}H\}$ NMR spectrum of **3a** taken at 300 K consists of at least 11 resonances; the ^{1}H NMR spectrum (Fig. 6) also clearly shows that there are many isomers present in solution. The hydride resonances are observed to lie between δ −17.1 and −22.3 ppm. The IR spectrum of **3a** recorded in a number of solvents: hexane, toluene, tetrachloromethane, dichloromethane, tetrahydrofuran and acetonitrile, shows no variation with solvent that may suggest a change in isomer distribution with solvent polarity. This is also corroborated by the ^{1}H NMR spectrum of **3a** in d_8-toluene, which does not show significant variations in relative peak intensities from that in $CDCl_3$.

A total of seven isomeric structures have been assigned with reasonable certainty based on the NMR data of the six disubstituted derivatives studied (see Supplementary Information). In our tentative assignments of the solution structures, we have assumed that the various isomers could be attributed to different relative arrangements of the phosphorus and hydride ligands only, and that the CO ligands are in rapid exchange. The latter is corroborated by the ambient temperature $^{13}C\{^{1}H\}$ NMR spectra of **3a**, **3f** and **3h**, which show no distinct CO resonances; this is indicative of rapid fluxionality of the carbonyls in solution. The IR spectra also show broad, and most often no, bridging carbonyl signals although these groups are present in the solid-state structures. The proposed structures for the six isomers of **3a** are given in Fig. 7, and the tentative structural and NMR assignments for all the derivatives studied are given in Table 3.

The arsine and stibine analogues of **3a** exhibit similar isomerism to **3a**, while the other derivatives generally exhibit an appreciably smaller number of isomers. For Ru,Ru-**3h**, which represents the seventh isomeric form for the disubstituted derivatives, it was observed to isomerise over days to Ru,Os-**3h**; the NMR spectra taken a month later showed that Ru,Ru-**3h** was completely absent. The results suggest that Ru,Ru-**3h** is the kinetic product, and that there is preferential substitution at the Ru vertex; this is also in accord with observations on the $RuOs_2(CO)_{12}$ system [10]. In addition, it appears that substitution of a second ligand at the substituted vertex is electronically favoured, and that substitution at a different second site is primarily a consequence of steric reasons. Subsequent isomerisation to the thermodynamically more stable isomers of Ru,Os-**3h** presumably proceeded via phosphine migration. A similar site selectivity was also observed with **3d** (cone angle for P(*n*-Bu)$_3$ = 132°).

As may be expected, the isomers are rapidly interconverting; the ^{31}P and ^{1}H EXSY spectra of **3a** are given in Figs. 8 and 9, respectively. Unlike in the monosubstituted analogue, there is no reversible PPh_3 migration between Ru and Os vertices, and no intra-isomer hydride exchanges are observed; the ^{31}P exchange crosspeaks are ascribable to "virtual" exchanges due to hydride migrations. These observations appear to be general for all the disubstituted compounds studied. Like its monosubstituted analogue, a variable temperature ^{1}H NMR experiment on **3f** indicated broadening of the main resonances below 273 K which is ascribable to the slowing down of restricted rotation about the metal–phosphorus bond.

3.3. Comparisons with the $FeRu_3$ system

An outstanding feature of the analogous $FeRu_3$ system is that the positions of the two bridging hydrides and the two bridging carbonyls in the parent cluster remain unchanged even after mono- and disubstitution. At most two types of isomers (labelled C_S and C_1 in the original paper) have been noted for the monosubstituted derivatives and only one for the disubstituted derivatives [1]. The isomers in the $RuOs_3$ system arise not only from differences in the position of the PR_3 ligand, but also from the locations of the bridging hydrides.

No derivatives disubstituted at the same vertex were observed in the $FeRu_3$ system, even with the relatively small PMe_3 ligand. In both systems, there is an interesting tendency towards substitution at a ruthenium vertex. For the monosubstituted $FeRu_3$ derivatives, it has been found that the C_S/C_1 isomer ratio is dependent on ligand size and basicity, as well as the solvent employed. In contrast, we have not observed any solvent effect on the isomeric distribution in the $RuOs_3$ system.

4. Concluding remarks

In this study, we have shown that the substitution of carbonyl ligands in the heteronuclear cluster $RuOs_3(\mu\text{-}H)_2(CO)_{13}$ by group 15 ligands can give rise to a very large number of isomers which depend on the nature of the group 15 ligand. These isomers are largely a consequence of the different arrangements, and relative orientations, of the group 15 ligands and metal hydrides, and are probably a reflection of the well-established similarity in chemistry (electronic properties and size) of the two metals, viz., ruthenium and osmium. There is a clear preference for structures in which one group 15 ligand is substituted at a ruthenium and another at an osmium vertex; the five such isomeric forms include all possible combinations of hydride positions in which the two hydrides share a common vertex and bridge M–M edges where at least one group 15 ligand is at the vertices of those edges. This disposition of ligands has also been observed for similar derivatives of the other group 8 clusters [1,11]. The three derivatives of the triphenyl group 15 ligands,

viz., **3a**–**c**, present the largest number of isomers – six each. Clusters **3d** and **3h** are the only ones in which isomers with both trialkyl phosphine ligands on the same vertex are observed, and has probably to do with the relatively small cone angles ($\theta = 118°$ and 132° for PMe_3 and $P(n\text{-}Bu)_3$, respectively) and similar electronic parameters ($\chi = 8.0$ and 4.2, respectively) [12]. Evidence has been presented that the initial substitution appears to be predominantly at the ruthenium vertex and subsequently isomerisation proceeds via migration of the group 15 ligand(s).

Acknowledgements

This work was supported by the National University of Singapore (Research Grant No. R143-000-149-112) and one of us (L.J.P.) thanks the University for a Research Scholarship.

Appendix A. Supplementary information available

Selected ^1H, $^{31}P\{^1H\}$, COSY and EXSY NMR spectra, and details of the tentative NMR assignment of the solution structures and fluxionality studies. CCDC Nos. 283362–283368 contains the supplementary crystallographic data for this paper. These data can be obtained free of charge from The Cambridge Crystallographic Data Centre via www.ccdc.cam.ac.uk/data_request/cif. Supplementary data associated with this article can be found, in the online version, at doi:10.1016/j.poly.2006.02.012.

References

[1] (a) J.R. Fox, W.L. Gladfelter, T.G. Wood, J.A. Smegal, T.K. Foreman, G.L. Geoffroy, I. Tavaniepour, V.W. Day, C.S. Day, Inorg. Chem. 20 (1981) 3214;
(b) W.L. Gladfelter, J.R. Fox, J.A. Smegal, T.G. Wood, G.L. Geoffroy, Inorg. Chem. 20 (1981) 3223;
(c) W.L. Gladfelter, G.L. Geoffroy, Inorg. Chem. 19 (1980) 2574;
(d) J.R. Fox, W.L. Gladfelter, G.L. Geoffroy, Inorg. Chem. 19 (1980) 2579.
[2] L. Pereira, W.K. Leong, J. Organomet. Chem. (in press).
[3] SMART version 5.628, Bruker AXS Inc., Madison, WI, USA, 2001.
[4] SAINT+ version 6.22a, Bruker AXS Inc., Madison, WI, 2001.
[5] G.M. Sheldrick, SADABS, 1996.
[6] SHELXTL version 5.1, Bruker AXS Inc., Madison, WI, 1997.
[7] Orpen, A.G., XHYDEX, School of Chemistry, University of Bristol, UK, 1997.
[8] P.J. Dyson, J.S. McIndoe, Transition Metal Carbonyl Cluster Chemistry, Gordon and Breach, Amsterdam, 2000.
[9] (a) M.I. Bruce, M.J. Liddell, C.A. Hughes, B.W. Skelton, A.H. White, J. Organomet. Chem. 347 (1988) 157;
(b) M.I. Bruce, M.J. Liddell, C.A. Hughes, J.M. Patrick, B.W. Skelton, A.H. White, J. Organomet. Chem. 347 (1988) 181;
(c) M.I. Bruce, M.J. Liddell, O. Shawkataly, I. Bytheway, B.W. Skelton, A.H. White, J. Organomet. Chem. 369 (1989) 217;
(d) K. Biradha, V.M. Hansen, W.K. Leong, R.K. Pomeroy, M.J. Zaworotko, J. Cluster Sci. 11 (2000) 285.
[10] F.W. Vergeer, M. Lutz, A.L. Spek, J. Calhorda, D.J. Stufkens, F. Hartl, Eur. J. Inorg. Chem. (2005) 2206.
[11] (a) C.R. Eady, B.F.G. Johnson, J. Lewis, J. Chem. Soc., Dalton Trans. 5 (1977) 477;
(b) E.W. Burkhardt, G.L. Geoffroy, J. Organomet. Chem. 198 (1980) 179;
(c) J.A. Krause, U. Siriwardane, T.A. Salupo, J.R. Wermer, D.W. Knoeppel, S.G. Shore, J. Organomet. Chem. 454 (1993) 263.
[12] C.A. Tolman, Chem. Rev. 77 (1977) 313.

The present study reports the improved conditions of the synthesis and also the structural characterization of the crystalline phases formed in the $Ba(OH)_2$–MeOH system.

2. Experimental

Anhydrous $Ba(OH)_2$ was prepared by dehydration of $Ba(OH)_2 \cdot 8H_2O$, and BaO by decomposition of BaO_2, at 400 and 800 °C, respectively. Methanol was dehydrated by refluxing over $Mg(OMe)_2$, and was subsequently applied in preparation of solutions with exact concentrations of water. All operations were carried out in dry argon or nitrogen atmosphere. The barium concentration was determined by acidimetric titration with Methyl Orange as indicator (using distilled water, purified from carbon dioxide by prolonged refluxing under an inert atmosphere). FTIR spectra have been recorded with the dry powders of the samples between KBr pellets on a Perkin–Elmer FTIR 1600 Instrument.

2.1. Crystallography

The crystals were placed in glass capillaries, and sealed under nitrogen gas. The data were collected for compounds **1** and **2** using a SMART CCD 1k instrument at room temperature (295 K) using graphite monochromated Mo Kα radiation, $\lambda = 0.71073$ Å. The experimental details are summarized in Table 1. The structures were solved by direct methods. Barium atoms were located from the initial solutions, and the other non-hydrogen atoms were isolated in subsequent difference Fourier syntheses. All non-hydrogen atoms were refined by least squares techniques on F^2, first in isotropic and then in anisotropic approximations. The coordinates of hydrogen atoms were added geometrically and applied in isotropic approximations riding on the corresponding carbon atoms. Hydrogen atoms of the OH-groups and solvating water molecules within the metal–oxygen cores could not be objectively located in the Fourier syntheses and the assignment of the nature of oxygen atoms was made on the basis of bond distances in comparison with the literature data (see below). Doubtless location of hydrogen atoms in the structures of barium hydroxide solvates or halide solvates can be achieved only in low temperature neutron diffraction experiments. The residual electron density 2.364 e/Å^3 for **1** and 5.426 e/Å^3 for **2** was located in the proximity of the barium atoms.

Table 1
Crystallographic data for complexes **1** and **2**

Compound	**1**, Plates	**2**, Needles
Formula	$C_2H_{14}O_6Ba$	$C_3H_{14}O_5Ba$
Formula weight	271.48	253.46
Crystal size, mm	$0.35 \times 0.10 \times 0.10$	$0.55 \times 0.35 \times 0.10$
Crystal system	tetragonal	monoclinic
Space group	$I\bar{4}$	$P2(1)/c$
a (Å)	4.6297(6)	10.8208(14)
b (Å)	4.6297(6)	18.711(3)
c (Å)	22.404(5)	8.1899(19)
α (°)	90	90
β (°)	90	99.497(3)
γ (°)	90	90
V (Å^3)	480.20(13)	1635.4(5)
Z	2	8
Reflections collected	1457	6469
Independent reflections [R_{int}]	557 [0.2154]	2126 [0.1317]
Data/restraints/parameters	557/0/23	2126/0/153
Goodness-of-fit on F^2	1.194	0.855
Final R indices [$I > 2\sigma(I)$]	$R_1 = 0.0656$, $wR_2 = 0.1628$	$R_1 = 0.0634$, $wR_2 = 0.1725$
R indices (all data)	$R_1 = 0.0659$, $wR_2 = 0.1644$	$R_1 = 0.0789$, $wR_2 = 0.1874$
Absolute structure parameter	0.1(3)	

2.2. Synthesis and isolation of *1* and *2*

Preparation of the crystals was carried out using solutions of BaO or $Ba(OH)_2$ in anhydrous MeOH and also in MeOH containing up to 10% water (for comparison). After long-term stirring at 0 °C with the Ba-containing reactant, taken in large excess, the concentration of solutions achieved 20–23 mass% in relation to $Ba(OH)_2$. The solutions were removed from the residual solids by decantation and concentrated in vacuum or in a dessicator with P_2O_5 until crystallization commenced. The obtained crystalline samples were washed with anhydrous MeOH and dried in vacuum at room temperature. Crystallo-optical investigation of the samples revealed normally the presence of several types of crystals. In addition to the compounds **1** and **2** described below, there have been also observed "rectangular rods" (described in [5]), which could not be isolated in the form of single crystals suitable for X-ray studies. Phases of the same type could only be isolated under controlled conditions as described below.

2.2.1. *[Ba(OH)$_2$(H$_2$O)$_2$](MeOH)$_2$ (1)*

Crystallized as rectangular plates from solutions of BaO in 90–95% methanol at 20 °C (this phase was isolated from solutions of BaO in 90%-methanol according to [5]). *Anal.* Calc. for $BaC_2H_{14}O_6$: Ba, 50.6. Found: Ba, 50.3%. IR, cm^{-1}: 3575 s, 3483 s, 3360 vs br, 2914 vs, 2860 vs, 2783 s sh, 1645 w, 1473 s, 1154 s, 1060 m, 836 vs, 720 m.

2.2.2. *[Ba(OH)$_2$(MeOH)$_2$](MeOH) (2)*

Crystallized as thin needles from 98% to 100% methanol solutions of BaO or $Ba(OH)_2$ subjected to reflux for 2–3 h with subsequent cooling to 0–20 °C. *Anal.* Calc. for $BaC_3H_{14}O_5$: Ba, 51.3. Found: Ba 51.0%. IR, cm^{-1}: 3580 vw, 3386 vs br, 2915 s, 2851 s, 2780 m, 1655 sh, 1439 sh, 1176 vw, 1141 w, 1062 vs, 824 vs, 720 w. (The needle-shaped form described in [5] as $Ba(OH)_2 \cdot 2MeOH \cdot H_2O$, crystallized from solutions not subjected to reflux at 20 °C).

The total concentration of $Ba(OH)_2$ in the mother liquors over **1** and **2** was about 20%, but the isolated crystalline products are almost insoluble in MeOH or $MeOC_2H_4OH$.

3. Results and discussion

The obtained synthetic results permitted the conclusion that the composition of the products crystallizing from the $Ba(OH)_2$–MeOH system is, in contradiction to the data reported in [5], not dependent on the nature of the starting reagent – BaO or $Ba(OH)_2$. Preliminary refluxing of the solution can supposedly influence the equilibrium of replacement of the inner-sphere water molecules with those of methanol, enhancing the transformation of $[Ba(OH)_2(H_2O)_2](MeOH)_2$ (**1**) into $[Ba(OH)_2(MeOH)_2](MeOH)$ (**2**). Anhydrous barium oxide, BaO, is evidently only a metastable solid phase in this system. The total concentration of the mother liquor with respect to barium hydroxide over it at 0 °C is rather high, up to ~20%, which permits the use of these solutions in sol–gel processes, but decreases with the increase in temperature, supposedly due to the following equilibria:

$$BaO + 2MeOH \rightleftharpoons Ba(OMe)_2 + H_2O$$

$$Ba(OMe)_2 + 2H_2O \rightleftharpoons Ba(OH)_2 + 2MeOH$$

and subsequent formation of the stable barium hydroxide phase, almost insoluble in the alcohol. It should be noted that the hydrated barium hydroxide, $Ba(OH)_2 \cdot 8H_2O$, displays rather high solubility at 20 °C even in anhydrous methanol (~25% $Ba(OH)_2$).

The structure of $[Ba(OH)_2(H_2O)_2](MeOH)_2$ (**1**) (see Fig. 1, Table 2) consists of planar layers of tetragonally distorted $[Ba(OH)_{4/2}(H_2O)_{4/2}]$ cubes, sharing edges situated along the *c*-axis (Fig. 1). Barium atoms form in this way a regular square net. Methanol molecules are placed only between the layers, perpendicularly to them and parallel to the *c*-axis. This "distancing" of the layers from each other results in a much longer axial *c*-parameter (22.404 Å) compared to the basal ones, $a = b = 4.6297$ Å in the observed tetragonal cell. The extinctions in the collected data permitted a comparably broad choice of possible space groups from $I\bar{4}$ to $I4/mmm$, with a combined figure of merit strongly favoring the choice of $I\bar{4}$. The structure could be solved using a higher symmetry group (in particular $I4/mmm$), but the refinement could not converge as the high symmetry imposed equivalence between hydroxide groups and water molecules, which resulted in an anomalous distribution of the electron density (maximum corresponding to the potential unique oxygen atom was localized at an abnormally low distance of 2.45 Å from the barium atom). We consider therefore that the lower symmetry, permitting these groups to be distinguished clearly and localized at reasonable distances from the barium atoms at 2.763(9) and 2.918(15) Å, does really represent the true structure of this compound. The bridges are asymmetric and the bonding roles within the core are equivalent. The hydrogen bonding to the interlayer alcohol molecules, however, permits them to be distinguished as the O(1)–O(2) distance is considerably shorter, 2.546(9) Å, in comparison with O(1)–O(3) distance, 2.666(9) Å, which gives a hint that O(2) stays for an OH-group and O(3) for the water molecule. Thus each alcohol molecule is hydrogen bonding to an OH-group and a water molecule in the nearest hydroxide layer.

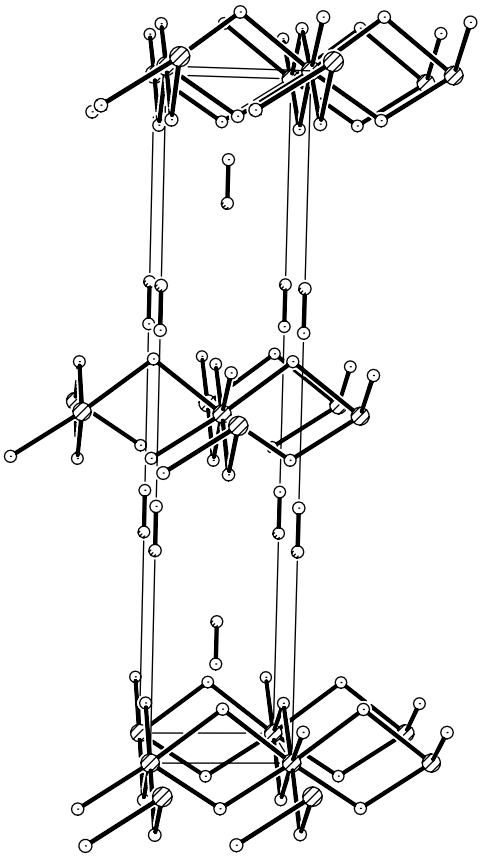

Fig. 1. Fragment in the crystal structure of $[Ba(OH)_2(H_2O)_2](MeOH)_2$ (**1**).

Table 2
Selected bond distances (Å) and angles (°) in the structure of $[Ba(OH)_2(H_2O)_2](MeOH)_2$ (**1**)

Ba(1)–O(3)#1	2.763(9)	Ba(1)–O(2)	2.918(15)
O(3)#1–Ba(1)–O(3)#2	107.3(3)	O(2)#4–Ba(1)–O(2)#3	111.8(4)
O(3)#1–Ba(1)–O(3)#3	113.8(6)	O(2)#4–Ba(1)–O(2)	105.0(8)
O(3)#1–Ba(1)–O(2)#4	175.6(5)	O(3)#2–Ba(1)–O(2)#4	70.6(2)

Symmetry transformations used to generate equivalent atoms: #1 $y, -x-1, -z$; #2 $x+1, y, z$; #3 $y, -x, -z$; #4 $x, y+1, z$; #5 $y+1, -x, -z$; #6 $x, y-1, z$; #7 $x-1, y, z$.

The task of distinguishing between the hydroxide and water ligands in general is very much dependent on the nature of the considered compounds and the structural functions of the groups. In the structures of barium halide hydrates, such as $BaCl_2 \cdot H_2O$ [7], $BaCl_2 \cdot 2H_2O$ [8], $BaBr_2 \cdot H_2O$ [7], $BaBr_2 \cdot 2H_2O$ [9], $BaI_2 \cdot H_2O$ [7] and $BaI_2 \cdot 2H_2O$ [10], the water molecules occupy a terminal positions in relation to the barium atoms, which results in rather uniform Ba–O distances in the range 2.84–2.87 Å, which are intermediate values for the distances in the structure of **1**. The structures of hydroxide halides, such as Ba(OH)Cl [11], $Ba(OH)Cl \cdot 2H_2O$ [12] or $Ba(OH)I \cdot 4H_2O$ [13], contain hydroxide groups together with halide

ones in the bridging positions, while the water molecules occupy the sites in the layer not attached directly to barium atoms and connected to the hydroxide groups through hydrogen bonding. The bond length variations for these compounds are in the range 2.69–2.79 Å and cover one of the two distances (for each oxygen atom) in **1**. Incorporation of two hydroxide ligands per barium atom leads normally to formation of highly asymmetric bridges, which already in the structure of the water-free $Ba(OH)_2$ [14] vary in length between 2.72 and 2.92 Å and thus cover the observed variation in **1**. In the structure of $Ba(OH)_2 \cdot 8H_2O$ [15], where the water molecules are connected exclusively to the barium atoms, while the hydroxide anions in contrast are attached to the solvated cations via hydrogen bonding, the Ba–$O(H)_2$ bond lengths vary in the interval 2.73–2.81 Å in both the solid state and in the water solution of this compound. In the structures of mono- and tri-hydrates of barium hydroxide, i.e. $Ba(OH)_2 \cdot H_2O$ [16] and $Ba(OH)_2 \cdot 3H_2O$ [17], the hydroxide ligands form shorter contacts to barium atoms, of about 2.70 Å, while the water molecules coordinated by the metal atoms and involved also in the hydrogen bonding with OH-groups and each other are situated in the range 2.78–2.93 Å from the barium atoms, covering thus the variation observed in **1**. In view of this comparison, the strategy of identification of the nature of groups via additional hydrogen bonding appears reliable.

The structure of $[Ba(OH)_2(MeOH)_2](MeOH)$ (**2**) (see Figs. 2–4, Table 3) is formed by planar layers of distorted antiprisms connected to each other via four opposite edges. The antiprisms around two different symmetrically independent barium atoms have equally long diagonals, but their centers are replaced in such way that the basis of one antiprism is formed by two shorter, and the basis of the other – two longer Ba–OH bonds. The structure of the layer is displayed in the Figs. 2 and 3. Both antiprisms have coplanar upper and lower planes, for Ba(1) with a ±0.122 Å margin for the upper plane (O2A, O3A, O5, O6) and with a ±0.030 Å margin for the lower one (O1, O2, O3, O4), for Ba(2) with a ±0.001 Å margin for the upper plane (O1, O8, O1A, O8A) and with a ±0.039 Å margin for the lower one (O5, O7, O5A, O7A). The angles between the planes are 8.7° and 0.7° for Ba(1) and Ba(2), respectively. Both Ba-atoms are displaced towards the "lower" planes from the geometric centers of the prisms. The distance from the planes are 1.734 and 1.101 Å, respectively, for Ba(1) and 1.830 and 0.956 Å, respectively, for Ba(2) (see Fig. 4). The structure of **2** contains also interlayer alcohol molecules but they are relatively strongly hydrogen-bonded to the layers (2.65 and 2.82 Å) and not placed along the axis perpendicular to the layer (*a*-axis for this structure).

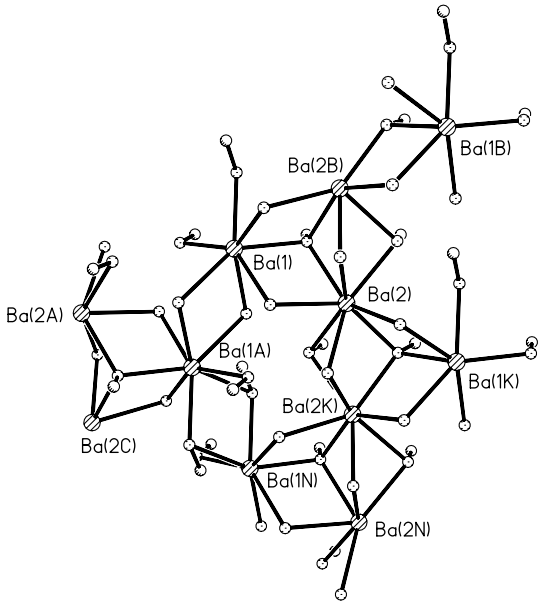

Fig. 2. Fragment of the metal–oxygen core in the layered structure of $[Ba(OH)_2(MeOH)_2](MeOH)$ (**2**).

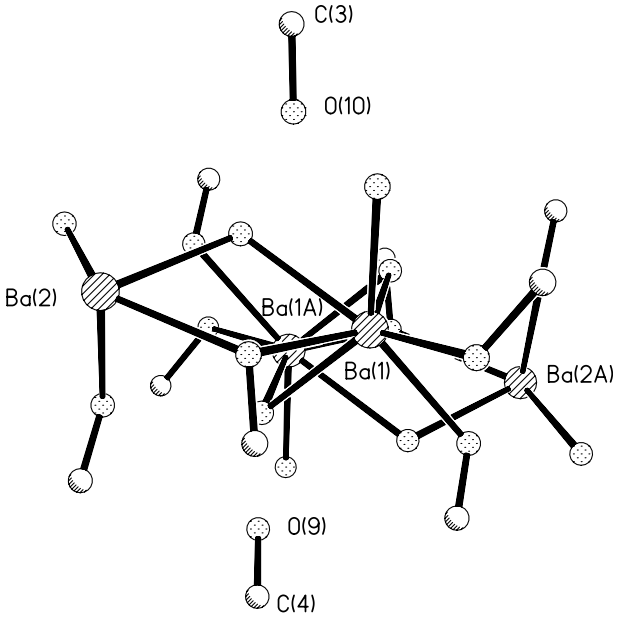

Fig. 3. View of $[Ba(OH)_2(MeOH)_2](MeOH)$ (**2**) along the *c*-axis.

The major difference between the two structures is that the alcohol molecules in the structure of **1** are situated between the $Ba(OH)_2$ layers, while in **2** they are incorporated in the coordination sphere of the Ba atoms within the layer. The four coordinated MeOH molecules have different functions in the coordination spheres of the two symmetrically independent atoms: one tridentate, two bidentate and one terminal for Ba(1), i.e. $[Ba(\mu_3\text{-}ROH)(\mu\text{-}OH)_4(\mu\text{-}ROH)_2(ROH)]$, and two tridentate and two bidentate for Ba(2), i.e. $[Ba(\mu_3\text{-}ROH)_2(\mu\text{-}ROH)_2(\mu\text{-}OH)_4]$.

The difference between compounds **1** and **2** can be traced in the positions of the *ν*-O–H bands in the IR spectra of these two complexes. The structure of **1** involves MeOH molecules situated only in the interlayer space, which is reflected by the presence of three intensive bands in its spectrum at 3575, 3483 and 3360 cm^{-1}. The first two of them are narrow and have their origin in the hydrogen bonds formed by more loosely connected alcohol mol-

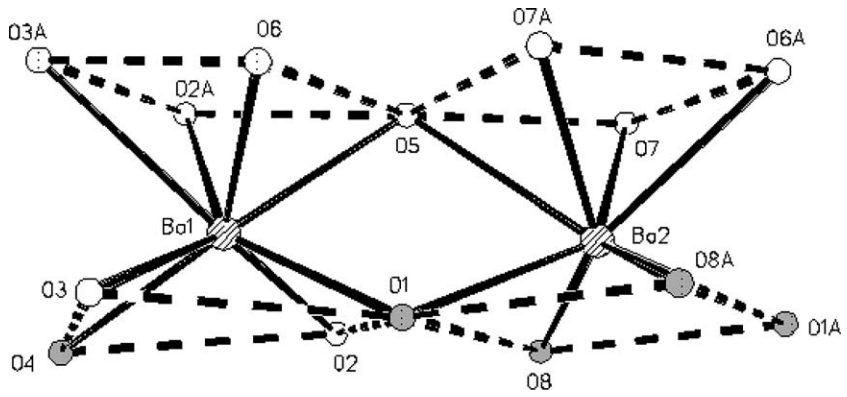

Fig. 4. Atom numbering scheme for the two symmetrically independent prismatic fragments in the structure of $[Ba(OH)_2(MeOH)_2](MeOH)$ (**2**). Oxygen atoms of the alcohol molecules are identified by the grey color.

Table 3
Selected bond distances (Å) and angles (°) in the structure of $[Ba(OH)_2(MeOH)_2]\cdot MeOH$ (**2**)

Ba(1)–O(1)	2.658(9)	Ba(2)–O(1)	2.746(9)
Ba(1)–O(4)	2.710(9)	Ba(2)–O(1)#4	2.745(9)
Ba(1)–O(6)	2.763(9)	Ba(2)–O(7)	2.791(8)
Ba(1)–O(2)	2.768(10)	Ba(2)–O(7)#3	2.792(9)
Ba(1)–O(3)	2.759(10)	Ba(2)–O(8)#3	2.835(9)
Ba(1)–O(5)	2.796(9)	Ba(2)–O(8)	2.866(9)
Ba(1)–O(2)#2	2.927(9)	Ba(2)–O(6)#4	2.888(9)
Ba(1)–O(3)#1	2.984(10)	Ba(2)–O(5)	2.926(9)
Ba(1)–C(5)	3.269(17)	O(6)–Ba(2)#3	2.888(9)
O(1)–Ba(2)#3	2.745(9)	O(7)–Ba(2)#4	2.792(9)
O(3)–Ba(1)#1	2.984(10)	O(8)–Ba(2)#4	2.835(9)
O(1)–Ba(1)–O(4)	125.7(3)	O(1)–Ba(2)–O(1)#4	139.3(4)
O(1)–Ba(1)–O(6)	74.6(3)	O(1)–Ba(2)–O(7)	135.1(3)
O(4)–Ba(1)–O(6)	139.3(3)	O(1)#4-Ba(2)–O(7)	75.8(3)
C(2)#1–Ba(1)–O(2)	108.8(15)	O(1)#4-Ba(2)–O(7)#3	135.4(3)
O(1)–Ba(1)–O(2)	80.6(3)	O(7)–Ba(2)–O(7)#3	96.0(3)
O(4)–Ba(1)–O(2)	80.9(3)	O(1)–Ba(2)–O(8)#3	72.4(3)
O(6)–Ba(1)–O(2)	139.7(3)	O(1)#4-Ba(2)–O(8)#3	94.0(3)
C(2)#1–Ba(1)–O(3)	94.4(13)	O(7)–Ba(2)–O(8)#3	145.6(3)
O(1)–Ba(1)–O(3)	81.0(3)	O(7)#3-Ba(2)–O(8)#3	68.1(3)
O(4)–Ba(1)–O(3)	80.0(3)	O(1)–Ba(2)–O(8)	94.3(3)
O(6)–Ba(1)–O(3)	68.3(3)	O(1)#4-Ba(2)–O(8)	72.0(3)
O(2)–Ba(1)–O(3)	138.2(3)	O(7)–Ba(2)–O(8)	67.7(3)
O(1)–Ba(1)–O(5)	74.6(3)	O(7)#3-Ba(2)–O(8)	145.6(3)
O(4)–Ba(1)–O(5)	139.9(3)	O(8)#3-Ba(2)–O(8)	140.8(3)
O(6)–Ba(1)–O(5)	75.0(3)	O(1)–Ba(2)–O(6)#4	138.1(2)
O(2)–Ba(1)–O(5)	68.0(3)	O(1)#4-Ba(2)–O(6)#4	71.4(3)
O(3)–Ba(1)–O(5)	140.1(3)	O(7)–Ba(2)–O(6)#4	66.7(3)
O(4)–Ba(1)–O(2)#2	80.2(3)	O(7)#3-Ba(2)–O(6)#4	65.4(3)
O(6)–Ba(1)–O(2)#2	105.2(3)	O(8)#3-Ba(2)–O(6)#4	78.9(2)
O(2)–Ba(1)–O(2)#2	75.6(3)	O(8)–Ba(2)–O(6)#4	126.6(3)
O(5)–Ba(1)–O(2)#2	68.2(3)	O(1)–Ba(2)–O(5)	71.3(3)
O(1)–Ba(1)–O(3)#1	141.3(3)	O(1)#4-Ba(2)–O(5)	138.6(2)
O(4)–Ba(1)–O(3)#1	80.9(3)	O(8)#3-Ba(2)–O(5)	126.2(3)
O(6)–Ba(1)–O(3)#1	67.9(3)	O(8)–Ba(2)–O(5)	80.2(3)
Ba(1)–O(1)–Ba(2)	110.0(3)	O(6)#4-Ba(2)–O(5)	104.1(3)

Symmetry transformations used to generate equivalent atoms: #1 $-x, -y, -z$; #2 $-x, -y, -z+1$; #3 $x, -y+1/2, z-1/2$; #4 $x, -y+1/2, z+1/2$; #5 $x, y, z+1$; #6 $x, y, z-1$.

ecules, while the third broad one corresponds to vibrations associated with the OH or H_2O fragments involved in the coordination sphere of the barium atoms. At the same time, in the spectrum of **2** the lower frequency bands are rather weak, while the band with the maximum at 3360 cm^{-1}, corresponding to the vibration of the O–H fragments of coordinated polydentate molecules, is the most intensive one.

It is interesting to compare the structures of **1** and **2** with those of known hydrates of barium hydroxide, i.e. $Ba(OH)_2\cdot 3H_2O$ and $Ba(OH)_2\cdot H_2O$. The first of them contains chains of distorted antiprisms, *cis*-$[Ba(OH)_2(H_2O)_{6/2}]$, and the second – a network of nine-vertex polyhedra, $[Ba(OH)_{6/.3}(H_2O)_{3/3}]$, where seven bonds within the polyhedron are much shorter than those to the interlayer molecules of water (2.69–2.91 and 3.14 Å). The Ba–OH distance in **1** and **2** fall in the same range as those in the hydrate structures and all have the same structural function – doubly bridging. It is noteworthy that the alcohol molecules coordinated by the barium atoms in **2** all have different types of functions – μ_3-O(1) with the distances 2.655–2.757 Å, μ_2-O(8) 2.849–2.870 Å and terminal O(4) 2.718 Å. It can be concluded that this family of compounds has a well pronounced electrostatic character of bonding with the bond length determined to a greater extent by the packing effects rather than by the bonding mode of the coordinated ligands.

4. Supplementary materials

Supplementary data are available from the CCDC, 12 Union Road, Cambridge, CB2 1EZ, UK, fax: +44 1223 366 033, e-mail: deposit@ccdc.ac.uk or on the web www: http://www.ccdc.cam.ac.uk. on request, quoting the deposition numbers CCDC 286852 and 286853 for **1** and **2**, respectively.

References

[1] N.Ya. Turova, E.P. Turevskaya, V.G. Kessler, M.I. Yanovskaya, The Chemistry of Metal Alkoxides, Kluwer AP, Boston, 2002, p. 129.
[2] A. Brasseur, B. Michaux, R. Pirard, O. VanCantfort, J.P. Pirard, A.J. Lecloux, J. Sol–Gel Sci. Technol. 9 (1997) 5.
[3] Y. Yuasa, H. Tsuruta, Y. Yuasa, Org. Process Res. Dev. 2 (1998) 412, C.A. 133, 333343 (2000).

[4] N.Ya. Turova, A.V. Novoselova, Russ. Chem. Rev. (Uspechi Khimii) 34 (1965) 161.
[5] R. Scholder, M. Kreutz, Liebigs Ann. Chem. 653 (1962) 1.
[6] K.T. Ranjit, K.J. Klabunde, Chem. Mater. 17 (2005) 65.
[7] H.D. Lutz, W. Buchmeier, B. Engelen, Acta Crystallogr. B 43 (1987) 71.
[8] V.M. Padmanabhan, W.R. Busing, H.A. Levy, Acta Crystallogr. B 34 (1978) 2290.
[9] H.D. Lutz, B. Engelen, C. Freiburg, Acta Crystallogr. B 36 (1980) 437.
[10] K.M. Fromm, Angew. Chem. (Intl Ed.) 36 (1997) 2799.
[11] H. Moeller, K. Beckenkamp, T. Kellersohn, H.D. Lutz, J.K. Cockcroft, Z. Kristallog. 209 (1994) 157.
[12] H.D. Lutz, T. Kellersohn, K. Beckenkamp, Z. Naturforsch. B 44 (1989) 928.
[13] T. Kellersohn, K. Beckenkamp, H.D. Lutz, Z. Naturforsch. B 46 (1991) 1279.
[14] H. Lueke, Acta Crystallogr. B 24 (1968) 1705.
[15] I. Persson, M. Sandström, H. Yokoyama, M. Chaudhry, Z. Naturforsch. A 50 (1995) 21.
[16] H.D. Lutz, T. Kellersohn, T. Vogt, Acta Crystallogr. C 46 (1990) 361.
[17] W. Buchmeier, H.D. Lutz, Z. Anorg. Allgem. Chem. 538 (1986) 131.

(napy) in place of ppy to form the $(napy)_2Ir(acac)$ complex and shifted the emission to 595 nm which is 71 nm longer than that of $(ppy)_2Ir(acac)$ [17].

In the present work, the (napy) ligand was modified by incorporating a trifluoromethyl group onto the pyridine ring to produce a new ligand, 2-naphthalen-1-yl-*n*-trifluoromethyl-pyridine (*n*-fnapy). It is expected that the introduction of the trifluoromethyl group would generate a larger bathochromic effect on the emission wavelength of the corresponding Ir-complexes. The effects of the trifluoromethyl substituent and the importance of its position are described.

2. Experimental

2.1. Equipment

^1H NMR and ^{13}C NMR in $CDCl_3$ or d_6-acetone were recorded using a Bruker (Avance 300) spectrometer at 400 MHz and 100 MHz, respectively. High-resolution mass spectra were recorded using a Finnigan MAT-95XL in EI mode. Elemental analyses were carried out on an Elementar vario EL III analyzer. Absorption spectra (in CH_2Cl_2) were recorded on a Agilent 8453 spectrophotometer, and concentrations were 1×10^{-5} M to obtain the extinction coefficient. Emission spectra (1×10^{-3} M in CH_2Cl_2) were recorded on a HITACHI model F-2500 FL Spectrophotometer. Cyclic votlammetry (CV) was performed in 1.0 mM CH_2Cl_2 solution with a Valtammetric Analyzer CV-50 W. All oxidation CV measurements were carried out in CH_2Cl_2 containing 0.1 M tetrabutylammonium perchlorate (n-Bu_4NClO_4) as a supporting electrolyte. A Pt disk electrode was used as a working electrode, a Pt wire as a counter electrode, and $Ag/AgNO_3$ as a reference electrode. The ferrocenium/ferrocene redox couple in CH_2Cl_2/$n$$Bu_4NClO_4$ occurred at $E^{0'} = +0.35$ V vs. $Ag/AgNO_3$. The oxidation potential of the Ir complexes were determined against the ferrocenium/ferrocene redox couple.

2.2. Reagents

All chemicals were of reagent grade and used as purchased. $IrCl_3 \cdot nH_2O$ was purchased from Alfa Aesar, USA, 1-naphthylboronic acid and 2-chloro-trifluoromethyl-pyridine from Lancaster Chemicals, USA, and the remaining compounds from Aldrich Chemicals, USA.

2.3. Syntheses

2.3.1. 2-Naphthalen-1-yl-3-trifluoromethyl-pyridine (3-fnapy)

Add 1-naphthylboronic acid 0.75 g (4.4 mmol), 2-chloro-3-trifluoromethyl-pyridine 0.53 g (2.9 mmol), PPh_3 79 mg (0.30 mmol), and Cs_2CO_3 2.33 g into 15 mL 1,4-dioxane. Stir the mixture under nitrogen. Heat the mixture to 60 °C and add $Pd(OAC)_2$ 17 mg (0.075 mmol), and keep on refluxing for 4 h. After removing the solvent, extract the mixture twice with H_2O and ethyl acetate. Remove the ethyl acetate, and purify with a chromatographic column using ethyl acetate–hexane (1:5) as the eluant to obtain 0.66 g (83%) of a yellow liquid. EI-HRMS: *m*/*z* calcd 272.0765, found 272.0699 $[M]^+$, ^1H NMR (d-acetone, 300 MHz) δ 8.95 (d, $J = 4.7$ Hz, 1H), 8.34 (d, $J = 7.8$ Hz), 8.00 (m, 2H), 7.72 (m, 1H), 7.58 (t, $J = 7.8$ Hz, 1H), 7.52 (t, $J = 7.2$ Hz, 1H), 7.39 (m, 2H), 7.28 (d, $J = 8.4$ Hz, 1H).

2.3.2. 2-Naphthalen-1-yl-4-trifluoromethyl-pyridine (4-fnapy)

Yield 92%, yellow liquid. EI-HRMS: *m*/*z* calcd 272.0765, found 272.0701 $[M]^+$, ^1H NMR (d-acetone, 300 MHz) δ 9.04 (d, $J = 5.1$ Hz, 1H), 8.11 (d, $J = 7.8$ Hz, 1H), 8.04 (d, $J = 8.7$ Hz, 1H), 7.78 (m, 2H), 7.70 (d, $J = 6.2$ Hz, 1H), 7.62 (t, $J = 7.78$ Hz, 2H), 7.56 (m, 2H).

2.3.3. 2-Naphthalen-1-yl-5-trifluoromethyl-pyridine (5-fnapy)

Yield 87%, yellow solid. M.p.: 58 °C. EI-HRMS: *m*/*z* calcd 272.0765, found 272.0707 $[M]^+$, ^1H NMR ($CDCl_3$, 400 MHz) δ 9.07 (s, 1H), 8.07 (t, $J = 8.2$ Hz, 2H), 7.96 (m, 2H), 7.74 (d, $J = 8.2$ Hz, 1H), 7.62 (m, 2H), 7.54 (m, 2H).

2.3.4. 2-Naphthalen-1-yl-6-trifluoromethyl-pyridine (6-fnapy)

Yield 83%, yellow liquid. EI-HRMS: *m*/*z* calcd 272.0765, found 272.0696 $[M]^+$, ^1H NMR ($CDCl_3$, 500 MHz) δ 8.12 (d, $J = 2.4$ Hz, 1H), 7.95 (m, 3H), 7.75 (d, $J = 7.8$ Hz, 1H), 7.72 (d, $J = 7.8$ Hz, 1H), 7.66 (d, $J = 7.2$ Hz, 1H), 7.59 (d, $J = 7.8$ Hz, 1H), 7.54 (m, 2H).

2.3.5. bis[2-Naphthalen-1-yl-4-trifluoromethyl-pyridine-N,$C^{2'}$]-iridium(acetylacetonate)(4-fnapy)$_2$ Ir(acac)

The synthesis process can be found in [16]. Yield 63%, orange solid, EI-HRMS: *m*/*z* calcd 836.1449, found 836.1452 $[M]^+$, ^1H NMR (CD_2Cl_2, 300 MHz) δ 8.74 (s, 2H), 8.70 (t, $J = 7.3$ Hz, 2H), 8.47 (d, $J = 8.0$ Hz, 2H), 7.65 (d, $J = 8.0$ Hz, 2H), 7.53 (t, $J = 7.3$ Hz, 2H), 7.29 (m, 4H), 7.09 (d, $J = 8.0$ Hz, 2H), 6.28 (d, $J = 8.0$ Hz, 2H), 5.28 (s, 1H), 1.81(s, 6H). ^{13}C NMR (CD_2Cl_2, 75 MHz) δ 185.4, 170.5, 157.0, 149.3, 139.2, 138.7, 136.7, 131.9, 131.6, 131.2, 130.0, 127.2, 122.9, 120.7, 117.9, 116.0, 100.7, 28.625. *Anal.* Calc. for $C_{37}H_{25}F_6IrN_2O_2$: C, 53.17; H, 3.01; N, 3.35. Found: C, 53.35; H, 3.42; N, 3.35%.

2.3.6. bis[2-Naphthalen-1-yl-5-trifluoromethyl-pyridine-N,$C^{2'}$]-iridium(acetylacetonate)(5-fnapy)$_2$ Ir(acac)

Yield 78%, orange solid, EI-HRMS: *m*/*z* calcd 836.1449, found 836.1458 $[M]^+$, ^1H NMR (CD_2Cl_2, 300 MHz) δ 8.79 (s, 2H), 8.62 (d, $J = 8.7$ Hz, 2H), 8.47 (d, $J = 8.7$ Hz, 2H), 7.99 (d, $J = 8.7$ Hz, 2H), 7.64 (d, $J = 8.0$ Hz, 2H), 7.48 (t, $J = 8.0$ Hz, 2H), 7.26 (m, 2H), 7.09 (d, $J = 8.0$ Hz, 2H), 6.30 (d, $J = 8.7$ Hz, 2H), 5.31 (s, 1H), 1.82 (s, 6H). ^{13}C NMR (CD_2Cl_2, 75 MHz) δ 185.6, 172.6, 158.6, 145.6,

136.5, 134.2, 132.3, 131.9, 131.2, 130.3, 130.0, 127.1, 124.7, 122.9, 122.5, 122.0, 121.7, 121.1, 120.9, 100.9, 28.5. *Anal.* Calc. for $C_{37}H_{25}F_6IrN_2O_2$: C, 53.17; H, 3.01; N, 3.35. Found: C, 53.31; H, 3.30; N, 3.22%.

2.4. OLED fabrication and testing

EL devices were fabricated with a similar structure to [Ir(ppy)$_3$] as reported by Thompson et al. [18] by vacuum-deposition techniques. The device structure used in this work was a typical multi-layer, employing indium tin oxide (ITO) as the anode, 4,4′-bis[*N*-(1-naphthyl)-*N*-phenyl-amino]biphenyl (NPB)(50 nm) as the hole-transport material, and 4,4′-di(carbazole-9-yl)biphenyl (CBP) as the host material (30 nm). Bathocuproine (BCP) (10 nm) was applied as the hole-blocking material, tris(8-quinolinolato)aluminum (Alq_3) (30 nm) as the electron-injection layer, and Al as the cathode.

2.5. X-ray crystallographic analyses

Crystals of (napy)$_2$Ir(acac) and (4-fnapy)$_2$Ir(acac) were obtained from solutions of CH_2Cl_2-Ether. The crystal data were selected for indexing and intensity data collection on a Siemens SMART CCD diffractometer equipped with a normal focus, 3-kW sealed tube X-ray source at 21–23 °C. No significant decay was observed for all samples during the data collection. Data were process on a PC using the Bruker AXS SHELXTL NT software package. Neutral atom scattering factors were taken from Cromer and Waber. The crystals of (napy)$_2$Ir(acac) and (4-fnapy)$_2$Ir(acac) belong to the monoclinic space group $P2(1)/n$ and triclinic space group $P\bar{1}$, respectively. All structure were solved by direct methods. All non-hydrogen atoms were refined anisotropically. The positions for all hydrogen atoms were either calculated or located directly from different Fourier maps and their contributions in structural factor calculation were included. The crystallographic data of (napy)$_2$Ir(acac) and (4-fnapy)$_2$Ir(acac) are given in Table 3, and selected bond lengths and angles are summarized in Table 4.

3. Results and discussion

The trifluoromethyl-substituted napy ligands were synthesized by the reaction of 1-naphthylboronic acid with the corresponding 2-chloro-*n*-trifluoromethyl-pyridine in the presence of Cs_2CO_3, $Pd(OAc)_2$, and PPh_3 (Scheme 1). The synthesized ligands including 2-naphthalen-1-yl-3-trifluoromethyl-pyridine (*3*-fnapy), *4*-fnapy, *5*-fnapy, and *6*-fnapy were reacted with $IrCl_3$ and acetylacetone in the presence of 2-ethoxyethanol and Na_2CO_3 in order to prepare the corresponding (*n*-fnapy)$_2$Ir(acac) complexes (Scheme 1). All the ligands and the Ir-complexes were characterized by HRMS, ^{1}H and ^{13}C NMR. Due to the steric hindrance effect of the bulky trifluoromethyl group, stable

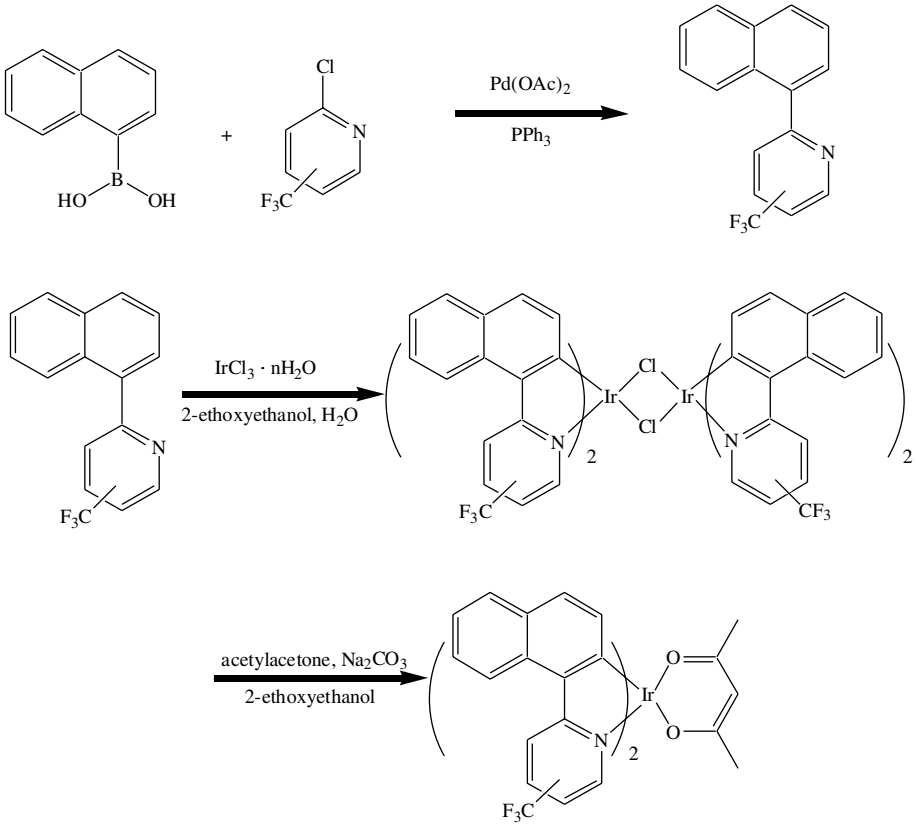

Scheme 1. Synthesis route of iridium complexes.

(*3*-fnapy)$_2$Ir(acac) and (*6*-fnapy)$_2$Ir(acac) complexes could not be obtained. Stable ((3-fnapy)$_2$IrCl)$_2$ could be prepared but the naphthalene and pyridine ring had to be in the same plane in order to form the (*3*-fnapy)$_2$Ir(acac) complex. The trifluoromethyl group on the 3-position, however, suppresses this possibility. In the case of 6-fnapy ligand, the trifluoromethyl group directly faces to the bridging chloride of the $IrCl_3$, preventing the active site of the ligand from approaching the active site of $IrCl_3$, and as a result no desired product can be obtained. Thus, this discussion will focus on (*4*-fnapy)$_2$Ir(acac) and (*5*-fnapy)$_2$Ir(acac).

Fig. 1 shows the UV–Vis absorption spectrum of 1×10^{-5} M of (4-fnapy)$_2$Ir(acac) and (5-fnapy)$_2$Ir(acac) complexes in dichloromethane. The absorption spectra of the ligands and (napy)$_2$Ir(acac) complex are also included for comparison. The data taken from these spectra are collected in Table 1. As can be seen, the spectra of the two iridium complexes are fairly similar in terms of peak position. Weak absorption bands between 330 nm to 560 nm that are observed for both (4-fnapy)$_2$Ir(acac) and (5-fnapy)$_2$Ir(acac) complexes are not observed for the pure ligands. These weak bands can be assigned to singlet and triplet metal to ligand charge transfer (MLCT) transitions. The intense absorption bands at wavelengths shorter than 350 nm are due to the π–π^* transition of the fnapy ligands. Note that the differences observed between the spectra of the pure fnapy ligands and their corresponding iridium complexes indicates that coordination between ligands and iridium ions had indeed taken place. Compared to the corresponding absorption spectra of the ligands, the peaks of π–π^* transition from (4-fnapy)$_2$Ir(acac) and (5-fnapy)$_2$Ir(acac) complexes have blue-shifted approximately 20 nm.

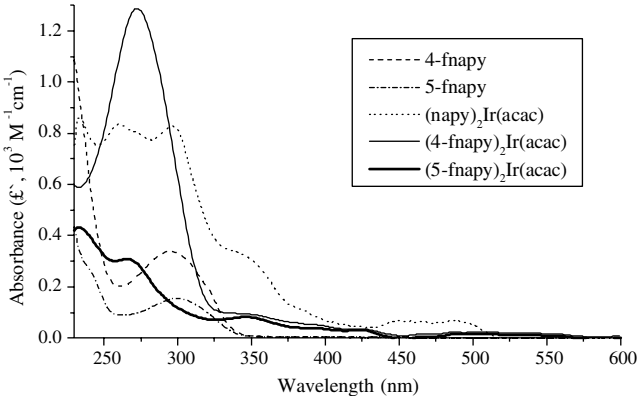

Fig. 1. UV–Vis spectra of ligands and iridium complexes which were collected in CH_2Cl_2 solution (1×10^{-5} M).

Table 1
UV–Vis (1×10^{-5} M) and photoluminescence (1×10^{-3} M) data of compound in CH_2Cl_2 solution

	UV–Vis absorption	Photoluminescence
Compound	λ (nm) {ε, 10^3 M^{-1} cm^{-1}}	emission λ_{max}(nm)
4-fnapy	230(108.0), 294(33.7)	
5-fnapy	229(44.8), 298(14.8)	
(napy)$_2$Ir(acac)	296(84.04), 448(7.7), 486(8.20)	590
(4-fnapy)$_2$Ir(acac)	273(128.32), 347(8.18), 395(3.45), 424(2.43), 502(1.50)	617
(5-fnapy)$_2$Ir(acac)	233(82.82), 266(59.22), 394(3.37), 423(2.78), 502(1.52)	613

Fig. 2 shows the photoluminescence spectra of 1×10^{-3} M of (4-fnapy)$_2$Ir(acac) and (5-fnapy)$_2$Ir(acac) complexes in dichloromethane. For comparison, the spectra of (napy)$_2$Ir(acac) is also included in this figure. The data taken from these spectra are summarized in Table 1. It can be seen that (4-fnapy)$_2$Ir(acac) and (5-fnapy)$_2$Ir(acac) emit red light at 617 and 613 nm, respectively. With regard to (napy)$_2$Ir(acac), which emits orange light at 595 nm, it is clear that the incorporation of the trifluoromethyl group leads to a 20 nm bathochromic shift. The trifluoromethyl group changes the π–π conjugation of the cyclometalated ligand and lowers the triplet energy level, thus lowering the lowest unoccupied molecular orbital (LUMO) level. Under the same excitation condition, the intensity of the emission of (4-fnapy)$_2$Ir(acac) and (5-fnapy)$_2$Ir(acac) are the same and the full width at half maximum (FWHM) is 40 nm for both complexes, which is about the same as the FWHM for the (napy)$_2$Ir(acac) which contains no trifluoromethyl group.

Cyclic voltammetry experiments were carried out for the (napy)$_2$Ir(acac), (4-fnapy)$_2$Ir(acac) and (5-fnapy)$_2$Ir(acac) iridium complexes in dichloromethane and the data taken from the cyclic voltammograms are summarized in Table 2. Due to the limited electrochemical window of the solvent, only the oxidation process for the complexes was obtained. For the electrochemical behavior of Ir(ppy)$_3$ analogues it is generally accepted that the oxidation process involves the iridium moiety of the complexes, and the highest occupied molecular orbital (HOMO) levels are mostly due to the d orbital of iridium with some π-orbital contributions from the ligand. Fig. 3 shows that both (4-fnapy)$_2$Ir(acac) and (5-fnapy)$_2$Ir(acac) exhibit reversible oxidation waves at potential more

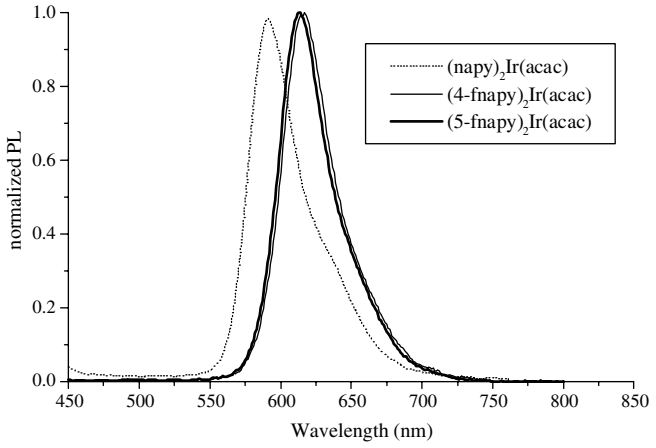

Fig. 2. Normalized photoluminescence spectra of iridium which were collect in CH_2Cl_2 solution (1×10^{-3} M).

Table 2
Electrochemical data, absorption edge, HOMO, LUMO, and energy gap of $(napy)_2Ir(acac)$, $(4\text{-}fnapy)_2Ir(acac)$, and $(5\text{-}fnapy)_2Ir(acac)$

Complex	$E_{1/2}$ (mV)[a]	ΔE_p (mV)	Adsorption edge (nm)[b]	HOMO (eV)	LUMO (eV)	Energy gap (eV)
$(napy)_2Ir(acac)$	340	64	520	−5.1	−2.7	2.4
$(4\text{-}fnapy)_2Ir(acac)$	528	68	570	−5.3	−3.1	2.2
$(5\text{-}fnapy)_2Ir(acac)$	528	64	572	−5.3	−3.1	2.2

[a] $E_{1/2}$ vs. ferrocene/ferrocenium.
[b] Data were collected in CH_2Cl_2 solution by UV–Vis spectrophotometer.

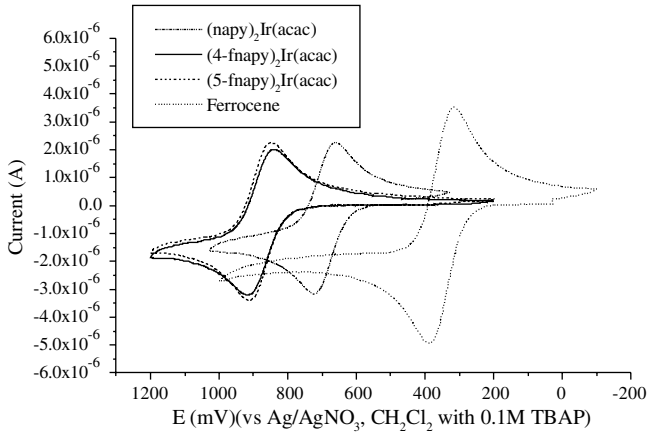

Fig. 3. The cyclic voltammograms of $(napy)_2Ir(acac)$, $(4\text{-}fnapy)_2Ir(acac)$, $(5\text{-}fnapy)_2Ir(acac)$ at the concentration 1×10^{-3} M in CH_2Cl_2. The scan rate is 50 mV/s.

positive than (napy), indicating the relative difficulty of oxidation. This can be ascribed to the electron-withdrawing ability of the trifluoromethyl group. Based on method in the literature [19], the HOMO values for the iridium complexes were calculated by using the oxidation potentials collected from cyclic voltammograms. The calculated HOMO values are presented in Table 2. This table shows that $(4\text{-}fnapy)_2Ir(acac)$ and $(5\text{-}fnapy)_2Ir(acac)$ have the same HOMO value, −5.3 eV, while the HOMO level of $(napy)_2Ir(acac)$ is −5.1 eV. From the spectroscopy absorption edge it is found that $(4\text{-}fnapy)_2Ir(acac)$ and $(5\text{-}fnapy)_2Ir(acac)$ have the same energy gap, 2.2 eV. According to the theory presented by Burrows et al. [20] the LUMO energy level for the iridium complexes are determined from the energy gap and the HOMO energy level. As shown in Table 2, $(4\text{-}fnapy)_2Ir(acac)$ and $(5\text{-}fnapy)_2Ir(acac)$ have the same LUMO energy, −3.1 eV, while the LUMO level of $(napy)_2Ir(acac)$ is −2.7 eV. These results indicate that the trifluoromethyl group has a stronger influence on lowering the LUMO levels than on the HOMO levels.

Some studies regarding the substituent effect of the trifluoromethyl group on the cyclometalated Ir(III) complexes have been discussed in the literature [21,22]. It has been concluded that when the substitution is on the electron-deficient ring, like pyridine or pyrimidine, red shift in the emission wavelength often occurs due to the lowering of the LUMO energy level. Recently, Chi et al. [23] demonstrated that when the pyridine ring of the $(napy)_2[Ir]$ complex was replaced by a CF_3 substituted pyrimidine to form the $(fnapm)_2[Ir]$ complex (Scheme 2) a significant decrease in the LUMO energy level occurred and the emission wavelength shifted from 590 nm of $(napy)_2[Ir]$ to 618 nm of $(fnapm)_2[Ir]$. They attributed this to the effect of the electronegative nitrogen of the pyrimidine fragment. However, they may have overlooked the effect of the CF_3 group, because our data indicate that simply introducing a CF_3 group to the pyridine ring shifts the emission wavelengths to 617 $(4\text{-}fnapy)_2Ir(acac)$ and 613 nm $(5\text{-}fnapy)_2Ir(acac)$ which are very close to that of $(fnapm)_2Ir(acac)$. Since there is such a small difference between the emission wavelength of the $(n\text{-}fnapy)_2Ir(acac)$ and that of the $(fnapm)_2Ir(acac)$, the bathochromic effect of the nitrogen on the pyrimidine should be much weaker than Chi et al. expected.

ORTEP diagrams of $(napy)_2Ir(acac)$ and $(4\text{-}fnapy)_2Ir(acac) \cdot CH_2Cl_2$ are shown in Fig. 4, and the X-ray diffraction data are listed in Table 3. The iridium complexes were dissolved in CH_2Cl_2 by slowly adding ethylether, and letting the mixture stand for crystallization for 2 days. In the case of $(4\text{-}fnapy)_2Ir(acac) \cdot CH_2Cl_2$, each unit cell contains two $(4\text{-}fnapy)_2Ir(acac)$ and two CH_2Cl_2 molecules. In the $(napy)_2Ir(acac)$ crystals, each unit cell contains four $(napy)_2Ir(acac)$ molecules and no solvent molecule. Apparent stacking phenomenon was observed in the

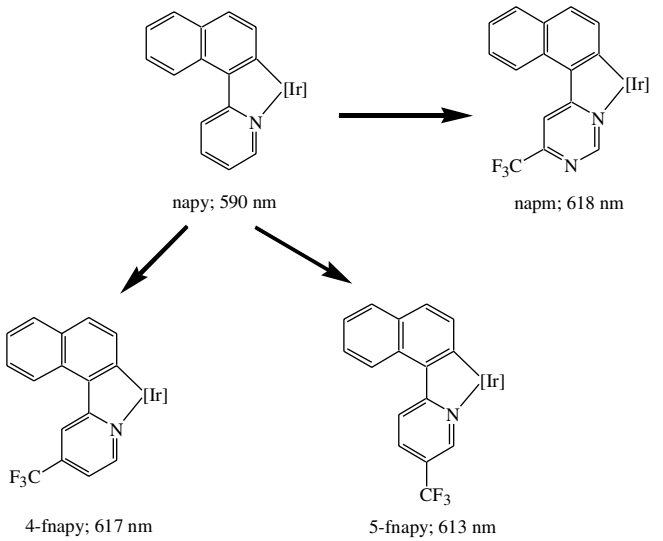

Scheme 2.

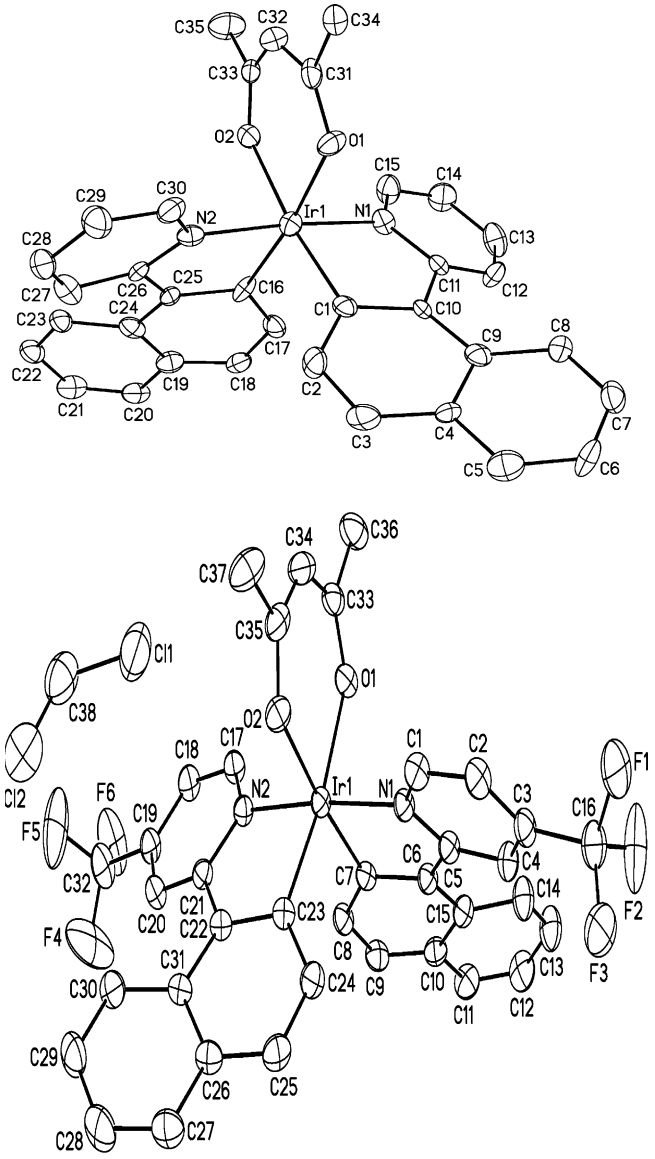

Fig. 4. ORTEP diagram with 50% probability thermal ellipsoids of $(napy)_2Ir(acac)$ (up) and $(4\text{-}fnapy)_2Ir(acac) \cdot CH_2Cl_2$ (down).

$(napy)_2Ir(acac)$ crystal; the complex molecules are so close to each other that there is not enough space for the incorporation of other solvent molecules. On the other hand, the $(4\text{-}fnapy)_2Ir(acac)$ molecules spread in a dimension structure and the CH_2Cl_2 molecules are distributed between the one dimension chains. The trifluoromethyl group seems to keep the $(4\text{-}fnapy)_2Ir(acac)$ molecules from gathering together, and this fact would help to lower the concentration quenching effect in the OLED device. The distorted octahedral geometry around the iridium is a consequence of the ligand structure, two mutually *trans* pyridyl and two *cis* naphthalenyl rings connected to the iridium atom. The average Ir–C (1.98) and Ir–N (2.02) distances are normal when compared to other Ir(III) bis-ppy derivatives [24]. The bond lengths and angles around the iridium atom are listed in Table 4.

Table 3
Crystal data and structure refinement for $(napy)_2Ir(acac)$ and $(4\text{-}fnapy)_2Ir(acac) \cdot CH_2Cl_2$

	$(napy)_2Ir(acac)$	$(4\text{-}fnapy)_2Ir(acac) \cdot CH_2Cl_2$
Formula	$C_{35}H_{27}IrN_2O_2$	$C_{38}H_{27}Cl_2F_6Ir\ N_2O_2$
Formula weight	699.79	920.72
Crystal system	monoclinic	triclinic
Space group	$P2(1)/n$	$P\bar{1}$
a (Å)	7.4940(4)	9.8483(6)
b (Å)	15.7345(1)	14.0018(8)
c (Å)	22.8672(19)	14.3758(8)
α (°)	90	114.708(1)
β (°)	93.588(2)	90.727(1)
γ (°)	90	102.466(1)
Volume (Å^3)	2691.1(4)	1746.52(18)
Z	4	2
Density (calculated) (Mg/m^3)	1.727	1.751
Goodness-of-fit on F^2	0.429	1.019
Final R indices $[I > 2\alpha(I)]$	R_1[a] = 0.0309, wR_2[b] = 0.0352	R_1[a] = 0.0236, wR_2[b] = 0.0615
R indices (all data)	R_1[a] = 0.1048, wR_2[b] = 0.0396	R_1[a] = 0.0267, wR_2[b] = 0.0624

[a] $R_1 = \sum|F_o| - |F_c| / \sum F_o|$.
[b] $wR_2 = [\sum w[(F_o^2 - F_c^2)^2] / \sum[w(F_o^2)^2]]^{1/2}$ $(w = 1/\sigma^2(F_o^2) + (0.075P)^2)$, where $P = [\mathrm{Max}(F_o^2, 0) + 2F_c^2]/3)$.

The peak wavelengths of the EL spectrum for the devices using $(4\text{-}fnapy)_2Ir(acac)$ and $(5\text{-}fnapy)_2Ir(acac)$ were 615 and 611 nm, respectively. There were no characteristic

Table 4
Selected bond lengths (Å) and bond angles (deg) for $(napy)_2Ir(acac)$ and $(4\text{-}fnapy)_2Ir(acac) \cdot CH_2Cl_2$

	$(napy)_2Ir(acac)$	$(4\text{-}fnapy)_2Ir(acac) \cdot CH_2Cl_2$
Bond lengths		
Ir–C	1.972(6)	1.981(3)
	1.993(6)	1.985(3)
Ir–N	2.015(5)	2.022(2)
	2.024(5)	2.026(2)
Ir–O	2.130(4)	2.129(2)
	2.160(4)	2.142(2)
Bond angles		
O(1)–Ir–O(2)	87.9(2)	87.55(8)
N(1)–Ir–N(2)	175.1(2)	174.92(8)
C(1)–Ir–C(16)/ C(7)–Ir–C(23)	93.6(2)	93.9(1)
O(1)–Ir–N	92.0(2)	89.81(8)
	92.5(2)	93.32(8)
O(2)–Ir–N	89.9(2)	90.86(8)
	92.5(2)	93.28(8)
O(1)–Ir–C	89.7(2)	91.77(9)
	172.7(2)	171.83(8)
O(2)–Ir–C	89.5(2)	87.54(9)
	172.9(2)	173.32(8)
N(1)–Ir–C	80.9(2)	80.1(1)
	95.0(2)	97.0(1)
N(2)–Ir–C	80.7(2)	80.22(9)
	96.9(2)	95.8(1)

Table 5
OLED performance of $(4\text{-napy})_2\text{Ir(acac)}$ and $(5\text{-fnapy})_2\text{Ir(acac)}$

	$(4\text{-napy})_2\text{Ir(acac)}$	$(5\text{-fnapy})_2\text{Ir(acac)}$
EL color	red	red
Peak wavelength (nm)	615	611
CIE-*x*	0.66	0.65
CIE-*y*	0.34	0.35
Turn-on voltage (V)	5.3	4.8
Luminance (cd/m^2) at 10 mA/cm^2	680	830
Drive voltage (V) at 10 mA/cm^2	7.9	6.8
Luminous efficiency (cd/A) at 10 mA/cm^2	6.82	8.43
Power efficiency (lm/W) at 10 mA/cm^2	2.73	3.81
Luminance (cd/m^2) at 10.5 V	3600	8600
Current density (mA/cm^2) at 10.5 V	85.3	200
Luminous efficiency (cd/A) at 10.5 V	4.24	4.29
Power efficiency (lm/W) at 10.5 V	1.26	1.28

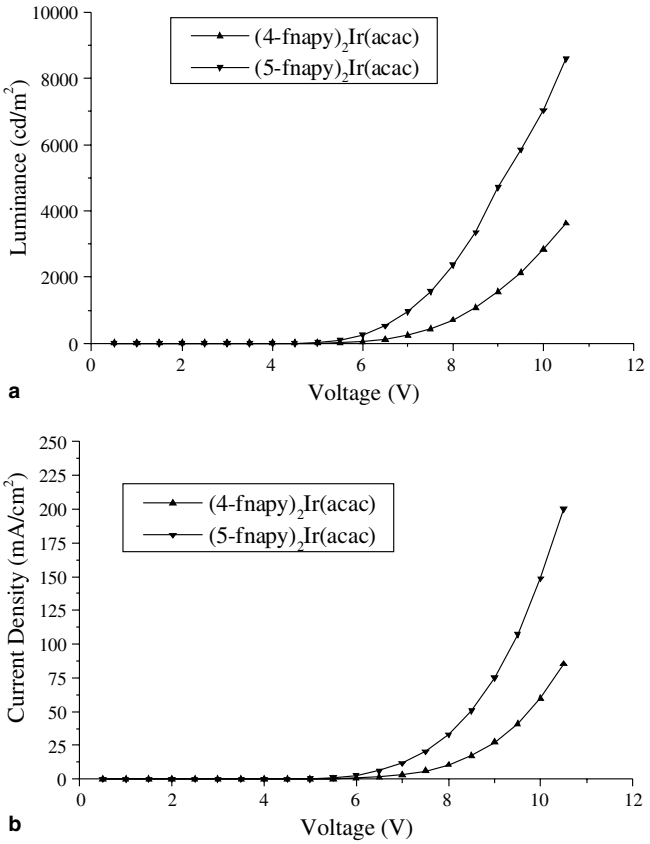

Fig. 5. (a) The luminance-voltage characteristics of OLED devices. (b) The current density-voltage characteristics of OLED devices.

emission peaks from CBP or Alq_3, indicating that the emission originates mostly from the dopant. Electrophosphorescence data for the iridium complexes are summarized in Table 5. The EL performances of the device are presented in Fig. 5. The turn-on voltage of the two OLED devices for emission were both about 5.0 V. The maximum efficiency and brightness of $(5\text{-fnapy})_2\text{Ir(acac)}$ are almost twice that of $(4\text{-fnapy})_2\text{Ir(acac)}$. The luminance of 3600 cd m^{-2} at 10.5 V and efficiency of 4.2 cd A^{-1} at 85 mA cm^{-2} was achieved by using $(4\text{-fnapy})_2\text{Ir(acac)}$ at 6 wt% doping level. The higher luminance of 8600 cd m^{-2} at 10.5 V and efficiency of 4.3 cd A^{-1} at 200 mA cm^{-2} was achieved by using $(5\text{-fnapy})_2\text{Ir(acac)}$. Due to the weaker Forster energy transfer [12,25] efficiency from CBP to the iridium complex, there is a downward tendency in quantum efficiencies with a red-shift of the emission peak. At the same applied volatge, the luminance of $(5\text{-fnapy})_2\text{Ir(acac)}$ is apparently higher than $(4\text{-fnapy})_2\text{Ir(acac)}$. High luminous efficiency of this series of iridium complexes has been confirmed. Due to the decrease of triplet–triplet annihilation, a gradual increase in the external quantum efficiency along with a decrease in the current density was observed for each device. At a current density of 10 mA cm^{-2}, the luminous efficiencies were reached at 6.82 and 8.43 cd A^{-1}. The emission of Commission Internationale de L'Eclairage (CIE) coordinates are (0.66, 0.34) and (0.65, 0.35). The colors emitted are both belong to red in the OLED devices.

4. Conclusions

A series of trifluoromethyl-substituted 2-naphthalen-1-yl-pyridine ligands and the corresponding iridium complexes have been synthesized and characterized by spectroscopic methods as well as by X-ray crystallography. The photoluminescent and electrochemical properties of these red-emitting Ir(III) complexes were measured. Significant bathochromic shift was observed with the incorporation of trifluoromethyl group. We have demonstrated that the emission wavelength of $(napy)_2\text{(acac)}$ can be tuned to more than 20 nm so that the color is close to pure red. Using $(5\text{-fnapy})_2\text{Ir(acac)}$ as the red dopant in CBP, the device has a maximum efficiency of 8.43 cd A^{-1} and a brightness of 830 cd m^{-2} at 10 mA cm^{-2}.

Acknowledgements

This work was supported by the National Science Council of the Republic of China, Taiwan (NSC 94-2113-M-006-017).

Appendix A. Supplementary data

Crystallographic data (excluding structure factors) for $(napy)_2\text{Ir(acac)}$ and $(4\text{-fnapy})_2\text{Ir(acac)} \cdot CH_2Cl_2$ have been deposited with the Cambridge Crystallographic Data Centre as supplementary publication numbers CCDC 260872 and 260873, respectively. Copies of the data can be obtained, free of charge, on application to CCDC, 12 Union Road, Cambridge CB2 1EZ, UK. Supplementary data associated with this article can be found, in the online version, at doi:10.1016/j.poly.2006.02.003.

References

[1] C.W. Tang, S.A. VanSlyke, C.H. Chen, J. Appl. Phys. 65 (1989) 3610.
[2] M.A. Baldo, D.F. O'Brien, Y. You, A. Shoustikov, S. Sibley, M.E. Thompson, S.R. Forrest, Nature 395 (1998) 151.
[3] J. Kido, H. Hayase, K. Hongawa, K. Nagai, K. Okuyame, Appl. Phys. Lett. 65 (1994) 2124.
[4] M. Pope, C.E. Swenberg, Electronic Process in Organic Crystals and Polymers, Oxford University Press, New York, 1999.
[5] C. Adachi, M.A. Baldo, M.E. Thompson, S.R. Forrest, J. Appl. Phys. 90 (2001) 5048.
[6] M. Ikai, S. Tokito, Y. Sakamoto, T. Suzuki, Y. Taga, Appl. Phys. Lett. 79 (2001) 156.
[7] C. Adachi, M.A. Baldo, S.R. Forrest, M.E. Thompson, Appl. Phys. Lett. 77 (2000) 904.
[8] M.C. DeRosa, D.J. Hodgson, G.D. Enright, B. Dawson, C.E.B. Evans, R.J. Crutchley, J. Am. Chem. Soc. 126 (2004) 7619.
[9] B.W. D'Andrade, J. Brooks, V. Adamovich, M.E. Thompson, S.R. Forrest, Adv. Mater. 14 (2002) 1032.
[10] K. Kalyanasundaram, M. Gretzel, Coord. Chem. Rev. 177 (1998) 347.
[11] Y.L. Tung, P.C. Wu, C.S. Liu, Y. Chi, J.K. Yu, Y.H. Hu, P.T. Chou, S.M. Peng, G.H. Lee, Y. Tao, A.J. Carty, C.F. Shu, F.I. Wu, Organometallics 23 (2004) 3745.
[12] M.A. Baldo, M.E. Thompson, S.R. Forrest, Nature 403 (2000) 750.
[13] K.C. Tang, K.L. Liu, I.C. Chen, Chem. Phys. Lett. 386 (2004) 437.
[14] A.B. Tamayo, B.D. Alleyne, P.I. Djurovich, S. Lamansky, I. Tsyba, N.N. Ho, R. Bau, M.E. Thompson, J. Am. Chem. Soc. 125 (2003) 7377.
[15] T. Tsuzuki, N. Shirasawa, T. Suzuki, S. Tokito, Adv. Mater. 15 (2003) 1455.
[16] C.H. Yang, C.C. Tai, I.W. Sun, J. Mater. Chem. 14 (2004) 947.
[17] W. Zhu, M. Zhu, Y. Ke, L. Su, M. Yuan, Y. Cao, Thin Solid Films 446 (2004) 128.
[18] M.A. Baldo, S. Lamansky, P.E. Burrows, M.E. Thompson, S.R. Forrest, Appl. Phys. Lett. 75 (1999) 4.
[19] H.M. Koepp, H. Wendt, H.Z. Strehlow, Electrochemistry 64 (1960) 483.
[20] P.E. Burrows, Z. Shen, V. Bulovic, D.M. McCarty, S.R. Forrest, J. Appl. Phys. 79 (1996) 7991.
[21] A. Tsuboyama, H. Iwawaki, M. Furugori, T. Mukaide, J. Kamatani, S. Igawa, T. Moriyama, S. Miura, T. Takiguchi, S. Okada, M. Hoshino, K. Ueno, J. Am. Chem. Soc. 125 (2003) 12971.
[22] V.V. Grushin, N. Herron, D.D. LeCloux, W.J. Marshell, V.A. Petrov, Y. Wang, Chem. Commun. (2001) 1494.
[23] F.M. Hwang, H.Y. Chen, P.S. Chen, C.S. Liu, Y. Chi, C.F. Shu, F.I. Wu, P.T. Chou, S.M. Peng, G.H. Lee, Inorg. Chem. 44 (2005) 1344.
[24] P.J. Hay, J. Phys. Chem. A 106 (2002) 1634.
[25] M. Klessinger, J. Michl, Excited States and Photochemistry of Organic Molecules, VCH Publishers, New York, 1995.

example $[MoO(N_3)(CN)_4]^{3-}$ [5], $[WO(F)(CN)_4]^{3-}$ [6] and $[ReO(NCS)(CN)_4]^{2-}$ [7].

An excellent relationship exists between the pK_{a1}-values obtained from the different $[MO(OH_2)(CN)_4]^{n-}$ complexes, the M–OH_2 bond distances and the formal metal ion charge. Thus the pK_{a1} decreased from 10.0 for the molybdenum(IV) complex [8] (Mo–OH_2 bond distance 2.271(4) Å) to 1.4 for the rhenium(V) complex [9] (Re–OH_2 bond distance 2.142(7) Å). The profound effect of the central metal ion on the chemistry of these complexes was also demonstrated by the rate of substitution of the aqua ligand. A decrease of a factor 10^4 was observed for the substitution of the aqua ligand by NCS^- in $[ReO(OH_2)(CN)_4]^-$ [10] compared to the same reaction for $[WO(OH_2)(CN)_4]^{2-}$ [11].

One of the major differences between the chemistry of the $[MO(H_2O)(CN)_4]^{n-}$ complexes (M = Mo and W) and the iso-electronic $[ReO(OH_2)(CN)_4]^-$ complex was the ability of the former to react with bidentate ligands, substituting the aqua as well as one of the cyanide ligands to form the corresponding $[MO(LL)(CN)_3]^{n-}$ complexes, e.g., $[MoO(phen)(CN)_3]^-$ [12] and $[WO(pic)(CN)_3]^{2-}$ [13]. The absence of bidentate substitution reactions for the $[ReO(OH_2)(CN)_4]^-$ complex (pK_{a1} 1.4) is attributed to the protonation of the bidentate ligand at low pH-values.

The same protonation behaviour (Eq. (2)) was observed for $[MN(H_2O)(CN)_4]^{n-}$, (M = Re(V) and Os(VI)) [14,15] with the exception that the $[MN(O)(CN)_4]^{n-}$ type complex was never observed.

$$[MN(HO)(CN)_4]^{(n+1)-} \underset{+H^+}{\overset{-H^+;K_{a1}}{\rightleftharpoons}} [MN(H_2O)(CN)_4]^{n-} \qquad (2)$$

These studies highlighted the influence of the nitrido ligand compared to that of oxygen as terminal ligand. The nitrido ligand had a large influence on the pK_{a1} value. The pK_{a1} increased from 1.4 for $[ReO(OH_2)(CN)_4]^-$ to 11.6(2) for $[ReN(OH_2)(CN)_4]^{2-}$. The same large increase in pK_{a1} value was observed for the osmium (VI) complexes [15]. These studies also indicated a large labilising effect by the N^{3-} ligand [16]. This substantial increase in the pK_{a1}-values prompted the research for the isolation and the kinetic study of possible reactions using bidentate ligands with the nitrido complexes. The first step in this search was the investigation of the photolytic reaction between $[ReN(H_2O)(CN)_4]^{2-}$ and ethylenediamine [17]. Contrary to the expected di-hapto behaviour, a novel ethanediamine bridged rhenium complex, $[\{ReN(CN)_4\}_2(\mu\text{-en})]^{2-}$, was isolated.

With the above in mind and the still elusive bidentate ligand behaviour for the rhenium-nitrido complex as our aim, we continued investigating the possible reactions between $[ReN(H_2O)(CN)_4]^{2-}$ and different bidentate ligands. In this paper we report the successful preparation and identification of the first $[ReN(LL')(CN)_3]^{n-}$ complex as $[ReN(\eta^2\text{-pic})(CN)_3]^{2-}$ (pic = pyridine-2-carboxylato ion) as well as the kinetic study of the reactions involved in the formation of the final complex.

2. Experimental

All the preparations were performed in an efficient fume cupboard. The UV–Vis spectra were recorded on a Varian Carey (model 50 Conc) or a Hitachi (model 150–20) spectrophotometer at room temperature. IR spectra were recorded as powder or crystals on a Digilab Merlin FTIR spectrophotometer.

2.1. Syntheses of the complexes

2.1.1. $K_2[ReN(CN)_4]\cdot H_2O$

$K_2[ReN(CN)_4]\cdot H_2O$ was synthesised according to the literature method [18]. Spectral data: ν(R≡N), 993, 966 cm^{-1}; ν(CN), 2117 cm^{-1}; % yield = 58.

2.1.2. $(Ph_4As)_2[ReN(\eta^2\text{-pic})(CN)_3]\cdot 4H_2O$

$K_2[ReN(CN)_4]\cdot H_2O$ (0.5 g, 0.12 mmol) was dissolved in H_2O (2 ml). Picolinic acid (0.75 g, 6.1 mmol) and Na_2CO_3 (0.33 g, 3.1 mmol) were dissolved in H_2O (10 ml), and added to the first solution after the effervescence has ceased. The reaction mixture was heated at 80 °C for 6 h. The volume of the solution was kept constant at 12 ml by adding distilled water from time to time. $AsPh_4Cl\cdot H_2O$ (0.82 g, 0.19 mmol) was dissolved in H_2O (2 ml) and added to the cooled reaction mixture. The yellow-orange crystals were obtained after about 10 h. These crystals were suitable for X-ray analysis.

Spectral data. ν(Re≡N), 1061 cm^{-1}; ν(C≡N), 2106 cm^{-1}; $\lambda_{max} = 400$ nm; $\varepsilon_{(400)} = 2.3\times10^3$ mol^{-1} dm^3 cm^{-1}; $\lambda_{max} = 355$ nm; $\varepsilon_{(355)} = 2.0\times10^3$ mol^{-1} dm^3 cm^{-1} (see Table 1).

2.2. Kinetics

All reagents and chemicals were of analytical grade and distilled H_2O was used in all the experiments. Picolinic acid was recrystallised from hot ethanol. All pH measurements were performed on a Hannah model 8519 pH meter with a combined glass/calomel electrode using standard buffer solutions for calibration and an ionic strength 5.0 M KCl. Kinetic measurements were made on a Hitachi model 150–20 and Varian Carey (model 50 Conc) spectrophotometer. Temperature control of the reaction solutions was maintained by means of a Labcon CPE 50 circulating water bath system and APPA-51 Digital thermometer (accurate within 0.1–1.0°). The kinetic reactions were measured aerobically under pseudo first-order conditions with at least 100-fold excess of the ligand concentration. All the reactions were monitored at 400 nm with 1.00 ± 0.001 cm tandem quartz cells. The absorbance versus time spectra showed two distinctive reactions, a fast reaction with a half-life of a few seconds followed by a second slow reaction with a half-life of 10–20 min. Each kinetic run and pH titration for the slow reaction was performed at least two times and an average of both values

Table 1
Crystal data and structure refinement for $(Ph_4As)_2[ReN(pic)(CN)_3]\cdot 4H_2O$

Identification code	repic
Empirical formula	$C_{57}H_{52}As_2N_5O_6Re$
Formula weight	1239.08
Temperature (K)	293(2)
Wavelength (Å)	0.71073
Crystal system	triclinic
Space group	$P\bar{1}$
Unit cell dimensions	
a (Å)	13.586(2)
b (Å)	13.726(2)
c (Å)	17.100(3)
α (°)	87.972(3)
β (°)	69.659(3)
γ (°)	62.209(3)
Volume (Å^3)	2614.1(7)
Z	2
D_{calc} (mg m^{-3})	1.574
D_{meas} (mg m^{-3})	1.53
Absorption coefficient (mm^{-1})	3.636
$F(000)$	1236
Crystal size (mm)	$0.45\times0.23\times0.13$
θ Range for data collection (°)	1.29–25.00
Index ranges	$-16\leqslant h\leqslant 16$, $-16\leqslant k\leqslant 10$, $-19\leqslant l\leqslant 20$
Reflections collected/unique [R_{int}]	14322, 9129 [0.0188]
Completeness to $\theta = 25.00$(°)	28.29–96.2
Absorption correction	semi-empirical from equivalents
Maximum and minimum transmission	0.6233 and 0.3111
Refinement method	full-matrix least-squares on F^2
Data/restraints/parameters	9129/0/630
Goodness-of-fit on F^2	1.005
Final R indices [$I>2\sigma(I)$]	$R_1 = 0.0286$, $wR_2 = 0.0742$
R indices (all data)	$R_1 = 0.0363$, $wR_2 = 0.0770$
Largest differential peak and hole (e Å^{-3})	1.731 and −0.801

was taken. Kinetic runs and pH titrations for the fast reaction were monitored on a stopped-flow (model 05–109 Photophysics) spectrophotometer coupled with a personal computer (SX 18 MV) capable of performing least-square analyses on absorbance versus time data. Data of 150 points per trace were collected and at least 120 points for each trace were analyzed by least-square fit to give the rate constant. The reported rate constants are an average of 4–12 runs The Scientist program was used to fit the data to selected functions. Linear plots of $\ln(A_\infty - A_t)$ versus time were obtained for at least two half-lives under all conditions. The solid line in the figures present computer least-square fits of the data while the experimentally determined values are presented by the dots.

2.3. X-ray crystallography

Intensity data were collected on a Bruker SMART 1K CCD area detector diffractometer (Jan Boeyens Structural Chemistry Laboratory, School of Chemistry, University of the Witwatersrand) with graphite monochromated Mo Kα radiation (50 kV, 30 mA). The collection method involved ω-scans of width 0.3°. Data reduction was carried out using the program SAINT+ [19] and absorption corrections were made using the program SADABS [20].

The crystal structure was solved by direct methods using SHELXTL [21]. Non-hydrogen atoms were first refined isotropically followed by anisotropic refinement by full matrix least-squares calculations based on F^2 using SHELXTL. With exception of the H-atoms attached to the water molecules all H-atoms were first located in the difference map then positioned geometrically and allowed to ride on their respective parent atoms. In addition to the Re molecule and two $AsPh_4^-$ counter ions the structure also contains four water molecules. Two of these (O1W and O2W) were successfully refined anisotropically while the other two (O3W and O4W) were refined isotropically. Where possible H-atom positions were calculated for water molecules involved in hydrogen bonding. However, it was not possible to unambiguously calculate a position for one H-atom on O2W, O3W and O4W, respectively. The contribution of these has however been added to the sum formula, moiety formula, crystal density and $F(000)$. Diagrams and publication material were generated using SHELXTL and PLATON [22].

3. Results and discussion

3.1. Synthesis

The IR stretching frequencies of the product corresponds very well with the other rhenium-nitrido complexes that were prepared and identified previously. The ν(Re≡N) stretching frequency of 1061 cm^{-1} of the title complex is almost identical to the value of 1060 cm^{-1} that was obtained for $[ReN(H_2O)(CN)_4]^{2-}$ but significantly different from 1040 cm^{-1} that was obtained for $[ReN(CN)_5]^{3-}$. The difference in stretching frequency is indicative of the relative *trans* influence of the group *trans* to the nitrido ligand [16]. These results clearly indicate that the *trans* influence of the H_2O in $[ReN(H_2O)(CN)_4]^{2-}$ and the oxo group of the picolinate anion in $[ReN(\eta^2\text{-pic})(CN)_3]^{2-}$ are compatible. The ν(CN) of 2106 cm^{-1} is also in good agreement with the cyano stretching frequencies of the other rhenium-nitrido complexes.

3.2. Crystal structure

The most important bond lengths and angles of both the cation and anion are listed in Table 2. The numbering scheme of the $[ReN(\eta^2\text{-pic})(CN)_3]^{2-}$ anion is shown in the perspective drawing, Fig. 1. The structure consists of discrete $[ReN(\eta^2\text{-pic})(CN)_3]^{2-}$ anions and $AsPh_4^+$ cations. The As atoms are tetrahedrally surrounded by four phenyl rings. The average As–P bond distance is 1.915(4) Å while the C–As–C bond angles range between 107.3(2)° and 111.0(2)°. These results are in good agreement with those found in other structures containing $AsPh_4^+$ cations (1.911(8) Å, 107.6–111.5° [23], 1.912(11) Å, 107.3(4)–111.6(4)° [24], 1.889 Å, 109.5° [25] and 1.906 Å, 109.5° [12]).

Table 2
Selected bond lengths (Å) and angles (°) for $(Ph_4As)_2[ReN(pic)(CN)_3]\cdot 4H_2O$

Re–N(5)	1.655(3)	C(71)–As(2)	1.921(4)
C(2)–Re	2.067(5)	C(9)–O(2)	1.226(5)
C(1)–Re	2.111(4)	C(9)–O(1)	1.285(5)
C(3)–Re	2.105(4)	C(4)–N(4)	1.352(5)
Re–N(4)	2.169(3)	C(2)–N(2)	1.158(5)
Re–O(1)	2.289(3)	C(7)–C(8)	1.395(7)
C(21)–As(1)	1.914(4)	C(8)–C(9)	1.501(7)
C(31)–As(1)	1.914(4)	C(6)–C(7)	1.366(8)
C(41)–As(1)	1.916(4)	C(5)–C(6)	1.365(7)
C(11)–As(1)	1.917(4)	C(8)–N(4)	1.355(5)
C(81)–As(2)	1.912(4)	C(3)–N(3)	1.146(5)
C(61)–As(2)	1.907(4)	C(1)–N(1)	1.150(5)
C(51)–As(2)	1.916(4)	C(4)–C(5)	1.378(5)
N(5)–Re–O(1)	166.5(1)	N(1)–C(1)–Re	175.7(4)
N(5)–Re–C(1)	100.6(2)	N(2)–C(2)–Re	178.0(4)
N(5)–Re–C(2)	99.6(2)	N(3)–C(3)–Re	174.8(4)
N(5)–Re–C(3)	99.1(2)	C(9)–O(1)–Re	117.7(3)
C(2)–Re–C(1)	87.6(2)	N(4)–C(8)–C(7)	121.1(4)
C(2)–Re–C(3)	86.1(2)	N(4)–C(8)–C(9)	115.5(4)
C(3)–Re–C(1)	160.1(2)	C(7)–C(8)–C(9)	123.5(4)
N(5)–Re–N(4)	94.2(2)	O(2)–C(9)–O(1)	125.2(5)
C(2)–Re–N(4)	166.1(1)	O(2)–C(9)–C(8)	119.5(4)
C(1)–Re–N(4)	88.6(1)	O(1)–C(9)–C(8)	115.3(4)
C(3)–Re–N(4)	93.1(1)	C(5)–C(6)–C(7)	119.1(5)
C(2)–Re–O(1)	93.9(1)	C(6)–C(7)–C(8)	120.2(5)
C(1)–Re–O(1)	80.7(1)	C(6)–C(5)–C(4)	119.1(5)
C(3)–Re–O(1)	80.7(1)	C(8)–N(4)–Re	119.0(3)
N(4)–Re–O(1)	72.4(1)	N(4)–C(4)–C(5)	123.1(4)
C(4)–N(4)–C(8)	117.5(4)	C(4)–N(4)–Re	123.4(3)

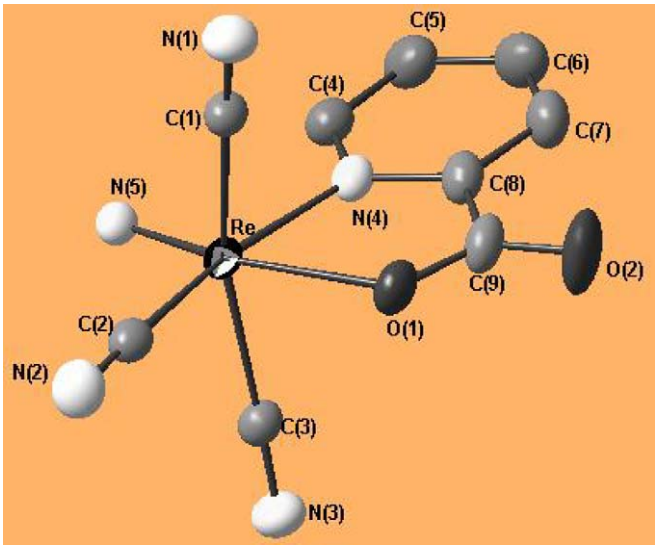

Fig. 1. Perspective view of the $[ReN(\eta^2\text{-pic})(CN)_3]^{2-}$ ion with atomic labeling scheme.

The rhenium atom has a distorted octahedral geometry and is surrounded by the nitrido ligand, three cyano groups an a picolinate anion that is bonded bidentally via the oxygen and nitrogen atoms. The distortion has two main features namely a displacement of 0.2979(2) Å of the rhenium from the equatorial C(1), C(2), C(3) and N(4) plane towards the nitrido ligand and a 13.3° distortion of the Re–O(1) bond from the expected linear N(5)–Re–O(1) axis. The latter is mainly the result of bite angle restrictions due to the five-membered chelate ring. The former displacement is typical for $[MO(L)(CN)_4]^{m-}$ or $[MN(L)(CN)_4]^{n-}$ complexes where different bond strengths along the *trans* O=M–L or N≡M–L moieties prevail [26]. The Re≡N(5) bond distance is 1.655(3) Å and may be compared with the corresponding bond length in $[ReN(N_3)(CN)_4]^{3-}$ [27] (1.65(2) Å), $[ReN(H_2O)(CN)_4]^{2-}$ [24] (1.639(8) Å) and $[ReN(CN)_5]^{3-}$ [28] (1.68(1) Å). The Re–O(1) bond length of 2.289(3) Å is significantly shorter than the 2.496(7) Å of the Re–O bond length in $[ReN(H_2O)(CN)_4]^-$ [24], but longer than the same bond in the $[WO(\eta^2\text{-pic})(CN)_3]^{2-}$ and the $[MoO(\eta^2\text{-pic})(CN)_3]^{2-}$ anions [13,29] (2.171(8) and 2.191(2) Å, respectively). The latter result fits in well with the general tendency where the bond distances in the rhenium-nitrido complexes are longer than the corresponding bonds in the molybdenum(IV), tungsten(IV) and rhenium(V) oxo complexes [30–32]. The carboxylate oxygen of the picolinate ligand is bonded *trans* to the nitrido ligand with a N(5)≡Re–O(1) bond angle of 166.5(1)°. This value corresponds well with the bond angles of 164.7(5)° and 162.0(1)° which was obtained for the same bonds in $[WO(\eta^2\text{-pic})(CN)_3]^{2-}$ and the $[MoO(\eta^2\text{-pic})(CN)_3]^{2-}$, respectively. The pyridine nitrogen of the picolinate ligand with a N(5)–Re–N(4) bond angle of 94.2(2)° and a Re–N(4) bond distance of 2.169(3) Å compares favourably with the data of $[WO(\eta^2\text{-pic})(CN)_3]^{2-}$ (92.2(5)° and 2.188(13) Å). The rest of the bond distances and angles in the picolinate ligand are normal and agrees well with those found in other complexes containing the same bidentate ligand [13,29].

The Re–C–N chains are nearly linear (ranging between 174.8(4)° and 178.0(4)°). Another interesting aspect of this structure is that the rhenium cyano bond length *trans* to the pyridine nitrogen of the picolinate anion is shorter than the other two metal cyano bond lengths (*trans* with respect of one another). The Re–C(2) is 2.067(5) Å compared to the 2.105(4) and 2.111(4) Å of the other two metal cyano bond lengths. The same tendency was observed for the corresponding tungsten complex. The phenomenon is attributed to weak or no π-bonding capability of the pyridine nitrogen of the picolinate anion. This leads to extensive π-shortening of the Re–C bond due to back-bonding from the metal to the π^*-orbital of the cyanide ligand. This shortening of the metal cyanide bond can also be explained in terms of the thermodynamic *trans*-influence of the different ligands. The cyanide ligand has a greater thermodynamic *trans* influence than the nitrogen of the picolinate anion. This will also lead to a shortening of the Re–C bond *trans* to the nitrogen compared to the two *trans*-orientated cyanide ligands.

This structure determination is the first rhenium-nitrido cyano complex in which a bidentate ligand is bonded to the metal center.

3.3. Kinetics

The UV/Vis spectra taken at 80 °C of the reaction between $[ReN(H_2O)(CN)_4]^{2-}$ and pic^- (Fig. 2) showed the formation of two distinctive peaks, one at 355 nm (B) and the other at 400 nm (C). It was decided to follow the substitution reaction at 400 nm. The formation of these peaks correspond to formation of the final complex, $[ReN(\eta^2\text{-pic})(CN)_3]^{2-}$. Two different reactions were observed at close inspection of absorbance versus time spectra at this temperature. The first reaction was relatively fast and resulted in a decrease in absorption at 400 nm (A in Fig. 2). The second reaction was much slower (B and C in Fig. 2) and yielded the UV/Vis spectrum which was identical to that of the final product. A reaction mechanism is proposed in Scheme 1 for all the reactions which are possible under the experimental conditions that prevailed during the study.

The low solubility of the picolinic acid at pH values lower than 5 ($pK_{a(picH)} = 5.52$ [33]) restricted the concentration range in which the reactions could be performed and no reactions were observed between the rhenium complex and the picolinic acid at or below a pH of 4. This completely eliminates the k_4 and k_{-4} pathway from the final rate law.

The crystal structure determination clearly indicates that both the aqua and a cyano ligand are replaced during the substitution reaction. Previous studies [27,28] have indicated that the substitution of the aqua ligand from $[ReN(H_2O)(CN)_4]^{2-}$ by ligands such as $CN^-$and N_3^- are relatively fast, while the ring-closure step was found to be rate-determining [13] for the reaction between $[WO(H_2O)(CN)_4]^{2-}$ and pic^-. The fast reaction that was observed in this study is thus also regarded as the substitution of the aqua ligand to form the mono substituted $[ReN(\eta^1\text{-pic})(CN)_4]^{2-}$ complex.

Figs. 3 and 4 illustrate the pH dependence on rate of the reaction for both the fast and slow reactions, respectively, while Fig. 5 illustrates the effect of pH on the absorbance of the reaction mixture. Figs. 6 and 7 illustrate the temperature and $[pic]_T$ dependence of the fast and slow reactions at low pH (pH ~8), respectively, while Fig. 8 illustrates the temperature and $[pic]_T$ dependence of the slow reaction at high pH (pH ~12.5). The influence of pH on the reactivity of the incoming ligand was investigated at low pH (between 4 and 8) and these results are given in Fig. 9.

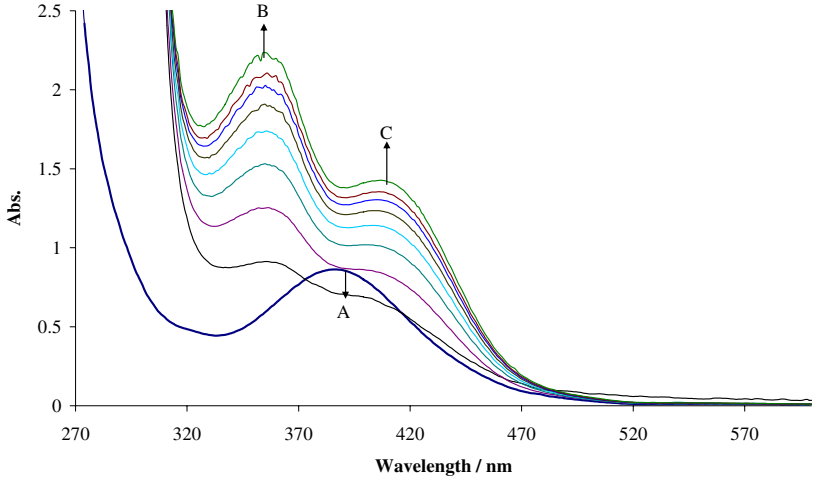

Fig. 2. UV–Vis spectral changes during the reaction between $[ReN(H_2O)(CN)_4]^{2-}$ and picolinic acid ($[pic]_T$), $T = 80.3$ °C, pH 8.04, $[ReN(H_2O)(CN)_4{}^{2-}] = 1.0 \times 10^{-3}$ M, $[pic]_T = 1.0$ M: A = initial fast reaction, B and C = subsequent slow reaction. Time intervals 1.0 min.

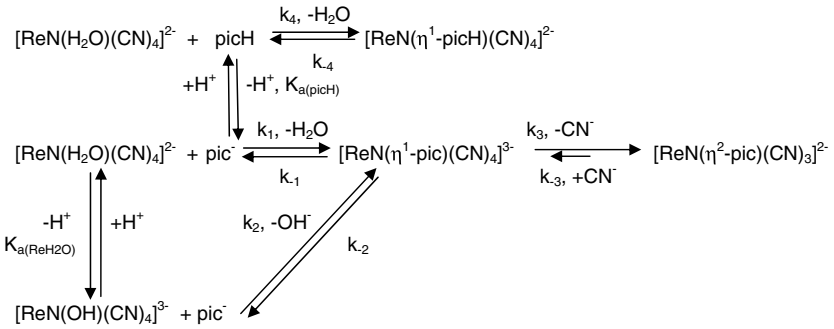

Scheme 1.

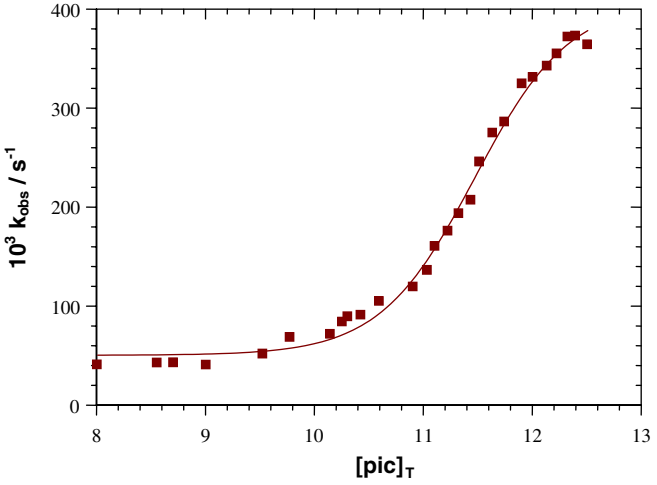

Fig. 3. Plot of k_{obs} vs. pH, $T = 40.3$ °C, $[ReN(H_2O)(CN)_4^{2-}] = 1.0 \times 10^{-2}$ M, $[pic]_T = 0.1$ M, $\lambda = 400$ nm, $\mu = 1.0$ M $NaClO_4$.

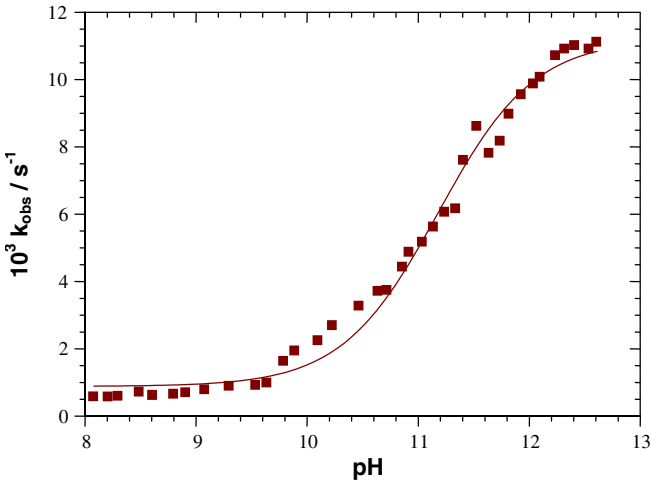

Fig. 4. Plot of k_{obs} vs. pH, $T = 80.2$ °C, $[ReN(H_2O)(CN)_4^{2-}] = 1.0 \times 10^{-3}$ M, $[pic]_T = 0.1$ M, $\lambda = 400$ nm, $\mu = 1.0$ M $NaClO_4$.

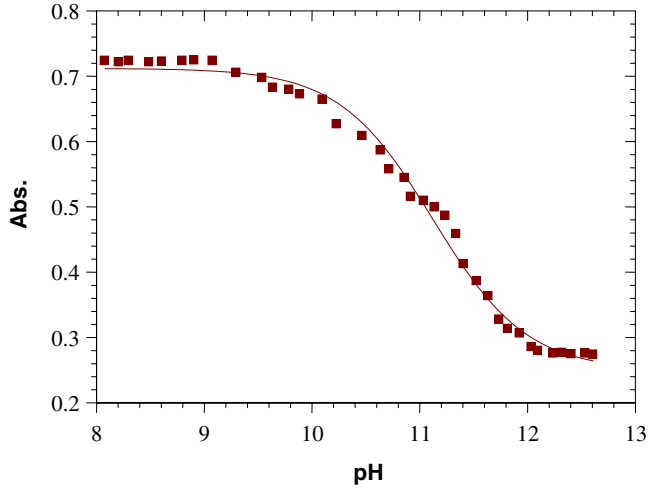

Fig. 5. Plot of absorbance vs. pH, $T = 80.2$ °C, $[ReN(H_2O)(CN)_4^{2-}] = 1.0 \times 10^{-3}$ M, $[pic]_T = 0.1$ M, $\lambda = 400$ nm, $\mu = 1.0$ M $NaClO_4$.

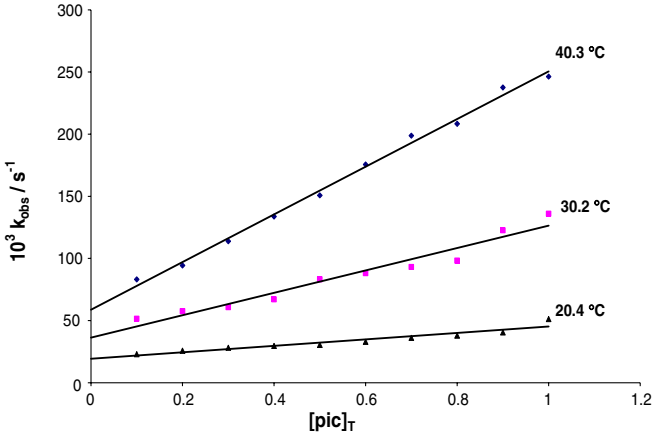

Fig. 6. Plot of k_{obs} vs. $[pic]_T$ at different temperatures, pH 8.05, $[ReN(H_2O)(CN)_4^{2-}] = 1.0 \times 10^{-2}$ M, $\lambda = 400$ nm, $\mu = 1.0$ M $NaClO_4$.

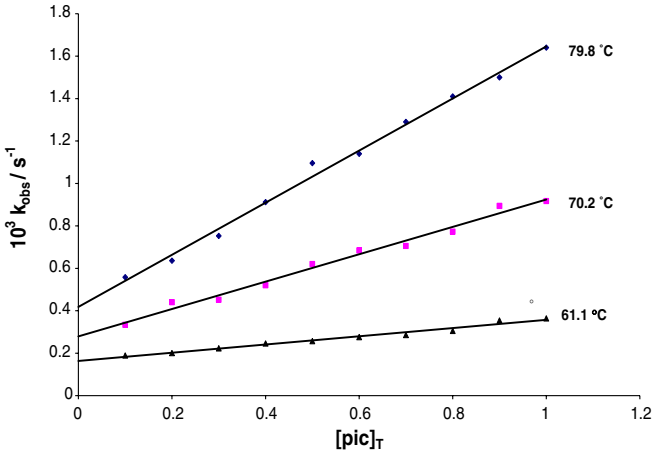

Fig. 7. Plot of k_{obs} vs. $[pic]_T$ at different temperatures, pH 8.06, $[ReN(H_2O)(CN)_4^{2-}] = 1.0 \times 10^{-3}$ M, $\lambda = 400$ nm, $\mu = 1.0$ M $NaClO_4$.

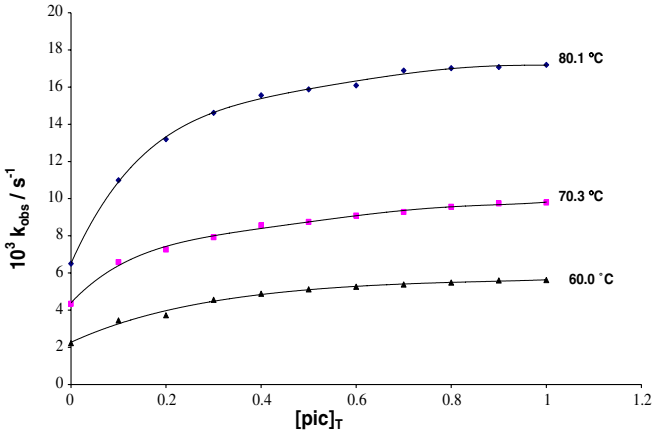

Fig. 8. Plot of k_{obs} vs. $[pic]_T$ at different temperatures, pH 12.6, $[ReN(H_2O)(CN)_4^{2-}] = 1.0 \times 10^{-3}$ M, $\lambda = 400$ nm, $\mu = 1.0$ M $NaClO_4$.

The stability constant (K_{eq}, Table 4) for the overall reaction was spectrophotometrically determined by a least-square fit of absorbance versus $[pic]_T$ to Eq. (3) and

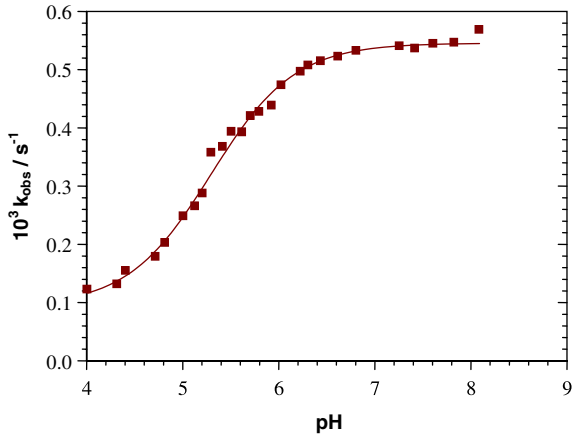

Fig. 9. Plot of k_{obs} vs. pH, $T = 80.3$ °C, $[ReN(H_2O)(CN)_4^{2-}] = 1.0 \times 10^{-3}$ M, $[pic]_T = 0.1$ M, $\lambda = 400$ nm, $\mu = 1.0$ M $NaClO_4$.

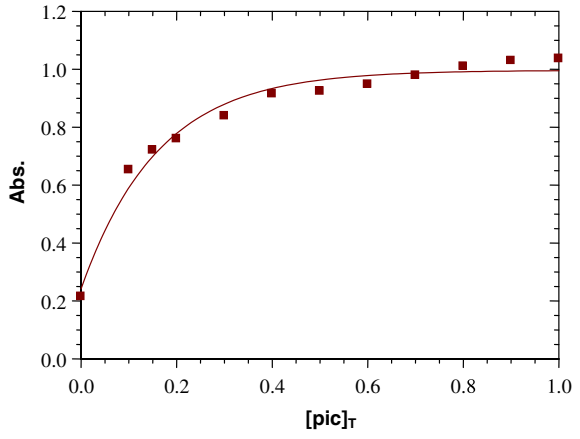

Fig. 10. Plot of absorbance vs. $[pic]_T$, $T = 79.8$ °C, pH ≈8.06, $[ReN(H_2O)(CN)_4^{2-}] = 1.0 \times 10^{-3}$ M, $\lambda = 400$ nm, $\mu = 1.0$ M $NaClO_4$.

illustrated in Fig. 10. This equation is derived using Beer's law, mass balance as well as the definition of K'' for the overall reaction.

$$A = \frac{A_{ReH_2O} + A_{Repic}K''[pic]_T}{1 + K''[pic]_T}, \quad (3)$$

where A_{ReH_2O} = absorbance of $[ReN(H_2O)(CN)_4]^{2-}$, A_{Repic} = absorbance of $[ReN(\eta^2\text{-pic})(CN)_3]^{2-}$ and $[pic]_T$ = analytical concentration of picolinic acid.

The acid dissociation constant for the $[ReN(H_2O)(CN)_4]^{2-}$ complex, $K_{a(ReH_2O)}$, were calculated from the experimental data in Fig. 5 which were fitted to Eq. (4) and the value for $K_{a(ReH_2O)}$ is reported in Table 4

$$A = \frac{A_{ReH_2O}K_{a(ReH_2O)} + A_{ReOH}[H^+]}{K_{a(ReH_2O)} + [H^+]}, \quad (4)$$

where A_{ReH_2O} = absorbance of $[ReN(H_2O)(CN)_4]^{2-}$ and A_{ReOH} = absorbance for $[ReN(OH)(CN)_4]^{3-}$.

3.4. Fast reaction

The rate law corresponding to the fast reaction in the biphasic time–concentration data, taking into account that the formation of the final product ($[ReN(\eta^2\text{-pic})(CN)_3]^{2-}$) is much slower (more so at the lower temperatures at which these reactions were followed) and does not influence the rate of the $[ReN(\eta^1\text{-pic})(CN)_4]^{3-}$ formation, is given in Eq. (5)

$$\begin{aligned}\text{Rate} = {} & k_1[ReN(H_2O)(CN)_4^{2-}][pic^-] \\ & + k_2[ReN(OH)(CN)_4^{3-}][pic^-] \\ & + k_4[ReN(H_2O)(CN)_4^{2-}][picH] \\ & - k_{-1}[ReN(\eta^1\text{-pic})(CN)_4^{3-}] \\ & - k_{-2}[ReN(\eta^1\text{-pic})(CN)_4^{3-}][OH^-] \\ & - k_{-4}[ReN(\eta^1\text{-picH})(CN)_4^{2-}]. \end{aligned} \quad (5)$$

At a pH between 4 and 6 ($[H^+] \gg K_{a(ReH_2O)}$, and k_2, $k_{-2} \sim 0$), the pseudo first-order rate constant is given by

$$\begin{aligned} k_{obs} = {} & (k_1 + k_4[H^+]/K_{a(picH)})(1 + [H^+]/K_{a(picH)})[pic]_T \\ & + (k_{-1} + k_{-4}[H^+]/K_{a(picH)})/(1 + [H^+]/K_{a(picH)}), \end{aligned} \quad (6)$$

where $[pic]_T$ represents the total picolinate/picolinic acid concentration.

The pseudo first-order rate constant ($[pic]_T > [Re]_t$) at higher pH (pH between 8 and 13) is given by

$$\begin{aligned} k_{obs} = {} & (k_1 + k_2K_{a(ReH_2O)}/[H^+])/(1 + K_{a(ReH_2O)}/[H^+]) \\ & \times [pic]_T + k_{-1} + k_{-2}[OH^-]. \end{aligned} \quad (7)$$

Eq. (7) simplifies to Eq. (8) at a pH < 9 ($pK_{a(ReH_2O)} \sim 11.6$)

$$k_{obs} = k_1[pic]_T + k_{-1}. \quad (8)$$

Eq. (8) predicts a straight line with slope k_1 and an intercept of k_{-1} ($[OH^-]$ very small). The experimental k_{obs} versus $[pic]_T$ data obtained at the three different temperatures (Fig. 6) were used to calculate the values for k_1 and k_{-1} using a least-squares fit to Eq. (8) and these values are reported in Table 3. The values of k_2, $K_{a(ReH_2O)}$ and k_{-2} were calculated from Eq. (7), using the k_1 and k_{-1} values from the pH variation (Fig. 3) and are also reported in Table 3.

3.5. Slow reaction

From Scheme 1 the overall rate law for the slow reaction is given by

$$\begin{aligned}\text{Rate} = {} & k_3[ReN(\eta^1\text{-pic})(CN)_4^{3-}] - k_{-3}[CN^-] \\ & \times [ReN(\eta^2\text{-pic})(CN)_4^{2-}] \\ = {} & k_{obs}([ReN(\eta^1\text{-pic})(CN)_4^{3-}] \\ & + [ReN(H_2O)(CN)_4^{2-}] \\ & + [ReN(OH)(CN)_4^{3-}]) - k_{-3}[CN^-]. \end{aligned} \quad (9)$$

The pseudo first-order rate constant ($[pic]_T > [Re]_T$) is given by

Table 3
Kinetic data for the fast reaction between $[ReN(H_2O)(CN)_4]^{2-}$ and $[pic]_T$, $\lambda = 400$ nm $\mu = 1.0$ M ($NaClO_4$)

Temperature (°C)	Constant	Value
40.3	k_1 (M^{-1} s^{-1})[a]	$1.92(5) \times 10^{-1}$
	k_1 (M^{-1} s^{-1})[b]	$5.3(3) \times 10^{-1}$
	k_{-1} (s^{-1})[a]	$5.9(3) \times 10^{-2}$
	k_{-1} (s^{-1})[b]	$5.9(3) \times 10^{-2}$
	K_1 (M^{-1})[c]	3.3(1)
	k_2 (M^{-1} s^{-1})[b]	4.1(2)
	k_{-2} (s^{-1})[b]	$1.0(1) \times 10^{-3}$
30.2	k_1 (M^{-1} s^{-1})[a]	$8.98(7) \times 10^{-2}$
	k_{-1} (s^{-1})[a]	$3.65(5) \times 10^{-2}$
	K_1 (M^{-1})[c]	2.46(1)
20.4	k_1 (M^{-1} s^{-1})[a]	$2.1(1) \times 10^{-2}$
	k_{-1} (s^{-1})[a]	$2.11(5) \times 10^{-2}$
	K_1 (M^{-1})[c]	1.0(2)
	$pK_{a(ReH_2O)}$[b]	11.43(2)
	$\Delta H^{\neq}$ (k_1) kJ mol^{-1}	82.5(2)
	$\Delta S^{\neq}$ (k_1) J K^{-1} mol^{-1}	5.01(6)
	$\Delta H^{\neq}$ (k_{-1}) kJ mol^{-1}	36.8(1)
	$\Delta S^{\neq}$ (k_{-1}) J K^{-1} mol^{-1}	−151.4(1)

[a] Slope and intercept, Fig. 6, Eq. (8).
[b] Data in Fig. 3, Eq. (7).
[c] $K_1 = k_1/k_{-1}$.

$$k_{obs} = (k_3K_1 + k_3K_2K_{a(ReH_2O)}/[H^+])[pic]_T/(K_1[pic]_T + K_2[pic]_TK_{a(ReH_2O)}/[H^+] + K_{a(ReH_2O)}/[H^+] + 1) + k_{-3}. \quad (10)$$

Eq. (10) predicts a non-linear relationship between k_{obs} and $[pic]_T$. The experimental results obtained from the plot of k_{obs} versus $[pic]_T$ in Fig. 7 (at pH ~8) clearly show a linear relationship between these two variables indicating that the term $K_1[pic]_T \ll 1$, Eq. (10) simplifies to Eq. (11)

$$k_{obs} = (k_3K_1 + k_3K_2K_{a(ReH_2O)}/[H^+]) \times [pic]_T/(K_2[pic]_TK_{a(ReH_2O)}/[H^+] + K_{a(ReH_2O)}/[H^+] + 1) + k_{-3}. \quad (11)$$

At a pH well below the $pK_{a(ReH_2O)}$, Eq. (11) simplifies further to

$$k_{obs} = k_3K_1[pic]_T + k_{-3}. \quad (12)$$

This equation predicts a straight line with slope k_3K_1 and intercept k_{-3}. The experimental results in Fig. 7 were fitted to Eq. (12) to yield the slopes and intercepts. The values for the different rate constants are reported in Table 4.

The reaction was also followed at a pH (between 4 and 8) where the incoming ligand changed from the protonated picolinic acid (picH) to the free picolinate anion (pic^-). These results are shown in Fig. 9 and the values for k_3K_1 and $pK_{a(picH)}$ were fitted to Eq. (13), where $K_{a(picH)}$ represents the acid dissociation constant of picolinic acid and are reported in Table 4

$$k_{obs} = k_3K_1[pic]_T/(1 + [H^+]/K_{a(picH)}) + k_{-3}, \quad (13)$$

where $[pic]_T = [pic^-] + [picH]$.

Table 4
Kinetic data for the slow reaction between $[ReN(H_2O)(CN)_4]^{2-}$ and $[pic]_T$, $\lambda = 400$ nm $\mu = 1.0$ M ($NaClO_4$)

Temperature (°C)	Constant	Value
80	k_3K_1 (M^{-1} s^{-1})[a]	$1.23(3) \times 10^{-3}$
	k_3 (s^{-1})[b]	$1.84(2) \times 10^{-2}$
	k_3 (s^{-1})[c]	$1.85(2) \times 10^{-2}$
	k_3 (s^{-1})[d]	$6.8(1) \times 10^{-2}$
	k_{-3} (M^{-1} s^{-1})[a]	$4.2(2) \times 10^{-4}$
	k_{-3} (M^{-1} s^{-1})[c]	$7.72(1) \times 10^{-4}$
	k_{-3} (M^{-1} s^{-1})[d]	$9.3(1) \times 10^{-5}$
	K_1 (M^{-1})[c]	$6.6(1) \times 10^{-2}$
	K_1 (M^{-1})[d]	$6.6(1) \times 10^{-2}$
	K_1 (M^{-1})[e]	$6.6(1) \times 10^{-2}$
	K_2 (M^{-1})[b]	14.8(1)
	K_2 (M^{-1})[c]	13.99(3)
	K_3[f]	731(1)
	K_{eq}[g]	5.2(4)
	$pK_{a(Re\text{-}H_2O)}$[c]	11.54(6)
	$pK_{a(picH)}$[d]	5.29(2)
	$pK_{a(pic)}$	5.52 [33]
	$pK_{a(ReH_2O)}$[h]	11.09(3)
70	k_3K_1 (M^{-1} s^{-1})[a]	$6.3(3) \times 10^{-4}$
	k_3 (s^{-1})[b]	$1.01(2) \times 10^{-2}$
	k_{-3} (M^{-1} s^{-1})[a]	$2.8(1) \times 10^{-4}$
	K_1 (M^{-1})[e]	$6.3(1) \times 10^{-2}$
	K_2 (M^{-1})[b]	14.1(2)
60	k_3K_1 (M^{-1} s^{-1})[a]	$1.96(6) \times 10^{-4}$
	k_3 (M^{-1} s^{-1})[b]	$6.04(1) \times 10^{-3}$
	k_{-3} (M^{-1})[a]	$1.7(4) \times 10^{-4}$
	K_1 (M^{-1})[e]	$3.2(5) \times 10^{-2}$
	K_2 (M^{-1})[b]	9.5(1)
	$\Delta S^{\neq}$ (k_3) J K^{-1} mol^{-1}	−133.4(3)
	$\Delta H^{\neq}$ (k_3) kJ mol^{-1}	51.7(5)

[a] From slope and intercept, Fig. 7, Eq. (12).
[b] Data in Fig. 4, Eq. (11).
[c] Data in Fig. 7, Eq. (11).
[d] Data Fig. 9, Eq. (13).
[e] $K_1 = k_3K_1/k_3$.
[f] $K_3 = k_3/k_{-3}$.
[g] Data in Fig. 10, Eq. (3).
[h] Data in Fig. 5, Eq. (4).

The non-linear experimental data reported in Fig. 8 was fitted to Eq. (11) (pH between 8 and 12) and the final rate and equilibrium constants calculated are reported in Table 4. As was the case for the fast reaction, it appeared that the complex is also reactive at the pH where $[ReN(OH)(CN)_4]^{3-}$ is the predominant species in solution.

The reactivity of the final product $[ReN(\eta^2\text{-pic})(CN)_3]^{2-}$ towards CN^- ions was confirmed with the addition of free CN^- to a solution containing the final product (Fig. 11), but these results not only point to the reverse reaction, k_{-3}, but also to successive further cyanide substitution of the picolinate anion from the coordination sphere [14].

The $\Delta H^{\neq}$ and $\Delta S^{\neq}$ values for the k_1, k_{-1} and k_3 paths were obtained from a least-squares fit of the k_3 versus temperature data to the Eyring–Polanyi equation and are reported in Tables 3 and 4.

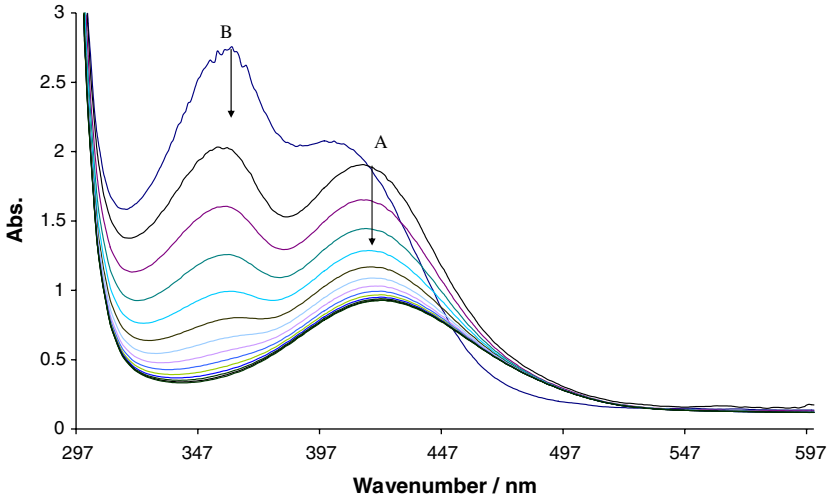

Fig. 11. UV/Vis spectral changes during the reaction between $[ReN(\eta^2\text{-pic})(CN)_3]^{2-}$ (1.0×10^{-3} M), with [NaCN] = 1.0 M, $T = 70.3$ °C, pH ≈8.01. Time intervals of 0.1 min.

4. Discussion

The reaction between $[ReN(H_2O)(CN)_4]^{2-}$ and picolinate, as presented in Scheme 12, is largely based on the results obtained from previous kinetic and structural studies. Monodentate substitution reactions between $[ReN(H_2O)(CN)_4]^{2-}$ and CN^- or N_3^- [27,28] clearly indicate that only the aqua ligand is substituted in a relatively fast reaction and that the rest of the coordination sphere is left unchanged (except for an increase in octahedral distortion [14,27]). A comparison between the aqua substitution rate for the $[ReX(H_2O)(CN)_4]^{n-}$ complexes ($k_1 = 3.48(4) \times 10^{-3}\ M^{-1}\ s^{-1}$ at 25 °C for NCS^- for $X = O^{2-}$ and $k_1 = 7.2(4) \times 10^3\ M^{-1}\ s^{-1}$ for CN^- at 25 °C for $X = N^{3-}$) clearly indicated that the Re–OH_2 bond lengths (2.142(7) and 2.496(7) Å for $[ReO(H_2O)(CN)_4]^-$ and $[ReN(H_2O)(CN)_4]^{2-}$, respectively) is a very good indicator of the lability of the complex towards substitution reactions. The relatively large *trans* influence of the terminal ligand, resulting in the labilisation of the *trans* ligand, is clearly illustrated by the *cis* and *trans* cyano bond lengths in the $[ReN(CN)_5]^{3-}$ complex. The average equatorial Re–CN bond length is equal to 2.12(1) Å while the apical Re–CN bond length is equal to 2.39(1) Å.

The final products for these reactions, as well as a number of other iso-electronic complexes all revealed that the incoming group is situated *trans* with respect to the strongly bonded terminal ligand. It is well known [34] and in accordance with the present structure determination that the carboxylate group in the picolinate ion will coordinate before the pyridine nitrogen atom. It is therefore concluded that the first step in the reaction between the starting complex and the picolinate ion in this study is the substitution of the aqua ligand by the carboxylate oxygen and the subsequent ring-closure step (slow) with the displacement of a cyano group with bonding of the pyridine nitrogen to the metal center.

The rate of aqua substitution in the $[ReN(H_2O)(CN)_4]^{2-}$ complex by the picolinate anion was determined as $2.1(1) \times 10^{-2}\ M^{-1}\ s^{-1}$ at 20.4 °C which is substantially slower (factor 10^5) than the corresponding reaction when CN^- was the incoming group. This is due to the difference in the coordination capability of the two ligands which is also manifested in the stability constant for the two different complexes which were determined as $471(1)\ M^{-1}$ for $[ReN(CN)_5]^{3-}$ and $1.0(2)\ M^{-1}$ (k_1/k_{-1}) for the $[ReN(\eta^1\text{-pic})(CN)_4]^{3-}$, respectively, indicating the weak σ-donating ability of the COO^- group compared to that of the cyano group. The same tendency was observed for the corresponding reaction between $[WO(H_2O)(CN)_4]^{2-}$ and picolinate where a decrease in substitution rate with a factor of 2.5 was observed when compared to the rate with CN^- as incoming group [23] . A decrease of a factor of 10^3 was also observed for the stability constant of $[WO(H_2O)(CN)_4]^{2-}$ and picolinate when compared to that of the reaction between $[WO(H_2O)(CN)_4]^{2-}$ and CN^- [23] .

A very interesting result from this study is the reactivity of the $[ReN(OH)(CN)_4]^{3-}$ complex towards the picolinate anion. Results obtained in the pH variation as indicated in Fig. 3 clearly indicate acceleration in the substitution rate with an increase in pH. The calculated k_2 value at 40.3 °C of $4.1(2)\ M^{-1}\ s^{-1}$ is a factor 20 faster than the corresponding aqua reaction. These results are quite novel in the sense that in all the previous studies, except maybe for the substitution between $[ReN(H_2O)(CN)_4]^{2-}$ and CN^-, indications are that the hydroxo complexes are normally inert with respect to substitution. In the case of the reaction between $[ReN(H_2O)(CN)_4]^{2-}$ and CN^- [14] a hydroxo substitution rate of $1.5(4) \times 10^1\ M^{-1}\ s^{-1}$ was obtained, but due to the large error was interpreted as zero and therefore non-reactive towards the incoming ligand.

The acid dissociation constant, $pK_{a(ReH_2O)}$ for the $[ReN(H_2O)(CN)_4]^{2-}$ complex was kinetically determined as 11.43(2) (Fig. 3) and spectrophotometrically as

11.09(3) (Fig. 5). These values correspond very favourably with the 11.6(2) that was previously determined [14].

The relatively small activation enthalpy and entropy (Table 3) for the forward reaction is compatible with the $\Delta H^{\neq} = 70(9)$ kJ mol^{-1} and $\Delta S^{\neq} = -12(31)$ J K^{-1} mol^{-1} values that was obtained for the corresponding reaction between $[WO(H_2O)(CN)_4]^{2-}$ and picolinate.

The substitution of the CN^- group by the pyridine nitrogen atom of the picolinate anion (slow reaction) was substantially slower than the aqua substitution and these reactions were studied at much higher temperatures. It is anticipated that the stronger bonded cyano ligand would be much more difficult to substitute than the more labile aqua ligand, hence the slower ring-closure step. The value for the ring-closure step for the $[ReN(\eta^1\text{-pic})(CN)_4]^{3-}$ to form the final $[ReN(\eta^2\text{-pic})(CN)_3]^{2-}$ complex at 80 °C was determined as $1.84(2) \times 10^{-2}$ s^{-1}. The pH variation as indicated in Fig. 4 also clearly illustrates the increase in substitution rate with an increase in pH. The stability constants calculated from these kinetic results clearly show that the k_2 pathway ($K_2 = 14.8$ M^{-1} compared to $K_1 = 6.6(1) \times 10^{-2}$ M^{-1}) is favoured above the k_1 pathway for the fast reaction, while the K_3 value of 731(1) M (slow reaction) is substantially larger than the previous two (K_1 and K_2) stability constants. These results clearly indicate an increase towards thermodynamic stability which is normally associated with chelation reactions. The $pK_{a(ReH_2O)}$ value for the $[ReN(H_2O)(CN)_4]^{2-}$ complex of 11.54(6) is also in good agreement with the values obtained for the fast reaction.

The reaction between the $[ReN(H_2O)(CN)_4]^{2-}$ and picolinate/picolinic acid, see Fig. 9, at low pH values (k_4, $k_{-4} \sim 0$) yielded a $pK_{a(picH)}$ value of 5.29(2) for the picolinic acid which agrees also very well with the literature value of 5.52.

The activation entropy, $\Delta S^{\neq}$, for the slow reaction (Table 4) is clearly negative (−133.4(3) J K^{-1} mol^{-1}), indicating associative activation during the last step of the reaction. It is anticipated that the strongly bonded cyano group will not dissociate easily and that substantial bond formation between the picolinate anion and the metal complex takes place before the dissociation of the cyanide group. An increase in coordination number for these transition metal complexes is well known, for example the isolation of the $[Re(CN)_7]^{4-}$ complex [35]. The free energy of activation, $\Delta G^{\neq}$, for the fast reaction (81.1 kJ mol^{-1}) has a very large contribution from the activation enthalpy (82.5 kJ mol^{-1}) indicating that this particular reaction is mainly enthalpy driven whilst the reverse process is more entropy driven. The $\Delta G^{\neq}$ for the slow reaction of 98.8 kJ mol^{-1} (80 °C) on the other hand has a large activation entropy component (47.1 kJ mol^{-1}), pointing to a substantial entropy contribution resulting from stereochemical changes in the final reaction.

Additional free cyanide ions was added to a solution containing $[ReN(\eta^2\text{-pic})(CN)_3]^{2-}$ complex in an effort to investigate the reverse reaction of the slow chelating step (k_{-3} in Scheme 12). A relatively fast reaction was observed (see Fig. 11) and a $[CN^-]_T$ variation clearly showed a linear dependence [36] in cyanide concentration. The slope in the plot of k_{obs} versus $[CN^-]_T$ (suppose to be k_{-3}) is however orders of magnitude smaller than the values obtained in this study while the intercept (suppose to be k_3) is orders of magnitude larger than the present values obtained for the k_3 pathway. The final spectrum (Fig. 11) with absorption maximums at 273 and 420 nm corresponds very well with the values of 272.2 (not shown in Fig. 11 due to large extinction coefficient) and 422 nm obtained for the $[ReN(CN)_5]^{3-}$ complex in a previous study [14]. These results suggested that the reaction sequence between $[ReN(\eta^2\text{-pic})(CN)_3]^{2-}$ and CN^- ions is as follows:

$$[ReN(\eta^2\text{-pic})(CN)_3]^{2-} + CN^- \rightarrow [ReN(\eta^1\text{-pic})(CN)_4]^{3-} \rightarrow [ReN(CN)_5]^{3-} + pic^- \quad (14)$$

and that the picolinato anion is completely substituted from the coordination sphere.

Acknowledgement

The authors thank the Research Fund of this University for financial support.

Appendix A. Supplementary data

Supplementary data are available from the CCDC, 12 Union Road, Cambridge CB2 1EZ, UK on request, CCDC No. 282758. Supplementary data associated with this article can be found, in the online version, at doi:10.1016/j.poly.2006.02.004.

References

[1] J.G. Leipoldt, S.S. Basson, A. Roodt, Adv. Inorg. Chem. 40 (1993) 297.
[2] V.W. Day, J.L. Hoard, J. Am. Chem. Soc. 90 (1968) 3374.
[3] S.J. Lippard, B.J. Russ, Inorg. Chem. 6 (1967) 1943.
[4] K. Weighardt, G. Backes-Dahmann, W.J. Holzbach, W.J. Swiridoff, J. Weiss, Z. Anorg. Allg. Chem. 499 (1983) 44.
[5] S.S. Basson, J.G. Leipoldt, I.M. Potgieter, A. Roodt, Inorg. Chim. Acta 103 (1985) 121.
[6] J.G. Leipoldt, S.S. Basson, A. Roodt, I.M. Potgieter, S. Afr. J. Chem. 39 (1986) 179.
[7] W. Purcell, A. Roodt, S.S. Basson, J.G. Leipoldt, Transition Met. Chem. 14 (1989) 369.
[8] A. Roodt, J.G. Leipoldt, E.A. Duetsch, J.C. Sullivan, Inorg. Chem. 31 (1992) 1080.
[9] W. Purcell, A. Roodt, S.S. Basson, J.G. Leipoldt, Transition Met. Chem. 15 (1990) 239.
[10] W. Purcell, A. Roodt, S.S. Basson, J.G. Leipoldt, Transition Met. Chem. 14 (1989) 224.
[11] A. Roodt, J.G. Leipoldt, S.S. Basson, I.M. Potgieter, Transition Met. Chem. 13 (1988) 336.
[12] S.S. Basson, J.G. Leipoldt, I.M. Potgieter, Inorg. Chim. Acta 87 (1984) 71.
[13] J.G. Leipoldt, S.S. Basson, A. Roodt, I.M. Potgieter, Transition Met. Chem. 11 (1986) 323.

[14] L.J. Damoense, W. Purcell, J.G. Leipoldt, Transition Met. Chem. 19 (1994) 619.
[15] H.J. Van der Westhuizen, S.S. Basson, J.G. Leipoldt, W. Purcell, Polyhedron 13 (1994) 717.
[16] H.J. Van der Westhuizen, S.S. Basson, J.G. Leipoldt, W. Purcell, Polyhedron 13 (5) (1994) 717.
[17] H.J. VanderWesthuizen, W. Purcell, S.S. Basson, Transition Met. Chem. 27 (2002) 506.
[18] N.P. Johnson, J. Chem. Soc. A (1969) 1843.
[19] Bruker, SAINT+. Version 6.02 (includes XPREP and SADABS), Bruker AXS Inc., Madison, WI, 1999.
[20] G.M. Sheldrick, SADABS, University of Göttingen, Germany, 1996.
[21] Bruker, SHELXTL. Version 5.1. (includes XS, XL, XP, XSHELL), Bruker AXS Inc., Madison, WI, 1999.
[22] A.L. Spek, J. Appl. Crystallogr. 36 (2003) 7.
[23] J. Smith, W. Purcell, G.J. Lamprecht, J.G. Leipoldt, Polyhedron 14 (1995) 1795.
[24] W. Purcell, I.M. Potgieter, L.J. Damoense, J.G. Leipoldt, Transition Met. Chem. 17 (1992) 387.
[25] J.L. Martin, J. Takas, Inorg. Chem. 14 (1975) 1358.
[26] A. Roodt, A. Abou-Hamdan, H.P. Engelbrecht, A.E. Merbach, Adv. Inorg. Chem. 49 (2000) 59.
[27] W. Purcell, I.M. Potgieter, L.J. Damoense, J.G. Leipoldt, Transition Met. Chem. 195 (1992) 217.
[28] W. Purcell, I.M. Potgieter, L.J. Damoense, J.G. Leipoldt, Transition Met. Chem. 16 (1991) 473.
[29] J. Szklarzewicz, A. Makula, D. Matoga, J. Fawcet, Inorg. Chim. Acta 358 (2005) 1749.
[30] A. Roodt, S.S. Basson, J.G. Leipoldt, Polyhedron 13 (1994) 599.
[31] W. Purcell, L.J. Damoense, J.G. Leipoldt, Inorg. Chim. Acta 195 (1992) 217.
[32] R.K. Murmann, E.O. Schlemper, Inorg. Chem. 10 (1971) 2352.
[33] B. Garcia, S. Ibeas, J.M. Leal, J. Phys. Org. Chem. 9 (1996) 593.
[34] D. Margerum, G. Caley, D. Weatherburn, D. Pagenkopf, in: A. Martell (Ed.), Coordination Chemistry, ACS Monograph 174, Washington, DC, 1978 (Chapter 1).
[35] J.-M. Manoli, C. Potvin, J.C.S. Brégeault, Dalton (1980) 192.
[36] T.N. Mtshali, W. Purcell, H.G. Visser, S.S. Basson (in press).

2. Experimental

2.1. Materials

Kpiv was synthesized in water by treatment of Hpiv with KOH in 1:1 molar ratio. Admtrz and adetrz were prepared according to the literature methods [13]. All other chemicals were commercial products and used as received.

2.2. Synthesis

2.2.1. $[Ni_2(\mu\text{-}H_2O)(\mu\text{-admtrz})_2(piv)_4(H_2O)_2]\cdot 13H_2O$ ($\mathbf{1}\cdot 13H_2O$)

To a 10 mL ethanol solution of $NiCl_2\cdot 6H_2O$ (0.2 g, 0.84 mmol) was added Kpiv (0.353 g, 2.52 mmol) and admtrz (0.094 g, 0.84 mmol) while stirring. The solution was stirred at room temperature for 17 h and then filtered. Green crystals of $\mathbf{1}\cdot 13H_2O$ were obtained by slow evaporation of the resulting solution, which readily lost lattice water molecules to give product **1** when they left their mother liquor at room temperature. The dried powder sample of product **1** was used for its characterization and magnetic study. Yield 0.050 g (15%). *Anal.* Calc. for **1** $C_{28}H_{58}N_8Ni_2O_{11}$: C, 42.03; H, 7.31; N, 14.00. Found: C, 41.74; H, 7.54; N, 13.72%. IR (KBr pellet, cm^{-1}): 3459 (m), 3300 (m), 3184 (m), 2962 (s), 2929 (m), 2871 (w), 1648 (w), 1528 (vs), 1485 (s), 1458 (w), 1415 (m), 1362 (m), 1268 (w), 1226 (m), 1098 (w), 1049 (w), 1029 (w), 905 (w), 879 (w), 792 (w), 608 (w), 554 (w).

2.2.2. $[Ni_2(\mu\text{-}H_2O)(\mu\text{-adetrz})_2(piv)_4]\cdot 3H_2O$ ($\mathbf{2}\cdot 3H_2O$)

To a 10 mL ethanol solution of $NiCl_2\cdot 6H_2O$ (0.2 g, 0.84 mmol) was added Kpiv (0.236 g, 1.68 mmol) and adetrz (0.236 g, 1.68 mmol) while stirring. The solution was stirred at room temperature for 17 h and then filtered. Green crystals of $\mathbf{2}\cdot 3H_2O$ were obtained by slow evaporation of the resulting solution, which readily lost lattice water molecules to give product **2** when they left their mother liquor at room temperature. The dried powder sample of product **2** was used for its characterization and magnetic study. Yield 0.034 g (10%). *Anal.* Calc. for **2** $C_{32}H_{62}N_8Ni_2O_9$: C, 46.86; H, 7.62; N, 13.66. Found: C, 46.89; H, 7.84; N, 13.37%. IR (KBr pellet, cm^{-1}): 3295 (m), 3216 (m), 3191 (m), 2977 (s), 2929 (m), 2873 (w), 1655 (m), 1525 (vs), 1486 (s), 1459 (m), 1434 (s), 1412 (m), 1372 (w), 1360 (m), 1285 (w), 1227 (m), 1142 (w), 1095 (w), 1054 (w), 904 (w), 878 (w), 791 (w), 609 (w).

2.3. Crystal structure determination

Data for $\mathbf{1}\cdot 13H_2O$ and $\mathbf{2}\cdot 3H_2O$ were collected on a Bruker SMART-CCD diffractometer with graphite monochromated Mo Kα ($\lambda = 0.71073$ Å) and corrected for absorption using SADABS program [14]. These two structures were solved by direct methods and refined on F^2 against all reflections by full-matrix least-squares methods with SHELXTL program [15]. The hydrogen atoms in two compounds were positioned geometrically and refined in the riding-model approximation. All non-hydrogen atoms were refined anisotropically. Some disorders were detected for the carbon atoms of the *t*-butyl groups in $\mathbf{1}\cdot 13H_2O$, which were refined over two sites, yielding occupation factors of 0.647(7), 0.647(7) and 0.647(7) for C8, C9 and C10, respectively. Crystal data and structure refinement details for $\mathbf{1}\cdot 13H_2O$ and $\mathbf{2}\cdot 3H_2O$ are summarized in Table 1. The selected bond distances and bond angles for $\mathbf{1}\cdot 13H_2O$ and $\mathbf{2}\cdot 3H_2O$ are given in Tables 2 and 3, respectively. The selected hydrogen bond distances and angles for $\mathbf{1}\cdot 13H_2O$ and $\mathbf{2}\cdot 3H_2O$ are given in Table 4.

2.4. Measurements

Elemental analyses (C, H and N) were carried out on a Perkin–Elmer 240C analytical instrument. IR spectra were recorded on a VECTOR 22 Bruker spectrophotometer with KBr pellets in the 4000–400 cm^{-1} region. Magnetic susceptibilities on powder samples of **1** and **2** were carried out with a Quantum Design MPMS-XL SQUID magnetometer in the 1.8–300 K range. The applied magnetic field was 0.2 T and diamagnetic corrections were made with Pascal's constants as -586×10^{-6} emu mol^{-1} for **1** and -595×10^{-6} emu mol^{-1} for **2**.

Table 1
Crystal data and structure refinement for $\mathbf{1}\cdot 13H_2O$ and $\mathbf{2}\cdot 3H_2O$

	$\mathbf{1}\cdot 13H_2O$	$\mathbf{2}\cdot 3H_2O$
Empirical formula	$C_{28}H_{84}N_8Ni_2O_{24}$	$C_{32}H_{68}N_8Ni_2O_{12}$
Formula weight	1034.45	874.36
T (K)	293(2)	293(2)
λ (Å)	0.71073	0.71073
Crystal system	monoclinic	trigonal
Space group	$P2/n$	$P3_221$
Unit cell dimensions		
a (Å)	16.423(4)	25.004(3)
b (Å)	9.890(2)	25.004(3)
c (Å)	17.093(4)	14.039(2)
β (°)	105.991(4)	
V (Å^3)	2669(1)	7601(2)
Z	2	6
D_{calc} (g cm^{-3})	1.287	1.146
μ(Mo Kα) (cm^{-1})	0.783	0.797
F(000)	1112	2808
Crystal size (mm)	$0.30\times0.12\times0.10$	$0.27\times0.13\times0.11$
θ Range (°)	2.02–26.00	1.63–26.00
Reflections collected	13 823	41 382
Independent reflections [R_{int}]	5207 [0.049]	9934 [0.054]
Reflections observed [$I > 2\sigma(I)$]	3740	8753
Parameters	320	535
Goodness-of-fit on F^2	1.045	1.073
R_1[a]	0.0891	0.0604
wR_2[b]	0.1289	0.1217
Largest difference peak and hole (e Å^{-3})	0.38 and −0.47	0.53 and −0.29

[a] $R_1 = \sum ||F_o| - |F_c|| / \sum |F_o|$.
[b] $wR_2 = [\sum w(|F_o|^2 - |F_c|^2) / \sum w|F_o|^2]^{1/2}$.

Table 2
Selected bond distances (Å) and angles (°) for $\mathbf{1}\cdot 13H_2O$[a]

Ni(1)–N(1)	2.084(3)	Ni(1)–O(2)	2.078(3)
Ni(1)–O(1)	2.095(2)	Ni(1)–O(4)	2.053(3)
Ni(1)–O(3)	2.066(3)	Ni(1)–N(2)$^{\#1}$	2.112(3)
Ni(1)···Ni(1)$^{\#1}$	3.444(2)		
O(3)–Ni(1)–O(1)	178.0(1)	O(2)–Ni(1)–O(1)	88.9(1)
O(4)–Ni(1)–O(3)	86.6(1)	N(1)–Ni(1)–O(1)	84.1(1)
O(4)–Ni(1)–O(2)	87.8(1)	O(4)–Ni(1)–N(2)$^{\#1}$	177.9(1)
O(3)–Ni(1)–O(2)	92.8(1)	O(3)–Ni(1)–N(2)$^{\#1}$	94.9(1)
O(4)–Ni(1)–N(1)	90.3(1)	O(2)–Ni(1)–N(2)$^{\#1}$	90.6(1)
O(3)–Ni(1)–N(1)	94.1(1)	N(1)–Ni(1)–N(2)$^{\#1}$	91.1(1)
O(2)–Ni(1)–N(1)	172.7(1)	O(1)–Ni(1)–N(2)$^{\#1}$	86.1(1)
O(4)–Ni(1)–O(1)	92.5(1)	Ni(1)$^{\#1}$–O(1)–Ni(1)	108.2(2)
N(2)–N(1)–Ni(1)	119.0(2)	N(1)–N(2)–Ni(1)$^{\#1}$	117.0(2)

[a] Symmetry transformations used to generate equivalent atoms: #1, $-x+3/2$, y, $-z+3/2$.

Table 3
Selected bond distances (Å) and angles (°) for $\mathbf{2}\cdot 3H_2O$[a]

A			
Ni(1)–O(2)	2.024(3)	Ni(1)–O(4)	2.084(2)
Ni(1)–N(2)$^{\#1}$	2.042(3)	Ni(1)–N(1)	2.097(3)
Ni(1)–O(1)	2.049(2)	Ni(1)–O(5)	2.121(3)
Ni(1)···Ni(1)$^{\#1}$	3.312(1)		
O(2)–Ni(1)–N(2)$^{\#1}$	94.8(1)	O(4)–Ni(1)–N(1)	97.1(1)
O(2)–Ni(1)–O(1)	89.6(1)	O(2)–Ni(1)–O(5)	86.9(1)
N(2)$^{\#1}$–Ni(1)–O(1)	87.6(1)	N(2)$^{\#1}$–Ni(1)–O(5)	164.6(1)
O(2)–Ni(1)–O(4)	86.4(1)	O(1)–Ni(1)–O(5)	107.7(1)
N(2)$^{\#1}$–Ni(1)–O(4)	103.8(1)	O(4)–Ni(1)–O(5)	61.0(1)
O(1)–Ni(1)–O(4)	168.2(1)	N(1)–Ni(1)–O(5)	93.1(1)
O(2)–Ni(1)–N(1)	176.1(1)	O(1)–Ni(1)–N(1)	86.6(1)
N(2)$^{\#1}$–Ni(1)–N(1)	86.2(1)	Ni(1)–O(1)–Ni(1)$^{\#1}$	107.8(2)
N(2)–N(1)–Ni(1)	117.6(2)	N(1)–N(2)–Ni(1)$^{\#1}$	112.8(3)
B			
Ni(2)–N(5)	1.996(3)	Ni(2)–O(9)	2.068(3)
Ni(2)–O(7)	2.047(3)	Ni(2)–O(8)	2.120(3)
Ni(2)–O(6)	2.063(2)	Ni(2)–N(6)$^{\#2}$	2.157(3)
Ni(2)···Ni(2)$^{\#2}$	3.340(1)		
N(5)–Ni(2)–O(7)	102.2(1)	O(7)–Ni(2)–O(9)	86.7(1)
N(5)–Ni(2)–O(6)	85.3(1)	O(6)–Ni(2)–O(9)	89.5(1)
O(7)–Ni(2)–O(6)	171.8(1)	N(5)–Ni(2)–O(8)	163.1(1)
N(5)–Ni(2)–O(9)	92.5(1)	O(7)–Ni(2)–O(8)	61.0(1)
O(6)–Ni(2)–O(8)	111.5(1)	O(6)–Ni(2)–N(6)$^{\#2}$	87.1 (1)
O(9)–Ni(2)–O(8)	85.7(1)	O(9)–Ni(2)–N(6)$^{\#2}$	176.6(1)
N(5)–Ni(2)–N(6)$^{\#2}$	87.9(1)	O(8)–Ni(2)–N(6)$^{\#2}$	95.0(1)
O(7)–Ni(2)–N(6)$^{\#2}$	96.5(1)	Ni(2)$^{\#2}$–O(6)–Ni(2)	108.1(2)
N(6)–N(5)–Ni(2)	121.7(2)	N(5)–N(6)–Ni(2)$^{\#2}$	113.0(2)

[a] Symmetry transformations used to generate equivalent atoms: #1, $x-y+1$, $-y+2$, $-z+4/3$; #2, $x-y+1$, $-y+2$, $-z+7/3$.

3. Results and discussion

3.1. Synthesis

Compounds $\mathbf{1}\cdot 13H_2O$ and $\mathbf{2}\cdot 3H_2O$ were obtained from the reaction of $NiCl_2\cdot 6H_2O$, Kpiv and the corresponding triazoles in ethanol at room temperature with 10–15%. A reaction mixture of $NiCl_2\cdot 6H_2O$, Kpiv and admtrz in a molar ratio of 1:3:1 gave pure $\mathbf{1}\cdot 13H_2O$ while $\mathbf{2}\cdot 3H_2O$ was synthesized from a reaction mixture of $NiCl_2\cdot 6H_2O$, Kpiv and adetrz in a molar ratio of 1:2:2. Some green uncharacterized powder samples were formed after the isolation of $\mathbf{1}\cdot 13H_2O$ and $\mathbf{2}\cdot 3H_2O$, which might be responsible for the low yields (10–15%). It was further found that the reaction mixture of the correct stoichiometric molar ratio (Ni:piv:triaz = 1:2:1) did not yield $\mathbf{1}\cdot 13H_2O$ and $\mathbf{2}\cdot 3H_2O$.

Table 4
Selected hydrogen bond distances (Å) and angles (°) for $\mathbf{1}\cdot 13H_2O$ and $\mathbf{2}\cdot 3H_2O$[a]

D–H···A	D–H	H···A	D···A	D–H···A
1 $\cdot 13H_2O$				
O(2)–H(2A)···O(6)	0.85	1.82	2.565(4)	146.0
O(1)–H(1A)···O(5)$^{\#1}$	0.85	1.93	2.595(3)	134.0
O(8)–H(8G)···O(3)$^{\#1}$	0.85	2.19	3.039(4)	178.9
O(9)–H(9H)···O(8)$^{\#1}$	0.85	2.38	2.882(4)	118.6
O(11)–H(11D)···O(7)$^{\#2}$	0.85	1.95	2.793(4)	170.5
O(2)–H(2C)···O(10)$^{\#3}$	0.85	1.94	2.746(4)	159.0
O(7)–H(7A)···O(5)$^{\#4}$	0.85	2.23	2.854(4)	130.5
N(4)–H(4A)···O(6)$^{\#4}$	0.89	2.14	3.030(4)	178.3
2 $\cdot 3H_2O$				
O(1)–H(1C)···O(3)	0.85	1.65	2.441(3)	154.7
O(6)–H(6C)···O(10)	0.85	1.72	2.528(3)	157.0
N(8)–H(8D)···O(5)	0.89	2.27	3.059(4)	148.0
N(8)–H(8F)···O(3)$^{\#1}$	0.89	2.23	3.053(4)	154.6
N(4)–H(4E)···O(8)$^{\#3}$	0.89	2.12	2.924(5)	150.6
O(16)–H(16F)···N(4)$^{\#4}$	0.85	2.42	2.951(8)	121.4
O(11)–H(11D)···O(12)$^{\#5}$	0.85	2.23	2.962(9)	144.7

[a] Symmetry transformations used to generate equivalent atoms: #1, $-x+3/2$, y, $-z+3/2$; #2, $x+1/2$, $1-y$, $z+1/2$; #3, x, $y+1$, z; #4, $x-1/2$, $1-y$, $z-1/2$ for $\mathbf{1}\cdot 13H_2O$; #1, $1+x-y$, $2-y$, $-z+4/3$; #3, y, $1+x$, $2-z$; #4, x, $y-1$, z; #5, $1+x-y$, $2-y$, $-z+1/3$ for $\mathbf{2}\cdot 3H_2O$.

3.2. IR spectroscopy

The IR spectra show an absorption peak at 1648 cm^{-1} for **1** and 1655 cm^{-1} for **2**, which can be assigned to the C=O stretching vibration of the pivalate ligand. And the *t*-butyl groups appear at frequencies at 1362 and 1226 cm^{-1} for **1**, and at 1372, 1360, and 1227 cm^{-1} for **2**. The IR spectra also exhibit a series of signals at 1528, 1485 and 1458 cm^{-1} for **1**, and at 1525, 1486 and 1459 cm^{-1} for **2**, which can be attributed to the triazole ring.

3.3. Crystal structures

3.3.1. $[Ni_2(\mu\text{-}H_2O)(\mu\text{-admtrz})_2(piv)_4(H_2O)_2]\cdot 13H_2O$ ($\mathbf{1}\cdot 13H_2O$)

The crystal structure of $\mathbf{1}\cdot 13H_2O$ consists of a dinuclear nickel compound **1** and thirteen lattice water molecules. The structure determination reveals that **1** has two six-coordinated Ni(II) centers, both with a distorted octahedral geometry, which are held together by two bridged admtrz ligands and one bridging water molecule (see Fig. 1). There is a twofold rotation axis going through O1 atom and the middle center of Ni1–Ni1$^{\#1}$ [symmetry

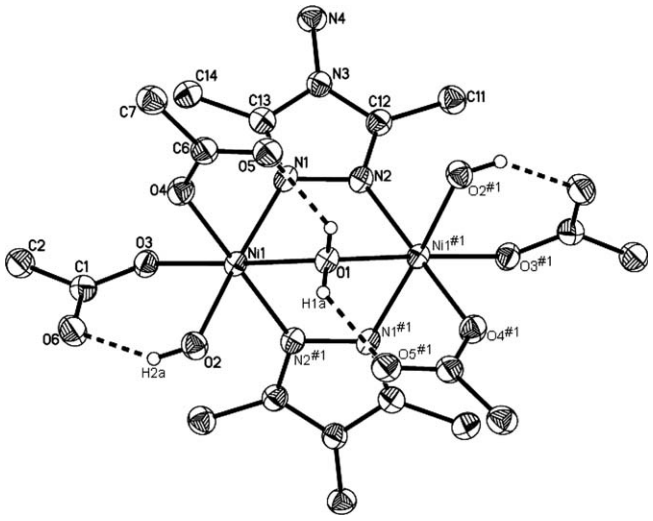

Fig. 1. ORTEP drawing (30% probability level) of $\mathbf{1} \cdot 13H_2O$, showing the atom-labeling scheme; all hydrogen atoms (except the hydrogen atoms involving the intramolecular hydrogen bonds), lattice water, and methyl groups in pivalates have been omitted for clarity [symmetry code: #1, $-x + 3/2$, y, $-z + 3/2$]. Dashed lines indicate the intramolecular hydrogen bonds.

code: #1, $-x + 3/2$, y, $-z + 3/2$]. Ni1 atom is coordinated by one oxygen atom (O1) from the bridging water molecule (Ni1–O1 = 2.095(2) Å), one oxygen atom (O2) from a terminally coordinated water molecule (Ni1–O2 = 2.078(3) Å), two oxygen atoms (O3 and O4) from two terminally coordinated pivalate ligands (Ni1–O3 = 2.066(3), Ni1–O4 = 2.053(3) Å) and two nitrogen atoms (N1 and $N2^{\#1}$) from the bridged admtrz groups (Ni1–N1 = 2.084(3), Ni1–$N2^{\#1}$ = 2.112(3) Å). The Ni1–N1 and Ni1–$N2^{\#1}$ bonds are somewhat longer than those in the reported dinuclear Ni(II) complexes with double and triple triazole bridges (2.013–2.074 Å) [9,10]. The bond angles N2–N1–Ni1 and N1–N2–$Ni1^{\#1}$ are 119.0(2)° and 117.0(2)°, respectively, smaller than those in the reported dinuclear Ni(II) compounds with double and triple triazole bridges (124.3–138.8°) [9,10]. The Ni1···$Ni1^{\#1}$ distance in $\mathbf{1} \cdot 13H_2O$ is 3.444(2) Å, much shorter than those observed in the previously reported dinickel(II) complexes with only double triazole bridge (4.10–4.14 Å) [9]. These differences can be attributed to the additional water molecule bridge between the two Ni(II) centers in $\mathbf{1} \cdot 13H_2O$. There are two types of intramolecular O–H···O hydrogen bonds: one hydrogen bond with the O···O distance of 2.595(3) Å

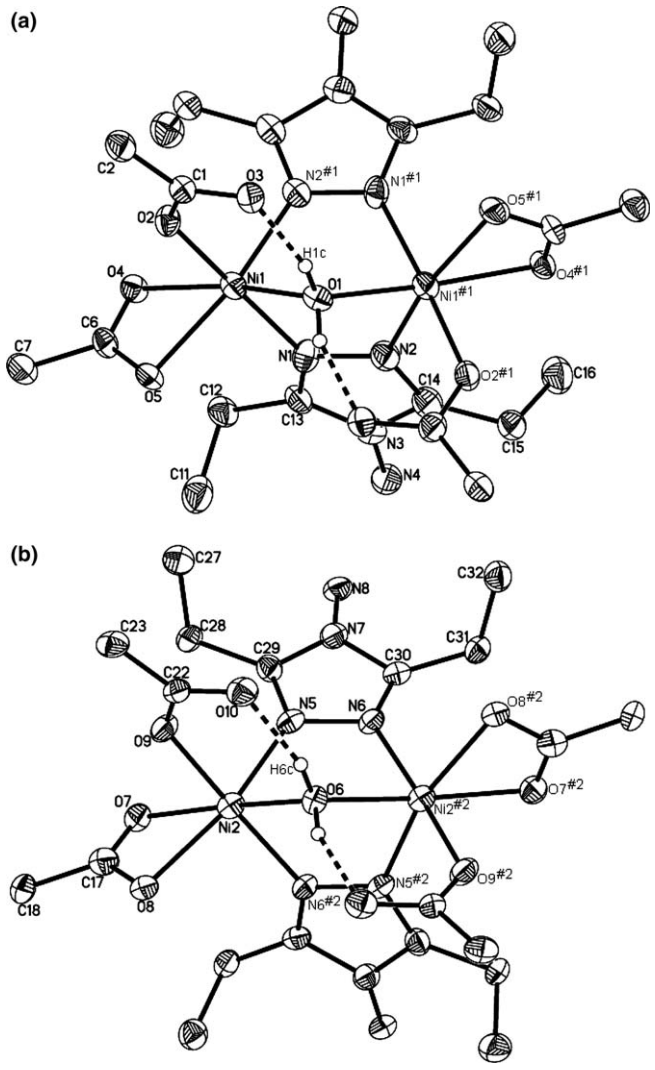

Fig. 3. ORTEP drawing (30% probability level) of **A** (a) and **B** (b), showing the atom-labeling scheme; all hydrogen atoms (except the hydrogen atoms involving the intramolecular hydrogen bonds), lattice water, and methyl groups in pivalates have been omitted for clarity [symmetry codes: #1, $x - y + 1$, $-y + 2$, $-z + 4/3$; #2, $x - y + 1$, $-y + 2$, $-z + 7/3$]. Dashed lines indicate the intramolecular hydrogen bonds.

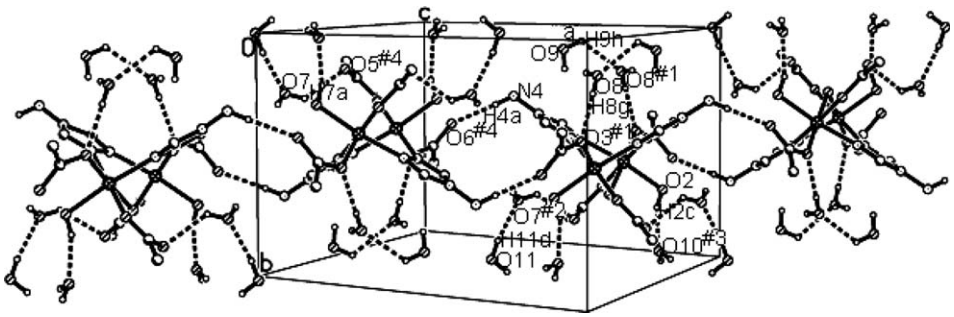

Fig. 2. The one-dimensional chain structure of $\mathbf{1} \cdot 13H_2O$ in the crystal lattice. The isolated water molecules and methyl groups in pivalates and admtrz have been omitted for clarity [symmetry codes: #1, $-x + 3/2$, y, $-z + 3/2$; #2, $x + 1/2$, $1 - y$, $z + 1/2$; #3, x, $y + 1$, z; #4, $x - 1/2$, $1 - y$, $z - 1/2$]. Dashed lines indicate the intermolecular hydrogen bonds.

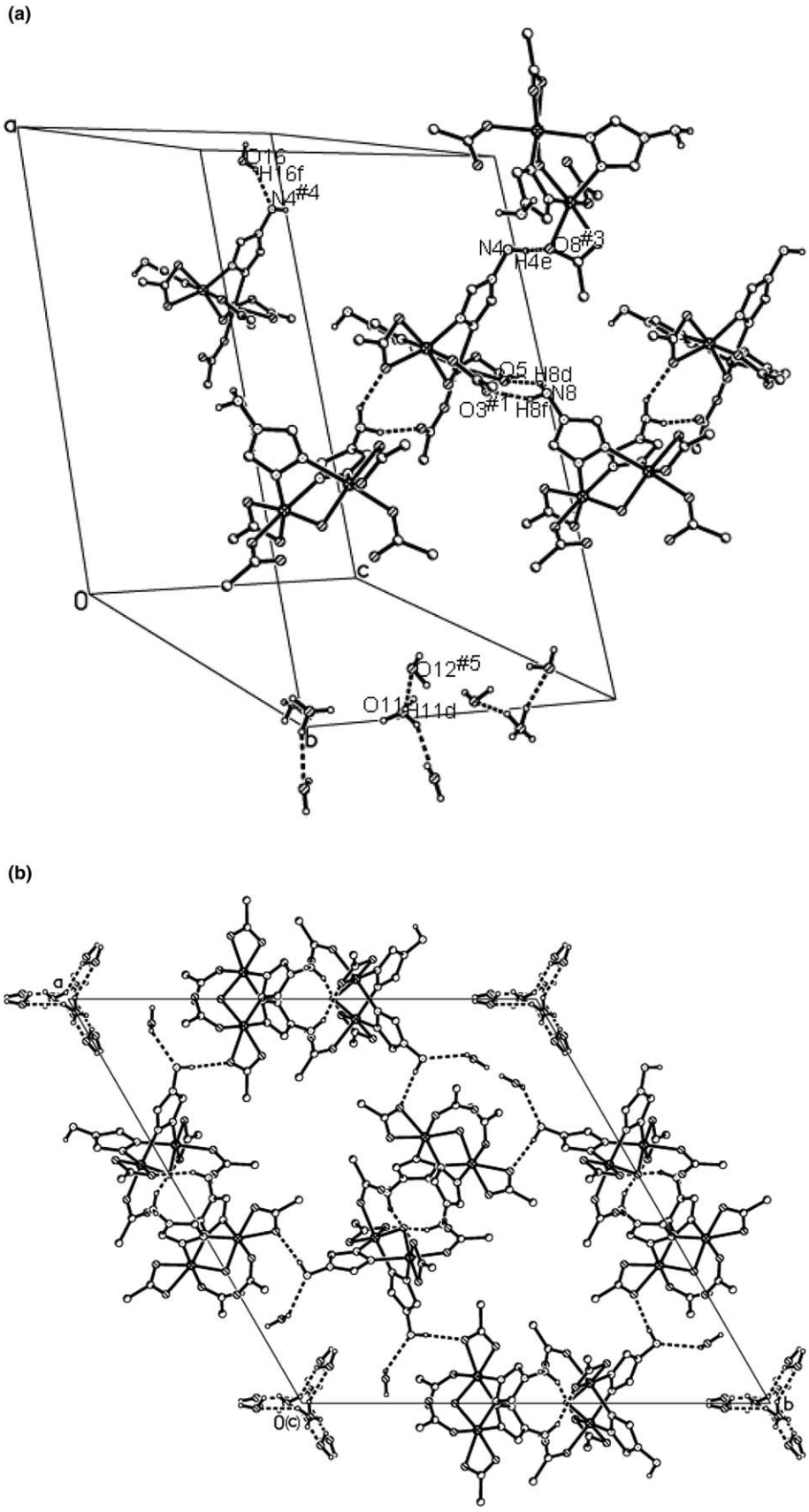

Fig. 4. (a) The intermolecular hydrogen bonds of $\mathbf{2}\cdot 3H_2O$ [symmetry codes: #1, $1+x-y$, $2-y$, $-z+4/3$; #3, y, $1+x$, $2-z$; #4, x, $y-1$, z; #5, $1+x-y$, $2-y$, $-z+1/3$]. (b) Projection showing the three-dimensional network for $\mathbf{2}\cdot 3H_2O$ viewed down the c axis. The ethyl groups in adetrz and methyl groups in pivalates have been omitted for clarity. Dashed lines indicate intermolecular hydrogen bonds.

between the bridging water molecule O1 and O5$^{\#1}$ atom from the terminally coordinated pivalate ligand and the other hydrogen bond with the O···O distance of 2.565(4) Å between the terminally coordinated water molecule O2 and O6 atom from the terminally coordinated pivalate ligand (see Table 4). The molecular packing of **1** · 13H_2O in the crystal lattice is shown in Fig. 2. The adjacent dinuclear molecules are linked through the intermolecular N4–H4a···O6$^{\#4}$ hydrogen bond along the [1 0 1] direction, leading to one-dimensional chains of molecules. The one-dimensional chain is surrounded by three lattice water molecules (O7, O8 and O10$^{\#3}$) via three types of intermolecular hydrogen bonds, i.e., O7–H7a···O5$^{\#4}$, O8–H8g···O3$^{\#1}$ and O2–H2c···O10$^{\#3}$. O8$^{\#1}$ and O7$^{\#2}$ are further connected with another two water molecules (O9 and O11) via intermolecular hydrogen bonds O9–H9h···O8$^{\#1}$ and O11–H11d···O7$^{\#2}$ [symmetry codes: #1, $-x+3/2$, y, $-z+3/2$; #2, $x+1/2$, $1-y$, $z+1/2$; #3, x, $y+1$, z; #4, $x-1/2$, $1-y$, $z-1/2$] (see Table 4). The other lattice water molecules are isolated in the crystal structure.

3.3.2. [$Ni_2(\mu$-$H_2O)(\mu$-adetrz$)_2$(piv$)_4$] · 3H_2O (**2** · 3H_2O)

In the crystal structure of **2** · 3H_2O, there are two types of crystallographically independent molecules (**A** and **B**) in addition to the lattice water molecules, which have the same structure except the different orientation of ethyl groups of the bridged adetrz (see Fig. 3). Both **A** and **B** have a twofold rotation axis passing the oxygen atom of bridging water molecule and the middle center of Ni–Ni [Ni1–Ni1$^{\#1}$ for **A** and Ni2–Ni2$^{\#2}$ for **B**, symmetry codes: #1, $x-y+1$, $-y+2$, $-z+4/3$; #2, $x-y+1$, $-y+2$, $-z+7/3$]. The bond length parameters in **A** and **B** are not significantly different. Therefore only the structural detail of **A** is discussed here. Similar to the structure of **1**, **A** has a dinuclear Ni(II) unit bridged with one water molecule and two adetrz ligands. Besides the occurrence of one terminally coordinated pivalate ligand, the other two remaining donor atoms around Ni(II) ion are different in **1** and **A**. As discussed above, the two coordination sites of Ni(II) ion in **1** are completed by one oxygen atom from the pivalate ligand and one oxygen atom from the terminal water molecule. In **A**, the two coordination sites are occupied by two oxygen atoms (O4 and O5) from one pivalate ligand with the O4–Ni1–O5 angle of 61.0(1)°, which leads to more seriously distorted octahedral geometry of Ni(II) center than that in **1**. The bond angles N2–N1–Ni1 and N1–N2–Ni1$^{\#1}$ (117.6(2)° and 112.8(3)°) are comparable to those in **1**. The Ni1···Ni1$^{\#1}$ distance is 3.312(1) Å. There are two symmetrically related intramolecular O–H···O hydrogen bonds with the O···O distance of 2.441 Å between the bridging water molecule (O1) and O3 or O3$^{\#1}$ atom from the terminally coordinated pivalate ligand (see Table 4). The molecular packing of **2** · 3H_2O in the crystal lattice is shown in Fig. 4. **A** and adjacent **B** are linked through the intermolecular N8–H8d···O5 and N8–H8f···O3$^{\#1}$ hydrogen bonds, leading the assembly of

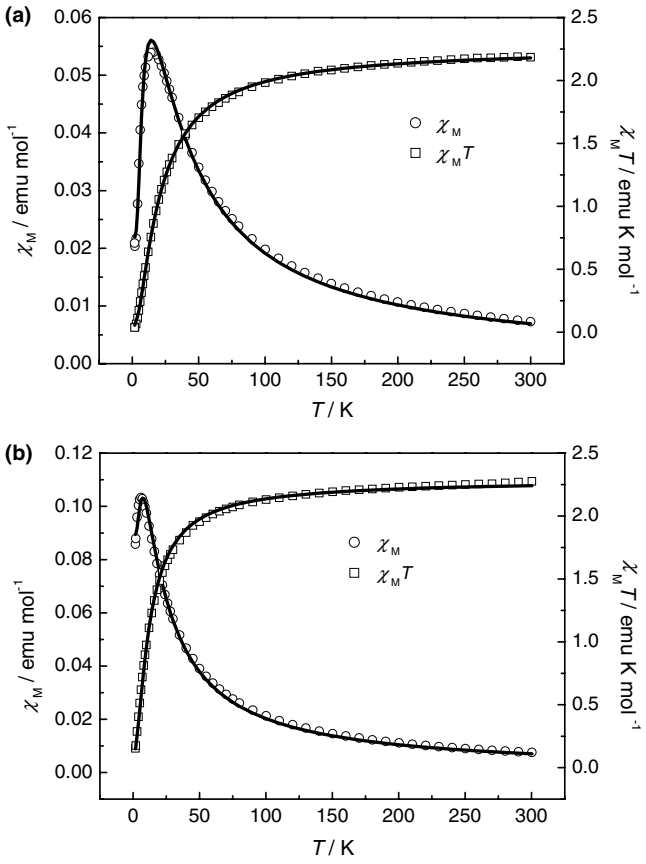

Fig. 5. Plots of χ_m (○) and $\chi_m T$ (□) vs. temperature for **1** (a) and **2** (b), where the solid line represents the theoretical curve.

one-dimensional zigzag chains of molecules along the c axis (see Fig. 4(a)). Neighboring chains of molecules are connected through the intermolecular N4–H4e···O8$^{\#3}$ hydrogen bond, resulting in a three-dimensional network (see Fig. 4(b)). One water molecule (O16) interacts with the amino group via the intermolecular O16–H16f···N4$^{\#4}$ hydrogen bond. Besides, there are two water molecules O11 and O12$^{\#5}$ clustered together via the intermolecular O11–H11d···O12$^{\#5}$ hydrogen bond in the crystal lattice [symmetry codes: #1, $1+x-y$, $2-y$, $-z+4/3$; #3, y, $1+x$, $2-z$; #4, x, $y-1$, z; #5, $1+x-y$, $2-y$, $-z+1/3$] (see Table 4). The other lattice water molecules are isolated in the crystal structure.

3.4. Magnetic properties

The powder samples of **1** and **2**, in which the lattice water molecules are completely removed, but the bridging water molecule remains in its place and in the case of **1** also two terminal water molecules, were used for magnetic study. The temperature dependence of the magnetic susceptibility of **1**, in the form of χ_m and $\chi_m T$, is shown in Fig. 5(a), χ_m being the magnetic susceptibility per dinuclear Ni(II) compound and T the temperature. The room-temperature $\chi_m T$ product is 2.18 cm^3 K mol^{-1} for **1**, which is slightly larger than that expected for two magnetically

isolated Ni(II) ions ($2.0\ cm^3\ K\ mol^{-1}$). The $\chi_m T$ value decreases slowly upon cooling till about 100 K, then decreases rapidly and reaches $0.04\ cm^3\ K\ mol^{-1}$ at 2 K. The magnetic behavior reveals the antiferromagnetic interactions between two Ni(II) centers in **1** and the ground state is $S = 0$. The magnetic data was analysed on the basis of the model including the zero-field splitting developed by Ginberg et al. [16]. The best fit leads to $g = 2.198$, $D = -10.03\ cm^{-1}$, and $J = -6.88\ cm^{-1}$ with the agreement factor $R = 1.1 \times 10^{-6}$ ($R = \sum |(\chi_m T)_{exp} - (\chi_m T)_{calc}|^2 / \sum (\chi_m T)^2_{exp}$). The χ_m and $\chi_m T$ versus T plot of **2** is very similar to that of **1** (see Fig. 5(b)). The room temperature $\chi_m T$ value of $2.28\ cm^3\ K\ mol^{-1}$ is close to that of **1** ($2.23\ cm^3\ K\ mol^{-1}$). The $\chi_m T$ value decreases rapidly below 75 K, which indicates weak antiferromagnetic interactions between two Ni(II) centers. The best fitting result is $g = 2.143$, $D = -12.31\ cm^{-1}$, and $J = -5.63\ cm^{-1}$ with $R = 6.0 \times 10^{-4}$. Since **1** and **2** are the first group dinuclear Ni(II) compounds with one water and two triazole bridges, it is difficult to rationalize their magnetic properties due to limited data available. More closely related compounds will be needed together with their magnetic studies.

4. Conclusions

In this paper the syntheses, structures and magnetic properties of two new water bridged dinuclear nickel(II) complexes containing derivatives of 1,2,4-triazole and pivalate ligands, namely, $[Ni_2(\mu\text{-}H_2O)(\mu\text{-admtrz})_2(piv)_4(H_2O)_2] \cdot 13H_2O$ (**1** · $13H_2O$) (admtrz = 4-amino-3,5-dimethyl-1,2,4-triazole, piv = pivalate anion) and $[Ni_2(\mu\text{-}H_2O)(\mu\text{-adetrz})_2(piv)_4] \cdot 3H_2O$ (**2** · $3H_2O$) (adetrz = 4-amino-3,5-diethyl-1,2,4-triazole), have been reported. They have similar structural features with unprecedented dinuclear Ni(II) units bridged by one water molecule and two triazole ligands. Variable temperature magnetic susceptibility measurements for the solid samples of **1** and **2** in the range of 1.8–300 K show that weak antiferromagnetic interactions occur in **1** and **2**.

5. Supplementary data

Crystallographic data of **1** · $13H_2O$ and **2** · $3H_2O$ in the CIF format have been deposited with the Cambridge Crystallographic Data Center as supplementary publication Nos. CCDC 279103 for **1** · $13H_2O$ and CCDC 279104 for **2** · $3H_2O$. Copies of the data can be obtained free of charge on application to CCDC, 12 Union Road, Cambridge CB2 1EZ, UK, fax: +44 1223 336 003, e-mail: deposit@ccdc.cam.ac.uk or http://www.ccdc.cam.ac.uk.

Acknowledgements

We thank the reviewers for their helpful comments. This work was supported by Natural Science Grant of Jiangsu Province (BK 2004087), Foundation of Nature Science Foundation of China (20001004) and Grant of Instruments of Nanjing University.

References

[1] O. Kahn, Molecular Magnetism, VCH, New York, 1993.
[2] J.R. Lancester Jr., Bioinorganic Chemistry of Nickel, VCH, New York, 1988.
[3] R.P. Hausinger, Biochemistry of Nickel, Plenum Press, New York, 1993.
[4] A.M. Barrios, S.J. Lippard, Inorg. Chem. 40 (2001) 1250.
[5] D. Ghosh, S. Mukhopadhyay, S. Samanta, K.-Y. Choi, A. Endo, M. Chaudhury, Inorg. Chem. 42 (2003) 7189.
[6] (a) B.-H. Ye, I.D. Williams, X.-Y. Li, J. Inorg. Biochem. 92 (2002) 128;
(b) D. Lee, P.-L. Hung, B. Spingler, J.S. Lippard, Inorg. Chem. 41 (2002) 521;
(c) D. Volkmer, B. Hommerich, K. Greisar, W. Haase, B. Krebs, Inorg. Chem. 35 (1996) 3792.
[7] (a) J.G. Haasnoot, Coord. Chem. Rev. 200–202 (2000) 131;
(b) M.H. Klingele, S. Brooker, Coord. Chem. Rev. 241 (2003) 119;
(c) U. Beckmann, S. Brooker, Coord. Chem. Rev. 245 (2003) 17.
[8] (a) S. Ferrer, P.J. van Koningsbruggen, J.G. Haasnoot, J. Reedijk, H. Kooijman, A.L. Spek, L. Lezama, A.M. Arif, J.S. Miller, J. Chem. Soc., Dalton Trans. (1999) 4269;
(b) P.M. Slangen, P.J. van Koningsbruggen, K. Goubitz, J.G. Haasnoot, J. Reedijk, Inorg. Chem. 33 (1994) 1121;
(c) P.M. Slangen, P.J. van Koningsbruggen, J.G. Haasnoot, J. Jansen, S. Gorter, J. Reedijk, H. Kooijman, W.J.J. Smeets, A.L. Spek, Inorg. Chim. Acta 212 (1993) 289;
(d) W.M.E. Koomen-van Oudenniel, R.A.G. de Graaff, J.G. Haasnoot, R. Prins, J. Reedijk, Inorg. Chem. 28 (1989) 1128;
(e) M.H. Klingele, B. Moubaraki, J.D. Cashion, K.S. Murray, S. Brooker, J. Chem. Soc., Chem. Commun. (2005) 987.
[9] (a) P.J. van Koningsbruggen, M.W. Gluth, V. Ksenofontov, D. Walcher, D. Schollmeyer, G. Levchenko, P. Gütlich, Inorg. Chim. Acta 273 (1998) 54;
(b) F.S. Keij, R.A.G. de Graaff, J.G. Haasnoot, J. Reedijk, J. Chem. Soc., Dalton Trans. (1984) 2093;
(c) M.H. Klingele, P.D.W. Boyd, B. Moubaraki, K.S. Murray, S. Brooker, Eur. J. Inorg. Chem. (2005) 910.
[10] G. Vos, A.J. de Kok, G.C. Verschoor, Z. Naturforsch. 36b (1981) 809.
[11] (a) I.L. Eremenko, M.A. Golubnichaya, S.E. Nefedov, A.A. Sidorov, I.F. Golovaneva, V.I. Burkov, O.G. Ellert, V.M. Novotortsev, L.T. Eremenko, A. Sousa, M.R. Bermejo, Russ. Chem. Bull. (1998) 725;
(b) T.B. Mikhailova, I.G. Fomina, A.A. Sidorov, I.F. Golovaneva, G.G. Aleksandrov, V.M. Novotortsev, V.N. Ikorskii, I.L. Eremenko, Russ. J. Inorg. Chem. 48 (2003) 1648;
(c) T.O. Denisova, G.G. Aleksandrov, O.P. Fialkovskii, S.E. Nefedov, Russ. J. Inorg. Chem. 48 (2003) 1476;
(d) I.L. Eremenko, S.E. Nefedov, A.A. Sidorov, M.A. Golubnichaya, P.V. Danilov, V.N. Ikorskii, Y.G. Shvedenkov, V.M. Novotortsev, I.I. Moiseev, Inorg. Chem. 38 (1999) 3764;
(e) G. Chaboussant, R. Basler, H.U. Güdel, S. Ochsenbein, A. Parkin, S. Parsons, G. Rajaraman, A. Sieber, A.A. Smith, G.A. Timco, R.E.P. Winpenny, J. Chem. Soc., Dalton Trans. (2004) 2758.
[12] J.-H. Zhou, R.-M. Cheng, Y. Song, Y.-Z. Li, Z. Yu, X.-T. Chen, Z.-L. Xue, X.-Z. You, Inorg. Chem. 44 (2005) 8011.
[13] R.M. Herbst, J.A. Garrison, J. Org. Chem. 18 (1953) 872.
[14] G.M. Sheldrick, Program for Empirical Absorption Correction, University of Göttingen, Germany, 2000.
[15] G.M. Sheldrick, Program for Crystal Structure Solution and Refinement, University of Göttingen, Germany, 2000.
[16] A.P. Ginsberg, R.L. Martin, R.W. Brookes, R.C. Sherwood, Inorg. Chem. 11 (1972) 2884.

novel transition metal complexes, hydroquinone complexes and Ni(dmit)$_2$ salts of verdazyl radicals have also been studied [17–21].

Although the spin distribution in verdazyl radicals has been mainly studied by ESR [6,7,22–24], other techniques such as electron–nuclear double resonance, ENDOR [25], electron–electron double resonance, ELDOR [26], and nuclear magnetic resonance (NMR) [27] have also been used.

The synthesis and spectroscopic characterization of 6-(4-acetamidophenyl)-1,4,5,6-tetrahydro-2,4-dimethyl-1,2,4,5-tetrazin-3(2*H*)-one (**1**) has been reported previously [28]. This free radical, as a monohydrate, forms stable red crystals that were accidentally left for five years in a sample vial before a crystal structure and magnetic measurements were undertaken. This is some eighteen years less than the length of time that Koelsch's free radical was left prior to characterization but nevertheless illustrates the exceptional stability of this free radical [29,30].

Here we present the crystal structure of the radical **1**, solved by synchrotron radiation due to the small size of the single crystals, as well as its complete magnetic characterization (thermal variation of the magnetic susceptibility and the solid-state and solution Q-band ESR spectra). These magnetic studies show the presence of weak antiferromagnetic coupling between the radicals in the solid state and the spin distribution in the radical.

2. Crystal structure

The radical crystallizes as a monohydrate. The radical itself is essentially planar except for hydrogen atoms, with an r.m.s. deviation of 0.041 Å, and has unremarkable internal geometry; its structure is shown in Fig. 1, which also includes the water molecule of the asymmetric unit. Molecules are stacked parallel to each other along the crystallographic *b*-axis (Figs. 2 and 3). Within the stack, pairs of molecules form dimers with a high degree of overlap (Fig. 2), and successive dimers display a significant lateral offset (Fig. 3). The spacing in the stacks is uniform, the difference between perpendicular distances within (3.349 Å) and between (3.345 Å) dimers being insignificant.

The molecules within a stack do not lie perpendicular to the stacking direction, but are inclined to it. Successive adjacent stacks in the crystallographic *c* direction have alternating directions of inclination, to give an overall criss-cross pattern when viewed in this direction (Fig. 4). Lateral interactions between stacks are further supported by hydrogen bonds mediated by the water molecules, with O···O and N···O distances between 2.841 and 2.922 Å, and near-linearity at the H atoms (161–178°). Both oxygen atoms of the radical act as acceptors for water O–H bonds, and the N–H group serves as a donor to water; there are no hydrogen bonds directly between radicals. Fig. 4 shows the overall packing arrangement including these interactions.

3. Magnetic properties

The thermal variation of the product of the molar magnetic susceptibility times the temperature ($\chi_m T$) of the title compound shows at room temperature a value of ca. 0.38 emu K mol^{-1}, which is the expected value for a radical with one unpaired electron ($S = 1/2$) with a *g* value close to 2. On lowering the temperature, $\chi_m T$ remains constant down to ca. 50 K and then smoothly decreases to reach a value of ca. 0.16 emu K mol^{-1} at 2 K (Fig. 5). This behavior indicates that the title compound behaves essentially as an $S = 1/2$ paramagnet with weak antiferromagnetic interactions. Since the structure of this compound shows the presence of short distances between the two molecules forming the eclipsed dimer in the solid state and also between the molecules of different dimers, we can envisage three possible exchange schemes: (i) that this antiferromagnetic coupling takes place between the two molecules forming the almost eclipsed dimer, neglecting the interdimer interactions; that the coupling also takes place between dimers, leading either to (ii) a regular antiferromagnetic $S = 1/2$ chain (if the intra- and interdimer exchange are equal); or to (iii) a dimerised chain (a chain of dimers or alternating chain, if the intra- and interdimer exchange are different). A close inspection of the intermolecular distances also reveals short distances between molecules of different "chains of dimers" and therefore (iv) an isotropic exchange scheme can also be envisaged. According to these possible exchange schemes, we have fitted the magnetic data to the four aforementioned schemes with the following models: (i) an $S = 1/2$ dimer [31], (ii) a regular antiferromagnetic chain [32], (iii) an alternating antiferromagnetic $S = 1/2$ chain

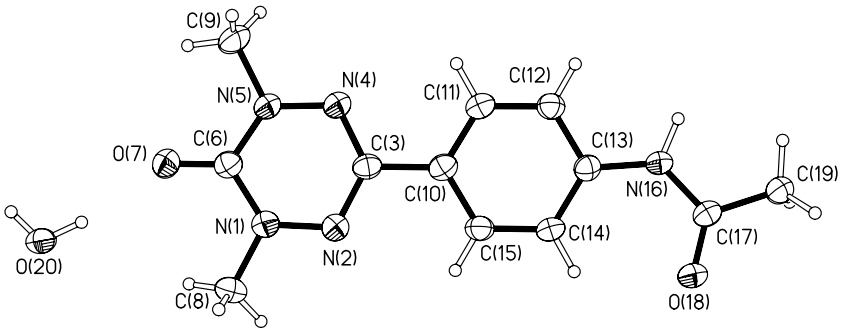

Fig. 1. The asymmetric unit of the crystal structure, with 50% probability displacement ellipsoids for non-hydrogen atoms.

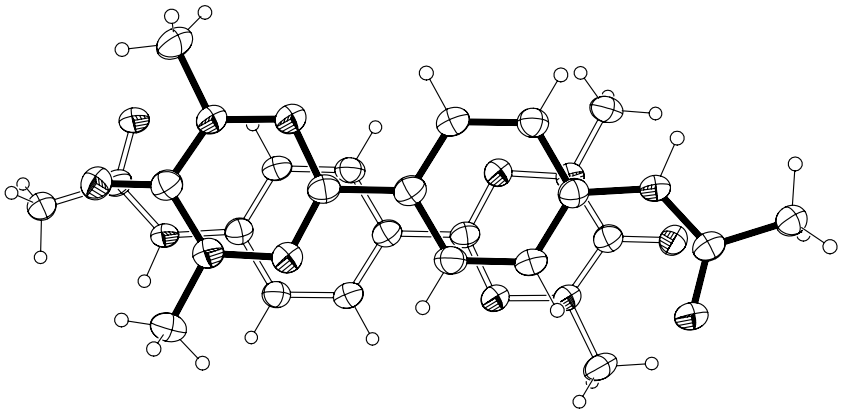

Fig. 2. The overlap of pairs of radicals to form dimers within a stack. The view direction, as for Fig. 1, is perpendicular to the mean plane of each individual radical. The further radical is shown with open bonds for greater clarity.

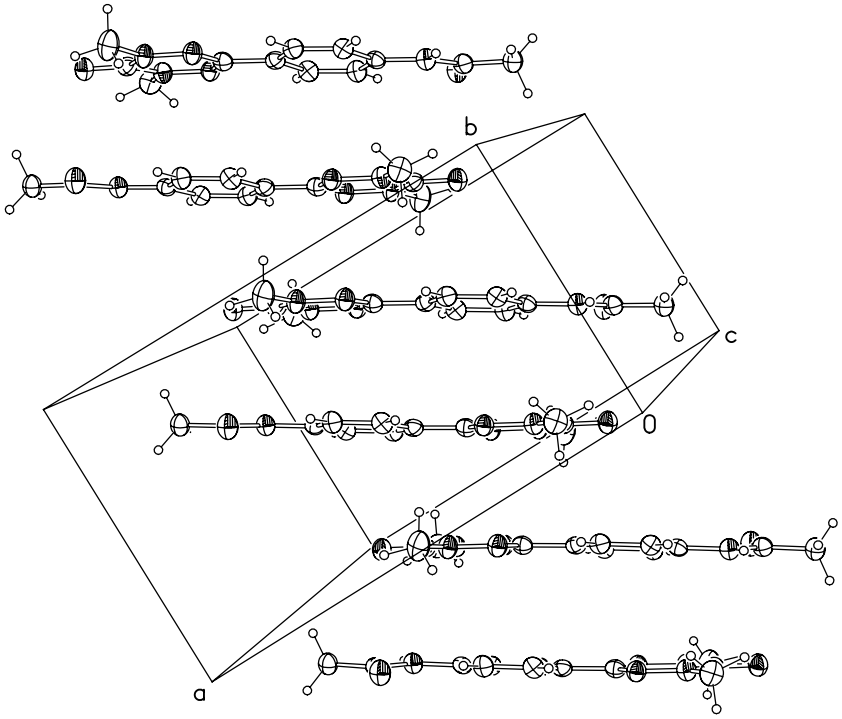

Fig. 3. Part of a stack of radicals, showing three successive dimers and the unit cell outline.

[33], and (iv) a simple Curie–Weiss law: $\chi = C/T - \theta$. Although the general behavior of the magnetic data can be well reproduced with any of these four models with g values very close to 2, and with θ, J (intradimer or intrachain) and J' (interdimer) values in the -1.5 to -2.5 K range, the best fit is obtained for the antiferromagnetic regular chain (solid line in Fig. 5). This model reproduces very satisfactorily the magnetic moment over the whole temperature range with the following parameters: $g = 2.012(1)$ and $J = -1.54(1)$ K $= -1.07(1)$ cm^{-1} (the Hamiltonian is written as $H = -2J\Sigma J_i J_{i+1}$). This result agrees with the perpendicular distances between mean planes of the stacked molecules in the title compound, which are essentially identical (3.349 Å for the intra- and 3.345 Å for the interdimer distance). A further confirmation of the spin ground state and the presence of antiferromagnetic interactions is provided by the isothermal magnetization of the title compound at 2 K, which shows an almost linear behavior that can be well reproduced with a Brillouin function for an $S = 1/2$ spin ground state with a reduced g value that accounts for the antiferromagnetic interactions (Fig. 6).

The ESR spectrum of the title compound shows a single narrow feature at $g = 2.0049$ with a line-width (ΔH) of ca. 14.1 G at room temperature (Fig. 7). Both the position and the line-width are typical of this kind of radical. The intensity of the ESR signal increases when lowering the temperature, whereas both the ΔH and g values remain almost

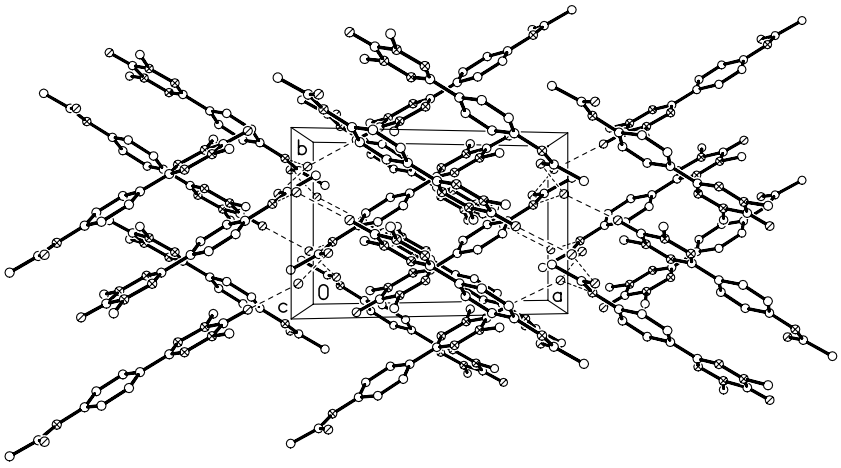

Fig. 4. The crystal structure, viewed along the *c*-axis, showing hydrogen bonds as dashed lines.

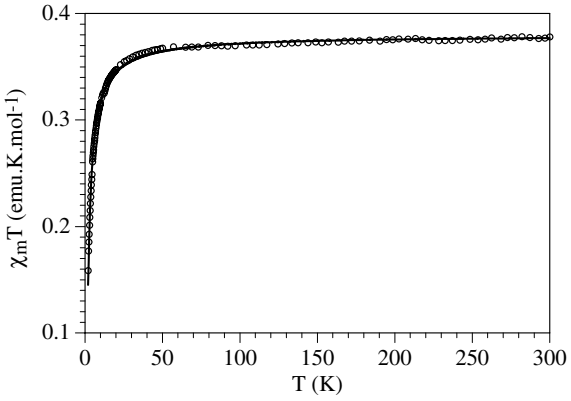

Fig. 5. Thermal variation of the $\chi_m T$ product for the title compound. The solid line is the best fit to the regular antiferromagnetic $S = 1/2$ chain (see text).

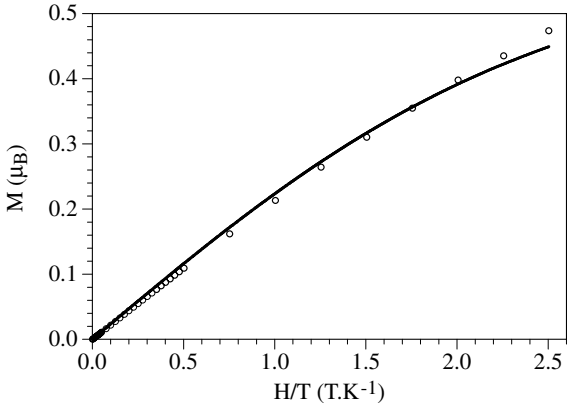

Fig. 6. Isothermal magnetization at 2 K of the title compound. Solid line shows the best fit to a Brillouin function with $S = 1/2$ (see text).

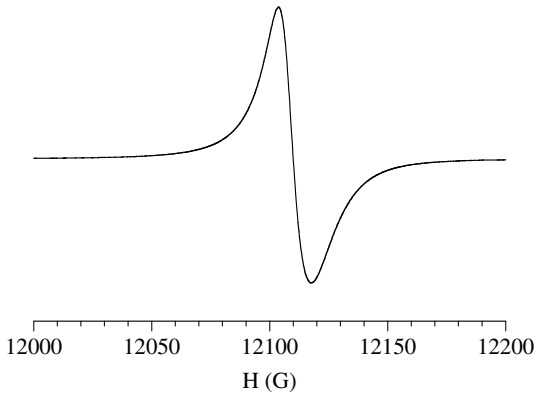

Fig. 7. Q-band solid state ESR spectrum at room-temperature of the title compound.

constant (ΔH and g smoothly increase up to ca. 16.7 G and ca. 2.0082, respectively, at low temperatures). The area of the ESR signal (proportional to the spin susceptibility) follows a "Curie–Weiss like" law with a negative Weiss temperature, as observed in the static susceptibility magnetic measurements. Note that the precision in the determination of the ESR area precludes the discrimination among any of the four aforementioned magnetic models. This behavior confirms the presence of an unpaired electron in the title compound as well as the paramagnetic behavior with weak antiferromagnetic interactions.

Besides the solid-state ESR spectra, we have also obtained ESR spectra of the title compound in CH_3CN and toluene solutions. The spectrum in CH_3CN solution shows a single feature with the same g value as in the solid and a lower line width (7.2 G). When the temperature is decreased, the g and ΔH values follow similar variations to those observed in the solid. The lower line width indicates that the radical in solution has fewer spin relaxation pathways (or less effective) than in the solid state and suggests the formation of small aggregates in solution. More interesting is the ESR spectrum of the toluene solution, since this radical is much less soluble in toluene, precluding the formation of aggregates. Thus, the ESR spectra of a dilute toluene solution show a hyperfine structure centred at $g = 2.00505$ (value obtained from the simulation), very close to the value obtained in the ESR spectrum of the solid at room temperature (2.0049, see above). This hyperfine structure shows up to 13 main signals above the freezing point of the solvent (180 K). Furthermore, most

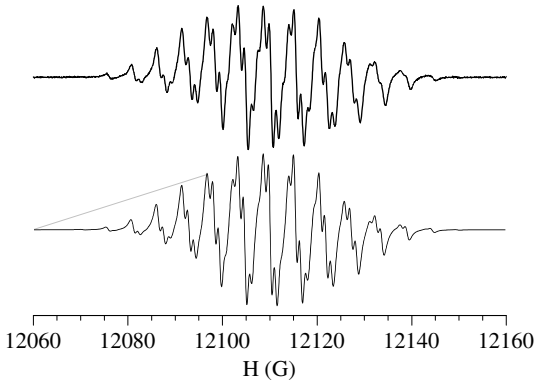

Fig. 8. Top: Q-band ESR spectrum at room temperature of a toluene solution of the title compound. Bottom: the simulated spectrum with $g = 2.0050$, $a(N_{2,4}) = 6.5$ G, $a(N_{1,5}) = 5.4$ G and $a(H_{1,5}) = 5.3$ G.

of these 13 signals are split into four or more, rendering a very complex spectrum, as can be seen in Fig. 8(top). A very satisfactory simulation of the shape, intensity and position of all the lines in this spectrum (Fig. 8, bottom) can be obtained by taking into account a hyperfine coupling with the two groups of two equivalent nitrogen atoms (N1–N5 and N2–N4) (^{14}N, $I = 1$, natural abundance = 99.635%) plus an additional coupling with the six hydrogen atoms of the two methyl groups bonded to the N1 and N5 atoms in the verdazyl ring (^{1}H, $I = 1/2$, natural abundance = 99.9844%). The hyperfine coupling constants obtained are: $a(N_{2,4}) = 6.5\ \text{G} = 6.08 \times 10^{-4}\ \text{cm}^{-1}$, $a(N_{1,5}) = 5.4\ \text{G} = 5.05 \times 10^{-4}\ \text{cm}^{-1}$ and $a(H_{1,5}) = 5.3\ \text{G} = 4.96 \times 10^{-4}\ \text{cm}^{-1}$ for the six equivalent hydrogen atoms. These values are very similar to those obtained by Neugebauer et al. [22b]. According to Neugebauer et al. [22], the larger hyperfine coupling is assigned to the two 2-coordinated nitrogen atoms (N2 and N4), indicating that the unpaired electron is mainly delocalized over the N=C–N group of the verdazyl ring, rather than over the Me–N–CO–N–Me group. It is important to indicate that a change from six to four hydrogen atoms does not change significatively the simulated spectrum and, therefore, it is not possible to unambiguously determine if the superhyperfine structure observed in the ESR spectrum is due to the four hydrogens on the phenyl ring or to the six hydrogen atoms of the two methyl groups of the verdazyl ring. Albeit, previous NMR measurements have shown that the coupling constants with the hydrogen atoms of the phenyl ring are well below 1 G and, therefore, the observed coupling can be assigned to the six hydrogen atoms of the two methyl groups of the verdazyl ring [27].

4. Conclusion

The structural and magnetic characterization of the title compound five years after its synthesis indicate that it is a very stable radical. The magnetic susceptibility measurements confirm the presence of one unpaired electron per molecule with weak antiferromagnetic exchange interactions that can be well reproduced with a regular antiferromagnetic chain model, in agreement with the structural data. ESR spectra in solid state and in solution confirm that the title compound is a radical whose unpaired electron is delocalized over the verdazyl ring, showing hyperfine coupling with the four nitrogen atoms of the verdazyl ring and the six hydrogen atoms of the two methyl groups bonded to the verdazyl ring.

5. Experimental

5.1. Magnetic properties

Variable-temperature susceptibility measurements were carried out in the temperature range 2–300 K at an applied magnetic field of 0.1 T on a polycrystalline sample with a Quantum Design MPMS-XL-5 SQUID magnetometer. The susceptibility data were corrected for the sample holder previously measured using the same conditions and for the diamagnetic contributions of the salt as deduced by using Pascal's constant tables. Isothermal magnetization measurements were performed at 2 K with magnetic fields up to 5 T. ESR spectra were recorded in Q band (33.98 GHz) with a Bruker E-500 ELEXSYS spectrometer in the temperature range 4–300 K on a polycrystalline sample and on toluene and acetonitrile solutions. The simulation of the toluene solution spectrum at room temperature was performed with the Win-EPR SimFonia software from Bruker.

5.2. X-ray crystal structure determination

Crystallographic data for $C_{12}H_{14}N_5O_2 \cdot H_2O$: $a = 12.616(3)$ Å, $b = 7.904(2)$ Å, $c = 14.122(4)$ Å, $\beta = 111.682(3)°$ at 120 K, with $Z = 4$ in the monoclinic space group $P2_1/c$. $R = 0.051$ for F values of 1539 reflections with $F^2 > 2\sigma(F^2)$, $R_w = 0.139$ for all 2290 unique F^2 values (7543 data measured, $2\theta < 48.6°$, $R_{int} = 0.044$) and 197 refined parameters, GOF = 1.039 on F^2. Data were collected with synchrotron radiation ($\lambda = 0.6902$ Å) and a Bruker APEX2 diffractometer at station 9.8 of the SRS, Daresbury Laboratory, from a crystal of size $0.08 \times 0.06 \times 0.01$ mm. Structure solution was by direct methods. A final difference synthesis contained no features outside ± 0.25 e Å^{-3}. Programs were standard Bruker APEX2, SAINT and SHELXTL.

6. Supplementary material

Supplementary data are available from the CCDC, 12 Union Road, Cambridge CB2 1EZ, UK on request, quoting the deposition number 297266. Crystallographic data are in CIF format. This material is also available free of charge via the Internet at http://pubs.acs.org.

Acknowledgements

C.J.G.G. thanks the Generalitat Valenciana for financial support (Projects GV04B-078 and IIARC0-2004-159).

References

[1] (a) K. Awaga, Y. Maruyama, Chem. Phys. Lett. 158 (1989) 556;
(b) K. Awaga, T. Inabe, U. Nagashima, Y. Maruyama, J. Chem. Soc., Chem. Commun. (1989) 1617.
[2] (a) D.A. Dougherty, Acc. Chem. Res. 24 (1991) 88;
(b) W.T. Borden, H. Iwamura, J.A. Berson, Acc. Chem. Res. 27 (1994) 109.
[3] B.D. Koivisto, R.G. Hicks, Coord. Chem. Rev. 249, 2612.
[4] (a) H. Oshio, T. Ito, Coord. Chem. Rev. 198 (2000) 329;
(b) D. Luneau, P. Rey, Coord. Chem. Rev. 249, 2591.
[5] F.A. Neugebauer, H. Fischer, C. Krieger, J. Chem. Soc., Perkin Trans. 2 (1993) 535.
[6] C.L. Barr, P.A. Chase, R.G. Hicks, M.T. Lemaire, C.L. Stevens, J. Org. Chem. 64 (1999) 8893.
[7] R.M. Fico Jr., M.F. Hay, S. Reese, S. Hammond, E. Lambert, M.A. Fox, J. Org. Chem. 64 (1999) 9386.
[8] R.K. Kremer, B. Kanellakopulos, P. Bele, H. Brunner, F.A. Neugebauer, Chem. Phys. Lett. 230 (1994) 255.
[9] S. Tomiyoshi, T. Yano, N. Azuma, M. Shoga, K. Yamada, J. Yamauchi, Phys. Rev. B 49 (1994) 16031.
[10] M. Mito, H. Nakano, T. Kawae, M. Hitaka, S. Takagi, H. Deguchi, K. Suzuki, K. Mukai, K. Takeda, J. Phys. Soc. Jpn. 66 (1997) 2147.
[11] K. Mukai, K. Konishi, K. Nedachi, K. Takeda, J. Phys. Chem. 100 (1996) 9658.
[12] K. Takeda, T. Hamoro, T. Kawae, M. Hidaka, M. Takahashi, K. Kawasaki, K. Mukai, J. Phys. Soc. Jpn. 64 (1995) 2343.
[13] M. Mito, K. Takeda, K. Mukai, N. Azuma, M.R. Gleiter, C. Kreiger, F.A. Neugebauer, J. Phys. Chem. B 101 (1997) 9517.
[14] K. Mukai, M. Matsubara, H. Hisatou, Y. Hosokoshi, K. Inove, N. Azuma, J. Phys. Chem. B 106 (2002) 8632.
[15] K. Mukai, N. Wada, J.B. Jamali, N. Achiwa, Y. Narumi, K. Kindo, T. Kobayashi, K. Amaya, Chem. Phys. Lett. 257 (1996) 538.
[16] K. Mukai, Y. Shimobe, J.B. Jamali, N. Achiwa, J. Phys. Chem. B 103 (1999) 10876.
[17] D.J.R. Brook, V. Lynch, B. Conklin, M.A. Fox, J. Am. Chem. Soc. 119 (1997) 5155.
[18] D.J.R. Brook, S. Fornell, J.E. Stevens, B. Noll, T.H. Kock, W. Eisfeld, Inorg. Chem. 39 (2000) 562.
[19] R.G. Hicks, M.T. Lemaire, L.K. Thompson, T.M. Barclay, J. Am. Chem. Soc. 122 (2000) 8077.
[20] R.G. Hicks, M.T. Lemaire, L. Ohrstrom, J.F. Richardson, L.K. Thompson, Z. Xu, J. Am. Chem. Soc. 123 (2001) 7154.
[21] K. Mukai, N. Senba, T. Hatanaka, H. Minakuchi, K. Ohara, M. Taniguchi, Y. Misaki, Y. Hosokoshi, K. Inonue, N. Azuma, Inorg. Chem. 43 (2004) 566.
[22] (a) F.A. Neugebauer, H. Fischer, Angew. Chem., Int. Ed. Engl. 19 (1980) 724;
(b) F.A. Neugebauer, H. Fischer, R. Siegel, Chem. Ber. 121 (1988) 815.
[23] Y. Morita, E. Miyazaki, J. Kawai, K. Sato, D. Shiomi, T. Takui, K. Nakasuji, Polyhedron 22 (2003) 2219.
[24] Y. Morita, S. Nishida, T. Kobayashi, K. Fukui, K. Sato, D. Shiomi, T. Takui, K. Nakasuji, Org. Lett. 6 (2004) 1397.
[25] K. Mukai, T. Yamamoto, M. Kohno, N. Azuma, K. Ishizu, Bull. Chem. Soc. Jpn. 47 (1974) 1797.
[26] K. Mukai, H. Shikata, N. Azuma, K. Kuwata, J. Magn. Reson. 35 (1979) 133.
[27] (a) F.A. Neugebauer, H. Brunner, Tetrahedron 30 (1974) 2841;
(b) F.A. Neugebauer, H. Brunner, K.H. Hausser, Tetrahedron 27 (1971) 3623.
[28] M.J. Plater, J.P. Sinclair, S. Kemp, T. Gelbrich, M.B. Hursthouse, C.J. Gómez-García, J. Chem. Res. (in press).
[29] C.F. Koelsch, J. Am. Chem. Soc. 79 (1957) 4439.
[30] M.J. Plater, S. Kemp, E. Lattmann, J. Chem. Soc., Perkin Trans. 1 (2000) 971.
[31] B. Bleaney, K.D. Bowers, Proc. Roy. Soc. (Lond.) Ser. A 214 (1952) 451.
[32] D.B. Brown, J.A. Donner, J.W. Hall, S.R. Wilson, R.B. Wilson, D.J. Hodgson, W.E. Hatfield, Inorg. Chem. 18 (1979) 2635.
[33] J.W. Hall, W.E. Marsh, R.R. Weller, W.E. Hatfield, Inorg. Chem. 20 (1981) 1033.

$n = 4$, 6 and 8, respectively [10]. We have also investigated the reaction of UCl_4 or $U(OSO_2CF_3)_4$ with homooxacalix[*n*]arenes ($n = 4$, 6, 8) in pyridine, with the unexpected finding of homooxacalixarene cleavage to give di- or triphenoxide species, likely as a result of nucleophilic attack by pyridine on the benzylic ether carbon atom of the macrocycle, assisted by initial uranium coordination to the ether groups [11]. New uranium(IV) [11a] and uranyl [11b] complexes with acyclic polyphenoxide ligands were thus obtained. In order to avoid this cleavage reaction, we turned to macrocycles in the related homocalixarene family, in which the ether links present in homooxacalixarenes are replaced by aliphatic linkages [12]. We report herein the crystal structure of the complexes obtained by reaction of UCl_4 with *p-tert*-butylhomocalix[*n*]arenes ($n = 4$ and 6), or, more precisely, *p-tert*-butyltetrahydroxy[3.1.3.1]- and *p-tert*-butylhexahydroxy[2.1.2.1.2.1]metacyclophanes, denoted H_4L^1 and H_6L^2, respectively (Scheme 1), as well as that of the uncoordinated form of the latter. These macrocycles differ from the calix[*n*]arenes by both the length of the aliphatic linkage and the presence of the *p-tert*-butyl groups. The uranyl complex of the tetraanionic L^1 ligand has been reported previously; its crystal structure was the first to be determined for a complex of a homocalix[4]arene [13].

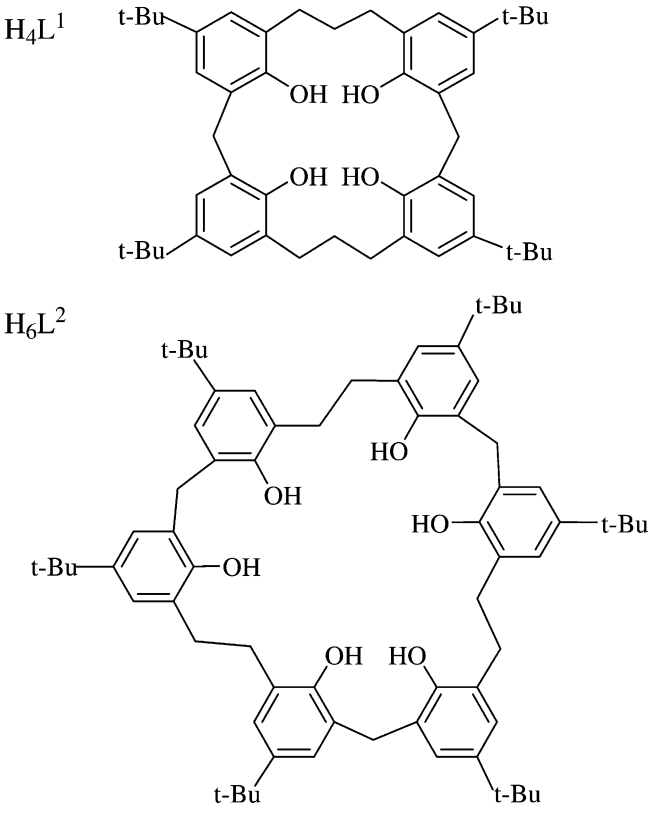

Scheme 1. The *p-tert*-butylhomocalixarenes H_4L^1 and H_6L^2.

2. Experimental

2.1. Syntheses

All reactions were carried out under argon (<5 ppm oxygen or water) using standard Schlenk-vessel and vacuum-line techniques or in a glove box. Solvents were dried by standard methods and distilled immediately before use. The uranium salts UCl_4 and $U(acac)_4$ were synthesized as reported in the literature [14]. The ^1H NMR spectra were recorded on a Bruker DPX 200 instrument and referenced internally using the residual protio solvent resonances relative to tetramethylsilane.

The homocalixarenes H_4L^1 (6,13,22,29-tetra-*tert*-butyl-9,16,25,32-tetrahydroxy[3.1.3.1]metacyclophane) and H_6L^2 (5,12,20,27,35,42-hexa-*tert*-butyl-8,15,23,30,38,45-hexahydroxy[2.1.2.1.2.1]metacyclophane) were synthesized as previously described [15,16]; ^1H NMR (C_5D_5N, 200 MHz, $T = 23$ °C): $\delta = 1.27$ (36H, *t*Bu), 1.73 (4H, $-CH_2-$), 2.84 (8H, $-CH_2-$), 4.20 (4H, $-CH_2-$), 7.08 and 7.53 (2×4H, aromatic H), 10.71 (4H, OH) and ^1H NMR (thf, 200 MHz, $T = 23$ °C): $\delta = 1.60$ (54H, *t*Bu), 3.10 (12H, $-CH_2-$), 4.20 (6H, $-CH_2-$), 7.29 and 7.56 (2×6H, aromatic H), 8.48 (6H, OH) for H_4L^1 and H_6L^2, respectively. Single crystals of $H_6L^2 \cdot 5py$ (**1**) were obtained by slow evaporation of a pyridine solution of H_6L^2.

[Hpy][UCl$_2$(L^1)] · 2.5py (**2**). An NMR tube was charged with H_4L^1 (5 mg, 0.0071 mmol) and UCl_4 (2.7 mg, 0.0071 mmol) in C_5D_5N (0.4 ml). Immediately, the ^1H NMR spectrum of the resulting brown solution indicated the complexation of the ligand: δ (200 MHz, $T = 23$ °C) = 1.5 (br, 52H, $-CH_2-$ and *t*Bu), 11.9 (br, 2H, aromatic H), 12.8 (br, 4H, aromatic H), 26.9 (br, 2H, aromatic H). δ (200 MHz, $T = -20$ °C) = −9.71 and −3.48 (2×2H, $-CH_2-$), −0.63 (18H, *t*Bu), 0.93, 1.21 and 1.85 (3×2H, $-CH_2-$), 2.15 (4H, $-CH_2-$), 3.36 (18H, *t*Bu), 5.07 (2H, $-CH_2-$), 11.67, 13.35, 14.41 and 15.35 (4×1H, aromatic H), 18.33 (2H, aromatic H), 25.03 and 26.12 (2×1H, aromatic H). Prolonged heating at 110 °C led to the formation of a mixture of dark brown crystals of compound **2** and colourless crystals of HpyCl which were deposited at the bottom of the tube. When the reaction was performed with $U(acac)_4$ (acac = acetylacetonato) instead of UCl_4, or in thf, no reaction occurred and the NMR spectra showed only the signals of the uncomplexed ligand H_4L^1, even at high temperature.

[U$_4$Cl$_2$O$_2$(L^2)$_2$(H$_2$O)(thf)] · 3thf (**3**). An NMR tube was charged with H_6L^2 (7 mg, 0.0069 mmol) and UCl_4 (5.2 mg, 0.0138 mmol) in tdf (0.4 ml). Adventitious traces of water probably entered the reaction flask during prolonged heating at 80 °C, which resulted in the formation of dark brown needles of compound **3** from the brown solution. Attempts to prepare this complex in a controlled way, by introducing measured quantities of water into the reaction mixture, were unsuccessful. The crystals could not be characterized by ^1H NMR because of their insolubility in organic solvents.

2.2. Crystallography

The data were collected on a Nonius Kappa-CCD area detector diffractometer [17] using graphite-monochromated Mo Kα radiation ($\lambda = 0.71073$ Å). The crystals were introduced in glass capillaries with a protecting "Paratone-N" oil (Hampton Research) coating. The unit cell parameters were determined from ten frames, then refined on all data. A 180° φ-range was scanned with 2° steps during data collection, with a crystal-to-detector distance fixed to 28 or 30 mm. The data were processed with HKL2000 [18]. The structures were solved by direct methods with SHELXS-97 and subsequent Fourier-difference synthesis and refined by full-matrix (**1** and **2**) or blocked matrix (**3**) least-squares on F^2 with SHELXL-97 [19]. Absorption effects in **2** and **3** were corrected empirically with the program DELABS in PLATON [20]. All non-hydrogen atoms were refined with anisotropic displacement parameters. The hydrogen atoms bound to oxygen atoms in **1** and to nitrogen atoms in **2** were found on Fourier-difference maps, whereas those of the water molecule in **3** were not found, nor introduced. The other hydrogen atoms were introduced at calculated positions and all were treated as riding atoms with a displacement parameter equal to 1.2 (OH, NH, CH, CH_2) or 1.5 (CH_3) times that of the parent atom. For compound **2**, some restraints on displacement parameters were applied for the terminal carbon atoms of one *tert*-butyl group and some atoms of the pyridine solvent molecules; the highest residual electron density is located near the uranium atom. The very low quality of the crystals of compound **3**, and the resulting low quality of the diffraction data only enabled a rough structure determination to be obtained. In particular, some short H···H contacts indicate that some parts of the complex, particularly the *tert*-butyl groups, are not perfectly described. However, the main features of the structure are unambiguously determined. Restraints on bond lengths and/or displacement parameters had to be applied, particularly for the *tert*-butyl groups and the tetrahydrofuran molecules. Some large voids in the lattice indicate the presence of other, unresolved solvent molecules. Crystal data and structure refinement parameters are given in Table 1. The molecular plots were drawn with SHELXTL [21].

3. Results and discussion

The ligand H_6L^2 crystallizes in pyridine to give the compound $H_6L^2 \cdot 5py$ (**1**) in which three pyridine molecules are associated with the macrocycle by hydrogen bonding (Fig. 1). The H_6L^2 molecule, which has no crystallographic symmetry but only a pseudo-trigonal geometry, assumes a rather flat shape, with the three methylene-linked diphenolic subunits in "butterfly" conformation and with their concave side oriented in the same direction, giving to the macrocycle the shape of a very shallow cone. The dihedral angles between the aromatic rings in these diphenolic units are 63.1(2)°, 72.1(2)° and 67.3(2)°, whereas the dihedral angles between adjacent aromatic rings linked by an ethylene bridge are much smaller, 1.28(12)°, 11.7(2)° and 26.7(2)°. The C(arom)–C–C–C(arom) torsion angles defined by the ethylene bridges are all *anti*, with values of 176.3(4)°, 173.8(5)° and 175.8(5)°, whereas all the

Table 1
Crystal data and structure refinement details

	$H_6L^2 \cdot 5py$ (**1**)	$[Hpy][UCl_2(L^1)] \cdot 2.5py$ (**2**)	$[U_4Cl_2O_2(L^2)_2(H_2O)(thf)] \cdot 3thf$ (**3**)
Chemical formula	$C_{94}H_{115}N_5O_6$	$C_{65.5}H_{78.5}Cl_2N_{3.5}O_4U$	$C_{154}H_{202}Cl_2O_{19}U_4$
M (g mol^{-1})	1410.91	1287.75	3380.18
Crystal system	triclinic	monoclinic	triclinic
Space group	$P\bar{1}$	$P2_1/n$	$P\bar{1}$
a (Å)	15.6211(17)	20.5557(6)	18.092(2)
b (Å)	16.3945(12)	19.6241(4)	19.633(3)
c (Å)	17.4244(19)	30.9189(8)	23.134(4)
α (°)	84.679(6)	90	89.801(8)
β (°)	88.638(3)	103.8670(10)	84.060(10)
γ (°)	68.254(6)	90	69.551(8)
V (Å^3)	4126.7(7)	12108.8(5)	7653(2)
Z	2	8	2
D_{calc} (g cm^{-3})	1.135	1.413	1.467
μ(Mo Kα) (mm^{-1})	0.070	2.818	4.314
F(000)	1524	5232	3360
Total reflections	29989	78606	48276
Independent reflections	14339	22575	25785
Observed reflections ($I > 2\sigma(I)$)	5438	1510	10107
R_{int}	0.082	0.097	0.131
Parameters	964	1393	1648
R_1 (observed data)	0.091	0.047	0.098
wR_2 (all data)	0.242	0.112	0.262
S	0.996	1.016	0.965
$\Delta\rho_{min}$ (e Å^{-3})	−0.29	−0.83	−1.12
$\Delta\rho_{max}$ (e Å^{-3})	0.30	2.02	1.48

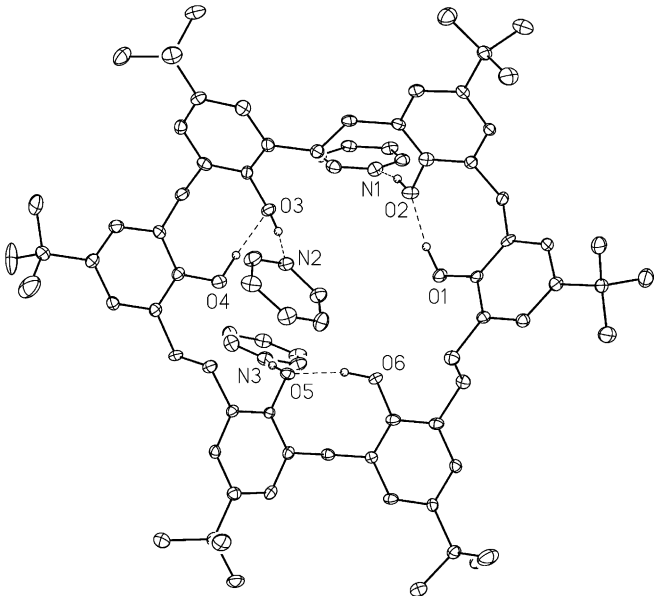

Fig. 1. View of the structure of $H_6L^2 \cdot 5py$ (**1**). The hydrogen atoms and solvent molecules not involved in hydrogen bonding are omitted for clarity. Hydrogen bonds are shown as dashed lines. Displacement ellipsoids are drawn at the 30% probability level.

C(arom)–C(arom)–C–C torsion angles are in the range 81.9(6)–103.0(6)°. The ethylene-bridged rings are thus nearly parallel to one another, albeit not coplanar. Each methylene-bridged diphenolic unit is associated with an intramolecular O–H···O hydrogen bond (Table 2), the second phenolic proton being diverted to form a hydrogen bond with a pyridine solvent molecule. Two of these three pyridine molecules (N1 and N3) are located on the convex side of the macrocycle and the third one (N2) in the concave cavity. The crystal packing further unites the molecules in slightly offset pairs related by a symmetry centre, with their concave sides facing each other and encompassing the two pyridine molecules, which are likely involved in C–H···π interactions (shortest H···centroid distance 2.73 Å) [22].

The reaction between UCl_4 and H_4L^1 in pyridine gives the mononuclear uranium(V) complex $[Hpy][UCl_2(L^1)] \cdot 2.5py$ (**2**); this result contrasts with the synthesis in thf, at room temperature, of the $[UCl_2(calix[4]arene\text{-}2H)(thf)_2]$ uranium(IV) complex recently reported [10]. The uranium(V) centre is bound to the four phenoxide groups and retains also two chlorine atoms (Fig. 2). The asymmetric unit contains two independent but nearly identical complex molecules. By contrast with the uranyl complex of the same ligand [13], in which the macrocycle is in the cone conformation and the four phenoxide oxygen atoms are in a plane so as to match the tetra-coordinated equatorial environment suitable for this ion, the macrocycle in **2** is distorted so as to provide, together with the chlorine atoms in adjacent positions, a slightly distorted octahedral environment for the uranium centre (Table 3). The U–O bond lengths are in the range 2.072(4)–2.113(4) Å [mean value 2.093(14) Å], i.e., lower than those in the other uranium(V) complex with a calixarene [7a] [mean value 2.15(3) Å], whereas the U–Cl bond lengths are in the range 2.6342(15)–2.6472(16) Å [mean value 2.639(5) Å], which corresponds to the largest values for U(V)–Cl bond lengths reported in the Cambridge Structural Database [23] [range 2.467–2.640, mean value 2.52(5) Å]. The macrocycle adopts a distorted cone conformation. The two 1,3-propylene bridges assume different geometries; in both molecules A and B, one of the bridges corresponds to C(arom)–C(arom)–C–C and C(arom)–C–C–C torsion angles which are roughly *gauche*, in the range 48.5–95.3°, whereas the other bridge contains two C(arom)–C–C–C torsion angles nearer to *syn* or *anti* geometries (larger and smaller values 36.5° and 169.4°, respectively). The complex unit $[UCl_2(L^1)]$ is monoanionic and its charge is compensated by the presence of one pyridinium ion, involved in a hydrogen bond with a pyridine molecule (Table 2). As shown in Fig. 2, the two [Hpy]py ensembles thus formed in the asymmetric unit are located in the cavity formed by the two macrocycles facing each other, in which they are held by various weak interactions. The two hydrogen bonded [Hpy]py assemblies are reversed with respect to one another and are thus possibly held together by dipole-dipole interactions. They may also be involved in two weak π–π interactions, each of them associating a pyridinium and a pyridine rings, with centroid···centroid distances of

Table 2
Hydrogen bonding geometry in compounds **1**–**3**: distances (Å) and angles (°)

	D···A		D–H		H···A		D–H···A	
1	O1···O2	2.724(5)	O1–H1	0.98	H1···O2	1.75	O1–H1···O2	171
	O2···N1	2.645(6)	O2–H2	1.01	H2···N1	1.65	O2–H2···N1	166
	O3···N2	2.672(6)	O3–H3	1.01	H3···N2	1.67	O3–H3···N2	169
	O4···O3	2.766(5)	O4–H4	0.97	H4···O3	1.91	O4–H4···O3	146
	O5···N3	2.687(6)	O5–H5	0.99	H5···N3	1.75	O5–H5···N3	158
	O6···O5	2.695(5)	O6–H6	0.99	H6···O5	1.73	O6–H6···O5	163
2	N1···N3	2.660(7)	N1–H1	0.85	H1···N3	1.83	N1–H1···N3	165
	N4···N2	2.653(7)	N4–H4	0.96	H4···N2	1.70	N4–H4···N2	174
3[a]	O3···O5	2.68(2)						
	O3···O6	2.68(2)						

[a] Hydrogen atoms not found.

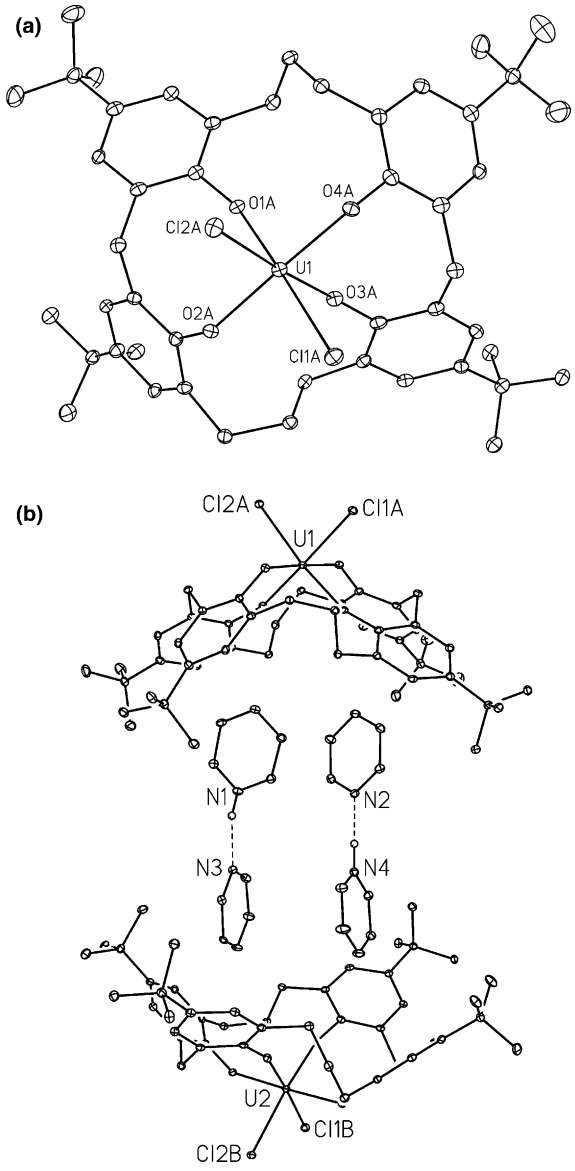

Fig. 2. (a) View of one of the two independent molecules of the monoanionic complex $[UCl_2(L^1)]$ in **2**. Hydrogen atoms are omitted for clarity. Displacement ellipsoids are drawn at the 20% probability level. (b) View showing the dimerization in **2**. The hydrogen atoms and solvent molecules not involved in hydrogen bonding are omitted for clarity. Displacement ellipsoids are drawn at the 10% probability level.

4.087(4) and 4.025(4) Å, dihedral angles of 18° and 11° and centroid offsets of 1.7 and 1.5 Å, for the ring pairs containing N1, N2 and N3, N4, respectively. The cohesion of the whole assembly seems to involve numerous CH–π interactions [22], in addition to cation-anion interactions. Seven such interactions can be found, which associate the protons of the pyridinium/pyridine moieties and the aromatic rings of the homocalixarenes, with H···centroid distances shorter than 2.9 Å and as low as 2.45 Å and C–H···centroid angles in the range 126–160°. Similar situations have been found in uranyl complexes of homooxacalixarenes with an included protonated [2.2.2]cryptand [24]. However, by contrast with these other cases, cation–π interactions [25] do not seem to be present in **2**, since no short contact is found between the protonated nitrogen atoms or their α-carbon atoms and the centroids of the aromatic rings. As a matter of fact, an evaluation of the relative importance of these weak interactions in such complex systems is unattainable on the basis of limited structural data alone [26].

When reacted with UCl_4 in tetrahydrofuran, H_6L^2 gives the neutral tetranuclear complex $[U_4Cl_2O_2(L^2)_2(H_2O)(thf)]\cdot 3thf$ (**3**), the structure of which is represented in Fig. 3. No crystallographic symmetry is present and the complex only possesses a pseudo-inversion centre at the intersection of the U1–U3 and U2–U4 lines. Complete deprotonation of the two macrocycles implies that **3** is a mixed valence compound comprising two U^{IV} and two U^{V} centres. The four metal atoms are at the apexes of an elongated rhombus which contains two μ_3-oxo ions and further bridging is ensured by two chlorine and two phenoxide groups. The average side length of the rhombus is 3.85(9) Å and the two diagonals are 6.6004(14) Å (U1···U3) and 3.9597(14) Å (U2···U4). This U_4O_2 assemblage can also be viewed as two coplanar U_3O triangles sharing a common edge, U2 and U4 being bound to both μ_3-oxo ions. These six atoms define a plane with an rms deviation of 0.08 Å, which also contains the chlorine and phenoxide bridges. Such tetranuclear planar arrangements around two μ_3-oxo centres are somewhat frequent in uranyl chemistry [27], and some examples are also found among uranium(IV) complexes [28]; in one case, two uranyl and two uranium(V) centres are involved [29]. In complex **3**, the μ_3-oxo ions are not perfectly trigonal, which is due to the differences in U–O bond lengths (see below) and to the enlargement by ca. 14° of the U–O–U angles associated with the chlorine bridges. Two uranium atoms are located within the ring defined by the six oxygen atoms of each macrocycle (U1 and U2 in the ligand denoted A, U3 and U4 in B). In addition to the μ_3-oxo ion and the bridging chlorine atoms, each metal atom is bound to three adjacent phenoxide oxygen atoms from the same calixarene, and U1 and U3 are also bound to one bridging phenoxide (O5A and O5B) from the other calixarene. The resulting coordination number is six for U1 and U3, with a distorted octahedral environment, whereas U2 and U4 are bound to an extra ligand, water for U2 and tetrahydrofuran for U4, which results in seven-coordinate environments with a distorted pentagonal bipyramidal geometry (O4A, O6A and O4B, O6B in axial positions for U2 and U4, respectively). The two pairs of atoms (U1 and U3) and (U2 and U4) show further differences when the average bond lengths are considered. ⟨U–O(oxo)⟩, ⟨U–O(terminal phenoxide)⟩, ⟨U–O(bridging phenoxide)⟩ and ⟨U–Cl⟩ are respectively equal to 2.04(2), 2.09(2), 2.28(4), 2.734(6) Å for (U1 and U3) and 2.36(3), 2.116(17), 2.46(2), 2.947(12) Å for (U2 and U4). Apart from the values for ⟨U–O(terminal phenoxide)⟩ which are not significantly different for the two sets of atoms and close to the values in the uranium(V) complex **2** and in the uranium(IV) complexes with *p-tert*-butylcalix[*n*]arene [2.125(12)–2.15(4) Å]

Table 3
Selected bond lengths (Å) and bond angles (°) in compounds **2** and **3**

$[Hpy][UCl_2(L^1)] \cdot 2.5py$ (**2**)	U1–O1A	2.098(4)	U2–O1B	2.074(4)
	U1–O2A	2.113(4)	U2–O2B	2.098(4)
	U1–O3A	2.072(4)	U2–O3B	2.095(4)
	U1–O4A	2.082(4)	U2–O4B	2.110(4)
	U1–Cl1A	2.6472(16)	U2–Cl1B	2.6342(15)
	U1–Cl2A	2.6343(15)	U2–Cl2B	2.6404(15)
	O1A–U1–Cl1A	178.26(12)	O1B–U2–Cl1B	175.27(12)
	O2A–U1–O4A	177.19(16)	O2B–U2–O4B	177.56(15)
	O3A–U1–Cl2A	173.00(12)	O3B–U2–Cl2B	177.12(12)
$[U_4Cl_2O_2(L^2)_2(H_2O)(thf)] \cdot 3thf$ (**3**)	U1–O1A	2.106(15)	U3–O1B	2.116(14)
	U1–O2A	2.072(15)	U3–O2B	2.053(14)
	U1–O3A	2.089(15)	U3–O3B	2.114(16)
	U1–O5B	2.317(17)	U3–O5A	2.245(14)
	U1–O1	2.017(13)	U3–O2	2.058(16)
	U1–Cl1	2.740(7)	U3–Cl2	2.728(6)
	O1A–U1–O3A	163.6(6)	O1B–U3–O3B	160.0(6)
	O2A–U1–O1	170.1(6)	O2B–U3–O2	170.0(4)
	O5B–U1–Cl1	149.5(4)	O5A–U3–Cl2	148.9(3)
	U2–O4A	2.099(15)	U4–O4B	2.128(15)
	U2–O5A	2.482(12)	U4–O5B	2.440(15)
	U2–O6A	2.099(13)	U4–O6B	2.136(13)
	U2–O1	2.351(14)	U4–O1	2.377(14)
	U2–O2	2.385(17)	U4–O2	2.312(14)
	U2–O3	2.451(15)	U4–O4	2.421(18)
	U2–Cl1	2.959(6)	U4–Cl2	2.934(6)
	O4A–U2–O6A	163.6(6)	O4B–U4–O6B	161.7(6)
	U1–Cl1–U2	87.11(18)	U3–Cl2–U4	88.30(18)
	U1–O5B–U4	104.4(6)	U2–O5A–U3	105.5(5)
	U1–O1–U2	128.1(7)	U2–O2–U3	115.7(6)
	U1–O1–U4	117.4(7)	U2–O2–U4	114.9(7)
	U2–O1–U4	113.7(5)	U3–O2–U4	129.1(8)

[10] (but slightly smaller than those in the uranium(IV) complexes with acyclic polyphenoxides [2.138(4)–2.208(6) Å]), all the bond lengths are larger, by ca. 0.2–0.3 Å, for the (U2 and U4) pair. The differences in U–Cl and U–O bond lengths between uranium(IV) and uranium(V) are 0.10 and 0.17 Å, respectively, for the structures reported in the Cambridge Structural Database (terminal chlorine ligands only since there is no example of a bridging chlorine bound to U^V). Besides, the ionic radii reported for uranium(IV) with a coordination number of seven and uranium(V) with a coordination number of six are 0.95 and 0.76 Å, respectively [30]. It can also be noticed that the U^V–O(μ_3-oxo) bond length in the other example reported is 2.08(2) Å [29], close to the value relative to U1 and U3 in the present case and that the average U^{IV}–O(μ_3-oxo) bond length is 2.23(8) Å [8], smaller than the value for U2 and U4, but closer to it than to the previous one. All this allows to consider that complex **3** is a mixed-valence species with uranium(IV) and uranium(V) centres localized at the (U2 and U4) and (U1 and U3) sites, respectively. This is the third example of a uranium mixed-valence complex involving a calixarene-like ligand, the other ones being the localized U^{III}/U^{IV} species obtained with the calix[4]tetrapyrrole tetraanion [9], and the delocalized U^V/U^{VI} complex with *p-tert*-butylcalix[4]arene [7a].

As stated above, each macrocycle encompasses two uranium ions (one U^{IV} and one U^V) within the ring defined by its six phenoxide groups. This is in agreement with previous observations relative to the number of uranyl ions included versus the size of macrocycles in the calixarene and homooxacalixarene families [31]. The ligand $[L^2]^{6-}$ provides an hexa-phenoxide coordination site surrounded by a 27-membered bond array and it is thus roughly equivalent in this respect to *p-R*-calix[7]arene and *p-R*-tetrahomodioxacalix[6]arene, which present a 28-membered array. Mononuclear uranyl complexes have been obtained with these two latter ligands, but *p*-benzylcalix[7]arene has also been shown to behave as a ditopic ligand for uranyl ions [27]. However, it must be noted that the geometrical requirements of uranyl and $U^{IV,V}$ ions are very different, as well as the finer geometry of the ligands. In compound **3**, the six oxygen atoms of each macrocycle define mean planes with rms deviations of 0.34 and 0.36 Å, the atoms O5A,B and O6A,B being the most displaced out of the plane; both planes are nearly parallel to one another, with a dihedral angle of 1.1(3)°, and perpendicular to the U_4O_2 central core, with dihedral angles of 88.5(3)° and 89.5(3)°. The conformation of the macrocycle can be seen as a shallow cone, as in the uncomplexed form **1**, but of course the pseudo-trigonal geometry observed in the latter is replaced

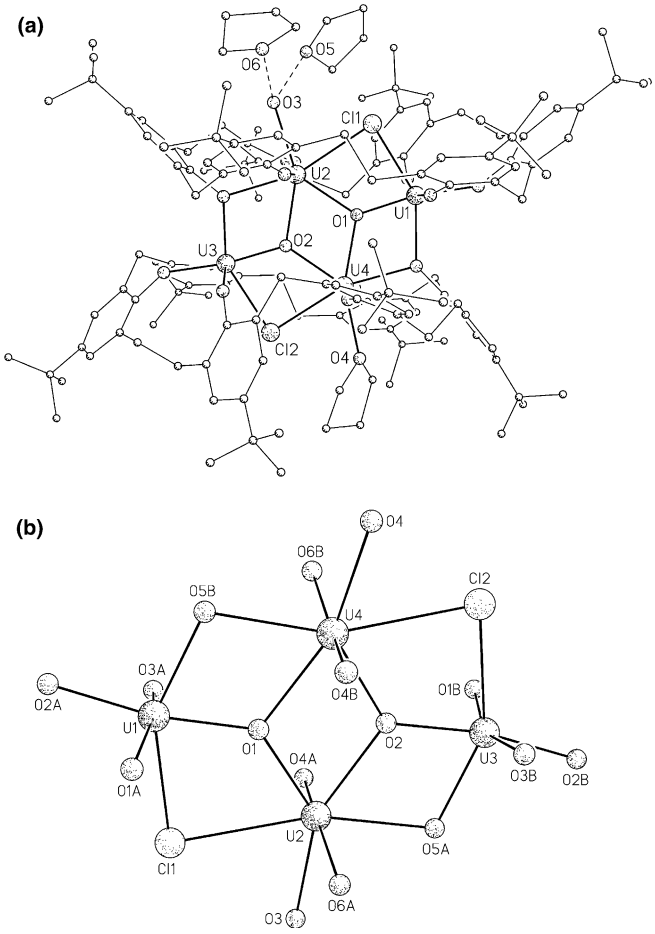

Fig. 3. (a) View of the complex $[U_4Cl_2O_2(L^2)_2(H_2O)(thf)]\cdot 3thf$ (**3**). The hydrogen atoms and the isolated thf molecule are omitted. For the sake of clarity, the atoms are represented as spheres, the carbon ones being arbitrarily reduced. Hydrogen bonds are shown as dashed lines. (b) View of the uranium atoms environment.

by a more elongated, roughly elliptical one, due to the inclusion of the two metal atoms. As in **1**, the dihedral angles between adjacent aromatic rings are larger for the rings separated by a methylene bridge [57.4(7)–86.1(7)°] than for those separated by an ethylene bridge [8.2(10)–30.2(9)°]. As in **1** also, the C(arom)–C–C–C(arom) torsion angles defined by the ethylene bridges are close to *anti* conformations, with values in the range 142(2)–165(2)°, while the C(arom)–C(arom)–C–C torsion angles are in the range 72(3)–112(3)°. The chlorine atoms and the coordinated water and tetrahydrofuran molecules are located in the calixarene cavities and the water molecule (O3) is further hydrogen bonded to two tetrahydrofuran molecules.

4. Conclusion

Compounds **2** and **3** provide rare examples of structural characterization of complexes involving homocalixarenes and they also extend the limited family of uranium (uranyl excepted) complexes of calixarene-like molecules. Unfortunately, they cannot be compared with the complexes obtained by reaction of UCl_4 with the closely related homooxacalixarenes, due to the macrocycle cleavage observed with the latter. Both compounds **2** and **3** confirm the ready metal oxidation previously encountered in attempts to complex uranium(IV) with calixarenes [7], since only in **3** half the metal centres remain in this oxidation state. As frequently observed in calixarene complexes, large assemblies are obtained, either through weak interactions involving the counter-ions and the solvent molecules (**2**) or as a result of metal aggregation due to the polytopic nature of the macrocycle and the presence of additional bridging species (**3**). Eventually, compound **2** is the first U(V) mononuclear complex with a calixarene ligand and it could be used as a starting material for the synthesis of derived complexes by substitution of the two chlorine atoms.

Appendix A. Supplementary material

Crystallographic data for the structural analysis have been deposited with the Cambridge Crystallographic Data Centre, CCDC Nos. 296822–296824. Copies of this information may be obtained free of charge from The Director, CCDC, 12 Union Road, Cambridge CB2 1EZ, UK (fax: +44 1223 336 033; e-mail: deposit@ccdc.cam.ac.uk or www: http://www.ccdc.cam.ac.uk). Supplementary data associated with this article can be found, in the online version, at doi:10.1016/j.poly.2006.02.006.

References

[1] T. Nagasaki, K. Kawano, K. Araki, S. Shinkai, J. Chem. Soc., Perkin Trans. 2 (1991) 1325.
[2] (a) J. Harrowfield, Gazz. Chim. Ital. 127 (1997) 663;
(b) P. Thuéry, M. Nierlich, J. Harrowfield, M. Ogden, in: Z. Asfari, V. Böhmer, J. Harrowfield, J. Vicens (Eds.), Calixarenes 2001, Kluwer Academic Publishers, Dordrecht, 2001 (Chapter 30) and references therein.
[3] (a) P. Thuéry, B. Masci, Dalton Trans. (2003) 2411, and references therein;
(b) X. Delaigue, C.D. Gutsche, J.M. Harrowfield, M.I. Ogden, B.W. Skelton, D.F. Stewart, A.H. White, Supramol. Chem. 16 (2004) 603, and references therein.
[4] R. Ludwig, K. Kunogi, N. Dung, S. Tachimori, Chem. Commun. (1997) 1985.
[5] Q. Lu, J.H. Callahan, G.E. Collins, Chem. Commun. (2000) 1913.
[6] J.M. Harrowfield, M.I. Ogden, A.H. White, J. Chem. Soc., Dalton Trans. (1991) 2625.
[7] (a) P.C. Leverd, M. Nierlich, Eur. J. Inorg. Chem. (2000) 1733;
(b) P.C. Leverd, D. Rinaldo, M. Nierlich, J. Chem. Soc., Dalton Trans. (2002) 829.
[8] J. Old, A.A. Danopoulos, S. Winston, New J. Chem. 27 (2003) 672.
[9] (a) I. Korobkov, S. Gambarotta, G.P.A. Yap, Organometallics 20 (2001) 2552;
(b) I. Korobkov, S. Gambarotta, G.P.A. Yap, L. Thompson, P.J. Hay, Organometallics 20 (2001) 5440.
[10] L. Salmon, P. Thuéry, M. Ephritikhine, Chem. Commun. (2006) 856.
[11] (a) L. Salmon, P. Thuéry, M. Ephritikhine, B. Masci, Dalton Trans. (2003) 2405;
(b) L. Salmon, P. Thuéry, M. Ephritikhine, B. Masci, Acta Crystallogr., Sect. C 60 (2004) m27.

[12] B. Masci, in: Z. Asfari, V. Böhmer, J. Harrowfield, J. Vicens (Eds.), Calixarenes 2001, Kluwer Academic Publishers, Dordrecht, 2001 (Chapter 12) and references therein.
[13] P. Thuéry, J.T. Gil, T. Yamato, Supramol. Chem. 15 (2003) 359.
[14] (a) J.A. Hermann, J.F. Suttle, Inorg. Synth. 5 (1957) 143;
(b) A. Vallat, E. Laviron, A. Dormond, J. Chem. Soc., Dalton Trans. (1990) 921.
[15] (a) T. Yamato, Y. Saruwatari, S. Nagayama, K. Maeda, M. Tashiro, J. Chem. Soc., Chem. Commun. (1992) 861;
(b) T. Yamato, Y. Saruwatari, M. Yasumatsu, J. Chem. Soc., Perkin Trans. 1 (1997) 1725.
[16] T. Yamato, Y. Saruwatari, L.K. Doamekpor, K. Hasegawa, M. Koike, Chem. Ber. 126 (1993) 2501.
[17] Kappa-CCD Software, Nonius B.V., Delft, The Netherlands, 1998.
[18] Z. Otwinowski, W. Minor, Methods Enzymol. 276 (1997) 307.
[19] G.M. Sheldrick, SHELXS-97 and SHELXL-97, University of Göttingen, Germany, 1997.
[20] A.L. Spek, PLATON, University of Utrecht, The Netherlands, 2000.
[21] G.M. Sheldrick, SHELXTL, Version 5.1, Bruker AXS, Inc., Madison, WI, USA, 1999.
[22] (a) H. Takahashi, S. Tsuboyama, Y. Umezawa, K. Honda, M. Nishio, Tetrahedron 56 (2000) 6185;
(b) H. Suezawa, T. Yoshida, M. Hirota, H. Takahashi, Y. Umezawa, K. Honda, S. Tsuboyama, M. Nishio, J. Chem. Soc., Perkin Trans. 2 (2001) 2053.
[23] F.H. Allen, Acta Crystallogr., Sect. B 58 (2002) 380.
[24] B. Masci, M. Nierlich, P. Thuéry, New J. Chem. 26 (2002) 766.
[25] J.C. Ma, D.A. Dougherty, Chem. Rev. 97 (1997) 1303.
[26] J. Harrowfield, D. Matt, J. Incl. Phenom. Macr. Chem. 50 (2004) 133, and references therein.
[27] P. Thuéry, M. Nierlich, B. Souley, Z. Asfari, J. Vicens, J. Chem. Soc., Dalton Trans. (1999) 2589, and references therein.
[28] (a) F. Calderazzo, G. dell'Amico, M. Pasquali, G. Perego, Inorg. Chem. 17 (1978) 474;
(b) N. Brianese, U. Casellato, F. Ossola, M. Porchia, G. Rossetto, P. Zanella, R. Graziani, J. Organomet. Chem. 365 (1989) 223.
[29] A.J. Zozulin, D.C. Moody, R.R. Ryan, Inorg. Chem. 21 (1982) 3083.
[30] R.D. Shannon, Acta Crystallogr., Sect. A 32 (1976) 751.
[31] P. Thuéry, M. Nierlich, J. Vicens, B. Masci, J. Chem. Soc., Dalton Trans. (2001) 867.

absorption and Raman spectroscopy and emission spectroscopy. The crystal structures of the ADA and AZA complexes were also determined.

2. Experimental

2.1. Syntheses

Uranyl benzoylacetonate (ba) was prepared by reacting 1-3-diphenyl-1,3-propanedione (dibenzoylmethane, Aldrich) in ethanolic solution, in slight excess, with uranyl carbonate in aqueous suspension, under stirring. Typical preparations involved ca. 100 mg of uranyl carbonate in suspension in ca. 5 mL of distilled water and a slight stoichiometric excess of dibenzoylmethane dissolved in ca. 10 mL of absolute ethanol. Precipitation was immediate. The suspension was filtered after 1 h, to ensure complete precipitation, washed with water and dried in vacuo in a desiccator with anhydrous calcium chloride. Yields obtained were typically 97%. This compound was characterized by IR spectroscopy.

The complexes were prepared as follows: uranyl ba dissolved in acetone (50 mg in ca. 5 mL) was added to methanolic solutions of the corresponding neutral ligands in a slight stoichiometric excess (typically 50 mg in 5 mL of analytical grade methanol). Precipitation was observed after some minutes, but the suspensions were left for one day before filtering. The precipitates were filtered, washed with methanol and dried in vacuo over anhydrous calcium chloride. Recrystallization from methanol, by slow solvent evaporation, yielded crystals suitable for structure determinations. Typical yields were 80%. Characterization procedures involved elemental analyses, IR, Raman and emission spectroscopy. They are described below in Section 3.

2.2. Instrumentation

Elemental analyses were carried out in a Perkin–Elmer 240 microanalyzer. Infrared absorption spectra were recorded in a Nicolet FT-IR-510 spectrometer using KBr pellets. Visible emission spectra were recorded in a modified Hitachi–Perkin–Elmer MPF4 spectrofluorimeter at 298 and 77 K. Raman spectra were recorded in a FT-Raman Bruker FRS-100 S spectrometer, using a Nd/YAG laser (Coherent Compass 1064-500 N) for excitation at $\lambda = 1064$ nm and 40 mW power, using an InGaAs detector.

2.3. X-ray crystallography

Suitable crystals were mounted on glass fibers and aligned on an Enraf-Nonius CAD-4 diffractometer. Data were obtained with graphite-monochromated Mo Kα radiation ($\lambda = 0.71073$ Å) and 2ω–2θ scan mode, at room temperature, in the ranges 1.59–25.01° (ADA complex) and 2.02–27.50° (AZA complex).

Table 1
Crystallographic data and details of the structure refinement for (**1**) and (**2**)

Compound	**1**	**2**
Empirical formula	$C_{42}H_{38}NO_7U$	$C_{38}H_{36}NO_7U$
Formula weight	906.76	856.71
Temperature (K)	293(2)	293(2)
Crystal size (mm)	$0.25 \times 0.10 \times 0.10$	$0.20 \times 0.15 \times 0.10$
Crystal system, space group	orthorhombic, *Pbca*	monoclinic, $P2_1/n$
Z	8	8
a (Å)	14.730(1)	16.7695(4)
b (Å)	20.980(2)	13.2783(3)
c (Å)	25.536(2)	31.1403(7)
β (°)		93.572(1)
Volume (Å^3)	7891.7(1)	6920.6(3)
D_{calc} (g/cm^3)	1.526	1.644
Absorption coefficient (mm^{-1})	4.162	4.740
$F(000)$	3560	3352
θ Range data collection (°)	1.59–25.01	2.02–27.50
Limiting indices (h,k,l)	$-1 \leqslant h \leqslant 17$, $0 \leqslant k \leqslant 24$, $-30 \leqslant l \leqslant 0$	$-21 \leqslant h \leqslant 21$, $-15 \leqslant k \leqslant 17$, $-25 \leqslant l \leqslant 40$
Reflections collected	7524	26032
Independent reflections (R_{int})	6942 (0.0334)	13853 (0.0330)
Observed reflections [$I > 2\sigma(I)$]	3450	11053
Refinement method	full-matrix least-squares on F^2	full-matrix least-squares on F^2
Data/restraints/parameters	6942/0/461	13853/0/847
Goodness-of-fit on F^2	0.916	0.996
SHELX-97 weight parameters	0.0809/0	0.0228/28.384
Final R/wR [$I > 2\sigma(I)$]	0.0522/0.1145	0.0452/0.0914
R/wR (all data)	0.1412/0.1539	0.0642/0.1014
Largest difference in peak and hole (e/Å^3)	0.966/−1.722	0.257/−0.247

During data collection, the intensities of three selected reflections (for both crystals) were monitored each 1800 s of X-ray exposure, showing no significative decay. Data were corrected for Lorentz-polarization and absorption.

Structures were solved by the standard heavy-atom Patterson method, using SHELX-86 program [19], followed by normal difference Fourier techniques that yielded the positions of the remaining non-H atoms. These latter were located on stereochemical grounds and refined with fixed geometry, each riding on a carrier atom with an isotropic displacement parameter amounting to 1.2 times the value of the equivalent isotropic displacement parameter of the atom to which they are attached. Structures were refined anisotropically by full-matrix least-squares methods on F^2, using SHELXL-97 program [20]. Molecular displays were carried out by ZORTEP program [21]. Table 1 reports crystal data and refinement parameters for the two complexes.

3. Results and discussion

Microanalytical results were the following: for the ADA complex, calculated (experimental) percent values were: C, 55.6 (56.3); H, 4.2 (4.7); N, 1.5 (1.1); for the AZA complex, C, 53.3 (53.6); H, 4.2 (4.5); N, 1.6 (1.4); for the TPPO

Table 2
Selected IR and Raman bands of $UO_2(ba)_2L$ complexes (cm^{-1})

Compound	$UO_2(\nu_1)$	$UO_2(\nu_2)$	$UO_2(\nu_3)/\nu CC + \nu CO$	$\nu CC + \nu CO$	$\nu CC + \nu CO$
(a) Infrared					
$UO_2(ba)_2$ TPPO	829w		938w	1540s	1349m
$UO_2(ba)_2$ ADA	815w		941w	1541s	1359m
$UO_2(ba)_2$ AZA	811w		941w	1539s	1351m
Compound	$UO_2(\nu_1)$	$UO_2(\nu_2)$	$UO_2(\nu_3)/\nu CC + \nu CO$	$\delta CH + \nu CC$	C_6H_6 ring stretching
(b) Raman					
$UO_2(ba)_2$ TPPO	830s	211w	942m	1185m	1597s
$UO_2(ba)_2$ ADA	816m	212w	943m	1191s	1597s
$UO_2(ba)_2$ AZA	814s		943m	1185m	1598s

complex, C, 57.6 (58.0); H, 5.2 (4.9). These results indicate the general composition $UO_2(ba)_2L$ (L = ADA, AZA, TPPO). The small difference in the CHN percents observed for the ADA complex was explained when its crystal structure was determined. This complex has one crystallization solvent molecule (methanol) per unit cell.

Table 2 shows some selected frequencies obtained from infrared absorption and Raman spectra. Benzoylacetonate bands were assigned according to the literature [22–25]. The $\nu CC + \nu CO$ acetonate bands are in the same region of the UO_2 ν_3 mode. These acetonate bands point out to O-bonded complexes. On the other hand, if the complexes were C-bonded, the C=O frequency would be around 1650–1620 cm^{-1} [26–28].

The uranyl ion frequencies observed (for the same complex) in IR and Raman spectra are identical within 4 cm^{-1}; this difference can be due to calibrations of the respective spectrometers. The appearance of $\nu_2(UO_2^{2+})$ in the Raman spectra can be explained by the asymmetric field created by the ligands; the same explanation holds for the appearance of $\nu_1(UO_2^{2+})$ in the infrared spectra [29]. Since UO_2^{2+} is a symmetric linear ion, ν_3 should also be absent in the Raman spectra. In this case, since the $\nu CC + \nu CO$ (acetonate combination bands) fall in the same region, no such verification could be made. Since the bands observed in the Raman spectra at 942–943 cm^{-1} are of medium intensity, it is reasonable to assign them to the $\nu CC + \nu CO$ combination band.

In all Raman spectra the most intense bands appear at ca. 1597 cm^{-1}. This band has been assigned to benzene ring stretching [30].

Table 3 shows some bands related to the neutral ligands, which appear in the infrared spectra. A comparison is also made with the corresponding free ligands. In all cases it can be verified that the CO or PO stretching frequencies are shifted to lower frequencies. These shifts point out to bondings through the respective CO and PO oxygen atoms.

All complexes are luminescent and their emission spectra present several vibronic bands. This is a common feature in uranyl compounds. It is believed that the emitting state is one in which an electron has been transferred from an UO_2^{2+} molecular orbital to a 5f U atomic orbital (in other words, a charge transfer) [31]. A strong argument in favor of this excited state is the pronounced radical-like activity of these excited molecules [6].

Table 3
Selected IR bands related to the neutral ligands (cm^{-1})

Compound	νCO	νPO
$UO_2(ba)_2$ ADA	1626	
ADA	1649	
$UO_2(ba)_2$ AZA	1630	
AZA	1643	
$UO_2(ba)_2$ TPPO		1119
TPPO		1127

All emission spectra were obtained with excitation at $\lambda = 370$ nm. Excitation spectra show only a broad band with maxima near that wavelength.

For the three complexes, even at 77 K the emission bands are broad, with poorly resolved vibronic structures. For the TPPO complex, five bands appear, with maxima at 482, 503, 535, 560 and 586 nm; for the ADA complex, only one broad band appears, with maxima at 542, 566, a shoulder at 589 and a smaller maximum at 606 nm; for the AZA complex, three bands appear at 417, 440 and 467 nm, and a more intense, broader band with maximum intensity at 541 nm and a smaller peak at 567 nm. The mean energy separations are: for TPPO, 818; for ADA, 810 and for AZA, 784 cm^{-1}.

The different values for these energy separations point out to differences in the uranyl ions immediate environments in the different complexes. It is important to emphasize that the uranyl nitrate complexes previously studied in this laboratory [16,18] emit more strongly than the ba complexes described in this paper. It is known that the most intense uranyl emission bands are zero-phonon transitions, which are magnetic dipole allowed when the U atom is situated in a centrosymmetrical environment [32]. Such is indeed the case for the complexes described in Refs. [16,18]. In the complexes here described (heptacoordinated) no center of symmetry exists.

Comparing the values of energy separations of the emission bands with the corresponding IR and Raman spectra (Table 2), it is apparent that more than one vibrational

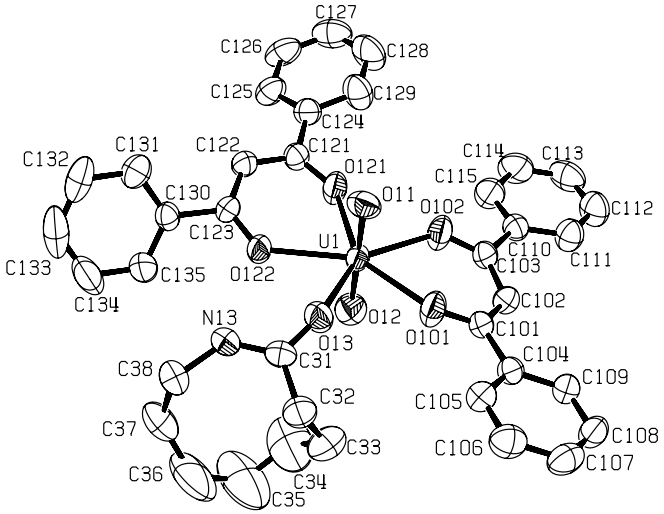

Fig. 1. ORTEP plot of the structure of compound **1**.

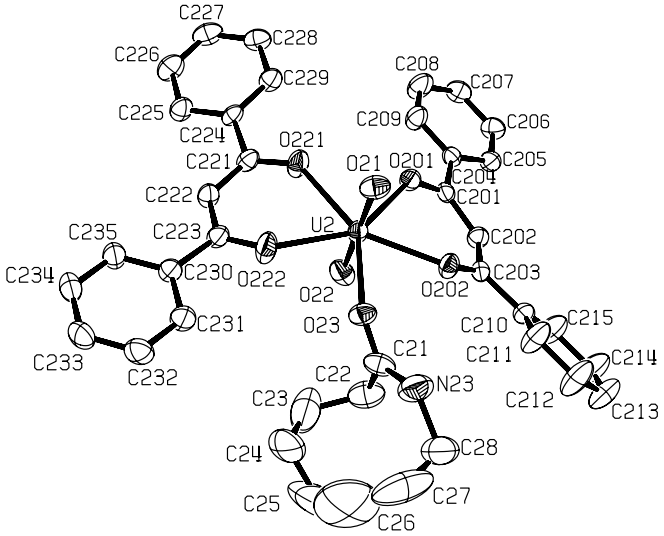

Fig. 2. ORTEP plot of the structure of compound $\mathbf{2_1}$.

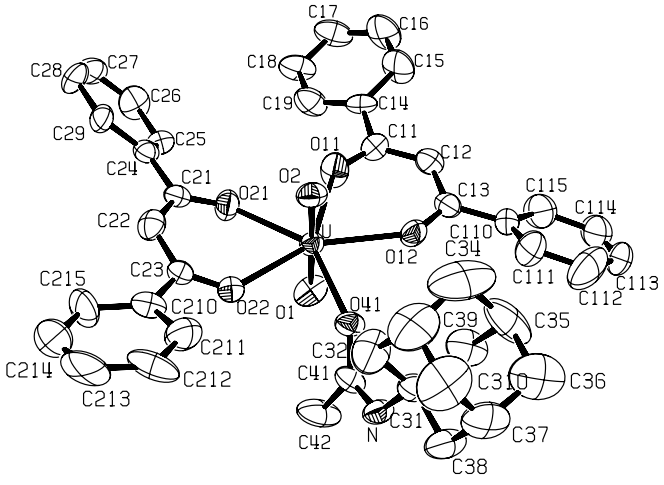

Fig. 3. ORTEP plot of the structure of compound $\mathbf{2_2}$.

Table 4
Selected bond distances (Å) and angles (°) for **1** and **2**

(1)			
U–O(1)	1.753(9)	O(1)–U–O(2)	178.7(4)
U–O(2)	1.763(8)	O(1)–U–O(11)	92.0(4)
U–O(11)	2.319(8)	O(2)–U–O(11)	89.2(4)
U–O(22)	2.345(8)	O(1)–U–O(22)	92.5(4)
U–O(21)	2.354(8)	O(2)–U–O(22)	86.3(4)
U–O(41)	2.383(8)	O(11)–U–O(22)	141.9(3)
U–O(12)	2.393(8)	O(1)–U–O(21)	88.5(4)
		O(2)–U–O(21)	91.4(3)
		O(11)–U–O(21)	72.4(3)
		O(22)–U–O(21)	69.9(3)
		O(1)–U–O(41)	86.0(3)
		O(2)–U–O(41)	93.3(3)
		O(11)–U–O(41)	144.9(3)
		O(22)–U–O(41)	73.1(3)
		O(21)–U–O(41)	142.3(3)
		O(1)–U–O(12)	92.6(4)
		O(2)–U–O(12)	88.3(3)
		O(11)–U–O(12)	69.9(3)
		O(22)–U–O(12)	147.5(3)
		O(21)–U–O(12)	142.3(3)
		O(41)–U–O(12)	75.2(3)
(2_1)			
U(1)–O(12)	1.759(5)	O(12)–U(1)–O(11)	178.5(2)
U(1)–O(11)	1.769(5)	O(12)–U(1)–O(102)	89.1(2)
U(1)–O(102)	2.333(4)	O(11)–U(1)–O(102)	92.3(2)
U(1)–O(121)	2.355(5)	O(12)–U(1)–O(121)	94.2(2)
U(1)–O(101)	2.354(4)	O(11)–U(1)–O(121)	86.8(2)
U(1)–O(13)	2.367(5)	O(102)–U(1)–O(121)	75.23(16)
U(1)–O(122)	2.393(4)	O(12)–U(1)–O(101)	89.3(2)
		O(11)–U(1)–O(101)	90.5(2)
		O(102)–U(1)–O(101)	69.82(16)
		O(121)–U(1)–O(101)	144.81(16)
		O(12)–U(1)–O(13)	92.4(2)
		O(11)–U(1)–O(13)	86.06(19)
		O(102)–U(1)–O(13)	142.14(16)
		O(121)–U(1)–O(13)	142.17(15)
		O(101)–U(1)–O(13)	72.37(16)
		O(12)–U(1)–O(122)	85.6(2)
		O(11)–U(1)–O(122)	93.8(2)
		O(102)–U(1)–O(122)	144.08(16)
		O(121)–U(1)–O(122)	69.81(15)
		O(101)–U(1)–O(122)	145.36(16)
		O(13)–U(1)–O(122)	73.65(15)
(2_2)			
U(2)–O(22)	1.743(6)	O(22)–U(2)–O(21)	179.6(3)
U(2)–O(21)	1.783(5)	O(22)–U(2)–O(201)	87.6(2)
U(2)–O(201)	2.341(4)	O(21)–U(2)–O(201)	92.1(2)
U(2)–O(222)	2.349(5)	O(22)–U(2)–O(222)	88.3(3)
U(2)–O(202)	2.359(4)	O(21)–U(2)–O(222)	92.1(3)
U(2)–O(221)	2.369(5)	O(201)–U(2)–O(222)	144.94(16)
U(2)–O(23)	2.392(4)	O(22)–U(2)–O(202)	88.7(2)
		O(21)–U(2)–O(202)	91.0(2)
		O(201)–U(2)–O(202)	69.61(15)
		O(222)–U(2)–O(202)	145.06(17)
		O(22)–U(2)–O(221)	90.2(2)
		O(21)–U(2)–O(221)	89.8(2)
		O(201)–U(2)–O(221)	75.10(16)
		O(222)–U(2)–O(221)	70.11(18)
		O(202)–U(2)–O(221)	144.71(17)
		O(22)–U(2)–O(23)	89.59(19)
		O(21)–U(2)–O(23)	90.56(19)
		O(201)–U(2)–O(23)	141.47(16)
		O(222)–U(2)–O(23)	73.26(17)
		O(202)–U(2)–O(23)	71.92(16)
		O(221)–U(2)–O(23)	143.36(17)

Table 5
Hydrogen-bonding geometry (Å, °) for **1** and **2**

D–H···A	D–H	H···A	D···A	D–H···A
(1)				
C17–H17···O1^{i}	0.93	2.68	3.28(2)	123
C214–H214···O1^{ii}	0.93	2.61	3.34(2)	135
C25–H25···Cg(1)^{iii}	0.93	2.91	3.759	152
C37–H7···Cg(2)^{iv}	0.98	2.78	3.715	160
(2)				
C131–H131···O22^{v}	0.93	2.43	3.291(9)	154
C215–H215···O11^{vi}	0.93	2.52	3.43(1)	169
C35–H35B···Cg(1)^{vii}	0.97	2.99	3.50	114
C213–H213···Cg(3)^{viii}	0.93	2.73	3.65	172

Symmetry code: (i) $1-x, 1-y, -z$; (ii) $1/2-x, -1/2+y, z$; (iii) $1-x, -y, 1-z$; (iv) $-1/2+x, y, 1/2-z$; (v) $1/2+x, 1/2-y, -1/2+z$; (vi) $-1/2+x, 1/2-y, 1/2+z$; (vii) $1-x, 1-y, -z$; (viii) $-1+x, y, z$. Cg(1_1): C14–C19; Cg(2_1): C24–C29. Cg(1_2): C104–C109; Cg(3_2): C124–C129.

mode of the UO_2^{2+} ion may be involved in the observed progressions, for the three complexes.

The crystal structures of the ADA and AZA complexes were determined. In the ADA complex (compound **1**) there is a disordered molecule of solvent (methanol) per unit cell which could not be modeled, and that is the reason for the high residual electron density. In the AZA complex (compound **2**) there are two independent molecules in the asymmetric unit. The structures are shown in Figs. 1 (compound **1**), 2 (compound $\mathbf{2_1}$) and 3 (compound $\mathbf{2_2}$). Selected bond distances and angles are listed in Table 4. The structure shows that, in all cases, the U atom is surrounded by seven O atoms, four of ba, one of the other ligand and the two uranyl O atoms. The U–O_{uranyl} distances are in the range of other seven coordinated similar compounds; in fact, a search in Cambridge Structural Database [33] showed that for 118 distances, the mean value is 1.76 Å. The U–O_{ba} distances are in good agreement, to within experimental accuracy, with the ones found in the literature ([9] and references therein). The overall bond lengths and angles show that the U atom is in a distorted pentagonal bipyramidal geometry coordination, with O (uranyl) occupying the apices. Regarding the basal plane, the maximum deviation of the oxygens from the best least-square plane through them are 0.138(3), 0.172(3) and 0.055(3) Å, for (**1**), ($\mathbf{2_1}$) and ($\mathbf{2_2}$), respectively. In the ba ligands the benzene rings are not coplanar, forming different dihedral angles: 40.4(5)° and 42.3(5)° in (**1**) and 9.8(2)° and 64.2(2)° in ($\mathbf{2_1}$) and 24.7(3)° and 17.3(2)° in ($\mathbf{2_2}$). The molecular packing is stabilized by intermolecular C–H···O interactions involving the aromatic rings (Table 5).

Acknowledgements

The authors wish to thank Prof. Marcia L.A. Temperini (Laboratório de Espectroscopia Molecular, Instituto de Química, Universidade de São Paulo) for the recording of Raman spectra. Prof. M. Martinez-Ripoll is gratefully acknowledged for making possible the use of the CSD. This work was partially supported by CNPq and FAPESP.

Appendix A. Supplementary data

The structures reported in this paper and all pertinent Supplementary data have been deposited at the Cambridge Crystallographic Date Centre under Register Nos. 294835 and 294836. Supplementary data associated with this article can be found, in the online version, at doi:10.1016/j.poly.2006.02.009.

References

[1] G. Folcher, N. Keller, J. Paris, Solar Energ. Mater. 10 (1984) 303.
[2] C.K. Jörgensen, R. Reisfeld, Struct. Bond. (Berl.) 50 (1982) 121.
[3] C.G. Roffey, Photopolymerisation of Surface Coatings, Wiley, Chichester, 1985, p. 123.
[4] S.L. Suib, K.A. Carrado, Inorg. Chem. 24 (1984) 200.
[5] E. Rabinovitch, R.L. Belford, Spectroscopy and Photochemistry of Uranium Compounds, Pergamon, Oxford, 1964.
[6] H.D. Burrows, T.J. Kemp, Chem. Soc. Ver. 3 (1974) 139.
[7] H.G.F. Güsten, Gmelin Handbook of Inorganic Chemistry, vol. Ac, Springer, Berlin, 1983 (Chapter 3).
[8] C. Moulin, P. Decambox, V. Moulin, J.G. Decaillon, Anal. Chem. 67 (1995) 348.
[9] M. Alagar, K. Rajagopal, R.V. Krishnakumar, M. Subha Nandhini, S. Kannan, S. Natarajan, Acta Crystallogr. E59 (2003) m524.
[10] M. Alagar, S. Kannan, K. Rajagopal, V. Venugopal, R.V. Krishnakumar, M. Subha Nandhini, S. Natarajan, Acta Crystallogr. E60 (2004) m773.
[11] K. Rajagopal, R.V. Krisnakumar, M. Subha Nandhini, S. Kannan, S. Natarajan, Acta Crystallogr. E58 (2002) m316.
[12] H.K. Fun, S. Kannan, A. Usman, I.A. Razak, S. Chantrapromma, Acta Crystallogr. C58 (2002) m368.
[13] H.K. Fun, S. Kannan, S. Chantrapromma, I.A. Razak, A. Usman, Acta Crystallogr. E58 (2002) m463.
[14] A.L. Rodgers, L.R. Nassimbeni, R.A. Paupitt, G. Orpen, J.M. Haigh, Acta Crystallogr. B33 (1977) 3110.
[15] N.W. Alcock, D.J. Flanders, Acta Crystallogr. C43 (1987) 1480.
[16] A.R. Aquino, G. Bombieri, P.C. Isolani, G. Vicentini, J. Zukerman-Schpector, Inorg. Chim. Acta 306 (2000) 101.
[17] A.R. Aquino, P.C. Isolani, J. Zukerman-Schpector, L.B. Zinner, G. Vicentini, J. Alloys Comp. 323–324 (2001) 18.
[18] K.C.S. Almeida, T.S. Martins, P.C. Isolani, G. Vicentini, J. Zukerman-Schpector, J. Solid State Chem. 171 (2003) 230.
[19] G.M. Sheldrick, Acta Crystallogr. A46 (1990) 467.
[20] G.M. Sheldrick, SHELXL-97, Program for Crystal Structure Refinement, University of Göttingen, Germany, 1997.
[21] L.J. Farrugia, J. Appl. Crystallogr. 30 (1997) 565.
[22] M. Mikami, I. Nakagawa, T. Shimanouchi, Spectrochim. Acta 23A (1967) 1037.
[23] R.E. Hester, R.A. Plane, Inorg. Chem. 3 (1964) 513.
[24] P.X. Armendarez, L.S. Forster, J. Chem. Phys. 40 (1964) 273.
[25] S. Mizumi, N. Iwasaki, Bull. Chem. Soc. Jpn. 40 (1967) 550.
[26] J. Lewis, R.F. Long, C. Oldham, J. Chem. Soc. (1965) 6740.
[27] D. Gibson, J. Lewis, C. Oldham, J. Chem. Soc. (1966) 1453.
[28] D. Gibson, J. Lewis, C. Oldham, J. Chem. Soc. (1967) 72.
[29] J. Sutton, Nature 169 (1952) 235.
[30] A.J. Hubert, A.C. Gonzalez, E.J. Baran, O. Sala, J. Raman Spectrosc. 20 (1989) 555.
[31] C.P. Baird, T.J. Kemp, Prog. React. Kin. 22 (1997) 87.
[32] P.A. Tanner, Appl. Spectrosc. 47 (1993) 1949.
[33] F.H. Allen, O. Kennard, Chem. Des. Auto. News 8 (1993) 131 (CSD version 5.24, updated to April 2003).

number of extensive studies that have been reported in the literature dealing with the formation of micelles in aqueous surfactant solutions. Increasing attention is being devoted to the study of the incorporation or solubilization of neutral molecules into micelle in aqueous solution. The nature of a cosolvent determines the direction of changes in the CMC of surfactants. The effect of different cosolvents having an –OH group, such as PEG, sucrose, ethylene glycol and alcohols, on the micellization process has been studied [11,12]. Some of the most studied solubilizates are alcohols, because of the important role they have in the preparation of microemulsions. An excellent review of earlier work on the effect of *n*-alcohols on micellar solutions was given by Leung and Shah [13] and Zana [14]. Addition of alcohol can strongly influence the behaviour of the micelles and increase or decrease the micellar size depending upon the hydrophilic/hydrophobic character of alcohol [15,16]. Whereas the hydrophilic alcohols (methanol to propanol) mainly solubilize in aqueous solution and affect the micellization process by modifying the solvent, the more hydrophobic alcohol molecules (butanol, pentanol and higher alcohols) take part in the micellization process and become unique components of the micelle aggregate. To differentiate them from "inverted micelles which are formed in non-polar organic solvents, the term "solvophobic" has been applied by various researchers [17–20] to organic solvents, in analogy with the "hydrophobic interactions" causing micellization in aqueous media. The micelle formed due to a "solvophobic interaction" in polar non-aqueous solvents are similar in many respects to the micelles that are formed in aqueous media, although in general, micelle formation is not as favoured in non-aqueous solvents (with a low dielectric constant) as in water for a given surfactant [17–20].

In the present work, efforts have been made to study the effect of temperature variations on the CMC of metallosurfactants in non-aqueous solvents using a conductivity technique. Various aspects of the interaction of these surfactants in formamide during micelle formation in the presence of alcohols with various chain lengths are also discussed. In addition, the thermodynamic parameters, Gibbs free energy changes (ΔG^0_{mic}), enthalpies (ΔH^0_{mic}) and entropies (ΔS^0_{mic}), have also been estimated and analyzed for Cr^{III} metallosurfactants in non-aqueous solvents.

2. Experimental methods

2.1. Materials

Surface active Cr^{III} complexes, *cis*-$[Cr(en)_2(C_{12}H_{25}NH_2)F](ClO_4)_2$, *cis*-$[Cr(en)_2(C_{12}H_{25}NH_2)Cl](ClO_4)_2$ and *cis*-$[Cr(en)_2(C_{12}H_{25}NH_2)Br](ClO_4)_2$ used in the present work were prepared similar to those complexes reported earlier [3]. Their purity was tested by UV–Vis spectroscopy and CHN analysis. All other chemicals were obtained from Fluka and were used without purification.

Safety note: caution. Perchlorate salts of Cr^{III} complexes containing organic ligands are potentially explosive! Although we have experienced no problems with the compounds reported in this work, they should only be handled in small quantities and never scraped from sintered glass frits nor heated in the solid state.

2.2. Determination of CMC

CMC values of the complexes were calculated using electrical conductance data measured using a digital conductivity meter (Metrohm 712). The conductivity cell (dip-type with a cell constant of 1.0) was calibrated with KCl solutions in the appropriate concentration range. The cell constant was calculated using molar conductivity data for KCl published by Barthel et al. [21]. Various concentrations of Cr^{III}–surfactant complexes were prepared in the range 10^{-6}–10^{-2} mol dm^{-3}. All the measurements were done in a jacketed vessel, which was maintained at the desired temperature (±0.1 °C) with a circulating water thermostat bath. The conductivity of these solutions was measured at 293–313 K. The conductance was measured after thorough mixing and temperature equilibrium at each dilution. The measurement was started with a dilute solution and the subsequent concentrated solutions were prepared by adding a previously prepared stock solution. Establishment of equilibrium was checked by taking a series of readings after 15 min intervals until no significant change occurred.

3. Results and discussion

3.1. Temperature dependence of CMC

The CMC values of metallosurfactants in *n*-alcohol–formamide mixtures of different compositions and at various temperatures were determined from conductance measurements. Fig. 1. shows representative plots of specific conductivity corrected by that of the solvent $k–k_o$, as a function of the surfactant concentration at a fixed solvent composition and at different temperatures. Similar plots (not shown) were obtained in all the cases studied. The specific conductance of the solution in *n*-alcohol increases with increasing surfactant concentration. The increase seems to be due to the tendency of the metallosurfactants to form aggregates at higher surfactant concentration. It may be also attributed to the combined effect of ionic atmosphere, solvation of ions and decrease of mobility and ionization with the formation of micelles. When the conductivity of solutions with increasing concentration of surfactant is measured, the specific conductivity–surfactant concentration plots show two straight lines with different slopes. The first one corresponds to the concentration range below the CMC, when only monomers of surfactant exist in solution. Micelles start to form and a change of slope appears because the conductivity increases in a different manner. The intersection of these two straight lines was taken as the CMC value of the surfactant. The CMC values were computed from the slope of [Cr(III)] versus specific

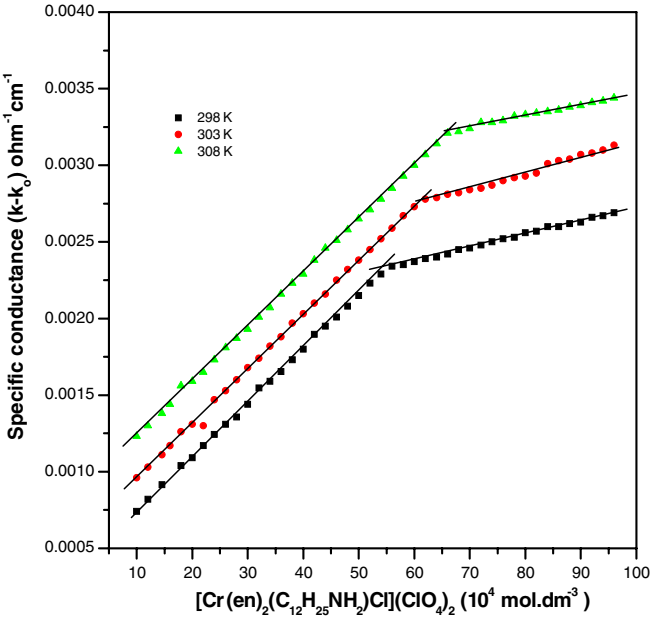

Fig. 1. Electrical conductivity vs. [Cr(III)] in methanol solution.

conductance data. At all temperatures a break in the conductance versus concentration plots, characteristic of micelle formation, was observed. The CMC values were determined by fitting the data points above and below the break to two equations of the form $y = mx + c$ and solving the two equations simultaneously to obtain the point of intersection. Least-squares analysis was employed and correlation coefficients were greater than 0.98 in all the cases. The conductivity measurements at different temperatures have been repeated three times and the accuracy of the CMC values are found to be within ±3% error. Tables 1 and 2 show the values of the CMCs of Cr^{III} ethylenediamine surfactant as a function of temperature. It is found that the CMC values increase on increasing the temperature for a given system. It is observed that by changing the ion from F^- to Br^-, the CMC decreases. It may be due to the increase in the size of the ion in the coordination sphere, which makes it more weakly hydrated. Weakly hydrated ions can be adsorbed more readily in the micellar surface which decreases the charge repulsion between the polar groups and thus facilitates the micellization.

3.2. Effect of the solvent on the CMC

It is well known that micellar properties of surfactants are significantly influenced by solvents. The physicochemical properties of solvents, dielectric constant, hydrogen bonding ability and cohesiveness parameters all play vital roles [22–24]. An increase in CMC is seen (Table 1, Figs. 1 and 2) for methanol and ethanol and a decrease in CMC is observed for higher alcohols when compared with the CMC obtained for aqueous solution [3]. Decrease in CMC on addition of *n*-propanol, *n*-butanol, *n*-pentanol and *n*-hexanol may result from the penetration of alcohol molecules into the micelle. The decrease in CMC can be explained as follows: it is known that the major factor that determines the inter-micellar solubility of long chain alcohols is the change in hydrophilic balance of the micelle during the inclusion of alcohol in it [25,26]. Moreover, the solvophobic effect associated with the solvophobic moiety of alcohol molecules favours micellization and increases as the length of the hydrocarbon chain of the alcohol increases. This explains the increased lowering of the CMC as the number of carbon atom increases in the alcohol series. Herein we report the micellization of metallosurfactants in binary combinations of the *n*-alcohol–formamide mixture. The changes in CMC with increasing concentration of methanol, ethanol, *n*-propanol, *n*-butanol and *n*-pentanol in formamide are reported in Table 2. Fig. 3 shows the critical aggregation concentration as a function of molar concentrations of alcoholic hydroxyl group in methanol, ethanol, *n*-propanol, *n*-butanol, *n*-pentanol in formamide (as representative for C1–C5 containing one hydroxyl group, respectively). The increase in CMC on addition of methanol and ethanol is due to the solvent power of the formamide–alcohol mixture. All the other surfactants gave similar behaviour for methanol and ethanol CMC increases on increasing its concentration in formamide which can be explained on the basis of increased solubility of the non-polar part of the surfactants in a non-aqueous medium. This is because the addition of methanol and ethanol disrupts the formamide structure or solvates the solute molecules preferentially. Similar behaviour was found for simple surfactants in formamide in the presence of alcohols for various chain lengths [26,27].

Table 1
Critical micelle concentration values of Cr^{III} complexes in various solvents

Solvents	CMC (10^3 mol dm^{-3})														
	$[Cr(en)_2(C_{12}H_{25}NH_2)F]^{2+}$					$[Cr(en)_2(C_{12}H_{25}NH_2)Cl]^{2+}$					$[Cr(en)_2(C_{12}H_{25}NH_2)Br]^{2+}$				
	293 K	298 K	303 K	308 K	313 K	293 K	298 K	303 K	308 K	313 K	293 K	298 K	303 K	308 K	313 K
Water	4.1	4.3	4.5	4.6	4.6	3.9	4.2	4.3	4.4	4.5	3.8	4.1	4.2	4.2	4.3
Methanol	5.0	5.5	6.3	7.2	7.8	4.8	5.4	6.1	6.6	7.0	4.5	5.3	5.9	6.2	6.7
Ethanol	4.8	5.3	6.0	6.8	7.4	4.5	5.2	5.7	6.4	6.8	4.3	4.9	5.6	6.1	6.5
n-Propanol	3.7	3.9	4.1	4.4	4.6	2.9	3.3	3.7	4.0	4.3	2.5	2.8	3.2	3.7	4.0
n-Butanol	2.9	3.2	3.6	3.9	4.3	2.7	3.0	3.2	3.7	4.1	2.2	2.7	3.1	3.5	3.9
n-Pentanol	2.7	3.0	3.3	3.6	4.0	2.4	2.7	3.0	3.4	3.7	1.7	2.2	2.8	3.2	3.6
n-Hexanol	2.5	2.9	3.1	3.4	3.7	1.9	2.3	2.6	3.0	3.3	1.5	1.9	2.4	2.7	3.1
Formamide	1.0	1.4	1.8	2.0	2.4	0.3	0.8	1.2	1.5	2.0	0.09	0.4	0.7	1.3	1.8

Table 2
Critical micelle concentration values of Cr^{III} complexes in formamide in the presence of various alcohol mixtures

Solvents (v/v %)	CMC (10^3 mol dm^{-3})								
	$[Cr(en)_2(C_{12}H_{25}NH_2)F]^{2+}$			$[Cr(en)_2(C_{12}H_{25}NH_2)Cl]^{2+}$			$[Cr(en)_2(C_{12}H_{25}NH_2)Br]^{2+}$		
	303 K	308 K	313 K	303 K	308 K	313 K	303 K	308 K	313 K
Methanol									
80	5.7	6.4	7.0	5.5	6.0	6.5	5.1	5.7	6.2
60	5.2	5.9	6.4	4.7	5.4	6.1	4.5	5.0	5.6
40	4.5	5.1	5.7	4.0	4.9	5.5	3.8	4.6	5.2
20	3.7	4.0	5.0	3.4	3.8	4.7	3.0	3.5	4.3
Ethanol									
80	5.4	6.1	6.6	5.0	5.9	6.1	4.8	5.4	5.9
60	4.8	5.5	6.0	4.3	5.2	5.8	4.0	4.7	5.3
40	4.0	4.7	5.4	3.6	4.3	5.0	3.2	4.0	4.6
20	3.2	3.8	4.7	2.7	3.1	4.2	2.4	3.0	3.7
n-Propanol									
80	3.6	4.0	4.3	3.3	3.7	4.0	2.9	3.4	3.8
60	3.1	3.5	3.9	2.9	3.3	3.6	2.5	3.0	3.3
40	2.8	3.1	3.6	2.5	2.9	3.3	2.0	2.6	2.9
20	2.4	2.7	3.2	2.0	2.6	3.0	1.6	2.1	2.5
n-Butanol									
80	3.2	3.6	4.0	2.9	3.3	3.7	2.7	3.2	3.6
60	2.9	3.3	3.7	2.6	3.0	3.3	2.3	2.8	3.3
40	2.5	3.0	3.4	2.2	2.6	2.9	1.8	2.2	2.7
20	2.2	2.7	3.1	1.9	1.5	2.5	1.3	1.7	2.2
n-Pentanol									
80	3.0	3.4	3.7	2.7	3.0	3.4	2.4	2.7	3.1
60	2.7	3.1	3.5	2.4	2.6	3.0	2.0	2.4	2.7
40	2.4	2.7	3.2	2.0	2.4	2.7	1.5	2.0	2.3
20	2.0	2.3	2.8	1.6	1.9	2.3	1.0	1.6	2.0

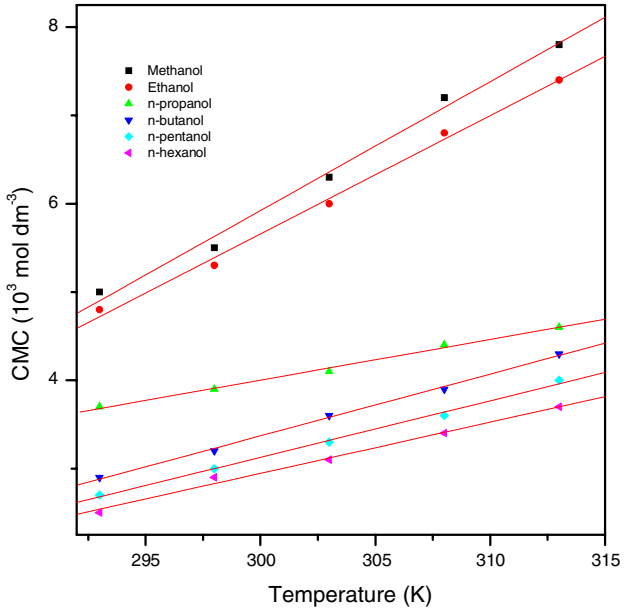

Fig. 2. Plot of CMC vs. temperature for *cis*-$[Cr(en)_2(C_{12}H_{25}NH_2)F]^{2+}$ in different solvents.

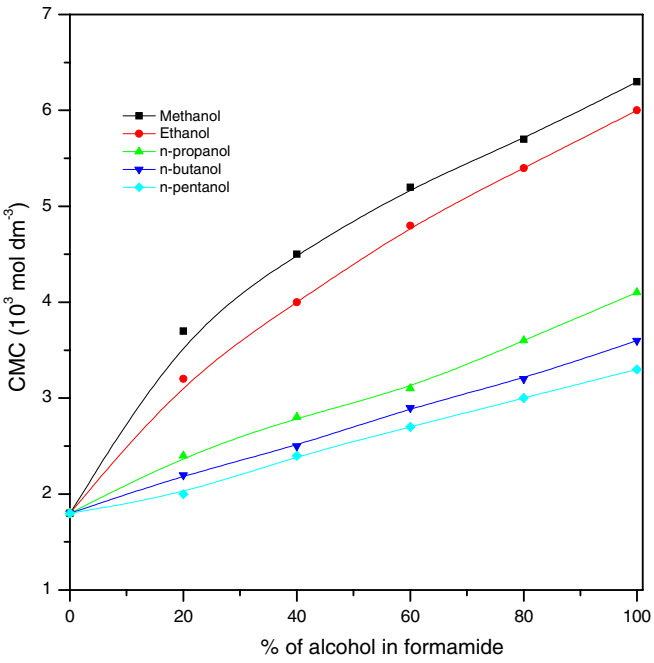

Fig. 3. Effect of different alcohols in formamide on the CMC values for *cis*-$[Cr(en)_2C_{12}H_{25}NH_2F]^{2+}$ at 303 K.

3.3. Effect of dielectric constant on the CMC

Furthermore, the CMC value of the metallosurfactant is a function of the dielectric constant of the medium. In alcohols the CMC values were in the order methanol > ethanol > *n*-propanol > *n*-butanol > *n*-pentanol > *n*-hexanol, whereas the dielectric constant decreases from methanol to *n*-hexanol [28]. The decrease in CMC with the

change in dielectric constant is due to a less favourable interaction between the polar groups of the surfactant molecules and the solvent causing micellization to occur at relatively lower concentrations. The effect of van der Waals interactions, which will of course be different in each case, is difficult to predict but it is obvious that it is the interaction between polar groups and solvent (affected by the dielectric constant) which mainly controls the variations of the CMC [13].

In alcohol–formamide mixtures, a similar variation in CMC is also observed. The CMC for these surfactants in formamide was much lower than water. Since, the dielectric constant of water is lower than the dielectric constant of formamide; it seems that the dielectric constant plays a more dominant role in micelle formation than the dipole moment [29,30]. The ionization of the surfactant in formamide is higher than in water, therefore there is a tendency of forming micelles at a lower concentration. Further the observation that the CMC decreases with the decrease in dielectric constant (methanol to *n*-pentanol) also shows that the degree of ionization of micellar units changes with solvent and in solvents of low dielectric constant, smaller micelles would form. This is because if the degree of ionization of micellar units is constant with a change in dielectric constant, then a decrease of the dielectric constant would surely imply an increase in CMC since the repulsion between charged groups of micelle would increase [31,32].

3.4. Thermodynamics of micelle formation

The study of CMC versus temperature is often undertaken to obtain information on hydrophobic and head group interactions. This involves driving various thermodynamic parameters of micelle formation. Two models are generally used, the mass-action or equilibrium model and the phase separation or pseudo-phase model [33–35]. The mass-action model assumes that an equilibrium exists between the monomeric surfactant and the micelles. The phase separation model assumes that the aggregates with their counterions in the surrounding atmosphere are in a separate phase. According to these models, the standard Gibbs free energy of micelle formation per mole of monomer, ΔG^0_m, is given by

$$\Delta G^0_m = RT \ln \mathrm{CMC} \quad (1)$$

where R and T are the gas constant and absolute temperature, respectively, even though the size of the micelle is not known at present.

The standard enthalpy of micelle formation, ΔH^0_m, can be obtained from the temperature variation of CMC by applying the Gibbs–Helmholtz equation to Eq. (1):

Table 3
Thermodynamic parameters in kJ mol^{-1} for metallosurfactants in formamide in the presence of various alcohols

Solvents (v/v %)	$[Cr(en)_2(C_{12}H_{25}NH_2)F]^{2+}$			$[Cr(en)_2(C_{12}H_{25}NH_2)Cl]^{2+}$			$[Cr(en)_2(C_{12}H_{25}NH_2)Br]^{2+}$		
	$-\Delta G^0_{mic}$	$-\Delta H^0_{mic}$	$T\Delta S^0_{mic}$	$-\Delta G^0_{mic}$	$-\Delta H^0_{mic}$	$T\Delta S^0_{mic}$	$-\Delta G^0_{mic}$	$-\Delta H^0_{mic}$	$T\Delta S^0_{mic}$
Methanol	12.7 ± 0.2	1.7 ± 0.2	11.0 ± 0.2	12.8 ± 0.3	1.8 ± 0.1	11.0 ± 0.2	12.9 ± 0.3	2.0 ± 0.1	10.9 ± 0.1
80	13.0 ± 0.1	1.9 ± 0.1	11.1 ± 0.4	13.1 ± 0.1	2.4 ± 0.3	10.7 ± 0.2	13.2 ± 0.2	3.3 ± 0.2	9.9 ± 0.1
60	13.2 ± 0.2	2.2 ± 0.1	11.0 ± 0.2	13.5 ± 0.2	4.4 ± 0.2	9.1 ± 0.2	13.6 ± 0.3	5.0 ± 0.3	8.6 ± 0.2
40	13.6 ± 0.1	3.4 ± 0.3	10.2 ± 0.5	13.9 ± 0.4	5.8 ± 0.1	8.1 ± 0.2	14.0 ± 0.1	6.3 ± 0.1	7.7 ± 0.3
20	14.1 ± 0.2	7.2 ± 0.1	6.9 ± 0.1	14.3 ± 0.1	7.6 ± 0.2	6.7 ± 0.1	14.6 ± 0.1	8.4 ± 0.1	6.2 ± 0.2
Ethanol	12.8 ± 0.1	1.9 ± 0.2	10.9 ± 0.2	13.0 ± 0.1	2.0 ± 0.2	11.0 ± 0.2	13.0 ± 0.2	2.2 ± 0.2	10.8 ± 0.1
80	13.1 ± 0.2	3.0 ± 0.2	10.1 ± 0.1	13.3 ± 0.2	4.1 ± 0.1	9.2 ± 0.1	13.4 ± 0.1	4.9 ± 0.1	8.5 ± 0.4
60	13.4 ± 0.1	4.7 ± 0.1	8.7 ± 0.1	13.7 ± 0.1	5.6 ± 0.1	8.1 ± 0.3	13.9 ± 0.1	6.4 ± 0.2	7.5 ± 0.2
40	13.9 ± 0.3	6.3 ± 0.2	7.6 ± 0.3	14.1 ± 0.3	7.1 ± 0.2	7.0 ± 0.2	14.4 ± 0.2	7.6 ± 0.2	6.8 ± 0.3
20	14.4 ± 0.4	7.7 ± 0.4	6.7 ± 0.1	14.8 ± 0.2	8.0 ± 0.2	6.8 ± 0.1	15.1 ± 0.3	8.7 ± 0.1	6.4 ± 0.2
n-Propanol	13.8 ± 0.2	1.8 ± 0.2	12.0 ± 0.1	14.1 ± 0.2	1.7 ± 0.2	12.4 ± 0.1	14.4 ± 0.3	2.0 ± 0.2	12.4 ± 0.1
80	14.1 ± 0.2	3.7 ± 0.1	10.4 ± 0.2	14.3 ± 0.1	4.6 ± 0.1	9.7 ± 0.2	14.7 ± 0.2	5.3± 0.1	9.4 ± 0.1
60	14.5 ± 0.1	5.4 ± 0.1	9.1 ± 0.1	14.7 ± 0.1	6.9 ± 0.1	7.8 ± 0.1	15.0 ± 0.1	7.3 ± 0.1	7.7 ± 0.1
40	14.8 ± 0.3	7.6 ± 0.2	7.2 ± 0.3	15.0 ± 0.2	8.0 ± 0.1	7.0 ± 0.2	15.6 ± 0.3	8.8 ± 0.3	6.8 ± 0.2
20	15.1 ± 0.1	8.2 ± 0.1	6.9 ± 0.4	15.6 ± 0.1	8.6 ± 0.1	7.0 ± 0.1	16.2 ± 0.1	9.3 ± 0.2	6.9 ± 0.1
n-Butanol	14.1 ± 0.2	2.5 ± 0.3	11.6 ± 0.1	14.4 ± 0.2	3.0 ± 0.2	11.4 ± 0.1	14.5 ± 0.1	3.7 ± 0.2	10.8 ± 0.1
80	14.4 ± 0.3	4.1 ± 0.2	10.3 ± 0.1	14.7 ± 0.1	5.3 ± 0.1	9.4 ± 0.3	14.8 ± 0.1	6.4 ± 0.1	8.4 ± 0.1
60	14.7 ± 0.1	6.0 ± 0.1	8.7 ± 0.2	14.9 ± 0.2	7.2 ± 0.1	7.7 ± 0.1	15.3 ± 0.1	8.2 ± 0.3	7.1 ± 0.2
40	15.0 ± 0.1	8.2 ± 0.1	6.8 ± 0.2	15.4 ± 0.2	8.9 ± 0.3	6.5 ± 0.3	15.9 ± 0.3	9.5 ± 0.4	6.4 ± 0.3
20	15.4 ± 0.1	8.7 ± 0.2	6.7 ± 0.1	15.7 ± 0.2	9.5 ± 0.1	6.2 ± 0.2	16.7 ± 0.2	10.4 ± 0.1	6.3 ± 0.2
n-Pentanol	14.3 ± 0.1	4.3 ± 0.1	10.0 ± 0.1	14.6 ± 0.2	5.6 ± 0.1	9.0 ± 0.1	14.8 ± 0.2	6.3 ± 0.2	8.5 ± 0.1
80	14.6 ± 0.2	5.4 ± 0.2	9.2 ± 0.1	14.8 ± 0.1	7.0 ± 0.1	7.8 ± 0.3	15.1 ± 0.1	7.9 ± 0.1	7.2 ± 0.1
60	14.8 ± 0.2	6.5 ± 0.1	8.3 ± 0.2	15.1 ± 0.1	8.3 ± 0.1	6.8 ± 0.3	15.6 ± 0.1	9.2 ± 0.3	6.4 ± 0.2
40	15.1 ± 0.1	8.6 ± 0.2	6.5 ± 0.3	15.6 ± 0.3	10.2 ± 0.2	5.4 ± 0.2	16.3 ± 0.3	11.4 ± 0.2	4.9 ± 0.4
20	15.6 ± 0.4	9.4 ± 0.4	6.2 ± 0.4	16.2 ± 0.1	11.3 ± 0.3	4.9 ± 0.1	17.4 ± 0.1	12.7 ± 0.1	4.7 ± 0.2
n-Hexanol	14.5 ± 0.2	7.6 ± 0.3	6.9 ± 0.2	14.9 ± 0.3	8.4 ± 0.2	6.5 ± 0.3	15.1 ± 0.1	9.2 ± 0.3	5.9 ± 0.3
Formamide	15.9 ± 0.3	10.2 ± 0.1	5.7 ± 0.1	16.9 ± 0.1	12.7 ± 0.2	4.2 ± 0.2	18.3 ± 0.1	13.9 ± 0.4	4.4 ± 0.1

$$\Delta H^0_m = -RT^2 \mathrm{d}\ln\ \mathrm{CMC}/\mathrm{d}T \quad (2)$$

Once the Gibbs free energy and the enthalpy of micelle formation are obtained, obviously the entropy of micelle formation can be determined by

$$\Delta S^0_m = (\Delta H^0_m - \Delta G^0_m)/T \quad (3)$$

Also the low CMC values in *n*-alcohols may invalidate the use of the above mentioned equations, because the monomer activity would be quite different from the monomer concentration. Moreover, since the changes of CMC with temperature are small, the values of ΔG^0_m, ΔH^0_m and ΔS^0_m must be rather inaccurate. Therefore, the thermodynamic parameters in Table 3 must be viewed only as approximate. Nevertheless, from the present data some generalization can be extracted. The observed more negative Gibbs free energy of micellization for the surfactants with increasing head polarity indicates more favoured micellization. It also suggests that a strong solvophobic interaction takes place for long alkyl chains in formamide. Our data show that the free energy of micellization is negative in all cases and becomes less negative with increasing concentration of co-solvents. As can be seen from Table 3, the standard Gibbs free energy of micelle formation decreases as the number of carbon atoms in the alkyl chains of various alcohols increases, as shown in Fig. 4. It suggests that a strong solvophobic interaction take place for long alkyl chains in formamide. It is also observed that the enthalpy of micellization (ΔH^0_m) is negative and becomes smaller as the co-solvent increases. Negative values of enthalpy of micellization indicate an exothermic nature of the micellization process. Nusselder and Engberts [36] have suggested that for negative ΔH^0_m, the London-dispersion forces play a major role in the micellar process. The entropic contribution of micelle formation, ΔS^0_m, presents positive values and are larger than ΔH^0_m, showing the importance of solvophobic interactions in the micelle formation process. Therefore, the fact that ΔS^0_m values decrease as the formamide content increases indicates that the presence of formamide in the system produces a weakening of the solvent cohesiveness, thereby increasing the solubility of the hydrocarbon tails and decreasing the solvophobic effect. It is evident from Table 3 that in all cases micellization is exothermic. This may be interpreted as a consequence of the decrease in energy required to break up the iceberg structure surrounding the hydrocarbon chains of the monomeric surfactants. It is also observed that in the presence of higher alcohols (*n*-butanol, *n*-pentanol and *n*-hexanol) the enthalpy was more negative and entropy was less positive. Therefore, the contribution of the enthalpy to the micellization becomes increasingly important with the lengthening of the carbon chain length of the alcohol in contrast to the predominance of the entropy in the aqueous solution. Similar behaviour of a more negative enthalpy in the presence of organic additives has been observed [26,37].

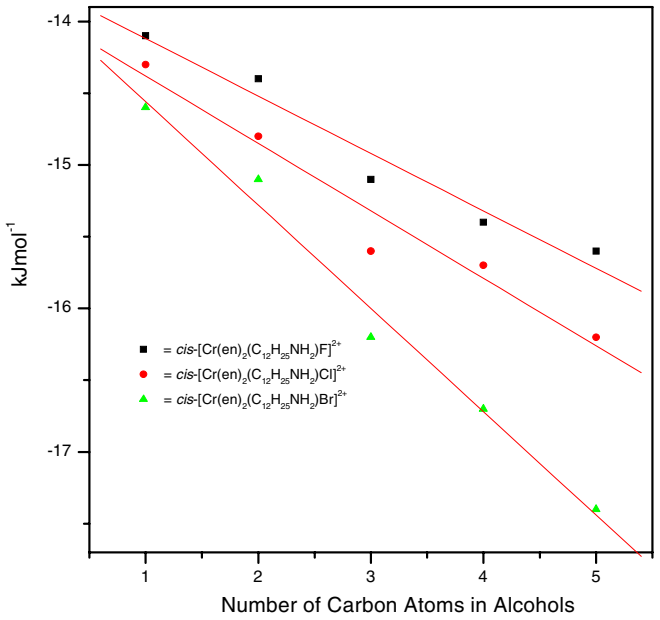

Fig. 4. Gibbs energy change of Cr(III) metallosurfactants in formaide in presence of 20% of various *n*-alcohols.

References

[1] M.J. Rosen, Surfactants and Interfacial Phenomena, 2nd ed., Wiley, New York, 1989.
[2] T.F. Tadros, Applied Surfactants, 1st ed., Wiley–VCH, Germany, 2005.
[3] N. Kumaraguru, S. Arunachalam, M.N. Arumugham, K. Santhakumar, Transit. Metal Chem. 31 (2006) 250.
[4] C.A. Behm, I. Creaser, B. Daszkiewicz, R.J. Geue, A.M. Sargeson, G.W. Walker, J. Chem. Soc., Chem. Commun. 24 (1993) 1844.
[5] C.A. Behm, P.F.L. Boreham, I.I. Creaser, B. Korybut-Daszkiewicz, D.J. Maddalena, A.M. Sargeson, G.M. Snowdown, Aust. J. Chem. 48 (1995) 1009.
[6] G. Ghirlanda, P. Scrimin, P. Tecilla, A. Toffoletti, Langmuir 14 (1998) 1646.
[7] C. Treiner, A.A. Khodja, A. Mayaffre, J. Colloid Interface Sci. 115 (1987) 573.
[8] M.S. Bakshi, Bull. Chem. Soc. Jpn. 69 (1996) 2723.
[9] A.K. Jain, R.B.B. Singh, J. Colloid Interface Sci. 86 (1982) 575.
[10] W.U. Malik, A.K. Jain, M.J. Siddiqui, Indian J. Chem. 14 (1976) 124.
[11] K.K. Ghosh, S. Roy, Indian J. Chem. 37B (1998) 875.
[12] M.L. Corrin, W.D. Harkins, J. Chem. Phys. 14 (1946) 640.
[13] R. Leung, D.O. Shah, J. Colloid Inteface Sci. 113 (1986) 484.
[14] R. Zana, Adv. Colloid Interface Sci. 57 (1995) 1.
[15] S.M. Stephany, T.M. Kole, M.R. Fisch, J. Phys. Chem. 8 (1994) 11126.
[16] G.M. Forland, J. Samseth, H. Hoiland, K. Mortensen, J. Colloid Interface Sci. 164 (1994) 163.
[17] A.J. Fryar, S. Kaufman, J. Colloid Interface Sci. 29 (1969) 444.
[18] M. Salim Akhter, S.M. Alawi, Colloids Surf. A 173 (2000) 95.
[19] G.J. Olofsson, Chem. Soc. Faraday Trans. 87 (1991) 3037.
[20] A. Couper, G.P. Gladden, B.T. Ingram, Faraday Discuss. 59 (1976) 63.
[21] J. Barthel, F. Feuerlein, R. Neueder, R. Wachter, J. Sol. Chem. 9 (1980) 209.
[22] R. Nagarajan, Adv. Colloid Interface Sci. 26 (1986) 205.
[23] K. Mukherjee, D.C. Mukherjee, S.P. Moulik, J. Phys. Chem. 98 (1994) 4713.
[24] K.S. Sharma, A.K. Rakshit, Bull. Chem. Soc. Jpn. 78 (2005) 771.
[25] H.N. Singh, S. Swarup, R.P. Singh, S.M. Saleem, Indian J. Chem. 20 (1981) 292.

[26] S. Miyagishi, Bull. Chem. Soc. Jpn. 47 (1974) 2972;
Bull. Chem. Soc. Jpn. 48 (1975) 2349.
[27] M. Salim Akhter, S.M. Alawi, Colloids Surf. A 196 (2002) 163, and reference therein.
[28] G. Akerlof, J. Am. Chem. Soc. 54 (1932) 4125.
[29] J.A. Riddck, W.B. Bunger, Techniques of Chemistry, vol. II, Wiley–Interscience, New York, 1970, p. 444.
[30] R.C. Weast, M.J. Astle, Handbook of Chemistry and Physics, 63 ed., CRC Press, Boca Raton, FL, 1982/1983.
[31] M. Salim Akhther, S.M. Alawi, Colloids Surf. A 175 (2000) 311.
[32] M. Salim Akhther, S.M. Alawi, Colloids Surf. A 219 (2003) 281.
[33] P. Mukerjee, Adv. Colloid Interface Sci. 1 (1961) 241.
[34] J.J. Galan, A. Gonzalez-Perez, J.R. Rodriguez, J. Therm. Anal. Calorim. 72 (2003) 465.
[35] A. Gonzalez-Perez, J.C. Del Castillo, T. Czapkiewicz, J.R. Rodriguez, Colloid Polym. Sci. 280 (2002) 503.
[36] J.J.H. Nusselder, J.B.F.N. Engberts, J. Colloid Interface Sci. 148 (1992) 353.
[37] H.N. Singh, S.M. Sakeem, R.P. Singh, J. Phys. Chem. 84 (1980) 2191.

polydentate salicylidenimines [12–15]. It was reported on the synthesis and structure of μ-oxo-dioxotetrakis(*N*-methylsalicylidenimine) dimolybdenum(V) binuclear complex with the bridging oxygen [16]. However, there are no reports on di-μ-oxo-molybdenum(V) complexes with alkylsalicylidenimine ligands.

2. Experimental

2.1. Synthesis

Chemicals were purchased from commercial sources and used without further purification. The starting complex $[Mo_2O_3(OCOCH_3)_3Cl]_2 \cdot (CH_3CO)_2O$ was synthesised as previously reported in [17].

2.1.1. General procedure for synthesis of $RNH_3[Mo_2O_4(N\text{-}R\text{-}salim)_2OCOCH_3] \cdot C_6H_6 \cdot CH_3COOH$

The same procedure was followed for the preparations of all complexes (Scheme 1). The products were obtained from $[Mo_2O_3(OCOCH_3)_3Cl]_2 \cdot (CH_3CO)_2O$ and freshly prepared *N*-R-salicylidenimines in molar ratio 1:16. Since the starting compound is a tetranuclear complex that includes eight potentially exchangeable ligand sites, the molar ratio should be 1:8. To facilitate the ligand exchange higher molar ratio was used. Imines were prepared by the simple condensation reaction of salicylaldehyde and appropriate alkylamine in equimolar ratio at room temperature. The mixture of these compounds (16 mmol of each) was left for 2 h, afterwards was added in small portions the well powdered Mo-starting complex. After stirring of 2–3 h at 35 °C, the dark red "sticky mass" was formed and left overnight at room temperature. A small volume of benzene was added and the crystalline products were filtered off, washed with ether and dried in vacuo. For preparation of imines with R = Me and Et, the gaseous amines, produced from amine water solutions by sodium hydroxide, were brought into aldehyde. Water present in the imines was not removed. Yields were between 60% and 70%.

2.1.2. Synthesis of $BuNH_3[Mo_2O_4(N\text{-}Bu\text{-}salim)_2OCOCH_3] \cdot C_6H_6 \cdot CH_3COOH$

Representative procedure for synthesis of butyl derivate: a mixture of 1 g (1 mmol) $[Mo_2O_3(OCOCH_3)_3Cl]_2 \cdot (CH_3CO)_2O$ and freshly prepared *N*-Bu-salimH ($C_6H_4(OH)CHNC_4H_9$) (ca. 16 mmol) was stirred for 2 h. A very viscous dark mixture was left overnight, 3 mL of C_6H_6 were added, and after stirring a crystalline product was isolated. Yield (based on the initial Mo complex): 1.15 g (68%). IR data (KBr, cm^{-1}) 3424 w-m br [ν(OH)], 3200–2330 w br, [$\nu(NH_3^+)$], 2959 w-m, 2931 w-m and 2871 w [$\nu(CH_3)$, $\nu(CH_2)$], 1700 w [ν(C=O)], 1628 vs [ν(C=N), $\nu_{as}(OCO_b)_{acetate}$], 1600 m [$\nu$(C=C), $\delta(NH_3^+)$], 1549 s [ν(C=C), $\nu(C\text{–}O)_{phenolate}$], 1302 s br [$\nu_s(OCO_b)_{acetate}$], 954 s and 935 sh [$\nu(Mo{=}O)_t$], 756 m and 740 m [$\nu_{as}(Mo\text{–}O\text{–}Mo)_b$], 612 w-m [$\nu$(Mo–N)], 471 w-m and 456 sh [$\nu(Mo\text{–}O)_{acetate}$]. UV/Vis [DMF, λ_{max}/nm ($\varepsilon/M^{-1}\,cm^{-1}$)] 312 (15170), 377 (4656).

2.2. Physical measurements

The infrared spectra in the region 4000–400 cm^{-1} were recorded as KBr pellets on a Perkin–Elmer spectrum BX FTIR System. UV/Vis spectra were measured on a Perkin–Elmer lambda 35 spectrophotometer. Magnetic susceptibilities in the solid state were measured at room temperature by the standard Gouy method using a Cahn-Ventron RM-balance and $CuSO_4 \cdot 5H_2O$ as the susceptibility standard. Elemental analyses were performed on a Carlo Erba instrument.

2.3. X-ray crystallography and data collection

The crystal used for data collection was an orange prism, dimensions $0.3 \times 0.15 \times 0.1$ mm. Three intensity control reflections measured every 120 min did not show any significant loss of intensity during the data collection, which was performed on an Enraf Nonius CAD4 diffractometer with a graphite monochromated Cu Kα (1.54179 Å) radiation at temperature of 150 (2) K (cooled by a stream of dry nitrogen gas using Oxford Cryostream 700 series). The crystal data are shown in Table 1. The WinGX standard procedure was applied for data reduction [18]. Cell parameters were calculated from 25 reflections (θ range 8.15–17.1°). An absorption correction based on eight Ψ-scan reflections was performed [19]. The structure was solved using the Patterson method implemented in SHELXS97 [20] and refined with SHELXL97 [21]. Molecular geometry calculations were performed with PLATON [22], and molecular graphics were prepared using ORTEP-3 [23],

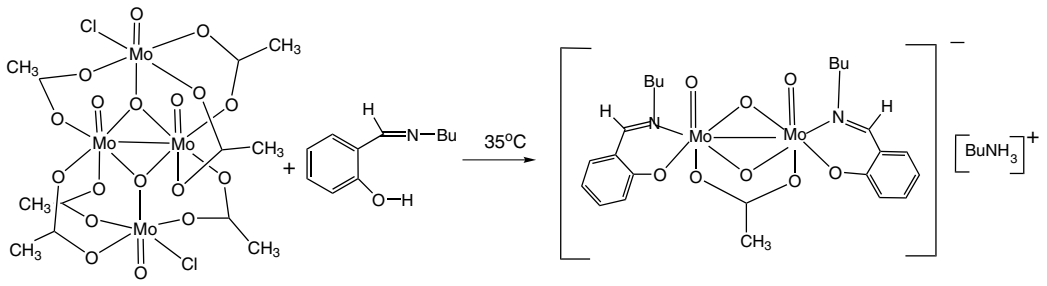

Scheme 1.

Table 1
Crystal and structure refinement data

Chemical formula	$C_{36}H_{53}Mo_2N_3O_{10}$
Molecular weight	877.69
Crystal system	triclinic
Space group	$P\bar{1}$
a (Å)	12.0658(10)
b (Å)	12.8168(7)
c (Å)	14.6612(13)
α (°)	100.94(1)
β (°)	95.52(1)
γ (°)	114.60(1)
V (Å^3)	1984.7(3)
Z	2
D_{calc} (g cm^{-3})	1.496
μ (Cu Kα) (mm^{-1})	5.655
Absorption correction	psi-scans
T_{min}, T_{max}	0.2898, 0.4376
Crystal size (mm)	$0.1 \times 0.15 \times 0.3$
T (K)	150(2)
Reflections measured	8717
Unique reflections	8306
Θ_{max} (°)	76.3
R_{int}	0.059
R_σ	0.037
Refinement on	$\|F\|^2$
Number of parameters refined	461
$R(F)$ $[I > 2\sigma(I)]$	0.0425
$R_w(F^2)$	0.1175
S	0.961
$\Delta\rho_{min}$, $\Delta\rho_{max}$ (e Å^{-3})	−1.691, 1.467

and CCDC-Mercury [24]. The model was refined using the full-matrix least-squares refinement on $|F|^2$ with hydrogen atoms refined as the riding entities, their initial positions calculated according to stereochemistry. All non-hydrogen atoms except C24 were refined anisotropically. Disorder of C23 and C24 can explain the residual electron density (Table 1). The atomic scattering factors were those included in SHELXL97 [21].

3. Results and discussion

3.1. Synthesis and spectroscopic studies

The reaction of $[Mo_2O_3(OCOCH_3)_3Cl]_2 \cdot (CH_3CO)_2O$ with Schiff base ligands, derived from salicylaldehyde and alkyl amines, gave complexes generally formulated as $RNH_3[Mo_2O_4(N\text{-R-salim})_2OCOCH_3] \cdot C_6H_6 \cdot CH_3COOH$.

Syntheses of some complexes, either Mo(VI) or Mo(V) with Schiff bases, reported in the literature [12–15] were carried out in the presence of suitable solvents or solvent mixtures. The syntheses of the title complexes were performed without solvents but in high excess of the imine ligands. Water present in imines has not biased reactions; even more, water destabilised starting complex and assisted replacement of acetate by imines.

The complexes are diamagnetic compounds moderately stable in the air, except the very hygroscopic complex with *N*-Me-salim ligand. Solubility of complexes decreases as R of imines increases; solubility in solvents decreases as follows:

$$CH_2Cl_2 > CHCl_3 > (CH_3)_2CO > C_6H_6 > n\text{-}C_6H_{14}$$

The structural characterisation of the title complexes: coordinated di-μ-oxo-dimolybdate(V) and small alkyl ammonium cation, is based on analytical data, infrared and visible spectra and X-ray structure analysis of $BuNH_3[Mo_2O_4(N\text{-Bu-salim})_2OCOCH_3] \cdot C_6H_6 \cdot CH_3COOH$. The efforts to prepare crystals of all complexes suitable for X-ray structure determinations failed. Nevertheless, the analytical and spectral data indicated analogy among their structures.

The IR spectra of the complexes are very complicated with extensive vibrational coupling and overlapping of absorption bands. In spite of this, the results obtained clearly point to modes of the metal–ligand coordination in these compounds, and agree well with the X-ray analysis of complex derived from butyl derivative. The great similarity in spectra of the complexes suggests that their structure is also similar (see Table 2). The bonding of the Schiff base in the anionic form through the azomethine nitrogen and the deprotonated phenolic oxygen is supported by the presence of very strong absorption at ca. 1630 cm^{-1} and strong band at 1550 cm^{-1} assigned to ν(C=N) and phenolic ν(C–O) vibration, respectively [25,26]. In the former region appears also the acetate ν_{as}(OCO) absorption while in the later frequency region are displayed also the aromatic ν(C=C) vibrations. A weak to medium band at around 612 cm^{-1} may be attributed to the Mo–N stretching of the coordinating azomethine nitrogen [27]. Besides the phenolic oxygen, there are three other groups with the oxygen donor atoms in the complexes. A strong absorption in the 960–930 cm^{-1} region confirms the presence of the terminal oxo ligands [16]. A strong band at 954 cm^{-1} with a shoulder on the lower frequency side about 940 cm^{-1} in the butyl complex or a closely spaced doublet in the same region in all other complexes assignable to terminal ν(Mo=O) vibration is consistent with

Table 2
Analytical and selected IR data of $RNH_3[Mo_2O_4(N\text{-R-salim})_2OCOCH_3] \cdot C_6H_6 \cdot CH_3COOH$

R	Colour	Found (calcd.) %				ν(C=N)	ν(Mo–O–Mo)	ν(Mo=O)
		Mo	C	H	N			
CH_3	brownish-yellow	26.23 (25.46)	41.09 (43.03)	4.22 (4.68)	5.73 (5.58)	1630	760, 753, 741	950, 936
C_2H_5	brownish-orange	24.57 (24.12)	43.98 (45.29)	4.22 (5.19)	4.98 (5.28)	1626	762, 754, 741	950, 932
C_3H_7	orange-red	22.70 (22.90)	44.62 (47.32)	6.40 (5.62)	4.98 (5.02)	1630	758, 753, 738	961, 946
C_4H_9	orange-red	22.05 (21.81)	49.31 (49.15)	5.97 (6.07)	4.49 (4.78)	1628	756, 740	954, 940

Abbreviations. *N*-R-salim, *N*-alkyl substituted salicylidenimine; Me, methyl; Et, ethyl; Pr, propyl; Bu, butyl. IR bands are in cm^{-1}.

syn arrangement of two oxo ligands relative to the central Mo_2O_2 core. The splitted band of medium intensity with two or three maxima between 762 and 739 cm^{-1} of the stretching vibrations of the bridging Mo–O–Mo group, are characteristic for the doubly bridged Mo_2O_2 moiety. The reduced symmetry of the complexes may cause complexity and splitting of metal–ligand bands. A weak to medium band at around 470 cm^{-1} with shoulder on the lower frequency side may be ascribed to the acetate bridging Mo–O stretching vibrations. A marked lengthening of the bridged Mo–$O_{acetate}$ bonds in the complexes gives rise that differences between the C–O asymmetric and symmetric frequencies is increased with respect to values expected for the acetato bridging complexes [28]. Thus the ν_{as}(OCO) absorption superimposed upon that of the ν(C=N) absorption gives a very strong band at around 1630 cm^{-1} while a strong and broad band at 1303 cm^{-1} may be assigned to the corresponding ν_s(OCO) vibration. A broad ν(OH) absorption around 3425 cm^{-1} and ν(C=O) band at 1700 cm^{-1} indicate the presence of the undissociated acetic acid in the complexes that is hydrogen bonded both to the alkylammonium cation and the anionic complex. The ammonium asymmetric and symmetric stretching vibrations in the spectra of complexes give a very broad complex progression of the combination of absorptions covering the whole 3200–2350 cm^{-1} frequency region, overlapping the weak aromatic C–H stretching absorption normally expected below 3080 cm^{-1} as well as the alkane C–H stretching region with three weak to medium sharp bands between 2960 and 2870 cm^{-1}. The complexity of this absorption arises from hydrogen bond interactions with the solvate acetic acid and oxygen atoms of the anionic complex.

The electronic absorption spectra of complexes in DMF are characterised by a strong absorption at 312 nm along with less intense band at around 377 nm, which may be assigned to metal–ligand charge transfers, possible superposed by ligand internal π–π^* and n–π^* transitions [25]. A decrease in the intensity of both these absorptions takes place very slowly on time; therefore it may be presumed that complexes are stable towards solvolysis in DMF solution.

3.2. Crystal structure of butylammonium di-μ-oxo-μ-acetato-bis[(N-butylsalicylideniminato-N,O) oxomolybdenum(V)] benzene acetic acid solvate

The anionic complex (Fig. 1) is dinuclear, with both molybdenum atoms having a slightly distorted octahedral coordination (Table 3). Each Mo atom is coordinated by a terminal oxo ligand and chelated by a *N*-butylsalicylideniminate ion. Further, Mo atoms are bridged by two μ_2-oxygen atoms and a μ_2-acetato group. Mo–Mo distance is 2.5675 (5) Å, corresponding to a single Mo–Mo bond. Mean bond lengths of Mo–O and Mo–N (O and N of the *N*-butylsalicylideniminate ligands) are 2.050(3) and 2.192(3) Å, respectively. They agree to the values of

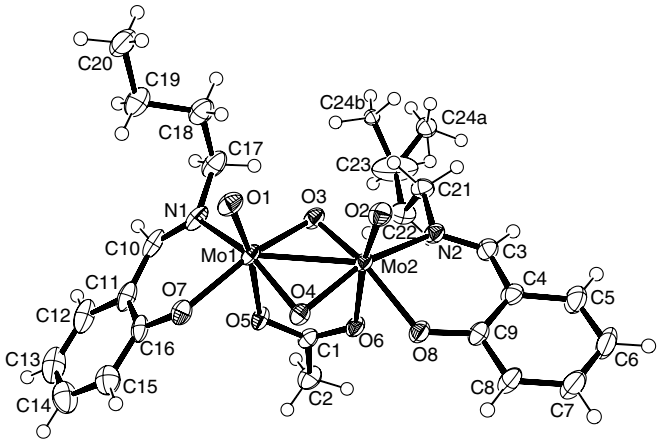

Fig. 1. Di-μ-oxo-μ-acetato-bis[(*N*-butylsalicylideniminato-*N*,*O*)oxomolybdenum(V)] anion. Thermal ellipsoids are drawn at 50% probability. Hydrogen atoms are depicted as spheres of arbitrary radii.

Table 3
Selected geometric parameters (Å, °)

Mo1–Mo2	2.5675 (5)
Mo1–O4	1.951 (3)
Mo1–O7	2.049 (3)
Mo1–O5	2.325 (3)
Mo1–O3	1.929 (3)
Mo1–N1	2.195 (4)
Mo1–O1	1.683 (3)
Mo2–O4	1.943 (3)
Mo2–O8	2.051 (3)
Mo2–N2	2.189 (4)
Mo2–O6	2.353 (3)
Mo2–O3	1.938 (3)
Mo2–O2	1.679 (4)
O1–Mo1–O3	104.60(13)
O1–Mo1–O4	105.82(12)
O3–Mo1–O4	95.70(11)
O1–Mo1–O7	96.26(12)
O3–Mo1–O7	157.94(11)
O4–Mo1–O7	85.26(10)
O1–Mo1–N1	95.38(13)
O3–Mo1–N1	85.34(12)
O4–Mo1–N1	157.70(12)
O7–Mo1–N1	85.65(12)
O1–Mo1–O5	169.73(12)
O3–Mo1–O5	80.69(10)
O4–Mo1–O5	82.10(10)
O7–Mo1–O5	77.62(10)
N1–Mo1–O5	76.08(11)
O2–Mo2–O3	104.91(12)
O2–Mo2–O4	105.98(12)
O3–Mo2–O4	95.47(11)
O2–Mo2–O8	98.66(12)
O3–Mo2–O8	155.36(11)
O4–Mo2–O8	84.70(10)
O2–Mo2–N2	94.50(12)
O3–Mo2–N2	85.50(11)
O4–Mo2–N2	158.43(11)
O8–Mo2–N2	85.60(11)
O2–Mo2–O6	172.01(11)
O3–Mo2–O6	79.49(10)
O4–Mo2–O6	79.94(10)
O6–Mo2–O8	172.0(2)
N2–Mo2–O6	79.07(10)

Mo–O and Mo–N distances found in μ-glycine-O:O′-di-μ-oxo-bis[(glycinato-*N*,*O*)oxomolybdenum(V)] [29], whereas Mo-μ-O and Mo=O distances agree with the values observed in similar binuclear Mo(V) species such as $[Mo_2O_4(C_2O_4)_2(H_2O)_2]^{2-}$ [30,31]. However, $Mo–O_{acetato}$ bonds, *trans* to the terminal O atoms, are significantly longer than other Mo–O single bonds, indicating a *trans* influence of the terminal O atoms (Table 3). The coordination polyhedra are slightly distorted octahedra; their equatorial L–Mo–L angles are 85(1)°. The octahedra of the title complex are more regular than others observed in binuclear Mo(V) complexes [30,31].

A static disorder is present in one of the pendant *N*-butyl moieties. Therefore, the atom C24 is split between two positions (C24a and C24b) with occupancies about 0.75 and 0.25, respectively. Their temperature parameters were refined isotropically. The atom C23 is also disordered over two positions, however, they are very close to each other, producing a rather elongated ellipsoid.

An asymmetric unit consists of a di-μ-oxo-μ-acetato-bis[(*N*-butylsalicylideniminato-*N*,*O*)oxomolybdenum(V)] anion, a butylammonium cation, a molecule of benzene and a molecule of undissociated acetic acid (Fig. 2). Hydrogen bonds (Table 4, Fig. 2) connect the anionic complex, butylammonium cation and a molecule of acetic acid. The $[BuNH_3]^+$ is hydrogen bonded to the acetic acid via N40–H401···O51 and through N40–H402···O4 (bridging oxygen) to the complex. The acetic acid molecule is hydrogen bonded to the complex through O50–H50···O6. Two such groups link to each other via N40–H400···O7 hydrogen bond and form a centrosymmetric "supra-dimer". The hydrogen bond O50–H50···O6 of 2.595 (4) Å is a relatively short one [32]. The significant elongation of O50–H50 covalent bond can be deduced from a location of H50 in a difference Fourier map.

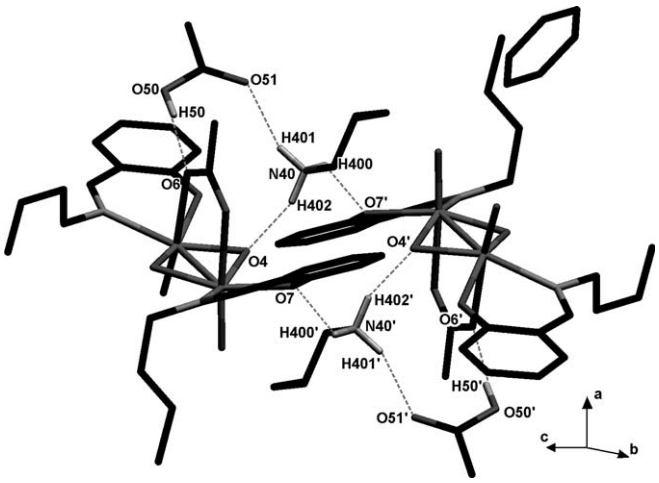

Fig. 2. Crystal structure with hydrogen bonding pattern of butylammonium di-μ-oxo-μ-acetato-bis[(*N*-butylsalicylideniminato-*N*,*O*)oxomolybdenum(V)]benzene, acetic acid solvate. Hydrogen bonds are drawn as dashed lines. Hydrogen atoms which do not participate in hydrogen bonding are omitted for clarity. Separation distance between the aromatic rings is larger than 7 Å and too far for π···π stacking interaction.

Table 4
Hydrogen-bonding geometry (Å, °)

D–H···A	D–H	H···A	D···A	D–H···A
N40–H402 ··· O4	0.890 (4)	1.896 (3)	2.721 (5)	143.5 (3)
N40–H401 ··· O51	0.890 (4)	2.071 (3)	2.917 (5)	158.6 (3)
O50–H50 ··· O6	1.09 (6)	1.52 (6)	2.595 (4)	168 (7)
N40–H400 ··· O7	0.890 (4)	2.217 (4)	2.908 (6)	134.2 (3)

4. Conclusion

The Mo(V) Schiff base complexes derived from alkylamines and salycilaldehyde, $RNH_3[Mo_2O_4(N–C_4H_9\text{-salim})_2OCOCH_3]\cdot xC_6H_6\cdot xCH_3COOH$ (R = Me, Et, Pr, Bu) were prepared and characterised by elemental analysis, magnetic measurements, and spectroscopic methods. The structure of butylammonium cation complex was determined by X-ray structure analysis: it is composed of a di-μ-oxo-μ-acetato-bis[(*N*-butylsalicylideniminato-*N*,*O*)-oxomolybdenum(V)] anion, cation and two solvent molecules, benzene and acetic acid. The Mo atoms of this dinuclear complex [with Mo–Mo bond of 2.5675(5) Å] exhibit the octahedral geometry.

Acknowledgments

This work was supported by Ministry of Education and Science, Sarajevo Canton, Project No. 11-14-22850, and Federal Ministry of Education of Bosnia and Herzegovina, project 04-39-3988/03 (E.K.) and Ministry of Science, Education and Sport of Croatia, Project Nos. 0098036 (K.M. and B.K.-P.) and 0098035 (Lj.T.-B.). Thanks are also due to Prof. Dr. B. Korpar-Čolig and Prof. Dr. B. Kamenar Faculty of Science, University of Zagreb, Croatia for support and offered facilities to one of the authors (E.K.) during her stay at the Faculty of Science, Zagreb.

Appendix A. Supplementary material

Crystallographic data (excluding structure factors) have been deposited with The Cambridge Crystallographic Data Centre as Supplementary Publication No. CCDC-264410. Copies of this information can be obtained free of charge from The Director, CCDC, 12, Union Road, Cambridge CB2 1EZ, UK (fax: +44 1223 336033; e-mail: deposit @ccdc.cam.ac.uk or http://www.ccdc.cam.ac.uk, www.ccdc.cam.ac.uk/conts/retrieving.html). Supplementary data associated with this article can be found, in the online version, at doi:10.1016/j.poly.2006.02.008.

References

[1] R.J.P. Williams, J.J.R.F. da Silva, Biochem. Res. Commun. 292 (2002) 293.
[2] E.I. Stiefel, Science 272 (1996) 1599.

[3] D. Sellman, Angew. Chem., Int. Ed. 32 (1993) 64.
[4] J. Kim, D. Wood, D.C. Ress, Biochemistry 32 (1993) 7104.
[5] E.T.K. Haupt, C. Wontorra, D. Rehder, A. Müller, Chem. Commun. (2005) 3912.
[6] S.F. Gheller, J.R. Bradbury, M.F. Mackay, A.G. Wedd, Inorg. Chem. 20 (1981) 3899.
[7] K. Yamanouchi, S. Yamada, J.H. Emmark, Inorg. Chim. Acta 85 (1984) 129.
[8] J.A. Craig, E.W. Harlan, B.S. Synder, M.A. Whitener, R.H. Holm, Inorg. Chem. 28 (1989) 2082.
[9] R. Laï, O. Desbois, F. Zamkotsian, R. Faure, J. Feneau-Dupont, J.-P. Declerq, Organometallics 14 (1995) 2145.
[10] L.-Z. Cai, L.-J. Song, H.-Y. Zeng, Z.-C. Dong, G.-C. Guo, J.-S. Huang, Inorg. Chim. Acta 344 (2003) 61.
[11] F.H. Allen, Acta Crystallogr. Sect. B58 (2002) 380.
[12] C.A. Rice, C.G. Benson, C.A. McAuliffe, Inorg. Chim. Acta 59 (1982) 33.
[13] C.A. McAuliffe, F.P. McCullough, M.J. Parrott, C.A. Rice, B.J. Sayle, J. Chem. Soc., Dalton Trans. (1977) 1762.
[14] D. Kamalendy, R.K. Maiti, J.K. Bhar, Trans. Met. Chem. 6 (1981) 346.
[15] J.R. Dilworth, C.A. McAuliffe, B.J. Sayle, J. Chem. Soc., Dalton Trans. (1977) 849.
[16] K. Yamanouchi, S. Yamada, Inorg. Chim. Acta 9 (1974) 83.
[17] B. Kamenar, B. Korpar-Čolig, M. Penavić, J. Chem. Soc., Dalton Trans. (1981) 311.
[18] K. Harms, S. Wocadlo, XCAD-4, Program for Processing CAD4 Diffractometer Data, University of Marburg, Germany, 1995.
[19] A.C.T. North, D.C. Phillips, F.S. Mathews, Acta Crystallogr. Sect. A24 (1968) 351.
[20] G.M. Sheldrick, SHELXS97. Program for Crystal Structure Solution, Universität Göttingen, Germany, 1997.
[21] G.M. Sheldrick, SHELXL97: Program for the Refinement of Crystal Structures, Universität Göttingen, Germany, 1997.
[22] A.L. Spek, PLATON98: A Multipurpose Crystallographic Tool, 120398 Version, University of Utrecht, Utrecht, The Netherlands, 1998.
[23] L.J. Farrugia, J. Appl. Crystallogr. 30 (1997) 565.
[24] F.H. Allen, O. Kennard, Chem. Des. Automat. News 8 (1) (1993), 1 and 31.
[25] Y.-L. Zhai, X.-X. Xu, X. Wang, Polyhedron 11 (1992) 415.
[26] S.K. Dutta, D.B. McConville, W.J. Youngs, M. Chaudhury, Inorg. Chem. 36 (1997) 2517.
[27] B. Korpar-Čolig, M. Cindrić, D. Matković-Čalogović, V. Vrdoljak, B. Kamenar, Polyhedron 21 (2002) 147.
[28] K. Nakamoto, Infared and Raman Spectra of Inorganic and Coordination Compounds, Part B: Applications in Coordination Organometallic and Bioinorganic Chemistry, 5th ed., Wiley-Interscience, New York, 1997.
[29] J. Liu, Y.-G. Wei, Q. Liu, S.-W. Zhang, Acta Crystallogr. Sect. C56 (2000) 822.
[30] B. Kamenar, B. Kaitner, N. Strukan, Croat. Chem. Acta 64 (1991) 329.
[31] N. Strukan, M. Cindrić, B. Kamenar, Acta Crystallogr. Sect. C56 (2000) 639.
[32] T. Steiner, W. Saenger, Acta Crystallogr. Sect. B50 (1994) 348.

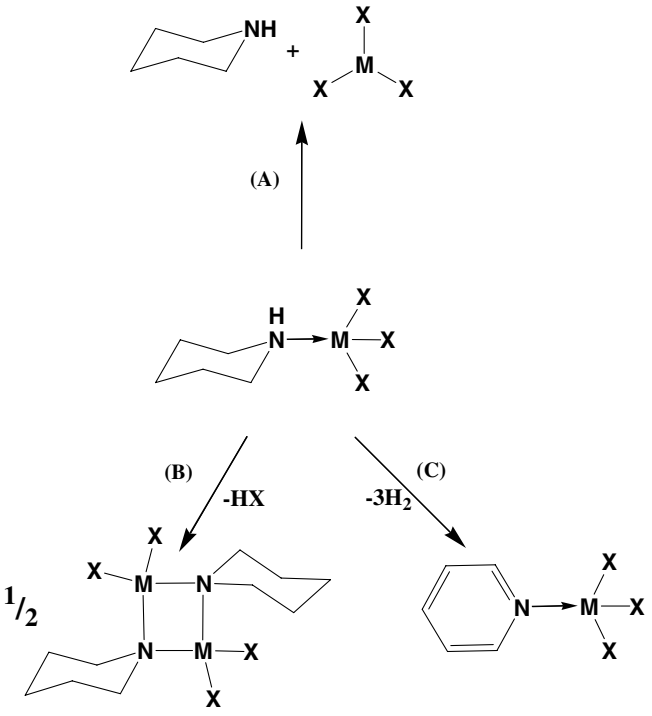

Scheme 1. The three decomposition pathways of $MX_3 \cdot$ pip adducts considered in the present work.

2. Computational details

All structures have been fully optimized at the B3LYP/LANL2DZ(d,p) level of theory [9,10] and verified to be minima on the potential energy surface. The LANL2DZ(d,p) basis set is identical to that used in previous research [3] and was constructed from the standard LANL2DZ basis [11] by adding the following polarization functions: p-function for H (1.0), and d-functions for C (0.75), N (0.8), Al (0.4), Ga (0.16), Cl (0.56), and I (0.15). The GAUSSIAN 98 program package [12] has been employed throughout. Standard enthalpies were obtained taking into account zero point energies and thermal corrections. Zero point energies, thermal corrections and standard entropies have been computed by standard statistical thermodynamic methods using the ideal gas rigid rotor – harmonic oscillator approximations using optimized geometries and computed vibrational frequencies (unscaled).

It was earlier shown that the B3LYP/LANL2DZ(d,p) level of theory satisfactory predicts the dissociation enthalpies of complexes between group 13 metal halides and ammonia [3]. However, in recent work [13] Gilbert has reported that the B3LYP/6-311++G(d,p) level of theory significantly underestimates the B–N bond energies in molecular complexes of BX_3 with ammonia and methylamines. Therefore, a more detailed assessment of the performance of the theoretical method for the DA complexes of the heavier analogs of boron is desirable.

A comparison between available experimental and theoretical data for model compounds and reactions is presented in Tables 1 and 2. Computed standard entropies of compounds are in good agreement with the experimental data, with mean absolute deviation 2 J mol^{-1} K^{-1} (Table 1). Agreement between predicted and experimental standard enthalpies is less satisfactory. Hydrogen elimination from piperidine (reaction 1) is underestimated by 15–20 kJ mol^{-1}. Large differences (30–55 kJ mol^{-1}) are found for the standard enthalpies of reactions of gaseous Al and Ga with HCl and HI (reactions 2–5), which are both overestimated and underestimated at the B3LYP/LANL2DZ(d,p) level of theory. This may be attributed to the known deficiency of DTF methods for the description of isolated atoms [15]. When a halogen exchange reaction (6) is considered, the B3LYP/LANL2DZ(d,p) endothermicity is underestimated by 15 kJ mol^{-1}. Table 2 summarizes theoretical and experimental dissociation enthalpies and entropies of donor–acceptor complexes with ammonia (reactions 7–9), pyridine (10–13) and piperidine (process 14). With the exception of the $AlCl_3 \cdot NH_3$ complex, the B3LYP/LANL2DZ(d,p) level of theory underestimates the dissociation enthalpies. Surprisingly good agreement is found for the case of $GaCl_3$, where the differences between theoretical and experimental values for the complexes with ammonia, pyridine and piperidine are all less then 4 kJ mol^{-1}. However, this may be due to a fortuitous cancellation of errors for this particular acceptor. Note that use of more extensive all-electron 6-311G++G** basis set with diffuse functions leads to worse agreement with experiment. Thus, at the B3LYP/6-311++G** level of theory the dissociation enthalpy of the $AlCl_3 \cdot NH_3$ complex [14] is 120 kJ mol^{-1} and is underestimated by 17 kJ mol^{-1}. The dissociation enthalpy of the $GaCl_3 \cdot NH_3$ complex is predicted to be 96 kJ mol^{-1} and it is underestimated by 38 kJ mol^{-1} [14]. A joint experimental and theoretical study of the $GaCl_3 \cdot$ pyrazine adduct showed that at the B3LYP/pVDZ level of theory the dissociation enthalpy is underestimated by 8 kJ mol^{-1} [7,8]. For the AlI_3 and GaI_3 complexes with pyridine, the dissociation energies predicted at the B3LYP/LANL2DZ(d,p) level of theory are underestimated by 15–20 kJ mol^{-1}.

Thus, from comparison with available experimental results we conclude that underestimation of the dative bond energy at the B3LYP/6-311++G(d,p) level of theory, reported recently by Gilbert for the B–N complexes [13],

Table 1
Comparison of theoretical and experimental standard gas phase entropies S^0_{298} J mol^{-1} K^{-1}

Compound	B3LYP/LANL2DZ(d,p)	Experiment
H_2	130.3	130.7 [16]
Al	155.6	164.6 [16]
Ga	167.3	169.0 [16]
HCl	186.6	186.8 [16]
HI	206.3	206.5 [16]
py (C_5H_5N)	281.9	283.0 [16]
$AlCl_3$	312.7	313.8 ± 1.7 [17]
AlI_3	374.4	376.1 ± 3.3 [17]

Table 2
Comparison of theoretical and experimental standard enthalpies ΔH^0_{298} (kJ mol^{-1}) and standard entropies ΔS^0_{298} (J mol^{-1} K^{-1}) of model gas phase reactions

N	Process	ΔH^0_{298}		ΔS^0_{298}	
		Theory	Experimental	Theory	Experimental
1	pip = py + $3H_2$	172.8	187.4 [16] 193 ± 2.1 [17]	362.5	
2	Al + 3HCl = $AlCl_3$ + $1.5H_2$	−625.9	−638.1 [17]	−207.3	−214.6 [17]
3	Ga + 3HCl = $GaCl_3$ + $1.5H_2$	−469.1	−439.4 [17]	−205.7	
4	Al + 3HI = AlI_3 + $1.5H_2$	−562.6	−617.8 [17]	−204.8	−211.9 [17]
5	Ga + 3HI = GaI_3 + $1.5H_2$	−468.4	−496.5 [17]	−204.1	
6	$AlCl_3$ + GaI_3 = AlI_3 + $GaCl_3$	62.6	77.4 [17]	0.8	
7	$AlCl_3 \cdot NH_3$ = $AlCl_3$ + NH_3	156.7 [3]	137.1 ± 5.9 (744 K) [20]	136.1 [3]	120.4 ± 6.3 (744 K) [20]
8	$GaCl_3 \cdot NH_3$ = $GaCl_3$ + NH_3	137.8 [3]	134.2 ± 2.5 (743 K) [20]	127.3 [3]	141.3 ± 3.8 (743 K) [20]
9	$AlI_3 \cdot NH_3$ = AlI_3 + NH_3	141.3 [3]	134[a] [20]	136.5 [3]	
10	$AlCl_3 \cdot$ py = $AlCl_3$ + py	157.5	166 ± 6 [21] 193 ± 8 [26]	142.1	
11	$GaCl_3 \cdot$ py = $GaCl_3$ + py	138.4	141 ± 8 [22] 147 ± 8 [26]	137.0	
12	$AlI_3 \cdot$ py = AlI_3 + py	133.4	156 ± 7 (709 K) [23,24]	146.2	146 ± 9 (709 K) [23,24]
13	$GaI_3 \cdot$ py = GaI_3 + py	110.5	140 ± 7 [18,19] 124 ± 7 (625 K) [18,19]	145.4	143 ± 7 (625 K) [18,19]
14	$GaCl_3 \cdot$ pip = $GaCl_3$ + pip	157.1	159 ± 8 [26]	158.2	

B3LYP/LANL2DZ(d,p) level of theory.
[a] Estimated value.

holds for the Al–N and Ga–N complexes as well. However, the role of the basis set is also of great importance: while the dissociation enthalpies are strongly overestimated with the LANL2DZ basis set without polarization functions [3], they are strongly underestimated with the 6-311++G** basis set that includes both diffuse and polarization functions [13,14]. Results obtained with LANL2DZ(d,p) and pVDZ basis sets fall between the two, and the B3LYP/LANL2DZ(d,p) level of theory is able to predict the reaction enthalpies of donor–acceptor complexes with an error of about 4–15 kJ mol^{-1}.

3. Results and discussion

3.1. Thermodynamics of the decomposition reactions of $MX_3 \cdot$ pip adducts

Three major reaction pathways have been considered (Scheme 1):

(**A**) dissociation of the complex:

$$MX_3 \cdot \text{pip (g)} = MX_3 \text{ (g)} + \text{pip (g)}$$

(**B**) elimination of HX with formation of amidodimers:

$$MX_3 \cdot \text{pip (g)} = \tfrac{1}{2}[MX_2C_5H_{10}N]_2 \text{ (g)} + HX \text{ (g)}$$

(**C**) elimination of H_2 with formation of pyridine (py, C_5H_5N) complexes:

$$MX_3 \cdot \text{pip (g)} = MX_3 \cdot \text{py (g)} + 3H_2 \text{ (g)}$$

The thermodynamic characteristics of the processes considered are given in Table 3. The dissociation enthalpies of piperidine complexes are about 20 kJ mol^{-1} higher compared to the analogous complexes with pyridine (Table 2). Thus, the complexes with piperidine are more stable with respect to dissociation of the donor–acceptor bond, in agreement with the early experimental findings of Greenwood and Perkins [26].

Elimination of HX from the DA complexes with formation of monomeric $MX_2C_5H_{10}N$ amido compounds is strongly endothermic. Note that subsequent dimerization of amido monomers is highly exothermic (by −150 to 230 kJ per mole of dimer), but does not fully compensate the unfavorability of the HX elimination. The dimerization enthalpies are decreasing in order Al > Ga and Cl > I.

Analysis of the thermodynamic characteristics of the three processes (**A**–**C**) shows that all reactions are strongly endothermic but favored by entropy. At the standard temperature 298 K all the processes are thermodynamically unfavorable. As the entropies of the decomposition reactions are positive, temperature elevation results in lowering the ΔG^0_T values for all reactions. Process (**C**) (molecular hydrogen elimination) is the most favorable from entropic considerations, and it becomes thermodynamically favorable above 500 K. Both the HCl and HI elimination reactions are highly endothermic and remain unfavorable even at high temperatures. On the basis of our thermodynamic analysis, the formation of $MX_3 \cdot$ py complexes is expected as a result of the thermolysis of source $MX_3 \cdot$ pip compounds above 500 K. Alternative pathways (dissociation into components or hydrogen halide elimination) require much higher temperatures.

To test the validity of these theoretical predictions, we have carried out an experimental study of the thermal

Table 3
Predicted at B3LYP/LANL2DZ(d,p) thermodynamic characteristics of the gas phase dissociation processes (**A**–**C**) in Scheme 1 of $MX_3 \cdot pip$ complexes

Process	ΔH^0_{298}	ΔS^0_{298}	ΔG^0_{298}	ΔG^0_{500}	ΔG^0_{1000}
$AlCl_3 \cdot pip = AlCl_3 + pip$	173.8	158.5	126.5	94.5	15.3
$AlCl_3 \cdot pip = AlCl_3 \cdot py + 3H_2$	189.1	378.9	76.2	−0.3	−189.8
$AlCl_3 \cdot pip = Cl_2AlNC_5H_{10} + HCl$	228.5	149.7	183.9	153.7	78.8
$2Cl_2AlNC_5H_{10} = [Cl_2AlNC_5H_{10}]_2$	−234.0	−233.2	−164.6	−117.6	−0.8
$AlCl_3 \cdot pip = 1/2[Cl_2AlNC_5H_{10}]_2 + HCl$	111.5	33.1	101.6	94.9	78.4
$AlI_3 \cdot pip = AlI_3 + pip$	151.5	157.2	104.7	72.9	−5.6
$AlI_3 \cdot pip = AlI_3 \cdot py + 3H_2$	191.0	373.5	79.7	4.3	−182.5
$AlI_3 \cdot pip = I_2AlNC_5H_{10} + HI$	188.4	146.7	144.7	115.1	41.7
$2I_2AlNC_5H_{10} = [I_2AlNC_5H_{10}]_2$	−183.2	−235.2	−113.2	−65.8	52.0
$AlI_3 \cdot pip = 1/2[I_2AlNC_5H_{10}]_2 + HI$	96.8	29.1	88.1	82.2	67.7
$GaCl_3 \cdot pip = GaCl_3 + pip$	157.1	158.2	110.0	78.0	−1.1
$GaCl_3 \cdot pip = GaCl_3 \cdot py + 3H_2$	191.5	383.7	77.2	−0.3	−192.2
$GaCl_3 \cdot pip = Cl_2GaNC_5H_{10} + HCl$	203.4	146.9	159.6	130.0	56.5
$2Cl_2GaNC_5H_{10} = [Cl_2GaNC_5H_{10}]_2$	−194.8	−225.6	−127.6	−82.0	30.8
$GaCl_3 \cdot pip = 1/2[Cl_2GaNC_5H_{10}]_2 + HCl$	106.0	34.1	95.8	89.0	71.9
$GaI_3 \cdot pip = GaI_3 + pip$	129.9	155.4	83.6	52.3	−25.4
$GaI_3 \cdot pip = GaI_3 \cdot py + 3H_2$	192.3	372.4	81.3	6.1	−180.1
$GaI_3 \cdot pip = I_2GaNC_5H_{10} + HI$	183.6	143.9	140.7	111.6	39.7
$2I_2GaNC_5H_{10} = [I_2GaNC_5H_{10}]_2$	−152.6	−230.8	−83.8	−37.2	78.2
$GaI_3 \cdot pip = 1/2[I_2GaNC_5H_{10}]_2 + HI$	107.3	28.5	98.8	93.0	78.8

Standard enthalpies ΔH^0_{298} and Gibbs energies ΔG^0_T in kJ mol^{-1} and standard entropies ΔS^0_{298} in J mol^{-1} K^{-1}.

decomposition of the $GaCl_3 \cdot pip$ adduct. This complex has been previously reported by Greenwood and Wade [25], but its thermal decomposition was not studied.

3.2. Experimental studies of the thermal decomposition of the $GaCl_3 \cdot pip$ adduct

Due to the high air and moisture sensitivity of gallium trichloride and its complexes, all experiments have been performed in a glass apparatus under a vacuum ($\sim 10^{-5}$ Torr). $GaCl_3$ has been synthesized from its elements and purified by multiple (no less than four times) resublimations in a vacuum. Piperidine was dried above KOH, distilled, degassed in vacuum, stored above the mixture of zeolites (NaA, CaX), and distilled in vacuum before use. Purity control of the samples was performed by means of mass spectrometry and vapor pressure measurements. The adduct was synthesized by direct reaction of the components in the vacuum and purified by multiple sublimations in vacuum at 120–140 °C. The chemical composition of the complex was verified to be $GaCl_3 \cdot pip$ from the chemical analysis. Measured by the thermography method, the melting point is 140 °C (literature value 134 °C) [25]. Mass spectrometry (MS) studies have been carried out using a standard MX1321 mass spectrometer with direct probe introduction. The temperature of the ionization chamber was 200 °C, electron energy 70 and 19 eV, and the temperature of the vaporization chamber 120 °C. Major ions in MS (relative intensity, %) were: $GaCl_2C_5H_{11}N^+$ (44); $GaCl_2C_5H_{10}N^+$ (11); $GaCl_2CH_3N^+$ (8); $GaCl_2^+$ (23); $GaCl^+$ (5); $C_5H_{11}N^+$ (59); $C_5H_{10}N^+$ (100); Ga^+ (8); HCl^+ (31); Cl^+ (8).

Tensimetry studies were performed by a static method with a glass membrane as null-manometer. The $GaCl_3 \cdot pip$ complex (55.55 mg) was introduced into the measurement chamber (volume 42.28 ml), and the system was heated in a furnace with a speed of about 0.5–1 °C per minute. The temperature was controlled by means of two chromel–alumel thermocouples, and the vapor pressure was measured with a mercury manometer. The vapor pressure–temperature dependence for the first two heating/cooling runs over $GaCl_3 \cdot pip$ complex is given in Fig. 1. For the

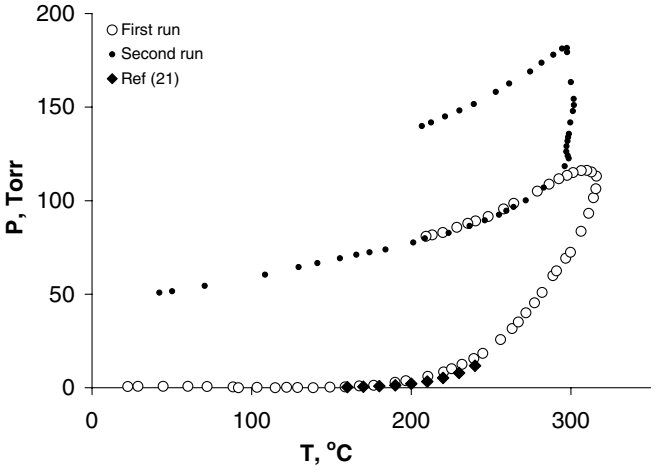

Fig. 1. Vapor pressure–temperature dependence for the $GaCl_3 \cdot pip$ complex. For the first run the lower circles refer to heating up to 316 °C. The upper curve circles for the first run refer to cooling for temperatures below 316 °C. For the second run the lower set of small solid dots refer to heating up to 298 °C. The upper set of small solid dots refers to cooling for temperatures below 298 °C.

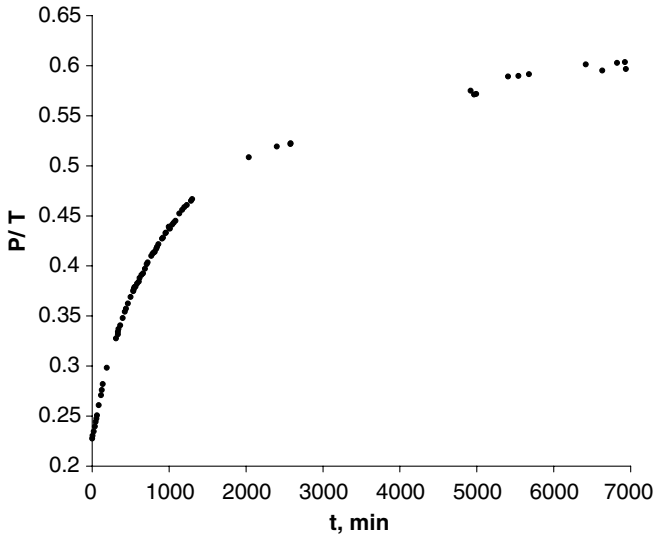

Fig. 2. Dependence of the P/T value on the decomposition time.

first run the measured vapor pressure is in agreement with the reported literature data [25]. In the temperature range 190–275 °C the vapor pressure is approximated by the equation $\lg P(\text{Torr}) = 8.003 \pm 0.022 - (3491 \pm 11)/T$. The vaporization enthalpy $\Delta H^{0\,\text{vap}}_{505} = 66.8 \pm 0.2$ kJ mol^{-1} lies below the literature value of $\Delta H^{0\,\text{vap}}_{473} = 85.9$ kJ mol^{-1} [25]; vaporization entropy $\Delta S^{0\,\text{vap}}_{505} = 98.1 \pm 0.4$ J mol^{-1} K^{-1}. As may be seen from Fig. 1, heating above 275 °C results in an irreversible pressure increase. The decomposition process proceeds slowly, as can be seen from Fig. 2, which displays the P/T – time dependence at 299 ± 4 °C. The P/T value is proportional to gas concentration ($P/T = nR/V$). The P/T – time dependence falls close to the logarithmic law. MS analysis of the volatile products after the thermal decomposition reveals the disappearance of the ions $GaCl_2C_5H_{11}N^+$, $GaCl_2C_5H_{10}N^+$, $C_5H_{11}N^+$ and $C_5H_{10}N^+$, indicating complete thermal destruction of the $GaCl_3 \cdot$ pip complex. Major species detected by MS after pyrolysis are: $GaCl_2NH_3^+$ (100); $GaCl_2C_5H_5N^+$ (53) and its homologues $GaCl_2C_5H_5(CH_2)_xN^+$ (with relative intensities 50; 17; 4; 2; 3; 2; 0.6 for $x = 1, 2, 3, 4, 5, 6, 7$, respectively) and the products of dissociative ionization $GaCl_2^+$ (54); $GaCl^+$ (21); Ga^+ (70); C_5H_5N (35); and $C_5H_5(CH_2)_xN^+$ (with relative intensities 78; 40; 6; 3; 5 for $x = 1, 2, 3, 4, 5$, respectively). Thus, formation of the DA complex $GaCl_3 \cdot$ py is observed experimentally, and it is accompanied by formation of DA complexes with methyl pyridines, which are probably originate from the Friedel–Crafts reactions in the condensed phase, catalyzed by $GaCl_3$.

4. Conclusions

Dissociation enthalpies of donor–acceptor complexes obtained at the B3LYP/LANL2DZ(d,p) level of theory are usually underestimated by 4–15 kJ mol^{-1}. Thus, the underestimation of the dative bond energy at B3LYP level of theory, reported recently by Gilbert for the B–N complexes [13], holds for the Al–N and Ga–N complexes as well. The present theoretical study of three possible thermal decomposition pathways of $MX_3 \cdot$ pip adducts suggests that hydrogen elimination with formation of $MX_3 \cdot$ py complexes is expected at temperatures near 500 K. Dissociation into components and hydrogen halide elimination requires much higher temperatures. In agreement with these expectations, experimental study of thermal decomposition of $GaCl_3 \cdot$ pip revealed the evolution of hydrogen gas and formation of the $GaCl_3 \cdot$ py complex and its homologues due to Friedel–Crafts reactions in the condensed phase.

Acknowledgements

A.Y.T. is grateful to the St. Petersburg administration for the partial financial support of this work (Grant PD05-1.3-071) and Alexander-von-Humboldt foundation for the award of a return fellowship. Work at the University of Georgia was supported by NSF Grant CHE-0451445.

References

[1] O.-S. Joo, K.-D. Jung, S.-H. Cho, J.-H. Kyoung, C.-K. Ahn, S.-C. Choi, Y. Dong, H. Yun, S.-H. Han, Chem. Vapor Depos. 8 (2002) 273.
[2] A.Y. Timoshkin, H.F. Schaefer, Chem. Rec. 2 (2002) 319.
[3] A.Y. Timoshkin, A.V. Suvorov, H.F. Bettinger, H.F. Schaefer, J. Am. Chem. Soc. 121 (1999) 5687.
[4] A.Y. Timoshkin, A.V. Suvorov, H.F. Schaefer, Russ. J. Gen. Chem. 69 (1999) 1204.
[5] A.Y. Timoshkin, A.V. Suvorov, H.F. Schaefer, Zh. Obsh. Khim. 69 (1999) 1250.
[6] E.A. Berezovskaya, A.Y. Timoshkin, T.N. Sevastianova, A.D. Misharev, A.V. Suvorov, H.F. Schaefer, J. Phys. Chem. B 108 (2004) 9561.
[7] A.Y. Timoshkin, E.A. Berezovskaya, A.V. Suvorov, A.D. Misharev, Russ. J. Gen. Chem. 75 (2005) 1173.
[8] A.Y. Timoshkin, E.A. Berezovskaya, A.V. Suvorov, A.D. Misharev, Zh. Obsh. Khim. 75 (2005) 1239.
[9] A.D. Becke, J. Chem. Phys. 98 (1993) 5648.
[10] C. Lee, W. Yang, R.G. Parr, Phys. Rev. B 37 (1988) 785.
[11] P.J. Hay, W.R. Wadt, J. Chem. Phys. 82 (1985) 270.
[12] M.J. Frisch, G.W. Trucks, H.B. Schlegel, G.E. Secures, M.A. Robb, J.R. Cheeseman, V.G. Zakrzewski, J.A. Montgomery, R.E. Stratmann, J.C. Burant, S. Dapprich, J.M. Millam, A.D. Daniels, K.N. Kudin, M.C. Strain, O. Farkas, J. Tomasi, V. Barone, M. Gossi, M. Cammi, B. Mennucci, C. Pomelli, C. Adamo, S. Clifford, J. Ochterski, G.A. Petersson, P.Y. Ayala, Q. Cui, K. Morokuma, D.K. Malick, A.D. Rabuck, K. Raghavachari, J.B. Foresman, J. Cioslowski, J.V. Ortiz, B.B. Stefanov, G. Liu, A. Liashenko, P. Piskorz, I. Komaromi, R. Gomperts, R.L. Martin, D.J. Fox, T. Keith, M.A. Al-Laham, A. Nanayakkara, C. Gonzales, M. Challacombe, P.M.W. Gill, B.G. Johnson, W. Chen, M.W. Wong, J.L. Andres, C. Gonzalez, M. Head-Gordon, J.A. Pople, GAUSSIAN 98, Revision A.3, Gaussian Inc., Pittsburgh, PA, 1998.
[13] T.M. Gilbert, J. Phys. Chem. A 108 (2004) 2550.
[14] A. Ogava, H. Fujimoto, Inorg. Chem. 41 (2002) 4888.
[15] J.M. Galbraith, H.F. Schaefer, J. Chem. Phys. 105 (1996) 862.
[16] NIST Standard Reference Database Number 69, June 2005. Internet: <http://webbook.nist.gov/chemistry/>.

[17] V.S. Yungman (Ed.), Electronic database "Thermal Constants of Substances", Version 24.07.2004. Internet: <http://www.chemnet.ru/cgi-bin/tkv.pl?show=welcome.html>.
[18] A.Y. Timoshkin, A.A. Grigoriev, A.V. Suvorov, Russ. J. Gen. Chem. 65 (1995) 1634.
[19] A.Y. Timoshkin, A.A. Grigoriev, A.V. Suvorov, Zh. Obsh. Khim. 65 (1995) 1634.
[20] V.I. Trusov, Ph.D. Thesis, Leningrad State University, 1974.
[21] A.A. Grigoriev, Ph.D. Thesis, Leningrad State University, 1987.
[22] S.D. Ershov, Ph.D. Thesis, Leningrad State University, 1982.
[23] A.Y. Timoshkin, A.V. Suvorov, A.D. Misharev, Russ. J. Gen. Chem. 72 (2002) 1874.
[24] A.Y. Timoshkin, A.V. Suvorov, A.D. Misharev, Russ. Zh. Obsh. Khim. 72 (2002) 1980.
[25] N.N. Greenwood, K. Wade, J. Chem. Soc. (1958) 1671.
[26] N.N. Greenwood, P.G. Perkins, J. Chem. Soc. (1960) 1145.

through both *N*,*O*- and *O*,*O*-chelating fashions, as shown by the crystal structure of $[Eu(picOH)_2(\mu\text{-}HpicO)(H_2O)]\cdot 3H_2O$ [6]. The 2-hydroxynicotinate ion coordinates through *O*,*O*-chelation to lanthanides as registered for the complexes $[Ln(HnicO)_2(\mu\text{-}HnicO)(H_2O)]\cdot nH_2O$ (Ln = Eu, Tb) [7]. Lanthanide complexes with pyridine-carboxylic acids usually form polymeric structures, with the carboxylate group establishing a bridge between lanthanide ions [5–7,13–15,17]. In this work, the coordination modes of the pyridine-carboxylic ligands, as *N*,*O*- or *O*,*O*-chelators, together with the photoluminescence of the Sm^{3+} in these complexes have been investigated.

2. Results and discussion

2.1. Crystal structure of $K_2[Sm_2(pic)_6(\mu\text{-}pic)_2]\cdot 7.5H_2O$ (1)

The crystal structure of $K_2[Sm_2(pic)_6(\mu\text{-}pic)_2]\cdot 7.5H_2O$ (**1**) shares striking similarities with the compounds recently reported by Sendor et al. [17] belonging to the $X[Ln(pic)_4]\cdot nH_2O$ family (where $X = Na^+$ or NH_4^+, and $Ln^{3+} = Eu^{3+}$, Gd^{3+}, Tb^{3+} and Ho^{3+}), in the sense that the one-dimensional anionic $[Sm_2(pic)_6(\mu\text{-}pic)_2]_n^{2n-}$ coordination polymer present in **1** is structurally similar to those found in the above mentioned compounds. More recently, the same material containing Tb^{3+} cations could also be isolated and was described elsewhere [18]. However, crystal solution and refinement of **1** proved to be a challenge (see Section 3 dedicated to crystallography), not because of poor data quality (crystal data were collected several times from crystals isolated from different batches), but most probably due to the presence of the larger, and sterically bulkier, K^+ cations in **1**. While all compounds reported by Sendor et al. [17] were solved and refined in either the $P6_122$ or $P6_522$ space groups, which ultimately led to only one crystallographically unique Ln^{3+} cation in their crystal structures, compound **1** could only produce a reasonable structural model when the overall symmetry was reduced to that of the $P6_5$ space group (even though structural tests for missed symmetry elements, with the ADDSYMM routines provided with PLATON [19,20], still indicate an overall pseudo-symmetry identical to that of $P6_522$ space group).

The crystal structure contains two crystallographically independent Sm^{3+} sites, Sm(1) and Sm(2), both coordinated to four *N* and five *O*-donor atoms from five distinct picolinate (pic^-) ligands (Fig. 1a), leading to a nine-coordination fashion, $\{SmN_4O_5\}$, resembling a highly distorted tricapped trigonal prism, in close agreement with the geometries described by Sendor et al. [17] for the $X[Ln(pic)_4]\cdot nH_2O$ family. For Sm(1), the basal planes of the trigonal prism are formed by O(1)···O(3)···O(7) and O(5)···O(15)···N(2) (dihedral angle between planes of ca. 23.8°), with N(1), N(3) and N(8) capping the lateral faces [N–Sm–N angles found within the 100.3(4)–136.6(4)° range; see Fig. 1a and Table 1]. For Sm(2), the basal planes are instead formed by O(13)···O(16)···N(5) and N(4)···N(6)···O(11) (dihedral angle between planes of ca. 14.1°) with, in this case, O(8), O(9) and N(7) capping the lateral faces [(O,N)–Sm–(O,N) angles found within the 108.6(4)–130.0(4)° range; see Fig. 1a and Table 1]. The Sm–N and Sm–O bond distances are found within the 2.640(10)–2.752(9) Å and 2.355(13)–2.437(11) Å [for Sm(1)], and 2.634(1)–2.760(9) Å and 2.358(13)–2.452(10) Å [for Sm(2)] ranges, respectively. These values are in good agreement with those typically found in related compounds, as revealed by a search in the Cambridge Structural Database (CSD) (Version 5.25, November 2003) [21,22]: while the typical Sm–N bond distances are in the 2.12–2.98 Å range (from 294 entries with a median of 2.54 Å), the $Sm–O_{carboxylate}$ bond distances are instead in the 2.19–3.08 Å bond range (from 61 entries with a median of 2.41 Å).

As usually found in related compounds [5,13,16], particularly those belonging to the above mentioned $X[Ln(pic)_4]\cdot nH_2O$ family [17], all picolinate ligands in **1** are coordinated to the Sm^{3+} metal centres through the typical *N*,*O*-chelation mode, with average bite angles of ca. 63.6° and 63.4° for Sm(1) and Sm(2), respectively (Table 1, Fig. 1 and Scheme 1a). However, one picolinate residue further establishes a *skew*-bridge [via O(7); see Fig. 1 and Scheme 1b] with the neighbouring Sm^{3+}, thus completing the nine-coordination sphere of the metal centre and leading to the formation of a one-dimensional (1D) anionic coordination polymer, $[Sm_2(pic)_6(\mu\text{-}pic)_2]_n^{2n-}$, running along the [0 1 0] direction (Fig. 1b and c). The *skew*-bridge is also responsible for the zigzag distribution of the Sm^{3+} metal centres along the aforementioned crystallographic direction, imposing an intermetallic Sm(1)···Sm(2) separation of 6.462(2) Å.

2.2. Crystal structure of $[Sm(picOH)_2(\mu\text{-}HpicO)(H_2O)]\cdot 3H_2O$ (2)

While investigating the luminescent properties of lanthanide complexes containing 3-hydroxypicolinic acid (HpicOH) residues, we have also described in a previous study the structural properties of the series of materials with empirical formula $[Ln(picOH)_2(\mu\text{-}HpicO)(H_2O)]\cdot 3H_2O$ (where $Ln^{3+} = Eu^{3+}$, Tb^{3+} and Er^{3+}) [6]. In this manuscript we report the synthesis of the analogous compound containing Sm^{3+}, providing details on the coordination environment of Sm^{3+} and the coordination modes of the organic ligand.

Compound **2** contains a single Sm^{3+} centre, which appears coordinated to four HpicOH residues (of which only three are crystallographically independent) and one water molecule, $\{SmN_2O_6\}$, with an eight-coordination geometry closely resembling a distorted dodecahedron (Fig. 2a), in which the Sm–N [2.583(5)–2.597(5) Å] and Sm–O [2.313(3)–2.423(3) Å] bonds (Table 2) are well within the expected ranges found by the in-depth survey of the CSD (see above). Two $picOH^-$ residues (*trans*-positioned in the coordination sphere – see Fig. 2a) are coordinated to the metallic centre forming a typical *N*,*O*-chelate with an aver-

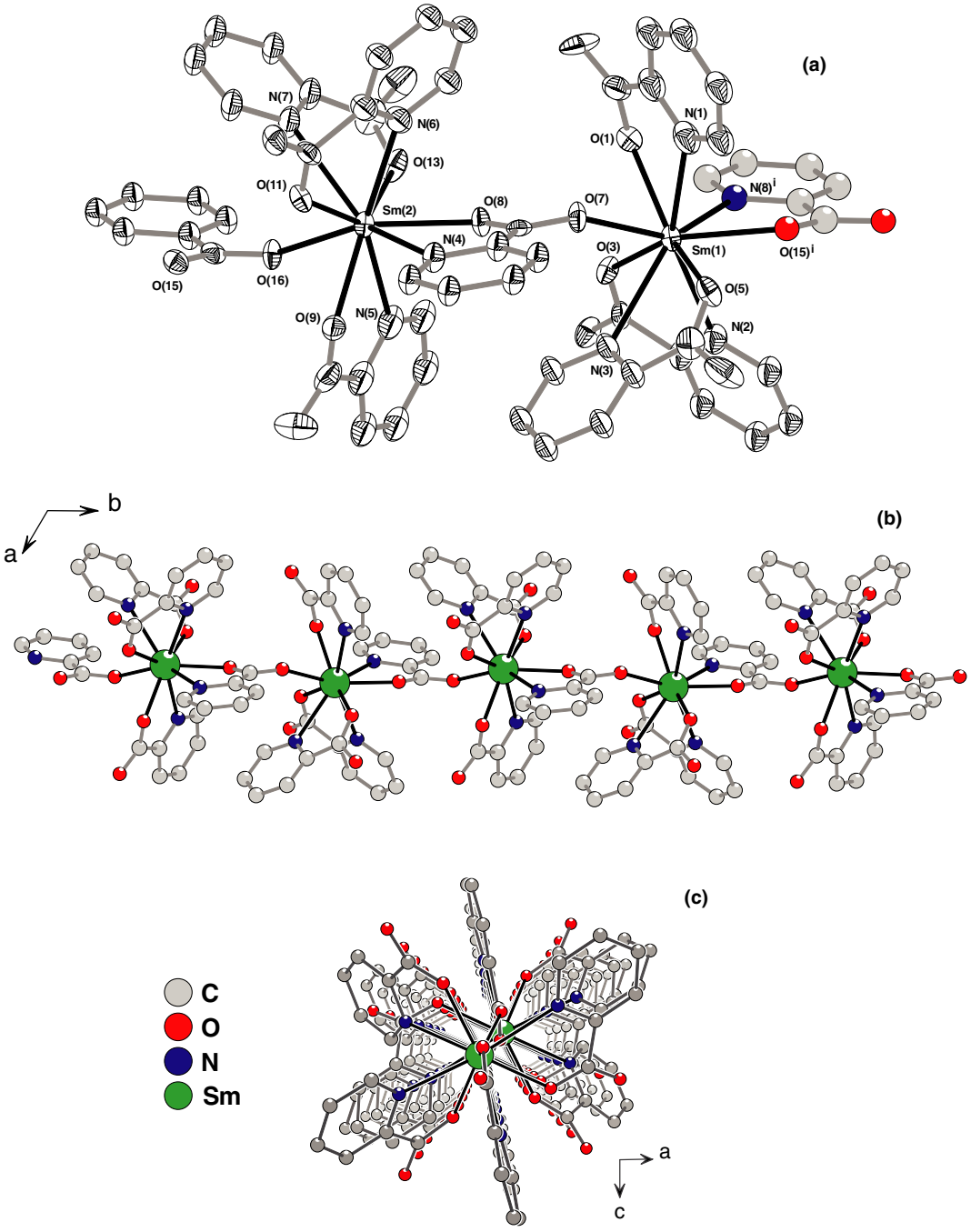

Fig. 1. (a) Tricapped trigonal prismatic coordination environments of Sm(1) and Sm(2) in $K_2[Sm_2(pic)_6(\mu\text{-pic})_2]\cdot 7.5H_2O$ (**1**), showing the labelling scheme for the atoms belonging to the first coordination sphere. Thermal ellipsoids are drawn at the 30% probability level. (b and c) Perspective views of the one-dimensional anionic $[Sm_2(pic)_6(\mu\text{-pic})_2]_n^{2n-}$ coordination polymer viewed along the [0 1 0] and [0 0 1] directions of the unit cell. Hydrogen atoms have been omitted for clarity purposes. For selected bond lengths and angles see Table 1. Symmetry code used to generate equivalent atoms: (i) x, $1+y$, z.

age bite angle of ca. 64.6° (Scheme 1c). The remaining crystallographically independent organic ligand (μ-HpicO$^-$) is, on the one hand, forming a six-membered chelate ring but, in this case, via the deprotonated phenolic and carboxylic acid groups (*O*,*O*-chelate) with a bite angle of 71.85(11)° (Fig. 2a); on the other hand, the deprotonated carboxylate group if further establishing a physical bridge (of the *syn*,*anti*-μ_2 type – Scheme 1d) with a neighbouring Sm^{3+}, imposing an intermetallic Sm(1)···Sm(1)^i separation of 6.963(1) Å [symmetry code: (i) x, $1.5-y$, $1/2+z$]. Once again, this latter bridging coordination fashion is responsible for the formation of the one-dimensional neutral $[Sm(picOH)_2(\mu\text{-HpicO})(H_2O)]$ coordination polymer (Fig. 2b), running parallel to the *c*-axis of the unit cell (Fig. 2c). As expected, this hybrid polymer is very much similar to those found for the $[Ln(picOH)_2(\mu\text{-HpicO})(H_2O)]\cdot 3H_2O$ (where $Ln^{3+} = Eu^{3+}$, Tb^{3+} and Er^{3+}) materials [6].

Table 1
Selected bond lengths (in Å) and angles (in degrees) for the Sm^{3+} coordination environments present in $K_2[Sm_2(pic)_6(\mu\text{-pic})_2] \cdot 7.5H_2O$ (**1**)[a]

Sm(1)–O(1)	2.377(13)	Sm(2)–O(8)	2.452(10)
Sm(1)–O(3)	2.379(12)	Sm(2)–O(9)	2.385(13)
Sm(1)–O(5)	2.355(13)	Sm(2)–O(11)	2.358(13)
Sm(1)–O(7)	2.406(13)	Sm(2)–O(13)	2.383(13)
Sm(1)–O(15)^{i}	2.437(11)	Sm(2)–O(16)	2.401(12)
Sm(1)–N(1)	2.665(10)	Sm(2)–N(4)	2.681(9)
Sm(1)–N(2)	2.640(10)	Sm(2)–N(5)	2.659(10)
Sm(1)–N(3)	2.752(9)	Sm(2)–N(6)	2.634(10)
Sm(1)–N(8)^{i}	2.672(9)	Sm(2)–N(7)	2.760(9)
O(1)–Sm(1)–O(3)	78.0(4)	O(8)–Sm(2)–N(4)	63.4(4)
O(1)–Sm(1)–O(7)	73.8(5)	O(8)–Sm(2)–N(5)	75.4(4)
O(1)–Sm(1)–O(15)^{i}	108.6(4)	O(8)–Sm(2)–N(6)	76.3(4)
O(1)–Sm(1)–N(1)	63.2(5)	O(8)–Sm(2)–N(7)	121.2(4)
O(1)–Sm(1)–N(2)	131.9(4)	O(9)–Sm(2)–O(8)	108.6(4)
O(1)–Sm(1)–N(3)	130.0(4)	O(9)–Sm(2)–O(13)	143.7(5)
O(1)–Sm(1)–N(8)^{i}	69.3(4)	O(9)–Sm(2)–O(16)	74.2(4)
O(3)–Sm(1)–O(7)	91.8(4)	O(9)–Sm(2)–N(4)	69.4(4)
O(3)–Sm(1)–O(15)^{i}	130.0(4)	O(9)–Sm(2)–N(5)	63.4(5)
O(3)–Sm(1)–N(1)	139.6(5)	O(9)–Sm(2)–N(6)	131.9(4)
O(3)–Sm(1)–N(2)	65.4(4)	O(9)–Sm(2)–N(7)	130.0(4)
O(3)–Sm(1)–N(3)	73.7(4)	O(11)–Sm(2)–O(8)	129.5(4)
O(3)–Sm(1)–N(8)^{i}	74.5(4)	O(11)–Sm(2)–O(9)	78.5(4)
O(5)–Sm(1)–O(1)	143.1(5)	O(11)–Sm(2)–O(13)	132.7(5)
O(5)–Sm(1)–O(3)	133.5(4)	O(11)–Sm(2)–O(16)	92.5(4)
O(5)–Sm(1)–O(7)	85.0(5)	O(11)–Sm(2)–N(4)	74.1(4)
O(5)–Sm(1)–O(15)^{i}	68.5(4)	O(11)–Sm(2)–N(5)	140.6(5)
O(5)–Sm(1)–N(1)	81.1(5)	O(11)–Sm(2)–N(6)	64.9(4)
O(5)–Sm(1)–N(2)	84.3(4)	O(11)–Sm(2)–N(7)	73.8(4)
O(5)–Sm(1)–N(3)	62.4(4)	O(13)–Sm(2)–O(8)	68.5(4)
O(5)–Sm(1)–N(8)^{i}	129.8(4)	O(13)–Sm(2)–O(16)	84.9(5)
O(7)–Sm(1)–O(15)^{i}	138.2(4)	O(13)–Sm(2)–N(4)	129.6(4)
O(7)–Sm(1)–N(1)	67.9(4)	O(13)–Sm(2)–N(5)	81.6(5)
O(7)–Sm(1)–N(2)	134.3(4)	O(13)–Sm(2)–N(6)	83.7(4)
O(7)–Sm(1)–N(3)	66.9(4)	O(13)–Sm(2)–N(7)	61.9(4)
O(7)–Sm(1)–N(8)^{i}	142.5(4)	O(16)–Sm(2)–O(8)	137.9(4)
O(15)^{i} –Sm(1)–N(1)	76.2(4)	O(16)–Sm(2)–N(4)	143.0(4)
O(15)^{i} –Sm(1)–N(2)	76.3(4)	O(16)–Sm(2)–N(5)	68.7(4)
O(15)^{i} –Sm(1)–N(3)	121.2(4)	O(16)–Sm(2)–N(6)	134.2(4)
O(15)^{i} –Sm(1)–N(8)^{i}	63.4(4)	O(16)–Sm(2)–N(7)	66.5(4)
N(1)–Sm(1)–N(3)	123.0(4)	N(4)–Sm(2)–N(7)	136.6(4)
N(2)–Sm(1)–N(1)	152.1(4)	N(5)–Sm(2)–N(4)	99.8(4)
N(2)–Sm(1)–N(3)	68.8(4)	N(5)–Sm(2)–N(7)	123.5(4)
N(2)–Sm(1)–N(8)^{i}	71.5(4)	N(6)–Sm(2)–N(4)	71.3(4)
N(8)^{i} –Sm(1)–N(1)	100.3(4)	N(6)–Sm(2)–N(5)	151.2(4)
N(8)^{i} –Sm(1)–N(3)	136.6(4)	N(6)–Sm(2)–N(7)	69.0(4)

[a] Symmetry transformations used to generate equivalent atoms: (i) $x, 1+y, z$.

2.3. Crystal structure of $[Sm(HnicO)_2(\mu\text{-}HnicO)(H_2O)] \cdot 5H_2O$ (3)

In another recent study, we have described the crystal structures of $[Tb(HnicO)_2(\mu\text{-}HnicO)(H_2O)] \cdot 1.75H_2O$ and $[Eu(HnicO)_2(\mu\text{-}HnicO)(H_2O)] \cdot 1.25H_2O$ [7]. When Sm^{3+} cations were added to the reactive system, the systematic poor quality of the isolated crystals (usually very thin and long needles) avoided the collection of good-quality X-ray data, both of powder and single-crystal. Only recently its structure could be fully elucidated by collecting crystal data at the low temperature of 180(2) K in a diffractometer with a much higher CCD sensitivity (see section dedicated to single-crystal X-ray diffraction). Indeed, and as expected, $[Sm(HnicO)_2(\mu\text{-}HnicO)(H_2O)] \cdot 5H_2O$ (**3**) proved to be structurally identical to the above mentioned materials with Eu^{3+} and Tb^{3+}, with the major difference between the three compounds being the amount of water molecules of crystallisation accounted in their crystal structures.

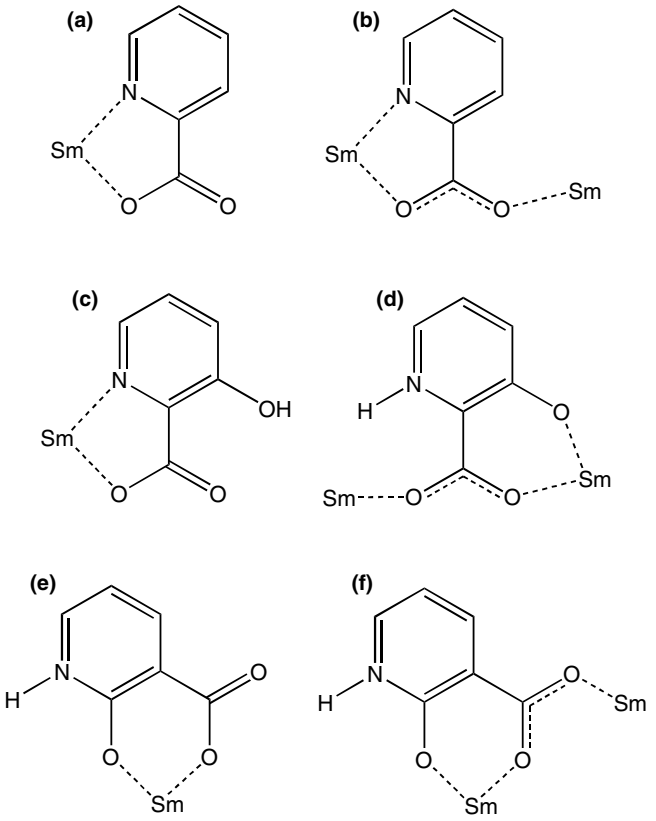

Scheme 1. Coordination modes of the ligands present in compounds **1**–**3**: (a and b) picolinic acid, (c and d) 3-hydroxypicolinic acid, and (e and f) 2-hydroxynicotinic acid.

As observed for the analogous materials with Eu^{3+} and Tb^{3+}, compound **3** contains only one crystallographically unique Sm^{3+} metallic centre, coordinated to four 2-hydroxynicotinic acid (H_2nicO) residues and one water molecule, $\{SmO_8\}$, in an eight-coordination geometry which, as for **2**, is best described as a distorted dodecahedron (Fig. 3a). The Sm–O bonds are found within 2.362(5)–2.490(7) Å, well within the expected bond range (see above).

The various functional groups present in the H_2nicO residues confer richness to the coordination flexibility of this organic molecule. On the one hand, the three crystallographically unique $HnicO^-$ ligands appear in the crystal structure with both phenolic and carboxylic acid groups deprotonated and coordinated to the Sm^{3+} centres, in a typical *O*,*O*-chelating coordination fashion (Scheme 1e) with an average bite angle of ca. 70.7° (Table 3). Even though the latter value is slightly smaller than that registered for the previous compound, it is also well within the range of values typically found in related materials as

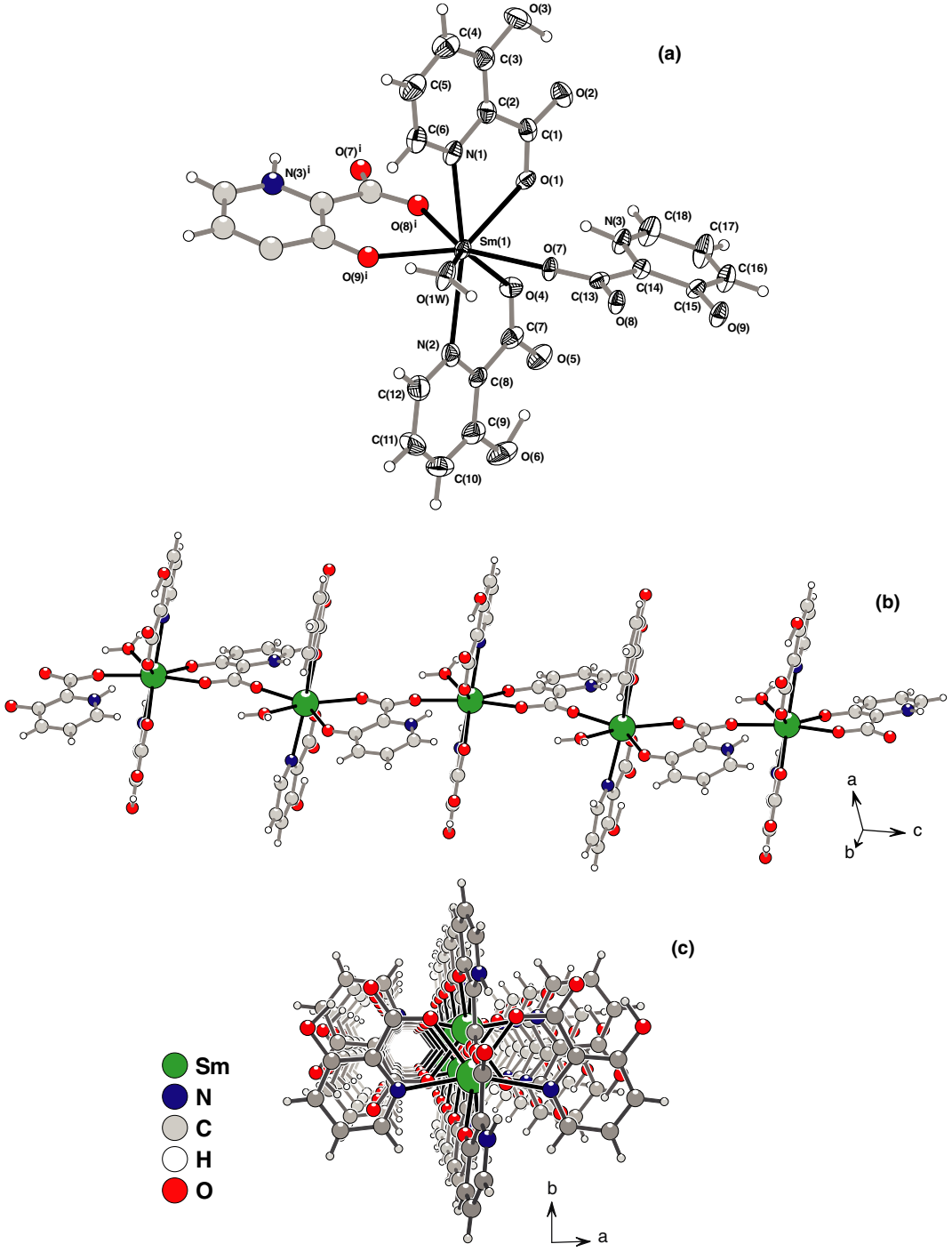

Fig. 2. (a) Distorted dodecahedral coordination environment of Sm(1) in $[Sm(picOH)_2(\mu\text{-}HpicO)(H_2O)]\cdot 3H_2O$ (**2**), showing the labelling scheme for all non-hydrogen atoms belonging to asymmetric unit. Thermal ellipsoids are drawn at the 50% probability level. (b and c) Perspective views of the one-dimensional $[Sm(picOH)_2(\mu\text{-}HpicO)(H_2O)]$ coordination polymer. For selected bond lengths and angles see Table 2. Symmetry code used to generate equivalent atoms: (i) x, $1.5 - y$, $1/2 + z$.

revealed by a search in the CSD (from 8 database entries, with values found in the ca. 61.0–74.1° range; median of ca. 69.2°) [21,22]. On the other hand, and as observed in the two previously described structures, a carboxylate group from one of these *O*,*O*-chelating $HnicO^-$ residues establishes a physical *syn, anti*-bridge with a neighbouring Sm^{3+} cation (μ-$HnicO^-$ – see Scheme 1f), thus forming a one-dimension neutral $[Sm(HnicO)_2(\mu\text{-}HnicO)(H_2O)]$ coordination polymer which runs parallel to the [1 0 0] direction of the unit cell (Fig. 3b and c). Such coordination fashion for the μ-$HnicO^-$ moiety imposes significant steric constrain in the carboxylate group, leading to a dihedral angle (with respect to the aromatic ring) of ca. 26.4° (see Fig. 3b). The minimum $Sm(1)\cdots Sm(1)^i$ intermetallic separation

Table 2
Selected bond lengths (in Å) and angles (in degrees) for the Sm^{3+} coordination environment present in $[Sm(picOH)_2(\mu\text{-}HpicO)(H_2O)]\cdot 3H_2O$ (**2**)[a]

Sm(1)–O(1)	2.423(3)	Sm(1)–O(9)^{i}	2.313(3)
Sm(1)–O(4)	2.381(3)	Sm(1)–O(1W)	2.400(3)
Sm(1)–O(7)	2.388(3)	Sm(1)–N(1)	2.583(5)
Sm(1)–O(8)^{i}	2.399(3)	Sm(1)–N(2)	2.597(5)
O(1)–Sm(1)–N(1)	64.44(12)	O(8)^{i}–Sm(1)–O(1W)	141.08(11)
O(1)–Sm(1)–N(2)	135.49(12)	O(8)^{i}–Sm(1)–N(1)	82.88(13)
O(4)–Sm(1)–O(1)	72.20(11)	O(8)^{i}–Sm(1)–N(2)	107.01(13)
O(4)–Sm(1)–O(7)	78.65(12)	O(9)^{i}–Sm(1)–O(1)	136.62(12)
O(4)–Sm(1)–O(8)^{i}	78.07(12)	O(9)^{i}–Sm(1)–O(4)	123.57(12)
O(4)–Sm(1)–O(1W)	135.76(13)	O(9)^{i}–Sm(1)–O(7)	144.19(11)
O(4)–Sm(1)–N(1)	136.02(12)	O(9)^{i}–Sm(1)–O(8)^{i}	71.85(11)
O(4)–Sm(1)–N(2)	64.76(13)	O(9)^{i}–Sm(1)–O(1W)	72.14(12)
O(7)–Sm(1)–O(1)	73.44(11)	O(9)^{i}–Sm(1)–N(1)	86.14(13)
O(7)–Sm(1)–O(8)^{i}	143.91(11)	O(9)^{i}–Sm(1)–N(2)	79.92(13)
O(7)–Sm(1)–O(1W)	72.85(11)	O(1W)–Sm(1)–O(1)	127.88(13)
O(7)–Sm(1)–N(1)	95.33(13)	O(1W)–Sm(1)–N(1)	80.49(14)
O(7)–Sm(1)–N(2)	87.22(13)	O(1W)–Sm(1)–N(2)	80.54(14)
O(8)^{i} –Sm(1)–O(1)	73.38(11)	N(1)–Sm(1)–N(2)	159.17(13)

[a] Symmetry transformations used to generate equivalent atoms: (i) x, $1.5 - y$, $1/2 + z$.

imposed by this organic ligand is of 6.521(1) Å [symmetry code: (i) $-1 + x$, y, z], a distance very much equivalent to those registered for the analogous Eu^{3+} and Tb^{3+} materials [7].

In compound **3** the *N*-donor atoms from the aromatic rings are not engaged in any type of coordination to the metal centres. Indeed, even though both *N*,*O*-chelation [23] and *N*-unidentate [24] coordination fashions are commonly observed for transition metal centres, in the case of lanthanides, coordination involving the nitrogen atom is even yet to be observed [7].

2.4. Vibrational spectra

Selected vibrational data and the molecular formulae for all complexes studied in this paper are supplied in Table 4, and are in accordance with the crystallographic studies summarised in the previous subsections. Infrared and Raman vibrational bands have been tentatively assigned, for Hpic, HpicOH, H_2nicO and their lanthanide complexes [5–7]. In Table 4 only the bands sensitive to metal coordination are reported. In the spectra of the picolinate and 3-hydroxypicolinate complexes, the asymmetric mode $\nu_{as}(CO_2)$ shifts (up to 106 cm^{-1}) to lower wavenumber, whereas the symmetric mode $\nu_s(CO_2)$ shifts to higher wavenumber (up to 40 cm^{-1}) when compared to the respective free ligands. Opposite shifts are observed for the 2-hydroxynicotinate complex. In the IR and Raman spectra of the complexes **1** and **2** the pyridine ν(CN) and ν(CC) stretches of the pyridinic ring show shifts to lower wavenumber (up to 23 cm^{-1}) when compared to Hpic and HpicOH. These shifts are in accordance with the *N*,*O*-chelation, as seen in the crystal structures of the complexes **1** and **2**. As expected, no shifts were observed for pyridine stretches in complex **3** because the coordination to the Sm^{3+} does not involve the nitrogen atom. Shifts of 21 cm^{-1} observed in the spectra of **2** for the band assigned to the $\nu(C–O)_h$ stretch are a result of the *O*,*O*-chelation of one ligand ($HpicO^-$). Similar shifts in the vibrational bands have been reported in the literature for other lanthanide complexes with aromatic ambidentate ligands [5–7].

2.5. Photoluminescence spectra

Fig. 4 shows the room-temperature emission spectra for the solid samarium complexes **1**–**3** under excitation at 325 nm. The emission spectra of the complexes are composed of a series of straight lines assigned to the Sm^{3+} intra-$4f^5$ transitions, $^4G_{5/2} \rightarrow {}^6H_{5/2,7/2,9/2,11/2}$ and of a large broad band in the range 380–550 nm for complexes **1** and **2**, and 380–680 nm for complex **3**, which may arise from the ligands excited states. The large broad bands observed in the emission spectra of the complexes **2** and **3** are blue-shifted comparatively with the previous reported for the Gd^{3+}-based complexes [7]. For all the complexes the more intense straight line characteristic of the Sm^{3+} is the magnetic dipole transition $^4G_{5/2} \rightarrow {}^6H_{7/2}$. Changes are detected in the energy, number of Stark components and in the full-width at half-maximum of the intra-$4f^5$ lines, reflecting the different Sm^{3+}-local coordination sites in each complex. For the three complexes a series of intra-$4f^5$ self-absorptions superimposed on the large broad band are also detected. The relative intensity between the broad band and the Sm^{3+} emission lines suggests that the efficiency of the energy transfer ligand-to-metal process is not efficient for the three complexes. Only compound **1** showed room-temperature emission under a Xe lamp (not shown) allowing the measurement of the correspondent excitation spectrum of the solid compound, monitored around the cation's more intense line at 595 nm, Fig. 5. The spectrum displays a large broad band between 250 and 325 nm associated with Hpic ligand [6], and a series of sharp lines assigned to transitions between the ground multiplet ($^6H_{5/2}$) and several excited states of the Sm^{3+}. The lower relative intensity of the ligand band indicates that the Sm^{3+} ions are essentially excited via direct metal excitation, rather than by an efficient sensitised process.

3. Experimental

3.1. Preparation of samarium (III) complexes

All chemicals were supplied by Aldrich and used as received.

The syntheses of samarium (III) complexes were performed as earlier described for the other lanthanide complexes with picolinic [5], 3-hydroxypicolinic [6] and 2-hydroxynicotinic [7] acids.

Compound **1** was prepared by adding an aqueous solution (5 ml) of the samarium salt ($SmCl_3 \cdot 6H_2O$, 1 mmol,

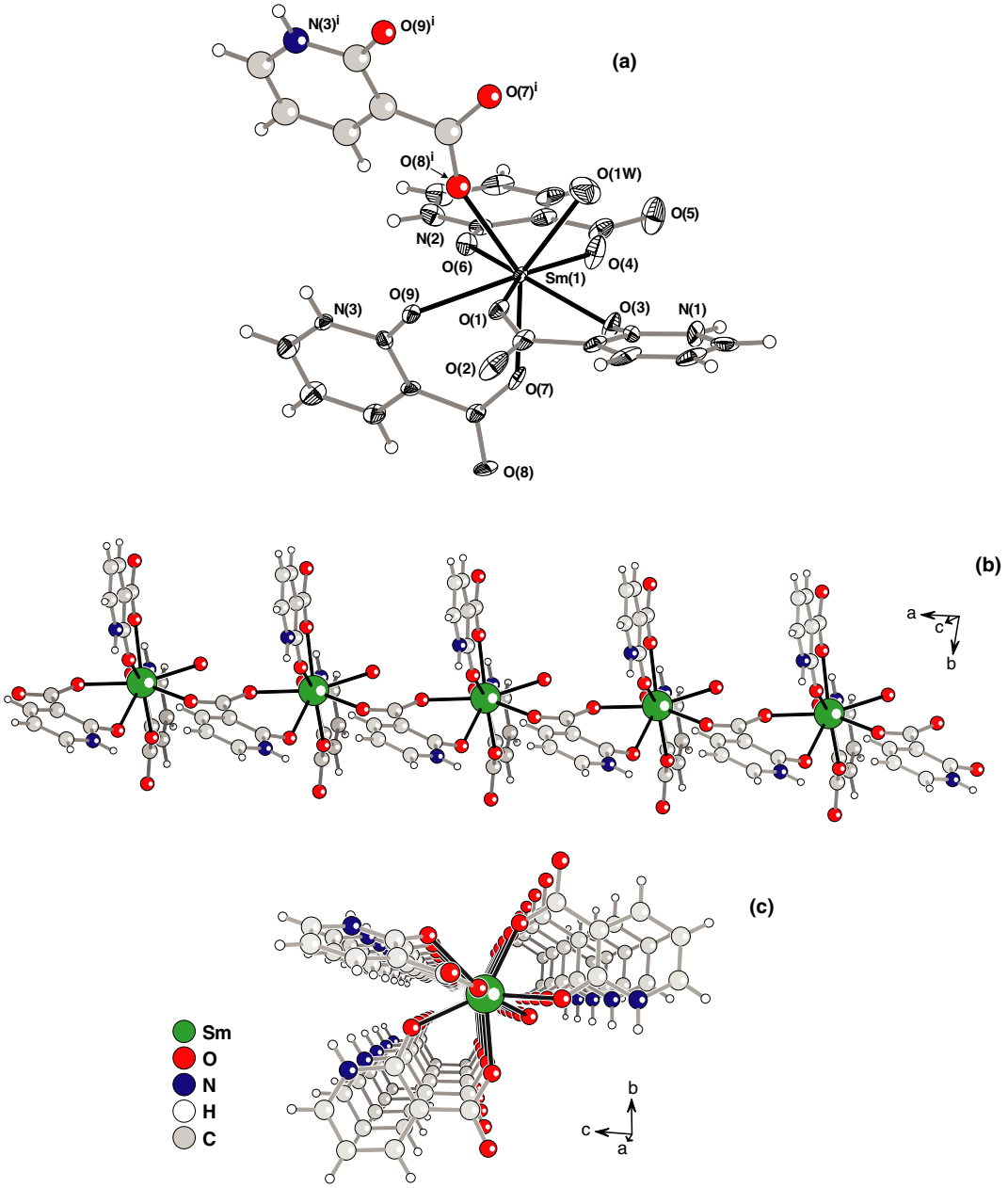

Fig. 3. (a) Slightly distorted dodecahedral coordination environment of Sm(1) in $[Sm(HnicO)_2(\mu\text{-}HnicO)(H_2O)] \cdot 5H_2O$ (**3**), showing the labelling scheme for selected non-hydrogen atoms belonging to asymmetric unit. Thermal ellipsoids are drawn at the 50% probability level. (b and c) Perspective views of the one-dimensional $[Sm(HnicO)_2(\mu\text{-}HnicO)(H_2O)]$ coordination polymer. For selected bond lengths and angles see Table 3. Symmetry code used to generate equivalent atoms: (i) $-1 + x, y, z$.

364 mg) to an aqueous solution (20 ml, pH ~ 6.7) of picolinic acid (Hpic, 4 mmol, 492 mg) and KOH (4 mmol, 224 mg). After stirring the mixture during approximately 1 h, an aqueous solution (5 ml) of tetrabutylammonium chloride hydrate ($^n Bu_4NCl \cdot nH_2O$, 4 mmol, 1.12 g) was added dropwise. The resulting solution was then heated (~100 °C), leading to the isolation of a white precipitate which was collected by filtering, followed by washing with distilled water. The materials were dried over silica gel. Colourless crystals with hexagonal habit of $K_2[Sm_2(pic)_6(\mu\text{-}pic)_2] \cdot 7.5H_2O$ were obtained from the mother solution by slow evaporation of the solvent during 3 days.

Compound **2** was synthesised by adding an aqueous solution (8 ml) of KOH (4.5 mmol, 252 mg) to an equal volume of a second aqueous solution containing the samarium salt ($SmCl_3 \cdot 6H_2O$, 1.5 mmol, 546 mg). The resulting mixture was stirred during approximately 90 min, after which time it was filtered, washed thoroughly with distilled water and added to an aqueous solution (25 ml) containing 3-hydroxypicolinic acid (4 mmol, 556 mg). This mixture was stirred during 1 h, heated for 30 min at 80 °C, and further stirred

Table 3
Selected bond lengths (in Å) and angles (in degrees) for the Sm^{3+} coordination environment present in $[Sm(HnicO)_2(\mu\text{-}HnicO)(H_2O)]\cdot 5H_2O$ (**3**)[a]

Sm(1)–O(1)	2.359(5)	Sm(1)–O(7)	2.391(5)
Sm(1)–O(3)	2.362(5)	Sm(1)–O(8)^{i}	2.369(5)
Sm(1)–O(4)	2.375(6)	Sm(1)–O(9)	2.454(5)
Sm(1)–O(6)	2.401(5)	Sm(1)–O(1W)	2.490(7)
O(1)–Sm(1)–O(3)	71.46(19)	O(4)–Sm(1)–O(7)	84.9(2)
O(1)–Sm(1)–O(6)	140.63(18)	O(4)–Sm(1)–O(9)	134.7(2)
O(1)–Sm(1)–O(7)	94.89(18)	O(4)–Sm(1)–O(1W)	78.8(3)
O(1)–Sm(1)–O(8)^{i}	83.74(19)	O(6)–Sm(1)–O(9)	70.08(18)
O(1)–Sm(1)–O(4)	149.4(2)	O(6)–Sm(1)–O(1W)	115.2(2)
O(1)–Sm(1)–O(9)	72.50(18)	O(7)–Sm(1)–O(6)	84.11(18)
O(1)–Sm(1)–O(1W)	85.7(2)	O(7)–Sm(1)–O(9)	70.73(17)
O(3)–Sm(1)–O(4)	79.0(2)	O(7)–Sm(1)–O(1W)	147.7(2)
O(3)–Sm(1)–O(6)	143.9(2)	O(8)^{i}–Sm(1)–O(4)	113.7(2)
O(3)–Sm(1)–O(7)	75.3(2)	O(8)^{i}–Sm(1)–O(6)	75.2(2)
O(3)–Sm(1)–O(8)^{i}	136.1(2)	O(8)^{i}–Sm(1)–O(7)	144.25(19)
O(3)–Sm(1)–O(9)	127.15(19)	O(8)^{i}–Sm(1)–O(9)	74.87(18)
O(3)–Sm(1)–O(1W)	74.4(2)	O(8)^{i}–Sm(1)–O(1W)	68.0(2)
O(4)–Sm(1)–O(6)	69.9(2)	O(9)–Sm(1)–O(1W)	138.6(2)

[a] Symmetry transformations used to generate equivalent atoms: (i) $-1+x, y, z$.

over 8 h at room temperature. The isolated solid material was filtered, washed thoroughly with distilled water and dried over silica gel. Single-crystals of $[Sm(picOH)_2(\mu\text{-}HpicO)(H_2O)]\cdot 3H_2O$ were obtained from the filtrate after slow evaporation over a period of 3 days.

Compound **3** was prepared by adding an aqueous solution (5 ml) of the samarium salt ($SmCl_3\cdot 6H_2O$, 0.5 mmol, 182 mg), to an aqueous solution (15 ml, pH 6.0) of 2-hydroxynicotinic acid (2 mmol, 278 mg) and KOH (2 mmol, 112 mg). After stirring the mixture at ambient temperature for 1 h, the solid which was formed was collected by filtering, and then washed thoroughly with distilled water. The material was dried over silica gel. Single-crystals of $[Sm(HnicO)_2(\mu\text{-}HnicO)(H_2O)]\cdot 3H_2O$, were obtained by recrystallisation from aqueous solution.

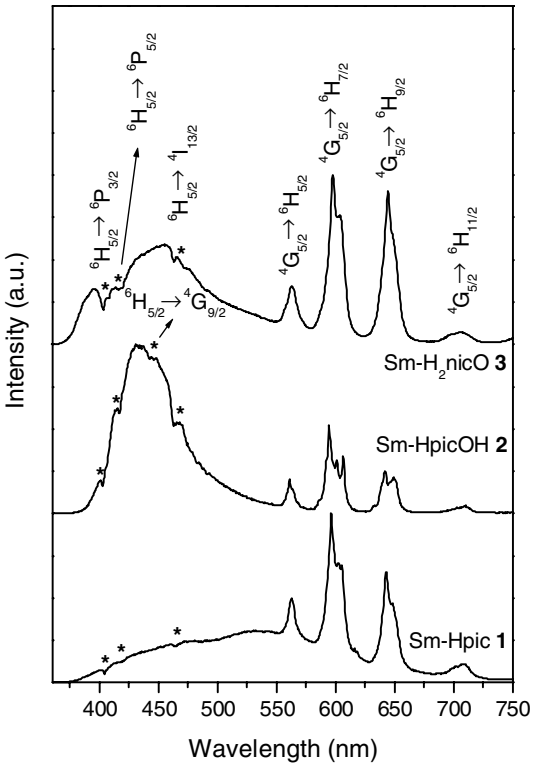

Fig. 4. Room-temperature emission spectra of compounds **1**–**3** excited at 325 nm. The asterisks denote intra-$4f^5$ self-absorptions.

3.2. Crystallography

Suitable single-crystals of $K_2[Sm_2(pic)_6(\mu\text{-}pic)_2]\cdot 7.5H_2O$ (**1**), $[Sm(picOH)_2(\mu\text{-}HpicO)(H_2O)]\cdot 3H_2O$ (**2**) and $[Sm(HnicO)_2(\mu\text{-}HnicO)(H_2O)]\cdot 5H_2O$ (**3**) were mounted on glass fibres using perfluoropolyether oil [25]. Data for **1** and **2** were collected at 180(2) K on a Nonius Kappa charge coupled device (CCD) area-detector diffractrometer (Mo Kα graphite-monochromated radiation, $\lambda = 0.7107$ Å), equipped with an Oxford Cryosystems cryostream

Table 4
Analytical and spectroscopic data for samarium complexes of pyridine-carboxylic acid derivatives and the free ligands

Compound	Analysis[a] (%)			Vibrational spectra[b] (cm^{-1})			
	C	N	H	$\nu_{as}(CO_2)$	ν(CN), ν(CC)	$\nu_s(CO_2)$	$\nu(C\text{–}O)_h$
Picolinic acid				1722 s	1608 s	1344 vs	
				1692 w	*1620* w	*1358* w	
$K_2[Sm_2(pic)_6(\mu\text{-}pic)_2]\cdot 7.5H_2O$ (**1**)	38.7 (38.7)	8.2 (7.5)	2.1 (3.2)	1621 vs	1585 vs	1382 vs	
					1596 w	*1383* vw	
3-Hydroxypicolinic acid				1702 s	1608 s	1320 s	1284 vs
					1612 m	*1323* w	*1286* vw
$[Sm(picOH)_2(\mu\text{-}HpicO)(H_2O)]\cdot 3H_2O$ (**2**)	34.8 (34.0)	6.8 (6.6)	2.1 (3.2)	1621 vs	1592 vs	1344 s	1263 s
				1619 vw	*1594* vw		*1258* vw
2-Hydroxynicotinic acid				1629 vs	1550 vs	1413 vs	
				1628 vw	*1554* vs	*1422* vw	
$[Sm(HnicO)_2(\mu\text{-}HnicO)(H_2O)]\cdot 5H_2O$ (**3**)	32.9 (32.1)	6.8 (6.3)	2.6 (3.6)	1637 vs	1552 vs	1386 s	
					1553 vs	*1372* vw	

[a] Calculated values in parentheses.
[b] Infrared and Raman (in italics) data; vs – very strong, s – strong, m – medium, w – weak, vw – very weak.

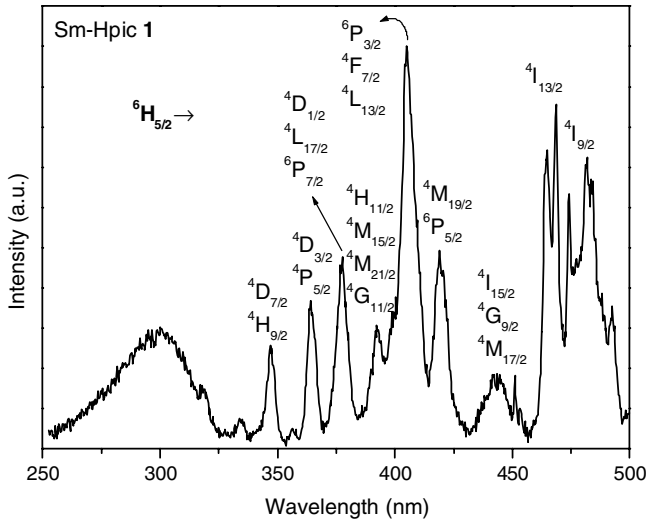

Fig. 5. Room-temperature excitation spectrum of compound **1** monitored at 595 nm.

and controlled by the Collect software package [26]. Images were processed using the software packages Denzo and Scalepack [27], and data were corrected for absorption by the empirical method employed in Sortav [28,29]. Data for **3** were collected at 100(2) K (at the Unidade de Raios-X, RIAIDT, University of Santiago de Compostela, Spain) on a Bruker SMART 1000 charge coupled device (CCD) area-detector diffractometer (Mo Kα graphite-monochromated radiation, $\lambda = 0.7107$ Å), controlled by the SMART software package [30]. Images for **3** were processed using the SAINTPlus software package [31], and data were corrected for absorption by using the semi-empirical method of SADABS [32]. All structures were solved using SHELXS-97 [33], and refined by full-matrix least-squares on F^2 using SHELXL-97 [34].

Information concerning crystallographic data collection and structure refinement details are summarised in Table 5. Selected bond lengths and angles are given in Tables 1–3 for structures **1**–**3**, respectively.

3.2.1. Structure solution and refinement details for $K_2[Sm_2(pic)_6(\mu\text{-}pic)_2]\cdot 7.5H_2O$ (1)

Systematic absences, inspected using the interface *XPREP*, suggested four possible non-centrosymmetric and chiral space groups for **1**: $P6_1$, $P6_5$, $P6_122$ and $P6_522$. The structure was solved in $P6_5$ (all other space groups led to unrealistic solutions) using Patterson synthesis which allowed the initial location of the Sm^{3+} and K^+ cations. The remaining non-hydrogen atoms were located from difference Fourier maps calculated in successive least-squares refinements. All non-hydrogen atoms were successfully refined using anisotropic displacement parameters.

Table 5
Crystal and structure refinement data for $K_2[Sm_2(pic)_6(\mu\text{-}pic)_2]\cdot 7.5H_2O$ (**1**), $[Sm(picOH)_2(\mu\text{-}HpicO)(H_2O)]\cdot 3H_2O$ (**2**) and $[Sm(HnicO)_2(\mu\text{-}HnicO)(H_2O)]\cdot 5H_2O$ (**3**)

Compound	**1**	**2**	**3**
Formula	$C_{48}H_{47}K_2N_8O_{23.5}Sm_2$	$C_{18}H_{20}N_3O_{13}Sm$	$C_{18}H_{24}N_3O_{15}Sm$
Formula weight	1490.84	636.72	672.75
Crystal system	hexagonal	monoclinic	triclinic
Space group	$P6_5$	$P2_1/c$	$P\bar{1}$
a (Å)	12.7777(18)	9.0597(18)	6.5210(13)
b (Å)	12.7777(18)	18.705(4)	13.093(3)
c (Å)	62.202(12)	13.554(3)	14.529(3)
α (°)	90	90	82.37(3)
β (°)	90	104.34(3)	80.71(3)
γ (°)	120	90	82.37(3)
Volume (Å^3)	8795(2)	2225.3(8)	1205.5(4)
Z	6	4	2
D_{calc} (g cm^{-3})	1.689	1.901	1.853
μ(Mo Kα) (mm^{-1})	2.210	2.714	2.517
F(000)	4446	1260	670
Crystal size (mm)	$0.21\times0.18\times0.05$	$0.12\times0.07\times0.05$	$0.15\times0.10\times0.08$
Crystal type	colourless hexagonal plates	colourless blocks	colourless needles
θ Range	3.58–22.44	3.55–27.50	3.61–26.46
Index ranges	$-13\leqslant h\leqslant 11$; $-13\leqslant k\leqslant 13$; $-66\leqslant l\leqslant 66$	$-11\leqslant h\leqslant 11$; $-24\leqslant k\leqslant 24$; $-17\leqslant l\leqslant 17$	$-8\leqslant h\leqslant 8$; $-16\leqslant k\leqslant 16$; $-18\leqslant l\leqslant 18$
Reflections collected	26556	13036	13533
Independent reflections	7074 ($R_{int} = 0.0643$)	5087 ($R_{int} = 0.0649$)	4920 ($R_{int} = 0.0524$)
Data completeness	to $\theta = 22.44°$, 98.2%	to $\theta = 27.50°$, 99.6%	to $\theta = 26.46°$, 98.9%
Final R indices [$I > 2\sigma(I)$]	$R_1 = 0.0657$, $wR_2 = 0.1512$	$R_1 = 0.0425$, $wR_2 = 0.0783$	$R_1 = 0.0558$, $wR_2 = 0.1349$
Final R indices (all data)	$R_1 = 0.0801$, $wR_2 = 0.1575$	$R_1 = 0.0829$, $wR_2 = 0.0890$	$R_1 = 0.0700$, $wR_2 = 0.1422$
Absolute structure parameter	0.07(3)		
Largest difference in peak and hole (e Å^{-3})	1.541 and −0.960	1.137 and −0.955	2.443 and −2.079

The eight crystallographically unique aromatic rings were refined with geometry heavily restrained to ensure a chemically reasonable structural model for these moieties: on the one hand, the *intra*-ring distances were restrained to common values, one for direct connections [ca. 1.37(1) Å], and another two for those which are one [ca. 2.37(1) Å] and two [ca. 2.73(1) Å] bonds apart; on the other hand, the six atoms of each aromatic ring were restrained to lie in a common plane using the *FLAT* instruction, and to share common anisotropic displacement parameters (*EADP* instruction). Hydrogen atoms attached to carbon were located at their idealised positions using the *HFIX 43* instruction in SHELXL, and included in the refinement in riding-motion approximation with an isotropic thermal displacement parameter fixed at 1.2 times U_{eq} of the carbon atom to which they are attached.

The seven and a half crystallographically unique water molecules of crystallisation were directly located from difference Fourier maps and refined with a common thermal isotropic displacement parameter. Even though no attempt was made to either locate the hydrogen atoms associated with these molecules, or to place them in calculated positions, the hydrogen atoms were included in the empirical formula of the compound (see Table 5).

The last difference Fourier map synthesis showed the highest peak (1.541 e $Å^{-3}$) located at 0.08 Å from O(1W), and the deepest hole (−0.960 e $Å^{-3}$) at 0.99 Å from Sm(2).

3.2.2. Structure solution and refinement details for $[Sm(picOH)_2(\mu\text{-}HpicO)(H_2O)] \cdot 3H_2O$ (**2**)

The structure was solved using direct methods, which allowed the location of the majority of non-hydrogen atoms. The remaining atoms were located from difference Fourier maps calculated in successive least-squares refinement cycles. All non-hydrogen atoms were successfully refined using anisotropic displacement parameters.

The four crystallographically unique water molecules were directly located from difference Fourier maps and refined successfully using anisotropic displacement parameters. Hydrogen atoms associated with the coordinated O(1W) and the lattice O(3W) water molecules were successfully located from difference Fourier maps, and refined with the O–H and H···H distances restrained to 0.84(1) Å and 1.37 Å, respectively (in order to ensure a chemically reasonable geometry for these molecules), and using a riding model with an isotropic displacement parameter fixed at 1.5 times U_{eq} of the atom to which they are attached. Hydrogen atoms from O(2W) and O(4W) could not be located and, even though no attempt was made to place these in calculated positions, they have been included in the empirical formula (Table 5).

Despite the hydrogen atoms associated with the hydroxyl groups were markedly visible in difference Fourier maps, their position in the structure was constrained using the *HFIX 147* instruction with isotropic thermal displacement parameters fixed at 1.5 times U_{eq} of the parent oxygen atom. Hydrogen atoms attached to carbon (from the three single 3-hydroxypicolinate aromatic residues) were located at their idealised positions using the *HFIX 43* instruction, and included in the refinement in riding-motion approximation with an isotropic thermal displacement parameter fixed at 1.2 times U_{eq} of the carbon atom to which they are attached.

One 3-hydroxypicolinate aromatic residue needs to be protonated so to balance the crystal charge. A close inspection of the crystal structure reveals that only the bridging 3-hydroxypicolinate ligand has the nitrogen atom not directly bound to a metal centre. Moreover, one *Q* peak neighbouring the mentioned nitrogen was markedly visible in difference Fourier maps. This hydrogen atom was subsequently refined with the N–H distance restrained to 0.95(1) Å and U_{iso} fixed at $1.5 \times U_{eq}$(N).

The last difference Fourier map synthesis showed the highest peak (1.137 e $Å^{-3}$) located at 1.19 Å from H(4), and the deepest hole (−0.955 e $Å^{-3}$) at 0.82 Å from Sm(1).

3.2.3. Structure solution and refinement details for $[Sm(HnicO)_2(\mu\text{-}HnicO)(H_2O)] \cdot 5H_2O$ (**3**)

The position of the crystallographically unique Sm^{3+} centre was located using Patterson synthesis, and the remaining non-hydrogen atoms were located from difference Fourier maps calculated in successive least-squares refinement cycles. Non-hydrogen atoms belonging to the neutral [Sm(HnicO)$_2$(μ-HnicO)(H$_2$O)] coordination polymer were successfully refined using anisotropic displacement parameters.

Hydrogen atoms bound to carbon were located at their idealised position using the *HFIX 43* instruction in SHELXL, and were included in subsequent refinement cycles in riding-motion approximation with U_{iso} fixed at $1.2 \times U_{eq}$ of the carbon atom to which they are attached. So to balance the crystal charge, three positive charges per Sm^{3+} cation were required. As the *N*-donor atoms from the three crystallographically independent 2-hydroxynicotinic acid residues are not bound to the Sm^{3+} metallic centres, and following the structural assumptions previously reported for the Tb^{3+} and Eu^{3+} analogue materials [7], the required hydrogen atoms were attached to the nitrogen atoms using the *HFIX 43* instruction in SHELXL. As for the aromatic hydrogen atoms, these were refined in riding-motion approximation with U_{iso} fixed at $1.2 \times U_{eq}$(N). The last difference Fourier map synthesis showed the highest peak (2.443 e $Å^{-3}$) located at 0.85 Å from Sm(1), and the deepest hole (−2.079 e $Å^{-3}$) at 0.11 Å from O(10W).

Eleven independent crystallographic sites, ascribed to highly disordered water molecules of crystallisation, could be directly located from difference Fourier maps. In good agreement with the values calculated in unrestrained refinement cycles (so to produce chemically reasonable temperature factors for the oxygen atoms), these water molecules were refined with fixed rates of occupancy of 50% [from O(2W) to O(10W)] and 25% [O(11W) and O(12W)]. Moreover, these moieties were refined using a common isotropic thermal displacement parameter.

Hydrogen atoms associated with the coordinated water molecule and those belonging to the crystal lattice were not visible in difference Fourier maps, mainly due to the smeared-out electron density associated with the latter moieties. However, the hydrogen atoms were included in the empirical formula (see Table 5).

In order to further validate the refined structural model, and since the collected crystal data showed strong evidence for the existence of extensive thermal disorder associated with all water molecules of crystallisation, the contribution of these moieties to the total electron density was removed by using the SQUEEZE [35] subroutine included with the crystallographic software package PLATON [19]. The calculated solvent-free reflection data were used in subsequent least-squares refinement cycles, converging to a structural model which does not differ significantly from that already obtained using the original reflection data set. As expected, using the solvent-free reflection data the global reliability factors improved, with R_1 $[I > 2\sigma(I)] = 0.0444$ and wR_2 (all data) = 0.1074. PLATON estimated that the unit cell contains ca. 304 Å^3 of total accessible solvent area (ca. 25% of the total volume), located in only one large cavity centred at (−0.010 0.500 0.000), totally containing ca. 83 electrons. These values are in good agreement with the total amount of just about 5 water molecules of crystallisation which were included in the final structural model of **3**.

3.3. Instrumentation

Infrared spectra were measured as KBr disks using a Mattson 7000 FT instrument. Raman spectra were recorded using a Bruker RFS100/S FT-Raman spectrometer (Nd:YAG laser, 1064 nm excitation). Elemental analysis (C, H and N) were measured in the Department of Chemistry, University of Aveiro. Solid-state room-temperature luminescence spectra were recorded on a Jobin Yvon-Spex spectrometer (HR 460) coupled to a R928 Hamamatsu photomultiplier. A He–Cd laser beam (325 nm and P = 30 mW) and a Xe-arc lamp (150 W) were used as excitation sources. All the emission spectra were corrected for the response of the detector.

4. Conclusions

New Sm^{3+} complexes of three pyridine-carboxylic acid derivatives (picolinic, 3-hydroxypicolinic and 2-hydroxynicotinic acids) were obtained and structurally characterised. The X-ray crystal structures show one-dimensional polymeric chains for all complexes presenting *N*,*O*- or *O*,*O*-chelation for the ligands. Four picolinate ligands coordinate to Sm^{3+} through *N*,*O*-chelation in complex **1**, with an one-dimensional chain being formed by a carboxylate bridge from one of the pic^- ligands. In the 3-hydroxypicolinate complex **2** *N*,*O*-chelation is observed for two $picOH^-$ ligands and the third ligand $HpicO^-$ coordinates through *O*,*O*-chelation and forms the carboxylate bridge of the chain. The coordination sphere of complex **2** is completed by one water molecule as also happens for complex **3**. In the 2-hydroxynicotinate complex **3** *O*,*O*-chelation is observed for the three ligands bonded to lanthanide centre, one of which forms the carboxylate bridge of the chain. In complexes **2** and **3** Sm^{3+} is eight-coordinated, while in complex **1** a coordination number of nine was obtained through four chelating ligands and a carboxylate bridge, thus avoiding water coordination. All complexes show room-temperature photoluminescence.

Acknowledgements

The authors thank to Fundação para a Ciência e a Tecnologia (Portugal) for funding under the POCI program and FEDER, and for the Grant SFRH/BPD/14954/2004 to P.C.R.S.S.

Appendix A. Supplementary data

Supplementary data are available from the CCDC, 12 Union Road, Cambridge CB2 1EZ, UK [Fax: (+44) 1223 336033; e-mail: deposit@ccdc.cam.ac.uk] on request, quoting the deposition numbers 290110 (for **1**), 231999 (for **2**), and 290111 (for **3**). Supplementary data associated with this article can be found, in the online version, at doi:10.1016/j.poly.2006.03.002.

References

[1] J.M. Lehn, Angew. Chem., Int. Ed. Engl. 29 (1990) 1304.
[2] D. Parker, J.A.G. Williams, J. Chem. Soc., Dalton Trans. (1996) 3613.
[3] A.P. Bassett, S.W. Magennis, P.B. Glover, D.J. Lewis, N. Spencer, S. Parsons, R.M. Williams, L. De Cola, Z. Pikramenou, J. Am. Chem. Soc. 126 (2004) 9413.
[4] S. Quici, M. Cavazzini, G. Marzanni, G. Accorsi, N. Armaroli, B. Ventura, F. Barigelletti, Inorg. Chem. 44 (2005) 529.
[5] P.C.R. Soares-Santos, H.I.S. Nogueira, V. Félix, M.G.B. Drew, R.A. Sá Ferreira, L.D. Carlos, T. Trindade, Inorg. Chem. Commun. 6 (2003) 1234.
[6] P.C.R. Soares-Santos, H.I.S. Nogueira, V. Félix, M.G.B. Drew, R.A. Sá Ferreira, L.D. Carlos, T. Trindade, Chem. Mater. 15 (2003) 100.
[7] P.C.R. Soares-Santos, H.I.S. Nogueira, J. Rocha, V. Félix, M.G.B. Drew, R.A. Sá Ferreira, L.D. Carlos, T. Trindade, Polyhedron 27/22 (2003) 3529.
[8] H.F. Brito, O.L. Malta, M.C.F.C. Felinto, E.E.S. Teotonio, J.F.S. Menezes, C.F.B. Silva, C.S. Tomiyama, C.A.A. Carvalho, J. Alloys Compd. 344 (2002) 393.
[9] S. Petoud, S.M. Cohen, J.-C.G. Bünzli, K.N. Raymond, J. Am. Chem. Soc. 125 (2003) 13324.
[10] P.C.R. Soares-Santos, H.I.S. Nogueira, F.A. Almeida Paz, R.A. Sá Ferreira, L.D. Carlos, J. Klinowski, T. Trindade, Eur. J. Inorg. Chem. 19 (2003) 3609.
[11] B.-L. An, M.-L. Gong, M.-X. Li, J.-M. Zhang, J. Mol. Struct. 687 (2004) 1.
[12] B. Yan, Q. Wie, J. Mol. Struct. 688 (2004) 73.
[13] P. Starynowicz, Acta Cryst. C 47 (1991) 32.
[14] P. Starynowicz, Acta Cryst. C 47 (1991) 294.
[15] P. Starynowicz, Acta Cryst. C 49 (1993) 1895.
[16] M. Jian-Fang, H. Ning-Hai, N. Jia-Zuan, Polyhedron 15 (1996) 1797.
[17] D. Sendor, M. Hilder, T. Juestel, P. Junk, U. Kynast, New J. Chem. 27 (2003) 1070.

[18] F.A. Almeida Paz, P.C.R. Soares-Santos, J. Klinowski, T. Trindade, H.I.S. Nogueira, Acta Cryst. E, submitted for publication.
[19] A.L. Spek, J. Appl. Crystallogr. 36 (2003) 7.
[20] A.L. Spek, Acta Cryst. A 46 (1990) C34.
[21] F.H. Allen, Acta Cryst. B 58 (2002) 380.
[22] F.H. Allen, W.D.S. Motherwell, Acta Cryst. B 58 (2002) 407.
[23] S. Chattopadhyay, P.E. Fanwick, R.A. Walton, Inorg. Chim. Acta 357 (2004) 764.
[24] S.M.O. Quintal, H.I.S. Nogueira, V. Félix, M.G.B. Drew, Polyhedron 21 (2002) 2783.
[25] T. Kottke, D. Stalke, J. App. Cryst. 26 (1993) 615.
[26] R. Hooft, Nonius B.V., Delft, The Netherlands, 1998.
[27] Z. Otwinowski, W. Minor, in: C.W. CarterJr., R.M. Sweet (Eds.), Methods in Enzymology, Academic Press, New York, 1997, p. 307.
[28] R.H. Blessing, Acta Cryst. A 51 (1995) 33.
[29] R.H. Blessing, J. Appl. Crystallogr. 30 (1997) 421.
[30] SMART, Bruker Molecular Analysis Research Tool v 5.054 © Bruker AXS, Madison, WI, USA, 1997–1998.
[31] SAINTPlus, Data Reduction and Correction Program v. 6.01 © Bruker AXS, Madison, WI, USA, 1997–1998.
[32] G.M. Sheldrick, SADABS v.2.01, Bruker/Siemens Area Detector Absorption Correction Program Bruker AXS, Madison, WI, USA, 1998.
[33] G.M. Sheldrick, SHELXS-97, Program for Crystal Structure Solution, University of Göttingen, Göttingen, 1997.
[34] G.M. Sheldrick, SHELXL-97, Program for Crystal Structure Refinement, University of Göttingen, Göttingen, 1997.
[35] P. van der Sluis, A.L. Spek, Acta Cryst. A 46 (1990) 194.

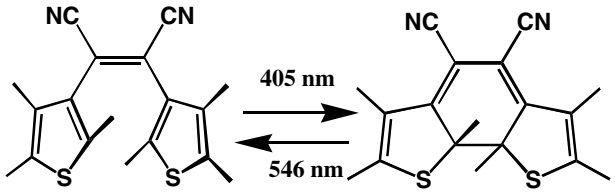

Scheme 1. Photochromic reaction of *cis*-dbe.

properties of Rh(II), dirhodium pivalate was selected as the metal salt in this work and three novel Rh(II) complexes were prepared, which are different from the previously dirhodium trifluoroacetate complexes [28] both in coordination modes and in conformation. Furthermore it was found that the dirhodium complex with the closed-dbe, where the metal atom has a direct coordination with the thienyl ring, is transferred to the open-form upon excitation with 529 nm light during the cycloreversion reaction.

2. Experimental

2.1. General methods

Unless otherwise indicated, all starting materials were used as received from commercial suppliers (Aldrich and Wako Chemicals). All reactions and manipulations were carried out under an argon atmosphere prior to use. Solvents were dried using standard procedures and distilled under an argon atmosphere. $[Rh_2(O_2CC(CH_3)_3)_4]$ was prepared according to the known literature procedure [29]. Closed-dbe was obtained by separating a *cis*-dbe hexane solution irradiated with 405 nm light.

Infrared spectra were recorded using KBr disks on a JASCO FT/IR-430 spectrometer. Absorption spectra in the crystalline state were measured by diffuse reflection using the Kubelka–Munk method on a SHIMADZU UV-2450 spectrometer, and barium sulfate was used as a reference. Photoirradiation was carried out using a 150 W Xe lamp and monochromatic light was obtained by passing the light through a monochromator.

2.2. Syntheses

2.2.1. $[Rh_2(O_2CC(CH_3)_3)_4(cis\text{-}dbe)_2]$ (1)

$[Rh_2(O_2CC(CH_3)_3)_4]$ (15.3 mg, 0.03 mmol) and *cis*-dbe (8.2 mg, 0.03 mmol) were dissolved in 5 mL benzene, and the resultant solution was carefully introduced into a 7 mm glass tube, which afforded complex **1** as green brick crystals after standing in the dark at an ambient temperature for 1 week. IR (KBr pellet, range 4000–400 cm^{-1}): 2965 (m), 2920 (m), 2864 (m), 2214 (m), 1578 (s), 1547 (w), 1484 (w), 1457 (w), 1439 (w), 1416 (m), 1376 (w), 1363 (w).

2.2.2. $[Rh_2(O_2CC(CH_3)_3)_4]$ (trans-dbe)$](CH_2Cl_2)_4$ (2)

Red-brown brick crystals were obtained similarly to those of complex **1** using dichloromethane instead of benzene. Yield: 63.8%. $Rh_2S_2O_8N_2C_{39.5}H_{57}Cl_3$: C, 44.58; H, 5.40; N, 2.63. Found: C, 44.42; H, 5.33; N, 2.61%. IR (KBr pellet, range 4000–400 cm^{-1}): 2987 (m), 2958 (m), 2923 (m), 2867 (m), 2237 (w), 1585 (s), 1484 (m), 1454 (w), 1415 (s), 1376 (m), 1363 (w).

2.2.3. $[Rh_2(O_2CC(CH_3)_3)_4]$ (closed-dbe) (3)

Red brick crystals were obtained similarly to those of complex **1** using closed-dbe in place of *cis*-dbe. Yield: 70.0%. *Anal.* Calc. for $Rh_2S_2O_8N_2C_{38}H_{54}$: C, 48.72; H, 5.81; N, 2.99. Found: C, 47.78; H, 5.51; N, 2.90%. IR (KBr pellet, range 4000–400 cm^{-1}): 3446 (m), 2959 (m), 2928 (m), 2904 (m), 2871 (m), 1584 (s), 1540 (w), 1505 (m), 1483 (s), 1457 (w), 1444 (w), 1414 (s), 1375 (m), 1363 (m).

2.3. X-ray data collection and structure solution and refinement

Diffraction data for complexes **1**–**3** were collected on a Rigaku MSC Mercury CCD diffractometer with graphite monochromated Mo Kα radiation ($\lambda = 0.71069$ Å). Intensity data were collected at 150 K using the ω scanning technique and a total of 6623, 6235 and 12071 reflections were collected for complexes **1**–**3**, respectively. No decay correction was applied. The linear absorption coefficients μ for the Mo Kα radiation were 7.28, 10.62 and 7.38 cm^{-1}, respectively.

The structures were solved by direct methods followed by subsequent Fourier calculations [30]. The non-hydrogen atoms were refined anisotropically for all complexes. For complex **1** the hydrogen atoms were located from difference density maps and their coordinates were refined. The C—H and O—H bonds lengths are 0.69(3)–1.14(3) Å. For complexes **2** and **3** the hydrogen atoms were introduced as fixed contributors. The final cycle of the full-matrix least squares refinement was based on 6059, 5809 and 9635 observed reflections and 442, 307 and 470 variable parameters for **1**–**3**, respectively, converged with the unweighted and weighted agreement factors of $R = \sum ||F_o| - |F_c|| / \sum |F_o|$ and $R_w = [\sum w(F_o^2 - F_c^2)^2 / \sum w(F_o^2)^2]^{1/2}$. The atomic scattering factors and anomalous dispersion terms were taken from the International Tables for X-ray Crystallography, vol. IV [31]. All calculations were performed using the TEXSAN crystallographic software package [32]. Details of the X-ray experiments and crystal data are summarized in Table 1. Selected bond lengths and bond angles are given in Table 2.

3. Results and discussion

3.1. Structural characterizations

The structures of the three Rh(II) coordination compounds were determined by X-ray crystallographic analyses and are showed in Figs. 1–3. The crystallographic data and lengths and angles of selected bonds of complexes **1**–**3** are listed in Tables 1 and 2.

Table 1
Crystallographic data for complexes **1**–**3**

	1	**2**	**3**
Formula	$Rh_2S_4O_8N_4C_{56}H_{72}$	$Rh_2S_2O_8N_2C_{42}H_{62}Cl_8$	$Rh_2S_2O_8N_2C_{38}H_{54}$
FW	1263.26	1276.52	936.78
Crystal system	triclinic	monoclinic	orthorhombic
Space group	*P*1(#2)	*C*2/*c*(#15)	*Fdd*2(#43)
a (Å)	10.212(4)	17.992(2)	36.112(3)
b (Å)	12.968(8)	17.224(2)	51.701(5)
c (Å)	13.042(6)	18.549(2)	11.379(1)
α (°)	93.40(2)		
β (°)	104.29(3)	88.817(6)	
γ (°)	112.20(2)		
V (Å^3)	1527(1)	5746(1)	21245(3)
Z	1	4	16
D (g cm^{-3})	1.374	1.475	1.171
μ (Cu Kα)	7.28	10.62	7.38
Observed reflections ($I > 2\sigma(I)$)	6059	5809	9635
R[a]	0.034	0.046	0.068
R_w[b]	0.088	0.120	0.204
Goodness-of-fit	1.05	1.08	1.05

[a] $R = \sum \| |F_o| - |F_c| \| / \sum |F_o|$.
[b] $R_w = \{\sum w(F_o^2 - F_c^2)^2 / \sum w(F_o^2)^2\}^{1/2}$.

Table 2
Selected bond lengths (Å) and angles (°) for complexes **1**–**3**

Complex ***1***			
Rh(1)—Rh(1*)	2.394(1)	Rh(1)—O(2*)	2.030(2)
Rh(1)—S(1)	2.544(1)	Rh(1)—O(3)	2.042(2)
Rh(1)—O(1)	2.033(2)	Rh(1)—O(4*)	2.032(2)
Rh(1*)—Rh(1)—S(1)	175.40(2)		
Complex ***2***			
Rh(1)—Rh(1*)	2.3802(4)	Rh(1)—O(4*)	2.037(2)
Rh(1)—O(1)	2.039(2)	N(1)—C(6)	1.140(4)
Rh(1)—O(2*)	2.029(2)	Rh(1)—N(1)	2.137(3)
Rh(1)—O(3)	2.034(2)		
Rh(1)—N(1)—C(6)	163.9(3)	Rh(1*)—Rh(1)—N(1)	176.46(7)
Complex ***3***			
Rh(1)—Rh(2)	2.3987(8)	Rh(1)—O(1)	2.041(6)
Rh(1)—S(1)	2.585(2)	Rh(1)—O(3)	2.044(6)
Rh(2′)—N(2)	2.155(7)	Rh(1)—O(5)	2.048(6)
C(3)—N(1)	1.16(1)	Rh(1)—O(7)	2.021(6)
C(4)—N(2)	1.14(1)		
Rh(2)—Rh(1)—S(1)	176.30(5)	Rh(2′)—N(2)—C(4)	173.1(7)

In complex **1** it was found that two Rh(II) ions are coordinated with two S atoms of thienyl groups from two different ligands to give a 2:1 mononuclear complex with a dirhodium unit and the two thienyl groups of the ligand are arranged in a parallel conformation (Fig. 1). As in Rh(II) trifluoroacetate complexes the metal ions have no interaction with the thieophene rings of the bisthienylethenes, this implies the coordination mode and conformation of the crystals are influenced by the carboxylates. Complex **1** is also quite distinguished from the structures of Ag(I) complexes with *cis*-dbe [27] where the metal center is coordinated with one cyano group as well as one thienyl S atom of different bisthienylethene molecules.

The crystals of complex **2** were synthesized similarly to complex **1** using dichloromethane instead of benzene. The X-ray crystallographic analyses show *cis*-dbe is changed to *trans*-dbe to coordinate with Rh(II). Each Rh(II) atom is coordinated to one cyano group of the *trans*-dbe with a bond length of 2.173(3) Å, which lead to an almost straight 1-D chain (Fig. 2). The coordination environment around the rhodium ions of complex **2** is notably different from that of complex **1**. In comparison with a Cu(I) complex with *trans*-dbe [26], both metal atoms are coordinated with two cyano groups from two different *trans*-dbe. The Rh—Rh bond length has a slightly change from 2.394(1) Å in complex **1** to 2.3802(4) Å in complex **2**.

Complex **3** was synthesized in the same manner as complex **1** using rigid closed-dbe, of which two thienyl groups are almost in the same plane, in the place of the flexible *cis*-dbe. The X-ray crystallographic analyses found the metal atoms are coordinated with one cyano group and one thienyl S atom from two different closed-dbe molecules to give a 1-D chain structure (Fig. 3). The Rh—S bond distance in both complexes coordinated to at least one thienyl group, namely complexes **1** and **3** is 2.544(1) Å and 2.588(2) Å, respectively. The short Rh—S bond distance in complex **3** is considered less favorable in photogenerated reactions based on the free rotation of the two thienyl groups. The Rh—Rh distance is 2.394(1) Å in complex **1** and 2.3987(8) Å in complex **3**, which are slightly longer values than that of the parent compound $[Rh_2(O_2CC(CH_3)_3)_4]$ (2.371(1) Å).

In conclusion, three Rh(II) complexes with *cis*, *trans* and closed-dbe were synthesized in which the coordination modes are different. In addition there are some differences in structures and conformations of three complexes: complexes **2** and **3** are coordination polymers whereas complex **1** is a mononuclear complex. In fact only complex **1** in this

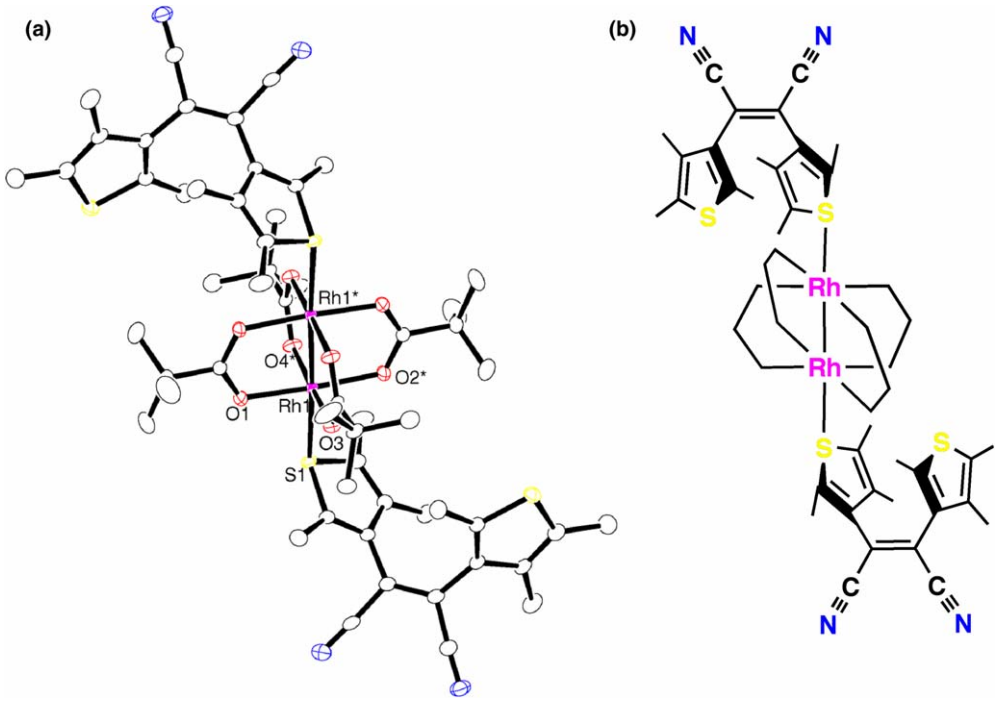

Fig. 1. Crystal structure of complex **1** ([$Rh_2(O_2CCMe_3)_4$(*cis*-dbe)$_2$]). (a) ORTEP view with the atomic labelling scheme, showing 50% thermal ellipsoids. Hydrogen atoms have been omitted for clarity. (b) Schematic figure.

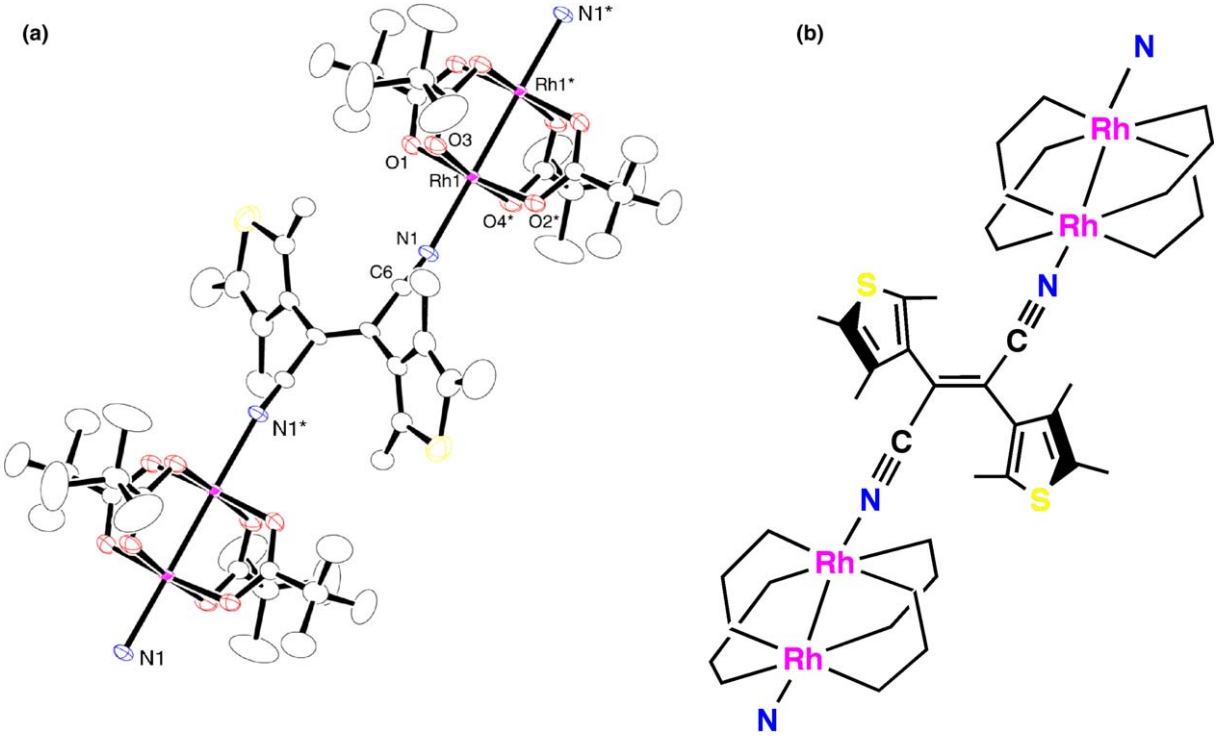

Fig. 2. Crystal structure of complex **2** ([$Rh_2(O_2CCMe_3)_4$(*trans*-dbe)](CH_2Cl_2)$_4$). (a) ORTEP view with the atomic labelling scheme, showing 50% thermal ellipsoids. Hydrogen atoms have been omitted for clarity. (b) Schematic figure.

work is not a chain structure, unlike the five dirhodium(II) trifluoroacetate and other pivalate complexes. A detailed comparison of Rh(II) complexes with *cis*-dbe or closed-dbe is summarized in Table 3.

3.2. Photochromism in the crystalline phase

The green complex [$Rh_2(O_2CC(CH_3)_3)_4$] (*cis*-dbe) **1** was synthesized in benzene. The most remarkable feature of **1** is

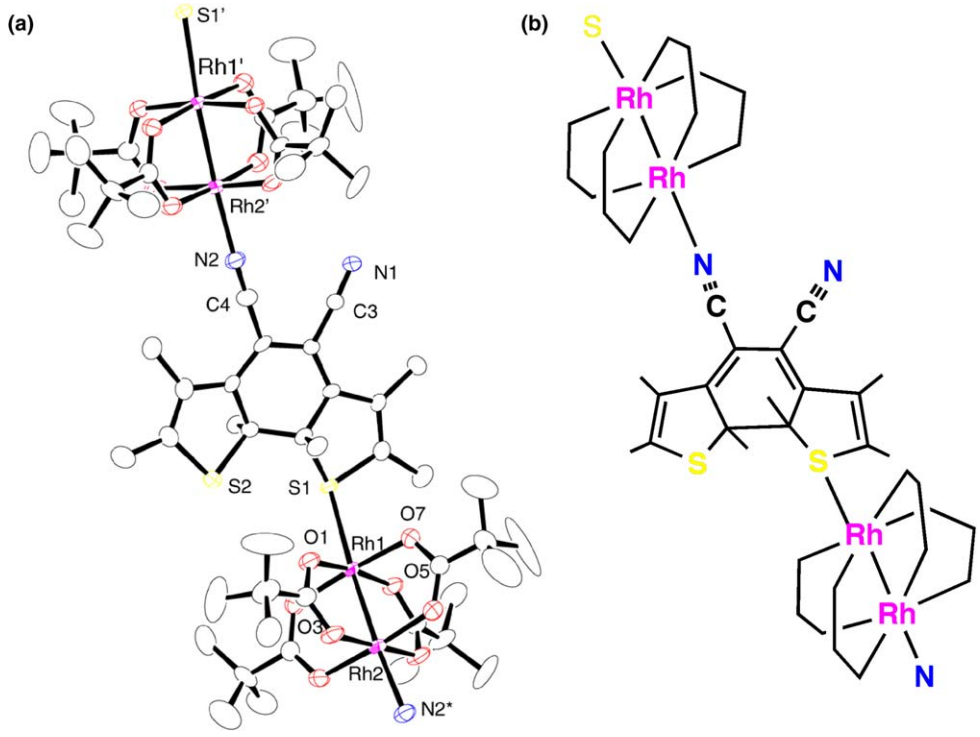

Fig. 3. Crystal structure of complex **3** ([$Rh_2(O_2CCMe_3)_4$(closed-dbe)]). (a) ORTEP view with the atomic labelling scheme, showing 50% thermal ellipsoids. Hydrogen atoms have been omitted for clarity. (b) Schematic figure.

Table 3
Rh(II) complexes with dbe

Complex	Anion	Ligand	Bridging	Conformation	Reference
[$Rh_2(O_2CCF_3)_4$(*cis*-dbe)](benzene)	$O_2CCF_3^{2-}$	*cis*-dbe	two cyano groups	three kinds	[28]
[$Rh_2(O_2CCF_3)_4$(closed-dbe)](*p*-xylene)	$O_2CCF_3^{2-}$	closed-dbe	two cyano groups	antiparallel	[28]
[$Rh_2(O_2CC(CH_3)_3)_4$(*cis*-dbe)]	$O_2CC(CH_3)_3^{2-}$	*cis*-dbe	two thienyl groups	parallel	this work
[$Rh_2(O_2CC(CH_3)_3)_4$ (*trans*-dbe)](CH_2Cl_2)$_4$	$O_2CC(CH_3)_3^{2-}$	*cis*-dbe	two cyano groups	*trans*	this work
[$Rh_2(O_2CC(CH_3)_3)_4$ (closed-dbe)]	$O_2CC(CH_3)_3^{2-}$	closed-dbe	one thienyl group and one cyano group	antiparallel	this work

one thienyl group of *cis*-dbe is coordinated to Rh to give two thienyl groups in a parallel conformation, which suppress the photocyclization reaction proceeding (Scheme 2). A bisthienylethene molecule could exist in two conformations: (i) parallel, in which the two thiophene rings are in mirror symmetry; (ii) antiparallel, in which the rings are in C_2 symmetry. According to the Woodward–Hoffmann rules, photochromic performance of diarylethene derivatives in crystals strongly depends on the

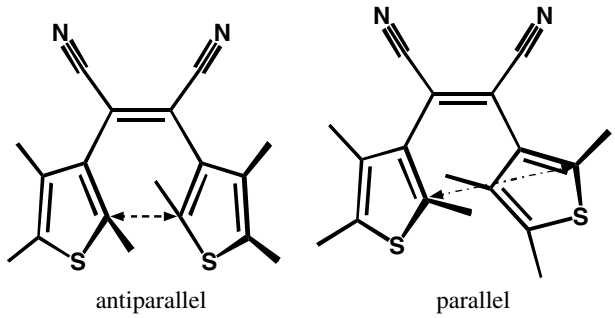

Scheme 2. Antiparallel and parallel conformations.

conformation of the molecules and the photocyclization reaction can only occur from the antiparallel conformation [1]. Further the distance between the reactive carbon atoms C(5) and C(9) in parallel complex **1** is 4.174 Å, which is too long for a covalent C—C single bond formation [1]. Thus in complex **1** a photocyclization reaction could not happen without the necessary antiparallel conformation and short distances between the reactive carbons. In contrast to Rh(II) trifluoroacetates complexes [28], of which each metal ion of the dimetal trifluoroacetates is coordinated with a cyano group of *cis*-dbe and three kinds of conformations coexist in the compound, each Rh(II) ion is coordinated with one thienyl group from each ligand and only a parallel conformation is packed in complex **1**. This phenomenon shows that the carboxylates influence not only the coordination mode but also the conformation of the ligand, and subsequently the photoinduced behavior.

Complex **2** was synthesized in dichloromethane using the same ligand. *cis*-dbe is changed to *trans*-dbe accompanying the coordination of two cyano groups to different Rh(II) atoms and the formation of molecular packing

including dichloromethane molecules. This shows the solvent has a close correlation with the coordination mode and conformation of dbe in the complex. Further investigation on NMR spectra of the free *cis*-dbe ligand in deuterated benzene and deuterated dichloromethane shows the signals of the methyl protons in different solvents are quite different (see Supplementary Information). This result suggests the existence of both *cis* and *trans* conformations in solution, which is agreeable with the previous examination of *cis*-dbe in deuterated CCl_4 solution [9], but there is different equilibrium between the two conformers in both solvents. The interesting solvent effect responsible for the different conformation in complexes **1** and **2** may be decided by which conformer, *cis* or *trans*, is superior in benzene or dichloromethane, and in which the metal complex is predominantly crystallized. Similarly to the previously reported Cu(I) complex with *trans*-dbe [26], complex **2** shows no visible color change upon any reasonable period of irradiation. The λ_{max} of complex **2** is 539 nm and is shifted to 570 nm after irradiation with 405 nm light for 30 min, indicating that the structure of complex **2** is changed with the irradiation.

The reddish purple complex **3** was prepared by using closed-dbe to avoid the rotation of *cis-trans* isomerization and the parallel conformation of two thienyl groups of *cis*-dbe. The most interesting feature of this complex is that one thienyl group, as well as one cyano group of *cis*-dbe, is coordinated to the rhodium atoms. Fig. 4 shows the absorption spectra changes of complex **3** in the crystalline phase. Before irradiation complex **3** has strong absorptions in the UV region and at 529 nm. Upon irradiation, the reddish purple complex **3** of closed-ring form is transformed to the green open-ring form and the 529 nm peak gradually flattens. The spectrum changed showing two constant isosbestic points (456 and 632 nm), and subsequently indicates that the transformation is occurring without the decomposition of the original and resulting complexes. The shoulder band around 529 nm did not disappear by further irradiation, indicating completeness of the conversion. The open-form of complex **3** shows a new absorption band with a λ_{max} value of 593 nm due to a $\pi^* \rightarrow \sigma^*$ transition band, which is at 683 nm in $[Rh_2(O_2CC(CH_3)_3)_4]$, as shown in Fig. 5.

It is noted that in this work the closed-dbe of antiparallel conformation in complex **3** is transferred to the ring-open isomer in spite of the special coordination environment of Rh(II). It is known that the photocycloreversion reaction of bisthienylethene in the crystalline phase varies depending on the molecular structure [2], but the details have not been clarified at present. The conversion of the closed-form to the open-form in complex **3** clearly suggests that the photocycloreversion reaction of bisthienylethene complexes could proceed with metal atoms being coordinated with a thienyl group. It is expected that this finding is useful to further understand the photochromic behavior of bisthienylethene coordination compounds in the crystalline phase.

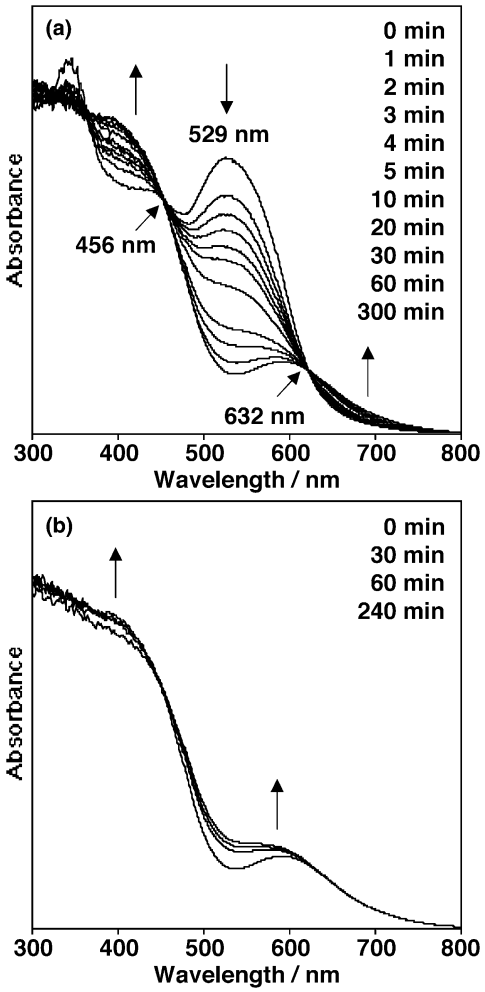

Fig. 4. Absorption spectral changes of complex **3** ($[Rh_2(O_2CC(CH_3)_3)_4$ (closed-dbe)]) by photoirradiation in the crystalline phase: (a) the closed-form was transformed to the open-form with 529 nm light and irradiation times are 0, 1, 2, 3, 4, 5, 10, 20, 30, 60 and 300 min; (b) the open-form was not transformed to the closed-form with 405 nm light and irradiation times are 0, 30, 60 and 240 min.

However, the resultant open-form of complex **3** is not converted to the initial closed-form on exposure to 405 nm light. The precise mechanism of the cyclization reaction remains unknown, while some consideration is necessary. Generally, a rotational motion encounters steric hindrance in the crystal. Therefore, the cyclization reaction in crystalline phases is dependent on the conformation and crystal packing [33]. In the previous report [27] we found that Ag(I) complexes with *cis*-dbe were transferred to the closed form where two thienyl S atoms were coordinated with metal atoms. No transformation of the open-form to the closed-form in complex **3** may be attributable to the steric hindrance of pivalate to the rotation of the thiophene rings.

It is well established that UV–Vis spectroscopy is the most common and effective detection method used in the solid state by far, where the photochromic states are identified by measuring the absorption bands characteristic of the open and closed isomers [4,14,26–28]. The photoreaction of the closed-dbe of complex **3** with irradiation of light

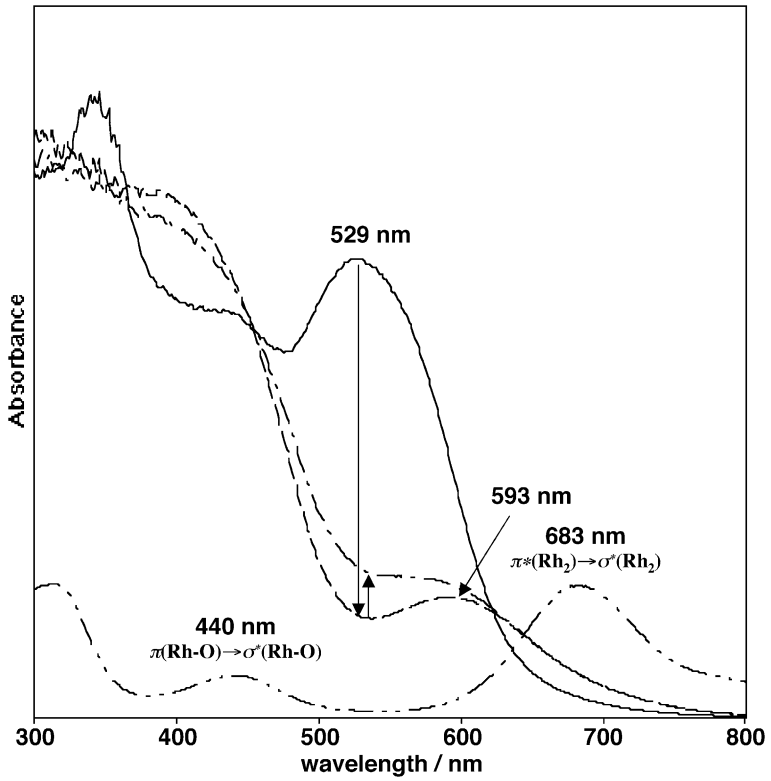

Fig. 5. Absorption spectral changes of complex **3** by photoirradiation in the crystalline phase: before irradiation (—), irradiation with 529 nm light for 300 min (---) and in the photostationary state under irradiation with 405 nm light for 240 min (-··-). Absorption spectrum of $[Rh_2(O_2CC(CH_3)_4)$ (-···-), $\lambda_{max} = 311$, 440, 683 nm.

occurs only on the surface of the crystals and subsequently the small amount of product (open-ring form) may not be detected by MAS NMR spectroscopy. Despite the limited monitoring method the green open form of complex **3** is considered not identical to complex **1**. The crystals of complex **3** are packed in a fixed orientation in the crystalline phase and a marked transformation from antiparallel to parallel is unacceptable. Also the open form of complex **3** seems not to decompose on exposure to 405 nm light which shows two constant isosbestic points judging from the UV spectra (Fig. 4(b)).

In contrast, λ_{max} of the metal-free closed-dbe (484 nm) < complex **3** (529 nm) < $[Rh_2(O_2CCF_3)_4$ (closed-dbe)] (574 nm). The absorption maximum is shifted much with coordination of both cyano groups compared to coordination with one cyano group and one thienyl group.

4. Conclusions

Three novel Rh(II) pivalate complexes were prepared where the dirhodium moieties are linked via 1,2-dicyano-1,2-bis(2,4,5-trimethyl-3-thienyl)ethene of *cis*, *trans* and closed forms. X-ray crystallographic analyses demonstrated that dirhodium pivalate leads to three kinds of coordination mode, that is the metal ions can be coordinated with two thienyl groups (complex **1**), two cyano groups (complex **2**) and one cyano group as well as one thienyl group (complex **3**). The three coordination modes are of interest in connection with the syntheses of photochromic complexes with bisthienylethene. *cis*-dbe is coordinated to Rh(II) accompanied by parallel conformation and *trans* isomerization to generate complex **1** and **2**, respectively. On the other hand, the closed-dbe of complex **3** shows typical spectral changes to the open-form on irradiation at 529 nm in spite of the Rh(II) being coordinated to both thienyl and cyano groups.

Acknowledgments

This work was partially supported by a Grant-in-Aid for Science Research (Nos. 14340211 and 13874084) from the Ministry of Education, Science, Sports and Culture in Japan.

Appendix A. Supplementary data

NMR spectra of the free ligand in benzene and dichloromethane can be obtained as supplementary material. Crystallographic data for the X-ray crystal structural analysis have been deposited with Cambridge Crystallographic Data Center, Nos. (0580) 289367–289369 for complexes **1**–**3**, respectively. Copies of this information may be obtained free of charge from The Director, CCDC, 12 Union Road, Cambridge, CB2 1EZ, UK (fax: +44 1233 336033); e-mail: deposit@ccdc.cam.ac.uk or http://www.ccdc.cam.ac.uk. Supplementary data associated with

this article can be found, in the online version, at doi:10.1016/j.poly.2006.02.013.

References

[1] S. Kobatake, K. Uchida, E. Tsuchida, M. Irie, Chem. Commun. (2002) 2804.
[2] M. Morimoto, S. Kobatake, Chem. Eur. J. 9 (2003) 621.
[3] S. Kobatake, M. Irie, Bull. Chem. Soc. Jpn. 77 (2004) 195.
[4] S. Kobatake, S. Kuma, M. Irie, Bull. Chem. Soc. Jpn. 77 (2004) 945.
[5] H. Tian, S.J. Yang, Chem. Soc. Rev. 33 (2004) 85.
[6] M. Irie, T. Lifka, K.S. Kobatake, Y. Shindo, Chem. Commun. (1999) 747.
[7] S.H. Kawasi, S.L. Gilat, R. Ponsinet, Chem. Eur. J. 1 (1995) 285.
[8] K. Higashiguchi, K. Matsuda, M. Irie, Angew. Chem., Int. Ed. 42 (2003) 3537.
[9] M. Irie, M. Mohri, J. Org. Chem. 53 (1988) 803.
[10] B. Qin, R.X. Yao, X.L. Zhao, H. Tian, Org. Biomol. Chem. 12 (2003) 2187.
[11] S.L. Gilat, S.H. Kawasi, J.-M. Lehn, Chem. Eur. J. 1 (1995) 275.
[12] M. Irie, T. Lifka, S. Kobatake, N. Kato, J. Am. Chem. Soc. 122 (2000) 4871.
[13] S. Fraysse, C. Coudret, J.-P. Launay, Eur. J. Inorg. Chem. 39 (2000) 1581.
[14] T. Yamada, S. Kobatake, K. Muto, M. Irie, J. Am. Chem. Soc. 122 (2000) 1589.
[15] N. Tanio, M. Irie, Jpn. J. Appl. Phys. 33 (1994) 1550.
[16] Y. Kaneuchi, T. Kawai, M. Hamaguchi, K. Yoshino, M. Irie, Jpn. J. Appl. Phys. 36 (1997) 3736.
[17] T. Kawai, T. Koshido, K. Yoshino, Appl. Phys. Lett. 67 (1995) 795.
[18] K. Takashi, K. Tsuyoshi, Y. Katsumi, J. Phys. Chem. 99 (1995) 6110.
[19] H. Ishitobi, Z. Sekkat, M. Irie, S. Kawata, J. Am. Chem. Soc. 122 (2000) 12802.
[20] K. Horie, S. Murase, S. Takahashi, M. Teramoto, H. Furukawa, Macromol. Symp. 195 (2003) 201.
[21] Z.Z. Gu, T. Iyoda, A. Fujishima, O. Sato, Adv. Mater. 13 (2001) 1295.
[22] M. Toshiko, M. Hiroyuki, X.L. Mo, T. Nobutaka, H. Takashi, Thin Solid films 499 (2006) 114.
[23] T. Kawai, T. Koshido, M. Nakazono, K. Yoshino, Chem. Lett. (1993) 697.
[24] W.Y. Duan, M. Fijiwara, Y. Tanimoto, Jpn. J. Appl. Phys. Part 1 43 (2004) 8213.
[25] T. Kawai, T. Koshido, Y. Kaneuchi, K. Yoshino, Thin Solid Films 273 (1996) 195.
[26] M. Munakata, L.P. Wu, T. Kuroda-Sowa, M. Maekawa, Y. Suenaga, K. Furuichi, J. Am. Chem. Soc. 118 (1996) 3305.
[27] H. Konaka, L.P. Wu, M. Munakata, T. Kuroda-Sowa, M. Maekawa, Y. Suenaga, Inorg. Chem. 42 (2003) 1928.
[28] J. Han, H. Konaka, T. Kuroda-Sowa, M. Maekawa, Y. Suenaga, H. Isihara, M. Munakata, Inorg. Chim. Acta 359 (2006) 99.
[29] F.A. Cotton, T.R. Felthouse, Inorg. Chem. 19 (1980) 323.
[30] P.T. Beurskens, G. Admiraal, G. Beurskens, W.P. Bosman, R. de Gelder, R. Israel, J.M.M. Smits, The DIRDIF-94 Program System, Technical report of the crystallography laboratory, University of Nijmegen, The Netherlands, 1994.
[31] D.T. Cromer, J.T. Waer, International Tables for X-ray Crystallography, vol. IV, The Kynoch Press, Birmingham, England, 1974.
[32] Crystal Structure Analysis Package, Molecular Structure Corporation, 1985 and 1992.
[33] S. Kobatake, M. Yamada, T. Yamada, M. Irie, J. Am. Chem. Soc. 121 (1999) 8450.

pane) [10] contain the corresponding fragments bonded to cyclic $(V_4O_{12})^{4-}$ units. In $[\{Co(phen)_2\}_2(V_6O_{17})]_n$ [11], the $Co(phen)_2$ fragments are covalently bonded to $\{V_6O_{17}\}_n^{n-}$ chains which are composed of alternate $V_4O_{12}^{4-}$ and $V_4O_7^{4-}$ building units.

Specifically, the $CuSO_4$–*phen*–V_2O_5–H_2O system yielded under hydrothermal conditions the compound $[\{Cu(phen)_2\}_4V_{10}O_{29}]\cdot 6H_2O$. The structure of this compound consists of discrete tetradeca-nuclear clusters built up from $V_{10}O_{29}^{8-}$ moieties and four $[Cu(phen)_2]^{2+}$ fragments [11]. The compound $[Cu(phen)(H_2O)(V_2O_6)]$ [12] was isolated after the hydrothermal reaction in the similar $Cu(NO_3)_2$–*phen*–Na_3VO_4 system. The structure of this compound consists of ribbon-like chains composed of $V_4O_{12}^{4-}$ clusters connected by $Cu(phen)(H_2O)$ fragments.

Nearly all these complexes were prepared by hydrothermal methods. In addition to the evident advantages of hydrothermal methods of syntheses of inorganic–organic hybrid compounds (increased solubility of the reactants, enhanced crystallization of metastable phases) they also have some drawbacks. Hydrothermal methods often lead to the formation of mixtures of several compounds that are hard to separate, and study of their properties, with the exception of X-ray diffraction analysis of mechanically separated monocrystals, is then questionable. There is also a limited ability to follow the course of reactions, and the relationship between the conditions of syntheses, composition and structure of the products is not very clear.

This paper is a part of our study dealing with the influence of some reaction conditions on the composition and structure of inorganic–organic hybrid compounds. We have chosen a simple Cu(II)–1,10-phenanthroline–oxovanadate system to avoid possible ambiguities in the ligand–metal bonding. 1,10-Phenanthroline represents a relatively rigid compound, which is usually bound as a bidentate chelate ligand in the *cis*-positions of a coordination polyhedron.

2. Experimental

2.1. Materials, instruments and analytical methods

KVO_3 was prepared according to Ref. [13]. All other chemicals were used as supplied (Lachema, Aldrich). The IR spectra were measured on a Nicolet Magna 750 spectrophotometer as nujol mulls or KBr pellets.

C, H, N were estimated on a CHN analyser (Carlo Erba). Vanadium(V) was determined by titration with $FeSO_4$.

2.2. Syntheses

2.2.1. $[Cu_2(H_2O)_2(OH)_2(phen)_2][Cu_2(OH)_2(phen)_2(V_4O_{12})]\cdot 6H_2O$ (**3**)

Hot solutions of $CuSO_4\cdot 5H_2O$ (1.25 g, 5 mmol in 100 ml H_2O) and 1,10-phenathroline (0.90 g, 5 mmol in 100 ml H_2O) were mixed. The obtained solution was added to a hot solution of KVO_3 (1.38 g, 10 mmol in 600 ml H_2O), the pH of which was adjusted to 12 using KOH (10%). A dark blue solution and brown-yellow precipitate were formed. On standing at room temperature, the precipitate gradually dissolved and the solution decolorized. The pH of the solution after 1 month decreased to 9.6. Blue crystals were isolated after 1 month. *Anal.* Calc. for $C_{48}H_{52}N_8O_{24}Cu_4V_4$ (1582.92): C, 36.4; H, 3.3; N, 7.1; V, 12.9. Found: C, 36.4; H, 2.9; N, 7.4; V, 13.2%.

2.2.2. $[Cu_2(phen)_4(V_4O_{12})]\cdot 4H_2O$ (**4**)

About 20 g KCl was dissolved in water (170 ml) and solid $CuSO_4\cdot 5H_2O$ (0.25 g, 1 mmol) was added. The yellow-green solution obtained was mixed with a hot solution of KVO_3 (1.65 g, 12 mmol in 30 ml H_2O). Finally, solid 1,10-phenanthroline (0.360 g, 2 mmol) was added. After a short reflux (30 min), the solution was left to crystallize at room temperature, the initial pH was 8.1. Blue crystals were isolated after 3 months and the final pH value was 6.9. *Anal.* Calc. for $C_{48}H_{40}N_8O_{16}Cu_2V_4$ (1315.73): C, 43.8; H, 3.1; N, 8.5; V, 15.5. Found: C, 44.2; H, 2.9; N, 8.6; V, 15.1%.

2.2.3. $[Cu_2(phen)_4(V_4O_{12})]\cdot 6H_2O$ (**5**)

Solutions of $CuSO_4\cdot 5H_2O$ (0.125 g, 0.5 mmol in 250 ml H_2O) and KVO_3 (0.138 g, 1 mmol in 250 ml H_2O) were mixed and a hot solution of 1,10-phenanthroline (0.180 g, 1 mmol in 50 ml H_2O) was added. The solution was refluxed (20 h) and the small amount of precipitate formed was filtered off. The filtrate was heated at 80 °C and blue green crystals were isolated after 30 h of heating. The final pH value at 25 °C was 7.1. *Anal.* Calc. for $C_{48}H_{44}N_8O_{18}Cu_2V_4$ (351.77): C, 42.6; H, 3.3; N, 8.3; V, 15.1. Found: C, 42.0; H, 3.0; N, 8.2; V, 14.8%.

2.2.4. $[Cu_2(phen)_4(VO_3)_4]\cdot 10H_2O$ (**6**)

Solution A: $CuSO_4\cdot 5H_2O$ (0.5 g, 2 mmol) was dissolved in water (200 ml). The solution was warmed and 1,10-phenanthroline (0.72 g, 4 mmol) was added and dissolved. The pH was adjusted to 8 using KOH (10%). Solution B: KVO_3 (1.6 g, 11.6 mmol) was dissolved in water (300 ml). Hot solutions A and B were mixed, the pH was adjusted to 11 with KOH (10%) and, after cooling to room temperature, ethanol (200 ml) was added. Large blue crystals were isolated after 3 months. *Anal.* Calc. for $C_{48}H_{52}N_8O_{22}Cu_2V_4$ (1423.837): C, 40.5; H, 3.7; N, 7.9; V, 14.3. Found: C, 40.4; H, 3.2; N, 7.6; V, 13.8%.

2.2.5. $[Cu(phen)_3]_2V_4O_{12}\cdot phen\cdot 22H_2O$ (**7**)

A mixture of $CuSO_4\cdot 5H_2O$ (0.25 g, 1 mmol), KVO_3 (0.276 g, 2 mmol), 1,10-phenanthroline (0.72 g, 4 mmol) and H_2O (400 ml) was refluxed for 10 h. Blue crystals of compound **12** were filtered off from the hot solution. After cooling the solution, grey crystals with a metallic shine crystallized out from the solution (pH 7.4). *Anal.* Calc. for $C_{84}H_{100}N_{14}O_{34}Cu_2V_4$ (2180.62): C, 46.3; H, 4.6; N, 9.0; V, 9.3. Found: C, 46.7; H, 4.1; N, 8.8; V, 8.8%.

*2.2.6. [Cu(phen)(VO$_3$)$_2$] (**9**)*

$CuSO_4 \cdot 5H_2O$ (0.25 g, 1 mmol), KVO_3 (0.276 g, 2 mmol), 1,10-phenanthroline (0.18 g, 1 mmol) and H_2O (70 ml) were refluxed for 25 h. After several minutes of refluxing, green needle-like crystals formed, which were then isolated after 25 h. The final pH (25 °C) was 6.4. For a given ratio $n(phen)/n(Cu) = 1$, the variation of the $n(V)/n(Cu)$ ratio in the interval 2–12 had no effect on the composition of the final product. The crystals were too small for X-ray structure determination. *Anal.* Calc. for $C_{12}H_8N_2O_6CuV_2$ (441.63): C, 32.6; H, 1.8; N, 6.3; V, 23.1. Found: C, 32.7; H, 1.8; N, 6.4; V, 22.8%.

*2.2.7. [Cu$_2$(phen)$_4$(V$_4$O$_{12}$)] · 4H$_2$O (**12**)*

A mixture of $CuSO_4 \cdot 5H_2O$ (0.25 g, 1 mmol), KVO_3 (0.414 g, 3 mmol), 1,10-phenanthroline (0.36 g, 2 mmol) and H_2O (300 ml) was refluxed for 10 h. The blue crystals of **12** were then isolated from the solution (pH 7.2, 25 °C). If the ratio $n(phen)/n(Cu) = 2$ was maintained, a change in the $n(V)/n(Cu)$ ratio in the interval 2–24 had no influence on the composition of the final product. *Anal.* Calc. for $C_{48}H_{40}N_8O_{16}Cu_2V_4$ (1315.73): C, 43.8; H, 3.1; N, 8.5; V, 15.5. Found: C, 44.3; H, 2.8; N, 8.5; V, 15.1%.

2.3. Crystal structure determination

X-ray measurements on the selected crystals of compounds **3**, **5**, **6**, **7** and **12** were performed on a Enraf–Nonius KappaCCD diffractometer equipped with a Oxford Cryostream Cooler using Mo Kα radiation ($\lambda = 0.71073$ Å) and a graphite monochromator. The data sets were corrected for Lorentz and polarization effects. All the data collection, cell refinement, data reduction and correction procedures were carried out using purchased software.

The X-ray measurement of compound **4** was performed on a Kuma KM-4 four-circle κ-axis diffractometer equipped with a Oxford Cryostream Cooler. Mo Kα radiation ($\lambda = 0.71073$ Å), a graphite monochromator and a CCD detector under a nitrogen atmosphere were used. The data set was corrected for Lorentz and polarization effects. All data collection, cell refinement, data reduction and correction procedures were performed using the CRYSALIS CCD and CRYSALIS RED software.

The phase problem was solved by direct methods using SIR-97 [14] (compounds **3**, **5**, **6**, **7** and **12**) and SHELXS-97 [15] (compound **4**) software. SHELXL-97 [16] was used to refine all the structures by full-matrix least-squares on F^2. All atoms other than the hydrogens were refined as independent atoms using anisotropic thermal parameters. Details of refinement are commented in supplemental CIF files.

3. Results and discussion

3.1. Syntheses

The formation of compounds **1**–**12** (Table 2) is a result of the interaction of oxovanadate ions with $[Cu(phen)_x(H_2O)_y]^{2+}$ complexes. There are at least five factors which influence the composition and structure of the reaction products: the $n(phen)/n(Cu)$ molar ratio, pH, concentration, temperature and reaction time.

Although we were not able to clarify fully the effect of these factors, some distinct tendencies were observed. The key factor determining the composition of the products is the $n(phen)/n(Cu)$ ratio (denoted here as R). If we suppose a coordination number of 5 or 6 for Cu(II) in these compounds, then in the case that R is smaller than 3, all the *phen* ligands are evidently coordinated to the central atom, leaving one or two positions (for $R = 2$, compounds **1**, **4**, **5**, **6**, **12**) and three or four positions (for $R = 1$, compounds **2**, **3**, **9** and **10)** vacant in the coordination sphere of the copper atom. These free positions (eventually occupied by weakly bonded molecules of water) are available for bonding of oxovanadate entities. For some R values we changed the $n(V)/n(Cu)$ ratio, but we did not observe any dependence of composition of the solid products on this ratio.

A variety of species may be present in these solutions, the least soluble of which will crystallize out. Obviously, both the relative stability of the solution species and their relative solubilities will decide the composition of the solid products. The ionic form of the vanadate ions is mainly dependent on the pH value. In the pH range 4–12 used in this study, monomeric HVO_4^- and $H_2VO_4^{2-}$ ions are predominant at lower vanadium concentrations and $HV_2O_7^{3-}$, $V_4O_{12}^{4-}$ and $H_xV_{10}O_{28}^{(6-x)-}$ (the latter anions for pH < 6.3) species at higher vanadium concentrations. We obtained most of the products from approximately neutral and slightly alkaline solutions where the $V_4O_{12}^{4-}$ ion prevails. We did not observe formation of any divanadates for pH > 9.5, although the HVO_4^{2-}, $V_2O_7^{4-}$ and $HV_2O_7^{3-}$ ions dominate in this pH range [17]. On the other hand, a relatively high pH can lead to the formation of hydroxo complexes of copper, as was observed in the case of compound **3**. At pH < 6 we obtained the solid product ($[Cu(phen)_2Cl]_3H_3V_{10}O_{28} \cdot 7H_2O$ [18]) only when HCl was used for acidification. From ten Cu–*phen*–V compounds prepared in our laboratory, six contain the $V_4O_{12}^{4-}$ group, three include an endless anionic chain $(VO_3)_n^{n-}$ and one compound is a decavanadate [18]. A preferential formation of compounds containing the $V_4O_{12}^{4-}$ unit is surprising as all metavanadates with simple inorganic cations are constructed from $(VO_3)_n^{n-}$ chains.

So far we have not been able to reveal how the composition of the products depends on reaction time and temperature.

3.2. Infrared spectra

The characteristic bands in the IR spectra enable the polymeric $(VO_3)_n^{n-}$ chain and $V_4O_{12}^{4-}$ group to be unequivocally distinguished (Table 3). In addition to the bands at 958, 939, 910 and 894 cm^{-1}, corresponding to

Table 1
Crystallographic and refinement data

Compound	**3**	**4**	**5**	**6**	**7**	**12**
Chemical formula (summary)	$C_{48}H_{52}N_8O_{24}Cu_4V_4$	$C_{48}H_{40}N_8O_{16}Cu_2V_4$	$C_{48}H_{44}N_8O_{18}Cu_2V_4$	$C_{48}H_{54}N_8O_{23}Cu_2V_4$	$C_{84}H_{100}N_{14}O_{34}Cu_2V_4$	$C_{48}H_{40}N_8O_{16}Cu_2V_4$
CCDC number	287858	288599	288645	186331	186330	186329
Colour/shape	green-blue prism	blue prism	cyan fragment	cyan prism	blue/grey bar	blue bar
Crystal dimensions (mm)	$0.1 \times 0.08 \times 0.03$	$0.3 \times 0.25 \times 0.15$	$0.25 \times 0.15 \times 0.08$	$0.3 \times 0.2 \times 0.025$	$0.83 \times 0.3 \times 0.08$	$0.1 \times 0.1 \times 0.05$
M_r (g mol^{-1})	1582.92	1315.72	1419.66	1441.84	2180.62	1315.73
Crystal system/ space group	triclinic, $P\bar{1}$	triclinic, $P\bar{1}$	triclinic, $P\bar{1}$	triclinic, $P\bar{1}$	triclinic, $P\bar{1}$	monoclinic, $P2_1/n$
Unit cell parameters						
a (Å)	10.9790(4)	9.7168(8)	10.1330(3)	11.0850(5)	12.9040(4)	14.7640(7)
b (Å)	11.5830(6)	10.1107(9)	11.2000(4)	16.0390(6)	17.5760(5)	13.4410(6)
c (Å)	12.4140(6)	12.9463(11)	13.2050(4)	17.4260(6)	23.3640(6)	25.6720(11)
α (°)	109.140(2)	107.978(8)	106.269(2)	94.130(2)	105.9810(15)	90
β (°)	93.870(2)	91.412(7)	92.916(2)	92.916(2)	91.2340(18)	106.279(2)
γ (°)	107.819(2)	94.068(7)	106.538(2)	98.8500(19)	106.9010(15)	90
V (Å^3)	1394.93(11)	1205.29(18)	1365.14(8)	2911.8(2)	4844.3(2)	4890.2(4)
Z	2	2	1	2	2	4
T (K)	293	120	293	293	293	293
D_{calc} (g cm^{-3})	1.875	1.813	1.746	1.624	1.495	1.787
Absorption coefficient (mm^{-1})	2.225	1.694	1.514	1.416	0.889	1.669
Reflections measured	18009	6465	18157	10283	23869	8612
Independent/observed reflections [$I \geqslant 2\sigma(I)$]	6376/4178	4105/3596	6228/4568	10283/7858	15749/11316	8612/5276
Refined parameters/restraints	398/0	352/0	391/0	776/0	1243/0	718/0
Absolute structure parameter, $F(000)$	788	662	718	1444	2160	2616
Goodness of fit on F^2	1.017	1.052	1.036	1.067	1.039	1.080
Final R indices [$I \geqslant 2\sigma(I)$] (%)	$R_F = 4.94$, $R_{wF2} = 11.54$	$R_F = 3.35$, $R_{wF2} = 9.27$	$R_F = 4.52$, $R_{wF2} = 11.40$	$R_F = 5.76$, $R_{wF2} = 14.30$	$R_F = 5.31$, $R_{wF2} = 13.39$	$R_F = 8.64$, $R_{wF2} = 16.68$
Final R indices (all data) (%)	$R_F = 9.21$, $R_{wF2} = 13.69$	$R_F = 3.71$, $R_{wF2} = 9.54$	$R_F = 6.94$, $R_{wF2} = 12.96$	$R_F = 8.34$, $R_{wF2} = 16.50$	$R_F = 8.24$, $R_{wF2} = 15.49$	$R_F = 15.53$, $R_{wF2} = 20.56$

Table 2
Compounds prepared from the Cu–*phen*–vanadate system

Number	Compound	*n*(Cu):*n*(*phen*)[a]	Colour	References
1	$[\{Cu(phen)_2\}_4V_{10}O_{29}]\cdot 6H_2O$	1:2	blue	[11]
2	$[Cu(phen)(H_2O)(V_2O_6)]$	1:1	blue	[12]
3	$[Cu_2(H_2O)_2(OH)_2(phen)_2][Cu_2(OH)_2(phen)_2(V_4O_{12})]\cdot 6H_2O$	1:1	blue	this work
4	$[Cu_2(phen)_4(V_4O_{12})]\cdot 4H_2O$	1:2	blue	this work
5	$[Cu_2(phen)_4(V_4O_{12})]\cdot 6H_2O$	1:2	blue-green	this work
6	$[Cu_2(phen)_4(VO_3)_4]\cdot 10H_2O$	1:2	blue	this work
7	$[Cu(phen)_3]_2V_4O_{12}\cdot phen\cdot 22H_2O$	1:4	grey	this work
8	$[Cu(phen)_2Cl]H_3V_{10}O_{28}\cdot H_2O$	1:2	green	[18]
9	$[Cu(phen)(VO_3)_2]$	1:1	green needles	this work
10	$[Cu_2(phen)_2(V_4O_{12})]\cdot 5H_2O$	1:1	green	[19]
11	$[Cu(phen)_3](VO_3)_2\cdot 20H_2O$	1:2.22	blue	[19]
12	$[Cu_2(phen)_4(V_4O_{12})]\cdot 4H_2O$	1:2	blue	this work

[a] Molar ratio used in synthesis.

Table 3
Characteristic IR bands (cm^{-1}) of the V_4O_{12} groups and the $(VO_3)_n^{n-}$ chains in vanadium(V) compounds

Compound	ν_{as}(V–O–V)	ν_s(V–O–V)	References
$(CH_3)_3(CNH_3)_4V_4O_{12}$	810, 735	660	[21]
$(cyclamH_2)_2V_4O_{12}$	805, 740	675	[22]
3 $[Cu_2(H_2O)_2(OH)_2(phen)_2]$ $[Cu_2(OH)_2(phen)_2(V_4O_{12})]\cdot 6H_2O$	800, 777	641	this work
4 $[Cu_2(phen)_4(V_4O_{12})]\cdot 4H_2O$	809, 794, 757	680, 644	this work
5 $[Cu_2(phen)_4(V_4O_{12})]\cdot 6H_2O$	811, 795, 757	679, 644	this work
7 $[Cu(phen)_3]_2V_4O_{12}\cdot phen\cdot 22H_2O$	821, 803	644	this work
10 $[Cu_2(phen)_2(V_4O_{12})]\cdot 5H_2O$	773	654	[19]
12 $[Cu_2(phen)_4(V_4O_{12})]\cdot 4H_2O$	787, 769	649, 642	this work
6 $[Cu_2(phen)_4(VO_3)_4]\cdot 10H_2O$	643	507	this work
9 $[Cu(phen)(VO_3)_2]$	616	518	this work
11 $[Cu(phen)_3](VO_3)_2\cdot 20H_2O$	662	509	[19]

stretching vibrations of the terminal V=O groups, the infrared spectrum of compound **6** exhibits bands at 643 (vs, broad) and 507 (w) cm^{-1} (Fig. 1) which can be assigned to the υ_{as}(VOV) and υ_s(VOV) vibrations and which are characteristic for the polymeric chain structure $(VO_3)_n^{n-}$ consisting of VO_4 tetrahedra [20]. The strong band at 785 cm^{-1}, which is absent in the IR spectra of vanadates with isolated $(VO_3)_n^{n-}$ chains (KVO_3, NH_4VO_3) [20], was assigned to the stretching vibrations of the V–O–Cu groups. A similar spectral pattern is exhibited by other compounds containing a pyroxene-like chain (**9** – see Fig. 1, **11**).

In addition to the characteristic υ(V=O) bands, the infrared spectrum of compound **12** (Fig. 2) and similarly the spectra of compounds **3**, **4**, **5**, **7** (Fig. 2) and **10** [19] exhibit bands in the 820–730 cm^{-1} interval and at about 650 cm^{-1}, which we assigned to υ_{as}(VOV) and υ_s(VOV), respectively. These bands seem to be characteristic for the presence of the V_4O_{12} group in the structure (Table 3), irrespective of whether this cluster is isolated or coordinated to a central atom. The relatively high wavenumbers of these bands are probably due to the shorter V–O–V bonds and the larger V–O–V angles in the V_4O_{12} fragment [21, this work] in comparison with the bonds and angles in the endless pyroxene-type chain that was found, e.g. in KVO_3 [23].

3.3. Crystal structures

3.3.1. $[Cu_2(H_2O)_2(OH)_2(phen)_2][Cu_2(OH)_2(phen)_2(V_4O_{12})]\cdot 6H_2O$ (3)

The structure of compound **3** consists of binuclear $[Cu_2(H_2O)_2(OH)_2(phen)_2]^{2+}$ cations and $[Cu_2(OH)_2(phen)_2(V_4O_{12})]^{2-}$ units forming the anionic chain. In both structural parts, Cu(II) has the coordination number 5, and the coordination polyhedra are trigonal bipyramidal distorted square based pyramids (TBDSBP) according to τ-factors 0.34 (Cu1) and 0.11 (Cu2). The cations are formed by two $[Cu(H_2O)(phen)]^{2+}$ units connected through two OH^- bridging ligands in a binuclear complex (Fig. 3a). The $[Cu_2(OH)_2(phen)_2(V_4O_{12})]^{2-}$ units form an anionic chain in the direction of the *x* axis (Fig. 3b). They consist of binuclear $[Cu_2(OH)_2(phen)_2]$ fragments, in which OH^- acts again as a bridging ligand. The Cu(II) atoms attain the coordination number 5 via the formation of Cu–O–V bonds, in which the oxygen atom is the terminal atom of the $(V_4O_{12})^{4-}$ ring, formed by four VO_4 tetrahedra joined at the apices. Two binuclear $[Cu_2(OH)_2(phen)_2]$ units are mutually bonded through the tetravanadate ligand $(V_4O_{12})^{4-}$, which forms a μ_2^1-bridge.

Each binuclear unit is bonded through Cu(II) atoms to two different tetravanadate $(V_4O_{12})^{4-}$ bridging ligands,

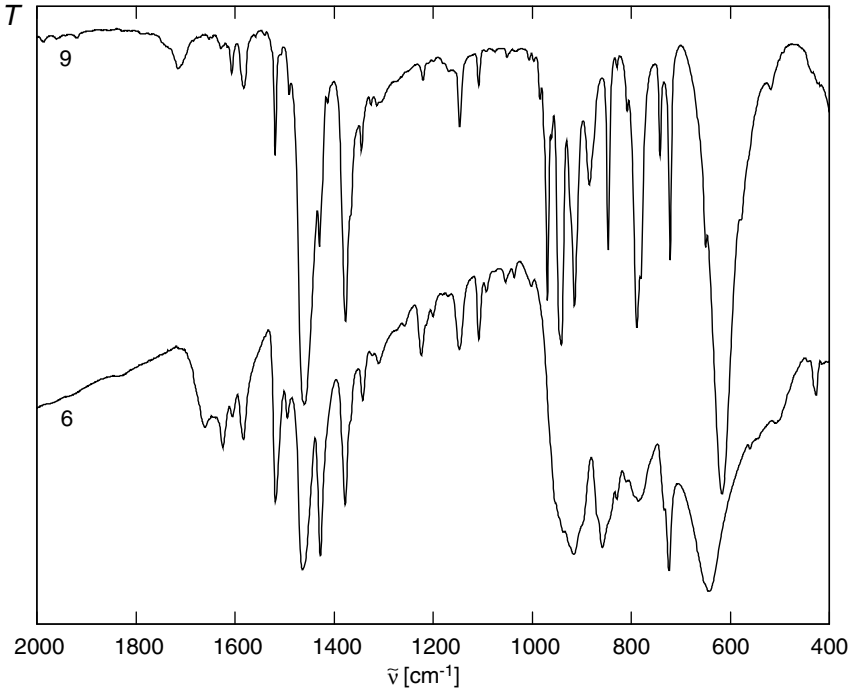

Fig. 1. IR spectra of $[Cu_2(phen)_4(VO_3)_4]\cdot 10H_2O$ (**6**) and $[Cu(phen)(VO_3)_2]$ (**9**).

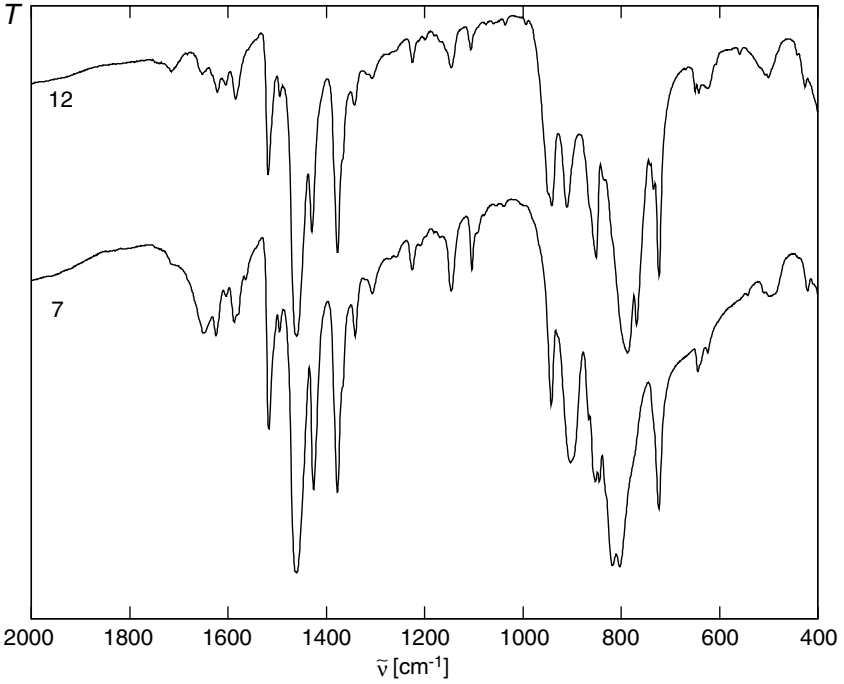

Fig. 2. IR spectra of $[Cu(phen)_3]_2V_4O_{12}\cdot phen\cdot 22\ H_2O$ (**7**) and $[Cu_2(phen)_4(V_4O_{12})]\cdot 4H_2O$ (**12**).

forming an endless anionic chain. Discrete $[Cu_2(H_2O)_2(OH)_2(phen)2]^{2+}$ binuclear complex cations are located between the anionic chains. Molecules of water of crystallization occupy the cavities in the structure (Fig. 3c); radii of these intersectioning voids were calculated by the PLATON suite and lie in the interval 1.45–1.83 Å.

3.3.2. $[Cu_2(phen)_4(V_4O_{12})]\cdot 4H_2O$ (*4*)

The basic structural units in the structure of compound **4** are neutral binuclear $[Cu_2(phen)_4V_4O_{12}]$ complexes. They are formed of two $[Cu(phen)_2]^{2+}$ units bonded through a cyclic μ^1_2-$V_4O_{12}{}^{4-}$ bridge. The CuN_4O coordination polyhedron has the TBDSBP shape with $\tau = 0.35$. An

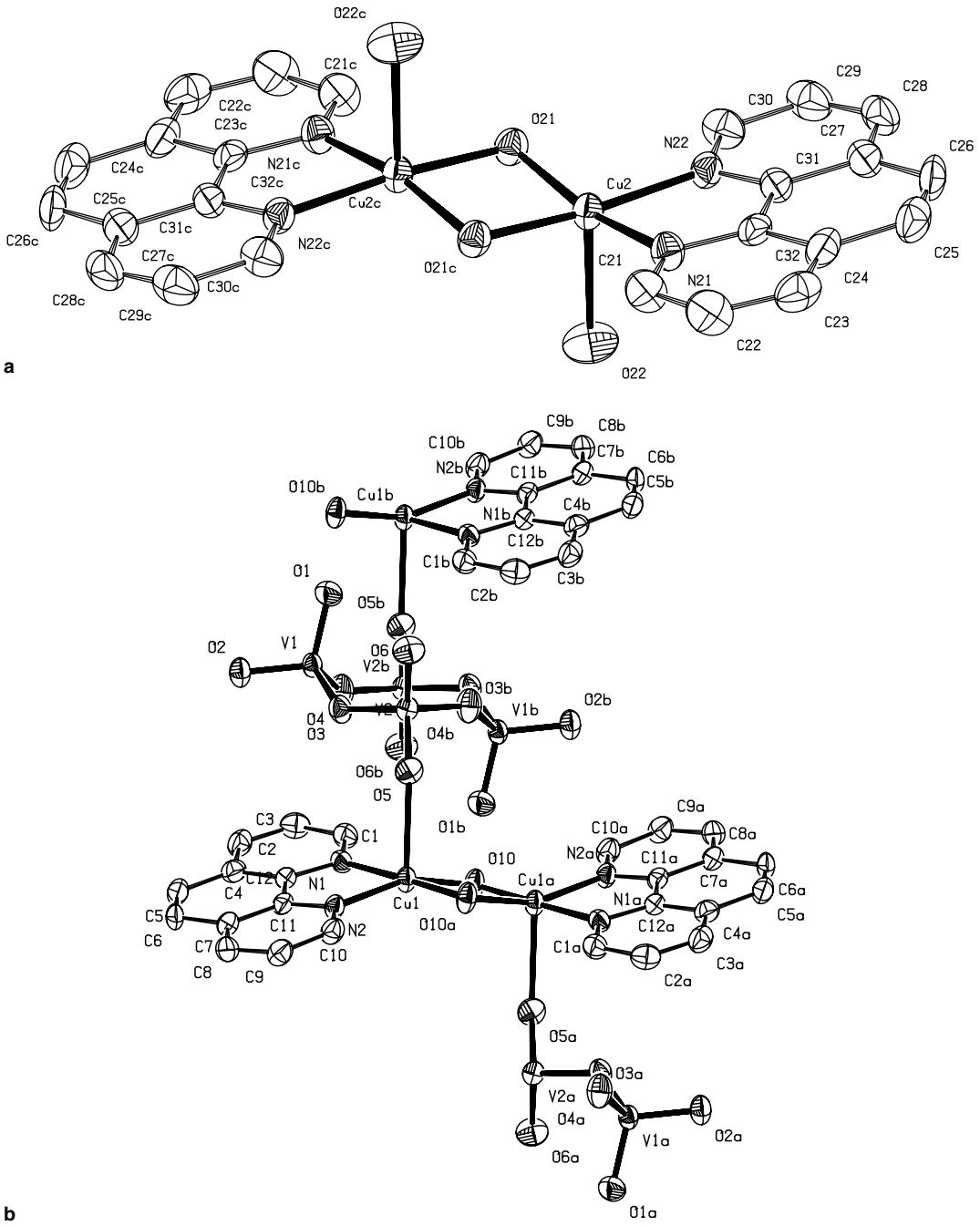

Fig. 3. ORTEP drawings of the cationic dimers (a) and anionic chains (b) of compound **3** with the numbering system and PLUTON packing diagram (c, view in the direction of the *x* axis). (All the H atoms are excluded for clarity, non-H atoms in ORTEP drawings are drawn as 50% probability ellipsoids).

interesting feature of the structure is the formation of chains between the $V_4O_{12}^{4-}$ tetravanadate rings in the direction along the *z* axis through strong hydrogen bonds (donor–acceptor distances between 2.78 and 2.99 Å), with participation of molecules of water of crystallization (Fig. 4).

3.3.3. $[Cu_2(phen)_4(V_4O_{12})]\cdot 6H_2O$ (**5**)

The structural units in the structure of compound **5**, similar to those in compound **4**, are neutral binuclear $[Cu_2(phen)_4V_4O_{12}]$ complexes. However, in compound **5**, the $V_4O_{12}^{4-}$ ligand is a μ_2^2-bridge. This means that every Cu(II) atom is bonded to two terminal atoms of the neighbouring VO_4 tetrahedra of the $V_4O_{12}^{4-}$ ring. Thus, the Cu(II) atoms have a coordination number of 6 and the CuN_4O_2 coordination polyhedron has the shape of a deformed octahedron (Fig. 5). Molecules of water of crystallization are located in the cavities.

3.3.4. $[Cu_2(phen)_4(VO_3)_4]\cdot 10H_2O$ (**6**)

The metavanadate anion $(VO_3)_n^{n-}$ forms a pyroxene type chain along the *x* axis. The structural units of the

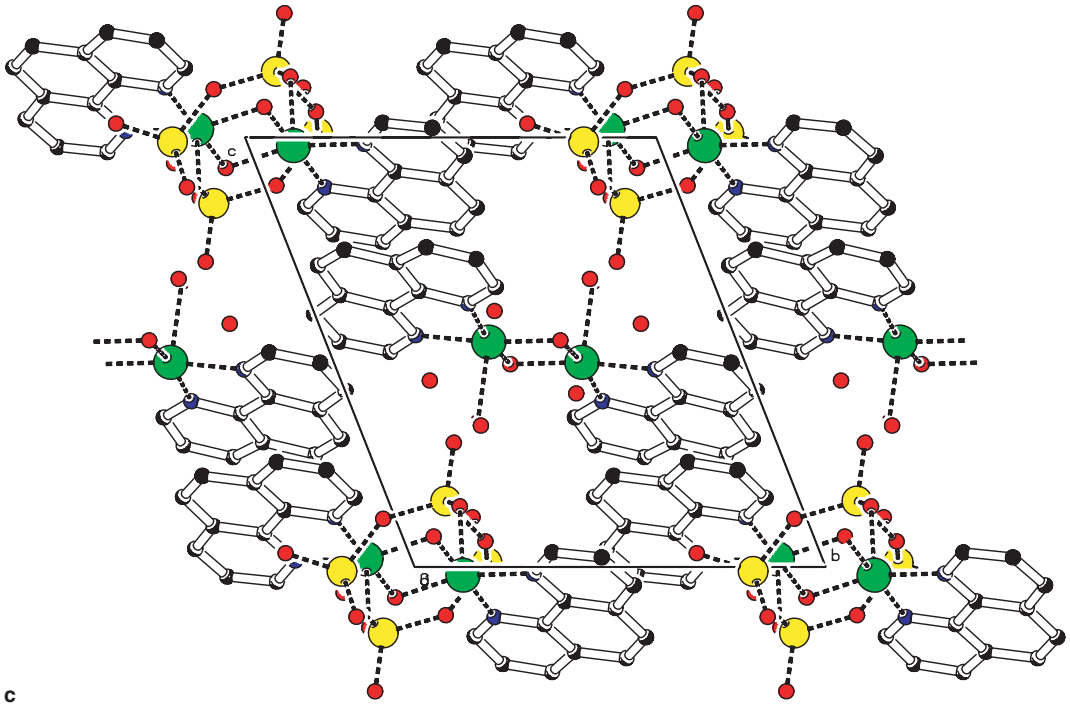

Fig. 3 (*continued*)

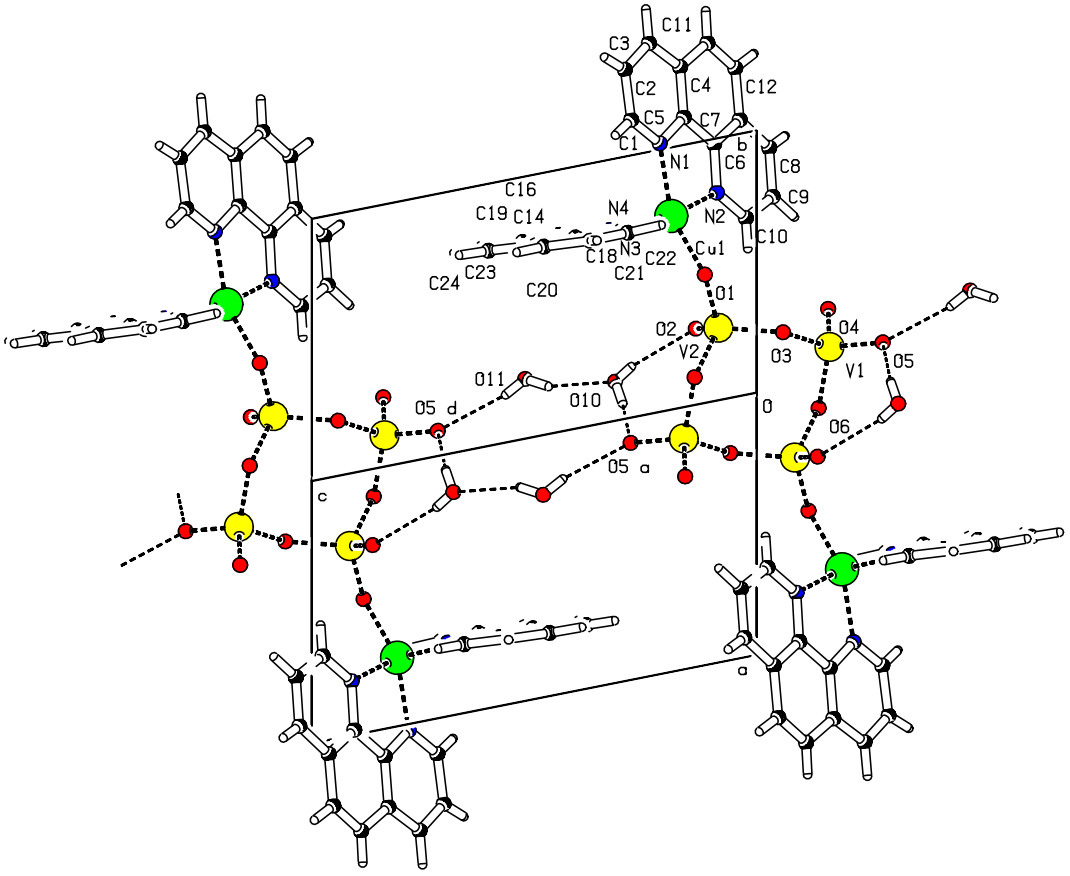

Fig. 4. PLUTON drawing of the unit cell of compound **4** (view perpendicular to the [1 1 0] plane) with the hydrogen bonds network and numbering system.

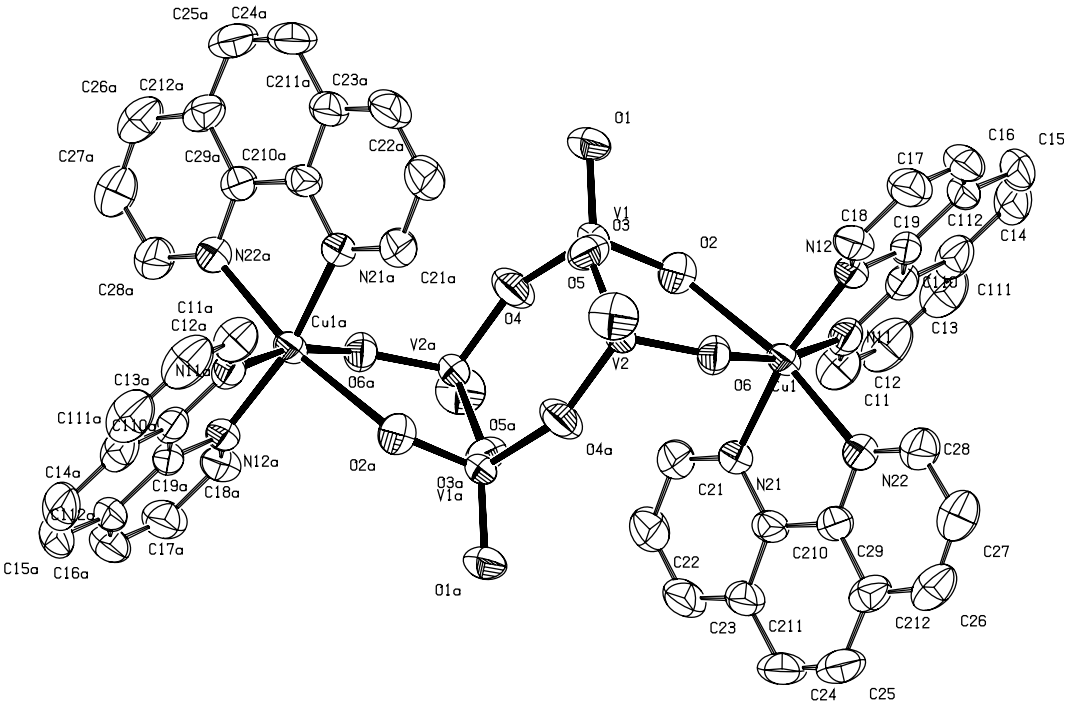

Fig. 5. ORTEP drawing of the $[Cu_2(phen)_4(V_4O_{12})]$ complex in compound **5**, showing the chair conformation of μ_2^2-$V_4O_{12}{}^{4-}$ bridge with the numbering system. (All the H atoms are excluded for clarity, non-H atoms are drawn as 50% probability ellipsoids.)

chain are VO_4 tetrahedra connected through two apices. The charge on the chain is compensated by formation of Cu–O–V bonds with the $[Cu(phen)_2]^{2+}$ units. These units are bonded to the terminal oxygen atoms of two neighbouring VO_4 tetrahedra on both sides of the chain, where two VO_4 tetrahedra, without bonded cations, are located between them (Fig. 6). This bonding mode of the complex units to the anionic $(VO_3)_n{}^{n-}$ chain has not been observed previously. The CuN_4O coordination polyhedron has the TBDSBP arrangement with τ-factors practically identical for both Cu1 and Cu2 atoms ($\tau = 0.38$). The water molecules are located between the chains.

3.3.5. *[Cu(phen)$_3$]$_2$V$_4$O$_{12}$ · phen · 22H$_2$O (7)*

The structure of this substance contains two layers parallel to the [0 0 1] plane: cationic and anionic. The cationic

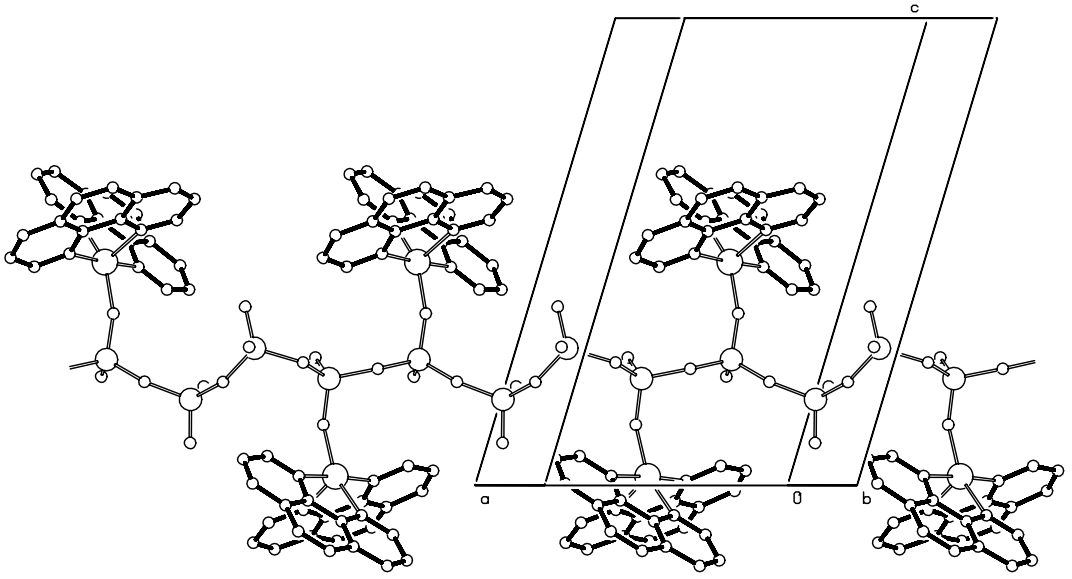

Fig. 6. PLUTON drawing of the pyroxene-like chain $(VO_3)_n{}^{n-}$ in compound **6**, illustrating the binding mode of complex $[Cu(phen)_2]^{2+}$ to the oxygen atoms of the vanadium–oxygen chain (view in the direction of the *y* axis; all the H atoms are excluded for clarity).

layer is formed by $[Cu(phen)_3]^{2+}$ cations and molecules of uncoordinated phenanthroline occupying the cavities in the layer. The anionic layer consists of cyclic $V_4O_{12}^{4-}$ anions, with water molecules located between them in the same layer (Fig. 7). This type of structure was also determined for two other compounds $[M(II)(phen)_3]_2V_4O_{12} \cdot phen \cdot 22H_2O$, where M(II)=Co or Ni [24]. The number of molecules of water of crystallization was determined in all three substances by studying their thermal decomposition [25].

3.3.6. $[Cu_2(phen)_4(V_4O_{12})] \cdot 4H_2O$ (12)

The structure of compound **12** contains neutral $[Cu_2(phen)_4(V_4O_{12})]$ complexes formed by connection of two $[Cu_2(phen)_4]^{2+}$ units through a μ_2^1-$V_4O_{12}^{4-}$ bridge. Cu(II) forms two types of CuN_4O chromophores with TBDSBP geometry and τ-factors 0.24 (Cu1) and 0.39 (Cu2). The cavities in the structure are occupied by water molecules (Fig. 8).

The basic structural motifs of substances **12** and **4** are similar. In substance **12**, the positions of the oxygen atoms in the tetravanadate ligand $V_4O_{12}^{4-}$ are somewhat disordered and they could not be described on the basis of two different positions of the VO_4 tetrahedra. A measurement at a lower temperature led to destruction of the crystal. The main difference between the structures lies in the following fact: while in the structure of **4** the hydrogen bonds between the $V_4O_{12}^{4-}$ rings and water molecules lead to the formation of chains, in substance **12** the hydrogen bonding network is more complicated due to disorder and formation of a 3D framework by water molecules.

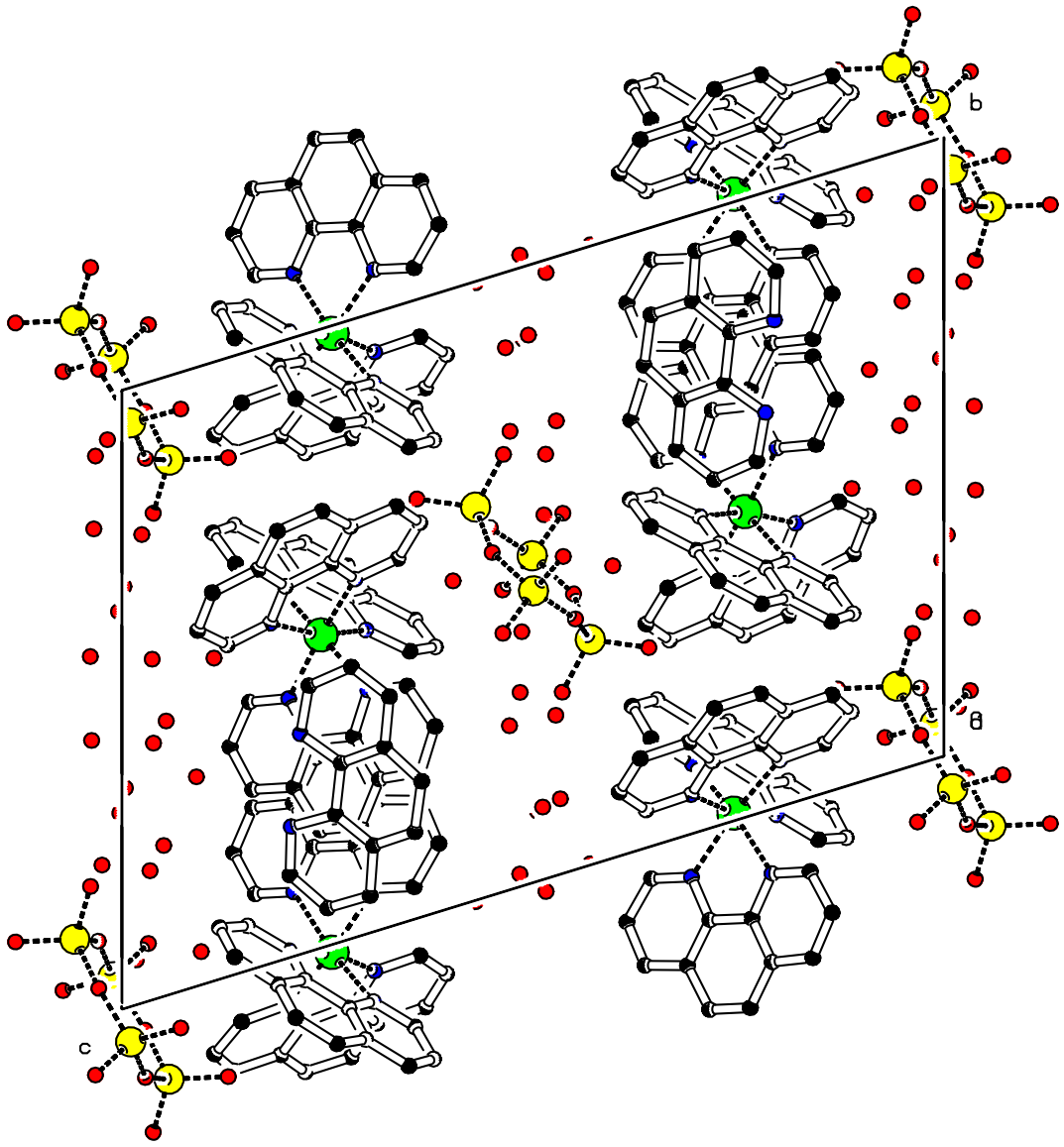

Fig. 7. PLUTON packing diagram for compound **7** showing alternate anionic and cationic layers (view in *x* axis direction; all H atoms are excluded for clarity).

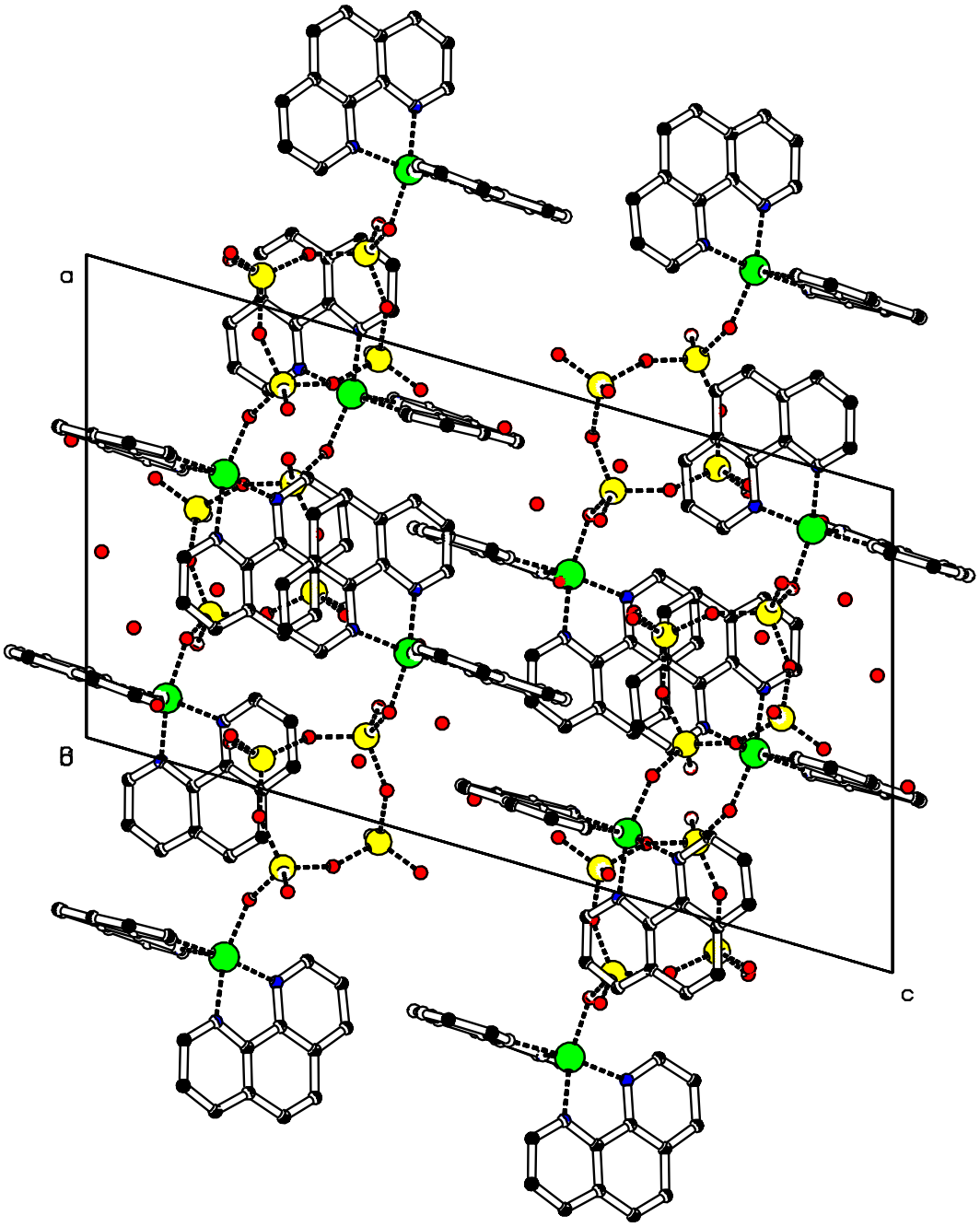

Fig. 8. PLUTON packing diagram for compound **12** (view in the direction of the *x* axis; all the H atoms are excluded for clarity).

All copper(II)–phenanthroline compounds described in this work could be classified as metavanadates, as the ratio n(V):n(O) = 1:3 indicates the presence of the metavanadate anion $(V_nO_{3n})^{n-}$. One of them, the substance **6**, contains the metavanadate anion as a chain of the pyroxene type. An anionic chain of the pyroxene type formed by mutually connected VO_4 tetrahedra is also present in other metavanadates containing Cu(II) complexes with organic ligands, e.g. [Cu(*en*)(V_2O_6)], [Cu(*bpy*)(V_2O_6)] and [Cu(*bpy*)$_2$(V_2O_6)] [8]. In the latter compound, the organocopper fragments form covalent Cu–O–V bonds at the terminal oxygens of every second VO_4 tetrahedron of the chain, while in compound **6**, described here, the $[Cu(phen)_2]^{2+}$ fragments are bonded to two neighbouring VO_4 tetrahedra and the next two do not bind any fragment.

The other compounds characterized in this work contain in their structure a cyclic $V_4O_{12}^{4-}$ anion, forming an 8-membered V_4O_4 ring. In the structure of substance **7**, this anion is present as an isolated structural unit. In the structures of the other prepared compounds, $V_4O_{12}^{4-}$ is a bridging ligand, which bonds two copper fragments. In substance **5**, the μ_2^2-bridge has a chair conformation, so that every Cu(II) atom is also bonded through two terminal oxygen atoms to two neighbouring VO_4 tetrahedra.

The boat conformation of the μ_2^2-$V_4O_{12}^{4-}$ bridge is also known, e.g. in the structure of $[\{Co(phen)_2\}_2(V_4O_{12})]\cdot H_2O$ [26]. In this compound, the tetravanadate anion is bonded to the cobalt atom through two terminal oxygen atoms which do not belong to the neighbouring but opposing VO_4 tetrahedra. The boat conformation of the bridge has not yet been found in phenanthroline–copper vanadates. The $V_4O_{12}^{4-}$ anion is a μ_2^1-bridge in all other compounds (**3**, **4** and **12**). Devi et al. found in the structure of $[Cu(phen)(H_2O)(V_2O_6)]$ [12] another type of bridge, namely the μ_4^1-$V_4O_{12}^{4-}$ anion. Here, the tetravanadate anion is bonded through the terminal oxygen atoms of all tetrahedra on four Cu(II) atoms.

Amongst the formerly prepared inorganic–organic hybrid phenanthroline-copper compounds, there are two which contain a decavanadate anionic unit. The first, $[\{Cu(phen)_2\}_4V_{10}O_{29}]\cdot 6H_2O$, was described by Zhang et al. [11]. The $V_{10}O_{29}^{8-}$ unit is formed of two V_4O_{12} rings connected by a V_2O_7 bridge. The structure of $[Cu(phen)_2Cl]$-$H_3V_{10}O_{28}\cdot 7H_2O$, prepared in our laboratory, contains $H_3V_{10}O_{28}^{3-}$ as an isolated structural unit consisting of 10 VO_6 octahedra [18].

The coordination polyhedra of Cu(II), CuN_4O, in all the compounds prepared (except **5** and **7**), are variously deformed tetragonal pyramids, characteristic for copper(II); in compound **5** this is a deformed CuN_4O_2 octahedron, while in compound **7** it is a CuN_6 octahedron. From a chemical point of view, compound **3** is interesting, as it contains two kinds of bridging ligands, hydroxide and $V_4O_{12}^{4-}$ anions. The hydroxide anions form two kinds of binuclear copper complexes, while the $V_4O_{12}^{4-}$ anions bond only one kind of these binuclear complexes in endless anionic chains.

From the standpoint of the supramolecular architecture, hydrogen bonds play a very important role in structures of the prepared compounds; in some compounds (e.g. in compound **4**), interesting structural motifs, chains of $V_4O_{12}^{4-}$ rings, are formed. Various types of π–π interactions between the phenanthroline rings, which were found in the structures of all these compounds, are also of great importance in the stabilization of the structure.

Acknowledgements

This work was supported by Grant No. 087/2004 based on an Agreement between the Governments of the Slovak Republic and the Czech Republic on Cooperation in Science and Technology and by the Ministry of Education of the Slovak Republic (Grant No. 1/1375/04).

Appendix A. Supplementary data

Supplementary crystallographic data (excluding structure factors) for the structures reported in this paper are available from the Cambridge Crystallographic Data Centre, 12 Union Road, Cambridge, CB2 1EZ, UK (fax: +44 1223 366 033, e-mail: deposit@ccdc.ac.uk or on the web www: http://www.ccdc.cam.ac.uk) on request, quoting the deposition number(s) mentioned in Table 1. Supplementary data associated with this article can be found, in the online version, at doi:10.1016/j.poly.2006.02.020.

References

[1] V. Day, W.G. Klemperer, O.M. Yaghi, J. Am. Chem. Soc. 111 (1989) 5959.
[2] D. Hou, K.S. Hagen, C.L. Hill, J. Am. Chem. Soc. 114 (1992) 5864.
[3] D. Hou, K.S. Hagen, C.L. Hill, J. Chem. Soc., Chem. Commun. (1993) 426.
[4] L.F. Nazar, B.E. Koene, J.F. Britten, Chem. Mater. 8 (1996) 327.
[5] P.J. Hagrman, R.C. Finn, J. Zubieta, Solid State Sci. 3 (2001) 745.
[6] Y. Zhang, P.J. Zapf, L.M. Meyer, R.C. Haushalter, J. Zubieta, Inorg. Chem. 36 (1997) 2159.
[7] S.X. Liu, B.Z. Lin, S. Lin, Inorg. Chim. Acta 304 (2000) 33.
[8] J.R.D. DeBord, Y. Zhang, R.C. Haushalter, C.J. O'Connor, J. Solid State Chem. 122 (1996) 251.
[9] T. S-C. Law, I.D. Williams, Chem. Mater. 12 (2000) 2070.
[10] T. S-C. Law, H.H.Y. Sung, I.D. Williams, Inorg. Chem. Commun. 3 (2000) 420.
[11] X.M. Zhang, M.L. Tong, X.M. Chen, Chem. Commun. (2000) 1817.
[12] R.N. Devi, J. Zubieta, Inorg. Chim. Acta 343 (2003) 313.
[13] M. Sivák, D. Joniaková, P. Schwendt, Transition Met. Chem. 18 (1993) 304.
[14] A. Altomare, M.C. Burla, M. Camalli, G. Cascarano, C. Giacovazzo, A. Guagliardi, A G.G. Moliterni, G. Polidori, R. Spagna, J. Appl. Cryst. 32 (1998) 115.
[15] G.M. Sheldrick, SHELXS-97. Program for Crystal Structure Determination, University of Göttingen, Germany, 1997.
[16] G.M. Sheldrick, SHELXL-97. Program for crystal structure refinement, University of Göttingen, Germany, 1997.
[17] L. Pettersson, B. Hedmann, I. Andersson, N. Ingri, Chem. Scripta 22 (1983) 254.
[18] E. Rakovský, D. Joniaková, R. Gyepes, P. Schwendt, Z. Mička, Cryst. Res. Technol. 40 (2005) 719.
[19] P. Schwendt, D. Joniaková, R. Gyepes, Z. Mička, Solid State Phenom. 90–91 (2003) 423.
[20] S. Onodera, Y. Ikegami, Inorg. Chem. 19 (1980) 615.
[21] P. Roman, A.S. Jose, A. Luque, J.M. Gutiérrez-Zorilla, Inorg. Chem. 32 (1993) 775.
[22] V. Suchá, M. Sivák, Monatsh. Chem. 127 (1996) 1.
[23] M. Petrášová, J. Mad'ar, F. Hanic, Chem. Zvesti 12 (1958) 410.
[24] L'. Žúrková, R. Kucsera, R. Gyepes, M. Sivák, Monatsh. Chem. 134 (2003) 1071.
[25] R. Kucsera, D. Joniaková, L'. Žúrková, J. Therm. Anal. Calorim. 78 (2004) 263.
[26] Y. Lu, E. Wang, M. Yuan, Y. Li, Ch. Hu, N. Hu, H. Iia, J. Mol. Struct. 607 (2002) 189.

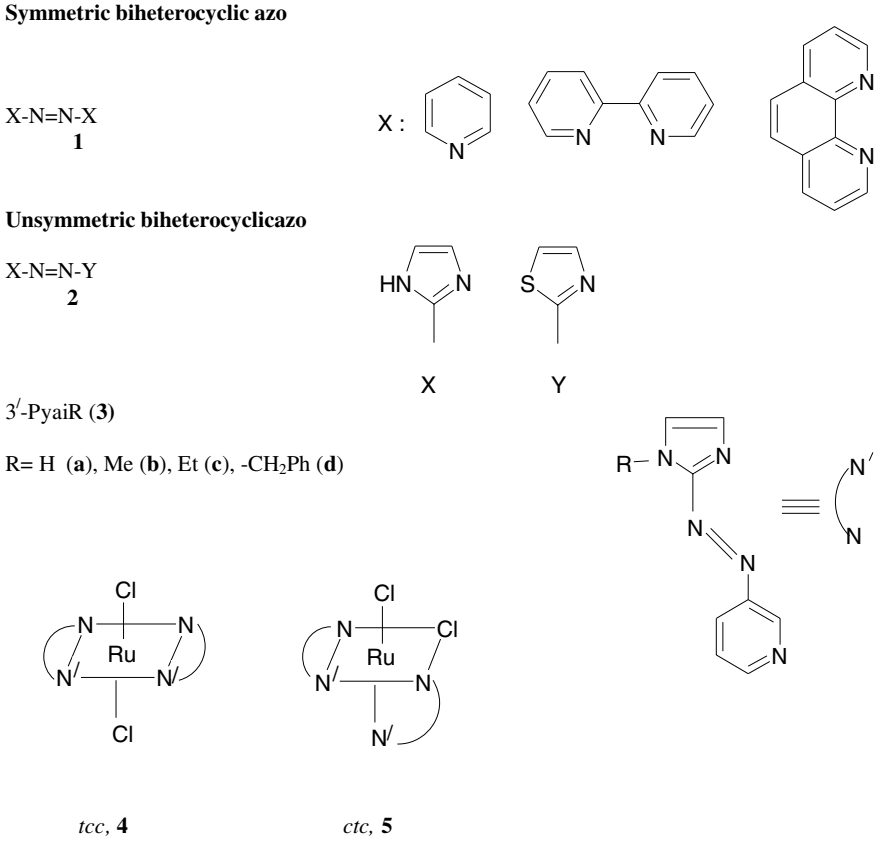

Scheme 1.

ruthenium trichloride and ruthenium phosphine carbonyl compounds, $Ru(CO)_3(PPh_3)_2$. The structure in one case has been confirmed by X-ray diffraction study.

2. Result and discussion

2.1. Ruthenium(II) coordination complexes and their isomer characterisation

2-(3′-Pyridylazo)imidazole (3′-PyaiH, **3a**) and 1-alkyl-2-(3′-pyridylazo)imidazoles (3′-PyaiR: R = Me (**3b**), Et (**3c**), CH_2Ph (**3d**)) have been used in the synthesis of coordination complexes of ruthenium(II). An ethanolic solution of 3′-PyaiR reacts with $RuCl_3$ under dinitrogen and affords the complexes, $Ru(3'\text{-PyaiR})_2Cl_2$ (**4**,**5**) via spontaneous reductive chelation (Eq. (1)). Dark colored crystalline compounds are collected from the cold solution. Two isomers, green and blue-violet have been separated from the mixture by chromatographic separation. The pseudo-octahedral complexes of the formula, $Ru(N,N')_2Cl_2$ with unsymmetric chelating ligands may exist in five geometrically isomeric forms [14]. The isomers are assigned in terms of sequences of coordination of pairs of Cl; N(imidazole) and N(azo): two isomers *trans–trans–trans* and *trans–cis–cis* belong to *trans*-$RuCl_2$ and three isomers *cis–trans–cis*, *cis–cis–trans* and *cis–cis–cis* belong to *cis*-$RuCl_2$ configurations. In this case the green (**4**) and blue-violet (**5**) complexes are assigned to *trans–cis–cis* (tcc) and *cis–trans–cis* (ctc) $Ru(3'\text{-PyaiR})_2Cl_2$. The complexes are diamagnetic (t_{2g}^6) and non-conducting. The microanalytical data support their composition. The spectroscopic data determine the structure of these complexes. The reaction between 3′-PyaiH and $RuCl_3$ in refluxing ethanol under a N_2 environment has separated dark coloured insoluble compounds. Because of the insolubility of the complexes we would not proceed further to identify the compounds.

$$RuCl_3 + 2\,3'\text{-PyaiR} \xrightarrow{\text{EtOH/boil}} Ru(3'\text{-PyaiR})_2Cl_2 + Cl^- \qquad (1)$$

Infrared spectra of the free ligands and complexes were compared to assign the major frequencies. The complexes exhibit stretching frequencies ν(N=N) and ν(C=N) at 1370–1380 and 1550–1580 cm^{-1}, respectively, and ν(N=N) has been shifted to shorter wavelength by 10–15 cm^{-1} compared to the free ligand value. The green isomers (**4**) display a single ν(Ru–Cl) stretch at 320–325 cm^{-1}; blue-violet isomers (**5**) exhibit two stretches at 310–315 and 320–325 cm^{-1}. These values support the *trans*-$RuCl_2$ and *cis*-$RuCl_2$ configuration of **4** and **5**, respectively. We have not been attempted to assign all other stretches; however they are shifted to higher frequency compared to free ligand spectra.

The electronic spectral data were collected in MeCN (Table 1, Fig. 1). The transitions <400 nm are of the intra-ligand charge transfer type and are not considered

Table 1
UV–Vis spectral[a] and cyclic voltammetric[b] data of the ruthenium complexes

Compounds	λ_{max}, nm ($10^{-3}\varepsilon$, $M^{-1}\,cm^{-1}$)	Metal oxidation Ru(III)/Ru(II)	Ligand reduction
tcc-Ru(3′-PyaiMe)$_2$Cl$_2$ (**4b**)	644 (1.82), 364 (10.61)	0.724 (90)	−0.651 (100), −0.851 (120), −1.28[d]
tcc-Ru(3′-PyaiEt)$_2$Cl$_2$ (**4c**)	662 (6.29), 392 (8.47), 344 (11.36)	0.812 (100)	−0.635 (120), −0.825 (120), −1.26[d]
tcc-Ru(3′-PyaiBz)$_2$Cl$_2$ (**4d**)	660 (6.18), 390 (10.44), 330 (12.30)	0.75 (100)	−0.642 (100), −0.835 (100), −1.25[d]
ctc-Ru(3′-PyaiMe)$_2$Cl$_2$ (**5b**)	556 (3.34), 366 (10.01)	0.845 (120)	−0.622 (100), −0.818 (120), −1.27[d]
ctc-Ru(3′-PyaiEt)$_2$Cl$_2$ (**5c**)	554 (7.70), 376 (26.04), 358 (22.75)	0.768 (100)	−0.618 (110), −0.800 (120), −1.25[d]
ctc-Ru(3′-PyaiBz)$_2$Cl$_2$ (**5d**)	552 (2.85), 366 (9.04)	0.865 (120)	−0.600 (100), −0.805 (100), −1.24[d]
Ru(3′-PyaiH)(CO)(PPh$_3$)$_2$ (**6a**)	472 (8.25), 376 (6.06), 340 (5.47)	1.20[c]	−0.75 (120), −0.91 (140)
Ru(3′-PyaiMe)(CO)(PPh$_3$)$_2$ (**6b**)	478 (7.14), 374 (18.15), 362 (17.52)	1.28[c]	−0.729 (110), −0.85 (100)
Ru(3′-PyaiEt)(CO)(PPh$_3$)$_2$ (**6c**)	472 (3.44), 384 (8.58)	1.32[c]	−0.72 (120), −0.80 (100)
Ru(3′-PyaiBz)(CO)(PPh$_3$)$_2$ (**6d**)	472 (4.24), 374 (18.35), 360 (17.58)	1.15[c]	−0.74 (140), −1.10 (140)
[Ru(3′-PyaiH)(CO)(Cl)(PPh$_3$)$_2$](ClO$_4$) (**7a**)	506 (10.25), 388 (9.76)	0.785 (130)	−0.610 (120), −0.821 (140)
[Ru(3′-PyaiMe)(CO)(Cl)(PPh$_3$)$_2$](ClO$_4$) (**7b**)	516 (11.99), 398 (11.36), 280 (19.70)	0.778 (120)	−0.628 (130), −0.798 (140)
[Ru(3′-PyaiEt)(CO)(Cl)(PPh$_3$)$_2$](ClO$_4$) (**7c**)	504 (8.53), 384 (7.35)	0.770 (130)	−0.620 (130), −0.804 (160)
[Ru(3′-PyaiBz)(CO)(Cl)(PPh$_3$)$_2$](ClO$_4$) (**7d**)	506 (9.25), 386 (8.16)	0.788 (120)	−0.610 (120), −0.815 (140)

[a] Solvent: CH_3CN.
[b] Solvent: MeCN, platinum disk milli electrode, SCE reference, [Bu_4N][ClO_4] supporting electrolyte, scan rate 50 mV s^{-1}. Potentials are expressed in V, $E_{1/2}$, $\Delta E_p = |E_{pa} - E_{pc}|$, mV.
[c] E_{pa} (anodic peak potential).
[d] E_{pc} (cathodic peak potential).

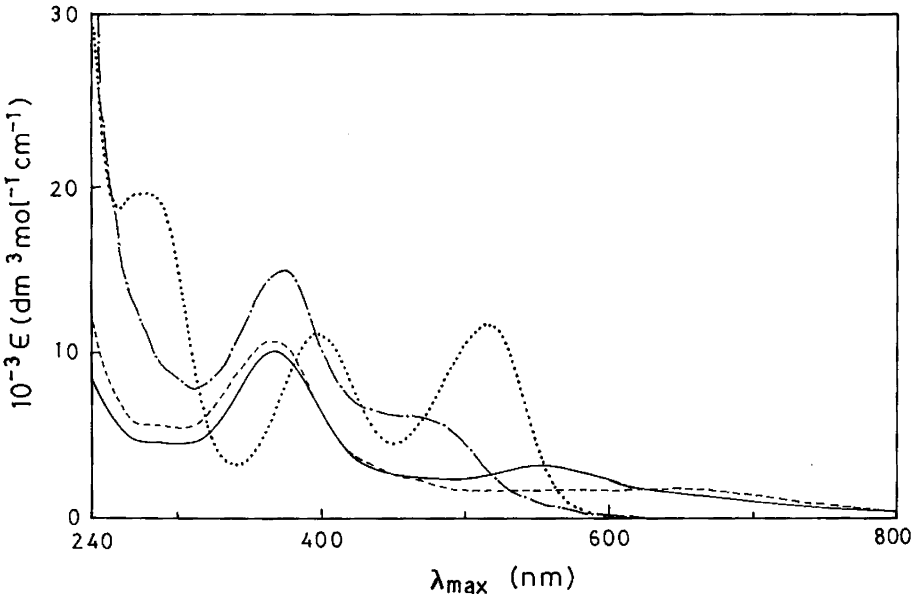

Fig. 1. UV–Vis spectra of ctc-Ru(3′-PyaiMe)$_2$Cl$_2$ (**5b**) (—); tcc-Ru(3′-PyaiMe)$_2$Cl$_2$ (**4b**) (---); Ru(3′-PyaiMe)(CO)(PPh$_3$)$_2$ (**6b**) (—·—·—); [Ru(3′-PyaiMe)(CO)(Cl)(PPh$_3$)$_2$](ClO$_4$) (**7b**) (···).

further. *tcc*-Ru(3′-PyaiR)$_2$Cl$_2$ (**4**) show high intense transitions ($\varepsilon \sim 10^4$ dm^3 mol^{-1} cm^{-1}) in the region 640–660 nm while the blue-violet isomers, ctc-Ru(3′-PyaiR)$_2$Cl$_2$ (**5**) give transitions at higher energies 550–560 nm (Fig. 2). These are assigned to the MLCT transitions.

The stereochemistry of the complexes is supported by ^{1}H NMR spectral data (Table 2) collected in $CDCl_3$. The signals were assigned on the basis of the spin–spin interaction and on comparing with free ligand values. The N(1)–R signals are as follows. The N–Me signal appears at 4.2 and 4.1 ppm in the green (**4a**) and blue-violet (**5a**) complexes, respectively. The methylene, –N–CH_2–(CH_3) appears as a quartet at 4.4 ppm (^2J, 10.0 Hz) and the methyl, (–N–CH_2)–CH_3 shows a triplet signal at 1.6 ppm ($^2J = 8.0$ Hz) for the green complexes (**4b**). The methylene of –N–CH_2–(Ph) of green **4c** appears as a singlet at 5.5 ppm. The difference in the stereochemical description of the two chelating azoimine groups in the blue-violet isomer, **5**, has been ascribed from the inequivalent AB type splitting of –CH_2– in –N–CH_2–(CH_3) (**5b**) and –N–CH_2–(Ph) (**5c**). There are, however, neither neighbouring chiral centers nor any appreciable bond rotational barrier but a distorted coordination around the metal centre does exist. This overall distortion may lead to molecular dissymmetry [14,20].

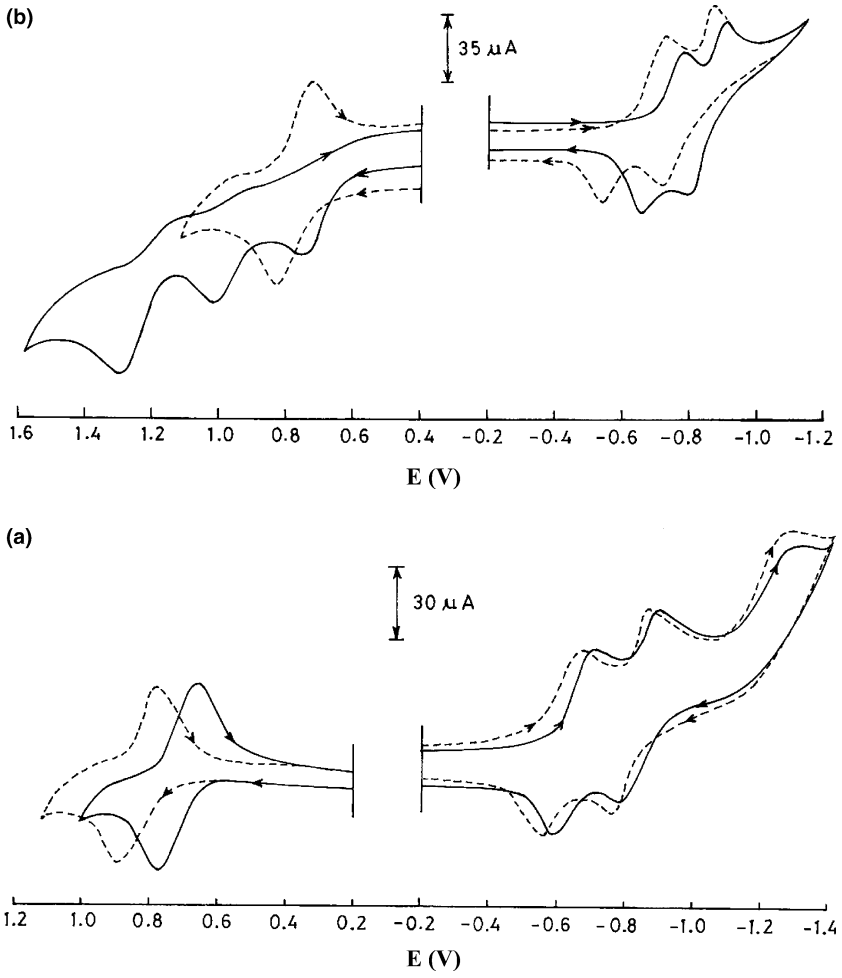

Fig. 2. Cyclic voltammogram of (a) **4b** (—), **5b** (---); (b) **6b** (—), **7b** (---).

Table 2
^{1}H NMR data[a] recorded of ruthenium complexes (**4**–**7**) at 298 K

Compounds	δ, ppm (J, Hz)							
	4-H[b]	5-H[b]	7-H[c]	9-H[b]	10-H[d]	11-H[b]	N(1)–R	PPh_3-protons[e]
(**4b**)	7.20 (7.0)	7.07 (7.0)	8.65	7.84 (9.0)	7.50 (9.0)	8.33 (9.0)	4.10[f]	
(**4c**)	7.21 (7.0)	7.06 (7.0)	8.61	7.82 (8.5)	7.51 (9.0)	8.35 (8.5)	4.44 (12.0),[g] 1.58 (8.0)[d]	
(**4d**)	7.18 (7.0)	7.00 (7.0)	8.60	7.78 (9.0)	7.46 (9.0)	8.35 (9.0)	5.35[h]	
(**5b**)	7.22 (7.0)	7.05 (7.0)	8.62	7.80 (9.0)	7.45 (9.0)	8.32 (9.0)	4.14[f]	
(**5c**)	7.25 (7.0)	7.10 (7.0)	8.68	7.85 (8.5)	7.53 (9.0)	8.41 (8.5)	4.35 (12.0),[g] 1.48 (8.0)[d]	
(**5d**)	7.22 (7.0)	7.06 (7.0)	8.65	7.82 (9.0)	7.48 (9.0)	8.39 (9.0)	5.54, 5.27 (22.0)[g]	
(**6a**)	7.15 (6.0)	7.02 (6.0)	8.51	7.62 (9.0)	7.42 (9.0)	8.36 (6.0)	5.97[i]	7.30–7.50
(**6b**)	7.16 (6.0)	7.05 (6.0)	8.55	7.65 (9.0)	7.46 (9.0)	8.35 (6.0)	4.22[f]	7.30–7.45
(**6c**)	7.18 (6.0)	7.08 (6.0)	8.57	7.66 (9.0)	7.47 (9.0)	8.34 (6.0)	4.50 (12.0),[g] 1.48 (8.0)[d]	7.30–7.45
(**6d**)	7.29 (7.0)	7.09 (7.0)	8.56	7.69 (9.0)	7.49 (9.0)	8.33 (6.0)	6.00[h]	7.25–7.50
(**7a**)	7.22 (7.0)	7.08 (7.0)	8.55	7.70 (9.0)	7.50 (9.0)	8.41 (7.0)	5.80[i]	7.30–7.50
(**7b**)	7.18 (7.0)	7.05 (7.0)	8.58	7.72 (9.0)	7.48 (9.0)	8.42 (7.0)	4.20[f]	7.30–7.45
(**7c**)	7.16 (7.0)	7.05 (7.0)	8.56	7.70 (9.0)	7.47 (9.0)	8.43 (7.0)	4.45 (12.0),[g] 1.60 (8.0)[d]	7.30–7.45
(**7d**)	7.22 (7.0)	7.07 (7.0)	8.61	7.75 (9.0)	7.54 (9.0)	8.45 (7.0)	5.85[h]	7.25–7.50

[a] In $CDCl_3$.
[b] Doublet.
[c] Singlet.
[d] Triplet.
[e] Multiplet.
[f] 1-CH_3.
[g] Quartet for –CH_2–.
[h] 1-CH_2(Ph), and δ(Ph): 7.4–7.5 ppm.
[i] N(1)–H, broad.

Imidazole 4-H and 5-H appear as doublet signals at 7.1–7.2 and 7.0–7.1 ppm, respectively. A singlet signal appearing at the most downfield position, 8.6 ppm, is unambiguously assigned to 7-H. The second highest chemical shift is observed at 8.3 ppm which is a doublet signal ($^2J = 9.0$ Hz) and is assigned to 11-H. Two other protons 9-H and 10-H appear as a doublet and triplet at ca. 7.8 and 7.5 ppm, respectively.

Redox activities of the complexes have been examined by cyclic voltammetry. Fig. 2 shows four redox responses in the potential range 1.2 to −1.4 V versus SCE (Table 1) in MeCN. A couple positive to SCE at 0.7–0.8 V is oxidative in nature. This is quasireversible in nature as evident from ΔE_p values (>90 mV). This is referred to the Ru(III)/Ru(II) couple. Three reduction responses appear negative to SCE and are quasireversible in nature. The chelated azoimine (–N=N–C=N–) groups are well known π-acidic agents which have low lying azo-centered π^*-molecular orbitals. Thus, the reductions are referred to electron accommodation at LUMOs characterized by the azo function.

The potential data (Table 1) related to the blue-violet isomers (**5**) exhibit higher redox potentials by 0.1–0.2 V than those of the green isomers (**4**). An increase in stability of the Ru(II) state in the blue-violet isomer (**5**) may be due to a cisoid orientation of the azoimine function. In *ctc*-$Ru(3'\text{-PyaiR})_2Cl_2$ (**5**) the back bonding interaction may in turn occur with two different dπ-orbitals, while in the *trans*-orientation two groups will compete for the same dπ-orbitals. This may be associated with the increase in effective charge on the ruthenium in **5** and may shift the Ru(III)/Ru(II) couple to more positive values than in **4**. The present set of Ru(III)/Ru(II) redox potential data are higher than $Ru(RaaiR')_2Cl_2$ (RaaiR′ = 1-alkyl-2-(arylazo)imidazole) [14] but lower than $Ru(aapm)_2Cl_2$ (aapm = 2-(arylazo)pyrimidine) [19]. This suggests that the π-acidity order of the ligands is as follows: arylazoimidazole < pyridylazoimidazole < arylazopyrimidine.

2.2. Ruthenium carbonyl complexes of 3′-PyaiR

2.2.1. Synthesis and formulation

$Ru(CO)_3(PPh_3)_2$ has been used as a starting material in the synthesis of mixed ligand Ru(0)-carbonyl compounds. In extremely moisture free conditions under a dinitrogen atmosphere, $Ru(CO)_3(PPh_3)_2$ has been reacted with 3′-PyaiR in MeCN under reflux for 2–2.5 h.

$$Ru(CO)_3(PPh_3)_2 + 3'\text{-PyaiR} \rightarrow \underset{\mathbf{6}}{Ru(CO)_3(3'\text{-PyaiR})(PPh_3)_2} + 2CO \quad (2)$$

3′-PyaiR is an efficient π-acidic chelating agent and acts as an effective CO supplement in the stabilization of low metal oxidation states. The product isolated after filtration has been purified by a chromatography process. The complexes are extremely stable and remain unchanged upon exposure to air even in solution for a month. The composition of the complexes, $Ru(CO)(3'\text{-PyaiR})(PPh_3)_2$ (**6**) has been supported by microanalytical data. The complexes are non-electrolytes and are diamagnetic.

2.2.2. X-ray structure determination

The X-ray structure of $Ru(CO)(3'\text{-PyaiH})(PPh_3)_2$ (**6a**) has been determined and is shown in Fig. 3. Selected bond parameters are listed in Table 3. The molecule consists of a central Ru atom surrounded by five coordination centers and the arrangement is quite a regular square pyramid. The atomic arrangement involves two *trans*-phosphines, cheated pyridylazo-imidazole and a CO within the RuP_2N_2C coordination sphere. The atomic group Ru, N(1), C(1), N(4), N(3) constitute a chelate plane (rms deviation ⩽0.031 Å). The 3′-pyridyl ring is inclined at an angle of 37.38(15)° with the chelate ring. The *trans*-phosphine angle, P(1)–Ru–P(2) is 167.62 (2)° and lies in the lower

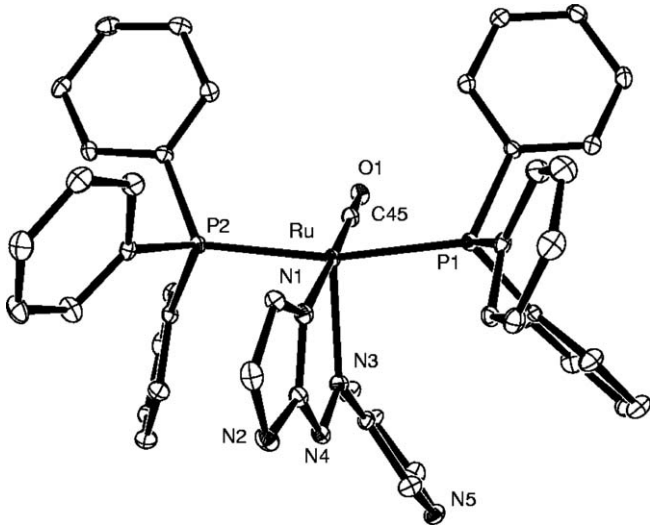

Fig. 3. X-ray structure of $Ru(3'\text{-PyaiH})(CO)(PPh_3)_2$ (**6a**).

Table 3
Selected bond distances (Å) and angles (°) for $[Ru(CO)(3'\text{-PyaiH})(PPh_3)_2]$ (**6a**) along with their esd in parentheses

Distances (Å)		Angles (°)	
Ru–C(45)	1.8545(13)	N(1)–Ru–N(3)	73.79(8)
Ru–N(1)	2.111(2)	N(1)–Ru–C(45)	176.04(7)
Ru–N(3)	2.1938(19)	N(3)–Ru–C(45)	103.79(7)
Ru–P(1)	2.3605(7)	N(1)–Ru–N(3)	73.79(8)
Ru–P(2)	2.3478(7)	Ru–N(1)–C(1)	112.97(16)
N(3)–N(4)	1.284(3)	Ru–N(3)–N(4)	117.93(15)
N(1)–C(1)	1.347(3)	P(1)–Ru–P(2)	167.62(2)
		P(1)–Ru–C(45)	88.54(4)
		P(2)–Ru–C(45)	89.10(4)
		P(1)–Ru–N(1)	94.79(6)
		P(1)–Ru–N(3)	95.40(5)
		P(2)–Ru–N(1)	88.10(6)
		P(2)–Ru–N(3)	96.96(5)

range of reported data [27–34]. This large deviation from *trans*-angle values may be due to steric crowding. The chelate bite angle N(1)–Ru–N(3) is 73.79(8)°. Other angles around Ru define a distorted quite regular pyramidal geometry.

The Ru–N(3) (N(3) is the azo–N) bond length of 2.194(2) Å is slightly longer than Ru–N(1) (N(1) is imidazole) (2.112(3) Å). This is unusual to the structural chemistry of Ru–azoheterocycles [14–18]. The N=N distance is 1.284(3) Å and is longer than the free ligand value (1.268(2) Å) [32]. It is elongated due to $d\pi(Ru) \rightarrow \pi^*(azo)$ charge transfer. The observed Ru–P distances are very short (2.3478(7), 2.3605(7) Å) in the series of $Ru(PPh_3)$ chemistry [30–33]. Ru(0) may be associated with PPh_3 by strong π-back bonding which causes shortening of the Ru–P distances. Ru(0) is a better donor than Ru(II) and this may support the shortening of the Ru–P distances.

The Ru–C bond length (1.8545(13) Å) is comparable with the data reported for the Ru(II)-carbonyl system [27,33,34]. This shows that the Ru(0) oxidation state has little influence on the Ru–CO distance. The C–O bond length is 1.141(4) Å and is also insignificantly influenced by the zero oxidation state of ruthenium. The EHMO results also support this data (Fig. 4).

2.2.3. Spectra and bonding

The complexes $[Ru(CO)(3'\text{-PyaiR})(PPh_3)_2]$ (**6**) show a sharp stretch at ca. 1925 cm^{-1} that corresponds to ν(CO). Presence of a single ν(CO) band is in support of a 'Ru(CO)' type carbonyl derivative [33,34]. Other significant stretchings are ν(N=N) and ν(C=N) at 1410–1415 and 1580–1600 cm^{-1}, respectively. Comparisons of the infrared data for monocarbonyl ruthenium/osmium complexes of other heterocyclic–N chelators [27,33,34] also helped us to identify the present series of complexes.

The complexes are sparingly soluble in non-polar solvents but reasonably soluble in polar solvents. The electronic spectra of the complexes in MeCN show a high intense transition at 360–380 nm (inter-ligand charge transfer) with a reasonably intense shoulder at 460–470 nm (Table 1, Fig. 1). The absorption at 460–470 nm may be assigned to a transition involving metal orbitals, e.g., d–d, MLCT/LMCT type. Upon excitation at 365 nm the complexes give an observable emission at the longer wavelength of 418–426 nm in MeCN, which originates from the (π–π^*) type.

To explain the electronic properties of the complexes, extended Huckel calculation were performed using crystallographic parameters of $[Ru(CO)(3'\text{-PyaiH})(PPh_3)_2]$. Some

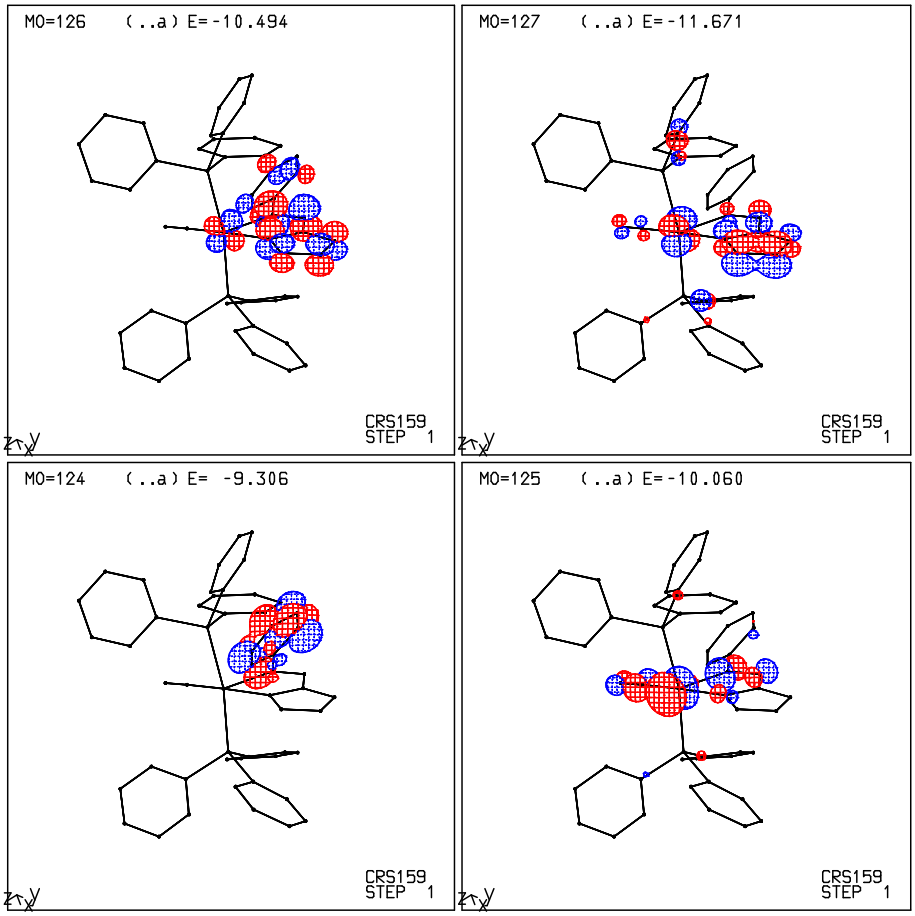

Fig. 4. EHMO plots of HOMO − 1, HOMO, LUMO, LUMO + 1 MO = 127 (HOMO − 1) Ru 46%, 3′-PyaiH = 33%, azo = 10%; MO = 126 (HOMO) Ru = 16%, 3′-PyaiH = 78%, azo = 48%; MO = 125 (LUMO) Ru = 63%, 3′-PyaiH = 19%, azo = 17%, CO = 10%; MO = 124 (LUMO + 1) Ru = 0%, 3′-PyaiH = 99%.

of the MOs are shown in Fig. 4. The transition HOMO → LUMO may be assigned to a LMCT transition; since the HOMO is composed of 78% ligand function and the LUMO brings 63% metal function. Thus the electronic transition at 460–470 nm may be assigned to a LMCT and the intense band at 370–380 comprises intra-ligand transitions. Emission spectra observed upon excitation at 365 nm thus originate from a ligand centered π–π* state.

The ^{1}H NMR spectra of the complexes (**6**) were carried out in $CDCl_3$. Data are set out in Table 2. Imidazole protons, 4- and 5-H, appear as a pair of doublets at 7.2–7.4 and 7.0–7.1 ppm, respectively. A singlet appears at 8.5 ppm and is assigned to 7-H. Other signals are also assigned on comparing with the free ligand data [26]. The 1-R signals appear in their usual positions. 1-Me appears as a singlet at 4.2 ppm; 1-CH_2-CH_3 gives a quartet (4.5 ppm, ($J = 12.0$ Hz)) and a triplet (1.5 ppm ($J = 8.0$ Hz)); 1-CH_2-(Ph) gives a singlet at 6.00 ppm. PPh_3 shows multiplets at 7.3–7.5 ppm. Because of the low solubility in $CDCl_3$ we could not perform ^{13}C NMR spectral measurements.

2.2.4. Electrochemistry

The redox data are summarised in Table 1 and a representative voltammogram is shown in Fig. 2. An initial scan (+ve to SCE) from 0.0 to 1.8 V shows three responses at 0.6–0.7, 0.9–1.0 and 1.2–1.3 V. Scan reversal does not give cathodic peak potentials and suggests irreversibility of the electrochemical reaction. The nature of the redox program does not change with scan rate (50–250 mV S^{-1}). Ru(0) in the complexes **6** can sequentially exhibit Ru(I)/Ru(0), Ru(II)/Ru(I) and Ru(III)/Ru(II) redox processes. We do not have any definite proof to the existence of these redox couples. Because of small difference in E_{pa} (peak potential) values we could not perform coulometric oxidation at a definite potential, and oxidation at the highest potential (>1.4 V) does not complete the coulomb count. This may be due to participation of the solvent in oxidation. The solution colour changes to bright brown red. We did not proceed further.

On scanning to the negative direction (0 to −1.8 V) three redox responses are observed. First two responses are quasireversible ($\Delta E_p \geqslant 100$ mV) and the third one appears at <−1.2 V which is irreversible in nature. The chelated ligand belongs to a π-acidic family and can accommodate two electrons centered at the azo group (–N=N–). On comparing with literature information [14–20], we may assign the first two reductive responses (−0.7 and −0.9 V) as azo reductions [–N=N–]/[–NN---N]$^-$ and [–NN---N]$^-$/[–N–N–]$^{2-}$.

2.2.5. Reaction with Cl_2

$$\mathrm{Ru(CO)(3'\text{-}PyaiR)(PPh_3)_2} + \mathrm{Cl_2} \xrightarrow[\mathrm{NaClO_4(aq)}]{\mathrm{MeCN}} \underset{\mathbf{7}}{[\mathrm{Ru(CO)Cl(3'\text{-}PyaiR)(PPh_3)_2}](\mathrm{ClO_4})} \quad (3)$$

A MeCN solution of the complex was stirred with a Cl_2 saturated solution in the same solvent for 15 min. The solution colour changed from brown to red-brown within a few minutes. The solution was evaporated to dryness, washed with cold water and extracted with chloroform. The solution was chromatographed and eluted by MeCN–MeOH (3:2, v/v). To a methanolic solution of the brown mass $NaClO_4$(aq) was added and a dark coloured precipitate was filtered and then washed with cold water.

The dry mass was chromatographed over silica gel, prepared in benzene. An orange brown band was eluted by MeCN and evaporated slowly in air. Crystalline compound **7** (40–50%) was then separated. A black mass was adhered on the column head and rejected. The molar conductance data in MeCN solutions ($\Lambda_M = 70$–$90\ \Omega^{-1}\ M^{-1}\ cm^{-1}$) suggested a 1:1 electrolyte. The complex may exist in two different isomeric forms. However, we could not separate them by the chromatographic process. So the spectral property may be referred to the mixture of isomeric data. Infrared spectra of the complexes show a strong sharp stretch at 1085–1090 cm^{-1} along with a weak transmission at 625–630 cm^{-1}. This corresponds to $\nu(ClO_4)$. A sharp strong stretch at 1953–1965 cm^{-1} is assigned to ν(CO), which is blue shifted by 30–35 cm^{-1} compared to ν(CO) of the precursor, [Ru(CO)$(PPh_3)_2$(3′-PyaiR)]. This is obviously due to weakening of the π-back donation ability of Ru(II) in the product compared to Ru(0). Additionally, a weak stretch is observed at 310–320 cm^{-1} which is absent in precursor. This is assigned to a ν(Ru–Cl) stretch. Other significant stretchings are ν(N=N) at 1410–1400 and ν(C=N) at 1590–1600 cm^{-1}. We could not crystallize this complex to get a good single crystal for X-ray analysis.

The solution electronic spectra of these complexes exhibit absorptions at 500–510, 400–390 and 350–280 nm (Table 1, Fig. 1). The longer wavelength band, which is absent in the precursor, is assigned to a $d\pi(Ru) \rightarrow \pi^*$ (3′-PyaiR), MLCT transition. Other transitions may be ligand centered (LC) transitions. The cyclic voltammogram of [Ru(CO)Cl(3′-PyaiR)$(PPh_3)_2$](ClO_4) (**5**) shows a quasireversible oxidative response at >0.7 V. This refers to the Ru(III)/Ru(II) redox process (Fig. 2). Ligand centered reductions are observed at <−0.6 V and correspond to electron addition to the –N=N– bond.

3. Conclusion

Pyridylazoimidazole (3′-PyaiR) stabilizes the Ru(0) state in collaboration with CO and PPh_3. The structure shows quite a regular square pyramid of the formula Ru(CO)-$(PPh_3)_2$(3′-PyaiR) (**6**). Cl_2 oxidation has isolated the Ru(II) complex [Ru(CO)Cl(3′-PyaiR)$(PPh_3)_2$](ClO_4) (**7**). Upon oxidation ν(CO) is blue shifted by 30–35 cm^{-1}. The electronic and ^{1}H NMR spectra are also reported. Cyclic voltammograms shows irreversible oxidations corresponding to Ru(0) → Ru(I), Ru(I) → Ru(II) and Ru(II) → Ru(III) while **6** shows a quasireversible Ru(II) → Ru(III) oxidation. Ligand reductions are usually observed at the azo centre. Ru(II) complexes of the formula Ru(3′-PyaiR)$_2$$Cl_2$ are isolated from the reaction between $RuCl_3$ and 3′-PyaiR.

Two isomers, green tcc-Ru(3′-PyaiR)$_2$Cl$_2$ and blue-violet ctc-Ru(3′-PyaiR)$_2$Cl$_2$ are also characterised.

4. Experimental

4.1. Materials and methods

3-Aminopyridine was purchased from Lancaster, UK. Imidazole and all other organic chemicals and inorganic salts were available from the Sisco Research Lab, Mumbai, India. Ru(CO)$_3$(PPh$_3$)$_2$ was synthesized as in the reported procedure [33]. For the solution spectral studies, spectroscopic grade solvents were used from Lancaster, UK. Microanalyses (C, H, N) were performed using a Perkin–Elmer 2400 CHNO elemental analyzer. Spectroscopic measurements were carried out using the following instruments: UV–Vis spectra, JASCO UV–Vis/NIR model V-570; IR spectra (KBr disk, 4000–200 cm^{-1}), JASCO FT-IR model 420; ^{1}H NMR spectra in CDCl$_3$ and CD$_3$CN Bruker 300 MHz FT-NMR spectrometers in the presence of TMS as internal standard. Molar conductances (Λ_M) were measured in a Systronics conductivity meter 304 model using ca. 10^{-3} M solutions in DMSO. Silver is measured gravimetrically. Emission was examined by a F-4500 Hitachi spectrofluorimeter at room temperature (298 K) in MeCN under non-degassed conditions.

4.1.1. Synthesis of the ligands 3′-(pyridyazo)imidazole

Pyridylazoimidazole is a new class of unsymmetric biheterocycle and has been synthesized by coupling the diazonium salt of 3-aminopyridine with imidazole in Na$_2$CO$_3$ solution. N(1)-alkylation has been performed by the reported method using RX in dry THF in the presence of NaH. The chromatographic process has been used to purify the N(1)-alkylated product. Detailed procedures have been reported earlier [26].

4.1.2. Preparation and separation of tcc- and ctc-[Ru(3′-PyaiMe)$_2$Cl$_2$] (**4** and **5**)

A degassed dry ethanol (10 ml) solution of 3-PyaiMe (0.25 g, 1.34 mmol) was added slowly using a pressure equalising funnel to a green Ru(II) solution (prepared by reduction of RuCl$_3 \cdot 3$H$_2$O (0.17 g, 65 mmol) in 10 ml dry ethanol and refluxed for 3 h under nitrogen environment). The volume of the solution was reduced to half of its original volume by nitrogen bubbling and was kept in refrigerator overnight. The precipitate so obtained was filtered and washed with water, cold ethanol and finally with ether. It was then dried over CaCl$_2$. A CH$_2$Cl$_2$ solution of the dry mass was chromatographed over silica gel prepared in petroleum ether (60–80 °C). A green band was eluted by toluene–acetonitrile (9:1 v/v) and a blue violet band was collected using toluene–acetonitrile (3:2 v/v). The solutions were evaporated in air and crystalline products were isolated in 35% and 20% yields.

The microanalytical data of the complexes are as follows: *Anal.* Calc. for C$_{18}$H$_{18}$N$_{10}$Cl$_2$Ru (**4b**): C, 39.47; H, 3.39; N, 25.71. Found: C, 39.56; H, 3.30; N, 25.64%. *Anal.* Calc. for C$_{22}$H$_{22}$N$_{10}$Cl$_2$Ru (**4c**): C, 41.74; H, 3.88; N, 24.30. Found: C, 41.81; H, 3.83; N, 24.39%. *Anal.* Calc. for C$_{30}$H$_{26}$N$_{10}$Cl$_2$Ru (**4d**): C, 51.65; H, 3.66; N, 20.00. Found: C, 51.58; H, 3.72; N, 20.06%. *Anal.* Calc. for C$_{18}$H$_{18}$N$_{10}$Cl$_2$Ru (**5b**): C, 39.50; H, 3.25; N, 25.70. Found: C, 39.56; H, 3.30; N, 25.64%. *Anal.* Calc. for C$_{22}$H$_{22}$N$_{10}$Cl$_2$Ru (**5c**): C, 41.78; H, 3.78; N, 24.30. Found: C, 41.81; H, 3.83; N, 24.39%. *Anal.* Calc. for C$_{30}$H$_{26}$N$_{10}$Cl$_2$Ru (**5d**): C, 51.65; H, 3.66; N, 20.00. Found: C, 51.58; H, 3.72; N, 20.06%.

4.1.3. Preparation of [Ru(CO)(PPh$_3$)$_2$(3′-PyaiH)] (**6a**)

To a solution of [Ru(CO)$_3$(PPh$_3$)$_2$] (0.200 g, 0.282 mmol) in MeCN (20 ml) was added 3′–PyaiH (0.05 g, 0.289 mmol) in acetonitrile. The solution was stirred for 8 h. The yellow solution turned red. The solution was filtered and evaporated slowly. Red coloured crystals developed after four days. The crystals were collected by filtration, washed with cold water–acetonitrile (1:1, v/v) and dried over CaCl$_2$ in vacuo. The yield was 0.16 g (78%). The microanalytical data of the complexes are as follows: *Anal.* Calc. for C$_{45}$H$_{37}$N$_5$OP$_2$Ru (**6a**): C, 65.37; H, 4.48; N, 8.47. Found: C, 65.29; H, 4.43; N, 8.39%. *Anal.* Calc. for C$_{46}$H$_{39}$ C$_{46}$H$_{39}$N$_5$OP$_2$Ru (**6b**): C, 65.71; H, 4.64; N, 8.33. Found: C, 65.66; H, 4.60; N, 8.27%. *Anal.* Calc. for C$_{47}$H$_{41}$N$_5$OP$_2$Ru (**6c**): C, 66.04; H, 4.80; N, 8.20. Found: C, 65.96; H, 4.76; N, 8.15%. *Anal.* Calc. for C$_{52}$H$_{43}$ N$_5$OP$_2$Ru (**6d**): C, 68.12; H, 4.69; N,7.64. Found: C, 68.06; H, 4.65; N, 7.58%.

4.1.4. Oxidation of [Ru(CO)(PPh$_3$)$_2$(3′-PyaiMe)] by Cl$_2$ (**6b**)

To a MeCN solution (15 ml) of [Ru(CO)(PPh$_3$)$_2$(3′-PyaiMe)] (0.2 g, 0.24 mmol) 3 ml of Cl$_2$ saturated MeCN solution was added, dropwise, and stirred. The solution colour changed immediately from brown red to orange red. The solution was stirred for 30 min and then evaporated in air to reduce its volume to half of its original value. Upon addition of a 2 ml saturated solution of NaClO$_4$ to this solution, a dark coloured compound precipitated. This was then filtered, washed with water and dried over CaCl$_2$. The CH$_2$Cl$_2$ solution of the dry mass was chromatographed over silica gel prepared in petroleum ether (60–80 °C). A deep orange red band was eluted by MeCN–toluene (1:3, v/v) and a black mass was attached on the column head. The solution was evaporated via rotary evaporation and the solid product was recrystallised by diffusion of a CH$_2$Cl$_2$ solution to hexane. Yield, 0.14 g, 60%.

The other compounds were prepared by an identical procedure and the yield varied from 60% to 65%.

The microanalytical data of the complexes are as follows: *Anal.* Calc. for C$_{45}$H$_{37}$N$_5$O$_5$P$_2$Cl$_2$Ru (**7a**): C, 56.26; H, 3.80; N, 7.17. Found: C, 56.19; H, 3.85; N, 7.28%. *Anal.*

Table 4
Summarised crystallography data for [Ru(CO)(3′-pyaiH)(PPh_3)$_2$] (**6a**)

Crystal parameters	
Empirical formula	$C_{45}H_{37}N_5OP_2Ru$
Formula weight	826.81
Crystal system	monoclinic
Space group	*Cc*
a (Å)	12.2952 (8)
b (Å)	19.3393 (8)
c (Å)	16.7572 (8)
β (°)	104.0670 (10)
Size	$0.25 \times 0.20 \times 0.10$
V (Å^3)	3865.0 (4)
λ (Å)	0.71073
ρ_{calc} (Mg m^{-3})	1.421
Z	4
T (K)	295 (2)
μ(Mo Kα) (mm^{-1})	0.531
2θ	$4.02 \leqslant 2\theta \leqslant 56.7$
hkl	$-15 \leqslant h \leqslant 16$, $-25 \leqslant k \leqslant 24$, $-22 \leqslant l \leqslant 22$
Reflection collected	20133
Observed data ($I > 2\sigma(I)$)	7363
Refined parameters	481
R	0.0293
wR_2	0.0462
Goodness-of-fit[a]	0.832

$w = 1/[\sigma^2(F_o^2) + (0.0214P)^2]$, where $P = (F_o^2 + 2F_c^2)/3$.
[a] Goodness-of-fit is defined as $[w(F_o^2 - F_c^2)/(n_0 - n_v)]^{1/2}$ where n_0 and n_v denote the number of data and variables, respectively.

Calc. for $C_{46}H_{39}N_5O_5P_2Cl_2Ru$ (**7b**): C, 56.57; H, 4.08; N, 7.07. Found: C, 56.73; H, 4.00; N, 7.19%. *Anal*. Calc. for $C_{47}H_{41}N_5O_5P_2Cl_2Ru$ (**7c**): C, 57.07; H, 4.08; N, 7.23. Found: C, 57.14; H, 4.15; N, 7.09%. *Anal*. Calc. for $C_{52}H_{43}N_5O_5P_2Cl_2Ru$ (**7d**): C, 59.40; H, 4.17; N, 6.75. Found: C, 59.49; H, 4.10; N, 6.67%.

4.2. X-ray diffraction study

Crystals of [Ru(CO)(3′-PyaiH)(PPh_3)$_2$] (**6a**) were grown by slow diffusion of a CH_2Cl_2 solution of the complex into hexane. Crystal parameters and refinement results are summarized in Table 4. Data were collected on a Bruker SMART CCD diffractometer using graphite monochromatised Mo Kα radiation ($\lambda = 0.71073$ Å) at 295(2) K. Data collections were performed in the 2θ range 4–56°. Empirical absorption corrections were carried out based on ψ and ω-scans. The structure was solved by direct methods and refined by full-matrix least-squares refinement based on F_o^2 and including all reflections. All non-hydrogen atoms were refined anisotropically. Data reduction, structure solution and refinement were performed with SHELX-97.

5. Supporting information available

Crystallographic data for structural analysis are available from the Cambridge Crystallographic Data Centre, 12 Union Road, Cambridge CB2 1EZ, UK, fax: +44 1223 336 033 (e-mail: deposit@ccdc.cam.ac.uk or www:http://www.ccdc.cam.ac.uk) on request, quoting the CCDC No. 256887.

Acknowledgements

The financial support has been received from the University Grants Commission and Department of Science and Technology, New Delhi, India. Miss. Chun Yu Chen of the National Science Council in Taiwan is acknowledged for her data collection of X-ray diffraction.

References

[1] E.A. Seddon, K.R. Seddon, The Chemistry of Ruthenium, Elsevier, Amsterdam, 1984.
[2] J. Reedijk, in: G. Wilkinson, J.A. Mcclerverty (Eds.), Comprehensive Coordination Chemistry, Pergamon, Oxford, UK, 1987.
[3] K. Kalyansundaram, Coord. Chem. Rev 46 (1982) 159.
[4] B.K. Ghosh, A. Chakravorty, Coord. Chem. Rev. 95 (1989) 239.
[5] S. Serroni, S. Campagna, F. Puntoriero, C.D. Pietro, N.D. Mcclenaghan, F. Loisean, Chem. Soc. Rev. 30 (2001) 367.
[6] A.C.G. Hotze, H. Kooijman, A.L. Spek, J.G. Haasnoot, J. Reedijk, New J. Chem. 28 (2004) 565.
[7] R.E. Shepherd, Coord. Chem. Rev. 247 (2002) 147.
[8] C. Das, A. Saha, C.-H. Hung, G.-H. Lee, S.-M. Peng, S. Goswami, Inorg. Chem. 42 (2003) 198.
[9] B.K. Santra, G.K. Lahiri, J. Chem. Soc., Dalton Trans. 1 (1998) 1613.
[10] G.K. Lahiri, S. Bhattacharya, S. Goswami, A. Chakravorty, J. Chem. Soc., Dalton Trans. (1990) 561.
[11] S. Goswami, R.N. Mukherjee, A. Chakravorty, Inorg. Chem. 22 (1983) 2825.
[12] R.A. Krause, K. Krause, Inorg. Chem. 23 (1984) 2195.
[13] E.C. Constable, Coord. Chem. Rev. 93 (1989) 205.
[14] T.K. Misra, D. Das, C. Sinha, P. Ghosh, C.K. Pal, Inorg. Chem. 37 (1998) 1672.
[15] P. Byabartta, Sk. Jasimuddin, B.K. Ghosh, C. Sinha, A.M.Z. Slawin, J.D. Woollins, New J. Chem. 26 (2002) 1415.
[16] P. Byabartta, J. Dhinda, P.K. Santra, C. Sinha, K. Panneerselvam, F.-L. Liao, T.-H. Lu, J. Chem. Soc., Dalton Trans. (2001) 2825.
[17] S. Pal, T.K. Misra, C. Sinha, A.M.Z. Slawin, J.D. Woollinns, Polyhedron 19 (2000) 1925.
[18] Sk. Jasimuddin, P. Byabartta, C. Sinha, G. Mostafa, T.-H. Lu, Inorg. Chim. Acta 357 (2004) 2015.
[19] P.K. Santra, T.K. Misra, D. Das, C. Sinha, A.M.Z. Slawin, J.D. Woollins, Polyhedron 18 (1999) 2869.
[20] P. Byabartta, P.K. Santra, T.K. Misra, C. Sinha, C.H.L. Kennard, Polyhedron 20 (2001) 905.
[21] J. Otsuki, N. Onokawa, K. Yochiba, I. Yoshikawa, T. Akasaka, T. Suerobu, T. Takido, K. Araki, S. Fukuzumi, Inorg. Chem. 42 (2003) 3057, and references therein.
[22] W. Kaim, Coord. Chem. Rev. 219 (2001) 463.
[23] L. Carlucci, G. Ciani, D.M. Proserpio, S. Rizzato, New J. Chem. 27 (2003) 483.
[24] T. Akasaka, T. Mutai, J. Otsuki, K. Araki, J. Chem. Soc., Dalton Trans. (2003) 1537.
[25] P.-O. Astrand, K.L. Bak, S.P.A. Sauer, Chem. Phys. Lett 343 (2001) 171.
[26] T. Mathur, Sk. Jasimuddin, H. Milton, J.D. Woollins, C. Sinha, Inorg. Chim. Acta 357 (2004) 3503.
[27] M. Shivakumar, K. Pramanik, A. Chakravorty, Inorg. Chem. Commun. 7 (2004) 729.
[28] P.K. Santra, C. Sinha, W.J. Sheen, F.-L. Liao, T.-H. Lu, Polyhedron 20 (2001) 599.

[29] M. Menon, A. Pramanik, N. Bag, A. Chakravorty, J. Chem. Soc., Dalton Trans. (1995) 1417.
[30] T.-G. Gottschalk, J.C. Huffman, G. Geard, O. Eisenstein, G.K. Caulton, Inorg. Chem. 39 (2000) 3957.
[31] K.R. Flower, G.L. Leal, R.G. Pritchard, Inorg. Chem. Commun. 7 (2004) 729.
[32] T. Mathur, U.S. Ray, B.N. Baruri, C. Siha, J. Coord. Chem. 58 (2005) 399.
[33] M. Herberhold, K. Bauer, W. Milius, J. Organomet. Chem. 563 (1998) 227, and references therein.
[34] B.K. Panda, K. Ghosh, S. Chattopadhyay, A. Chakravorty, J. Organomet. Chem. 674 (2003) 107.

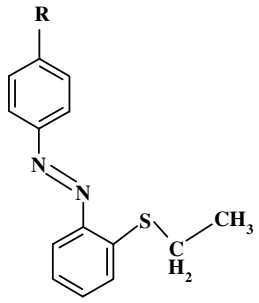

	R
L^1H	H
L^2H	Me
L^3H	Cl

2

2. Experimental

2.1. Materials

Platinum chloride was purchased from Arrora Mathey, Calcutta, India. Dipotassium tetrachloroplatinate(II) was prepared by a reported method [7]. Dipotassium tetraiodoplatinate (K_2PtI_4) was obtained from SRL. 2-Ethyl sulfanyl aniline was synthesized by reacting ethyl bromide with 2-aminothiophenol [5]. All other chemical and solvents were reagent grade and used as received from E-Marck, Calcutta, India. Silica gel (60–120 mesh) was used for the column chromatography.

2.2. Syntheses of ligands

The ligand L^1H, L^2H and L^3H were prepared by a similar procedure. The detailed method is given below for L^1H.

2.2.1. L^1H

0.5 g (3.26 mmol) of 2-(ethylsulfanyl) aniline was dissolved in (15 cm^3) glacial acetic acid and 0.35 g (3.26 mmol) of nitrosobenzene was added pinchwise within 10 min. Stirring was continued for 3 h, maintaining the temperature at 70 °C, the dark mass thus obtained was dissolved in benzene and subjected to column chromatography over silica gel (60–120 mesh). The first fraction eluted by pet. ether (60–80 °C) afforded the solid L^1H ligand upon evaporation of the solvent. Yield: 70%. *Anal.* Calc. for $C_{14}H_{14}N_2S$: C, 69.42; H, 5.78; N, 11.57. Found: C, 69.45; H, 5.73; N, 11.55%. UV–Vis (CH_2Cl_2) $\lambda_{max}/\varepsilon$ nm (/M^{-1} cm^{-1}): 397(4951), 321(17660), 278(13030), 268(14218), 233(16339). IR (KBr): $\nu_{N=N}$ 1450 cm^{-1}.

2.2.2. L^2H and L^3H

The other ligands (L^2H and L^3H) were prepared similarly using *p*-methyl nitrosobenzene and *p*-chloro nitrosobenzene in place of nitrosobenzene. Yield for L^2H: 70% and L^3H: 65%. *Anal.* Calc. for $C_{15}H_{16}N_2S$: C, 70.31; H, 6.25; N, 10.93. Found: C, 70.25; H, 6.30; N, 11.00%. UV–Vis (CH_2Cl_2) $\lambda_{max}/\varepsilon$ nm (/M^{-1} cm^{-1}): 407(4096), 328(19267), 268(10240), 238(14920). IR (KBr): $\nu_{N=N}$ 1454. *Anal.* Calc. for $C_{14}H_{13}N_2SCl$: C, 60.75; H, 4.70; N, 10.12. Found: C, 60.71; H, 4.73; N, 10.55%. UV–Vis (CH_2Cl_2) $\lambda_{max}/\varepsilon$ nm (/M^{-1} cm^{-1}): 405(5327), 327(18267), 266(12442), 235(16460). IR (KBr): $\nu_{N=N}$ 1454 cm^{-1}.

2.3. Syntheses of complexes

2.3.1. $Pt(L^1)Cl$

To an aqueous solution (5 cm^3) of K_2PtCl_4 (0.05 g, 0.121 mmol), a methanolic solution of L^1H (0.03 g, 0.121 mmol) was added. The mixture was stirred for 12 h. The dark solid precipitate was separated by filtration and purified by column chromatography using silica gel (60–120 mesh). The eluent was toluene–acetonitrile mixed solvent (80/20 v/v) and upon evaporation of the solvent, the dark red solid $Pt(L^1)Cl$ was obtained. Yield: 80%. *Anal.* Calc. for $C_{14}H_{13}N_2SPtCl$: C, 35.63; H, 2.75; N, 5.93. Found: C, 35.60; H, 2.80; N, 5.90%. UV–Vis (CH_2Cl_2) $\lambda_{max}/\varepsilon$ nm (/M^{-1} cm^{-1}): 234(7903), 260(5540), 360(3878), 381(4332), 410(3878), 472(1800). IR (KBr): $\nu_{N=N}$ 1361, ν_{Pt-Cl} 335 cm^{-1}.

2.3.2. $Pt(L^2)Cl$ and $Pt(L^3)Cl$

The other complexes $Pt(L^2)Cl$ and $Pt(L^3)Cl$ were prepared by a similar method using L^2H and L^3H in place of L^1H. Yield for $Pt(L^2)Cl$: 70% and $Pt(L^3)Cl$: 65%. *Anal.* Calc. for $C_{15}H_{15}N_2SPtCl$: C, 36.92; H, 3.07; N, 5.74. Found: C, 36.95; H, 3.10; N, 5.75%. UV–Vis (CH_2Cl_2) $\lambda_{max}/\varepsilon$ nm (/M^{-1} cm^{-1}): 581(330), 490(705), 417(2220), 381(2070), 362(1744), 342(1410), 264(2682), 228(3865). IR (KBr): $\nu_{N=N}$ 1365, ν_{Pt-Cl} 340 cm^{-1}. *Anal.* Calc. for $C_{14}H_{12}N_2SPtCl_2$: C, 33.20; H, 2.37; N, 5.53. Found: C, 33.24; H, 2.41; N, 5.50%. UV–Vis (CH_2Cl_2) $\lambda_{max}/\varepsilon$ nm (/M^{-1} cm^{-1}): 573(2207), 496(2348), 415(12702), 381(13035), 362(11878), 261(15075), 231(13207). IR (KBr): $\nu_{N=N}$ 1357 ν_{Pt-Cl} 345 cm^{-1}.

2.3.3. $Pt(L^1)I_3$

To an aqueous solution (5 cm^3) of K_2PtI_4 (0.05 g, 0.064 mmol) a methanolic solution of L^1H (0.015 g, 0.064 mmol) was added. The mixture was stirred for 12 h. The dark solid precipitate was separated by filtration and purified by column chromatography using silica gel (60–120 mesh). The eluent was pet. ether–toluene mixed solvent (80/20 v/v) and upon evaporation of the solvent, the dark red solid $Pt(L^1)I_3$ was obtained. Yield: 80%. *Anal.* Calc. for $C_{14}H_{13}N_2SPtI_3$: C, 20.63; H, 1.59; N, 3.43. Found: C, 20.65; H, 1.63; N, 3.48%. UV–Vis (CH_2Cl_2) $\lambda_{max}/\varepsilon$ nm (/M^{-1} cm^{-1}): 425(9881), 390(9920), 332(7800), 268(26610), 230(21900). IR (KBr): $\nu_{N=N}$ 1387 cm^{-1}.

2.3.4. $Pt(L^2)I_3$ and $Pt(L^3)I_3$

The other complexes, $Pt(L^2)I_3$ and $Pt(L^3)I_3$, were prepared by a similar method using L^2H and L^3H in place of L^1H. Yield for $Pt(L^2)I_3$: 70% and $Pt(L^3)I_3$: 65%. *Anal.* Calc. for $C_{15}H_{15}N_2SPtI_3$: C, 21.73; H, 1.81; N, 3.38. Found: C, 21.76; H, 1.85; N, 3.35%. UV–Vis (CH_2Cl_2) $\lambda_{max}/\varepsilon$ nm (/M^{-1} cm^{-1}): 422(9881), 393(9928), 335(7885), 264(26615), 230(21936). IR (KBr): $\nu_{N=N}$ 1385 cm^{-1}. *Anal.* Calc. for $C_{14}H_{12}N_2SPtI_3Cl$: C, 19.79; H, 1.41; N, 3.29. Found: C,

Table 1
Crystallographic data for $Pt(L^3)I_3$

Chemical formula	$C_{14}H_{12}ClI_3N_2PtS$
Formula weight	851.56
Space group	$P2_1/n$
Crystal system	monoclinic
a (Å)	19.075(8)
b (Å)	9.1689(18)
c (Å)	22.505(13)
β (°)	93.80(4)
λ (Å)	0.71073
V (Å^3)	3927(3)
Z	8
Temperature (K)	293
ρ_{calc} (Mg m^{-3})	2.881
μ (mm^{-1})	12.102
$F(000)$	3040
R^a	0.0936
$wR_2{}^c$	0.2753
Goodness-of-fit (GOF)[b]	1.06

[a] $R_1 = \sum||F_o| - |F_o||/\sum|F_o|$.
[b] $GOF = [\sum[w(F_o^2 - F_c^2)^2]/(n-p)]^{1/2}$.
[c] $wR_2 = [\sum[w(F_o^2 - F_c^2)^2]/\sum[w(F_o^2)^2]]^{1/2}$ where $w = 1/\sigma^2(F_o^2) + (aP)^2 + bP$, $P = (F_o^2 + 2F_c^2)/3$.

19.75; H, 1.45; N, 3.35%. UV–Vis (CH_2Cl_2) $\lambda_{max}/\varepsilon$ nm ($/M^{-1}$ cm^{-1}): 429(22936), 387(23210), 339(18636), 264(61278), 230(48295). IR (KBr): $\nu_{N=N}$ 1385 cm^{-1}.

2.4. Physical measurements

Microanalysis (C, H, N) was performed using a Perkin–Elmer 240C elemental analyzer. Fourier transforms IR spectra were obtained on a Nicolet spectrophotometer with samples prepared as KBr pellets. Electronic spectra were recorded using a Hitachi U-2001 spectrophotometer. ^1H NMR spectra were obtained on Brucker AC-200 and Brucker Avance DPX 300 spectrometers in $CDCl_3$, using TMS as the internal standard.

2.5. Crystallography

Crystals of $Pt(L^3)I_3$ were grown by slow diffusion of hexane into dichloromethane solutions at 25 °C. Data were collected by the ω-scan technique on an Enraf-Nonius CAMX-3 diffractometer with Mo Kα radiation, monochromated by a graphite crystal. The structure solution was done by a direct method with the SHELXS-97 program. Full-matrix least-square refinements were performed using the SHELX-97 program (PC version). All non-hydrogen atoms were refined anisotropically using reflections $I > 2\sigma(I)$. Hydrogen atoms were included in calculated positions. The crystal data and data collection parameters are listed in Table 1.

3. Results and discussion

3.1. Synthesis

The ligands LH were synthesized by treating 2-ethyl sulfanyl aniline (prepared by reacting 2-amino thiophenol with ethyl bromide in sodium ethoxide) with the appropriate nitrosoarenes in glacial acetic acid in the following equation [8]:

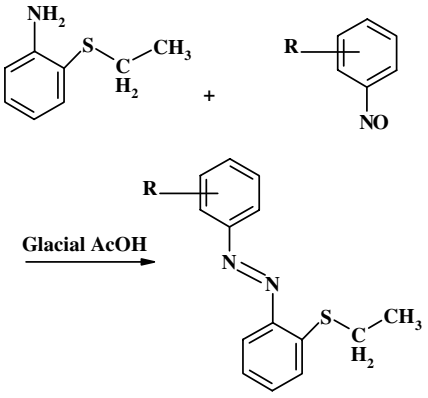

(1)

Reactions of K_2PtCl_4 with the LH ligands afforded the orthometallated complexes of bivalent platinum as shown in **3**.

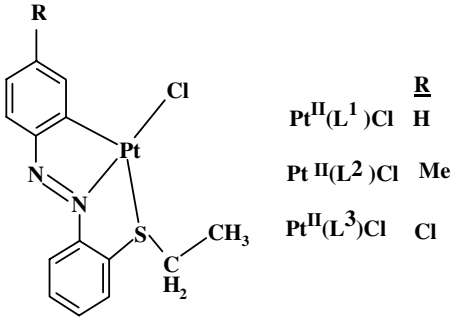

3

On the contrary, the reaction of LH with K_2PtI_4 (in warm methanol) afforded the Pt(IV) orthometallated species as shown in **4**. It is believed that in the case of K_2PtI_4, the reactions proceeded either via oxidative addition of LH or addition of I_2 that was generated in situ due to aerial oxidation of I^- which was released from K_2PtI_4 upon the initial formation of Pt(L)I. We tried our best to obtain Pt(L)I, performing the reaction in a nitrogen atmosphere, but always ended up with $Pt(L)I_3$. However, these $Pt(L)I_3$ compounds are examples of new Pt(IV) orthometallated azobenzene complexes [5,6].

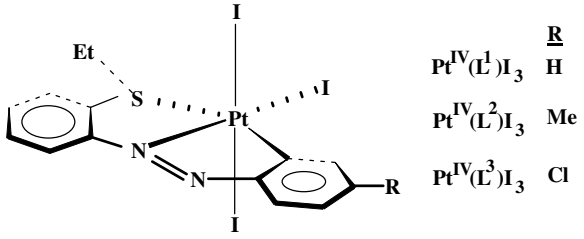

4

All the complexes, Pt(L)Cl and Pt(L)I_3, are non-electrolytic, diamagnetic and soluble in common organic solvents.

3.2. Characterization

The ligands and complexes display characteristic UV–Vis spectra. Representative spectra of L^3H, Pt(L^3)Cl and Pt(L^3)I_3 are shown in Fig. 1. Data are collected in Section 2.

The LH ligands exhibit $\nu_{N=N}$ near 1454 cm^{-1} in the IR spectra, which shifts to the lower energy range 1357–1365 cm^{-1} for Pt(L)Cl and 1385–1387 for Pt(L)I_3 upon complex formation, indicating coordination of the azo nitrogen [5]. The ν_{Pt-Cl} of Pt(L)Cl were observed at ~350 cm^{-1}. The significant IR data are collected in Section 2.

In the ^1H NMR spectra of LH, 13-H and 14-H (atom numbering scheme is shown in Fig. 2) resonances of the ethyl group of the thioether fragment appeared near δ 3.0 and δ 1.7 as a quartet and triplet, respectively. The total proton counts matched well with the composition. The *p*-Me protons of L^2H were observed at δ 2.44. The chemical shift values and integrations of the aromatic protons are collected in Table 2. The downfield shifting of 13-H (~δ 0.4) upon complexation [5] indicated S coordination. The resonance at δ 7.9 for two equivalent protons in the case of L^1H has been assigned for 2-H and 6-H. This signal shifts a little in the downfield region (δ 8.1) for Pt(L^1)Cl and the proton count is matched with one equivalent

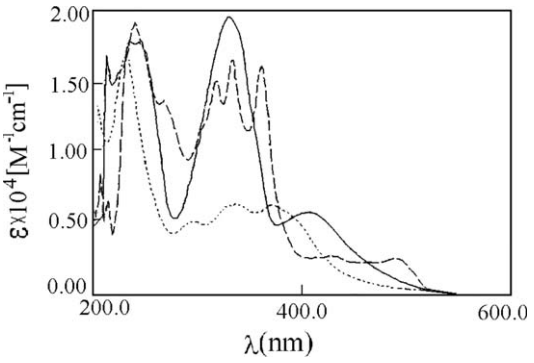

Fig. 1. UV–Vis spectra of (L^3H) (——), Pt(L^3)Cl (-----) and Pt(L^3)I_3 (···).

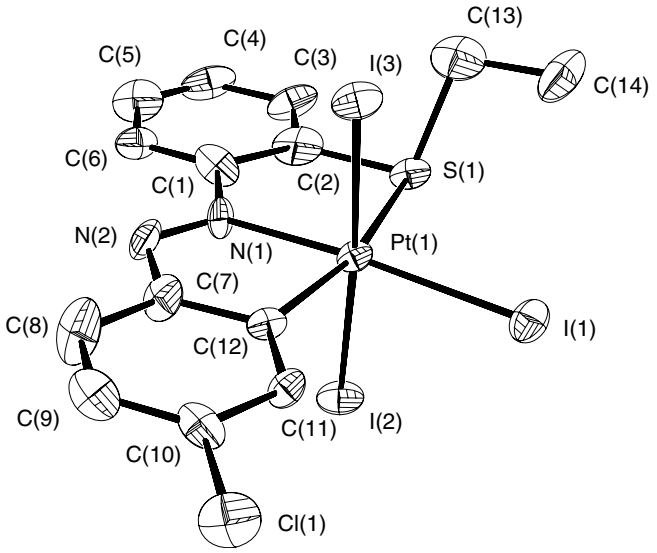

Fig. 2. Perspective view of Pt(L^3)I_3 with the atom numbering scheme. Hydrogen atoms are omitted for clarity.

Table 2
^1H NMR spectra of all the ligands (LH), complexes Pt(L)Cl and Pt(L)I_3 in $CDCl_3$

Compound	δ^b (X, *n*H)[a]		
	Aromatic protons	Non-aromatic protons	R (CH_3)
L^1H	7.94(d, 2H), 7.67(d, 1H), 7.55–7.43(m, 4H), 7.36(d, 1H), 7.19(t, 1H)	3.06–2.94(q, 2H), 1.41(t, 3H)	
L^2H	7.84(d, 2H), 7.65(d, 1H), 7.35–7.26(m, 4H), 7.16(t, 1H)	3.07–2.95(q, 2H), 1.43(t, 3H)	2.44(s, 3H)
L^3H	7.91(d, 2H), 7.68(d, 1H), 7.49–7.45(m, 2H), 7.38–7.32(m, 2H), 7.16(t, 1H)	3.07–2.96(q, 2H), 1.44(t, 3H)	
Pt(L^1)Cl	8.21(d, 1H), 7.97(d, 1H), 7.78(d, 1H), 7.72(t, 1H), 7.60–7.27(m, 3H), 7.18(t, 1H),	3.50–3.47(q, 2H), 1.44(t, 3H)	
Pt(L^2)Cl	8.19(d, 1H), 7.87(d, 1H), 7.74–7.64(m, 2H), 7.57–7.47(m, 2H), 7.03(d, 1H)	3.48–3.41(q, 2H), 1.43(t, 3H),	2.34(s, 3H)
Pt(L^3)Cl	8.33(d, 1H), 7.92(d, 1H), 7.82–7.70(m, 2H), 7.65–7.45(m, 2H), 7.20(d, 1H)	3.49–3.46(q, 2H), 1.43(t, 3H)	
Pt(L^1)I_3	8.43(d, 1H), 8.37(d, 1H), 8.31(d, 1H), 7.82(d, 1H), 7.70(t, 1H), 7.58(t, 1H), 7.50(t, 1H), 7.28(t, 1H)	4.16(b, 1H), 3.65(b, 1H), 1.70(t, 3H)	
Pt(L^2)I_3	8.35(d, 1H), 8.19(d, 1H), 7.85(d, 1H), 7.71–7.57(m, 3H), 7.02(d, 1H)	4.21(b, 1H), 3.64(b, 1H), 1.73(t, 3H)	2.56(s, 3H)
Pt(L^3)I_3	8.40(d, 1H), 8.25(d, 1H), 7.84(d, 1H), 7.72(d, 1H), 7.69–7.53(d, 2H), 7.24(t, 1H)	4.25(b, 1H), 3.66(b, 1H) 1.74(t, 3H)	

[a] X = multiplicity (m, multiplet; s, singlet; d, doublet; t, triplet; b, broad; q, quartet), *n*, proton count.
[b] In ppm.

proton, unlike L^1H (two equivalent protons), indicating dissociation of a C–H proton due to M–C bond formation. An important feature of $Pt(L)I_3$ complexes in the ^1H NMR spectra is the non-equivalent nature of the methylene (13-H) protons of the ethyl group on sulfur. Two resonances at $\sim\delta$ 3.65 and $\sim\delta$ 4.15 appeared for these two protons with a separation of $\sim\delta$ 0.5. This is characteristic for all the $Pt(L)I_3$ complexes and may be attributed to the non-equivalent magnetic environment about the two methylene protons due to three bulkier I^- ligands within the coordination sphere.

3.3. X-ray structure of $Pt(L^3)I_3$

Crystals suitable for X-ray studies were grown by slow diffusion of dichloromethane into hexane. The platinum is hexacoordinated in a distorted octahedral geometry indicating the tetravalent platinum. The deprotonated ligand, $[L^3]^-$, binds the metal in a tridentate (C, N, S) fashion and it is meridionally oriented. Three I^- ligands satisfy the hexacoordination about platinum (IV). The asymmetric unit contains two molecules. During the anisotropic refinement, N(4) and C(25) showed non-positive thermal parameters. Thus those two atoms were not refined anisotropically. However, the bond parameters, within the coordination sphere of Pt, of the two molecules were similar. Only the azo N(3)–N(4) distance (1.26(3) Å) of one molecule did not match with the azo N(1)–N(2) distance (1.21(3) Å) of the other. Thus we considered only the N(1)–N(2) distance for the discussion as more reliable than N(3)–N(4) since N(4) could not be refined anisotropically. A perspective view of the molecular structure is shown in Fig. 2. Selected bond distances and bond angles are collected in Table 3.

The Pt–N(azo), Pt–C and Pt–I lengths are within the normal values for Pt(IV) species [5]. The N=N(azo) length (1.20 (3) Å) is also within the normal value. However, the Pt–S (thioether) distance (2.430(7) Å) is larger than the expected Pt–S length (2.25 Å) due to the strong *trans* influence of the aryl carbon atom [5].

Table 3
Selected bond distances (Å) and bond angles (°) for $Pt(L^3)I_3$

Distances			
Pt(1)–I(1)	2.636(3)	S(1)–C(2)	1.80(3)
Pt(1)–I(2)	2.667(2)	C(1)–C(2)	1.38(4)
Pt(1)–I(3)	2.655(2)	N(1)–C(1)	1.49(3)
Pt(1)–S(1)	2.430(7)	N(1)–N(2)	1.20(3)
Pt(1)–N(1)	2.031(18)	N(2)–C(7)	1.41(4)
Pt(1)–C(12)	2.01(3)	C(7)–C(12)	1.44(4)
Angles			
I(1)–Pt(1)–I(2)	90.73(7)	I(3)–Pt(1)–S(1)	95.74(17)
I(1)–Pt(1)–I(3)	92.18(7)	I(3)–Pt(1)–N(1)	88.6(6)
I(1)–Pt(1)–S(1)	98.35(15)	I(3)–Pt(1)–C(12)	85.9(6)
I(1)–Pt(1)–N(1)	174.4(5)	S(1)–Pt(1)–N(1)	87.1(5)
I(1)–Pt(1)–C(12)	97.0(7)	S(1)–Pt(1)–C(12)	164.5(7)
I(2)–Pt(1)–I(3)	175.99(8)	N(1)–Pt(1)–C(12)	77.5(9)
I(2)–Pt(1)–S(1)	86.54(17)	N(2)–N(1)–Pt(1)	123.5(18)
I(2)–Pt(1)–N(1)	88.2(6)	I(2)–Pt(1)–C(2)	91.0(6)
C(1)–N(1)–Pt(1)	117.3(15)		

4. Conclusions

The reaction of 1-arylazo-2-ethyl sulfanyl benzene (LH) with K_2PtCl_4 and K_2PtI_4 has been studied. In both the cases orthoplatinated compounds were isolated and characterized. K_2PtCl_4 afforded Pt(II) complexes, Pt(L)Cl, while K_2PtI_4 produced the Pt(IV) compounds, $Pt(L)I_3$. The oxidation of Pt in the case of $Pt(L)I_3$ is believed to occur as a result of oxidative addition of LH.

5. Supplementary data

Crystallographic data for the structural analysis have been deposited with the Cambridge Crystallographic Data Centre, CCDC reference number CCDC280164. Copies of this information may be obtained free of charge from The Director, CCDC, 12 Union Road, Cambridge CB2 1EZ, UK. E-mail: deposite@ccdc.cam.ac.uk.

Acknowledgments

We are thankful to the Council of Scientific and Industrial Research, (CSIR), New Delhi, for funding and fellowship to BS. We are also thankful to DST (New Delhi) for funding and fellowship to J.P. (No. SR/S1/IC-09/2003). We acknowledge the help of Dr. S. Pal of the University of Hyderabad for X-ray studies.

References

[1] (a) M. Lersch, M. Tilset, Chem. Rev. 105 (2005) 2471, and references therein;
(b) C.B. Pamplin, P. Legzdins, Acc. Chem. Res. 36 (2003) 223, and references therein;
(c) V. Ritleng, C. Sirlin, M. Pfeffer, Chem. Rev. 102 (2002) 1731;
(d) W.D. Jones, Acc. Chem. Res. 36 (2003) 140, and references therein;
(e) R.H. Carbtree, Chem. Rev. 95 (1995) 987;
(f) W.D. Jones, Activation of Unreactive Bonds and Organic Synthesis, Springer, Berlin, 1999 (Chapter 2);
(g) A.F. Heyduk, T.G. Driver, J.A. Labinger, J.E. Bercaw, J. Am. Chem. Soc. 126 (2004) 15034.
[2] D.St.C. Black, G.B. Deacon, G.L. Edwards, Aust. J. Chem. 47 (1994) 217, and references therein.
[3] (a) A.C. Cope, R.W. Siekman, J. Am. Chem. Soc. 87 (1965) 3272;
(b) R.C. Elder, R.D.P. Cruea, R.F. Morrison, Inorg. Chem. 15 (1976) 1623.
[4] (a) I. Omae, Chem. Rev. 79 (1979) 287;
(b) J. Pratihar, N. Maiti, S. Chattopadhyay, Inorg. Chem. 44 (2005) 6111;
(c) J. Pratihar, N. Maiti, P. Pattanayak, S. Chattopadhyay, Polyhedron 24 (2005) 1953;
(d) J. Pratihar, D. Patra, S. Chattopadhyay, J. Organomet. Chem. 690 (2005) 4816;
(e) S. Nag, P. Gupta, J.R. Butcher, S. Bhattacharya, Inorg. Chem. 43 (2004) 4814.
[5] (a) S. Chattopadhyay, C. Sinha, A. Basu, A. Chakravorty, J. Organomet. Chem. 414 (1991) 421;

(b) S. Chattopadhyay, C. Sinha, A. Basu, A. Chakravorty, Organometallics 10 (1991) 1135, and references therein.
[6] M. Ghedini, D. Pucci, A. Crispini, G. Barberio, Organometallics 18 (1999) 2116.
[7] S.E. Livingstone, Synth. React. Inorg. Met.-Org. Chem. 1 (1971) 1.
[8] A.K. Mahapatra, D. Banbyopadhyay, P. Bandyopadhyay, A. Chakravorty, Inorg. Chem. 25 (1986) 2214.

X-ray crystal analysis, grew after the reaction mixture was left overnight.

2.1.1. $[(C_6H_6)RuCl_2(\alpha\text{-pic})_2]$

Yield: 78%. Colour: red. IR (KBr): 3056 $\nu_{CH\text{-phen}}$; 2933 $\nu_{CH\text{-phenyl}}$; 1605 ν_{CN}; 1481 $\delta_{(C–CH\text{ in the plane})}$; 1436 $\nu_{C=C}$; 1303 ν_{ring}; 1117 δ_{CH}; 1064 δ_{CH}; 832 $\nu_{Ru–N}$; 719 δ_{pic}. ^{1}H NMR (δ, $CDCl_3$): 8.59 (dd H6 pic); 7.20 (t H5 pic); 7.67 (td H4 pic); 7.16 (d H3 pic); 5.69 (s C_6H_6); 3.16 (s CH_3). UV–Vis (CH_2Cl_2, λ, nm): 434.6 (2.88), 346.2 (3.05), 263.0 (3.56), 227.0 (3.69) *Anal.* Calc. for $C_{12}H_{13}Cl_2NRu$: C, 51.31; H, 4.55; Cl, 16.83; N, 3.32; Ru, 23.99. Found: C, 51.41; H, 4.35; N, 3.33%.

2.1.2. $[(C_6H_6)RuCl_2(\beta\text{-pic})_2]$

Yield: 81%. Colour: orange. IR (KBr): 3060 $\nu_{CH\text{-phen}}$; 2949 ν_{CH3}; 1605 ν_{CN}; 1478 $\delta_{(C–CH\text{ in the plane})}$; 1433 $\nu_{C=C}$; 1112 δ_{CH}; 1049 δ_{CH}; 841 $\nu_{Ru–N}$; 700 δ_{pic}. ^{1}H NMR (δ, $CDCl_3$): 8.85 (H2 pic); 7.33 (d H4 pic); 7.31 (dd H5 pic); 8.80 (d H6 pic); 5.89 (s C_6H_6); 2.19 (s CH_3). UV–Vis (CH_2Cl_2, λ, nm): 409.8 (2.93), 256.8 (3.90), 224.4 (3.96), 213.4 (4.02). *Anal.* Calc. for $C_{12}H_{13}Cl_2NRu$: C, 51.31; H, 4.55; Cl, 16.83; N, 3.32; Ru, 23.99. Found: C, 51.42; H, 4.37; N, 3.32%.

2.1.3. $[(C_6H_6)RuCl_2(\gamma\text{-pic})_2]$

Colour: yellow-orange. Yield: 82%. Colour: orange. IR (KBr): 3032 $\nu_{CH\text{-phen}}$; 2947 $\nu_{CH\text{-phenyl}}$; 1613 ν_{CN}; 1494 $\delta_{(C–CH\text{ in the plane})}$; 1423 $\nu_{C=C}$; 1107 δ_{CH}; 1041 δ_{CH}; 815 $\nu_{Ru–N}$; 721 δ_{pic}.^{1}H NMR (δ, $CDCl_3$): 8.50 (d H2, H6 pic); 7.25 (d H3, H5 pic); 5.98 (s C_6H_6); 2.61 (s CH_3). UV–Vis (CH_2Cl_2, λ, nm): 402.4 (2.66), 249.8 (3.98), 220.4 (3.99), 218.0 (4.06). *Anal.* Calc. for $C_{12}H_{13}Cl_2NRu$: C, 51.31; H, 4.55; Cl, 16.83; N, 3.32; Ru, 23.99. Found: C, 51.40; H, 4.32; N, 3.31%.

2.2. Physical measurements

Infrared spectra were recorded on a Nicolet Magna 560 spectrophotometer in the spectral range 4000–400 cm^{-1} with the sample in the form of a KBr pellet. Electronic spectra were measured on a spectrophotometer Lab Alliance UV–Vis 8500 in the range 800–200 nm in deoxygenated dichloromethane solution. Elemental analyses (C, H, N) were performed on a Perkin–Elmer CHN-2400 analyzer. The ^{1}H NMR spectra were recorded on a INOVA 300 spectrometer in $CDCl_3$ solutions.

2.3. Crystal structure determination and refinement

A red needle crystal was mounted on a KM-4-CCD automatic diffractometer equipped with CCD detector, and was used for data collection. X-ray intensity data were collected with graphite monochromated Mo Kα radiation ($\lambda = 0.71073$ Å) at the temperature 293(2) K, with the ω scan mode. A 16.00 seconds exposure time was used and all reflections of the Ewald sphere were collected up to $2\theta = 63.12°$. The unit cell parameters were determined from least-squares refinement of the setting angles of 7033 strongest reflections. Details concerning crystal data and refinement are given in Table 1. Examination of 52 reflections on two reference frames monitored after each 20 frames measured showed 2.31% loss of the intensity. During the data reduction the above decay correction coefficient was taken into account. Lorentz, polarization and numerical absorption [5] corrections were applied. The structure was solved by direct methods and subsequently completed by difference Fourier recycling. All the non-hydrogen atoms were refined anisotropically using the full-matrix, least-squares technique on F^2. All the hydrogen atoms were found from the difference Fourier synthesis after four cycles of anisotropic refinement, and refined as ''riding'' on the adjacent carbon atom with an individual isotropic temperature factor equal to 1.2 times the value of the equivalent temperature factor of the aromatic parent carbon atom and equal to 1.5 times the value of equivalent temperature factor of the methyl parent carbon atom. The methyl group was allowed to rotate during refinement about its local threefold axis. SHELXS 97 [6], SHELXL 97 [7] and SHELXTL [8] programs were used for all the calculations. Atomic scattering factors were those incorporated in the computer programs.

2.4. Computational details

The GAUSSIAN 03 program [9] was used in the calculations. The geometry optimisation was carried out with

Table 1
Crystal data and structure refinement details of $[(C_6H_6)RuCl_2(\alpha\text{-pic})]$

Empirical formula	$C_{12}H_{13}Cl_2NRu$
Formula weight	343.20
Temperature (K)	293(2)
Crystal system	monoclinic
Space group	$P2_1/n$
Unit cell dimensions	
a (Å)	14.8628(8)
b (Å)	7.2851(4)
c (Å)	23.1613(12)
β (°)	95.363(4)
Volume (Å^3)	2496.9(2)
Z	8
Calculated density (Mg/m^3)	1.826
Absorption coefficient (mm^{-1})	1.654
$F(000)$	1360
Crystal dimensions (mm)	$0.432 \times 0.196 \times 0.081$
θ Range for data collection (°)	2.87–31.56
Index ranges	$-10 \leqslant h \leqslant 20$ $-8 \leqslant k \leqslant 10$ $-28 \leqslant l \leqslant 33$
Reflections collected	28 687
Independent reflections	7215 [$R_{(int)} = 0.0259$]
Data/restraints/parameters	7215/0/356
Goodness-of-fit on F^2	1.128
Final R indices [$I > 2\sigma(I)$]	$R_1 = 0.0394$ $wR_2 = 0.0828$
R indices (all data)	$R_1 = 0.0527$ $wR_2 = 0.0875$
Largest different in peak and hole (e Å^{-3})	0.924 and −0.763

the DFT method with the use of the B3LYP functional [10,11]. The electronic spectrum was calculated with the TDDFT method [12]. The calculations were performed using the DZVP basis set [13] with f functions with exponents 1.94722036 and 0.748930908 on the ruthenium atom and polarization functions to all other atoms: 6-31g(2d,p) – chlorine, 6-31g** – carbon, nitrogen and 6-31g(d,p) on hydrogen atoms.

3. Results and discussion

Refluxing the ruthenium(II) benzene complex $[(C_6H_6)RuCl_2]_2$ with an excess of 2, 3 and 4-methylpyridine in methanol leads to the half-sandwich complexes $[(C_6H_6)RuCl_2(pic)]$, where pic = α-, β-, γ-picoline. The elemental analyses of the complexes are in good agreement with their formulation. Infrared spectra of the complexes exhibit characteristic bands due to picoline ring vibrations. The $\nu_{C=N}$ band in the complexes appear around 1605 (complex with α- and β-picoline) and 1613 cm^{-1} ($[(C_6H_6)RuCl_2(\gamma\text{-pic})]$). The $\nu_{C=C}$ absorption bands are visible at 1436, 1433, and 1423 cm^{-1}, respectively. The absorption bands at 832 cm^{-1} (complex with α-picolne), 841 cm^{-1} (β-picoline) and 915 (γ-picoline) are due to ν_{Ru-N}. The ^1H NMR spectra of the complexes confirm the presence of picoline molecules in the coordination spheres. The positions of the ^1H NMR signals and their assignment are given in the experimental part of the paper.

The obtained complexes were crystallized from methanolic solution but only the complex with α-picoline gave well-shaped crystals suitable for X-ray analysis.

The complex $[(C_6H_6)RuCl_2(\alpha\text{-pic})]$ crystallizes in the monoclinic space group $P2_{1/n}$ and the crystal structure is built up of two independent molecules in the asymmetric unit. The relative orientation of the molecules is depicted in Fig. 1, which also shows the displacement ellipsoids of the non-hydrogen atoms. The picoline substituent of the molecule indicated by Ru(2) atom is statically disordered over two sites with participation of domains in the ratio 3:1. Both domain atoms are coplanar, and are rotated along the axis going through the Ru(2) atom and perpendicular to the picoline atoms weighted least squares plane. The second molecule picoline substituent also shows signs of disorder, but it is rather dynamical in character. Selected bond lengths and angles are given in Table 2. The distances and the angles between the appropriate atoms in the two molecules are similar. The most different distance is Ru(1)–Cl(2) 2.438(8) Å and Ru(2)–Cl(52) 2.423(9) Å, and most different angles are N(1)–Ru(1)–Cl(2) 89.98(8)° and N(51)–Ru(2)–Cl(52) 96.0(6)°; N(1)–Ru(1)–C(10) 161.62(13)° and N(51)–Ru(2)–C(60) 167.0(6)°; C(8)–Ru(1)–N(1) 110.77(15)° and C(58)–Ru(2)–N(51) 105.5(6)°. The coordination about ruthenium is formally six and the structure adopts a distorted piano-stool type of geometry with angles (average value) around the ruthenium of 85.54(17)° (Cl(1)–Ru–Cl(2)), 89.52(8)° (N(1)–Ru–Cl(1)), 92.99(3)° (N(1)–Ru–Cl(2)).

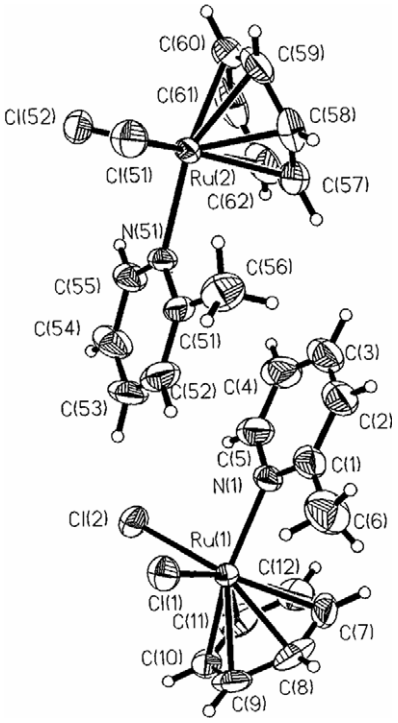

Fig. 1. ORTEP drawing of $[(C_6H_6)RuCl_2(\alpha\text{-pic})]$ with 50% probability displacement ellipsoids. The disordered part of picoline substituent is omitted for clarity.

The Ru–Cl bonds length are of the same order as in related compounds [14]. The picoline ligand displays a Ru–N distance of 2.188(3) Å for Ru(1)–N(1) and 2.184(7) Å for Ru(2)–N(51), which are similar and in the range of Ru–N distances. The ruthenium atom is π-bonded to the benzene ring with an average Ru–C distance of 2.176(4) Å (2.173(4) Å for Ru(1)–C to 2.178(4) Å for Ru(2)–C), whereas the distance between the ruthenium atom and the centroid of the ring varies from 1.665(9) Å (Ru(1)) to 1.671(2) Å (Ru(2)) and is consistent with those reported for other Ru(II) η^6-arene complexes [15,16].

The bond valences were computed as $v_{ij} = \exp[(R_{ij} - d_{ij})/b]$ [17–19], where R_{ij} is the bond-valence parameter (in the formal sense the R_{ij} parameter value can be considered as an idealised single-bond length between i and j atoms). The R_{Ru-N}, $R_{Ru-\pi}$, R_{Ru-Cl} values were taken as 1.656, 1.731 and 1.932 [20], respectively, and b was taken as 0.37 [17]. The computed bond valences of ruthenium are $v_{Ru-N} = 0.237$, 0.240; $v_{Ru-\pi} =$ 1.195, 1.176; $v_{Ru-Cl} = 0.267$, 0.268 and 0.255, 0.265 v.u. (valence units) which means that the Ru–π bond is almost four times stronger than the other bonds, and the Ru–N bond is the weakest one. The valence sum rule states that the sum of the valences of the bonds formed by an atom is equal to the valence of the atom. The computed total valence of the Ru(1) atom is 1.954 and of Ru(2) – 1.949 v.u., which agree with the formal oxidation state and confirm the correctness of the coordination sphere solution.

The two intermolecular hydrogen bonds [21–23] linking the chlorine ligand and picoline C(3)–H(3)...Cl(52)(1# x, $y+1$, z) (D···A distance 3.611(5) Å, D–H···A angle

Table 2
Selected bond lengths (Å) and angles (°) for $[(C_6H_6)RuCl_2(\alpha\text{-pic})]$

Experimental				Calculated
Bond lengths (Å)				
Ru(1)–Cl(1)	2.421(8)	Ru(2)–Cl(51)	2.419(9)	2.423
Ru(1)–Cl(2)	2.438(8)	Ru(2)–Cl(52)	2.423(9)	2.435
Ru(1)–N(1)	2.188(3)	Ru(2)–N(51)	2.184(7)	2.242
Ru(1)–C(11)	2.166(3)	Ru(2)–C(61)	2.167(4)	2.219
Ru(1)–C(7)	2.168(4)	Ru(2)–C(57)	2.169(4)	2.232
Ru(1)–C(8)	2.169(4)	Ru(2)–C(58)	2.176(4)	2.255
Ru(1)–C(9)	2.170(3)	Ru(2)–C(59)	2.177(4)	2.213
Ru(1)–C(10)	2.179(3)	Ru(2)–C(60)	2.188(4)	2.216
Ru(1)–C(12)	2.188(4)	Ru(2)–C(62)	2.188(4)	2.260
Bond angles (°)				
C(8)–Ru(1)–N(1)	110.77(15)	C(58)–Ru(2)–N(51)	105.5(6)	111.50
C(10)–Ru(1)–N(1)	161.62(13)	C(60)–Ru(2)–N(51)	167.0(6)	165.47
C(12)–Ru(1)–N(1)	94.80(13)	C(62)–Ru(2)–N(51)	99.6(5)	98.86
C(8)–Ru(1)–Cl(1)	95.66(13)	C(58)–Ru(2)–Cl(51)	95.04(12)	97.58
C(10)–Ru(1)–Cl(1)	109.39(11)	C(60)–Ru(2)–Cl(51)	111.46(14)	107.06
C(12)–Ru(1)–Cl(1)	163.81(13)	C(62)–Ru(2)–Cl(51)	161.77(15)	164.09
C(8)–Ru(1)–Cl(2)	159.21(12)	C(58)–Ru(2)–Cl(52)	158.23(13)	159.78
C(10)–Ru(1)–Cl(2)	92.38(10)	C(60)–Ru(2)–Cl(52)	92.53(13)	92.78
C(12)–Ru(1)–Cl(2)	109.90(14)	C(62)–Ru(2)–Cl(52)	112.90(15)	85.36
N(1)–Ru(1)–Cl(1)	88.96(7)	N(51)–Ru(2)–Cl(51)	90.07(17)	87.46
N(1)–Ru(1)–Cl(2)	89.98(8)	N(51)–Ru(2)–Cl(52)	96.0(6)	88.21
Cl(1)–Ru(1)–Cl(2)	85.80(3)	Cl(51)–Ru(2)–Cl(52)	85.28(3)	87.43
C(8)–Ru(1)–C(10)	67.52(15)	C(58)–Ru(2)–C(60)	67.04(17)	67.01
C(8)–Ru(1)–C(12)	68.27(18)	C(58)–Ru(2)–C(62)	67.62(18)	66.53
C(10)–Ru(1)–C(12)	67.27(15)	C(60)–Ru(2)–C(62)	68.02(17)	67.00

146.3°), C(8)–H(8)...Cl(1)(2# $-x+1/2, y+1/2, -z+1/2$) (D···A distance 3.660(4) Å, D–H···A angle 174.3°) atoms are observed. Four other intramolecular weak hydrogen bonds are presented in the structure of the complex between picoline C(5)–H(5) and Cl(2) (D···A distance 3.210(4) Å, D–H···A angle 122.9°), C(6)–H(6A)···Cl(1) (D···A distance 3.423(5) Å, D–H···A angle 146.6°), and C(55)–H(55)...Cl(52) (D···A distance 3.178(8) Å, D–H···A angle 116.7°), C(56)–H(56C)...Cl(51) (D···A distance 3.341(7) Å, D–H···A angle 143.5°). In this way an infinite three-dimensional hydrogen-bonded net has been created (see Table 3). In the molecule two C–H···π interactions can also be found, which, according to Desiraju and Steiner [21] can be classified as weak hydrogen bonds: C(2)–H(2)···Cg(picoline$_{(N51)}$# $-x+1, -y+1, -z$) and C(59)–H(59)··· Cg(benzene$_{(C7)}$# $-x+1/2, y+1/2, -z+1/2$) with D···A distances 3.417(8), 3.241(5) Å, and D–H···A angles 89.55°, 74.21°, respectively. The structure is stabilised by intermolecular stacking interactions between almost coplanar benzene rings: indicated by C(7) and C(57# $-x+3/2, y+1/2, -z+1/2$) atoms with a Cg···Cg# distance 3.542(5) Å, angle between Cg···Cg# vector and normal to plane Cg# equal to 24.2(3)° and perpendicular distance of Cg on ring Cg# 3.231(5) Å.

Table 3
Hydrogen bonds for $[(C_6H_6)RuCl_2(\alpha\text{-pic})]$ (Å and °)

D–H···A	*d*(D–H)	*d*(H···A)	*d*(D···A)	∠(DHA)
C(3)–H(3)...Cl(52)#1	0.93	2.80	3.611(5)	146.3
C(5)–H(5)...Cl(2)	0.93	2.61	3.210(4)	122.9
C(6)–H(6A)...Cl(1)	0.96	2.58	3.423(5)	146.6
C(8)–H(8)...Cl(1)#2	0.93	2.73	3.660(4)	174.3
C(55)–H(55)...Cl(52)	0.93	2.65	3.178(8)	116.7
C(56)–H(56C)...Cl(51)	0.96	2.52	3.341(7)	143.5

Symmetry transformations used to generate equivalent atoms: #1 $x, y+1, z$; #2 $-x+1/2, y+1/2, -z+1/2$.

3.1. Geometry and electronic structure

The optimised geometry parameters for the complex with α-picoline are given in Table 2. The optimized bond distances and angles of $[(C_6H_6)RuCl_2(\alpha\text{-pic})_2]$ agree with the experimental values. The largest differences were found for the ruthenium–benzene carbons distances. The calculated Ru–benzene distance is 1.7219 Å. Although the X-ray structures of the complexes with β- and γ-picoline were not determined, their geometries, electronic transitions and IR frequencies were calculated. A good agreement of the calculated spectroscopic properties of $[(C_6H_6)RuCl_2(\beta\text{-pic})_2]$ and $[(C_6H_6)RuCl_2(\gamma\text{-pic})_2]$ with the experimental ones indicates the calculated geometries correspond to the real structures. The maximum error between the calculated and experimental IR frequencies is about 4.8% for the complex with β-picoline and 3.5% for $[(C_6H_6)RuCl_2(\gamma\text{-pic})]$.

The formal charge of ruthenium is +2 in these complexes. The calculated charges on the ruthenium atoms, obtained from natural population analysis, are equal to 0.735 for the complex with α-picoline, 0.745 for β- and γ-picoline The charges on the chloride ligands are higher

than −1 (−0.516, −0.525 for α-picoline; −0.528 for β-picoline; −0.527, −0.529 for γ-picoline); the charge on the picoline nitrogen atom is negative and amounts to −0.453, −0.431 and −0.442 for complexes with α-, β- and γ-picoline, respectively. The HOMO–LUMO gap is 4.06 eV for $[(C_6H_6)RuCl_2(\alpha\text{-pic})]$, 4.03 eV for $[(C_6H_6)RuCl_2(\beta\text{-pic})]$ and 4.04 eV for $[(C_6H_6)RuCl_2(\gamma\text{-pic})]$.

The bonding between benzene and ruthenium, formed by the two π orbitals of e_{1g} symmetry (π_2 and π_3) and the empty d_{xz} and d_{yz} orbitals of the metal atom (donation from benzene to ruthenium), is visible in the HOMO − 12 and HOMO − 13 molecular orbitals and the antibonding are LUMO and LUMO + 1. In the back-donation (metal to ligand), the occupied $d_{x^2-y^2}$ and d_{xy} metal orbitals and empty π_4^*, π_5^* benzene orbitals participate (HOMO − 1, HOMO and LUMO + 3, LUMO + 5). The HOMO − 2 is a combination of d ruthenium and π chlorine orbitals. HOMO − 3 is a π chlorine orbital. The chlorine orbitals have a contribution, with the d metal orbitals, in the HOMO − 4, HOMO − 7 and HOMO − 8 molecular orbitals. The picoline ligand has a significant contribution in the HOMO − 5 (with the π chlorine), HOMO − 10 and HOMO − 11 molecular orbitals. The LUMO + 2 and LUMO + 4 molecular orbitals are composed of picoline rings.

3.2. Electronic spectrum

The experimental spectra of the investigated complexes show bands at 434.6, 346.2, 263.0, 227.0 nm for $[(C_6H_6)RuCl_2(\alpha\text{-pic})]$, 409.8, 256.8, 224.4, 213.4 nm for $[(C_6H_6)RuCl_2(\beta\text{-pic})]$ and 402.4, 249.8, 220.4, 218.0 nm for $[(C_6H_6)RuCl_2(\gamma\text{-pic})]$. The measured (solid line) and calculated (dashed line) electronic spectrum of $[(C_6H_6)RuCl_2(\alpha\text{-pic})]$ is shown in Fig. 2. Each calculated transition in Fig. 2 was represented by a Gaussian function with the height equal to the oscillator strength and width equal to 0.05. With the use of the TDDFT method 90 electronic transitions were calculated for these complexes using the DZVP with f functions basis set on the ruthenium atom and the polarization functions on the other atoms. The calculated spectra are in good agreement with the experimental ones.

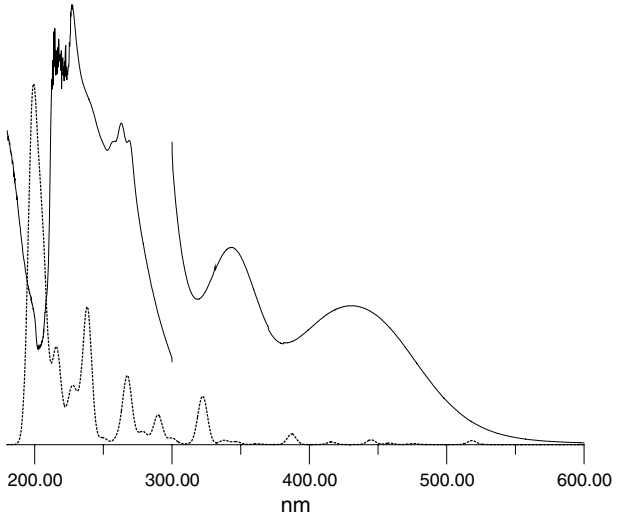

Fig. 2. The UV–Vis spectrum of the $[(C_6H_6)RuCl_2(\alpha\text{-pic})]$ complex.

In the calculated electronic spectra of $[(C_6H_6)RuCl_2(picoline)]$ the lowest energy transitions (above 400 nm) are of d → d origin and they are characterised with small oscillator strengths. The experimental bands at 346.2 nm for the complex with α-picoline, 256.8 nm for β-picoline and 249.8 nm for γ-picoline correspond to the MLCT ($d \rightarrow \pi^*_{pic}$) and LMCT ($Cl \rightarrow d$) transitions. The higher energy bands at 263.0, 224.4, 220.4 nm and 227.0, 213.4, 218 nm for complexes with α-, β- and γ-picoline complexes, respectively, are of LLCT type (inter and intraligand) and consist of $\pi_{Cl} \rightarrow \pi^*_{Cl}$, $\pi_{pic} \rightarrow \pi^*_{pic}$, $\pi_{Cl} \rightarrow \pi^*_{pic}$, $\pi_{pic} \rightarrow \pi^*_{Cl}$ transitions. The $\pi_{benz} \rightarrow d$ (LMCT) excitation is visible in the highest energy bands.

4. Supplementary material

More details of the crystal structure determination have been deposited with the Cambridge Crystallographic Data Centre with the deposition number: CCDC 264833. Copies of this information can be obtained from the Director, CCDC, 12 Union Road, Cambridge CB2 1EZ, UK, fax: +44 1223 336 033, e-mail deposit@ccdc.cam.ac.uk or on the www.ccdc.cam.ac.uk.

Acknowledgements

The crystallographic part was financed by funds allocated by the Ministry of Scientific Research and Information Technology to the Institute of General and Ecological Chemistry, Technical University of Łódź. The GAUSSIAN 03 calculations were carried out in the Wrocław Centre for Networking and Supercomputing, WCSS, Wrocław, Poland under calculational Grant No. 51/96.

References

[1] (a) H. Le Bozec, D. Touchard, P.H. Dixneuf, Adv. Organomet. Chem. 29 (1989) 163;
(b) R.M. Moriarty, U.S. Gill, Y.-Y. Ku, J. Organomet. Chem. 350 (1988) 157;
(c) R. Noyori, S. Hashiguchi, Acc. Chem. Res. 30 (1997) 97;
(d) M.A. Bennett, in: E.W. Abel, F.G.A. Stone, G. Wilkinson (Eds.), Comprehensive Organometallic Chemistry II, vol. 7, Pergamon Press, Oxford, 1995;
(e) M.A. Bennett, Coord. Chem. Rev. 166 (1997) 225;
(f) Y.N.V. Gopal, A.K. Kondapi, J. Biosci. 26 (2001) 271;
(g) Y.N.V. Gopal, N. Konuru, A.K. Kondapi, Arch. Biochem. Biophys. 401 (2002) 53.
[2] G. Winkhaus, H. Singer, J. Organomet. Chem. 7 (1967) 487.
[3] (a) I. de los Rios, M.J. Tenerio, M.A.J. Tenorio, M.C. Puerta, P. Valerga, J. Organomet. Chem. 525 (1996) 57;
(b) A. Schlüter, K. Bieber, W.S. Sheldrick, Inorg. Chim. Acta 340 (2002) 35;
(c) Y. Chen, M. Valentini, P.S. Pregosin, A. Albinati, Inorg. Chim. Acta 327 (2002) 4;

(d) A. Singh, N. Singh, D.S. Pandey, J. Organomet. Chem. 642 (2002) 48.
[4] M.A. Bennett, T.-N. Huang, T.W. Matheson, A.K. Smith, Inorg. Synth. 21 (1982) 74.
[5] X-RED, Version 1.18, STOE & Cie GmbH, Darmstadt, Germany, 1999.
[6] G.M. Sheldrick, Acta Cryst. A 46 (1990) 467.
[7] G.M. Sheldrick, SHELXL 97. Program for the Solution and Refinement of Crystal Structures, University of Göttingen, Germany, 1997.
[8] G.M. Sheldrick, SHELXTL: release 4.1 for Siemens Crystallographic Research Systems, 1990.
[9] M.J. Frisch, G.W. Trucks, H.B. Schlegel, G.E. Scuseria, M.A. Robb, J.R. Cheeseman, J.A. Montgomery Jr., T. Vreven, K.N. Kudin, J.C. Burant, J.M. Millam, S.S. Iyengar, J. Tomasi, V. Barone, B. Mennucci, M. Cossi, G. Scalmani, N. Rega, G.A. Petersson, H. Nakatsuji, M. Hada, M. Ehara, K. Toyota, R. Fukuda, J. Hasegawa, M. Ishida, T. Nakajima, Y. Honda, O. Kitao, H. Nakai, M. Klene, X. Li, J.E. Knox, H.P. Hratchian, J.B. Cross, C. Adamo, J. Jaramillo, R. Gomperts, R.E. Stratmann, O. Yazyev, A.J. Austin, R. Cammi, C. Pomelli, J.W. Ochterski, P.Y. Ayala, K. Morokuma, G.A. Voth, P. Salvador, J.J. Dannenberg, V.G. Zakrzewski, S. Dapprich, A.D. Daniels, M.C. Strain, O. Farkas, D.K. Malick, A.D. Rabuck, K. Raghavachari, J.B. Foresman, J.V. Ortiz, Q. Cui, A.G. Baboul, S. Clifford, J. Cioslowski, B.B. Stefanov, G. Liu, A. Liashenko, P. Piskorz, I. Komaromi, R.L. Martin, D.J. Fox, T. Keith, M.A. Al-Laham, C.Y. Peng, A. Nanayakkara, M. Challacombe, P.M.W. Gill, B. Johnson, W. Chen, M.W. Wong, C. Gonzalez, J.A. Pople, GAUSSIAN 03, Revision B.03, Gaussian, Inc., Pittsburgh, PA, 2003.
[10] A.D. Becke, J. Chem. Phys. 98 (1993) 5648.
[11] C. Lee, W. Yang, R.G. Parr, Phys. Rev. B 37 (1988) 785.
[12] M.E. Casida, in: J.M. Seminario (Ed.), Recent Developments and Applications in Modern Density Functional Theory, Theoretical and Computational Chemistry, vol. 4, Elsevier, Amsterdam, 1996.
[13] N. Godbout, D.R. Salahub, J. Andzelm, E. Wimmer, Can. J. Chem. 70 (1992) 560.
[14] F.B. McCormick, D.D. Cox, W.B. Gleason, Organometallics 12 (1993) 610.
[15] U. Beck, W. Hummel, H.B. Burgi, A. Ludi, Organometallics 6 (1993) 20.
[16] F.B. McCormick, D.D. Cox, W.B. Gleason, Organometallics 12 (1993) 610.
[17] I.D. Brown, Acta Crystallogr., Sect., B 48 (1992) 553.
[18] I.D. Brown, Acta Crystallogr., Sect., B 53 (1997) 381.
[19] M. O'Keeffe, N.E. Brese, J. Am. Chem. Soc. 113 (1991) 3226.
[20] J.G. Małecki, J.O. Dzigielewski, M. Jaworska, R. Kruszynski, T.J. Bartczak, Polyhedron 23 (5) (2004) 885.
[21] G.R. Desiraju, T. Steiner, The Weak Hydrogen Bond in Structural Chemistry and Biology, Oxford University Press, Oxford, 1999.
[22] G.A. Jeffrey, W. Saenger, Hydrogen Bonding in Biological Structures, Springer-Verlag, Berlin, 1994.
[23] R. Taylor, O. Kennard, J. Am. Chem. Soc. 104 (1982) 5063.

followed by water (40 ml). The dichloromethane layer was separated and dried over anhydrous sodium sulfate. Distillation of dichloromethane extract gave *N*-benzoylimidazole (yield 90%) a colorless pasty liquid. IR (neat, cm^{-1}) 3150(s), 2843(s), 1711(s), 1603(s), 1552(s), 1383(s), 1327(m), 1327(m), 1276(s), 1178(m), 1071(s), 835(s), 717(s); ^1H NMR ($CDCl_3$) 7.84(s, 1H) 7.76–7.69(m, 1H), 7.56–7.53(m,2H), 7.46–7.42(m, 1H) 7.33–7.29(m, 2H), 6.918(s, 1H); ^{13}C NMR ($CDCl_3$) 137.48, 132.86, 131.12, 130.95, 129.06, 128.26, 127.65, 126.92; GC mass (*m/e*) 344 (for dimer), 277, 176, 116, 106, 78, 49, 38.

2.2. Synthesis of N-benzoyl 3,5-dimethylpyrazole (*II*)

To a solution of benzoylchloride (700 mg, 5 mmol) in dichloromethane (5 ml), triethylamine (606 mg, 6 mmol) was added. To this solution another solution of 3,5-dimethylpyrazole (480 mg, 5 mmol) in dichloromethane (6 ml) was added dropwise at room temperature. The solution was stirred for 3.5 h and to the reaction mixture dichloromethane (20 ml) was added, followed by addition of water (40 ml). The dichloromethane layer was separated by a separating funnel and dried over anhydrous sodium sulfate. Distillation of the dichloromethane extract gave the crude product. The crude product was washed with hexane (10 ml) to remove any hexane soluble impurity. The residue was filtered and the residue was found to be *N*-benzoyl 3,5-dimethylpyrazole (yield 92%). IR (neat, cm^{-1}) 3068(w), 2981(m), 2935(m), 1700(s), 1598(s), 1459(s), 1413(s), 1342(s), 1280(s), 1193(m), 1127(m), 1039(m), 978(s), 922(s), 804(m), 712(s). ^1H NMR ($CDCl_3$) 7.96–7.94(m, 2H), 7.58–7.40(m, 1H), 7.39–7.37(m, 2H), 6.0(s, 1H), 2.59(s, 3H), 2.20(s, 3H); ^{13}C NMR ($CDCl_3$): 167.82, 151.59, 144.59, 132.96, 131.96, 130.95, 127.40, 110.72, 14.17, 13.69. GC mass (*m/e*) 202, 172, 115, 105, 77, 59, 39.

2.3. Synthesis of imidazolium benzoate (*III*)

N-benzoylimidazole (176 mg 1 mmol) was dissolved in ethyleneglycol (1 ml). To this solution water (0.2 ml) was added. Standing for two days gave white crystals of imidazoliumbenzoate (60 mg). IR(KBr, cm^{-1}): 3401(bs), 3139(s), 2842(s), 1710(s), 1598(s), 1547(s), 1465(s), 1383(s), 1306(s), 1255(s), 1183(s), 1070(s), 1024(s), 896(s), 717(s). Elemental *Anal*. Calc. for $C_{10}H_{10}N_2O_2$: C, 63.13; H, 5.30; N, 14.73. Found: C, 63.58; H, 5.28; N, 14.26%. ^1H NMR ($CDCl_3$): 13.5(s,1H), 8.00–7.96(m, 1H), 7.67–7.65(m, 2H), 7.45–7.34(m,1H), 7.30–7.28(m, 2H), 7.06–7.01(m, 2H).

2.4. Synthesis of cis-$(pz)_2Cu(OBz)_2 \cdot$ trans-$(pz)_2Cu(OBz)_2H_2O$ (*B*)

To a solution of copper(II) nitrate trihydrate (242 mg, 1 mmol) in acetonitrile (3 ml) *N*-benzoyl 3,5-dimethylpyrazole (404 mg, 2 mmol) was added. The mixture was stirred to obtain a homogeneous solution. To this solution water (1 ml) was added. A blue crystalline precipitate appeared after 7 days (30 mg) on standing. The crystals were picked out and the structure was determined by X-ray diffraction. Elemental *Anal*. Calc. for $C_{48}H_{54}N_8O_9Cu_2$: C, 56.83; H, 5.37; N, 11.05. Found: C, 57.05; H, 5.56; N, 10.95; IR(KBr, cm^{-1}): 3206(m), 3145(m), 3047(w), 1628(s), 1582(m), 1531(s), 1403(s), 1296(m), 1183(w), 1070(w), 860(w), 804(w), 717(s). Crystal parameters of **B:** Monoclinic, space group *C2/c*, $a = 39.461(5)$, $b = 16.2272(17)$, $c = 11.6867(12)$ Å, $\alpha = 90.00°$, $\beta = 94.998(7)°$, $\gamma = 90.00°$, $V = 7455.1(15)$ Å^3, $Z = 4$, $T = 296$ K.

2.5. Copper(II) catalyzed benzoylation of alcohols by N-benzoylimidazole

In a typical experiment *N*-benzolylimidazole (115 mg, 1 mmol), copper(II) nitrate trihydrate (12 mg, 0.05 mmol) and nitric acid (0.01 M, 0.1 ml) were mixed together in methanol (2 ml) and stirred at room temperature. After 2 h of stirring, water (20 ml) was added to the reaction mixture and the organic products were extracted with dichloromethane (40 ml). The dichloromethane layer was separated using a separating funnel and dried over anhydrous sodium sulfate. Removal of dichloromethane from this extract under reduced pressure gave methylbenzoate as the only product. The compound was characterized by recording its ^1H NMR and IR spectra and comparing them with an authentic sample. Products from similar reactions with other alcohols were also confirmed by recording ^1H NMR and GC–MS spectra. For benzoylation of solid alcohols dry acetonitrile was used as the solvent. From a similar reaction of ethyleneglycol with *N*-benzoylimidazole under catalytic conditions only the mono-benzoylated ester was obtained. Spectral details of $C_6H_5COOCH_2CH_2OH$: IR (neat, cm^{-1}) 3416(bs), 1716(s), 1603(m), 1347(s), 1265(s), 1117(s), 707(s). ^1H NMR ($CDCl_3$): 8(m, 2H), 7.55(m, 1H), 7.4(m, 2H), 4.4(m, 2H), 3.9(m, 2H), 2.4(bs, exchangeable, 1H). GC–MS: (*m/e*), 167, 148, 135, 105, 77, 51.

3. Results and discussions

N-benzoylimidazole reacts with copper(II) nitrate trihydrate in methanol to form methylbenzoate and tetra-(imidazole)copper(II) nitrate (**A**) (Eq. (1)) under ambient conditions. Complex **A** has been characterized by determining its crystal structure by single crystal X-ray diffraction. The structure of this complex tallies with the one reported in the literature [28]. This reaction is a stoichiometric reaction. From this reaction, we could prepare the corresponding ester of methanol by using 1/4 molar ratio of copper(II) nitrate with respect to the *N*-benzoylimidazole. However, we had an important observation at this stage, if a drop of dilute nitric acid is added to the reaction mixture the esterification reaction worked catalytically. Inspired by this observation, we carried out a series of

benzoylation reactions by *N*-benzoylimidazole with different alcohols (Eq. (2)). The results showing the reaction time and yield obtained from these esterification reactions catalyzed by copper(II) under ambient conditions are listed in Table 1. In order to ascertain that the copper(II) nitrate, along with nitric acid, acts as a catalyst, we have carried out reactions under identical conditions without the catalyst and observed no significant reaction in this case. It is worth mentioning that the reaction of *N*-benzoylimidazole with nitric acid without copper(II) nitrate led to the formation of benzoic acid (1 ml, 0.1 M HNO_3, approximately 2 h for conversion of 1 mmol of *N*-benzoylimidazole). However, we used a lesser amount of the acid in our reactions; namely 0.1 ml of 0.01 M nitric acid for conversion of 1 mmol of *N*-benzoylimidazole to ester. These results clearly indicate that the catalytic ability of the copper(II) nitrate trihydrate is enhanced by the presence of the nitric acid. This probably happens because of protonation of the imidazole that is formed in the reaction by C–N bond cleavage. Imidazole in the absence of an acid can otherwise coordinate strongly to the copper(II) ion. This is further confirmed by adding nitric acid to tetra(imidazole)copper(II) nitrate in an independent experiment, which led to decomposition of this complex.

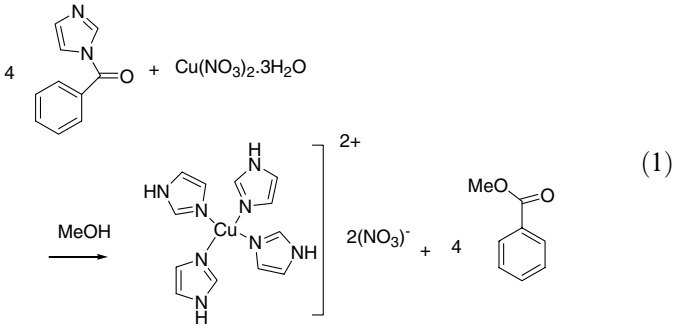

(1)

In addition to the primary alcohols, secondary alcohols such as isopropyl alcohol reacted very well to give the corresponding esters. The reaction does not work with tertiary alcohols such as *tert*-butanol. We also examined the reaction of *N*-benzoylimidazole with methanol in the presence of *tert*-butanol under catalytic conditions to ascertain if *tert*-butanol has a retarding effect on the rate. In this reaction only methylbenzoate was formed. It showed that *tert*-butanol does not hinder the benzolyation and also it does not itself give the corresponding ester under ambient conditions. Different allylic esters from allylic alcohols were also prepared by this copper(II) catalyzed reaction. However, in the case of decanol the reaction had to be carried out by suspending copper(II) nitrate trihydrate under heterogeneous conditions, as the later is not soluble in decanol. This solubility problem could be overcome by using complex **A** with very dilute nitric acid as a catalyst in acetonitrile as the solvent. Thus, the use of tetra(imidazole)copper(II) nitrate (**A**) as a catalyst instead of copper(II) nitrate trihydrate has an advantage as it minimizes the solubility problem in the case of long chain alcohols. Complex **A** is soluble in common solvents such as methanol, ethanol, acetonitrile; so the benzoylation reactions using complex **A** as a catalyst could be carried out in solvents other than the alcohols. The copper complex **A** does not have any water of crystallization, so the water content in the reaction is minimized and also the side reaction to give benzoic acid. Two illustrative examples using complex **A** as a catalyst are given in Table 1 (last two rows). Since our interest is on an alternative reagent for benzoylchloride, it is essential to know the stability of *N*-benzoylimidazole. *N*-benzoylimidazole itself gets hydrolytically cleaved in methanol/water mixture (1:1) in 24 h to give methylbenzoate and benzoic acid. However, it undergoes slow hydrolysis in ethyleneglycol. When *N*-benzoylimidazole was dissolved in ethyleneglycol containing traces of water; the water present in the ethyleneglycol reacted with it. After two days of reaction, we obtained white crystals of imidazoliumbenzoate from the reaction mixture. The role of ethyleneglycol in this salt formation reaction is presumably to provide a medium for the reaction to control the crystallization process. This fact is supported by the observation that an aqueous methanolic solution of *N*-benzoylimidazole on standing under ambient conditions gave benzoic acid as a crystalline product after five days. The reaction of ethyleneglycol with *N*-benzoylimidazole in the presence of a catalytic amount of copper(II) nitrate trihydrate and nitric acid gave the mono-benzolylated derivative of ethyleneglycol. It was earlier reported [18] that 1-(benzoyl)benzotriazole can be used for benzoylation of different diols in methylenechloride to give mono-benzoylated derivatives. These reactions were carried out in basic

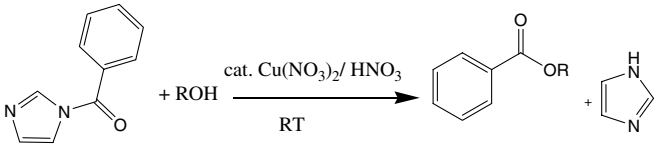

R = Methyl, Ethyl, *iso*-propyl, benzyl, allyl, crotyl, propargyl etc.

(2)

Table 1
The results on copper(II) nitrate catalyzed benzoylation

Alcohol	Product	Time, yield (%)
CH_3OH	$C_6H_5COOCH_3$	2 h, 95
CH_3CH_2OH	$C_6H_5COOCH_2CH_3$	1.5 h, 86
$CH_3(CH_2)_3OH$	$C_6H_5COO(CH_2)_3CH_3$	2 h, 68
$(CH_3)_2CHOH$	$C_6H_5COOCH(CH_3)_2$	2 h, 94
$C_6H_5CH_2OH$	$C_6H_5COOCH_2C_6H_5$	2 h, 90
$CH_2{=}CHCH_2OH$	$C_6H_5COOCH_2CH{=}CH_2$	3 h, 56
$CH_3CH{=}CHCH_2OH$	$C_6H_5COOCH_2CH{=}CHCH_3$	2 h, 90
$CHCCH_2OH$	$C_6H_5COOCH_2CCH$	2 h, 86
$C_6H_5CH{=}CHCH_2OH$	$C_6H_5COOCH_2CH{=}CHC_6H_5$	2 h, 76
Cyclo-$C_6H_{11}OH$	C_6H_5COO(cyclo-C_6H_{11})	2 h, trace
CH_2OHCH_2OH	$C_6H_5COOCH_2CH_2OH$	1 h, 92
$CH_3(CH_2)_7OH$	$C_6H_5COO(CH_2)_7CH_3$	3 h, trace
CH_3OH[a]	$C_6H_5COOCH_3$	1 h, 95
CH_3CH_2OH[a]	$C_6H_5COOCH_2CH_3$	1 h, 97

[a] With a catalytic amount of tetra(imidazole)copper(II) nitrate.

medium in the presence of triethylamine. Our copper catalyzed benzoylation reactions of *N*-benzoylimidazole with diols also gave only the mono-benzoylated product, but the difference is that the copper(II) catalyzed reactions were carried out under acidic conditions.

N-benzoyl 3,5-dimethylpyrazole on reaction with copper(II) nitrate trihydrate (2:1 molar ratio) in aqueous methanol at 25 °C for three days gave an interesting mixed copper(II) benzoate complex having the composition *cis*-$(pz)_2Cu(OBz)_2 \cdot$ *trans*-$(pz)_2Cu(OBz)_2H_2O$ (**B**) (where pz = 3,5-dimethylpyrazole and OBz = benzoate anion). The compound is structurally important (Fig. 1) as it has the distinction of having a unique lattice in which both *cis* and *trans* coordination of 3,5-dimethylpyrazole are present around two independent copper(II) centers. From this structure, the process can be understood to be co-crystallization of two inorganic neutral molecules in the form of an adduct. It is interesting to note that each of the two independent units, namely *cis*-$(pz)_2Cu(OBz)_2$ and *trans*-$(pz)_2Cu(OBz)_2H_2O$, is not held by any common weak interactions such as hydrogen-bonding, π-interactions or C–H···O interactions in the lattice but probably they are held by dipolar interactions due to a difference in the dipole moment of two the units. Such a difference in dipole moments is obvious from the orientation of the ligand as well as the coordination number of the two counterparts. The adduct (**B**) can also easily be prepared by the reaction of copper(II) acetate with benzoic acid in the presence of 3,5-dimethylpyrazole in methanol. However, reactions of copper(II) acetate with *o*-chlorobenzoic acid or *o*-nitrobenzoic acid and 3,5-dimethylpyrazole gives monomeric bis-3,5-dimethylpyrazole copper(II) *o*-chlorobenzoate or bis-3,5-dimethylpyrazole copper(II) *o*-nitrobenzoate respectively. Complex **B** has an interesting packing pattern, as shown in Fig. 2. It forms a parallel layered structure and the layers are formed by H-bonding interactions among the *cis*-$(pz)_2Cu(OBz)_2$ and *trans*-$(pz)_2Cu(OBz)_2H_2O$, independently. The layers are held by H-bonding interactions between the NH groups of the 3,5-dimethylpyrazole and the carboxylate oxygen atoms of each independent *cis*-$(pz)_2Cu(OBz)_2$ unit. In the *trans* counterpart, the H-bonding interactions occurs through the carboxyl oxygens with coordinated water and also through N–H···O interactions among carboxyl groups and N–H protons of the 2,3-dimethylpyrazole ligands.

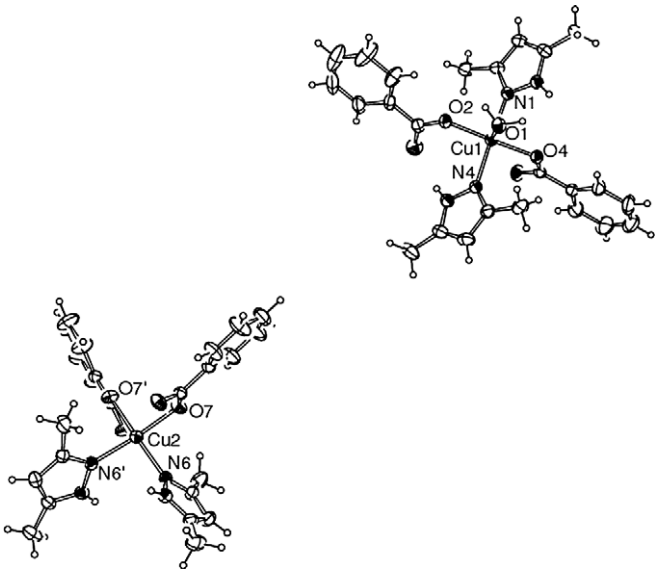

Fig. 1. Crystal structure of the adduct *cis*-$(pz)_2Cu(OBz)_2 \cdot$ *trans*-$(pz)_2Cu(OBz)_2H_2O$ (**B**).

All these results show that the formation of complex **A** is one of the driving forces for catalysis of *N*-benzoylimidazole, but in the case of *N*-benzoyl 3,5-dimethylpyrazole, such reactions gave a catalytically inactive complex **B**.

In conclusion we have shown that C–N bond cleavage by copper(II) complexes are not only useful for catalytic

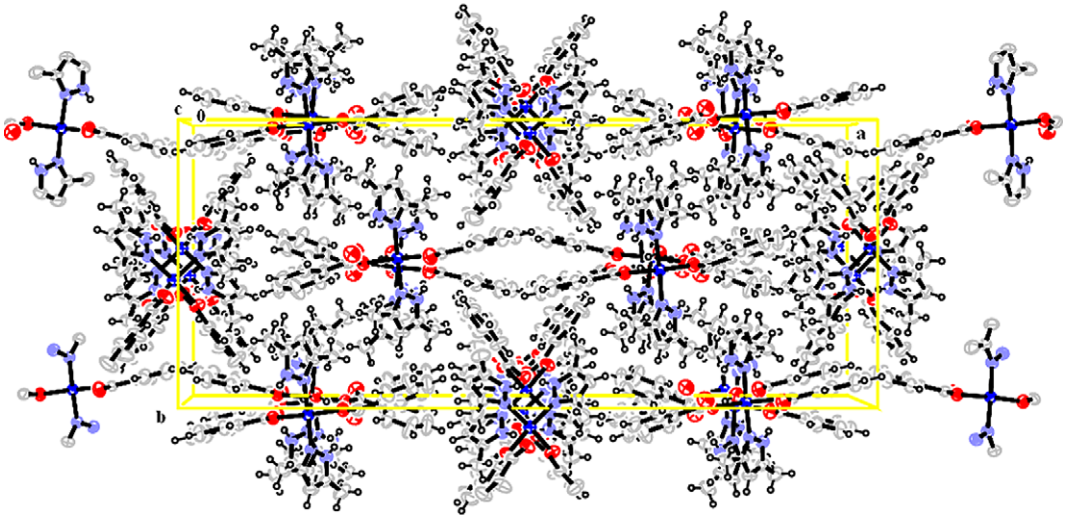

Fig. 2. The crystal packing in the adduct **B** viewed along crystallographic *c*-axis.

benzoylation reactions but also provide a method for the preparation of metal complexes.

Acknowledgments

The authors thank DST (New Delhi, India) for funding and the X-ray diffractometer facility. We thank Mr. R.J. Sarma for help with the crystallography.

Appendix A. Supplementary material

Crystallographic data for the structure have been deposited with the Cambridge Crystallographic Data Centre, CCDC No. 281721. Copies of this information can be obtained from the Director, CCDC, 12 Union Road, Cambridge CB2 1EZ, UK, e-mail: deposit@ccdc.cam.ac.uk.

The GC mass of the *N*-benzoylimidazole and *N*-benzoyl 3,5-dimethylpyrazole are also available. Supplementary data associated with this article can be found, in the online version, at doi:10.1016/j.poly.2006.02.019

References

[1] P.J. Kocienski, Protecting Groups, Theime, Stuttgart, 1994.
[2] T.W. Greene, P.G.M. Wutz, Protective Groups in Organic Synthesis, third ed., Wiley, New York, 1999.
[3] J. Otera, Esterification: Methods, Reactions and Applications, Wiley-VCH, Weinheim, 2003.
[4] A.K. Prasad, V. Kumar, J. Maity, Z.W. Wang, V.T. Ravikumar, Y.S. Sanghvi, V.S. Parmar, Syn. Commun. 35 (2005) 935.
[5] J.K. Murthy, U. Gross, S. Rudiger, E. Kemnitz, Appl. Catal. A 278 (2004) 133.
[6] H.A. Prescott, M. Wloka, E. Kemnitz, J. Mol. Catal. A 223 (2004) 67.
[7] H. Nakamura, K. Arata, Bull. Chem. Soc. Japan 77 (2004) 1893.
[8] U.B. Gangadharmath, A.V. Demchenko, Synlet (2004) 2191.
[9] H.S. Wang, J. She, L.H. Zhang, X.S. Ye, J. Org. Chem. 69 (2004) 5774.
[10] S.M. Landge, M. Chidambaram, A.P. Singh, J. Mol. Catal. A 213 (2004) 257.
[11] P. Ciuffreda, L. Alessandrini, G. Terraneo, E. Santaniello, Molecules (2003) 374.
[12] Y. Matsumura, T. Maki, S. Murakami, O. Onomura, J. Am. Chem. Soc. 125 (2003) 2052.
[13] T. Iwata, Y. Miyake, Y. Nishibayashi, S. Uemura, J. Chem. Soc., Perkin Trans. 1 (2002) 1548.
[14] I. Mohammadpoor-Baltork, H. Aliyan, A.R. Khosropour, Tetrahedron 57 (2001) 5851.
[15] R.R. Mukti, H. Nur, S. Endud, H. Hamdan, in: E. Van Steen, L.H. Callanan, M. Claeys (Eds.), Studies in Surface Science and Catalysis, vol. 154, Elsevier, Amsterdam, 2004, p. 2767.
[16] E. Santaniello, S. Casati, P. Ciuffreda, L. Gamberoni, Tetrahedron Asym. 15 (2004) 3177.
[17] G.L. Rebeiro, B.M. Khadilkar, Syn. Commun. 30 (2000) 1605.
[18] T. Wang, Z.X. Zhang, N.A. Meanwell, Tetrahedron Lett. 40 (1999) 6745.
[19] B. Bhat, Y.S. Sanghvi, Abstract of papers of the Am. Chem. Soc. 213, 105-carb part 1, April 13, 1997.
[20] A.J. Moczulska, Carbohydrate Chem. 13 (1994) 1179.
[21] S. Kim, H. Chang, W. Kim, J. Org. Chem. 50 (1985) 1751.
[22] S. Paul, P. Nanda, R. Gupta, Tetrahedron Asym. 14 (2003) 3197.
[23] T. Sano, K. Ohashi, T. Oriyama, Synthesis (1999) 1141.
[24] M.S. Wolfe, Syn. Commun. 27 (2004) 2975.
[25] H.J. Koh, K.L. Han, I. Lee, J. Org. Chem. 64 (1999) 4783.
[26] O.A. El Seoud, M. Ferreira, W.A. Rodrigues, M.F. Ruasse, J. Phys. Org. Chem. 18 (2005) 173.
[27] O.A. El Seoud, M.F. Ruasse, W.A. Rodrigues, J. Chem. Soc., Perkin Trans. 2 (2002) 1053.
[28] D.L. McFadden, A.T. McPhail, C.D. Garner, F.E. Mabbs, J. Chem. Soc., Dalton Trans. (1976) 47.

starting from aminomethylferrocene and substituted benzaldehydes [8a]. As a part of our current research related to the cyclo-metallation of ferrocenylamines[8b], in this communication, we wish to report the synthesis of ferrocenylamines [(η^5-C_5H_5)Fe(η^5-$C_5H_4CH_2N(CH_3)CH_2$-C_6H_4R-4)] (R = CH_3(**b**), Cl(**d**)), starting from ferrocenylcarboxaldehyde and *p*-substituted benzylamines, and the cycloplatination reactions of these five ferrocenylamines as mentioned above (Scheme 1) and to try to elucidate the relationship between the structures of the substrates and their selectivities.

2. Results and discussion

2.1. Synthesis of *6a–e*

Condensations of ferrocenylcarboxaldehyde and *p*-methyl (**2b**) or *p*-chloroaniline (**2d**) in methanol at room temperature produced the corresponding aldimines **3b**, **d**, which followed by reduction with lithium aluminum hydride in THF afforded quantitatively **4b**, **d**, respectively. Methylation of **4b**, **d** with sodium cyanoborohydride, aqueous formaldehyde and acetic acid [9] at room temperature gave the aliphatic tertiary ferrocenylamines **5b**, **d** [8] in good yield. Like their analogues, compounds **5b**, **d** are very stable in air, and they are normally liquid or solid with low melting points.

The reactions of **5a–e** and *cis*-[Pt(DMSO)$_2$Cl$_2$] were carried out in methanol under nitrogen. The mixtures were refluxed and stirred for 30 min and cooled down to room temperature. The solvent was evaporated in vacuo and water was then added. Extraction of the water phase with dichloromethane three times (3×30 cm^3) and removal of solvent afforded residues which were further purified by column chromatography (silica gel, ethyl acetate/hexane = 1:5 (v/v)) to give **6a–e** as orange-yellow solids. The yields of **6a–e** are relevant to the character of the substituents on the phenyl ring. For instance, when the substituents are methoxy (**5a**) or methyl (**5b**), the yields of **6a**, **b** are moderate (65%, 60%, respectively), whereas when the substituents are chloro (**5d**) or nitro (**5e**), lower yields of **6d**, **e** (55%, 40%, respectively) are normally obtained. Complexes **6a–e** are very stable in air and are easily soluble in most organic solvents, but are poorly soluble in hexane.

2.2. Spectral characterization of *6a–e*

Compounds **3b–5b**, **3d–5d** and **6a–e** were characterized by elemental analyses, IR and ^{1}H NMR. Elemental analyses for these compounds are in good agreement with the proposed formula. The IR and ^{1}H NMR spectra of compounds **3b–5b**, **3d–5d** are very similar to their analogues, e.g., **3a–5a** [8]. The IR spectra of **6a–6e** all display two medium absorption bands around ν 1100 and 1000 cm^{-1}, indicating that the cycloplatination of **5a–e** occurs at the substituted cyclopentadienyl (Cp) rings [10]. In the ^{1}H NMR spectra, the δ values of N—CH_3 range from 3.02 (**6a**) to 2.81 (**6b**), suggesting that N—Pt coordination exists in these molecules. Also in the ^{1}H NMR spectra of **6**, a doublet and multiplet around δ4.10 ppm are assigned to H5 and H4, respectively, and a singlet around δ4.20 ppm is attributed to H3. In addition, H11 exhibit a typical AB spin–spin coupling system (δ3.62 ppm) due to the formation of a five membered platinocycle (in **6a**, the chemical shifts of H11 are overlapped with those of H19 and H20). It seems that H12 have a similar coupling system (around δ4.00 ppm) to that for H11. The protons in *p*-substituted phenyl rings all give their corresponding AA′XX′ splitting patterns.

2.3. Chemoselectivity and stereoselectivity

In all cases, a preferred cycloplatination occurred at the Cp ring over the phenyl ring in **5** (Scheme 2). According to the rule of cyclometallation, the reactions of **5** and *cis*-[Pt(DMSO)$_2$Cl$_2$] form initially the coordinated complexes **7** (Scheme 2) which then direct the platinum to activate its adjacent C—H bonds and hence give the cycloplatinated

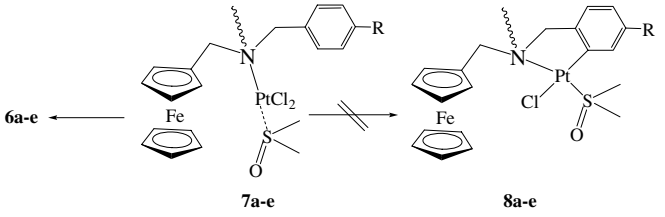

Scheme 2. The preferred activation of C—H bond in Cp ring over that in phenyl ring.

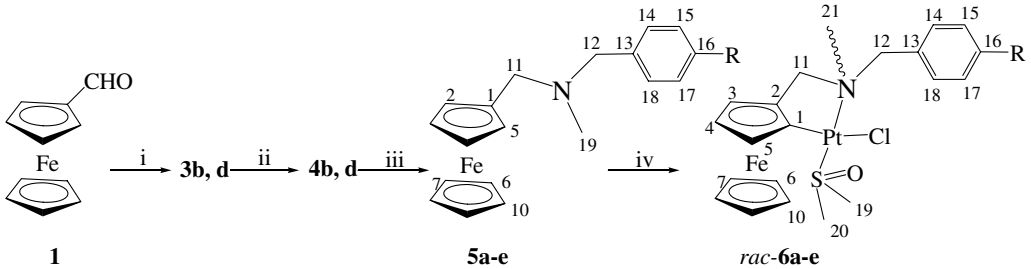

Scheme 1. (i) Amines **2**: 4-R$C_6H_4CH_2NH_2$, R = CH_3O(**a**); CH_3(**b**); H(**c**) Cl(**d**), NO_2(**e**), methanol, room temperature. (ii) $LiAlH_4$, THF, reflux. (iii) $NaCNBH_3$, HCHO(aq), AcOH, room temperature. (iv) *cis*-[Pt(DMSO)$_2$Cl$_2$], methanol, reflux 30 min.

compounds. It should be noted that two kinds of C—H bonds are present in **5**, i.e., the $C_{ferrocenyl}$—H bond and the C_{phenyl}—H bond, and activation of both C—H bonds could afford the corresponding stable five membered platinocycles **6a**–**e** and **8a**–**e**, respectively. In fact, only **6a**–**e** were isolated in our experiment. The compounds **8a**–**e** resulting from activation of C_{phenyl}—H bonds in **7a**–**e** were not observed. The preferred activation of the $C_{ferrocenyl}$—H bond over the C_{phenyl}—H bond is consistent with Lopez's observations [7], and this phenomenon is easily explained by the fact that electrophilic substitution of platinum is more facile on a ring with a high electron density (Cp ring) than on one with a low electron density (phenyl ring) [11].

Surprisingly, of the cycloplatinated complexes **6a**–**e** only **6a** crystallizes in two forms, i.e., prismatic crystal and plate, which are difficult to separate from each other in the mixture. A prismatic crystal suitable for X-ray diffraction was carefully picked out of the mixture and its configuration was determined to be R_NR_P [12] (Fig. 1). The optical rotations of **6a**–**e** have been determined to be zero at a given wavenumber ($\lambda = 5893$ Å) and conditions (CH_2Cl_2, $T = 298$ K), implying that complexes **6** are probably composed of racemers. It is possible that each form of **6a** corresponds to one isomer of the racemers. This result may be echoed by the possible mechanism for the formations of **6** as shown in Scheme 3.

Theoretically, an orbital reversion at nitrogen is present between the two isomers **5α** and **5β** (Scheme 3) and each isomer will possess the same stable conformation as that of [(*N*-methyl-*N*-4-methylbenzyl)amino]methyl-ferrocene [13]. Thus, coordination of platinum and **5α**,**β** will afford

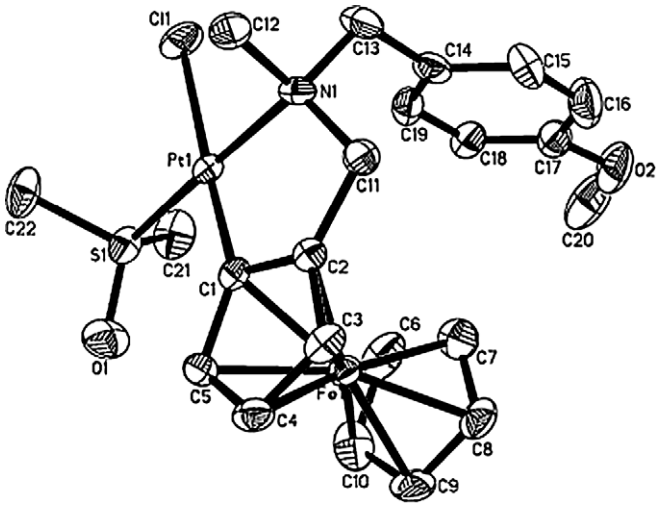

Fig. 1. Crystal structure of **6a** with the numbering scheme (H atoms are omitted for clarity).

the corresponding intermediates **7α**,**β** with a similar conformation to that of the coordinated Pt—FcN complex [5]. When platinum in **7α**,**β** activates the C2(5)—H bonds, a pair of racemers **6α**,**β** will be generated. Alternatively, the N—Pt moiety in **7α**,**β** could rotate freely around the axis of the C1—C11 bond and subsequently activate the C5(2)—H bonds to give another pair of racemers **6γ**,**δ**. Obviously, cycloplatination of **5** will produce two pairs of enantiomers, and moreover, the pair **6α**,**β** are the diastereomers of the other pair **6γ**,**δ**.

On the other hand, the orientation of platinum in **7α**,**β** approaches the C2—H, C5—H bonds, respectively [5], the

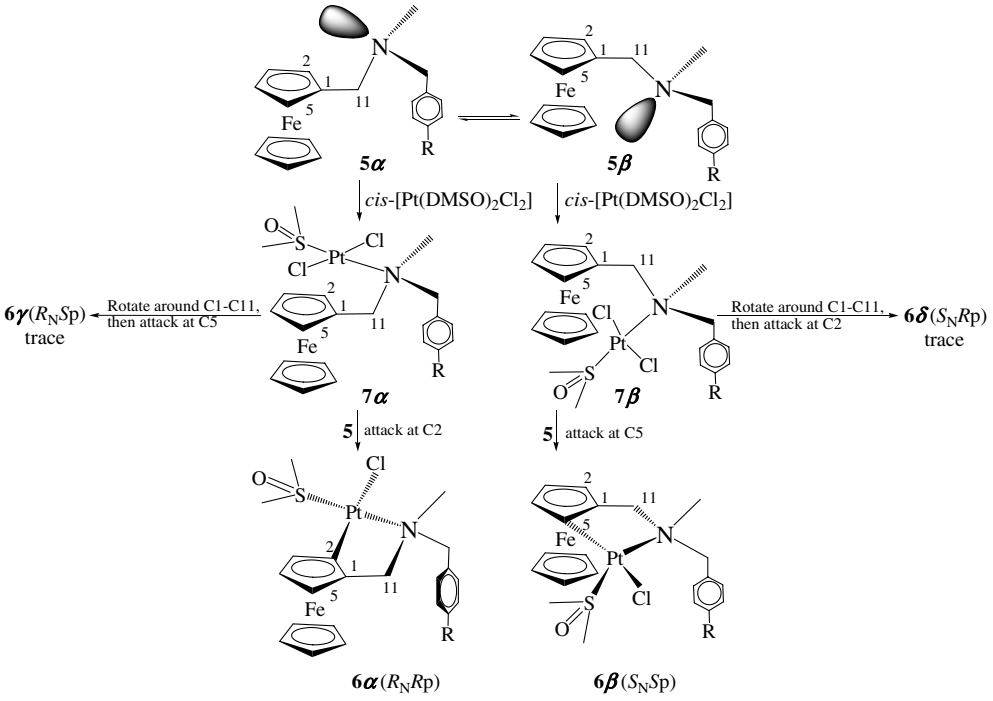

Scheme 3. The possible mechanism for the formation of **6**.

Table 1
Crystallographic data for **6a**

Compound	**6a**
Empirical formula	$C_{22}H_{28}ClFeNO_2PtS$
M	656.90
Crystal dimensions (mm)	$0.28 \times 0.20 \times 0.16$
Crystal system, space group	orthorhombic, $P2(1)2(1)2(1)$
a (Å)	9.4664(5)
b (Å)	12.5579(7)
c (Å)	18.9943(1)
α (°)	90
β (°)	90
γ (°)	90
V (Å^3)	2258.0(2)
Z	4
$\rho_{calc.}$ (g cm^{-3})	1.932
μ (mm^{-1})	7.060
θ Range for data collection	$2.14° \leqslant \theta \leqslant 25.02°$
Limiting indices	$-11 \leqslant h \leqslant 11$, $-14 \leqslant k \leqslant 14$, $-13 \leqslant l \leqslant 22$
Reflections collected/unique (R_{int})	12027/3952 (0.0209)
Data/restraints/parameters	3952/0/266
Final R_1, wR_2	0.0155, 0.0359
Largest difference peak and hole (e Å^{-3})	0.458, −0.850

Table 2
Selected bond lengths (Å) and angles (°) for compound **6a**

Bond lengths (Å)			
Pt(1)—N(1)	2.128(3)	S(1)—C(22)	1.772(4)
Pt(1)—Cl(1)	2.4148(1)	C(1)—C(2)	1.424(5)
Pt(1)—C(1)	1.985(3)	C(2)—C(11)	1.495(5)
Pt(1)—S(1)	2.1919(1)	N(1)—C(11)	1.505(5)
S(1)—O(1)	1.465(3)	N(1)—C(13)	1.512(5)
Angles (°)			
C(1)—Pt(1)—Cl(1)	173.15(1)	C(11)—N(1)—Pt(1)	111.4(2)
N(1)—Pt(1)—S(1)	178.20(9)	C(13)—N(1)—Pt(1)	115.9(2)
N(1)—Pt(1)—Cl(1)	92.09(9)	C(2)—C(11)—N(1)	108.2(3)
C(1)—Pt(1)—N(1)	81.79(1)	C(14)—C(13)—N(1)	115.4(3)

activation of these two C—H bonds to produce **6α,β** by platinum will be favored. However, this orientation may disfavor the activation of C5(2)—H bonds to generate **6γ,δ** probably because the free rotation of the N—Pt moiety around the axis of the C1—C11 bond is retarded by the steric hindrance between the phenyl group and the H atom in the Cp ring. Diastereomers are easily separated by column chromatography, and we indeed obtained a trace product (probably **6γ,δ**) of insufficient quantity to identify. Based upon the discussion as mentioned above and the configuration of **6a** (Fig. 1), it is suggested that **6** consists probably of **6α,β**.

2.4. Crystal structure of *6a*

The structure of **6a** was also confirmed by X-ray single crystal diffraction (Fig. 1). Crystallographic data for **6a** are presented in Table 1, selected bond lengths and angles are listed in Table 2. X-ray diffraction studies for **6a** (Fig. 1) demonstrate that the structure of **6a** consists of discrete molecules σ-Pt[(η^5-C_5H_5)Fe(η^5-$C_5H_3CH_2N(CH_3)CH_2C_6H_4OCH_3$-4)]-Cl(DMSO) separated by van der Waals distances in which platinum is in a slight distorted square-planar environment, bonded to Cl1, S1, N1 and C1. The deviations of the atoms from the mean plane defined by the former five atoms in **6a** are Pt1 0.0218, Cl1 −0.0317, S1 0.0225, N1 0.0272 and C1 −0.0398 Å. In **6a**, the DMSO moiety adopts a *trans* configuration to the N1 atom with a bond angle N1–Pt1–S1 178.20(9)° and this array is very common in platinum complexes [5,6a]. **6a** contains two fused five-membered rings, i.e., the substituted pentagonal ring of the ferrocenyl fragment and a five-membered platinocycle with an envelope-like conformation. The bond length of N1—Pt1 (2.128(3) Å) is shorter than that in cycloplatinated FcN (2.141(6) Å) [5]. The metallated Cp and phenyl rings are nearly perpendicular with an angle of 89.7°. The bond length of Pt1—C1 (1.985(3) Å) is nearly the same as that in cycloplatinated FcN (1.988(7) Å) [5]. The average C—C bond length in the pentagonal rings (1.410 Å) is similar to the values reported for other ferrocene derivatives [10]. The Fe—C (Cp ring) bond lengths range from 1.381(6) to 1.424(5) Å. The two pentagonal rings of the ferrocenyl moiety are planar and nearly parallel (interplanar angle 2.2°). In addition, the Cp rings are also nearly eclipsed and they are skewed from the eclipsed conformation with an angle of 2.56°.

3. Conclusion

Stereoselective cycloplatination of ferrocenylamines of the formula $FcCH_2NMeCH_2Ar$ produced the corresponding two pairs of racemers in which the pair R_NR_P, S_NS_P was the major product. No products resulting from the activation of C_{phenyl}—H bonds were observed. It is anticipated that cyclometallation of ferrocenylamines such as $FcCHRN(CH_3)CH_2Ar$ or $FcCH_2N(CH_3)CHRAr$ will afford four diastereomers which can be easily separated by column chromatography.

4. Experimental

4.1. Materials and instruments

Ferrocenylamines **5a**, **c**, **e** [8] and *cis*-[Pt(DMSO)$_2$Cl$_2$] [14] were prepared according to the literature procedure. Ferrocenylcarboxaldehyde, *p*-methylbenzylamine, *p*-chlorobenzylamine, lithium aluminum hydride, aqueous formaldehyde, sodium cyanoborohydride, acetic acid were obtained commercially and used without further purification. All of the solvents were purified by the standard methods prior to use. Melting points were obtained from a Yanaco micro melting point apparatus and were uncorrected. Elemental analyses were obtained from a Carlo Erba 1106 Elemental analyzer. IR spectra were taken on BIO-RAD 3000 and Digilab FTIR spectrometers. ^{1}H NMR spectra were measured with a Bruker AV-400 spectrometer

by using $CDCl_3$ as a solvent and TMS as the internal standard.

4.2. Synthesis of [(η^5-C_5H_5)Fe(η^5-$C_5H_4CH_2N$-(CH_3)$CH_2C_6H_4R$-4)] (**5b, d**)

4.2.1. [(η^5-C_5H_5)Fe(η^5-$C_5H_4CH{=}NCH_2C_6H_4CH_3$-4)] (**3b**)

3b was prepared by condensation of ferrocenyl-carboxaldehyde and 4-methylaniline in methanol at room temperature under nitrogen. Red brown solid. Yield 54%. M.p. 70–72 °C. *Anal*. Calc. for $C_{19}H_{19}FeN$: C, 71.94; H, 6.04; N, 4.42. Found: C, 71.84; H, 6.01; N, 4.42%. FT-IR(KBr): *v* 3092(w), 2935(w), 2888(w), 1636(vs), 1516(s), 1340(m), 1246(w), 1167(s), 1106(m), 1000(m), 809(s) cm^{-1}. ^1H NMR ($CDCl_3$): δ 2.10(s, 3H, Ar—CH_3), 3.84(d, 2H, H2, H5), 4.14(m, 2H, H3, H4), 4.17(s, 5H, η^5-C_5H_5), 4.50(s, 2H, H12), 7.70–7.89 (AA′XX′, 4H, H15, H17, H14, H18), 8.10(s, 1H, H11) ppm.

4.2.2. [(η^5-C_5H_5)Fe(η^5-$C_5H_4CH{=}NCH_2C_6H_4Cl$-4)] (**3d**)

3d was prepared with the same procedure as that for **3b**. Red brown solid. Yield 88%. M.p. 57–59 °C. *Anal*. Calc. for $C_{18}H_{16}ClFeN$: C, 64.03; H, 4.78; N, 4.15. Found: C, 63.98; H, 4.76; N, 4.13%. FT-IR(KBr): *v* 3085(w), 2917(w), 2823(w), 1638(vs), 1449(s), 1240(w), 1105(m), 1001(m), 817(s) cm^{-1}. ^1H NMR ($CDCl_3$): δ 3.86(d, 2H, H2, H5), 4.15(m, 2H, H3, H4), 4.18(s, 5H, η^5-C_5H_5), 4.51(s, 2H, H12), 7.81–7.93 (AA′XX′, 4H, H14, H18, H15, H17), 8.15(s, 1H, H11) ppm.

4.2.3. [(η^5-C_5H_5)Fe(η^5-$C_5H_4CH_2NHCH_2C_6H_4CH_3$-4)] (**4b**)

4b was prepared by reduction of imine **3b** with lithium aluminum hydride in THF under nitrogen. Yellow solid, Yield 80%. M.p. 28–30 °C. *Anal*. Calc. for $C_{19}H_{21}FeN$: C, 71.49; H, 6.63; N, 4.39. Found: C, 71.45; H, 6.60; N, 4.38%. FT-IR (KBr): *v* 3329(s), 3093(s), 2920(s), 2814(m), 1514(vs), 1449(s), 1354(w), 1105(vs), 1001(s), 809(vs) cm^{-1}. ^1H NMR($CDCl_3$): δ 1.88(s, 1H, NH), 2.11(s, 3H, Ar—CH_3), 3.47(s, 2H, H11), 3.71(s, 2H, H12), 3.80(d, 2H, H2, H5), 4.09(s, 5H, η^5-C_5H_5), 4.13(t, 2H, H3, H4), 6.85–7.23 (AA′XX′, 4H, H15, H17, H14, H18) ppm.

4.2.4. [(η^5-C_5H_5)Fe(η^5-$C_5H_4CH_2NHCH_2C_6H_4Cl$-4)] (**4d**)

4d was prepared with the same procedure as that for **4b**. Yellow liquid. Yield 80%. *Anal*. Calc. for $C_{18}H_{18}ClFeN$: C, 63.65; H, 5.34; N, 4.12. Found: C, 63.41; H, 5.24; N, 4.11%. FT-IR (KBr): *v* 3298(w), 3086(s), 2911(s), 2828(m), 1487(m), 1452(s), 1104(vs), 1000(vs), 818(vs) cm^{-1}. ^1H NMR($CDCl_3$): δ 1.90(s, 1H, NH), 3.49(s, 2H, H11), 3.72(s, 2H, H12), 3.81(d, 2H, H2, H5), 4.11(s, 5H, η^5-C_5H_5), 4.15(t, 2H, H3, H4), 6.93–7.45 (AA′XX′, 4H, H14, H18, H15, H17) ppm.

4.2.5. [(η^5-C_5H_5)Fe(η^5-$C_5H_4CH_2N(CH_3)$-$CH_2C_6H_4CH_3$-4)] (**5b**)

5b was prepared according to the literature method [9]. Yellow solid. Yield 80%. M.p. 32–34 °C. *Anal*. Calc. for $C_{20}H_{23}FeN$: C, 72.08; H, 6.96; N, 4.20. Found, C, 71.99; H, 6.94; N, 4.21%. FT-IR (KBr): *v* 3091(w), 2928(w), 1513(s), 1453(s), 1361(w), 1105(s), 1020(vs), 805(vs) cm^{-1}. ^1H NMR ($CDCl_3$): δ 2.12(s, 3H, Ar—CH_3), 2.34(s, 3H, N—CH_3), 3.40(s, 2H, H11), 3.43(s, 2H, H12), 4.09(s, 5H, η^5-C_5H_5), 4.12(m, 2H, H2, H5), 4.18(d, 2H, H3, H4), 7.20–7.28 (AA′XX′, 4H, H15, H17, H14, H18) ppm.

4.2.6. [(η^5-C_5H_5)Fe(η^5-$C_5H_4CH_2N(CH_3)$-$CH_2C_6H_4Cl$-4)] (**5d**)

5d was prepared with the same procedure as that for **5b**. Yellow solid. Yield 72%. M.p. 38–40 °C. *Anal*. Calc. for $C_{19}H_{20}ClFeN$: C, 64.52; H, 5.70; N, 3.96: Found, C, 64.33; H, 5.68; N, 3.95%. FT-IR (KBr): *v* 3085(m), 2929(s), 2834(s), 1492(s), 1452(s), 1361(w), 1105(s), 1022(vs), 1000(vs), 818(vs) cm^{-1}. ^1H NMR ($CDCl_3$): δ 2.12(s, 3H, N—CH_3), 3.42(s, 4H, H11, H12), 4.06(s, 5H, η^5-C_5H_5), 4.10(m, 2H, H2, H5), 4.16(d, 2H, H3, H4), 7.12–7.19 (AA′XX′, 4H, H14, H18, H15, H17) ppm.

4.3. Synthesis of σ-Pt[(η^5-C_5H_5)Fe(η^5-$C_5H_3CH_2N(CH_3)$-$CH_2C_6H_4$-R-4)]Cl(DMSO) (**6a–e**)

General procedure: To a stirred solution of amine (0.5 mmol) in methanol (20 cm^3) was added *cis*-[Pt($DMSO)_2Cl_2$] (105 mg, 0.25 mmol). The mixture was stirred and refluxed for 30 min under nitrogen and cooled down to room temperature. The solvent was removed in vacuo and water was then added. The mixture was extracted with dichloromethane (3×30 cm^3) and separated. The organic layer was dried over anhydrous sodium sulfate and filtered. Removal of solvent gave the crude product which was further purified by column chromatography (silica gel, ethyl acetate/hexane = 1:5 (v/v)) to afford **6**.

4.3.1. σ-Pt[(η^5-C_5H_5)Fe(η^5-$C_5H_3CH_2N(CH_3)$-$CH_2C_6H_4OCH_3$-4)]Cl(DMSO) (**6a**)

Yellow powder. Yield 65%. M.p. 218–220 °C. *Anal*. Calc. for $C_{22}H_{28}ClFeNO_2PtS$: C, 40.22; H, 4.30; N, 2.13. Found: C, 40.18; H, 4.29; N, 2.13%. FT-IR (KBr): *v* 3091(w), 1610(s), 1511(vs), 1455(m), 1253(s), 1132(s, S═O), 1101(m), 1000(m), 819(s) cm^{-1}. Far IR (Nujol): *v* 272(Pt—Cl), 352(Pt—S) cm^{-1}. ^1H NMR ($CDCl_3$): δ 3.02(s, 3H, H21), 3.18(s, 3H, OCH_3), 3.55(m, 8H, H19, H20, H11), 3.72(AB, 2H, $J = 14.8$ Hz, H12), 3.82(d, 1H, $J_{Pt-H} = 33.2$ Hz, H5), 4.00(s, 5H, η^5-C_5H_5), 4.11(m, 1H, H4), 4.22(s, 1H, H3), 6.86–6.94 (AA′XX′, 4H, H15, H17, H14, H18) ppm.

4.3.2. σ-Pt[(η^5-C_5H_5)Fe(η^5-$C_5H_3CH_2N(CH_3)$-$CH_2C_6H_4CH_3$-4)]Cl(DMSO) (**6b**)

Yellow powder. Yield 60%. M.p. 184–186 °C. *Anal.* Calc. for $C_{22}H_{28}ClFeNOPtS$: C, 41.23; H, 4.40; N, 2.19. Found: C, 41.18; H, 4.38; N, 2.18%. FT-IR (KBr): *v* 3094(w), 2917(w), 1457(m), 1411(s), 1132(vs, S=O), 1103(m), 1000(m), 807(s) cm^{-1}. Far IR (Nujol): *v* 273(Pt—Cl), 353(Pt—S) cm^{-1}. ^{1}H NMR ($CDCl_3$): *δ* 2.32(s, 3H, Ar—CH_3), 2.81(s, 3H, H21), 3.53(s, 3H, H19), 3.57(s, 3H, H20), 3.62(AB, 2H, $J = 12.8$ Hz, H11), 4.04(AB, 2H, $J = 14.8$ Hz, H12), 4.12(s, 5H, η^5-C_5H_5), 4.16(d, 1H, $J_{Pt-H} = 33.2$ Hz, H5), 4.25(m, 1H, H4), 4.31(s, 1H, H3), 6.89–7.77 (AA′XX′, 4H, H15, H17, H14, H18) ppm.

4.3.3. σ-Pt[(η^5-C_5H_5)Fe(η^5-$C_5H_3CH_2N(CH_3)$-CH_2-C_6H_5)]Cl(DMSO) (**6c**)

Yellow powder. Yield 56%. M.p. 210–212 °C. *Anal.* Calc. for $C_{21}H_{26}ClFeNOPtS$: C, 40.24; H, 4.18; N, 2.23. Found: C, 40.19; H, 4.16; N, 2.20%. FT-IR (KBr): *v* 3092(w), 1559(w), 1457(m), 1130(vs, S=O), 1102(m), 1000(m) cm^{-1}. Far IR (Nujol): *v* 274(Pt—Cl), 353(Pt—S) cm^{-1}. ^{1}H NMR ($CDCl_3$): *δ* 1.55(s, 3H, H21), 2.83(s, 3H, H21), 3.54(s, 3H, H19), 3.57(s, 3H, H20), 3.62(AB, 2H, $J = 12.8$ Hz, H11), 4.10(AB, 2H, $J = 14.8$ Hz, H12), 4.13(s, 5H, η^5-C_5H_5), 4.21(d, 1H, $J_{Pt-H} = 33.2$ Hz, H5), 4.29(m, 1H, H4), 4.34(s, 1H, H3), 7.04–7.94 (m, 5H, H14, H15, H16, H17, H18) ppm.

4.3.4. σ-Pt[(η^5-C_5H_5)Fe(η^5-$C_5H_3CH_2N(CH_3)$-$CH_2C_6H_4Cl$-4)]Cl(DMSO) (**6d**)

Yellow powder. Yield 55%. M.p. 181–183 °C. *Anal.* Calc. for $C_{21}H_{25}Cl_2FeNOPtS$: C, 38.14; H, 3.81; N, 2.12. Found: C, 38.00; H, 3.78; N, 2.11%. FT-IR (KBr): *v* 3081(w), 2915(w), 1455(m), 1407(w), 1130(vs, S=O), 1103(m), 1002(m), 806(m) cm^{-1}. Far IR (Nujol): *v* 272(Pt—Cl), 352(Pt—S) cm^{-1}. ^{1}H NMR ($CDCl_3$): *δ* 2.91(s, 3H, H21), 3.49(s, 3H, H19), 3.55(s, 3H, H20), 3.60(AB, 2H, $J = 12.8$ Hz, H11), 4.02(AB, 2H, $J = 14.8$ Hz, H12), 4.12(s, 5H, η^5-C_5H_5), 4.15(d, 1H, $J_{Pt-H} = 33.2$ Hz, H5), 4.24(m, 1H, H4), 4.30(s, 1H, H3), 7.94–8.27 (AA′XX′, 4H, H14, H18, H15, H17) ppm.

4.3.5. σ-Pt[(η^5-C_5H_5)Fe(η^5-$C_5H_3CH_2N(CH_3)$-$CH_2C_6H_4NO_2$-4)]Cl(DMSO) (**6e**)

Yellow powder. Yield 40%. M.p. 176–179 °C. *Anal.* Calc. for $C_{21}H_{25}ClFeN_2O_3PtS$: C, 37.54; H, 3.75; N, 4.17. Found: C, 37.44; H, 3.73; N, 4.16%. FT-IR (KBr): *v* 3092(w), 2914(w), 1522(vs), 1458(m), 1344(s), 1137(m, S=O), 1103(m), 1000(m), 810(m) cm^{-1}. Far IR (Nujol): *v* 271(Pt—Cl), 352(Pt—S) cm^{-1}. ^{1}H NMR ($CDCl_3$): *δ* 2.84(s, 3H, H21), 3.51(s, 3H, H19), 3.58(s, 3H, H20), 3.64(AB, 2H, $J = 12.8$ Hz, H11), 4.06(AB, 2H, $J = 14.8$ Hz, H12), 4.14(s, 5H, η^5-C_5H_5), 4.18(d, 1H, $J_{Pt-H} = 33.2$ Hz, H5), 4.27(m, 1H, H4), 4.33(s, 1H, H3), 8.22–8.38 (AA′XX′, 4H, H14, H18, H15, H17) ppm.

4.4. X-ray determination of **6a**

The prismatic single crystal of **6a** suitable for X-ray analysis was obtained by slow evaporation of a mixture of ethyl acetate and hexane at room temperature over a period of one week. This single crystal was mounted on a Bruker SMART CCD diffractometer equipped with graphite monochromated Mo Kα ($\lambda = 0.71073$ Å) radiation at ambient temperature ($T = 293$ K) using the *ω*-2*θ* multi-scans technique for data collection. Semi-empirical absorption corrections were applied using the SABABS program [15]. The structure was solved by direct methods and refined by full-matrix least-squares procedure on F^2 using the SHELX suite of programs [16].

5. Supplementary materials

Crystallographic data (excluding structure factors) for the structure of **6a** in this paper has been deposited with the Cambridge Crystallographic Data Centre as supplementary publication no. CCDC 286580. Copies of the data can be obtained, free of charge, on application to CCDC, 12 Union Road, Cambridge CB2 1EZ, UK (fax: +144 1223 336033 or e-mail: deposit@ccdc.cam.ac.uk).

Acknowledgement

We are grateful to the Natural Scientific Foundation of Tianjin City, People's Republic of China, for financial support for this project (Project No. 033609011).

References

[1] (a) J. Dupont, C.S. Consort, J. Spencer, Chem. Rev. 105 (2005) 2527;
(b) A. Togni, L.M. Venanzi, Angew. Chem., Int. Ed. 33 (1994) 497;
(c) A.D. Ryabov, Chem. Rev. 90 (1990) 403;
(d) V.V. Dunina, O.A. Zalevskaya, V.M. Potatov, Russ. Chem. Rev. 57 (1988) 250;
(e) I. Omae, Coord. Chem. Rev. 83 (1988) 137;
(f) G.R. Newkome, W.E. Puckett, V.K. Gupta, G.E. Kiefer, Chem. Rev. 86 (1986) 451;
(g) I. Omae, Chem. Rev. 79 (1979) 287;
(h) M.I. Brice, Angew. Chem., Int. Ed. 10 (1977) 73.
[2] J.S. Fossy, C.J. Richards, Organometallics 18 (1999) 2116.
[3] (a) M. Ghedini, D. Pucci, A. Crispini, G. Barberio, Organometallics 18 (1999) 2116;
(b) J. Buey, L. Diez, P. Espinet, H.S. Kitzerow, J.A. Miguel, Chem. Mater. 8 (1996) 2375.
[4] M.D. Meijer, E. de Wolf, M. Lutz, A.L. Spek, G.P.M. van Klink, G. van Koten, Organometallics 20 (2001) 4198.
[5] P.R.R. Ranatunge-Bandarage, B.H. Robinson, J. Simpson, Organometallics 13 (1994) 500.
[6] (a) A.D. Ryabov, I.M. Panyashkina, V.A. Polyakov, J.A.K. Howard, L.G. Kuz'mina, M.S. Datt, C. Sacht, Organometallics 17 (1998) 3615;
(b) A.D. Ryabov, I.M. Panyashkina, V.A. Polyakov, A. Fischer, Organometallics 21 (2002) 1633;
(c) A.D. Ryabov, S. Otto, P.V. Samuleev, V.A. polyakov, L. Alexandrova, G.M. Kazankov, S. Shova, M. Revenco, J. Lipkowski, H. Johansson, Inorg. Chem. 41 (2002) 4286;

(d) J.M. Vila, M.T. Pereira, J.M. Ortigueira, D. Lata, M.L. Torres, J.J. Fernandez, A. Fernandez, H. Adams, J. Organomet. Chem. 566 (1998) 93;
(e) G.W.V. Cave, F.P. Fanizzi, R.J. Deeth, W. Errington, J.P. Pourke, Organometallics 19 (2000) 1355;
(f) M. Crespo, C. Grande, A. Klein, M. Font-Bardia, X. Solans, J. Organomet. Chem. 563 (1998) 179;
(g) C.R. Baar, H.A. Jenkins, J.J. Vittal, G.P.A. Yap, R.J. Puddephatt, Organometallics 17 (1998) 2805;
(h) X. Riera, A. Caubet, C. Lopez, V. Moreno, X. Solans, M. Font-Barida, Organometallics 19 (2000) 1384;
(i) M. Crespo, J. Granell, X. Solans, M. Font-Bardia, Organometallics 21 (2002) 5140.

[7] (a) R. Bosque, C. Lopez, J. Sales, J. Organomet. Chem. 498 (1995) 147;
(b) C. Lopez, J. Sales, X. Solans, R. Zquiak, J. Chem. Soc., Dalton Trans. 15 (1992) 2321;
(c) R. Bosque, C. Lopez, J. Sales, X. Solans, M. Font-Bardia, J. Chem. Soc., Dalton Trans. 5 (1994) 735.

[8] (a) H.X. Wang, H.F. Wu, H.C. Zhou, F.Y. Geng, R.Q. Gao, J. Xu, Y.J. Li, R. Jin, W.Q. Zhang (unpublished results);
(b) H.X. Wang, Y.J. Li, R. Jin, J.R. Niu, H.F. Wu, H.C. Zhou, J. Xu, R.Q. Gao, F.Y. Geng, J. Organomet. Chem. 691 (2006) 987.

[9] R.F. Borch, A.I. Hassid, J. Org. Chem. 37 (1972) 1673.

[10] M. Rosenblum, R.B. Woodward, J. Am. Chem. Soc. 80 (1958) 5443.

[11] M. Rosenblum, J.O. Santer, W.G. Howells, J. Am. Chem. Soc. 85 (1963) 1450.

[12] R.S. Cahn, C. Ingold, V. Prelog, Angew. Chem., Int. Ed. 4 (1966) 385, and references therein.

[13] H.X. Wang, H.F. Wu, F.Y. Geng, R.Q. Gao, H.C. Zhou, Acta Cryst. E62 (2006) m14.

[14] J.M. Price, A.N. Williamson, R.F. Schramm, B.B. Wayland, Inorg. Chem. 11 (1972) 1280.

[15] G.M. Sheldrick, SADABS, University of Göttingen, 1996.

[16] G.M. Sheldrick, SHELXS-97 and SHELXL-97, Programs for Crystal Structure Solution and Refinement, University of Göttingen, 1997.

$(PPh_3)_2](ReO_4)\cdot\frac{1}{2}H_2O$ ($\mathbf{2}\cdot\frac{1}{2}H_2O$). The reaction of $ReOCl_3(AsPh_3)(OAsPh_3)$] with 1,10-phenanthroline in acetone leads to the [$ReOCl_3$(phen)] complex. Similarly, the diimine ligands pyox and pyth react with [$ReOCl_3(PPh_3)_2$] in benzene to give oxo species of the [$ReOCl_3$(N–N)] type [11]. However, the refluxing of [$ReOCl_3(PPh_3)_2$] with phen in ethanol affords [$ReCl_2$(phen)$(PPh_3)_2$](ReO_4) (**2**). Likewise, the complexes with biimidazole and 2(2-pyridyl)benzimidiazole, $[ReX_2(PPh_3)_2(biimH_2)]^+$ and $[ReX_2(PPh_3)_2$-(pbimz)]$^+$, are obtained from [$ReOX_2$(OEt)$(PPh_3)_2$] or [$ReOX_3(PPh_3)_2$] and the ligand [12,13]. It can be supposed that an endeavour in this area would lead to a new families of variable-valence rhenium compounds.

The electronic structures of **1** and **2** have been determined on the basis of results of density functional theory (DFT) calculations. The spin-allowed electronic transitions of the $[ReCl_2(phen)(PPh_3)_2]^+$ cation, ReO_4^- anion and [$ReOCl_3$(phen)] complex have been calculated with the the time-dependent DFT method (TDDFT), and the UV–Vis spectra of the title compounds have been discussed on this basis.

The recent calculations with the TD-DFT method for open- and closed-shell 5d-metal complexes (including rhenium complexes) have supported the TD-DFT method to be applicable for such systems giving good assignment of experimental spectra [14–16].

2. Experimental

2.1. General procedure

All the reagents used in the synthesis were commercially available and were used without further purification. The $ReOCl_3(AsPh_3)(OAsPh_3)$] and [$ReOCl_3(PPh_3)_2$] complexes were prepared according to the literature methods [17,18].

IR spectra were recorded on a Nicolet Magna 560 spectrophotometer in the spectral range 4000–400 cm^{-1} with the samples in the form of KBr pellets. Electronic spectra were measured on a spectrophotometer Lab Alliance UV-VIS 8500 in the range 900–200 nm in deoxygenated dichloromethane solution. Elemental analyses (C H N) were performed on a Perkin–Elmer CHN-2400 analyzer.

2.2. Preparation of [$ReOCl_3$(phen)] (1)

A mixture of $ReOCl_3(AsPh_3)(OAsPh_3)$] (0.5 g, 0.53 mmol), phen (0.20, 1.0 mmol) and acetone (50 ml) was stirred for 12 h. 30 ml of acetone was distilled off and 100 ml of diethyl ether was added. [$ReOCl_3$(phen)] was filtered off, washed with ethanol, diethyl ether and dried. Yield 70%. The green crystals of **1** for X-ray investigation were obtained by recrystallization from acetonitrile.

IR (KBr): 1628 (w), 1605(m), 1575 (w), 1520 (m) ν_{CN} and $\nu_{C=C}$; 985 (s) $\nu_{Re=O}$.

Anal. Calc. for $C_{12}H_8Cl_3N_2ORe$: C, 29.49; H, 1.65; N, 5.73. Found: C, 29.45; H, 1.55; N, 5.80%.

2.3. Preparation of [$ReCl_2$(phen)$(PPh_3)_2$](ReO_4) (2)

[$ReOCl_3(PPh_3)_2$] (0.83 g, 1 mmol) was added to phenanthroline (0.40 g, 2.0 mmol) in ethanol (100 ml) and the reaction mixture was refluxed overnight. 60 ml of ethanol was distilled off and 100 ml of diethyl ether was added and the precipitate of **2** was collected by filtration. Yield 50%.

Red crystals of water solvate $\mathbf{2}\cdot\frac{1}{2}H_2O$ were obtained by slow evaporation of a chloroform–ethanol solution of **2** in air.

IR (KBr): 1633 (m, br), 1570 (w) ν_{CN} and $\nu_{C=C}$; 1480 (m) δ(C–CH in the plane); 1438 $\nu_{Ph(P-Ph)}$; 912(vs) $\nu_{Re=O(ReO4)}$. *Anal.* Calc. for $C_{48}H_{38}Cl_2N_2O_4P_2Re_2$: C, 47.56; H, 3.16; N, 2.31. Found: C, 47.8; H, 3.25; N, 2.41%.

2.4. Crystal structure determination and refinement

The X-ray intensity data of **1** and $\mathbf{2}\cdot\frac{1}{2}H_2O$ were collected on a KM-4-CCD automatic diffractometer equipped with a CCD detector. 32 and 38 s exposure time was used, respectively, and reflections were collected up to $\theta = 25°$. The unit cell parameters were determined from least-squares refinement of the setting angles of 4065 and 4325 strongest reflections, respectively, for **1** and $\mathbf{2}\cdot\frac{1}{2}H_2O$. Details concerning crystal data and refinement are given in Table 1. Lorentz, polarization and numerical absorption corrections [19] were applied. The structure was solved by the Patterson method and subsequently completed by difference Fourier recycling. All the non-hydrogen atoms were refined anisotropically using the full-matrix, least-squares technique. The hydrogen atoms were treated as ''riding'' on their parent carbon atoms and assigned isotropic temperature factors equal to 1.2 times the value of equivalent temperature factor of the parent atom. SHELXS97 [20], SHELXL97 [21] and SHELXTL [22] programs were used for all the calculations. Atomic scattering factors were those incorporated in the computer programs.

3. Computational details

The GAUSSIAN03 program [23] was used in the calculations. The geometry optimisations of the $[ReCl_2(phen)(PPh_3)_2]^+$ cation, ReO_4^- anion and [$ReOCl_3$-(phen)] complex were carried out with the DFT method with the use of the B3LYP functional [24,25]. The electronic spectra of the $[ReCl_2(phen)(PPh_3)_2]^+$ cation, ReO_4^- anion and [$ReOCl_3$(phen)] complex were calculated with the TDDFT method [26]. The LANL2DZ basis set [27] with additional d (with exponent $\alpha = 0.3811$) and f (with exponent $\alpha = 2.033$) functions was used on the rhenium, 6-31g* on the chlorine, phosphorous, nitrogen and carbon atoms and 6-31g basis on the hydrogen atoms in the calculations.

Natural bond orbital (NBO) calculations were performed with the NBO code [28] included in Gaussian03.

Table 1
Crystal data and structure refinement for the complexes **1** and **2** · $\frac{1}{2}H_2O$

	1	**2** · $\frac{1}{2}H_2O$
Empirical formula	$C_{12}H_8Cl_3N_2ORe$	$C_{48}H_{39}Cl_2N_2O_{4.50}P_2Re_2$
Formula weight	488.75	1221.05
Temperature (K)	293(2)	293(2)
Wavelength (Å)	0.71073	0.71073
Crystal system	monoclinic	triclinic
Space group	$P2_1/c$	$P\bar{1}$
Unit cell dimensions		
a (Å)	7.9499(5)	9.7372(5)
b (Å)	17.9305(10)	12.6595(10)
c (Å)	10.1244(8)	19.4648(15)
α (°)		87.689(5)
β (°)	106.991(6)	80.306(5)
γ (°)		75.457(5)
Volume (Å^3)	1380.19(16)	2289.3(3)
Z	4	2
D_{calc} (Mg/m^3)	2.352	1.771
Absorption coefficient (mm^{-1})	9.375	5.516
F(000)	912	1182
Crystal size (mm)	0.14 × 0.07 × 0.07	0.47 × 0.25 × 0.14
θ Range for data collection (°)	3.10–25.10	3.06–25.10
Index ranges	$-9 \leqslant h \leqslant 9$, $-21 \leqslant k \leqslant 21$, $0 \leqslant l \leqslant 12$	$-11 \leqslant h \leqslant 11$, $-15 \leqslant k \leqslant 15$, $-23 \leqslant l \leqslant 23$
Reflections collected	4825	24751
Independent reflections	2456 ($R_{int} = 0.0288$)	8155 ($R_{int} = 0.0433$)
Completeness to 2θ (%)	96.4	99.8
Maximum and minimum transmission	0.670 and 0.225	0.499 and 0.124
Data/restraints/parameters	2456/0/172	8155/0/561
Goodness-of-fit on F^2	1.115	1.101
Final R indices [$I > 2\sigma(I)$]	$R_1 = 0.0560$, $wR_2 = 0.1204$	$R_1 = 0.0445$, $wR_2 = 0.0938$
R indices (all data)	$R_1 = 0.0710$, $wR_2 = 0.1292$	$R_1 = 0.0562$, $wR_2 = 0.0993$
Largest difference peak and hole (e Å^{-3})	4.146 and −2.639	2.212 and −2.358

3.1. Magnetic measurement

The magnetic measurements of the powdered samples were measured over the temperature range 1.8–300 K using a Quantum Design SQUID – based MPMSXL-5-type magnetometer. The superconducting magnet was generally operated at a field strength ranging from 0 to 5 T. Measurements of samples of the compounds were made at a magnetic field of 0.5 T.

The SQUID magnetometer was calibrated with a palladium rod sample. Corrections are based on subtracting the sample-holder signal and contribution χ_D estimated from the Pascal constants [29], equal to 610×10^{-6} cm^3 mol^{-1} for the complex $[ReCl_2(phen)(PPh_3)_2](ReO_4)$ (**2**). The effective magnetic moment was calculated from the equation $\mu_{eff} = 2.83(\chi_M T)^{1/2}$ (BM).

4. Results and discussion

4.1. Preparation

Treatment of the *mer*,*cis*-$[ReOCl_3(AsPh_3)(OAsPh_3)]$ oxo compound with an excess of 1,10-phenanthroline in acetone at ambient temperature leads to the $[ReOCl_3(phen)]$ complex (**1**), whereas the refluxing of *mer*,*trans*-$[ReOCl_3(PPh_3)_2]$ with phen in ethanol affords $[ReCl_2(phen)(PPh_3)_2](ReO_4)$ (**2**). The formation of **2** is accompanied by disproportionation of Re(V) into Re(III) and Re(VII), similar to that taking place in the synthesis of $[Re(bipy)_3](ReO_4)_2$ from K_2ReF_6 and bipy [30].

4.2. Infrared data

The IR spectrum of **1** exhibits a strong band at 985 cm^{-1} assignable to the ν(Re=O) mode. This value compares well with those reported for rhenium(V) complexes containing a chelating ligand in the coordination sphere: $[ReOBr_3(dppen)]$ [dppen = *cis*-$Ph_2PCH{=}CHPPh_2$] – 984 cm^{-1}, $[ReOBr_3(dppm)]$ [dppm = $Ph_2PCH_2PPh_2$] – 980 cm^{-1} and $[ReOBr_3(dppe)]$ [dppe = $Ph_2PCH_2CH_2PPh_2$] – 982 cm^{-1} [31]. A strong absorption band at 912 cm^{-1} in the IR spectrum of **2** corresponds to the ν(Re=O) mode of the perrhenate anion and its location is in agreement with the literature value of ν_3(Re–O) 918 cm^{-1} for ReO_4^- [32].

The characteristic bands corresponding to the ν(CN), ν(C=C) modes of the phen ligand appear in the range 1640–1570 cm^{-1} in the IR spectra of complexes **1** and **2**.

4.3. Crystal structures

The complex **2** crystallises as the solvate **2** · $\frac{1}{2}H_2O$, with a water molecule multipositionally disordered around the special position b of the $P\bar{1}$ space group at 0, 0, $\frac{1}{2}$ (one water molecule per unit cell). The crystal data for **1** and **2** · $\frac{1}{2}H_2O$ are given in Table 1. The molecular structures of **1** and **2** are presented in Figs. 1 and 2, respectively. For complex **2** · $\frac{1}{2}H_2O$, there are no significant contacts involving either the cation or anion, with the possible exception of some rather weak hydrogen bonds from the perrhenate anion to the phenyl rings. The weak intra- and intermolecular hydrogen bonds [33,34] of **1** and **2** · $\frac{1}{2}H_2O$ are presented in Table 2. The most important angles and bond lengths for **1** and **2** are reported in Tables 3 and 4, respectively.

The rhenium atom in **1** is in a distorted octahedral environment with the three chloride ligands arranged in a *meridional* fashion. The pseudooctahedral environment of the Re center in **1** shows clear distortions, induced by the multiple bonding ligand (oxo) and narrow bite angle of the chelating 1,10-phenanthroline. The high concentration

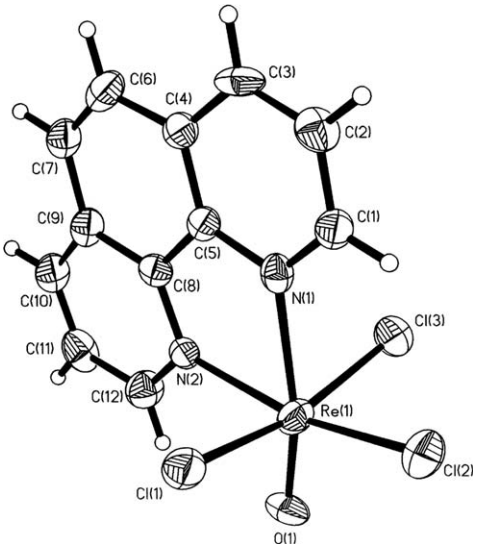

Fig. 1. The molecular structure of $[ReOCl_3(phen)]$.

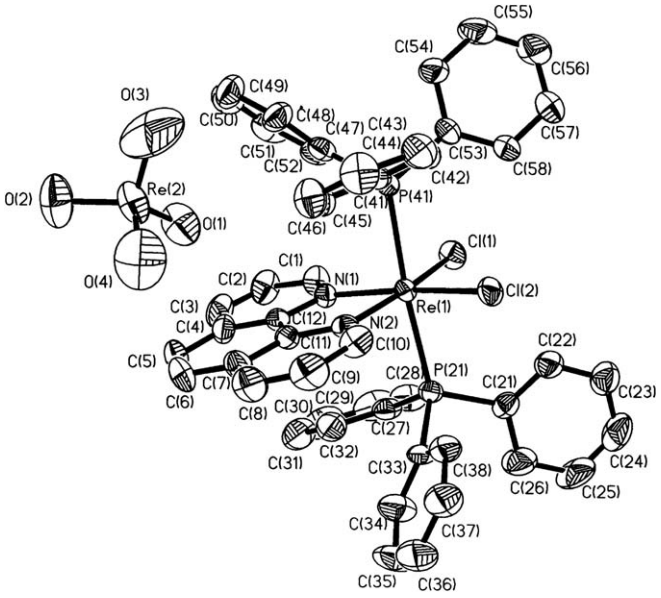

Fig. 2. The molecular structure of $[ReCl_2(phen)(PPh_3)_2](ReO_4)$.

of electronic density along the Re–O axis strongly influences the positions of the adjacent chlorine atoms, which are pushed away – the mean of the O–Re–Cl angles is 99.5°. This also can explain the local electron density distortion inside the rhenium radii [35] (the highest peak and deepest hole on the difference Fourier synthesis are located respectively at 0.87 and 0.76 Å from rhenium atom centre). The Re–O bond in **1** is a typical example of reported terminal multiple $Re–O_{oxo}$ distances in mononuclear $[ReO]^{3+}$ compounds and indicates the presence of a triple Re≡O bond [36]. The Re(1)–N(1) distance is affected by the *trans* influence of the oxo ligand and therefore it is significantly longer than the Re–N(2) bond length located in a *trans* position to the chloride ligand. The large structural *trans* effect of the oxo ligand has been documented for many transition metal complexes [37]. The shortest Re···Re distance is 5.916 Å (second Re atom obtained by x, $-y+1/2$, $z+1/2$ symmetry transformation).

The chloride ions and phen molecule of the $[ReCl_2(phen)(PPh_3)_2]^+$ cation in the structure $\mathbf{2}\cdot\frac{1}{2}H_2O$ hold

Table 2
Hydrogen bonds for **1** and **2**

D	A	H···A	D···A	D–H···A
1				
C(1)	Cl(2)	2.73	3.319(13)	122.1
C(3)	Cl(1)#1	2.78	3.599(13)	147.5
C(11)	Cl(1)#2	2.79	3.483(13)	131.9
C(12)	O(1)	2.53	3.018(16)	112.9
2				
C(1)	Cl(1)	2.68	3.281(7)	123.1
C(3)	O(1)#3	2.51	3.378(10)	156.2
C(6)	O(2)#4	2.41	3.284(12)	156.2
C(10)	Cl(2)	2.73	3.308(8)	121.5
C(22)	Cl(1)	2.77	3.455(8)	131.0
C(38)	Cl(2)	2.72	3.569(8)	152.5
C(42)	Cl(2)#5	2.79	3.572(7)	142.5
C(51)	O(4)#6	2.51	3.389(13)	157.9
C(58)	Cl(2)	2.72	3.503(8)	142.9

#1: $-x$, $-y$, $-z+1$; #2: $x+1$, $-y+0.5$, $z+0.5$; #3: $-x+1$, $-y+1$, $-z+1$; #4: $-x$, $-y+1$, $-z+1$; #5: $-x+1$, $-y+1$, $-z$; #6: $x+1$, y, z.

Table 3
The experimental and optimized bond lengths (Å) and angles (°) for **1**

Bond lengths	Experimental	Optimized	Bond angles	Experimental	Optimized
Re(1)–O(1)	1.720(8)	1.665	O(1)–Re(1)–N(1)	165.6(4)	162.8
Re(1)–N(1)	2.260(10)	2.314	O(1)–Re(1)–N(2)	92.4(4)	89.6
Re(1)–N(2)	2.143(9)	2.140	N(2)–Re(1)–N(1)	73.3(4)	73.2
Re(1)–Cl(1)	2.347(3)	2.429	O(1)–Re(1)–Cl(1)	97.6(3)	100.6
Re(1)–Cl(2)	2.305(3)	2.380	O(1)–Re(1)–Cl(2)	104.0(3)	107.4
Re(1)–Cl(3)	2.362(3)	2.429	O(1)–Re(1)–Cl(3)	97.0(3	100.6
			N(1)–Re(1)–Cl(1)	83.5(2)	79.6
			N(1)–Re(1)–Cl(2)	90.3(3)	89.8
			N(1)–Re(1)–Cl(3)	81.8(2)	79.6
			N(2)–Re(1)–Cl(1)	87.8(3)	89.3
			N(2)–Re(1)–Cl(2)	163.5(3)	163.0
			N(2)–Re(1)–Cl(3)	89.5(3)	89.3
			Cl(2)–Re(1)–Cl(1)	88.49(13)	87.5
			Cl(2)–Re(1)–Cl(3)	90.06(13)	87.5
			Cl(1)–Re(1)–Cl(3)	165.20(13)	158.6

Table 4
The experimental and optimized bond lengths (Å) and angles (°) for **2**

Bond lengths	Experimental	Optimized	Bond angles	Experimental	Optimized
Re(1)–N(1)	2.119(5)	2.123	N(1)–Re(1)–N(2)	77.6(2)	77.18
Re(1)–N(2)	2.120(5)	2.123	N(1)–Re(1)–Cl(1)	91.16(15)	91.46
Re(1)–Cl(1)	2.3742(16)	2.421	N(1)–Re(1)–Cl(2)	169.58(15)	168.59
Re(1)–Cl(2)	2.3642(16)	2.421	N(2)–Re(1)–Cl(1)	168.66(15)	168.59
Re(1)–P(21)	2.5105(17)	2.575	N(2)–Re(1)–Cl(2)	92.02(15)	91.46
Re(1)–P(41)	2.5038(17)	2.575	Cl(2)–Re(1)–Cl(1)	99.26(6)	99.91
			N(1)–Re(1)–P(21)	90.45(15)	93.58
Re(2)–O(1)	1.719(6)	1.727	N(1)–Re(1)–P(41)	94.04(15)	93.06
Re(2)–O(2)	1.705(6)	1.727	Cl(1)–Re(1)–P(41)	89.74(6)	88.03
Re(2)–O(3)	1.593(10)	1.727	Cl(2)–Re(1)–P(41)	86.31(6)	86.50
Re(2)–O(4)	1.719(8)	1.727	N(2)–Re(1)–P(41)	92.16(14)	93.58
			N(2)–Re(1)–P(21)	89.56(14)	93.06
			Cl(1)–Re(1)–P(21)	89.40(6)	86.50
			Cl(2)–Re(1)–P(21)	89.41(6)	88.03
			P(41)–Re(1)–P(21)	175.44(5)	171.50
			O(2)–Re(2)–O(1)	109.0(3)	109.52
			O(3)–Re(2)–O(1)	110.8(4)	109.55
			O(4)–Re(2)–O(1)	108.8(4)	109.36
			O(3)–Re(2)–O(2)	108.6(5)	109.50
			O(3)–Re(2)–O(4)	110.8(5)	109.42
			O(2)–Re(2)–O(4)	108.8(4)	109.46

the equatorial positions. The axial positions of the distorted octahedron of the cation are occupied by triphenylphosphine molecules. Likewise in **1**, the narrow phen bite angle causes a strong departure from an ideal octahedron. The Re–N bond lengths (2.119(5) and 2.120(5) Å) of the title complex are similar to those found for the rhenium(III) polypyridyl compounds: in $[ReCl_2(bipy)_2]PF_6$ – 2.094(5) and 2.096(5) Å [38] and in the $[ReL(terpy)_2]^{2+}$ (L = Cl, OH, NCS) complexes – about 2.10 Å [39]. These values are significantly shorter than comparable distances for saturated amine complexes, where metal-to-ligand π-back bonding is not possible, for instance, the Re–NH_2 distance in the compound $[Re(N_2)(ampy)(tbpy)(PPh_3)]PF_6$ is 2.197(7) [40]. A lengthening of the Re–N_{phen} distances in the Re(V) complex (2.143(9) and 2.260(10) Å) in comparison with **2** is consistent with the notion of the greatest M–L back bonding occurring when the metal is most electron-rich. The shortest Re···Re distance is 5.914 Å (first Re(2) atom and second Re(2) atom obtained by $-x$, $-y$, $-z$ symmetry transformation).

4.4. Geometry optimisation

The geometries of **1** and **2** were optimised by the DFT method with the B3LYP functional. For the $[ReCl_2(phen)(PPh_3)_2]^+$ cation, the geometry optimisation was carried out in triplet and singlet states. The energy of the singlet state is 13.8 kcal higher. The geometries of $[ReOCl_3(phen)]$ and ReO_4^- were optimised in a singlet state. The optimised geometric parameters of **1** and **2** are gathered in Tables 3 and 4, respectively. In general, the predicted bond lengths and angles are in agreement with the values based upon the X-ray crystal structure data, and the general trends observed in the experimental data are well reproduced in the calculations.

4.5. Charge distribution and NBO analysis

Table 5 presents the atomic charges from the natural population analysis (NPA) for complexes **1** and **2**. The calculated charges on the rhenium atoms in $[ReOCl_3(phen)]$, $[ReCl_2(phen)(PPh_3)_2]^+$ and ReO_4^- are considerable lower than the formal charges +5, +3 and +7. This is a result of significant charge donation from the ligands. There are large positive charges on the P atoms, and the negative charges on the chloride and oxo ligands are significantly smaller than −1 and −2, respectively.

Three natural bond orbitals were detected for the Re–O bond in complex **1**. Each natural bond orbital (NBO) σ_{AB}

Table 5
Atomic charges from the natural population analysis (NPA) for **1** and **2**

Atom	**1**	**2**
Re(1)	1.113	0.406
Cl(1)	−0.401	−0.375
Cl(2)	−0.338	−0.375
Cl(3)	−0.401	
N(1)	−0.481	−0.462
N(2)	−0.443	−0.462
O(1)	−0.385	
P(21)		1.374
P(42)		1.374
Re(2)		2.197
O(1)		−0.799
O(2)		−0.799
O(3)		−0.799
O(4)		−0.799

Table 6
The occupancies and hybridization of the calculated natural bond orbitals (NBOs) between the rhenium and the oxo ligands for **1**

BD	Occupancy	Hybridization of NBO	BD*	Occupancy
Re–O_t	1.968	$0.496(sd^{4.22})_{Re} + 0.868(sp^{2.21})_O$	$0.868(sd^{4.22})_{Re} - 0.496(sp^{2.21})_O$	0.264
Re–O_t	1.884	$0.519(d)_{Re} + 0.855(p)_O$	$0.855(d)_{Re} - 0.519(p)_O$	0.243
Re–O_t	1.968	$0.563(d)_{Re} + 0.826(p)_O$	$0.826(d)_{Re} - 0.563(p)_O$	0.251

BD denotes 2-center bond. * denotes antibond NBO.

can be written in terms of two directed valence hybrids (HHOs) h_A and h_B on atoms A and B:

$$\sigma_{AB} = c_A h_A + c_B h_B$$

where c_A and c_B are polarization coefficients. Each valence bonding NBO must in turn be paired with a corresponding valence *anti*-bonding NBO:

$$\sigma^*_{AB} = c_B h_A - c_A h_B$$

to complete the span of the valence space [41]. In the case of the $[ReOCl_3(phen)]$ complex, three Re–O_t natural bond orbitals were detected. The occupancies and hybridization of the calculated Re–O_t natural bond orbitals (NBOs) are given in Table 6. The σ and π Re–O bonds are clearly polarized towards the oxygen end. The s and p oxygen orbitals and s and d rhenium orbitals take part in the σ_{Re-Ot} bond formation, whereas the π_{Re-Ot} bond orbitals result from overlapping of the empty d_{xy} and d_{yz} rhenium orbitals with the occupied p_x and p_z orbitals of the terminal oxygen ligands.

The Re–N natural bonds were not detected in **1** and $[ReCl_2(phen)(PPh_3)_2]^+$, indicating predominant Coulomb-type interactions between the central ion and the phen ligand [42].

4.6. Electronic structure

The energies, characters and contours of several lowest unoccupied molecular orbitals (LUMO or L) and highest occupied molecular orbitals (HOMO or H) of **1** are presented in Figs. 3a and 3b, respectively. The HOMO–LUMO gap is 2.84 eV. The highest occupied MO of **1** is of d_{xz} type with antibonding contributions from p_π chlorine orbitals. The remaining four d-type orbitals of rhenium are found among unoccuppied MOs. It confirms the d^2 configuration of the rhenium atom. The rhenium–oxygen interac-

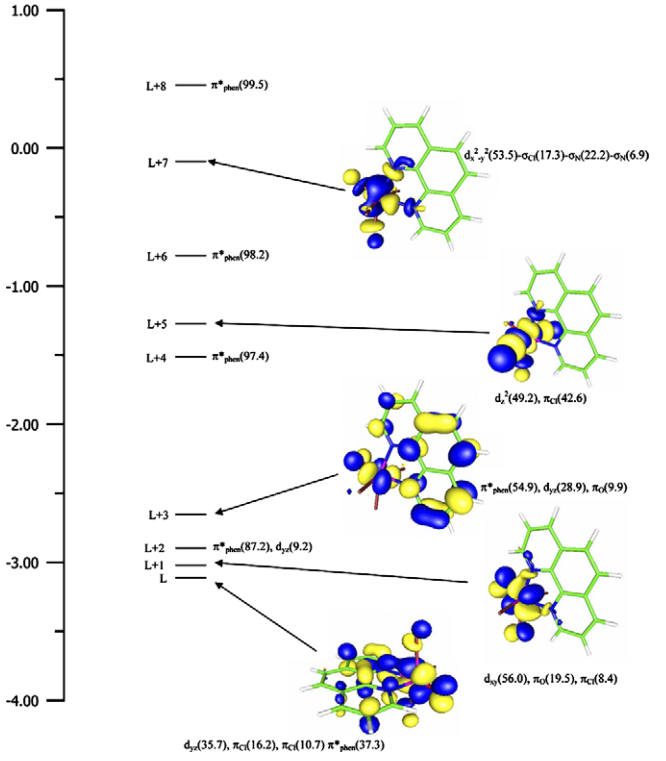

Fig. 3a. The energy (eV), character and some contours of the unoccupied molecular orbitals of **1**. Positive values of the orbital contour are represented in yellow (0.04 a.u.) and negative values are represented in blue (−0.04 a.u.). (For interpretation of the references to colour in this figure legend, the reader is referred to the web version of this article.)

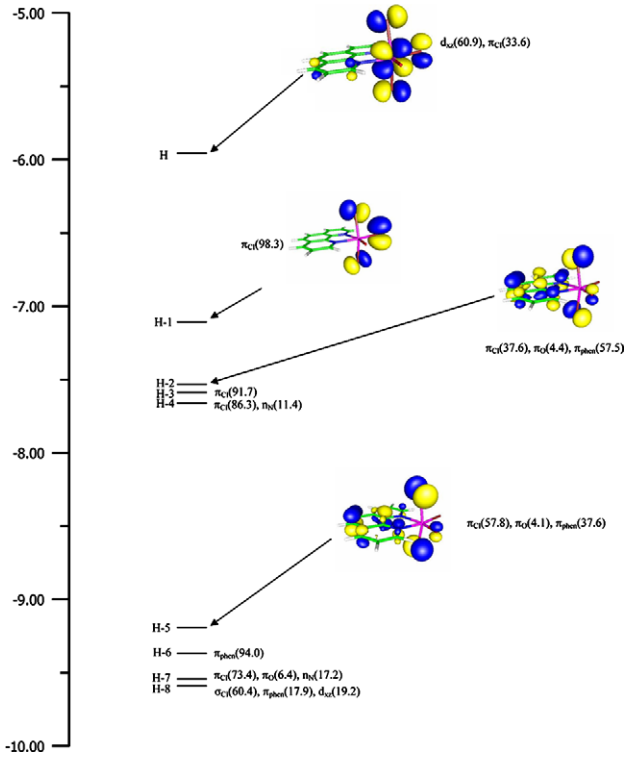

Fig. 3b. The energy (eV), character and some contours of the unoccupied molecular orbitals of **1**. Positive values of the orbital contour are represented in yellow (0.04 a.u.) and negative values are represented in blue (−0.04 a.u.). (For interpretation of the references to colour in this figure legend, the reader is referred to the web version of this article.)

Table 7
The energy and character of the selected occupied (HOMO) and unoccupied (LUMO) spin orbitals α and β for the triplet state of the $[ReCl_2(phen)(PPh_3)_2]^+$ cation

α Spin orbitals	*E* (eV)	Character	β Spin orbitals	*E* (eV)	Character
HOMO − 15	−9.681	$\pi_{phen}(60.8)$; $\pi_{Cl}(20.7)$	HOMO − 15	−9.979	$\pi_{Ph}(28.6)$; $\pi_{phen}(26.2)$; $\pi_{Cl}(21.4)$, $n_P(13.9)$
HOMO − 14	−9.420	π_{Ph}	HOMO − 14	−9.977	π_{phen}
HOMO − 13	−9.406	π_{Ph}	HOMO − 13	−9.655	$\pi_{phen}(58.1)$; $\pi_{Ph}(28.0)$; $\pi_{Cl}(11.1)$
HOMO − 12	−9.289	$\pi_{Ph}(78.8)$; $d_{z^2}(14.5)$	HOMO − 12	−9.415	π_{Ph}
HOMO − 11	−9.245	π_{Ph}	HOMO − 11	−9.401	π_{Ph}
HOMO − 10	−9.235	π_{Ph}	HOMO − 10	−9.261	π_{Ph}
HOMO − 9	−9.162	π_{Ph}	HOMO − 9	−9.230	π_{Ph}
HOMO − 8	−9.142	π_{Ph}	HOMO − 8	−9.224	π_{Ph}
HOMO − 7	−8.957	$\pi_{Ph}(55.8)$; $d_{xz}(33.0)$	HOMO − 7	−9.161	π_{Ph}
HOMO − 6	−8.945	π_{Ph}	HOMO − 6	−9.131	π_{Ph}
HOMO − 5	−8.766	π_{Ph}	HOMO − 5	−8.936	π_{Ph}
HOMO − 4	−8.764	π_{Ph}	HOMO − 4	−8.827	π_{Ph}
HOMO − 3	−8.626	$d_{xz}(41.5)$; $\pi_{Cl}(26.3)$; $\pi_{Ph}(27.4)$	HOMO − 3	−8.760	π_{Ph}
HOMO − 2	−8.515	$\pi_{Ph}(55.4)$; $n_P(20.7)$; $\pi_{Cl}(12.8)$	HOMO − 2	−8.759	π_{Ph}
HOMO − 1	−8.481	$d_{xy}(59.7)$; $\pi_{Cl}(33.2)$	HOMO − 1	−8.491	$\pi_{Ph}(58.5)$; $n_P(25.5)$; $\pi_{Cl}(8.7)$
HOMO	−8.417	$d_{yz}(62.5)$; $\pi_{Cl}(10.3)$; $\pi_{Ph}(15.8)$	HOMO	−7.815	$d_{xz}(64.0)$; $\pi_{Cl}(12.9)$; $\pi_{phen}(17.9)$
LUMO	−4.927	π^*_{phen}	LUMO	−5.712	$d_{yz}(64.3)$; $\pi_{Cl}(12.5)$; $\pi_{Ph}(14.7)$
LUMO + 1	−4.768	π^*_{phen}	LUMO + 1	−5.178	$d_{xy}(74.2)$; $\pi_{Cl}(17.3)$
LUMO + 2	−3.594	$d_{z^2}(35.5)$–$\sigma_P(32.6)$; $\pi^*_{Ph}(24.9)$	LUMO + 2	−4.880	$\pi^*_{phen}(81.2)$; $d_{xz}(12.6)$
LUMO + 3	−3.475	π^*_{phen}	LUMO + 3	−4.700	π^*_{phen}
LUMO + 4	−2.990	$\pi^*_{Ph}(70.0)$, P(19.1)	LUMO + 4	−3.446	π^*_{phen}
LUMO + 5	−2.953	$\pi^*_{Ph}(68.9)$, P(8.7)	LUMO + 5	−3.345	$d_{z^2}(34.5)$–$\sigma_P(28.1)$; $\pi^*_{Ph}(33.3)$
LUMO + 6	−2.845	$\pi^*_{Ph}(83.1)$, P(9.6)	LUMO + 6	−2.981	$\pi^*_{Ph}(71.5)$, P(19.3)
LUMO + 7	−2.818	π^*_{phen}	LUMO + 7	−2.934	$\pi^*_{Ph}(76.9)$, P(11.0)
LUMO + 8	−2.746	$d_{x^2-y^2}(45.0)$–$\sigma_N(16.3)$–$\sigma_{Cl}(26.0)$	LUMO + 8	−2.843	$\pi^*_{Ph}(83.6)$, P(9.5)
LUMO + 9	−2.741	$\pi^*_{Ph}(78.5)$, P(16.8)	LUMO + 9	−2.791	$\pi^*_{phen}(57.9)$; $\pi^*_{Ph}(31.6)$, P(6.1)
LUMO + 10	−2.620	π^*_{Ph}	LUMO + 10	−2.660	$\pi^*_{Ph}(60.0)$, P(9.8); $\pi^*_{phen}(20.6)$
LUMO + 11	−2.505	π^*_{Ph}	LUMO + 11	−2.619	$\pi^*_{Ph}(77.6)$, P(10.4)
LUMO + 12	−2.495	π^*_{Ph}	LUMO + 12	−2.496	π^*_{Ph}

HOMO – highest occupied molecular orbital.
LUMO – lowest unoccupied molecular orbital.

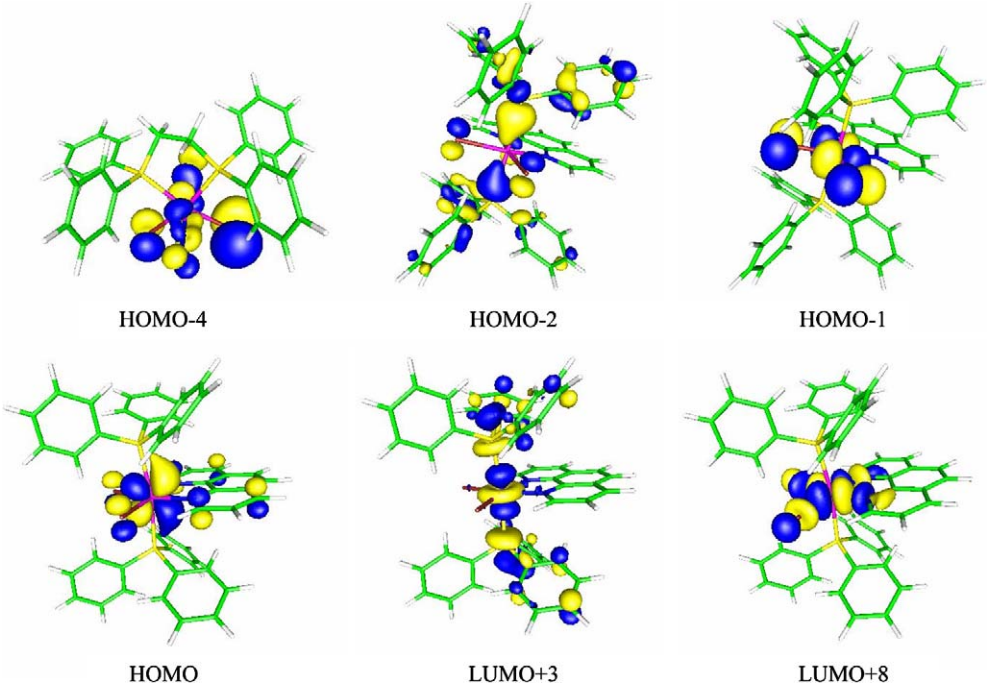

Fig. 4. The selected occupied (HOMO) and LUMO orbitals with α-spin for $[ReCl_2(phen)(PPh_3)_2]^+$. Positive values of the orbital contour are represented in yellow (0.04 a.u.) and negative values are represented in blue (−0.04 a.u.). (For interpretation of the references to colour in this figure legend, the reader is referred to the web version of this article.)

tion in **1** is described as a triple bond. The $\pi_{Re\equiv O}$ bonds arise from overlap of the two occupied oxygen p_π orbitals with the empty d_{xy} and d_{xz} metal orbitals. The contribution of the π^*_{Re-O} orbitals are visible in the LUMO, LUMO + 1 and LUMO + 3 orbitals. The LUMO and LUMO + 3 orbitals, however, also have an admixture of π-antibonding phenanthroline orbitals. The percent participations of the atomic orbitals in the HOMO and LUMO orbitals are given in round brackets. The LUMO + 5 and LUMO + 7 orbitals are predominantly of d_{z^2} and $d_{x^2-y^2}$ rhenium orbital character, respectively.

The energies and characters of several highest occupied and lowest unoccupied α(spin-up) and β(spin-down) molecular orbitals of $[ReCl_2(phen)(PPh_3)_2]^+$ are presented in Table 7. The percent participations of the atomic orbitals in the molecular orbitals are given in round brackets. The selected α molecular orbitals of $[ReCl_2(phen)(PPh_3)_2]^+$ are depicted in Fig. 4. The d_{xz}, d_{yz} and d_{xy} metal orbitals make main contributions into the HOMO − 3, HOMO − 1 and HOMO with α spin and HOMO, LUMO and LUMO + 1 with β spin. In all these molecular orbitals, the d_{xz}, d_{yz} and d_{xy} rhenium orbitals bear antibonding character towards the p_π orbitals of the chloride ligands. The remaining two d-type orbitals of rhenium are found among unoccuppied MOs of high energy. It confirms the $(d_{xz})^2(d_{yz})^1(d_{xy})^1$ configuration of the rhenium atom in the $[ReCl_2(phen)(PPh_3)_2]^+$ cation. The HOMO − 3, and HOMO with α spin and LUMO with β spin also display some contribution of π-antibonding phenyl orbitals, whereas the HOMO with β spin has admixture of π_{phen} orbitals. The LUMO orbital with α-spin has predominantly π^*phen character. In some of the lowest unoccupied molecular orbitals of $[ReCl_2(phen)(PPh_3)_2]^+$, the contribution of the phosphorous orbitals is visible. In classical

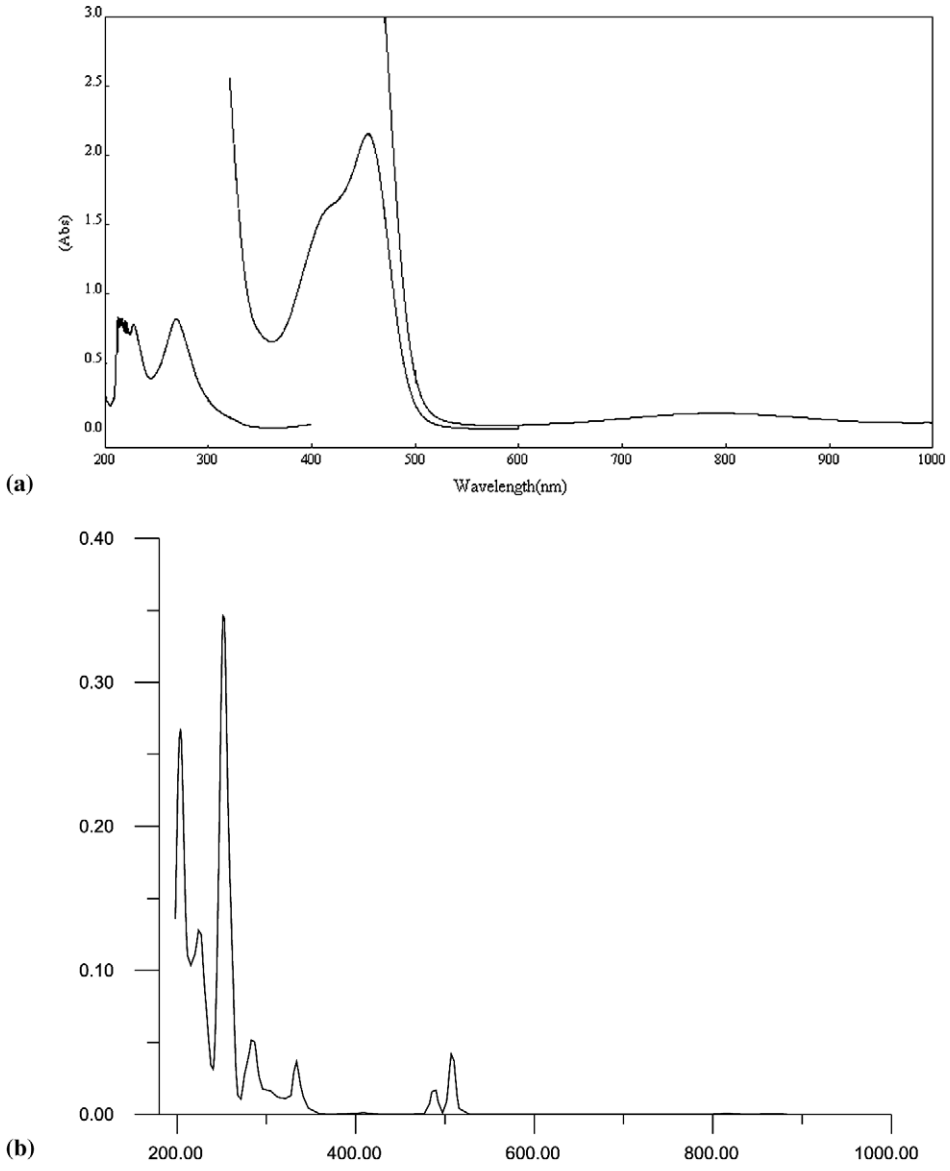

Fig. 5. The experimental (a) and calculated (b) electronic absorption spectra of **1**.

concepts, empty phosphorous 3d orbitals are used in π-back bonding between the metal center and the phosphine ligand. Now it is generally recognised that the d orbitals are very high in energy and play only a minor role in π_{M-PR3} bond formation [43]. In the π-back bonding between the metal center and the phosphine ligand are involved the σ^*(P–C) orbitals.

4.7. Electronic spectra

The experimental electronic spectra of **1** and **2** are presented in Figs. 5a and 6a, respectively. Figs. 5b and 6b present the calculated electronic spectra of $[ReOCl_3(phen)]$ and $[ReCl_2(phen)(PPh_3)_2]^+$. Each calculated transition in Figs. 5b and 6b was represented by a gaussian function $y = ce^{-bx^2}$ with height (c) equal to the oscillator strength and b equal to 0.04 nm^{-2}.

For the perrhenate anion, electronic transitions of π(O) → d character were calculated at ~225 and 197 nm.

Tables 8 and 9 present the position of the experimental absorption bands of **1** and **2** and the spin-allowed electronic transitions calculated with the TDDFT method for $[ReOCl_3(phen)]$ and $[ReCl_2(phen)(PPh_3)_2]^+$, respectively. The calculations result in many transitions with very small oscillator strengths. Except for the low energy part of the spectrum, only transitions with oscillator strengths larger than 0.010 for **1** and 0.005 for **2** are listed in Tables 8 and 9.

The assignment for complex **2** is not complete. The $[ReCl_2(phen)(PPh_3)_2]^+$ cation is of large size (882 basis

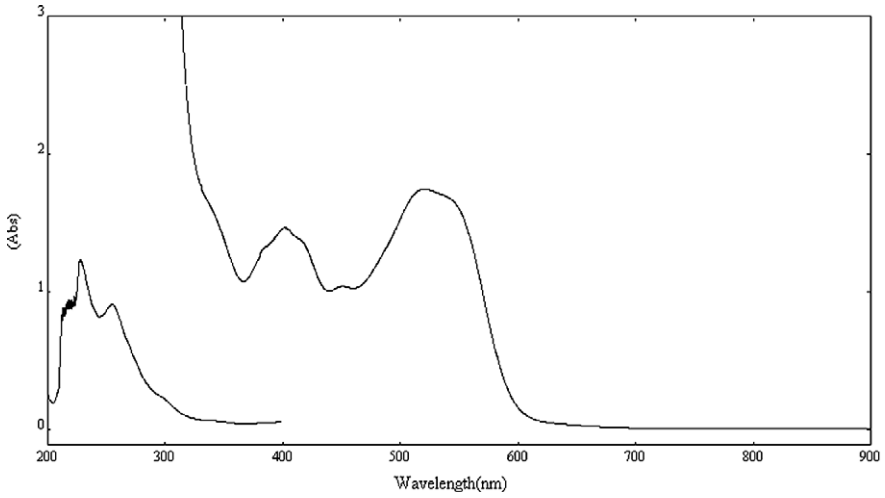

Fig. 6a. The experimental electronic absorption spectrum of **2**.

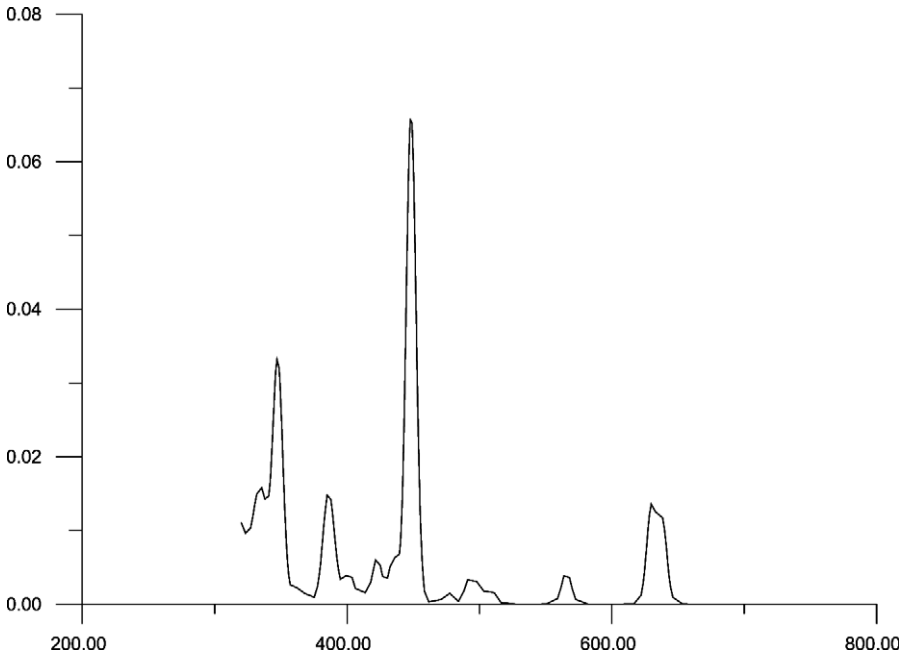

Fig. 6b. The electronic absorption spectrum of $[ReCl_2(phen)(PPh_3)_2]^+$.

Table 8
The energy and molar absorption coefficients of experimental absorption bands and the electronic transitions calculated with the TDDFT method for **1**

The most important orbital excitations	Character	λ (nm)	E (eV)	f	Experimental Λ (nm)(E (eV))ε
H → L + 1	d → d	869.0	1.43	*0.0002*	807.4 (1.54) 75
H → L	d → d	817.3	1.52	*0.0007*	
H → L + 2 H → L + 3	d → π*(phen)	508.0	2.44	*0.0434*	459.6 (2.70) 2160
H → L + 2 H → L + 3	d → π*(phen)	487.7	2.54	*0.0201*	416.6 (2.98) 1680
H − 4 → L	π(Br) → d	332.9	3.72	*0.0310*	
H − 5 → L	π(Br)/π(phen) → d	320.5	3.87	*0.0108*	
H − 2 → L + 2	π(Br)/π(O)/π(phen) → π*(phen)	310.2	4.00	*0.0128*	
H − 7 → L	π(Br)/π(O) → d	304.1	4.08	*0.0117*	
H − 4 → L + 2	π(Br) → π*(phen)				
H − 6 → L	π(phen) → d	286.2	4.33	*0.0322*	270.6 (4.58) 7470
H − 5 → L + 3	π(Br)/π(phen) → π*(phen)				
H − 5 → L + 2 H − 5 → L + 3	π(Br)/π(phen) → π*(phen)	283.0	4.38	*0.0247*	
H → L + 6	d → π*(phen)	276.5	4.48	*0.0256*	
H − 8 → L	σ(Br)/π(O) → d	262.3	4.73	*0.0149*	
H − 6 → L + 3	π(phen) → π*(phen)	259.8	4.77	*0.0992*	
H − 6 → L + 3	π(phen) → π*(phen)	252.4	4.91	*0.2999*	
H − 1 → L + 4	π(Br) → π*(phen)	247.7	5.00	*0.0724*	
H − 8 → L + 2	σ(Br)/π(O) → π*(phen)	245.5	5.05	*0.0300*	
H − 4 → L + 5	π(Br) → d	233.6	5.31	*0.0124*	
H − 12 → L + 1	π(Br)/π(O) → π*(phen)	232.1	5.45	*0.0276*	
H − 4 → L + 5	π(Br) → d				
H − 2 → L + 4	π(Br)/π(O)/π(phen) → π*(phen)	226.0	5.49	*0.0371*	228.8 (5.42) 7250
H − 9 → L + 2	π(Br)/π(phen) → π*(phen)	221.2	5.61	*0.0371*	
H − 5 → L + 4	π(Br)/π(phen) → π*(phen)	218.8	5.67	*0.0346*	
H − 5 → L + 5	π(Br)/π(phen) → d	215.3	5.76	*0.0216*	
H − 7 → L + 5	π(Br)/π(O) → d	214.8	5.77	*0.0106*	
H − 11 → L	π(O)/π(phen) → d	211.8	5.85	*0.0303*	
H − 11 → L + 2	π(O)/π(phen) → π*(phen)				
H − 13 → L	π(Br)/π(O)/π(phen) → d	208.5	5.95	*0.0206*	
H − 6 → L + 4	π(phen) → π*(phen)	204.9	6.05	*0.1394*	212.4 (5.84) 7330
H − 2 → L + 6	π(Br)/π(O)/π(phen) → π*(phen)				
H − 2 → L + 6	π(Br)/π(O)/π(phen) → π*(phen)	204.4	6.07	*0.0279*	
H − 11 → L + 2	π(O)/π(phen) → π*(phen)	201.5	6.15	*0.0636*	
H − 14 → L + 1	σ(O) → d	200.1	6.19	*0.0612*	

ε – molar absorption coefficient ($dm^3\ mol^{-1}\ cm^{-1}$).
f – oscillator strength.
H – highest occupied molecular orbital.
L – lowest unoccupied molecular orbital.

functions), and 90 calculated electron transitions do not comprise all the experimental absorption bands. As solution spectra of PPh_3 and 1,10-phenanthroline exhibit intense absorption bands in 260–200 nm region, some additional intraligand and interligand transitions are expected to be found at higher energies in the calculations for $[ReCl_2(phen)(PPh_3)_2]^+$.

The assignment of the calculated transitions to the experimental bands is based on the criterion of the energy and oscillator strength of the calculated transitions. In the description of the electronic transitions the main components of the molecular orbital are used.

The UV–Vis spectrum of **1** exhibits a few intense absorption bands in the range 500–200 nm and a weak absorption in the low energy range, at 807.4 nm.

The longest wavelength experimental band of **1** is attributed to the transitions of d → d character with small oscillator strengths, calculated at 869.0 and 817.3 nm.

The absorption bands at 459.6 and 416.6 nm are assigned to the electronic transitions calculated at 508.0 and 487.7 nm, respectively. They have MLCT (metal–ligand charge transfer) character and originate from the d_{Re} orbitals to the π^*_{phen} orbitals.

The experimental bands below 300 nm result from ligand–metal charge transfer: (π(Br)/π(O)/π(phen) → d) and ligand–ligand charge transfer: (π(Br)/π(O)/π(phen) → π*(phen) transitions. Nevertheless, the main contribution can be assigned to the LLCT excitations. The oscillator strengths of the LLCT transitions are considerable larger than those of LMCT transitions.

Table 9
The energy and molar absorption coefficients of experimental absorption bands of **2** and electronic transitions calculated with the TDDFT method for $[ReCl_2(phen)(PPh_3)_2]^+$

The most important orbital excitations		Character	λ (nm)	E (eV)	f	Experimental λ (nm) (E (eV))ε
α molecular orbitals	β molecular orbitals					
	H − 1 → L	π(Ph)/n(P) → d	638.2	1.94	*0.0110*	540.8 (2.29) 4240
	H → L + 2	d → π*(phen)	629.9	1.97	*0.0129*	
	H → L + 3	d → π*(phen)	565.8	2.19	*0.0044*	
	H − 1 → L + 1	π(Ph)/n(P) → d	508.7	2.44	*0.0020*	
	H − 3 → L	π(Ph) → d	498.2	2.49	*0.0020*	
	H − 4 → L	π(Ph) → d	492.2	2.52	*0.0031*	
	H − 8 → L	π(Ph) → d	450.5	2.97	*0.0135*	411.0 (3.02) 3530
H → L		d → π*(phen)	448.1	2.77	*0.0454*	
H → L + 1		d → π*(phen)	446.6	2.78	*0.0110*	
H − 3 → L + 1						
	H − 6 → L	π(Ph) → d	435.2	2.85	*0.0057*	
H − 3 → L		d → π*(phen)	422.5	2.93	*0.0058*	
H → L + 1						
	H − 12 → L	π(Ph) → d	401.5	3.09	*0.0042*	
	H → L + 5	d → d	391.7	3.17	*0.0014*	
H − 3 → L + 1		d → π*(phen)	386.4	3.21	*0.0082*	
	H − 13 → L	π(phen)/π(Ph) → d	383.2	3.24	*0.0055*	
	H − 1 → L + 3	π(Ph)/n(P) → π*(phen)				
H → L + 2		d → d	350.3	3.54	*0.0035*	331.0 (3.75) 4520
	H − 14 → L	π(phen) → d	347.5	3.57	*0.0254*	
	H → L + 4	d → π*(phen)				
H − 1 → L + 2		d → d	338.8	3.66	*0.0010*	
H − 1 → L + 8		d → d	333.8	3.71	*0.0001*	
H − 7 → L + 1	H − 4 → L + 3	π(Ph) → π*(phen)	333.2	3.72	*0.0058*	
H − 9 → L + 1		π(Ph) → π*(phen)	318.5	3.89	*0.0065*	300.0 (4.13) 16850
						256.0 (4.84) 41130
						228.8 (5.42) 55670

ε – molar absorption coefficient ($dm^3\ mol^{-1}\ cm^{-1}$).
f – oscillator strength.
H – highest occupied molecular orbital.
L – lowest unoccupied molecular orbital.

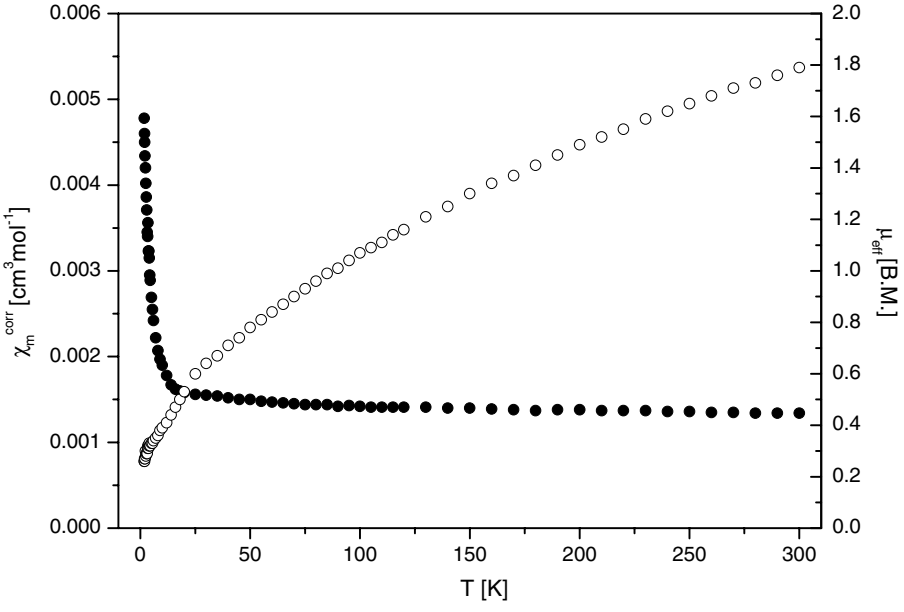

Fig. 7. Plots of the experimental magnetic data χ_M (•) and μ_{eff} (○) vs. T for the complex $[ReCl_2(phen)(PPh_3)_2](ReO_4)$ (**2**).

The broad intense asymmetric experimental band of **2** with a maximum at 540.8 nm is attributed to the three electronic transitions calculated at 638.2, 629.9 and 565.8 nm. The first one has LMCT and originates from triphenylphosphine orbitals to the d_{yz} rhenium orbital. The next two calculated excitations are of $d \rightarrow \pi^*_{phen}$ (MLCT) character.

The MLCT transitions from the d rhenium orbitals to the π^*_{phen} orbitals and LMCT excitations from triphenylphosphine orbitals to the d_{Re} orbitals are also responsible for the experimental bands at 411.0 and 331.0 nm. The LF (ligand field) electronic transitions calculated in the range 395–330 nm have small oscillator strengths and they do not contribute significantly to the overall shape of the absorption band at 331 nm.

4.8. Magnetic properties

The magnetic properties of the $[ReCl_2(phen)(PPh_3)_2](ReO_4)$ (**2**) complex under the form χ_M versus T and μ_{eff} versus T (χ_M being the molar magnetic susceptibilities and μ_{eff} the effective magnetic moment) are shown in Fig. 7. The rhenium(III) complex shows a room temperature magnetic moment of 1.79 BM (0.401 $cm^3\,mol^{-1}\,K$). The magnetic moment of the solid complex is temperature independent between 300 and 90 K. This value is characteristic of a mononuclear complex with low-spin rhenium(III) (d^4) ions in an O_h field ($^3T_{1g}$ ground state) [44–52] and arises because of the large spin–orbit coupling ($\zeta = 2500\ cm^{-1}$ [53]), which gives a diamagnetic ground state.

5. Supplementary data

Supplementary data for $C_{12}H_8Cl_3N_2ORe$ and $C_{48}H_{39}Cl_2N_2O_{4.50}P_2Re_2$ are available from the CCDC, 12 Union Road, Cambridge CB2 1EZ, UK on request, quoting the deposition numbers 297650 and 297651.

Acknowledgements

The Gaussian03 calculations were carried out in the Wrocław Centre for Networking and Supercomputing, WCSS, Wrocław, Poland.

The crystallographic part was financed by funds allocated by the Ministry of Scientific Research and Information Technology to the Institute of General and Ecological Chemistry, Technical University of Łódź.

References

[1] R.H. Holm, Chem. Rev. 87 (1987) 1401.
[2] C.C. Romä, F.E. Kühn, W.A. Hermann, Chem. Rev. 97 (1997) 3197.
[3] W.A. Hermann, F.E. Kühn, Acc. Chem. Res. 30 (1997) 169.
[4] W. Volkert, W.F. Goeckeler, G.J. Ehrhardt, A.R. Ketring, J. Nucl. Med 32 (1991) 174.
[5] E.A. Deutsch, K. Libson, J.L. Vanderheyden, Technetium and Rhenium in Chemistry and Nuclear Medicine, Raven Press, New York, 1990.
[6] L. Wallace, C. Woods, D.P. Rillema, Inorg. Chem. 34 (1995) 2875.
[7] E. Hevia, J. Pérez, V. Riera, D. Miguel, S. Kassel, A. Rheingold, Inorg. Chem. 41 (2002) 4673.
[8] S. Ranjan, S.Y. Lin, K.Ch. Hwang, Y. Chi, W.L. Ching, Ch.S. Liu, Y.T. Tao, Ch.H. Chien, S.M. Peng, G.H. Lee, Inorg. Chem. 42 (2003) 1248.
[9] K.A. Conner, R.A. Walton, Comprehensive Coordination Chemistry, vol. 4, Pergamon Press, Oxford, 1987.
[10] U. Abram, in: J.A. McClevery, T.J. Mayer (Eds.), Comprehensive Coordination Chemistry II, vol. 5, Elsevier, Oxford, 2004.
[11] J. Gangopadhyay, S. Sengupta, S. Bhattacharyya, I. Chakraborty, A. Chakravorty, Inorg. Chem. 41 (2002) 2616.
[12] S. Fortin, A.L. Beauchamp, Inorg. Chem. 40 (2001) 105.
[13] M.N. Sokolov, N.E. Fedorova, E.V. Peresypkina, R. Pätow, V.E. Fedorov, D. Fenske, Inorg. Chim. Acta 358 (2005) 3914.
[14] M.C. Aragoni, M. Arca, T. Cassano, C. Denotti, F.A. Devillanova, F. Isaia, V. Lippolis, D. Natali, L. Niti, M. Sampietro, R. Tommasi, G. Verani, Inorg. Chem. Commun. 5 (2002) 869.
[15] P. Romaniello, F. Lelj, Chem. Phys. Lett. 372 (2003) 51.
[16] P. Norman, P. Cronstrand, J. Ericsson. Chem. Phys. 285 (2002) 207.
[17] T.J. Bartczak, W. Czurak, J.O. Dzięgielewski, B. Machura, A. Jankowska, J. Kusz, J. Warczewski, J. Coord. Chem. 52 (2001) 361.
[18] G. Rouschias, G. Wilkinson, J. Chem. Soc. A (1966) 465.
[19] STOE & Cie, X-RED Version 1.18, STOE & Cie GmbH, Darmstadt, Germany, 1999.
[20] G.M. Sheldrick, Acta Crystallogr., Sect. A 46 (1990) 467.
[21] G.M. Sheldrick, SHELXL97. Program for the Solution and Refinement of Crystal Structures, University of Göttingen, Germany, 1997.
[22] G.M. Sheldrick, SHELXTL: release 4.1 for Siemens Crystallographic Research Systems, 1990.
[23] M.J. Frisch, G.W. Trucks, H.B. Schlegel, G.E. Scuseria, M.A. Robb, J.R. Cheeseman, J.A. Montgomery Jr., T. Vreven, K.N. Kudin, J.C. Burant, J.M. Millam, S.S. Iyengar, J. Tomasi, V. Barone, B. Mennucci, M. Cossi, G. Scalmani, N. Rega, G.A. Petersson, H. Nakatsuji, M. Hada, M. Ehara, K. Toyota, R. Fukuda, J. Hasegawa, M. Ishida, T. Nakajima, Y. Honda, O. Kitao, H. Nakai, M. Klene, X. Li, J.E. Knox, H.P. Hratchian, J.B. Cross, C. Adamo, J. Jaramillo, R. Gomperts, R.E. Stratmann, O. Yazyev, A.J. Austin, R. Cammi, C. Pomelli, J.W. Ochterski, P.Y. Ayala, K. Morokuma, G.A. Voth, P. Salvador, J.J. Dannenberg, V.G. Zakrzewski, S. Dapprich, A.D. Daniels, M.C. Strain, O. Farkas, D.K. Malick, A.D. Rabuck, K. Raghavachari, J.B. Foresman, J.V. Ortiz, Q. Cui, A.G. Baboul, S. Clifford, J. Cioslowski, B.B. Stefanov, G. Liu, A. Liashenko, P. Piskorz, I. Komaromi, R.L. Martin, D.J. Fox, T. Keith, M.A. Al-Laham, C.Y. Peng, A. Nanayakkara, M. Challacombe, P.M.W. Gill, B. Johnson, W. Chen, M.W. Wong, C. Gonzalez, J.A. Pople, GAUSSIAN 03, Revision B.03, Gaussian, Inc., Pittsburgh, PA, 2003.
[24] A.D. Becke, J. Chem. Phys. 98 (1993) 5648.
[25] C. Lee, W. Yang, R.G. Parr, Phys. Rev. B 37 (1988) 785.
[26] M.E. Casida, in: J.M. Seminario (Ed.), Recent Developments and Applications in Modern Density Functional Theory, Theoretical and Computational Chemistry, vol. 4, Elsevier, Amsterdam, 1996.
[27] P.J. Hay, W.R. Wadt, J. Chem. Phys. 82 (1985) 299.
[28] E.D. Glendening, A.E. Reed, J.E. Carpenter, F. Weinhold, NBO (version 3.1).
[29] E. König, Magnetic Properties of Coordination and Organometallic Transition Metal Compounds, Springer, Berlin, 1966.
[30] M. Stebler, A. Gutierrez, A. Ludi, H.B. Buergi, Inorg. Chem. 26 (1987) 1449.
[31] X.L.R. Fontaine, E.H. Fowles, T.P. Layzell, B.L. Shaw, M. Thornton-Pett, J. Chem. Soc., Dalton Trans. (1991) 1519.
[32] K. Nakamoto, Infrared Spectra of Inorganic and Coordination Compounds, second ed., Wiley–Interscience, New York, 1970, p.111.
[33] G.A. Jeffrey, W. Saenger, Hydrogen Bonding in Biological Structures, Springer, Berlin, 1994.

[34] G.R. Desiraju, T. Steiner, The Weak Hydrogen Bond in Structural Chemistry and Biology, Oxford University Press, Oxford, 1999.
[35] J.O. Dziegielewski, S. Michalik, M. Jaworska, R. Kruszynski, J. Kusz, Ann. Pol. Chem. Soc. (2003) 588.
[36] J.M. Mayer, Inorg. Chem. 27 (1988) 3899.
[37] B.J. Coe, S.J. Glenwright, Coord. Chem. Rev. 203 (2000) 5.
[38] L.E. Helberg, S.D. Orth, M. Sabat, W.D. Harman, Inorg. Chem. 35 (1996) 5584.
[39] J. Rall, F. Weingart, D.M. Ho, M.J. Heeg, F. Tisato, E. Deutsch, Inorg. Chem. 33 (1994) 3442.
[40] S.D. Orth, J. Barrerra, M. Sabat, W.D. Harman, Inorg. Chem. 33 (1994) 3026.
[41] A.E. Reed, L.A. Curtiss, F. Weinhold, Chem. Rev. 88 (1988) 899.
[42] M.L. Kuznestov, A.J.L. Pombeiro, J. Chem. Soc., Dalton Trans. (2003) 738.
[43] A. Vogler, H. Kunkely, Coord. Chem. Rev. 230 (2002) 243.
[44] J.E. Fergusson, Coord. Chem. Rev. 1 (1966) 459.
[45] B.N. Figgis, J. Lewis, Prog. Inorg. Chem. 6 (1964) 37.
[46] B.N. Figgis, Introduction to Ligand Field, Wiley–Interscience, New York, 1966, p. 248.
[47] J. Chatt, G.J. Leigh, D.M.P. Mingos, E.W. Randall, D. Shaw, J. Chem. Soc., Chem. Commun. (1968) 419.
[48] H.P. Gunz, G.J. Leigh, J. Chem. Soc (1971) 2229.
[49] B. Coutinho, J.R. Dilworth, P. Jobanputra, R.M. Thompson, S. Schmidt, J. Strähle, C.M. Archer, J. Chem. Soc., Dalton Trans. (1995) 1663.
[50] M. Hirsch-Kuchma, T. Nicholson, A. Davison, W.M. Davis, A.G. Jones, Inorg. Chem. 36 (1997) 3237.
[51] C.A. McConnachie, E.I. Stiefel, Inorg. Chem. 36 (1997) 6144.
[52] C. Pearson, A.L. Beauchamp, Can. J. Chem. 75 (1997) 220.
[53] A. Earnshaw, B.N. Figgis, J. Lewis, R.D. Peacock, J. Chem. Soc. (1961) 3132.

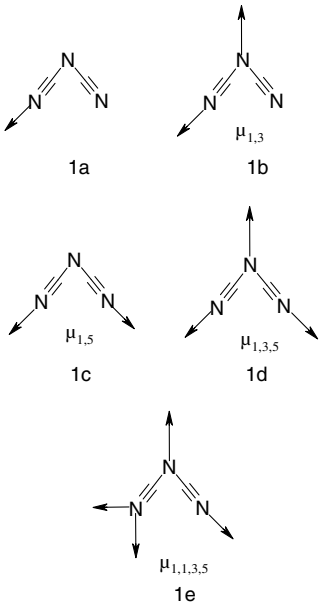

Scheme 1.

nitrogen, bidentate mode through two nitrile nitrogen atoms with end-to-end bridging, tris–monodentate bridging of three metal atoms, as well as an unusual μ-4 coordination where one nitrile nitrogen binds to two metal atoms. The coordination properties thus allow for the preparation of compounds with a large variety of architectures: mononuclear, dinuclear, as well as one-, two- and three-dimensional (nD, $n = 1$–3) networks [5] and therefore both its homo- and heteroleptic complexes have rich topologies and excellent magnetic properties [6]. A series of binary compounds of the general formula $[M^{II}(dca)_2]$, with a 3D rutile type structure, have gained much interest as several of these have been shown to be ferromagnetic (Co, $T_c = 9$ K; Ni, $T_c = 20$ K; Fe, $T_c = 19$ K), antiferromagnetic (Cr, $T_N = 47$ K; Mn, $T_N = 16$ K; Fe, $T_N = 19$ K) and paramagnetic [3]. Introduction of auxiliary ligands into the M^{II}–dca system has allowed the syntheses of several ternary systems, $[M^{II}L_x(dca)_y]$ (L = organic ligand, $x = 1$ or 2, $y = 1$ or 2), with a wide variety of topologies [7]. Coordination compounds with extended networks have been widely reported exhibiting different combinations of metallic cations, dipyridyl-type organic ligands and dca ligands [8]. A literature survey reveals the fact that dca-complexes in combination with 2,4,6-tris(2-pyridyl)-1,3,5-triazine (tptz) are rare. We have chosen tptz for its flexible coordination sites [9]. We have recently reported some novel observations utilising dca in the synthesis of chain structures with single, symmetrical, $\mu_{1,5}$-dca bridged Cu(II) and Ni(II) polymers [10]. In the present work, we describe the syntheses and crystal structures of three new supramolecular frameworks with dca and the auxiliary ligand, 2,4,6-tris(2-pyridyl)-1,3,5-triazine (tptz): $[Mn(ac)(tptz)(dca)(H_2O)] \cdot (H_2O)_2$ (**1**) (where ac = acetate anion), $[Zn(tptz)(dca)_2] \cdot (H_2O)_2$ (**2**) and $[Cd_2(tptz)_2(dca)_2(H_2O)_2] \cdot (ClO_4)_2$ (**3**). To date, a number of higher-dimensional architectures of different transition metals have been reported using dca as a bridging ligand, but the number of dinuclear compounds with bridging dca, are scarce [11]. To the best of our knowledge, this is the first dinuclear complex of Cd(II) using dca as a bridging ligand.

2. Experimental

2.1. Physical techniques

The infrared spectra of the complexes were recorded on a Perkin–Elmer RX 1 FT-IR spectrometer with a KBr disc. The electronic spectrum of **1** was recorded on a Perkin–Elmer Lambda 40 (UV–Vis) spectrophotometer in methanol. Elemental analyses were carried out using a Perkin–Elmer 2400 II elemental analyser. The electrochemical study was performed on a CH 600A cyclic voltammeter instrument for complex **1** in dimethylformamide solvent and using tetrabutylammonium perchlorate as the supporting electrolyte. The magnetic susceptibility was measured on a powder sample in a vibrating sample magnetometer for **1** using mercury(tetrathiocyanato)cobaltate as the standard.

2.2. Materials

All the chemicals and solvents used for the syntheses were of reagent grade. Manganese acetate tetrahydrate, zinc nitrate hexahydrate, cadmium perchlorate hydrate (Merck), 2,4,6-tris(2-pyridyl)-1,3,5-triazine (Aldrich) and sodium dicyanamide ($NaN(CN)_2$) (Fluka) were used as received. *Caution*! Although no problems were encountered in this work, perchlorate salts are potentially explosive. They should be prepared in small quantities and handled with care.

2.3. Synthesis

2.3.1. Synthesis of $[Mn(ac)(tptz)(dca)(H_2O)] \cdot (H_2O)_2$ (**1**)

Complex **1** was synthesised by adding 1 mmol (0.312 g) of tptz to a solution of 1 mmol (0.246 g) of manganese acetate tetrahydrate in 10 ml of methanol, followed by the dropwise addition of 1 mmol (0.089 g) of sodium dicyanamide dissolved in the minimum quantity of water. The resulting clear yellow solution was filtered off and left to stand in air. After 3 days, yellow needles of **1** were obtained that were suitable for X-ray determination. Yield: 0.41 g (74.6%). *Anal.* Calc. for $C_{22}H_{21}MnN_9O_5$: C, 48.31; H, 3.84; N, 23.06. Found: C, 48.25; H, 3.79; N, 22.97%.

2.3.2. Synthesis of $[Zn(tptz)(dca)_2] \cdot (H_2O)_2$ (**2**)

Crystals of complex **2** were separated as a pale yellow crystalline solid by adding 1 mmol (0.089 g) aqueous solution of sodium dicyanamide to a methanolic solution containing a mixture of zinc nitrate hexahydrate (1 mmol, 0.297 g) and tptz (0.312 g, 1 mmol). Yield: 0.39 g (72%).

Anal. Calc. for $C_{22}H_{16}N_{12}ZnO_2$: C, 48.36; H, 2.93; N, 30.77. Found: C, 48.32; H, 2.87; N, 30.71%.

2.3.3. Synthesis of $[Cd_2(tptz)_2(dca)_2(H_2O)_2]\cdot(ClO_4)_2$ (**3**)

Complex **3** was obtained as pale yellow hexagonal crystals by the reaction of 20 ml methanolic solution containing cadmium perchlorate hydrate (0.311 g, 1 mmol) and tptz (0.312 g, 1 mmol) with 10 ml aqueous of sodium dicyanamide (0.089 g, 1 mmol). Yield: 0.46 g (75%). *Anal.* Calc. for $C_{20}H_{14}CdClN_9O_5$: C, 39.32; H, 2.30; N, 20.64. Found: C, 39.23; H, 2.26; N, 20.51%.

2.4. X-ray crystallography

Experimental details for **1** and **3** are given in Table 1. The data processing was performed by the Kappa CCD analysis software [12] and the lattice constants were refined by least-square refinement. No absorption correction was applied to the data sets. The unit-cell parameters, crystal system, space group and refinement details are summarised in Table 1. The structures were solved by direct methods (SIR97 program [13]) combined with Fourier difference syntheses and refined against F using reflections with $[I/\sigma(I) > 3]$ (CRYSTALS program [14]). All non-hydrogen atoms were successfully refined anisotropically.

Intensity data for **2** were collected on a Bruker SMART APEX diffractometer, equipped with a CCD area detector and graphite monochromated Mo-Kα radiation ($\lambda =$ 0.71073 Å), controlled by a Pentium-based PC running the SMART software package [15]. Single crystals were mounted and measured at room temperature. All data were corrected for Lorentz and polarization effects. Semi-empirical absorption corrections were applied using the SADABS program [16]. Both data processing programs were integrated with the Bruker SAINTPLUS program [17]. The structure was solved by the Patterson method, completed by difference Fourier techniques and refined by full-matrix least-squares on F^2 (SHELXL/97) [18] with initial isotropic, but subsequently anisotropic thermal parameters. Hydrogen atoms were included in calculated positions and refined riding on carbon atoms with free isotropic displacement parameters. The hydrogen atoms of the two water molecules were located from the difference Fourier map, and their positions were refined with a restrained O–H = 0.9 Å distance [18]. Further details are given in Table 1.

3. Results and discussion

3.1. Description of the crystal structures

3.1.1. $[Mn(ac)(tptz)(dca)(H_2O)]\cdot(H_2O)_2$ (**1**)

The molecular structure of **1** is shown in Fig. 1. Selected bond distances and bond angles are presented in Table 2. Each manganese atom is hepta-coordinated, with a coordination polyhedron close to a pentagonal bipyramid. Hepta-coordination is achieved by means of three N atoms belonging to the tptz ligand (N10, N21 and N33) and two

Table 1
Crystallographic data of complexes **1**–**3**

	1	**2**	**3**
Chemical formula	$C_{22}H_{21}MnN_9O_5$	$C_{22}H_{16}N_{12}ZnO_2$	$C_{20}H_{14}CdCl_1N_9O_5$
Formula weight	546.40	545.84	608.24
Crystal system	monoclinic	triclinic	triclinic
Temperature (K)	293	295	293
Space group	$C2/c$	$P\bar{1}$	$P\bar{1}$
a (Å)	14.668(5)	9.250(9)	7.956(5)
b (Å)	13.394(3)	10.558(10)	10.751(5)
c (Å)	26.821(9)	13.354(13)	14.043(5)
α (°)	90	110.758(10)	72.295(5)
β (°)	99.613(1)	98.480(2)	80.237(5)
γ (°)	90	100.659(2)	83.170(5)
V (Å^3)	5195.7(3)	1166.0(2)	1125(1)
Z	8	2	2
Reflections collected	10988	8572	6697
Independent reflections	5908	5035	5493
R_{int}	0.029	0.018	0.02
Density (calculated) (Mg m^{-3})	1.361	1.555	1.796
Absorption coefficient (mm^{-1})	0.555	1.101	1.143
$F(000)$	2248	548	604
Crystal size (mm)	$0.01\times0.01\times0.06$	$0.42\times0.39\times0.27$	$0.01\times0.01\times0.09$
θ Range for data collection	1.5–27.6	1.7–28.0	1.5–30.2
Number of restraints	9	6	3
R indices (all data)	$R_1 = 0.1179$	$R_1 = 0.0493$	$R_1 = 0.0887$
	$wR_2 = 0.1148$	$wR_2 = 0.1076$	$wR_2 = 0.0951$
Final R indices $[I > 3\sigma(I)$ for **1** and **3**] and $[I > 2\sigma(I)$ for **2**]	$R_1 = 0.0498$	$R_1 = 0.0409$	$R_1 = 0.0480$
	$wR_2 = 0.0595$	$wR_2 = 0.1026$	$wR_2 = 0.0527$
Largest difference in peak and hole (e Å^3)	0.57, −0.52	0.52, −0.35	0.65, −0.61

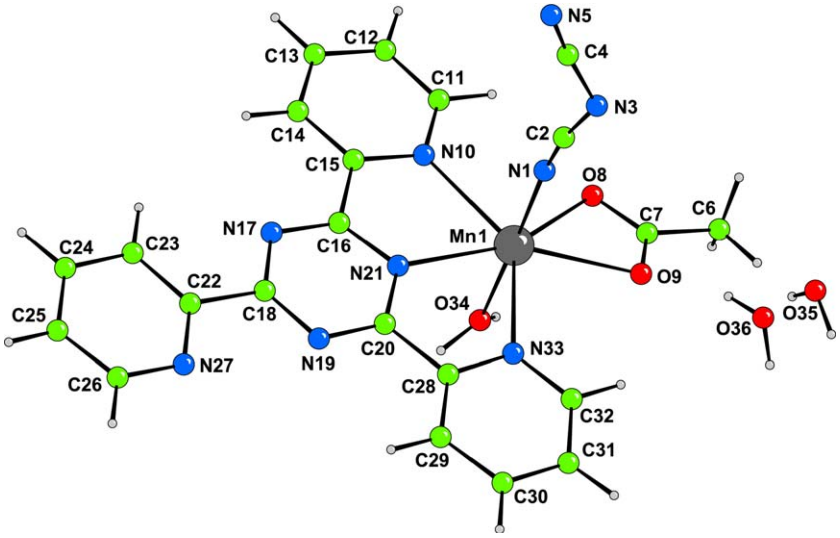

Fig. 1. Coordination environment of the metal in complex **1** with the atom numbering scheme.

Table 2
Selected bond distances (Å) and bond angles (°) for complex **1**

Mn1–O8	2.291(3)	C13–C14	1.387(6)
Mn1–O9	2.347(3)	C16–N17	1.324(5)
Mn1–O34	2.137(3)	C18–N19	1.331(5)
Mn1–N1	2.184(5)	C22–C23	1.387(6)
Mn1–N10	2.415(4)	C25–C26	1.369(7)
Mn1–N21	2.292(3)	C28–C29	1.370(5)
Mn1–N33	2.390(3)	C31–C32	1.369(6)
N1–C2	1.094(6)	C11–C12	1.380(6)
N3–C2	1.279(8)	C14–C15	1.375(6)
N3–C4	1.290(9)	C23–C24	1.389(6)
N5–C4	1.097(9)	C26–N27	1.341(6)
C15–C16	1.488(5)	C29–C30	1.392(7)
C18–C22	1.497(6)	C32–N33	1.340(5)
C20–C28	1.476(5)	C12–C13	1.366(7)
O8–Mn1–O9	55.76(9)	O34–Mn1–N1	177.48(13)
O8–Mn1–O34	85.66(10)	O34–Mn1–N10	90.23(10)
O8–Mn1–N1	96.82(14)	O34–Mn1–N21	85.82(11)
O8–Mn1–N10	85.95(10)	O34–Mn1–N33	84.76(10)
O8–Mn1–N21	152.76(10)	N1–Mn1N10	89.52(13)
O8–Mn1–N33	136.13(10)	N1–Mn1–N21	91.77(13)
O9–Mn1–O34	94.79(10)	N1–Mn1–N33	93.71(13)
O9–Mn1–N1	86.98(13)	N10–Mn1–N21	68.26(11)
O9–Mn1–N10	140.71(10)	N10–Mn1–N33	136.71(11)
O9–Mn1–N21	150.92(10)	N21–Mn1–N33	68.50(10)
O9–Mn1–N33	82.58(9)		

oxygen atoms from the bidentate acetato ligand (O8 and O9), which determine the equatorial plane and finally the nitrogen N1 atom from the terminal dicyanamido ligand and a water molecule (O34) are in a *trans* disposition (yielding N1–Mn1–O34 as the *trans-axial* angle 177.48(13)°).

The shorter bond lengths, 2.184(5) and 2.137(3) Å, correspond to the axial positions occupied by the terminal monodentate dca ligand, Mn1–N1 and water molecule Mn1–O34, respectively, whereas the equatorial sites show similar bond lengths in the 2.291(3)–2.415(4) Å range which are more or less comparable to similar systems [9,19]. The deviation from ideal pentagonal-bipyramidal geometry is indicated by the difference in the basal angles which vary from 85.95(10)° to 55.76(9)°. The source of distortion primarily comes from the bites taken by the ligand, smaller than the ideal value of 72°, because of the constraint imposed in the five-membered chelate rings. Three kinds of bond angles may be found in the equatorial plane: the lower of 55.76(9)° corresponds to the bidentate acetate ligand O8–Mn1–O9 bond angle, two intermediate ones of 68.50(10)° and 68.26(11)° corresponding to the N(tptz)–Mn1–N(tptz) bond angles and two greater O(acetate)–Mn1–N(tptz) bond angles of 85.95(10)° and 82.58(9)°. These values are consistent with those found for related complexes [20]. The bond distance of Mn(II) to the middle nitrogen N21 is significantly shorter than the Mn1–N10 and Mn1–N33 distances, which is usually observed in tptz-type ligands [19]. The tptz ligand is almost planar; the angles between the central triazine ring and the attached pyridyl rings are 2.5(1)°, 2.1(1)° and 3.5(1)° which are in accordance with the values reported in the literature in related systems [9,21] and the tptz plane is inclined by an angle of 15.7(1)° to the bidentate acetate plane. In tptz, the $C(sp^2)$–$C(sp^2)$ distances within the ring are normal (1.45 Å) and the exterior bonds (C16–C15, 1.48(5) Å; C20–C28, 1.47(5) Å; C18–C22, 1.49(6) Å) are also normal. The manganese atom is 0.071(1) Å out of the basal pentagonal plane. The deviations of the atoms N10, N21, N33, O8 and O9 from the mean basal plane are 0.097(3), −0.003(3), −0.092(3), 0.195(3) and 0.194(3) Å, respectively. The dihedral angles between the equatorial plane and the plane of the tptz and dca groups are 3.11(5)° and 86.6(2)°, respectively.

The structure also contains uncoordinated water molecules in the lattice. Both hydrogen atoms of the coordinated water molecule (O34) are involved in making hydrogen bonds with (i) the oxygen atom of an uncoordinated water molecule (O35) and with (ii) the oxygen atom (O8) of the counter anion ($CH_3CO_2^-$) which belongs to a

Table 3
Hydrogen bonds for **1** (Å and °)

D–H···A	*d*(D–H)	*d*(H···A)	*d*(D···A)	⟨(DHA)⟩
O34–H341···O8^{i}	0.89(2)	1.80(3)	2.678(4)	173(4)
O34–H342···O35^{ii}	0.89(3)	1.82(3)	2.693(4)	170(3)
O35–H351···O36	0.89(3)	1.84(3)	2.720(6)	168(2)
O35–H352···N27^{iii}	0.88(3)	2.06(3)	2.906(6)	160(3)
O36–H361···N5^{iv}	0.90(3)	2.01(3)	2.875(8)	160(3)
O36–H362···O9	0.89(3)	1.93(3)	2.791(6)	166(3)
C11–H101···O8	1.0100	2.5900	3.243(5)	122.00
C23–H221···N5^{v}	1.0200	2.5900	3.504(9)	149.00
C29–H281···O35^{vi}	1.0100	2.4700	3.471(6)	172.00
C32–H284···O9	1.0100	2.4100	3.103(5)	125.00

Symmetry transformations used to generate equivalent atoms: (i) $2-x, y, 1/2-z$; (ii) $1/2+x, 1/2+y, z$; (iii) $3/2-x, -1/2-y, -z$; (iv) $1/2+x, -1/2+y, z$; (v) $1/2+x, 1/2+y, z$; (vi) $3/2-x, -1/2-y, -z$.

neighbouring manganese-complex. Thus, infinite chains are formed. The second oxygen atom (O9) of the $CH_3CO_2^-$ anion makes a hydrogen bond with one of the hydrogen atoms of the other lattice water molecule (O36). O36 is also connected to N5 (the terminal nitrogen atom of the $N(CN)_2^-$ ligand) and is further involved in hydrogen bonding interactions to the other neighbouring terminal nitrogen atom and thus connects the 1D chains together to form 2D sheets which lie in the [1 0 0] plane. O35 is connected via hydrogen bonds to O36 and to N27 (nitrogen atoms belonging to the external ring of the tptz ligand connected to another manganese-complex), connecting the sheets together to form a 3D supramolecular network. Due to the presence and the number of uncoordinated water molecules inside this structure, many hydrogen bonds are formed connecting isolated complexes together and thus the structure can be assumed to be a pseudo 3D network (Table 3, Fig. 2). This hydrogen bonding network is reinforced by two types of weak C–H···O interactions (Table 3). This weak hydrogen bonding is possibly a contributing factor in the supramolecular assembly and stabilisation of the lattice, however, the strong O–H···O interactions are obviously the dominant intermolecular interactions. The significant π–π stacking distance between the two parallel planar rings of the tptz ligand is 3.76(1) Å. This distance is very similar to other π–π stacked systems [22].

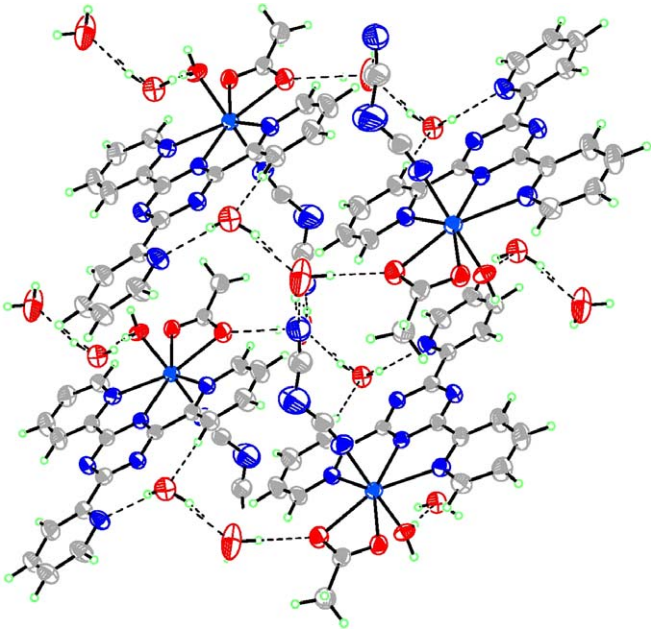

Fig. 2. Hydrogen bonds building 3D networks in **1**.

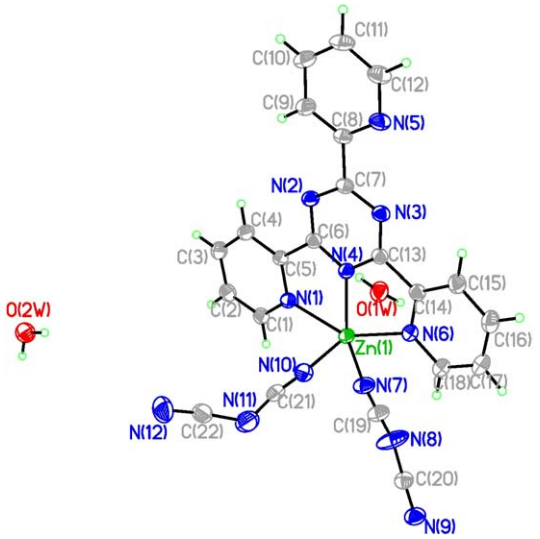

Fig. 3. Local coordination environment of the metal in complex **2** with the atom numbering scheme.

3.1.2. $[Zn(tptz)(dca)_2]\cdot(H_2O)_2$ (**2**)

The structure of **2** consists of the neutral mononuclear unit, $[Zn(tptz)(dca)_2]\cdot(H_2O)_2$ (Fig. 3), in which the three tptz nitrogen atoms and a terminal dca nitrogen bind to zinc in equatorial positions (Zn1–N1, 2.216(2) Å; Zn1–N4, 2.077(2) Å; Zn1–N6, 2.225(2) Å and Zn1–N7, 1.974(3) Å), and another terminal dca nitrogen resides in an apical position (Zn–N10, 2.064(2) Å). Considering these bonds, the zinc coordination geometry may be described as distorted square pyramidal, the trigonality parameter τ being 0.21 [23].

Selected bond distances and bond angles are summarised in Table 4. The Zn–pyridyl bond distances are comparable and the values are similar to those found in similar systems [24]. The deviation from the ideal square pyramid is indicated by the difference in *cisoid* (63.53(8)–110.29(10)°) and *transoid* angles (147.62(7)–160.22(11)°). The source of distortion primarily comes from the bites taken by the ligand; the bite angles N1–Cd1–N4 and N4–Cd1–N6 are 74.21(7)° and 73.53(8)°, respectively, significantly smaller than the ideal value of 90°. The deviations of the atoms N1, N4, N6 and N7 from the mean basal plane are −0.0850, +0.1121, −0.0910 and 0.0638 Å, respectively, and the zinc atom is displaced by 1.1202 Å from the plane towards the apical dca. The dihedral angles between the equatorial plane and the plane of the tptz and two dca groups are 8.5°, 62.7° (apical) and 58.4°, respectively. The

Table 4
Selected bond distances (Å) and bond angles (°) for complex **2**

Zn1–N1	2.216(2)	C7–C8	1.482(4)
Zn1–N4	2.077(2)	C1–C2	1.370(4)
Zn1–N6	2.225(2)	C2–C3	1.395(4)
Zn1–N7	1.974(3)	C3–C4	1.381(4)
Zn1–N10	2.064(2)	C4–C5	1.380(3)
N7–C19	1.143(4)	C8–C9	1.375(4)
N8–C20	1.300(3)	C9–C10	1.376(4)
N8–C19	1.277(4)	C10–C11	1.377(5)
N9–C20	1.138(3)	C11–C12	1.368(4)
N10–C21	1.126(4)	C13–C14	1.480(3)
N11–C22	1.284(4)	C14–C15	1.379(4)
N11–C21	1.287(4)	C15–C16	1.386(4)
N12–C22	1.120(5)	C16–C17	1.380(5)
C5–C6	1.483(3)	C17–C18	1.372(5)
N1–Zn1–N4	74.21(7)	N4–Zn1–N7	160.22(11)
N1–Zn1–N6	147.62(7)	N4–Zn1–N10	101.08(9)
N1–Zn1–N7	110.29(10)	N6–Zn1–N7	99.30(10)
N1–Zn1–N10	90.83(9)	N6–Zn1–N10	97.92(10)
N4–Zn1–N6	73.53(8)	N7–Zn1–N10	98.14(11)

pyridyl rings of tptz are planar and the angles between the central triazine ring and the attached pyridyl rings are 1.8° (Py–N1), 2.7° (Py–N5) and 2.4° (Py–N6). The tptz group acts as a tridentate ligand through its three nitrogen atoms, the zinc to triazine-nitrogen (N4) bond being significantly shorter than the two zinc to pyridyl-nitrogen ones (Zn1–N1 and Zn1–N6 distances), a pattern usually observed in this type of three point attachment of tptz-type ligands [25]. The average $C(sp^2)$–$C(sp^2)$ bond lengths in the tptz ligand within the ring are normal and the exterior bonds (C5–C6, 1.483(3) Å; C7–C8, 1.482(4) Å; C13–C14, 1.480(3) Å) are also in agreement with those reported previously [26] and with complexes **1** and **3** also.

There are extensive arrays of hydrogen bonding interactions involving the dicyanamide, tptz moieties and lattice water molecules yielding a 1D supramolecular chains-like architecture (Fig. 4, Table 5). The two lattice water molecules with their centrosymmetric homologous are linked by strong hydrogen bonds, giving rise to quadrilateral frameworks (O1W–H2W···O2W = 2.864(3) Å and O2W–H4W···O1W = 2.854(3) Å). The four remaining hydrogen atoms bind, respectively, to two terminal nitrogen atoms of $N(CN)_2^-$ ligands and two pyridyl nitrogen atoms (belonging to the external ring of the tptz ligand) of the neighbouring zinc complex (Fig. 4 and Table 5). The resulting supramolecular network thus can be described as layers of complexes with the aromatic ligands lying parallel to (1 0 1) planes linked by hydrogen bonds provided by the water molecules. There are also weak π–π interactions between tptz ligands (closest non-hydrogen contact is 3.644 (2) Å).

3.1.3. $[Cd_2(tptz)_2(dca)_2(H_2O)_2]\cdot(ClO_4)_2$ (**3**)

A perspective view of complex **3** with the atom numbering scheme is shown in Fig. 5. Selected bond distances and bond angles are summarised in Table 6. Two dca groups bridge the metal atoms in a symmetric end-to-end fashion.

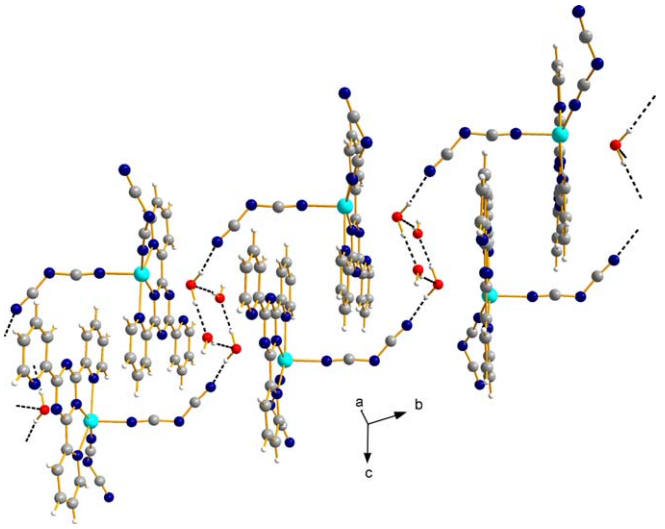

Fig. 4. Perspective view of **2** showing 1D-layers formed by the hydrogen bond interaction in the [0 1 0] plane. Hydrogen atoms are omitted for clarity.

Table 5
Hydrogen bonds for **2** (Å and °)

D–H···A	*d*(D–H)	*d*(H···A)	*d*(D···A)	⟨(DHA)⟩
O1W–H1W···N12^{i}	0.88(4)	1.96(4)	2.836(4)	169(4)
O1W–H2W···O2W^{ii}	0.99(4)	1.88(4)	2.864(3)	172(3)
O2W–H3W···N3^{iii}	0.90(4)	2.62(4)	3.439(3)	152(4)
O2W–H3W···N5^{iii}	0.90(4)	2.21(5)	2.944(3)	138(4)
O2W–H4W···O1W^{iv}	0.87(4)	2.01(4)	2.854(3)	165(4)
C3–H3···N9^{v}	0.93	2.53	3.445(4)	167.00
C9–H9···N2	0.93	2.48	2.796(3)	100.00

Symmetry transformations used to generate equivalent atoms: (i) x, $1+y$, z; (ii) $-x$, $1-y$, $2-z$; (iii) $1-x$, $1-y$, $2-z$; (iv) x, $-1+y$, z; (v) x, y, $1+z$.

Complex **3** is an unusual dinuclear entity bridged by dca. One nitrogen from triazine and two from pyridyl moieties along with the two dca anions and one water molecule form the distorted octahedral geometry around each Cd(II). Three nitrogen atoms (N18, N1 and N12) from the tptz ligand and one bridging dca (N25) form the mean equatorial base, while O35 from water and N29 from another bridging dicyanamide occupy the axial positions.

The bond lengths are in accordance with those observed in the literature [27]. The deviation from ideal octahedral geometry is indicated by the difference in *cisoid* (67.97(15)–122.9(2)°) and *transoid* angles (136.84(14)–172.75(19)°). The deviations of the atoms N1, N12, N18 and N25 from the mean basal plane are 0.073(4), −0.070(5), −0.057(4) and 0.076(6) Å. The source of distortion primarily comes from the bites taken by the ligand; the bite angles N18–Cd1–N1 and N1–Cd1–N12 are 67.97(15)° and 68.87(15)°, respectively, significantly smaller than the ideal value of 90°. The bond distance of Cd(II) to the middle nitrogen N1 (2.330(4) Å) is significantly shorter than the Cd1–N18 (2.426(4) Å) and Cd1–N12 (2.378(6) Å) distances, a pattern observed for complexes **1**–**3**, and the values are comparable for these types of bonds [28]. The

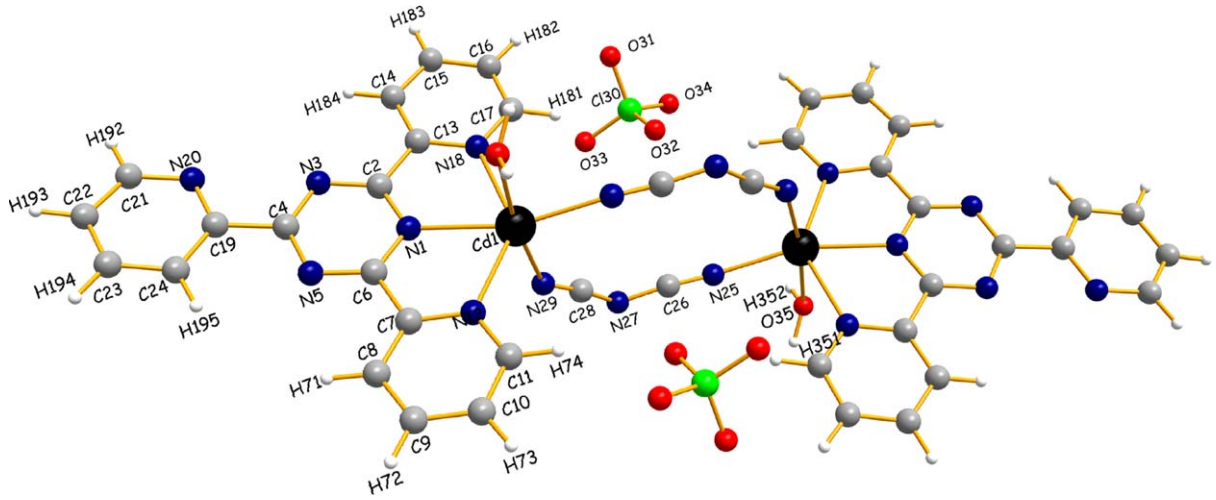

Fig. 5. Perspective view of the dinuclear unit in **3** showing the atom numbering scheme.

Table 6
Selected bond distances (Å) and bond angles (°) for complex **3**

Cd1–O35	2.365(5)	C21–C22	1.391(9)
Cd1–N1	2.330(4)	C22–C23	1.359(9)
Cd1–N12	2.378(6)	C23–C24	1.390(9)
Cd1–N18	2.426(4)	C19–C24	1.389(8)
Cd1–N25	2.199(7)	C13–C14	1.382(8)
Cd1–N29	2.287(6)	C14–C15	1.395(9)
N25–C26	1.130(10)	C15–C16	1.374(9)
N27–C28	1.275(10)	C16–C17	1.370(8)
N27–C26	1.260(10)	C13–C14	1.382(8)
N29–C28	1.133(9)	C7–C8	1.378(9)
C6–C7	1.486(7)	C8–C9	1.375(10)
C2–C13	1.483(7)	C9–C10	1.380(11)
C4–C19	1.495(7)	C10–C11	1.385(11)
O35–Cd1–N1	84.35(16)	N1–Cd1–N29	102.32(17)
O35–Cd1–N12	90.94(18)	N12–Cd1–N18	136.84(14)
O35–Cd1–N18	85.28(16)	N12–Cd1–N25	122.9(2)
O35–Cd1–N25	84.5(2)	N12–Cd1–N29	94.10(18)
O35–Cd1–N29	172.75(19)	N18–Cd1–N25	99.6(2)
N1–Cd1–N12	68.87(15)	N18–Cd1–N29	94.55(17)
N1–Cd1–N18	67.97(15)	N25–Cd1–N29	88.4(2)
N1–Cd1–N25	163.9(2)		

Table 7
Hydrogen bonds for **3** (Å and °)

D–H···A	*d*(D–H)	*d*(H···A)	*d*(D···A)	⟨(DHA)⟩
N27–H272···N27^{i}	1.00	2.61	3.13(8)	112.00
O35–H351···O34^{ii}	0.95(6)	1.89(6)	2.797(10)	160(4)
O35–H352···N20^{iii}	0.94(4)	2.07(5)	2.954(7)	155(4)
C8–H71···O31^{iv}	1.0200	2.4700	3.383(11)	149.00
C11–H74···O34	1.0200	2.3400	3.249(11)	148.00
C16–H182···O31^{v}	1.0200	2.4400	3.190(12)	130.00
C15–H183···O33^{vi}	1.0200	2.4900	3.464(11)	161.00
C14–H184···O35^{iii}	1.0200	2.4800	3.444(8)	158.00

Symmetry transformations used to generate equivalent atoms: (i) $2-x$, $-y$, $2-z$; (ii) $1-x$, $1-y$, $2-z$; (iii) $1-x$, $1-y$, $1-z$; (iv) $-x$, $1-y$, $2-z$; (v) $1-x$, $-y$, $2-z$; (vi) x, y, $-1+z$.

Cd1–N(dca) distances vary from 2.199(7) to 2.287(6) Å and Cd1–O(water) is 2.365(5) Å. In the ligand tptz, the C(sp^2)–C(sp^2) distances within the ring are normal (in the range 1.272(10)–1.486(7) Å) and the exterior bond distances (C6–C7, 1.486(7) Å; C2–C13, 1.483(7) Å; C4–C19, 1.495(7) Å) are also normal. The tptz ligands do not deviate much from planarity [24,29]; the three pyridyl rings are twisted with respect to the central triazine ring by angles of 0.8(1)°, 4.5(1)° and 4.6(1)°, with the non-coordinating ring displaying the highest degree of twisting. The cadmium···cadmium separation within the dinuclear unit is 7.537(5) Å, and the shortest inter-dimer cadmium···cadmium distance is 7.713(1) Å. Each dimer is connected to each other via hydrogen bonding interactions, building infinite neutral chains running along the following vector: [0.08; −0.47; 0.87]. The structural cohesion between these chains is then assumed by coulombic interactions. Both the hydrogen atoms of O35 are involved in hydrogen bonding interactions: (i) with the oxygen atom of the ClO_4^- counter anion; (ii) with one nitrogen atom (N20) of the external pyridyl ring of the tptz ligand belonging to the neighbouring cadmium. The later hydrogen bond allows the connection between dimers to form infinite chains. These 1D chains are further connected into supramolecular 2D sheets along the *bc*-plane (Table 7, Fig. 6). There exist weak π–π interactions between the tptz ligands (closest non-hydrogen contact is equal to 3.77(2) Å). The directed H-bond, which gives this complex an overall 2D structure, may be responsible for the stabilisation of the coordinated dinuclear form.

3.2. Infrared spectra

Complexes **1**–**3** exhibit strong absorptions in the region 2325–2155 cm^{-1} that correspond to $\nu_{C\equiv N}$ modes for dca groups, attributed to $\nu_{as} + \nu_s(C\equiv N)$ combination modes, $\nu_{as}(C\equiv N)$ and $\nu_s(C\equiv N)$. The shift towards higher wave numbers for the peaks of dca in **1**–**3** when compared to those of free dicyanamide is consistent with the coordination of dca in the complexes. These three bands appear at 2293, 2239, 2177 cm^{-1} for complex **1**, at 2299, 2237, 2178 cm^{-1} for complex **2**, and at 2312, 2245, 2183 cm^{-1}

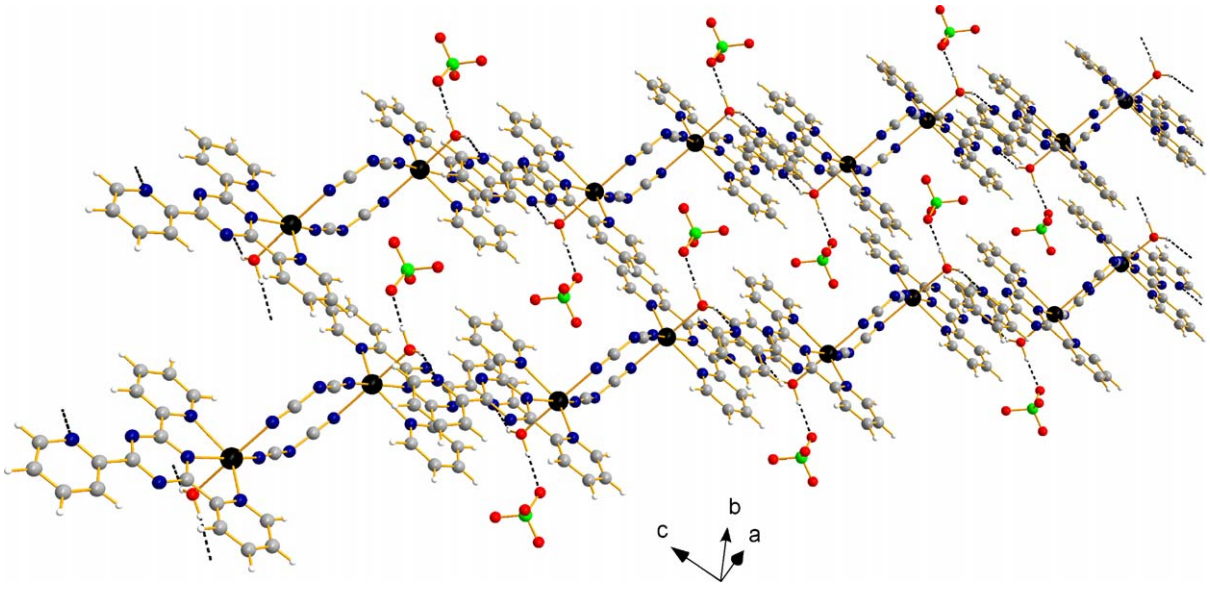

Fig. 6. 3D-supramolecular architecture formed by the hydrogen bonding interactions in **3**.

for complex **3** [1,5,11,30]. Bands dealing with the ν_{as}(C–N) stretching frequencies (1400–1300 cm^{-1} region) and the ν_s(C–N) stretch (950–900 cm^{-1} region) occur in all the spectra. Additionally, pyridyl ring breathing signals have been detected around 1050 cm^{-1} for these compounds. Complex **1** shows a broad signal at about 3400 cm^{-1} which corresponds to coordinated water and indicates the presence of hydrogen bonding [1a]. A strong and broad absorption at 3340 cm^{-1} (O–H stretching of water) in the infrared spectrum of **3** is due to the presence of coordinated water with hydrogen bonds [30b]. Strong bands at 1560 and 1520 cm^{-1} for **1**, 1564 and 1519 cm^{-1} for **2** and 1572 and 1524 cm^{-1} for **3** correspond to the coordinated tptz ligand. Peaks at 1625, 1593, 1530, 1479, 1461, 1443, 1369 and 973 cm^{-1} present in **1**–**3** can be assigned to the C=C and C=N ring stretching vibrations [19]. Peaks are also observed at 766 cm^{-1} (C–H stretching) and 586 cm^{-1} (pyridyl out-of-ring deformation) for all the three complexes [31]. The characteristic strong bands of carboxylate groups appeared at 1560 (for asymmetric stretching) and 1416 cm^{-1} (for symmetric stretching) [19,31]. The difference ($\Delta\nu = 144\ cm^{-1}$) between $\nu_{asym}(COO^-)$ and $\nu_{sym}(COO^-)$ bands suggests the presence of a chelating acetate group linked with the metal center for complex **1**. Broad intense bands at ca. 1100 cm^{-1} due to ClO_4^- show no splitting, indicating the absence of coordinated ClO_4^- in **1** [32].

3.3. Electronic spectrum

The electronic spectrum of **1** was recorded in dimethylformamide and showed two strong bands at about 240 and 265 nm which are clearly charge transfer in origin and an absorption band observed at 295 nm can be assigned to charge transfer from the coordinated ligand to Mn(II). The complex does not show any d–d transitions [33].

3.4. Electrochemical study

An electrochemical study of complex **1** was performed using dimethylformamide as solvent and tetrabutylammonium perchlorate as the supporting electrolyte at a scan rate of 50 mV s^{-1}. One irreversible reductive response at −1.05 V versus SCE was observed, which is attributed to a ligand-centered reduction. No oxidation response was found on the positive side of SCE.

3.5. Magnetic study

The effective magnetic moment at 20 °C for complex **1** is 5.98 BM, which is near to the spin-only value of the manganese(II) ion relative to mercury(tetrathiocyanato)cobaltate as the standard.

4. Conclusion

We have synthesised three dicyanamido complexes obtained from room temperature reactions. Complexes **1** and **2** are mononuclear and complex **3** is a dicyanamide-bridged dinuclear complex. To the best of our knowledge, complex **3** is the first example of a dicyanamide-bridged dinuclear cadmium(II) system. In fact, dca has a strong tendency to form polymeric complexes and that is why dinuclear dicyanamido-bridged complexes are rare in the literature. The difference in preferred coordination number between manganese (5–7), zinc (4–6) and cadmium (2–8) inspires significant differences in their respective structures. Here, the numerous hydrogen bonding interactions

involving the constituent materials enhance the stability of all the complexes and lead to the supramolecular architectures.

5. Supplementary material

Crystallographic data for the structural analysis have been deposited with the Cambridge Crystallographic Data Centre, CCDC Nos. 284526–284528 for **1**–**3**, respectively. Copies of this information may be obtained free of charge from The Director, 12 Union Road, Cambridge, CB2 1EZ, UK (fax: +44 1223 336 033; e-mail: deposit@ccdc.cam.ac.uk or http://www.ccdc.cam.ac.uk).

Acknowledgements

The research was supported by grant from DST, New Delhi, India. We thank Dr. Andrés Ibañez for the structural data analysis and the diagrams.

References

[1] (a) C.-B. Liu, M.-X. Yu, X.-J. Zheng, L.-P. Jin, S. Gao, S.-Z. Lu, Inorg. Chim. Acta 358 (2005) 2687;
(b) C.R. Peŕez, P.L. Luis, M.H. Molina, M.M. Laz, Fernando S. Delgado, P. Gili, M. Julve, Eur. J. Inorg. Chem. (2004) 3873.
[2] H. Casellas, C. Massera, P. Gamez, A.M.M. Lanfredi, Jan Reedijk, Eur. J. Inorg. Chem. (2005) 2902.
[3] W. Dong, Q.-L. Wang, Z.-Q. Liu, D.-Z. Liao, Z.-H. Jiang, S.-P. Yan, P. Cheng, Polyhedron 22 (2003) 3315.
[4] J. Carranza, C. Brennan, J. Sletten, F. Lloret, M. Julve, J. Chem. Soc., Dalton Trans. (2002) 3164.
[5] B. Vangdal, J. Carranza, F. Lloret, M. Julve, J. Sletten, J. Chem. Soc., Dalton Trans. (2002) 566.
[6] Y.-Q. Xu, J.-H. Luo, D.-Q. Yuan, Y. Xu, R. Cao, M.-C. Hong, J. Mol. Struct. (2003) 658.
[7] I. Riggio, G.A. van Albada, D.D. Ellis, A.L. Spek, J. Reedijk, Inorg. Chim. Acta 313 (2001) 120.
[8] S. Martín, M.G. Barandika, J.M. Ezpeleta, R. Cortés, J.I.R. de Larramendi, L. Lezama, T. Rojo, J. Chem. Soc., Dalton Trans. (2002) 4275.
[9] A. Majumder, C.R. Choudhury, S. Mitra, C. Marschner, J. Baumgartner, Z. Naturforsch. 60b (2005) 99.
[10] (a) R. Karmakar, C.R. Choudhury, D.L. Hughes, G.P.A. Yap, M.S. El Fallah, C. Desplanches, J.-P. Sutter, S. Mitra, Inorg. Chim. Acta 359 (2006) 1184;
(b) S. Sen, P. Talukder, S. Mitra, G. Rosair, G. Yap, V. Gramlich, J. Kim, T. Matsushita, C. Desplanches, J.-P. Sutter, Inorg. Chim. Acta 358 (2005) 4534.
[11] D. Ghoshal, H. Bialas, A. Escuer, M. Font-Bardía, T.K. Maji, J. Ribas, X. Solans, R. Vicente, E. Zangrando, N. Ray Chaudhuri, Eur. J. Inorg. Chem. (2003) 3929.
[12] Nonius COLLECT, DENZO, SCALEPACK, SORTAV: KappaCCD Program us B.V., Delft, The Netherlands, 1999.
[13] G. Cascarano, A. Altomare, C. Giacovazzo, A. Guagliardi, A.G.G. Moliterni, D. Siliqi, M.C. Burla, G. Polidori, M. Camalli, Acta Crystallogr., Sect. A 52 (1996) C-79.
[14] D.J. Watkin, C.K. Prout, J.R. Carruthers, P.W. Betteridge, CRYSTAL Issue 11, Chemical Crystallography Laboratory, Oxford, UK, 1999.
[15] Bruker, SMART-NT Version 5.629 Bruker AXS Inc., Madison, WI, USA, 2000.
[16] G.M. Sheldrick, SADABS, University of Göttingen, Germany, 1996.
[17] Bruker, SAINT-NT Version 6.45 Bruker AXS Inc., Madison, WI, USA, 2000.
[18] G.M. Sheldrick, SHELXTL/PC, Version 6.10 Bruker AXS Inc., Madison, WI, USA.
[19] A. Escuer, F.A. Mautner, Nuŕia Sanz, R. Vicente, Inorg. Chim. Acta 340 (2002) 163.
[20] (a) C.W. Chan, C.M. Che, S.M. Peng, Polyhedron 12 (1993) 2169;
(b) A. Claramunt, A. Escuer, F.A. Mautner, N. Sanz, R. Vicente, J. Chem. Soc., Dalton Trans. (2000) 2627;
(c) M.K. Kabir, M. Kawahara, H. Kumagai, K. Adachi, S. Kawata, T. Ishii, S. Kitagawa, Polyhedron 20 (2001) 1417;
(d) M.K. Kabir, M. Kawahara, K. Adachi, S. Kawata, T. Ishii, S. Kitagawa, Mol. Cryst. Liq. Cryst. 376 (2002) 65;
(e) Y.G. Yin, K.K. Cheung, W.T. Wong, Chem. J. Chin. Univ. 21 (2000) 5.
[21] J. Kim, S. Han, Acta Crystallogr., Sect. C 58 (2002) m521.
[22] C. Janiak, J. Chem. Soc., Dalton Trans. (2000) 3885.
[23] A.W. Addison, T.N. Rao, J. Reedijk, J.V. Rijn, G.C. Verschoor, J. Chem. Soc., Dalton Trans. (1984) 1349.
[24] P. Gamez, P. de Hoog, M. Lutz, W.L. Driessen, A.L. Spek, J. Reedijk, Polyhedron 22 (2003) 205.
[25] (a) M.A. Harvey, S. Baggio, R. Baggio, Acta Crystallogr., Sect. C 60 (2004) m498;
(b) F. Marandia, A.A. Soudia, A. Morsali, R. Kempe, Z. Anorg. Allg. Chem. 631 (2005) 3070.
[26] M. Harvey, S. Baggio, S. Russi, R. Baggio, Acta Crystallogr., Sect. C 59 (2003) m171.
[27] (a) J. Luo, M. Hong, J. Weng, Y. Zhao, R. Cao, Inorg. Chim. Acta 329 (2002) 59;
(b) O.V. Nesterova (Pryma), S.R. Petrusenko, V.N. Kokozay, B.W. Skelton, W. Linert, Inorg. Chem. Commun. 7 (2004) 450;
(c) J.-H. Luo, M.-C. Hon, R. Cao, Y.-C. Liang, Y.-J. Zhao, R.-H. Wang, J.-B. Weng, Polyhedron 21 (2002) 893.
[28] (a) G.A. Barcley, R.S. Vagg, E.C. Watton, Acta Crystallogr., Sect. B 34 (1978) 1833;
(b) B.N. Figgis, E.S. Kucharski, S. Mitra, B.W. Skelton, A.H. White, Aust. J. Chem 43 (1990) 1269.
[29] S.A. Cotton, V. Franckevicius, J. Fawcett, Polyhedron 21 (2002) 2055.
[30] (a) J. Carranza, J. Sletten, F. Lloret, M. Julve, Inorg. Chim. Acta 357 (2004) 3304;
(b) S.R. Marshall, A.L. Rheingold, L.N. Dawe, W.W. Shum, C. Kitamura, J.S. Miller, Inorg. Chem. 41 (2002) 3599.
[31] K. Nakamoto, Infrared and Raman Spectra of Inorganic and Coordination Compounds, Wiley, New York, 1997.
[32] (a) X.-Y. Xu, Q.-H. Luo, M.-C. Shen, X.-Y. Huang, Q.-J. Wu, Polyhedron 16 (1997) 915;
(b) H. Keypour, S. Salehzadeh, R.G. Pritchard, R.V. Parish, Polyhedron 19 (2000) 1633.
[33] A.B.P. Lever, Inorganic Electronic Spectroscopy, 2nd ed., Elsevier Science, Amsterdam, 1984.

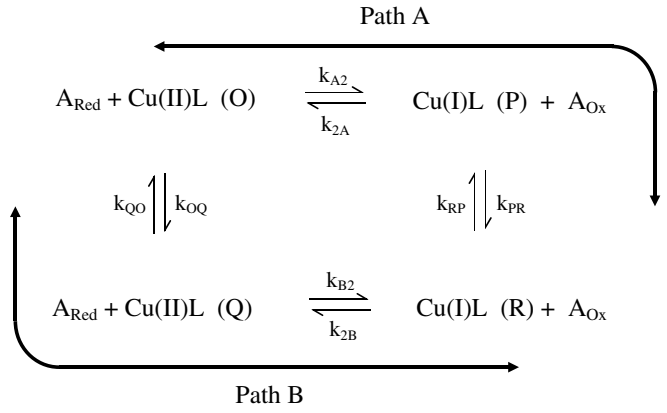

Fig. 1. The dual-pathway square scheme [1].

15,18-dithia-9,24-diaza-cyclohexadeca-9,23-diene, possible model systems of blue copper proteins. $[Cu^{I}(bite)](BF_4)$ (Fig. 2) reveals a distorted tetrahedral N_2S_2 coordination about copper, with highly unequal Cu–S distances (2.194(2) and 2.323(2) Å). The distortions from perfect C_2 symmetry may be related to the unusually high redox potential of the $[Cu^{I/II}(bite)]^{+/2+}$ couple. $[Cu^{II}(bite)](BF_4)_2$ reveals an approximately square-planar CuN_2S_2 structure of C_2 symmetry (Fig. 3) with two distant axial BF_4^- anions (Cu–F distance of 2.546(4) Å) in the solid state. However, the spectral data indicate the existence of only four-coordinate $[Cu^{I/II}(bite)]^{+/2+}$ complexes in acetone and dichloromethane solutions [3].

Cyclic voltammetry experiments [3] of the $[Cu^{I/II}(bite)](BF_4)_{1,2}$ redox couple in acetonitrile show only quasi-reversible behavior with wide peak-to-peak separation. Copper(I/II) electron self-exchange kinetics measured by ^1H NMR line broadening of $[Cu^{I}(bite)]^+$ in the presence

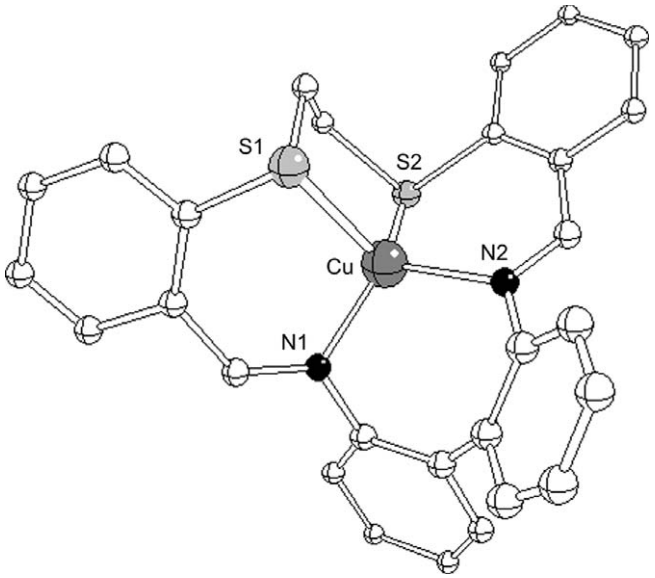

Fig. 2. The structure of quasi-tetrahedral $Cu(bite)^+$ (H atoms omitted) [3].

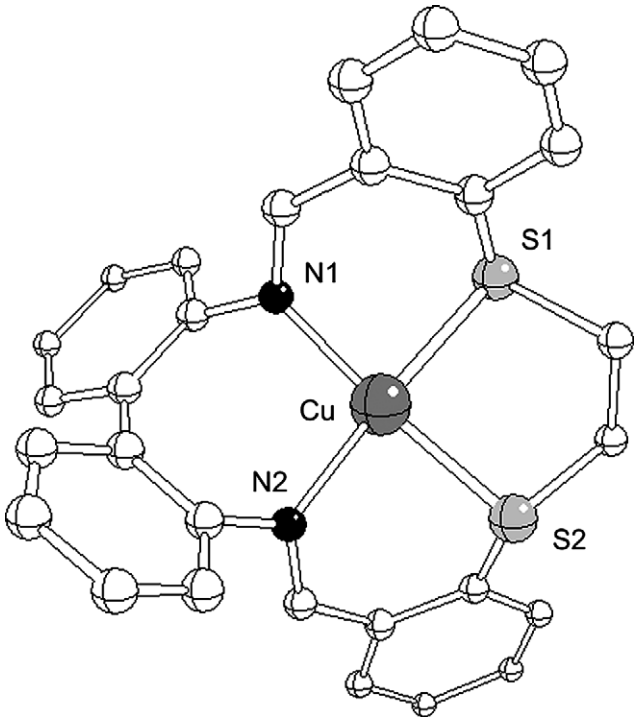

Fig. 3. The structure of quasi-square planar $Cu(bite)^{2+}$ (H atoms omitted) [3].

of $[Cu^{II}(bite)]^{2+}$ reveal an overall first-order process with a rate constant of $21.7 \pm 1.9\ s^{-1}$ at 295 K in acetone-d_6, which corresponds to fully gated electron transfer [3].

Electron-transfer kinetics of the $[Cu(bite)]^{+/2+}$ redox couple with Co(II), Ru(II) and Fe(III) complexes in acetonitrile has been studied by UV–Vis stopped-flow methods and explained in terms of a dual-pathway square mechanism (Fig. 1). All of the cross-reactions proceed through the same intermediate, and the outer-sphere self-exchange reaction should fulfill a second-order rate law with a rate constant of $0.01\ M^{-1}\ s^{-1}$ [4].

The preferable electron transfer to the pseudo-tetrahedral $[Cu^{I}(bite)]^+$ as an initial step in the anodic oxidation of $[Cu^{I}(bite)]^+$ has been observed by in situ ESR/UV–Vis–NIR cyclovoltammetry at different temperatures in various solutions [5]. Domination of the more stable square-planar $[Cu^{II}(bite)]^{2+}$ structure, observed during the oxidation of $[Cu^{I}(bite)]^+$ even at 230 K, indicates very fast transformation of metastable tetrahedral $[Cu^{II}(bite)]^{2+}$ to square-planar $[Cu^{II}(bite)]^{2+}$. In dichloromethane, where no adsorption phenomena arise, the rate constant for heterogeneous electron transfer, $k = 2 \times 10^{-4}$ cm s^{-1}, has been estimated.

In the first part of this study [6] the geometry and corresponding electronic structure parameters of DFT optimized tetrahedral and square-planar $Cu(bite)^q$ complexes, $q = +1$ and $+2$, have been investigated and compared with experimental data. A simple change of the cation charge does not cause a qualitative change of Cu coordination, which indicates an energy barrier for the

tetrahedral ↔ square-planar coordination transition during oxidation. Substantial differences in Cu–S bond lengths, observed in the tetrahedral reduced complex, are of intrinsic origin (mechanical strain of the bite ligand). Due to the plasticity of the central Cu atom, the energy effects implied by mechanical strain are low but the geometry deformations of the Cu coordination polyhedron may substantially change the composition as well as the relative energy of the frontier molecular orbitals and thus decrease the Franck–Condon barrier. The first order rate constant ($21.7 \pm 1.9\ s^{-1}$ at 295 K in acetone-d_6) obtained by ^{1}H NMR line broadening kinetic studies [3] corresponds to oxidation in the tetrahedral geometry (path B of Fig. 1).

Many experts (such as most referees of biochemical and biophysical journals) denote the macrocyclic compounds as very poor model systems of blue copper proteins (blue copper proteins cannot be modelled by strained complexes, their electronic structure is quite different, their electron transfer rate is very low, etc.). One of their arguments is the large mechanical strain in comparison with real blue copper proteins. The aim of this study is to evaluate the strain and reorganization energy in the $[Cu(bite)]^{+/2+}$ system and to compare them with analogous data for tetracoordinate copper complexes with monodentate imidazole and thiolate ligands that are used as model systems for blue copper proteins [2].

2. Calculations

As in the first part of this study [6], the standard DFT method of quantum chemistry (Amsterdam Density Functional – ADF program package) [7] with Vosko–Wilk–Nussair parameterization for the local density approximation (LDA), and Becke exchange and Perdew correlation gradient corrections has been used in order to find the optimal geometries of tetrahedral and square-planar $Cu(bite)^q$, $q = +1$ or $+2$ (denoted as R/Q and P/O structures, respectively – see Table 1 and Figs. 1–3) as well as of the bite ligand alone (tetrahedral T and square-planar S structures). No symmetry restrictions were applied. Cu(II) systems were treated within the unrestricted formalism. The geometries of the individual model systems starting from experimental structures were optimized until the maximum and the root-mean-squared gradients were below 0.01 and 0.007 Hartree/Å and the maximum and root-mean-squared changes in geometry were below 0.01 and 0.007 Å, respectively. For H, C, N and S atoms, standard basis sets III (of DZP type) from the ADF library have been used (with the 1s orbitals of C, N and S and

Table 1
Selected structure data (DFT optimized geometries)

	Tetrahedral geometry			Square-planar geometry		
Compound	$Cu(bite)^+$	$Cu(bite)^{2+}$	$Bite^0$	$Cu(bite)^+$	$Cu(bite)^{2+}$	$Bite^0$
Geometry notation	R	Q	T	P	O	S
Interatomic distances (Å)						
Cu–S1	2.278	2.271		2.443	2.341	
Cu–S2	2.347	2.279		2.445	2.344	
Cu–N1	1.943	1.964		2.023	2.022	
Cu–N2	1.944	1.968		2.025	2.020	
S1–S2	3.481	3.380	3.413	3.350	3.279	3.171
N1–N2	3.252	3.263	3.185	3.158	3.054	3.261
S1–N1	3.277	3.205	3.024	3.051	3.007	2.949
S1–N2	3.788	3.810	3.473	4.454	4.354	4.381
S2–N1	3.717	3.802	3.442	4.454	4.361	4.321
S2–N2	3.235	3.206	2.998	3.054	2.999	2.921
Angles (°)						
S1–Cu–S2	97.6	95.9		86.5	88.8	
S1–Cu–N1	101.5	98.1		85.6	86.8	
S1–Cu–N2	127.3	127.9		170.9	173.6	
S2–Cu–N1	119.8	127.2		170.9	174.1	
S2–Cu–N2	97.4	97.7		85.6	86.5	
N1–Cu–N2	113.5	112.2		102.5	98.2	
S1–S2–N1–N2	−87.3	−91.7	−81.3	171.2	172.1	174.2
Distances from phenyl plane 1 (Å)						
Cu	0.645	0.603		1.563	1.417	
S1	0.165	0.194	0.091	0.189	0.202	0.117
N1	0.320	0.192	0.012	0.525	0.485	0.527
Distances from phenyl plane 2 (Å)						
Cu	1.041	0.728		1.551	1.423	
S2	0.178	0.180	0.106	0.207	0.214	0.111
N2	0.489	0.256	0.110	0.520	0.485	0.500

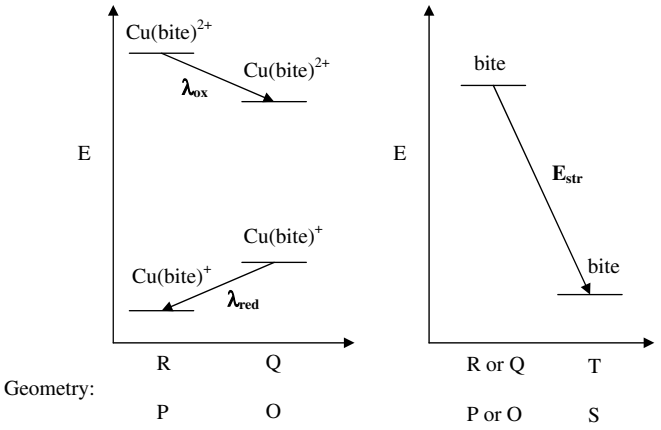

Fig. 4. Schematic illustration of reorganization (λ_{ox}, λ_{red}) and strain (E_{str}) energies.

the 2p orbitals of the S atoms frozen). For copper, a similar (IV) type basis set (containing only 4p polarization functions) has been enhanced with 4d and 4f functions (with frozen 2p orbitals) with exponent values of 1.70 (4d) and 1.05 (4f) , respectively [8].

For the sake of simplicity, the values of the total energy of the molecule, E_{tot}, are related to the total energy of the most stable tetrahedral *R* conformation of $Cu(bite)^+$ complex cation , $\Delta E_{tot} = E_{tot} - E_{tot}(R)$. Using the E_{tot} values of the individual systems under study, some energy characteristics of the $Cu(bite)^{+/2+}$ redox system are estimated [2].

The inner-sphere reorganization energy for the oxidized complex, λ_{ox}, is calculated as the difference in energy of the Cu(II) system at its optimal geometry and at the optimal geometry of the reduced complex. Likewise, the reorganization energy for the reduced complex, λ_{red}, is calculated as the energy of the Cu(I) system at its optimal geometry minus the energy of the Cu(I) complex calculated at the geometry optimal for the Cu(II) complex (see Fig. 4). The total inner-sphere reorganization energy for a self-exchange reaction, λ_i, is the sum of λ_{ox} and λ_{red}.

The strain energy, E_{str}, is the energy of the ligand molecule (i.e., without the Cu ion) in the optimal geometry of the complex related to the optimal geometry of the ligand alone (see Fig. 4) [2].

3. Results and discussion

As mentioned in [6], the results of the geometry optimization of $Cu(bite)^+$ (R and P structures), $Cu(bite)^{2+}$ (Q and O structures) and $bite^0$ (T and S structures) starting from experimental quasi-tetrahedral and quasi-planar geometries (Table 1) exhibit no qualitative changes in the starting S_2N_2 polyhedron. This indicates an energy barrier for the tetrahedral ↔ square-planar coordination transition. The geometry and electronic structure of the tetrahedral and square-planar $Cu(bite)^q$ complexes has been discussed in the first part of this study [6]. Substantial differences in Cu–S bond lengths may be observed in the tetrahedral reduced (R) complex only. As proposed by Flanaghan and and co-workers [3], higher non-equivalence of Cu-phenyl non-planarity (such as higher differences in Cu distances from the phenyl plane) in Cu(I) systems than in Cu(II) ones implies that the origin of this ligand geometry perturbation is in mechanical strain caused by the larger Cu(I) ion in the same macrocyclic bite ligand. Thus, we described the Cu volume by the surrounding S_2N_2 tetrahedron dimensions (Table 1) and compared them with these dimensions in the optimized geometry of the free bite molecule. The resulting bite geometry is different for starting tetrahedral and square-planar S_2N_2 arrangements. It may be expected that the edges of the S_2N_2 tetrahedron in the free bite molecule (i.e., without the central copper atom) are shorter than in the corresponding $Cu(bite)^q$ complexes but this relation has many exceptions (see the S1–S2, N1–N2 and S1–N2 distances in Table 1) . Analogously, these edges need not be longer for Cu(I) than for Cu(II) in quasi-tetrahedral systems. Such a behavior is reflected by bond angles, too. The extent of non-planarity of the phenyl rings bonded to S atoms (Cu, S and N atoms distances from phenyl planes) in the free bite ligands may substantially differ from the corresponding Cu complexes (up to 0.11 Å in the T model versus over 0. 18 Å in R and Q models).

As mentioned in the first part of this study [6], the most stable reduced structure is tetrahedral (R) whereas the most stable oxidized one is square-planar (O) in agreement with the dual-pathway square scheme [1]. The total energy of the quasi-tetrahedral *R* conformation of $Cu(bite)^+$ is taken as the reference energy value in Table 2.

Calculated values of reorganization and strain energies are presented in Table 3. The total inner-sphere reorganization energy is higher within quasi-tetrahedral conformations (28.3 kJ/mol) in comparison with the square-planar ones (23.5 kJ/mol). If the tetrahedral ↔ planar structural change is accounted for, the reorganization energy increases ca. 3–4 times (93.7 kJ/mol). A similar increase of the strain energy is not observed, its highest value corresponds to the tetrahedral Cu(I) system (36.5 kJ/mol). It

Table 2
Calculated energy data of $Cu(bite)^q$ cations and bite ligands (for geometry notation see Table 1, energy data are related to the total energy of the *R* conformation of $Cu(bite)^+$)

Compound		Geometry	Charge *q*	ΔE_{tot} (kJ/mol)
$Cu(bite)^q$	tetrahedral	R	+1	0.0
		R	+2	967.6
		Q	+1	3.2
		Q	+2	942.5
	square-planar	P	+1	33.5
		P	+2	930.9
		O	+1	45.5
		O	+2	919.4
Bite	tetrahedral	R	0	−106.6
		Q	0	−111.3
		T	0	−143.1
	square-planar	P	0	−112.2
		O	0	−109.1
		S	0	−126.1

Table 3
The calculated reorganization and strain energy data

Transition	Reorganization energy (kJ/mol)			Strain energy (kJ/mol)	
	λ_{red}	λ_{ox}	λ_i	Cu(I)	Cu(II)
Tetrahedral ↔ tetrahedral	3.2	25.0	28.3	36.5[c]	31.8[c]
Planar ↔ planar	12.0	11.5	23.5	13.9[d]	17.1[d]
Tetrahedral ↔ planar	45.5[a]	48.2[b]	93.7	30.9[c]	34.0[c]
				19.6[d]	14.9[d]

[a] O–R energy difference for $Cu(bite)^{+}$.
[b] R–O energy difference for $Cu(bite)^{2+}$.
[c] Related to the tetrahedral T geometry.
[d] Related to the square-planar S geometry.

means that Cu(I) in this system causes the largest deformation of the bite ligand (evaluated in energy units) that should increase the reactivity of this system as a whole.

Table 4 presents similar data for some copper protein model systems with monodentate imidazole (Im) and thiolate (SCH_3^- and $S(CH_3)_2$) ligands in vacuo [2d] or in which a substantially larger environment has been included by QM/MM treatment at the B3LYP level of theory [2e]. It may be seen that $Cu(bite)^{+,2+}$ reorganization energies within the same coordination type (24–28 kJ/mol) in vacuo are comparable with those for $Cu(Im)_2(SCH_3)(S(CH_3)_2)^{0/+}$ in various environments (27–57 kJ/mol) and are significantly lower than these ones in vacuo (62–78 kJ/mol). Only the $Cu(bite)^{+,2+}$ reorganization energy for the tetrahedral ↔ planar transition is higher (94 kJ/mol). The strain energy data calculated for $Cu(bite)^{+,2+}$ (14–37 kJ/mol) are comparable or lower than for $Cu(Im)_2(SCH_3)(S(CH_3)_2)^{0/+}$ in various environments (34–66 kJ/mol). It may be expected that the environment effect inclusion should decrease the above quantities also for $Cu(bite)^{+,2+}$ model systems.

Table 4
Comparison of the reorganization and strain energy data of $Cu(Im)_2(SCH_3)(S(CH_3)_2)^{0/+}$ in various environments [2d]

Environment type	Environment fixation	Reorganization energy (kJ/mol)			Strain energy (kJ/mol)	
		λ_{red}	λ_{ox}	λ_i	Cu(I)	Cu(II)
Trigonal symmetry						
Vacuo		32.7	28.8	61.5		
Reduced plastocyanin	yes	23.4	3.7	27.2	50.6	36.1
	no	25.7	0.4	29.7	44.7	34.7
Oxidized plastocyanin	yes	18.9	19.0	37.9	58.2	36.0
	no	26.0	5.1	31.1	46.8	32.6
Tetragonal symmetry						
Vacuo		37.7	39.8	77.5		
Nitrite reductase	yes	21.9	9.2	31.1	58.6	40.7[a]
	no	28.9	5.2	34.1	53.8	40.6[a]
Cucumber basic protein	yes	18.4	8.2	26.6	51.0	33.8[b]
	no	15.4	41.5	57.0	66.4	44.9[b]

[a] The tetragonal structure obtained in vacuo with the $Cu(Im)_2(SH)(S(CH_3)_2)^+$ model.
[b] The structure intermediate between trigonal and tetragonal that cannot be found in vacuo.

The inner-sphere reorganization energy λ_i in the real proteins azurin and plastocyanin has been estimated to 19 kJ/mol [9] and 18 kJ/mol [10], respectively. It is evident that our λ_i results for the case of the preserved coordination polyhedra type (28.3 kJ/mol for tetrahedral ↔ tetrahedral and 23.5 kJ/mol for square-planar ↔ square-planar coordination transitions in vacuo, see Table 3, should be lowered in the above mentioned environments, too) agree very well with these experimental data as well. It might be an indirect proof that the Cu coordination polyhedron type is preserved during the oxidation/reduction of blue copper proteins. Nevertheless, it must be kept in mind that the self-exchange reactions of Cu(II)/Cu(I) model complexes, in general, tend to have large inner-sphere reorganization barriers in comparison with copper proteins just owing to the different geometric preferences of the two oxidation states [11].

4. Conclusions

Our results indicate that the reorganization and strain energy of the macrocyclic bite ligand are comparable with simple monodentate ligands of blue copper proteins model systems. This may be explained by the plasticity of the central copper atom. On the contrary to monodentate imidazole and thiolate ligands where the ligand positions are determined by the central atom properties and to a lower extent by the mutual ligands repulsion, the mechanical strain in the bite ligand forces the N and S atoms to adopt such positions that are determined prevailingly by the ligand sterical demands and are only influenced to a lower extent by the central Cu atom. It may result in unusual Cu–S bond lengths, bond angles deformations as well as significant changes of molecular orbitals. The deformations of the electronic structure of the active center may be crucial for the electron transfer. Consequently, thermal vibrations with minimal energy demands may lead to the active center geometry possessing molecular orbitals with energies and symmetry properties suitable for oxidation/reduction and thus reducing the Franck–Condon energy barrier.

As mentioned above, many experts denote the macrocyclic compounds as very poor model systems of blue copper proteins due to many reasons. The aim of this study cannot be the polemics with them. Nevertheless, our results indicate that large mechanical strain cannot be the argument against these model systems.

Acknowledgments

We thank Prof. P. Coppens (SUNY at Buffalo, USA) for helpful discussions and valuable suggestions. This work has been supported by National Science Foundation, USA (Project No. NSF-CHE9981864) and by Slovak Grant Agency, Slovakia (Project Nos. 1/2449/05 and 1/3566/

06). Computational support has been provided by the Center for Computational Research of SUNY-Buffalo, USA, which is supported by grant DBI9871132 from the US National Science Foundation.

References

[1] (a) B.C. Dunn, L.A. Ochrymowycz, D.B. Rorabacher, Inorg. Chem. 36 (1997) 3253;
(b) N.M. Villeneuve, R.R. Schroeder, L.A. Ochrymowycz, D.B. Rorabacher, Inorg. Chem. 36 (1997) 4475;
(c) B.C. Dunn, P. Wijetunge, J.R. Vyvyan, T.A. Howard, A.J. Grall, L.A. Ochrymowycz, D.B. Rorabacher, Inorg. Chem. 36 (1997) 4484;
(d) E.A. Ambundo, M.-V. Deydier, A.J. Grall, N. Aguera-Vega, L.T. Dressel, T.H. Cooper, M.J. Heeg, L.A. Ochrymowycz, D.B. Rorabacher, Inorg. Chem. 38 (1999) 4233;
(e) K. Krylova, Ch.P. Kulatilleke, M.J. Heeg, C.A. Salhi, L.A. Ochrymowycz, D.B. Rorabacher, Inorg. Chem. 38 (1999) 4322;
(f) P. Wijetunge, Ch.P. Kulatilleke, L.T. Dressel, M.J. Heeg, L.A. Ochrymowycz, D.B. Rorabacher, Inorg. Chem. 39 (2000) 2897;
(g) Q. Yu, C.A. Salhi, E.A. Ambundo, M.J. Heeg, L.A. Ochrymowycz, D.B. Rorabacher, J. Am. Chem. Soc. 123 (2001) 5720.

[2] (a) U. Ryde, M.H.M. Olsson, K. Pierloot, B.O. Roos, J. Mol. Biol. 261 (1996) 586;
(b) K. Pierloot, J.O.A. De Kerpel, U. Ryde, B.O. Roos, J. Am. Chem. Soc. 119 (1997) 218;
(c) M.H.M. Olsson, U. Ryde, B.O. Roos, K. Pierloot, J. Biol. Inorg. Chem. 3 (1998) 109;
(d) M.H.M. Olsson, U. Ryde, B.O. Roos, Protein Sci. 7 (1998) 2659;
(e) U. Ryde, M.H.M. Olsson, Int. J. Quantum Chem. 81 (2001) 335;
(f) U. Ryde, M.H.M. Olsson, B.O. Roos, J.O.A. De Kerpel, K. Pierloot, J. Biol. Inorg. Chem. 5 (2000) 565.

[3] S. Flanagan, J. Dong, K. Haller, S. Wang, W.R. Scheidt, R.A. Scott, T.R. Webb, D.M. Stanbury, L.J. Wilson, J. Am. Chem. Soc. 119 (1997) 8857.

[4] B. Xie, L.J. Wilson, D.M. Stanbury, Inorg. Chem. 40 (2001) 3606.

[5] P. Rapta, J. Kožíšek, M. Breza, M. Gembický, L. Dunsch, J. Electroanal. Chem. 566 (2004) 123.

[6] M. Breza, J. Kožíšek, J. Mol. Struct. (Theochem.) 718 (2005) 175.

[7] (a) G. te Velde, F.M. Bickelhaupt, S.J.A. van Gisbergen, C. Fonseca Guerra, E.J. Baerends, J.G. Snijders, T. Ziegler, J. Comput. Chem. 22 (2001) 931;
(b) C. Fonseca Guerra, J.G. Snijders, G. te Velde, E.J. Baerends, Theor. Chem. Acc. 99 (1998) 391;
(c) Program ADF2002.01, SCM, Theoretical Chemistry, Vrije Universiteit, Amsterdam, The Netherlands, Available from: <http://www.scm.com>.

[8] M. Breza, J. Kožíšek, P. Coppens, Challenges for coordination chemistry in the new century, in: M. Melnik, A. Sirota (Eds.), Monograph Series of the International Conference on Coordination Chemistry, Slovak Technical University Press, Bratislava, Slovakia, 2001, p. 115.

[9] E. Fraga, M.A. Webb, G.R. Loppnow, J. Phys. Chem. 100 (1996) 3278.

[10] G.R. Loppnow, E. Fraga, J. Am. Chem. Soc. 119 (1997) 896.

[11] G.B. Jameson, J.A. Ibers, in: I. Bertini, H.B. Gray, S.J. Lippard, J.S. Valentine (Eds.), Bioinorganic Chemistry, University Science Books, Mill Valley, CA, USA, 1994, p. 167.

under nitrogen over Na\benzophenone and distilled before use. Methylene chloride, *n*-hexane and petroleum ether were refluxed under nitrogen over calcium hydride and distilled before use. Methylaluminoxane (MAO, 10 wt.% solution in toluene, $M = 800\ g\ mol^{-1}$, Al = 5.3 wt.%) was purchased from Wtico, *n*-butyl lithium, methyl lithium, phenyl lithium trimethylchlorosilane and titanium tetrachloride were purchased from Aldrich. ^1H and ^{13}C NMR spectra were recorded on a Varian Mercury-300 NMR spectrometer with $CDCl_3$ as solvent and TMS as an internal standard. IR spectra were recorded on a Nicolet Impact 410 FTIR spectrometer using KBr pellets. Elemental analyses were performed on a Perkin–Elmer 240c element analyzer. The crystal structure was determined with a CCD diffraction apparatus. Viscosity-average molecular weights of the polystyrenes were determined in *o*-dichlorobenzene at 135 °C using a Schott Gerate Mod. AVS/T2 Ubbelohde viscosimeter. Melting transition temperatures (T_m) of the polystyrenes were determined by DSC (Du Pont 910 differential scanning calorimeter) at a heating rate of 10 °C min^{-1}.

2.2. Synthesis of ligands

1,2-Diphenyl-4-methylcyclopentadiene (**1**) and 1,2,4-triphenylcyclopentadiene (**3**) were synthesized according to the literature procedures [19,20]. Compound **1** was obtained as a white crystalline material after purification by column chromatography through silica (methylene chloride/petroleum ether, 1:4 in v/v). Yield: 68%. ESI-MS, *m*/*z*: 232.4 $[M]^+$, 178.1 $[M-CH_3-C_3H_3]^+$. ^{13}C NMR ($CDCl_3$, 75 MHz): δ 16.4 (CH_3), 49.1, 132.3, 137.6, 141.6, 144.3 (C_5H_3), 126.2, 127.1, 127.9, 128.4, 128.6, 137.6, 137.8 (C_6H_5).

Compound **3** was purified by column chromatography through silica (methylene chloride/petroleum ether, 1:5 in v/v) as a white solid. Yield: 61%. ESI-MS, *m*/*z*: 294.3 $[M]^+$, 178.2 $[M-C_6H_5-C_3H_3]^+$. ^{13}C NMR ($CDCl_3$, 75 MHz): δ 45.2, 132.1, 137.1, 142.3, 145.3 (C_5H_3), 125.2, 126.8, 127.2, 127.4, 128.0, 128.5, 128.7, 128.8, 129.0, 136.0, 137.4, 139.6 (C_6H_5).

1,2-Diphenyl-4-*n*-butylcyclopentadiene (**2**) was synthesized by a similar procedure as follows: To a solution of butyl lithium (27.7 mmol) in THF (20 mL) was slowly added a solution of 3,4-diphenyl-2-cyclopentenone (7.03 g, 30 mmol) in THF (40 mL) under nitrogen with stirring at 0 °C. The resulting solution was allowed to warm to room temperature slowly and stirred overnight. The reaction mixture was quenched with ice-water (60 mL), treated with concentrated hydrochloric acid (9 mL) and the organic layer was separated. The aqueous layer was extracted with diethyl ether (3 × 20 mL). The combined organic layers were washed with 80 mL of saturated aqueous solution of sodium chloride, dried over anhydrous $MgSO_4$, filtered and evaporated under reduced pressure. The pure product (5.15 g, 62.5%) was obtained by column chromatography through silica (methylene chloride/petroleum ether, 1:4 in v/v) as a yellowish oil. ESI-MS, *m*/*z*: 274.4 $[M]^+$, 232.3 $[M-C_3H_6]^+$, 178.2 $[M-CH_3-C_3H_3]^+$. ^1H NMR ($CDCl_3$, 300 MHz): δ 0.96 (s, 3H, CH_3), 1.41 (q, 2H, CH_2), 1.52 (q, 2H, CH_2), 2.47 (t, 2H, CH_2), 3.46 (s, 2H, C_5H_3), 6.34 (s, 1H, C_5H_3), 7.10–7.41 (m, 10H, C_6H_5). ^{13}C NMR ($CDCl_3$, 75 MHz): δ 14.2, 22.8, 30.7, 31.9 (*n*-Bu), 47.5, 131.2, 137.6, 141.4, 149.4 (C_5H_3), 126.2, 127.1, 127.9, 128.4, 128.6, 128.6, 137.6, 137.8 (C_6H_5).

2.3. Synthesis of 1,2-diphenyl-4-methylcyclopentadienyltitanium trichloride (*4*)

To a solution of 1,2-diphenyl-4-methyl-cyclopentadiene (1.16 g, 5.0 mmol) in diethyl ether (40 mL) was slowly added a solution of *n*-BuLi (5.1 mmol) in *n*-hexane (20 mL) at −78 °C with stirring. After 1 h, the reaction mixture was allowed to warm to room temperature and stirred overnight. The solvent was removed under vacuum and the residue was washed with dry *n*-hexane (3 × 20 mL). The obtained white powder was dissolved in THF (30 mL), and Me_3SiCl (5.1 mmol) was slowly added at −78 °C. The reaction mixture was allowed to warm to room temperature and stirred for 2 h. The solvent and excess Me_3SiCl were removed under reduced pressure. The residue was extracted with toluene (20 mL) and slowly added to a solution of $TiCl_4$ (4.75 mmol) in 30 mL of toluene at −78 °C. The reaction mixture was allowed to warm to room temperature and stirred for 24 h. The precipitate was filtered off and the solvent was removed to leave a red solid. Recrystallization from methylene chloride/*n*-hexane (1:3 in v/v) gave pure **4** (1.30 g, 68.2%). *Anal.* Calc. for $C_{18}H_{16}Cl_3Ti$ (385.54): C, 56.08; H, 3.92. Found: C, 56.00; H, 3.98%. IR (KBr, cm^{-1}): 3100w, 2957w, 2925m, 2850w, 1491m, 1453w, 1424m, 1163w, 1079w, 1050w, 1022w, 889m, 769vs, 706vs, 676m, 663m. ^1H NMR ($CDCl_3$, 300 MHz): δ 2.59 (s, 3H, CH_3), 7.12 (s, 2H, C_5H_2), 7.56–7.35 (m, 10H, C_6H_5). ^{13}C NMR ($CDCl_3$, 75 MHz): δ 18.4 (CH_3), 129.4, 132.8, 140.5 (C_5H_2), 124.3, 128.4, 129.4, 138.4 (C_6H_5).

2.4. Synthesis of 1,2-diphenyl-4-n-butylcyclopentadienyltitanium trichloride (*5*)

Complex **5** was synthesized in almost the same manner as complex **4** except that 1,2-diphenyl-4-butyl-cyclopentadiene (1.37 g, 5.0 mmol) was used as the starting material and its deprotonation reaction was carried out in *n*-hexane. Pure **5** (1.32 g, 61.5%) was obtained as red crystals by recrystallization from methylene chloride/*n*-hexane (1:4 in v/v). *Anal.* Calc. for $C_{21}H_{21}Cl_3Ti$ (427.62): C, 58.98; H, 4.95. Found: C, 59.05; H, 4.89. IR (KBr, cm^{-1}): 3086w, 2960m, 2932m, 2875w, 1494m, 1452w, 1427m, 1156w, 1079w, 1030w, 923w, 885m, 853m, 796s, 772vs, 757vs, 729m, 698s, 670m, 606m. ^1H NMR ($CDCl_3$, 300 MHz): δ 0.98 (t, $^3J_{HH} = 7.5$ Hz, 3H, CH_3), 1.47 (m, $^3J_{HH} = 7.4$ Hz, 2H, CH_2), 1.73 (m, $^3J_{HH} = 7.3$ Hz, 2H, CH_2), 2.93 (t, $^3J_{HH} = 7.5$ Hz, 2H, CH_2), 7.13 (s, 2H, C_5H_2), 7.36–7.57

(m, 10H, C_6H_5). ^{13}C NMR ($CDCl_3$, 75 MHz): δ 13.8, 22.5, 32.2, 32.5 (C_4H_9), 129.4, 132.9, 145.9 (C_5H_2), 123.4, 128.4, 129.5, 138.3 (C_6H_5).

2.5. Synthesis of 1,2,4-triphenyl-cyclopentadienyltitanium trichloride (6)

Complex **6** was synthesized in the same manner as complex **4** with 1,2,4-triphenylcyclopentadiene (1.47 g, 5.0 mmol) as the starting material. Pure **6** (1.36 g, 60.6%) was obtained as red crystals by recrystallization from methylene chloride/*n*-hexane (1:3 in v/v). *Anal.* Calc. for $C_{23}H_{17}Cl_3Ti$ (447.61): C, 61.72; H, 3.83. Found: C, 61.55; H, 3.78%. IR (KBr, cm^{-1}): 3079w, 2959w, 2931m, 2867w, 1487m, 1452w, 1425m, 1157w, 1072w, 1018w, 924w, 882w, 875m, 854m, 792s, 773vs, 759vs, 726m, 699s, 669m, 661m, 609m. ^1H NMR (300 MHz, $CDCl_3$): δ 7.08 (C_5H_2), 7.24–7.55 (C_6H_5). ^{13}C NMR ($CDCl_3$, 75 MHz): δ 123.2, 132.4 (C_5H_2), 123.8, 128.5, 129.6, 138.3 (C_6H_5).

2.6. X-ray structural determination of complex 4

Single crystals of complex **4** suitable for X-ray diffraction were grown from a saturated solution in methylene chloride/*n*-hexane (1:4, v/v) at room temperature. A red crystal of dimensions $0.37 \times 0.31 \times 0.26$ mm sealed in a glass capillary was used. Data collection was performed using a standard Siemens SMART CCD diffractometer with graphite monochromated Mo Kα radiation. The data were integrated using the siemens SAINT program with intensities corrections for lorentz factor, polarization and air absorption [21]. The structure was solved by the direct method and was refined by full-matrix least squares techniques [22]. All non-hydrogen atoms were refined with anisotropic thermal parameters, while all hydrogen atoms were placed by geometrical considerations and refined isotropically. Crystallographic data, details of the data collection and refinement parameters are summarized in Table 1.

2.7. Polymerization of styrene

Styrene polymerization experiments were carried out in a 250 mL Schlenk flask with magnetic stirring. Fifty milliliters of toluene, 5 mL of freshly distilled styrene and an appropriate amount of MAO were added to the flask that was placed in an oil bath at the desired temperature and the mixture was stirred for 10 min. The titanium catalyst (2.5 μmol in toluene) was injected into the flask and the polymerization was performed at 25, 50 or 75 °C for 30 or 60 min periods. The polymerization was terminated by addition of 10% HCl in methanol. The precipitated polymer was washed three times with methanol and dried at 100 °C in vacuo to a constant weight. The polymer was extracted with refluxing 2-butanone for 24 h in a Soxhlet extractor to remove atactic polymer and dried again at 100 °C for 24 h.

Table 1
Crystal data and structure refinement for complex 1,2-Ph_2-4-Me-$CpTiCl_3$

Formula	$C_{18}H_{15}Cl_3Ti$
F_w	385.55
Temperature (K)	293(2)
Crystal system	orthorhombic
Space group	$P2_12_12_1$
a (Å)	6.6086(10)
b (Å)	12.2932(3)
c (Å)	21.8492(5)
α (°)	90
β (°)	90
γ (°)	90
V (Å^3)	1775.05(7)
Z	4
D_c (g cm^{-3})	1.443
$F(000)$	784
Absorption coefficient (mm^{-1})	0.926
Crystal size (mm^3)	$0.37 \times 0.31 \times 0.26$
Collect range (°)	$1.86 \leqslant \theta \leqslant 23.25$
Collection region	$-7 \leqslant h \leqslant 7$
	$-13 \leqslant k \leqslant 6$
	$-24 \leqslant l \leqslant 24$
Absorption correction	empirical
Maximum and minimum transmission	0.5093 and 0.4542
Number of reflections	8620
Number of independent reflections	2547
R_{int}	0.0286
Number of data/restraints/parameters	2547/0/200
Final R indices [$I > 2\sigma(I)$]	$R_1 = 0.0240$
	$wR_2 = 0.0636$
R indices (all data)	$R_1 = 0.0260$
	$wR_2 = 0.0645$
Goodness-of-fit	1.072
Largest difference in peak and hole (e/Å^{-3})	0.210 and −0.157

3. Results and discussion

3.1. Synthesis of ligands

1,2-Diphenyl-4-methyl-1,3-cyclopentadiene (**1**) and 1,2,4-diphenyl-1,3-cyclopentadiene (**3**) were synthesized according to the literature procedures [19,20] and characterized by ^1H and ^{13}C NMR as well as mass spectroscopy. The ^1H NMR data are identical to that reported. The ^{13}C NMR and mass spectroscopy data are in agreement with the structures of compounds **1** and **3**. 1,2-Diphenyl-4-butyl-1,3-cyclopentadiene (**2**) was synthesized in similar way via the 1,2-addition reaction of 3,4-diphenyl-2-cyclopentenone with butyllithium, followed by dehydration of the 1-hydroxy-1-butyl-3,4-diphenyl-2-cyclopentene with concentrated HCl. Compound **2** was also characterized by ^1H and ^{13}C NMR as well as mass spectroscopy. These spectroscopy data are consistent with the structure of compound **2**.

3.2. Synthesis of titanium complexes

Complexes **4**, **5** and **6** were synthesized in similar way to the published procedure [23,24]. Treatment of compounds **1**, **2** and **3** with *n*-butyl lithium, followed by reaction with trimethylchlorosilane, produced the trimethylsilyl substituted derivatives of **1**, **2** and **3**, respectively. The

deprotonation reaction of compounds **1** and **3** was carried out in diethyl ether, while the same reaction of compound **2** was conducted in *n*-hexane since **2** has pretty good solubility in *n*-hexane and the produced lithium salt readily precipitated from *n*-hexane, which resulted in the easy separation of the lithium salt. Reactions of the trimethylsilyl substituted derivatives with $TiCl_4$ in toluene (Scheme 1) gave the corresponding complexes **4**, **5** and **6**, respectively. These titanium complexes are quite soluble in benzene, toluene and methylene chloride, whilst being slightly soluble in *n*-pentane and *n*-hexane. Therefore, they can be recrystallized from a mixture of methylene chloride and *n*-hexane. These complexes were found to be relatively stable to air and moisture in the solid state, and could be exposed to air for several hours without obvious decomposition, but they decomposed readily in solution when exposed to air.

3.3. The crystal structure of complex *4*

The crystal structure of the complex **4** is shown in Fig. 1, and selected bond distances and angles are summarized in Table 2. The coordination geometry about the Ti atom can be described as a distorted tetrahedron, formed by the substituted Cp ring and three Cl atoms, which is similar to that of known titanium complexes (η^5-C_9H_7)$TiCl_3$ and (η^5-C_9Me_7)$TiCl_3$ [8j,25]. The distances of Ti–C1 (2.388(2) Å) and Ti–C2 (2.405(3) Å) are longer than those of known Ti–Cp-ring carbon distances [8j,8k], which could be obviously attributed to the steric effect of the two phenyl groups on the Cp-ring. The C–C distances in the substituted Cp ring range from 1.396(4) to 1.430(3) Å, and the C1–C2 bond length (1.430(3) Å) is the longest among these values, which could also be explained by the steric and conjugate effects of the two phenyl groups on the Cp-ring. The average Ti–Cl distance of 2.2347(9) Å is close to that of 2.2308(1) Å in (η^5-C_9H_7)$TiCl_3$ [8j]. The Cl–Ti–Cl angles in complex **4** are in the range of 101.19(4)°–103.66(3)°. The two phenyl groups on the Cp-ring construct a partially crowded environment around the metal center, which might have a greater or lesser effect on the polymerization of styrene (see Table 2).

3.4. Styrene polymerization

Upon activation with MAO, complexes **4**, **5** and **6** can all catalyze the polymerization of styrene to form syndiotactic polystyrene. The results of styrene polymerization catalyzed by these complexes under different conditions are summarized in Table 3. For comparison, polymerization experiments catalyzed by $CpTiCl_3$/MAO were also carried out under identical conditions. As can be seen from Table 3, the **4**–**6**/MAO systems show better catalytic performance than the $CpTiCl_3$/MAO system for styrene polymerization in terms of catalytic activity, syndiotacticity, melting temperature and molecular weight of the produced polystyrene. It has been known that the phenyl substituent

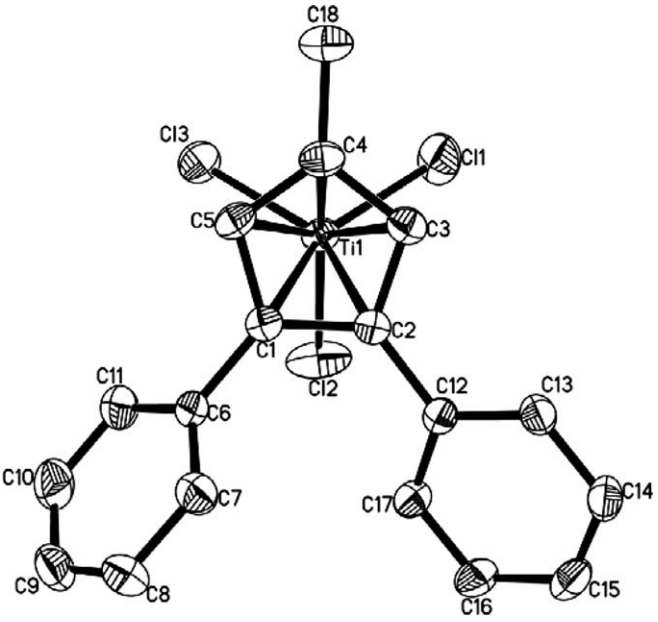

Fig. 1. Structure of complex **4**.

Table 2
Selected bond lengths (Å) and angles (°) for complex **4**

Complex **4**			
Ti(1)–Cl(1)	2.2437(9)	Ti(1)–C(1)	2.388(2)
Ti(1)–Cl(3)	2.2466(8)	Ti(1)–centroid	2.028(3)
Ti(1)–Cl(2)	2.2138(9)	C(1)–C(2)	1.430(3)
Ti(1)–C(3)	2.338(3)	C(2)–C(3)	1.419(3)
Ti(1)–C(4)	2.334(3)	C(3)–C(4)	1.417(3)
Ti(1)–C(5)	2.327(3)	C(4)–C(5)	1.396(4)
Ti(1)–C(2)	2.405(3)		
Cl(1)–Ti(1)–Cl(2)	103.27(4)	Cl(1)–Ti(1)–centroid	115.8(2)
Cl(1)–Ti(1)–Cl(3)	103.66(3)	Cl(2)–Ti(1)–centroid	116.0(3)
Cl(3)–Ti(1)–Cl(2)	101.19(4)	Cl(3)–Ti(1)–centroid	115.0(3)

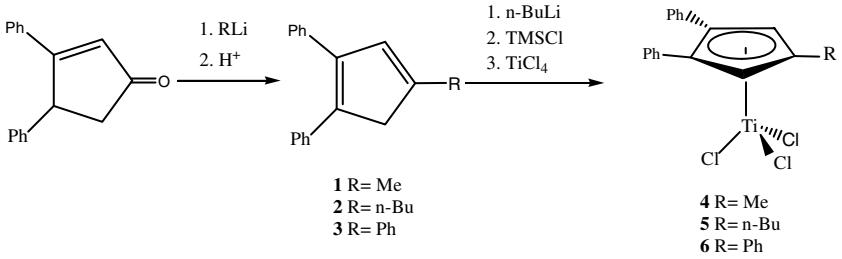

Scheme 1. Synthetic procedure of complexes **4**–**6**.

Table 3
Styrene polymerization catalyzed by complexes **4**, **5** and **6**, activated by MAO[a]

No.	Catalyst	Time (min.)	T_p (°C)	A[b] ($\times 10^{-7}$)	SY[c] (%)	T_m[d] (°C)	M_η[e] ($\times 10^{-5}$)
1	**4**	30	25	0.71	92.1	273.8	1.69
2		30	50	1.32	96.8	269.5	1.63
3		30	75	1.05	94.0	270.6	1.55
4		60	50	1.10	94.6	272.3	1.58
5	**5**	30	25	0.67	93.2	273.4	1.65
6		30	50	1.20	96.1	270.3	1.54
7		30	75	1.12	95.0	271.5	1.38
8		60	50	1.03	95.5	272.4	1.44
9	**6**	30	25	0.56	94.5	272.1	1.45
10		30	50	1.05	96.1	269.5	1.24
11		30	75	0.75	95.0	267.7	1.26
12		60	50	0.92	96.0	270.8	1.31
13	$CpTiCl_3$	30	25	0.61	83.1	263.2	1.26
14		30	50	1.14	87.5	261.6	1.21
15		30	75	0.95	84.3	259.0	1.05
16		60	50	1.05	86.7	260.9	1.17

[a] Polymerization conditions: [Ti] = 50 μM; [Al]/[Ti] = 3000; reaction time = 0.5 or 1 h; [styrene] = 0.87 M.
[b] A (activity) = (g bulk polymer)/(mol Ti)(mol monomer)(h).
[c] Percentage s-PS = [(g of 2-butanone insoluble polymer)/(g of butanone polymer)] × 100.
[d] T_m, melting temperature of s-PS, determined with DSC at a heating rate of 10 °C min^{-1}.
[e] M_η, measured in *o*-dichlorobenzene at 135 °C.

on the cyclopentadienyl group of similar titanium catalysts can improve the catalytic property due to the increased resonance stabilization [8l,26].

For all complexes **4**, **5** and **6**, the catalytic activity increases with the increase in polymerization temperature, and reaches the highest value at about 50 °C. Further increase in the polymerization temperature results in a decrease in the catalytic activity. All catalytic systems exhibit higher catalytic activities for 30 min polymerization experiments than 60 min ones, which indicates that the active catalysts deactivate during the polymerization. The results in Table 3 also demonstrate the substituent effect of the R group on the cyclopentadienyl ligand of complexes **4**, **5** and **6** on their catalytic properties. The catalytic activity of these complexes is in the order of **6** < **5** < **4**, which implies that both the electronic and steric factors of the R group play roles in determining the catalytic activity of these complexes. In addition, in comparison with the $CpTiCl_3$ catalyst system, the syndiotacticity of polystyrenes produced with the **4**, **5** or **6** catalyst system is higher, which might be attributed to the relatively crowded environment around the metal center of **4**, **5** and **6**.

4. Conclusions

We have synthesized and characterized 1,2-diphenyl-4-R-cyclopentadienyl titanium trichloride (R = Me (**4**), *n*-Bu (**5**), Ph (**6**)). The molecular structure of complex **4** has been confirmed by X-ray crystallography. When activated with MAO, these titanium complexes are efficient catalysts for the syndioselective polymerization of styrene.

Acknowledgement

This work was supported by the National Natural Science Foundation of China (No. 20374023).

Appendix A. Supplementary data

Crystallographic data (excluding structure factors) for the structure reported in this paper have been deposited with the Cambridge Crystallographic Data Center as Supplementary Publication No. CCDC-260775. Copies of the data can be obtained free of charge from The Director, CCDC, 12 Union Road, Cambridge CB2 1EZ, UK, fax: +44 1223 336 033, e-mail: deposit@ccdc.cam.ac.uk or www: http://www.ccdc.cam.ac.uk. Supplementary data associated with this article can be found, in the online version, at doi:10.1016/j.poly.2006.03.006.

References

[1] W. Kaminsky, M. Arndt, Adv. Polym. Sci. 127 (1997) 143.
[2] H.H. Brintzinger, D. Fischer, R. Mülhaupt, B. Rieger, R.M. Waymouth, Angew. Chem., Int. Ed. Engl. 34 (1995) 1143.
[3] T. Keii, K. Soga (Eds.), Catalytic Polymerization of Olefins, Elsevier, New York, 1986.
[4] M. Bochmann, J. Chem. Soc., Dalton Trans. (1996) 255.
[5] E.J. Thomas, J.C.W. Chien, M.D. Rausch, Organometallics 18 (1999) 1439.
[6] (a) J.C.W. Chien (Ed.), Coordination Polymerization, Academic press, New York, 1975;
(b) W. Kaminsky, K. Külper, H.H. Brintzinger, F.R.W.P. Wild, Angew. Chem. 97 (1985) 507;
(c) W. Kaminsky, Catalytic Polymerization of Olefins, in: T. Keli, K. Soga (Eds.), Kodansha-Elsevier, Tokyo, 1986, p. 293;
(d) J.A.M. Canich, Eur. Pat. Appl. Ep 420436-A1, 1991 (Exxon).;
(e) J.A.M. Canich, G.F. Licciard, US Patent 5,057,475, 1991 (Exxon).

[7] (a) N. Ishihara, T. Seimiya, M. Kuramoto, M. Uoi, Macromolecules 19 (1986) 2464;
(b) N. Ishihara, M. Kuramoto, M. Uoi, Macromolecules 21 (1988) 3356.
[8] (a) A. Zambelli, L. Oliva, C. Pellechia, Macromolecules 22 (1989) 2129;
(b) J.C.W. Chien, Z. Salajka, S. Dong, Macromolecules 25 (1992) 3199;
(c) A. Zambelli, C. Pellechia, L. Oliva, P. Longo, A. Grassi, Makromol. Chem. 192 (1991) 223;
(d) A. Kucht, H. Kucht, S. Barry, J.C.W. Chien, M.D. Rausch, Orgnometallics 12 (1993) 3075;
(e) H. Kucht, A. Kucht, J.C.W. Chien, M.D. Rausch, Appl. Organomet. Chem. 8 (1994) 393;
(f) R. Quyoum, Q. Wang, M.J. Tudoret, M.C. Baird, D.J. Gillis, J. Am. Chem. Soc. 116 (1994) 6435;
(g) T.E. Ready, R.O. Day, J.C.W. Chien, M.D. Rausch, Macromolecules 26 (1993) 5822;
(h) Idemitsu, Eur. Pat. Appl. 275943, 276801, 322663, 1988.;
(i) Dow Chemical, Int. Pat. Appl. WO. 88/10275, 1988.;
(j) T.E. Ready, J.C.W. Chien, M.D. Rausch, J. Organomet. Chem. 519 (1996) 21;
(k) N. Schneider, M.H. Prosenc, H.H. Brintzinger, J. Organomet. Chem. 545 (1997) 291;
(l) P.F. Foster, J.C.W. Chien, M.D. Rausch, Organometallics 15 (1996) 2404;
(m) C. Pellechia, A. Immirzi, D. Pappalardo, A. Peluso, Organometallics 13 (1994) 3773.
[9] K. Nomura, N. Naga, M. Miki, K. Yanagi, A. Imai, Organometallics 17 (1998) 2152.
[10] S.J. Lancaster, O.B. Robinson, M. Bochmann, Organometallics 14 (1995) 2456.
[11] N. Ishihara, M. Kuramoto, Syntheses and properties of syndiotactic polystyrene, in: K. Soga, M. Terano (Eds.), Catalyst Design for Tailor-Made Polyolefins, Kodansha, Tokyo, 1994, pp. 350–359.
[12] J.C. Flores, J.S. Wood, J.C.W. Chien, M.D. Rausch, Organometallics 15 (1996) 4944.
[13] Q. Wang, R. Quyoum, D.J. Gillis, M.J. Tudoret, D. Jeremic, B.K. Hunter, M.C. Baird, Organometallics 15 (1996) 693.
[14] N. Schneider, M.E. Huttenloch, U. Stehling, R. Kirsten, F. Schaper, H.H. Brintzinger, Organometallics 16 (1997) 3413.
[15] M.S. Blais, J.C.W. Chien, M.D. Rausch, Organometallics 17 (1998) 3775.
[16] W. Kaminsky, S. Lenk, Macromol. Symp. 118 (1997) 45.
[17] B.Y. Lee, J.W. Han, Y.K Chung, S.W. Lee, J. Organomet. Chem. 587 (1999) 181.
[18] Y. Kim, B.H. Koo, Y. Do, J. Organomet. Chem. 527 (1997) 155.
[19] F. Zhang, Y. Mu, L. Zhao, Y. Zhang, W. Bu, J. Organomet. Chem. 613 (2000) 68.
[20] F. Zhang, Y. Mu, J. Wang, Z. Shi, W. Bu, S. Hu, Y. Zhang, S. Feng, Polyhedron 19 (2000) 1941.
[21] SMART and SAINT Software Packages, Siemens Analytical X-ray Instruments, Inc., Madison, WI, 1996.
[22] SHELXTL, Version 5.1, Siemens Industrial Automation, Inc., 1997.
[23] G.H. Llinas, M. Mena, F. Palacios, R. Serrano, J. Organomet. Chem. 340 (1988) 37.
[24] M. Bjorgvinsson, S. Halldorsson, I. Arnason, J. Magull, D. Fenske, J. Organomet. Chem. 544 (1997) 207.
[25] D. O'Hare, V. Murphy, G.M. Diamond, P. Arnold, P. Mountford, Organometallics 13 (1994) 4689.
[26] B.Y. Lee, J.W. Han, H. Seo, I.S. Lee, Y.K. Chung, J. Organomet. Chem. 627 (2001) 233.

The magnetic properties of the compound have been investigated as well.

2. Experimental

2.1. Synthesis and characterization

The reactants V_2O_5 (0.182 g, 1 mmol), H_3PO_3 (0.410 g, 5 mmol) and *N*,*N*′-dimethylpiperazine, (0.3 ml, 4.48 mmol) were added to 2 ml (166 mmol) distilled water. The initial pH was 4.2. The mixture was placed in a 23 ml capacity teflon-lined stainless steel hydrothermal bomb, under autogenous pressure, heated at 160 °C for 120 h, followed by slow cooling to room temperature. The pH of the mixture was 5.6. The product was washed with deionized water and dried at room temperature.

The synthesis was carried out in a 23 mL teflon-lined stainless steel vessel under autogenous pressure with a filling capacity of ~10%. The elemental analysis was performed on a Perkin–Elmer 2400 element analyzer and the inductively coupled plasma (ICP) analysis was performed on a Perkin–Elmer Optima 3300 DV ICP spectrometer. Magnetic susceptibility data were collected over the temperature range 2.4–300 K at a magnetic field of 5 kG on a Quantum Design MPMS-7 SQUID magnetometer.

2.2. Determination of crystal structure

A suitable single crystal with dimensions $0.20 \times 0.20 \times 0.14$ mm was selected for X-ray diffraction analysis. The intensity data collected on a Siemens SMART CCD diffractometer with graphite-monochromatic Mo Kα ($\lambda = 0.71073$ Å) radiation at a temperature of 293 ± 2 K. A hemisphere of data was collected using a narrow-frame method with scan widths of 0.30° in ω and an exposure time of 30 s/frame. Data processing was accomplished with the SAINT processing program [25]. The structure was solved by direct methods using the SHELXTL crystallographic software package [26]. The zinc and phosphorus atoms were first located, whereas the carbon, nitrogen and oxygen atoms were found in the difference Fourier maps. The hydrogen atoms residing on the amine molecules and the phosphorus were placed geometrically. A total of 2692 reflection intensities, of which 1594 were independent ($R_{int} = 0.0338$), were collected within the range $2.40° < \theta < 23.23°$ ($-8 \leqslant h \leqslant 8$, $-8 \leqslant k \leqslant 9$, $-10 \leqslant l \leqslant 8$) for the compound. The final cycle of refinement performed on F_o^2 afforded residuals $R = 0.0372$ and $R_w = 0.0981$. A summary of the crystallographic data is presented in Table 1.

Table 1
Crystal data and structure refinement for $(C_6H_{16}N_2)[V^{III}(OH)_2(V^{IV}O)_2(HPO_3)_4]\cdot H_3O$

Empirical formula	$C_6H_{25}N_2V_3P_4O_{17}$
fw	673.98
T (K)	293(2)
λ (Å)	0.71073
Space group	$P\bar{1}$
a (Å)	7.9258(4)
b (Å)	8.4892(4)
c (Å)	9.4253(5)
α (°)	108.276(2)
β (°)	103.124(3)
γ (°)	103.090(3)
V (Å^3)	555.23(5)
Z	1
$\rho_{calc.}$ (Mg/m^{-3})	2.016
μ (mm^{-1})	1.606
R_1[a] [$I>2\theta(I)$]	0.0372
wR_2[b] [$I>2\theta(I)$]	0.0981

[a] $R_1 = \sum\|F_o| - |F_c\|/\sum|F_o|$.
[b] $wR_2 = \{\sum[w(F_o^2 - F_c^2)^2]/\sum[w(F_o^2)^2]\}^{1/2}$.

3. Results and discussion

3.1. Characterization

The elemental analysis found (wt%): V, 23.01; P, 18.41; C, 10.52; N, 4.23; H, 3.51%. These are consistent with the calculated values from the formula of $(C_6H_{16}N_2)[V^{III}(OH)_2(V^{IV}O)_2(HPO_3)_4]\cdot H_3O$: V, 22.66; P, 18.40; C, 10.68; N, 4.15; H, 3.71%.

The powder X-ray diffraction pattern for $(C_6H_{16}N_2)[V^{III}(OH)_2(V^{IV}O)_2(HPO_3)_4]\cdot H_3O$ was consistent with the simulated one on the basis of the single-crystal structure, as shown in Fig. 1. The diffraction peaks on both patterns correspond well in position, indicating the phase purity of the synthesized sample. The difference in reaction intensities between the simulated and experimental patterns was due to the variation in crystal orientation for the power sample.

The IR spectrum of the product exhibited medium bands at 2995, 2923 and 1629 cm^{-1} due to the terminal NH_3^+ stretch, and the stretching vibrations of —CH_2— groups were at 2854 cm^{-1}. The bands at 2389 and 1074 cm^{-1} were attributed to the terminal P—H stretch

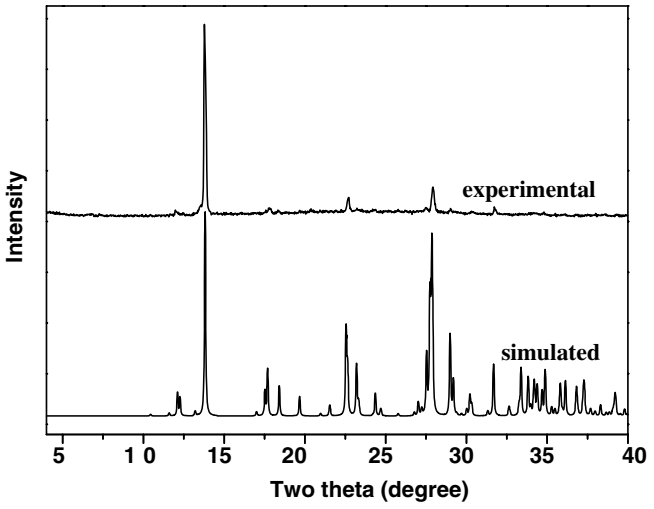

Fig. 1. Simulated and experimental powder X-ray diffraction patterns of the compound **1**.

and deformation. Absorptions at 1154, 626, 567 cm^{-1} can be attributed to P—O vibrations. The IR results showed clearly the vibrations from the [HPO_3^{2-}] phosphite group and the template molecule.

3.2. Description of the structure

The structure of the compound consists of V—O—P layers, the interlamellar space of which is occupied by protonated water molecules and double protonated *N*,*N*′-dimethylpiperazine cations. Final atomic positional and thermal parameters for $(C_6H_{16}N_2)[V^{III}(OH)_2(V^{IV}O)_2(HPO_3)_4]\cdot H_3O$ are given in Table 2, and selected bond distance and bond angle data are summarized in Table 3. The asymmetric unit of **1** is presented in Fig. 2.

There are 17 non-hydrogen atoms in compound **1**, 12 of which belong to the ''framework'' (two V, two P and eight O atoms) and five to the guest (three C, one N and O). In this structure two independent vanadium atoms present two different coordination geometries. V(1) is square pyramidal coordinated by five oxygen atoms, two connections to the P(1) atom and two connections to P(2) via oxygen and one classical short-bond V=O(5) bond (1.581 Å). V(2) is octahedral coordinated by six oxygen atoms, two occur as terminal V—O(8)H, two make V—O—P(1) linkages and the remaining two form V—O—P(2) linkages. As expected, the two distinct P atoms form the centre of pseudo pyramid hydrogen phosphite groups. P(1) has two connections to the V(1) atom via oxygen atoms (O1 and O3) and one connection to the V(2) atom via oxygen atom O6. The atom P(2) has its three oxygen atoms bonded to two V(1) and one V(2) atom. The infinite V/P/O layer is constructed from VO_6 octahedral, VO_5 square pyramids and $[HPO_3]^{2-}$ pseudo pyramids by sharing vertices. The framework structure of $(C_6H_{16}N_2)[V^{III}(OH)_2(V^{IV}O)_2(HPO_3)_4]\cdot H_3O$ consists of alternate inorganic and organic layers. Fig. 3 shows the inorganic layer viewed down the [1 0 0] direction. The inorganic layer, with the composition $[V(OH)_2(VO)(HPO_3)_2]^-$, is constructed by connecting $[(VO)(HPO_3)_2]^{2-}$ chains through bridging $V(OH)_2$ frag-

Table 2
Atomic coordinates (×10^4) and equivalent isotropic displacement parameters (Å^2 × 10^3) for $(C_6H_{16}N_2)[V^{III}(OH)_2(V^{IV}O)_2(HPO_3)_4]\cdot H_3O$

	x	*y*	*z*	*U* (eq)
V(1)	4032(1)	−7(1)	7185(1)	25(1)
V(2)	0	−5000	0	42(1)
P(1)	2297(2)	−1833(2)	3471(1)	24(1)
P(2)	2693(2)	−1821(2)	9427(2)	36(1)
O(1)	3004(4)	−2022(4)	5044(3)	26(1)
O(2)	2843(5)	−1794(5)	7837(4)	39(1)
O(3)	6343(4)	404(4)	6717(4)	31(1)
O(4)	5463(5)	1444(4)	9429(4)	39(1)
O(5)	2852(5)	1184(5)	6840(4)	46(1)
O(6)	1720(5)	−3609(5)	2162(4)	42(1)
O(7)	1356(6)	−3553(6)	−896(4)	68(2)
O(8)	1497(8)	−6553(7)	−300(6)	96(2)
O(1W)	5000	−5000	0	133(4)
N(1)	3151(6)	−5260(6)	5060(6)	39(1)
C(1)	4713(8)	−4928(8)	6451(7)	46(2)
C(2)	3507(8)	−6138(7)	3578(7)	46(2)
C(3)	1398(8)	−6311(8)	5126(9)	60(2)

Table 3
Bond lengths (Å) and angles (deg) for $(C_6H_{16}N_2)[V^{III}(OH)_2(V^{IV}O)_2(HPO_3)_4]\cdot H_3O$

V(1)—O(1)	2.030(3)	V(2)—O(6) (×2)	1.976(3)
V(1)—O(2)	1.941(3)	V(2)—O(7) (×2)	1.960(4)
V(1)—O(3)	1.960(3)	V(2)—O(8) (×2)	1.963(6)
V(1)—O(4)	1.980(3)		
V(1)—O(5)	1.581(4)		
P(1)—O(1)	1.533(3)	P(2)—O(2)	1.537(3)
P(1)—O(3)#2	1.515(3)	P(2)—O(4)#4	1.503(4)
P(1)—O(6)	1.506(4)	P(2)—O(7)#3	1.498(4)
P(1)—H(1)	1.42(6)	P(2)—H(2)	1.56(6)
O(2)—V(1)—O(1)	82.29(13)	O(6)#1—V(2)—O(6)	180.0(2)
O(2)—V(1)—O(3)	130.07(16)	O(7)—V(2)—O(6)	92.66(15)
O(2)—V(1)—O(4)	88.82(14)	O(7)—V(2)—O(6)#1	87.34(15)
O(3)—V(1)—O(1)	85.45(13)	O(7)—V(2)—O(7)#1	180.0(2)
O(3)—V(1)—O(4)	87.83(14)	O(7)—V(2)—O(8)	90.9(2)
O(4)—V(1)—O(1)	161.34(15)	O(7)#1—V(2)—O(8)	89.1(2)
O(5)—V(1)—O(2)	113.97(19)	O(8)—V(2)—O(6)	89.10(19)
O(5)—V(1)—O(1)	99.16(16)	O(8)—V(2)—O(6)#1	90.90(19)
O(5)—V(1)—O(3)	115.72(18)	O(8)—V(2)—O(8)#1	180.0
O(5)—V(1)—O(4)	99.44(18)	O(4)#4—P(2)—O(2)	111.3(2)
O(3)#2—P(1)—O(1)	112.31(19)	O(7)#3—P(2)—O(2)	107.7(2)
O(6)—P(1)—O(1)	108.1(2)	O(7)#3—P(2)—O(4)#4	113.5(3)
O(6)—P(1)—O(3)#2	114.3(2)	O(7)#3—P(2)—H(2)	107(2)
O(6)—P(1)—H(1)	111(2)	O(4)#4—P(2)—H(2)	110(2)
O(1)—P(1)—H(1)	110(3)	O(2)—P(2)—H(2)	106(2)
O(3)#2—P(1)—H(1)	102(3)	P(2)#4—O(4)—V(1)	138.7(2)
P(1)—O(1)—V(1)	124.48(19)	P(2)—O(2)—V(1)	134.1(2)
P(1)#2—O(3)—V(1)	139.4(2)	P(2)#5—O(7)—V(2)	146.1(3)
P(1)—O(6)—V(2)	141.1(3)	V(2)—O(8)—H(8)	109.5

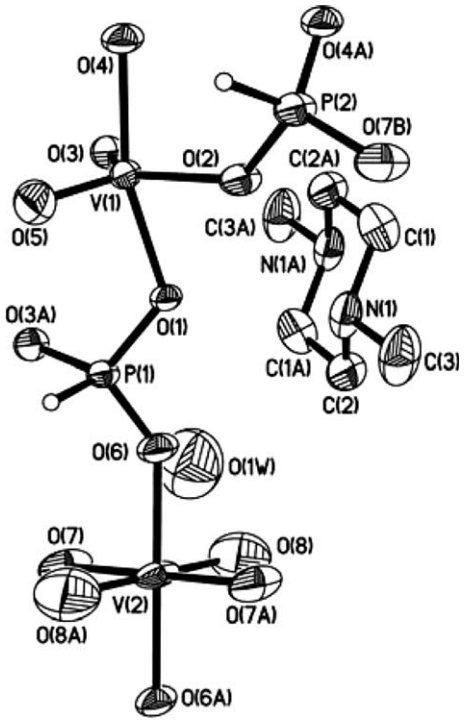

Fig. 2. Asymmetric unit of $(C_6H_{16}N_2)[V^{III}(OH)_2(V^{IV}O)_2(HPO_3)_4]\cdot H_3O$ with thermal ellipsoids shown at 50% probability.

ments. The chains are composed of vertex-sharing $[VO_5]$ square pyramids and $[HPO_3]^{2-}$ pseudo-pyramids, fused together via V—O—P bonds. Each $[VO_5]$ group forms four V—O—P links, resulting in polyhedral "four-rings" with strict alternation of the V and P species. The polyhedral chain-linkage pattern of vertex-linked $[VO_5]$/$[HPO_3]$ four-rings is similar to that found in $[CN_3H_6][VO(H_2O)(HPO_4)(H_2PO_4)]\cdot H_2O$ [27], $Ba_2VO(PO_4)_2\cdot H_2O$ [28] and $VO(H_2PO_4)_2\cdot H_2O$ [29] with a one-dimensional chain structure.

Fig. 4 shows the stacking of the inorganic layer with the intercalated organic cations viewed along the [1 1 0] direction. The inorganic layers are stacked exactly one over the other in an AAAA fashion. The double protonated *N*,*N*′-dimethylpiperazine is intercalated between the layers with hydrogen bonding. As in many inorganic framework compounds, $(C_6H_{16}N_2)[V^{III}(OH)_2(V^{IV}O)_2(HPO_3)_4]\cdot H_3O$ exhibits significant hydrogen bond interactions between *N*,*N*′-dimethylpiperazine cations and framework oxygens. The *N*,*N*′-dimethylpiperazine cation is situated between two vanadium phosphite layers and interacts with the layers though N—H···O hydrogen bonds (Fig. 5). The water molecule connects with the inorganic layer via hydrogen bonds as evidenced by the short O(8)···O(1W) distances of 2.698 Å.

3.3. Physical data

The magnetic susceptibility of **1** was measured between 4 and 300 K in a 5000 G field and the temperature-dependence of χ_M and reciprocal molar magnetic susceptibility χ^{-1} are shown in Fig. 6. The molar magnetic susceptibility, χ_M, increases with decreasing temperature, which shows paramagnetic behavior in compound **1**. The thermal evolution of χ_M follows the Curie–Weiss law $[\chi_M = C_m/(T-\theta)]$ above 50 K, with $C_m = 0.391$ emu K^{-1} mol^{-1} and $\theta = -38.99$ K. At 300 K the magnetic moment (μ_{eff}) per vanadium, determined from the equation $\mu_{eff} = 2.828(\chi_M T)^{1/2}$, is 1.73 μB which is slightly lower than that expected for a trivalent/tetravalent system with $\mu_{eff} = 1.75$ μB. The magnetic susceptibility confirmed the valances of the vanadium atoms to be mixed valence of +3/+4 for compound **1**.

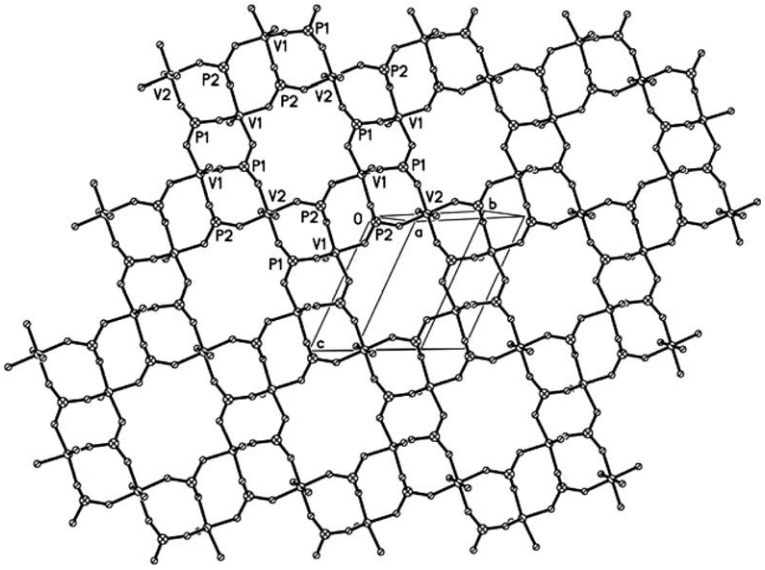

Fig. 3. The inorganic layer structure of compound **1** viewed along the [0 1 0] direction.

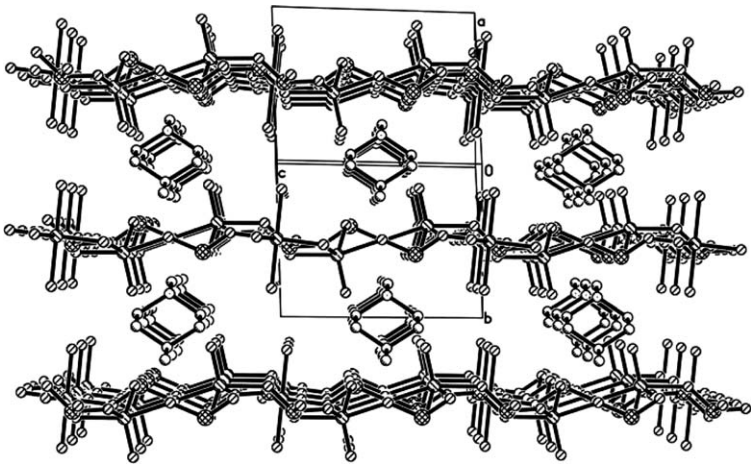

Fig. 4. The stacking of the layers with the intercalated organic cations viewed along the [1 1 0] direction.

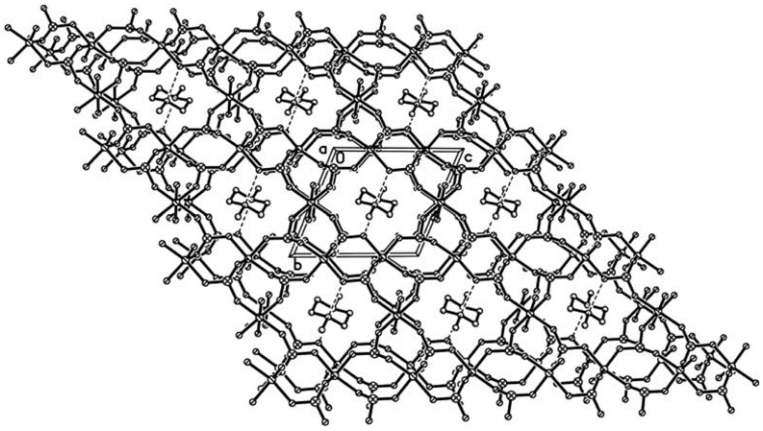

Fig. 5. View the structure of compound **1** along [1 0 0]. Dotted lines represent the various hydrogen bond interactions.

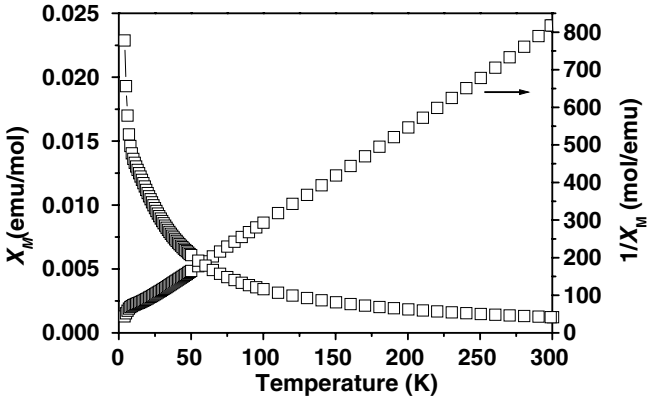

Fig. 6. Thermal dependence of χ_M (open block) and $\chi_M T$ (solid block) for compound **1**.

4. Conclusions

In summary, a novel open-framework vanadium phosphite $(C_6H_{16}N_2)[V^{III}(OH)_2(V^{IV}O)_2(HPO_3)_4]\cdot H_3O$ was obtained as good quality single crystals by the hydrothermal method. The structure of compound **1** is built up from alternate V(III)O_6 octahedra, V(IV)O_5 square pyramids and [HPO_3^{2-}] pseudo pyramids by sharing vertices. This organically templated vanadium phosphite possesses alternate inorganic and organic layers, formed by four- and eight-membered rings. The *N*,*N*′-dimethylpiperazine cation acts as a template for directing occupies between two vanadium phosphite layers and interacts with the layers though N—H···O hydrogen bonds.

5. Supplementary material

The supplementary material in the form of a CIF file has been deposited with the Cambridge Crystallographic Data Centre, 12 Union Road, Cambridge CB2 IEZ, UK, as supplementary material No. CCDC-266817 and can be obtained by contacting the CCDC (fax: +44 1223 336 033; e-mail: deposit@ccdc.cam.ac.uk) quoting the article details and the corresponding SUP number.

Acknowledgement

This work was supported by the Natural Science Foundation of Chongqing (No. CSTC2005BB4203).

References

[1] J.W. Johnson, D.C. Johnson, A.J. Jacobson, J.R. Brody, J. Am. Chem. Soc. 106 (1984) 8123.
[2] D. Beltran-Porter, P. Amoros, R. Ibanez, E. Martinez, A. Beltran-Porter, A. Le Bail, G. Ferey, G. Villeneuve, Solid State Ionics 57 (1989) 32.
[3] K.-H. Lii, J. Chin. Chem. Soc. 39 (1992) 569.
[4] J. Do, R.P. Bontchev, A.J. Jacobson, J. Solid State Chem. 154 (2000) 514.
[5] D. Beltran, A. Beltran, P. Amoros, R. Ibanez, E. Martinez, G. Ferey, G. Villeneuve, Eur. J. Solid State Inorg. Chem. 28 (1991) 131.
[6] V. Soghomonian, Q. Chen, Y. Zhang, R.C. Haushalter, C.J. O'Connor, C. Tao, J. Zubieta, Inorg. Chem. 34 (1995) 3509.
[7] G. Centi, F. Trifiro, J.R. Enber, V.M. Franchetti, Chem. Rev. 88 (1988) 55.
[8] V. Soghomonian, Q. Chen, R.C. Haushalter, J. Zubieta, C.J. O'Connor, Science 259 (1993) 1596.
[9] Z. Shi, S. Feng, S. Gao, L. Zhang, G. Yang, J. Hua, Angew. Chem., Int. Ed. 39 (2000) 2325.
[10] M.I. Khan, L.M. Meyer, R.C. Haushalter, A.L. Schweitzer, J. Zubieta, J.L. Dye, Chem. Mater. 8 (1996) 43.
[11] G. Bonavia, J. Debord, R.C. Haushalter, D. Rose, J. Zubieta, Chem. Mater. 7 (1995) 1995.
[12] S. Fernandez, J.L. Pizarro, J.L. Mesa, L. Lezama, M.I. Arriortua, R. Olazcuaga, T. Rojo, Chem. Mater. 14 (2002) 2300.
[13] S. Fernandez, J.L. Pizarro, J.L. Mesa, L. Lezama, M.I. Arriortua, T. Rojo, Int. J. Inorg. Mater. 3 (2001) 331.
[14] S. Fernandez, J.L. Pizarro, J.L. Mesa, L. Lezama, M.I. Arriortua, R. Olazcuaga, T. Rojo, Inorg. Chem. 40 (2001) 3476.
[15] S. Fernandez, J.L. Mesa, J.L. Pizarro, L. Lezama, M.I. Arriortua, R. Olazcuaga, T. Rojo, Chem. Mater. 12 (2000) 2092.
[16] J.A. Rodgers, W.T.A. Harrison, Chem. Commun. (2000) 2385.
[17] W.T.A. Harrison, M.L.F. Phillips, T.M. Nenoff, Int. J. Inorg. Mater. 3 (2001) 1033.
[18] W.T.A. Harrison, M.L.F. Phillips, T.M. Nenoff, J. Chem. Soc., Dalton Trans. 2459 (2001).
[19] W.T.A. Harrison, Int. J. Inorg. Mater. 3 (2001) 187.
[20] W.T.A. Harrison, M.L.F. Phillips, J. Stanchfield, T.M. Nenoff, Inorg. Chem. 40 (2001) 895.
[21] W.T.A. Harrison, J. Solid State Chem. 160 (2001) 4.
[22] S. Fernandez, J.L. Mesa, J.L. Pizarro, L. Lezama, M.I. Arriortua, T. Rojo, Angew. Chem., Int. Ed. 41 (2002) 3683.
[23] Z. Shi, G. Li, S. Feng, Inorg. Chem. 42 (2003) 2357.
[24] Z. Shi, D. Zhang, S. Feng, J. Solid State Chem. 172 (2003) 464.
[25] SMART and SAINT, Siemens Analytical X-ray Instruments, Inc., Madison, WI, 1996.
[26] SHELXTL,Version 5.1, Siemens Industrial Automation, Inc., 1997.
[27] Z. Bircsak, A.K. Hall, W.T.A. Harrison, J. Solid State Chem. 142 (1999) 168.
[28] W.T.A. Harrison, S.C. Lim, J.T. Vaughey, A.J. Jacobson, D.P. Goshorn, J.W. Johnson, J. Solid State Chem. 113 (1994) 444.
[29] A. Le Bail, M.D. Marcos, P. Amoros, Inorg. Chem. 33 (1994) 2607.

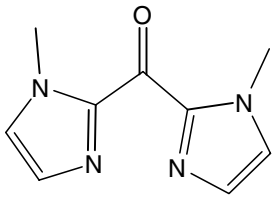

bik

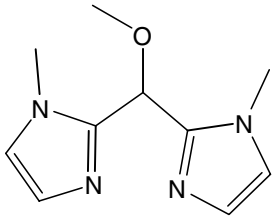

bimm

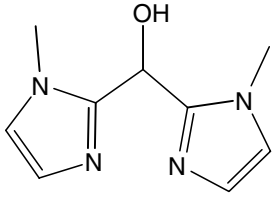

bihm

Scheme 1.

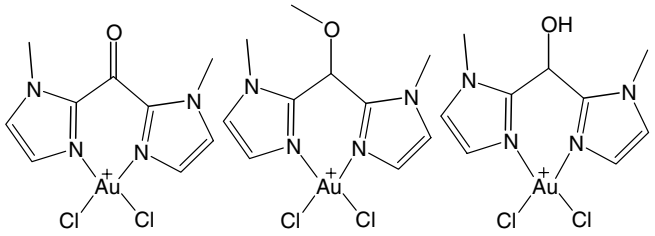

1 2 3

Scheme 2.

spectra in the X band were recorded with a Bruker System ESP 300 equipped with a Bruker ER035M gaussmeter and a HP 5350B microwave counter. Cyclic voltammetry was carried out at a 100 mV/s scan rate in dichloromethane/0.1 M Bu_4NPF_6 using a three-electrode configuration (glassy carbon electrode, Pt counter electrode, Ag/AgCl reference) and a PAR 273 potentiostat and function generator. A two-electrode capillary was used in radical complex generation for X band EPR studies [9].

2.2. Syntheses

The ligand bik was synthesized according to the literature [3], single crystals were grown in DMF at −30 °C. The ligands bis(1-methyl-2-imidazolyl)methoxymethane (bimm) and bis(1-methyl-2-imidazolyl)hydroxymethane (bihm) were obtained as described previously [4,10].

2.2.1. *[$AuCl_2$(bik)]Cl, (**1**)Cl*

A solution of $KAuCl_4$ (262 mg: 0.69 mmol) in 15 mL methanol was added to a 15 mL methanol solution of bik (131 mg: 0.69 mmol) in the dark and stirred for 18 h at ambient temperature. The yellow solid formed was filtered and washed with methanol to obtain the product in 69% yield (236 mg). Single crystals suitable for X ray diffraction could be grown as methanol solvates by slow evaporation from an acetonitrile solution. *Anal.* Calc. for $C_{10}H_{14}AuCl_3N_4O_2$ (525.57): C, 22.85; H, 2.69; N, 10.66. Found: C, 22.83; H, 2.48; N, 10.58%. ^{1}H NMR (DMSO-d_6): 4.08 (s, 6H, NCH_3), 7.6 (s, 2H, CH), 7.9 (s, 2H, CH). ^{13}C NMR (DMSO-d_6): 36.9 (NCH_3), 125.8 (C im), 129.8 (C im), 138.65 (C im), 165.6 (CO). IR (KBr): 1684 cm^{-1} (CO).

2.2.2. *[$AuCl_2$(bimm)]($AuCl_2$), (**2**)($AuCl_2$)*

A solution of $KAuCl_4$ (126 mg: 0.33 mmol) in 15 mL methanol was added to a methanol solution of bimm (72 mg: 0.34 mmol) in the dark and stirred for 18 h. The precipitated product (59 mg, 48%), insoluble in methanol, was isolated and gave suitable crystals for X ray analysis after slow evaporation from a dichloromethane solution. *Anal.* Calc. for $C_{10}H_{14}Au_2Cl_4N_4O$ (741.99): C, 16.19; H, 1.90; N, 7.55. Found: C, 16.23; H, 1.89; N, 7.51%. ^{1}H NMR (DMSO-d_6): 3.41 (s, 3H, OCH_3), 4.00 (s, 6H, NCH_3), 6.29 (CH), 7.59 (s, 2H, im), 7.77 (s, 2H, im). ^{13}C NMR (DMSO-d_6): $\delta = 35.44$ (NCH_3), 56.85 (CHOMe), 63.04 (OCH_3), 123.96 (C im), 125.22 (C im), 138.9 (C im).

2.2.3. *[$AuCl_2$(bihm)]Cl, (**3**)Cl*

A solution of $KAuCl_4$ (307 mg: 0.81 mmol) in 20 mL of THF was added to a THF solution (80 mL) of bihm (155 mg: 0.806 mmol) in the dark and stirred for 25 h. The resulting yellow suspension was cooled to −30 °C to cause the yellow solid product to settle down which was then filtered to yield 301 mg (75%) of a THF hemi-solvate. *Anal.* Calc. for $C_{11}H_{16}AuCl_3N_4O_{1.5}$ (531.54): C, 24.86; H, 3.03; N, 10.54. Found: C, 24.88; H, 3.07; N, 9.14%. ^{1}H NMR (DMSO-d_6): 1.73 (m, 4H, CH_2 from THF), 3.59 (m, 4H, CH_2 from THF), (3.99 s, 6H, NCH_3), 6.22 (d, CH), 6.35 (d, COH), 7.68 (s, 2H, im), 7.73 (s, 2H, im). ^{13}C NMR (CD_3OD): 38.59 (NCH_3), 60.67 (COH), 127.8 (C im), 128.8 (C im), 145 (C im). IR (KBr): 3430 cm^{-1} (OH). The analogous reaction was carried out in methanol from which suitable solvent-containing crystals for X ray analysis could be grown by slow evaporation.

2.3. Crystallography

Single crystals of bik were obtained from a DMF solution kept at −30 °C. A colorless crystal of 0.6 × 0.3 × 0.1 mm size was used to collect data at 293 K with a Siemens P3 diffractometer. Single crystals of (**1**)Cl, (**2**)($AuCl_2$) and (**3**)Cl were obtained, partially as methanol solvates, by slow evaporation from solutions as described above. Data were collected of selected specimens (yellow platelets

Table 1
Crystallographic data for bik and for the complexes **1**–**3**

Complex	bik	(**1**)Cl · CH_3OH	(**2**)($AuCl_2$)	(**3**)Cl · 1/2CH_3OH
Empirical formula	$C_9H_{10}N_4O$	$AuC_9Cl_3H_{10}N_4O \cdot (CH_3OH)$	$Au_2C_{10}Cl_4H_{14}N_4O$	$AuC_9Cl_3H_{12}N_4O \cdot 1/2CH_3OH$
Formula weight	190.21	525.57	741.99	511.56
T (K)	293	100	293	100
Space group	$P2_1/c$	Cc	$C2/c$	$P2_1/c$
a (Å)	10.043(2)	7.6249(2)	18.8757(4)	7.520(4)
b (Å)	7.3246(15)	26.6680(9)	11.5032(3)	27.894(2)
c (Å)	13.045(3)	7.7076(2)	16.6746(4)	7.4368(4)
β (°)	108.33(3)	118.478(2)	90.327(2)	118.720(4)
V (Å^3)	910.9(3)	1377.63(7)	3620.5(2)	1368.1(1)
Z	4	4	8	4
ρ_{calc} (g cm^{-3})	1.387	2.534	2.722	2.484
μ (mm^{-1})	0.097	11.27	16.78	11.34
R_1	0.0431	0.038	0.046	0.118
wR_2	0.1078	0.102	0.074	0.131

in each case, $0.1 \times 0.1 \times 0.04$ mm (**1**)Cl · CH_3OH, $0.15 \times 0.1 \times 0.04$ (**2**)($AuCl_2$), and $0.2 \times 0.2 \times 0.06$ mm (**3**)Cl · 1/2CH_3OH) with a NONIUS Kappa CCD diffractometer at 100 K ((**1**)Cl · CH_3OH, (**3**)Cl · 1/2CH_3OH), and 293 K ((**2**)($AuCl_2$)), respectively. Additional crystallographic information is given in Table 1. The structures were solved using direct methods with refinement by full-matrix least-squares of F^2, employing the program system SHELXL-97 in connection with absorption correction [11]. Except for C10 from the methanol molecule in (**1**)Cl · 1/2CH_3OH all non-hydrogen atoms were refined anisotropically, hydrogen atoms were introduced at appropriate positions.

2.4. DFT calculations

Density functional (DFT) calculations were carried out using the program package GAUSSIAN [12], the hybrid functional B3LYP with 6-31G* or LANL2DZ basis sets was employed. The latter was used for the calculations involving metal complexes although this basis systematically yielded slightly longer bonds. Energy and bond parameter differences between conformers were calculated with very similar results for both basis sets.

3. Results and discussion

3.1. Crystal structure of bik

Although bik has been used several times as a ligand in biomimetic coordination chemistry [3] no crystal structure had been reported so far. Crystallographic data for bik as obtained from crystallization from DMF at −30 °C are summarized in Table 1, selected data and their reproduction by DFT calculations are listed in Table 2. Fig. 1 shows the molecular structure in the crystal, the N1–C1–C5–O1 and N3–C6–C5–O1 torsional angles are 31.0° and 27.5°, respectively (calculated: 27.9°). The C1–N1–C3–C2–N2 plane has an angle of 49.4° with respect to the plane of the other methylimidazole ring (C6–N3–C8–C7–N4). The conformation adopted reflects an approximate *s-trans*/*s-trans* arrangement of the π accepting (N=C)–(C=O)–(C=N) bonds.

On reduction to bik$^{\bullet-}$ the major bond length change calculated is a lengthening of the C–O bond as befits a ketyl-type radical (Table 2).

Table 2
Selected experimental and calculated bond lengths (Å) and angles (°) for bik and bik$^{\bullet-}$ (see Scheme 3 for numbering)

	bik		bik$^{\bullet-}$
	Experimental	DFT	DFT
Bond lengths (Å)			
O1–C5	1.223(2)	1.273	1.339
N3–C6	1.331(2)	1.353	1.368
N3–C8	1.365(2)	1.380	1.388
C5–C1	1.474(2)	1.470	1.457
C5–C6	1.472(2)	1.470	1.457
N4–C9	1.462(2)	1.473	1.464
N4–C7	1.360(2)	1.382	1.401
Bond angles (°)			
C1–N2–C4	128.8(1)	122.6	127.7
O1–C5–C1	120.9(1)	120.6	119.5
C6–N3–C8	105.1(1)	106.1	106.3
O1–C5–C6	121.3(1)	120.6	119.5

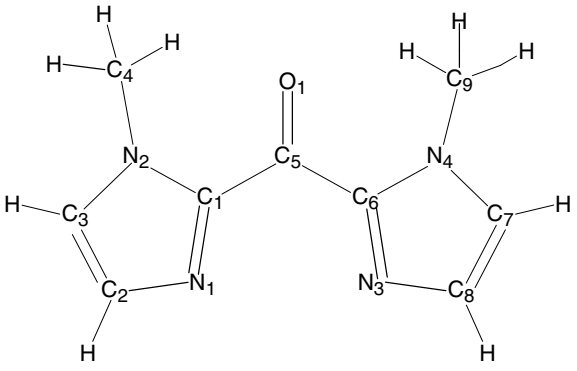

Scheme 3.

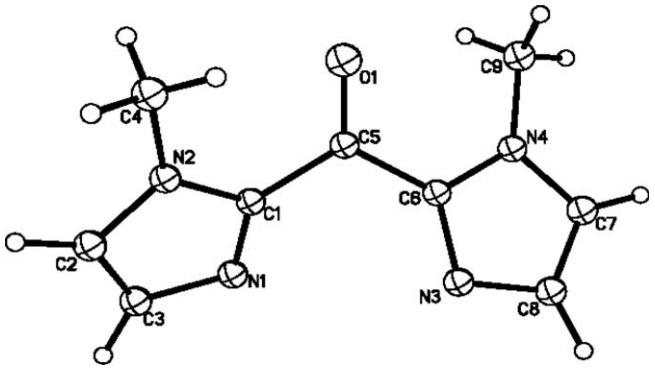

Fig. 1. Structure of bik in the crystal.

3.2. Synthesis, structure, spectroscopy and electrochemistry of complexes $[AuCl_2(L)](X)$

The gold(III) complex cations **1**–**3** were obtained from reacting $KAuCl_4$ with bik, bimm or bihm, respectively. Two of the cationic complexes have Cl^- as the counter ion while the complex with bimm contains the reductively generated dichlorogold(I) anion, the result from elemental analyses being supported by X ray crystallography. The equivalence of the downfield shifted imidazole protons in the ^1H NMR spectra suggests Au^{III} coordination to both N atoms in each case. At 1684 cm^{-1} the IR carbonyl stretching frequency for complex **1** is 50 cm^{-1} higher than that of free bik. Similar effects were found for a previously reported dimethylgold(III) complex of bik [3a]. The presence of a broad O–H stretching band at 3430 cm^{-1} is indicative of a non-coordinating OH group in **3**.

The results from the X ray diffraction analyses (Table 1) for the gold(III) complexes are summarized in Table 3. Fig. 2 shows the molecular structures.

In all three cases **1**–**3** the N,N′ coordination of nearly square planar Au^{III} with the formation of six-membered chelated rings was observed. While there are slight differences of the bond distances between Au^{III} and the nitrogen atoms, the Au–Cl bond lengths are almost invariant. The six-membered chelate rings adopt a distorted boat conformation as specified for **1**–**3** and as calculated for **1** (Table 3).

The Au–N–C–C torsional angles within the six-membered rings are smaller than 11°. The dihedral (''boat'') angles Au–N1–C1–C5/C5–C6–N3–Au reflect considerable structural flexibility as evident from the experimental variation between **1** or **3** (ca. 17°) and **2** (ca. 45°) and from the difference between the experimental and the calculated value (0°) for system **1**. The experimentally observed boat conformation for **1** is calculated to lie 0.167 eV (3.85 kcal/mol) higher than the planar energy minimum conformation, supporting the notion of a flat energy surface. Otherwise, the structure of **1** is reasonably reproduced by DFT calculations, however, the calculated bond distances involving the metal are typically too long relative to the experiment. The N,O coordination alternative with a five-membered Au–N–C–C–O chelate ring is calculated

Table 3
Selected bond lengths (Å) and angles (°) for gold complexes

	(**1**)Cl · CH_3OH	**1**[a]	(**1**$^{\cdot-}$)[a]	(**2**)($AuCl_2$)	(**3**)Cl · 1/2CH_3OH
Bond lengths (Å)					
Au–N3	2.040(7)	2.082	2.241	2.014(5)	2.04(1)
Au–N1	2.030(7)	2.082	2.241	2.020(5)	2.03(1)
Au–Cl1	2.261(2)	2.386	2.501	2.259(2)	2.259(3)
Au–Cl2	2.260(2)	2.386	2.501	2.260(2)	2.260(3)
N3–C6	1.30(1)	1.367	1.360	1.326(7)	1.32(2)
N1–C1	1.34(1)	1.367	1.360	1.329(7)	1.32(2)
C5–C6	1.46(1)	1.472	1.470	1.501(8)	1.50(2)
C5–C1	1.46(1)	1.472	1.470	1.510(8)	1.51(2)
C5–O1	1.21(1)	1.262	1.271	1.422(7)	1.38(2)
N4–C9	1.47(1)	1.487	1.478	1.463(8)	1.48(2)
N2–C4	1.50(1)	1.487	1.478	1.464(9)	1.50(2)
O1–C10		n.a.	n.a.	1.415(8)	
Bond angles (°)					
N1–Au–N3	90.1(3)	90.2	83.5	89.1(2)	90.0(4)
Cl1–Au–N1	177.5(2)	178.0	174.3	178.7(2)	177.9(3)
Cl2–Au–N3	178.5(2)	178.0	174.3	179.6(2)	178.1(3)
Cl1–Au–N3	92.1(2)	91.8	90.8	90.2(1)	92.0(3)
Cl2–Au–N1	91.2(2)	91.8	90.8	90.7(2)	91.5(3)
Cl1–Au–Cl2	86.51(7)	86.2	94.9	89.96(7)	86.6(1)
Torsional angles (°)					
Au–N1–C1–C5	−8(1)	0.0	0.0	−5.3(8)	1(2)
Au–N3–C6–C5	4(1)	0.0	0.0	10.2(8)	2(2)
Dihedral angles (°)					
Au–N1–C1–C5/C5–C6–N3–Au	17.8(8)	0.0	0.0	44.8(3)	17.4(7)

[a] From DFT calculations.

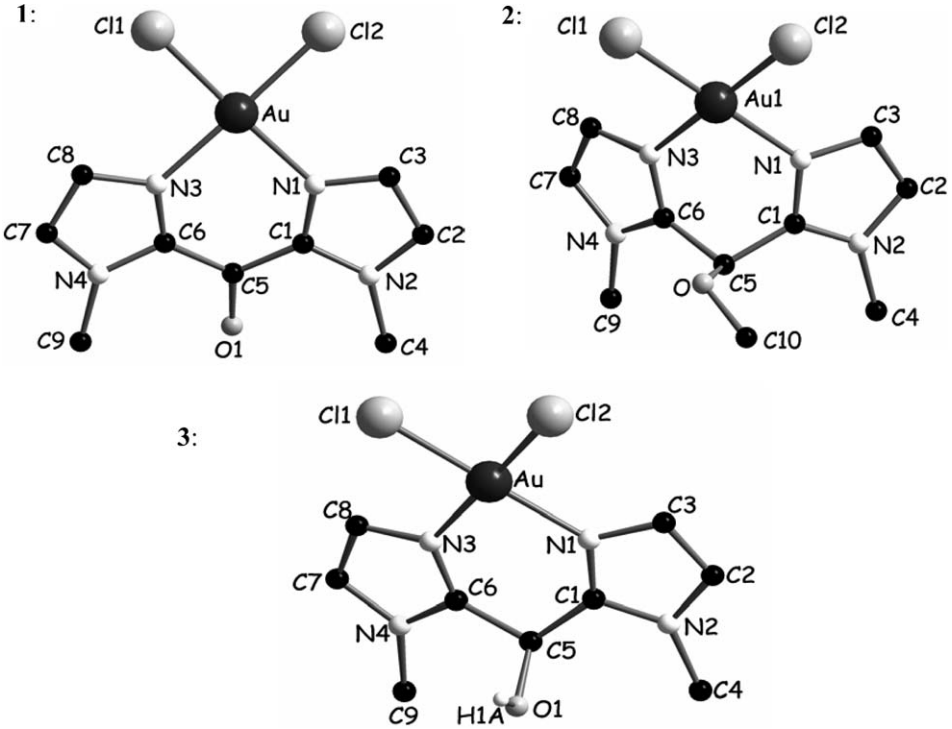

Fig. 2. Structures of the complex cations **1**, **2** and **3** in corresponding crystals (**1**)Cl, (**2**)($AuCl_2$) and (**3**)Cl.

to lie 25.0 kcal/mol higher than the six-membered chelate ring configuration with N,N′ coordination.

3.3. Cyclic voltammetry and EPR spectroscopy

The cyclic voltammetry of complexes (**1**)Cl and (**3**)Cl at 20 °C in CH_2Cl_2/0.1 M Bu_4NPF_6 gave only irreversible waves for the cathodic reduction. Reversibility corresponding to $i_c/i_a \approx 1.0$ and $\Delta E_{pp} \approx 120$ mV was achieved only by cooling to 195 K; a very negative potential of −3.03 V versus ferrocene/ferrocenium was measured for (**3**)Cl while complex (**1**)Cl reacted with the reference. There was no detectable EPR signal for complex **1**$^{\cdot}$ after in situ reduction at 195 K and measurement at 4 K. This result signifies chemical lability of the neutral species [(bik)$AuCl_2$]$^{\cdot}$ and/or rapid EPR relaxation because of strong contributions from the heavy atom; DFT calculation results for the [(bik)$AuCl_2$]$^{+}$/[(bik)$AuCl_2$]$^{\cdot}$ pair (Table 3, Fig. 3) serve to rationalize these observations.

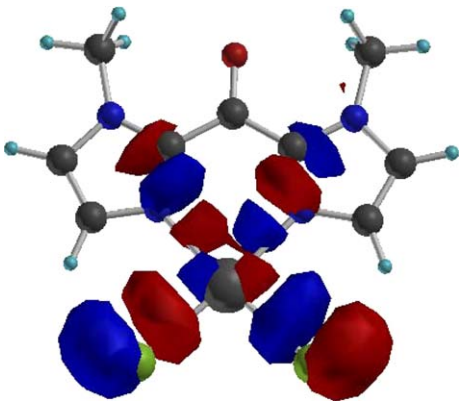

Fig. 3. DFT calculated SOMO of [(bik)$AuCl_2$]$^{\cdot}$.

The lowest unoccupied MO of **1** which is related to the singly occupied MO, SOMO, of [(bik)$AuCl_2$]$^{\cdot}$ shows almost no contributions from the organic ligand (Fig. 3), the bonds affected in terms of considerable elongation are those involving the metal. Metal–ligand dissociation is thus expected to occur on reduction at higher temperatures, consistent with the DFT results.

4. Supplementary data

CCDC 271455–271457, 604458 contain the supplementary crystallographic data for this paper. These data can be obtained free of charge from The Cambridge Crystallographic Data Centre via www.ccdc.cam.ac.uk/data_request/cif.

Acknowledgement

This work was supported by the Land Baden-Württemberg.

References

[1] (a) I. Bertini, A. Sigel, H. Sigel (Eds.), Handbook on Metalloproteins, Marcel Dekker, New York, 2001;
(b) A. Messerschmidt, Handbook of Metalloproteins, Wiley, New York, 2004;
(c) W. Kaim, B. Schwederski, Bioinorganic Chemistry, Wiley, Chichester, 1994.

[2] (a) I. Sóvágó, K. Várnagy, K. Ösz, Comments Inorg. Chem. 23 (2002) 149;
(b) S. Abuskhuna, M. McCann, J. Briody, M. Devereux, V. McKee, Polyhedron 23 (2004) 1731;
(c) T. Ruether, K.J. Cavell, N.C. Braussaud, B.W. Skelton, A.H. White, J. Chem. Soc., Dalton Trans. (2002) 4684;
(d) R. Bhalla, M. Helliwell, R.L. Beddoes, D. Collison, C.D. Garner, Inorg. Chim. Acta 273 (1998) 225.
[3] (a) P.K. Byers, A.J. Canty, L.M. Engelhardt, J.M. Patrick, A.H. White, J. Chem. Soc., Dalton Trans. (1985) 981;
(b) X.M. Chen, Z.-T. Xu, T.C. Mak, Polyhedron 14 (1995) 319;
(c) M. Grehl, B. Krebs, Inorg. Chem. 33 (1994) 3877;
(d) H. Engelking, S. Karentzopoulos, G. Reusmann, B. Krebs, Chem. Ber. 127 (1994) 2355;
(e) G. Reusmann, M. Grehl, W. Reckordt, B. Krebs, Z. Anorg. Allg. Chem. 620 (1994) 199;
(f) A.F. Stange, W. Kaim, Z. Anorg. Allg. Chem. 622 (1996) 1116;
(g) S. Elgafi, L.D. Field, B.A. Messerle, T.W. Hambley, P. Turner, J. Chem. Soc., Dalton Trans. (1997) 2341;
(h) F.M. Hornung, O. Heilmann, W. Kaim, S. Zalis, J. Fiedler, Inorg. Chem. 39 (2000) 4052;
(i) C.J. Burns, L.D. Field, T.W. Hambley, T. Lin, D.D. Ridley, P. Turner, M.P. Wilkinson, ARKIVOC (2001) 157;
(j) S. Elgafi, L.D. Field, B.A. Messerle, P. Turner, T.W. Hambley, J. Organomet. Chem. 588 (1999) 69;
(k) A. Bousseksou, C. Place, J. Linares, F. Varret, J. Magn. Magn. Mater. 104–107 (1992) 225;
(l) L. Bénisvy, J.-C. Chottard, J. Marrot, Y. Li, Eur. J. Inorg. Chem. (2005) 999;
(m) J. Rall, W. Kaim, J. Chem. Soc., Faraday Trans. 90 (1994) 2905.
[4] (a) S.M. Gorun, G.C. Papaefthymiou, R.B. Frankel, S.J. Lippard, J. Am. Chem. Soc. 109 (1987) 4244;
(b) S.M. Gorun, S.J. Lippard, Inorg. Chem. 27 (1988) 149;
(c) , See alsoW.B. Tolman, A. Bino, S.J. Lippard, J. Am. Chem. Soc. 111 (1989) 8522;
(d) M.J. Bloemink, H. Engelking, S. Karentzopoulos, B. Krebs, J. Reedijk, Inorg. Chem. 35 (1996) 619.
[5] A. Kumar, I.Yu. Galaev, B. Mattiasson, Bioseparation 7 (1998) 185.
[6] C.J. Jones, D. Taube, V.R. Ziatdinov, R.A. Periana, R.J. Nielsen, J. Oxgaard, W.A. Goddart III, Angew. Chem. 116 (2004) 4726.
[7] C.J. Jones, D. Taube, V.R. Ziatdinov, R.A. Periana, R.J. Nielsen, J. Oxgaard, W.A. Goddart III, Angew. Chem., Int. Ed. 43 (2004) 4626.
[8] (a) A.S.K. Hashmi, J.P. Weyrauch, M. Rudolph, E. Kurpejović, Angew. Chem. 116 (2004) 6707;
(b) A.S.K. Hashmi, J.P. Weyrauch, M. Rudolph, E. Kurpejović, Angew. Chem., Int. Ed. 43 (2004) 6545;
(c) , Cf. alsoA.S.K. Hashmi, Angew. Chem. 117 (2005) 7150;
(d) A.S.K. Hashmi, Angew. Chem., Int. Ed. 44 (2005) 6990.
[9] W. Kaim, S. Ernst, V. Kasack, J. Am. Chem. Soc. 112 (1990) 173.
[10] A. Stange, Ph.D. Thesis, Universität Stuttgart, 1996.
[11] (a) G.M. Sheldrick, Program System SHELXL-97, Göttingen, Germany, 1997;
(b) W. Herrendorf, H. Bärnighausen, Program HABITUS, Karlsruhe, Germany, 1993.
[12] M.J. Frisch, G.W. Trucks, H.B. Schlegel, G.E. Scuseria, M.A. Robb, J.R. Cheeseman, V.G. Zakrewski, J.A. Montgomery, R.E. Stratmann, J.C. Burant, S. Dapprich, J.M. Millam, A.D. Daniels, K.N. Kudin, M.C. Strain, O. Farkas, J. Tomasi, V. Barone, M. Cossi, R. Cammi, B. Mennuci, C. Pomelli, C. Adamo, S. Clifford, J. Ochterski, G.A. Petersson, P.Y. Ayala, Q. Cui, K. Morokuma, D.K. Malick, A.D. Rabuck, K. Raghavachari, J.B. Foresman, J. Cioslowski, J.V. Ortiz, B.B. Stefanov, G. Liu, A. Liashenko, P. Piskorz, A. Komaromi, R. Gompertz, R.L. Martin, D.J. Fox, T. Keith, M.A. Al-laham, J.Y. Peng, A. Nanayakkara, C. Gonzales, M. Challacombe, P.M.W. Gill, B.G. Johnson, W. Chen, M.W. Wong, J.L. Andres, M. Head-Gordon, E.S. Replogle, J.A. Pople, Gaussian, Inc., Pittsburgh PA, 1998.

few are simple paramagnets [9,10]. That alternating cation–anion arrangement and π–π cation–anion stacking are necessary for observing bulk magnetic order in this class of compound has been demonstrated by some negative examples [9–12] which, although S···S cation–anion contacts are present, are simple paramagnets down to 2 K. Continuing our efforts in this line, we chose another anion based on a much bigger conjugated system containing a tetradentate Schiff base containing five aromatic rings, hoping to increase the π–π interactions and enhance the π–d magnetic exchange. Compared to the anions reported before, $[Cr(NAOP)(NCS)_2]^{2-}$ ($NAOP^{2-} = N,N'$-(1,2-phenylenebis(nitrilomethylidyne))bis-2-naphtholate) is sterically more demanding, more delocalized and has only two isothiocyanates *trans* to each other. Herein, we report the preparation of the precursor complexes, $(Bu_4N)[Cr(NAOP)(NCS)_2]$ (**1**) and $(Bu_4N)[Cr(SALEN)(NCS)_2]\cdot CH_3OH$ (**2**), the crystal structures and magnetic properties of [TTF][Cr(NAOP)(NCS)$_2$] (**3**), [BEDT-TTF][Cr(NAOP)-(NCS)$_2$]$\cdot$ 1.5CH_2Cl_2 (**4**), [HMET][Cr(NAOP)(NCS)$_2$]$\cdot$ 2.5CH_2Cl_2 (**5**) and $[TTF]_3[Cr(SALEN)(NCS)_2]_3\cdot 4CH_2Cl_2\cdot H_2O$ (**6**) (where $NAOP^{2-} = N,N'$-(1,2-phenylenebis (nitrilomethylidyne))bis(2-naphtholate), $SALEN^{2-} = N,N'$-ethylenebis(salicylideneiminate), TTF = tetrathiafulvalene, BEDT-TTF = ethylenedithio(tetrathiafulvalene) and HMET = hydroxymethyl-ethylenedithio(tetrathiafulvalene)). The following scheme shows the structural formulae of the donors and the metal-complex anions.

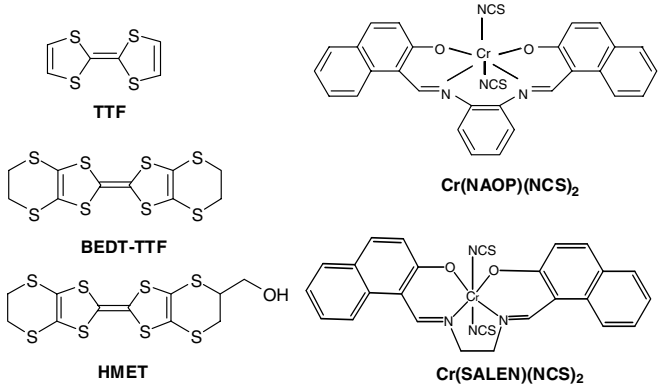

2. Experimental

2.1. Syntheses

All the chemicals were analytical grade and purchased from Aldrich. The Schiff base NAOP-H_2 (*N*,*N*′-bis(2-hydroxy-1-naphthylmethylene)-1,2-phenylenediamine) was prepared by refluxing 2-hydroxy-1-naphthaldehyde and 1,2-phenylenediamine in 2:1 in absolute ethanol. $[Cr(SALEN)(H_2O)_2]Cl$ [13], $(TTF)_3(BF_4)_2$ [14] and HMET [15] were prepared by the published methods.

2.2. Physical measurements

Variable temperature DC magnetization experiments were made with a Quantum Design MPSM1 SQUID magnetometer using randomly orientated polycrystalline material in a gelatine capsule. Magnetization was recorded from 2 to 300 K with an applied field of 100–500 G. Two-probe DC transport measurements were made with an Oxford instruments Mag Lab 2000 equipped with an EP probe. Gold wire electrodes (0.0025 mm diameter) were attached to the crystals using Au paste. Reflective Raman spectra were recorded at room temperature with a Renishaw InVia Raman microscope equipped with a diode laser (785 nm) and a 1200 l/mm grating using a laser power of ca 1 mW. The reported spectra are the result of 20 accumulations of 5 s each. The X-ray diffraction measurements were performed with a Nonius KappaCCD area detector at 120 K using ϕ scans and ω scans to fill asymmetric unit sphere for compounds **3**–**6**. All structures were solved by direct methods using the program SHELXS-97 and refined on F^2 by full-matrix least-squares procedures using SHELXL-97.

2.2.1. $[Cr(NAOP)(H_2O)_2]Cl$

A modification of the procedure described in the Ref. [13] was adapted. To a solution of $CrCl_3\cdot 6H_2O$ (0.01 mol) in ethylene glycol–water–methanol (1:1:3, 100 ml) were added NAOP-H_2 (0.01 mol). After the mixture was heated at 110 °C for about 30 min, sodium carbonate (0.007 mol) was added in small portions to the solution, followed by refluxing the solution for 4 h. On concentrating the solution, a brown precipitate was obtained. The precipitate was recrystallized from methanol to give dark brown crystal of the desirable complex used directly for the next reaction. Yield: 86%. *Anal*. Calc. for $C_{28}H_{22}N_2O_4ClCr$: C, 62.51; H, 4.13; N, 5.21. Found: C, 63.39; H, 4.40; N, 4.77%.

2.2.2. $(Bu_4N)[Cr(NAOP)(NCS)_2]$ (**1**)

The method described for $[Cr(SALEN)(NCS)_2K\cdot H_2O]$ [16] ($SALEN^{2-} = N,N'$-ethylenebis(salicyldeneiminate)) was adapted here. To a methanol solution (100 ml) was added $[Cr(NAOP)(H_2O)_2]Cl$ (0.005 mol) and tetrabutylammonium thiocyanate (0.02 mol). The resulting mixture was refluxed for 4 h with stirring. Some red brown solid was obtained when cooled to room temperature, which was filtered and washed with cold methanol. Dark red brown crystals were obtained after recrystallizing the solid from acetonitrile. Yield: 73%. *Anal*. Calc. for $C_{46}H_{54}N_5O_2S_2Cr$: C, 66.95; H, 6.61; N, 8.49. Found: C, 67.02; H, 6.58; N, 8.49%. IR (KBr, cm^{-1}): 2061s ($\nu_{C\equiv N}$) and 2089m ($\nu_{C\equiv N}$).

2.2.3. $(Bu_4N)[Cr(SALEN)(NCS)_2]\cdot CH_3OH$ (**2**)

The method described for $[Cr(SALEN)(NCS)_2K\cdot H_2O]$ [16] ($SALEN^{2-} = N,N'$-ethylenebis(salicyldeneiminate)) was adapted. To a methanol solution (15 ml) was added $[Cr(SALEN)(H_2O)_2]Cl$ (0.001 mol) and tetrabutylammonium thiocyanate (0.004 mol). The resulting mixture was

refluxed for 4 h with stirring. Red orange crystals were obtained when cooled to room temperature, which was filtered and washed with cold ether. Yield: 83%. *Anal*. Calc. for $C_{35}H_{54}N_5O_3S_2Cr$: C, 59.32; H, 7.63; N, 9.89. Found: C, 59.47; H, 7.48; N, 10.06%. IR (KBr, cm^{-1}): 2078s ($\nu_{C=N}$) and 2102m ($\nu_{C=N}$).

2.2.4. *[TTF][Cr(NAOP)(NCS)$_2$] (3)*

A dilute solution of $(TTF)_3(BF_4)_2$ (12 mg) in hot acetonitrile (40 ml) was filtered and to it was added an acetonitrile solution (10 ml) of $(Bu_4N)[Cr(NAOP)(NCS)_2]$ (25 mg). Storage at room temperature overnight afforded black needle-like crystals of the desired salt. Yield: 64% based on [Cr]. *Anal*. Calc. for $C_{36}H_{22}N_4O_2S_6Cr$: C, 54.93; H, 2.82; N, 7.12. Found: C, 54.55; H, 2.88; N, 7.33%. IR (KBr, cm^{-1}): 2071s ($\nu_{C=N}$).

2.2.5. *[BEDT-TTF][Cr(NAOP)(NCS)$_2$] · 1.5CH$_2$Cl$_2$ (4)*

The charge transfer salt was prepared by in situ oxidation of BEDT-TTF (5 mg), placed in the anode of an H-shaped electrochemical cell. The remainder of the cell was filled with a filtered solution of $(Bu_4N)[Cr(NAOP)(NCS)_2]$ (15 mg) in freshly distilled CH_2Cl_2 (30 ml). 0.5 μA was applied across the cell for a week giving about 1 mg of dark brown needle-like crystals which grew on the anode. *Anal*. Calc. for $C_{40}H_{26}N_4O_2S_{10}Cr$ (corresponding to complete loss of volatile solvent dichloromethane): C, 49.66; H, 2.71; N, 5.79. Found: C, 49.30; H, 2.77; N, 5.53%. IR (KBr, cm^{-1}): 2074s ($\nu_{C=N}$).

2.2.6. *[HMET][Cr(NAOP)(NCS)$_2$] · 2.5CH$_2$Cl$_2$ (5)*

The HMET charge transfer salt was prepared using an identical method to that which gave the BEDT-TTF salt. About 0.5 mg of black needle-like crystals was grown on the anode after twelve days. *Anal*. Calc. for $C_{41.5}H_{28}N_4O_3S_{10}CrCl$ (corresponding to loss of two volatile solvent dichloromethane): C, 48.00; H, 2.70; N, 5.40. Found: C, 48.14; H, 2.84; N, 5.35%. IR (KBr, cm^{-1}): 2077s ($\nu_{C=N}$).

2.2.7. *[TTF]$_3$[Cr(SALEN)(NCS)$_2$]$_3$ · 4CH$_2$Cl$_2$ · H$_2$O (6)*

TTF (10 mg) was placed in the anode of an H-shaped electrochemical cell. The remainder of the cell was filled with a filtered solution of $(Bu_4N)[Cr(SALEN)(NCS)_2]\cdot CH_3OH$ (30 mg) in freshly distilled CH_2Cl_2 (30 ml). 1.5 μA was applied across the cell for three days giving about 0.5 mg of black needle-like crystals which grew on the anode. *Anal*. Calc. for $C_{72}H_{56}N_{12}O_7S_{18}Cr_3$ (corresponding to complete loss of volatile solvent dichloromethane): C, 44.72; H, 2.90; N, 8.70. Found: C, 44.57; H, 2.81; N, 8.53%. IR (KBr, cm^{-1}): 2071s ($\nu_{C=N}$).

3. Results and discussion

3.1. Crystal structures

Single crystals of salts **3**–**6** were found to be suitable for single crystal X-ray diffraction. Standard ORTEP drawings of compound **3** and **4** are shown in Figs. 1, 2 with the atom numbering scheme and 50% thermal ellipsoids. A molecular structure of compound **6** is shown in Fig. 3. The crystal and refinement data are given in Table 1. Selected bond lengths of the donors are listed in Table 2.

The asymmetric unit of **3** contains one $TTF^{+\cdot}$ and one $[Cr(NAOP)(NCS)_2]^-$ (Fig. 1). The Cr atom is six-coordinate with the tetradentate ligand $NAOP^{2-}$ in the equatorial plane and two NCS in the axial positions coordinated via the N atoms. The Cr–N and Cr–O ($NAOP^{2-}$) distances are in good agreement with those observed in other Cr^{III} Schiff base complexes [16] and slightly shorter than those to N of NCS (i.e., Cr1–N1, Cr1–N2, Cr1–O1 and Cr1–O2 are 1.998(3), 2.004(3), 1.936(2) and 1.918(2) Å, respectively, as compared to 2.030(3) and 2.018(3) Å for Cr1–N31 and Cr1–N32, respectively). The bond angles of O1–Cr1–N2 and O2–Cr1–N1 are 173.45(10)° and 173.59(10)°, respectively, showing the Cr atom is slightly displaced from the equatorial plane. The NCS bond angles (175.6(3)–178.8(3)°) are nearly linear, whereas Cr1–N32–C32 (163.2(3)°) is much smaller than Cr1–N31–C31 (176.5(3)°). In $TTF^{+\cdot}$, both the C–S bond lengths (1.712(3)–1.727(3) Å) and C=C bond lengths (C43=C44, C41=C42, C45=C46 are 1.387(4), 1.338(5) and 1.332(5) Å, respectively) are in good agreement with those observed in other $TTF^{+\cdot}$ charge transfer salts [3,4,17].

A crystal packing diagram for compound **3**, showing the *ab*-plane and viewed in the *c*-direction, is given in Fig. 4. The $TTF^{+\cdot}$ and the $[Cr(NAOP)(NCS)_2]^-$ are segregated into layers and linked by hydrogen bonds and van der Waals forces. There is π–π stacking between TTF^+ and the $NAOP^{2-}$ ligand in the *c*-direction. Their planes are nearly parallel, e.g., the one bounded by S41, S43 and S44 makes an angle of 13.32° to the plane C6–C15–C23.

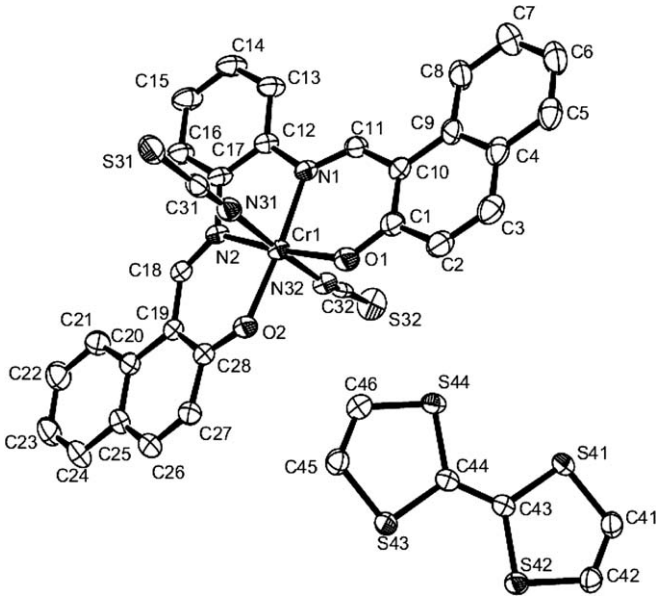

Fig. 1. ORTEP diagram with 50% probability for compound **3**.

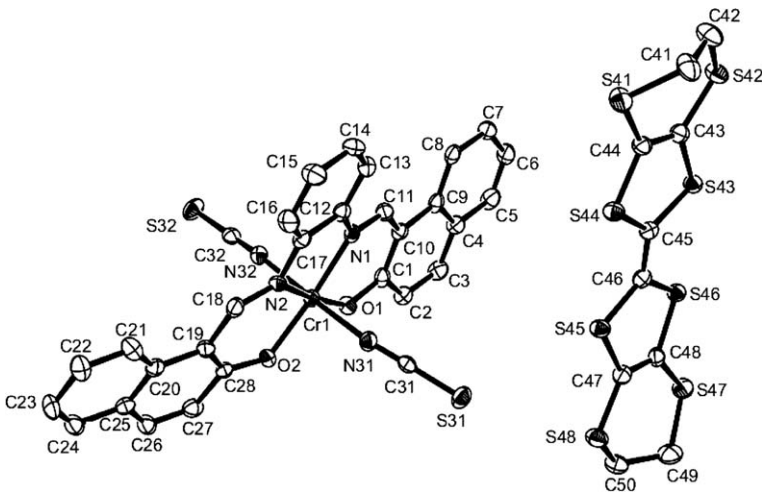

Fig. 2. ORTEP diagram with 50% probability for compound **4**, the solvate dichloromethane molecules and hydrogen atoms have been omitted for clarity.

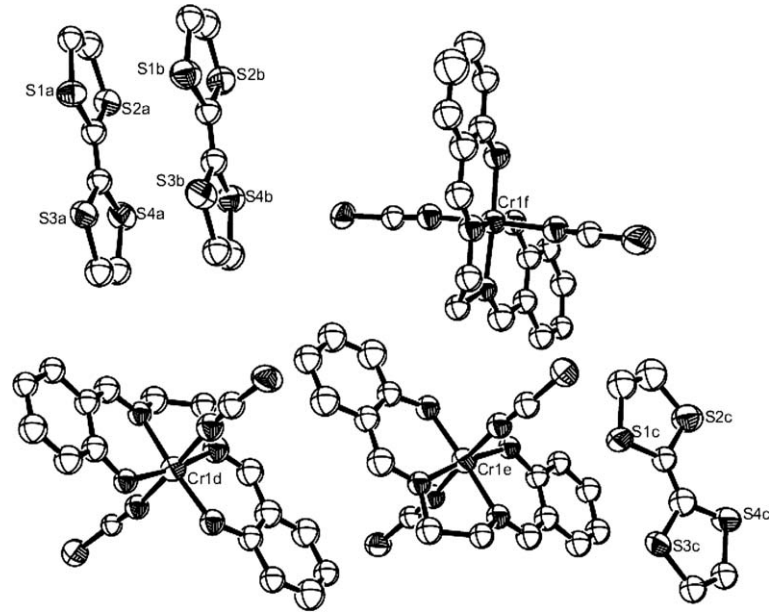

Fig. 3. Molecular structure for compound **6**; only the heavier atoms (Cr, Cl and S) were refined anisotropically. The solvate dichloromethane, water molecules and hydrogen atoms are omitted for clarity.

There are two kinds of S···S close contacts between $TTF^{+\cdot}$ and the anion, one (3.431 Å) between S31 and S41 involving π stacking and another (3.356 Å) between S32 and S42 not involving π stacking, both shorter than the S···S van der Waals distance of 3.6 Å. The $TTF^{+\cdot}$ occur as dimers with inter-cation distances of 3.282 Å (S41···S43) and 3.368 Å (S42···S44) but the shortest S···S distance between the dimers is very long (6.386 Å), much longer than in other TTF salts (4.33 Å) [17]. In addition there are also close S···S contacts between anions (e.g., S31···S31, 3.521 Å) and many other kinds of short contacts, such as weak C14–H14···C31 interactions between the non parallel anions and C–H···S (C16–H16···S32) with H16···S32 of 2.960 Å. The shortest distance between the parallel anions is 3.517 Å but there is no obvious π stacking among them.

Like compound **3**, compound **4** also shows many close contacts between the donor BEDT-TTF and the anion (S31···S43, 3.346 Å; S31···S42, 3.527 Å and S32···S47, 3.425 Å) (Fig. 5). The plane bounded by S44, S45 and S46 makes an angle of 28.78° to the plane C6–C15–C23. Unfortunately, the BEDT-TTF in compound **4** also form dimers with the shortest intermolecular distances of 3.439 Å (S43···S45) and 3.422 Å (S44···S46). From the well-known correlation between C–S and C=C bond lengths and donor charges for BEDT-TTF salts [18], the

Table 1
Crystal and refinement data for compounds **3**–**6**

	3	**4**	**5**	**6**
Formula	$C_{36}H_{22}CrN_4O_2S_6$	$C_{41.50}H_{29}Cl_3CrN_4O_2S_{10}$	$C_{43.5}H_{33}Cl_5CrN_4O_3S_{10}$	$C_{76}H_{64}Cl_{18}Cr_3N_{12}O_7S_{18}$
Formula weight	786.94	1094.64	1209.6	2274.19
Crystal system	monoclinic	orthorhombic	orthorhombic	monoclinic
Space group	$P2_1/c$	*Pbca*	*Pbca*	$P2_1/c$
a (Å)	11.5029(18)	15.4512(13)	15.3546(12)	13.510(3)
b (Å)	17.988(3)	21.546(4)	21.6989(16)	57.434(11)
c (Å)	16.2851(15)	27.380(4)	28.252(2)	13.0413(19)
α (°)	90	90	90	90
β (°)	101.961(10)	90	90	111.137(7)
γ (°)	90	90	90	90
Z	4	8	8	4
V (Å^3)	3296.5(8)	9115(2)	9412.9(12)	9438(3)
D_{calc} (g cm^{-3})	1.586	1.595	1.71	1.600
T (K)	120(2)	120(2)	120(2)	120(2)
λ (Å)	0.71073	0.71073	0.71073	0.71073
μ (mm^{-1})	0.770	0.928	1.02	1.022
F(000)	1608	4456	4920	4624
hkl Range	$-14 \leqslant h \leqslant 14$	$-20 \leqslant h \leqslant 10$	$-19 \leqslant h \leqslant 19$	$-15 \leqslant h \leqslant 16$
	$-23 \leqslant k \leqslant 22$	$-27 \leqslant k \leqslant 27$	$-28 \leqslant k \leqslant 24$	$-68 \leqslant k \leqslant 59$
	$-21 \leqslant l \leqslant 20$	$-16 \leqslant l \leqslant 35$	$-36 \leqslant l \leqslant 36$	$-15 \leqslant l \leqslant 13$
Collected	45857	45529	10504	61736
Unique	7541	4490	7239	15974
Parameters	442	568	594	647
Goodness-of-fit	1.023	1.085	1.162	1.143
R_1 [$I > 2\sigma(I)$]	0.0534	0.0774	0.1600[a]	0.1946[a]
wR_2 [$I > 2\sigma(I)$]	0.1151	0.1175	0.2830[a]	0.3719[a]
(D map) maximum/minimum [e Å^{-3}]	0.782/−0.869	0.596/−0.530	1.294/−1.230	1.193/−0.797

[a] $F_o > 4\sigma(F_o)$.

Table 2
Bond lengths (Å) used for the donor charge calculation for compounds **3**–**5**

3		**4**		**5**	
C41–C42	1.338(5)	C41–C42	1.484(7)	C1–S1	1.82(2)
C41–S41	1.717(3)	C41–S41	1.799(5)	C2–S2	1.756(19)
C42–S42	1.719(3)	C42–S42	1.837(5)	C3–S1	1.754(14)
C43–C44	1.387(4)	C43–C44	1.363(7)	C4–S2	1.743(14)
C43–S41	1.712(3)	C43–S43	1.727(5)	C3–S3	1.738(13)
C43–S42	1.722(3)	C43–S42	1.747(5)	C4–S4	1.760(16)
C44–S43	1.717(3)	C44–S44	1.739(5)	C5–S3	1.697(13)
C44–S44	1.727(3)	C44–S41	1.747(5)	C5–S4	1.713(13)
C45–C46	1.332(5)	C45–C46	1.379(6)	C6–S5	1.745(12)
C45–S43	1.723(3)	C45–S43	1.725(5)	C6–S6	1.747(13)
C46–S44	1.718(3)	C45–S44	1.723(5)	C7–S5	1.757(14)
		C46–S46	1.722(5)	C8–S6	1.767(14)
		C46–S45	1.732(5)	C7–S7	1.745(14)
		C47–C48	1.353(7)	C8–S8	1.728(14)
		C47–S48	1.739(5)	C9–S7	1.847(16)
		C47–S45	1.750(5)	C10–S8	1.82(2)
		C48–S47	1.744(5)	C3–C4	1.340(17)
		C48–S46	1.748(5)	C5–C6	1.375(18)
		C49–C50	1.494(7)	C7–C8	1.344(17)
		C49–S47	1.813(5)	C1–C2	1.31(2)
		C50–S48	1.812(5)	C9–C10	1.34(2)

charge on the BEDT-TTF in **4** can be estimated as 0.9 ± 0.1, which is in agreement with the stoichiometry and Raman data [19]. Furthermore, there are weak C–H···S interactions between the dimerized donors with a C50–H50B···S42 angle of 138.42° and H50B···S42 of 2.991 Å. If we define a plane bounded by C6, C15 and C23 then the anions are parallel to each other with the shortest inter-anion distance being 3.249 Å, similar to compound **3**, but the anions are arranged side by side and there is no π stacking between them. Thus, the 'dimerized' anions and the dimerized donors form a two-dimensional lattice via many kinds of weak interactions (hydrogen bonds and van der Waals forces). Solvent CH_2Cl_2 molecules are situated between the layers.

The crystal structure of compound **5** shows that it is a 1:1 salt, with CH_2Cl_2 molecules included in the lattice. The HMET and anions form a layer structure parallel to the *ab*-plane (Fig. 6). The structure was resolved in the *Pbca* space group, and its overall cell dimensions and structural arrangement closely resemble compound **4**, which could also be solved in the same space group to $R = 7.7\%$. However, in compound **5** the total structure is not as well defined ($R = 16\%$) since there is disorder in the point of attachment of the hydroxymethyl-sidechain. This necessarily affects the positions of the adjacent CH_2Cl_2 molecules, which are also disordered. Nevertheless, it is clear that the HMET donor molecules occur in pairs, face to face, but isolated from other donor molecules. This is the first structure containing the hydroxymethyl-ET molecule.

The unit-cell contents and relative dispositions of the molecules in the crystal of compound **6** were obtained

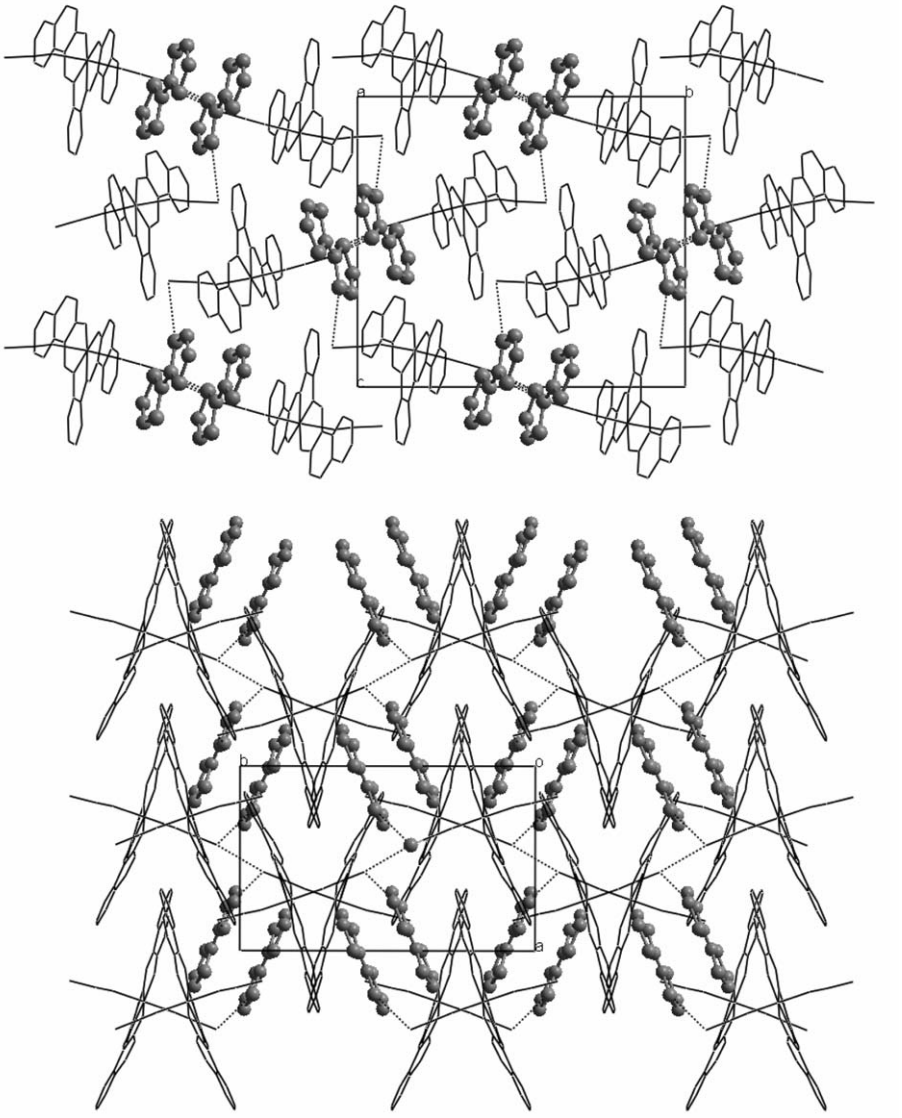

Fig. 4. Crystal packing diagrams for compound **3** viewed in the *a* (top) and *c* (bottom) directions, showing the S···S cation–anion and anion–anion close contacts and the cation dimers.

by single crystal X-ray diffraction. However the quality of the data ($R_{int} = 0.313$) meant that no full refinement was possible and only the heavier atoms (Cr, Cl and S) were refined anisotropically in a model with final *R*-value of 0.1946. It should be noted that the monoclinic *b*-axis is particularly long (57.434 Å). Nevertheless, it is clear that the asymmetric unit contains three $TTF^{+\cdot}$, three $[Cr(SALEN)(NCS)_2]^-$, four CH_2Cl_2 molecules and one disordered H_2O (Fig. 3). In $[Cr(SALEN)(NCS)_2]^-$, the Cr atom is coordinated with the tetradentate ligand $SALEN^{2-}$ in the equatorial plane and two NCS in the axial positions via the N atoms. The Cr–N and Cr–O (of $SALEN^{2-}$) distances are in good agreement with those observed in $[Cr(SALEN)(NCS)_2K \cdot H_2O]$ [16] and $[Cr(NAOP)(NCS)_2]^-$. A crystal packing diagram viewed along the *a*-direction is given in Fig. 7. As is common in this type of compound, the anions and the cations are linked together by many kinds of short contacts and H bonds which include the cation–anion S···S and $S \cdots O_{SALEN^{2-}}$ contacts. All the TTF cations are present as dimers with the shortest S···S distances in the range 3.227–3.394 Å. Compared to $[Cr(NAOP)(NCS)_2]^-$, $[Cr(SALEN)(NCS)_2]^-$ is much smaller in size with less extensive conjugation, which may diminish the possibilities of π–π stacking between the anions. Indeed, in compound **6**, there are no π–π stacking interactions between the anions and the nearest two anions are situated in the opposite positions. Finally, as shown in Fig. 7, the dimerized $TTF^{+\cdot}$ and the two nearest anions are arranged alternately and propagate approximately along the *b*-direction.

3.2. Magnetic properties

As was expected from the structures, no long-range magnetic ordering was observed down to 2 K among

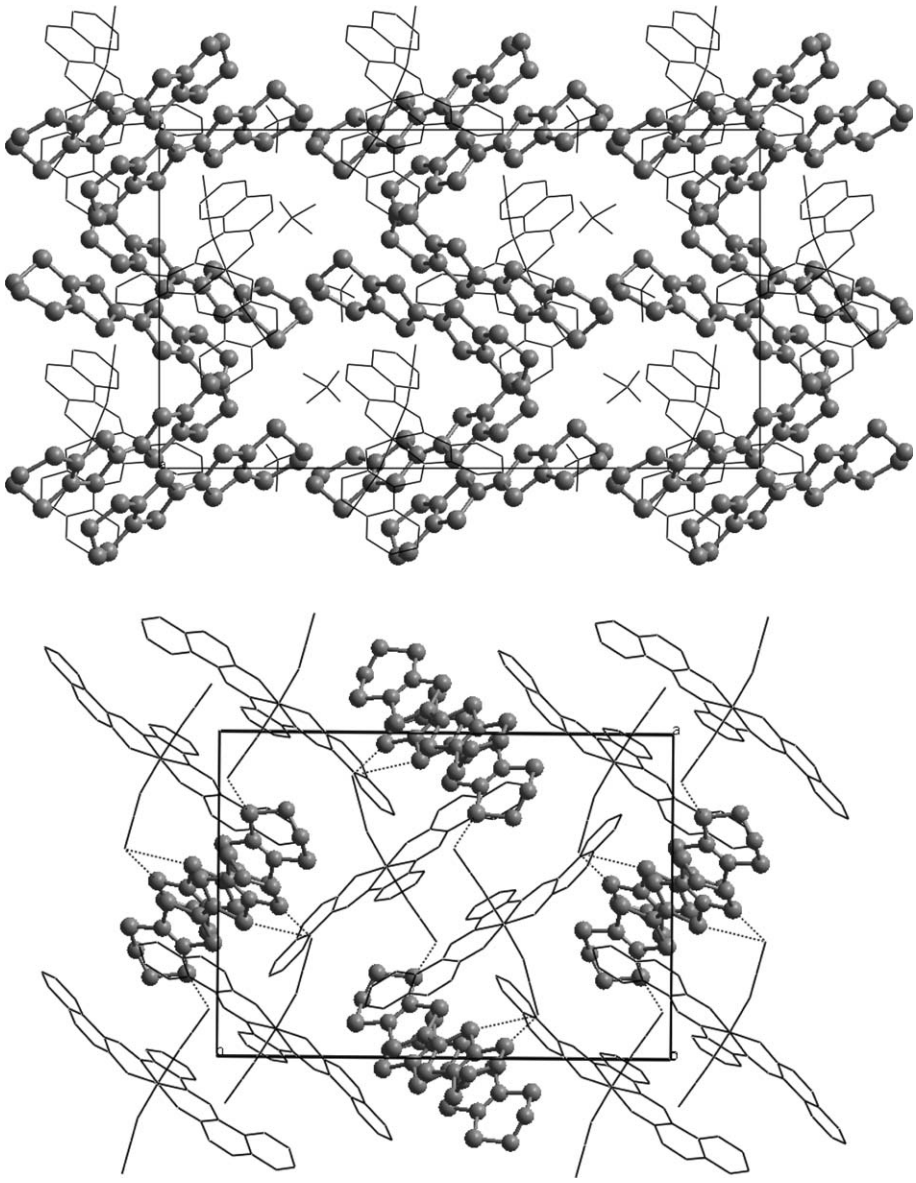

Fig. 5. Crystal packing diagram for compound **4** viewed in the *a*-direction, showing the cation–anion layered structure and dichloromethane molecules are situated between the layers (top); one layer viewed in the *c*-direction showing the S···S contacts between the donor and the anion (bottom).

all these charge transfer salts due to the lack of alternating cation–anion π–π contacts. Table 3 gives details of the Curie and Weiss constants of these compounds, determined from fits to the Curie–Weiss law $\chi_m = C/(T-\theta)$ from 2 to 300 K. The magnetic susceptibility of compound **3** is typical of a simple paramagnet (Fig. 8). The temperature variation of χ_m^{-1} follows the Curie–Weiss law over the whole temperature range with a Curie constant of 1.79 emu mol^{-1} K and a very small Weiss constant of +0.11 K. The C value is slightly lower than the spin-only value of 1.875 emu mol^{-1} K expected for one magnetically isolated Cr^{III} ($S = 3/2$) and the low temperature magnetization is dominated by the individual metal centers of the anions. For compounds **4**–**6**, the Weiss constants (−1.2 to −1.4 K) indicate the presence of weak antiferromagnetic interactions between the anions.

Two-probe DC transport measurements were made on compounds **3**–**6**. As expected, none of the compounds is a conductor; they are insulators with room temperature resistance higher than the largest that could be measured with the instrumentation (10^9 Ω).

3.3. Raman spectroscopy

Reflective Raman spectroscopy is used as a rapid means for determining or confirming the charge on the donor molecule by comparing the ν_3 and ν_4 of the symmetrical

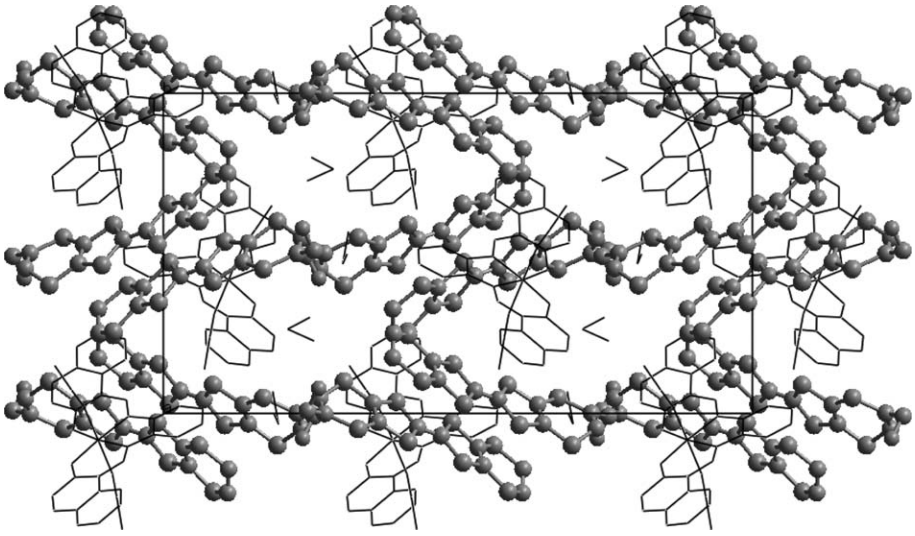

Fig. 6. Crystal packing diagram for compound **5** viewed in the *b*-direction, showing the layer stacking and dichloromethane molecules are situated between the layers. Only one orientation is shown for the donor and each solvent molecule.

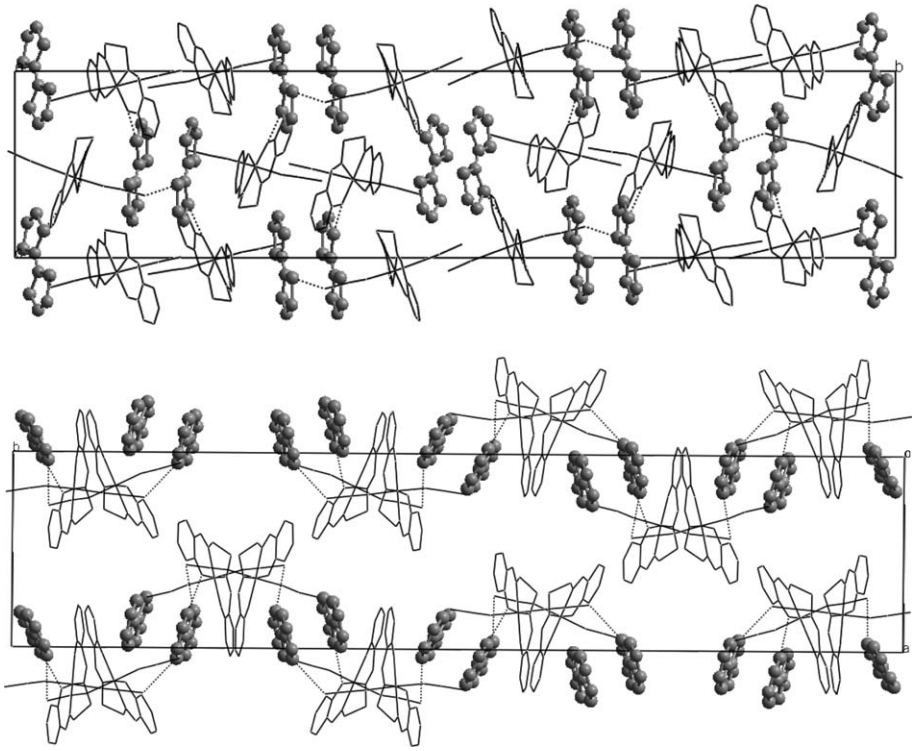

Fig. 7. Crystal packing diagram for compound **6** viewed in the *a* (top) and *c* (bottom) directions, showing the S···S and S···O ($SALEN^{2-}$) close contacts between the donor and the anion.

central C=C bond in the range of 1400–1480 cm^{-1} [19]. Compound **4** shows two peaks at 1420.9 and 1450.9 cm^{-1} and two weak and broad peaks are at 1535.7 and 1574.5 cm^{-1}. The two prominent peaks correspond to a charge of +0.9, which agrees well with that calculated from bond lengths for the donor ET^{+} in **4**. For compound **5**, there are two very prominent peaks at 1414 (ν_4) and 1456.1 (ν_3) cm^{-1} and three very weak peaks at 1533.0, 1575.2 and 1601.8 cm^{-1}. Using the formula in [19], the calculated charge of the TTF is +1.0, in agreement with the value 1.0 ± 0.1 from the bond length–charge correlation [18] and the stoichiometry.

Table 3
Curie and Weiss constants for compounds **3**–**6**

	3	**4**	**5**	**6**
Curie constant, C (emu mol^{-1} K)	1.79	1.79	1.80	1.85
Weiss constant, θ (K)	0.11	−1.4	−1.2	−1.3

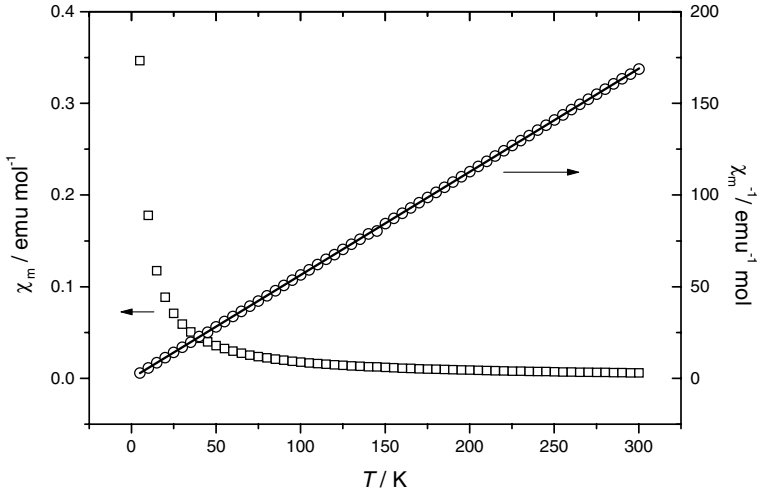

Fig. 8. Plots of temperature dependence of χ_m (open squares) and χ_m^{-1} (open circles) measured at 500 G field for **3**; the solid line represents the best fit to Curie–Weiss law from 2 to 300 K for χ_m^{-1}.

4. Conclusions

We have described the synthesis of two precursors, $(Bu_4N)[Cr(NAOP)(NCS)_2]$ and $(Bu_4N)[Cr(SALEN)(NCS)_2]\cdot CH_3OH$, and the synthesis and crystal structures of four new charge transfer salts with stoichiometry [donor][Cr(SA)(NCS)$_2$] where SA = $NAOP^{2-}$ for donor = TTF, ET and HMET and SA = $SALEN^{2-}$ for donor = TTF. Anions $[Cr(NAOP)(NCS)_2]^-$ and $[Cr(SALEN)(NCS)_2]^-$ which have a tetradentate Schiff base in the equatorial plane and two isothiocyanates *trans* to each other are different from $[M(phen)(NCS)_4]^-$ and [M(isoquinoline)$(NCS)_4]^-$ (M = Cr or Fe) both in shape and size. Some charge transfer salts which contain the latter anions and various donors have been proved to show long-range π–d ferrimagnetic ordering at low temperature because of the alternating cation–anion arrangement in at least two directions. As for $[Cr(NAOP)(NCS)_2]^-$, increasing the size of the donor from TTF to ET and HMET was not sufficient to inhibit dimerization of the cations, with loss of the cation moment, and formation of alternating cation–anion stacks. It could mean that the shape of this anion plays an important role in directing the final crystal structures or it might be worth trying some bigger donors with more rings and more sulphur atoms.

It is not easy to find common features among the structures of this family of Schiff-base charge transfer salts; nevertheless with TTF as the donor, the structures do all contain alternate stacks consisting of segregated cations and anions with the $TTF^{+\cdot}$ separated clearly from the anions because of its smaller size. With ET and HMET, however, cations and anions are interleaved. To explore the crystal chemistry of the charge transfer salts containing this class of anion further, and in an effort to match the donor cation size with that of the anions, we chose $[Cr(SALEN)(NCS)_2]^-$ which is smaller and contains three fewer aromatic rings than $[Cr(NAOP)(NCS)_2]^-$. However the TTFs in $[TTF]_3[Cr(SALEN)(NCS)_2]_3\cdot 4CH_2Cl_2\cdot H_2O$ are also present as dimers. The arrangement of the donors and anions is quite similar to that in [TTF][Cr(NAOP)(NCS)$_2$]. It seems probable that it is primarily the overall shape of the anion that determines the arrangement of the anions and cations in the final structures. Summarizing, the challenge in designing new charge transfer salts with long-range π–d ferrimagnetic order remains open. From the crystal engineering point of view, the compounds described here should provide useful information for further design and investigation on this elusive class of π–d magnets.

Acknowledgements

This work has been supported in part by the UK Engineering and Physical Sciences Research Council. Shi Wang wishes to thank the Royal Society for a postdoctoral fellowship at the Royal Institution. We are grateful to Drs. Lee Martin and Simon Carling for assistance with the measurements and useful discussions. The Royal Institution group is part of the European Commission Framework 6 Programme Network of Excellence MAGMANet.

Appendix A. Supplementary material

Crystallographic data have been deposited with the Cambridge Crystallographic Center, CCDC Nos. 295734, 295735, 295736 and 295737. Copies of this information may be obtained free of charge from The Director, CCDC, 12 Union Road, Cambridge, CB2 1EZ, UK (fax: +44 1223 336 033; email: deposit@ccdc.cam.ac.uk or www:http://www.ccdc.cam.ac.uk). Supplementary data associated with this article can be found, in the online version, at doi:10.1016/j.poly.2006.03.010.

References

[1] J.M. Williams, J.R. Ferraro, R.J. Thorn, K.D. Carlson, U. Geiser, H.H. Wang, A.M. Kini, M.-H. Whangbo, Organic Superconductors (Including Fullerenes) Synthesis, Structure, Properties, Theory, Prentice-Hall, New Jersy, 1992.

[2] S.S. Turner, P. Day, J. Mater. Chem. 15 (2005) 23, and the references therein.

[3] S.S. Turner, C. Michaut, S. Durot, P. Day, T. Gelbrich, M.B. Hursthouse, J. Chem. Soc., Dalton Trans. (2000) 905.

[4] S.S. Turner, D.L. Pévelen, P. Day, K. Prout, J. Chem. Soc., Dalton Trans. (2000) 2739.

[5] F. Setifi, S. Golhen, L. Ouahab, A. Miyazaki, K. Okabe, T. Enoki, T. Toita, J. Yamada, Inorg. Chem. 41 (2002) 3786.

[6] M. Mas-Torrent, S.S. Turner, K. Wurst, J. Vidal-Gancedo, X. Ribas, J. Veciana, P. Day, C. Rovira, Inorg. Chem. 42 (2003) 7544.

[7] F. Setifi, L. Ouahab, S. Golhen, A. Miyazaki, T. Enoki, J. Yamada, C. R. Chim. 6 (2003) 309.

[8] S.S. Turner, S.G. Carling, P. Day, C.J. Gómez-Garcia, E. Coronado, J. Phys. IV (Paris) 114 (2004) 585.

[9] F. Setifi, S. Golhen, L. Ouahab, S.S. Turner, P. Day, Cryst. Eng. Commun. 4 (2002) 1.

[10] F. Setifi, A. Ota, L. Ouahab, S. Golhen, H. Yamochi, G. Saito, J. Solid State Chem. 168 (2002) 450.

[11] S.S. Turner, P. Day, T. Gelbrich, M.B. Hursthouse, J. Solid State Chem. 159 (2001) 385.

[12] S.S. Turner, D.L. Pévelen, P. Day, K. Prout, J. Solid State Chem. 168 (2002) 573.

[13] S. Yamada, K. Iwasaki, Inorg. Chim. Acta 5 (1971) 3.

[14] F. Wudl, J. Am. Chem. Soc. 97 (1975) 1962.

[15] (a) F. Leurquin, T. Ozturk, M. Pilkington, J.D. Wallis, J. Chem. Soc., Perkin Trans. 1 (1997) 3173;
(b) T. Ozturk, N. Saygili, S. Ozkara, M. Pilkington, C.R. Rice, D.A. Tranter, F. Turksoy, J.D. Wallis, J. Chem. Soc., Perkin Trans. 1 (2001) 407;
(c) N. Saygili, R.J. Brown, P. Day, R. Hoelzl, P. Kathirgamanathan, E.R. Mageean, T. Ozturk, M. Pilkington, M.M.B. Qayyum, S.S. Turner, L. Vorwerg, J.D. Wallis, Tetrahedron 57 (2001) 5015.

[16] H. Li, Z.J. Zhong, X.-Z. You, W. Chen, Polyhedron 16 (1997) 1119.

[17] B. Zhang, Z. Wang, H. Fujiwara, H. Kobayashi, M. Kurmoo, K. Inoue, T. Mori, S. Gao, Y. Zhang, D. Zhu, Adv. Mater. 17 (2005) 1988.

[18] P. Guionneau, C.J. Kepert, G. Bravic, D. Chasseau, M.R. Truter, M. Kurmoo, P. Day, Synth. Met. 86 (1997) 1973.

[19] H.H. Wang, J.R. Ferraro, J.M. Williams, U. Geiser, J.A. Schlueter, J. Chem. Soc., Chem. Commun. (1994) 1893.

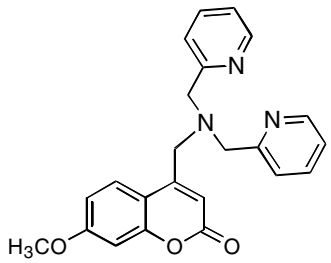

1

A large number of fluorescent PET sensors that follow the basic design principle of a chromophore-spacer-receptor architecture have been reported to date [4]. The signaling process of these sensors depends on a molecular recognition event to inhibit, or initiate PET between a covalently linked chromophore and a receptor, leading to the generation (off–on), or quenching (on–off) of fluorescence. The role of the saturated spacer unit in these assemblies is to preserve the independence of the chromophore and the receptor in the electronic ground state.

The modular nature of this design has led to the development of a large number of molecules that are capable of functioning as sensors for a variety of cations. We have previously reported a fluorescent PET sensor based on the bis-(2-picolyl)amine receptor, that is capable of generating a fluorescence signal upon binding zinc ions [5]. In this paper we report a new sensor that is based on a coumarin chromohore and the same receptor, and also extend our cation binding studies to several transition and post transition metal ions [6].

The PET process responsible for the signaling in **1**, occurs from the receptor (tertiary amine) to the excited chromophore (coumarin), quenching the fluorescence of the coumarin. The driving force for this process (ΔG_{et}) can be expressed by modified Weller equation as follows:

$$\Delta G_{et} = -E_s - E_{red.chrom} + E_{ox.receptor},$$

where E_s, $E_{red.chrom}$ and $E_{ox.receptor}$ are the singlet energy, reduction potential of the chromophore and the oxidation potential of the receptor, respectively [4]. An increase in the oxidation potential of the receptor, caused by the binding of a cation, will increase the ΔG_{et}, which will decrease and eventually quench the PET process. This in turn will allow the excited chromophore to relax by fluorescence, and will result in the generation of a fluorescent signal in **1** due to cation binding.

2. Experimental

Nuclear magnetic resonance spectra were recorded on a Bruker Avance 300/300MHz FT-NMR Spectrometer. All NMR spectra were obtained in $CDCl_3$ at room temperature and the chemical shifts are reported in δ values (ppm) relative to TMS. High Resolution mass spectra were obtained at the Mass Spectrometry Service Laboratory at the Department of Chemistry, University of Minnesota. Elemental analysis was carried out at Robertson-Microlit Laboratories, Madison, New Jersey. Ultraviolet and visible spectra were recorded on Cary 300 Bio UV–Vis Spectrophotometer and Agilent 8453 Spectrophotometers. Excitation and emission spectra were recorded on a Cary Eclipse Fluorescence Spectrophotometer. Cation binding studies were carried out in anhydrous acetonitrile using metal perchlorate salts. Ionic strength of all solutions was maintained at 0.1 M using sodium perchlorate. (*Warning! Metal perchlorate salts are potentially explosive; the isolated salts should never be dried and should not be subjected to shock!*).

2.1. 4-[(Bis(pyridin-2-ylmethyl)amino)methyl]-7-methoxychromen-2-one (1)

A mixture of 4-(bromomethyl)-7-methoxycoumarin (1.102 g, 4.095 mmol), 2,2′dipicolylamine (0.808 g, 4.095 mmol), triethylamine (0.816 g, 8.08 mmol) in ethanol (77 mL) was refluxed for two days. After cooling to room temperature, dichloromethane (30 mL) was added and the mixture was washed with 3 M hydrochloric acid (4×30 mL). The aqueous layer was neutralized with sodium carbonate and extracted into dichloromethane (50 mL). The organic layer was dried over magnesium sulfate, filtered, and evaporated to give an oily residue. Purification by column chromatography (silica: methanol/ethyl acetate 5:95) gave **1** as a viscous residue (1.01 g, 53%). ^{1}H NMR ($CDCl_3$): δ 8.35–8.30 (m, 2H), 7.50–7.25 (m, 5H), 7.00–6.90 (m, 2H), 6.60–6.50 (m, 2H), 6.42 (s, 1H), 3.71 (s, 4H), 3.69 (s, 2H), 3.61 (s, 3H). ^{13}C NMR ($CDCl_3$): δ 161.96, 160.77, 157.89, 154.94, 152.62, 148.63, 136.09, 125.18, 122.63, 121.84, 111.71, 111.44, 110.92, 100.27, 60.01, 55.17, 54.16. HRMS (ESI) for $C_{23}H_{21}N_3O_3$ (M + Na) calculated 410.1475, found 410.1475. *Anal.* Calc. for $C_{23}H_{21}N_3O_3$: C, 71.29; H, 5.47; N, 10.85. Found: C, 71.02; H, 6.16; N, 10.87%.

3. Results and discussion

The fluorescence of **1** is quenched due to the thermodynamically favored PET between the tertiary amine and the excited chromophore. Increasing the oxidation potential of the tertiary amine due to cation binding prevents this PET and regenerates the fluorescence of the chromophore [5]. Three metal ions, Zn^{2+}, Cd^{2+} and Pb^{2+} show a significant fluorescence enhancement of **1**. No fluorescence enhancement was observed with Hg^{2+}, Ag^{+} and Cu^{2+}. The Job's plot data indicated that the ligand:metal binding ratio is 1:1 (see Figs. 1 and 2).

Sensor **1**, when dissolved in acetonitrile showed two peaks at 262 and 321 nm on the UV–Vis spectrum. On binding of Zn^{2+}, Cd^{2+} and Pb^{2+}, the peak at 262 nm remained the same while a small bathochromic shift was observed for the peak at 321 nm. For Cd^{2+} and Zn^{2+}, the new peak was observed at 328 nm while for lead it was 331 nm. This indicates the possibility of an interaction

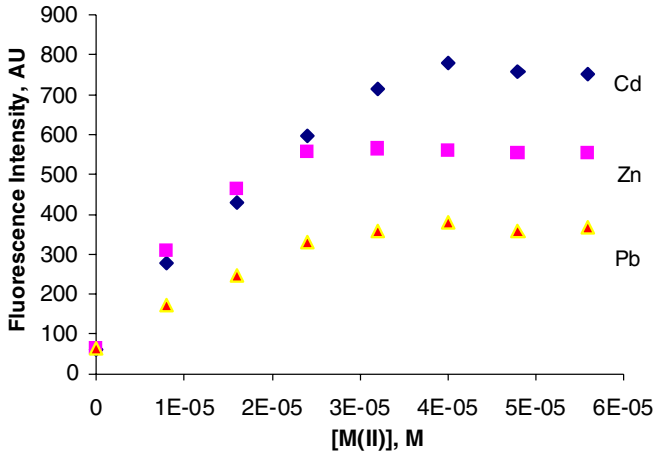

Fig. 1. Fluorescence intensity (I_f) of **1** (4.0×10^{-5} M) vs. metal ion concentration (0–5.6×10^{-5} M) in acetonitrile ($\lambda_{ex} = 330$, $\lambda_{em} = 410$ nm).

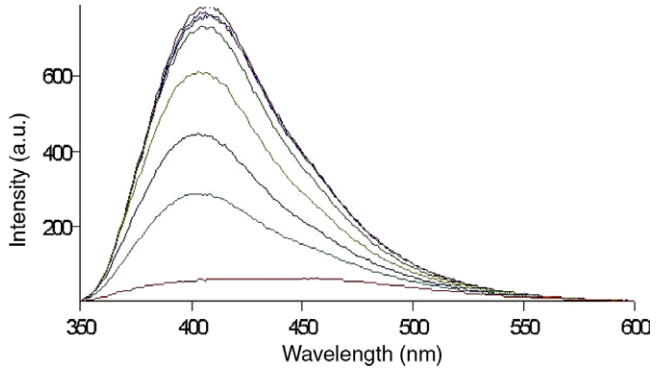

Fig. 2. Fluorescence emission spectra of **1** (4.0×10^{-5} M) with 0, 0.8, 1.6, 2.4, 3.2, 4.0, 4.8, 5.6 ($\times 10^{-5}$ M) of [Cd^{2+}] (in order of increasing intensity) in acetonitrile ($\lambda_{ex} = 330$ nm, $\lambda_{em} = 350$–600 nm).

between the metal bound ligand and the coumarin. The extinction coefficients (ε) of Zn^{2+}, Cd^{2+} and Pb^{2+} complexes were found to be 9434, 9832, 11 977 cm^{-1} M^{-1}, respectively.

Similar shifts attributed to the formation of charge transfer complexes between the cation bound receptor and the chromophore are documented [4a]. The binding constants ($\log \beta$) for these metal ions with **1** were measured, and found to be 6.10 ± 0.4, 6.37 ± 0.3, and 5.67 ± 0.3, respectively [7]. These values calculated from fluorescence measurements are in agreement with binding constants reported in the literature [5,6,11]. These results also indicate that **1** preferentially binds cadmium over zinc or lead.

Cadmium and lead are toxic heavy metal pollutants in the environment. It is believed that much of the physiological action of cadmium arises from its chemical similarity to zinc [8]. Specifically, cadmium may replace zinc in some zinc enzymes, thereby altering the stereostructure of the enzyme and impairing its catalytic activity [8]. Lead poisoning is one of the most common pediatric health problems in the US [9], and in particular in New York City. These factors make the detection and quantification of cadmium and lead in the environment a significant area of research.

Zinc is an integral part of many biologically important enzymes [10]. Interestingly, the adverse effects of both cadmium and lead are known to arise due to their ability to replace zinc from zinc-binding enzymes. Therefore, we were interested in comparing the binding properties of **1** with all three cations in order to compare its binding and sensing preference. We have observed that **1** preferentially binds cadmium over zinc or lead and we plan to carry out further studies to investigate this observation. Although there are many elegant examples of zinc [6a,6b,11] and lead [12] sensors reported to date, there are only a very few cadmium sensors reported [4d,13].

In summary, we have presented a fluorescent PET sensor that can function as a fluorescent off–on switch for Zn^{2+}, Cd^{2+}, and Pb^{2+}. Importantly, this cation sensor shows preferential binding and sensing for Cd^{2+}. The coumarin chromophore is expected to make this sensor more cell permeable than our previous sensor based on an anthracene chromophore. We are currently working on fluorescent PET sensors that would be more selective towards these cations, and more water soluble. We also hope to evaluate the signaling capabilities of these sensors in vivo.

Acknowledgements

This work was supported by PSC-CUNY Grants 66400-00 35, 67875-00 36 and Montclair Sate University. We thank Dr. J.L. Isidor for obtaining NMR spectra.

References

[1] Y.E. Spichiger-Keller, US-Sensors and Biosensors for Medical and Biological Applications, Wiley-VCH, New York, 1998.
[2] C.F. Mason, Biology of Freshwater Pollution, 2nd ed., Longman, New York, 2002.
[3] (a) A.P. de Silva, N.D. McClenaghan, Chem. Eur. J. 10 (2004) 574;
(b) A.P. de Silva, B. McCaughan, B.O.F. McKinney, M. Querol, J. Chem. Soc., Dalton Trans. (2003) 1902;
(c) R. Martinez-Manez, F. Sancenon, Chem. Rev. 103 (2003) 4419;
(d) T.D. James, S. Shinkai, Top. Curr. Chem. 218 (2002) 159;
(e) W. Wang, X. Gao, B. Wang, Curr. Org. Chem. 6 (2002) 1285;
(f) R. Ballardini, V. Balzani, A. Credi, M.T. Gandolfi, M. Venturi, Acc. Chem. Res. 34 (2001) 445;
(g) S.L. Wiskur, H. Ait-Haddou, J.J. Lavigne, E.V. Anslyn, Acc. Chem. Res. 34 (2001) 963.
[4] (a) A.P. de Silva, D.B. Fox, A.J.M. Huxley, T.S. Moody, Coord. Chem. Rev. 205 (2000) 41;
(b) A.P. de Silva, H.Q.N. Gunaratne, T. Gunnlaugsson, A.J.M. Huxley, C.P. McCoy, J.T. Rademacher, T.E. Rice, Chem. Rev. 119 (1997) 7891;
(c) A.J. Bryan, A.P. de Silva, S.A. de Silva, R.A.D.D. Rupasinghe, K.R.A.S. Sandanayake, Biosensors 4 (1989) 169;
(d) T. Gunnlaugsson, T.C. Lee, R. Parkesh, Tetrahedron 60 (2004) 11239.
[5] (a) S.A. de Silva, A. Zavaleta, D.E. Baron, O. Allam, E.V. Isidor, N. Kashimura, J.M. Percarpio, Tetrahedron Lett. 38 (1997) 2237;
(b) S.A. de Silva, M.L. Kasner, M.A. Whitener, S.L. Pathirana, Int. J. Quantum Chem. 100 (2004) 753.

[6] (a) Several fluorescent sensors for zinc ions based on the bis-(2-picolyl)-amine receptor have been reported recently: G.K. Walkup, S.H. Burdette, S.J. Lippard, R.Y. Tsien, J. Am. Chem. Soc. 122 (2000) 5644;
(b) S.C. Burdette, C.J. Frederickson, W. Bu, S.J. Lippard, J. Am. Chem. Soc. 125 (2003) 1778;
(c) Several fluorescent sensors for zinc ions based on the coumarin chromophore, including one that utilizes a bis-(2-picolyl)-amine were reported recently: N.C. Lim, J.V. Schuster, M.C. Porto, M.A. Tandura, L. Yao, H.D. Freake, C. Bruckner, Inorg. Chem. 44 (2005) 2018;
(d) N.C. Lim, L. Yao, H.C. Freake, C. Bruckner, Biorg. Med. Chem. Lett. 13 (2003) 2251.
[7] (a) Calculated according to: A.P. de Silva, H.Q.N. Gunaratne, G.E.M. Maguire, J. Chem. Soc., Chem. Commun. (1994) 1213;
(b) A.P. de Silva, K.R.A.S. Sandanayake, J. Chem. Soc., Chem. Commun. (1989) 1183.
[8] S.E. Manahan, Environmental Chemistry, 8th ed., CRC Press, New York, 2005.
[9] H.A. Godwin, Curr. Opin. Biol. Chem. 5 (2) (2001) 223.
[10] A.S. Prasad, Biochemistry of Zinc, Plenum Press, New York, 1993.
[11] (a) T. Hirano, K. Kikuchi, Y. Urano, T. Higuchi, T. Nagano, J. Am. Chem. Soc. 122 (2000) 12399;
(b) J. Wang, Y. Xiao, Z. Zhang, X. Qian, Y. Yang, Q. Xu, J. Mater. Chem. 15 (2005) 2839;
(c) S.C. Burdette, S.J. Lippard, Inorg. Chem. 41 (2002) 6816;
(d) P. Wang, N. Onozawa-Komatsuzaki, Y. Himeda, H. Sugihara, H. Arakawa, K. Kasuga, Tetrahedron Lett. 42 (2001) 9199;
(e) G. Xue, J.S. Bradshaw, N.K. Dalley, P.B. Savage, R.M. Izatt, L. Prodi, M. Montalti, N. Zaccheroni, Tetrahedron 58 (2002) 4809;
(f) H.A. Godwin, J.M. Berg, J. Am. Chem. Soc. 118 (1996) 6514;
(g) K. Kubo, A. Mori, J. Mater. Chem. 15 (2005) 2902.
[12] (a) J.Y. Kwon, Y.J. Jang, Y.J. Lee, K.M. Kim, M.S. Seo, W. Nam, J. Yoon, J. Am. Chem. Soc. 127 (2005) 10107;
(b) S. Deo, H.A. Godwin, J. Am. Chem. Soc. 122 (2000) 174.
[13] (a) L. Prodi, M. Montalti, N. Zaccheroni, J.S. Bradshaw, R.M. Izaat, P.B. Savage, Tetrahedron Lett. 42 (2001) 2941;
(b) T. Gunnlaugsson, T.C. Lee, R. Parkesh, Tetrahedron 60 (2004) 11239;
(c) A.M. Costero, R. Andreu, E. Monrabal, R. Martinez-Manez, F. Sancenon, J. Soto, J. Chem. Soc., Dalton Trans. (2002) 1769;
(d) L. Prodi, F. Boletta, M. Montalti, N. Zaccheroni, Eur. J. Inorg. Chem. 3 (1999) 455;
(e) M.E. Huston, C. Engleman, A.W. Czarnik, J. Am. Chem. Soc. 112 (1990) 7054;
(f) N. Ertas, E.U. Akkkaya, O.Y. Ataman, Talanta 51 (2000) 693;
(g) S. Charles, S. Yunus, F. Dubois, E. Vander Donckt, Anal. Chim. Acta 440 (2001) 37;
(h) M. Choi, M. Kim, K.D. Lee, K.N. Han, I.A. Yoon, H.J. Chung, J. Yoon, Org. Lett. 3 (2001) 3455.

peptide O atom to a third copper(II) ion. Only in the Cu(II) complexes with glycyl-amino acid dipeptides, 1:1 and 1:2 metal:ligand stoichiometries have been found, showing monomeric and dimeric compounds [16,17]. When the dipeptides contain side chains with additional donor atoms, such as histidine, those groups also participate in the coordination [18,19]. However, there is still lack of systematic studies.

On the other hand, the structure of copper complexes in solution is an issue that has not received proper attention, especially in the case of labile metal complexes such as those of copper(II). Relevant to the rationalization of the molecular structure–biological activity relationship in solution, is the atomic-resolution information provided by solid state structural determinations. In spite of the fact that there are several studies that present stability constant data and stoichiometry of the species in solution [2,3], it is necessary to have additional structural data before inferring the structures in solution from their crystal counterpart. In fact, there are some antecedents where combined potentiometric and EPR studies were instrumental in disclosing the molecular structure of species in solution.

As a continuation to our studies of copper(II) complexes with amino acids [20–22] and oligopeptides [10,11,23], the synthesis, analytical, structural and spectroscopic characterization of four new Cu(II) dipeptide complexes with gly-val, val-gly, val-phe and phe-phe as ligands are described in this work. The crystallographic analyses of the four Cu(II) complexes are presented. A preliminary characterization of their structures in solution, based on EPR and electronic spectroscopic techniques is also reported.

2. Experimental

2.1. Synthesis of the complexes and analytical characterization

The copper (II) complexes of stoichiometry [Cu(L-dipeptide)] · nH$_2$O were obtained by adding 0.15 mmol of CuCO$_3$ to 5 mL of an aqueous solution containing 0.1 mmol of dipeptide (dipeptide: L-gly-L-val, L-val-L-gly, L-val-L-phe, L-phe-L-phe, SIGMA). After stirring, the remaining excess of carbonate was filtered off and the obtained blue solution was concentrated by slow evaporation until the formation of crystals. They were separated by filtration and washed with small portions of a 1:2 water:acetone mixture. In all the studied complexes, the yield of the reactions was about 70%.

The composition of the complexes was confirmed by elemental analysis. *Anal.* Calc. for [Cu(gly-val)] · $\frac{1}{2}$H$_2$O (C$_7$H$_{13}$N$_2$O$_{3.5}$Cu): C, 34.35; H; 5.35; N, 11.45. Found: C, 34.52; H, 5.53; N, 11.51%. *Anal.* Calc. for [Cu(val-gly)] (C$_7$H$_{12}$N$_2$O$_3$Cu): C, 35.67; H, 5.13; N, 11.88. Found: C, 35.92; H, 5.58; N, 11.96%. *Anal.* Calc. for [Cu(val-phe)] (C$_{14}$H$_{18}$N$_2$O$_3$Cu): C, 51.60; H, 5.57; N, 8.60. Found: C, 51.96; H, 6.01; N, 8.60%. *Anal.* Calc. for [Cu(phe-phe)] (C$_{18}$H$_{18}$N$_2$O$_3$Cu): C, 57.82; H, 4.85; N, 7.49. Found: C, 57.42; H, 4.76; N, 7.57%.

2.2. Spectroscopic measurements

Electronic absorption spectra were recorded on aqueous solutions of the complexes with a Milton Roy Spectronic 3000 spectrophotometer, employing 1 cm quartz cells.

FTIR spectra, in the range between 4000 and 200 cm^{-1}, were measured as KBr pellets on a BOMEN MB 102 instrument.

2.3. Crystal structure determination

The X-ray diffraction data were collected on an Enraf-Nonius Kappa-CCD diffractometer with graphite-monochromated Mo Kα radiation ($\lambda = 0.71073$ Å). Bragg reflections were collected up to 50° in 2θ, with a redundancy of 4 in all cases. The final unit cell parameters were determined by least-squares refinement of the angular settings for all collected reflections. The measurements were performed at low temperature, which was controlled with an Oxford Cryosystem device. Data collections were made using the COLLECT program [24]; integration and scaling of the reflections were performed with the HKL DENZO-SCALEPACK system of programs [25]. Absorption corrections were carried out using the multi-scan method [26]. The structures were solved using direct methods with SHELXS-97 [27]. The models were refined by full-matrix least-squares procedures on F^2 using SHELXL-97 [28]. The H atoms of the phenyl and methyl groups were positioned stereo chemically and refined with fixed individual displacement parameters [U_{iso}(H) = 1.2U_{eq}(C) or 1.5U_{eq}(C$_{methoxy}$)] using the SHELXL riding model with C–H length ranging from 0.93 to 0.98 Å. The WINGX program was used to analyze and prepare the data for publication [29]. The ORTEP3 for Windows [30] was used to prepare the molecular graphics. Crystal data, data collection procedures, structure determination methods and refinement results are summarized in Table 1.

2.4. EPR measurements

X-band (9.5 GHz) EPR measurements were carried out on aqueous solutions both at room temperature and at 77 K (as frozen solutions), and on solid samples at 77 K, using a Varian E109 spectrometer and cavities with 100 kHz field modulation. The g-values were obtained from spectral simulations using the QPOW [31,32] and the SimFonia [33] programs.

3. Results and discussion

3.1. Crystal structure of the complexes

The copper–dipeptide complexes crystallized in different spatial groups ($C2$, $P2_12_12_1$ and $P2_1$) as shown in Table 1. Figs. 1–4 show ORTEP plots from part of the unit cell of

Table 1
Crystal data and structural refinement parameters

Compound	[Cu(gly-val)] · $\frac{1}{2}H_2O$	[Cu(val-gly)]	[Cu(val-phe)]	[Cu(phe-phe)]
Empirical formula	$[C_7H_{12}CuN_2O_3] \cdot \frac{1}{2}(H_2O)$	$C_7H_{12}N_2O_3Cu$	$C_{14}H_{18}N_2O_3Cu$	$C_{18}H_{18}N_2O_3Cu$
Formula weight	244.73	235.73	325.84	373.88
Temperature (K)	295(2)	120(2)	120(2)	120(2)
Crystal system	monoclinic	orthorhombic	orthorhombic	monoclinic
Space group	*C*2	$P2_12_12_1$	$P2_12_12_1$	$P2_1$
Unit cell dimensions				
a (Å)	19.257(1)	8.7746(3)	5.4627(1)	5.5355(2)
b (Å)	9.343(1)	9.8369(3)	9.0931(2)	8.9581(3)
c (Å)	5.430(1)	10.6744(3)	27.2711(8)	16.0027(5)
β (°)	93.31(1)			92.687(2)
Volume (Å^3)	975.3(2)	921.36(5)	1354.63(6)	792.66(5)
Z	4	4	4	2
D_{calc} (Mg/m^3)	1.667	1.699	1.598	1.566
Absorption coefficient (mm^{-1})	2.223	2.346	1.621	1.397
F(000)	504	484	676	386
Crystal size (mm^3)	$0.14 \times 0.12 \times 0.06$	$0.20 \times 0.14 \times 0.12$	$0.15 \times 0.09 \times 0.04$	$0.20 \times 0.06 \times 0.03$
Index ranges	$-22,21$; $-11,9$; $-6,5$	0,10; 0,11; $-12,12$	0,6; 0,10; $-31,32$	$-6,6$; $-10,10$; 0,19
Reflections collected	2915	1618	2367	2772
Independent reflections [R_{int}]	1567 [0.0407]	1618 [0.0567]	2367 [0.1028]	2772 [0.0701]
Completeness (%)	99.6	99.9	99.4	99.6
Maximum and minimum transmission	0.858 and 0.802	0.7660 and 0.6512	0.9380 and 0.7931	0.9593 and 0.7676
Data/restraints/parameters	1567/3/129	1618/0/120	2367/0/183	2772/1/217
Goodness-of-fit on F^2	1.065	1.060	1.067	1.066
Final *R* indices [$I > 2\sigma(I)$]	R_1[a] = 0.0293, wR_2[b] = 0.0696	R_1[a] = 0.0352, wR_2[b] = 0.0944	R_1[a] = 0.0396, wR_2[b] = 0.0818	R_1[a] = 0.0379, wR_2[b] = 0.0885
R indices (all data)	R_1[a] = 0.0316, $wR_2 = 0.0713$	R_1[a] = 0.0364, wR_2[b] = 0.0959	R_1[a] = 0.0521, wR_2[b] = 0.0863	R_1[a] = 0.0437, wR_2[b] = 0.0923
Absorption structure parameters	0.00(2)	−0.02(2)	−0.02(2)	−0.03(2)
Largest difference in peak and hole (e Å^{-3})	0.408 and −0.437	0.413 and −0.671	0.367 and −0.624	0.318 and −0.658

[a] $R_1 = \sum\|F_o| - |F_c\|/\sum|F_c|$.
[b] $wR_2 = \{\sum[w(F_o^2 - F_c^2)^2]/\sum[w(F_o^2)^2]\}^{1/2}$, $w = 1/[\sigma^2(F_o^2) + (s1 * P)^2 + s2 * P]$; $P = (F_o^2 + 2F_c^2)/3$.

the Cu(II) complexes with gly-val, val-gly, val-phe and phe-phe, respectively.

In the four studied complexes the Cu(II) has a pyramidal square-based coordination geometry. The copper occupies the centre of the square base, being equatorially coordinated to a dipeptide molecule acting as a tridentate ligand through the N-atom of the terminal NH_2 group, the deprotonated N-atom from the amide group, and one of the oxygen atoms of the carboxylate group. The fourth equatorial ligand is a carboxylate oxygen of a second

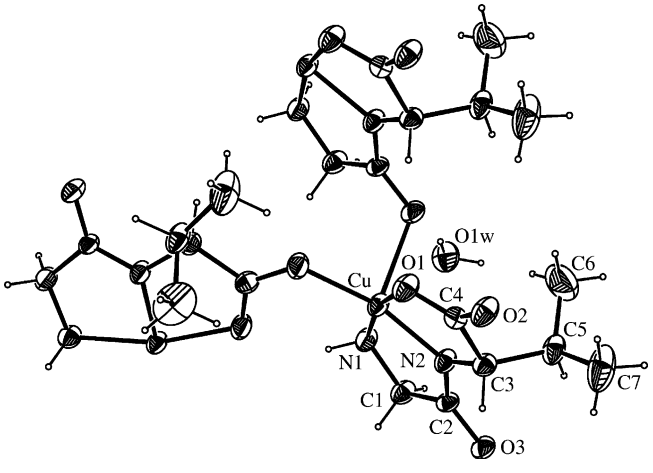

Fig. 1. ORTEP view of the asymmetric unit content of [Cu(gly-val)]·$\frac{1}{2}H_2O$, showing the labelling of the non-H atoms and their displacement ellipsoids at the 50% probability level.

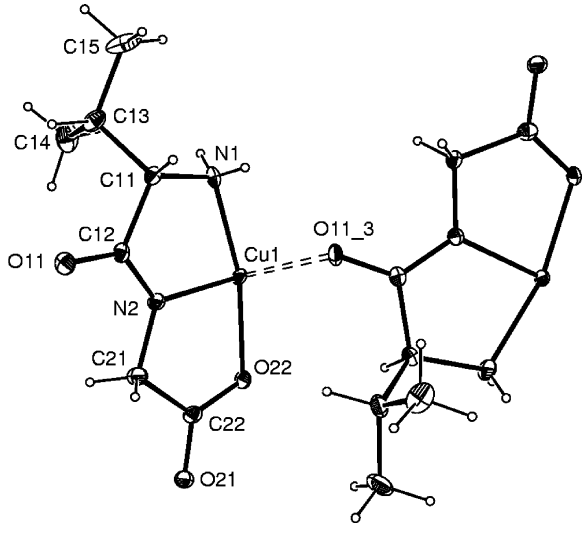

Fig. 2. ORTEP view of the asymmetric unit content of [Cu(val-gly)].

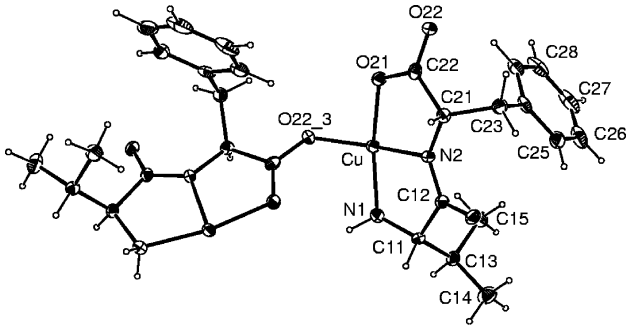

Fig. 3. ORTEP view of the asymmetric unit content of [Cu(val-phe)].

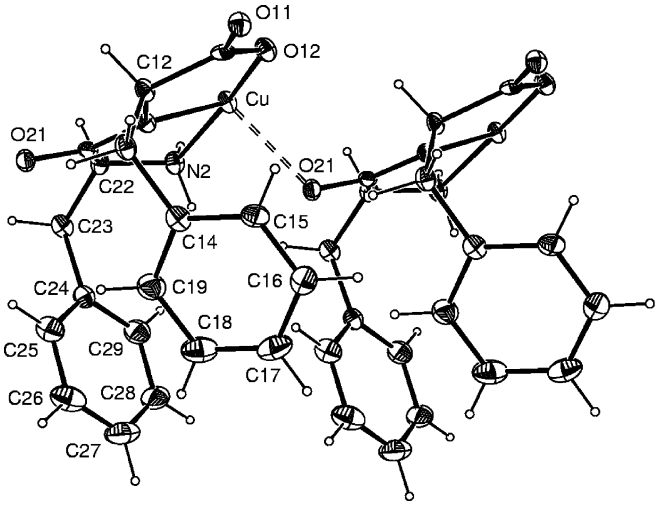

Fig. 4. ORTEP view of the asymmetric unit content of [Cu(phe-phe)].

dipeptide molecule, giving rise to carboxylate bridged polymeric chains. The pyramid apex is occupied by an oxygen atom of the amide bond belonging to a third dipeptide molecule which, in turn, links adjacent chains through amidate bridges. The configuration around the copper ion, even in the case of copper complexes with glycyl dipeptides, is similar to those previously reported for related Cu-dipeptide complexes with non-coordinating side-chains [10]. The bond distances and angles around the copper centre are summarized in Tables 2–5.

The bond lengths are similar to those found in previously reported complexes [10–14]. The distances between

Table 2
Bond distances (Å) and bond angles (°) around copper in [Cu(gly-val)] · $\frac{1}{2}H_2O$

CuN(2)	1.902(3)	CuN(1)	2.030(3)
CuO(2)^{i}	1.962(3)	CuO(3)^{ii}	2.331(3)
CuO(1)	2.013(3)		
N(2)CuO(2)^{i}	162.8(1)	O(1)CuN(1)	165.0(1)
N(2)CuO(1)	82.0(1)	N(2)CuO(3)^{ii}	108.6(1)
O(2)^{i}CuO(1)	92.7(1)	O(2)^{i}CuO(3)^{ii}	88.0(1)
N(2)CuN(1)	83.5(1)	O(1)CuO(3)^{ii}	94.0(1)
O(2)^{i}CuN(1)	100.2(1)	N(1)CuO(3)^{ii}	94.1(1)

Symmetry transformations used to generate equivalent atoms: (i) $-x+1/2$, $y-1/2$, $-z+2$; (ii) x, y, $z+1$.

Table 3
Bond lengths (Å) and bond angles (°) around copper in [Cu(val-gly)]

Cu(1)N(2)	1.898(3)	Cu(1)N(1)	2.025(3)
Cu(1)O(21)^{i}	1.967(3)	Cu(1)O(11)^{ii}	2.285(2)
Cu(1)O(22)	2.016(2)		
N(2)Cu(1)O(21)^{i}	159.0(1)	O(22)Cu(1)N(1)	165.6(1)
N(2)Cu(1)O(22)	82.6(1)	N(2)Cu(1)O(11)^{ii}	111.5(1)
O(21)^{i}Cu(1)O(22)	91.6(1)	O(21)^{i}Cu(1)O(11)^{ii}	89.4(1)
N(2)Cu(1)N(1)	83.0(1)	O(22)Cu(1)O(11)^{ii}	104.40(9)
O(21)^{i}Cu(1)N(1)	101.9(1)	N(1)Cu(1)O(11)^{ii}	81.1(1)

Symmetry transformations used to generate equivalent atoms: (i) $x+1/2$, $-y+1/2$, $-z+1$; (ii) $-x$, $y+1/2$, $-z+1/2$.

Table 4
Bond lengths (Å) and bond angles (°) around copper in [Cu(val-phe)]

Cu(1)N(2)	1.904(3)	Cu(1)O(21)	1.993(2)
Cu(1)O(22)^{i}	1.975(3)	Cu(1)O(11)^{ii}	2.345(3)
Cu(1)N(1)	1.985(3)		
N(2)Cu(1)O(22)^{i}	163.3(1)	N(1)Cu(1)O(21)	166.5(1)
N(2)Cu(1)N(1)	83.7(1)	N(2)Cu(1)O(11)^{ii}	114.4(1)
O(22)^{i}Cu(1)N(1)	97.9(1)	O(22)^{i}Cu(1)O(11)^{ii}	82.3(1)
N(2)Cu(1)O(21)	83.3(1)	N(1)Cu(1)O(11)^{ii}	84.4(1)
O(22)^{i}Cu(1)O(21)	93.6(1)	O(21)Cu(1)O(11)^{ii}	104.1(1)

Symmetry transformations used to generate equivalent atoms: (i) $-x+2$, $y-1/2$, $-z+1/2$; (ii) $x+1$, y, z.

Table 5
Bond lengths (Å) and bond angles (°) around copper in [Cu(phe-phe)]

CuN(1)	1.917(3)	CuN(2)	2.012(3)
CuO(11)^{i}	1.960(3)	CuO(21)^{ii}	2.333(2)
CuO(12)	1.999(3)		
N(1)CuO(11)^{i}	160.6(1)	O(12)CuN(2)	164.3(1)
N(1)CuO(12)	83.2(1)	N(1)CuO(21)^{ii}	117.6(1)
O(11)^{i}CuO(12)	93.4(1)	O(11)^{i}CuO(21)^{ii}	81.9(1)
N(1)CuN(2)	81.8(1)	O(12)CuO(21)^{ii}	100.8(1)
O(11)^{i}CuN(2)	102.3(1)	N(2)CuO(21)^{ii}	82.3(1)

Symmetry transformations used to generate equivalent atoms: (i) $-x+2$, $y+1/2$, $-z+2$; (ii) $x+1$, y, z.

two adjacent Cu(II) ions of the same chain linked by carboxylate bridges are 5.248, 5.087, 5.192 and 5.275 Å for [Cu(gly-val)] · $\frac{1}{2}H_2O$, [Cu(val-gly)], [Cu(val-phe)] and [Cu(phe-phe)], respectively, while the distances between neighbouring copper ions on different chains linked by amidate bridges are longer: 5.430, 5.770, 5.463 and 5.535 Å, respectively.

In spite of the common features exhibited by the four structures, there are some significant structural differences. The distances of the copper ion to the mean plane determined by the four equatorial ligands and the dihedral angles between adjacent planes are shown in Table 6. While the Cu(II) ion departs from the equatorial plane in distances that vary from 0.1444 Å (for the phe-phe complex) to 0.1950 Å (in the val-gly complex), the dihedral angle

Table 6
(1) Distances of the copper atom to the equatorial plane of ligands, and (2) dihedral angles between consecutive least-square planes

Compound	(1) Distance (Å)	(2) Angle (°)
[Cu(gly-val)] · $\frac{1}{2}H_2O$	0.1913	31.9
[Cu(val-gly)]	0.1950	77.4
[Cu(val-phe)]	0.1857	0.0
[Cu(phe-phe)]	0.1444	56.8

between adjacent planes varies from 0° (val-phe complex) to 77° (val-gly complex).

Consideration of the crystal packing shows that the aromatic rings in [Cu(phe-phe)] and [Cu(val-phe)] are planar to within experimental error and are parallel to the corresponding equivalent in the other molecule. It is interesting to note that the arrangement of the ligands in the lattice gives rise to hydrophobic layers of aromatic rings alternated with hydrophilic layers defined by the copper and the hetero-atoms of the ligands. In the case of [Cu(gly-val)] · $\frac{1}{2}H_2O$ a similar layered structure was found although this is now interrupted by water molecules near the glycine residues sites. In contrast, the crystal packing of [Cu(val-gly)] does not show these differentiated regions.

3.2. Infrared spectra

A tentative assignment of the most characteristic bands out of the band-rich infrared spectra of the complexes was carried out. In order to find such distinctive pattern of bands, the spectra of the copper complexes were studied and compared to those of the free dipeptides, and also to those found in our previous work on amino acids and dipeptide copper complexes [10,11,20,22,34]. The positions of the IR bands of the new copper-dipeptide complexes are presented in Table 7.

The free dipeptides exist as zwitterions in the solid state, as evidenced by the presence of a medium intensity band near the 2100 cm^{-1} region, which has been assigned to the combination of $\delta(NH_3^+)$ and $\rho(NH_3^+)$ [35]. This band disappears upon reaction with copper and the N–H stretching vibration of the NH_2 group is displaced to higher energies in relation to the free dipeptides. These spectroscopic facts signal the copper binding to the NH_2 group.

The N–H stretching band of the amido group disappears after coordination, in agreement with the deprotonation process that this group undergoes.

The two carboxylate stretching modes suffer only small changes upon coordination compared to the free dipeptide, in agreement with the usual behaviour exhibited by bridging carboxylate groups. The differences between $\nu_{as}(COO^-)$ and $\nu_s(COO^-)$ also support this coordination mode [36].

3.3. EPR spectra of solid samples

The powder EPR spectra of [Cu(gly-val)] · $\frac{1}{2}H_2O$, [Cu(val-gly)] and [Cu(phe-phe)] complexes are very similar. Fig. 5 shows the spectrum of [Cu(phe-phe)]. The EPR spectra do not show any hyperfine structure. This is probably due to exchange interactions between the paramagnetic ions mediated by the carboxylate bridges, which are known to provide relatively strong exchange couplings [37,38]. In such cases, exchange interaction may average out other interactions such as hyperfine [39]. This is in agreement with the polymeric structure found in the complexes.

Remarkably, in the case of [Cu(val-phe)], the EPR spectrum shows three lines that can not be explained in terms of a $S = 1/2$ spin (Fig. 6).

3.4. EPR spectra of solutions

The EPR spectra of frozen 1 mM solutions of all the studied compounds are very similar. Fig. 7 shows the spectra of

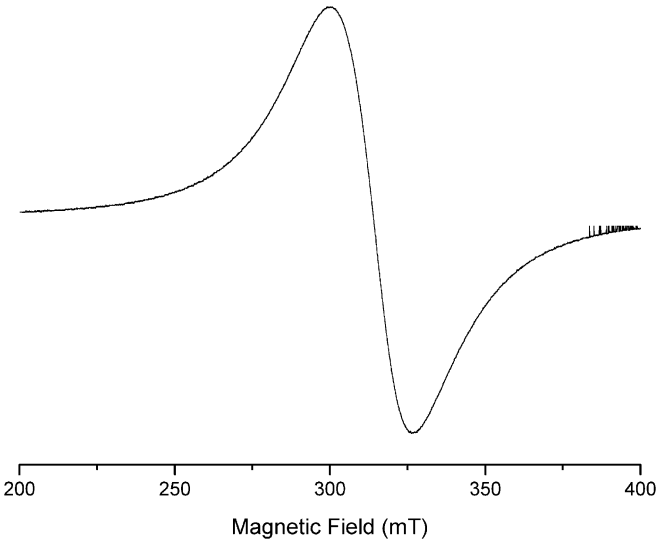

Fig. 5. EPR spectrum of [Cu(phe-phe)].

Table 7
Characteristic IR bands (cm^{-1}) of complex spectra

[Cu(gly-val)] · $\frac{1}{2}H_2O$	[Cu(val-gly)]	[Cu(val-phe)]	[Cu(phe-phe)]	Assignment
3392s/3260sh	3365s/3296m	3351m/3281m	3357m/3281w	$\nu(NH_2)$
1580s	1585s	1576s	1574s	ν(C=O)amide I
1600m	1626s/1613s	1611sh	1616m	$\delta(NH_2)$
1538s	1551s	1543s	1547s	$\nu_{as}(COO^-)$
1464m	1461m	1431m	1453m	$\nu_s(COO^-)$

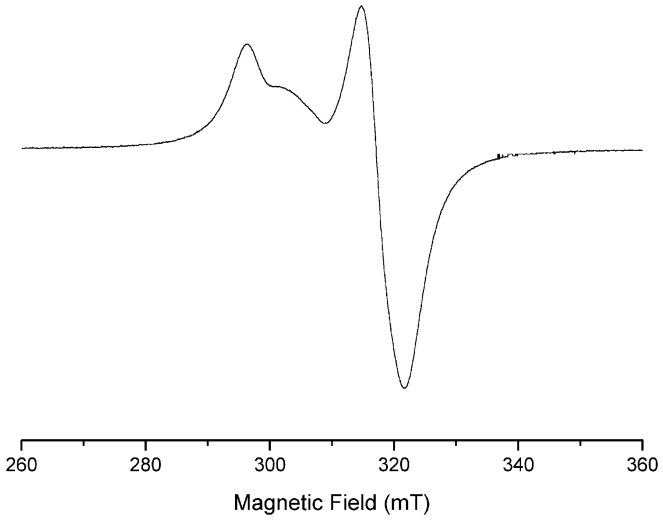

Fig. 6. EPR spectrum of [Cu(val-phe)].

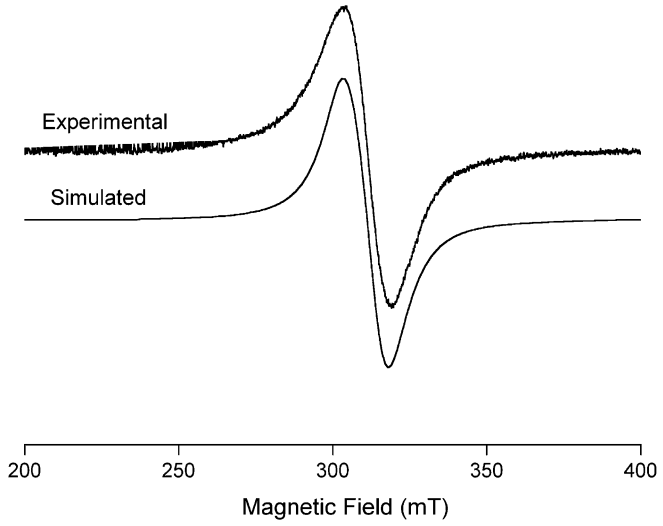

Fig. 7. EPR spectrum of a frozen 1 mM solution of the [Cu(phe-phe)] complex.

[Cu(phe-phe)], along with a simulation obtained with the QPOW program. Table 8 shows the parameters which fitted best the experimental spectra.

These results are typically found in the spectra of exchange coupled copper complexes [39].

In order to observe some hyperfine structure, it is necessary to reduce the concentration to about 0.5 mM. These results suggest that in the frozen solutions the complexes exist mostly as polymeric species, with exchange operating

Table 8
g-Parameters which gave the best simulations

Compound	$g_{\parallel}$	$g_{\perp}$
[Cu(gly-val)] · $\frac{1}{2}H_2O$	2.165	2.076
[Cu(val-gly)]	2.155	2.070
[Cu(val-phe)]	2.160	2.065
[Cu(phe-phe)]	2.150	2.075

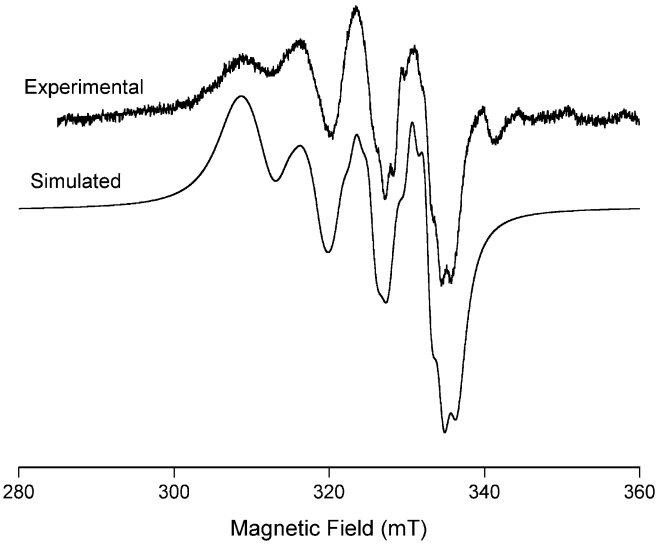

Fig. 8. EPR spectrum of a 0.5 mM solution of [Cu(val-phe)].

between their copper centres, while at lower concentrations the EPR spectrum is mainly due to uncoupled monomeric species.

In an attempt to determine whether these results reflect the composition of the solution at room temperature, additional spectra were recorded at 25 °C.

Fig. 8 shows the spectrum, at room temperature, of 0.5 mM solution of [Cu(val-phe)] and its simulated spectrum using the SIMFONIA program. The spectra of the other complexes are similar to the spectrum of [Cu(val-phe)].

In the spectrum shown in Fig. 8, the hyperfine structure due to the copper nuclear spin and the super-hyperfine structure due to the nitrogen nuclear spin can be clearly observed. This indicates that there is no exchange coupling between the copper atoms. Therefore, at room temperature the solution contains mostly uncoupled monomeric species. In addition, the extra peaks in the high-field line indicate the coordination through two equivalent nitrogens.

Summing up, it can be concluded that solutions of 0.5 mM, at room temperature, mostly contain monomeric species. On the other hand, at lower temperatures, the equilibrium is displaced towards the formation of the polymeric complexes, perhaps as a result of the concentration of solutes in small pockets. This idea has been previously suggested by Sigel et al. [2].

3.5. Electronic spectra

The electronic spectra of 5 mM aqueous solution of all the complexes at room temperature are very similar to one another. Table 9 shows the λ_{max} and the ε_M values of the complexes.

The complexes containing glycine residues present an absorption band near 635 nm while those containing bigger N-terminal residues show absorption band maxima at slightly minor wavelengths. These spectra are characteristic of Cu(II) in an octahedral environment and the main

Table 9
λ_{max} (nm) and ε_M (M^{-1} cm^{-1}) of the complexes

Compound	λ_{max} (nm)	ε_M (M^{-1} cm^{-1})
[Cu(gly-val)]	635	80
[Cu(val-gly)]	636	70
[Cu(val-phe)]	627	90
[Cu(phe-phe)]	626	100

absorption can be assigned to the $d_{xy} \rightarrow d_{x^2-y^2}$ transition [40].

The λ_{max} of these compounds lie close to those of the previously studied [Cu(ala-val)] and other Cu-dipeptide complexes [10,11].

The EPR spectroscopic results show that the monomeric moiety is the dominant species in diluted solutions of the copper complexes. Assuming that each copper ion is coordinated only to one dipeptide through the carboxylate oxygen atom, the amide nitrogen and the amine nitrogen atoms, and that the rest of the coordination positions are occupied by water, then, according to the empirical equation proposed by Prenesti et al. [41], the calculated λ_{max} would be 627 nm. This wavelength is similar to that found for [Cu(val-phe)] and [Cu(phe-phe)] complexes. In the case of complexes containing the glycine residue, where the experimental λ_{max} is slightly higher, it is possible that the molecules undergo further hydrolysis processes.

Acknowledgements

The authors are especially grateful to Prof. Dr. Otaciro Nascimento for the very helpful advice and discussion of the EPR spectra. The authors thank PEDECIBA-Química (Uruguayan Organization) for financial support. G. Facchin thanks PEDECIBA-Química for a doctoral scholarship and AMSUD/Pasteur for financial support. E.J. Baran and O.E. Piro are members of the Research Career from CONICET (Argentina). A.J. Costa-Filho and J. Ellena thank CNPq for financial support. A.J. Costa-Filho thanks to PRONEX/FAPESP/CNPq (Grant No. 03/09859-2) for financial support.

Appendix A. Supplementary data

Supplementary Crystallographic data for the structures reported in this paper have been deposited with the Cambridge Crystallographic Data Centre as supplementary publication Nos. CCDC 266051–266053 for [Cu(gly-val)] · $\frac{1}{2}H_2O$, [Cu(val-gly) and [Cu(val-phe)] respectively, and CCDC 266055 for [Cu(phe-phe)]. Copies of available material can be obtained, free of charge, on application to the Director, CCDC, 12 Union Road, Cambridge CH2 1EZ, UK, fax: +44 1223 336 033 or e-mail: deposit@ccdc.cam.ac.uk or http://www.ccdc.cam.ac.uk. Supplementary data associated with this article can be found, in the online version, at doi:10.1016/j.poly.2006.03.012.

References

[1] H.C. Freeman, in: G.L. Eichrorn (Ed.), Inorganic Biochemistry, vol. 1, Elsevier, New York, 1973, pp. 121–166.
[2] H. Sigel, R.B. Martin, Chem. Rev. 82 (1982) 385.
[3] H. Kozlowski, W. Bal, M. Dyba, T. Kowalic-Jankowska, Coord. Chem. Rev. 184 (1999) 319.
[4] R.H. Holm, P. Kennepohl, E. Solomon, Chem. Rev. 96 (1996) 2239.
[5] J.E. Weder, C.T. Dillon, T.W. Hambley, B.J. Kennedy, P.A. Lay, J.R. Biffin, H.L. Regtop, N.M. Davies, Coord. Chem. Rev. 232 (2002) 95.
[6] N. Farrell, Transition Metal Complexes as Drugs and Chemoterapeutic Agents, Kluwer Academic Publishers Group, Dordrecht, 1989.
[7] N.P. Farrell, Uses of Inorganic Chemistry in Medicine, The Royal Society of Chemistry, Cambridge, 1999.
[8] R. Ruiz, C. Surville-Barland, A. Aukauloo, E. Anoxolabehere-Mallart, Y. Journaux, J. Cano, M.C. Muñoz, J. Chem. Soc. Dalton Trans. (1997) 745.
[9] H.C. Freeman, M.J. Healy, M.L. Scudder, J. Biol. Chem. 252 (1977) 8840.
[10] G. Facchin, M.H. Torre, E. Kremer, O.E. Piro, E.E. Castellano, E.J. Baran, Z. Naturforsch. 55b (2000) 1157.
[11] G. Facchin, M.H. Torre, E. Kremer, O. Piro, E.E. Castellano, E.J. Baran, J. Inorg. Biochem. 89 (2002) 174.
[12] O.R. Nascimento, M. Tabak, J. Inorg. Biochem. 23 (1985) 13.
[13] O.R. Nascimento, A.J. Costa-Filho, D.I.D. Morais, J. Ellena, L.F. Delboni, Inorg. Chim. Acta 312 (2001) 133.
[14] M.B. Hursthouse, S.A.A. Jayaweera, H. Milburn, A. Quick, J. Chem. Soc. Dalton Trans. (1975) 2569.
[15] R. Baggio, N.M.C. Casado, R. Calvo, R.E. Rapp, M.T. Garland, Acta Crystallogr., Sect. C 61 (2005) 250.
[16] A. Sugihara, T. Ashida, Y. Sasada, M. Kakudo, Acta Crystallogr., Sect. B. 24 (1968) 203.
[17] T. Glowiak, I. Podgorska, Acta Crystallogr., Sect. C 43 (1987) 53.
[18] J.F. Blount, K.A. Fraser, H.C. Freeman, J.T. Szymanski, Acta Crystallogr. 22 (1967) 396.
[19] G. Fusch, E.C. Hillgeris, B. Lippert, Inorg. Chim. Acta 217 (1994) 33.
[20] A. Cuevas, I. Viera, M.H. Torre, E. Kremer, S.B. Etcheverry, E.J. Baran, Acta Farmacéutica Bonaerense 17 (1998) 213.
[21] A. Cuevas, I. Viera, M.H. Torre, E. Kremer, E. Baran, Afinidad 475 (1998) 183.
[22] A. Cuevas, I. Viera, M.H. Torre, E. Kremer, S.B. Etcheverry, E.J. Baran, Afinidad 482 (1999) 263.
[23] G. Facchin, M.H. Torre, I. Viera, E. Kremer, E.J. Baran, in: L. Khassanova, P. Collery, I. Maymard, Z. Khassanova, J.-C. Étienne (Eds.), Sod-like Activity and Lipophilicity of Copper Chelates with Aminoacids and Peptides, Metal Ions in Biology and Medicine, vol. 7, John Libbey Eurotext, Paris, 2002, pp. 11–14.
[24] Enraf-Nonius COLLECT; Nonius BV: Delft, The Netherlands (1997–2000).
[25] Z. Otwinowski, W. Minor, in: C.W. Carter, R.M. Sweet (Eds.), *HKL* DENZO and SCALEPACK, vol. 276, Academic Press, New York, 1997, pp. 307–326.
[26] R.H. Blessing, Acta Crystallogr., Sect. A 51 (1995) 33.
[27] G.M. Sheldrick, SHELXL-97. Program for Crystal Structures Resolution, University of Göttingen, Göttingen, 1997.
[28] G.M. Sheldrick, SHELXL-97. Program for Crystal Structures Analysis, University of Göttingen, Göttingen, 1997.
[29] L.J. Farrugia, J. Appl. Cryst. 32 (1999) 837.
[30] L.J. Farrugia, J. Appl. Cryst. 30 (1997) 565.
[31] R.L. Belford, M.J. Nilges, Computer Simulation of Powder Spectra, Denver, CO, 1979.
[32] A.M. Maurice, PhD Thesis, University of Illinois: Urbana, IL, 1979.
[33] Bruker SIMFONIA: Madison, WI, 1996.
[34] G. Facchin, M.H. Torre, E. Kremer, E.J. Baran, A. Mombrú, H. Pardo, M.P. Araujo, A.A. Batista, A.J. Costa-Filho, Inorg. Chim. Acta 355 (2003).

[35] D. Lin-Vien, N.B. Colthup, W.G. Fately, J.G. Grasselli, The Handbook of Infrared and Raman Characteristic Frequencies of Organic Molecules, Academic Press Inc., San Diego, 1991.
[36] K. Nakamoto, Infrared and Raman Spectra of Inorganic and Coordination Compounds. Part B, 5 edn., John Wiley and Sons, New York, 1997.
[37] E. Colacio, M. Ghazi, R. Kivekas, J.M. Moreno, Inorg. Chem. 39 (2000) 2882.
[38] A.J. Costa-Filho, O.R. Nascimento, L. Ghievelder, R. Calvo, J. Phys. Chem. B 105 (2001) 5039.
[39] A. Bencini, D. Gatteschi, EPR of Exchange Coupled Systems, Springer-Verlag, Berlin, 1990.
[40] A.B.P. Lever, Inorganic Electronic Spectroscopy, 2nd edn., Elsevier, Amsterdam, 1984.
[41] E. Prenesti, P.G. Daniele, M. Prencipe, G. Ostacoli, Polyhedron 18 (1999) 3233.

$[Zn(4,4'\text{-bipy})_2(H_2O)_4](ClO_4)_2 \cdot 2(4,4'\text{-bipy})$ (**1**), $[Zn_3(4,4'\text{-bipy})_4(OAc)_4](ClO_4)_2 \cdot 2(H_2O)$ (**2**), $[Zn_3(4,4'\text{-bipy})_3(OAc)_4(H_2O)_2](ClO_4)_2 \cdot (H_2O)$ (**3**), $[Zn(4,4'\text{-bipy})(ClO_4)(H_2O)(OH)]$ (**4**), $[Zn(4,4'\text{-bipy})(DMSO)_4](ClO_4)_2$ (**5**), and $[Zn(4,4'\text{-bipy})_3(DMSO)_2](ClO_4)_2 \cdot 2(4,4'\text{-bipy}) \cdot (H_2O)$ (**6**). The series of compounds provides a clear illustration of the versatility of bipy as a spacer ligand when assembling transition metal ions into coordination polymers, providing examples of monomeric, linear chain, zig-zag chain, ladder, and two-dimensional network structures (Scheme 1). Varied structural topologies often appear from the same synthesis, differing in the weak hydrogen bonding and π-stacking interactions that are also present. A review of Zn(II) coordination polymers, including those containing bipy, has recently been published by Erxleben [17].

2. Experimental

2.1. Materials

The starting materials zinc(II) perchlorate hexahydrate (98%) and 4,4′-bipyridine (98%) were purchased from Aldrich Chemical Co. Dimethyl sulfoxide (99.9%) was purchased from Fisher Scientific. Absolute ethanol was purchased from Aaper Chemical Co. All reagents were used without further purification.

Caution! Perchlorate salts of metal complexes with organic ligands are potentially explosive. Although no explosive decomposition of compounds **1**–**6** has been observed in experiments performed up to 150 °C, caution should still be exercised when handling perchlorate salts.

2.2. Synthesis of $[Zn(4,4'\text{-bipy})_2(H_2O)_4](ClO_4)_2 \cdot 2(4,4'\text{-bipy})$ (**1**), $[Zn_3(4,4'\text{-bipy})_4(OAc)_4](ClO_4)_2 \cdot 2(H_2O)$ (**2**), and $[Zn_3(4,4'\text{-bipy})_3(OAc)_4(H_2O)_2](ClO_4)_2 \cdot (H_2O)$ (**3**)

A solution was prepared by dissolving 741 mg of $Zn(ClO_4)_2 \cdot 6H_2O$ (2.0×10^{-3} mol) in 10 mL of water contained within a Teflon canister. Addition of 934 mg of 4,4′-bipyridine (6.0×10^{-3} mol) and 2 mL of absolute ethanol produced in a white suspension. The Teflon canister was sealed within a homemade, stainless steel, hydrothermal autoclave, purged with argon gas, and heated to 150 °C for 5 days. The container was subsequently cooled to room temperature over a period of 24 h without any specific control over the rate of cooling. From this reaction mixture, colorless plates of **1** were obtained as the majority product and colorless needles of **2** and **3** crystallized as the minority products. The crystals were washed with water before further characterization. The composition of the products was determined by X-ray structure analysis.

2.3. Synthesis of $[Zn(4,4'\text{-bipy})(ClO_4)(H_2O)(OH)]$ (**4**) and $[Zn(4,4'\text{-bipy})(DMSO)_4](ClO_4)_2$ (**5**)

A solution containing 741 mg of $Zn(ClO_4)_2 \cdot 6H_2O$ (2.0×10^{-3} mol) dissolved in 10 mL of DMSO was combined with a solution containing 467 mg of 4,4′-bipyridine (3.0×10^{-3} mol) dissolved in 10 mL of DMSO. The resulting colorless solution, contained within an evaporating dish, produced colorless plates of **1** as the majority product and colorless crystals of **4** and **5** as the minority products within 2–4 weeks of solvent evaporation. The crystals were

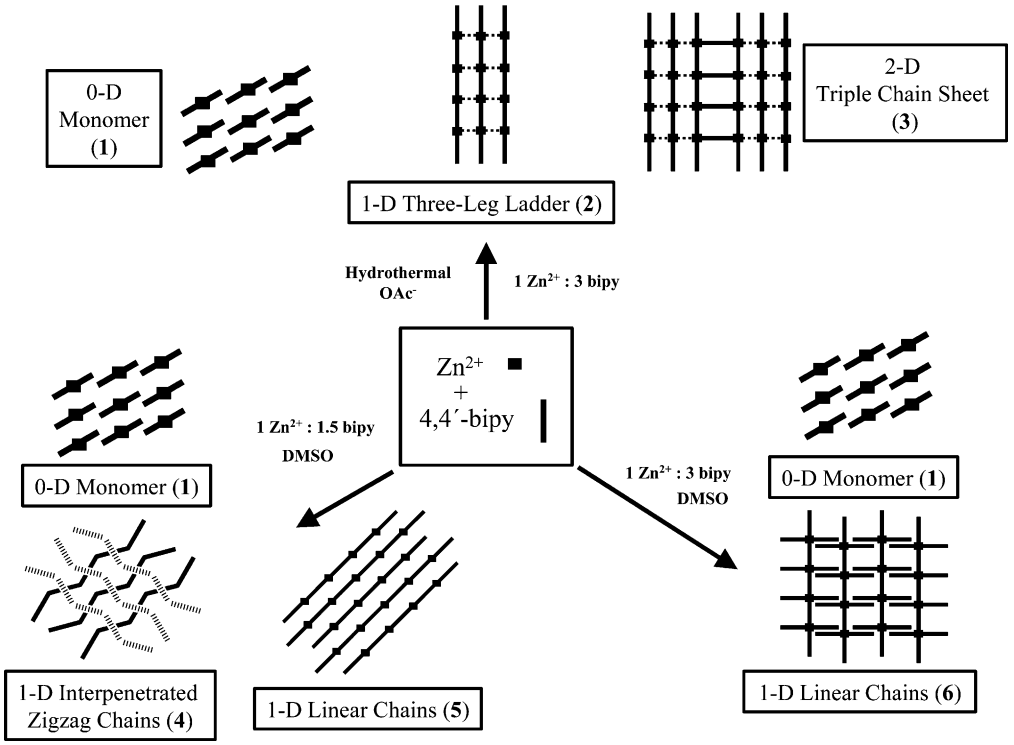

Scheme 1.

washed with DMSO before further characterization. The composition of the products was determined by X-ray structure analysis.

2.4. Synthesis of [Zn(4,4′-bipy)$_3$(DMSO)$_2$](ClO$_4$)$_2$ · 2(4,4′-bipy) · (H$_2$O) (6)

A solution containing 741 mg of $Zn(ClO_4)_2 \cdot 6H_2O$ (2.0×10^{-3} mol) dissolved in 10 mL of DMSO was combined with a solution containing 934 mg of 4,4′-bipyridine (6.0×10^{-3} mol) dissolved in 10 mL of DMSO. The resulting colorless solution, contained within an evaporating dish, produced colorless plates of **1** as the majority product and colorless blocks of **6** as the minority product within 2 weeks of solvent evaporation. The crystals were washed with DMSO before further characterization. The composition of the products was determined by X-ray structure analysis.

2.5. X-ray structure determination

A colorless plate of compound **1** ($0.17 \times 0.21 \times 0.30$ mm^3), a needle of **2** ($0.04 \times 0.33 \times 0.51$ mm^3), a needle of **3** ($0.11 \times 0.15 \times 0.18$ mm^3), a plate of **4** ($0.07 \times 0.10 \times 0.12$ mm^3), a plate of **5** ($0.04 \times 0.20 \times 0.23$ mm^3), and block of **6** ($0.08 \times 0.19 \times 0.20$ mm^3) were selected for X-ray analysis. Each crystal was mounted on a glass fiber under nitrogen gas. The same data collection procedures were used for each sample. Data were collected at 173 K on a Siemens SMART PLATFORM equipped with a CCD area detector and a graphite monochromator utilizing Mo Kα radiation ($\lambda = 0.71073$ Å). Cell parameters were refined using 8192 reflections. A hemisphere of data (1381 frames) was collected using the ω-scan method (0.3° frame width). The first 50 frames were re-measured at the end of data collection to monitor instrument and crystal stability (maximum correction of I was <1%). Absorption corrections by integration were applied based on measured indexed crystal faces.

All structures were solved by the direct methods in SHELLXTL6 [18] and refined using full-matrix least squares. The non-H atoms were treated anisotropically, whereas the hydrogen atoms were calculated in ideal positions and were refined by riding on their respective carbon atoms. For compound **1**, the asymmetric unit consists of a Zn(II) ion, three 4,4′-bipy molecules, two water molecules, and one perchlorate anion. A total of 411 parameters were refined with F^2 in the final cycle using 6416 reflections with $I > 2\sigma(I)$ to yield $R_1 = 3.85\%$ and $wR_2 = 9.79\%$. For compound **2**, the asymmetric unit consists of two Zn(II) ions, two 4,4′-bipy molecules, two acetate molecules, a water molecule, and a perchlorate anion. Both acetate ligands are disordered and refined in two parts. Their site occupation factors were dependently refined to 0.49(7) and 0.50(3) for the first and second parts, respectively. A total of 362 parameters were refined with F^2 in the final cycle using 5939 reflections with $I > 2\sigma(I)$ to yield $R_1 = 4.59\%$ and $wR_2 = 11.12\%$. For compound **3**, the asymmetric unit consists of two Zn(II) ions, 1.5 4,4′-bipy molecules, two acetate molecules, a water molecule, and a perchlorate anion. A total of 329 parameters were refined with F^2 in the final cycle using 5088 reflections with $I > 2\sigma(I)$ to yield $R_1 = 3.63\%$ and $wR_2 = 9.08\%$. For compound **4**, the asymmetric unit consists of a Zn(II) ion, one 4,4′-bipy molecule, one water molecule, one hydroxide ion, and one coordinated perchlorate anion. The hydroxide proton is disordered and was refined in two positions, obtained from a difference Fourier map, with their site occupation factors fixed at 50% and their thermal parameters set at 1.5 that of their parent O atom. A total of 190 parameters were refined with F^2 in the final cycle using 2827 reflections with $I > 2\sigma(I)$ to yield $R_1 = 3.13\%$ and $wR_2 = 7.73\%$. For compound **5**, the asymmetric unit consists of two Zn(II) ions, one 4,4′-bipy molecule, four DMSO molecules, and two perchlorate anions. A total of 363 parameters were refined with F^2 in the final cycle using 6951 reflections with $I > 2\sigma(I)$ to yield $R_1 = 2.74\%$ and $wR_2 = 6.71\%$. For compound **6**, the asymmetric unit consists of a Zn(II) ion, five 4,4′-bipy molecules, two DMSO molecules, one water molecule, and two perchlorate anions. One of the 4,4′-bipyridine molecules is disordered and refined in two parts. Their site occupation factors were dependently refined to 0.54(1) for the major part, and consequently 0.46(1) for the minor part; C53 was found to be common to both parts. Both perchlorate counter ions were found to be disordered and each was refined in two parts with each pair's site occupation factors dependently refined to 0.62(1)/0.38(1) for the first and 0.53(1)/0.47(1) for the second, respectively. A 0.4 occupancy water molecule was found midway between the perchlorate ions. A total of 717 parameters were refined with F^2 in the final cycle using 11994 reflections with $I > 2\sigma(I)$ to yield $R_1 = 4.72\%$ and $wR_2 = 11.38\%$.

3. Results and discussion

3.1. Compound synthesis

Compounds **1**, **2**, and **3** resulted from the direct combination of one equivalent of $Zn(ClO_4)_2 \cdot 6H_2O$ with three equivalents of 4,4′-bipyridine under hydrothermal conditions (Scheme 1). Since 4,4′-bipy is relatively insoluble in water, elevated temperatures (150 °C) and pressures are necessary for the dissolution of the Zn–bipy suspension. Compound **1** is the majority product and crystallizes as colorless plates. Only relatively small quantities of **2** and **3** were obtained, both as colorless needles of similar morphology. To prevent the formation of unwanted side-products, such as high oxidation state metal oxides, the reaction mixtures were purged with argon gas and treated with a small quantity of ethanol (acting as a mild reducing agent) before heating. However, the ethanol itself was apparently oxidized, accounting for the presence of acetate ligands in **2** and **3**. Note that while compounds **1** and **3**

Table 1
Crystallographic data for $[Zn(4,4'\text{-bipy})_2(H_2O)_4](ClO_4)_2 \cdot 2(4,4'\text{-bipy})$ (**1**), $[Zn_3(4,4'\text{-bipy})_4(OAc)_4](ClO_4)_2 \cdot 2(H_2O)$ (**2**), $[Zn_3(4,4'\text{-bipy})_3(OAc)_4(H_2O)_2](ClO_4)_2 \cdot (H_2O)$ (**3**) $[Zn(4,4'\text{-bipy})(ClO_4)(H_2O)(OH)]$ (**4**), $[Zn(4,4'\text{-bipy})(DMSO)_4]_n(ClO_4)_{2n}$ (**5**), and $[Zn(4,4'\text{-bipy})_3(DMSO)_2](ClO_4)_2 \cdot 2(4,4'\text{-bipy})(H_2O)$ (**6**)

Compound	**1**	**2**	**3**	**4**	**5**	**6**
Empirical formula	$C_{60}H_{56}Cl_2N_{12}O_{12}Zn$	$C_{24}H_{24}ClN_4O_9Zn_{1.5}$	$C_{38}H_{44}Cl_2N_6O_{20}Zn_3$	$C_{10}H_{12}ClN_2O_6Zn$	$C_{18}H_{32}Cl_2N_2O_{12}S_4Zn$	$C_{54}H_{52.80}Cl_2N_{10}O_{10.40}S_2Zn$
Formula mass	1273.44	645.98	1171.80	357.04	732.97	1208.65
Crystal system	triclinic	triclinic	triclinic	monoclinic	triclinic	monoclinic
Color and habit	colorless plates	colorless needles	colorless needles	colorless prism	colorless plate	colorless plate
Space group	$P\bar{1}$ (no. 2)	$P\bar{1}$ (no. 2)	$P\bar{1}$ (no. 2)	$P2_1/n$ (no. 14)	$P\bar{1}$ (no. 2)	Cc (no. 9)
a (Å)	7.7199(4)	11.2274(9)	9.1166(6)	7.585(1)	8.3491(4)	18.6657(8)
b (Å)	14.1985(8)	11.4636(9)	11.3249(7)	15.485(2)	9.3154(4)	11.4524(5)
c (Å)	14.8386(8)	11.9610(9)	11.6350(7)	10.690(2)	19.4783(8)	25.783(1)
α (°)	63.539(1)	106.453(1)	80.800(1)	90	86.677(1)	90
β (°)	88.295(1)	109.417(1)	80.664(1)	98.757(2)	89.337(1)	94.525
γ (°)	81.940(1)	100.529(1)	74.162(1)	90	89.421(1)	90
V (Å^3)	1440.7(1)	1325.6(2)	1131.9(1)	1240.9(3)	1512.2(1)	5494.4(4)
Z	1	2	1	4	2	4
T (°C)	173(2)	173(2)	173(2)	173(2)	173(2)	173(2)
λ (Å)	0.71073	0.71073	0.71073	0.71073	0.71073	0.71073
ρ_{calc} (g cm^{-3})	1.468	1.618	1.719	1.906	1.610	1.461
μ (Mo Kα, mm^{-1})	0.595	1.528	1.782	2.222	1.323	0.689
$R(F)$ for $F_o^2 > 2\sigma(F_o^2)$[a]	0.0385	0.0459	0.0363	0.0317	0.0274	0.0472
$R_w(F_o^2)$[b]	0.0979	0.1112	0.0908	0.0793	0.0671	0.1138

[a] $R(F) = \sum ||F_o| - |F_c|| / \sum |F_o|$.
[b] $R_w(F_o^2) = [\sum[w(F_o^2 - F_c^2)^2] / \sum wF_o^4]^{1/2}$.

Table 2
Selected bond distances (Å) and angles (°) for $[Zn(4,4'\text{-bipy})_2(H_2O)_4](ClO_4)_2 \cdot 2(4,4'\text{-bipy})$ (**1**)

Zn–O1	2.1503(13)	Zn–O2A[a]	2.1300(14)
Zn–O1A[a]	2.1503(13)	Zn–N1	2.1215(15)
Zn–O2	2.1300(14)	Zn–N1A[a]	2.1215(15)
O2–Zn–O2A[a]	180.00(8)	O2A[a]–Zn–O1	89.18(6)
O2–Zn–N1A[a]	89.16(6)	N1A[a]–Zn–O1	90.62(6)
O2A[a]–Zn–N1A[a]	90.84(6)	N1–Zn–O1	89.38(6)
O1–Zn–O1A[a]	180.00(8)	O2–Zn–O1A[a]	89.18(6)
O2–Zn–N1	90.84(6)	O2A[a]–Zn–O1A[a]	90.83(6)
O2A[a]–Zn–N1	89.16(6)	N1A[a]–Zn–O1A[a]	89.38(6)
N1A[a]–Zn–N1	180.00(8)	N1–Zn–O1A[a]	90.62(6)
O2–Zn–O1	90.82(6)		

Symmetry transformations used to generate equivalent atoms: (a) $-x+1, -y+1, -z+1$.

Table 3
Selected bond distances (Å) and angles (°) for $[Zn_3(4,4'\text{-bipy})_4(OAc)_4](ClO_4)_2 \cdot 2(H_2O)$ (**2**)

Zn1–N1	2.189(2)	Zn2–N2	2.170(2)
Zn1–N1′A[a]	2.187(2)	Zn2–N2A[b]	2.170(2)
Zn1–N3	2.137(3)	Zn2–O43	2.148(4)
Zn1–O42	2.200(5)	Zn2–O43′	2.091(4)
Zn1–O42′	1.983(5)	Zn2–O43A[b]	2.148(4)
Zn1–O43	2.241(4)	Zn2–O43′A[b]	2.091(4)
Zn1–O52	2.224(5)	Zn2–O53	2.125(4)
Zn1–O52′	1.965(5)	Zn2–O53A[b]	2.125(4)
Zn1–O53	2.238(4)	Zn2–O53′	2.066(4)
		Zn2–O53′A[b]	2.066(4)
N1–Zn1–N1′A[a]	177.62(10)		
N1–Zn1–N3	91.84(10)	N2–Zn2–N2A[b]	180.00
N1′A[a]–Zn1–N3	88.46(10)	N2–Zn2–O43	89.80(13)
N1–Zn1–O42	89.10(14)	N2A[b]–Zn2–O43	90.20(13)
N1′A[a]–Zn1–O42	88.52(14)	N2–Zn2–O43A[b]	90.20(13)
N3–Zn1–O42	94.55(17)	N2A–Zn2–O43A[b]	89.80(13)
N1–Zn1–O42′	89.79(16)	N2–Zn2–O43′	90.43(14)
N1′A[a]–Zn1–O42′	87.85(16)	N2A[b]–Zn2–O43′	89.57(14)
N3–Zn1–O42′	105.7(2)	N2–Zn2–O43′A[b]	89.57(14)
N1–Zn1–O43	89.17(13)	N2A–Zn2–O43′A[b]	90.43(14)
N1′A[a]–Zn1–O43	89.51(13)	N2–Zn2–O53	89.15(13)
N3–Zn1–O43	153.35(13)	N2A[b]–Zn2–O53	90.85(13)
N1–Zn1–O52	91.49(14)	N2–Zn2–O53A[b]	90.85(13)
N1′A[a]–Zn1–O52	90.87(14)	N2A–Zn2–O53A[b]	89.15(13)
N3–Zn1–O52	89.35(16)	N2–Zn2–O53′	89.66(14)
N1–Zn1–O52′	90.86(16)	N2A[b]–Zn2–O53′	90.34(14)
N1′A[a]–Zn1–O52′	91.40(16)	N2–Zn2–O53′A[b]	90.34(14)
N3–Zn1–O52′	101.3(2)	N2A–Zn2–O53′A[b]	89.66(14)
N1–Zn1–O53	90.30(12)	O43–Zn2–O43A[b]	180.00
N1′A[a]–Zn1–O53	90.71(12)	O43′–Zn2–O43′A[b]	180.00
N3–Zn1–O53	147.84(13)	O53–Zn2–O53A[b]	180.00
O42–Zn1–O43	58.84(18)	O53′–Zn2–O53′A[b]	180.00
O42–Zn1–O52′	164.1(2)	O43–Zn2–O53′	90.48(17)
O42′–Zn1–O52	164.8(2)	O43–Zn2–O53′A[b]	89.52(17)
O42′–Zn1–O53	106.4(2)	O43A[b]–Zn2–O53′	89.52(17)
O43–Zn1–O52′	105.3(2)	O43A[b]–Zn2–O53′A[b]	90.48(17)
O52–Zn1–O53	58.51(18)	O43′–Zn2–O53	88.38(16)
		O43′–Zn2–O53A[b]	91.62(17)
		O43′A[b]–Zn2–O53	91.62(17)
		O43′A[b]–Zn2–O53A	88.38(17)

Symmetry transformations used to generate equivalent atoms: (a) $x, y+1, z$, (b) $-x+1, -y+1, -z+2$.

Table 4
Selected bond distances (Å) and angles (°) for $[Zn_3(4,4'\text{-bipy})_3(OAc)_4(H_2O)_2](ClO_4)_2 \cdot (H_2O)$ (**3**)

Zn1–N1	2.116(2)	Zn2–N2	2.135(2)
Zn1–N1A[a]	2.116(2)	Zn2–N2′A[b]	2.131(2)
Zn1–O1	2.1255(18)	Zn2–O2	2.0403(19)
Zn1–O1A[a]	2.1255(18)	Zn2–O3	2.2716(18)
Zn1–O3	2.1540(18)	Zn2–O4	2.1683(19)
Zn1–O3A[a]	2.1540(18)	Zn2–O5	2.052(2)
N1–Zn1–N1A[a]	180.00	N2–Zn2–N2′A[b]	174.82(8)
N1–Zn1–O1	89.91(8)	N2–Zn2–O2	89.45(8)
N1–Zn1–O1A[a]	90.09(8)	N2–Zn2–O3	91.11(7)
N1A[a]–Zn1–O1A[a]	89.91(8)	N2[a]–Zn2–O4	88.62(8)
N1A[a]–Zn1–O1	90.09(8)	N2–Zn2–O5	87.71(9)
O1–Zn1–O1A[a]	180.00	N2′A[b]–Zn2–O2	91.40(8)
N1–Zn1–O3	90.05(8)	N2′A[b]–Zn2–O3	93.80(7)
N1A[a]–Zn1–O3	89.95(8)	N2′A[b]–Zn2–O4	92.48(8)
O1–Zn1–O3	89.70(7)	N2′A[b]–Zn2–O5	87.11(9)
O1A[a]–Zn1–O3	90.30(7)	O2–Zn2–O3	99.26(7)
N1–Zn1–O3A[a]	89.95(8)	O2–Zn2–O4	158.04(7)
N1A[a]–Zn1–O3A[a]	90.05(8)	O2–Zn2–O5	102.96(9)
O1A[a]–Zn1–O3A[a]	89.70(7)	O3–Zn2–O4	58.93(7)
O1–Zn1–O3A[a]	90.30(7)	O3–Zn2–O5	157.75(9)
O3–Zn1–O3A[a]	180.00	O4–Zn2–O5	98.82(9)

Symmetry transformations used to generate equivalent atoms: (a) $-x+1, -y+1, -z+1$, (b) $x, y+1, z$.

Table 5
Selected bond distances (Å) and angles (°) for $[Zn(4,4'\text{-bipy})(ClO_4)(H_2O)(OH)]$ (**4**)

Zn–O1	2.244(2)	Zn–N1	2.043(2)
Zn–O2	2.096(2)	Zn–N2	2.031(2)
Zn–O3	1.9594(18)		
O3–Zn–N2	124.89(9)	N1–Zn–O2	91.44(9)
O3–Zn–N1	121.82(9)	O3–Zn–O1	85.03(9)
N2–Zn–N1	112.84(9)	N2–Zn–O1	92.65(9)
O3–Zn–O2	88.10(8)	N1–Zn–O1	85.90(9)
N2–Zn–O2	97.38(9)	O1–Zn–O2	169.89(8)

Table 6
Selected bond distances (Å) and angles (°) for $[Zn(4,4'\text{-bipy})(DMSO)_4]_n(ClO_4)_{2n}$ (**5**)

Zn1–O1	2.1276(12)	O2–Zn1–N1	92.60(5)
Zn1–O1A[a]	2.1276(12)	O2A–Zn1–N1[a]	87.40(5)
Zn1–O2	2.1487(13)	N1A–Zn–N1[a]	180.0
Zn1–O2A[a]	2.1487(13)	O2–Zn1–O1	94.07(5)
Zn1–N1	2.1282(14)	O2A–Zn1–O1[a]	85.93(5)
Zn1–N1A[a]	2.1282(14)	N1A–Zn1–O1[a]	90.00(5)
S1–O1	1.5105(13)	N1–Zn1–O1	90.00(5)
S2–O2	1.5215(13)	O2–Zn1–O1A[a]	85.93(5)
O2–Zn1–O2A[a]	180.0	O2A–Zn1–O1A[a]	94.07(5)
O2–Zn1–N1A[a]	87.40(5)	N1A–Zn1–O1A[a]	90.00(5)
O2A–Zn1–N1A[a]	92.60(5)	N1–Zn1–O1A[a]	90.00(5)
O1–Zn1–O1A[a]	180.0	S1–O1–Zn1	139.45(8)
		S2–O2–Zn1	128.55(8)

Symmetry transformations used to generate equivalent atoms: (a) $-x, -y, -z+1$.

Table 7
Selected bond distances (Å) and angles (°) for $[Zn(4,4'\text{-bipy})_3(DMSO)_2](ClO_4)_2 \cdot 2(4,4'\text{-bipy})(H_2O)$ (**6**)

Zn–O1	2.160(3)	O2–Zn–N1	91.04(13)
Zn–O2	2.164(3)	O2–Zn–N1′A[a]	89.50(14)
Zn–N1	2.168(2)	O2–Zn–N2	85.66(14)
Zn–N1′A[a]	2.200(2)	O2–Zn–N3	95.46(13)
Zn–N2	2.136(3)	N1–Zn–N1′A[a]	176.80(16)
Zn–N3	2.163(3)	N2–Zn–N3	178.61(15)
S1–O1	1.524(3)	N1–Zn–N2	92.68(13)
S2–O2	1.491(4)	N1–Zn–N3	88.13(13)
O1–Zn–O2	177.69(11)	N1′A[a]–Zn–N2	90.51(14)
O1–Zn–N1	90.82(13)	N1′A[a]–Zn–N3	88.68(13)
O1–Zn–N1′A[a]	88.71(14)	S1–O1–Zn1	139.01(8)
O1–Zn–N2	92.89(13)	S2–O2–Zn1	141.9(2)
O1–Zn–N3	85.96(13)		

Symmetry transformations used to generate equivalent atoms: (a) $x, y-1, z$.

incorporate three equivalents of bipy per Zn(II) ion within their structures, **2** has four equivalents of bipy instead.

Compounds **4** and **5** were crystallized from DMSO by the combination of one equivalent of $Zn(ClO_4)_2 \cdot 6H_2O$ with 1.5 equivalents of bipy under ambient laboratory conditions while **6** was obtained using three equivalents of bipy (Scheme 1). From these reactions, compound **1** also co-crystallized as the major product while **4**, **5** (both present as colorless plates of similar morphology), and **6** (colorless blocks) were the minor products. Note that the initial Zn:bipy stoichiometries do not reflect those contained within the products. Additionally, reducing the relative quantity of bipy has no apparent effect on the quantity of **1** produced but favors the formation of compounds **4** and **5** compared to **6**. None of the compounds **1**–**6** are sensitive to loss of solvent or inclusions.

3.2. Description of the structures

Crystallographic and structural refinement data for the title compounds are given in Table 1. Selected bond distances and angles for **1**, **2**, **3**, **4**, **5** and **6** are shown in Tables 2–7, respectively.

3.3. $[Zn(4,4'\text{-bipy})_2(H_2O)_4](ClO_4)_2 \cdot 2(4,4'\text{-bipy})$ (1)

Compound **1** consists of sheet-like arrays of monomeric $[Zn(4,4'\text{-bipy})_2(H_2O)_4]^{2+}$ cations connected by intermediary, uncoordinated bipy molecules arranged to form hydrophobic, triangular channels. The ZnN_2O_4 unit (Fig. 1a) adopts a slightly distorted octahedral geometry, being coordinated axially by two *trans*-related 4,4′-bipyridine ligands with the equatorial sites occupied by four aqua ligands. The pyridyl rings of the bipy ligands are not coplanar but twisted along the central C–C bonds at angles of 27.9° with respect to one another. The monomeric $[Zn(4,4'\text{-bipy})_2(H_2O)_4]^{2+}$ cations form stacks along the *a*-axis. The uncoordinated pyridyl rings of the bipy ligands interdigitate with those in adjacent stacks giving

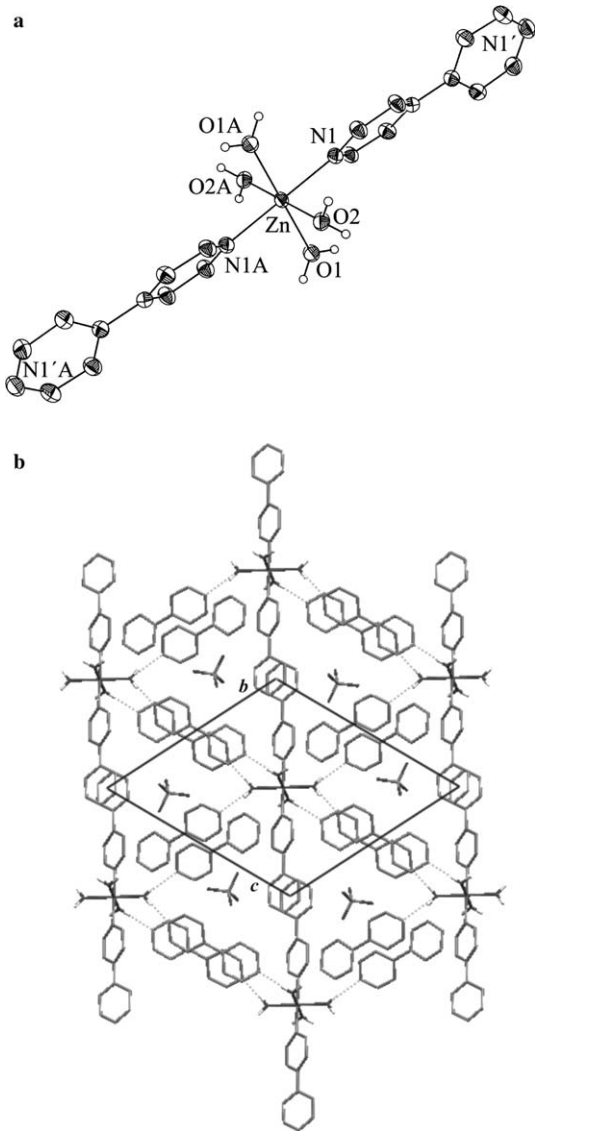

Fig. 1. Crystal structure of $[Zn(4,4'\text{-bipy})_2(H_2O)_4](ClO_4)_2 \cdot 2(4,4'\text{-bipy})$ (**1**): (a) ORTEP plot (drawn to encompass 50% of electron density) of a $[Zn(4,4'\text{-bipy})_2(H_2O)_4]^{2+}$ monomer with atomic numbering scheme and (b) perspective view parallel to the *a*-axis depicting the layered structure and triangular channels. All aromatic hydrogen atoms have been omitted for clarity.

rise to pseudo two-dimensional sheets. The offset face-to-face distances range from ≈3.1 to 3.5 Å indicative of relatively strong π-stacking interactions sustaining the sheets.

The sheets of monomers are well separated by uncoordinated bipy molecules and perchlorate counterions (Fig. 1b). The uncoordinated bipy's crosslink the sheets through an extensive array of N···H–O hydrogen bonds (1.98–2.08 Å) between the uncoordinated pyridyl nitrogen atoms and nearby aqua ligands, ultimately giving rise to a three-dimensional hydrogen-bonded network. The stacks of bipy guests define triangular, hydrophobic channels along the *a*-axis that clathrate perchlorate counterions. Two- and three-dimensional hydrogen-bonded networks

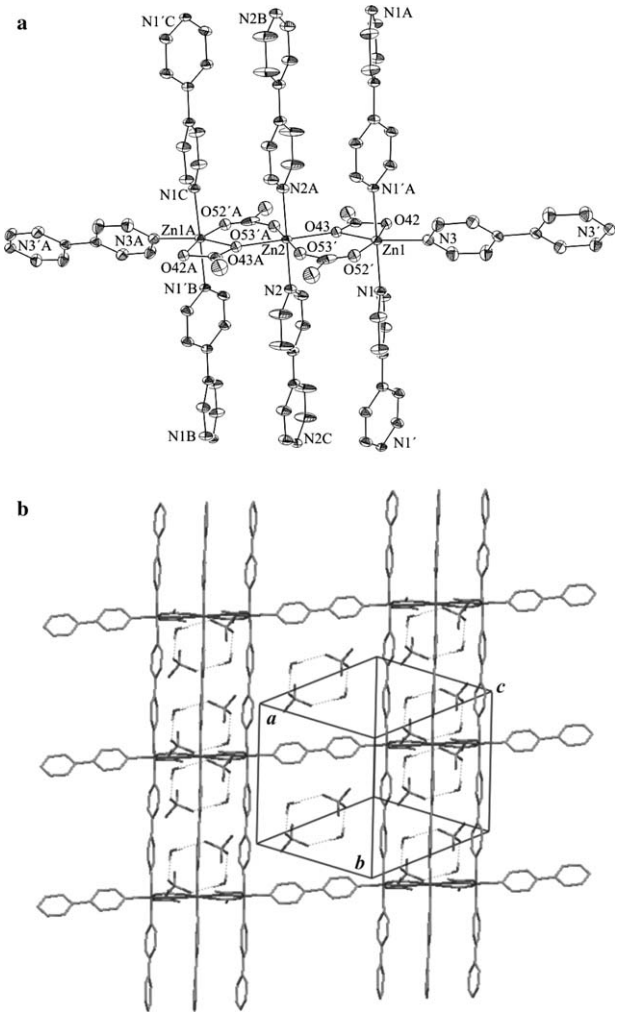

Fig. 2. Crystal structure of $[Zn_3(4,4'\text{-bipy})_4(OAc)_4](ClO_4)_2 \cdot 2(H_2O)$ (**2**): (a) ORTEP plot (drawn to encompass 50% of electron density) of a $[Zn_3(4,4'\text{-bipy})_8(OAc)_4]^{2+}$ moiety with atomic numbering scheme and showing only one orientation of the disordered acetate ligands and (b) perspective view of a sheet within the *ac*-plane depicting the prismatic and rectangular cavities as well as the cyclic, hydrogen-bonded perchlorate-water moieties. All aromatic and aliphatic hydrogen atoms have been omitted for clarity.

sustained through intermediary, uncoordinated bipy molecules have also been reported for $[Zn(4,4'\text{-bipy})(H_2O)_4](NO_3)_2 \cdot (4,4'\text{-bipy})$, $[Zn(4,4'\text{-bipy})(H_2O)_4](NO_3)_2 \cdot 2(4,4'\text{-bipy}) \cdot 3(H_2O)$ [2], and $[Zn(4,4'\text{-bipy})(H_2O)_3(ClO_4)](ClO_4) \cdot (4,4'\text{-bipy}) \cdot 1.5(H_2O)$ [19,20].

3.4. $[Zn_3(4,4'\text{-bipy})_4(OAc)_4](ClO_4)_2 \cdot 2(H_2O)$ (**2**)

The structure of compound **2** consists of cationic, two-dimensional $[Zn_3(4,4'\text{-bipy})_4(OAc)_4]^{2+}$ sheets that feature hydrophobic rectangular and prismatic cavities. The basic repeating units within the sheets are centrosymmetric, planar, $[Zn_3(OAc)_4]$ trimers that contain Zn(II) metal centers connected by *syn–syn* bridging acetate ligands (Fig. 2a). The peripheral Zn(II) ions are connected to the central metals each through unsymmetrical bridging (η-1,1) and bridging/chelating (η-1,3) acetate anions. The acetates are disordered in two parts about the central carbon atoms: one orientation consists of the η-1,1-mode and the other part is the η-1,3-chelate/bridge.

There are two distinct types of Zn(II) ions within the $[Zn_3(OAc)_4]$ trimers and the local coordination environments of the metal centers are depicted in Fig. 2a. For the peripheral Zn(II) ions, the $Zn1N_3O_3$ unit adopts a highly distorted octahedral geometry. The equatorial *cis*- and *trans*-N–Zn1–O and O–Zn1–O angles deviate significantly from the expected 90° and 180°, respectively, due to the chelating acetate ligands. The bite angles of the four-member chelating acetate rings (O42–Zn1–O43 and O52–Zn1–O53) are 58.8° and 58.5°, respectively. The central $Zn2N_2O_4$ site is also distorted, being coordinated axially by two *trans*-related 4,4′-bipyridine ligands and equatorially by oxygen atoms from four disordered acetate ligands. The Zn1–O43 (43A)–Zn2 and Zn1–O53 (O53A)–Zn2 bridging angles are 119.1° and 120.3°, respectively.

The axial bipy ligands link adjacent $[Zn_3(OAc)_4]$ trimers to form Zn–bipy triple chains which extend along the *b*-axis. The Zn–bipy–Zn distances along the three chains are all equal (11.464 Å). While the pyridyl rings of the outer chain bipy's are twisted 30.1° along the central C–C bonds, those of the central bipy ligands are coplanar. Adjacent aromatic rings participate in weak, offset π-stacking interactions with face-to-face contacts of ≈3.8 Å, reflecting the Zn1–Zn2 and Zn1A–Zn2 separation distances of 3.784 Å. The close approach of the aromatic rings causes slight distortions along both the peripheral and central bipy chains.

The equatorial bipy ligands further link the peripheral Zn(II) ions of the trimers perpendicular to the chains to form two-dimensional, cationic sheets (Fig. 2b). The sheets possess two distinct types of cavities. Narrow, prismatic cavities (3.78×11.64 Å^2) within the triple chains and larger, rectangular hydrophobic cavities (11.46×11.59 Å^2) are found between the triple chains. Sheet topologies exhibiting a related connectivity as well as possessing both prismatic and rectangular cavities similar to **2** are observed in $[M_8(ip)_8(4,4'\text{-bipy})_8]$ (M = Ni, Cd; ip = isophthalate) [21] and [M(tp)(4,4′-bipy)] (M = Co, Cd, Zn; tp = terephthalate) [22], all of which incorporate carboxylate-bridged, metal–bipy double chains rather than the triple chains observed for **2**.

Adjacent sheets are offset, super-positioning the prismatic cavities within the triple chains toward the faces of the rectangular, hydrophobic cavities on adjacent sheets. The space between the sheets is occupied by anionic, cyclic, dimeric units (Fig. 2b) comprised of two perchlorate counterions and two lattice water molecules that are sustained by two short (1.99 Å) and two long (2.22 Å) O···H–O hydrogen bonds. Similar clusters have been observed in $[Cd(4,4'\text{-bipy})_2(H_2O)_2] \cdot (NO_3)_2 \cdot 4(H_2O)$ [23].

3.5. $[Zn_3(4,4'\text{-bipy})_3(OAc)_4(H_2O)_2](ClO_4)_2 \cdot (H_2O)$ (3)

The structure of compound **3** consists cationic $[Zn_3(4,4'\text{-bipy})_3(OAc)_4(H_2O)_2]^{2+}$ three-leg ladders containing hydrophobic, prismatic cavities. The basic repeating units within the ladders are centrosymmetric, planar, $[Zn_3(OAc)_4]$ trimers, similar to those in **2**, that contain Zn(II) metal centers connected by *syn–syn* bridging acetate ligands (Fig. 3a). In contrast to **2**, the peripheral $Zn2N_2O_4$ moiety contains an equatorial aqua ligand (O5) in place of the bridging bipy.

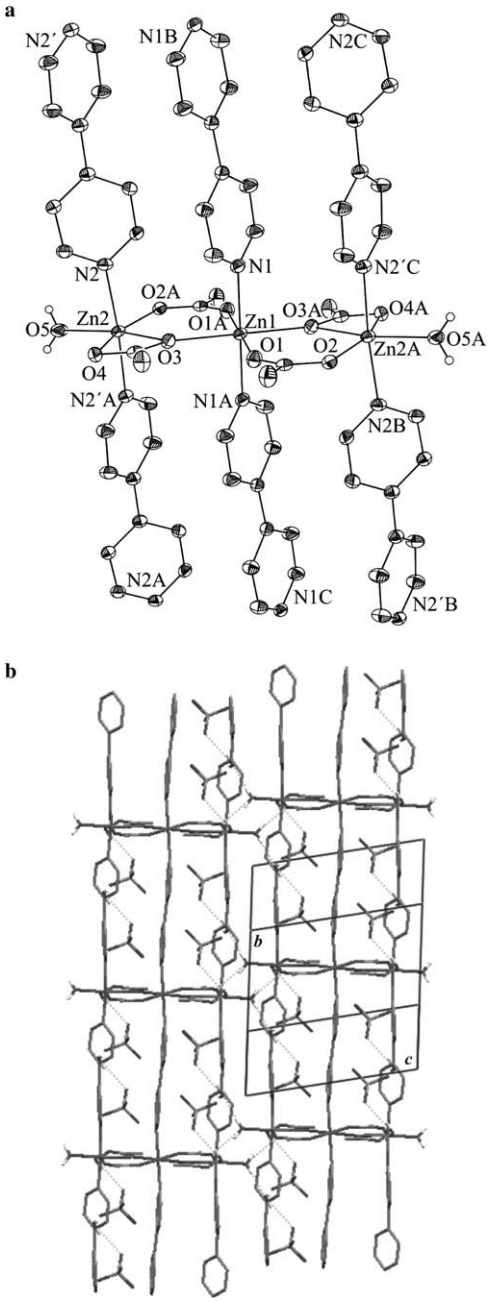

Fig. 3. Crystal structure of $[Zn_3(4,4'\text{-bipy})_3(OAc)_4(H_2O)_2](ClO_4)_2 \cdot (H_2O)$ (**3**): (a) ORTEP plot (drawn to encompass 50% of electron density) of a $[Zn_3(4,4'\text{-bipy})_6(OAc)_4(H_2O)_2]^{2+}$ moiety with atomic numbering scheme and (b) perspective view of a sheet of three-leg ladders within the *bc*-plane depicting prismatic cavities. All aromatic and aliphatic hydrogen atoms have been omitted for clarity.

The bipy ligands coordinated above and below the plane containing the $[Zn_3(OAc)_4]$ moieties link adjacent trimers together to form three-leg ladders which extend along the crystallographic *b*-axis (Fig. 3b). The Zn–bipy triple chains act as the legs and the $[Zn_3(OAc)_4]$ moieties act as the rungs. The replacement of the equatorial bridging bipy ligands in **2** by aqua ligands prevents **3** from extending along the *c*-axis to form two-dimensional sheets. The Zn–bipy–Zn distances along the three chains are all equal (11.325 Å). While the pyridyl rings of the outer leg bipy's are twisted 36.7° along the central C–C bonds, those of the central bipy ligands are coplanar. Adjacent aromatic rings participate in weak, offset π-stacking interactions with face-to-face contacts ranging from ≈3.8 to 4.0 Å. The close approach of the twisted aromatic rings causes a significant distortion along the central bipy chains. In contrast, the peripheral chains experience only a slight distortion. Narrow, prismatic cavities (3.89×11.33 Å^2) are present within the three-leg ladders. Adjacent three-leg ladders are juxtaposed on a side-by-side fashion to form pseudo two-dimensional sheets sustained by double, inter-ladder hydrogen bonds (O···H–O, 1.98 Å) between the aqua and acetate ligands on adjacent ladders. The sheets adopt a layered topology, similar to that in **2**. The interlayer space is occupied by lattice waters and perchlorate counterions. Acetate-bridged, three-leg ladder coordination polymers similar to **3** have been reported for $[Zn_3(OAc)_4(4,4'\text{-bipy})_3\{N(CN)_2\}_2]$ [24] and $[Co_3(OAc)_4(bpe)_3(dca)_2]$ (bpe = 1,2-bis-(4-pyridyl)ethane, dca = dicyanamide) [25] while $[Cu(4,4'\text{-bipy})(OAc)_2]_2 \cdot 2.5(H_2O)$ and $[Zn(4,4'\text{-bipy})(OAc)_2]_2$ [26] are analogous two-leg ladders.

3.6. Structure of $[Zn(4,4'\text{-bipy})(ClO_4)(H_2O)(OH)]$ (4)

Compound **4** is a network of neutral, interpenetrating, zig-zag chains. The ZnN_2O_3 unit (Fig. 4a) adopts a distorted trigonal bipyramidal geometry, being coordinated axially by aqua (O1) and hydroxide (O2) ligands while the equatorial sites are occupied by two 4,4′-bipyridine ligands and a monodentate perchlorate anion (O3). The Zn–O bond distances exhibit considerable variation. The Zn–O3 bond (1.96 Å) is short compared to the distances reported for other Zn(II)–monodentate ClO_4^- complexes (2.32–2.38 Å) however, the equatorial coordination of perchlorate in **4** would account for this discrepancy [20]. Similarly, the long Zn–O1 (2.24 Å) and intermediate Zn–O2 (2.09 Å) bonds are longer than those distances reported for aqua-Zn(II) (2.12–2.19Å) [2] and hydroxo-Zn(II) (1.94–1.97 Å) [27] complexes due to their axial coordination. The intermediate Zn–O2 bond is reasonable for a coordinated hydroxide ion rather than an aqua ligand based on bond distance and charge balance considerations.

Compound **4** exhibits a form of inclined interpenetration with the zig-zag chains weaving a three-dimensional network in the *bc* plane, intersecting at an angle of ≈80° (Fig. 4b). The sheets then stack along the *a* axis, held together by hydrogen bonds (O···H–O, 1.92 Å) between

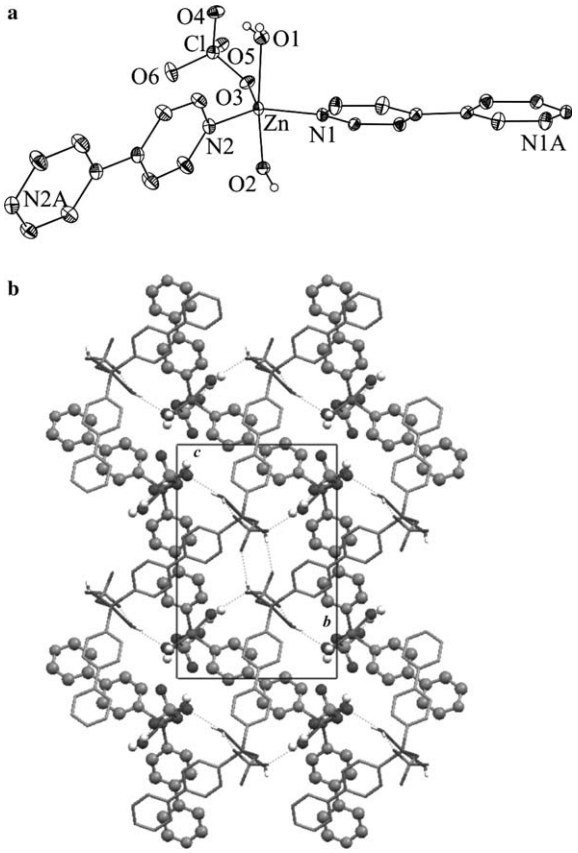

Fig. 4. Crystal structure of $[Zn(4,4'\text{-bipy})(ClO_4)(H_2O)(OH)]$ (**4**): (a) ORTEP plot (drawn to encompass 50% of electron density) of a $[Zn(4,4'\text{-bipy})_2(ClO_4)(H_2O)(OH)]$ fragment with atomic numbering scheme and (b) perspective view parallel to the *a*-axis depicting the network of mutually interpenetrated chains; adjacent parallel chains are shown in tube form and adjacent inclined chains are shown as ball-and-stick representation. All aromatic hydrogen atoms have been omitted for clarity.

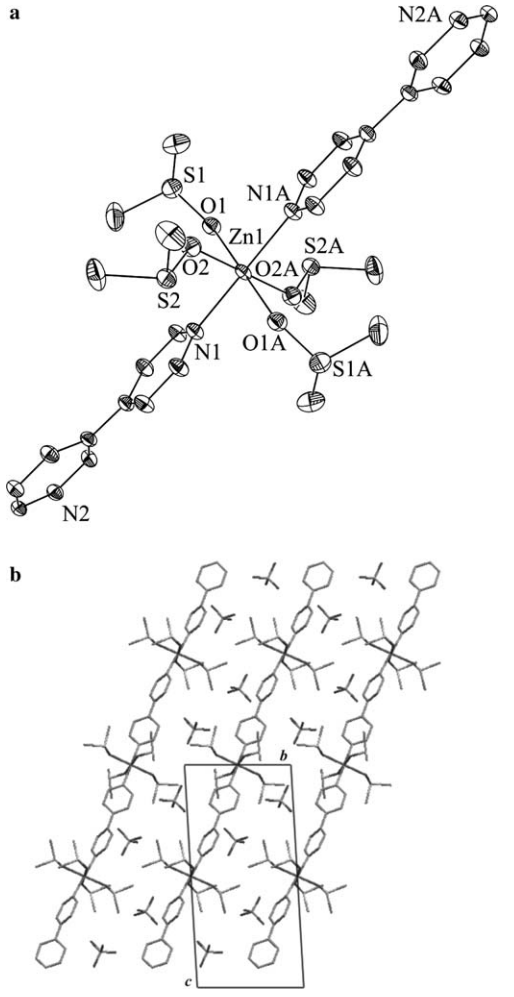

Fig. 5. Crystal structure of $[Zn(4,4'\text{-bipy})(DMSO)_4](ClO_4)_2$ (**5**): (a) ORTEP plot (drawn to encompass 50% of electron density) of a $[Zn(4,4'\text{-bipy})_2(DMSO)_4]^{2+}$ fragment with atomic numbering scheme and (b) perspective view parallel to the *a*-axis depicting the linear chains. All aromatic and aliphatic hydrogen atoms have been omitted for clarity.

the hydroxide and perchlorate oxygen atoms on adjacent chains. This self-inclusion reduces the volume of void space so that no lattice guests or counterions are present. Interpenetration to fill void space within a lattice is now a common feature of coordination polymers [28]. Some related examples include $[Cu(bpe)_2][Cu(bpe)(H_2O)_2(SO_4)_2]\cdot 2H_2O$ (bpe = *trans*-1,2-bis(4-pyridyl)ethylene), which is a three-dimensional interpenetrated network resulting from one-dimensional $[Cu(bpe)_2]$ chains threading through and filling void space within the rhombic channels of adjacent two-dimensional $[Cu(4,4'\text{-bpe})(H_2O)_2(SO_4)_2]$ grids [29]. Additionally, $[Cu(bpe)(H_2O)(SO_4)]$ is a mutually interpenetrated, three-dimensional network resulting from the inclusion of undulating, two-dimensional grids into the rhombic channels of adjacent sheets [29].

3.7. Structure of $[Zn(4,4'\text{-bipy})(DMSO)_4](ClO_4)_2$ (5)

Compound **5** consists of cationic, one-dimensional $[Zn(4,4'\text{-bipy})(DMSO)_4]^{2+}$ chains. The ZnN_2O_4 unit (Fig. 5a) adopts a slightly distorted octahedral geometry, being coordinated axially by two *trans*-related bipy ligands while the equatorial sites are occupied by four DMSO ligands. As shown in Fig. 5b, the *trans*-coordination of the bridging bipy ligands produces linear chains that extend along the [0 −1 1] direction. The pyridyl rings and the bipy ligands are not coplanar but twisted at an angle of 38.0°. Adjacent chains are arranged in a staggered fashion (Fig. 5b) with perchlorate anions tying them together via weak O···H–C contacts (2.43–2.67 Å) with nearby methyl and aromatic hydrogen atoms.

3.8. $[Zn(4,4'\text{-bipy})_3(DMSO)_2](ClO_4)_2\cdot 2(4,4'\text{-bipy})(H_2O)$ (6)

The structure of compound **6** consists of cationic, one-dimensional $[Zn(4,4'\text{-bipy})_3(DMSO)_2]^{2+}$ chains. The ZnN_4O_2 unit (Fig. 6a) is a slightly distorted octahedron with axial DMSO ligands and four equatorial bipy ligands. Two *trans* bipy ligands bridge the Zn(II) ions to form infinite linear chains (Fig. 6b) whereas the other *trans* pair are

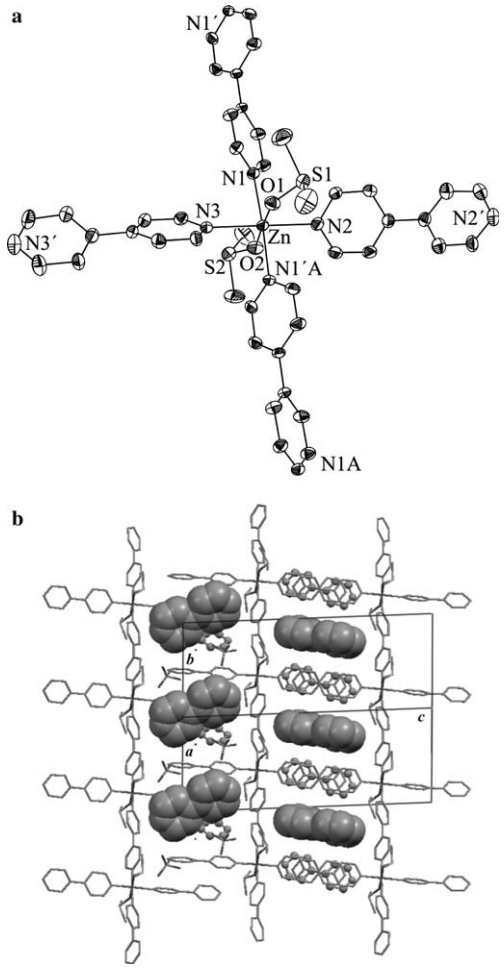

Fig. 6. Crystal structure of $[Zn(4,4'\text{-bipy})_3(DMSO)_2](ClO_4)_2 \cdot 2(4,4'\text{-bipy}) \cdot (H_2O)$ (**6**): (a) ORTEP plot (drawn to encompass 50% of electron density) of a $[Zn(4,4'\text{-bipy})_4(DMSO)_2]^{2+}$ moiety with atomic numbering scheme and (b) perspective view depicting the hydrophobic channels that extend along the [1 1 0] and [−1 1 0] directions as well as the intercalating, non-disordered guest molecules (in ball-and-stick representation) and disordered guest molecules (in space filling representation). All aromatic and aliphatic hydrogen atoms have been omitted for clarity. Only one orientation of the disordered bipy molecules is shown.

monocoordinate, accounting for the 1:3 metal:bipy stoichiometry within the host.

Adjacent Zn–bipy chains are linked by overlapping the monocoordinate bipy ligands to form two-dimensional sheets (Fig. 6b). The closest face-to-face distance between the aromatic rings is ≈3.6 Å indicating strong π-stacking interactions sustaining the sheets. One set of the uncoordinated bipy molecules intercalates between pairs of the monocoordinate bipy ligands to link adjacent sheets in the *a* direction with similarly strong π-stacking interactions (3.6–3.9 Å). Compound **6** is nearly isostructural with the previously reported copper analog, $[Cu(4,4'\text{-bipy})_3(DMSO)_2](ClO_4)_2 \cdot 2(4,4'\text{-bipy})$ [30].

The characteristic alignment of the Zn–bipy chains produces hydrophobic, rectangular cavities of dimensions of 11.45×12.89 Å^2 within the sheets. The offset superpositioning of the sheets aligns the hydrophobic cavities to form oblique channels that extend along the [1 1 0] and [−1 1 0] directions. The void space within the channels is occupied by a set of disordered uncoordinated bipy molecules, lattice waters, and perchlorate counterions. The disordered bipy's are partially stabilized by edge-to-face C–H···π facial interactions (close contacts ≈2.8–2.9 Å) with the edges of nearby non-disordered bipy molecules and pairs of monodentate bipy ligands. Compound **6** is related to a number of porous metal–bipy coordination polymers possessing hydrophobic cavities that clathrate guests. The compounds $[Ni(4,4'\text{-bipy})_3(H_2O)_2](ClO_4)_2 \cdot 1.4(4,4'\text{-bipy}) \cdot 3(H_2O)$, $[Co(4,4'\text{-bipy})_3(H_2O)_2](ClO_4)_2 \cdot 1.4(4,4'\text{-bipy}) \cdot 3(H_2O)$ [30], $[Zn(4,4'\text{-bipy})(H_2O)_4](NO_3)_2 \cdot 2(4,4'\text{-bipy}) \cdot 3H_2O$ [2], and $[Cu(4,4'\text{-bipy})(H_2O)_2(BF_4)_2] \cdot (4,4'\text{-bipy})$ [31] consist of one-dimensional chains that form porous, layered, sheet-like topologies, similar to that in **6**, sustained by various hydrogen bonding and hydrophobic interactions. In contrast, in $[Cd(4,4'\text{-bipy})_2(H_2O)_2] \cdot (NO_3)_2 \cdot 4(H_2O)$ [8,23], $[Zn(4,4'\text{-bipy})_2(H_2O)_2](ClO_4)_2 \cdot 2(2,4'\text{-bipy}) \cdot (H_2O)$, and $[Cu(4,4'\text{-bipy})_2(H_2O)_2](ClO_4)_4 \cdot (4,4'\text{-}H_2\text{bipy})$ [19], the monodentate bipy's are replaced by bridging bipy's to form two-dimensional grids, but the rectangular, hydrophobic cavities similar to those in **6** that clathrate bipy guests are retained.

4. Conclusions

This paper reports the crystal structures of six novel zinc(II)–4,4′-bipyridine coordination polymers that exhibit a diverse array of structural topologies common in supramolecular chemistry. The compounds $[Zn(4,4'\text{-bipy})_2(H_2O)_4](ClO_4)_2 \cdot 2(4,4'\text{-bipy})$ (**1**), $[Zn_3(4,4'\text{-bipy})_4(OAc)_4](ClO_4)_2 \cdot 2(H_2O)$ (**2**), and $[Zn_3(4,4'\text{- bipy})_3(OAc)_4(H_2O)_2](ClO_4)_2 \cdot (H_2O)$ (**3**) were crystallized under hydrothermal conditions. Compound **1** contains hydrogen-bonded, sheet-like arrays of discreet monomers connected by uncoordinated bipy molecules arranged into stacks of hydrophobic, triangular channels. Compounds **2** and **3** consist of acetate-bridged, Zn–bipy triple chains arranged in layered, two-dimensional sheets and three-leg ladders, respectively, with hydrophobic, prismatic channels. In contrast, $[Zn(4,4'\text{-bipy})(ClO_4)(H_2O)(OH)]$ (**4**), $[Zn(4,4'\text{-bipy})(DMSO)_4](ClO_4)_2$ (**5**), and $[Zn(4,4'\text{-bipy})_3(DMSO)_2](ClO_4)_2 \cdot 2(4,4'\text{-bipy}) \cdot (H_2O)$ (**6**) were crystallized from DMSO under ambient laboratory conditions. Compound **4** is a mutually interpenetrated network of hydrogen-bonded, one-dimensional Zn–bipy zig-zag chains while compound **5** exists as isolated, linear chains. Compound **6** is a porous, three-dimensional network of Zn–bipy chains, sustained by π-stacking interactions between bipy ligands and guests, which possess clathrated, hydrophobic channels. The title compounds not only demonstrate the ability of bipy to create novel and diverse coordination solids, but also show that weak hydrogen-bonding and π-stacking interactions in addition to covalent bonds can be employed to assemble supramolecular networks and porous solids.

Acknowledgments

This work was partially supported by the National Science Foundation through Grants DMR-9900855 and DMR-0543362 (D.R.T.). Partial support from the Petroleum Research Fund, administered by the ACS, is gratefully acknowledged (D.R.T.). K.A.A. wishes to acknowledge the National Science Foundation and the University of Florida for funding of the purchase of the X-ray equipment.

Appendix A. Supplementary material

Crystallographic data for the structural analysis have been deposited with the Cambridge Crystallographic Data Centre, CCDC 289243–289248 for compounds **1**–**6**, respectively. Copies of this information may be obtained free of charge from The Director, CCDC, 12 Union Road, Cambridge, CB2 1EZ, UK (fax: +44 1223 336 033; email: deposit@ccdc.cam.ac.uk or www: http://www.ccdc.cam.ac.uk). Supplementary data associated with this article can be found, in the online version, at doi:10.1016/j.poly.2006.03.013.

References

[1] M.J. Zaworotko, Chem. Commun. (2001) 1.
[2] L. Carlucci, G. Ciani, D.M. Proserpio, A. Sironi, J. Chem. Soc., Dalton Trans. (1997) 1801.
[3] R.H. Groeneman, L.H. MacGillivray, J.L. Atwood, Inorg. Chem. 38 (1999) 208.
[4] M.J. Zaworotko, Chem. Soc. Rev. (1994) 283.
[5] B.D. Wagner, G.J. McManus, B. Moulton, M.J. Zaworotko, Chem. Commun. 18 (2002) 2176.
[6] O.M. Yaghi, H. Li, T.L. Groy, Inorg. Chem. 36 (1997) 4292.
[7] M. Fujita, Y.J. Kwon, S. Washizu, K. Ogura, J. Am. Chem. Soc. 116 (1994) 1151.
[8] M.-L. Tong, S.-L. Zheng, X.-M. Chen, Polyhedron 19 (2000) 1809.
[9] R.W. Gable, B.F. Hoskins, R. Robson, J. Chem. Soc., Chem. Commun. (1990) 1677.
[10] T. Soma, H. Yuge, T. Iwamoto, Angew. Chem., Int. Ed. Engl. 33 (1994) 1655.
[11] S. Subramanian, M.J. Zaworotko, Angew. Chem., Int. Ed. Engl. 34 (1995) 2127.
[12] G.B. Gardner, D. Venkataraman, J.S. Moore, S. Lee, Nature 374 (1995) 792.
[13] M. Kondo, M. Shimamura, S.I. Noro, S. Minakoshi, A. Asami, K. Seki, S. Kitagawa, Chem. Mater. 12 (2000) 1288.
[14] O.M. Yaghi, H. Li, J. Am. Chem. Soc. 118 (1996).
[15] J.S. Seo, D. Whang, H. Lee, S.I. Jun, J. Oh, Y.J. Jeon, K. Kim, Nature 404 (2000) 982.
[16] T. Sawaki, T. Dewa, Y. Aoyama, J. Am. Chem. Soc. 120 (1998) 8639.
[17] A. Erxleben, Coord. Chem. Rev. 246 (2003) 203.
[18] G.M. Sheldrick, Bruker-AXS, Madison, WI, USA, 2000.
[19] M.-L. Tong, B.-Y. Ye, J.-W. Cai, X.-M. Chen, S.W. Ng, Inorg. Chem. 37 (1998) 2645.
[20] M.-L. Tong, J.-W. Cai, X.-L. Yu, X.-M. Chen, S.W. Ng, T.C.W. Mak, Aust. J. Chem. 51 (1998) 637.
[21] J. Tao, X.-M. Chen, R.-B. Huang, L.-S. Zheng, J. Solid State Chem. 170 (2003) 130.
[22] J. Tao, M.-L. Tong, X.-M. Chen, J. Chem. Soc., Dalton Trans. (2000) 3669.
[23] M. Aoyagi, K. Biradha, M. Fujita, Bull. Chem. Soc. Jpn. 73 (2000) 1369.
[24] B.-W. Sun, S. Gao, Z.-M. Wang, Chem. Lett. (2001) 2.
[25] D. Ghoshal, G. Mostafa, T.K. Maji, E. Zangrando, T.-H. Lu, J. Ribas, N.R. Chaudhuri, New. J. Chem. 28 (2004) 1204.
[26] B. Conerney, P. Jensen, P.E. Kruger, B. Moubaraki, K.S. Murray, CrystEngComm 5 (2003) 454.
[27] R. Stahl, C. Jung, H.D. Lutz, W. Kockelmann, H. Jacobs, Z. Anorg. Allg. Chem. 624 (1998) 1130.
[28] S.R. Batten, R. Robson, Angew. Chem., Int. Ed. Engl. 37 (1998) 1460.
[29] D. Hagrman, R.P. Hammond, R. Haushalter, J. Zubieta, Chem. Mater. 10 (1998) 2091.
[30] J.D. Woodward, R. Backov, K.A. Abboud, H. Ohnuki, M.W. Meisel, D.R. Talham, Polyhedron 22 (2003) 2821.
[31] A.J. Blake, S.J. Hill, P. Hubberstey, W.-S. Li, J. Chem. Soc., Dalton Trans. (1997) 913.

that for a given ligand coordination environment, the more highly organized structure will have lower spin-state crossover temperatures and more abrupt crossovers than those with less highly or more "loosely" organized structures. In contrast, we have shown that differences in the molecular, rather than supramolecular, structure of the two crystallographically independent molecules in $Fe[(p\text{-}HC{\equiv}CC_6H_4)B(3\text{-}Mepz)_3]_2$ can have an impact on the temperature and abruptness of the observed spin-state crossover.

Herein we report the synthesis, solid-state structure, and magnetic and Mössbauer spectral properties of $Fe[(C_6H_5)B(3\text{-}Mepz)_3]_2$, the parent complex of the $Fe[(p\text{-}R\text{-}C_6H_4)B(3\text{-}Mepz)_3]_2$ complexes referred to above. Analyses of these results provide interesting new insight into the factors that control the spin-crossover behavior of this class of compounds.

2. Experimental

2.1. General considerations

Unless otherwise specified, all operations were carried out under a nitrogen atmosphere by using either standard Schlenk techniques or a Vacuum Atmospheres HE-493 inert atmosphere dry box. Solvents for synthetic procedures and spectroscopic studies were dried by conventional methods and distilled under a N_2 atmosphere immediately prior to use. All chemicals were purchased from Aldrich Chemicals. 3-Methylpyrazole was distilled under vacuum before use. Robertson Microlit Laboratories performed all elemental analyses. Melting point determinations were made on samples contained in glass capillaries using an Electrothermal 9100 apparatus and are uncorrected. Mass spectrometric measurements recorded in ESI(±) mode were obtained on a Micromass Q-Tof spectrometer. NMR spectra were recorded by using a Varian Gemini 300. Chemical shifts were referenced to solvent resonances at δ_H 7.26 for $CDCl_3$, and δ_H 3.31 for CD_3OD.

Magnetic susceptibilities were measured between 4 and 300 K in an applied field of 0.5 T using a Quantum Design MPMS XL SQUID magnetometer. The sample was measured in a gelatin capsule whose very small diamagnetic susceptibility made a negligible contribution to the overall observed susceptibility. The molar magnetic susceptibility of $Fe[(C_6H_5)B(3\text{-}Mepz)_3]_2$ was calculated with a molecular mass of 718.26 g/mol and was corrected by -364.5×10^{-6} emu/mol for the diamagnetism of the complex, a value which was obtained from tables of Pascal's constants.

The Mössbauer spectral absorber contained 42 mg/cm^2 of crushed but unground crystals of $Fe[(C_6H_5)B(3\text{-}Mepz)_3]_2$ mixed with boron nitride. The spectra were measured at 4.2, 78, and 295 K on a constant-acceleration spectrometer which utilized a room temperature rhodium matrix cobalt-57 source and was calibrated at room temperature with α-iron foil. The spectra have been fit with a single symmetric quadrupole doublet and the estimated relative errors of the fitting parameters are ±0.005 mm/s for the isomer shifts and ±0.01 mm/s for the quadrupole splittings and line widths. The absolute errors are approximately twice as large.

2.2. $Na[(C_6H_5)B(3\text{-}Mepz)_3]$ (1)

In the drybox, neat BBr_3 (3.76 g, 15.0 mmol. *Caution*. The vapors of neat boron tribromide are very corrosive toward stopcock grease and plastics) was added by pipette to neat phenyltrimethylsilane (2.04 g, 13.6 mmol) contained in a PTFE-stopcock Schlenk flask and was capped with a PTFE-taped glass stopper. The stopper of the Schlenk flask was reinforced with rubber bands, taken out of the dry box, and placed in a 60 °C oil bath, with the stopcock closed, for 4.5 h (*Caution*. Adequate shielding must be used at this point because a closed system is being heated; the rubber bands, in conjunction with the glass stopper, act as a check valve for pressure build-up). After the reaction was complete, the volatile components were removed by vacuum distillation at room temperature to yield 3.16 g (94%) of crude $C_6H_5BBr_2$ as an off-white solid. The glass stopper was replaced with a rubber septum, and the $C_6H_5BBr_2$ (3.16 g, 12.8 mmol) was dissolved, in situ, in 50 mL toluene. The $C_6H_5BBr_2$ solution was added via cannula to a solution of 3-methylpyrazole (3.14 g, 38.3 mmol) and NEt_3 (3.55 mL, 25.6 mmol) in toluene (150 mL). After the resulting cloudy suspension was stirred at room temperature overnight, the toluene solution [presumably containing $(C_6H_5)B(3\text{-}Mepz)_2(3\text{-}MepzH)$] was transferred to a 500 mL Schlenk flask by cannula filtration thereby removing the colorless precipitate of $(HNEt_3)Br$ (4.38 g, 94%). A solution of NaO^tBu (1.23 g, 12.8 mmol) in 1:1 toluene/THF (50 mL) was added by cannula to the solution of "$(C_6H_5)B(3\text{-}Mepz)_2(3\text{-}MepzH)$" and the resulting suspension was stirred for 12 h. The colorless solid was separated by filtration, washed with hexanes (2 × 100 mL) and was dried under vacuum to leave 4.00 g (85%, from phenyltrimethylsilane) of $Na[(C_6H_5)B(3\text{-}Mepz)_3]$ as a white solid. Mp, 282 °C sinters; 300 °C dec. black liquid. ^{1}H NMR (300 MHz, CD_3OD, 25 °C): $\delta = 7.25$ (m, 2H, *meta*-H), 7.11 (m, 3H, *ortho*-H and *para*-H), 7.05 (d, $J = 1.5$ Hz, 3H, H_5-pz), 5.86 (d, $J = 1.5$ Hz, 3H, H_4-pz), 2.23 (s, 9H, CH_3); ^{13}C NMR (125.79 MHz, CD_3OD, 25 °C): $\delta = 149.23$, 136.78, 135.14, 134.14, 127.28, 125.74 (C_3- and C_5-pz, aryl) 103.67 (C_4-pz), 13.44 (–CH_3) High Res. ESI(−)MS, Calc. (Obs.) for anion: 331.1843 (331.1844).

2.3. $Fe[(C_6H_5)B(3\text{-}Mepz)_3]_2$ (2)

Under inert atmosphere, the addition of an aqueous solution (50 mL) of $FeCl_2\cdot4H_2O$ (0.153 g, 0.77 mmol) to a methanol solution (20 mL) of **1** (0.546 g, 1.54 mmol) yielded a copious amount of colorless solid that was isolated by filtration. The solid was then taken up in CH_2Cl_2, the solution was dried over $MgSO_4$, filtered, and the

$MgSO_4$ was extracted with boiling benzene (2×100 mL, caution) and filtered hot. After cooling, the solvent was removed from the combined organic fractions by rotary evaporation to yield 0.360 g (65%) of pure $Fe[(C_6H_5)B(3\text{-}Mepz)_3]_2$ as a colorless solid. Recrystallization of this solid by layering a CH_2Cl_2 solution of the complex with methanol and allowing the solvents to diffuse slowly over two days yielded 0.280 g (78% from 0.360 g) of X-ray quality, colorless block crystals. Mp, 289 °C slowly darkens; 293–294 °C dec. charred, black solid. *Anal.* Calc. for $C_{36}H_{40}B_2FeN_{12}$: C, 60.20; H, 5.61; N, 23.40. Found: C, 60.42; H, 5.78; N, 23.25. ^1H NMR (300 MHz, $CDCl_3$, 25 °C) 45.6, 43.4, 23.8, 4.4, 2.9, −5.9. High Res. ESI(+)MS, Calc. (Obs.): 718.3047 (718.3052).

2.4. X-ray structure determination of $Fe[(C_6H_5)B(3\text{-}Mepz)_3]_2$ at 90 and 294 K

Two X-ray intensity data sets were measured at 90(1) and 294(1) K on a Bruker SMART APEX CCD-based diffractometer [4] with Mo Kα radiation at $\lambda = 0.71073$ Å. The same prismatic crystal was used for both measurements. At higher temperatures, the crystal is light green, whereas, upon cooling, a gradual, barely noticeable, transition occurs to a light pink color. There is no change in crystal system or space group (see below) between 90 and 294 K. Raw data frame integration and Lp corrections were performed with SAINT+ [4]. Final unit cell parameters were determined by least-squares refinement of all reflections with $I > 5\sigma(I)$ from each data set. Analysis of the data showed negligible crystal decay during data collection. The data were not corrected for absorption. Direct methods structure solution, difference Fourier calculations and full-matrix least-squares refinement against F^2 were performed with SHELXTL [5].

$Fe[(C_6H_5)B(3\text{-}Mepz)_3]_2$ (**2**) crystallizes in the triclinic system, and the $P\bar{1}$ space group was confirmed by the successful solution and refinement of both data sets. Half of one $Fe[(C_6H_5)B(3\text{-}Mepz)_3]_2$ complex, situated on an inversion center, is present in the asymmetric unit at both temperatures. All non-hydrogen atoms were refined with anisotropic displacement parameters. Hydrogen atoms were placed in geometrically idealized positions and included as riding atoms.

3. Results

3.1. Tris(pyrazolyl)borate chemistry

The new ligand, sodium tris(3-methylpyrazolyl)phenylborate (**1**), was prepared according to a previous synthetic scheme for an analogous ligand [3a] by using commercially obtained phenyltrimethylsilane as the starting material. $Na[(C_6H_5)B(3\text{-}Mepz)_3]$ was then used to prepare $Fe[(C_6H_5)B(3\text{-}Mepz)_3]_2$ (**2**) in acceptable yield by the salt metathesis reaction between two equivalents of the ligand and iron(II) chloride (Eq. 1), resulting in a slightly off-white powder. The crystals of **2**, grown as discussed below, were colorless which corresponds to a high-spin iron(II) complex. Low spin, octahedral iron(II) complexes of this type are usually purple. Prior to X-ray structural analysis, a few of the crystals of **2** were placed in liquid nitrogen in order to determine whether a spin-state crossover occurred; no color change to purple was observed (vide infra), indicating that no crossover occurred upon cooling to 78 K.

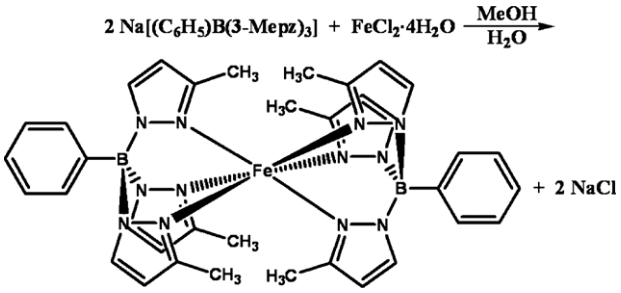

(1)

3.2. Structural analysis

The $Fe[(C_6H_5)B(3\text{-}Mepz)_3]_2$ (**2**) complex was obtained as exquisite crystals by layering a methylene chloride solution with methanol and allowing the two solvents to slowly diffuse. The crystallization process is best performed in the absence of light, thus reducing the formation of iron(III) impurities [3a]. Crystallographic information and selected bond distances and angles are given in Tables 1 and 2. The molecular structure of **2** was determined at 90 and 294 K; as is indicated in Table 2, the two structures are nearly identical. An ORTEP diagram of **2** from the structure obtained at 294 K is shown in Fig. 1.

The complex consists of two negatively charged *tris*-(3-methylpyrazolyl)phenylborate ligands κ^3-bonded to the iron(II) center in the required facial arrangement. The average Fe–N bond distances in both structures of approximately 2.18 Å clearly indicate that the complex is high spin in the solid state at both temperatures (Table 2). Low-spin complexes tend to have shorter Fe–N bond distances of ca. 1.98 Å, whereas high-spin complexes have distances of 2.17–2.19 Å as a result of the antibonding character of the partially filled e_g^* orbitals in the high-spin complexes. The FeN_6 octahedral core is only slightly distorted by the restrictions in the intraligand bond angles caused by the chelate rings.

Although the crystal structure shows that the FeN_6 core has only small distortions from pseudooctahedral geometry, because the bite angles of tris(pyrazolyl)borate ligands are generally fixed by the tetrahedral central boron atom, there are other subtle distortions of the ligand framework that occur on binding to large metal ions. In order to bond to larger metals, tris(pyrazolyl)-borate and tris(pyrazolyl)methane ligands that have a fourth group bonded to the boron other than hydrogen

Table 1
Crystallographic data for $Fe[(C_6H_5)B(3\text{-}Mepz)_3]_2$ at 294 and 90 K

Formula	$C_{36}H_{40}B_2FeN_{12}$	$C_{36}H_{40}B_2FeN_{12}$
Formula weight (g/mol)	718.27	718.27
Space group	$P\bar{1}$	$P\bar{1}$
Crystal system	triclinic	triclinic
a (Å)	10.0266(6)	9.9604(5)
b (Å)	10.1334(6)	10.0319(5)
c (Å)	10.4753(6)	10.3639(k)
α (°)	107.3300(10)	107.8380(10)
β (°)	117.7410(10)	117.8900(10)
γ (°)	93.0300(10)	92.0560(10)
V (Å^3)	875.83(9)	851.31(7)
Z	1	1
Crystal color, habit	colorless, block	light pink, block
D_{calc} (g cm^3)	1.362	1.401
Temperature (K)	294(1)	90(1)
Diffractometer	Bruker SMART APEX CCD	
Radiation	Mo Kα ($\lambda = 0.71073$ Å)	
$R(F)$ (%)[a]	3.91	3.41
$R(wF^2)$ (%)[a]	11.72	9.25

[a] Quantity minimized: $R(F) = \sum[F_o - F_c]/\sum[F_o]$; $R(wF^2) = \sum[w(F_o^2 - F_c^2)^2]/\sum[(wF_o^2)]^{1/2}$.

Table 2
Selected bond distances (Å) and bond angles (°)

Atom connectivity	Fe–N bond distances (294 K)	Fe–N bond distances (90 K)
Fe1–N11	2.193(1)	2.188(1)
Fe1–N21	2.138(1)	2.132(1)
Fe1–N31	2.232(1)	2.227(1)
	N–Fe–N angles (294 K)	N–Fe–N angles (90 K)
N11–Fe1–N11a	180	180
N11–Fe1–N21	84.94(5)	84.69(4)
N11–Fe1–N21a	95.06(5)	95.31(4)
N11–Fe1–N31	88.15(4)	88.14(4)
N21–Fe1–N21a	180	180
N21–Fe1–N31	85.17(5)	85.43(4)
N21a–Fe1–N31	94.83(5)	94.57(4)
N11a–Fe1–N31	91.85(4)	91.86(4)
N31–Fe1–N31a	180	180

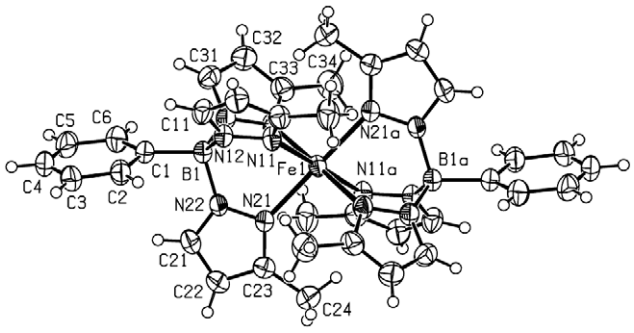

Fig. 1. The molecular structure of $Fe[(C_6H_5)B(3\text{-}Mepz)_3]_2$ (**2**) at 294 K with partial atom numbering; displacement ellipsoids drawn at the 50% probability level.

undergo a twisting of the pyrazolyl rings from the ideal C_{3v} symmetry. The MN(n1)–N(n2)B torsion angles, where n is the pyrazolyl ring number, describes the degree of twisting [6]. When these ligands bind to smaller metals, e.g., to low-spin iron(II), the MN–NB torsion angles approach their ideal values of 0°. In contrast, when they bind to larger metals, e.g., to high-spin iron(II), the MN–NB angles increase in magnitude [3]. This twisting is best visualized in Fig. 2, which shows the molecule oriented down the pseudo threefold axis. As indicated in Table 3, the pyrazolyl rings are highly distorted in this high-spin complex, with the 3-ring (shown vertically in Fig. 2) severely twisted by 22.3° away from the ideal torsion angle of 0°. It is important to note that this extreme twisting of the 3-ring also correlates with the long Fe–N31 bond distance.

In contrast to the $Fe[(p\text{-}R\text{-}C_6H_4)B(3\text{-}Mepz)_3]_2$ derivatives studied previously [3], an analysis of the intermolecular structure of **2** revealed no supramolecular organization within the crystal. The molecules are held together within the crystal only by van der Waals forces.

3.3. Magnetic studies

The temperature dependence of the magnetic susceptibility of **2** has been measured between 4 and 300 K, and the results, in terms of the inverse magnetic susceptibility and the magnetic moment, are shown in Fig. 3. The inset to this figure indicates that **2** is a dilute high-spin paramagnetic iron(II) complex that exhibits Curie law behavior with a Curie constant of 3.21 (Kemu)/mol, a corresponding magnetic moment of 5.06 μ_B, and a zero susceptibility intercept of 0.86 K, a value which is very close to the expected zero Kelvin value. No change or hysteresis was observed in the magnetic susceptibility upon repeated cooling and reheating.

At room temperature, the observed magnetic moment of 5.06 μ_B for **2** is slightly higher than the spin-only moment of 4.9 μ_B expected for a high-spin iron(II) complex and indicates the expected [7] presence of a small orbital contribution to the moment. This moment is also in good agreement with the room temperature moments observed in related high-spin iron(II) complexes such as $Fe[HB(3,5\text{-}Me_2pz)_3]_2$, which exhibits a moment of 5.0 μ_B at 298 K [8].

Upon cooling, the magnetic moment of **2** increases linearly from 5.06 μ_B at 300 K to 5.12 μ_B at 30 K, and then decreases more substantially below ca. 20 K. However, as may be seen in the inset of Fig. 3, $1/\chi$ versus T is linear even at the lowest temperatures. The decrease in the moment below ca. 20 K is exactly that expected [7,9] from zero field splitting in a magnetically dilute high-spin iron(II) complex in a distorted octahedral coordination environment. Thus the decrease in moment of **2** at the lowest temperatures is not associated with any change in the spin state of the iron(II) ion, i.e., **2** is a magnetically dilute high-spin paramagnetic iron(II) complex at all temperatures above 4 K.

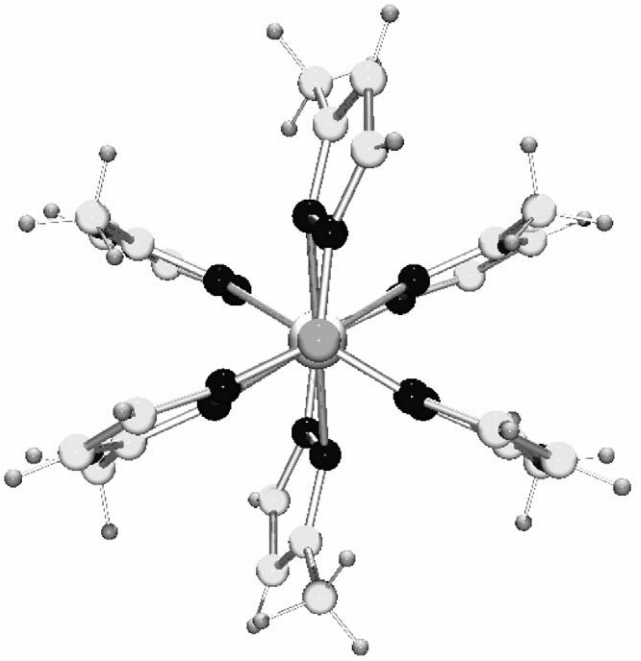

Fig. 2. View of $Fe[(C_6H_5)B(3\text{-}Mepz)_3]_2$ (**2**) down the pseudo-threefold axis at 294 K.

Table 3
Torsion angles of the pyrazolyl rings in $Fe[(C_6H_5)B(3\text{-}Mepz)_3]_2$

Atoms	Torsion angle (°)	
	294 K	90 K
Fe1–N11–N12–B1	0.2	1.0
Fe1–N21–N22–B1	13.0	14.5
Fe1–N31–N32–B1	22.3	23.2

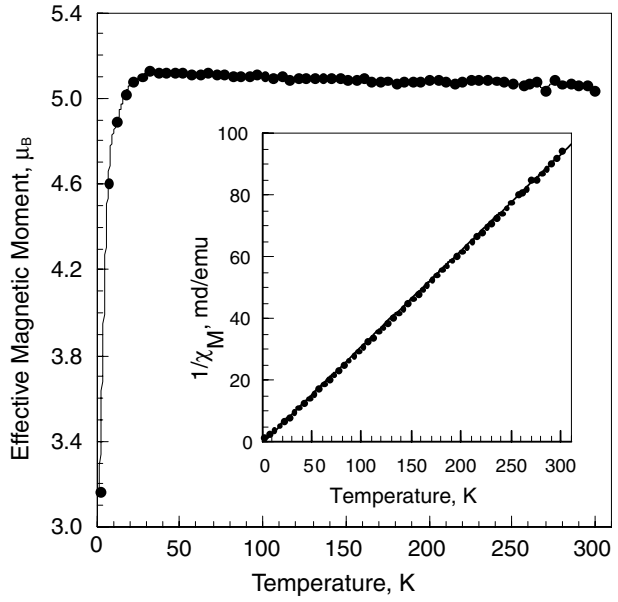

Fig. 3. The temperature dependence of the effective magnetic moment and the inverse molar magnetic susceptibility (inset) of $Fe[(C_6H_5)B(3\text{-}Mepz)_3]_2$ (**2**).

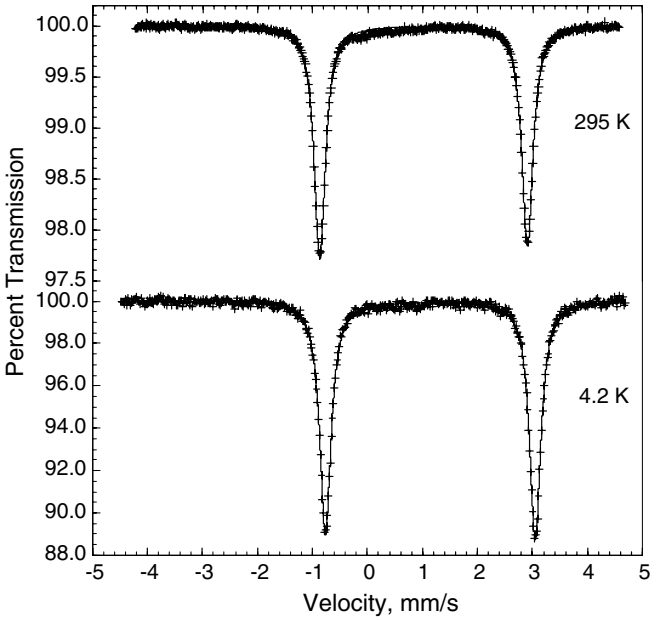

Fig. 4. Mössbauer spectra of $Fe[(C_6H_5)B(3\text{-}Mepz)_3]_2$ (**2**) obtained at 4.2 and 295 K.

Table 4
Mössbauer spectral hyperfine parameters for $Fe[(C_6H_5)B(3\text{-}Mepz)_3]_2$

T (K)	δ (mm/s)[a]	ΔE_Q (mm/s)	Γ (mm/s)
295	1.015	3.77	0.24
78	1.106	3.82	0.29
4.2	1.142	3.81	0.25

[a] The isomer shifts are given relative to room temperature α-iron foil.

3.4. Mössbauer spectral studies

The same sample used for the magnetic studies was subsequently used for Mössbauer spectral studies and the resulting spectra are shown in Fig. 4. The spectra have been fit with a single symmetric quadrupole doublet and the resulting hyperfine parameters are given in Table 4.

The 4.2, 78, and 295 K spectra of fine unground, but crushed, crystals of **2** indicate that this complex is high-spin at these temperatures. The observed hyperfine parameters are very similar to those observed for the high-spin iron(II) component in $Fe[HB(3,5\text{-}Me_2pz)_3]_2$ at the same temperatures [10]. There is a slight decrease in the isomer shift and increase in the quadrupole splitting of **2** as compared with $Fe[HB(3,5\text{-}Me_2pz)_3]_2$, changes that may be related to small differences in the coordination geometry in the complexes.

4. Discussion

We have carefully studied [3] the spin-state crossover properties of several $Fe[(p\text{-}R\text{-}C_6H_4)B(3\text{-}Mepz)_3]_2$ derivatives because they all have very similar FeN_6 coordination environments; changes in the distal *para* position of the phenyl ring attached to boron should have a minimal direct

electron and steric impact on the iron(II) coordination environments and, hence, its electronic spin state. In contrast, by systematically introducing R-groups in these "third generation" tris(pyrazolyl)borate ligands that can enter into supramolecular interactions, we anticipated delineating the relationship between the inter- and intramolecular structure and the spin-crossover phenomenon. Mössbauer spectral data, in conjunction with magnetic susceptibility and X-ray crystallographic data, clearly demonstrate that **2**, the parent molecule of this family of complexes, remains at least 98% high spin down to 4 K (the crystals color slightly at 90 K, but no low-spin signals are detected in the Mössbauer spectra). In contrast, all but one of the Fe[(*p*-R-C_6H_4)B(3-Mepz)$_3$]$_2$ derivatives, where R is I, —C≡C—H, —C≡C—$SiMe_3$, or —C≡C—C_6H_5 undergo a spin-state crossover at low temperatures.

In our previous work, two factors have been shown to influence the temperature at which the various molecules undergo a spin crossover: the type of supramolecular structure observed and the degree of pyrazolyl ring twisting in the molecular structure. As most clearly indicated by the behavior of the two polymorphs of Fe[(*p*-IC_6H_4)-B(3-Mepz)$_3$]$_2$, one of which does and one of which does not undergo a spin-state crossover at low temperatures, we proposed that highly organized three-dimensional supramolecular structures can energetically "lock in" the high-spin state, even at very low temperatures. The lack of an R-functional group in **2** that can undergo π–π, C–H···π, and other weak hydrogen bonding interactions has produced a structure in which no supramolecular forces are observed, making this issue moot.

In contrast, it appears that the degree of twisting of the pyrazolyl rings in the high temperature structure explains the lack of a spin-state crossover for **2**. Our best previous evidence that greater twisting in the high-spin form leads to spin-state crossover at lower temperatures was with the two independent molecules in the structure of Fe-[(*p*-HC≡CC_6H_4)B(3-Mepz)$_3$]$_2$. Table 5 gives the torsion angles along with the Fe–N bond distances for the known Fe[(*p*-R-C_6H_4)B(3-Mepz)$_3$]$_2$ complexes. In the case of Fe[(*p*-HC≡CC_6H_4)B(3-Mepz)$_3$]$_2$, the molecule containing Fe2, the one showing the lesser ring twisting undergoes a spin-state crossover at a higher temperature than those containing Fe1, the one showing the greater ring twisting. In this case, the two-dimensional supramolecular structures of each of the crystallographically distinct iron(II) sites were very similar leading to the conclusion that the ring twisting issue dominated the spin-crossover behavior.

In the case of **2** reported herein, it is clear that the supramolecular structure is not an issue in the spin-state crossover behavior. As indicated in Table 5, this complex has the

Table 5
A structural comparison of known Fe[(*p*-R-C_6H_4)B(3-Mepz)$_3$]$_2$ complexes

Compound	Atom connectivity	Torsion angle (°)	Average torsion angle (°)	Fe–N distance (Å)	Average Fe–N distance (Å)
Fe[(*p*-HC≡CC_6H_4)B(3-Mepz)$_3$]$_2$, Fe1[a]	Fe1–N11–N12–B1	5.6	9.2	2.137	2.179
	Fe1–N21–N22–B1	12.4		2.213	
	Fe1–N31–N32–B1	9.6		2.186	
Fe[(*p*-HC≡CC_6H_4)B(3-Mepz)$_3$]$_2$, Fe2[a]	Fe2–N41–N42–B2	0.6	6.0	2.078	2.101
	Fe2–N51–N52–B2	4.8		2.120	
	Fe2–N61–N62–B2	12.5		2.104	
Fe[(*p*-Me_3SiC≡CC_6H_4)B(3-Mepz)$_3$]$_2$, 200 K	Fe1–N11–N12–B1	0.1	7.9	2.109	2.165
	Fe1–N21–N22–B1	12.1		2.201	
	Fe1–N31–N32–B1	11.6		2.185	
Fe[(*p*-C_6H_5C≡CC_6H_4)B(3-Mepz)$_3$]$_2$, 294 K	Fe1–N11–N12–B1	10.3	10.5	2.132	2.172
	Fe1–N21–N22–B1	1.0		2.170	
	Fe1–N31–N32–B1	20.3		2.215	
Fe[(p-IC_6H_4)B(3-Mepz)$_3$]$_2$, form A[b], SCO[c], 100 K	Fe1–N11–N12–B1	11.0	5.0	1.963	1.963
	Fe1–N21–N22–B1	3.6		1.953	
	Fe1–N31–N32–B1	0.4		1.974	
Fe[(*p*-IC_6H_4) B(3-Mepz)$_3$]$_2$, form A, SCO, 294 K	Fe1–N11–N12–B1	2.6	8.6	2.124	2.175
	Fe1–N21–N22–B1	13.0		2.207	
	Fe1–N31–N32–B1	10.2		2.195	
Fe[(p-IC_6H_4)B(3-Mepz)$_3$]$_2$, form B[b], NSCO[c],150 K	Fe1–N11–N12–B1	6.6	9.3	2.137	2.184
	Fe1–N21–N22–B1	3.8		2.206	
	Fe1–N31–N32–B1	17.4		2.208	
Fe[(C_6H_5)B(3-Mepz)$_3$]$_2$, 294 K	Fe1–N11–N12–B1	0.2	12.0	2.193	2.188
	Fe1–N21–N22–B1	13.0		2.138	
	Fe1–N31–N32–B1	22.3		2.232	

[a] Denotes non-equivalent iron sites.
[b] Form label denotes polymorph.
[c] SCO, spin crossover; NSCO, non-spin crossover.

highest degree of ring twisting of any of the known Fe[(*p*-R-C_6H_4)B(3-Mepz)$_3$]$_2$ complexes. Especially notable is the large distortion of the 3-ring at 22.3°, a twisting which is accompanied by the longest Fe–N bond distance. We propose that this *pyrazolyl ring twisting is the reason for the lack of a spin-state crossover in this complex*; the ligand rearrangement needed to lower this ring twisting as the bonds would shorten to the normal low-spin values is a barrier to the spin crossover. This result strengthens our earlier proposals that indicated the degree of pyrazolyl ligand ring twisting in the high-spin structure is an important factor controlling the spin-state crossover behavior of poly(pyrazolyl)borate [3] and poly(pyrazolyl)methane complexes [11b]. Significant twisting of the rings energetically favors the larger high-spin complexes because it favors the longer Fe–N bond distances such that **2** does not undergo the crossover even at 4 K because of the extreme degree of twisting. These results are parallel to those observed with {Fe[HC(3,5-Me_2pz)$_3$]$_2$}-(BF_4)$_2$, in which a phase transition at low temperature converts the equivalent iron(II) sites in the high temperature structure to two non-equivalent sites [11]. One of the sites has highly twisted pyrazolyl rings, and this site remains high spin; it does not undergo spin crossover down to 4 K. In contrast, for the other site, the rings are not twisted and the iron(II) exhibits a spin-state crossover to the low-spin state at the temperature of the phase transition.

It is interesting to note that the molecule in Table 5 with the second most twisted rings, Fe[(*p*-$C_6H_5C{\equiv}C{-}C_6H_4$)B(3-Mepz)$_3$]$_2$, also has an organized three-dimensional supramolecular structure, but undergoes spin crossover at low temperatures [3b]. In this case, as with {Fe[HC-(3,5-Me_2pz)$_3$]$_2$}(BF_4)$_2$ [11] and Fe[(*p*-$Me_3SiC{\equiv}C{-}C_6H_4$)-B(3-Mepz)$_3$]$_2$ [3b], a phase change is observed at the same temperature that spin crossover occurs. Clearly, phase changes will dominate the more subtle influences of ring twisting and the relatively weak supramolecular interactions that are present in these complexes. The detailed analysis of the importance of the more subtle effects of ring twisting reported herein was possible because **2** does not undergo a structural phase change upon cooling from 294 to 90 K and, most likely, not below 90 K.

5. Supplementary material

Crystallographic data for the structures reported in this paper have been deposited at the Cambridge Crystallographic Data Center, CCDC 290338 (294 K) and 290339 (90 K). Copies of the information may be obtained free of charge from the Director, CCDC, 12 Union Road, Cambridge, CB2 1EZ, UK, fax: +44 1223 336 033, email: data_request@ccdc.cam.ac.uk or www: http://www.ccdc.cam.ac.uk.

Acknowledgements

The authors acknowledge with thanks the financial support of the US National Science Foundation through Grant CHE-0414239 for D.L.R. and the financial support of the Ministère de la Région Wallonne through Grant RW/115012 for F.G. and L.R.

References

[1] (a) R.N. Muller, L. Van der Elst, S. Laurent, J. Am. Chem. Soc. 125 (2003) 8405;
(b) O. Kahn, C.J. Martinez, Science 279 (1998) 44.
[2] (a) For leading reviews, see: J.A. Real, A.B. Gaspar, V. Niel, M.C. Muñoz, Coord. Chem. Rev. 236 (2003) 121;
(b) P. Gütlich, Y. Garcia, H.A. Goodwin, Chem. Soc. Rev. 29 (2000) 419;
(c) P. Gütlich, A. Hauser, H. Spiering, Angew. Chem., Int. Ed. Engl. 33 (1994) 2024;
(d) E. König, G. Ritter, S.K. Kulshreshtha, Chem. Rev. 85 (1985) 219.
[3] (a) D.L. Reger, J.R. Gardinier, M.D. Smith, A.M. Shahin, G.J. Long, L. Rebbouh, F. Grandjean, Inorg. Chem. 44 (2005) 1852;
(b) D.L. Reger, J.R. Gardinier, W.R. Gemmill, M.D. Smith, A.M. Shahin, G.J. Long, L. Rebbouh, F. Grandjean, J. Am. Chem. Soc. 127 (2005) 2303.
[4] SMART Version 5.625 and SAINT+ Version 6.22. Bruker Analytical X-ray Systems, Inc., Madison, WI, USA, 2001.
[5] G.M. Sheldrick, SHELXTL Version 6.1; Bruker Analytical X-ray Systems, Inc., Madison, WI, USA, 2000.
[6] (a) D.S. Frohnapfel, P.S. White, J.L. Templeton, H. Ruegger, P.S. Pregosin, Organometallics 16 (1997) 3737;
(b) D.L. Reger, T.D. Wright, C.A. Little, J.J.S. Lamba, M.D. Smith, Inorg. Chem. 40 (2001) 3810.
[7] B.N. Figgis, Introduction to Ligand Fields, Wiley–Interscience, New York, 1966, p. 274.
[8] (a) J.J.A. Kolnaar, M.I. De Heer, H. Kooijman, A.L. Spek, G. Schmitt, V. Ksenofontov, P. Gütlich, J.G. Haasnoot, J. Reedijk, Eur. J. Inorg. Chem. 5 (1999) 881;
(b) Y. Garcia, P.J. van Koningsbruggen, E. Codjovi, R. Lapouyade, O. Kahn, L. Rabardel, J. Mater. Chem. 7 (1997) 857;
(c) J.P. Jesson, J.F. Weiher, S. Trofimenko, J. Chem. Phys. 48 (1968) 2058.
[9] G.J. Long, W.A. Baker Jr., J. Chem. Soc. A (1971) 2956.
[10] G.J. Long, B.B. Hutchinson, Inorg. Chem. 26 (1987) 608.
[11] (a) D.L. Reger, C.A. Little, V.A. Young Jr., M. Pink, Inorg. Chem. 40 (2001) 287;
(b) D.L. Reger, C.A. Little, M.D. Smith, G.J. Long, Inorg. Chem. 41 (2002) 4453.

witnessed as model complexes. Hence, the synthesized heterobinuclear complexes are used for modeling the properties of the active site of the metallobiosites. In our earlier works [16,17] we have reported the spectral, electrochemical and kinetic properties of homobinuclear copper(II) complexes and in this work we rationalize how the heterobinuclear complexes behave differently from homobinuclear complexes.

2. Experimental

Elemental analysis was carried out on a Carlo Erba Model 1106 elemental analyzer. ^{1}H NMR spectra were recorded using FX-80-Q Fourier transition NMR spectrometer. Electronic spectral studies were carried out on a Hitachi 320 spectrophotometer in the range 200–800 nm. IR spectra were recorded on a Hitachi 270-50 spectrophotometer on KBr disks in the range 4000–250 cm^{-1}. The mass spectra were obtained on JEOL DX-303 mass spectrometer. Cyclic Voltammograms were obtained on CHI600A (CHI Instruments Co., USA) electrochemical analyzer using DMF. The measurements were carried out under oxygen free condition by purging nitrogen gas, using a three electrode cell in which glassy carbon electrode was working electrode, saturated Ag/AgCl electrode was reference electrode and platinum wire was used as auxiliary electrode. Glassy carbon electrode surface was pretreated by metallographic polishing with alumina on a velvet cloth (abraded with fine grade of emery paper), followed by ultrasonic cleaning in double distilled water and washing with small amount of highly diluted acid and DMF. Ferrocene/ferrocenium (1+) couple was used as standard and $E_{1/2}$ of the Ferrocene/ferrocenium (Fc/Fc^+) couple under the experimental condition is 470 mV in DMF and ΔE_p for Fc/Fc^+ is 70 mV. Tetra (*n*-butyl)ammonium perchlorate (TBAP) was used as supporting electrolyte. The kinetic investigation of catechol oxidation and hydrolysis of 4-nitrophenyl phosphate was carried out spectrophotometrically by choosing the strongest absorbance at appropriate wavelength and monitoring the increase in the absorbance at this wavelength as a function of time. A plot of log $(A_\infty/A_\infty - A_t)$ versus time was made for each complexes and the rate constant was calculated. All the kinetic studies were carried out in DMF solvent at room temperature (25 °C).

2.1. Materials

5-Methylsalicylaldehyde [18], 3-chloromethyl-5-methylsalicylaldehyde [19] and 3,4:9,10-dibenzo-1,12-diaza-5,8-dioxocyclotetradecane [20,21] were prepared from the literature methods. TBAP used as supporting electrolyte in electrochemical measurement was purchased from Fluka and recrystallised from hot methanol. (Caution! TBAP is potentially explosive; hence care should be taken in handling the compound). DMF and CH_3CN were obtained from E. MERCK. All other chemicals and solvents were of analytical grade and were used as received without any further purification.

2.2. Synthesis of precursor compound

2.2.1. 3,4:9,10-Dibenzo-1,12[N,N′-bis{(3-formyl-2-hydroxy-5-methyl)benzyl}diaza]-5,8-dioxocyclotetradecane [16] (precursor compound)

A mixture of 3,4:9,10-dibenzo-1,12-diaza-5,8-dioxocyclotetradecane (0.95 g, 3.2 mmol) and triethylamine (1.32 g, 6.4 mmol) in 30 ml of THF was added slowly to a stirred solution of 3-chloromethyl-5-methylsalicylaldehyde (1.16 g, 6.4 mmol) in 30 ml of THF. After the addition was over the stirring was continued further for one more hour. The whole solution was then refluxed under water bath for 3 h and was allowed to cool on standing at room temperature. Copious water was added to this solution to dissolve any salt obtained. Then the required compound was extracted in organic medium using chloroform. The extraction was repeated for two to three times. A pale yellow compound was obtained on evaporation of solvent at room temperature (25 °C). Light yellow microcrystals were obtained on recrystallization from chloroform. Yield: 1.82 g (80%), m.p.: 100 °C. *Anal.* Calc. for $C_{36}H_{38}O_6N_2$: C, 60.50; H, 5.32; N, 3.92. Found: C, 60.72; H, 5.36; N, 3.98%. IR data (ν cm^{-1}): 1678 (νC=O, s), 3448 (νOH, br). ^{1}H NMR (δ ppm in $CDCl_3$): 10.0 (s, 2H, CHO protons), 7.0 (m, 12H, aromatic protons), 4.7 (m, 4H, methylene protons attached to oxygen atom), 3.8 (m, 8H, benzylic protons), 3.5 (s, 4H, methylene protons attached to nitrogen atom), 2.3 (s, 6H, CH_3 protons attached to aromatic ring). Mass (EI) *m*/*z*: 594 (m^+).

2.3. Synthesis of macrobicyclic heterobinuclear complexes

2.3.1. $[CuZnL^1](ClO_4)_2$

A methanolic solution (20 ml) of zinc(II)perchlorate hexahydrate (0.707 g, 1.9 mmol) [Caution! zinc(II) perchlorate salt is potentially explosive; hence care should be taken in handling the compound] was added to the hot solution of mononuclear copper(II) complex [16] $[CuL^1](ClO_4)$ (1.562 g, 1.9 mmol) in 25 ml of methanol followed by the addition triethylamine (0.192 g, 1.9 mmol) in 5 ml of methanol. The solution was refluxed on water bath for 24 h. After the reaction was over, the solution was filtered at hot condition and allowed to stand at room temperature. After slow evaporation of the solvent at 25 °C, the dark green compound obtained was washed with methanol and dried in vacuum. Yield: 1.48 g (80%). *Anal.* Calc. $C_{42}H_{46}O_{12}N_6Cl_2CuZn$: C, 49.17; H, 4.48; N, 8.19. Found: C, 49.28; H, 4.62; N, 8.20%. Selected IR (KBr): 1628 (s), 1100 (s), 622 (s) cm^{-1}. λ_{max} (nm) (ε/M^{-1} cm^{-1}) in CH_3CN: 565 (121), 372 (16870), 272 (37200).

2.3.2. $[CuZnL^2](ClO_4)_2$

$[CuZnL^2](ClO_4)_2$ was synthesized by following the previously described procedure for $[CuZnL^1](ClO_4)_2$, using the

mononuclear complex $[CuL^2](ClO_4)$ instead $[CuL^1](ClO_4)$. The compound obtained was dark green. Yield: 1.44 g (77%). *Anal*. Calc. for $C_{43}H_{48}O_{12}N_6Cl_2CuZn$: C, 49.66; H, 4.61; N, 8.08. Found: C, 49.79; H, 4.73; N, 8.20%. Selected IR (KBr): 1620 (s), 1100 (s), 626 (s) cm^{-1}. λ_{max} (nm) ($\varepsilon/M^{-1}\,cm^{-1}$) in CH_3CN: 595 (131), 352 (14 590), 271 (37 160).

2.3.3. $[CuZnL^3](ClO_4)_2$

$[CuZnL^3](ClO_4)_2$ was synthesized by following the previously described procedure for $[CuZnL^1](ClO_4)_2$, using the mononuclear complex $[CuL^3](ClO_4)$ instead $[CuL^1](ClO_4)$. The compound obtained was dark green. Yield: 1.49 g (79%). *Anal*. Calc. for $C_{44}H_{50}O_{12}N_6Cl_2CuZn$: C, 50.14; H, 4.74; N, 7.97. Found: C, 50.22; H, 4.84; N, 8.11%. Selected IR (KBr): 1622 (s), 1101 (s), 627 (s) cm^{-1}. λ_{max} (nm) ($\varepsilon/M^{-1}\,cm^{-1}$) in CH_3CN: 625 (125), 355 (15 440), 273 (32 400).

2.3.4. $[CuZnL^4](ClO_4)_2$

$[CuZnL^4](ClO_4)_2$ was synthesized by following the previously described procedure for $[CuZnL^1](ClO_4)_2$, using the mononuclear complex $[CuL^4](ClO_4)$ instead $[CuL^1](ClO_4)$. The compound obtained was blackish green. Yield: 1.51 g (78%). *Anal*. Calc. for $C_{46}H_{46}O_{12}N_6Cl_2CuZn$: C, 51.44; H, 4.28; N, 7.82. Found: C, 51.62; H, 4.41; N, 7.93%. Selected IR (KBr): 1628 (s), 1100 (s), 625 (s) cm^{-1}. λ_{max} (nm) ($\varepsilon/M^{-1}\,cm^{-1}$) in CH_3CN: 605 (110), 412 (13 400), 375 (12 300), 275 (33 500).

2.3.5. $[CuZnL^5](ClO_4)_2$

$[CuZnL^5](ClO_4)_2$ was synthesized by following the previously described procedure for $[CuZnL^1](ClO_4)_2$, using the mononuclear complex $[CuL^5](ClO_4)$ instead $[CuL^1](ClO_4)$. The compound obtained was blackish green. Yield: 1.62 g (80%). *Anal*. Calc. for $C_{50}H_{48}O_{12}N_6Cl_2CuZn$: C, 53.52; H, 4.28; N, 7.49, Found: C, 53.59; H, 4.37; N, 7.59%. Selected IR (KBr): 1624 (s), 1101 (s), 625 (s) cm^{-1}. λ_{max} (nm) ($\varepsilon/M^{-1}\,cm^{-1}$) in CH_3CN: 635 (140), 401 (15 300), 368 (18 300), 268 (34 000).

In all cases we could obtain only microcrystals and attempts to obtain the crystals suitable for X-ray analysis were unsuccessful.

3. Results and discussion

Schiff's base condensation of the precursor compounds with diamines in the presence of metal ion by template method results into various macrobicyclic hetero binuclear Cu(II)—Zn(II) complexes. Scheme 1 represents the synthetic pathway of hetero binuclear Cu(II)—Zn(II) complexes. In our previous study [16] the crystal structures of mono and binuclear copper(II) complexes have been rationalized. Hence, in accordance with this, it is proposed that the geometry around copper(II) and zinc(II) ion is distorted square planar. Extensive spectral, electrochemical and kinetic studies of the heterobinuclear complexes were carried out and discussed.

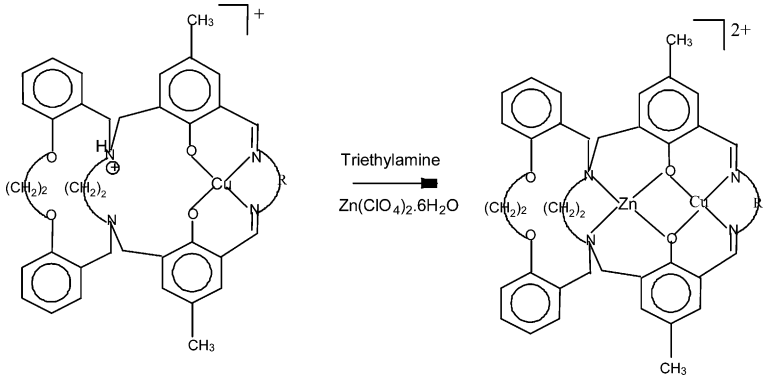

R	
L^1	$-(CH_2)_2-$
L^2	$-(CH_2)_3-$
L^3	$-(CH_2)_4-$
L^4	
L^5	

Scheme 1. Synthesis of macrobicyclic heterobinuclear Cu(II)—Zn(II) complexes.

3.1. Spectral studies

The IR spectra of the complexes show ν(C=N) peak [22] at 1620–1630 cm^{-1}. The peaks appeared near 1100 and 620 cm^{-1} are characteristics of the uncoordinated perchlorate ion. The electronic spectra of the complexes show three main transitions. A weak band observed in the range 565–635 nm is due to *d–d* transition of the Cu(II) ion presents in the heterobinuclear complexes. On moving from the complexes of ligand L^1 to L^3 and L^4 to L^5, an increase in λ_{max} (red shift) [23] of the *d–d* transition of Cu(II) ion in the complexes was observed. A moderate intensive band observed in the range 352–375 nm is due to ligand-to-metal charge transfer transition and the strong band observed in the range 268–275 nm is due to intraligand charge transfer transition [24]. Apart from these, additional peaks are observed for the complexes of ligands L^4 to L^5 due to the presence of aromatic ring in the imine nitrogen compartment.

The solid state ESR spectra of the heterobinuclear Cu(II)—Zn(II) complexes show four line hyperfine splittings due to Cu(II) ion with a nuclear hyperfine spin of 3/2. Fig. 1 represents the ESR spectrum of the complex $[CuZnL^1](ClO_4)_2$ with $g_{\|}$ value 2.14 and $g_{\perp}$ value 2.02.

3.2. Electrochemistry

The electrochemical properties of the complexes reported in the present work were studied by cyclic voltammetry in the potential range 0 to −1.4 V in dimethylformamide containing 10^{-1} M tetra(*n*-butyl)ammonium perchlorate and the data are represented in Table 1. All the heterobinuclear Cu(II)—Zn(II) complexes undergo one quasi reversible reduction at negative potential. Fig. 2 depicts the cyclic voltammograms of the heterobinuclear Cu(II)—Zn(II) complexes and the redox processes are assigned as follows:

$$Cu^{II}Zn^{II} \rightleftharpoons Cu^{I}Zn^{II}$$

The interesting feature connoted for heterobinuclear complexes is shifting of reduction potential towards anodic from −0.98 to −0.78 as we move from complexes of ligand L^1 to L^3. This is because of the reason that the increase in chain length in imine nitrogen compartment increases the macrocyclic ring size and hence causes more flexibility [25–27] which, in turn makes the reduction of the complexes easier. In our earlier work [16] we have reported the reduction potentials of the corresponding mono and

Table 1
Electrochemical data[a] of heterobinuclear Cu(II)—Zn(II) complexes in DMF medium (reduction)

Complexes	E^1_{pc} (V)	E^1_{pa} (V)	$E^1_{1/2}$ (V)	ΔE (mV)
$[CuZnL^1](ClO_4)_2$	−0.98	−0.88	−0.93	100
$[CuZnL^2](ClO_4)_2$	−0.82	−0.75	−0.79	130
$[CuZnL^3](ClO_4)_2$	−0.78	−0.69	−0.74	90
$[CuZnL^4](ClO_4)_2$	−1.08	−0.95	−1.04	130
$[CuZnL^5](ClO_4)_2$	−0.90	−0.79	−0.84	110

[a] Measured by CV at 25 mV/s. E vs. Ag/AgCl conditions: GC working and Ag/AgCl reference electrodes; supporting electrolyte TBAP; concentration of complex 1×10^{-3} M, concentration of TBAP 1×10^{-1} M.

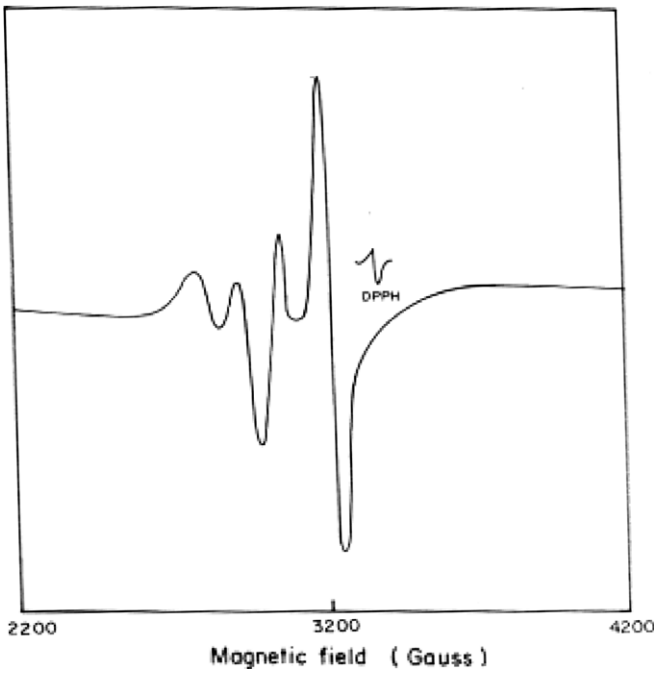

Fig. 1. ESR spectrum of complex $[CuZnL^1](ClO_4)_2$.

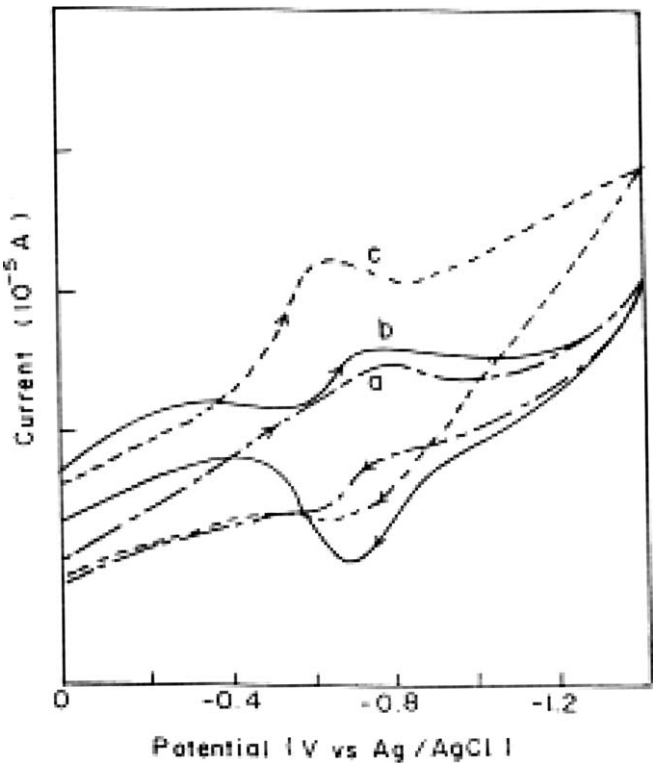

Fig. 2. Cyclic voltammograms of heterobinuclear complexes (1×10^{-3}M) (a) $[CuZnL^1](ClO_4)_2$ (b) $[CuZnL^2](ClO_4)_2$ (c) $[CuZnL^3](ClO_4)_2$.

binuclear copper(II) complexes and in the case of heterobinuclear Cu(II)—Zn(II) complexes the observed reduction potentials fall in the vicinity of the potentials of the corresponding mononuclear copper(II) complexes. Hence, it is worthwhile to assign this potential to the corresponding Cu(II) ion presents in the imine nitrogen compartment. The Zn(II) ion presents in the tertiary nitrogen compartment does not undergo reduction in this potential range. Thus, cyclic voltammetric technique is a useful tool to assign the site specificity of metal ion in the heterobinuclear complexes.

An inspection on the reduction potential of the heterobinuclear Cu(II)—Zn(II) complexes reveals that the observed reduction potentials are comparatively lesser than the corresponding homobinuclear [16] Cu(II) complexes. This clearly indicates that the interaction between two metal ions in homobinuclear Cu(II) complexes is effective when compared to the heterobinuclear Cu(II)—Zn(II) complexes. Because of this, heterobinuclear complexes have more or less the same reduction potential as mononuclear Cu(II) complexes.

3.3. Kinetic studies

All the heterobinucler Cu(II)—Zn(II) complexes were subjected for both catecholase activity and phosphate hydrolysis. The investigation of the kinetic studies of the heterobinuclear Cu(II)—Zn(II) complexes implies that the complexes act as model for catecholase and phosphate hydrolase. The kinetics of the catecholase activity was carried out using 10^{-3} M of complex and 10^{-1} M of 3,5-di-*tert*-butylcatechol in DMF. The product *o*-quinone is fairly stable and has a strong absorbance at 390 nm. The kinetics of the hydrolysis of 4-nitrophenyl phosphate was carried out using an equal concentration of the complex catalyst and tetramethylammonium hydroxide (10^{-3} M) and 4-nitrophenyl phosphate (10^{-1} M) in DMF. The chromophore leaving group 4-nitrophenolate, which is the hydrolysis product of the substrate was monitored at 420 nm. The course of the reaction in both cases was followed nearly 45 min at regular time interval. The slope was determined by monitoring the growth of the band of the corresponding product.

Plots of $\log(A_\infty/A_\infty - A_t)$ versus time for both catecholase activity and phosphate hydrolysis are obtained and shown in Figs. 3 and 4, respectively. The rate constant values are also reported in Table 2. The first apparent result was that the reactivities of the complexes differ significantly, as the size of macrocycle increases. In both kinetics, the catalytic activities of heterobinuclear Cu(II)—Zn(II) complexes are found to increase as the macrocyclic ring size increases due to the intrinsic flexibility. The catalytic activity of the complexes containing aromatic diimines is found to be less than that of the complexes containing aliphatic diimines. This can be explained that the planarity, which is associated with aromatic ring, imparts less catalytic efficiency due to the rigidity of the systems as observed in the

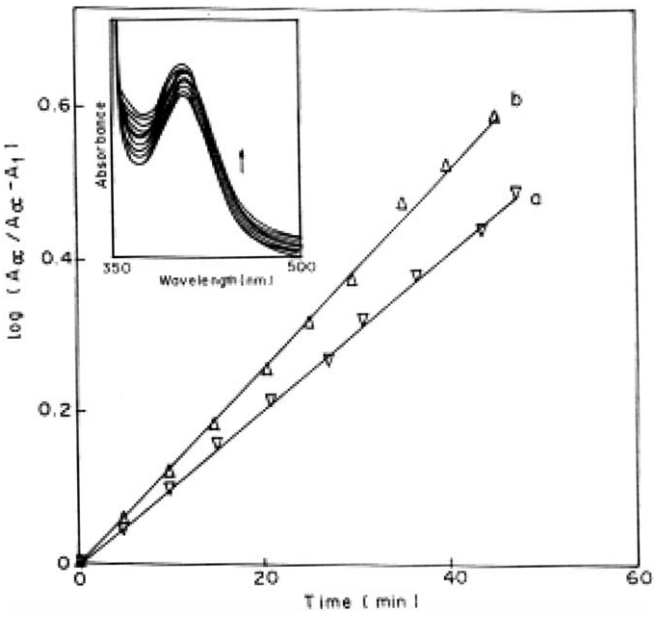

Fig. 3. Catecholase activity of heterobinuclear complexes (a) $[CuZnL^1](ClO_4)_2$ (b) $[CuZnL^2](ClO_4)_2$.

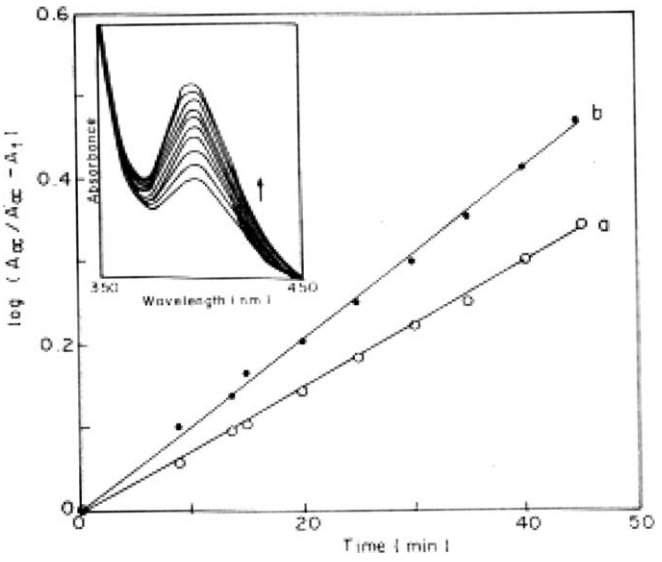

Fig. 4. Catalytic activity of heterobinuclear complexes for hydrolysis of 4-nitrophenylphosphate (a) $[CuZnL^1](ClO_4)_2$ (b) $[CuZnL^2](ClO_4)_2$.

Table 2
Catalytic activity[a] of heterobinuclear Cu(II)—Zn(II) complexes for catecholase activity and hydrolysis of 4-nitrophenyl phosphate

Complexes	Rate constant (min^{-1})	
	Catecholase activity	Hydrolysis activity
$[CuZnL^1](ClO_4)_2$	2.91×10^{-3}	1.75×10^{-2}
$[CuZnL^2](ClO_4)_2$	3.05×10^{-3}	2.27×10^{-2}
$[CuZnL^3](ClO_4)_2$	3.39×10^{-3}	3.43×10^{-2}
$[CuZnL^4](ClO_4)_2$	2.81×10^{-3}	1.68×10^{-2}
$[CuZnL^5](ClO_4)_2$	2.89×10^{-3}	2.12×10^{-2}

[a] Measured spectrophotometrically in DMF medium.

case of electrochemical reduction of the complexes. It seems interesting to observe that the rate constant values of heterobinuclear Cu(II)—Zn(II) for catecholase activities are less when compared to the rate constant values of corresponding mono and homobinuclear [16] Cu(II) complexes.

4. Conclusion

This work involves the synthesis of lateral macrobicyclic compartmental heterobinuclear Cu(II)—Zn(II) complexes with phenolate bridging atoms. Their extensive spectral, electrochemical and catalytic studies were carried out with slight modification in the ligand framework and compared with their corresponding mono and homobinuclear Cu(II) complexes. The increase in macrocyclic ring size in the ligand framework influences the spectral, electrochemical and catalytic properties of the complexes. Electronic spectral studies indicate that the *d–d* transition of Cu(II) ion is responsible for the appearance of band in the visible region. Electrochemical studies imply that the Zn(II) ion does not undergo reduction in the given potential range.

Acknowledgements

The author M.T. gratefully appreciates the financial support received from CSIR and UGC major project sanctioned to M.K., New Delhi.

References

[1] M. Yonemura, H. Okawa, M. Ohba, D.E. Fenton, L.K. Thompson, Chem. Commun. (2000) 817.
[2] G.T. Babcock, L.E. Vickery, G. Palmer, J. Biol. Chem. 253 (1978) 2400.
[3] P.A. Vigato, S. Tamburini, D.E. Fenton, Coord. Chem. Rev. 106 (1990) 25.
[4] F. Arena, C. Floriani, A.C. Villa, C. Guastini, Inorg. Chem. 25 (1986) 4589.
[5] Y. Aratake, H. Okawa, E. Asato, H. Sakiyama, M. Kodera, S. Kida, M. Sakamoto, J. Chem. Soc., Dalton Trans. (1990) 2941.
[6] H. Okawa, J. Nishio, M. Ohba, M. Tadokoro, N. Matsumoto, M. Koikawa, S. Kida, D.E. Fenton, Inorg. Chem. 32 (1993) 2949.
[7] M. Yonemura, K. Arimura, K. Inoue, N. Usuki, M. Ohba, H. Okawa, Inorg. Chem. 41 (2002) 582.
[8] H. Okawa, H. Furutachi, D.E. Fenton, Coord. Chem. Rev. 174 (1998) 51.
[9] M. Yonemura, N. Usuki, Y. Nakamura, H. Okawa, J. Chem. Soc., Dalton Trans. (2000) 3624.
[10] J.R. Morrow, W.C. Trogler, Inorg. Chem. 27 (1998) 3387.
[11] N.P. Sadler, C.C. Chuang, R.M. Milburn, Inorg. Chem. 34 (1995) 402.
[12] I.M. Atkinson, L.F. Lindoy, Coord. Chem. Rev. (2000) 200.
[13] P. Hendry, A.M. Sargeson, Inorg. Chem. 29 (1990) 92.
[14] N. Strater, T. Klaubunde, P. Tucker, H. Witzel, B. Krebs, Science 268 (1995) 1489.
[15] M.P. Engloff, P.T.W. Coher, P. Reimer, D. Barfard, J. Mol. Biol. 254 (1995) 942.
[16] M. Thirumavalavan, P. Akilan, M. Kandaswamy, K. Chinnakali, G. Senthil Kumar, H.K. Fun, Inorg. Chem. 42 (2003) 3308.
[17] M. Thirumavalavan, P. Akilan, M. Kandaswamy, Inorg. Chem. Commun. 5 (2002) 422.
[18] J.C. Duff, J. Chem. Soc. (1941) 547.
[19] J.D. Crane, D.E. Fenton, J.M. Latour, A.J. Smith, J. Chem. Soc., Dalton Trans. (1991) 2279.
[20] L.G. Armstrong, L.F. Lindoy, Inorg. Chem. 14 (1975) 1322.
[21] P.G. Grimsley, L.F. Lindoy, H.C. Lip, R.J. Smith, J.T. Baker, Aust. J. Chem. 30 (1977) 2095.
[22] G. Das, R. Shukala, S. Mandal, R. Singh, P.K. Bharadwaj, J.V. Singh, K.U. Whitmire, Inorg. Chem. 36 (1997) 323.
[23] R. Bhalla, M. Helliwell, C.D. Garner, Inorg. Chem. 36 (1997) 2944.
[24] P. Amudha, M. Kandaswamy, L. Govindaswamy, D. Velmurugan, Inorg. Chem. 37 (1998) 4490.
[25] E. Gao, W. Bu, G. Yang, D. Liao, Z. Jiang, S. Yan, G. Way, J. Chem. Soc. Dalton Trans. (2000) 1431.
[26] P.A. Connick, K.A. Macor, Inorg. Chem. 30 (1991) 4654.
[27] H. Okawa, M. Tadokora, T.Y. Aratake, M. Ohba, K. Shindom, M. Mitsumi, M. Koikawa, M. Tomono, D.E. Fenton, J. Chem. Soc., Dalton Trans. (1993) 253.

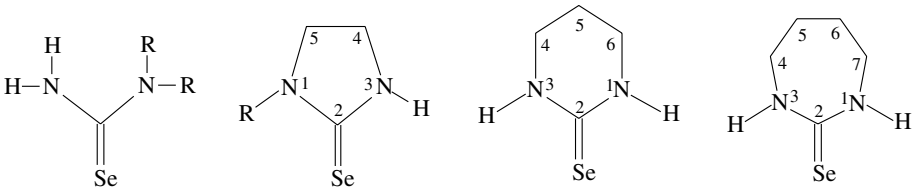

(a-b) (c-d) (e) (f)

Scheme 1. (a) R = H; selenourea (SeU) (b) R = CH_3; *N*,*N*-dimethylselenourea (DmSeU) (c) R = H; Imidazolidine-2-selone (ImSe) (d) R = CH_3; *N*-methylimidazolidine-2-selone (MeImSe); R = *i*-C_3H_7; *N*-isopopylimidazolidine-2-selone (*N*-*i*-PrImSe) (e) 1,3-diazinane-2-selone (DiazSe) (f) 1,3-diazipine-2-selone (DiapSe).

2.2. Spectroscopic measurements

The solid state IR spectra of the ligands and their mercury(II) complexes were recorded on a Perkin–Elmer FTIR 180 spectrophotometer using KBr pellets over the range 4000–400 cm^{-1}.

All NMR measurements were carried out on a Jeol JNM-LA 500 NMR spectrophotometer at 297 K. The ^{1}H NMR spectra were recorded at a frequency of 500.00 MHz. The ^{13}C NMR spectra were obtained at a frequency of 125.65 MHz with ^{1}H broadband decoupling and relative to TMS. The spectral conditions were: 32 k data points, 0.967 s acquisition time, 1.00 s pulse delay and 45° pulse angle.

The ^{15}N NMR spectrum was recorded at 50.55 MHz using $^{15}NH_4NO_3$ as external reference, which lies at −358.63 ppm relative to pure $MeNO_2$. The spectral conditions for ^{15}N were: 32 K data points, 0.721 s acquisition time, 2.50 s delay time, 60° pulse angle and approximately 5000 scans. ^{77}Se NMR spectra were recorded at 95.35 MHz, using 0.160 s acquisition time and a 2.00 s pulse delay. Chemical shifts were measured relative to external SeO_2 at 1301 ppm [20].

Natural abundance ^{13}C solid state NMR spectra were obtained on a JEOL LAMBDA 500 spectrometer operating at 125.65 MHz (11.74 T), at ambient temperature of 25 °C. Samples were packed into 6 mm zirconium oxide rotors. Cross-polarization and high power decoupling were employed. Pulse delay of 7.0 s and a contact time of 5.0 ms were used in the CPMAS experiments. The magic angle spinning rates were from 2 kHz to 5 kHz. Carbon chemical shifts were referenced to TMS by setting the high frequency isotropic peak of solid adamantane to 38.56 ppm. Solid state cross-polarization magic-angle spinning (CP MAS) $^{199}Hg\{^{1}H\}$ NMR spectra were obtained at ambient temperature on the same spectrometer operating at a frequency of 89.30 MHz. Contact time of 20 ms was used with a proton pulse width of 6 μs, with a recycle delay of 10 s. Approximately 5000 FID's were collected and transformed with a line broadening of 100 Hz. Chemical shifts were referenced using an external sample of solid $[Hg(DMSO)_6](O_3SCF_3)_2$ ($\delta Hg = -2313$ ppm from Me_2Hg) [21]. CP MAS ^{77}Se spectra were obtained on the same instrument operating at a frequency of 95.35 MHz. The contact time of 5 ms with proton pulse width of 6.0 μs, with a recycle delay of 12 s were used. Sample was spun at 3 and 5 kHz at the magic angle to determine the isotropic peaks. Approximately 5000 scans were employed. ^{77}Se chemical shifts are referenced using an external solid ammonium selenate ($\delta_{Se} = 1040.2$ ppm relative to liquid Me_2Se at 23 °C) [22]. Center band signals were located by varying the spinning speed. The CP MAS spectra (^{199}Hg and ^{77}Se) containing spinning side-band manifolds were analyzed using a program based on Maricq and Waugh and developed by Durham University, UK, using an iterative method, to yield shielding tensor values [23]. Calculated tensor values and the isotropic chemical shifts are shown in Table 3. Errors in the shielding tensor parameters for ^{77}Se are considered high (±30 ppm) because of the high noise level and base line correction. Errors in ^{199}Hg tensors are estimated to be around 20 ppm. For some complexes only the isotropic chemical shifts are reported as the quality of spectra did not allow the calculation of individual shielding tensors.

2.3. Synthesis of the complexes

The complexes were prepared by adding selones in acetonitrile to mercuric chloride solution in acetone in the molar ratios of 2:1 or 4:1 and stirring for 15–20 min [12]. The resulting white precipitates were filtered and washed with acetone.

The elemental analysis of these complexes is given in Table 1.

2.4. X-ray data collection and structure determination

A crystal of the complex (N-*i*-PrImSe)$_2HgCl_2$ was mounted on a glass fiber. Diffraction data were recorded on a Bruker-Axs Smart Apex system equipped with a graphite monochromatized Mo Kα radiation (λ = 0.71073 Å). The data were collected using SMART [24]. The data integration was performed using SAINT [25]. An empirical absorption correction was carried out using SADABS [26]. The structure was solved with the direct methods and refined by full-matrix least-square methods based on F^2, using the structure determination and graphics package SHELXTL [27] based on SHELX 97 [28]. Hydrogen atoms were included at calculated positions using a riding

Table 1
Elemental analysis and IR frequencies, $\nu(cm^{-1})$ of L_xHgCl_2 complexes (where $x = 2$, 3 or 4)

Complex	Found (Calcd) %			M.p. (°C)	ν(C═Se)
	C	H	N		
Bis complexes					
$(SeU)_2HgCl_2$	5.13 (4.64)	1.66 (1.56)	11.54 (10.83)	189–192	562 (736)[a]
$(DmSeU)_2HgCl_2$	12.78 (12.56)	2.92 (2.81)	10.21 (9.77)	198–199	528 (594)[a]
$(ImSe)_2HgCl_2$	13.05 (12.65)	2.13 (2.12)	10.13 (9.84)	219–221	565 (558)[a]
$(MeImSe)_2HgCl_2$	15.6 (16.08)	2.68 (2.70)	9.50 (9.37)	185–188.5	628 (580)[a]
$(DiazSe)_2HgCl_2$	16.39 (16.08)	2.79 (2.70)	9.73 (9.37)	188.5–190	715 (602)[a]
$(DiapSe)_2HgCl_2$	18.72 (19.2)	3.29 (3.22)	9.14 (8.95)	196–197.5	615 (614)[a]
Tris complexes					
$(ImSe)_3HgCl_2$	14.84 (15.04)	2.53 (2.52)	11.67 (11.7)	206–207.5	572
$(MeImSe)_3HgCl_2$	18.16 (18.95)	3.29 (3.18)	11.26 (11.05)	186–187	589
$(DiazSe)_3HgCl_2$	18.92 (18.95)	3.23 (3.18)	11.22 (11.05)	207–209	796
$(DiapSe)_3HgCl_2$	22.71 (22.40)	3.96 (3.77)	10.78 (10.47)	169–171.5	612
Tetrakis complexes					
$(SeU)_4HgCl_2$	6.35 (6.29)	2.14 (2.11)	14.58 (14.68)	194.5–195.5	584

[a] Values for the free ligands.

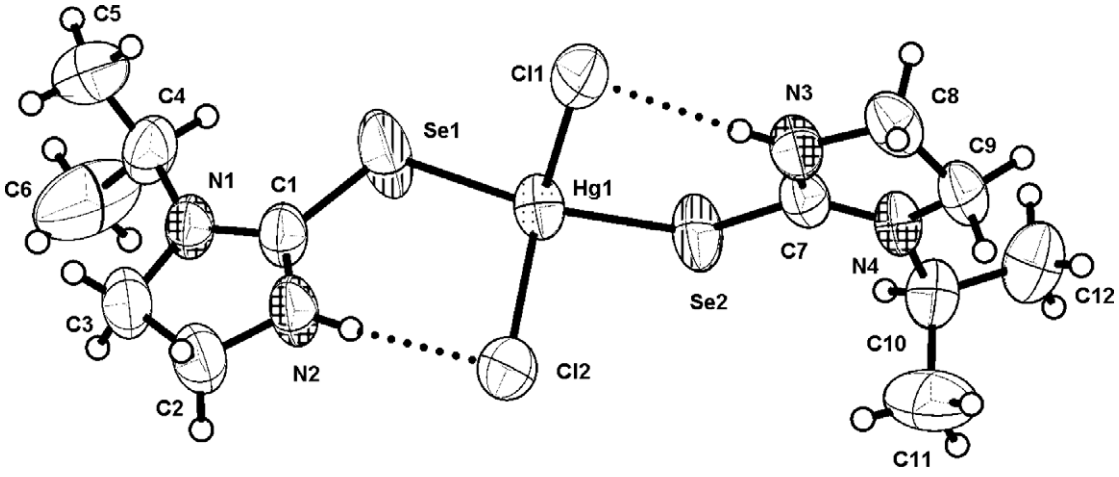

Fig. 1. Molecular structure of $(N\text{-}i\text{-}PrImSe)_2HgCl_2$.

model and an sp^2 hybridization was assumed for the nitrogen atoms of the NH groups. The crystallographic data are given in Table 4. Selected bond lengths and angles are given in Table 5. Complete bond lengths and bond angles, anisotropic thermal parameters and calculated hydrogen coordinates are deposited as supplementary materials. The ORTEP atomic labeling scheme is given in Fig. 1.

3. Results and discussion

The complexes were synthesized by reacting $HgCl_2$ with selones in 1:2 or 1:4. However, the elemental analyses of the complexes showed that except for selenourea a tetrakis complex (M:L = 1:4) could not be obtained and for other selones; maximum three ligands could coordinate to Hg(II) resulting in tris complexes, $[(\rangle C{=}Se)_3HgCl]Cl$ [12]. For DmSeU only a bis complex, $[Hg(DmSeU)_2Cl_2]$ was isolated. The NMR results also showed that for the complex prepared with M:L = 1:4, the resonances appeared at the same positions as observed for $[Hg(DmSeU)_2Cl_2]$. The steric hindrance offered by methyl groups seems to be a major factor due to which a tris or tetrakis complex could not be obtained.

3.1. IR spectroscopic studies

In the IR spectra of the complexes, the ν(C═Se) vibration, which occurs around 600 cm^{-1} for the free ligands shifts towards lower frequency upon complexation, in accordance with the data observed for selone complexes of other metal ions [15,16,29]. There are also strong absorptions around 3200 cm^{-1} corresponding to ν(NH) mode. The presence of a band around 3200 cm^{-1} in free ligands as well as in the complexes indicates the existence of the selone form of the ligands in the solid state. The IR frequencies of the complexes are given in Table 1.

3.2. ^1H and ^{13}C NMR solution studies

The ^1H and ^{13}C NMR chemical shifts of the complexes in DMSO-d_6 are summarized in Table 2. In ^1H NMR spectra of the complexes, the N—H signal of thiones became

less intense upon coordination and shifted downfield by 0.5–1.1 ppm from their positions in free ligands. Deshielding of the N—H proton is related to an increase of the π electron density in the C—N bond upon complexation [8,15,16]. The appearance of N—H signal in ^{1}H NMR shows that the ligands are coordinating in the selone form in solution [15,16].

In all complexes, the C-2 resonance of selones appears upfield by 6–12 ppm compared to free ligands as observed for other complexes of Ag(I) and Au(I) with selones [15,16]. The upfield shift is attributed to a lowering of the >C=S bond order upon coordination and a shift of N → C electron density producing partial double bond character in the C—N bond [8,13,15]. The upfield shift decreases as the number of ligands attached to mercury(II) increases from two in $[L_2HgCl_2]$ to three in $[L_3HgCl]Cl$ or four in $[L_4Hg]Cl_2$ (Table 2). This is because of the increase in number of electronegative groups attached to metal ion. This observation is demonstrated for number of complexes e.g. $Hg(ImSe)_2Cl_2$, $Hg(ImSe)_3Cl_2$; $Hg(MeImSe)_2Cl_2$, $Hg(MeImSe)_3Cl_2$; $Hg(Diaz)_2Cl_2$, $Hg(Diaz)_3Cl_2$; in all these complexes the bis complex show more ^{13}C shift compare to tris complex. A small shift of about 1 ppm is observed in other carbon atoms, which shows that nitrogen atoms are not involved in coordination. In the complexes of ImSe and MeImSe, a deshielding effect is observed at C-4/5 while in the DiazSe complexes, a deshielding effect is observed at C-4 and C-6 (C-4 and C-7 in DiapSe), but C-5 bears a shielding effect. The deshielding at C-4/6 is due to an increase in π character of the C–N bond [13]. Similar observation was made for ^{13}C chemical shift of the >C=Se resonance of SeU in $Ag(SeU)NO_3$ which was shifted by 12 ppm upfield compared to free SeU ligand, while in $Ag(SeU)_2NO_3$, the upfield shift was only by 7 ppm. The upfield shift is attributed to a lowering of >C=Se bond order upon coordination and a shift of N → C electron density producing a partial double bond character in the C—N bond, as observed in metal complexes of thiourea [29].

The ^{13}C NMR shift difference for the C-2 resonance of selones upon complexation is related to the strength of the metal-selenium bond [8]. The C-2 shift of 12 ppm is the highest in $[(DiapSe)_2HgCl_2]$ showing that the Hg—Se bond in $[(DiapSe)_2HgCl_2]$ should be the strongest among these complexes. It can be seen from Table 2 that as the ring size of the ligand is increased the shift difference at C-2 also increases. Thus DiapSe forms more stable complexes with mercury(II) compared to ImSe and DiazSe which shifted by approximately 8.90 ppm for both complexes.

Table 2
^{1}H, ^{13}C and ^{77}Se chemical shifts (ppm) of selones and their complexes in DMSO-d_6

Species	N—H	C-2	C-4	C-5	C-6	δ^{77}Se	δ^{15}N	δ^{199}Hg
SeU	7.55	179.92				215.3	−262.00[a]	
$(SeU)_2HgCl_2$	8.66	170.46				166.42	−251.01	
	+1.11	−9.46				−48.88		
$(SeU)_4HgCl_2$	8.42	172.67				178.30	−250.07	
	+0.97	−7.25				−37.0		
DmSeU	7.53	177.81				231.40		
$(DmSeU)_2HgCl_2$	8.30	168.30				167.40		
	+0.77	−9.51				−64.0		
ImSe	8.48	177.09	44.94	44.94		88.79		
$(ImSe)_2HgCl_2$	8.99	168.31	45.39	45.39		61.82		
	+0.51	−8.78	+0.45	+0.45		−26.97		
$(ImSe)_3HgCl_2$	9.35	170.47	45.31	45.31		66.98		
	+0.87	−6.62	+0.37	+0.37		−21.81		
MeImSe	8.47	178.67	42.07	50.35		88.00		
$(MeImSe)_2HgCl_2$	9.35	169.2	43.23	51.34		44.19		−1114.6
	+0.88	−9.47	+1.16	+0.99		−43.81		
$(MeImSe)_3HgCl_2$	9.12	172.13	42.91	51.05		55.75		
	−0.23	−6.54	+0.84	+0.70		−32.25		
N-i-PrImSe	8.43	177.18	42.28	47.72	42.26 (N—C1)			
$(N\text{-}i\text{-}PrImSe)_2HgCl_2$		168.02	43.49	49.22	43.08 (N—C1); 19.47 (—CH_3)	45.76		−1093.9
DiazSe	8.23	169.14	40.10	18.76	40.10	214.93		
$(DiazSe)_2HgCl_2$	9.34	160.24	40.37	18.03	40.37			−1051.1
	+1.11	−8.90	+0.27	−0.73	+0.27			
$(DiazSe)_3HgCl_2$	9.36	161.39	40.38	18.18	40.38	173.73		
	+1.02	−7.75	+0.28	−0.58	+0.28	−41.20		
DiapSe	8.21	180.98	45.12	26.63	26.63	292.70		
$(DiapSe)_2HgCl_2$	9.29	168.97	45.57	25.82	25.82	221.33		
	+1.08	−12.01	+0.45	−0.81	−0.81	−71.37		
$(DiapSe)_3HgCl_2$	9.19	170.48	45.49	25.98	25.98	227.93		−1095.5
	+0.98	−10.5	+0.37	−0.65	−0.65	−64.77		

[a] From Ref. [34].

3.3. ^{15}N NMR solution studies

^{15}N NMR could be recorded for SeU complexes only because the ligand contains ~5% enriched ^{13}C and ^{15}N. The ^{15}N signal for NH_2 resonance of SeU appears downfield by 4–5 ppm in the complexes compared to free ligand (Table 2). The downfield shift is consistent with an increase in double bond character of the C—N bond [8,13,21]. A smaller downfield, instead of a large upfield shift in ^{15}N NMR rules out the binding of selones to mercury(II) via nitrogen [13,22]. There is no significant difference between ^{15}N resonances of $(SeU)_2HgCl_2$ and $(SeU)_4HgCl_2$ probably because N is far from the Hg(II) and it also suggest that —NH_2 of the ligand is not involved in the binding to Hg(II).

3.4. ^{77}Se NMR solution studies

^{77}Se NMR seems to be the most effective technique for characterizing these complexes because in ^{77}Se NMR a large upfield shift is observed for all the ligands upon complexation. On coordination selenium resonances are shielded by about 22–71 ppm. This very large shielding provides a clear evidence for selenium binding to mercury(II). A decrease in the upfield shift is observed as the number of coordinating ligands increases. The less upfield shift in the tris or tetrakis complexes is because each ligand is sharing approx. 1/3 or 1/4 metal ion, compared to that in $[L_2HgCl_2]$ where each L is sharing 1/2 ion. As observed in ^{13}C NMR, the shift difference in ^{77}Se NMR is highest for DiapSe complexes suggesting that the Hg—Se bond is the strongest in these complexes. It is also observed that the shift difference increases with the ring size of the ligand. This again suggests that DiapSe forms more stable complexes with mercury(II) compared to ImSe and DiazSe. This observation is consistent with ^{13}C NMR data as indicated earlier, both ^{77}Se and ^{13}C NMR data show $[(DiapSe)_2HgCl_2]$ is the most stable complex.

We measured ^{199}Hg NMR spectra for the few complexes as reported in Table 2 because of the solubility of these complexes. However, there is no trend observed, therefore, some solid ^{199}Hg NMR spectra were measured and discussed below.

3.5. ^{199}Hg and ^{77}Se CP MAS NMR studies

The ^{199}Hg and ^{77}Se CPMAS spectra of the complex $(N\text{-}i\text{-}PrImSe)_2HgCl_2$ are shown in Figs. 2 and 3 respectively with the calculated spectra shown as stick plots. The ^{199}Hg, ^{77}Se and ^{13}C chemical shifts and some shielding anisotropies for the complexes are shown in Table 3, along with the corresponding data for the free ligand. While solid-state ^{199}Hg NMR spectroscopy reports of thiolate complexes are somewhat common [30], those of selone complexes are scarce in the literature [12]. The chemical shift of Hg nucleus is determined by the arrangement of atoms directly bonded to the Hg atom while the arrangement of the other atoms in the ligand plays a minor role

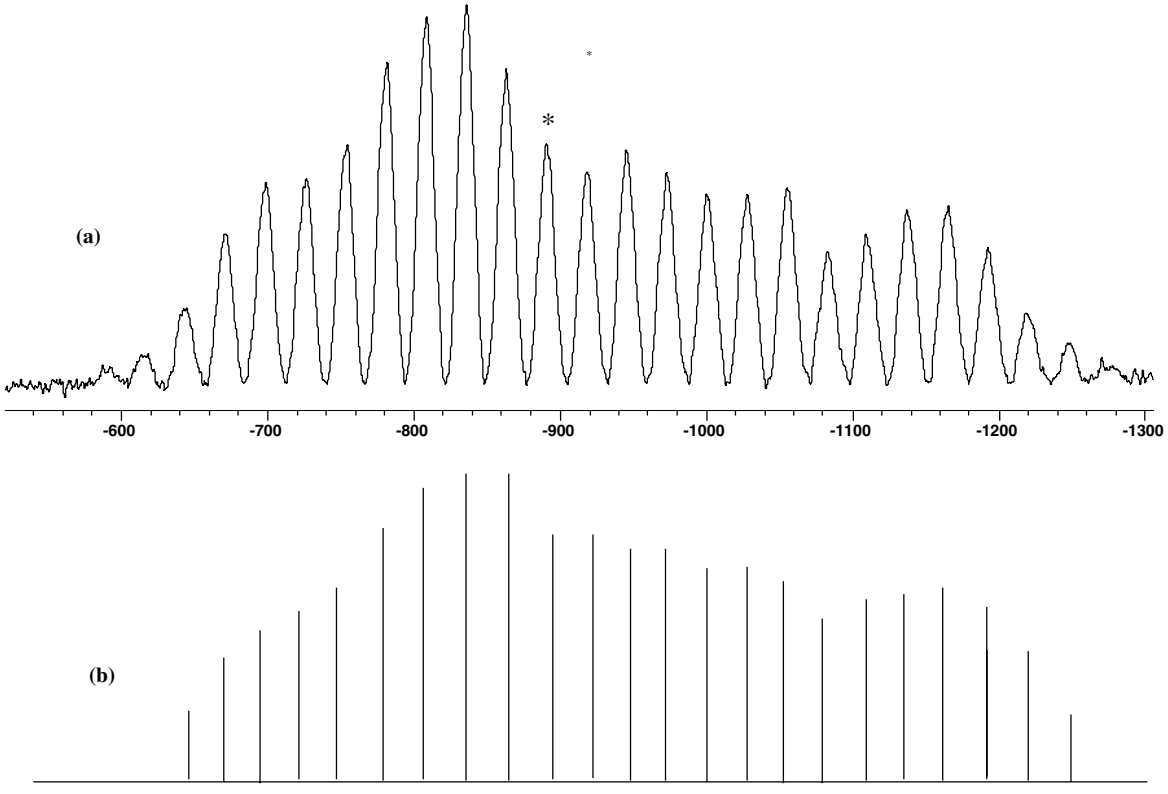

Fig. 2. ^{199}Hg CPMAS spectrum of $(N\text{-}i\text{-}PrImSe)_2HgCl_2$. (a) Observed and (b) calculated. The * denotes the isotropic peak.

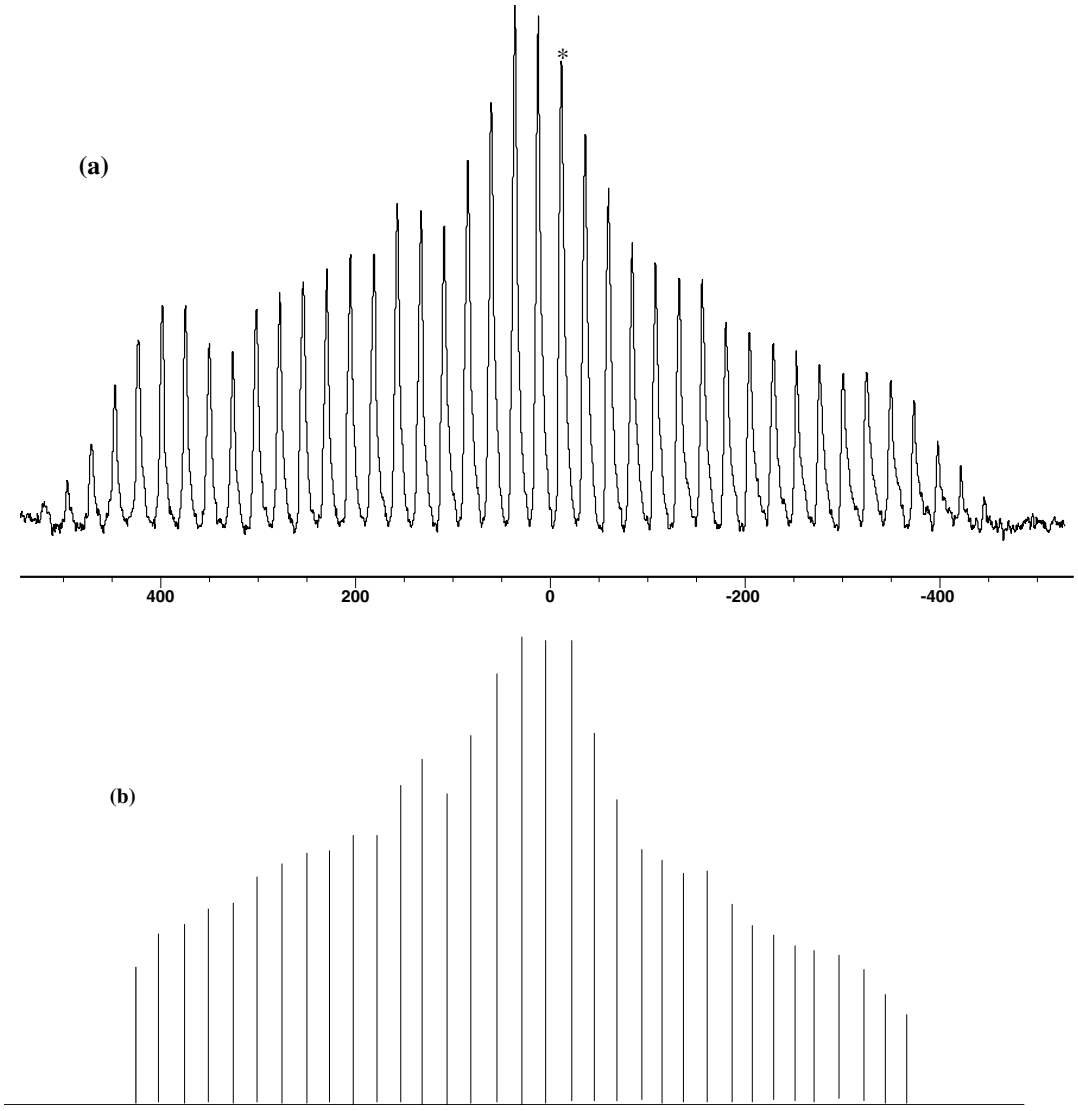

Fig. 3. The ^{77}Se CPMAS spectrum of (*N*-*i*-PrImSe)$_2$HgCl$_2$. (a) Observed and (b) calculated. The * denotes the isotropic peak.

[31]. The Hg nucleus in the tris complexes are more shielded by about 100 ppm compared to the bis complexes. The linear Hg(SeCN)$_2$ complex shows a large shielding anisotropy ($\Delta\sigma$) of 2520 ppm [31]. It has been found that the magnitude of the shielding anisotropy of mercury decreases from linear through trigonal planar to a perfect tetrahedral geometry, where it approaches a value of zero. A larger anisotropy is shown by the *bis* complex (N-*i*-PrImSe)$_2$HgCl$_2$, compared to the *tris* complexes. The asymmetry parameters for the complexes indicate that the point symmetry of site occupied by mercury atom is away from the axial symmetry (see Table 3).

An analysis of the orientation of the three orthogonal principal axes of the chemical shift tensor with respect to the molecular framework can be attempted. This is based on the criteria that the shielding effect of a given M—L bond is maximal in the direction perpendicular to the M—L vector and that the Se is the most deshielding atom [32]. On the basis of above, the most deshielded component σ_{11} should be disposed nearly collinear with the Hg—Cl axis in the *tris* complexes, whereas in the (N-*i*-PrImSe)$_3$HgCl$_2$ complex the component σ_{11} should be disposed perpendicular to the planes containing the two selenium atoms and the mercury atom.

The three different selenium environments are shown by the *tris* complexes and two different environments are shown by the *bis* complexes. However, in (N-*i*-PrImSe)$_2$HgCl$_2$ complex, we were able to see only one selenium environment in the NMR (Fig. 3). This may be due to an accidental degeneracy of the chemical shifts for the two selenium sites. The selenium chemical shift tensors calculated for (N-*i*-PrImSe)$_2$HgCl$_2$ are then an average for the two sites. Better overlap of the filled Hg orbitals with lowest unoccupied orbitals of Se should lead to shielding of the Se nucleus. Hence we can assign Se shifts based on their bond length to the mercury atom. With the shortest bond length leading to largest shielding. In the case of the ImSe complexes we observe a deshielding of the selenium upon

Table 3
Solid-state ^{199}Hg, ^{77}Se and ^{13}C isotropic chemical shifts (δ_{iso}) and principal shielding tensors (σ_{xx})[a] of the complexes

Compound	δ_{iso}	σ_{11}	σ_{22}	σ_{33}	$\Delta\sigma$	η
^{199}Hg Chemical shifts						
$(MeImSe)_3HgCl_2$	−1092.9	881	1050	1346	380	0.67
$(N\text{-}i\text{-}PrImSe)_2HgCl_2$	−890.6	242	830	1599	1062	0.83
$(ImSe)_3HgCl_2$	−1058.9	740	1037	1399	510	0.87
$(ImSe)_2HgCl_2$	−999.5					
$(DiazSe)_2HgCl_2$	−954.2					
^{77}Se Chemical shifts						
ImSe[b]	59.8					
$(ImSe)_2HgCl_2$	102.2, 94.62					
$(ImSe)_3HgCl_2$	112.2, 125.0, 130.2					
MeImSe[b]	68.7	213	52	−471	−604	0.40
$(MeImSe)_3HgCl_2$[c]	i. 7.8	−304	−187	468	714	0.25
	ii 83.6	−548	−116	413	746	0.87
	iii 92.4	−636	−520	878	1426	0.12
N-*i*-PrImSe[b]	57.1	225	55	−451	−591	0.43
$(N\text{-}i\text{-}PrImSe)_2HgCl_2$	12.5	−578	−443	983	1494	0.14
DiazSe[b]	173.1					
$(DiazSe)_2HgCl_2$	124.4, 138.2					
^{13}C Chemical shifts						
ImSe[b]	175.0					
$(ImSe)_2HgCl_2$	171.5, 172.1					
$(ImSe)_3HgCl_2$	167.2, 170.2, 172.4					
N-*i*-PrImSe[b]	175.6					
$(N\text{-}i\text{-}PrImSe)_2HgCl_2$	168.2, 169.9					
DiazSe[b]	174.0					
$(DiazSe)_2HgCl_2$	161.2, 166.3					

[a] Isotropic shielding, $\sigma_i = (\sigma_{11} + \sigma_{22} + \sigma_{33})/3$; $\Delta\sigma = \sigma 33 - 0.5(\sigma_{11} + \sigma_{22})$; $\eta = 3(\sigma_{22} - \sigma_{11})/2\Delta$.
[b] From Ref. [19].
[c] Ref. [12].

Table 4
Crystallographic data for $(N\text{-}i\text{-}PrImSe)_2HgCl_2$

Empirical formula	$C_{12}H_{24}Cl_2HgN_4Se_2$
Formula weight	653.76
Crystal system	triclinic
Space group	$P\bar{1}$
Temperature (K)	296
Radiation Mo Kα (Å)	($\lambda = 0.71073$)
ρ_{calc} (g cm^{-3})	2.137
a (Å)	8.3722(13)
b (Å)	9.3929(15)
c (Å)	13.865(2)
α (°)	76.116(2)
β (°)	76.971(2)
γ (°)	77.494(3)
V (Å^3)	1015.9(3)
Z	2
R_1 ($I > 2\sigma(I)$)	0.0410
wR_2 ($I > 2\sigma(I)$)	0.0891

Table 5
Selected bond lengths (Å) and bond angles (°) for $(N\text{-}i\text{-}PrImSe)_2HgCl_2$

Bond lengths			
Hg1—Cl1	2.5173(19)	Se1—C1	1.850(6)
Hg1—Cl2	2.5370(17)	Se2—C7	1.881(5)
Hg1—Se1	2.5706(9)	N1—C1	1.306(7)
Hg1—Se2	2.5989(8)	N2—C1	1.328(7)
Bond angles			
Cl1—Hg1—Cl2	105.89(7)	Cl2—Hg1—Se2	108.22(5)
Cl1—Hg1—Se1	110.64(5)	Se1—Hg1—Se2	111.87(3)
Cl2—Hg1—Se1	111.73(4)	C1—Se1—Hg1	104.08(18)
Cl1—Hg1—Se2	108.24(5)	C7—Se2—Hg1	103.89(19)

complexation. For the complexes we observe positive ^{77}Se anisotropy, while the ligands show a negative anisotropy. This arises because of apparent swapping of the components σ_{11} and σ_{33}.

The ^{13}C NMR spectra also showed the three distinct environments for the selone carbons in the tris complexes and two distinct environments in the bis complexes. On complexation, the selenocarbonyl carbon atoms are more shielded, and this shielding is largest in the case of $(DiazSe)_2HgCl_2$ complex.

3.6. Crystal structure of $(N\text{-}i\text{-}PrImSe)_2HgCl_2$

The complex $(N\text{-}i\text{-}PrImSe)_2HgCl_2$ adopts a distorted tetrahedral geometry. The Se—Hg—Cl bond angles range from 108.22(5)° to 111.73(4)° while the remaining bond angles are Cl1—Hg1—Cl2 105.89(7)° and Se1—Hg1—Se2 111.87(3)°. The average Hg—Se and Hg—Cl bond lengths are 2.585(1) Å and 2.527(2) Å, respectively. To the best of our knowledge, this structure represents the first X-ray structure reported so far for a mononuclear selone mercury (II) complex with $[Se_2Cl_2]$ coordination sphere. The Hg—Se

and Hg—Cl bond distances are in the same range as those reported for the complexes $[HgCl(py)(SeEt)]_4$ [33] and $[Hg(MeImSe)_3Cl]^+$ [12]. Short N···Cl contacts take place (N2···Cl2: 3.168 Å and N3···Cl1: 3.187 Å), suggesting intramolecular NH···Cl hydrogen bonding between the NH groups of the two imidazoline rings and the two chlorine atoms.

The distortion from the ideal tetrahedral geometry is stabilized by hydrogen bonding interactions. As a matter of fact, the existing hydrogen bonding scheme gives rise to two six-membered rings namely $Hg_1Se_2C_7N_3H_3Cl_1$ and $Hg_1Se_1C_1N_2H_2Cl_2$. Both rings adopt a pseudo half-boat conformation in which the five atom Se—C—N—H—Cl fragment, excluding the metal ion, is essentially planar. The metal ion displacement from this mean plane is 0.699(3) Å and 0.311(4) Å for the former and later ring respectively. The half boat conformation is thus less pronounced in the $Hg_1Se_1C_1N_2H_2Cl_2$ ring resulting in more strain and a higher Se1—Hg1—Cl2 bond angle (111.73(4)°) compared to Se2—Hg1—Cl1 bond angle (108.24(5)°).

4. Conclusion

In this study, we have shown that a series of selones react with $HgCl_2$ to form complexes of the type HgL_2Cl_2, HgL_3Cl_2 and HgL_4Cl_2 in which the ligands exist in selone form both in solution as well as in the solid state. The X-ray structures of $(N\text{-}i\text{-}PrImSe)_2HgCl_2$ complex revealed a distorted tetrahedral geometry. The ^{13}C and ^{77}Se solution NMR data clearly indicate that as the ring size of the ligand is increased, the chemical shift difference for the free and bound resonance also increases. Thus DiapSe forms more stable complexes with mercury(II) compared to ImSe and DiazSe. The chemical shifts for different complexes presented here are useful, especially if the ^{77}Se NMR is used to study the metal–ligand interactions in biological systems.

5. Supplementary materials

The supplementary X-ray data are available from the CCDC, 12 Union Road, Cambridge CB2 1EZ, UK (fax: +44 1223 366 033, e-mail: deposit@ccdc.ac.uk or on the web www: http://www.ccdc.cam.ac.uk) on request, quoting the deposition No. 268447.

Acknowledgements

This research was supported by the KFUPM Research Committee under project no. CY/NMR-STUDIES/277.

References

[1] W. Eikens, C. Kienitz, P.G. Jones, C. Thone, J. Chem. Soc., Dalton Trans. (1994) 83.
[2] S. Ahmad, A.A. Isab, A.R. Al-Arfaj, A.P. Arnold, Polyhedron 21 (2002) 2099.
[3] A.P. Arnold, K.S. Tan, D.L. Rabenstein, Inorg. Chem. 25 (1986) 2433.
[4] F.A. Devillanova, G. Verani, Transit. Met. Chem. 2 (1977) 9.
[5] C.J. Dillard, A.L. Tappel, J. Inorg. Biochem. 28 (1986) 13.
[6] C. Sasakura, K.T. Suzuki, J. Inorg. Biochem. 71 (1998) 159.
[7] A.A. Isab, H.P. Perzanowski, Polyhedron 15 (1996) 2397.
[8] Z. Popovic, G. Pavlovic, D. Matkovic-Calogovic, Z. Soldin, M. Rajic, D. Vikic-Topic, D. Kovacek, Inorg. Chim. Acta 306 (2000) 142.
[9] A.M. Hutchings, N.E. McConnel, R.A. Faucher, D. VanDerveer, D.J. Williams, J. Chem. Crystallgr. 33 (2003) 619.
[10] D.M. Calogovic, D.M. Sermek, Z. Popovic, Z. Soldin, Acta Crystallogr., Sect. C 60 (2004) m44.
[11] V.W. Yam, Y.L. Pui, K.K. Cheung, J. Chem. Soc., Dalton Trans. 3658 (2000).
[12] A.D. Al-Amri, M. Fettouhi, M.I.M. Wazeer, A.A. Isab, Inorg. Chem. Commun. 8 (2005) 1109.
[13] A.A. Isab, S. Ahmad, M. Arab, Polyhedron 21 (2002) 1267.
[14] S. Ahmad, A.A. Isab, H.P. Perzanowski, Can. J. Chem. 80 (2002) 1279.
[15] S. Ahmad, A.A. Isab, A.P. Arnold, J. Coord. Chem. 56 (2003) 539.
[16] M.I.M. Wazeer, A.A. Isab, Spectrochim. Acta (A) 62 (2005) 880.
[17] W. Ashraf, S. Ahmad, A.A. Isab, Transit. Met. Chem. 29 (2004) 400.
[18] F. Cristiani, F.A. Devillanova, G. Verani, J. Chem. Soc. Perkin II Trans. (1977) 324.
[19] M.I.M. Wazeer, A.A. Isab, H.P. Perzanowski, Magn. Res. Spectrosc. 41 (2003) 1026.
[20] J. Milne, Mag. Res. Chem. 31 (1993) 652.
[21] J.M. Hook, P.A.W. Dean, L.C.M. van Gorkom, Magn. Reson. Chem. 33 (1995) 77.
[22] M.J. Collins, C.I. Ratcliffe, J.A. Ripmeester, J. Magn. Reson. 68 (1986) 172.
[23] M. Maricq, J. Waugh, J. Chem. Phys. 70 (1979) 3300.
[24] SMART APEX software (5.05) for SMART APEX detector, Bruker Axs Inc., Madison, WI, USA.
[25] SAINT software (5.0) for SMART APEX detector, Bruker Axs Inc., Madison, WI, USA.
[26] G.M. Sheldrick, SADABS. Program for Empirical Absorption correction of Area detector Data, University of Gottingen, Germany, 1996.
[27] G.M. Sheldrick, SHELXTL V5.1 Software, Bruker AXS, Inc., Madison, WI, USA, 1997.
[28] G.M. Sheldrick, University of Gottingen, Germany, 1997.
[29] S. Ahmad, A.A. Isab, Inorg. Chem. Commun. 5 (2002) 355.
[30] R.A. Santos, E.S. Gruff, S.A. Koch, G.S. Harbison, J. Am. Chem. Soc. 113 (1991) 469.
[31] G.A. Bowmaker, A.V. Churakov, R.K. Harris, J.A.K. Howard, D.C. Apperley, Inorg. Chem. 37 (1998) 1734.
[32] E. Riviera, P.D. Ellis, Inorg. Chem. 31 (1992) 2096.
[33] A.P. Arnold, A.J. Canty, B.W. Skelton, A.H. White, J. Chem. Soc., Dalton Trans. (1982) 607.
[34] A.A. Isab, M.I.M. Wazeer, J. Coord. Chem. 58 (2005) 529.

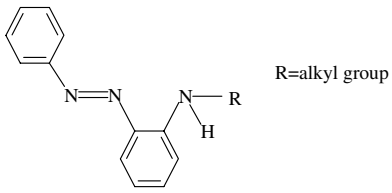

2 (HL[a])

2. Results and discussion

2.1. Syntheses

The 1*N*-(2-pyridyl-2-methyl)-2-arylazo aniline, HL (**1**), ligands were prepared by refluxing 2-(arylazo) aniline with 2-chloromethyl pyridine in acetonitrile in the presence of potassium carbonate and a catalytic amount of potassium iodide (Scheme 1). The ligands were isolated as orange solids.

The reactions of the new HL ligands with Na_2PdCl_4 in methanol afforded pink complexes of palladium (II) of the composition (L)PdCl (**3**) incorporating a new tridentate (*N*,*N*,*N*) ligand (Scheme 1). The deprotonated secondary amino and the azo nitrogens bind the metal, forming a six membered diazoketiminato chelate, while the other 1*N*-alkyl-2-arylazo aniline, HL[a] (**2**) [7] produced the orthopalladated species (L[a])PdCl (**4**) upon treatment with Na_2PdCl_4. Formation of a six membered azoimine chelate in the case of HL has been attributed to the delocalisation of the negative charge within the ligand backbone.

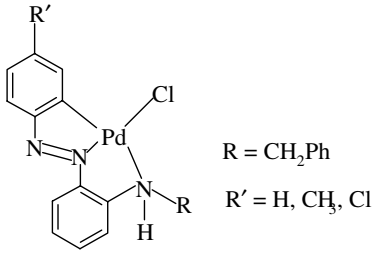

4

The general mechanism of the formation of orthopalladated azobenzene was described to proceed via initial coordination of azo nitrogen followed by electrophilic substitution at the pendant aryl ring [11]. This mechanism was plausible in the cases of HL[a] since these ligands also underwent facile orthopalladation upon treatment with Na_2PdCl_4 (Scheme 2). Whereas reaction of HL with Na_2PdCl_4 did not afford the orthopalladated product and the reaction pathway has been proposed as shown in Scheme 3. Coordination of the amino nitrogen upon concomitant dissociation of its proton was assumed to occur as a result of prior binding of the pyridyl nitrogen to Pd(II). These preceding coordinations of pyridyl and amido nitrogens enabled the ligand to form the diazoketiminato chelate upon subsequent binding through the azo nitrogen and delocalisation of negative charge, which grows upon amino proton dissociation.

2.2. Characterisation

All the ligands displayed characteristic UV–Vis spectra with an absorption near 325 nm for the n–π^* transition of azo compounds [6]. The (L)PdCl complexes exhibited a characteristic low energy absorption near 560 nm, which was assigned to a MLCT transition. Representative UV–Vis spectra of the ligand HL[3]and (L[3])PdCl are shown in Fig. 1. Relevant data are collected in Section 3.

The IR spectra of HL display a sharp singlet near 3189 cm^{-1} for ν_{N-H} which was absent in spectra of (L)PdCl, indicating dissociation of the amino proton on complexation. The $\nu_{N=N}$ band of the ligands ($\sim$1510 cm^{-1}) shifts to lower frequency after formation of the Pd(II) chelates (1350–1400 cm^{-1}), consistent with coordination of the azo nitrogen [6]. The ν_{Pd-Cl} of the palladium complexes appear in the range 290–333 cm^{-1} [7]. Relevant data are included in Section 3.

The ^1H NMR spectra of the ligands and the corresponding palladium complexes are consistent with the formulae and structures. Although the amino proton of HL appears as a broad signal, due to the vicinal coupling of the methylene protons its splitting into a broadened triplet can be observed. On the other hand, the methylene proton resonance also splits as a doublet due to vicinal coupling of the N–H proton. In contrast, the ^1H NMR spectra of (L)PdCl do not display the N–H resonance and the methylene protons appear as a singlet (the vicinal coupling of N–H is absent), signifying the dissociation of the amino proton upon complexation. The methylene proton reso-

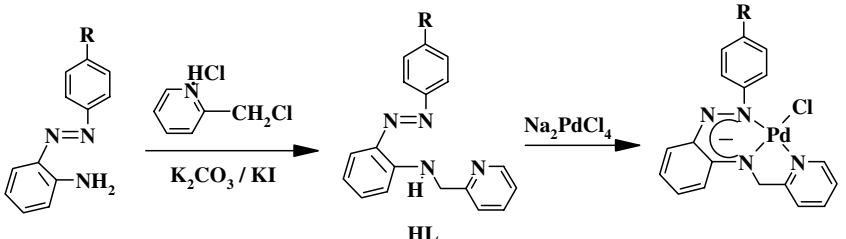

Scheme 1.

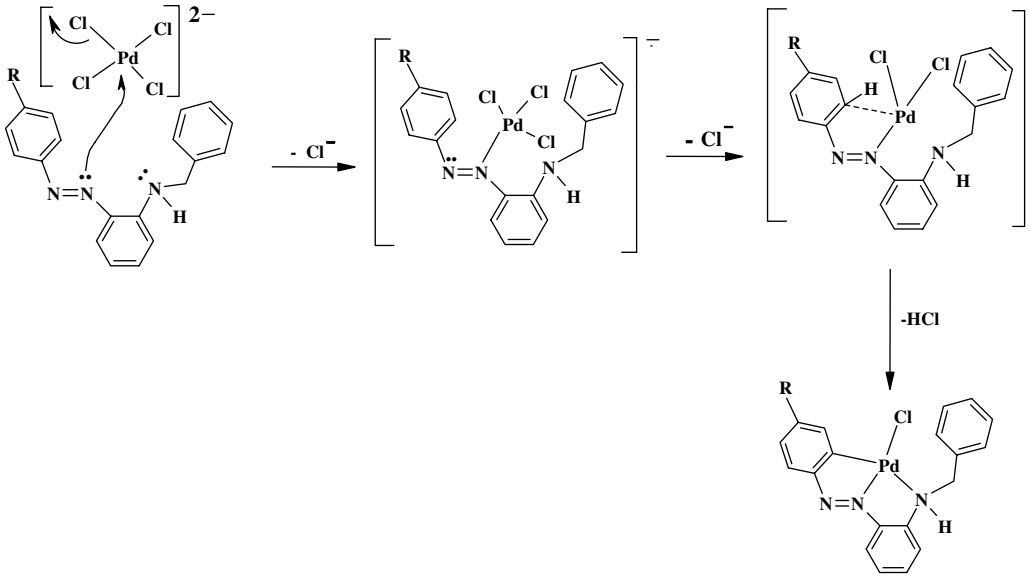

Scheme 2.

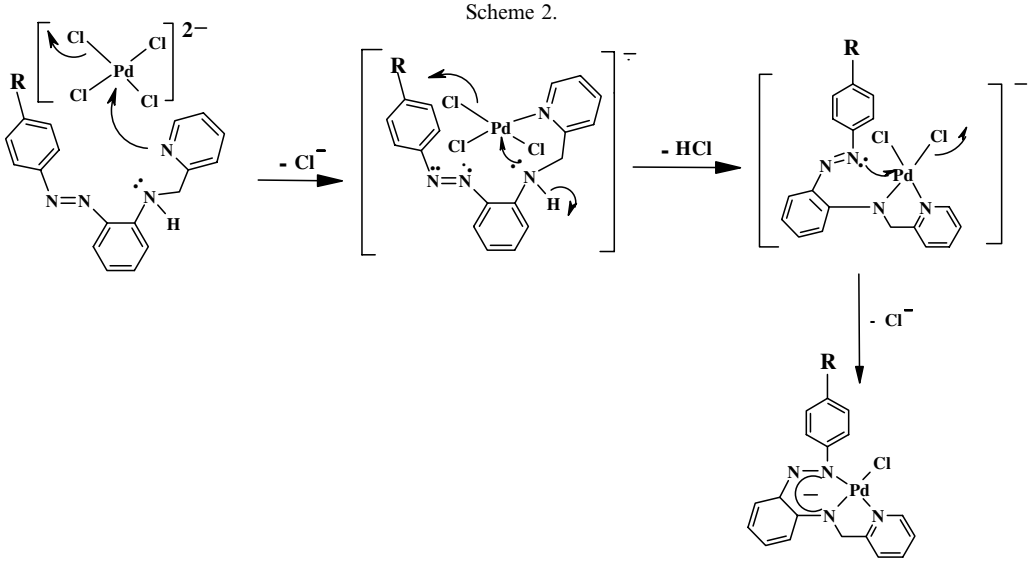

Scheme 3.

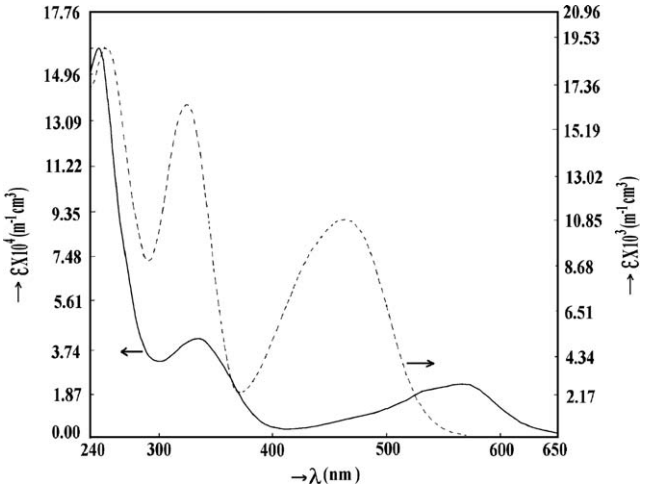

Fig. 1. UV–Vis spectra of HL^3 (---) and $(L^3)PdCl$ (—). The arrows indicate scales of the corresponding spectrum.

nance of (L)PdCl (~δ 5.24) is shifted downfield compared to that of the HL ligands (~δ 4.68). The ^{1}H NMR data are given in Section 3.

2.3. X-ray structure

Suitable crystals of $(L^1)PdCl$ were grown by slow diffusion of hexane into a dichloromethane solution. The X-ray structure of the complex was determined and the perspective view of the $(L^1)PdCl$ molecule, along with the atom numbering scheme, is shown in Fig. 2. Selected bond distances and angles are collected in Table 1. The geometry about palladium is distorted square planar, where the mono anionic deprotonated ligand $(L^1)^-$ binds in a tridentate (*N*,*N*,*N*) fashion. A chloride ligand satisfies the tetracoordination. Three chelating nitrogens are: azo (*N*(azo)), pyridyl (*N*(py)) and amino (*N*(am)). The Pd–*N*(azo), Pd–*N*(py) and Pd–Cl lengths (1.988(4) Å, 2.037(5) Å and

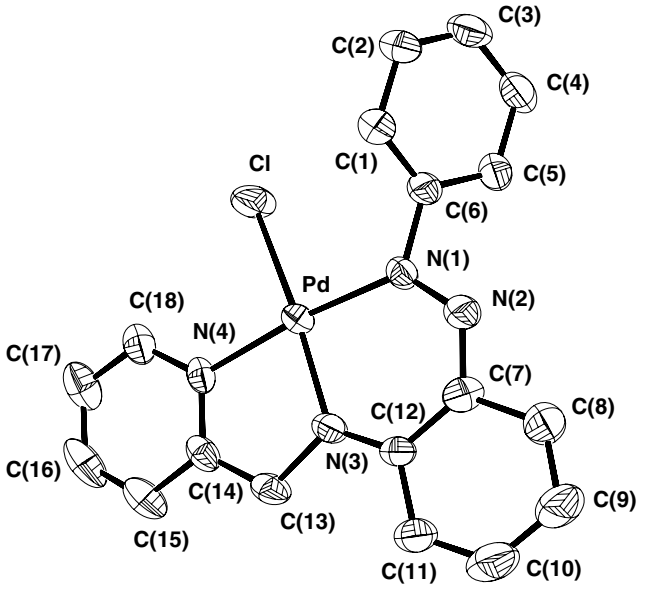

Fig. 2. Perspective view of (L^1)PdCl with the atom numbering scheme. Hydrogen atoms are omitted for clarity.

Table 1
Selected bond distances (Å) and angles (°) for (L^1)PdCl

Pd–N(4)	2.037(5)	N(3)–C(12)	1.330(9)
Pd–N(1)	1.988(4)	C(7)–C(8)	1.429(9)
Pd–N(3)	1.968(5)	C(8)–C(9)	1.349(10)
Pd–Cl	2.330(2)	C(9)–C(10)	1.385(13)
N(1)–C(6)	1.454(8)	C(10)–C(11)	1.368(12)
N(1)–N(2)	1.284(7)	C(11)–C(12)	1.419(10)
N(2)–C(7)	1.346(8)	N(3)–C(13)	1.466(8)
C(7)–C(12)	1.421(1)	C(13)–C(14)	1.454(10)
C(7)–C(8)	1.344(2)	C(14)–N(4)	1.350(9)
N(4)–Pd–N(3)	82.3(2)	N(1)–N(2)–C(7)	124.6(5)
N(1)–Pd–N(4)	173.7(2)	C(13)–C(14)–N(4)	118.0(6)
N(1)–Pd–Cl	94.8(2)	C(14)–N(4)–Pd	113.4(4)
N(3)–Pd–Cl	172.2(3)	Pd–N(1)–N(2)	126.7(4)
C(6)–N(1)–Pd	123.9(4)	C(7)–C(12)–N(3)	121.5(6)
C(13)–N(3)–Pd	114.6(4)	C(12)–N(3)–Pd	126.6(5)

2.330(2) Å, respectively) are within the normal range [9a]. The geometry about palladium is planar (mean deviation 0.042 Å) justifying the oxidation state of Pd(II) and the uninegative ligand since the complex is a non-electrolyte.

The delocalisation of the negative charge within the ligand backbone causes the bond lengths to be suitably altered [6]. The C(12)–N(3) length (1.330(9) Å) is shorter compared to the C–N single bond (N(1)–C(6), 1.454(8) Å) in the same molecule and is similar to the imine (C=N) distance [6]. Also the effect of imine formation due to delocalisation has been reflected in the adjacent phenyl ring (C(7), C(8), C(9), C(10), C(11) and C(12)) which is distorted with two short (~1.35 Å) and four long (~1.4 Å) bonds. Thus the formation of an azoimine chelate could be inferred from the X-ray studies [6] and the structural formula of (L^1)PdCl has been drawn accordingly in **3** of Scheme 1 (vide supra). All the non-hydrogen atoms of (L^1)PdCl, excluding the pendant phenyl ring (C(1)–C(6)), make a good plane (mean deviation 0.114 Å).

3. Experimental

3.1. Materials

The solvents used in the reactions were of reagent grade, obtained from E. Merck, Kolkata, India and purified and dried by reported procedures [6]. 2-(Arylazo) anilines were prepared according to the reported procedure [6]. Palladium chloride and potassium carbonate were purchased from E. Merck, Kolkata, India. 2-(Chloromethyl) pyridine hydrochloride was purchased from Lancaster, England. Disodium tetrachloropalladate was prepared by a reported procedure [6a].

3.2. Syntheses of the ligands

All the ligands, HL^1, HL^2 and HL^3, were prepared following similar procedures. A representative procedure for HL^1 is given below.

3.2.1. HL^1

A mixture of 2-(phenylazo) aniline (0.3 g, 1.52 mmol), 2-chloromethyl pyridine hydrochloride (0.25 g, 1.52 mmol), 1 g of K_2CO_3 and a catalytic amount of KI (0.01 g, 0.06 mmol) in 30 cm^3 dry acetonitrile was refluxed for 3 h. The orange solid mass that was obtained after evaporation of the solvent, afforded the ligand, HL^1, which was isolated by column chromatography on silica gel (60–120 mesh) using the eluent petroleum ether–benzene (3/1 v/v). Upon evaporation of the solvent after chromatography, the orange-red solid of pure HL^1 was obtained. Yield: 0.262 g, 60%. *Anal.* Calc. for $C_{18}H_{16}N_4$, HL^1: C, 75.00; H, 5.20; N, 19.44. Found: C, 74.42; H, 5.35; N, 19.35%. UV–Vis (λ_{max}/nm (ϵ/M^{-1} cm^{-1}) in dichloromethane): 465 (1620), 420 (9430), 325 (10 570). IR (KBr pellets, cm^{-1}): ν_{N-H} 3189, $\nu_{N=N}$ 1512. ^1H NMR ($CDCl_3$): $\delta = 9.50$ (b, NH); 8.66 (d, 1H, $J = 6.0$); 7.90 (d, 3H, $J = 9.0$); 7.66 (t, 1H, $J = 8.5$); 7.49 (t, 2H, $J = 7.5$); 7.41 (d, 1H, $J = 7.2$); 7.36 (t, 1H, $J = 6.0$); 7.28 –7.20 (m, 2H); 6.81 (t, 1H, $J = 7.2$); 6.73 (d, 1H, $J = 8.4$); 4.69 (d, 2H, $J = 4.5$).

3.2.2. HL^2 and HL^3

Ligands HL^2 and HL^3 were prepared using 2-(*p*-tolylazo) aniline and 2-(*p*-chlorophenylazo) aniline in place of 2-(phenylazo) aniline, respectively. Yield: HL^2, 62% and HL^3, 65%.

Anal. Calc. for $C_{19}H_{18}N_4$, HL^2: C, 75.50; H, 5.96; N, 18.54. Found: C, 75.42; H, 6.00; N 18.60%. UV–Vis (λ_{max}/nm (ϵ/M^{-1} cm^{-1}) in dichloromethane): 451 (37 287), 419 (32 681), 321 (61 303). IR (KBr pellets, cm^{-1}): ν_{N-H} 3196, $\nu_{N=N}$ 1512. ^1H NMR ($CDCl_3$): $\delta = 9.37$ (b, NH); 8.65 (d, 1H, $J = 5.0$); 7.86 (d, 1H, $J = 8.0$); 7.79 (d, 1H, $J = 8.5$); 7.64 (t, 1H, $J = 7.5$); 7.35 (d, 1H, $J = 10.0$); 7.29 (d, 2H, $J = 8.0$); 7.24–7.19 (m, 3H); 6.79 (t, 1H, $J = 7.5$); 6.73 (d, 1H, $J = 8.5$); 4.68 (d, 2H, $J = 5.5$); 2.42 (s, 3H).

Anal. Calc. for $C_{18}H_{15}N_4Cl$, HL^3: C, 66.97; H, 4.65; N, 17.37. Found: C, 66.50; H, 4.70; N, 17.25%. UV–Vis (λ_{max}/nm (ϵ/M^{-1} cm^{-1}) in dichloromethane): 461 (10854), 426 (8483), 324 (17123), 253 (19435). IR (KBr pellets, cm^{-1}): ν_{N-H} 3196, $\nu_{N=N}$ 1511. ^1H NMR ($CDCl_3$): $\delta = 9.55$ (b, NH); 8.66 (d, 1H, $J = 4.0$); 7.88 (d, 1H, $J = 8.0$); 7.84 (d, 2H, $J = 7.0$); 7.66 (t, 1H, $J = 7.5$); 7.46 (d, 2H, $J = 9.0$); 7.33 (d, 1H, $J = 7.5$); 7.25 (m, 1H); 7.22 (t, 1H, $J = 6.5$); 6.83 (t, 1H, $J = 8.0$); 6.75 (d, 1H, $J = 8.5$); 4.68 (d, 2H, $J = 5.0$).

3.3. Syntheses of the complexes

All the complexes, $(L^1)PdCl$, $(L^2)PdCl$ and $(L^3)PdCl$ were prepared following similar procedures. A representative procedure for $(L^1)PdCl$, is given below.

3.3.1. $(L^1)PdCl$

A solution of HL^1 (0.150 g, 0.52 mmol) in 10 cm^3 methanol was added to a solution of Na_2PdCl_4 (0.153 g, 0.52 mmol) in 5 cm^3 methanol. The mixture was stirred for 5 h. The dark solid precipitate was separated by filtration and purified by column chromatography using silica gel (60–120 mesh). The eluent was benzene–acetonitrile (19/1 v/v) mixed solvent. Upon evaporation of the solvent, a violet solid of pure $(L^1)PdCl$ was obtained. Yield: 0.122 g, 55%. *Anal.* Calc. for $C_{18}H_{15}N_4PdCl$, $(L^1)PdCl$: C, 50.32; H, 3.49; N, 13.04. Found: C, 50.35; H, 3.50; N, 13.00%. UV–Vis (λ_{max}/nm (ϵ/M^{-1} cm^{-1}) in dichloromethane): 565 (14660), 525 (3230), 325 (31870). IR (KBr pellets, cm^{-1}): $\nu_{N=N}$ 1357, ν_{Pd-Cl} 333. ^1H NMR ($CDCl_3$): $\delta = 9.39$ (d, 1H, $J = 6.0$); 7.86 (t, 2H, $J = 7.2$); 7.52 (d, 1H, $J = 7.8$); 7.45–7.30 (m, 7H); 7.02 (d, 1H, $J = 9.0$); 6.68 (t, 1H, $J = 7.8$); 5.24 (s, 2H).

3.3.2. $(L^2)PdCl$ and $(L^3)PdCl$

Complexes $(L^2)PdCl$ and $(L^3)PdCl$ were prepared using the ligands HL^2 and HL^3 in place of HL^1, respectively. Yield: $(L^2)PdCl$, 55% and $(L^3)PdCl$, 55%.

Anal. Calc. for $C_{19}H_{17}N_4PdCl$, $(L^2)PdCl$: C, 51.46; H, 3.83; N, 12.64. Found: C, 51.40; H, 3.90; N, 12.70%. UV–Vis (λ_{max}/nm (ϵ/M^{-1} cm^{-1}) in dichloromethane): 563 (25711), 529 (22733), 460 (19844), 327 (37666). IR (KBr pellets, cm^{-1}): $\nu_{N=N}$ 1354, ν_{Pd-Cl} 332. ^1H NMR ($CDCl_3$): $\delta = 9.40$ (d, 1H, $J = 5.5$); 7.86 (m, 2H); 7.53 (d, 1H, $J = 8.0$); 7.43 (t, 1H, $J = 7.0$); 7.35–7.31 (m, 3H); 7.18 (d, 2H, $J = 8.0$); 7.01 (d, 1H, $J = 8.5$); 6.67 (t, 1H, $J = 7.5$); 5.22 (s, 2H); 2.39 (s, 3H).

Anal. Calc. for $C_{18}H_{14}N_4PdCl_2$, $(L^3)PdCl$: C, 46.60; H, 3.02; N, 12.08. Found: C, 46.55; H, 3.00; N, 12.10%. UV–Vis (λ_{max}/nm (ϵ/M^{-1} cm^{-1}) in dichloromethane): 566 (21488), 534 (18813), 334 (40348), 247 (159395). IR (KBr pellets, cm^{-1}): $\nu_{N=N}$ 1357, ν_{Pd-Cl} 333. ^1H NMR ($CDCl_3$): $\delta = 9.35$ (d, 1H, $J = 5.5$); 7.86 (t, 1H, $J = 7.5$); 7.79 (d, 1H, $J = 8.5$); 7.53 (d, 1H, $J = 7.5$); 7.44–7.32 (m, 6H); 7.02 (d, 1H, $J = 9.0$); 6.68 (t, 1H, $J = 7.5$), 5.23 (s, 2H).

Table 2
Crystallographic data for $(L^1)PdCl$

Chemical formula	$C_{18}H_{15}ClN_4Pd$
Formula weight	429.21
Space group	*Pna*21 cab (no. 33)
Crystal system	orthorhombic
a (Å)	6.9300(11)
b (Å)	13.3390(13)
c (Å)	17.738(2)
λ (Å)	0.71073
V (Å^3)	1639.7(4)
Z	4
Temperature (K)	293
ρ_{calc} (Mg/m^3)	1.739
μ (mm^{-1})	1.301
F (000)	856
R_1	0.0300
Unique reflections/[$I > 2\sigma(I)$]	1448/1269
wR_2	0.0805
Goodness-of-fit	1.04

3.4. Physical measurements

Microanalyses (C,H,N) were performed using a Perkin–Elmer 240C elemental analyser. Infrared spectra were recorded on a Perkin–Elmer L120-00A FT-IR spectrometer with the samples prepared as KBr pellets. Electronic spectra were recorded on a Shimadzu UV-2401 PC spectrophotometer. ^1H NMR spectra were obtained on Brucker Avance DPX 300 and Brucker RPX 500 NMR spectrometers in $CDCl_3$, using TMS as the internal standard.

3.5. Crystallography

A crystal of $C_{18}H_{15}N_4PdCl$ was grown by slow diffusion of hexane into a dichloromethane solution at 298 K. Data were collected by the ω-scan technique on a Enraf–Nonius CAD4 diffractometer with Mo Kα radiation monochromated by a graphite crystal. The structure solution was done by the direct method with the SHELXS-97 program. Full matrix least square refinements were performed using the SHELX-97 program (PC version). All non-hydrogen atoms were refined anisotropically using reflections $I > 2\sigma(I)$. Hydrogen atoms were included in calculated positions. The crystal data and data collection parameters are listed in Table 2.

4. Conclusion

Reactions of transition metal substrates with preformed ligands describe the actual metal–ligand interaction which is important to rationalise several biological and catalytic processes. The work presented here is a unique example in this regard. In this report we have described that the M–C interaction in polyfunctional organic molecules may be influenced not only electronically but also by suitable arrangements of the hetero donor atoms. The *N*-alkylated arylazo anilines, HL^a, were demonstrated to be appropriate for C–H bond activation via orthometallation [7] while

reactions of the newly synthesised ligands, HL with Na_2PdCl_4 afforded the remarkable azoimine chelates. A plausible rationale has been given considering the logical progress of the reactions.

Acknowledgments

We are thankful to the DST (New Delhi) for funding and fellowship to J.P. under the DST-SERC project. The necessary laboratory and infrastructural facility are provided by the Department of Chemistry, University of Kalyani. We are thankful to Prof. G.K. Lahiri (IIT, Mumbay) for his continuous help. The support of the DST under the FIST program to the Department of Chemistry, University of Kalyani is acknowledged.

Appendix A. Supplementary data

Figs. S1–S6, UV–Vis spectra; Figs. S7–S12, IR spectra and Figs. S13–S18, ^{1}H NMR spectra are supplied as supplementary material. Crystallographic data for the structural analysis have been deposited with the Cambridge Crystallographic Data Center, CCDC reference number 250543. Copies of this information may be obtained free of charge from The Director, CCDC, 12 Union Road, Cambridge CB2 1EZ, UK, e-mail: deposite@ccdc.cam.ac.uk or www: http://www.ccdc.cam.ac.uk. Supplementary data associated with this article can be found, in the online version, at doi:10.1016/j.poly.2006.03.019.

References

[1] A.C. Cope, R.W. Siekman, J. Am. Chem. Soc. 87 (1965) 3272.
[2] (a) S. Ganguly, S. Chattopadhyay, C. Sinha, A. Chakravorty, Inorg. Chem. 39 (2000) 2954;
(b) S. Ganguly, V. Manivannan, A. Chakravorty, J. Chem. Soc., Dalton Trans. (1998) 461;
(c) S. Karmakar, S.B. Choudhury, S. Ganguly, A. Chakravorty, J. Chem. Soc., Dalton Trans. (1997) 585, and references therein.
[3] (a) R. Acharyya, S.-M. Peng, G.-H. Lee, S. Bhattacharya, Inorg. Chem. 42 (2003) 7378;
(b) S. Nag, P. Gupta, R.J. Butcher, S. Bhattacharya, Inorg. Chem. 43 (2004) 4814;
(c) P. Gupta, R.J. Butcher, S. Bhattacharya, Inorg. Chem. 42 (2003) 5405;
(d) R. Aharyya, F. Basuli, R.Z. Wang, T.C. Mak, S. Bhattacharya, Inorg. Chem. 43 (2004) 704, and references therein.
[4] (a) A.H. Velders, K. van der Schilden, A.C.G. Hotze, J. Reedijk, H. Kooijman, A.L. Spek, J. Chem. Soc., Dalton Trans. (2004) 448;
(b) M. Shivakumar, V. Pramanik, I. Bhattacharyya, A. Chakravorty, Inorg. Chem. 39 (2000) 4332;
(c) S. Banerjee, S. Bhattacharyya, B.K. Dirghangi, M. Menon, A. Chakravorty, Inorg. Chem. 39 (2000) 6;
(d) C. Das, A. Saha, C.H. Hung, G.-H. Lee, S.-M. Peng, S. Goswami, Inorg. Chem. 42 (2003) 198.
[5] (a) P. Byabartta, J. Dinda, P.K. Santra, C. Sinha, K. Panneerselvam, F.L. Liao, T.H. Lu, J. Chem. Soc., Dalton Trans. (2001) 2825;
(b) I. Chakraborty, S. Bhattacharyya, S. Banerjee, B.K. Dirghangi, A. Chakravorty, J. Chem. Soc., Dalton Trans. (1999) 3747;
(c) T.K. Misra, T.K. Das, C. Sinha, P. Ghosh, C.K. Pal, Inorg. Chem. 37 (1998) 167.
[6] (a) N. Maiti, S. Pal, S. Chattopadhyay, Inorg. Chem. 40 (2001) 2204, and references therein;
(b) N. Maiti, B.K. Dirghangi, S. Chattopadhyay, Polyhedron 22 (2003) 3109;
(c) N. Maiti, S. Chattopadhyay, Indian J. Chem. 42A (2003) 2327.
[7] J. Pratihar, N. Maiti, P. Pattanayak, S. Chattopadhyay, Polyhedron 24 (2005) 1953.
[8] (a) S. Chattopadhyay, C. Sinha, A. Basu, A. Chakravorty, J. Organomet. Chem. 414 (1991) 421;
(b) S. Chattopadhyay, C. Sinha, A. Basu, A. Chakravorty, Organometallics 10 (1991) 1135, and references therein.
[9] (a) K.K. Kamar, S. Das, C.-H. Hung, A. Castineiras, M.D. Kuzmin, C. Rillo, J. Bartolome, S. Goswami, Inorg. Chem. 42 (2003) 5367;
(b) C. Das, S.-M. Peng, G.-H. Lee, S. Goswami, New. J. Chem. 26 (2002) 222.
[10] (a) T. Yitaka, M. Kurihara, K. Kubo, H. Nishihara, Inorg. Chem. 39 (2000) 3438;
(b) M. Kurihara, H. Nishihara, Coord. Chem. Rev. 226 (2002) 125, and references therein.
[11] J. Dupont, C.S. Consorti, J. Spencer, Chem. Rev. 105 (2005) 2527.

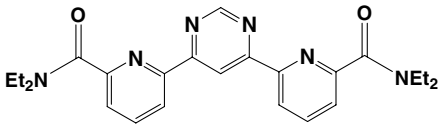

Fig. 1. Structure of ligand **L**.

appropriate metal ions, we observed that complexes of different architectures were obtained depending mainly on the kind of metal ions used for coordination, as a consequence of preferred coordination geometry.

Herein we report new investigations into the coordination chemistry of ligand **L** with transition metal ions and show that it is able to form novel polynuclear complexes.

2. Experimental

2.1. Measurements

NMR spectroscopic data were run on a Varian Gemini 300 MHz spectrometer, were calibrated against the residual protonated solvent signal ([D_6]DMSO: $\delta = 2.50$) and are given in ppm. Mass spectra were determined by a Waters Micromass ZQ spectrometer in acetonitrile. The samples were run in the positive-ion mode. The concentrations of the compounds were about 10^{-4} mol dm^{-3}. Sample solutions were introduced into the mass spectrometer source with a syringe pump with a flow rate of 40 μL min^{-1} with a capillary voltage of +3 kV and a desolvation temperature of 300 °C. Source temperature was 120 °C. Cone voltage (V_c) was set to 30 V to allow transmission of ions without fragmentation processes. Scanning was performed from $m/z = 200$ to 1000 for 6 s, and 10 scans were summed to obtain the final spectrum. Microanalyses were obtained using a Perkin–Elmer 2400 CHN microanalyzer. IR spectra were obtained with a Perkin–Elmer 580 spectrophotometer and are reported in cm^{-1}.

2.2. Preparation of Mn(II) complex (*1*)

An equimolar mixture of $Mn(ClO_4)_2 \cdot 6H_2O$ (8.4 mg, 23 μmol) and ligand **L** (10.0 mg, 23 μmol) in MeCN (5 cm^3) was stirred at RT for 24 h. The solvent was evaporated under reduced pressure to give a quantitative yield a yellowish powder. Slow diffusion of toluene into solution of **1** in acetonitrile over period of 2 months in air gave the single crystals of **1**. ^{1}H NMR (300 MHz, DMSO): $\delta = 9.46$, 9.25, 8.56, 8.18, 7.77, 5.31, 4.22, 3.51, 3.34, 2.91, 1.98, 1.77, 1.23, 1.18, 0.85, 0.19 ppm. ESI-MS *m/z* (%) = 586 (30 [Mn**L**(ClO$_4$)]$^+$), 460 (40 [Mn$\mathbf{L}_2$]$^{2+}$), 433 (2 [**L**]$^+$), 358 (30 [Mn$_2\mathbf{L}_2$(ClO$_4$)]$^{3+}$), 244 (100 [Mn**L**]$^{2+}$). IR (KBr [cm^{-1}]): $\bar{\nu} = 3364$, 3094, 2980, 1598, 1570, 1493, 1438, 1388, 1362, 1290, 1262, 1239, 1142, 1122, 1089, 1021, 993, 951, 834, 757, 636, 626, 574, 521, 464, 409. *Anal.* Calc. for $Mn_n(\mathbf{L})_n(ClO_4)_n \cdot (C_7H_8)$ (778.50): C, 47.83; H, 4.66; N, 10.80. Found: C, 47.91; H, 4.67; N, 10.81%.

2.3. Preparation of Cu(I) complex (*2a*)

An equimolar mixture of [Cu(CH$_3$CN)$_4$]PF$_6$ (9.7 mg, 26 μmol) and ligand **L** (11.3 mg, 26 μmol) in MeCN (5 cm^3) was stirred at room temperature for 24 h. The solvent was evaporated under reduced pressure to give a quantitative yield of **2a** as purple-violet powder. Slow diffusion of methanol into solution of **2a** in acetonitrile over period of 2 months in air gave the single crystals of **2a**. ^{1}H NMR (300 MHz, DMSO): $\delta = 9.85$ (s), 9.35 (s), 9.18 (d, $J = 8.1$ Hz), 8.53 (t, $J = 8.1$ Hz), 8.03 (d, $J = 8.1$ Hz), 3.35 (q, $J = 6.6$ Hz), 1.23 (t, $J = 6.6$ Hz), 0.87 (t, $J = 6.6$ Hz) ppm. ESI-MS: $m/z = 928$ (5 [Cu$\mathbf{L}_2$]$^+$), 496 (100 [Cu$_4\mathbf{L}_4$]$^{4+}$), 433 (7 [**L**]$^+$). IR (KBr [cm^{-1}]): $\bar{\nu} = 3429$, 3105, 2978, 1636, 1597, 1567, 1492, 1435, 1385, 1366, 1303, 1266, 1249, 1213, 1125, 1090, 1011, 950, 841, 751, 715, 655, 557, 492, 403. *Anal.* Calc. for $Cu_4(\mathbf{L})_4(PF_6)_4 \cdot (CH_3OH)_{0.5} \cdot H_2O$ (2598.15): C, 44.61; H, 4.50; N, 12.94. Found: C, 44.51; H, 4.53; N, 12.98%.

2.4. Preparation of Cu(I) complex (*2b*)

A solution of ligand **L** (10.2 mg, 24 μmol) and $(CuCF_3SO_3)_2 \cdot C_6H_6$ (5.9 mg, 12 μmol) in MeCN (3 cm^3) was stirred at room temperature for 24 h. The violet complex **2b** was isolated in quantitative yield upon evaporation of the solvent. ^{1}H NMR (300 MHz, DMSO): $\delta = 9.49$ (s), 9.27 (s), 8.58 (d, $J = 8.4$ Hz), 8.19 (t, $J = 8.4$ Hz), 7.80 (d, $J = 8.4$ Hz), 3.36 (q, $J = 7.2$ Hz), 3.04 (q, $J = 7.2$ Hz), 1.24 (t, $J = 7.2$ Hz) ppm. ESI-MS: $m/z = 928$ (5 [Cu$\mathbf{L}_2$]$^+$), 495 (100 [Cu$_4\mathbf{L}_4$]$^{4+}$), 433 (2 [**L**]$^+$). IR (KBr [cm^{-1}]): $\bar{\nu} = 3081$, 2978, 1636, 1567, 1488, 1438, 1382, 1368, 1278, 1257, 1224, 1159, 1127, 1031, 947, 824, 756, 638, 572, 516, 475, 408. *Anal.* Calc. for $Cu_4(\mathbf{L})_4(CF_3SO_3)_4$ (2580.53): C, 46.54; H, 4.37; N, 13.03; S, 4.97. Found: C, 46.51; H, 4.36; N, 13.11; S, 4.99%.

2.5. Preparation of Ag(I) complex (*3a*)

A solution of ligand **L** (12.0 mg, 28 μmol) and $AgBF_4$ (5.4 mg, 28 μmol) in MeCN (5 cm^3) was stirred at room temperature for 24 h. The pale yellow complex **3a** was isolated in quantitative yield by evaporation of the solvent. ^{1}H NMR (300 MHz, DMSO): $\delta = 9.48$ (s), 9.26 (s), 8.57 (d, $J = 8.1$ Hz), 8.19 (t, $J = 7.8$ Hz), 7.79 (d, $J = 7.8$ Hz), 3.34 (q, $J = 7.2$ Hz), 1.22 (t, $J = 4.5$ Hz) ppm. ESI-MS: $m/z = 974$ (3 [Ag$\mathbf{L}_2$]$^+$), 539 (100 [Ag$_4\mathbf{L}_4$]$^{4+}$), 433 (2 [**L**]$^+$). IR (KBr, [cm^{-1}]): $\bar{\nu} = 3439$, 3081, 2978, 1636, 1572, 1534, 1486, 1438, 1382, 1365, 1268, 1220, 1081, 1033, 827, 756, 656, 522. *Anal.* Calc. for $Ag_4(\mathbf{L})_4(BF_4)_4$ (2508.76): C, 45.96; H, 4.50; N, 13.40. Found: C, 45.39; H, 4.43; N, 13.25%.

2.6. Preparation of Ag(I) complex (*3b*)

A solution of ligand **L** (17.0 mg, 39 μmol) and $AgCF_3SO_3$ (10.1 mg, 39 μmol) in MeCN (5 cm^3) was stirred

Table 1
Crystal data, data collection and structure refinement

Compound	**1**	**2a**
Formula	$(C_{24}H_{28}MnN_6O_2)^{2n+} \cdot 2n(ClO_4)^- \cdot (C_7H_8)$	$(C_{96}H_{112}Cu_4N_{24}O_8)^{4+} \cdot 4(PF_6)^- \cdot 1/2(CH_3OH) \cdot H_2O$
Formula weight	778.50	2598.16
Crystal system	monoclinic	orthorhombic
Space group	*C*2/*c*	*Pbca*
a (Å)	30.362(6)	17.938(3)
b (Å)	9.026(2)	35.937(5)
c (Å)	26.254(5)	34.479(6)
β (°)	105.42(3)	90
V (Å^3)	6936(3)	22226(6)
Z	8	8
D_x (g cm^{-3})	1.49	1.55
F(000)	3224	10 640
μ(mm^{-1})	0.60	00.92
Crystal size (mm)	0.2 × 0.15 × 0.05	0.2 × 0.07 × 0.05
Θ Range (°)	2–25	2–25
h k l range	$-36 \leqslant h \leqslant 33$	$-21 \leqslant h \leqslant 17$
	$-9 \leqslant k \leqslant 10$	$-42 \leqslant k \leqslant 42$
	$-30 \leqslant l \leqslant 31$	$-38 \leqslant l \leqslant 41$
Reflections		
Collected	23 576	170 930
Unique (R_{int})	6089 (0.13)	19 543 (0.3)
Final $R(F)$ [$I > 3\sigma(I)$]	0.104	0.118
Final $wR(F^2)$ [all data]	0.313	0.46
Goodness-of-fit	1.18	1.11
Maximum/minimum Δ*ρ* (e Å^{-3})	1.01/−0.60	1.07/−0.95

at room temperature for 24 h. The pale yellow complex **3b** was isolated in quantitative yield by evaporation of the solvent. ^{1}H NMR (300 MHz, DMSO): $\delta = 9.48$ (s), 9.26 (s), 8.57 (d, $J = 8.1$ Hz), 8.19 (t, $J = 7.8$ Hz), 7.79 (d, $J = 7.8$ Hz), 3.53 (q, $J = 6.9$ Hz), 1.22 (t, $J = 6.9$ Hz) ppm. ESI-MS: $m/z = 974$ (5 $[AgL_2]^+$), 539 (100 $[Ag_4L_4]^{4+}$), 433 (15 $[L]^+$). IR (KBr [cm^{-1}]): $\bar{\nu} = 3441$, 2980, 1636, 1537, 1487, 1468, 1378, 1364, 1279, 1258, 1224, 1158, 1031, 947, 829, 758, 638, 574, 517, 408. *Anal*. Calc. for $Ag_4(L)_4(CF_3SO_3)_4$ (2757.82): C, 43.55; H, 4.09; N, 12.19; S, 4.65. Found: C, 43.71; H, 4.03; N, 12.35; S, 4.65%.

2.7. Crystal structure determination of complexes *1* and *2a*

The crystals of both compounds were of poor quality. We decided to lower the temperature of data collection, and the diffraction data for **1** and **2a** were therefore collected at 100(1) K by the ω-scan technique up to $2\theta = 50°$, on a KUMA-KM4CCD diffractometer [44] with graphite-monochromatized Mo Kα radiation ($\lambda =$ 0.71073 Å). Temperature was controlled by an Oxford Cryosystems cooling device. The data were corrected for Lorentz-polarization effects [45]. Unit-cell parameters were determined by the least-squares fit of 1356 (**1**) and 2300 (**2a**) reflections of highest intensity, chosen from the whole experiment. The structures were solved with SHELXS97 [46] (in both structures additional solvent molecules were found: in **1** toluene, in **2a** water and disordered methanol), and refined with the full-matrix least-squares procedure on F^2 by SHELXL97 [47,48]. Scattering factors incorporated in SHELXL97 were used. All non-hydrogen atoms were refined anisotropically; hydrogen atoms were placed geometrically in idealized positions and refined as rigid groups; U_{iso} of hydrogen atoms were set as 1.2 (1.3 for CH_2 and CH_3 groups) times U_{eq} of the appropriate carrier atom. A number of constraints had to be applied during refinement. However, these constraints were not applied to the geometry of main structural elements (complexes and counterions); therefore, despite the relatively high *R*-factors the discussion of the composition and structure of the complexes formed seems to be reasonable. Relevant crystal data are listed in Table 1, together with refinement details.

3. Results and discussion

In view of the successful synthesis of Fe(II), Co(II), Zn(II) [43], Sm(III), Eu(III), Tb(III) and Dy(III) [49] complexes with **L** (Scheme 1), we investigated the preparation of complexes with Mn(II) (**1**), Cu(I) (**2a**, **2b**) and Ag(I) (**3a**, **3b**). Scheme 1 shows that ligand **L** forms a variety of polynuclear coordination architectures and coordination modes.

In previous papers we carried out studies of self-assembly of ligand **L** in the presence of metal ions with preferred octahedral coordination geometry, such as Fe(II), Co(II) and Zn(II), and found out that the ligand is correctly preorganized for the assembly of tetranuclear grid-type complexes [43]. Initial investigations into the lanthanide complexation behaviour of **L** focussed upon the reaction between 1:1 stoichiometric combinations of M^{3+}:L ($M^{3+} = Sm^{3+}$, Eu^{3+}, Tb^{3+}, Dy^{3+}) in the hope of obtaining $[M_4L_4]^{12+}$ grid-type products. Evidence for the existence of

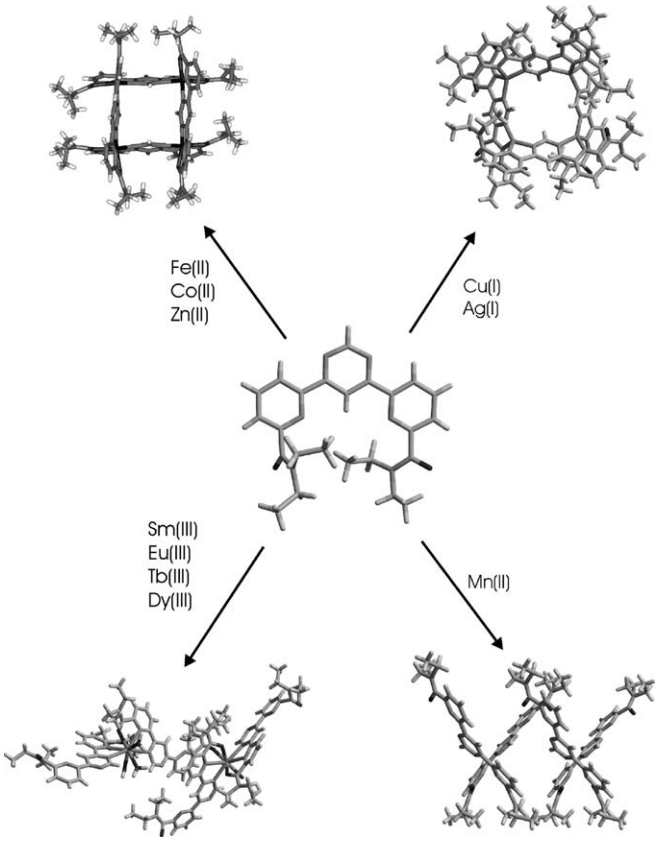

Scheme 1.

$[M_4L_4]^{12+}$ species which may be of a grid-type structure was obtained for the $M^{3+} = Eu^{3+}$ system using ESI-MS. The result of ESI-MS indicated that many kinds of multinuclear structures co-existed in solution, in the form of grids or helicates. Since we could not obtain crystals suitable for X-ray analysis, and thereby confirm the structural identity of the components in the mixture, we decided to change the molar ratio of M^{III}:**L** to 3:2 and we obtained intricate dinuclear complexes of Sm(III), Eu(III), Tb(III) and Dy(III): $[M_2L_4(CF_3SO_3)_6]$ [49]. As a continuation of this work, herein we report the use of ligand **L** in the complexation with manganese(II) ion whose tendency to form polymeric complexes is well-known, and we observed the formation of a new linear coordination polymer complex: $[MnL]_n$ (**1**). In reaction with tetrahedrally coordinated metal ions such as Cu(I) (**2a**, **2b**) and Ag(I) (**3a**, **3b**) ligand **L** acts in a bidentate fashion and generates of $[2 \times 2]$ grids. The new compounds have been characterized on the basis of spectroscopic data in solution (IR, ^{1}H NMR, ESI-MS), and confirmed in the solid state in the case of complexes **1** and **2a** by X-ray crystallography.

3.1. Synthesis and characterization of the polymeric complex of Mn(II)

An equimolar reaction of manganese(II) perchlorate with amide ligand **L** provided a new polymeric zigzag complex **1**. Each ion in this chain is situated in a distorted octahedral coordination environment comprising two N,N,O ligand donor sets.

The ^{1}H NMR spectrum of paramagnetic complex of manganese(II) shows strongly shifted signals. In addition to NMR and elemental analysis, the complex was also characterized with electrospray ionization mass spectrometry. The ESI-MS spectrum of complex **1** showed the signals at $m/z = 586$ $[MnL(ClO_4)]^+$, 460 $[MnL_2]^{2+}$, 433 $[L]^+$, 358 $[Mn_2L_2(ClO_4)]^{3+}$, 244 $[MnL]^{2+}$. While this may indicate the presence of some smaller linear oligomers in solutions, the peaks may be fragments of a high mass polymeric species [50].

3.2. Crystal data for complex *1*

Crystals of the manganese complex **1** were obtained by diffusion of toluene into a solution of the complex in acetonitrile and its structure was determined by X-ray crystallography (Fig. 2). Complex **1** in the solid state turned out to be a polymeric structure. The Mn(II) ions are six-coordinated (by ring nitrogen atoms, but also by carbonyl oxygen atoms), and the coordination is close to octahedral (Table 2). The Mn–N and Mn–O bond lengths are typical, but lie among smaller values found in similar complexes.

In the free ligand [43] the disposition of three rings was *trans–trans* (with respect to nitrogen atoms), and the amide oxygen atoms were *trans* with respect to nitrogen atoms of the neighbouring ring. The formation of the complex molecule changes this conformation basically: Three rings are in *cis–cis* orientation, as can be seen from the values of dihedral angles N–C–C–N of 0.2° and −3.2°, and the oxygen atoms are also close to *cis* positions: the N(ring)–C–C–O torsion angles are 15.6° and 21.9°. This conformation makes three-dentate "bay area" N,N,O; two such fragments from two consecutive, almost perpendicular, ligand

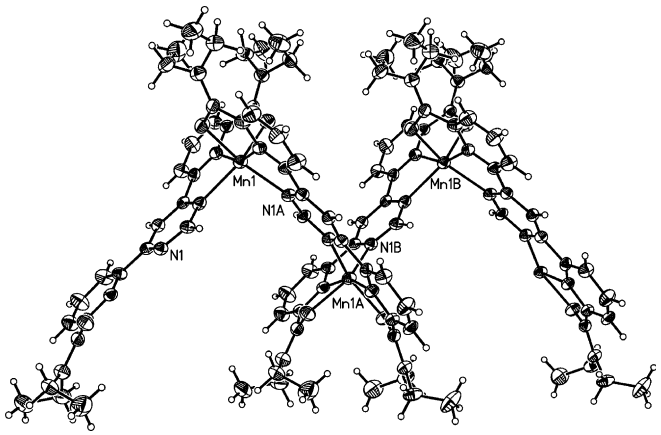

Fig. 2. Anisotropic-ellipsoid representation of a fragment of polymer **1**. The ellipsoids are drawn at the 33% probability level, hydrogen atoms are represented by spheres of arbitrary radii. The counterions are omitted for clarity.

Table 2
Selected geometrical parameters of the polymeric structure **1**

Polymer 1			
Bond lengths			
Mn1–O20	2.121(5)	Mn1–O27^{i}	2.188(5)
Mn1–N8^{i}	2.188(6)	Mn1–N14	2.206(5)
Mn1–N3	2.278(6)	Mn1–N1^{i}	2.286(6)
Bond angles (°)			
O20–Mn1–O27^{i}	92.5(2)	O20–Mn1–N8^{i}	93.8(2)
O27^{i}–Mn1–N8^{i}	71.5(2)	O20–Mn1–N14	73.2(2)
O27^{i}–Mn1–N14	89.5(2)	N8^{i}–Mn1–N14	156.8(2)
O20–Mn1–N3	144.7(2)	O27^{i}–Mn1–N3	92.3(2)
N8^{i}–Mn1–N3	120.8(2)	N14–Mn1–N3	71.9(2)
O20–Mn1–N1^{i}	95.7(2)	O27^{i}–Mn1–N1^{i}	143.3(2)
N8^{i}–Mn1–N1^{i}	72.3(2)	N14–Mn1–N1^{i}	127.0(2)
N3–Mn1–N1^{i}	100.9(2)		

Symmetry code: $^{i}3/2 - x, 1/2 + y, 1/2 - z$.

molecules fulfill the coordination of one Mn ion. Further, the approximate C_2 symmetry of the ligand allows for the polymer formation (Fig. 2). The rings are planar within the experimental error, and the dihedral angles between them are small, comparable with the free ligand molecule (3.1–9.6°). In the crystal structure there are also perchlorate counterions, and solvent–toluene molecules. These molecules fill the voids between the ligand molecules and are kept by weak π-stacking interactions; the distance between the ring planes is ca. 3.3 Å.

The subsequent units in the polymer are organized in a zigzag fashion (Fig. 2), and the neighbouring zigzag ribbons are connected through perchlorate ions by weak hydrogen bonds C–H···O.

3.3. Synthesis and characterization of the grid-type complexes of Cu(I) and Ag(I)

A multitopic ligand with N,N,O type donor sets has only infrequently been employed in the metal ion directed assembly of coordination architectures. Ligand **L** was found to form complexes with Cu(I) and Ag(I) ions, giving $[2 \times 2]$ grid-type structures with each metal ion tetrahedrally coordinated by two N,N donor atoms.

The self-assembly of $[2 \times 2]$ grid-type compounds was achieved by reaction at room temperature in acetonitrile, using ligand **L** and tertakis(acetonitrile)copper(I) hexafluorophospate (**2a**), copper(I) triflate (**2b**), silver(I) tetrafluroborate (**3a**) and silver(I) triflate (**3b**), respectively. The complexation reactions were followed by ESI-MS, IR and NMR spectroscopy.

For the complex of **3a**, three charge-states were observed in the ESI mass spectrum at $m/z = 974$ $[AgL_2]^{+}$, 539 $[Ag_4L_4]^{4+}$, 433 $[L]^{+}$. These data confirm the presence of grid **3a** in solution. The spectra of all the grid-type complexes include the following signals: $[ML_2]^{+}$, $[M_4L_4]^{4+}$, $[L]^{+}$, which means that in solution significant dissociation of the grid complexes to mononuclear species and ligand molecules occurs [31,51].

3.4. Crystallographic characterization of grid complex **2a**

Crystals of complex **2a** were obtained by diffusion of methanol into a solution of the complex in acetonitrile and its structure was determined by X-ray crystallography at 100 K (Figs. 3 and 4). It shows that it is a $[2 \times 2]$ grid-type (Fig. 3), stable from 100 K, at least to room temperature. The unit cell contains, besides the grid molecules, counterions PF_6^{-}, water molecule and disordered solvent (methanol) molecules.

The shape of the grid is close to a square, the lengths of diagonals are 0.83 and 0.86 nm. The Cu(I) are four-coordinated (by ring nitrogen atoms only), and the coordination polyhedra are distorted tetrahedra (Table 3). On complexation, the conformation of the ligand had to change from *transoid*, observed in free ligand **L** [43], to *cisoid*, as was also observed in the formation of Zn(II) and Co(II) complexes [43].

In the free ligand the three rings do not deviate seriously from coplanarity; the maximum value of the dihedral angle between the ring planes being ca. 12° [43]; in the grid the dihedral angles between the ring planes are larger (up to 23.5°), in order to allow grid formation. The amide planes are almost perpendicular to the ring planes, the dihedral angles between these planes are in the range of 54–88°.

In the crystal structure the grids are connected – by means of relatively short C–H···F hydrogen bonds – via hexafluorophosphate counterions. Two such counterions lie below and above the grid plane (Fig. 4), and all four counterions act as 'glue' for the 3D structure.

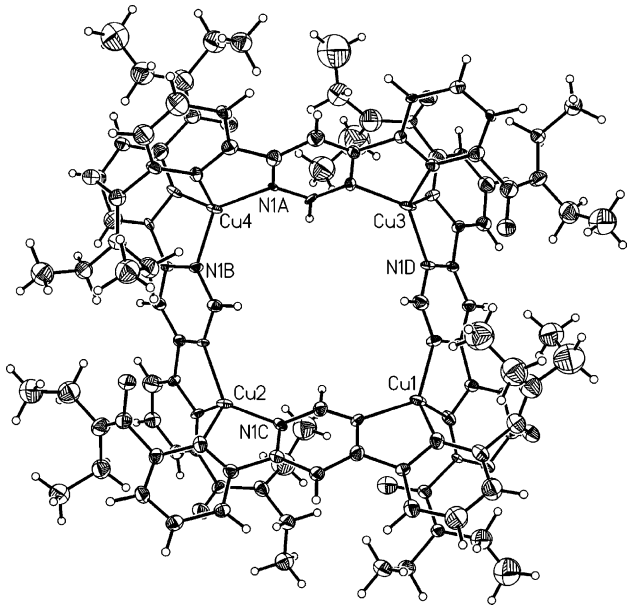

Fig. 3. Anisotropic-ellipsoid representation of grid **2a**. The ellipsoids are drawn at the 33% probability level, hydrogen atoms are represented by spheres of arbitrary radii. The counterions and solvent molecules are omitted for clarity.

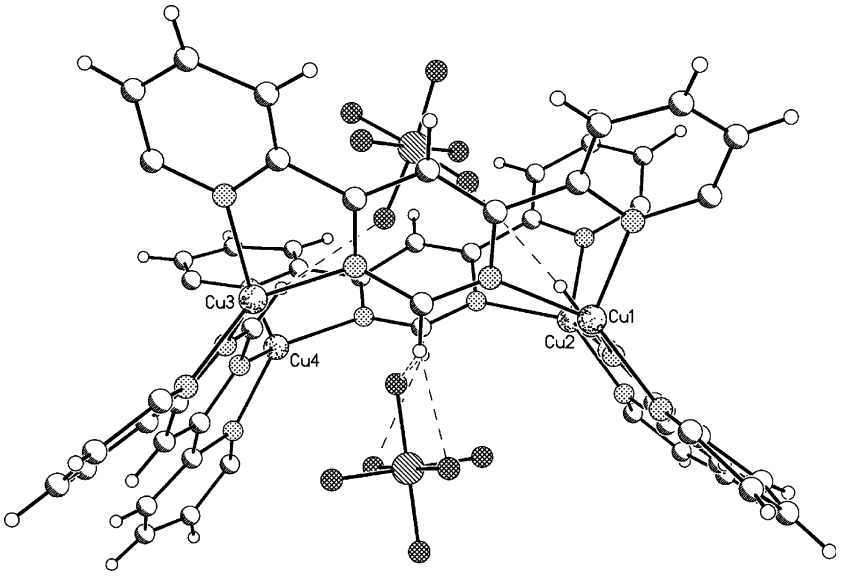

Fig. 4. Fragment of the 3D structure of complex **2a** with PF_6^- counterions below and above the Cu-plane. Weak hydrogen bonds are drawn as dashed lines.

Table 3
Selected geometrical parameters of the [2 × 2] grid-type complex **2a**

Grid 2a			
Bond distances (Å)			
Cu1–N3D	2.004(1)	Cu3–N1D	1.984(1)
Cu1–N14C	2.014(1)	Cu3–N3A	2.005(1)
Cu1–N14D	2.017(1)	Cu3–N14A	2.037(1)
Cu1–N3C	2.019(1)	Cu3–N8D	1.984(1)
Cu2–N8C	1.985(1)	Cu4–N1A	1.964(1)
Cu2–N3B	2.032(1)	Cu4–N8A	1.965(1)
Cu2–N1C	1.965(1)	Cu4–N8B	1.967(1)
Cu2–N14B	2.059(1)	Cu4–N1B	1.982(1)
Bond angles (°)			
N3D–Cu1–N14C	135.5(1)	N8D–Cu3–N1D	80.6(1)
N3D–Cu1–N14D	82.2(1)	N8D–Cu3–N3A	128.2(1)
N14C–Cu1–N14D	109.9(1)	N1D–Cu3–N3A	130.9(1)
N3D–Cu1–N3C	125.9(1)	N8D–Cu3–N14A	114.2(1)
N14C–Cu1–N3C	81.7(4)	N1D–Cu3–N14A	126.3(1)
N14D–Cu1–N3C	127.0(1)	N3A–Cu3–N14A	81.6(1)
N1C–Cu2–N8C	80.6(1)	N1A–Cu4–N8A	81.7(1)
N1C–Cu2–N3B	130.9(1)	N1A–Cu4–N8B	132.8(1)
N8C–Cu2–N3B	125.6(1)	N8A–Cu4–N8B	106.5(1)
N1C–Cu2–N14B	132.1(1)	N1A–Cu4–N1B	129.9(1)
N8C–Cu2–N14B	112.3(1)	N8A–Cu4–N1B	128.9(1)
N3B–Cu2–N14B	80.2(1)	N8B–Cu4–N1B	81.2(1)

4. Conclusion

We report the synthesis of new grid-type complexes of Cu(I), Ag(I) and a polymeric complex of Mn(II) with ligand **L**, comprising two tridentate N,N,O(carbonyl) binding subunits. The Mn(II) ions present octahedral, and Cu(I) and Ag(I) ions distorted tetrahedral geometry.

The present results demonstrate that ligand **L** is flexible, versatile and capable of stabilizing complexes with metals in different coordination environments. These assemblies are potentially useful for example as functional components in molecular electronics [52,53] and they could find various applications in nanotechnology [54] and catalysis [55].

5. Supplementary material

Crystallographic data (excluding structure factors) for the structural analysis have been deposited with the Cambridge Crystallographic Data Centre, Nos. CCDC-290966 (**1**), and CCDC-290965 (**2a**). Copies of this information may be obtained free of charge from: The Director, CCDC, 12 Union Road, Cambridge, CB2 1EZ, UK, fax: +44 1223 336 033, e-mail: deposit@ccdc.cam.ac.uk, or www: www.ccdc.cam.ac.uk.

Acknowledgments

This research was carried out as part of the Polish Ministry of Education and Science project (Grant No. 4 T09A 049 24).

References

[1] J.-M. Lehn, A. Rigault, J. Siegel, J. Harrowfield, B. Chevrier, D. Moras, Proc. Natl. Acad. Sci. USA 84 (1987) 2565.
[2] J.-M. Lehn, Supramolecular Chemistry-Concepts and Perspectives, VCH, Weinheim, 1995.
[3] C. Piguet, G. Bernardinelli, G. Hopfgartner, Chem. Rev. 97 (1997) 2005.
[4] P. Molenveld, J.F.J. Engbersen, D.N. Reinhoudt, Chem. Soc. Rev. 29 (2000) 75.
[5] S. Leininger, B. Olenyuk, P.J. Stang, Chem. Rev. 100 (2000) 853.
[6] G.F. Swiegers, T.J. Malefetse, Chem. Rev. 100 (2000) 3483.
[7] L.M. Greig, D. Philp, Chem. Soc. Rev. 30 (2001) 287.
[8] M. Albrecht, Chem. Rev. 101 (2001) 3457.
[9] M. Ruben, J. Rojo, F.J. Romero-Salguero, L.H. Uppadine, J.-M. Lehn, Angew. Chem., Int. Ed. 43 (2004) 3644.
[10] F. Würthner, C.-C. You, C.R. Saha-Möller, Chem. Soc. Rev. 33 (2004) 133.

[11] M.A.R. Meier, U.S. Schubert, Chem. Commun. (2005) 4610.
[12] N. Koga, S. Karasawa, Bull. Chem. Soc. Jpn. 78 (2005) 1384.
[13] J.L.C. Rowsell, O.M. Yaghi, Microporous Mesoporus Mater. 73 (2004) 3.
[14] C. Li, X. Wang, Q. Peng, Y. Li, Inorg. Chem. 44 (2005) 6641.
[15] I. Imaz, G. Bravic, J.-P. Sutter, Dalton Trans. (2005) 2681.
[16] S.J. Hong, J.Y. Ryu, J.Y. Lee, C. Kim, Y. Kim, S.-J. Kim, Dalton Trans. (2004) 2697.
[17] M.A.R. Meier, J.-F. Gohy, C.-A. Fustin, U.S. Schubert, J. Am. Chem. Soc. 126 (2004) 11517.
[18] R. Pothiraja, M. Sathiyendiran, R.J. Butcher, R. Murugavel, Inorg. Chem. 44 (2005) 6314.
[19] C. Ma, C. Chen, Q. Liu, F. Chen, D. Liao, L. Li, L. Sun, Eur. J. Inorg. Chem. (2005) 2872.
[20] M.U. Triller, W.Y. Hsieh, V.L. Pecoraro, A. Rompel, B. Krebs, Inorg. Chem. 41 (2002) 5544.
[21] M.D. Godbole, M. Kloskowski, R. Hage, A. Rompel, A.M. Mills, A.L. Spek, E. Bouwman, Eur. J. Inorg. Chem. (2005) 305.
[22] N. Reddig, D. Pursche, M. Kloskowski, C. Slinn, S.M. Baldeau, A. Rompel, Eur. J. Inorg. Chem. (2005) 879.
[23] M.-T. Youinou, N. Rahmouni, J. Fischer, J.A. Osborn, Angew. Chem., Int. Ed. 31 (1992) 733.
[24] M. Schmittel, V. Kalsani, J.W. Bats, Inorg. Chem. 44 (2005) 4115.
[25] R. Hoogenboom, G. Kickelbick, U.S. Schubert, Eur. J. Org. Chem. (2003) 4887.
[26] Y. Lan, D.K. Kennepohl, B. Moubaraki, K.S. Murray, J.D. Cashion, G.B. Jameson, S. Brooker, Chem. Eur. J. 9 (2003) 3772.
[27] J.R. Nitschke, M. Hutin, G. Bernardinelli, Angew. Chem., Int. Ed. Eng. 43 (2004) 6724.
[28] A.J. Blake, N.R. Champness, P. Hubberstey, W.-S. Li, M.A. Whitersby, M. Schroder, Coord. Chem. Rev. 183 (1999) 117.
[29] E.C. Constable, C.E. Housecroft, M. Neuburger, S. Reymann, S. Schaffner, Chem. Commun. (2004) 1056.
[30] H.-L. Hu, C.-W. Yeh, J.-D. Chen, Eur. J. Inorg. Chem. (2004) 4696.
[31] V. Patroniak, A.R. Stefankiewicz, J.-M. Lehn, M. Kubicki, Eur. J. Inorg. Chem. (2005) 4168.
[32] C. Shimokawa, S. Itoh, Inorg. Chem. 44 (2005) 3010.
[33] P.N.W. Baxter, J.-M. Lehn, J. Fisher, M.-T. Youinou, Angew. Int. Ed. Engl. 33 (1994) 2284.
[34] P.N.W. Baxter, J.-M. Lehn, G. Baum, D. Fenske, Chem. Eur. J. 6 (2000) 4510.
[35] M.-C. Brandys, R.J. Puddephatt, Chem. Commun. (2001) 1508.
[36] I. Weissbuch, P.N.W. Baxter, S. Cohen, H. Cohen, K. Kjaer, P.B. Howes, J. Als-Nielsen, G.S. Hanan, U.S. Schubert, J.-M. Lehn, L. Leiserowitz, M. Lahav, J. Am. Chem. Soc. 120 (1998) 4850.
[37] I. Weissbuch, P.N.W. Baxter, I. Kuzmenko, H. Cohen, S. Cohen, K. Kjaer, P.B. Howes, J. Als-Nielsen, J.-M. Lehn, L. Leiserowitz, M. Lahav, Chem. Eur. J. 6 (2000) 725.
[38] B. Wiley, Y. Sun, B. Mayers, Y. Xia, Chem. Eur. J. 11 (2005) 454.
[39] P. Jiang, Z. Guo, Coord. Chem. Rev. 248 (2004) 205.
[40] W.-Y. Sun, B.-L. Fei, T.-a. Okamura, W.-X. Tang, N. Ueyama, Eur. J. Inorg. Chem. (2001) 1855.
[41] C.S. Campos-Fernández, B.L. Schottel, H.T. Chifotides, J.K. Bera, J. Bacsa, J.M. Koomen, D.H. Russell, K.R. Dunbar, J. Am. Chem. Soc. 127 (2005) 12909.
[42] A. Petitjean, N. Kyritsakas, J.-M. Lehn, Chem. Eur. J. 11 (2005) 6818.
[43] V. Patroniak, P.N.W. Baxter, J.-M. Lehn, M. Kubicki, M. Nissinen, K. Rissanen, Eur. J. Inorg. Chem. (2003) 4001.
[44] Oxford Diffraction. CrysAlisCCD, User Guide v.171. Oxford Diffraction Poland Sp., Wrocław, Poland, 2003.
[45] Oxford Diffraction. CrysAlisRed, CCD data reduction GUI v.171. Oxford Diffraction Poland Sp., Wrocław, Poland, 2003.
[46] R.H. Blessing, J. Appl. Crystallogr. 22 (1989) 396.
[47] G.M. Sheldrick, Acta Crystallogr., Sect. A 46 (1990) 467.
[48] G.M. Sheldrick, SHELX97 – Programs for Crystal Structure Analysis (Release 97-2), Institüt für Anorganische Chemie der Universität, Göttingen, Germany, 1998.
[49] V. Patroniak, P.N.W. Baxter, J.-M. Lehn, Z. Hnatejko, M. Kubicki, Eur. J. Inorg. Chem. (2004) 2379.
[50] O. Mamula, A. von Zelewsky, T. Bark, G. Bernardinelli, Angew. Chem., Int. Ed. 38 (1999) 2945.
[51] P.N.W. Baxter, R.G. Khoury, J.-M. Lehn, G. Baum, D. Fenske, Chem. Eur. J. 6 (2000) 4140.
[52] P.J. Low, Dalton Trans. (2005) 2821.
[53] M.S. Alam, S. Strömsdörfer, V. Dremov, P. Müller, J. Kortus, M. Ruben, J.-M. Lehn, Angew. Chem., Int. Ed. Engl. 44 (2005) 7896.
[54] J.-M. Lehn, Science 295 (2002) 2400.
[55] M.L. Merlau, M.P. Mejia, S.T. Nguyen, J.T. Hupp, Angew. Chem., Int. Ed. 40 (2001) 4239.

2.2. Synthesis of $[Cu^{I}Cu^{II}(n\text{-}Pr_2dtc)Cl_2]_2[Cu^{II}_2(n\text{-}Pr_2dtc)_2Cl_2]_2$ (**1**)

Complex **1** was synthesized by the reaction of a 20 ml $CHCl_3$ solution of $Cu(n\text{-}Pr_2dtc)_2$ (0.0416 g, 0.1 mmol) and a 20 ml acetone solution of $CuCl_2 \cdot 2H_2O$ (0.0170 g, 0.1 mmol). The black single crystals, suitable for X-ray diffraction, were obtained from the mixture by recrystallization with hexane in a glass tube over a period of more than 1 week. *Anal.* Calc. for $C_{42}H_{84}Cl_8Cu_8N_6S_{12}$: C, 27.27; H, 4.58; N, 4.54. Found: C, 27.30; H, 4.50; N, 4.54%.

2.3. X-ray structure determination

Single crystal X-ray data collection was performed on a RIGAKU R-AXIS RAPID imaging plate area detector with graphite monochromated Mo Kα (0.71069 Å) radiation. The intensity data were collected at angles up to 55° at room temperature. The crystal data and experimental parameters are listed in Table 1. The structure was solved by a direct method (SHELX97) [24] and expanded using Fourier techniques (DIRDIF99) [25]. Non-hydrogen atoms were refined anisotropically, whereas hydrogen atoms were introduced as fixed contributors. All calculations were performed using the CRYSTALSTRUCTURE crystallographic software package [26].

2.4. Magnetic measurement

The magnetic susceptibilities of the polycrystalline sample of **1** were studied in a field of 10000 Oe using a Quantum Design MPMS SQUID Magnetometer. Diamagnetic corrections were estimated from Pascal's constants.

Table 1
Crystallographic data and data collection parameters for $[Cu^{I}Cu^{II}(n\text{-}Pr_2dtc)Cl_2]_2[Cu^{II}_2(n\text{-}Pr_2dtc)_2Cl_2]_2$ (**1**)

Formula	$C_{21}H_{42}N_3S_6Cu_4Cl_4$
Formula weight	924.94
Color of crystal	black
Crystal system	monoclinic
Space group	$P2_1/c$ (#14)
a (Å)	15.836(16)
b (Å)	15.861(17)
c (Å)	15.887(12)
α (°)	
β (°)	115.93(13)
γ (°)	
V (Å^3)	3589(6)
Z	4
D_{calc} (g cm^{-3})	1.712
μ (cm^{-1})	30.03
Number of collected reflections	34027
Number of unique reflections	8162
R_{int}	0.019
Number of observations ($I > 2\sigma(I)$)	5355
Number of variables	395
Reflection/parameter ratio	13.56
R_1[a]	0.0309
wR_2[b]	0.0740
Goodness-of-fit	1.017

[a] $R_1 = \sum||F_o| - |F_c||/\sum|F_o|$.
[b] $wR_2 = [\sum(w(F_o^2 - F_c^2)^2)/\sum w(F_o^2)^2]^{1/2}$.

3. Results and discussion

The X-ray structural analysis reveals an octanuclear cluster structure of **1**, which is shown in Fig. 1. Complex **1** consists of two chloride-bridged dinuclear units, $Cu_2(n\text{-}Pr_2dtc)_2Cl_2$, and one tetranuclear unit, $[Cu_2(n\text{-}Pr_2dtc)Cl_2]_2$. In the dinuclear units, the $n\text{-}Pr_2dtc^-$ ligand coordinates to each copper ion with a four-membered chelate ring, and the two copper ions are bridged by the two chloride ions. The copper ions Cu(1) and Cu(2) have distorted square-pyramidal coordination geometries. The apical positions of the Cu(1) and Cu(2) ions are respectively occupied by a chloride ion and a sulfur atom from the nearest neighbor chloride bridged dinuclear unit in the crystallographically equivalent octanuclear cluster, with weak Cu(1)···Cl(2**) (2.9178(8) Å) and Cu(2)···S(1**) (3.0116(9) Å) coordination bonds, which are significantly longer than the Cu–S and Cu–Cl distances in the basal plane. Based on the weak coordination bonds, the octanuclear cluster creates an infinite one-dimensional assembly as shown in Fig. 2(a). In this one-dimensional assembly, a dimer of $[Cu_2(n\text{-}Pr_2dtc)_2Cl_2]_2$ which is formed by the two chloride-bridged dinuclear units, and the tetranuclear unit of $[Cu_2(n\text{-}Pr_2dtc)Cl_2]_2$ are alternately aligned. Fig. 2(a) shows the two adjacent one-dimensional assemblies. There are no open spaces between the assemblies because the spaces created by the one-dimensional assemblies are actually filled by the alkyl groups of the $n\text{-}Pr_2dtc^-$ ligand. The tetranuclear unit of $[Cu_2(n\text{-}Pr_2dtc)Cl_2]_2$ includes two crystallographically equivalent dinuclear copper units, in which the Cu(3) and Cu(4) ions have distorted tetrahedral and square-pyramidal coordination geometries, respectively. The Cu(3) and Cu(4) ions are bridged by two chloride ions. The Cu(4) ion is coordinated by a Pr_2dtc^- ligand with a four-membered chelate ring, and the Cu(3) ion is coordinated by a sulfur atom of the chloride-bridged dinuclear unit, $Cu_2(n\text{-}Pr_2dtc)_2Cl_2$. The apical position of the Cu(4) ion is occupied by one of the bridging chloride ions in the centrosymmetric tetranuclear unit with a weak Cu(4)···Cl(3*) coordination bond (2.8389(11) Å).

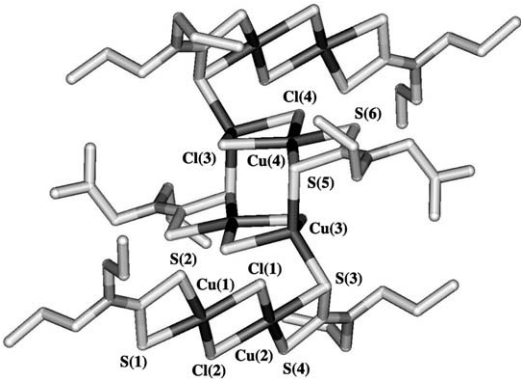

Fig. 1. The structure of $[Cu^{I}Cu^{II}(n\text{-}Pr_2dtc)Cl_2]_2[Cu^{II}_2(n\text{-}Pr_2dtc)_2Cl_2]_2$.

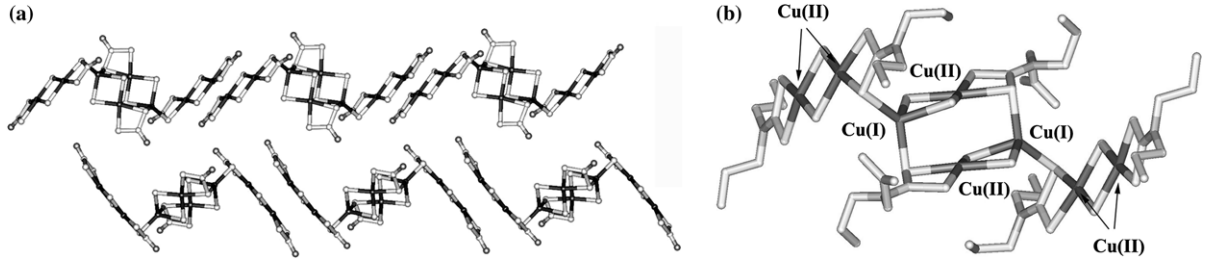

Fig. 2. A view of the one-dimensional assembly (a) and the valence states of the copper ions (b) for $[Cu^{I}Cu^{II}(n\text{-}Pr_2dtc)Cl_2]_2[Cu^{II}_2(n\text{-}Pr_2dtc)_2Cl_2]_2$.

For the dinuclear unit, $Cu_2(n\text{-}Pr_2dtc)_2Cl_2$, the dihedral angles between the planes of S(1)–Cu(1)–S(2) and Cl(1)–Cu(1)–Cl(2) in the Cu(1) coordination sphere and between the planes of Cl(1)–Cu(2)–Cl(2) and S(3)–Cu(2)–S(4) in the Cu(2) coordination sphere are 13.295° and 5.216°, respectively. While for the tetranuclear unit, $Cu_4(n\text{-}Pr_2dtc)_2Cl_4$, the dihedral angles between the planes of S(3)–Cu(3)–S(5) and Cl(3*)–Cu(3)–Cl(4*) in the Cu(3) coordination sphere and between the planes of S(5)–Cu(4)–S(6) and Cl(3)–Cu(4)–Cl(4) in the Cu(4) coordination sphere are 85.712° and 14.963°, respectively, indicating that the Cu(3) ion, having a large distortion, could be ascribed as a Cu(I) ion. Although the other copper ions of Cu(1), Cu(2) and Cu(4) also have apparent distortions, this is common for Cu(II)-dithiocarbamate complexes with square-pyramidal coordination geometry; for example, $Cu(Et_2dtc)_2$ [27], $Cu(n\text{-}Pr_2dtc)_2$ [23], $Cu(n\text{-}Bu_2dtc)_2$ [23], $Cu(Bz_2dtc)_2$ [23] and $Cu(EtOH_2dtc)_2$ [28], which have square-pyramidal coordination geometry by the dimerization of the mononuclear Cu(II) complexes, have largely distorted basal planes in which the dihedral angles are 18.89°, 19.00°, 17.71°, 10.84° and 20.86°, respectively. Meanwhile, the distortion of Cu(II) complexes with square-planar coordination geometry, such as $Cu(i\text{-}Pr_2dtc)_2$ [23], Cu(BuEt-dtc)$_2$ [23] and Cu(Piperidine-dtc)$_2$ [29], is almost zero, that is they have flat basal planes.

The Cu–S bond lengths in the basal planes are 2.2604(14)–2.2912(10) Å for Cu(1), 2.2518(12)–2.3195(8) Å for Cu(2), 2.2709(8)–2.2896(11) Å for Cu(3) and 2.2722(12)–2.3362(9) Å for Cu(4), in which no remarkable differences between the tetrahedral Cu(3) ion and the other distorted square-pyramidal Cu(1), Cu(2) and Cu(4) ions could be found. The distances are similar to those of other Cu(II)-dithiocarbamate mononuclear complexes, such as $Cu(Et_2dtc)_2$ (2.312 Å (av.)) [27], Cu(EtPr-dtc)$_2$ (2.284 Å (av.)) [23], $Cu(Bu_2dtc)_2$ (2.308 Å (av.)) [23] and $Cu(Bz_2dtc)_2$ (2.293 Å (av.)) [23]. However there are apparent differences in the Cu–Cl bond distances, that is the Cu–Cl bond distances in the copper spheres are 2.3153(10)–2.3252(12) Å for Cu(1), 2.2755(13)–2.3486(12) Å for Cu(2), 2.3805(10)–2.4431(8) Å for Cu(3) and 2.3063(8)–2.3186(9) Å for Cu(4), in which the Cu–Cl bond distances in the Cu(3) basal plane are significantly larger than the other Cu–Cl bond distances. Assuming that the distorted tetrahedral Cu(3) ion having long Cu–Cl distances is monovalent and the distorted square-pyramidal Cu(1), Cu(2) and Cu(4) ions are divalent, the total charge would be zero, consistent with the results of the X-ray study and magnetic measurements mentioned below. Namely, this complex is a mixed-valence Cu(I)–Cu(II) octanuclear cluster consisting of a mixed-valence Cu(I)–Cu(II) tetranuclear unit and two chloride-bridged Cu(II) dinuclear units, and it would formally be represented as $[Cu^{I}Cu^{II}(n\text{-}Pr_2dtc)Cl_2]_2[Cu^{II}_2(n\text{-}Pr_2dtc)_2Cl_2]_2$ (see Table 2, Fig. 2(b)).

Magnetic susceptibilities were measured from 300 to 2.0 K and plotted in Fig. 3 as the molar magnetic susceptibility χ_M and the effective magnetic moment μ_{eff} vs. temperature. The χ_M value increases with decreasing temperature without any peaks concerned with an antiferromagnetic phase transition, while the μ_{eff} value decreases with decreasing temperature because of the existence of the strong antiferromagnetic interaction between the

Table 2
Selected bond distances (Å) for $[Cu^{I}Cu^{II}(n\text{-}Pr_2dtc)Cl_2]_2$-$[Cu^{II}_2(n\text{-}Pr_2dtc)_2Cl_2]_2$ (**1**)

Cu(1)–Cl(1)	2.3153(10)	Cu(1)–Cl(2)	2.3252(12)
Cu(1)–S(1)	2.2912(10)	Cu(1)–S(2)	2.2604(14)
Cu(2)–Cl(1)	2.2755(13)	Cu(2)–Cl(2)	2.3486(9)
Cu(2)–S(3)	2.3195(8)	Cu(2)–S(4)	2.2518(12)
Cu(3)–Cl(3)[a]	2.4431(8)	Cu(3)–Cl(4)[a]	2.3805(10)
Cu(3)–S(3)	2.2709(8)	Cu(3)–S(5)	2.2896(11)
Cu(4)–Cl(3)	2.3186(9)	Cu(4)–Cl(4)	2.3063(8)
Cu(4)–S(5)	2.3362(9)	Cu(4)–S(6)	2.2722(12)

[a] $-X+1, -Y, -Z+1$.

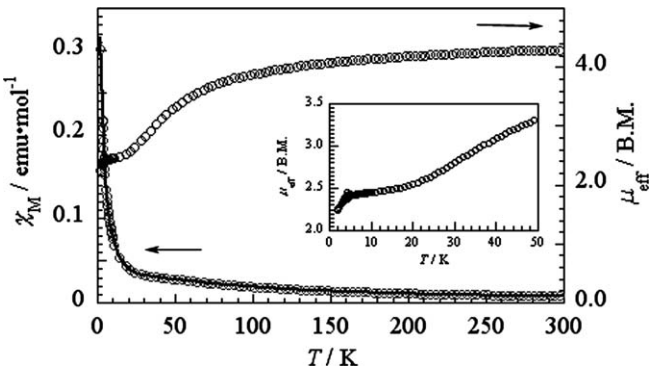

Fig. 3. Temperature dependence of the molar magnetic susceptibility χ_M and the effective magnetic moment μ_{eff} of $[Cu^{I}Cu^{II}(n\text{-}Pr_2dtc)Cl_2]_2$-$[Cu^{II}_2(n\text{-}Pr_2dtc)_2Cl_2]_2$.

Cu(II) ions in the one-dimensional assembly. The effective magnetic moment at 300 K is 4.28 B.M., in accordance with the expected value (4.24 B.M.) for the six Cu(II) ions in the mixed-valence Cu(I)–Cu(II) octanuclear $[Cu^{I}Cu^{II}(n\text{-}Pr_2dtc)Cl_2]_2[Cu^{II}_2(n\text{-}Pr_2dtc)_2Cl_2]_2$, as characterized by the X-ray study. It is expected that the exchange interaction between the Cu(1) and Cu(2) ions of the dinuclear units, $Cu^{II}_2(n\text{-}Pr_2dtc)_2Cl_2$, is the largest, because the magnetic orbitals, $d_{x^2-y^2}$, of the two copper ions would effectively overlap through the chloride ions since they lie in the same plane of the dinuclear unit. Meanwhile, the other interactions between Cu(1)···Cu(1**), Cu(1)···Cu(2**) and Cu(4)···Cu(4*) must be much smaller since the magnetic orbitals are not in the same planes and the weak Cu···S or Cu···Cl bonds to the apical sites are included between the Cu(II) ions as described in the structural part. The Cu(2)···Cu(4) interaction via the d^{10} Cu(3) ion would also provide a small antiferro- or ferro-magnetic interaction. The effective magnetic moment in the low temperature region gradually approaches the value (2.45 B.M.) of the two remaining paramagnetic Cu(II) ions, Cu(4) and Cu(4*), with decreasing temperature as shown in the inset of the Fig. 3, and decreases again with decreasing temperature below 5 K because of the weak antiferromagnetic interactions. The exchange interactions of complex **1** were estimated with the following equation:

$$\chi_M = 2 \times \frac{N_A g^2 \mu_B^2}{3k_B(T-\theta)} \frac{2}{1+1/3\exp(-2J/k_BT)} + 2 \times \frac{N_A g^2 \mu_B^2}{4k_B(T-\theta)} + N\alpha,$$

where N_A, g, μ_B and k_B have the usual meaning, and $N\alpha$ is the temperature independent paramagnetism. In this equation, the magnetic interaction between the Cu(1) and Cu(2) ions in the chloride-bridged dinuclear units $[Cu^{II}_2(n\text{-}Pr_2dtc)_2Cl_2]_2$ and the paramagnetic species of the magnetically isolated Cu(II) ions in the tetranuclear unit $[Cu^{I}Cu^{II}(n\text{-}Pr_2dtc)Cl_2]_2$ were treated with the Bleany–Bowers equation [30] in the first term and the equation in the second term, respectively, both of which included the Weiss constant θ in order to treat the other weak magnetic interactions between Cu(1)···Cu(1**), Cu(1)···Cu(2**), Cu(2)···Cu(4) and Cu(4)···Cu(4*). Least-squares analysis of the data for complex **1** led to $J = -35.6\ cm^{-1}$, $\theta = -0.53$ K and $g = 2.07$. The agreement factor R[1] was equal to 0.99993. The estimated J value is a little smaller than those of the chloride-bridged dinuclear Cu(II) complexes, $Cu^{II}_2(Bz_2dtc)_2Cl_2$, $Cu^{II}_2(n\text{-}Pr_2dtc)_2Cl_2$, $Cu^{II}_2(n\text{-}Bu_2dtc)_2Cl_2$, $Cu^{II}_2(n\text{-}Pen_2dtc)_2Cl_2$, $Cu^{II}_2(Hex_2dtc)_2Cl_2$ and $Cu^{II}_2(Bz\text{-}n\text{-}Pr\text{-}dtc)_2Cl_2$ in which the estimated exchange interactions were −49, −55, −65, −70, −68 and −50 cm^{-1}, respectively [31].

[1] $R = \sum_i (x_i - \bar{x})(y_i - \bar{y}) / \left(\sqrt{\sum_i (x_i - \bar{x})^2} \sqrt{\sum_i (y_i - \bar{y})^2} \right)$.

4. Conclusions

We found a simple synthetic method to create a new Cu(I)–Cu(II) mixed-valence octanuclear cluster, $[Cu^{I}Cu^{II}(n\text{-}Pr_2dtc)Cl_2]_2[Cu^{II}_2(n\text{-}Pr_2dtc)_2Cl_2]_2$, from a mononuclear Cu(II) complex, $Cu(n\text{-}Pr_2dtc)_2$, and copper(II) chloride. This mixed-valence Cu(I)–Cu(II) cluster has been structurally and magnetically characterized. The exploitation of such mixed-valence metal-assembled complexes could be important for new functional materials based on inter-valence charge transfer, therefore this simple synthetic method for the mixed-valence Cu(I)–Cu(II) cluster might be useful for generating a variety of functional mixed-valence metal-assembled complexes.

Acknowledgement

This work was supported by the Science and Technology Research Grant Program for Young Researchers from the Ministry of Education, Culture, Sports, Science and Technology of Japan.

Appendix A. Supplementary material

CCDC-295375 contains the supplementary crystallographic data for this paper. These data can be obtained free of charge at www.ccdc.cam.ac.uk/conts/retrieving.html (or from the Cambridge Crystallographic Data Center, 12 Union Road, Cambridge, CB2 1EZ, UK, fax: +44 1223 366 033, e-mail: deposit@ccdc.ac.uk or on the web www: http://www.ccdc.cam.ac.uk). Supplementary data associated with this article can be found, in the online version, at doi:10.1016/j.poly.2006.03.023.

References

[1] D.D. LeCloux, R. Davydov, S.J. Lippard, Inorg. Chem. 37 (1998) 6814.
[2] C. He, S.J. Lippard, Inorg. Chem. 39 (2000) 5225.
[3] S.B. Harkins, J. Peters, J. Am. Chem. Soc. 126 (2004) 2885.
[4] J.-C. Liu, G.-C. Guo, J.-S. Hung, X.-Z. You, Inorg. Chem. 42 (2003) 235.
[5] P. Drevensek, T. Zupancic, B. Pihlar, R. Jerala, U. Kolitsch, A. Plaper, I. Turel, J. Inorg. Biochem. 99 (2005) 432.
[6] S.M.-F. Lo, S.S.-Y. Chui, L.-Y. Shek, Z. Lin, X.-X. Zhang, G.-h. Wen, I.D. Williams, J. Am. Chem. Soc. 122 (2000) 6293.
[7] S. Brooker, J.D. Ewing, T.K. Ronson, C.J. Harding, J. Nelson, D.J. Speed, Inorg. Chem. 42 (2003) 2764.
[8] R. Ahlrichs, C.E. Anson, D. Fenske, O. Hampe, A. Rothenberger, M. Sierka, Angew. Chem. Int. Ed. Engl. 42 (2003) 4036.
[9] H. Zhao, Z. Qu, Q. Ye, X.-S. Wang, J. Zhang, R.-G. Xiong, B.F. Abrahams, X.-Z. You, Inorg. Chem. 43 (2004) 1813.
[10] L.-M. Zheng, P. Yin, X.-Q. Xin, Inorg. Chem. 41 (2002) 4084.
[11] E. Colacio, R. Kivekas, F. Lloret, M. Sunberg, J. Suarez-Varela, M. Bardaji, A. Laguna, Inorg. Chem. 41 (2002) 5141.
[12] M.-L. Tong, L.-J. Li, K. Mochizuki, H.-C. Chang, X.-M. Chen, Y. Li, S. Kitagawa, Chem. Commun. (2003) 428.

[13] Y.-H. Wen, J.-K. Cheng, Y.-L. Feng, J. Zhang, Z.-J. Li, Y.-G. Yao, Inorg. Chim. Acta 358 (2005) 3347.
[14] C.-M. Liu, D.-Q. Zhang, J.-L. Luo, N.-L. Wang, H.-M. Hu, D.-B. Zhu, Eur. J. Inorg. Chem. (2003) 3618.
[15] T.K. Maji, D. Ghoshal, E. Zangrando, J. Ribas, N.R. Chaudhuri, Cryst. Eng. Commun. 6 (2004) 623.
[16] G. Dong, Q. Chun-qi, D. Chun-ying, P. Ke-liang, M. Qing-jin, Inorg. Chem. 42 (2003) 2024.
[17] L.-M. Zheng, P. Yin, X.-Q. Xin, Inorg. Chem. 41 (2002) 4084.
[18] H.-Z. Kou, B. Chuan, R.-J. Wang, J. Organomet. Chem. 689 (2004) 369.
[19] K. Schulbert, M. Rainer, Z. Naturforschung. B 1993 (1993) 1227.
[20] R.M. Golding, A.D. Rae, B.J. Ralph, L. Sulligoi, Inorg. Chem. 13 (1974) 2499.
[21] A.R. Hendrickson, R.L. Martin, D. Taylor, J. Chem. Soc., Chem. Commun. (1975) 843.
[22] T. Okubo, R. Kawajiri, T. Mitani, T. Shimoda, J. Am. Chem. Soc. 127 (2005) 17598.
[23] S.C. Ngo, K.K. Banger, M.J. DelaRosa, P.J. Toscano, J.T. Welch, Polyhedron 22 (2003) 1575.
[24] G.M. Sheldrick, SHELX97, 1997.
[25] P.T. Beurskens, G. Admiraal, G. Beurskens, W.P. Bosman, R. de Gelder, R. Israel, J.M.M. Smits, Technical Report of the Crystallography Laboratory, University of Nijmegen, The Netherlands, 1999.
[26] CRYSTALSTRUCTURE 3.7.0: Crystal Structure Analysis Package, Rigaku and Rigaku/MSC (2000–2005), 9009 New Trails Dr., The Woodlands, TX 77381, USA.
[27] F. Jian, Z. Wang, Z. Bai, X. You, H.-K. Fun, K. Chinnakali, I.A. Razak, Polyhedron 18 (1999) 3401.
[28] A. Radha, M. Seshasayee, K. Radha, G. Aravamudan, C. Subramanyam, Acta Crystallogr., Sect. C 41 (1985) 1166.
[29] A. Radha, M. Seshasayee, G. Aravamudan, Acta Crystallogr., Sect. C 44 (1988) 1378.
[30] B. Bleany, D.K. Bowers, Proc. R. Soc. Lond. A 214 (1952) 451.
[31] R.H. Furneaux, E. Sinn, Inorg. Chem. 16 (1977) 1809.

Table 1
Magnetic and structural data known for $Ln(DMF)_4(H_2O)_3M(CN)_6 \cdot H_2O$ (M = Co and Fe)

	Configurations and terms	Magnetism [16]	Bridging Ln–N (Å)	Bridging Ln–N–C (°)	Structures reference
Ce–Co	$^2F_{5/2}$–$^1A_{1g}$		2.579(2)	163.0(2)	[16]
Nd–Co	$^4I_{9/2}$–$^1A_{1g}$		2.543(5)	165.1(4)	[22]
Sm–Co	$^6H_{9/2}$–$^1A_{1g}$		2.513(3)	163.5(5)	[16]
Gd–Co	$^8S_{7/2}$–$^1A_{1g}$		2.516(10)	167.5(9)	[22]
Tb–Co	$^7F_6$–$^1A_{1g}$		2.448(5)	162.6(4)	this work
Dy–Co	$^6H_{15/2}$–$^1A_{1g}$		2.431(6)	162.9(4)	this work
Ho–Co	$^5I_8$–$^1A_{1g}$		2.422(4)	163.2(4)	this work
Er–Co	$^4I_{15/2}$–$^1A_{1g}$		2.410(4)	163.7(3)	this work
Ce–Fe	$^2F_{5/2}$–$^2T_{2g}$	antiferro	2.568(9)	165.3(9)	[17]
Nd–Fe	$^4I_{9/2}$–$^2T_{2g}$	antiferro	2.523(6)	162.3(6)	[7]
Sm–Fe	$^6H_{9/2}$–$^2T_{2g}$	negligible	2.505(5)	165.0(4)	[18]
Gd–Fe	$^8S_{7/2}$–$^2T_{2g}$	antiferro	2.51(1)	164(1)	[18]
Tb–Fe	$^7F_6$–$^2T_{2g}$	ferro			
Dy–Fe	$^6H_{15/}$–$^2T_{2g}$	antiferro			
Ho–Fe	$^5I_8$–$^2T_{2g}$	ferro			
Er–Fe	$^4I_{15/2}$–$^2T_{2g}$	negligible	2.398(14)	165.2(14)	[20]

bimetallic assemblies, $Ln(DMF)_4(H_2O)_3Co(CN)_6 \cdot H_2O$ (DMF = *N*,*N*′-dimethylformamide, Ln = Tb, Dy, Ho and Er), and X-ray photoelectron spectroscopy (XPS) studies of several analogous 3d–4f complexes, $Ln(DMF)_4(H_2O)_3Co(CN)_6 \cdot H_2O$ (Ln = Ce, Nd, Sm, Gd, Tb, Dy, Ho and Er; M = Co and Fe). We also discuss both structural and electronic factors changed by substitution of metal elements for a series of cyano-bridged 3d–4f systems in order to elucidate the reasons for photo-induced magnetization.

2. Experimental

2.1. Materials and physical measurements

Chemicals of the highest commercial grade available (Aldrich and Wako) were used as received without further purification. Elemental analyses (C, H, N) were carried out on an Elementar Vario EL analyser at Keio University. Infrared spectra were recorded as KBr pellets on a JASCO FT-IR 660 plus spectrophotometer in the range of 4000–400 cm^{-1} at 298 K. Diffuse reflectance electronic spectra were measured on a JASCO V-560 spectrophotometer equipped with an integrating sphere in the range of 850–220 nm at 298 K. Emission spectra were measured with a JASCO FP-6500 spectrofluorometer in the solid state at 298 K. The mass concentration of Ln^{III} and Fe^{III} or Co^{III} ions was measured with a HORIBA X-ray analytical microscope XGT-2700 using X-ray fluorescence analyses. XPS spectra were recorded with a JEOL JPS-9000MX at 298 K. Powder samples were pressed as pellets and put under UHV to reach the 10^{-8} Pa range. The non-monochromatized Mg Kα source was used at 10 kV and 10 mA, as a flood gun to compensate for the non-conductive samples. The binding energy of the spectra was calibrated in relation to the C1s binding energy (284.0 eV), which was applied as an internal standard.

2.2. Preparations

The complexes were prepared according to the literature procedure [18,22]. Characterization was carried out by elemental analyses, IR spectroscopy (Table S1) and X-ray fluorescence analyses (Table S2) for the 16 complexes investigated.

2.3. X-ray crystallography

The previously unknown crystal structures of **Tb–Co**, **Dy–Co**, **Ho–Co** and **Er–Co** have been determined, and their crystallographic data are summarized in Table 2. The single crystals of prismatic morphology suitable for X-ray crystallography were mounted on a glass fiber coated with epoxy glue. The intensity data were collected on a Rigaku AFC-7R diffractometer with graphite monochromated Mo Kα ($\lambda = 0.7073$ Å) radiation using ω–2θ scan techniques at 297 K. The calculations were performed on an SGI O2 workstation with the TEXSAN [35] software package. Empirical absorption corrections were applied based on ψ scans. No significant decay in the intensity of three standard reflections was observed throughout the data collection. The structures were solved by direct methods using SIR-92 [36] and refined on F^2 anisotropically for non-hydrogen atoms by full-matrix least-squares methods with SHELXL-97 [37]. The hydrogen atoms, except for hydrogen atoms connected with O5, O6, O7 and O8 as water molecules, were added at geometrically expected positions with bond distances of 0.96 Å, and they were refined isotropically as riding models. Residual electron density could not found in the difference Fourier maps completely. The refinement with the models containing additional water molecules resulted in an increase of *R* values. Therefore, only one oxygen atom was assigned as water molecules of crystallization for the refinement carried out.

Table 2
Crystallographic data for **Tb–Co**, **Dy–Co**, **Ho–Co** and **Er–Co**

Compound	Tb–Co	Dy–Co	Ho–Co	Er–Co
Formula	$C_{18}H_{36}CoN_{10}O_8Tb$	$C_{18}H_{36}CoDyN_{10}O_8$	$C_{18}H_{36}CoHoN_{10}O_8$	$C_{18}H_{36}CoErN_{10}O_8$
Molecular weight	738.40	742.00	744.41	746.74
Crystal system	monoclinic	monoclinic	monoclinic	monoclinic
Space group	$P2_1/a$ (#14)	$P2_1/a$ (#14)	$P2_1/a$ (#14)	$P2_1/a$ (#14)
a (Å)	24.826(16)	24.79(4)	24.770(5)	24.722(4)
b (Å)	8.872(5)	8.870(9)	8.8633(18)	8.858(1)
c (Å)	13.931(6)	13.92(1)	13.918(2)	13.893(2)
β (°)	96.34(4)	96.4(1)	96.279(15)	96.36(1)
V (Å^3)	3050(3)	3042(6)	3037.3(10)	3023.7(7)
Z	4	4	4	4
D_{calc} (g cm^{-3})	1.608	1.619	1.628	1.640
$F(000)$	1480	1484	1488	1492
μ (mm^{-1})	2.898	3.036	3.190	3.355
Crystal size (mm)	0.50 × 0.20 × 0.20	0.30 × 0.30 × 0.30	0.30 × 0.30 × 0.30	0.50 × 0.50 × 0.50
Unique reflections	7013	6977	6993	6935
Observed reflections ($I > 2\sigma(I)$)	5554	6138	5612	6273
Parameters	343	343	343	343
R_1[a], R_w[b], S	0.0399, 0.1189, 0.982	0.0404, 0.1431, 1.253	0.0364, 0.1121, 0.958	0.0340, 0.1290, 1.160
Minimum and maximum residual densities (e/Å^3)	3.469 and −1.393	2.094 and −1.466	2.783 and −1.812	1.242 and −1.240

[a] $R_1 = \sum \| F_o | - | F_c \| / \sum | F_o |$.
[b] $R_w = (\sum w(|F_o| - |F_c|)^2 / \sum w|F_o|^2)^{1/2}$, $w = 1/(\sigma^2(F_o) + (0.1P)^2)$ where $P = (F_o^2 + 2|F_c^2|)/3$.

3. Results and discussion

3.1. Crystal structures

The molecular structures of **Tb–Co** are depicted in Fig. 1. Selected bond lengths and angles for **Tb–Co**, **Dy–Co**, **Ho–Co** and **Er–Co** are given in Table 3. The isostructural four heterometallate complexes crystallize in the monoclinic space group $P2_1/a$ with $Z = 4$, showing slight differences of cell parameters and geometrical parameters. The Ln^{III} ions are eight-coordinated with a distorted dodecahedral geometry, which consists of seven oxygen atoms (four DMF ligands and three coordinated water molecules) and one nitrogen atom of the bridging cyanide ligand. The former Ln–O bond distances are shorter than the latter Ln–N6 ones. The order of the Ln–O bond distances are **Tb–Co** > **Dy–Co** > **Ho–Co** > **Er–Co**, which is attributed to the typical lanthanoid contraction [38]. The features are also similar to the related **Ln–Fe** complexes

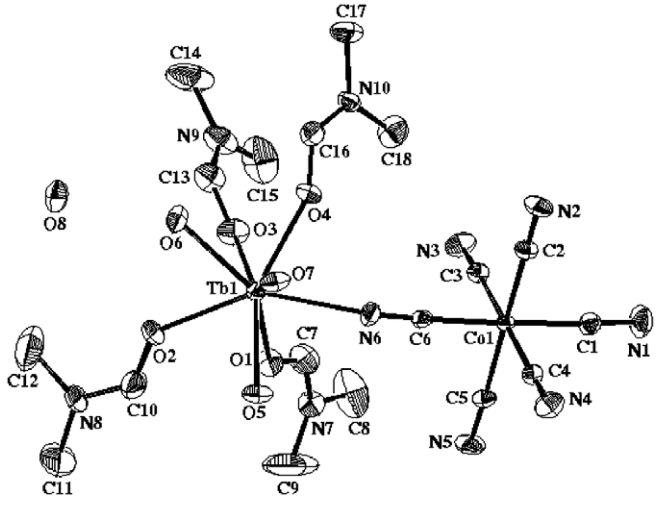

Fig. 1. The molecular structure of **Tb–Co** showing the atomic labelling scheme. Displacement ellipsoids are drawn at the 30% probability level. H atoms are omitted for clarity.

Table 3
Selected geometric parameters (Å, °) for **Tb–Co**, **Dy–Co**, **Ho–Co** and **Er–Co**

Compound	Tb–Co	Dy–Co	Ho–Co	Er–Co
Ln1–O1	2.364(4)	2.355(4)	2.355(4)	2.343(3)
Ln1–O2	2.358(4)	2.353(5)	2.347(4)	2.329(3)
Ln1–O3	2.375(5)	2.371(5)	2.358(4)	2.352(4)
Ln1–O4	2.346(4)	2.338(4)	2.328(4)	2.318(3)
Ln1–O5	2.398(4)	2.386(4)	2.384(3)	2.359(3)
Ln1–O6	2.390(4)	2.370(4)	2.368(3)	2.351(4)
Ln1–O7	2.411(4)	2.406(4)	2.389(3)	2.382(3)
Ln1–N6	2.448(5)	2.431(6)	2.422(4)	2.410(4)
Co1–C1	1.898(6)	1.887(6)	1.890(5)	1.894(5)
Co1–C2	1.890(5)	1.890(5)	1.892(5)	1.890(4)
Co1–C3	1.912(6)	1.911(6)	1.906(5)	1.907(4)
Co1–C4	1.907(6)	1.891(6)	1.896(5)	1.885(4)
Co1–C5	1.899(5)	1.891(5)	1.894(5)	1.895(4)
Co1–C6	1.887(5)	1.886(5)	1.886(5)	1.887(4)
C≡N (mean)	1.145	1.151	1.148	1.150
C6–N6	1.146(7)	1.150(7)	1.145(6)	1.142(5)
Co1–C1–N1	177.0(6)	176.8(6)	176.8(6)	176.4(5)
Co1–C2–N2	178.5(5)	178.5(5)	178.5(5)	177.3(4)
Co1–C3–N3	177.5(5)	178.2(5)	177.3(5)	177.6(4)
Co1–C4–N4	179.3(5)	179.7(5)	179.3(5)	179.6(5)
Co1–C5–N5	178.4(5)	178.0(5)	178.3(4)	178.9(4)
Co1–C6–N6	177.0(5)	176.8(4)	177.1(4)	176.8(4)
Co–C≡N (mean)	178.0	178.0	178.9	177.8
Ln1–N6–C6	162.6(4)	162.9(4)	163.2(4)	163.7(3)

[16–20]. The magnitude of the Ln1–C6–N6 bond angles of the bridging cyanide ligands is similar, as follows: 162.6(4)°, 162.9(4)°, 163.2(4)° and 163.7(3)° for **Tb–Co**, **Dy–Co**, **Ho–Co** and **Er–Co**, respectively. However, it should be noted that the Ln1–C6–N6 bond angles in the **Nd–Co** and **Nd–Fe** complexes showed exceptional values, that is **Ce–Co** (163.0(2)°) < **Nd–Co** (165.1(4)°) > **Sm–Co** (163.5(5)°), while **Ce–Fe** (165.3(9)°) > **Nd–Fe** (162.3(6)°) < **Sm–Fe** (165.0(4)°). These characteristic bent-bond features are similar to the proposed photo-excited structures of **Nd–M** complexes by powder XRD patterns [7]. The $[Co(CN)_6]^{3-}$ moieties adopt a slightly distorted octahedral coordination environment and no obvious differences are observed among the four complexes. Because hydrogen atoms could not be introduced completely, we cannot discuss intramolecular or intermolecular hydrogen bonding interactions at present. Intramolecular hydrogen bonds are formed around the DMF ligands (O1–O4) and coordination water (O5–O7) atoms. Intermolecular hydrogen bonds are formed along the crystallographic *a* axis via solvent water (O8) to create the two-dimensional networks. Possible intermolecular hydrogen bonding distances between the cyanide nitrogen and solvent water $O8\cdots N4^{i}$ are 2.824(7), 2.848(7), 2.851(5) and 2.831(6) Å for **Tb–Co**, **Dy–Co**, **Ho–Co** and **Er–Co**, respectively [symmetry code: (i) $x-3/2, -y+1/2, z$]. On the other hand, possible intermolecular hydrogen bonds between the cyanide nitrogen and coordinated water of the adjacent molecules $N5\cdots O5^{ii}$ are 2.712(5), 2.717(5), 2.719(4) and 2.715(5) Å for **Tb–Co**, **Dy–Co**, **Ho–Co** and **Er–Co**, respectively [symmetry code: (ii) $-x+5/2, y+1/2, -z+2$].

3.2. X-ray photoelectron spectroscopy (XPS)

The intensity is plotted by arbitrary scales for XPS in this paper. The C 1s, N 1s and O 1s peaks for 16 **Ln–M** complexes are summarized in Table 4, and the corresponding spectra for eight **Ln–Fe** and **Ln–Co** complexes are shown in Figs. S1 and S2, respectively. For example, distinct and sharp peaks of the XP spectra for **Tb–Co** can be assigned as follows: Tb $4d_{3/2}$ around 154 eV, C 1s at 284 eV, N 1s at 397 eV, O 1s at 531 eV, Co $2p_{3/2}$ at 781 eV, Co $2p_{3/2}$ at 796 eV [39–41]. No significant differences could be observed for the C 1s, N 1s and O 1s peaks of the ligand moieties.

Table 4
The XPS C 1s, N 1s and O 1s peaks (eV) for **Ln–M** complexes

Compound	C 1s	N 1s	O 1s
Ce–Co	284	396	529
Nd–Co	284	396	530
Sm–Co	284	395	530
Gd–Co	284	395	530
Tb–Co	284	397	531
Dy–Co	284	397	531
Ho–Co	284	397	531
Er–Co	284	397	530
Ce–Fe	284	397	531
Nd–Fe	284	397	530
Sm–Fe	284	397	530
Gd–Fe	284	396	530
Tb–Fe	284	396	530
Dy–Fe	284	396	530
Ho–Fe	284	396	530
Er–Fe	284	396	530

The narrow survey XPS of Co $2p_{3/2}$ for **Ln–Co** and Fe $2p_{3/2}$ for **Ln–Fe** complexes are shown in Figs. S3–S6, respectively. The Co $2p_{3/2}$ peak binding energies are at 785.1, 784,7, 785.0, 784.8, 785.4, 785.3, 785.4 and 785.1 eV for **Ce–Co**, **Nd–Co**, **Sm–Co**, **Gd–Co**, **Tb–Co**, **Dy–Co**, **Ho–Co** and **Er–Co**, respectively. While the Fe $2p_{3/2}$ peak binding energies are at 712.7, 712.3, 712.0, 711.7, 712.6, 712.1, 711.9, 712.5 eV and the Fe $2p_{1/2}$ peaks are at 726.4, 724.8, 725.3, 724.7, 725.9, 726.9, 726.3, 726.6 eV for **Ce–Fe**, **Nd–Fe**, **Sm–Fe**, **Gd–Fe**, **Tb–Fe**, **Dy–Fe**, **Ho–Fe** and **Er–Fe**, respectively. These peaks are ascribed to Co^{III} (or Fe^{III}) oxidation states. Thus, no remarkable shift of peaks could be observed for Fe^{III} or Co^{III} ions regardless of the Ln^{III} ions. Furthermore, we could not clearly observe shake-up satellites, typical features of anti-bonding π molecular orbitals (π–π* transitions).

Figs. 2–5 show the narrow survey Ce and Nd (Fig. 2), Sm and Gd (Fig. 3), Tb and Dy (Fig. 4), and Ho and Er (Fig. 5) $4d_{3/2}$ XPS for 16 **Ln–M** complexes. The Ce $4d_{3/2}$ peak binding energies are at 114.0 and 114.7 eV for **Ce–Co** and **Ce–Fe**, Nd $4d_{3/2}$ are at 124.7 and 125.4 eV for **Nd–Co** and **Nd–Fe**, Sm $4d_{3/2}$ are at 134.6 and 135.8 eV for **Sm–Co** and **Sm–Fe**, Gd $4d_{3/2}$ are at 144.3 and 145.4 eV for **Nd–Co** and **Nd–Fe**, Tb $4d_{3/2}$ are at 153.7 and 153.1 eV for **Tb–Co** and **Tb–Fe**, Dy $4d_{3/2}$ are at 159.7 and 159.2 eV for **Dy–Co** and **Dy–Fe**, Ho $4d_{3/2}$ are at 165.6 and 165.3 eV for **Ho–Co** and **Ho–Fe**, Er $4d_{3/2}$ are at 172.2 and 171.8 eV for **Er–Co** and **Er–Fe**, respectively. These peaks are ascribed to Ln^{III} oxidation states, and the binding energies of **Ln–Co** complexes are lower than that of **Ln–Fe** complexes for Ln = Ce, Nd, Sm and Gd (the number of 4f electrons are less than 7). In contrast, the binding energies of **Ln–Co** complexes are similar or higher than that of **Ln–Fe** complexes for Ln = Tb, Dy, Ho and Er (the number of 4f electrons are more than 7).

Commonly, XPS was used to investigate valence states of metal ions and coordination bonding natures in the field of coordination chemistry [42,43]. For example, it has been reported that XPS binding energies indicate good correlations between substituted groups in Au complexes [44], mixed valence in Au complexes [45], electron transfer in tungsten complexes [46], magnetic properties in copper complexes [47,48] and Moessbauer isomer shift in iron complexes [49]. Recently, inorganic solids containing Ln^{III} ions were also measured by using synchrotron radiation [50]. According to them, the bonds with more electronegative atoms would result in greater positive XPS chemical shifts. The peaks of higher oxidized ions would appear with

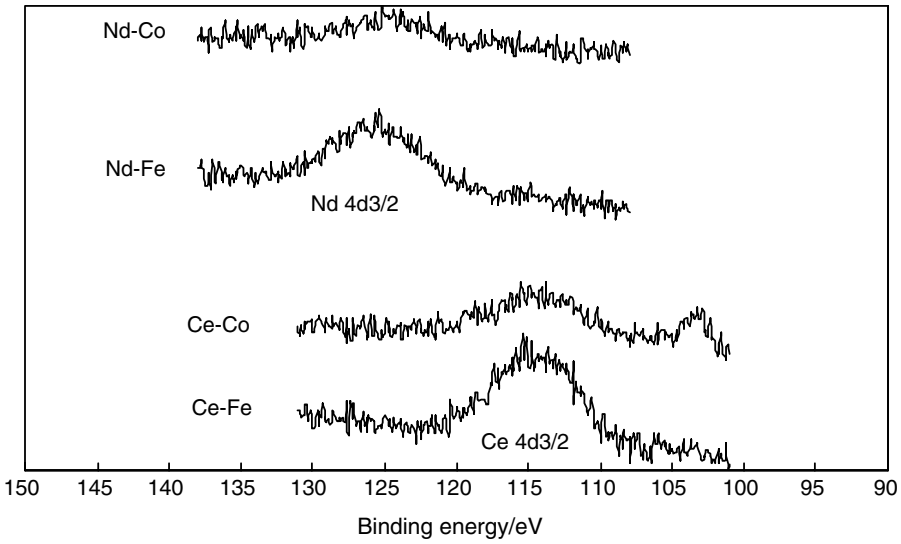

Fig. 2. Narrow survey Ce or Nd $4d_{3/2}$ XPS for **Ce–M** or **Nd–M** (M = Co and Fe).

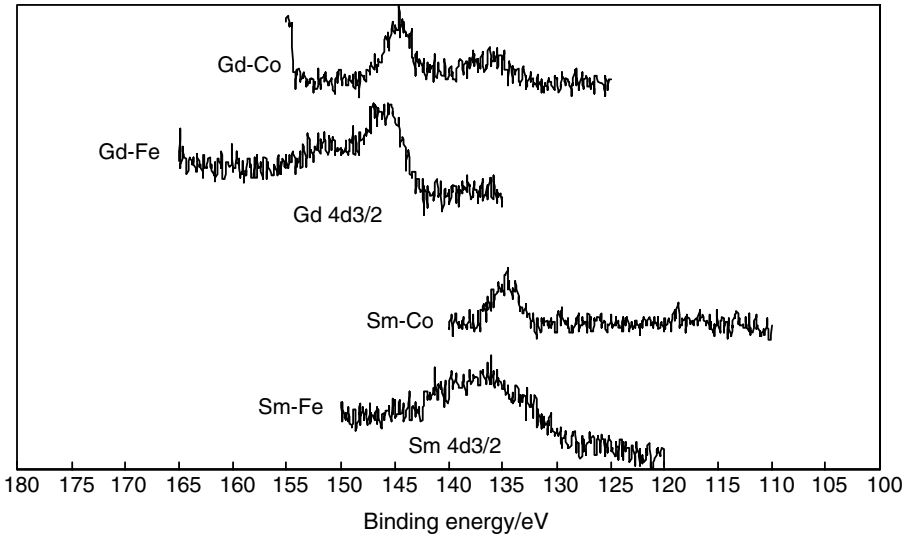

Fig. 3. Narrow survey Sm or Gd $4d_{3/2}$ XPS for **Sm–M** or **Gd–M** (M = Co and Fe).

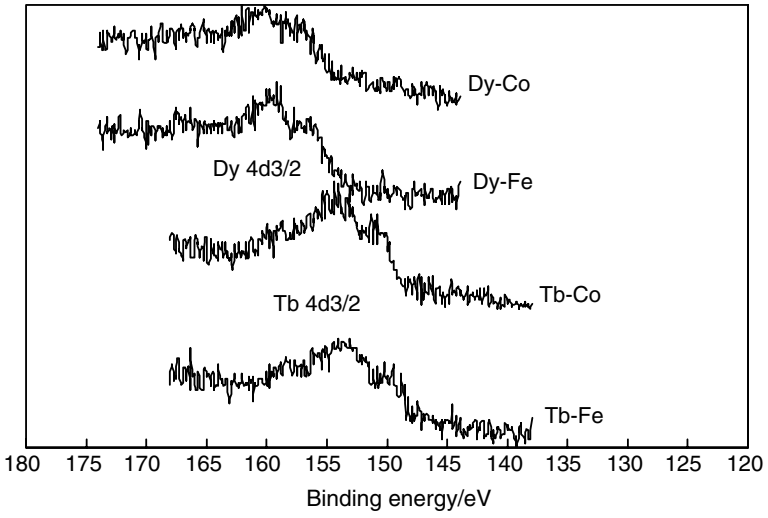

Fig. 4. Narrow survey Tb or Dy $4d_{3/2}$ XPS for **Tb–M** or **Dy–M** (M = Co and Fe).

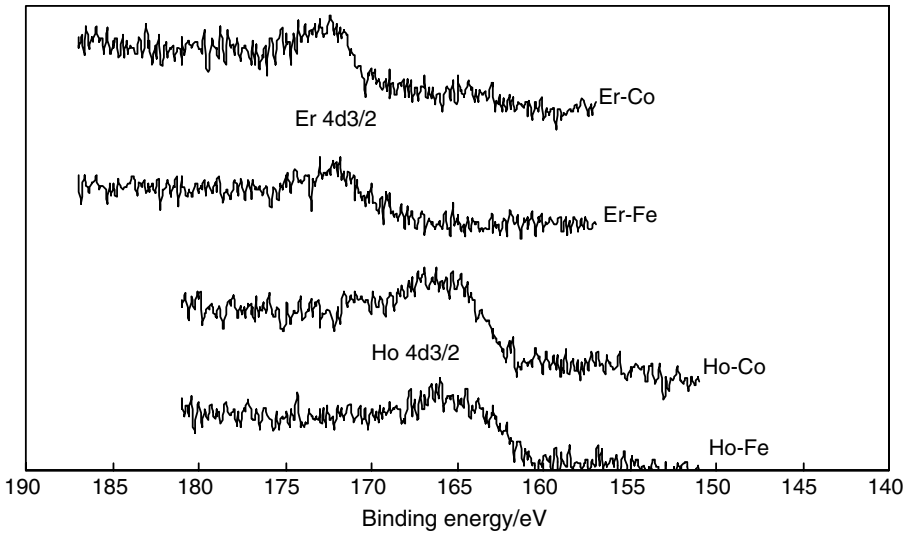

Fig. 5. Narrow survey Ho or Er $4d_{3/2}$ XPS for **Ho–M** or **Er–M** (M = Co and Fe).

higher binding energies. Accordingly, two kinds of Ln $4d_{3/2}$ XPS peak shifts suggest that the cyano-bridged Ln ions of **Ln–Fe** complexes for Ln = Ce, Nd, Sm and Gd easily release electrons even under these conditions. In other words, these selected Ln ions are easy to take mixed-valence states.

3.3. IR and electronic spectra

As listed in Table 1, cyanide stretching bands of the IR spectra of **Ln–Co** and **Ln–Fe** complexes are in the range of 2127–2137 cm^{-1} and 2123–2128 cm^{-1}, respectively. As for the simple $K_3[Fe(CN)_6]$ complex in O_h point group, normal vibration modes were assigned as follows: 2315 cm^{-1} (A_{1g}), 2130 cm^{-1} (E_g) and 2118 cm^{-1} (F_{1u}) [51]. Despite being sensitive to valence or spin states, the present values are comparable to analogous 3d–4f bimetallic assemblies. By comparing with the related 3d–3d or 3d–4f complexes [52], spectral shift features, that is substitution of Co^{III} and Fe^{III} ions, is more effective than substitution of Ln^{III} ions. The spectral features of the IR spectra should also correspond to shifts in the charge transfer absorption bands between the 3d orbitals of M^{III} ions and the unoccupied π^* orbitals of bridging cyanide ligands. The splitting by bridged and uncoordinated cyanide ligands was unclear for the present cases.

On the other hand, electronic spectra (Figs. S7–S10) exhibit strong and broad bands in the UV region due to π–π^* transitions from ligands of both DMF and low-spin $[Co(CN)_6]^{3-}$ or low-spin $[Fe(CN)_6]^{3-}$ moieties. The electronic spectra for the **Ln–Fe** complexes show two peaks around 23 000–32 000 cm^{-1} and 30 000–34 000 cm^{-1}, while **Ln–Co** complexes show a peak around 28 000–32 000 cm^{-1}. The spectral shapes of the UV region depend on the electronic states of the $[M(CN)_6]^{3-}$ moieties. In addition, several sharp peaks could be observed in the visible region for **Nd–M** (Nd^{3+}: $^4I_{9/2}$ ground state), **Dy–M** (Dy^{3+}: $^6H_{15/2}$ ground state), **Ho–M** (Ho^{3+}: $^5I_8$ ground state) and **Er–M** (Er^{3+}: $^4I_{15/2}$ ground state) (M = Co and Fe). In this way, visible light-sensitivity depends on Ln ions for these complexes. Although we have also tried to measure emission spectra (λ_{ex} = 250, 300 and 350 nm) in the solid states at 298 K, we could not detect emission from these complexes under these experimental conditions.

3.4. Electronic properties of 3d–4f cyanide-bridged systems

The effect of interaction between Ln^{III} and M^{III} ions through cyano-bridges can lead to a different charge distribution, overshadowing the decreasing extent of π-back-donation. As elucidated in the present results, this effect is mixed by both structural factors and electronic factors and appeared for specific Ln^{III} elements remarkable for the ground states of these complexes.

As for 3d–3d Prussian blue analogues, the electron configurations corresponding to the strongest ferromagnetic interaction are t_{2g}^3–$t_{2g}^6e_g^2$, while weak antiferromagnetic interaction are t_{2g}^m–$t_{2g}^ne_g^1$ or t_{2g}^m–$t_{2g}^ne_g^2$. Unpaired electrons in the t_{2g} orbitals can be used for superexchange interactions through unoccupied π^* orbitals of cyanide bridging ligands. So oxidation states as well as the kind of 3d elements are important for the mechanism of these magnetic interactions. Indeed, it has been elucidated that in cyano-bridged Mo–M systems, containing $[Mo(CN)_8]^{n-}$ moieties, Mo^{III} ions show larger exchange coupling constants than the equivalent compounds with first transition series elements due to the more diffuse character of the 4d orbitals in comparison with the 3d orbitals [15].

The nature of the coordination bonds of the $[Fe(CN)_6]^{3-}$ moiety is π-backdonation, in which five 3d electrons occupying t_{2g} orbitals are provided to unoccupied π^* orbitals of the cyanide ligands. Recently, detailed electronic states have been confirmed by means of X-ray absorption spectra [53–56]. In O_h symmetry, the electron

configuration of the Fe^{III} ion is $t_{2g}^5 e_g^0$ and irreducible representations of 2π orbitals of the cyanide ligands are t_{1g}, t_{1u}, t_{2g} and t_{2u}. Qualitatively speaking, the formation of a $[Fe(CN)_6]^{3-}$ complex results in molecular orbitals which are split into occupied t_{2g}, degenerated t_{1g}, t_{1u} and t_{2u}, and t_{2g} orbitals and unoccupied degenerated t_{1g}, t_{1u} and t_{2u}, e_g and t_{2g} orbitals. When the electrons of cyanides are excited to π^* orbitals (formed from unoccupied t_{1g}, t_{1u} and t_{2u} orbitals) associated with metal to ligand charge transfer from the t_{2g}^5 orbital in the Fe^{III} ion to unoccupied π^* orbitals in cyanide ligands [56], π-backdonation may be weaken because of electronic repulsion of electrons in the unoccupied π^* orbitals.

4. Conclusion

Consequently, we can point out characteristic structural and electronic features for photo-induced magnetization of **Nd–M** complexes. Systematic crystal structures revealed that gradually changes of isostructural crystals due to lanthanoid contraction lead to remarkable Ln–O coordination bond distances or a decrease of the cell volume. However, only **Nd–Fe** and **Nd–Co** complexes show exceptional bent Ln–N–C bond angles, which may be proposed photo-excited structures of bent-bonds. The patterns of Ln $4d_{3/2}$ XPS peak shifts for Ln = Ce, Nd, Sm and Gd differ from that of Ln = Tb, Dy, Ho and Er, which suggests that the cyano-bridged Ln^{III} ions of **Ln–Fe** complexes for Ln = Ce, Nd, Sm and Gd easily become mixed-valence states. In addition, absorption spectra exhibit that π-backdonation of cyano-bridging ligands uses unoccupied π^* orbitals and unoccupied t_{2g} orbitals in $[Fe(CN)_6]^{3-}$ moieties. Further studies on the structural and electronic natures of other cyano-bridging heterometallic assemblies are in progress in order to rationalize the design of multi-functional materials which consist of (transition) metal complexes.

Acknowledgements

This work was supported by a Grant-in-Aid for the 21st Century COE program 'KEIO Life Conjugate Chemistry' form the Ministry of Education, Culture, Sports, Science, and Technology, Research Foundation for Opto-Science and Technology, and Japan and Mizuho Foundation for the Promotion of Science.

Appendix A. Supplementary data

Crystallographic information is available (CCDC Nos. 279742, 279743, 279744 and 279745 for **Tb–Co**, **Dy–Co**, **Ho–Co** and **Er–Co**, respectively) from the Cambridge Crystallographic Data Centre, 12 Union Road, Cambridge CB2 1EZ, UK (e-mail: deposit@ccdc.cam.ac.uk). Characterization data, XPS and diffuse reflectance electronic spectra have been deposited as supplementary data. Supplementary data associated with this article can be found, in the online version, at doi:10.1016/j.poly.2006.03.026.

References

[1] O. Sato, Acc. Chem. Res. 36 (2003) 692.
[2] O. Sato, S. Hayami, Y. Einaga, Z.-Z. Gu, Bull. Chem. Soc. Jpn. 76 (2003) 443.
[3] O. Sato, T. Iyoda, A. Fujishima, K. Hashimoto, Science 272 (1996) 704.
[4] J.M. Herrera, V. Marcaud, M. Verdaguer, J. Marrot, M. Kalisz, C. Mathoniere, Angew. Chem., Int. Ed. 43 (2004) 5468.
[5] C. Mathoniere, R. Podgajny, P. Guionneau, C. Labrugre, B. Sieklucka, Chem. Mater. 17 (2005) 442.
[6] S. Bonhommeau, G. Molnar, A. Galet, A. Zwick, J.-A. Real, J.J. McGarvey, A. Bousseksou, Angew. Chem., Int. Ed. 44 (2004) 4069.
[7] G. Li, T. Akitsu, O. Sato, Y. Einaga, J. Am. Chem. Soc. 125 (2003) 12396.
[8] G. Li, O. Sato, T. Akitsu, Y. Einaga, J. Solid State Chem. 177 (2004) 2835.
[9] G. Li, T. Akitsu, O. Sato, Y. Einaga, Hyperfine Interact. 156/157 (2004) 143.
[10] G. Li, P. Yan, O. Sato, Y. Einaga, J. Solid State Chem. 178 (2005) 36.
[11] M. Nishino, Y. Yoshioka, K. Yamaguchi, Chem. Phys. Lett. 297 (1998) 51.
[12] M. Nishino, S. Kubo, Y. Yoshioka, A. Nakamura, K. Yamaguchi, Mol. Cryst. Liq. Cryst. 205 (1997) 109.
[13] M. Ohba, H. Okawa, Coord. Chem. Rev. 198 (2000) 313.
[14] H. Okawa, M. Ohba, Bull. Chem. Soc. Jpn. 75 (2002) 1191.
[15] E. Ruiz, A. Rodriguez-Fortea, S. Alcarez, M. Verdaguer, Chem. Eur. J. 11 (2005) 2135.
[16] S. Figuerola, C. Diaz, J. Ribas, V. Tangoulis, J. Granell, F. Lloret, J. Mahia, M. Maestro, Inorg. Chem. 42 (2003) 641.
[17] J.A. Kautz, D.F. Mullica, B.P. Cunningham, R.A. Combs, J.M. Farmer, J. Mol. Struct. 523 (2000) 175.
[18] G. Li, T. Akitsu, O. Sato, Y. Einaga, J. Coord. Chem. 57 (2004) 855.
[19] H.-Z. Kou, G.-M. Yang, D.-Z. Liao, P. Cheng, Z.-H. Jiang, S.-P. Yan, X.-Y. Huang, G.-L. Wang, J. Chem. Crystallogr. 28 (1998) 303.
[20] D.F. Mullica, J.M. Farmer, B.P. Cunningham, J.A. Kautz, J. Coord. Chem. 49 (2000) 239.
[21] B.P. Cunningham, J.A. Kautz, J. Chem. Crystallogr. 30 (2000) 671.
[22] G. Li, T. Akitsu, O. Sato, Y. Einaga, J. Coord. Chem. 57 (2004) 189.
[23] R.A. Combs, J.M. Farmer, J.A. Kautz, Acta Crystallogr., Sect. C 56 (2000) 1420.
[24] H.-Z. Kou, S. Gao, X.L. Jin, Inorg. Chem. 40 (2001) 6295.
[25] H.-Z. Kou, S. Gao, B.-W. Sun, J. Zhang, Chem. Mater. 13 (2001) 1431.
[26] B.-Q. Ma, S. Gao, G. Su, G.-X. Xu, Angew. Chem., Int. Ed. Engl. 40 (2001) 434.
[27] C. Yang, G.-C. Guo, H.-W. Ma, J.-C. Liu, X. Zhang, F.-K. Zheng, S.-H. Lin, G.-W. Zhou, J.-G. Mao, J.-S. Huang, Chin. J. Struct. Chem. 20 (2001) 229.
[28] J.-R. Li, L.-Z. Cai, R.-Q. Zou, G.-W. Zhou, G.-C. Guo, X.-H. Bu, J.-S. Huang, Acta. Crystallogr., Sect. E 58 (2002) m686.
[29] J.-R. Li, G.-C. Guo, M.-S. Wang, G.-W. Zhou, X.-H. Bu, J.-S. Huang, Chin. J. Struct. Chem. 22 (2003) 182.
[30] A. Figuerola, C. Diaz, J. Ribas, V. Tangoulis, J. Granell, F. Lloret, J. Mahia, M. Maestro, Inorg. Chem. 42 (2003) 641.
[31] J.-R. Li, L.-Z. Cai, Y. Zheng, G.-C. Guo, X.-H. Bu, J.-S. Huang, Chin. J. Inorg. Chem. 19 (2003) 91.
[32] W.-T. Chen, L.-Z. Cai, A.-Q. Wu, G.-C. Guo, J.-S. Huang, Chin. J. Struct. Chem. 23 (2004) 1282.
[33] J.-R. Li, L.-Z. Cai, G.-C. Guo, X.-H. Bu, J.-S. Huang, Acta. Crystallogr., Sect. E 60 (2004) m259.
[34] W.-T. Chen, L.-Z. Cai, A.-Q. Wu, G.-C. Guo, J.-S. Huang, Z.-C. Dong, A. Matsushita, Chin. J. Inorg. Chem. 20 (2004) 693.
[35] Molecular Structure Corporation. TEXSAN. Version 1.11., MSC, 9009 New Trails Drive, The Woodlands, TX 77381-5209, USA, 2001.
[36] A. Altomare, G. Cascarano, C. Giacovazzo, A. Guagliardi, M.C. Brurla, G. Polidori, M. Camalli, J. Appl. Crystallogr. 27 (1994) 435.

[37] G.M. Sheldrick, SHELXL97: Program for the Refinement of Crystal Structures, University of Göttingen, Göttingen, Germany, 1997.
[38] A. Bondi, J. Phys. Chem. 68 (1964) 441.
[39] J.A. Bearden, A.F. Burr, Rev. Mod. Phys. 39 (1967) 125.
[40] M. Cardona, L. Lay (Eds.), Photoemission in Solids I: General Principles, Springer, Berlin, 1978.
[41] J.C. Fugggle, N. Martensson, J. Electron. Spectrosc. Relat. Phenom. 12 (1980) 275.
[42] W.L. Jolly, Coord. Chem. Rev. 12 (1974) 47.
[43] R.A. Walton, Coord. Chem. Rev. 21 (1976) 63.
[44] P.G. Gassman, C.H. Winter, Organometallics 10 (1991) 1592.
[45] H. Kitagawa, N. Kojima, T. Nakajima, J. Chem. Soc., Dalton Trans. (1991) 3121.
[46] B. Sieklucka, R. Dziembaj, S. Witkowski, Inorg. Chim. Acta 187 (1991) 5.
[47] C. Furlani, G. Polzonetti, C. Preti, G. Tosi, Inorg. Chim. Acta 73 (1983) 105.
[48] H. Hu, J.-L. Du, R.C. Thompson, D.C. Frost, Inorg. Chim. Acta 179 (1991) 113.
[49] W. Linert, V. Gutmann, O. Baumgartner, G. Wiesinger, H. Kirchmayr, Inorg. Chim. Acta 74 (1983) 123.
[50] A.P. Holm, T.C. Ozawa, S.M. Kauzlarich, S.A. Morton, G.D. Waddill, J.G. Tobin, J. Solid State Chem. 178 (2005) 262.
[51] W.P. Griffith, G.T. Turner, J. Chem. Soc. A (1970) 888.
[52] B. Yan, Z. Chen, Helv. Chim. Acta 84 (2001) 817.
[53] G.K. Wertheim, A. Rosencwaig, J. Chem. Phys. 54 (1971) 3235.
[54] R.J. Emrich, L. Traynor, W. Gambofi, E. Buhks, J. Vac. Sci. Technol. A5 (1987) 1307.
[55] Y.F. Jia, Q. Zhu, K.M. Thomas, Chem. Phys. Lett. 371 (2003) 105.
[56] A.S. Vinogradov, A.B. Preobrajenski, A. Knop-Gericke, S.L. Molodtsov, S.A. Krasnikoc, S.V. Nekipelov, R. Szargan, M. Havecker, R. Schlogl, J. Electron. Spectrosc. Relat. Phenom. 114–116 (2001) 813.

complexes) have supported the TD-DFT method to be applicable for such systems giving good assignment of experimental spectra [10–16].

2. Experimental

2.1. General procedure

All synthetic manipulations were carried out open to the atmosphere. The solvents were of reagent grade and were used as received. Ammonium perrhenate, Ph_3P and PPh_2py were purchased from Aldrich and used as received. $[ReOX_3(PPh_3)_2]$ (X = Cl, Br) were prepared according to the literature methods [17].

IR spectra were recorded on a Nicolet Magna 560 spectrophotometer in the spectral range 4000–400 cm^{-1} with the samples in the form of KBr pellets. Electronic spectra were measured on a Lab Alliance UV–VIS 8500 spectrophotometer in the range 900–200 nm in deoxygenated dichloromethane solution. Elemental analyses (C, H, N) were performed on a Perkin–Elmer CHN-2400 analyzer.

2.2. Preparation of *[$ReCl_3(PPh_3)(OPPh_2py$-O,N)]* (*1*)

$[ReOCl_3(PPh_3)_2]$ (0.83 g, 1 mmol) and PPh_2py (0.26 g, 1 mmol) were suspended in acetone (100 cm^3) and stirred for 5 h. The volume was condensed to 10 cm^3 and a dark red precipitate was filtered off. The product was washed with diethyl ether and dried in vacuo. Yield 90%. Slow evaporation of the acetonitrile solution of **1** gave red crystals of the acetonitrile solvate (**1** · **CH_3CN**).

IR (KBr, cm^{-1}) 3055(m), 1986(w), 1915(w), 1836(w), 1776(w), 1647(w), 1618(w), 1585(m), 1570(sh), 1481(m), 1435(s), 1367(w), 1313(w), 1284(w), 1230(w), 1190(w), 1120(s), 1092(m), 1042(s), 1021(m), 996(m), 918(w), 738(s), 693(s), 566(s), 531(s), 510(sh), 493(m), 459(w), 428(w).

Anal. Calc. for $C_{35}H_{29}NP_2Cl_3ORe$: C, 50.40; H, 3.50; N, 1.68. Found: C, 50.55; H, 3.60; N, 1.75%.

2.3. Preparation of *[$ReBr_3(PPh_3)(OPPh_2py$-O,N)]* (*2*)

A procedure similar to that for **1** was used with $[ReOBr_3(PPh_3)_2]$ (0.97 g, 1 mmol) and PPh_2py (0.26 g, 1 mmol). A dark red crystalline precipitate of **2** was collected in 80% yield. Crystals of **2** suitable for X-ray investigation were obtained by recrystallization from a mixture of chloroform–ethanol.

IR (KBr, cm^{-1}) 3049(m), 1963(w), 1896(w), 1817(w), 1768(w), 1668(w), 1586(m), 1481(m), 1433(s) 1333(w), 1313(w), 1284(w), 1234(w), 1186(w), 1118(s), 1091(m), 1043(s), 1023(m), 997(w), 924(w), 845(w), 738(s), 691(s), 563(s), 531(s), 518(sh), 492(m), 454(w), 427(m), 502(s), 465(m), 450(sh).

Anal. Calc. for $C_{35}H_{29}NP_2Br_3ORe$: C, 43.45; H, 3.02; N, 1.45. Found: C, 43.35; H, 3.08; N, 1.36%.

2.4. Crystal structure determination and refinement

The X-ray intensity data of **1** · **CH_3CN** and **2** were collected on a KM-4-CCD automatic diffractometer equipped with a CCD detector, with 20 and 60 s exposure time being used receptively. The unit cell parameters were determined from least-squares refinement of the setting angles of 12909 and 4387 strongest reflections respectively for **1** · **CH_3CN** and **2**. Details concerning crystal data and refinement are given in Table 1. Lorentz, polarization and numerical absorption corrections [18] were applied. The structures were solved by the Patterson method and subsequently completed by difference Fourier recycling. All the non-hydrogen atoms were refined anisotropically using the full-matrix, least-squares technique. The aromatic ring hydrogen atoms were found by difference Fourier synthesis and they were refined as "riding" on their parent carbon atoms [d(C–H) = 0.93 Å] and assigned isotropic temperature factors equal to 1.2 times the value of the equivalent temperature factor of the parent carbon atom. The methyl group hydrogen atoms were also found by difference

Table 1
Crystal data and structure refinement for **1** · **CH_3CN** and **2**

	1 · **CH_3CN**	**2**
Empirical formula	$C_{37}H_{32}Cl_3N_2OP_2Re$	$C_{35}H_{29}Br_3NOP_2Re$
Formula weight	875.14	967.46
Temperature (K)	293(2)	293(2)
Wavelength (Å)	0.71073	0.71073
Crystal system	monoclinic	monoclinic
Space group	$P2_1/c$	$P2_1/n$
Unit cell dimensions		
a (Å)	10.5760(4)	12.0145(9)
b (Å)	9.8982(7)	16.7188(12)
c (Å)	33.5696(12)	17.7049(19)
β (°)	95.252(3)	106.358(7)
Volume (Å^3)	3499.4(3)	3412.4(5)
Z	4	4
Density (calculated) (Mg/m^3)	1.661	1.883
Absorption coefficient (mm^{-1})	3.826	7.196
F(000)	1728	1856
Crystal size (mm)	0.49 × 0.41 × 0.40	0.18 × 0.17 × 0.09
θ Range for data collection (°)	3.19–25.13	3.01–25.11
Index ranges	$-12 \leqslant h \leqslant 12$; $-11 \leqslant k \leqslant 1$; $-39 \leqslant l \leqslant 39$	$-14 \leqslant h \leqslant 13$; $-19 \leqslant k \leqslant 19$; $0 \leqslant l \leqslant 21$
Reflections collected	34655	11840
Independent reflections (R_{int})	6232 (0.0446)	6073 (0.0833)
Completeness to 2θ (%)	93.6	96.2
Maximum and minimum transmission	0.182 and 0.305	0.560 and 0.361
Data/restraints/parameters	6232/0/416	6073/0/388
Goodness-of-fit on F^2	1.267	0.967
Final R indices [$I > 2\sigma(I)$]	$R_1 = 0.0279$ $wR_2 = 0.0527$	$R_1 = 0.0677$ $wR_2 = 0.1430$
R indices (all data)	$R_1 = 0.0298$ $wR_1 = 0.0531$	$R_1 = 0.1172$ $wR_2 = 0.1621$
Largest different peak and hole (e Å^{-3})	0.500 and −0.862	1.455 and −1.972

Fourier synthesis and refined as "riding" on their parent carbon atoms [d(C–H) = 0.96 Å] and they were assigned isotropic temperature factors equal to 1.5 times the value of equivalent temperature factor of the parent carbon atom. The methyl group was allowed to rotate about its local threefold axis. SHELXS97 [19] and SHELXL97 [20] programs were used for the calculations. Atomic scattering factors were those incorporated in the computer programs.

2.5. Computational details

The Gaussian03 program [21] was used in the calculations. The geometry optimization was carried out with the DFT method with the use of the B3LYP functional [22,23]. The electronic spectrum of **1** was calculated with the TDDFT method [24]. The calculations were performed using the ECP basis set on the rhenium atom, the standard 6-31+g(2d) basis for chlorine, 6-31+g** for oxygen and nitrogen, 6-31+g* for carbon and 6-31G basis for hydrogen atoms. The Xe core electrons of Re were replaced by an effective core potential and DZ quality Hay and Wadt Los Alamos ECP basis set (LANL2DZ) [25] was used for the valence electrons. An additional d function with exponent $\alpha = 0.3811$ and f function with exponent $\alpha = 2.033$ were added on the rhenium atom.

2.6. Magnetic measurements

The magnetic measurements of the powdered samples were measured over the temperature range 1.8–300 K using a Quantum Design SQUID – based MPMSXL–5-type magnetometer. The superconducting magnet was generally operated at a field strength ranging from 0 to 5 T. Measurements of samples of the compounds were made at magnetic field of 0.5 T.

The SQUID magnetometer was calibrated with a palladium rod sample. Corrections are based on subtracting the sample – holder signal and contribution χ_D estimated from Pascal constants [26] and equal -467×10^{-6} cm^3 mol^{-1} for complex [$ReCl_3(PPh_3)(OPPh_2py$-O,N)] (**1**) and -497×10^{-6} cm^3 mol^{-1} for complex [$ReBr_3(PPh_3)(OPPh_2py$-O,N)] (**2**). The effective magnetic moments were calculated from the equation, $\mu_{eff} = 2.83(\chi_M T)^{1/2}$(B.M.).

3. Results and discussion

The [$ReCl_3(PPh_3)(OPPh_2py$-O,N)] (**1**) and [$ReBr_3(PPh_3)$-($OPPh_2py$-O,N)] (**2**) complexes have been obtained in high yield in the reactions of [$ReOX_3(PPh_3)_2$] (X = Cl, Br) with diphenyl(2-pyridyl)phosphine in acetone at room temperature (Eq. (1)):

$$[ReOX_3(PPh_3)_2] + PPh_2py \rightarrow [ReX_3(PPh_3)(OPPh_2py - O, N)] + PPh_3 \quad (1)$$

The well-known capacity of phosphines to interact with the Re≡O bond in rhenium(V) oxo-complexes explains the course of the reactions between [$ReOX_3(PPh_3)_2$] and PPh_2py.

The elemental analyses of complexes **1** and **2** are in good agreement with their formulations. The IR spectra of **1** and

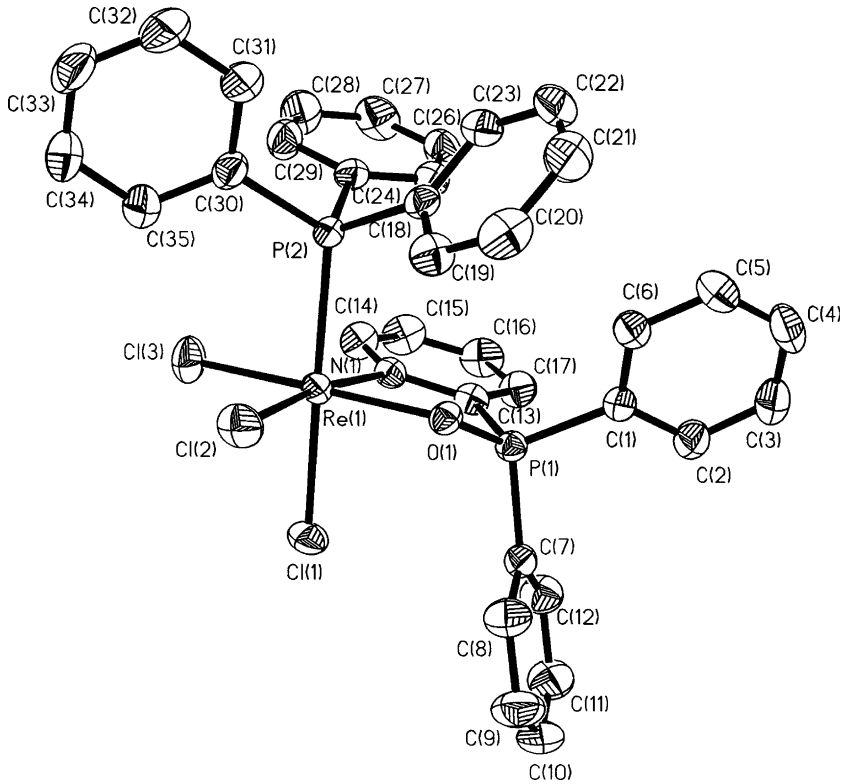

Fig. 1. The molecular structure of **1**. The hydrogen atoms of the phenyl rings are omitted for clarity.

2 are governed by the vibrations of the phosphine ligands. The absence of the characteristic strong ν(Re=O) band at $\sim$980 cm^{-1} is a clear indication that there is no oxo-Re(V) starting material left in the samples of **1** and **2**. A strong band corresponding to the stretching vibration of the P=O group appears in **1** and **2** at 1120 and 1118 cm^{-1}, respectively. The absorption bands at $\sim$1580 cm^{-1} are typical of C=N stretching modes [27].

3.1. X-ray structures

The chloride complex crystallises as the solvate **1** · MeCN. The acetonitrile molecule from crystallization is not bonded to any other atom, with the exception of some rather weak hydrogen bonds [28,29].

A perspective drawing of **1** is given in Fig. 1. The rhenium atoms of both complexes are in a distorted octahedral environment with two halogen ions and the bidentate ligand – diphenyl(2-pyridyl)phosphine oxide – in the equatorial plane. Deviations from an ideal octahedron can be ascribed to the bite angle of the five membered chelate ring.

The X-ray structures of a few [$ReCl_3(PPh_3)L$] and [$ReCl_3(PPh_3)L_2$] complexes are known. The $ReCl_3$ fragments have *fac* and *mer* geometries. The geometrical preferences of the $ReCl_3$ unit can be rationalized in terms of the electronic nature of the L ligands. Triphenylphosphine is a π-accepting ligand, σ^*(P–C) phosphine orbitals are involved in π-back bonding between the metal center and the phosphine ligand. Trivalent rhenium is prone to back-bonding. When the L ligand is a π-acid, the facial geometry is expected to be favored. Assuming an idealized octahedral geometry, the back bonding has $t_{2g}(Re) \rightarrow \sigma^*(P–C)$ and $t_{2g}(Re) \rightarrow \pi^*(L–L)$ components. This bonding is maximized when the acceptor ligands are *facially* disposed so that competition between ligands for identical metal orbitals is minimal [30–37]. Back bonding is believed

Table 3
Atomic charges from the Natural Population Analysis (NPA) for **1**

Atom	**1**
Re(1)	0.551
Cl(1)	−0.467
Cl(2)	−0.428
Cl(3)	−0.345
P(1)	2.287
O(1)	−1.086
P(2)	1.360
N(1)	−0.459

Table 2
The experimental bond lengths [Å] and angles [°] for **1** and **2**, and optimized bond lengths [Å] and angles [°] for **1**

Bond lengths	Experimental	Optimized	Bond angles	Experimental	Optimized
1					
Re(1)–Cl(1)	2.4330(9)	2.443	O(1)–Re(1)–N(1)	81.67(10)	80.08
Re(1)–Cl(2)	2.3818(9)	2.424	O(1)–Re(1)–Cl(3)	173.19(7)	172.85
Re(1)–Cl(3)	2.3416(9)	2.374	N(1)–Re(1)–Cl(3)	91.84(8)	93.63
Re(1)–O(1)	2.128(2)	2.130	O(1)–Re(1)–Cl(2)	91.67(7)	88.84
Re(1)–N(1)	2.132(3)	2.137	N(1)–Re(1)–Cl(2)	171.64(8)	166.80
Re(1)–P(2)	2.4307(9)	2.489	Cl(3)–Re(1)–Cl(2)	94.60(4)	97.81
O(1)–P(1)	1.534(2)	1.533	O(1)–Re(1)–P(2)	92.16(6)	91.25
			N(1)–Re(1)–P(2)	93.47(7)	97.18
			Cl(3)–Re(1)–P(2)	90.26(3)	86.13
			Cl(2)–Re(1)–P(2)	91.83(3)	90.16
			O(1)–Re(1)–Cl(1)	87.54(6)	89.35
			N(1)–Re(1)–Cl(1)	84.94(8)	83.23
			Cl(3)–Re(1)–Cl(1)	89.85(3)	93.30
			P(2)–Re(1)–Cl(1)	178.41(3)	179.32
			P(1)–O(1)–Re(1)	115.68(13)	116.71
2					
Re(1)–Br(1)	2.6014(15)		O(1)–Re(1)–N(1)	81.0(4)	
Re(1)–Br(2)	2.5503(14)		O(1)–Re(1)–P(2)	93.1(2)	
Re(1)–Br(3)	2.4891(16)		N(1)–Re(1)–P(2)	90.8(3)	
Re(1)–O(1)	2.113(8)		O(1)–Re(1)–Br(3)	177.5(2)	
Re(1)–N(1)	2.141(10)		N(1)–Re(1)–Br(3)	96.8(3)	
Re(1)–P(2)	2.438(3)		P(2)–Re(1)–Br(3)	88.20(9)	
O(1)–P(1)	1.525(8)		O(1)–Re(1)–Br(2)	88.9(2)	
			N(1)–Re(1)–Br(2)	168.0(3)	
			P(2)–Re(1)–Br(2)	96.27(9)	
			Br(3)–Re(1)–Br(2)	93.02(5)	
			O(1)–Re(1)–Br(1)	87.9(2)	
			N(1)–Re(1)–Br(1)	83.3(2)	
			P(2)–Re(1)–Br(1)	173.81(9)	
			Br(3)–Re(1)–Br(1)	90.52(6)	
			Br(2)–Re(1)–Br(1)	89.84(5)	
			P(1)–O(1)–Re(1)	120.4(5)	

Table 4
The energies and characters of selected molecular orbitals with α and β spins for **1**

	α MO		β MO	
	E (eV)	Character	*E* (eV)	Character
HOMO − 15	−7.647	π_{Ph}(OPPh$_2$py)	−7.662	π_{Ph}(OPPh$_2$py); π(Cl)
HOMO − 14	−7.482	π_{Ph}(OPPh$_2$py); π(Cl)	−7.650	π_{Ph}(OPPh$_2$py); π(Cl)
HOMO − 13	−7.361	π(Cl); π_{Ph}(PPh$_3$)	−7.530	π(Cl); π(O)
HOMO − 12	−7.305	π_{Ph}(OPPh$_2$py); π_{Ph}(PPh$_3$)	−7.468	π_{Ph}(OPPh$_2$py); π(Cl)
HOMO − 11	−7.274	π_{Ph}(OPPh$_2$py); π_{Ph}(PPh$_3$); π(Cl); π(O)	−7.305	π_{Ph}(PPh$_3$); π_{Ph}(OPPh$_2$py)
HOMO − 10	−7.134	π(pzH), π(Cl)	−7.289	π_{Ph}(OPPh$_2$py); π_{Ph}(PPh$_3$); π(Cl)
HOMO − 9	−6.985	π_{Ph}(PPh$_3$)	−7.241	π_{Ph}(PPh$_3$); π(Cl)
HOMO − 8	−6.920	π(Cl); π_{Ph}(PPh$_3$)	−7.130	π_{Ph}(PPh$_3$)
HOMO − 7	−6.715	π(Cl); π_{Ph}(PPh$_3$)	−6.979	π_{Ph}(PPh$_3$)
HOMO − 6	−6.678	π_{Ph}(PPh$_3$); *n*(P); π(Cl)	−6.726	π_{Ph}(PPh$_3$); π(Cl)
HOMO − 5	−6.567	π_{Ph}(PPh$_3$)	−6.620	π_{Ph}(PPh$_3$); *n*(P); π(Cl)
HOMO − 4	−6.408	π_{Ph}(PPh$_3$); *n*(P); π(Cl)	−6.567	π_{Ph}(PPh$_3$); *n*(P); π(Cl)
HOMO − 3	−6.118	π (Cl); *n*(P)	−6.529	π(Cl); π_{Ph}(PPh$_3$)
HOMO − 2	−5.350	d_{xz}(Re); π(Cl); π(O)	−6.249	π (Cl); *n*(P)
HOMO − 1	−5.198	d_{yz}(Re); π(Cl); π(O)	−6.073	π (Cl); *n*(P)
HOMO	−4.991	d_{xy}(Re); π(Cl)	−4.371	d_{xy}(Re); π(Cl)
LUMO	−1.981	π*(py); π^*_{Ph}(OPPh$_2$py)	−2.235	d_{xz}(Re); π(Cl); π(O); π(py)
LUMO + 1	−1.567	π^*_{Ph}(OPPh$_2$py)	−2.073	d_{yz}(Re); π(Cl); π*(py)
LUMO + 2	−1.348	π*(py); π^*_{Ph}(OPPh$_2$py)	−1.752	d_{yz}(Re); π(Cl); π(O); π*(py)
LUMO + 3	−1.055	π^*_{Ph}(OPPh$_2$py)	−1.548	π^*_{Ph}(OPPh$_2$py); π*(py)
LUMO + 4	−0.932	π^*_{Ph}(OPPh^{2}py); π*(py)	−1.366	π*(py); π^*_{Ph}(OPPh$_2$py)
LUMO + 5	−0.885	π^*_{Ph}(PPh$_3$); $d_{x^2-y^2}$	−1.038	π^*_{Ph}(OPPh$_2$py); π*(py)
LUMO + 6	−0.812	π^*_{Ph}(PPh$_3$)	−0.932	π^*_{Ph}(OPPh$_2$py); π*(py)
LUMO + 7	−0.536	π^*_{Ph}(OPPh$_2$py)	−0.820	π^*_{Ph}(PPh$_3$)
LUMO + 8	−0.510	π^*_{Ph}(PPh$_3$); d_z^2	−0.768	π^*_{Ph}(PPh$_3$); d_z^2
LUMO + 9	−0.376	π^*_{Ph}(PPh$_3$)	−0.533	π^*_{Ph}(OPPh$_2$py)
LUMO + 10	−0.174	d_z^2(Re)-σ (Cl)-σ(O); π^*_{Ph}(PPh$_3$)	−0.476	π^*_{Ph}(PPh$_3$)
LUMO + 11	−0.036	d_z^2(Re)-σ (Cl)-σ(O); π^*_{Ph}(PPh$_3$)	−0.364	π^*_{Ph}(PPh$_3$)
LUMO + 12	0.220	π^*_{Ph}(PPh$_3$)	−0.098	π^*_{Ph}(PPh$_3$)
LUMO + 13	0.316	$d_{x^2-y^2}$(Re)-σ(Cl)-σ(N)-σ(P)	0.223	π^*_{Ph}(PPh$_3$)

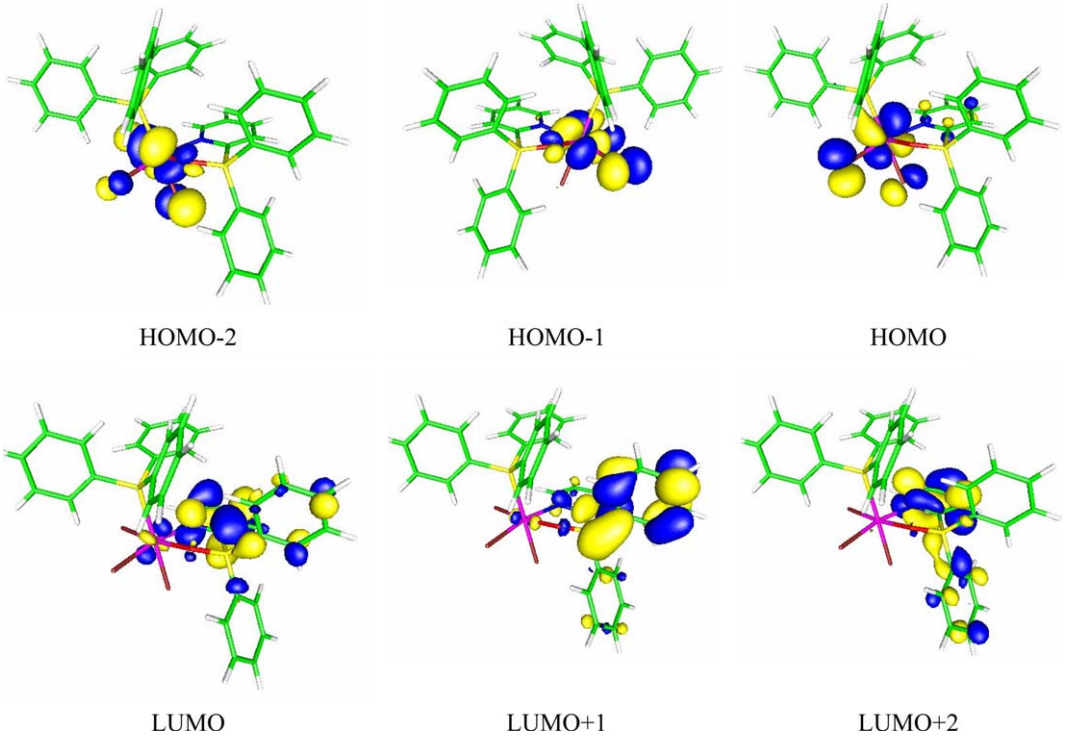

Fig. 2. Selected HOMO and LUMO orbitals with α-spin for **1**.

to sustain the *fac* geometry in **1** and **2** by more than offsetting the steric and electrostatic advantages of the *mer* geometry, as has been observed in related species.

The most important experimental bond lengths and angles for **1** and **2** are reported in Table 2. In both complexes, a notable *trans* influence of triphenylphosphine ligand is observed; the Re–X(1) bond lengths are longer in comparison to the corresponding Re–X(2) and Re–X(3) distances. Furthermore, the Re–X(2) bond lengths in the *trans* position to the N atom of the bidentate ligand are considerable longer in comparison with the Re–X(3) bonds opposite the O atom of the PPh_2py molecule. The shortest Re···Re distances are 8.601(1) and 9.394(1) Å respectively for **1** · MeCN and **2**.

The bond valences were computed as $v_{ij} = \exp[(R_{ij} - d_{ij})/b]$ [38–40], where R_{ij} is the bond-valence parameter (in the formal sense the R_{ij} parameter value can be considered as the idealised single-bond length between i and j atoms). R_{Re-N}, R_{Re-P}, R_{Re-O}, R_{Re-Cl} and R_{Re-Br} were taken as 2.06, 2.46, 1.97, 2.23 and 2.45 [41] respectively, and b was taken as 0.37 [40]. The computed bond valences of the rhenium are $v_{Re-N} = 0.82$; $v_{Re-P} = 1.08$, $v_{Re-O} = 0.65$; $v_{Re-Cl} = 0.58$, 0.66 and 0.74 v.u. (valence units) for **1** and $v_{Re-N} = 0.80$; $v_{Re-P} = 1.06$, $v_{Re-O} = 0.68$; $v_{Re-Br} =$ 0.66,

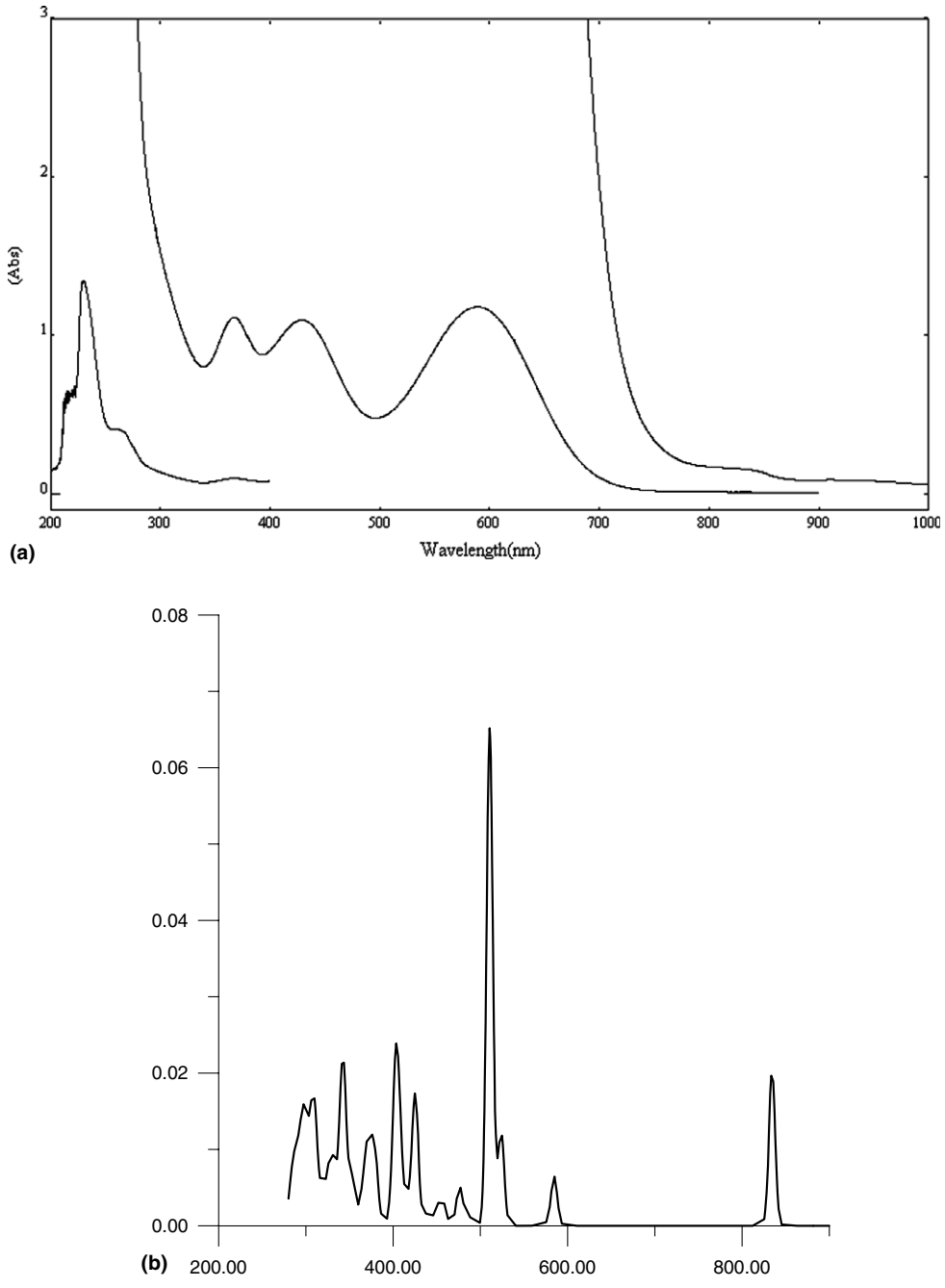

Fig. 3. The experimental (a) and calculated (b) electronic absorption spectra of **1**.

0.76 and 0.90 v.u for **2,** which means the Re–P bonds are the strongest ones and Re–O Re–X(1) bonds are the weakest ones (X(1) notation as above).

3.2. Optimized geometry

The geometry of **1** was optimized in triplet and singlet states using the DFT method with the B3LYP functional. The energy of the singlet state is 14.5 kcal/mol higher. The optimized geometric parameters of the triplet state of **1** are gathered in Table 2. In general, the predicted bond lengths and angles are in good agreement with the values based upon the X-ray crystal structural data, and the general trends observed in the experimental data are well reproduced in the calculations.

3.3. Charge distribution

Table 3 presents the atomic charges from the Natural Population Analysis (NPA) for **1**. The calculated charge on the rhenium atom is considerable lower than the formal charge +3. It results from charge donation from the chloride ions and triphenylphosphine ligand. There is large positive charge on the P atom, and the charges on the chloride ions are significantly smaller than –1. Some differences in the values of the charges can be noticed for the halogen

Table 5
The energy and molar absorption coefficients of absorption bands and the electronic transitions calculated with the TDDFT method for **1**

The most important orbital excitations	Character	λ (nm)	E (eV)	f	Experimental λ (nm) (E (eV))ε
H(β) → L + 1(β) H(β) → L + 2(β)	d → d/π*(py)	834.5	1.49	0.0203	819.8(1.51)180
H(β) → L + 4(β)	d → π*($OPPh_2py$)	584.6	2.12	0.0065	591.4(2.10)3850
H − 1(α) → L(α)	d → π*($OPPh_2py$)	523.9	2.37	0.0123	
H(α) → L(α)	d → π*($OPPh_2py$)	510.8	2.43	0.0652	
H − 1(α) → L(α)	d → π*($OPPh_2py$)				
H − 2(α) → L(α)	d → π*($OPPh_2py$)	485.3	2.55	0.0015	432.4(2.87)3580
H(β) → L + 5(β)	d → π*($OPPh_2py$)	475.9	2.61	0.0052	
H(β) → L + 5(β)	d → π*($OPPh_2py$)	458.2	2.71	0.0019	
H(α) → L + 1(α)	d → π*($OPPh_2py$)	453.4	2.73	0.0029	
H(β) → L + 8(β)	d → π*(PPh_3)				
H − 1(β) → L(β)	π(Cl)/*n*(P) → d/π*(py)	442.0	2.81	0.0016	
H(α) → L + 2(α)	d → π*($OPPh_2py$)	425.1	2.92	0.0169	
H(β) → L + 7(β)	d → π*(PPh_3)	417.4	2.97	0.0017	
H(β) → L + 3(β)	d → π*($OPPh_2py$)	415.4	2.98	0.0015	
H(α) → L + 5(α)	d → π*(PPh_3)	407.8	3.04	0.0075	
H − 1(β) → L + 1(β)	π(Cl)/*n*(P) → d/π*(py)	404.0	3.07	0.0103	
H − 2(β) → L(β)	π(Cl)/*n*(P) → d/π*(py)	402.2	3.08	0.0105	
H − 1(α) → L + 5(α)	d → π*(PPh_3)	380.5	3.26	0.0021	380.2(3.26)3250
H − 2(α) → L + 2(α)	d → π*($OPPh_2py$)	378.4	3.28	0.0054	
H − 5(β) → L(β)	π_{Ph}(PPh_3)/*n*(P)/π(Cl) → d/π*(py)	373.9	3.32	0.0024	
H − 3(β) → L(β)					
H − 4(β) → L(β)	π_{Ph}(PPh_3)/*n*(P)/π(Cl) → d/π*(py)	371.0	3.34	0.0075	
H(β) → L + 11(β)	d → π*(PPh_3)	365.6	3.39	0.0024	
H − 3(α) → L(α)	π(Cl)/*n*(P) → π*($OPPh_2py$)	353.4	3.51	0.0035	
H − 1(α) → L + 3(α)	d → π*($OPPh_2py$)	344.4	3.60	0.0028	
H(α) → L + 4(α)	d → π*($OPPh_2py$)	342.5	3.62	0.0083	
H(α) → L + 6(α)	d → π*(PPh_3)				
H − 3(β) → L + 1(β)	π(Cl)/*n*(P)/π_{Ph}(PPh_3) → d/π*(py)	341.7	3.63	0.0075	
H − 4(α) → L(α)	π_{Ph}(PPh_3)/*n*(P)/π(Cl) → π*($OPPh_2py$)	329.8	3.76	0.0032	
H − 2(α) → L + 3(α)	d → π*($OPPh_2py$)	327.7	3.78	0.0024	
H − 2(α) → L + 4(α)	d → π*($OPPh_2py$)	319.1	3.88	0.0029	
H − 1(α) → L + 8(α)	d → π*(PPh_3)	309.8	4.00	0.0029	261.4(4.74)21400
H − 3(β) → L + 1(β)	π(Cl)/π_{Ph}(PPh_3) → d/π*(py)				
H − 1(α) → L + 9(α)	d → π*(PPh_3)	309.4	4.01	0.0022	
H − 3(α) → L + 1(α)	π(Cl)/*n*(P) → π*($OPPh_2py$)	309.1	4.01	0.0028	
H − 3(α) → L + 1(α)	π(Cl)/*n*(P) → π*($OPPh_2py$)	308.6	4.02	0.0034	
H(α) → L + 9(α)	d → π*(PPh_3)	305.1	4.06	0.0037	
H − 7(β) → L(β)	π_{Ph}(PPh_3) → d/π*(py)	302.1	4.10	0.0021	
H − 3(α) → L + 2(α)	π(Cl)/*n*(P) → π*($OPPh_2py$)	298.7	4.15	0.0042	
H − 2(β) → L + 3(β)	π(Cl)/*n*(P) → π*($OPPh_2py$)	297.9	4.16	0.0022	
H − 7(β) → L(β)	π_{Ph}(PPh_3) → d/π*(py)	297.0	4.17	0.0021	
H − 4(α) → L + 1(α)	π_{Ph}(PPh_3)/*n*(P)/π(Cl) → π*($OPPh_2py$)	286.8	4.32	0.0027	
					231.2(5.36)70300

ligands – the least negative is the chloride ion in the *trans* position to the oxygen atom of the PPh_2py ligand, whereas the most negative is Cl(1) in the *trans* position to the PPh_3 molecule. It corresponds to differences in the Re–Cl bonds lengths.

3.4. Molecular orbitals

The energies and characters of selected MOs of **1** are presented in Table 4, and the selected contours of the HOMO and LUMO orbitals with α spin are depicted in Fig. 2. The rhenium atom possesses a $(d_{xy})^2(d_{xz})^1(d_{yz})^1$ configuration. The metal d_{xz}, d_{yz} and d_{xy} orbitals make the main contributions into HOMO − 2, HOMO − 1 and HOMO with α spin and HOMO, LUMO, LUMO + 1 and LUMO + 2 with β spin. In all these molecular orbitals the rhenium d_{xz}, d_{yz} and d_{xy} orbitals bear antibonding character towards the p_π orbitals of the chloride ligands. The HOMO − 2 and HOMO − 1 orbitals with α spin and LUMO and LUMO + 2 with β spin also have an admixture of π oxygen orbitals, and some contribution of the π-antibonding pyridine ring orbitals is visible in the LUMO, LUMO + 1 and LUMO + 2 with β spin. The LUMO with α spin is composed of π-antibonding of the pyridine and phenyl rings of the $OPPh_2py$ ligand.

3.5. Electronic spectrum from the TDDFT calculations

The experimental and calculated electronic spectra of the chloro complex are represented graphically in Fig. 3. Each calculated transition in Fig. 3b is represented by a gaussian function with the height equal to the oxidator strength and width equal to 0.04. The solution spectrum of **1** exhibits a very weak absorption band at 819.8 nm and some more absorptions in the low energy range at 591.4, 432.4, 380.2, 261.4 and 231.2 nm. The shape of the UV–Vis spectrum of **2** is the same as for the chloro analogue; the absorption bands of the bromo complex were recorded at 820.0, 589.4, 431.0, 341.0, 260.0 and 231.2 nm.

Table 5 shows the energy and molar absorption coefficients of the experimental absorption bands of **1** and the spin-allowed triplet–triplet electronic transitions calculated with the TDDFT method. The assignment of the calculated transitions to the experimental absorption bands was based on the criterion of the energy and oscillator strength of the calculated transitions.

The investigated complex is of a large size; the number of basis functions is equal to 743. A hundred electron transitions calculated by the TDDFT method do not comprise all the experimental absorption bands. The UV–Vis spectrum of **1** was calculated to ~285 nm, so the shortest wavelength experimental band is not assigned to the calculated transitions, and the assignment to the band at 261.4 nm is probably not complete. As the solution spectra of PPh_3 and PPh_2py exhibit intense absorption bands in 280–200 nm region, some additional intraligand and interligand transitions are expected to be found at higher energies in the calculations for **1**.

The longest wavelength weak experimental band at 819.8 nm is assigned to the transitions from HOMO(β) to LUMO + 1(β) and LUMO + 2(β) orbitals. As the LUMO + 1 and LUMO + 2 orbitals have a substantial admixture of π^* orbitals of the pyridine ring, these transitions are classified as $d \rightarrow d/\pi^*(py)$. It explains the relatively high value of the oscillator strength of the calculated excitation at 834.5 nm.

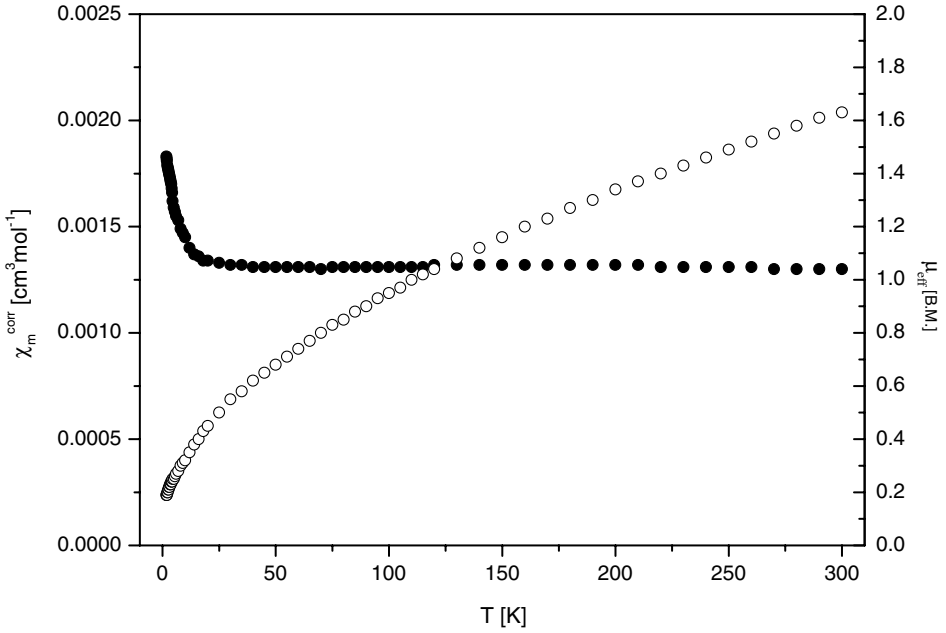

Fig. 4. Plots of the experimental magnetic data χ_M(●) and μ_{eff} (○) vs. *T* for the complex $[ReCl_3(PPh_3)(OPPh_2py\text{-}O,N)]$ (**1**).

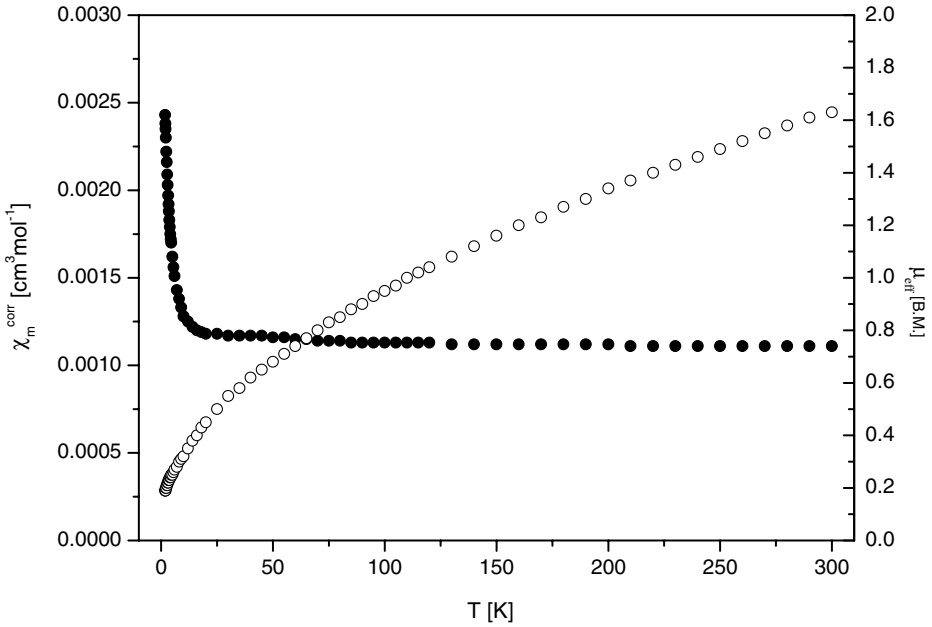

Fig. 5. Plots of the experimental magnetic data χ_M(●) and μ_{eff}(○) vs. T for the complex [$ReBr_3(PPh_3)(OPPh_2py$-O,N)] (**2**).

The experimental absorption band at 591.4 nm is attributed to the transitions calculated between 590 and 510 nm. These are excitations from central metal d orbitals to the π^* orbitals of the chelate ligand.

The absorption bands at 432.4 and 380.2 nm are ascribed to the metal–ligand charge transfer transitions ($d \rightarrow \pi^*_{OPPh_2py}$ and $d \rightarrow \pi^*_{PPh_3}$) and transitions of $\pi(Cl)/n(P)/\pi_{Ph}(PPh_3) \rightarrow d/\pi^*(py)$ character. The last ones occur mainly from chloride and phosphine ligand orbitals to the d rhenium orbitals. However, due to significant participation of π^* pyridine orbitals in the unoccupied molecular orbitals, the character of these excitations is formally ascribed as $\pi(Cl)/n(P)/\pi_{Ph}(PPh_3) \rightarrow d/\pi^*(py)$.

The experimental absorption band at 261.4 nm is mainly attributed to the transitions of LLCT type, although some MLCT and LMCT excitations are also calculated below 310 nm.

3.6. Magnetic properties

The magnetic properties of the [$ReCl_3(PPh_3)(OPPh_2py$-O,N)] (**1**) and [$ReBr_3(PPh_3)(OPPh_2py$-O,N)] (**2**) complexes under the form χ_M vs. T and μ_{eff} vs. T (χ_M being the molar magnetic susceptibility and μ_{eff} the effective magnetic moment) are shown in Figs. 4 and 5, respectively. The chloro and bromo Re(III) complexes show room temperature magnetic moments of 1.77 BM (0.389 cm^3 mol^{-1} K) and 1.63 BM (0.333 cm^3 mol^{-1} K), respectively. The magnetic moments of the solids are temperature independent between 300 and 50 K. These values are characteristic of mononuclear d^4 low-spin octahedral Re(III) complexes ($^3T_{1g}$ ground state) [42–50] and arise because of the large spin–orbit coupling ($\zeta = 2500$ cm^{-1} [51]), which gives a diamagnetic ground state.

4. Conclusions

Two novel Re(III) compounds – [$ReCl_3(PPh_3)(OPPh_2$-py-O,N)]$\cdot CH_3CN$ (**1**) and [$ReBr_3(PPh_3)(OPPh_2py$-O,N)] (**2**) – have been prepared and structurally as well as spectroscopically characterized. The well-known capacity of phosphines to interact with the Re≡O bond in the rhenium(V) oxo-complexes explains the formation of the title complexes in the reactions of [$ReOX_3(PPh_3)_2$] with PPh_2py. The DFT studies confirm the $(d_{xy})^2(d_{xz})^1(d_{yz})^1$ configuration of the central metal, and these results are in good agreement with the magnetic measurements.

5. Supplementary data

Supplementary data for $C_{37}H_{32}Cl_3N_2OP_2Re$ and $C_{35}H_{29}Br_3NP_2Re$ are available from the CCDC, 12 Union Road, Cambridge CB2 1EZ, UK on request, quoting the deposition numbers: 297775 for **1** and 297776 for **2**.

Acknowledgements

The Gaussian03 calculations were carried out in the Wrocław Centre for Networking and Supercomputing, WCSS, Wrocław, Poland.

The crystallographic part was financed by funds allocated by the Ministry of Education and Science to the Institute of General and Ecological Chemistry, Technical University of Łódź.

References

[1] J.R. Dilworth, S.J. Parrott, Chem. Soc. Rev. 27 (1998) 43.
[2] S.S. Jurisson, J.D. Lydon, Chem. Rev. 99 (1999) 2205.
[3] S. Liu, D.S. Edwards, Chem. Rev. 99 (1999) 2235.

[4] J.M. de Klerk, B.A. Zonnenberg, H.G. Krouwer, G.H. Blijham, A. van Dijk, A.D. van het Schip, J. van Die, P.P. van Rijk, J. Nucl. Med. 37 (1996) 465.
[5] E.S. Mull, V.J. Sattigeri, A.L. Rodriguez, J.A. Katzenellenbogen, Bioorg. Med. Chem. 10 (2002) 1381.
[6] H.R. Maxon, L.E. Schroder, L.C. Washburn, S.R. Thomas, R.C. Samaratunga, D. Biniakiewicz, J.S. Moulton, D. Cummings, G.J. Ehrhardt, V. Morris, J. Nucl. Med. 39 (1998) 659.
[7] B. Machura, J.O. Dzięgielewski, S. Michalik, R. Kruszynski, T.J. Bartczak, J. Kusz, Transit. Met. Chem. 28 (2003) 939.
[8] B. Machura, J.O. Dzięgielewski, R. Kruszynski, T.J. Bartczak, J. Kusz, Inorg. Chim. Acta 357 (2004) 1011.
[9] B. Machura, J.O. Dzięgielewski, R. Kruszynski, T.J. Bartczak, Polyhedron 22 (2003) 2869.
[10] M.C. Aragoni, M. Arca, T. Cassano, C. Denotti, F.A. Devillanova, F. Isaia, V. Lippolis, D. Natali, L. Niti, M. Sampietro, R. Tommasi, G. Verani, Inorg. Chem. Commun. 5 (2002) 869.
[11] P. Romaniello, F. Lelj, Chem. Phys. Lett. 372 (2003) 51.
[12] P. Norman, P. Cronstrand, J. Ericsson. Chem. Phys. 285 (2002) 207.
[13] J. Bossert, N.B. Amor, A. Strich, C. Daniel, Chem. Phys. Lett. 342 (2001) 617.
[14] C.E. Powell, M.P. Cifuentes, A.M. McDonagh, S.K. Hurst, N.T. Lucas, C.D. Delfs, R. Stranger, M.G. Humphrey, S. Houbrechts, I. Asselberghs, A. Persoons, D.C.R. Hockless, Inorg. Chim. Acta 352 (2003) 9.
[15] J.P. Morral, C.E. Powell, R. Stranger, M.P. Cifuentes, M.G. Humphrey, G.A. Heath, J. Organomet. Chem. 670 (2003) 248.
[16] P. Romaniello, F. Lelj, J. Mol. Struct. Theochem. 636 (2003) 23.
[17] G. Rouschias, G. Wilkinson, J. Chem. Soc. A (1966) 465.
[18] STOE & Cie, X-RED. Version 1.18. STOE & Cie GmbH, Darmstadt, Germany, 1999.
[19] G.M. Sheldrick, SHELXS-97, Program for the Solution of Crystal Structures, University of Göttingen, Germany, 1997.
[20] G.M. Sheldrick, SHELXL-97, Program for the Refinement of Crystal Structures, University of Göttingen, Germany, 1997.
[21] M.J. Frisch, G.W. Trucks, H.B. Schlegel, G.E. Scuseria, M.A. Robb, J.R. Cheeseman, J.A. Montgomery Jr., T. Vreven, K.N. Kudin, J.C. Burant, J.M. Millam, S.S. Iyengar, J. Tomasi, V. Barone, B. Mennucci, M. Cossi, G. Scalmani, N. Rega, G.A. Petersson, H. Nakatsuji, M. Hada, M. Ehara, K. Toyota, R. Fukuda, J. Hasegawa, M. Ishida, T. Nakajima, Y. Honda, O. Kitao, H. Nakai, M. Klene, X. Li, J.E. Knox, H.P. Hratchian, J.B. Cross, C. Adamo, J. Jaramillo, R. Gomperts, R.E. Stratmann, O. Yazyev, A.J. Austin, R. Cammi, C. Pomelli, J.W. Ochterski, P.Y. Ayala, K. Morokuma, G.A. Voth, P. Salvador, J.J. Dannenberg, V.G. Zakrzewski, S. Dapprich, A.D. Daniels, M.C. Strain, O. Farkas, D.K. Malick, A.D. Rabuck, K. Raghavachari, J.B. Foresman, J.V. Ortiz, Q. Cui, A.G. Baboul, S. Clifford, J. Cioslowski, B.B. Stefanov, G. Liu, A. Liashenko, P. Piskorz, I. Komaromi, R.L. Martin, D.J. Fox, T. Keith, M.A. Al-Laham, C.Y. Peng, A. Nanayakkara, M. Challacombe, P.M.W. Gill, B. Johnson, W. Chen, M.W. Wong, C. Gonzalez, J.A. Pople, Gaussian 03, Revision B.03, Gaussian, Inc., Pittsburgh, PA, 2003.
[22] A.D. Becke, J. Chem. Phys. 98 (1993) 5648.
[23] C. Lee, W. Yang, R.G. Parr, Phys. Rev. B 37 (1988) 785.
[24] M.E. Casida, in: J.M. Seminario (Ed.), Recent Developments and Applications in Modern Density Functional Theory, Theoretical and Computational Chemistry, vol. 4, Elsevier, Amsterdam, 1996.
[25] P.J. Hay, W.R. Wadt, J. Chem. Phys. 82 (1985) 299.
[26] E. König, Magnetic Properties of Coordination and Organometallic Transition Metal Compounds, Springer Verlag, Berlin, 1966.
[27] K. Nakamoto, Infrared and Raman Spectra of Inorganic and Coordination Compounds, fourth ed., Wiley-Interscience, New York, 1986.
[28] G.A. Jeffrey, W. Saenger, Hydrogen Bonding in Biological Structures, Springer Verlag, Berlin, 1994.
[29] G.R. Desiraju, T. Steiner, The Weak Hydrogen Bond in Structural Chemistry and Biology, Oxford University Press, Oxford, 1999.
[30] S. Bhattacharyya, S. Banerjee, B.K. Dirghangi, M. Menon, A. Chakravorty, J. Chem. Soc., Dalton Trans. (1999) 155.
[31] I. Chakraborty, S. Bhattacharyya, S. Banerjee, B.K. Dirghangi, A. Chakravorty, J. Chem. Soc., Dalton Trans. (1999) 3747.
[32] C. Pearson, A.L. Beauchamp, Can. J. Chem. 75 (1999) 220.
[33] S. Bhattacharyya, I. Chakraborty, B.K. Dirghangi, A. Chakravorty, Inorg. Chem. 40 (2001) 286.
[34] Y. Miyashita, N. Mahboob, S. Tsuboi, Y. Yamada, K. Fujisawa, K. Okamoto, Acta Crystallogr. C 57 (2001) 558.
[35] F. Tisato, F. Refosco, C. Bolzati, A. Cagnolini, S. Gatto, G. Bandoli, J. Chem. Soc., Dalton Trans. (1997) 1421.
[36] C. Pearson, A.L. Beauchamp, Inorg. Chem. 37 (1998) 1242.
[37] A. Vogler, H. Kunkely, Coord. Chem. Rev. 230 (2002) 243.
[38] I.D. Brown, Acta Crystallogr. B 48 (1992) 553.
[39] I.D. Brown, Acta Crystallogr. B 53 (1997) 381.
[40] M. O'Keeffe, N.E. Brese, J. Am. Chem. Soc. 113 (1991) 3226.
[41] N.E. Brese, M. O'Keeffe, Acta Crystallogr. B 47 (1991) 192.
[42] J.E. Fergusson, Coord. Chem. Rev. 1 (1966) 459.
[43] B.N. Figgis, J. Lewis, Prog. Inorg. Chem. 6 (1964) 37.
[44] B.N. Figgis, Introduction to Ligand field, Wiley Interscience, New York, 1966, p. 248.
[45] J. Chatt, G.J. Leigh, D.M.P. Mingos, E.W. Randall, D. Shaw, J. Chem. Soc., Chem. Commun. (1968) 419.
[46] H.P. Gunz, G.J. Leigh, J. Chem. Soc. (1971) 2229.
[47] B. Coutinho, J.R. Dilworth, P. Jobanputra, R.M. Thompson, S. Schmidt, J. Strähle, C.M. Archer, J. Chem. Soc., Dalton Trans. (1995) 1663.
[48] M. Hirsch-Kuchma, T. Nicholson, A. Davison, W.M. Davis, A.G. Jones, Inorg. Chem. 36 (1997) 3237.
[49] C.A. McConnachie, E.I. Stiefel, Inorg. Chem. 36 (1997) 6144.
[50] C. Pearson, A.L. Beauchamp, Can. J. Chem. 75 (1997) 220.
[51] A. Earnshaw, B.N. Figgis, J. Lewis, R.D. Peacok, J. Chem. Soc. (1961) 3132.

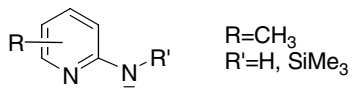

Scheme 1.

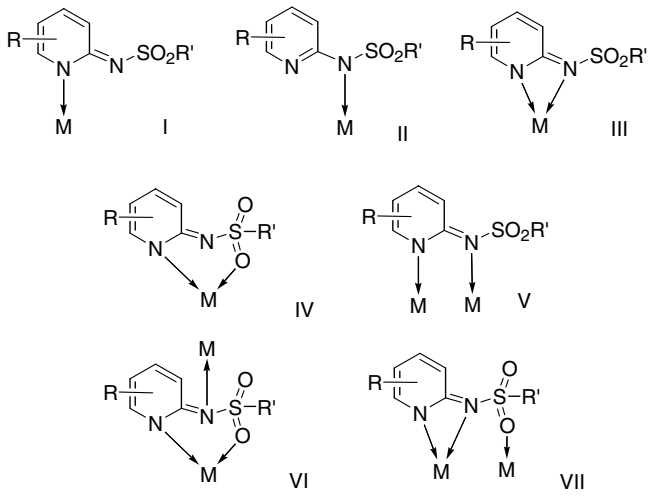

Scheme 2.

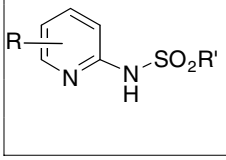

Code	R'	R
HTs3mepy	4-MeC_6H_4	3-Me
HMs3mepy	2,4,6-$Me_3C_6H_2$	3-Me
HTs6mepy	4-MeC_6H_4	6-Me
HMs6mepy	2,4,6-$Me_3C_6H_2$	6-Me

Scheme 3.

coligand, 2,2′-bipyridine or 1,10-phenanthroline. The presence in the electrolytic cell of the two species allows the synthesis of mixed compounds in one step.

2. Experimental

Acetonitrile, dichloromethane, 2-amino-3-picoline, 2-amino-6-picoline, *p*-toluenesulfonyl chloride, 2-mesitylenesulfonyl chloride, 2,2′-bipyridine, 1,10-phenanthroline monohydrate and all other reagents were commercial products and were used as supplied. Cobalt (Aldrich) was used as 2×2 cm plates.

2.1. Preparation of ligands

Ligands were prepared by reaction of the corresponding amine and the sulfonyl chloride in 1:1 ratio following a previously described method [14]. Analytical and spectroscopic data for the ligands are given below.

2.1.1. HMs6mepy

Anal. Calc. for $C_{15}N_2H_{18}O_2S$: C, 62.1; H, 6.2; N, 9.6; S, 11.0. Found: C, 62.3; H, 6.4; N, 9.5; S, 10.9%. ^{1}H NMR ($CDCl_3$, ppm) 2.24(s), 3H, CH_3(*p*-tolyl); 2.37(s), 3H, CH_3(py); 2.69(s) 6H, CH_3(*o*-tolyl); 6.55(d), 1H, py; 6.74(d), 1H, py; 6.88(s), 2H, tolyl; 7.37(d), 1H, py; 9.40(b), 1H, NH. IR (KBr, cm^{-1}): 3236(w), 2931(w), 1616(vs), 1533(m), 1362(vs), 1136(vs). EI MS: *m*/*z*: 291 (4%, M^+); 108 (13%, $M^+-\{O_2S$-mesityl$\}$).

2.1.2. HTs6mepy

Anal. Calc. for $C_{13}N_2H_{14}O_2S$: C, 59.5; H, 5.4; N, 10.7; S, 12.2. Found: C, 58.8; H, 5.6; N, 10.6; S, 12.3%. ^{1}H NMR ($CDCl_3$, ppm) 2.41(s), 3H, CH_3(py); 2.36(d), 3H, CH_3(tolyl); 6.60(d), 1H, py; 7.46(dd), 1H, py; 7.06(d), 1H, py; 7.22(d), 2H, tolyl; 7.79(d), 2H, tolyl; 9.95(b), 1H, NH. IR (KBr, cm^{-1}): 3231(w), 2958(w), 1612(vs), 1534(m), 1369(s), 1134(s). EI MS: *m*/*z*: 262 (6%, M^+); 108 (3%, $M^+-\{O_2S$-tolyl$\}$).

2.1.3. HTs3mepy

Anal. Calc. for $C_{13}N_2H_{14}O_2S$: C, 59.5; H, 5.4; N, 10.7; S, 12.2. Found: C, 58.7; H, 5.7; N, 10.2; S, 11.8%. ^{1}H NMR ($CDCl_3$, ppm) 2.15(s), 3H, CH_3(py); 2.35(d), 3H, CH_3(tolyl); 6.50(d), 1H, py; 7.40(d), 1H, py; 7.49(d), 1H, py; 7.85(d), 2H, tolyl; 7.21(d), 2H, tolyl; 12.14(b), 1H, NH. IR (KBr, cm^{-1}): 3248(m), 2951(w), 1594(s), 1544(s), 1342(s), 1126(s). EI MS: *m*/*z*: 262 (8%, M^+); 108 (20%, $M^+-\{O_2S$-tolyl$\}$).

2.1.4. HMs3mepy

Anal. Calc. for $C_{15}N_2H_{18}O_2S$: C, 62.1; H, 6.2; N, 9.6; S, 11.0. Found: C, 61.3; H, 6.0; N, 9.3; S, 11.2%. ^{1}H NMR ($CDCl_3$, ppm) 2.15(s), 3H, CH_3(py); 2.25(s), 3H,

Table 1
Experimental conditions for the electrochemical synthesis

Compound expected	Proligand HL	Coligand L′	Amount of HL (g)	Amount of L′ (g)[a]	Initial Voltaje (V)[b]	Metal dissolved (mg)	Electrochemical efficiency (mol F^{-1})
[Co(Ts3mepy)$_2$bipy]	HTs3mepy	bipy	0.150	0.045	8	14.4	0.44
[Co(Ts3mepy)$_2$phen]	HTs3mepy	phen	0.150	0.052	7	15.9	0.48
[Co(Ms3mepy)$_2$bipy]	HMs3mepy	bipy	0.165	0.045	10	15.3	0.46
[Co(Ms3mepy)$_2$phen]	HMs3mepy	phen	0.165	0.052	11	15.9	0.48
[Co(Ts6mepy)$_2$bipy]	HTs6mepy	bipy	0.150	0.045	8	15.9	0.48
[Co(Ts6mepy)$_2$phen]	HTs6mepy	phen	0.150	0.052	7	15.1	0.45
[Co(Ms6mepy)$_2$bipy]	HMs6mepy	bipy	0.165	0.045	8	18.4	0.56
[Co(Ms6mepy)$_2$phen]	HMs6mepy	phen	0.165	0.052	7	16.8	0.50

[a] Plus $[NMe_4]ClO_4$ (ca. 20 mg).
[b] Voltage to produce a current of 10 mA.

CH_3(*p*-tolyl); 2.71(s), 6H, CH_3(*o*-tolyl); 6.47(d), 1H, py; 6.89(s), 2H, tolyl; 7.36(d), 1H, py; 7.42(d), 1H, py; 12.33(b), 1H, NH. IR (KBr, cm^{-1}): 3222(m), 2940(w), 1595(s), 1544(s), 1338(s), 1098(s). EI MS: *m*/*z*: 291 (100%, M^+); 108 (10%, $M^+-\{O_2S$-mesityl$\}$).

2.2. Preparation of complexes: general procedure

The complexes were obtained by an electrochemical procedure [18]. A solution of a mixture of the sulfonamide and the coligand, with a small amount of tetraethylammonium perchlorate (ca. 10 mg) as a current carrier, was electrolyzed using a platinum wire as the cathode and a cobalt plate (suspended from another platinum wire) as the sacrificial anode. The cell was a 100 mL tall-form beaker fitted with a rubber bung through which the electrochemical leads entered. Direct current was obtained from a purpose-built d.c. power supply. Applied voltages of 5–15 V allowed sufficient current flow for smooth dissolution of the cobalt metal. The current was maintained at 10 mA during one hour. In all cases, hydrogen was evolved at the cathode. These cells can be summarized as $Co_{(+)}/CH_3CN + HL + L'/Pt_{(-)}$, where L and L′ represent the corresponding sulfonamide and coligand, respectively. On completion of the electrolysis the colored solutions were filtered to remove any possible metal particle and then left to concentrate. This procedure yielded crystalline products. The solids were washed with acetonitrile and diethyl ether and dried at room temperature. The solution compositions and experimental conditions are given in Table 1.

2.3. Physical measurements

The C, N, H and S contents of the compounds (Table 2) were determined on a Carlo-Erba EA 1108 microanalyser. IR spectra (Table 2) were recorded as KBr mulls on a Bruker Vector-22 spectrophotometer. The ^1H NMR spectra of the ligands were recorded on a Bruker ARX-400 MHz spectrometer using $CDCl_3$ as solvent. Solid state electronic spectra were recorded on a Shimadzu UV 3101 PC. EI mass spectra were recorded on a Micromass instrument (70 eV, 250 °C). LSI mass spectra were recorded on a VG Autospec-M Micromass instrument using 2-nitrobenzyl alcohol (2-NBA) as the matrix material.

2.4. Crystal structure determination

The data collections were taken on a SIEMENS Smart CCD area-detector diffractometer with graphite-monochromated Mo Kα radiation. Absorption corrections were carried out using SADABS [19]. All of the structures were solved by direct methods and refined by full-matrix least-squares based on F^2 [20]. All non-hydrogen atoms were refined with anisotropic displacement parameters. Hydrogen atoms were included in idealised positions and refined with isotropic displacement parameters. Atomic scattering

Table 2
Analytical, spectroscopic and magnetic data for the compounds

	Found (Calc.) (%)				IR data					
	C	N	H	S	$\nu(CH_3)$	$\nu(C{=}N)$	$\nu(C{=}C)$	$\nu_{as}(S{=}O)$	$\nu_s(S{=}O)$	ν(bipy/phen)
[Co(Ts3mepy)$_2$bipy] ($C_{36}H_{34}N_4O_4S_2Co$)	56.16 (58.60)	11.15 (11.40)	4.55 (4.65)	8.03 (8.67)	2918(m)	1597(s)	1413(s)	1324(s)	1081(vs)	769(s), 734(m)
[Co(Ts3mepy)$_2$phen]2CH_3CN ($C_{42}H_{40}N_8O_4S_2Co$)	59.81 (59.84)	12.53 (12.21)	4.16 (4.65)	7.73 (7.97)	2924(m)	1599(s)	1416(s)	1326(s)	1113(vs)	1517(m), 845(m), 728(m)
[Co(Ms3mepy)$_2$bipy] ($C_{40}H_{42}N_6O_4S_2Co$)	59.60 (60.51)	9.79 (10.59)	5.25 (5.34)	10.16 (8.06)	2924(m)	1608(s)	1447(s)	1315(m)	1172(m)	769(s), 736(m)
[Co(Ms3mepy)$_2$phen]CH_3CN ($C_{44}H_{45}N_7O_4S_2Co$)	59.04 (61.53)	10.43 (11.41)	5.10 (5.28)	7.13 (7.47)	2919(m)	1597(s)	1414(s)	1341(s)	1178(m)	1519(m), 844(m), 727(m)
[Co(Ts6mepy)$_2$bipy] ($C_{36}H_{34}N_6O_4S_2Co$)	57.70 (58.60)	11.49 (11.40)	4.73 (4.65)	8.69 (8.67)	2921(w)	1592(s)	1457(s)	1322(s)	1119(s)	766(s), 736(m)
[Co(Ts6mepy)$_2$phen]CH_3CN ($C_{40}H_{37}N_7O_4S_2Co$)	60.03 (59.84)	12.65 (12.21)	4.48 (4.65)	8.26 (7.97)	2922(w)	1590(s)	1456(s)	1321(s)	1139(s)	1517(m), 853(m), 727(m)
[Co(Ms6mepy)$_2$bipy] ($C_{40}H_{42}N_6O_4S_2Co$)	61.38 (60.51)	10.74 (10.59)	5.66 (5.34)	8.38 (8.06)	2931(w)	1591(s)	1455(s)	1319(s)	1130(vs)	766(s), 734(w)
[Co(Ms6mepy)$_2$phen] ($C_{42}H_{42}N_6O_4S_2Co$)	61.20 (61.68)	10.56 (10.28)	5.33 (5.18)	7.57 (7.84)	2934(w)	1590(s)	1455(s)	1232(s)	1130(s)	1516(m), 846(m), 726(m)

Table 3
Summary of crystal data and structure refinement

Compound	[Co(Ts3mepy)bipy]	[Co(Ts3mepy)phen]	[Co(Ms3mepy)phen]	[Co(Ts6mepy)$_2$bipy]	[Co(Ts6mepy)$_2$phen]	[Co(Ms6mepy)$_2$phen]
Empirical formula	$C_{36}H_{34}CoN_6O_4S_2$	$C_{42}H_{40}CoN_8O_4S_2$	$C_{44}H_{45}CoN_7O_4S_2$	$C_{36}H_{34}CoN_6O_4S_2$	$C_{40}H_{37}CoN_7O_4S_2$	$C_{42}H_{42}CoN_6O_4S_2$
Formula weight	737.74	843.86	858.92	737.74	802.82	817.87
Temperature (K)	293(2)	293(2)	293(2)	173(2)	173(2)	293(2)
Wavelength (Å)	0.71073	0.71073	0.71073	0.71073	0.71073	0.71073
Crystal system	orthorhombic	orthorhombic	monoclinic	orthorhombic	triclinic	monoclinic
Space group	$Pna2_1$	$Pcca$	$P2_1$	$Pbc2_1$	$P\bar{1}$	$P2_1/c$
Unit cell dimensions						
a (Å)	11.3095(18)	16.0317(9)	14.8657(11)	22.9894(16)	10.1462(15)	17.4668(11)
b (Å)	18.324(3)	14.2467(8)	8.6577(6)	14.3933(10)	13.535(2)	11.6772(7)
c (Å)	17.178(3)	18.3541(10)	17.2097(13)	10.4728(7)	15.889(2)	19.7359(12)
α (°)				90	110.013(3)	90
β (°)	90	90	109.628(2)	90	90.021(3)	103.4120(10)
γ (°)				90	101.344(3)	90
Volume (Å^3)	3559.9(10)	4192.1(4)	2086.2(3)	3465.4(4)	2004.8(5)	3915.6(4)
Z	4	4	2	4	2	4
D_{calc} (Mg/m^3)	1.377	1.337	1.367	1.414	1.330	1.387
Absorption coefficient (mm^{-1})	0.647	0.560	0.563	0.664	0.581	0.596
$F(000)$	1532	1756	898	1532	834	1708
Crystal size (mm^3)	$0.25 \times 0.18 \times 0.08$	$0.42 \times 0.36 \times 0.32$	$0.35 \times 0.21 \times 0.14$	$0.32 \times 0.18 \times 0.09$	$0.34 \times 0.13 \times 0.05$	$0.50 \times 0.45 \times 0.45$
θ Range for data collection (°)	1.62–28.18	2.21–28.04	1.45–28.05	1.67–28.04	1.37–28.07	2.04–27.99
Index ranges	$-14 \leqslant h \leqslant 14$, $-16 \leqslant k \leqslant 24$, $-22 \leqslant l \leqslant 22$	$-20 \leqslant h \leqslant 19$, $-18 \leqslant k \leqslant 13$, $-24 \leqslant l \leqslant 24$	$-19 \leqslant h \leqslant 19$, $-11 \leqslant k \leqslant 10$, $-22 \leqslant l \leqslant 19$	$-29 \leqslant h \leqslant 30$, $-17 \leqslant k \leqslant 19$, $-13 \leqslant l \leqslant 12$	$-13 \leqslant h \leqslant 13$, $-17 \leqslant k \leqslant 11$, $-17 \leqslant l \leqslant 20$	$-22 \leqslant h \leqslant 15$, $-15 \leqslant k \leqslant 14$, $-25 \leqslant l \leqslant 24$
Reflections collected	18 774	22 657	12 882	19 945	10 985	21 441
Independent reflections (R_{int})	7482 (0.1211)	4940 (0.0341)	7955 (0.0481)	7548 (0.0856)	7722 (0.0756)	8699 (0.0462)
Completeness to θ (%)	96.8	97.0	94.9	98.3	79.3	92.0
Maximum and minimum transmission	0.950 and 0.682	0.836 and 0.617	0.924 and 0.751	0.942 and 0.707	0.971 and 0.797	0.765 and 0.488
Data/restraints/parameters	7482/1/446	4940/0/260	7955/1/523	7548/1/446	7722/0/492	8699/0/504
Goodness-of-fit on F^2	0.723	1.065	0.799	0.787	0.87 4	0.850
Final R indices [$I > 2\sigma(I)$]	$R_1 = 0.0526$, $wR_2 = 0.0704$	$R_1 = 0.0461$, $wR_2 = 0.1195$	$R_1 = 0.0459$, $wR_2 = 0.0753$	$R_1 = 0.0526$, $wR_2 = 0.0620$	$R_1 = 0.0766$, $wR_2 = 0.1907$	$R_1 = 0.0455$, $wR_2 = 0.0952$
R indices (all data)	$R_1 = 0.1912$, $wR_2 = 0.0914$	$R_1 = 0.0836$, $wR_2 = 0.1287$	$R_1 = 0.0968$, $wR_2 = 0.0854$	$R_1 = 0.1306$, $wR_2 = 0.0747$	$R_1 = 0.2139$, $wR_2 = 0.2349$	$R_1 = 0.1016$, $wR_2 = 0.1075$
Absolute structure parameter			0.024(15)	0.096(16)		
Largest difference in peak and hole (e Å^{-3})	0.292 and −0.482	0.402 and −0.280	0.473 and −0.264	0.904 and −0.437	1.569 and −0.398	0.399 and −0.375

factors and anomalous dispersion corrections for all atoms were taken from International Tables for X-ray Crystallography [21]. Details of crystal data and structural refinement are given in Table 3.

3. Results and discussion

The analytical results (Table 2) show that the electrochemical procedure described above is an effective method for the synthesis of cobalt complexes with these sulfonamide ligands and the method represents a simple alternative to other standard chemical procedures. The compounds are of the general formula $[CoL_2L']$. The electrochemical efficiency value (Table 1) is defined as the amount of metal dissolved per Faraday of charge and was close to 0.5 mol F^{-1} in all cases. This fact, along with the evolution of hydrogen gas at the cathode, is compatible with a reaction mechanism involving the anodic oxidation to cobalt(II) and the deprotonation of the ligand at the cathode.

Anode: $Co \rightarrow Co^{2+} + 2e^-$
Cathode: $2HL + 2e^- \rightarrow 2L^- + H_2$
Overall: $Co + 2HL + L' \rightarrow [CoL_2L'] + H_2$
where L′ is 2,2′-bipyridine or 1,10-phenanthroline.

The sulfonamide compounds were obtained by air concentration of the resulting acetonitrile solution. These compounds are air stable compounds that are soluble in common organic solvents.

3.1. Description of the structures

3.1.1. Crystal structure of [Co(Ts3mepy)$_2$bipy] and [Co(Ts3mepy)$_2$phen]

The molecular structures of [Co(Ts3mepy)$_2$bipy] and [Co(Ts3mepy)$_2$phen] are shown in Fig. 1 together with the atomic numbering scheme. Selected bond lengths and angles are given in Table 4.

[Co(Ts3mepy)$_2$phen] crystallized with two molecules of acetonitrile, which are not shown in the figure since they do not interact with the complex molecule to any significant degree.

Both complexes consist of discrete molecules with the six-coordinate cobalt atoms coordinated by a 2,2′-bipyridine or 1,10-phenanthroline, which act as N,N′-bidentate ligands, and two anionic sulfonamide ligands acting as

Table 4
Selected bond lengths (Å) and angles (°) for [Co(Ts3mepy)$_2$bipy] and [Co(Ts3mepy)$_2$phen]

[Co(Ts3mepy)$_2$bipy]		[Co(Ts3mepy)$_2$phen]	
Co–O(11)	2.040(5)	Co–O(11)	2.0751(16)
Co–O(21)	2.113(4)	Co–O(11^i)	2.0751(16)
Co–N(11)	2.189(5)	Co–N(11)	2.1483(19)
Co–N(21)	2.158(5)	Co–N(21)	2.171(2)
Co–N(31)	2.166(6)	Co–N(11^i)	2.1483(19)
Co–N(32)	2.136(6)	Co–N(21^i)	2.171(2)
O(11)–Co–O(21)	93.46(19)	O(11^i)–Co–O(11)	94.71(10)
O(11)–Co–N(32)	169.3(2)	O(11^i)–Co–N(21)	170.99(8)
O(21)–Co–N(32)	96.7(2)	O(11)–Co–N(21)	94.29(7)
O(11)–Co–N(21)	86.5(2)	O(11^i)–Co–N(11)	87.73(7)
O(11)–Co–N(31)	94.2(2)	O(11^i)–Co–N(21^i)	94.29(7)
O(21)–Co–N(31)	172.0(2)	O(11)–Co–N(21^i)	170.99(8)
O(21)–Co–N(21)	85.1(2)	O(11)–Co–N(11^i)	87.73(7)
O(11)–Co–N(11)	85.7(2)	O(11^i)–Co–N(11^i)	86.19(7)
N(32)–Co–N(21)	97.6(2)	N(12^i)–Co–N(21)	94.42(7)
N(32)–Co–N(11)	91.3(2)	N(11)–Co–N(21)	92.62(7)
N(21)–Co–N(11)	169.6(2)	N(11)–Co–N(11^i)	171.03(10)
O(21)–Co–N(11)	88.4(2)	O(11)–Co–N(11)	86.19(7)
N(21)–Co–N(31)	93.0(2)	N(11^i)–Co–N(21^i)	92.62(7)
N(31)–Co–N(11)	94.5(2)	N(12)–Co–N(21^i)	94.42(7)
N(32)–Co–N(31)	75.8(2)	N(21)–Co–N(21^i)	76.71(11)

Symmetry transformations used to generate equivalent atoms: i: $-x$, y, $1/2 - z$.

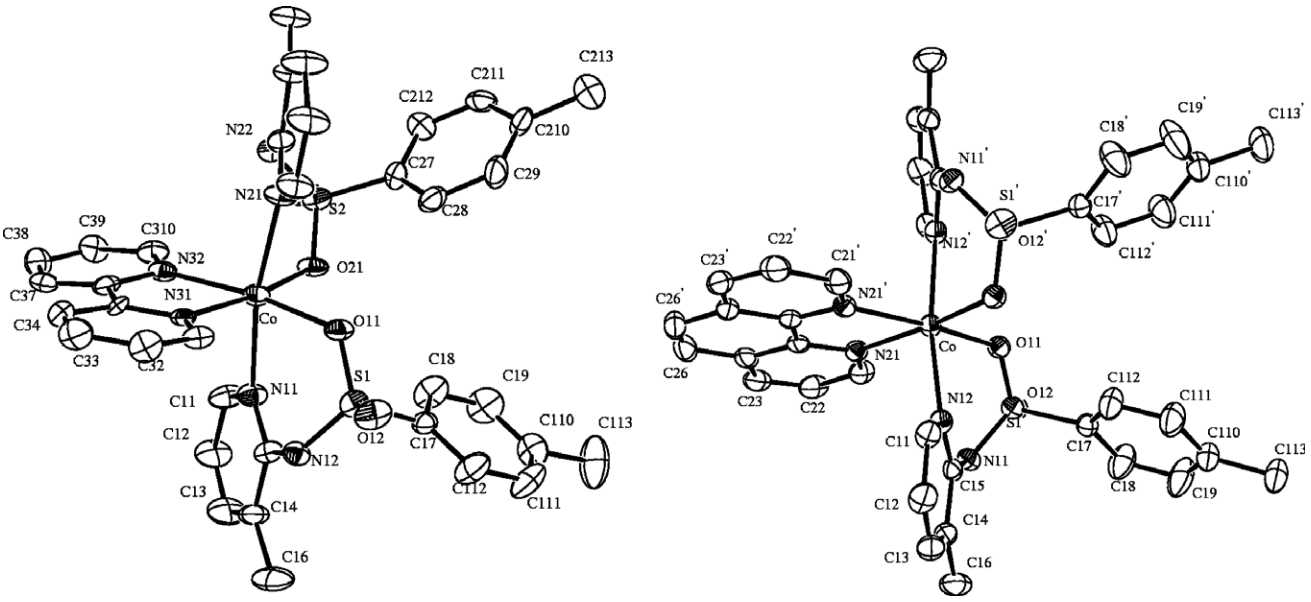

Fig. 1. The molecular structures of [Co(Ts3mepy)$_2$bipy] and [Co(Ts3mepy)$_2$phen].

N_{py},O-bidentate systems. The coordination polyhedron around the metal is best described as an octahedron, with the oxygen atoms in *cis* positions and the pyridine nitrogen atoms in *trans* positions. Such an arrangement implies a two-fold axis, which is crystallographic in [Co(Ts3mepy)$_2$-phen]. In the case of [Co(Ts3mepy)$_2$bipy] the arrangement is more distorted and, for example, the dihedral angle between the two pyridine rings in the bipyridine moiety is 9.7(4)°. In the case of [Co(Ts3mepy)$_2$phen], the phenanthroline moiety forms a dihedral angle of only 0.94(5)° with the equatorial plane, whereas in [Co(Ts3mepy)$_2$bipy] this angle is 7.6(2)°. For symmetry reasons, the best equatorial plane contains the cobalt atom in [Co(Ts3mepy)$_2$phen] and the defining atoms are only 0.005(1) Å out of this plane (RMS, 0.005). However, in [Co(Ts3mepy)$_2$bipy] the best plane (RMS, 0.0563) is at 0.008(3) Å from the cobalt(II) atom and the defining atoms are up to 0.061(2) Å out of the plane. The distortion of an octahedron can also be measured using the values of the dihedral angles α between bidentate coordination planes (related by a three-fold axis in a regular octahedron). The average values for the angle α are 84.9(2)° and 86.92(7)° in [Co(Ts3mepy)$_2$bipy] and [Co(Ts3mepy)$_2$phen], respectively, and these are not very far from 90° [22].

The pyridine ring plane and the benzene ring plane of the sulfonamide ligand form dihedral angles of 75.6(1)° for [Co(Ts3mepy)$_2$phen] and 51.4(3)° and 75.9(2)° for [Co(Ts3mepy)$_2$bipy]. These angles again highlight the differences found in the latter complex but are not significantly different from those found in the free ligand [10].

The Co–N bond distances, which range from 2.136(6) to 2.189(5) Å, and the Co–O distances, 2.040(5)–2.113(4) Å, also show the greater level of distortion in [Co(Ts3mepy)$_2$-bipy] than [Co(Ts3mepy)$_2$phen]. These values are, however, all in the range expected for hexacoordinated cobalt(II) complexes. The Co–N bond lengths are very similar to those found in the octahedrally coordinated complexes with four pyridine nitrogen donor atoms and two oxygen atoms in *cis* positions [23,24]. The average Co–O bond length is 2.076 Å for [Co(Ts3mepy)$_2$(bipy)], which is virtually the same as the symmetry imposed value of 2.075(2) Å for [Co(Ts3mepy)$_2$(phen)]. These values are very close to the Co–O bond length found for the cationic aquo complex $[Co(H_2O)_2(phen)_2]^{2+}$, 2.077(3) Å (average) [23], but are slightly shorter than that found in the neutral DMF complex [Co(Tspy)$_2$(DMF)$_2$], 2.1635(14) Å [11], or in the triflate complex [Co(triflate)$_2$(phen)$_2$], 2.215(4) Å [25].

3.1.2. Description of the structure of [Co(Ms3mepy)$_2$phen]

The molecular structure of [Co(Ms3mepy)$_2$phen] is shown in Fig. 2 together with the atomic numbering scheme. Selected bond lengths and angles are given in Table 5.

[Co(Ms3mepy)$_2$phen] crystallized with an acetonitrile solvent molecule, which is not shown in the figure since it does not interact significantly with the complex molecule.

The structure of [Co(Ms3mepy)$_2$phen] is similar to those described above, with the sulfonamide ligands acting as N_{py},O-bidentate donors and the neutral ligand as an N,N bidentate system. However, the dispositions of the ligands are different, as in this case the oxygen atoms are in an axial disposition and the pyridine nitrogen atoms of the sulfonamide ligands are in a *cis* disposition. This arrangement allows a π,π-stacking interaction between one of the mesitylene rings and the phenanthroline moiety, with a dihedral angle of 1.4(1)° and distances between rings of about 3.6 Å.

The pyridine ring plane and the benzene ring plane of this sulfonamide ligand form dihedral angles of 89.3(1)°

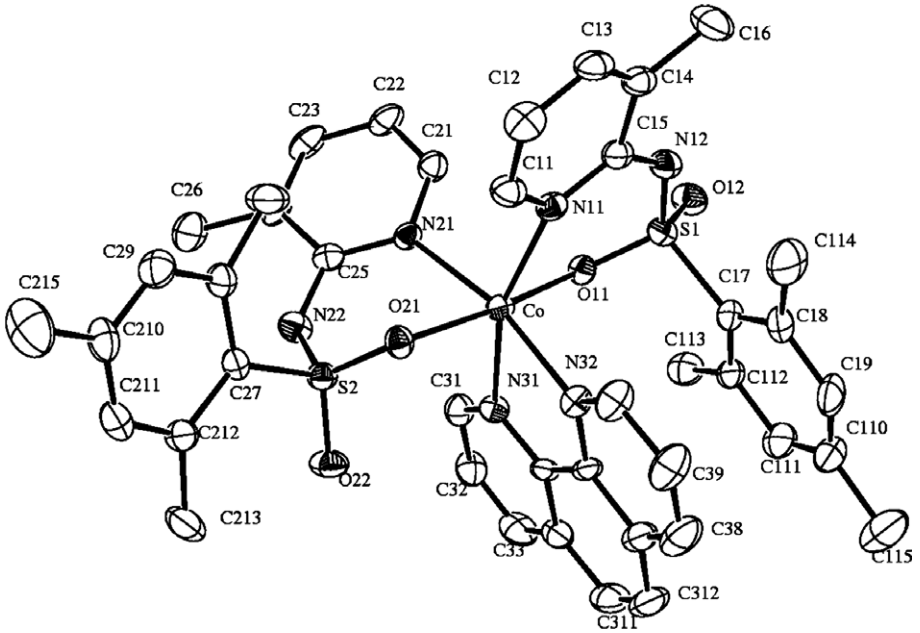

Fig. 2. The molecular structure of [Co(Ms3mepy)$_2$phen].

Table 5
Selected bond lengths (Å) and angles (°) for [Co(Ms3mepy)$_2$phen]

Co–O(11)	2.084(3)	Co–O(21)	2.114(3)
Co–N(21)	2.133(4)	Co–N(31)	2.149(3)
Co–N(32)	2.154(4)	Co–N(11)	2.157(4)
O(11)–Co–O(21)	172.46(12)	O(11)–Co–N(21)	89.62(13)
O(21)–Co–N(21)	83.13(13)	N(21)–Co–N(11)	96.27(13)
O(11)–Co–N(31)	80.33(12)	O(21)–Co–N(31)	98.49(12)
N(21)–Co–N(31)	97.30(14)	N(21)–Co–N(32)	167.87(14)
O(11)–Co–N(32)	99.82(13)	O(21)–Co–N(32)	87.10(12)
O(11)–Co–N(11)	85.98(13)	O(21)–Co–N(11)	96.83(13)
N(32)–Co–N(11)	92.01(14)	N(31)–Co–N(11)	160.60(14)
N(31)–Co–N(32)	77.00(14)		
Some staking interactions			
N(32)–C(17)	3.456(5)	C(19)–C(38)	3.579(8)
C(18)–C(310)	3.491(7)	C(110)–C(37)	3.562(7)
C(111)–C(37)	3.640(7)	C(112)–C(36)	3.574(6)

and these are larger than those found in the free ligand [14] or in the other ligand [74.8(1)° in the complex]. A π,π-stacking interaction has already been found in similar complexes of copper, zinc and cadmium, but only when the ligand contains a mesitylene ring. This is probably due to the electron-donating effect of the three methyl groups in the ring as well as the increase in the overall size of the group.

The average value for the angle α (vide supra) is 81.61(12)°, which deviates significantly from regularity towards a trigonal prism. In addition, the best equatorial plane defined by the four nitrogen donor atoms has an RMS deviation of 0.231, with the N32 atom up to 0.255(2) Å out of the plane. The cobalt atom is, however, only 0.047(2) Å out of this plane.

The Co–N bond distances, which are in the range 2.133(4)–2.157(4) Å, are very similar to those found in the previously described complexes. The Co–O distances, 2.084(3) and 2.114(3) Å, are slightly longer than those found in the previously described complexes, but are still shorter than those described in the literature [25].

3.1.3. Description of the structures of [Co(Ts6mepy)$_2$bipy], [Co(Ts6mepy)$_2$phen] and [Co(Ms6mepy)$_2$phen]

The molecular structures of these compounds are shown in Figs. 3–5, respectively, together with the atomic numbering schemes. Selected bond lengths and angles for the molecules are given in Tables 6 and 7. Once more, [Co(Ts6mepy)$_2$phen] crystallized with an acetonitrile solvent molecule, which is not shown in the figure since it does not interact with the complex molecule to any significant degree.

The coordination behavior of the anionic ligands in these complexes is quite different from the previous examples described in this paper. In these cases, the sulfonamide anionic ligands are N_{py},N_{amide}-bidentate ligands. A neutral 2,2′-bipyridine or 1,10-phenanthroline, both of which act as N,N-donors, completes the coordination sphere of the metal. Consequently, the coordination polyhedron around the cobalt(II) is best described as a highly distorted octahedron [CoN_6]. However, some differences can be found between the structures in terms of the disposition of the ligands around the metal. In all cases, the pyridine nitrogen atoms are in *cis* positions and in the same equatorial plane as the bipyridine moiety. The small chelate angles of the sulfonamide ligands are the main source of distortion, with angles ranging from 62.04(7)° to 62.9(3)°. The axial angles (theoretical value of 180°) range from 156.72(14)° to 165.62(14)°.

In [Co(Ts6mepy)$_2$bipy] the average value for the angle α (vide supra) is 85.5(1)° and this is close to the theoretical 90°. Another measurement of the distortion of the octahedron is

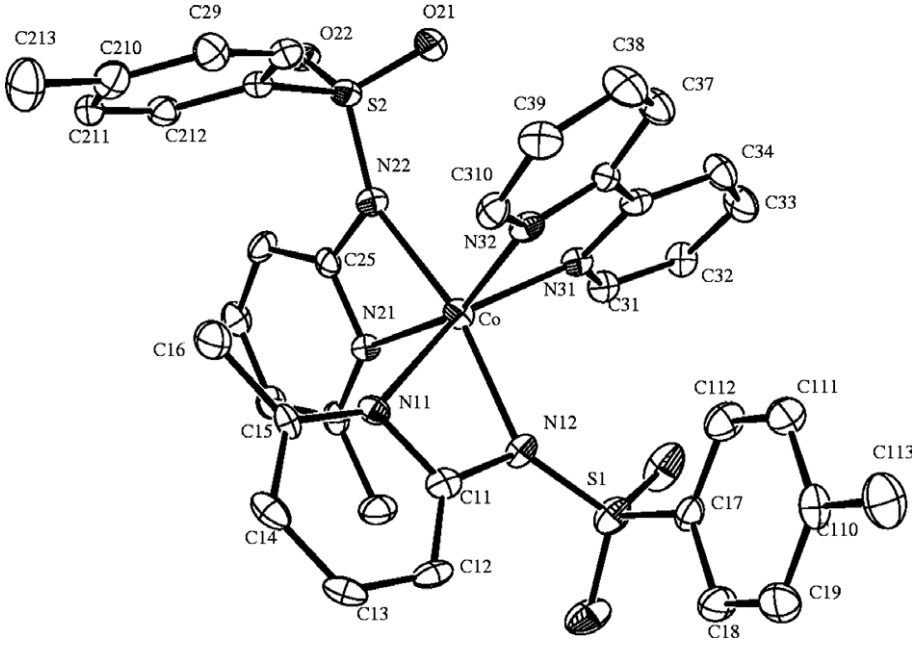

Fig. 3. Molecular structure of [Co(Ts6mepy)$_2$bipy].

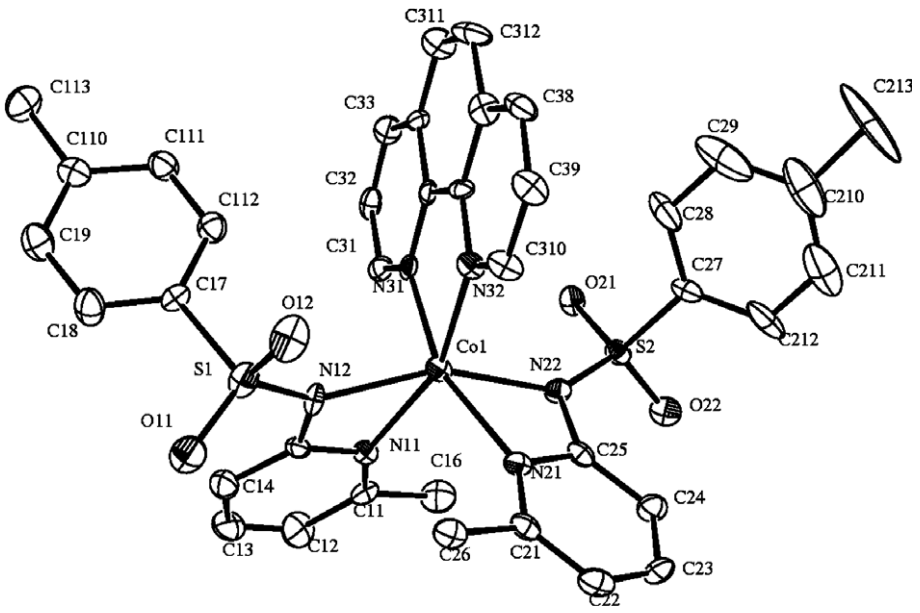

Fig. 4. Molecular structure of [Co(Ts6mepy)$_2$phen].

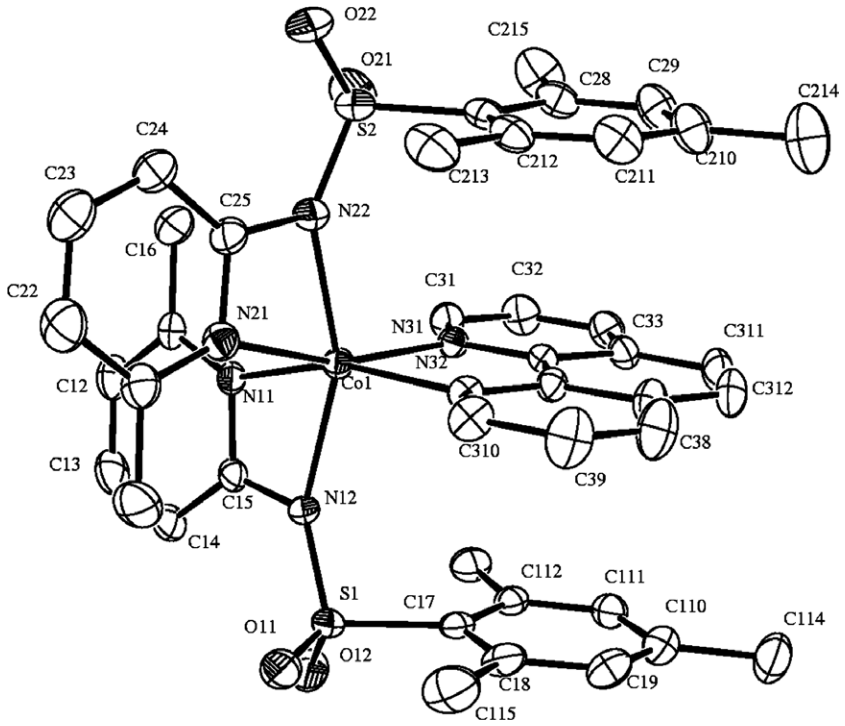

Fig. 5. Molecular structure of [Co(Ms6mepy)$_2$phen].

the angle ϕ, defined as the twist angle between the two triangles of nitrogen atoms perpendicular to a trigonal axis (Scheme 4). Unfortunately, in this compound these triangular planes are not parallel and they form dihedral angles of 20.2(2)°, 18.1(2)° and 15.5(2)°. If we consider the latter two triangles, we have N31, N21 and N12 and N32, N22 and N11 – i.e., one sulfonamide nitrogen atom, one pyridine nitrogen atom from a different ligand and a bipyridine nitrogen atom – and the values for the angle ϕ are −39.3(2)°, −39.5(2)° and −45.2(2)°.

The planarity of the equatorial plane can also be a criterion to assess the distortion of the octahedron. The best calculated plane formed by the pyridine nitrogen atoms and the nitrogen atoms of the bypiridine moiety shows an RMS deviation of 0.3898, and the atom N32 is up to 0.431(2) Å out of the plane. The cobalt(II) atom is 0.014(2) Å out of the plane.

In the case of [Co(Ts6mepy)$_2$phen], the arrangement of the ligands around the metal gives rise to an α angle with an average value of 82.4(3)°, which shows greater distortion

Table 6
Selected bond lengths (Å) and angles (°) for [Co(Ts6mepy)$_2$bipy] and [Co(Ts6mepy)$_2$phen]

	[Co(Ts6mepy)$_2$bipy]	[Co(Ts6mepy)$_2$phen]
Co–N(11)	2.216(4)	2.194(7)
Co–N(12)	2.131(4)	2.121(7)
Co–N(21)	2.122(3)	2.137(6)
Co–N(22)	2.163(4)	2.149(7)
Co–N(31)	2.088(4)	2.120(6)
Co–N(32)	2.117(3)	2.101(7)
N(31)–Co–N(32)	78.28(14)	78.3(3)
N(31)–Co–N(21)	103.98(13)	158.2(3)
N(32)–Co–N(21)	158.10(14)	101.6(3)
N(31)–Co–N(12)	96.41(13)	97.7(2)
N(32)–Co–N(12)	97.24(14)	97.4(2)
N(21)–Co–N(12)	104.06(14)	104.1(3)
N(31)–Co–N(22)	91.11(14)	96.4(2)
N(32)–Co–N(22)	96.28(13)	99.0(3)
N(21)–Co–N(22)	62.09(13)	62.9(3)
N(12)–Co–N(22)	165.62(14)	157.0(2)
N(31)–Co–N(11)	156.72(14)	92.2(2)
N(32)–Co–N(11)	94.90(13)	159.9(3)
N(21)–Co–N(11)	90.67(13)	97.7(2)
N(12)–Co–N(11)	62.06(14)	61.9(3)
N(22)–Co–N(11)	111.86(15)	99.6(3)

Table 7
Selected bond lengths (Å) and angles (°) for [Co(Ms6mepy)$_2$phen]

Co–N(11)	2.1514(18)	Co–N(22)	2.124(2)
Co–N(12)	2.1905(18)	Co–N(31)	2.117(2)
Co–N(21)	2.192(2)	Co–N(32)	2.1236(19)
N(31)–Co–N(32)	78.05(8)	N(31)–Co–N(11)	95.75(7)
N(31)–Co–N(22)	101.75(8)	N(32)–Co–N(11)	161.49(7)
N(32)–Co–N(22)	96.93(8)	N(22)–Co–N(11)	101.43(8)
N(31)–Co–N(12)	95.22(7)	N(22)–Co–N(12)	157.61(8)
N(32)–Co–N(12)	100.82(7)	N(11)–Co–N(12)	62.04(7)
N(31)–Co–N(21)	163.51(7)	N(22)–Co–N(21)	62.19(8)
N(32)–Co–N(21)	99.24(8)	N(11)–Co–N(21)	91.47(8)
N(12)–Co–N(21)	101.26(8)		
Some staking interactions			
C(19)–C(37)	3.576(4)	C(211)–C(36)	3.796(4)
C(211)–C(38)	3.699(5)	C(110)–C(37)	3.586(4)
C(28)–C(35)	3.609(3)	C(111)–C(34)	3.647(3)
C(211)–C(37)	3.673(4)	C(112)–C(35)	3.479(3)

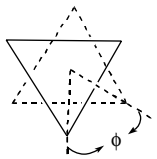

Scheme 4.

than the former complex, and values for the ϕ angle of −35.4(3)°, −38.2(3)° and −36.2(3)°. The increase in the distortion is probably due to packing reasons and also to a twist in the N22–S2 bond. However, when the planarity of the equatorial plane is considered, the RMS deviation is 0.3324 and the N31 atom is 0.372(4) Å out of the plane. The cobalt(II) atom is 0.045(4) Å out of the plane.

The coordination polyhedron around the cobalt(II) in [Co(Ms6mepy)$_2$phen] is, once again, best described as an octahedron, with dihedral α angles between bidentate coordination planes (related by three-fold axis in a regular octahedron) of 88.90(8)°, 84.49(6)° and 85.52(7)°, average 86.30(8)°, which is close to the theoretical 90° [22]. The angles ϕ, defined as above, have values of 38.94(8)°, 41.45(8)° and 39.07(9)°. The planarity of the equatorial plane is better than in the last two complexes, with an RMS deviation of 0.2981, and the N31 atom is 0.327(1) Å out of the plane. The cobalt(II) atom is only 0.004(1) Å out of the plane.

Once again, significant intermolecular "π–π stacking" stabilization is produced between the 1,10-phenanthroline unit and the benzene rings of both sulfonamide ligands. This interaction does not appear to occur in an intermolecular manner. The dihedral angles between the rings involved in these interactions are 0.74(12)° and 3.77(13)° and several short distances are shown in Table 7. It is worth noting the difference found between this compound and the complex [Cu(Ms6mepy)$_2$phen]; in the copper compound the distances in the axis N12–Cu–N22 are longer than those in the equatorial plane and the angle is nearer to 180° [average 171.2(2)°]. In the cobalt compound, the distances in the axis N12–Co–N22 are similar to those in the equatorial plane and the angle shows more distortion, 157.61(8)°.

Dihedral angles between the pyridine ring and the mesytilene ring for each ligand are 77.48(8)° and 81.69(8)°, values similar to those found in the free ligand.

The average Co–N$_{py}$ [2.169(7) Å], Co–N$_{amide}$ [2.146(7) Å] and Co–N$_{phen}$ or Co–N$_{bipy}$ [2.111(7) Å] bond lengths are similar in all of the complexes and are very close to those found in other octahedral cobalt(II) complexes with pyridine and amide nitrogen donor ligands; for example, 2.150 (9) Å is the average value for CoL_2 (HL = 1-[(4-methylphenyl)-sulfonamido]-2-[(2-pyridylmethyleneamino)benzene]) [26].

3.2. Spectroscopic studies

The IR spectra of these complexes (Table 2) do not contain the band observed in the ligand at 3248–3222 cm^{-1}, which is attributed to ν(N–H) stretching. This observation indicates that the ligand is in the anionic amidate form in the complex. The spectra also show bands in the aromatic region due to ν(C=N) (1615–1590 cm^{-1}) and ν(C=C) (1459–1413 cm^{-1}). These bands appear in similar positions to those for the free ligand in the complexes with Ts3Mepy$^-$ and Ms3Mepy$^-$ but are shifted to lower frequencies in the Ts6Mepy$^-$ and Ms6mepy$^-$ complexes as result of coordination through the sulfonamide nitrogen atom. The spectra also show bands in the region 1342–1319 cm^{-1}, which are attributed to ν_{as}(S=O), and bands in the range 1178–1081 cm^{-1}, which are attributed to the ν_{sym}(S=O) vibrations. A band is also observed at 2938–2918 cm^{-1} and this corresponds to ν(CH$_3$). In addition, the IR spectra show absorptions typical of coordinated

2,2′-bipyridine (769–766 and 736–734 cm^{-1}) [27] and 1,10-phenanthroline (1519–1517, 853–844 and 728–726 cm^{-1}) [27,28].

The solid state electronic spectra between 20 000 and 5000 cm^{-1} of all the heteroleptic complexes $[Co(Me3mepy)_2L']$ contain three bands in the regions 8700–9500 and 18 900-21 000 cm^{-1}, assigned to $^4T_{1g}(F) \rightarrow {}^4T_{2g}(\nu_1)$ and $^3T_{1g}(F) \rightarrow {}^4T_{2g}(\nu_3)$ transitions, respectively, in a distorted octahedral field. A band assignable to $^4T_{1g}(F) \rightarrow {}^4A_{2g}(\nu_2)$ [except for the $[Co(Me3mepy)_2bipy]$ (14 500 cm^{-1})] was not observed, probably because such a band must be very weak and obscured by the ν_3 transition [29].

Acknowledgements

This work was supported by the Xunta de Galicia (Spain) (Grant PGIDT00PXI20305PR) and by the Ministerio de Ciencia y Tecnología (Spain) (Grant BQU2002-01819) and the Universidade de Vigo, under the Grant C221 122F 64102. We thank fergus.uvigo.es (http://fergus.uvigo.es/) for X-ray solution and refinement facilities.

Appendix A. Supplementary material

The atomic positions, full list of bond lengths and angles and other crystallographic data are available on request to J.C. Crystallographic data have been deposited in the Cambridge Crystallographic Data Centre, and can be obtained free of charge at www.ccdc.cam.ac.uk/conts/retrieving.html [or from the Cambridge Crystallographic Data Centre, 12 Union Road, Cambridge CB2 1EZ, UK; Fax: (intrnat.) +44 1223 336 033; e-mail: deposit@ccdc.cam.ac.uk] quoting the deposition numbers CCDC 295055–295060. Supplementary data associated with this article can be found, in the online version, at doi:10.1016/j.poly.2006.03.004.

References

[1] R. Kempe, Eur. J. Inorg. Chem. (2003) 191, and references therein.
[2] M. Polamo, M. Leskel, J. Chem. Soc., Dalton Trans. (1996) 4345.
[3] R. Clerac, F.A. Cotton, K.R. Dunbar, C.A. Murillo, I. Pascual, X. Wang, Inorg. Chem. 38 (1999) 2655.
[4] L.M. Engelhardt, M.G. Gardiner, C. Jones, P.C. Junk, C.L. Raston, A.H. White, J. Chem. Soc., Dalton Trans. (1996) 3053.
[5] C.L. Raston, B.W. Skelton, V.A. Tolhurst, A.H. White, Polyhedron 17 (1998) 935.
[6] A. Spannenberg, P. Arndt, R. Kempe, Angew. Chem., Int. Ed. 37 (1998) 832.
[7] A. Spannenberg, H. Fuhrmann, P. Arndt, W. Baumann, R. Kempe, Angew. Chem., Int. Ed. 37 (1998) 3363, and references therein.
[8] C.A. Otter, S.M. Couchman, J.C. Jeffery, K.L.V. Mann, E. Psillakis, M.D. Ward, Inorg. Chim. Acta 278 (1998) 178.
[9] S. Cabaleiro, J. Castro, J.A. García-Vázquez, J. Romero, A. Sousa, Acta Crystallogr., Sect. C 56 (2000) 293.
[10] I. Beloso, J. Castro, J.A. García-Vázquez, P. Pérez-Lourido, J. Romero, A. Sousa, Polyhedron 22 (2003) 1099.
[11] S. Cabaleiro, J. Castro, J.A. García-Vázquez, J. Romero, A. Sousa, Polyhedron 19 (2000) 1607.
[12] S. Cabaleiro, J. Castro, E. Vázquez-López, J.A. García-Vázquez, J. Romero, A. Sousa, Polyhedron 18 (1999) 1669.
[13] I. Beloso, J. Castro, J.A. García-Vázquez, P. Pérez-Lourido, J. Romero, A. Sousa, Z. Anorg. Allg. Chem. 629 (2003) 275.
[14] I. Beloso, J. Borrás, J. Castro, J.A. García-Vázquez, P. Pérez-Lourido, J. Romero, A. Sousa, Eur. J. Inorg. Chem. (2004) 635.
[15] C.-F. Lee, S.-M. Peng, J. Chin. Chem. Soc. (Taipei) 38 (1991) 559.
[16] H.-Y. Cheng, P.-H. Cheng, C.-F. Lee, S.-M. Peng, Inorg. Chim. Acta 181 (1991) 145.
[17] S. Cabaleiro, J. Castro, E. Vázquez-López, J.A. García-Vázquez, J. Romero, A. Sousa, Inorg. Chim. Acta 294 (1999) 87.
[18] D.G Tuck, Pure Appl. Chem. 51 (1979) 2005.
[19] G.M. Sheldrick, SADABS: An Empirical Absorption Correction Program for Area Detector Data, University of Göttingen, Göttingen, Germany, 1996.
[20] G.M. Sheldrick, SHELX-97: Program for the Solution and Refinement of Crystal Structures, University of Göttingen, Göttingen, Germany, 1997.
[21] International Tables for X-ray Crystallography, vol. C, Kluwer, Dordrecht, 1992.
[22] P.B. Donaldson, P.A. Tasker, N.W. Alcock, J. Chem. Soc., Dalton Trans. (1977) 1160.
[23] R. Carballo, B. Covelo, E.M. Vázquez-López, E. García-Martínez, Z. Anorg. Allg. Chem. 629 (2003) 244.
[24] A. Moghimi, R. Alizadeh, A. Shokrollahi, H. Aghabozorg, M. Shamsipur, A. Shockravi, Inorg. Chem. 42 (2003) 1616.
[25] M.-T. Youinou, R. Ziessel, J.-M. Lehn, Inorg. Chem. 30 (1991) 2144.
[26] A. Sousa, M.R. Bermejo, M. Fondo, A. Garcia-Deibe, A. Sousa-Pedrares, O. Piro, New J. Chem. 25 (2001) 647.
[27] A.A. Schilt, R.C. Taylor, J. Inorg. Nucl. Chem. 9 (1959) 211.
[28] R.G. Inskeep, J. Inorg. Nucl. Chem. 24 (1963) 763.
[29] A.B.P. Lever, Inorganic Electronic Spectroscopy, 2nd ed., Elsevier, Amsterdam, 1984.

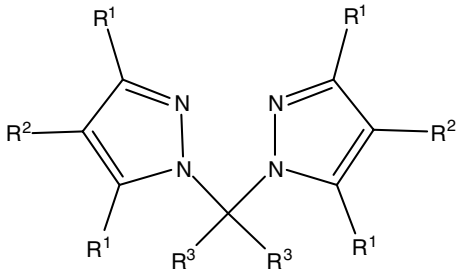

L^1: R^1=H; R^2=H; R^3=H
L^2: R^1=CH_3; R^2=H; R^3=H
L^3: R^1=H; R^2=H; R^3=CH_3
L^4: R^1=CH_3; R^2=CH_3; R^3=H
L^5: R^1=H; R^2=CH_3; R^3=H
L^6: R^1=H; R^2=I; R^3=H
L^7: R^1=CH_3; R^2=I; R^3=H

Fig. 1. Bis(pyrazol-1-yl)methane derivatives.

prepared by Pettinari et al. [5]. It was noted that in the case of the complexes of CdI_2 and $HgCl_2$ displacement of the L^4 ligand is observed under analogous conditions. Nevertheless, L^4 reacts with mercury(II) acetate in the presence of saccharine (*o*-sulfobenzoic acid imide, SacH) in aqueous solution with the formation of a mixed-ligand complex $Hg(L^4)(Sac^-)_2$ [5].

The same authors [5] also report that ligand L^4 is displaced from the complexes $Zn(L^4)X_2$ ($X = Cl^-$, Br^-) and $Cd(L^4)Br_2$ upon their reaction with various monodentate ligands (pyrazole, *N*-methylimidazole, 4-phenylimidazole) and 2,2′-bipyridyl. Similarly, when $Hg(L^5)Cl_2$ was reacted with triphenylphosphine (PPh_3) and 2,2′-bipyridyl (bipy), only $Hg(PPh_3)_2Cl_2$ and $Hg(bipy)Cl_2$ compounds were isolated [6].

A considerable quantity of 3*d*-transition-metal mixed-ligand complexes with bis(pyrazol-1-yl)methane derivatives involves copper(I) ions. Thus, $[Cu(NO_3)(PPh_3)_2]$ reacts with L^1 [7] or L^5 [8] to form mixed-ligand adducts $[Cu(L)(PPh_3)_2](NO_3)$ ($L = L^1$, L^5). It is interesting to note that the same reaction was observed even in the case of strongly electron-deficient bis(4-nitropyrazol-1-yl)methane [7]. Similarly, complexes containing other counter-ions, namely $[Cu(L)(PPh_3)X]$ ($L = L^1$, L^2; $X = Cl^-$, Br^-) [8], $[Cu(L)(PPh_3)_2](ClO_4)$ ($L = L^1$, L^2, L^5) [9], $[Cu(L^2)(PPh_3)](ClO_4)$ [10] and $[Cu(L^1)(MeCN)_n](ClO_4)$ ($n = 1$, 2) [11] have been reported.

A binuclear mixed-ligand copper(I) complex with a bridging bidentate heterocyclic ligand, $[Cu_2(L^2)_2(MeCN)_2(\mu\text{-Prz})](ClO_4)_2$, was prepared by the reaction of $[Cu(L^2)(MeCN)](ClO_4)$ with pyrazine (Prz) in dichloromethane solution [10].

As it is seen from the literature, no copper(II) mixed-ligand complexes containing bis(pyrazol-1-yl)methane derivatives together with any other organic ligands are known.

In this contribution we report the preparation of complexes of L^1, L^2 ligands and novel bis(4-iodopyrazol-1-yl)methane (L^6) and bis(3,5-dimethyl-4-iodopyrazol-1-yl)methane (L^7) ligands with copper(II) nitrate and chloride. The reactivity of the complexes obtained with various mono- and bidentate ligands is investigated.

2. Experimental

2.1. Syntheses

Commercial reagents and solvents were used as received.

Bis(pyrazol-1-yl)methane (L^1) was prepared as previously described [12]. Briefly, 5.00 g (73.5 mmol) of 1*H*-pyrazole were dissolved in 30 ml of DMSO, and 16.46 g (294.0 mmol) of finely powdered KOH were added. The suspension was vigorously stirred for 1 h at 60 °C, and 6.40 g (2.6 ml, 36.8 mmol) of dibromomethane in 20 ml of DMSO were added dropwise over 30 min. Stirring at 60 °C was continued for an additional 4 h, and the reaction mixture was poured into 300 ml of water and extracted with chloroform (6 × 30 ml). The extract was washed with water (2 × 20 ml) and dried over anhydrous calcium chloride. Removal of the solvent produced 4.45 g (yield 82%) of solid product. M.p. 107–107.5 °C (benzene–hexane, 1:1, lit. m.p. 108 °C [13]). *Anal.* Calc. for $C_7H_8N_4$: C, 56.74; H, 5.44; N, 37.81. Found: C, 56.36; H, 5.67; N, 38.05%. ^{1}H NMR spectrum corresponds to literature data [14]. IR bands, cm^{-1}: 1610, 1510, 1450 (ν_{ring} – pyrazole ring stretching vibrations); 1355 (βCH – in-plane C–H bending vibrations); 1045 (pyrazole ring breathing); 940, 740 (δ_{C-H}). UV–Vis bands (EtOH), λ_{max}, nm (ε, $dm^3\ cm^{-1}\ mol^{-1}$): 222 (8860), 203 (sh).

Bis(3,5-dimethylpyrazol-1-yl)methane (L^2) was prepared similarly. Yield 92%, m.p. 105–105.5 °C (benzene–hexane, 1:1, lit. m.p. 105 °C [13]). *Anal.* Calc. for $C_{11}H_{16}N_4$: C, 64.68; H, 7.89; N, 27.43. Found: C, 63.88; H, 8.03; N, 26.82%. ^{1}H NMR spectrum corresponds to literature data [14]. IR bands, cm^{-1}: 1550, 1450 (ν_{ring}); 1345 (βCH); 1125; 1020 (pyrazole ring breathing); 955, 765, 700. UV–Vis bands (EtOH), λ_{max}, nm (ε, $dm^3\ cm^{-1}\ mol^{-1}$): 222 (6790), 206 (5900).

Bis(4-iodopyrazol-1-yl)methane (L^6) was prepared as previously described [15]. Briefly, a suspension of 3.50 g (23.6 mmol) of L^1, 4.80 g (18.9 mmol) of powdered iodine, 1.65 g (9.4 mmol) of HIO_3 in 30 ml of glacial acetic acid and 3 ml 30% aqueous H_2SO_4 was vigorously stirred for 15 min at 70 °C until the reaction mixture became colorless. The mixture was then poured into 250 ml of water, the precipitate formed was filtered, washed with H_2O, and dried to yield 9.25 g (98%) of compound L^6. M.p. 165–165.5 °C (benzene–hexane, 4:1), *Anal.* Calc. for $C_7H_6N_4I_2$: C, 21.02; H, 1.51; N, 14.01. Found: C, 21.47; H, 1.93; N, 13.99%. ^{1}H NMR ($CDCl_3$): δ, ppm: 6.15 (s, 2H, CH_2), 7.49 (s, 2H, H^3), 7.62 (s, 2H, H^5). IR bands, cm^{-1}: 1520 (ν_{ring}); 1395 (βCH); 1310; 1000 (pyrazole ring breathing). UV–Vis bands (EtOH), λ_{max}, nm (ε, $dm^3\ cm^{-1}\ mol^{-1}$): 238 (8410), 202 (8410).

Bis(3,5-dimethyl-4-iodopyrazol-1-yl)methane (L^7) was prepared similarly. Yield 94%, m.p. 183–184 °C (EtOH). *Anal.* Calc. for $C_{11}H_{14}N_4I_2$: C, 29.27; H, 3.09; N, 12.28. Found: C, 29.34; H, 3.04; N, 12.08%. ^{1}H NMR ($CDCl_3$):

δ, ppm: 2.12 (s, 6H, 3-CH_3), 2.40 (s, 6H, 5-CH_3), 6.08 (s, 2H, CH_2). IR bands, cm^{-1}: 1525, 1460 (ν_{ring}); 1370; 1335 (βCH); 1050 (pyrazole ring breathing). UV–Vis bands (EtOH), λ_{max}, nm (ε, $dm^3\,cm^{-1}\,mol^{-1}$): 238 (6790), 204 (6560).

2.1.1. Bis(pyrazol-1-yl)methanedinitratocopper(II) monohydrate (*1*)

A solution of 0.752 g (4.0 mmol) of L^1 in 6 ml of acetone was added to a solution of 0.592 g (4.0 mmol) of $Cu(NO_3)_2 \cdot 3H_2O$ in 3 ml of the same solvent. The immediately formed light-blue precipitate was filtered after 30 min, thoroughly washed with acetone and dried in vacuo at 40 °C. The yield of compound **1** was 0.800 g (57%).

Complexes **2**–**5**, **7**, **9**, **10** were obtained similarly, whilst a 2:1 ligand to metal ratio was used in case of compounds **6** and **8**.

2.1.2. Bis(pyrazol-1-yl)methane-2,2′-bipyridyl-nitratocopper(II) nitrate (*11*)

A solution of 0.078 g (0.5 mmol) 2,2′-bipyridyl in 1 ml of acetone was added to a warmed-up (40 °C) solution of 0.168 g (0.5 mmol) of the complex $[Cu(L^1)(O_2NO)_2] \cdot H_2O$ (**1**) in 15 ml of acetone. The precipitated light-blue crystals of compound **11** (yield 0.170 g, 69%) were filtered, washed with acetone and dried in vacuo.

Compounds **12**–**14** were prepared similarly from copper complexes **2** or **3** and bidentate ligands (2,2′-bipyridyl or acetylacetone) in a 1:1 ratio. Mixed-ligand complexes **15**–**18** were obtained upon mixing one equivalent of complex **2** with two equivalents of the corresponding monodentate ligand in ethanol (compound **15**), acetone (complexes **16**, **17**) or isopropyl alcohol (compound **18**).

2.2. Analytical data

2.2.1. Bis(pyrazol-1-yl)methanedinitratocopper(II) monohydrate (*1*)

$Cu(L^1)(NO_3)_2 \cdot H_2O$. Yield 57%; m.p. 207 °C; molar conductivity $\lambda = 27.5\ \Omega^{-1}\,cm^2\,mol^{-1}$ (acetone). *Anal.* Calc. for $C_7H_{10}CuN_6O_7$: C, 23.77; H, 2.85; N, 23.76. Found: C, 24.04; H, 2.86; N, 24.10%. IR bands, cm^{-1}: 3400br (ν_{O-H}, H_2O); 2354, 2167 ($\nu_1 + \nu_3$ of NO_3^-); 1788, 1757 ($\nu_1 + \nu_4$ of NO_3^-); 1618 (δ_{O-H}, H_2O); 1514 (ν_{ring}); 1464 (ν_3 mode of NO_3^-); 1398 (ν_{ring}); 1321 (βCH); 1285 (ν_3 mode of NO_3^-); 1045 (pyrazole ring breathing); 1017 (ν_1 mode of NO_3^-); 809 (ν_2 mode of NO_3^-); 760, 729 (ν_4 mode of NO_3^-). UV–Vis bands (ethanol), λ_{max}, nm (ε, $dm^3\,cm^{-1}\,mol^{-1}$): 935 (sh), 685 (120), 338 (sh), 256 (sh), 219 (16 580). Cyclic voltammetry, $E_{1/2} = -214$ mV, $\Delta E = 182$ mV.

2.2.2. Bis(3,5-dimethylpyrazol-1-yl)methanedinitratocopper(II) (*2*)

$Cu(L^2)(NO_3)_2$. Yield 93%; m.p. 230–231 °C; $\lambda = 19.1\ \Omega^{-1}\,cm^2\,mol^{-1}$ (acetone). *Anal.* Calc. for $C_{11}H_{16}CuN_6O_6$: C, 33.72; H, 4.12; N, 21.45. Found: C, 34.20; H, 4.45; N, 20.98%. IR bands, cm^{-1}: 1540 (ν_{ring}); 1500 (ν_3 mode of NO_3^-); 1455 (ν_{ring}); 1370 (βCH); 1280 (ν_3 mode of NO_3^-); 1040 (pyrazole ring breathing); 995 (ν_1 mode of NO_3^-); 820 (ν_2 mode of NO_3^-); 730, 690 (ν_4 mode of NO_3^-). UV–Vis bands (ethanol), λ_{max}, nm (ε, $dm^3\,cm^{-1}\,mol^{-1}$): 935 (sh); 685 (120); 338 (sh); 256 (sh); 219 (16 580). $E_{1/2} = -137$ mV, $\Delta E = 112$ mV.

2.2.3. Bis(4-iodopyrazol-1-yl)methanedinitratocopper(II) (*3*)

$Cu(L^6)(NO_3)_2$. Yield 77%; m.p. 229–230 °C. *Anal.* Calc. for $C_7H_6CuI_2N_6O_6$: C, 14.31; H, 1.03; N, 14.30. Found: C, 14.77; H, 1.30; N, 14.00%. IR bands, cm^{-1}: 1742, 1703 ($\nu_1 + \nu_4$ of NO_3^-); 1521 (ν_{ring}); 1454 (ν_3 mode of NO_3^-); 1433 (ν_{ring}); 1329 (βCH); 1293 (ν_3 mode of NO_3^-); 1032 (pyrazole ring breathing); 1003 (ν_1 mode of NO_3^-); 827 (ν_2 mode of NO_3^-); 782, 735 (ν_4 mode of NO_3^-).

2.2.4. Bis(3,5-dimethyl-4-iodopyrazol-1-yl)methanedinitratocopper(II) dihydrate (*4*)

$Cu(L^7)(NO_3)_2 \cdot 2H_2O$. Yield 94%; m.p. 222–223 °C; $\lambda = 14.5\ \Omega^{-1}\,cm^2\,mol^{-1}$ (acetone). *Anal.* Calc. for $C_{11}H_{18}CuI_2N_6O_8$: C, 19.44; H, 2.67; N, 12.37. Found: C, 19.82; H, 2.95; N, 12.09%. IR bands, cm^{-1}: 3400br (ν_{O-H}, H_2O); 1620 (δ_{O-H}, H_2O); 1520 (ν_3 mode of NO_3^-); 1470 (ν_{ring}); 1370 (βCH); 1265 (ν_3 mode of NO_3^-); 1070 (pyrazole ring breathing); 1000 (ν_1 mode of NO_3^-); 835 (ν_2 mode of NO_3^-); 725, 700 (ν_4 mode of NO_3^-). UV–Vis bands (ethanol), λ_{max}, nm (ε, $dm^3\,cm^{-1}\,mol^{-1}$): 1030 (sh); 722 (50.0); 342 (sh); 234 (13 860); 204 (27 650). $E_{1/2} = -176$ mV, $\Delta E = 183$ mV.

2.2.5. Bis(pyrazol-1-yl)methanedichlorocopper(II) (*5*)

$Cu(L^1)Cl_2$. Yield 93%; m.p. 266–267 °C (lit. m.p. 264–265 [3]); $\lambda = 15.0\ \Omega^{-1}\,cm^2\,mol^{-1}$ (acetone). *Anal.* Calc. for $C_7H_8Cl_2CuN_4$: C, 29.75; H, 2.85; N, 19.82. Found: C, 29.55; H, 2.60; N, 20.10%. IR bands, cm^{-1}: 1500 (ν_{ring}); 1260 (βCH); 1050 (pyrazole ring breathing). UV–Vis bands (ethanol), λ_{max}, nm (ε, $dm^3\,cm^{-1}\,mol^{-1}$): 940 (sh); 765 (73); 334 (sh); 260 (sh); 215 (11630). $E_{1/2} = -169$ mV, $\Delta E = 128$ mV.

2.2.6. Bis{bis(pyrazol-1-yl)methane}copper(II) dichloride dihydrate (*6*)

$Cu(L^1)_2Cl_2 \cdot 2H_2O$. Yield 90%; m.p. 180–182 °C; $\lambda = 11.7\ \Omega^{-1}\,cm^2\,mol^{-1}$ (acetone). *Anal.* Calc. for $C_{14}H_{20}Cl_2CuN_8O_2$: C, 36.02; H, 4.32; N, 24.00. Found: C, 36.03; H, 4.16; N, 23.60%. IR bands, cm^{-1}: 3400br (ν_{O-H}, H_2O); 1630 (δ_{O-H}, H_2O); 1500, 1450 (ν_{ring}); 1390 (βCH); 1045 (pyrazole ring breathing). UV–Vis bands (ethanol), λ_{max}, nm (ε, $dm^3\,cm^{-1}\,mol^{-1}$): 1040 (sh); 765 (82); 337 (sh); 319 (163); 268 (2175); 220 (12120). $E_{1/2} = -111$ mV, $\Delta E = 45$ mV.

2.2.7. Bis(3,5-dimethylpyrazol-1-yl)methanedichlorocopper(II) (*7*)

$Cu(L^2)Cl_2$. Yield 78%; m.p. 200–202 °C; $\lambda = 52.3\ \Omega^{-1}\,cm^2\,mol^{-1}$ (acetone). *Anal.* Calc. for $C_{11}H_{16}Cl_2CuN_4$: C, 39.00; H, 4.76; N, 16.54. Found: C, 38.60; H, 4.78; N,

16.90%. IR bands, cm^{-1}: 1540 (ν_{ring}); 1260 (βCH); 1015 (pyrazole ring breathing). UV–Vis bands (ethanol), λ_{max}, nm (ε, $dm^3\,cm^{-1}\,mol^{-1}$): 950 (sh); 740 (102); 335 (sh); 268 (2433); 222 (10260). $E_{1/2} = -179$ mV, $\Delta E = 140$ mV.

2.2.8. Bis{bis(3,5-dimethylpyrazol-1-yl)methane}-copper(II) dichloride dihydrate (**8**)

$Cu(L^2)_2Cl_2 \cdot 2H_2O$. Yield 73%; m.p. 174–175 °C; $\lambda = 52.1\ \Omega^{-1}\,cm^2\,mol^{-1}$ (acetone). *Anal.* Calc. for $C_{22}H_{36}Cl_2CuN_8O_2$: C, 45.63; H, 6.27; N, 19.35. Found: C, 45.62; H, 5.86; N, 19.20%. IR bands, cm^{-1}: 3430br (ν_{O-H}, H_2O); 1610 (δ_{O-H}, H_2O); 1550, 1460 (ν_{ring}); 1370 (βCH); 1020 (pyrazole ring breathing). UV–Vis bands (ethanol), λ_{max}, nm (ε, $dm^3\,cm^{-1}\,mol^{-1}$): 945 (sh); 715 (168); 351 (sh); 265 (sh); 225 (30950). $E_{1/2} = -202$ mV, $\Delta E = 140$ mV.

2.2.9. Bis(4-iodopyrazol-1-yl)methanedichlorocopper(II) (**9**)

$Cu(L^6)Cl_2$. Yield 93%; m.p. 267–269 °C; $\lambda = 18.6\ \Omega^{-1}\,cm^2\,mol^{-1}$ (acetone). *Anal.* Calc. for $C_7H_8Cl_2CuI_2N_4$: C, 15.73; H, 1.13; N, 10.48. Found: C, 15.80; H, 1.19; N, 10.90%. IR bands, cm^{-1}: 1500, 1430 (ν_{ring}); 1360 (βCH); 1005 (pyrazole ring breathing). UV–Vis bands (ethanol), λ_{max}, nm (ε, $dm^3\,cm^{-1}\,mol^{-1}$): 870 (38.7); 228 (15800).

2.2.10. Bis(3,5-dimethyl-4-iodopyrazol-1-yl)methane-dichlorocopper(II) dihydrate (**10**)

$Cu(L^7)Cl_2 \cdot 2H_2O$. Yield 88%; m.p. 229 °C; $\lambda = 22.7\ \Omega^{-1}\,cm^2\,mol^{-1}$ (acetone). *Anal.* Calc. for $C_{11}H_{18}Cl_2CuI_2N_4O_2$: C, 21.09; H, 2.90; N, 8.94. Found: C, 21.33; H, 3.10; N, 8.49%. IR bands, cm^{-1}: 3300br (ν_{O-H}, H_2O); 1690 (δ_{O-H}, H_2O); 1585, 1520, 1470 (ν_{ring}); 1345 (βCH); 1070 (pyrazole ring breathing). UV–Vis bands (ethanol), λ_{max}, nm (ε, $dm^3\,cm^{-1}\,mol^{-1}$): 820 (67); 341 (sh); 238 (14460). $E_{1/2} = -180$ mV, $\Delta E = 164$ mV.

2.2.11. Bis(pyrazol-1-yl)methane-2,2′-bipyridyl-nitratocopper(II) nitrate (**11**)

$Cu(L^1)(bipy)(NO_3)_2$. Yield 69%; m.p. 194–196 °C; $\lambda = 52.6\ \Omega^{-1}\,cm^2\,mol^{-1}$ (acetone). *Anal.* Calc. for $C_{17}H_{16}CuN_8O_6$: C, 41.51; H, 3.28; N, 22.78. Found: C, 41.90; H, 2.90; N, 22.30%. IR bands, cm^{-1}: 2371, 2278 ($\nu_1 + \nu_3$ of NO_3^-); 1743, 1712 ($\nu_1 + \nu_3$ of NO_3^-); 1610, 1601 (ν_{ring} of pyridine); 1567 (ν_{ring}); 1475 (ν_3 mode of NO_3^-); 1343 (βCH); 1279 (ν_3 mode of NO_3^-); 1160 (βCH of pyridine ring); 1032 (pyrazole ring breathing); 1016 (ν_1 mode of NO_3^-); 902 (γCH – out-of-plane C–H bending vibrations of pyridine ring); 831, 812 (ν_2 mode of NO_3^-); 731, 705 (ν_4 mode of NO_3^-). UV–Vis bands (ethanol), λ_{max}, nm (ε, $dm^3\,cm^{-1}\,mol^{-1}$): 880 (sh); 695 (65.3); 336 (sh); 312 (16270); 300 (17370); 242 (sh); 213 (32850). $E_{1/2} = -153$ mV, $\Delta E = 121$ mV.

2.2.12. Bis(3,5-dimethylpyrazol-1-yl)methane-2,2′-bipyridylnitratocopper(II) nitrate (**12**)

$Cu(L^2)(bipy)(NO_3)_2$. Yield 81%; m.p. 229–231 °C; $\lambda = 81.6\ \Omega^{-1}\,cm^2\,mol^{-1}$ (acetone). *Anal.* Calc. for $C_{21}H_{24}CuN_8O_6$: C, 46.03; H, 4.41; N, 20.45. Found: C, 45.76; H, 4.45; N, 20.93%. IR bands, cm^{-1}: 2392, 2283 ($\nu_1 + \nu_3$ of NO_3^-); 1744, 1713 ($\nu_1 + \nu_4$ of NO_3^-); 1601 (ν_{ring} of pyridine); 1567 (ν_{ring}); 1477 (ν_3 mode of NO_3^-); 1334 (βCH); 1288 (ν_3 mode of NO_3^-); 1159 (βCH of pyridine ring); 1041 (pyrazole ring breathing); 1018 (ν_1 mode of NO_3^-); 902 (γCH of pyridine ring); 833, 808 (ν_2 mode of NO_3^-); 732, 705 (ν_4 mode of NO_3^-). UV–Vis bands (ethanol), λ_{max}, nm (ε, $dm^3\,cm^{-1}\,mol^{-1}$): 910 (sh); 685 (74.4); 341 (sh); 313 (12410); 302 (13060); 243 (sh); 210 (35740). $E_{1/2} = -190$ mV, $\Delta E = 157$ mV.

2.2.13. Bis(4-iodopyrazol-1-yl)methane-2,2′-bipyridyl-nitratocopper(II) nitrate (**13**)

$Cu(L^6)(bipy)(NO_3)_2$. Yield 46%; m.p. 203–206 °C; $\lambda = 76.5\ \Omega^{-1}\,cm^2\,mol^{-1}$ (acetone). *Anal.* Calc. for $C_{17}H_{14}CuI_2N_8O_6$: C, 27.45; H, 1.90; N, 15.07. Found: C, 27.74; H, 2.07; N, 14.96%. IR bands, cm^{-1}: 2371, 2282 ($\nu_1 + \nu_3$ of NO_3^-); 1743, 1716 ($\nu_1 + \nu_4$ of NO_3^-); 1610, 1601 (ν_{ring} of pyridine); 1567 (ν_{ring}); 1497 (ν_3 mode of NO_3^-); 1445 (ν_{ring}); 1331 (βCH); 1293 (ν_3 mode of NO_3^-); 1160 (βCH of pyridine ring); 1032 (pyrazole ring breathing); 1014 (ν_1 mode of NO_3^-); 902 (γCH of pyridine ring); 831, 812 (ν_2 mode of NO_3^-); 734, 706 (ν_4 mode of NO_3^-). UV–Vis bands (ethanol), λ_{max}, nm (ε, $dm^3\,cm^{-1}\,mol^{-1}$): 910 (sh); 705 (107); 336 (sh); 311 (26460); 308 (30370); 290 (sh); 232 (sh); 210 (53520). $E_{1/2} = -150$ mV, $\Delta E = 127$ mV.

2.2.14. Bis(3,5-dimethylpyrazol-1-yl)methaneacetyl-acetonatonitratocopper(II) (**14**)

$Cu(L^2)(acac)(NO_3)$. Yield 67%; m.p. 177–178 °C; $\lambda = 67.9\ \Omega^{-1}\,cm^2\,mol^{-1}$ (acetone). *Anal.* Calc. for $C_{16}H_{23}CuN_5O_5$: C, 44.80; H, 5.40; N, 16.33. Found: C, 44.35; H, 5.12; N, 16.78%. IR bands, cm^{-1}: 2392, 2283 ($\nu_1 + \nu_3$ of NO_3^-); 1744, 1709 ($\nu_1 + \nu_4$ of NO_3^-); 1556 (ν_{ring}); 1478 (ν_3 mode of NO_3^-); 1475 (ν_{ring}); 1335 (βCH); 1288 (ν_3 mode of NO_3^-); 1041 (pyrazole ring breathing); 1018 (ν_1 mode of NO_3^-); 836, 807 (ν_2 mode of NO_3^-); 741, 704 (ν_4 mode of NO_3^-). UV–Vis bands (ethanol), λ_{max}, nm (ε, $dm^3\,cm^{-1}\,mol^{-1}$): 1020 (sh); 680 (54.1); 340 (sh); 295 (5970); 245 (sh); 219 (sh). $E_{1/2} = -187$ mV, $\Delta E = 114$ mV.

2.2.15. Bis(3,5-dimethylpyrazol-1-yl)methane-bis(triphenylphosphine)nitratocopper(II) nitrate (**15**)

$Cu(L^2)(PPh_3)_2(NO_3)_2$. Yield 77%; m.p. 184–185 °C; $\lambda = 88.1\ \Omega^{-1}\,cm^2\,mol^{-1}$ (acetone). *Anal.* Calc. for $C_{47}H_{46}CuN_6O_6P_2$: C, 61.60; H, 5.06; N, 9.17. Found: C, 61.65; H, 5.07; N, 8.75%. IR bands, cm^{-1}: 1557 (ν_{ring}); 1479 (ν_3 mode of NO_3^-); 1465 (ν_{ring}); 1435 ($\nu_{C=C}$); 1332 (βCH); 1281 (ν_3 mode of NO_3^-); 1097; 1049 (pyrazole ring breathing); 1022 (ν_1 mode of NO_3^-); 836, 810 (ν_2 mode of NO_3^-); 743, 705 (ν_4 mode of NO_3^-); 694 (δ-mode of PPh_3); 521 (ν_{C-P}); 503 (γ-mode of PPh_3). UV–Vis bands (methanol), λ_{max}, nm (ε, $dm^3\,cm^{-1}\,mol^{-1}$): 700 (16.8); 340 (sh); 256 (sh); 215 (80910). $E_{1/2} = -171$ mV, $\Delta E = 145$ mV; $E_{1/2} = -829$ mV, $\Delta E = 244$ mV.

*2.2.16. Bis(3,5-dimethylpyrazol-1-yl)methane-bis{1H-benzimidazole}nitratocopper(II) nitrate (**16**)*

$Cu(L^2)(BImH)_2(NO_3)_2$. Yield 84%; m.p. 312 °C; $\lambda = 55.6\ \Omega^{-1}\ cm^2\ mol^{-1}$ (ethanol). *Anal.* Calc. for $C_{25}H_{28}CuN_{10}O_6$: C, 47.81; H, 4.49; N, 22.30. Found: C, 47.50; H, 4.08; N, 22.11%. IR bands, cm^{-1}: 3380br (ν_{N-H} in BImH); 2388 ($\nu_1 + \nu_3$ of NO_3^-); 1712 ($\nu_1 + \nu_4$ of NO_3^-); 1624 (ν_{C-C}); 1595, 1557 (ν_{ring}); 1479 (ν_3 mode of NO_3^-); 1465 (ν_{ring}); 1332 (βCH); 1290 (ν_3 mode of NO_3^-); 1041 (pyrazole ring breathing); 1012 (ν_1 mode of NO_3^-); 835, 808 (ν_2 mode of NO_3^-); 748, 705 (ν_4 mode of NO_3^-). UV–Vis bands (ethanol), λ_{max}, nm (ε, $dm^3\ cm^{-1}\ mol^{-1}$): 1060 (sh); 670 (68.2); 339 (sh); 279 (14710); 273 (13320); 267 (sh); 250 (12720); 244 (13720); 213 (26440). $E_{1/2} = -171$ mV, $\Delta E = 159$ mV; $E_{1/2} = -509$ mV, $\Delta E = 294$ mV.

*2.2.17. Bis(3,5-dimethylpyrazol-1-yl)methane-bis{1H -benzotriazole}nitratocopper(II) nitrate (**17**)*

$Cu(L^2)(BtaH)_2(NO_3)_2$. Yield 43%; m.p. >330 °C. *Anal.* Calc. for $C_{23}H_{26}CuN_{12}O_6$: C, 43.84; H, 4.16; N, 26.68. Found: C, 43.86; H, 3.87; N, 27.00%. IR bands, cm^{-1}: 3380br (ν_{N-H} in BtaH); 1763, 1720 ($\nu_1 + \nu_4$ of NO_3^-); 1560 (ν_{ring}); 1470 (ν_3 mode of NO_3^-); 1465 (ν_{ring}); 1332 (βCH); 1283 (ν_3 mode of NO_3^-); 1195, 1153; 1049 (pyrazole ring breathing); 1011 (ν_1 mode of NO_3^-); 839, 830 (ν_2 mode of NO_3^-); 692 (ν_4 mode of NO_3^-).

*2.2.18. Bis(3,5-dimethylpyrazol-1-yl)methanebis-{3,5-dimethyl-1H-pyrazole}nitratocopper(II) nitrate (**18**)*

$Cu(L^2)(Me_2PyrH)_2(NO_3)_2$. Yield 50%; m.p. 237–238 °C; $\lambda = 52.5\ \Omega^{-1}\ cm^2\ mol^{-1}$ (ethanol). *Anal.* Calc. for $C_{21}H_{32}CuN_{10}O_6$: C, 43.18; H, 5.52; N, 23.98. Found: C, 42.95; H, 5.70; N, 24.02%. IR bands, cm^{-1}: 3300br (ν_{N-H} in Me_2PyrH); 2393, 2283 ($\nu_1 + \nu_3$ of NO_3^-); 1747, 1713 ($\nu_1 + \nu_4$ of NO_3^-); 1557 (ν_{ring}); 1479 (ν_3 mode of NO_3^-); 1467 (ν_{ring}); 1333 (βCH); 1288 (ν_3 mode of NO_3^-); 1042 (pyrazole ring breathing); 1017 (ν_1 mode of NO_3^-); 835, 809 (ν_2 mode of NO_3^-); 733, 705 (ν_4 mode of NO_3^-). UV–Vis bands (ethanol), λ_{max} nm (ε, $dm^3\ cm^{-1}\ mol^{-1}$): 1030 (sh); 685 (59.6); 340 (sh); 280 (sh); 215 (26150). $E_{1/2} = -193$ mV, $\Delta E = 162$ mV; $E_{1/2} = -559$ mV; $E_{1/2} = -722$ mV, $\Delta E = 41$ mV.

2.3. Physical measurements

Conductivities of solutions ($c = 1.0 \times 10^{-3}$ mol/dm^3 in acetone or ethanol) were measured in a temperature-controlled cell with stainless steel electrodes, cell constant $\varphi = 0.251\ cm^{-1}$.

Elemental analyses were carried out on a Carlo Erba analyzer.

IR spectra of solid samples as KBr pellets were recorded on Specord 71 IR (in the range of 4600–650 cm^{-1}) and Nicolet 5700 (4000–400 cm^{-1}) spectrophotometers.

Electronic absorption spectra were registered on Perkin–Elmer 124 (in the range of 200–800 nm) and SF-26 (800–1200 nm) spectrophotometers.

NMR spectra were recorded on a Bruker AV300 instrument.

Cyclic voltammograms were obtained on a TA-4 voltammetric analyzer (Tomanalyt, Tomsk, Russia). The three-electrode electrochemical cell consisted of a mercury-film working electrode and saturated Ag/AgCl reference and auxiliary electrodes. The concentration of the sample in the cell was 1.0×10^{-4} mol/dm^3, and 0.1 mol/dm^3 KCl was used as a supporting electrolyte. The potential was varied in the range 0 to −1.3 V at 50 mV s^{-1} scan rate. Oxygen was removed from the solutions by bubbling nitrogen through immediately before any measurements. Formal potentials were calculated as $E_{1/2} = (E_{p.c.} + E_{p.a.})/2$.

3. Results and discussion

3.1. Synthesis of the ligands

Bis(pyrazol-1-yl)methanes L^1 and L^2 were first prepared by Trofimenko [14]. We have developed a new procedure for double alkylation of azoles via the reaction of 1*H*-pyrazole or 3,5-dimethyl-1*H*-pyrazole with dibromomethane in a superbasic medium (DMSO-KOH). Iodo-derivatives L^6 and L^7 were obtained by oxidative iodination of L^1 and L^2 by an I_2–HIO_3–H_2SO_4 mixture in acetic acid.

3.2. Synthesis and characterization of bis(pyrazol-1-yl)-methane complexes

The complexes were prepared by the reaction of the ligands with copper(II) nitrate or chloride in acetone solution. In the case of $Cu(NO_3)_2$, independent of the metal to ligand ratio used (1:1 or 1:2), complexes **1**–**4** of 1:1 composition were formed. The same feature was observed for the reaction of copper(II) chloride with the ligands L^6 and L^7 (complexes **9** and **10** were obtained). When $CuCl_2$ reacted with the ligands L^1 and L^2, 1:1 complexes **5** and **7**, as well as 1:2 complexes **6** and **8** were isolated depending on the reagent ratio.

All of the coordination compounds obtained gave satisfactory elemental analysis and were characterized by molar conductivity, infra-red and electronic spectroscopy.

The complexes of copper(II) nitrate, **1**, **2** and **4**, are weak electrolytes in acetone, therefore both of the NO_3^- ions are bound to the central ion. The solubility of complex **3** was insufficient for conductivity measurements.

Bis(pyrazol-1-yl)alkanes are bidentate in most of their complexes, so the same coordination mode is to be expected for the investigated compounds with L^1, L^2, L^6 and L^7. Bidentate coordination of bis(pyrazol-1-yl)methane derivatives in the prepared complexes can be assumed from the absence of the splitting of pyrazole ring vibrational bands in the IR spectra. This splitting should have occurred if only one of pyrazole rings in bis(pyrazol-1-yl)methane ligand was coordinated to the copper(II) ion. The possibility of formation of polymeric complexes, in which metal ions are connected by bridging ligands, can

be ruled out by sharp melting points of the compounds obtained. In the copper(II) nitrate complexes, the NO_3^- ions may be coordinated in a mono- or bidentate fashion. The coordination modes of nitrate ions can be established by means of IR spectroscopy [16–19].

Bands corresponding to all of the vibrational modes of the nitrate ion were detected in the IR spectra of complexes **1**–**4** (Table 1). Two intense bands in the 1455–1500 and 1265–1295 cm^{-1} regions were assigned to stretching vibrations of N–O bonds in a NO_3^- ion (ν_3) belonging to the C_{2v} symmetry group [17]. The bands of in-plane bending vibrations (ν_4) appear at 690–735 and 725–780 cm^{-1}. Large splitting of these bands ($\Delta(\nu_3) > 160$ and $\Delta(\nu_4) > 25$ cm^{-1}) confirms the presence of bidentate nitrate ions in all of the four complexes. For monodentate coordination of NO_3^- the splitting of the ν_3 band is not higher than 120 cm^{-1} and that of ν_4 is less than 20 cm^{-1} [17].

Single bands around 820 cm^{-1} (out-of-plane bending vibrations ν_2) as well as bands of medium intensity at about 1000 cm^{-1} (symmetric stretching vibrations ν_1) were observed in IR spectra of complexes **1**–**4** [17]. The occurrence of the latter band gives further evidence for the nitrate ions coordination, since the vibrational transition ν_1 in the free NO_3^- is symmetry-forbidden, so this band does not appear in IR spectra or has a very minute intensity [16].

Furthermore, weak combination bands ($\nu_1 + \nu_4$) and ($\nu_1 + \nu_3$) with the splitting values $\Delta(\nu_1 + \nu_4)$ and $\Delta(\nu_1 + \nu_3)$ in accord with those expected for bidentate nitrate ion coordination [18] were detected in the spectra of the complexes **1** and **3**.

Therefore, in nitrate complexes **1**–**4** the bidentate organic ligands occupy two coordination places, also each of the nitrate ions occupies two places. Consequently, the copper(II) ions in these complexes are hexacoordinated. Locations of absorption bands in the region of d–d* transitions in the electronic spectra of the complexes (a shoulder in the 930–1030 nm area and a band around 685–720 nm) correspond very well to the literature values for octahedrally surrounded Cu^{2+} [20]. For example, the already mentioned $[Cu(L^2)_2(O_2NO)](NO_3)$ exhibits an absorption at 694 nm with a shoulder at 1042 nm [2].

3.3. Preparation of mixed-ligand complexes

We have also studied the reactivity of the synthesized complexes towards various mono- and bidentate ligands,

Table 1
Characteristic frequencies of nitrate ion vibrations

Compound	Formula	ν_1	ν_2	ν_3	$\Delta(\nu_3)$	ν_4	$\Delta(\nu_4)$	$\nu_1 + \nu_4$	$\Delta(\nu_1 + \nu_4)$	$\nu_1 + \nu_3$	$\Delta(\nu_1 + \nu_3)$
1	$Cu(L^1)(NO_3)_2 \cdot H_2O$	1017	809	1464 1285	179	760 729	31	1788 1757	31	2354 2167	187
2	$Cu(L^2)(NO_3)_2$	1040	820	1500 1280	220	730 690	40				
3	$Cu(L^6)(NO_3)_2$	1003	827	1454 1293	161	782 735	47	1742 1703	39		
4	$Cu(L^7)(NO_3)_2 \cdot 2H_2O$	1000	835	1520 1265	255	725 700	25				
11	$Cu(L^1)(bipy)(NO_3)_2$	1016	831 812	1475 1279	196	731 705	26	1743 1712	31	2371 2278	93
12	$Cu(L^2)(bipy)(NO_3)_2$	1018	833 808	1477 1288	199	732 705	27	1744 1713	31	2392 2283	109
13	$Cu(L^6)(bipy)(NO_3)_2$	1014	831 812	1497 1293	204	734 706	28	1743 1716	27	2371 2282	89
14	$Cu(L^2)(acac)(NO_3)$	1018	836 807	1478 1288	190	741 704	37	1744 1709	35	2392 2283	109
15	$Cu(L^2)(PPh_3)_2(NO_3)_2$	1022	836 810	1479 1281	198	743 705	38				
16	$Cu(L^2)(BImH)_2(NO_3)_2$	1012	835 808	1479 1290	189	748 705	43	1712		2388	
17	$Cu(L^2)(BtaH)_2(NO_3)_2$	1011	839 830	1470 1283	187	692		1763 1720	43		
18	$Cu(L^2)(Me_2PyrH)_2(NO_3)_2$	1017	835 809	1479 1288	191	733 705	28	1747 1713	34	2393 2283	110

namely 2,2′-bipyridyl (bipy), acetylacetone (Hacac), triphenylphosphine (PPh_3), benzimidazole (BImH), benzotriazole (BtaH) and 3,5-dimethylpyrazole (Me_2PyrH). These compounds represent four different types of ligands – phosphorus-containing, *O*,*O*-bidentate, *N*,*N*-bidentate and monodentate nitrogen-containing heterocycles, which are widely spread among important biologically active substances. Mixed-ligand complexes with such compounds may serve as models for metalloenzymes [21] and as building blocks for supramolecular systems [22].

We have found that the complexes of copper(II) nitrate **1**–**3** react with 2,2′-bipyridyl with the formation of mixed-ligand complexes **11**–**13**, comprising of coordinated molecules of bis(pyrazol-1-yl)methane derivatives as well as those of 2,2′-bipyridyl. Moreover, complex **2** reacts with other above-mentioned compounds also forming mixed-ligand complexes **14**–**18**. At the same time, copper(II) chloride complexes **5**–**10**, as well as the nitrate complex **4** undergo a displacement of bis(pyrazol-1-yl)methanes from the coordination sphere yielding homoligand complexes. These complexes are identical by melting points and spectral characteristics to the compounds prepared under the same conditions using copper(II) chloride or nitrate instead of bis(pyrazol-1-yl)methane-copper(II) complexes.

Bands due to bis(pyrazol-1-yl)methane ligand vibrations as well as due to additional ligands were observed in the IR-spectra of the mixed-ligand complexes **11**–**18**. Strong bands in the area of 1550–1560 cm^{-1} account for pyrazole ring stretching vibrations and bands at 1030–1050 cm^{-1} correspond to ring breathing vibrations in bis(pyrazol-1-yl)methane derivatives [23]. Absorption in the 1600 and 1610 cm^{-1} regions of 2,2′-bipyridyl mixed-ligand complexes **11**–**13** spectra correspond to pyridine ring stretching vibrations [24,25]. Triphenylphosphine characteristic bands at 503 and 694 cm^{-1} [26] were detected in the spectra of the PPh_3 derivative **15**. Broad bands in the area of 3300–3500 cm^{-1} corresponding to N–H stretching vibrations were detected in the spectra of the complexes **16**–**18**, comprising of nitrogen-unsubstituted heterocycles. Strong broadening of these bands may be explained by intramolecular hydrogen-bonding with coordinated nitrate ions. The presence of these bands indicates that the heterocycles are coordinated in their neutral, not anionic forms.

Acetylacetonate and 2,2′-bipyridyl, as well as bis(pyrazol-1-yl)methane derivatives are certainly bidentate ligands. It can be assumed that the coordination sphere of the complexes **11**–**14** consists of two organic bidentate ligands and one nitrate ion is also coordinated in a bidentate fashion as follows from the IR data (see example in Fig. 2). The central copper(II) ion in these complexes is therefore hexacoordinated, and the second nitrate ion remains uncoordinated. This is consistent with the detection of two bands in the out-of-plane bending vibrations area (800–830 cm^{-1}, Table 1). Presumably, one of them is related to bound NO_3^- ions and the other is due to the free nitrate ions. Apparently, the remaining bands of the free nitrate ions overlap with the bands of organic ligands and were not registered.

The same conclusions about hexacoordination of the copper(II) ion can be made for the complexes **15**–**18** containing two monodentate molecules of triphenylphosphine or nitrogen-containing heterocycle, one bidentate molecule of L^2 ligand and one bidentate nitrate-ion, while the second NO_3^- ion remains in the outer sphere (Fig. 3).

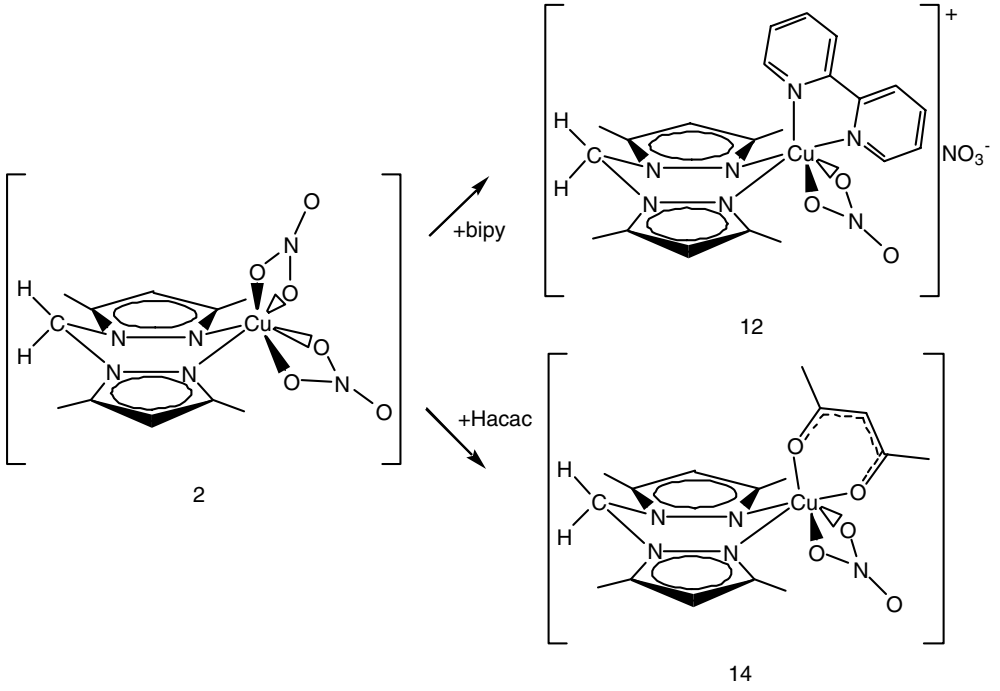

Fig. 2. Synthesis of bis(pyrazol-1-yl)methane-copper(II) mixed-ligand complexes with bidentate ligands.

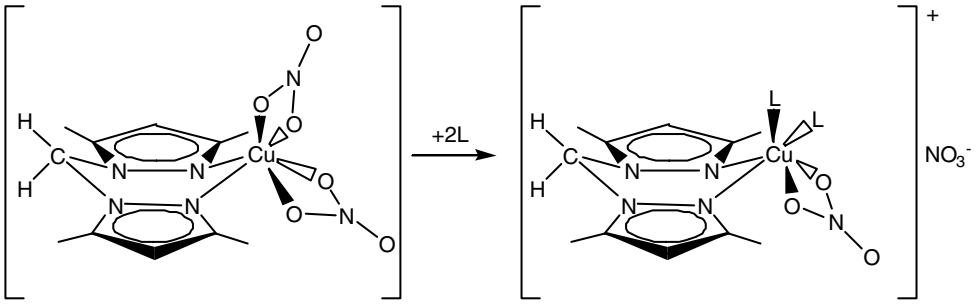

Fig. 3. Synthesis of bis(pyrazol-1-yl)methane-copper(II) mixed-ligand complexes with monodentate ligands.

3.4. Cyclic voltammetry

We have also carried out a cyclic voltammetric study of the synthesized homo- and mixed-ligand coordination compounds. Complexes of copper(II) nitrate and chloride **1**–**10** as well as mixed-ligand complexes **11**–**18** undergo a quasi-reversible (or reversible in case of the complex **6**) reduction on a mercury-film electrode in the range of potentials from −111 to −214 mV. Furthermore, cyclic voltammograms of several mixed-ligand complexes demonstrate additional peaks which are probably associated with the electrochemical activity of the organic ligands. Thus, the complex $[Cu(L^2)(PPh_3)_2(O_2NO)](NO_3)$ (**15**) undergoes a quasi-reversible reduction at a formal potential of −829 mV (relative to the saturated Ag/AgCl electrode) and the complex $[Cu(L^2)(BImH)_2(O_2NO)](NO_3)$ (**16**) is reduced at −509 mV. In the case of $[Cu(L^2)(Me_2PyrH)_2(O_2NO)](NO_3)$ (**18**) an irreversible reduction wave at −559 mV and a reversible one at a formal potential of −722 mV were observed.

Many copper complexes can mimic metalloenzymes, superoxide dismutase (SOD) being one of them. Li et al. pointed out that in order to act as a SOD mimic, the copper complex should have a redox potential in the range −0.36 ... +0.69 V (vs. the saturated Ag/AgCl electrode) [27]. Furthermore, the higher the redox potential $E_{1/2}$ and the greater the reversibility of the electrode process (characterized by the $\Delta E = E_{p.a.} - E_{p.c.}$ value), the higher the antioxidant activity of a given complex. As is seen from our cyclic voltammetry data, all of the complexes meet the specified requirements, and the highest SOD-like activity should be expected for complexes **6, 2**, **13**, **11** (in descending order of activity). A detailed study of the antioxidant properties of bis(pyrazol-1-yl)methane–copper(II) complexes will be reported elsewhere.

4. Conclusions

In summary, novel coordination compounds of copper(II) with bis(pyrazol-1-yl)methane derivatives are reported in this paper. The complexes synthesized reacted with a number of mono- and bidentate ligands yielding mixed-ligand complexes. No examples of bis(pyrazol-1-yl)methane mixed-ligand complexes with these ligands have been reported previously.

References

[1] C. Pettinari, R. Pettinari, Coord. Chem. Rev. 249 (2005) 663.
[2] J. Reedijk, J. Verbiest, Transit. Met. Chem. 4 (1979) 239.
[3] M. Mesubi, F. Anumba, Transit. Met. Chem. 10 (1985) 5.
[4] M. Mesubi, J. Coord. Chem. 13 (1984) 179.
[5] C. Pettinari, G. Lobbia, A. Lorenzotti, A. Cingolani, Polyhedron 14 (1995) 793.
[6] C. Pettinari, C. Santini, D. Leonesi, P. Cecchi, Polyhedron 13 (1994) 1553.
[7] F. Bonati, A. Cingolani, G. Lobbia, D. Leonesi, A. Lorenzotti, C. Pettinari, Gazz. Chim. Ital. 120 (1990) 341.
[8] C. Pettinari, G. Lobbia, G. Sclavi, D. Leonesi, M. Colapietro, G. Portalone, Polyhedron 14 (1995) 1709.
[9] C. Pettinari, F. Marchetti, R. Polimante, A. Cingolani, G. Portalone, M. Colapietro, Inorg. Chim. Acta 249 (1996) 215.
[10] C–C. Chou, C–C. Su, A. Yeh, Inorg. Chem. 44 (2005) 6122.
[11] C–C. Chou, C–C. Su, H-L. Tsai, K-H. Lii, Inorg. Chem. 44 (2005) 628.
[12] A.S. Potapov, A.I. Khlebnikov, Izv. vuzov. Ser. Khim i khim. technol. 7 (2003) 66.
[13] S. Julia, P. Sala, J. del Mazo, M. Sancho, C. Ochoa, J. Elguero, J.-P. Fayet, M.-C. Vertut, J. Heterocycl. Chem. 19 (1982) 1141.
[14] S. Trofimenko, J. Am. Chem. Soc. 70 (1970) 5118.
[15] A.S. Potapov, A.I. Khlebnikov, S.F. Vasilevsky, Russ. J. Org. Chem., accepted for publication.
[16] B.M. Gatehouse, S.E. Livingstone, R.S. Nyholm, J. Chem. Soc. (1957) 4222.
[17] N.F. Curtis, Y.M. Curtis, Inorg. Chem. 4 (1965) 804.
[18] A.B.P. Lever, E. Mantovani, B.S. Ramaswamy, Can. J. Chem. 49 (1971) 1957.
[19] K. Nakamoto, Infrared Spectra of Inorganic and Coordination Compounds, Wiley, New York, 1986.
[20] A.B.P. Lever, Inorganic Electronic Spectra, Elsevier, Amsterdam, 1984.
[21] M. Afzaal, E. Flynn, M.A. Malik, P. O'Brien, M. Motevalli, Polyhedron 24 (2005) 1101.
[22] N. Gianneschi, M. Masar III, C. Mirkin, Acc. Chem. Res. 38 (2005) 825.
[23] C.S. Rondetvedt, P.K. Chang, J. Am. Chem. Soc. 77 (1955) 6532.
[24] R.C. Lord, A.L. Marston, F.A. Miller, Spectrochim. Acta 9 (1957) 113.
[25] B. Stuart, Infrared Spectroscopy, Wiley, New York, 2004.
[26] G. Davidson (Ed.), Spectroscopic Properties of Inorganic and Organometallic Compounds, vol. 34, Royal Society of Chemistry, 2001.
[27] D. Li, S. Li, D. Yong, J. Yu, J. Huang, Y. Li, W. Tang, Inorg. Chem. 24 (2003) 6071.

dried over NaK and vacuum transferred prior to use. ^{1}H, ^{13}C, ^{19}F, ^{207}Pb NMR spectra were recorded with Bruker DRX 400 MHz and Omega 500 MHz spectrometers. ^{19}F NMR spectra were referenced to $FCCl_3$ in C_6D_6 ($\delta = 0$). ^{207}Pb NMR spectra were referenced to $Pb(NO_3)_2$ 1 M in H_2O ($\delta = -2961.2$) [14]. Infrared spectra were recorded as thin films from benzene using a Perkin–Elmer 2000 FTIR spectrometer. Elemental analyses were performed by Desert Analytics (Tucson, AZ). MS (ES) analyses were recorded on a Micromass LCT spectrometer.

2.2. Synthesis of Pb(hfac)$_2$(diglyme) (1)

Hexafluoroacetylacetone (493 mg, 2.37 mmol) in ca 15 mL of toluene was added dropwise to a stirred suspension of PbO (210 mg, 0.94 mmol) in diglyme (148 mg, 1.10 mmol). The solution rapidly became clear and light yellow within 30 min. Solvent was removed in vacuo to give a yellow powder. Crystals of **1** (458 mg, 0.60 mmol, 64%) suitable for X-ray diffraction were obtained from diethyl ether at room temperature; m.p.: 69 °C. Complex **1** sublimes at 35 °C at 2×10^{-5} Torr. *Anal.* Calc. for $C_{16}H_{16}F_{12}O_7Pb$: C, 25.43; H; 2.12; F, 30.16; Pb, 27.43. Found: C, 25.43; H, 2.62; F, 30.26; Pb, 26.82%. ^{1}H NMR (C_6D_6): δ 2.91 (8 H, OCH_2CH_2O), 3.06 (6 H, OCH_3), 6.13 (2 H, $OCCHCO$); ^{13}C (C_6D_6): δ 58.76 (OCH_3), 70.15, 71.15 (OCH_2CH_2O), 91.78 ($OCCHCO$), 121.23 (q, CF_3), 176.62 (q, $CCOCF_3$); ^{19}F NMR (C_6D_6): δ −79.52. ^{207}Pb NMR (C_6D_6): δ −2097.9. IR 3138 w, 3002 w, 2933 s, 2846 m, 1952 w, 1913 w, 1729 w, 1673 s, 1641 s, 1594 m, 1552 s, 1532 s, 1492 s, 1463 s, 1381 w, 1354 w, 1340 m, 1319 m, 1255 vs, 1200 vs, 1145 vs, 1088 s, 1010 m, 944 m, 857 m, 830 m, 798 s, 768 m, 740 m, 662 s, 580 s, 523 m cm^{-1}. MS (ES) 415 $[Pb(hfac)]^+$, 549 $[Pb(hfac)(diglyme)]^+$.

2.3. Synthesis of [(18-crown-6)K(hfac)]$_n$ (2)

K (4 mg, 0.10 mmol) was added to ca 5 mL of toluene containing 18-crown-6 (28 g, 0.11 mmol) and stirred for 2 h. The resulting mixture was added dropwise to $Pb(hfac)_2$(diglyme) (84 g, 0.11 mmol) in 5 mL of toluene. The solution immediately formed a gray-black precipitate which turned drab green within an hour and was allowed to stir overnight. The resulting orange solution was separated from gray-black insolubles by centrifugation. Removal of solvent in vacuo left an orange powder. Crystals of $[(18\text{-crown-6})K(hfac)]_n$ were obtained from a toluene solution of the orange powder at −35 °C.

2.4. X-ray data collection, structure solution and refinement

A colorless crystal of **1** of approximate dimensions $0.28 \times 0.30 \times 0.32$ mm and a yellow crystal of **2** of approximate dimensions $0.15 \times 0.28 \times 0.29$ mm were each mounted on a glass fiber and transferred to a Bruker CCD platform diffractometer. The SMART [15] program package was used to determine the unit-cell parameters and for data collection (25 sec/frame scan time for a sphere of diffraction data). The raw frame data were processed using SAINT [16] and SADABS [17] to yield the reflection data file. Subsequent calculations were carried out using the SHELXTL [18] program. There were no systematic absences nor any diffraction symmetry other than the Friedel condition. The centrosymmetric triclinic space group $P\bar{1}$ was assigned for both **1** and **2** and was later determined to be correct (see Table 1).

Table 1
X-ray data collection parameters for $[Pb(hfac)_2(\mu\text{-}\eta^3{:}\eta^1\text{-diglyme})]_2$ (**1**) and $[(18\text{-crown-6})K(hfac)]_n$ (**2**)

Empirical formula	$C_{16}H_{16}F_{12}O_7Pb$ (**1**)	$C_{17}H_{25}F_6O_8K$ (**2**)
Formula weight	755.48	510.47
Temperature (K)	163(2)	163(2)
Crystal system	triclinic	triclinic
Space group	$P\bar{1}$	$P\bar{1}$
a (Å)	10.0794(10)	8.7662(16)
b (Å)	10.7790(11)	9.2344(17)
c (Å)	11.9284(12)	14.376(3)
α (°)	74.665(2)	71.996(3)
β (°)	70.677(2)	89.864(3)
γ (°)	85.778(2)	87.148(3)
Volume (Å^3)	1179.3(2)	1105.3(4)
Z	2	2
ρ_{calc} (Mg/m^3)	2.128	1.534
μ (mm^{-1})	7.282	0.331
R_1 [$I > 2.0\sigma(I)$]	0.0275	0.0694
wR_2 (all data)	0.0783	0.1850

The structures were solved by direct methods and refined on F^2 by full-matrix least-squares techniques. The analytical scattering factors [19] for neutral atoms were used throughout the analysis. Hydrogen atoms were included using a riding model. In **2**, the fluorine atoms F(4), F(5) and F(6) were disordered and included using multiple components with partial site-occupancy-factors.

3. Results and discussion

3.1. Synthesis of Pb(hfac)$_2$(diglyme) (1)

A hexafluoroacetylacetonate complex of lead can be readily synthesized in air by reacting hexafluoroacetylacetone [H(hfac)] with lead(II) oxide and diglyme in toluene, Eq. (2). This synthesis is analogous to the preparation of Ln(hfac)$_3$(diglyme) [1–3], Eq. (1). The solution turns yellow almost immediately as the suspension of PbO is rapidly consumed leaving a clear solution. The reaction reaches completion typically within an hour at room temperature. In contrast, the Ln(hfac)$_3$(diglyme) syntheses require several hours at reflux [1–3], which is typical of syntheses of other metal hfac complexes [1–4,20,21]. Crystallization from diethyl ether of the yellow powder obtained from the reaction mixture gives crystals of $[Pb(hfac)_2(\mu\text{-}\eta^3{:}\eta^1\text{-diglyme})]_2$ (**1**) suitable for X-ray analysis, Fig. 1

$$PbO + \text{diglyme} + 2Hhfac \rightarrow Pb(hfac)_2(\text{diglyme}) + H_2O \quad (2)$$

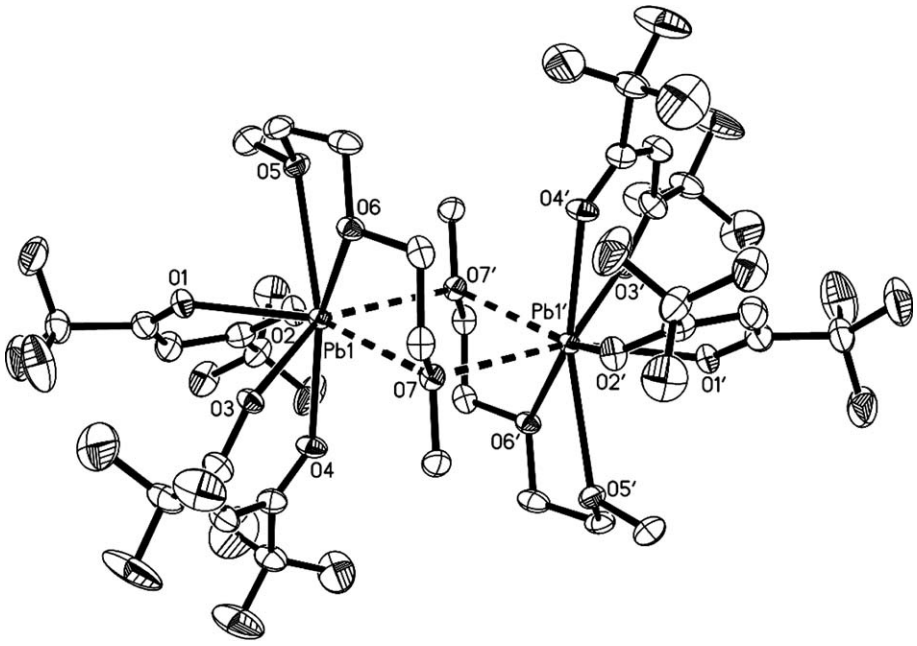

Fig. 1. Thermal ellipsoid plot of the $[Pb(hfac)_2(\mu\text{-}\eta^3{:}\eta^1\text{-diglyme})]_2$ dimer (**1**) with hydrogen atoms omitted for clarity and ellipsoids drawn at the 50% probability level.

Elemental analysis as well as NMR spectroscopy were consistent with the composition $Pb(hfac)_2(diglyme)$. The ^1H and ^{13}C NMR spectra of **1** in C_6D_6 contained a single set of signals for the diglyme protons (methylene hydrogens at δ 2.91 ppm and the methyl hydrogens at δ 3.06 ppm) and carbons (methyl carbon at δ 58.76 ppm and methylene carbons at δ 70.15 and 71.15 ppm). In an HMQC-NMR experiment, both of the methylene carbons in the ^{13}C NMR spectrum correlated with the single peak in the ^1H NMR. The ^{19}F and ^{207}Pb NMR spectra each contained single signals at δ −79.52 and −2098 ppm, respectively. Complex **1** has a ^{207}Pb resonance consistent with an oxygen coordinated ligand system [14]. The closest divalent lead complex with a fluorinated oxygen bound ligand [14] is $Pb(O_2CC_6F_5)_2$, which has a ^{207}Pb resonance at δ −1044 ppm [22]. The more negative value for **1** suggests that $Pb(hfac)_2(diglyme)$ has a coordination number greater than four [14], thus indicating at least some coordination of the diglyme to the lead in solution.

3.2. Structure of $[Pb(hfac)_2(\mu\text{-}\eta^3{:}\eta^1\text{-diglyme})]_2$ (**1**)

In the solid state, **1** exists as a racemic pair of enantiomers in which one diglyme oxygen of one monomeric unit is oriented toward the lead of the other, Figs. 1 and 2. Selected bond distances and angles are given in Table 2.

Each lead in **1** is coordinated by two hfac ligands with Pb–O distances in the range 2.417(3)–2.497(3) Å. Comparison of these distances with two other lead(II) β-diketonates shows a wide range of Pb–O lengths in these compounds. The Pb–O distances in **1** are up to 0.2 Å longer than those in bis(2,2,6,6,-tetramethylheptane-3,5-dionato)lead, $Pb(Me_3CCOCH_2COCMe_3)_2$, which has Pb–O distances of 2.287(9)–2.303(8) Å [20]. Bis(2,2-dimethyl-6,6,7,7,8,8,8-heptafluorooctane-3,5-dionato)lead, $Pb(CF_3CF_2CF_2COCH_2COCMe_3)_2$, has a range of Pb–O distances, 2.272(6)–2.410(5) Å [20], that overlaps those in both complexes. The Pb–O distances are shorter than the Ln–O distances of $Ln(hfac)_3(diglyme)$ (Ln = La, Sm, Eu, Gd, Tb) complexes [1–3] after correcting for variations in atomic radii [11]. For example, $Sm(hfac)_3(diglyme)$ has Sm–O distances of 2.386(1)–2.437(1) Å. Since the 1.079 Å eight coordinate radius of Sm is 0.21 Å shorter than that of Pb^{2+} [11], the comparable lead length in **1** would be 2.596–2.647 Å.

All of the Pb–O(diglyme) distances are longer than the Pb–O(hfac) distances. The Pb–O distances of 2.706(3) and 2.759(3) Å for the diglyme oxygen atoms, O(5) and O(6), respectively, are distinctly shorter than that of the third diglyme oxygen, O(7), which is found 2.851(3) Å from Pb(1). However, each O(7) is also oriented towards the other lead center, Pb(1′), at a distance of 3.021(3) Å.

If the long bridging Pb–O linkages are included in the coordination sphere of each metal, the formal coordination number is eight. These eight donor atoms do not describe one of the typical eight coordinate geometries [23], a result that may be due to the effect of a stereoactive lone pair. Lead complexes with this effect are described as "hemidirected" as opposed to "holo-directed" [4] when no void or perturbation is found in the sphere around the metal. The most open area in the coordination sphere of **1** is shown in the view in Fig. 3. It can be seen from this orientation that part of the coordination sphere contains no donor atoms.

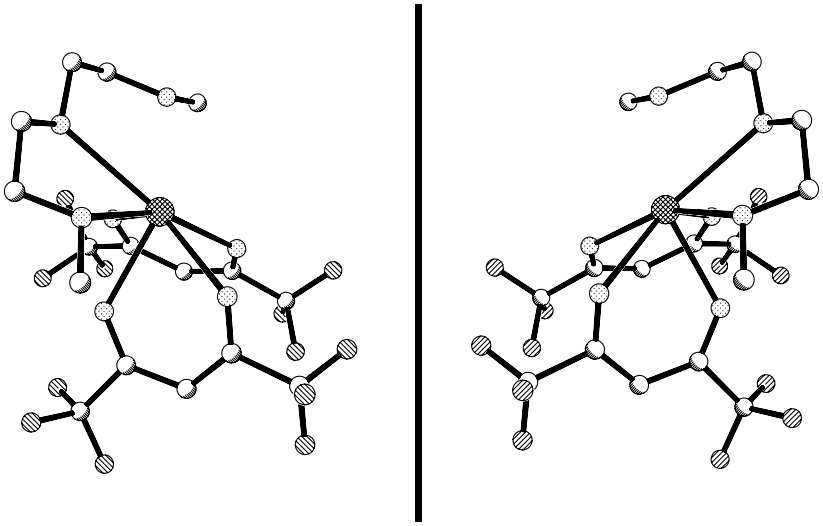

Fig. 2. The two enantiomeric units of $Pb(hfac)_2(diglyme)$ (**1**) shown as mirror images.

Table 2
Selected bond distances (Å) and angles (°) for $[Pb(hfac)_2(\mu\text{-}\eta^3{:}\eta^1\text{-diglyme})]_2$ (**1**)

Compound **1**	
Pb(1)–O(1)	2.417(3)
Pb(1)–O(2)	2.497(3)
Pb(1)–O(3)	2.476(3)
Pb(1)–O(4)	2.444(3)
Pb(1)–O(5)	2.706(3)
Pb(1)–O(6)	2.759(3)
Pb(1)–O(7)	2.851(3)
Pb(1)–O(7′)	3.021(3)
O(6)–Pb(1)–O(7′)	101.68(9)
O(1)–Pb(1)–O(2)	72.54(11)
O(4)–Pb(1)–O(3)	72.56(11)
O(5)–Pb(1)–O(6)	61.32(11)
O(6)–Pb(1)–O(7)	60.83(10)
O(7)–Pb(1)–O(7′)	83.94(9)
Pb(1)–O(7)–Pb(1′)	96.07

The unsymmetrical nature of the coordination sphere of **1** can best be evaluated by comparing it to the structure of the closely related $[Ba(thd)_2(diglyme)]_2$ (**3**) [24] Fig. 3 (thd = ^{t}BuC(O)CHC(O)^{t}Bu). The barium complex not only has the same composition, but the diglyme ligand bridges in a similar $\eta^3{:}\eta^1$ manner. Fig. 3 presents a view of **3** analogous to that of **1**, which shows how the full coordination sphere of a metal can be filled by this ligand set.

The differences in the orientation of diglyme in **1** versus that in **3** can be seen in several structural features. The O(6)–Pb(1)–O(7′) in **1** is 101.68(9)° compared to the analogous angle of 89.4(2)° in **3**. Similarly, the 83.94(9)° O(7)–Pb(1)–O(7′) angle in **1** is wider than the corresponding 64.4(2)° angle between the bridging oxygens and the metal in **3**. These angles show that even though lead is the smaller metal, the diglyme oxygens in **1** bend away from this part of the coordination sphere. In addition, the 2.851(3) Å Pb(1)–O(7) distance of the bridging diglyme oxygen in **1**

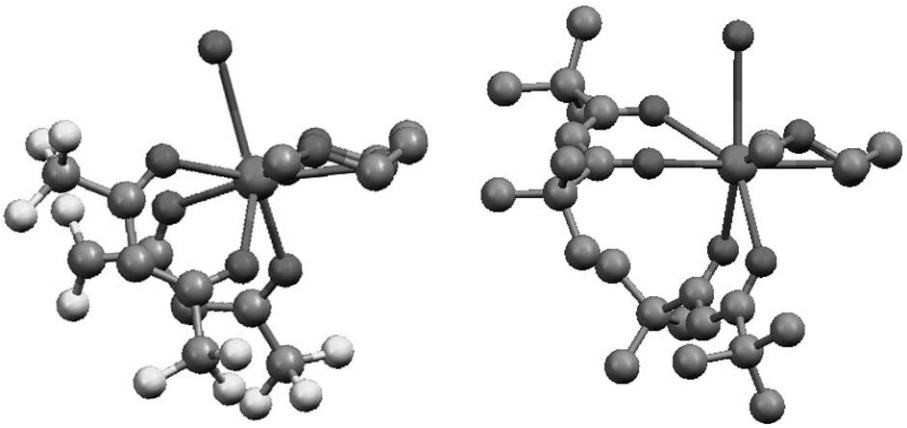

Fig. 3. Comparison of monomer units of $[Pb(hfac)_2(\mu\text{-}\eta^3{:}\eta^1\text{-diglyme})]_2$ (**1**, left) and $[Ba(thd)_2(diglyme)]_2$ (**3**, right). Both views show the coordinated diglyme oxygen in the top center. The barium complex had its ligands oriented more globally around the metal than the lead complex, which has open space in the upper right quadrant.

is much longer than either Pb(1)–O(6) or Pb(1)–O(5) at 2.759(3) and 2.706(3) Å, respectively. In contrast, the Ba–O(diglyme) distances in **3** are in the narrow range of 2.857(6)–2.888(6) Å.

3.3. Stability and volatility of Pb(hfac)$_2$(diglyme) (*1*)

The addition of diglyme to the coordination sphere of Pb(hfac)$_2$ appears to make **1** both more thermally stable and more resistant to coordination of water. Only a simple recrystallization is necessary to obtain a water-free diglyme complex, whereas Pb(hfac)$_2$ will coordinate water, even in the solid state [20]. In addition, crystals of **1** are stable at ambient temperatures for months compared to Pb(hfac)$_2$ which has a more limited lifetime [20].

Complex **1** shows a melting point of 69 °C, which is significantly lower than the 156 °C value of Pb(hfac)$_2$ [9,20]. Consistent with this, the volatility of complex **1** is high: it sublimes at 35 °C (ca 2×10^{-5} Torr). This combination of stability and volatility is not always found with metal hfac complexes [5,6,20,21], although it is consistent with the stabilizing presence of diglyme as a ligand [1–3,25], as in the Ln(hfac)$_3$(diglyme) series.

3.4. Reactivity of *1* with potassium

The addition of potassium to Ln(hfac)$_3$(diglyme) complexes containing both redox active (Eu, Sm, Nd) and traditionally redox inactive (Gd) metals has previously been found to lead to C–F bond activation and cleavage [1] with the formation of fluoride "ate" salts, Eq. (3).

$$2\mathrm{Ln(hfac)_3(diglyme)} + 2\mathrm{K} \rightarrow [\mathrm{LnF(hfac)_3K(diglyme)}]_2 \quad (3)$$

In order to compare this reactivity with that of the lead complex, **1** was treated with K and 18-crown-6 in toluene. The reaction generates a series of color changes

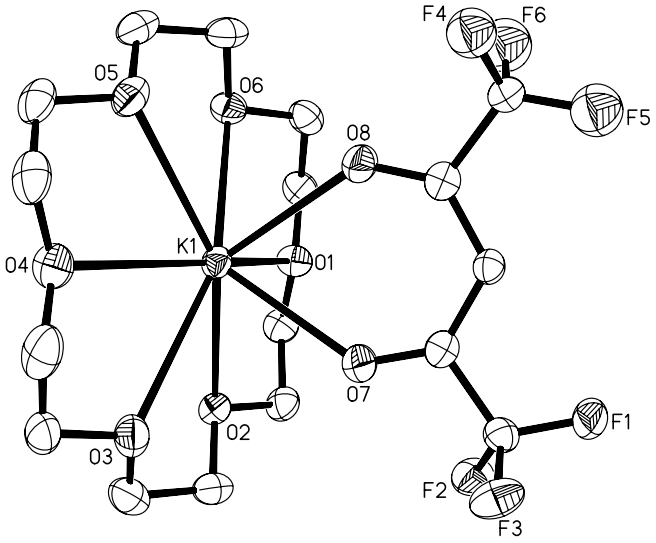

Fig. 4. Thermal ellipsoid plot of the monomer of [(18-crown-6)K(hfac)]$_n$ (**2**) with hydrogen atoms omitted for clarity and ellipsoids drawn at the 50% probability level.

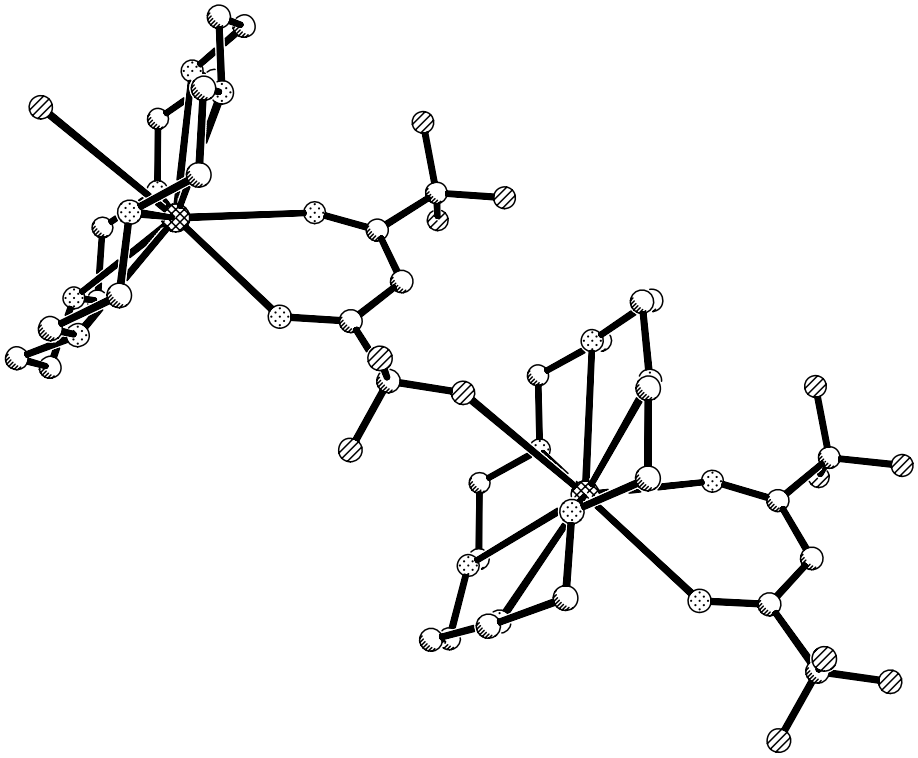

Fig. 5. Ball and stick representation of the polymer chain of [(18-crown-6)K(hfac)]$_n$ (**2**).

Table 3
Selected bond distances (Å) and angles (°) for $[(18\text{-crown-6})K(hfac)]_n$ (**2**)

Compound **2**	
K(1)–O(1)	2.802(3)
K(1)–O(2)	2.898(3)
K(1)–O(3)	2.953(3)
K(1)–O(4)	2.876(3)
K(1)–O(5)	2.864(3)
K(1)–O(6)	2.941(3)
K(1)–O(7)	2.690(3)
K(1)–O(8)	2.770(3)
K(1)–F(5B′)[a]	2.934(7)
K(1)–F(5′)	3.081(6)
O(7)–K(1)–O(8)	65.10(8)
C(17)–F(5)–K(1′)	147.0(4)
C(17)–F(5B)–K(1′)[a]	155.4(5)

[a] F5B is one of the disordered positions of F5.

as well as a complex ^1H NMR spectrum that suggest that this is a complicated reaction system. The only product definitively identified from the mixture was $[(18\text{-crown-6})K(hfac)]_n$ (**2**) which was characterized by X-ray crystallography, Fig. 4. Since K(hfac) is not readily soluble in toluene, the crown ether evidently brought this ligand into solution.

Only one other solid state structure of an 18-crown-6 adduct of a potassium β-diketonate is in the literature: (18-crown-6)K[$Me_3C(O)CHCO_2Et$] [26] (**4**). The K–O (crown ether) distances in **2** and **4** are similar, as are the K–O(acetylacetonate) lengths: 2.690(3) and 2.770(3) Å for K(1)–O(7) and K(1)–O(8), respectively, in **2**, and 2.650 and 2.732 Å in **4**. Complex **2** is different from **4** in that it contains a short F(5B)–K(1′) distance, 2.934(7) Å, that is comparable to the K(1)–O(3) and K(1)–O(6) crown ether distances of 2.953(3) and 2.941(3) Å, respectively. This produces the chain structure shown in Fig. 5. No short intermolecular contacts were found in **4** (see Table 3).

4. Conclusion

An hfac diglyme complex of lead can be prepared from PbO and Hhfac more easily than the analogous syntheses of Ln(hfac)$_3$(diglyme) complexes. The $[Pb(hfac)_2(\mu\text{-}\eta^3{:}\eta^1\text{-diglyme})]_2$ complex exists in the solid state as a dimer of chiral enantiomers connected with the third diglyme oxygen of one unit oriented toward the Pb of the other. Despite the dimeric structure, the complex is quite volatile. Treatment of $[Pb(hfac)_2(\mu\text{-}\eta^3{:}\eta^1\text{-diglyme})]_2$ with K/18-crown-6 forms $[(18\text{-crown-6})K(hfac)]_n$ that exists in the solid state as a linear polymeric chain via CF_3–K interactions.

Acknowledgements

We thank the Chemical Sciences, Geosciences, and Biosciences Division of the Office of Basic Energy Sciences of the Department of Energy for support and Dr. Philip R. Dennison for assistance with the ^{207}Pb NMR spectra.

Appendix A. Supplementary material

Crystallographic data for **1** (CCDC No. 290349) and **2** (CCDC No. 290350) have been deposited with the Cambridge Crystallographic Data Centre. These data can be obtained free of charge via www.ccdc.cam.ac.uk, or by contacting The Cambridge Crystallographic Data Centre, 12 Union Road, Cambridge CB2 1EZ, UK; fax: +44 1223 336033 (e-mail: deposit@ccdc.cam.ac.uk). Supplementary data associated with this article can be found, in the online version, at doi:10.1016/j.poly.2006.03.011.

References

[1] W.J. Evans, D.G. Giarikos, M.A. Johnston, M.A. Greci, J.W. Ziller, J. Chem. Soc., Dalton Trans. (2002) 520.
[2] G. Malandrino, C. Benelli, F. Catelli, I.L. Fragalà, Chem. Mater. 10 (1998) 3434.
[3] G. Malandrino, O. Inoctro, F. Castelli, I.L. Fragalà, Chem. Mater. 8 (1996) 1292.
[4] L. Shimoni-Livny, J.P. Glusker, C.W. Bock, Inorg. Chem. 37 (1998) 1853.
[5] N. Kuzimina, M. Ryazanov, S. Troyanov, Polyhedron 18 (1999) 2177.
[6] V.V. Krisyuk, A.E. Turgambaeva, I.K. Igumenov, Chem. Vap. Depos. 4 (1998) 43.
[7] W.J. Evans, D.G. Giarikos, D. Josell, J.W. Ziller, Inorg. Chem. 42 (2003) 8266.
[8] J.A. Darr, M. Poliakoff, A.J. Blake, W.-S. Li, Inorg. Chem. 37 (1998) 5491.
[9] G.K. Schweitzer, B.P. Pullen, Y.-H. Fang, Anal. Chim. Acta 43 (1968) 332.
[10] G. Malandrino, I.L. Fragalà, S. Aime, W. Dastrù, R. Gobetto, C. Benelli, J. Chem. Soc., Dalton Trans. (1998) 1509.
[11] R.D. Shannon, Acta. Crystallogr. A32 (1976) 751.
[12] R.D. Hancock, M.S. Shaikjee, S.M. Dobson, J.C.A. Boeyens, Inorg. Chim. Acta 154 (1988) 229.
[13] D.J. Teff, J.C. Huffman, K.G. Caulton, Inorg. Chem. 34 (1995) 2491.
[14] B. Wrackmeyer, K. Horschler, Ann. Rep. NMR Spectrosc. 22 (1989) 249.
[15] SMART Software Users Guide, Version 5.1, Bruker Analytical X-ray Systems, Inc., Madison, WI, 1999.
[16] SAINT Software Users Guide, Version 6.0, Bruker Analytical X-ray Systems, Inc., Madison, WI, 1999.
[17] G.M. Sheldrick, SADABS, Version 2.10, Bruker Analytical X-ray Systems, Inc., Madison, WI, 2002.
[18] G.M. Sheldrick, SHELXTL, Version 6.12, Bruker Analytical X-ray Systems, Inc., Madison, WI, 2001.
[19] International Tables for X-ray Crystallography, vol. C., Kluwer Academic Publishers, Dordrecht, 1992.
[20] M.A. Malik, P. O'Brian, M. Motevalli, A.C. Jones, T. Leedham, Polyhedron 18 (1999) 1641.
[21] V.V. Krisuk, S.V. Sysoev, N.E. Fedotova, I.K. Igumenov, N.V. Grigorieva, Thermochim. Acta 307 (1997) 107.
[22] P.G. Harrison, M.A. Healy, A.T. Steel, J. Chem. Soc., Dalton Trans. (1983) 1845.
[23] D.L. Kepert, Prog. Inorg. Chem. 24 (1978) 179.
[24] S.R. Drake, M.B. Hursthouse, K.M. Abdul Malik, S.A.S. Miller, Inorg. Chem. 32 (1993) 4653.
[25] (a) G. Malandrino, I.L. Fragalà, D.A. Neumayer, C.L. Stern, B.J. Hinds, T.J. Marks, J. Mater. Chem. 4 (1994) 1061;

(b) S.-J. Kang, Y.S. Jung, Y.S. Sohn, Bull. Korean Chem. Soc. 18 (1997) 75;
(c) G. Malandrino, F. Castellli, I.L. Fragalà, Inorg. Chim. Acta 224 (1994) 203;
(d) G. Malandrino, R. Licata, F. Castelli, I.L. Fragalà, Inorg. Chem. 34 (1995) 6233.
[26] C. Cambillau, G. Bram, J. Corset, C. Riche, C. Pascard-Billy, Tetrahedron 34 (1978) 2675.

formed to one in which it is greatly weakened. In this case, even if the lability of the amines is still linearly related to their basicity, the constant *b* for unhindered pyridines, that is their lability, is smaller than the one of other sp^3 aliphatic N-donors bases and evidences have been presented for a significant contribution of a π interaction between the filled d orbitals of the metal and the empty antibonding orbitals of the pyridine ring, that contributes to the stabilization of the ground state of the substrates. This suggestion seems to be in agreement with further deviations observed for pyridines having a *para*-substituent able to contribute to the π system [1,3]. In order to improve these experimental observations and the range of applicability of the proposed interpretation, we have now extended our study to five-membered nitrogen donors (thiazoles and isostructural species such as oxazole, isoxazole, imidazole and pyrazoles) by measuring the kinetics of the forward and reverse steps of the process (1).

$$[Pt(terpy)Cl]^+ + nu \rightleftharpoons [Pt(terpy)(nu)]^{2+} + Cl^- \quad (1)$$

(nu = thiazole, 4-methylthiazole, 4,5-dimethylthiazole, 5-methylthiazole, oxazole, isoxazole, imidazole, 3,5-dimethylpyrazole, pyrazole and only for the reverse reaction 2-aminothiazole and benzothiazole). The kinetics were carried out in methanol at 25 °C in order to directly compare the results with those obtained with other nitrogen donors under the same experimental conditions [3] and to widen and complete our precedent study regarding only two unhindered five-membered N-donors [5]. The great importance of ligand substitution reactions on $[Pt(terpy)L]^{n+}$ substrates is underlined by the recent publication of a number of papers regarding kinetics and mechanism of the reactions between biologically relevant ligands and the $[PtCl(terpy)]^+$ or $[Pt(H_2O)(terpy)]^{2+}$ cations [6–8].

2. Experimental

2.1. Materials

2,2′,6,2″-Terpyridine was purchased from Aldrich. Pure reagent-grade LiCl, CH_3SO_3Na, CH_3SO_3H, $AgClO_4$ (Aldrich) were used without further purification. The thiazoles, oxazole, isoxazole, imidazole and pyrazoles were recrystallized or distilled before use when necessary. Anhydrous MeOH was obtained by distillation over Mg wires, but traces of water did not appear to have any appreciable effect upon the reactions.

2.2. Instruments

Electronic spectra and kinetic measurements were obtained on a Perkin–Elmer Lambda 15 spectrophotometer. ^{1}H NMR spectra were taken on Bruker Avance 300 or Bruker AC 200 spectrometers. Elemental analyses were performed by the Microanalytical Laboratory of the University of Padua.

2.3. Preparation of complexes

$[Pt(terpy)Cl]ClO_4$ was prepared starting from *cis*/*trans*-$[PtCl_2(SMe_2)_2]$ as reported in the literature [9].

All other complexes of the type $[Pt(terpy)(nu)](ClO_4)_2$ (nu = thiazole, 4-methylthiazole, 3,5-dimethylthiazole, 5-methylthiazole, $2NH_2$-thiazole, benzothiazole, oxazole, isoxazole, imidazole, pyrazole and 3,5-dimethypyrazole) were prepared as follows. $AgClO_4$ (0.103 g, 0.5 mmol) was added, under stirring in the dark, to a warm mixture (10 ml, 50 °C) of $[Pt(terpy)Cl]ClO_4$ (0.281 g, 0.5 mmol) in nitromethane. After 10 min, the AgCl formed was filtered off and the solution was treated with 0.5 mmol of the nitrogen ligand, stirred for 15 min and finally diethylether (50 ml) was added. The powdery product precipitated was filtered off, washed twice with diethylether and dried in vacuo. Yields >80% in all cases. Analytical and ^{1}H NMR data for the complexes are collected in Tables 1 and 2, respectively.

^{1}H NMR for coordinated five-membered N-donors are given according to Scheme 1.

2.4. Kinetics

The reactions were initiated by adding a 0.05 mol dm^{-3} dimethylformamide solution (2–20 μl) of the substrate complex, $[Pt(terpy)Cl]^+$ or $[Pt(terpy)(nu)]^{2+}$ to a methanolic solution (3 cm^{-3}) of the appropriate reagent, the nitrogen donor or chloride ion respectively, previously brought to the reaction temperature (25 °C) in a thermostatted cell in

Table 1
Analytical data

Complex	Analysis[a] (%)		
	C	H	N
$[Pt(terpy)Cl](ClO_4)$	31.7 (32.0)	2.13 (1.97)	7.41 (7.46)
$[Pt(terpy)(thiazole)](ClO_4)_2$	30.5 (30.3)	1.84 (1.98)	7.75 (7.86)
$[Pt(terpy)(4\text{-methylthiazole})](ClO_4)_2$	31.3 (31.4)	2.07 (2.22)	7.68 (7.71)
$[Pt(terpy)(4,5\text{-dimethylthiazole})](ClO_4)_2$	32.2 (32.4)	2.38 (2.45)	7.39 (7.57)
$[Pt(terpy)(5\text{-methylthiazole})](ClO_4)_2$	31.56 (31.42)	2.02 (2.22)	7.83 (7.71)
$[Pt(terpy)(2\text{-aminothiazole})](ClO_4)_2$	30.0 (29.7)	2.14 (2.08)	9.51 (9.63)
$[Pt(terpy)(benzothiazole)](ClO_4)_2$	35.6 (35.6)	1.98 (2.21)	7.12 (7.23)
$[Pt(terpy)(oxazole)](ClO_4)_2$	31.2 (31.0)	2.24 (2.03)	8.12 (8.05)
$[Pt(terpy)(isoxazole)](ClO_4)_2$	31.1 (31.0)	2.17 (2.03)	7.91 (8.05)
$[Pt(terpy)(pyrazole)](ClO_4)_2$	31.3 (31.1)	2.22 (2.17)	10.2 (10.1)
$[Pt(terpy)(3,5\text{-dimethylpyrazole})](ClO_4)_2$	32.9 (33.2)	2.79 (2.65)	9.52 (9.68)
$[Pt(terpy)(imidazole)](ClO_4)_2$	29.8 (31.1)	1.87 (2.17)	9.85 (10.1)

[a] Calculated values in parentheses.

Table 2
^{1}H NMR[a] data of the complexes

Compound	^{1}H NMR (δ, ppm; J, Hz; CD_3NO_2, 298 K)
[Pt(terpy)(thiazole)](ClO$_4$)$_2$	9.85 (dd, 1H, $^4J_{H-H} = 2.2$, $^4J_{H-H} = 1.0$, $^3J_{Pt-H} = 22$, thiazole-H$_2$); 8.70–7.30 (m, 11H, terpy); 8.58 (dd, 1H, $^3J_{H-H} = 3.5$, $^4J_{H-H} = 1.0$, thiazole-H$_4$); 8.33 (dd, $^3J_{H-H} = 3.5$, $^4J_{H-H} = 2.2$, thiazole-H$_5$)
[Pt(terpy)(4-methylthiazole)](ClO$_4$)$_2$	9.75 (d, 1H, $^4J_{H-H} = 2.4$, $^3J_{Pt-H} = 22$, thiazole-H$_2$); 8.70–7.70 (m, 11H, terpy); 7.93 (dq, $^4J_{H-H} = 2.4$, $^4J_{H-H} = 1.2$, thiazole-H$_5$); 2.89 (d, 3H, $^4J_{H-H} = 1.2$, $^4J_{Pt-H} = 6$, thiazole-Me$_4$)
[Pt(terpy)(5-methylthiazole)](ClO$_4$)$_2$	9.60 (d, 1H, $^4J_{H-H} = 1.0$, $^3J_{Pt-H} = 22$, thiazole-H$_2$); 8.70–7.79 (m, 11H, terpy); 8.26 (qt, 1H, $^4J_{H-H} = 1.3$, $^4J_{H-H} = 1.0$, thiazole-H$_4$); 2.75 (d, 3H, $^4J_{H-H} = 1.3$, thiazole-Me$_5$)
[Pt(terpy)(2-aminothiazole)](ClO$_4$)$_2$	8.70–7.80 (m, 11H, terpy); 7.57, 7.12 (AB spin system, 2H, $^3J_{AB} = 4.3$, thiazole-H$_{4,5}$); 7.06 (s, br, 2H, thiazole-NH$_2$)
[Pt(terpy)(4,5-dimethylthiazole)](ClO$_4$)$_2$	9.50 (s, 1H, $^3J_{Pt-H} = 22$, thiazole-H$_2$); 8.70–7.30 (m, 11H, terpy); 2.80 (s, 3H, $^4J_{Pt-H} = 6$, thiazole-Me$_4$); 2.65 (s, 3H, thiazole-Me$_5$)
[Pt(terpy)(benzothiazole)](ClO$_4$)$_2$	10.15 (s, 1H, $^3J_{Pt-H} = 24$, thiazole-H$_2$); 8.86–7.34 (m, 15H, terpy + benzothiazole)
[Pt(terpy)(oxazole)](ClO$_4$)$_2$	9.28 (s, 1H, $^3J_{Pt-H} = 10$, thiazole-H$_2$); 8.80–7.20 (m, 13H, terpy+oxazole)
[Pt(terpy)(isoxazole)](ClO$_4$)$_2$	9.37 (d, 1H, $^3J_{H-H} = 2.2$, isoxazole-H$_3$); 9.30 (d, 1H, $^3J_{H-H} = 2.0$, isoxazole-H$_5$); 8.76–7.76 (m, 11H, terpy); 7.28 (dd, 1H, $^3J_{H-H} = 2.2$, $^3J_{AB} = 2.0$ Hz, isoxazole-H$_4$)
[Pt(terpy)(imidazole)](ClO$_4$)$_2$	^{1}H NMR: 8.57 (t, 1H, $^4J_{H-H} = 1.8$, imidazole-H$_2$); 8.71–7.76 (m, 11H, terpy); 7.72 (dd, 1H, $^3J_{H-H} = 2.4$, $^4J_{H-H} = 1.8$, imidazole-H$_4$); 7.65 (dd, 1H, $^3J_{H-H} = 2.4$, $^4J_{H-H} = 1.8$, imidazole-H$_5$). NH observed in d^6-DMSO, 3.33 ppm, br.
[Pt(terpy)(pyrazole)](ClO$_4$)$_2$	8.70–7.75 (m, 11H, terpy); 8.37 (d, 1H, $^3J_{H-H} = 2.4$, pyrazole-H$_3$); 8.33 (d, 1H, $^3J_{H-H} = 2.4$, pyrazole-H$_5$); 7.46 (s, br, 1H, NH); 7.00 (t, 1H, $^3J_{H-H} = 2.4$, pyrazole-H$_4$)
[Pt(terpy)(3,5-dimethylpyrazole)](ClO$_4$)$_2$	8.72–7.75 (m, 12H, terpy + NH); 6.53 (s, 1H, pyrazole-H$_4$); 2.62 (s, 3H, $^4J_{Pt-H} = 6$, pyrazole-Me$_3$); 2.56 (s, 3H, pyrazole-Me$_5$)

[a] Chemical shifts for ^{1}H NMR are reported by reference to TMS.

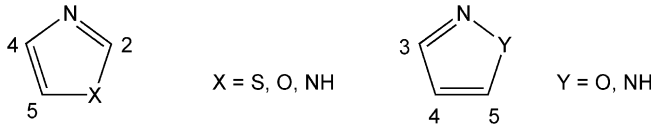

Scheme 1. Numeration of the considered five-membered N-donor heterocycles.

the spectrophotometer. The concentration of the entering group was always large enough to provide pseudo-first-order conditions. After preliminary repetitive scan experiments in the range 240–360 nm to search for isosbestic points and spectral changes, the kinetics were studied by measuring the changing absorbance at suitable wavelengths as a function of time. Pseudo first-order-rate constants (k_{obs}/s^{-1}) were obtained either from the gradients of plots of $\log(D_t - D_\infty)$ vs. time or from a non-linear least-squares fit of experimental data to $D_t = D_\infty + (D_0 - D_\infty)\exp(-k_{obs}t)$ with D_0, D_∞ and k_{obs} as the parameters to be optimized (D_0 = absorbance after mixing the reactants, D_∞ = absorbance at completion of the reaction). Rate constants were accurate to within 5%.

All the prepared complexes follow the Lambert–Beer equation in the considered concentration range and experimental conditions, so the presence of π-stacking effects [10] can be reasonably excluded.

3. Results and discussion

Thiazoles, oxazole, isoxazole, imidazole and pyrazoles are potentially ambidentate ligands and it is necessary to ascertain the site of binding to Pt(II) in its complexes, but there is considerable evidence to indicate bonding through nitrogen of which the following are probably the most important: (i) thiazoles and oxazoles bind to the analogous soft d^8 Au(III) through nitrogen [11]; (ii) thiazole ligands were found to be bonded to platinum through the nitrogen atom from data in the literature [12,13]; (iii) further proof of the Pt–N bond comes from the crystal structure of solid *trans*-[Pt(dmso)(thiazole)Cl$_2$] determined by X-ray diffraction [14]; (iv) there is a general similarity of the behaviour of these complexes with the corresponding R-py (N-containing six-membered heterocycles), that depends only upon the basicity of the nitrogen.

3.1. Kinetics of displacement of chloride by nitrogen donors from [Pt(terpy)Cl]$^+$

The spectrophotometric changes observed in repetitive scanning of the spectrum of the reaction mixture are characteristic of a single chemical stage, with well maintained isosbestic points. Careful examination of the spectral changes (subsequent changes have never been observed) which occur after the reagents are mixed and the close similarity of the spectra at the end of the reaction with those of authentic samples of the expected reaction products demonstrate that all the reactions that have been studied kinetically involve the displacement of coordinated chloride by the nitrogen base. The rate constants were determined in the usual way from the change

in absorbance as a function of time at a convenient wavelength within the region 300–340 nm. All the reactions were studied in the presence of a sufficient excess of nucleophile over the substrate to provide pseudo-first-order conditions and the observed rate constants, k_{obs}, collected in Table 3, obey to the general relationship $k_{obs} = k_1^f + k_2^f[nu]$, which is usual for nucleophilic substitution at planar four coordinate d^8 metal complexes [15].

Table 3
First-order rate constants, k_{obs}[a] for the reaction $[Pt(terpy)Cl]^+ + nu \rightarrow [Pt(terpy)(nu)]^{2+} + Cl^-$ in methanol at 25 °C

Nucleophile	[nu] (mol dm^{-3})	$10^3\,k_{obs}$ (s^{-1})
Thiazole	0.05	21.9
	0.08	32.7
	0.10	44.1
	0.12	54.1
	0.15	68.0
5-Methylthiazole	0.02	12.1
	0.04	26.4
	0.06	39.1
	0.08	53.2
	0.10	63.1
Imidazole	0.003	21.0
	0.005	34.0
	0.008	56.8
	0.010	67.1
	0.015	101.7
4,5-Dimethylthiazole	0.033	16.3
	0.066	28.5
	0.099	48.8
	0.132	65.1
	0.166	80.3
3,5-Dimethylpyrazole	0.01	7.43
	0.02	14.7
	0.03	23.2
	0.04	29.0
	0.05	37.4
4-Methylthiazole	0.05	17.4
	0.10	34.1
	0.15	52.9
	0.20	66.9
	0.25	89.8
Oxazole	0.15	27.9
	0.20	36.2
	0.25	47.2
	0.30	55.5
	0.35	65.4
Isoxazole	0.05	9.79
	0.10	21.1
	0.15	31.2
	0.20	42.3
	0.25	49.5
Pyrazole	0.001	0.48
	0.003	1.44
	0.006	2.80
	0.008	3.75
	0.010	4.92

[a] Errors on individual k_{obs} determinations are in the ±5% range.

3.2. Kinetics of displacement of nitrogen donors by chloride from $[Pt(terpy)(nu)]^{2+}$

In all the reactions with an excess of chloride ion the spectrophotometric changes are characteristic of a single chemical stage, with the same isosbestic points observed for the forward reactions. The spectra at the end of the reactions coincide with those of authentic samples of the expected products at the same concentration, so that the displacement of the coordinated nitrogen donor by chloride is assured. The reactions were studied in the presence of 0.05 mol dm^{-3} CH_3SO_3H at constant ionic strength ($I = 0.1$ mol dm^{-3}, CH_3SO_3Na). Preliminary experiments showed that, at constant chloride concentration, the rate of reaction was independent of the concentration of the acid over the range 0.02–0.2 mol dm^{-3}. The acid simply serves to protonate the released nu and to prevent the reverse reaction. For the weakest bases, oxazole and isoxazole, the acid concentration is not sufficient to ensure complete protonation of the released ligand. However, because of their low basicity these species are poor ligands towards Pt(II) complexes and also in these cases a careful comparison of the spectra at the end of the reactions with the spectra of an authentic sample of $[Pt(terpy)Cl]^+$ and nu at the same concentration and acidity confirms the completion of the reactions. The observed rate constants, k_{obs}, collected in Table 4, obey the general relationship $k_{obs} = k_1^r + k_2^r[Cl^-]$, where k_1^r and k_2^r have the usual meaning, and k_2^r values at $I = 0.1$ mol dm^{-3} are reported in Table 5 together with the corresponding values k_2^{0r} extrapolated to zero ionic strength. The extrapolation to zero ionic strength uses the Debye–Hückel relationship, $\log k_2^{0r} = \log k_2^r - 2\alpha ZaZbI^{1/2}/(1 + \beta I^{1/2})$ with $Za = +2$, $Zb = -1$, $\alpha = 1.90$ and $\beta = 1.55$ (estimated from the relative permittivity of methanol at 25 °C). [16] Preliminary experiments showed that the rate of the processes between the monocationic $[Pt(terpy)Cl]^+$ complex and the neutral nitrogen donor is not influenced by primary salt effects over the range 0.0–0.5 mol dm^{-3} ionic strength, whereas that of the reverse reactions between the bis-cationic species $[Pt(terpy)\ (nu)]^{2+}$ and chloride ion depends upon the ionic strength. As a consequence the equilibrium constants, K, also depend upon the ionic strength and in Table 5 the values $K = k_2^f/k_2^r$ and $K^0 = k_2^f/k_2^{0r}$, determined from the ratios of the second-order rate constants for the forward and reverse reactions, are reported.

The data obtained from the reaction $[Pt(terpy)Cl]^+ + nu \rightarrow [Pt(terpy)(nu)]^{2+} + Cl^-$ are compared to the entry of pyridines and other nitrogen donors, under the same experimental conditions [3], and are reported in Fig. 1, where the values of $\log k_2^f$ are plotted against the pK_a of the entering nucleophiles. As far as the unhindered thiazole, 5-methylthiazole, oxazole, isoxazole, imidazole and pyrazole are concerned, it is evident that the data fit quite nicely the linear free-energy relationships $\log k_2^f = 0.23\,pK_a + \text{constant}$ already observed for the entry of unhin-

Table 4
First-order rate constants, k_{obs}[a] for the reaction $[Pt(terpy)(nu)]^{2+} + Cl^- \rightarrow [Pt(terpy)Cl]^+ + nu$ in methanol at 25 °C ($I = 0.1$ mol dm^{-3}, CH_3SO_3Na)

nu	$10^3[Cl^-]$ (mol dm^{-3})	$10^3 k_{obs}$ (s^{-1})
Thiazole	0.25	8.20
	0.37	12.3
	0.75	25.7
	1.50	44.5
5-Methylthiazole	0.40	8.41
	0.60	11.8
	1.00	16.5
	1.50	25.7
4,5-Dimethylthiazole	0.20	0.78
	0.40	1.50
	0.60	2.26
	1.00	3.54
2-Aminothiazole	0.60	0.12
	1.00	0.22
	1.50	0.31
	2.00	0.41
	2.50	0.49
Pyrazole	0.20	7.80
	0.40	14.9
	0.60	24.3
	0.80	31.6
	1.00	38.7
3,5-Dimethylpyrazole	0.50	0.91
	1.00	1.89
	1.50	2.58
	2.00	3.72
	2.50	4.67
4-Methylthiazole	0.50	3.03
	0.75	4.45
	1.25	6.85
	1.50	9.69
	2.50	16.1
Oxazole	0.08	12.2
	0.10	15.2
	0.12	19.7
	0.15	23.5
	0.20	30.9
	0.25	38.7
Isoxazole	0.20	20.3
	0.30	30.5
	0.40	41.0
	0.50	50.8
	0.60	58.7
Benzothiazole	0.20	9.65
	0.40	14.9
	0.60	22.8
	1.00	34.2
	1.50	50.0
Imidazole	5.0	0.29
	10.0	0.57
	30.0	1.71
	50.0	2.95

[a] Errors on individual k_{obs} determinations are in the ±5% range.

dered pyridines on $[Pt(terpy)Cl]^+$ [3], whereas the nucleophilicity is higher ($\Delta \log k_2^f \cong 0.60$, corresponding to a difference of about 3.4 kJ mol^{-1}) and this fact can be reasonably ascribed to the smaller C–N–X (X = C, O, N) angle (≅108°) of the five-membered N-donors with respect to that of the pyridine (C–N–C ≅ 120°), which implies a decrease of congestion in the trigonal bipyramidal transition state. Another difference between the five-membered nucleophiles (unhindered thiazoles, oxazole, isoxazole, imidazole and pyrazoles) and pyridines in the entry reaction is the amount of steric retardation, as measured from the parameter Δ[1] attributable to the presence of a methyl group in the α-position with respect to the N-donor atom. In the case of α-methylpyridines the parameter Δ_{f1} is about 1.5, corresponding to a difference of about 8.6 kJ mol^{-1}, and it reduces to $\Delta_{f2} \cong 0.25$ (1.4 kJ mol^{-1}) for the entry of 4-methylthiazole, 4,5-dimethylthiazole and 3,5-dimethylpyrazole on the same complex.

The amount of steric retardation is related to the free rotation of the ligand molecule around the Pt–N bond, which leads to steric interference with the pyridine rings of the terpy ligand placed in the axial position in the trigonal bipyramidal transition state. For this reason, the differences in reactivity can be explained by considering the different structures of the pyridines compared to that of the five-membered N-donors (Scheme 2), which leads to a decrease in steric congestion in the latter compounds if compared to the former.

As far as the reverse reaction is concerned, the replacement of the N-ligands by Cl^-, the differences between the five-membered heterocycles and the pyridines groups are quite evident. In the replacement reactions of the N-ligand from the bis-cationic Pt-terpy substrate by chloride, the six five-membered N-donors are significantly less labile than the unhindered pyridines (Fig. 2).

The dependence of the lability of the two kinds of ligands upon basicity is almost the same and the data fit nicely the free-energy relationship $\log k_2^r = -0.51\ pK_a$ + constant already reported [3] for the displacement of unhindered pyridines, and the decrease in lability corresponds to a difference of about 3 kJ mol^{-1} between the free energy of activation of the two reacting systems. The lability of the five-membered N-donor heterocycles is considerably lower than that of pyridines, strongly suggesting that, in addition to possible but unlikely solvatation effects, the Pt–N bond in the case of five-membered N-donors may be reinforced by π bonding. It seems reasonable to conclude that the π system of five-membered N-donors can interact in the ground state with the filled d orbitals of Pt(II) better than pyridines. The fact that the thiazoles are weaker σ donors but fairly better π acceptors than pyridines once coordinated to Pt(II) has been pointed out in a work concerning hydrogen isotope exchange in Pt(II)-thiazole systems [18]. Also in the present study, for the pyridines system, the relatively large dependence of the

[1] Δ can be regarded as the steric effect due to the introduction of a methyl group *ortho* to the nitrogen in the entering nucleophiles without any interference from the basicity change that might arise from the presence of the substituent.

Table 5
Second-order rate constants[a] and equilibrium constants for the reaction $[Pt(terpy)Cl]^+ + nu \underset{k_1^r+k_2^r[Cl^-]}{\overset{k_1^f+k_2^f[nu]}{\rightleftharpoons}} [Pt(terpy)nu]^{2+} + Cl^-$

Nucleophile	$10^2k_2^f$ (dm^3 mol s^{-1})	$10^2k_2^r$ (dm^3 mol s^{-1})	$10^2k_2^{0r}$ (dm^3 mol s^{-1})	$10^2K(k_2^f/k_2^r)$	$10^2K^0(k_2^f/k_2^r)$	pK_a of nuH$^+$
Thiazole	47 ± 2	2800 ± 200	114800	1.6 ± 0.2	0.041	2.55
4-Methylthiazole	36 ± 1	660 ± 40	27060	5.5 ± 0.9	0.133	3.26
4,5-Dimethylthiazole	49 ± 1	345 ± 9	14145	14.2 ± 0.6	0.346	3.73
Imidazole	670 ± 10	5.9 ± 0.9	241.9	11300 ± 300	2.769	7.65
Benzothiazole		3120 ± 60	127920			1.2
Oxazole	18.8 ± 0.4	15400 ± 400	631400	0.122 ± 0.006	0.003	0.8
2-Aminothiazole		19.5 ± 0.7	799.5			5.36
5-Methylthiazole	64 ± 2	1500 ± 100	61500	4.3 ± 0.4	0.104	3.12
Pyrazole	48 ± 1	3900 ± 100	159900	1.23 ± 0.06	0.030	2.48
3,5-Dimethylpyrazole	74 ± 2	150 ± 20	6150	49 ± 8	1.203	4.38
Isoxazole	20.1 ± 0.1	9700 ± 300	397700	0.207 ± 0.007	0.005	1.30

pK_a values were taken from Ref. [17].
[a] Determined by weighted linear regression of k_{obs} values vs. nucleophile concentration.

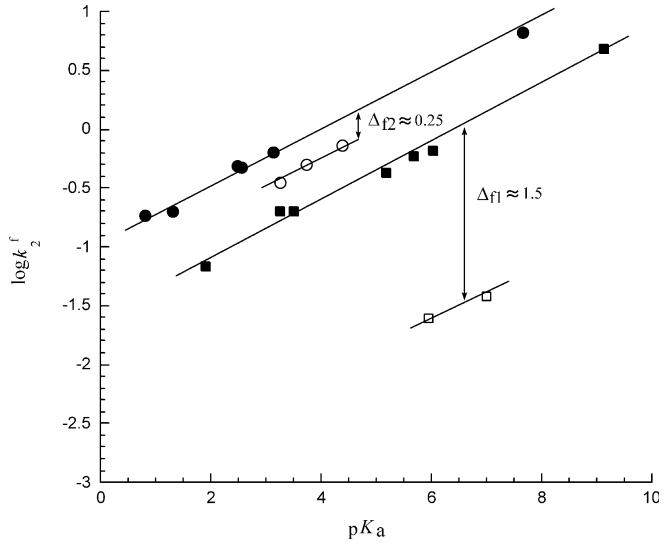

Fig. 1. $\log k_2^f$ for the reaction $[Pt(terpy)Cl]^+ + nu \rightarrow [Pt(terpy)(nu)]^{2+} + Cl^-$ plotted against pK_a of nuH$^+$: ●, oxazole, isoxazole, pyrazole, thiazole, 5-methylthiazole, imidazole; ○, 4-methylthiazole, 4,5-dimethythiazole, 3,5-dimethylpyrazole; ■, 4-cyanopyridine, 4-acetylpyridine, methylisonicotinate, pyridine, 4-methylpyridine, 3-methylpyridine, 4-aminopyridine; □, 2-methylpyridine, 2,4-dimethylpyridine; data for all the pyridines were taken from Ref. [3].

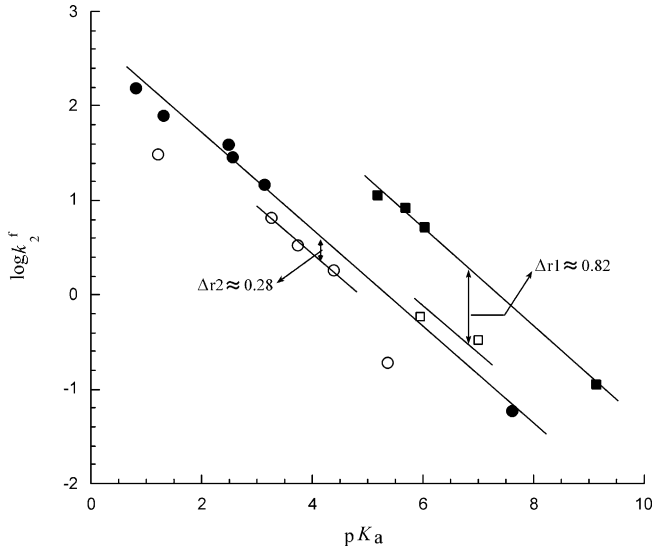

Fig. 2. $\log k_2^r$ for the reaction $[Pt(terpy)(nu)]^{2+} + Cl^- \rightarrow [Pt(terpy)Cl]^+ + nu$ plotted against pK_a of nuH$^+$: ●, oxazole, isoxazole, pyrazole, thiazole, 5-methylthiazole, imidazole; ○, 4-methylthiazole, 4,5-dimethythiazole, 3,5-dimethylpyrazole; ■, pyridine, 4-methylpyridine, 3-methylpyridine, 4-aminopyridine; □, 2-methylpyridine, 2,4-dimethylpyridine; data for all the pyridines were taken from Ref. [3].

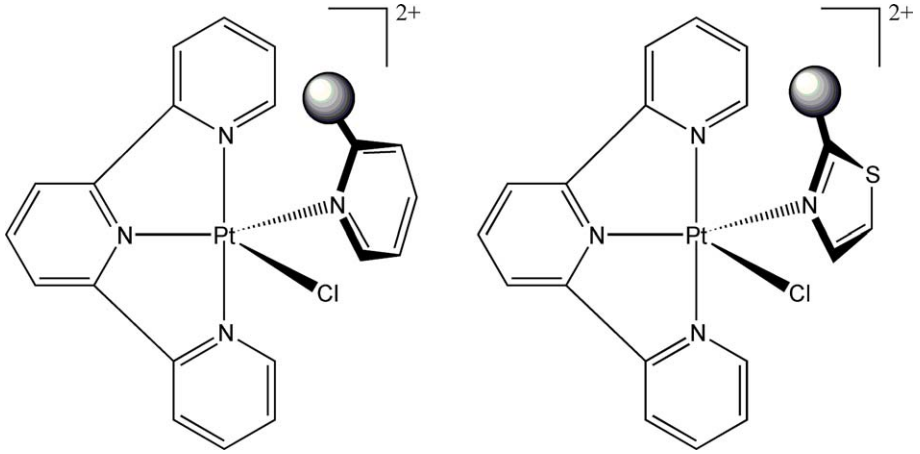

Scheme 2. Steric congestion in the trigonal bipyramidal transition state for substituted pyridines and thiazoles.

substitution lability upon ligand basicity suggests that the formation of the transition state requires a considerable change in the Pt–N bond, confirming therefore the observation already reported [1,4] that the transition state can be described as a structure containing a well formed Pt–Cl bond and a weak Pt–N bond. As far as the lability of hindered five-membered N-donors (4-methylthiazole, 4,5-dimethylthiazole and 3,5-dimethypyrazole) in the reverse reactions of process (1) is concerned, a lower (as expected, see above) steric effect for five-membered N-donors ($\Delta \cong 0.28$, 1.4 kJ mol^{-1}) than for pyridines ($\Delta \cong 0.82$, 4.6 kJ mol^{-1}) has been observed (Fig. 2). Not only α-methyl-substituted five-membered heterocycles, but also other ligands such as 2-aminothiazole and benzothiazole were considered. For these substrates the Δ value is higher (0.70, 3.9 kJ mol^{-1}) than that measured for 4-methylthiazole, 4,5-dimethylthiazole and 3,5-dimethylpyrazole. This difference is due to the greater congestion on the metal centre caused by the NH_2- and benzo-substituents, which disfavours the platinum–chloride bond formation. The ratio between the second-order rate constants for the forward and reverse reactions gives the corresponding equilibrium constants for the systems:

$$[Pt(terpy)Cl]^+ + nu \rightleftharpoons [Pt(terpy)(nu)]^{2+} + Cl^-$$

and the actual values of K at $I = 0.1$ mol dm^{-3} and K^0 at zero ionic strength are reported in Table 5. The plot of $\log K^0$ versus pK_a (Fig. 3) is linear for the group of five-membered N-donors formed by thiazole, 5-methylthiazole, oxazole, isoxazole, imidazole and pyrazole, and the free energy relationship $\log K^0 = (0.74)pK_a + \text{constant}$ can be derived.

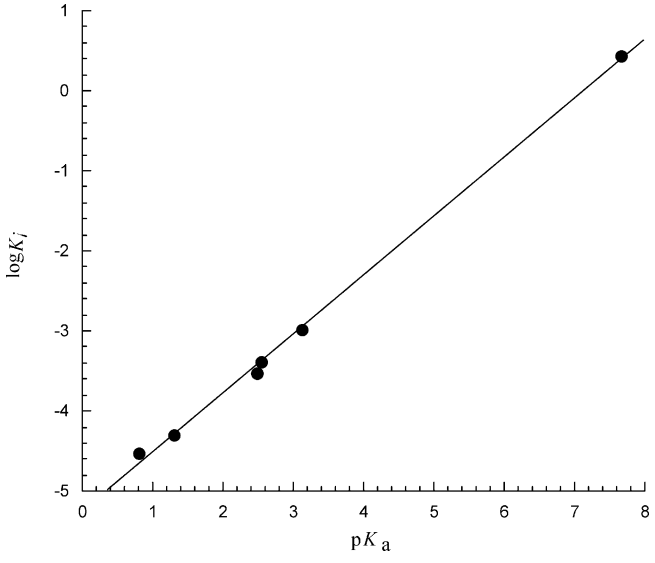

Fig. 3. $\log K^0$ for the reaction $[Pt(terpy)Cl]^+ + nu \rightleftharpoons [Pt(terpy)(nu)]^{2+} + Cl^-$ plotted against pK_a of nuH^+: ●, oxazole, isoxazole, pyrazole, thiazole, 5-methylthiazole, imidazole.

The dependence of the stability of the complexes upon the basicity of the ligands is the same as that measured for pyridines under the same experimental conditions [3]. However, the values of the equilibrium constants are higher than those found in the previous case. Such a difference may reflect a greater tendency of five-membered N-donors, in comparison with pyridines, to give π back-donation from the filled orbitals of the metal to the antibonding orbitals of the ligand, leading to a relative stabilization of the ground state of the products.

Acknowledgements

We thank the Italian Ministry of University for financial support.

References

[1] B. Pitteri, G. Marangoni, L. Cattalini, J. Chem. Soc., Dalton Trans. (1994) 3539.
[2] B. Pitteri, G. Marangoni, L. Cattalini, Polyhedron 14 (1995) 2331.
[3] B. Pitteri, G. Marangoni, F. Visentin, L. Cattalini, T. Bobbo, Polyhedron 17 (1997) 475.
[4] M. Bellicini, L. Cattalini, G. Marangoni, B. Pitteri, J. Chem. Soc., Dalton Trans. 12 (1994) 1805.
[5] M. Bonivento, L. Cattalini, G. Marangoni, B. Pitteri, T. Bobbo, Trans. Met. Chem. 22 (1997) 46.
[6] Z. Bugarčić, G. Liehr, R. Van Eldik, J. Chem. Soc., Dalton Trans. (2002) 2825.
[7] Z. Bugarčić, F.W. Heinemann, R. Van Eldik, J. Chem. Soc., Dalton Trans. (2004) 279.
[8] Z. Bugarčić, T. Soldatović, R. Jelić, B. Aguleró, A. Grandas, J. Chem. Soc., Dalton Trans. (2004) 3869.
[9] G. Annibale, B. Pitteri, Inorg. Synth. 34 (2004) 78.
[10] P. Moore, G.U. Priimov, Inorg. React. Mech. 5 (2003) 21, and references therein.
[11] L. Canovese, L. Cattalini, M. Tomaselli, M.L. Tobe, J. Chem. Soc., Dalton Trans. (1991) 307.
[12] M. Van Beusichem, N. Farrel, Inorg. Chem. 31 (1991) 634.
[13] M.M. Muir, M.E. Cadiz, A. Baez, Inorg. Chim. Acta 151 (1988) 209.
[14] A. Cornia, A.C. Fabretti, M. Bonivento, L. Cattalini, Inorg. Chim. Acta 255 (1997) 405.
[15] F. Basolo, R.G. Pearson, Mechanism of Inorganic Reactions, 2nd ed., Wiley, New York, 1967.
[16] R.A. Robinson, R.H. Stokes, Electrolyte Solutions, second ed., Butterworths, London, 1959, p. 231.
[17] D.D. Perrin, Dissociation Constants of Organic Bases in Aqueous Solution, Butterworths, London, 1965.
[18] E. Buncel, O. Clement, J. Chem. Soc., Perkin Trans. (1995) 1333.

produce clusters of Mo(III) magnetically coupled to Ni(II) ions [10]. These clusters show higher magnetic anisotropy and better orbital overlap compared with the analogous compounds containing Cr(III) substituted for Mo(III). Other examples such as 2D $K_2Mn(II)_3(H_2O)_6[Mo(III)(CN)_7]_2 \cdot 6H_2O$ have used $Mo(III)(CN)_7^{4-}$ as a building block [11].

Examples of low-dimensional ruthenium(III) based polymers are rare however, having been limited until very recently [12] to M(II)Ru(III)oxalato complexes (M is a 3d ion) which typically adopt a 2D network [13,14]. Initially the sign of the exchange coupling in the M(II)Ru(III)oxalato complex (M = Cu(II)) was thought not to obey simple symmetry considerations [13], but an alternative interpretation showed that the interaction does indeed conform to symmetry-based expectations [14]. We report here the first example of a structurally characterized 1D cyano-bridged coordination polymer containing Ru(III). The magnetic coupling in this compound conforms to symmetry-based expectations, showing ferromagnetic coupling between Ru(III) and Ni(II). No long-range ordering or slow relaxation of the magnetization was observed above 3 K.

2. Experimental

2.1. General

[Ni(cyclam)]$(ClO_4)_2$ was prepared according to the literature procedure [15]. Mass spectra were obtained by infusing a methanolic solution of the compound into a Varian 1200 L single quadrupole mass spectrometer. Infrared spectra were recorded of KBr pellets using a Biorad FTS-60 FTIR spectrometer. Elemental analyses were performed by Desert Analytics (Tucson, AZ). Variable temperature magnetic susceptibility measurements were taken of powder samples on a Quantum Design MPMS SQUID magnetometer in the temperature range of 2–300 K. Susceptibilities were corrected for the sample holder and the diamagnetism of the sample calculated from Pascal's constants. Heat capacity measurements were performed in zero applied field on a Quantum Design PPMS.

2.2. Synthesis

Na[Ru(salen)$(CN)_2$], (**2**) was prepared according to Leung and Che [16]. IR (KBr pellet) $\nu_{CN} = 2099\ cm^{-1}$. MS (ESI) m/z $(M-Na)^-$ 420.1. *Anal.* Calc. for $C_{18}H_{14}N_4NaO_2Ru \cdot 1.5H_2O$ C, 46.06; H, 3.65; N, 11.94. Found: C, 46.04; H, 3.64; N, 11.67%. Blue crystalline plates of **2** were grown from slow evaporation of a methanolic solution.

[Ru(III)(salen)$(CN)_2$][Ni(II)(cyclam)](ClO_4), (**1**): [Ni(cyclam)]$(ClO_4)_2$ (104 mg; 0.226 mmol) in 5 mL of acetonitrile were added dropwise to a solution of 100 mg (0.226 mmol) **2** in 5 mL of water. The resulting blue precipitate was isolated by centrifugation, washed with water and acetronitrile and dried in vacuo yielding 126 mg **1** (72%). IR (KBr pellet) $\nu_{CN} = 2126\ cm^{-1}$. *Anal.* Calc. for $C_{28}H_{38}ClN_8NiO_6Ru$: C, 43.23; H, 4.92; N, 14.41. Found: C, 43.39; H, 5.11; N, 14.09%. Blue needle-like crystals of **1** suitable for X-ray diffraction resulted from slow diffusion of Ni(II)(cyclam)$(ClO_4)_2$ in acetonitrile into an aqueous solution of **2**.

2.3. X-ray crystallography

Crystallographic data were collected on a Bruker SMART 1000 X-ray diffractometer with CCD detector using graphite monochromated Mo Kα radiation ($\lambda = 0.71073$ Å). Data sets for **1** and **2** were obtained at 153(2) K. For **2** the data were collected with a θ range of 1.91–29.12°. Data were obtained in 0.3° oscillations with 10 s exposures. For **1**, the θ range for data collection was 1.46–28.65° and data were collected in 0.3° oscillations with 25 s exposures. The crystal-to-detector distance was 50.00 mm with the detector at the 28° swing position for both **1** and **2**. Data were processed using SAINT-NT from Bruker and were corrected for Lorentz and polarization effects. The structures were solved by direct methods [17], expanded using Fourier techniques and refined by full-matrix least-squares on F^2 [18]. The non-hydrogen atoms were refined anisotropically. Hydrogen atoms were included in idealized positions but not refined with the exception of the hydroxyl hydrogen in the methanol solvate of **2** and the hydrogen atoms of the water solvent molecule in **1**. These H-atoms could not be located in reasonable positions. Crystallographic data for **1** and **2** are tabulated in Table 1 with selected bond lengths and angles given in Tables 2 and 3 for **2** and **1**, respectively.

Table 1
Crystallographic data for **1** and **2**

	1 · H_2O · MeCN	**2** · MeOH
Empirical formula	$C_{30}H_{43}ClN_9NiO_7Ru$	$C_{19}H_{18}N_4NaO_3Ru$
Formula weight	836.93	474.43
Crystal system	triclinic	monoclinic
Space group	*P*-1	$P2_1/c$
a (Å)	9.6253(11)	7.3220(9)
b (Å)	14.2047(17)	12.4263(16)
c (Å)	14.2607(17)	20.662(3)
α (°)	94.109(2)	90
β (°)	99.171(2)	92.362(2)
γ (°)	107.940(2)	90
V (Å^3)	1816.1(4)	1878.3(4)
Z	2	4
ρ (calc) (g cm^{-3})	1.531	1.674
μ (mm^{-1})	1.064	0.886
Reflections collected/ unique [R_{int}]	16822/8465 [0.0381]	17596/4667 [0.0411]
Reflections observed [$I > 2\sigma(I)$]	6322	4062
Data/restraints/parameters	8465/0/446	4667/0/254
Goodness-of-fit on F^2	1.085	1.072
Final *R* indices [$I > 2\sigma(I)$]	$R_1 = 0.0600$, $wR_2 = 0.1547$	$R_1 = 0.0235$, $wR_2 = 0.0608$
R indices (all data)	$R_1 = 0.0831$, $wR_2 = 0.1748$	$R_1 = 0.0286$, $wR_2 = 0.0624$

Table 2
Selected bond lengths (Å) and bond angles (°) for compound **2** · MeOH

Ru(1)–N(2)	1.9818(14)	Na(1)–O(1)	2.3104(13)
Ru(1)–N(1)	1.9844(14)	Na(1)–O(3)	2.3621(18)
Ru(1)–O(2)	2.0305(12)	Na(1)–N(3)#1	2.4162(19)
Ru(1)–O(1)	2.0159(12)	Na(1)–N(4)#2	2.4916(18)
Ru(1)–C(17)	2.0745(18)	Na(1)–O(2)	2.6157(15)
Ru(1)–C(18)	2.0773(18)	N(3)–C(17)	1.153(2)
Ru(1)–Na(1)	3.2777(8)	N(4)–C(18)	1.150(2)
N(2)–Ru(1)–N(1)	83.69(6)	N(3)–C(17)–Ru(1)	170.45(16)
N(2)–Ru(1)–O(1)	175.63(5)	N(4)–C(18)–Ru(1)	172.18(16)
N(1)–Ru(1)–O(1)	92.34(5)	C(17)–Ru(1)–C(18)	172.88(7)
N(2)–Ru(1)–O(2)	93.03(6)	O(1)–Na(1)–O(3)	143.52(7)
N(1)–Ru(1)–O(2)	176.25(5)	O(1)–Na(1)–N(3)#1	114.84(6)
O(1)–Ru(1)–O(2)	91.00(5)	O(3)–Na(1)–N(3)#1	101.30(7)
N(2)–Ru(1)–C(17)	84.72(6)	O(1)–Na(1)–N(4)#2	92.19(5)
N(1)–Ru(1)–C(17)	94.12(6)	O(3)–Na(1)–N(4)#2	76.21(6)
O(1)–Ru(1)–C(17)	93.77(6)	N(3)#1–Na(1)–N(4)#2	115.05(6)
O(2)–Ru(1)–C(17)	87.37(6)	O(1)–Na(1)–O(2)	71.42(4)
N(2)–Ru(1)–C(18)	89.01(6)	O(3)–Na(1)–O(2)	95.90(6)
N(1)–Ru(1)–C(18)	88.54(6)	N(3)#1–Na(1)–O(2)	104.03(6)
O(1)–Ru(1)–C(18)	92.72(6)	N(4)#2–Na(1)–O(2)	140.91(6)
O(2)–Ru(1)–C(18)	89.59(6)	Ru(1)–O(1)–Na(1)	98.28(5)
		Ru(1)–O(2)–Na(1)	88.81(5)

Symmetry transformations used to generate equivalent atoms: #1 $1-x$, $-1/2+y$, $1/2-z$; #2 $1+x$, y, z.

Table 3
Selected bond lengths (Å) and bond angles (°) for compound **1** · MeCN · H_2O

Ru(1)–N(2)	1.994(4)	Ni(1)–N(5)	2.068(4)
Ru(1)–N(1)	2.001(3)	Ni(1)–N(6)	2.075(4)
Ru(1)–O(2)	2.016(3)	Ni(1)–N(3)	2.080(4)
Ru(1)–O(1)	2.026(3)	Ni(2)–N(8)	2.057(4)
Ru(1)–C(17)	2.058(4)	Ni(2)–N(7)	2.072(4)
Ru(1)–C(18)	2.072(4)	Ni(2)–N(4)	2.134(4)
N(3)–C(17)	1.135(6)	N(4)–C(18)	1.144(5)
N(2)–Ru(1)–N(1)	82.64(15)	N(3)–C(17)–Ru(1)	179.6(4)
N(2)–Ru(1)–O(1)	171.97(14)	N(4)–C(18)–Ru(1)	173.5(4)
N(1)–Ru(1)–O(1)	89.79(13)	C(17)–Ru(1)–C(18)	177.14(16)
N(2)–Ru(1)–O(2)	90.96(15)		
N(1)–Ru(1)–O(2)	172.45(14)	N(5)–Ni(1)–N(6)	94.62(16)
O(1)–Ru(1)–O(2)	96.78(13)	N(5)–Ni(1)–N(3)	89.61(14)
N(2)–Ru(1)–C(17)	92.16(15)	N(6)–Ni(1)–N(3)	89.73(15)
N(1)–Ru(1)–C(17)	86.98(14)	N(8)–Ni(2)–N(7)	85.78(17)
O(1)–Ru(1)–C(17)	90.09(14)	N(8)–Ni(2)–N(4)	87.14(15)
O(2)–Ru(1)–C(17)	89.27(14)	N(7)–Ni(2)–N(4)	91.67(14)
N(2)–Ru(1)–C(18)	86.91(15)	C(17)–N(3)–Ni(1)	175.6(4)
N(1)–Ru(1)–C(18)	95.58(16)	C(18)–N(4)–Ni(2)	159.9(4)
O(1)–Ru(1)–C(18)	91.19(14)		
O(2)–Ru(1)–C(18)	88.04(15)		

3. Results and discussion

3.1. Synthesis and structural characterization

Crystals of Na[Ru(salen)$(CN)_2$] (**2**) [16] suitable for X-ray diffraction were grown from slow evaporation of a methanolic solution (Tables 1 and 2 and Fig. 1). The sodium counterion interacts with cyanide atom N3#1 from one adjacent Ru(III) complex (at $1-x$, $-1/2+y$, $1/2-z$) and cyanide N4#2 from another nearby Ru(III) complex (at $1+x$, y, z) giving rise to a 2D layered structure (Fig. 2). As a result, the C17–Ru1–C18 angle is 172.88(7)°, while Ru1–C17–N3 and Ru1–C18–N4 display angles of 170.45(16)° and 172.18(16)°, respectively. The coordination sphere of sodium is completed by salen oxygens O1 and O2 and a methanol solvent molecule. Comparison with *trans*-NBu_4[Ru(III)(salen)$(CN)_2$] shows the significant distortion arising from the sodium counterion. As a tetrabutylammonium salt, there is no interaction between Ru(III) centers resulting in nearly linear angles for C17–Ru1–C18 (178.3(7)°), Ru1–C17–N3 (178(1)°), and Ru1–C18–N4 (176(1)°) [12]. The Ru–C and C≡N bond lengths for **2** fall within the range observed by Yeung et al.

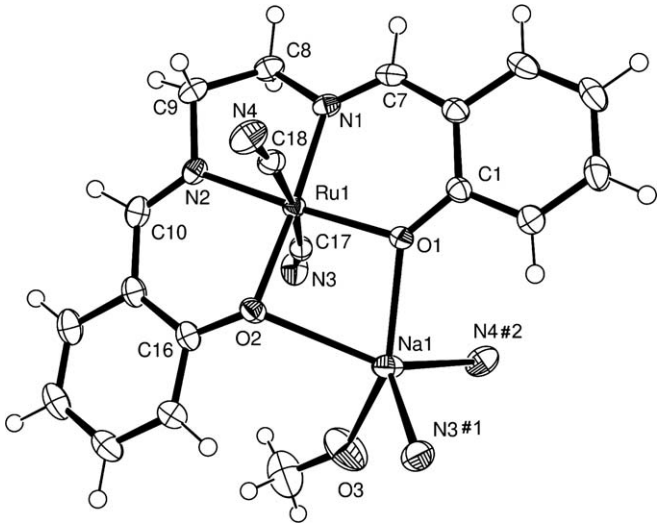

Fig. 1. Thermal ellipsoid (50%) plot of **2** · MeOH.

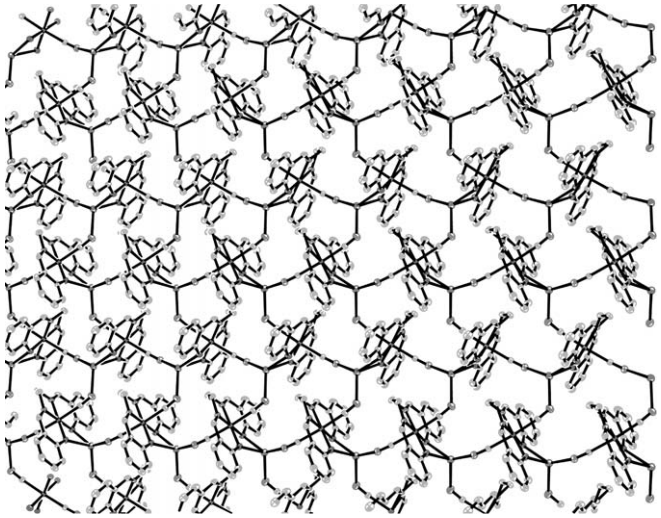

Fig. 2. View of 2D plane of **2** · MeOH with MeOH solvates removed for clarity. The 2D network lies in the plane defined by the crystallographic *a* and *b* axes.

Reaction of equimolar Ni(II)(cyclam) perchlorate [15] in solvents such as water, acetone and acetonitrile with **2** in water resulted in immediate precipitation of a fine steel blue particulate of formulation [Ru(III)(salen)(CN)$_2$][Ni(II)-(cyclam)](ClO$_4$) (**1**). X-ray quality needles of **1** resulted from slow diffusion of Ni(II)(cyclam)(ClO$_4$)$_2$ in acetonitrile into an aqueous solution of **2** (Tables 1 and 3, Fig. 3). The C≡N stretching frequency shifts to higher energy from 2099 cm^{-1} in **2** to 2126 cm^{-1} in **1**, with concomitant bond shortening of the cyano moiety from 1.153(2) Å for N3–C17 and 1.150(2) Å for N4–C18 in **2** to 1.135(6) and 1.144(5) Å, respectively, in compound **1**. These results are comparable to that seen by Yeung et al. upon addition of $NiCl_2$ and cyclam to $Ru(acac)_2(CN)_2^-$ and are consistent with N coordination to the Ni(cyclam) subunit. The Ru1–C17 distance in **1** is 2.058(4) Å while Ru1–C18 is similar to that in **2** at 2.072(4) Å. Around Ni, the Ni1–N3 distance is 2.080(4) Å while Ni2–N4 is 2.134(4) Å. With the exception of Ni2–N4, these distances are identical to those reported for the trimeric Ni(cyclam)[Ru(acac)$_2$(CN)$_2$]$_2$ [12].

The presence of the perchlorate anion results in a deviation from linearity of the –(Ru–CN–Ni–NC)– fragment giving rise to two different Ni(II) sites. The two Ni atoms lie on independent inversion centers. Along the metal cyanide axis, the Ni1 site is nearly linear with an angle of 175.6(4)° between Ni1–N3–C17 and an angle of 179.6(4)° between N3–C17–Ru1. The analogous measurements around Ni2 display a more bent shape with 159.9(4)° for Ni2–N4–C18 and 173.5(4)° between N4–C18–Ru1.

3.2. Magnetic properties

The results of variable temperature magnetic susceptibility measurements performed on powder samples of compounds **1** and **2** in a field of 1 kOe are shown in Fig. 4. At room temperature $\chi_M T$ for **2** is 0.51 cm^3 mol^{-1} K, considerably higher than the calculated spin-only value of 0.38 cm^3 mol^{-1} K for $S = 1/2$, but comparable to other monomeric Ru(III) complexes such as *trans*-Ph$_4$P[Ru(III)(acac)$_2$(CN)$_2$] [19] and Ru(III)(acac)$_3$ [20]. The shape of the curve closely resembles that observed for *trans*-Ph$_4$P[Ru(III)(acac)$_2$(CN)$_2$] and polymeric [CoCp$_2$*][ZnRu(ox)$_3$] [13], all of which display a gradual decrease in $\chi_M T$ from 300 K to approximately 15 K with a subsequent steep drop below 15 K. Correction for a temperature independent paramagnetism (TIP) contribution of 5×10^{-4} cm^3 mol^{-1} renders $\chi_M T$ independent of temperature from 300 to 100 K with a value of 0.36 cm^3 mol^{-1} K in agreement with the spin only value. As noted by Coronado et al. [13], the low temperature behavior below 15 K arises from spin–orbit coupling and incomplete quenching of the orbital contribution to the magnetic moment and can cause difficulties in the interpretation of susceptibility data containing Ru(III) ions as seen below.

For chain **1**, $\chi_M T$ is 1.57 cm^3 mol^{-1} K at 300 K, higher than the calculated spin only value of 1.38 cm^3 mol^{-1} K for uncorrelated $S = 1$ Ni(II) and $S = 1/2$ Ru(III) ions, but in good agreement with the calculated result of 1.51 cm^3 mol^{-1} K using the data obtained for **2**. Applying the same TIP correction used in the analysis of **2** gives a $\chi_M T$ of 1.42 cm^3 mol^{-1} K at 300 K but does not remove the minimum at 55 K. The presence of the minimum would seem to indicate an antiferromagnetic interaction between Ru(III) and Ni(II). This conclusion was drawn from simi-

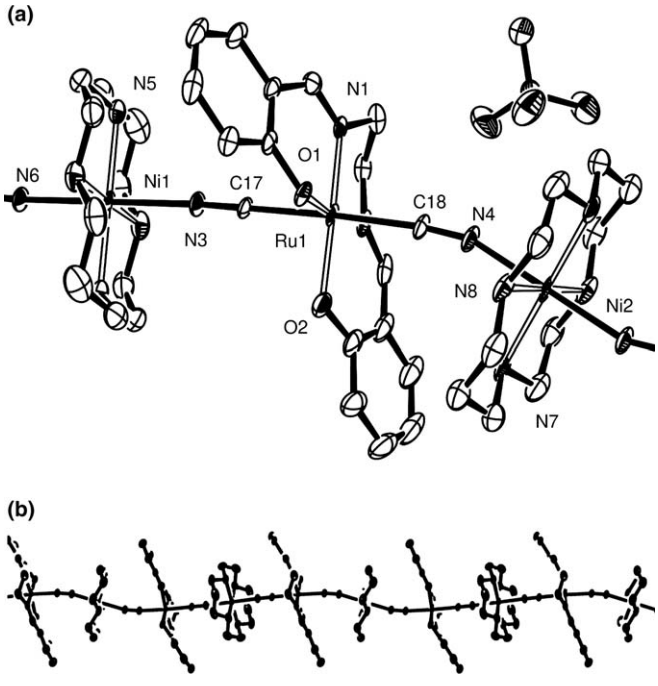

Fig. 3. (a) Thermal ellipsoid plot (50%) of [Ru(III)(salen)(CN)$_2$][Ni(II)-(cyclam)](ClO$_4$) · H$_2$O · MeCN (**1** · H$_2$O · MeCN). Water and MeCN solvates and hydrogen atoms have been removed for clarity. (b) View of cationic portion of **1** · H$_2$O · MeCN perpendicular to crystallographic *a* axis showing several repeat units. The chain axis runs along the vector difference of the crystallographic *b* and *c* axes.

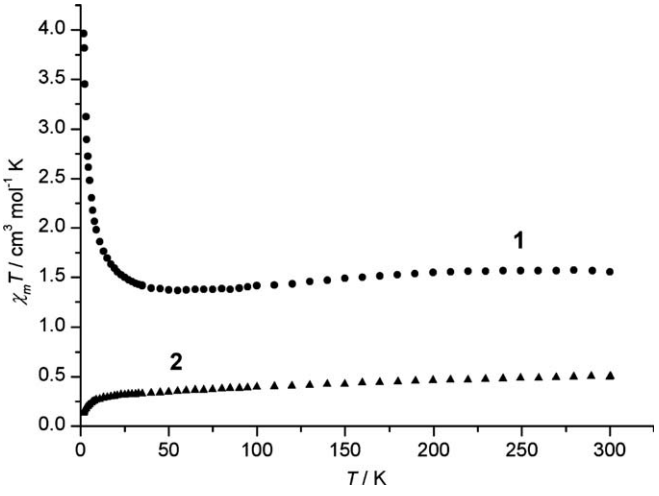

Fig. 4. The product of temperature and magnetic susceptibility as a function of temperature for compounds **1** and **2** in the range of 2–300 K at an applied field of 1 kOe. TIP correction is not included.

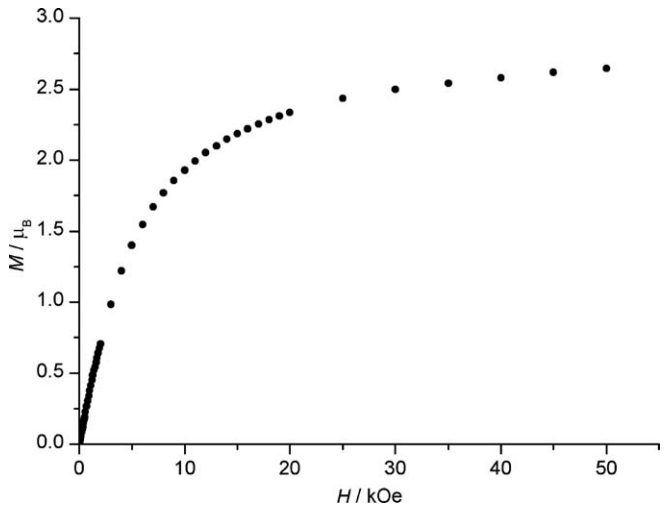

Fig. 5. Magnetization of **1** as a function of applied field at 2.0 K.

lar data by Kahn and co-workers for the 2D (NBu_4)-[Cu(II)Ru(III)$(ox)_3$] framework [14]. An alternative interpretation that appears to be more applicable in this case attributes the minimum to the anisotropic Ru(III) ion and indicates that the type of coupling must be determined through examination of the low temperature field-dependent magnetization data [13].

The magnetization of **1** as a function of applied field at 2 K is depicted in Fig. 5. At 50 kOe, the magnetization is nearly saturated with a value of 2.46 μ_B. The calculated saturation magnetization (M_s) for a spin-only system consisting of ferromagnetically coupled Ni(II) ($S = 1$) and Ru(III) ($S = 1/2$) is 3 μ_B. Antiferromagnetic coupling of the two ions results in a calculated M_s of 1 μ_B. The experimentally observed value clearly indicates ferromagnetic coupling, a conclusion that agrees with the results of Coronado et al. and with the expected orthogonality of magnetic orbitals between Ni(II) and Ru(III) [12,13]. The lower than expected saturation value can be attributed to the Ru(III) ion [13,20].

Zero-field cooled (zfc) and field-cooled (fc) magnetization experiments performed on **1** in applied fields of 3 and 50 Oe show no inflection point and little difference down to 3 K. These measurements indicate a lack of any type of long-range magnetic order above 3 K. Further evidence for the absence of 3D ordering above 2 K is given by the lack of a λ-peak in the heat capacity measurements of **1** indicating that there is no magnetic phase transition. Compound **1** displays negligible hysteresis at 2 K.

Although **1** does not display slow relaxation of the magnetization above 3 K, the salen ligand is readily amenable to synthetic modification which could be used to affect the magnetism of the compound through changes in the electronics at the Ru(III) center. It is interesting to note that a similar species, Ni(cyclam)[$Ru(acac)_2(CN)_2]_2$, is trimeric [12], reflecting the marked effect small structural changes can have on the dimensionality of the resulting mixed metal system. The current results demonstrate that Ru(III) can be incorporated into a 1D coordination polymer and provide further evidence that simple symmetry considerations can be used to predict whether the ion will display a ferro- or antiferromagnetic exchange interaction.

Acknowledgement

We acknowledge Dr. Oleksandr Chernyashevskyy for assistance with the magnetic measurements. This research was supported by NIH R01-A147003.

Appendix A. Supplementary material

Crystallographic data for structural analysis (cif files for the two structures) have been deposited with the Cambridge Crystallographic Data Centre, 12 Union Road, Cambridge CB2 1EZ, UK, fax: +44 1223 336 033 or e-mail: deposit@ccdc.cam.ac.uk or http://www.ccdc.cam.ac.uk. Refer to CCDC number 286496 for **1** and number 286497 for **2**. Supplementary data associated with this article can be found, in the online version, at doi:10.1016/j.poly.2006.03.024.

References

[1] E. Coronado, F. Palacio, J. Veciana, Angew. Chem., Int. Ed. Engl. 42 (2003) 2570.
[2] T.-F. Liu, D. Fu, S. Gao, Y.-Z. Zhang, H.-L. Sun, G. Su, Y.-J. Liu, J. Am. Chem. Soc. 125 (2003) 13976.
[3] H. Tamaki, Z.J. Zhong, N. Matsumoto, S. Kida, M. Koikawa, N. Achiwa, Y. Hashimoto, H. Okawa, J. Am. Chem. Soc. 114 (1992) 6974.
[4] S. Decurtins, H.W. Schmalle, H.R. Oswald, A. Linden, J. Ensling, P. Gütlich, A. Hauser, Inorg. Chim. Acta 216 (1994) 65.
[5] S. Decurtins, H.W. Schmalle, P. Schneuwly, R. Pellaux, J. Ensling, Mol. Cryst. Liq. Cryst. Sec. A 273 (1995) 605.
[6] L.M.C. Beltran, J.R. Long, Acc. Chem. Res. 38 (2005) 325.
[7] K.R. Dunbar, R.A. Heintz, Prog. Inorg. Chem. 45 (1997) 283.
[8] L.M. Toma, R. Lescouëzec, F. Lloret, M. Julve, J. Vaissermann, M. Verdaguer, Chem. Commun. (2003) 1850.
[9] S. Wang, J.-L. Zuo, S. Gao, Y. Song, H.-C. Zhou, Y.-Z. Zhang, X.-Z. You, J. Am. Chem. Soc. 126 (2004) 8900.
[10] M.P. Shores, J.J. Sokol, J.R. Long, J. Am. Chem. Soc. 124 (2002) 2279.
[11] J. Larionova, O. Kahn, S. Gohlen, L. Ouahab, R. Clérac, J. Am. Chem. Soc. 121 (1999) 3349.
[12] W.-F. Yeung, P.-H. Lau, T.-C. Lau, H.-Y. Wei, H.-L. Sun, S. Gao, Z.-D. Chen, W.-T. Wong, Inorg. Chem. 44 (2005) 6579.
[13] E. Coronado, J.R. Galán-Mascarós, C.J. Gómez-García, J.M. Martínez-Agudo, E. Martínez-Ferrero, J.C. Waerenborgh, M. Almeida, J. Solid State Chem. 159 (2001) 391.
[14] J. Larionova, B. Mombelli, J. Sanchiz, O. Kahn, Inorg. Chem. 37 (1998) 679.
[15] B. Bosnich, M.L. Tobe, G.A. Webb, Inorg. Chem. 4 (1965) 1109.
[16] W.H. Leung, C.M. Che, Inorg. Chem. 28 (1989) 4619.
[17] G.M. Sheldrick, SHELXS-97, Program for Crystal Structure Determination, University of Göttingen, Germany, 1997.
[18] G.M. Sheldrick, SHELXL-97, Program for the Refinement of Crystal Structures, University of Göttingen, Germany, 1997.
[19] W.-F. Yeung, W.-L. Man, W.-T. Wong, T.-C. Lau, S. Gao, Angew. Chem., Int. Ed. Engl. 40 (2001) 3031.
[20] B.N. Figgis, P.A. Reynolds, K.S. Murray, B. Moubaraki, Aust. J. Chem. 51 (1998) 229.

the effect of different transition metal ions (Co^{3+} and Ni^{2+}), *trans*-ligands (NO_2^- and Cl^-) and length of the alkylene bridge ($n = 2$ and $n = 4$) were studied. Therefore four complexes were synthesized and characterized by crystal structure, ^{1}HNMR and FTIR spectra.

2. Experimental

2.1. Materials and instruments

All chemicals are commercially available (CarloErba Co., Fluka, Sigma, BDH chemical Co., EKA Nobel. AB Co., May&Baker LTD., Merck Co. and Mallinck vodt Co.) and were used without further purification. All X-ray data were collected on a Siemens-Smart CCD Diffractometer. Magnetic susceptibility measurements were carried out at room temperature on a magnetic susceptibility balance model Magway MSB Mk1. The infrared spectra were measured as KBr disks on a Perkin–Elmer Model system 2000 spectrophotometer. Proton NMR were recorded on a JEOL Model INM-A500 FTNMR 500 MHz spectrometer with deuterated-chloroform (d^1-$CHCl_3$) as solvent for complexes **1** and **2**, deuterated DMSO (d^6-DMSO) for EnH_2 and complex **3**, deuterated acetone (d^6-acetone) for BnH_2 and complex **4**, and TMS was used as an internal standard.

2.2. Syntheses

2.2.1. 3,3′-(1,4-Butanediyldinitrilo)bis(2-butanone)-dioxime(BnH_2)

Ligand BnH_2 was prepared using the method described in the literature [24,25], with a slight modification. 2,3-Butanedione (20.23 g, 0.20 mole) in 50 ml of methanol was added to 1,4-diaminobutane (10.00 ml, 0.10 mole). The resulting solution was stirring at room temperature. After 15 min, a white solid precipitated. It was then isolated by vacuum filtration and washed with cool methanol, then diethyl ether and dried in a desiccator. The yield was 76%. BnH_2 has a melting point of 148–150 °C (the literature value is 149–151 °C). This ligand was identified by infrared and NMR spectra which gave a good agreement with the literature data [24]. The proton NMR spectral data are listed in Table 5.

2.2.2. 3,3′-(1,2-Ethanediyldinitrilo)bis(2-butanone)-dioxime(EnH_2)

This ligand was prepared by a similar procedure as BnH_2 using 1,2-diaminoethane instead of 1,4-diaminobutane. Its melting point is 160–161 °C. The proton NMR spectral data are listed in Table 5.

2.2.3. Complex **1**: trans-dinitro(3,3′-(1,4-butanediyldinitrilo)bis(2-butanonedioximato)cobalt(III), [Co(BnH)(NO_2)$_2$]

Solid BnH_2 (1.26 g, 5.0 mmole) was added to an aqueous solution of hydrated cobalt(II) chloride (1.19 g, 5.0 mmole in 10 ml. water). Sodium nitrite solution (0.77 g, 11.0 mmoles in 5 ml of 1 mmole sodium hydroxide) was added to the Co–BnH_2 solution. After bubbling air through the mixture for 3 h with stirring, a yellow-orange precipitate was obtained. The precipitate was collected, washed with cool water, then with diethylether and dried in a desiccator. The yield was 43%. The yellow-orange single crystal was crystallized from a mixture of water:acetone (1:3). *Anal*. Calc. C, 35.62; H, 5.24; N, 20.79. Found: C, 36.32; H, 5.14; N, 21.55%.

2.2.4. Complex **2**: trans-dichloro(3,3′-(1,4-butanediyldinitrilo)bis(2-butanonedioximato)cobalt(III), [Co(BnH)Cl_2]

Solid BnH_2 (1.26 g, 5.0 mmole) was added to cobalt(II) chloride hexahydrate (1.19 g, 5.0 mmole) in 15 ml of methanol. The mixture was stirred at room temperature with air bubbling, giving a dark green precipitate. The green solid was collected, washed with cool methanol, then with diethyl ether and dried in a desiccator. The yield was 43%. The dark green single crystals were crystallized from a mixture of water:acetone (1:3). *Anal*. Calc. C, 37.62; H, 5.52; N, 14.62. Found: C, 38.14; H, 5.45; N, 14.99%.

2.2.5. Complex **3**: trans-dichloro(3,3′-(1,2-ethanediyldinitrilo)bis(2-butanonedioximato)cobalt(III), [Co(EnH)Cl_2)]

Cobalt(II) chloride hexahydrate in 10 ml of methanol was added to a hot methanol solution of EnH_2 (1:1 molar ratio). The mixture was stirred at room temperature with air bubbling, giving a dark green precipitate. The precipitate was collected by filtration, washed with ethanol, then diethyl ether and dried in a desiccator. The dark green crystals were crystallized from a mixture of water:acetone (1:3). *Anal*. Calc. C, 33.82; H, 4.83; N, 15.77. Found: C, 33.93; H, 4.51; N, 15.99%.

2.2.6. Complex **4**: 3,3′-(1,4-butanediyldinitrilo)-bis(2-butanonedioximato)nickel(II)perchlorate, [Ni(BnH)]ClO_4

The ligand BnH_2 was added to a water:acetone mixture (1:3) containing nickel(II) chloride ($NiCl_2$) (1:1 molar ratio). This mixture was stirred until the solution was homogeneous. An aqueous solution of sodium perchlorate was added to the reaction mixture and stirred well. After the reaction mixture was allowed to stand at room temperature for 2 days, orange-red crystals formed. The crystals were collected and dried in a desiccator. *Anal*. Calc. C, 35.03; H, 5.14; N, 13.62. Found: C, 34.97; H, 5.12; N, 13.23%.

2.3. X-ray crystallographic analyses

The diffraction data for all complexes with appropriately sized crystal were collected at 298(2) K on a 1K BRUKER SMART CCD area detector diffractometer using ω rotation scans with a scan width of 0.3° and graphite monochromated Mo Kα radiation ($\lambda = 0.71073$ Å). For data

Table 1
Crystallographic data

	1	2	3	4
Complex	$[Co(BnH)(NO_2)_2]$	$[Co(BnH)Cl_2]$	$[Co(EnH)Cl_2]$	$[Ni(BnH)]ClO_4$
Formula	$C_{12}H_{21}N_6O_6Co$	$C_{12}H_{21}N_4O_2Cl_2Co$	$C_{10}H_{17}N_4O_2Cl_2Co$	$C_{12}H_{21}N_4O_6ClNi$
Crystal system	orthorhombic	orthorhombic	monoclinic	triclinic
Space group	$P2_12_12_1$	$P2_12_12_1$	$P2_1/c$	$P1$
a (Å)	7.4396(2)	8.0095(16)	8.1953(2)	6.5421(2)
b (Å)	10.1192(3)	14.031(3)	13.3987(4)	10.8561(2)
c (Å)	23.0488(7)	29.050(6)	13.4361(3)	12.9977(3)
α (°)	90	90	90	103.561(1)
β (°)	90	90	99.367(1)	95.740(1)
γ (°)	90	90	90	103.161(1)
V (Å^3)	1735.18(9)	3264.6(11)	1455.70(6)	862.26(4)
Z	4	8	4	1
D_m (g cm^{-3}), flotation	1.551	1.555	not measured	unable to measure
D_c (g cm^{-3})	1.548	1.559	1.620	1.585
μ (mm^{-1})	1.031	1.387	1.548	1.316
$2\theta_{max}$ (°)	60.96	56.76	60.88	61.00
No. reflections measured	12944	22231	10642	6456
Independent	5034	8033	4144	5487
R[a]	0.0573	0.0343	0.0445	0.0373
R_w [b]	0.1336	0.0703	0.1137	0.0955

[a] $R = \sum\|F_o| - |F_c\|/\sum|F_o|$.
[b] $R_w = \sum w(F_o^2 - F_c^2)^2/\sum w(F_o^2)^2]^{1/2}$.

collections and data integration, the SMART and SAINT programs were used [26] and empirical absorption correction was done by using the program SADABS [27]. The structures were solved by direct methods using the SHELXTL program system [28] and were refined by full-matrix least-squares first with isotropic and then with anisotropic thermal parameters for all non hydrogen atoms. For all complexes the hydrogen atoms were located from a Fourier difference map and refined. Two oxygen atoms in the perchlorate ions were disordered, as can be recognized from the large values of the temperature factor. They were not refined anisotropically. Crystal data and refinement results of all the complexes are listed in Table 1. Selected bond lengths and bond angles for complexes **1**–**4** are summarized in Table 2.

3. Results and discussion

3.1. Crystal structures of the complexes

Complex **1**, $[Co(BnH)(NO_2)_2]$, and complex **2**, $[Co(BnH)Cl_2]$, are isomorphous, crystallizing in the orthorhombic system whereas complex **3**, $[Co(EnH)Cl_2]$, crystallizes in the monoclinic system. Complex **1** is a neutral mononuclear cobalt(III) complex. The distorted octahedron about the cobalt is completed by two *cis* oxime nitrogens, two *cis*-imine nitrogens and two nitro ligands in *trans* positions (Fig. 1). All atoms on the square planes are almost coplanar. The molecule consists of two five-membered imineoxime chelate rings and one seven-membered butylene chelate ring. Two nitro groups are in a staggered configuration. The bond length of Co—N(5) is shorter than that of Co—N(6) and the N(5)—Co—N(6) angle is 177.05(17)°. In one nitro group the N(5)—O(3) and N(5)—O(4) bond lengths are quite different (1.228(6) and 1.179 (6) Å) while in the other nitro group the N—O bond lengths are similar (1.217(5) and 1.226(5) Å). The shorter Co—N(5) bond distance brings one nitro oxygen atom close to the diiminedioxime square plane so that weak hydrogen bonding between the nitro oxygen and oxime hydrogen occurs. Consequently the intramolecular hydrogen bonding between *cis* oxime groups becomes weakened. A short intramolecular hydrogen bond with an O—O distance of 2.434(5) Å for this complex was observed.

The crystal structure of complex **2** consists of a neutral distorted octahedrally coordinated cobalt(III) complex (Fig. 2). There are two molecules per asymmetric unit. These two molecules are not related by any symmetry. The cobalt atom is coordinated to four nitrogen atoms of the diiminedioxime ligands and two *trans* chloro ligands, resulting in a distorted octahedral geometry. The square plane about the cobalt is slightly distorted as evident by the result of the least square plane analysis. One set of *trans*-nitrogens are below the best plane through the cobalt and four diiminedioxime nitrogens while the other set are above this plane, within 0.0240. The Co—Cl bond lengths are slightly different. No weak interaction between the chloro ligand and oxime hydrogen was observed. This complex exhibits an intramolecular hydrogen bond with an O—O distance of 2.423(4) Å in molecule 1 and 2.414(3) Å in molecule 2. This is similar to that observed for $[Co(BnH)Cl_2]$ reported by Choo [29].

In $[Co(EnH)Cl_2]$ the octahedron about the cobalt is completed by four nitrogens of the tetradentate ligand and two *trans*-chloro ligands (Fig. 3). The four Co—N bond lengths are shorter than those in $[Co(BnH)Cl_2]$, but the Co—Cl bond lengths are longer. The average

Table 2
Selected bond lengths (Å) and bond angles (°) for compounds **1**–**4**

Compound ***1***			
Co(1)—N(1)	1.910(4)	Co(1)—N(2)	1.961(4)
Co(1)—N(4)	1.958(3)	Co(1)—N(3)	1.899(3)
Co(1)—N(5)	1.951(4)	Co(1)—N(6)	1.965(4)
O(1)—N(1)	1.321(6)	O(2)—N(3)	1.330(5)
O(3)—N(5)	1.228(6)	O(4)—N(5)	1.179(6)
O(5)—N(6)	1.217(5)	O(6)—N(6)	1.226(5)
O(1)—O(2)	2.434(5)	N(3)—Co(1)—N(1)	95.86(17)
N(3)—Co(1)—N(5)	88.96(15)	N(1)—Co(1)—N(5)	90.69(16)
N(3)—Co(1)—N(4)	81.31(15)	N(1)—Co(1)—N(4)	177.13(16)
N(5)—Co(1)—N(4)	88.81(16)	N(3)—Co(1)—N(2)	176.49(15)
N(1)—Co(1)—N(2)	80.81(17)	N(5)—Co(1)—N(2)	89.97(15)
N(4)—Co(1)—N(2)	102.01(16)	N(3)—Co(1)—N(6)	88.62(14)
N(1)—Co(1)—N(6)	87.88(15)	N(5)—Co(1)—N(6)	177.05(17)
N(4)—Co(1)—N(6)	92.49(15)	N(2)—Co(1)—N(6)	92.35(15)
Compound ***2***			
Co(1)—N(1)	1.903(2)	Co(1)—N(2)	1.951(2)
Co(1)—N(3)	1.974(2)	Co(1)—N(4)	1.904(2)
Co(2)—N(5)	1.903(2)	Co(2)—N(6)	1.950(2)
Co(2)—N(7)	1.962(2)	Co(2)—N(8)	1.900(2)
Co(1)—Cl(1)	2.2325(8)	Co(1)—Cl(2)	2.2448(8)
Co(2)—Cl(3)	2.2373(7)	Co(2)—Cl(4)	2.2367(8)
O(1)—N(1)	1.325(3)	O(2)—N(4)	1.320(3)
O(3)—N(5)	1.332(3)	O(4)—N(8)	1.338(6)
O(1)—O(2)	2.423(4)	O(3)—O(4)	2.414(3)
N(1)—Co(1)—N(4)	96.18(11)	N(1)—Co(1)—N(2)	80.54(10)
N(4)—Co(1)—N(2)	176.43(10)	N(1)—Co(1)—N(3)	176.50(10)
N(4)—Co(1)—N(3)	80.67(10)	N(2)—Co(1)—N(3)	102.64(9)
N(1)—Co(1)—Cl(1)	91.78(8)	N(4)—Co(1)—Cl(1)	89.69(8)
N(2)—Co(1)—Cl(1)	89.01(7)	N(3)—Co(1)—Cl(1)	89.74(7)
N(1)—Co(1)—Cl(2)	87.41(8)	N(4)—Co(1)—Cl(2)	88.94(8)
N(2)—Co(1)—Cl(2)	92.30(7)	N(3)—Co(1)—Cl(2)	90.99(7)
Cl(1)—Co(1)—Cl(2)	178.33(3)	N(8)—Co(2)—N(5)	96.13(11)
N(8)—Co(2)—N(6)	176.68(10)	N(5)—Co(2)—N(6)	80.56(11)
N(8)—Co(2)—N(7)	80.47(9)	N(5)—Co(2)—N(7)	176.08(10)
N(6)—Co(2)—N(7)	102.84(10)	N(8)—Co(2)—Cl(4)	88.71(7)
N(5)—Co(2)—Cl(4)	87.20(7)	N(6)—Co(2)—Cl(4)	90.99(7)
N(7)—Co(2)—Cl(4)	90.77(7)	N(8)—Co(2)—Cl(3)	90.64(7)
N(5)—Co(2)—Cl(3)	91.40(7)	N(6)—Co(2)—Cl(3)	89.58(7)
N(7)—Co(2)—Cl(3)	90.58(7)	Cl(4)—Co(2)—Cl(3)	178.38(3)
Compound ***3***			
Co—N(1)	1.8732(17)	Co—N(2)	1.8385(17)
Co—N(4)	1.8892(17)	Co—N(3)	1.8618(17)
Co—Cl(1)	2.2518(6)	Co—Cl(2)	2.2526(6)
O(1)—N(1)	1.309(2)	O(2)—N(4)	1.362(2)
O(1)—O(2)	2.708(2)	N(1)—Co—N(2)	84.36(8)
N(1)—Co—N(4)	104.31(8)	N(1)—Co—N(3)	173.26(8)
N(4)—Co—N(2)	171.07(8)	N(3)—Co—N(2)	88.93(8)
N(3)—Co—N(4)	82.42(8)	N(1)—Co—Cl(2)	89.18(6)
N(2)—Co—Cl(2)	89.08(6)	N(4)—Co—Cl(2)	88.93(6)
N(3)—Co—Cl(2)	91.45(6)	N(1)—Co—Cl(1)	89.82(6)
N(2)—Co—Cl(1)	90.68(6)	N(4)—Co—Cl(1)	91.45(6)
N(3)—Co—Cl(1)	89.53(6)	Cl(2)—Co—Cl(1)	178.99(2)
Compound ***4***			
Ni(1)—N(1)	1.920(6)	Ni(2)—N(5)	1.831(7)
Ni(1)—N(2)	1.894(7)	Ni(2)—N(6)	1.902(7)
Ni(1)—N(3)	1.868(7)	Ni(2)—N(7)	1.964(6)
Ni(1)—N(4)	1.904(6)	Ni(2)—N(8)	1.842(7)
O(1)—N(1)	1.273(9)	O(2)—N(4)	1.321(8)
O(3)—N(5)	1.387(8)	O(4)—N(8)	1.379(9)
O(1)—O(2)	2.473(8)	O(3)—O(4)	2.390(9)
N(1)—Ni(1)—N(2)	81.5(3)	N(5)—Ni(2)—N(6)	82.6(3)
N(1)—Ni(1)—N(3)	174.0(4)	N(5)—Ni(2)—N(7)	174.3(3)
N(1)—Ni(1)—N(4)	96.1(3)	N(5)—Ni(2)—N(8)	95.5(3)
N(2)—Ni(1)—N(3)	100.8(3)	N(6)—Ni(2)—N(7)	101.9(3)
N(2)—Ni(1)—N(4)	166.1(3)	N(6)—Ni(2)—N(8)	166.6(4)
N(3)—Ni(1)—N(4)	83.0(3)	N(7)—Ni(2)—N(8)	80.9(3)

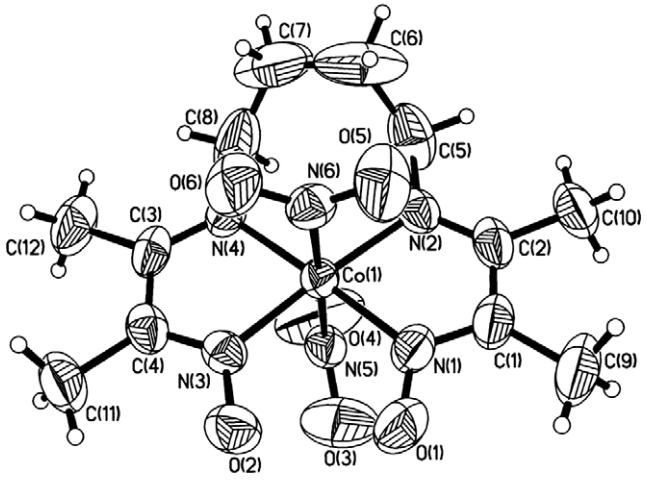

Fig. 1. Perspective view of $[Co(BnH)(NO_2)_2]$ (**1**), showing thermal ellipsoids (50% probability) and atom labelling.

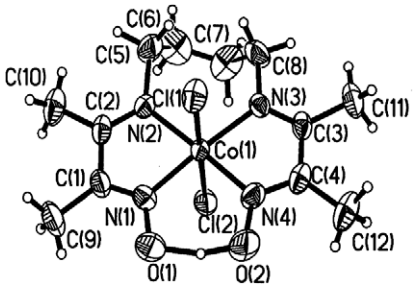

Fig. 2. Perspective view of $[Co(BnH)Cl_2]$ (**2**) showing thermal ellipsoids (50% probability) and atom labelling.

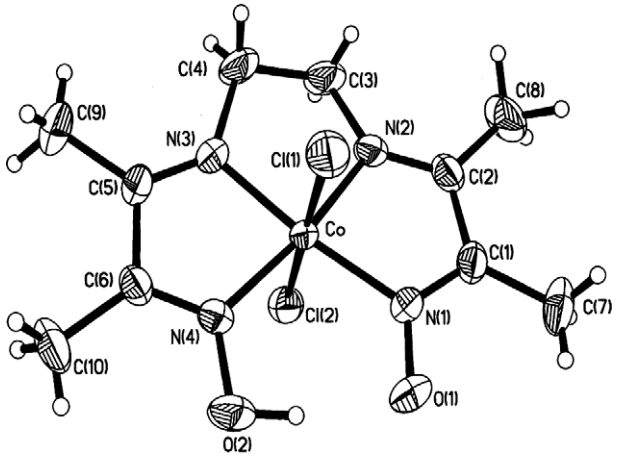

Fig. 3. Perspective view of $[Co(EnH)Cl_2]$ (**3**) showing thermal ellipsoids (50% probability) and atom labelling.

Co—$N_{(imine)}$ and Co—$N_{(oxime)}$ bond distances of $[Co(BnH)(NO_2)_2]$ and $[Co(BnH)Cl_2]$ in this study are the longest among diiminedioxime cobalt(III) complexes. A similar result was found in the diaminedioxime complexes. This is probably indicative of a weaker metal—ligand interaction in the BnH_2 complex compared with the EnH_2 and $PreH_2$ complexes. The shortest metal—nitrogen bond distances exhibited by EnH_2 suggested that this ligand forms the strongest complex with Co(III). This might be expected on the basis of chelate effects exerted by the three five-membered chelate rings in the EnH_2 complex as compared to a combination of one six-membered and five-membered chelate rings in the $PreH_2$ complex, and one seven-membered and two five-membered chelate rings in the BnH_2 complex. On the basis of cobalt—nitrogen bond distances, the relative ligand field strength of diiminedioximes for complex formation would be $EnH_2 > PreH_2 > BnH_2$ (similar to EnAO > PnAO > BnAO). In the sequence of the EnH_2, $PreH_2$ and BnH_2 complexes, the O—O distances and $N_{(oxime)}$—Co—$N_{(oxime)}$ bond angles decrease, but the $N_{(imine)}$—Co—$N_{(imine)}$ bond angles, and Co—$N_{(imine)}$ and Co—$N_{(oxime)}$ bond distances increase. Similar results were observed in EnAO, PnAO and BnAO complexes [16–21]. The $N_{(imine)}$—Co—$N_{(imine)}$, $N_{(oxime)}$—Co—$N_{(oxime)}$ and $N_{(oxime)}$—Co—$N_{(imine)}$ bond angles in this study are very close to the corresponding angles in $[Co(BnH)Cl_2]$ [29]. The longest O—O distance of 2.708(2) Å is found in $[Co(EnH)Cl_2]$ indicating no weak intramolecular hydrogen bonding. The elongation of the O—O distances in the diiminedioxime complexes of Co(III) agrees with the degree of constraint of the alkylene bridge between the two imine nitrogens. The degree of constraint follows the order: $BnH_2 < PreH_2 < EnH_2$. In $[Co(BnH)Cl_2]$ the butylene bridge between the two imine-nitrogens imposes less constraint on the ligand resulting in a larger $N_{(imine)}$—Co—$N_{(imine)}$ angle when compared to $PreH_2$ and EnH_2 complexes which impose more constraints on the complex geometry. Consequently the $N_{(imine)}$—Co—$N_{(imine)}$ angle for the $[Co(EnH)Cl_2]$ complex is smaller than that of $[Co(BnH)Cl_2]$. Hence, the longest O—O distance of 2.708 (2) Å is found in $[Co(EnH)Cl_2]$.

The crystal structure of $[Ni(BnH)]ClO_4$ consists of a distorted square planar $[Ni(BnH)]^+$ cation and a perchlorate

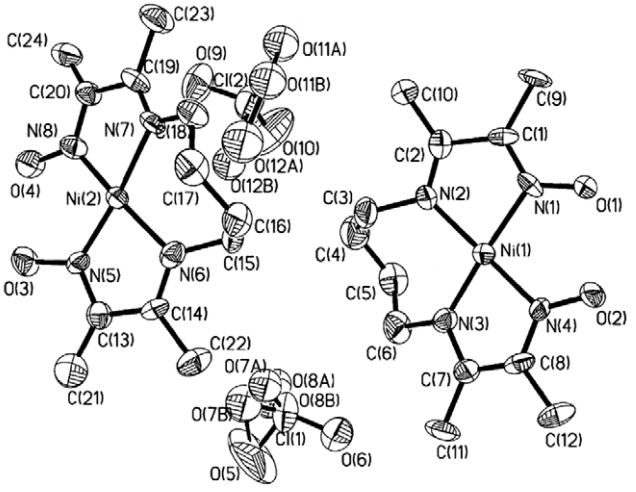

Fig. 4. Perspective view of $[Ni(BnH)]ClO_4$ (**4**) showing thermal ellipsoids (50% probability) and atom labelling for nonhydrogen atom.

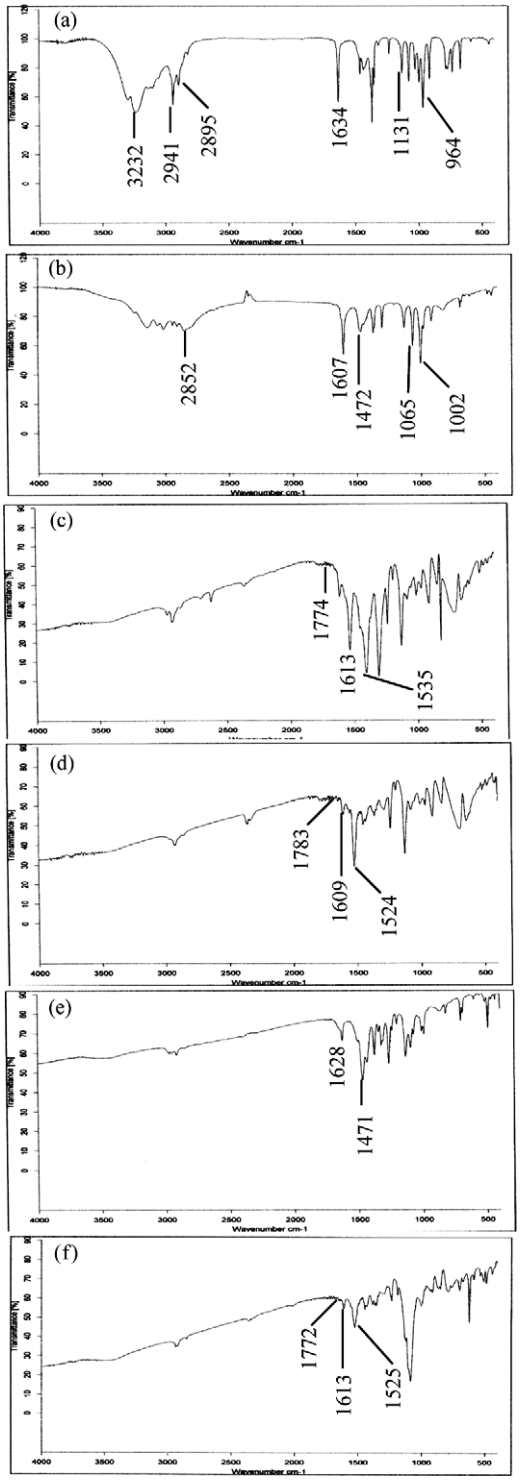

Fig. 5. FTIR spectra of (a) BnH_2 (b) EnH_2 (c) $[Co(BnH)(NO_2)_2]$ (d) $[Co(BnH)Cl_2]$ (e) $[Co(EnH)Cl_2]$ and (f) $[Ni(BnH)]ClO_4$.

counter ion (Fig. 4). There are two molecules per asymmetric unit. A least squares plane through the nickel and the four coordinate nitrogens show that two *trans*-nitrogens are above the plane, within 0.150 Å, and the other two *trans*-nitrogen are below the plane, within −0.170 Å. The O—O distances for complex **4** are 2.390(9) in molecule 1 and 2.473(8) Å in molecule 2. The average O—O distance 2.432 Å is about the same as those of $[Co(BnH)(NO_2)_2]$ and $[Co(BnH)Cl_2]$. Therefore changing Co^{3+} to the Ni^{2+} ion does not play a pronounced effect on the O—O distance. It is due to the comparable size of Co^{3+} (69 pm) and Ni^{2+} (63 pm) ions [30].

Table 3
The vibrational frequencies for the C—N bond in the free ligands and complexes **1**–**4**

	EnH_2	BnH_2	Complex			
			1	**2**	**3**	**4**
ν_{CN}	1607	1634	1613 (m) 1535 (s)	1609 (m) 1524 (s)	1628 (w) 1471 (m)	1613 (w) 1525 (m)

Table 4
Comparison of O—O distances, stretching frequencies and chemical shifts of the intermolecular hydrogen bond in various complexes

Compound	O—O (Å)	δ_{OH} (ppm)	ν_{OHO} (cm^{-1})	Reference
BnH_2		10.43		this work
EnH_2		11.43		this work
$[Co(BnH)Cl_2]$[a]	2.420 (10) 2.390 (9)			[29]
$[Co(BnAO)(NO_2)_2]$[b]	2.412 (3)	19.35	1790	[20]
$[Ni(BnAO)]I \cdot H_2O$[b]	2.417 (7)	18.50	1798	[23]
$[Co(BnH)Cl_2]$[a]	2.423 (4) 2.414 (3)	19.58	1783 (w,b)	this work
$[Co(PnAO)(NO_2)_2]$[b]	2.432 (3)	18.40	1780	[17]
$[Ni(BnH)]ClO_4$[a]	2.390 (9) 2.473 (8)	18.00	1772 (w,b)	this work
$[Co(BnH)(NO_2)_2]$	2.434 (5)	19.03	1774 (w,b)	this work
$[Co(PreH)Cl_2]$	2.448 (5)	19.35	1772	[22]
$[Co(EnAO)(NO_2)_2]$[b]	2.554 (6)	7.35	1720	[20]
$[Co(EnH)Cl_2]$	2.708 (2)			this work

[a] Crystallizes as two molecules per asymmetric unit.
[b] EnAO, PnAO and BnAO are the abbreviation of the corresponding diaminedioxime.

3.2. Magnetic susceptibility

The square planar geometry around Ni^{2+} in $[Ni(BnH)ClO_4]$ is also evident by the magnetic measurement. According to the valence bond theory, the Ni^{2+} hybridization is dsp^2 meaning that there is no unpaired electron. The measured χ_g, χ_m and μ_{eff} values for this complex are 9.29×10^{-7} c.g.s, 3.82×10^{-4} and 0.9939 BM, respectively. The calculated number of unpaired electron is zero.

3.3. Infrared spectra

The vibrational frequencies for particular bonds in the free ligand and the complexes are summarized in Fig. 5. When the complex is formed, two C=N bonds are distinguishable. Two $\nu_{C=N}$ are observed at lower frequencies than that in the free ligand, supporting the coordination at oxime and imine nitrogens (Table 3). The vibrational frequencies for weak intramolecular hydrogen bonding ν_{OHO} in the complexes occur at 1772–1783 cm^{-1}, as observed in other diiminedioxime complexes (Table 4). For $[Co(EnH)Cl_2]$, no peak was observed in this region indicating that no intramolecular hydrogen bond was formed. It was found that the O—O distances vary inversely with the ν_{OHO} value.

3.4. Nuclear magnetic resonance spectra

The proton NMR peaks for $[Co(BnH)Cl_2]$ exhibits downfield shifts when compared to the corresponding peaks for $[Co(BnH)(NO_2)_2]$ (Table 5). This may be due to the inductive effect of the chloride compared to the nitro group [31]. The intramolecular hydrogen bridge proton between two oxime groups is expected to resonate at a very low field as reported for other diaminedioxime and diiminedioxime complexes [1–22]. The signals at 19.03, 19.58 and 18 ppm are assigned to the hydrogen bridge protons in complexes **1**, **2** and **4**, respectively. No oxime hydrogen bridge proton signal is observed in the $[Co(EnH)Cl_2]$ spectrum. This is probably indicative of an exchange phenomena taking place in the complex. The oxime hydrogen easily exchanges with the water hydrogen (solvent impurity) and exchange is so rapid that no hydrogen proton resonance is detected.

Table 5
^1H NMR spectral data for the free ligands and complexes **1**–**4** δ (ppm)

		Solvent	a	b	c	d	e
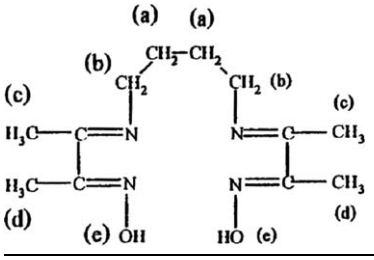	BnH_2	d^6-acetone	1.79	3.46	2.00	2.01	10.43
	EnH_2	d^6-acetone		3.69	1.88	2.01	11.43
	$[Co(BnH)(NO_2)_2]$	d^1-$CHCl_3$	1.91	4.12	2.49	2.54	19.03
	$[Co(BnH)Cl_2]$	d^1-$CHCl_3$	2.33	4.24	2.57	2.60	19.58
	$[Ni(BnH)]ClO_4$	d^6-acetone	2.0	3.6	2.1	2.2	18.0

Consequently, the signal collapses with the water hydrogen signal. There is no correlation between O—O distance and oxime hydrogen signal (Table 4).

4. Conclusions

Comparison of crystal structures for diiminedioxime (BnH_2 and EnH_2) complexes of Co(III) and Ni(II) indicates that introduction of a propylene bridge opposite the hydrogen bond imposes no significant constraint but the ethylene bridge impose significant constraint. Hence the O—O distance of $[Co(EnH)Cl_2]$ is much longer than those for $[Co(BnH)(NO_3)_2]$ and $[Co(BnH)Cl_2]$. Due to the comparable size of Co^{3+} and Ni^{2+} there is no pronounced effect on the O—O distance. The observed O—O distances for $[Co(BnH)(NO_3)_2]$ are longer than that for $[Co(BnH)Cl_2]$ due to the presence of a weak interaction between the nitro oxygen and oxime hydrogen. The ν_{OHO} frequencies of all the complexes were observed at 1772–1783 cm^{-1}. A decrease in the O—O distance tends to shift the ν_{OHO} band to high energy. The proton NMR spectra of all the complexes shows all methyl and methylene protons resonances with the expected chemical shifts and integrated intensities. The intramolecular hydrogen bond proton resonance appears at 19.03 ppm in $[Co(BnH)(NO_3)_2]$, 19.58 ppm in $[Co(BnH)Cl_2]$ and 18 ppm in $[Ni(BnH)ClO_4]$. It was found that there is an inverse relationship between the O—O distances and ν_{OHO} but no relationship between the O—O distance and oxime proton resonance.

5. Supplementary data

CCDC Nos. 294384 – 294387 contain the supplementary crystallographic data for this paper. The data can be obtained free of charge from the CCDC, 12 Union Road, Cambridge CB2, 1EZ, UK, fax: +44 1223 336 033; or e-mail: deposit@ccdc.cam.ac.uk or http://www.ccdc.cam.ac.uk on request.

Acknowledgements

The authors thank Department of Chemistry, Faculty of Science, Kasetsart University and TRF fund (RTA 4880008) for financial support.

References

[1] R.K. Murman, J. Am. Chem. Soc. 79 (1957) 521.
[2] D.E. Williams, G. Wohlauer, R.E. Rundle, J. Am. Chem. Soc. 81 (1959) 755.
[3] E.O. Schlemper, Inorg. Chem. 7 (1968) 1130.
[4] A. Vacciago, L. Zandaecio, J. Chem. Soc. A (1970) 218.
[5] F.A. Cotton, J.G. Norman Jr., J. Am. Chem. Soc. 93 (8) (1970) 1914.
[6] S. Bruckner, L. Randaecio, J. Chem. Soc., Dalton Trans. (1974) 1017.
[7] E.O. Schlemper, C.K. Fair, Acta Crystallogr., Sect. B 33 (1977) 2482.
[8] E.O. Schlemper, S.I. Laplace, B.R. Paris, W.C. Hamilton, Acta Crystallogr., Sect. B 34 (1978) 918.
[9] M.S. Hussain, B.E.V. Salinas, E.O. Schlemper, Acta Crystallogr., Sect. B 35 (1979) 628.
[10] S. Siripaisarnpipat, E.O. Schlemper, Inorg. Chem. 23 (1984) 330.
[11] R. Dreos, G. Tauzher, S. Geremia, L. Randaceio, F. Asaro, G. Pellizer, C. Tavagnacco, G. Costa, Inorg. Chem. 33 (1994) 5404.
[12] M. Kubiak, T. Glowiak, M. Moszner, J.J. Ziolkowski, F. Asaro, G. Costa, G. Pellizer, C. Tavagnacco, Inorg. Chim. Acta 236 (1995) 141.
[13] A.K. Das, S.M. Peng, S. Bhattacharya, Polyhedron 20 (2001) 327.
[14] C.H. Li, R.J. Wang, H.Z. Kou, Y.D. Li, Inorg. Chem. Commun. 5 (2002) 403.
[15] X.W. Liu, S. Chu, X.Q. Wang, Y. Zhang, R. Wang, G.Q. Shen, D.Z. Shen, Inorg. Chem. Commun. 5 (2002) 1086.
[16] H. Goff, S. Kidwell, J. Lauer, R.K. Murmann, Inorg. Chem. 12 (11) (1973) 2631.
[17] R.K. Murmann, E.O. Schlemper, Inorg. Chem. 12 (1975) 2625.
[18] C.K. Fair, E.O. Schlemper, Acta Crystallogr., Sect. B 34 (1978) 436.
[19] D.P. Gavel, E.O. Schlemper, Inorg. Chem. 18 (1979) 283.
[20] S. Siripaisarnpipat, Synthesis and structural studies of rhodium(III) and cobalt(III) complexes with intramolecular hydrogen bonds. Ph.D. Dissertion, University of Missouri-Columbia.
[21] S. Siripaisarnpipat, E.O. Schlemper, Inorg. Chem. 22 (1983) 282.
[22] S. Siripaisarnpipat, E.O. Schlemper, J. Coord. Chem. 13 (1984) 281.
[23] I. Pal, R.K. Murmann, E.O. Schlemper, C.K. Fair, M.S. Hussian, Inorg. Chim. Acta 115 (1986) 153.
[24] R.R. Gange, J.L. Allison, M. Ingle, Inorg. Chem. 18 (10) (1979) 2767.
[25] J.W.L. Martin, J.H. Timmons, A.E. Martell, P. Rudolf, A. Clearfield, Inorg. Chem. 20 (3) (1981) 814.
[26] SMART, Data Collection Software, Version 4.0 and SAINT, Data integration Software, Version 4.0, Bruker AXS, Inc., Madison, WI, 1997.
[27] G.M. Sheldrick, SADABS, Program for Empirical Absorption, University of Göttingen, Germany, 1996.
[28] G.M. Sheldrick, SHELXTL version 5.1, University of Göttingen, Germany, 1993.
[29] P.L. Choo, A.M. Mulichak, R.W. Bacon, V.B. Pett, D.E. Zacharias, Inorg. Chim. Acta 171 (1990) 183.
[30] G.L. Miessler, D.A. Tarr, Inorganic Chemistry, 3rd ed., International Editor (Appendix B).
[31] R.V. Parish, NMR NQR EPR and Mossbauer Spectroscopy in Inorganic Chemistry, Ellis Horwood Limited, West Sussex, 1990, pp. 59.

Table 1
Crystal data and refinement data for **1**

	1
Empirical formula	$C_9H_7Cl_3N_7Fe$
Molecular mass	375.42
Temperature (K)	233(2)
Crystal system	monoclinic
Space group	$P2_1/c$
a (Å)	9.276(4)
b (Å)	19.754(8)
c (Å)	7.368(3)
β (°)	93.172(3)
V (Å^3)	1348.1(9)
Z, $\rho_{calcd.}$ (Mg m^{-3})	4, 1.850
μ (Mo Kα) (mm^{-1})	1.712
$F(000)$	748
Crystal size (mm)	$0.22 \times 0.14 \times 0.08$
Goodness-of-fit	1.143
R_1 [$I > 2\sigma(I)$]	0.0763
wR_2 [$I > 2\sigma(I)$]	0.1338

used as received without further purification. Infrared spectra were recorded on a Nicolet AVATAR 360 FT-IR instrument as KBr plates. Elemental analysis (C, H, N) was performed with Element Analysis system EA 1112 CE Instruments by the Korea Basic Science Institute.

2.2. Synthesis of $[Fe(btp)Cl_3]_n$ (1)

A solution of $FeCl_3 \cdot 6H_2O$ (0.015 g, 0.052 mmol) in acetone (20 ml) was allowed to diffuse into a solution of btp (0.0106 g, 0.05 mmol) in CH_2Cl_2(20 ml) slowly. After a few weeks, green crystals were separated and air-dried. Yield: 0.014 g (74.6%, based on btp). $C_9H_7Cl_3N_7Fe$ (375.42): Calc. C 50.70, H 3.31, N 45.99%; Found: C 50.35, H 3.40, N 45.96%. Selected IR data (cm^{-1}): 3137 (m), 3106 (m), 1604 (s), 1585 (s), 1522 (s), 1469 (s), 1444 (m), 1366 (m), 1283 (m), 1212 (s), 1137 (s), 1064 (m), 810 (m), 775 (m), 670 (m), 639 (m).

2.3. Crystal structure and determination

X-ray diffraction measurements were performed on a Bruker SMART diffractometer equipped with CCD area detector with graphite-monochromated Mo Kα radiation ($\lambda = 0.71073$ Å) at 233(2) K for **1**. The reflections were successfully indexed by an automated indexing routine built in the SMART program [10]. The solution was solved by direct methods and refined by full-matrix least-squares calculations on F^2 with SHELX-97 [11]. All non-hydrogen atoms were refined anisotropically. All hydrogen atoms were located in the calculated positions using the riding model. Crystallographical data and refinement details for **1** are listed in Table 1.

3. Results and discussion

2,6-Bis(*N*1-1,2,4-triazolyl)pyridine (btp) is a versatile ligand which has the potential to show various coordination modes: bridging two metal centres, chelating a metal ion as a terdentate ligand or functioning with the two cases simultaneously [9].

The reaction of btp with an equivalent of $FeCl_3 \cdot 6H_2O$ afforded 1D infinite chains. The btp ligands connect the ferric centres as shown in Fig. 1. Even when 1:2 or 1:3 ligand-to-metal ions ratios were employed, only the 1:1 mol ratio complex **1** was obtained. X-ray single crystal structure analysis [12] of complex **1** reveals that the geometry of the iron centre has a trigonal bipyramidal environment comprising two nitrogen atoms located on the apical sites and three chloride ligands occupying three vertices of a trigonal plane. To the best of our knowledge, there are only two examples of which the structures are fully characterized with the TBP geometry on the ferric centre; $[Fe(N_3)_5]^{2-}$ [12] and $FeCl_3(4\text{-cpy})_2$(4-cpy = 4-cyanopyridine) [13]. Until now no more TBP ferric complexes have been observed.

The average Fe–Cl bond length of 2.214(2) Å is similar to those found in $FeCl_3(4\text{-cpy})_2$[2.215(1) Å]. The deviation of Cl–Fe–Cl and N–Fe–N angles from ideal D_{3h} point symmetry is commonly observed in the case of the TBP MX_3L_2 system. The Fe–N bond lengths of 2.162(2) and 2.189(6) Å are shorter than those in $FeCl_3(4\text{-cyb})_2$ [2.214(3) and 2.231(3) Å] [13]. This is partly because the nitrogen atoms of triazole experience less steric repulsion against Cl ligands in approaching the iron centre due to a

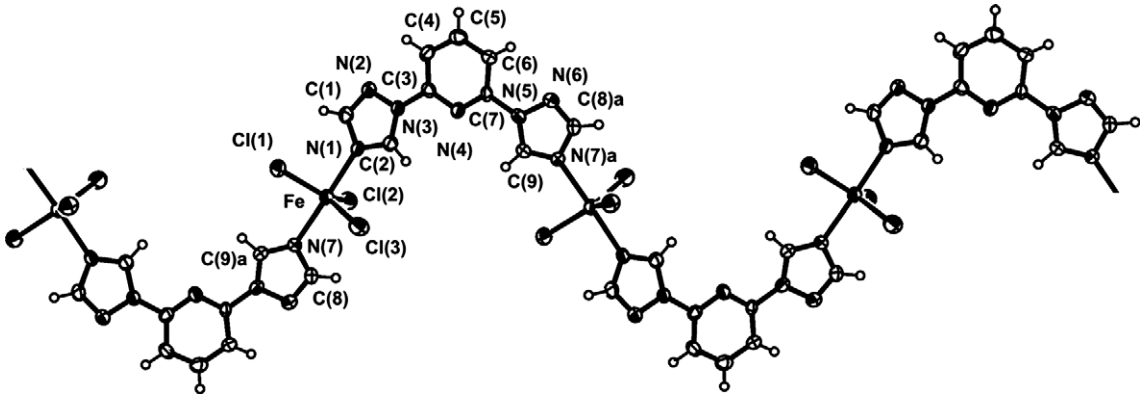

Fig. 1. 1-D zigzag chain of complex **1**. Symmetry code (a): $-x$, $0.5 + y$, $0.5 - z$.

Table 2
Selected bond lengths (Å) and bond angles (°) for **1**

Fe–N(1)	2.162(6)	Fe–N(7)	2.189(6)
Fe–Cl(1)	2.210(2)	Fe–Cl(2)	2.219(2)
Fe–Cl(3)	2.213(2)	Cu1–O4	1.979(2)
N(1)–Fe–N(7)	177.3(2)	Cl(1)–Fe–Cl(2)	127.85(9)
Cl(1)–Fe–Cl(3)	117.76(1)	Cl(2)–Fe–Cl(3)	114.39(1)

small inner angle of the triazole ring compared with pyridine. The selected bond lengths and angles are listed in Table 2.

As shown in Fig. 2, the stacking pattern of the 1D chains implies that there are non-classical C–H···Cl hydrogen bonds, which get 1D chains to form a 2D architecture. The chloride ligand (Cl(2)) bound to the ferric ion pro-

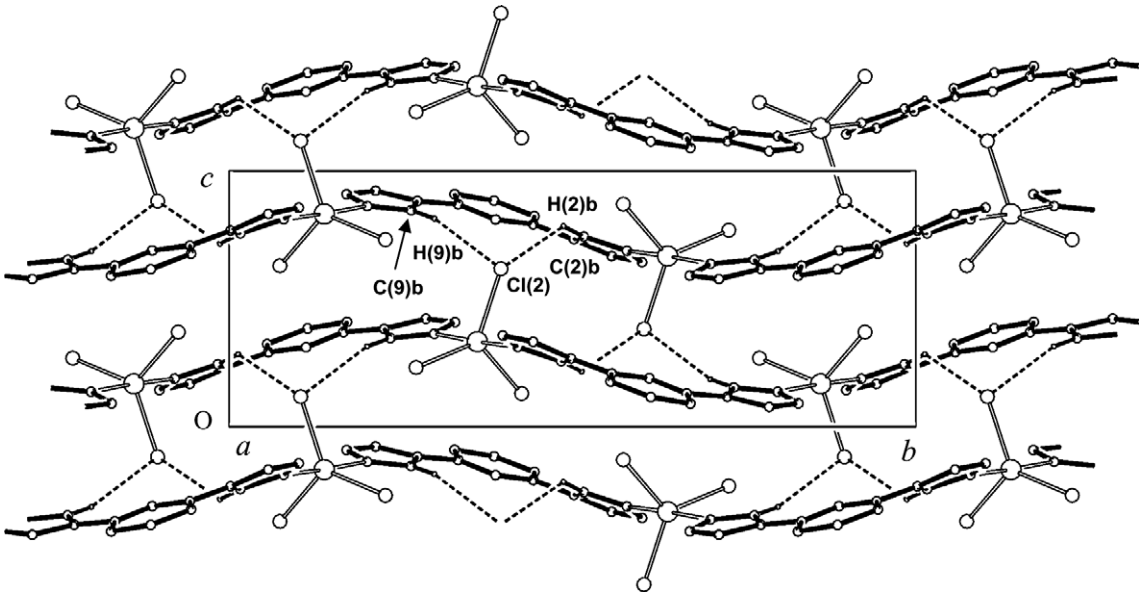

Fig. 2. Stacking diagram of **1** parallel to *x*-axis. C–H···Cl hydrogen bonds are represented as dashed lines. All hydrogen atoms except H(2) and H(9) and C–H···N hydrogen bonds are omitted for clarity. Symmetry code (b): $-x$, $1-y$, $1-z$.

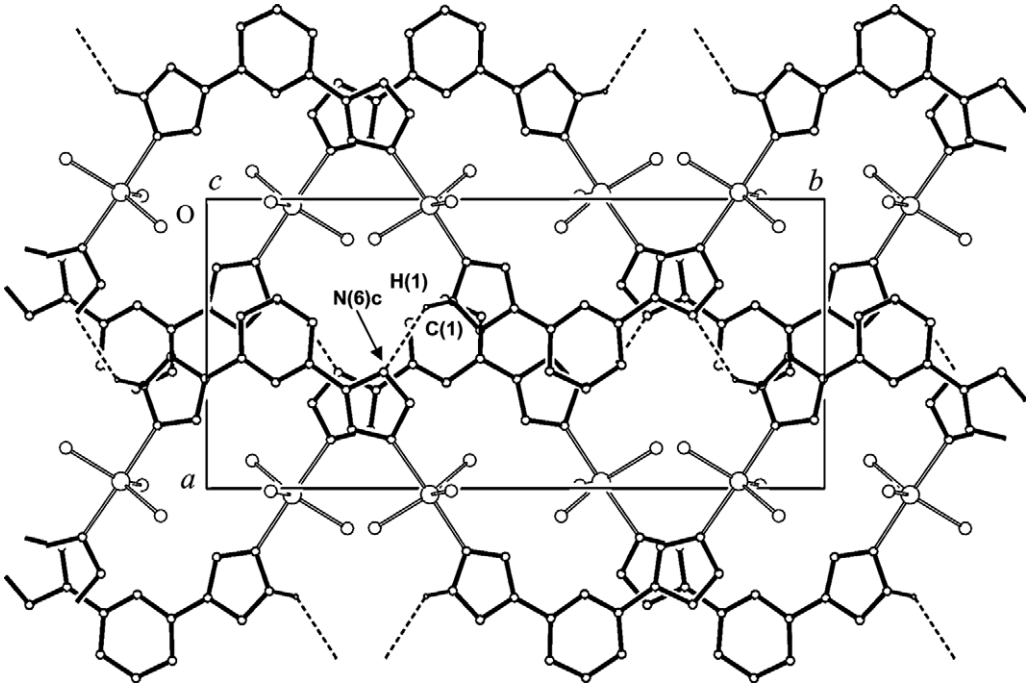

Fig. 3. Stacking diagram of **1** parallel to *z*-axis. C–H···N hydrogen bonds are represented as dashed lines. All hydrogen atoms except H(1) and C–H···Cl hydrogen bonds are omitted for clarity. Symmetry code (c): $1-x$, $-0.5+y$, $0.5-z$.

trudes into the inter-space of 1D chains along the *c*-axis so as to participate in bifurcated hydrogen bonding with two C–H groups *ortho* to the nitrogen atoms, leading to the 2D brick wall architecture. The C–H···Cl interaction is reasonably regarded as hydrogen bonding nature [4,8]. As far as we are aware, C–H units *ortho* to nitrogen frequently function as hydrogen donors and form weak hydrogen bonds with halogen atoms. In these cases, the H···Cl distances fall below the sum of van der Waals radii (2.95 Å) and the C–H···Cl angles are larger than 130°. The H···Cl distances of 2.74 and 2.80 Å and the C–H···Cl angles of 134.7° and 163.6° are in the compatible range of those reported previously [5,6,8].

On the other hand, 1D zigzag chains propagate along with the crystallographic *c*-axis as shown in Fig. 3. These sinusoidal chains are linked to one another via the C–H···N hydrogen bonds. C–H units make the hydrogen bonds with two nitrogens (N(6)) of triazole rings belonging to neighbouring chains, showing a distance of 2.48 Å and C–H···N angle of 132.0°. These values lie in the range considered as C–H···N hydrogen bonds [14]. At last, the 2D sheet parallel with the [0 0 1] plane results as depicted in Fig. 3.

Consequently, 1D sinusoidal chains formed by coordination bonds are connected with one another by two kinds of non-classical hydrogen bonds, resulting in the 3D architecture.

Acknowledgement

The authors acknowledge the financial support of the Korea Science and Engineering Foundation (Grant No. RO1-2001-00053).

Appendix A. Supplementary material

Crystallographic data for complex **1** have been deposited at the Cambridge Crystallographic Data Centre as a supplementary publication (CCDC-297541). These data can be obtained free of charge from The Director, CCDC, 12 Union Road, Cambridge, CB2 1EZ, UK (fax: +44 1223 336 033; e-mail: deposit@ccdc.cam.ac.uk or www.ccdc.cam.ac.uk/conts/retrieving.html). Supplementary data associated with this article can be found, in the online version, at doi:10.1016/j.poly.2006.03.028.

References

[1] (a) O.M. Yaghi, H. Li, C. Davis, D. Richadson, T.L. Groy, Acc. Chem. Res. 31 (1998) 474;
(b) B.F. Abrahams, S.R. Batten, M.J. Grannas, H. Hamit, B.F. Hoskins, R. Robson, Angew. Chem., Int. Ed. 38 (1999) 1475;
(c) J. Lu, A. Mondal, B. Moulton, M.J. Zaworotko, Angew. Chem., Int. Ed. 40 (2001) 2113;
(d) B. Moulton, M.J. Zaworotko, Chem. Rev. 101 (2001) 1629;
(e) M. Eddaoudi, B. Moler, H. Ji, B. Chen, T.M. Reineke, M. O'Keeffe, O.M. Yaghi, Acc. Chem. Res. 34 (2001) 319;
(f) T.J. Prior, M.J. Rosseinsky, Chem. Commun. (2001) 495.

[2] (a) M. Munakata, L.P. Wu, M. Yamamoto, T. Kuroda-Sowa, M. Maekawa, J. Am. Chem. Soc. 118 (1996) 3117;
(b) H.J. Choi, M.P. Suh, J. Am. Chem. Soc. 120 (1998) 10622;
(c) M.J. Allen, A.D. Burrows, M.J. Mahon, J. Chem. Soc., Dalton Trans. (1999) 215;
(d) J.C. Macdonald, P.C. Dorrestein, M.M. Pilley, M.M. Foote, J.L. Lundburg, R.W. Henning, A.J. Schultz, J.L. Manson, J. Am. Chem. Soc. 122 (2000) 11692;
(e) Y.-B. Dong, M.D. Smith, H.-C. zur Loye, Inorg. Chem. 39 (2000) 1943;
(f) C.J. Kuehl, F.M. Tabellion, A.M. Arif, P.J. Stang, Organometallics 20 (2001) 1956;
(g) L.-G. Zhu, S. Kitagawa, K. Seki, Chem. Lett. 32 (2003) 588.

[3] (a) R.K.O. Sigel, E. Freisinger, S. Metzger, B. Lippert, J. Am. Chem. Soc. 120 (1998) 12000;
(b) L.D. Gibb, E.D. Stevens, B.C. Gibb, J. Am. Chem. Soc. 123 (2001) 5849;
(c) T. Spaniel, H. Görls, J. Scholz, Angew. Chem., Int. Ed. 37 (1998) 1862;
(d) Z. Shirin, J. Thompson, L. Liable-Sands, G.P.A. Yap, A.L. Rheingold, A.S. Borovik, J. Chem. Soc., Dalton Trans. (2002) 1714;
(e) L. Brammer, Chem. Soc. Rev. 33 (2004) 476;
(f) A. Angeloni, P.C. Crawford, A.G. Orpen, T.J. Podesta, B.J. Shore, Chem. Eur. J. 10 (2004) 3783;
(g) C. Janiak, T.G. Scharmann, Polyhedron 22 (2003) 1123.

[4] (a) O. Navon, J. Bernstein, V. Khodorkovsky, Angew. Chem. Int. Ed. Engl. 36 (1997) 601;
(b) C.B. Aakeröy, T.A. Evans, K.R. Seddon, J. Pálinkó, New J. Chem. 23 (1999) 145.

[5] M. Freytag, P.G. Jones, Chem. Commun. (2000) 277.

[6] R. Taylor, O. Kennard, J. Am. Chem. Soc. 104 (1982) 5063.

[7] (a) G.R. Desiraju, Acc. Chem. Res. 29 (1996) 441;
(b) D. Braga, F. Grepioni, G.R. Desiraju, J. Organomet. Chem. 548 (1997) 33;
(c) T. Steiner, Angew. Chem., Int. Ed. 41 (2002) 48.

[8] (a) P.G. Jones, B. Ahrens, Chem. Commun. (1998) 2307;
(b) L. Brammer, E.A. Bruton, P. Sherwood, Cryst. Growth Des. 1 (2001) 277.

[9] (a) K.-T. Youm, H.C. Kang, G.-B. Lee, H.K. Woo, Y.J. Park, N.-K. Lee, J. Ko, M.-J. Jun, Polyhedron 25 (2006) in press;
(b) Y. Kim, S.-J. Kim, A.J. Lough, Polyhedron 20 (2001) 3073;
(c) S.-K. Yoo, J.Y. Ryu, J.Y. Lee, C. Kim, S.-J. Kim, Y. Kim, J. Chem. Soc., Dalton Trans. (2003) 1454;
(d) J.Y. Ryu, J.Y. Lee, J.S. Seo, C. Kim, Y. Kim, Appl. Organometal. Chem. 17 (2003) 805;
(e) J.Y. Ryu, J.Y. Lee, S.H. Choi, C. Kim, Y. Kim, S.-J. Kim, Inorg. Chim. Acta 338 (2005) 3398;
(f) S.J. Hong, J.S. Seo, J.Y. Ryu, J.H. Lee, C. Kim, S.-J. Kim, Y. Kim, A.J. Lough, J. Mol. Struct. 751 (2005) 22;
(g) J.Y. Ryu, J.H. Han, J.Y. Lee, S.J. Hong, S.H. Choi, C. Kim, S.-J. Kim, Y. Kim, Inorg. Chim. Acta 358 (2005) 3659.

[10] SMART Area-Detector Software Package, Bruker AXS, Inc., Madison, WI, 1995.

[11] G.M. Sheldrick, SHELX-97: A Program for Structure Determination, University of Göttingen, Göttingen, Germany, 1997.

[12] J. Drummond, J.S. Wood, J. Chem. Soc., Chem. Commun. (1969) 1373.

[13] J.-C. Daran, Y. Jeannin, L.M. Martin, Inorg. Chem. 19 (1980) 2935.

[14] (a) M.J. Mascal, Chem. Commun. (1998) 303;
(b) C.E. Marjo, R. Bishop, D.C. Craig, M.L. Scudder, Eur. J. Org. Chem. (2001) 863.

it was found that paramagnetic centers interact through extended bridging ligands, other applications are optic, electronic materials [17–20], ion exchange, catalysis and separation [21,22].

In the present work, we have used the *p*-aminobenzoate ligand (PAB) to prepare a 1D nickel polymer. The ligand contains a carboxylate group that can act as terminal or bridging, monodentate or bidendate, and also a monodentate amino group in the para position. The crystal structures of some *p*-aminobenzoate metals complexes have been previously determined. The studies demonstrate different ligating behavior of the *p*-aminobenzoate ion, indicating rich coordination chemistry for the complexes from monomeric to polymeric structures. In the complex bis(*p*-aminobenzoato)zinc hydrate $[Zn(4\text{-}NH_2C_6H_4COO)_2]_n \cdot 1.5nH_2O$, the zinc atoms are in a distorted tetrahedral coordination with two N atoms and two O atoms from four aminobenzoate groups, which link the complex into a polymeric structure [23]. The coordination number of lead is 6 in $[Pb(4\text{-}NH_2C_6H_4CO_2)_2]_n$. The carboxylate groups form chelate rings to the lead atom, other groups bridge two metal atoms. The nitrogen atoms of amine groups are not coordinated to the lead atom [24]. While in $[Pb(4\text{-}NH_2C_6H_4CO_2)NO_3]_n$, additional coordination by three oxygen atoms from two nitrate groups and a nitrogen atom from the amino group of PAB brings the coordination number of the lead atom to 8 [25]. The molecular structure of silver(I) *p*-aminobenzoate $[4\text{-}NH_2\text{-}C_6H_4CO_2Ag]$ consists of two types of polymeric chains: the silver atoms are linked by CO_2 groups in the first type, while in the second type the silver atoms are linked by both CO_2 and NH_2 groups of PAB [26]. Both cobalt atoms of $[Co(4\text{-}NH_2C_6H_4CO_2)_2(H_2O)_4]$ and manganese atoms of $[Mn(4\text{-}NH_2C_6H_4CO_2)_2(H_2O)_4]$ are in distorted octahedral coordination with four oxygen atoms from four H_2O molecules, and two oxygen atoms from PAB are *trans* to each other [27,28]. The nickel atoms of the diaquabis(*p*-aminobenzoato)nickel(II) complex occupy centers of symmetry and are coordinated to two oxygen atoms and two nitrogen atoms of both *p*-aminobenzoate molecules in addition to two water molecules, H-bonding makes the structure polymeric [29]. The dimer $[Cu(4\text{-}NH_2C_6H_4CO_2)(phen)(H_2O)]_2\text{-}(NO_3)_2 \cdot 2(4\text{-}NH_2C_6H_4CO_2H) \cdot 2H_2O$ has been synthesized and its X-ray structure studied (phen = phenanthroline). The dimer results through bridging of two symmetrically related *p*-aminobenzoate molecules by bidentate carboxylic groups giving a Cu–Cu distance of 3.060 Å [30].

Although the molecular structures of the above compounds have been well determined, their magnetic properties remain unexplored. Only the dimer $[Cu(p\text{-}NH_2\text{-}C_6H_4CO_2)(phen)(H_2O)]_2(NO_3)_2 \cdot 2(4\text{-}NH_2C_6H_4CO_2H) \cdot 2\,H_2O$ was characterized by EPR spectra and by magnetic measurement [30]. Excellent luminescence properties were obtained for rare-earth Eu^{3+} and Tb^{3+} complexes with *p*-aminobenzoic acid and phenanthroline incorporated into a silica gel matrix [31]. The formation constants of *p*-aminobenzoic acid with the metals Be^{2+}, Zn^{2+}, Fe^{3+}, Th^{4+} and Zr^{4+} have also been determined using potentiometric techniques [32].

As part of our investigations into the synthesis of new polymeric complexes containing the *p*-aminobenzoate ligand, a crystal of the title compound **1** was obtained and its structure, magnetic and thermal properties were studied. The formation constant and thermodynamic parameters of Ni(II) with *p*-aminobenzoic acid were also evaluated.

2. Experimental

2.1. Synthesis of $[Ni(4\text{-}NH_2C_6H_4CO_2)_2\text{-}(CH_3OH)_2] \cdot CH_3OH$ (1)

$NiCl_2 \cdot 6H_2O$ (0.56 g, 2.36 mmol) in methanol (25.0 ml) was added to sodium 4-amino benzoate (0.75 g, 4.70 mmol) in methanol (50.0 ml). The mixture was refluxed for 2 h. Light green crystals of **1** were formed within one week. The typical yield was 95% based on $NiCl_2 \cdot 6H_2O$. *Anal.* Calc. for $C_{17}H_{24}N_2NiO_7$: C, 47.81; H, 5.67, N, 6.56. Found: C, 46.60; H, 5.54; N, 6.72%.

IR (KBr): 3493.2 (m), 3368.9 (m), 3297.3 (m), 3265.9 (m), 3186.4 (m), 2956.7 (w), 2831.3 (w), 1604.7 (s), 1525.6 (s), 1430.2 (m), 1386.7 (s), 1303.8 (w), 1240.1 (m), 1180.4 (m), 1143.7 (w), 1095.5 (w), 1040.5 (m), 1016.4 (m), 970.1 (m), 851.4 (m), 785.0 (m), 698.2 (w), 632.6 (w), 588.2 (w), 559.3 (w), 515.0 (w), 430.1 (w).

2.2. Potentiometry

The potentiometric measurements were carried out using Denver instrument Model 225 pH – ion selective electrode meter fitted with a combined glass electrode (reading to ±0.01 pH unit). The cell compartment was kept constant by using a thermostatic Model Heto HMT 200 in the temperature range 20–40 °C (±0.01 °C). The K_a values of *p*-aminobenzoic acid (PABH) and the stability constants with nickel were computed using an acid–base titration technique in 50% ethanol with ionic strength 0.30 M KCl [33]. The dissociation constant was determined by titrating 50.00 ml of the acid (1.00×10^{-3} M) versus standard NaOH (1.00×10^{-2} M). The stability constant at each temperature was computed from the obtained K_a values and pH readings of the titration of a 50.00 ml solution of nickel(II) ion (5.00×10^{-4} M) with PABH ligand (1.00×10^{-3} M) versus 1.00×10^{-2} M NaOH solution.

2.3. Physical measurements

Elemental analysis of C, H, N was performed at the Elemental Analysis Lab – University of Surrey. Infrared data were collected on a Schimadzu 8300 FTIR spectrophotometer using the KBr pellet method. The magnetic susceptibility of crystalline samples was measured on an Oxford Maglab 2000 magnetic measurement system. Diamagnetic corrections were applied using Pascal's constants. Thermal

analysis was performed on a Setaram-Labsys instrument using the TG-DTA module. The heating rate was 7 °C/min. Dry nitrogen was passed over 15 mg of the sample placed in a platinum crucible.

2.4. Crystallography

2.4.1. X-ray experiment

A pale blue-green prismatic crystal of the complex having approximate dimensions of $0.20 \times 0.12 \times 0.08$ mm was mounted on a glass fiber. All measurements were made with graphite monochromated Mo Kα radiation. Cell parameters were obtained from 2359 reflections with θ ranging from 2.67° to 28.31°. Cell constants and an orientation matrix for data collection were obtained from a least-squares refinement using the angle $\theta_{max} = 28.31°$. The structure was solved using Fourier techniques. The non-hydrogen atoms were refined anisotropically. Hydrogen atom positions were calculated using a riding mode and were refined isotropically. A summary of data collection and structure refinement is given in Table 1, and selected bond lengths and bond angles are given in Table 2.

2.4.2. Data collection

Bruker SMART; cell refinement: Bruker SMART/SAINTPLUS diffractometer; data reduction: Bruker SAINTPLUS; program(s) used to solve structure: SHELXS-97 (Sheldrick, 1990); program(s) used to refine structure: SHELXL97 (Sheldrick, 1997); molecular graphics: Bruker SHELXTL; computing publication materials: Bruker SHELXTL.

Table 1
Crystal data and structure refinement for $[Ni(4\text{-}NH_2\text{-}C_6H_4CO_2)_2\text{-}(CH_3OH)_2] \cdot CH_3OH$ (**1**)

	1
Empirical formula	$C_{17}H_{24}N_2Ni_1O_7$
Color	pale blue-green
M (g mol^{-1})	426.7
T (K)	297(2)
Crystal system	monoclinic
θ (°)	2.67–28.31
Space group	P2(1)/n
a (Å)	9.0903(5)
b (Å)	10.9059(5)
c (Å)	9.9994(5)
α (°)	90.00
β (°)	106.6880(10)
γ (°)	90.00
V (Å^3)	949.57(8)
Z	4
ρ_{calc} (g cm^{-3})	1.473
μ (mm^{-1})	1.062
Crystal size (mm)	$0.20 \times 0.12 \times 0.08$
Number of unique reflections/parameters	2359/124
Number of reflections $I > 2\sigma(I)$	2117
Goodness-of-fit on F^2	1.064
R, wR_2 (all data)	0.0423, 0.1075
Residual (e Å^{-3})	0.619

Table 2
Selected geometric parameters: interatomic distances (Å) and bond angles (°) for **1**

Ni1–O4	2.0432(13)
Ni1–O17	2.0686(15)
Ni1–N1	2.1557(17)
O4–C9	1.258(2)
O5–C9	1.254(3)
O15–C15	1.076(12)
C15–O15	1.433(12)
O4–Ni1–O4	180.00(7)
O4–Ni1–O17	90.66(6)
O4–Ni1–O17	89.34(6)
O17–Ni1–O17	180.0
O4–Ni1–N1	86.49(6)
O4–Ni1–N1	93.51(6)
O17–Ni1–N1	94.31(7)
O17–Ni1–N1	85.69(7)
N1–Ni1–N1	180.0
C9–O4–Ni1	129.23(13)
C8–N1–Ni1	117.66(12)
O5–C9–O4	124.85(18)
O5–C9–C4	118.15(18)
O4–C9–C4	116.97(18)
C11–O17–Ni1	131.93(16)

3. Results and discussion

3.1. Description of the structure

3.1.1. One-dimensional linear chain structure

The title compound $[Ni(4\text{-}NH_2C_6H_4CO_2)_2(CH_3OH)_2] \cdot CH_3OH$ (**1**) consists of Ni(II) atoms linked by PAB ligands into one-dimensional chains. The repeating unit of **1** with the atom numbering scheme is shown in Fig. 1. Each unit of **1** contains one Ni(II) center with a N_2O_4 binding set in which the Ni(1) atom coordinates to two oxygen atoms O(4) and O(4A) of carboxylate groups of two PAB anions in a monodentate fashion, two nitrogen atoms N(1) and

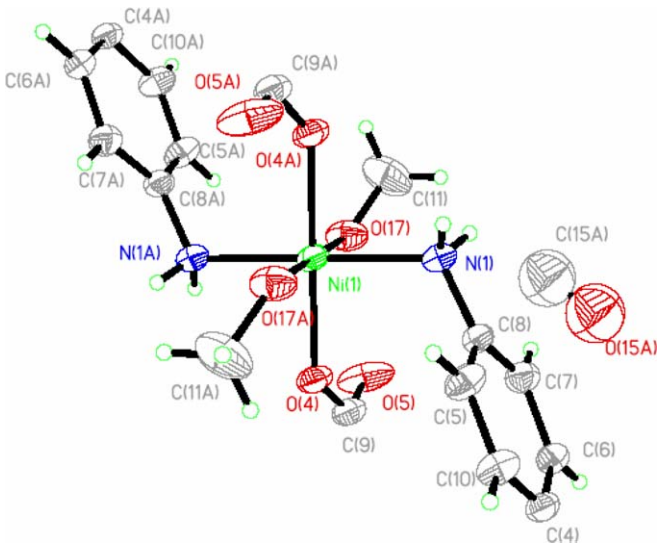

Fig. 1. Thermal ellipsoids of the repeat unit structure of compound **1**.

N1(A) of amino groups from two different PAB ligands, and two methanol oxygen atoms O(17) and O(17A). Ni(1) is thus in an elongated octahedral environment in a *trans* configuration with two long Ni–N(amino) bonds 2.1557(17) Å, two short Ni–O(methanol) bonds 2.0686(15) Å, and two short Ni–O(carboxylate) bonds 2.0432(13) Å.

Each of the *trans* bonds N(1)–Ni(1)–N(1A), O(4)–Ni(1)–O(4A), O(17)–Ni(1)–O(17A) in compounds **1** are linear with coordination angles 180.00(7)°, while the *cis* bonds in **1** form coordination angles ranging from 85.69(7)° to 94.31(7)°. The aromatic rings of two facing bridging PAB ligands are planar to one another with an angle of 180.00° (see Fig. 2). The nitrogen atom of the NH_2 group and carbon atom of the CO_2 group of PAB are not coplanar with the aromatic ring, instead the N and C atoms are bent out of the aromatic plane by 6.27° and 5.70°, respectively, towards the side of the nickel atoms. The rotation angle of the phenyl group relative to the CO_2 moiety in PAB is $\phi_{rot} = 3.12°$, Fig. 2.

The bidentate PAB ligands doubly bridge the metal ions forming infinite ribbons along the crystallographic *a*-axis. Within these ribbons the Ni–Ni distance is 9.090 Å, Fig. 2. Each of the nickel atoms in a central chain has eight neighboring nickel atoms, two from each of the four adjacent chains. The separating distances between interchain nickel atoms are 7.90 and 9.40 Å. Fig. 3 shows the chains in a cross-sectional view down the *a*-axis on the *bc* plane. The chains are packed in an –ABAB– stacking sequence along the *b*-axis on the *ab* plane, Fig. 4. The lattice includes methanol molecules occupy space between the parallel chains, Figs. 1 and 3. The guest methanol molecules are disordered and the two orientations are well resolved hinting at statistical disorder.

A linear 1D chain structure closely related to compound **1** is $[Ni(imbz)_2(H_2O)_2]_n$, where $imbz^- =$ the 4′-(imidazol-1-ylmethyl)benzoate anion. The two nickel(II) atoms, with a distance of 10.91 Å, are connected by two imbz ligands resulting in a dinuclear macrocyclic framework [34]. Another 1D chain structure is $[(\mu_{N,S}\text{-}SCN)_2\{Ni(ampy)\}]_n$ in which each nickel(II) ion is linked to two of its neighbors by two end-to-end μ-thiocyanato ligands. The neighbor Ni···Ni intrachain distance is 5.684(2) Å and the shortest Ni···Ni interchain separation is 6.833(4) Å [35]. The 1D polymeric structure of the nickel azido pyrazolate complex contains alternating dinickel(II) building units in which both pyrazolate and μ-1,3 azido bridge two metal ions in one dinuclear unit and a double μ-1,3 azido linkage bridge the next dinuclear unit resulting in two intrachain nickel···nickel distances of 4.469 and 5.183 Å [36].

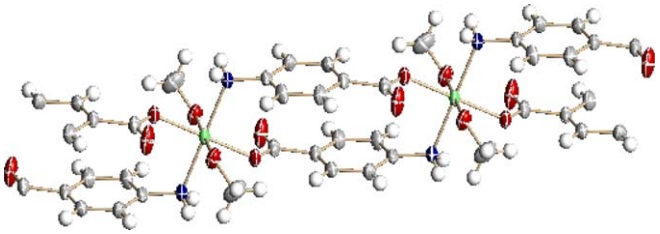

Fig. 2. View of the chain in **1** propagating along the *a*-axis.

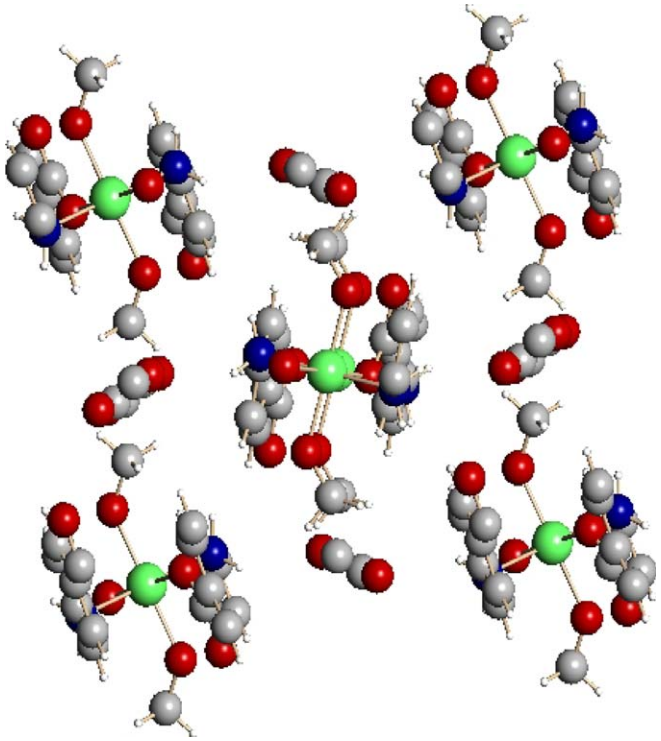

Fig. 3. Cross-sectional view of **1** down the *a*-axis on the *bc* plane. Each chain is surrounded by four other chains.

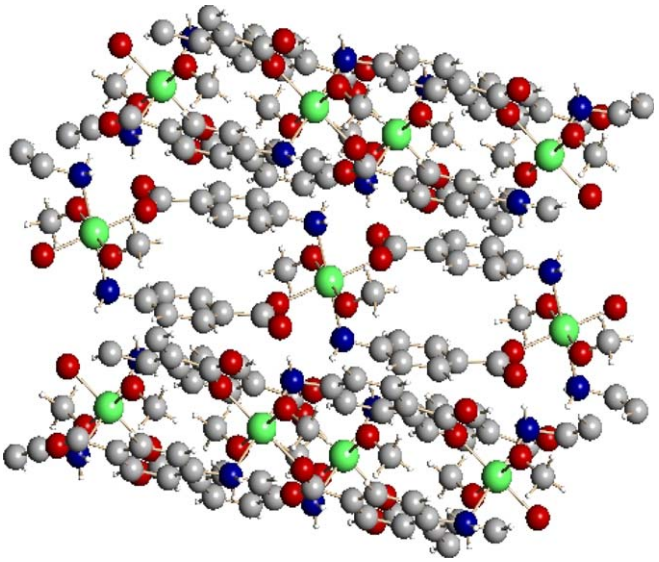

Fig. 4. View down the *c*-axis on the *ab* plane. The chains are packed in **1** in an ABAB fashion along the *b*-axis.

3.1.2. H-bonds

There is a short distance between O(17) of a coordinated methanol and O(5) of the carboxylate group of a PAB ligand: (O5···O17 = 2.563 Å), which suggests the presence of an intrachain H-bond. Each Ni octahedral unit is

involved in four interchain H-bonds. Thus each chain of type I interacts by H-bonds with four chains of type II forming a 3D network structure. Atom N(1) of an amino group of one Ni octahedral unit acts as a H-bond donor via H(1A) to O(5) of the carboxylate group of a second Ni octahedral unit. The bonds distances and angles involved in H-bonds are: N(1)···O(5), 2.979 Å; H(1A)···O(5), 2.250 Å; N(1)–H(1A)···O(5), 137.76°, Fig. 5.

3.1.3. π–π Interactions

Intrachain π–π interactions are observed between the aromatic rings of two *p*-aminobenzoate ligands bridging two adjacent nickel atoms. The aromatic rings are parallel displaced in an offset or slipped arrangement and have a centroid separation of 3.920 Å. The interplanar spacing is 3.607 Å. The interplanar angle between the arene rings is 180.00°, Fig. 6. The obtained distance between the arene rings is in agreement with the experimental value of 3.66 Å, measured for π–π stacking in a copper *p*-chlorobenzoate complex. The interaction energy for the parallel *p*-chlorobenzoic acid dimer complex is calculated to be 5.1 kcal mol^{-1} [37]. π–π Stacking interactions govern the self-assembly of a variety of complexes and interlocked molecular compounds. It occurs between π-donors rings (electron-rich) and π-accepting ring (electron-deficient) [38,39]. It is also observed between similar aromatic rings [37,40–44].

The aromatic rings in the chain are slipped so that the carboxylate group of one ring overlaps the facing ring at the edge carrying the NH_2 group. Carboxylate and amine substituents perturb the uniform charge distribution in benzene. Partial atomic charges and permanent dipoles result which introduce electrostatic dipole–dipole and dipole-induced dipole π–π interactions. Also π–σ attractions can dominate between the positively charged hydrogen atoms and the π-electrons of the rings. These van der Waals interactions are attractive and their potentials fall off rapidly with distance, $1/r^6$. The attractive forces overcome the π–π Pauli repulsions in an offset π-stacked geometry (Hunter–Sanders rule). Pauli repulsion is caused by the filled electron clouds of interacting molecules that overlap at short distances [38,43]. The separation of 3.607 Å of the rings in complex **1** falls in the usual range (3.3–3.8 Å), and it is the result of medium π–π interactions. The order of stability in the interaction of two π systems is π-deficient–π-deficient > π-deficient–π-rich > π-rich–π-rich [43]. The presence of the two substituents, carboxylate (electron-acceptor) and amine (electron-donor) in PAB of compound **1** causes an intermediate π-electron density ring and therefore intermediate π–π interactions.

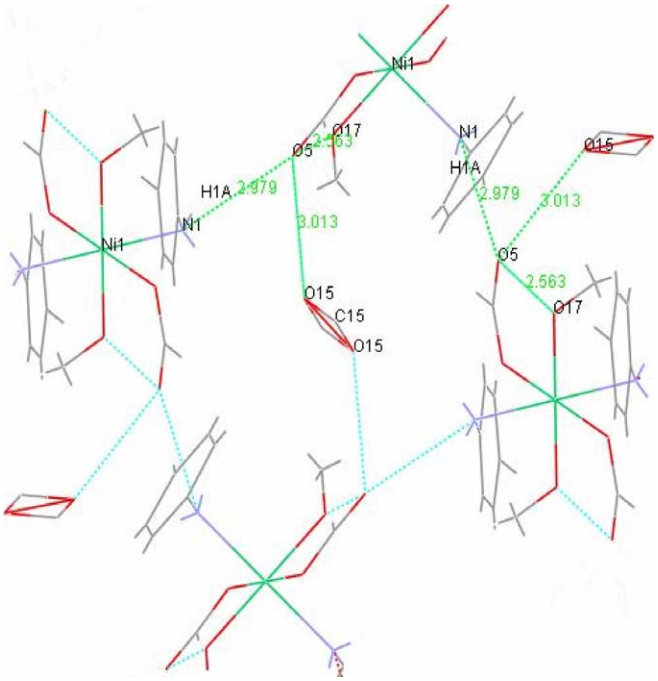

Fig. 5. H-bonding in **1**.

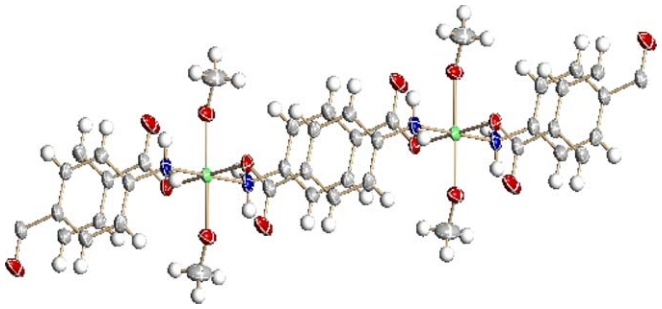

Fig. 6. Intrachain π–π interactions in **1** between aryl rings of bridging *p*-aminobenzoate ligands, centroids separation = 3.920 Å.

3.2. Discussion on IR spectra

Two carbon–oxygen stretching frequencies of the carboxylate group have been observed in compound **1**: $\nu_{asym}(CO_2) = 1525.6\ cm^{-1}$ and $\nu_{sym}(CO_2) = 1386.7\ cm^{-1}$, with $\Delta = 138.9\ cm^{-1}$. Unidentate coordination removes the equivalence of the two oxygen atoms. The carbon–oxygen bond orders are affected. This should increase $\nu_{asym}(CO_2)$ and decrease $\nu_{sym}(CO_2)$ and thus increase the separation Δ between the νCO_2 frequencies. Δ Values $>200\ cm^{-1}$ for acetate complexes appear generally associated with unidentate coordination [45]. However, exceptions to this rule have been found in two nickel complexes $Ni(O_2CMe_2)(H_2O)_2$ ($\nu_{asym}(CO_2) = 1550\ cm^{-1}$, $\nu_{sym}(CO_2) = 1425\ cm^{-1}$, $\Delta = 125\ cm^{-1}$) [46] and $Ni(O_2CMe)_2(H_2O)_2(py)_2$, ($\nu_{asym}(CO_2) = 1550\ cm^{-1}$, $\nu_{sym}(CO_2) = 1412\ cm^{-1}$, $\Delta = 138\ cm^{-1}$) [45]. The low values of Δ have been attributed to the involvement of CO_2's uncoordinated oxygen in hydrogen bonding with a water ligand. A similar situation has been found in compound **1** where also the CO_2's uncoordinated oxygen is hydrogen bonded to the amino group. Little difference has been found in bond distances of the carboxylate group of **1**;

C(9)–O(4) = 1.258 (2) Å for the uncoordinated oxygen and C(9)–O(5) = 1.254 (3) Å for the coordinated oxygen, which can explain the small value of Δ.

3.3. Magnetic study

The temperature dependence of the magnetic susceptibility ($\chi_M T$ versus T) for compound **1** in the range 3–300 K is shown in Fig. 7. The $\chi_M T$ value is approximately constant (1.38 $cm^3\,K\,mol^{-1}$) in the temperature range 100–300 K, but below 100 K it increases slightly to reach a maximum of 1.53 $cm^3\,K\,mol^{-1}$ at 9 K. This behavior is indicative of ferromagnetic intramolecular coupled nickel ions. The value of $\chi_M T$ at room temperature is greater than that expected for the spin only formula, which indicates that an orbital contribution and/or ferromagnetic coupling are involved. In the low temperature region 3–10 K, a decrease in the $\chi_M T$ value is the signature of single-ion zero field splitting D. The experimental data of the magnetic susceptibility (χT) were fitted to the analytical expression given by de Neef [47,48,35] for $S = 1$, based on a spin-Hamiltonian taking into account both the intramolecular exchange coupling (J) and the single-ion zero field splitting (D):

$$H = -2J\sum_{i=1}^{n-1} S_i S_{i+1} - D\sum_{i=1}^{n}\left(S_{iz}^2 - \frac{2}{3}\right) \quad (1)$$

and

$$\chi(J,D) = g^2\mu_B^2 \sum_{i\geqslant 1} \frac{d_i J^{i-1}}{(k_B T)^{-i}(3^i i!)} + \frac{2g^2\mu_B^2}{k_B T(2+e^{-D/k_B T})} + \frac{g^2\mu_B^2}{3k_B T}\sum_{i,j} b_{i,j}\frac{J^i D^j}{(3k_B T)^{i+j}(i+j)!} - \frac{2g^2\mu_B^2}{3k_B T} \quad (2)$$

where μ_B is the bohr magneton, k_B is the Boltzman constant, g is the Landé factor and d_i, $b_{i,j}$ are the coefficients of the susceptibility expansion given by de Neef [49]. The best least square fitting of the experimental data to Eq. (2) leads to the values of $J/k_B = 1.07$ K ($\sim 0.74\ cm^{-1}$), $D/k_B = -3.58$ K ($\sim -2.48\ cm^{-1}$) and $g = 2.35$ with an agreement factor $R = (\chi_{cal} - \chi_{exp})^2/\chi_{exp}^2 = 2.4 \times 10^{-4}$. The magnetic data for representative ferromagnetic 1D Ni polymers are listed for comparison in Table 3. It is worth noting that antiferromagnetic data has been also obtained in 1D polymeric nickel(II) complexes that contain end-to-end azido bridges as in [Ni(4-ethylpyridine)$_4$(N$_3$)][(PF$_6$) [51] and in a nickel azido pyrazolate complex [36].

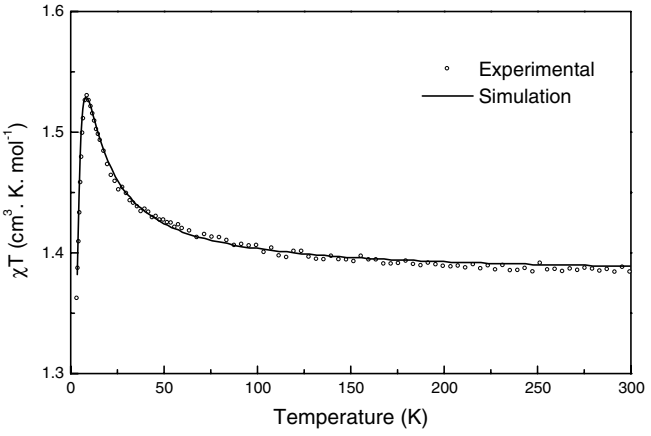

Fig. 7. The variation of $\chi_M T$ as a function of temperature for compound **1**. The symbols represent the experimental data and the continuous line represents the best fit to Eq. (2).

3.4. Thermal analysis

The results of thermogravimetric analysis for compound **1** are shown in Figs. 8 and 9. The compound was heated to 1000 °C, all relevant weight losses were complete by 600 °C. The TGA curve reveals that the polymer is stable up to 150 °C after which a weight loss due to the removal of one lattice-included methanol molecule and one half CO group occurs in the range 150–185 °C (observed loss 10.46%, theoretical loss 10.78%). The dTG curve indicates that the inflexion temperature occurred at 174.94 °C, Fig. 8. An endothermic peak is observed at the same temperature in the DTA curve with an enthalpy value equal to 165.25 kJ/mol, Fig. 9. A sharp weight loss of one PAB ligand is centered at 387.42 °C (observed loss 31.62%, theoretical loss 31.88%). The heat flow peak associated with the process reveals that it is endothermic with $\Delta H = 94.86$ kJ/mol. Loss of two coordinated methanol molecules occurred at a higher temperatures (489.20 °C) with $\Delta H = 29.78$ kJ/mol. The experimental and theoretical losses are 15.14% and 15.00%, respectively. Fragmentation of the PAB ligand further occurred at 550.73 °C with loss of 0.25$C_6H_4NH_2$ group ($\Delta H = 20.08$ kJ/mol). Material decomposition of the complex continues at higher temperature with the formation of nickel (II) oxide, Figs. 8 and 9.

3.5. Formation constant and thermodynamic parameters

The point-wise method [33,52,53] was used to calculate the dissociation constant of the *p*-aminobenzoic acid ligand, based on evaluation of the average proton number associated with the ligand n_A at different pH values, Table 4. On plotting the pK values versus $1/T$, straight lines are obtained with a slope of $\Delta H/2.303$ R, from which the ΔH

Table 3
Magnetic parameters for some representative ferromagnetic 1D Ni polymers

Compound	Parameters			Ref.
	J (cm^{-1})	g	D (cm^{-1})	
[Ni(PAB)$_2$(CH$_3$OH)$_2$] · CH$_3$OH	0.74	2.35	−2.48	this work
{catena-($\mu_{N,S}$-NCS)[Ni(Medien)(NCS)]}	0.96	2.18		[48]
[($\mu_{N,S}$-SCN)$_2${Ni(ampy)}]$_n$	1.4	2.06	2.6	[35]
{catena-($\mu_{N,S}$-NCS)[Ni(en)$_2$]}(PF$_6$)	0.20	2.19	−1.83	[50]

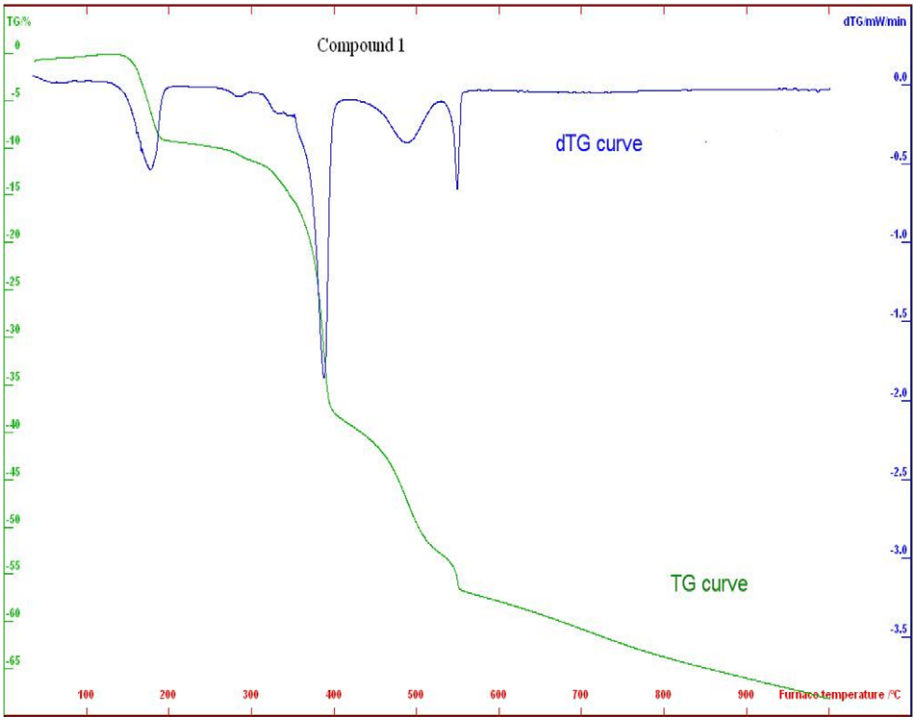

Fig. 8. TG and dTG curves in the thermogravimetric analysis of compound **1**.

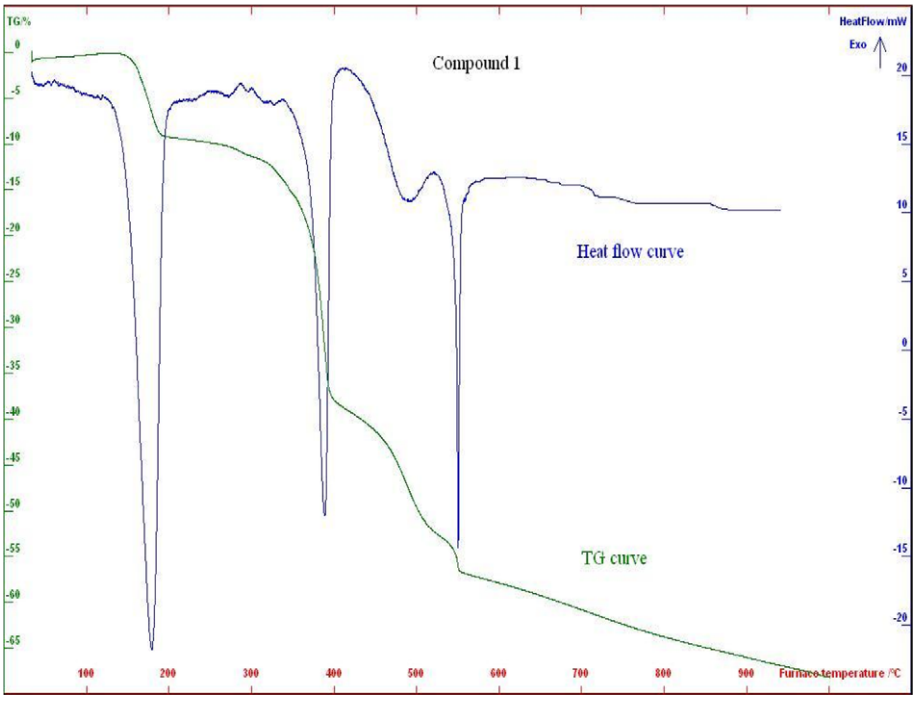

Fig. 9. TG and heat flow curves in the thermogravimetric analysis of **1**.

values (kcal mol^{-1}) are computed (Van't Hoff method). The free energy values ΔG (kcal mol^{-1}) are calculated using the equation $\Delta G = 2.303RT\,pK$, whereas the entropy term ΔS (eu) is given as $\Delta S = 10^3(\Delta H - \Delta G)/T$. The thermodynamics of ionization of *p*-aminobenzoic acid are evaluated in the temperature range 20–40 °C, Table 4. The pK_a values decrease with increasing temperature. The positive ΔH value indicates that the acid dissociation is an endothermic mechanism. The negative ΔS value in 50% ethanol is attributed to the presence of intermolecular hydrogen bonding with the solvent that promotes a higher degree of ordering [54].

Table 4
pK values and thermodynamic parameters for *p*-aminobenzoic acid in 50% ethanol–water

T (°C)	p$K_a \pm 0.03$	ΔG (kcal mol^{-1}) ± 0.04	ΔS (cal mol^{-1} K) ± 0.20
20	6.23	8.50	−16.00
25	6.18	8.43	−15.76
30	6.13	8.36	−15.53
35	6.10	8.32	−15.40
40	6.05	8.26	−15.19

ΔH (kcal mol^{-1}) $= 3.73 \pm 0.07$.

The stability constants of the nickel complexes can be calculated using the modified Bjerrum's method [33,53,55]. The pH measurements during titration of the solution of the chelating agent in the presence and absence of metal ions with alkali could be used to calculate the free ligand exponent (pA) and the degree of formation of the system (n). [A^{-2}] is the concentration of free ligand anion and n is the average number of moles of ligand bound per mole of metal ion. By plotting the values of n versus pA, $\log K_{f1}$ and $\log K_{f2}$ values are obtained at the pA values equivalent to 0.5 and 1.5, respectively, Table 5 [33,53]

$$[A^{-2}] = \frac{(2-a)C_A - [H^+] + [OH^-]}{\frac{2[H^+]^2}{K_1K_2} + \frac{[H^+]}{K_2}}$$

$$\overline{n} = \frac{1}{C_M}\left(C_A - \left[\frac{[H^+]^2}{K_1K_2} + \frac{[H^+]}{K_2} + 1\right][A^{-2}]\right)$$

The thermodynamic parameters for metal complexation are also listed in Table 5. The enthalpy of complexation, ΔH (kcal mol^{-1}) values were determined from the plot of $\log K_f$ versus $1/T$. Straight lines were obtained with a slope of $-\Delta H/2.303$ R. The free energy ΔG (kcal mol^{-1}) was calculated from the relation $\Delta G = -2.303RT \log K_f$. The entropy ΔS (eu) is given as $\Delta S = 10^3(\Delta H - \Delta G)/T$.

The negative values of ΔG indicate that the formation of 1:1 and 1:2 metal ligand complexes is a thermodynamically favored process. The high negative value of ΔH indicates that the enthalpy effect is more dominant than the entropy effect. In the case of PAB bridging two metal atoms, the highly unfavorable entropy due to steric effects can be overcome by the large stabilization energy from π–π interactions. The formation of a mononuclear *p*-aminobenzoate nickel complex has been confirmed by X-ray [29], while in the present studies the linear doubly bridged polymer has been obtained. During the synthesis of **1**, the initially formed mononuclear NiL_2, with L = PAB coordinated through the carboxylate group to Ni(II), acts as a ligand to another NiL_2 through the NH_2 group forming dinuclear and similarly trinuclear species until reaching a more thermodynamically stable situation by forming a 1D polynuclear complex. Thus, the system under equilibrium forms and breaks bonds, sifts through various possibilities until reaching the most stable product, complex **1**.

Table 5
$\log K_{f1}$ and ($\log K_{f2}$) values and thermodynamic parameters for the nickel complex with *p*-aminobenzoic acid in 50% ethanol–water

T (°C)	$\log K_{f1}$ ($\log K_{f2}$) ± 0.04	ΔG (kcal mol^{-1}) ± 0.06	ΔS (cal mol^{-1} K) ± 0.40
20	3.39(1.45)	−4.63(−1.98)	−17.44(−69.93)
25	3.24(1.21)	−4.42(−1.65)	−18.15(−71.04)
30	3.11(0.84)	−4.24(−1.14)	−18.75(−72.75)
35	3.08(0.69)	−4.20(−0.94)	−18.88(−73.42)
40	2.89	−3.94	−19.76

ΔH (kcal mol^{-1}) $= -9.83 \pm 0.20$ for K_{f1} and ΔH (kcal mol^{-1}) $= -22.83 \pm 0.40$ for K_{f2}.

Acknowledgements

Dr. Joanna Clark and the Center for Materials Research at the University of Nebraska-Lincoln are thanked for single crystal X-ray diffraction data and analysis on the Bruker SMART Apex was provided by the National Science Foundation, CHE-0092004. Amer Ghanoum and Nadine Khalil are thanked for assistance.

Appendix A. Supplementary data

CCDC 210116 contains the supplementary crystallographic data for this paper. These data can be obtained free of charge at www.ccdc.cam.ac.uk/conts/retrieving.html, or from the Cambridge Crystallographic Data Centre (CCDC), 12 Union Road, Cambridge CB2 1EZ, UK (fax: + 44 1223 336 033; e-mail: deposit@ccdc.cam.ac.uk). Supplementary data associated with this article can be found, in the online version, at doi:10.1016/j.poly.2006.03.029.

References

[1] R. Robson, B.F. Abrahams, S.R. Batteen, R.W. Gable, B.F. Hoskins, J. Liu, in: T. Bein, (Ed.), Supramolecular Architecture, ACS Symposium Series, vol. 499, Washington, DC, 1992 (Chapter 19).
[2] (a) K.T. Holman, H.H. Hammud, S. Isber, M. Tabbal, Polyhedron 24 (2005) 221;
(b) M.J. Zaworotko, Chem. Soc. Rev. (1994) 283.
[3] R.W. Gable, B.F. Hoskins, R.J. Robson, J. Chem. Soc., Chem. Commun. (1990) 1677.
[4] S. Subramanian, M.J. Zaworotko, Angew. Chem., Int. Ed. Engl. 34 (1995) 2127.
[5] L. Carlucci, G. Ciani, D.M. Proserpio, A. Sironi, Angew. Chem., Int. Ed. Engl. 34 (1995) 1895.
[6] L. Carlucci, G. Ciani, D.M. Prosperio, A. Sironi, Inorg. Chem. 34 (1995) 5698.
[7] L. Carlucci, G. Ciani, D.M. Proserpio, A. Sironi, J. Am. Chem. Soc. 117 (1995) 4562.
[8] P. Jensen, S.R. Batten, G.D. Fallon, B. Moubaraki, K.S. Murray, D.J. Price, Chem. Commun. (1999) 177.
[9] S.R. Batten, P. Jensen, C.J. Kepert, M. Kurmoo, B. Moubaraki, K.S. Murray, D.J. Price, J. Chem. Soc., Dalton Trans. (1999) 2987.
[10] A.M. Kutabi, S.R. Batten, A.R. Harris, B. Moubaraki, K.S. Murray, Aust. J. Chem. 55 (2002) 311.
[11] L. Jager, Ch. Wagner, M. Korabik, A. Zygmunt, J. Mrozinski, J. Mol. Struct. 570 (2001) 159.
[12] J.L. Manson, A.M. Arif, J.S. Miller, J. Mater. Chem. 9 (1999) 979.

[13] I. Riggio, G.A. van Albada, D.D. Ellis, A.L. Spek, J. Reedjik, Inorg. Chim. Acta 313 (2001) 120.
[14] J.L. Manson, Q.Z. Huang, J.W. Lynn, H.J. Koo, M.H. Whamgbo, R. Bateman, T. Otsuka, N. Wada, D.N. Argyriou, J.S. Miller, J. Am. Chem. Soc. 123 (2001) 162.
[15] L. Karanovic, D. Poleti, J. Rogan, G.A. Bogdanovic, A. Spasojevic-de Bire, Acta Crystallogr., Sect. C (2002) m275.
[16] L. Pan, B.S. Finkel, X. Huang, J. Li, Chem. Commun. (2001) 105.
[17] B.F. Abrahams, B.F. Hoskins, D.M. Michael, R. Robson, Nature 369 (1994) 727.
[18] S. Kitagawa, M. Kondo, Bull. Chem. Soc. Jpn. 71 (1998) 1.
[19] O.M. Yaghi, G. Li, H. Li, Nature 378 (1995) 703.
[20] S.S.Y. Chui, S.M.F. Lo, J.P.H. Charmant, A.G. Orpen, I.D. Williams, Science 283 (1999) 1148.
[21] M. Fujita, Y.J. Kwon, S. Washizu, K. Ogura, J. Am. Chem. Soc. 116 (1994) 1151.
[22] M. Kondo, T. Yoshitomi, K. Seki, H. Matsuzaka, S. Kitagawa, Angew. Chem., Int. Ed. Engl. 36 (1997) 1725.
[23] I.R. Amiraslanov, G.N. Nadzhafov, B.T. Usubaliev, A.A. Musaev, E.M. Movsumov, Kh.S. Mamedov, J. Struct. Chem. Engl. Transl. 21 (3) (1980) 363.
[24] I.R. Amiraslanov, N.Kh. Dzhafarov, G.N. Nadzhafov, Kh.S. Mamedov, E.M. Movsumov, B.T. Usubaliev, J. Struct. Chem. Engl. Transl. 21 (1) (1980) 104.
[25] I.R. Amiraslanov, N.Kh. Dzhafarov, G.N. Nadzhafov, Kh.S. Mamedov, E.M. Movsumov, B.T. Usubaliev, J. Struct. Chem. Engl. Transl. 21 (1) (1980) 109.
[26] I.R. Amiraslanov, B.T. Usubaliev, G.N. Nadzhafov, A.A. Mussaev, E.M. Movsumov, Kh.S. Mamedov, Zh. Strukt. Khim. 21 (5) (1980) 112.
[27] I.R. Amiraslanov, Kh.S. Mamedov, E.M. Movsumov, F.N. Mussaev, G.N. Nadzhafov, Zh. Strukt. Khim. 20 (6) (1979) 1075.
[28] I.R. Amiraslanov, Kh.S. Mamedov, E.M. Movsumov, F.N. Mussaev, G.N. Nadzhafov, Zh. Strukt. Khim. 19 (6) (1978) 1120.
[29] I.R. Amiraslanov, Kh.S. Mamedov, E.M. Movsumov, F.N. Musaev, A.N. Shnulin, G.N. Nadzhafov, Zh. Strukt. Khim. 19 (6) (1978) 1129.
[30] L.P. Battaglia, A.C. Bonamartini, S. Ianelli, M.A. Zoroddu, G.J. Sanna, J. Chem. Soc., Faraday Trans. 87 (24) (1991) 3863.
[31] B. Yan, H. Zhang, S. Wang, J.A. Ni, Mater. Res. Bull. 33 (10) (1998) 1517.
[32] S. Parveen, K.P. Dubey, Proc. Natl. Acad. Sci. India Sect. A 51 (3) (1981) 337.
[33] M.S. Masoud, H.H. Hammud, H. Beidas, Thermochim. Acta 381 (2002) 119.
[34] J. Fan, Y-A. Zhang, T. Okamura, Z.H. Zou, N. Ueyama, W.Y. Sun, Inorg. Chem. Commun. 4 (2001) 501.
[35] T.K. Maji, I.R. Laskar, G. Mostafa, A.J. Welch, P.S. Mukherjee, N.R. Chaudhuri, Polyhedron 20 (2001) 651.
[36] F. Meyer, H. Pritzkow, Inorg. Chem. Commun. 4 (2001) 305.
[37] D. Sundholm, M.R. Sundberg, R. Uggla, J. Phys. Chem. A 102 (36) (1998) 7137.
[38] C.G. Claessens, J.F. Stoddart, J. Phys. Org. Chem. 10 (1997) 254.
[39] A.T. Kabbani, G.N. La Mar, J. Magn. Reson. 43 (1981) 90.
[40] C. Glidewell, R.A. Howie, J.N. Low, J.M.S. Skakle, S.V. Wardell, J.L. Wardell, Acta Crystallogr., Sect. B 58 (2002) 864.
[41] M.-L. Tong, W. Li, X.-M. Chen, S.-L. Zheng, S.W. Ng, Acta Crystallogr., Sect. C 58 (2002) m232.
[42] S.J. Garden, S.P. Fontes, J.L. Wardell, J.M.S. Skakle, J.N. Low, C. Glidewell, Acta Crystallogr., Sect. B 58 (2002) 701.
[43] C. Janiak, J. Chem. Soc., Dalton Trans. (2000) 3885.
[44] A.T. Kabbani, M.J. Zaworotko, H. Abourahma, R.D.B. Walsh, H.H. Hammud, J. Chem. Crystallogr. 34 (11) (2004) 749.
[45] G.B. Deacon, R.J. Philips, Coord. Chem. Rev. 33 (1980) 227.
[46] D.A. Edwards, R.N. Hayward, Can. J. Chem. 46 (1968) 3443.
[47] T. de Neef, Phys. Rev. B 13 (9) (1976) 4141.
[48] A. Escuer, S.B. Kumar, F. Mautner, R. Vicente, Inorg. Chim. Acta 269 (1998) 313.
[49] (a) T. de Neef, Ph.D. Thesis, Eindhoven, Netherlands, 1975.;
(b) http://alexandria.tue.nl/extra1/PRF2B/7707037.pdf.
[50] M. Montfort, C. Bastos, C. Diaz, J. Ribas, Inorg. Chim. Acta 218 (1994) 185.
[51] M.A.S. Goher, A. Escuer, F.A. Mautner, N.A. Al-Salem, Polyhedron 21 (2002) 1871.
[52] M.A. El-Dessouky, M.S. Masoud, Afinidad 416 (1988) 321.
[53] M.J. Zaworototko, H.H. Hammud, I. Abbas, V. Kravtsov, M.S. Masoud, J. Coord. Chem. (2006) 65.
[54] E.A. Daniell, F.C. Marek, H.K. Powell, W.T. Robinson, J.M. Russell, Aust. J. Chem. 31 (1978) 723.
[55] A.E. Martell, R.J. Motekaitis, Determination and Use of Stability Constants, 2nd ed., VCH, New York, 1992.

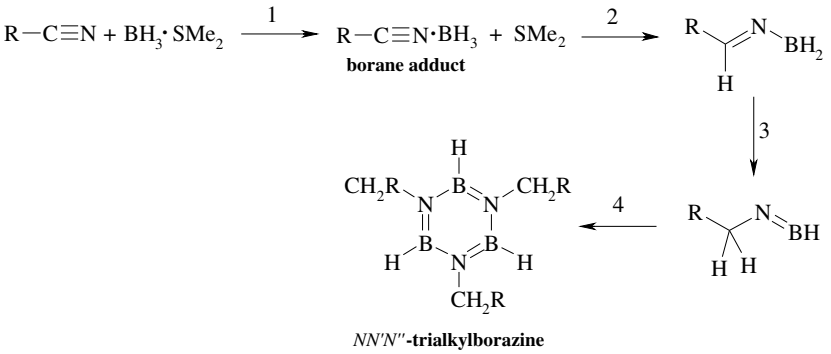

Scheme 1.

affording 35–40% *NN′N″*-triethylborazine [9]. In addition, a further 25–37% of the product distribution has been attributed to bicyclic compounds [10].

Complexes of borane with ethers (e.g., $BH_3 \cdot THF$ and $BH_3 \cdot OEt_2$) effectively convert nitriles to their corresponding amines after hydrolysis [3,4,11]. The reduction is, however, more sluggish with the dimethyl sulfide complex [12,13]. While the greater stability of the borane–dimethyl sulfide complex ($BH_3 \cdot SMe_2$) towards dissociation was cited as a reason for the retardation in reactivity, its stability towards decomposition and better handling characteristics are the reason for the choice of this complex in hydroboration and reduction reactions [13]. An improved procedure for enhancing the reactivity of the borane–dimethyl sulfide complex towards nitriles has been published and its general applicability toward nitrile reduction established [5,14]. Tetrabutylammonium borohydrides have also been used for the reduction of nitriles [15], while various strategies for the enhancement of the reactivity and selectivity of sodium borohydrides toward the reduction of nitrile compounds have also been developed [16].

The conventionally adopted method for investigating the reactivity of nitriles toward reduction by borane–Lewis base adducts has been the determination of residual hydridic hydrogen at the end of the reaction period [17]. This technique, while adequate for comparison of the relative reactivity of various boranes toward nitriles, cannot be used to determine precise kinetic and activation parameters. The applicability of infrared spectroscopy to the investigation of the hydroboration reaction has been demonstrated for some time in the literature [18–25]. Yet, ^{11}B NMR spectroscopy has not received much attention in the field of hydroboration kinetics, with the technique usually relegated to a qualitative role [26,27]. The non-destructive nature of the technique coupled with its real-time analysis, shows the potential of its use for the determination of kinetic data for various reactions. The aim of this investigation was, thus, to determine kinetic and activation parameters for the reduction of acrylonitrile using ^{11}B NMR spectroscopy.

2. Experimental

2.1. General

Borane dimethyl sulfide (1 M in dichloromethane, Sigma–Aldrich) was used without further purification. Acrylonitrile, propionitrile and benzonitrile (all Sigma–Aldrich) were dried by percolating over activated 3 Å molecular sieve before use. Nitrile and borane dimethyl sulfide solutions were diluted to the relevant concentrations with dichloromethane (Merck) distilled over calcium hydride.

Standard techniques for handling of air- and moisture-sensitive materials were used for handling syringes, needles, canulae, glassware, quartz NMR tubes and reagents [28,29].

2.2. Kinetic measurements

^{11}B NMR spectra were recorded at 160 MHz and referenced externally against $BF_3 \cdot OEt_2$ (0 ppm) on a Varian Unity Inova 500 spectrometer in 5 mm quartz tubes with proton decoupling (Waltz-16). A proton-coupled spectrum of the reaction was also recorded in order to identify reaction intermediates and products. A 1-min delay was allowed for mixing and temperature equilibration in the spectrometer, after which arrayed spectra were recorded at set time intervals. The temperature of the spectrometer was controlled at an accuracy of ±0.5 °C. The kinetic data were obtained by monitoring the signal area of the borane dimethyl sulfide peak with time. The following peaks were identified over time in the ^{11}B NMR spectrum: $BH_3 \cdot SMe_2$ [quartet, $\delta^{11}B = -20.3$ ppm, $J_{B-H} = 110$ Hz], $CH_2{=}CH{-}C{\equiv}N \cdot BH_3$ [quartet, $\delta^{11}B = -25.7$ ppm, $J_{B-H} = 104$ Hz] and vinylimino borane [triplet, $\delta^{11}B = -16.3$ ppm, $J_{B-H} = 111$ Hz], $EtC{\equiv}N \cdot BH_3$ [quartet, $\delta^{11}B = -26.2$ ppm, $J_{B-H} = 102$ Hz] and $C_6H_5C{\equiv}N \cdot BH_3$ [quartet, $\delta^{11}B = -25.8$ ppm, $J_{B-H} = 102$ Hz]. Also identified in the spectrum were impurities in the $BH_3 \cdot SMe_2$ solution [singlet, $\delta^{11}B = -10.9$ ppm; singlet, $\delta^{11}B = -13.5$ ppm; singlet, $\delta^{11}B = -17.3$ ppm; singlet, $\delta^{11}B = -15.4$ ppm; singlet, singlet, $\delta^{11}B = -23.2$ ppm; $\delta^{11}B = -29.2$ ppm].

The concentration dependence study of the reduction of acrylonitrile was carried out under pseudo-first-order conditions with the concentration of the nitrile in at least 10-fold excess over that of the borane. Pseudo-first-order rate constants were calculated from single-exponential kinetic traces of integral data from arrayed NMR spectra on Origin 5.0 software. The activation parameters, $\Delta H^{\neq}$ and $\Delta S^{\neq}$, were determined from temperature studies of k_2' over the temperature range 15–30 °C.

3. Computational modelling

Computational calculations were performed on Spartan '04 [30] computational software. The reaction profile was generated from the B3LYP/6-31G* [31–33] single point energies of SE/AM1-optimised geometries. Electrostatic charges and thermodynamic parameters were determined at the B3LYP/6-31G* level.

4. Results and discussion

No reduction was observed for the reaction involving borane dimethyl sulfide with propionitrile and benzonitrile. These compounds formed borane–nitrile adducts, $C_6H_5C{\equiv}N \cdot BH_3$ ($\delta^{11}B = -25.8$ ppm) and $CH_3CH_2C{\equiv}N \cdot BH_3$ ($\delta^{11}B = -26.2$ ppm), identifiable as quartets in the ^{11}B spectrum. Surprisingly, there are no NMR chemical shifts reported in the literature for these types of adducts. Both ^1H and ^{11}B NMR spectroscopy showed the equilibrium between the $Me_2S \cdot BH_3$ and the $RC{\equiv}N \cdot BH_3$ adducts to favour the former, with ^1H NMR investigation revealing $K = (7.45 \pm 0.20) \times 10^{-3}$ and $K = (1.16 \pm 0.02) \times 10^{-2}$ for $C_6H_5C{\equiv}N \cdot BH_3$ and $EtC{\equiv}N \cdot BH_3$, respectively. The weak equilibrium constants for nitrile–borane adduct formation may be responsible for the lack of reactivity, reduction in this case, of these two compounds. For reduction to occur, a stable adduct would first need to be formed.

It was, however, possible to monitor the kinetics of the reaction up to the first reduction of acrylonitrile (steps 1 and 2 in Scheme 1) through ^{11}B NMR spectroscopy (Fig. 1). The borane–nitrile adduct formed between acrylonitrile and BH_3 ($\delta^{11}B = -25.7$ ppm, $J_{B-H} = 107$ Hz) was completely depleted after 500 s and was generally present in such small concentrations that no meaningful kinetic data could be obtained for it. This is not surprising, as these have been reported to be unstable at room temperature [7]. It can, therefore, be concluded that borane–nitrile adduct formation and depletion are very fast processes. Kinetic investigation of the two hydride shifts prior to

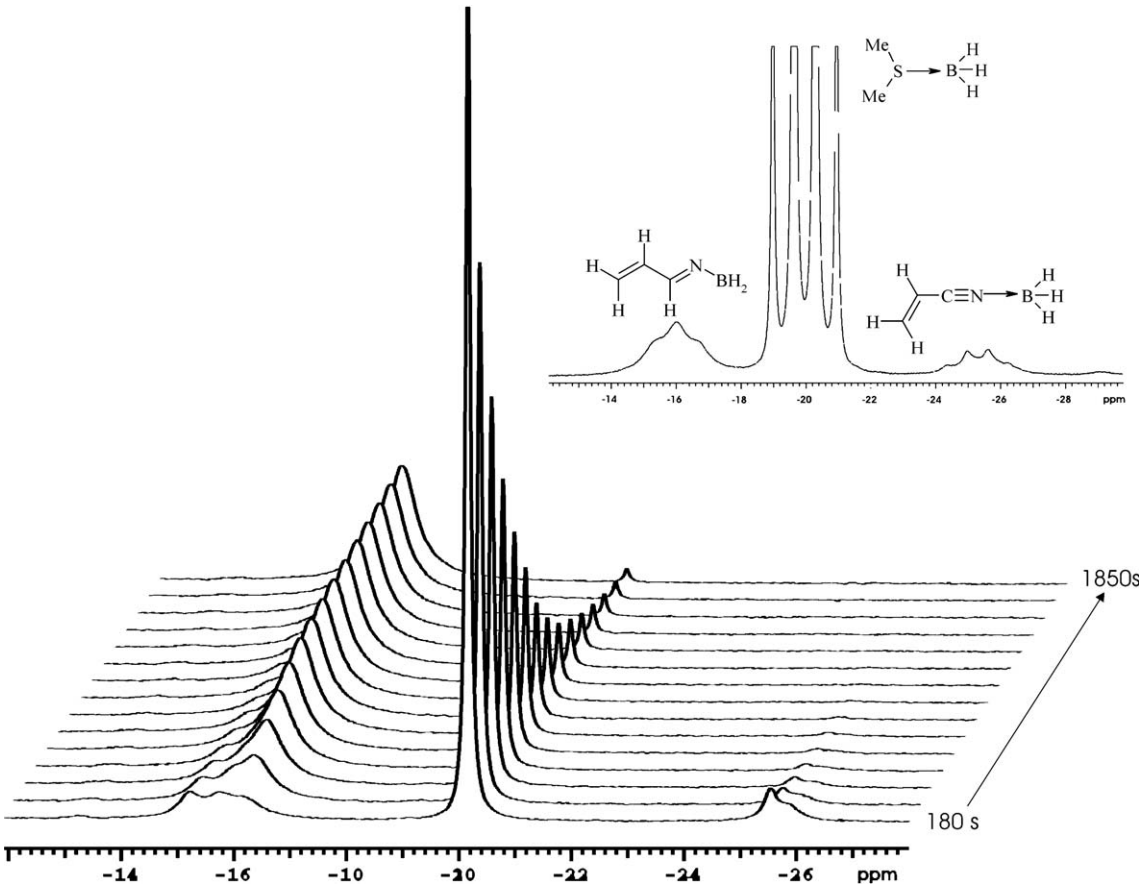

Fig. 1. Arrayed ^{11}B–{^1H} spectrum for reduction of acrylonitrile with borane dimethyl sulfide complex (0.16 M) in CH_2Cl_2 at 25 °C and ^{11}B spectrum (inset) showing species identified during reaction.

borazine formation (steps 3 and 4 in Scheme 1) was not possible owing to the polymerisation of the acrylonitrile. This polymerisation is expected under the reaction conditions of the study [34,35]. Analysis of the arrayed spectra shows that the reduction of acrylonitrile did not proceed to the borazine and carbozara stages. No peaks consistent with those reported for *NN′N″*-tri-*n*-alkylborazines [36] and carbozara derivatives [10] were identified in the ^{11}B NMR spectrum at the end of reaction. The relatively high field shift of the aldiminoborane indicates a shielded boron atom in a four-coordinate environment suggestive of a dimeric aldiminoborane species. This is supported by the literature precedents that show that aldiminoboranes are, in general, dimeric rather than monomeric [37–39].

4.1. Kinetic measurements

Pseudo-first-order rate constants, k_{obs}, for the reduction of acrylonitrile by the borane–dimethyl sulfide complex (0.16 M) at various concentrations (3–8 M) and temperatures (15–30 °C) were obtained from ^{11}B NMR arrayed experiments and subsequent integration of the borane and vinyliminoborane peaks. These resulted in the kinetic plot shown in Fig. 2.

A first-order exponential decay curve was then fitted over the data points for the depletion of the borane dimethyl sulfide complex in order to generate the pseudo-first-order rate constants, k_{obs}. These were then plotted against acrylonitrile concentration, resulting into a linear dependence of k_{obs} on the concentration of acrylonitrile with no meaningful *y*-intercept as shown in Fig. 3.

The results imply that k_{obs} can be expressed by

$$k_{obs} = k'_2[\text{acrylonitrile}]. \quad (1)$$

On the basis of the observed ^{11}B NMR data and kinetics, we propose the following pre-equilibrium mechanism that involves a dissociative step (Eqs. (2) and (3)):

$$BH_3 \cdot SMe_2 \rightleftharpoons BH_3 + SMe_2 \quad (2)$$

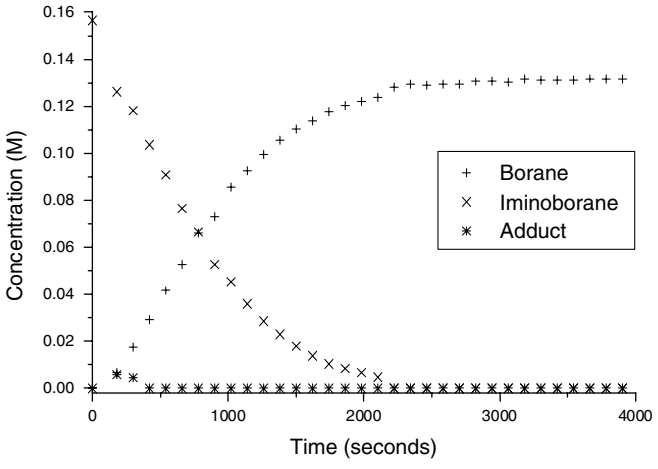

Fig. 2. Kinetic plot for reduction of acrylonitrile with borane dimethyl sulfide complex (0.16 M) in CH_2Cl_2 at 25 °C.

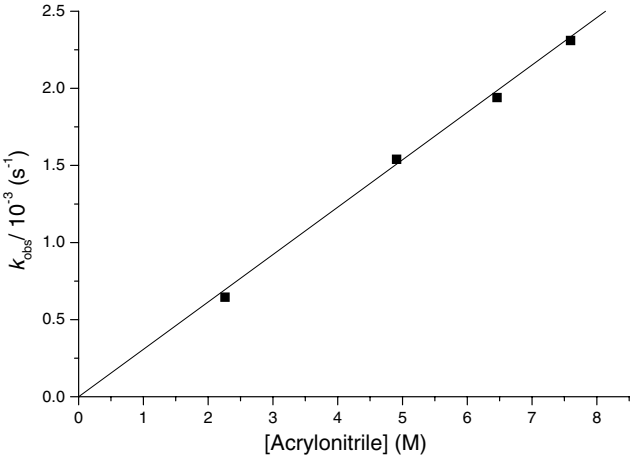

Fig. 3. Concentration dependence of k_{obs} on acrylonitrile concentration in the reduction of acrylonitrile with borane dimethyl sulfide complex (0.16 M) in CH_2Cl_2 at 25 °C.

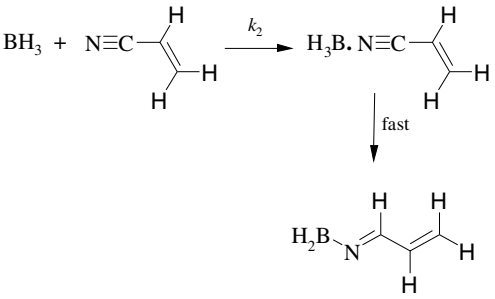

(3)

The rate for this mechanism can be expressed as shown in Eq. (4)

$$k_{obs} = \frac{k_1 k_2[\text{acrylonitrile}]}{k_{-1}[SMe_2] + k_2[\text{acrylonitrile}]}. \quad (4)$$

In the presence of excess dimethyl sulfide, $k_{-1}[SMe_2]$ becomes greater than k_2[acrylonitrile]. Hence, Eq. (4) reduces to Eq. (5) since $[SMe_2]$ is constant

$$k_{obs} = \frac{k_1 k_2}{k_{-1}[SMe_2]}[\text{acrylonitrile}] = k'_2[\text{acrylonitrile}]. \quad (5)$$

To determine whether the $BH_3 \cdot SMe_2$ complex obtained from Sigma–Aldrich had any excess SMe_2, ^1H NMR spectrum of the complex was determined. The integration of the relevant signals showed that free SMe_2 was present at an excess of 12.5%.

The rate constants obtained for acrylonitrile are summarised in Table 1.

The temperature dependence of the reduction of acrylonitrile was also investigated. Since Fig. 3 showed the absence of a reverse reaction, a single concentration (4.911 M) of acrylonitrile was investigated. The values of activation enthalpy, $\Delta H^{\neq}$, and activation entropy, $\Delta S^{\neq}$, were determined from the Eyring plot shown in Fig. 4; which shows a linear correlation over the investigated temperature range. The values of the activation parameters, $\Delta H^{\neq}$ and $\Delta S^{\neq}$, are tabulated in Table 1.

The negative $\Delta S^{\neq}$ value indicates that the overall mechanism of the reduction of acrylonitrile by $BH_3 \cdot SMe_2$ in the

Table 1
Kinetic data for the reduction of acrylonitrile in CH_2Cl_2

Temperature (°C)	$k'_2/10^{-3}$ ($M\ s^{-1}$)[a]	Thermodynamic data
15.0	0.47 ± 0.01	$\Delta H^{\neq} = 58 \pm 3$ kJ mol^{-1}
20.0	1.16 ± 0.04	
25.0	1.54 ± 0.04	
30.0	2.42 ± 0.09	$\Delta S^{\neq} = -71 \pm 10$ J K^{-1} mol^{-1}
k_1(25 °C)[b]	$(2.52 \pm 0.57) \times 10^{-3}$ s^{-1}	

[a] $k'_2 = k_2k_1/k_{-1}[SMe_2]$.
[b] From $[SMe_2]$ dependence study, [acrylonitrile] = 4.911 M.

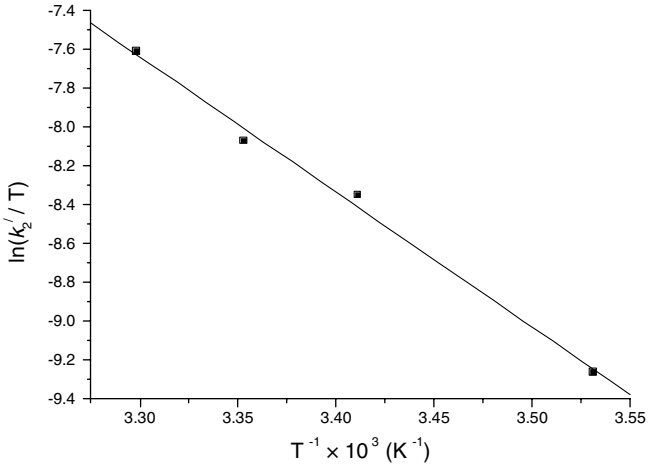

Fig. 4. Eyring plot illustrating the temperature dependence of k'_2 for the depletion of borane dimethyl sulfide complex (0.16 M) in the first step of the reduction of acrylonitrile in CH_2Cl_2.

presence of excess dimethyl sulfide is associative. The dissociation of the dimethyl sulfide prior to reduction has a positive entropy contribution, which must be smaller than the negative entropy contribution of the reduction process.

To test the mechanism further, Eq. (5) was expressed differently as shown in

$$\frac{1}{k_{obs}} = \frac{k_{-1}}{k_1k_2[\text{acrylonitrile}]}[SMe_2] + \frac{1}{k_1}. \quad (6)$$

This equation was used to analyse the k_{obs} data obtained when the acrylonitrile concentration was held constant (4.911 M) while that of excess dimethyl sulfide was varied from 0.019 to 0.193 M. Plotting $1/k_{obs}$ against $[SMe_2]$ resulted in the linear plot shown in Fig. 5. This confirms that the first step in the reaction sequence is the dissociation of the Lewis base from BH_3 as proposed in the mechanism.

4.2. Computational study

The reduction of acrylonitrile, propionitrile, hydrogen cyanide and benzonitrile was modelled at the B3LYP/6-31G* level of theory in order to account for the observed

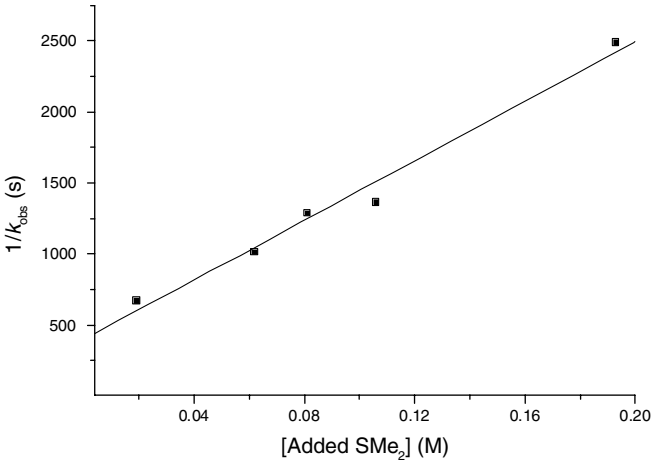

Fig. 5. Concentration dependence of k_{obs} on dimethyl sulfide concentration in the reduction of acrylonitrile with borane dimethyl sulfide complex (0.16 M) in CH_2Cl_2 at 25 °C.

reactivities. The energy profile for the reaction is depicted in Fig. 6 where, in contrast to the MNDO results of Ray and Chadha [40], there was no transition state found for the formation of a borane–nitrile adduct. The B3LYP calculations support the observation by Emeléus and Wade [7] that the stability of the borane–nitrile adducts affects their reactivities, with adduct of acrylonitrile and BH_3 being about 6–8 kJ mol^{-1} more stable than those of benzonitrile and propionitrile. A stable adduct is more likely to undergo step 2 of Scheme 1.

The concepts of absolute hardness, η, and electronegativity, χ^0, as defined by Eq. (7) can be revoked to explain the weakness of the BH_3 adducts of benzonitrile and propionitrile by accounting for the effect of the HOMO–LUMO gap [41].

$$\eta = \frac{(I-A)}{2} \quad \text{and} \quad \chi^0 = \frac{(I+A)}{2}. \quad (7)$$

Molecular orbital theory shows that $I = -E_{LUMO}$ and $A = -E_{HOMO}$ in eV such that combining η and χ^0 to determine the transfer of electron density possible from a Lewis base to a Lewis acid, ΔN as defined in Eq. (8), puts the stability of the nitrile–BH_3 adducts in perspective

$$\Delta N = \frac{(\chi^0_A - \chi^0_B)}{2(\eta_A + \eta_B)}. \quad (8)$$

The results in Table 2 show that acrylonitrile is the most similar to BH_3 in terms of hardness with a large degree of electron transfer to BH_3 in the nitrile–BH_3 adduct, thereby explaining the relative stability of the complex. Propionitrile, by contrast, is in fact harder than BH_3, implying a much larger HOMO–LUMO gap, with hardly any transfer of electron density. Though benzonitrile has a similar level of electron transfer to acrylonitrile, it is softer than BH_3 suggests a much larger HOMO–LUMO gap (the HOMO of acrylonitrile is 0.61 eV higher in energy than that of benzonitrile), which has implications for the ener-

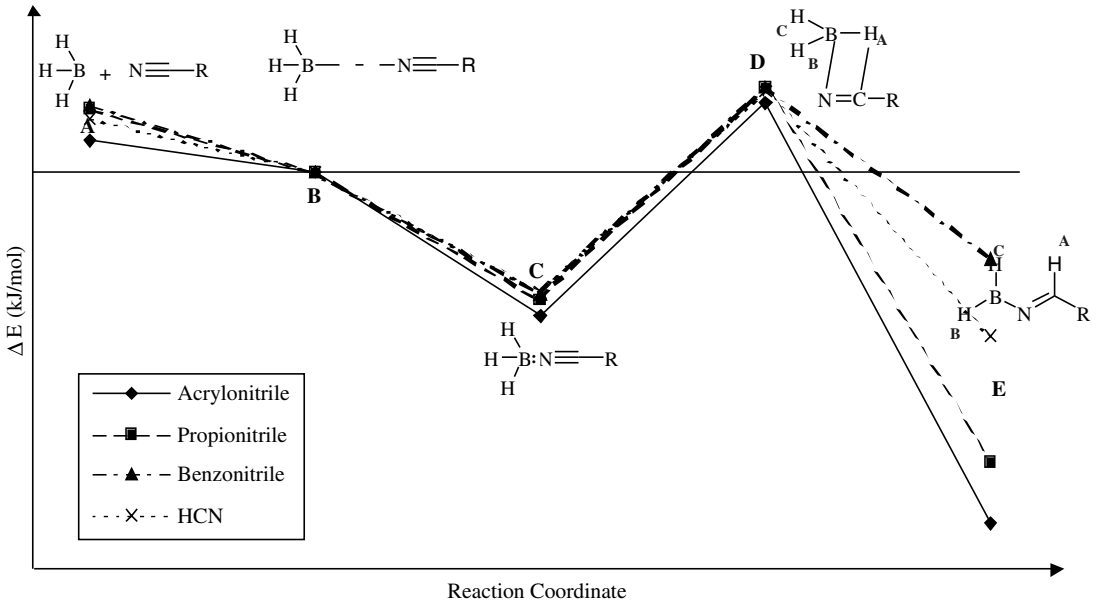

Fig. 6. B3LYP/6-31G* energy profile of stationary points for the reaction of BH_3 with acrylonitrile, propionitrile and benzonitrile.

Table 2
B3LYP/6-31G* calculated absolute hardness, absolute negativity and electron density transfer in adducts of selected nitriles with BH_3

	η (eV)	χ^0 (eV)	ΔN
BH_3	3.89	5.67	
$H_2C{=}CH{-}C{\equiv}N$	3.17	4.70	0.734
$C_6H_5{-}C{\equiv}N$	2.93	4.34	0.734
$H_3C{-}CH_2{-}C{\equiv}N$	4.83	3.93	0.550
$H{-}C{\equiv}N$	5.17	4.61	0.567

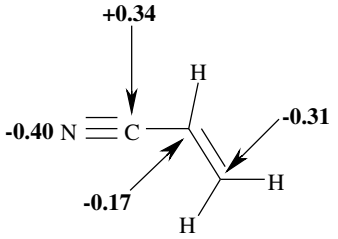

Fig. 7. B3LYP/6-31G* calculated electrostatic charge distribution in the acrylonitrile molecule.

getic requirements of adduct formation. Table 3 shows that the change in energy of complex formation, $\Delta_{complexation}E$, is greatest for the formation of the acrylonitrile–BH_3 adduct at -75.1 kJ mol^{-1}.

In addition to the relative stability of the adducts, depicted in Fig. 7, the activation energy requirements are critical for reduction to take place. As summarised in Table 3, the overall energy barriers ($\Delta_{activation}E$) for the reduction of propionitrile (42.7 kJ mol^{-1}), hydrogen cyanide (40.7 kJ mol^{-1}) and benzonitrile (42.3 kJ mol^{-1}) are higher than the energy barrier (34.7 kJ mol^{-1}) for the reduction of acrylonitrile. The B3LYP method gives a better account of the reaction with energy barriers calculated in the present work being substantially lower and, thus, more reasonable than those calculated by Ray and Chadha's MNDO study [40].

Table 3
B3LYP/6-31G* calculated energies for the reaction of selected nitriles with BH_3

Adduct	$\Delta_{complexation}E$ (kJ mol^{-1})	$\Delta_{activation}E$ (kJ mol^{-1})
$H_2C{=}CH{-}C{\equiv}N$	-75.1	34.7
$H_3C{-}CH_2{-}C{\equiv}N$	-64.3	42.7
$C_6H_5{-}C{\equiv}N$	-61.4	42.3
$H{-}C{\equiv}N$	-60.8	40.7
$H{-}C{\equiv}N$ [40]	-66.9	89.1

The B3LYP results for charge transfer (Table 4) bear out with those of Ray and Chadha [40] in that there is a reversal of charge in the nitrile–BH_3 adduct for the atoms that make up the borane and the nitrogen and carbon atoms in the nitrile. These transfers of charge are of the similar magnitude where 0.8 units of charge are transferred to the boron atom from the borane protons and the nitrogen and carbon atoms of the nitrile functionality.

An interesting question arises when considering the preference of reduction at the nitrile as opposed to the alkene functionality of acrylonitrile, especially in relation to Brown and Kortnyk's [5] observation that, in solution, nitriles are less reactive than alkenes towards hydroboration/reduction. A look into the distribution of electrostatic charge in the acrylonitrile molecule (Fig. 7) reveals that the nitrogen atom carries most of the electrostatic charge in the molecule and, as such, is the point most susceptible to electrophilic attack.

Table 4
Changes in electrostatic charges of atoms in the stationary points C (nitrile–BH_3 adduct) on the reaction surface

Atom	$H_2C{=}CH{-}C{\equiv}N$	$H_3C{-}CH_2{-}C{\equiv}N$	$C_6H_5{-}C{\equiv}N$	$H{-}C{\equiv}N$
B	0.79	0.78	0.82	0.74
H_A	−0.12	−0.11	−0.12	−0.11
H_B	−0.12	−0.11	−0.12	−0.11
H_C	−0.12	−0.11	−0.12	−0.11
N	−0.52	−0.56	−0.62	−0.53
C	0.17	0.22	0.27	0.20

Note. Original charge on the boron atom of the free borane is +0.30, thus if the boron atom gains 0.79 units of negative charge from acrylonitrile its final charge will be −0.49 in the borane–acrylonitrile adduct.

5. Summary

In summary, the results obtained in this study indicate that the overall reduction of acrylonitrile with $BH_3 \cdot SMe_2$ is associative. In addition, the importance of the dissociation of the dimethyl sulfide from borane to the reduction process has also been illustrated. The lack of reaction with propionitrile and benzonitrile at 25 °C can be attributed to lack of stability of their adducts as demonstrated by the low equilibrium constants for the formation of their adducts with borane and further illustrated in Fig. 6 in their higher energies than the acrylonitrile–borane adduct. Furthermore, these compounds would have higher activation barriers, as shown in Table 3.

The applicability of ^{11}B NMR spectroscopy to physical organic chemistry has been demonstrated. To our knowledge, this is the first time that a detailed mechanistic study of these types of complexes has been undertaken.

Acknowledgements

The authors acknowledge financial support from Sastech R&D, DTI/Thrip and the University of KwaZulu-Natal. The authors also wish to thank Mr. C. D. Grimmer of the University of KwaZulu-Natal for assistance with recording NMR spectra, as well as Mr. A. de Klerk and Dr. H. Strauss of Sasol Ltd. for the constructive discussions.

Appendix A. Supporting information

The crystal data can be found in the Cambridge Crystallographic Data Centre (CCDC), 12 Union Road, Cambridge CB2 1EZ, UK, fax: +44 1223 336 033, e-mail: deposit@ccdc.cam.ac.uk, or on the web www.ccdc.cam.ac.uk. Supplementary data associated with this article can be found, in the online version, at doi:10.1016/j.poly.2006.04.002.

References

[1] For a review of early developments see: H.I. Schlessinger, A.B. Burg, Chem. Rev. 31 (1942) 1.
[2] F.G.A. Stone, J. Emeléus, J. Chem. Soc. (1950) 2755.
[3] H.C. Brown, B.C. Subba Rao, J. Org. Chem. 22 (1957) 1135.
[4] H.C. Brown, B.C. Subba Rao, J. Am. Chem. Soc. 82 (1960) 681.
[5] H.C. Brown, W. Kortnyk, J. Am. Chem. Soc. 82 (1960) 3866.
[6] H.C. Brown, P. Heim, M.M. Yoon, J. Am. Chem. Soc. 92 (1970) 1637.
[7] J. Emeléus, K. Wade, J. Chem. Soc. (1960) 2614.
[8] A.B. Burg, Rec. Chem. Prog. (Kresge-Hooker Sci. Lab.) 15 (1954) 159 (Chem. Ab., 1955, 49, 35313).
[9] J.R. Jennings, K. Wade, J. Chem. Soc. A (1968) 1946.
[10] R. Coult, M.A. Fox, B. Rand, K. Wade, A.V.K. Westwood, J. Chem. Soc., Dalton Trans. (1997) 3411.
[11] J.S. Fowler, R.R. MacGregor, A.N. Ansari, H.L. Atkins, A.P. Wolf, J. Med. Chem. 17 (1974) 246.
[12] L.M. Braun, R.A. Braun, H.R. Crissman, M. Opperman, R.M. Adams, J. Org. Chem. 36 (1971) 2388.
[13] C.F. Lane, Adrichim. Acta 8 (1976) 20.
[14] H.C. Brown, Y.M. Choi, S. Narasimhan, J. Org. Chem. 47 (1981) 3153.
[15] T. Wakamatsu, H. Inaki, A. Ogawa, M. Watanabe, Y. Ban, Heterocycles 4 (1980) 1437.
[16] M. Periasamy, M. Thirumalaikumar, J. Organomet. Chem. 69 (2000) 137.
[17] For a recent example see: H.C. Brown, J.V.B. Kanth, M. Zaidlewicz, J. Org. Chem. 63 (1998) 5154.
[18] H.C. Brown, J. Chandrasekharan, Orgamometallics 2 (1983) 1261.
[19] H.C. Brown, J. Chandrasekharan, D.J. Nelson, J. Am. Chem. Soc. 106 (1984) 3768.
[20] H.C. Brown, L.T. Murray, Inorg. Chem. 23 (1984) 2746.
[21] H.C. Brown, J. Chandrasekharan, J. Org. Chem. 50 (1985) 518.
[22] H.C. Brown, J. Chandrasekharan, Gazz. Chim. Ital. 117 (1987) 517.
[23] H.C. Brown, J. Chandrasekharan, J. Org. Chem. 53 (1988) 4811.
[24] H.C. Brown, N. Ravindran, J. Am. Chem. Soc. 106 (1984) 1863.
[25] K.K. Wang, H.C. Brown, J. Org. Chem. 45 (1980) 5303.
[26] For some examples see: H.C. Brown, J.V.B. Kanth, P.V. Dalvi, M. Zaidlewicz, J. Org. Chem. 64 (1999) 64.
[27] H.C. Brown, J.V.B. Kanth, P.V. Dalvi, M. Zaidlewicz, J. Org. Chem. 65 (2000) 4655.
[28] D.F. Shriver, The Manipulation of Air-sensitive Compounds, McGraw-Hill Inc., New York, 1969.
[29] G.W. Kramer, A.B. Levy, M.M. Midland, in: H.C. Brown (Ed.), Organic Synthesis via Boranes, John Wiley and Sons, Inc., New York, 1975, pp. 191–261.
[30] Spartan '04, Wavefunction, Inc., Irvine, CA. Available from: <http://www.wavefun.com>.
[31] B3LYP Method: P.J. Stevens, J.F. Devlin, C.F. Chabalowski, M.J. Frisch, J. Phys. Chem. 98 (1994) 11623.
[32] 6-31G* basis method: W.J. Hehre, R. Ditchfield, A.J. Pople, J. Chem. Soc. 56 (1972) 2257.
[33] P.C. Hariharan, J.A. Pople, Theor. Chim. Acta 28 (1973) 213.
[34] D.R. Schultz, J. Polym. Sci. 1B (1963) 613.
[35] (a) Y. Ogata, Y. Minoura, Kogyo Kagaku Zasshi 66 (1963) 1707; (b) Y. Ogata, Y. Minoura, Kogyo Kagaku Zasshi 66 (1963) 1710; (c) Y. Ogata, Y. Minoura, Kogyo Kagaku Zasshi 66 (1963) 1714.
[36] H.C. Brown, J.V.B. Kanth, M. Zaidlewicz, J. Org. Chem. 63 (1998) 5154.
[37] M.F. Hawthorne, Tetrahedron 17 (1962) 117.
[38] J.E. Lloyd, K. Wade, J. Chem. Soc. (1961) 649.
[39] J.R. Jennings, R. Snaith, M.M. Mahmoud, S.C. Wallwork, S.J. Bryan, J. Halfpenny, E.A. Petch, K. Wade, J. Organomet. Chem. 249 (1983) C1.
[40] R. Chadha, Naba K. Ray, J. Indian Chem. Soc. (1982) 204.
[41] R.G. Pearson, Chemical Hardness: Applications from Molecules to Solids, Wiley-VCH, Weinheim, 1997.

We chose the ligand L^1H, to get a carboxylato bridged manganese complex as there has been significant research interest in the chemistry of manganese carboxylato complexes owing to their relevance to the biological Mn sites [2,3] and the realisation of single-molecular magnets which are cluster complexes having abnormally large values of ground state spin [26,27]. Dinuclear manganese(II) complexes are of special attraction, since such systems are known to exist at the active centres of some manganese containing enzymes [28]. Recently, dinuclear units with one to three carboxylato bridges were suggested to be a plausible structure of the dinuclear sites in Mn catalases [28]. Using the same ligand, we have already reported one quasi-tetrahedral Cu_4 cluster and a helical-chain copper(II) complex [29], and two novel zinc(II) helical chain polymers in our earlier articles [30]. In the present case we get a rare double $\mu_{1,1}$-carboxylato bridged five coordinated dinuclear manganese(II) complex. On the other hand a salen type ligand L^2H_2 has been employed for the preparation of complex **2**. Though the ligand L^2H_2 is very similar with the ligand stated in our previous report [25], here we get a monomeric manganese(III) complex, which forms a dimer through hydrogen bonds.

The present paper describes the synthesis, spectral characterisation and crystal structures of two new Mn(II) and Mn(III) complexes using two different Schiff base ligands (L^1H and L^2H_2). The magnetic behaviour for **1** is driven by a weak antiferromagnetic interaction.

2. Experimental

2.1. Materials and measurements

Pyridine 2-carboxyldehyde, anthranilic acid (Aldrich), 1,3-diaminopropane, *o*-vanillin, manganese(II) nitrate tetrahydrate, manganese(II) perchlorate hexahydrate (Fluka), sodium thiocyanate, sodium azide(Aldrich) were used as received. The solvents used were of reagent grade.

Elemental analyses were carried out using a Perkin–Elmer 2400 II elemental analyser. The infrared spectra were recorded on a Perkin–Elmer FT-IR spectrophotometer with a KBr disc. The electronic spectrum was recorded (for complex **2**) on a Perkin–Elmer Lambda 40 (UV–Vis) spectrophotometer in methanol. Electrochemical study (for complex **2**) was performed on a CH600A cyclic voltammeter (CV) using tetrabutyl ammonium perchlorate (TBAP) as the supporting electrolyte. The magnetic measurement for **1** was carried out on polycrystalline sample using a Quantum Design SQUID MPMS-XL magnetometer in the temperature range 300–2K with an applied field of 3000G. The contribution of the sample holder was determined separately in the same temperature range and field. Diamagnetic corrections were estimated from Pascal's constants. Room temperature magnetic susceptibility was measured in vibrating sample magnetometer using mercury(tetrathiocyanato)cobaltate as the standard. As the complex **1** is insoluble, electronic spectrum and electrochemical study were not performed for this complex. Magnetic susceptibility for **2**, at room temperature was measured in a vibrating sample magnetometer using mercury(tetrathiocyanato)cobaltate as the standard. As complex **1** is insoluble, electronic spectrum and electrochemical studies were not performed for this complex.

2.2. Synthesis of ligands and metal complexes

2.2.1. $[C_5H_4NC{=}NC_6H_4(COOH)]$ (L^1H)

The Schiff base ligand (L^1H) was prepared by refluxing pyridine 2-carboxyldehyde (10 mmol) and anthranilic acid (10 mmol) in 50 ml of methanol for 30 min. The resulting brownish red solution containing the ligand was used without further purification.

2.2.2. $[(OMe)(OH)C_6H_3C{=}NCH_2CH_2CH_2N{=}CC_6H_3(OH)(OMe)]$ (L^2H_2)

The Schiff base ligand L^2H_2 was obtained by the condensation of *o*-vanillin (20 mmol) with 1,3-diaminopropane (10 mmol) in 50 ml methanol under refluxing conditions for 30 min. The resulting orange yellow solution of the ligand was used without further purification.

2.2.3. $[Mn_2(L^1)_2(NCS)_2]$ (**1**)

To a methanolic solution (20 ml) of manganese nitrate tetrahydrate (0.251 g, 1 mmol), the liquid Schiff base (L^1H) (2 mmol) was added, followed by the addition of a solution of sodium thiocyanate (0.081 g, 1 mmol) in a minimum volume of methanol with constant stirring for 30 min. The resulting mixture was kept in a refrigerator yielding light orange, hexagonal crystals suitable for X-ray diffraction after 15 days. The crystals were collected by filtration and air-dried. Yield – 60%. *Anal.* Calc. for $C_{28}H_{18}Mn_2N_6O_4S_2$: C,49.7; H, 2.7; N, 12.4. Found: C, 49.6; H, 2.6; N, 12.1%.

2.2.4. $[Mn(L^2)(N_3)(H_2O)]$ (2)

To a methanolic solution (15 ml) of manganese perchlorate hexahydrate (0.365 g, 1 mmol), a methanolic solution of the Schiff base (L^2H_2) (1 mmol) was added. Then a solution of sodium azide (0.065 g, 1 mmol) in a minimum volume of water was added with constant stirring. The resulting solution was stirred for 20 min at room temperature. Deep brown, hexagonal crystals suitable for X-ray diffraction were obtained after 9 days. The crystals were collected by filtration and air-dried. Yield – 72 %. *Anal.* Calc. for $C_{19}H_{22}MnN_5O_5$: C, 43.7; H, 4.9; N, 12.1. Found: C, 43.6; H, 4.8; N, 12.1%.

Caution. Perchlorate salts are potentially explosive and should be used in small quantities with much care.

2.3. X-ray crystallographic studies

X-ray single-crystal diffraction data for **1** and **2** were collected at low temperature (163(2) K) with a Nonius Kappa CCD diffractometer equipped with a normal

Table 1
Crystallographic data for **1** and **2**

	1	**2**
Empirical formula	$C_{28}H_{18}Mn_2N_6O_4S_2$	$C_{19}H_{22}MnN_5O_5$
Formula weight	676.48	455.36
Temperature (K)	163(2)	298(2)
Wavelength (Å)	0.71073	0.71073
Crystal system	monoclinic	monoclinic
Space group	$P2_1/n$	$P2_1/c$
a (Å)	10.8252(5)	23.0024(4)
b (Å)	8.7628(4)	12.4365(2)
c (Å)	15.7444(10)	13.9569(2)
α (°)	90	90
β (°)	109.174(2)	94.1220(10)
γ (°)	90	90
Volume (A^3)	1410.65(13)	3982.31(11)
Z	2	8
Density (g/cm^3) (calculated)	1.593	1.519
Absorption coefficient (mm^{-1})	1.090	0.706
Crystal size (mm)	$0.10 \times 0.10 \times 0.10$	$0.50 \times 0.30 \times 0.10$
Θ range (°)	2.01–27.41	1.86–27.48
Reflections collected	5257	15505
Independent reflections [R_{int}]	3187 [0.0565]	8978 [0.0407]
Maximum and minimum transmission	0.8989 and 0.8989	0.9328 and 0.7192
Goodness-of-fit on F^2	1.049	0.959
Final R indices [$I > 2\sigma(I)$]	$R_1 = 0.0620$, $wR_2 = 0.1524$	$R_1 = 0.0510$, $wR_2 = 0.1354$
R indices (all data)	$R_1 = 0.1020$, $wR_2 = 0.1833$	$R_1 = 0.0952$, $wR_2 = 0.1610$
Residual electron density (e Å^{-3})	0.605 and −0.634	0.435 and −0.454

monochromatised focus X-ray tube having a molybdenum target. The data were collected using the COLLECT software (Nonius BV, 1997–2000) and then were processed through the DENZO reduction software (Otwinowski and Minor, 1997). The structures were solved and refined on F^2 using the SHELXTL software. All non-hydrogen atoms were refined with anisotropic thermal parameters. The hydrogen atoms were included in the final refinement model in calculated positions with isotropic thermal parameters. Crystal structure and refinement data are summarised in Table 1.

3. Results and discussion

3.1. Description of the structures

3.1.1. $[Mn_2(L1)_2(NCS)_2]$ (1)

Fig. 1 shows the molecular structure of **1** with atom labelling scheme and the relevant bond lengths and angles are summarised in Table 2. The structure consists of a centro-symmetric dimer where each equivalent manganese atoms is associated with a terminal thiocyanate ligand and a tridentate Schiff base bonded through imine nitrogen, pyridine nitrogen and carboxylato oxygen (NNO) atoms. The two μ_2-carboxylato O-atoms bridge the two manganese centres and link the two halves of the dimer about a pseudo twofold symmetry axis which lies normal to the almost planar Mn_2O_2 rhombus. For a pentacoordinated metal centre, the distortion of the structure from trigonal bipyramidal (TBP) to square pyramidal (SP) can be evaluated by the Addision distortion index τ [31,32]: $\tau = |\beta - \alpha|/60°$, α and β being the two largest angles around the central atom; values for τ in perfect polyhedra are 1.0 for TBP and 0.0 for SP. Here, the five coordinated manganese(II) ions exhibit a distorted square pyramidal geometry ($\tau = 0.0603$) with the thiocyanate nitrogen occupying the apical sites and two bridging carboxylato oxygen, one pyridine and one imine nitrogen atoms of the coordinated

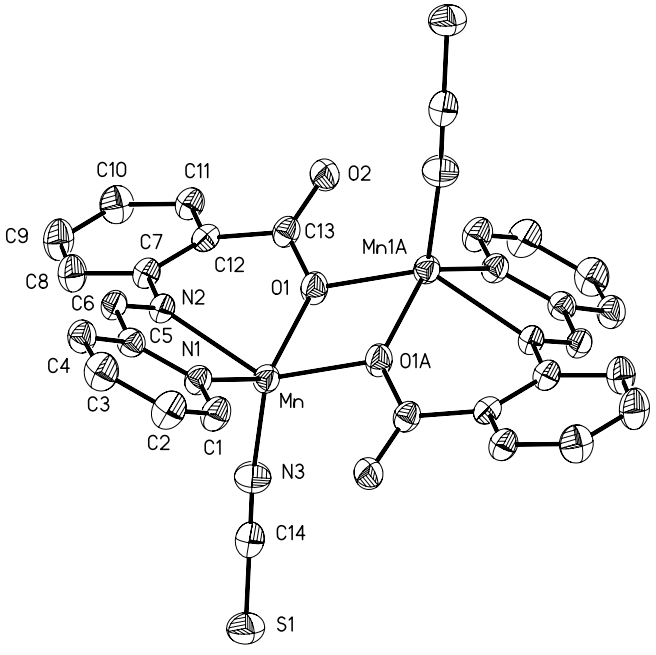

Fig. 1. Molecular view of **1** with atom labelling and ellipsoids at 30% probability.

Table 2
Bond lengths (Å) and bond angles (°) for **1** and **2**

1		**2**			
		A		**B**	
Mn–N3	2.054(4)	Mn1–O4A	1.8970(18)	Mn2–O4B	1.905(2)
Mn–O1A	2.125(3)	Mn1–O3A	1.895(2)	Mn2–O3B	1.900(2)
Mn–O1	2.170(3)	Mn1–N1A	2.006(2)	Mn2–N1B	2.030(3)
Mn–N1	2.218(3)	Mn1–N2A	2.057(3)	Mn2–N2B	2.070(3)
Mn–N2	2.241(3)	Mn1–N5A	2.228(3)	Mn2–N5B	2.176(3)
		Mn1–O2WA	2.282(3)	Mn2–O2WB	2.268(2)
N3–Mn–O1A	114.88(13)	O4A–Mn1–O3A	87.61(8)	O4B–Mn2–O3B	86.13(9)
N3–Mn–O1	110.97(14)	O4A–Mn1–N1A	176.39(10)	O4B–Mn2–N1B	171.85(10)
O1A–Mn–O1	74.00(11)	O3A–Mn1–N1A	89.69(9)	O3B–Mn2–N1B	89.42(10)
N3–Mn–N1	112.24(15)	O4A–Mn1–N2A	90.33(9)	O4B–Mn2–N2B	89.33(10)
O1A–Mn–N1	101.98(11)	O3A–Mn1–N2A	174.65(10)	O3B–Mn2–N2B	175.12(9)
O1–Mn–N1	133.58(12)	N1A–Mn1–N2A	92.15(10)	N1B–Mn2–N2B	94.87(11)
N3–Mn–N2	105.44(14)	O4A–Mn1–N5A	91.97(10)	O4B–Mn2–N5B	99.02(10)
O1A–Mn–N2	137.20(11)	O3A–Mn1–N5A	97.95(10)	O3B–Mn2–N5B	95.25(10)
O1–Mn–N2	78.88(10)	N1A–Mn1–N5A	90.77(11)	N1B–Mn2–N5B	88.18(11)
N1–Mn–N2	74.11(11)	N2A–Mn1–N5A	87.06(11)	N2B–Mn2–N5B	87.23(11)
		O4A–Mn1–O2WA	89.81(9)	O4B–Mn2–O2WB	90.08(10)
		O3A–Mn1–O2WA	91.78(10)	O3B–Mn2–O2WB	88.50(9)
		N1A–Mn1–O2WA	87.87(10)	N1B–Mn2–O2WB	82.97(10)
		N2A–Mn1–O2WA	83.27(11)	N2B–Mn2–O2WB	89.72(11)
		N5A–Mn1–O2WA	170.17(11)	N5B–Mn2–O2WB	170.36(11)

Symmetry operations used for equivalent atoms **A**: $1-x, -1/2+y, 1/2-z$ and **B**: $1-x, 1-y, 1-z$.

Schiff base ligands forming a good mean plane from which the manganese centres are deviated by 0.797 Å towards the thiocyanate ligand. The Mn…Mn separation (3.431 Å) and the bond distances and angles associated with Mn_2O_2 fragment are comparable to similar systems (Table 4, Scheme 1). The thiocyanate ligand is almost linear (N3–C14–S1 = 178.9(4)°) but it coordinates with the metal centre in bent fashion (C14–N3–Mn = 165.1(4)°).

3.1.2. *[Mn(L²)(N₃)(H₂O)] (2)*

The ORTEP presentation of **2** is shown in Fig. 2 and relevant bond lengths and angles are summarised in Table 2. The structure consists of two crystallographically independent six coordinated Mn(III) complexes labelled **A** and **B**. In both independent units **A** and **B**, the manganese(III) ion adopts a distorted octahedral geometry where the coordination sites of the Schiff base ligand, i.e. two imine nitrogen and two phenolic-oxygen atoms form an equatorial plane and the axial sites are occupied by the azido nitrogen atom and an oxygen atom from the coordinated water molecule. The square base of each octahedron is nearly planar with the Mn(III) centres being deviated by 0.077 and 0.064 Å from the mean plane containing the four basal atoms for **A** and **B**, respectively. The axial Mn–N and Mn–O bonds [2.228(3)–2.282(3) Å/2.176(2)–2.268(2) Å] are longer than the corresponding equatorial bonds [1.895(2)–2.057(3) Å/1.900(2)–2.070(3) Å] because of the Jahn Teller effect, as anticipated for high spin Mn(III) complexes. The azide group is almost linear with a N–N–N angle 179.3(4)°/177.8(5)°, indicating sp hybridisation of the central azide N-atom, and it connects with the Mn(III) centre in a bent fashion making an angle N4A–N5A–Mn1 = 127.9(2)°/N4B–N5B–Mn2 = 127.7(3)°. The three six membered rings, which are formed around each manganese centre, are puckered. Each hydrogen atom of the coordinated water molecule forms strong H-bonds with the non-coordinated methoxy oxygen and coordinated phenolato oxygen atoms of another similar mononuclear unit (i.e. **A** connected to **A** and **B** connected to **B**). In this way each mononuclear complex gives rise to a dimeric structure (**A**–**A**/**B**–**B**) (Fig. 3, Table 3). The distance between the two Mn atoms connected through H-bonding is 5.1092(8) Å.

3.2. Infrared spectra

The strong absorption bands corresponding to $\nu_{C=N}$ of the thiocyanato ligand for **1** and $\nu_{N=N}$ of the azido ligand for **2** appear at 2075 and 2029 cm^{-1}, respectively. The bands at 1626 and 1611 cm^{-1} for **1** and **2**, respectively, are attributable to $\nu_{C=N}$ (imine bond) and these bands shift to a lower frequency region compared to that obtained for the respective free ligands [at 1640 (L^1H) and 1633 cm^{-1} (L^2H_2)]. For complex **1**, the bands at 1412 and 1545 cm^{-1} are assigned to $\nu_s(CO_2)$ and $\nu_{as}(CO_2)$ vibrations. The difference of these two frequencies, Δ [$\Delta = \nu_s(CO_2) - \nu_{as}(CO_2) = 133\ cm^{-1}$] indicates the bridging coordination modes of the carboxylate group of the Schiff base [36]. Ligand coordination with the manganese ion is substantiated by two types of bands at 439(**1**), 445(**2**) cm^{-1} and 361(**1**), 371(**2**) cm^{-1}, corresponding to ν_{Mn-N} and ν_{Mn-O}, respectively. Some additional bands are obtained only in the spectrum of **2**, due to the presence of the coordinated water molecule. A broad absorption band around 3410 cm^{-1} appears due to the ν_{sym} and ν_{asym} vibration of

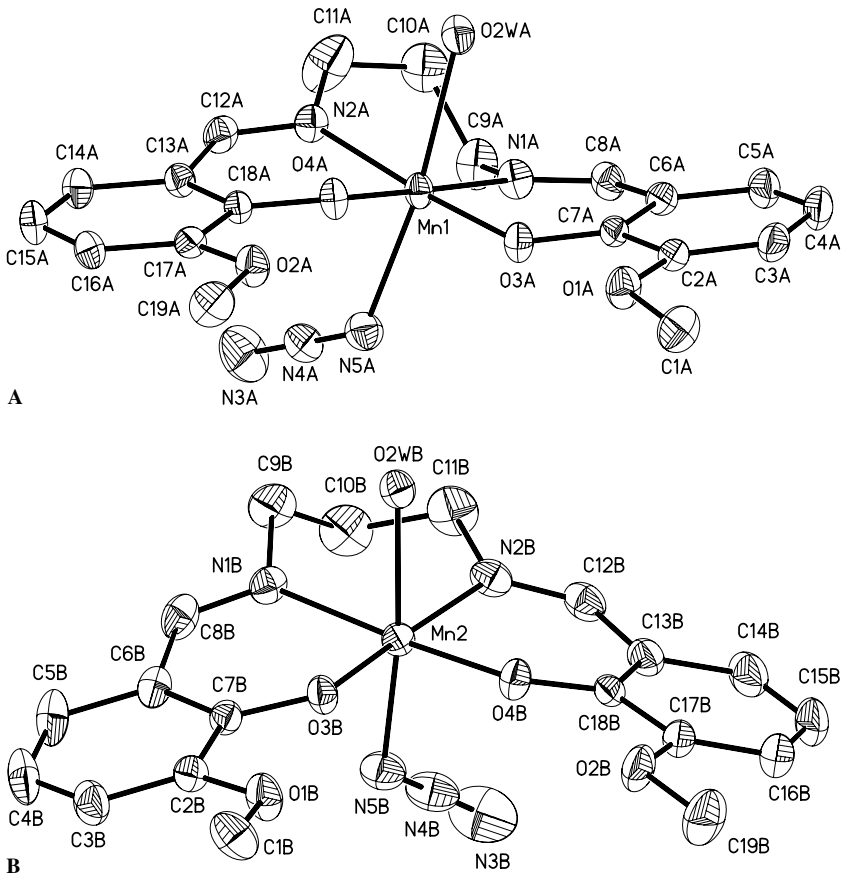

Fig. 2. Molecular view of **2** (**A** and **B**) with atom labelling and ellipsoids at 30% probability.

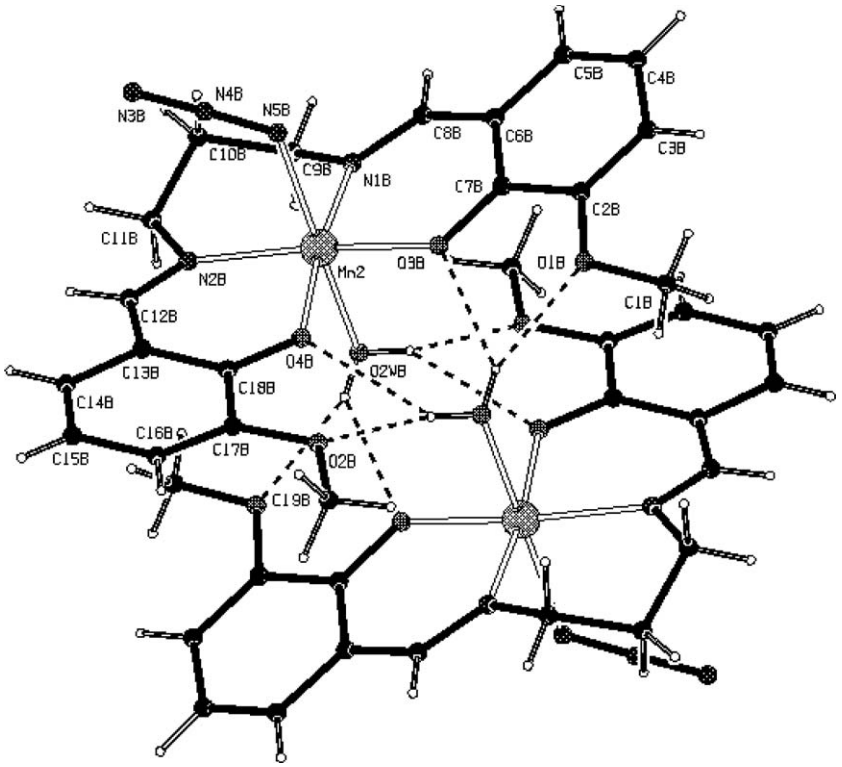

Fig. 3. Dimeric view of complex **2** through H-bonding (for the sake of clarity only one crystallographic unit, **B** is shown).

Table 3
Hydrogen bond dimensions (bond lengths in Å and angles in °) for **2**

D–H...A	*d*(D–H)	*d*(H...A)	*d*(D...A)	∠(DHA)
O2WA–H1WA...O2A	0.65(4)	2.31(4)	2.882(4)	149(4)
O2WA–H1WA..O4A	0.65(4)	2.43(4)	2.954(4)	140(4)
O2WA–H2WA...O1A	0.88(5)	2.02(5)	2.896(4)	173(4)
O2WB–H2WB...O1B	0.74(4)	2.11(4)	2.761(3)	147(4)
O2WB–H1WB...O2B	0.77(4)	2.20(4)	2.852(4)	144(4)
O2WB–H1WB...O4B	0.77(4)	2.39(4)	3.029(3)	142(4)

Symmetry operations used for equivalent atoms **A**: $1-x$, $-1/2+y$, $1/2-z$ and **B**: $1-x$, $1-y$, $1-z$.

the OH group of the water molecule. The scissoring motion for the coordinated water appears at 1560 cm^{-1}.

3.3. Electronic spectrum

Complex **2** displays two strong absorption bands in the region 230 ($\varepsilon = 1100\ mol^{-1}\ cm^{-1}$) and 275 nm ($\varepsilon = 1150\ mol^{-1}\ cm^{-1}$), which can be assigned to charge transfer from the ligand to the Mn(III) centre. The spectrum also shows low-intensity absorption bands associated with d–d transitions in the range 490–500 ($\varepsilon = 390\ mol^{-1}\ cm^{-1}$) nm.

3.4. Electrochemical study

The cyclic voltammetry of complex **2** shows one irreversible oxidative and one irreversible reductive response at 1.33 and −0.42 V due to Mn(III)/Mn(IV) and Mn(II)/Mn(III) redox couples.

3.5. Magnetic studies

The overall magnetic behaviour of complex **1** corresponds to weak antiferromagnetically coupled systems (Fig. 4). At room temperature, $\chi_M T$ shows a value of 8.395 $cm^3\ K\ mol^{-1}$ which is as expected for two manganese(II) ions (8.655 $cm^3\ mol^{-1}\ K$ per two Mn(II) with $g = 2.0$). When the sample is cooled, the $\chi_M T$ value remains constant, and below approximately 80 K decreases quickly to 6.020 $cm^3\ K\ mol^{-1}$ at very low temperatures (5 K). The χ_M value increases continuously on cooling from 0.029 $cm^3\ mol^{-1}$ to reach a maximum value of 1.204 $cm^3\ mol^{-1}$ at 5 K. To determine the exchange parameters via the double η^1:μ-$O_{carboxylate}$ bridge, (Fig. 5) χ_MT was fitted to the equation Eq. (1) for an isotropically coupled pair of $S = 5/2$ ions [48], where N is Avogadro's number, μ_B is the Bohr magneton and k_B is the Boltzmann constant. The best fit parameters for reproducing satisfactorily the experimental data, as shown in Fig. 4, are $J_1 = -0.41 \pm 0.029\ cm^{-1}$, and $g = 2.0$ with $R = 3.2 \times 10^{-5}$ ($R = \sum_i(\chi T_{icalc} - \chi T_{iexp})^2 / (\chi T_{iexp})^2$).

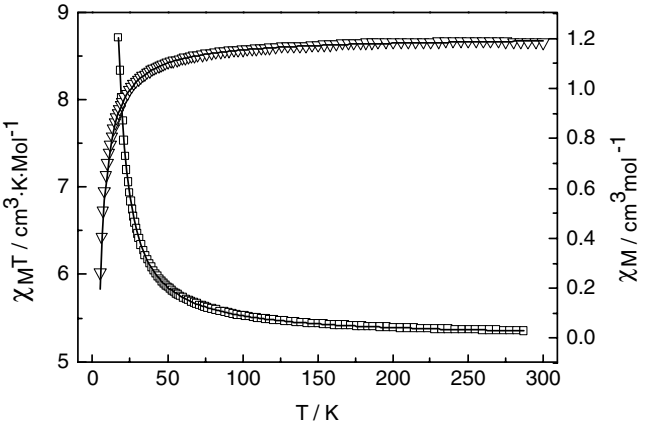

Fig. 4. Plot of the $\chi_M T$ product (△) and χ_M (□) vs. T for compound **1**. Solid line shows the best fit of the data (see text).

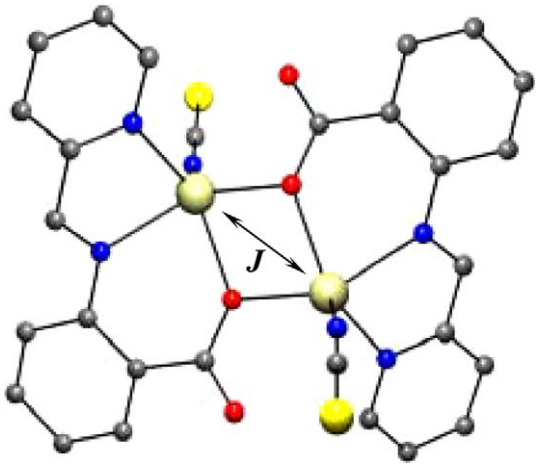

Fig. 5. Dinuclear structure of complex **1**. The schematic magnetic interaction is indicated.

It is well known that the magnetic coupling in M(II)-oxo bridged systems is mainly governed by the M–O–M angle [49]. In complex **1** this angle is close to 106.0°, which should correspond to a small and negative J value. The weak antiferromagnetic coupling found in complex **1** is compared to that previously reported in the literature for similar complexes [37,40] and also for complexes where two Mn(II) ions are bridged by two phenolate ligands [50–53]. This feature can be checked from Table 4, where the J value of $-0.41\ cm^{-1}$ for complex **1** matches those shown in this Table for complexes with similar M–O–M angles.

The X-band powder spectrum at room temperature is shown in Fig. 6. This spectrum is the addition of the spectra for $S = 1, 2, 3, 4$ and 5 excited states. Considering the small J value, all S states are populated at room temperature

$$\chi_M T = \frac{Ng^2\mu_B^2}{k_B} \cdot \frac{2\exp(J/k_B) + 10\exp(3J/k_B) + 28\exp(6J/k_B) + 60\exp(10J/k_B) + 110\exp(15J/k_B)}{1 + 3\exp(J/k_B) + 5\exp(3J/k_B) + 7\exp(6J/k_B) + 9\exp(10J/k_B) + 11\exp(15J/k_B)} \quad (1)$$

Table 4
Selected structural parameters of the fragment [Mn–O_2–Mn] (Scheme 1) in double μ_2-carboxylato bridged manganese complexes according to the structural database (CSD version 5.26, update August 2005)

Compound[i]	Mn1···Mn2 (Å)	Mn1–O1 (Å)	Mn1–O2 (Å)	O1–Mn1–O2 (°)	Mn1–O1–Mn2 (°)	Mn1–O2–Mn2 (°)	Mn–O1–Mn2–O2 (°)	J (cm^{-1})	Reference
a	4.091	2.591	2.231	64.110	115.890	115.890	0.000	−1.31	[33]
b	3.525	2.348	2.447	85.393	94.607	94.607	0.000	*	[34]
c	3.795	2.287	2.370	71.426	105.974	111.352	5.816	*	[35]
d	3.633	2.210	2.204	69.172	110.828	110.828	0.000	−8.95(J_1), −0.60(J_2), −3.37(J_3)	[36]
e	3.711	2.232	2.252	71.637	109.808	109.111	0.145	−0.631	[37]
f	3.589	2.230	2.293	74.961	105.039	105.039	0.000	*	[38]
	3.546	2.224	2.291	76.486	103.514	103.514	0.000		
g	3.740	2.316	2.236	69.096	107.738	107.426	−22.968	*	[39]
h	3.460	2.174	2.207	76.328	105.039	102.770	−1.320	−0.20	[40]
j	3.537	2.266	2.238	76.479	103.521	103.521	0.000	*	[41]
k	3.531	2.297	2.177	75.780	104.220	104.220	0.000	*	[42]
l	3.672	2.312	2.250	72.470	106.439	108.382	0.077	*	[43]
m	3.652	2.231	2.306	72.806	107.194	107.194	0.000	*	[44]
n	3.473	2.198	2.150	73.989	106.011	106.011	0.000	*	[45]
o	3.289	2.241	2.246	78.366	94.713	94.138	−28.153	−1.43	[46]
p	3.803	2.313	2.312	69.386	110.614	110.614	0.000	*	[47]
Complex **1**	3.431	2.170	2.125	74.00	106.00	106.00	0.000	−0.39	present study

* J value not reported.

[i] (a) bis(μ_2-*N*-methyl-*N*′-carboxymethyl-*N*,*N*′-bis(2-pyridylmethyl)ethane-1,2-diamine)-diaqua-di-manganese(ii) diperchlorate; (b) bis(μ_2-2,4,5-trichlorophenoxyacetato-*O*)-bis(*trans*-diaqua-(2,4,5-trichlorophenoxyacetato)-manganese(ii)); (c) bis(μ_2-*N*,*N*-bis(2-pyridylmethyl)-(S)-histidinate)-dimanganese (ii) diperchlorate trihydrate; (d) bis(μ_2-pyridine-2-carboxylato-*N*,*O*,*O*)-bis(acetato-*O*)-bis(pyridine-2-aldoxime-*N*,*N*′)-di-manganese(ii); (e) bis(μ_2-(bis-(2-pyridylmethyl)amino)acetato-*N*,*N*′,*N*″,*O*,*O*)-tetra-aqua-di-manganese(ii) diperchlorate monohydrate; (f) bis(μ_2-2,6-dimethoxybenzoato-*O*,*O*)-diaqua-bis(2,6-dimethoxybenzoato)-bis(4,7-dimethyl-1,10-phenanthroline)-di-manganese(ii) ethanol solvate; (g) (μ_3-2,6-pyridinedicarboxylato)-(μ_2-2,6-pyridinedicarboxylato)-tris(2,2′-bipyridyl)-(2,6-pyridinedicarboxylato)-tri-manganese(ii)nonahydrate; (h) catena-(bis((μ_3-(bis(methylthio)methylene)malonato-*O*,*O*,*O*′,*O*″)-(2,2′-bipyridyl-*N*,*N*′)-manganese(ii))); (j) (bis(μ_2-1,4,7,10-tetra-azacyclododecane-1,4-diacetato)-manganese(ii)) methanol solvate; (k) bis-((μ_2-2,6-dimethoxybenzoato-*O*,*O*)-aqua-(2,2′-bipyridine)-(2,6-dimethoxybenzoato-*O*)-manganese(ii)) bipyridine solvate; (l) bis((μ_2-*N*,*N*-bis((1-methylimidazol-2-yl)methyl)glycinato)-diaqua-manganese(ii)) bis(hexafluorophosphate) monohydrate; (m) catena-(bis(μ_3-oxydiacetato)-(μ_2-aqua)-di-aqua-di-manganese(ii)); (n) bis(μ_2-3-methyl-2,6-dioxo-1,2,3,6-tetrahydro-pyrimidine-4-carboxylato-*O*,*O*′)-hexa-aqua-di-manganese(ii); (o) bis((μ_2-acetato-*O*,*O*′)-(μ_2-2,2′-bipyridyl-3,3′-dicarboxylato-*O*,*O*,O′,O′)-aqua-dipyridyl)-tri-manganese hemihydrate; (p) bis((μ_2-pyridine-2,6-carboxylato-*N*,*O*,*O*,*O*′)-triaqua-manganese(ii)) bis(pyridine-2,6-dicarboxylic acid).

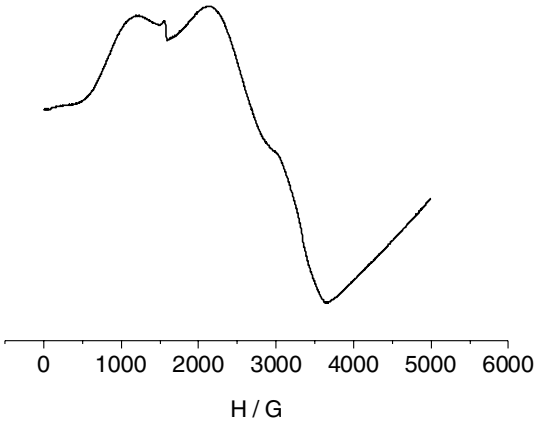

Fig. 6. EPR spectra of compound **1** at room temperature.

($E_{S=5} = -15J = -15 \times -0.39 \approx 6\ cm^{-1}$). Each state has its own D value, very small in manganese(II) complexes. This is the reason of the width of the spectrum (5000 G approximately).

The room temperature magnetic moment value for **2** is 2.64 BM and the value is very much consistent with that of other low spin manganese(III) complexes [54]. The value

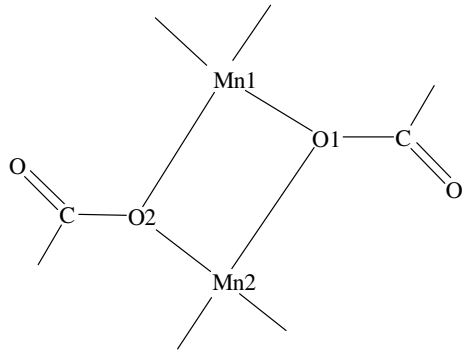

Scheme 1.

indicates that there is no interaction between the two manganese centres connected through hydrogen bonds.

4. Conclusion

One dinuclear five coordinated Mn(II) complex and a mononuclear octahedral Mn(III) complex (**1** and **2**) are obtained from a tridentate and a tetradentate Schiff base, respectively. A very weak antiferromagnetic interaction has been observed for **1**. Complex **2** forms a dimer through

H bonds, but no significant magnetic interaction is found for this complex. In the case of **2**, there is no direct bonding between the two crystallographically independent monomeric units present in the lattice, and this may be due to the occurrence of two bulky methoxy groups in the coordinated Schiff base.

5. Supplementary data

CCDC-289532 (**1**) and 289533 (**2**) contain the supplementary crystallographic data for this paper. These data can be obtained free of charge at www.ccdc.cam.ac.uk [or from the Cambridge Crystallographic Data Center, 12, Union Road, Cambridge CB2 1EZ, UK; e-mail: deposit @ccdc.cam.ac.uk].

Acknowledgements

We acknowledge the financial assistance to S. Sen from the CSIR (New Delhi, India). The magnetic measurement of complex **1** is supported by grants given by the Ministerio de Educación y Ciencia (Programa Ramón y Cajal) and BQU2003/00539.

References

[1] V.L. Pecoraro (Ed.), Manganese Redox Enzymes, VCH, New York, 1992.
[2] G. Christou, Acc. Chem. Res. 22 (1989) 328.
[3] K. Wieghardt, Angew. Chem., Int. Ed. Engl. 28 (1981) 1153.
[4] L. Que, A.E. True, Prog. Inorg. Chem. 38 (1990) 97.
[5] K. Weighardt, Angew. Chem., Int. Ed. Engl. 28 (1989) 1153.
[6] G.C. Dismukes, Chem. Rev. 96 (1996) 2909.
[7] W. Ruttinger, G.C. Dismukes, Chem. Rev. 97 (1997) 1.
[8] O. Kahn, Molecular Magnetism, VCH, New York, 1993.
[9] D. Gatteschi, O. Kahn, J.S. Miller, F. Palacio, Magnetic Molecular Materials, NATO ASI, Kluwer, Dordrecht, 1991.
[10] M.A.M. Abu-Youssef, M. Drillon, A. Escuer, M.A.S. Goher, F.A. Mautner, R. Vicente, Inorg. Chem. 39 (2000) 5022.
[11] J.-P. Costes, F. Dahan, B. Donnadieu, M.-J. Rodriguez Douton, A. Bousseksou, J.-P. Tuchagues, Inorg. Chem. 43 (2004) 2736.
[12] N. Matsumoto, Y. Sunatsuki, H. Miyasaka, Y. Hashimoto, D. Luneau, J.-P. Tuchagues, Angew. Chem., Int. Ed. Eng. 38 (1999) 171.
[13] K.R. Reddy, M.V. Rajasekharan, J.-P. Tuchagues, Inorg. Chem. 37 (1998) 5978.
[14] R. Sessoli, H.-L. Tsai, A.R. Schake, S. Wang, J.B. Vincent, K. Folting, D. Gatteschi, G. Christou, D.N. Hendrickson, J. Am. Chem. Soc. 115 (1993) 1804.
[15] R. Sessoli, D. Gatteschi, A. Caneschi, M. Novak, Nature 365 (1993) 141.
[16] C. Palopoli, B. Chansou, J.-P. Tuchagues, S. Signorella, Inorg. Chem. 39 (2000) 1458.
[17] H.L. Shyu, H.-H. We, Y. Wang, Inorg. Chim. Acta 290 (1990) 8, references therein.
[18] Y. Cringh, S.W. Gordon-Wylie, R.E. Norman, G.R. Clark, S.T. Weintraub, C.P. Horwitz, Inorg. Chem. 36 (1997) 1805.
[19] F.M. Ashmawy, C.A. McAuliffe, R.V. Parish, J. Tames, J. Chem. Soc., Dalton Trans. (1985) 1391.
[20] R. Ramraraj, A. Kira, M. Kaneko, Angew. Chem., Int. Ed. Engl. 25 (1986) 825.
[21] J. Limburg, J.S. Vrettos, L.M. Liable-Sands, A.L. Rheingold, R.H. Crabtree, G.W. Brudvig, Science 283 (1999) 1524.
[22] N. Auranzeb, C.E. Helme, C.A. McAuliffe, R.G. Pritchard, M. Watkinson, R. Bermejo, A. Sousa, J. Chem. Soc., Chem. Commun. (1994) 1153.
[23] K. Oyaizu, T. Nakagawa, E. Tsuchida, Inorg. Chim. Acta 305 (2000) 184.
[24] M. Maneiro, M.R. Bermejo, A. Sousa, M. Fondo, A.M. Gonzalez, A. Sousa-Pedrares, C.A. McAuliffe, Polyhedron 19 (2000) 47.
[25] R. Karmakar, C.R. Choudhury, G. Bravic, J.-P. Sutter, S. Mitra, Polyhedron 13 (2004) 949.
[26] E.M. Chudnovsky, Science 274 (1996) 938.
[27] G. Aromi, S.M.J. Aubin, M.A. Bolcar, G. Christou, H.J. Eppley, K. Folting, D.N. Hendrickson, J.C. Huffman, R.C. Squire, H.-L. Tsai, S. Wang, M.W. Wemple, Polyhedron 17 (1998) 3005.
[28] P.-R. Wei, Q. Li, W.-P. Leung, T.C.W. Mak, Polyhedron 16 (1997) 897.
[29] S.K. Dey, N. Mondal, M.S. El Fallah, R. Vicente, A. Escuer, X. Solans, M. Font-Bardia, T. Matsushita, V. Gramlich, S. Mitra, Inorg. Chem. 43 (2004) 2427.
[30] C.R. Choudhury, A. Datta, V. Gramlich, G.M. Golzar Hossain, K.M.A. Malik, S. Mitra, Inorg. Chem. Commun. 6 (2003) 790.
[31] A.W. Addison, T.N. Rao, J. Reedijik, J. van Rijn, C.G. Verscoor, J. Chem. Soc., Dalton Trans. (1984) 1349.
[32] H. Miyasaka, N. Matsumoto, N. Re, E. Gallo, E. Floriani, Inorg. Chem. 36 (1997) 670.
[33] C. Baffert, M.-N. Collomb, A. Deronzier, S. Kjaergaard-Knudsen, J.-M. Latour, K.H. Lund, C.J. McKenzie, M. Mortensen, L.P. Nielsen, N. Thorup, J. Chem. Soc., Dalton Trans. (2003) 1765.
[34] C.H.L. Kennard, G. Smith, E.J. O'Reilly, W. Chiangjin, Inorg. Chim. Acta 69 (1983) 53.
[35] K. Yamato, I. Miyahara, A. Ichimura, K. Hirotsu, Y. Kojima, H. Sakurai, D. Shiomi, K. Sato, T. Takui, Chem. Lett. (1999) 295.
[36] C.J. Milios, E. Kefalloniti, C.P. Raptopoulou, A. Terzis, A. Escuer, R. Vicente, S.P. Perlepes, Polyhedron 23 (2004) 83.
[37] H. Iikura, T. Nagata, Inorg. Chem. 37 (1998) 4702.
[38] E. Garribba, G. Micera, M. Zema, Inorg. Chim. Acta 357 (2004) 2038.
[39] C. Ma, C. Chen, Q. Liu, D. Liao, L. Li, Eur. J. Inorg. Chem. (2003) 1227.
[40] J. Kim, J.M. Lim, M.C. Suh, H. Yun, Polyhedron 20 (2001) 1947.
[41] A. Bianchi, L. Calabi, C. Giorgi, P. Losi, P. Mariani, D. Palano, P. Paoli, P. Rossi, B. Valtancoli, J. Chem. Soc., Dalton Trans. (2001) 917.
[42] T. Glowiak, H. Kozlowski, L.S. Erre, G. Micera, Inorg. Chim. Acta 236 (1995) 149.
[43] C. Policar, S. Durot, F. Lambert, M. Cesario, F. Ramiandrasoa, I. Morgenstern-Badarau, Eur. J. Inorg. Chem. (2001) 1807.
[44] C. Jiang, X. Zhu, Z.-P. Yu, Z.-Y. Wang, Inorg. Chem. Commun. 6 (2003) 706.
[45] F. Nepveu, M. Berkaoui, P. Castan, L. Walz, Z. Kristallogr. 209 (1994) 351.
[46] Z.J. Zhong, X.-Z. You, T.C.W. Mak, Polyhedron 13 (1994) 2157.
[47] N. Okabe, N. Oya, Acta Crystallogr., Sect. C: Cryst. Struct. Commun. 56 (2000) 1416.
[48] C.J. O'Connor, Prog. Inorg. Chem. 29 (1982) 203.
[49] E. Ruiz, P. Alemany, S. Alvarez, J. Cano, J. Am. Chem. Soc. 119 (1997) 1297, and references therein.
[50] D.P. Kessissoglou, W.M. Butler, V.L. Pecoraro, Inorg. Chem. 26 (1987) 495.
[51] E. Gallo, E. Solari, N. Re, C. Floriani, A. Chiesi-Villa, C. Rizzoli, J. Am. Chem. Soc. 119 (1997) 5144.
[52] D. Coucouvanis, K. Greiwe, A. Salifoglou, P. Challen, A. Simopoulos, A. Kostikas, Inorg. Chem. 27 (1988) 593.
[53] T.C. Higgs, K. Spartalian, C.J. O'Connor, B.F. Matzanke, C.J. Carrano, Inorg. Chem. 37 (1998) 2263.
[54] R.L. Dutta, A. Syamal, Elements of Magnetochemistry, S Chand & Company Ltd, New Delhi, India, 1982.

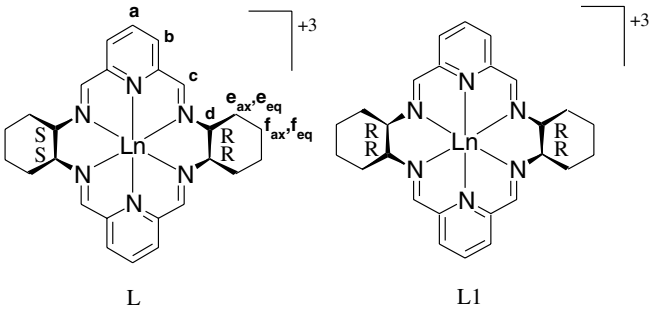

Scheme 1. The general structure and the labelling scheme of the Ln(III) complexes of the macrocycles L and L1.

complexes. In particular, it has been established that chirality of the tetraazamacrocycles strongly influences the properties of their complexes. The complexes of the *meso*-type tetraazamacrocycles differ from their chiral isomers not only in structure, but also in the reactivity and spectroscopic properties [8]. Typical examples of such tetraazameacrocyclic isomers are the *meso*- and chiral racemic *rac*-forms of 5,7,7,12,14,14-hexamethyl-1,4,8,11-tetraazacyclotetradeca-4,11-diene [8a,8c,8g]. In contrast, very few *meso*- and *rac*-isomers of the lanthanide(III) complexes with the larger hexaazamacrocycles are known [9], and their comparison is limited. In this report we present the synthesis and characterisation of a new series of lanthanide(III) complexes with the *meso*-hexaazamacrocycle L, and compare their structure, stability and paramagnetic NMR spectra with those of the analogous complexes of the isomeric chiral macrocycle L1.

2. Experimental

2.1. Synthesis

2,6-Diformylpyridine was obtained by oxidation of 2,6-pyridinedimethanol [10]. Macrocycle L was synthesised as described in Ref. [7]. All other reagents (Aldrich) were reagent grade and used as received.

2.1.1. Method A

A solution of 17 mmol of (+/−)-*trans*-1,2-diaminocyclohexane (1.941 g) in 5 mL of methanol was combined with a solution of 17 mmol of 2,6-diformylpyridine (2.297 g) in 165 mL of methanol and the mixture was refluxed for 48 h. The white precipitate of a mixture of 2 + 2 and 4 + 4 macrocycles was filtered off, washed with methanol and dried under vacuum. The combined product (3.523 g) was obtained in 97.2% yield. 256 mg of the above mixture (containing 0.45 mmol of L and 0.075 mmol of macrocycle 4 + 4, as determined by NMR integration of the sample) was suspended in 40 mL of dichloromethane and solution of the appropriate lanthanide nitrate hydrate (0.6 mmol) in 20 mL of methanol was added. The mixture was stirred for 1 h at room temperature. The dichloromethane was removed on rotary evaporator and the volume reduced to ca. 20 mL. The mixture was filtered to remove the unreacted 4 + 4 macrocycle and the volume of the filtrate was further reduced to 2–10 mL, depending on Ln(III) ion, until a new precipitate appeared. The mixture was placed in the freezer and the crystalline product obtained the next day was filtered, washed with small amount of cold methanol and dried under vacuum.

$LaL(NO_3)_3 \cdot 0.5H_2O$: Yield 67% (based on L). Required for: $C_{52}H_{62}N_{18}O_{19}La_2$ C, 41.06; H, 4.11; N, 16.58. Found: C, 41.13; H, 3.87; N, 16.76%. Electrospray MS (MeOH): *m/z* 690 $LaL(NO_3)_2^+$, 314 $LaL(NO_3)^{+2}$.

$CeL(NO_3)_3 \cdot 1.5H_2O$: Yield 80%. Required for: $C_{52}H_{66}N_{18}O_{21}Ce_2$ C, 40.05; H, 4.27; N, 16.17. Found: C, 39.73; H, 3.95; N, 16.06%. Electrospray MS (MeOH): *m/z* 691 $CeL(NO_3)_2^+$, 314 $CeL(NO_3)^{+2}$.

$PrL(NO_3)_3 \cdot 3H_2O$: Yield 55%. Required for: $C_{26}H_{36}N_9O_{12}Pr$ C, 38.67; H, 4.49; N, 15.61. Found: C, 38.29; H, 4.19; N, 15.32%. Electrospray MS (MeOH): *m/z* 692 $PrL(NO_3)_2^+$, 315 $PrL(NO_3)^{+2}$.

$NdL(NO_3)_3 \cdot 3H_2O$: Yield 75%. Required for: $C_{26}H_{36}N_9O_{12}Nd$ C, 38.51; H, 4.47; N, 15.55. Found: C, 38.33; H, 4.36; N, 15.26%. Electrospray MS (MeOH): *m/z* 694 $NdL(NO_3)_2^+$, 316 $NdL(NO_3)^{+2}$.

$SmL(NO_3)_3 \cdot 2H_2O$: Yield 82%. Required for: $C_{26}H_{34}N_9O_{11}Sm$ C, 39.09; H, 4.29; N, 15.78. Found: C, 39.10; H, 4.48; N, 15.62%. Electrospray MS (MeOH): *m/z* 704 $SmL(NO_3)_2^+$, 320 $SmL(NO_3)^{+2}$.

$EuL(NO_3)_3 \cdot 2H_2O$: Yield 51.24%. Required for: $C_{26}H_{34}N_9O_{11}Eu$ C, 39.01; H, 4.28; N, 15.75. Found: C, 39.23; H, 4.00; N, 15.39%. Electrospray MS (MeOH): *m/z* 703 $EuL(NO_3)_2^+$, 320 $EuL(NO_3)^{+2}$.

$GdL(NO_3)_3 \cdot 2H_2O$: Yield 60%. Required for: $C_{26}H_{34}N_9O_{11}Gd$ C, 38.75; H, 4.25; N, 15.64. Found: C, 39.01; H, 4.32; N, 15.40%. Electrospray MS (MeOH): *m/z* 708 $GdL(NO_3)_2^+$, 323 $GdL(NO_3)^{+2}$.

$TbL(NO_3)_3 \cdot 2H_2O$: Yield 72.35%. Required for: $C_{26}H_{34}N_9O_{11}Tb$ C, 38.67; H, 4.24; N, 15.61. Found C, 39.03; H, 4.33; N, 15.45%. Electrospray MS (MeOH): *m/z* 710 $TbL(NO_3)_2^+$, 324 $TbL(NO_3)^{+2}$.

$DyL(NO_3)_3 \cdot 3H_2O$: Yield 50%. Required for: $C_{26}H_{36}N_9O_{12}Dy$ C, 37.66; H, 4.38; N, 15.20. Found: C, 37.69; H, 4.27; N, 14.82%. Electrospray MS (MeOH): *m/z* 714 $DyL(NO_3)_2^+$, 326 $DyL(NO_3)^{+2}$.

$HoL(NO_3)_3 \cdot 2H_2O$: Yield 57%. Required for: $C_{26}H_{34}N_9O_{11}Ho$ C, 38.39; H, 4.21; N, 15.50. Found: C, 38.51; H, 4.07; N, 15.14%. Electrospray MS (MeOH): *m/z* 716 $HoL(NO_3)_2^+$, 326 $HoL(NO_3)^{+2}$.

$ErL(NO_3)_3 \cdot 2H_2O$: Yield 43%. Required for: $C_{26}H_{34}N_9O_{11}Er$ C, 38.28; H, 4.20; N, 15.45. Found: C, 38.54; H, 4.03; N, 15.20%. Electrospray MS (MeOH): *m/z* 717 $ErL(NO_3)_2^+$, 327 $ErL(NO_3)^{+2}$.

$TmL(NO_3)_3 \cdot 2H_2O$: Yield 37%. Required for: $C_{26}H_{34}N_9O_{11}Tm$ C, 38.20; H, 4.19; N, 15.42. Found: C, 38.54; H, 4.11; N, 15.21%. Electrospray MS (MeOH): *m/z* 719 $TmL(NO_3)_2^+$, 328 $TmL(NO_3)^{+2}$.

$YbL(NO_3)_3 \cdot 2.5H_2O$: Yield 31.86%. Required for: $C_{52}H_{70}N_{18}O_{23}Yb_2$ C, 37.60; H, 4.25; N, 15.18. Found: C,

37.87; H, 4.09; N, 14.91%. Electrospray MS (MeOH): *m/z* 724 $YbL(NO_3)_2^+$, 330 $YbL(NO_3)^{+2}$.

$LuL(NO_3)_3 \cdot 2.5H_2O$: Yield 41%. Required for: $C_{52}H_{70}N_{18}O_{23}Lu_2$ C, 37.51; H, 4.24; N, 15.14. Found: C, 37.73; H, 4.01; N, 14.89%. Electrospray MS (MeOH): *m/z* 725 $LuL(NO_3)_2^+$, 332 $LuL(NO_3)^{+2}$.

2.1.2. Method B

256 mg (0.6 mmol) of pure macrocyle L was suspended in 40 mL of dichloromethane and solution of the appropriate lanthanide nitrate hydrate (0.6 mmol) in 20 mL of methanol was added. The mixture was stirred for 1 h at room temperature to give a clear solution. The dichloromethane was removed on a rotary evaporator and the volume reduced (to ca. 10 mL for Eu(III) and Er(III), to ca. 2–3 mL for Yb(III)) until solid product started to appear. The mixture was placed in the freezer and the crystalline product obtained next day was filtered, washed with small amount of cold methanol and dried under vacuum. The properties of Eu(III), Er(III) and Yb(III) complexes obtained in this way were identical to those prepared according to method A.

2.2. Methods

The NMR spectra were taken on Bruker Avance 500 and AMX 300 spectrometers. The spectra were acquired using 200 ms to 2 s repetition times, depending on the kind of lanthanide ion studied. The chemical shifts were referenced to the residual solvent signal. The COSY and HMQC spectra were acquired using 256×1 K data points and zero filled to $1\text{ K} \times 1\text{ K}$ matrix. The isotropic shifts were calculated by using diamagnetic Lu(III) complexes as a reference. The resulting isotropic shifts were fit to Eq. (7) using a non-linear least squares fit of D_1 and D_2 parameters and the angle α determining the orientation of the principal axes of the magnetic susceptibility tensor within the symmetry plane of the complex. The calculations were accomplished by minimising the agreement factor: $R = [\sum(\delta_{obs}^{iso} - \delta_{dip}^{calc})^2 / \sum(\delta_{iso}^{obs})^2]^{0.5}$. The geometric factors for each proton were derived from the coordinates of the crystal structure of Sm(III) complex. The experimental isotropic shifts were treated as averaged shifts of pairs of protons such as a and a′, b and b′, etc. Electrospray mass spectra were obtained using Finnigan TSQ-700 instrument equipped with EST ion source. The elemental analyses were carried out on a Perkin–Elmer 2400 CHN elemental analyser.

2.3. X-ray data collection and structure determination

Crystals of both complexes were grown by slow evaporation of a methanol–chloroform solutions. The data were collected at 100 K using a KM4 CCD diffractometer and graphite-monochromated Mo Kα radiation generated from Diffraction X-ray tube operated at 50 kV and 35 mA. The images were indexed, integrated, and scaled using the Oxford Diffraction data reduction package [11]. The experimental details together with crystal data are given in Table 1. The structure was solved by the heavy atom method using SHELXS97 [12] and refined by the full-matrix least-squares method on all F^2 data [13]. The lattice parameters were calculated for refinement of positions of all measured reflections. The data were corrected for absorption [14].

Table 1
Crystal data and structures refinement for $[LaL(NO_3)_2(CH_3OH)](NO_3) \cdot (CH_3OH)$ and $[SmL(NO_3)_2(CH_3OH)](NO_3) \cdot (CH_3OH)$

Empirical formula	$C_{27}H_{33}N_8O_7La$, CH_4O, NO_3	$C_{27}H_{33}N_8O_7Sm$, CH_4O, NO_3
Formula weight	813.57	826.03
Temperature (K)	100(2)	100(2)
Wavelength (Å)	0.71073	0.71073
Crystal system	triclinic	triclinic
Space group	*P*-1	*P*-1
Unit cell dimensions		
a (Å)	8.788(2)	8.799(2)
b (Å)	13.422(3)	13.353(3)
c (Å)	14.916(3)	14.806(3)
α (°)	94.08(3)	93.93(3)
β (°)	105.08(3)	104.37(3)
γ (°)	101.05(3)	100.87(3)
V (Å^3)	1653.6(6)	1642.7(6)
Z	2	2
Density calculated (Mg m^{-3})	1.636	1.670
Absorption coefficient (mm^{-1})	1.364	1.860
T_{min}/T_{max}	0.678/0.896	0.789/0.876
F(000)	826	836
Crystal size (mm)	$0.10 \times 0.08 \times 0.06$	$0.06 \times 0.10 \times 0.10$
Diffractometer	Kuma KM4CCD	Kuma KM4CCD
θ Range for data collection (°)	3.11–28.45	3.09–28.46
Ranges of *h*, *k*, *l*	$-11 \leqslant h \leqslant 11$, $-17 \leqslant k \leqslant 17$, $-19 \leqslant l \leqslant 19$	$-11 \leqslant h \leqslant 11$, $-17 \leqslant k \leqslant 17$, $-19 \leqslant l \leqslant 18$
Reflections collected	19066	22979
Independent reflections (R_{int})	7616 (0.0338)	7693 (0.0451)
Data/parameters	7616/503	7693/452
Goodness-of-fit (F^2)	1.080	1.085
Final R_1/wR_2 indices [$I > 2\sigma(I)$]	0.0322/0.0597	0.0346/0.0654
Largest difference in peak/hole (e Å^{-3})	0.836/−0.797	0.857/−0.700

3. Results and discussion

3.1. Synthesis and stability of the complexes

The $[LnL](NO_3)_3 \cdot nH_2O$ complexes can be synthesized both from the pure macrocycle L [7] (method B) as well as from the mixture (method A) of L and another macrocycle that is a 4 + 4 condensation product. This mixture can be easily obtained in the condensation of racemic *trans*-1,2-diaminocyclohexane and 2,6-diformylpyridine [7]. In method A, the 4 + 4 macrocycle is separated from the methanol solution of the complex as poorly soluble product. This method is more practical, because it allows to omit the purification of L by fractional crystallisation. In both methods care should be taken to use relatively mild conditions and short reaction times, otherwise admixture

of lanthanide(III) complexes of L1 is obtained. In fact the L1 complexes were main product of the reaction, when the above mixture of macrocycles was refluxed for several days in methanol with the lanthanide(III) nitrates or chlorides (for this reason we were initially convinced that the above macrocyclic substrate L was a free form of chiral ligand L1). This observation indicates that the complexes of L1 are thermodynamically more stable. Presumably, they are formed as a result of hydrolytic cleavage of the Schiff base macrocycle L of RRSS configuration, and rearrangement of the diamine fragments into racemic *RRRR*/*SSSS* form of the more stable complexed macrocyle L1.

To further test this hypothesis, we have investigated the stability of pure $[LnL](NO_3)_3 \cdot nH_2O$ complexes in solution. The complexes are relatively stable in CD_3OD or $CD_3OD/CDCl_3$ 1:2 v/v solutions at room temperature. For instance the ^1H NMR spectrum of the Eu(III) complex obtained after 30 days indicates only traces of the EuL1 complex as well as of hydrolytic decomposition products such as dimeric μ-hydroxo complexes of L. The decomposition is somewhat more pronounced at elevated temperatures and in aqueous solutions. The hydrolytic decomposition is much faster for the complexes of L with heavier lanthanides, such as Yb(III), than for the complexes with lighter lanthanide(III) ions. The conversion of complexes of L into complexes of L1 is further accelerated by the presence of additional free lanthanide(III) nitrate. For instance almost complete transition of $[YbL](NO_3)_3$ into $[YbL1](NO_3)_3$ is observed when the $CD_3OD/CDCl_3$ 1:2 v/v solution of the former complex is heated at 50 °C in the presence of 2 equiv. of Yb(III) nitrate for 9 days (Supplementary Fig. 1). This experiment corresponds to reaction conditions under which impure products are obtained. The effect of excess of Ln(III) ion and elevated temperature is in accord with the hydrolytic mechanism of the rearrangement of L into L1. The formation of imine bond (accompanied by release of water molecule) is partially reversible and is catalysed by acids. For this reason, the reverse reaction is faster in the acidic conditions resulting form the hydrolysis of the free Ln(III) salt, in the presence of additional amount of water introduced with the lanthanide salts, or possibly is catalysed by the free Ln(III) ion itself. The transformation of $[LnL]^{3+}$ complexes into $[LnL1]^{3+}$ complexes is consistent with the fact that complexes of L are not formed in a template synthesis. In this synthesis only the complexes of L1 are obtained from the racemic form to the diamine. This preference for the chiral form of the hexaazamacrocycle is not observed in the case of derivatives of substituted ethylenediamines. In this case, mixtures of *meso* and chiral *rac* hexaazamacrocycles were obtained in reactions of racemic diamine templated by Ln(III), Ca(II) and Sr(II) ions [9].

The identity of the complexes has been confirmed by elemental analyses and mass spectra. The ESI-MS+ of methanol solutions of the $[LnL](NO_3)_3 \cdot nH_2O$ complexes show peaks at m/e corresponding to ions $[LnL](NO_3)^{+2}$ and $[LnL](NO_3)_2{}^{+}$. The presence of these species indicates axial coordination of nitrate anions rather than clusterisation of ions under the conditions of ESI-MS measurements. The binding of anions is also evident from titration of the $[LnL](NO_3)_3 \cdot nH_2O$ complex with sodium acetate monitored by NMR spectroscopy (vide infra).

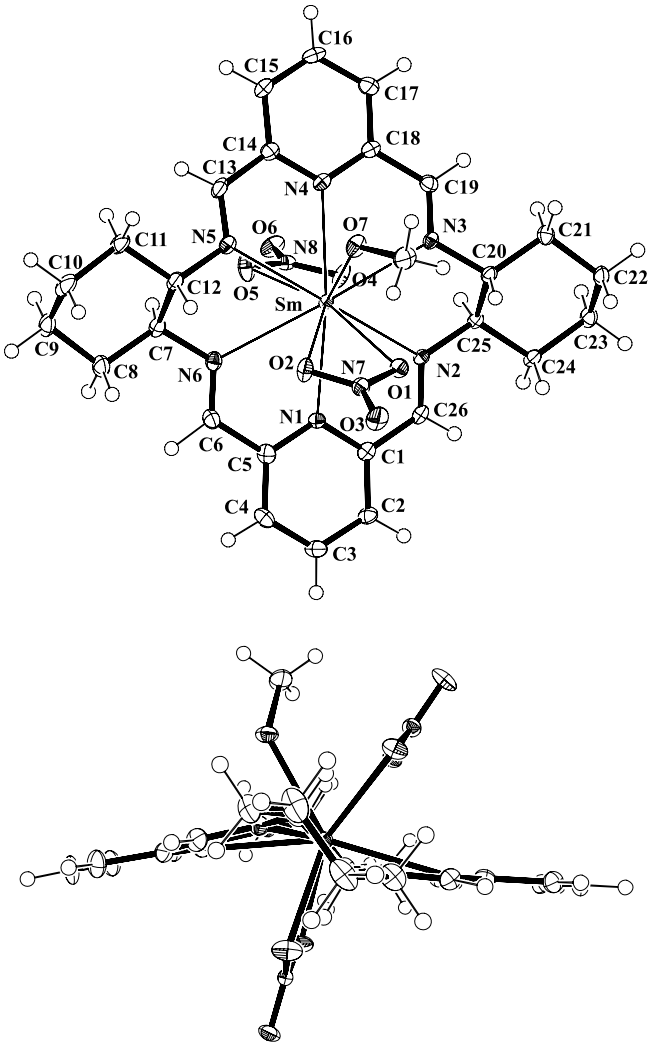

Fig. 1. Front and side view of the complex cation $[SmL(NO_3)_2(CH_3OH)]^+$.

4. Crystal structure of $[SmL(NO_3)_2(CH_3OH)](NO_3) \cdot CH_3OH$ and $[LaL(NO_3)_2(CH_3OH)](NO_3) \cdot CH_3OH$ complexes

Crystals of $[SmL(NO_3)_2(CH_3OH)](NO_3) \cdot CH_3OH$ and the isomorphic $[LaL(NO_3)_2(CH_3OH)](NO_3) \cdot CH_3OH$ complexes have been obtained by slow evaporation of the $[LnL](NO_3)_3 \cdot nH_2O$ solutions in chloroform/methanol mixture. The asymmetric unit of the samarium(III) complex is composed of the complex cation $[SmL(NO_3)_2(CH_3OH)]^+$, nitrate anion and additional methanol molecule. The samarium(III) ion is coordinated in the centre of the macrocycle by six nitrogen atoms of the ligand L (Fig. 1, Table 2). The coordination sphere of Sm(III) is

completed by axial ligands: on one side of the macrocycle by bidentate nitrate anion and on the other side by bidentate nitrate anion and methanol molecule. The coordination sphere of the Sm(III) ion defines irregular polyhedron. The $[SmL(NO_3)_2(CH_3OH)](NO_3)CH_3OH$ complex represents a rare example of the 11-coordinate samarium(III) ion, which prefers smaller coordination numbers. On the other hand, this coordination number is not unusual for the larger La(III) ion and was previously observed for the La(III) complexes with hexaazamacrocycles [2]. The fact that the La(III) and Sm(III) complexes are isostructural is not expected for the hexaazamacrocyclic complexes. For this class of compounds the larger La(III) ion typically has higher coordination number than the ions belonging to the middle of the series of lanthanide(III) ions [2]. The structure of the Sm(III) and La(III) $[LnL](NO_3)_3 \cdot nH_2O$ complexes is different to that of the $[LnL1](NO_3)_3 \cdot nH_2O$ complexes [3d]. The latter complexes are 10-coordinate and have two bidentate axial nitrate anions bound in axial position. The most striking difference is that the Sm(III) complex of L is 11-coordinate, while the L1 complex of the larger Nd(III) ion is 10-coordinate. This difference results from different steric requirements of the two isomeric macrocycles and reflects the influence of the structure of the macrocyclic equatorial ligand on the axial ligation.

The macrocycle L in its La(III) and Sm(III) complexes adopts flatter conformation in comparison with the free form [7], but it preserves some features of the stepped conformation (Fig. 1). In the free form the two pyridine rings are placed on two parallel planes separated by 5.37 Å, while in the complexed form these two rings are inclined at 13.38° for Sm(III) and 13.70° for La(III) complexes, respectively and are closer to being positioned in one plane. This angle between the pyridine rings describes also the overall bending of the macrocycle.

Table 2
Bond lengths (Å) and bond angles (°) for $[LaL(NO_3)_2(CH_3OH)](NO_3) \cdot (CH_3OH)$ and $[SmL(NO_3)_2(CH_3OH)](NO_3) \cdot CH_3OH$

Bond lengths			
La–N(1)	2.710(2)	Sm–N(1)	2.691(3)
La–N(2)	2.772(2)	Sm–N(2)	2.754(3)
La–N(3)	2.709(2)	Sm–N(3)	2.673(3)
La–N(4)	2.671(2)	Sm–N(4)	2.613(3)
La–N(5)	2.709(2)	Sm–N(5)	2.653(3)
La–N(6)	2.769(2)	Sm–N(6)	2.760(3)
La–O(1)	2.629(2)	Sm–O(1)	2.524(2)
La–O(2)	2.666(2)	Sm–O(2)	2.588(2)
La–O(4)	2.641(2)	Sm–O(4)	2.545(2)
La–O(5)	2.699(2)	Sm–O(5)	2.643(2)
La–O(7)	2.609(2)	Sm–O(7)	2.532(2)
Bond angles			
N(1)–La–N(2)	59.58(7)	N(1)–Sm–N(2)	60.06(8)
N(1)–La–N(6)	59.92(7)	N(1)–Sm–N(6)	59.51(8)
N(3)–La–N(2)	59.83(7)	N(3)–Sm–N(2)	59.56(8)
N(4)–La–N(3)	61.07(7)	N(4)–Sm–N(3)	61.43(8)
N(4)–La–N(5)	60.91(7)	N(4)–Sm–N(5)	61.95(8)
N(5)–La–N(6)	59.76(7)	N(5)–Sm–N(6)	59.81(8)
O(1)–La–O(2)	48.27(6)	O(1)–Sm–O(2)	50.24(7)
O(1)–La–O(7)	70.92(6)	O(1)–Sm–O(7)	70.49(7)
O(4)–La–O(5)	47.55(6)	O(4)–Sm–O(5)	48.90(7)
O(7)–La–O(2)	68.91(7)	O(7)–Sm–O(2)	69.28(8)

The hexaazamacrocycles adopt their conformation to the size and coordination requirements of the coordinated lanthanide(III) ions [2]. This is achieved by combination of various degree of bending and helical twisting of the macrocycle. In the case of nitrate derivatives of the lanthanide(III) complexes with the isomeric chiral macrocycle L1, practically no bending is observed and the helical twist determines the macrocycle conformation. It should be noted that helical twist of the hexaazamacrocyle is usually observed also for the achiral macrocycles, e.g., for the derivatives of ethylenediamine and 2,6-diacetylpyridine [2]. In this way chiral complexes are formed from macrocycles devoid of stereogenic centres. In the case of L, however, the *RR* and *SS* configuration of the two diaminocyclohexane rings imposes C_s symmetry of the macrocycle. For this reason, the $[LnL](NO_3)_3 \cdot nH_2O$ complexes exhibit no helical twist. This is manifested, e.g., by the angle formed between the two vectors defined by the opposite pairs of diamine nitrogen atoms N2N3 and N5N6 which is close to zero (0.68°). This twist is even better reflected by the improper torsion angle C2C4C15C17 equal to 1.87°. For 13 out of 86 structures [15] of related complexes of lanthanide and transition metal ions with hexaaza and hexaoxaaza macrocyles containing two pyridine rings, this angle was close to zero (less than 3°). The majority of these complexes exhibit various degrees of helical twist; for the remaining 73 structures this angle varies from 5° to 88.66° including values of 22.73° and 27.83° for the Nd(III) and Tm(III) complexes of macrocyle L1. The helical twist can be also measured by the torsional angle determined by two C–N bonds of the opposite pyridine fragments. In the present case this angle is nonzero (6.8°), this value results from the stepped conformation and not from helical twist.

4.1. ^1H NMR spectroscopy

The investigated compounds give rise to eight signals of intensity 1:2:2:2:2:2:2:2 in their ^1H NMR spectra (Table 3), and seven signals in ^{13}C NMR spectra. The number of resonances corresponds to effective C_{2h} symmetry of the $[LnL](NO_3)_3 \cdot nH_2O$ complexes. This symmetry results from fast on the NMR time scale, dynamic exchange of axial ligands on the two sides of the macrocycle, accompanied by conformational averaging of the C_s-symmetric structure of the macrocycle L observed for the solid state. For this latter symmetry 16 ^1H NMR signals should be observed. Similar dynamic averaging of the axial ligation of macrocyclic lanthanide complexes was observed previously [3c,16]. The exchange process is slowed down at 183 K as indicated by doubling of some resonances and observation of more complicated spectra. Unfortunately, line broadening did not allow for detailed analysis of the spectra recorded at low temperatures.

Table 3
^{1}H NMR chemical shifts of the $[LnL(NO_3)_3]\cdot nH_2O$ complexes ($CD_3OD/CDCl_3$ 1:2 v/v solution, 298 K)

	a	b	c	d	e_{eq}	e_{ax}	f_{eq}	f_{ax}
$[LaL(NO_3)_3]\cdot 0.5H_2O$	8.29	7.96	8.63	3.78	2.42	1.7	2.06	1.46
$[CeL(NO_3)_3]\cdot 1.5H_2O$	9.54	9.57	15.66	9.79	4.98	5.14	3.65	3.27
$[PrL(NO_3)_3]\cdot 3H_2O$	9.89	10.82	24.01	14.61	6.70	7.47	4.92	4.50
$[NdL(NO_3)_3]\cdot 3H_2O$	8.81	9.63	24.72	14.12	5.79	6.15	4.75	4.18
$[SmL(NO_3)_3]\cdot 2H_2O$	8.36	8.08	8.16	4.89	3.03	2.49	2.27	1.86
$[EuL(NO_3)_3]\cdot 2H_2O$	6.96	4.66	−18.38	−5.80	−0.05	−1.65	−0.82	−0.69
$[TbL(NO_3)_3]\cdot 2H_2O$	17.37	20.44	−14.05	14.77	20.44	18.26	5.72	7.70
$[DyL(NO_3)_3]\cdot 3H_2O$	18.80	22.45	−5.44	1.43	15.70	12.73	3. 66	3.90
$[HoL(NO_3)_3]\cdot 2H_2O$	9.45	13.36	12.18	46.25	25.69	27.67	11.93	14.76
$[ErL(NO_3)_3]\cdot 2H_2O$	−0.75	1.48	16.68	74.69	27.65	33.12	16. 04	20.65
$[TmL(NO_3)_3]\cdot 2H_2O$	−2.08	−7.15	−22.99	5.36	−5.57	−3.36	0.24	0.57
$[YbL(NO_3)_3]\cdot 2.5H_2O$	6.06	4.76	4.00	1.57	0.01	−0.24	1.57	1.07
$[LuL(NO_3)_3]\cdot 2.5H_2O$	8.32	7.97	8.67	3.63	2.31	1.69	2.04	1.51

The spectra of $CD_3OD/CDCl_3$ 1:2 v/v solutions of the paramagnetic Ce(III), Pr(III), Nd(III), Eu(III) and Yb(III) $[LnL](NO_3)_3\cdot nH_2O$ complexes were assigned on the basis of COSY and HMQC experiments (Fig. 2, Supplementary Fig. 2). In the remaining cases the signals were assigned on the basis of the linewidth dependence on the reverse sixth power of the proton–Ln(III) distance [17]. Analysis of crystal structures of $[LnL](NO_3)_3\cdot nH_2O$ complexes enables calculation of the relative ratios of linewidths, increasing in the order $\mathbf{f}_{eq}$, **a**, $\mathbf{f}_{ax}$, **b**, $\mathbf{e}_{eq}$, $\mathbf{e}_{ax}$, **c**, **d** (see Scheme 1 for the labelling).

The chemical shifts of the various paramagnetic $[LnL](NO_3)_3\cdot nH_2O$ complexes span a wide range of values (Table 3), reflecting differences in magnetic properties of these ions. There is an interesting comparison between

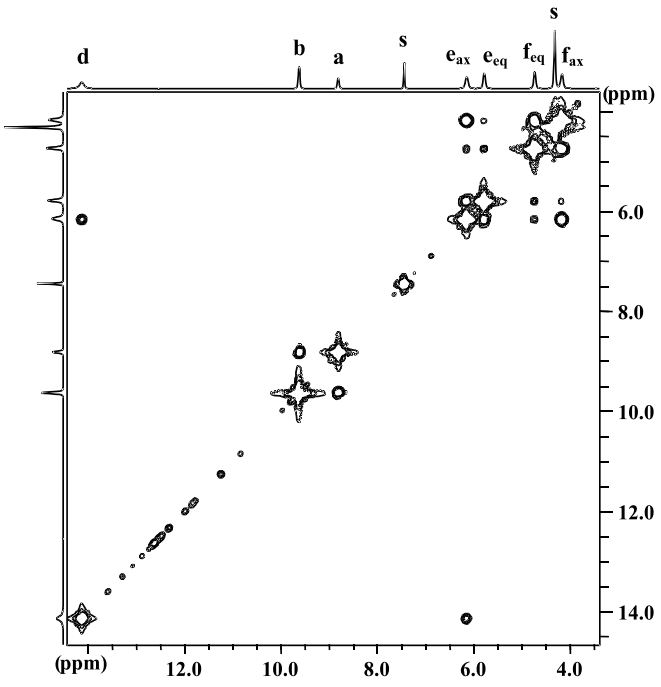

Fig. 2. The COSY spectrum ($CD_3OD/CDCl_3$ 1:2 v/v solution, 298 K) of $[NdL(NO_3)_3]\cdot 3H_2O$ complex.

the spectra of $[LnL](NO_3)_3\cdot nH_2O$ and the isomeric $[LnL1](NO_3)_3\cdot nH_2O$ complexes measured in the same solvent (Fig. 3). In the case of diamagnetic La(III) and Lu(III) derivatives the spectra are almost identical. This is a consequence of the fact that L and L1 are isomers and despite the difference in configuration of chiral carbon atoms the chemical nature of the two compounds is similar. In the case of Eu(III) derivatives (Fig. 3), as well as in the case of Ce(III), Pr(III), Nd(III), and Sm(III)), the overall spectral patterns of the two types of complexes bear some similarity, but the differences in the shift values are clear. Yet in the case of Tb(III), Dy(III), Ho(III), Er(III), Tm(III) and Yb(III) derivatives completely different spectral patterns are observed for the complexes of L and the corresponding complexes of L1 (Fig. 3, Supplementary Fig. 1).

In paramagnetic metal complexes the observed nucleus experiences additional shift, called the isotropic shift, δ_{iso}, that arises from the interaction of the nuclear and electronic spins [17]. In the case of lanthanide complexes this paramagnetic shift is often called lanthanide induced shift (LIS). The isotropic shift can be separated into through-space dipolar contribution (called also pseudocontact) δ_{dip} and through-bonds contact contribution δ_{con}:

$$\delta_{iso} = \delta_{dip} + \delta_{con}. \quad (1)$$

In the case of lanthanide complexes [18] the dipolar contribution is given by:

$$\delta_{dip} = C_j G, \quad (2)$$

where constant C_j depends on the Ln(III) ion, while G contains the information about crystal field parameters of the complex and geometric factors G' determined by position in space of given nucleus.

The contact shift is given by the formula [19,20]:

$$\delta_{con} = A\langle S_z\rangle/\gamma\hbar B_0 = A'\langle S_z\rangle, \quad (3)$$

where A is the hyperfine coupling constant, and $\langle S_z\rangle$ is the spin expectation value.

An estimation of the contact and dipolar contributions to the paramagnetic shift can be made on the basis of the Reilley method [21], which combines the Eqs. (1)–(3) into:

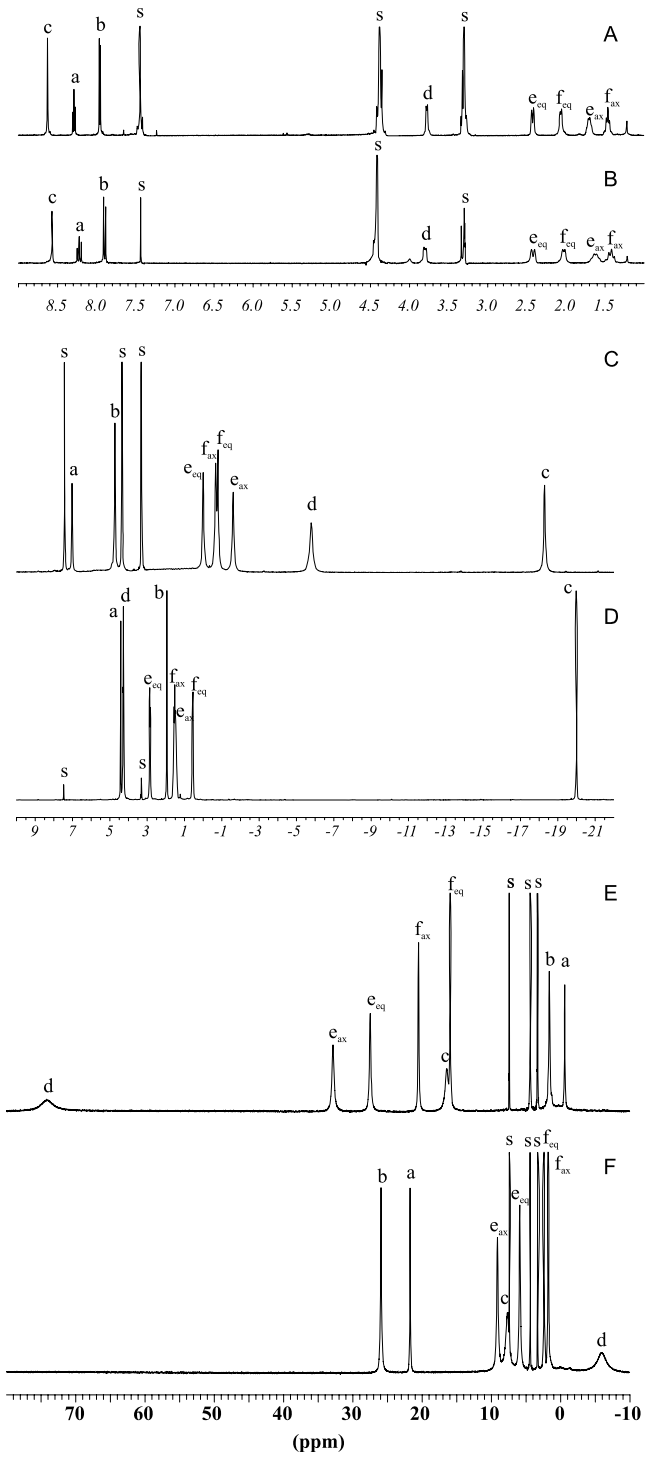

Fig. 3. The comparison of the ^{1}H NMR spectra ($CD_3OD/CDCl_3$ 1:2 v/v solution, 298 K) of complexes of L and L1: (A) $[LaL(NO_3)_3]\cdot 0.5H_2O$; (B) $[LaL1(NO_3)_3]$; (C) $[EuL(NO_3)_3]\cdot 2H_2O$; (D) $[EuL1(NO_3)_3]$; (E) $[ErL(NO_3)_3]\cdot 2H_2O$; (F) $[ErL1(NO_3)_3]$.

$$\delta_{ij}/C_j = G_i + A'_i\langle S_z\rangle_j/C_j, \quad (4)$$

$$\delta_{ij}/\langle S_z\rangle_j = A'_i + G_iC_j/\langle S_z\rangle_j, \quad (5)$$

where index i denotes given nucleus and index j refers to series of lanthanide ions. In the idealised situation of the exactly isostructural series of Ln(III) complexes, the crystal field parameters, geometrical factors and hyperfine coupling constants are equal in each complex and hence are the constants G and A'. Since the values of $\langle S_z\rangle$ and C_j are known [18–20], the linear fit of the Eq. (5) or Eq. (6), written for a set of Ln(III) complexes, gives the constants G and A' for each position. The crystal-field dependent method described above was refined into so called crystal-field independent approach based on analysis of shifts of two given protons along the lanthanide series [22–24]. In this method the crystal field parameters are factored out, and the ratios of geometric factors, $R_{ik} = G'_i/G'_k = G_i/G_k$, of nuclei i and k, are obtained in the linear fit of the equation:

$$\delta_{ij}/\langle S_z\rangle_j = (A'_i - R_{ik}A'_k) + R_{ik}\delta_{kj}/\langle S_z\rangle_j. \quad (6)$$

For series of isostructural Ln(III) complexes plots according to dependence (6) should be linear even when crystal field parameters are not constant along the series.

In order to check the isostructurality of the series of lanthanide(III) complexes of L in solution, the isotropic shifts were fit to Eqs. (4) and (5). As often observed, the plots according to Eq. (5) give better correlation in comparison with those based on Eq. (4). The plots based on Eq. (5) show three branches corresponding to series Ce(III)–Eu(III), Tb(III)–Ho(III) and Tm(III)–Yb(III) (Fig. 4). The points for Tb(III) (and to a lesser degree for Dy(III)) lie on the intersection of the first two branches, so alternatively they can be included in the second branch. In the case of plots corresponding to position **a** and **b** the first two branches are very close, giving the false impression of a correlation along the Ce(III)–Ho(III) series (Fig. 4). Each observed branch corresponds to a series of isostructural complexes. The presence of the first branch is in full agreement with the X-ray crystal data indicating that the La(III) and Sm(III) complexes are isomorphous.

The ''breaks'' observed in the middle of lanthanide ion series are often observed [17,22–24], and are ascribed to the abrupt change of the geometry of the complexes related to the gradual decrease of the ion radius. This change usually corresponds to the variation of coordination number. In the present case, the ''breaks'' reflect at least two changes of axial ligation along the series of lanthanide(III) complexes of the macrocycle L. The lighter lanthanides Ce–Eu form 11-coordinate complexes described above. The next series of Tb–Ho complexes are likely to lose coordinated solvent molecule and form 10-coordinate complexes with two bidentate nitrate anions on the two sides of the macrocyle. The coordination number is further decreased for the Tm(III) and Yb(III) complexes, e.g., as a result of coordination of monodentate nitrate anion or replacement of bidentate nitrate anion by solvent molecule. The correlation concerning two experimental points (Tm(III) and Yb(III)) is not meaningful, so these two complexes may further vary in geometry.

The data for Sm(III) complexes were not taken into account in the analysis, since the isotropic shifts as well as $\langle S_z\rangle$ value of Sm(III) exhibit the largest relative errors,

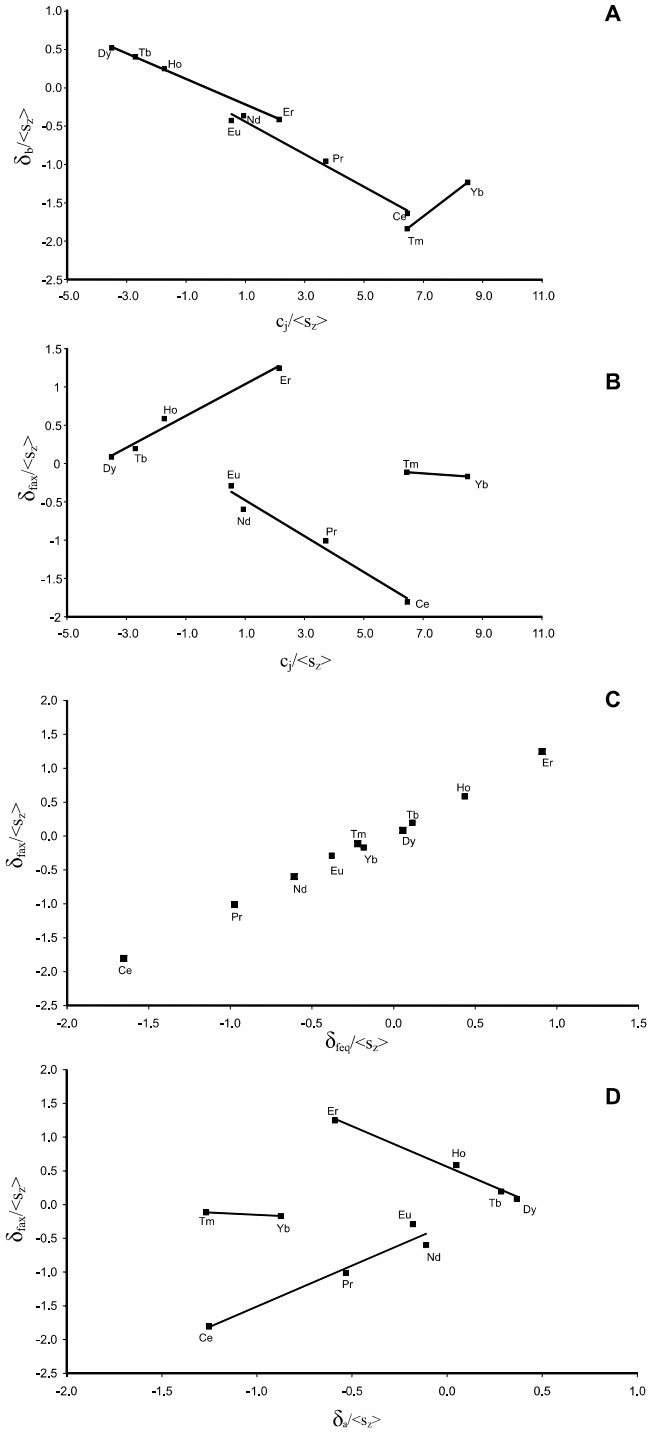

Fig. 4. Plots of $\delta_{ij}/\langle S_z\rangle_j$ vs. $C_j/\langle S_z\rangle_j$ for protons **b** (plot **A**) and $\mathbf{f}_{ax}$ (plot **B**) in the $[LnL](NO_3)_3 \cdot nH_2O$ complexes ($CD_3OD/CDCl_3$ 1:2 v/v solution, 298 K). Plots of $\delta_{ij}/\langle S_z\rangle_j$ vs. $\delta_{kj}/\langle S_z\rangle_j$ for the pairs of protons $i = \mathbf{f}_{ax}$, $k = \mathbf{f}_{eq}$ (plot **C**) and $i = \mathbf{f}_{ax}$, $k = \mathbf{a}$ (plot **D**) in the $[LnL](NO_3)_3 \cdot nH_2O$ complexes ($CD_3OD/CDCl_3$ 1:2 v/v solution, 298 K).

and as often observed [17], the data for Sm(III) complexes exhibit larger deviations in the plots. The data for Gd(III) complexes were also not analysed, because the severe broadening of the lines precluded observation and assignment of NMR signals.

The calculated values of G and A' (Table 4) allow in turn calculation of the dipolar and contact contributions to the isotropic shifts on the basis of Eqs. (2) and (3), respectively. The contact contribution dominates the paramagnetic shifts of the $[EuL](NO_3)_3 \cdot 2H_2O$ complex, in particular, the large contact shift −23.43 ppm of the azomethine proton is similar to the corresponding shift of $[EuL1](NO_3)_3$ complex [3a]. The G values are very different for the series of complexes of L and L1 of the heavier lanthanide ions, reflecting the very different dipolar contributions.

The results discussed above were verified using a crystal-field independent method [22–24]. When the shifts of pairs of remote protons, e.g., the pair of protons **a** and $\mathbf{f}_{ax}$ are analysed on the basis of the Eq. (6) (Fig. 4) similar breaks are obtained in the plots to those observed for plots based on Eq. (5). Thus the crystal-field independent method confirms the presence of structural changes. On the other hand, for the pairs of neighbouring protons, such as the pair of signals $\mathbf{f}_{ax}$ and $\mathbf{f}_{eq}$ (Fig. 4), linear plots following the Eq. (6) are obtained for the whole series of paramagnetic lanthanide ions. These correlations reflect parallel changes of geometric factors for the pairs of close nuclei [3a], rather than the presence of one series of isostructural complexes.

The shifts of $[YbL(NO_3)_3]_2 \cdot 2.5H_2O$ complex are expected to be dominated by dipolar contribution. The dipolar shift [17] is given by the Eq. (7):

$$\delta_{dip} = D_1 G_1 + D_2 G_2 = \frac{(\bar{\chi} - \chi_{zz})}{2N}\left\langle \frac{1 - 3\cos^2\theta}{r^3} \right\rangle + \frac{(\chi_{xx} - \chi_{yy})}{2N}\left\langle \frac{\sin^2\theta\cos 2\varphi}{r^3} \right\rangle, \quad (7)$$

where χ_{xx}, χ_{yy} and χ_{zz} are the principal components of magnetic susceptibility tensor and r, θ and φ are polar coordinates of the given nucleus. The ^{1}H NMR spectrum of this complex is rather unusual, because all the signals are in practically diamagnetic region −0.24 to 6.06 ppm. For other macrocyclic Yb(III) complexes a wide range of sizable paramagnetic shifts is observed [3a,3b, 3e,25,26], e.g., for the $[YbL1](NO_3)_3$ complex of ligand L1 the signals span the 0.55–25.84 ppm range. The small range of paramagnetic shifts of $[YbL](NO_3)_3 \cdot 2.5H_2O$ indicate small magnetic anisotropy of Yb(III) ion in this complex. The values of magnetic anisotropy parameters D_1 and D_2 have been varied in the computer simulation of Eq. (7) to obtain the best agreement between the calculated dipolar shifts and the experimental isotropic shifts. The values obtained for D_1 and D_2 were −500 and 260 ppm × Å^3, respectively, indeed much smaller than the values obtained for the related $[YbL1(NO_3)_3]_2$ complex. A satisfactory agreement factor ($R = 0.097$) was obtained in the calculation. The magnetic z axis is rotated by $\alpha = 19°$ from the direction perpendicular to the macrocycle plane. Similar values ($D_1 = -540$ ppm Å^3, $D_2 = 190$ ppm Å^3, $\alpha = 15°$ and $R = 0.084$) were obtained in a simplified calculations taking into account only one quarter of the macrocycle.

Table 4
Calculated A' and G values, as well as correlation coefficients R, for the $[LnL](NO_3)_3$ complexes

	a	b	c	d	e_{ax}	e_{eq}	f_{ax}	f_{eq}
Ce–Eu								
A'	0.02144	−0.23769	−3.09548	−1.13449	−0.31532	−0.2266	−0.2438	−0.3224
G	−0.18516	−0.21149	−0.61426	−0.78062	−0.48703	−0.3785	−0.2344	−0.1993
R	−0.97721	−0.99184	−0.99557	−0.98417	−0.99052	−0.9881	−0.9855	−0.9881
Tb–Er								
A'	−0.22167	−0.06107	0.15477	2.9081	1.45288	1.23333	0.82611	0.60177
G	−0.17272	−0.16595	0.19913	0.84075	0.29667	0.21036	0.20716	0.15367
R	−0.99778	−0.99962	0.87265	0.98991	0.98161	0.97813	0.98801	0.98292

On the other hand the range of paramagnetic shifts is larger for the acetate (−23.73 to 28.06 ppm) and mixed acetate/nitrate (−10.40 to 23.84 ppm) Yb(III) complexes of L. These complexes were generated in solution during titration of the $[YbL](NO_3)_3 \cdot 2.5H_2O$ complex with sodium acetate monitored by NMR spectroscopy. Analogous complexes were observed during titration of Eu(III) derivative (Supplementary Fig. 3). Addition of 1 equiv. of acetate results in formation of a mixture containing $[LnL](AcO)(NO_3)^+$ species. The addition of two or more equivalents of acetate leads to complete formation of $[LnL](AcO)_2^+$derivatives. The formation of these complexes is easily observed, since, as previously noticed [3b,25,26], the NMR spectra of macrocyclic complexes of paramagnetic Ln(III) ions strongly depend on axial ligation. The formation of mixed acetate/nitrate species is not accompanied by doubling of the number of lines observed for analogous complexes of L1 [3b]. This difference reflects faster exchange of axial ligands for the complexes of L, resulting in higher effective symmetry, as discussed above.

5. Conclusions

The crystal structures of La(III) and Sm(III) complexes of the macrocycle L show 11-coordinate metal ion bound in the centre of the macrocycle. The NMR results confirm that the complexes of L with the lighter lanthanide(III) ions are isostructural, but the complexes with heavier lanthanides differ in axial ligation. The comparison of complexes of the *meso*-macrocycle L with the complexes of the chiral isomeric macrocycle L1 shows the effect of the configuration of the stereogenic carbon atoms on the properties of lanthanide(III) complexes. The main differences are:

1. The complexes of the macrocycle L are thermodynamically less stable.
2. The steric requirements of L are related to higher coordination number of the bound Ln(III) ion.
3. The macrocycle L adopts bent conformation in its Ln(III) complexes, while L1 adopts helically twisted conformation.
4. The chemical shifts of the complexes of L and L1 with the same paramagnetic Ln(III) are drastically different as a result of completely different dipolar contribution to the paramagnetic shift.

Acknowledgement

This work was supported by MNiI Grant 1 T09A 143 30.

Appendix A. Supplementary data

Supplementary Figures 1–3 are available on request. Supplementary data for structure of La(III) and Sm(III) complexes are available from the Cambridge Crystallographic Data Centre, 12 Union Road, Cambridge, CB2 1EZ, UK (fax: +44 1223 366 033, e-mail: deposit@ccdc.ac.uk or on the web www: http://www.ccdc.cam.ac.uk) on request, quoting the deposition numbers CCDC 290780 and CCDC 290781, respectively. Supplementary data associated with this article can be found, in the online version, at doi:10.1016/j.poly.2006.04.001.

References

[1] (a) H.C. Aspinall, Chem. Rev. 102 (2002) 1807;
(b) D. Parker, R.S. Dickins, H. Puschmann, C. Crossland, J.A.K. Howard, Chem. Rev. 102 (2002) 1977;
(c) V. Jacques, J.F. Desreux, Top. Curr. Chem. 221 (2002) 123;
(d) M. Komiyama, N. Takeda, H. Shigekawa, Chem. Commun. (1999) 1443.
[2] (a) W. Radecka-Paryzek, V. Patroniak, J. Lisowski, Coord. Chem. Rev. 249 (2005) 2156;
(b) P.A. Vigato, S. Tamburini, Coord. Chem. Rev. 248 (2004) 1717;
(c) V. Alexander, Chem. Rev. 95 (1995) 273.
[3] (a) J. Lisowki, J. Gregoliński, M. Świtalska, K. Wiglusz, Inorg. Chim. Acta 358 (2005) 3015;
(b) J. Lisowski, S. Ripoli, L. Di Bari, Inorg. Chem. 43 (2004) 1388;
(c) J. Lisowski, J. Mazurek, Polyhedron 21 (2002) 811;
(d) J. Lisowski, P. Starynowicz, Polyhedron 19 (2000) 465;
(e) J. Lisowski, Magn. Reson. Chem. 37 (1999) 287;
(f) T. Tsubomura, K. Yasaku, T. Sato, M. Morita, Inorg. Chem. 31 (1992) 447.
[4] (a) P.M. Fitzsimmons, S.C. Jackels, Inorg. Chim. Acta 246 (1996) 301;
(b) S.W.A. Bligh, N. Choi, E.G. Evagorou, W.-S. Li, M. McPartlin, Chem. Commun. (1994) 2399.
[5] (a) S.W.A. Bligh, N. Choi, E.G. Evagorou, M. McPartlin, K.N. White, Dalton Trans. (2001) 3169;
(b) S.W.A. Bligh, N. Choi, W.J. Cummins, E.G. Evagorou, J.D. Kelly, M. McPartlin, Dalton Trans. (1994) 3369;
(c) J. Lisowski, P. Starynowicz, Inorg. Chem. Commun. 6 (2003) 593.
[6] (a) A. Gonzalez-Alvarez, I. Alfonso, F. Lopez-Oritz, A. Aguirre, S. Garcia-Granda, V. Gotor, Eur. J. Org. Chem. (2004) 1117;

(b) N. Kuhnert, G.M. Rossignolo, A. Lopez-Periago, Org. Biomol. Chem. 1 (2003) 1157.
[7] J. Gregoliński, J. Lisowski, T. Lis, Org. Biomol. Chem. 3 (2005) 3161.
[8] (a) For some recent examples see: C. Creutz, M.H. Chou, E. Fujita, D.J. Szalda, Coord. Chem. Rev. 249 (2005) 375;
(b) X. Liang, P.J. Sadler, Chem. Soc. Rev. 33 (2004) 246;
(c) E. Madej, O. Monsted, P. Kita, J. Chem. Soc., Dalton Trans. (2002) 2361;
(d) R.I. Haines, D.R. Hutchings, T.M. McCormack, J. Inorg. Biochem. 85 (2001) 1;
(e) N.F. Curtis, Inorg. Chim. Acta 317 (2001) 27;
(f) J.M. Slocik, M.S. Ward, R.E. Shepherd, Inorg. Chim. Acta 317 (2001) 290;
(g) D.A. House, J. Browning, J.R. Pipal, W.T. Robinson, Inorg. Chim. Acta 292 (1999) 73.
[9] (a) F. Benetollo, G. Bombieri, A.M. Adeyga, K.K. Fonda, W.A. Gootee, K.M. Samaria, L.M. Vallarino, Polyhedron 21 (2002) 425;
(b) F. Benetollo, G. Bombieri, W.A. Gootee, K.K. Fonda, K.M. Samaria, L.M. Vallarino, Polyhedron 17 (1998) 3633;
(c) F. Benetollo, G. Bombieri, K.M. Samaria, L.M. Vallarino, J.W. Williams, Polyhedron 20 (2001) 3143;
(d) L.M. Vallarino, J. Alloys. Compd 249 (1997) 69.
[10] N.W. Alcock, R.G. Kingston, P. Moore, C. Pierpoint, Dalton Trans. (1984) 1937.
[11] Oxford Diffraction Poland Sp., CCD Data Collection and Reduction GUI, Version 1.173.13 beta (release 14.11.2003) Copyright 1995–2004.
[12] G.M. Sheldrick, SHELXS97 Program for Solution of Crystal Structure, University of Goettingen, Germany, 1997.
[13] G.M. Sheldrick, SHELXL97 Program for Refinement of Crystal Structure, University of Goettingen, Germany, 1997.
[14] CrysAlis_RED 1.171.13 Oxford Diffraction Poland Sp., Copyright 1995–2005.
[15] Cambridge Structural Database, Conquest 1.7 Version, November 2004.
[16] J. Mazurek, J. Lisowski, Polyhedron 22 (2003) 2877.
[17] (a) For NMR of paramagnetic complexes see: G.N. La Mar, W.DeW HorrocksJr., R.H. Holm (Eds.), NMR of Paramagnetic Molecules, Academic Press, New York, 1973;
(b) I. Bertini, C. Luchinat, NMR of Paramagnetic Molecules in Biological Systems, Benjamin/Cummings, Menlo Park, CA, 1986;
(c) I. Bertini, P. Turano, A.J. Vila, Chem. Rev. 93 (1993) 2833;
(d) I. Bertini, C. Luchinat, Coord. Chem. Rev. 150 (1996) 1;
(e) A.D. Sherry, C.F.G.C. Geraldes, in: J.-C.G. Bunzli (Ed.), Lanthanide Probes in Life, Chemical and Earth Sciences, Theory and Practice, Elsevier, Amsterdam, 1989 (Chapter 4);
(f) J.A. Peters, J. Huskens, D.J. Raber, J. Prog. NMR Spectrosc. 28 (1996) 283.
[18] (a) B. Bleaney, J. Magn. Reson. 8 (1972) 91;
(b) B. Bleaney, C.M. Dobson, B.A. Levine, R.B. Martin, R.J.P. Williams, A.V.J. Xavier, Chem. Commun. (1972) 791.
[19] R.M. Golding, M.P. Halton, Aust. J. Chem. 25 (1972) 2577.
[20] A.A. Pinkerton, M. Rossier, S. Spiliadis, J. Magn. Reson 64 (1985) 420.
[21] C.N. Reilley, B.W. Good, R.D. Allendoerfer, Anal. Chem. 48 (1976) 1446.
[22] C.F.G.C. Geraldes, S. Zhang, A.D. Sherry, Inorg. Chim. Acta 357 (2004) 381.
[23] C. Platas, F. Avecilla, A. de Blas, C.F.G.C. Geraldes, T. Rodriguez-Blas, H. Adams, J. Mahia, Inorg. Chem. 38 (1999) 3190.
[24] J. Reuben, J. Magn. Reson. 50 (1982) 233.
[25] J. Lisowski, J.L. Sessler, V. Lynch, T.D. Mody, J. Am. Chem. Soc. 117 (1995) 2273.
[26] V. Patroniak, M. Kubicki, A. Mondry, J. Lisowski, W. Radecka-Paryzek, Dalton Trans. (2004) 3295.

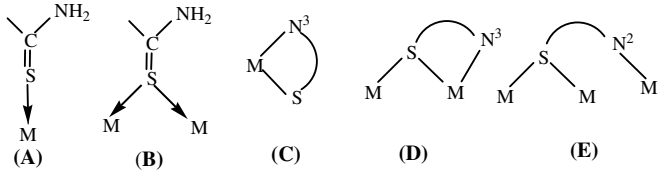

Chart 1.

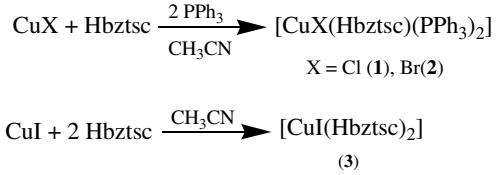

Scheme 1.

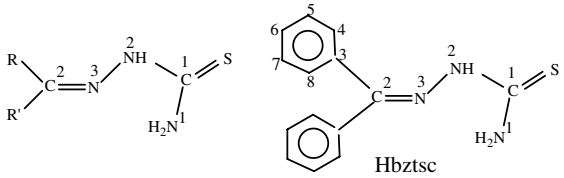

Chart 2.

analyzer. Infrared spectra were recorded as KBr pellets in the range 4000–200 cm^{-1} on Pye–Unicam SP-3-300 spectrophotometer. The melting points were determined with a Gallenkamp electrically heated apparatus. ^1H NMR were recorded on a JEOL AL-300 FT spectrometer operating at a frequency of 300 MHz using $CDCl_3$ as solvent with TMS as internal reference. ^{13}C NMR spectra were recorded at a frequency of 200 MHz using $CDCl_3$ as solvent and TMS as an internal reference. ^{31}P NMR spectra were recorded on a Bruker ACP-300 spectrometer operating at a frequency of 121.5 MHz with $(CH_3O)_3P$ as external reference set at zero value.

2.2. Preparation of ligand (Hbztsc)

To a solution of thiosemicarbazide (2.5 g, 0.027 mol) in hot distilled water (50 mL) and glacial acetic acid (5 mL), was slowly added benzophenone (4.99 g, 0.027 mol) dissolved in methanol (30 mL). The contents were refluxed for 30 h. and the clear solution containing yellowish orange oily layer, was poured in a beaker and stirred vigorously with a glass rod. The yellow solid formed was dried and recrystallised using methanol. Slow evaporation of the solution gave clear yellow crystals. (25%, m.p. 160–162 °C). *Anal.* Calc. for $C_{14}H_{13}N_3S$: C, 65.79; H, 5.09; N, 16.45. Found: C, 65.66; H, 4.93; N, 16.25%. Main IR peaks (KBr, cm^{-1}): ν(N–H) 3412 s, 3346 s, 3247 m, (–NH_2–) 3151 s (–NH–); 1608b, 1437b ν(C=N) + δNH_2 + ν(C=C); 1070 s, 1026 s, 846 s (thioamide moiety). ^1H NMR ($CDCl_3$, δ ppm) 8.68 (–N^2H), 7.81 s, 6.45 sb (N^1H_2), 7.27–7.61 m (Ph). ^{13}C NMR ($CDCl_3$, δ ppm, J, Hz): 178.8 (C^1); 151.0 (C^2); 136.3, 131.0 (C^3); 130.3, 130.23 (C^6); 129.86, 127.7 ($C^{4,8}$); 128.4 ($C^{5,7}$).

2.3. Synthesis of complexes

2.3.1. [CuCl(η^1-S-Hbztsc)(PPh_3)$_2$] · CH_3CN (1)

To a solution of CuCl (0.025 g, 0.25 mmol) in dry acetonitrile (15 mL) was added solid Hbztsc (0.064 g, 0.25 mmol) and the contents were stirred for 3 h at room temperature. During stirring, a yellow solid formed was separated. To this solid suspended in acetonitrile was added PPh_3 (0.132 g, 0.50 mmol) and stirring was continued for further 1 h followed by refluxing for 10 min. Clear light yellow solution formed was filtered and allowed to evaporate at room temperature. Slow evaporation of solution gave clear light yellow crystals. Complex is soluble in chloroform, dichloromethane and hot acetonitrile (60%, m.p. 182–184 °C). *Anal.* Calc. for $C_{50}H_{43}ClCuN_3P_2S \cdot CH_3CN$: C, 67.83; H, 5.00; N, 6.08. Found: C, 67.58; H, 5.04; N, 5.52%. Main IR peaks (KBr, cm^{-1}): ν(N–H) 3336 s, 3238 m (–NH_2–), 3144 m (–NH–); 1602 m, 1585 sh ν(C=N) + $\delta(NH_2)$ + ν(C=C); 1072 s, 1024 s, 841 s (thioamide moiety); 1093 s ν(P–C_{Ph}). ^1H NMR ($CDCl_3$, δ ppm) 9.11 b (–N^2H), 8.57 s, 6.91 s (–N^1H_2), 7.29–7.69 m (Ph + PPh_3). ^{13}C NMR ($CDCl_3$, δ ppm, J, Hz) 176.9 (C^1); 157.9 (C^2); 136.3, 131.1 (C^3); 130.4 (C^6); 129.8, 127.8 ($C^{4,8}$); 128.6 ($C^{5,7}$); 133.9 (*i*-C, PhP); 133.9 (*o*-C, $J_{P-C} = 15.1$, PhP); 129.4 (*p*-C, PhP); 128.4 (*m*-C, $J_{P-C} = 8.8$, PhP). ^{31}P NMR ($CDCl_3$, δ ppm): −112.16 ppm, $\Delta\delta(\delta_{complex} - \delta_{ligand}) = 0.991$ ppm. Compound **2** was prepared in the similar manner.

2.3.2. [CuBr(η^1-S-Hbztsc)(PPh_3)$_2$] · CH_3CN (2)

Crystals were grown from an acetonitrile solution at room temperature. Complex is soluble in chloroform, dichloromethane and hot acetonitrile (61%, m.p. 184–186 °C). *Anal.* Calc. for $C_{50}H_{43}BrCuN_3P_2S \cdot CH_3CN$: C, 64.70; H, 4.76; N, 5.80. Found: C, 64.82; H, 5.15; N, 5.31%. Main IR peaks (KBr, cm^{-1}): ν(N–H) 3344 s, 3236m (–NH_2–), 3157 m (–NH–); 1602 s, 1585 m ν(C=N) + $\delta(NH_2)$ + ν(C=C); 1025 s, 837 s (thioamide moiety); 1091 s ν(P–C_{Ph}). ^1H NMR ($CDCl_3$, δ ppm) 9.02 b (–N^2H), 8.46 s (–N^1H_2), 7.20–7.66 m (–N^1H_2 + Ph + PPh_3). ^{13}C NMR ($CDCl_3$, δ ppm, J, Hz) 176.6 (C^1); 151.7 (C^2); 136.3, 131.1 (C^3); 130.4 (C^6); 129.5, 127.8 ($C^{4,8}$); 128.5 ($C^{5,7}$); 133.4 (*i*-C, PhP), 133.9 (*o*-C, $J_{P-C} = 14.7$, PhP),129.4 (*p*-C, PhP), 128.4 (*m*-C, $J_{P-C} = 9.1$, PhP). ^{31}P NMR ($CDCl_3$, δ ppm): −112.73, $\Delta\delta(\delta_{complex} - \delta_{ligand}) = 0.427$ ppm.

2.3.3. [CuI(η^1-S-Hbztsc)$_2$] (3)

To a solution of CuI (0.025 g, 0.13 mmol) in dry acetonitrile (20 mL) was added solid Hbztsc (0.067 g, 0.26 mmol) and contents were stirred for 4 h. Clear yellow solution was filtered and allowed to evaporate at room temperature. Slow evaporation of solution gave clear

yellow crystalline needles. Complex is soluble in chloroform, dichloromethane and hot acetonitrile. (68.5%, m.p. 210–212 °C). *Anal.* Calc. for $C_{28}H_{26}CuIN_6S_2$: C, 47.92; H, 3.71; N, 11.98. Found: C, 48.53; H, 3.84; N, 11.81%. Main IR peaks (KBr, cm^{-1}): ν(N–H) 3390 s, 3346 s, 3223 m (–NH_2–) 3149 s (–NH–); 1595 sh, 1583 m, 1500 m ν(C=N) + δ(NH) + ν(C=C); 1072 s, 1026 s, 831 s (thioamide moiety). ^{1}H NMR ($CDCl_3$, δ ppm), 8.78 s (–N^2H), 8.06 sb (–N^1H_2), 7.28–7.60 m (N^1H_2 + Ph).

2.4. X-ray crystallography

Suitable light yellow crystals of Hbztsc and compounds **1**, **2** and **3** were mounted on an automatic Enraf Nonius CAD-4 diffractometer equipped with graphite monochromator and Mo Kα radiation ($\lambda = 0.71073$ Å). The unit cell dimensions and intensity data were measured at 93 K for Hbztsc, **1**, **2** and 100 K for **3**. The structures were solved by direct methods and refined by full matrix least squares method based on F^2. All nonhydrogen atoms were refined anisotropically using XCAD-49 (data reduction) and SHELXL. The hydrogen atoms were calculated using structure factor calculations in their idealized positions. The crystallographic data is summarized in Table 1.

3. Results and discussion

3.1. Synthesis and infrared spectroscopy

Reaction of copper(I) chloride/copper(I) bromide with benzophenone thiosemicarbazone (Hbztsc, Ph_2C=N–NH–C(=S)–NH_2) in the molar ratio of 1:1 in MeCN formed an insoluble product of stoichiometry {CuX-(Hbztsc)} which after addition of two moles of PPh_3 yielded a monomeric tetrahedral complex [CuX(Hbztsc)(PPh_3)$_2$] (X = Cl, **1**; Br, **2**) (Scheme 1). Reaction of copper(I) iodide with Hbztsc in the presence of two moles of PPh_3 did not form similar complex, rather it formed a known cubane complex, {$Cu_4I_4(PPh_3)_4$}. However copper(I) iodide with Hbztsc in MeCN in the absence of PPh_3, formed a trigonal complex [CuI(Hbztsc)$_2$] (**3**). All these complexes have melting points in the range of 182–210 °C. Complexes **1** and **2** are readily soluble in chloroform while **3** is sparingly soluble.

The IR spectra of ligand (Hbztsc) shows ν(N–H) in the range of 3412–3247 cm^{-1} (–NH_2) and at 3151 s (–NH–). In all the complexes, ν(N–H) ranges from 3390–3236 cm^{-1} (–NH_2) and 3160–3140 cm^{-1} (–NH–). It suggests the neutral monodentate (η^1-S) nature of ligand Hbztsc. The thioamide bands ν(C–S) + ν(C–N) appear in the range of 846–1085 cm^{-1} in Hbztsc. These modes appear in the region of 830–1090 cm^{-1} in the complexes. Medium to broad peaks appear at 1608 b, 1473 b cm^{-1} in free ligand corresponding to ν(C=N), δ(NH_2) and ν(C=C). However, they appear in the range of 1500–1605 cm^{-1} in all the complexes. A characteristic ν(P–C_{Ph}) peak at 1093 s cm^{-1} in (**1**) and 1091 s cm^{-1} in (**2**) confirms the presence of PPh_3 in the coordinated form in the complexes.

3.2. Crystal structures of ligand and complexes *1–3*

The atomic numbering schemes for molecular structures of ligand and complexes **1**, **2** and **3** are shown in Figs. 1–4 and the selected bond lengths and angles are given in Table 2.

Table 1
Crystallographic data for compounds **1**, **2**, **3** and ligand

	1	**2**	**3**
Empirical formula	$C_{50}H_{43}ClCuN_3P_2S \cdot CH_3CN$	$C_{50}H_{43}BrCuN_3P_2S \cdot CH_3CN$	$C_{28}H_{26}CuIN_6S_2$
MW	919.92	964.38	701.11
Crystal colour	yellow	yellow	yellow
Crystal system	triclinic	triclinic	monoclinic
Space group	$P\bar{1}$	$P\bar{1}$	$P2/c$
a (Å)	12.3639(8)	10.356(7)	16.4147(14)
b (Å)	13.9423(8)	14.480(11)	6.1106(17)
c (Å)	14.8040(9)	17.684(13)	31.3870(7)
V (Å^3)	2255.8(2)	2311(3)	2893.2(8)
α (°)	113.9130(10)	66.206(12)	90
β (°)	100.6420(10)	79.346(14)	113.22
γ (°)	94.9190(10)	72.729(13)	90
Z	2	2	4
D (Mg m^{-3})	1.354	1.386	1.610
μ(Mo Kα) (mm^{-1})	0.702	1.492	1.995
Reflections collected	18082	18915	10863
Unique reflections, R_{int}	10732, 0.0450	10975, 0.0365	10897, 0.0000
Final R indices R_1 and wR_2	0.0490, 0.1006	0.0502, 0.114	0.0379, 0.0937

Crystal data for $C_{14}H_{13}N_3S$: 255.33; monoclinic; $C2/c$; $a = 26.5443(16)$ Å; $b = 6.0935(4)$ Å; $c = 16.7931(10)$ Å; $V = 2649.2(3)$ Å^3; $\alpha = 90°$; $\beta = 102.7580(10)°$; $\gamma = 90°$; $V = 2649.2(3)$ Å^3; $Z = 8$; $D = 1.280$ Mg m^{-3}; μ(Mo Kα) (mm^{-1}) = 0.229; reflections collected = 9934; unique reflections = 3227; $R_{int} = 0.0297$; $R = 0.0453$.

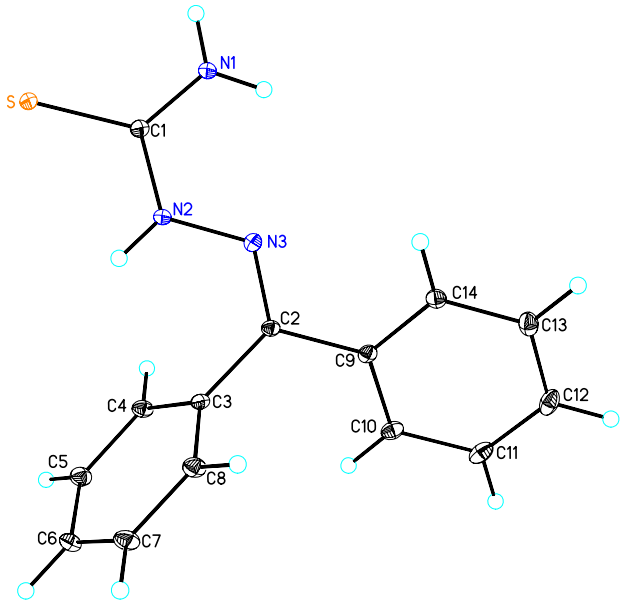

Fig. 1a. The structure of ligand (Hbztsc) with numbering scheme.

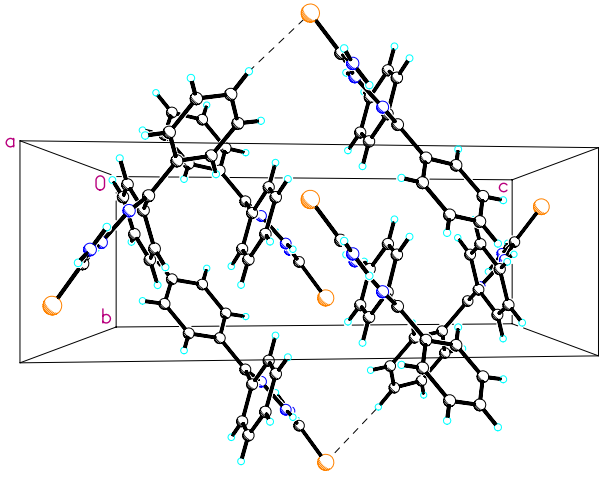

Fig. 1b. Packing diagram of the ligand (Hbztsc).

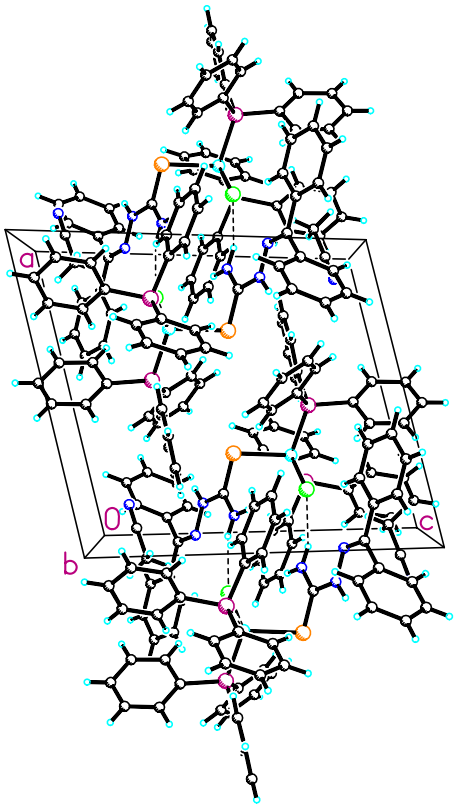

Fig. 2b. Packing diagram of [CuCl(η^1-S-Hbztsc)(PPh_3)$_2$] · CH_3CN (**1**).

3.2.1. Ligand

The ligand (Hbztsc) crystallized in the monoclinic space group *C*2/*c*. The S and the hydrazinic N(3) atoms are *trans* with respect to C(1)–N(2) bond and thus ligand has *E* configuration. The C(1)–S bond distance, 1.6866(17) Å is close to a double bond, and comparable with ca.1.69 Å in salicylaldehyde thiosemicarbazone and 2-hydroxyacetophenone [43,44]; other bonds, C(2)–N(3), C(1)–N(1), C(1)–N(2), N(2)–N(3) are also comparable with the literature data

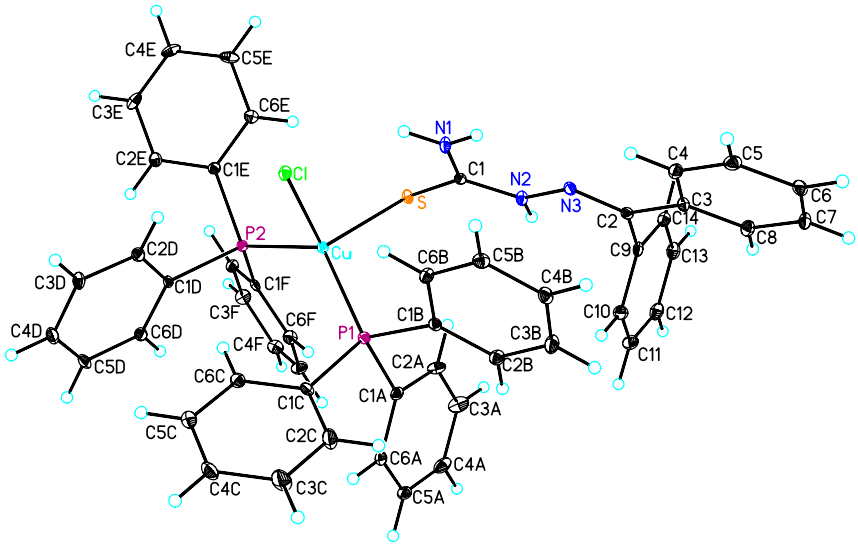

Fig. 2a. The structure of [CuCl (η^1-S-Hbztsc)(PPh_3)$_2$] · CH_3CN (**1**) with numbering scheme.

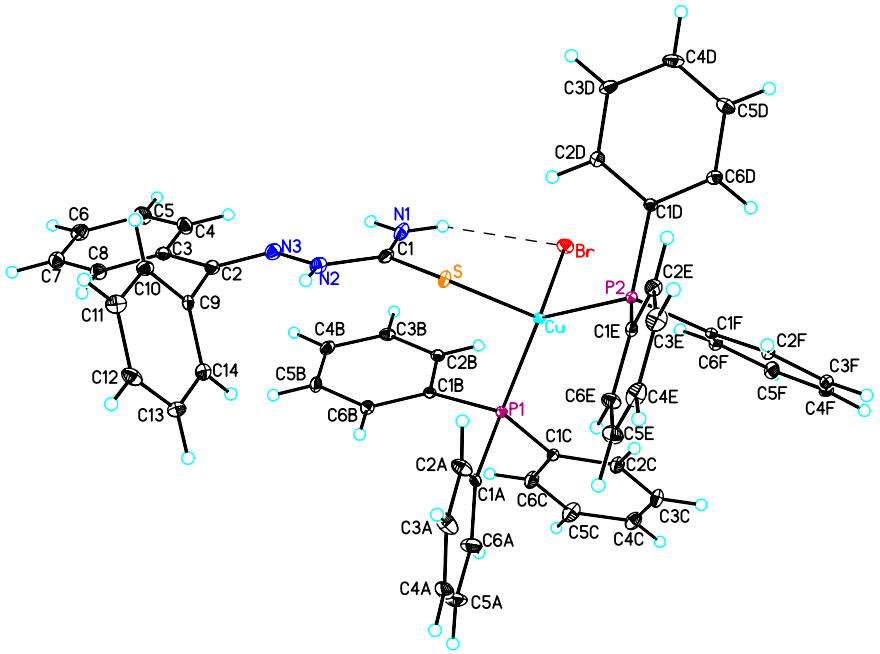

Fig. 3a. The structure of $[CuBr(\eta^1\text{-S-Hbztsc})(PPh_3)_2]\cdot CH_3CN$ (**2**) with numbering scheme.

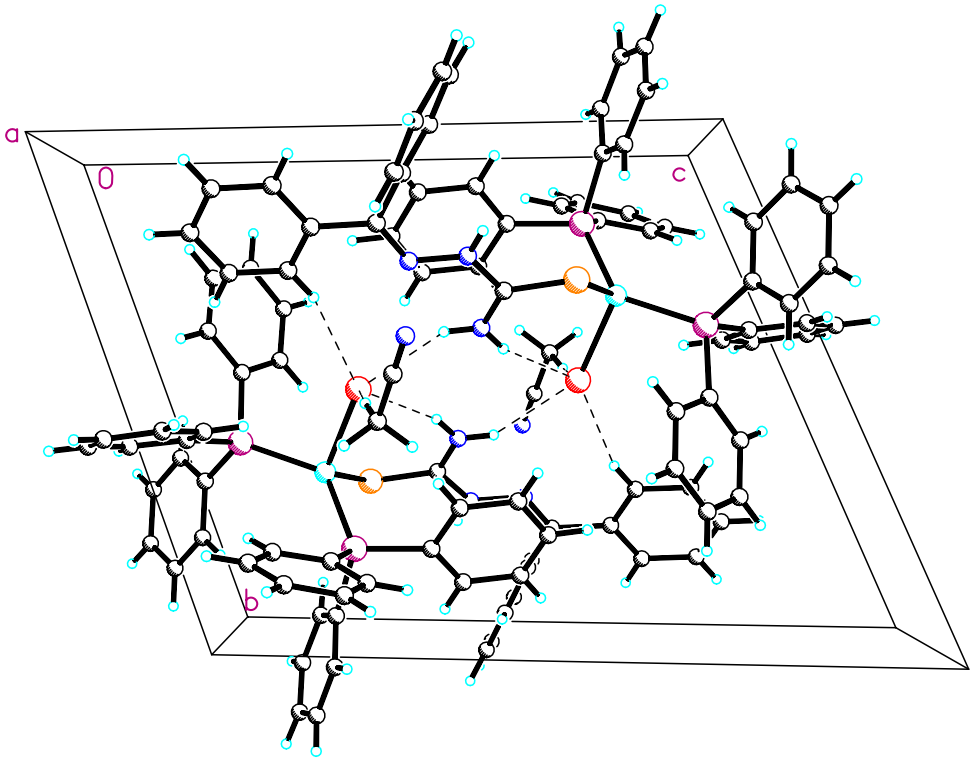

Fig. 3b. Packing diagram of $[CuBr(\eta^1\text{-S-Hbztsc})(PPh_3)_2]\cdot CH_3CN$ (**2**).

[43–45]. There is a moderately strong intermolecular N(1)–H(1B)···S* bond [2.49 Å] {cf. sum of van der Waals radii of H and S, 3.0 Å [46]} and a long range C–H_{Ph}···S intermolecular hydrogen bonding leading to formation of dimer as shown in Fig. 1b.

3.2.2. Complexes *1–3*

Complexes **1** and **2** have the triclinic space groups, while complex **3** has monoclinic space group. The E-configuration of free ligand is unchanged in the complexes. In complex **1**, copper is bonded to one S atom of the ligand

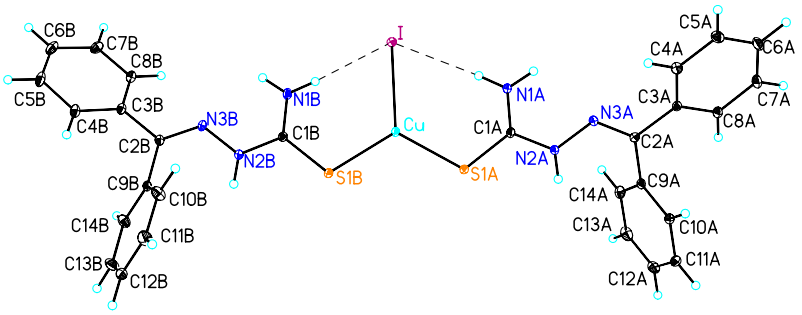

Fig. 4a. The structure of $[CuI(\eta^1\text{-S-Hbztsc})_2]$ (**3**) with numbering scheme.

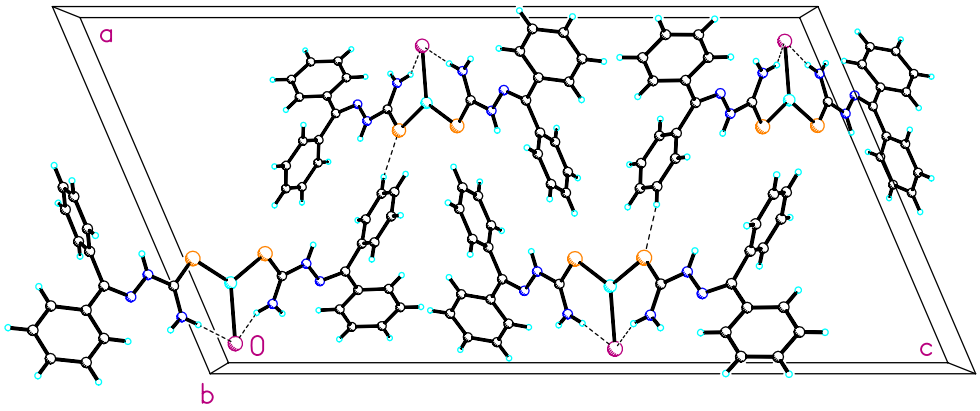

Fig. 4b. Packing diagram of $[CuI(\eta^1\text{-S-Hbztsc})_2]$ (**3**).

(Hbztsc) with Cu–S bond distance of 2.3606(8) Å; two P atoms from PPh_3 ligands {Cu–P(1), 2.2665(8) Å; Cu–P(2), 2.2505(8) Å}, and one chlorine atom at Cu–Cl bond distance of 2.3757(7) Å. Complex **2** has similar bond parameters, viz., Cu–S, 2.3542(17) Å; Cu–P(1), 2.2749 (17) Å; Cu–P(2), 2.2552(16) Å; Cu–Br, 2.4863(12) Å. The angles around Cu lie in the ranges, 102.55(3)–126.00(3)° and 99.49(6)–131.56(4)° in compounds **1** and **2**, respectively, with P(2)–Cu–P(1) being the largest, and P(2)–Cu–X {X = Cl, Br} being the smallest. This reveals a distorted tetrahedral geometry around Cu atom in both the complexes. Finally in complex **3**, each Cu is bonded to two S atoms of two Hbztsc ligands with Cu–S distances of 2.2269(7), 2.2321(7) Å, and to one iodine atom with Cu–I bond distance of 2.5441(4) Å. The angles around Cu range from 118.95(2)° to 121.42(2)°, indicating a trigonal geometry around copper center. The C–S bond distances in these complexes are marginally longer vis-à-vis free ligand, and reveal weakening of pπ–pπ bond. It may be noted that trends of variation in Cu–P, Cu–S and C–S distances are analogous to the literature values [19,21,24a]. The absence of PPh_3 in trigonal planar complex **3** makes a stronger Cu–S bond. Further, Cu–X distances in the complexes are much less than the sum of the ionic radii of Cu^+ and X^- (Cu^+, Cl^-, 2.58 Å; Cu^+, Br^-, 2.73 Å; Cu^+, I^-, 2.97 Å [46]).

In the solid state, amino (–HN^1H) hydrogen atom of thiosemicarbazone is involved in hydrogen bonding in all the complexes (Table 3). In complex (**1**), one hydrogen of amino group is engaged in intramolecular –$HN^1H\cdots$Cl hydrogen bonding while other hydrogen is involved in intermolecular –$HN^1H\cdots$Cl hydrogen bonding forming a dimer (Fig. 2b). Similar trend of bonding is seen in complex **2** except for the presence of additional long range C–H_{Ph}(Hbztsc)$\cdots$Br contact resulting in the formation of 8 membered ring in the center of the dimer. Two molecules of CH_3CN are present as solvent of crystallization per unit cell in the crystal packing but are not involved in any sort of hydrogen bonding at all and also do not appear in the analysis (Fig. 3b). However, in complex **3**, one hydrogen of amino group is engaged in intramolecular –$HN^1H\cdots$I hydrogen bonding while other hydrogen remains free. In addition, long range intermolecular C–H_{Ph}(Hbztsc)$\cdots$S hydrogen bonding is present forming a dimer (Fig. 4b).

A comparison of P–Cu–P, S–Cu–X and Cu–S–C bond angles is made for various Cu^I-complexes with analogous thiosemicarbazones (Table 4). The groups at C^2 carbon appear to play significant role in affecting the above angles which are correlated with the electronegativity of halogen atoms. When py, H (**4**–**6**) [24a] ; and Ph, H (**7**, **8**) [24a] are bonded to C^2 carbon, angles Cu–S–C and S–Cu–X increase with change in X from chloride to iodide; and the corresponding P–Cu–P bond angles decrease. The halogens are engaged in intramolecular –$N^2H\cdots$X, or –$N^1H_2\cdots$X hydrogen bonds and strengths of these bonds obviously vary with the electronegativity of halogen atoms. Chart 3 exhibits how the amino and imino hydrogen atoms

Table 2
Selected bond distances (Å) and bond angles (°) for ligand (Hbztsc) and complexes **1**, **2** and **3**

Bond distances			
Hbztsc			
S–C(1)	1.6866(17)	N(3)–C(2)	1.289(2)
N(1)–C(1)	1.321(2)	C(2)–C(3)	1.496(2)
N(2)–C(1)	1.358(2)	C(2)–C(9)	1.481(2)
N(2)–N(3)	1.3766(19)		
1			
Cu–S	2.3606(8)	N(2)–C(1)	1.351(3)
Cu–P(1)	2.2665(8)	N(2)–N(3)	1.374(3)
Cu–P(2)	2.2505(8)	N(2)–C(2)	1.296(4)
Cu–Cl	2.3757(7)	C(2)–C(3)	1.479(4)
S–C(1)	1.702(3)	C(2)–C(9)	1.495(4)
N(1)–C(1)	1.314(3)		
2			
Cu–S	2.3542(17)	N(2)–C(1)	1.395(4)
Cu–P(1)	2.2749(17)	N(2)–N(3)	1.357(4)
Cu–P(2)	2.2552(16)	N(3)–C(2)	1.291(5)
Cu–Br	2.4863(12)	C(2)–C(3)	1.499(5)
S–C(1)	1.699(4)	C(2)–C(9)	1.513(5)
N(1)–C(1)	1.292(5)		
3			
Cu–I	2.5441(4)	N(2A)–N(3A)	1.378(3)
Cu–S(1A)	2.2269(7)	N(2B)–N(3B)	1.378(3)
Cu–S(1B)	2.2321(7)	N(3A)–C(2A)	1.288(3)
S(1A)–C(1A)	1.712(7)	N(3B)–C(2B)	1.289(3)
S(1B)–C(1B)	1.708(2)	C(2A)–C(3A)	1.479(3)
N(1A)–C(1A)	1.306(3)	C(2A)–C(9A)	1.493(3)
N(1B)–C(1B)	1.306(3)	C(2B)–C(3B)	1.480(3)
N(2A)–C(1A)	1.346(3)	C(2B)–C(9B)	1.493(3)
N(2B)–C(1B)	1.352(3)		
Bond angles			
Hbztsc			
C(1)–N(2)–N(3)	119.71(13)	N(2)–C(1)–S	118.58(12)
C(2)– N(3)–N(2)	117.42(14)	N(3)–C(2)–C(3)	124.33(14)
N(1)–C(1)–S	124.71(13)	N(3)–C(2)–C(9)	116.68(14)
1			
P(2)–Cu–P(1)	126.00(3)	C(1B)–P(1)–Cu	115.40(9)
P(2)–Cu–S	106.49(3)	C(1C)–P(1)–Cu	117.17(10)
P(1)–Cu–S	107.17(3)	C(1A)–P(1)–Cu	112.85(10)
P(2)–Cu–Cl	102.55(3)	C(1F)–P(2)–Cu	117.60(9)
P(1)–Cu–Cl	106.96(3)	C(1D)–P(2)–Cu	113.17(9)
S–Cu–Cl	106.21(3)	C(1E)–P(2)–Cu	114.27(10)
C(1)–S–Cu	101.93(10)		
2			
P(2)–Cu–P(1)	131.56(4)	C(1B)–P(1)–Cu	109.40(10)
P(2)–Cu–S	104.64(4)	C(1C)–P(1)–Cu	120.06(11)
P(1)–Cu–S	103.34(4)	C(1A)–P(1)–Cu	115.35(12)
P(2)–Cu–Br	99.49(6)	C(1F)–P(2)–Cu	116.31(11)
P(1)–Cu–Br	105.27(6)	C(1D)–P(2)–Cu	112.30(11)
S–Cu–Br	112.38(4)	C(1E)–P(2)–Cu	117.45(11)
C(1)–S–Cu	108.19(12)		
3			
S(1A)–Cu–S(1B)	119.62(3)	C(1A)–N(2A)–N(3A)	118.8(2)
S(1A)–Cu–I	121.42(2)	C(2A)–N(3A)–N(2A)	117.6(2)
S(1B)–Cu–I	118.95(2)	C(1B)–N(2B)–N(3B)	118.0(2)
C(1A)–S(1A)–Cu	110.62(8)	C(2B)–N(3B)–N(2B)	117.6(2)
C(1B)–S(1B)–Cu	110.30(9)	N(1A)–C(1A)–(N2A)	117.6(2)

are involved in hydrogen bonding with halogens. A stronger $-N^2H\cdots X$ or $-N^1H_2\cdots X$ hydrogen bond shortens the Cu–S–C bond angle, which leads to opening of P–Cu–P angle. The trend for *p*-HOC_6H_5, H groups (**9**, **10**) [21] bonded to C^2 is similar except for S–Cu–X which decreased and this may be due to the packing effect or presence of solvent of crystallization. Due to rigidity of isatin groups (**11**, **12**) [19], the above trends are less significant.

The most significant observation is found when two Ph groups are bonded to C^2 carbon. Both Cu–S–C and S–Cu–X angles increase as noted for above complexes. However, P–Cu–P angle increases with change in halide from chloride (121°) to bromide (131°) in complexes **1** and **2**, unlike the expected decreasing trend. The increased P–Cu–P bond angle in complex **2** is due to the steric effect of two Ph groups at C^2 carbon with large bromide group. In case of still bulky iodide group in complex **3**, this steric effect becomes very large and this explains lack of formation copper(I) iodide complex containing PPh_3 ligands similar to **1** or **2**.

3.3. NMR spectroscopy

The ^1H NMR of ligand Hbztsc in $CDCl_3$ shows a singlet at 8.68 ppm (N^2H), which shifted downfield to 9.11 ppm in complex **1**, 9.02 ppm in complex **2** and 8.78 ppm in complex **3**. This is in accordance with the coordination behaviour of thiosemicarbazones [24a], and its presence in the spectra of complexes indicates that N^2H protons are not deprotonated. The N^1H_2 protons of free ligand Hbztsc exhibit two sets of signals, one broad peak (unresolved) at 6.45 ppm and a doublet at 7.81 ppm. This can be attributed to the restricted rotation about C^1–N^1 bond axis due to delocalization of lone pairs of electrons on N^1H_2 nitrogen. A pair of broad signals corresponding to N^1H_2 protons appear downfield at 6.91 ppm and 8.56 ppm in complex **1**. However, a single broad signal is observed at 8.47 ppm in complex **2** and 8.06 ppm in complex **3**. The second signal is probably obscured by the protons of phenyl rings. This may be attributed to intermolecular as well as intramolecular $-HN^1H\cdots X$ (X = Cl, Br, I) hydrogen bonding in the solid state which may be operative even in the solution phase. The phenyl protons in free ligand show a series of multiplets in the region of 7.27–7.61 ppm. Ph_3P signals in the complexes merged with the signals of phenyl protons of ligand and show a series of doublets and multiplets in the region of 7.29–7.69 ppm in **1** and 7.20–7.66 ppm in **2**. In complex **3**, phenyl protons appeared unchanged at 7.28–7.60 ppm.

The ^{13}C NMR spectra provide more convincing information about the monodentate behaviour of Hbztsc moiety in the complexes. The C^1 carbon signal appears at δ 176.9 ppm in **1** and at δ 176.5 ppm in **2**, which are upfield relative to the free ligand (δ 178.8 ppm). Further, C^2 carbon signal at δ 157.9 ppm in **1** and δ 151.7 ppm in **2** shifts downfield relative to the free ligand (δ 150.98 ppm), the former carbon showing more pronounced shift. This behaviour is similar to that observed for related complexes

Table 3
Hydrogen bonds (Å) for complexes **1**–**3**

Complex no.	D–H...A	*d*(D–H)	*d*(H...A)	*d*(D...A)	∠(DHA)
1	N(1)–H(1A)...Cl#1	0.88	2.44	3.230(2)	149.3
	N(1)–H(1B)...Cl	0.88	2.54	3.281(3)	142.7
2	N(1)–H(1A)...Br#1	0.88	2.63	3.407(4)	147.3
	N(1)–H(1B)...Br	0.88	2.64	3.494(4)	163.1
3	N(1A)–(H1AA)...I#1	0.88	3.08	3.570(2)	117.2
	N(1A)–H(1AB)...I	0.88	2.65	3.503(2)	164.0
	N(1B)–H(1BA)...I#2	0.88	3.19	3.764(2)	125.2
	N(1B)–H(1BB)...N(1A)#2	0.88	2.67	3.157(3)	116.2
	N(1B)–H(1BB)...I	0.88	2.75	3.509(2)	145.7

Table 4
Comparison of bond angles (°) of complexes **1**–**3** with related complexes

S. no.	Ligand	Complexes	C(1)–S–Cu	P–Cu–P	S–Cu–X	Hydrogen bonding (H···X)
	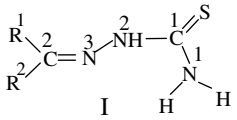 I					
	R^1, R^2					
1	Py, H	Cl (**4**)	103.13(8)	120.92(2)	103.13(8)	–NH–
		Br (**5**)	105.82(15)	122.39(5)	107.76(4)	–NH–
		I (**6**)	115.85(18)	117.21(5)	113.41(4)	$–NH_2–$
2	Ph, H	Br (**7**)	110.52(8)	123.31(2)	109.93(18)	$–NH_2–$
		I (**8**)	115.73(7)	118.11(2)	115.42(2)	–NH–
3	*p*-OHC_6H_5, H	Br (**9**)	107.0(11)	135.4(1)	114.81(9)	–NH–
		I (**10**)	112.1(4)	123.1(1)	110.18(9)	–NH–
4	Ph, Ph	Cl (**1**)	101.93(10)	126.00(3)	108.22(17)	$–NH_2–$
		Br (**2**)	108.19(12)	131.56(4)	112.38(4)	$–NH_2–$
		I (**3**)	110.62(8), 110.30(9)		121.42(2), 118.95(2)	$–NH_2–$
5	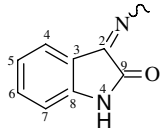	Br (**11**)	113.30(12)	121.97(3)	109.22(3)	$–NH_2–$
		I (**12**)	115.50(2)	124.09(5)	112.13(4)	$–NH_2–$

(**1**)–(**3**) this work; [CuCl(Hpytsc)$(PPh_3)_2$] (**4**) [CuBr(Hpytsc)$(PPh_3)_2$] (**5**) [CuI(Hpytsc)$(PPh_3)_2$] (**6**) (Hpytsc = pyridine-2-carbaldehyde thiosemicarbazone), [CuBr(Hbtsc)$(PPh_3)_2$] (**7**), [CuI(Hbtsc)$(PPh_3)_2$]. (**8**) (Hbtsc = Benzaldehyde thiosemicarbazone) [24a]; [CuBr(L)$(PPh_3)_2$] (**9**), [CuI(L)$(PPh_3)_2$] (**10**) (L = 4 hydroxybenzaldehyde thiosemicarbazone) [21]; [CuBr(H_2istsc)$(PPh_3)_2$] (**11**); [CuI(H_2istsc)$(PPh_3)_2$] (**12**) (H_2istsc = Isatin-3-carbaldehyde thiosemicarbazone) [19].

[24a]. C^3 carbon in free ligand shows a pair of low intensity signals at δ 136.3 ppm and δ 131.0 ppm. This can be attributed to the fact that the two phenyl rings at C^2 carbon in the free ligand as well as in complexes are not coplanar rather at an angle with respect to each other. Thus carbon atoms of two phenyl rings at C^2 carbon are in different chemical environments due to different spatial arrangement of phenyl rings, also revealed by the X-ray structure of the ligand (Fig. 1a). Similarly, $C^{4,8}$ and C^6 carbon atoms show pairs of signals at δ 129.8, 127.7 ppm and δ 130.3, 130.2 ppm, respectively. A single broad signal at δ 128.4 ppm is observed for $C^{5,7}$ carbons. Similar signals are observed for ligand ring carbons (C^3,$C^{4,8}$,$C^{5,7}$,C^6) in the complexes **1** and **2** showing no significant shift. Various signals due to *ipso* carbon, *ortho*, *meta* and *para* carbons of phosphine ligands are well resolved in both the complexes. The *i*-C, *ortho*, *meta* and *para* carbon signals of Ph rings of

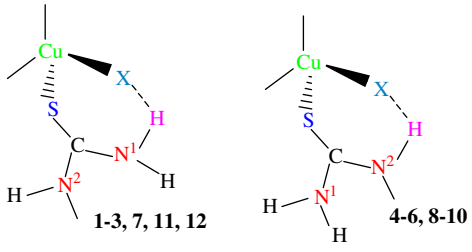

Chart 3.

PPh_3 in **1** appear as separate and are similar to the corresponding signals in **2**.

The ^{31}P NMR signal of free Ph_3P appears at −113.153 ppm. A single broad signal is observed in the complexes **1** and **2** indicating the equivalence of two PPh_3 groups. This signal shifted downfield to −112.16 ppm in **1** and −112.73 ppm in **2** with coordination shifts ($\delta_{complex} - \delta_{ligand}$) of 0.99 and 0.43 ppm, respectively. Such low coordination shifts can be attributed to the equilibrium between coordinated PPh_3 and the free PPh_3 in the solution phase, and similar behaviour was observed in the literature [24b].

4. Supplementary material

Supplementary data is available from CCDC, 12 Union Road, Cambridge CB2 1EZ, UK (fax: +44 12336033; e-mail: deposit@ccdc.cam.ac.uk, or on the web www.ccdc.cam.ac.uk) on request quoting the deposition number CCDC 297906 for (**1**), 297907 for (**2**), 297908 for (**3**) and 297909 for Hbztsc.

Acknowledgements

Financial assistance from CSIR, New Delhi (F. No. 9/254(159)/2005-EMR-I) and research facilities to one of us (Sonia) by the university are gratefully acknowledged.

References

[1] D.X. West, S.B. Padhye, P.B. Sonaware, Struct. Bond. (Berlin) 76 (1991) 4.
[2] M.J.H. Campbell, Coord. Chem. Rev. 15 (1975) 279.
[3] S. Padhye, G.B. Kauffman, Coord. Chem. Rev. 63 (1985) 127.
[4] D.X. West, A.E. Liberta, S.B. Padhye, R.C. Chilate, P.B. Sonaware, A.S. Kumbhar, R.G. Yerande, Coord. Chem. Rev. 123 (1993) 49.
[5] J.S. Casas, M.S. Garcia-Tasende, J. Sordo, Coord. Chem. Rev. 209 (2000) 197.
[6] D.R. Smith, Coord. Chem. Rev. 164 (1997) 575.
[7] R.K. Mahajan, I. Kaur, T.S. Lobana, Talanta 59 (2003) 101.
[8] D.X. West, J.J. Ingram, N.M. Kozub, G.A. Bain, A.E. Liberta, Transition Met. Chem. 21 (1996) 213.
[9] E.W. Ainscough, A.M. Brodie, J.D. Ransford, J.M. Waters, J. Chem. Soc., Dalton. Trans. (1997) 1251.
[10] M.A. Ali, A.H. Mirza, A.M.S. Hossain, M. Nazimuddin, Polyhedron 20 (2001) 1045.
[11] D.X. West, M.M. Salberg, G.A. Bain, A.E. Liberta, J.-V. Martinez, S.H. Ortega, Transition Met. Chem. 21 (1996) 206.
[12] E.W. Ainscough, A.M. Brodie, J.D. Ransford, J.M. Waters, J. Chem. Soc., Dalton. Trans. (1991) 2125.
[13] M. Baldini, M.B. Ferrari, F. Bisceglie, G. Pelosi, S. Pinelli, P. Tarasconi, Inorg. Chem. 42 (2003) 2049.
[14] E.W. Ainscough, A.M. Brodie, J.D. Ransforsd, J.M. Waters, J. Chem. Soc., Dalton. Trans. (1991) 1737.
[15] M.B. Ferrari, F. Bisceglie, G. Pelosi, P. Tarasconi, R. Albertini, G.G. Fava, S. Pinelli, J. Inorg. Biochem. 89 (2002) 36.
[16] M.E. Hossain, M.N. Alam, J. Begum, M.A. Ali, M. Nazimuddin, F.E. Smith, R.C. Hynes, Inorg. Chim. Acta 249 (1996) 247.
[17] D.X. West, A.M. Stark, G.A. Bain, A.E. Liberta, Transition Met. Chem. 21 (1996) 289.
[18] M.B. Ferrari, F. Bisceglie, G. Pelosi, P. Albertini, P.P. Dall'Aglio, A. Bergamo, G. Sava, S. Pinelli, J. Inorg. Biochem. 98 (2004) 301.
[19] T.S. Lobana, Rekha, B.S. Sidhu, A. Castineiras, E. Bermejo, T. Nishioka, J. Coord. Chem. 58 (2005) 803.
[20] T.S. Lobana, Rekha, R.J. Butcher, Transition Met.Chem. 29 (2004) 291.
[21] H.G. Xeng, D.X. Zeng, X.Q. Xin, W.T. Wong, Polyhedron 16 (1997) 3499.
[22] M.B. Ferrari, G.G. Fava, M. Lanfranchi, C. Pellizzi, P. Tarasconi, Inorg. Chim. Acta 181 (1991) 253.
[23] M.B. Ferrari, A. Bonardi, G.G. Fava, C. Pellizi, P. Tarasconi, Inorg. Chim. Acta 223 (1994) 77.
[24] (a) T.S. Lobana, Rekha, R.J. Butcher, A. Castineiras, E. Bermejo, P.V. Bharatam, Inorg. Chem. 45 (2006) 1535;
(b) T.S. Lobana, Seema Paul, A. Castineiras, Polyhedron 16 (1997) 4023.
[25] S. Lhuachan, S. Siripaisarnpipat, N. Chaichat, Eur. J. Inorg. Chem. (2003) 263.
[26] G. Argay, A. Kalman, L. Parkanyl, V.M. Laovac, I.D. Braski, P.N. Radivojsa, J. Coord. Chem. 51 (2000) 9.
[27] L.A. Ashfield, A.R. Cowley, J.R. Dilworth, P.S. Donnely, Inorg. Chem. 43 (2004) 4121.
[28] Y.P. Tian, W.T. Yu, C.Y. Zhao, M.-H. Jiang, Z.G. Cai, H.K. Fun, Polyhedron 21 (2002) 1217.
[29] P. Souza, L. Sanz, V. Fernandez, A. Monge, Z. Naturoforsch B: Chem. Sci. 46 (1991) 767.
[30] C.-Y. Duan, Y.-P. Tian, C.-Y. Zhao, T.C.W. Mak, Polyhedron 16 (1997) 2857.
[31] Y.P. Tian, C.-Y. Duan, C.-Y. Zhao, X. Zhao, Inorg. Chem. 36 (1997) 1247.
[32] D.V. Garcia, A. Fernandez, J.J. Fernandez, M.L. Tornes, J.M. Origueria, J.M. Vila, H.A. Adams, J. Organomet. Chem. 595 (2000) 199.
[33] P. Dapporto, G. Demunno, A.A.G. Tomnlinsonb, J. Chem. Res. 40 (1984) 501.
[34] J.S. Casas, E.E. Castellano, J. Ellena, M.S.G. Tasende, A. Sanchez, J. Sordo, M.J. Vidarte, Inorg. Chem. 42 (2003) 2584.
[35] M. Bonamino, G. Dessy, V. Fares, L. Scaramuza, Cryst. Struct. Commun. 4 (1975) 629.
[36] R.P. John, A. Sreekanth, M.R.P. Kurup, S.M. Mobin, Polyhedron 21 (2002) 2515.
[37] D.K. Darezzeizi, N.K. Mells, D.X. West, J.V. Martinez, S. Hermande, Z. Orega, Eur. J. Inorg. Chem. (1998) 861.
[38] E. Labisbal, K.D. Haslow, K.S. Pednares, J.V. Martinez, S.H. Ortega, D.X. West, Polyhedron 22 (2003) 2831.
[39] N.T. Akinchan, R. Akinchamn, V.J. Ibok, L.P. Batlagilia, A.B. Corrada, J. Crystallogr. Spectrosc. Res. 22 (1992) 741.
[40] Y.P. Tian, W.T. Yu, M.H. Jiang, S.S.S. Raj, P. Yang, H.K. Fun, Acta Crystallogr. Sect. C: Cryst. Struct. Commun. 55 (1999) 1639.
[41] U. Abram, K. Ortner, R. Gust, K. Sommer, Dalton (2000) 735.
[42] G. Brauer, Handbook of Preparative Chemistry, 2nd ed., vol. 2, Academic Press, New York, 1965.
[43] D. Chattopadhyay, S.K. Mazumdar, T. Banerjee, S. Ghosh, T.C.W. Mak, Acta Crystallogr. C44 (1988) 1025.
[44] M.S. Garcia, J.V. Martinez, R.A. Toscano, Acta Crystallogr. C44 (1988) 1247.
[45] E. Labisbal, K.D. Haslow, A.S. Pedrares, J.V. Martinez, S.H. Ortega, D.X. West, Polyhedron 22 (2003) 2831.
[46] J.E. Huheey, E.A. Keiter, R.L. Keiter, Inorganic Chemistry: Principles of Structure and Reactivity, 4th ed., Harper Collins, New York, 1993.

self-assembly of metal, bidentate azoimine blocker and pseudohalide, we have been successful in isolating and characterizing tetranuclear complexes with the formula $[Cu(RaaiR')(N_3)_2]_4$ [RaaiR′; R = H (**3**), Me (**4**); R′ = Me (**a**), Et (**b**)]. The structure has been confirmed by a single crystal X-ray diffraction study of $[Cu(HaaiMe)(N_3)_2]_4$ (**3a**). Variable temperature magnetic measurements of **3a** show the occurrence of ferromagnetic ($J_1 = +25.3\ cm^{-1}$) and antiferromagnetic ($J_2 = -4.7\ cm^{-1}$) interactions through the double and single end-on azido bridges, respectively. Addition of excess of RaaiR′ to the respective tetranuclear copper(II) complex in 2-methoxy ethanol has enabled the cluster to be split into a mononuclear copper(II) complex of the composition $[Cu(RaaiR')_2(N_3)_2]$. The structure and magnetism are detailed below.

2. Results and discussion

2.1. The complexes

The complexes are synthesized by the reaction of 1-alkyl-2-(arylazo)imidazole (RaaiR′), $Cu(OAc)_2 \cdot H_2O$ and NaN_3 in MeOH in a 1:1:2 mole proportion at 298 K. The ligand is an unsymmetric, N,N′-bidentate chelator where N and N′ refer to N(imidazole) and N(azo) donor centres, respectively. The azide (N_3^-) is a bridging ligand showing its versatile coordination motifs. The composition, $[Cu(RaaiR')(N_3)_2]_4$ (R = H (**3**), Me (**4**); R′ = Me (**a**), (**b**)) has been confirmed by X-ray crystal structure determination of one of the compounds, $[Cu(HaaiMe)(N_3)_2]_4$ (**3a**). The tetranuclear cluster is dissociated into a mono-copper complex, $[Cu(RaaiR')_2(N_3)_2]$ (**5**, **6**) upon addition of excess of RaaiR′ to a 2-methoxy ethanol solution of the complex. The structure of the mononuclear copper(II) compound has also been established by X-ray structure study in one case, $[Cu(HaaiEt)_2(N_3)_2]$ (**6a**), and by comparing with previously reported results [16].

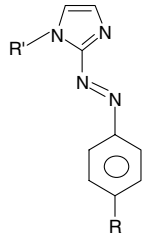

RaaiR′

R = H (**a**), Me (**b**); R′ = Me (**1**), Et (**2**)

2.2. Spectral studies

Infrared spectral data were assigned on comparing with the free ligand data and on comparing with $[Cu(RaaiR')_2(N_3)_2]$ [16]. The most significant observation is the appearance of strong sharp stretches at 2069–2082, 2045–2050 and 2026–2028 cm^{-1} for **3** and **4**. These correspond to $\nu_{asym}(N_3)$. This supports a bridging end-on type binding of N_3 in the complexes **3** and **4** [9,11,22]. Moderately intense stretchings at 1583–1598 and 1438–1448 cm^{-1} are due to ν(C=N) and ν(N=N), respectively [14].

Because of the insolubility of the complexes in common organic solvents, the electronic spectra of the complexes have been recorded in *N*,*N*-dimethyl formamide (DMF) solution in the UV–Vis region (200–900 nm). The complexes (**3**, **4**) exhibit four weak transitions around 715, 585, 475 and 450 nm. The position and intensity of the bands may not only be of d–d origin rather an admixture of d–d and MLCT ($d\pi(Cu) \rightarrow \pi^*$(ligand)) transitions. The bands $\leqslant$400 nm are presumably due to intra-ligand π–π^* and n–π^* transitions.

2.3. Crystal structures

2.3.1. $[Cu(HaaiMe)(N_3)_2]_4$ (**3a**)

The X-ray structure (Fig. 1) reveals that complex **3a** is a neutral tetranuclear copper(II) derivative, comprising a dimer-of-dinuclear copper(II) subunits. Selected bond lengths and angles are given in Table 1. There are two crystallographically unique copper(II) environments; one of them is a five-coordinated square-based pyramid with a CuN_5 donor set and other is a six-coordinated distorted octahedral CuN_6 type. The dinuclear core unit is generated by a two $\mu_{1,1}$-N_3 bridging scheme. Dimerisation of the dinuclear motif is carrying out by $\mu_{1,1}$-N_3-group bridging. Thus, an arrangement of four copper atoms is formed. Each copper centre has been chelated with a HaaiMe ligand in which the ligand acts as an unsymmetric bidentate N,N′-donor type where N(imidazole) and N(azo) refer to N and N′, respectively.

The atomic groups Cu(1), N(5), C(13), N(7), N(8) and Cu(2), N(1), C(3), N(3), N(4) constitute two chelate planes of mean deviation $\leqslant$0.02 Å. The pendant phenyl ring makes a dihedral angle of about 8° with the chelating

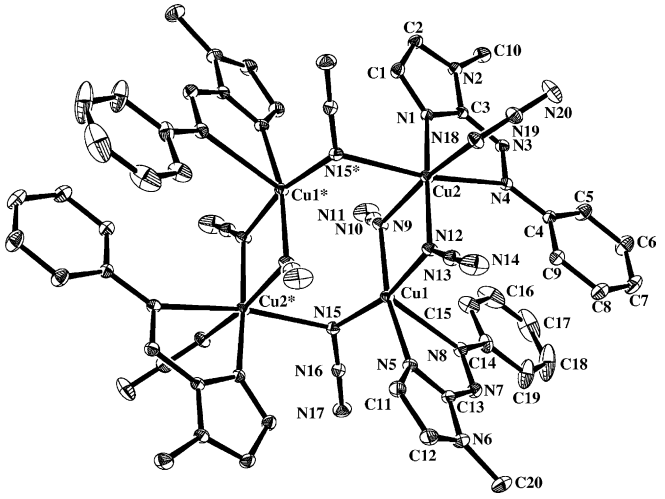

Fig. 1. ORTEP view of **3a** showing the metal environment and the atom labelling.

Table 1
Selected bond distances (Å) and angles (°) for $[Cu(HaaiMe)(N_3)_2]_4$ (**3a**)

Cu(1)–N(5)	2.002(2)	N(5)–Cu(1)–N(9)	168.06(10)
Cu(1)–N(8)	2.639(1)	N(5)–Cu(1)–N(12)	92.35(10)
Cu(1)–N(9)	2.017(2)	N(5)–Cu(1)–N(15)	97.47(10)
Cu(1)–N(12)	1.973(2)	N(9)–Cu(1)–N(12)	77.77(10)
Cu(1)–N(15)	1.961(3)	N(9)–Cu(1)–N(15)	93.52(10)
Cu(2)–N(1)	1.973(2)	N(12)–Cu(1)–N(15)	165.59(12)
Cu(2)–N(4)	2.632(3)	N(8)–N(7)–C(13)	113.2(3)
Cu(2)–N(9)	2.051(2)	Cu(1)–N(8)–N(7)	107.24
Cu(2)–N(12)	1.980(2)	Cu(1)–N(5)–C(13)	120.7(2)
Cu(2)–N(18)	1.967(3)	Cu(1)–N(15)–N(16)	122.6(2)
N(3)–N(4)	1.260(3)	N(1)–Cu(2)–N(9)	95.87(10)
N(1)–C(3)	1.325(4)	N(1)–Cu(2)–N(12)	169.23(11)
N(3)–C(3)	1.387(4)	N(1)–Cu(2)–N(18)	94.00(10)
N(7)–N(8)	1.243(4)	N(9)–Cu(2)–N(12)	76.82(10)
N(5)–C(13)	1.332(5)	N(9)–Cu(2)–N(18)	170.03(10)
N(7)–C(13)	1.372(5)	N(12)–Cu(2)–N(18)	93.21(11)
N(9)–N(10)	1.213(4)	Cu(2)–N(1)–C(3)	121.4(2)
N(10)–N(11)	1.168(5)	N(1)–C(3)–N(3)	128.1(3)
N(12)–N(13)	1.195(4)	N(15)–N(16)–N(17)	178.0(3)
N(13)–N(14)	1.126(5)	N(4)–N(3)–C(3)	112.0(3)
N(15)–N(16)	1.191(4)	Cu(1)–N(15)–Cu(2_a)*	100.59(12)
N(16)–N(17)	1.143(8)	Cu(1)–N(9)–N(10)	124.5(2)
N(18)–N(19)	1.182(4)	Cu(2)–N(9)–N(10)	127.2(2)
N(19)–N(20)	1.152(5)	N(9)–N(10)–N(11)	177.9(4)
Cu(1)···Cu(2)	3.130	Cu(1)–N(12)–Cu(2)	104.71(12)
Cu(1)···Cu(2_a)#	3.592	Cu(1)–N(12)–N(13)	131.3(2)
		Cu(2)–N(12)–N(13)	123.8(2)
		N(12)–N(13)–N(14)	177.8(3)
		N(8)–Cu(1)–N(9)	107.01(10)
		N(1)–Cu(2)–N(4)	69.54(9)
		N(5)–Cu(1)–N(8)	68.75(10)

Symmetry code: $2-x, 1-y, 1-z$.

plane. The chelate angles of —Cu—N=N—C=N— are N(1)–Cu(2)–N(4), 69.54(9)°, N(5)–Cu(1)–N(8), 68.75(10)°. From the respective basal plane, the Cu(1) and Cu(2) centres are moved in same direction by −0.168(1) and −0.123(1) Å. These two planes are inclined at a dihedral angle of 87.22(10)°. In the dinuclear motif the bridging unit Cu_2N_2 is a four armed distorted plane of mean deviation ~0.02 Å. The Cu–N distances in the Cu_2N_2 unit reveal the distortion of the tetraatomic cycle: Cu(1)–N(1), 2.017(2); Cu(2)–N(1), 2.051(2); Cu(1)–N(12), 1.973(2); Cu(2)–N(12), 1.980(2) Å. The bridge angles are 100.60(11)° and 104.71(12)°. The other two angles (N(9)–Cu(1/2)–N(12)) are 77.77(10)° and 76.82(10)°. The chelate and bridge planes are inclined at an angle of 76.30(13)°. Double bridged azide groups are inclined at an acute angle with the bridge plane [N(9)–N(10)–N(11) makes 55° and N(12)–N(13)–N(14) makes 15° angle with Cu_2N_2]. The single-bridged azido group [N(15)–N(16)–N(17)] lies at an angle of 61° with the Cu_2N_2 motif. Dimerisation of the dicopper core generates the Cu_2N bridge unit (Cu(2_a)*–N(15)–Cu(1)) (* symmetry: $2-x, 1-y, 1-z$) of angle 106.59(12)°. The geometrical arrangement reflects the distorted orientation of the groups around the bridge. In the CuN_6 arrangement the donor centres are as follows: chelating HaaiMe gives two N-donor centres; three end-on azido bridged-N centres and a terminal azido-N donor. The bond parameters around the CuN_6 coordination environment shows a distorted octahedral arrangement. In the TBP CuN_5, the triangular base is constituted by N(8), N(13), N(15), Cu(1) and apical positions are occupied by N(9) and N(5). The azido bridge angles in the dinuclear copper(II) unit (Cu(1)–$\{\mu_{1,1}$-$N_3\}_2$–Cu(2)) are 100.60(11)° and 104.72(12)° and lie in the range of reported values [9,11,27]. The bridge angle has a major effect on the spin-exchange phenomena (evaluated from the exchange parameter J). Planarity of the Cu_2N_2 unit, chelate angle of the capping agent, dihedral angle between two coordination planes, steric and electronic factors of the ligand significantly control the magnetic properties of the complexes. The two dinuclear copper(II) cores (Cu(1)···Cu(2) unit) are bridged by a $\mu_{1,1}$-N_3 group in an inverted fashion (Cu(1) of core-1 is bridged by $\mu_{1,1}$-N_3 to Cu(2a)* (* symmetry: $2-x, 1-y, 1-z$) of core-2 and vice versa) to constitute an eight-member ring. The Cu(1)···Cu(2) distance is 3.13 Å and is similar to reported azido bridged (end-on) dicopper complexes [13] but shorter than oxobridged (Cu–O–Cu) phenolato compounds [7a]. In the single azido bridged (Cu(1)–$\{\mu_{1,1}$-$N_3\}$–Cu(2_a)*) (* symmetry: $2-x, 1-y, 1-z$) dinuclear copper(II) unit the Cu···Cu separation is 3.59(2) Å and is longer than the double azido bridged dicopper unit.

There are three types of (azido) N_3-groups present in the tetranuclear copper(II) unit: two N_3-units bridge two Cu(II)-centres in the dimeric core; one N_3-function serves to bridge two dimer cores and the last N_3-unit coordinates as a monodentate donor with one of the two copper centres in the dimer. Other N-donor centres are N(imidazole) and N(azo) from the chelated HaaiMe. Out of them, the N(azo) requires considerably more room than the other N-donors [23]. There are at least two steric reasons for this. First, the N(azo) belongs to an exocyclic N=N along with a pendant aryl group; thus the van der Waals repulsion will be greater than N(imidazole). Second, the N(azido) has larger s-character compared to N(azo) and thus N(azo) is more space demanding. The Cu–N(azo) distances are the longest in the series and are Cu(1)–N(8), 2.639(1) and Cu(2)–N(4), 2.632(3) Å. However, the Cu–N(azo) distances are less than the sum of the van der Waals radii of Cu(II) and N(azo) [24]. This implies a covalent interaction of N(azo) and Cu(II). Cu(II) has some preference to bind to N(imidazole) [25] compared to N(azo) and is shortened by 0.6 Å. The azido bond lengths lie in the range 1.12–1.21 Å. The azo N=N distances in the two chelated HaaiMe of the dimer are N(3)–N(4), 1.260(3) and N(7)–N(8), 1.243(4) Å, which are near to the free ligand value (1.250(1) Å) [26].

2.4. Magnetic study

The variable temperature magnetic susceptibility data for complex **3a** was recorded between 300 and 2 K. A plot of $\chi_M T$ versus T for the four copper(II) ions is shown in Fig. 2. At 300 K, the $\chi_M T$ value is 1.64 $cm^3\ mol^{-1}$ K, which

is close to that expected for four uncoupled spins, with $g = 2.09$. The value increases slightly on lowering the temperature and reaches a maximum (1.83 $cm^3\ mol^{-1}\ K$) at 22 K. Below this temperature $\chi_M T$ decreases to a value of 1.38 $cm^3\ mol^{-1}\ K$ at 2 K. The shape of this curve indicates dominant ferromagnetic coupling until 22 K and below this temperature $\chi_M T$ decreases from 1.8 to 1.4 $cm^3\ mol^{-1}\ K$, which is the signature of antiferromagnetic exchange and/or the presence of the ZFS of the ground state. To analyze the magnetic pathways it is necessary to schematize them as is shown in Fig. 3. This scheme matches with the structure that, as indicated above, can be considered as a dimer of dimers. The J_1 corresponds to the double end-on azido bridges with an equatorial–equatorial (short–short) coordination mode, whereas J_2 corresponds to the single end-on azido bridge, but in equatorial–axial (short–long) coordination mode. Thus, considering these two different J values, the analysis of the experimental susceptibility values has been performed using the following expression:

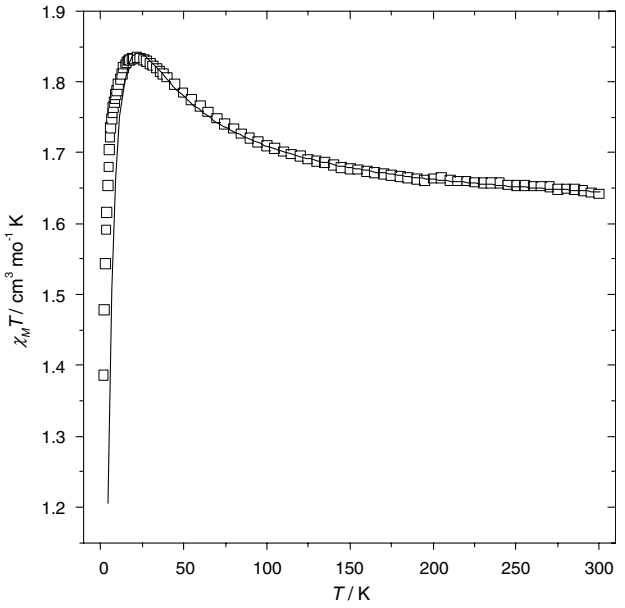

Fig. 2. Plot of the $\chi_M T$ vs. T data for complex **3a**. Solid line represents the best fit (see text).

$$\chi_M = Ng^2\beta^2/KT[A/B], \quad (1)$$

where $A = [30\exp(-E_1/kT) + 6\exp(-E_2/kT) + 6\exp(-E_3/kT) + 6\exp(-E_4/kT)]$, $B = 5[\exp(-E_1/kT) + 3\exp(-E_2/kT) + 3\exp(-E_3/kT) + 3\exp(-E_4/kT) + \exp(-E_5/kT) + \exp(-E_6/kT)]$.

E_n values can be obtained using the Kambe method from the Hamiltonian:

$$H = -J_1(S_1 \cdot S_2 + S_3 \cdot S_4) - J_2(S_1 \cdot S_3 + S_2 \cdot S_4)$$
$$E_1 = (-J_1 - J_2)/2, \quad E_2 = (-J_1 + J_2)/2,$$
$$E_3 = (J_1 + J_2)/2, \quad E_4 = (J_1 - J_2)/2,$$
$$E_5 = (J_1 + J_2)/2 + (J_1^2 + J_2^2 - J_1J_2)^{1/2},$$
$$E_6 = (J_1 + J_2)/2 - (J_1^2 + J_2^2 - J_1J_2)^{1/2}$$

where J_i parameters correspond to those given in Fig. 4. The best fit parameters found are: $J_1 = +25.3\ cm^{-1}$, $J_2 = -4.7\ cm^{-1}$, $g = 2.07$ and $R = 1.6 \times 10^{-4}$, where $R = \sum[(\chi_M T)_{exp} - (\chi_M T)_{cal}]^2 / \sum(\chi_M T)^2_{exp}$. Attempts to fit the experimental data introducing D, zJ' or θ parameters in the expression (1) did not improve the R factor.

The values of the superexchange parameters are $J_1 = +25.3\ cm^{-1}$ and $J_2 = -4.7\ cm^{-1}$ which are typical for such Cu(II) complexes with these structural features. The bonding pattern of Cu–(N_3)–Cu is unique in this example, having one single end-on and double end-on azide bridging, and is different from so far reported end-on azido bridged Cu(II) complexes (Table 2). Indeed, for the equatorial–equatorial coordination mode (such as in the J_1 pathway), the magnetic behavior of copper-azide bridged complexes in end-on mode is well-known [28–35] and the general trends of their magnetic properties are well-correlated to the structural parameters of the bridge (mainly Cu–N_{azide}–Cu angle). Currently, the end-on or ($\mu_{1,1}$) double bridges are usually associated with ferromagnetic behavior [5], although for angles out of the range 96–104° the interaction can be antiferromagnetic [27,36]. However, for azido anions bridging in an end-on fashion at the axial–equatorial position (such in the J_2 case, Fig. 3), the reported J values are always small and they can be ferromagnetic or antiferromagnetic [37–42], depending on the Cu–N distance and the τ parameter ($\tau = 0$ for square pyramidal or elongated octahedral geometries and

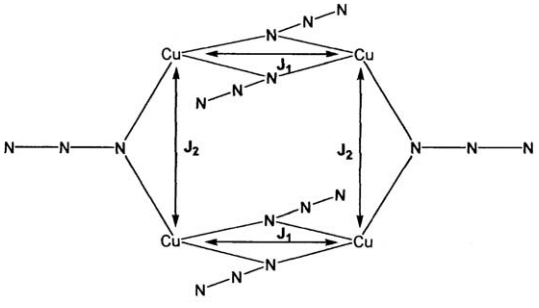

Fig. 3. Magnetic interaction pathways J_1 and J_2 between the different copper(II) centres.

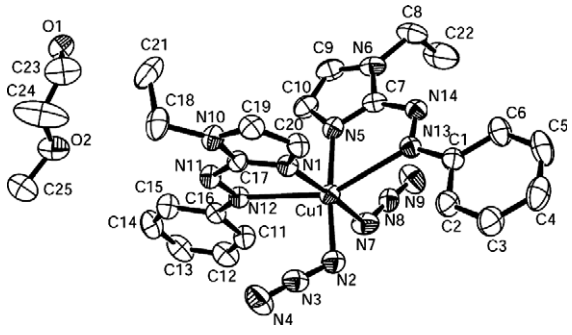

Fig. 4. ORTEP view of **6a** · $C_3H_8O_2$ showing the metal environment and the atom labelling.

Table 2
Selected structural and magnetic data of some single- and double end-on azido bridged Cu(II) complexes

Complex[a]	Cu–N (Å)	Cu–N–Cu (°)	J (cm^{-1})	Ref.
Double end-on azido bridged Cu(II) complexes				
$[Cu_2(OBISDIEN)(\mu_2\text{-}N_3)_2(N_3)_2]$	1.990, 2.043	105.5, 101.6	70	[28]
$[Cu_2(t\text{-Bupy})4(\mu_2\text{-}N_3)_2](ClO_4)_2$	1.99	100.5	105	[29]
$[Cu_2(tbz)_2(\mu_2\text{-}N_3)_2(N_3)_2]\cdot 2CH_3OH$	2.059, 1.97	104.7	23	[31]
$[Cu_2(DMPTD)(\mu_2\text{-}N_3)_2(N_3)_2]$	1.995, 2.043	98.3, 101.9	85	[36]
$[Cu_2(\mu_{1,1}N_3)_2(4\text{-Etpy})_4(\mu\text{-}NO_3)_2]$	1.996, 2.004	98.3	230	[11b]
$[Cu_2(\mu_{1,1}N_3)_2(3\text{-ampy})_4(\mu\text{-}NO_3)_2]\cdot C_2H_5OH$	2.000, 2.006	97.5	223	
$[Cu_3(\mu_{1,1}N_3)_4(Meinic)_2(N_3)_2(DMF)_2]$	1.998, 2.012	100.8, 99.2	47.3	
$[Cu(L^1)(N_3)]_2$	2.215, 2.174	90.93	1.03	[33]
$[Cu_4(bpm)_2(N_3)_8]_n$	2.002, 1.998	101.4	11.7	[34]
	2.023, 2.010	102.3		
$[Cu(4\text{-Etpy})(N_3)_2]$	1.970, 1.979	103.0	weak ferro	[11c]
$[Cu_4(L^2)(\mu_2\text{-}N_3)_4](PF_6)_4$	2.012, 1.996	98.1, 96.6	94	[35]
Single end-on azido bridged Cu(II) complexes				
$[Cu_2(terpy)_2\text{-}\mu\text{-}(N_3)_4Cu_2\text{-}\mu\text{-}N_3)_2(N3)_2]$	1.943, 2.374	107.11	−100	[42a]
$Cu_3(SE)_2(N_3)_4(DMF)_2$	2.001, 2.042	102.33	32.6	[42b]
$[Cu_2(\mu\text{-oxen})(\mu_{1,1}\text{-}N_3)_2(Br)]_n$	1.98, 1.95	112.5	−85.7	[42c]
$[Cu_4(\mu\text{-oxen})_2(\mu_{1,1}\text{-}N_3)_2(\mu\text{-}1,3\text{-}N_3)]_n(ClO_4)_n$	1.98, 1.98	111.8		[4]
	2.41, 1.95	97.3		
$[Cu_2(hppz)_2(N_3)_2(\mu_{1,1}\text{-}N_3)(\mu_{1,3}\text{-}N_3)]_n$	2.28, 2.01	130.0	−11.5	[42d]
$[Cu_2(L^3)_2(N_3)_2(\mu_{1,1}\text{-}N_3)(\mu_{1,3}\text{-}N_3)]_n$	2.34, 1.99	116.6	14.1	[42e]
$[Cu_2(Me\text{-}L^4)(\mu_{1,1}\text{-}N_3)_4]_n$	2.30, 1.97	110.9		
$[Cu(L^5)(N_3)(\mu_{1,1}\text{-}N_3)]_n$	2.42, 1.96	113.6	−2.2	[42f]
$[Cu(L^6)(N_3)(\mu_{1,1}\text{-}N_3)]_n$	2.60, 1.95	107.1	−3.7	
Single- and double end-on azido bridged, together, in compound ***1***				
Compound **3a**	1.973, 2.017	104.7, 100.6	25.3	this work
	2.051, 1.961	106.59	−4.7	

[a] OBISDIEN = 1,13-dioxa-4,7,10,16,19,23-hexaazacyclotetracosane; *t*-bupy = 4-*tert*-butylpyridine; (tbz = bis(2-benzimidazolyl)propane; DMPDT = 2,5-bis-((pyridylmethy1)thio)thiadiazole; 4-Etpy = 4-ethylpyridine; 3-ampy = 3-aminopyridine; Meinic = methylisonicotinate; HL^1 = 1-(2-hydroxybenzyl)-1,5-diazacicloctane; bpm = bis(pyrazol-1-yl)methane; L^2 = 1,2,4,5-tetrakis-(1,4,7-triazacyclonon-1-ylmethyl)benzene, terpy = 2,2′:6,2″-terpyridine; SE = result from the condensation of *N*,*N*-dimethylethylenediamine with salicylaldehyde; H_2oxen = *N*,*N*′-bis(2-aminoethyl)oxamide; hppz = homopiperazine; L^3 = 2-(pyrazol-1-yl-methyl)pyridine; Me-L^4 = 2-(3-methylpyrazol-1-ylmethyl)pyridine. L^5 and L^6 are obtained from the condensation of 2-pyridylaldehyde with aniline and *p*-chloroaniline, respectively.

$\tau = 1$ for trigonal bipyramidal geometry). Thus, the J_2 value of $-4.7\ cm^{-1}$ (small for copper(II) ions), can be unequivocally assigned to the monobridge azido ligand (equatorial–axial). The two J values found in **3a** match with those shown in Table 2.

2.4.1. Reaction of excess ligand with $[Cu(RaaiR')(N_3)_2]_4$

To a 2-methoxy-ethanol solution of the tetranuclear complex, an excess of the ligand (the same ligand as is present in the tetranuclear copper(II) complex) was added and stirred for a few minutes. Upon addition of water to this solution a brown product was separated. It was then purified by recrystallisation from the mixture of methanol and 2-methoxy ethanol (1/1 v/v). Infrared spectra of the complex show a sharp single band at an average of $2045\ cm^{-1}$. This supports the presence of terminal N_3-bonding. Moderately intense stretchings at 1585–1595 and 1440–1450 cm^{-1} are referred to ν(C=N) and ν(N=N), respectively. These complexes are non-conducting and sufficiently soluble in common organic solvents like chloroform, dichloromethane and acetonitrile. The UV–Vis spectra are recorded in acetonitrile solution and show weak absorptions at 706–730 and 570–580 nm. The structural confirmation has been carried out in one case by a single crystal X-ray structure study and is given below in detail. Room temperature (298 K) magnetic data of mononuclear complexes **5** and **6** show the typical values of $\chi_M T$ for one unpaired electron (d^9), around 0.4 $cm^3\ mol^{-1}$ K.

2.4.2. $Cu(HaaiEt)_2(N_3)_2\cdot C_3H_8O_2$ (**6a**$\cdot C_3H_8O_2$)

Crystals are obtained on slow evaporation of a mixture of 2-methoxy ethanol and a methanol solution of $[Cu(HaaiEt)_2(N_3)_2]_4$ and HaaiEt (in excess). An ORTEP view of $Cu(HaaiEt)_2(N_3)_2\cdot C_3H_8O_2$ is shown in Fig. 4. Selected bond lengths and angles are given in Table 3. In the discrete molecule, copper(II) is surrounded by two ligands and two azido groups. The ligand serves as an unsymmetric N,N′-chelating agent (N refers to imidazole-N and N′ refers to azo-N donor centres) and two ligands chelate in a manner to give *cis*-N,N and *trans*-N′,N′ arrangements. Two N_3^- coordinate in a *cis*-fashion around Cu(II). Thus, the coordination sequence of azides, imidazole-N(N) and azo-N(N′) describe a *cis–cis–trans* stereochemical orientation. The geometry of the copper ion is an axially elongated octahedron; the equatorial plane is formed by two imidazole-N (each from an individual ligand) and two azido-N

Table 3
Bond distances (Å) and bond angles (°) of $Cu(HaaiEt)_2(N_3)_2 \cdot C_3H_8O_2$ (**6a** · $C_3H_8O_2$)

Cu(1)–N(1)	2.003(3)	N(1)–Cu(1)–N(12)	70.28(10)
Cu(1)–N(5)	2.018(3)	N(2)–Cu(1)–N(13)	105.40(13)
Cu(1)–N(12)	2.541(3)	N(5)–Cu(1)–N(7)	90.13(14)
Cu(1)–N(13)	2.569(3)	N(5)–Cu(1)–N(8)	70.84 (12)
Cu(1)–N(2)	1.985(4)	N(5)–Cu(1)–N(12)	88.04 (12)
Cu(1)–N(7)	1.994(3)	N(5)–Cu(1)–N(13)	69.60 (12)
N(1)–C(17)	1.319(5)	N(7)–Cu(1)–N(12)	106.21(12)
N(11)–C(17)	1.396(4)	N(7)–Cu(1)–N(13)	90.48(13)
N(11)–N(12)	1.264(4)	N(12)–Cu(1)–N(13)	152.30(10)
N(13)–N(14)	1.269(5)	N(1)–Cu(1)–N(12)	70.28(10)
N(2)–N(3)	1.201(6)	N(1)–Cu(1)–N(13)	93.35(11)
N(3)–N(4)	1.153(6)	Cu(1)–N(1)–C(17)	119.5(2)
N(7)–N(8)	1.164(6)	Cu(1)–N(2)–N(3)	120.0(3)
N(8)–N(9)	1.159(6)	N(2)–N(3)–N(4)	177.9(5)
N(5)–C(7)	1.326(5)	Cu(1)–N(5)–C(7)	119.0(3)
N(14)–C(7)	1.383(5)	N(1)–Cu1–N2	91.00(13)
		N1–Cu(1)–N(7)	176.16(14)
		N(2)–Cu(1)–N(5)	174.63(15)
		N(2)–Cu(1)–N(7)	87.90(15)
		Cu(1)–N(12)–N(11)	111.6(2)

donor centres. The two axial positions are occupied by two azo-N donor centres of two HaaiEt. The N–Cu–N bond angles subtended by the chelating ligands are N(1)–Cu–N(12), 70.28(10)° and N(5)–Cu–N(13), 69.60(12)° which are close to the precursor tetranuclear copper(II) compound. The arylazoimidazole moiety is almost planar with a deviation from the least square plane <0.04 Å. The chelate rings constitute good planes (mean deviation ~0.03 Å). The pendant aryl ring makes small a dihedral angle with the chelate plane and lie in the range 7–8°. The proposed molecular planes in the octahedral geometry are found to be heavily distorted in this structure. The distortion in CuN_6 coordination is supported from the bond parameters of the structures (Table 3).

There are three types of N-donor centres: N(imidazole), N(azo) and N(azido). Usually Cu–N(azo) distances are longer than the other distances and lie in the range of 2.6–2.7 Å. The reasons of more space of N(azo) have been accounted for earlier (see above) [23–25]. The structural distortion is not only of electronic origin (Jahn–Teller distortion for d^9, Cu(II)) but also arises from the steric effect of N-donor centres. The lowering in overall symmetry is manifested by the elongation of axial bonds and the two N(azo) donor centres occupy two axial positions. There is a small difference (~0.01 Å) between two Cu–N(imidazole) distances [Cu(1)–N(1), 2.003(3); Cu(1)–N(5), 2.018(3) Å]. The sum of the equatorial bond angles (plane is constituted by two imidazole-N and two azido-N donor centres) at Cu is 360.31°. It shows that the metal ion is essentially in the mean plane. A significant deviation from the *trans* angle is observed for the two axial N-donors, more than that of the equatorial N-donors in the chelated fragment Cu(HaaiEt). In the equatorial plane the *trans* angles are >170° [N(1)–Cu(1)–N(7), 176.16(14)°; N(2)–Cu(1)–N(5), 174.63(15)°]. The axial ∠N–Cu–N is >150° [N(12)–Cu(1)–N(13), 152.30(10)°]. The large deviation (~35°) from the *trans* angle (180°) is undoubtedly from the combined contribution of short chelate angle, lifting of the inherent degeneracy of the d^9 configuration and the steric requirement of azo-N centres. The azido bond lengths and angles are within the range for reported data [9–13]. The azo, N=N, distances lie between 1.26–1.27 Å which is longer than the free ligand value (1.250(1) Å) [26].

3. Experimental

3.1. Materials

$Cu(OAc)_2 \cdot H_2O$, NaN_3 were purchased from Sisco Research Lab, India, and 1-alkyl-2-arylazoimdazoles (RaaiR′) were prepared following the literature procedures [20]. All other chemicals and solvents were analytical reagent grade. Solvents were used after drying. For spectral studies solvents of spectroscopic grade were purchased from Lancaster, UK. The reaction conditions have been set up following the procedure of synthesis of $[Mn(MeaaiEt)(N_3)_2]_n$ [14].

Caution! Azido complexes of transition metal ions containing organic ligands are potentially explosive. Only a small amount of material should be prepared, and it should be handled with care.

3.2. Physical measurements

Microanalyses (C, H, N) were performed using a Perkin–Elmer 2400 CHNO/S elemental analyzer. Copper analyses were carried out by iodometric titration [43]. Spectroscopic measurements were carried out using the following instruments: UV–Vis spectra, reflectance spectra, JASCO UV–Vis/NIR model V-570; IR spectra (KBr disk, 4000–200 cm^{-1}), JASCO FT-IR model 420. The room temperature magnetic moment was measured using a vibrating sample PAR-155 magnetometer at 298 K. Molar conductances (Λ_M) were measured in a Systronics conductivity meter 304 model using ca. 10^{-3} M solutions in MeOH. The magnetic susceptibility of a powdered sample was measured using a SQUID Magnetometer in the temperature range 300–2 K at an applied field of 0.1 T. The contribution of the sample holder was determined separately in the same temperature range and field. Diamagnetic corrections were estimated from Pascal's constants. The magnetic susceptibility was fitted by least square techniques.

3.3. Syntheses

3.3.1. *[Cu(HaaiMe)(N3)2]4 (**3a**)*

A solution of 1-methyl-2-(phenylazo)imidazole (HaaiMe) (0.045 g, 0.24 mmol) in methanol (10 ml) was added dropwise to a stirred solution of $Cu(OAc)_2 \cdot H_2O$ (0.05 g, 0.25 mmol per copper) in MeOH (10 ml) at 298 K. The greenish brown solution was stirred for 15 min. NaN_3 (0.033 g, 0.51 mmol) in MeOH (10 ml) was

added to this solution. The colour changed from greenish brown to red brown. The solution was filtered and left undisturbed for a few days. The dark brown crystalline compounds were collected, washed with aqueous methanol (1:1, v/v) and finally with ether. It was dried in vacuo. Yield was 0.063 g (74%). The microanalytical data of the two complexes is as follows, $[Cu(HaaiMe)(N_3)_2]_4$ (**3a**): *Anal.* Calc. for $C_{40}H_{40}N_{40}Cu_4$: C, 35.97; H, 2.99; N, 41.97; Cu, 19.05. Found: C, 35.86; H, 3.05; N, 41.84; Cu, 18.91%. $[Cu(MeaaiMe)(N_3)_2]_4$ (**3b**) (yield, 65%). *Anal.* Calc. for $C_{44}H_{48}N_{40}Cu_4$: C, 37.98; H, 3.45; N, 40.28; Cu, 18.28. Found: C, 37.89; H, 3.39; N, 40.37; Cu, 18.14%. $[Cu(HaaiEt)(N_3)_2]_4$ (**4a**) (yield, 67%). *Anal.* Calc. for $C_{44}H_{48}N_{40}Cu_4$: C, 37.98; H, 3.45; N, 40.28; Cu, 18.28. Found: C, 37.92; H, 3.51; N, 40.33; Cu, 18.17%. $[Cu(MeaaiEt)(N_3)_2]_4$ (**4b**) (yield, 72%). *Anal.* Calc. for $C_{48}H_{56}N_{40}Cu_4$: C, 39.83; H, 3.87; N, 38.73; Cu, 17.57. Found: C, 39.89; H, 3.81; N, 38.68; Cu, 17.45%.

3.3.2. Reaction of HaaiMe with $[Cu(HaaiMe)(N_3)_2]_4$

To a well-stirred suspension of $[Cu(HaaiMe)(N_3)_2]_4$ (**3a**) (0.1 g, 0.30 mmol) in 2-methoxy ethanol (5 ml), a small excess to one equivalent (with reference to per copper atom) of HaaiMe (0.60 g, 0.32 mmol) in methanol (10 ml) was added and stirred continuously for 30 min. By this time the solution colour changed to brown violet. It was then filtered through a G-4 crucible, to reject any residue, and left undisturbed for slow evaporation. Dark coloured crystals appeared after a week. These were then filtered, washed with cold methanol and dried in vacuo over $CaCl_2$. Yield was 0.09 g (58%). $[Cu(HaaiMe)_2(N_3)_2]$ (**5a**): *Anal.* Calc. for $C_{20}H_{20}N_{14}Cu$: C, 35.97; H, 2.99; N, 41.97; Cu, 19.05. Found: C, 35.86; H, 3.05; N, 41.84; Cu, 18.91%.

$[Cu(MeaaiMe)_2(N_3)_2]$ (**5b**) (yield, 55%). *Anal.* Calc. for $C_{22}H_{24}N_{14}Cu$: C, 37.98; H, 3.45; N, 40.28; Cu, 18.28. Found: C, 37.89; H, 3.39; N, 40.37; Cu, 18.14%. $[Cu(HaaiEt)_2(N_3)_2]$ (**6a**) (yield, 60%). *Anal.* Calc. for $C_{22}H_{24}N_{14}Cu$: C, 37.98; H, 3.45; N, 40.28; Cu, 18.28. Found: C, 37.92; H, 3.51; N, 40.33; Cu, 18.17%. $[Cu(MeaaiEt)_2(N_3)_2]$ (**6b**) (yield, 58%). *Anal.* Calc. for $C_{24}H_{28}N_{14}Cu$: C, 39.83; H, 3.87; N, 38.73; Cu, 17.57. Found: C, 39.89; H, 3.81; N, 38.68; Cu, 17.45%.

3.4. Crystallographic data collection and refinement of the structure

Good quality and stable to X-ray crystals for both the complexes were collected from slow evaporation of synthetic mixtures in methanol and 2-methoxy ethanol. Data were collected with a Siemens SMART CCD diffractometer using fine focus sealed graphite-monochromatized Mo Kα radiation ($\lambda = 0.71073$ Å). Unit cell parameters were determined from least-squares refinement of setting angles of 6529 reflections at 293 K for $[Cu(HaaiMe)(N_3)_2]_4$ (**3a**) and 7195 reflections for $[Cu(HaaiEt)_2(N_3)_2]\cdot C_3H_8O_2$ (**6a**) at 294 K. Data were collected with 2θ in the range $4.04 \leqslant 2\theta \leqslant 56.54°$ (for **3a**) and $2.6 \leqslant 2\theta \leqslant 56.6°$ (for **6a**).

Table 4
Summarized crystallographic data for **3a** and **6a** · $C_3H_8O_2$

Compound	**3a**	**6a** · $C_3H_8O_2$
Empirical formula	$C_{40}H_{40}N_{40}Cu_4$	$C_{25}H_{32}N_{14}O_2Cu$
Formula weight	1335.32	624.19
Temperature (K)	293	294
Crystal system	orthorhombic	orthorhombic
Space group	*Pbca*	*Pbca*
Crystal size $(mm)^3$	$0.10 \times 0.08 \times 0.05$	$0.15 \times 0.20 \times 0.20$
a (Å)	19.2947(14)	12.5670(7)
b (Å)	14.9915(11)	15.8577(9)
c (Å)	19.2947(14)	31.2045(18)
β (°)	90	90
V $(Å)^3$	5581.1(7)	6218.5(6)
Z	8	8
λ (Å)	0.71073	0.71073
μ (Mo Kα) (mm^{-1})	1.576	0.750
D_{calc} $(Mg\,m^{-3})$	1.589	1.134
Refined parameters	379	383
Reflection number total	31 861	35 918
Unique reflections	6529	7195
R_1[a] $[I > 2\sigma(I)]$	0.0444	0.0652
wR_2[b]	0.0970	0.1322
Goodness-of-fit	0.92	0.83

[a] $R = \sum(|F_o - F_c|)/\sum|F_o|$.
[b] $wR = [\sum w(F_o^2 - F_c^2)/\sum w(F_o)^2]^{1/2}$, $w = 1/[\sigma^2(F_o)^2 + (0.0462P)^2]$ for **3a** and $w = 1/[\sigma^2(F_o)^2 + (0.0659P)^2]$ for **6a**, where $P = ((F_o)^2 + 2(F_c)^2)/3$.

A summary of the crystallographic data and structure refinement parameters is given in Table 4. Reflection data were recorded using the ω scan technique. Data were corrected for Lorentz polarization effects and for linear decay using the SAINT program. Semi-empirical absorption corrections based on ψ-scans were applied. The structure was solved by direct methods using SHELXS-97 [44,45] and successive difference Fourier syntheses. All non-hydrogen atoms were refined anisotropically. The hydrogen atoms were fixed geometrically and refined using the riding model. In the final difference Fourier map the residual maxima and minima were 0.396 and −0.206 for **3a** and 0.313 and −0.230 for **6a**.

4. Conclusion

In this research we demonstrate the synthesis of tetranuclear $[Cu(RaaiR')(N_3)_2]_4$ complexes from the reaction of $Cu(OAc)_2\cdot H_2O$, RaaiR′ and NaN_3 in a 1:1:2 mole ratio. Addition of RaaR′ (a slight excess of one equivalent) to a 2-methoxy ethanol solution of the tetranuclear compound has degraded it to a mono-copper compound of composition, $[Cu(RaaiR')_2(N_3)_2]$. In each case, the structural confirmation has been done by X-ray diffraction studies. The tetranuclear arrangement has been achieved by end-on sharing of N_3-groups in the dimers in which six-coordinated CuN_6 and five-coordinated CuN_5 units are associated via two end-on-N_3 bridging groups. IR spectra also distinguish the bonding pattern. Variable temperature magnetic susceptibility measurement (300–2 K) shows both anti- and ferromagnetic interactions for $[Cu(HaaiMe)(N_3)_2]_4$.

Acknowledgements

Financial support from the Council of Scientific and Industrial Research, and Department of Science and Technology, New Delhi are gratefully acknowledged. C.S. also acknowledges UGC for providing him a Visiting Associateship to I.I.Sc., Bangalore. M.S.F. is also grateful for the grant given by the Spanish Ministerio de Ciencia y Tecnologia (Programa Ramon y Cajal). Our sincere thanks are due to Prof. J. Ribas, Universitat de Barcelona, Spain for his helpful discussion on magnetism of the complexes.

Appendix A. Supplementary material

UV–Vis and infrared spectral data are submitted in Supplementary Table. Crystallographic data for the structures have been deposited with the Cambridge Crystallographic Data Centre, CCDC No. 249036 for $Cu(HaaiEt)_2(N_3)_2 \cdot C_3H_8O_2$ and 249037 for $[Cu(HaaiMe)(N_3)_2]_4$. Copies of this information may be obtained free of charge from the CCDC, 12 Union Road, Cambridge CB2 1EZ, UK (e-mail: deposit@ccdc.cam.ac.uk or www: http://www.ccdc.cam.ac.uk). Supplementary data associated with this article can be found, in the online version, at doi:10.1016/j.poly.2006.04.007.

References

[1] M. Melnik, Coord. Chem. Rev. 42 (1982) 259.
[2] S. Sain, T.K. Maji, D. Das, J. Cheng, T.-H. Lu, J. Ribas, M.S. El Fallah, N.R. Chaudhuri, J. Chem. Soc., Dalton Trans. (2002) 1302.
[3] (a) T.K. Maji, P.S. Mukherjee, G. Mostafa, T. Mallah, J. Cano-Boquera, N.R. Chaudhuri, Chem. Commun. (2001) 1012;
(b) T.K. Maji, P.S. Mukherjee, S. Koner, G. Mostafa, J.P. Tuchangues, N.R. Chaudhuri, Inorg. Chim. Acta 314 (2001) 111.
[4] P.S. Mukherjee, T.K. Maji, G. Mostafa, T. Mallah, N.R. Chaudhuri, Inorg. Chem. 39 (2000) 5147.
[5] (a) O. Kahn, Molecular Magnetism, VCH, New York, 1993;
(b) O. Kahn (Ed.), Magnetism: A Supramolecular Function, NATO Series C 484, Kluwer Academic, Dordrecht, 1996.
[6] (a) J.S. Miller, M. Drillon (Eds.), Magnetism: Molecules to Materials II, Molecule-based Materials, Wiley–VCH, Weinheim, 2001;
(b) M.M. Turnbull, T. Sugimoto, L.K. Thompson (Eds.), Molecular-based Magnetic Materials: Theory, Techniques and Applications, ACS Symposium Series, American Chemical Society, Washington, DC, 1996, p. 644.
[7] (a) A. Mukherjee, M.K. Saha, I. Rudra, S. Ramsesha, M. Nethaji, A.R. Chakravarty, Inorg. Chim. Acta 357 (2004) 1077;
(b) S.K. Dey, B. Bag, K.M. Abdul Malik, M.S. El Fallah, J. Ribas, S. Mitra, Inorg. Chem. 42 (2003) 4029;
(c) J.D. Crane, A.Mc. Laughlin, Inorg. Chem. Commun. 7 (2004) 499;
(d) J. Ribas, M. Monfort, R. Costa, X. Solans, Inorg. Chem. 32 (1993) 695, and references therein;
(e) J. Pons, F.J. Sanchez, J. Casabo, A. Alvarez-Larena, J.F. Piniella, J. Ros, Inorg. Chem. Commun. 6 (2003) 833.
[8] D.M. Ciurtin, M.D. Smith, H.-C. Zurloye, J. Chem. Soc., Dalton Trans. (2003) 1245.
[9] (a) Y. Nishida, S. Kida, J. Chem. Soc., Dalton Trans. (1986) 2633;
(b) K. Geetha, M. Nethaji, N.Y.V. Vasanthaacharya, A.R. Chakravorty, J. Coord. Chem. 47 (1999) 77.
[10] (a) F. Averseng, P.G. Lacroix, I. Malfant, N. Perisse, C. Lepetit, K. Nakatani, Inorg. Chem. 40 (2001) 3797;
(b) H. Oshio, Y. Saito, T. Ito, Angew. Chem., Int. Ed. 36 (1997) 2673.
[11] (a) D.A. Buckingham, Coord. Chem. Rev. 587 (1994) 135;
(b) A. Escuer, M.A.S. Goher, F.A. Mautner, R. Vicente, Inorg. Chem. 39 (2000) 2107;
(c) M.A.S. Goher, A. Escuer, F.A. Mautner, N. Al-Salem, Polyhedron 20 (2001) 2971;
(d) R. Costa, M.K. Urtiaga, L. Lezama, J. Ignacio, R. Larramendi, M.I. Arriortua, T. Rojo, J. Chem. Soc., Dalton Trans. (1993) 3685;
(e) J. Ribas, A. Escuer, M. Monfort, R. Vicente, R. Costa, L. Lezama, T. Rojo, Coord. Chem. Rev. 193–195 (1999) 1027.
[12] P. Manikandan, R. Muthukumaran, K.R.J. Tomas, B. Varghese, G.V.R. Chandramouli, P.T. Manoharan, Inorg. Chem. 40 (2001) 2378.
[13] S. Koner, S. Saha, K.-I. Okamoto, J.P. Tuchagues, Inorg. Chem. 42 (2003) 4668.
[14] U.S. Ray, Sk. Jasimuddin, B.K. Ghosh, M. Monfort, J. Ribas, G. Mostafa, T.-H. Lu, C. Sinha, Eur. J. Inorg. Chem. (2004) 250.
[15] (a) T.K. Misra, D. Das, C. Sinha, Polyhedron 16 (1997) 4163;
(b) P.K. Santra, T.K. Misra, C. Sinha, Indian J. Chem. 38a (1999) 82;
(c) J. Dinda, U.S. Ray, G. Mostafa, T.-H. Lu, A. Usman, I.A. Razak, S. Chantrapromma, H.-K. Fun, C. Sinha, Polyhedron 22 (2003) 247.
[16] U.S. Ray, D. Banerjee, G. Mostafa, T.-H. Lu, C. Sinha, New J. Chem. 28 (2004) 1432.
[17] U.S. Ray, B.G. Chand, G. Mostafa, J. Chang, T.-H. Lu, C. Sinha, Polyhedron 22 (2003) 2587.
[18] (a) T.K. Misra, D. Das, C. Sinha, P. Ghosh, C.K. Pal, Inorg. Chem. 37 (1998) 1672;
(b) S. Pal, T.K. Misra, C. Sinha, A.M.Z. Slawin, J.D. Woollins, Polyhedron 19 (2000) 1925;
(c) P. Byabartta, S. Pal, T.K. Misra, C. Sinha, F.-L. Liao, K. Panneerselvam, T.-H. Lu, J. Coord. Chem. 55 (2002) 479.
[19] (a) J. Dinda, D. Das, P.K. Santra, C. Sinha, L.R. Falvello, J. Organomet. Chem. 629 (2001) 28;
(b) S. Pal, D. Das, C. Sinha, C.H.L. Kennard, Inorg. Chim. Acta 313 (2001) 21;
(c) S. Pal, D. Das, P. Chattopadhyay, C. Sinha, K. Pannerselvam, T.-H. Lu, Polyhedron 19 (2000) 1263.
[20] U.S. Ray, B.G. Chand, A.K. Dasmahapatra, T.-H. Lu, G. Mostafa, C. Sinha, Inorg. Chem. Commun. 6 (2003) 634.
[21] (a) B.G. Chand, U.S. Ray, J. Chang, T.-H. Lu, C. Sinha, Polyhedron 22 (2003) 1213;
(b) B.G. Chand, U.S. Ray, G. Mostafa, T.-H. Lu, C. Sinha, J. Coord. Chem. 57 (2004) 627;
(c) B.G. Chand, U.S. Ray, G. Mostafa, T.-H. Lu, L.R. Falvello, T. Soler, M. Tomás, C. Sinha, Polyhedron 22 (2003) 3161;
(d) B.G. Chand, U.S. Ray, G. Mostafa, T.-H. Lu, C. Sinha, Polyhedron 23 (2004) 1669;
(e) B.G. Chand, U.S. Ray, P.K. Santra, G. Mostafa, T.-H. Lu, C. Sinha, Polyhedron 22 (2003) 1205.
[22] K. Nakamoto, Infrared and Raman Spectra of Inorganic and Coordination Compounds: Part B, 5th ed., Wiley, New York, 1997.
[23] J.E. Huheey, E.A. Keiter, R.L. Keiter, Inorganic Chemistry, 4th ed., Harper Collins (Addison-Wesley Publishing Company), Reading, MA, 2000.
[24] A.G. Orpen, L. Brammar, F.K. Allen, O. Kennard, D.G. Watson, R. Taylor, J. Chem. Soc., Dalton Trans. 1 (1989) S1.
[25] K.D. Karlin, J. Zubieta (Eds.), Copper Coordination Chemistry: Biochemical and Inorganic Perspectives, Adenine Press, Guilderland, NY, 1983.
[26] D. Das, Ph.D. Thesis, Burdwan University, Burdwan-713104, India, 1998.
[27] E. Ruiz, J. Cano, S. Alvarez, P. Alemany, J. Am. Chem. Soc. 120 (1998) 11122.
[28] J. Comarmond, P. Plumeré, J.M. Lehn, Y. Agnus, R. Louis, R. Weiss, O. Kahn, I. Morgenstern-Badarau, J. Am. Chem. Soc. 104 (1982) 6330.

[29] (a) S. Sikorav, I. Bkouche-Waksman, O. Kahn, Inorg. Chem. 23 (1984) 490;
(b) M.L. Boillot, Y. Jornaux, A. Bencini, D. Gatteschi, O. Kahn, Inorg. Chem. 24 (1985) 263.
[30] M.A. Aebersold, B. Gillon, O. Plantevin, L. Pardi, O. Kahn, P. Bergerat, I. von Seggern, F. Tuczek, L. Ohrström, A. Grand, E. Levièvre-Berna, J. Am. Chem. Soc. 120 (1998) 5238.
[31] G.A. van Albada, M.T. Lakin, N. Veldman, A.L. Spek, J. Reedijk, Inorg. Chem. 34 (1995) 4910.
[32] F. Tuczek, W. Bensch, Inorg. Chem. 34 (1995) 1482.
[33] X.H. Bu, M. Du, Z.-L. Shang, R.-H. Zhang, D.-Z. Liao, M. Shionoya, T. Clifford, Inorg. Chem. 39 (2000) 4190.
[34] L. Zhang, L.-F. Tang, Z.-H. Wang, M. Du, M. Julve, F. Lloret, J.-T. Wang, Inorg. Chem. 40 (2001) 3619.
[35] B. Graham, M.T.W. Hearn, P.C. Junk, C.M. Kepert, F.E. Mabbs, B. Moubaraki, K.S. Murray, L. Spiccia, Inorg. Chem. 40 (2001) 1536.
[36] S.S. Tandon, L.K. Thompson, M.E. Manuel, J.N. Bridson, Inorg. Chem. 33 (1994) 5555.
[37] G. De Munno, M.G. Lombardi, M. Julve, F. Lloret, J. Faus, Inorg. Chim. Acta 282 (1998) 82.
[38] J.P. Costes, F. Dahan, J. Ruiz, J.P. Laurent, Inorg. Chim. Acta 239 (1995) 53.
[39] L. Li, D. Liao, Z. Jiang, S. Yan, Polyhedron 20 (2001) 681.
[40] K. Matsumoto, S. Ooi, K. Nakatsuka, W. Mori, S. Suzuki, A. Nakahara, Y. Nakao, J. Chem. Soc., Dalton Trans. (1985) 2095.
[41] H. Shen, W. Bu, E. Gao, D. Liao, Z. Jiang, S. Yan, X. Wang, Angew. Chem., Int. Ed. 39 (2000) 3633.
[42] (a) J.D. Woodward, R.V. Backov, K.A. Abboud, D. Dai, H.-J. Koo, M.-H. Whangbo, M.W. Meisel, D.R. Talham, Inorg. Chem. 44 (2005) 638;
(b) Y.-B. Jiang, H.-Z. Kou, R.-J. Wang, A.-L. Cui, Eur. J. Inorg. Chem. (2004) 4608;
(c) E.-Q. Gao, S.-Q. Bai, C.-F. Wang, Y.-F. Yue, C.-H. Yan, Inorg. Chem. 42 (2003) 8456;
(d) Z.-N. Chen, H.-X. Zhang, K.-B. Yu, B.-S. Kang, Chem. Lett. (1998) 275;
(e) Z.-N. Chen, J. Qiu, Z.-K. Wu, D.G. Fu, K.-B. Yu, W.X. Tang, J. Chem. Soc., Dalton Trans. (1994) 1923;
(f) E.-Q. Gao, Y.-F. Yue, S.-Q. Bai, Z. He, C.-H. Yan, Cryst. Growth Des. 5 (2005) 1119.
[43] A.I. Vogel, A Text Book of Quantitative Inorganic Analysis, 3rd ed., ELBS, Longman, London, 1975, p. 433.
[44] G.M. Sheldrick, SHELXL-97: Program for Refinement of Crystal Structures; SHELXS-97: Program for the Solution of Crystal Structures, University of Gottingen, Gottingen, Germany, 1997.
[45] A.L. Spek, PLATON: Molecular Geometry Program, University of Utrecht, Netherlands, 1999.

elimination of RH is accompanied by formation of binuclear and polynuclear compounds containing bridging bpy ligand in which both pyridyl rings are 3-metallated [19].

We were using some dimeric rhodium(II) complexes ($[Rh_2(RCOO)_2(N–N)_2(H_2O)_2](RCOO)_2$ and $[Rh_2X_2(RCOO)_2(N–N)_2]$ where R = H, CH_3, Me, Et, *n*-Bu, PhCH(OH), X = Cl^-, Br^-, I^- and N–N = 2,2′-bipyridine or 1,10-phenanthroline) as very active homogeneous hydrogenation catalysts of ketones [20] and olefins [21]. The reaction takes place in basic methanolic solutions. In order to understand better reactivity of these catalytic systems we have decided to investigate 'in situ' generated catalysts using ^1H and ^{13}C NMR. The NMR experiments were run in the solution of $[Rh_2\{\mu\text{-}(S)\text{-}PhCH(OH)COO\}_4(H_2O)_2]$ (**1**) and $[Rh_2(\mu\text{-}CH_3COO)_4(H_2O)_2]$ with 2,2′-bipyridine and 4,4′-dimethyl-2,2′-bipyridine in CD_3ONa/CD_3OD as well as $[Rh(bpy)_2]Cl$ (**2**) in the same CD_3ONa/CD_3OD solution. ^1H and ^{13}C NMR experiments for **1** in the solution of CD_3ONa/CD_3OD have shown that C–H bond activation in the coordinated bpy ligand takes place. As a result of this reaction H–D exchange occurs. To our knowledge this is the first example of deuterium exchange of **H3,3′**-protons in 2,2′-bipyridine complexes of rhodium.

2. Experimental

The complexes $[Rh_2\{\mu\text{-}(S)\text{-}PhCH(OH)COO\}_4(H_2O)_2]$ (**1**) [22], $[Rh_2(\mu\text{-}CH_3COO)_4(H_2O)_2]$ [23], and $[Rh(bpy)_2]Cl$ (**2**) [24] were prepared according to the published methods. The CD_3ONa/CD_3OD solutions were prepared by dissolving sodium metal in oxygen-free CD_3OD. NMR experiments were performed using the following conditions: Na:Rh molar ratio = 20:1–60:1; [Rh] = 10^{-2} M–4×10^{-2} M; bpy: Rh molar ratio = 2:1; temperature = 25–50 °C. All manipulations were performed under Ar. ^1H and ^{13}C NMR spectra were recorded on a Bruker AM400 and AMX300 spectrometers. ^{13}C NMR spectra were performed using ca. 50 000–60 000 scans. Chemical shifts are reported in ppm relative to tetramethylsilane, using the residual solvent proton resonance (methanol, $\delta = 3.31$ ppm) as an internal standard. The procedure with **1** as a starting compound was as follows: the appropriate amount of **1** and bpy was placed in NMR tube, and the tube was filled with argon. Then the known amount of CD_3ONa/CD_3OD solution was added under argon to the NMR tube. The solid reagents dissolve over a period of about 15–30 min at room temperature to give a deep violet solution. At this moment the measurements of the NMR spectra have been started. In the case of 4,4′-Me_2-bpy the solution of the ligand in CD_3ONa/CD_3OD was prepared first. Then this solution was transported under argon to the NMR tube containing the known amount of **1**. Again NMR measurements were started when the solution turned deep violet. The procedure with **2** was analogous. In the case of this reaction the solution of ligand in CD_3ONa/CD_3OD was added to the tube containing rhodium complex **2**.

3. Results and discussion

Dissolution of $[Rh_2\{\mu\text{-}(S)\text{-}PhCH(OH)COO\}_4(H_2O)_2]$ – bpy mixture (bpy: Rh molar ratio = 2:1) in the CD_3ONa/CD_3OD as a solvent (under Ar) affords a violet solution over a period of about 10–30 min which depends mainly on the temperature. At higher temperatures (50 °C) it takes about 10 min to get the violet colour. The NMR spectra of the resultant solutions exhibit two general characteristic features:

(i) At the beginning of reaction there are four signals present in the "bipyridine region": **H6,6′** (8.66 ppm, d $^3J_{5,6} = 5.6$ Hz); **H3,3′** (8.28 ppm, d, $^3J_{3,4} = 8.0$ Hz); **H4,4′** (7.93 ppm, t, $^3J_{3,4} = {}^3J_{4,5} = 8.0$ Hz); **H5,5′** (7.44 ppm, dd, $^3J_{4,5} = 8.0$ Hz, $^3J_{5,6} = 5.6$ Hz). The doublet due to **H3,3′** protons is slowly diminishing during the reaction and finally completely vanishes. The substitution is completed within 2–3 days at room temperature, and within 0.5–1 h when the solution is heated at 50 °C. At the same time, the signal due to 4,4′-protons (δ 7.93 ppm) undergoes transformation from triplet to doublet (exhibiting the fine structure due to H–D coupling) and the signals due to the 5,5′ – and 6,6′ – protons remain essentially unchanged (Fig. 1).

Under analogous reaction conditions, free bpy is unreactive. These observations are in accord with complete

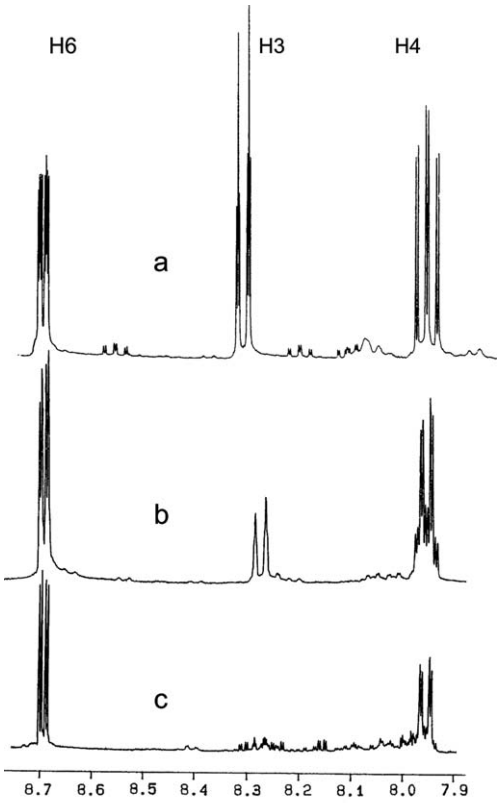

Fig. 1. A part of ^1H NMR spectrum measured in the time of reaction. (a) 20 min after adding CD_3ONa/CD_3OD solution to the solution of **1** with bpy in CD_3OD. (b) Spectrum recorded after 10 h of reaction and (c) final spectrum after two days of reaction. Reaction was made at 298 K.

exchange of the 3,3′ protons for deuterium. This exchange has been also followed using ^{13}C NMR. After complete exchange of **H3,3′** protons the **C3,3′** resonance at 122.7 ppm also decreases and finally disappears due to the lack of the Nuclear Overhauser Effect and the new, very low intensity triplet centered at 122.2 ppm appears (Fig. 2).

The slight shift towards a higher field is due to the isotope effect. During the diminishing of **H3,3′** resonances several new, low intensity signals in the "bipyridine region" are observed. Two of them are shifted towards higher fields; 6.84 ppm (d) and 6.64 ppm (dd). The analogous patterns with similar chemical shifts have been observed for well defined $[Ir(Hbpy\text{-}C^3,N')(bpy\text{-}N,N')_2]^{3+}$ in $Me_2SO\text{-}d_6$ (6.8 ppm (d) and 7,16 ppm (dd)) [16] and for $[Ir(bpy\text{-}C^3,N')^{-}(bpy\text{-}N,N')_2]^{2+}$ in 50% D_2O – 50% $Me_2SO\text{-}d_6$ (6.8 ppm (d) and 7.12 ppm (dd)) [15], for some Pd cyclometallated complexes with 6- substituted bipyridine (the observed chemical shifts were 6.73 and 6.84 ppm for H5, and 7.29 and 7.33 for H4 protons in complexes of the type $[Pd(L)(PPh_3)Cl]\cdot HBF_4$ [25], or in similar platinum(II) complexes [26]. Therefore we suggest that complexes of the type (**II**) (see Scheme 1) are formed during H–D exchange reaction.

(ii) During the deuterium exchange reaction several hydride resonances appear. They have been observed in the range of −14 to −28 ppm. The number and intensity of the signals in hydride region are strongly dependent upon the reaction temperature. Hydride signals at higher fields (about −26 to −28 ppm) are observed only at low temperatures, below −60 °C. The most stable Rh hydride resonance is a doublet at −15.94 ppm ($^1J_{Rh-H} = 27.5$ Hz). It can be assigned to the orthometallated Rh(III) complex

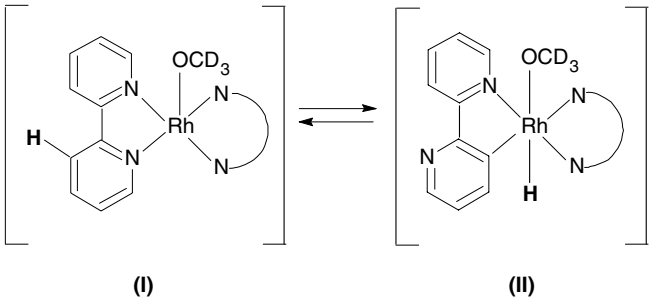

(I) (II)

Scheme 1.

which should be kinetically inert due to the d^6 electronic configuration of the central atom (Fig. 3).

It must be emphasized that the only hydrogen source are coordinated 2,2′-bipyridine ligands because the experiments have been performed under Ar and in solution of CD_3ONa in CD_3OD. The process of hydride formation is rather slow and the time after which hydride resonances can be observed depends strongly on the reaction conditions (especially on the temperature of reaction). At 50 °C the −15.94 ppm resonance is observed after about 5–10 min. Within this period of time the solution becomes violet, suggesting the formation of the square planar Rh(I) compounds [24] which may undergo oxidative addition giving hydrido complexes of Rh(III). The hydride signals are of very low intensity as compared to the very strong resonances of the 2,2′-bipyridine protons of the "main" rhodium complex present in solution. The hydride resonances are approximately four times less intense than signals at 6.64 ppm and 6.84 ppm characteristic for complexes obtained in the reaction of "roll over metallation" [25,26].

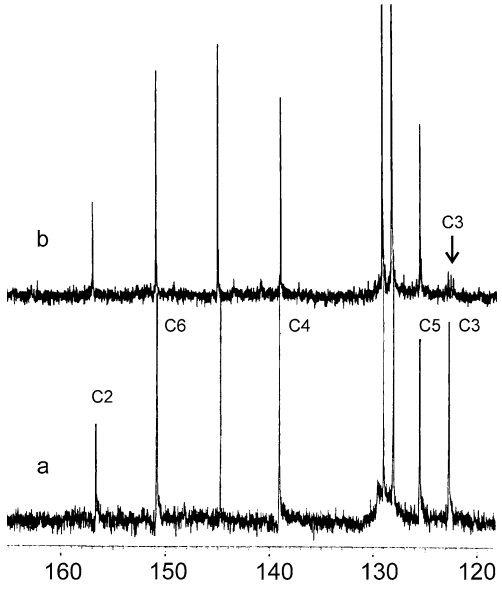

Fig. 2. Fragment of ^{13}C NMR spectrum for the same solution as in Fig. 1. (a) The beginning of the reaction and (b) spectrum recorded after complete exchange of **H3,3′** protons.

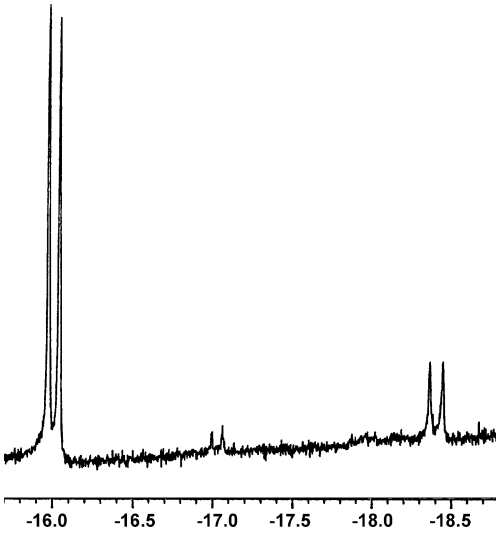

Fig. 3. 3 Part of ^1H NMR spectrum in "hydride" region. The doublet at −15.94 ppm ($J_{Rh-H} = 27.5$ Hz) belongs to the most stable hydrido complex.

The chemical shifts observed for hydride resonances in these "in situ" experiments are; −13.97 ppm (d, $^1J_{Rh-H} = 27.2$ Hz) and −15.94 ppm (d $^1J_{Rh-H} = 27.5$ Hz). The signal at −13.97 ppm (always present at the beginning of experiment) slowly decreases while the −15.94 ppm doublet is growing. This higher field signal is present in the spectrum until the **H3,3′–D3,3′** exchange is completed. The observed chemical shifts and coupling constants are quite similar to those reported for some rhodium(III) complexes with ethylenediamine as a chelating ligand [27]: $\delta = -16.3$ to −22.6 ppm; $^1J_{Rh-H} = 19$ to 30 Hz.

Above observations strongly suggest that oxidative addition reaction according to the Scheme 1 takes place.

In the first step of the reaction the carboxylate bridges are broken and coordination of the [OCD_3^-] anions and 2,2′-bipyridine occurs. It has been recently confirmed for [$Pt(bpy)_2$] complex in aqueous alkaline solution that at these conditions an attack of OH^- at the metal center takes place [37]. As a result of this reaction, a six-coordinate rhodium(III) hydride (abbreviated as (**II**)) is formed, and it should play the crucial role as a kinetically inert intermediate in the deuterium exchange reaction. We postulate that at this step of the reaction hydride resonances in NMR spectra are observed. The analogous pathway have been postulated for the cyclometallation of [$Pt(Me)_2$(6-R-bpy)], where R = alkyl or aryl [26].

In order to simplify the system under investigation we have prepared [$Rh(bpy)_2$]Cl (**2**) [24]. The ^{1}H NMR (300 MHz) spectrum of this complex (10^{-2} M) in CD_3ONa/CD_3OD solution (under Ar) exhibits only one hydride resonance of low intensity at −15.94 ppm (d, $^1J_{Rh-H} = 27.4$ Hz). As in the case of "in situ" reactions for this compound **H3,3′–D3,3′** exchange is also observed (the **H3,3′** doublet ($\delta = 8.29$ ppm) and 122.6 ppm resonance in ^{13}C are lowering their intensities with time). Square planar complexes of the type $[Rh(bpy)_2]^+$ are well known [24,28–33] and have been used in some interesting catalytic reactions as for instance: hydrogen production [29,30], wgsr [33], selective hydrogenation of ketones and hydrogenation of ketones with isopropanol as a hydrogen source [34,35].

On the basis of NMR experiments we postulate one of the possible mechanisms of the **H3,3′–D3,3′** exchange in the system under investigations (Scheme 2).

As it has been mentioned earlier during the "in situ" reactions several hydride resonances are observed which suggest a few different rhodium species (all signals are of low intensity). It is well known that $[Rh(bpy)_2]^+$ forms several different species which is pH and concentration dependent [24]. These species may form different hydrides.

We would like to emphasize that when the reaction mixture is heated to 50 °C for a long period of time (several hours) **H4,4′–D4,4′** and **H5,5′–D5,5′** exchange has also been observed. This suggests that other exchange mechanisms are also possible, as was proposed for ruthenium compound with bpy [3,36].

In order to establish how substituents in bpy influence the reactivity of H–D exchange we performed the "in situ" reaction of **1** with 4,4′-Me_2-bpy. We have noticed unexpectedly that in this case there were no H–D exchange reaction in bpy rings. However this system shows considerable activity of methyl protons towards the H–D exchange reaction, although under similar reaction conditions free 4,4′-Me_2-bpy is unreactive. During the reactions no hydrides have been observed. Therefore the mechanism of this exchange should be different from that proposed for 2,2′-bipyridine.

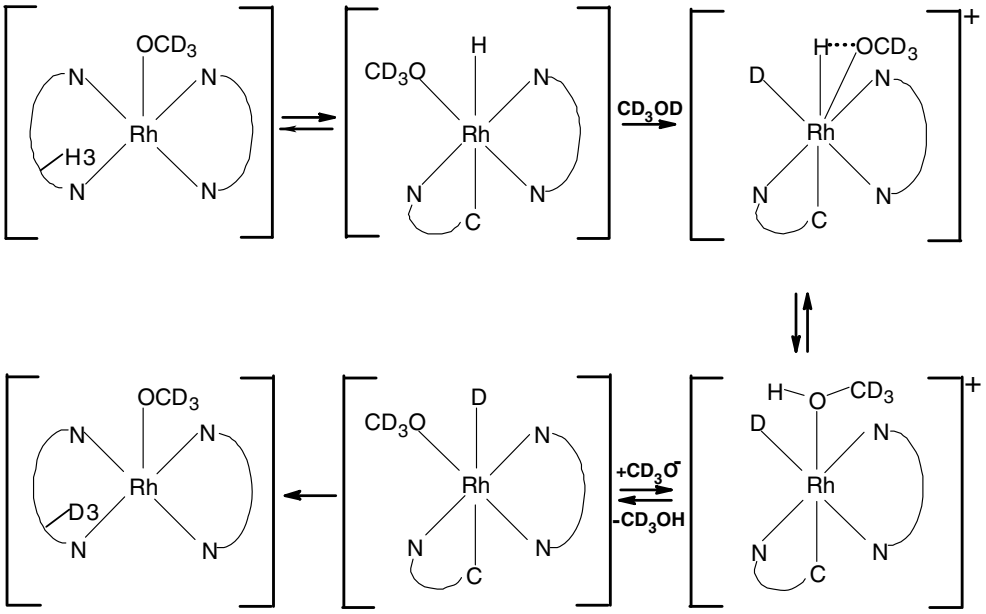

Scheme 2.

References

[1] E.C. Constable, K.R. Seddon, J. Chem. Soc., Chem. Commun. (1982) 34.
[2] O. Wernberg, J. Chem. Soc., Dalton Trans. (1985) 1993.
[3] E.C. Constable, J. Chem. Soc., Dalton Trans. (1985) 2687.
[4] (a) E.C. Constable, J.M. Holmes, J. Organomet. Chem. 301 (1986) 203; (b) F. Barigelletti, D. Sandrini, M. Maestri, V. Balzani, A. von Zalewsky, L. Chassot, P. Jolliet, U. Maeder, Inorg. Chem. 27 (1988) 3644; (c) K. Dedeian, P.I. Djurovich, F.O. Garces, G. Carlson, R.J. Watts, Inorg. Chem. 30 (1991) 1685; (d) E.C. Constable, A.M.W. Cargill Thompson, T.A. Leese, D.G.F. Reese, D.A. Tocher, Inorg. Chim. Acta 182 (1991) 93; (e) J.H. van Diemen, J.G. Haasnoot, R. Hage, J. Reedijk, J.G. Vos, R. Wang, Inorg. Chem. 30 (1991) 4038; (f) M.G. Colombo, T.C. Brunold, T. Riedener, H.U. Güdel, M. Förtsch, H.-B. Bürgi, Inorg. Chem. 33 (1994) 545.
[5] (a) E.C. Constable, R.P.G. Henney, T.A. Leese, D.A. Tocher, J. Chem. Soc., Dalton Trans. (1990) 443; (b) J.-P. Collin, M. Beley, J.-P. Sauvage, F. Barigelletti, Inorg. Chim. Acta 186 (1991) 91; (c) E.C. Constable, M.J. Hannon, Inorg. Chim. Acta 211 (1993) 101.
[6] E.C. Constable, S.J. Dunne, D.G.F. Rees, C.X. Schmitt, J. Chem. Soc., Chem. Commun. (1996) 1169.
[7] A.J. Deeming, R. Peters, M.B. Hursthouse, J.D.J. Backer-Dirks, J. Chem. Soc., Dalton Trans. (1982) 787.
[8] S. Dholakia, R.D. Gillard, F.L. Wimmer, Inorg. Chim. Acta 69 (1983) 179.
[9] S. Dholakia, R.D. Gillard, F.L. Wimmer, Inorg. Chim. Acta 65 (1982) L121.
[10] F.L. Wimmer, S. Wimmer, Transit. Met. Chem. Weinheim, Ger. 10 (1985) 238.
[11] P. Castan, F. Dahan, S. Wimmer, F.L. Wimmer, J. Chem. Soc., Dalton Trans. (1990) 2971.
[12] S. Wimmer, F.L. Wimmer, J. Chem. Soc., Dalton Trans. (1994) 879.
[13] L. Yang, F.L. Wimmer, S. Wimmer, J. Zhao, P.S. Braterman, J. Organomet. Chem. 525 (1996) 1.
[14] W.A. Wickramasinghe, P.H. Bird, N. Serpone, J. Chem. Soc., Chem. Commun. (1981) 1284.
[15] C. Nord, A.C. Hazell, R.G. Hazell, O. Farver, Inorg. Chem. 22 (1983) 3429.
[16] P.J. Spellane, R.J. Watts, C.J. Curtis, Inorg. Chem. 22 (1983) 4060.
[17] A.C. Hazel, R.G. Hazel, Acta Crystallogr., Sect. C 40 (1984) 806.
[18] F.O. Garces, R.J. Watts, Inorg. Chem. 29 (1990) 582.
[19] A.C. Skapski, V.F. Sutcliffe, G.B. Young, J. Chem. Soc., Chem. Commun. (1985) 609.
[20] (a) F.P. Pruchnik, Pure. Appl. Chem. 61 (1989) 795; (b) H. Pasternak, E. Lancman, F. Pruchnik, J. Mol. Catal. 16 (1975) 67.
[21] H. Pasternak, F. Pruchnik, K. Wajda-Hermanowicz, M. Zuber, Pol. J. Chem. 63 (1989) 619.
[22] F. Pruchnik, B.R. James, P. Kvintovics, Can. J. Chem. 64 (1986) 936.
[23] G.A. Rempel, P. Legzdins, H. Smith, G. Wilkinson, Inorg. Synth. 13 (1972) 90.
[24] M. Chou, C. Creutz, D. Mahajan, N. Sutin, A.P. Zipp, Inorg. Chem. 21 (1982) 3989.
[25] A. Zucca, M.A. Cinellu, M.V. Pinna, S. Stoccoro, G. Minghetti, Organometallics 19 (2000) 4295.
[26] G. Minghetti, S. Stoccoro, M.A. Cinellu, B. Soro, A. Zucca, Organometallics 22 (2003) 4770.
[27] K. Thomas, G. Wilkinson, J. Chem. Soc., A (1970) 356.
[28] Q.G. Mulazzani, S. Emmi, M.Z. Hoffman, M. Venturi, J. Am. Chem. Soc. 103 (1981) 3362.
[29] D. Morton, D.J. Cole-Hamilton, J. Chem. Soc., Chem. Commun. (1987) 248.
[30] D. Morton, D.J. Cole-Hamilton, I.D. Utuk, M. Paneque-Sosa, M. Lopez-Poveda, J. Chem. Soc., Dalton Trans. (1989) 489.
[31] B. Martin, W.R. McWhinnie, G.M. Waind, J. Inorg. Nucl. Chem. 23 (1961) 207.
[32] J.D. Miller, F.D. Olivier, J. Chem. Soc., Dalton Trans. (1972) 2473.
[33] D. Mahajan, C. Creutz, N. Sutin, Inorg. Chem. 24 (1985) 2063.
[34] G. Zassinovich, A. Camus, G. Mestroni, Inorg. Nucl. Chem. Lett. 12 (1976) 865.
[35] G. Mestroni, S. Spoligarich, A. Camus, F. Martinelli, G. Zassinovich, J. Organomet. Chem. 157 (1978) 345.
[36] E.C. Constable, Polyhedron 211 (1993) 101.
[37] C.S. McInnes, B.R. Clark, W.R. Redmond, C.R. Clark, A.G. Blackman, J. Chem. Soc., Dalton Trans. (2003) 2215.

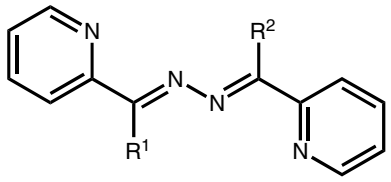

L^1: $R^1 = NH_2$; $R^2 = CH_3$

L^2: $R^1 = R^2 = CH_3$

Scheme 1. Bis(bidentate) diazine ligands L^1 and L^2.

magnetic coupling. The magnetic properties vary as a function of the rotation of the magnetic plane about the N–N bond [12b].

The present work describes the synthesis, structural characterization and magnetic properties of three triple-helicates. The general formula of Ni(II) triple-helicates is $[Ni_2(L^i)_3]\cdot(ClO_4)_4\cdot(H_2O)_3$ $(i = 1, 2)$, where L^1 and L^2 are 1,4-bis(2-pyridyl)-1-amino-4-methyl-2,3-diaza-1,3-butadiene and 2,5-bis(2-pyridyl)-3,4-diaza-2,4-hexadiene (Scheme 1), respectively, and the Mn(II) triple-helicate is $[Mn_2(L^1)_3]\cdot(ClO_4)_4\cdot(H_2O)_3$. The crystal structure of L^1 is also presented.

2. Experimental

2.1. Materials and synthesis

All the starting chemicals were of AR grade and used as purchased without further purification.

Caution! Although not encountered in our experiments, readers are cautioned about the potentially explosive nature of the perchlorate and azido complexes. Only a small amount of the material should be prepared, and it should be handled with care.

Ligands. The L^1 and L^2 ligands were prepared according to the literature procedures [14–17]. Recrystallization of L^1 from an ethanol solution afforded yellow crystals suitable for X-ray analysis.

*$[Ni_2(L^1)_3]\cdot(ClO_4)_4\cdot 3H_2O$ (**1**)*. A methanol solution (2 mL) of nickel(II) perchlorate hexahydrate (0.146 g, 0.4 mmol) was added with continuous stirring into 10 mL methanol solution of L^1 (0.144 g, 0.6 mmol). Slow evaporation of the resulting reddish-orange solution at room temperature yielded reddish-orange crystals within 1 week. The crystals were filtered off, washed quickly with water and ethanol, and dried in air. Yield: (0.137 g) 53.4%. $C_{39}H_{45}N_{15}Ni_2Cl_4O_{19}$ (Fw: 1287.12). *Anal.* Calc. C, 36.40; H, 3.52; N, 16.32. Found: C, 36.17; H, 3.66; N, 16.45%. Main IR bands (cm^{-1}): 3354m, 3208m, 1661vs, 1593m, 1421m, 1376m, 1100vs, 1021sh, 793m, 780m, 747m.

*$[Ni_2(L^2)_3]\cdot(ClO_4)_4\cdot 3H_2O$ (**2**)*. Crystals of **2** were obtained by the same method as for **1**, using L^2 instead of L^1. Slow evaporation of the reaction solution at room temperature yielded reddish-orange crystals of **2** within 1 week. Yield: (0.115 g) 44.7%. $C_{42}H_{48}N_{12}Ni_2Cl_4O_{19}$ (Fw: 1284.14). *Anal.* Calc. C, 39.37; H, 3.78; N, 13.13. Found: C, 39.55; H, 3.74; N, 13.26%. Main IR bands (cm^{-1}): 3079m, 2924m, 1659vs, 1596m, 1444m, 1375m, 1334m, 1261m, 1095 vs, 1020m, 776m, 745m.

*$[Mn_2(L^1)_3]\cdot(ClO_4)_4\cdot 3H_2O$ (**3**)*. A methanol solution (4 mL) containing L^1 (0.072 g 0.3 mmol) was added into one arm of an H-shaped tube and manganese(II) perchlorate hexahydrate (0.073 g 0.2 mmol) in the same solvent (2 mL) was added into the other arm, and then about 20 mL of methanol was carefully added so that the bridge of the tube was filled. Slow diffusion between the two solutions afforded orange crystals of **3** within 1 week. Yield: (0.095 g) 74.3%. $C_{39}H_{45}N_{15}Mn_2Cl_4O_{19}$ (Fw: 1279.58). *Anal.* Calc. C, 36.65; H, 3.55; N, 16.45. Found: C, 37.15; H, 3.69; N, 16.16%. Main IR bands (cm^{-1}): 3349m, 3213m, 1656vs, 1589m, 1417m, 1373m, 1098vs, 1017sh, 795m, 780m, 744m.

Table 1
Summary of crystallographic data for L^1 and the complexes **1**, **2** and **3**

	L^1	**1**	**2**	**3**
Formula	$C_{13}H_{13}N_5$	$C_{39}N_{15}H_{45}Ni_2Cl_4O_{19}$	$C_{42}N_{12}H_{48}Ni_2Cl_4O_{19}$	$C_{39}H_{45}N_{15}Mn_2Cl_4O_{19}$
Formula weight	239.28	1287.12	1284.14	1279.58
Crystal system	orthorhombic	cubic	cubic	cubic
Space group	*Pbca*	$Pa\bar{3}$	$Pa\bar{3}$	$Pa\bar{3}$
a (Å)	18.7892(3)	22.062(3)	22.275(3)	22.3701(8)
b (Å)	10.3215(3)	22.062(3)	22.275(3)	22.3701(8)
c (Å)	19.2061(4)	22.062(3)	22.275(3)	22.3701(8)
β (°)	90	90	90	90
U (Å^3)	3724.7(2)	10738(2)	11052(2)	11194.5(7)
Z	12	8	8	8
μ(Mo Kα) (mm^{-1})	0.882	0.981	0.949	0.725
T (K)	293(2)	293(2)	293(2)	293(2)
Reflections measured	57398	78786	51438	54166
Unique reflections/R_{int}	4255/0.0751	6803/0.1503	2402/0.0884	1390/0.0937
R_1	0.0619	0.0836	0.0559	0.0709
wR_2 (all data)	0.2084	0.3141	0.1542	0.2140

2.2. Physical measurements

Elemental analyses (C, H, N) were performed on an Elementar Vario EL analyzer. IR spectra were recorded on a Nicolet Magna-IR 750 spectrometer equipped with a Nic-Plan Microscope. Magnetic properties of the complexes **1**, **2** and **3** were carried out on a Quantum Design PPMS-9 magnetometer. Diamagnetic corrections were made with Pascal's constants [18].

2.3. Crystallographic studies

Diffraction intensity data of the single crystals were collected at room temperature on a Bruker Smart APEX CCD diffractometer (**1**), a Rigaku RAXIS RAPID IP diffractometer (**2**) and a Nonius Kappa CCD diffractometer (L^1 and **3**), all equipped with graphite-monochromated Mo Kα radiation ($\lambda = 0.71073$ Å). Empirical absorption corrections were applied using the SORTAV program [19] (for L^1 and **3**), the SADABS program (for **1**) [20] and the ABSCOR program (for **2**) [21]. All structures were solved by the direct method and refined by the full-matrix least-squares method on F^2 with anisotropic thermal parameters for all non-hydrogen atoms [22]. Hydrogen atoms were located geometrically and refined using the riding model. Pertinent crystallographic data and structure refinement parameters are summarized in Table 1. The diffraction intensity of **3** was very weak with poor resolution, and the measured maximum 2θ angle was only 37.05°. To confirm the structure, the powder XRD pattern of **3** was measured on a Rigaku D/MAX-2000 diffractometer using graphite-monochromated Cu Kα radiation ($\lambda = 1.5418$ Å), and compared with that calculated from the single-crystal data.

3. Results and discussion

3.1. Crystal structure of ligand L^1

The structure of L^1 is illustrated in Fig. 1, and selected bond distances and bond angles are listed in Table 2. The L^1 ligand crystallizes in an orthorhombic system with two crystallographically independent molecules included in the asymmetric unit. Each pyridylimine unit is planar and adopts a *transoid* conformation with respect to the Py–C bond to minimize the repulsive force of the electronic interactions between the lone pairs of N(pyridyl) and N(imine) [10a]. The two pyridylimine fragments in each molecule are also in *transoid* positions with respect to the central N–N bond to minimize the repulsive force between the amine group and the methyl group, but due to the rotational flexibility of the N–N bond, the relative orientation of two pyridylimine fragments is variable. For one set, the dihedral angle between the two pyridylimine fragments is 174.89° and the C–N–N–C torsion angle is 176.49°. For the other set, both angles are 180°, due to the presence of a crystallographic inversion center in the middle of the N–N bond. The centrosymmetry leads to a statistical disorder of the two substituent groups: both the amine group and the methyl group occupy the position of the X1 atom with occupancies of 0.5.

Table 2
Selected bond lengths (Å) and bond angles (°) for L^1

C(1)–N(1)	1.337(3)	N(2)–N(3)	1.412(2)
C(5)–N(1)	1.343(3)	C(19)–X(1)	1.430(3)
C(6)–N(2)	1.288(2)	C(14)–N(6)	1.361(4)
C(7)–N(3)	1.291(2)	C(19)–N(7)	1.291(3)
C(8)–N(4)	1.342(2)	N(7)–N(7)A	1.400(4)
C(12)–N(4)	1.338(3)		
N(2)–C(6)–N(5)	125.6(2)	N(7)–C(19)–X(1)	125.1(2)
N(2)–C(6)–C(5)	118.7(2)	N(7)–C(19)–C(18)	116.3(2)
N(5)–C(6)–C(5)	115.7(2)	X(1)–C(19)–C(18)	118.6(2)
N(3)–C(7)–C(13)	124.7(2)	C(6)–N(2)–N(3)	111.6(2)
N(3)–C(7)–C(8)	117.7(2)	C(7)–N(3)–N(2)	112.7(2)
C(13)–C(7)–C(8)	117.6(2)	C(19)–N(7)–N(7)A	112.5(2)

Symmetry code A: $-x+1, -y, -z+1$.

3.2. Crystal structure of the complexes

Crystal structure analyses revealed that complexes **1**, **2** and **3** are isomorphous and consist of cationic binuclear triple helicates with crystallographic C_3 symmetry. As shown in Fig. 2, the powder XRD pattern of **3** is in good agreement with those calculated from the single-crystal data of **1** and **3**, confirming that the single-crystal structural

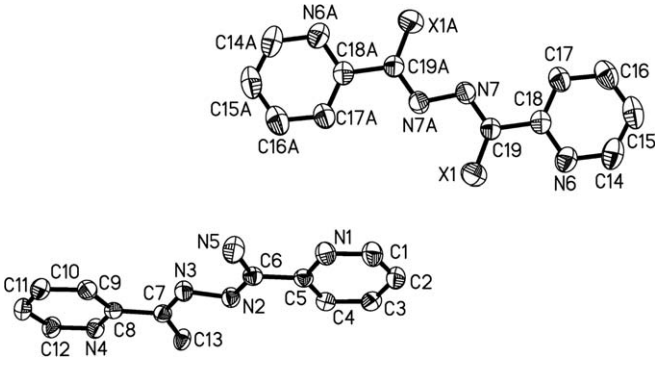

Fig. 1. Structures of the two crystallographically independent sets of molecules in L^1. Symmetry code A: $-x+1, -y, 1-z$.

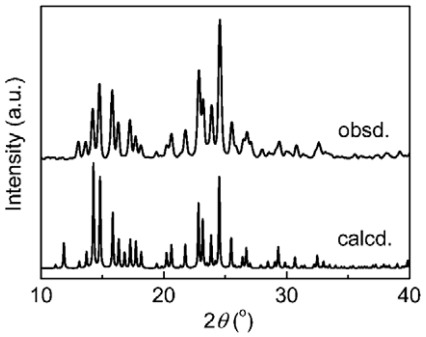

Fig. 2. The powder XRD pattern of **3**.

analysis of **3** is reasonable despite of the poor diffraction resolution.

3.2.1. $[Ni_2(L^1)_3]\cdot(ClO_4)_4\cdot 3H_2O$ (**1**)

The structure of **1** is illustrated in Fig. 3a, and selected bond distances and bond angles are listed in Table 3. In comparison with the "free" ligand, the ligand L^1 in complex **1** exhibits no appreciable differences in the N–N, C–C and C–N distances, but the conformation is completely different. The pyridine ring rotates by ca. 180° around the Py–C bond to place the pyridyl nitrogen and the imine nitrogen on the same side, so each pyridylimine group can act as a bidentate bite site. The pyridylimine groups are rotated around the N–N bond so that the C–N–N–C torsion angle and the dihedral angles between the two planar pyridylimine groups become 81.18° and 72.66°, respectively, giving rise to a twisted spiral conformation for the whole ligand.

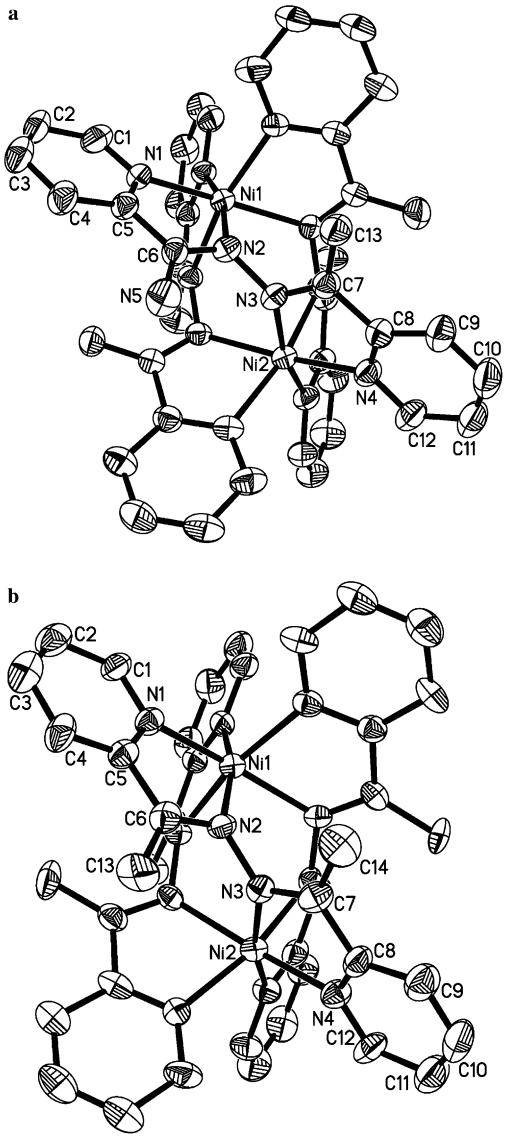

Fig. 3. (a) Molecular structure of complex **1**; (b) molecular structure of complex **2**.

Table 3
Selected bond lengths (Å) and bond angles (°) for the complexes **1**, **2** and **3**

	1	**2**	**3**
M(1)–N(1)	2.078(4)	2.063(6)	2.215(8)
M(1)–N(2)	2.079(3)	2.089(5)	2.249(7)
M(2)–N(4)	2.080(4)	2.065(6)	2.253(7)
M(2)–N(3)	2.086(4)	2.079(5)	2.206(8)
C(1)–N(1)	1.337(6)	1.329(8)	1.34(1)
C(5)–N(1)	1.342(6)	1.356(8)	1.34(1)
C(6)–N(2)	1.287(6)	1.284(8)	1.28(1)
C(7)–N(3)	1.302(6)	1.276(8)	1.30(1)
C(8)–N(4)	1.340(6)	1.319(9)	1.35(1)
C(12)–N(4)	1.338(6)	1.306(9)	1.34(1)
N(2)–N(3)	1.389(5)	1.400(7)	1.40(1)
N(1)–M(1)–N(2)A	166.3(1)	166.0(2)	97.2(3)
N(1)A–M(1)–N(2)	94.9(1)	95.2(2)	159.4(3)
N(1)–M(1)–N(2)	77.0(1)	77.0(2)	72.1(4)
N(2)A–M(1)–N(2)	90.3(1)	90.0(2)	88.3(3)
N(4)A–M(2)–N(4)	99.6(1)	99.1(2)	105.7(3)
N(4)–M(2)–N(3)A	94.0(1)	94.9(2)	161.2(3)
N(4)A–M(2)–N(3)	166.4(1)	166.0(2)	92.6(3)
N(4)–M(2)–N(3)	77.2(1)	77.2(2)	72.8(3)
N(3)A–M(2)–N(3)	89.7(1)	89.5(2)	88.5(3)

Symmetry code A: $-x+1$, $y+1/2$, $-z+3/2$.

The spiral twist induces chirality to the ligand, and three equivalent ligands wrap around two metal ions to yield a binuclear triple helicate (*M*-configured with *ΔΔ* metal centers in Fig. 2a) with a C_3 symmetry and a 3-fold axis along the two central Ni(II) ions. In the binuclear cation, each nickel(II) ion is ligated by three pyridylimine groups and adopts the octahedral geometry with a trigonal distortion and with the Ni–N distances in the narrow range of 2.07–2.09 Å. The Ni···Ni distance spanned by the triple N–N bridges is 3.679(1) Å, and the Ni–N–N–Ni torsion angle is 46.94°. The perchlorate ions and water molecules lie among the binuclear cations without any indication of hydrogen bonding. The nearest Ni···Ni distance between neighboring binuclear units is 7.9 Å between Ni1 and Ni2 ($-x$, $1-y$, $1-z$).

3.2.2. $[Ni_2(L^2)_3]\cdot(ClO_4)_4\cdot 3H_2O$ (**2**)

The structure of **2** is depicted in Fig. 3b. The bond distances and bond angles (Table 3) are similar to those in **1**, and the Ni···Ni distance spanned by the triple N–N bridge is 3.683(2) Å. The major differences lie in the twist of the diazine ligands. The C–N–N–C and Ni–N–N–Ni torsion angles are 87.37° and 50.11°, respectively, and the dihedral angles between the two planar pyridylimine groups is 72.0°.

3.2.3. $[Mn_2(L^1)_3]\cdot(ClO_4)_4\cdot 3H_2O$ (**3**)

Complex **3** is isostructural with complexes **1** and **2**. As expected, the Mn–N distances (av. 2.22 Å) are longer than the Ni–N distances in **1** and **2**. The Mn···Mn distance spanned by the triple N–N bridge is 3.95 Å. The C–N–N–C and Mn–N–N–Mn torsion angles are 99.9° and 49.1°, respectively, and the dihedral angles between the two planar pyridylimine groups is 75.6°.

3.3. Magnetism

The magnetic susceptibilities of complexes **1** and **2** were measured in the 5–300 K temperature range and are shown in Figs. 4 and 5, respectively. At 300 K, the experimental $\chi_M T$ values are 2.23 and 2.04 emu mol^{-1} K for **1** and **2**, respectively, which correspond to the spin-only value expected for two high-spin Ni(II) ions. Upon cooling, the $\chi_M T$ products decrease monotonically, and the χ_M values increase continuously to maxima of 0.099 emu mol^{-1} at 10 K and 0.054 emu mol^{-1} at 17 K for **1** and **2**, respectively. These observations indicate that an antiferromagnetic interaction is operative between the Ni(II) ions linked by the triple N–N bridges.

The data were fitted to the expression derived from the isotropic spin-coupling Hamiltonian $H = -J\hat{S}_1\hat{S}_2$ [23]

$$\chi_M = \frac{2Ng^2\beta^2}{kT}\frac{1+5\exp(2J/kT)}{3+5\exp(2J/kT)+\exp(-J/kT)}.$$

The simulations resulted in $J = -2.97$ with $g = 2.13$ and $J = -5.40$ cm^{-1} with $g = 2.07$ for **1** and **2**, respectively. Although several helical binuclear Ni(II) complexes with open-chain diazine bridges have been structurally characterized previously [10c,15,17,24], to our knowledge, only one of them, $[Ni_2(pahox)_3]\cdot(ClO_4)_4\cdot 4H_2O$ (pahox = butanedione-monoxime picolinamide hydrazone), has been investigated with variable-temperature magnetic measurements, and it was found to exhibit a weaker magnetic interaction [24]. Selected structural and magnetic data of the compound together with those of the present compounds are collected in Table 4. As can be seen, the difference in the magnitude of the magnetic interaction seems to be due to the different Ni–N–N–Ni torsion angles: larger magnetic exchange parameters are associated with larger torsion angles, although larger torsion angles lead to larger Ni···Ni distances.

The thermal variation of magnetic susceptibility for complex **3** is shown in Fig. 6. At room-temperature the experimental $\chi_M T$ value is 8.90 emu mol^{-1} K for **3**, which corresponds to the spin-only value expected for two high-spin Mn(II) ions. Upon cooling, the $\chi_M T$ product increases smoothly to 14.41 emu mol^{-1} K at 2 K. This behavior is consistent with a ferromagnetic interaction between the two metal centers linked by the triple N–N bridges. The field dependent magnetization data was measured at 2 K (Fig. 7), and the magnetization ($9.93N\beta$) at 5.5 T is very close to the saturation value. It is noted that the magnetization curve is in good agreement with that calculated from the Brillouin function for $S = 5$, suggesting a high spin ground state for the binuclear complex due to the ferromagnetic interaction.

The thermal variation of magnetic data were fitted to a simple isotropic exchange expression for two $S = 5/2$ spin states, derived from the exchange Hamiltonian $H = -J\hat{S}_1\hat{S}_2$ [25].

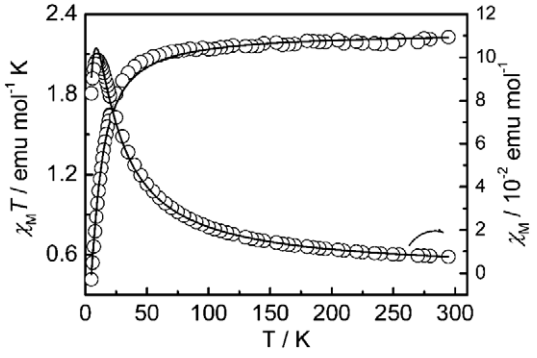

Fig. 4. χ_M vs. T and $\chi_M T$ vs. T plots for complex **1**. The solid lines represent the best fit of the experimental data.

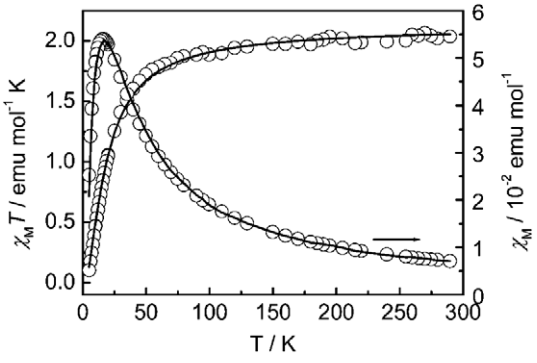

Fig. 5. χ_M vs. T and $\chi_M T$ vs. T plots for complex **2**. The solid lines represent the best fit of the experimental data.

Table 4
Structural and magnetic parameters for helical binuclear Ni(II) and Mn(II) complexes

Complex[a]	1	2	3	4	5	6
J (cm^{-1})	−2.97	−5.40	1.24	−0.77	1.04	−1.4
τ (°)[b]	46.94	50.11	49.1	41.40	44.2	86.2
M···M (Å)	3.679	3.682	3.944	3.654	3.946	4.821
Ref.	this work	this work	this work	[24]	[15]	[24]

[a] **4**, $[Ni_2(pahox)_3]\cdot(ClO_4)_4\cdot 4H_2O$ (pahox = butanedione-monoxime picolinamide hydrazone); **5**, $[Mn_2(pahap)_3]\cdot(ClO_4)_4\cdot 5H_2O$ (pahap = picolinamide azine); **6**, $[Mn_2(pahox)_2Cl4]\cdot H_2O$.
[b] Ni–N–N–Ni torsion angles.

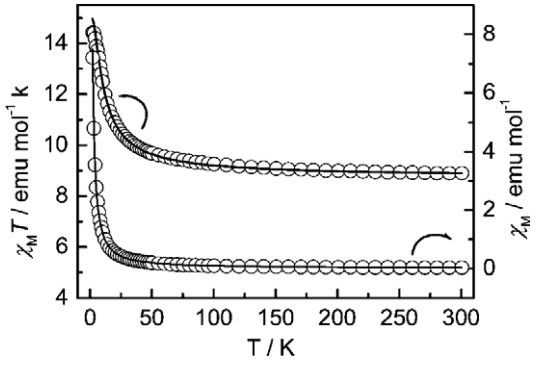

Fig. 6. χ_M vs. T and $\chi_M T$ vs. T plots for complex **3**. The solid lines represent the best fit of the experimental data.

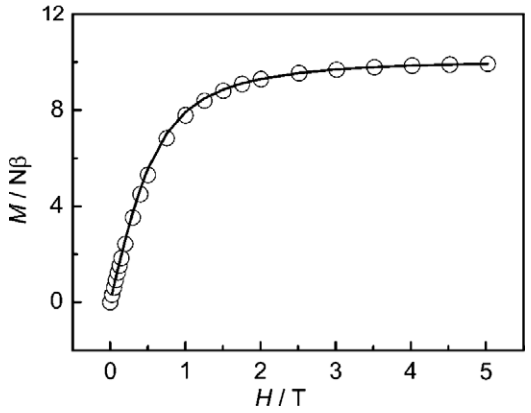

Fig. 7. Field dependence of magnetization of **3**; the solid line represents the best fit to the Brillouin function for $S = 5$, $g = 2.0$ at 2 K.

The deduced expression of the magnetic susceptibility is

$$\chi_M = \frac{2Ng^2\beta^2}{kT}\,\frac{55 + 30e^{5x} + 14e^{9x} + 5e^{12x} + e^{14x}}{11 + 9e^{5x} + 7e^{9x} + 5e^{12x} + 3e^{14x} + e^{15x}},$$

where $x = J/kT$. A reasonable data fit (Fig. 5) was obtained for $J = 1.24\ cm^{-1}$ and $g = 2.0$. The magnetic exchange in Mn(II) systems can also be related to the M–N–N–M torsion angles: the magnetic interaction in **3** is ferromagnetic ($J = 1.04\ cm^{-1}$). It is consistent with that for the reported $[Mn_2(pahap)_3]\cdot(ClO_4)_4\cdot 5H_2O$ (pahap = picolinamideazine) [15], in which the torsion angles (av. 44.2°) are close to that (49.1°) in **3**, but contrasts with the reported double helicate $[Mn_2(pahox)_2Cl4]\cdot H_2O$ [24], where the magnetic coupling is antiferromagnetic and the torsion angles are much larger (av. 86.2°). It seems that the magnetic differences might arise from the difference in the M–N–N–M torsion angles. With these limited data, however, it is unwarranted to conclude any unambiguous magneto-structural correlations. Other structural factors such as the coordination geometry around the metal ions may also contribute to the observed magnetic interactions. Complexes **1**–**3** and related binuclear triple helicates (**4** and **5**, Table 4) have comparable M–N–N–M angles and coordination environments, but the signs of the magnetic interactions for Ni(II) and Mn(II) are opposite, reflecting the significant influence of the different magnetic orbitals and exchange pathways involved for Ni(II) and Mn(II) in these triply diazine-bridged systems.

4. Conclusion

By employing open-chain diazine ligands with two bidentate pyridylimine groups, we successfully obtained three binuclear triple helicates with Ni(II) and Mn(II). In these complexes, three bis(bidentate) diazine ligands with a spiral conformation wrap around two metal cations, resulting in triple helicates with C_3 symmetry. Magnetic investigations revealed that the intramolecular magnetic interactions through the triple diazine bridges are antiferromagnetic for the Ni(II) triple helicates but ferromagnetic for the Mn(II) triple helicate. It seems that the magnetic interactions for the Ni(II) compounds are mainly dependent upon the degree of the twist of the ligands about the N–N bond. Further experimental and theoretical studies are needed to obtain more precise correlations.

Acknowledgments

We thank the NSFC (20221101, 90201014, and 20423005) and the MOST (2006CB601104) for financial support.

Appendix A. Supplementary material

Crystallographic data (X-ray data in *.cif files) for the structures reported in this paper have been deposited with the Cambridge Crystallographic Data Centre, CCDC No. 226505 for L^1, 226506 for compound **1**, 205607 for compound **2** and 293482 for compound **3**. Copies of this information may be obtained from the Director, CCDC, 12 Union Road, Cambridge, CB2 1EZ, UK (fax: +44 1223 336 033; e-mail: deposit@ccdc.cam.ac.uk or http://www.ccdc.cam.ac.uk). Supplementary data associated with this article can be found, in the online version, at doi:10.1016/j.poly.2006.04.008.

References

[1] (a) F.G. Gelalcha, M. Schulz, R. Kluge, J. Sieler, J. Chem. Soc., Dalton Trans. (2002) 2517;
(b) C. He, C.-Y. Duan, C.-J. Fang, Q.-J. Meng, J. Chem. Soc., Dalton Trans. (2000) 2419.
[2] Y. Cui, H.L. Ngo, W. Lin, Chem. Commun. (2003) 1388.
[3] M.J. Hannon, C.L. Painting, A. Jackson, J. Hamblin, W. Errington, Chem. Commun. (1997) 1807.
[4] (a) D. Philp, J.F. Stoddart, Angew. Chem., Int. Ed. Engl. 35 (1996) 1155;
(b) J. Xu, T.N. Parac, K.N. Raymond, Angew. Chem., Int. Ed. Engl. 38 (1999) 2878;
(c) C. Piguet, G. Bernardinelli, G. Hopfgartner, Chem. Rev. 97 (1997) 2005;
(d) R.P.K. Bowyer, K.A. Porter, A.D. Rae, A.C. Willis, S.B. Wild, Chem. Commun. (1998) 1153.
[5] M.J. Hannon, S. Bunce, A.J. Clarke, N.W. Alcock, Angew. Chem., Int. Ed. Engl. 38 (1999) 1277.
[6] (a) M. Albrecht, O. Blau, E. Wegelius, K. Rissanen, New J. Chem. 23 (1999) 667;
(b) M. Albrecht, Chem.-A Eur. J. 6 (2000) 3485;
(c) J.M. Lehn, Superamolecular Chemistry, VCH, Weinheim, 1995.
[7] D. Guo, K.-L. Pang, C.-Y. Duan, C. He, Q.-J. Meng, Inorg. Chem. 41 (2002) 5978.
[8] (a) S. Aravinda, N. Shamala, C. Das, A. Sriranjini, I.L. Karle, P. Balaram, J. Am. Chem. Soc. 125 (2003) 5308;
(b) J. Keegan, P.E. Kruger, M. Nieuwenhuyzen, J. O'Brien, N. Martin, Chem. Commun. (2001) 2192;
(c) J. Lacour, J.J. Jodry, D. Monchaud, Chem. Commun. (2001) 2302.
[9] T. Yano, R. Tanaka, T. Nishioka, I. Kinoshita, K. Isobe, L.J. Wright, T.J. Collins, Chem. Commun. (2002) 1396.
[10] (a) P.K. Bowyer, K.A. Porter, A.D. Rae, A.C. Willis, S.B. Wild, Chem. Commun. (1998) 1153;

(b) C.J. Matthews, S.T. Onions, G. Morata, L.J. Davis, S.L. Heath, D.J. Price, Angew. Chem., Int. Ed. 42 (2003) 3166;
(c) W.J. Stratton, Inorg. Chem. 9 (1970) 517.
[11] L.K. Thompson, Coord. Chem. Rev. 233–234 (2002) 193.
[12] (a) D. Guo, C. He, C.-Y. Duan, Q.-J. Meng, New J. Chem. 26 (2002) 796;
(b) Z. Xu, S. White, L.K. Thompson, D.O. Miller, M. Ohba, H. Okawa, C. Wilson, J.A.K. Howard, J. Chem. Soc., Dalton Trans. (2000) 1751.
[13] (a) E.-Q. Gao, Y.-F. Yue, S.-Q. Bai, Z. He, C.-H. Yan, J. Am. Chem. Soc. 126 (2004) 1419;
(b) E.-Q. Gao, S.-Q. Bai, Z.-M. Wang, C.-H. Yan, J. Am. Chem. Soc. 125 (2003) 4984.
[14] F.H. Case, J. Org. Chem. 30 (1965) 93.
[15] Z. Xu, L.K. Thompson, D.O. Miller, H.J. Clase, J.A.K. Howard, A.E. Goeta, Inorg. Chem. 37 (1998) 3620.
[16] D. Guo, C.-Y. Duan, C.-J. Fang, Q.-J. Meng, J. Chem. Soc., Dalton Trans. (2002) 834.
[17] (a) W.J. Stratton, D.H. Busch, J. Am. Chem. Soc. 80 (1958) 1286;
(b) W.J. Stratton, D.H. Busch, J. Am. Chem. Soc. 82 (1960) 4834.
[18] C.J. O'Connor, Prog. Inorg. Chem. 29 (1982) 203.
[19] (a) R.H. Blessing, Acta Crystallogr., Sect. A 51 (1995) 33;
(b) R.H. Blessing, J. Appl. Crystallogr. 30 (1997) 421.
[20] G.M. Sheldrick, Program for Empirical Absorption Correction of Area Detector Data, University of Göttingen, Germany, 1996.
[21] T. Higashi, ABSCOR, Empirical Absorption Correction based on Fourier Series Approximation, Rigaku Corporation, Tokyo, 1995.
[22] (a) G.M. Sheldrick, SHELXTL Version 5.1, Bruker Analytical X-ray Instruments, Inc., Madison, WI, USA, 1998;
(b) G.M. Sheldrick, SHELXL-97, PC Version, University of Göttingen, Germany, 1997.
[23] (a) A.P. Ginsberg, Inorg. Chim. Acta Rev. 6 (1971) 45;
(b) R.L. Martin, in: E.A.V. Ebsworth, A.G. Maddock, A.G. Sharpe (Eds.), New Pathways in Inorganic Chemistry, Cambridge University Press, New York, NY, 1968 (Chapter 9).
[24] Z. Xu, L.K. Thompson, D.A. Black, C. Ralph, D.O. Miller, M.A. Leech, J.A.K. Howard, J. Chem. Soc., Dalton Trans. (2001) 2042.
[25] O. Kahn, Molecular Magnetism, VCH, New York, 1993.

Perkin–Elmer FT-IR Espectrum One, as KBr pellets. UV spectra of 0.1 mM solutions were obtained with a UNICAM UV 300 and mass spectra were obtained with a VG Autospec mass spectrometer operating in the electron Impact (EI) mode and liquid secondary iron mass spectrometry (LSIMS) mode. Elemental compositions were analysed with a Perkin–Elmer 2400B. 4-(2-Thienyl)-1,3-dithiol-2-thione [20], 4-(3-thienyl)-1,3-dithiol-2-thione [20] and 4-(*p*-cyanophenyl)-1,3-dithiole-2-thione [18,20] were prepared by published methods. Electrochemical measurements were recorded on a EG&G 273 model and carried out in dry CH_2Cl_2 under argon using $[n\text{-}NBu_4]PF_6$ (0.1 M) as a background electrolyte, with a Pt disk electrode versus SCE (values in V).

2.2. 4-(2-Thienyl)-1,3-dithiole-2-one (*1*)

To a solution of 4-(2-thienyl)-1,3-dithiol-2-thione (216 mg, 1 mmol) in MeCN (10 ml) was added $Hg(OAc)_2$ (414 mg, 1.3 mmol). The mixture was refluxed for 6 h and after cooling the solvent was completely removed in vacuo. Purification was carried out by column chromatography (silica, CH_2Cl_2). The resulting solution was carefully washed with sat. Na_2CO_3 and water. After drying (Na_2SO_4) the solvent was evaporated in vacuo to afford a yellow solid. Yield: 85%. *Anal*. Calc. for $[C_7H_4OS_3]$: C, 41.93; H, 2.01; S, 47.92. Found: C, 41.95; H, 2.42; S, 47.52%. IR (KBr, cm^{-1}): ν(C=O) 1638. ^1H NMR (300 MHz, $CDCl_3$, 25 °C): δ 7.30–7.28 (m, 1H, *H_5-thienyl*), 7.07–7.03 (m, 2H, *$H_{3,4}$-thienyl*), 6.73 (s, 1H, *H_5-dithiole*) ppm. *m/z* (EI^+): 200 ($[M]^+$, 16%), 136 (100%).

2.3. 4-(3-Thienyl)-1,3-dithiole-2-one (*2*)

This compound was prepared as described for **1** using 4-(3-thienyl)-1,3-dithiol-2-thione (216 mg, 1 mmol). Yellow solid. Yield: 80%. *Anal*. Calc. for $[C_7H_4OS_3]$: C, 41.93; H, 2.01; S, 47.92. Found: C, 41.54; H, 2.40; S, 47.49%. IR (KBr, cm^{-1}): ν(C=O) 1628. ^1H NMR (300 MHz, $CDCl_3$, 25 °C): δ 7.42–7.18 (m, 1H, *H_2-thienyl*), 7.30–7.23 (m, 2H, *$H_{4,5}$-thienyl*), 6.77 (s, 1H, *H_5-dithiole*) ppm. *m/z* (EI^+): 200 ($[M]^+$, 100%), 172 ($[M–C–O]^+$, 52%), 140 ($[M–C–O–S]^+$, 12%).

2.4. [M{S_2C_2H-(*p*-CN-C_6H_4)}(dppe)], M = Ni (*3*), Pd (*4*)

4-(*p*-Cyanophenyl)-1,3-dithiole-2-thione (47 mg, 0.2 mmol) was suspended in MeOH (20 ml) under argon atmosphere. KOH (0.5 ml, 1 M in MeOH) was added and the reaction mixture was refluxed until the thione was dissolved (3 h). After cooling $[NiCl_2(dppe)]$ (106 mg, 0.2 mmol) or $[PdCl_2(dppe)]$ (115 mg, 0.2 mmol) was added. The reaction mixture was stirred for 24 h and the precipitate was subsequently collected by filtration and washed with diethyl ether. M = Ni (**3**), green solid. Yield: 45%. *Anal*. Calc. for $[C_{35}H_{29}NNiP_2S_2]$: C, 64.90; H, 4.51; N, 2.16; S, 9.90. Found: C, 64.68; H, 4.86; N, 2.09; S, 10.01%. IR (KBr, cm^{-1}): ν(C≡N) 2218, ν(C=C) 1597. ^1H NMR (300 MHz, $CDCl_3$, 25 °C): δ 7.80–7.66 (m, 10H), 7.46–7.36 (m, 14H), 7.30 (s, 1H), 2.38 (d, 4H, $J = 17.4$ Hz) ppm. $^{31}P\{^1H\}$ NMR: AB system $\delta_A = 58.6$, $\delta_B = 57.9$ ppm ($J_{AB} = 46.5$ Hz). *m/z* ($LSIMS^+$): 647 ($[M]^+$, 100%). M = Pd (**4**), orange solid. Yield: 65%. *Anal*. Calc. for $[C_{35}H_{29}NP_2PdS_2]$: C, 60.39; H, 4.20; N, 2.01; S, 9.21. Found: C, 59.99; H, 4.15; N, 1.96; S, 9.21%. IR (KBr, cm^{-1}): ν(C≡N) 2213, ν(C=C) 1599. ^1H NMR (300 MHz, $CDCl_3$, 25 °C): δ 7.84–7.73 (m, 10H), 7.52–7.40 (m, 14H), 7.20 (d, 1H, $J = 3.6$ Hz), 2.53 (d, 4H, $J = 20.7$ Hz) ppm. $^{31}P\{^1H\}$ NMR: AB system $\delta_A = 51.7$, $\delta_B = 51.6$ ppm (J_{AB}=36.1 Hz). *m/z* ($LSIMS^+$): 695 ($[M]^+$, 100%).

2.5. [M{S_2C_2H-(2-C_4H_3S)}(dppe)], M = Ni (*5*), Pd (*6*)

4-(2-Thienyl)-1,3-dithiole-2-one (**1**) (50 mg, 0.25 mmol) was suspended in EtOH (10 ml) under argon atmosphere, for M = Pd in THF (10 ml). NaOEt (2 ml, 0.4 M in EtOH) was added and the reaction mixture was refluxed until the ketone was dissolved (1.5 h). After cooling $[NiCl_2(dppe)]$ (132 mg, 0.25 mmol) or $[PdCl_2(dppe)]$ (144 mg, 0.25 mmol) was added. The reaction mixture was stirred for 24 h and then the solvent was reduced in vacuo to 5 ml. Hexane or diethyl ether (20 ml) was added to precipitate the corresponding compound which was filtered off. Purification was carried out by column chromatography. M = Ni (**5**), (silica, 60 ethyl acetate/40 hexane), green solid. Yield: 15%. *Anal*. Calc. for $[C_{32}H_{28}NiP_2S_3]$: C, 61.05; H, 4.45; S, 15.26. Found: C, 60.68; H, 4.06; S, 14.88%. IR (KBr, cm^{-1}): ν(C=C) 1633. ^1H NMR (300 MHz, $CDCl_3$, 25 °C): δ 7.77–7.70 (m, 8H), 7.45–7.19 (m, 12H), 6.92 (m, 2H), 6.84 (m, 1H), 6.72 (m, 1H), 2.35–2.27 (m, 4H) ppm. $^{31}P\{^1H\}$ NMR: AB system $\delta_A = 58.0$, $\delta_B = 57.5$ ppm ($J_{AB} = 34.8$ Hz). *m/z* ($LSIMS^+$): 628 ($[M]^+$, 100%), 431 ($[S(dppe)^+]$, 72%). M = Pd (**6**), (silica, dichloromethane), purple solid. Yield: 49%. *Anal*. Calc. for $[C_{32}H_{28}P_2PdS_3]$: C, 56.71; H, 4.13; S, 14.18. Found: C, 56.40; H, 4.43; S, 13.68%. IR (KBr, cm^{-1}): ν(C=C) 1634. ^1H NMR (300 MHz, $CDCl_3$, 25 °C): δ 7.77–7.68 (m, 9H), 7.37–7.33 (m, 11H), 6.99 (m, 1H), 6.89–6.83 (m, 2H), 6.72 (m, 1H), 2.42 (d, 4H, $J = 15.3$ Hz) ppm. $^{31}P\{^1H\}$ NMR: AB system $\delta_A = 50.9$, $\delta_B = 50.7$ ppm ($J_{AB} = 26.7$ Hz). *m/z* ($LSIMS^+$): 676 ($[M]^+$, 100%), 506 ([Pd(dppe)], 18%), 429 ([S(dppe)], 32%).

2.6. [M{S_2C_2H-(3-C_4H_3S)}(dppe)], M = Ni (*7*), Pd (*8*)

4-(3-Thienyl)-1,3-dithiole-2-one (**2**) (50 mg, 0.25 mmol) was suspended in THF (15 ml). NaOEt (2 ml, 0.4 M in EtOH) was added and the reaction mixture was refluxed until the ketone was dissolved (1.5 h). After cooling $[NiCl_2(dppe)]$ (132 mg, 0.25 mmol) or $[PdCl_2(dppe)]$ (144 mg, 0.25 mmol) was added. The reaction mixture was stirred for 24 h and then the solvent was reduced in

vacuo to 5 ml. Hexane (20 ml) was added to precipitate the corresponding compound which was filtered off. M = Ni (**7**), green solid. Yield: 44%. *Anal*. Calc. for [$C_{32}H_{28}NiP_2S_3$]: C, 61.05; H, 4.45; S, 15.26. Found: C, 60.67; H, 4.48; S, 14.84%. IR (KBr, cm^{-1}): ν(C=C) 1629. ^1H NMR (300 MHz, $CDCl_3$, 25 °C): δ 7.77–7.61 (m, 10H), 7.44–7.37 (m, 10H), 7.19–7.13 (m, 2H), 7.00 (m, 1H), 6.93 (s, 1H), 2.30 (d, 4H, $J = 13.2$ Hz) ppm. $^{31}P\{^1H\}$ NMR: AB system $\delta_A = 57.8$, $\delta_B = 57.6$ ppm ($J_{AB} = 34.1$ Hz). *m/z* (LSIMS$^+$): 628 ([M]$^+$, 100%), 431 ([S(dppe)$^+$], 25%). M = Pd (**8**), brown solid. Yield: 90%. *Anal*. Calc. for [$C_{32}H_{28}P_2PdS_3$]: C, 56.71; H, 4.13; S, 14.18. Found: C, 56.40; H, 4.21; S, 13.76%. IR (KBr, cm^{-1}): ν(C=C) 1638. ^1H NMR (300 MHz, $CDCl_3$, 25 °C): δ 7.80–7.71 (m, 8H), 7.43–7.35 (m, 12H), 7.21 (m, 2H), 7.03 (m, 1H), 6.85 (m, 1H), 2.43 (d, 4H, $J = 15.3$ Hz) ppm. $^{31}P\{^1H\}$ NMR: δ 50.5 (s) ppm. *m/z* (LSIMS$^+$): 676 ([M]$^+$, 100%), 476 (52%), 291 (72%).

2.7. Crystallographic studies

Crystals suitable for X-ray diffraction were obtained by slow diffusion of diethyl ether into dichloromethane solutions. A summary of the fundamental crystal and refinement data of compounds **4** and **6** is given in Table 3. The crystals were mounted on a glass fiber with inert oil and centered on a Bruker Nonius Kappa CCD diffractometer in the case of **4** and on a Bruker-Siemens Smart CCD diffractometer in **6** using monochromated Mo Kα radiation ($\lambda = 0.7107$ Å), scan type θ–2θ. The diffraction frames were integrated using the SAINT [21] package and corrected for absorption with SORTAV [22,23] or SADABS [24] programs. The structures were solved by direct methods using SHELXS [25]. Full-matrix least squares refinement was carried out using SHELXTL [26] minimising $\omega(F_o^2 - F_c^2)^2$. Hydrogen atoms were included using a riding model. Weighted *R* factors (R_w) and all goodness-of-fit *S* values are based on F^2; conventional *R* factors (*R*) are based on *F*.

3. Results and discussion

Deprotection of 4-(*p*-cyanophenyl)-1,3-dithiole-2-thione [18,20], 4-(2-thienyl)-1,3-dithiole-2-one (**1**) and 4-(3-thienyl)-1,3-dithiole-2-one (**2**) with a base in MeOH or in THF (to improve the solubility) leads to the formation in situ of the corresponding dithiolate salts. Curiously the formation of the dithiolates takes place starting from the thione (Scheme 1, (i)) in the case of *p*-cyanophenyl, though in the case of 2- and 3-thienyl the transformation is on the corresponding ketone, in order to improve the electrophilicity around the C atom in the 2 position, necessary as a previous reaction. Subsequent addition of [$NiCl_2$(dppe)] and [$PdCl_2$(dppe)] followed by purification work-up afforded the heteroleptic complexes as shown in Scheme 1.

The spectroscopic data of all the dithiolenes are in agreement with their formulation. In the ^1H NMR spectra, the proton of the S_2C_2H unit appears as a doublet or multiplet, possibly due to the coupling of this proton with the P atom in the *trans* position. More illustrative are the $^{31}P\{^1H\}$ NMR spectra, most of them show an AB system around 58 ppm for Ni complexes and 51 ppm for Pd complexes. This AB system is due to the closed resonances of the two inequivalent phosphorous atoms because of the lack of symmetry of the dithiolene ligand used in this work. The LSIMS$^+$ mass spectra exhibit the molecular peaks in all cases.

Crystals of the palladium complexes [Pd{S_2C_2H-(*p*-CN-C_6H_4)}(dppe)] (**4**) and [Pd{S_2C_2H-(2-C_4H_3S)}(dppe)] (**6**) were grown by slow diffusion of diethyl ether into a dichloromethane solution of each complex. Perspective drawings of the structures are shown in Figs. 1 and 2 respectively. Bond distances and angles are collected in Tables 1 and 2 and crystallographic data are collected in Table 3.

The crystalline structure of the two compounds is similar to that of other group 10 metallo-1,2-enedithiolate complexes [8,27–33]. Compound **6** crystallises as the water

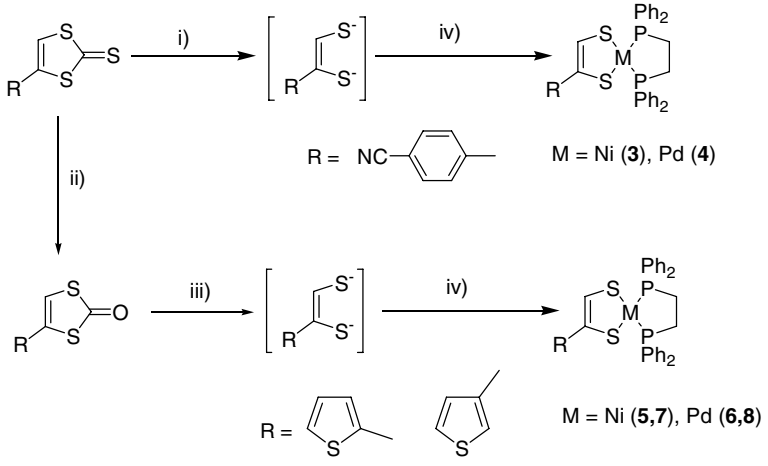

Scheme 1. Synthesis of heteroleptic dithiolene complexes.

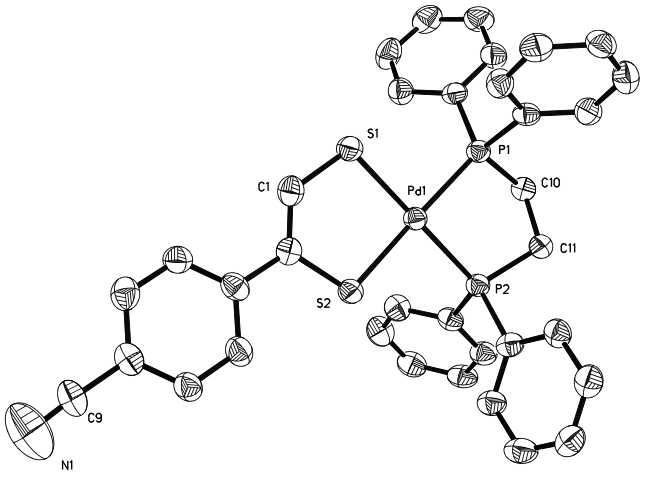

Fig. 1. Crystal structure of [Pd{S_2C_2H-(*p*-CN-C_6H_4)}(dppe)] (**4**). Thermal ellipsoids are drawn at the 50% probability level and H atoms have been omitted for clarity.

solvate with two independent molecules per unit cell. The P–Pd–P angles are very similar in both complexes, [P(1)–Pd(1)–P(2) = 86.09(5)° in **4** and P(1)–Pd(1)–P(2) = 85.00(6)°, P(4)–Pd(2)–P(3) = 84.71(6)° in **6**] as occurs with the S–Pd–S angles [S(1)–Pd(1)–S(2) = 88.34(5)° in **4** and S(1)–Pd(1)–S(2) = 89.31(5)°; S(5)–Pd(2)–S(4) = 88.48(6)° in **6**]. The metallo-1,2-enedithiolate consists of a planar five-membered ring in the two cases with the palladium atom deviating slightly from the least squares planes, 0.0143(6) Å in **4** and 0.0387(7), 0.0571(14) Å in the two independent molecules of **6**. The substituents *p*-cyanophenyl in **4** and 2-thienyl in **6** are also coplanar with the metallo-1,2-dithiolene unit with smaller torsion angles in the case of the two molecules of complex **6** [C(33)–C(34)–

Table 1
Bond lengths (Å) and angles (°) for [Pd{S_2C_2H-(*p*-CNC_6H_4)}(dppe)] (**4**)

Pd(1)–P(1)	2.2808(13)	Pd(1)–S(2)	2.2980(13)
Pd(1)–P(2)	2.2869(12)	N(1)–C(9)	1.094(8)
Pd(1)–S(1)	2.2893(12)		
P(1)–Pd(1)–P(2)	86.09(5)	P(2)–Pd(1)–S(1)	179.12(4)
P(1)–Pd(1)–S(1)	93.66(5)	P(1)–Pd(1)–S(2)	177.77(4)
P(2)–Pd(1)–S(2)	91.90(5)	C(21)–P(2)–Pd(1)	114.31(15)
S(1)–Pd(1)–S(2)	88.34(5)	C(31)–P(2)–Pd(1)	120.45(14)
C(51)–P(1)–Pd(1)	114.48(15)	C(11)–P(2)–Pd(1)	107.51(15)
C(41)–P(1)–Pd(1)	122.48(15)	C(1)–S(1)–Pd(1)	103.28(17)
C(10)–P(1)–Pd(1)	106.74(15)	C(2)–S(2)–Pd(1)	103.73(16)

Table 2
Bond lengths (Å) and angles (°) for [Pd{S_2C_2H-(2-C_4H_3S)}(dppe)] (**6**)

Pd(1)–P(1)	2.2716(16)	Pd(2)–S(5)	2.2969(17)
Pd(1)–P(2)	2.2778(15)	Pd(2)–S(4)	2.3068(17)
Pd(1)–S(1)	2.2935(14)	C(1)–C(2)	1.341(8)
Pd(1)–S(2)	2.3114(16)	C(5)–C(6)	1.312(12)
Pd(2)–P(4)	2.2721(17)	C(33)–C(34)	1.338(10)
Pd(2)–P(3)	2.2903(16)	C(39)–C(40)	1.531(9)
P(1)–Pd(1)–P(2)	85.00(6)	C(34)–S(4)–Pd(2)	103.5(2)
P(1)–Pd(1)–S(1)	90.84(5)	C(33)–S(5)–Pd(2)	102.9(2)
P(2)–Pd(1)–S(1)	167.89(6)	C(9)–P(1)–Pd(1)	118.9(2)
P(1)–Pd(1)–S(2)	175.92(6)	C(15)–P(1)–Pd(1)	112.81(18)
P(2)–Pd(1)–S(2)	95.65(6)	C(7)–P(1)–Pd(1)	108.1(2)
S(1)–Pd(1)–S(2)	89.31(6)	C(21)–P(2)–Pd(1)	124.4(2)
P(4)–Pd(2)–P(3)	84.71(6)	C(27)–P(2)–Pd(1)	109.45(19)
P(4)–Pd(2)–S(5)	89.91(6)	C(8)–P(2)–Pd(1)	108.1(2)
P(3)–Pd(2)–S(5)	171.91(6)	C(41)–P(3)–Pd(2)	113.4(2)
P(4)–Pd(2)–S(4)	177.97(6)	C(47)–P(3)–Pd(2)	123.85(19)
P(3)–Pd(2)–S(4)	97.01(6)	C(40)–P(3)–Pd(2)	107.7(2)
S(5)–Pd(2)–S(4)	88.48(6)	C(59)–P(4)–Pd(2)	117.3(2)
C(1)–S(1)–Pd(1)	102.4(2)	C(53)–P(4)–Pd(2)	113.7(2)
C(2)–S(2)–Pd(1)	102.5(2)	C(39)–P(4)–Pd(2)	107.3(2)

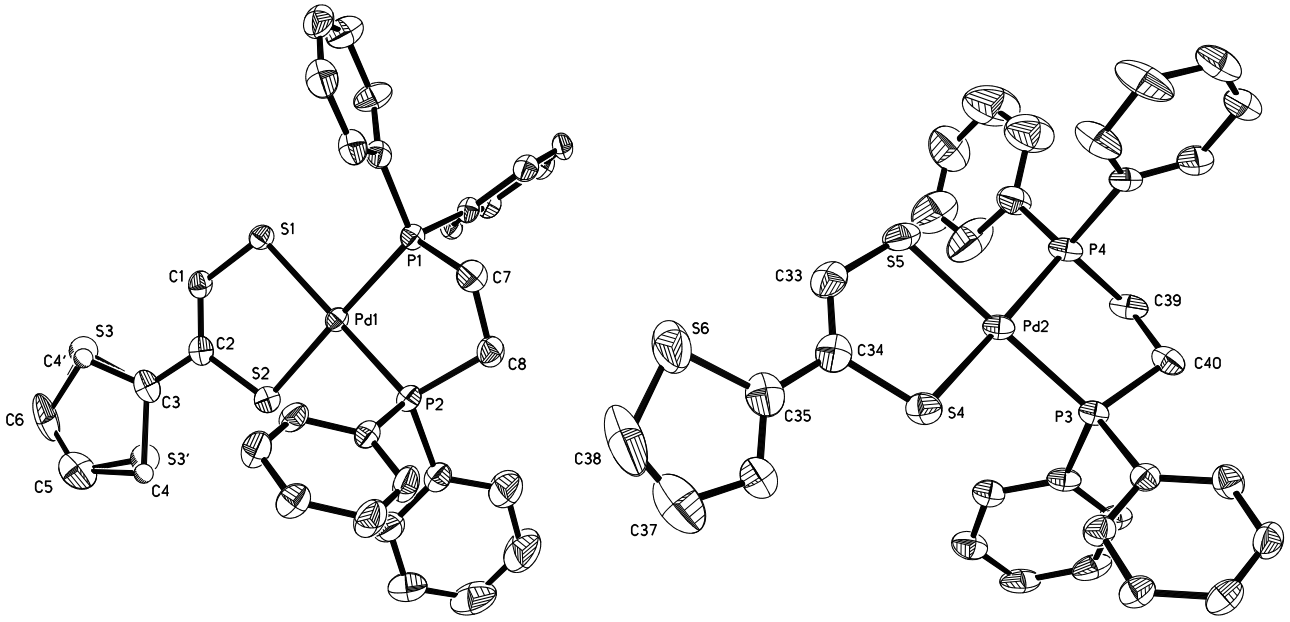

Fig. 2. Crystal structure of the two independent molecules of [Pd{S_2C_2H-(2-C_4H_3S)}(dppe)] (**6**). Thermal ellipsoids are drawn at the 50% probability level and H atoms have been omitted for clarity.

Table 3
Summary of the crystallographic data for complexes [Pd{S_2C_2H-(*p*-CNC_6H_4)}(dppe)] (**4**) and [Pd{S_2C_2H-(2-C_4H_3S)}(dppe)] (**6**)

	4	**6**
Empirical formula	$C_{35}H_{29}NP_2PdS_2$	$C_{64}H_{53}OP_4Pd_6$
Formula weight	696.05	1367.10
Temperature (K)	150(2)	100(2)
Crystal system	monoclinic	orthorhombic
Space group	$P2_1/c$	*Pbcn*
a (Å)	11.453(2)	49.977(5)
b (Å)	19.734(4)	15.397(5)
c (Å)	14.318(3)	16.191(5)
α (°)	90	90
β (°)	105.81(3)	90
γ (°)	90	90
V (Å^3)	3113.8(11)	112459(6)
Z	4	8
D_c (Mg/m^3)	1.485	1.460
μ (mm^{-1})	0.859	0.922
Crystal size (mm)	0.25 × 0.24 × 0.04	0.55 × 0.16 × 0.08
θ Range for data collection (°)	2.96–30.48	1.63–27.09
Number of data collected	20982	75856
Number of unique data [R_{int}]	7877 [0.0773]	13666 [0.0717]
R_1[a]($F^2 > 2\sigma(F^2)$)	0.0568	0.0647
ϖR_2[b] (all data)	0.1638	0.1679
S[c] (all data)	1.026	1.099
Residual ρ (e Å^3)	1.789, −1.539	1.736, −1.088

[a] $R_1(F) = \sum\|F_o| - |F_c\|/\sum|F_o|$.
[b] $\varpi R_2(F^2) = [\sum[\varpi(F_o^2 - F_c^2)^2]/\sum[w(F_o^2)^2]^{1/2}$; $w^{-1} = [\sigma^2(F_o^2) + (\alpha P)^2 + bP]$, where $P = [\max(F_o^2, 0) + 2F_c^2]/3$.
[c] $S = [\sum[\varpi(F_o^2 - F_c^2)^2]/(n-p)]^{1/2}$, where *n* is the number of reflections and *p* the number of refined parameters.

C(35)–S(6) = 9.1° and C(1)–C(2)–C(3)–S(2) = 9.5° in **6** and C(2)–C(3)–C(8)–S(2) = 13° in **4**]. The Pd–S bond lengths are in the range of other Pd-dithiolene complexes [31,34–37]. The C–C bonds in the dithiolene unit are best described as double bonds [C(1)–C(2) = 1.329(6) Å in **4** and C(1)–C(2) = 1.341(8), C(33)–C(34) = 1.338(10) Å in **6**] while the C–C bonds in the bisphosphine dppe are single bonds. One of the molecules in compound **6** shows some disorder in the thiophene ring between *syn* and *anti* conformers with respect to the proton of the dithiolene unit (S_2C_2H), in an equal distribution, while the thiophene in the other molecule displays a *syn* conformation.

*Electrochemical properties of complexes **3**–**8***. Cyclic voltammetry experiments display in all the new complexes one reversible one-electron oxidation due to the dithiolene unit, except in the case of the palladium complex **4** which shows an irreversible oxidation (Table 4). In the case of complexes **3** and **6** an additional irreversible oxidation process is observed at $E_{(ox)} = 1.07$ V (**4**) and 0.59 V (**6**), which can be assigned to a second oxidation of the dithiolenes (see Table 4).

Table 4
Cyclic voltammetric data for complexes **3**–**8** (V vs. SCE, Pt disk electrode in 0.1 M of NBu_4PF_6)

Compound	**3**	**4**	**5**	**6**	**7**	**8**
$E^1_{1/2}$	+0.39v	+0.52v(i)	+0.42v	+0.39v	+0.408v	+0.38v
$E^2_{1/2}$	+1.16v(i)			+1.11v(i)		

4. Concluding remarks

We have presented the synthesis and complete characterisation of heteroleptic nickel and palladium dithiolenes via deprotection of the corresponding starting thiones and subsequent addition of the metallic derivatives with 1,2-bis(diphenylphosphino)ethane as an ancillary ligand. The X-ray analyses of two Pd-dithiolenes show a planar five-membered ring involving the metallic center and the dithiolene unit.

Acknowledgment

We thank the Ministerio de Ciencia y Tecnología of Spain for financial support (CTQ2005-08099-C03-01).

Appendix A. Supplementary material

Crystallographic data for the structural analyses have been deposited with the Cambridge Crystallographic Data Centre, CCDC No. 600597 for compound **4** and CCDC No. 600598 for compound **6**. Copies of this information may be obtained free of charge from the Director, CCDC, 12 Union Road, Cambridge CB2 1EZ, UK, fax: +44 1223 336 033, e-mail: deposit@ccdc.cam.ac.uk or www: http://www.ccdc.cam.ac.uk. Supplementary data associated with this article can be found, in the online version, at doi:10.1016/j.poly.2006.04.010.

References

[1] U.T. Mueller-Westerhoff, B. Vance, in: G. Wilkinson, R.D. Gillard, J.A. McClverty (Eds.), Comprehensive Coordination Chemistry, vol. 2, Pergamon Press, Oxford, 1987, p. 595.
[2] E.I. Stiefel, in: K. Karlin (Ed.), Progress in Coordination Chemistry, vol. 52, Maryland, 2004.
[3] G.N. Schrauzer, V.P. Mayweg, J. Am. Chem. Soc. (1966) 3235.
[4] D.C. Olson, V.P. Mayweg, G.N. Schrauzer, J. Am. Chem. Soc. (1966) 4876.
[5] M.D. Ward, J.A. McCleverty, J. Chem. Soc., Dalton Trans. (2002) 275.
[6] M. Nomura, M. Fujii, K. Fukuda, T. Sugiyama, Y. Yokoyama, M. Kajitani, J. Organomet. Chem. 690 (2005) 1627.
[7] E. Canadell, Coord. Chem. Rev. 185–186 (1999) 629.
[8] R.M. Olk, B. Olk, W. Dietzsch, R. Kirmse, E. Hoyer, Coord. Chem. Rev. 117 (1992) 99.
[9] P. Cassoux, L. Valade, H. Kobayashi, A. Kobayashi, R.A. Clark, A.E. Underhill, Coord. Chem. Rev. 110 (1991) 115.
[10] P. Cassoux, Coord. Chem. Rev. (1999) 213.
[11] M.C. Aragoni, M. Arca, T. Cassano, C. Denotti, F.A. Devillanova, R. Frau, F. Isaia, F. Lelj, V. Lippolis, L. Nitti, P. Romaniello, R. Tommasi, G. Verani, Eur. J. Inorg. Chem. (2003) 1939.
[12] U.T. Mueller-Westerhoff, B. Vance, D.I. Yoon, Tetrahedron 47 (1991) 909.
[13] U.T. Mueller-Westerhoff, I.J.Q.K.H. Drexhage, E. QE-8, 1972, 759.
[14] U.T. Mueller-Westerhoff, K.H. Drexhage, U. Patent, 3, 964, 1973.
[15] A.E. Pullen, R.M. Olk, Coord. Chem. Rev. 188 (1999) 211.

[16] M. Fourmigué, Coord. Chem. Rev. 178–180 (1998) 823.
[17] M. Fourmigué, Acc. Chem. Res. 37 (2004) 179.
[18] E. Cerrada, J. Garrido, M. Laguna, N. Lardiés, I. Romeo, Synth. Met. 102 (1999) 1709.
[19] E. Cerrada, C. Diaz, M. Laguna, I. Romeo, H. Teruel, N. Urzay, Synth. Met. 120 (2001) 817.
[20] R.P. Clausen, J. Becher, Tetrahedron 52 (1996) 3171.
[21] SAINT, M. version 5.0 Bruker Analytical X-ray Systems, W.1.G.
[22] R.H. Blessing, Acta Crystallogr., Sect. A A51 (1995) 33.
[23] R.H. Blessing, J. Appl. Crystallogr. 30 (1997) 421.
[24] G.M. Sheldrick, SADABS Empirical Absorption Program, University of Göttingen, Göttingen, Germany, 1996.
[25] G.M. Sheldrick, Acta Crystallogr., Sect. A 46 (1990) 467.
[26] G.M. Sheldrick, Program for Crystal Structure Refinement, University of Göttingen, 1997.
[27] S.P. Kaiwar, J.K. Hsu, L.M. Liable-Sands, A.L. Rheingold, R.S. Pilato, Inorg. Chem. 36 (1997) 4234.
[28] S.P. Kaiwar, A. Vodacek, N.V. Blough, R.S. Pilato, J. Am. Chem. Soc. 119 (1997) 9211.
[29] K.A.v. Houten, D.C. Heath, C.A. Barringer, A.L. Rheingold, R.S. Pilato, Inorg. Chem. (1998) 37.
[30] J.M. Bevilacqua, J.A. Zuleta, R. Eisenberg, Inorg. Chem. 33 (1994) 258.
[31] B.W. Smucker, J.M. Hudson, M.A. Omary, K.R. Dunbar, Inorg. Chem. 42 (2003) 4714.
[32] M. Bousseau, L. Valade, J.-P. Legros, P. Cassoux, M. Garbauskas, L.V. Interrante, J. Am. Chem. Soc. 108 (1986) 1908.
[33] N.G. Connelly, J.G. Crossley, A.G. Orpen, Chem. Commun. (1992) 1568.
[34] M. Bousseau, L. Valade, J.-P. Legros, P. Cassoux, M. Garbauskas, L.V. Interrante, J. Am. Chem. Soc. 108 (1986) 1908.
[35] K.A.v. Houten, D.C. Heath, C.A. Barringer, A.L. Rheingold, R.S. Pilato, Inorg. Chem. 37 (1998) 4647.
[36] N.G. Connelly, J.G. Crossley, A.G. Orpen, Chem. Commun. (1992) 1568.
[37] M.C. Aragoni, M. Arca, C. Denotti, F.A. Devillanova, E. Grigiotti, F. Isaia, F. Laschi, V. Lippolis, L. Pala, A.M.Z. Slawin, P. Zanello, J.D. Woollins, Eur. J. Inorg. Chem. (2003).

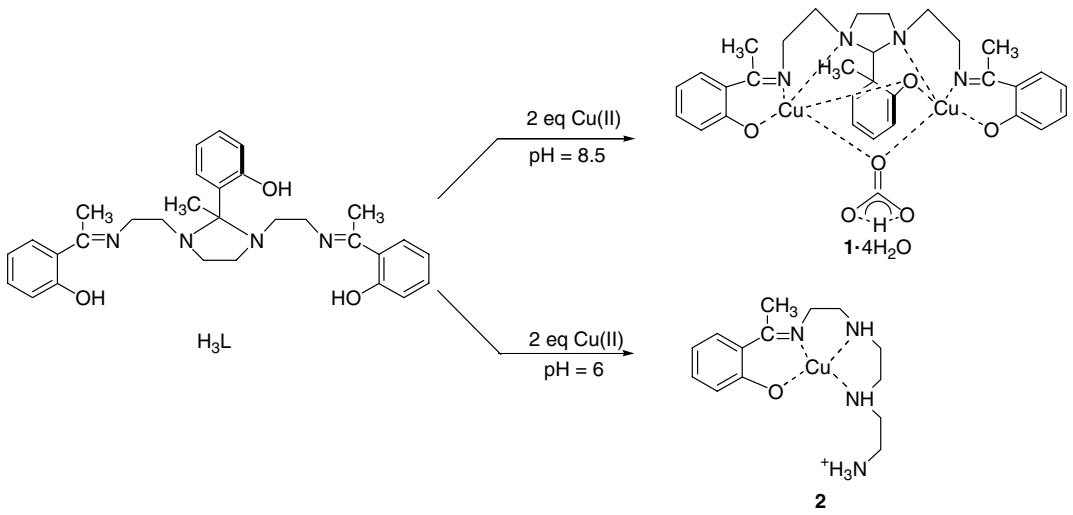

Scheme 1.

bridging groups by occupying the vacant positions. 2-Methyl(2′-hydroxyphenyl)imidazolidine group can function as a spacer in the μ-bis(tetradenate) imine phenol ligand H_3L (Scheme 1).

2. Experimental

2.1. Physical measurements

The chemicals used were obtained from the following sources: triethylenetetramine from S.D. Fine Chem., India. 2-Hydroxy acetophenone from Spectrochem, Mumbai, India. Copper(II) perchlorate hexahydrate was prepared by treating Copper(II) carbonate with 1:1 $HClO_4$ and crystallized after concentration on water bath. All other chemicals and solvents were reagent grade materials and were used as received without further purification. The elemental analyses (C, H, N) were performed with a Perkin–Elmer model 240 C elemental analyzer. ^1H and ^{13}C NMR spectra of the ligand were obtained on a Bruker AC 200 NMR spectrometer using TMS as the internal standard. ^1H NMR spectra of the complex were collected on a 250 MHz Bruker DXR 250 spectrometer. In all cases, the protio-solvent signal was used as reference and chemical shifts were quoted on the δ scale (down field shifts are positive). IR spectra were recorded on a Perkin–Elmer 883 spectrophotometer. The solution electrical conductivity and electronic spectra were obtained using a Unitech type U131C digital conductivity meter with a solute concentration of about 10^{-3} M and a Shimadzu UV 3100 UV–Vis–NIR spectrophotometer, respectively. The room temperature magnetic susceptibilities in the solid state were measured using a home built Gouy balance fitted with a polytronic d.c. power supply. The experimental magnetic susceptibilities were corrected for the diamagnetic response using Pascal's constants [10]. Magnetic measurements were carried out at the "Servei de Magnetoquímica (Universitat de Barcelona)" on polycrystalline samples (ca. 40 mg) using a Quantum Design MPMS XL-5 SQUID susceptometer operating at a constant magnetic field of 1 T between 2 and 300 K. The experimental magnetic moment was corrected for the diamagnetic contribution from the sample holder. X-band and EPR measurements (9.7857 GHz) were performed at various temperatures on powdered samples a Bruker Spectrometer (ESR 300E), working with an oxford liquid helium cryostat for variable temperature.

2.2. Preparation of H_3L

A solution of triethylenetetramine (3.7 g, 25.32 mmol) in methanol (25 ml) was dropwise added to a methanolic solution (25 ml) of 2-hydroxyacetophenone (10.2 g, 74.90 mmol) with stirring at room temperature. The yellow solution was then refluxed for 5 h. The solvent was evaporated in air. The yellow solid was separated by filtration through G4 sintered bed and washed thoroughly with hexane and water. Finally, the isolated compound was dried in vacuo over P_4O_{10}. Yield 9.3 g (75%), m.p. 184–186 °C. *Anal.* Calc. for $C_{30}H_{36}N_4O_3$: C, 71.97; H, 7.25; N, 11.19. Found: C, 71.51; H, 7.62; N, 11.49%. Mass spectrum (EI): m/z 500 ($M^+ = L^+$). Infrared spectrum (cm^{-1}, KBr disk): ν(phenolic OH) 3443(w); ν(C=N) 1616(s); ν(phenolic C–O) 1371(s); $\nu(CH_2)$ 835(m); ν(aromatic CH) 745(m). ^1H NMR ($CDCl_3$, ppm): δ (terminal phenolic OH) 16.13(s, 2H); (pendant phenolic OH) 12.03(s, 1H); (H_{2-5}) 7.21–7.48(m, 8H); (H_{15-18}) 6.74–6.89(m, 4H); (H_8) 3.47–3.55(m, 4H); (H_9) 2.86(t, 4H); (H_{10} and H_{11}) 2.74–2.80(m, 4H); ($H_{terminal\ methyl}$) 2.21(s, 6H); ($H_{central\ methyl}$) 1.138(s, 3H). ^{13}C NMR ($CDCl_3$, ppm): δ (C_7) 164.29; ($C_{1,14}$) 162.38; (C_6) 132.48; ($C_{16,18}$) 130.68; ($C_{3,5}$) 128.00; (C_{17}) 119.18; (C_4) 118.88; ($C_{2,15}$) 118.39; (C_{12}) 116.83; (C_8) 49.61; (C_9) 49.44; (C_{10}) 49.10; ($C_{terminal\ methyl}$) 26.58; ($C_{central\ methyl}$) 14.51.

Table 1
Crystallographic data for complexes $1 \cdot 4H_2O$ and **2**

Molecular formula	$C_{31}H_{42}N_4O_{10}Cu_2$	$C_{14}H_{24}N_4O_9CuCl_2$
Molecular weight	757.78	526.80
Crystal system	orthorhombic	monoclinic
Space group	*Pnam*	$P2_1/n$
a (Å)	13.627(2)	8.647(18)
b (Å)	14.261(2)	11.133(10)
c (Å)	17.877(3)	22.280(3)
α (°)	90.00	90.00
β (°)	90.00	90.980(2)
γ (°)	90.00	90.00
U (Å^3)	3474.2(18)	2145.0(6)
D_c (g cm^{-3})	1.493	1.632
Z	4	2
$F(000)$	1604	1084
Crystal size (mm)	$0.32 \times 0.28 \times 0.16$	$0.28 \times 0.20 \times 0.15$
μ (mm^{-1})	1.290	1.321
θ Range (°)	1.83–24.97	1.83–25.05
R_1, wR_2 $[I > 2\sigma(I)]$	0.0639, 0.1301	0.0787, 0.2187
Goodness-of-fit on F^2	1.019	1.038
Final difference map		
Maximum and minimum (e Å^{-3})	0.649, −0.394	0.908, −0.822

$R_1 = \sum(||F_o| - |F_c||)/\sum|F_o|$. $wR_2 = [\sum w(|F_o| - |F_c|)^2/\sum w(F_o)^2]^{1/2}$, $w = 0.75/(\sigma^2(F_o) + 0.0010F_o^2)$.

Table 2
Selected bond lengths (Å) and bond angles (°) in $1 \cdot 4H_2O$ and **2**

$1 \cdot 4H_2O$		**2**	
Bond lengths (Å)			
Cu(1)–O(1)	1.885(4)	Cu(1)–O(1)	1.884(5)
Cu(1)–O(2)	1.978(4)	Cu(1)–N(1)	1.953(6)
Cu(1)–N(1)	1.947(6)	Cu(1)–N(2)	2.002(8)
Cu(1)–N(2)	2.092(5)	Cu(1)–N(3)	2.074(8)
Cu(1)–O(3)	2.307(6)	C(13)–N(4)	1.504(12)
C(20)–O(3)	1.240(15)		
C(20)–O(4)	1.319(13)		
Bond angles (°)			
O(1)–Cu(1)–N(1)	92.8(2)	O(1)–Cu(1)–N(1)	94.7(2)
O(1)–Cu(1)–O(2)	89.9(2)	O(1)–Cu(1)–N(2)	179.1(4)
N(1)–Cu(1)–O(2)	159.7(2)	N(1)–Cu(1)–N(2)	86.0(3)
O(1)–Cu(1)–N(2)	177.0(2)	O(1)–Cu(1)–N(3)	95.4(3)
N(1)–Cu(1)–N(2)	86.1(2)	N(1)–Cu(1)–N(3)	166.7(3)
O(2)–Cu(1)–N(2)	90.1(2)	N(2)–Cu(1)–N(3)	84.0(4)
O(1)–Cu(1)–O(3)	92.6(2)		
N(1)–Cu(1)–O(3)	121.8(2)		
O(2)–Cu(1)–O(3)	78.1(2)		
N(2)–Cu(1)–O(3)	90.3(2)		
O(3)–C(20)–O(4)	120.4(8)		
O(4)–C(20)–O(4)#1	119.1(17)		

2.3. Preparation of $1 \cdot 4H_2O$

To the solution of H_3L (0.50 g, 1.00 mmol) in acetonitrile (20 ml) was added aqueous solution of NaOH (0.12 g, 3.00 mmol) followed by aqueous solution of $Cu(ClO_4)_2 \cdot 6H_2O$ (0.74 g, 2.00 mmol) with magnetic stirring in air at ambient temperature. The reaction mixture was then stirred for two more hours. The resulting dark green color solution was then left for evaporation in the air. The dark green color crystals separated out were isolated and dried in vacuo. Yield: 0.56 g (75%). *Anal.* Calc. for $C_{31}H_{42}N_4O_{10}Cu_2$: C, 49.13; H, 5.58; N, 7.39; Cu, 16.77. Found: C, 49.41; H, 5.48; N, 7.51; Cu, 17.12%. IR (KBr, cm^{-1}): $\nu = 3395$(b), 2920(b), 1590(s), 1531(s), 1441(s), 1338(s), 1242(s), 1113(s), 850(s), 747(s). Molar conductance, Λ_M: (MeCN solution) 45 ohm^{-1} cm^2 mol^{-1}. UV–Vis spectra [λ_{max}, nm (ε, l mol^{-1} cm^{-1})]: (MeCN solution) 635 (338), 395 (2700), 366 (6886), 309(8627). Room temperature μ_{eff} (tot.): 2.29 μ_B; μ_{eff}/Cu: 1.62 μ_B.

2.4. Preparation of **2**

To the solution of H_3L (0.50 g, 1.00 mmol) in acetonitrile (20 ml) was added aqueous solution of $Cu(ClO_4)_2 \cdot 6H_2O$ (0.74 g, 2.00 mmol) with magnetic stirring in air at room temperature. The resulting blue violet solution was then stirred for 1hour and left in the air for solvent evaporation. The dark blue violet solid that separated out was filtered washed with water and dried in the vacuo. Yield: 0. 37 g (70%). *Anal.* Calc. for $C_{14}H_{24}N_4O_9CuCl_2$: C, 31.91; H, 4.59; N, 10.63; Cu, 12.06. Found: C, 32.13; H, 4.48; N, 10.85; Cu, 12.37%. IR (KBr, cm^{-1}): $\nu = 2928$(b), 1607(vs), 1589(s), 1323(s), 1091(s), 963(s), 738(s). Molar conductance, Λ_M: (MeCN solution) 235 ohm^{-1} cm^2 mol^{-1}. UV–Vis spectra [λ_{max}, nm (ε, l mol^{-1} cm^{-1})]: (MeCN solution) 567 (290), 351 (8445), 268 (27 265), 239 (30 605). Room temperature μ_{eff} 1.75 μ_B.

2.5. X-ray crystallographic procedures for $1 \cdot 4H_2O$ and **2**

Suitable crystals of $1 \cdot 4H_2O$ and **2** were grown from acetonitrile/H_2O and acetonitrile/dichloromethane solution of the complexes, respectively, at room temperature over a period of 5–10 days. The single crystal data were collected on Bruker-Nonius Mach3 CAD4 X-ray diffractometer that uses graphite monochromated Mo Kα radiation ($\lambda = 0.71073$ Å) by ω-scan method. The structure was solved by direct methods and refined by least-square methods on F^2 using SHELX-97 [11]. Non-hydrogen atoms were refined anisotropically and hydrogen atoms on C-atoms were fixed at calculated positions and refined using a riding model. Whereas H-atoms on water molecules in $1 \cdot 4H_2O$ could not be located. The details of crystal data are given in Table 1. The selected bond lengths are summarized in Table 2.

3. Results and discussion

3.1. Syntheses and characterization

The μ-bis(tetradentate) ligand H_3L was synthesized by the known imidazolidine ring formation reaction with 2-hydroxy acetophenone and triethylenetetramine in 3:1 molar ratio under reflux for 5 h, and isolated in the solid form following a modified Bailer route [12]. The resulting Schiff base incorporated an imidazolidine ring from the

reaction of the third ketone with the two inner adjacent secondary amine nitrogens of trine [13]. In the IR spectrum of the ligand H_3L, the phenolic O–H stretching of the two terminal rings are observed at 3443 cm^{-1}. The C=N stretching frequency is observed at 1616 cm^{-1}. In the EI-MS of the ligand, the molecular ion peak (m/z) was observed at 500, confirming the formation of the desired imidazolidine ring containing ligand. In ^1H NMR spectra the characteristic central methyl protons and terminal methyl protons both appear as singlets at 1.38 and 2.21 ppm, respectively. The signals due to aromatic ring protons were observed in the 6.74–7.40 ppm region. The hydrogens on the imidazolidine backbone appeared as a complex set of overlapping triplet resonance signals at 2.74–2.80 ppm. The characteristic central methyl carbon and terminal methyl carbons appear at 14.51 and 26.58 ppm, respectively, in ^{13}C NMR spectra. The imidazolidine ring carbon at the hydroxyphenyl substitution appears at 116.83 ppm. The imine carbon appears at 164.29 ppm. Both ^1H and ^{13}C NMR data are comparable with the literature values [14,15]. The reaction of H_3L with $Cu(ClO_4)_2 \cdot 6H_2O$ in air leads to complex $\mathbf{1} \cdot 4H_2O$ after fixation and transformation of carbon dioxide, possibly resulting from the initial formation of the corresponding dinuclear complex with vacant coordination sites. Utilization of methylimine ligand (H_3L) instead of the corresponding (unsubstituted) imine ligand increases the ease of substitution of the apical bridging ligands in dicopper complexes. We have found that the aqua bridged complex, $[Cu^{II}_2(\mu\text{-}L)(\mu\text{-}H_2O)]ClO_4$, which represents the starting point of this investigation, fixes carbon dioxide in the form of the $\mu\text{-}\eta^2 : HCO_3^-$ bridged complex $\mathbf{1} \cdot 4H_2O$ in nearly quantitative yield (Scheme 2). The product was identified by IR spectroscopy and X-ray crystal structure analysis. Any carbonate bridged complex was not obtained at this pH. In moderate basic medium the fixation of carbon dioxide as hydrogencarbonate is possible when a nucleophilic M–OH unit attacks the electrophilic carbon atom of the CO_2 molecule. A proposed mechanism for the formation of $\mathbf{1} \cdot 4H_2O$ is suggested in Scheme 2. Possibly the bridged aqua ligand is activated by two Lewis-acidic Cu^{II} centers, favouring its deprotonation to give the μ-OH intermediate. Bridging water, which has no access for nucleophilic attack to the imidazolidine carbon and imine carbon of L^{3-}, is responsible for CO_2 activation.

The aqua bridged complex, formed initially in solution, thus exhibits remarkably high affinity for CO_2. The hydrogencarbonate group is generated in situ by reaction of atmospheric CO_2 without the need of bubbling CO_2 into the solution. On the other hand if a water molecule is present as a terminal ligand, it can hydrolyze the central imidazolidine part and terminal salicylimine end of the ligand. Attack of H_2O to the tertiary carbon of the imidazolidine ring and protonation of one imidazolidine nitrogen may be responsible for the ring hydrolysis. Further attack of H_2O to one of the imine bond gives the mononuclear complex $[Cu^{II}(HL^1)] \cdot 2ClO_4$ (**2**) with the loss of second 2-hydroxyacetophenone molecule as shown in Scheme 3.

The dicopper complex is bridged by endogenous L^{3-} and by the oxygen atom of an exogenous hydrogencarbonate. Only one $\mu\text{-}\eta^1 : \eta^1\text{-}O,O'$-hydrogencarbonate bridged

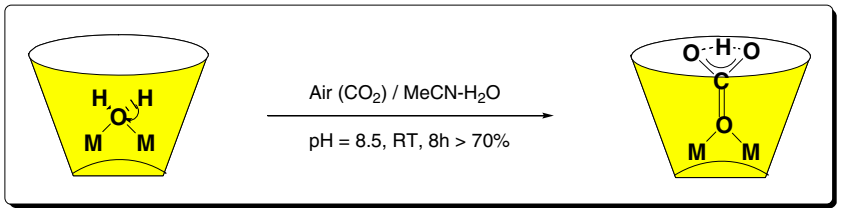

Scheme 2.

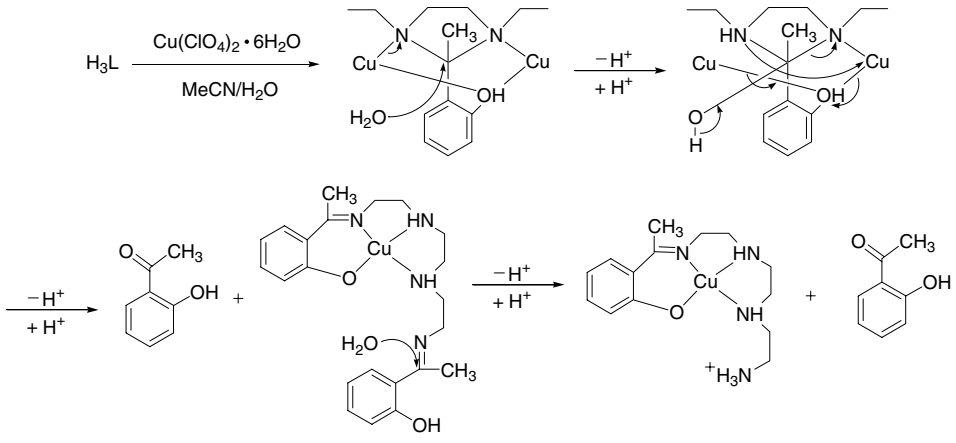

Scheme 3.

dicopper(II) complex has been reported till date [16]. Complex $\mathbf{1}\cdot 4H_2O$ is the first example where the hydrogencarbonate bridges between two copper centers through the single oxygen of one C=O group. Four possible bridging modes for hydrogencarbonate/carbonate bridged dinuclear metal systems are shown in Scheme 4. Mode A for hydrogencarbonate is reported for the first time in $\mathbf{1}\cdot 4H_2O$.

Complex $\mathbf{1}\cdot 4H_2O$ is obtained from the reaction of H_3L with $Cu(ClO_4)_2\cdot 6H_2O$ and NaOH (pH 8.5) in 1:2:3 molar ratio in acetonitrile–water (1:1 vol) at room temperature in air. In MeCN the solution conductivity measurement ($45\ \Omega^{-1}\ cm^2\ mol^{-1}$, 28 °C) shows non-electrolytic behavior, confirming the nature of the bridging group as HCO_3^-. The IR spectrum of the complex showed a strong absorption band at $1590\ cm^{-1}$ which is the characteristic stretching vibration of ν(C=O) of this group [17]. Fixation of atmospheric CO_2 as CO_3^{2-} or HCO_3^- bridged dinuclear or polynuclear Cu^{II} complexes has been described previously [18]. A broad peak at $3395\ cm^{-1}$ is due to uncoordinated water molecules. Of all dicopper compounds made from ligands related to H_3L, $\mathbf{1}\cdot 4H_2O$ is only the third example featuring a single exogenous oxygen bridging ligand (Scheme 5) [19,20] and the first example for any kind of neutral oxygen bridging reported till date.

Electronic spectra of the complex in acetonitrile solutions show several intense absorption bands in the visible region. A strong broad band at 635 nm region with molar extinction coefficient of $340\ l\ mol^{-1}\ cm^{-1}$ is characteristic of d–d transitions. Higher intensity charge transfer transitions are obtained at 395, 366 and 309 nm with molar extinction coefficients of 2700, 6885 and $8625\ l\ mol^{-1}\ cm^{-1}$, respectively.

Complex **2** was obtained as a blue violet solid in 70% yield from the reaction of H_3L with $Cu(ClO_4)_2\cdot 6H_2O$ in 1:2 molar ratio in air and in absence of base (pH 6) in MeCN–water mixture at room temperature. The complex behaves as a 1:2 electrolyte in acetonitrile solution ($\Lambda_M = 235\ ohm^{-1}\ cm^2\ mol^{-1}$). The IR spectrum of the complex showed strong absorption bands at 2928 and $1607\ cm^{-1}$, characteristic of the ν(NH) and ν(C=N) stretching vibrations. The strong unsplit band for $\nu(ClO_4^-)$ at around $1091\ cm^{-1}$ suggests no coordination of perchlorate ions [17]. The electronic spectra of the complex shows a d–d transition band at 567 nm with molar extinction coefficient of $290\ l\ mol^{-1}\ cm^{-1}$ and several charge transfer transitions in the 351–239 nm range with molar extinction coefficient of 8455–$30605\ l\ mol^{-1}\ cm^{-1}$. The structure of **2** shows that during the reaction, the ligand H_3L undergoes copper(II) mediated imidazolidine ring and one terminal imine bond hydrolysis simultaneously. It is interesting to note that the corresponding bis(amide) ligand is stable towards this type of coordination driven hydrolysis reaction [21].

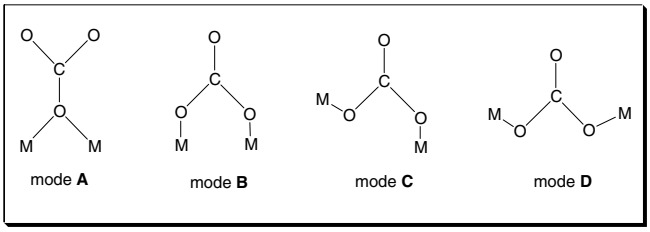

Scheme 4.

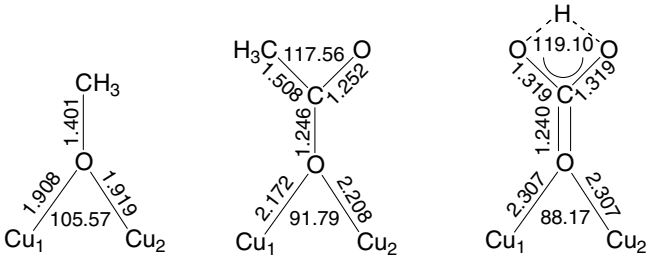

Scheme 5.

3.2. X-ray structure of $[Cu_2^{II}(L)(HCO_3)]\cdot 4H_2O$ ($\mathbf{1}\cdot 4H_2O$) and $[Cu^{II}(HL^1)]\cdot 2ClO_4$ (**2**)

The molecular structure of $\mathbf{1}\cdot 4H_2O$ (Fig. 1a) consists of two Cu^{II} ions chelated and bridged by one L^{3-} ligand, which are related by a crystallographic plane of symmetry.

The bridging moieties of this ligand are one μ-η^1:η^1-*N*,*N*′-imidazolidine fragment and the single oxygen of the central phenoxide group, the imine N-atoms and the oxygen from terminal phenoxide groups completing the donation from L^{3-}. In addition, the metals are bridged by one μ-η^2-HCO_3^- group, which completes the triply bridging motif in the dicopper complex. Thus, each Cu^{II} ion exhibits a distorted square pyramidal ($\tau = 0.28$) [22] coordination geometry (N_2O_3) where the two N-atoms (imine and amine) and two O-atoms (terminal and bridging phenoxide groups, respectively) form the basal square plane and the C=O oxygen from the hydrogencarbonate ligand occupies the fifth (apical) coordination position. Bridging of hydrogencarbonate within a dicopper system by a C=O single oxygen is very uncommon.

Each *meridional* half of the ligand L^{3-} forms one five-membered (N–Cu–N) and two six-membered (N–Cu–O) chelate rings. The chelate bite angles are 86.1(2)° for the five-membered ring and 92.8(2)° (terminal phenoxide) and 90.1(2)° (bridging phenoxide) for the six-membered rings. The bond distances from Cu^{II} to the bridging oxygen atoms are 1.978(4) (phenolate) and 2.307(6) Å (hydrogencarbonate). The Cu···Cu distance is 3.210(6) Å, which is in the normal range for other molecules with a triply bridging motif [23,24]. The Cu–O–Cu bond angles for bridging phenol and hydrogencarbonate are 108.4(3)° and 88.2(3)°, respectively. The Cu–N_{imine} and Cu–N_{amine} distances are distinctly different; the longer Cu–N_{amine} distance (2.092(5) Å) compared to that of the Cu–N_{imine} bond (1.947(6) Å) is mainly due to the different states of

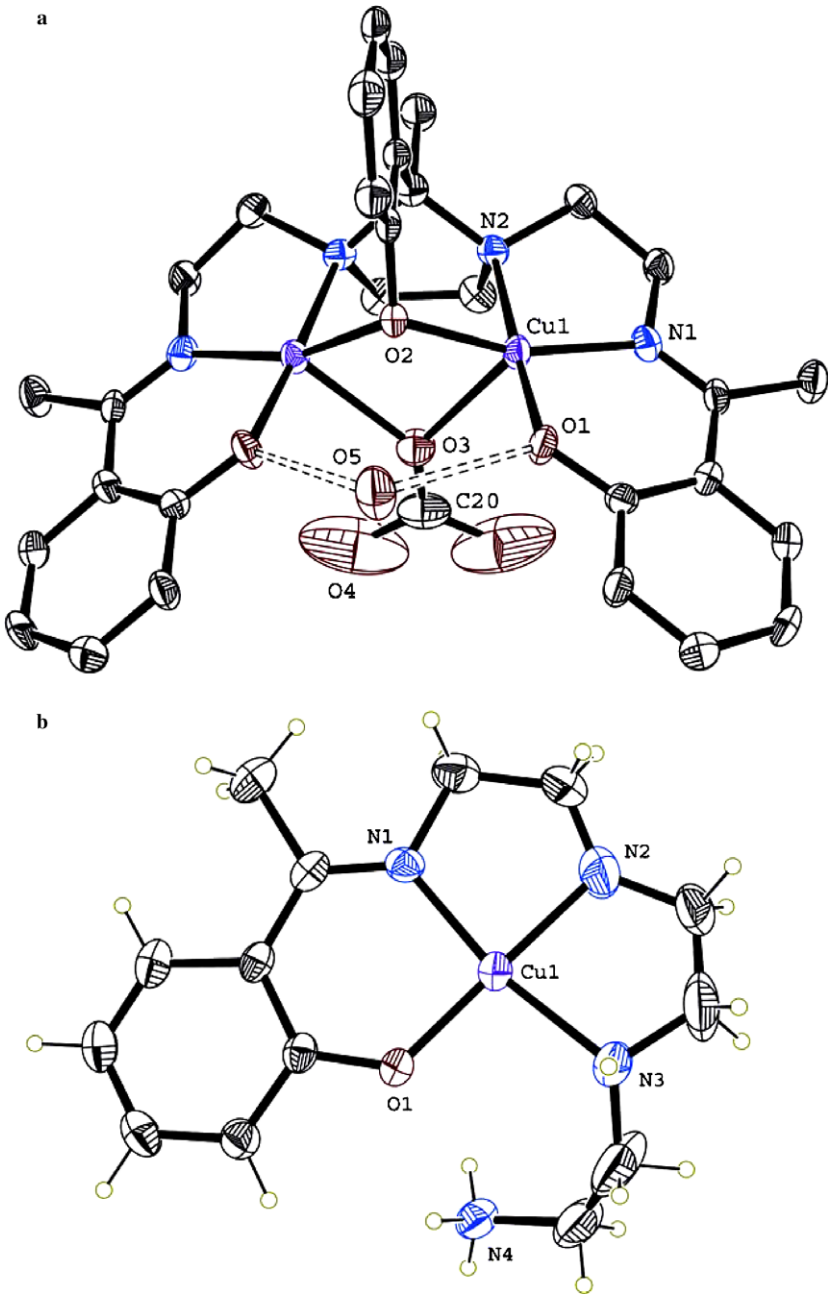

Fig. 1. Labeled ORTEP view of $\mathbf{1} \cdot 4H_2O$ with H-bond indicated as dashed lines (a), and cationic part of **2** (b). Ellipsoids are drawn at 30% probability. Hydrogen atoms are omitted for clarity in (a).

hybridization of the coordinating N atoms in the molecule. The Cu–N_{amine} distance is in the usual range for a bivalent metal ion and is not longer due to their participation in bridging. The C=O distance (1.240(15) Å) of the bridging hydrogencarbonate moiety is short in comparison to other reported C=O(carbonate) bridged dicopper complexes, proving the enhanced double-bond character of the carbon–oxygen bond in complex $\mathbf{1} \cdot 4H_2O$ [18b,25]. The other C–O distance in this moiety (C20–O4) is 1.319(13) Å, whereas all the O–C–C angles are close to 120°. It is difficult to establish the presence of the proton attached to the hydrogencarbonate group. This is inferred by inspection of the C–O bond distances, and is required to ensure the charge balance within the system. To the best of our knowledge, this is the first reported structure of a neutral dicopper system bridged by hydrogencarbonate through one single oxygen atom. The average C–C and C–N bond distances fall in the usual range. There are two water molecules of crystallization within the crystal lattice. The first water molecule O(5) shows intramolecular interactions with both the terminal phenolic oxygen atoms O(1) and O(2) (Fig. 1a) [O(5)···O(1)/O(2) = 2.773(3) Å]. The hydrogen bonded water molecule provides a pseudo macrocyclic ligand environment around two copper(II) centers

(Fig. 1a). The second water molecule is further hydrogen bonded to the first one at a distance O(5)···O(6) = 2.740(3) Å, which is in the range found in regular ice (2.74–2.85 Å) [26]. The molecules of $[Cu_2(L)(HCO_3)]\cdot 4H_2O$ units form an extended array by a combination of π···π, C–H···O and O–H···O hydrogen bonds [27], leading to the formation of a 3D network with zigzag hydrophilic layers along the (0 1 0) direction (Fig. 2a). The guest water molecules occupy the interlayer space of dicopper complexes and form an intricate hydrogen bond scheme. According to the structural data, they belong to either of two categories: (i) tightly bonded molecules, anchored to the network by one or more hydrogen bonds involving the terminal phenol oxygen atoms; and (ii) loosely bonded molecules showing only contacts with other water molecules.

The molecular structure of **2** (Fig. 1b) shows a mononuclear complex of copper(II) in square planar N_3O environment of the hydrolyzed zwitterionic ligand H_2L^{1+}.

The donor atoms consist of three nitrogens (one imine and two amine) and one phenolic oxygen. The tetradentate ligand H_2L^{1+} forms two five membered (N–Cu–N) and one six membered (N–Cu–O) chelate rings with bite angles of 86.0(3)°, 84.0(4)° and 94.7(2)°, respectively. The three chelate planes around the copper(II) ion are almost planar with maximum deviations of 0.051 Å at atom O(1) for the O(1)C(2)C(1)C(7)N(1)Cu(1) ring, −0.088 Å at atom C(9) for the N(1)C(8)C(9)N(2)Cu(1) ring and −0.032 Å at atom C(11) for the N(2)C(10)C(11)N(3)Cu(1) ring. The $Cu–O_{phenol}$ bond length [1.884(5) Å] is comparable to those observed in other four coordinate Cu^{II} complexes [28]. As for complex **2**, the $Cu–N_{imine}$ distance (1.953(6) Å) is shorter than the average $Cu–N_{amine}$ distances (2.038(8) Å) due to the different states of hybridization of the coordinating N_{amine} atoms in the molecule. The bond near the pendant $-NH_3^+$ moiety [Cu(1)–N(3)] features the longer distance (2.074(8) Å) compared to the Cu(1)–N(2) distance (2.002(8)) of the other amine nitrogen atom. The C–C and C–N bond distances fall in the usual range. The uncoordinated pendant $-NH_3^+$ group of the complex shows three hydrogen bonds; one with the coordinated phenolic oxygen and two with oxygen atoms of the two uncoordinated perchlorate molecules, respectively. Of the three hydrogen bonds, that with the coordinated

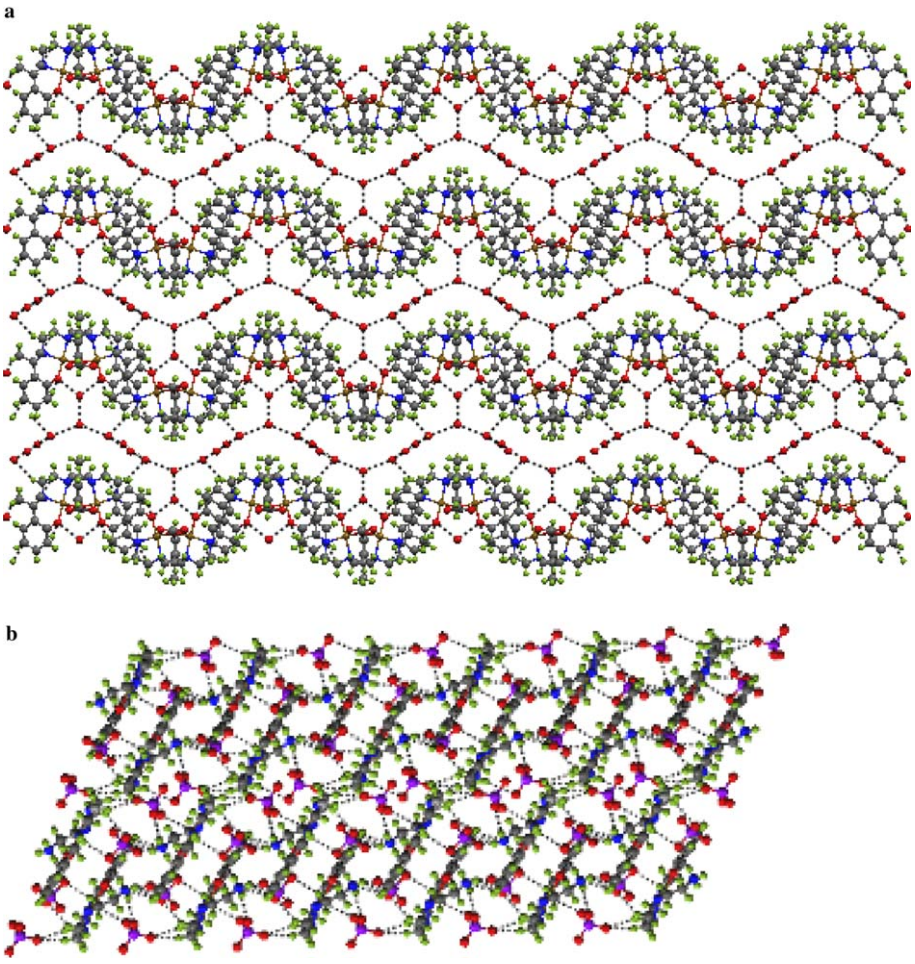

Fig. 2. (a) View of the packing of $\mathbf{1}\cdot 4H_2O$ along the (0 1 0) direction; guest water molecules give hydrogen bonded zigzag layers between the dinuclear units. (b) View of the packing of **2** along the (0 1 0) direction showing the formation of a 3D network with a step structure.

phenol (O(1)) is the shortest (with a N–H···O distance of 2.705 Å). The three observed hydrogen bonds again confirm the cationic nature of the pendant $-NH_3^+$ arm. The $[Cu^{II}(HL^1)]\cdot 2ClO_4$ units also form an extended array by a combination of C–H···O and O–H···O hydrogen bonds between the perchlorate anions and the ethylene backbone of the ligand, leading to the formation of a 3D network with a step structure along the (0 1 0) direction (Fig. 2b).

3.3. Magnetochemistry of $[Cu^{II}_2(L)(HCO_3)]\cdot 4H_2O$ ($\mathbf{1}\cdot 4H_2O$)

Bulk magnetization measurements on complex $\mathbf{1}\cdot 4H_2O$ under a constant magnetic field of 1 T were performed in the 2–300 K temperature range. The $\chi_M T$ versus T plot (Fig. 3) remains almost constant in almost all temperature range and only drops at a very low temperature, indicating that the magnetic exchange between Cu^{II} centers is very weak and antiferromagnetic.

A fit to the Bleaney-Bowers equation (for the Hamiltonian $H = -JS_1S_2$) provided a coupling constant of $J = -1.2\ cm^{-1}$. This is in contrast with the (much more significant) ferromagnetic nature of the coupling observed within a pair of carbonate bridged dimers previously reported with a ligand very similar to H_3L [18b]. The ferromagnetism in the latter case was explained, with help of DFT calculations, in terms of the counter-complementary effect between the various bridging moieties linking the Cu^{II} ions. However, in the present case, the coordination number and geometries of the metals are very different, and therefore, it is not possible to establish any analogy. This fit produced TIP and g values of $251\times 10^{-6}\ cm^3\ mol^{-1}$ and 1.94, respectively. The latter is slightly lower than expected for Cu^{II} and it could be due to an experimental error. A more reliable value ($g = 2.15$) could be obtained from variable temperature X-band solid state EPR (Fig. 4), as calculated from the rhombic signals $g_1 = 2.23$, $g_2 = 2.14$ and $g_3 = 2.08$. The existence of a signal even at 8 K is consistent with the very weak antiferromagnetic coupling existing between both Cu^{II} signals. The solution behavior of $\mathbf{1}\cdot 4H_2O$ was investigated by means of room temperature ^1H NMR in d_4-MeOH. The spectrum (Fig. 5) is similar to that obtained for a previously reported complex of H_3L, featuring bridging acetate instead of hydrogencarbonate.

For complex $\mathbf{1}\cdot 4H_2O$, however, the spectrum is much broader, to the point that many peaks escape detection. For this reason, only the peaks corresponding to the $-CH_3$ groups could be assigned in the present spectrum. A very broad peak, the integration of which is much larger than any other peak in the spectrum is attributed to exchangeable protons. This presumably reflects the fact that the antiferromagnetic coupling in $\mathbf{1}\cdot 4H_2O$ is weaker

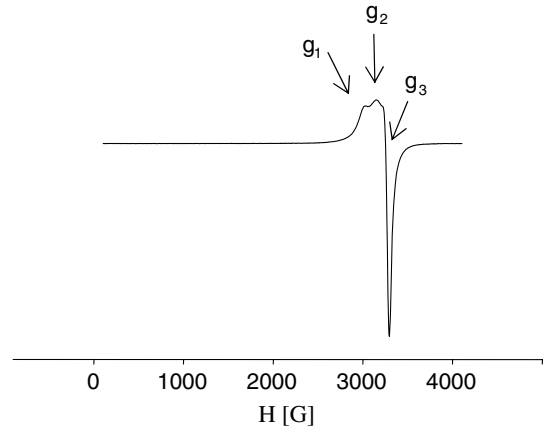

Fig. 4. Solid state powder EPR spectra (X-band) of $[Cu^{II}_2(L)(HCO_3)]\cdot 4H_2O$ ($\mathbf{1}\cdot 4H_2O$) at 8 K.

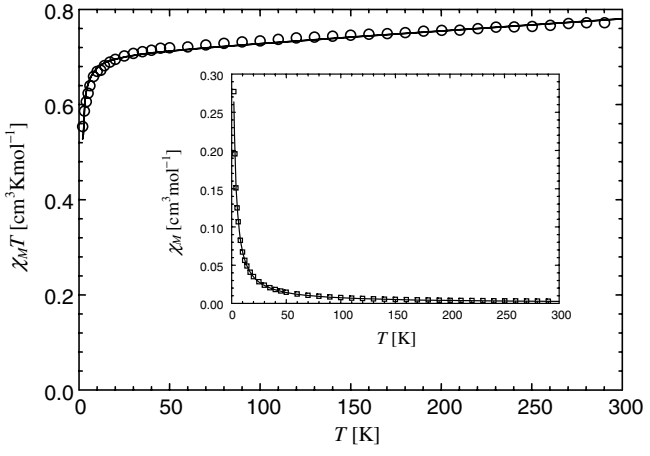

Fig. 3. Plot of $\chi_M T$ vs. T per molecule of $[Cu^{II}_2(L)(HCO_3)]\cdot 4H_2O$ ($\mathbf{1}\cdot 4H_2O$). The solid line is a fit to the experimental data using the Bleaney-Bowers equation. (Inset) Representation of experimental (squares) and calculated (solid line) χ_M vs. T data for ($\mathbf{1}\cdot 4H_2O$).

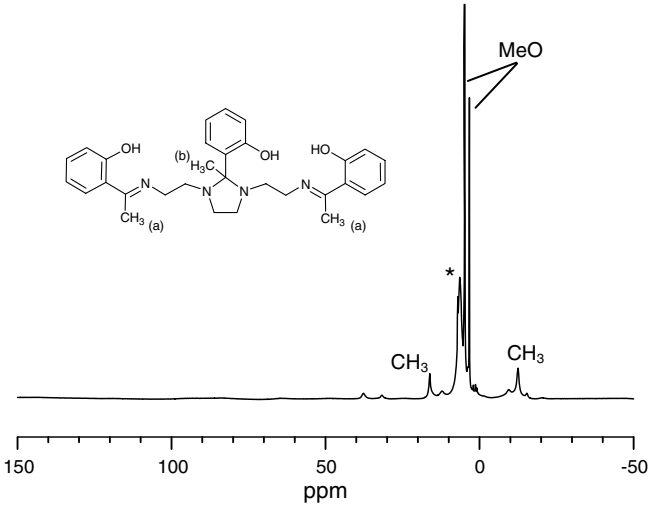

Fig. 5. Room temperature 250 MHz ^1H NMR spectrum of $[Cu^{II}_2(L)(HCO_3)]\cdot 4H_2O$ ($\mathbf{1}\cdot 4H_2O$) in d_4-MeOH. The signal labelled as '*' is attributed to exchangeable protons.

and also suggests that the solid state structure is maintained in solution (see Fig. 5).

4. Concluding remarks

In conclusion, we have described a ligand system that in the presence of Cu^{II} undergoes, depending on the pH conditions, either atmospheric CO_2 fixation and coordination upon formation of a dinuclear complex, or ligand hydrolysis leading to a mononuclear complex. The results presented here represent the first synthesis, structural description and magnetic characterization of a HCO_3^- neutral single oxygen bridged $Cu^{II}\cdots Cu^{II}$ complex. The magnetic coupling between the Cu^{II} ions is very weak and antiferromagnetic. This new $[Cu_2^{II}]$ complex shows a $[Cu_2(\mu\text{-imidazolidine})]^{4+}$ core and, currently, we are engaged in synthesizing analogues complexes of other 3d and 4d metal ions to scrutinize the effect that the nature of the exogenous bridging moiety has on the molecular structure and magnetism of new complexes.

Appendix A. Supplementary materials

Further details of the structure determinations, including atomic coordinates, bond lengths and bond angles and thermal parameters of all non-hydrogen atoms for the structure are available on request as supplementary material from The Director, Cambridge Crystallographic Data Center, 12, Union Road, Cambridge CB2 1EZ, UK (fax: +44 1223 336 033; e-mail: deposit@ccdc.cam.ac.uk) (CCDC deposition Nos. 283579 and 283580). Supplementary data associated with this article can be found, in the online version, at doi:10.1016/j.poly.2006.04.005.

References

[1] N. Kitajama, S. Hikichi, M. Tanaka, Y. Moro-oka, J. Am. Chem. Soc. 115 (1993) 5496.
[2] S. Inoue, H. Koinuma, Rev. Inorg. Chem. 6 (1984) 291.
[3] P. Braunstein, D. Malt, D. Nobel, Chem. Rev. 27 (1988) 747.
[4] A. Behr, Angew. Chem., Int. Ed. Engl. 27 (1988) 661.
[5] M. Yamashita, K. Goto, T. Kawashima, J. Am. Chem. Soc. 127 (2005) 7294.
[6] A. Escuer, E. Penalba, R. Vicente, X. Solans, M.J. Font-Badıa, J. Chem. Soc., Dalton Trans. (1997) 2315.
[7] A. Escuer, F.A. Mautner, E. Penalba, R. Vicente, Inorg. Chem. 37 (1998) 4190, and references therein.
[8] J. Sertucha, A. Luque, P. Romań, F. Lloret, M. Julve, Inorg. Chem. Commun. 2 (1999) 14.
[9] M. Rodrıguez, A. LLobet, M. Corbella, P. Muller, M.A. Uson, A.E. Martell, J. Reibenspens, J. Chem. Soc., Dalton Trans. (2002) 2900.
[10] R.L. Carlin, Magnetochemistry, Springer, New York, 1986.
[11] G.M. Sheldrick, SHELXS-97, Program for the Refinement of Crystal Structures, University of Göttingen, Germany, 1997.
[12] B.D. Sarma, J.C. Bailar Jr., J. Am. Chem. Soc. 77 (1955) 5476.
[13] D.F. Evans, D.A. Jakubovic, J. Chem. Soc., Dalton Trans. (1988) 2927.
[14] E. Wong, S. Liu, T. Lugger, F.E. Hahn, C. Orvig, Inorg. Chem. 34 (1995) 93.
[15] U. Mukhopadhay, L.R. Falvello, D. Ray, Eur. J. Inorg. Chem. (2001) 2823.
[16] Y. Nishida, A. Yatani, J.-I. Taka, S. Kashino, W. Mori, S. Suzuki, Chem. Lett. (1999) 135.
[17] K. Nakamoto, Infrared and Raman Spectra of Inorganic and Coordination Compounds, 4th ed., Wiley, New York, 1986, pp. 147–150, 227–233, 251–253.
[18] (a) G.A. vanAlbada, I. Mutikainen, O.S. Roubeau, U. Turpeinen, J. Reediijk, Eur. J. Inorg. Chem. (2000) 2179;
(b) M. Fondo, A.M. García-Deibe, M. Corbella, E. Ruiz, J. Tercero, J. Sanmartın, M.R. Bermejo, Inorg. Chem. 44 (2005) 5011.
[19] M. Fondo, A.M. García-Deibe, M. Corbella, J. Ribas, A. Llamas-Saiz, M.R. Bermejo, J. Sanmartín, Dalton Trans. (2004) 3503.
[20] M. Fondo, A.M. Garcıá-Deibe, J. Sanmartıń, M.R. Bermejo, L. Lezama, T. Rojo, Eur. J. Inorg. Chem. (2003) 3703.
[21] P.K. Nanda, D. Ray, J. Chem. Res–S., 2006, accepted for publication.
[22] A.W. Addison, T.N. Rao, J. Reedijk, J. Van Rijn, G.C. Verschoor, J. Chem. Soc., Dalton Trans. (1984) 1349.
[23] L.K. Thompson, S.S. Tandon, M.E. Manuel, Inorg. Chem. 34 (1995) 2356.
[24] D. Ajo, A. Bencini, F. Mani, Inorg. Chem. 27 (1988) 2437.
[25] R.P. Doyle, P.E. Kruger, B. Moubaraki, K.S. Murray, M. Nieuwenhuyzen, Dalton Trans. (2003) 4230.
[26] R. Ludwig, Angew. Chem. Int. Ed. 40 (2001) 1808.
[27] W. Grochala, A. Jagielska, K. Wozniak, A. Wiekowska, R. Bilewicz, B. Korybut-Daszkiewicz, J. Bukowska, L. Piela, J. Phys. Org. Chem. 14 (2001) 63.
[28] M. Bera, W.T. Wong, G. Aromí, J. Ribas, D. Ray, Inorg. Chem. 43 (2004) 4787.

above-mentioned connectivity-based indices and indices based on topological distances (Wiener's type indices) there are indices that use explicitly the electronic structure of the molecule, [21–23] or are obtained by the combination of basic topological indices [24,25]. Needless to say, the topological indices are frequently highly intercorrelated, [26] and can be interpreted in various ways in terms of elementary molecular properties (size and shape of a molecule, molecular volume or surface, etc.) [27].

Our expectation that topological indices should work for the estimation of stability constants of coordination compounds is not based only on their wide application in all branches of chemistry. There are many approaches aimed at systematic or ad hoc estimation of the stability of coordination compounds, ranging from molecular mechanics [28–31] and molecular dynamics [32], to the methods based on the continuous distribution of solvent [33,34] or on the overlapping-sphere volume [35,36]. The variety of methods employed indicates that the stability of coordination compounds is determined by many, often unrelated, factors: electronic (strength of the metal—ligand bond), stereochemical (mode of coordination) and sterical (conformational). Thermodynamic stability is also dependent on the energy of solvation (hydration) of the metal, ligand and the complex, etc. In such a complex situation it seems appropriate to rely on holistic models, like the models based on topological indices.

In our preliminary work on molecular graph models [37,38], we have found that the estimates of stability constants of copper(II) chelates with amino acids were fairly well correlated on topological indices, the connectivity indices [39] proved to be among the best. The results, however, also suggest that the estimate depends on the molecular species (constitutional formula). In order to propose a model of general validity, in this paper we aim to study the influence of the constitutional formula, from which a molecular graph is derived, on the success of the estimate. For this purpose, we chose copper(II) complexes of amino acids and diaminoethane, along with their derivatives, divided into four sets. Also, we directed our efforts to the mono- and (binary and ternary) bis-complexes of those ligands.

2. Methods

The calculations of topological indices were performed with a program system DRAGON 2.1, written by Todeschini and coworkers, [40] that is capable of yielding 262 topological indices in a single run, along with many other molecular descriptors.

The connectivity matrix was constructed with the program CORINA, [41] developed by J. Sadowski, C.H. Schwab and J. Gasteiger.

Preliminary calculations have, however, shown that generally the most consistent results were obtained with the Randić index $^3\chi^v$ (*the valence molecular connectivity index of the 3rd order*):

$$^3\chi^v = \sum_{\text{path}} \{\delta(i)\delta(j)\delta(k)\delta(l)\}^{-0.5} \quad (1)$$

where $\delta(i)$, $\delta(j)$, δ(k) and $\delta(l)$ are weights (valence-delta values) of vertices (atoms) i, j, k and l making up the path of length 3 (three consecutive chemical bonds) in a vertex-weighted molecular graph [39,42]. The valence-delta value, $\delta(i)$, of a vertex i is defined by:

$$\delta(i) = [Z^v(i) - H(i)]/[Z(i) - Z^v(i) - 1] \quad (2)$$

where $Z^v(i)$ is the number of valence electrons belonging to the atom i, $Z(i)$ is its atomic number and $H(i)$ is the number of hydrogen atoms attached to the atom i. For instance, delta values for primary, secondary, tertiary and quaternary carbon atoms are, 1, 2, 3 and 4, respectively; for oxygen in an OH group it is equal to 5, and for the NH_2 group $\delta(N) = 3$. (It has to be pointed out that $^3\chi^v$ is only a member of the family of valence connectivity indices, $^n\chi^v$, which differ from each other by path length, i.e. the number of factors $\delta(i)$'s in the summation term.)

In this paper four kinds of molecular formulas (graphs) were used for the calculation of the index $^3\chi^v$. Besides the graphs of free ligands (L models), we also used the graphs of their chelates in various representations (Figs. 1, 3 and 5). Graphs with or without two additionally bound water molecules were denoted with b, and were used in ML^{aq} and ML models, respectively. If an additional ligand coordination is proposed for a complex, the new graph is constructed and marked with a c, and was used in the ML^{cor} models instead of the corresponding graph b. For the sake of simplicity, only the graphs of mono-chelates are given in Figs. 1, 3 and 5, while the graphs of the corresponding bis-complexes that were used in ML_2, ML_2^{aq} and ML_2^{cor} models can be derived from them in a straightforward manner, assuming the maximum coordination number of copper is six.

Regression calculations, including the leave-one-out procedure of cross validation, *cv*, were done by the CROMRsel program [43]. The standard error of cross validation estimate is defined as:

$$SE_{cv} = \left(\sum \Delta X^2/N\right)^{0.5} \quad (3)$$

where ΔX and N denote *cv* residuals and number of reference points, respectively.

3. Results

3.1. Chelates of 1,2-diaminoethane and its derivatives

As the first test for our approach we have chosen a set consisting of 14 copper(II) mono- and bis-complexes of 1,2-diaminoethane and its *N*-alkylated (**2**–**6**), *N*,*N*′-dialkylated (**7**–**10**) and *C*-substituted (**11**–**14**) derivatives (Table 1). All experimental $\log\beta_1$ ($\log K_1$) and $\log\beta_2$ values were selected from the literature, and were determined with the same method (potentiometry) under the same experimental conditions ($T = 298$ K, $I = 0.5$ mol L^{-1}).

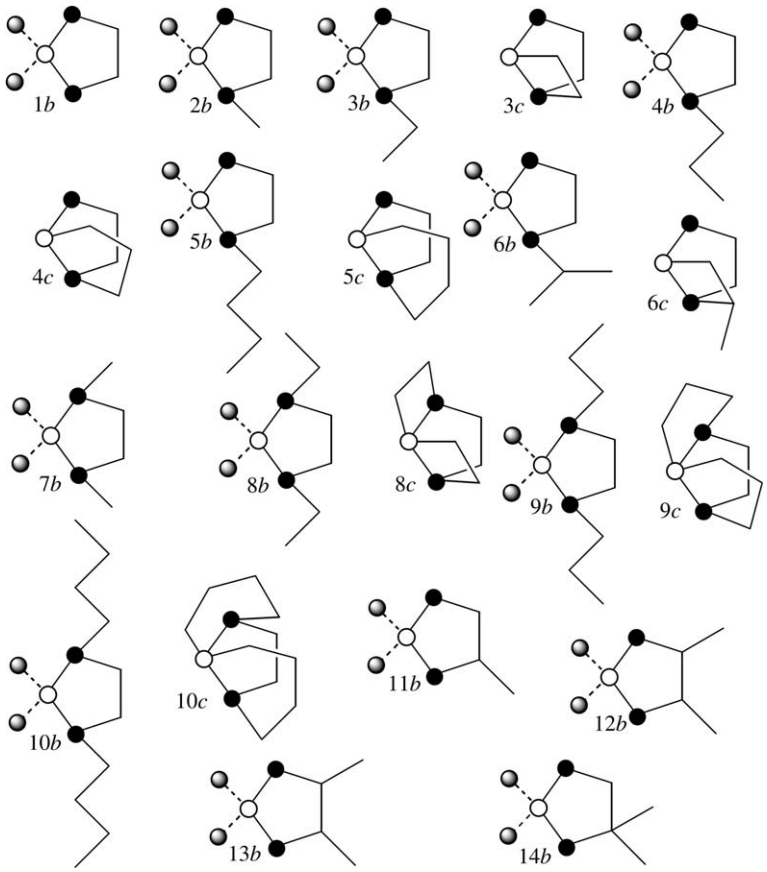

Fig. 1. The three kinds of molecular graphs of copper(II) mono-complexes of 1,2-diaminoethanes, as used in ML (*b*, without bonded H_2O), ML^{aq} (*b*, with bonded $2H_2O$) and ML^{cor}(*c*) models. Heteroatoms are marked with ○ (Cu), ● (N), ◍ (O).

Table 1
Stability constants ($\log\beta_1$ and $\log\beta_2$) of copper(II) mono- and bis-complexes with 1,2-diaminoethane and its derivatives

No.	Ligand	$\log\beta_1$	$\log\beta_2$	Reference
1	1,2-Diaminoethane	10.76	20.13	[50]
2	*N*-methyl-1,2-diaminoethane	10.55	19.11	[50]
3	*N*-ethyl-1,2-diaminoethane	10.19	18.57	[50]
4	*N*-propyl-1,2-diaminoethane	9.98	18.14	[50]
5	*N*-butyl-1,2-diaminoethane	9.94	18.21	[50]
6	*N*-isopropyl-1,2-diaminoethane	9.07	16.52	[50]
7	*N*,*N*′-dimethyl-1,2-diaminoethane	10.47	18.1	[51]
8	*N*,*N*′-diethyl-1,2-diaminoethane	9.30	15.62	[51]
9	*N*,*N*′-dipropyl-1,2-diaminoethane	8.79	14.34	[51]
10	*N*,*N*′-dibutyl-1,2-diaminoethane	8.67	13.51	[51]
11	1,2-Diaminopropane	10.78	20.06	[52]
12	(*R*,*S*)-2,3-diaminobutane	10.72	20.06	[52]
13	(*R*,*R*)-2,3-diaminobutane	11.39	21.21	[52]
14	2-Methyl-1,2-diaminopropane	10.53	19.58	[52]

Linear regression of $\log\beta_1$ on the connectivity index $^3\chi^v$ shows a distinct improvement of the results as the formula becomes more realistic; ML is a better representation than L, and ML^{aq} than ML (Table 2). Even better estimates were obtained when an additional coordination of the alkyl chains was proposed for all the *N*-substituents, except methyl. In this model, denoted as ML^{cor}, ligands **1**, **2**, **7** and **11**–**14** were assumed to be bidentate, **3**–**6** terdentate and **8**–**10** tetradentate (Fig. 1). The ML^{cor} model (No. 4, Fig. 2) proved to be the best; *r* rises to 0.903 and SE_{cv} drops to 0.38 $\log\beta$ units. Absolute values of cv residuals were in range from 0.00 (**5**) to 0.94 (**13**), which is very close to the range of model 3 (0.01–1.03 $\log\beta$ units), but substantially better than the range of model 2 (0.02–1.42 $\log\beta$ units), and especially of model 1 (0.07–1.48 $\log\beta$ units). The worst estimates for all the models were yielded for complexes **6**, *N*-isopropyl-1,2-diaminoethane, and **13**, (*R*,*R*)-2,3-diaminopropane, in contrast to its meso-isomer **12**, with the $\log\beta_1$

values reproduced in an absolute error range from 0.2 (model 4) to 0.75 $\log\beta$ units (model 1). It is interesting to note that model 4 equally well reproduced *b* and *c* set of molecules in terms of SE_{cv}, in contrast to models 2 and 3 with $SE_{cv}(b)/SE_{cv}(c)$ values of 1.59 and 1.37, respectively. (In models ML and ML^{aq} $SE_{cv}(c)$ stands for complexes for which an additional coordination in ML^{cor} model is proposed.)

In Table 2 seven models for the copper(II) bis-complexes with 1,2-diaminoethanes are also referred. Beside L, ML_2, ML_2^{aq} and ML_2^{cor} models (5–8), we checked the models based on the graphs of mono-complexes (9–11) for estimation of $\log\beta_2$ values. The best model proved to be model 11 ($r = 0.930$, $SE_{cv} = 0.93$ $\log\beta$ units), but the difference to other models is rather small. The two second to best are models 6 and 10, which yielded the same statistical parameters ($r = 0.918$, $SE_{cv} = 1.03$ $\log\beta$ units), and similar absolute cv residual range (0.03–2.21, 0.01–2.19 and 0.12–2.02 $\log\beta$ units for model 6, 10 and 11, respectively). Moreover, the models do not equally well reproduce *b* and *c* set of molecules. $SE_{cv}(b)/SE_{cv}(c)$ equals 1.63, 1.33, 2.00 and 1.62 for models 6, 7, 9 and 10, respectively. Models based on the ML^{cor} representation, however, yielded opposite trends; $SE_{cv}(b)/SE_{cv}(c)$ is 0.57 and 1.56 for model 8 and 11, respectively.

3.2. Chelates of aliphatic amino acids and N-alkylated glycines

The second set consists of altogether 11 ligands (Table 3): glycine (**1**), its seven *N*-alkylated and *N*,*N*-dialkylated derivatives (**5**–**11**) and three amino acids with alkylic side chains (**2**–**4**). All experimental values were obtained with the same method (potentiometry) and under the same experimental conditions ($T = 298$ K, $I = 0.1$ mol L^{-1}), except for leucine complexes, which were studied at $I = 0.01$ mol L^{-1}. In the ML^{cor} models, an additional coordination is assumed for complexes **7**–**11** (Fig. 3). The estimates for mono-complexes (Table 4) show a small difference between the models based on the assumption of ML, ML^{aq} or ML^{cor} structures. Model 14 appears to be the best, and the other two models yield equally good estimates; model 13 is superior to model 15 in terms of SE_{cv}, but model 15 is better than model 13 in terms of *r* and SE The best model in terms of absolute cv residual values is, however, model 13 (0.03–0.71 $\log\beta$ units), and this is slightly better than the residuals obtained by the "best" model 14 (0.00–0.74 $\log\beta$ units). The ML^{cor} model (No. 15) gave a $SE_{cv}(b)/SE_{cv}(c)$ value close to 1 (0.74), but model 13 yielded an even better value (1.20), in contrast to $SE_{cv}(b)/SE_{cv}(c) = 0.45$ for model 14.

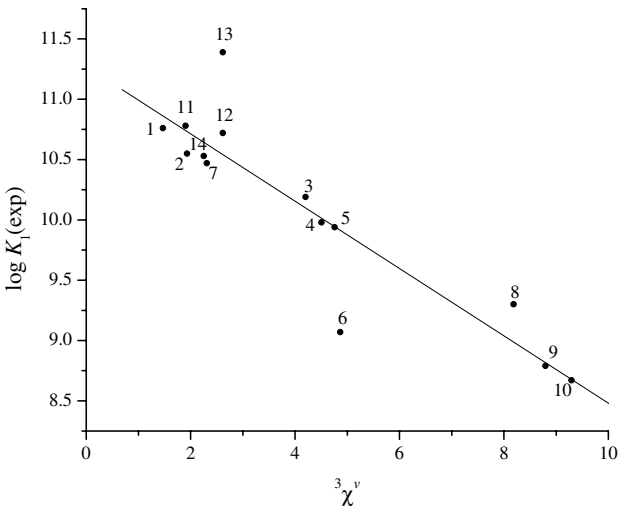

Fig. 2. The best linear regression (4, Table 2) of $\log K_1$ on the connectivity index $^3\chi^v$ for mono-complexes of 1,2-diaminoethane and its derivatives.

Table 3
Stability constants ($\log\beta_1$ and $\log\beta_2$) of copper(II) mono- and bis-complexes with aliphatic amino acids and glycine derivatives

No.	Ligand	$\log\beta_1$	$\log\beta_2$	Reference
1	Glycine	8.38	15.17	[52]
2	Alanine	8.15	14.82	[53]
3	Valine	8.11	14.79	[53]
4	Leucine	8.11	14.34	[54]
5	*N*-methylglycine	7.94	14.59	[52]
6	*N*,*N*-dimethylglycine	7.30	13.65	[52]
7	*N*-ethylglycine	7.34	13.55	[52]
8	*N*,*N*-diethylglycine	6.88	12.86	[52]
9	*N*-propylglycine	7.25	13.31	[52]
10	*N*-butylglycine	7.32	13.52	[52]
11	*N*-*iso*-propylglycine	6.70	12.45	[52]

Table 2
Linear regressions of $\log\beta_1$ and $\log\beta_2$ on the connectivity index $^3\chi^v$; ligands **1**–**14**, Table 1

Regression no.	Dependent variable	Independent variable	Intercept (SE)	Slope (SE)	*r*	SE	SE_{cv}
1	$\log\beta_1$	$^3\chi^v$ (L)	11.15(34)	−1.36(38)	0.714	0.56	0.62
2	$\log\beta_1$	$^3\chi^v$ (ML)	12.64(59)	−0.98(22)	0.792	0.49	0.54
3	$\log\beta_1$	$^3\chi^v$ (ML^{aq})	13.01(57)	−0.74(14)	0.837	0.44	0.49
4	$\log\beta_1$	$^3\chi^v$ (ML^{cor})	11.27(19)	−0.279(38)	0.903	0.34	0.38
5	$\log\beta_2$	$^3\chi^v$ (L)	21.30(85)	−4.10(95)	0.779	1.39	1.53
6	$\log\beta_2$	$^3\chi^v$ (ML_2)	27.8(12)	−1.20(15)	0.918	0.88	1.03
7	$\log\beta_2$	$^3\chi^v$ (ML_2^{aq})	27.2(13)	−0.85(12)	0.905	0.94	1.12
8	$\log\beta_2$	$^3\chi^v$ (ML_2^{cor})	22.34(75)	−0.348(55)	0.875	1.07	1.25
9	$\log\beta_2$	$^3\chi^v$ (ML)	25.6(15)	−2.87(54)	0.836	1.22	1.38
10	$\log\beta_2$	$^3\chi^v$ (ML^{aq})	27.0(11)	−2.25(28)	0.918	0.88	1.03
11	$\log\beta_2$	$^3\chi^v$ (ML^{cor})	21.5(45)	−0.795(91)	0.930	0.82	0.93

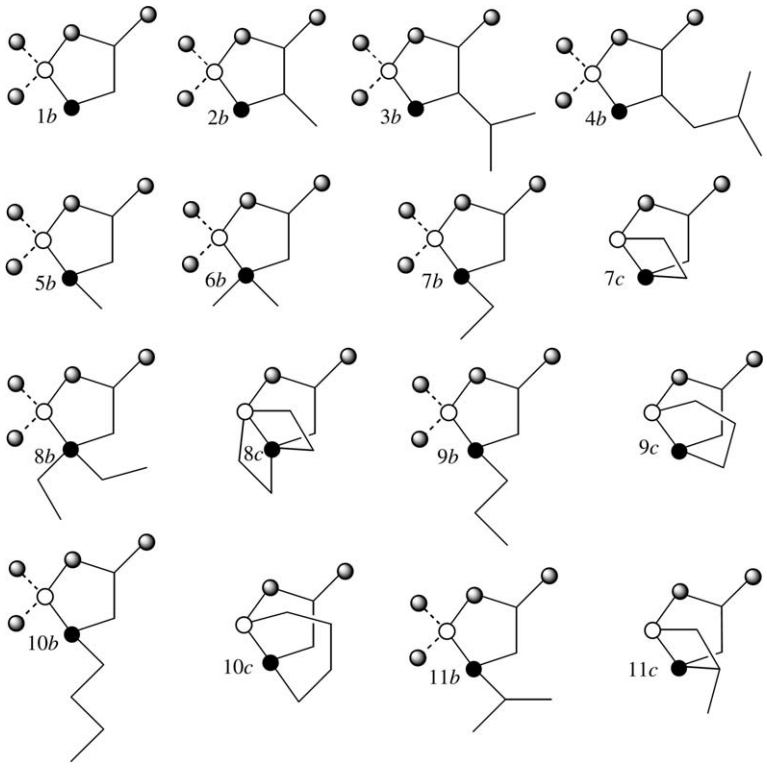

Fig. 3. The three kinds of molecular graphs of copper(II) mono-complexes of aliphatic amino acids and their *N*-alkylated derivatives; as used in ML (*b*, without bonded H_2O), ML^{aq}(*b*, with bonded $2H_2O$), and ML^{cor}(*c*) models. Heteroatoms are marked with ○ (Cu), ● (N), ◕ (O).

For the bis-complexes of this set of ligands, the same kinds of models are checked as for diaminoethane complexes (Table 4). The model based on the ML_2^{cor} representation (No. 19, Fig. 4), proved to be the best, and next to it are models 18 (ML_2^{aq}) and 21 (ML^{aq}). The best model (No. 19) also yielded a substantially better range of absolute cv residual values (0.03–0.88 $\log\beta$ units) than for the other two models (0.02–1.33 and 0.02–1.22 $\log\beta$ units, for models 18 and 21, respectively). The best $SE_{cv}(b)$/$SE_{cv}(c)$ values, 0.85 and 0.90, were obtained for models 19 and 20, respectively.

3.3. Chelates of naturally occurring amino acids

As a representative set for copper(II) chelates with naturally occurring amino acids, we choose glycine (**1**) followed by three alkylic (**2**, **4**, **6**), two hydroxy (**3**, **5**), two aromatic (**7**, **8**) and one sulfur-containing amino acid (**9**), Table 5. Stability constants were determined under the same experimental conditions ($T = 298$ K, $I = 0.05$ mol L^{-1}). The representation with additional coordination (*c*) was applied to ligands with hydroxy, aromatic, and sulfanyl groups (**3**, **5**, **7**, **8**, **9**, Fig. 5). In our decision, we were directed by the proposed ability of the side chains to interact with the central atom. The experimental findings support the assumed interactions of the hydroxy and aromatic group with the copper(II) in coordination compounds [44–46]. For methionine (**9**) the experimental findings are contradictory, because there is no evidence for Cu–S interactions in complexes of methionine [47], but such an interaction is observed in blue copper proteins [48]. Thus, for methionine complexes we proposed a

Table 4
Linear regressions of $\log\beta_1$ and $\log\beta_2$ on the connectivity index $^3\chi^v$; ligands **1**–**11**, Table 3

Regression no.	Dependent variable	Independent variable	Intercept (SE)	Slope (SE)	*r*	SE	SE_{cv}
12	$\log\beta_1$	$^3\chi^v$ (L)	7.99(39)	−0.59(51)	0.358	0.51	0.62
13	$\log\beta_1$	$^3\chi^v$ (ML)	9.03(49)	−0.74(25)	0.708	0.38	0.44
14	$\log\beta_1$	$^3\chi^v$ (ML^{aq})	9.64(42)	−0.68(14)	0.858	0.28	0.37
15	$\log\beta_1$	$^3\chi^v$ (ML^{cor})	8.32(22)	−0.251(65)	0.792	0.33	0.47
16	$\log\beta_2$	$^3\chi^v$ (L)	14.65(58)	−1.08(77)	0.423	0.76	0.91
17	$\log\beta_2$	$^3\chi^v$ (ML_2)	17.23(72)	−0.57(12)	0.845	0.45	0.61
18	$\log\beta_2$	$^3\chi^v$ (ML_2^{aq})	17.06(75)	−0.395(92)	0.819	0.48	0.57
19	$\log\beta_2$	$^3\chi^v$ (ML_2^{cor})	15.45(28)	−0.172(28)	0.898	0.37	0.44
20	$\log\beta_2$	$^3\chi^v$ (ML)	16.27(72)	−1.21(36)	0.749	0.56	0.66
21	$\log\beta_2$	$^3\chi^v$ (ML^{aq})	17.05(68)	−1.04(22)	0.845	0.45	0.59
22	$\log\beta_2$	$^3\chi^v$ (ML^{cor})	15.07(33)	−0.397(97)	0.806	0.50	0.75

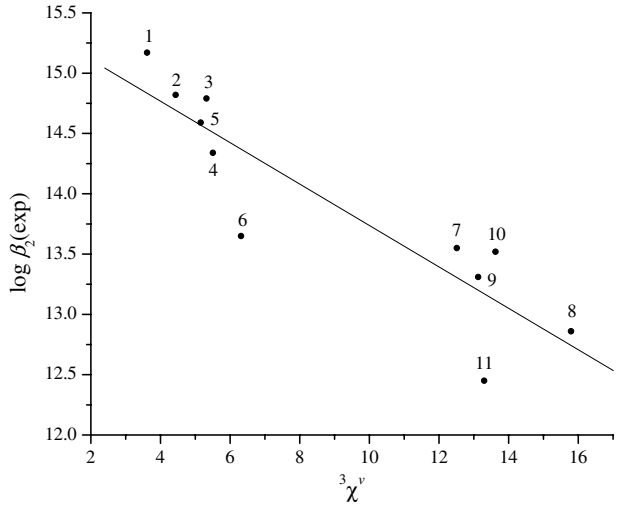

Fig. 4. The best linear regression (19, Table 4) of $\log\beta_2$ on the connectivity index $^3\chi^v$ for bis-complexes of aliphatic amino acids and *N*-alkylated glycines.

Table 5
Stability constants ($\log\beta_1$ and $\log\beta_2$) of copper(II) mono- and bis-complexes with a representative set of naturally occurring amino acids

No.	Ligand	$\log\beta_1$	$\log\beta_2$	Reference
1	Glycine	8.22	15.11	[55]
2	Alanine	8.18	14.99	[55]
3	Serine	7.93	14.57	[55]
4	Valine	8.05	14.91	[56]
5	Threonine	8.03	14.77	[55]
6	Leucine	8.19	15.13	[57]
7	Phenylalanine	7.86	14.77	[55]
8	Tyrosine	7.85	14.78	[55]
9	Methionine	7.85	14.53	[58]

structure with an apically bonded terminal aliphatic C-atom, reflecting sterical interactions of the bulky —S—CH_3 group with copper (9*c*, Fig. 5).

For the ML complexes, the best results were obtained for the ML^{cor} model (26, Table 6), which yielded $r = 0.888$ and $SE_{cv} = 0.08$ $\log\beta$ units (Fig. 6). Surprisingly, three other models yielded the same SE_{cv} values (0.11 $\log\beta$ units), and very slight differences in the values of the correlation coefficients ($r = 0.766$–0.771). The model 26 also reproduces the best experimental $\log\beta_1$ values, yielding absolute cv residuals from 0.01 to 0.14 $\log\beta$ units. It is significantly better than the other models, e.g. model 25 yielded 0.03–0.23 $\log\beta$ units. The quotient $SE_{cv}(b)/SE_{cv}(c)$ is close for all the models; it equals 1.2, 1.0 and 0.8 for models 24, 25 and 26, respectively.

For the bis-complexes, fairly good results were yielded by ML_2^{cor} and ML^{cor} models; $r = 0.786$, $SE_{cv} = 0.15$ $\log\beta$ units and $r = 0.743$, $SE_{cv} = 0.16$ $\log\beta$ units for models 30 and 33, respectively (Table 6). Assuming rather high standard errors of the slope for the other models, only models 30 and 33 appeared to be acceptable. They also have a similar range of absolute cv residual values, 0.01–0.32 vs. 0.00–0.35 $\log\beta$ units. In all the models, the worst estimate was yielded for serine (**3**). The same holds true for mono-complexes. The $SE_{cv}(b)/SE_{cv}(c)$ value is close to 0.8 for all the models.

3.4. Mixed complexes of naturally occurring amino acids

As the final proof of validity of our approach, we chose a set of 16 $\log\beta_2$ values for mixed (ternary) complexes of naturally occurring amino acids (Table 7). We derived two composite indices obtained by addition or subtraction

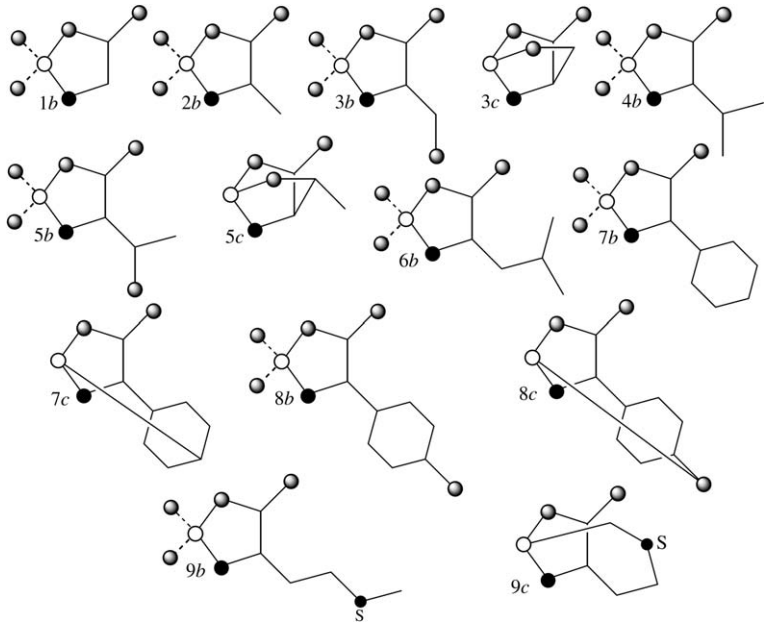

Fig. 5. The three kinds of molecular graphs of copper(II) mono-complexes of naturally occurring amino acids; as used in ML (*b*, without bonded H_2O), ML^{aq} (*b*, with bonded $2H_2O$), and ML^{cor}(*c*) models. Heteroatoms are marked with ○ (Cu), ● (N), ◍ (O).

Table 6
Linear regressions of $\log\beta_1$ and $\log\beta_2$ on the connectivity index $^3\chi^v$; ligands **1**–**9**, Table 5

Regression no.	Dependent variable	Independent variable	Intercept (SE)	Slope (SE)	r	SE	SE_{cv}
23	$\log\beta_1$	$^3\chi^v$ (L)	8.223(73)	−0.208(65)	0.771	0.09	0.11
24	$\log\beta_1$	$^3\chi^v$ (ML)	8.42(13)	−0.200(63)	0.768	0.09	0.11
25	$\log\beta_1$	$^3\chi^v$ (ML^{aq})	8.57(18)	−0.206(65)	0.766	0.09	0.11
26	$\log\beta_1$	$^3\chi^v$ (ML^{cor})	8.319(64)	−0.112(22)	0.888	0.07	0.08
27	$\log\beta_2$	$^3\chi^v$ (L)	15.00(14)	−0.17(13)	0.440	0.18	0.23
28	$\log\beta_2$	$^3\chi^v$ (ML_2)	15.29(35)	−0.083(64)	0.441	0.18	0.23
29	$\log\beta_2$	$^3\chi^v$ (ML_2^{aq})	15.40(45)	−0.083(66)	0.428	0.18	0.23
30	$\log\beta_2$	$^3\chi^v$ (ML_2^{cor})	15.19(11)	−0.043(13)	0.786	0.13	0.15
31	$\log\beta_2$	$^3\chi^v$ (ML)	15.17(26)	−0.16(12)	0.452	0.18	0.22
32	$\log\beta_2$	$^3\chi^v$ (ML^{aq})	15.29(35)	−0.17(13)	0.441	0.18	0.23
33	$\log\beta_2$	$^3\chi^v$ (ML^{cor})	15.19(13)	−0.131(45)	0.743	0.14	0.16

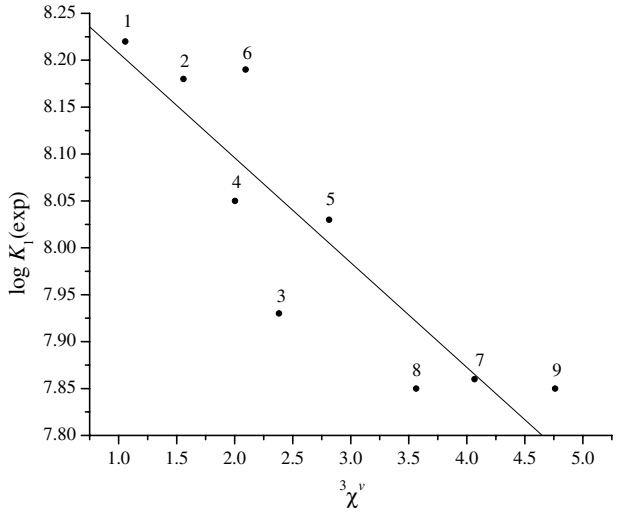

Fig. 6. The best linear regression (26, Table 6) of $\log K_1$ on the connectivity index $^3\chi^v$ for mono-complexes of naturally occurring amino acids.

of the $^3\chi^v$ indices for two chelate rings, ML and MA, constituting a mixed complex (MLA), assuming $^3\chi^v(\mathrm{ML}) > {}^3\chi^v(\mathrm{MA})$. There are many possibilities to draw a graph of a mixed complex in terms of additional coordination, thus we took into account only the combinations referred in Table 7. Bivariate linear regression (35, Table 8) based on additional coordination representation, yielded better statistical parameters, which are comparable to the parameters for binary complexes ($r = 0.786$, $SE_{cv} = 0.15$, model 30). The values of absolute cv residual are in the range 0.01–0.33 $\log\beta$ units, with the highest residual value for the mixed complex of serine and threonine (**11**). This again shows superiority of the ML^{cor} to ML model.

4. Discussion

The results presented above and summarized in Table 9, show that the $\log\beta_1$ values are reproduced, in terms of SE_{cv}, within the range 0.08–0.38, and $\log\beta_2$ values from 0.15 to 0.93 $\log\beta$ units. These results, referred to the best regression for a set, show also that generally the best results were obtained with the models based on the ML^{cor} (ML_2^{cor}) representation; the sole exception being model 14 (Table 4), based on the ML^{aq} representation. In spite of this, there is a small difference between the estimates obtained with the

Table 7
Stability constants ($\log\beta_2$) of copper(II) mixed bis-complexes with the set of amino acids defined in Table 5

No.	Ligands	$\log\beta_2$	Ring combinations in model 34	Ring combinations in model 35	Reference
1	Glycine, alanine	15.10	*bb*	*bb*	[55]
2	Glycine, serine	15.09	*bb*	*ba*	[55]
3	Glycine, threonine	15.13	*bb*	*ba*	[55]
4	Glycine, tyrosine	15.35	*bb*	*ba*	[55]
5	Glycine, phenylalanine	15.36	*bb*	*ba*	[55]
6	Alanine, serine	15.07	*bb*	*ba*	[55]
7	Alanine, threonine	15.08	*bb*	*ba*	[55]
8	Alanine, tyrosine	15.30	*bb*	*ba*	[55]
9	Alanine, phenylalanine	15.26	*bb*	*ba*	[55]
10	Valine, tyrosine	15.25	*bb*	*ba*	[58]
11	Serine, threonine	14.55	*bb*	*aa*	[55]
12	Serine, tyrosine	14.78	*bb*	*aa*	[55]
13	Serine, phenylalanine	14.77	*bb*	*aa*	[55]
14	Threonine, tyrosine	14.98	*bb*	*aa*	[55]
15	Threonine, phenylalanine	14.96	*bb*	*aa*	[55]
16	Tyrosine, phenylalanine	14.92	*bb*	*aa*	[58]

Table 8
Bivariate linear regressions of $\log\beta_2$ on the sum and the differences of the connectivity index $^3\chi^v$ of ML and MA; ligands **1**–16, Table 7

No.	Intercept (SE)	$^3\chi^v$ (ML) + $^3\chi^v$ (MA) Slope (SE)	$^3\chi^v$ (ML) − $^3\chi^v$ (MA) Slope (SE)	r	SE	SE_{cv}
34	15.06(27)	−0.041(69)	0.20(11)	0.468	0.19	0.23
35	15.04(18)	−0.053(30)	0.202(52)	0.764	0.14	0.18

Table 9
Comparison of the overlapping sphere (OS) method and the method based on topological indices ($^3\chi^v$)

	$^3\chi^v$	OS [34–36]	$^3\chi^v$ vs. OS	$^3\chi^v$ and OS (average)
1,2-Diaminoethanes				
Mono-complexes				
SE_{cv}	0.38	0.48	0.42	0.38
Absolute *cv* residual range	0–0.94	0.01–1.07	0.01–0.95	0.02–0.71
Bis-complexes				
SE_{cv}	0.93	0.94	1.24	0.70
Absolute *cv* residual range	0.12–2.02	0.12–1.97	0.04–3.71	0.01–1.37
Aliphatic and N-alkylated amino acids				
Mono-complexes				
SE_{cv}	0.37	0.27	0.21	0.30
Absolute *cv* residual range	0.00–0.70	0.00–0.60	0.04–0.38	0.02–0.58
Bis-complexes				
SE_{cv}	0.44	0.50	0.51	0.40
Absolute *cv* residual range	0.13–0.88	0.09–1.08	0.06–1.26	0.13–0.98
Naturally occurring amino acids				
Mono-complexes				
SE_{cv}	0.08	0.08	0.05	0.07
Absolute *cv* residual range	0.01–0.14	0.01–0.16	0.02–0.09	0.00–0.14
Bis-complexes				
SE_{cv}	0.15	0.17	0.06	0.16
Absolute *cv* residual range	0.01–0.32	0.04–0.36	0–0.10	0.02–0.34
Ternary complexes				
SE_{cv}	0.17	0.08	0.12	0.12
Absolute *cv* residual range	0.01–0.33	0–0.16	0.01–0.30	0.01–0.23

ML^{cor} and ML^{aq} models for the complexes of diaminoethanes and *N*-alkylated glycines. However, the very high superiority of the ML^{cor} models for complexes of naturally occurring amino acids should be explained by the higher affinity of the groups in the amino-acids side chains to the apical position. It is noteworthy that no model systematically reproduced a better *b* or *c* molecular subset, indicating that there is no substantial difference in molecules of both subsets.

The less successful reproduction of $\log\beta_2$ values has to be attributed mostly to the fact that they were generally determined with a higher error than the first constants. It is noteworthy that the difference between experimental values for $\log\beta$s amounts up to 0.3, although measured in the same way [49]. In judging the success of the estimate, one has also to keep in mind the range of experimental values ($\log\beta^{min}$–$\log\beta^{max}$) in the set. Taking as a measure of success the estimate quotient $SE_{cv}/(\log\beta^{max}–\log\beta^{min})$, models referred in Table 9 gave a quotient in the range from 0.12 to 0.26, with the same mean value (0.19) for both ML and ML_2 complexes.

The comparison of the best regressions in this paper with our previously published estimates obtained by the overlapping spheres (OS) method, [34–36] Table 9, clearly shows the quality of the results is virtually the same for both methods, in terms of SE_{cv} and the absolute cv residual range. This finding speaks in favor of the method based on topological indices, for the OS method is much more complicated. Internal comparison of the estimates shows that OS and $^3\chi^v$ methods often differ much more to each other than to the experimental results, pointing out that they would not be considered as equivalent. The reason for such a discrepancy, especially in the values of residuals, should be found in the fact there are some complexes whose stability constants are very hard to reproduce. For the $^3\chi^v$ method these are complexes of (*R*,*R*)-2,3-diaminobutane, *N*-isopropyl-1,2-diaminoethane, *N*,*N*′-diethylglycine, *N*-isopropylglycine and serine. For the OS models, the worst were reproduced for complexes of 1,2-diaminoethane, *N*,*N*′-dimethyl-1,2-diaminoethane, *N*-isopropylglycine and serine. Obviously, the OS method better reproduces the stability constants of the complexes of optical isomers, (*R*,*S*)- and (*R*,*R*)-2,3-diaminobutane, but *N*-isopropylglycine and serine were poorly reproduced by both methods.

A substantial improvement of the estimates was obtained by averaging the results of both methods (Table 9); SE_{cv}

dropped to 0.07–0.38 and 0.16–0.70 $\log\beta$ units for mono- and bis-complexes, respectively. The maximum error dropped even more; for the most poorly reproduced (bis-diaminoethane) complexes it descended from 2.02 ($^3\chi^v$, **13**) and 1.97 (OS, **7**) to 1.37 $\log\beta$ units (**10**). For the amino acid complexes, however, the complexes of *N*-isopropylglycine (**11**), and serine (**3**) were again reproduced worst.

As a conclusion of this paper, it can be stated that methods based on the topological indices fairly well reproduces the stability constants of coordination compounds, usually with an error less than 0.5 $\log\beta$ units. However, caution should be taken for the ''anomalous'' behavior of some ligands. The results should be substantially bettered by averaging the results obtained by other methods. Thus, the development of such a combinative approach will be the aim of our further research.

References

[1] H. Wiener, J. Am. Chem. Soc. 69 (1947) 17.
[2] E.V. Konstantinova, M.V. Diudea, Croat. Chem. Acta 73 (2000) 383.
[3] B. Lučić, S. Nikolić, N. Trinajstić, Croat. Chem. Acta 68 (1995) 417.
[4] A.T. Balaban, D. Mills, O. Ivanciuc, S.C. Basak, Croat. Chem. Acta 73 (2000) 923.
[5] D.H. Rouvray, W. Tatong, Z. Naturforsch. 41a (1986) 1238.
[6] N. Bošnjak, N. Adler, M. Perić, N. Trinajstić, On the structural origin of chromatographic retention data: alkanes and cycloalkanes, in: Z.B. Maksić (Ed.), Modelling of Structure and Properties of Molecules, Wiley, New York, 1987, p. 103.
[7] L.B. Kier, L.H. Hall, Molecular Connectivity in Chemistry and Drug Research, Academic Press, New York, 1976.
[8] L.H. Hall, L.B. Kier, Eur. J. Med. Chem. 16 (1981) 399.
[9] A. Sabljić, N. Trinajstić, Acta Pharm. 31 (1981) 189.
[10] M. Medić-Šarić, Ž. Maleš, S. Šarić, A. Brantner, Croat. Chem. Acta 69 (1996) 1603.
[11] S. Bajaj, S.S. Sambi, A.K. Madan, Croat. Chem. Acta 78 (2005) 165.
[12] C. Trindle, Croat. Chem. Acta 57 (1984) 1231.
[13] C.J. Suckling, K.E. Suckling, C.W. Suckling, Chemistry Through Models, Cambridge University Press, Cambridge, 1978.
[14] M.V. Diudea, I. Gutman, Croat. Chem. Acta 71 (1998) 21.
[15] N. Trinajstić, Chemical Graph Theory, second ed., CRC Press, Boca Raton, FL, 1992.
[16] M. Karelson, V.S. Lobanov, A.R. Katritzky, Chem. Rev. 96 (1996) 1027.
[17] Y.C. Martin, J. Med. Chem. 24 (1981) 229.
[18] S.V. Nizhniy, N.A. Epshteyn, Usp. Khim. 67 (1978) 739.
[19] N. Trinajstić, Chemical Graph Theory, first ed., CRC Press, Boca Raton, Florida, 1983.
[20] R. Todeschini, V. Consonni, Handbook of Molecular Descriptors, Wiley-VCH, Weinheim, 2000.
[21] S.E. O'Brien, P.L.A. Popelier, J. Chem. Inf. Comp. Sci. 41 (2001) 764.
[22] S.E. O'Brien, P.L.A. Popelier, Can. J. Chem. 77 (1999) 28.
[23] L. Pogliani, Croat. Chem. Acta 78 (2005) 189.
[24] L. Pogliani, J. Phys. Chem. 98 (1994) 1494.
[25] L. Pogliani, J. Phys. Chem. 100 (1996) 18065.
[26] B. Hollas, I. Gutman, N. Trinajstić, Croat. Chem. Acta 78 (2005) 489.
[27] N. Raos, Croat. Chem. Acta 76 (2003) 81.
[28] J. Sabolović, N. Raos, Polyhedron 9 (1990) 1277.
[29] J. Sabolović, N. Raos, Polyhedron 9 (1990) 2419.
[30] M. Zimmer, Chem. Rev. 95 (1995) 2629.
[31] A. Fedorowicz, J. Mavri, P. Bala, A. Koll, Chem. Phys. Lett. 289 (1998) 457.
[32] J. Tomasi, M. Persico, Chem. Rev. 94 (1994) 2027.
[33] R. Bonaccorsi, P. Palla, J. Tomasi, J. Am. Chem. Soc. 106 (1984) 1945.
[34] N. Raos, Croat. Chem. Acta 78 (2005) 175.
[35] A. Miličević, N. Raos, Croat. Chem. Acta 78 (2005) 525.
[36] A. Miličević, N. Raos, Croat. Chem. Acta 79 (2006) 281.
[37] B. Grgas, S. Nikolić, N. Paulić, N. Raos, Croat. Chem. Acta 72 (1999) 885.
[38] S. Nikolić, N. Raos, Croat. Chem. Acta 74 (2001) 621.
[39] M. Randić, J. Am. Chem. Soc. 97 (1975) 6609.
[40] http://www.disat.unimib.it/chm/.
[41] http://www2.chemie.uni-erlangen.de/software/corina/index.html.
[42] L.B. Kier, L.H. Hall, Molecular Connectivity in Structure–Activity Analysis, Wiley, New York, 1986.
[43] B. Lučić, N. Trinajstić, J. Chem. Inf. Comput. Sci. 39 (1999) 121.
[44] Z. Kralj, N. Paulić, N. Raos, V. Simeon, Croat. Chem. Acta 55 (1982) 337.
[45] T. Sugimori, H. Masuda, N. Ohata, K. Koiwai, A. Odani, O. Yamauchi, Inorg. Chem. 36 (1997) 576.
[46] S.H. Laurie, Amino acids, peptides and proteins, Comprehensive Coordination Chemistry, vol. 1, Pergamon Press, Oxford, 1987.
[47] H. Kozlowski, T. Kowalik, Inorg. Chim. Acta 34 (1979) L231.
[48] J.M. Guss, H.C. Freeman, J. Mol. Biol. 169 (1983) 521.
[49] D.D. Perrin, Stability Constants of Metal–Ion Complexes. Part B. Organic Ligands, Pergamon Press, Oxford, 1979.
[50] F. Basolo, R.K. Murmann, J. Am. Chem. Soc. 74 (1952) 5243.
[51] F. Basolo, R.K. Murmann, J. Am. Chem. Soc. 76 (1954) 211.
[52] F. Basolo, Y.T. Chen, R.K. Murmann, J. Am. Chem. Soc. 76 (1954) 956.
[53] T.P. I, G.H. Nancollas, Inorg. Chem. 11 (1972) 2414.
[54] P. Bretton, J. Chim. Phys. 54 (1957) 827.
[55] A. Gergely, I. Sovago, I. Nagypal, R. Kiraly, Inorg. Chim. Acta 6 (1972) 435.
[56] G. Brookes, L.D. Pettit, J. Chem. Soc. Dalton Trans. (1977) 1918.
[57] H. Sigel, R. Tribolet, K.H. Scheller, Inorg. Chim. Acta 100 (1985) 151.
[58] O. Yamauchi, A. Odani, Inorg. Chim. Acta 100 (1985) 165.

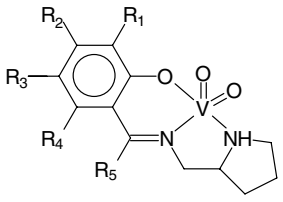

	R_1	R_2	R_3	R_4	R_5
1	H	H	H	H	H
2	H	H	CH_3	H	H
3	H	H	OCH_3	H	H
4	H	OCH_3	H	OCH_3	H
5	H	H	Br	H	H
6	H	H	NO_2	H	H
7	H	H	H	H	CH_3
8	H	H	H	H	C_6H_5
9	H	H	$-(CH)_4-$		H
10	$-(CH)_4-$		H	H	CH_3

Fig. 1. Structural formulae of dioxovanadium(V) Schiff base complexes.

spectra were obtained in DMSO-d_6 solutions at 50 °C with a Varian Mercury 400 BB (400 MHz) spectrometer using TMS (^{1}H) and $VOCl_3$ (^{51}V) as reference compounds. The circular dichroism spectra were recorded using a Jasco J-20 recording spectropolarimeter.

2.2. X-ray investigations

The structure of **7** was determined. Crystal data and refinement details are provided in Table 1. Data for the **7** complex were obtained with Mo Kα radiation using a Nonius-Kappa CCD diffractometer. Structure was solved using direct methods with SHELXS-97 [16] and refined by full-matrix least-squares using the SHELXL-97 [17] with anisotropic thermal parameters for the non-hydrogen atoms. Analysis utilized the program PLATON [18]. Hydrogen atoms bonded to C and O atoms were included in calculated positions. Selected bond lengths and bond angles are listed in Table 2.

Table 1
Crystal data and structure refinement for **7**

Moiety formula	$C_{26}H_{34}N_4O_6V_2 \cdot 2H_2O$
Formula weight	636.48
Temperature (K)	293(2)
Wavelength (Å)	0.71073
Crystal system	monoclinic
Space group	$P2_1/c$
Unit cell dimensions	
a (Å)	9.7420(3)
b (Å)	6.7430(2)
c (Å)	20.6960(8)
β (°)	94.903(1)
Volume (Å^3)	1354.55(8)
Z	2
D_{calc} (g cm^{-3})	1.561
Absorption coefficient (mm^{-1})	0.747
$F(000)$	664
Crystal size (mm)	$0.25 \times 0.20 \times 0.15$
θ Range for data collection (°)	3.00–27.50
Limiting indices	$-12 \leqslant h \leqslant 12$, $-7 \leqslant k \leqslant 8$, $-26 \leqslant l \leqslant 26$
Reflections collected/unique [R_{int}]	5347/2968 [0.028]
Completeness to $\theta = 27.45$ (%)	95.2
Refinement method	full-matrix least-squares on F^2
Data/restraints/parameters	2968/2/214
Goodness-of-fit on F^2	1.165
Final R indices [$I > 2\sigma(I)$]	$R_1 = 0.0609$, $wR_2 = 0.1658$
R indices (all data)	$R_1 = 0.0770$, $wR_2 = 0.1725$
Extinction coefficient	0.026(5)
Largest difference in peak and hole (e Å^{-3})	0.313 and −0.533

Table 2
Selected bond lengths (Å) and bond angles (°) for **7**

V1–O1	1.610(3)	O2–V1–N1	156.59(13)
V1–O2	1.665(2)	O2–V1–N2	94.06(14)
V1–O3	1.896(3)	O3–V1–N1	83.27(11)
V1–N1	2.219(3)	O3–V1–N2	156.00(15)
V1–N2	2.097(4)	N1–V1–N2	77.25(13)
V1–O2′	2.396(3)	O1–V1–O2′	171.25(13)
O1–V1–O2	106.95(15)	O2–V1–O2′	77.28(12)
O1–V1–O3	102.12(15)	O3–V1–O2′	84.57(12)
O1–V1–N1	95.37(14)	N1–V1–O2′	79.67(10)
O1–V1–N2	93.61(17)	N2–V1–O2′	78.31(14)
O2–V1–O3	98.46(12)	V1–O2–V1′	102.72(12)

The sign ′ denotes atom at $1 - x$, $-y$, $1 - z$.

2.3. Complexes

The complexes were prepared by methods analogous to the literature procedure of Root et al. [19]. Typically, 10 mmol of (*S*)-(+)-2-(aminomethyl)pyrrolidine in 10 ml of absolute ethanol was added with stirring to a freshly filtered solution of triethyl vanadate (10 mmol) in 250 ml of absolute ethanol producing a suspension of an intermediate. Then to that suspension was added slowly the desired aromatic *o*-hydroxyaldehyde (salicylaldehyde or its 5-methyl, 5-methoxy, 4,6-dimethoxy, 5-bromo, 5-nitro derivatives or 2-hydroxy-1-naphtaldehyde) or the *o*-hydroxyketone (2-hydrocyacetophenone, 2-hydroxybenzophenone or 1-hydroxy-2-acetonaphtone). After refluxing and stirring for 2 (aldehydes) or 10 h (ketones) the separated yellow solids were filtered off, washed several times with ethanol and Et_2O and then dried. Crystals suitable for X-ray analysis were obtained by slow crystallization of **7** from DMSO.

2.3.1. *N-(salicylidene)-(S)-(2-pyrrolidinylmethyl)amine dioxovanadium(V) (**1**)*

Yield: 60%. *Anal.* Calc. for $C_{12}H_{15}N_2O_3V$: C, 50.3; H, 5.3; N, 9.8. Found: C, 50.4; H, 5.3; N, 9.8%. IR (KBr, cm^{-1}): 3204 (ν_{N-H}); 1645, 1598 ($\nu_{C=N} + \nu_{C=C}$); 930, 843 ($\nu_{V=O}$). UV–Vis spectrum in DMSO [λ_{max} (nm), ε (M^{-1} cm^{-1})]: 371 (3800). CD spectrum in DMSO [λ_{max} (nm), $\Delta\varepsilon$ (M^{-1} cm^{-1})]: 276 (2.01), 353 (0.98). ^{1}H NMR (DMSO-d_6): 7.540 (1H, d, $^3J = 8$ Hz), 7.443 (1H, t, $^3J = 8$ Hz), 6.811 (1H, t, $^3J = 8$ Hz), 6.783 (1H, d, $^3J = 8$ Hz) (aromatic); 8.864 (1H, s) (azomethine); 6.288 (0.9H, br s), 5.822 (0.1H, s) (HN2); 4.014 (0.11H, dd, $^2J = 14$ Hz, $^3J = 5$ Hz), 4.008 (0.89H, dd, $^2J = 14$ Hz, $^3J = 5.5$ Hz), 3.869 (0.89H, dd, $^2J = 14$ Hz, $^3J = 9.4$ Hz), 3.690 (0.11H, br t) (CH_2N1); 3.476 (0.89H, m) (methine); 3.03–3.10 (ov) (CH_2N2); 2.000 (0.30H, m), 1.77–1.92

(2.72H, m), 1.624 (0.9H, m), 1.221 (0.1H, m) (CH_2CH_2). ^{51}V NMR (DMSO-d_6): −536 (0.86 V), −549 (0.14 V).

*2.3.2. N-(5-methylsalicylidene)-(S)-(2-pyrrolidinylmethyl)-amine dioxovanadium(V) (**2**)*

Yield: 54%. *Anal*. Calc. for $C_{13}H_{17}N_2O_3V \cdot H_2O$: C, 49.1; H, 6.0; N, 8.8. Found: C, 48.9; H, 5.8; N, 8.7%. IR (KBr, cm^{-1}): 3198 (ν_{N-H}); 1637, 1592 ($\nu_{C=N} + \nu_{C=C}$); 930, 842 ($\nu_{V=O}$). UV–Vis spectrum in DMSO [λ_{max} (nm), ε ($M^{-1}\,cm^{-1}$)]: 384 (3180). CD spectrum in DMSO [λ_{max} (nm), $\Delta\varepsilon$ ($M^{-1}\,cm^{-1}$)]: 288 (0.95), 364 (0.62). ^1H NMR (DMSO-d_6): 6.694 (1H, d, $^3J = 9$ Hz), 7.270 (1H, dd, $^3J = 9$ Hz, $^4J = 2$ Hz), 7.315 (1H, d, $^4J = 2$ Hz) (aromatic); 8.788 (1H, s) (azomethine); 6.260 (0.9H, br s), 6.572 (0.1H, s) (HN2); 3.973 (0.11H, dd, $^2J = 14$ Hz, $^3J = 5$ Hz), 3.990 (0.89H, dd, $^2J = 14$ Hz, $^3J = 5.9$ Hz), 3.845 (0.89H, dd, $^2J = 14$ Hz, $^3J = 8.6$ Hz), 3.673 (0.11H, br t) (CH_2N1); 3.457 (1H, m) (methine); 3.09–3.15 (ov) (CH_2N2); 1.995 (0.3H, m), 1.71–1.93 (2.9H, m), 1.56–1.67 (1H, m), 1.402 (0.1H, m) (CH_2CH_2). ^{51}V NMR (DMSO-d_6): −535 (0.95 V), −547 (0.05 V).

*2.3.3. N-(5-methoxysalicylidene)-(S)-(2-pyrrolidinylmethyl)-amine dioxovanadium(V) (**3**)*

Yield: 63%. *Anal*. Calc. for $C_{13}H_{17}N_2O_4V \cdot \frac{1}{2}H_2O$: C, 48.0; H, 5.6; N, 8.6. Found: C, 48.2; H, 5.4; N, 8.6%. IR (KBr, cm^{-1}): 3196 (ν_{N-H}); 1646, 1604 ($\nu_{C=N} + \nu_{C=C}$); 931, 845 ($\nu_{V=O}$). UV–Vis spectrum in DMSO [λ_{max} (nm), ε ($M^{-1}\,cm^{-1}$)]: 403 (3630). CD spectrum in DMSO [λ_{max} (nm), $\Delta\varepsilon$ ($M^{-1}\,cm^{-1}$)]: 284 (2.31), 374 (0.93). ^1H NMR (DMSO-d_6): 7.114 (1H, d, $^3J = 9$ Hz), 7.102 (1H, s) 6.735 (1H, d, $^3J = 9$ Hz) (aromatic), 8.831 (1H, s) (azomethine); 6.260 (1H, br s) (HN2); 3.988 (1H, dd, $^2J = 14$ Hz, $^3J = 5.6$ Hz), 3.845 (0.89H, dd, $^2J = 14$ Hz, $^3J = 9.2$ Hz) (CH_2N1); 3.459 (1H, m) (methine), 3.09–3.15 (ov) (CH_2N2); 1.71–1.95 (3H, m), 1.56–1.67 (1H, m), (CH_2CH_2). ^{51}V NMR (DMSO-d_6): −536 (0.95 V), −547 (0.05 V).

*2.3.4. N-(4,6-dimethoxysalicylidene)-(S)-(2-pyrrolidinyl-methyl)amine dioxovanadium(V) (**4**)*

Yield: 51%. *Anal*. Calc. for $C_{14}H_{19}N_2O_5V \cdot H_2O$: C, 46.2; H, 5.8; N, 7.7. Found: C, 46.0; H, 5.6; N, 7.6%. IR (KBr, cm^{-1}): 3207 (ν_{N-H}); 1625, 1600 ($\nu_{C=N} + \nu_{C=C}$); 928, 853 ($\nu_{V=O}$). UV–Vis spectrum in DMSO [λ_{max} (nm), ε ($M^{-1}\,cm^{-1}$)]: 319 (16940). CD spectrum in DMSO [λ_{max} (nm), $\Delta\varepsilon$ ($M^{-1}\,cm^{-1}$)]: 269 (0.23), 290 (0.24). ^1H NMR (DMSO-d_6): 5.981 (1H, d, $^4J = 1.6$ Hz), 5.950 (1H, d, $^4J = 1.6$ Hz) (aromatic); 8.896 (1H, s) (azomethine); 6.225 (0.9H, br d, $^3J = 5.6$ Hz), 5.803 (0.1H, br s) (HN2); 3.973 (1H, dd, $^2J = 14$ Hz, $^3J = 5.6$ Hz), 3.845 (0.89H, dd, $^2J = 14$ Hz, $^3J = 8.6$ Hz) (one of CH_2N1 protons); 3.852 (3.5H, s), 3.776 (3.5H, s) (six of two MeO groups which overlap the other of CH_2N1 protons); 3.428 (1H, m) (methine), 3.09–3.15 (ov) (CH_2N2); 1.90–1.98 (0.2H, m), 1.70–1.93 (2.8H, m), 1.55–1.62 (1H, m) (CH_2CH_2). ^{51}V NMR (DMSO-d_6): −533 (0.89 V), −545 (0.11 V).

*2.3.5. N-(5-bromosalicylidene)-(S)-(2-pyrrolidinyl-methyl)amine dioxovanadium(V) (**5**)*

Yield: 49%. *Anal*. Calc. for $BrC_{12}H_{14}N_2O_3V$: C, 39.6; H, 3.9; N, 7.7. Found: C, 39.4; H, 3.8; N, 7.7%. IR (KBr, cm^{-1}): 3205 (ν_{N-H}); 1656, 1587 ($\nu_{C=N} + \nu_{C=C}$); 936, 835 ($\nu_{V=O}$). UV–Vis spectrum in DMSO [λ_{max} (nm), ε ($M^{-1}\,cm^{-1}$)]: 378 (3430). CD spectrum in DMSO [λ_{max} (nm), $\Delta\varepsilon$ ($M^{-1}\,cm^{-1}$)]: 278 (1.73), 364 (0.63). ^1H NMR (DMSO-d_6): 7.745 (1H, d, $^4J = 2.5$ Hz), 7.527 (1H, dd, $^3J = 9$ Hz, $^4J = 2$ Hz), 6.754 (1H, d, $^3J = 9$ Hz) (aromatic); 8.835 (1H, s) (azomethine); 6.305 (0.9H, br s), 5.814 (0.1H, br s) (HN2); 3.990 (1H, dd, $^2J = 14$ Hz, $^3J = 6$ Hz), 3.741 (1H, dd, $^2J = 14$ Hz, $^3J = 9.6$ Hz), (CH_2N1); 3.488 (1H, m) (methine); 3.09–3.15 (ov) (CH_2N2); 1.72–2.02 (3H, m), 1.57–1.66 (1H, m) (CH_2CH_2). ^{51}V NMR (DMSO-d_6): −537 (0.95 V), −547 (0.05 V).

*2.3.6. N-(5-nitrosalicylidene)-(S)-(2-pyrrolidinyl-methyl)amine dioxovanadium(V) (**6**)*

Yield: 43%. *Anal*. Calc. for $C_{19}H_{25}N_2O_4V$: C, 43.5; H, 4.3; N, 12.7. Found: C, 43.7; H, 4.3; N, 12.6%. IR (KBr, cm^{-1}): 3233 (ν_{N-H}); 1650, 1602 ($\nu_{C=N} + \nu_{C=C}$); 936, 834 ($\nu_{V=O}$). UV–Vis spectrum in DMSO [λ_{max} (nm), ε ($M^{-1}\,cm^{-1}$)]: 354 (18560). CD spectrum in DMSO [λ_{max} (nm), $\Delta\varepsilon$ ($M^{-1}\,cm^{-1}$)]: 288 (1.75), 343 (−0.88). ^1H NMR (DMSO-d_6): 8.590 (1H, d, $^4J = 3$ Hz), 8.228 (1H, dd, $^3J = 9$ Hz, $^4J = 3$ Hz), 6.888 (1H, d, $^3J = 9$ Hz) (aromatic); 8.996 (1H, s) (azomethine); 6.303 (1H, br s) (HN2); 4.012 (1H, dd, $^2J = 14$ Hz, $^3J = 6$ Hz), 3.932 (1H, dd, $^2J = 14$ Hz, $^3J = 9.6$ Hz) (CH_2N1); 3.555 (1H, m) (methine); 3.09–3.15 (ov) (CH_2N2); 1.53–2.12 (3H, m), 1.26–1.40 (1H, m) (CH_2CH_2). ^{51}V NMR (DMSO-d_6): −534 (0.95 V), −545 (0.05 V).

*2.3.7. N-(7-methylsalicylidene)-(S)-(2-pyrrolidinyl-methyl)amine dioxovanadium(V) (**7**)*

Yield: 35%. *Anal*. Calc. for $C_{13}H_{17}N_2O_3V \cdot H_2O$: C, 49.1; H, 6.0; N, 8.8. Found: C, 49.2; H, 6.0; N, 8.9%. IR (KBr, cm^{-1}): 3204 (ν_{N-H}); 1602 ($\nu_{C=N} + \nu_{C=C}$); 925, 841 ($\nu_{V=O}$). UV–Vis spectrum in DMSO [λ_{max} (nm), ε ($M^{-1}\,cm^{-1}$)]: 351 (3510). CD spectrum in DMSO [λ_{max} (nm), $\Delta\varepsilon$ ($M^{-1}\,cm^{-1}$)]: 278 (−0.74), 308 (0.92), 352 (0.90), 394 (0.29). ^1H NMR (DMSO-d_6): 7.767 (1H, d, $^3J = 8$ Hz), 7.361 (1H, t, $^3J = 7.6$ Hz), 6.76–6.81 (2H, m) (aromatic); 6.194 (0.8H, br s), 5.613 (0.2H, br s) (HN2); 4.124 (0.2H, dd, $^2J = 14$ Hz, $^3J = 5.2$ Hz), 4.008 (0.8H, dd, $^2J = 14$ Hz, $^3J = 5.6$ Hz), 3.651 (0.8H, t) (CH_2N1); 3.508 (1H, m) (methine); 3.072 (1.7H, m), 2.881 (0.3H, m) (CH_2N2); 2.619 (2.3H, s), 2.586 (0.7H, s) (methyl); 1.40–2.20 (4H, m) (CH_2CH_2). ^{51}V NMR (DMSO-d_6): −539 (0.75 V), −547 (0.25 V).

*2.3.8. N-(7-phenylsalicylidene)-(S)-(2-pyrrolidinyl-methyl)amine dioxovanadium(V) (**8**)*

Yield: 44%. *Anal*. Calc. for $C_{18}H_{19}N_2O_3V \cdot H_2O$: C, 56.9; H, 5.6; N, 7.4. Found: C, 56.8; H, 5.6; N, 7.4%. IR (KBr, cm^{-1}): 3209 (ν_{N-H}); 1593 ($\nu_{C=N} + \nu_{C=C}$); 936, 848

($\nu_{V=O}$). UV–Vis spectrum in DMSO [λ_{max} (nm), ε ($M^{-1}\,cm^{-1}$)]: 367 (3450). CD spectrum in DMSO [λ_{max} (nm), $\Delta\varepsilon$ ($M^{-1}\,cm^{-1}$)]: 309 (0.82), 378 (−0.10), 410 (−0.04). ^{1}H NMR (DMSO-d_6): 7.56–7.64 (3H, m), 7.34–7.39 (3H, m), 6.842 (1H, d, $^3J = 8$ Hz), 6.750 (1H, d, $^3J = 7.6$ Hz), 6.614 (1H, t, $^3J = 7.6$ Hz) (aromatic); 6.296 (0.9H, br s), 5.704 (0.1H, br s) (HN2); 3.554 (1H, dd, $^3J = 9.6$ Hz) (CH_2N1); 3.34–3.39 (2H, m) (methine and one of CH_2N1 protons); 3.10–3.15 (ov) (CH_2N2); 1.65–1.95 (3H, m), 1.40–1.55 (1H, m) (CH_2CH_2). ^{51}V NMR (DMSO-d_6): −538 (0.9 V), −547 (0.1 V).

2.3.9. *N-(2-oxido-1-naphtyl)methylene-(S)-(2-pyrrolidinylmethyl)amine dioxovanadium(V)* (**9**)

Yield: 38%. *Anal.* Calc. for $C_{16}H_{17}N_2O_3V$: C, 57.1; H, 5.1; N, 8.3. Found: C, 57.3; H, 5.0; N, 8.3%. IR (KBr, cm^{-1}): 3199 (ν_{N-H}); 1625, 1543 ($\nu_{C=N} + \nu_{C=C}$); 925, 842 ($\nu_{V=O}$). UV–Vis spectrum in DMSO [λ_{max} (nm), ε ($M^{-1}\,cm^{-1}$)]: 322 (10120), 397 (5840). CD spectrum in DMSO [λ_{max} (nm), $\Delta\varepsilon$ ($M^{-1}\,cm^{-1}$)]: 283 (3.78), 310 (−0.10), 334 (0.86), 378 (1.53). ^{1}H NMR (DMSO-d_6): 8.363 (1H, d, $^3J = 6$ Hz), 7.989 (1H, d, $^3J = 9$ Hz), 7.854 (1H, td, $^3J = 7$ Hz, $^4J = 1.5$ Hz), 7.838 (1H, d, $^3J = 8$ Hz), 7.378 (1H, td, $^3J = 8$ Hz, $^4J = 1.2$ Hz), 7.036 (1H, d, $^3J = 9.8$ Hz) (aromatic); 9.689 (1H, s) (azomethine); 6.384 (1H, br s), (HN2); 4.211 (1H, dd, $^2J = 14$ Hz, $^3J = 5.4$ Hz), 4.015 (1H, dd, $^2J = 14$ Hz, $^3J = 8.2$ Hz) (CH_2N1); 3.533 (1H, m) (methine); 3.11–3.13 (ov) (CH_2N2); 1.75–1.95 (3H, m), 1.61–1.73 (1H, m) (CH_2CH_2). ^{51}V NMR (DMSO-d_6): −533 (0.95 V), −544 (0.05 V).

2.3.10. *N-(1-oxido-2-naphtyl)ethylidene-(S)-(2-pyrrolidinylmethyl)amine dioxovanadium(V)* (**10**)

Yield: 34%. *Anal.* Calc. for $C_{17}H_{19}N_2O_3V$: C, 58.3; H, 5.5; N, 8.0. Found: C, 58.2; H, 5.5; N, 8.0%. IR (KBr, cm^{-1}): 3211 (ν_{N-H}); 1621, 1585 ($\nu_{C=N} + \nu_{C=C}$); 930, 838 ($\nu_{V=O}$). UV–Vis spectrum in DMSO [λ_{max} (nm), ε ($M^{-1}\,cm^{-1}$)]: 327 (5480), 388 (5720). CD spectrum in DMSO [λ_{max} (nm), $\Delta\varepsilon$ ($M^{-1}\,cm^{-1}$)]: 281 (−0.27), 313 (−0.51), 373 (−0.63), 417 (0.40). ^{1}H NMR (DMSO-d_6): 8.300 (0.9H, d, $^3J = 8.4$ Hz), 8.876 (0.1H, d), 7.783 (2H, m), 7.571 (1H, t, $^3J = 9$ Hz, $^4J = 8.4$ Hz), 7.464 (1H, t, $^3J = 8$ Hz), 7.246 (1H, d, $^3J = 8.4$ Hz) (aromatic); 6.297 (0.77H, br s), 5.736 (0.23H, br s) (HN2); 4.168 (0.22H, dd, $^2J = 14.4$ Hz, $^3J = 5.2$ Hz), 4.077 (0.78H, dd, $^2J = 15$ Hz, $^3J = 5.7$ Hz), 3.713 (0.78H, dd, $^2J = 15$ Hz, $^3J = 8.6$ Hz) (CH_2N1); 3.579 (1H, m) (methine); 3.106 (2H, m) (CH_2N2); 2.696 (2.3H, s), 2.661 (0.7H, s) (methyl); 1.66–2.10 (3.77H, m), 1.459 (0.23H, m) (CH_2CH_2). ^{51}V NMR (DMSO-d_6): −538 (0.75 V), −543 (0.25 V).

3. Results and discussion

3.1. Crystal and molecular structure of 7

The crystal of **7** is built from two kinds of dimeric complex molecules $\mathbf{A}_2$ and $\mathbf{B}_2$ and water molecules. An ORTEP diagram illustrating the molecular structure of **7** is given in Fig. 2. The figure shows that vanadium(V) ion is six-coordinated through three bonds to oxo groups and through bonds to the tridentate Schiff base ligand. The six-coordination illustrates the strong propensity of vanadium to increase its coordination number via dimerisation of two pentadentate monomers. The geometry of the coordination environment resembles two edge shared octahedrons that are significantly distorted. The separation of O1 from V1 (1.610(3) Å) (Table 2) is typically for V=O which is not involved in donor–acceptor interactions [19–23]. The O2, V1, O2′, V1′ atoms are situated in edges of a parallelogram with the acute O2–V1–O2′ angle of 77.3(1)°. The tridentate ligand is coordinated meridionally, its oxygen (O3) and pyrrolidine ring nitrogen (N2) occupy axial positions. The six-membered chelate ring defined by V1, O3, N1, C1, C6, C7 atoms is planar (maximal deviation of plane defining atoms does not exceed 0.029 Å). In the final stage of anisotropic refinement conformation disorder of pyrrolidine and five-membered chelate rings was recognized. Two conformations of each of these rings could be distinguished. The disorder of C12, common for pyrrolidine and five-membered chelate rings, and of C11 of the pyrrolidine ring, is displayed in Fig. 2. Both the chelate and pyrrolidine five-membered rings adopt in **B** twist (half-chair) but in **A** the envelope conformations. The refined site occupancy values of 0.552(14) for C11B and C12B and of 0.447(14) for C11A and C12A indicate that the crystal of **7** is a solid solution of **B** (55%) and **A** (45%). These arrangements and the priority sequence rules of Cahn et al. [24] allow to assign the absolute configuration of C12A to *R* and that of C12B to *S*. The ligand sites in conformation isomers **A** and **B** are diastereotopic and therefore the crystal of **7** may be considered as a solid solution of two

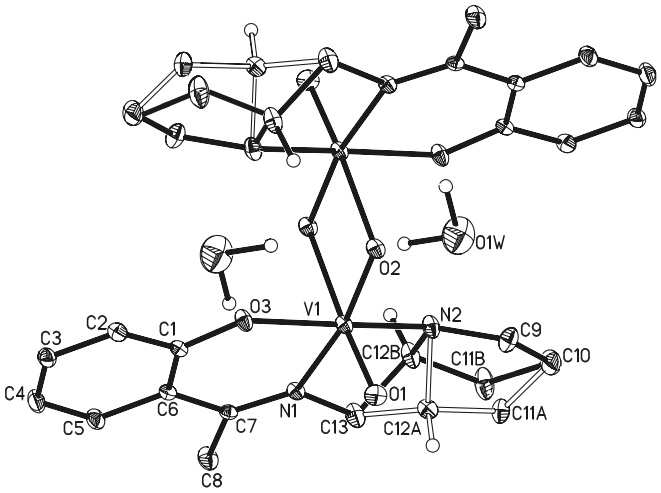

Fig. 2. An ORTEP drawing of the crystal structure of **7** with the atomic numbering scheme. H atoms, except those which are bound to C12A, C12B and of water molecules, are omitted for clarity. Displacement ellipsoids are drawn at the 10% probability level. The disordered conformation of five-membered ring is indicated by bonds drawn as parallel lines.

covalent diastereomers. A rare case of two diastereomers in one crystal was demonstrated earlier by Fulwood et al. [25] who resolved the crystal structure of the monooxovanadium(V) Schiff base complex solvate [VO(sal-L-ala)Bu^s]Bu^{s}OH. The steric demand of the space group symmetry prevents the inversion of rings so that only the most stable form of the molecule should be present in the crystal. The inconsistency of the crystal structure with that demand seems to be the result of sufficient similarity of **A** to **B** molecules, which quantified by the Kitaigorodski's isosterism coefficient [26] is $\varepsilon = 1 - v_{no}/v_o = 0.761 \pm 0.003$ (where v_{no} and v_o represent the non-overlap and overlap volumes of **A** and **B** molecules calculated on the basis of the average volumes of elements derived [27] from the analysis of the Cambridge Structural Database). The obtained ε value is somewhat smaller than the lower limit value of the reported 0.8–1 range [26] required for formation of a solid solution from two kinds of molecules. Partial transformation of **B** into **A** induced by crystallization occurs probably at the expense of the crystallization energy.

The diffraction experiment (due to its time and space averaging character) sees the structure of the crystal of **7**, containing the 45:55 mixture of two (**A** and **B**) conformers, centrosymmetric.

3.2. Spectroscopic studies

IR spectra of non-solvated complexes show a single band in the 3196–3233 cm^{-1} region designated to the N–H stretching mode of the coordinated secondary amino group, two bands in the 1585–1650 cm^{-1} range associated with ν(C=N) and ν(C=C) vibrations, two bands in the 839–936 cm^{-1} range which may be assigned to asymmetric and symmetric vibrations of VO_2 group. By analogy to the dissociation of the $[VO_2(1,2\text{-pnSal})]_2$ [19] and $[VO_2(MeenSal)]_2$ [20] dimers in DMSO solutions, which are weakly associated in the solid state [19,21], we felt it was likely that also the related dimeric complex **7** associated in the crystal through elongated O2–V1′ and O2′–V1 bonds (2.393(3) Å), and also the **1**–**6**, **8**–**10** complexes, are dissociated in DMSO at 50 °C to form monomeric compounds. In contrast to a single transition observed in the ^{51}V NMR spectrum of $[VO_2(1,2\text{-pnSal})]_2$ [19] and of $[VO_2(MeenSal)]_2$ [20] the **1**–**10** complexes exhibit two transitions in DMSO-d_6, one in the range from −532 to −539 ppm and the other approximately 8 ppm at higher field. The large separation of two ^{51}V resonances may be explained as the result of diastereomeric splitting which amounts ca. 7.5 ppm when the chiral centre containing asymmetric carbon atom is separated from the chiral vanadium centre by two bonds [28] like C12 from V1 in **7**. Intensities of ^{51}V NMR signals, as measured by areas they enclose, are in the ratios 3:1 for both **7** and **10** and in a greater number to one for the remaining compounds. The chemical shifts of both transitions from −531 to −556 ppm are in a range observed for five-coordinated V(V) complexes with similar O_3N_2 donor sets [19,20]. Since crystal structure conformations are generally good guides to conformational preferences in solution [29] we assigned two ^{51}V resonance signals to **A** and **B** diastereomers which were found in the crystal of **7**.

Chemical shifts, signal multiplicities and coupling constants of protons bonded to aromatic carbon atoms are comparable with the ^{1}H NMR data for related dioxovanadium(V) Schiff base complexes derived from analogous aromatic hydroxycarbonyl compounds and different diamines [20]. Protons of both five-membered rings of **1**–**10** give two sets of signals as illustrated in the part of the spectrum of the **5** compound (Fig. 3). Ratio's of signal intensities for corresponding protons from these sets are comparable with the **B**:**A** molar ratio's determined from ^{51}V NMR spectra. Two resonance signals of the ethylidene methyl group are observed in the spectra of **7** and **10** compounds. The integrated intensity ratio of these signals (3.24:1 for **7**, 3.45:1 for **10**) closely correlates with the molar ratio of **B**:**A** diastereomers in DMSO solution. Since the methyl group is not disordered two signals of its protons may be attributed to the van der Waals effect which result in a lower field shift of one of the signals relative to the other due to shorter H(C8) ⋯ H(C13) contact separation in **B** (stronger low field shift) than in **A**.

The methylene protons of the =N—CH_2—CH fragment have been analysed as two AB subspectra of the ABX system and the computations yield the values of a geminal coupling constant J_{AB} = 14–15 Hz, and vicinal couplings

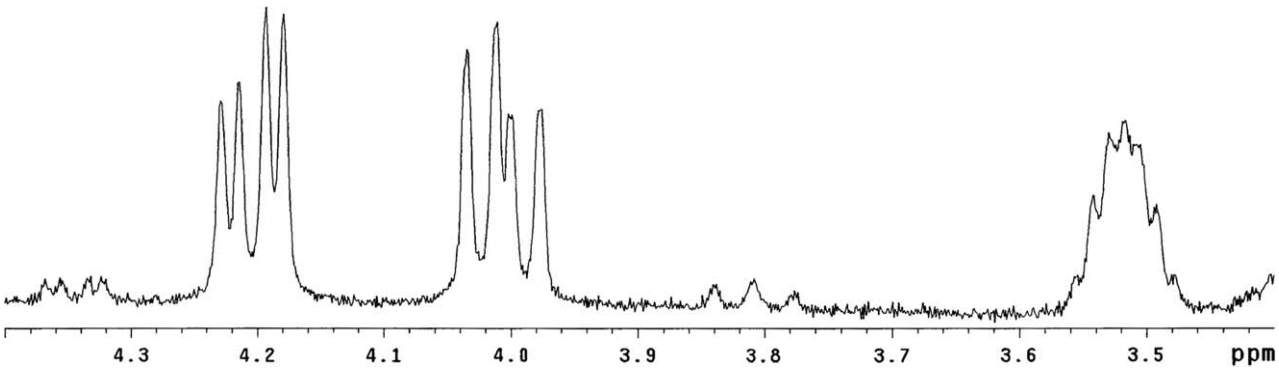

Fig. 3. Part of the ^{1}H NMR (400 MHz) spectrum of **5**.

$J_{AX} = 8$–10 Hz and $J_{BX} = 5$–6 Hz. The methine proton produces a seven-line multiplet (Fig. 3) with relative intensities of its components about 1:2:3:4:3:2:1 and this multiplicity may be interpreted as a triplet ($^3J = 10$ Hz) of triplets ($^3J = 5$ Hz) on the basis of first-order approximation. At 50 °C the AB system is in the region of slow exchange and the equilibrium constant $K = [\mathbf{B}]\backslash[\mathbf{A}]$ can be determined by integration of the separate resonance signals for **A** and **B**, particularly of NH, =N—CH_2 and CH_3—C=N protons. From the equation $-\Delta G^0 = RT \ln K$ the difference in free energy of the two conformations of **A** and **B** molecules is obtained. Its negative values $\Delta G^0(323) = -3.157 \pm 0.003$ kJ mol^{-1} for **10** and $\Delta G^0(323) = -3.325 \pm 0.003$ kJ mol^{-1} for **7** indicate that the compounds favour the twist conformation of both five-membered chelate rings.

The circular dichroism data for the complexes in DMSO are summarized in Section 2. Basing on the assumption that sign of the Cotton effect reflects the conformation of the five-membered chelate ring of a Schiff base complex [30] it may be concluded that the positive sign of all CD bands for **1**–**5** and **9** complexes is consistent with a high predominance of **B** form in DMSO solutions of complexes derived from aromatic hydroxyaldehydes.

3.3. Conclusions

A series of new Schiff base vanadium(V) complexes incorporating the pyrrolidine fragment have been obtained. The successfully determined structure of **7** is one of the rare case of vanadium complexes for which there are two diastereomers in one crystal and they appear in the diffraction experiment as one disordered molecule. The ratio of the diastereomer **B**, possessing the asymmetric carbon atom in the same absolute configuration as the parent (*S*)-(+)-2-(aminomethyl)pyrrolidine, to the diastereomer **A**, containing the corresponding carbon atom in *R* configuration, being 55:45 for the crystal of **7** changes to 3:1 in its DMSO solution and to a higher predominance of **B** over **A** in solutions of all of the remaining complexes. The free energy change value of transformation of *S*-diastereomer into its *R* analog in DMSO solution is particularly low for **7** and **10** complexes containing ethylidene substituent attached to the aromatic ring.

4. Supplementary material

Supplementary crystallographic data are available from the CCDC, Union Road, Cambridge CB2 1EZ, UK on request quoting the deposition number CCDC 292426 (fax: +44 1223 336 033; e-mail: deposit@ccdc.cam.ac.uk).

Acknowledgements

The research was supported by the University Grants BW/8000-5-0191-4, BW/8000-5-0277-5, BW/8000-5-0308-6 and DS/8210-4-0086-6. The Institute of Physical Chemistry, Polish Academy of Sciences, Warsaw, is acknowledged for its generous support with crystal structure determination.

References

[1] M.J. Jun, C.F. Liu, Inorg. Chim. Acta 15 (1975) 111.
[2] S. Kitagava, T. Murakami, M. Hatamo, Inorg. Chem. 14 (1975) 2387.
[3] M.J. Jun, C.F. Liu, J. Chem. Soc., Dalton Trans. (1976) 1031.
[4] M. Yamagouchi, S. Yano, M. Saburi, S. Yoshikawa, Inorg. Chem. 19 (1980) 2016.
[5] Z. Dokuzovic, N.K. Roberts, J.F. Sawyer, J. Wheland, B. Bosnich, J. Am. Chem. Soc. 108 (1986) 2034.
[6] K. Miyamura, K. Hata, T. Makino, M. Saburi, S. Yoshikawa, J. Chem. Soc., Dalton Trans. (1987) 1127.
[7] P.V. Bernhardt, P. Comba, T.V. Hambley, L.I. Martin, K. Varnagy, L. Zipper, Helv. Chim. Acta 75 (1992) 145.
[8] Y.N. Belokon, V.I. Maleev, S.O. Videnskaya, M.B. Saporovskaya, V.A. Tsarapkin, V.M. Belikov, Izv. Akad. Nauk SSSR, Ser. Khim. (1991) 126.
[9] S. Shibata, H. Matsushita, K. Kato, M. Noguchi, M. Saburi, S. Yoshikawa, Bull. Chem. Soc. Jpn. 52 (1979) 2938.
[10] F.H. Nielsen, in: H. Siegel, A. Siegel (Eds.), Metal Ions in Biological Systems. Vanadium and its Role in Life, vol. 31, M. Dekker, New York, 1995, p. 543.
[11] T. Hirao, Chem. Rev. 97 (1997) 2707.
[12] H.A. Messerschmidt, R. Wever, Proc. Natl. Acad. Sci. 93 (1996) 392.
[13] Y. Sun, B.R. James, S.J. Rettig, C. Orvig, Inorg. Chem. 15 (1996) 1667.
[14] D.C. Crans, J. Inorg. Biochem. 80 (2000) 123.
[15] D.C. Crans, J.J. Smee, E. Gaidamauskas, L. Yang, Chem. Rev. 104 (2004) 849.
[16] G.M. Sheldrick, SHELXS-97, Program for Crystal Structure Solution, University of Gottingen, Germany.
[17] G.M. Sheldrick, SHELXL-97, Program for Structure Refinement, University of Gottingen, Germany.
[18] A.L. Spek, J. Appl. Crystallogr. 36 (2003) 7.
[19] C.A. Root, J.D. Hoeschele, C.R. Cornman, J.F. Kampf, V.L. Pecoraro, Inorg. Chem. 32 (1993) 3955.
[20] E. Kwiatkowski, G. Romanowski, W. Nowicki, M. Kwiatkowski, K. Suwińska, Polyhedron 22 (2003) 1009.
[21] L.M. Mokry, C.J. Carrano, Inorg. Chem. 32 (1993) 6119.
[22] C.J. Carrano, C.M. Nunn, R. Quan, J.A. Bonadies, V.L. Pecoraro, Inorg. Chem. 29 (1990) 944.
[23] G. Asgedom, A. Sreedhara, J. Kivikoski, E. Kohlemainen, C.P. Rao, J. Chem. Soc., Dalton Trans. (1996) 93.
[24] R.S. Cahn, C. Ingold, A.V. Prelog, J. Chem. Soc. (1951) 612.
[25] R. Fulwood, H. Schmidt, D. Rehder, J. Chem. Soc., Chem. Commun. (1995) 1443.
[26] A.I. Kitaigorodski, Organic Chemical Crystallography, Consultants Bureau, New York, 1961, p. 210.
[27] D.M.W. Hofmann, Acta Crystallogr., Sect. B 58 (2002) 489.
[28] C. Weidemann, W. Priebsch, D. Rehder, Chem. Ber. 122 (1989) 235.
[29] F.H. Allen, W.D.S. Motherwell, Acta Crystallogr., Sect. B 58 (2002) 407.
[30] R.S. Downing, F.L. Urbach, J. Am. Chem. Soc. 91 (1959) 5977.

planar and/or axial positions: a frame of distorted octahedron is always available, although different visible spectrophotometric behaviour is recorded in event of planar or axial entrance of the donors in substitution of pre-existing water oxygen. Visible spectrophotometric response is then fundamental, since both calorimetric and stability data are usually unable to discriminate among equatorial and axial positions of donor groups, as well known.

As previously observed by various authors [4–6], a red shift in the visible λ_{max} position of a copper(II) complex appears when a donor group is located in an axial position, that is the so-called "pentammine effect". In our context of copper(II)–ligand interaction in aqueous solution, a "*red shift*" is the shift towards higher wavelengths (shorter energies) of the visible absorption maximum occurring when an equatorially co-ordinated copper(II) complex (λ_{max1}) acquires a donor in an axial position (λ_{max2}): the corresponding red shift is simply expressed as $\Delta\lambda_{max} = \lambda_{max2} - \lambda_{max1}$. Oxygen of water is considered as a donor, since its contribution to the ligand field of a copper(II) aqueous ion is quantitatively known [1,5]. The red shift is defined for each axial donor by means of a simple normalisation, $\Delta\lambda_{max}/n$, with $n = 2$ for a complex having two donors along the z-axis.

In this study we attempted to obtain reliable discriminating evidences, using literature findings as well, in order to formulate a simple spectrum–structure correlation test to hypothesize an axial co-ordination in a copper(II) complex. Since visible absorption spectra discussed in many papers were recorded without explicit reference to the chemical speciation, that is without strictly considering stability aspects and overlapping of the species, we are forced to exclude many potential axially co-ordinated copper(II) complexes by our treatment. The equation developed in [1] (see also Refs. therein), providing a link between the λ_{max} value of a copper(II) complex and its equatorial co-ordination environment, should now help us in seeking discriminating visible spectrophotometric features to formulate a well-documented hypothesis of axial co-ordination for copper(II) ion. In this connection, a series of visible spectra were recorded on copper(II)–2,2′-bipyridine system (various metal-to-ligand ratios and pH were tested), since this bidentate ligand is known for its ability to co-ordinate copper(II) in axial position as well. Copper(II) complex formation with L-aspartic acid (a potential tridentate ligand) was also investigated by combined pH-metric and visible spectrophotometric techniques to check the eventual axial co-ordination. The study is moreover strengthen by a computer-assisted calculation procedure, based on the Lambert–Beer law, which allow us to calculate a visible spectrum for each of the complexes formed in solution (almost those reaching a significant percentage of formation). As a consequence, the spectrum–structure correlation is thought on single species, avoiding the significant errors due to the presence of two or more species at the same pH value.

2. Experimental

2.1. Chemicals

2,2′-Bipyridine (bipy, H_2L^{2+}, 99.5%) was a BDH AnalaR product and L-aspartic acid (asp, H_3L^{+}, 99%) was a Merck product, both employed without any further purification.

The copper(II) chloride stock solution was standardized by means of complexometric titrations with EDTA, in the presence of the metallochromic indicator murexide. Standard solutions of NaOH, KOH, HCl and HNO_3 were prepared by diluting concentrated Merck ampoules and were standardised against potassium hydrogenphthalate or sodium carbonate, respectively. Grade A glassware and deionised and twice distilled water were used for all solutions. The ionic strength was adjusted to 0.1 M by addition of KCl. The purity of acid–base active reagents ($\geqslant$99%) was checked by pH-metric titrations followed potentiometrically.

2.2. Electromotive force measurements

The potentiometric measurements of pH were performed at $T = (25.0 \pm 0.1)$ °C and ionic strength $I = 0.1$ M (KCl) with an Amel 338 potentiometer equipped with a combined glass electrode provided by Metrohm (Switzerland), model 6.0222.100, internal Ag/AgCl reference electrode (filling electrolyte: 3 mol/l KCl). The couple was calibrated in $-\log[H_3O^+]$ units (pH) employing alkalimetric titrations of hydrochloric acid with standard, carbonate free, potassium hydroxide. The ionic strength of the calibrating solutions was the same as that of solutions being examined. The alkalimetric titrations were carried out in a stream of purified nitrogen. Temperature control was achieved by means of liquid circulation from a thermo cryostat (model D1-G Haake). The concentration ranges examined was from 3 to 6 mM for C_M (C means analytical concentration). The metal-to-ligand molar ratios were from 1:1 to 1:3 for Cu^{2+}–2,2′-bipyridine and from 1:1 to 1:5 for Cu^{2+}–L-aspartic acid.

2.3. Spectrophotometric measurements

The visible spectrophotometric determinations were carried out with a Jasco V-550 UV/Vis spectrophotometer from 400 to 800 nm (optical path length 1.000). The solution being examined was transferred from the potentiometric to an optical cell using a peristaltic pump in order to record spectra as a function of the pH value of the solution, avoiding any equilibrium inconvenience. The metal concentration and the metal-to-ligand molar ratios were the same with regard to potentiometric determinations.

2.4. Data analysis and calculations

The stability constants of the complexes are expressed by the general formula: $\beta_{pqr} = [Cu_pL_qH_r]/[Cu]^p[L]^q[H]^r$ (all over the paper charges of complexes are omitted for sake of

simplicity); their values were refined by means of the BSTAC [7] program, which minimizes the error squares sum on electromotive force values and takes into account eventual variations of ionic strength among and/or during titrations.

Spectrophotometric data were analysed by means of the least squares computer program MOLEX [8], which calculates the values of molar absorptivity (ε_λ/dm^3 mol^{-1} cm^{-1}) by using experimental spectra (absorbance, A, versus wavelength, λ/nm), analytical concentrations of each reagent and the chemical model (stoichiometric coefficients, $p\ q\ r$, and known stability constant values of all complexes) as input. After the calculation of the species distribution, the spectra are estimated for each complex formed in solution, only leaving out the species formed in negligible amount, by assuming the additivity of the absorbance in the investigated concentration range (Lambert–Beer law). No assumptions on the shape of the curves nor on the nature of electronic transitions are taken into account by the calculation program.

In all calculations the hydrolysis of copper(II) ion [9] was considered.

3. Results

3.1. Complexes of 2,2′-bipyridine

First, the formation constant of the dimer $Cu_2L_2H_{-2}$ (2 2 −2 using $p\ q\ r$ indexes) with 2,2′-bipyridine has been re-calculated using pH-metric data (alkalimetric titrations of acidified Cu/L mixtures): we found ($T = 25$ °C, $I = 0.1$ M) $\log\beta_{22-2} = 5.59 \pm 0.02$ (uncertainty is expressed as ±SD). The agreement with the value previously estimated (5.68 ± 0.04 [10]) is good. The refinement has been performed assuming as fixed the values of $\log\beta_{pqr}$ related to the following species [11]: CuL ($\log\beta_{110} = 8.12$), CuL_2 ($\log\beta_{120} = 13.63$) and CuL_3 ($\log\beta_{130} = 17.0$); protonation constant values were from Ref. [10] (see also Refs. therein).

Then, combined measurements of pH and visible absorption spectrophotometry were performed in order to get spectra in controlled experimental conditions, suitable for further high quality computer-assisted treatment. The visible absorption spectra, recorded as a function of pH on various solutions, are strongly dependent upon the metal-to-ligand molar ratio. The trend of these spectra (Figs. 1–3) strongly suggests the occupation of copper(II) axial positions when $Cu(bipy)_2$ and $Cu(bipy)_3$ are formed. Coupling the blend of experimental spectra and the chemical model (Table 1) we were able to calculate an absorption spectrum for each complex of the investigated binary system under the experimental conditions previously described. Fig. 4 shows the visible spectra calculated for single complexes of the Cu^{2+}–2,2′-bipyridine system; the results are collected in Table 1, also containing structural hypotheses under discussion below. Jorgensen [12] recorded some spectrophotometric data related to Cu^{2+}–2,2′-bipyridine and Cu^{2+}–*o*-phenantroline systems. If considering that: (i) pH values are not declared (and perhaps not stated), (ii) there are not thermodynamic data for solution speciation, (iii) 50% of ethanol is present in the solutions under measurement (which modify both species distribution and absorption features), and (iv) an attempt of deconvolution of experimental spectra was not made (the dimer is still present in excess of ligand), we have not considered the above report in the prosecution of our paper.

3.2. Complexes of L-aspartic acid

Copper(II) complex formation with L-aspartic was also investigated by coupled pH-metric and visible spectrophotometric techniques (25 °C and $I = 0.1$ M) to check the

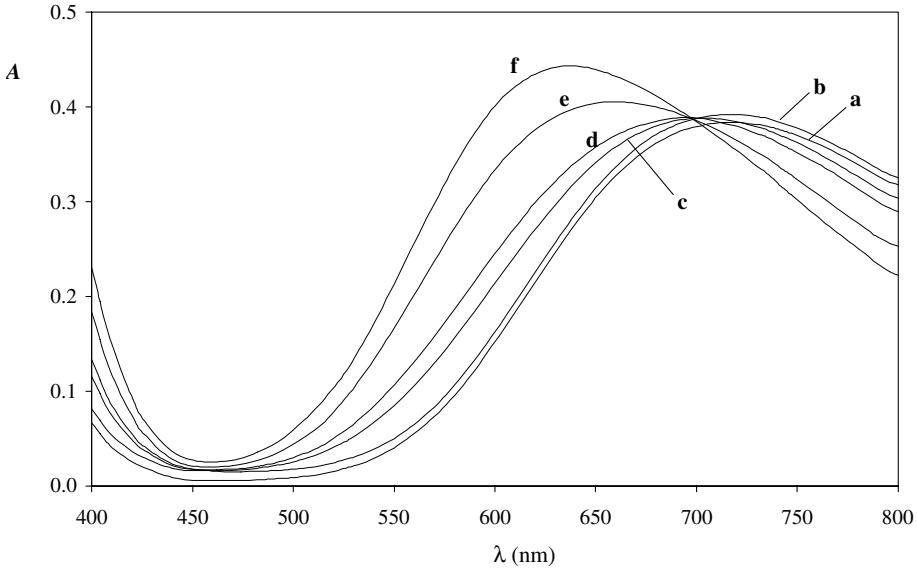

Fig. 1. Experimental visible spectra for Cu^{2+}–2,2′-bipyridine system. $C_{Cu} = 10.0$, $C_{bipy} = 10.0$ mM. a: pH 3.73; b: pH 5.21; c: pH 6.03; d: 6.19; e: pH 6.56; and f: pH 6.88.

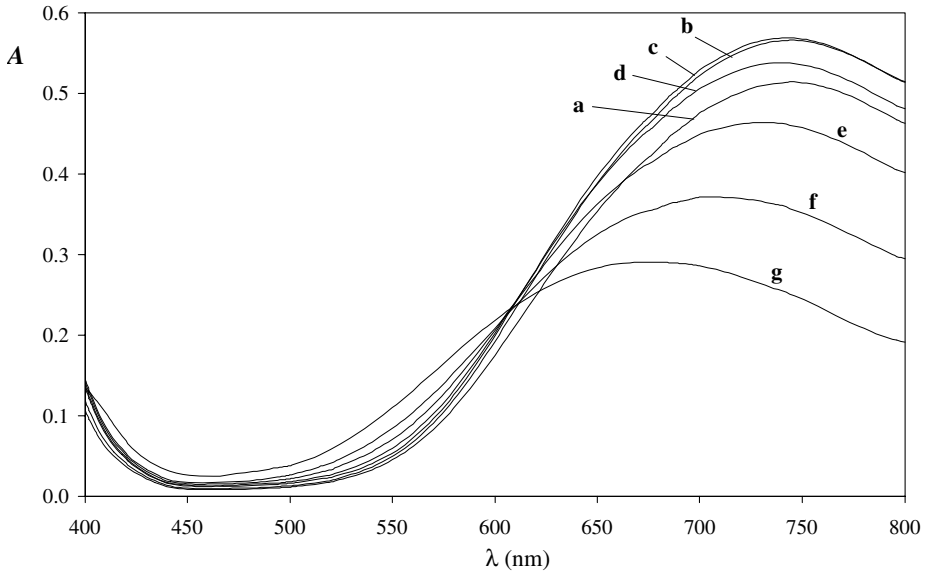

Fig. 2. Experimental visible absorption spectra Cu^{2+}–2,2′-bipyridine system. $C_{Cu} = 5.0$, $C_{bipy} = 10.0$ mM. a: pH 2.14; b: pH 2.99; c: pH 6.77; d: 7.31; e: pH 7.93; f: pH 8.61; and g: pH 9.68.

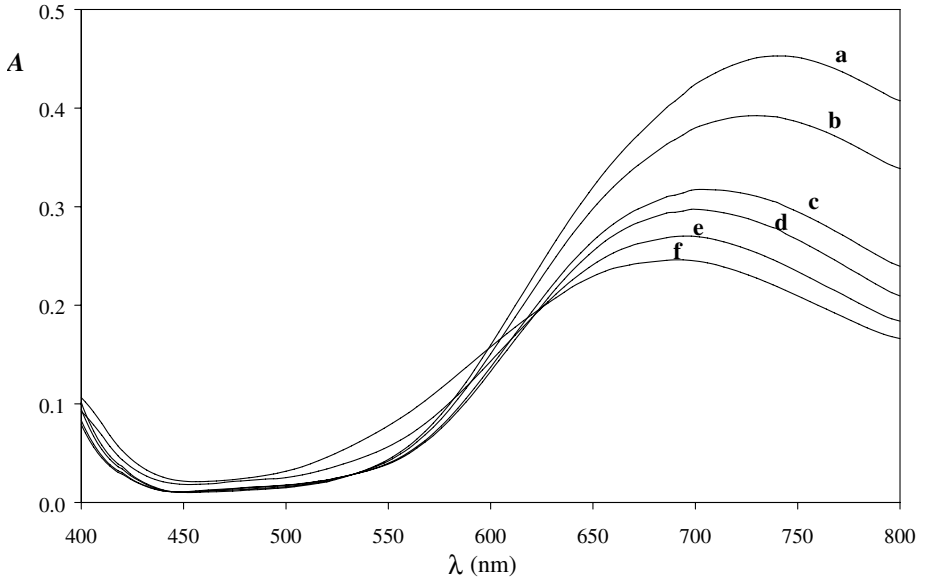

Fig. 3. Experimental visible absorption spectra Cu^{2+}–2,2′-bipyridine system. $C_{Cu} = 4.0$, $C_{bipy} = 12.0$ mM. a: pH 2.75; b: pH 3.37; c: pH 4.24; d: 5.02; e: pH 9.36; and f: pH 10.14.

eventual axial co-ordination. Stability constants (including protonation) was from Ref. [13]. In our current study, M:L molar ratio was forced towards the excess of ligand, to test the ability of the L-aspartic acid in acting as tridentate molecule, thus increasing the probability of an axial co-ordination. Solutions with M:L ratio from 1:1 to 1:5 were tested. Main complexes, as confirmed by the literature [11,13,14,16], are CuLH, CuL and CuL_2. The deconvolution of the wide blend of experimental spectra (recorded as a function of pH) allowed us to calculate a visible absorption spectrum for each complex species. We obtained: for CuLH $\lambda_{max} = 730$ nm and $\varepsilon_{730} = 34$ dm^3 mol^{-1} cm^{-1}, for CuL $\lambda_{max} = 685$ nm and $\varepsilon_{685} = 42$ dm^3 mol^{-1} cm^{-1} and for CuL_2 $\lambda_{max} = 630$ nm and $\varepsilon_{630} = 53$ dm^3 mol^{-1} cm^{-1} (with a ligand excess, solutions containing $Cu(asp)_2$ alone in the neutral-basic range of pH can be prepared).

4. Discussion

4.1. The model

The model to study the co-ordination chemistry of copper(II) ion in aqueous solution must unavoidably refer to two cases.

Table 1
Thermodynamic and visible spectrophotometric results (25 °C, $I = 0.1$ M) with structural hypotheses for copper(II) complexes with 2,2′-bipyridine in aqueous solution

Complex	*p q r*	Thermodynamic results	Spectrophotometric results		Structural hypotheses			
					Pure equatorial case		Mixed equatorial and axial case	
		$\log\beta_{pqr}$	λ_{max} [b]	ε_{max} [b]	Donor groups *per* copper(II) [c]	$\lambda_{max\ calc.}$ [d]	Planar donor groups *per* copper(II)	Axial donor groups *per* copper(II)
CuL	1 1 0	8.12	689	24	2pyn, 2wo	692		
$Cu_2L_2H_{-2}$	2 2 −2	5.59 ± 0.02 [a]	611	96	2pyn, 2ho	612		
CuL_2	1 2 0	13.63	750	138	3pyn, 1wo	634	2pyn	2pyn
CuL_3	1 3 0	17.0	670	54	4pyn	585	4pyn	2pyn

[a] Value optimized in this paper. Uncertainty expressed as ±SD.
[b] λ_{max} in nm; ε_{max} in $dm^3\ mol^{-1}\ cm^{-1}$.
[c] Pyridine nitrogen: pyn; hydroxide oxygen: ho; water oxygen: wo.
[d] Ref. [1].

For structural hypothesis of *pure equatorially co-ordinated* copper(II) complexes (the square planar case) the following equation [1] can be used:

$$\lambda_{max} = 10^3 / \sum_{i=1}^{4} n_i \bar{v}_i \quad (1)$$

where $\bar{v}_i$ represents the individual contribution of each donor group to the ligand field of the complex. The equation allows an estimation of the λ_{max} values of a copper(II) complex ($\lambda_{max\ calc.}$) by means of a simulation considering a planar hypothesis of co-ordination. It is noteworthy, for the meaning of this paper, that $\bar{v}_i$ values were optimized on the basis of experimental data of absorption spectra, thus the energies estimated for a planar co-ordination include intrinsically the contribution of the two water molecules along the *z*-axis of the copper(II) distorted octahedron. The donor groups considered, whit the related $\bar{v}_i$ values, are:

Amino nitrogen (an): 0.450; peptide nitrogen (pn): 0.495; imidazole nitrogen (in): 0.427; carboxylate oxygen (co): 0.353; alcoholate oxygen (ao): 0.39; hydroxide oxygen (ho): 0.39; water oxygen (wo): 0.296. The same $\bar{v}_i$ value was assumed in calculations for amide nitrogen (adn) with respect to that of peptide nitrogen and for pyridine nitrogen (pyn) with respect to that of imidazole nitrogen.

For structural hypothesis of *mixed equatorially and axially co-ordinated* copper(II) complexes – including both the square pyramid and the octahedron (or tetragonal bipyramid) cases – experience shows that d–d energies decrease if a position along the *z*-axis is occupied by a donor group substituting pre-existing water oxygen. The evaluation of the red shift (quantity defined in Section 1) must be carried out considering a reference complex showing the same planar co-ordination environment as that of the axially co-ordinated complex under study.

4.2. Complexes of 2,2′-bipyridine with molar ratios of 1:1

We found $\lambda_{max} = 689$ nm for CuL and $\lambda_{max} = 611$ nm for $Cu_2L_2H_{-2}$ (Table 1). If we assume for CuL a structure of bidentate complex with two nitrogen donors involved, we can estimate (Eq. (1) and [1]) $\lambda_{max} = 692$ nm. Moreover, if we hypothesise for $Cu_2L_2H_{-2}$ a structure corresponding to two CuL units connected by two bridged hydroxide groups – $Cu_2L_2(\mu\text{-}OH)_2$ – we obtain $\lambda_{max} =$ 612 nm [1], assuming two equivalent chromophores in the complex.

4.3. Complexes of 2,2′-bipyridine with molar ratios of 1:2 and 1:3

The situation is more complicated for CuL_2 and CuL_3. In fact, $\log\beta_{pqr}$ (Table 1) indicates an increase in stability, leading to the hypothesis of an increasing of

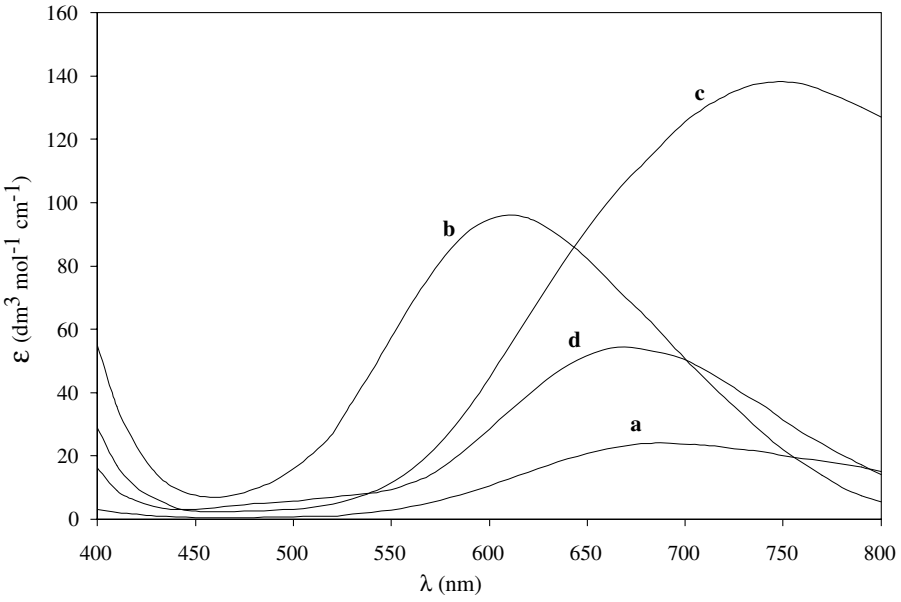

Fig. 4. Calculated visible absorption spectra for the individual complexes. a: Cu(bipy); b: $Cu_2(bipy)_2H_{-2}$; c: $Cu(bipy)_2$; and d: $Cu(bipy)_3$.

donor groups around copper(II) with respect to CuL. Moreover, also calorimetric data agree with a greater number of donor groups in CuL_2 and CuL_3 with respect to CuL. In fact, we have (25 °C, $I = 0.1$ M) $\Delta H = -46.0$, $\Delta H = -71.9$ and $\Delta H = -102$ kJ/mol for CuL, CuL_2 and CuL_3, respectively [11]. Nevertheless, a non-univocal trend of λ_{max} values, from CuL_2 and CuL_3, is clearly shown in Table 1 and in Fig. 4, inducing us to imagine a mixed equatorial and axial arrangement of the donors. Furthermore, calculation of λ_{max} [1] for CuL_2 and CuL_3, simply based on equatorial location of donors, fails (see Table 1, sixth column), although in accordance with stability and calorimetric findings. Then, axial hypotheses of donor arrangement must be formulated to fit our data with a coherent structure of these complexes in solution, accounting for the whole of the available indications. Particularly, for CuL_2 we can hypothesise each ligand disposed with a pyridine nitrogen in the equatorial plane and with the other one in an axial position. If only planar environment is considered, we have $\lambda_{max} = 689$ nm (as CuL), hence we can obtain the red shift *per* donor group as $(750 - 689)/2 = 31$ nm. Alternatively, even if considering only one nitrogen donor in axial position, we have $\lambda_{max} = 630$ nm [17] (calculated value with Eq. (1) is 634 nm) for a planar environment with three pyridine nitrogen and a water molecule; hence, the red shift should be $750 - 630 = 120$ nm, too big for one nitrogen atom along the *z*-axis, on the basis of current knowledge.

Moreover, for CuL_3 we can simply plan a fully occupied distorted octahedron of copper(II). Being the calculated λ_{max} for such a planar environment of 585 nm, we can obtain the red shift *per* donor group as $(670 - 585)/2 = 43$ nm. Fig. 5 shows the structures proposed for Cu(bipy), $Cu(bipy)_2$ and $Cu(bipy)_3$ (the ligand is schematised for sake of simplicity).

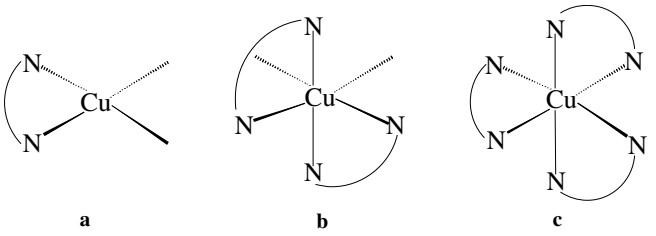

Fig. 5. Structure proposed for the complexes. a: Cu(bipy); b: $Cu(bipy)_2$; and c: $Cu(bipy)_3$. The ligand is schematised for sake of simplicity.

4.4. Complexes of L-aspartic acid

Some authors [13–15] have suggested a participation of the ω-carboxylate group of aspartate in co-ordination towards copper(II) ion, on the basis of thermodynamic data ($\log\beta_{110}$ and $\log\beta_{120}$ [10], ΔH and ΔS [14] values). Kinoshita et al. [15] underlined, via visible circular dichroism spectra, the important role played by the ω-carboxylate group of aspartate.

As for Cu(asp), our value of $\lambda_{max} = 685$ nm is fully compatible with a tridentate complex in the equatorial plane (two chelate rings of 5 and 6 terms are formed); a chromophore showing two carboxylate oxygen (α- and ω-carboxylate groups), one amino nitrogen and a water molecule allow us to calculate $\lambda_{max\ calc.} = 689$ nm with Eq. (1). The stability constants ($\log\beta_{110} = 8.83$ [13] or 8.89 [11] or 8.84 [16] at 25 °C and $I = 0.1$ M) is compatible with the hypothesis (for Cu(gly), $\log\beta_{110} = 8.14$ [13], gly = glycine). Claridge et al. [16] found for Cu(asp) $\lambda_{max} = 729$ nm. This value (declared ±5 nm by the authors) has been simply inferred by experimental spectra recorded on solution(s) containing Cu(asp) as major species; analogous treatment is forwarded for both Cu(asp)H ($\lambda_{max} = 733$ nm [16]) and $Cu(asp)_2$ ($\lambda_{max} = 621$ nm [16]) complexes (molar

absorptivity values are ignored by the authors). Unfortunately, it seems very hard to estimate the λ_{max} value for Cu(asp) from spectra at pH around 3.6 chosen by the authors. In fact, Cu(asp) and Cu(asp)H shows very similar molar concentration (M:L molar ratio 1:1 or 1:2), while the big amount of free copper(II) ion, with λ_{max} around 820 nm, shifts significantly the λ_{max} value of the solutions under measurement towards red. In this case, a Lambert–Beer-based deconvolution is inalienable.

The λ_{max} value we have obtained for Cu(asp)H is compatible with a glycine-like mode of co-ordination (calculated value with Eq. (1) is 717 nm). Visible absorption and ESR parameters reported in [16] indicate that the complexes Cu(asp)H have the α-amino carboxylate group co-ordinated to copper(II) ion.

The value of $\lambda_{max} = 630$ nm here determined for $Cu(asp)_2$ complex suggests a structure with two amino and two α-carboxylate groups in the equatorial plane together with a probable weak axial interaction from one ω-carboxylate (for amino acids without a co-ordinating side chain, the λ_{max} value of the $Cu(aminoacidate)_2$ complex is very close to 620 nm). An inspection of ΔS value reported for $Cu(asp)_2$ species confirms that the axial interaction from ω-carboxylate is weak. In fact, at 25 °C and $I = 0.1$ M, $\Delta S = 31.1$ cal/K mol for $Cu(asp)_2$ [11], while ΔS is 28.6 cal/K mol for $Cu(\text{L-alanine})_2$ [11], 58.5 cal/K mol [11] for Cu(EDTA). As a consequence of all the above considerations, the axial interaction, if any, from a ω-carboxylate group is weak and we have not considered this small red shift in the course of the paper.

4.5. Complexes of other ligands

A re-examination of a series of co-ordination hypothesis is analyzed in this paragraph.

As for multidentate ligands, such as the *N*-(phosphonomethyl)glycine (the widely used herbicide commercially known as *glyphosate*), various hypotheses for its CuL_2 complex ($\lambda_{max} = 715$ nm [18]) appear to be likely, although it is clear the involvement of both the nitrogen atoms of the ligand [18]. In Table 2 is proposed the structure involving an equatorial arrangement of the $Cu(aminoacidate)_2$ type, with a phosphonate donor group in axial position. Moreover, also for the CuL species ($\lambda_{max} = 730$ nm [18]) an axial co-ordination can be hypothesized (Table 2). The low value of λ_{max} can be suitably explained with an axial co-ordination, since $\log\beta_{110} = 11.80$ [18] is not compatible with a low co-ordination number. Hence, a red shift of apparently logic amplitude is estimated locating a phosphonate donor group in an axial position. The knowledge of the ligand field of the alcholate donor group, optimized in Ref. [1], strongly helped us in the actual structural definition.

Another multidentate ligand considered in the past, the oligopeptide hyppuryl-L-histidyl-L-leucine [24], is interesting for a structural re-discussion in the light of current findings. The equatorial arrangement of the donors in the species $CuLH_{-2}$ ($\lambda_{max} = 575$ nm) includes amide, N(3)-imidazole and deprotonated peptide nitrogens. As for the structure of the complex $CuLH_{-3}$ ($\lambda_{max} = 575$ nm), formed at more basic pH values, we can put forward a new hypothesis according to which in the deprotonation reaction to form $CuLH_{-3}$ there is a structural re-arrangement and in the equatorial plane we have one amido and two deprotonated peptide nitrogens with the carboxylate group, while N(3)-imidazole group occupies an axial position. For such a planar environment the calculations (Eq. (1)) leads to $\lambda_{max} = 544$ nm, hence the red shift results to be $575 - 544 = 31$ nm (Table 2).

In the paper of Bonomo et al. [25] the interaction of copper(II) with glycyl-L-histidyl-glycyl-L-histidine in aqueous solution is investigated. The structure of the complex $CuLH_{-2}$ ($\lambda_{max} = 575$ nm) can be explained assuming an equatorial plane fully occupied by one amino, two deprotonated peptide nitrogens and one imidazole nitrogen atoms (that of the C-terminal histidyl residue). Furthermore, one imidazole nitrogen atoms is located in an axial positions. The λ_{max} estimated for the planar co-ordination, considering the complex $CuLH_{-2}$ with glycyl-glycyl-L-histidyl-L-alanine, is 530 nm [26]. The red shift is $575 - 530 = 45$ nm, compatible with our current findings (Table 2).

The structure of the copper(II)–EDTA complex species is reported by Jorgensen [4], who indicates a pentadentate co-ordination as $Cu(EDTA)(H_2O)^{2-}$ ($\lambda_{max} = 734$ nm). Unfortunately, speciation is ignored while the author reports, for the mentioned complex, $\lambda_{max} = 734$ nm [4] and $\lambda_{max} = 730$ nm [12]. On the other side, structures of the copper(II)–EDTA complex(es) are investigated in the solid state. EDTA is considered as a pentadentate ligand with respect to copper(II) complex formation [27], owing to its capability to form only five-membered chelate rings. An EDTA-type ligand – 1,3-propanediamine-*N*,*N*′-diacetate-*N*,*N*′-di-3-propionate ion – able to form both five- and six-membred chelate rings, is reported [27] as exadentate towards copper(II) on the basis of X-ray data. As to EDTA, assuming a planar co-ordination as Cu(N,N,O,O), we should have a red shift of $734 - 620 = 114$ nm, enormous for a single donor (penta co-ordination), according to current knowledge on the topic. On the other hand, Billo [5] supposed a planar tridentate structure as $Cu(N,N,O)(H_2O)$, and two carboxylate groups in axial position: in such an arrangement we should have a red shift of $(734 - 646)/2 = 44$ nm, in agreement with the actual findings.

Jorgensen [12] considered CuL_3 complexes with ethylenediamine (en) or glycine (gly); he reported: $Cu(en)_3$, $\lambda_{max} = 610$ nm, $Cu(gly)_3$, $\lambda_{max} = 662$ nm, to be compared with the corresponding CuL_2 species, $\lambda_{max} = 549$ for $Cu(en)_2$ and $\lambda_{max} = 633$ for $Cu(gly)_2$. The mentioned data revealed a red shift from CuL_2 to CuL_3 species, in accordance with the theory here examined. Nevertheless, there are some aspects which make hard the interpretation of these data. In fact, the formation of the species $Cu(gly)_3$ is eventually possible only under extreme experimental conditions and the stability constant of this complex in not considered by the NIST database [11]. Hence, it is difficult

Table 2
Visible spectrophotometric λ_{max} values and structural hypotheses for single copper(II) complexes with probable axial co-ordination in aqueous solution

Equatorial donor groups	Axial donor group(s)[a]	Complex *p q r s*[b]	λ_{max} (nm)	Ligand(s) L, L′	Red shift *per* donor group[c]	Ref.
$4NH_3$		1 4 0 0	590	*ammonia*		[6]
	$1NH_3$	1 5 0 0	640	ammonia	640 − 590 = 50	
4an		1 2 0 0	549	*1,2-diaminoethane*		[19]
	2co	1 2 0 0	606	2,4-diaminobutyric acid	(606 − 549)/2 = 29	[20]
	$1NH_3$	1 2 1 0	599	1,2-diaminoethane, NH_3	599 − 549 = 50	[19]
	1ho	1 2 0 0	599	1,2-diaminoethane	599 − 549 = 50	[21]
	2an	1 2 0 0	630	diethylenetriamine	(630 − 549)/2 = 41	[4]
2an, 1co, 1wo			646	*calculated value*		[1]
	2co	1 1 0 0	734	EDTA	(734 − 646)/2 = 44	[4]
2an, 2co		1 2 0 0	620	L-alanine		[20]
	2ao	1 2 0 0	715	*N*-(phosphonomethyl)glycine	(715 − 620)/2 = 48	[18]
	2co	1 2 0 0	658	nitrilotriacetic acid	(658 − 620)/2 = 19	[4]
1an, 1co, 1ao, 1wo			672	*calculated value*		[1]
	1ao	1 1 0 0	730	*N*-(phosphonomethyl)glycine	730 − 672 = 58	[12]
3co, 1ao			690	*calculated value*		[1]
	1co	2 2 0 −2	730	citric acid	730 − 690 = 40	[22]
2an, 1co, 1in			595	*calculated value*		[1]
	1in, 1co	1 2 0 0	640	L-histidine	(640 − 595)/2 = 23	[17]
	1co	1 2 0 1	615	L-histidine	615 − 595 = 20	[17]
	1in, 1co	1 2 0 0	640	τ-methyl-L-histidine	(640 − 595)/2 = 23	[17]
	1co	1 2 0 1	622	τ-methyl-L-histidine	622 − 595 = 27	[17]
2an, 2adn		1 2 0 0	525	L-alaninamide		[23]
	2co	1 2 0 0	580	asparagine	(580 − 525)/2 = 28	[20]
1an, 1co, 2wo			717	*calculated value*		[1]
	2co	1 1 0 0	775	nitrilotriacetic acid	(775 − 717)/2 = 29	[4]
1adn, 2pn, 1co			544	*calculated value*		[1]
	1in	1 1 0 −3	575	hyppuryl-L-histidyl-L-leucine	575 − 544 = 31	[24]
1an, 2pn, 1in		1 1 0 −2	530	*glycyl-glycyl-L-histidyl-L-alanine*		[25]
	1in	1 1 0 −2	575	glycyl-L-histidyl-glycyl-L-histidine	575 − 530 = 45	[24]
4pyn			585	*calculated value*		[1]
	2pyn	1 3 0 0	670	2,2′-bipyridine	(670 − 585)/2 = 43	this paper
2pyn, 2wo		1 1 0 0	689	*2,2′-bipyridine*		this paper
	2pyn	1 2 0 0	750	2,2′-bipyridine	(750 − 689)/2 = 31	this paper

Structures, although reasonable, are not always univocally proven.

[a] Donor group(s) supposed along the *z*-axis. Symbols: Amino nitrogen: an; amide nitrogen: adn; imidazole nitrogen: in; peptide nitrogen: pn; pyridine nitrogen: pyn; carboxylate oxygen: co; alcoholate oxygen: ao; hydroxide oxygen: ho; water oxygen: wo.

[b] Indexes for the interaction among the metal ion and mixed ligands L and L′ (charges omitted) are referred to the reaction: $pCu + qL + rL' + sH \leftrightarrows Cu_pL_qL'_rH_s$.

[c] Red shift expressed as $\Delta\lambda_{max}$ (nm) for each donor group in axial position (see Section 1).

to hypothesize whether one or two donors are located along the *z*-axis. As to $Cu(en)_3$, Romano and Bjerrum [19] suggest that the participation of the third molecule of en involves only one of the two potential nitrogen donors. For these reasons we does not considered these species quantitatively but simply as a display of axial co-ordination (the link of the spectral data reported with the mentioned single complex molecules does not convince).

As to ammonia complexes, considering the paper of Bjerrum et al. [6] we have: $\lambda_{max} = 640$ nm for $Cu(NH_3)_5^{2+}$ and $\lambda_{max} = 590$ nm for $Cu(NH_3)_4^{2+}$ complex. A red shift of 50 nm results (Table 2). Furthermore, the species $Cu(NH_3)_6^{2+}$ with $\lambda_{max} = 640$ nm is also considered by Bjerrum et al. [6] with an anomalous spectral behaviour, since the sixth ammonia molecules in axial position does not cause further red shift. In addition to the explanations of Bjerrum et al., the species $Cu(NH_3)_6^{2+}$ cannot be used in this context, since it can be obtained only in liquid ammonia. In our previous paper on the relationship between λ_{max} and ε_{max} values [2], we attributed a $\lambda_{max} = 640$ nm to the $Cu(NH_3)_4^{2+}$ complex, which it is very probably due to $Cu(NH_3)_5^{2+}$.

5. Conclusive remarks

Unfortunately, literature is poor of well-characterised copper(II) complexes in aqueous solution, handled with

care for both stability and structural aspects. As well known, if speciation is neglected, structures cannot be surely referred to a single complex species and this can introduce dangerous noise when the structures in solution are discussed. Despite the mentioned severe limitations, an attempt to gain in the knowledge of this topic was pursued, providing an indicative criterion to support a hypothesis of axial co-ordination around the copper(II) ion in aqueous solution. Obviously, features of the ligand(s) involved, as steric hindrance of some donor group and number and dimension of the chelate ring(s), cannot be neglected in a correct structure assessment of a complex in solution.

Pyridine nitrogen and N(3) imidazole nitrogen donor groups, as summarised in Table 2, tend to exhibit values of red shift *per* axial donor group ranging between 31 and 45 nm (the value of 23 nm, found for CuL_2 with L-histidine or τ-methyl-L-histidine, is not considered in this discussion, since it has been obtained by mixed contributions, very probably due to both carboxylate oxygen and imidazole nitrogen).

A wide range of red shift values are observed for the axial displacement of a carboxylate donor group, ranging between 19 nm (L = nitrilotriacetic acid) and 44 nm (L = EDTA).

As for other donor groups listed in Table 2, namely hydroxide, amino (or ammonia) and alcoholate, we can estimate a red shift ranging between 41 nm (donor: amino group) and 58 nm (donor: hydroxide group) *per* axial donor group.

In spite of this attempt to rationalize the visible spectrophotometric results, it appears rather difficult to reach unambiguous identification of the red shift value for an individual donor group. In fact, effects attributable to the overall ligand structure (as those observed in [2]) cannot be excluded, so as the influence of the stability of the chemical bond on the red shift amplitude. Nevertheless, on the basis of all the red shifts handled in this paper, we calculated a mean value of 36 nm *per* axial donor group, while extreme values observed are 19 and 58 nm.

References

[1] E. Prenesti, P.G. Daniele, M. Prencipe, G. Ostacoli, Polyhedron 18 (25) (1999) 3233.
[2] E. Prenesti, P.G. Daniele, S. Toso, Anal. Chim. Acta 459 (2002) 323.
[3] B.N. Figgis, Introduction to Ligand Fields, Wiley–Interscience, New York, 1966.
[4] C.K. Jorgensen, Acta Chem. Scand. 10 (1956) 887.
[5] E.J. Billo, Inorg. Nucl. Chem. Lett. 10 (1974) 613.
[6] J. Bjerrum, C.J. Ballhausen, C.K. Jorgensen, Acta Chem. Scand. 8 (1954) 1275.
[7] C. De Stefano, P. Mineo, C. Rigano, S. Sammartano, Ann. Chim. (Rome) 83 (1993) 243.
[8] A. Sabatini, A. Vacca, personal communication.
[9] G. Arena, R. Calì, E. Rizzarelli, S. Sammartano, Thermochim. Acta 16 (1976) 315.
[10] G. Ostacoli, P.G. Daniele, A. Vanni, Ann. Chim. (Rome) 65 (1975) 197.
[11] R.M. Smith, A.E. Martell, R.J. Motekaitis, NIST Critical Selected Stability Constant of Metal Complexes Databases, Version 6.0, 2001.
[12] C.K. Jorgensen, Acta Chem. Scand. 9 (1955) 1362.
[13] P.G. Daniele, P. Amico, G. Ostacoli, Ann. Chim. (Rome) 74 (1984) 105.
[14] I. Nagypal, A. Gergely, E. Farkas, J. Inorg. Nucl. Chem. 36 (1974) 699.
[15] H. Kinoshita, Y. Yoshino, Scientific Papers of the College of General Education, University of Tokyo, 23(2) (1972) 99.
[16] R.F.C. Claridge, J.J. Kilpatrick, K.J. Powell, Aust. J. Chem. 33 (1980) 2757.
[17] E. Prenesti, P.G. Daniele, V. Zelano, M. Gulmini, Ann. Chim. (Rome) 89 (1999) 1.
[18] P.G. Daniele, C. De Stefano, E. Prenesti, S. Sammartano, Talanta 45 (1997) 425.
[19] V. Romano, J. Bjerrum, Acta Chem. Scand. 24 (1970) 1551.
[20] E.W. Wilson Jr., M.H. Kasperian, R.B. Martin, J. Am. Chem. Soc. 92 (1970) 5365.
[21] H.B. Jonassen, R.E. Reeves, L. Segal, J. Am. Chem. Soc. 77 (1955) 2748.
[22] P.G. Daniele, G. Ostacoli, O. Zerbinati, S. Sammartano, A. De Robertis, Transition Met. Chem. 13 (1988) 87.
[23] J.M. Tsangaris, R.B. Martin, J. Am. Chem. Soc. 92 (1970) 4255.
[24] P.G. Daniele, E. Prenesti, R. Aigotti, G. Ostacoli, J. Inorg. Biochem. 58 (1995) 139.
[25] R.P. Bonomo, F. Bonsignore, E. Conte, G. Impellizzeri, G. Pappalardo, R. Purrello, E. Rizzarelli, J. Chem. Soc., Dalton Trans. (1993) 1295.
[26] P.G. Daniele, E. Prenesti, O. Zerbinati, R. Aigotti, G. Ostacoli, Spectrochim. Acta A 49 (1993) 1373.
[27] B.V. Prelesnik, D.D. Radanovic, Z.D. Tomic, P.T. Djurdjevic, D.J. Radanovic, D.S. Veselinovic, Polyhedron 15 (1996) 3761.

CuO_6 chromophore. It has focused on the analysis of a disorder, noticed in large thermal ellipsoids of the coordinated atoms [5]. An impact of this disorder was correlated to changes in the ground state of the complex.

2. Experimental

All starting compounds and solvents were used as purchased, without any further purification. The title compound, *cis*-[Cu($C_8H_7O_3$)$_2$(H_2O)$_2$], was synthesized as described previously [4].

Diffraction data were collected on a Nonius Kappa CCD diffractometer with graphite monochromated Mo Kα radiation. The data were processed using the DENZO program [11]. The structure was solved by direct methods using SIR97 [12]. We employed full-matrix least-squares refinements on F magnitudes with anisotropic displacement factors for all non-hydrogen atoms using XTAL3.6 [13]. The hydrogen atoms were located from the difference Fourier maps. Their positions together with their isotropic displacement factors were refined using restraints on O—H and C—H distances. Crystal data: $C_{16}H_{18}CuO_8$, M_r = 401.86, monoclinic, a = 7.7401(1) Å, b = 10.4922(2) Å, c = 21.2398(3) Å, β = 95.6277(7)°, V = 1716.58(5) Å^3, T = 115(2) K, space group $P2_1/c$ (No. 14), Z = 4, μ = 1.313 mm^{-1}, crystal size 0.30 × 0.25 × 0.10 mm^3 (plate), 19814 reflections measured (integrated), θ_{max} 27.48°, 3921 unique (R_{int} = 0.031), 3244 observed [$F^2 > 2\sigma(F^2)$], R = 0.031 ($R = \sum(||F_o| - |F_c||)/\sum|F_o|$), wR = 0.026 ($wR = \sum(w||F_o| - |F_c||)/\sum(w|F_o|)$), 298 refined parameters, 3676 reflections.

Spectra of the powdered samples were recorded by a Bruker ESP-300 spectrometer, operating at X-band (9.59 GHz) at variable temperatures.

3. Results and discussion

X-ray data of the title compound *cis*-diaqua-bis(4-formyl-2-methoxyphenolato-*O*:*O*′)copper(II) were collected at 115 K and an analysis reveals two bidentate vanillinate anions (4-formyl-2-methoxyphenolate) and two water molecules in a *cis* orientation around the central copper(II) ion (Fig. 1). The vanillinates are coordinated through methoxy (Cu—O1a 2.151(1), Cu—O1b 2.354(1) Å) and deprotonated hydroxy (Cu—O2a 1.919(1), Cu—O2b 1.914(1) Å) oxygen atoms, while water molecules complete the octahedral coordination sphere (Cu—O1w 2.163(1), Cu—O2w 2.020(1) Å). The methoxy oxygen atoms and the water molecules are in *trans* positions with respect to the copper ion, thus forming two non-symmetrical axes O1a—Cu—O2w and O1b—Cu—O1w. The hydroxy oxygen atoms describe the third axis O2a—Cu—O2b.

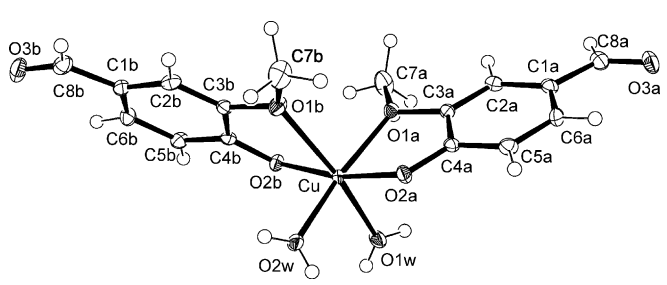

Fig. 1. An ORTEP molecular structure of *cis*-[Cu($C_8H_7O_3$)$_2$(H_2O)$_2$], 115 K [14,15]. Thermal ellipsoids are drawn at the 50% probability level.

The *cis* arrangement of the ligands is found also in the room temperature structure of the title compound. The whole conformation of the complex molecules is very similar in both structures, however at room temperature the complex posses a twofold symmetry axis, which is lost at 115 K (Table 1, Scheme 1) [5]. This is related with two O(methoxy)—Cu—O(water) coordination axes of the same length, and the third shorter O(hydroxy)—Cu—O(hydroxy) axis of the axial coordination sphere in the 293 K structure. Consequently, in spite of a similarity of the packing arrangement and the unit cell parameters, the symmetry of the space group $C2/c$ at room temperature is lowered to its sub-group $P2_1/n$ at 115 K. The unit cell parameters for the 293 and 115 K data, respectively, are: a = 22.0422(3), 23.3084(3) Å; b = 10.6891(2), 10.4922(2) Å; c = 7.6668(1), 7.7401(1) Å; β = 104.8463(8), 114.9252(7)°; V = 1746.08(5), 1716.58(5) Å^3 (The later set of parameters is transformed from that written in Section 2, using the 3 × 3 matrix (−1 0 1 0 1 0 1 0 0) and corresponds to the $P2_1/n$ space group, enabling a more adequate comparison of both structures. Initially, the $P2_1/c$ space group was chosen, since the corresponding β angle 95.6277(7)° is closer to 90° and thus favourable for computations reasons). The unit cell parameters show an anisotropic change, similarly as noticed for the coordination bond distances. It is interesting that the colour of the compound changes reversibly from orange at room temperature to yellow-green at 115 K.

Fig. 2 shows an ORTEP plot of the central coordination sphere of the title complex, determined from the 293 K dataset [5]. It can easily be seen that the thermal ellipsoids of the donor atoms mainly, as well as that of the central copper(II) atom, are large and significantly elongated. In the structure of the same complex measured at 115 K, an electron density distribution of these atoms is much more located (see Fig. 1). Since the thermal ellipsoids of the donor atoms are more perpendicular to the corresponding Cu—O bonds, a static distortion would in theory be suggested (for the dynamic disorder, the ellipsoids should be parallel to the Cu—O bond) [8,9]. However, such a disorder along a metal—ligand bond is not always evident in the visible shape of the thermal ellipsoids of the atoms concerned. Therefore, a more sensitive MSDA (mean-square displacement amplitude) analysis was applied [7,8,14,15]. Certain disordered bonds may show high $\langle d^2 \rangle$ values from the high temperature structure thermal motion data. If they are accompanied with significant reduction of $\langle d^2 \rangle$ for the low temperature data, it should be a proof for the dynamic disorder. Indeed, much higher $\langle d^2 \rangle$ values and their temperature dependence along

Table 1
Selected bond distances (Å), angles (°) and hydrogen-bonding geometry for *cis*-[$Cu(C_8H_7O_3)_2(H_2O)_2$] at two temperatures

293 K [5]		115 K			
Cu—O1	2.2603(12)	Cu—O1a	2.1513(8)	Cu—O1b	2.3541(8)
Cu—O2	1.9086(11)	Cu—O2a	1.9192(8)	Cu—O2b	1.9140(8)
Cu—O1w	2.0869(13)	Cu—O1w	2.1629(8)	Cu—O2w	2.0199(8)
O1—Cu—O1w	169.97(5)	O1a—Cu—O2w	172.08(3)	O1b—Cu—O1w	168.42(3)
O2—Cu—O2′	169.14(7)	O2a—Cu—O2b	168.43(3)		
O1—Cu—O1′	91.09(7)	O1a—Cu—O1b	93.62(3)		
O1w—Cu—O1w′	93.15(9)	O1w—Cu—O2w	91.11(3)		
O1—Cu—O2	77.31(4)	O1a—Cu—O2a	79.32(3)	O1b—Cu—O2b	75.57(3)
O2—Cu—O1′	95.00(5)	O1a—Cu—O2b	93.01(3)	O1b—Cu—O2a	96.12(3)
O1′—Cu—O1w′	88.74(6)	O1a—Cu—O1w	88.35(3)	O1b—Cu—O2w	88.49(3)
O2—Cu—O1w	92.71(6)	O2b—Cu—O2w	94.91(4)	O1w—Cu—O2a	95.45(4)
O2—Cu—O1w′	94.75(6)	O1w—Cu—O2b	92.94(3)	O2a—Cu—O2w	92.87(3)
D—H···A	D···A	D—H···A	D—H···A	D···A	D—H···A
293 K			115 K		
O1w—H11···O2[a]	2.759(2)	166(3)	O1w—H1w1···O3b[c]	2.780(2)	175(2)
			O2w—H1w2···O3a[d]	2.727(2)	174(2)
O1w—H12···O[b]	2.760(2)	168(2)	O1w—H2w1···O2b[e]	2.767(2)	166(2)
			O2w—H2w2···O2a[a]	2.713(2)	167(2)

[a] $-x, 1-y, 1-z$.
[b] $1/2+x, 1/2-y, 1/2+z$.
[c] $x, 3/2-y, 1/2+z$.
[d] $x, 3/2-y, -1/2+z$.
[e] $1-x, 1-y, 1-z$.

the Cu—O(methoxy) than for the other coordination bonds Cu—O(hydroxy) and Cu—O(water) were found (Scheme 1). A comparison with *cis*-diaqua-bis(methoxyacetato)zinc(II) of related geometry (295 K), does not show the same ellipsoid elongation effect of the related atoms [9]. This is in agreement with a Zn(II) d^{10} configuration, where the Jahn–Teller phenomenon is not expected. Altogether this indicates more towards a higher pseudo-Jahn–Teller fluxionality in the title Cu(II)-complex above 180 K, which is gradually frozen out by decreasing temperature (see Fig. 3). Thus, a librational dynamic disorder of the Jahn–Teller distorted axes leads to an equalisation of the determined bond lengths, imitating a higher symmetry in the structure at higher temperature. The herein described disorder may be induced with one type of a ligand (high $\langle d^2 \rangle$ only for Cu—O(methoxy)), but the consequences are certainly evident in both O(methoxy)—Cu—O(water) coordination axes, as a whole.

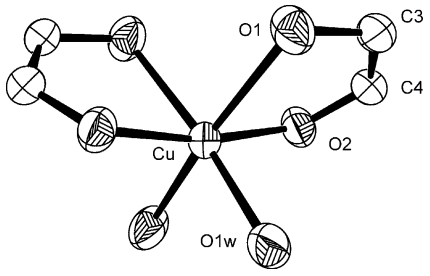

Fig. 2. An ORTEP-plot of the central coordination sphere of the title complex (293 K), showing 50% atomic displacement ellipsoids [5,14,15]. Other atoms are omitted for clarity.

EPR spectra of the *cis*-vanillinate title complex were measured in the temperature range from 298 to 115 K (Fig. 3). The room temperature spectrum shows an inverse axial symmetry pattern with $g_\perp(g_1 \sim g_2) > g_\parallel(g_3) = 2.005(3)$, while the 115 K spectrum shows rhombic symmetry with

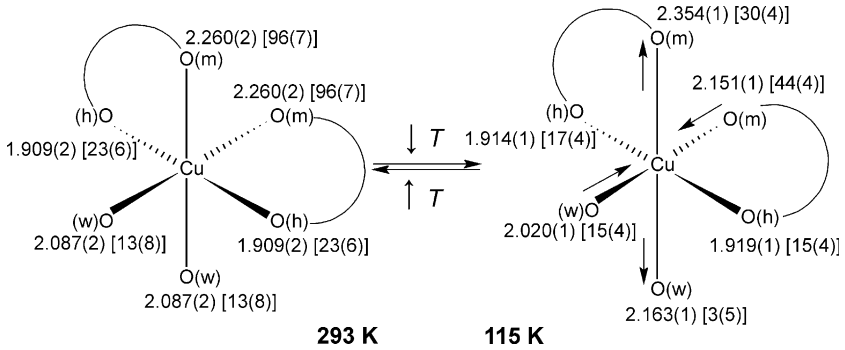

Scheme 1. A temperature induced reversible change of the Cu—O coordination bond distances (Å) in *cis*-[$Cu(C_8H_7O_3)_2(H_2O)_2$] (h – hydroxy, m – methoxy, w – water). Cu—O $\langle d^2 \rangle$ values ($\times 10^4$ Å^2) are in square brackets.

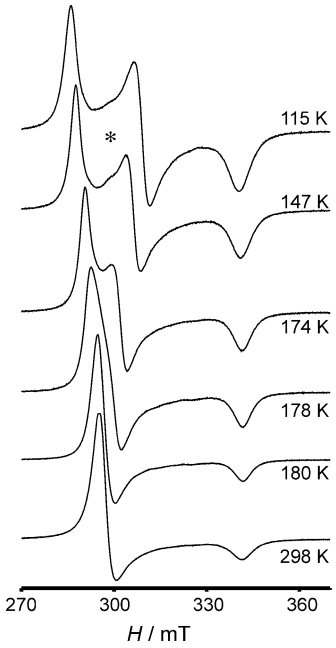

Fig. 3. Splitting of the $g_{1,2}$ signal to g_1 and g_2 in the EPR spectra of *cis*-$[Cu(C_8H_7O_3)_2(H_2O)_2]$, while cooling from 298 to 115 K. An asterisk marks a weak signal between dominant g_1 and g_2 noticed in the low temperature spectra.

$g_1 > g_2 > g_3 = 2.010(3)$ [5]. The g_{12} ($g_\perp$) signal is unchanged in the temperature range from 298 to 180 K, and further decrease of temperature shows its gradual splitting to g_1 and g_2 that probably continues below 115 K. This change between the low and the high temperature spectra is reversible (Scheme 1).

For a more detailed discussion of the complex electronic situation, an assignment of the axes orientation is necessary. In our case, we would orient the coordination system as follows: *x*-axis O1w′—Cu—O1(m), O1w—Cu—O1b(m); *y*-axis O1w—Cu—O1′(m), O2w—Cu—O1a(m); *z*-axis O2(h)—Cu—O2′(h), O2a(h)—Cu—O2b(h) (m – methoxy, h – hydroxy) for the high and the low temperature situation, respectively. Therefore, we have for the two compressed octahedral cases, a tetragonal and a rhombic stereochemistry with short *z*-axis and more or less elongated *x*- and *y*-axes. The resulting orbital splitting diagrams are given in Scheme 2.

Due to the non-equivalence of the six donor sites in the complex, a rhombic distortion of the coordination sphere is expected and the d-energy levels would not posses any degeneracy. However, at room temperature, the dynamic librational disorder of the molecule is fast enough to simulate degeneracy along the *x* and *y*-axes (see Scheme 2). This librational dynamics is fast in the X-ray and EPR timescales showing averaged bond lengths along these axes, and an 'inverse' axial (tetragonal) symmetry found in the X-ray structure analysis and EPR spectra $g_{1,2}(g_\perp) > g_3(g_\parallel, g_Z) \sim g_e$ (pseudo Jahn–Teller distortion). Due to the orbital splitting (see Scheme 2), the high temperature EPR spectrum and the low g_3 value (2.005), a $\{d_{z^2}\}^1$-ground state can be assumed (see Table 2).

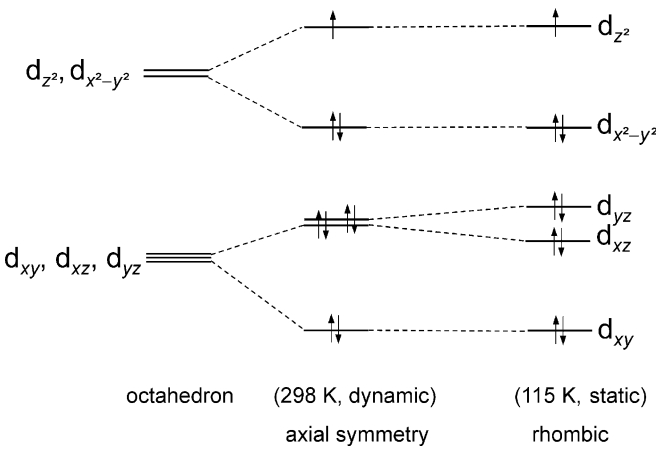

Scheme 2. An orbital splitting diagram of a Jahn–Teller compressed octahedron along the *z*-axis.

By decreasing temperature, the dynamic process will be frozen, thus adopting the true rhombic symmetry of the coordination sphere and splitting all degeneracy of the energy levels. As in the X-ray structure analysis (Scheme 1), this is also clearly observable in the EPR spectra, which are of rhombic symmetry below ~178 K, with $g_1(g_x) > g_2(g_y) > g_3(g_z)$ (see Fig. 3). The $g_3(g_z)$ value is more or less unchanged at different temperatures according to the relatively small changes of the bond distances along the *z*-axis, whereas $g_\perp$ splits into $g_1(g_x) > g_2(g_y)$, due to more static situation in the structure with the expected rhombic symmetry (D_{2h}). Therefore, a $\{d_{x^2-y^2}\}^1$ ground state of the title complex at low temperature might be suggested, but the unchanged signal for $g_3(g_z)$ indicates that the ground states at 293 and 115 K have a similar character. Furthermore, a mixing of the $d_{x^2-y^2}$ and the d_{z^2} orbital cannot be excluded for this symmetry. This can easily lead to miss-assignments of the ground state, especially if the structure is solved only from the room temperature data and no other complementary methods (EPR, UV–Vis, EXAFS, MSDA) with temperature variation are used [7]. Cu(II) complexes with a compressed octahedral symmetry and a $\{d_{z^2}\}^1$ ground state are therefore very rare [7,16–20].

Since the theory with a disorder in such cases is not fully clear-cut, an alternative explanation for related complexes was introduced. Namely, a switch of the ground state

Table 2
Temperature dependence of selected EPR parameters of the vanillinate complex with a CuO_6 chromophore

	298 K	115 K
H_1 (mT)	297.4	286.0
H_2 (mT)	297.4	309.2
H_3 (mT)	341.5	340.6
g_1	2.302	2.393
g_2	2.302	2.214
g_3	2.005	2.010

The estimated errors are $H \pm 0.5$ mT, $g \pm 0.003$.

from a $\{d_{z^2}\}^1$ at 295 K to a $\{d_{x^2-y^2}\}^1$ at 5 K for [Cu(2,6-bis(hydrazonomethyl)pyridine)$_2$](ClO$_4$)$_2$ and [Cu(2,6-bis-(oximomethyl)pyridine)$_2$](ClO$_4$)$_2$ was reported [7,10]. It was suggested that a temperature-dependent switching between two different ground states would be possible, if the distal Cu—ligand bond is inductively weakened, possibly by an electron withdrawing substituent. Through this perspective, the rigid vanillinate ion in *cis*-[Cu(C$_8$H$_7$O$_3$)$_2$-(H$_2$O)$_2$], due to its strong hydroxy coordination that would not allow the methoxy group to coordinate closer, was expected to be interesting for a possible switch. A small signal between g_1 and g_2 (see the low temperature spectra in Fig. 3), observed also in the spectra of the above mentioned two $\{d_{z^2}\}^1$ species [7,10] that was tentatively assigned as a small fraction of fluctional $\{d_{x^2-y^2}\}^1$ Cu(II) spins, could be in favour of the last explanation.

Additionally, it should not be forgotten that the title compound was isolated in a pure form only under specific conditions by quick and careful melting of vanillin, followed by its immediate dissolution in hot acidified Cu^{2+}(aq), since otherwise another isomer (*trans*) predominates [4]. Therefore, a high temperature was crucial during the synthesis, possibly enabling a sterical advantage of the compressed *cis* isomer against the elongated *trans* isomer. Maybe the complex was already formed in the $\{d_{z^2}\}^1$ state, which requires a specific geometry around the Cu(II) ion, later preserved after cooling to room temperature, due to specific conditions with a fixed *cis* coordination enabled by the rigid bidentate ligand with a withdrawing group. The preservation of a very similar conformation and packing of the molecules with a temperature change is seen also in only minor differences in the coordination sphere angles and H-bonding network (Table 1, and as well from a great similarity of the powder diffraction patterns). This would agree with the ligand imposed distortion or packing in the crystal.

4. Concluding remarks

X-ray structure analysis of *cis*-[Cu(C$_8$H$_7$O$_3$)$_2$(H$_2$O)$_2$] at 115 K reveals a *cis* coordination of vanillinate ions and water molecules, with three rhombic coordination axes. The distances and the symmetry of the coordination sphere differ importantly from the room temperature molecular structure, where compressed axial axes were determined. The MSDA thermal ellipsoid analysis confirms the vibrational disorder in the structure at high temperature, and its gradual freezing by decreasing temperature. These results are fully in agreement with the EPR spectra, showing also the reversibility of this change. Based on the EPR data, a $\{d_{z^2}\}^1$ ground state is proposed, although the room temperature spectrum suggests a 'normal' $\{d_{x^2-y^2}\}^1$ ground state, but with a small g_3 value (close to g_e). A careful analysis of the data in such cases is recommended.

Acknowledgements

The financial support of the MVZT P-6209, P1-0175 and X-2000, Republic of Slovenia, is gratefully acknowledged. We thank Dr. M. Šentjurc, EPR center, 'Jožef Stefan' Institute, Ljubljana, for EPR spectra.

Appendix A. Supplementary data

All atom parameters and other crystallographic data have been deposited with the Cambridge Crystallographic Data Center as supplementary material with the deposition number CCDC 296921. Copies of this information may be obtained free of charge from the Director, CCDC, 12 Union Road, Cambridge CB2 1EZ, UK (fax: +44 1223 336033; e-mail: deposit@ccdc.cam.ac.uk or http://www.ccdc.cam.ac.uk/conts/retrieving.html). Supplementary data associated with this article can be found, in the online version, at doi:10.1016/j.poly.2006.04.009.

References

[1] M. Petrič, F. Pohleven, I. Turel, P. Šegedin, A.J.P. White, D.J. Williams, Polyhedron 17 (1998) 255.
[2] M. Petrič, M. Pavlič, F. Pohleven, P. Šegedin, B. Kozlevčar, S. Polanc, B. Štefane, R. Lenaršič, Internat. Res. Group Wood Preserv., IRG/WP 99-30198, 1999.
[3] B. Kozlevčar, N. Lah, I. Leban, I. Turel, P. Šegedin, M. Petrič, F. Pohleven, A.J.P. White, D.J. Williams, G. Giester, Croat. Chem. Acta 72 (1999) 427.
[4] B. Kozlevčar, B. Mušič, N. Lah, I. Leban, P. Šegedin, Acta Chim. Slov. 52 (2005) 40.
[5] B. Kozlevčar, M. Humar, P. Strauch, I. Leban, Z. Naturforsch. 60b (2005) 1273.
[6] B. Kozlevčar, D. Odlazek, A. Golobič, A. Pevec, P. Strauch, P. Šegedin, Polyhedron 25 (2006) 1161.
[7] M.A. Halcrow, J. Chem. Soc., Dalton Trans. (2003) 4375.
[8] L.R. Falvello, J. Chem. Soc., Dalton Trans. (1997) 4463.
[9] K. Prout, A. Edwards, V. Mtetwa, J. Murray, J.F. Saunders, F.J.C. Rossotti, Inorg. Chem. 36 (1997) 2820.
[10] M.A. Halcrow, C.A. Kilner, J. Wolowska, E.J.L. McInnes, A.J. Bridgeman, New J. Chem. 28 (2004) 228.
[11] Z. Otwinowski, W. Minor, Methods Enzymol. 276 (1997) 307.
[12] A. Altomare, M.C. Burla, M. Camalli, G. Cascarano, C. Giacovazzo, A. Guagliardi, A.G.G. Moliterni, G. Polidori, R. Spagna, J. Appl. Cryst. 32 (1999) 115.
[13] S.R. Hall, D.J. du Boulay, R. Olthof-Hazekamp (Eds.), XTAL3.6 System, University of Western Australia, 1999.
[14] A.L. Spek, PLATON, University of Utrecht, The Netherlands, 2003.
[15] L.J. Farrugia, J. Appl. Cryst. 30 (1997) 565.
[16] G. Wingefeld, R. Hoppe, Z. Anorg. Allg. Chem. 516 (1984) 223.
[17] J.M. Holland, X. Liu, J.P. Zhao, F.E. Mabbs, C.A. Kilner, M. Thornton-Pett, M.A. Halcrow, J. Chem. Soc., Dalton Trans. (2000) 3316.
[18] Z. Mazej, I. Arčon, P. Benkič, A. Kodre, A. Tressaud, Chem. Eur. J. 10 (2004) 5052.
[19] N.K. Solanki, E.J.L. McInnes, F.E. Mabbs, S. Radojević, M. McPartlin, N. Feeder, J.E. Davies, M.A. Halcrow, Angew. Chem. Int. Ed. 37 (1998) 2221.
[20] I. Persson, P. Persson, M. Sandström, A.-S. Ullström, J. Chem. Soc., Dalton Trans. (2002) 1256.

(py) and on the basis of IR spectral data, suggested that the barbiturate ligands are coordinated to copper(II) through an oxygen atom. However, X-ray structures of $[M^{II}(barb)_2(im)_2]$ (M^{II} = Co and Zn; im = imidazole) [6], $[Ni(isoamylbarb)_2(im)_2]$ [7], $[Cu(barb)_2(py)_2]$ [8], $[Cu(barb)_2(pic)_2]\cdot 2H_2O$ [9] and $[Zn(barb)_2(pic)_2]$ (pic = picoline) [10] showed that in all these complexes, the barbital moiety is deprotonated and the donor site of the barbiturate anion is the deprotonated N atom. On the other hand, it was recently reported that in $[Cu(C_4N_2H_3)_2(H_2O)_3]$ [11], the barbiturate ligands were found to be O-coordinated. Furthermore, in the case of platinum metals, 1,3-dimethybarbiturate (dmbarb) exhibited linkage isomerism. For example, in $[Pd(en)_2(dmbarb)_2]\cdot 5.5H_2O$ [12] and $[Pt(en)_2(dmbarb)_2]$ (en = ethylenediamine) [13], one barbiturate ligand coordinates at the deprotonated carbon atom and the other at a deprotonated enol oxygen, while both barbiturate ligands in $[Pt(en)_2(dmbarb)_2]\cdot 2H_2O$ [13] are C-bonded.

The presence of several potential donor atoms such as two amine nitrogen atoms and three carbonyl oxygen atoms makes barbiturates very interesting and polyfunctional ligands in coordination chemistry. They have often been used as building blocks in ordered organic supramolecular assemblies with specific and directional hydrogen bonds [14–18], and they also seem to be capable of bridging metal centres to form polymeric structures. However, a literature survey indicates that metal complexes of barbiturates are rare. Recently, we have reported the synthesis, thermal, spectral and structural characterization of two new copper and cadmium complexes of barb with en, namely *cis*-$[Cu(barb)_2(en)]$ [19] and $\{[Cd(barb)_2(\mu\text{-}en)]\cdot 2H_2O\}_n$ [19]. The barb ligand in both complexes acts as a bidentate chelating ligand via the negatively charged imino N atom and one of the carbonyl O atoms adjacent to the imino N atom. In the case of zinc, $[Zn(barb)_2(en)]$ and $[Zn(barb)_2(bpy)]\cdot H_2O$ (bpy = 2,2′-bipyridine) complexes were obtained [20], and both barb ligands in $[Zn(barb)_2(en)]$ are N-bonded. It was shown that the barbiturate coordination modes depend on the nature of the barbiturate anion (Scheme 1). This has prompted us to study the Ag^I-barb system to probe the coordination modes of barb with silver(I) in the solid state, and herein we report the syntheses, crystal structures, thermal behaviors and spectroscopic properties of three novel Ag^I-barb frameworks containing en and *trans*-1,2-bis-(4-pyridyl)ethylene (bpe), namely $Na_3[Ag_3(\mu\text{-}barb)_6]$ (**1**), $\{[Ag_2(\mu\text{-}barb)_2][Ag_2(\mu\text{-}en)_2]\cdot 5H_2O\}_n$ (**2**) and $[Ag(barb)(\mu\text{-}bpe)]_n$ (**3**). The structures of the complexes were determined by single-crystal X-ray diffraction and also supported by IR, ^1H NMR and thermal decomposition studies. The antimicrobial activity of the ligands and complexes was also studied.

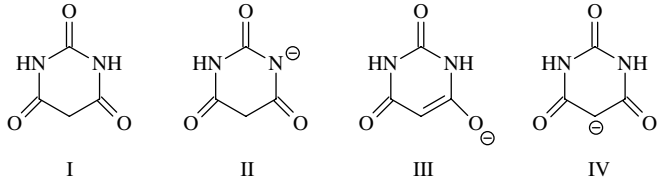

Scheme 1. Barbiturate and its anions.

2. Experimental

2.1. Materials and measurements

All commercial reagents were used as supplied. Elemental analyses for C, H, and N were performed using a Carlo Erba 1106 microanalyser. IR spectra were recorded with a Jasco FTIR-430 spectrophotometer with samples as KBr pellets in the 4000–400 cm^{-1} range. ^1H NMR spectra were recorded at room temperature (298 K) with a Bruker AC200 spectrometer. Thermal analysis curves (TG and DTA) were obtained using a Rigaku TG8110 thermal analyzer in a static air atmosphere with a heating rate of 10 °C min^{-1} and a sample size of 5–10 mg.

2.2. Preparation of $Na_3[Ag_3(\mu\text{-}barb)_6]$ (1)

A solution of $AgNO_3$ (0.34 g, 2 mmol) in distilled water (10 mL) was mixed with a solution of Nabarb (5,5-diethylbarbituric acid sodium salt) (0.41 g, 2 mmol) in distilled water (10 mL) with continuous stirring at room temperature. The solution immediately became milky. The addition of *N*-(2-hydroxyethyl)ethylenediamine (0.21 mL) together with 10 mL of 2-propanol to the milky suspension resulted in a clear solution. The resulting solution was allowed to stand in darkness at room temperature and colorless prisms of **1** were obtained after 3 days. Yield 72%. *Anal.* Calc. for $C_{48}H_{66}N_{12}O_{18}Ag_3Na_3$: C, 38.65; H, 4.46; N, 11.27. Found: C, 38.53; H, 4.59; N, 11.39%. IR (solid KBr pellet): ν (cm^{-1}) 3184 sb, 3058 vw, 2970 vw, 1697 vs, 1666 vs, 1558 vs, 1464 s, 1411 s, 1376 s, 1311 vs, 1265 vs, 1043 m, 937 m, 841 vs, 793 m, 752 m, 652 m, 522 m, 476 m, 443 m. ^1H NMR (200 MHz, [D6]DMSO, 25 °C): $\delta = 0.69$ (t, 3H, CH_3), 1.75 (q, 2H, CH_2), 10.66 (s, H, NH) ppm.

2.3. Preparation of $\{[Ag_2(\mu\text{-}barb)_2][Ag_2(\mu\text{-}en)_2]\cdot 5H_2O\}_n$ (2)

The preparation method of **2** was the same as described for **1** with ethylenediamine (en) replacing *N*-(2-hydroxyethyl)ethylenediamine. The colorless crystals were obtained after 2 days. Yield 56%. *Anal.* Calc. for $C_{20}H_{46}N_8O_{11}Ag_4$: C, 23.87; H, 4.61; N, 11.13. Found: C, 23.73; H, 4.52; N, 11.25%. IR (solid KBr pellet): ν (cm^{-1}) 3197 sb, 3088 vw, 2973 w, 1676 sh, 1615 vs, 1431 vs, 1337 vs, 1258 s, 1013 s, 951 w, 829 m, 768 m, 543 m, 451 m, 420 w. ^1H NMR (200 MHz, [D6]DMSO, 25 °C): $\delta = 0.65$ (t, 3H, CH_3), 1.72 (q, 2H, CH_2), 2.80 (s, 2H, $\underline{CH_2}$–NH_2), 3.37 (s, H, NH_2) ppm.

2.4. Preparation of [Ag(barb)(μ-bpe)]$_n$ (3)

Compound **3** was synthesized in a similar manner to **2** except that *trans*-1,2-bis(4-pyridyl)ethylene (bpe) was used instead of en. Colorless crystals suitable for X-ray were formed by slow evaporation of the resulting solution in darkness at room temperature after a few days. Yield 87%. *Anal.* Calc. for $C_{20}H_{21}N_4O_3Ag$: C, 50.74; H, 4.47; N, 11.84. Found: C, 50.85; H, 4.57; N, 11.72%. IR (solid KBr pellet): ν (cm^{-1}) 3170 sb, 2979 w, 1677 vs, 1584 vs, 1414 vs, 1347 vs, 1275 sh, 987 s, 837 s, 760 m, 554 s, 452 m, 410 w. ^1H NMR (200 MHz, [D6]DMSO, 25 °C): $\delta = 0.69$ (t, 3H, CH_3), 1.75 (q, 2H, CH_2), 7.57 (s, H, CH=CH), 7.63 (dd, 2H, py ring), 8.62 (dd, 2H, py ring), 10.65 (s, H, NH) ppm.

2.5. Antimicrobial testing

For antimicrobial activities, the compounds were tested against standard strains of Gram-negative *Escherichia coli* MC4100 and *Pseudomonas aeruginosa* ATCC27853, Gram-positive *Bacillus subtilis* and *Staphylococcus aureus* ATCC 43300, and two yeasts *Candida albicans* ATCC 10231 and *C. parapsilosis* ATCC 22019. Antimicrobial activity tests were carried out using the broth dilution method. For the broth dilution method, cultures were started inoculating a single colony from a freshly grown culture on nutrient broth agar (Acumedia) and grown overnight in nutrient broth (Acumedia) at 37 °C for 18 h in an orbital shaker incubator (GLF, Germany) shaking at 200 rpm. These cultures were used as starter cultures. Approximately, 10^6 cells from starter cultures were inoculated in 5 ml nutrient broth media. For *Candida* strains cultures were initially grown on PDA plates (Merck) 37 °C for 48 h and used for inoculation in fresh nutrient broth medium. The inoculum amount was same as that of bacterial strains. All the test cultures were grown at 37 °C in the shaker incubator. The incubation period was 24 h for bacterial strains and 48 h for fungal strains. Nutrient broth containing test tubes first supplemented with various amounts of each compound, made serial dilutions in nutrient broth from 100 to 0.1 μg/ml. The compounds were first tested in 10-fold serial dilution; eventually the ranges were narrowed to define more exact values. The minimum inhibitor concentration, at which no growth was observed, was taken as the MIC value (μg/ml), and represents the mean of at least three determinations. Ampicillin (Applichem) was used as a reference inhibitor for bacterial strains and nystatin (BDH) for fungal strains. For comparison, $AgNO_3$ was tested for MIC values. All the ligands and the solvents used were also tested for antimicrobial activity.

2.6. X-ray crystallography

The intensity data of the complexes **1**–**3** were collected using a STOE IPDS 2 diffractometer with graphite-monochromated Mo Kα radiation ($\lambda = 0.71073$). Complexes **1** and **2** were measured at 100 K, while complex **3** was measured at 293 K. The structures were solved by direct methods and refined on F^2 with the SHELXL-97 program [21]. All non-hydrogen atoms were found from the difference Fourier map and refined anisotropically. All hydrogen atoms

Table 1
Crystallographic data and structure refinement for **1**–**3**

	1	**2**	**3**
Empirical formula	$C_{48}H_{66}N_{12}O_{18}Ag_3Na_3$	$C_{20}H_{46}N_8O_{11}Ag_4$	$C_{20}H_{21}N_4O_3Ag$
Formula mass	1491.71	1006.13	473.28
Crystal system	monoclinic	triclinic	monoclinic
Space group	*C*2/*c*	*P*1	$P2_1/c$
a (Å)	12.8963(6)	7.9379(6)	7.6546(6)
b (Å)	13.7160(6)	10.3408(8)	20.9540(17)
c (Å)	33.0661(14)	10.5210(8)	14.0053(12)
α (°)	90.00	101.660(6)	90.00
β (°)	98.211(3)	96.451(6)	118.072(5)
γ (°)	90.00	102.091(6)	90.00
V (Å^3)	5789.0(4)	816.16(11)	1982.1(3)
Z	4	1	4
D_{calc} (g/cm^3)	1.712	2.047	1.586
μ (mm^{-1})	1.108	2.428	1.045
F(000)	3024	498	960
Crystal size (mm^3)	0.38 × 0.27 × 0.14	0.36 × 0.27 × 0.24	0.20 × 0.16 × 0.08
θ Range (°)	2.18–25.03	2.00–27.81	1.91–26.00
Index range (*h*,*k*,*l*)	−15/15, −16/16, −39/39	−10/10, −13/13, −13/13	−9/9, −25/25, −17/15
Reflections collected	31400	13058	23617
Independent reflections	5098 ($R_{int} = 0.159$)	7134 ($R_{int} = 0.066$)	3094 ($R_{int} = 0.163$)
Absorption correction	numerical	numerical	numerical
Data/parameters	5098/380	7134/394	3094/253
Goodness-of-fit on F^2	1.102	0.858	0.992
Final *R* indices [$I > 2\sigma(I)$]	0.0528	0.0235	0.0599
$\Delta\rho_{max/min}$ (e Å^{-3})	1.188/−1.096	0.917/−1.142	1.086/−0.651

were included using a riding model. The details of data collection, refinement and crystallographic data are summarized in Table 1.

3. Results and discussion

3.1. Synthetic aspects

Silver complexes **1**–**3** were obtained by the direct reaction of sodium barbital with $AgNO_3$ in the presence of the co-ligands. Initially, we aimed to prepare mixed-ligand silver(I)-barb complexes with some diamine ligands such as *N*-(2-hydroxyethyl)ethylenediamine (heen), en and bpe. However, in the case of heen, the desired silver(I) complex could not be prepared since the coordination of the ligand seemed to be unsuccessful in the present conditions. Instead, a new anionic complex, $Na_3[Ag_3(\mu\text{-barb})_6]$ (**1**), was obtained. The direct synthesis of **1** from sodium barbital and $AgNO_3$ in the absence of heen was attempted, but the reaction resulted in the rapid precipitation of a polycrystalline powder, presumably $[Ag(barb)]_n$ which is barely soluble in known solvents.

Complexes **1**–**3** are air stable and do not exhibit a melting point, but decompose at 310, 36 and 232 °C, respectively. They were obtained in reasonably high yields (over 55%). The analytical data are consistent with the proposed formulation of the complexes. All three complexes are highly soluble in a 4:1 mixture of water and 2-propanol, and slightly soluble in pure water and common alcohols such as methanol, ethanol and 2-propanol.

3.2. IR and ^1H NMR spectra

The IR spectra (KBr disks) of complexes **1**–**3** were recorded in KBr in the 4000–400 cm^{-1} range. For comparative purposes the IR spectra of the free ligands were also obtained. The complexes display the characteristic bands of the ligands, somewhat modified by coordination. The strong and broad absorption bands at 3170–3197 cm^{-1} in the spectra of the complexes indicate the presence of the NH groups. The relatively weak bands in the 2970–3080 cm^{-1} range are attributed to the C–H stretching vibrations. The sharp absorption bands in the frequency range 1560–1700 cm^{-1} characterize vibrations of the carbonyl groups. The barb ligand exists in the triketo form and all carbonyl groups interact with sodium(I) in Na(barb) [3]. As will be discussed later, similar interactions of the carbonyl groups with the sodium(I) ion were observed in **1** and, therefore, the IR spectra of Na(barb) and **1** both possess two sharp bands at 1697 and 1666 cm^{-1}, in accord with the presence of two different carbonyl groups. Two types of strong absorption bands of the carbonyl group were also observed at 1676 and 1615 cm^{-1} for **2**, whereas only a single band was found at 1677 cm^{-1} in the spectrum of **3**. In **2** and **3**, carbonyl groups do not participate in coordination and the apparent red-shifts may be associated with strong hydrogen bonding. The strong bands at 1584 and 1558 cm^{-1} in the spectra of **1** and **3**, respectively, are due to N–H deformation vibrations of the barb ligand. The absence of this band in the spectrum of **2** clearly suggests the complete deprotonation of both amine groups. These conclusions are supported by the results of X-ray diffraction studies. The bands with strong intensity between 1464 and 1311 cm^{-1} correspond to the C–H deformation vibrations and the band centered around 1265 cm^{-1} is attributed to the C–N stretching vibrations [5]. The weak or medium intensity bands in the region 455–410 cm^{-1} can be assigned to the Ag–N stretching vibration.

The ^1H NMR spectra of complex **1** show all expected resonances of the barb moiety. The signal at 10.66 ppm was assigned to the NH proton of barb and was shifted to downfield by about 1 ppm, compared to Na(barb). The NH proton appears as a sharp band in DMSO and is absent in the spectra of complex **2**, confirming deprotonation of the barb monoanion to a dianion, also proposed above from its IR spectra. In the NMR spectra of **2**, signals at 2.80 and 3.37 ppm correspond to the CH_2–NH_2 and NH_2 groups, respectively, and are shifted upfield compared to those of free en; this is quite similar to findings reported for platinum complexes with en derivatives [22]. The protons of the water molecules appear as a broad band centered at 3.65 ppm. For complex **3**, the ^1H NMR spectra are similar to that of complex **1**, the only differences arising from the py rings of the bpe ligand. The spectra show that the chemical shifts of the protons of the py ring exhibit two sets of signal at 7.64 ppm, as a doublet, and 8.62 ppm, also as a doublet. Moreover, the protons of the ethylene moiety appear at 7.57 ppm as a singlet.

3.3. Thermal studies

To study the thermal decomposition behaviors and thermal stabilizes of complexes **1**–**3**, thermogravimetric (TG) and differential thermal analyses (DTA) of the compounds were performed in an atmosphere of air in the temperature range 20–900 °C. The final decomposition residues were identified by elemental analysis and also confirmed by mass loss calculations. Complex **1** shows a very high thermal stability and begins to decompose at 309 °C. Its thermal stability is comparable to $Na[Ag(sac)_2]$ (sac = saccharinate) [23]. The degradation of the barb moiety is completed in a single step with a continuous mass loss in the TG curve between 309 and 450 °C, and the DTA curve presents an endothermic peak at 330 °C and three highly exothermic peaks at 377, 398 and 439 °C, giving a final decomposition product containing silver, sodium and oxygen.

Complex **2** shows a two-step decomposition process and in the first step, it starts to lose water molecules between 36 and 198 °C with a mass loss of 8.57% (calc. 8.94%). The initial temperature of dehydration is relatively low and suggests that the water molecules are uncoordinated. In the second step, the anhydrous compound begins to decompose at 204 °C with a continuous mass loss and due to

overlapping decomposition processes of both en and barb ligands it is impossible to calculate mass loss values for the elimination of each ligand. However, the overall mass loss of the second step is 49.05% (calc. 48.11%). The end product at 398 °C was presumably silver oxide.

Complex **3** is thermally stable up to 232 °C, a significantly lower temperature than that of **1**. It shows a continuous decomposition in the temperature range 232–381 °C. The endothermic peak at 309 °C corresponds to the decomposition of the bpe ligands, while the violently exothermic peak at 356 °C characterizes the decomposition of the barb ligands. The total weight loss value of 74.46% is in agreement with the calculated value 75.52%. The end decomposition product was suggested to be silver oxide.

3.4. Description of the structures

3.4.1. $Na_3[Ag_3(\mu\text{-barb})_6]$ (1)

The asymmetric unit of **1** is shown in Fig. 1 and selected bond lengths and angles are listed in Table 2. Complex **1** is a coordination polymer, in which the barb anions simultaneously bridge the silver and sodium cations giving rise to a 3D network. The structure of **1** contains two different silver and Na atoms, as depicted in Fig. 1. Both silver(I) ions are linearly coordinated by the negatively charged N atoms of the two barbital ions. In contrast to atom Ag1, atom Ag2 is coordinated a barb ligand and its symmetry-equivalent partner. All Ag–N bond distances are almost identical, resulting in an average value of 2.075(4) Å. The barb anions act as a bridge between the sodium(I) cations through their carbonyl groups. The coordination mode of the three distinct barb ligands in **1** differs: ligands barb1 and barb2 with atoms N1, and N3, respectively, behave as tridentate ligands through a N and two carbonyl O atoms, while ligand barb3 with atom N5 acts as a bidentate bridging ligand via one of the carbonyl O and a N atom. To the best of our knowledge, the simultaneous presence of two coordination modes of the barb ligand has not been reported until now.

Table 2
Selected bond lengths (Å) and angles (°) for **1**[a]

Ag1–N1	2.078(4)	O6–Na1–O1	116.28(14)
Ag1–N3	2.075(4)	O6–Na1–O1^{iv}	73.61(13)
Ag2–N5	2.073(4)	O6–Na1–O6^{iv}	91.14(14)
Na1–O1	2.630(3)	O6–Na1–O5^{vi}	95.73(16)
Na1–O5^{i}	2.455(4)	O5^{v}–Na1–O1	87.88(12)
Na1–O6	2.376(4)	O5^{v}–Na1–O1^{vi}	82.60(12)
Na2–O2^{i}	2.459(4)	O5^{v}–Na1–O5^{vi}	87.39(16)
Na2–O3	2.370(4)	O5^{v}–Na1– O6^{iv}	95.73(16)
Na2–O4	2.679(4)	O4–Na2–O7	171.97(16)
Na2–O7	2.700(4)	O3–Na2–O2^{i}	161.36(15)
Na2–O8^{ii}	2.467(5)	O9^{iii}–Na2–O8^{ii}	160.67(16)
Na2–O9^{iii}	2.333(5)	O2^{i}–Na2–O8^{ii}	85.36(16)
Ag1–Na1	3.537(2)	O3–Na2–O8^{ii}	94.79(16)
Ag1–Na2	3.651(2)	O8^{ii}–Na2–O4	88.96(15)
Ag2–Na2	3.638(2)	O8^{ii}–Na2–O7	86.53(13)
N1–Ag1–N3	179.44(17)	O9^{iii}–Na2–O2^{i}	91.50(16)
N5–Ag2– N5^{iii}	180.00(17)	O9^{iii}–Na2–O3	94.20(18)
O1–Na1–O1^{iv}	166.84(12)	O9^{iii}–Na2–O4	71.81(15)
O6–Na1–O5^{v}	155.84(12)	O9^{iii}–Na2–O7	112.30(15)
O6^{iv}–Na1–O5^{vi}	155.84(13)		

H-bonds	N···O (Å)	N–H···O (°)
N2–H2···O4^{v}	2.817(6)	155
N4–H4···O1^{i}	2.802(6)	164
N6–H6···O7^{ii}	2.778(6)	179

[a] Symmetry operations: (i) $1/2+x,1/2+y,z$; (ii) $1-x,1-y,1-z$; (iii) $3/2-x,1/2-y,1-z$; (iv) $1-x,y,1/2-z$; (v) $x-1/2,y-1/2,z$; (vi) $3/2-x,y-1/2,1/2-z$.

In contrast to the tetrahedrally coordinated sodium(I) ions in Nabarb [3], in **1** both sodium(I) ions are octahedrally coordinated by the carbonyl O atoms from six different barb ligands with Na–O bond distances ranging from 2.333(5) to 2.700(4) Å and *cis*-O–Na–O bond angles ranging between 71.81(15) and 112.30(15), as listed in Table 2. The Na–O bond distances were found to be

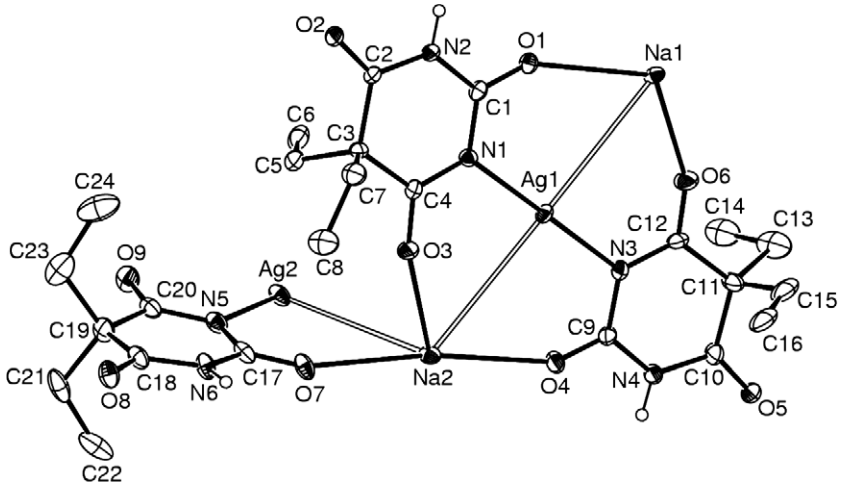

Fig. 1. View of the asymmetric unit of **1**, showing coordination environments of silver and sodium atoms (30% probability thermal ellipsoids; C–H hydrogen atoms were omitted for clarity).

significantly longer than those reported for Nabarb [3]. Since the total van der Waals radii of sodium and silver ($r_{Na} = 2.27$ Å and $r_{Ag} = 1.72$ Å) is 3.99 Å, the Ag···Na separations of 3.537(2), 3.651(2) and 3.638(2) Å may indicate a kind of 'metallophilic' interactions between silver(I) and sodium(I) ions. The minimum Ag···Ag and Na···Na distances are 5.733 and 7.188 Å, respectively.

The pyrimidine rings in the three barb ligands are essentially planar and the three carbonyl groups are not significantly displaced from the mean planes of their attached pyrimidine ring. The dihedral angle between the barb1 and barb2 mean planes is 5.90(18)°, indicating the co-planarity of these barb ligands. Conformation, bond lengths and angles of the barb ligands in **1** are similar to those of the barb ion [3,4]. The two ethyl groups in barb2 are disordered over two positions with approximately equal occupancy. Fig. 2 shows the packing of anionic $[Ag(barb)_2]$ units in the absence of sodium(I) ions. $[Ag(barb)_2]$ units are linked by N–H···O hydrogen bonds generating a 2D supramolecular framework and the sodium(I) cations further connect these layers to a 3D network (Fig. 2).

3.4.2. $\{[Ag_2(\mu\text{-}barb)_2][Ag_2(\mu\text{-}en)_2]\cdot 5H_2O\}_n$ (2)

The asymmetric unit of complex **2** is shown in Fig. 3, and Table 3 lists selected bond length and angles together with the hydrogen bonding geometry. The asymmetric unit contains four crystallographically unique Ag atoms, each having a significantly different environment. As shown in

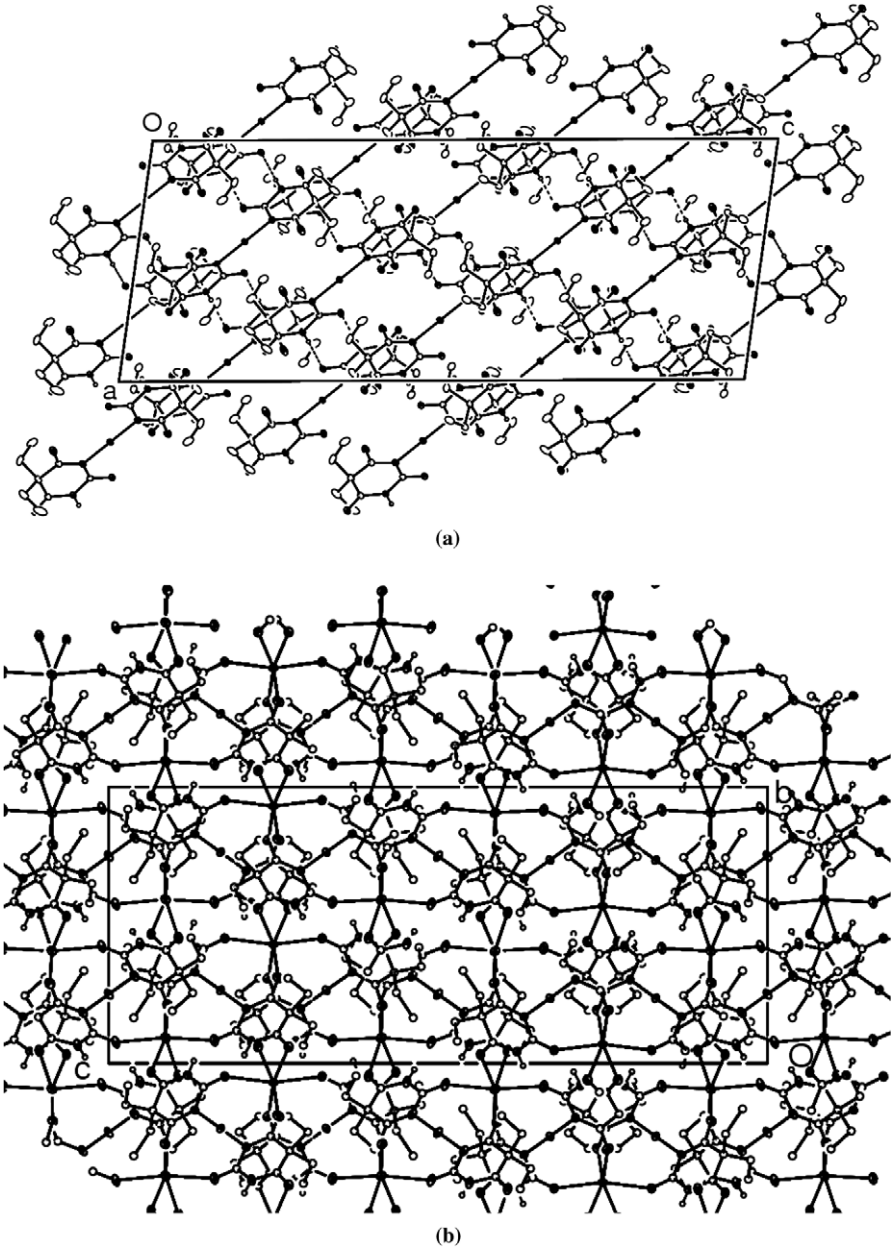

Fig. 2. (a) Interaction of $[Ag(barb)_2]$ units in **1** via hydrogen bonds (Na and C–H hydrogen atoms were omitted for clarity). (b) View of the crystal packing of **1**, viewed along the *a* axis.

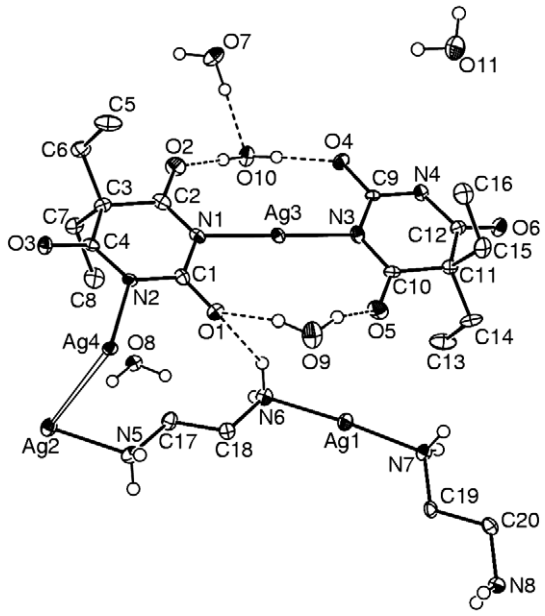

Fig. 3. View of the asymmetric unit of **2**, showing coordination environments of silver atoms (30% probability thermal ellipsoids; C–H hydrogen atoms were omitted for clarity).

Fig. 4, complex **2** consists of two different chains: an anionic 1D linear chain with [Ag(μ-barb)] units and a cationic 1D zig-zag chain containing [Ag(μ-en)] units. These anionic and cationic chains are interconnected by way of Ag···Ag interactions to form an unusual 2D framework, in which the chains interact each other leading to a rectangle-grid motif with dimensions of 17.04×34.55 Å^2 (Fig. 4). In complex **2**, the barb ligand is further deprotonated to form a dianion, which acts as a bidentate bridging ligand via both negatively charged N atoms. Again, to the best of our knowledge, this is the first example of a barb dianion coordinating to a metal ion, and the *N*,*N*′-bridging coordination mode of the ligand has also been observed for the first time in this work. As a result, Scheme 1 should be extended to include the new anionic form of barb.

In both anionic and cationic units, each Ag^I center has a slightly distorted linear $\{AgN_2\}$ coordination geometry. The average Ag–N_{en} bond distance of 2.13(5) Å is similar to that observed in $[Ag_2(sac)_2(en)(H_2O)]_n$ [24], but is noticeably longer than the Ag–N_{barb} bond distances in **2**. The silver atoms appear to be interacting based on the Ag–Ag distances of 3.236(1) and 3.404(1) Å, which are significantly shorter than twice the van der Waals radius of silver (3.44 Å) and clearly indicate a bonding interaction as observed in $[Ag_2(sac)_2(en)(H_2O)]_n$ [24]. The intra-chain Ag–Ag distances are 5.827(5) and 7.449(4) Å in the anionic and cationic chains. Ag···Ag interactions have been a subject of discussion: Jansen [25] suggested a upper limit value of 3.30 Å for an Ag···Ag contact in silver(I) coordination compounds, but Dance et al. [26] argued that since the linear geometry around silver(I) indicates the fulfillment of its coordination requirements, there is no bonding interaction between silver(I) centers as close to each other as 2.886 Å in $[Ag(SCMeEt)_2]_n$. However, although the closed d^{10} configuration of silver(I) appears to cancel any intermetallic bonding in silver(I) complexes, there are many examples of silver(I) complexes with definite Ag···Ag attractive forces known as 'argentophilic' interactions [27].

Both barb ligands are almost planar, but the C atoms bearing the two ethyl groups deviate from the mean plane by 0.2 Å. The barb rings are co-planar with a dihedral angle of 3.98(15)°. The torsion angle of 178.6(7)° suggests that the non-hydrogen atoms of en lie in the same plane. Complex **2** exhibits a number of intra- and intermolecular N–H···O and O–H···O hydrogen bonds as listed in Table 3. The amine hydrogen atoms of en participate in

Table 3
Selected bond lengths (Å) and angles (°) for **2**[a]

Ag1–N6	2.138(5)		Ag4–N4^{ii}	2.085(6)	
Ag1–N7	2.122(5)		Ag1–Ag4^{iii}	3.236(1)	
Ag2–N5	2.157(5)		Ag2–Ag4	3.404(1)	
Ag2–N8^{i}	2.156(5)		N6–Ag1–N7	175.0(3)	
Ag3–N1	2.081(5)		N5–Ag2–N8^{i}	177.3(2)	
Ag3–N3	2.081(5)		N3–Ag3–N1	179.7(3)	
Ag4–N2	2.097(6)		N2–Ag4–N4^{ii}	178.9(3)	
H–bonds	O···N (Å)	N–H···O (°)		O···O (Å)	O–H···O (°)
N5–H1···O6^{ii}	3.282(7)	173	O7–H9···O10	2.775(6)	179
N5–H2···O4^{iv}	3.206(7)	135	O7–H10···O11^{viii}	2.818(6)	180
N6–H3···O1	3.049(7)	140	O8–H11···O3^{iii}	2.775(5)	180
N6–H4···O3^{iii}	3.043(7)	176	O8–H12···O7^{iv}	2.821(5)	179
N7–H5···O9^{iii}	3.213(8)	153	O9–H13···O1	2.689(7)	165
N7–H6···O8^{v}	2.896(7)	164	O9–H14···O5	2.836(8)	153
N8–H7···O11^{vi}	3.116(7)	132	O10–H15···O4	2.704(7)	176
N8–H8···O10^{vii}	3.000(7)	156	O10–H16···O2	2.717(7)	180
			O11–H17···O6^{ix}	2.875(6)	180
			O11–H18···O9^{x}	2.837(7)	180

[a] Symmetry operations: (i) $1+x,y,z-1$; (ii) $1+x,1+y,z$; (iii) $x-1,y,z$; (iv) $x,1+y,z$; (v) $x,y,1+z$; (vi) $x-1,1+y,z$; (vii) $x,1+y,1+z$; (viii) $x,y,z-1$; (ix) $1+x,y,z$; (x) $x,y-1,z$.

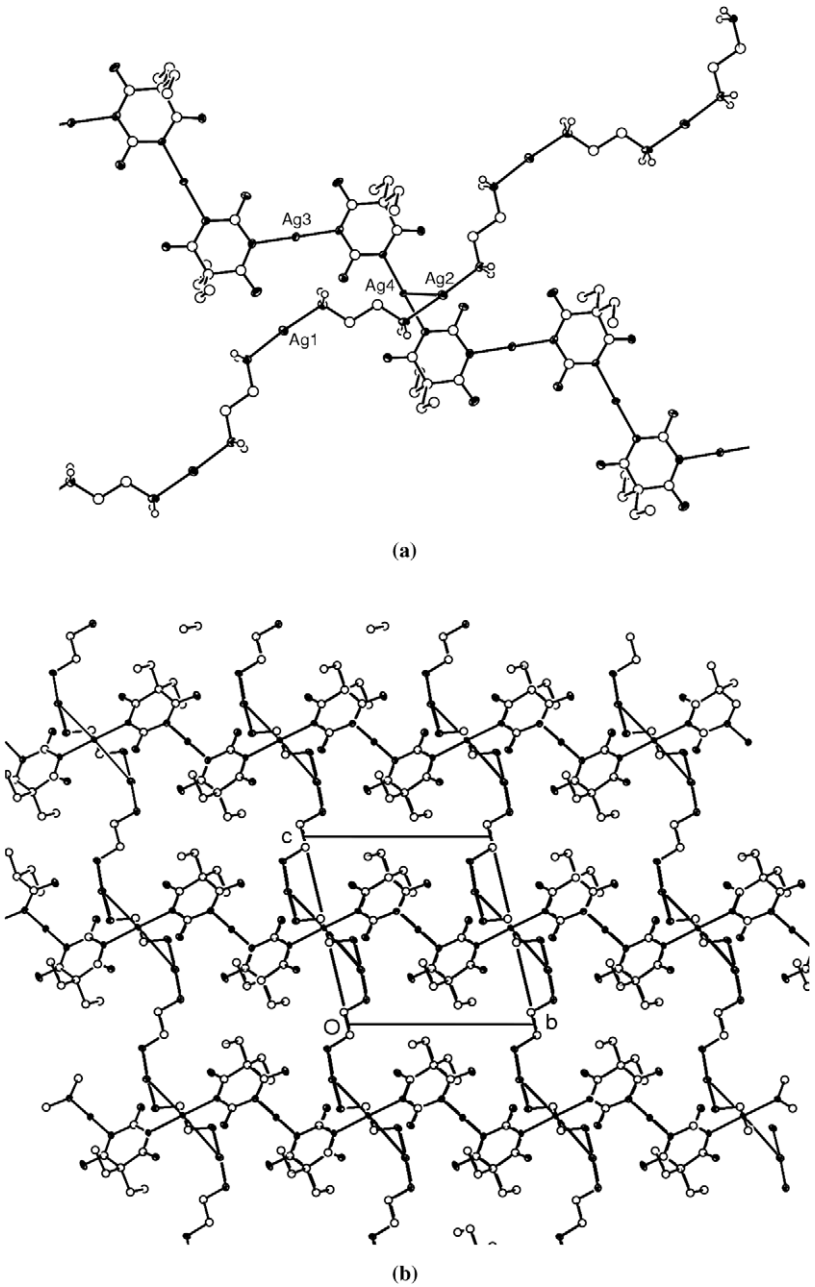

Fig. 4. (a) Interaction of individual anionic and cationic chains in **2** by way of Ag–Ag interactions (C–H hydrogen atoms were omitted for clarity). (b) Perspective view of the 2D layer structure of **2** (water molecules are omitted for clarity).

weak hydrogen bonding with the O atoms of barb ligands and water molecules. The water O atoms do not participate in coordination with silver(I) and their hydrogen atoms form strong hydrogen bonds with the O atoms of barb ligands and water molecules. Thus, the 2D layers of **2** are linked by these hydrogen bonds into a 3D network with open channels (Fig. 5). Calculations with PLATON [28] show that in the absence of the water molecules, the structure of **2** has solvent accessible voids with a volume of 73.7 $Å^3$, which is approximately 9% of the total cell volume, indicating that the channels are filled with water molecules.

*3.4.3. [Ag(barb)(μ-bpe)]$_n$ (**3**)*

The X-ray crystal structure shows that complex **3** is an infinite 1D coordination polymer. The coordination environment around the silver(I) ion is shown in Fig. 6. The N–Ag–N bond angles in Table 4 suggest that the local AgN_3 geometry is between trigonal and T-shape. The basic building blocks in the extended structure are [Ag(barb)(bpe)], which are bridged by the two N atoms of the bpe ligand, generating a helical chain running along the *a* axis (Fig. 7). The barb ligands are *N*-coordinated through the negatively charged N atom. The Ag–N_{barb} bond distances are slightly longer than the Ag–N_{bpe} bond

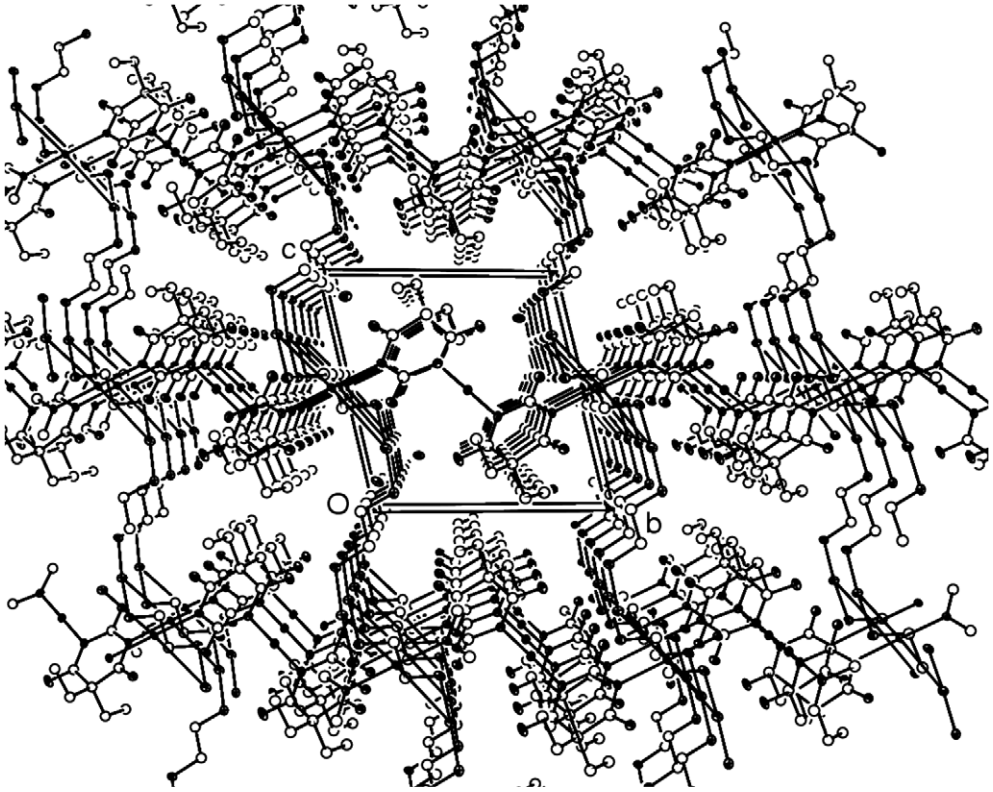

Fig. 5. View of the stacking sheets along the *a* axis of **2**.

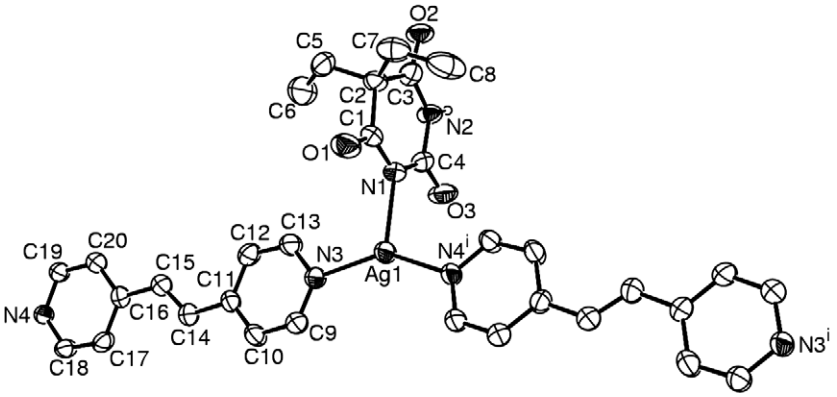

Fig. 6. View of the coordination environment of silver atoms in **3**, symmetry code (i): $x-2, 1/2-y, z-1/2$ (30% probability thermal ellipsoids; C–H hydrogen atoms were omitted for clarity).

distances, but significantly longer than the corresponding bond distances in **1** and **2**. The Ag–Ag distance within a chain separated by a bpe ligand is 13.783 Å.

The ring systems of barb and bpe are planar and the pyrimidine and py rings are almost perpendicular to each other with a dihedral angle of 84.17(15)°. Although the

Table 4
Selected bond lengths (Å) and angles (°) for **3**[a]

Ag1–N1	2.299(5)		N1–Ag1–N3	105.02(19)	
Ag1–N3	2.222(5)		N1–Ag1–N4^{i}	109.52(18)	
Ag2–N4^{i}	2.205(5)		N3–Ag3–N4^{i}	145.40(18)	
H–bonds	N···O (Å)	N–H···O (°)		C···O (Å)	C–H···O (°)
N2–H2···O3^{ii}	2.861(7)	177	C17–H17···O1^{iii}	3.262(10)	154
			C19–H19···O2^{iv}	3.295(9)	167

[a] Symmetry operations: (i) $x-2, 1/2-y, z-1/2$; (ii) $-x, 1-y, 1-z$; (iii) $1+x, 1/2-y, 1/2+z$; (iv) $-x, -1/2+y, 1/2-z$.

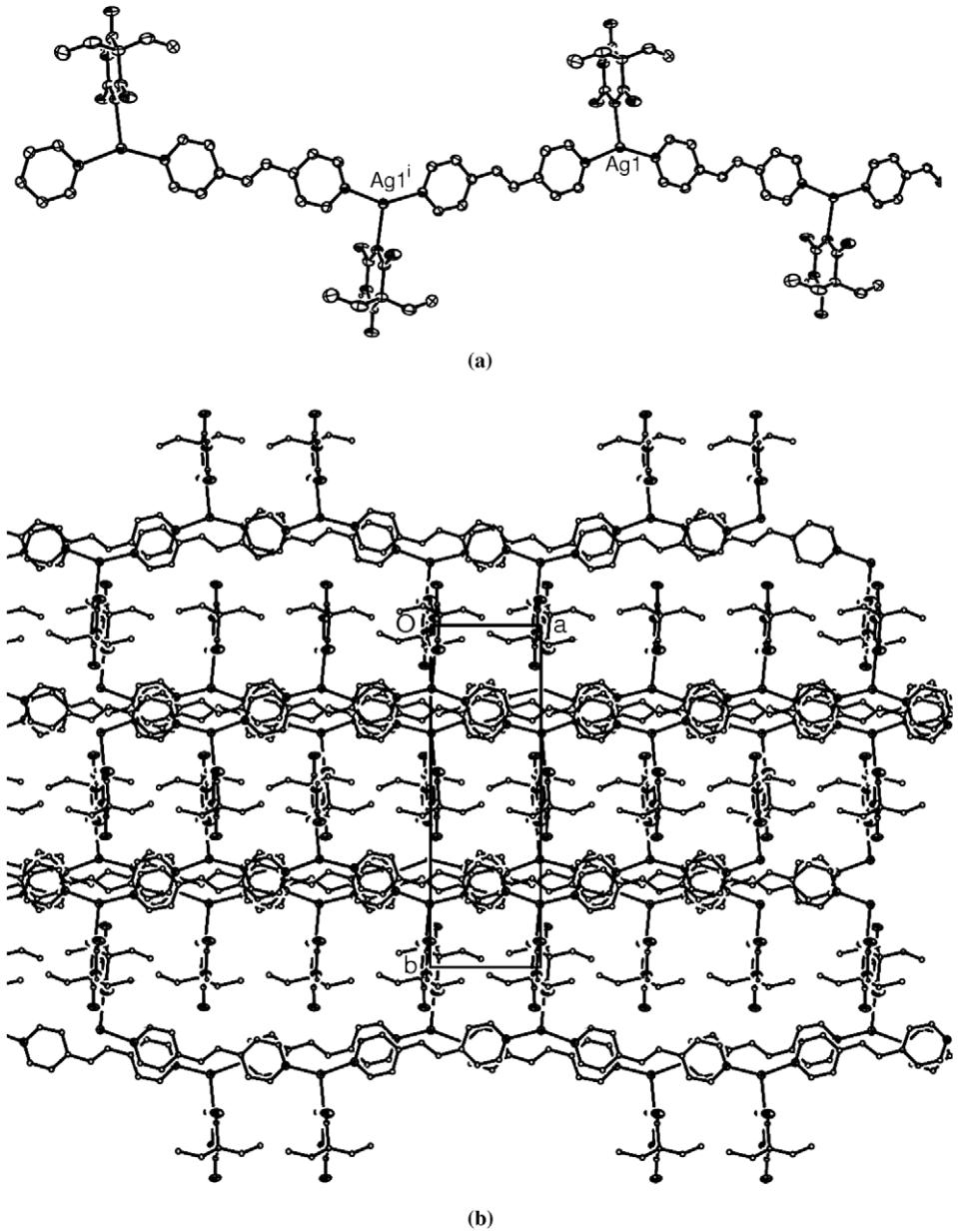

Fig. 7. (a) A fragment of the 1D chain in **3**, symmetry code (i): $x, y - 1/2, z + 1/2$. (b) Perspective view of the stacking of the 2D layers via aromatic π–π stacking interactions along the *c* axis.

bpe molecule is basically flat, the py rings within a bpe molecule are tilted by about 6.5°. Individual chains are connected by N–H···O hydrogen bonds between the barb ligands into 2D layers, which are further linked by aromatic π–π stacking interactions between the py rings of the bpe ligands [$C_g \cdots C_g^i = 3.543$ Å; i = $1 + x, y, z$ and $C_g \cdots C_g^{ii} = 3.558$ Å; (ii) $-1 + x, y, z$; C_g is the centroid on the benzene ring] to generate a 3D framework as shown in Fig. 7.

3.5. Antimicrobial activities

The metal-free ligands and their silver(I) complexes were tested for their in vitro antimicrobial activities against two Gram-positive bacteria, *B. subtilis* and *S. aureus*, two Gram-negative bacteria, *E. coli* and *P. aeruginosa*, and two fungi *C. albicans* and *C. parapsilosis*. The results are presented in Table 5 as minimum inhibitor concentration (MIC) values (μg/ml) which is the minimum concentration to inhibit the growth of bacteria or fungi.

The free ligands and solvents showed no antimicrobial activity against either bacterial or fungal strains tested at a concentration of 100 μg/ml, but the ligands in the form of silver complexes had significant levels of activity due to facts that in general silver(I) complexes are kinetically labile and a ligand exchange process is quite likely to occur. The antimicrobial activity of $AgNO_3$ was, almost without exception, superior to that of complexes **1**–**3** across all of

Table 5
Antimicrobial activity of compounds evaluated by minimum inhibitory concentration (MIC = μg/ml)

Compound	*P. aeruginosa*	*E. coli*	*B. subtilis*	*S. aureus*	*C. albicans*	*C. parapsilosis*
Na(barb)	>100	>100	>100	>100	>100	>100
en	>100	>100	>100	>100	>100	>100
bpe	>100	>100	>100	>100	>100	>100
$AgNO_3$	1.5	1.5	1.5	2	8	6
1	12	23	27	25	25	15
2	13	15	47	15	35	35
3	42	42	43	43	38	47
Ampicillin	>100	50	55	10		
Nystatin					7	3

the bacterial and the fungal strains studied. Complex **1** had a higher activity on all the strains especially against *P. aeruginosa* and *C. parapsilosis*. The MICs for four strains, *E. coli*, *B. subtilis*, *S. aureus* and *C. albicans*, were ca. 25 μg/ml, while the growth of the other two strains, *P. aeruginosa* and *C. parapsilosis*, was inhibited more effectively at ca. 12 μg/ml. For complex **2**, the growth of the strains *P. aeruginosa*, *E. coli* and *S. aureus* was inhibited at a concentration of ca. 15 μg/ml of the complex, while the MICs were 47 μg/ml for *B. subtilis* and 35 μg/ml for both fungal strains. Complex **3** showed similar MIC values for all the strains. Compared to complexes **1** and **2**, the MICs of **3** were found to be noticeably higher and this may be consequence of the slow precipitation tendency of this complex in the growth medium. Among the three silver-barbital complexes, complex **2** seems to be more effective against all bacterial strains. Compared to ampicillin, all three complexes demonstrated a remarkable microbial activity on bacterial strains with exception of *S. aureus*. It is interesting to note that *P. aeruginosa* was significantly affected by complexes **1** and **2**. These facts are consistent with recently observed results for polymeric silver(I) complexes containing Ag–N and Ag–O bonds [29–32]

Nystatin and $AgNO_3$ inhibited the growth of the fungi at MIC values less than 10 μg/ml. Complexes **1**–**3** are remarkably active against both the *Candida* strains. Both strains were more susceptible to complex **1**, while similar MIC values were found for the other two complexes conclusively, having less activity than $AgNO_3$ and nystatin.

In the case of silver(I) complexes, two key factors were proposed for a wide range of antimicrobial activities: (i) the type of the coordinating ligands around silver(I), and (ii) the ease of their replacement with biological ligands such as proteins, enzymes, amino acids and nucleic acids [33–36]. As can be seen from Tables 1–3, the silver(I) ion has a AgN_3 core in complexes **1**–**3** and the Ag–N bond lengths increase in the order of **1**, **2** and **3**. Although complex **3** seems to have higher ligand exchange ability among the three complexes, its precipitation in the growth medium makes complex **2** a good inhibitory agent. On the other hand, there are contrasting effects regarding drug solubility. For example, a water-insoluble polymeric complex, sulfadiazinesilver(I) (commercially known as silvadene or flamazine), is used to treat burn wounds [37] and its antimicrobial activity is mainly attributed to the slow liberation of silver. In conclusion, the title complexes show effective antimicrobial inhibition and their low solubility in water promises some potential antibacterial and antifungal applications.

Supplementary material

Crystallographic data for the structures reported in this paper have been deposited at the CCDC as supplementary data, CCDC-290101 (**1**), -290102 (**2**) and -290103 (**3**). Copies of the data can be obtained on application to CCDC, 12 Union Road, Cambridge CB2 1EZ, UK. E-mail: deposit@ccdc.cam.ac.uk.

Acknowledgment

Financial support from the research fund of Ondokuz Mayis University is gratefully acknowledged.

References

[1] J.N. Delgado, W.A. Remers, J.B. Lippincott (Eds.), Wilson and Gisvold's Textbook of Organic Medicinal and Pharmaceutical Chemistry, ninth ed., Lippincott-Raven, Philadelphia, 1991, p. 39, 341, 376.
[2] B.M. Craven, E.A. Vizzini, M.M. Rodrigues, Acta Crystallogr., Sect. B 25 (1969) 1978.
[3] B. Berking, B.M. Craven, Acta Crystallogr., Sect. B 27 (1971) 1107.
[4] B. Berking, Acta Crystallogr., Sect. B 28 (1972) 98.
[5] L. Levi, C.E. Hubley, Anal. Chem. 28 (1956) 1591.
[6] B.C. Wang, B.M. Craven, J. Chem. Soc., Chem. Commun. (1971) 290.
[7] L.R. Nassimbeni, A. Rodgers, Acta Crystallogr., Sect. B 30 (1974) 2593.
[8] M.R. Caira, G.V. Fazakerley, P.W. Linder, L.R. Nassimbeni, Acta Crystallogr., Sect. B 29 (1973) 2898.
[9] G.V. Fazakerley, P.W. Linder, L.R. Nassimbeni, A.L. Rodgers, Inorg. Chim. Acta 9 (1974) 193.
[10] L. Nassimbeni, A. Rodgers, Acta Crystallogr., Sect. B 30 (1974) 1953.
[11] Y. Xiong, C. He, T.C. An, C.H. Cha, X.H. Zhu, Transition Met. Chem. 28 (2003) 69.
[12] K. Noguchi, H. Yuge, T.K. Miyamato, Acta Crystallogr., Sect. C 56 (2000) e40.
[13] K. Noguchi, T. Tamura, H. Yuge, T.K. Miyamato, Acta Crystallogr., Sect. C 56 (2000) 171.
[14] J.A. Zerkowski, C.T. Seto, D.A. Wierda, G.M. Whitesides, J. Am. Chem. Soc. 112 (1990) 9025.
[15] J.A. Zerkowski, J.P. Mathias, D.A. Wierda, G.M. Whitesides, J. Am. Chem. Soc. 116 (1994) 4305.

[16] J.-M. Lehn, M. Mascal, A. Decian, J. Fischer, J. Chem. Soc., Chem. Commun. (1990) 479.
[17] K.C. Russell, J.-M. Lehn, N. Kyritsakas, A. DeCian, J. Fischer, New J. Chem. 22 (1998) 123.
[18] P.V. Bernhardt, Inorg. Chem. 38 (1999) 3481.
[19] F. Yimaz, V.T. Yilmaz, C. Kazak, Z. Anorg. Allg. Chem. 631 (2005) 1536.
[20] F. Yilmaz, V.T. Yilmaz, E. Bicer, O. Büyükgüngör, Z. Naturforsch., Teil B 61B (2006) 275.
[21] G.M. Sheldrick, SHELXL97. Programs for Crystal Structure Analysis, University of Göttingen, Germany, 1997.
[22] M.V. de Almeida, E.T. Cesar, E.de C.A. Felicio, A.P.S. Fontes, M.R. Gero, J. Braz. Chem. Soc. 11 (2000) 154.
[23] V.T. Yilmaz, S. Hamamci, C. Thone, Z. Anorg. Allg. Chem. 630 (2004) 1641.
[24] V.T. Yilmaz, S. Hamamci, C. Kazak, Z. Anorg. Allg. Chem. 631 (2005) 1961.
[25] M. Jansen, Angew. Chem. Int. Ed. 26 (1987) 1098.
[26] I.G. Dance, L.J. Fitzpatrick, A.D. Rae, M.L. Scudder, Inorg. Chem. 22 (1983) 3785.
[27] P. Pyykkö, Chem. Rev. 97 (1997) 597.
[28] A.L. Spek, PLATON, A Multipurpose Crystallographic Tool, Utrecht University, Utrecht, The Netherlands, 1998.
[29] B.S. Creaven, D.A. Egan, K. Kavanagh, M. McCann, M. Mahon, A. Noble, B. Thati, M. Walsh, Polyhedron 24 (2005) 949.
[30] K. Nomiya, A. Yoshizawa, K. Tsukagoshi, N.C. Kasuga, S. Hirakawa, J. Watanabe, J. Inorg. Biochem. 98 (2004) 46.
[31] N.C. Kasuga, A. Sugie, K. Nomiya, J. Chem. Soc., Dalton Trans. 21 (2004) 3732.
[32] M. McCann, B. Coyle, J. Briody, F. Bass, N. O'Gorman, M. Devereux, K. Kavanagh, V. McKee, Polyhedron 22 (2003) 1595.
[33] K. Nomiya, K. Tsuda, T. Sudoh, M. Oda, J. Inorg. Biochem. 68 (1997) 39.
[34] K. Nomiya, K. Tsuda, Y. Tanabe, H. Nagano, J. Inorg. Biochem. 69 (1998) 9.
[35] K. Nomiya, K. Tsuda, N.C. Kasuga, J. Chem. Soc., Dalton Trans. (1998) 1653.
[36] K. Nomiya, R. Noguchi, M. Oda, Inorg. Chim. Acta 298 (2000) 24.
[37] N.C. Baenziger, A.W. Struss, Inorg. Chem. 15 (1976) 1807.

2. Experimental

2.1. Materials

Solvents (benzene, alcohols, dichloromethane, *n*-hexane, acetone and diethyl ether, etc.) were dried and purified according to the literature methods [24]. Phosphorous pentasulfide (E. Merck) was used as received. Ethane-1,2-dithiol (E. Merck), antimony trichloride (S. D. Fine), glycols [butane-2,3-diol (E. Merck) and 2,3-dimethylbutane-2,3-diol (Aldrich)] were distilled before use. 2-Chloro-1,3-dithia-2-stibacyclopentane [25] and the alkylene-/diorganodithiophosphoric acids and their sodium/ammonium salts were synthesized by earlier reported methods [2,5].

2.2. Measurements

The elemental analysis (C and H) was performed on a Perkin–Elmer 2400 elemental analyzer. Sulfur was estimated gravimetrically as barium sulfate and antimony was estimated iodometrically titrating against standard sodium thiosulfate solution [6,7]. Molecular weights were determined cryoscopically in benzene. IR spectra were recorded in KBr discs on a Perkin–Elmer 557 spectrophotometer in the region 4000–200 cm^{-1}. The UV spectra were recorded in chloroform solution at room temperature on a Shimadzu UV-1601 UV–Vis spectrophotometer within the range 500–200 nm. ^{1}H, ^{13}C and ^{31}P spectra of all these newly synthesized complexes were recorded in $CDCl_3$ solution using TMS and 85% H_3PO_4 as standards, respectively. The ^{1}H and ^{13}C NMR spectra were operated at 300.13 and 75.49 MHz respectively, on a Bruker AC-300F NMR spectrophotometer at the Sophisticated Analytical Instrument (SAIF) Facility, Punjab University, Chandigarh and ^{31}P NMR spectra were operated at 121.50 MHz on a DRX-300 NMR spectrophotometer, SAIF, Central Drug Research Institute (CDRI), Lucknow.

The single crystal X-ray diffraction analysis was performed on a STOE IPDS (imaging plate system) diffractometer at 25 °C, using graphite monochromated Mo Kα X-ray radiation ($\lambda = 0.71073$ Å). A suitable crystal, grown from a toluene–isopropyl alcohol solution, was sealed in a glass capillary under dry nitrogen atmosphere and mounted on the goniometer head. The data collection was performed at room temperature using the ω–θ scan technique. The crystal structure was solved by direct methods and refined by full-matrix least squares on F^2 using the SHELXS software package for crystal structure solution and refinement. All non-hydrogen atoms were refined with anisotropic thermal parameters in the later cycles of refinement. The hydrogen atoms were placed in idealized positions and refined using the riding model with general isotropic temperature factors. The data collection was performed only up to 27.87°. Selected atomic parameters are collected in Tables 2 and 3, and the crystallographic numbering scheme is shown in Fig. 1.

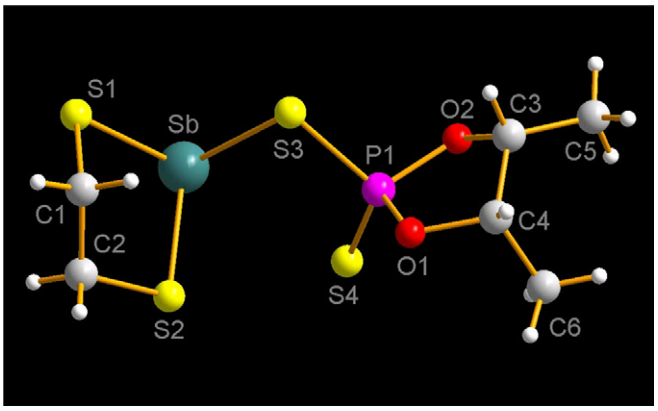

Fig. 1. X-ray single crystal structure of 1,3-dithia-2-stibacyclopentane 2,3-butylenedithiophosphate.

2.3. Antimicrobial studies

The following strains of bacteria and fungi were used: *Staphylococcus aureus* (ATCC 9144), *Bacillus subtilis* (ATCC 6051), *Escherichia coli* (ATCC 9637), *Pseudomonas aeruginosa* (ATCC 25619), *Aspergillus niger* (ATCC 9029) and *Penicillium chrysogenum* (ATCC 10106). Antimicrobial activities were evaluated by the disc diffusion method [27–29] for the tested compounds as follows.

A 0.5 mL (containing 10^6–10^7 microorganisms mL^{-1}) of each of the investigated organisms was added to a sterile agar medium just before solidification, then poured into sterile petri dishes (9 cm in diameter) and left to solidify.

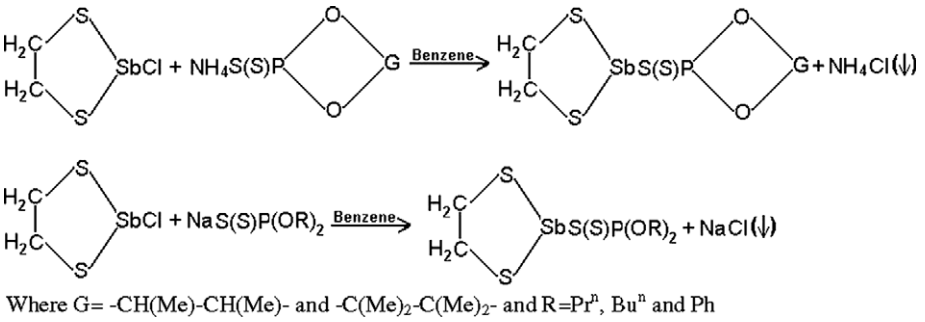

Scheme 1. Reaction of 2-chloro-1,3-dithia-2-stibacyclopentane with sodium/ammonium dithiophosphates in an equimolar ratio.

Using a sterile cork borer (6 mm in diameter), three holes (wells) were made in each dish, then 0.1 ml of tested compounds dissolved in DMF (50, 100 and 200 μg mL^{-1}) were poured into these holes. Finally the dishes were incubated at 37 °C for 24 h (for bacteria) and at 30 °C for 72 h (for fungi), then inhibition zones were detected around each hole.

A quantity of 0.1 ml DMF alone was also tested under the same conditions for each organism and it was found that DMF had no effect on the organisms at the concentrations studied.

2.4. Synthesis of mixed 1,3-dithia-2-stibacyclopentane alkylene-/dialkyl-dithiophosphate derivatives

2.4.1. Synthesis of 1,3-dithia-2-stibacyclopentane 2,3-butylenedithiophosphate

A benzene solution (30 ml) of 2-chloro-1,3-dithia-2-stibacyclopentane (0.72 g, 2.88 mmol) was added to the ammonium salt of 2,3-butylenedithiophosphoric acid (0.58 g, 2.88 mmol) in an equimolar ratio (Scheme 1). The reaction mixture was refluxed with stirring for ~5 h followed by cooling to room temperature. The precipitated ammonium chloride (0.15 g) was removed by filtration. The removal of the solvent from the filtrate under reduced pressure afforded a yellow crystalline compound, which was recrystallised in dichloromethane (yield: 1.13 g, 98%).

The other complexes were synthesized by adopting a similar method. Pertinent analytical and physico-chemical data for these complexes are listed in Table 1.

3. Results and discussion

3.1. Synthesis of antimony(III) complexes

1,3-Dithia-2-stibacyclopentane derivatives with alkylene-/dialkyl-dithiophosphate have been synthesized by the reactions of 2-chloro-1,3-dithia-2-stibacyclopentane with the ammonium/sodium salts of alkylene-/dialkyl-dithiophosphoric acids in an equimolar (1:1) ratio in refluxing benzene ~5 h.

All these newly synthesized derivatives are either yellow crystalline solids or yellow sticky solids and are soluble in common organic solvents like benzene, chloroform, acetone, dichloromethane, DMF and DMSO, etc., but decompose in water.

3.2. Electronic spectra

In the electronic absorption spectra [12–15,26], all the 1,3-dithia-2-stibacyclopentane dithiophosphate derivatives absorb strongly in the region 230–235 nm, corresponding to a π–π^* transition. Another rather weak absorption occurs at 304–309 nm, which may be due to a n–π^* transition. These dithiophosphates also absorb in these regions.

Table 1
Physical and analytical data of the 1,3-dithia-2-stibacyclopentane alkylene-/dialkyl-dithiophosphate complexes

Reactants (g; mmol)		Empirical formula; yield = g (%)	Mol. wt. found (calc.)	Colour and state; m.p. (°C)	Analysis (%) found (calculated)				
	Ligand (dithiophosphates)				C	H	P	S	Sb
0.72 (2.88)	0.58 (2.88)	$C_6H_{12}PO_2S_4Sb$; 1.13 (98)	386 (397.35)	yellow crystalline solid; 85	18.09 (18.14)	2.98 (3.04)	7.64 (7.80)	32.20 (32.28)	30.57 (30.64)
0.56 (2.25)	0.52 (2.25)	$C_8H_{16}PO_2S_4Sb$; 0.93 (97)	410 (425.21)	yellow crystalline solid; 103	22.55 (22.60)	3.72 (3.79)	7.13 (7.29)	30.09 (30.16)	28.59 (28.65)
0.55 (2.20)	$NaS_2P(OPr^n)_2$ 0.52 (2.20)	$C_8H_{18}PO_2S_4Sb$; 0.89 (95)	412 (427.22)	yellow sticky solid;	22.41 (22.49)	4.29 (4.25)	7.14 (7.26)	29.94 (30.02)	28.46 (28.51)
0.69 (2.76)	$NaS_2P(OBu^n)_2$ 0.73 (2.76)	$C_{10}H_{22}PO_2S_4Sb$; 1.23 (97)	439 (455.27)	yellow sticky solid;	26.27 (26.38)	4.79 (4.87)	6.71 (6.81)	28.08 (28.17)	26.68 (26.75)
0.68 (2.71)	$NaS_2P(OPh)_2$ 0.81 (2.70)	$C_{14}H_{14}PO_2S_4Sb$; 1.26 (94)	482 (495.26)	yellow sticky solid;	33.89 (33.95)	2.82 (2.85)	6.12 (6.26)	25.78 (25.89)	24.52 (24.59)

Table 2
Crystal data and refinement details for 1,3-dithia-2-stibacyclopentane 2,3-butylenedithiophosphate

Compound	$\overline{SCH_2CH_2SSb}\overline{S_2POCH(CH_3)CH(CH_3)O}$
Formula	$C_6H_{12}O_2PS_4sSb$
Formula weight	397.12
Crystal system	monoclinic
Space group	$P2_1/n$
a (Å)	11.641(2)
b (Å)	10.528(2)
c (Å)	12.472(2)
α (°)	90
β (°)	117.78(3)
γ (°)	90
V (Å^3)	1352.4(4)
Z	4
Crystal size (mm^3)	$0.28 \times 0.2 \times 0.15$
D_c (Mg m^{-3})	1.950
$F(000)$	776
Reflection collected	12095
θ_{max} (°)	2.67–27.87
Maximum and minimum transmission	0.48 and 0.30
Final R indices [$I > 2\sigma$ (I)]	
R_1	0.0366
wR_2	0.1007
R indices (all data)	
R_1	0.0384
wR_2	0.1020
Residual ρ_{max} (e Å^3)	0.928
Residual ρ_{min} (e Å^3)	−0.702

Table 3
Selected bond distances (Å) and bond angles (°) for 1,3-dithia-2-stibacyclopentane 2,3-butylenedithiophosphate

Bond distances	
Sb(1)–S(2)	2.4485(9)
Sb(1)–S(1)	2.4491(10)
Sb(1)–S(3)	2.5566(13)
S(1)–C(1)	1.834(3)
S(2)–C(2)	1.842(3)
S(3)–P(1)	2.0541(12)
S(4)–P(1)	1.9456(16)
P(1)–O(1)	1.602(2)
P(1)–O(2)	1.608(3)
O(1)–C(4)	1.477(4)
O(2)–C(3)	1.481(4)
C(1)–C(2)	1.504(6)
C(3)–C(5)	1.519(5)
C(3)–C(4)	1.525(5)
C(4)–C(6)	1.513(5)
Bond angles	
S(2)–Sb(1)–S(1)	87.80(3)
S(2)–Sb(1)–S(3)	94.83(4)
S(1)–Sb(1)–S(3)	92.17(4)
C(1)–S(1)–Sb(1)	97.97(11)
C(2)–S(2)–Sb(1)	100.36(11)
P(1)–S(3)–Sb(1)	95.79(5)
O(1)–P(1)–O(2)	97.52(13)
O(1)–P(1)–S(4)	116.06(12)
O(2)–P(1)–S(4)	112.98(12)
O(1)–P(1)–S(3)	105.68(10)
O(2)–P(1)–S(3)	109.30(12)
S(4)–P(1)–S(3)	113.89(6)
C(4)–O(1)–P(1)	111.40(19)
C(3)–O(2)–P(1)	109.48(19)
C(2)–C(1)–S(1)	111.6(2)
C(1)–C(2)–S(2)	112.0(3)
O(2)–C(3)–C(5)	109.2(3)
O(2)–C(3)–C(4)	104.1(3)
C(5)–C(3)–C(4)	116.2(3)
O(1)–C(4)–C(6)	109.3(3)
O(1)–C(4)–C(3)	103.5(3)
C(6)–C(4)–C(3)	116.1(3)

3.3. Infra-red spectra

These newly synthesized complexes show medium to strong intensity bands in the regions 1000–1030 cm^{-1} and 830–860 cm^{-1} which are assigned due to ν\{(P)–O–C\} and ν\{P–O–(C)\}, respectively [5–8,17,18]. A broad band in the region 690–720 cm^{-1} (alkylenedithiophosphates) and 660–690 cm^{-1} (dialkyldithiophosphates) due to ν(P=S), present in the free phosphoric acids, is shifted towards lower frequencies in the spectra of all these complexes and is present in the regions 650–660 and 635–645 cm^{-1} respectively, this also overlaps with the ν(C–S) vibrations of dithiolate moieties in these complexes. A sharp band present in the region 925–930 cm^{-1} in the corresponding alkylenedithiophosphate may be assigned to the ring vibrations of the dioxaphospholane ring [30]. The bands of medium to weak intensity in the regions 530–540 and 310–320 cm^{-1} are assigned to ν(P–S) and ν(Sb–S), respectively [17].

3.4. NMR spectral data

3.4.1. ^{1}H NMR spectra

The chemical shifts corresponding to the protons of mixed 1,3-dithia-2-stibacyclopentane derivatives with alkylene-/dialkyl-dithiophosphate are listed in Table 4. In the ^{1}H NMR spectra of these compounds, a sharp singlet observed in the region δ 3.61–3.74 ppm is due to four CH_2S protons of the 1,3-dithia-2-stibacyclopentane ring [17,18], indicating that these protons are equivalent. In addition, these compounds also exhibit the characteristic proton resonances [5–18] for the corresponding protons of dithiophosphate moieties (Table 4). In a few of the alkylene-/dialkyl-dithiophosphate derivatives, OCH and OCH_2 protons couple with ^{31}P nuclei and appear as a multiplets and doublets of triplets.

3.4.2. ^{13}C NMR spectra

The ^{13}C NMR spectra of the ethane-1,2-dithiolate moiety show only one sharp singlet signal in the region δ 41.41–42.40 ppm due to SCH_2 carbons [17,18] indicating that these two carbon atoms are magnetically equivalent, thus supporting the results of the ^{1}H NMR spectra. In addition, these derivatives also exhibit the expected signals due to the carbons of dithiophosphate moieties [5–17]. The methylene carbons attached to P–O and P–O–C groups

Table 4
^{1}H, $\{^{1}H\}^{13}C$ and ^{31}P NMR spectral data of 1,3-dithia-2-stibacyclopentane alkylene-/dialkyl-dithiophosphate complexes

Compound (No.)	^{1}H Chemical shifts (δ ppm)	^{13}C Chemical shifts (δ ppm)	^{31}P Chemical shifts (δ ppm)
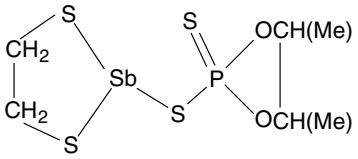 (1)	1.31 (6H, d ($J = 6.3$ Hz), CH_3) 3.71 (4H, s, CH_2S) 4.65–4.70 (2H, m, OCH)	15.46 (s, Me) 42.40 (s, CH_2S) 79.10 (s, OCH)	108.14
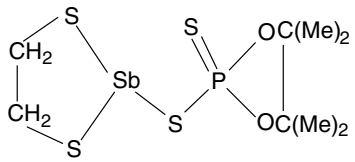 (2)	1.45 (12H, s, $OCMe_2$) 3.74 (4H, s, CH_2S)	24.17 (s, Me_2) 42.14 (s, CH_2S) 90.92 (s, OC)	103.7
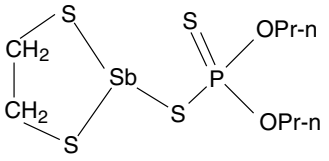 (3)	0.93 (6H, t ($J(CH_3\text{-}CH_2) = 7.35$ Hz), $OCCCH_3$dtp) 1.69 (4H, m, $OCCH_2$-dtp) 3.69 (4H, s, CH_2S) 4.02 {4H, dt ($J(OCH_2\text{-}CH_2) = 6.54$ Hz and $J(PO\text{-}CH_2) = 9.34$ Hz), OCH_2-dtp}	9.73 (s, $OCCCH_3$-dtp) 22.75 (s, $OCCH_2$-dtp) 41.41 (s, CH_2S) 68.67 (s, OCH_2-dtp)	90.90
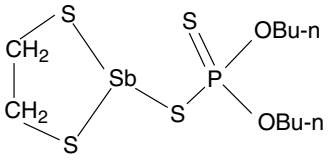 (4)	0.88 (6H, t ($J(CH_3\text{-}CH_2) = 7.37$ Hz), $OCCCCH_3$dtp) 1.36 (4H, m, $OCCCH_2$-dtp) 1.64 (4H, m, $OCCH_2$-dtp) 3.67 (4H, s, CH_2S) 4.06 {4H, dt ($J(OCH_2\text{-}CH_2) = 6.49$ Hz and $J(PO\text{-}CH_2) = 9.19$ Hz), OCH_2-dtp}	13.61 (s, $OCCCCH_3$-dtp) 18.76 (s, $OCCCH_2$-dtp) 31.88 (d ($J = 8.60$ Hz), $OCCH_2$-dtp) 42.03 (s, CH_2S) 67.60 (d ($J = 7.17$ Hz), OCH_2-dtp)	90.89
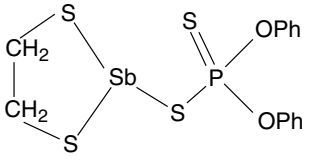 (5)	3.61 (4H, s, CH_2S) 7.19–7.37 (10H, m, OC_6H_5)	42.26 (s, CH_2S) 122.08 (s, *m*-C of C_6H_5) 125.85 (s, *o*-C of C_6H_5) 129.49 (s, *p*-C of C_6H_5)	88.13

Where b = broad, s = singlet, d = doublet, t = triplet, q = quartet, dt = doublet of triplets and m = multiplet.

give rise to a doublet for compound No. 4 due to the coupling with ^{31}P nuclei [9] (Table 4).

3.4.3. ^{31}P NMR spectra

The proton decoupled ^{31}P NMR spectra show only one sharp singlet between δ 103.7–108.1 ppm (in alkylenedithiophosphate derivatives). Chemical shift values appear to be downfield by about δ 10–13 ppm with respect to their parent alkylene dithiophosphoric acids (δ 93.07–95.49 ppm) indicating the bidentate behaviour of these dithiophosphate ligands. The corresponding complexes with dialkyldithiophosphate ligands show a ^{31}P signal in the region δ 88–91 ppm. Glidewell [31] concluded that diorganodithiophosphate complexes showing their ^{31}P NMR signals in the range δ 82–101 exhibit a bidentate mode of attachment of the ligands, thus indicating the bidentate mode of binding of diorganodithiophosphate ligands in these synthesized complexes. It is valid for many cases, however doubts have been made about the universality of the above generalization [32,33].

3.5. Crystal structure

The solid-state structure of the compound 1,3-dithia-2-stibacyclopentane 2,3-butylenedithiophosphate has been established by single crystal X-ray analysis, which revealed a monomeric unit. The molecular structure of 1,3-dithia-2-stibacyclopentane 2,3-butylenedithiophosphate is shown in

Fig. 1 and selected interatomic parameters are collected in Table 3. The antimony atom forms three close contacts, two to the ethane-1,2-dithiolato sulfur atoms, Sb(1)–S(2) (2.4485 Å) and Sb(1)–S(1) (2.4491 Å), and one to the dithiophosphato sulfur atom, Sb(1)–S(3) (2.5566 Å). If these three close contacts were considered to define the coordination geometry, the dithiophosphate ligand behaves in a monodentate fashion. Considering the observed Sb–S interactions, the environment about the antimony would be best described as trigonal pyramidal with the lone pair of electrons being stereochemically active, but with non-equivalent S–Sb–S bond angles [87.80(3)°, 92.17(4)° and 94.83(4)°] (Table 3) [34]. The phosphorus atom is tetrahedrally coordinated to two sulfur and two oxygen atoms, which are further attached with carbon atoms of the alkylene group (Fig. 1). The crystal structure shows that the heteroalkylene ring is markedly non-planar and that the configuration of the bonds about the antimony atom is nearly orthogonal.

The structure of this compound is unique as in this compound the 2,3-butylenedithiophosphate ligand is exhibiting monodentate behaviour. However, in most alkylenedithiophosphate derivatives of main group metals, bismuth(III) [20] and organotin(IV) [22,23], the bidentate behaviour of these alkylenedithiophosphate ligands has been reported. However, in (2,9-dimethyl-1,10-phenanthroline) *bis*(4,4,5,5-tetramethyl-1,3,2-dioxaphospholane-2-thione-2-thiolato)-nickel(II), one ligand is unidentate and the other one is bidentate [21]. It is also noticeable here that diorganodithiophosphate and dithiophosphinate ligands exhibited a bidentate as well as a bidentate triconnective chelating nature in their antimony(III) complexes [2,3].

3.6. Antimicrobial activity

The free ligands and their antimony(III) complexes were screened to evaluate their antimicrobial activity against *S. aureus*, *B. subtilis*, *E. coli*, *P. aeruginosa*, *A. niger* and *P. chrysogenum* at three different concentrations, and results are listed in Table 5. The antibacterial activities of some earlier reported antibiotics [29] were compared with the free ligands and their antimony(III) complexes.

The results showed that the antimony(III) complexes exhibit higher antibacterial and antifungal activity than the free diorganodithiophosphate ligands (dtp). It is noticeable here that *E. coli* and *P. aeruginosa* are resistant to the free dtp ligands. It may be concluded that the free ligands and antimony complexes inhibit the growth of bacteria to a greater extent as the concentration is increased. Nevertheless, it is difficult to make out an exact structure and activity relationship between microbial activity and the structure of these complexes.

A comparison of the antimicrobial activities of the free ligands and synthesized complexes with some previously investigated antibiotics [29] shows the following results:

(i) The free ligands (dtp) and their antimony(III) compounds show a greater effect towards *S. aureus* compared to amikacin, septrin, cefobid, ampicillin and traivid. However, the free ligands (dtp) and antimony(III) compounds show a lesser effect towards *S. aureus* compared to doxycllin, augmantin, sulperazon, unasyn, nitrofurantion and erythromycin.

Table 5
Antimicrobial activity[a] of the free dithiophosphate ligands and 1,3-dithia-2-stibacyclopentane alkylene-/dialkyl-dithiophosphate complexes

Compounds	Fungi						Gram (+ve) bacteria						Gram (−ve) bacteria					
	A. niger			*P. chysogenum*			*S. aureus*			*B. subtilis*			*E. coli*			*P. aeruginosa*		
	Conc. (μg/mL)			Conc. (μg/mL)			Conc. (μg/mL)			Conc. (μg/mL)			Conc. (μg/mL)			Conc. (μg/mL)		
	50	100	200	50	100	200	50	100	200	50	100	200	50	100	200	50	100	200
$(CH_3CH_2CH_2O)_2PS_2Na$	+	+	++	+	+	++	+	+	+	+	+	+	0	0	0	0	0	0
$(CH_3CH_2CH_2CH_2O)_2PS_2Na$	+	+	++	+	+	++	+	+	+	+	+	+	0	0	0	0	0	0
$(C_6H_5O)_2PS_2NH_4$	+	+	++	+	+	++	+	+	+	+	+	++	0	0	0	0	0	0
	+	+	++	+	+	+	+	+	+	+	+	++	0	0	0	0	0	0
$\overline{OCH(CH_3)CH(CH_3)O}PS_2NH_4$	+	+	+	+	+	+	+	+	+	+	+	+	0	0	0	0	0	0
$\overline{OC(CH_3)_2C(CH_3)_2O}PS_2NH_4$																		
(1)	+	++	+++	+	++	+++	++	+++	+++	+	+++	+++	+	++	+++	+	++	+++
(2)	+	++	+++	+	++	+++	++	+++	+++	+	++	+++	+	++	+++	+	++	+++
(3)	+	++	+++	+	++	+++	++	+++	+++	+	++	+++	+	++	+++	+	++	+++
(4)	+	++	++	+	++	++	++	++	+++	++	++	+++	+	+	+	++	++	+++
(5)	+	++	++	+	++	++	+	++	++	++	++	+++	+	+	+	+	+	++
Chloroamphenicol	−	−	−	−	−	−	+	+	++	+	+	++	+	++	+++	+	++	+++
Terbinafin	+	++	++	+	++	++	−	−	−	−	−	−	−	−	−	−	−	−

[a] The test was done using the diffusion agar technique, well diameter = 6 mm, inhibition values beyond control are + = 1–5 mm, ++ = 6–10 mm, +++ = 11–15 mm, 0 = not active and − = not tested.

(ii) The antimony(III) compounds show a greater antibacterial effect towards *P. aeruginosa* than doxycillin, augmantin, unasyn, septrin, cefobid, nitrofurantion, traivid, erythromycin and free dtp ligands. However, the antimony(III) compounds show a lesser effect towards *P. aeruginosa* compared to amikacin, sulperazon and chloroamphenicol.
(iii) The antimony(III) complexes show a greater effect towards *E. coli* compared to unasyn, cefobid, ampicillin, erythromycin and dtp ligands (resistance to *E. coli*). However, the antimony(III) compounds show a lesser effect towards *E. coli* compared to amikacin, doxycllin, augmantin, sulperazon, nitrofurantion, traivid and chloroamphenicol.
(iv) Some of the antimony(III) compounds exhibit an equal antimicrobial effect as that of some antibiotics.

From all of the above results we can conclude that some of the free ligands and their antimony complexes show greater antibacterial effects to some of the investigated antibiotics.

4. Conclusions

Present study describes a series of 1,3-dithia-2-stibacyclopentane complexes with alkylene-/dialkyl-dithiophosphate. On the basis of physico-chemical and spectroscopic data we propose a monodentate behaviour of these ligands in these complexes, which is further confirmed by the X-ray crystal structure of 1,3-dithia-2-stibacyclopentane 2,3-butylenedithiophosphate.

Biological activity of the free ligands and their antimony(III) derivatives has been studied by the disc diffusion method on various microorganisms. All antimony(III) complexes exhibit greater antimicrobial activity compared to that of the free ligands. The free alkylene-/dialkyldithiophosphate and their mixed antimony compounds exhibited a higher antibacterial effect than the some of the previously investigated antibiotics.

5. Supplementary materials

Crystallographic data, tables of atomic coordinates, thermal parameters, bond lengths and bond angles of the structure have been deposited with the Cambridge Crystallographic Data Centre, with the deposition number: 604201. Copies of this are available free of charge from the Director, CCDC, 12 Union Road, Cambridge, CB2 1EZ, UK (fax: +44 1223 336 033; deposit@ccdc.cam.ac.uk or www: http://www.ccdc.cam.ac.uk).

Acknowledgements

Elemental analyses as well as spectral studies were carried out at the SAIF of the CDRI, Lucknow and Punjab University, Chandigarh. The authors are also thankful to S. Srivastava, Holkar Science College, for providing facilities for antimicrobial studies and to Dr. D. Buddhi for UV–Vis spectra.

References

[1] R.C. Mehrotra, G. Srivastava, B.P.S. Chauhan, Coord. Chem. Rev. 55 (1984) 207.
[2] S.S. Garje, V.K. Jain, Coord. Chem. Rev. 236 (2003) 35.
[3] H.P.S. Chauhan, Coord. Chem. Rev. 173 (1998) 1.
[4] C. Silvestru, I. Haiduc, Coord. Chem. Rev. 147 (1996) 117.
[5] H.P.S. Chauhan, C.P. Bhasin, G. Srivastava, R.C. Mehrotra, Phosphorus Sulfur 15 (1983) 99.
[6] H.P.S. Chauhan, G. Srivastava, R.C. Mehrotra, Polyhedron 3 (1984) 1337.
[7] H.P.S. Chauhan, G. Srivastava, R.C. Mehrotra, Polyhedron 2 (1983) 359.
[8] R.K. Gupta, A.K. Rai, R.C. Mehrotra, V.K. Jain, Inorg. Chim. Acta 88 (1984) 201.
[9] S.K. Pandey, G. Srivastava, R.C. Mehrotra, Synth. React. Inorg. Met.-Org. Chem. 19 (1989) 795.
[10] S.K. Pandey, G. Srivastava, R.C. Mehrotra, J. Ind. Chem. Soc. 66 (1989) 558.
[11] S.K. Pandey, G. Srivastava, R.C. Mehrotra, Ind. J. Chem. 29 (1990) 339.
[12] C.P. Bhasin, G. Srivastava, R.C. Mehrotra, Inorg. Chim. Acta 131 (1987) 195.
[13] C.P. Bhasin, G. Srivastava, R.C. Mehrotra, Inorg. Chim. Acta 144 (1988) 157.
[14] C.P. Bhasin, G. Srivastava, R.C. Mehrotra, Inorg. Chim. Acta 77 (1983) L131.
[15] C.P. Bhasin, G. Srivastava, R.C. Mehrotra, Inorg. Chim. Acta 128 (1987) 69.
[16] R. Ratnani, G. Srivastava, R.C. Mehrotra, Phosphorus Sulfur Silicon 48 (1990) 245.
[17] H.P.S. Chauhan, B. Porwal, R.K. Singh, Phosphorus Sulfur Silicon 160 (2000) 93.
[18] H.P.S. Chauhan, S. Lunkad, Main Group Met. Chem. 17 (1994) 313.
[19] N.A. Chadaeva, G. Kamai, K.A. Mamakov, Zh. Obschch. Khim. 36 (1966) 1994.
[20] R. Bohra, H.P.S. Chauhan, G. Srivastava, R.C. Mehrotra, Phosphorus Sulfur Silicon 60 (1991) 167.
[21] C.P. Bhasin, R. Bohra, G. Srivastava, R.C. Mehrotra, Inorg. Chim. Acta 164 (1989) 11.
[22] H. Preut, V.-D. Ngo, F. Huber, Acta Crystallogr. C42 (1986) 809.
[23] H. Preut, V.-D. Ngo, F. Huber, Acta Crystallogr. C43 (1987) 164.
[24] J.A. Riddick, W.B. Bunger, Techniques of Chemistry, Organic Solvents, vol. 2, Wiley Interscience, New York, 1970.
[25] R.E.D. Clark, J. Chem. Soc. (1932) 1826.
[26] B.P. Singh, G. Srivatawa, R.C. Mehrotra, J. Organomet. Chem. 171 (1979) 35.
[27] M. Jain, S. Gaur, V.P. Singh, R.V. Singh, Appl. Organometal. Chem. 18 (2004) 73.
[28] H.P.S. Chauhan, N.M. Shaik, J. Inorg. Biochem. 99 (2005) 538.
[29] M.M. Mashaly, Z.H. Abd-Elwahab, A.A. Faheim, Synth. React. Inorg. Met.-Org. Chem. 34 (2004) 233.
[30] J. Cason, W. Baxter, W. De Acetis, J. Org. Chem. 24 (1959) 247.
[31] C. Glidewell, Inorg. Chim. Acta 25 (1997) 159.
[32] H.C. Clark, V.K. Jain, R.C. Mehrotra, B.P. Singh, G. Srivastava, T. Birchall, J. Organomet. Chem. 279 (1985) 385.
[33] B.P. Singh, G. Srivastava, R.C. Mehrotra, Synth. React. Inorg. Met.Org. Chem. 12 (1982) 105.
[34] R.K. Gupta, A.K. Rai, R.C. Mehrotra, V.K. Jain, B.F. Hoskins, E.R.T. Tiekink, Inorg. Chem. 24 (1985) 3280.

acid, however without cleavage of the Pd–$S_{chelating}$ bond. Therefore, in view of these findings and in our efforts to succeed in devising a route aimed at the preparation of cyclometallated thiosemicarbazone complexes with chelating diphosphines we reasoned that reaction of the tetranuclear palladacycles with a strong chelating diphosphine, plus concentrated hydrochloric acid, should suffice to yield the aforementioned species, and the results of this enterprise are presented herein.

2. Results and discussion

The ligands **a**–**d** were synthesized by reaction of 4-methyl or 4-ethyl-3-thiosemicarbazide with 2′-chloro- or 2′-bromoacetophenone as appropriate, in good yields, and were adequately characterized (see Section 6). The most prominent features were the characteristic ν(N–H) bands in the IR spectra ca. 3350 and 3200 cm^{-1}, assigned to the NHR and NH groups, respectively; distinctive ν(C=N) and ν(C=S) stretches appeared in the ranges 1620–1590 and 840–800 cm^{-1}, also, respectively. The NHR and NH proton resonances in the ^{1}H NMR appeared ca. δ 8.6 and 7.5 ppm, respectively. Reaction of the ligands by any one of the two alternative methods described, i.e., (a) lithium tetrachloropalladate and sodium acetate in methanol; or (b) palladium(II) acetate in glacial acetic acid, resulted in all cases in tetranuclear species, $[Pd\{2\text{-}XC_6H_3C(Me)=NN=C(S)NHR\}]_4$ (X/R: Cl/Me, **1a**; Cl/Et, **1b**; Br/Me, **1c**; Br/Et, **1d**) as air-stable solids, with the ligand in the *E*,*Z* configuration, which were fully characterized by microanalytical, mass spectra, IR and ^{1}H NMR determinations (see Section 6). The mass spectrum (FAB) showed peaks at *m*/*z* 1384 (**1a**), 1441 (**1b**), 1563 (**1c**) and 1620 (**1d**) for the molecular ion whose isotopic composition suggests a tetranuclear complex of the formula $C_{40}H_{40}Cl_4N_{12}Pd_4S_4$ (**1a**), $C_{44}H_{48}Cl_4N_{12}Pd_4S_4$ (**1b**), $C_{40}H_{40}Br_4N_{12}Pd_4S_4$ (**1c**) and $C_{44}H_{48}Br_4N_{12}Pd_4S_4$ (**1d**) (see Section 6).

The ν(C=N) band was shifted to lower wavenumbers ca. 30 cm^{-1} [24] indicating palladium coordination to the C=N moiety through the nitrogen lone pair [25,26]. The absence of the N*H* proton resonance in the ^{1}H NMR spectra was in agreement with deprotonation of the hydrazinic nitrogen atom [27,28]; accordingly, the C=S double bond character was minimized as confirmed by the non-existence of the ν(C=S) band [29]. Metallation of the ligands was

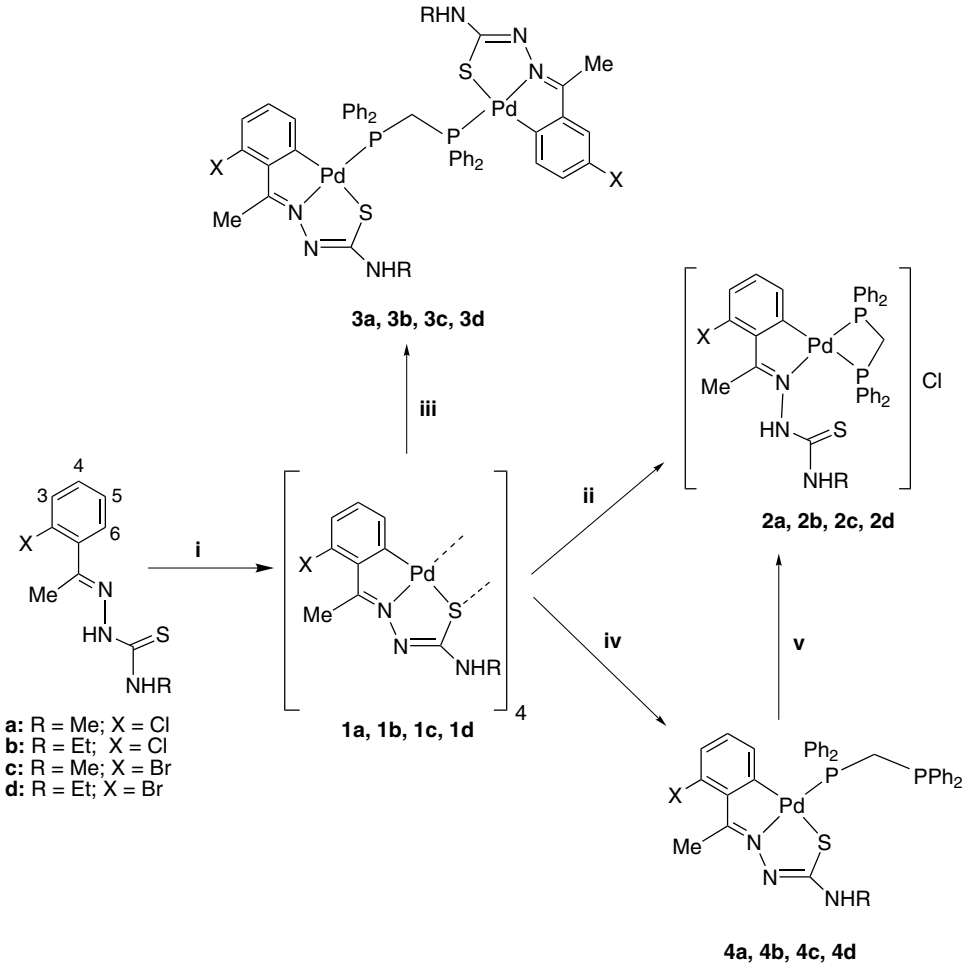

Scheme 1. (i) $Li_2[PdCl_4]$/NaAcO/MeOH; $Pd(AcO)_2$/AcOH; (ii) $Ph_2PCH_2PPh_2$/$HCl_{(aq)}$/acetone/1:4; (iii) $Ph_2PCH_2PPh_2$/acetone/1:2; (iv) $Ph_2PCH_2PPh_2$/acetone/1.4; (v) $HCl_{(aq)}$/acetone.

clear from the absence of the four proton ABCD spin system of the *ortho*-substituted phenyl ring; in the spectra of the complexes only three resonances were observed, which were unambiguously assigned to the H3, H4 and H5 protons (see Section 6).

3. Reactivity of the complexes

The reactions of **1a**–**1d** with $Ph_2PCH_2PPh_2$ in a 1:4 molar ratio and concentrated hydrochloric acid gave the hitherto unknown complexes [Pd{2-$XC_6H_3C(Me)$=NN(H)–C(=S)NHR}($Ph_2PCH_2PPh_2$-P,P)](Cl) **2a**–**2d** which were fully characterized (Section 6 and Scheme 1). Conductivity measurements in dry acetonitrile showed they were 1:1 electrolytes, with Λ_m values of ca. 130 ohm^{-1} cm^2 mol^{-1}. The most noticeable feature of these compounds was that protonation occurred at the hydrazinic nitrogen atom as shown by a broad resonance signal at ca. 8.80 ppm in the ^1H NMR spectra, and a band assignable to the ν(C=S) mode at ca. 8.35 cm^{-1} in the IR spectra. The ^{31}P–{^1H} NMR spectra showed two doublets for the two non-equivalent phosphorus nuclei. The resonance at lower frequency was assigned to the phosphorus nucleus *trans* to the phenyl carbon atom in accordance with the higher *trans* influence of the latter with respect to the C=N nitrogen atom [30]. The *H*C=N resonance was only coupled to the ^{31}P nucleus *trans* to nitrogen. This was confirmed by selective decoupling experiments on the ^{31}P atoms. Alternatively, compounds **2a**–**2d** could be prepared by stirring a mixture of **4a**–**4d** and concentrated hydrochloric acid at room temperature. Unfortunately, the yields were rather low in these cases, ca. 25%, and the final product contained unreacted starting material, and so far pure **2a**–**2d** could not be made by this additional route.

Treatment of the tetranuclear species with $Ph_2PCH_2PPh_2$ in the absence of acid gave dinuclear and mononuclear compounds with a bridging or monocoordinate phosphine ligand, respectively. Thus, reaction of **1a**–**1d** and the phosphine in a 1:2 molar ratio produced compounds [{Pd[2-$XC_6H_3C(Me)$=NN=C(S)NHR]}$_2$(μ-$Ph_2PCH_2PPh_2$)] (**3a**–**3d**) as pure air-stable solids, which were completely characterized (see Section 6). The symmetric nature of the complexes was evident from the ^1H NMR data, which showed only one set of signals; and consequently, only one singlet was observed in the ^{31}P–{^1H} spectra showing two equivalent phosphorus nuclei, with a δ value pointing

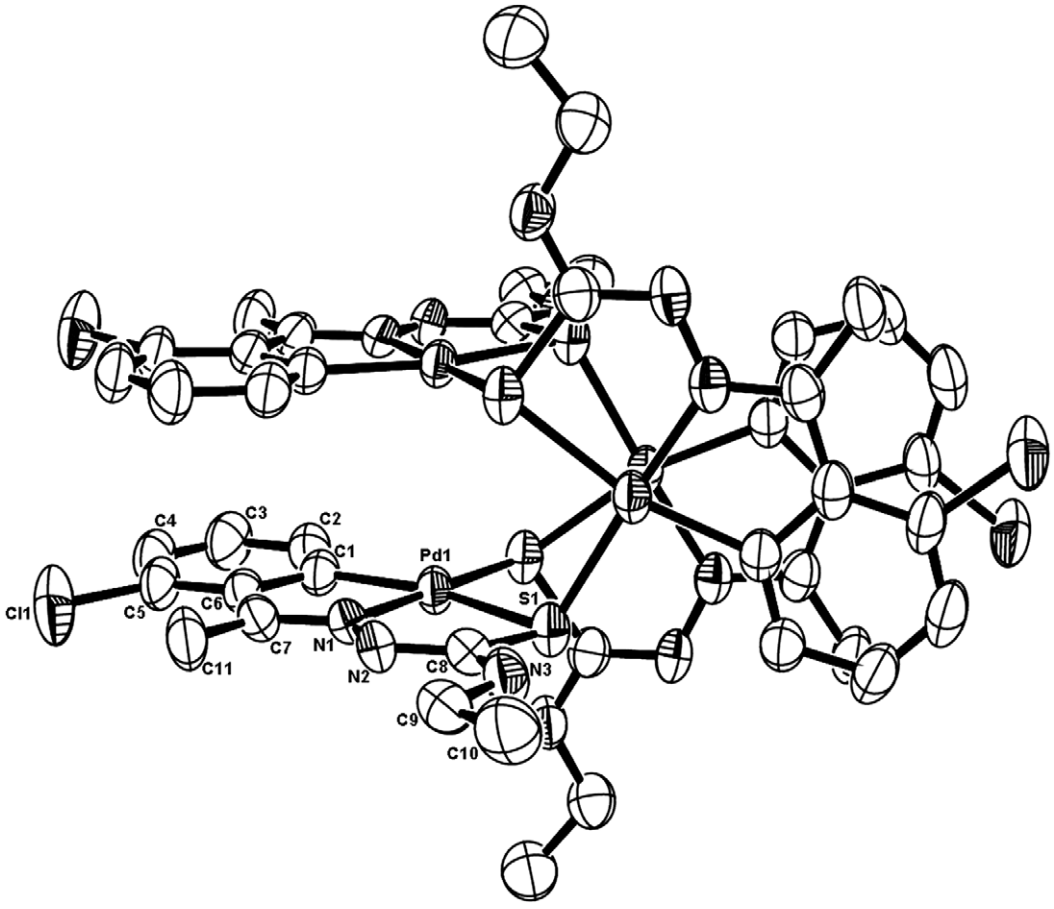

Fig. 1. An ORTEP drawing of the molecular structure for **1b** with the labelling scheme (50% probability). Hydrogen atoms have been omitted for clarity. Selected bond lengths (Å) and angles (°): Pd(1)–N(1) 1.989(4), Pd(1)–C(1) 2.007(5), Pd(1)–S(1)#1 2.3186(16), Pd(1)–S(1) 2.3551(16), S(1)–C(8) 1.792(6), N(1)–C(7) 1.316(6), N(1)–N(2) 1.385(6), N(2)–C(8) 1.308(6), C(6)–C(7) 1.469(8); N(1)–Pd(1)–C(1) 80.9(2), N(1)–Pd(1)–S(1)#1 177.11(13), C(1)–Pd(1)–S(1)#1 96.44(17), N(1)–Pd(1)–S(1) 84.10(13), C(1)–Pd(1)–S(1) 164.66(17), S(1)#1–Pd(1)–S(1) 98.52(4).

towards a phosphorus *trans* to nitrogen geometry [31,32]. The H5 resonance was low frequency shifted by ca. 1.5 ppm, showing coupling to the ^{31}P nucleus, also sustaining a P *trans* to N arrangement [33].

Reaction of **1a**–**1d** with $Ph_2PCH_2PPh_2$ in a 1:4 molar ratio gave the air-stable compounds [Pd{2-XC_6H_3C(Me)=NN=C(S)NHR}($Ph_2PCH_2PPh_2$-P)] (**4a**–**4d**). Characteristic microanalytical and spectroscopic data are given in Section 6. Even when excess diphosphine was used, only cleavage of the Pd–$S_{bridging}$ bonds was produced, therefore yielding species with coordination of the phosphine to the metal atom only through one phosphorus atom. The two doublets in the ^{31}P–{^1H} spectra were assigned to the two non-equivalent phosphorus nuclei with the signal for the phosphorus nucleus bonded to the metal center at higher frequency. The proton part of the *PCH_2P* ABXY spin system appeared as an apparent doublet at ca. 3.2 ppm.

4. Structural studies

4.1. Crystal structures of complexes *1b*, *1d*, *4c* and *4d*

Suitable crystals were grown by slowly evaporating chloroform/*n*-hexane solutions. The crystal structures are shown in Figs. 1–4. Crystal data are given in Table 1.

4.1.1. [Pd{2-XC_6H_3C(Me)=NN=C(S)NHEt}]$_4$ (X = Cl, *1b*; X = Br, *1d*)

The palladium(II) atoms in each structure are in slightly distorted square-planar environments (rms = 0.0132 **1b** and rms = 0.0132 **1d**), with small deviations from the coordination plane (±0.0412 **1b** and ±0.0437 **1d**), and are associated to two fused five-membered chelate rings: the C,N metallacycle and the N,S-chelate moiety, as a consequence of bonding to a terdentate C,N,S ligand. An eight-membered ring of palladium and sulfur atoms, with alternating Pd–$S_{bridging}$ and Pd–$S_{chelating}$ bonds compiles the central part of the molecule; the other two coordination positions at the metal are occupied by a phenyl carbon atom and the nitrogen atom of the C=N group (Figs. 1 and 2).

The angles between adjoining atoms in the coordination sphere are close to the theoretical value of 90°; with the most noteworthy strain in the C(1)–Pd(1)–N(1) values due to chelation of the ligand [22,23] [80.9(2)° **1b**; 81.4(3)° **1d**]. The Pd–C [2.007(5) Å **1b**, 1.990(7) Å **1d**] and Pd–N [1.989(4) Å **1b**, 1.988(6) Å **1d**] bond lengths are shorter than the expected values of 2.081 Å and 2.01 Å [34], respectively, probably induced by partial multiple-bond character [19,35]. The differing *trans* influence of the phenyl carbon and the azomethine nitrogen atoms is

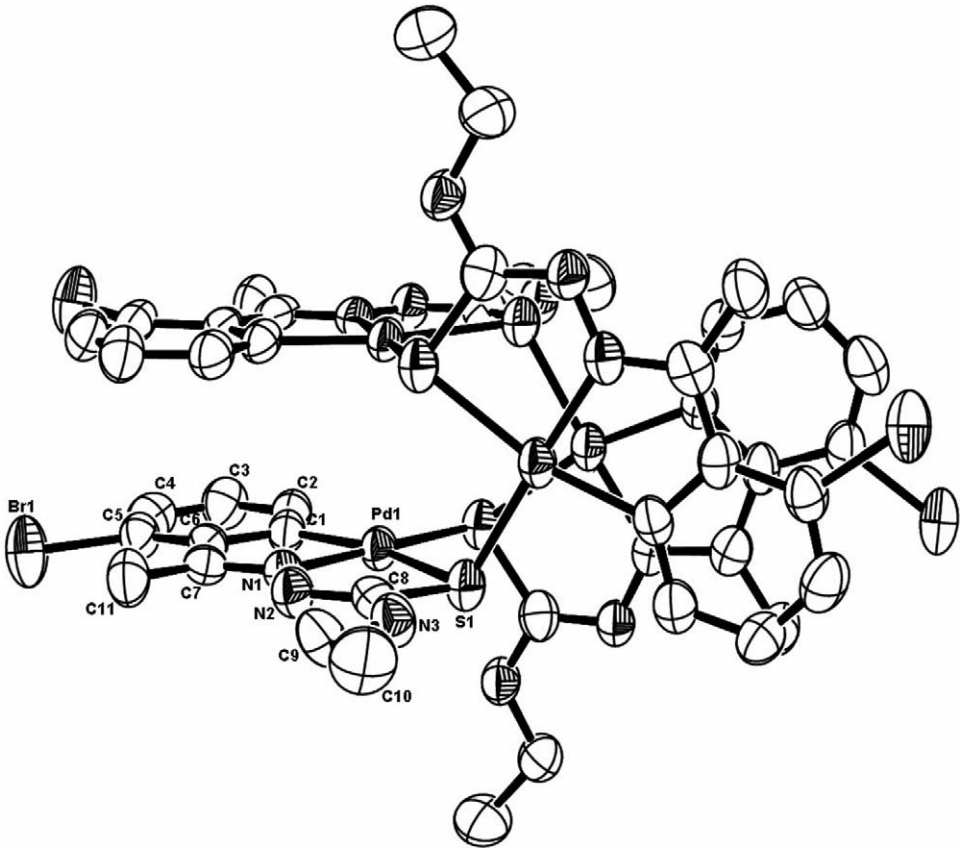

Fig. 2. An ORTEP drawing of the molecular structure for **1d** with the labelling scheme (50% probability). Hydrogen atoms have been omitted for clarity. Selected bond lengths (Å) and angles (°): Pd(1)–N(1) 1.988(6), Pd(1)–C(1) 1.990(7), Pd(1)–S(1)#1 2.315(2), Pd(1)–S(1) 2.355(2), S(1)–C(8) 1.794(7), N(1)–C(7) 1.330(8), N(1)–N(2) 1.381(8), N(2)–C(8) 1.304(8); N(1)–Pd(1)–C(1) 81.4(3), N(1)–Pd(1)–S(1)#1 177.48(17), C(1)–Pd(1)–S(1) 96.2(2), N(1)–Pd(1)–S(1) 84.01(19), C(1)–Pd(1)–S(1)#1 165.0(2), S(1)#1–Pd(1)–S(1) 98.27(7).

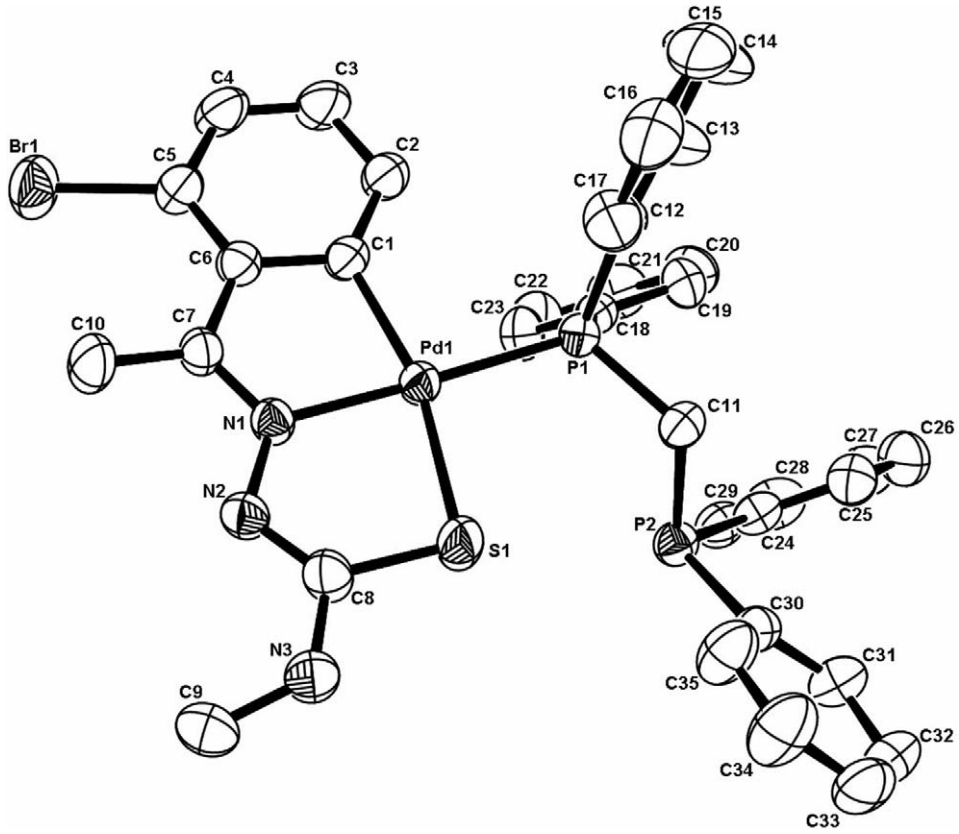

Fig. 3. An ORTEP drawing of the molecular structure for **4c** with the labelling scheme (50% probability). Hydrogen atoms and solvent molecules have been omitted for clarity. Selected bond lengths (Å) and angles (°): Pd(1)–N(1) 2.018(2), Pd(1)–C(1) 2.026(3), Pd(1)–P(1) 2.2626(8), Pd(1)–S(1) 2.3192(9), P(1)–C(18) 1.823(3), P(1)–C(12) 1.828(3), P(1)–C(11) 1.838(3), S(1)–C(8) 1.754(3), N(1)–C(7) 1.303(4), N(1)–N(2) 1.388(3), N(2)–C(8) 1.307(4), C(6)–C(7) 1.472(4); N(1)–Pd(1)–C(1) 80.77(7), N(1)–Pd(1)–P(1) 177.29(8), C(1)–Pd(1)–P(1) 97.94(2), N(1)–Pd(1)–S(1) 83.23(7), C(1)–Pd(1)–S(1) 163.95(9), P(1)–Pd(1)–S(1) 97.99(3).

put forward in the distinct values of the Pd–$S_{bridging}$ and Pd–$S_{chelating}$ distances [Pd(1)–S(1) 2.3551(16) Å, Pd(1)–S(1)#1 2.3186(16) Å **1b**; Pd(1)–S(1) 2.355(2) Å, Pd(1)–S(1)#1 2.315(2) Å **1d**]. The S(1)–C(8) [1.792(6) Å **1b**; 1.794(7) Å **1d**] and N(2)–C(8) [1.308(6) Å **1b**; 1.304(8) Å **1d**] distances, are consistent with increased single- and double-bond character, respectively, in the deprotonated form. The Pd–Pd lengths of 3.3725(7) Å **1b**, and 3.3596(16) Å **1d**, preclude any Pd–Pd interactions.

*4.1.2. [Pd{2-BrC$_6$H$_3$C(Me)=NN=C(S)NHR}-(Ph$_2$PCH$_2$PPh$_2$-P)] (R: Me **4c**; Et **4d**)*

The crystals consist of discrete molecules and $CHCl_3$, separated by normal van der Waals distances. The palladium coordination sphere is defined by an assorted set of four atoms arising from a terdentate C,N,S thiosemicarbazone and a η^1-diphosphine: the aryl C(1) carbon, the imine N(1) nitrogen, the thioamide S(1) sulfur and the phosphorus P(1) atoms, in a slightly distorted square-planar coordination, [N(1), S(1), C(1), P(1), plane 1] (r.m.s. = 0.0064 Å) **4c**, (Fig. 3), [N(1), S(1), C(1), P(1), plane 1] (r.m.s. = 0.0153 Å) **4d**, (Fig. 4), from which the palladium atom deviates by ±0.0382 Å **4c** and ±0.0328 Å **4d**.

As for the bond distances and the angles at palladium, the data observed for both structures show analogous values that are in accordance with the known theoretical data, with the most noticeable difference being in the Pd–N bond, which displays a marked lengthening due to the *trans* influence of the phosphine ligand [Pd(1)–N(1), 2.018(2) Å **4c**, 2.015(3) Å, **4d**], and the somewhat diminished C(1)–Pd(1)–N(1) angle, 80.77(7)° **4c**, 80.54(14)° **4d** (vide supra). The palladium coordination plane [Pd(1), C(1), N(1), S(1)], and the P(1)C(11)P(2), **4c**, and P(1)C(12)P(2), **4d**, planes are at angles of 68.72° and 69.70°, respectively.

5. Conclusions

We have shown that thiosemicarbazone ligands may yield tetranuclear palladacycles with two distinct Pd–$S_{bridging}$ and Pd–$S_{chelating}$ bonds; the strength of the latter hinders opening of the coordination ring, PdNNCS, bearing the Pd–$S_{chelating}$ bond, and upon reaction with $Ph_2PCH_2PPh_2$, in the absence of acid, only dinuclear and mononuclear compounds were obtained with bridging or monodentate phosphine ligands, respectively, and with the thiosemicarbazone ligand as a terdentate ligand [C,N,S]. However, when concentrated hydrochloric acid

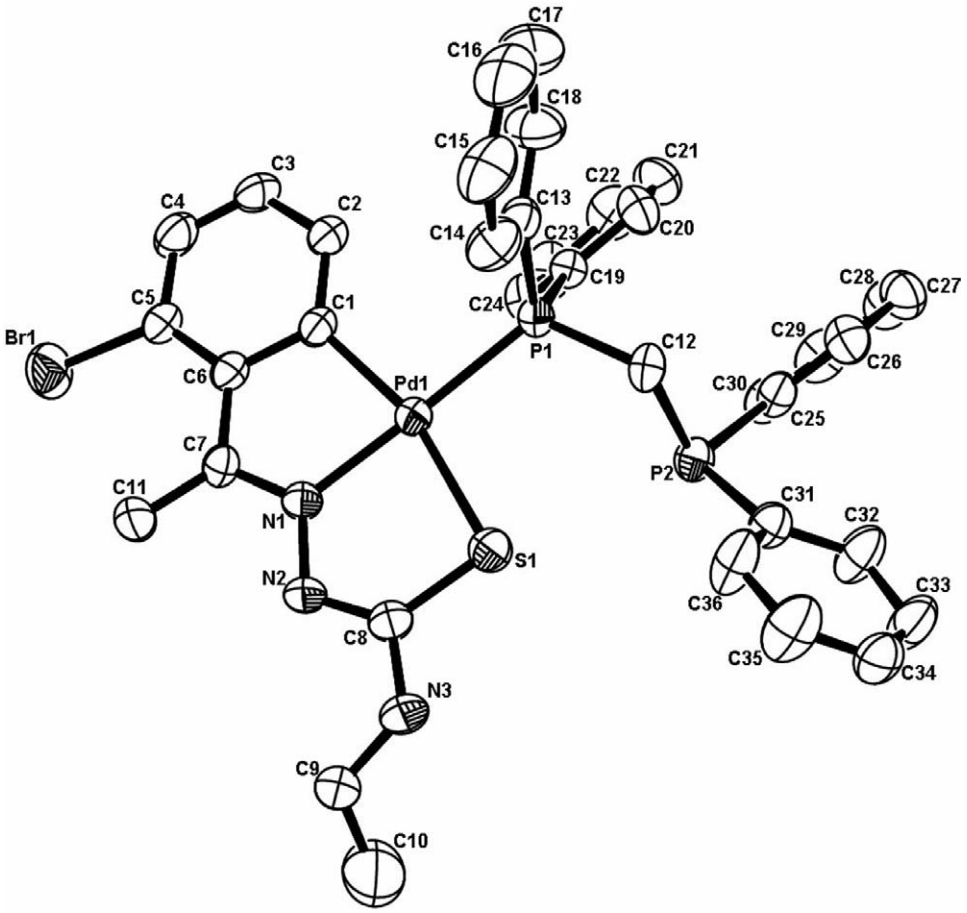

Fig. 4. An ORTEP drawing of the molecular structure for **4d** with the labelling scheme (50% probability). Hydrogen atoms and solvent molecules have been omitted for clarity. Selected bond lengths (Å) and angles (°): Pd(1)–N(1) 2.015(3), Pd(1)–C(1) 2.022(4), Pd(1)–P(1) 2.2659(10), Pd(1)–S(1) 2.3231(11), S(1)–C(8) 1.746(4), P(1)–C(13) 1.833(4), P(1)–C(19) 1.819(4), P(1)–C(12) 1.834(4), N(1)–C(7) 1.302(5), N(1)–N(2) 1.396(4), N(2)–C(8) 1.307(5), C(6)–C(7) 1.467(5); N(1)–Pd(1)–C(1) 80.54(14), N(1)–Pd(1)–P(1) 177.26(9), C(1)–Pd(1)–P(1) 98.33(12), N(1)–Pd(1)–S(1) 83.51(9), C(1)–Pd(1)–S(1) 164.05(12), P(1)–Pd(1)–S(1) 97.59(4).

was added to the reaction mixture, cleavage of the Pd–$S_{chelating}$ bond was produced, with protonation of the thiosemicarbazone and subsequent chelation of the diphosphine ligand, yielding the new thiosemicarbazone palladacycles as 1:1 electrolytes. These could also be made, although impure, by treatment of the compounds with η^1-diphosphine with hydrochloric acid.

6. Experimental

6.1. General procedures

Solvents were purified by standard methods [36]. Chemicals were reagent grade. Lithium tetrachloropalladate was prepared in situ by treatment of palladium(II) chloride with lithium chloride in methanol. Palladium(II) acetate and palladium(II) chloride were purchased from Alfa Products. The diphosphine $Ph_2PCH_2PPh_2$ (dppm) was purchased from Aldrich-Chemie. Microanalyses were carried out at the Servicio de Análisis Elemental at the Universidad of Santiago using a Carlo Erba Elemental Analyzer Model EA1108. IR spectra were recorded as Nujol mulls or KBr discs with Perkin–Elmer 1330, IR-FT Mattson Model Cygnus-100 and Bruker Model IFS-66V spectrophotometers. NMR spectra were obtained as $CDCl_3$ solutions and referenced to $SiMe_4$ (^1H) or H_3PO_4 (^{31}P–{^1H}) and were recorded with Bruker AMX 300, AMX 500 and WM250 spectrometers. All chemical shifts are reported downfield from standards. The FAB mass spectra were recorded with a Fisons Quatro mass spectrometer with a Cs ion gun; 3-nitrobenzyl alcohol was used as the matrix. Conductivity measurements were made on a CRISON GLP 32 conductivimeter using 10^{-3} mol dm^{-3} solutions in dry acetonitrile.

6.2. Syntheses

6.2.1. Preparation of thiosemicarbazone 2-$ClC_6H_4C(Me)$=$NN(H)C(=S)NHMe$ (**a**)

2′-Chloroacetophenone (147 mg, 9.51 mmol) and hydrochloric acid (35%, 0.65 cm^3) were added to a suspension of 4-methyl-3-thiosemicarbazide (100 mg, 9.51 mmol) in water (25 cm^3) to give a clear solution, which was stirred at room temperature for 4 h. The white solid that precipitated was

filtered off, washed with cold water and dried in air. Yield: 209 mg, 91%. *Anal.* $C_{10}H_{12}ClN_3S$ (241.7 g/mol) requires C, 49.7; H, 5.0; N, 17.4; S, 13.3. Found: C, 49.4; H, 5.0; N, 17.4; S, 13.2%. IR (cm^{-1}): *v*(N–H) 3357s, 3239m; *v*(C=N) 1591w; *v*(C=S) 834m. ^1H NMR ($CDCl_3$, δ ppm, *J* Hz): 8.62 (s, 1H, NH), 7.53 (br, 1H, N*H*Me), 7.36 (dd, 1H, H6, ^3J(H6H5) = 7.8, ^4J(H6H4) = 1.4), 7.26 (m, 3H, H3, H4, H5), 3.15 (d, 3H, NH*Me*, ^3J(HH) = 4.6), 2.22 (s, 3H, *Me*C=N). FAB-MS: *m*/*z* 242 $[M]^+$.

6.2.2. Thiosemicarbazones (*b*–*d*)

These were synthesized following a similar procedure.

6.2.2.1. 2-$ClC_6H_4C(Me)$=NN(H)C(=S)NHEt (*b*).

Yield: 165 mg, 77%. *Anal.* $C_{11}H_{14}ClN_3S$ (255.8 g/mol) requires C, 51.7; H, 5.5; N, 16.4; S, 12.5. Found: C, 51.5; H, 5.5; N, 16.3; S, 12.5%. IR (cm^{-1}): *v*(N–H) 3367s, 3201m; *v*(C=N) 1592w; *v*(C=S) 827m. ^1H NMR ($CDCl_3$, δ ppm, *J* Hz): 8.59 (s, 1H, NH), 7.53 (br, 1H, N*H*Et), 7.37 (m, 4H, H6, H3, H4, H5), 3.72 (dq, 2H, NH$CH_2$$CH_3$, ^3J(HH) = 7.4 Hz, ^3J(H–NH) = 5.5), 2.27 (s, 3H, *Me*C=N), 1.26 (t, 3H, NHCH$_2$$CH_3$, ^3J(HH) = 7.4). FAB-MS: *m*/*z* 256 $[M]^+$.

6.2.2.2. 2-$BrC_6H_4C(Me)$=NN(H)C(=S)NHMe (*c*).

Yield: 233 mg, 86%. *Anal.* $C_{10}H_{12}BrN_3S$ (286.2 g/mol) requires C, 42.0; H, 4.2; N, 14.7; S, 11.2. Found: C, 41.8; H, 4.3; N, 14.9; S, 11.0%. IR (cm^{-1}): *v*(N–H) 3357s, 3179s; *v*(C=N) 1586w; *v*(C=S) 833m. ^1H NMR ($CDCl_3$, δ ppm, *J* Hz): 8.63 (br, 1H, NH), 7.61 (dd, 1H, H6, ^3J(H6H5) = 7.9, ^4J(H4H6) = 1.4), 7.54 (br, 1 H, N*H*Me), 7.36 (dd, 1H, H3, ^3J(H3H4) = 7.9 Hz, ^4J(H3H5) = 1.4), 7.30 (td, 1H, H4, ^3J(H4H3) = 7.9 Hz, ^3J(H4H5) = 7.9 Hz, ^4J(H4H6) = 1.4), 7.25 (ddd, 1H, H5, ^3J(H6H5) = 7.9, ^3J(H5H4) = 7.9, ^4J(H5H3) = 1.4), 3.21 (d, 3H, NH*Me*, ^3J(HH) = 4.6), 2.27 (s, 3H, *Me*C=N). FAB-MS: *m*/*z* 287 $[MH]^+$.

6.2.2.3. 2-$BrC_6H_4C(Me)$=NN(H)C(=S)NHEt (*d*).

Yield: 204 mg, 81%. *Anal.* $C_{11}H_{14}BrN_3S$ (300.2 g/mol) requires C, 44.0; H, 4.7; N, 14.0; S, 10.7. Found: C, 43.9; H, 4.7; N, 14.2; S, 10.5%. IR (cm^{-1}): *v*(N–H) 3367s, 3208m; *v*(C=N) 1588w; *v*(C=S) 826m. ^1H NMR ($CDCl_3$, δ ppm, *J* Hz): 8.60 (br, 1H, NH), 7.61 (dd, 1H, H6, ^3J(H6H5) = 7.9, ^4J(H4H6) = 1.4), 7.54 (br, 1H, N*H*Et), 7.37 (dd, 1H, H3, ^3J(H3H4) = 7.9, ^4J(H3H5) = 1.4), 7.31 (td, 1H, H4, ^3J(H4H3) = 7.9, ^3J(H4H5) = 7.9, ^4J(H4H6) = 1.4), 7.25 (ddd, 1H, H5, ^3J(H6H5) = 7.9, ^3J(H5H4) = 7.9, ^4J(H5H3) = 1.4), 3.72 (dq, 2H, NH$CH_2$$CH_3$, ^3J(HH) = 7.4, ^3J(H–NH) = 5.5), 2.26 (s, 3H, *Me*C=N), 1.25 (t, 3H, NHCH$_2$$CH_3$, ^3J(HH) = 7.4 Hz). FAB-MS: *m*/*z* 300 $[M]^+$.

6.2.3. Preparation of [Pd{2-$ClC_6H_3C(Me)$=NN=C(S)-NHMe}]$_4$ (*1a*)

Method 1. Ligand **a** (286 mg, 1.18 mmol, 5% excess) and sodium acetate (185 mg, 2.26 mmol) were added to a stirred solution of palladium(II) chloride (200 mg, 1.13 mmol) and lithium chloride (96 mg, 2.26 mmol) in methanol (40 cm^3). The mixture was stirred for 48 h at room temperature under nitrogen. The yellow precipitate which formed was filtered off, washed with methanol and dried in vacuo. Yield: 346 mg, 89%. *Anal.* $C_{40}H_{40}Cl_4N_{12}Pd_4S_4$ (1384.6 g/mol) requires C, 34.7; H, 2.9; N, 12.1; S, 9.3. Found: C, 34.6; H, 2.9; N, 11.9; S, 9.2%. IR (cm^{-1}): *v*(N–H) 3425s, *v*(C=N) 1558s. ^1H NMR ($CDCl_3$, δ ppm, *J* Hz): 7.44 (dd, 1H, H5, ^3J(H5H4) = 7.9, ^4J(H5H3) = 0.9), 6.96 (dd, 1H, H3, ^3J(H3H4) = 7.9, ^4J(H3H5) = 0.9), 6.84 (t, 1H, H4, ^3J(H4H3) = 7.9, ^3J(H4H5) = 7.9), 5.07 (q, 1H, N*H*Me, ^3J(NH–H) = 4.6), 2.98 (d, 3H, N*Me*, ^3J(H–NH) = 4.6), 2.22 (s, 3H, *Me*C=N). FAB-MS: *m*/*z* 1384 $[M]^+$.

Method 2. Ligand **a** (226 mg, 0.94 mmol, 5% excess) and palladium(II) acetate (200 mg, 0.89 mmol) were added to glacial acetic acid (45 cm^3) to give a clear solution, which was heated to 60 ° C under nitrogen for 24 h. After cooling to room temperature, the yellow precipitate which formed was filtered off, washed with ethanol and dried in vacuo. Yield: 294 mg, 95%.

6.2.4. Compounds *1b*–*1d*

These were synthesized following a similar procedure.

6.2.4.1. [Pd{2-$ClC_6H_3C(Me)$=NN=C(S)NHEt}]$_4$ (*1b*).

Method 1. Yield: 347 mg, 85%. *Anal.* $C_{44}H_{48}Cl_4N_{12}Pd_4S_4$ (1440.7 g/mol) requires C, 36.7; H, 3.4; N, 11.7; S, 8.9. Found: C, 36.6; H, 3.3; N, 11.8; S, 9.1%. IR (cm^{-1}): *v*(N–H) 3429m, *v*(C=N) 1559s. ^1H NMR ($CDCl_3$, δ ppm, *J* Hz): 7.45 (dd, 1H, H5, ^3J(H5H4) = 7.9, ^4J(H5H3) = 0.9), 6.97 (dd, 1H, H3, ^3J(H3H4) = 7.9, ^4J(H3H5) = 0.9), 6.84 (t, 1H, H4, ^3J(H4H3) = 7.9, ^3J(H4H5) = 7.9), 5.08 (t, 1H, N*H*Et, ^3J(NH–H) = 5.5), 3.40 (m, 2H, NH$CH_2$$CH_3$), 2.19 (s, 3H, *Me*C=N), 1.24 (t, 3H, NHCH$_2$$CH_3$, ^3J(HH) = 7.4). FAB-MS: *m*/*z* 1441 $[M]^+$.

Method 2. Yield: 284 mg, 89%.

6.2.4.2. [Pd{2-$BrC_6H_3C(Me)$=NN=C(S)NHMe}]$_4$ (*1c*).

Method 1. Yield: 365 mg, 83%. *Anal.* $C_{40}H_{40}Br_4N_{12}Pd_4S_4$ (1562.4 g/mol) requires C, 30.8; H, 2.6; N, 10.8; S, 8.2. Found: C, 30.7; H, 2.4; N, 10.6; S, 8.1%. IR (cm^{-1}): *v*(N–H) 3417m, *v*(C=N) 1561s. ^1H NMR ($CDCl_3$, δ ppm, *J* Hz): 7.49 (dd, 1H, H5, ^3J(H5H4) = 7.9, ^4J(H5H3) = 0.9), 7.22 (dd, 1H, H3, ^3J(H3H4) = 7.9, ^4J(H3H5) = 0.9), 6.75 (t, 1H, H4, ^3J(H4H3) = 7.9, ^3J(H4H5) = 7.9), 5.08 (q, 1H, N*H*Me, ^3J(NH–H) = 4.6), 2.98 (d, 3H, NH*Me*, ^3J(H–NH) = 4.6), 2.24 (s, 3H, *Me*C=N). FAB-MS: *m*/*z* 1563 $[MH]^+$.

Method 2. Yield: 283 mg, 81%.

6.2.4.3. [Pd{2-$BrC_6H_3C(Me)$=NN=C(S)NHEt}]$_4$ (*1d*).

Method 1. Yield: 353 mg, 77%. *Anal.* $C_{44}H_{48}Br_4N_{12}Pd_4S_4$ (1618.5 g/mol) requires C, 32.7; H, 3.0; N, 10.4; S, 7.9. Found: C, 32.5; H, 2.9; N, 10.3; S, 8.0%. IR (cm^{-1}):

Table 1
Crystal data and structure refinement data for **1b**, **1d**, **4c** and **4d**

Compound	**1b**	**1d**	**4c**	**4d**
Empirical formula	$C_{44}H_{48}Cl_4N_{12}Pd_4S_4$	$C_{11}H_{12}BrN_3PdS$	$C_{36}H_{33}BrCl_3N_3P_2PdS$	$C_{36}H_{34}BrN_3P_2PdS$
Formula weight	1440.58	404.61	894.31	788.97
Temperature (K)	293(2)	293(2)	293(2)	293(2)
Wavelength (Å)	0.71073	0.71073	0.71073	0.71073
Crystal system	tetragonal	tetragonal	triclinic	triclinic
Space group	$I4_1/a$	$I4_1/a$	$P\bar{1}$	$P\bar{1}$
Unit cell dimensions				
a (Å)	17.196(4)	17.249(10)	10.5638(1)	10.7529(5)
b (Å)	17.196(4)	17.249(10)	11.8823(1)	11.9801(6)
c (Å)	16.917(5)	17.228(11)	15.9816(1)	15.9998(8)
α (°)			88.569(1)	89.3630(10)
β (°)			80.760(1)	80.5180(10)
γ (°)			69.257(1)	69.6490(10)
Volume (Å^3)	5002(2)	5126(5)	1850.56(3)	1903.67(16)
Z	4	16	2	2
Density (calculated) (Mg/m^3)	1.913	2.097	1.605	1.376
Absorption coefficient (mm^{-1})	1.843	4.709	1.971	1.703
$F(000)$	2848	3136	896	796
Crystal size (mm^3)	$0.28\times0.24\times0.24$	$0.36\times0.32\times0.20$	$0.60\times0.50\times0.50$	$0.40\times0.30\times0.20$
θ Range for data collection (°)	2.37–29.96	2.36–25.82	1.29–28.28	1.29–28.29
Index ranges	$0/h/24$, $-24/k/0$, $0/l/23$	$-8/h/21$, $-14/k/17$, $-21/l/17$	$-8/h/14$, $-8/k/15$, $-19/l/21$	$-10/h/14$, $-13/k/15$, $-18/l/21$
Reflections collected	3849	5194	12 634	13 248
Independent reflections [R_{int}]	3626 [0.0633]	2484 [0.1207]	8738 [0.0148]	9102 [0.0240]
Completeness to θ (%)	99.8	100.0	95.3	96.1
Absorption correction	multi-scan	multi-scan	multi-scan	multi-scan
Maximum and minimum transmission	0.643 and 0.603	0.309 and 0.200	0.373 and 0.319	0.711 and 0.547
Refinement method	full-matrix least-squares on F^2	full-matrix least-squares on F^2	full-matrix least-squares on F^2	full-matrix least-squares on F^2
Data/restraints/parameters	3626/0/157	2484/0/156	8738/0/434	9102/12/400
Goodness-of-fit on F^2	0.935	0.956	1.026	1.038
Final R indices [$I>2\sigma(I)$]	$R_1=0.0424$, $wR_2=0.0755$	$R_1=0.0358$, $wR_2=0.0690$	$R_1=0.0394$, $wR_2=0.0898$	$R_1=0.0506$, $wR_2=0.1024$
R indices (all data)	$R_1=0.2227$, $wR_2=0.1026$	$R_1=0.1615$, $wR_2=0.0926$	$R_1=0.0534$, $wR_2=0.0982$	$R_1=0.0823$, $wR_2=0.1148$
Largest differential peak and hole (e Å^{-3})	0.543 and −0.790	0.557 and −0.660	0.757 and −0.642	0.595 and −0.530

ν(N–H) 3425m, ν(C=N) 1557s. ^{1}H NMR ($CDCl_3$, δ ppm, J Hz): 7.50 (dd, 1H, H5, ^3J(H5H4) = 7.9, ^4J(H5H3) = 0.9), 7.22 (dd, 1H, H3, ^3J(H3H4) = 7.9, ^4J(H3H5) = 0.9), 6.75 (t, 1H, H4, ^3J(H4H3) = 7.9, ^3J(H4H5) = 7.9), 5.09 (t, 1H, N*H*Et, ^3J(NH–H) = 5.5), 3.40 (dq, 2H, NHCH_2CH$_3$, ^3J(HH) = 7.4, ^3J(H–NH) = 5.5), 2.21 (s, 3H, *Me*C=N), 1.24 (t, 3H, NHCH$_2$$CH_3$, ^3J(HH) = 7.4). FAB-MS: m/z 1620 [MH]$^+$.

Method 2. Yield: 302 mg, 84%.

6.2.5. *[(Pd{2-ClC$_6$H$_3$C(Me)=NN=C(S)NHMe})-(Ph$_2$PCH$_2$PPh$_2$)-P,P](Cl) (**2a**)*

The diphosphine $Ph_2PCH_2PPh_2$ (17.0 mg, 0.044 mmol) was added to a suspension of complex **1a** (15 mg, 0.011 mmol) in acetone (15 cm^3), and the mixture was treated with two drops of concentrated hydrochloric acid (35%). The resulting solution was stirred for 4 h and the yellow solid formed was filtered off and dried in vacuo. Yield: 19.6 mg, 42%. *Anal*. $C_{35}H_{33}Cl_2N_3P_2PdS$ (767.0 g/mol) requires C, 54.8; H, 4.3; N, 5.5; S, 4.2. Found: C, 54.7; H, 4.2; N, 5.5; S, 4.1%. IR (cm^{-1}): ν(N–H) 3440s, 3210; ν(C=N) 1557m. ^{1}H NMR($CDCl_3$, δ ppm, J Hz): 6.69 (dd, 1H, H3, ^3J(H3H4) = 7.9, ^4J(H3H5) = 0.9), 6.21 (t, 1H, H4, ^3J(H4H3) = 7.9, ^3J(H4H5) = 7.9), 6.05 (dd, 1H, H5, ^3J(H5H4) = 7.9, ^4J(H5H3) = 0.9), 4.82 (q, 1H, N*H*Me, ^3J(NH–H) = 5.1), 3.61 (d, 1H, PCH_2P, ^2J(HP) = 9.2), 3.57 (d, 1H, PCH_2P, ^2J(HP) = 9.2), 3.01 (d, 3H, NH*Me*, ^3J(H–NH) = 5.1), 2.69 (s, 3H, *Me*C=N). ^{31}P–{^{1}H} ($CDCl_3$, δ ppm, J Hz): 24.4 (d, 1P, ^2J(PP) = 13.1), 22.8 (d, 1P, ^2J(PP) = 13.3). Λ_m = 133.1 ohm^{-1} cm^2 mol^{-1} (in acetonitrile).

Compounds **2b**–**2d** were synthesized similarly.

6.2.6. *[(Pd{2-ClC$_6$H$_3$C(Me)=NN=C(S)NHEt})-(Ph$_2$PCH$_2$PPh$_2$)-P,P](Cl) (**2b**)*

Yield: 15.4 mg, 34%. *Anal*. $C_{36}H_{35}Cl_2N_3P_2PdS$ (781.0 g/mol) requires C, 55.4; H, 4.5; N, 5.4; S, 4.1. Found: C, 55.4; H, 4.4; N, 5.4; S, 4.0%. IR (cm^{-1}): ν(N–H) 3432s; ν(C=N) 1558m. ^{1}H NMR ($CDCl_3$, δ ppm, J Hz): 6.77 (dd, 1H, H3, ^3J(H3H4) = 7.9, ^4J(H3H5) = 1.4), 6.32 (t, 1H, H4,

^3J(H4H3) = 7.9, ^3J(H4H5) = 7.9), 6.02 (ddd, 1H, H5, ^3J(H5H4) = 7.9 Hz, ^4J(H5P) = 5.1, ^4J(H5H3) = 1.4), 4.81 (t, 1H, N*H*Et, ^3J(NH–H) = 5.5), 3.60 (d, 1H, P CH_2P, ^2J(HP) = 9.2), 3.56 (d, 1H, PCH_2P, ^2J(HP) = 9.2), 3.42 (dq, 2H, NHCH_2CH$_3$, ^3J(HH) = 7.4 Hz, ^3J(H–NH) = 5.5), 2.67 (s, 3H, *Me*C=N), 1.20 (t, 3H, NHCH$_2$$CH_3$, ^3J(HH) = 7.4). ^{31}P–{^{1}H} NMR ($CDCl_3$, δ ppm, J Hz): 24.3 (d, 1P, ^2J(PP) = 13.1), 22.7 (d, 1P, ^2J(PP) = 13.1). Λ_m = 132.7 ohm^{-1} cm^2 mol^{-1} (in acetonitrile).

6.2.7. [(Pd{2-BrC$_6$H$_3$C(Me)=NN=C(S)NHMe})-(Ph$_2$PCH$_2$PPh$_2$)-P,P](Cl) (**2c**)

Yield: 33.0 mg, 74%. *Anal.* $C_{35}H_{33}BrClN_3P_2PdS$ (811.5 g/mol) requires C, 51.8; H, 4.1; N, 5.2; S, 4.0. Found: C, 51.6; H, 4.0; N, 5.1; S, 3.9%. IR (cm^{-1}): ν(N–H) 3426m; ν(C=N) 1559s. ^{1}H NMR ($CDCl_3$, δ ppm, J Hz): 7.01 (d, 1H, H3, ^3J(H3H4) = 7.9), 6.22 (t, 1H, H4, ^3J(H4H3) = 7.9 Hz, ^3J(H4H5) = 7.9), 6.10 (m, 1H, H5), 4.83 (br, 1H, N*H*Me), 3.72 (d, 1H, PCH_2P, ^2J(HP) = 9.2), 3.68 (d, 1H, PCH_2P, ^2J(HP) = 9.2), 2.98 (d, 3H, NH*Me*, ^3J(H–NH) = 5.1), 2.70 (s, 3H, *Me*C=N). ^{31}P–{^{1}H} NMR ($CDCl_3$, δ ppm, J Hz): 24.1 (d, 1P, ^2J(PP) = 13.1), 22.7 (d, 1P, ^2J(PP) = 13.1). Λ_m = 125.6 ohm^{-1} cm^2 mol^{-1} (in acetonitrile).

6.2.8. [(Pd{2-BrC$_6$H$_3$C(Me)=NN=C(S)NHEt})-(Ph$_2$PCH$_2$PPh$_2$)-P,P](Cl) (**2d**)

Yield: 13.2 mg, 30%. *Anal.* $C_{36}H_{35}BrClN_3P_2PdS$ (825.5 g/mol) requires C, 52.4; H, 4.3; N, 5.1; S, 3.9. Found: C, 52.3; H, 4.3; N, 5.0; S, 3.9%. IR (cm^{-1}): ν(N–H) 3428m; ν(C=N) 1557m. ^{1}H NMR ($CDCl_3$, δ ppm, J Hz): 7.01 (dd, 1H, H3, ^3J(H3H4) = 7.9, ^4J(H3H5) = 0.9), 6.22 (t, 1H, H4, ^3J(H4H3) = 7.9 Hz, ^3J(H4H5) = 7.9), 6.10 (m, 1H, H5), 4.82 (br, 1H, N*H*Et), 3.60 (d, 1H, PCH_2P, ^2J(HP) = 9.2), 3.56 (d, 1H, PCH_2P, ^2J(HP) = 9.2), 3.41 (dq, 2H, NHCH_2CH$_3$, ^3J(HH) = 7.4 Hz, ^3J(H–NH) = 5.5), 2.68 (s, 3H, *Me*C=N), 1.20 (t, 3H, NHCH$_2$$CH_3$, ^3J(HH) = 7.4). ^{31}P–{^{1}H} NMR ($CDCl_3$, δ ppm, J Hz): 24.2 (d, 1P, ^2J(PP) = 13.7), 22.8 (d, 1P, ^2J(PP) = 14.5). Λ_m = 130.2 ohm^{-1} cm^2 mol^{-1} (in acetonitrile).

6.2.9. [(Pd{2-ClC$_6$H$_3$C(Me)=NN=C(S)NHMe})$_2$-(μ-Ph$_2$PCH$_2$PPh$_2$)] (**3a**)

The diphosphine $Ph_2PCH_2PPh_2$ (17.8 mg, 0.046 mmol) was added to a suspension of complex **1a** (30 mg, 0.023 mmol) in acetone (15 cm^3). The mixture was stirred for 4 h. and the resulting yellow solid was filtered off and dried in vacuo. Yield: 19.6 mg, 42%. *Anal.* $C_{45}H_{42}Cl_2N_6P_2Pd_2S_2$ (1076.7 g/mol) requires C, 50.2; H, 3.9; N, 7.8; S, 6.0. Found: C, 50.1; H, 3.9; N, 7.7; S, 5.8%. IR (cm^{-1}): ν(N–H) 3440s; ν(C=N) 1557m. ^{1}H NMR ($CDCl_3$, δ ppm, J Hz): 6.69 (dd, 1H, H3, ^3J(H3H4) = 7.9 Hz, ^4J(H3H5) = 0.9), 6.21 (t, 1H, H4, ^3J(H4H3) = 7.9 Hz, ^3J(H4H5) = 7.9), 6.05 (dd, 1H, H5, ^3J(H5H4) = 7.9, ^4J(H5H3) = 0.9), 4.82 (q, 1H, N*H*Me, ^3J(NH–H) = 5.1), 3.73 (t, 1H, PCH_2P, ^2J(HP) = 10.2), 3.01 (d, 3H, NH*Me*, ^3J(H–NH) = 5.1), 2.69 (s, 3H, *Me*C=N). ^{31}P–{^{1}H} NMR ($CDCl_3$, δ ppm): δ = 23.7s.

Compounds **3b**–**3d** were prepared analogously.

6.2.10. [(Pd{2-ClC$_6$H$_3$C(Me)=NN=C(S)NHEt})$_2$-(μ-Ph$_2$PCH$_2$PPh$_2$)] (**3b**)

Yield: 15.4 mg, 34%. *Anal.* $C_{47}H_{46}Cl_2N_6P_2Pd_2S_2$ (1104.7 g/mol) requires C, 51.1; H, 4.2; N, 7.6; S, 5.8. Found: C, 51.3; H, 4.5; N, 7.5; S, 5.7%. IR (cm^{-1}): ν(N–H) 3432s; ν(C=N) 1558m. ^{1}H NMR ($CDCl_3$, δ ppm, J Hz): 6.77 (dd, 1H, H3, ^3J(H3H4) = 7.9, ^4J(H3H5) = 1.4), 6.32 (t, 1H, H4, ^3J(H4H3) = 7.9, ^3J(H4H5) = 7.9), 6.02 (ddd, 1H, H5, ^3J(H5H4) = 7.9, ^4J(H5P) = 5.1, ^4J(H5H3) = 1.4), 4.81 (t, 1H, N*H*Et, ^3J(NH–H) = 5.5), 3.58 (t, 1H, PCH_2P, ^2J(HP) = 9.2), 3.42 (dq, 2H, NHCH_2CH$_3$, ^3J(HH) = 7.4, ^3J(H–NH) = 5.5), 2.67 (s, 3H, MeC=N), 1.20 (t, 3H, NHCH$_2$$CH_3$, ^3J(HH) = 7.4). ^{31}P–{^{1}H} NMR ($CDCl_3$, δ ppm): 22.9s.

6.2.11. [(Pd{2-BrC$_6$H$_3$C(Me)=NN=C(S)NHMe})$_2$-(μ-Ph$_2$PCH$_2$PPh$_2$)] (**3c**)

Yield: 33.0 mg, 74%. *Anal.* $C_{45}H_{42}Br_2N_6P_2Pd_2S_2$ (1165.6 g/mol) requires C, 46.4; H, 3.6; N, 7.2; S, 5.5. Found: C, 46.1; H, 3.7; N, 6.9; S, 5.4%. IR (cm^{-1}): ν(N–H) 3426m; ν(C=N) 1559s. ^{1}H NMR ($CDCl_3$, δ ppm, J Hz): 7.01 (d, 1H, H3, ^3J(H3H4) = 7.9), 6.22 (t, 1H, H4, ^3J(H4H3) = 7.9 Hz, ^3J(H4H5) = 7.9), 6.10 (m, 1H, H5), 4.83 (br, 1H, N*H*Me), 3.71 (t, 1H, PCH_2P, ^2J(HP) = 10.2), 2.98 (d, 3H, NH*Me*, ^3J(H–NH) = 5.1), 2.70 (s, 3H, MeC=N). ^{31}P–{^{1}H} NMR ($CDCl_3$, δ ppm): 23.6s.

6.2.12. [(Pd{2-BrC$_6$H$_3$C(Me)=NN=C(S)NHEt})$_2$-(μ-Ph$_2$PCH$_2$PPh$_2$)] (**3d**)

Yield: 13.2 mg, 30%. *Anal.* $C_{47}H_{46}Br_2N_6P_2Pd_2S_2$ (1193.6 g/mol) requires C, 47.3; H, 3.9; N, 7.0; S, 5.4. Found: C, 47.1; H, 3.9; N, 6.7; S, 5.2%. IR (cm^{-1}): ν(N–H) 3428m; ν(C=N) 1557m. ^{1}H NMR ($CDCl_3$, δ ppm, J Hz): 7.01 (dd, 1H, H3, ^3J(H3H4) = 7.9 Hz, ^4J(H3H5) = 0.9), 6.22 (t, 1H, H4, ^3J(H4H3) = 7.9, ^3J(H4H5) = 7.9), 6.10 (m, 1H, H5), 4.82 (br, 1H, N*H*Et), 3.58 (t, 1H, PCH_2P, ^2J(HP) = 9.2), 3.41 (dq, 2H, NHCH_2CH$_3$, ^3J(HH) = 7.4, ^3JH–NH = 5.5), 2.68 (s, 3H, *Me*C=N), 1.20 (t, 3H, NHCH$_2$$CH_3$, ^3J(HH) = 7.4). ^{31}P–{^{1}H} NMR ($CDCl_3$, δ ppm): 23.7s.

6.2.13. [Pd{2-ClC$_6$H$_3$C(Me)=NN=C(S)NHMe}-(Ph$_2$PCH$_2$PPh$_2$-P)] (**4a**)

The diphosphine $Ph_2PCH_2PPh_2$ (59.5 mg, 0.155 mmol) was added to a suspension of complex **1a** (50 mg, 0.038 mmol) in acetone (15 cm^3). The mixture was stirred for 4 h. The resulting yellow solid was filtered off and dried in vacuo. Yield: 130 mg, 78%. *Anal.* $C_{35}H_{32}ClN_3P_2PdS$ (730.5 g/mol) requires C, 57.5; H, 4.4; N, 5.8; S, 4.4. Found: C, 57.7; H, 4.5; N, 5.5; S, 4.3%. IR (cm^{-1}): ν(N–H) 3431m; ν(C=N) 1555m. ^{1}H NMR ($CDCl_3$, δ ppm, J Hz): 6.75 (d, 1H, H3, ^3J(H3H4) = 7.9), 6.31 (t, 1H, H4,

^3J(H4H3) = 7.9, ^3J(H4H5) = 7.9), 6.15 (m, 1H, H5), 4.81 (br, 1H, N*H*Me), 3.22 (d, 2H, P*CH*$_2$P, ^2J(HP) = 9.5), 2.97 (d, 3H, NH*CH*$_3$, ^3J(H–NH) = 5.1), 2.67 (s, 3H, *Me*C=N). ^{31}P–{^{1}H} NMR ($CDCl_3$, δ ppm, J Hz): 24.1 (d, 1P, P_A, ^2J(PP) = 79.8), −26.7 (d, 1P, P_B, ^2J(PP) = 79.8).

Compounds **4b**–**4d** were prepared analogously.

6.2.14. [Pd{2-ClC$_6$H$_3$C(Me)=NN=C(S)NHEt}-(Ph$_2$PCH$_2$PPh$_2$-P)] (**4b**)

Yield: 127 mg, 70%. *Anal.* $C_{36}H_{34}ClN_3P_2PdS$ (744.6 g/mol) requires C, 58.1; H, 4.6; N, 5.6; S, 4.3. Found: C, 57.9; H, 4.7; N, 5.7; S, 4.2%. IR (cm^{-1}): ν(N–H) 3423s; ν(C=N) 1555m. ^{1}H NMR ($CDCl_3$, δ ppm, J Hz): 6.74 (d, 1H, H3, ^3J(H3H4) = 7.9), 6.31 (t, 1H, H4, ^3J(H4H3) = 7.9, ^3J(H4H5) = 7.9), 6.15 (m, 1H, H5), 4.81 (br, 1H, N*H*Et), 3.41 (m, 2H, NH*CH*$_2$CH$_3$), 3.24 (d, 2H, P*CH*$_2$P, ^2J(HP) = 9.5), 2.67 (s, 3H, *Me*C=N), 1.18 (t, 3H, NHCH$_2$*CH*$_3$, ^3J(HH) = 7.4). ^{31}P–{^{1}H} NMR ($CDCl_3$, δ ppm, J Hz): 23.7 (d, 1P, P_A, ^2J(PP) = 79.8), −26.7 (d, 1P, P_B, ^2J(PP) = 79.8).

6.2.15. [(Pd{2-BrC$_6$H$_3$C(Me)=NN=C(S)NHMe})$_2$-(Ph$_2$PCH$_2$PPh$_2$-P)] (**4c**)

Yield: 64.1 mg, 73%. *Anal.* $C_{35}H_{32}BrN_3P_2PdS$ (775.0 g/mol) requires C, 54.2; H, 4.2; N, 5.4; S, 4.1. Found: C, 54.5; H, 4.4; N, 5.3; S, 4.0%. IR (cm^{-1}): ν(N–H) 3428m; ν(C=N) 1558m. ^{1}H NMR ($CDCl_3$, δ ppm, J Hz): 6.98 (m, 1H, H3), 6.21 (m, 1H, H4), 6.11 (m, 1H, H5), 4.83 (br, 1H, N*H*Me), 3.23 (d, 2H, P*CH*$_2$P, ^2J(HP) = 9.7), 2.98 (d, 3H, NH*CH*$_3$, ^3J(H–NH) = 5.1), 2.69 (s, 3H, *Me*C=N). ^{31}P–{^{1}H} NMR ($CDCl_3$, δ ppm, J Hz): 23.9 (d, 1P, P_A, ^2J(PP) = 79.8), −26.8 (d, 1P, P_B, ^2J(PP) = 79.8).

6.2.16. [Pd{2-BrC$_6$H$_3$C(Me)=NN=C(S)NHEt}-(Ph$_2$PCH$_2$PPh$_2$-P)] (**4d**)

Yield: 149 mg, 86%. *Anal.* $C_{36}H_{34}BrN_3P_2PdS$ (789.0 g/mol) requires C, 54.8; H, 4.3; N, 5.3; S, 4.1. Found: C, 55.0; H, 4.5; N, 5.0; S, 3.9%. IR (cm^{-1}): ν(N–H) 3418m; ν(C=N) 1556m. ^{1}H NMR ($CDCl_3$, δ ppm, J Hz): 6.97 (m, 1H, H3), 6.21 (m, 1H, H4), 6.12 (m, 1H, H5), 4.81 (br, 1H, N*H*Et), 3.42 (m, 2H, NH*CH*$_2$CH$_3$), 3.24 (d, 2H, P*CH*$_2$P, ^2J(HP) = 9.7), 2.68 (s, 3H, *Me*C=N), 1.22 (t, 3H, NHCH$_2$*CH*$_3$, ^3J(HH) = 7.4 Hz). ^{31}P–{^{1}H} NMR ($CDCl_3$, δ ppm, J Hz): 23.6 (d, 1P, P_A, ^2J(PP) = 75.1), −26.7 (d, 1P, P_B, ^2J(PP) = 75.1).

7. Crystal structures

Crystals of complexes **1b**, **1d**, **4c** and **4d**, were mounted on a glass fibre and transferred to the diffractometer. Three dimensional, room temperature X-ray data were collected with CAD4 Enraf Nonius (**1b** and **1d**) and Siemens (**4c** and **4d**) diffractometers by the omega scan method, using monochromated Mo K_α radiation. All the measured reflections were corrected for Lorentz and polarization effects and for absorption by semi-empirical methods based on symmetry-equivalent and repeated reflections [T_{max}/T_{min} = 0.643/0.603 (**1b**), 0.309/0.200 (**1d**), 0.373/0.319 (**4c**) and 0.711/0.547 (**4d**)]. The structures were solved by direct methods and refined by full matrix least squares on F^2. Hydrogen atoms were included in calculated positions and refined using the riding mode. The structure of **4d** contains 1 symmetry related void of 297.00 Å^3 containing unresolvable solvent, this was treated using the squeeze method lowering the R_1 value by 5.76% [37]. Refinement converged at a final R = 0.0424 (**1b**), 0.0358 (**1d**), 0.0394 (**4c**) and 0.0506 (**4d**) (observed data, F), and wR_2 = 0.1026 (**1b**), 0.0926 (**1d**), 0.0982 (**4c**) and 0.1148 (**4d**) (all unique data, F^2), with allowance for thermal anisotropy of all non-hydrogen atoms. Minimum and maximum final electron densities: −0.790 and 0.543 (**1b**), −0.660 and 0.557 (**1d**), −0.642 and 0.757 (**4c**), −0.530 and 0.595 e Å^{-3} (**4d**). The structure solutions and refinements were carried out with the SHELX-97 [38] program package.

Acknowledgements

We thank the DGESIC (Ministerio de Ciencia y Tecnología) Proyecto BQU2002-04533-C02-01 and the Xunta de Galicia, incentive PGIDIT03PXIC20912PN, for financial support. J. Martínez acknowledges a fellowship from the Ministerio de Ciencia y Tecnología (Grant No. PB98-0638-C02-01/02).

Appendix A. Supplementary data

Crystallographic data (excluding structure factors) for the structures reported in this paper have been deposited with the Cambridge Crystallographic Data Centre as supplementary publication numbers 292962 (**1b**), 292963 (**1d**), 292965 (**4c**) 29294 (**4d**). Copies of the data can be obtained free of charge on application to CCDC, 12 Union Road, Cambridge CB2 1EZ, UK (fax: +44 12336033; e-mail: deposit@ccdc.cam.ac.uk, or on the web www.ccdc.cam.ac.uk). Supplementary data associated with this article can be found, in the online version, at doi:10.1016/j.poly.2006.04.013.

References

[1] I. Omae, in: Organometallic Intramolecular Coordination Compounds, Elsevier Science, Amsterdam–New York, 1986.
[2] V.V. Dunina, O.A. Zalevskaya, V.M. Potapov, Russ. Chem. Rev. 571 (1984) 250.
[3] G.R. Newkome, W.E. Puckett, W.K. Gupta, G.E. Kiefer, Chem. Rev. 86 (1986) 451.
[4] A.D. Ryabov, Chem. Rev. 90 (1990) 403.
[5] M. Pfeffer, Recl. Trav. Chim. Pays-Bas 109 (1990) 567.
[6] (a) M. Pfeffer, J.P. Sutter, M.A. Rottevel, A. de Cian, J. Fischer, Tetrahedron 48 (1992) 2427;
(b) J. Dupont, M. Pfeffer, J. Spencer, Eur. J. Inorg. Chem. (2001) 1917.
[7] A.D. Ryabov, R. van Eldik, G. Le Borgne, M. Pfeffer, Organometallics 12 (1993) 1386.
[8] B.S. Wild, Coord. Chem. Rev. 166 (1997) 291.

[9] S.Y.M. Chooi, P.H. Leung, C.C. Lim, K.F. Mok, G.H. Quek, K.Y. Sim, M.K. Tan, Tetrahedron: Asymmetry 3 (1992) 529.
[10] (a) P. Espinet, M.A. Esteruelas, L.A. Oro, J.L. Serrano, E. Sola, Coord. Chem. Rev. 17 (1992) 215;
(b) M. Marcos, in: J.L. Serrano (Ed.), Metallomesogens. Synthesis, Properties and Applications, VCH, Weinheim, 1996.
[11] C. Navarro-Ranninger, I. López solera, J. Rodríguez, J.L. García-Ruano, P.R. Raithby, J.R. Masaguer, C. Alonso, J. Med. Chem. 36 (1993) 3795.
[12] C. Navarro-Ranninger, I. López-Solera, V.M. Gonzalez, J.M. Pérez, A. Alvarez-Valdés, A. Martin, P.R. Raithby, J.R. Masaguer, C. Alonso, Inorg. Chem. 35 (1996) 5181.
[13] (a) A. Bose, C.H. Saha, J. Mol. Catal. 49 (1989) 271;
(b) W.A. Herrmann, C. Brossmer, K. Oefele, C.P. Reisinger, T. Priermeier, M. Beller, H. Fischer, Angew. Chem., Int. Ed. Engl. 34 (1995) 1844.
[14] M. López-Torres, A. Fernández, J.J. Fernández, S. Castro-Juiz, A. Suárez, J.M. Vilay, M.T. Pereira, Organometallics 20 (2001) 1350.
[15] J.M. Vila, M. Gayoso, M.T. Pereira, M. López-Torres, J.J. Fernández, A. Fernández, J.M. Ortigueira, J. Organomet. Chem. 532 (1997) 171.
[16] J.M. Vila, M.T. Pereira, J.M. Ortigueira, D. Lata, M. López-Torres, J.J. Fernández, A. Fernández, H. Adams, J. Organomet. Chem. 566 (1998) 93.
[17] A. Fernández, J.J. Fernández, M. López-Torres, A. Suárez, J.M. Ortigueira, J.M. Vila, H. Adams, J. Organomet. Chem. 612 (2000) 85.
[18] A. Fernández, P. Uría, J.J. Fernández, M. López-Torres, A. Suárez, D. Vázquez-García, M.T. Pereira, J.M. Vila, J. Organomet. Chem. 620 (2001) 8.
[19] J.M. Vila, T. Pereira, J.M. Ortigueira, M. López-Torres, A. Castiñeiras, D. Lata, J.J. Fernández, A. Fernández, J. Organomet. Chem. 556 (1998) 21.
[20] A. Fernández, M. López-Torres, A. Suárez, J.M. Ortigueira, T. Pereira, J.J. Fernández, J.M. Vila, H. Adams, J. Organomet. Chem. 598 (2000) 1.
[21] A. Amoedo, M. Graña, J. Martinez, T. Pereira, M. Lopez-Torres, A. Fernandez, J.J. Fernandez, J.M. Vila, Eur. J. Inorg. Chem. (2002) 613.
[22] J.M. Vila, T. Pereira, J.M. Ortigueira, M. Graña, D. Lata, A. Suarez, J.J. Fernandez, A. Fernandez, M. Lopez-Torres, H. Adams, J. Chem. Soc., Dalton Trans. (1999) 4193.
[23] J. Martinez, M.T. Pereira, I. Buceta, G. Alberdi, A. Amoedo, J.J. Fernandez, M. Lopez-Torres, J.M. Vila, Organometallics 22 (2003) 5581.
[24] D.X. West, D.X.J.S. Ives, G.A. Bain, A.E. Liberta, J. Valdés-Martínez, K.H. Ebert, S. Hernández-Ortega, Polyhedron 16 (1997) 1995.
[25] H. Onoue, I. Moritani, J. Organomet. Chem. 43 (1972) 431.
[26] H. Onoue, K. Minami, K. Nakawaga, Bull. Chem. Soc. Jpn. 43 (1970) 3480.
[27] D. Kovala-Demertzi, A. Domopoulou, M.A. Demertzis, C.P. Raptopoulou, A. Terzis, Polyhedron 13 (1994) 1917.
[28] D. Kovala-Demertzi, A. Domopoulou, M.A. Demertzis, J. Valdés-Martínez, S. Hernández-Ortega, G. Espinosa-Pérez, D.X. West, M.M. Salberg, G.A. Bain, P.D. Bloom, Polyhedron 15 (1996) 665.
[29] T.S. Lobana, A. Sánchez, J.S. Casas, A. Castiñeiras, J. Sordo, M.S. García-Tasende, E.M. Vázquez-López, J. Chem. Soc., Dalton Trans. (1997) 4289.
[30] P.S. Pregosin, R.W. Kuntz, in: ^{31}P and ^{13}C NMR of Transition Metal Phosphine Complexes, in: P. Diehl, E. Fluck, R. Kosfeld (Eds.), NMR, vol. 16, Springer, Berlin, 1979.
[31] J. Albert, M. Gómez, J. Granell, J. Sales, Organometallics 9 (1990) 1405.
[32] J. Albert, J. Granell, J. Sales, M. Font-Bardía, X. Solans, Organometallics 14 (1995) 1393.
[33] J. Vicente, J.A. Abad, A.D. Frankland, M.C. Ramirez de Arellano, Chem. Eur. J. 5 (1999) 3067.
[34] L. Pauling, The Nature of the Chemical Bond, 3rd ed., Cornell University Press, New York, 1960.
[35] J.M. Vila, T. Pereira, J.M. Ortigueira, A. Amoedo, M. Graña, G. Alberdi, M. López-Torres, A. Fernandez, J. Organomet. Chem. 663 (2002) 239.
[36] D.D. Perrin, W.L.F. Armarego, Purification of Laboratory Chemicals, 4th ed., Butterworth-Heinemann, London, 1996.
[37] P. van der Slius, A.L. Spek, Acta Crystallogr., Sect. A 46 (1990) 194.
[38] G.M. Sheldrick, SHELX-97, An Integrated System for Solving and Refining Crystal Structures from Diffraction Data, University of Göttingen, Germany, 1997.

some bimetallic enzymes [22–24]. The catecholase activity of binuclear Cu(II) complexes was studied to identify functional as well as structural models for type III copper enzymes like tyrosinase and catechol oxidase [25–27]. Hydrolysis is found to be the key process in the active sites of a number of enzymes, namely urease, carbon monoxide dehydrogenase, superoxide dismutase, etc., mediated by nickel ions [28] and carboxy peptidase, alkaline phosphatase and β-lactanase mediated by zinc ions [29,30]. The hydrolysis of phosphate mono-, di- and tri-esters by metal complexes such as Cu(II), Zn(II), Cd(II), etc., are used in the development of artificial nucleases for use in molecular genetics and genetic engineering [31–33]. A variety of 'end-off' binuclear complexes containing an endogenous phenolato bridge with either one or two exogenous bridging units, such as acetato, hydroxo, azido and cyano groups, have already been reported [34–38].

Thus, in the present work, we have synthesized a new 'end-off' binucleating ligand (L) by the Mannich base reaction. The ligand contains a highly reactive aldehyde group, which may lead to the extension of its structure into a supramolecular moiety. Synthesis and electrochemical studies of such supramolecular moieties are also in progress. The structure of ligand (L) has been solved by the X-ray crystallographic method. The ligand has been used to prepare Cu(II), Ni(II) and Zn(II) mononuclear complexes and μ-phenoxo endogenous and bis-μ-acetato exogenous tribridged binuclear complexes. The spectral, electrochemical, magnetic and catalytic studies of these complexes are also discussed.

2. Experimental

2.1. Physical measurements

Elemental analysis of the complexes was obtained using a Haereus C, H, N rapid analyzer. ^{1}H NMR spectra were recorded using a JEOL GSX 400 MHz NMR spectrometer. Electronic spectral studies were carried out on a Hitachi 320 spectrophotometer in the range 200–800 nm. IR spectra were recorded on a Shimadzu FT-IR 8300 series spectrophotometer on KBr disks in the range 4000–400 cm^{-1}. Mass spectra were obtained on a JEOL DX-303 Mass spectrometer. Molar conductivity was measured by using an Elico digital conductivity bridge model CM-88 using a freshly prepared solution of the complex in dimethyl formamide. Cyclic voltammograms were obtained on CHI-600A electrochemical analyzer. The measurements were carried out under oxygen free conditions using a three-electrode cell in which a glassy carbon electrode was the working electrode, a saturated Ag/AgCl electrode was the reference electrode and a platinum wire was used as the auxiliary electrode. A ferrocene/ferrocenium (1+) couple was used as an internal standard and $E_{1/2}$ of the ferrocene/ferrocenium (Fc/Fc^+) couple under the experimental conditions is 470 mV. Tetra(*n*-butyl)ammonium perchlorate (TBAP) was used as the supporting electrolyte. The room temperature magnetic moment was measured on a PAR vibrating sample magnetometer Model-155. The variable-temperature magnetic moment was measured on an EG&G Princeton applied research VSM model 4500. X-band ESR spectra were recorded at 25 °C on a Varian EPR-E 112 spectrometer using diphenylpicrylhydrazine (DPPH) as the reference. The atomic absorption spectral data were recorded using a Varian spectra AA-200 model atomic absorption spectrophotometer. The catalytic oxidation of catechol to *o*-quinone by the copper complexes and the hydrolysis of 4-nitrophenylphosphate by the copper, nickel and zinc complexes were studied in a 10^{-3} M dimethylformamide solution. The reaction was followed spectrophotometrically by choosing the strongest absorbance of *o*-quinone at 390 nm and monitoring the increase in the absorbance, and the hydrolysis of *p*-nitrophenyl phosphate was monitored by following the UV absorbance change at 390 nm (assigned to the 4-nitrophenolate anion) as a function of time. A plot of $\log(A\alpha/A\alpha - A_t)$ versus time was made for each complex and the rate constant for the catalytic oxidation and the hydrolysis of 4-nitrophenyl phosphate was calculated.

The crystal data of ligand L were measured on a CAD4 diffractometer using the $\omega/2\theta$ scan mode. The stability of the crystal was checked by monitoring three standard reflections after every 200 reflections. Unit cell parameters were determined by least-squares refinement of 18 reflec-

Table 1
Summary of crystallographic data for ligand (L)

Empirical formula	$C_{19}H_{33}Cl_3N_4O_{17}$
Formula weight (g mol^{-1})	695.84
Temperature (K)	293(2)
Wavelength (Å)	0.71073
Crystal system	triclinic
Space group	$P\bar{1}$
Unit cell dimensions	
a (Å)	9.848(3)
b (Å)	10.679(5)
c (Å)	15.645(8)
α (°)	93.50(4)
β (°)	99.96(4)
γ (°)	104.55(3)
V (Å^3)	1559.1(12)
Z	2
D_{calc} (Mg m^{-3})	1.482
Absorption coefficient (mm^{-1})	0.373
$F(000)$	724
Crystal size (mm)	$0.60 \times 0.32 \times 0.25$
θ Range for data collection (°)	1.33–28.97
Index ranges	$-13 \leqslant h \leqslant 13$, $-14 \leqslant k \leqslant 14$, $0 \leqslant l \leqslant 21$
Reflections collected/unique (R_{int})	8758/8257 (0.075)
Refinement method	full-matrix least-squares on F^2
Data/restraints/parameters	8257/0/404
Goodness-of-fit on F^2	1.438
Final R indices [$I > 2\sigma(I)$]	$R_1 = 0.119$, $wR_2 = 0.345$
R indices (all data)	$R_1 = 0.162$, $wR_2 = 0.376$
Largest difference in peak and hole (e Å^{-3})	1.442 and −0.683

Table 2
Selected bond lengths (Å) and angles (°)

Atoms	Bond length (Å)	Atoms	Angle (°)
C1–O1	1.347(4)	O2–C7–C4	124.5(4)
C7–O2	1.219(6)	C12–N1–C9	109.4(3)
C8–N1	1.466(5)	C10–N2–C11	109.8(3)
C9–N1	1.488(5)	C18–N3–C15	109.1(3)
C10–N2	1.491(6)	C16–N4–C17	109.7(3)
C11–N2	1.494(6)		
C12–N1	1.456(5)		
C13–N2	1.492(6)		
C14–N3	1.499(5)		
C15–N3	1.509(5)		
C16–N4	1.492(5)		
C17–N4	1.504(6)		
C18–N3	1.501(4)		
C19–N4	1.545(6)		

tions in the range 7.29–13.52°. The ranges of *h*, *k* and *l* are −13–13, −14–14 and 0–21, respectively.

The structure was solved by direct methods using the program SHELXS-97 [39]. All non-hydrogen atoms were refined anisotropically [39] by full-matrix least-squares procedures with the weight $w = 1/[\sigma^2(F_o^2) + (0.2000P)^2]$, where $P = (F_o^2 + 2F_c^2)/3$. All hydrogen atoms were fixed geometrically and allowed to ride along with the corresponding non-hydrogen atoms during the refinement. The crystal data and structure refinement details for ligand L are given in Table 1, whereas selected bond lengths and angles are listed in Table 2.

2.2. Materials and safety note

Formaldehyde solution, *N*-methyl piperazine and *p*-hydroxybenzaldehyde were purchased from Qualigens and used as such. Methanol, acetonitrile and dimethyl formamide were purchased from Qualigens and distilled before usage. TBAP, used as the supporting electrolyte in electrochemical measurements, was purchased from Fluka and recrystallised from hot methanol. (*Caution!* TBAP is potentially explosive; hence care should be taken in handling the compound). All other chemicals and solvents were of analytical grade and were used as received without any further purification.

2.3. Synthesis of the ligand, 2,6-bis[(N-methyl piperazine-1-yl)methyl]-4-formyl phenol (L)

The ligand (L) was synthesized by taking *p*-hydroxybenzaldehyde (4.27 g, 0.035 mol) in methanol (100 ml) mixed with *N*-methyl piperazine (7.76 ml, 0.07 mol) and the solution was refluxed for 1 h. Then formaldehyde solution (37%) (5.28 ml, 0.07 mol) was added slowly with stirring and the resulting solution was kept at this temperature for 24 h. Two 5 ml portions of formaldehyde were added at approximately 8 h intervals. After that time, methanol was evaporated under vacuum and the resulting oil was extracted with chloroform and recrystallised with diethylether (Scheme 1). A colourless compound was obtained. Yield: 8.1 g (67%), m.p.: 96 °C. Mass (EI) *m*/*z*: 346.47. *Anal.* Calc. for $C_{19}H_{30}N_4O_2$: C, 65.87; H, 8.73; N, 16.17. Found: C, 65.97; H, 8.62; N, 16.29%. Selected IR data (KBr disc, ν/cm^{-1}): 1680 (C=O) s, 3398 (OH) br, 1456 (N–CH_3) br. ^1H NMR (δ ppm in $CDCl_3$) ~2.22 (s, 6H, N–CH_3), ~2.45 (broad S, 16H, methylene protons), ~3.64 (s, 4H, benzylic protons), ~7.3 (s, 2H, Ar–H), 9.8 (s, 1H, –CHO proton). UV–Vis [λ_{max} (nm) (ε, $M^{-1}\,cm^{-1}$)] in MeOH: 286 (21 900).

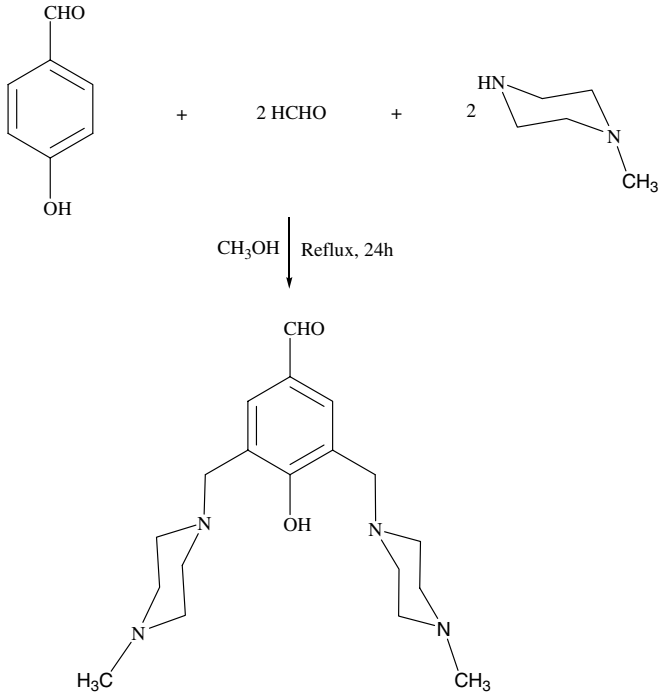

Scheme 1.

2.4. Synthesis of the mononuclear complexes

2.4.1. Synthesis of the [CuL(OAc)] · H_2O complex

To a 40 ml methanol solution of the ligand (L) (1.039 g, 0.003 mol) was added $Cu(OAc)_2 \cdot H_2O$ (0.598 g, 0.003 mol) dissolved in 20 ml of methanol, and the resulting solution was refluxed for 4 h. After the reaction was over, the solution was filtered when hot and allowed to stand at room temperature. After slow evaporation of the solvent at 25 °C, a dark green compound was obtained. The compound was recrystallised from acetonitrile. Yield: 1.32 g (75%). *Anal.* Calc. for $[C_{21}H_{32}N_4O_4Cu] \cdot H_2O$: C, 51.89; H, 7.05; N, 11.53; Cu, 13.07. Found: C, 51.81; H, 7.12; N, 11.47; Cu, 13.13%. Selected IR data (KBr disc, ν/cm^{-1}): 3449, 1680, 1450, 1103, 651. UV–Vis [λ_{max} (nm) (ε, $M^{-1}\,cm^{-1}$)] in MeOH: 590 (125), 352 (17 200), 288 (23 500), $g_{\|} = 2.21$, $g_{\perp} = 2.09$ and $A_{\|} = 180$. $\mu_{eff} = 1.72$ BM.

2.4.2. Synthesis of the [NiL(OAc)] · H_2O complex

The Ni(II) complex was prepared by following the above procedure using the ligand (L) (1.039 g, 0.003 mol)

and $Ni(OAc)_2 \cdot 4H_2O$ (0.746 g, 0.003 mol). A light green compound was obtained on recrystallisation from acetonitrile. Yield: 1.38 g (79%). *Anal.* Calc. for $[C_{21}H_{32}N_4O_4Ni] \cdot H_2O$: C, 52.41; H, 7.12; N, 11.64; Ni, 12.20, Found: C, 52.44; H, 7.06; N, 11.67; Ni, 12.16%. Selected IR data (KBr disc, ν/cm^{-1}): 3451, 1680, 1453, 1106, 653. UV–Vis [λ_{max} (nm) (ε, $M^{-1}\,cm^{-1}$)] in MeOH: 574 (143), 356 (16100), 289 (21700).

2.4.3. Synthesis of the $[ZnL(OAc)(H_2O)_2]$ complex

The Zn(II) complex was prepared by following the above procedure using the ligand (L) (1.039 g, 0.003 mol) and $Zn(OAc)_2 \cdot 2H_2O$ (0.658 g, 0.003 mol). A colourless compound was obtained on recrystallisation from acetonitrile. Yield: 1.25 g (71%). *Anal.* Calc. for $[C_{21}H_{32}N_4O_4Zn(H_2O)_2]$: C, 49.85; H, 7.17; N, 11.07; Zn, 12.92. Found: C, 49.81; H, 7.21; N, 11.15; Zn, 12.83%. Selected IR data (KBr disc, ν/cm^{-1}): 3451, 1680, 1455, 1108, 649. UV–Vis [λ_{max} (nm) (ε, $M^{-1}\,cm^{-1}$)] in MeOH: 286 (21600).

2.5. Synthesis of the binuclear complexes

2.5.1. Synthesis of the $[Cu_2L(OAc)_2](ClO_4) \cdot 2H_2O$ complex

A solution of the ligand (L) (0.693 g, 0.002 mol) in MeOH (40 ml) was added to $Cu(OAc)_2 \cdot H_2O$ (0.798 g, 0.004 mol) in MeOH (20 ml), and the resulting solution was refluxed for 7 h. The mixture was then reacted with one equivalent of $NaClO_4$ dissolved in 10 ml of methanol and refluxed for a further hour. A dark green precipitate was collected on evaporation of the resulting solution to half the volume and then cooling by standing at room temperature (25 °C). A dark green coloured compound was obtained on recrystallisation from acetonitrile. Yield: 1.13 g (78%). *Anal.* Calc. for $[C_{23}H_{35}N_4O_6Cu_2](ClO_4) \cdot 2H_2O$: C, 38.04; H, 5.41; N, 7.72; Cu, 17.50. Found: C, 38.09; H, 5.36; N, 7.62, Cu; 17.38%. Selected IR data (KBr disc, ν/cm^{-1}): 3447, 1680, 1485, 1105, 654. Conductance ($\Lambda_m/S\,cm^2\,mol^{-1}$) in DMF 84. UV–Vis [$\lambda_{max}$ (nm) (ε, $M^{-1}\,cm^{-1}$)] in MeOH: 662 (118), 358 (15800), 284 (24600). $g = 2.1$. $\mu_{eff} = 1.58$ BM.

2.5.2. Synthesis of the $[Ni_2L(OAc)_2(H_2O)_2]ClO_4$ complex

The Ni(II) complex was prepared by following the above procedure by using the ligand (L) (0.693 g, 0.002 mol) and $Ni(OAc)_2 \cdot 4H_2O$ (0.995 g, 0.004 mol). A light green compound was obtained on recrystallisation from acetonitrile. Yield: 1.04 g (73%). *Anal.* Calc. for $[C_{23}H_{35}N_4O_6Ni_2(H_2O)_2](ClO_4)$: C, 38.56; H, 5.49; N, 7.82; Ni, 16.38. Found: C, 38.43; H, 5.38; N, 7.97; Ni, 16.33%. Selected IR data (KBr disc, ν/cm^{-1}): 3449, 1680, 1467, 1104, 653. Conductance ($\Lambda_m/S\,cm^2\,mol^{-1}$) in DMF 89. UV–Vis [$\lambda_{max}$ (nm) (ε, $M^{-1}\,cm^{-1}$)] in MeOH: 800 (105), 618 (140), 561 (225), 363 (16700), 286 (23100).

2.5.3. Synthesis of the $[Zn_2L(OAc)_2(H_2O)_2]ClO_4$ complex

The Zn(II) complex was prepared by following the above procedure using the ligand (L) (0.693 g, 0.002 mol) and $Zn(OAc)_2 \cdot 2H_2O$ (0.878 g, 0.004 mol). A colourless compound was obtained on recrystallisation from acetonitrile. Yield: 1.02 g (70%). *Anal.* Calc. for $[C_{23}H_{35}N_4O_6Zn_2(H_2O)_2](ClO_4)$: C, 36.07; H, 5.66; N, 7.31; Zn, 17.08. Found: C, 36.18; H, 5.54; N, 7.42; Zn, 17.05%. Selected IR data (KBr disc, ν/cm^{-1}): 3451, 1680, 1475, 1108, 652. Conductance ($\Lambda_m/S\,cm^2\,mol^{-1}$) in DMF 81. UV–Vis [$\lambda_{max}$ (nm) (ε, $M^{-1}\,cm^{-1}$)] in MeOH: 286 (22500).

3. Results and discussion

A new end-off type ligand has been synthesized by the usual procedure of the Mannich reaction (Scheme 1) and characterized. Using this end-off ligand, mono and binuclear Cu(II), Ni(II) and Zn(II) complexes were prepared as shown in Scheme 2. The complexes were characterized by spectral studies. Their magnetic, electrochemical and catalytic behaviors are discussed.

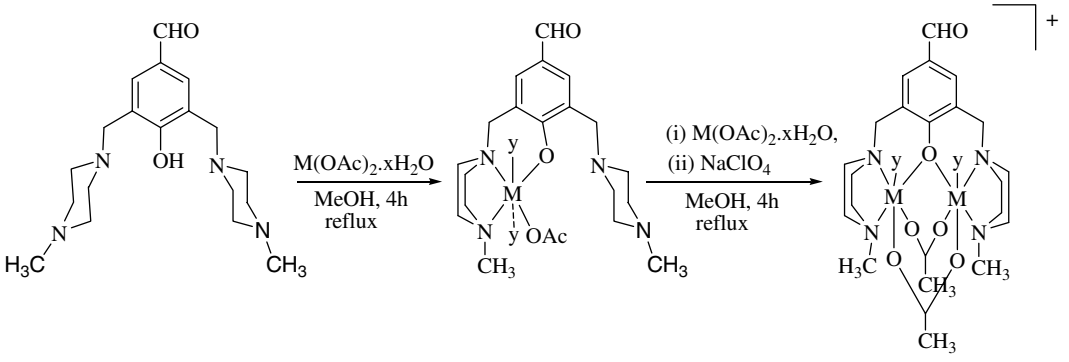

Complexes	M	x	y
1	Cu	1	-
2	Ni	4	-
3	Zn	2	H_2O

Complexes	M	x	y
4	Cu	1	-
5	Ni	4	H_2O
6	Zn	2	H_2O

Scheme 2.

3.1. The structure of ligand (L)

Crystals of the ligand L of X-ray quality were obtained from 1% perchloric acid in methanol by slow evaporation at room temperature. The ORTEP diagram of the ligand is shown in Fig. 1. The average C_{sp^2}–C_{sp^2} [1.395(2) Å] in the phenyl ring and C_{sp^3}–N [1.481(2) Å] bond distances are comparable with the corresponding values reported by Allen et al., in 1987 [40] [1.397(9) Å and 1.499(18) Å]. The piperazine rings adopt a chair conformation, which is confirmed by puckering parameters [41] and asymmetry parameters [42] [$Q_T = 0.579(8)$ and $\theta = 179.1(7)°$]. The mirror and twofold symmetry pass through N1 ($\Delta C_s = 0.006(4)$), C9 ($\Delta C_s = 0.002(4)$) and C10 ($\Delta C_s = 0.007(4)$) atoms and N1–C12 ($\Delta C_s = 0.006(3)$), C9–N1 ($\Delta C_2 = 0.004(3)$) and C10–C9 ($\Delta C_2 = 0.004(3)$) bonds, respectively. N–H···O, O–H···O and C–H···O hydrogen bonds stabilize the crystal packing. The O8 atom of the perchlorate is involved in C–H···O hydrogen bonds [H11A···$O8^i$ = 2.53 Å; C11···$O8^i$ = 3.380(1) Å and C11–H11A···$O8^i$ = 134°; i = −1 + *x*, *y*, *z*] and the O9 atom is involved in bifurcated hydrogen bonds C14–H14A···O9···H15B–C15 = 42.7(1)°. Neighboring molecules linked through N–H···O hydrogen bonds run along the '*ac*' plane, stabilizing the unit cell packing.

3.2. Spectral studies

The IR spectrum of the ligand shows a broad band at 3398 cm^{-1} due to the presence of the phenolic OH group. A sharp band at 1680 cm^{-1} shows the presence of an aromatic aldehyde in the ligand and the fact it remains unchanged in all the complexes indicates that the aromatic aldehyde group does not change on complexation. The absence of a peak around 3398 cm^{-1} in all the complexes indicates the absence of ν(OH) due to deprotonation followed by complexation [43a]. The strong $\nu(CO_2)$ bands at around 1450 cm^{-1} in the mononuclear complexes indicates the presence of an acetate linkage. The biacetato bridged binuclear complexes showed strong $\nu(CO_2)$ bands at 1460–1490 cm^{-1} [43b]. A broad band in the region around 3450 cm^{-1} indicates the presence of ν(OH) of water molecules for all the complexes. The presence of uncoordinated perchlorate anions in all complexes **1**–**6** are inferred from a single broad band around 1100 cm^{-1} (ν_3-antisymmetric stretching), which is not split, and a band around 650 cm^{-1} (ν_4-antisymmetric bending). The band around 930 cm^{-1} (ν_2-symmetric stretching) due to coordinated perchlorate is not observed and this vividly indicates that no perchlorate ions are coordinated in the complexes [44,45].

The electronic spectra of the mono and binuclear Cu(II) complexes and the mononuclear Ni(II) complex exhibit three main transitions. The moderately intense peak observed in the range 280–300 nm is probably due to an intra-ligand charge transfer transition [46]. A peak or shoulder in the range 350–365 nm is due to phenolato to copper(II) charge transfer transitions [47]. The mononuclear Cu(II) complex shows a λ_{max} at 590 nm due to a d–d transition, which is characteristic of a square planar geometry, and the d–d transition for the binuclear Cu(II) complex, observed at 662 nm, is indicative of a distorted square-pyramidal geometry [37,48]. The binuclear

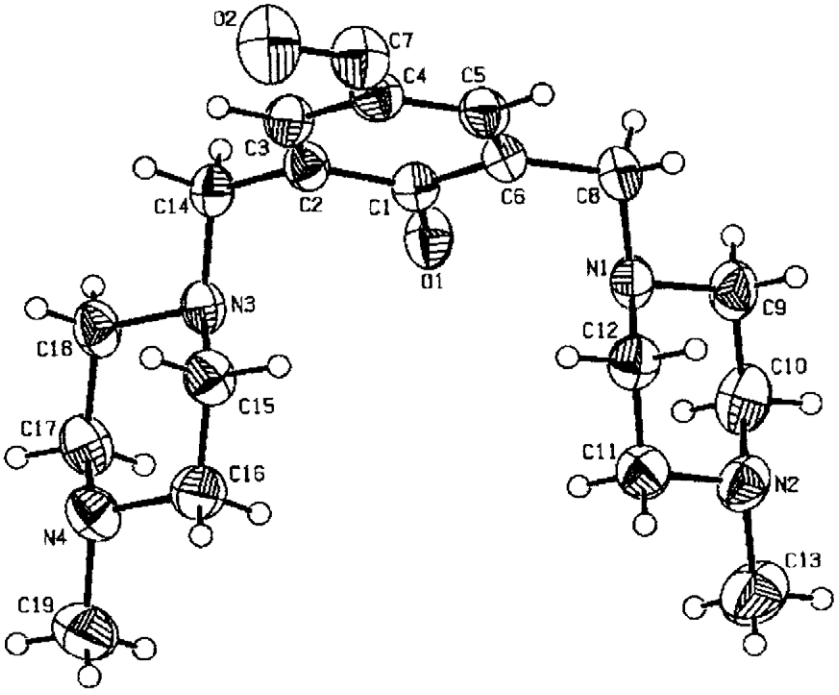

Fig. 1. ORTEP diagram of the ligand L with atom labels and numbering scheme (perchlorate and water molecules are omitted for clarity). The probability level for the ORTEP plot is 35%.

copper(II) complexes with exogenous diacetato bridges suggest that the endogenous bridging phenolate oxygen adopts the more strained pyramidal geometry. The bridging acetate groups in binuclear complexes present in a semi-bridging mode is primarily the result of the overall steric strain induced by the ligand, perhaps combined with the presence of two bridging acetate groups rather than one [37]. The mononuclear Ni(II) complex shows a single weak d–d band observed at 574 nm due to an $^1A_{1g} \rightarrow {}^1A_{2g}$ transition and this indicates that the complex has a square planar geometry [49,50]. The binuclear Ni(II) complex shows three d–d transitions at 800 nm, 618 nm and 561 nm assigned to $^3A_{2g} \rightarrow {}^3T_{2g}$, $^3A_{2g} \rightarrow {}^3T_{1g}$, $^3A_{2g} \rightarrow {}^3T_{1g}(P)$ spin allowed electronic transitions, which are characteristic of Ni^{2+} in an octahedral site [51,52]. The mono and binuclear Zn(II) complexes display only ligand centered charge transfer transitions in the UV region [53].

3.3. ESR spectra

The solid state ESR spectra of the copper(II) complexes were recorded at room temperature in the X-band region. The ESR spectra of the mononuclear complex $[CuL(OAc)]\cdot H_2O$ and the binuclear complex $[Cu_2L(OAc)_2]ClO_4\cdot 2H_2O$ are shown in Fig. 2. The ESR spectra of the mononuclear copper (II) complex shows four lines [54] with nuclear hyperfine spin 3/2 due to hyperfine splitting. The observed $g_{\|}$ value is 2.21, $g_{\perp} = 2.09$ and $A_{\|}$ is 180. A broad [55] spectrum with no hyperfine splitting was obtained for the dicopper complex with $g = 2.1$, indicating the presence of an anti-ferromagnetic interaction between the two copper ions. Owing to the favorable relative orientation of the magnetic orbitals and in spite of the Cu–Cu separation, an anti-ferromagnetic interaction is observed.

3.4. Magnetic studies

The magnetic moment values of the mono and binuclear complexes were calculated at room temperature. The magnetic moment value for the mononuclear copper(II) complex $[CuL(OAc)]\cdot H_2O$ is 1.72 BM, which is very close to that of the spin only value (1.73 BM) expected for complexes having one copper(II) ion [56] with a single unpaired electron sited in an essentially $d_{x^2-y^2}$ orbital. The value of the magnetic moment observed at room temperature for the binuclear copper (II) complex $[Cu_2L(OAc)_2]ClO_4\cdot 2H_2O$ is 1.58 BM. This confirms the presence of an anti-ferromagnetic interaction between the two copper(II) ions [57]. To evaluate the singlet–triplet energy separation ($-2J$), a variable-temperature magnetic study of the binuclear copper complex (Fig. 3) was carried out in the temperature range 77–300 K and the experimental magnetic susceptibility values were fitted to the modified Bleaney–Bowers equation [58]

$$\chi_m = (Ng^2\beta^2/3kT)[3 + \exp(-2J/kT)]^{-1}(1 - P) + (0.45P/T) + N_\alpha,$$

where χ_m is the paramagnetic susceptibility per metal atom after the correction for diamagnetism, N is Avogadro's number, β is the Boltzmann constant, g is the average gyromagnetic ratio and P is the fraction of monomeric copper(II) impurities. $-2J$ is the singlet–triplet energy separation, N_α is the temperature independent fraction, usually assumed to be 120×10^{-6} cgs units for copper (II) compounds. The value of the exchange integral $-2J$ for the binuclear copper complex is 134 cm^{-1}, indicative of weak antiferromagnetic coupling between the copper (II) ions. With few exceptions, magneto-structural correlations [59] for several phenoxo bridged dicopper complexes show that the major factor controlling the exchange interactions is the Cu–O–Cu bridge angle, however, other factors such as degree of distortion from planarity [60] and the dihedral angle [61] between the two copper planes also have an influence on the extent of the spin–spin interaction.

The position of the maximum in χ_{Cu} for the bis(μ-acetato) complex occurs at much lower temperatures because of weak exchange coupling. The acetate groups in the binuclear copper complex may connect the basal plane ($d_{x^2-y^2}$)

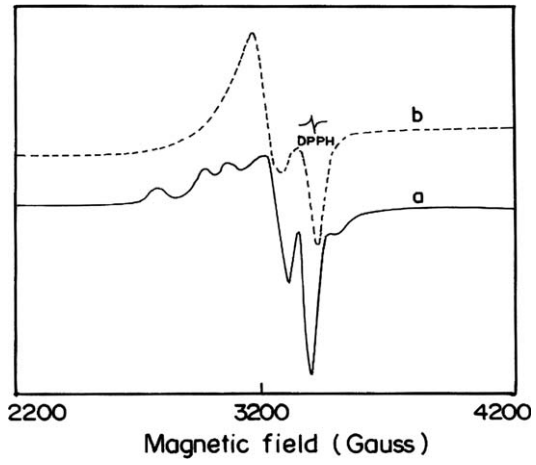

Fig. 2. ESR spectra of mononuclear: (a) $[CuL(OAc)]\cdot H_2O$ (**1**) and binuclear: (b) $[Cu_2L(OAc)_2]ClO_4\cdot 2H_2O$ (**4**) complexes.

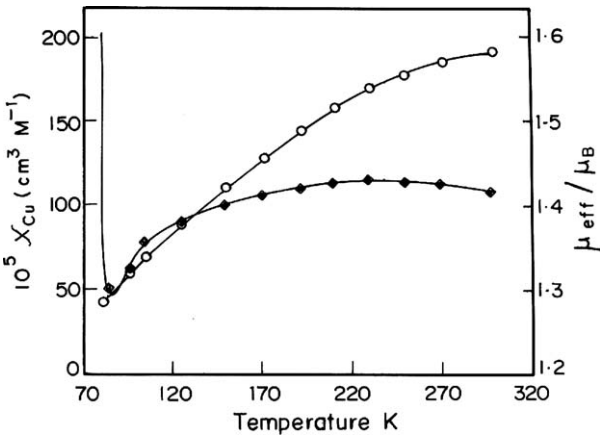

Fig. 3. Temperature-dependence magnetic properties for complex $[Cu_2L(OAc)_2]ClO_4\cdot 2H_2O$, where ○ is μ_{eff}/μ_B, ◆ is χ.

positions on one Cu with the apical (d_{z^2}) positions on the other, which will lead to a low overall J value, probably because of J_{ferro} contributions from these pathways [37]. Any contributions from the counter complementary effects of phenolate versus acetate bridging orbitals, proposed by Reed et al. [62] and Nishida and Kida [63], will be small in the complex because of the relative disposition of the Cu ($d_{x^2-y^2}$) orbitals. The mononuclear Ni(II) complex has a square planar geometry and is diamagnetic [56]. The binuclear Ni(II) complex has a magnetic moment value of 2.98 BM, characteristic of Ni^{2+} in an octahedral site [52,64].

3.5. Electrochemistry

3.5.1. Reduction process at negative potential

Conductivity measurements for the binuclear complexes were carried out in DMF, which showed conductance values in the range 80–90 (Λ_m/S cm^2 mol^{-1}), indicating that they are of 1:1 electrolyte type [65]. The electrochemical properties of the complexes were studied by cyclic voltammetry in the potential range 0 to −1.7 V in DMF, containing 0.1 M TBAP as the supporting electrolyte, and the data are summarized in Table 3. The electronegativity and hard nature of the phenoxide ligands influence the electrochemical properties of the complexes [66–68]. In general, this type of end-off complexes shows irreversible reduction waves in the cathodic potential region [37]. The cyclic voltammograms for mono and binuclear nickel(II) and zinc(II) complexes are depicted in Figs. 4 and 5, respectively. Cyclic voltammograms with different scan rates show no corresponding anodic peak in the cathodic direction, which indicates the electrode process is irreversible in nature. The mononuclear copper(II), nickel(II) and zinc(II) complexes **1**–**3** show an irreversible one-electron transfer reduction in the cathodic region. The binuclear copper(II), nickel(II) and zinc(II) complexes **4**–**6** show two-step irreversible one-electron transfer reductions. Controlled potential electrolysis was also carried out for the complexes at 100 mV s^{-1} more negative to the cathodic peak, consuming one electron per molecule ($n = 0.95$), which reports that each wave corresponds to a one-electron transfer process. So the two reduction processes are assigned generally as follows:

Table 3
Electrochemical data[a] for the complexes (reduction at cathodic potential)

Number	Complexes	E^1_{pc} (V)	E^2_{pc} (V)
1	$[CuL(OAc)]\cdot H_2O$	−0.74	
2	$[NiL(OAc)]\cdot H_2O$	−0.83	
3	$[ZnL(OAc)(H_2O)_2]$	−0.84	
4	$[Cu_2L(OAc)_2](ClO_4)\cdot 2H_2O$	−0.76	−1.21
5	$[Ni_2L(OAc)_2(H_2O)_2](ClO_4)$	−0.73	−1.35
6	$[Zn_2L(OAc)_2(H_2O)_2](ClO_4)$	−0.74	−1.61

[a] Measured by CV at 50 mV/s. E vs. Ag/AgCl conditions: GC working and Ag/AgCl reference electrodes; supporting electrolyte TBAP; concentration of complex 1×10^{-3} M, concentration of TBAP 1×10^{-1} M.

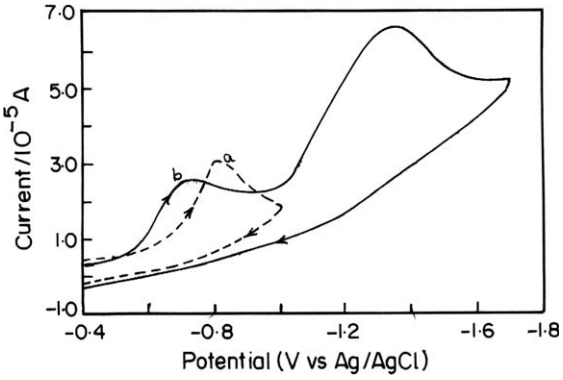

Fig. 4. Cyclic voltammograms of the mono and binuclear nickel(II) complexes: (a) $[NiL(OAc)]\cdot H_2O$ (**2**); (b) $[Ni_2L(OAc)_2(H_2O)_2]ClO_4$ (**5**) (reduction process).

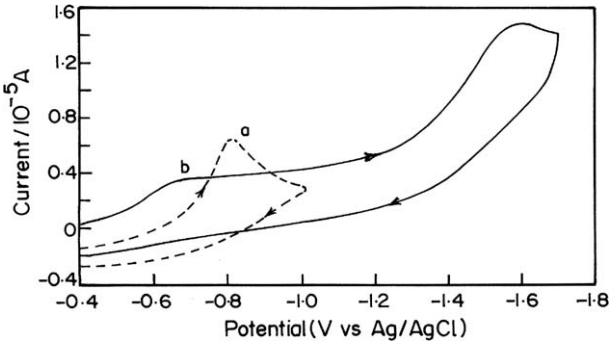

Fig. 5. Cyclic voltammograms of the mono and binuclear zinc(II) complexes: (a) $[ZnL(OAc)(H_2O)_2]$ (**3**); (b) $[Zn_2L(OAc)_2(H_2O)_2](ClO_4)$ (**6**) (reduction process).

$$M^{II}M^{II} \rightarrow M^{II}M^{I} \rightarrow M^{I}M^{I}.$$

3.5.2. Oxidation process at anodic potential

The cyclic voltammogram of the nickel(II) complexes **2** and **4** in the anodic potential region is given in Fig. 6. The mononuclear Ni(II) complex shows an irreversible oxidation wave in the positive potential at +0.76 V. The binuclear Ni(II) complex shows a two-step one-electron transfer processes in the potential range +0.82 V and +1.40 V and both are found to be irreversible in nature. The two oxidation processes are assigned generally as follows:

$$M^{II}M^{II} \rightarrow M^{III}M^{II} \rightarrow M^{III}M^{III}.$$

3.6. Kinetic studies

3.6.1. Oxidation of pyrocatechol (catecholase activity)

Measurement of the catecholase activity of both mono and binuclear copper(II) complexes synthesized in the present work was carried out using pyrocatechol as the convenient model substrate for the identification of functional models for the metalloenzymes [25,26]. For this purpose,

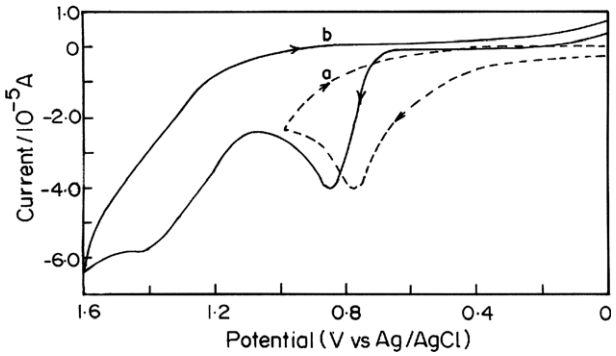

Fig. 6. Cyclic voltammograms of the mono and binuclear nickel(II) complexes: (a) $[NiL(OAc)]\cdot H_2O$ (**2**); (b) $[Ni_2L(OAc)_2(H_2O)_2](ClO_4)$ (**5**) (oxidation process).

10^{-3} mol dm^{-3} solutions of the complexes in dimethylformamide were treated with 100 equivalents of pyrocatechol in the presence of air. The course of the reaction was followed spectrophotometrically at 390 nm for nearly 45 min at regular time intervals of 5 min. The slope was determined by the method of initial rates by monitoring the growth of the 390 nm band of the product *o*-quinone. A linear relationship for initial rate and the complex concentration obtained for both the copper(II) complexes shows a first-order dependence on the complex concentration for the systems.

Plots of $\log(A_\infty/A_\alpha - A_t)$ versus time for catecholase activity of the mono and binuclear complexes are obtained and shown in Fig. 7. The observed initial rate constant value for the mononuclear and binuclear copper(II) complexes is given in Table 4. It is found that the binuclear copper(II) complex show higher reactivity than its mononuclear complex. This is due to the fact that the oxidation of pyrocatechol to *o*-quinone requires two metal ions in close proximity [27]; hence the rate constant for the binuclear copper complex is high.

Table 4
Hydrolysis of 4-nitrophenylphosphate[a] and catecholase activity[a]

Number	Complexes	Rate constant, k ($\times 10^{-3}$ min^{-1})	
		NPP	Catecholase
1	$[CuL(OAc)]\cdot H_2O$	4.60	6.40
2	$[NiL(OAc)]\cdot H_2O$	4.90	
3	$[ZnL(OAc)(H_2O)_2]$	4.30	
4	$[Cu_2L(OAc)_2](ClO_4)\cdot 2H_2O$	11.10	12.80
5	$[Ni_2L(OAc)_2(H_2O)_2](ClO_4)$	12.5	
6	$[Zn_2L(OAc)_2(H_2O)_2](ClO_4)$	9.60	

[a] Measured spectrophotometrically in DMF. Concentration of the complexes: 1×10^{-3} M; concentration of 4-nitrophenylphosphate: 1×10^{-1} M; concentration of pyrocatechol: 1×10^{-1} M.

3.6.2. Kinetic studies of hydrolysis of 4-nitrophenylphosphate

The catalytic activity of the mono and binuclear copper(II), nickel(II) and zinc(II) complexes on the hydrolysis of 4-nitrophenylphosphate was determined spectrophotometrically by monitoring the increase of the 4-nitrophenolate anion characteristic absorption at 420 nm over the time in DMF at 25 °C. For this purpose, 10^{-3} mol dm^{-3} solutions of the complexes in dimethylformamide and a 2.5×10^{-3} M solution of tetramethylammonium hydroxide were treated with 100 equivalents of nitrophenylphosphate in the presence of air.

The course of the reaction was followed at 420 nm for nearly 45 min at regular time intervals. The slope was determined by the method of initial rates by monitoring the growth of the 420 nm band of the product, the 4-nitrophenolate anion. A linear relationship for all the complexes shows a first-order dependence on the complex concentration for the systems. Plots of $\log(A_\infty/A_\alpha - A_t)$ versus time for the hydrolysis of 4-nitro phenyl phosphate activity of the complexes are obtained and shown in Fig. 8. The observed initial rate constant value for the mononuclear and binuclear copper(II) complexes is given in Table 4. It

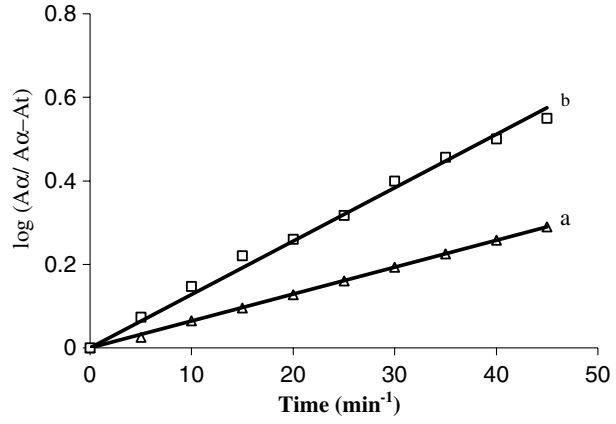

Fig. 7. Catecholase activity of the copper (II) complexes: (a) $[CuL(OAc)]\cdot H_2O$ (**1**); (b) $[Cu_2L(OAc)_2](ClO_4)\cdot 2H_2O$ (**4**).

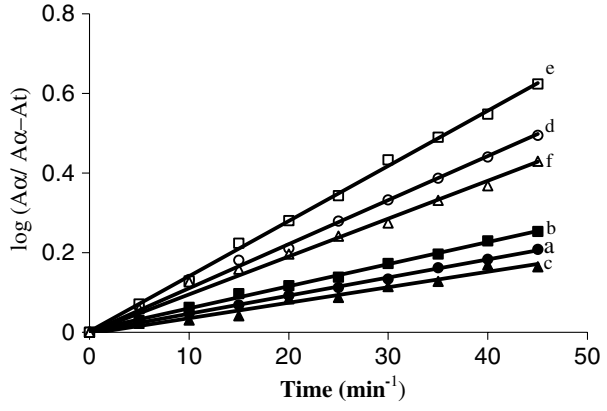

Fig. 8. Hydrolysis of 4-nitrophenylphosphate by copper(II), nickel(II) and zinc(II) complexes. (a) $[CuL(OAc)]\cdot H_2O$ (**1**); (b) $[NiL(OAc)]\cdot H_2O$ (**2**); (c) $[ZnL(OAc)(H_2O)_2]$ (**3**); (d) $[Cu_2L(OAc)_2](ClO_4)\cdot 2H_2O$ (**4**); (e) $[Ni_2L(OAc)_2(H_2O)_2](ClO_4)$ (**5**); and (f) $[Zn_2L(OAc)_2(H_2O)_2](ClO_4)$ (**6**).

is found that the binuclear complexes show higher reactivity than their corresponding mononuclear complexes due to the fact that this kind of mechanism requires two metal ions in close proximity. The mechanism of action has already been explained with the help of model complexes [69,70].

On the comparison of the hydrolysis of 4-nitrophenylphosphate by the copper(II), nickel(II) and zinc(II) complexes, the nickel(II) complexes have a higher rate constant value than the copper(II) and zinc(II) complexes. It is similar to the result of higher catalytic activity of the Ni(II)(tren) complex than the copper(II)(tren) and zinc(II)(tren) complexes reported by De Rosch and Trogler [32]. From the results, it is found that the catalytic activity of copper(II) complexes towards oxidation of pyrocatechol is more than that of the phosphate hydrolysis.

4. Supplementary material

Full crystal data and structure refinement details for ligand L have been deposited with the Cambridge Crystallographic Data Centre, CCDC No. 272757. Copies of this information may be obtained free of charge from The Director, CCDC, 12 Union Road, Cambridge CB2 1EZ, UK (fax: +44 1223 336 033; e-mail: deposit@ccdc.cam.ac.uk or www.ccdc.cam.ac.uk).

Acknowledgement

Financial support from the University Grants Commission, New Delhi is gratefully acknowledged.

References

[1] R. Breslow, D. Berger, D.-L. Huang, J. Am. Chem. Soc. 112 (1990) 3686.
[2] T. Gadja, R. Kramer, A. Jancso, Eur. J. Inorg. Chem. (2000) 1635.
[3] S.O. Kang, M. Kim, J. Am. Chem. Soc. 125 (2003) 4684.
[4] V.M. Shelton, J.R. Morrow, Inorg. Chem. 30 (1991) 4295.
[5] X. Xu, A.R. Lajmi, J.W. Canary, Chem. Commun. (1998) 2701.
[6] D.M. Bassani, J.-M. Lehn, K. Fromm, D. Fenske, Angew. Chem., Int. Ed. 41 (2002) 4041.
[7] Y.-B. Dong, M.D. Smith, H.-C. Zur Loye, Inorg. Chem. 39 (2000) 4927.
[8] W.A. Alves, S.A. de Almeida, R.H. de Almeida Santos, A.M. Costa Ferreira, Inorg. Chem. Commun. 6 (2003) 294.
[9] J.-M. Lehn, Supramolecular Chemistry, VCH, Weinheim, 1995.
[10] Y.S. Xie, X.T. Liu, M. Zhang, K.J. Wei, Q.L. Liu, Polyhedron 24 (2005) 165.
[11] P.D. Beer, E.J. Hayes, Coord. Chem. Rev. 240 (2003) 167.
[12] S.-S. Sun, A.J. Lees, P.J. Zavalij, Inorg. Chem. 42 (2003) 3445.
[13] S.L. Tobey, B.D. Jones, E.V. Anslyn, J. Am. Chem. Soc. 125 (2003) 4026.
[14] B. Hasenknopf, J.-M. Lehn, B.O. Kneisel, G. Baum, D. Fenske, Angew. Chem., Int. Ed. 35 (1996) 1838.
[15] Z. Tang, A.M. Guloy, J. Am. Chem. Soc. 121 (1999) 452.
[16] M. Fujita, S. Nagao, K. Ogura, J. Am. Chem. Soc. 117 (1995) 1649.
[17] B. Linton, A.D. Hamilton, Chem. Rev. 97 (1997) 1669.
[18] T.F. Pauwels, W. Lippens, P.W. Smet, G.G. Herman, A.M. Goeminne, Polyhedron 18 (1999) 1029.
[19] J. Chin, S.S. Lee, K.J. Lee, S. Park, D.H. Kim, Nature 401 (1999) 254.
[20] M.J. Young, J. Chin, J. Am. Chem. Soc. 117 (1995) 10577.
[21] T. Humphry, M. Forconi, N.H. Williams, A.C. Hengge, J. Am. Chem. Soc. 124 (2002) 14860.
[22] H. Ōkawa, H. Furutachi, D.E. Fenton, Coord. Chem. Rev. 174 (1998) 51.
[23] S.R. Collinson, D.E. Fenton, Coord. Chem. Rev. 148 (1996) 19.
[24] P.A. Vigato, S. Tamburini, D.E. Fenton, Coord. Chem Rev. 106 (1990) 25.
[25] K. Moore, G.S. Vigee, Inorg. Chim. Acta 66 (1982) 125.
[26] D. Bolus, G.S. Vigee, Inorg. Chim. Acta 67 (1982) 19.
[27] A. Neves, L.M. Rossi, A.J. Bortoluzzi, B.S. Szpoganicz, C. Wiezbicki, E. Schwingel, W. Haase, S. Ostrovsky, Inorg. Chem. 41 (2002) 1788.
[28] G.J. King, B. Zerner, Inorg. Chim. Acta 225 (1997) 381.
[29] T.W. Reid, I.B. Wilson, in: P.D. Boyer (Ed.), The Enzymes, 3rd ed., vol. 4, Academic Press, New York, 1971, p. 373.
[30] T. Hall, J.A. Porter, P.A. Blachy, D.J. Leahy, Nature 378 (1995) 212.
[31] B.F. Baler, P.B. Dervan, J. Am. Chem. Soc. 111 (1989) 2700.
[32] M.A. De Rosch, W.C. Trogler, Inorg. Chem. 29 (1990) 2409.
[33] R.G. Clewley, H. Slebocka-Tilk, R.S. Brown, Inorg. Chim. Acta 157 (1989) 233.
[34] H.P. Berends, D.W. Stephan, Inorg. Chim. Acta 99 (1985) L55.
[35] M.L. Boillot, O. Kahn, C.J. O'Connor, J. Gouteron, S. Jeannin, Y. Jeannin, J. Chem. Soc., Chem. Commun. (1985) 178.
[36] T. Mallah, O. Kahn, J. Gouteron, S. Jeannin, Y. Jeannin, C.J. O'Connor, Inorg. Chem. 26 (1987) 1375.
[37] K. Bertoncello, G.D. Fallon, J.H. Hodgkin, K.S. Murray, Inorg. Chem. 27 (1988) 4750.
[38] M.J. Hossain, M. Yamasaki, M. Mikuriya, A. Kuribayashi, H. Sakiyama, Inorg. Chem. 41 (2002) 4058.
[39] G.M. Sheldrick, SHELXS-97 and SHELXL-97, University of Göttingen, Göttingen, Germany, 1997.
[40] F.H. Allen, O. Kennard, D.G. Watson, L. Brammer, A.G. Orpen, R.J. Taylor, J. Chem. Soc., Perkin Trans. 2 (1987) S1.
[41] J.A. Cremer, J. Pople, J. Am. Chem. Soc. 97 (1975) 1354.
[42] M. Nardelli, Acta Crystallogr., Sect. C 39 (1983) 1141.
[43] (a) D. Saravanakumar, N. Sengottuvelan, G. Priyadarshni, M. Kandaswamy, H. Okawa, Polyhedron 23 (2004) 665;
(b) G.B. Deacon, R. Phillips, J. Coord. Chem. Rev. 33 (1980) 227.
[44] K. Nakamoto, Infrared and Raman Spectra of Inorganic and Coordination Compounds, Wiley–Interscience, New York, 1978.
[45] B.J. Hathaway, A.E. Underhill, J. Chem. Soc. (1961) 3091.
[46] J. Manonmani, M. Kandaswamy, V. Narayanan, R. Thirumurugan, S. Shanmuga Sundara Raj, G. Shanmugam, M.N. Ponnuswamy, H.K. Fun, Polyhedron 20 (2001) 3039.
[47] K.J. Oberhausen, J.F. Richardson, R.M. Buchnan, J.K. McCusker, D.N. Hendrickson, J.M. Latour, Inorg. Chem. 30 (1991) 1357.
[48] D. Reinen, C. Friebel, Inorg. Chem. 23 (1984) 791.
[49] A.B.P. Lever, Inorganic Electronic Spectroscopy, 2nd ed., Elsevier, Amsterdam, 1984.
[50] S. Bhattacharyya, T.J.R. Weakley, M. Chaudhury, Inorg. Chem. 38 (1999) 633.
[51] M.F. Cabral, B. Murphy, J. Nelson, Inorg. Chim. Acta 90 (1984) 169.
[52] T.C. Higgs, C.J. Carrano, Inorg. Chem. 36 (1997) 298.
[53] F. Yilmaz, V.T. Yilmaz, S. Topcu, N. Menek, J. Coord. Chem. 56 (2003) 903.
[54] S. Zhu, F. Kon, H. Lin, C. Lin, M. Lin, Y. Chen, Inorg. Chem. 35 (1997) 3851.
[55] R.C. Agarwal, N.K. Singh, R.P. Singh, Inorg. Chem. 20 (1981) 2794.
[56] A. Bottcher, H. Elias, E. Jager, H. Lanffelderova, M. Mazur, L. Mullor, H. Paulas, P. Pelikan, M. Rudolph, M. Valko, Inorg. Chem. 32 (1993) 4131.
[57] L.M. Liable-Sands, C. Incarvito, A.L. Rheingold, C. Jin Qin, A. Gavrilova, B. Bosnich, Inorg. Chem. 40 (2001) 2147.
[58] B. Bleaney, K.D. Bowers, Proc. R. Soc. Lond. Ser. A 214 (1952) 451.
[59] J.D. Crane, D.E. Fenton, J.M. Latour, A.J. Smith, J. Chem. Soc., Dalton Trans. (1991) 2279.

[60] H. Okawa, J. Nishio, M. Ohba, M. Tadokoro, N. Matsumoto, M. Koikawa, S. Kida, D.E. Fenton, Inorg. Chem. 32 (1993) 2949.
[61] S.L. Lambert, D.N. Hendrickson, J. Am. Chem. Soc. 105 (1983) 1513.
[62] V. McKee, M. Zragulis, C.A. Reed, Inorg. Chem. 24 (1985) 2914.
[63] Y. Nishida, S. Kida, J. Chem. Soc., Dalton Trans. (1986) 2633.
[64] M.P. Suh, B.Y. Shim, T.S. Yoon, Inorg. Chem. 33 (1994) 5509.
[65] W.J. Geary, Coord. Chem. Rev. 7 (1971) 81.
[66] A. Benzekeri, P. Dubourdeaux, J.M. Latour, P. Rey, J. Langier, J. Chem. Soc., Dalton Trans. (1991) 3359.
[67] P. Zanello, S. Tamburini, P.A. Vigato, G.A. Mazzocchin, Coord. Chem. Rev. 77 (1987) 165.
[68] F. Azevedo, C.T. Carrondo, B. Caseto, M. Convery, D. Domingues, C. Freire, T. Durate, K. Neilson, C. Santos, Inorg. Chim. Acta 219 (1994) 43.
[69] C.D. Toia, S. Menage, J.M. Vincent, M.T.V. Pouchot, M. Fontecave, Inorg. Chem. 36 (1997) 6148.
[70] M. Yamami, H. Furutachi, T. Yokohama, H. Ōkawa, Inorg. Chem. 37 (1998) 6832.

energy transfer from the resulting ligand-based triplet state [2i,3]. This is the usual basis for achieving sensitized emission from Eu(III) and Tb(III) [2]. Recently there have been intense efforts directed at attaching chromophores with relatively long wavelength absorption maxima (in the visible region), e.g., suitably functionalized organic dyes that have particularly low-energy π–π transitions [4] or d-metal complexes that have very strong charge-transfer absorptions at a range of wavelengths that span the visible region [5], to near-IR-emissive Ln^{III} ions, such as Yb(III), Nd(III), Pr(III) and Er(III).

The chances of identifying new 4f-metal complexes with interesting photophysical properties will benefit from the development of new reaction systems with suitable organic ligands. With this in mind we have started a systematic study of the coordination properties of complexing agents capable of efficiently sensitizing Eu(III) and Tb(III) emission. Our ligand design will employ simple units, based on strong binding sites for Ln^{III} coordination and bulky aromatic groups, to play the dual role of antenna and solvent shield, and to thus form – if possible – a hydrophobic shell around the metal ion. It should be mentioned at this point that species containing high-energy oscillators, such as C–H and O–H bonds (typically found in the ligand, coordinated solvent and moisture), are able to quench the metal excited states non-radiatively, leading to decreased luminescence intensities and shorter excited-state lifetimes [6]. In the ligands we plan to use, the binding and antenna domains may be or may not be independent of each other; in the former case this will allow the sensitizing group to be energetically optimized for a particular Ln^{III} ion without changing the binding characteristics of the ligand [2a].

In this paper, we describe our initial studies in this area based on the ligand di-2-pyridyl ketone, $(py)_2CO$ (Fig. 1). Our groups [7,8] and others [9] have been exploring reaction systems involving Mn, Fe, Co, Ni, Cu and Zn ions, and either (i) the monoanion, $(py)_2C(OH)O^-$, or the dianion, $(py)_2CO_2^{2-}$, of the *gem*-diol form (derivative), $(py)_2C(OH)_2$, of di-2-pyridyl ketone, $(py)_2CO$, or (ii) the monoanion, $(py)_2C(OR)O^-$ (R = Me, Et, etc.) of the hemiacetal form (derivative), $(py)_2C(OR)(OH)$, of di-2-pyridyl ketone. The formulae of these ligands and their abbreviations are shown in Fig. 1. The general goal of these efforts is the isolation of polynuclear complexes with interesting magnetic and optical properties. There is a chemical characteristic of $(py)_2CO$ that makes this molecule special as ligand; this is its carbonyl group. Water and alcohols (ROH) have been shown to add to the carbonyl group *upon coordination of the carbonyl oxygen and/or the 2-pyridyl rings* forming the ligands $(py)_2C(OH)_2$ (the *gem*-diol form of $(py)_2CO$) and $(py)_2C(OR)(OH)$ (the hemiacetal form of $(py)_2CO$), respectively [7]. Interesting coordination modes are seen when the ligands $(py)_2C(OH)_2$ and $(py)_2C(OR)(OH)$ are deprotonated. The presence of deprotonated hydroxyl group(s) leads to a great coordinative flexibility, due to the well known ability of the negatively charged oxygen atom to bridge two or three (μ_3) metal ions, while the dianionic form can bridge as many as five metal sites (μ_5). The immense structural diversity displayed by the 3d-metal complexes reported stems in part from the ability of $(py)_2C(OH)O^-$, $(py)_2CO_2^{2-}$ and $(py)_2C(OR)O^-$ to exhibit no less than ten distinct bridging coordination modes [7].Employment of carboxylates, β-diketonates or inorganic anions (NO_3^-, SO_4^{2-}, N_3^-, $N(CN)_2^-$, etc.) as ancillary ligands in the reaction mixtures gives an extraordinary structural flexibility in the mixed-ligand systems, allowing the preparation of a variety of 3d-metal clusters with nuclearities ranging from 3 to 26 [7], and with interesting physical properties including single-molecule magnetism [8d].

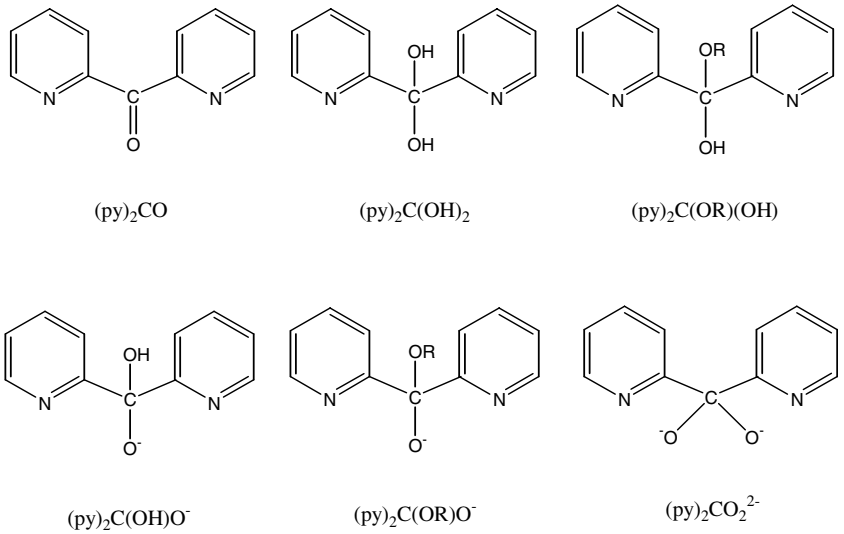

Fig. 1. The formulae of the ligands discussed in the text; note that $(py)_2C(OH)_2$, $(py)_2C(OR)(OH)$ and all four anions do not exist as free species but exist only in their respective metal complexes (R = Me, Et, etc.).

Surprisingly, however, $(py)_2CO$-based ligands have been practically ignored in 4f-metal chemistry. We have recently extended the reactions of $(py)_2CO$ in lanthanide(III) chemistry and investigated the $Er^{III}/SCN^-/(py)_2CO$ reaction mixtures in alcohols (MeOH, EtOH). Depending on the OH^- concentration in the reaction system, we were able to isolate and structurally characterize complexes $[Er(NCS)_3\{(py)_2C(OR)(OH)\}_3]$ and $[Er_2(NCS)_3\{(py)_2C(OMe)O\}_3(MeOH)]$ [10a]. We suspected that there might be a number of other Ln_x^{III} species accessible and have therefore been investigating the reactions of $(py)_2CO$ with lanthanide(III) nitrates under a variety of conditions; the products of these reactions are the subject of this report. It should be mentioned at this point that lanthanide(III) nitrate complexes of the somewhat similar ligand methyl-2-pyridyl ketone benzoyl hydrazone have been recently prepared [10b]; tentative structures for the complexes were proposed based on spectroscopic techniques.

2. Experimental

2.1. General and physical measurements

All manipulations were performed under aerobic conditions using materials (reagent grade) and solvents as received. Hydrated lanthanide(III) nitrates were purchased from Alfa Aesar.

Microanalyses (C, H, N) were performed by the University of Ioannina (Greece) Microanalytical Laboratory using an EA 1108 Carlo Erba analyzer. The metal content was determined volumetrically with ethylenediaminetetra-acetate using Xylenol Orange as indicator. IR spectra (4000–400 cm^{-1}) were recorded on a Perkin–Elmer 16 PC FT-spectrometer with samples prepared as KBr pellets; the spectra were also recorded as Nujol and hexachlorobutadiene mulls between CsI discs. Magnetic susceptibilities were measured at room temperature using the Faraday method with a Cahn-Ventron RM-2 balance standardized with $HgCo(NCS)_4$; diamagnetic corrections were estimated from Pascal's constants. Solid-state (diffuse reflectance, DRS) spectra in the 200–800 nm range were recorded on a Varian Cary 3 spectrometer equipped with an integration sphere under high-resolution detection conditions. Powders of the samples were used. Luminescence was recorded using an Ocean Optics S-2000 diode array spectrophotometer. The excitation source was a pulsed N_2 laser (336 nm). Luminescence was collected with an optical fiber. The excitation spectra were recorded using a Cary Eclipse fluorescence spectrophotometer.

2.2. Compound preparation

2.2.1. $[Pr_2(NO_3)_3\{(py)_2C(OMe)O\}_2\{(py)_2C(OH)O\}]$ (**1**)

Solids $(py)_2CO$ (0.037 g, 0.20 mmol) and $LiOH \cdot H_2O$ (0.0084 g, 0.20 mmol) were dissolved in MeOH (3 ml) resulting in a colourless solution. This was added to a pale green solution of $Pr(NO_3)_3 \cdot 6H_2O$ (0.086 g, 0.20 mmol) in EtOH (5 ml). The resulting new pale green solution was stirred for about 1 h during which time a precipitate formed. The solid was collected by filtration, washed with cold MeOH (2×2 ml) and Et_2O (2×5 ml), and dried in vacuo over silica gel. Yield: 21% (based on the ligand). *Anal.* Calc. for $C_{35}H_{31}Pr_2N_9O_{15}$: C, 38.23; H, 2.85; N, 11.47; Pr, 25.63. Found: C, 37.99; H, 2.90; N, 11.62; Pr, 26.13%. IR (KBr pellet, cm^{-1}): 3410 mb, 2975 w, 2912 w, 1599 m, 1569 w, 1476 s, 1464 s, 1438 s, 1384 s, 1304 m, 1284 m, 1233 w, 1224 w, 1154 w, 1112 sh, 1104 m, 1075 s, 1049 m, 1035 sh, 1012 m, 815 m, 766 m, 748 sh, 683 m, 661 w, 633 m, 541 w, 432 sh, 417 m. μ_{eff} (BM) per Pr^{III}: 3.44 (22 °C). DRS (nm): 268, 280, 340, 449, 474, 485, 599.

2.2.2. $[Eu_2(NO_3)_3\{(py)_2C(OMe)O\}_2\{(py)_2C(OH)O\}]$ (**2**)

Using $Eu(NO_3)_3 \cdot 6H_2O$, slightly different solvent volumes (MeOH: 7 ml, EtOH: 2 ml) and following exactly the same procedure as that described for the corresponding praseodymium(III) complex, a white microcrystalline material was isolated. Yield: 25% (based on the ligand). *Anal.* Calc. for $C_{35}H_{31}Eu_2N_9O_{15}$: C, 37.48; H, 2.79; N, 11.24; Eu, 27.10. Found: C, 37.62; H, 2.69; N, 11.38; Eu, 26.31%. IR (KBr pellet, cm^{-1}): 3399 mb, 2980 w, 2942 w, 1600 m, 1568 w, 1482 s, 1465 s, 1439 m, 1384 s, 1308 m, 1266 sh, 1232 w, 1222 w, 1154 w, 1111 sh, 1105 m, 1078 s, 1051 m, 1036 sh, 1015 m, 815 m, 767 m, 749 sh, 684 m, 662 w, 634 m, 542 w, 433 w, 417 m. μ_{eff} (BM) per Eu^{III}: 3.40 (20 °C). DRS (nm): 265, 281, 338, 363, 397.

2.2.3. $[Tb_2(NO_3)_3\{(py)_2C(OMe)O\}_2\{(py)_2C(OH)O\}]$ (**3**)

Solids $(py)_2CO$ (0.037 g, 0.20 mmol) and $LiOH \cdot H_2O$ (0.0084 g, 0.20 mmol) were dissolved in MeOH (6 ml) resulting in a colourless solution. This was added to a pale pink solution of $Tb(NO_3)_3 \cdot 6H_2O$ (0.087 g, 0.19 mmol) in a solvent mixture comprising MeOH (3 ml) and EtOH (3 ml). No noticeable colour change occurred. The resulting solution was stirred for about 1 h and layered with a mixture of Et_2O and *n*-hexane (20 ml, 1:1 v/v). Slow mixing gave a white microcrystalline solid, which was collected by filtration, washed with cold MeOH (2×3 ml) and Et_2O (2×5 ml), and dried in vacuo over silica gel. Yield: 19% (based on the ligand). *Anal.* Calc. for $C_{35}H_{31}Tb_2N_9O_{15}$: C, 37.02; H, 2.76; N, 11.10; Tb, 27.99. Found: C, 37.18; H, 2.80; N, 11.01; Tb, 28.63%. IR (KBr pellet, cm^{-1}): 3400 mb, 2985 w, 2930 w, 1601 m, 1568 w, 1480 s, 1467 s, 1439 m, 1384 s, 1309 m, 1285 m, 1267 sh, 1233 sh, 1224 w, 1155 w, 1112 sh, 1106 m, 1079 s, 1051 m, 815 m, 1035 sh, 1015 m, 815 m, 767 m, 750 sh, 684 m, 665 w, 634 m, 543 w, 437 w, 420 m. μ_{eff} (BM) per Tb^{III}: 9.59 (25 °C). DRS (nm): 266, 282, ~330, 373, 492.

2.2.4. $[Er_2(NO_3)_3\{(py)_2C(OMe)O\}_2\{(py)_2C(OH)O\}]\cdot 0.8EtOH\cdot 0.4MeOH$ ($\mathbf{4}\cdot 0.8EtOH\cdot 0.4MeOH$)

Solids $(py)_2CO$ (0.037 g, 0.20 mmol) and $LiOH\cdot H_2O$ (0.0084 g, 0.20 mmol) were dissolved in MeOH (5 ml) resulting in a colourless solution. This was added to a pale pink solution of $Er(NO_3)_3\cdot 5H_2O$ (0.090 g, 0.20 mmol) in a solvent mixture comprising MeOH (2 ml) and EtOH (3 ml). The resulting new pinkish solution was stirred for about 90 min and stored at 5 °C. After 8 days, pale pink (almost colourless), X-ray quality prisms formed; they were collected by filtration, washed with cold MeOH (2×2 ml) and Et_2O (2×5 ml) and dried in vacuo over silica gel. Yield: 39% (based on the ligand). A sample for crystallography was kept in contact with the mother liquor to prevent interstitial solvent loss. The dried sample analysed as solvent-free. *Anal.* Calc. for $C_{35}H_{31}Er_2N_9O_{15}$: C, 36.48; H, 2.72; N, 10.94; Er, 29.03. Found: C, 36.70, H, 2.65; N, 11.13; Er, 30.00%. IR (KBr pellet, cm^{-1}): 3380 mb, 2983 w, 2935 w, 1602 m, 1570 m, 1506 s, 1475 sh, 1438 m, 1384 m, 1298 m, 1284 m, 1260 sh, 1226 m, 1156 m, 1116 m, 1084 m, 1050 m, 1016 sh, 814 m, 786 sh, 762 m, 684 m, 666 w, 636 m, 532 w, 454 m, 425 m. μ_{eff} (BM) per Er^{III}: 9.54 (20 °C). DRS (nm): 262, 277, ~330, 370 sh, 380, 492, 520, 524, 530 sh, 542, 652, 657.

2.3. Single-crystal X-ray crystallography

A crystal of $\mathbf{4}\cdot 0.8EtOH\cdot 0.4MeOH$ was mounted in capillary. Diffraction measurements were made on a Crystal Logic Dual Goniometer diffractometer using graphite-monochromated Mo radiation. Complete crystal data and parameters for data collection and processing are reported in Table 1. Unit cell dimensions were determined and refined by using the angular settings of 25 automatically centered reflections in the range $11 < 2\theta < 23°$. Three standard reflections monitored every 97 reflections showed less than 3% variation and no decay. Lorentz, polarization and Ψ-scan absorption corrections were applied using Crystal Logic software.

The structure was solved by direct methods using SHELXS-86 [11a] and refined by full-matrix least-squares techniques on F^2 with SHELXL-97 [11b]. All hydrogen atoms were introduced at calculated positions as riding on bonded atoms and were refined isotropically. All non-hydrogen atoms were refined using anisotropic thermal parameters, except of the solvent molecules, which were refined isotropically.

Table 1
Crystallographic data for complex $\mathbf{4}\cdot 0.8EtOH\cdot 0.4MeOH$

Formula	$C_{37}H_{37.4}Er_2N_9O_{16.2}$
Formula weight	1201.88
Crystal colour, habit	colourless, prism
Crystal dimensions (mm)	$0.04\times 0.12\times 0.40$
Crystal system	monoclinic
Space group	$P2_1/c$
Unit cell dimensions	
a (Å)	11.261(5)
b (Å)	21.560(10)
c (Å)	18.669(8)
β (°)	101.46(1)
V (Å^3)	4442(3)
Z	Z
ρ_{calc} (g cm^{-3})	1.797
Radiation, λ (Å)	Mo Kα, 0.71073
Temperature (K)	298
Scan mode/speed (° min^{-1})	θ–2θ/1.5
$2\theta_{max}$ (°)	50.0
μ (mm^{-1})	3.832
Reflections collected/unique (R_{int})	8073/7817 (0.0338)
Data with $I > 2\sigma(I)$	5150
Parameters refined	584
$(\Delta\rho)_{max}$, $(\Delta\rho)_{min}$ (e Å^{-3})	0.908, −0.679
Goodness-of-fit (on F^2)	1.072
R_1,[a] wR_2[b] (all data)	0.1106, 0.1262
R_1,[a] wR_2[b] ($I > 2\sigma(I)$)	0.0569, 0.1067

[a] $R_1 = \sum(|F_o| - |F_c|)/\sum(|F_o|)$.

[b] $wR_2 = \{\sum[w(F_o^2 - F_c^2)^2]/\sum[w(F_o^2)^2]\}^{1/2}$.

3. Results and discussion

3.1. Synthetic comments

The 1:1:1 reactions between $Ln(NO_3)_3\cdot xH_2O$ (Ln = Pr, Eu, Tb, Er; $x = 5$ or 6), OH^- and $(py)_2CO$ in MeOH–EtOH gave the dinuclear complexes $[Ln_2(NO_3)_3\{(py)_2C(OMe)O\}_2\{(py)_2C(OH)O\}]$(**1**–**4**); the erbium(III) compound was crystallographically identified as $\mathbf{4}\cdot 0.8EtOH\cdot 0.4MeOH$. The formation of these lanthanide(III) complexes can be summarized in the general balanced Eq. (1).

$$2Ln(NO_3)_3\cdot xH_2O + 3(py)_2CO + 3LiOH\cdot H_2O + 2MeOH \xrightarrow{MeOH\text{–}EtOH} [Ln_2(NO_3)_3\{(py)_2C(\underset{\mathbf{1-4}}{OMe})O\}_2\{(py)_2C(OH)O\}] + 3LiNO_3 + (2x+5)H_2O \quad (1)$$

The Ln^{III}-mediated addition of solvent (MeOH, H_2O from the solvents and the starting materials) to $(py)_2CO$ to give the monoanion of the hemiacetal form of di-2-pyridyl ketone, $(py)_2C(OMe)O^-$ (Fig. 1), and the monoanion of the *gem*-diol form of this ligand, $(py)_2C(OH)O^-$ (Fig. 1), in **1**–**4** involves a nucleophilic attack of the MeOH and H_2O molecules on the carbonyl group [7]. The electrophilic character of the carbonyl group of $(py)_2CO$ is increased by coordination of the carbonyl oxygen to the metal ion (direct polarization) and/or coordination of the more remote 2-pyridyl sites (induced polarization) [7].

Several features of the general reaction represented by Eq. (1) deserve comments. First, the "wrong" reaction ratio employed for the preparation of **1**–**4** (see Section 2.2), compared to the stoichiometric ratio required by Eq. (1), obviously did not prove detrimental to the formation of the complexes. With the identities of **1**–**4** established, the "correct" stoichiometric ratio, i.e., Ln(III): OH^-:$(py)_2CO$ = 2:3:3, was employed and led to pure compounds in satisfactory yields. Second, use of bases other than $LiOH\cdot H_2O$ leads again to the same complexes. Thus,

the 2:3:3 $Ln(NO_3)_3 \cdot xH_2O/(py)_2CO/Et_3N$ reaction mixtures in MeOH–EtOH (the detailed procedures are not given in Section 2.2) lead to the isolation of **1**–**4** in yields higher than 30% according to Eq. (2). Third, the incorporation of the monoanions of *both* the hemiacetal and the *gem*-diol forms of $(py)_2CO$ as ligands in **1**–**4** was rather unexpected, given the fact that the complexes were isolated from alcohols. For example, the products isolated from the $Er^{III}/SCN^-/(py)_2CO$ reaction mixtures in MeOH contain *only* $(py)_2C(OMe)(OH)$ or $(py)_2C(OMe)O^-$ species as ligands [10a]. With hindsight this can be explained by the presence of H_2O (from the starting materials and from the moisture of the organic solvents) in the reaction mixtures. One possible reason for the presence of both $(py)_2C(OMe)O^-$ and $(py)_2C(OH)O^-$ is the satisfaction of the crystal lattice. It is likely that the reaction solution contains a complicated mixture of several species in equilibrium, with factors such as relative solubility, lattice energy and crystallization kinetics – amongst others – determining the identity of the isolated product. It should be mentioned at this point that the presence of both $(py)_2C(OH)O^-$ and $(py)_2C(OR)O^-$ in the same complex is rare in d-metal chemistry [9c,9f,12]. Forth, complexes **1**–**4** seem to be the only isolable products from the $Ln(NO_3)_3 \cdot xH_2O/OH^-/(py)_2CO$ reaction systems in MeOH of MeOH–EtOH. The Ln^{III} to ligand reaction ratio, the presence/absence of counter-cations or – anions (e.g., NBu^n_4 or ClO_4^-), and the precipitation/crystallization method have no influence on the identity of the products. With the identity of compounds **1**–**4** established we also tried similar reactions but employing a large excess of OH^- as a means of obtaining complexes containing the doubly deprotonated ligand $(py)_2CO_2^{2-}$ (Fig. 1) [7]. However, these yielded the same complexes $[Ln_2(NO_3)_3\{(py)_2C(OMe)O\}_2\{(py)_2C(OH)O\}]$ and/or amorphous hydroxo materials with poor analytical results. Fifth, the full synthetic investigation of the $Ln(NO_3)_3 \cdot xH_2O/LiOH \cdot H_2O$ or $Et_3N/(py)_2CO$ reaction systems in H_2O, MeCN or $MeCN/H_2O$ led to non-crystalline solids with non-reproducible analytical results. Sixth, the employment of EtOH as co-solvent is beneficial only for the isolation of crystalline solids in the case of **1**–**3** and single crystals of $\mathbf{4} \cdot 0.8EtOH \cdot 0.4MeOH$; in other words, its presence does not affect the identity of the product, but only its crystallization. The employment of EtOH might imply the presence of the monoanion $(py)_2C(OEt)O^-$ in the complexes. Although this is possible *in solution*, only the $(py)_2C(OMe)O^-$ and $(py)_2C(OH)O^-$ ligands are present in the *solid* complexes **1**–**4**. This result is difficult to be rationalized; suffice it to say that complexes **1**–**4** are the thermodynamically stable products from the $Ln(NO_3)_3 \cdot xH_2O/OH^-/(py)_2CO$ reaction system in a solvent mixture comprising non-absolute MeOH *and* EtOH. And seventh, despite our efforts, we could not isolate mononuclear complexes containing the neutral or anionic ligand, e.g., $Ln(NO_3)_3\{(py)_2C(OR)(OH)\}_x$ ($x = 1$ or 2) and $Ln(NO_3)_2\{(py)_2C(OR)O\}$. In the absence of external base, the $Er^{III}/SCN^-/(py)_2CO$ reaction mixture in alcohols (MeOH, EtOH) yielded [10a] the mononuclear complexes $[Er(NCS)_3\{(py)_2C(OR)(OH)\}_3]$ (R = Me, Et).

$$2Ln(NO_3)_3 \cdot xH_2O + 3(py)_2CO + 3Et_3N + 2MeOH \xrightarrow{MeOH–EtOH} [Ln_2(NO_3)_3\{(py)_2C(OMe)O\}_2\{(py)_2C(OH)O\}] + 3Et_3NHNO_3 + (2x-1)H_2O \quad (2)$$

3.2. Description of structure

A partially labelled plot of the dinuclear molecule present in complex $\mathbf{4} \cdot 0.8EtOH \cdot 0.4MeOH$ is shown in Fig. 2. A graphical representation of this complex appears in Fig. 3. The coordination polyhedra of the two Er^{III} atoms are shown in Fig. 5. Selected interatomic distances and angles are listed in Table 2.

The crystal structure of $\mathbf{4} \cdot 0.8EtOH \cdot 0.4MeOH$ consists of discrete dinuclear $[Er_2(NO_3)_3\{(py)_2C(OMe)O\}_2\{(py)_2C(OH)O\}]$ molecules and solvate molecules; the latter will not be further discussed. In the dinuclear molecule, the

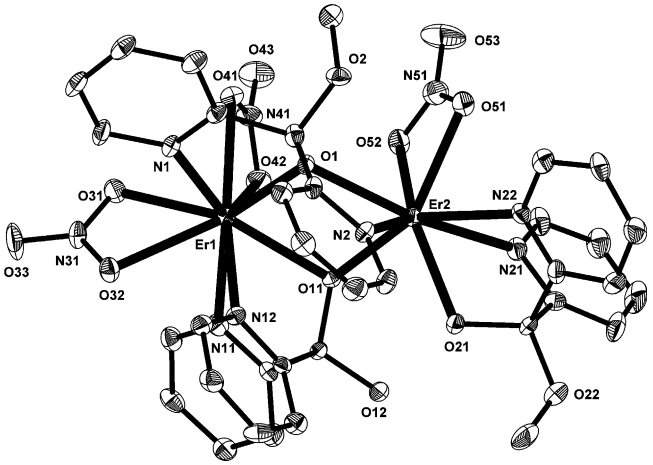

Fig. 2. The structure of the dinuclear molecule present in complex $\mathbf{4} \cdot 0.8EtOH \cdot 0.4MeOH$.

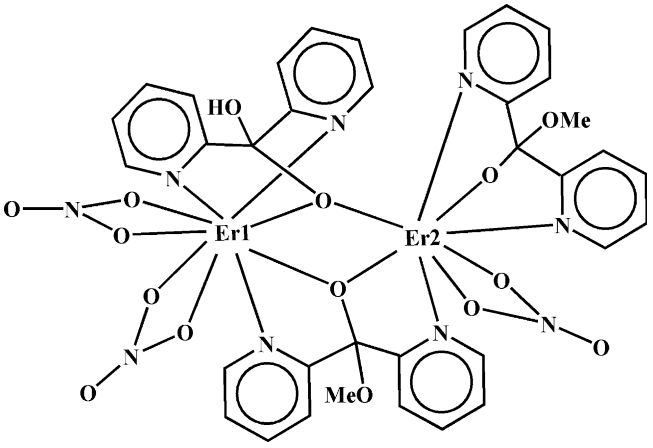

Fig. 3. An informative graphical representation of **4**.

Table 2
Selected interatomic distances (Å) and bond angles (°) for complex **4** · 0.8EtOH · 0.4MeOH

Er(1)···Er(2)	3.681(2)	Er(1)–N(12)	2.479(9)
Er(1)–O(1)	2.253(6)	Er(2)–O(1)	2.293(6)
Er(1)–O(11)	2.330(7)	Er(2)–O(11)	2.258(6)
Er(1)–O(31)	2.447(8)	Er(2)–O(21)	2.222(8)
Er(1)–O(32)	2.465(7)	Er(2)–O(51)	2.380(9)
Er(1)–O(41)	2.466(8)	Er(2)–O(52)	2.451(9)
Er(1)–O(42)	2.411(8)	Er(2)–N(2)	2.496(9)
Er(1)–N(1)	2.572(9)	Er(2)–N(21)	2.539(9)
Er(1)–N(11)	2.531(9)	Er(2)–N(22)	2.497(9)
O(1)–Er(1)–O(11)	71.9(2)	O(1)–Er(2)–O(11)	72.5(2)
O(1)–Er(1)–O(31)	139.9(3)	O(1)–Er(2)–O(51)	89.0(3)
O(1)–Er(1)–N(11)	138.2(3)	O(1)–Er(2)–N(22)	128.9(3)
O(11)–Er(1)–O(42)	81.7(3)	O(11)–Er(2)–O(21)	82.6(3)
O(11)–Er(1)–O(32)	125.4(3)	O(11)–Er(2)–O(51)	132.4(3)
O(11)–Er(1)–N(12)	66.6(3)	O(11)–Er(2)–N(2)	99.3(3)
O(31)–Er(1)–O(32)	52.0(3)	O(21)–Er(2)–O(52)	136.5(3)
O(31)–Er(1)–N(12)	121.3(3)	O(21)–Er(2)–N(21)	67.3(3)
O(32)–Er(1)–O(41)	118.5(3)	O(21)–Er(2)–N(22)	67.5(3)
O(32)–Er(1)–N(11)	73.2(3)	O(51)–Er(2)–O(52)	53.4(3)
O(41)–Er(1)–O(42)	52.1(3)	O(51)–Er(2)–N(21)	79.8(3)
O(41)–Er(1)–N(12)	159.6(3)	O(52)–Er(2)–N(2)	140.4(3)
O(42)–Er(1)–N(11)	73.0(3)	O(52)–Er(2)–N(22)	122.2(3)
N(1)–Er(1)–N(11)	146.8(3)	N(2)–Er(2)–N(21)	142.8(3)
N(1)–Er(1)–N(12)	86.7(3)	N(2)–Er(2)–N(22)	77.1(3)
N(11)–Er(1)–N(12)	76.7(3)	N(21)–Er(2)–N(22)	72.7(3)
Er(1)–O(1)–Er(2)	108.1(3)	Er(2)–O(11)–Er(1)	106.7(3)

monoanion of the *gem*-diol form of di-2-pyridyl ketone, $(py)_2C(OH)O^-$, and one monoanionic hemiacetal form of the organic ligand, $(py)_2C(OMe)O^-$, bridge the metal centers through their deprotonated hydroxyl groups. Thus, the two Er^{III} atoms are doubly bridged by the deprotonated hydroxyl oxygen atoms O(1) and O(11). The Er(1) atom is in a nine-coordinate ligand environment comprising the two just mentioned hydroxyl oxygen atoms, four oxygen atoms from two chelating nitrato ligands (O(31), O(32), O(41), O(42)), the two 2-pyridyl nitrogen atoms from the $(py)_2C(OH)O^-$ ligand (N(11), N(12)) and one 2-pyridyl nitrogen atom from the bridging $(py)_2C(OMe)O^-$ ligand (N(1)). Two oxygen atoms from the remaining chelating nitrato ligand (O(51), O(52)), the second nitrogen atom from the bridging $(py)_2C(OMe)O^-$ ligand (N(2)) and the N(21), N(22), O(21) triad of atoms from the tridentate chelating (i.e., terminal) $(py)_2C(OMe)O^-$ ligand complete eight-coordination at Er(2).

The coordination modes of the organic ligands of complex **4** · 0.8EtOH · 0.4MeOH are shown in Fig. 4. The $(py)_2C(OH)O^-$ anion behaves as an $\eta^1{:}\eta^2{:}\eta^1{:}\mu_2$ ligand or in a 2.201_11_1 mode (as described using Harris notation [13]). According to the latter, the binding mode of a ligand is referred to as $X.Y_1Y_2Y_3\cdots Y_n$, where X is the overall number of metals bound by the whole ligand and each value of Y refers to the metal ions attached to the different donor atoms. The ordering of Y is listed by the Cahn–Ingold–Prelog priority rules, hence here O before N. In the case of chelating/bridging ligands, to distinguish between several alternatives, a subscript number is included

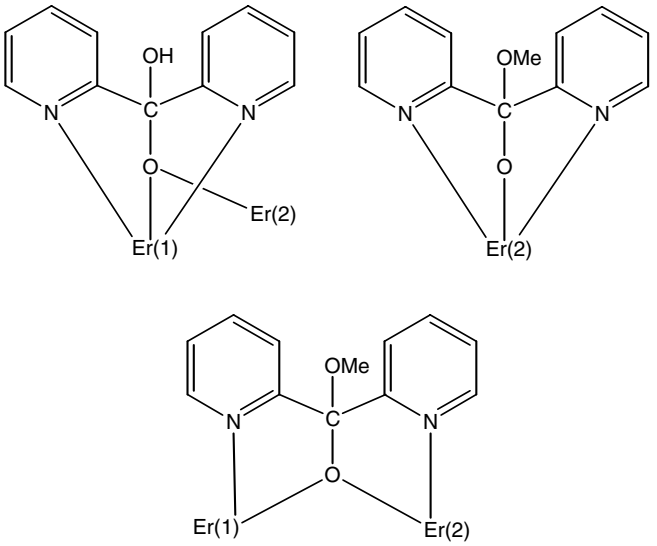

Fig. 4. The crystallographically established coordination modes of the organic ligands $(py)_2C(OH)O^-$ and $(py)_2C(OMe)O^-$ in complex **4** · 0.8EtOH · 0.4MeOH, and the Harris notation [13] that describes these modes.

to show to which metal ion the donor is attached. The bridging $(py)_2C(OMe)O^-$ anion behaves as an $\eta^1{:}\eta^2{:}\eta^1{:}\mu_2$ (or as 2.201_11_2 using Harris notation [13]) ligand, while the terminal $(py)_2C(OMe)O^-$ ligand is tridentate chelating ($\eta^1{:}\eta^1{:}\eta^1$ or 1.1011). The methoxy oxygen atom of both the $(py)_2C(OMe)O^-$ ligands and the hydroxyl oxygen atom of the $(py)_2C(OH)O^-$ ligand remain unbound to the metals. Ligands based on the *gem*-diol or the hemiacetal forms of di-2-pyridyl ketone have been observed in numerous ligation modes over the years [7]. The observed terminal and bridging ligation modes of $(py)_2C(OMe)O^-$ are common in the coordination chemistry of the hemiacetal forms of di-2-pyridyl ketone [7]. On the contrary, the observed 2.201_11_1 coordination mode of $(py)_2C(OH)O^-$ (Fig. 4) is extremely rare and has crystallographically been identified only in the dinuclear complex $[Bi_2(O_2CCF_3)_4\{(py)_2C(OH)O\}_2(THF)_2]$ [14].

The presence of two monoatomic bridges (O(1), O(11)) causes the Er(1)···Er(2) distance to be relatively short (3.681(2) Å). The Er–N distances are in the relatively narrow range 2.478(9)–2.572(9) Å; this range is typical for eight- and nine-coordinate Er(III) complexes [2f,2k,5c,13]. The Er–O bond lengths fall into two distinct categories; those involving the organic ligands (2.222(8)–2.330(7) Å) and those involving the nitrato ligands (2.380(9)–2.466(8) Å). The bridging Er–O distances involving O(1) and O(11) are asymmetric, e.g., Er(1)–O(11) = 2.330(7) Å and Er(2)–O(11) = 2.258(6) Å. The Er(2)–O bond distance for the bridging alkoxo-type oxygen atom of $(py)_2C(OMe)O^-$ (Er(2)–O(1) = 2.293(6) Å) is longer than the Er(2)–O distance exhibited by the terminal oxygen atom of $(py)_2C(OMe)O^-$ (Er(2)–O(21) = 2.222(8) Å). The Er(2)–O(alkoxo-type) distances have an average value of 2.258(8) Å, which is shorter than the corresponding value

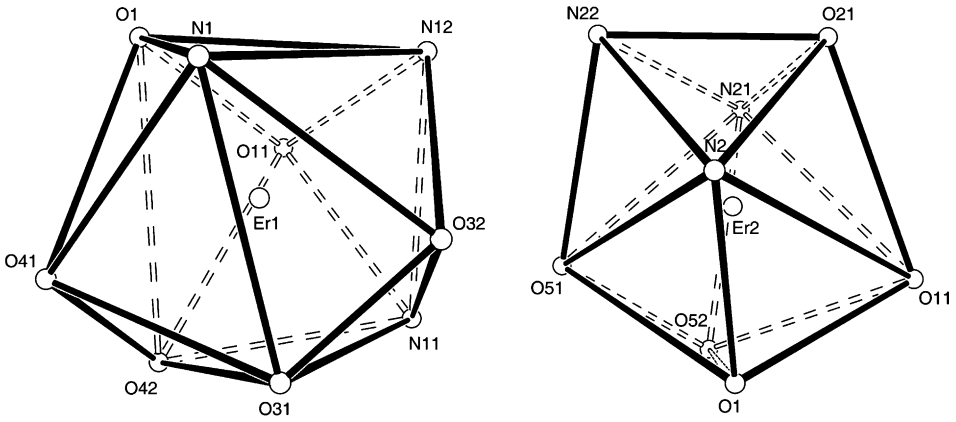

Fig. 5. Views of the inner coordination polyhedra of **4** · 0.8EtOH · 0.4MeOH showing the tricapped trigonal prismatic coordination of Er(1) and the dodecahedral stereochemistry about Er(2).

for the Er(1)–O (alkoxo-type) distances (2.292(7) Å); the decreased Er–O distances for Er(2) may be a consequence of the lower coordination number of this metal ion compared to that for Er(1) (eight versus nine). An analogous trend holds true for the Er–O(nitrato) bond distances; the average Er(1)–O(nitrato) and Er(2)–O(nitrato) distances are 2.447(8) and 2.416(9) Å, respectively. The nitrato ligands are planar, as indicated by the sum of O–N–O angles (359.7–360.0°), and almost symmetrically chelated. The Er–O(nitrato) bond lengths agree well with the values reported [15] for other eight- and nine-coordinate erbium(III) nitrate complexes.

The coordination polyhedron of Er(1) (Fig. 5) is best described as a distorted tricapped trigonal prism with the alkoxo-type oxygen atom, O(11), and the nitrate oxygen atoms O(32) and O(41) forming the three rectangular face caps. The angle sum subtended by the three capping atoms at Er(1) is 357.8°. It may be emphasized that in each nitrato ligand, the capping atom forms a slightly weaker bond to Er(1) than the non-capping atom, e.g., Er(1)–O(41) = 2.466(8) Å versus Er(1)–O(42) = 2.411(8) Å. The coordination polyhedron of the eight donor atoms about Er(2) (Fig. 5) is best described [10a] as a distorted dodecahedron. Atoms N(22), O(21), O(1), O(52) constitute a distorted tetrahedron that has been elongated along the fourfold inversion axis of the idealized polyhedron, whereas the set of atoms N(2), N(21), O(11), O(51) form a distorted tetrahedron that has been squashed along the same axis. An alternative way of viewing the dodecahedron about Er(2) is to consider it [16] as two interpenetrating planar trapezoids N(22)O(21)O(11)O(51) and N(2)N(21)O(1)O(52).

The distances O(12)···O(21) and O(ethanol)···O(42) ($-x+2$, $y+1/2$, $-z+3/2$) are only 2.557 and 2.985 Å, respectively, raising the possibility of the presence of hydrogen bonds. However, due to the fact that the hydrogen atoms of the structure were not located, the hydrogen bonds can not be considered in detail. The crystal structure is stabilized by four, crystallographically independent π–π stacking interactions (one intramolecular, three intermolecular). The intramolecular interaction involves the two 2-pyridyl rings that possess N(2) and N(12), the intercentroid distance (Cg···Cg*) and the dihedral angle being 3.740 Å and 10.1°, respectively. The corresponding perpendicular distances from Cg and Cg* to the best least-squares ring planes of the other stacking moieties are 3.490 and 3.549 Å. The first type of intermolecular interaction involves the two 2-pyridyl rings that possess N(11) and N(22) (the symmetry code is $x+1$, y, z), the intercentroid distance and the dihedral angle being 3.795° and 5.5°, respectively. The corresponding perpendicular distances from Cg and Cg* to the best least-squares ring planes of the other stacking moieties are 3.439 and 3.575 Å. The other intermolecular π–π stacking interactions involve the rings that possess N(2) and N(21) (x, $-y+1/2$, $z+1/2$), and the rings that possess N(1) and N(1) ($-x+2$, $-y+1$, $-z+1$).

The structural comparison of the dinuclear complexes $[Er_2(NO_3)_3\{(py)_2C(OMe)O\}_2\{(py)_2C(OH)O\}]$ (**4**) and $[Er_2(NCS)_3\{(py)_2C(OMe)O\}_3(MeOH)]$ [10a] reveals the following differences: (i) The former possesses two different types of monoanionic $(py)_2CO$-based ligands, whereas the latter only one; (ii) the organic ligands in **4** exhibit three *different* coordination modes (one terminal and two bridging), whereas the three $(py)_2C(OMe)O^-$ ligands in the isothiocyanate complex exhibit the same coordination mode; (iii) the two Er^{III} atoms are doubly bridged by deprotonated hydroxyl oxygens in **4** but triply bridged in the isothiocyanate compound [10a], and as a result the Er···Er distance is longer in the former (3.681(2) Å) than in the latter (3.380(2) Å), and (iv) the two Er^{III} atoms in the nitrate complex **4** have different coordination numbers (eight and nine) and hence two different coordination geometries (dodecahedral and tricapped trigonal prismatic), whereas the coordination number for both Er^{III} atoms in the isothiocyanate complex is the same (eight).

Complex **4** · 0.8EtOH · 0.4MeOH is the third structurally characterized lanthanide(III) complex with a $(py)_2CO$-based ligand (see Section 1) and joins only a handful of complexes of any metal that contain both $(py)_2C(OH)O^-$ and $(py)_2C(OR)O^-$ ions as ligands [9c,9f,12].

It also covers a gap in the erbium(III) literature in being the first crystallographically characterized dinuclear nitrate complex.

3.3. Magnetic moments, electronic and IR spectra

The experimental, room-temperature effective magnetic moment (μ_{eff}) values per Ln^{III} atom for complexes **1**–**4** (see Section 2.2) show very little deviation from the theoretical values (Pr^{III}, 3.62 BM; Eu^{III}, 3.5 BM; Tb, 9.7 BM; Er, 9.6 BM) predicted by Eq. (3), suggesting that the 4f electrons in the complexed Ln^{III} atoms are well-shielded by the outermost 5s and 5p electrons [16]

$$\mu_{eff} = g[J(J+1)]^{1/2} \quad (3)$$

The solid-state (diffuse reflectance) electronic spectra of the prepared complexes involve intraligand and f–f transitions. Detailed assignments (based on the literature data [17]) of the observed weak f–f bands are given in Table 3. The shape and the fine structure of the f–f band assigned to the "hypersensitive" transition $^4I_{15/2} \rightarrow {}^2H_{11/2}$ (Er-I) in the spectrum of **4** are sensitive to the coordination number [18]. By comparing the spectrum of **4** with the spectra of Er(III) complexes of known structures [10a,18,19] in the region of this transition (520–530 nm), it is confirmed that the metal ions are eight- or/and nine-coordinate.

The values of the bonding parameters $\bar{\beta}$ (nephelauxetic ratio), δ (Sinha's parameter) and $b^{1/2}$ (covalent factor) for complexes **1** and **4**, calculated from the solid-state f–f spectra by standard equations [10a,19,20] and listed in Table 4, indicate that the interaction between Pr^{III} and Er^{III} and the ligands is essentially electrostatic and that there is a minor participation of the 4f orbitals in bonding [20].

The IR spectra of vacuum-dried samples of **1**–**4** exhibit a medium intensity band at 3410–3380 cm^{-1}, assignable to the ν(OH) vibration of the $(py)_2C(OH)O^-$ ligand [8b]. The spectra of the four complexes do not exhibit bands in the region expected for the carbonyl stretching vibration (ν(C=O), at 1684 cm^{-1} for free $(py)_2CO$) with the nearest IR absorption at ~1600 cm^{-1} assigned as a 2-pyridyl stretching mode raised from 1582 cm^{-1}, as observed earlier on complex formation involving hydration or alcoholysis of $(py)_2CO$ [8b,21]. The bands at ~1050, ~765 and ~635 cm^{-1} can be assigned [22] to pyridyl ring breathing, pyridyl C–H out-of-plane bending and in-plane pyridyl ring deformation vibrations, respectively.

Diagnostic IR bands assigned to nitrate vibrations are listed in Table 5. The cited nitrate frequencies in Table 5 arise from spectra obtained as Nujol and hexachlorobutadiene mulls (whereas those cited in Section 2.2 arise from KBr pellets), since it is well known that pressing a pellet affects the nitrate coordination [23]; the organic ligands' frequencies are identical in both the KBr and mull spectra. The IR spectra of **1**–**4** in KBr are indicative of the presence of ionic nitrates (although the X-ray structure of **4** · 0.8EtOH · 0.4MeOH revealed no nitrate counterions); their existence in the KBr pellet is deduced from the appearance of the $\nu_3(E')(\nu_d(NO))$ mode of the D_{3h} ionic nitrate at 1384 cm^{-1} [24], suggesting [23] that a certain amount of nitrato ligands are replaced by bromides (thus generating ionic nitrates) in the KBr matrix. In the mull spectra of **1**–**4**, the bands at ~1475 and ~1285 cm^{-1} are assigned [24] to the $\nu_1(A_1)$ and $\nu_5(B_2)$ (under C_{2v} symmetry) stretching modes of the nitrato ligands, respectively. Their separation is large (~190 cm^{-1}) suggesting (**1**–**3**) or confirming (**4**) the bidentate character of the nitrato ligands [24]. The 1700–1800 cm^{-1} region is viewed as the key to

Table 3
Solid-state f–f bands for complexes **1**–**4**

λ (nm)	Assignment
Complex ***1***	
449	$^3H_4 \rightarrow {}^3P_2$
474	$^3H_4 \rightarrow {}^3P_1$
485	$^3H_4 \rightarrow {}^3P_0$
599	$^3H_4 \rightarrow {}^1D_2$
Complex ***2***	
363	$^7F_0 \rightarrow {}^5D_4$
397	$^7F_0 \rightarrow {}^5L_6$
Complex ***3***	
373	$^7F_6 \rightarrow {}^5G_6$
492	$^7F_6 \rightarrow {}^5D_4$
Complex ***4***	
370 sh, 380	$^4I_{15/2} \rightarrow {}^4G_{11/2}$ (Er-II)[a]
492	$^4I_{15/2} \rightarrow {}^4F_{7/2}$
520, 524, 530 sh	$^4I_{15/2} \rightarrow {}^2H_{11/2}$ (Er-I)[a]
542	$^4I_{15/2} \rightarrow {}^4S_{3/2}$
652, 657	$^4I_{15/2} \rightarrow {}^4F_{9/2}$

[a] These transitions are "hypersensitive".

Table 4
Bonding parameters[a] for the Pr(III) and Er(III) complexes **1** and **4**

Complex	β	δ (%)	$b^{1/2}$
1	0.994	+0.60	0.055
4	0.996	+0.40	0.045

[a] Calculated from the solid-state f–f spectra taking into account the wavenumbers of the transitions mentioned in Table 3.

Table 5
Diagnostic IR bands (cm^{-1}) of the NO_3^- ligands present in complexes **1**–**4**[a,b]

Complex	$\nu_1(A_1') + \nu_4(E')$[c]	$\nu_1(A_1)$[d]	$\nu_5(B_2)$[e]
1	1754, 1725	1474 s	1284 m
2	1749, 1712	1480 s	1283 m
3	1753, 1715	1480 s	1287 m
4	1758, 1716	1473 m	1282 m

[a] The cited wavenumbers arise from spectra recorded as Nujol and hexachlorobutadiene mulls.
[b] The spectra of these complexes in KBr exhibit a medium to strong intensity band at 1384 cm^{-1} (see text in Section 3.3).
[c] These terms refer to the free NO_3^-; $\nu_1(A_1')$ and $\nu_4(E')$ are the ν_s(NO) and δ_d(ONO) vibrations, respectively.
[d] ν(N=O).
[e] $\nu_{as}(NO_2)$.

differentiate between bidentate and monodentate nitrate coordination [15d,23–25]. Lever et al. [25] proposed the combination band $\nu_1(A_1') + \nu_4(E')$ of free NO_3^-, which appears in the 1700–1800 cm^{-1} region, as a spectroscopic criterion for structural diagnosis. Upon coordination, ν_4 (E′, in-plane bending) near 700 cm^{-1} splits into two bands, and the magnitude of the splitting is expected to be larger for bidentate than for monodentate ligands. This is reflected in the separation of the two ($\nu_1 + \nu_4$) weak bands in the 1700–1800 cm^{-1} region. The separation of the combination bands is 29–42 cm^{-1} (see Table 5) in our complexes and these values indicate bidentate nitrato ligands [15d,23–25]. As it has been observed by Fukuda et al. [15d], the value of this splitting parameter increases with decreasing ionic size across the lanthanide series.

3.4. Photoluminescence properties of the Eu(III) and Tb(III) complexes

Excitation and luminescence spectra of complex **2** and the luminescence spectrum of complex **3**, recorded in the solid state at 295 K, are shown in Figs. 6 and 7, respectively. Excitation at 336 nm into the lowest energy ligand-centered absorption band results in the luminescence characteristic of the Ln^{3+} ion (Ln = Eu, Tb).

The strong red emission of **2** is assigned to the characteristic $^5D_0 \rightarrow {}^7F_j$ ($j = 0$–4) transitions or Eu^{3+}. Specific assignments [2a,2j,26] are as follows: $^5D_0 \rightarrow {}^7F_0$ (580 nm), $^5D_0 \rightarrow {}^7F_1$ (587 nm), $^5D_0 \rightarrow {}^7F_2$ (615 nm), $^5D_0 \rightarrow {}^7F_3$ (652 nm) and $^5D_0 \rightarrow {}^7F_4$ (688 nm). The appearance of a slight structure in the symmetry-forbidden emission $^5D_0 \rightarrow {}^7F_0$ may indicate that more than one coordination environments are present for Eu(III) [2j,26a,26b]. The Eu^{3+} ion is unique in that both the ground state $^7F_0$ and the excited emissive state $^5D_0$ are non-degenerate. Since the $^5D_0 \rightarrow {}^7F_0$ transition occurs between non-degenerate energy levels, neither of which can be split by a ligand field, a single environment gives rise to only a single transition; if more than one Eu^{III} environments are present, each will have its own characteristic transition energy [2j]. The dominant band in the emission spectrum is the hypersensitive $^5D_0 \rightarrow {}^7F_2$ transition, which shows signs of splitting. The higher intensity of this transition compared to that of the magnetic-dipole allowed $^5D_0 \rightarrow {}^7F_1$ transition indicates that this complex has a structure with no imposed symmetry [26a]. As a matter of fact, complexes with a centrosymmetric coordination sphere have $(^5D_0 \rightarrow {}^7F_2)/(^5D_0 \rightarrow {}^7F_1)$ intensity ratios lower than 0.7 [26a,26c].

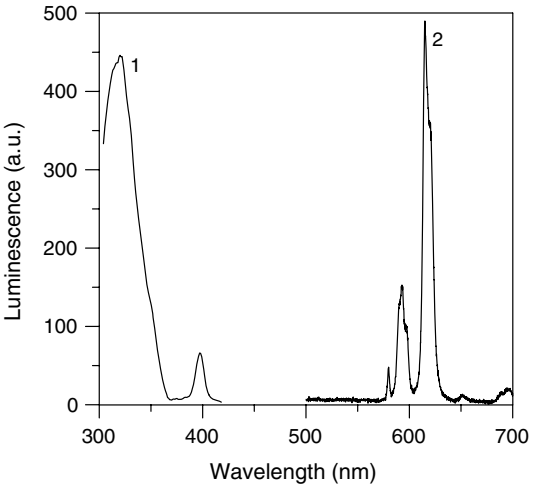

Fig. 6. Excitation (emission at 616 nm) (1) and emission (excitation at 336 nm) (2) spectra of **2** in the solid state at room temperature.

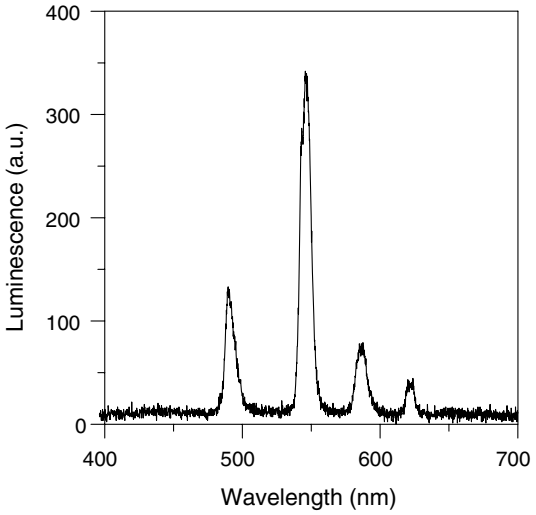

Fig. 7. The emission spectrum of **3** in the solid state at room temperature (excitation at 336 nm).

The Tb(III) complex **3** gives an entirely typical Tb^{3+} emission spectrum containing the expected sequence of $^5D_4 \rightarrow {}^7F_j$ transitions, with the $j = 3$–6 components being visible. Specific assignments [2a,26a,27] are as follows: $^5D_4 \rightarrow {}^7F_6$ (489 nm), $^5D_4 \rightarrow {}^7F_5$ (546 nm), $^5D_4 \rightarrow {}^7F_4$ (586 nm) and $^5D_4 \rightarrow {}^7F_3$ (622 nm). The spectrum is dominated by the $^5D_4 \rightarrow {}^7F_5$ transition, which gives an intense green luminescence output for the solid sample.

Generally, it is possible to obtain detectable luminescence for Eu(III) and Tb(III) only be direct excitation at their absorption peaks (at 396 and 370 nm, respectively) [28]. The fact that, for both **2** and **3**, strong luminescence was observed by excitation at 336 nm indicates that we have succeeded to increase the absorption cross-section of both lanthanides by excitation of the ligand(s) and energy transfer to the Ln^{III} ion, i.e., by an indirect process (antenna effect).

It is well known that the antenna-to-cation sensitization process, which seems to be general in Eu(III) and Tb(III) complexes, includes a sequence of steps [1j,2a,2e,2k]: (i) Light absorption to produce an excited singlet (S) from the ground singlet state in the organic ligand(s). (ii) Intersystem crossing (ISC) to populate the lowest-lying triplet (T) state by a radiationless process; competing with this are organic fluorescence and radiationless deactivation of the excited singlet as thermal energy. (iii) Radiationless

transfer of energy from the triplet state to one (or more) lanthanide-centered excited levels; the requirement for effective transfer is that the triplet state should be close in energy to or above the 4f levels concerned, and (iv) Emission of energy if one of the 4f levels excited by the transfer has an allowed transition to a lower 4f level.

4. Concluding comments and perspectives

The present work extends the body of results that emphasize the ability of the monoanionic ligands $(py)_2C(OH)O^-$ and $(py)_2C(OMe)O^-$ to form structurally interesting 4f-metal complexes. The use of the $(py)_2CO/NO_3^-$ "blend" in erbium(III) chemistry has provided access to the new complex $[Er_2(NO_3)_3\{(py)_2C(OMe)O\}_2\{(py)_2C(OH)O\}]$ (**4**) which has been structurally characterized; this complex has the $\{Er_2(\mu\text{-}OR)(\mu\text{-}OR')\}^{4+}$ core, where $R = (py)_2C(OH)-$ and $R' = (py)_2C(OMe)-$. Thus, complex **4** becomes the third structurally characterized lanthanide(III) complex with $(py)_2CO$-based ligands. Contrary to the previously characterized complexes $[Er(NCS)_3\{(py)_2C(OEt)(OH)\}_3]$ and $[Er_2(NCS)_3\{(py)_2C(OMe)O\}_3(MeOH)]$ [10], compound **4** possesses two different types of $(py)_2CO$-based ligands, i.e., $(py)_2C(OH)O^-$ and $(py)_2C(OMe)O^-$, that exhibit three distinct coordination modes. Thus, the principal objective of our studies, i.e., new structural types in $Ln(III)/(py)_2CO$ chemistry, has been realized. Based on analytical and spectroscopic studies, it seems that complexes **1**–**3** have a similar molecular structure with that of **4**. In this paper we have also demonstrated that the coordination of $(py)_2C(OH)O^-$ and $(py)_2C(OMe)O^-$ leads to complexes with efficient Ln(III) luminescence sensitization for Eu^{III} and Tb^{III} that emit in the visible region. This can be attributed to several factors such as the shielding of the metal ion from water and/or alcohol ligands, the lack of any strong ligand-to-metal charge-transfer bands that are usually responsible for the weak emission of the more readily reduced Eu(III), the lack of any energy back-transfer from the sensitizer triplet state, etc.

The nitrate terminal ligands present in **1**–**4** could have future utility as a means to access higher-nuclearity neutral or cationic clusters using bis(bidentate) bridging ligands, including aromatic heterocycles and dicarboxylates; such chemistry might alter the photophysical properties of the products. The ability of the *gem*-diol form of di-2-pyridyl ketone, "$(py)_2C(OH)_2$" (Fig. 1), to act as a dianionic ligand ($(py)_2CO_2^{2-}$, Fig. 1) and to bridge 3, 4 or 5 transition metal ions [7] gives also hopes for the isolation of high-nuclearity Ln(III) clusters if we find the right synthetic conditions for the formation of $(py)_2CO_2^{2-}$. A ligand "blend" that might prove successful for this synthetic purpose is $(py)_2CO/RCO_2^-$ [7]. Although only mononuclear and dinuclear complexes have been discovered from our work to date with lanthanide isothiocyanates and nitrates, clearly the $Ln^{III}/(py)_2CO$ chemistry warrants further study and also expansion to other inorganic anions with a higher charge and a higher bridging ability, e.g., SO_4^{2-}. Such synthetic efforts are in progress. In addition, we plan to try to design ligands in which the binding and antenna domains will be independent of each other; this will offer a wealth of possibilities for further derivatisation on the antenna part of the organic ligand, whilst maintaining binding properties, leading to improved photoluminescence properties of the resultant lanthanide(III) complexes.

5. Supplementary data

Full crystallographic details have been deposited with the Cambridge Crystallographic Data Centre. Copies of the data can be obtained free of charge on request from The Director, CCDC, 12 Union Road, Cambridge CB2 1EZ, UK (fax : +44 1233 336033; e-mail: deposit@ccdc.cam.ac.uk or http://www.ccdc.cam.ac.uk) quoting the deposition number CCDC 295807 ($\mathbf{4} \cdot 0.8EtOH \cdot 0.4MeOH$).

Acknowledgement

K.A.T. and S.P.P. thank The Research Committee of the University of Patras (K. CARATHEODORY Program No. 3016) for financial support of this work.

References

[1] (a) For example, see: A. Mayer, S. Neuenhofer, Angew. Chem., Int. Ed. Engl. 33 (1994) 1044;
(b) J. Kido, Y. Okamoto, Chem. Rev. 102 (2002) 2357;
(c) M. Montalti, I. Prodi, N. Zaccheroni, L. Charbonniere, L. Douce, R. Ziessel, J. Am. Chem. Soc. 123 (2001) 12694;
(d) D. Parker, R.S. Dickins, H. Puschmann, C. Crossland, J.A.K. Howard, Chem. Rev. 102 (2002) 1977;
(e) V.W.W. Ham, K.K.W. Lo, Coord. Chem. Rev. 184 (1999) 157;
(f) H. Tsukube, S. Shinoda, H. Tamiaki, Coord. Chem. Rev. 226 (2002) 227;
(g) K. Binnemans, C. Görller-Walrand, Chem. Rev. 102 (2002) 2303;
(h) S. Faulkner, J.L Matthews, in: J.A. McCleverty, T.J. Meyer (Eds.), Comprehensive Coordination Chemistry II, vol. 9, Elsevier, Amsterdam, 2004, p. 913;
(i) J. Silver, in: J.A. McCleverty, T.J. Meyer (Eds.), Comprehensive Coordination Chemistry II, vol. 9, Elsevier, Amsterdam, 2004, p. 689;
(j) K. Kuriki, Y. Koike, Y. Okamoto, Chem. Rev. 102 (2002) 2347;
(k) V. Vicinelli, P. Ceroni, M. Maestri, V. Balzani, M. Gorka, F. Vögtle, J. Am. Chem. Soc. 124 (2002) 6461.
[2] (a) Few representative references: S.W. Magennis, S. Parsons, Z. Pikramenou, Chem. Eur. J. 8 (2002) 5761;
(b) A.P. Basset, S.W. Magennis, P.B. Glover, D.J. Lewis, N. Spencer, S. Parsons, R.M. Williams, L. De Cola, Z. Pikramenou, J. Am. Chem. Soc. 126 (2004) 9413;
(c) K.-L. Wong, M.-M. Kwok, W.-T. Wong, D.L. Phillips, K.-W. Cheah, Angew. Chem., Int. Ed. 43 (2004) 4659;
(d) A. de Bettencourt-Dias, Inorg. Chem. 44 (2005) 2734;
(e) I. Nasso, C. Galaup, F. Havas, P. Tisnes, C. Picard, S. Laurent, L.V. Elst, R.N. Muller, Inorg. Chem. 44 (2005) 8293;
(f) A. Bellusci, G. Barberio, A. Crispini, M. Ghedini, M. La Deda, D. Pucci, Inorg. Chem. 44 (2005) 1818;
(g) L.S. Natrajan, A.J. Blake, C. Wilson, J.A. Weinstein, P.L. Arnold, Dalton Trans. (2004) 3748;
(h) J.B. Lamture, Z.H. Zhou, A.S. Kumar, Th.G. Wensel, Inorg. Chem. 34 (1995) 864;

(i) G.F. De Sá, L.H.A. Nunes, Z.-M. Wang, G.R. Choppin, J. Alloys Compd. 196 (1993) 17;
(j) V. Patroniak, P.N.W. Baxter, J.-M. Lehn, Z. Hnatejko, M. Kubicki, Eur. J. Inorg. Chem. (2004) 2379;
(k) S. Quici, G. Marzanni, A. Forni, G. Accorsi, F. Barigelletti, Inorg. Chem. 43 (2004) 1294.

[3] N. Sabbatini, M. Guardigli, J.-M. Lehn, Coord. Chem. Rev. 123 (1993) 201.

[4] (a) W.M. Shavaleev, S.J.A. Pope, Z.R. Bell, S. Faulkner, M.D. Ward, Dalton Trans. (2003) 808;
(b) G.A. Hebbink, L. Grave, L.A. Woldering, D.N. Reinhoudt, F.C.J.M. van Veggel, J. Phys. Chem. A 107 (2003) 2483.

[5] (a) J.-C.G. Bünzli, C. Piguet, Chem. Rev. 102 (2002) 1897;
(b) N.M. Shavaleev, G. Accorsi, D. Virgili, Z.R. Bell, Th. Lazarides, G. Calogero, N. Armaroli, M.D. Ward, Inorg. Chem. 44 (2005) 61;
(c) N.M. Shavaleev, L.P. Moorcraft, S.J.A. Pope, Z.R. Bell, S. Faulkner, M.D. Ward, Chem. Eur. J. 9 (2003) 5283;
(d) S.I. Klink, H. Keizer, F.C.J.M. van Veggel, Angew. Chem., Int. Ed. 39 (2000) 4319;
(e) A. Beeby, R.S. Dickins, S. Fitzgerald, L.J. Govenlock, C.L. Maupin, D. Parker, J.P. Riehl, G. Siligardi, J.A.G. Williams, Chem. Commun. (2000) 1183;
(f) D. Imbert, M. Cantuel, J.-C.G. Bünzli, G. Bernardinelli, C. Piguet, J. Am. Chem. Soc. 125 (2003) 15698;
(g) M.A. Subhan, H. Nakata, T. Suzuki, J.-H. Choi, S. Kaizaki, J. Lumin. 101 (2003) 307;
(h) S.J. Pope, B.J. Coe, S. Faulkner, Chem. Commun. (2004) 1550;
(i) S.A. Pope, B.J. Coe, S. Faulkner, E.V. Bichenkova, X. Yu, K.T. Douglas, J. Am. Chem. Soc. 126 (2004) 9490;
(j) D. Guo, C.-Y. Duan, F. Lu, Y. Hasegawa, Q.-J. Meng, S. Yanagida, Chem. Commun. (2004) 1486;
(k) P.D. Beer, F. Szemes, P. Passaniti, M. Maestri, Inorg. Chem. 43 (2004) 3965;
(l) P.B. Glover, P.R. Ashton, L.J. Childs, A. Rodger, M. Kercher, R.M. Williams, L. De Cola, Z. Pikramenou, J. Am. Chem. Soc. 125 (2003) 9918.

[6] G. Mancino, A.J. Ferguson, A. Beeby, N.J. Long, T.S. Jones, J. Am. Chem. Soc. 127 (2005) 524.

[7] For a review, see: G.S. Papaefstathiou, S.P. Perlepes, Comments Inorg. Chem. 23 (2002) 249.

[8] (a) Recent selected literature: C.G. Efthymiou, C.P. Raptopoulou, A. Terzis, R. Boča, M. Korabic, J. Mrozinski, S.P. Perlepes, E.G. Bakalbassis, Eur. J. Inorg. Chem., in press;
(b) E. Katsoulakou, V. Bekiari, C.P. Raptopoulou, A. Terzis, P. Lianos, E. Manessi-Zoupa, S.P. Perlepes, Spectrochim. Acta Part A 61 (2005) 1627;
(c) G.S. Papaefstathiou, A. Escuer, F.A. Mautner, C. Raptopoulou, A. Terzis, S.P. Perlepes, R. Vicente, Eur. J. Inorg. Chem. (2005) 879;
(d) A.K. Boudalis, B. Donnadieu, V. Nastopoulos, J. Modesto Clemente-Juan, A. Mari, Y. Sanakis, J.-P. Tuchagues, S.P. Perlepes, Angew. Chem., Int. Ed. 43 (2004) 2266;
(e) A.K. Boudalis, F. Dahan, A. Bousseksou, J.-P. Tuchagues, S.P. Perlepes, Dalton Trans. (2003) 3411;
(f) C.J. Milios, E. Kefalloniti, C.P. Raptopoulou, A. Terzis, R. Vicente, N. Lalioti, A. Escuer, S.P. Perlepes, Chem. Commun. (2003) 819.

[9] (a) Recent selected literature: Y.-M. Li, J.-J. Zhang, R.-B. Fu, S.-C. Xiang, T.-L. Sheng, D.-Q. Yuan, X.-H. Huang, X.-T. Wu, Polyhedron 25 (2006) 1618;
(b) C. Kanaras, B.L. Westcott, G. Crundwell, J.B. Updegraff III, M. Zeller, A.D. Hunter, S.O. Sommerer, Z. Kristallogr. 219 (2004) 1;
(c) G. Crundwell, B.L. Westcott, R. Coffey, M. Zeller, A.D. Hunter, Inorg. Chim. Acta 355 (2003) 432;
(d) S. Zhu, W.W. Brennessel, R.G. Harrison, L. Que Jr., Inorg. Chim. Acta 337 (2002) 32;
(e) M.-L. Tong, S.-L. Zheng, J.-X. Shi, Y.-X. Tong, H.K. Lee, X.-M. Chen, J. Chem. Soc., Dalton Trans. (2002) 1727;
(f) S.B. Jedner, H. Schwöppe, H. Nimir, A. Rompel, D.A. Brown, B. Krebs, Inorg. Chim. Acta 340 (2002) 181.

[10] (a) K.A. Thiakou, V. Nastopoulos, A. Terzis, C.P. Raptopoulou, S.P. Perlepes, Polyhedron 25 (2006) 539;
(b) X. Tai, H. Wang, X. Sun, M. Tan, Spectrosc. Lett. 38 (2005) 497.

[11] (a) G.M Sheldrick, SHELXS-86, Structure Solving Program, University of Göttingen, Germany, 1986;
(b) G.M Sheldrick, SHELXL-97, Program for the Refinement of Crystal Structures from Diffraction Data, University of Göttingen, Germany, 1997.

[12] (a) G.S. Papaefstathiou, A. Escuer, C.P. Raptopoulou, A. Terzis, S.P. Perlepes, R. Vicente, Eur. J. Inorg. Chem. (2001) 1567;
(b) Z.E. Serna, L. Lezama, M.K. Urtiaga, M.I. Arriortua, M.G. Barandika, R. Cortés, T. Rojo, Angew. Chem., Int. Ed. 39 (2000) 344;
(c) Z.E. Serna, M.K. Urtiaga, M.G. Barandika, R. Cortés, S. Martin, L. Lezama, M.I. Arriortua, T. Rojo, Inorg. Chem. 40 (2001) 4550.

[13] R.A. Coxall, S.G. Harris, D.K. Henderson, S. Parsons, P.A. Tasker, R.E.P. Winpenny, J. Chem. Soc., Dalton Trans. (2000) 2349.

[14] S.R. Breeze, S. Wang, J.E. Greedan, N.P. Raju, Inorg. Chem. 35 (1996) 6944.

[15] (a) For example, see: D.M.L. Goodgame, A.M. Khaled, D.J. Williams, Polyhedron 10 (1991) 1079;
(b) S.A. Cotton, P.R. Raithby, Inorg. Chem. Commun. 2 (1999) 86;
(c) Y.-C. Tan, X.-M. Gan, J.L. Stanchfield, E.N. Duesler, R.T. Paine, Inorg. Chem. 40 (2001) 2910;
(d) Y. Fukuda, A. Nakao, K. Hayashi, J. Chem. Soc., Dalton Trans. (2002) 527;
(e) M.G.B. Drew, M.J. Hudson, P.B. Iveson, C. Madic, M.L. Russell, J. Chem. Soc., Dalton Trans. (2000) 2711.

[16] S. Liu, L. Gelmini, S.J. Rettig, R.C. Thompson, C. Orvig, J. Am. Chem. Soc. 114 (1992) 6081.

[17] (a) For example, see: W.T. Carnall, P.R. Fields, K. Rajnak, J. Chem. Phys. 49 (1968) 4424, 4443, 4447, 4450;
(b) J.L. Ryan, C.K. Jørgensen, J. Phys. Chem. 70 (1966) 2845;
(c) S.P. Perlepes, Th.F. Zafiropoulos, J.K. Kouinis, A.G. Galinos, Z. Naturforsch. 36b (1981) 697.

[18] (a) D.G. Karraker, Inorg. Chem. 6 (1967) 1863;
(b) D.G. Karraker, Inorg. Chem. 7 (1968) 473.

[19] (a) A. Messimeri, V. Nastopoulos, A. Terzis, C.P. Raptopoulou, C. Papadimitriou, S.P. Perlepes, Inorg. Chem. Commun. 8 (2005) 578;
(b) A. Messimeri, C.P. Raptopoulou, V. Nastopoulos, A. Terzis, S.P. Perlepes, C. Papadimitriou, Inorg. Chim. Acta 336 (2002) 8.

[20] (a) C.K. Jørgensen, Modern Aspects of Ligand Field Theory, North-Holland, Amsterdam, 1971;
(b) S.P. Sinha, Spectrochim. Acta 22 (1966) 57;
(c) D.E. Henrie, G.R. Choppin, J. Chem. Phys. 49 (1968) 477.

[21] P.K. Byers, A.J. Canty, L.M. Engelhardt, J.M. Patrick, A.H. White, J. Chem. Soc., Dalton Trans. (1985) 981.

[22] Z.E. Serna, R. Cortés, M.K. Urtiaga, M.G. Barandika, L. Lezama, M.I. Arriortua, T. Rojo, Eur. J. Inorg. Chem. (2001) 865.

[23] G.J. Kleywegt, W.G.R. Wiesmeijer, G.J. Van Driel, W.L. Driessen, J. Reedijk, J.H. Noordik, J. Chem. Soc., Dalton Trans. (1985) 2177.

[24] K. Nakamoto, Infrared and Raman Spectra of Inorganic and Coordination Compounds, 4th ed., Wiley, New York, 1986, p. 121, 254.

[25] A.B.P. Lever, E. Mantovani, B.S. Ramaswamy, Can. J. Chem. 49 (1971) 1957.

[26] (a) C. Tedeschi, J. Azéma, H. Gornitzka, P. Tisnes, C. Picard, Dalton Trans. (2003) 1738;
(b) J.A. Fernandes, R.A.S. Ferreira, M. Pillinger, L.D. Carlos, J. Jepsen, A. Hazell, P. Ribeiro-Claro, I.S. Goncalves, J. Lumin. 113 (2005) 50;
(c) Y.-Q. Sun, J. Zhang, Y.-M. Chen, G.-Y. Yang, Angew. Chem. Int. Ed. 44 (2005) 5814.

[27] M. Elhabiri, R. Scopelliti, J.-C.G. Bünzli, C. Piguet, J. Am. Chem. Soc. 121 (1999) 10747.

[28] (a) M. Dejneka, E. Snitzer, R.E. Riman, J. Lumin. 65 (1995) 227;
(b) B.C. Joshi, J. Non-Cryst. Solids 180 (1995) 217.

(d_{001}) of about 18 Å and specific area of 200–300 m^2/g were reported by Pinnavaia [18] and Vaughan et al. [19]. These studies proposed that the intercalated species that give rise to this stable basal spacing is the so-called Keggin,s ion ($Al_{13}O_4(OH)_{24}(H_2O)_{12}^{7+}$), which has been characterized by angle X-ray scattering technique and by ^{27}Al nuclear magnetic resonance (^{27}Al NMR) data.

The chemical, surface, and structural properties of PILCs determine and can limit the potential applications which fall mainly into two categories: catalytic and adsorption processes. Presently, those materials can be used in a wide range of catalysis reactions, such as cracking, cycle hexane conversion, toluene with methanol alkylation, and propylene oligomerization. They are also commonly employed in the petroleum industry for long-chain hydrocarbons filtering and azeotropic cracking [20–30].

The aim of the present investigation is to study the structural and physical–chemical characteristics of two different types of smectites, such as natural and pillared clays, which were developed with $Al_{13}O_4(OH)_{24}(H_2O)_{12}^{7+}$ intercalation. This study investigated various parameters (chemical composition of the matrices, temperature of calcination, method of synthesis of the PILCs and effect of the acid activation) and their application into adsorption process with butylamine. Their adsorptive capacity was examined through adsorption isotherms, and the influence of the variation of parameters on PILCs texture was analyzed by different techniques.

2. Experimental

2.1. Raw material

Clay samples used in this investigation were obtained from the ''Serra do Maicuru'' area Para state, north of Brazil. Two different samples were used in this paper as starting materials and are named as A_1 and A_2. The particles that were lesser than 2 μm fraction of the sample were separated by sedimentation. The cation-exchange capacity (CEC) was ensured in order to evaluate the potential use of those clays for intercalation, following the ammonium acetate method by using a concentration of 2 mol dm^{-3} at pH 8. The results obtained were 9.2 mmol g^{-1} (A_1) and 10.5 mmol g^{-1} (A_2) on an air-dried basis and pointed for the continuation of the study. Mineralogical and chemical characterizations were carried out using the analytical techniques that will be described further.

2.2. Sample preparation and preliminary characterization

The samples were dried at 60 °C up to humidity between 12% and 15%. They were ground and passed in USS sieve No. 200 (74 mm) and examined through powder X-ray diffraction to confirm the presence of smectite clays by conventional sample preparation procedures, such as air-dried oriented mounts, ethylene glycol solvated and heated at 300 and 500 °C.

2.3. Synthesis of the pillaring solution and pillaring processes

Two distinct methods were used in the preparation of PILC materials:

(A) Method 1: The samples were saturated with Na_2CO_3 by adding the solution to dry materials at room temperature. This treatment was carried out using saturated solution of Na_2CO_3 (0.20 g cm^{-3}) in proportion of 1.00 mmol g^{-1} of sample. The mixture was homogenized and left standing for 12 h. The intercalating solution was obtained by slow addition of NaOH (0.2 mol dm^{-3}) in a $AlCl_3 \cdot 6H_2O$ (0.2 mol dm^{-3}) solution, with a basicity relationship OH/Al = 2. The sodium hydroxide solution was incorporated drop by drop in the aluminum chloride solution, which was maintained under vigorous stirring at 60 °C. The resultant solution was aged under reflux during 24 h. The polymeric solution was incorporated drop by drop in a suspension composed by 5% of Na-montmorillonite in a mixture of deionized water and ethanol. The amount of oligocation incorporated exhibited 20 mmol of Al per gram of natural clay. The resultant solution (polymeric solution and Na-montmorillonite) was filtrated and washed with deionized water. The sample was calcinated at 450 and 600 °C for 2 h. The resultant material was called Al-$PILC_1$.

(B) Method 2: The aluminum oligocation was prepared by using a solution of the following commercial product: Locron® $Al(NO_3)_3$ (0.2 mol dm^{-3}). The intercalating solution was obtained by slowly adding NaOH (0.2 mol dm^{-3}) into a $Al(NO_3)_3$ (0.2 mol dm^{-3}) solution, which was incorporated drop by drop into a suspension made with 50% of natural clay into a mixture of water, ethylene glycol and glycerin. The basicity ratio was 2 and quality of Al (0.2 M) was 20 mmol per gram of natural clay. The final solution containing clay, aluminum nitrate and sodium hydroxide was continuously stirred for 4 h and allowed to stand for 5 days. Finally, the material was washed with deionized water and calcinated at 450 and 600 °C. The resulting material was called Al-$PILC_1$ (450 °C) and Al-$PILC_1$ (600 °C), for sample A1 and Al-$PILC_2$ (450 °C) and Al-$PILC_2$ (600 °C), for sample A2.

2.4. Acid treatment

The pillared clays were activated with HCl in concentrations of 0.6 mol dm^{-3} by slowly adding the solutions to dry materials at room temperature, with continuous stirring for 2 h. The resultant solutions obtained (HCl and pillared clays) were filtrated and the resultant materials were washed with deionized water and dried at 60 °C. The resulting materials were called Al-PILC.

2.5. Adsorption process with butylamine

The adsorption process was carried out by suspending about 0.60 mg of the pillared clay in aqueous solution of each butylamine at room temperature. The isotherms of

concentration versus time were obtained through a batch method [31]. The number of moles adsorbed per gram (n_f) is calculated by the difference between the initial (n_i) and the supernatant (n_s) number of moles of amine divided by mass (m) of the compound used, $n_f = (n_i - n_s)/m$. The number of moles of butylamine adsorbed (n_f) increased with time (t) as a function of the concentration of the supernatant (C_s), until the plateau related total saturation of the acid center in the layered structure was obtained.

2.5.1. Adsorption isotherms

The most commonly used isotherms are the Langmuir isotherms, which have been originally derived for the adsorption of gases on plane surfaces such as glass, mica, and platinum; however, this adsorption process is applied to heavy metal ions adsorption in porous surfaces in the classical Langmuir form, where the quantity q_i of an adsorbate i adsorbed is related to the equilibrium solution concentration of the adsorbate c_i by the parameters K and b, the steepness of the isotherm is determined by K. It can be looked upon as a measure of the adsorbate for the surface. The value of b is the upper limit for q_i and represents the maximum adsorption of i determined by the number of reactive surface adsorption data by converting Eq. (1) into the linear form:

$$[C_s/N_f] = [1/(K \times b)] + [C_s/b] \quad (1)$$

Then the ratio $c_i/q_i = C_s/N_f$, the so-called distribution coefficient Kd, can be plotted against q_i. If the Langmuir equation can be applied, the measured data should fall on a straight line with slope of $-K$ and intercept of Kb, where $1/Kb$ is angular coefficient and $1/b$ is linear coefficient.

Another fitting for the adsorption process is established by Freundlich equation which has the form:

$$N_f = KfC^{1/n} \quad (2)$$

where Kf and n are adjustable positive valued parameters with n ranging only between 0 and 1. For $n = 1$ the linear C-type isotherms would be produced. The parameters are estimated by plotting $\log c_i$ with the resulting straight line having a y intercept of $\log a$ and a slope of n. The Temkin equation was also applied for solid/liquid interface:

$$N_f = A \ln C + B \quad (3)$$

where A and B are parameters of equation, estimating by plotting N_f against $\ln C$. The values are obtained for A and B, where B is the linear coefficient and A is the angular coefficient of the straight line. The coefficients obtained from these equations were used to adjust the theoretical model to the experimental data.

2.6. Analytical techniques

X-ray powder diffraction (XDR) patterns were recorded with a Philips PW 1050 diffractometer using Cu Kα (1.54060 Å) radiation in the region between 2° and 65° 2θ at a speed of 2° per minute and a step of 0.05°.

For the infrared spectroscopy, the samples were oven-dried at 120 °C to remove any adsorbed water. Each sample of about 0.200 g was finely ground for 1 min, combined with oven-dried spectroscopic grade KBr (0.0013 g) and pressed with 7 ton into a disc under vacuum. The spectrum of each sample was recorded in triplicate by accumulating 64 scans at 4 cm^{-1} resolution between 400 and 4000 cm^{-1}, using the Perkin–Elmer 1760X Fourier transform infrared spectrometer (FTIR).

The ^{27}Al MAS NMR spectra of the solid material were obtained on an AC 300/P Bruker spectrometer at room temperature at 75.5 MHz. A conical Andrew type rotor was used, and the spinning frequency was in the range of 4.5 kHz, with $Al(H_2O)_6^{3+}$ being used as an external standard.

Thermal analysis was carried out in a Stanton Redcroft 1000/1500 coupled to a DC ampler and temperature controller. Data from DTA-TG were obtained in all cases at a heating rate of 20 °C/min between 40 and 900 °C and under static air atmosphere.

BET surface areas and porosity measurements of the Al-PILC samples were determined using a Quantachome/Nova Surface Area Pore Volume Analyzer, Model 1200/5.01. The mesopore size distribution was obtained by applying the Barret–Joyner–Halenda (BJH) method to the adsorption branch of the isotherm.

The natural clays (A_1 and A_2), Al-$PILC_1$ and Al-$PILC_2$, were analyzed by induced coupled plasma-atomic emission spectrometry (ICP-AES), using an ARL 34000 instrument. The oven-dried powdered sample weighing exactly 0.231 g, 0.254 g, 0.241 g and 0.234 g, respectively, were placed separately on glass weighing dishes and transferred quantitatively to pre-cleaned nitric acid digestion bottles. The samples were then digested with 7 cm^3 of mixture of one part of nitric acid, three parts of hydrochloric acid and fifteen parts of hydrofluoric acid, and allowed to stand for five days. The samples were cooled in an ice-bath and 25 cm^3 of boric acid was added with stirring. Then, 50 cm^3 of deionized water was added and the solution was diluted to 100 cm^3. For each sample, a blank and a set of elemental standards were run to calibrate the instrument.

The samples for scanning electron microscopy (SEM) and micro-analysis (dispersive-energy system – EDS) were prepared in orientated blades at 25 °C and sputtered with gold. The used instrument was a model LEO-ZEISS, 430 Vp, in conditions of analysis using secondary images obtained to 20 KV, with distance of work of 11 mm.

3. Results and discussion

3.1. X-ray powder diffraction

Total mineralogical composition of the starting materials, A_1 and A_2 clays, was carried out in no oriented mounts

which exhibited mainly nontronite and goethite, besides the existence of kaolinite.

The results obtained for the d_{001} values are shown in Table 1. Figs. 1 and 2 show the X-ray powder diffractions for natural A_1 and A_2 clays and pillared/activated clays ($AlPILC_1$ and $AlPILC_2$) are given in a molar ratio of 2. It was observed that the pillared matrices obtained an increase in their interlayer distances after pillared process, with a *d* value of 18.97 Å for the sample $ALPILC_1$ and 18.86 Å for the sample $AlPILC_2$. It was also observed that the sample $ALPILC_1$ presented a slightly broader peak, in comparison with $ALPIC_2$, representing differences in the degree of crystallinity (calculated using the Biscaye's [13] equation, results shown in Table 1), related to interferences with the pillaring process. This fact can be explained based on the hypothesis of the existence of different species in the interlayer region that makes the entrance of the intercalation ion difficult, resulting in a structure distortion. Another possibility is the inadequate entrance of the ion in the interlayer region. When the matrix is submitted to a high temperature of calcination, it will exhibit a premature dehydroxylation of its pillars at a certain point of the interlayer region, resulting in a partial pillaring process of this matrix. In all cases, well-pillared samples showed approximately the same (d_{001}) basal spacing. The great influence of the number of pillars in interlayer spacing on the constitution and distribution of the pillars has been previously indicated in the literature [7–9].

3.2. Thermal analysis (DTA-TG)

The thermal curves are depicted in Figs. 3 and 4 in the 298–1273 °C range. The curves correspond to the starting natural clays, $AlPILC_1$ and $ALPIC_2$, after equilibrating in a desiccator, at room temperature and after a 2-h thermal treatment at 450 °C, temperature of calcination. The general feature of thermal curves clearly reveals two steps: (1) in the 25–300 °C and (2) in the 200–400 °C temperature ranges. The first step with natural clays A1 and A2 and pillared clays has been ascribed to physisorption of the hydrating water, whereas the second step is due to dehydroxylation of silicate structure. Sometimes, this step occurs dissociated into two,

Table 1
Basal spacing and textural properties of smectite and aluminum-pillared samples and activated with HCl

Sample	d_{001} (Å)	Surface area[a] (m^2/g)	Micropore area[b] (m^2/g)	Crystallinity[c]	Average pore diameter[b] (Å)	Pore volume[d] (cm^3 (PTN)/g)
A_1	15.6	44	18.21	0.80	25	0.12
A_2	15.2	51	17.09	0.92	23	0.06
Al-$PILC_1$-450	19.17	199	281.08	0.70	42	0.23
Al-$PILC_1$-600	18.96	177	254.82	0.65	40	0.21
Al-$PILC_2$-450	18.89	171	287.07	0.75	43	0.22
Al-$PILC_2$-600	18.56	138	244.75	0.56	41	0.19

[a] Determined from nitrogen adsorption isotherms using the BET equation.
[b] Determined from nitrogen adsorption isotherms.
[c] Calculated from diffraction of XDR and analyses using the Biscaye's [13] equation.
[d] Determined from nitrogen adsorption isotherms using BJH method.

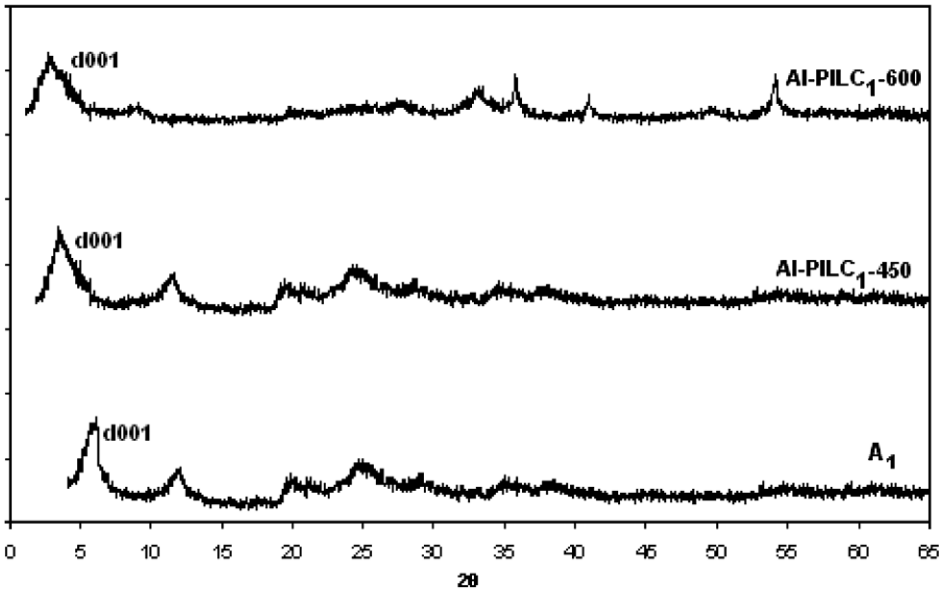

Fig. 1. X-ray pattern of A_1; Al-$PILC_1$-450; $AlPILC_1$-600 with acid activation (HCl 0.6 mol dm^{-3}).

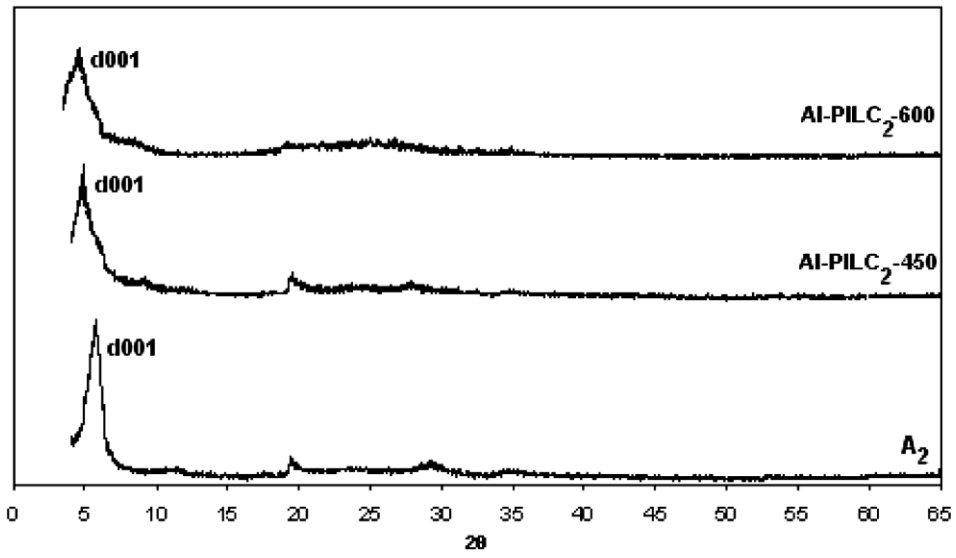

Fig. 2. X-ray pattern of A_2; Al-PILC$_2$-450; AlPILC$_2$-600 with acid activation (HCl 0.6 mol dm^{-3}).

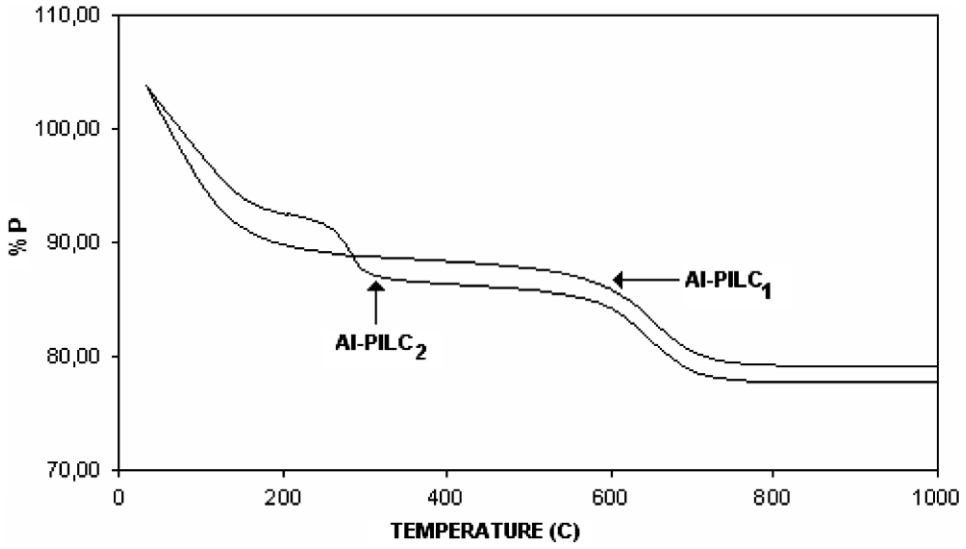

Fig. 3. TG analysis of the pillared/activated clays.

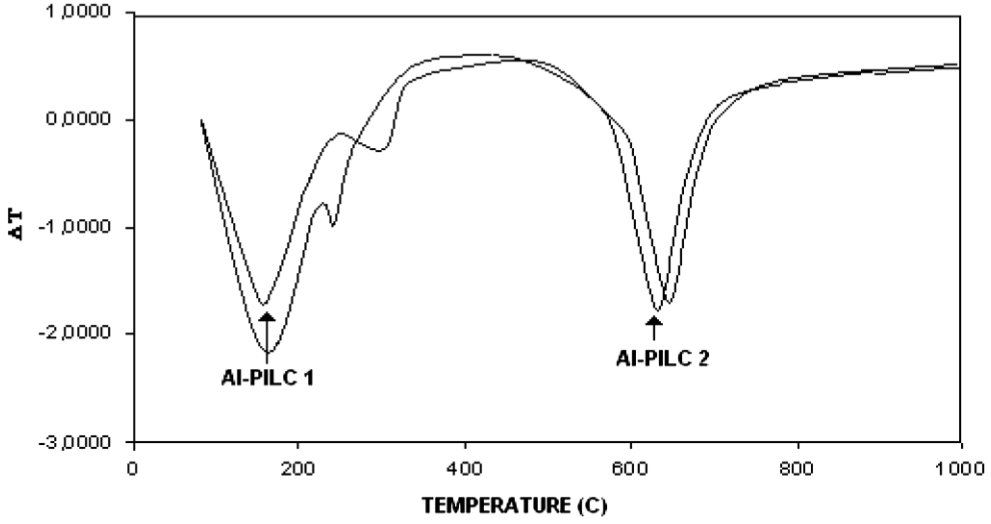

Fig. 4. DTG curves of the pillared/activated clays.

which is not well visible here but is clearly shown in the corresponding DTG and, more so, in the TGA curve (Fig. 4), denoting dehydroxylation of the silicate structure in two different environments. For Al and Mg, pillared materials, the net isomorphic substitution in the clay with different bonding strengths between the oligocations and the surrounding oxygen (or hydroxyl) ions can be observed. Dehydroxylation continues between 500 and 700 °C and is also detected to approximately 680 °C in an important step. This step is related with the stability of the pillars, since an important decrease in the basal spacing values occurs at this temperature, indicating the collapse of the clay structure. Therefore, the thermogravimetric analyses are in agreement with the aforementioned thermal stability of the synthesized pillared clay up to 600 °C.

3.3. Fourier-transformed infrared spectroscopy

Fig. 5 shows the infrared spectra of the $AlPILC_1$ and $AlPILC_2$ calcinated in a temperature of 450 °C. The low frequency regions of the infrared spectra of the $AlPILC_1$ and $AlPILC_2$ are very similar but the latter show a very small low intensity band around 667 cm^{-1} (Fig. 6). The lattice vibration at 667 cm^{-1} can be ascribed to the Al–O bond of tetrahedrally coordinated Al cations in the center of the Al_{13} pillars. The infrared spectra of natural clays presented bands in the region of 1787–1740 cm^{-1}, attributed to hydrating water. Similar results were reported by Kloprogge et al. [27], after using $Al(NO_3)_3$ as the aluminum source.

At high frequency regions of the infrared spectra (Fig. 7), the samples show a band at 3744 cm^{-1} related to the OH stretching of SiOH, corresponding to silanol groups, which adsorb at 3747 cm^{-1} on silica or on the external surfaces of zeolite [24,25]. Such hydroxyls are either located at corners and fractures of sheets or are formed by the processes of tetrahedral inversion. For Al-$PILC_1$-450 sample a new band is found at 3738 cm^{-1} (Fig. 6), which is probably produced by the change of position of the SiOH group in the structure of the smectite. The original position was altered by the entrance of the Al ion in the smectite structure, which is likely to be due to SiOH species perturbed by pillars, and

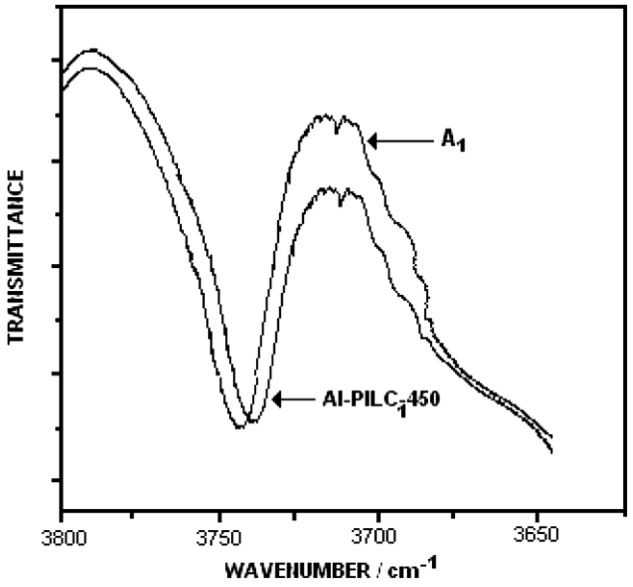

Fig. 6. FTIR spectra of the Al-$PILC_1$-450 and A_1.

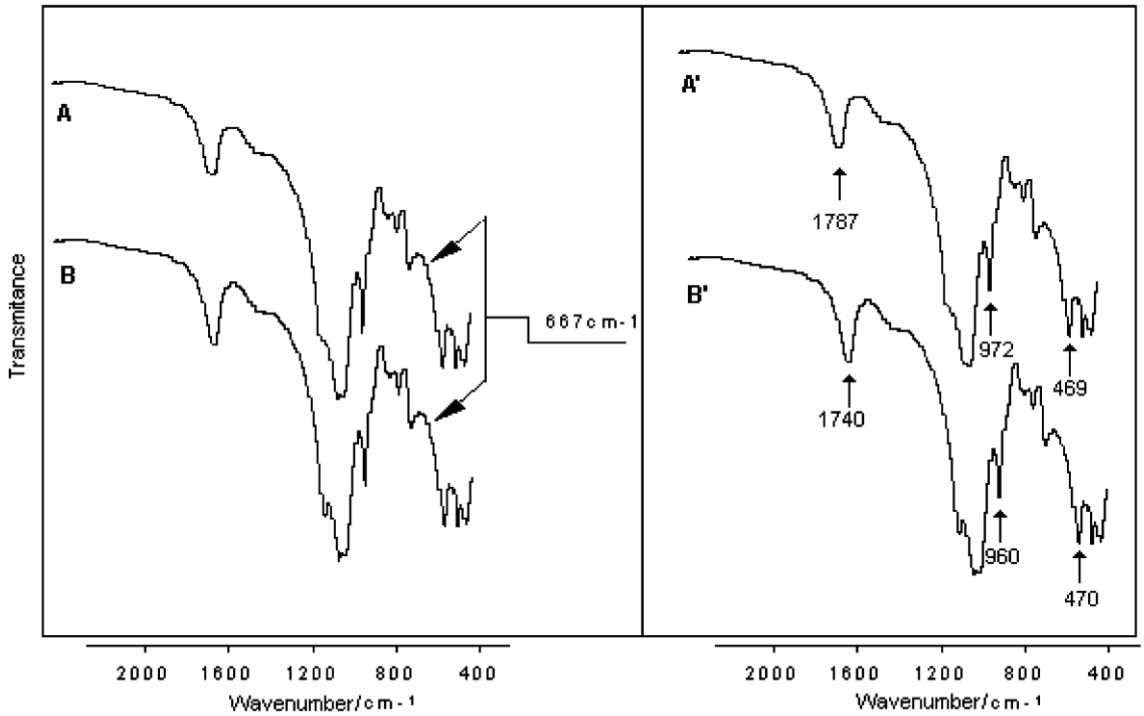

Fig. 5. FTIR spectra of (A) $AlPILC_1$-450; (B) $AlPILC_2$-450; (A′) A_1 and (B′) A_2.

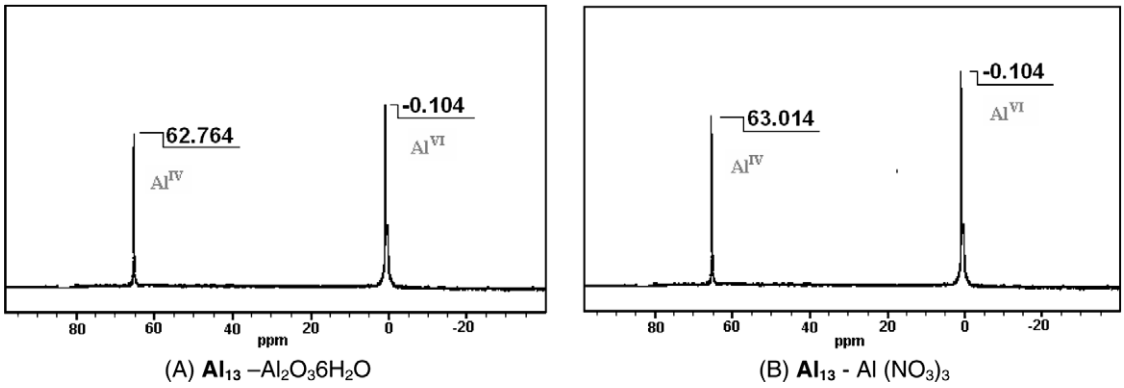

Fig. 7. ^{27}Al MAS NMR spectra of the aluminum polyhydroxypolymer solutions (Al_{13}).

designated as SiOH*, and similar results were previously reported by Bodoardo et al. [30].

A weak shoulder at 3715 cm^{-1} is observed in all clays, which is characteristic of isolated hydroxyl group on octahedral aluminum in Al_2O_3. A similar interpretation was proposed by Bodoardo et al. [30], but involving cations in the octahedral sheet and possibly in pillars in the case of Al-PILC$_1$-450 and Al-PILC$_1$-450 samples. Accordingly, the hydroxyl species were also denominated as $Al^{VI}OH$.

3.4. ^{27}Al and ^{29}Si MAS NMR

Fig. 7 shows the ^{27}Al MAS NMR spectra of the aluminum polyhydroxypolymer solutions. Most of the samples used Al_2O_3 as the aluminum source and the others were prepared with $Al(NO_3)_3$. These solutions exhibit two types of resonances corresponding to octahedral and tetrahedral-coordinated aluminum with a broad signal centered at 2.5 and 60 ppm, respectively.

Fig. 8 presents the ^{27}Al MAS NMR spectra. Signals were observed in the tetrahedral position ($\delta = 68$ ppm) and in Al in the octahedral position ($\delta = 0$ ppm) with percentages of 15% and 85%, respectively, which can indicate a possible charge deficiency in the tetrahedral layer. Also, a small signal was checked in the region of 58.7 ppm. This signal can be attributed to the tetrahedral aluminum that can be connected with the presence of the Keggin's ion (Al_{13}) in the interlayer region. After calcination, significant change was not observed in the spectra. In Fig. 9 are presented the of ^{29}Si MAS NMR spectra. Signals were observed in the −80 ppm attributed to the crystalline structure and signals in the 105 ppm attributed to the presence of quartz in the sample. After intercalation and pillaring processes, significant differences were not observed in the of ^{29}Si MAS NMR spectra.

3.5. Textural analysis

The nitrogen adsorption–desorption isotherms of pillared and activated clays are shown in Fig. 10. All isotherms are type IV of the BDDT classification and correspond to a microporous network formed in the interlayer spacing, with a well-defined H4 hysteresis loop, in accordance with Boer's classification that can be related to these micropores which

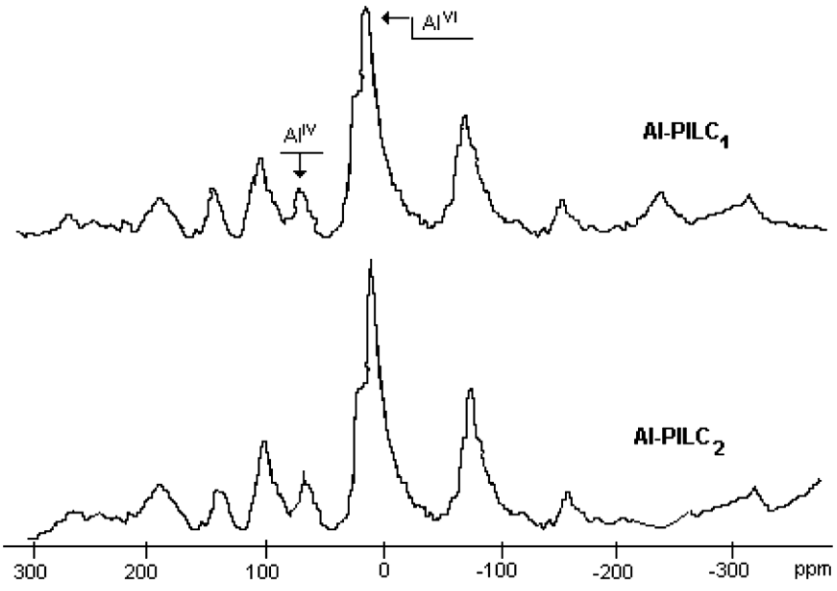

Fig. 8. ^{27}Al MAS NMR spectra of the pillared samples with Al_{13} and activated with HCl.

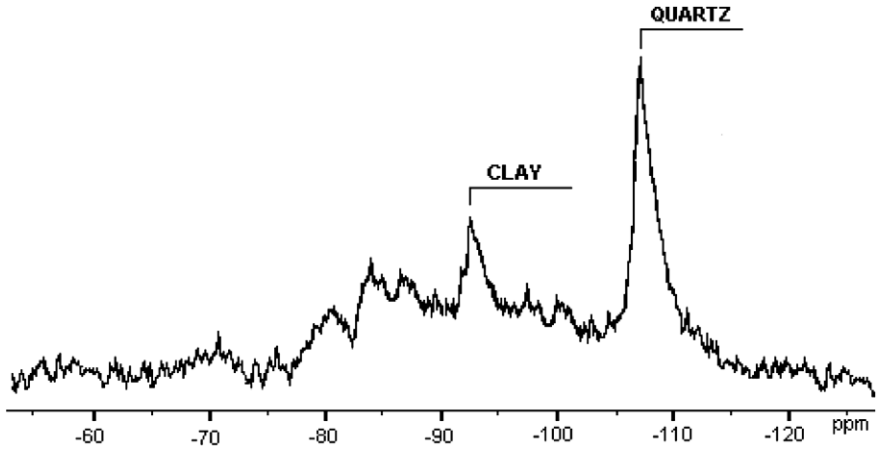

Fig. 9. ^{29}Si MAS NMR spectra of the pillared samples (Al-PILC$_2$) with Al_{13} and activated with HCl.

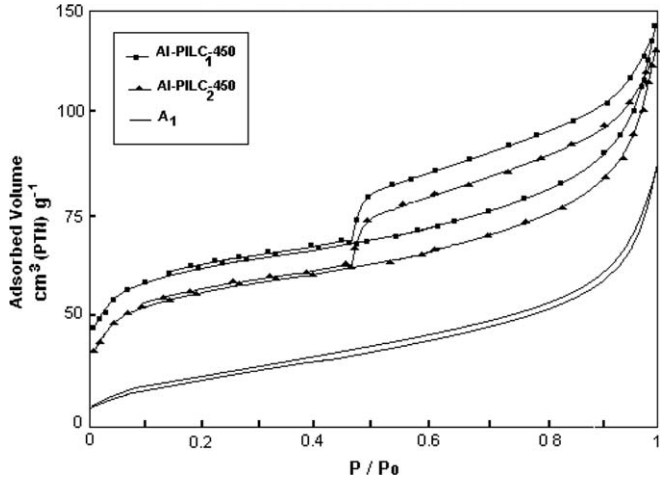

Fig. 10. N_2 adsorption–desorption isotherms of natural clay and pillared/activated samples.

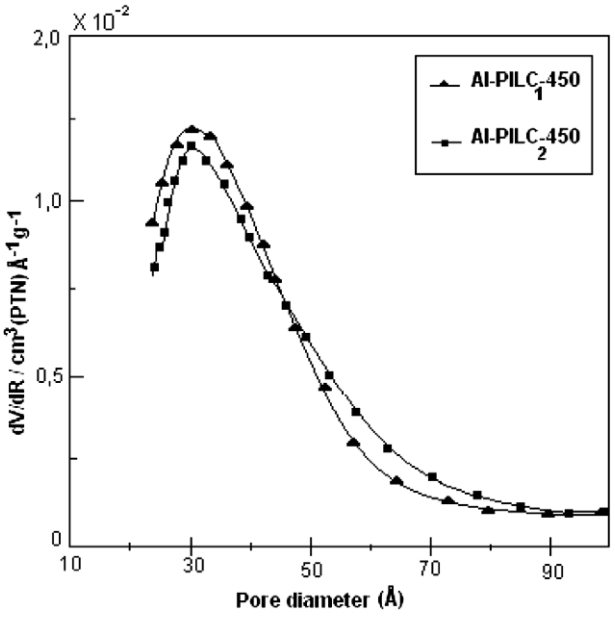

Fig. 11. Pore size distribution curve of pillared/activated samples.

are capillaries due to the interlayer space between parallel walls of aluminosilicate units [13].

Table 1 gathers the values for the surface area and micropore volume after BET equation and the BJH method along with the H–J standard curve. Also shown is $V_{0.98}$ where the total pore volume reached up to $p/p^0 = 0.98$.

Pore size distribution in Al series varies depending on the raw material source and particle size. Thus, AlPILC$_1$ and AlPILC$_2$ show unimodal distributions with pore sizes as listed in Table 1 and shown in Fig. 11.

3.6. Elemental analysis

The ICP-AES analyses of all samples are reported in Table 2. The results are consistent with nontronite being the major clay mineral containing significant amounts of iron and aluminum in its structure. The elemental analysis for AlPILC$_1$ and ALPILC$_2$ was obtained with major values for Al and significant variations of Ca, K and Ti of the present study. The results confirmed the entrance of the Al ion in the smectite structure.

Table 2
Elemental analyses (wt.%) of the clay samples and pillared clays

Samples	Al_2O_3	CaO	Na_2O	K_2O	TiO_2
A_1	17.89	4.78	1.20	1.80	4.90
A_2	12.01	5.03	1.70	1.91	5.21
Al-PILC$_1$	26.90	0.94	0.17	0.72	2.42
Al-PILC$_2$	25.95	1.08	0.19	0.75	3.14

3.7. Scanning electron microscopy with energy dispersive system

In the analysis of the results of the scanning electron microscopy (SEM) for the pillared matrix in a molar ratio of 2, it is possible to affirm that the pillaring process does not produce any change in the crystal form and crystalline size of the original smectites. It was observed that in all the experiments the smectite remained in the primitive crystal form, presenting itself in the foliated form with illite crys-

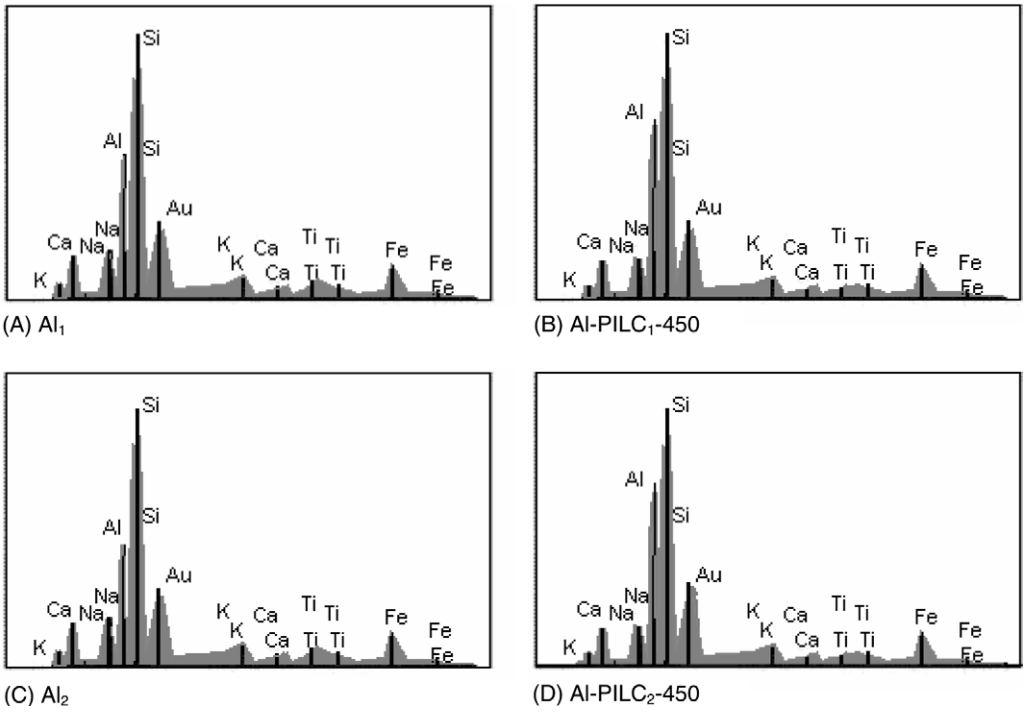

Fig. 12. EDS analysis of the natural clays and pillared samples.

tals in the extremities. Semi-quantitative analysis using EDS is shown in Fig. 12 exhibiting high aluminum concentration, related to the pillared matrix, which can be explained by the existence of pillars in the structure.

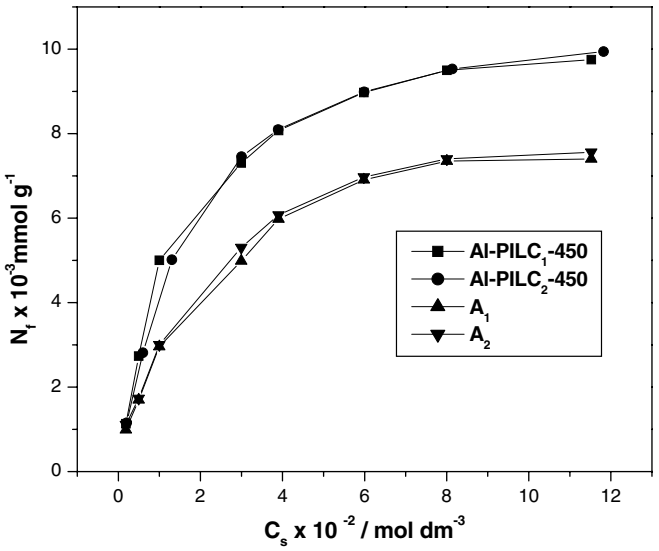

Fig. 13. Experimental values of butylamine adsorption.

3.8. Butylamine adsorption

In Fig. 13, the results of the experiments obtained of the butylamine adsorption are shown. The influence of acid activation was observed through adsorption values of saturation in matrices. In Table 3 and Figs. 14 and 15, the results of the linear correlation coefficients obtained from the Langmuir, Freundlich and Temkin equations are displayed. They indicate that three models of adsorption can be used to explain the significant capacity of the pillared matrix to quantify the adsorbed butylamine. The Langmuir model presents a significant advantage in comparison with the other models. It allows to quantify the adsorption's capacity of the present ions in the structure of the matrix and to evaluate the constant related to the bonding energy.

The complexation of metallic ions with bridgings immobilized external and internal surfaces of smectite structures, besides the external part of the pillars, is governed by the microenvironment around those bridgings, which are usually acidic centers. They are formed as accessories in the pillars and hydroxyls that still exist in the surfaces, mainly in the internal structure of hydration. Such hydroxyls act as bridgings for H^+ groups that result from the matrix acidi-

Table 3
Parameters of the Langmuir, Freundlich and Temkin equations used in the butylamine adsorption in Al_{13} pillared clay

Sample	Langmuir			Freundlich			Temkin		
	b	*K*	*r*	*kf*	*n*	*R*	*B*	*A*	*r*
Al-PILC$_1$-450	11.0816	0.6858	0.999	3.6297	0.5054	0.962	4.7811	2.2277	0.996
Al-PILC$_2$-450	11.4969	0.5786	0.999	3.5586	0.5220	0.956	4.5803	2.3425	0.994

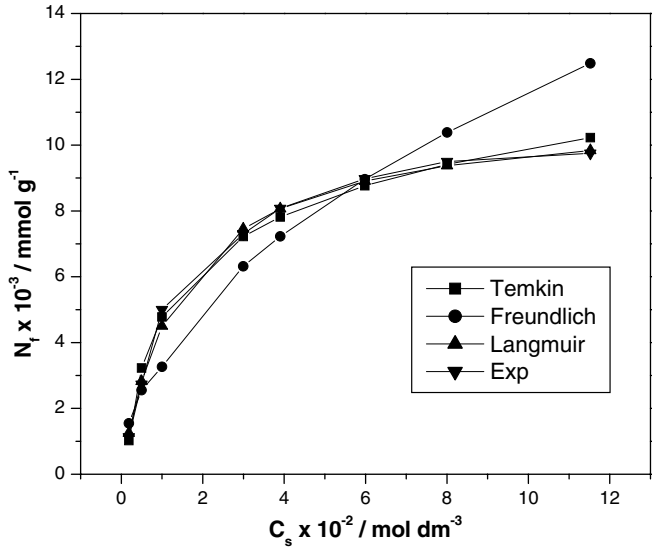

Fig. 14. Experimental value of butylamine adsorption and values obtained with Langmuir, Freundlich and Temkin equations – Al-PILC$_1$-450 with acid activation.

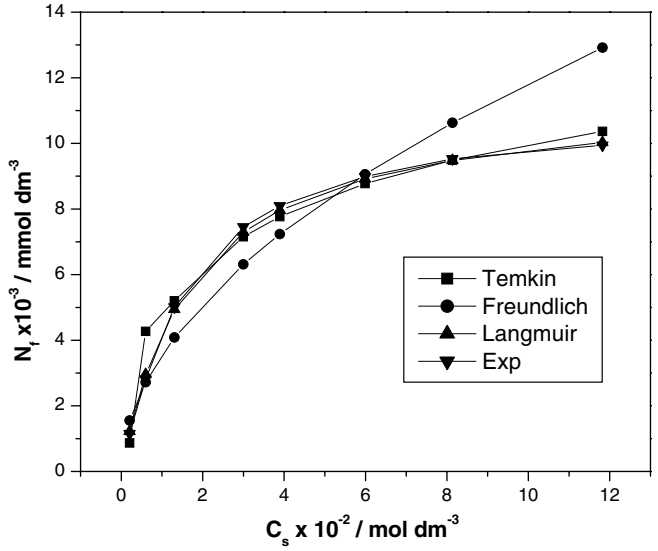

Fig. 15. Experimental value of butylamine adsorption and values obtained with Langmuir, Freundlich and Temkin equations – Al-PILC$_2$-450 with acid activation.

fication. Water removal in such surfaces becomes difficult due to the octahedral and tetrahedral sheet positions and also by the remaining hydroxyl groups from the primitive clay structure. Finally, quimisorption process is controlled by the positioning and amount of hydroxyl groups in the outer regions, as in lamellae borders and central structure.

4. Conclusions

The results of this investigation show that the clay deposits from Amazon region, Brazil, mainly montmorillonite (nontronite) present variations in the amounts of quartz, kaolinite and goethite as impurities. The results obtained by means of XRD powder diffraction confirmed an expansion of the original smectites to a thermally stable d_{001} spacing of 18.97 Å (Al-PILC$_1$-450), which requires a rather well defined Al polymer, such as the so-called Al_{13} species. The permanence of the d_{001} peak proved the resistance of the pillared matrix to support high temperature of calcinations (600 °C).

FTIR analysis confirmed the formation of Al-pillars in the pillared samples by the two methods employed. A weak shoulder at 667 cm^{-1} is observed in pillared clays. This low intensity band is observed in the pillared samples also by means of the two synthetic methods used. The presence of a band in the 3738 cm^{-1} region also proves the entrance of the Keggin's ion in the matrix structures.

The analyses of ^{27}Al MAS NMR demonstrated the formation of Al in the tetrahedral and octahedral positions in the pillaring solutions. The pillared matrix is shown with a signal in the region of 58.7 ppm. This signal can be attributed to the tetrahedral aluminum that can be connected with the presence of the Keggin's ion in the interlayer region.

The textural analysis of the pillared samples evaluated from the obtained isotherms pointed to the production of material containing mesopores and micropores, according to the Boer classification. The specific area of the pillared samples obtained grows in the two adopted methods. This growth is attributed to several factors: the production of Keggin's ions, the entrance of these ions in the interlayer, density of the pillars and number of pillars.

The models used of the isotherms' evaluation exhibited constant values similar to those observed for the experimental isotherm. A greater variation was observed in the Freundlich model. The results obtained using linear equations are very close to those obtained from the literature that frequently use a non-linear computational method based on the "Enzefitte" system. With the adsorption results obtained, it is possible to establish a relationship between the number of adsorbed ions and the number of acid sites produced after pillaring process. In this work, the K and b values from the Langmuir and Freundlich equations exhibited small variations when a "flat" was observed. In other words, this fact implies a saturation of the acid centers in the new smectite system produced after pillaring process, which stabilizes the two mathematical variables that drive the process.

The linear regression method used in this work did not produce significant systematic deviation of the adjusted isotherms. Therefore, it certainly can be used to describe ionic exchange processes related to metallic ions removal present in industrial sludges and from the mineral extraction.

Acknowledgement

The authors are indebted to CNPq for fellowships and financial support.

References

[1] F. Figueras, Catal. Ver. Sci. Eng. 30 (1988) 457.
[2] S. Moreno, E. Guitierrez, A. Alvarez, N.G. Papayannakos, G. Poncelet, Appl. Catal. 165 (1997) 103.
[3] M.L. Occelli, R.M. Tindwa, Clays Clay Miner. 32 (1983) 22.
[4] L. Storaro, M. Lenarda, A. Rinaldi, Micropor. Mesopor. Mater. 6 (1996) 55.
[5] P. Cañizares, J.L. Valverde, M.R. Sun Kou, C.B. Molina, Micropor. Mesopor. Mater. 29 (1999) 267.
[6] N. Maes, I. Hielen, P. Cool, E.F. Vansant, Appl. Clay Sci. 12 (1997) 43.
[7] M.R. Sun Kou, S. Mendioroz, M.L. Guijarrro, Thermochim. Acta 323 (1998) 142.
[8] C. Volzone, Micropor. Mesopor. Mater. 49 (2001) 197.
[9] M. Sychev, M. Rozwadowski, A.P.B. Sommen, V.H.J. Beer, R.A. van Santen, Micropor. Mesopor. Mater. 37 (2004) 187.
[10] S.M. Blandey, R.A. Kydd, J. Catal. 141 (1993) 239.
[11] D.M. Moore, R.C. Reynolds Jr., X-ray Diffraction and the Identification and Analysis of Clay Minerals, 2nd ed., Oxiford University Press, Oxford, 1997.
[12] S.B.C. Pergher, A. Corma, V. Fornes, Química Nova 22 (1999) 693.
[13] C.F. Gomes, Argilas - o que são e para que servem, Fund. Caloust Gulbenkian, Lisboa, 1988.
[14] P.S. Santos, Ciência e Tecnologia de Argilas, 2nd ed., vol. 1, Edgard Blücher, São Paulo, 1989.
[15] K. Ohtsuka, Chem. Mater. 9 (1997) 20035.
[16] B.M. Coudary, M.L. Kantam, M. Sateesh, k.k. Rao, P.L. Santhi, Appl. Catal. 149 (1997) 257.
[17] G.W. Brindley, R.E. Sempels, Clay Miner. 12 (1977) 229.
[18] T.J. Pinnavaia, Science 220 (1983) 595.
[19] D.E.W. Vanghan, R.J. Lussier, J.S. Magee, U.S. Patent 4, 176,090, 1979.
[20] J.F. Luna, U. Schuchardt, Química Nova 22 (1999) 104.
[21] M.L. Occelli, J.T. Hsu, L.G. Galya, J. Mol. Catal. 33 (1985) 371.
[22] A. Bahamonde, F. Mohino, M. Rebollar, M. Yates, P. Avila, S. Mendioroz, Catal. Today 69 (2001) 233.
[23] K.B. Brandt, R.A. Kydd, Appl. Catal. 165 (1997) 327.
[24] N.D. Hutson, M.J. Hoesksta, R.T. Yang, Micropor. Mesopor. Mater. 28 (1999) 267.
[25] B.C. Pergher, A. Corma, V. Fornes, Química Nova 22 (5) (1999) 693.
[26] J. Sterte, Pillared clays, in: R. Burch (Ed.), Catal. Today 2 (1988) 219.
[27] J.T. Kloprogge, R. Evans, L. Hickey, R.L. Frost, Appl. Clay Sci. 20 (2002) 157.
[28] E.P. Barret, L.G. Joyner, P.P. Halenda, J. Am. Chem. Soc. 73 (1953) 373.
[29] J.Y. Bottero, M. Axelos, D. Tchoubar, J.M. Cases, J.J. Fripiat, F. Fiessinger, J. Colloid Interface Sci. 47 (1987) 117.
[30] S. Bordoardo, F. Figueiras, E. Garrone, J. Catal. 147 (1994) 223.
[31] A.W. Adamson, Physical Chemistry of Surfaces, Wiley, New York, 1990.

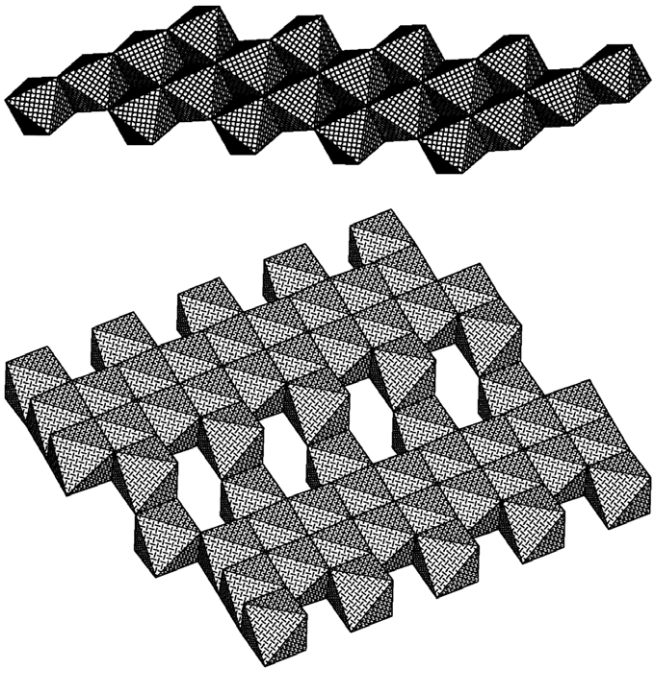

Fig. 1. Top: the $(Cd_4Cl_{12})_n^{4n-}$ ribbon in $(CH_3NH_2C_2H_4NH_3)_2Cd_4Cl_{12} \cdot 2H_2O$. Bottom: the fused serrated $(Cd_3Br_9)_n^{3n-}$ ribbons in $(CH_3NH_2C_2H_4NH_3)Cd_3Br_8 \cdot xH_2O$.

$(CdBr_2)] \cdot H_2O$, was prepared by mixing [DEA]Br (0.171 g, 1 mmol) and $CdBr_2$ (0.819 g, 3 mmol) in a solution of deionized water (10 mL) and methanol (3 mL). Short, clear, colorless needles formed after one week.

2.2. X-ray structure analysis

Crystals were removed from solution and immediately placed in hydrocarbon oil to prevent the crystalline material from possible deterioration due to solvent loss. A suitable crystal was selected, attached to a glass fiber, and placed immediately in the low-temperature nitrogen stream [7]. Data was collected at ca. 86(2) K using a Bruker/Siemens SMART APEX instrument (Mo Kα radiation, $\lambda = 0.71073$ Å) equipped with a Cryocool NeverIce low temperature device. Data were measured using omega scans of 0.3° per frame, and a full sphere of data was collected. The first 50 frames were recollected at the end of the data collection to monitor for decay. Cell parameters were retrieved using SMART [8] software and refined using SAINTPLUS [9] on all observed reflections. Data reduction and correction for Lp and decay was performed using the SAINTPLUS [9] software. Absorption corrections were applied using SADABS [10]. The structure was solved by direct methods and refined by the least squares method on F^2 using the SHELXTL program package [11]. No decomposition was observed during data collection. The pendant $CdBr_2$ group was disordered with occupancies of 95% for Cd5, Br9, and Br10 and 5% for Cd6, Br11, and Br12. The major moiety was refined anisotropically. It was not possible to resolve the disorder in the organic groups, so

Table 1
Data collection and refinement parameters for $[DEA]_2[Cd_3Br_8(CdBr_2)] \cdot H_2O$

Empirical formula	$C_8H_{26}Br_{10}Cd_4N_2O$
Formula weight	1415.01
Temperature (K)	86(2)
Description	colorless needle
Size (mm^3)	$0.39 \times 0.07 \times 0.06$
System	triclinic
Space group	$P\bar{1}$
Z	2
a (Å)	7.9884(8)
b (Å)	12.6197(13)
c (Å)	15.3982(16)
α (°)	80.031(2)
β (°)	84.339(2)
γ (°)	76.587(2)
V ($Å^3$)	1484.4(3)
Exposure (s)	5
D_{calc} ($Mg\ m^{-3}$)	3.166
Reflections used	5301
Goodness-of-fit	1.027
R indices $[I > 2\sigma(I)]$[a]	$R_1 = 0.0465$
	$wR_2 = 0.1012$
R indices (all data)	$R_1 = 0.0696$
	$wR_2 = 0.1094$

[a] $R_1 = \sum\|F_o| - |F_c\|/\sum|F_o|^2$; $wR_2 = \{\sum w(F_o^2 - F_c^2)^2 / \sum[w(F_c^2)^2]\}^{1/2}$.

Table 2
Atomic coordinates (×10^4) and equivalent isotropic displacement parameters ($Å^2 \times 10^3$) for the structure of $[DEA]_2[Cd_3Br_8(CdBr_2)] \cdot H_2O$

	x	y	z	U_{eq}
Cd(1)	10000	10000	10000	9(1)
Cd(2)	5000	10000	10000	9(1)
Cd(3)	8299(1)	8824(1)	8019(1)	9(1)
Cd(4)	13277(1)	8779(1)	8071(1)	9(1)
Cd(5)[a]	12085(1)	5670(1)	7351(1)	8(1)
Cd(6)[b]	6944(1)	5599(9)	7315(7)	8(1)
Br(1)	7436(1)	10779(1)	8796(1)	9(1)
Br(2)	12424(1)	10748(1)	8809(1)	9(1)
Br(3)	10756(1)	8080(1)	9298(1)	9(1)
Br(4)	5833(1)	8090(1)	9312(1)	9(1)
Br(5)	10789(1)	9511(1)	6926(1)	12(1)
Br(6)	8963(1)	6806(1)	7469(1)	15(1)
Br(7)	15683(1)	9552(1)	6934(1)	10(1)
Br(8)	14397(1)	6644(1)	7704(1)	13(1)
Br(9)[a]	12107(1)	3872(1)	8435(1)	12(1)
Br(10)[a]	12965(1)	5284(1)	5773(1)	17(1)
Br(11)[b]	7220(2)	3855(1)	8472(1)	9(1)
Br(12)[b]	8040(2)	5224(2)	5752(9)	9(1)
C(1)[a]	2251(1)	8388(9)	4650(7)	23(1)
C(2)[a]	3900(1)	8300(9)	5109(7)	23(1)
N(3)[a]	5188(9)	7305(6)	4901(5)	10(1)
C(4)[a]	6861(1)	7163(9)	5330(7)	23(1)
C(5)[a]	7813(1)	8048(9)	4930(7)	23(1)
C(6)[a]	7269(1)	4669(9)	9719(7)	23(1)
C(7)[a]	6883(1)	4014(9)	9045(7)	23(1)
N(8)[a]	7799(1)	4317(7)	8173(5)	10(1)
C(9)[a]	7544(1)	3715(9)	7462(7)	23(1)
C(10)[a]	8539(1)	4026(9)	6620(7)	23(1)
O(1)[a]	4428(1)	2336(6)	6934(5)	27(2)

U_{eq} is defined as one third of the trace of the orthogonalized U^{ij} tensor.
[a] Site occupancy factor set to 0.950.
[b] Site occupancy factor set to 0.050.

Table 3
Bond lengths (Å) and angles (°) for the structure of $[DEA]_2[Cd_3Br_8(CdBr_2)] \cdot H_2O$

Atoms	Distance	Atoms	Angle	Atoms	Angle
Cd(1)–Br(1)	2.789(9)	Cd(2)–Br(1)–Cd(1)	91.61(3)	Br(2)#2–Cd(2)–Br(1)	92.31(3)
Cd(1)–Br(2)	2.747(9)	Cd(2)–Br(1)–Cd(3)	92.98(3)	Br(2)#3–Cd(2)–Br(1)	87.69(3)
Cd(1)–Br(3)	2.739(9)	Cd(1)–Br(1)–Cd(3)	92.99(3)	Br(5)–Cd(3)–Br(7)#2	98.34(4)
Cd(2)–Br(1)	2.781(9)	Cd(1)–Br(2)–Cd(2)#1	92.52(3)	Br(5)–Cd(3)–Br(6)	93.42(4)
Cd(2)–Br(2)#2	2.780(9)	Cd(1)–Br(2)–Cd(4)	92.63(3)	Br(7)#2–Cd(3)–Br(6)	89.99(3)
Cd(2)–Br(4)	2.716(9)	Cd(2)#1–Br(2)–Cd(4)	92.79(3)	Br(5)–Cd(3)–Br(3)	87.19(3)
Cd(3)–Br(1)	2.840(1)	Cd(1)–Br(3)–Cd(3)	94.83(3)	Br(7)#2–Cd(3)–Br(3)	173.91(4)
Cd(3)–Br(3)	2.806(1)	Cd(1)–Br(3)–Cd(4)	93.09(3)	Br(6)–Cd(3)–Br(3)	92.23(3)
Cd(3)–Br(4)	2.852(1)	Cd(3)–Br(3)–Cd(4)	90.00(3)	Br(5)–Cd(3)–Br(1)	93.30(3)
Cd(3)–Br(5)	2.678(1)	Cd(2)–Br(4)–Cd(4)#2	94.29(3)	Br(7)#2–Cd(3)–Br(1)	92.18(3)
Cd(3)–Br(6)	2.741(1)	Cd(2)–Br(4)–Cd(3)	94.08(3)	Br(6)–Cd(3)–Br(1)	172.57(4)
Cd(3)–Br(7)#2	2.696(1)	Cd(4)#2–Br(4)–Cd(3)	90.22(3)	Br(3)–Cd(3)–Br(1)	84.92(3)
Cd(4)–Br(2)	2.823(1)	Cd(3)–Br(5)–Cd(4)	95.69(4)	Br(5)–Cd(3)–Br(4)	174.80(4)
Cd(4)–Br(3)	2.810(1)	Cd(6)–Br(6)–Cd(5)	108.6(3)	Br(7)#2–Cd(3)–Br(4)	86.50(3)
Cd(4)–Br(4)#1	2.818(1)	Cd(6)–Br(6)–Cd(3)	130.1(3)	Br(6)–Cd(3)–Br(4)	88.46(3)
Cd(4)–Br(5)	2.680(1)	Cd(5)–Br(6)–Cd(3)	120.15(4)	Br(3)–Cd(3)–Br(4)	87.89(3)
Cd(4)–Br(7)	2.706(1)	Cd(3)#1–Br(7)–Cd(4)	96.11(4)	Br(1)–Cd(3)–Br(4)	84.58(3)
Cd(4)–Br(8)	2.771(1)	Cd(6)#1–Br(8)–Cd(5)	105.7(2)	Br(5)–Cd(4)–Br(7)	93.48(3)
Cd(5)–Br(6)	2.579(1)	Cd(6)#1–Br(8)–Cd(4)	135.2(2)	Br(5)–Cd(4)–Br(8)	98.91(4)
Cd(5)–Br(8)	2.588(1)	Cd(5)–Br(8)–Cd(4)	117.33(4)	Br(7)–Cd(4)–Br(8)	93.52(3)
Cd(5)–Br(9)	2.571(1)	Br(3)#3–Cd(1)–Br(3)	180.00	Br(5)–Cd(4)–Br(3)	87.06(3)
Cd(5)–Br(10)	2.558(1)	Br(3)#3–Cd(1)–Br(2)	91.41(3)	Br(7)–Cd(4)–Br(3)	176.78(4)
Cd(6)–Br(6)	2.514(8)	Br(3)–Cd(1)–Br(2)	88.59(3)	Br(8)–Cd(4)–Br(3)	89.53(3)
Cd(6)–Br(8)#2	2.242(1)	Br(3)#3–Cd(1)–Br(1)	92.82(3)	Br(5)–Cd(4)–Br(4)#1	177.48(4)
Cd(6)–Br(11)	2.561(8)	Br(3)–Cd(1)–Br(1)	87.18(3)	Br(7)–Cd(4)–Br(4)#1	86.99(3)
Cd(6)–Br(12)	2.564(8)	Br(2)–Cd(1)–Br(1)	91.83(3)	Br(8)–Cd(4)–Br(4)#1	83.52(3)
		Br(2)#3–Cd(1)–Br(1)	88.17(3)	Br(3)–Cd(4)–Br(4)#1	92.33(3)
		Br(4)#4–Cd(2)–Br(2)#2	92.14(3)	Br(5)–Cd(4)–Br(2)	92.46(3)
		Br(4)–Cd(2)–Br(2)#2	87.86(3)	Br(7)–Cd(4)–Br(2)	91.12(3)
		Br(4)–Cd(2)–Br(1)#4	91.67(3)	Br(8)–Cd(4)–Br(2)	167.43(4)
		Br(4)–Cd(2)–Br(1)	88.33(3)		

Symmetry transformations used to generate equivalent atoms: #1 $-x, -y+2, -z+2$; #2 $-x-1, -y+2, -z+2$; #3 $x-1, y, z$; #4 $x+1, y, z$.

only the major components were included at 95% occupancies. Hydrogen atoms associated with water molecules were added geometrically to ensure optimal hydrogen bonding contacts. Data collection and refinement parameters are given in Table 1, atomic coordinates and equivalent isotropic thermal displacement parameters are given in Table 2 and pertinent bond distances and angles are given in Table 3.

3. Structure description

The unique structure of $[DEA]_2[Cd_3Br_8(CdBr_2)] \cdot H_2O$ is based on ribbons comprised of three infinite chains of edge-shared octahedra. These simple cadmium bromide ribbons can be envisioned as being cut from the original $CdBr_2$ parent hexagonal lattice by the $[DEA]^+$ cations. The edges of these ribbons have "fringed" edges consisting of $CdBr_4$ tetrahedra. These distinctive tetrahedral fringes, water molecules, and two crystallographically independent diethylammonium cations play an important role in linking these unique ribbons together.

The asymmetric unit is shown in Fig. 2. Differences in Cd–Br distances are observed throughout the body of the ribbon (Cd–Br range: 2.678(1)–2.840(1) Å) and in the octahedral angles (Br–Cd–Br range: 87.06(3)–98.34(4)°) due to the tetrahedral $CdBr_4$ fringe that caps the edges of each ribbon, as shown in Fig. 3. Significant angular distortion is also necessary within the tetrahedron in order to link two adjacent $CdBr_6$ octahedra. The Cd–Br bond distances in

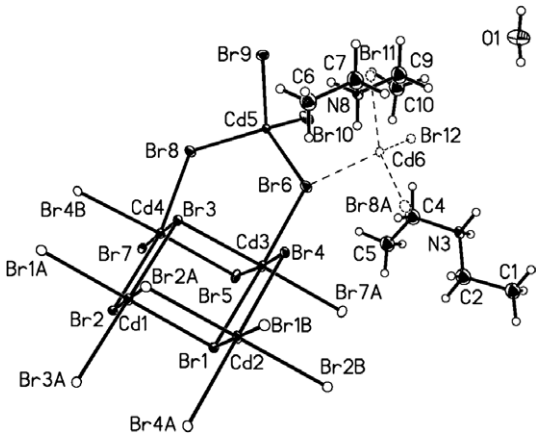

Fig. 2. Illustration of the asymmetric unit of the $[DEA]_2[Cd_3Br_8(CdBr_2)] \cdot H_2O$ structure. The disorder involving Cd5 and Cd6 is indicated by the dashed bonds surrounding Cd6. The octahedral coordination of each cadmium(II) atom has been completed with symmetry-related atoms (open ellipsoids). Thermal ellipsoids are shown at the 50% probability level.

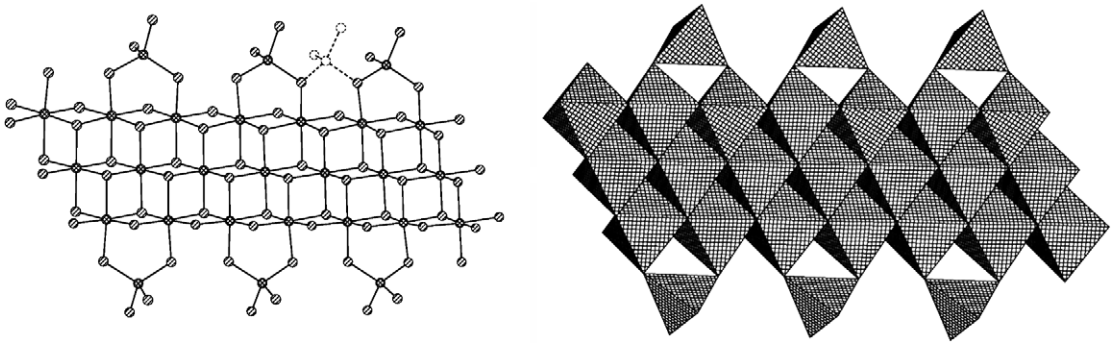

Fig. 3. Ball-and-stick (left) and polyhedral (right) illustrations showing the extended, fringed ribbon of the $[DEA]_2[Cd_3Br_8(CdBr_2)]\cdot H_2O$ structure which runs parallel to the *a*-axis. The ball-and-stick illustration also shows the location of a single disordered tetrahedral group (indicated by the dashed bonds).

the tetrahedra differ very little (av. 2.575 Å) while the Br–Cd–Br tetrahedral angles range from 105.7(2)° to 114.49(4)°. Additionally, disorder in the location of the tetrahedral fringe was observed, as discussed in Section 2. A small fraction (5%) bridge the other set of adjacent $CdBr_6$ octahedra as indicated by dashed lines in the asymmetric unit shown in Figs. 2 and 3.

Also present in this structure are lattice water molecules and two crystallographically independent $[DEA]^+$ cations. Cations lying almost perpendicular to the ribbon (thus virtually perpendicular to the *a* axis) have ethyl arms of *trans* conformations. Cations lying roughly parallel to the ribbons have one arm in the *gauche* conformation and the other in the *trans* conformation. These two different cations are illustrated in Fig. 4.

The isolated networks are linked together by a complex array of hydrogen bonding, involving the diethylammonium cations, water molecules and the bromide ions of the tetrahedral fringe, to stabilize the three dimensional structure (Fig. 5). Significant hydrogen bonding interactions are listed in Table 4 and a detailed diagram of the hydrogen bonding is shown in Fig. 6. Each cation lying perpendicular to the ribbons (labeled N8 in Fig. 6) hydrogen bonds to the $CdBr_4$ tetrahedra of a single ribbon, forming one normal (3.409(8) Å) and one bifurcated contact (with N–H···Br7 and N–H···Br5 bond distances of 3.447(8) and 3.533(8) Å, respectively). Thus, this type of

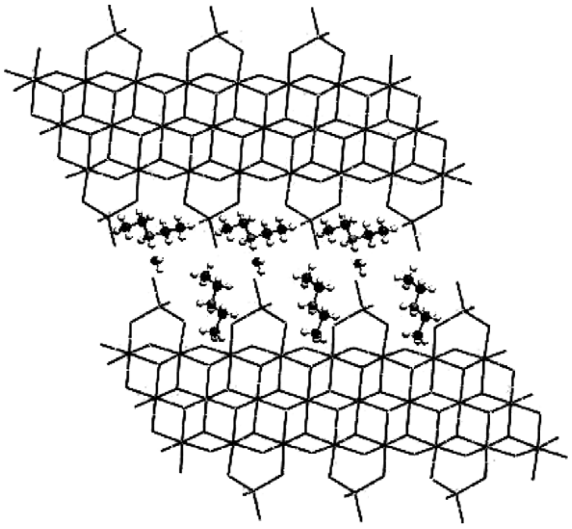

Fig. 5. Diagram of the $[DEA]_2[Cd_3Br_8(CdBr_2)]\cdot H_2O$ structure as viewed with the *a*-axis running horizontally to show the location of the $[DEA]^+$ cations and water molecules between the tetrahedral fringes. Only the cations and water molecules lying above the fringed gaps are shown.

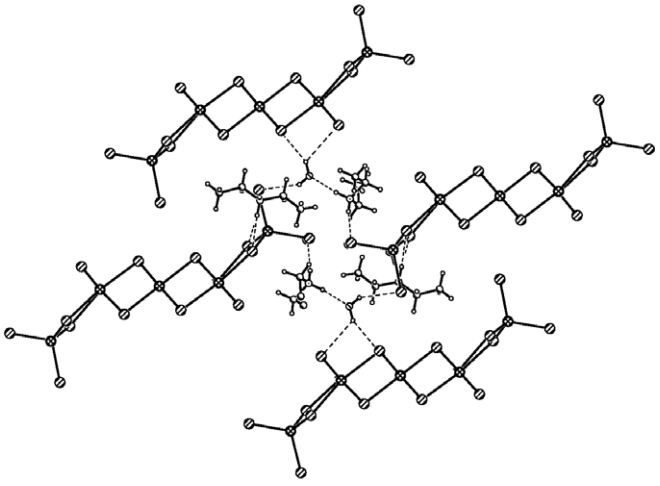

Fig. 4. Ball-and-stick packing diagram of the $[DEA]_2[Cd_3Br_8(CdBr_2)]\cdot H_2O$ structure as viewed along the *a*-axis to show the packing of the ribbons and the hydrogen bonding between water molecules and $[DEA]^+$ cations within the lattice.

Table 4
Hydrogen bonds for the structure of $[DEA]_2[Cd_3Br_8(CdBr_2)]\cdot H_2O$ (Å and °)

D–H···A	D–H (Å)	H···A (Å)	D···A (Å)	D–H···A (°)
N3–H1···O1	0.92	1.87	2.781(1)	171.5
N3–H2···Br4	0.92	2.55	3.451(8)	167.5
N8–H1···Br9A	0.92	2.49	3.409(8)	178.4
N8–H2···Br7	0.92	2.73	3.447(8)	135.7
N8–H2···Br5	0.92	2.78	3.533(8)	140.4
O1–H1···Br8	0.88	2.87	3.423(7)	122.5
O1–H1···Br9B	0.88	2.63	3.402(7)	147.7
O1–H2···Br2[a]	0.88	2.91	3.673(7)	146.8

[a] This hydrogen bond is not shown in Fig. 6.

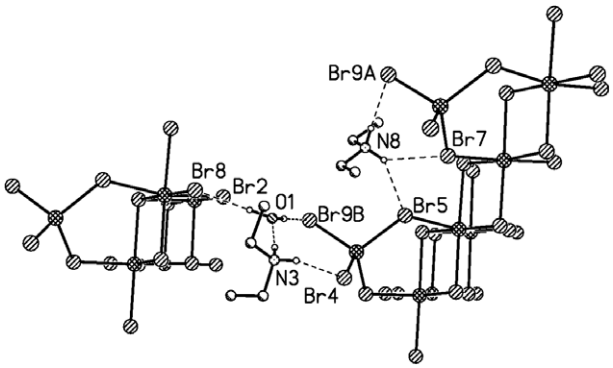

Fig. 6. Detailed diagram of the $[DEA]_2[Cd_3Br_8(CdBr_2)] \cdot H_2O$ structure to show the difference in hydrogen bonding between the two different types of cations. The hydrogen atoms on the $[DEA]^+$ cations have been removed and one of the bifurcated bonds (O1–H···Br2) is not shown for clarity.

cation is solely involved in providing partial charge balance for the ribbons. In contrast, cations containing N3 lie parallel to the ribbons and interact with water molecules to form a hydrogen bonding network which links the ribbons together. This type of cation forms a normal hydrogen bond to a terminal bromide ion on one ribbon via a N–H···Br4 (3.451(8) Å) contact and to a lattice water molecule via a N–H···O1 (2.781(1) Å) contact. The water molecule in turn forms a bifurcated hydrogen bond to two bridging bromide ions, labeled Br2 and Br8, on one ribbon and a normal hydrogen bond to a terminal bromide ion, Br9B, on an adjacent ribbon. In this manner, the three dimensional supramolecular structure is constructed.

4. Discussion

The decorated ribbon network found in this structure is a generalization of the decorated single chain network found in $(NH_3C_2H_4NH_3)[CdBr_4(CdBr_2)] \cdot 2H_2O$, illustrated in Fig. 7 [12]. In this structure, single chains of edge-shared CdX_6 octahedra are fringed by Cd ions in tetrahedral sites. These types of decorated ribbon structures can be considered as precursors to the perforated layer networks found in $Ca(H_2O)_8\{Cd_4Cl_{10}[Cd(H_2O)_2]\} \cdot 1.5H_2O$ [13] and $Ca(H_2O)_7\{Cd_4Cl_{10}[Cd_2Cl_2(H_2O)_2]\} \cdot H_2O$ [14], which are shown in polyhedral representations in Fig. 8. In these structures, ribbons composed of double chains of $CdCl_6$ octahedra are linked together via $CdCl_4(H_2O)_2$ octahedra and by pairs of $CdCl_5(H_2O)$ octahedra, respectively. The latter structure can be envisioned as arising from decorated $[Cd_2Cl_4(CdCl_2)]$ double chains via expansion of the coordination geometry of the $CdCl_4$ tetrahedra through fusion of the tetrahedra accompanied by the insertion of water molecules. In the former, expulsion of $CdCl_2$ fragments accompany the fusion process.

This process whereby the ribbons are augmented by the tetrahedral fringes can be understood on the basis of simple electrostatic arguments. A ribbon of $(Cd_nX_{2n+2})^{2n-}$ stoichiometry has an excess negative charge. This can be compensated in several ways: (a) strong, extensive

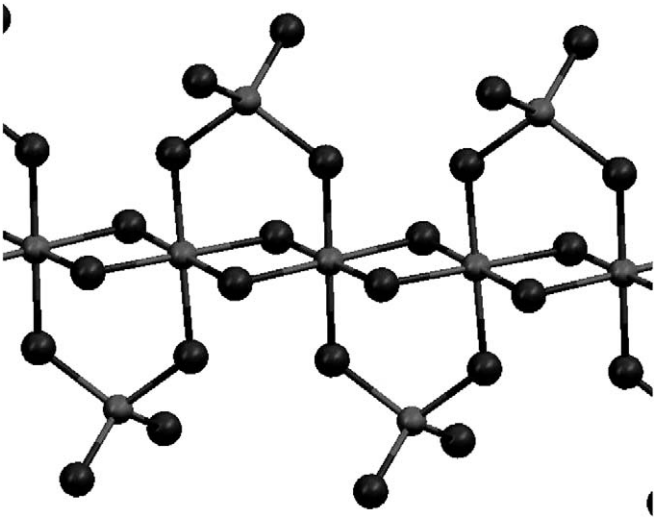

Fig. 7. Illustration of the fringed single network in $(NH_3C_2H_4NH_3)[CdBr_4(CdBr_2)] \cdot 2H_2O$.

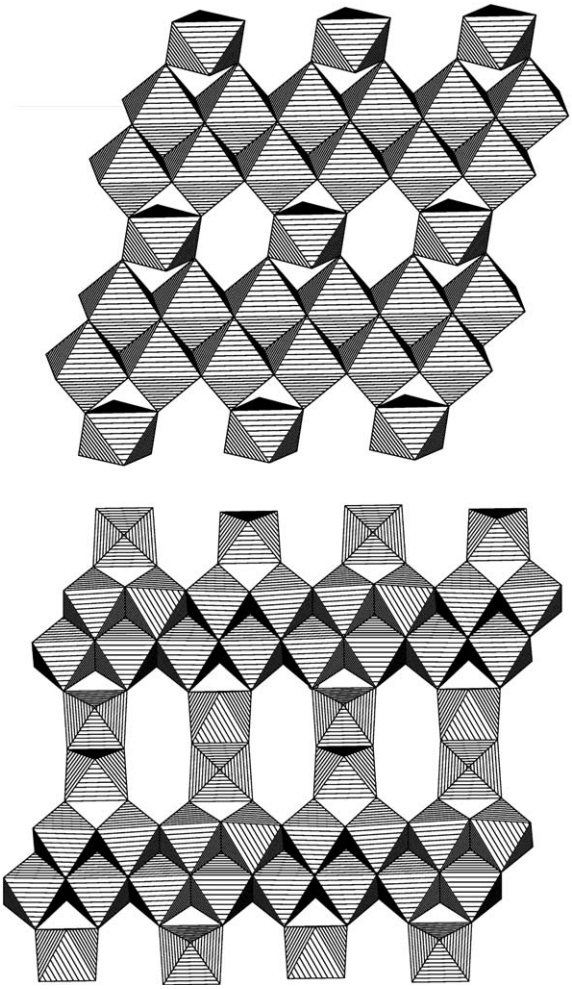

Fig. 8. Polyhedral representations of the perforated layer networks in (top) $Ca(H_2O)_8\{Cd_4Cl_{10}[Cd(H_2O)_2]\} \cdot 1.5H_2O$ and (bottom) $Ca(H_2O)_7\{Cd_4Cl_{10}[Cd_2Cl_2(H_2O)_2]\} \cdot H_2O$.

N–H···X and/or O–H···X hydrogen bonding, as in $(MEDA)_2Cd_4Cl_{12} \cdot 2H_2O$ [1]; (b) replacement of terminal halide ions by water or other solvent molecules, as in $(DEA)Cd_2Cl_5(H_2O) \cdot 2H_2O$ [6,15]; (c) addition of the CdX_2 decorations, as in the title structure. Here, the addition of the decorations reduces the X:Cd ration from 2.67 to 2.50, thus spreading the excess charge over more halide ions. In addition, the terminal halide ions are now part of tetrahedral species, rather than octahedral species, and thus are more accessible sterically for hydrogen bonding interactions.

Acknowledgements

The Bruker (Siemens) SMART APEX diffraction facility was established at the University of Idaho with the assistance of the NSF-EPSCoR program and the M.J. Murdock Charitable Trust, Vancouver, WA, USA. Work supported in part by ACS-PRF 34779-AC.

Appendix A. Supporting material

Crystal data in CIF format for structure has been deposited in the Cambridge Data Base: Reference CCDC 275807. Supplementary data associated with this article can be found, in the online version, at doi:10.1016/j.poly.2006.04.016.

References

[1] A. Thorn, R.D. Willett, B. Twamley, Cryst. Growth Des. 5 (2005) 673.
[2] (a) U. Geiser, R.D. Willett, M. Lindbeck, K. Emerson, J. Am. Chem. Soc. 108 (1986) 1173;
(b) M.R. Bond, R.D. Willett, Inorg. Chem. 28 (1989) 3267;
(c) R.D. Willett, Acta Crystallogr., Sect. A: Found Crystallogr. A49 (1993) 613;
(d) R.D. Willett, M.R. Bond, G. Pon, Inorg. Chem. 29 (1990) 4160;
(e) R.D. Willett, U. Geiser, Acta Chem. Croat. 57 (1984) 737.
[3] R.D. Willett, K.R. Maxcy, B. Twamley, Inorg. Chem. 41 (2002) 7024.
[4] E.G. Tulsky, J.R. Long, Chem. Mater. 13 (2001) 1149.
[5] A. Bonomartini-Corradi, M.R. Cramarossa, G.C. Pellacani, L.P. Battaglia, J. Giusti, Gazz. Chim. Ital. 124 (1994) 481.
[6] (a) A. Thorn, M.S. thesis, Washington State University, 2005;
(b) A. Thorn, R.D. Willett, B. Twamley, Cryst. Growth Des. 6 (2006) 1134.
[7] H. Hope, Prog. Inorg. Chem. 41 (1995) 1.
[8] SMART: v. 5.626, Bruker Molecular Analysis Research Tool, Bruker AXS, Madison, WI, 2002.
[9] SAINTPLUS: v. 6.36a, Data Reduction and Correction Program, Bruker AXS, Madison, WI, 2001.
[10] SADABS: v. 2.01, An Empirical Absorption Correction Program, Bruker AXS, Inc., Madison, WI, 2001.
[11] G.M. Sheldrick, SHELXTL: v. 6.10, Structure Determination Software Suite, Bruker AXS Inc., Madison, WI, 2001.
[12] V.G. Krishman, S.-Q. Dou, H. Paulus, A. Weiss, Ber. Bunsenges. Phys. Chem. 95 (1991) 1256.
[13] P.H. Leligny, J.C. Monier, Acta Crystallogr., Sect. C 37 (1983) 947.
[14] P.H. Leligny, J.C. Monier, Acta Crystallogr., Sect. B 45 (1989) 117.
[15] J.W. Bats, H. Fuess, A. Daoud, Acta Crystallogr., Sect. B 35 (1979) 1706.

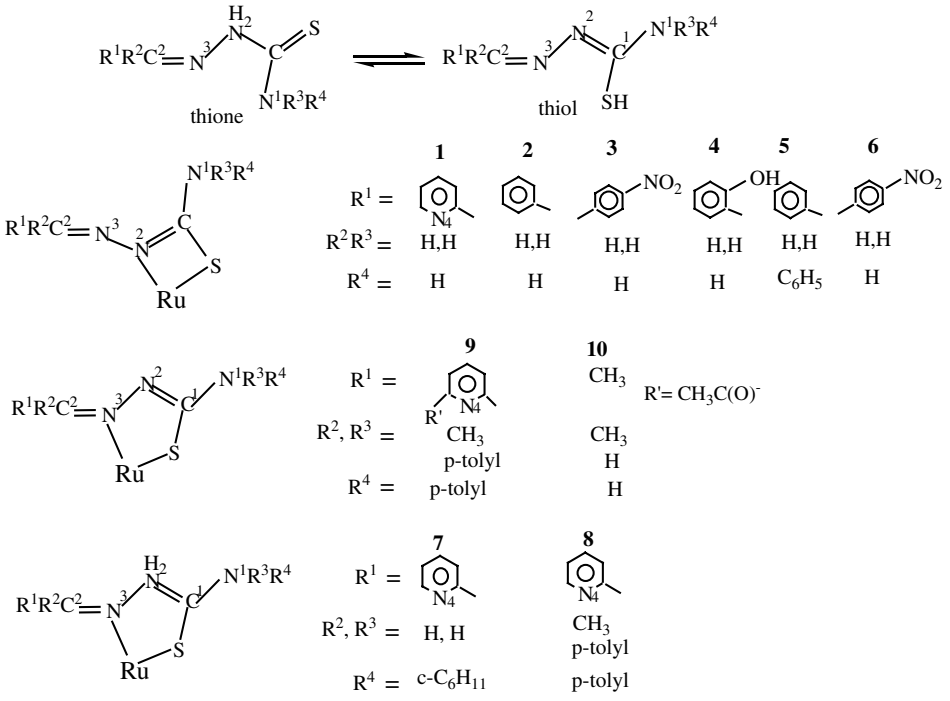

Chart 1.

coordination behaviour of these thiosemicarbazones is investigated under the influence of a potentially P,P-chelating diphosphine ligand $\{(C_6H_5)_2P–(CH_2)_4–P(C_6H_5)_2\}$ in compound **1**, and an unidenate PPh_3 ligand in compound **2**. To the best of our knowledge, compound **1** is the first example of a ruthenium(II)–thiosemicarbazone complex with a diphosphine ligand.

2. Experimental

2.1. Materials and techniques

The starting ruthenium(II) complexes, $RuCl_2(PPh_3)_3$ [12] and $Ru_2Cl_4(dppb)_3$ [13], were prepared by refluxing $RuCl_3 \cdot xH_2O$ and the suitable phosphine in dry ethanol for 5–6 h. Ligands benzaldehyde thiosemicarbazone and pyridine-2-carbaldehyde thiosemicarbazone were prepared by the reported methods [15]. Elemental analysis for C, H and N were carried out using a Thermoelectron FLASHEA1112 analyser. The melting points were determined with a Gallenkamp electrically heated apparatus. UV spectra were recorded using an UV-1601PC Shimadzu. IR spectra were recorded using KBr pellets on a Pye-Unicam SP3-300 spectrophotometer. ^{1}H NMR spectra were recorded on a JEOL AL300 FT spectrometer at 300 MHz in $CDCl_3$ with TMS as internal reference. ^{13}C NMR spectra were recorded at 75.45 MHz with TMS as internal reference. ^{31}P NMR spectra were recorded at 121.5 MHz with TMP $\{(CH_3O)_3P\}$ as external reference taken as zero position.

2.2. Synthesis of [Ru(pytsc)$_2$(dppb)] (1)

To a solution of Hpytsc (0.022 g; 0.12 mmol) in methanol (30 mL) was added solid $[Ru_2Cl_4(dppb)_3]$ (0.05 g; 0.03 mmol) followed by addition of NEt_3 (0.5 mL). The mixture was stirred for about 15 h. The red solid that formed was filtered, washed with methanol and dried. Crystals were grown from dichloromethane–acetonitrile–methanol. Yield: 51%, m.p. 172 °C. *Anal.* Calc. for $C_{42}H_{42}N_8P_2S_2Ru \cdot 2H_2O \cdot CH_3CN$: C, 54.6; H, 5.48; N, 13.02. Found: C, 54.0; H, 5.04; N, 13.25%. Main IR peaks (KBr, cm^{-1}): $\nu(NH_2) + \nu(OH_2)$ 3457m, 3360–3300m, 3150w; $\nu(C{=}N) + \delta NH_2 + \nu(C{=}C) + \delta(OH_2)$ 1585s, 1573sh, 1562sh; $\nu(C{=}S)$ 1047s; $\nu(P–C)$ 1093s; electronic spectra (CH_2Cl_2, $\lambda_{max/nm}$, ε/L mol^{-1} cm^{-1}) 391.50 (17600), 328.50 (24580), 245 (40000). ^{1}H NMR ($CDCl_3$): $\delta = 8.80$ (s, C^{2}H, 2H), 8.52 (d, C^{7}H, 2H), 7.10–7.66 (m, Ph–H + C^{4,5,6}H, 26H), 5.46 (s, NH_2, 4H), 1.26–2.89 (–CH_2–, 8 H) ppm; ^{13}C NMR ($CDCl_3$), $\delta = 182.0$ (C^1), 155.2 (C^3), 149.0 (C^7), 145.2 (C^2), 138.6–140.6 (*i*-C), 135.8 (C^5), 132.5 (*o*-C), 126.9–128.6 (*m*- and *p*-C), 122.4 (C^6), 120.7 (C^4), 30.1, 23.4 {–$(CH_2)_4$-carbons} ppm; ^{31}P NMR ($CDCl_3$), $\delta = -57.413$ ppm, $\Delta\delta(\delta_{complex} - \delta_{ligand}) = 66.48$ ppm.

2.3. Synthesis of [Ru(btsc)$_2$(Ph$_3$P)$_2$] (2)

This complex was prepared by the literature method [9]. To a solution of Hbtsc (0.0186 g; 0.1 mmol) in methanol (30 mL) was added solid $RuCl_2(Ph_3P)_3$ (0.05 g; 0.05 mmol) followed by NEt_3 base (0.5 mL). The mixture was stirred for 2 h and the yellow solid which separated was filtered,

washed with methanol and dried. The compound was recrystallized from dichloromethane–methanol solution. Yield: 60% m.p. 170 °C. Main IR peaks (KBr, cm^{-1}), $\nu(NH_2)$ 3483s, 3361s; $\nu(C{=}N) + \delta NH_2 + \nu(C{=}C)$ 1600s, 1577; $\nu(C{=}S)$ 1050s, 754 s; $\nu(P–C)$ 1087s. ^1H NMR ($CDCl_3$) $\delta = 8.88$ (s, C^2H, 2H), 5.03 (s, NH_2, 4H), 6.97–7.90 (m, $C^{2,4–6,8}H + 40H$, Ph). ^{13}C NMR ($CDCl_3$) 179.46 (C^1), 147.28 (C^2), 136.06 (C^3), 128.49 ($C^{4,8}$), 127.23 (C^5), 137.24 (*i*-C), 134.2 (t, *o*-C), 128.27 (d, *p*-C), 126.75 (t, *m*-C). ^{31}P NMR ($CDCl_3$), $\delta = -56.015$ ppm, $\Delta\delta(\delta_{complex} - \delta_{ligand}) = 57.13$ ppm.

2.3.1. Ligand NMR data

Hpytsc (dmso-d_6): ^1H NMR, $\delta = 11.57$ (s, N^2H, 1H), 8.47 (s, C^2H, 1H), 7.2–8.06 (6H, $C^{4,5,6,7} + Ph–H$) ppm. ^{13}C NMR 178.05 (C^1), 152.17 (C^3), 148.42 (C^2), 142.38 (C^7), 135.56 (C^5), 123.09 (C^6), 119.73 (C^4) ppm; Hbtsc [17] ^1H NMR $\delta = 7.27$, 6.60 (s, N^1H_2, 2H), 10.22 (s, N^2H, 1H), 9.26 (s, C_2H, 1H), 7.69 (m, $C^{4,8}H$, 2H), 7.43 (m, $C^{5,6,7}H$, 3H). ^{13}C NMR 178.86 (C^1), 143.94 (C^2), 133.99 (C^3), 130.87 (C^6), 128.96 ($C^{4,8}$), 127.54 ($C^{5,7}$); ^{31}P NMR of dppb: $\delta = -123.89$ ppm; ^{31}P NMR of PPh_3, $\delta = -113.15$ ppm.

2.4. X-ray crystallography

Suitable crystals of **1** and **2** were mounted on X-ray diffractomers (Bruker APEX II for **1**; CCD area detector for **2**), each equipped with graphite monochromators and a Mo Kα radiation source ($\lambda = 0.71073$ Å). The unit cell dimensions and intensity data were measured at 293 K. The structures were solved by direct methods and refined by full-matrix least-square methods based on F^2 with anisotropic thermal parameters for non-hydrogen atoms, using Bruker SMART (data collection and cell refinement), Bruker SHELXTL (data reduction and computing molecular graphics), SHELXS-97 (structure solution) and SHELXL-97 (structure refinement)] [16]. An empirical absorption correction was applied. Calculated positions for the H atoms were used in structure factor (SF) calculations. ω scans were to 56° (2θ). In compound **1**, one of the pyridine groups in each pytsc ligand was found to be disordered and these atoms were treated in an equal population model. One of the terminal pyridyl groups displayed disorder. During refinement the disorder in this group was resolved. Selected crystal data for compounds **1** and **2** are given in Table 1.

Table 1
Crystal data and refinement details for **1** and **2**

	1	**2**
Empirical formula	$C_{42}H_{44.5}N_8O_{1.5}P_2RuS_2$	$C_{52}H_{46}N_6P_2RuS_2$
M	912.49	982.08
T (K)	293(2)	293(2)
Crystal system	triclinic	triclinic
Space group	$P\bar{1}$	$P\bar{1}$
Unit cell dimensions		
a (Å)	9.7303(6)	12.715(3)
b (Å)	12.8038(8)	12.864(3)
c (Å)	19.3406(11)	16.286(4)
α (°)	85.2610(10)	72.184(5)
β (°)	84.9840(10)	72.621(5)
γ (°)	70.4980(10)	65.146(4)
V (Å^3)	2258.9(2)	2256.0(10)
Z	2	2
D_{calc} (g cm^{-3})	1.348	1.446
μ (mm^{-1})	0.552	0.556
Reflections collected	31 048	16 506
Unique reflections [R_{int}]	11 175 [0.0478]	10 455 [0.0740]
Reflections with [$I > 2\sigma(I)$]	6181	5602
Final *R* indices [$I > 2\sigma(I)$]	$R = 0.0448$, $wR = 0.1238$	$R = 0.0778$, $wR = 0.1274$

3. Results and discussion

3.1. Synthesis and IR spectroscopy

Scheme 1 shows the formation of complexes **1** and **2**. Reaction of $Ru_2Cl_4(dppb)_3$ {dppb = $Ph_2P–(CH_2)_4–PPh_2$} with pyridine-2-carbaldehyde thiosemicarbazone {$C_5H_4N–C(H){=}N^3–N^2H–C(=S)NH_2$, Hpytsc}, and that of $RuCl_2(PPh_3)_3$ with benzaldehyde thiosemicarbazone {$C_6H_5–C(H){=}N^3–N^2H–C(=S)–NH_2$, Hbtsc}, in the presence of Et_3N base led to loss of the $–N^2H–$ proton in each case, and yielded [Ru(pytsc)$_2$(dppb)] (**1**) and [Ru(btsc)$_2$(Ph_3P)$_2$] (**2**) [9], respectively. Both the complexes

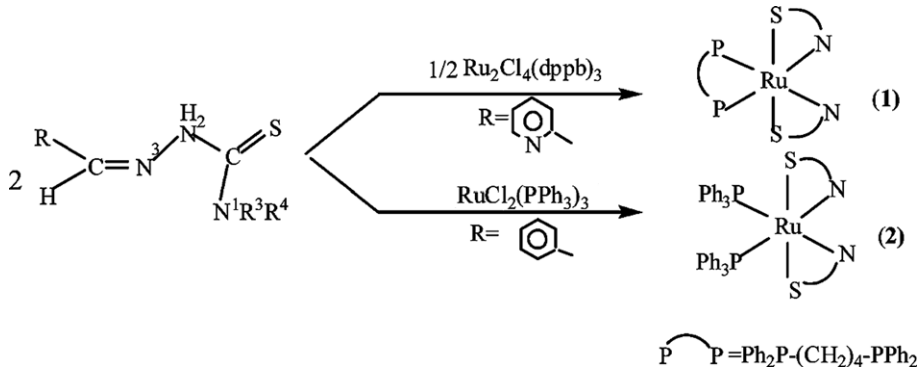

Scheme 1.

are soluble in dichloromethane, chloroform, acetone or toluene, but partially soluble in acetonitrile. The compounds are stable in air in the solid state; however in solution phase the complexes turn green on standing for a long time.

Due to the presence of H_2O in complex **1**, the ν(N–H) region has broad signals at 3457m, 3360–3300m and 3150w, and these peaks are attributed to ν(N–H) + ν(O–H). However in complex **2**, the ν(N–H) region shows sharp peaks at 3483s and 3361s. The free ligands show very strong signals due to ν(N–H) of the hydrazinic –N^2H– group in the region 3140–3150 cm^{-1} [14,18]. Thus in complex **2**, it is unequivocally established that deprotonation of the N^2H proton occurs after complexation; and in complex **1** due to obscuring of the ν(N–H) region by water, deprotonation of the N^2H proton appears less apparent. It may be pointed out here that in a series of complexes of copper(I) with neutral thiosemicarbazones, ν(N–H) of the hydrazinic –N^2H– group was clearly visible though shifted from the free ligand position [19]. Other important IR peaks are listed in the Section 2. The thioamide bands ν(C=S) + ν(C–N) appear in the range 1050–803 cm^{-1} (cf. free ligands, 1060–817 cm^{-1}), and on complexation, these shift to either lower energy or higher energy, but the shifts are not significant. The appearance of characteristic ν(P–C_{Ph}) bands at around 1090 cm^{-1} indicates the presence of Ph_3P and dppb in the complexes.

3.2. Crystal structures

The atomic numbering schemes for **1** and **2** are given in Figs. 1 and 2 respectively, and selected bond angles and bond lengths are listed in Table 2. Compounds **1** and **2** crystallized in triclinic crystal systems with the space group $P\bar{1}$ in each case. In compound **1**, the thiosemicarbazone ligand in its deprotonated form (pytsc$^-$) is chelating via its N^2, S-donor atoms, thus forming four membered chelate rings with average Ru(II)–N and Ru(II)–S distances of 2.202 Å and 2.418 Å, respectively, and the pyridyl group is pendant. The diphosphine ligand (dppb) is also chelating via its P,P donor atoms with an average Ru–P distance of 2.264 Å (Tables 2 and 3). The donor atoms around the Ru(II) center occupy *cis*:*cis*:*trans* N,N:P,P:S,S positions. The angles around the Ru(II) center lie in the range, 65–163°, with a N^2–Ru–S bite angle of 65.85°, N–Ru–N angle of 83.07° and *trans* S(1)–Ru–S(2) angle of 163.30°. The diphosphine ligand dppb forms a seven membered chelate ring with a P–Ru–P angle of 94.54°. Similarly, compound **2** has average Ru(II)–N, Ru(II)–S and Ru–P distances of 2.145, 2.410 and 2.301 Å, respectively. The average bond angles for N^2–Ru–S, N–Ru–N, S–Ru–S, P–Ru–P are 65.80°, 78.80°, 162.54° and 105.37°, respectively. The geometry of both the complexes is distorted octahedral.

On comparing the bond parameters of **1** and **2**, the most striking difference is found in their Ru–N and Ru–P distances. Interestingly, the Ru–P distances of **1** are shorter and its Ru–N distances are longer as compared to those of **2**. This shows the chelating effect of the dppb ligand which forms stronger Ru(II)–P bonds as compared to Ru(II)–PPh_3 bonds, which in turn affect the Ru(II)–N bonds *trans* to Ru–P bonds. The Ru–P distance for **1** is the shortest among all the complexes listed in Table 3. The Ru–S bonds remain unaffected by this change as can be seen by comparing the bonds in both the compounds. The C–S distances in both the compounds are similar, in

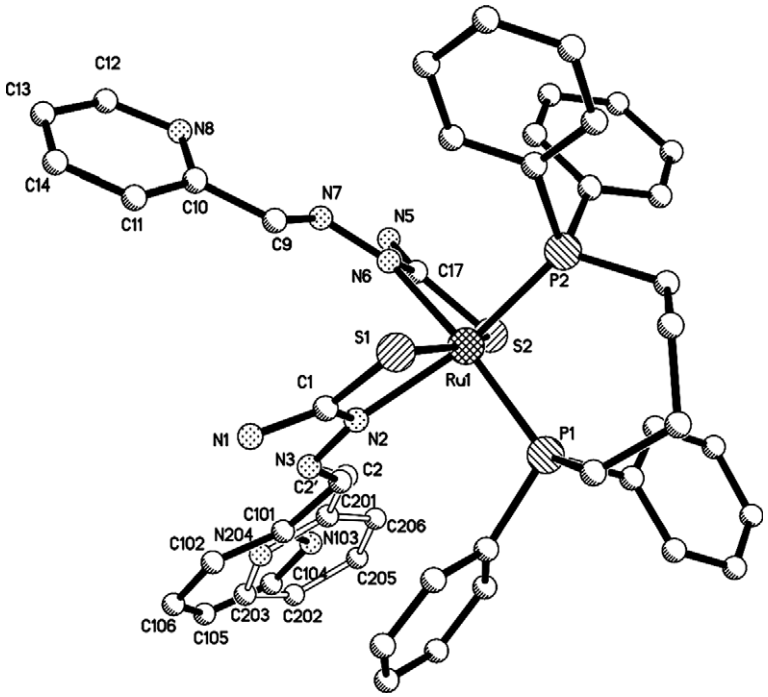

Fig. 1. The structure of [Ru(pytsc)$_2$(dppb)] (**1**) with the atomic numbering scheme.

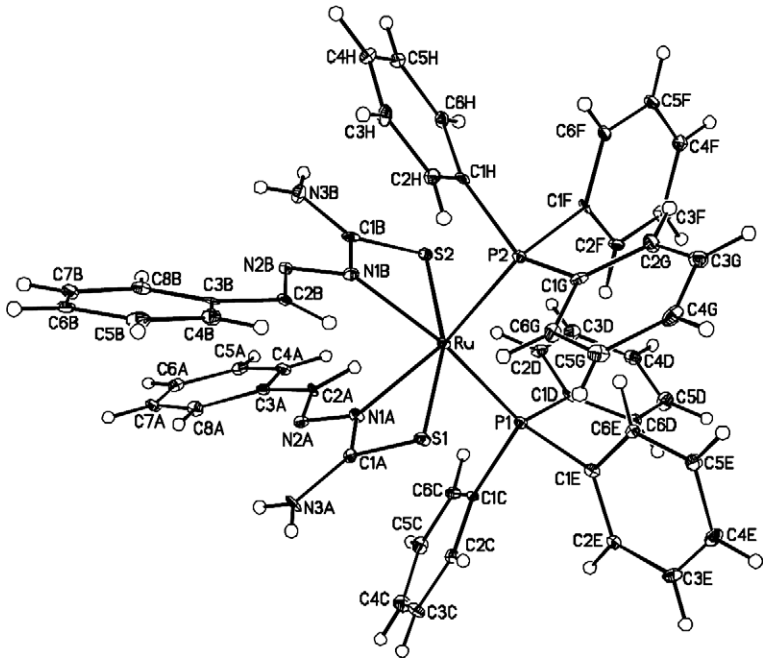

Fig. 2. The structure of $[Ru(btsc)_2(PPh_3)_2]$ (**2**) with the atomic numbering scheme.

Table 2
Selected bond lengths (Å) and bond angles (°) for **1** and **2**

1			
Ru(1)–N(2)	2.187(4)	Ru(1)–S(1)	2.4096(10)
Ru(1)–N(6)	2.218(3)	Ru(1)–S(2)	2.4270(10)
Ru(1)–P(1)	2.2582(9)	S(1)–C(1)	1.680(5)
Ru(1)–P(2)	2.2696(10)	S(2)–C(17)	1.718(4)
N(2)–Ru(1)–N(6)	83.06(12)	P(1)–Ru(1)–S(1)	91.20(3)
N(2)–Ru(1)–P(1)	92.07(9)	P(2)–Ru(1)–S(1)	97.49(4)
N(6)–Ru(1)–P(1)	163.99(8)	N(2)–Ru(1)–S(2)	101.64(13)
N(2)–Ru(1)–P(2)	162.42(13)	N(6)–Ru(1)–S(2)	65.55(9)
N(6)–Ru(1)–P(2)	94.57(9)	P(1)–Ru(1)–S(2)	100.83(3)
P(1)–Ru(1)–P(2)	94.54(3)	P(2)–Ru(1)–S(2)	93.10(4)
N(2)–Ru(1)–S(1)	66.06(13)	S(1)–Ru(1)–S(2)	163.30(4)
N(6)–Ru(1)–S(1)	100.62(9)		
2			
Ru–N(1A)	2.141(5)	Ru–S(1)	2.4083(17)
Ru–N(1B)	2.149(5)	Ru–S(2)	2.4131(17)
Ru–P(1)	2.2977(19)	S(1)–C(1A)	1.700(7)
Ru–P(2)	2.3044(18)	S(2)–C(1B)	1.712(7)
N(1A)–Ru–N(1B)	78.8(2)	N(1B)–Ru–S(1)	99.52(14)
N(1A)–Ru–P(1)	89.16(15)	P(1)–Ru–S(1)	87.19(6)
N(1B)–Ru–P(1)	162.18(14)	P(2)–Ru–S(1)	104.52(6)
N(1A)–Ru–P(2)	162.46(15)	N(1A)–Ru–S(2)	100.73(4)
N(1B)–Ru–P(2)	89.02(15)	N(1B)–Ru–S(2)	65.85(14)
P(1)–Ru–P(2)	105.37(7)	P(1)–Ru–S(2)	104.21(6)
N(1A)–Ru–S(1)	65.75(14)	P(2)–Ru–S(2)	85.43(6)
S(1)–Ru(1)–S(2)	162.54(6)		

the range 1.68–1.71 Å, which is shorter than a C–S single bond of 1.81 Å but longer than a C–S double bond of 1.62 Å, indicating a partial double bond character [20].

The second major difference lies in the P–Ru–P bond angle which is smaller for **1** as compared to that in **2**, and this is attributed to the presence of bulky PPh_3 ligands adjacent to each other which causes this angle to deviate towards the higher side. As a matter of fact, the P–Ru–P bond angle of **1** is the smallest among all the Ru(II) complexes of thiosemicarbazones reported to date. The N–Ru–N bond angle in **1** is bigger than that in **2**, and this variation is attributed to the scissoring effect of P–Ru–P angles. The S–Ru–S bond angles in both the complexes are comparable and are similar to other complexes reported in the literature (Table 3). From Table 3, it may be noted that parameters of **2** are very close to those of complexes **3**–**5**, but different from those of **1**. Complexes **1**–**5**, forming four-membered rings, have a bite angle of ca. 66°, which is small relative to the bite angles (ca. 81°) of complexes (**7**–**9**) which form five-membered rings.

Compounds **1**–**5** are analogous with four membered rings formed by the thiosemicarbazone, the steric bulk of the phosphines appears to favour N^2, S chelation irrespective of the substituents on the C^2 or N^1 atoms. Compound **7** has N^3, S chelation with five membered ring formation, despite the presence of bulky PPh_3 ligands in the *cis* position, and it is apparent that the presence of bulky groups at the N^1 atom appears to disfavour N^2, S chelation. In **8** and **9** the steric effect of PPh_3 is less demanding in view of the presence of one thiosemicarbazone ligand in each complex and this leads to a large P–Ru–P bond angle and also both have bulky R groups at N^1 and this leads to N^3, S chelation. As regards compound **6** and **10**, each have two bipyridine ligands and the only difference lies in the presence of substituents at the C^2 carbon while the substituents at $N^1$are identical (R^3, $R^4 = H$). This difference leads to N^2, S chelation in **6** and N^3, S chelation in **10**.

Table 3
Comparison of bond lengths (Å) and bond angles (°) of **1**, **2** and related complexes

	Ru–N	Ru–S	Ru–P	S–Ru–S	N–Ru–N	P–Ru–P	N–Ru–S	Ref.
1	2.202	2.418	2.264	163.30	83.07	94.54	65.85	this work
2	2.145	2.410	2.301	162.54	78.80	105.37	65.80	this work
3	2.181	2.440	2.299	162.77	80.42	99.24	65.90	[7]
4	2.152	2.426	2.323	161.23		105.95	65.74	[8]
5	2.140	2.439	2.314	160.65	80.50	97.76	65.45	[11]
7	2.146	2.369	2.382	170.81	81.4	101.74	81.65	[9]
8	2.035	2.386	2.399			175.2	83.3	[6]
9	1.981	2.398	2.371			165.8	81.5	[5]

3.3. NMR spectroscopy

The signals due to N^2H protons in the free ligands (see Section 2) were absent in the complexes **1** and **2**, and it showed that the ligands are uninegative. The NH_2 protons appear as single peaks in both the complexes due to free rotation of the N^1H_2 group along the C^1–N^1 bond axis, instead of two broad peaks as observed in the free ligands, due to the restricted rotation of the N^1H_2 group along the C^1–N^1 bond axis at room temperature [18]. All other protons appear in the aromatic region as multiplets and overlapping signals. The ^{13}C NMR spectra of both the compounds showed bands due to tsc^- anions and phosphine ligands (cf. Section 2). The C^1 carbons of both ligands move downfield, and it shows coordination via the S-donor atom, and likewise C^2 and C^3 move downfield, but the shift is small. All other tsc^- carbons show much smaller shifts. Various signals due to *ipso*, *ortho*, *meta* and *para* carbons of the phosphine ligands are resolved in the complexes. Finally, the ^{31}P NMR spectra of **1** and **2** showed coordination shifts $\{\Delta\delta(\delta_{complex}-\delta_{ligand})\}$ of 66.48 and 57.13 ppm, respectively, revealing that both the phosphorus atoms are equivalent in each case, and that the dppb ligand binds more strongly than PPh_3, in conformity with the structural data.

4. Conclusion

Compound **1** represents the first example of a ruthenium(II) complex with a chelating diphosphine, forming a stable seven membered P,P-chelate ring in the presence of a potentially tridentate pyridine-2-carbaldehyde thiosemicarbazonate anion coordinating via N^2, S-donor atoms, which is stable in solid and solution states. For R = Ph and py at the C^2 carbon of the tsc^- ligands, the mode of coordination remains same, viz., N^2, S.

Acknowledgements

Financial assistance from CSIR, New Delhi (F.No. 9/254(155)-EMR-II) and research facilities to one of us (Gagandeep) by the University are gratefully acknowledged.

Appendix A. Supplementary material

Supplementary data is available from CCDC, 12 Union Road, Cambridge CB2 1EZ, UK, fax: +44 1233 6033, e-mail:deposit@ccdc.cam.ac.uk on request quoting the deposition number CCDC 298895 for (**1**) and 298896 for (**2**). Supplementary data associated with this article can be found, in the online version, at doi:10.1016/j.poly.2006.04.018.

References

[1] S. Padhye, G.B. Kauffman, Coord. Chem. Rev. 63 (1985) 127.
[2] F.H. Allen, O. Kennard, R. Taylor, Acc. Chem. Res. 16 (1983) 146.
[3] M.J.H. Campbell, Coord. Chem. Rev. 15 (1975) 279.
[4] D.X. West, S. Padhye, P.B. Sonawane, Struct. Bond. (Berlin) 76 (1991) 4.
[5] (a) M. Maji, S. Ghosh, S.K. Chattopadhyay, T.C. Mak, Inorg. Chem. 36 (1997) 2938;
(b) L.J. Ashfield, A.R. Cowley, J.R. Dilworth, P.S. Donnelly, Inorg. Chem. 43 (2004) 4121;
(c) A.R. Cowley, J.R. Dilworth, P.S. Donnelly, E. Labisbal, A. Sousa, J. Am. Chem. Soc. 124 (2002) 5270.
[6] M. Maji, M. Chatterjee, S. Ghosh, S.K. Chattopadhyay, T.C. Mak, B.M. Wu, J. Chem. Soc., Dalton Trans. (1999) 135.
[7] F. Basuli, M. Ruf, C.G. Pierpont, S. Bhattacharya, Inorg. Chem. 37 (1998) 6113.
[8] F. Basuli, S.M. Peng, S. Bhattacharya, Inorg. Chem. 36 (1997) 5645.
[9] P.S. Gupta, R. Dinda, S. Ghosh, W.S. Sheldrick, Polyhedron 22 (2003) 447.
[10] F. Basuli, S.M. Peng, S. Bhattacharya, Inorg. Chem. 39 (2000) 1120.
[11] D. Mishra, S. Naskar, M.G.B. Drew, S.K. Chattopadhyay, Polyhedron 24 (2005) 1861.
[12] T.A. Stephenson, G.J. Wilkinson, J. Inorg. Nucl. Chem 28 (1966) 945.
[13] (a) M. Bressan, P. Rigo, Inorg. Chem. 14 (1975) 2286;
(b) T.S. Lobana, R. Singh, Polyhedron 14 (1995) 907.
[14] (a) E.W. Ainscough, A.M. Brodie, J.D. Ranford, J.M. Waters, J. Chem. Soc., Dalton Trans. (1997) 1251;
(b) P J.G. Tojal, J.G. Jaca, R. Cortes, T. Rojo, M.K. Urtiage, M.I. Arriortua, Inorg. Chim. Acta 249 (1996) 25;
(c) J.G. Tojal, L. Lezama, J.L. Pizarro, M. Insausti, M.I. Arriortua, T. Rojo, Polyhedron 18 (1999) 3703;
(d) J.S. Casas, E.E. Castellano, J. Ellena, M.S. Garcia-Tasende, A. Sanchez, J. Sordo, M.J. Vidarte, Inorg. Chem. 42 (2003) 2584;
(e) A.R. Cowley, J.R. Dilworth, P.S. Donnelly, J. Woollard-Shore, J. Chem. Soc., Dalton Trans. (2003) 748;
(f) J.S. Casas, A. Castineiras, M.C.R. Arguelles, A. Sanchez, J. Sordo, A.V. Lopez, S. Pinelli, P. Lunghi, P. Ciancianaini, A. Bonati, P.D. Aglio, R. Albertini, J. Inorg. BioChem. 76 (1999) 277;
(g) P. Sen Gupta, R. Dinda, S. Ghosh, W.S. Sheldrick, Polyhedron 22 (2003) 447.

[15] F.E. Anderson, C.J. Duca, J.V. Scudi, J. Am. Chem. Soc. 73 (1951) 4967.
[16] G.M. Sheldrick, SHELXL-97, Program for the Refinement of Crystal Structures, University of Gottingen, Gottingen, Germany, 1997.
[17] T.S. Lobana, A. Sanchez, J.S. Casas, A. Castineiras, J. Sordo, M.S. Garcia-Tasende, E.M. Vazquez-Lopez, J. Chem. Soc., Dalton Trans. (1997) 4289.
[18] T.S. Lobana, A. Castineiras, Polyhedron 21 (2002) 1603.
[19] T.S. Lobana, R. Rekha, P.V. Bharatam, A. Castineiras, E. Bermejo, R.J. Butcher, Inorg. Chem. 45 (2006) 1535.
[20] J.E. Huheey, E.A. Keiter, R.L. Keiter, Inorganic Chemistry: Principles of Structure and Reactivity, 4th ed., Harper Collins, NewYork, 1993.

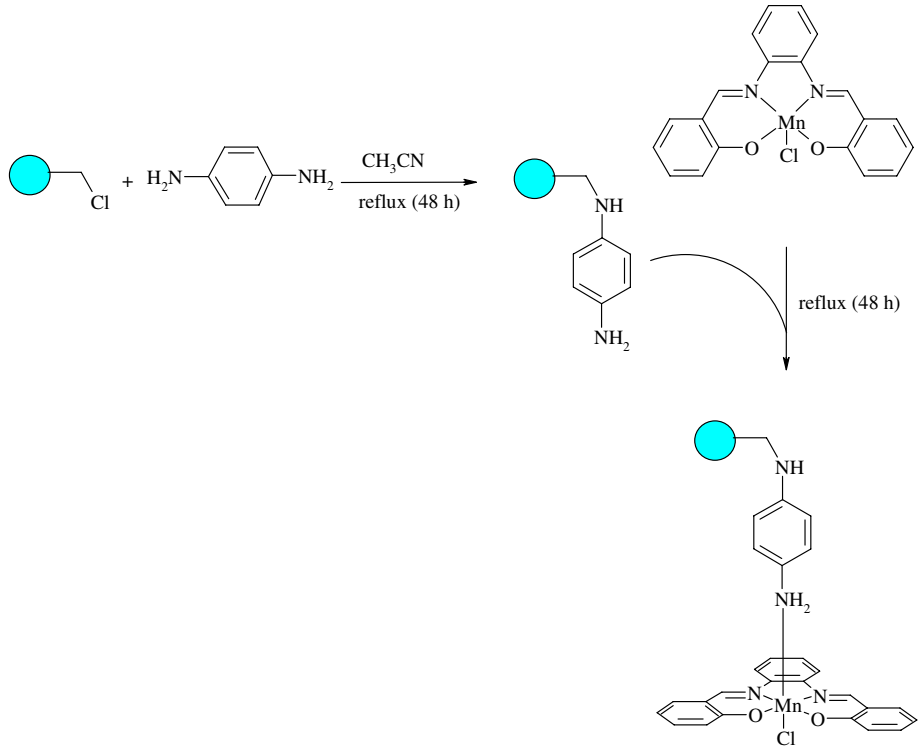

Scheme 1. Preparation of polymer supported catalyst, [Mn(salophen)Cl-PSP].

in many ways, namely: (a) non-covalent immobilization in zeolites, clay or siloxane membranes [22–25]; (b) covalent grafting onto inorganic supports such as silica or MCM-41 [26–30]; (c) co-polymerization of a functionalized salen monomer into an organic polymer [31]; and (d) attachment or build-up of a salen structure to a performed polymer [32–37]. Polymers, which are used as supports, have gained much attention being inert, non-toxic, non-volatile, insoluble and often recyclable. Imidazoles and pyridines were chosen since they ligate strongly to the axial positions of metallosalens in free solution [38,39], and furthermore, such a nitrogen base can increase the catalytic efficiency in the epoxidation with single oxygen atom donors.

This paper describes a catalytic system based on a chloromethylated polystyrene support modified with 1,4-phenylenediamine, which can act as an axial ligand for Mn(salophen) by covalent attachment (Scheme 1). The heterogeneous Mn(salophen) catalyst, [Mn(salophen)Cl-PSP], was characterized by FT-IR, UV–Vis and TG–DTG. Catalytic activity and reusability of this catalyst in the heterogeneous epoxidation of alkenes and hydroxylation of alkanes has also been demonstrated.

2. Results and discussion

2.1. Preparation of polymer-supported manganese salophen catalyst, [Mn(salophen)Cl-PSP]

Chloromethylated polystyrene (cross-linked with 2% divinylbenzene, 4–5% Cl content, 1.14–1.40 mmol/g Cl) was treated with an appropriate quantity of 1,4-phenylenediamine, using CH_3CN as solvent, and was refluxed for 48 h [40]. The supported [Mn(salophen)] was prepared by stirring a suspension of the support, (PSP), in a solution of Mn(salophen) in CH_3CN as solvent, because of better solvation and swelling of the polymer in it. The degree of incorporation of manganese salophen into the polymer was determined by neutron activation analysis (NAA). The covalent bonding of the polymer and the manganese salophen is so strong that Mn(III)-salophen is not eluted from the polymer with water and common organic solvents.

2.2. Characterization of catalyst

The prepared catalyst was characterized by IR, UV and TGA. [Mn(salophen)Cl-PSP] was characterized by elemental analysis. The amount of grafted Mn(salophen), which was calculated by neutron activation analysis (NAA), was 0.136 mmol/g base on Mn. The nitrogen content of this resin was 2.06%. According to this value, the degree of 1,4-phenylenediamine which was introduced into the polymer composition was 0.735 mmol/g of support. This shows that only 53–64% of the total chlorine was substituted by 1,4-phenylenediamine.

The diffuse reflectance spectra provide further evidence for the presence of the Mn(salophen) complex on the support. The absorption spectrum of [Mn(salophen)Cl-PSP] exhibits a broad peak near 450 nm which could be due to the d–d transition of Mn(III). Its homogeneous counterpart also shows a peak near 450 nm, which indicates the presence of the manganese catalyst on the polymer (Fig. 1).

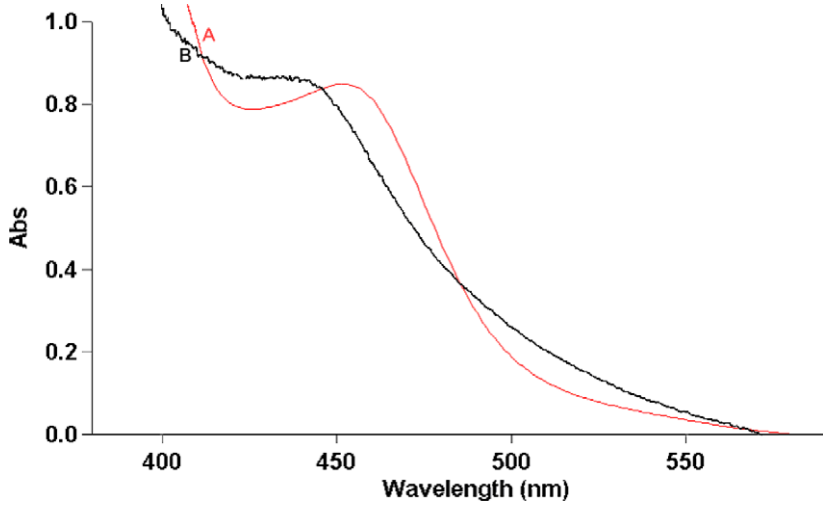

Fig. 1. UV–Vis spectra of: (a) Mn(salophen)Cl; (b) [Mn(salophen)Cl-PSP].

In order to ascertain the attachment of salophen on the polymer support, IR spectra were recorded in the (4000–400 cm^{-1}) regions. The sharp C–Cl peak (due to $–CH_2Cl$ groups) at 1264 cm^{-1} in the starting polymer (Fig. 2a) practically disappeared or was seen as a weak band after introduction of 1,4-phenylenediamine and manganese salophen on the polymer. The appearance of a band in the region of 1629–1550 cm^{-1}, assigned to $\nu_{C=N}$ (azomethine), and a medium intensity band due to stretching C–N at 1193 cm^{-1} clearly indicate the promotion of manganese salophen on the support (Fig. 2b and c).

Differential thermal analysis and thermogravimetric analysis have been used to characterize the immobilized of the metal complex. The decomposition behavior of the free complex and supported complex has been compared in order to understand the effect of the supporting (Fig. 3). The free complex shows a weight loss of 72% at a temperature 305 °C (Fig. 3a). However, for the corresponding supported complex, a 43% weight loss appears at the temperature 308 °C and a 54% weight loss appears at 418 °C (Fig. 3b). TG and DTA analysis for the free complex and supported complex indicated no change in thermal stability of the polymer after the complex is anchored, which may be due to the dissociation of covalently bound salophen ligand moieties or partial scission of the polymeric chain might be occurring at the same temperature [41]. These criteria indicate that the catalyst is thermally stable up to 200 °C.

2.3. The effect of terminal oxidants on the oxidations of cyclooctene catalyzed by Mn(salophen)Cl-PSP

In the catalytic epoxidation of alkenes the choice of oxygen donor and solvent is of crucial importance. In this study, we investigated the ability of different oxidants, such as NaOCl, $NaIO_4$, Bu_4NIO_4, H_2O_2, $KHSO_5$ and *tert*-butylhydroperoxide, urea–H_2O_2 (UHP), in the epoxidation of cyclooctene, catalyzed by the heterogeneous Mn(III) salophen. The results are summarized in Table 1. When NaOCl, H_2O_2, *tert*-butylhydroperoxide and urea–H_2O_2 (UHP) were used as the oxygen source, either in acetonitrile or dichloromethane, only small amounts of cyclooctene oxide was detected in the reaction mixture. The use of Oxone ($KHSO_5$) was not favored because of disadvantages such as needing a buffered media and the bleaching of the metal catalysts during the oxidation reactions.

The results show that in the presence of the Mn(salophen)Cl-PSP catalyst, $NaIO_4$ is the best oxygen source, because of good oxidation conversions, inertness in the absence of catalyst and high solubility in the CH_3CN/H_2O mixture.

2.4. The effect of solvent on the oxidation of cyclooctene catalyzed by [Mn(salophen)Cl-PSP]

The epoxidation of cyclooctene was studied in various solvents at room temperature (Table 2). Among the mixtures of methanol, ethanol, acetone, acetonitrile (single phase systems), chloroform, dichloromethane and carbontetrachloride (two phase systems with Bu_4NBr as a phase transfer catalyst) with water, the 2:1 mixture of acetonitrile/water mixture was chosen as the reaction medium, because a higher epoxidation yield was observed. The higher catalytic activity in aqueous acetonitrile is attributed to the polarity of the solvent, better swelling of the polymer and solubility of $NaIO_4$ in the solvent.

2.5. Catalytic alkene epoxidation with $NaIO_4$ catalyzed by Mn(salophen)Cl-PSP

It is well known that the catalytic ability of manganese Schiff bases is improved by the use of a nitrogen base as a co-catalyst [38,39]. In this study, the polystyrene-bound 1,4-phenylenediamine, was not only used as a support, but it also plays the axial ligand role in this catalytic system. Reactions were performed at room temperature

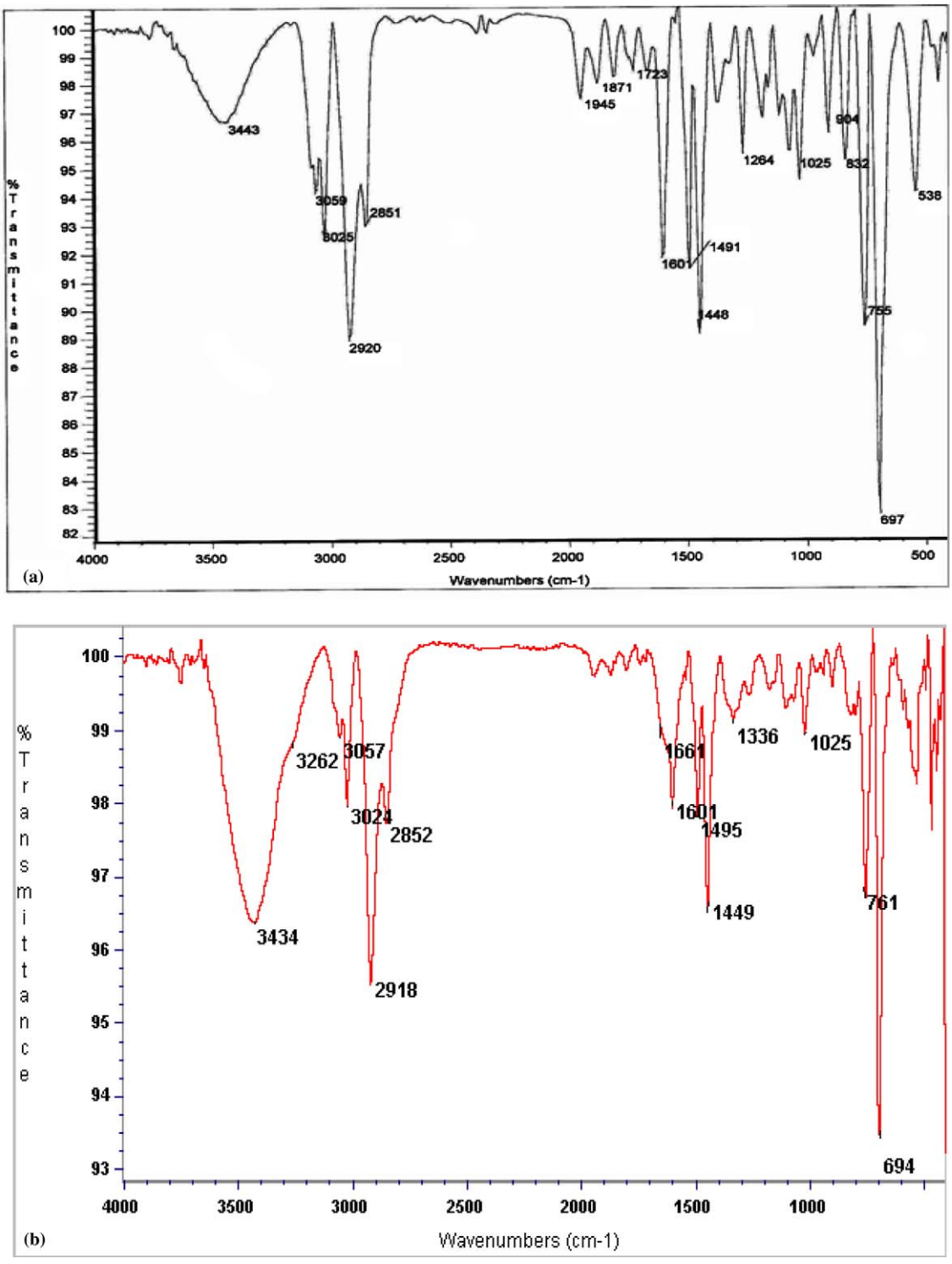

Fig. 2. (a) Chloromethylated polystyrene; (b) chloromethylated polystyrene modified with 1,4-phenylenediamine; (c) Mn(salophen)Cl-PSP; (d) recovered Mn(salophen)Cl-PSP.

under air in CH_3CN/H_2O containing the alkene, oxidant and catalyst. This catalytic system led to the epoxidation of various alkenes (Table 3) with good to excellent yields (64–99%). Cyclooctene was oxidized in the presence of this catalyst in high yield. Styrene and α-methylstyrene were oxidized to styrene oxide and α-methylstyrene oxide in 96% and 99% yield, respectively (see Table 3, entries 3 and 4). Under the heterogeneous Mn-catalyzed conditions and only traces of undesirable benzaldehyde and acetophenone were detected. Similarly, oxidation of cyclohexene was achieved in a high conversion yield and only 8% of cyclohexenone was produced. Epoxidation of

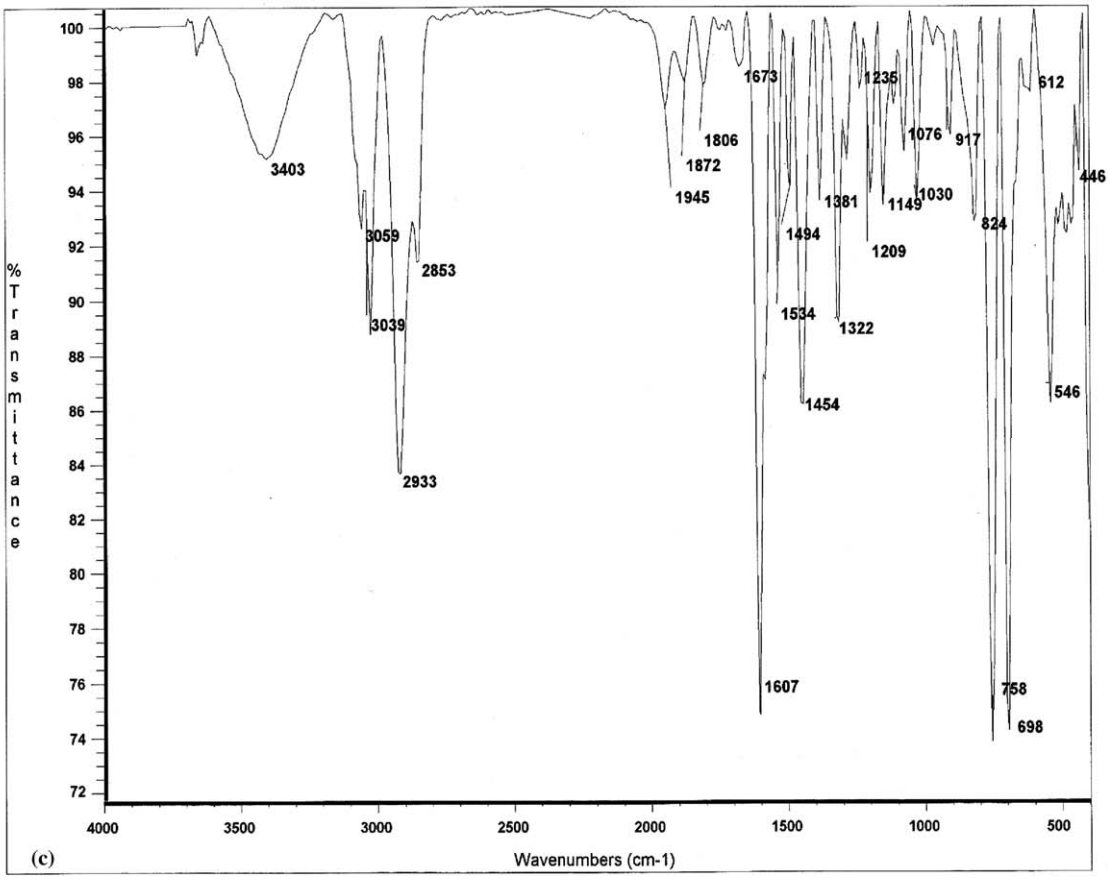

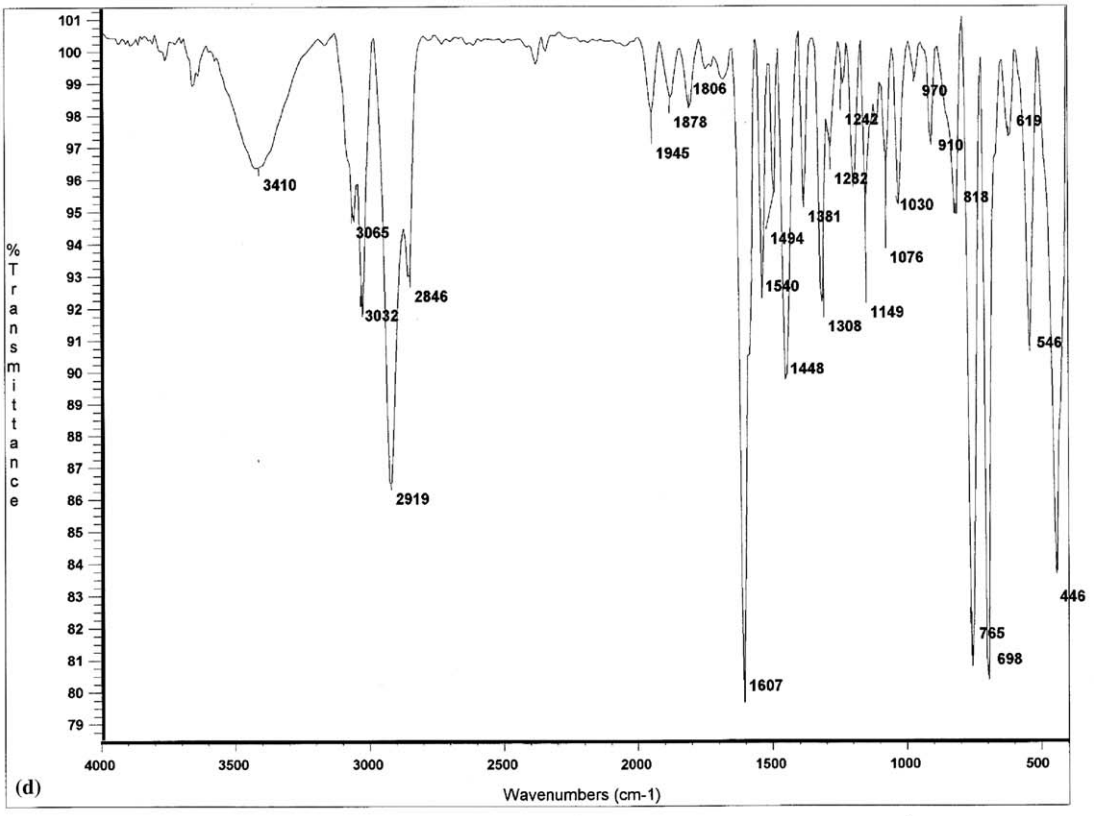

Fig. 2 (*continued*)

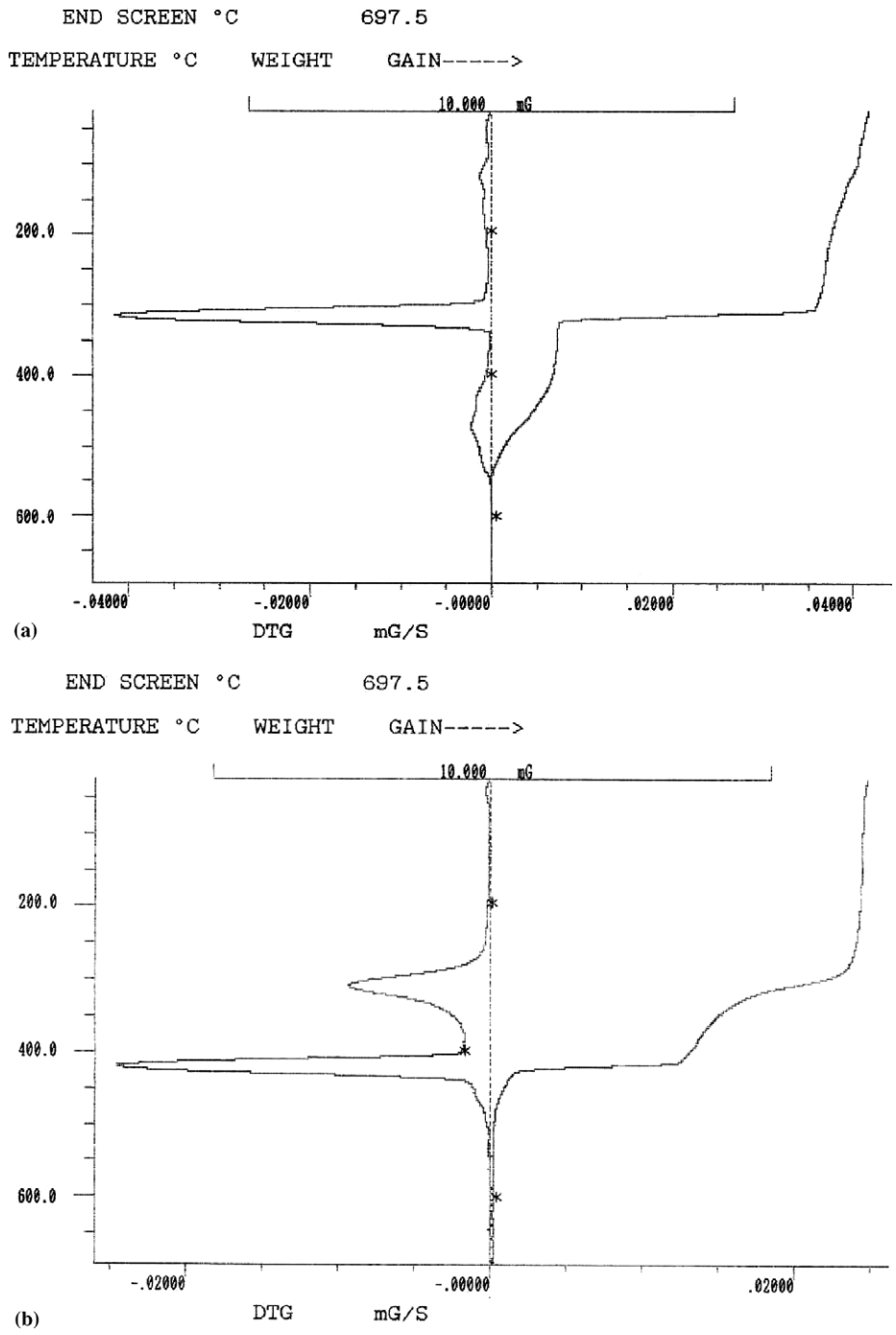

Fig. 3. TG–DTA curves of: (a) Mn(salophen)Cl; (b) Mn(salophen)Cl-PSP.

trans-stilbene proceed in a stereospecific manner with complete retention of configuration. In contrast, the epoxidation of *cis*-stilbene is associated with some loss of stereochemistry and affords 58% *cis*- and 23% *trans*-stilbene oxides, respectively. Apparently, formation of the thermodynamically more stable *trans*-stilbene oxide requires free rotation about the alkene C–C bond during some intermediate steps; such a rotation is expected to be more feasible using catalysts with less steric strain, as observed [42]. We used linear, cyclic and phenyl substituted olefins as substrates in this system. Electron-rich cyclic olefins are more active than the electron-poor terminal olefins. This reflects the electrophilic nature of oxygen transfer from the manganese-oxo intermediate to the olefinic double bond. This catalytic system shows a good activity in the epoxidation of linear alkenes such as 1-hexene and 1-dodecene. The Mn(salophen)Cl-PSP/$NaIO_4$ catalytic system exhibits good regioselectivity in the epoxidation of (*R*)-(+)-limonene. The ratio among 1,2- and 8,9-epoxide was found to be 2.4:1.

In the case of α-pinene, the major product is α-pinene oxide (93%), and allylic oxidation products, Verbenone

Table 1
The effect of oxidant on the epoxidation of cyclooctene catalyzed by Mn(salophen)Cl-PSP at room temperature[a]

Oxidant	Solvent	Epoxide yield (%) after 2.5 h[b]
$NaIO_4$	CH_3CN/H_2O	98
Oxone ($KHSO_5$)	CH_3CN/H_2O	88
H_2O_2	CH_3CN	42
H_2O_2/urea	CH_3CN	26
NaOCl	CH_3CN	47
tert-BuOOH	CH_3CN	21
Bu_4NIO_4	CH_3CN	49

[a] Cyclooctene (0.5 mmol), oxidant (1 mmol), catalyst (0.054 mmol), CH_3CN (5 ml), H_2O (2.5 ml).
[b] GLC yield based on starting cyclooctene.

Table 2
The effect of solvent on the epoxidation of cyclooctene with $NaIO_4$ catalyzed by Mn(salophen)Cl-PSP at room temperature[a]

Solvent	Epoxide yield (%) after 2.5 h[b]
CH_3CN/H_2O	98
CH_3COCH_3/H_2O	88
CH_3OH/H_2O	61
CH_3CH_2OH/H_2O	57
$CHCl_3/H_2O$	39
CH_2Cl_2/H_2O	35
CCl_4/H_2O	17

[a] Cyclooctene (0.5 mmol), $NaIO_4$ (1 mmol), catalyst (0.054 mmol), CH_3CN (5 ml), H_2O (2.5 ml).
[b] GLC yield based on starting cyclooctene.

Table 3
Epoxidation of alkenes with $NaIO_4$ catalyzed by Mn(salophen)Cl and Mn(salophen)Cl-PSP

Entry	Alkene	Conversion (%)[a]/time (h)		Epoxide yield (%)[a]	
		Heterogeneous	Homogeneous	Heterogeneous	Homogeneous
1		98/2.5	92/0.5	98	92
2		99[b]/2.5	91[b]/0.5	91	75
3	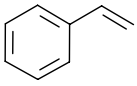	96[c]/2.5	75[c]/0.5	92	60
4	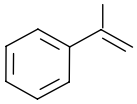	99[d]/2.5	92[d]/0.5	88	74
5	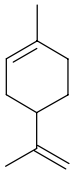	95/2.5	83/0.5	67 (1,2-epoxide)[e] 28 (8,9-epoxide)[e]	55 (1,2-epoxide)[e] 28 (8,9-epoxide)[e]
6	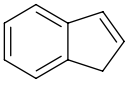	95/2.5	79/0.5	95	79
7	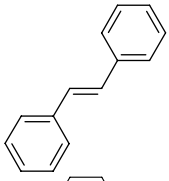	71/2.5	41/0.5	71 (*trans*-epoxide)[e]	41 (*trans*-epoxide)[e]
8	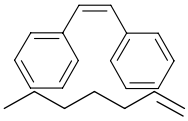	81/2.5	58/0.5	58 (*cis*-epoxide)[e] 23 (*trans*-epoxide)[e]	36 (*cis*-epoxide)[e] 22 (*trans*-epoxide)[e]
9	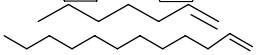	85/3	29/0.7	85	29
10		64/3	18/0.7	64	18
11	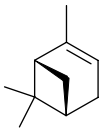	93[f]/2.5	75[f]/0.5	88	66

[a] GLC yield based on starting alkene.
[b] The by-product is 8% allylic ketone for the heterogeneous system and 16% for the homogeneous system.
[c] The by-product is 4% benzaldehyde for the heterogeneous system and 15% for the homogeneous system.
[d] The by-product is acetophenone.
[e] Both ^{1}HNMR and GLC data approved the reported yields.
[f] The by-products are 7% verbenone and 3% verbenol for the heterogeneous system and 3% verbenone and 2% verbenol for the homogeneous system.

(which is used as a building block of taxol) and Verbenol, were produced as minor products (Scheme 2).

A blank experiment in the presence of oxidant and using the same experimental conditions in the absence of catalyst was also investigated in the epoxidation of cyclooctene. The obtained results showed that $NaIO_4$ has poor ability to oxidize the cyclooctene. Also, no cyclooctene oxide was detected in the absence of oxidant in the reaction mixture.

The ability of aqueous manganese(II) salts, which was previously reported in the alkene epoxidation with H_2O_2 [43], was also investigated in the epoxidation of cyclooctene. The results indicated that these salts were unable to catalyze the epoxidation of cyclooctene with sodium periodate.

The polystyrene-bound 1,4-phenylenediamine modified with $Mn(II)ClO_4$ was also tested for its activity in the epoxidation of cyclooctene with $NaIO_4$. The amount of cyclooctene oxide after 6 h was 13%.

2.6. Oxidation of alkanes with $NaIO_4$ catalyzed by Mn(salophen)Cl-PSP

Direct oxidation of hydrocarbons is also one of the typical reactions of cytochrome P-450 [3]. The catalytic oxidation of alkanes with oxygen sources under mild conditions is an especially rewarding goal, since direct functionalization of inactivated C–H bonds in saturated hydrocarbons usually requires drastic conditions such as high pressure and high temperature. As shown in Table 4, we have found that the supported Mn(salophen)Cl is an efficient catalyst for the biomimetic functionalization of saturated hydrocarbons. Over oxidation of the alkane, the hydroxylation product is highly dependent on the nature of the hydrocarbon itself. Cyclooctane, cyclohexane, 1,2,3,4-tetrahydronaphthalene and adamantane were converted in high yields to their corresponding alcohols and ketones. In

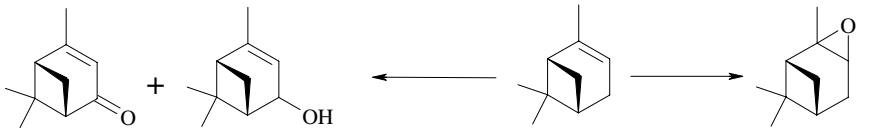

Verbenone Verbenol α-Pinene α-Pinene oxide

Scheme 2.

Table 4
Hydroxylation of alkanes with $NaIO_4$ catalyzed by Mn(salophen)Cl and Mn(salophen)Cl-PSP

Entry	Alkane	Conversion (%)[a]/time (h)		Ketone (%)[a]		Alcohol (%)[a]	
		Heterogeneous	Homogeneous	Heterogeneous	Homogeneous	Heterogeneous	Homogeneous
1		67/3	38/0.7	32	20	35	18
2		41/3	16/0.7	31	13	10	3
3	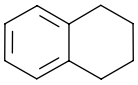	93[b]/3	60[b]/0.7	82	51	11	9
4	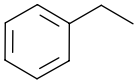	56[c]/3	18[c]/0.7	56	18		
5	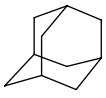	87/3	48/0.7	37	36	50	12
6	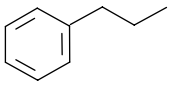	58[d]/3	21[d]/0.7	58	21		
7	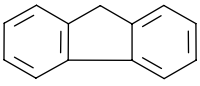	83/3	39/0.7	83	39		

[a] GLC yield based on starting alkane.
[b] Only the α-position was oxidized.
[c] The product is acetophenone.
[d] The product is ethylphenyl ketone.

contrast, ethylbenzene, propylbenzene and fluorene only produced the corresponding ketones. In the case of adamantane, 1-adamantanol and 2-adamantanone were produced in the reaction mixture.

2.7. Catalyst reuse and stability

To assess the long-term stability and reusability of [Mn(salophen)Cl-PSP], cyclooctene was used as a model substrate, and recycling experiments were carried out with a single sample of the catalyst. After each experiment, the catalyst was separated from the reaction mixture by simple filtration, washed with the methanol and dried carefully before using it in the subsequent run. After the use of the catalyst four consecutive times, the epoxide yields were 94%. No manganese was detectable in the filtrates by atomic absorption spectrometry (Table 5).

The nature of the recovered catalyst has been followed by IR. The results indicated that after reusing the catalyst several times, it showed no change in its IR spectra (Fig. 2c).

2.8. Comparison of homogeneous Mn(salophen)Cl and heterogeneous Mn(salophen)Cl-PSI in alkene epoxidation and alkane hydroxylation with sodium periodate

In order to demonstrate the effect of supporting on the catalytic activity of manganese (III) salophen in the alkene epoxidation and alkane hydroxylation with sodium periodate, we repeated all reactions under the same reaction conditions and with the same amounts of catalyst, substrate, $NaIO_4$ and imidazole as axial ligand in a CH_3CN:H_2O mixture. The obtained results are summarized in Tables 3 and 4 for alkene epoxidation and alkane hydroxylation, respectively.

In the alkene epoxidation, the production of by-products in the heterogenized system decreased in comparison with the homogeneous system. In the case of *R*-(+)-limonene, the ratio among 1,2- and 8,9-epoxide increased from 1.96 to 2.4. While, *cis–trans* isomerization decreased in the case of *cis*-stilbene, in which the ratio of *cis*/*trans* stilbene oxide increased from 1.64 to 2.52. The Mn(salophen)-PSP/$NaIO_4$ catalytic system showed a higher catalytic activity in the oxidation of linear alkenes (Table 3, entries 9 and 10).

Table 5
The results of [Mn(salophen)Cl-PSP] catalyst recovery and the manganese leached in the epoxidation of cyclooctene with sodium periodate

Run	Conversion (%)[a]	Epoxide yield (%)[a]	Mn leached (%)[b]
1	98	98	0
2	97	97	0
3	96	96	0
4	94	94	0

[a] GLC yield based on starting alkene.
[b] Determined by atomic absorption spectroscopy.

2.9. Conclusion

We have demonstrated that the supported manganese(III) salophen complex catalyst is featured by: (i) easy preparation and handling of the tethered catalyst; (ii) no need of axial ligand in the catalytic system; (iii) facile and effective recovery and recycling; (iv) catalyst efficiency comparable to that observed in the homogeneous phase.

3. Experimental

All materials were commercial reagent grade. Chloromethylated polystyrene (4–5% Cl and 2% cross-linked with divinylbenzene) was a product of Merck. Alkene, alkane and alkylaromatic compounds were obtained from Merck or Fluka. All of these compounds were passed through a column containing active alumina to remove peroxidic impurities.

3.1. Preparation of the salicylaldehyde-o-phenylenediimine(salophen) ligand

The Schiff base ligand was prepared by the standard procedure of refluxing ethanolic solutions of the corresponding diamine and salicylaldehyde derivative in a 1:2 molar ratio [44].

A stoichiometric amount of salicylaldehyde (2.44 g) in ethanol (25 mL) was added drop by drop to an alcoholic solution of *ortho*-phenylenediamine (1.08 g in 25 mL ethanol). The mixture was refluxed for 3 h and a bright yellow precipitate was separated by filtration, washed and dried in vacuum. It was then recrystallized from ethanol to yield the salophen ligand (2.8 g).

3.2. Preparation of Mn(III) salophen

The salophen ligand (1.58 g) was dissolved in hot absolute ethanol. Solid hydrated manganese(II) acetate (2.45 g) was added and the solution was refluxed for 1 h. Approximately, three equivalents of lithium chloride was then added, and the mixture was heated to reflux for an additional 0.5 h. Cooling the mixture to 273 K afforded the Mn(III) complex as dark brown crystals. Elemental analysis confirmed the obtained complex; [Mn(salophen)Cl], [*N*,*N*′-bis(salicylidine)-*o*-phenylenediaminato]manganese(III) chloride: UV–Vis, λ_{max}/nm: 285, 296, 330, ~430 (sh); FT-IR, ν/cm^{-1}: 1609 (vs), 1572 (vs), 1535 (vs), 1481 (m), 1445 (m), 1381 (m), 1313 (m), 1206 (m), 1152 (m), 888 (w), 816 (m), 756 (s), 657 (m), 548 (m) and 440 (w).

3.3. Preparation of polymer-supported manganese salophen

To a solution of 0.4 g manganese(III) salophen in acetonitrile (100 mL) was added chloromethylated polystyrene-bound 1,4-phenylenediamine (3 g). The mixture was vigorously stirred at 80 °C for 24 h. After cooling to room temperature, the brown resin was collected by filtration, washed thoroughly with acetonitrile, methanol and diethyl

ether, successively, and dried in vacuum at room temperature for several hours. The content of mangenese(III) salophen on the polymer support, which was calculated from the manganese content of the heterogenized catalyst, was determined by NAA.

3.4. Physico-chemical measurements

Diffuse reflectance spectra were recorded on a Shimadzu UV-265 instrument using optical grade $BaSO_4$ as reference. Thermogravimetric analysis of the catalyst was carried out on a Mettler TA4000 instrument. FT-IR spectra were obtained as potassium bromide pellets in the range 400–4000 cm^{-1} with a Nicolet-Impact 400D instrument. Gas chromatography experiments (GC) were performed with a Shimadzu GC-16A instrument using a 2 m column peaked with silicon DC-200 or Carbowax 20 m. ^1H NMR spectra were recorded on a Bruker-Arance AQS 300 MHz spectrometer.

3.5. General procedure for catalytic oxidation reactions catalyzed by [Mn(salophen)Cl-PSP]

All of the reactions were carried out at room temperature under air in a 25 ml flask equipped with a magnetic stirrer bar. A solution of $NaIO_4$ (1 mmol) in H_2O (2.5 ml) was added to a mixture of alkene or alkane (0.5 mmol), and Mn(salophen)-PSP (0.054 mmol) in CH_3CN (5 ml). The progress of the reaction was monitored by GLC. The reaction mixture was diluted with CH_2Cl_2 (20 ml) and filtered. The resin was thoroughly washed with CH_2Cl_2 and combined washings and filtrates were purified on silica-gel plates or a silica-gel column. IR and ^1HNMR spectral data confirmed the identities of the products. Blank experiments with each oxidant and using the same experimental conditions but without the catalyst were also performed.

3.6. General procedure for catalytic epoxidation of alkenes and hydroxylation of alkanes with sodium periodate catalyzed by Mn(salophen)Cl

To a 25 ml round-bottom flask containing alkene or alkane (0.5 mmol), Mn(salophen)Cl (0.05 mmol) and imidazole (0.05 mmol) in CH_3CN (5 ml) were added a solution of $NaIO_4$ (1 mmol) in H_2O (2.5 ml). The reaction progress was monitored by GLC. At the end of the reaction, the reaction mixture was diluted with water (20 ml) and the products and substrate were extracted with CH_2Cl_2 (2×10 ml). The extracts were purified on silica-gel plates or a silica-gel column. IR and ^1HNMR spectral data confirmed the identities of the products.

Acknowledgement

The support of this work by Isfahan University is acknowledged.

References

[1] W. Nam, S.-E. Park, I. K Lim, M.H. Lim, J. Hong, J. Kim, J. Am. Chem. Soc. 125 (2003) 14674.
[2] F.P. Guengerich, J. Biol. Chem. 266 (1991) 10019.
[3] P.R. Ortiz de Montellano, Cytochrome P-450, Structure, Mechanism and Biochemistry, 2nd ed., Plenum Press, New York, 1995.
[4] (a) T. Katsuki, Coord. Chem. Rev. 140 (1995) 189;
(b) T. Katsuki, J. Mol. Catal. A: Chem. 113 (1996) 87.
[5] C.T. Dalton, K.M. Ryan, V.M. Wall, C. Bousquet, D.G. Gilheany, Top. Catal. 5 (1998) 75.
[6] L. Canalai, D.C. Sherrington, Chem. Soc. Rev. 72 (1999) 603.
[7] M. Bandini, P.G. Gozzi, A. Umani-Ronchi, Chem. Commun. (2002) 919.
[8] H.-V. Blaser, Chem. Commun. (2003) 293.
[9] B.S. Lane, K. Burgess, Chem. Rev. 103 (2003) 2457.
[10] M. Costas, M.P. Mehn, M.P. Jensen, L. Que Jr., Chem. Rev. 104 (2004) 939.
[11] E.F. Di Mauro, A. Mamai, M.C. Kozlowski, Organometallics 22 (2003) 850.
[12] M. Palucki, G.J. McCormick, E.N. Jacobsen, Tetrahedron Lett. 36 (1995) 5457.
[13] R. Irie, N. Hosoya, T. Katasuki, Synlett (1994) 255.
[14] T. Linker, Angew. Chem., Int. Ed. Engl. 38 (1997) 2060.
[15] T. Hamada, H. Fukuda, T. Katsuki, Tetrahedron 52 (1996) 515.
[16] V. Mirkhani, S. Tangestaninejad, M. Moghadam, M. Moghbel, Bioorg. Med. Chem. 12 (2004) 903.
[17] V. Mirkhani, S. Tangestaninejad, M. Moghadam, M. Moghbel, Bioorg. Med. Chem. 12 (2004) 4673.
[18] R. Irie, T. Hashihayata, T. Katasuki, M. Akita, M. Moro-oka, Chem. Lett. (1998) 1041.
[19] T. Yamada, K. Imagawa, T. Nagata, T. Mukaiyama, Bull. Chem. Soc. Jpn. (1994) 67.
[20] J.P. Collman, V.J. Lee, C.J. Kellen-Yuen, X. Zhang, J.A. Brauman, J. Am. Chem. 117 (1995) 692.
[21] K. Srinivasan, P. Michaud, J.K. Kochi, J. Am. Chem. Soc. 108 (1986) 2309.
[22] J.M. Fraile, J.I. Garcia, J. Massam, J.A. Mayoral, J. Mol. Catal. A: Chem. 136 (1998) 47.
[23] M.R. Maurya, S.J. Titinchi, S. Chand, J. Mol. Catal. A: Chem. 377 (2002) 1.
[24] A. Heckel, D. Seebach, Helv. Chem. Acta 85 (2002) 913.
[25] D.A. Annis, E.N. Jacobsen, J. Am. Chem. Soc. 121 (1999) 4147.
[26] H. Zhang, S. Xiang, C. Li, Chem. Commun. (2005) 1209.
[27] S. Xiang, Y. Zhang, Q. Xin, C. Li, Chem. Commun. (2002) 2696.
[28] B.M. Choudary, M.L. Kantam, B. Bharathi, P. Sreekanth, F. Figueras, J. Mol. Catal. A: Chem. 159 (2000) 417.
[29] C. Baleizao, B. Gigante, H. Garcia, A. Corma, J. Catal. 215 (2003) 207.
[30] G.-J. Kim, S.-H. Kim, Catal. Lett. 57 (1999) 139.
[31] B.B. De, B.B. Lohray, S. Sivaram, P.K. Dhal, Tetrahedron: Asymm. 6 (1995) 2105.
[32] Y.R. de Miguel, J. Chem. Soc., Perkin Trans. 1 (2000) 4213.
[33] G. Kim, D.W. Park, Catal. Today 63 (2000) 537.
[34] F. Minutolo, D. Pini, A. Petri, P. Salvador, Tetrahedron: Asymm. 7 (1996) 2293.
[35] L. Canali, D.C. Sherrington, H. Deleuze, React. Funct. Polym. 40 (1999) 155.
[36] S.T. Regar, K.D. Janda, J. Am. Chem. Soc. 122 (2000) 6929.
[37] R.I. Kureshy, N.H. Khan, S.H.R. Abdi, P. Lyer, React. Funct. Polym. 34 (1997) 153.
[38] P.J. Collman, L. Zeng, I. Brauman, J. Inorg. Chem. 43 (2004) 2672.
[39] Z. Groos, S. Ini, J. Org. Chem. 62 (1997) 5514.
[40] (a) D.T. Gokak, B.V. Kamath, R.N. Ram, J. Appl. Polym. Sci. 35 (1988) 1528;

(b) M.L. Linares, N. Sanchez, R. Alajarin, J.J. Vaquero, J. Alvarez-Builla, Synthesis 3 (2001) 382.
[41] V.B. Valodkar, G.L. Tembe, M. Ravindranathan, R.N. Ram, H.S. Rama, J. Mol. Catal. A: Chem. 208 (2004) 21.
[42] D. Ostavic, T.C. Bruice, J. Am. Chem. Soc. 111 (1989) 6511.
[43] B.S. Lane, M. Vogt, V.J. DeRose, K. Burgess, J. Am. Chem. Soc. 124 (2002) 11946.
[44] (a) D. Chan, A.E. Martell, Inorg. Chem. 26 (1987) 1026;
(b) B.M. Trivedi, P.K. Bhattacharya, P.A. Ganeshpure, S. Satish, J. Mol. Catal. 75 (1992) 109.

result, as the biological chemistry of mercury is dominated by coordination to cysteine [13]. The preference of Hg for sulfur donor sites, due to its soft nature, is well known. In mercury thiolates, apart from the Hg–S bond, the possibility of a secondary mercury(II)–sulfur interaction has also been reported [14–16], which makes it difficult to anticipate the structures of such complexes.

2. Experimental

The C and H analyses were carried out with a Perkin–Elmer elemental analyzer 240 C. The ^{1}H and $^{13}C\{^{1}H\}$ NMR spectra were recorded on a Bruker Spectrospin DPX-300 NMR spectrometer at 300.13 and 75.47 MHz, respectively. $^{31}P\{^{1}H\}$ NMR spectra were recorded at 121.49 MHz using H_3PO_4 as an external indicator. IR spectra in the range 4000–250 cm^{-1} were recorded on a Nicolet Protége 460 FT-IR spectrometer as KBr pellets. The conductance measurements were made in acetonitrile (concentration ~1 mM) using an ORION conductivity meter model 162. The molecular weights (concentration ~5 mM) in chloroform were determined with a Knauer vapour pressure osmometer model A0280. The melting points determined in open capillary are reported as such. The Ph_2PCl and 2-chloroethyl ethyl sulfide were obtained from Aldrich (USA). $[RuCl_2(p\text{-cymene})]_2$ was synthesized by the reported method [17].

2.1. Synthesis of 1-(ethylthio)-2-(diphenylphosphino) ethane (*L*)

Chlorodiphenylphosphine solution (5.0 cm^3 of 1.0 M solution in THF) was added to lithium (0.63 g, 5.0 mmol) in dry THF (25 cm^3) at room temperature in a Schlenk flask. The mixture was stirred until the solution became dark red in colour, which indicated the formation of lithium diphenylphosphide. The PPh_2Li was then filtered and transferred to a Schlenk tube under nitrogen atmosphere and cooled to −78 °C. 2-Chloroethyl ethyl sulfide (0.62 g, 5.0 mmol) was added to it with constant stirring. The mixture was allowed to come to room temperature over ~12 h, after which all the THF was evaporated off from the mixture on a rotary evaporator and the residue was dissolved in deoxygenated dichloromethane (30 cm^3). The solution was again concentrated to ~10 cm^3on a rotary evaporator and mixed with hexane (30 cm^3). The resulting solid was then recrystallized with a dichloromethane–methanol mixture (1:1) to obtain **L** as a white crystalline solid. Yield ~85%; m.p. 45 °C. *Anal.* Calc.: C, 70.04, H, 6.98. Found: C, 70.01; H, 6.30%. ^{1}H NMR (δ vs TMS, $CDCl_3$, 25 °C): 1.17–1.22 (t, 3H, H_1), 2.30–2.35 (m, 2H, H_4), 2.49–2.62 (m, 4H, H_3 and H_2), 7.32–7.47 (m, 10H, Ar-H of PPh_2).

2.2. Synthesis of [CuBr(*L*)]$_2$ (*1*)

To a solution of **L** (0.13 g, 0.50 mmol) made in 10 cm^3 of chloroform was added Cu_2Br_2 (0.07 g, 0.50 mmol) dissolved in 10 cm^3 of nitromethane under nitrogen atmosphere. The resulting mixture was stirred under an inert nitrogen atmosphere for 2 h at room temperature. Thereafter, the solution was filtered through celite. The clear filtrate was concentrated to ~10 cm^3 on a rotary evaporator and mixed with hexane (20 cm^3). The resulting white solid was filtered, washed with hexane (3×20 cm^3) and dried in vacuo and stored under inert conditions. Complex **1** was recrystallized from chloroform–hexane mixture (1:1). Yield: 75%; m.p.: 78 °C (d). *Anal.* Calc.: C, 38.79, H, 3.81. Found: C, 38.72, H, 3.01%. Λ_m: 6.50 Ω^{-1} cm^2 mol^{-1}; ^{1}H NMR (δ vs TMS, $CDCl_3$, 25 °C) 1.21–1.26 (t, 3H, H_1), 2.58–2.60 (m, 2H, H_4), 2.69–2.76 (m, 2H, H_2), 2.83–2.88 (m, 2H, H_3), 7.30–7.47 (m, 10H, Ar-H of –PPh_2); $^{13}C\{^{1}H\}$ NMR (δ vs TMS, 25 °C), 13.5 (C_1), 26.5, 26.7 (C_4), 29.5, 29.7 (C_2), 30.1 (C_3), 128.7, 128.8, 130.8, 131.2, 132.5, 133.1, 133.3 (Ar-C of PPh_2).

2.3. Synthesis of [HgBr$_2$(*L*)] (*2*)

$HgBr_2$ (0.20 g, 0.55 mmol) was dissolved in acetone (20 cm^3) and mixed with a solution of **L** (0.15 g, 0.55 mmol) in chloroform (20 cm^3). The resulting mixture was stirred at room temperature until the ligand **L** was consumed (as monitored by TLC). The solvent was removed from the mixture on a rotary evaporator. The resulting residue was dissolved in 20 cm^3 of chloroform and filtered through celite. The filtrate was concentrated to 10 cm^3 on a rotary evaporator and mixed with 20 cm^3 of hexane. The white complex **2** was filtered, dried in vacuo and recrystallized from chloroform–hexane (1:1) mixture. Yield: 80%; m.p.: 135 °C. *Anal.* Calc.: C, 30.26, H, 2.29. Found: C, 30.04, H, 2.66%. Molecular weight; found: 659.0, calculated: 634.39; Λ_m: 4.60 Ω^{-1} cm^2 mol^{-1}; ^{1}H NMR (δ vs TMS, $CDCl_3$, 25 °C), 1.27–1.32 (t, 3H, H_1), 2.66–3.11 (m, 6H, H_4, H_3 and H_2), 7.59–7.80 (m, 10H, Ar-H of –PPh_2); $^{13}C\{^{1}H\}$ NMR (δ vs TMS, 25 °C), 13.8 (C_1), 26.3 (C_4), 27.4 (C_2), 30.1 (C_3), 129.9, 130.00, 132.9, 33.26, 134.00 (Ar-C of PPh_2).

2.4. Synthesis of [Ru(p-cymene)Cl$_2$(*L*)] (*3*)

$[RuCl_2(p\text{-cymene})]_2$ (0.61 g, 1.0 mmol) was taken in 20 cm^3 of dichloromethane and a solution of **L** (0.54 g, 2.0 mmol) in 10 cm^3 of dichloromethane was added to it. The mixture was stirred for 2 h at room temperature. The solvent was completely removed on a rotary evaporator under reduced pressure. The residue obtained was dissolved in dichloromethane (5 cm^3) and mixed with hexane (30 cm^3). The resulting red precipitate (**3**) was filtered, washed with hexane (3×20 cm^3) and dried in vacuo. It was recrystallized from dichloromethane–hexane (1:1) mixture. Yield: 80%; m.p.: 89 °C (d). *Anal.* Calc.: C, 53.78, H, 5.68. Found: C, 52.71, H, 5.25%. Molecular weight; found: 620.0, calculated: 580.07; Λ_m: 3.80 Ω^{-1} cm^2 mol^{-1}; ^{1}H NMR (δ vs TMS, $CDCl_3$, 25 °C), 1.22–1.33 (m, 9H, $H_1 + CH_3$ of *i*-Pr), 2.15 (s, 3H, CH_3 of *p*-cymene), 2.29

(m, 1H, CH of *p*-cymene), 2.81–3.06 (m, 6H, H_4, H_3 and H_2), 7.37–7.72 (m, 10H, Ar-H of $-PPh_2$); $^{13}C\{^1H\}$ NMR (δ vs TMS, 25 °C), 12.09 (C_1), 17.11 (CH_3 of *i*-Pr), 20.1 (C_4), 22.3 (CH_3 of *p*-cymene), 28.8 (C_2), 32.5 (CH of *p*-cymene), 33.1 (C_3), 87.9, 91.0 (Ar-C of *p*-cymene), 127.0, 128.3 129.9, 130.3, 132.2, 137.0 (Ar-C of PPh_2).

2.5. X-ray crystallography

The X-ray data for **2** were collected (at 120 K) on an Enraf Nonius Kappa CCD area detector diffractometer, with ϕ and ω scans chosen to give a complete asymmetric unit. Cell refinement [18,19] corresponds to an orthorhombic cell whose dimensions are given in Table 1, along with other experimental parameters. An absorption correction was applied [18,19]. The structure was solved by direct methods [20] and refined using the WinGX version [21] of SHELX-97 [22]. Hydrogen atoms were included in idealized positions with isotropic thermal parameters set at 1.2 times that of the carbon atom to which they were attached. Non-hydrogen atoms were treated anisotropically. The final cycle of full-matrix least-squares refinement for **2** was based on 4199 observed reflections (3243 for $F^2 > 4\sigma(F^2)$) and 191 variable parameters and converged (largest parameter shift was 0.001 times its esd). The molecular structure of **2** is displayed as an ORTEP diagram in Fig. 1. Its selected bond lengths and bond angles are given in Table 2.

Table 1
Crystal data and structure refinement for **2**

Empirical formula	$C_{16}H_{19}PSBr_2Hg$
Formula weight	634.75
Temperature (K)	120(2)
Wavelength (Å)	0.71073
Crystal system	orthorhombic
Space group	*Pbca*
a (Å)	13.567(1)
b (Å)	14.859(1)
c (Å)	18.095(1)
V (Å^3)	3647.6(6)
Z	8
D_{calc} (g/cm^3)	2.312
Absorption coefficient (mm^{-1})	13.014
F(000)	2368
Crystal size (mm^3)	$0.15 \times 0.08 \times 0.02$
θ Range for data collection (°)	3.30–27.53.
Index ranges	$-17 \leqslant h \leqslant 17$, $-19 \leqslant k \leqslant 19$, $-23 \leqslant l \leqslant 23$
Reflections collected	29610
Independent reflections (R_{int})	4199 (0.0602)
Maximum and minimum transmission	0.7808 and 0.2456
Refinement method	full-matrix least-squares on F^2
Data/restraints/parameters	4199/0/191
Goodness-of-fit on F^2	1.036
Final *R* indices [$F^2 > 4\sigma(F^2)$]	$R_1 = 0.0331$, $wR_2 = 0.0649$
R indices (all data)	$R_1 = 0.0526$, $wR_2 = 0.0711$
Largest difference in peak and hole (e Å^{-3})	1.001 and −1.162

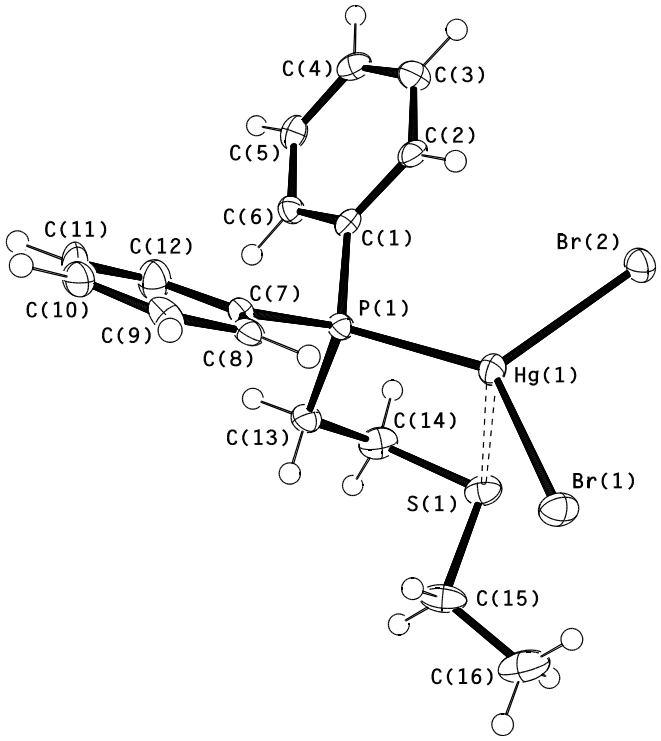

Fig. 1. Molecular structure of [$HgBr_2$(**L**)] (**2**).

Table 2
Selected bond lengths (Å) and angles (°) for **2**

Hg(1)–Br(1)	2.5152(6)	Hg(1)–Br(2)	2.5952(6)
Hg(1)–P(1)	2.415(1)	Hg(1)–S(1)	3.063(1)
S(1)–C(14)	1.811(5)	S(1)–C(15)	1.811(6)
P(1)–C(1)	1.809(5)	P(1)–C(7)	1.810(5)
P(1)–C(13)	1.825(5)		
Br(1)–Hg(1)–P(1)	135.52(4)	Br(2)–Hg(1)–P(1)	119.48(4)
Br(1)–Hg(1)–Br(2)	104.98(2)	P(1)–Hg(1)–S(1)	78.78(4)
Br(1)–Hg(1)–S(1)	92.22(3)	Br(2)–Hg(1)–S(1)	101.23(3)
Hg (1)–P(1)–C(1)	112.6(2)	Hg(1)–P(1)–C(7)	115.3(2)
Hg(1)–P(1)–C(13)	108.5(2)	C(14)–S(1)–C(15)	100.6(3)
C(1)–P(1)–C(7)	107.3(2)	C(1)–P(1)–C(13)	107.4(2)
C(7)–P(1)–C(13)	105.3(2)		
C(7)–C(8)–C(9)	120.0(5)	C(8)–C(9)–C(10)	120.4(5)
C(9)–C(10)–C(11)	120.0(5)	C(10)–C(11)–C(12)	120.6(5)
C(11)–C(12)–C(7)	119.6(5)	C(12)–C(7)–C(8)	119.3(4)

3. Results and discussion

The ligand **L**, obtained as white crystalline solid, is unstable and is moisture and air sensitive. It can be stored at low temperature ~5 °C in dry nitrogen atmosphere without appreciable decomposition for 2–3 months easily. It is soluble in common organic solvents such as chloroform, dichloromethane and acetone, but is insoluble in hexane. The crystals of **2** are not air and moisture sensitive, but **1** and **3** require storing in a refrigerator to avoid their decay. The complexes are soluble in common organic solvents such as chloroform, dichloromethane and acetone, but are insoluble in hexane. The molar conductance values Λ_m of the complexes **1**–**3** in acetonitrile at ~1 mM

concentration have been found to be between 3.8 and 6.5 Ω^{-1} cm^2 mol^{-1}, which are much lower than the values expected for a 1:1 electrolyte. The molecular weights of complexes **2**–**3**, determined in chloroform by the vapour pressure osmometric method, were found to be very close to the values calculated from their molecular formulae. This indicates that there is no appreciable dissociation of these complexes in solution. In the IR spectrum of **1**, the band at 248 cm^{-1} suggests the presence of bridging Cu–Br unit. The IR spectrum of **3** has ν_{sym}(Ru–Cl) and ν_{asym}(Ru–Cl) at 326 and 294 cm^{-1}, respectively [23,24]. In the ^{1}H NMR spectrum of **L**, signals of H_2 and H_3 protons are merged together and appear as a multiplet, whereas the signal of H_4 appears shielded in comparison to those of H_2 and H_3. In the ^{1}H NMR spectrum of **1**, the signals corresponding to H_2 and H_3 get separated and deshielding of the order of 0.2–0.3 ppm is found with respect to the corresponding signals of ligand **L**. The signal of H_4 appears deshielded by ~0.25 ppm in comparison to the corresponding signal of **L**. Signals for aromatic protons remain unchanged on the formation of **1**. In the ^{1}H NMR spectrum of **2**, signals corresponding to all –CH_2 protons merge at 2.66–3.11 ppm, showing deshielding of ~0.35–0.45 ppm. In the proton NMR spectrum of **3** also, signals of all the CH_2 protons are merged and the average deshielding was found to be ~0.5 ppm. The CH_3 signal of the ligand (**L**) appears to be merged with the CH_3 signal of the isopropyl group of the *p*-cymene ring in the ^{1}H NMR spectrum of **3**. No significant shift occurs in the aromatic protons.

In the carbon-13 NMR spectrum of **1**, the C_4 signal is deshielded by ~0.8 ppm as compared to that of free **L**. The signals for C_2 and C_1 appear to be deshielded by 1.9 and 1.6 ppm, respectively, with respect to the corresponding signals of free **L**. In the carbon-13 NMR spectrum of **2**, the C_4 signal appears deshielded by 0.68 ppm and the C_3 signal by 1.68 ppm in comparison to those of free **L**, whereas in the spectrum of **3**, the deshielding of the C_2 signal is ~1.2 ppm and the other signals do not undergo any significant change in their chemical shifts. The ^{31}P {^{1}H} NMR spectra of **L**, **1**, **2** and **3** all have a single peak at −17.0, 31.3, 20.16 and 28.9 ppm, respectively. The signals in the spectra of the complexes are deshielded with respect to that of the ligand. All these NMR data indicate that the interaction of **L** with Cu(I), Hg(II) and Ru(II) is through both phosphorous and sulfur. With sulfur it may be weak (secondary type), as found out in the case of **2** when its single crystal structure was determined. However, in the case of **1** and **3**, which did not give crystals suitable for X-ray diffraction, it could not be ascertained unequivocally.

3.1. Crystal structure

The molecular structure of **2** is shown in Fig. 1 and selected bond lengths and angles are given in Table 2. The ligand **L** coordinates through phosphorus only, resulting in a coordination number of three for Hg. The three coordination number for mercury is already known [25–28] and such examples include Hg arsine complexes [25]. The chemistry of Hg–phosphine complexes has been extensively studied by Bell et al. [30], including three coordinate Hg species containing phosphine ligands. However, **2** is the first example of a Hg–(P, S) ligand complex where Hg is three coordinated. The Hg(1)–P(1) bond length of 2.415(1) Å is consistent with the earlier reported values of 2.513(2) and 2.408(2)–2.437(2) Å [29,30]. The Hg(1)···S(1) bond distance [3.063(1)] is shorter than the sum of the van der Waal's radii (3.35 Å). The Hg(1)–Br(1) and Hg(1)–Br(2) bond lengths are 2.5152(6) and 2.5952(6) Å and these are consistent with our earlier observations [31] of 2.505(2)–2.700(2) Å, and 2.528(3) and 2.637(3) Å reported by Bell et al. [30]. The bond angles around Hg are in the range of 78.78(4)–135.52(4)°, with a Br(1)–Hg(1)–Br(2) angle of 104.98(2)° and P(1)–Hg(1)–S(1) angle of 78.78(4)°. However, the sum of the bond angles P(1)–Hg(1)–Br(1), P(1)–Hg(1)–Br(2) and Br(1)–Hg(1)–Br(2) is ≈360°. Therefore, the Hg, two Br and P atoms are coplanar and the geometry around Hg can be best described as essentially trigonal planar. There is a Hg···S secondary interaction in **2** and the S atom is nearly perpendicular to the plane of the three coordinate Hg-complex. In **2**, the C–C bond lengths and bond angles of all the phosphine rings were found to be normal.

4. Conclusion

A relatively simple method is reported for the synthesis of the (P, S) ligand 1-(ethylthio)-2-(diphenylphosphino) ethane (**L**). Its complexation with Cu(I), Hg(II) and organometallic species of Ru(II) have been explored. The single crystal structure of the Hg(II) complex has been determined. It is found to be a three coordinate species. The sum of the bond angles at Hg, viz. P(1)–Hg(1)–Br(1), P(1)–Hg(1)–Br(2) and Br(1)–Hg(1)–Br(2), is ≈360°, and consequently the geometry of Hg can be best described as trigonal planar. There exists a weak secondary interaction between Hg and the S donor site of the ligand [Hg(1)···S(1) bond distance 3.063(1) Å; sum of van der Waal's radii 3.35 Å].

5. Supplementary data

The CCDC No. 602402 contains the supplementary crystallographic data for **2**. These data can be obtained free of charge at www.ccdc.cam.ac.uk/conts/retrieving.html [or from the Cambridge Crystallographic Data Centre, 12 Union Road, Cambridge CB2 1EZ, UK; fax: (internat.) +44 1223 336 033; e-mail: deposit@ccdc.cam.ac.uk].

Acknowledgements

A.K.S. and G.S. thank the Department of Science and Technology (India) and Council of Scientific and Industrial Research, New Delhi (India) for financial support.

References

[1] P. Rigo, M. Bressan, M. Basato, Inorg. Chem. 18 (1979) 860.
[2] M. Bressan, F. Morandini, Inorg. Chim. Acta 77 (1983) L139.
[3] G.K. Anderson, R. Kumar, Inorg. Chem. 23 (1984) 4064.
[4] M. Bressan, L.D. Mas, F. Morandini, B. Prozzo, J. Organomet. Chem. 287 (1985) 275.
[5] A.D. Zotto, P. Rigo, J. Organomet. Chem. 315 (1986) 165.
[6] P. Rigo, M. Bressan, Inorg. Chem. 14 (1975) 1491.
[7] C. Bonuzzi, M. Bressan, F. Morandini, A. Morvillo, Inorg. Chim. Acta 154 (1988) 41.
[8] A.D. Zotto, P. Rigo, Inorg. Chim. Acta 147 (1988) 55.
[9] A.D. Zotto, A. Mezzetti, P. Rigo, Inorg. Chim. Acta 158 (1989) 151.
[10] A.D. Zotto, B.D. Ricca, E. Zangrando, P. Rigo, Inorg. Chim. Acta 261 (1997) 147.
[11] G.K. Anderson, R. Kumar, Inorg. Chim. Acta 97 (1985) L21.
[12] G.K. Anderson, R. Kumar, J. Organomet. Chem. 342 (1988) 263.
[13] A.L. Presa, M. Capdevila, P.G. Durate, Eur. J. Biochem. 271 (2004) 4872.
[14] I.G. Dance, Polyhedron 5 (1986) 1037.
[15] J.G. Wright, M.J. Natan, F.M. Macdonell, D.M. Ralston, T.V. O'Halloran, Prog. Inorg. Chem. 38 (1990) 323.
[16] N. Govindaswamy, J. Roy, M. Millar, S.A. Koch, Inorg. Chem. 26 (1992) 5343.
[17] M.A. Bennett, T.N. Huang, T.W. Matheson, A.K. Smith, Inorg. Synth. 21 (1982) 74.
[18] Z. Otwinowski, W. Minor, DENZO, in: C.W. CarterJr., R.M. Sweet (Eds.), Methods in Enzymology, Macromolecular Crystallography: Part A, vol. 276, Academic Press, York, 1997, p. 307.
[19] G.M. Sheldrick, SADABS V2.10, 2003.
[20] G.M. Sheldrick, Acta Crystallogr., Sect. A 46 (1990) 467.
[21] L.J. Farrugia, J. Appl. Crystallogr. 32 (1999) 837.
[22] G.M. Sheldrick, SHELXL-97, University of Gottingen, Gottingen, Germany.
[23] P. Govindaswamy, Y.A. Mozharivskyz, M.R. Kollipara, Polyhedron 23 (2004) 3115.
[24] R.S. Bates, M.J. Begley, A.H. Wright, Polyhedron 9 (1990) 1113.
[25] (a) B.M. Gatehouse, A.J. Canty, J. Chem. Soc., Chem. Commun. (1971) 443;
(b) R.C. Makhija, A.L. Beauchamp, R. Rivest, J. Chem. Soc., Chem. Commun. (1972) 1043.
[26] A.J. Canty, A. Marker, B.M. Gatehouse, J. Organomet. Chem. 88 (1975) C31.
[27] N. Guel, J.H. Nelson, J. Mol. Struct. 475 (1999) 121.
[28] Y.-Y. Kim, H.-J. Lee, H.-J. Nam, D.-Y. Noh, Bull. Korean Chem. Soc. 22 (2001) 17.
[29] D.W. Allen, N.A. Bell, S.T. Fong, L.A. March, I.W. Nowell, Inorg. Chim. Acta 99 (1985) 57.
[30] N.A. Bell, S.J. Coles, C.P. Constable, M.B. Hursthouse, M.E. Light, R. Mansor, N.J. Salvin, Polyhedron 21 (2002) 1845, and references therein.
[31] G. Singh, A.K. Singh, P. Sharma, J.E. Drake, M.B. Hursthouse, M.E. Light, J. Organomet. Chem. 688 (2003) 20.

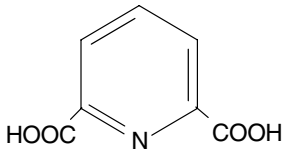

Fig. 1. Schematic structure of the dipicolinic acid (2,6-pyridinedicarboxilic acid).

this ligand and some derivatives form a variety of coordination compounds with vanadium in diverse oxidation states.

Dipicolinic acid shows various biological functions and is a suitable ligand for modeling potential pharmacological compounds because of its low toxicity and amphiphilic nature [12]. Recent results show that vanadium complexes of this compound have enhanced pharmacological activity as compared with the free ligand. Even though one of the desirable qualities of compounds for pharmaceutical use is its neutral charge, the insulin-like properties of the $[VO_2(dipic)]^-$ anion and its 4-hydroxydipicolinate derivative, $[VO_2(dipic)–OH]^-$, have been determined [12–14].

As part of our studies of the interaction of vanadium species with organic compounds displaying pharmacological activity, we have recently reported the synthesis, crystal structure and spectroscopic characterization of a new bis-oxo-bridge vanadium (V) compound of stoichiometry: $[CH_3NHC(NH_2)_2]_2[V_2O_4(dipic)_2]$. The two methyl guanidinium counterions stabilized the crystal structure by an extended H-bonds network [15]. The H-bond pattern gives rise to an eight-member ring, with irregular hexagonal geometry, similar to that described for the interaction between the guanidyl moiety of arginine and different oxoanion groups [16].

The aim of this work is the study of related compounds containing the monomeric anion $[VO_2(dipic)]^-$ with cations able to form intermolecular contacts mediated by H-bonding interactions. This kind of interlinkages is known to be relevant in biological systems involving metal containing moieties [4,17–19]. Herein, we report the synthesis and characterization of a new complex with the formula $C(NH_2)_3[VO_2(dipic)]\cdot 2H_2O$ and compare it with the corresponding ammonium salt. The later was selected as a reference compound due to its well-known therapeutic activity [12]. This complex has been previously prepared and characterized by different methods [12,14,20] and its crystal structure is reported here for the first time. Our structural data show a less symmetrical conformation that the one already reported for the cesium salt [21].

The guanidinium ion was chosen as counterion in $C(NH_2)_3[VO_2(dipic)]\cdot 2H_2O$, as it is present in a great number of naturally occurring and synthetic biologically and pharmacologically relevant systems. This highly resonance-stabilized ion remains protonated over a wide pH range including physiological pH (pK_a around 12.5). It is often used in molecular recognition in chemical and biological systems [22]. Its geometrical characteristics make it an efficient functional group in the binding of anionic species by means of strong non-covalent (H-bonding and charge-pairing) interactions. Specifically, the double hydrogen bond that forms the guanidinium group of arginine and the carboxylate moiety of aspartic acid is a determinant step in the interaction between the HIV virus and the cell primary receptor [23].

Finally, a geometry optimization and the corresponding vibrational analysis are carried out on the isolated vanadium (V) complex anion using tools based on the density functional theory. The optimized geometry is compared with the crystallographic data and the calculated vibrational frequencies are used to aid in the assignment of experimental vibrational modes. Some recent papers describe theoretical studies on vanadate complexes with biological activity. In particular, several works deal with the role of some complexes to model vanadium containing haloperoxidases. The B3LYP hybrid exchange-correlation functional was used to investigate structural and electronic properties of complexes that model the active site of the enzymes [24]. Peroxovanadate imidazole complexes, which can be thought of as models to investigate the oxidative chemistry of those systems, were also studied using the BP86 exchange-correlation within the density functional theory [25]. Furthermore, time-dependent density gradient-corrected density functional theory was used to calculate electronic excitations for vanadate species in different geometries and protonation states [26]. Other vanadium containing species with biological activity were also recently investigated. The study of the interaction of diperoxovanadate complexes with histidine-like ligands using the B3LYP method of the density functional theory has been recently reported [27]. The biological implications of several vanadium (V) peroxocomplexes with emphasis on several theoretical calculations that elucidate some of their properties have been also described [28]. However, in spite of those studies and to the best of our knowledge, there are no previous theoretical studies on the $[VO_2(dipic)]^-$ anion.

2. Experimental

2.1. Reagents and instrumentation

All chemicals were of analytical grade. V_2O_5 and NH_4VO_3 (Merck), dipicolinic acid and guanidine hydrochloride (Sigma), were used without further purification. IR spectra were recorded with a Bruker 113v FT-IR instrument, using the KBr pellet technique. Raman spectra were obtained with a Bruker IFS 66 FT-IR spectrophotometer, using the FRA 106 Raman accessory and the 1064 nm line of a Nd:YAG solid state laser for excitation. Elemental analysis (C, H, N) was performed using a Carlo Erba EA 1108 analyzer.

2.2. Synthesis of complexes

2.2.1. $C(NH_2)_3[VO_2(dipic)]\cdot 2H_2O$ (1)

1.5 g (8.2 mmol) of V_2O_5 and 2.76 g (16.5 mmol) of dipicolinic acid were dissolved in 65 ml of bidistilled water at 70 °C. To the resulting cooled (15 °C) and filtered solution, 1 drop of 100 vol. H_2O_2 was added to avoid V(V) reduction. A change to deep red color was immediately observed. Saturated guanidine hydrochloride aqueous solution was dropwise added until precipitation started. The system was then stored in the refrigerator during one week. The colorless obtained crystals (yield 18%) were filtered off and washed with cold water. In order to improve the yield of the reaction, the orange filtrate was concentrated by evaporation. The yellow solution obtained was afterwards cooled down to 0 °C. More guanidine hydrochloride saturated solution was added until opalescence appeared and the mixture was stored at room temperature. After several days, colorless prismatic crystals, suitable for X-ray structural analysis, were obtained.

Anal. Calc. for $C_8H_{13}N_4O_8V$: C, 27.9; H, 3.8; N, 16.3. Found: C, 27.2; H, 3.5; N, 15.8%.

2.2.2. $NH_4[VO_2(dipic)]$ (2)

The complex was prepared according to the reported procedure [20]. 2.9 g (24.8 mmol) of NH_4VO_3 and 4.17 g (24.9 mmol) of dipicolinic acid were dissolved in 25 ml of bidistilled water and heated at 80 °C until a yellow solution was obtained. After cooling it at 0 °C, a solid precipitates. It was separated by filtration and the filtrate was stored in the refrigerator. After one week, colorless plate shaped crystals of the complex were obtained, filtered off and washed with ethanol and ether (yield: 78%). *Anal.* Calc. for $C_7H_7N_2O_6V$: C, 31.6; H, 2.7; N, 10.5. Found: C, 31.2; H, 2.6; N, 10.1%. Both powder and crystals samples showed identical IR spectra.

2.3. X-ray diffraction data and crystal structure determination

Crystal data and refinement results for the two compounds are summarized in Table 1. Diffraction data of $C(NH_2)_3[VO_2(dipic)]\cdot 2H_2O$ were collected on an Enraf-Nonius Kappa CCD diffractometer with COLLECT [29] and reduced with DENZO and SCALEPACK [30] programs. The corresponding data for $NH_4[VO_2(dipic)]$ were collected on a Enraf-Nonius CAD4 diffractometer with EXPRESS [31] and reduced with XCAD4 [32]. Both data were corrected numerically for absorption with PLATON [33]. The structures were solved by direct and Fourier methods with SHELXS [34] program and its non-H atom refined by full-matrix least-squares with SHELXL [35] program. The hydrogen atoms of the organic molecules in both substances were positioned stereo-chemically and refined with the riding model. In $C(NH_2)_3[VO_2(dipic)]\cdot 2H_2O$, the dioxovanadium group showed rotational disorder with vanadium acting as pivotal atom. This gives rise to somewhat large atomic displacement parameters of the oxygen atoms and concomitant errors in the VO_2 bond distances and angle.

Table 1
Crystal data and structure solution methods and refinement results for $C(NH_2)_3[VO_2(dipic)]\cdot 2H_2O$ (**1**) and $NH_4[VO_2(dipic)]$ (**2**)

Compound	**1**	**2**
Chemical formula	$C_8H_{13}N_4O_8V$	$C_7H_7N_2O_6V$
Formula weight	344.16	266.09
Temperature (K)	150(2)	296(2)
Crystal system	monoclinic	orthorhombic
Space group	$P2_1$ (no. 4)	*Pnaa* (no. 56)
a (Å)	7.912(1)	7.714(1)
b (Å)	6.273(1)	13.529(2)
c (Å)	13.489(1)	18.815(2)
β (°)	102.47(1)	
V (Å^3)	653.7(1)	1963.6(4)
Z	2	8
D_{calc} (g cm^{-3})	1.749	1.800
Crystal size (mm)	$0.28\times0.23\times0.11$	$0.32\times0.28\times0.16$
μ (mm^{-1})	0.807	8.680
Radiation	Mo Kα, $\lambda = 0.71073$ Å	Cu Kα, $\lambda = 1.54184$ Å
$R_1(F_o)$[a] $[I>2\sigma(I)]$	0.0295	0.0323
$wR_2(F_o^2)$[b]	0.0776	0.0941

[a] $R_1 = \sum\|F_o| - |F_c\|/\sum|F_o|$.
[b] $wR_2 = [\sum w(|F_o|^2 - |F_c|^2)^2 / \sum w(F_o^2)^2]^{1/2}$.

The H-atoms of one crystallization water molecule of $C(NH_2)_3[VO_2(dipic)]\cdot 2H_2O$ were found in a difference Fourier map and refined isotropically with Ow–H and H···H distances restrained to target values of 0.86(1) and 1.36(1) Å, respectively. The other water molecule showed positional disorder. This was modeled in terms of two sites for the oxygen atom, which was refined anisotropically while keeping the sum of the occupational factors equal to one. The ammonium H-atoms of $NH_4[VO_2(dipic)]$ were located in a difference Fourier map and refined employing independent isotropic displacement parameters.

2.4. Theoretical calculations

Becke's three parameters hybrid exchange-correlation functional [36] as implemented in the GAUSSIAN-98 package [37] was used for the calculations. The Lee, Yang, and Parr density gradient-corrected correlation functional [38] was utilized then leading to the well-known B3LYP method. A basis set of triple-zeta quality in the valence space including both polarization and diffuse functions available as 6-311++G** in the GAUSSIAN-98 package was used for hydrogen, carbon, nitrogen, and oxygen. A $(14,9,5)/[8,5,3]/\{62111111,33111,311\}$ basis set including an additional p function with small orbital exponent was used for vanadium [39]. No scale factor was used in the calculated frequencies.

3. Results and discussion

3.1. Theoretical calculations

The geometry of the isolated $[VO_2(dipic)]^-$ anion was optimized using the density functional theory [40]. No

countercations were taken into account in the calculations. It should be stressed, then, that the optimized geometry obtained in this way must be strictly compared with gas phase experimental geometries. Thus, the discrepancies arising when comparing with solid state experimental geometries could be attributed to lattice effects (see below).

A vibrational analysis was performed to confirm that the optimized geometry is a true minimum on the molecular potential energy surface. Moreover, the assignment of experimental frequencies to molecular normal modes was accomplished with the help of the calculated vibrational spectrum.

3.2. Structure of the complex

Selected bond distances and angles around the vanadium (V) ion obtained from X-ray data and density functional calculations are compared in Table 2. Complete experimental and calculated geometrical parameters are available in Table S1. The ORTEP [41] drawings of the molecules are shown in Figs. 2 and 3.

Vanadium (V) shows a similar penta-coordinated environment in the guanidinium and ammonium salts of $[VO_2(dipic)]^-$. In the anion, the VO_2^+ group is coordinated to a $dipic^{2-}$ acting as a tridentate ligand through its carboxylic oxygen atoms [V–O distances of 1.983(2) and 1.988(2) Å in **1** and 1.974(2) and 1.978(2) Å in **2**] and the nitrogen atom [V–N distances of 2.086(2) (**1**) and 2.091(2) (**2**) Å]. The $dipic^{2-}$ ligand is planar [rms deviation of atoms from the least-squares plane of 0.012 (**1**) and 0.051 (**2**) Å] with the metal ion lying onto this plane in **1** [at 0.001(7) Å] and slightly above in **2** [at 0.136(1) Å]. The ligand plane of **1** bisects the dioxovanadium V=O double bonds whose lengths are 1.614(7) and 1.626(7) Å. This agrees with the structural data reported for the $[(VO_2)(dipic)]^-$ complex in $Cs[(VO_2)(dipic)]\cdot H_2O$ where

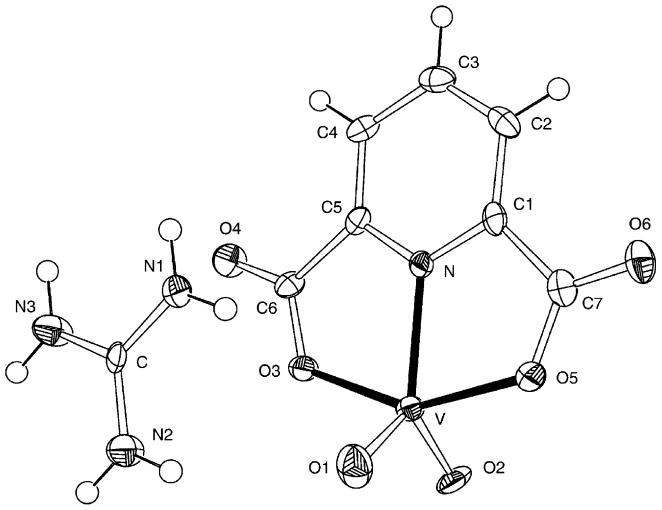

Fig. 2. Molecular plot of $C(NH_2)_3[VO_2(dipic)]\cdot 2H_2O$ showing the labeling of the non-H atoms and their displacement ellipsoids at the 50% probability level. Vanadium–ligand bonds are indicated by full lines. The crystallization water molecules are omitted for clarity.

the V=O double bond distances are 1.610(6) and 1.615(6) Å [18]. In contrast, the ligand plane of **2** structure departs appreciable from the O1=V=O2 bisector and the V–O1 bond distance is 0.012 Å (i.e. six times the rms error) longer than the V–O2 length [1.612(2) Å]. That difference in the VO distances is probably due to a pair of medium to strong N–H···O1 bonds with the NH_4^+ counter-ion (see below). We have recently reported an example of even more pronounced V=O bond asymmetry in the VO_2^+ group, namely in a bis oxo bridged binuclear vanadium (V) complex of stoichiometry $[CH_3NHC(NH_2)_2]_2[V_2O_4(dipic)_2]$ [15]. In this compound, the oxygen atom of the VO_2^+ moiety, laying near the coordination plane, bridges the two halves of a centro-symmetric dimer through a weak

Table 2
Selected experimental bond distances (Å) and angles (°) around vanadium (V) ion for $C(NH_2)_3[VO_2(dipic)]\cdot 2H_2O$ (**1**) and for $NH_4[VO_2(dipic)]$ (**2**)

	Experimental (**1**)	Experimental (**2**)	Calculated
Bond distances (Å)			
V–O(1)	1.614(7)	1.624(2)	1.613
V–O(2)	1.626(7)	1.612(2)	1.613
V–O(5)	1.983(2)	1.974(2)	2.051
V–O(3)	1.988(2)	1.978(2)	2.051
V–N	2.086(2)	2.091(2)	2.168
Bond angles (°)			
O(1)–V–O(2)	110.0(1)	107.69(9)	111.3
O(1)–V–O(5)	98.3(3)	101.38(9)	99.7
O(2)–V–O(5)	97.8(3)	98.49(9)	99.7
O(1)–V–O(3)	98.8(3)	98.40(8)	99.7
O(2)–V–O(3)	99.9(3)	97.66(8)	99.7
O(5)–V–O(3)	149.56(6)	149.22(7)	145.2
O(1)–V–N	124.6(4)	124.86(8)	124.3
O(2)–V–N	125.4(4)	124.86(8)	124.3
O(5)–V–N	74.82(6)	74.64(7)	72.6
O(3)–V–N	74.73(6)	74.72(7)	72.6

Calculated data for $[VO_2(dipic)]^-$ anion.

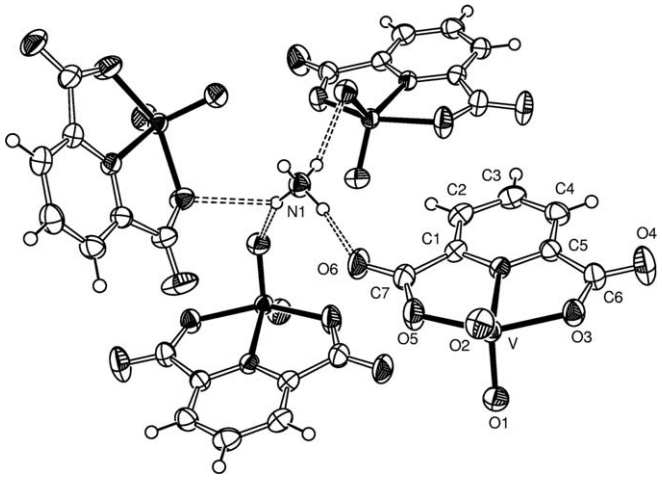

Fig. 3. Molecular diagram of $NH_4[VO_2(dipic)]$. The figure includes three additional, symmetry related, $[VO_2(dipic)]^-$ complexes to show the environment around the ammonium ion and the N–H···O bonding structure (in dashed lines).

axial V···O bond. As a consequence of this, the two V=O distances differ in 0.078(1) Å [d(V–O1) = 1.606(1) Å].

The carboxylic groups of the dipicolinate ligand of both complexes show, as expected, significant bond localization. In fact, the terminal C–O bond lengths are 0.07–0.10 Å shorter than the C–O distances corresponding to the oxygen atoms coordinated to the vanadium ion.

The optimized geometry of the $[VO_2(dipic)]^-$ anion shows a good general agreement with experimental data (Table S1). Nevertheless, it must be noted that several equivalent bond distances and bond angles are equal in the optimized geometry, in complete disagreement with experimental values as can be seen in Table 2. This result, however, is not surprising as the calculated geometry of the isolated anion corresponds to a low-pressure limit gas phase situation, with not allowance for lattice effects, whereas the anions interact with their counterions and, moreover, they are involved in hydrogen bonds when the complexes are formed in the solid state. Thus, the V=O distances are well reproduced within the experimental error for the $[VO_2(dipic)]^-$ anion in the guanidinium salt. On the other hand, for the ammonium salt, the present calculations are unable to reproduce the larger V–O1 distance, in agreement with the fact that the O1 atom is involved in an H-bonding interaction with neighboring NH_4^+ groups, as it was mentioned above. It can also be seen from Table 2 that the calculated O1–V–O2 bond angle overestimates the experimental value in the ammonium salt by ca. 4°. It is suggested that the larger V=O1 bond distance found in the solid **2** is the main responsible for the decreasing of the O1–V–O2 bond angle with respect to the calculated value.

The bond distances between the vanadium ion and the dipicolinate anion, namely V–N, V–O3, and V–O5, are overestimated by 0.06–0.08 Å. These discrepancies could be attributed both to deficiencies in the treatment of exchange and correlation effects within the B3LYP functional or to the fact that the basis sets used are not correlation consistent. More studies on related transition metal complexes are needed to shed light on this problem. The corresponding calculated bond angles are lower than experimental values by as much as 4°. This disagreement is consistent with the above mentioned differences found between calculated and experimental bond lengths.

The guanidinium cation shows three essentially equivalent C–N distances and C–N–C angles [average: 1.32 Å and 120°, respectively]. Its characteristic planar CN_3 skeleton, with a strong electronic delocalization, allows the cation to participate in an extended H-bonding network.

3.3. Hydrogen bonding interaction

3.3.1. $C(NH_2)_3[VO_2(dipic)]\cdot 2H_2O$

In this compound the planar guanidinium counterion lays parallel to the dipìc^{2-} ligand at a van der Waals contact distance of 3.1 Å. The $[VO_2(dipic)]^-$ and $[C(NH_2)_3]^+$ ions are arranged in the lattice along layers parallel to (0 1 0) crystallographic planes. These layers are stabilized by a network of medium to strong intra-layer N–H···O bonds involving the guanidinium NH_2 groups and carboxylic oxygen atoms of the dipic^{2-} ligand [N···O distances and N–H···O angles are found in the ranges 2.848–2.982 Å and 132.6–176.1°, respectively]. Two parallel N–H···O bonds are formed between the N2 and N3 atoms of the guanidinium ion and the carboxylate oxygens O3 and O4 of a neighboring anion. The interaction gives rise to an hexagonal pattern analogous to the observed in the bis-oxo-bridged V(V) complex [15] and similar to that found in a large number of H-bonded layered crystals and to that described for the interaction of phosphate, sulfonate, carboxylate and nitrate with this cation. In biological systems, this peculiar binding pattern is found in the interaction of the guanidinium group of L-arginine in some enzymes with the carboxylate group of aspartate or glutamate [16]. The N1 nitrogen atom of guanidinium interacts, through one of its hydrogen atoms, with the O6 oxygen from a carboxylate ion of another neighboring unit. The lattice is further stabilized by inter-layer H-bonds mediated by one crystallization water molecule held onto the layer by a N–H···Ow bond [the N···Ow distance and the N–H···Ow angle are 2.825 Å and 157.5°, respectively]. This molecule is acting as a donor in two Ow–H···O interactions with the dioxovanadium groups of neighboring layers [the corresponding Ow···O distances and Ow–H···O angles are 2.823 and 2.860 Å and 152.6° and 145.4°,

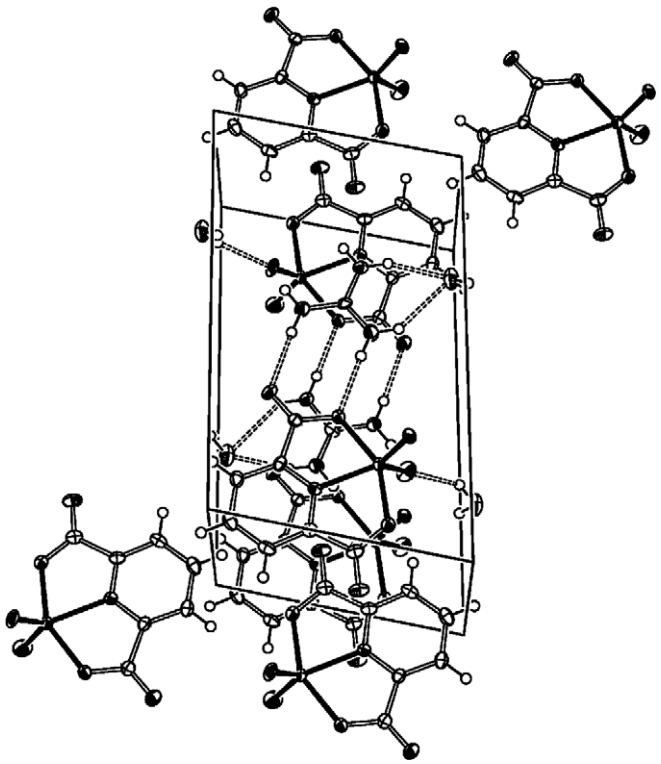

Fig. 4. Crystal packing of $C(NH_2)_3[VO_2(dipic)]\cdot 2H_2O$ showing the H-bonding interactions (dashed lines). The crystal unit cell a- and c-axis are along the horizontal and vertical directions, respectively.

respectively]. An ORTEP [41] drawing showing the crystal packing and the H-bonding network of compound **1** is presented in Fig. 4.

3.3.2. $NH_4[VO_2(dipic)]$

The crystal lattice of this compound is also stabilized by a network of N–H···O bonds. Each ammonium ion is linked to four $[VO_2(dipic)]^-$ units (see Fig. 3). To two of them with the VO_2^+ moiety through its O1 oxygen atom which, therefore, acts as a bifurcated H-bond acceptor [N···O1 distances and N–H···O1 angles are 2.873 and 2.984 Å and 155.6° and 159.7°, respectively]. To the other two units, through one of their carboxylate oxygens, namely O6 and O3 [N···O distances and N–H···O angles are 2.812 and 2.971 Å and 169.9° and 112.0°, respectively]. The NH_4^+ hydrogen atom bonded to the O3 atom on one unit forms a bifurcated H-bond as it is also linked to the O1 atom of another unit. Relevant hydrogen bonding interactions have been described also in other ammonium salts of dioxovanadium complexes, which were studied as structural models for the active site in vanadium-containing haloperoxidases [42,43]. The detailed H-bonding networks of compounds **1** and **2** are given in Tables S2 and S3.

3.4. Vibrational spectra

The solid-state properties of the compounds were examined by infrared (IR) and Raman spectroscopy. The spectra were compared with those of the free ligand and of guanidinium hydrochloride. In Table 3 we report the infrared and Raman frequencies of H_2dipic and the guanidinium and ammonium salts of $[VO_2(dipic)]^-$. Assignment of the more characteristic bands was performed with the help of the harmonic vibrational frequencies calculated in this work, which are also included in Table 3. Reported data of related compounds was also taken into account.

The IR spectrum of the free ligand shows a strong absorption in the 3100–2500 cm^{-1} range due to the O–H stretching mode of the COOH group, overlapped with the C–H stretching bands. The broad and irregular shape of this signal is indicative of a hydrogen-bonded dimer structure for the dipicolinic acid. The corresponding C–OH in-plane bending and out-of-plane OH···O deformation modes are located at 1417 and 927 cm^{-1}, respectively. The typical ν(C=O) stretch, due to the out-of-phase vibrations of the monomeric units in the dipicolinic acid dimer, appears as a broad and very strong IR band centered at 1705 cm^{-1}. The respective in-phase mode is situated at 1644 cm^{-1} in the Raman spectrum [44]. The ν(C–O) vibration is observed as two strong IR bands at 1332 and 1301 cm^{-1}, the corresponding Raman bands being at 1325 and 1296 cm^{-1}. Characteristic ring modes were also identified in the expected range [45].

The IR and Raman spectra of the complexes show very similar spectral pattern, except for the characteristic modes of the guanidinium and ammonium cations. This fact indicates similar coordination environments in both compounds as confirmed by crystal structural data. Compound **1** shows additional rather broad IR bands in the 3450–3100 cm^{-1} region that correspond to the O–H stretching vibrations of the crystallization water molecules and to N–H stretching modes of guanidinium. The position of these bands indicates that these groups are involved in H-bonds interactions. Characteristic bands of the guanidinium ion related to NH_2 in-plane and out-of-plane deformation are also present in the compound spectra. The strong Raman band at 1008 cm^{-1} corresponds to the symmetric stretching of the CN_3 skeleton of guanidinium [44,46]. The deformation mode of the water molecules are probably overlapped by the strong $\delta(NH_2)_{ip}$ IR band.

A weak band at 623 cm^{-1}, in the region of ring deformation modes, can be assigned to the water rocking motion. Compound **2** shows two IR bands of medium intensity at 3196 and 1401 cm^{-1}, attributed to the NH stretching and deformation of the NH_4^+ group, respectively.

In both compounds, $dipic^{2-}$ coordinates the VO_2^+ moiety as a tridentate ligand. The characteristic O–H bands of free carboxylate disappear, hence revealing the deprotonation of this group upon complex formation. This fact was also confirmed by the structural study.

The spectra exhibit strong IR absorption bands due to the symmetric and asymmetric stretching vibrations of the carboxylate anion. Each compound shows one strong IR band with a shoulder in the 1700–1650 cm^{-1} region, which can be assigned to the $\nu_{as}(COO^-)$ mode. The calculations clearly show that this splitting can be attributed to the in-phase (1733 cm^{-1}) and out-of-phase (1718 cm^{-1}) motions due to vibrational coupling between both terminal carboxylic groups. The symmetric stretch of carboxylate groups leads to a characteristic Raman line of medium intensity at 1337 cm^{-1} for compound **1** and at 1340 cm^{-1} for compound **2**. The corresponding IR bands are located at 1331 and 1337 cm^{-1}, respectively, whereas the calculated harmonic frequency is found at 1352 cm^{-1}, in excellent agreement with experimental values. The observed splitting in the IR bands (see Table 3) is consistent with the difference in the C–O distances of both coordinated carboxylate groups (see Table S1). This fact could be a consequence of different H-bond interactions with the counterion. The frequency difference between the asymmetric and symmetric vibrations for both complexes ($\Delta\nu > 300$ cm^{-1}) is in accordance with monodentate coordination of the carboxylate group [47]. As expected, the δ(COO) mode, which occurs in the free ligand as a strong band at 701 cm^{-1}, is shifted to higher frequency after coordination. Theoretical calculations show that it arises coupled with the in-plane ring deformation mode. Coordination through the heterocyclic nitrogen is evidenced by an intensity change and upward frequency shift of some skeletal vibration and in-plane and out-of-plane deformation ring modes (see below) [47].

The symmetric and asymmetric stretching vibrations of the VO_2^+ moiety are observed in the 960–940 cm^{-1} region for both compounds. Calculated harmonic vibrational frequencies for the asymmetric and symmetric modes of VO_2^+

Table 3
Assignment of some of the characteristic IR and Raman bands of dipicolinic acid [(H_2dipic)] and the compounds $C(NH_2)_3[VO_2(dipic)]\cdot 2H_2O$ (**1**) and in $NH_4[VO_2(dipic)]$ (**2**) compounds

H_2dipic		Compound **1**		Compound **2**		Calculated	Assignment
IR	Raman	IR	Raman	IR	Raman		
				3196 m			ν(NH) NH_4^+
3070 m	3097 w	3089 m	3084 vw	3082 m	3075 vw	3209 vw	ν(CH)
	3069 w	3055 sh		3050 m		3164 vw	
2800* s, b	2600* vw						ν(OH)
1705* vs, b	1644 m, b						ν(C=O)
		1703 s	1710 w	1679 s	1703 w	1733 s	$\nu_{as}(COO^-)$ip
		1683 sh	1688 w	1655 sh	1678 vw	1718 vs	$\nu_{as}(COO^-)$op
		1648 s					$\delta(NH_2)$ip
		1570 w					
		1544 sh					
1576 s	1576 m	1602 w	1602 w	1601 w	1603 w	1637 vw	ν(ring)
1460 m	1460 sh	1475 w	1586 w	1476 w	1581 w	1621 vw	
				1401 ms			$\delta(NH_4^+)$
1417 m							δ(OH)
1332 s	1325 w						ν(C–O)
1301 s	1296 w						
		1367 m	1373 sh				$\nu_s(COO^-)$
		1352 m		1358 sh		1352 s	
		1331 s	1337 m	1337 s	1340 m		
		1010 vw	1008 s				$\nu_s(CN_3)$
		953 sh	951 s	956 sh	955 vs	1015 s	$\nu(VO_2)$
		944 s	942 sh	940 s	928 w	1014 s	
927 m, b							γ(OH)
		887 m, b	864 m				$\delta(NH_2)$op
855 m	854 w	850 vw	836 w			855 vw	γ(CH) + γ(ring)
783 w	802 w	771 ms		774 ms		776 w	γ(CH)
753 s		753 ms		753 ms		750 w	δ(ring) + δ(COO)
701 s	762 s						δ(COO)
649 s	647 w	681 ms		679 ms		685 vw	δ(ring)
		623 w					$\rho_w H_2O$
587 w		596 w		594 w		594 vw	δ(ring)
419 vw		452 m	434 sh	451 m		449 vw	γ(ring)
		457 m	454 s	459 m	458 s	437 vw	ν(V–O)carb + δ(ring)
		422 w	410 vw	428 w		432 vw	$\delta(VO_2)$
		363 m		367 m, b	395 w	328 m	ν_a(V–O)carb + δ(V–N–C)
		352 m					
		293 w		294 sh		217 vw	ν(V–N)
		281 sh		276 w			
		254 vw	254 m		258 m	255 w	ν_s(V–O)carb + δ(N–C–COO^-)
		248 vw					

Band positions are in cm^{-1}.
vs: very strong, s: strong, m: medium, w: weak, sh: shoulder, b: broad; δ: in-plane deformation, γ: out-of-plane deformation, ρ: rocking, ip: in-phase, op: out-of-phase, * centered.

are located at 1015 and 1014 cm^{-1}, respectively. The corresponding $\delta(VO_2^+)$ appears as a very weak band at 422 (**1**) and 428 cm^{-1} (**2**), whereas the calculated value is found at 432 cm^{-1}.

Upon complex formation, changes in intensity and position of some of the ligand bands were observed. The vibrational modes corresponding to ν(CH) and skeletal ring vibration appear in the ranges 3100–3050 and 1600–1470 cm^{-1}, respectively, whereas the corresponding calculated values are found at 3200–3160 and 1640–1620 cm^{-1}. Between 1200 and 1030 cm^{-1} it was possible to identify the $\delta(CH)_{ip}$ and δ(ring) modes, the calculated frequencies being located at 1086 and 1044 cm^{-1}, respectively (data not shown). Out-of-plane CH and ring deformations appear in the 850–770 cm^{-1} range, while the in-plane ring modes are found between 750 and 590 cm^{-1}. On the theoretical side, the out-of-plane CH and ring deformations are calculated at 855 and 776 cm^{-1}, the in-plane ring modes at 750 and 594 cm^{-1}.

Furthermore, new bands were found between 460 and 250 cm^{-1}, which can be assigned to the stretching modes of the metal-to-ligand bonds, ν(V–O) and ν(V–N), respectively [48]. Calculated frequencies in the range 449–217 cm^{-1} clearly indicate that these modes are strongly coupled either with several out-of-plane and in-plane ligand deformations or with bending modes involving the five-member ring (VOCCN) formed with vanadium upon coordination (see Table 3). It is interesting to note that

the calculated metal-to-ligand ν(V–N) and ν(V–O) frequencies are found to be lower than experimental values, with downwards wavenumbers shifts of about 75 cm^{-1}. This fact seems to be consistent with the larger V–N and V–O bond distances calculated at the present level of theory as previously mentioned.

Acknowledgments

This work has been supported by CONICET, the National University of La Plata, and ANPCyT (PICT 06-06148) of Argentina and FAPESP of Brazil. Parts of the X-ray diffraction data were collected at LANADI (CONICET). B.S.P.-C., R.P.-D., O.E.P., and A.C.G.-B. are members of the Research Career from CONICET.

Appendix A. Supplementary materials

Tables containing complete information on atomic coordinates and equivalent isotropic displacement parameters, bond distances, angles, and anisotropic displacement parameters for the $C(NH_2)_3[VO_2(dipic)]\cdot 2H_2O$ and $NH_4[VO_2(dipic)]$ compounds are available from the authors upon request and have been deposited at the Cambridge Crystallographic Data Centre, 12 Union Road, Cambridge CB2 1EZ, UK (fax: (internat.) +44 1223 336 033; e-mail: deposit@ccdc.cam.ac.uk). These data can be obtained free of charge at www.ccdc.cam.ac.uk/conts/retrieving.html, reference numbers CCDC-288858 and CCDC-288859. Supplementary data associated with this article can be found, in the online version, at doi:10.1016/j.poly.2006.04.017.

References

[1] K.H. Thompson, C. Orvig, Coord. Chem. Rev. 219–221 (2001) 1033.
[2] Y. Shechter, I. Goldwaser, M. Mironchik, M. Fridking, D. Gefel, Coord. Chem. Rev. 237 (2003) 3.
[3] H. Siegel, A. Siegel (Eds.), Metal Ions in Biological Systems, Vanadium and its Role in Life, vol. 31, Marcel Dekker, New York, 1995.
[4] D. Rehder, Coord. Chem. Rev. 182 (1999) 297.
[5] E.J. Baran, J. Inorg. Biochem. 80 (2000) 1.
[6] H. Sakurai, Y. Kojima, Y. Yoshikawa, K. Kawabe, H. Yasui, Coord. Chem. Rev. 226 (2002) 187.
[7] A.G.J. Ligtenbarg, R. Hage, B.L. Feringa, Coord. Chem. Rev. 237 (2003) 89.
[8] D. Rehder, Inorg. Chem. Commun. 6 (2003) 604.
[9] M. Chatterjee, M. Maji, S. Ghosh, T.C.W. Mak, J. Chem. Soc., Dalton Trans. (1998) 3641.
[10] L. Yang, D.C. Crans, S.M. Miller, A. la Cour, O.P. Anderson, P.M. Kaszynski, M.E. Godzala III, L.D. Austin, G.R. Willsky, Inorg. Chem. 41 (2002) 4859.
[11] P. Lainé, A. Gourdon, J.P. Launay, Inorg. Chem. 34 (1995) 5129, 5138, 5150, 5156.
[12] (a) D.C. Crans, J. Inorg. Biochem. 80 (2000) 123;
(b) D.C. Crans, L. Yang, T. Jakusch, T. Kiss, Inorg. Chem. 39 (2000) 4409.
[13] D.C. Crans, M. Mahroof-Tahir, M.D. Johnson, P.C. Wilkins, L. Yang, K. Robbins, A. Johnson, J.A. Alfano, M.E. Godzala, L.T. Austin, G.R. Willsky, Inorg. Chim. Acta 356 (2003) 365.
[14] D.C. Crans, L. Yang, J.A. Alfano, L.H. Chi, W. Jing, M. Mahroof-Tahir, K. Robbins, M.M. Toloue, L.K. Chan, A.J. Plante, R.Z. Grayson, G.R. Willsky, Coord. Chem. Rev. 237 (2003) 13.
[15] A.C. González-Baró, E.E. Castellano, O.E. Piro, B.S. Parajón-Costa, Polyhedron 24 (2005) 49.
[16] (a) K.A. Schug, W. Lindner, Chem. Rev. 105 (2005) 67;
(b) A. Melo, M.J. Ramos, Chem. Phys. Lett. 245 (1995) 498;
(c) F.P. Schmidtchen, M. Berger, Chem. Rev. 97 (1997) 1609.
[17] W. Plass, Coord. Chem. Rev. 237 (2003) 205.
[18] M. Casny, D. Rehder, Chem. Commun. (2001) 921.
[19] C. Kimblin, X. Bu, A. Butler, Inorg. Chem. 41 (2002) 161.
[20] K. Wieghardt, Inorg. Chem. 17 (1978) 57.
[21] B. Nuber, J. Weiss, K. Wieghardt, Z. Naturforsch. B 33 (1978) 265.
[22] N. Ohata, H. Masuda, O. Yamauchi, Inorg. Chim. Acta 286 (1999) 37.
[23] P.D. Kwong, R. Wyatt, J. Robinson, R.W. Sweet, J. Sodroski, W.A. Hendrickson, Nature 393 (1998) 648.
[24] G. Zampella, J.Y. Kravitz, C.E. Webster, P. Fantucci, M.B. Hall, H.A. Carlson, V.L. Pecoraro, L. De Gioia, Inorg. Chem. 43 (2004) 4127.
[25] M. Bühl, R. Schurhammer, P. Imhof, J. Am. Chem. Soc. 126 (2004) 3310.
[26] M. Bangesh, W. Plass, J. Mol. Struct. (THEOCHEM) 725 (2005) 163.
[27] X.-Y. Yu, S.-H. Cai, X. Xu, Z. Chen, Inorg. Chem. 44 (2005) 6755.
[28] O. Bortolinia, V. Conte, J. Inorg. Biochem. 99 (2005) 1549, and references therein.
[29] Enraf-Nonius COLLECT, Nonius BV, Delft, The Netherlands, 1997–2000.
[30] Z. Otwinowski, W. Minor, in: C.W. Carter Jr., R.M. Sweets (Eds.), Methods in Enzymology, vol. 276, Academic Press, New York, 1997, pp. 307–326.
[31] CAD4 Express Software, Enraf-Nonius, Delft, The Netherlands, 1994.
[32] K. Harms, S. Wocadlo, XCAD4-CAD4 Data Reduction, University of Marburg, Marburg, Germany, 1995.
[33] A.L. Spek, PLATON: A Multipurpose Crystallographic Tool, Utrecht University, Utrecht, The Netherlands, 1998.
[34] G.M. Sheldrick, SHELXS-97: Program for Crystal Structure Resolution, University of Göttingen, Göttingen, Germany, 1997.
[35] G.M. Sheldrick, SHELXL-97: Program for Crystal Structures Analysis, University of Göttingen, Göttingen, Germany, 1997.
[36] A.D. Becke, J. Chem. Phys. 98 (1993) 5648.
[37] M.J. Frisch, G.W. Trucks, H.B. Schlegel, G.E. Scuseria, M.A. Robb, J.R. Cheeseman, V.G. Zakrzewski, J.A. Montgomery, R.E. Stratmann, J.C. Burant, S. Dapprich, J.M. Millam, A.D. Daniels, K.N. Kudin, M.C. Strain, O. Farkas, J. Tomasi, V. Barone, M. Cossi, R. Cammi, B. Mennucci, C. Pomelli, C. Adamo, S. Clifford, J. Ochterski, G.A. Petersson, P.Y. Ayala, Q. Cui, K. Morokuma, D.K. Malick, A.D. Rabuck, K. Raghavachari, J.B. Foresman, J. Cioslowski, J.V. Ortiz, A.G. Baboul, B.B. Stefanov, G. Liu, A. Liashenko, P. Piskorz, I. Komaromi, R. Gomperts, R.L. Martin, D.J. Fox, T. Keith, M.A. Al-Laham, C.Y. Peng, A. Nanayakkara, M. Challacombe, P.M.W. Gill, B. Johnson, W. Chen, M.W. Wong, J.L. Andres, C. Gonzalez, M. Head-Gordon, E.S. Replogle, J. Pople, GAUSSIAN-98, Revision A.9, Gaussian, Inc., Pittsburgh, PA, 1998.
[38] C. Lee, W. Yang, R.G. Parr, Phys. Rev. B 37 (1988) 785.
[39] A. Schäfer, H. Horn, R. Ahlrichs, J. Chem. Phys. 97 (1992) 2571.
[40] (a) P. Hohenberg, W. Kohn, Phys. Rev. 136 (1964) B864;
(b) W. Kohn, L.J. Sham, Phys. Rev. 140 (1965) A1133;
(c) R.G. Parr, W. Yang, Density Functional Theory of Atoms and Molecules, Oxford University Press, Oxford, 1989.
[41] C.K. Johnson, ORTEP-II. A Fortran Thermal-Ellipsoid Plot Program. Report ORNL-5318, Oak Ridge National Laboratory, Tennessee, USA, 1976.
[42] W. Plass, H.P. Yozgatli, Z. Anorg. Allg. Chem. 629 (2003) 65.
[43] A. Pohlmann, S. Nica, T.K. Luong, W. Plass, Inorg. Chem. Commun. 8 (2005) 289.

[44] D. Lin-Vien, N.B. Colthup, W.G. Fately, J.G. Grasselli, Infrared and Raman Characteristic Frequencies of Organic Molecules, Academic Press, Boston, 1991.
[45] P. Carmona, Spectrochim. Acta 36 (1979) 705.
[46] Z. Biresak, W.T.A. Harrison, Inorg. Chem. 37 (1998) 3204.
[47] K. Nakamoto, Infrared and Raman Spectra of Inorganic and Coordination Compounds, 5th ed., Wiley, New York, 1997.
[48] E.J. Baran, J. Coord. Chem. 54 (2001) 215.

effect), a co-ligand [10] or solvents [4,12] direct the course of the self-assembly processes. In search of the rational design of functional materials with extended architectures leading to supramolecular edifices, multicarboxylate ligands bearing differently oriented carboxylate groups with versatile coordination modes have been proved to be the most efficient ones [6,7,15–19] due to the considerably flexible steric orientation of the carboxylate groups enabling the carboxyl groups to connect metal ions in different directions, thus favoring the formation of helicate structures.

In view of the above-mentioned characteristics of multicarboxylate ligands, we thought it worthwhile to explore the possibility of ntp to generate supramolecular architectures, due to considerable flexibility and versatile coordination sites expected to exhibit both coordinate and non-covalent interactions. We report here the synthesis and characterization of coordination polymers of the type $[(H_2en)(ntpMCl_2)]_n$ and the single crystal structure and DNA binding studies of compound **1**. It seems to be the first report of its kind where en has dictated the formation of single stranded helical architectures. However, no interaction has been observed between MCl_2 and ntp in the absence of en, where ntp separates out leaving MCl_2 in solution.

2. Experimental

2.1. Physical measurements

The elemental analyses were obtained from the microanalytical laboratory of CDRI, Lucknow, India. The IR spectra (4000–200 cm^{-1}) of the compounds were recorded as nujol mulls on a Perkin–Elmer 2400 spectrophotometer using CsI optics. The ^1H NMR spectra of the compounds were recorded on a Jeol Eclipse 400 NMR spectrophotometer in D_2O. Metals and chlorides were determined volumetrically [20] and gravimetrically [21], respectively. The electrical conductivities of 10^{-3} M solutions in H_2O were obtained on a digital APX 185 conductivity bridge equilibrated at 25 ± 0.01 °C. Fluorescence measurements on the compound **1** were made on a Shimadzu RF-5301PC spectrofluorometer, equipped with a microcomputer. The fluorescence spectra were measured by three scans with a concentration of 50 μM with 1 cm cell path length. Excitation and emission slits were set at 5 nm each. The spectra were recorded in the 310–450 nm range and the excitation wavelength was set at 310 nm. All the stock solutions were filtered through 0.20 μm millipore filters prior to mixing, to minimize the inner filter effect [22].

2.2. Materials

The metal salts MCl_2 [M = Zn^{II} Cd^{II}, Hg^{II}], ethylenediamine, (All Aldrich) and 3,3′,3″-nitrilotripropionic acid, (TCI, Tokyo, Kasei) were commercially pure samples and used as received while MeOH (AR grade) was used without further purification. However, water was distilled before use.

2.3. Synthesis of the $[(H_2en)(ntpMCl_2)]_n$ polymers

An aqueous solution (20 ml) of ntp (6 mmol) was reacted with MCl_2 (3 mmol) [M = Zn^{II}, Cd^{II}, Hg^{II}] in MeOH (20 ml) followed by addition of en (6 mmol). The reaction contents were stirred at room temperature for about 18 h. The reaction mixture was allowed to stand at room temperature resulting in microcrystalline solids for Cd^{II} **2** and Hg^{II} **3**. However, good quality crystals appeared after a period of one week for Zn^{II} **1**.

2.4. Crystallographic data collection and refinement (*1*)

A colorless prismatic crystal of **1**, having approximate dimensions of $0.1 \times 0.25 \times 0.3$ mm, was mounted on a glass fibre. All measurements were made on a Rigaku AFC7R diffractometer with graphite monochromated radiation. Intensity data were corrected for Lorenz, polarization and absorption: the values for the mass attenuation coefficients are those of Creagh and Hubbel [23]. The structure was solved by heavy atom Patterson methods [24], expanded using Fourier techniques [25] and was refined on F by full-matrix least-squares. The non-hydrogen atoms were refined anisotropically. Hydrogen atoms were refined isotropically. Neutral atom scattering factors were taken from Cromer and Waber [26]. Anomalous dispersion effects were included in F_{cald} [27]; the values for $\Delta f'$ and $\Delta f''$ were those of Creagh and McAuley [28]. All calculations were performed using the TEXSAN [29] crystallographic software package of the molecular structure corporation. All crystallographic data are summarized in Table 1. Selected bond lengths and bond angles are given in Table 2.

2.5. Binding analysis (*1*)

The fluorescence intensity values at the emission maximum (325 nm) were used for calculating the relative fluorescence, considering the fluorescence intensity of the untreated control as 100. The least-square analysis of the initial linear points of relative fluorescence versus nucleotide to compound 1 molar ratio was used to determine the maximal quench, m (slope of the plot), from the following equation ($F = F_0 - mR$), where F is the fluorescence intensity at nucleotide to compound molar ratio (R) and F_0 is the fluorescence intensity of the nucleotide at zero compound concentration. Using the data points exhibiting deviations from the straight-line behavior, the fractional quench, Q, was determined at each nucleotide/compound molar ratio (R). This is obtained from the equation ($Q = F_0 - F/m$). The fractional quench Q is linearly related to the compound binding: (compound − nucleotide)/$(\text{compound})_T = Q$, where $(\text{compound})_T$ represents the total compound concentration. The binding affinity (K_a) and binding capacity (n) were determined from the slope and intercept on the X-axis of the straight line on the Scatchard plot Q versus $Q/(R - Q)$ $(\text{compound})_T$ [30].

Table 1
Crystal data, collection and refinement details for compound **1**

Empirical formula	$C_{11}H_{23}N_3Cl_2ZnO_6$
Formula weight	429.61
Crystal color, habit	colorless, prismatic
Crystal dimensions (mm)	$0.1 \times 0.25 \times 0.3$
Crystal system	monoclinic
Lattice type	primitive
Number of reflections used for unit cell	
Determination (2θ range, °)	25 (29.1–29.9)
Omega scan peak width at half-height (°)	0.38
Lattice parameters	
a (Å)	10.083(1)
b (Å)	11.426(2)
c (Å)	15.546(2)
β (°)	106.731(10)
V (Å^3)	1715.1(3)
Space group	$P2_1/c$ (# 14)
Z value	4
D_{calc} (g/cm^3)	1.664
F_{000}	888.00
μ (Mo Kα) (cm^{-1})	17.75
Diffractometer	Rigaku AFC7R
Radiation	Mo Kα ($\lambda = 0.71069$ Å) graphite monochromated
Attenuator	Zr foil (factors = 1.00,8.36,8.36,8.36)
Take-off angle (°)	6.0
Detector aperture	9.0 mm horizontal, 13.0 mm vertical
Crystal to detector distance (mm)	235
Temperature (K)	296
Scan type	ω–2θ
Scan rate (°/min)	8.0 (in ω)–up to 3 scans
Scan width (°)	$(1.15 + 0.30\tan\theta)$
$2\theta_{max}$ (°)	55.0
Number of reflections measured [R_{int}]	total: 4359 unique: 4133 [0.027]
Corrections	Lorentz-polarization absorption (transmission factors: 0.790–1.000)
Refinement	full-matrix least-squares
Function minimized	$\sum w(\|F_o\| - \|F_c\|)^2$
Least square weights	$1/\sigma^2(F_o) = 4F_o^2/\sigma^2(F_o^2)$
P-factor	0.00
Anomalous dispersion	all non-hydrogen atoms
Number of observations ($I > 3.00\sigma(I)$)	2656
Number of variables	300
Reflection/parameter ratio	8.85
Residuals: R; R_w	0.036; 0.038
Goodness-of-fit indicator	1.10
Maximum shift/error in final cycle	0.01
Maximum peak in final difference in map (e$^-$/Å^3)	0.46
Minimum peak in final difference in map (e$^-$/Å^3)	−0.58

Table 2
Selected bond lengths (Å) and bond angles (°) for compound **1**

Zn(1)–Cl(1)	2.230(1)	O(6)···H(16)	2.06(6)
Zn(1)–O(1)	1.987(3)	O(2)–C(3)	1.220(5)
Zn(1)–Cl(2)	2.277(1)	O(1)–C(3)	1.296(4)
Zn(1)–O(3)	1.977(3)	C(6)–O(3)	1.275(5)
Cl(1)–Zn(1)–Cl(2)	113.36(5)	O(1)–Zn(1)–O(3)	105.5(1)
Cl(1)–Zn(1)–O(1)	112.68(9)	Zn(1)–O(1)–C(3)	117.1(2)
Cl(1)–Zn(1)–O(3)	107.56(9)	Zn(1)–O(3)–C(6)	119.1(3)
Cl(2)–Zn(1)–O(1)	113.60(9)	Cl(2)–Zn(1)–O(3)	103.1(1)

Esds given in parentheses.

3. Results and discussion

The compounds **1**–**3** were stable to atmosphere and were found to be soluble in distilled water. The molar conductance values (Table 3) recorded in distilled water correspond to a 1:1 electrolytic nature of the compounds [31] while the analytical data of the compounds (Table 3) agree well with the proposed composition.

3.1. Infrared spectra

The mode of bonding, including hydrogen-bonding interactions, found in the solid state by X-ray diffraction studies were correlated with the IR study. The IR spectra of the compounds **1**–**3** consist of characteristic IR bands for protonated amine cations and carboxylate groups (Table 4). The ν(NH) absorption of the protonated amine consists [14,32,33] of a strong band around 3216–3210 cm^{-1} and a broad band around 3061–3051 cm^{-1} suggesting that one of the NH_3^+ groups of en is free while the other is involved in some hydrogen bonding interaction (H16···O6) which typically causes a broadening and shift to lower frequency. The appearance of an absorption band in the region 2948–2915 cm^{-1} may be assigned to the (NH^+) vibration expected for the zwitterion whose position is consistent [33] with the hydrogen bonding interactions [(N1H1···O2) = 2.49(5), (N1H1···O6) = 2.17(5) Å]. The IR spectra of all the compounds exhibit characteristic bands in the region 1625–1618 and 1371–1364 cm^{-1} corresponding to antisymmetric stretching ν_{as}(COO) and symmetric stretching ν_s(COO) modes of vibration, with a frequency difference (Δ) of ca. 254 cm^{-1} suggesting [34] the unidentate coordination mode of the carboxyl group which is further corroborated by X-ray data. However, the appearance of an additional band ca. 1525–1500 cm^{-1} in the IR spectra

Table 3
Yield (%), analytical data and molar conductance for the compounds (**1**–**3**)

Compound	Yield (%)	Found (Calc.)%					Molar conductivity (ohm^{-1} cm^{-2} mol^{-1})
		M	Cl	C	H	N	
$[H_2en]^{+2}[ntpZnCl_2]^{-2}$ (**1**)	60	15.1 (15.2)	16.3 (16.5)	30.6 (30.7)	5.3 (5.3)	9.8 (9.7)	69
$[H_2en]^{+2}[ntpCdCl_2]^{-2}$ (**2**)	58	23.4 (23.5)	14.6 (14.8)	27.6 (27.7)	4.8 (4.8)	8.7 (8.8)	65
$[H_2en]^{+2}[ntpHgCl_2]^{-2}$ (**3**)	45	33.3 (33.5)	12.4 (12.5)	23.1 (23.3)	4.0 (4.1)	7.3 (7.4)	61

Table 4
IR vibrational frequencies (cm^{-1}) of the compounds (**1**–**3**)

Compound	$\nu(N–H)_{en}$	$\nu(N–H)_{ntp}$	$\nu_{as}(COO)$	$\nu_{s}(COO)$	$\nu(M–Cl)$	$\nu(M–O)$
$[H_2en]^{+2}[ntpZnCl_2]^{-2}$ (**1**)	3216, 3058	2948	1618, 1500	1371	298	460
$[H_2en]^{+2}[ntpCdCl_2]^{-2}$ (**2**)	3211, 3051	2938	1620, 1520	1369	290	445
$[H_2en]^{+2}[ntpHgCl_2]^{-2}$ (**3**)	3210, 3061	2915	1625, 1525	1364	295	440

of all the compounds may reasonably be assigned [32] to ν(COO) for a non-coordinated carboxyl group. The lowering in frequency as compared to the coordinated one may be due to hydrogen bonding with the protonated en N2H16$\cdots$O6 = 2.06(6) Å. The absence of characteristic band ca. 1750–1700 cm^{-1} in all the compounds attributed [6,33] to a carboxylic group (–COOH) indicates the complete deprotonation of the carboxylic groups in the zwitterion, $[NH^{+}(CH_2CH_2COOH)_2(CH_2CH_2COO)^{-}]$. Medium intensity bands in the 298–290 and 460–440 cm^{-1} regions may be assigned to M–Cl and M–O vibrations.

3.2. ^1H NMR spectra

Further confirmation regarding the structure of the compounds was obtained by the ^1H NMR spectra which show the absence of a peak around 10.9–8.38 ppm corresponding [17,33] to protons of –COOH groups of the ntp ligand, thus indicating the deprotonation of the carboxylic groups of the zwitterion $[NH^{+}(CH_2CH_2COOH)_2(CH_2CH_2COO)^{-}]$. Singlets at 3.1, 3.4 and 3.2 ppm correspond [35] to the resonance peak for CH_2 protons of protonated en (4H, $H_3N^{+}–CH_2–CH_2–NH_3^{+}$) for **1**, **2** and **3** respectively. Owing to the close proximity of resonance frequencies corresponding to CH_2 protons adjacent to the carboxyl group (6H, C–CH_2–COO) and CH_2 protons adjacent to the tertiary nitrogen (6H, N–CH_2–C) of ntp^{2-} in all three compounds it was not possible to resolve their individual frequencies, rather a broad resonance signal around [33] 3.5–3.7 ppm was observed. The proton resonance signals expected for the protonated ethylenediamine moiety and the protonated tertiary amine group of ntp^{2-} could not be observed due to deuterium exchange leading to a breakdown of the helicate structure by loss of hydrogen bonding interactions.

3.3. Crystal structure of compound *1*

The X-ray analysis performed on a single crystal of **1** revealed a single stranded helical structure sustained by both coordinate and hydrogen bonds. The structure of the compound (Figs. 1 and 2) consists of Zn(II) ions which are sequentially linked by two of the carboxylate units of the ditopic ntp^{2-} ligand formed in situ due to the deprotonation of the zwitterion, $[NH^{+}(CH_2CH_2COOH)_2$-$(CH_2CH_2COO)^{-}]$ by en. This ditopic ligand ntp^{2-} coordinates in an antimonodentate manner to generate a polymeric coordinative chain, evident [34] from Zn–O bond distances [Zn1–O1 = 1.987(3) Å, Zn1–O3* = 1.977(3) Å]. Thus it appears that en shows a template effect which

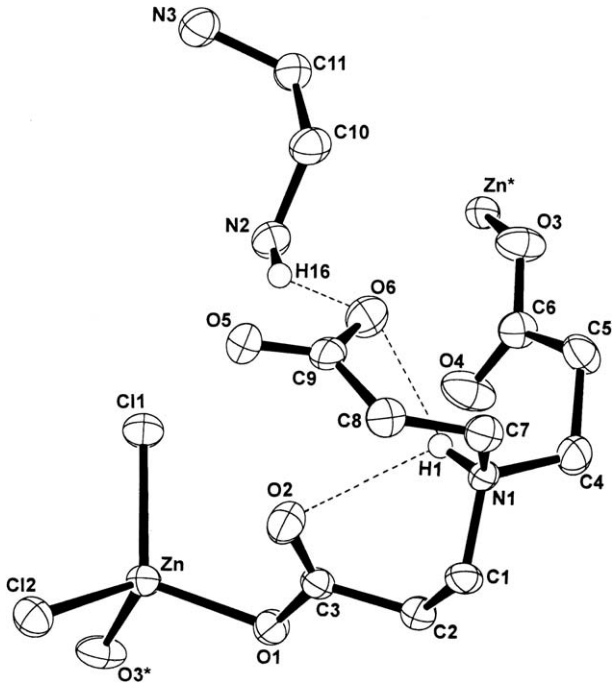

Fig. 1. Molecular structure of compound **1** showing the atom numbering scheme. H-atoms are drawn only for those that participate in hydrogen bonding. Broken lines denote hydrogen bonds. Displacement ellipsoids are drawn at 50% probability.

triggers formation of carboxylate bridged polynuclear compounds. This polymeric coordination compound is also sustained by hydrogen bonding interactions [H1$\cdots$O2 = 2.49(5), H1$\cdots$O6 = 2.17(5) Å]. Further, an intrastrand hydrogen bonding interaction between Cl1 and hydrogen atom H5 attached to the carbon atom C2 in the helical chain [H5$\cdots$Cl2 = 2.76(5) Å] plays an important role in stabilizing the resulted helical motif. As shown in Fig. 2, H_2en^{2+} molecules are incorporated into the groove of the helical chain by forming a hydrogen bond between the ammonium group N2 of en and the oxygen atom O6 of the metal-free carboxylate group of ntp [H16$\cdots$O6 = 2.06(6) Å].

In the crystal lattice, left-handed (M) and right-handed (L) helical chains co-exist with an equal molar ratio. The geometry around each zinc center is tetrahedral, defined by two oxygen donors from different ntp ligands and two chloride anions [Zn1–Cl1 = 2.230(1), Zn1–Cl2 = 2.277(1) Å]. Thus, the specific conformation of the ligand and therefore the compound itself is primarily governed by the interplay between possible versatile coordination modes and the flexibility of the ntp ligand and various hydrogen bonding interactions.

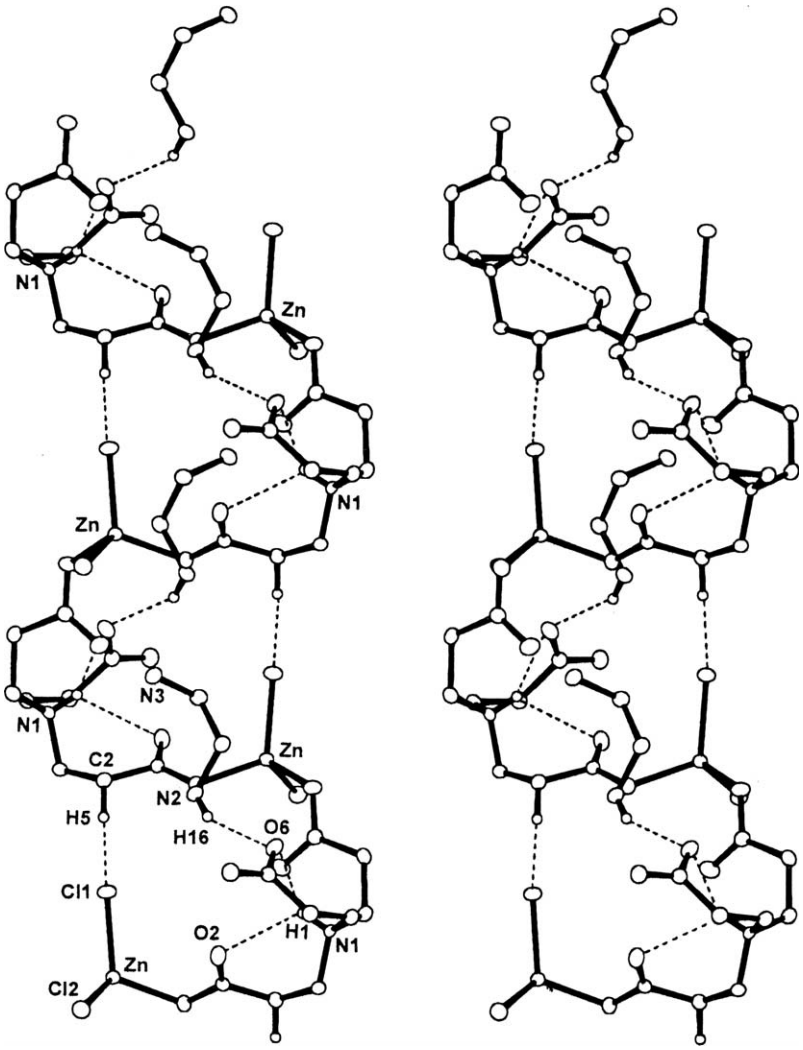

Fig. 2. Stereoview showing the formation of an infinite helical structure of compound **1** along a crystallographic twofold screw axis. H-atoms are drawn only for those that participate in hydrogen bonding. Broken lines denote hydrogen bonds. Note that H_2en^{2+} molecules are incorporated into the groove of the helical chain by forming the H16···O6 hydrogen bond.

3.4. Fluorescence measurements of the helical $[H_2en]^{+2}[ntpZnCl_2]^{-2}$ polymer

The interaction of compound **1** with calf thymus DNA was analyzed by measuring the changes in the intrinsic fluorescence of the compound at different nucleotide/compound molar ratios. A marked quenching effect was observed by the addition of DNA in the fluorescence emission spectra of the compound. The emission spectra observed was further interpreted as shown in Fig. 3. This showed a concentration dependent fluorescence quenching pattern of the compound. Fig. 4 shows the Scatchard [36] plot for the binding of the compound to calf thymus DNA. The slope and the intercept of the straight line obtained from Scatchard analysis gives the apparent association constant $(K_a) = 5.80 \times 10^3\ M^{-1}$ and the number of available binding sites per nucleotide phosphate $(n) = 0.19$, which is equivalent to ≈15 nucleotides per compound binding site.

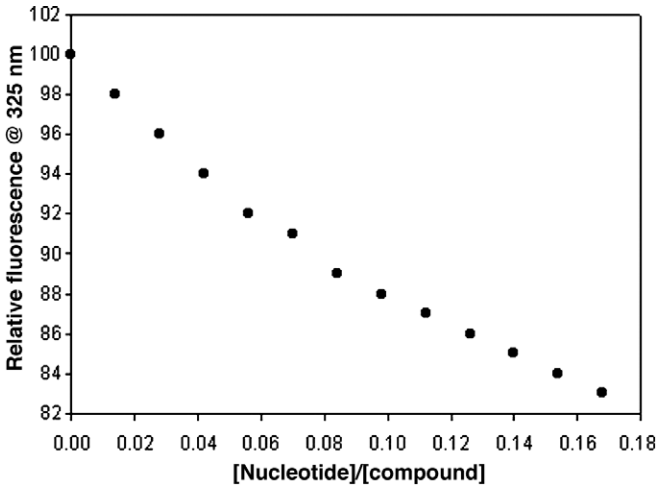

Fig. 3. Quenching effect of DNA at increasing concentration on the fluorescence of compound **1** (50 μM).

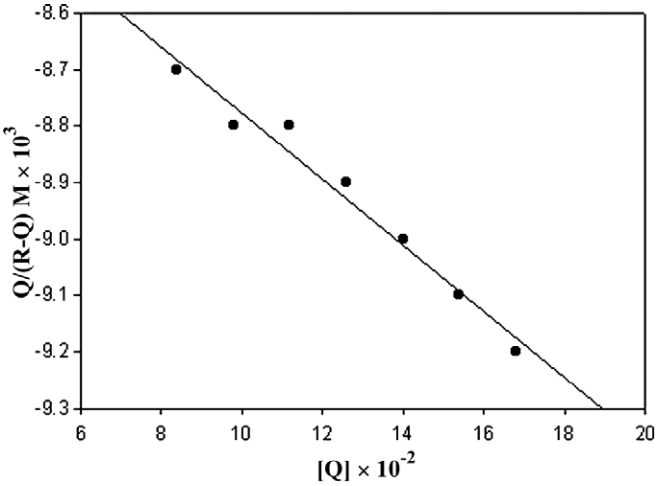

Fig. 4. Scatchard plot analysis for the binding of compound **1** with calf thymas DNA in 0.01 M in Tris–HCl buffer at 25 °C.

Our data suggests that the compound exhibits a good binding constant, which illustrates its binding ability to the DNA helix. This nature of the structure may also contribute to its better-fit position. This single stranded, helical structure of the compound with its tight binding to the DNA could be exploited to down regulate several undesirable expressed genes and so the technology might be analogous to antisense technology.

4. Supplementary data

Supplementary data are available from the CCDC, 12 Union Road, Cambridge CB2 IEZ, UK, quoting the Deposition number 272656.

Acknowledgements

The authors thank the Chairman, Department of Chemistry, Aligarh Muslim University, Aligarh, India for providing basic research facilities. Shama Parveen, SRF acknowledge the financial assistance from CSIR New Delhi (Project No. 01(1910)/04/EMR II).

References

[1] J.-W. Steed, J.L. Atwood, Supramolecular Chemistry, Wiley, New York, 2000.
[2] C. Piguet, G. Bernardinelli, G. Hopfgartner, Chem. Rev. 97 (1997) 2005.
[3] M. Albrecht, Chem. Rev. 101 (2001) 3457.
[4] D.L. Reger, R.F. Semeniuc, V. Rassolov, M.D. Smith, Inorg. Chem. 43 (2004) 537.
[5] R.L. Paul, S.M. Couchman, J.C. Jeffery, J.A. McCleverty, Z.R. Reeves, M.D. Ward, J. Chem. Soc., Dalton Trans. (2000) 845.
[6] X. Wang, C. Qin, E. Wang, Y. Li, N. Hao, C. Hu, L. Xu, Inorg. Chem. 43 (2004) 1850.
[7] S.K. Ghosh, P.K. Bharadwaj, Inorg. Chem. 43 (2004) 2293.
[8] Y.-B. Dong, M.D. Smith, R.C. Layland, H.-C.Z. Loye, J. Chem. Soc., Dalton Trans. (2000) 775.
[9] J.-M. Lehn, Supramolecular Chemistry, VCH, Weinheim, 1995.
[10] G. Guilera, J.W. Steed, Chem. Commun. (1999) 1563.
[11] R.L. Paul, S.P. Argent, J.C. Jeffery, L.P. Harding, J.M. Lynam, M.D. Ward, J. Chem. Soc., Dalton Trans. (2004) 3453.
[12] P. Diaz, D. Michael, P. Mingos, R. Vilar, A.J.P. White, D.J. Williams, Inorg. Chem. 43 (2004) 7597.
[13] L.P. Harding, J.C. Jeffery, T.R. Johannessen, C.R. Rice, Z. Zeng, Chem. Commun. (2004) 654.
[14] Z. Wang, B. Zhang, T. Otsuka, K. Inoue, H. Kobayashi, M. Kurmoo, J. Chem. Soc., Dalton Trans. (2004) 2209.
[15] N.J. Burke, A.D. Burrows, A.S. Donovan, R.W. Harrington, M.F. Mahon, C.E. Price, J. Chem. Soc., Dalton. Trans. (2003) 3840.
[16] E. Colacio, M. Ghazi, R. Kivekas, J.M. Moreno, Inorg. Chem. 39 (2000) 2882.
[17] B.-H. Ye, X.-Y. Li, I.D. Williams, X.-M. Chen, Inorg. Chem. 41 (2002) 6426.
[18] Z. Qin, M.C. Jennings, R.J. Puddephat, K.W. Muir, Inorg. Chem. 41 (2002) 5174.
[19] P. King, R. Clerac, W. Wernsdorfer, C.E. Anson, A.K. Powell, J. Chem. Soc., Dalton Trans. (2004) 2670.
[20] C.N. Reilly, R.W. Schmid, F.A. Sadak, J. Chem. Educ. 36 (1959) 619.
[21] A.I. Vogel, A Textbook of Quantitative Inorganic Analyses, Longmans, London, 1961, pp. 433.
[22] C.F. Chignell, Ann. NY. Acad. Sci. 226 (1973) 44.
[23] D.C. Creagh, J.H. Hubbell, in: A.J.C. Wilson (Ed.), International Tables for Crystallography, vol. C, Kluwer Academic Publisher, Boston, 1992, p. 200 (Table 4.2.4.3).
[24] PATTY: P.T. Beurskens, G. Admiraal, G. Beurskens, W.P. Bosman, S. Garcia-Granda, R.O. Gould, J.M.M. Smits, C. Smykalla. The DIRDIF Program System, Technical Report of the Crystallography Laboratory, University of Nijmegen, The Netherlands, 1992.
[25] DIRDIF 92: P.T. Beurskens, G. Admiraal, G. Beurskens, W.P. Bosman, S. Garcia-Granda, R.O. Gould, J.M.M. Smits, C. Smykalla. The DIRDIF Program System, Technical Report of the Crystallography Laboratory, University of Nijmegen, The Netherlands, 1992.
[26] D.T. Cromer, J.T. Waber, International Tables for X-ray Crystallography, vol. IV, The Kynoch Press, Birmingham, England, 1974 (Table 2.2A).
[27] I.A. Ibers, W.C. Hamilton, Acta. Crystallgr. 17 (1964) 781.
[28] D.C. Creagh, W.J. McAuley, in: A.J.C. Wilson (Ed.), International Tables for Crystallography, vol. C, Kluwer Academic Publisher, Boston, 1992, p. 219 (Table 4.2.6.8).
[29] TEXSAN: Crystal Structure Analysis Package, Molecular Structure Corporation, 1985, 1992.
[30] R.L. Levine, Clinical Chem. 23 (1977) 2292.
[31] W.J. Geary, Coord. Chem. Rev. 7 (1971) 81.
[32] N.F. Curtis, J. Chem. Soc. A (1968) 1579.
[33] E.R. Souaya, W.G. Hanna, E.H. Ismail, N.E. Milad, Molecules 5 (2000) 1121.
[34] G.B. Deacon, R.J. Phillips, Coord. Chem. Rev. 33 (1980) 227.
[35] W. Kemp, Organic Spectroscopy, Macmillan Press, London and Basingstoke, 1975.
[36] G. Scatchard, Ann. NY. Acad. Sci. 51 (1949) 660.

$K_{0.2}Co_{1.4}Fe(CN)_6 \cdot 6.9H_2O$ structure resulted in the formation of paramagnetic Co^{II}–NC–Fe^{III} units [25,26]. Promising photochromic properties based on a spin transition was detected on a Co–Fe polycyanide $Na_{0.34}Co_{1.33}Fe(CN)_6 \cdot 4.5H_2O$ [27]. Reversible light induced metal-to-metal and metal-to-ligand charge transfers were observed in dinuclear complexes of the $Na[(L_5)Co–CN-Fe(CN)_5] \cdot nH_2O$ type (L_5 = tetradentate macrocyclic ligand with amine pendant arm) [28–31] while the temperature dependent charge transfer, causing the spin transition, was identified in the pentanuclear $\{[Co(tmphen)_2]_3[Fe(CN)_6]_2\} \cdot 9H_2O$ complex [32]. In 2–4 M NaCl solutions with $[Co(en)_3]^{3+}$ or $[Co(NH_3)_6]^{3+}$ and $[Fe(CN)_6]^{4-}$ ions, a photo-induced ionic pair charge transfer can occur [33,34].

Surprisingly, only a few Co–Fe heterobimetallic complexes based on hexacyanoferrate(II,III) anions and bearing amine-type ligands have been structurally characterized to date. The majority of them exhibit ionic structures [35–38], in some cases they contain dinuclear [28–31] or pentanuclear cores [32], but no polymeric structure has been determined yet.

Mössbauer spectroscopy has been used for the study of the dehydration processes in hexacyanoferrates(III); it was found that uncoordinated water molecules in the vicinity of $[Fe(CN)_6]^{3-}$ anions exhibited a strong effect on the quadrupole splitting parameter due to the changes in the electronic population of the t_{2g} level [39–42]. Usually, the dehydration process in coordination compounds leads to destruction of the single crystal character of the starting material. To our knowledge, the inverse situation, i.e. preservation of the single crystal character during dehydration, was observed in 3D-coordination polymers of the type $\{[Me(H_2O)_2(\mu\text{-}C_4O_4)(\mu\text{-}4,4'\text{-}bipy)]\}_n \cdot H_2O$ (Me = Co, Ni, Fe) [43].

In this work, as a part of our systematic study of hexacyanoferrates(II, III) [44,45], we report on the synthesis, crystal structure, thermal behaviour and dehydration process in single crystals of a new Co(III)–Fe(III) heterobimetallic compound, $[Co(en)_3][Fe(CN)_6] \cdot H_2O$. As a unique result of this study, the anhydrous and thermally more stable complex, $[Co(en)_3][Fe(CN)_6]$, was prepared by a solid-state single crystal dehydration of **1**, and its X-ray structure has been determined.

2. Experimental

2.1. Materials

$K_3[Fe(CN)_6]$ (Merck Co.) and dimethylformamide (Lachema Co.) were used as received. $[Co(en)_3]Cl_3 \cdot 3H_2O$ was prepared by a slightly modified procedure to that described in the literature [46].

2.2. Synthesis of $[Co(en)_3][Fe(CN)_6] \cdot H_2O$ (1)

A solution of $K_3[Fe(CN)_6]$ (0.33 g, 1 mmol) in 20 ml of water was added to 10 ml of an aqueous solution of $[Co(en)_3]Cl_3 \cdot 3H_2O$ (0.31 g, 1 mmol) with stirring at room temperature. The yellow precipitate which formed immediately in the solution, was filtered off and recrystallized from a hot aqueous solution. Upon cooling, orange needles, suitable for a single crystal X-ray data collection, were obtained. The crystals were filtered off, washed with a small amount of water and dried under an infrared lamp at 40 °C for 2 h. Yield: 65%.

Anal. Calc. for $C_{12}H_{26}N_{12}CoFeO$: C, 30.6; H, 6.0; N, 35.7. Found: C, 30.5; H, 6.0; N, 35.4%. IR spectroscopy (cm^{-1}): ν(OH): 3510vs, 3439s; ν(NH): 3282s, 3211vs, 3097s; ν(CH): 2976w, 2910w; ν(C≡N): 2116s, 2100s; $\delta(OH_2)$: 1616m; $\delta(NH_2)$: 1579s, 1559s; $\delta(CH_2)$: 1460m; $\rho_w(CH_2)$: 1365m; $\rho_w(NH_2)$: 1325w, 1159m; $\rho_t(CH_2)$: 1294w; ν(C–N): 1120m; ν(C–C): 1055s; $\rho_t(NH_2)$: 1003w; $\rho_r(CH_2)$: 895vw; $\rho(OH_2)$: 777m, 741sh; δ(MCN): 585m; δ(N–C–C–N): 490w, 442m; ν(Fe–C): 398m; ν(Co–N): 379m.

The dehydrated $[Co(en)_3][Fe(CN)_6]$ compound **2** was prepared by a dynamic heating of a sample **1** up to 150 °C. *Anal.* Calc. for $C_{12}H_{26}N_{12}CoFe$: C, 31.9; H, 5.4; N, 37.3. Found: C, 31.8; H, 5.4; N, 37.1%. IR spectroscopy (cm^{-1}): ν(NH): 3277s, 3234vs, 3111s; ν(CH): 2988w, 2901w; ν(C≡N): 2111s; δ (NH_2) 1581s, 1561m; $\delta(CH_2)$: 1460m; $\rho_w(CH_2)$: 1369m; $\rho_w(NH_2)$: 1325w; $\rho_t(CH_2)$: 1284w; ν(C–N): 1142m; ν(C–C): 1055s; $\rho_t(NH_2)$: 1002w; $\rho_r(CH_2)$: 891vw; δ(MCN): 582m; δ(N–C–C–N): 498w, 433m;ν(Fe-C): 398m; ν(Co–N): 379m.

2.3. Physical measurements

Elemental analyses (C, H, N) were performed on a Flash EA 1112 Elemental Analyser (ThermoFinnigan). The IR spectra (400–4000 cm^{-1}) as well as far-IR spectra (100–600 cm^{-1}) were obtained on a NEXUS 670 FT-IR spectrometer (ThermoNicolet) using KBr tablets and polyethylene discs, respectively. The transmission Mössbauer spectra of **1** and **2** were collected at 300 K using a Mössbauer spectrometer in constant acceleration mode with a ^{57}Co(Rh) source. The isomer shift values are calibrated with respect to metallic α-Fe.

TG and DSC (thermogravimetric and differential scanning calorimetry) measurements of complex **1** were made in air atmosphere using a THASS TG/DSC XP-10 thermal analyser (THASS GmbH) with a sample weight of 10 mg and thermal gradient of 5 °C per minute.

2.4. X-ray structure analysis

X-ray experiments were carried out on a four-circle κ-axis Xcalibur2 diffractometer equipped with a CCD detector Sapphire2 (Oxford Diffraction) at 100(2) K. The CrysAlis software package [47] was used for data collection and reduction. The structures were solved by the SIR97 program [48] incorporated in the WinGX program package [49]. All non-hydrogen atoms of $[Co(en)_3][Fe(CN)_6] \cdot H_2O$ (**1**) and $[Co(en)_3][Fe(CN)_6]$ (**2**) were refined anisotropically by the

full-matrix least-squares procedure [SHELXL-97] [50] on F^2 with weight: $w = 1/[\sigma^2(F_o)^2 + (0.036P)^2 + 0.745P]$ for **1** and $w = 1/[\sigma^2(F_o)^2 + (0.103P)^2]$ for **2**, where $P = (F_o^2 + 2F_c^2)/3$. Hydrogen atoms in both **1** and **2** were located from difference Fourier maps and refined using a 'riding' model, except for those belonging to the water molecule in **1** which were refined freely with fixed U_{eq} parameters. The molecular structures of **1** and **2** are depicted in Figs. 1, and 2, respectively, and were drawn using the Diamond software [51]. Crystal data and structure refinements for **1** and **2** are summarized in Table 1, while selected bond lengths and angles are given in Table 2.

3. Results and discussion

3.1. Synthesis and thermal behaviour study

Formerly, $[Co(en)_3]$ $[Fe(CN)_6]\cdot 2H_2O$ was prepared from an aqueous system containing $[Co(en)_3]Cl_3$ and $K_3[Fe(CN)_6]$, and moreover, the product was also structurally characterized [38]. In this study, the $[Co(en)_3][Fe(CN)_6]\cdot H_2O$ complex **1** used as the starting compound was synthesized by a similar manner as previously but hot water (80 °C) was used for recrystallization yielding the monohydrate upon slow cooling of the mother liquor.

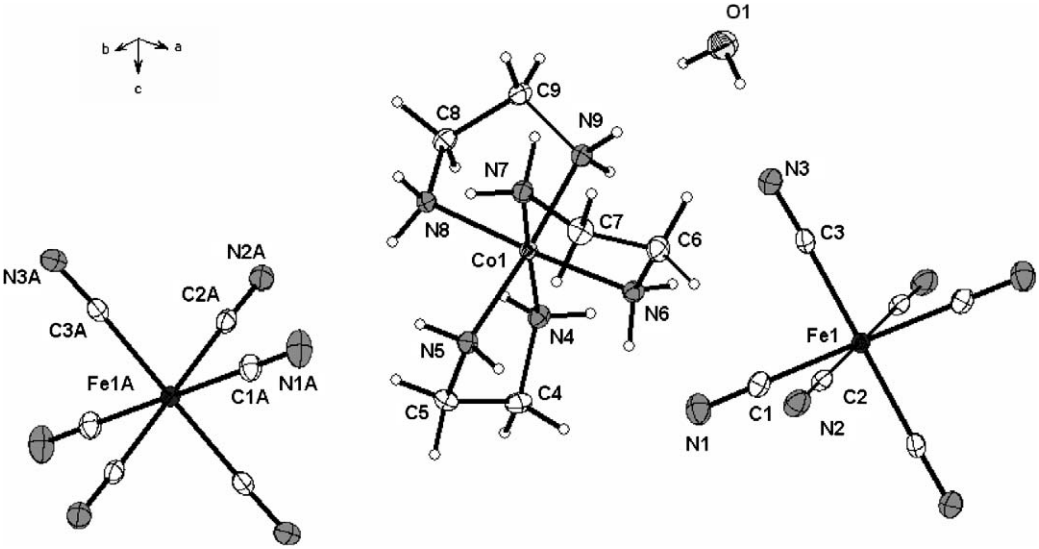

Fig. 1. The crystal structure of **1**. The thermal ellipsoids of non-hydrogen atoms are drawn at the 50% probability level. The H atoms are shown as small spheres of arbitrary radii.

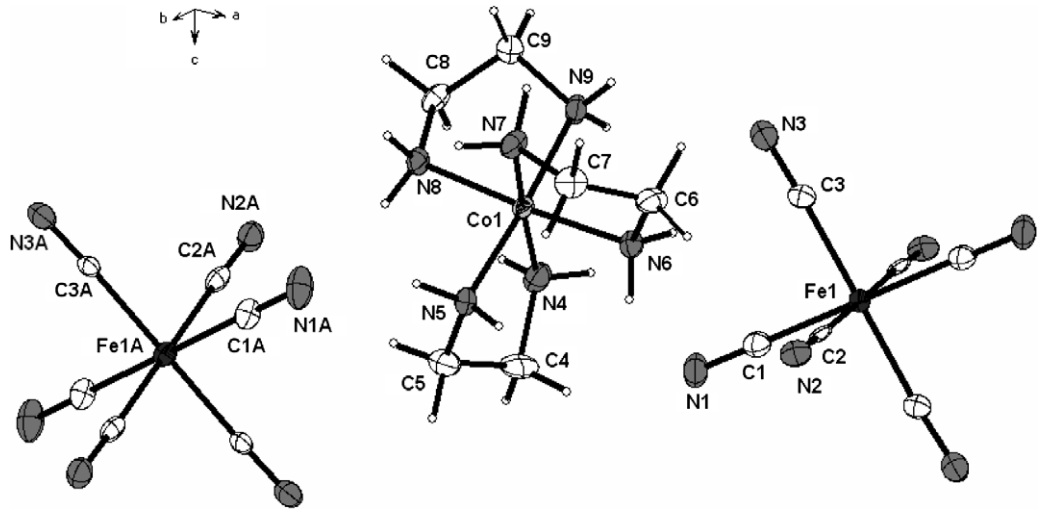

Fig. 2. The crystal structure of **2**. The thermal ellipsoids of non-hydrogen atoms are drawn at the 50% probability level. The H atoms are shown as small spheres of arbitrary radii.

Table 1
Crystal data and structure refinements for **1** and **2**

	1	**2**
Empirical formula	$C_{12}H_{26}CoFeN_{12}O$	$C_{12}H_{24}CoFeN_{12}$
Formula weight	469.23	451.21
Crystal system	monoclinic	monoclinic
Space group	$P2_1/c$	$P2_1/c$
Unit cell dimensions		
a (Å)	15.058(3)	15.034(5)
b (Å)	8.6670(17)	8.408(5)
c (Å)	15.113(3)	14.908(5)
β (°)	90.05(3)	90.258(5)
Z	4	4
v (Å^3)	1972.4(8)	1884.4(14)
$D_{calc.}$ (g cm^{-3})	1.580	1.590
T (K)	100	100
μ (mm^{-1})	1.607	1.674
Index ranges	$-17 \leqslant h \leqslant 17$; $-10 \leqslant k \leqslant 10$; $-16 \leqslant l \leqslant 17$	$-17 \leqslant h \leqslant 16$; $-9 \leqslant k \leqslant 7$; $-17 \leqslant l \leqslant 17$
θ Range for data collection	3.58–25.0	2.71–25.0
Reflection collected	12 206/3449	8407/3293
Independent reflections (R_{int})	6280 (0.0302)	3293 (0.0744)
Data/restrains/parameters	3449/2/253	3293/0/238
Goodness-of-fit on F^2	1.098	1.042
Final R indices [$I > 2\sigma(I)$]	$R_1 = 0.0272$, $wR_2 = 0.0647$	$R_1 = 0.0632$, $wR_2 = 0.1543$
R indices (all data)	$R_1 = 0.0316$, $wR_2 = 0.0666$	$R_1 = 0.0916$, $wR_2 = 0.1863$
Largest peak and hole (e Å^{-3})	0.559 and −0.232	1.359 and −0.605

It seems that a small change during the recrystallization process induced the formation of the monohydrated complex **1** instead of the dehydrated one. The existence of the monohydrated $[Co(en)_3][Fe(CN)_6] \cdot H_2O$ complex **1** follows not only from results of elemental analysis but mainly from single crystal X-ray analysis (see Section 3.2). The thermal stability interval of **1** lies between 25 and 70 °C (see Fig. 3). The complex starts to decompose and eliminate the water molecule at ca. 70 °C. This first step relating to one crystal water elimination is accompanied by a broad *endo*-effect observed on the DSC curve with the minimum at ca. 85 °C and it is finished at ca. 123 °C. Then, the anhydrous complex **2** remains thermally stable in the temperature interval of 125–215 °C (weight loss found/calcd.: 3.7/3.8%). Products of further thermal decomposition were not studied in detail. However, it is necessary to note that the thermal decomposition finishes at ca. 400 °C. The results following from this thermal study helped us to determine the thermal stability intervals both for **1** and **2**, and moreover, to suggest what solid-state synthetic route could be used for the preparation of single crystals of **2**.

Because the formation of an anhydrous complex by the dehydration of a hydrate is quite common, the formation and preservation of single crystals during the dehydration process was observed, to our knowledge, only in coordination polymers $\{[Me(H_2O)_2(\mu\text{-}C_4O_4)(\mu\text{-}4,4'\text{-}bipy)]\}_n \cdot H_2O$ (M = Co, Ni, Fe) [43]. Let us note that the anhydrous complex **2** is stable against secondary re-hydration when exposed to air humidity. This is not a common property

Table 2
Selected bond lengths (Å) and angles (°) of **1** and **2**

	1	**2**
Co1–N4	1.972(2)	1.962(5)
Co1–N5	1.967(2)	1.944(5)
Co1–N6	1.963(2)	1.967(5)
Co1–N7	1.958(2)	1.960 (5)
Co1–N8	1.970(2)	1.974(5)
Co1–N9	1.965(2)	1.977(5)
N4–Co1–N5	85.47(6)	85.8(2)
N6–Co1–N7	85.60(6)	85.0(2)
N9–Co1–N8	85.60(6)	85.3(2)
N7–Co1–N4	174.7(1)	174.5(2)
N6–Co1–N8	176.6(1)	175.6(2)
N5–Co1–N9	175.1(1)	176.4(2)
Fe1–C1	1.956(2)	1.941(6)
Fe1–C2	1.935(2)	1.910(7)
Fe1–C3	1.940(2)	1.936(7)
Fe1A–C1A	1.921(2)	1.917(7)
Fe1A–C2A	1.943(2)	1.937(7)
Fe1A–C3A	1.946(2)	1.943(6)
C2–Fe1–C3	87.8(1)	87.4(2)
C2–Fe1–C1	88.2(1)	89.1(3)
C3–Fe1–C1	88.8(1)	88.3(3)
C1A–Fe1A–C2A	87.0(1)	85.7(3)
C1A–Fe1A–C3A	91.2(1)	90.1(3)
C2A–Fe1A–C3A	90.9(1)	91.1(2)

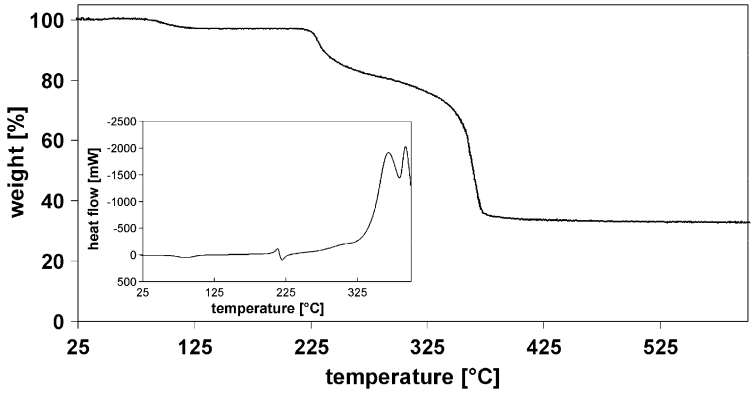

Fig. 3. TG and DSC (inside) curves of **1**.

of heterometallic cyano-based complexes as reported e.g. for $\{[Zn(en)_2Ni(CN)_4Zn(en)][Ni(CN)_4]\cdot 3H_2O\}_n$ [52].

3.2. X-ray structure analysis

The crystal structures of both **1** and **2** exhibit ionic structures and the respective unit cells are built up of $[Co(en)_3]^{3+}$ complex cations (Co1) and two halves of crystallographically independent $[Fe(CN)_6]^{3-}$ complex anions with Fe1 and Fe1A iron(III) ions occupying special positions (a centre of inversion). Moreover, one crystallographically independent water molecule of crystallization is present in the structure of the hydrate **1** (Figs. 1 and 2). From the chemical and crystallographic point of views, the crystal structures of **1** and **2** are very similar to that as determined for the dihydrate $[Co(en)_3][Fe(CN)_6]\cdot 2H_2O$ [38]. As would be anticipated, the unit cell parameters of the anhydrous complex **2** are slightly shorter than those of the complex **1**, resulting in the unit cell volume of **2** being smaller in comparison with **1** (see Table 1).

The Co(III) ions in both the complexes **1** and **2** are coordinated in deformed octahedral arrangements by six nitrogen atoms from three *en* ligands. The Co–N distances vary from 1.958(2) to 1.972(2) Å for **1**, and 1.944(5) to 1.977(5) Å for **2** (Table 2). These values are comparable to those found for similar compounds, e.g. *Λ*-$[Co(en)_3]P_3O_9\cdot 2H_2O$ {1.953(4)–1.972(3) Å} [53], $[Co(en)_3]_3[FeCl_6]Cl_6\cdot H_2O$ {1.954(4)–1.979(4) Å} [54] and $[Co(en)_3]_2(pip)[(HPO_4)_2O_{15}Mo_5]\cdot 6H_2O$, where *pip* = piperazinium {1.958(3)–1.979(2) Å} [55]. The remaining geometric parameters within the *en* ligands are as expected.

In both structures, the $[Co(en)_3]^{3+}$ cations exhibit the $\Lambda\lambda\delta\delta$ (oblel$_2$) conformation. Due to the presence of the centre of inversion in both structures, there are also present antipodes with the $\Delta\delta\lambda\lambda$ (*elob*$_2$) conformation. The distinct situation was found in the case of $[Co(en)_3][Fe(CN)_6]\cdot 2H_2O$, where the $[Co(en)_3]^{3+}$ cations exhibit $\Lambda\delta\delta\delta$ and $\Delta\lambda\lambda\lambda$ conformations [38]. At this point, it is necessary to emphasize that most of the *Λ*-$[M(en)_3]^{n+}$ cations exhibit the $\Lambda\delta\delta\delta$ conformation, which is the most stable one as follows from the order of decreasing stability $\Lambda\delta\delta\delta(lel_3) > \Lambda\lambda\delta\delta(oblel_2) > \Lambda\lambda\lambda\delta(oblel_2) \cong \Delta\lambda\lambda\lambda(ob_3)$. The enthalpy increment is approximately 1.6 ± 0.9 kJ/mol for each δ to λ ring inversion [56]. The stabilization of the observed conformations is probably caused by the presence of the hydrogen bond system.

Each of the crystallographically independent Fe(III) ions in both structures are coordinated by six carbon-to-iron oriented terminal cyano ligands. In **2**, both $[Fe(CN)_6]^{3-}$ octahedrons are slightly compressed, with Fe1–C2 1.910(7) Å and Fe1A–C1A 1.917(7) Å bond lengths. On the other hand, the distance of Fe1–C1 1.956(2) Å is slightly elongated in **1** and contrarywise, the Fe1A–C1A distance {1.921(2) Å} is slightly compressed, similarly as in **2**. Generally, Fe–C distances vary from 1.935(7) to 1.956(2) Å (for **1**) and from 1.917(7) to 1.943(6) Å (for **2**) and all corresponding bond lengths are shorter in **2** as compared to **1**. For all that, the Fe–C distances are comparable with those found in other hexacyanoferrates(III), e.g. in $[Hbet]_3[Fe(CN)_6]\cdot 4H_2O$ (*bet* = betaine) {1.921(4)–1.942(3) Å} [57] or [tams][Fe(CN)$_6$]·$8H_2O$ (tams = 2,4,6-tris(1,4-diazabicyclo(2.2.2.)octane-*N*-methyl)mesitylene^{3+}) {1.934(3)–1.952(3) Å} [58]. The maximal deviation of 4.3° from the "ideal" right angle for the *cis* C–Fe–C angles was observed in the Fe1A octahedron (see Table 2). A similar conclusion can be made in the case of [tams][Fe(CN)$_6$]·$8H_2O$ [58], where the above-mentioned *cis* angles vary from 86.25(2)° to 93.03(2)°.

As follows from the results of the single crystal X-ray analysis of both structures, only the water molecule of crystallization has an influence on the re-arrangement of complex ions in the crystal structure during the dehydration process. In contrast, no significant changes were observed in interatomic parameters between both structures. The most marked changes are as follows: (I) a shortening of the Co1–N5 distance was observed upon dehydration {from 1.967(2) to 1.944(5) Å}; the remaining Co–N distances are essentially the same within the level of significance; (II) the FeC_6 octahedron is slightly elongated with the Fe1–C1 bond in **1** {1.956(2) Å}, as compared to **2**, being the longest one, while the FeC_6 octahedron is compressed with the shortest distance Fe1–C2 1.910(7) Å in the anhydrous compound **2** (see Table 2).

Table 3
Possible hydrogen bonds for **1** and **2** (Å, °)

D–H···A	*d*(D–H)	*d*(H···A)	*d*(D···A)	∠(DHA)
For ***1***				
O1–H1V···N3^{I}	0.98(2)	1.93(2)	2.878(3)	164(2)
O1–H1W···N1A^{II}	0.94(2)	2.09(3)	2.845(3)	137(2)
N4–H4C···N2A^{III}	0.920	2.37	3.155(3)	143
N4–H4D···N1	0.920	2.49	3.240(3)	138
N5–H5C···N2^{iv}	0.920	2.17	2.993(3)	149
N5–H5D···N1A	0.920	2.39	3.221(3)	151
N6–H6C···N2^{iv}	0.920	2.15	3.025(3)	158
N6–H6D···N3	0.920	2.51	3.301(3)	144
N7–H7C···N1^{v}	0.920	2.23	3.070(3)	152
N7–H7D···O1^{vi}	0.920	2.01	2.848(3)	151
N8–H8C···N2A	0.920	2.31	3.114(3)	146
N8–H8D···N3A^{vii}	0.920	2.04	2.879(3)	150
N9–H9D···N1A^{vi}	0.920	2.17	3.012(3)	151
For ***2***				
N4–H4C···N2A^{III}	0.920	2.28	3.076(8)	144
N4–H4D···N1	0.920	2.43	3.158(8)	136
N5–H5C···N2^{iv}	0.920	2.18	2.986(8)	146
N5–H5D···N1A	0.920	2.16	3.037(8)	160
N6–H6C···N2^{iv}	0.920	2.12	2.993(8)	159
N6–H6D··· N3	0.920	2.40	3.235(8)	151
N7–H7C···N1^{v}	0.920	2.18	3.018(8)	151
N8–H8C···N2A	0.920	2.32	3.101(8)	142
N8–H8D···N3A^{vii}	0.920	2.07	2.890(8)	148
N9–H9D···N1A^{viii}	0.920	2.23	3.040(8)	146

Symmetry codes: (i) $x-1, -y-1/2, z-1/2$; (ii) $x-1, -y+1/2, z-1/2$; (iii) $-x+1, -y+1, -z+2$; (iv) $-x+2, -y+1, -z+2$; (v) $x, -y+1/2, z-1/2$; (vi) $x+1, -y+1/2, z+1/2$; (vii) $-x+1, y-1/2, -z+3/2$; (viii) $x, y-1, z$.

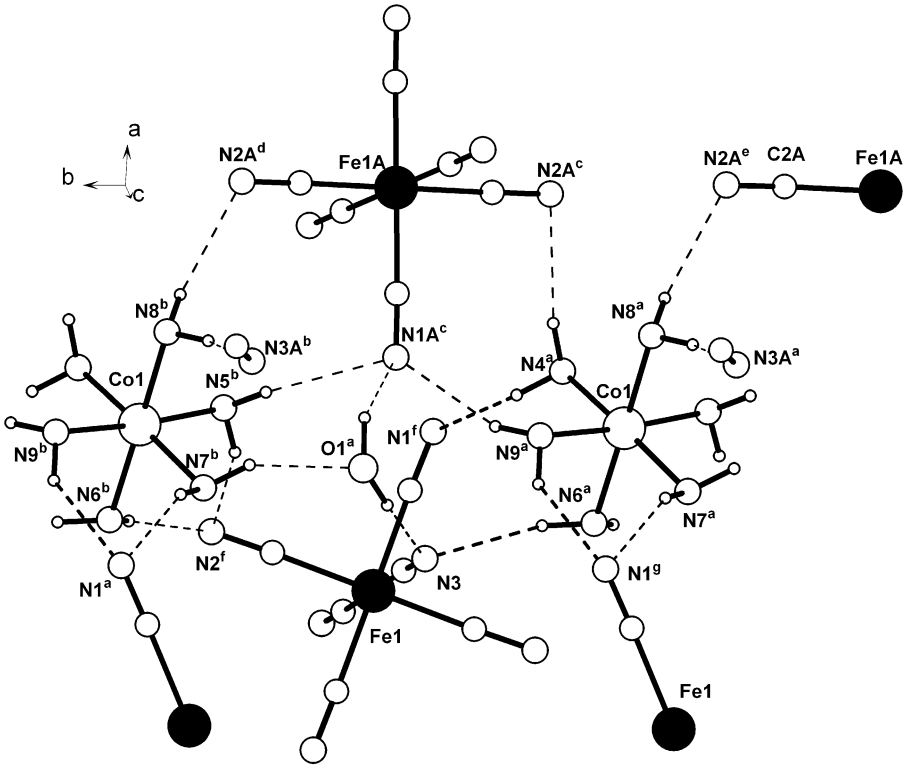

Fig. 4a. Hydrogen bond system in **1**. The methylene groups of ethylenediamine ligands were omitted for the sake of clarity. Symmetry codes: (a) $-x$, $1/2+y$, $1/2-z$; (b) $-x$, $3/2+y$, $1/2-z$; (c) $-x$, $-1-y$, $-z$; (d) $1+x$, $1+y$, z; (e) $1+x$, y, z; (f) $-x$, $-y$, $-z$; (g) $-x$, $-1/2+y$, $1/2-z$.

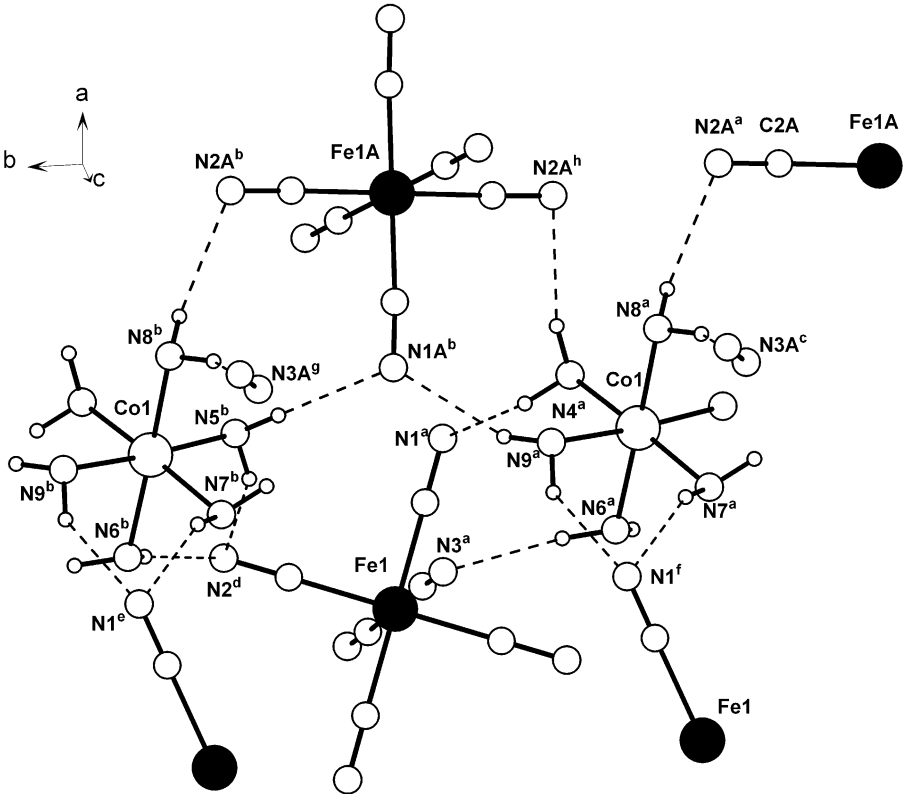

Fig. 4b. Hydrogen bond system in **2**. The methylene groups of ethylenediamine ligands were omitted for the sake of clarity. Symmetry codes: (a) $1-x$, $-y$, $1-z$; (b) $1-x$, $1-y$, $1-z$; (c) x, $1/2-y$, $-1/2+z$; (d) $1+x$, y, $-1+z$; (e) $1-x$, $1/2+y$, $3/2-z$; (f) $1-x$, $-1/2+y$, $3/2-z$; (g) x, $3/2-y$, $-1/2+z$; (h) x, $-1+y$, $-1+z$.

The crystal water molecule is situated in the space between both the complex ions in **1** and is involved in three hydrogen bonds. The oxygen atom of the water molecule acts as a donor in O–H···N hydrogen bonds and as an acceptor in N7–H7D···O1 ones (Table 3). The remaining hydrogen atoms from the amine group are involved in N–H···N(C) hydrogen bonds with N···N(C) distances in the range 2.848(3)–3.240(3) Å, and thus contribute to the stabilization of the crystal structure of **1**. In the anhydrous complex **2**, only N–H···N(C) hydrogen bonds are present with N···N(C) distances lying in the interval 2.890(8)–3.235(8) Å. A part of the crystal structure of **1** and **2** is depicted in Figs. 4a and 4b, respectively.

Additional structural information can be deduced from the comparison of hydrogen bond parameters in both compounds. As it can be seen from Table 3, almost all N–H···N(C) hydrogen bonds in compound **2** are shorter in comparison to **1**, indicating a somewhat higher contribution to the stabilization of the structure **2**, and moreover compensating the absence of the stabilization effect of the three medium hydrogen bonds in which the water molecules are involved in **1**. We assume that this ability to reinforce the hydrogen bond system after the loss of water molecules can be the reason for the fact that the crystal structure did not collapse during the heating process and the single crystal character was preserved. Moreover, the requirement to re-arrange the hydrogen bond system in **2** is most probably the reason for the above-mentioned changes in the coordination spheres of the Co1 and Fe1 central atoms.

3.3. Mössbauer study of *1* and *2*

The room temperature Mössbauer spectrum of $[Co(en)_3][Fe(CN)_6]\cdot H_2O$ (**1**) is depicted in Fig. 5. The room temperature Mössbauer spectra of both complex **1** and the dehydrated $[Co(en)_3][Fe(CN)_6]$ complex **2** reveal a doublet with almost the same isomer shift parameter

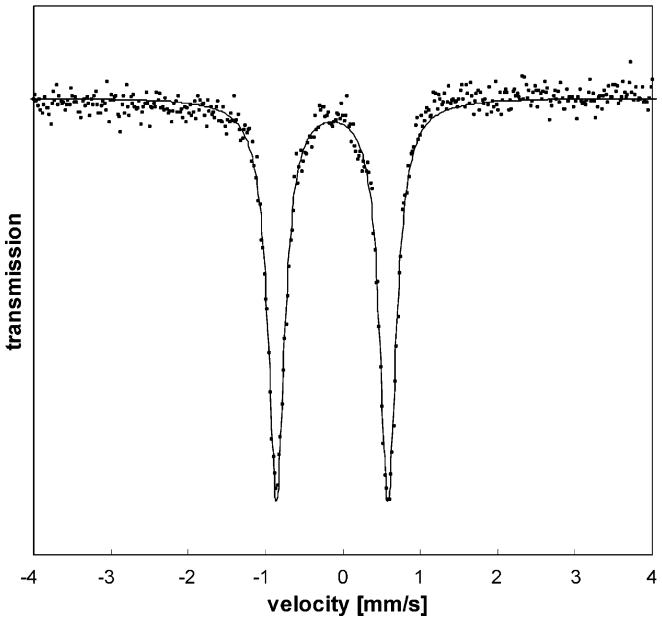

Fig. 5. The room temperature Mössbauer spectrum of **1**.

(−0.13 to −0.14 mm/s) characteristic for low-spin Fe^{3+} ions. Nevertheless, the dehydrated compound **2** exhibits significantly lower quadrupole splitting (0.99 mm/s) compared to the starting complex **1** (1.45 mm/s). This reflects an increase of the general symmetry of the iron environment due to the dehydration process. Such changes in quadrupole splitting parameters, depending on the number of water molecules and cation composition, were previously observed in Mössbauer spectra of various hexacyanoferrates(III) (see Table 4). The room temperature Mössbauer spectrum of the sample **1a** prepared by heating **1** up to 100 °C and occurring in an advanced dehydration stage (68%) is shown in Fig. 6. The fitting procedure gives clear evidence for the coexistence of both complexes **1** and **2**.

Table 4
Mössbauer parameters of **1** at room temperature and at ca. 100 °C (**1a**), and their comparison with the parameters of similar complexes involving $[Fe(CN)_6]^{3-}$ anions

Sample	δ (mm/s)	ΔE_Q (mm/s)	Γ (mm/s)	RA (%)	Assignment	Reference
1	−0.13	1.43	0.26	100	$[Co(en)_3][Fe(CN)_6]\cdot H_2O$	this work
1a	−0.13	1.45	0.26	32.0	$[Co(en)_3][Fe(CN)_6]\cdot H_2O$	this work
	−0.14	0.99	0.30	68.0	$[Co(en)_3][Fe(CN)_6]$	this work
	−0.14[a]	1.29	0.26	100	$Ba_3[Fe(CN)_6]_2$	[39]
	−0.16[a]	0.85	0.476	100	$Ni_3[Fe(CN)_6]_2$	[39]
	−0.16[a]	0.0		100	$La[Fe(CN)_6]\cdot 5H_2O$	[41]
	−0.16[a]	0.73		100	$La[Fe(CN)_6]\cdot 4H_2O$	[41]
	−0.15	0.54		100	$La[Fe(CN)_6]\cdot 3Gly\cdot 2H_2O$	[41]
	−0.09	1.40		100	$K[Mn(tmsalen)]_2[Fe(CN)_6]$	[59]
	−0.13	1.06		100	$\{N(C_2H_5)_4\}[Mn(salen)]_2[Fe(CN)_6]$	[59]

δ – isomer shift related to metallic iron, ΔE_Q – quadrupole splitting parameter, RA – relative spectrum area, Γ – full width of spectral line at a half maximum.

[a] δ values recalculated from sodium nitroprusside to metallic iron.

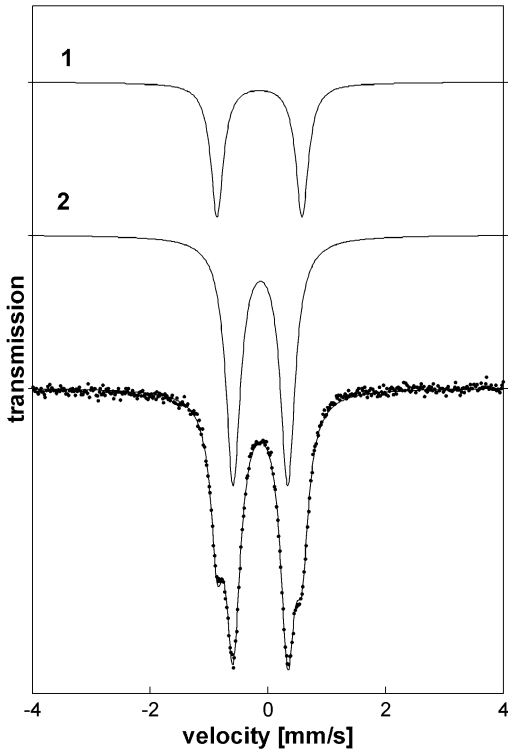

Fig. 6. A representative Mössbauer spectrum of sample **1a** prepared by dynamic heating of **1** up to 100 °C, exhibiting the coexistence of both complexes **1** [bottom] and **2** [top].

4. Supplementary materials

Crystallographic data for the compounds **1** and **2** have been deposited with the Cambridge Crystallographic Data Centre, CCDC nos. 290548 (for **1**) and 290549 (for **2**). Copies of the information may be obtained free of charge from The Director, CCDC, 12 Union Road, Cambridge CB2 1EZ, UK (fax: +44 122 3336033; e-mail: deposit@ccdc.cam.ac.uk or www: http://www.ccdc.cam.ac.uk).

Acknowledgements

We acknowledge the financial support from the Slovak Ministry of Education – VEGA (a Grant No. 1/3550/06), APVT (a Grant No. 20-05204), and The Czech Ministry of Education, Youth and Sports (Grant Nos. 1M6198959201 and MSM6198959218).

References

[1] M. Hartmann, E.W. Grabner, P. Bergveld, Sens. Actuat. 4 (1991) 333.
[2] A.A. Karyakin, Electroanalysis 13 (2001) 813.
[3] D.M. DeLongchamp, P.T. Hammond, Chem. Mater. 16 (2004) 4799(a).
[4] D.M. DeLongchamp, P.T. Hammond, Adv. Func. Mater. 14 (2004) 224(b).
[5] M. Pyrasch, A. Toutianoush, W.Q. Jin, J. Schnepf, B. Tieke, Chem. Mater. 15 (2003) 245.
[6] Y.T. Wang, J.Y. Zhu, R.J. Zhu, Z.Q. Zhu, Z.S. Lai, Z.Y. Chen, Meas. Sci. Technol. 14 (2003) 831.
[7] A.S. Kumar, P.Y. Chen, S.H. Chien, J.M. Zen, Electroanalysis 17 (2005) 210.
[8] I.L. de Mattos, L.V. Lukachova, L. Gorton, T. Laurell, A.A. Karyakin, Talanta 54 (2001) 963.
[9] P.A. Fiorito, V.R. Goncales, E.A. Ponzio, S.I.C. de Torresi, Chem. Commun. 3 (2005) 366.
[10] A. Malinauskas, R. Araminaite, G. Mickeviciute, R. Garjonyte, Mater. Sci. Eng. C 24 (2004) 513.
[11] C. Loos-Neskovic, M. Fedoroff, E. Garnier, D.J. Jones, Adv. Mater. Proces. Mat. Sci. Forum 282-2 (1998) 171.
[12] M. Phillippo, S. Gvozdanovic, D. Gvozdanovic, J.K. Chesters, E. Paterson, C.F. Mills, Veter. Record 122 (1988) 560.
[13] L. Roberts, Science 238 (1987) 1028.
[14] J. Larionova, S. Willemin, B. Donnadieu, B. Henner, Ch. Guerin, B. Gillon, A. Goujon, J. Phys. Chem. Solids 65 (2004) 677.
[15] W.T. Chen, L.Z. Cai, A.Q. Wu, G.C. Guo, J.S. Huang, Z.C. Dong, A. Matsushita, Chin. J. Inorg. Chem. 20 (2004) 693.
[16] X.P. Shen, S. Gao, G. Yin, K.B. Yu, Z. Xu, New J. Chem. 28 (2004) 996.
[17] M. Verdaguer, F. Villain, R. Ouahès, N. Galvez, R. Garde, G. Keller, F. Tournilhac, Polyhedron 24 (2005) 2906.
[18] S. Ferlay, R. Mallah, P. Ouahes, P. Veillet, M. Verdaguer, Nature 378 (1995) 701.
[19] S. Ohkoshi, T. Nuida, T. Matsuda, H. Tokoro, K. Hashimoto, J. Mater. Chem. 15 (2005) 3291.
[20] O. Sato, J. Photochem. Photobiol. C – Photochem. Rev. 5 (2004) 203.
[21] F. Varret, K. Boukheddaden, E. Codjovi, I. Maurin, H. Tokoro, S. Ohkoshi, K. Hashimoto, Polyhedron 24 (2005) 2857.
[22] A. Goujon, F. Varret, V. Escax, A. Bleuzen, M. Verdaguer, Polyhedron 20 (2001) 1339.
[23] N. Shimamoto, S. Ohkoshi, O. Sato, K. Hashimoto, Inorg. Chem. 41 (2002) 678.
[24] A. Bleuzen, V. Escax, A. Ferrier, F. Villain, M. Verdaguer, P. Munsch, J.P. Itie, Angew. Chem., Int. Ed. 43 (2004) 3728.
[25] O. Sato, T. Iyoda, A. Fujishima, K. Hashimoto, Science 272 (1996) 704.
[26] A. Bleuzen, C. Lomenech, A. Dolbecq, F. Villain, A. Goujon, O. Roubeau, M. Nogues, F. Varret, F. Baudelet, E. Dartyge, C. Giorgetti, J.J. Gallet, C. Cartier dit Moulin, M. Verdaguer, Mol. Cryst. Liq. Cryst. Technol. Sect. A 335 (1999) 965.
[27] M. Shimamoto, S. Ohkoshi, O. Sato, K. Hashimoto, Mol. Cryst. Liq. Cryst. 344 (2000) 95.
[28] P.V. Bernhardt, M. Martinez, Inorg. Chem. 38 (1999) 424.
[29] P.V. Bernhardt, B.P. Macpherson, M. Martinez, Inorg. Chem. 39 (2000) 5203.
[30] P.V. Bernhardt, B.P. Macpherson, M.J. Martinez, J. Chem. Soc., Dalton Trans. (2002) 1435.
[31] P.V. Bernhardt, F. Bozoglián, B.P. Macpherson, M. Martínez, Coord. Chem. Rev. 249 (2005) 1902.
[32] C.P. Berlinguette, A. Dragulescu-Andrasi, A. Sieber, J.R. Galán-Mascarós, H.U. Güdel, C. Achim, K.R. Dunbar, J. Am. Chem. Soc. 126 (2004) 6222.
[33] R. Billing, A. Vogler, J. Photochem. Photobiol. A 103 (1997) 239.
[34] C.H. Langford, R.L.P. Sasseville, Can. J. Chem. 59 (1981) 647.
[35] J.F. Jiang, A. Acunzo, S.A. Koch, J. Am. Chem. Soc. 123 (2001) 12109.
[36] D.B. Soria, M.E. Chacón Villalba, O.E. Piro, P.J. Aymonino, Polyhedron 21 (2002) 1767.
[37] B. Kersting, D. Siebert, D. Volkrner, M.J. Kolm, C. Janiak, Inorg. Chem. 38 (1999) 3871.
[38] L.D. Bok, J.G. Leipoldt, S.S. Basson, Z. Anorg. Allg. Chem. 389 (1972) 307.
[39] E. Reguera, J. Férnandez-Bertrán, Hyperfine Interact. 88 (1994) 49.
[40] E. Reguera, J. Férnandez-Bertrán, J. Radioanal. Nucl. Chem. Lett. 5 (1995) 443.

[41] J. Fernández-Bertrán, E. Reguera, A. Dago, C. López-Hernández, G. Infante, Polyhedron 15 (1996) 315.
[42] X.L. Xu, R.E. Emmenegger, F. Hulliger, Eur. J. Solid State Inorg. Chem. 27 (1990) 537.
[43] J. Greve, I. Jess, C. Nather, J. Sol. State. Chem. 175 (2003) 328.
[44] M. Mal'arová, J. Kuchár, J. Černák, W. Massa, Acta Crystallogr., Sect. C 59 (2003) m280.
[45] J. Kuchár, J. Černák, W. Massa, Acta Crystallogr., Sect. C 60 (2004) m418.
[46] W.C. Fernelius, Inorganic Syntheses, Vol. II, McGraw-Hill Book Company, New York, 1964, p. 221.
[47] Oxford Diffraction, CrysAlis RED and CrysAlis CCD software (Ver. 1.171.1), Oxford Diffraction Ltd., Abingdon, Oxfordshire, 2003, England.
[48] A. Altomare, M.C. Burla, M. Camalli, G.L. Cascarano, C. Giacovazzo, A. Guagliardi, A.G.G. Moliterni, G. Polidori, R. Spagna, J. Appl. Crystallogr. 32 (1999) 115.
[49] L.J. Farrugia, J. Appl. Crystallogr. 32 (1999) 837.
[50] G.M. Sheldrick, Institüt für Anorganische Chemie der Universität Göttingen, D-3400 Göttingen, Germany, 1998.
[51] K. Brandenburg, DIAMOND, Release 2.1e, Crystal Impact GbR, Bonn, Germany, 2000.
[52] J. Černák, I. Potočňák, J. Chomič, J. Therm. Anal. 39 (1993) 849.
[53] T. Nakashima, J. Mishiro, M. Ito, G. Kura, Z. Ikuta, N. Matsumoto, K. Nakajima, M. Kojima, Inorg. Chem. 42 (2003) 2323.
[54] M.C. Moron, F. Palacio, J. Pons, J. Casabo, X. Solans, K.E. Merabet, D. Huang, X. Shi, B.K. Teo, R.L. Carlin, Inorg. Chem. 33 (1994) 746.
[55] X. He, P. Zhang, T.Y. Song, Z.Ch. Mu, J.H. Yu, Y. Wang, J.N. Xu, Polyhedron 23 (2004) 2153.
[56] S.R. Nicketic, K.J. Rasmussen, Acta Chem. Scand. A32 (1978) 391.
[57] B. Yan, H.D. Wang, Z.D. Chen, J. Mol. Struct. 569 (2001) 65.
[58] A.M. Christofi, P.J. Garratt, G. Hogarth, A.J. Ibbett, Yu-Fai Ng, J.W. Steed, Tetrahedron 58 (2002) 4543.
[59] S. Iijima, F. Mizutani, H. Miyasaka, N. Matsumoto, H. Okawa, Z. Naturforch. 57 (2002) 603.

three complexes which show 1D and 2D polymeric structures, and found that weak interactions and hydrogen bonds, such as Ag···Ag, Ag···O, Cu···O, C–H···π and C–H···O, play important roles in linking the structures to form 3D supramolecular structures. The syntheses and crystal structures of $[Ag(PPIA)\cdot H_2O]_n$ (PPIA = 3-pyridinepropionic acid) (**1**), $[Cu(PPIA)_2\cdot 2H_2O]_n$ (**2**), and $[Zn(PPIA)_2(H_2O)_2]_n$ (**3**), form the subject of this report.

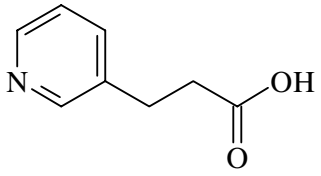

PPIA

2. Experimental

2.1. General procedures

The IR spectra were recorded on a Bio-Rad FTs-7 spectrometer. Elemental analyses were obtained from a PE 2400 series II CHNS/O analyzer, Perkin–Elmer CHN-2400 analyzer or HERAEUS VaruoEL analyzer.

2.2. Starting materials

The complexes $AgNO_3$, $Zn(NO_3)_2\cdot 6H_2O$ and $Cu(NO_3)_2\cdot 6H_2O$ were used as obtained from commercial sources without further purification. The reagent PPIA (PPIA = 3-pyridinepropionic acid) was purchased from Aldrich.

2.3. Preparation of $[Ag(PPIA)\cdot H_2O]_n$ (*1*)

$AgNO_3$ (0.17 g, 1.0 mmol) and PPIA (0.15 g, 1.0 mmol) were placed in a flask containing 15 mL CH_3OH. The mixture was stirred at room temperature for 20 h to yield a white precipitate. The solid was filtered out, washed with diethyl ether (2 × 10 ml) and dried under vacuum to give a white powder. Yield: 0.21 g, (76.1%). *Anal*. Calc. for $C_8H_{10}AgNO_3$ (MW = 276.04): C, 34.81; H, 3.65; N, 5.07. Found: C, 34.69; H, 3.46; N, 5.28%. IR (KBr disk, cm^{-1}): 3409(br), 3034(m), 2921(m), 2406(m), 1972(m), 1715(m), 1567(m), 1482(m), 1419(m), 1333(s), 1310(m), 1222(m), 1125(m), 1068(m), 1008(m), 909(m), 810(m), 699(m), 652(m), 634(m).

2.4. Preparation of $[Cu(PPIA)_2\cdot 2H_2O]_n$ (*2*)

$Cu(NO_3)_2\cdot 6H_2O$ (0.30 g, 1.0 mmol) was added to a MeOH solution (20 mL) containing PPIA (0.30 g, 2.0 mmol). The mixture was then refluxed for 20 h to afford

Table 1
Crystal data for **1**–**3**

Formula	$C_8H_{10}AgNO_3$	$C_{16}H_{20}CuN_2O_6$	$C_{16}H_{20}ZnN_2O_6$
F_w	276.04	399.88	401.71
Crystal system	triclinic	orthorhombic	monoclinic
Space group	$P\bar{1}$	*Pbca*	$P2_1/n$
a (Å)	4.8828(11)	9.0572(7)	9.5055(9)
b (Å)	8.2018(18)	11.195(3)	8.7994(6)
c (Å)	11.813(3)	31.898(2)	9.9916(12)
α (°)	100.548(4)	90	90
β (°)	98.494(3)	90	103.905(7)
γ (°)	104.797(4)	90	90
V (Å^3)	440.19(17)	3234.3(8)	811.23(14)
Z	2	8	2
D_{calc} (g/cm^3)	2.083	1.757	1.645
Crystal size (mm)	0.35 × 0.35 × 0.72	1.00 × 0.40 × 0.30	0.80 × 0.80 × 0.20
μ (Mo Kα) (mm^{-1})	2.261	1.611	1.551
Range (2θ) for data collection (°)	$5.28 \leqslant 2\theta \leqslant 50.02$	$5.10 \leqslant 2\theta \leqslant 49.98$	$5.32 \leqslant 2\theta \leqslant 48.98$
Temperature (°C)	25	25	25
Limiting indices	$-5 \leqslant h \leqslant 5$, $-9 \leqslant k \leqslant 8$, $-11 \leqslant l \leqslant 14$	$0 \leqslant h \leqslant 10$, $0 \leqslant k \leqslant 13$, $0 \leqslant l \leqslant 37$	$0 \leqslant h \leqslant 11$, $0 \leqslant k \leqslant 10$, $-11 \leqslant l \leqslant 11$
Independent reflections [R_{int}]	1544 [0.0225]	2810 [0.0000]	1448 [0.0350]
Refinement method	full-matrix least-squares on F^2	full-matrix least-squares on F^2	full-matrix least-squares on F^2
Data/restraints/parameters	1514/0/151	2810/0/199	1373/0/155
Quality-of-fit indicator[c]	1.008	1.232	1.030
Final R indices [$I > 2\sigma(I)$][ab]	$R_1 = 0.0220$, $wR_2 = 0.0493$	$R_1 = 0.0489$, $wR_2 = 0.1101$	$R_1 = 0.0313$, $wR_2 = 0.0661$
R indices (all data)	$R_1 = 0.0232$, $wR_2 = 0.0500$	$R_1 = 0.0646$, $wR_2 = 0.1201$	$R_1 = 0.0395$, $wR_2 = 0.0700$
Largest difference in peak and hole (e/Å^3)	0.689 and −0.423	1.147 and −0.560	0.327 and −0.654

[a] $R_1 = \sum||F_o| - |F_c||/\sum|F_o|$.

[b] $wR_2 = [\sum w(F_o^2 - F_c^2)^2/\sum w(F_o^2)^2]^{1/2}$. $w = 1/[\sigma^2(F_o^2) + (ap)^2 + (bp)]$, $p = [\max(F_o^2 \text{ or } 0) + 2(F_c^2)]/3$. $a = 0.0000$, $b = 1.1818$ for **1**; $a = 0.0000$, $b = 28.8445$ for **2**; $a = 0.0000$, $b = 1.7549$ for **3**.

[c] Quality-of-fit $= \left[\sum w(|F_o^2| - |F_c^2|)^2/N_{observed} - N_{parameters}\right]^{1/2}$.

a light blue solution and a blue solid. The precipitate was filtered and washed with ether (3×10 ml) and then dried under reduced pressure to give a blue solid. Yield: 0.45 g (56.3%). *Anal*. Calc. for $C_{16}H_{20}CuN_2O_6$ (MW = 399.88), C, 48.06; H, 5.04; N, 7.01; Found: C, 47.74; H, 5.03; N, 6.67%. IR (KBr disk, cm^{-1}): 3469(br), 3043(m), 2921(m), 2406(m), 1972(m), 1718(m), 1609(m), 1549(m), 1469(m), 1437(s), 1305(m), 1225(m), 1045(m), 1030(m), 771(m), 677(m). Blue crystals suitable for X-ray crystallography were obtained by slow diffusion of ether into a MeOH solution of **2**.

2.5. Preparation of $[Zn(PPIA)_2(H_2O)_2]_n$ (3)

$Zn(NO_3)_2 \cdot 6H_2O$ (0.297 g, 1.0 mmol) and PPIA (0.30 g, 2.0 mmol) were placed in a flask containing 15 mL CH_3OH. The mixture was stirred at room temperature for 20 h to yield a white precipitate. The solid was filtered out, washed with diethyl ether (2×10 ml) and dried under vacuum to give a white powder. Yield: 0.49 g (61.0%). *Anal*. Calc. for $C_{16}H_{20}ZnN_2O_6$ (MW = 401.71): C, 47.84; H, 5.02; N, 6.97. Found: C, 47.48; H, 4.96; N, 7.02%. IR (KBr disk, cm^{-1}): 3571(br), 3068(m), 2933(m), 2000(m), 1906(m), 1722(m), 1611(m), 1564(m), 1470(m), 1445(m), 1399(m), 1338(m), 1310(s), 1270(m), 1257(m), 1223(m), 1181(m), 1112(m), 1046(m), 981(m), 957(m), 836(m), 740(m), 676(m), 585(m). Colorless crystals suitable for X-ray crystallography were obtained by slow diffusion of diethyl ether into a MeOH solution of **3** over three days.

3. X-ray crystallography

The diffraction data of **1**–**3** were collected on a Siemens CCD diffractometer, which was equipped with graphite-monochromated Mo Kα (Kα = 0.71073 Å) radiation. Data reduction were carried by standard methods with the use of well-established computational procedures [10]. A colorless crystal of **1** was mounted on the top of a glass fiber with

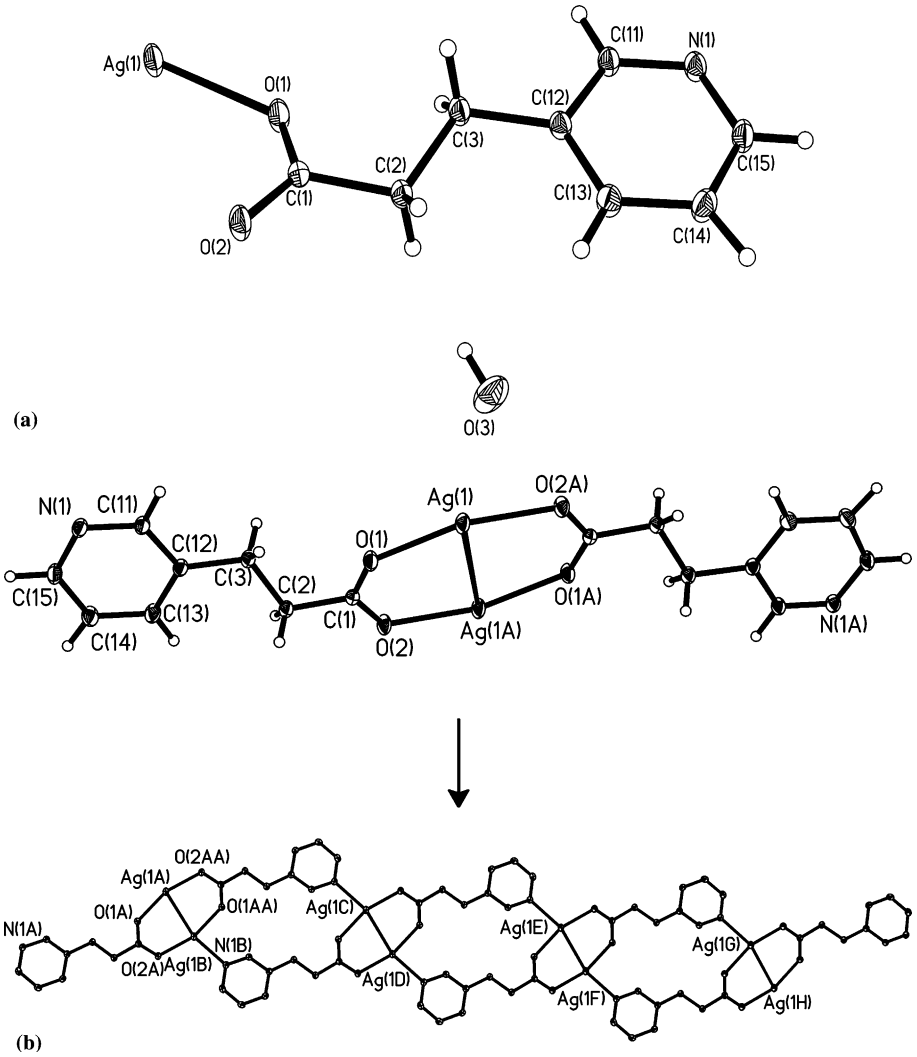

Fig. 1. (a) ORTEP drawing of the asymmetric unit of complex **1**. (b) An ORTEP drawing showing the coordination geometry of the silver metal center and the $Ag_2(PPIA)_2$ building blocks bound together by Ag–N bonds into a one-dimensional chain in **1**. Ellipsoids are scaled to enclose 20% of the electron density.

epoxy cement. The hemisphere data collection method were used to scan the data points at $5.28 < 2\theta < 50.02°$. The structure factors were obtained after Lorentz and polarization corrections. The positions of some of the heavier atoms, including the silver atom, were located by the direct method. The remaining atoms were found in a series of alternating difference Fourier maps and least-square refinements [11]. The final residuals of the final refinement were $R_1 = 0.0220$, $wR_2 = 0.0493$. The crystallographic procedures for **2** and **3** were similar to those for **1**. Basic information pertaining to crystal parameters and structure refinement is summarized in Table 1.

4. Results and discussion

4.1. Syntheses and spectroscopic studies

The reactions of 3-pyridinepropionic acid with $AgNO_3$, $Cu(NO_3)_2 \cdot 6H_2O$ and $Zn(NO_3)_2 \cdot 6H_2O$ in $MeOH/H_2O$ afforded complexes $[Ag(PPIA) \cdot H_2O]_n$ (PPIA = 3-pyridinepropionic acid) (**1**), $[Cu(PPIA)_2 \cdot 2H_2O]_n$ (**2**), and $[Zn(PPIA)_2(H_2O)_2]_n$ (**3**), respectively. For the complexes **1**–**3** and the PPIA ligand, the broad band centered at ca. 3400–3500 cm^{-1} indicates the O–H stretching of the carboxylic group or water molecules. The IR spectrum of the PPIA ligand suggests that the characteristic absorption bands of the COOH group occur at 1715 and 1482 cm^{-1}. For the complexes **1**–**3**, the peaks at 1567, 1609 and 1611 cm^{-1}, respectively, are attributed to the antisymmetric stretching vibrations, and 1419, 1399 and 1399 cm^{-1} to the symmetric vibrations of the carboxylic groups. Furthermore, the difference in values of the carboxylate group vibrations are 148, 210 and 212 cm^{-1} for **1**–**3**, respectively, agreeing with their solid state structural features [12].

4.2. Structure of $[Ag(PPIA) \cdot H_2O]_n$ (1)

Complex **1** crystallizes in the triclinic space group $P\bar{1}$. The asymmetric unit of **1**, Fig. 1(a), contains one Ag atom, one PPIA group and one included water molecule. The structure of complex **1**, emphasizing the environment around the silver, is shown in Fig. 1(b). Each Ag(I) center

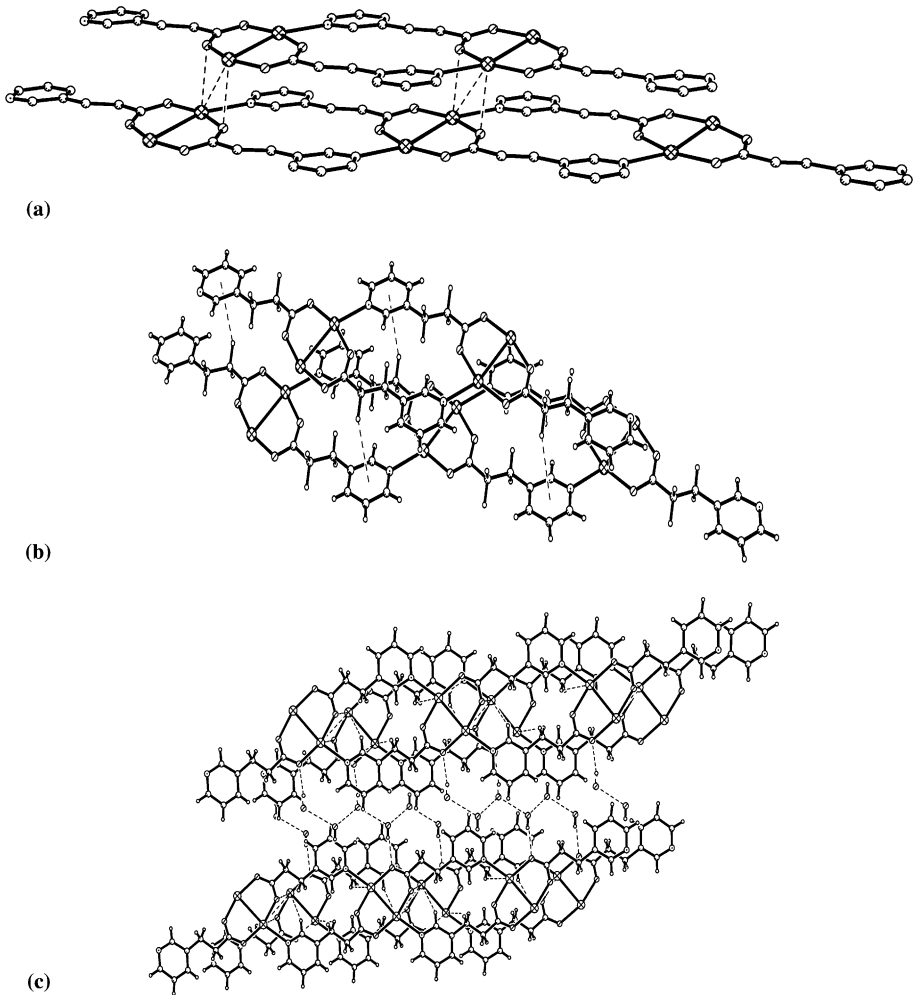

Fig. 2. (a) An ORTEP diagram showing the 1D chains penetrating into each other through Ag···Ag and Ag···O interactions in **1**. (b) An ORTEP diagram showing the set of one-dimensional chains stacking together through interchain C–H···π interactions in **1**. (c) An ORTEP diagram showing the 1D chains penetrating into each other through O–H···O interactions, forming a 3D supramolecular structure that is occupied by the water molecules in **1**.

lies in a distorted T-shaped coordination environment $\{AgNO_2\}$ consisting of one pyridyl nitrogen donor from one PPIA ligand (Ag(1)–N(1B) = 2.366(3) Å), and two oxygen atoms from different bridging carboxylate groups (Ag(1)–O(1) = 2.245(2) and Ag(1)–O(2A) = 2.216(2) Å). It is interesting that the tridentate PPIA ligand is coordinated to the silver center by the Ag–N bonds, linking $\{Ag_2(PPIA)_2\}$ building blocks into a one-dimensional polymeric chain (Fig. 1(b)). The Ag···Ag separation distance in the $\{Ag(PPIA)\}_2$ building block is 2.9203(7) Å, and the Ag···Ag separation distance in the 1D polymeric chain by the bridging PPIA ligand is 9.622 Å. The carboxylate groups of the PPIA ligand bridging silver centers form an eight-member ring $\{Ag_2O_4C_2\}$, while the 16-member ring $\{Ag_2O_2N_2C_{10}\}$ is formed by two silver atoms bonded to the pyridyl nitrogen donors and the carboxylate oxygen atoms of two bridging PPIA ligands in 1D chains.

The chains are further linked through extensive Ag···Ag and Ag···O weak interactions (Fig. 2(a)). The Ag···Ag distance is 3.539 Å, while the Ag···O distance is 2.977 Å, with the Ag(I) atom linking with the oxygen atom of a carboxylate group. The C–H···π type of interaction, from the methylene hydrogen atoms of the PPIA ligand to the center of the pyridyl ring of the other chain (H···π = 2.995 Å, ∠C–H···π = 145.8°), Fig. 2(b), were found in the structure. The hydrogen atoms of the water molecules also interact with the carboxylate oxygen atoms (H···O = 2.050 Å, ∠O–H···O = 168.7°) of the adjacent chains to form a 3D supramolecular structure. (Fig. 2(c)).

Complex **1** is in marked contrast to some Ag(I) complexes containing pyridine carboxylate ligands. The structure of $\{[Ag(Isonic)(HIsonic)]_{0.5}\cdot[Ag(Isonic)]\}_n$ (Isonic = the anion of isonicotinic acid) [13] consists two different of 1D chains; the hydrogen bonded assembly $[Ag(Isonic)(HIso)]_{0.5}$ and a wavy [Ag(Isonic)] polymeric chain. The complex $[Ag(nic)]_n$ (nic = the anion of nicotinic acid), [14] shows 1D zigzag chains of silver atoms, while each Ag atom is fivefold linked to two oxygen atoms of two different nicotinate ligands, to one nitrogen atom of a third nicotinate and to two other Ag atoms, having a dissymmetric

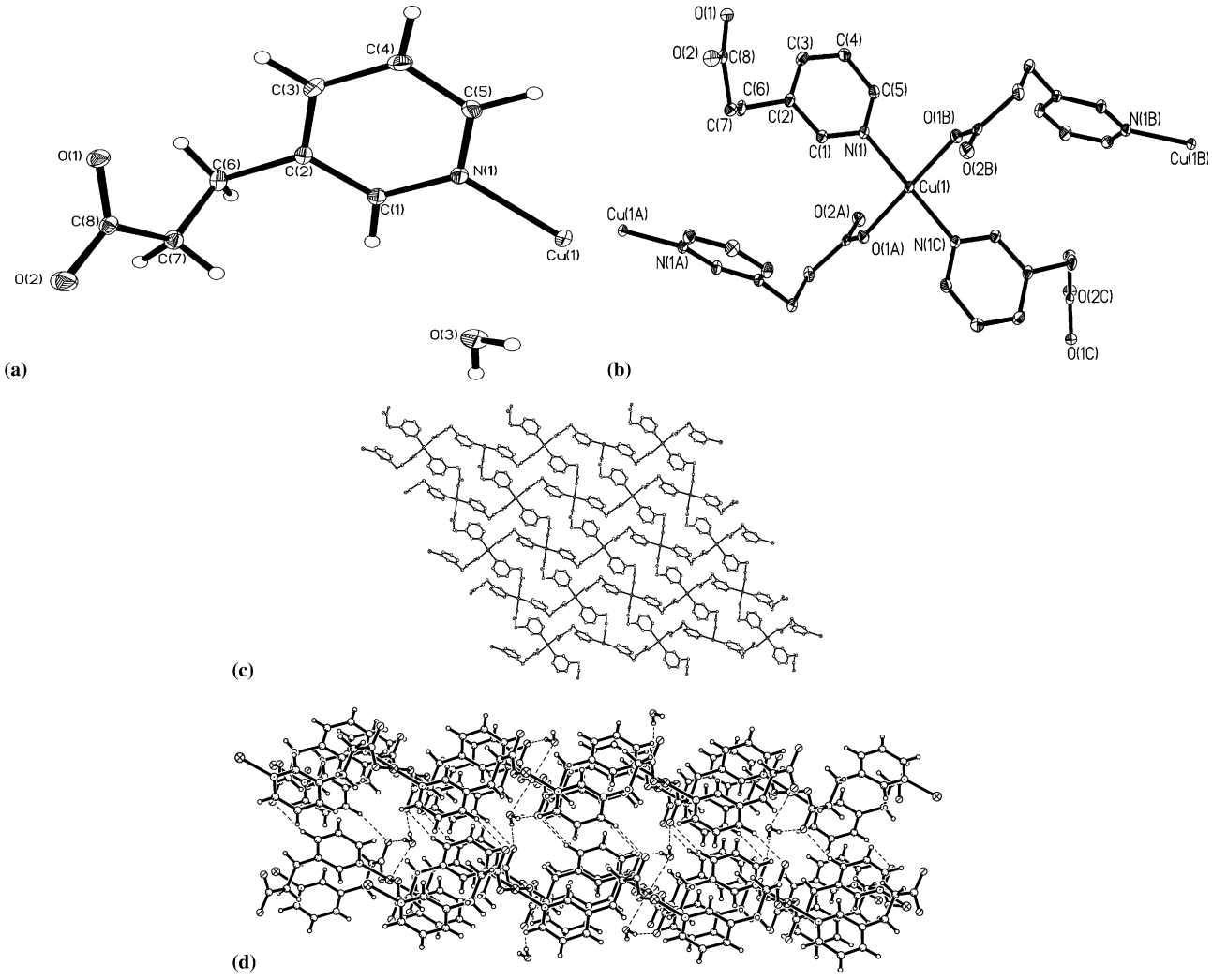

Fig. 3. (a) ORTEP drawing of the asymmetric unit of complex **2**. (b) An ORTEP drawing showing the coordination geometry of the copper metal center in **2**. (c) A 2D wave-like layer in **2** along the *c* axis. (d) Packing structure of **2** along the *b* axis showing the X–H···O (X = C or O) hydrogen bondings among the layers.

trigonal bipyramid geometry. The reaction of $AgBF_4$ with isonicotinic acid led to the polymeric structure $\{[Ag_3(Isonic)_2]BF_4\}_n$ [15] consisting of Ag_3 triangles linked together by two isonicotinate ligands. The structure of polymeric $[Ag(nic)]_n$ is based on three-coordinate silver complex units which form the 1D helical chain, while $\{NH_4[Ag(nic)_2]\cdot H_2O\}_n$ shows 1D zigzag chains with the Ag(I) center adopting a distorted trigonal planar geometry. [16] The structure of $H[Ag(nic)_2]$ can be described as a 1D polymeric chain consisting of $[Ag(nic)_2]^-$ monomers linked via O···H···O hydrogen bondings [17].

4.3. Structure of $[Cu(PPIA)_2\cdot 2H_2O]_n$ (2)

Complex **2** was solved in the orthorhombic space group *Pbca*. The Cu(II) ion is at the center of symmetry. Thus, each asymmetric unit of **2** consists of one Cu(II) atom, a PPIA group and one free water molecule (Fig. 3(a)). The central Cu(II) ion is coordinated by two *trans* monodentate carboxylate groups from different PPIA ligands (Cu(1)–O(1A) = 1.9968(12) Å), and two *trans* pyridyl nitrogen atoms (Cu(1)–N(1) = 2.0254(14) Å) (Table 2). The overall coordination geometry about Cu(II) is slightly distorted square planar, as shown in Fig. 3(b). PPIA acts as a bridging ligand, through its pyridyl nitrogen atom and monodentate carboxylate group, linking different Cu(II) centers.

Four PPIA ligands ,with a head-to-tail aggregation, link Cu(II) into a $\{Cu(PPIA)\}_4$ 32-member ring. In the $\{Cu(PPIA)\}_4$ ring, the four Cu(II) ions and four PPIA ligands are not coplanar, which may be due to the different arrangement of PPIA and the coordination geometry of the metal ion. The $\{Cu(PPIA)\}_4$ rings are further extended into a 2D layer by sharing Cu(II) joints and PPIA edges, Fig. 3(c). The complex shows a void space with a Cu···Cu separation of 8.648 Å. The layers are further linked through extensive O–H···O (H···O = 1.921–2.133 Å; ∠O–H···O = 161.4–176.0°) and C–H···O (H···O = 2.027 Å; ∠C–H···O = 175.3°) hydrogen bondings and weak Cu···O interactions (Cu···O = 2.467 Å) among the layers Fig. 3(d).

The structure of complex **3** is in marked contrast to that found in the complex $Cu(PPIA)_2(H_2O)_2$, where the flexibility of the aliphatic part of the ligand allows the copper centers' coordinated water molecules to form into buckled layers. [18] The complex $[Cu_{1.5}(3\text{-}PYD)_3(H_2O)]\cdot 1.5H_2O$ is a twofold interpenetrating 3D framework based on $\{Cu(3\text{-}PYD)\}_6$ rings formed through head-to head and

Table 2
Selected bond distances (Å) and angles (°) for **1**–**3**

1			
Bond distances			
Ag(1)–O(2A)	2.216(2)	Ag(1)–O(1)	2.245(2)
Ag(1)–N(1B)	2.366(3)	Ag(1)···Ag(1A)	2.9203(7)
Bond angles			
O(2A)–Ag(1)–O(1)	161.93(8)	O(2A)–Ag(1)–N(1B)	108.92(9)
O(1)–Ag(1)–N(1B)	88.85(9)	O(2A)–Ag(1)–Ag(1A)	87.68(6)
O(1)–Ag(1)–Ag(1A)	74.25(6)	N(1A)–Ag(1)–Ag(1A)	160.43(7)
2			
Bond distances			
Cu(1)–O(1A)	1.9968(12)	Cu(1)–N(1)	2.0254(14)
Bond angles			
O(1A)–Cu(1)–N(1)	90.14(5)		
3			
Bond distances			
Zn(1)–O(1A)	2.109(2)	Zn(1)–O(3)	2.150(2)
Zn(1)–N(1)	2.164(2)		
Bond angles			
O(1A)–Zn(1)–O(3)	93.26(9)	O(1B)–Zn(1)–O(3)	86.74(9)
O(1A)–Zn(1)–N(1)	90.71(9)	O(1B)–Zn(1)–N(1)	89.29(9)
O(3C)–Zn(1)–N(1)	91.55(9)	O(3)–Zn(1)–N(1)	88.45(9)

Symmetry transformations used to generate equivalent atoms: **1**: (A) $-x+2, -y+2, -z$; (B) $-x, -y+1, -z$. **2**: (A) $x+1/2, -y+1/2, z-1/2$; (B) $-x+1/2, y-1/2, -z+5/2$; (C) $-x+1, -y, -z+2$; (D) $-x+1/2, y+1/2, -z+5/2$. **3**: (A) $x-1/2, -y+1/2, z+1/2$; (B) $-x+5/2, y-1/2, -z+3/2$; (C) $-x+2, -y, -z+2$; (D) $-x+5/2, y+1/2, -z+3/2$.

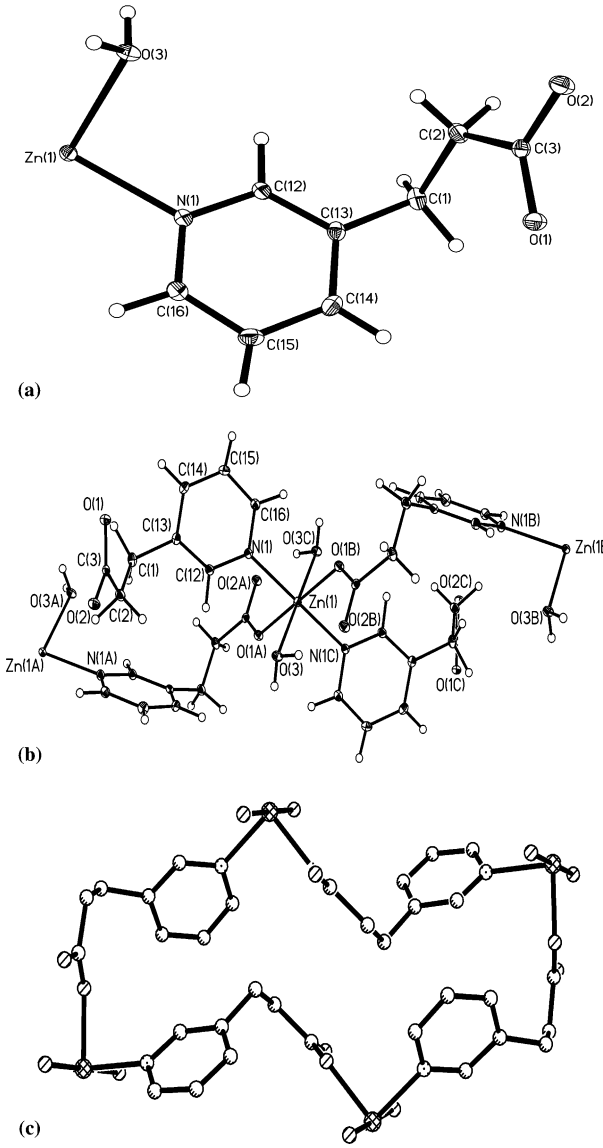

Fig. 4. (a) ORTEP drawing of the asymmetric unit of complex **3**. (b) An ORTEP drawing showing the coordination geometry of the zinc metal center in **3**. (c) $\{Zn(PPIA)\}_4$ rings from a head-to-tail arrangement of PPIA ligands. Ellipsoids are scaled to enclose 20% of the electron density.

head-to-tail mixed arrangements of 3-PYD [19]. The multidimensional Cu(II) coordination polymers $[Cu(Isonic)_2]\cdot EtOH$, $Cu(nic)_2$ [8f], $Cu(nic)_2$ [20], $\{[Cu_2(Isonic)_4\cdot 3H_2O]\cdot [Cu_2(Isonic)_4\cdot 2H_2O]\}\cdot 3H_2O$ [21] and $[Cu(Isonic)_2]\cdot 2H_2O$ [22] were synthesized by treating copper nitrate and copper chloride with isonicotinic acid and nicotinic acid under hydro(solvo)thermal conditions and they show rhombic open channels, pleated sheets, a perpendicular 24-member ring-like framework, mixed 2D and 3D open structures and chessboard tunnels, respectively.

4.4. Structure of $[Zn(PPIA)_2(H_2O)_2]_n$ (3)

Single-crystal X-ray diffraction analysis reveals that **3** is similar to **2**, showing a 2D supramolecular network consisting of $\{Zn(PPIA)\}_4$ rings derived from head-to-tail arranged PPIA ligands. Complex **3** was solved in the monoclinic space group $P2_1/n$. The asymmetric unit of **3**, Fig. 4(a), contains one Zn atom, one PPIA group and one bonded water molecule. Fig. 4(b) shows the coordination geometry about the Zn metal center. The zinc metal center adopts a distorted octahedral coordination geometry with the bond angles significantly deviated from 90° or 180° (Table 2). The Zn atom is bonded to two *trans* pyridyl nitrogen atoms (Zn(1)–N(1) = 2.164(2) Å) and two *trans* monodentate carboxylate groups (Zn(1)–O(1A) = 2.109(2) Å) in the equatorial plane. The Zn atom is also bonded to two H_2O ligands (Zn–O = 2.150(2) Å) in the axial positions to complete the distorted octahedral coordination geometry. Unlike complex **1**, the PPIA ligand bridges Zn(II) through the pyridyl nitrogen atoms and the oxygen atoms of the monodentate carboxylate groups, generating a head-to-tail aggregated $\{Zn(PPIA)\}_4$ 32-member ring, Fig. 4(c). In the $\{Zn(PPIA)\}_4$ ring, the four Zn(II) ions and four PPIA ligands are not coplanar, which may be due to the different arrangement of PPIA and the coordination geometry of the metal ion.

The $\{Zn(PPIA)\}_4$ rings are further extended into a 2D wave-like layer by sharing Zn(II) joints and PPIA edges, Fig. 5(a).The complex shows a void space with a Zn···Zn separation of 8.850 Å. The layers are further linked through extensive C–H···O (H···O = 2.369–2.441 Å; ∠C–H···O = 150.7–171.5°) and O–H···O (H···O = 2.027 Å; ∠O–H···O = 175.3°) hydrogen bondings, Fig. 5(b).

The nets in complex **3** are different from the chiral complex $Zn(nic)_2$ where the pyridine rings of the nicotinate groups intrude into the square cavities to result in interdigitation of the 2D square networks [23]. The noncentrosymmetric $[Zn(pecm)_2(H_2O)]_2\cdot CH_3CN\cdot 3H_2O$ (pecm = 4-[2-(4-pyridyl)ethenyl]cinnamate) adopts a caterpillar 1D chain structure [24] and the complex $[Zn(3\text{-}PYD)_2(H_2O)_2]$ (3-PYD = 3-(3-pyridyl)acrylic acid) shows a 3D supramolecular framework constructed by 1D {Zn(3-PYD)} chains through hydrogen-bonding interactions [19]. The complexes $Zn(nic)_2$ [25] and $Zn(Isonic)_2$ [26] were prepared by hydro(solvo)thermal reactions with 3-cyanopyridine or 4-cyanopyridine and $Zn(ClO_4)_2\cdot 6H_2O$, which exhibit complicated 2D grids with *exo*-tridentate nicotinate groups and 3D diamond-like networks.

5. Conclusion

Reactions of PPIA with different metal ions have afforded three coordination polymers based on $\{Ag(PPIA)\}_2$ and $\{M(PPIA)\}_4$ (M = Cu and Zn) rings or metal-carboxylate chains, respectively. Complex **1** forms 1D molecular chains through Ag···Ag, Ag···O interactions, C–H···π interactions and hydrogen bondings, to form 3D supramolecular structure. Complexes **2** and **3** form 2D layer structures which through hydrogen bondings form 3D

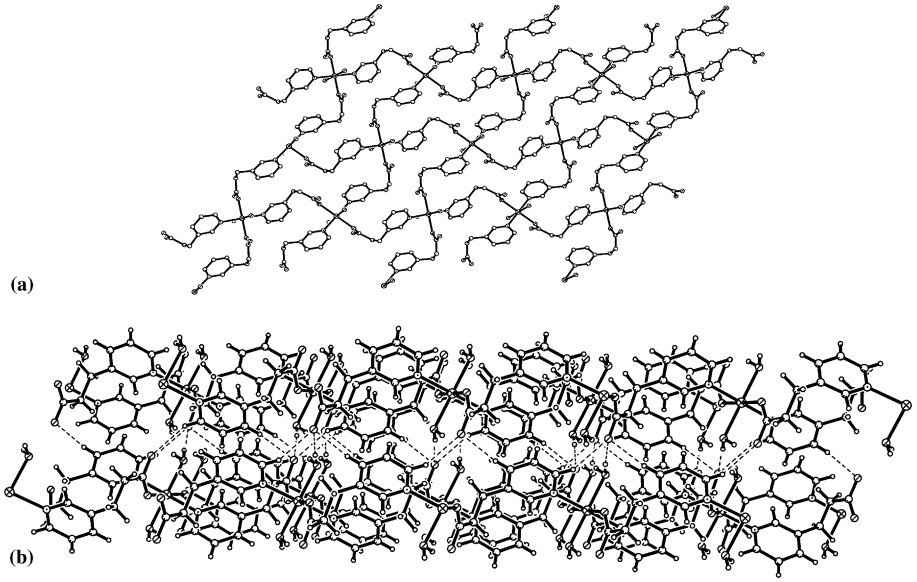

Fig. 5. (a) A 2D wave-like layer in **3** along the *c* axis. (b) Packing structure of **3** along the *b* axis showing the X–H···O (X = C or O) hydrogen bondings among the sheets.

supramolecular structures. Weak interactions like Ag···Ag, Ag···O interactions, C–H···π interactions and hydrogen bondings may play an important role in the self-assembly of such types of structures.

Acknowledgement

The researchers wish to thank the National Science Council of the Republic of China for support.

Appendix A. Supplementary material

Crystallographic data (excluding structure factors) for the structures in this paper has been deposited with the Cambridge Crystallographic Data Centre as supplementary publication numbers CCDC 275207–275209. Copies of the data can be obtained, free of charge, on application to CCDC, 12 Union Road, Cambridge CB2 1EZ, UK, fax: +44(0) 1223 336 033, or e-mail: deposit@ccdc.cam.ac.uk. Supplementary data associated with this article can be found, in the online version, at doi:10.1016/j.poly.2006.04.029.

References

[1] (a) R. Robson, B.E. Abrahams, S.R. batten, R.W. Gable, B.F. Hoskins, J. Lieu, Supramolecular Architecture, ACS Publications, Washington, DC, 1992;
(b) H. Gudbjartson, K. Biradha, K.M. Poirier, M.J. Zaworotko, J. Am. Chem. Soc. 121 (1999) 2599;
(c) S.-I. Noro, R. Kitauta, M. Kondo, S. Kitagawa, T. Ishii, H. Matauzaka, M. Yamashita, J. Am. Chem. Soc. 124 (2002) 2568;
(d) C. Janiak, J. Chem. Soc., Dalton Trans. (2003) 2781;
(e) S. Kitagawa, S. Masaoka, Coord. Chem. Rev. 246 (2003) 73;
(f) S.R. Batten, K.S. Murray, Coord. Chem. Rev. 246 (2003) 103;
(g) S.L. James, Chem. Soc. Rev. 32 (2003) 276.

[2] (a) E. Bakalbassis, C. Tsipis, A. Bozopoulos, W. Dreissig, H. Hartl, J. Mrozinski, Inorg. Chim. Acta 186 (1991) 113;
(b) J. Cano, G.D. Munno, J.L. Sanz, R. Ruiz, F. Lioret, J. Faus, M. Julve, J. Chem. Soc., Dalton Trans (1994) 3465;
(c) R.H. Groeneman, L.R. Macgillvrey, J.L. Atwood, Inorg. Chem. 38 (1999) 208;
(d) L. Deakin, A.M. Arif, J.S. Miller, Inorg. Chem 38 (1999) 5272;
(e) Y. Suenaga, T. Kuroda-Sowa, M. Maekawa, M. Munakata, Polyhedron 18 (1998) 191;
(f) M.-L. Tong, X.-M. Chen, S.W. Ng, Inorg. Chem. Commun. 3 (2000) 436;
(g) C. Richardson, P.J. Steel, Inorg. Chem. Commun. 1 (1998) 260;
(h) M.-L. Tong, X.-M. Chen, B.-H. Ye, S.W. Na, Inorg. Chem. 37 (1998) 5278.

[3] (a) E. Bakalbassis, P. Bergerat, O. Kahn, S. Jeannin, Y. Jeannin, Y. Dromzee, M. Guillot, Inorg. Chem. 31 (1992) 625;
(b) C.S. Hong, Y. Do, Inorg. Chem. 36 (1997) 5684;
(c) G.K.H. Shimizu, G.D. Enright, C.I. Ratcliffe, J.A. Ripmeester, Chem. Commun. (1999) 461;
(d) L. Carlucci, G. Ciani, D.M. Proserpio, Chem. Commun. (1999) 449.

[4] (a) H.J. Choi, M.P. Suh, Inorg. Chem. 38 (1999) 6309;
(b) H.-K. Fun, S.S.S. Raj, R.-G. Xiong, J.-L. Zuo, Z. Yu, X.-Z. You, J. Chem. Soc., Dalton Trans (1999) 1915;
(c) Y. Suenaga, T. Kamiya, T. Kuroda-Sowa, M. Maekawa, M. Munakata, Inorg. Chim. Acta 308 (2000) 17;
(d) W.-M. Bu, L. Ye, Y.-G. Fan, Inorg. Chem. Commun. 3 (2000) 194;
(e) X.-H. Bu, K. Biradha, T. Yamaguchi, M. Nishimura, T. Ito, K. Tanaka, M. Shionoya, Chem. Commun. (2000) 1953;
(f) L. Carlucci, G. Ciani, D.M. Proserpio, A. Sironi, Angew. Chem., Int. Ed. Engl 34 (1995) 1895.

[5] (a) A.J. Blake, N.R. Champness, P. Hubberstey, W.-S. Li, M.A. Withersby, M. Schröder, Coord. Chem. Rev. 183 (1999) 117;
(b) S. Muthu, J.H.K. Yip, J.J. Vittal, J. Chem. Soc., Dalton Trans. (2002) 4561;
(c) C.-W. Yeh, Y.-S. Yen, W.-B. Lin, C.-W. Su, J.-D. Chen, Ju-Chun Wang, Struct. Chem. 16 (2005) 141;
(d) H.-L. Hu, C.-W. Yeh, J.-D. Chen, Eur. J. Inorg. Chem. (2004) 4696.

[6] (a) C.-W. Su, C.-P. Wu, J.-D. Chen, L.-S. Liou, J.-C. Wang, Inorg. Chem. Commun. 5 (2002) 215;
(b) S.-H. Liu, J.-D. Chen, L.-S. Liou, J.-C. Wang, Inorg. Chem. 40 (2001) 6499;
(c) Y.-F. Hsu, J.-D. Chen, Eur. J. Inorg. Chem. (2004) 1488;
(d) C.-W. Yeh, H.-L. Hu, R.-H. Liang, K.-M. Wang, T.-Y. Yen, J.-D. Chen, J.-C. Wang, Polyhedron 24 (2005) 539.

[7] (a) M.-C. Suen, Y.-Y. Wu, G.-C. Dong, J.-D. Chen, T.-C. Keng, J.-C. Wang, J. Chin. Chem. Soc. 49 (2002) 331;
(b) M.-C. Suen, T.-C. Keng, J.-C. Wang, Polyhedron 21 (2002) 2705;
(c) M.-C. Suen, Y.-H. Wang, J.-C. Wang, J. Chin. Chem. Soc. 51 (2004) 43;
(d) C.-W. Yeh, M.-C. Suen, H.-L. Hu, J.-D. Chen, J.-C. Wang, Polyhedron 23 (2004) 1947;
(e) H.-L. Hu, M.-C. Suen, C.-W. Yeh, J.-D. Chen, Polyhedron 23 (2005) 1497.

[8] (a) D. Visinescu, G.I. Pascu, M. Andruh, J. Magull, H.W. Roesky, Inorg. Chim. Acta 340 (2002) 201;
(b) S. Sain, T.K. Maji, G. Mostafa, T.-H. Lu, N.R. Chaudhuri, New J. Chem. 27 (2003) 185;
(c) L. Carlucci, G. Ciani, D.M. Proserpio, S. Rizzato, Chem. Commun. (2001) 1198;
(d) H.-X. Zhang, B.-S. Kang, Z.-Y. Zhou, A.S.C. Chan, Z.-N. Chen, C. Ren, J. Chem. Soc., Dalton Trans (2001) 1664;
(e) P. Ayyappan, O.R. Evans, W. Lin, Inorg. Chem. 40 (2001) 4627;
(f) M.E. Chapman, P. Ayyappan, B.M. Foxman, G.T. Yee, W. Lin, Cryst. Grow. Des. 1 (2001) 159;
(g) D. Visinescu, M. Andruh, A. Müller, M. Schmidtmann, Y. Journaux, Inorg. Chem. Commun. 5 (2002) 42.

[9] (a) S.R. Batten, B.F. Hoskins, R. Robson, Chem. Eur. J. 6 (2000) 156;
(b) D.J. Chesnut, D. Plewak, J. Zubieta, J. Chem. Soc., Dalton Trans (2001) 2567;
(c) S.R. Batten, A.R. Harris, P. Jensen, K.S. Murray, A. Ziebell, J. Chem. Soc., Dalton Trans (2000) 3829;
(d) J.M. Knaust, S.W. Keller, Inorg. Chem. 41 (2002) 5650;
(e) J.Y. Lu, A.M. Babb, Inorg. Chem. 40 (2001) 3261;
(f) J.M. Knaust, S. Lopez, S.W. Keller, Inorg. Chim. Acta 324 (2001) 81.

[10] (a) XSCANS, Release, 2.1, Siemens Energy & Automation, Inc, Madison, WI, USA, 1995.;
(b) SMART/SAINT/ASTRO, Release 4.03, Siemens Energy & Automation, Inc., Madison, WI, USA, 1995.

[11] SHELXTL 5.10. Bruker Analytical X-ray Instruments Inc., Karlsruche, Germany, 1997.

[12] K. Nakamoto, Infrared and Raman Spectra of Inorganic and Coordination Compounds, Wiley, New York, 1986.

[13] B. Cova, A. Briceño, R. Atencio, New J. Chem 25 (2001) 1516.

[14] F. Jaber, F. Charbonnier, R. Faure, M. Petit-Ramel, Z. Krist. 209 (1994) 536.

[15] A.D. Burrows, M.F. Mahon, M.T. Palmer, J. Chem. Soc., Dalton Trans (1998) 1941.

[16] G. Smith, A.N. Reddy, K.A. Byriel, C.H. Kennard, Polyhedron 13 (1994) 2425.

[17] P.-O. Käll, J. Grin, M. Fahlman, F. Söderlind, Polyhedron 20 (2001) 2747.

[18] L.A. Brokowski, C.L. Cahill, Acta Crystallogr., Sect. E 59 (2003) m1127.
[19] X. Li, R. Cao, Y. Sun, W. Bi, X. Li, Y. Wang, Eur. J. Inorg. Chem. (2005) 321.
[20] J.Y. Lu, A.M. Babb, Inorg. Chem. Commun 4 (2001) 716.
[21] J.Y. Lu, A.M. Babb, Chem. Commun. (2001) 821.
[22] Y.-H. Liu, Y.-L. Lu, H.-L. Tsai, J.-C. Wang, K.-L. Lu, J. Solid State Chem 158 (2001) 315.
[23] J.Y. Lu, E.E. Kohler, Inorg. Chem. Commun. 5 (2002) 600.
[24] P. Ayyappan, G. Sirokman, O.R. Evans, T.H. Warren, W. Lin, Inorg. Chim. Acta 357 (2004) 3999.
[25] O.R. Evans, R.-G. Xiong, W. Lin, Z. Wang, J. Am. Chem. Soc 120 (1998) 13272.
[26] O.R. Evans, R.-G. Xiong, W. Lin, Z. Wang, G.K. Wong, Angew. Chem., Int. Ed 38 (1999) 536.

Teflon-lined stainless-steel autoclave and kept at 110 °C under autogenous pressure for 3 days. After cooling to room temperature, transparent prismatic crystals with suitable dimensions for crystallographic study were collected. The crystals were washed several times with distilled water and dried in the open air. They are stable for months under normal conditions of temperature and humidity. Schematically the reaction can be written as follows:

$$2.5ZnO + 3H_3PO_4 + C_6H_8N_2 + 5H_2O \rightarrow [Zn_{2.5}(HPO_4)_2(PO_4)][C_6N_2H_{10}] \cdot 5H_2O + 2.5H_2O$$

2.2. Investigation techniques

The title compound has been studied by various physico-chemical methods: X-ray diffraction, solid state NMR spectroscopy combined with ab initio calculations, infrared spectroscopy and thermal analysis.

2.2.1. X-ray diffraction

The intensity data collection was performed using a MACH3 Enraf Nonius diffractometer. The experimental conditions of data collection, the strategy followed for the structure determination and the final results are given in Table 1. The structure was solved by the SIR92 [16] program and refined by full matrix least-squares techniques based on F, using SHELXL97 [17]. Analytical empirical absorption corrections were made [18]. The structure factors were obtained after Lorentz polarization corrections. The positions of the heavier atoms, including the Zn atom, were located by the direct method. The remaining atoms were found in a series of alternating difference Fourier maps and least-square refinements. The positions of the hydrogen atoms of this hybrid compound were located directly from the difference Fourier maps. The drawings were made with DIAMOND [19].

2.2.2. NMR spectroscopy

All NMR spectra were recorded on a Bruker DSX-300 spectrometer operating at 75.49 MHz for ^{13}C and 121.51 MHz for ^{31}P with a classical 4 mm probehead allowing spinning rates up to 10 kHz. ^{13}C chemical shifts are given relative to tetramethylsilane and ^{31}P ones relative to 85% H_3PO_4 (external references, precision 0.5 ppm). The phosphorus spectrum was recorded under classical MAS conditions with high power proton decoupling while the carbon one was obtained by use of cross-polarization from protons (contact time 5 ms) and MAS. In all cases it was checked that there was a sufficient delay between the scans, allowing a full relaxation of the nuclei.

2.2.3. Ab initio calculations

DFT calculations (at the B3LYP/6-31+G* level) were made to allow the attribution of the ^{31}P and ^{13}C NMR signals to the various crystallographically unequivalent atoms. For phosphorus, the chemical shifts were determined by taking the coordinates of the PO_4 tetrahedra, found by X-ray diffraction, and calculating of the chemical shifts with the GIAO method. For carbon, the positions of the hydrogen atoms were first optimized at the same level of theory, the carbon and nitrogen atoms being frozen. All calculations were made with the GAUSSIAN 98 software.

Table 1
Crystal data and experimental parameters used for the intensity data collection

I. Crystal data	
Formula	$[Zn_{2.5}(HPO_4)_2(PO_4)][C_6N_2H_{10}] \cdot 5H_2O$
F_w	649.51
Crystal system	triclinic
Space group	$P\bar{1}$
a (Å)	9.841(4)
b (Å)	10.360(9)
c (Å)	12.852(4)
α (°)	111.07(5)
β (°)	90.72(3)
γ (°)	117.85(4)
V (Å^3)	1054.8(11)
Z	2
Refinement of unit-cell parameters with 25 reflection ($7° < \theta < 10°$)	
ρ_{calc} (g cm^{-3})	1.716
$F(000)$	556.00
Linear absorption factor: μ [Mo Kα] (cm^{-1})	2.471
Morphology	prism
Crystal size (mm)	$0.70 \times 0.35 \times 0.40$
Color	transparent
II. Intensity measurements	
Temperature (K)	293
Wavelength (Å) [Mo Kα]	0.7107
Diffractometer	Enraf-Nonius MACH 3
Scan mode	$\omega - 2\theta$
Monochromator	graphite plate
Theta range (°)	2.34–25.00
Measurement area	($\pm hkl$)
h_{max}; k_{max}; l_{max}	11; 12; 15
Number of scanned reflections (R_{int})	3679 (0.00)
Number of independent reflections	3516
Orientation and control reflections	2 −4 6 and 3 −5 4
III. Structure determination	
Lorentz and polarization corrections	
No absorption correction	
Program used	SHELX-97 [17]
Determination	direct methods
Hydrogen atoms located from difference Fourier maps and not refined	
Refined parameters	169
Absorption correction	analytical [18]
T_{min}, T_{max}	0.4167, 0.7088
Unique reflections included	(3516 ($I > 2\sigma$))
R; R_w	0.0449; 0.1333
Weighting scheme	σ
Goodness-of-fit on F^2	1.103
Residual Fourier density (Å^3)	$-1.77 < \rho < 2.66$
Largest shift/error	0.012
Drawings made with DIAMOND [19]	

Strategy and final results of the structure determination.

2.2.4. Thermal behavior

Thermal analysis was performed using the "multi-module 92 Setaram" analyzer operating from room temperature up to 500 °C at an average heating rate of 5 °C min^{-1} in a flowing drying argon atmosphere.

2.2.5. IR spectroscopy

Spectra were recorded in the range 4000–400 cm^{-1} with a "Perkin–Elmer FTIR" spectrophotometer 1000 using sample dispersed in a spectroscopically pure KBr pellet.

3. Results and discussion

3.1. Structure description

ZnP-2AMP exhibits a new type of layered structure. All non-hydrogen atoms occupy general positions in the unit cell, except the atom Zn(1) which is located in the special position 0, 1/2, 1/2 with half occupation. The three independent zinc atoms in ZnP-2AMP show distinct structural behaviour: Zn(2) and Zn(3) are tetrahedrally coordinated by O atoms with d_{av}[Zn(2)–O] = 1.940 Å and d_{av}[Zn(3)–O] = 1.939 Å. It is worth noting that Zn(1) with d_{av}[Zn(1)–O] = 2.092 Å is coordinated by two oxygen atoms, and four water molecules occupy the equatorial positions to form a slightly distorted octahedral coordination environment. The Zn(2) and Zn(3) atoms are both tetrahedrally coordinated and form Zn–O–P bonds via oxygen bridges, while Zn(1) forms only two Zn–O–P bonds. This environment yields rather larger displacement parameters for Zn(1) compared to Zn(2) and Zn(3). A similarly high coordination state of zinc atoms has been observed in other zinc phosphates [20,21]. The three independent P atoms represent three chemically distinct types of site; in each case the P atom is tetrahedrally coordinated to four oxygen atoms. The P(1) atom forms three P–O–Zn bonds via oxygen bridges and has one uncoordinated oxygen atom O(1) with a terminal –OH group (bond length d[P(1)–O(1)] = 1.580(5) Å). The P(2) atom makes the same linkages as P(1) (bond length d[P(2)–O(6)] = 1.591(5) Å). The P(3) atom makes linkages to three zinc atoms via bridging oxygen atoms and one terminal bond (bond length d[P(3)–O(11)] = 1.545(5) Å). There is one doubly protonated 2AMP molecule per asymmetric unit.

What is especially interesting about the framework structure of ZnP-2AMP is that it consists of one-dimensional tubes, linked together so as to form layers. The vertex linkage of ZnO_4, PO_4 and HPO_4 tetrahedra forms the building unit cage, which can been seen as building up of six 4-membered rings, two 8-membered rings and two 12-membered rings, as shown in Fig. 1, the octahedron pointing toward the interlayer space is the $ZnO_2(H_2O)_4$ group. It can also be considered as layers formed by two sheets, with 12-membered rings separated by about 4.1 Å. The linkage of the two sheets are made by P(2)–O(5)–Zn(2), P(3)–O(9)–Zn(3) and Zn(1)–O(4)–P(1) in a diagonal manner, as to form a regular sodalite cage built around the inversion center on which the octahedral $ZnO_2(H_2O)_4$ is located. The connection of the 12-membered cavity is similar to that of another zinc phosphate [22], and is shown in Fig. 1.

The inorganic sheets are anionic and the empirical formula of the layer is $[Zn_{2.5}(HPO_4)_2(PO_4)]_n^{2-}$, extended along the (a,b) plane. The neutrality is achieved by the incorporation of doubly protonated 2AMP. The inorganic–organic layers are shown in Fig. 2. The 2AMP and three water molecules [H_2O(3w), H_2O(4w), H_2O(5w)] occupy the interlayer spaces and are not bonded to each other. The 2AMP molecules serve as hydrogen bonding donors to the nearest oxygen framework atoms and balance the charge of anionic inorganic sheets. The interlayer hydrogen bonding between inorganic and organic layers

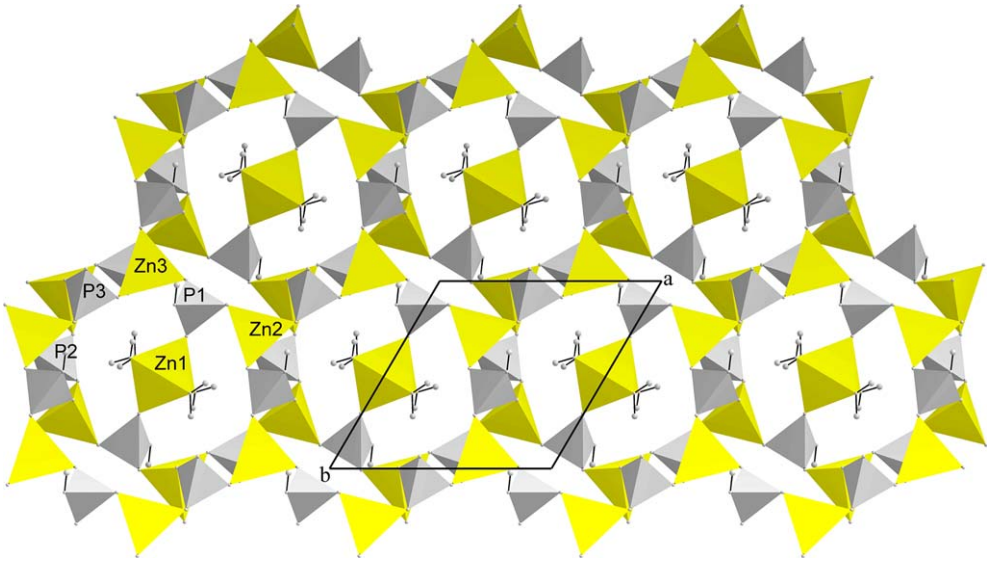

Fig. 1. Polyhedral representation of the framework $[Zn_{2.5}(HPO_4)_2(PO_4)][C_6N_2H_{10}] \cdot 5H_2O$, viewed down the c-direction.

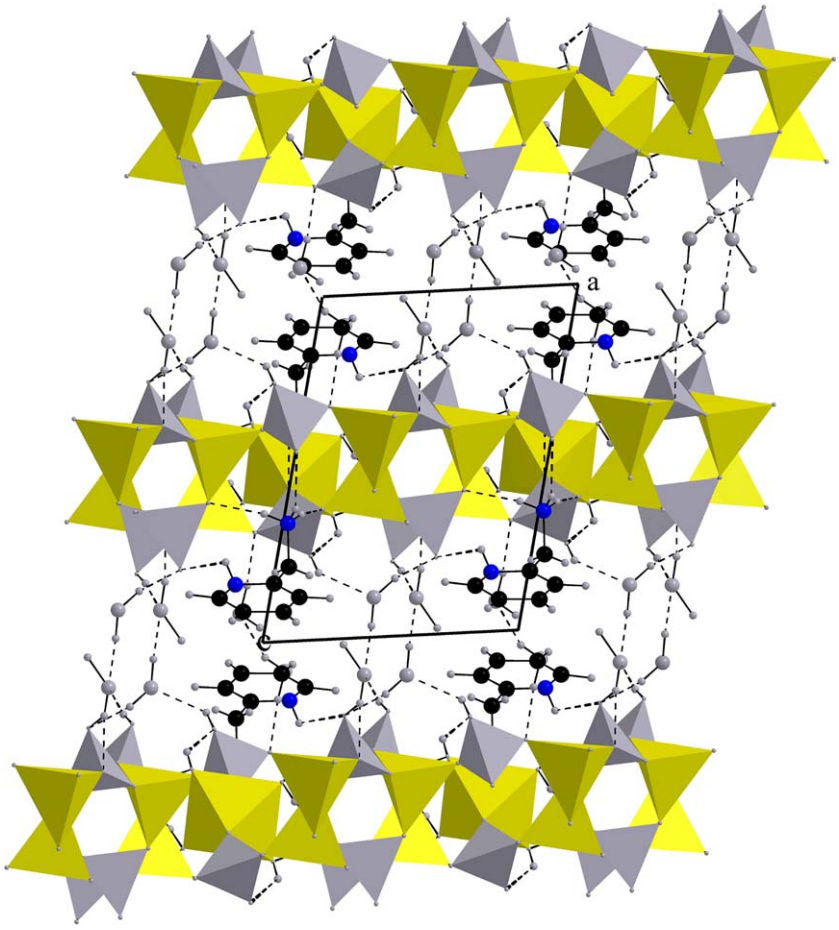

Fig. 2. Projection of $[Zn_{2.5}(HPO_4)_2(PO_4)][C_6N_2H_{10}]\cdot 5H_2O$ structure on the (a,c) plane.

and the intralayer hydrogen bonding between donor and acceptor in the same inorganic layer play an important role in stabilizing the ZnP-2AMP structure.

It can be pointed out that the structure of ZnP-2AMP is closely related to that of the metal phosphate $[Zn_{(2-x)}Co_x(HPO_4)_3]\cdot C_3N_2H_{12}$, $x = 0.05$ [23], in which the polyhedral connectivity of the MO_4 and HPO_4 centers leads to a layered structure with parallel 12-ring layers. The two dimensional sheets are built up from connecting infinite chains, through 4 rings, to form 12 rings; this type of chain contains triple edge-sharing 4-ring units. The latter have also been reported by Harrison et al. [22], and include edge sharing helixes of 4 rings in open-framework $NaZnPO_4\cdot H_2O$. The 12-ring layers presented in this paper are different from those reported by Harrison et al. [24,25]. First the linkage of 4-ring units that constitutes the 12-ring sheets is different and the orientation of the 12-ring sheets is distinct. Second, the 12 rings described here are linear and planar within a layer while those reported by Harrison et al. are split or "bifurcated".

3.2. NMR spectroscopy and ab initio calculations

Fig. 3 shows the proton-decoupled ^{31}P MAS NMR spectrum of crystalline monophosphate $[Zn_{2.5}(HPO_4)_2(PO_4)][C_6N_2H_{10}]\cdot 5H_2O$. This spectrum is in good agreement with the X-ray structure. Indeed, it exhibits three resonances at 0.5, 5.1 and 6.1 ppm, corresponding to three crystallographically independent phosphorus atoms. These chemical shift values agree well with those of monophosphates [26–31]. A tentative partial attribution of the NMR components to the phosphorus atoms P(1), P(2)

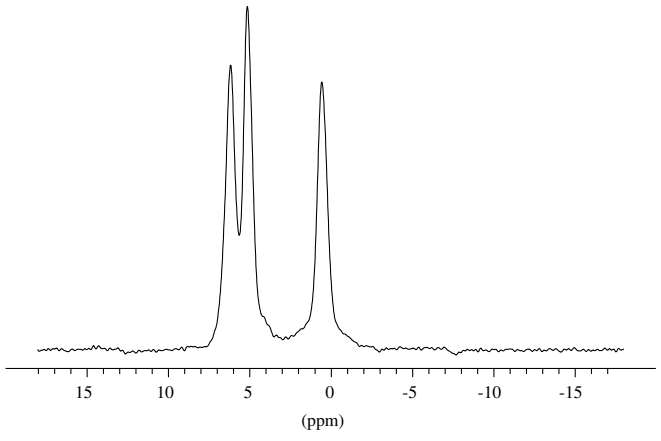

Fig. 3. ^{31}P MAS-NMR spectrum of crystalline $[Zn_{2.5}(HPO_4)_2(PO_4)][C_6N_2H_{10}]\cdot 5H_2O$.

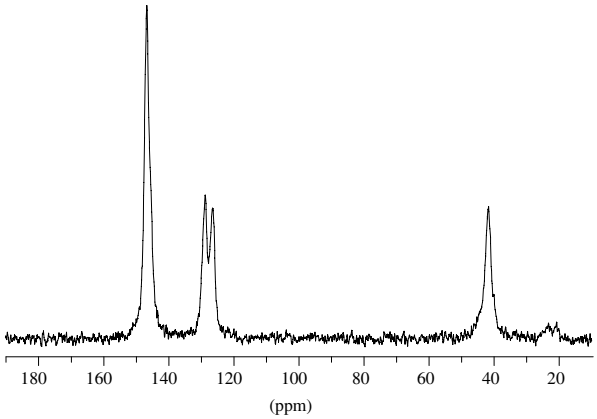

Fig. 4. ^{13}C CP-MAS-NMR spectrum of crystalline $[Zn_{2.5}(HPO_4)_2(PO_4)]\cdot[C_6N_2H_{10}]\cdot 5H_2O$.

and P(3) was done by using ab initio calculations. For this purpose, the isotropic chemical shifts of the three phosphorus atoms P(1), P(2) and P(3) in the three PO4 tetrahedra were calculated. The calculated values were the same for P(1) and P(2) and slightly shifted to lower ppm (with reference to H_3PO_4) for P(3). However the shift (ca. 1 ppm) was smaller than the experimental value (ca. 4 ppm), probably due to the fact that our calculations did not take into account the presence of the atoms in the outer coordination sphere. However we can reasonably attribute the signal at 0.5 ppm to P(3) and the two other signals to P(1) and P(2).

Fig. 4 shows the ^{13}C CP-MAS NMR spectrum of the title compound. The carbon atoms of the organic moiety are labelled as depicted below:

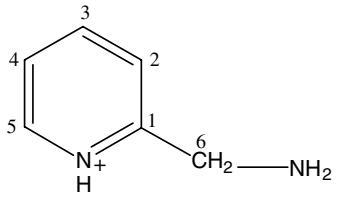

The signal at 41.6 ppm corresponds to the aliphatic carbon atom C6 and proves the presence of only one organic entity in the asymmetric unit of the compound. This result is in good agreement with the X-ray data. The other signals at higher chemical shifts are related to the pyridinium ring carbon atoms (C1, C2, C3, C4 and C5). As for phosphorus, a tentative attribution can be made by using ab initio calculations. As the hydrogen atoms were not refined during the X-ray determination, these atoms were first optimized at the B3LYP/6-31+G* level before calculation of the carbon chemical shifts. The values were then corrected to the value of tetramethylsilane. The calculated values agree well with the experimental ones for C2 (125.2 for 126.4), C4 (127.3 for 128.7) and C6 (36.3 for 41.6) atoms, but are strongly shifted (at least for C5 which is shifted by ca. 10 ppm, C2 being shifted by ca. 5 ppm) for the carbon atoms ortho and para to the nitrogen. C1 is probably not seen experimentally as it is not linked to protons and C2 and C5 correspond probably to the NMR signal at 146.7 ppm. The difference between theory and experiment is probably related to the bad location of the pyridinium proton which also interacts with other molecules in the crystal.

3.3. Thermal analysis

The DTA curve shows that the zinc phosphate ZnP-2AMP undertakes, between 50 and 280 °C, four endothermic peaks:

- The first one corresponds to the removal of water molecules Ow(3), Ow(4), Ow(5) located in the interlayer spaces which evaporate almost simultaneously at the relatively low temperature of about 80 °C, (weight loss calculated 8.31%, experimental 8.22%).
- The second and the third peaks correspond to the removal of water molecules Ow(1) and Ow(2). They depart less easily from octahedral coordination, and we can consider probably that the removal of Ow(1) occurs before that of Ow(2), because its hydrogen bonds are weaker, (weight loss calculated 5.54%, experimental 5.61%).
- The fourth peak corresponds to the removal of one water molecule arising from the irreversible dehydroxylation reaction due to the presence of terminal P–OH groups and deprotonation of the amine cations, above 224 °C (weight loss calculated 2.77%, experimental 2.86%), according to the following reaction:

$$[Zn_{2.5}(HPO_4)_2(PO_4)][C_6N_2H_{10}]\cdot 5H_2O \rightarrow Zn_2P_2O_7 + 1/2Zn(PO_3)_2 + C_6N_2H_8 + 7H_2O$$

Finally the weight loss, between 274 and 500 °C, corresponds to the degradation of the template molecule (organic entities), giving $Zn_2P_2O_7$ and $Zn(PO_3)_2$ as the final decomposition products. The observed total weight loss of (32.89%) agrees well with the calculated value (33.38%) for the loss of ZnP-2AMP. A grey solid is obtained, probably containing a carbon residue. The latter can be eliminated by calcination of the sample at 850 °C in air.

3.4. IR spectroscopy

The infrared absorption spectrum of the title compound shows the band vibrations of the 2-aminomethylpyridinium cation and monophosphoric anions (HPO_4^{2-} and PO_4^{3-}). To assign the IR peaks to vibrational modes, we have examined the modes and frequencies in similar compounds [32]. The broad bands between 3500 and 2300 cm^{-1} correspond to the stretching of the organic and hydroxyl groups [ν(N–H), ν(C–H) and ν(O–H) of P–OH groups]. The vibrations between 1650 and 1200 cm^{-1} are assigned to bending and stretching modes (δNH^+), $\nu C(=C)$). The observed shoulder at 1260 cm^{-1} and the weak band at 830 cm^{-1} are

assigned to the δ (P–O–H) in plane bending and δ(P–O–H) out of plane bending modes [33]. Various valency and bending vibration bands between 1200 and 300 cm^{-1}, are characteristic of a PO_4 tetrahedron [32]. In this case, the stretching vibration bands originating from both symmetric $\nu_1(A_1)$ and asymmetric $\nu_3(F_2)$ modes are, respectively, observed in the range [1000–800] and [1200–1000] cm^{-1}. The PO_4 tetrahedra has also bending vibrations as symmetric $\nu_4(F_2)$ and asymmetric $\nu_2(E)$, respectively observed in the frequency range [650–500] and [500–300] cm^{-1}. Supplementary frequencies in the $\nu_s(PO_4)$ domain are attributed to bending modes $\delta(C_{aryl}–H)_{ip}$ [34].

Acknowledgement

We thank the Ministry of Scientific Research Technology and Competing Development of Tunisia for its financial support.

Appendix A. Supplementary data

Supplementary crystal structure data were deposited with the CCDC under No. 603036, and are available on request to CCDC, 12 Union Road, Cambridge CB2 1EZ, UK (fax: (internat.) +44 1223/336 033; e-mail: deposit @ccdc.cam.ac.uk). Supplementary data associated with this article can be found, in the online version, at doi:10.1016/j.poly.2006.05.016.

References

[1] R.C. Haushalter, L.A. Mundi, Chem. Mater. 4 (1992) 31.
[2] K.H. Lii, Y.-F. Huang, V. Zima, C.-Y. Huang, H.-M. Lin, Y.-C. Jiang, F.-L. Liao, S.-L. Wang, Chem. Mater. 10 (1998) 2599.
[3] A.K. Cheetham, G. Férey, T. Loiseau, Angew. Chem., Int. Ed. 38 (1999) 3268.
[4] O. Terasaki, J.C. Barry, J.V. Sanders, J.M. Thomas, Nature 330 (1987) 58.
[5] G.A. Ozin, Adv. Mater. 4 (1992) 612.
[6] S.T. Wilson, B.M. Lok, C.A. Messina, T.R. Cannan, E.M. Flanigen, J. Am. Chem. Soc. 104 (1982) 1146.
[7] W.T.A. Harrison, L. Hannooman, J. Solid State Chem. 131 (1997) 363.
[8] A.A. Ayi, A. Choudhury, S. Natarajan, S. Neeraj, C.N.R. Rao, J. Mater. Chem. 11 (2001) 1181.
[9] W.T.A. Harrison, T.M. Nenoff, T.E. Gier, G.D. Stucky, Inorg. Chem. 32 (1993) 2437.
[10] W.T.A. Harrison, M.L.F. Phillips, Chem. Mater. 9 (1997) 1837.
[11] A. Choudhury, S. Natarajan, C.N.R. Rao, Inorg. Chem. 39 (2000) 4295.
[12] M. Wiebcke, J. Mater. Chem. 12 (2002) 143.
[13] T.E. Gier, G.D. Stucky, Nature 349 (1991) 508.
[14] K.O. Kongshaug, H. Fjellvag, K.P. Lillerud, Micropor. Mesopor. Mater. 39 (2000) 341.
[15] J. Yu, Y. Wang, Z. Shi, R. Xu, Chem. Mater. 13 (2001) 2972.
[16] A. Altomare, M. Cascarano, C. Giacovazzo, A. Gualiardi, J. Appl. Cryst. 26 (1993) 343.
[17] G.M. Sheldrick, SHELXS97 and SHELXL97. Program for Crystal Structure Solution and Refinement, University of Gottingen, Germany, 1997.
[18] J. De Meulenaer, H. Tompa, Acta Cryst. 19 (1965) 1014.
[19] K. Brandenburg, DIAMOND version 2.0 Impact GbR, Bonn., Germany, 1998.
[20] W.T.A. Harrison, J.T. Vaughey, L.L. Dussack, A.J. Jacobson, T.E. Maetin, G.D. Stucky, J. Solid State Chem. 114 (1995) 151.
[21] D. Whang, N.H. Hur, K. Kim, Inorg. Chem. 34 (1995) 3363.
[22] W.T.A. Harrison, T.E. Gier, G.D. Stucky, R.W. Broach, R.A. Bedard, J. Chem. Mater. 8 (1996) 145.
[23] Y. Liu, L. Na, G. Zhu, F.-S. Xiao, W. Pang, R. Xu, J. Solid State Chem. 149 (2000) 107.
[24] W.T.A. Harrison, Z. Bircsak, L. Hannooman, Z. Zhang, J. Solid State Chem. 136 (1998) 93.
[25] W.T.A. Harrison, T.M. Nenoff, T.E. Gier, G.D. Stucky, J. Solid State Chem. 113 (1994) 168.
[26] A.R. Grimmer, U. Haubenreisser, Chem. Phys. Lett. 99 (1983) 487.
[27] K. Cheetham, N.J. Clayden, C.M. Dobson, R.J.B. Jakemen, J. Chem. Soc., Chem. Commun. (1986) 195.
[28] I.L. Mudrakovskii, V.P. Shmochkova, N.S. Kentsarenko, V.M. Mastikhin, Phys. Chem. Solids 47 (1986) 335.
[29] L. Turner, K.A. Smith, R.J. Kirkpatrick, E.J. Oldfield, J. Magn. Reson. 70 (1986) 408.
[30] S. Prabhakar, K.J. Rao, C.N.R. Rao, Chem. Phys. Lett. 139 (1987) 96.
[31] P. Hartmann, J. Vogel, B. Schnabel, J. Magn. Reson. 111 (1994) 110.
[32] H. Naïli, T. Mhiri, A. Daoud, Int. J. Inorg. Mater. 3 (2001) 393.
[33] A.C. Chapman, L.E. Thirlwell, Spectrochim. Acta 20 (1964) 937.
[34] R.M. Silverstein, G.C. Bassler, T.C. Morill, Spectrometric Identification of Organic Compounds, 3rd ed., Wiley, New York, 1974.

polydentate 1,3,5-triazine-based N-donor ligands [25]. In the course of this study, it appeared that the architecture of these materials depends strongly on the reaction conditions, e.g. temperature and pressure [22,23]. This observation prompted us to study the influence of the reaction solvent on the topology of these complexes. In the present study, we selected *N*,*N*′-{2,4-di-[(di-pyridin-2-yl)amine]-1,3,5-triazine}ethylenediamine (L) as a flexible polydentate ligand and Zn(II) and Cd(II) metal centres, because only a few studies have been focused on late-transition metals so far. The ligand L reacts with Zn(II) and Cd(II) nitrate at 100 °C under autogenous pressure to afford either mononuclear complexes when the reaction is performed in methanol, or trinuclear species when the reaction is carried out in acetonitrile. The structures of these complexes are described in this report, as well as their spectroscopic characteristics.

2. Experimental

2.1. Syntheses

All commercially available reagents were used without further purification. The ligand L was prepared according to a reported method [26].

2.1.1. Preparation of coordination compounds *1* and *2*

Zinc(II) nitrate hexahydrate (20 mg, 0.066 mmol) or cadmium(II) nitrate tetrahydrate (20.8 mg, 0.067 mmol) was added to a suspension of L (15 mg, 0.016 mmol) in methanol (6 ml). The resulting colourless solutions were allowed to stand at 100 °C for 12 h under autogenous pressure in a sealed Pyrex tube to form in good yields **1**, or **2** as colourless single crystals.

*Analyses for **1**:* Yield 54% (10 mg). *Anal.* Calc.: C, 53.16; H, 3.50; N, 28.40. Found: C, 52.45; H, 3.54; N, 27.82%. Main IR absorption bands (cm^{-1}) 3300(w), 3085(w), 1604(w), 1583(s), 1557(s), 1538(w), 1367(s), 1303(s), 1020(m), 997(m), 808(s).

*Analyses for **2**:* Yield 48% (9 mg). *Anal.* Calc.: C, 50.95; H, 3.35; N, 27.22. Found: C, 49.84; H, 2.96; N, 26.53%. Main IR absorption bands (cm^{-1}) 3324(w), 3070(w), 1604(w), 1582(s), 1557(s), 1538(m), 1362(s), 1305(s), 1016(m), 997(m), 808(s).

2.1.2. Preparation of coordination compounds *3* and *4*

A similar procedure involving the same reactant quantities was followed but now using acetonitrile as solvent.

*Analyses for **3**:* Yield 41% (10.5 mg). *Anal.* Calc.: C, 39.92; H, 2.72; N, 25.12. Found: C, 40.04; H, 2.67; N, 25.19%. Main IR absorption bands (cm^{-1}) 3389(w), 3085(w), 1604(s), 1585(w), 1558(s), 1540(m), 1362(s), 1295(s), 1020(s), 809(s).

Analyses for ***4***: Yield 33% (9 mg). *Anal.* Calc.: C, 36.49; H, 2.49; N, 22.97. Found: C, 38.34; H, 2.61; N, 22.68%. Main IR absorption bands (cm^{-1}) 3382(w), 3085(w), 1600(s), 1581(w), 1558(s), 1540(m), 1367(s), 1300(s), 1017(s), 807(s).

2.2. Physical measurements

Elemental analyses for C, H and N were performed with a Perkin–Elmer 2400 analyser. FTIR spectra were recorded with a Perkin–Elmer Paragon 1000 FTIR spectrophoto-

Table 1
Crystallographic data and refinement details for $ZnL(NO_3)_2$ (**1**), $CdL(NO_3)_2$ (**2**) and $Zn_3L(NO_3)_6 \cdot CH_3CN$ (**3**)

	1	**2**	**3**
Formula	$ZnC_{48}H_{38}N_{22}O_6$	$CdC_{48}H_{38}N_{22}O_6$	$Zn_3C_{50}H_{41}N_{27}O_{18}$
FW	1084.37	1131.40	1504.21
Crystal system	monoclinic	monoclinic	monoclinic
Space group	*C*2/c	*C*2/c	*P*21/c
a (Å)	11.645(2)	11.729(5)	19.294(3)
b (Å)	23.145(3)	23.312(5)	8.960(2)
c (Å)	19.118(3)	19.268(5)	35.314(6)
β (°)	100.97(3)	101.91(5)	93.87(3)
V (Å^3)	5059(1)	5155(3)	6091(2)
Z	4	4	4
D_{calc} (g cm^{-3})	1.424	1.458	1.640
μ (mm^{-1})	0.558	0.495	1.267
F (000)	2232	2304	3056
Limiting indices	$-12 \leqslant h \leqslant 12$, $-25 \leqslant k \leqslant 25$, $-21 \leqslant l \leqslant 21$	$-13 \leqslant h \leqslant 13$, $-25 \leqslant k \leqslant 18$, $-17 \leqslant l \leqslant 21$	$-22 \leqslant h \leqslant 22$, $-10 \leqslant k \leqslant 10$, $-42 \leqslant l \leqslant 41$
θ Range for data collection (°)	1.99–23.30	2.05–23.27	1.51–25.02
Reflections collected/unique [R_{int}]	20559/3648 [0.0604]	10259/3645 [0.0940]	56087/10703 [0.0726]
Observed reflections	2405 [$F_o > 4.0\sigma(F_o)$]	1803 [$F_o > 4.0\sigma(F_o)$]	6385 [$F_o > 4.0\sigma(F_o)$]
Data/restraints/parameters	3648/0/354	3645/6/349	10703/5/890
Final *R* indices [$F_o > 4.0\sigma(F_o)$]	$R_1 = 0.0508$ $wR_2 = 0.1456$	$R_1 = 0.0671$ $wR_2 = 0.1409$	$R_1 = 0.0506$ $wR_2 = 0.1192$
R indices (all data)	$R_1 = 0.0815$ $wR_2 = 0.1591$	$R_1 = 0.1458$ $wR_2 = 0.1637$	$R_1 = 0.0983$ $wR_2 = 0.1354$
Goodness-of-fit on F^2	0.893	0.921	0.927

$R_1 = \sum||F_o| - |F_c||/\sum|F_o|$, $wR_2 = [\sum w(F_o^2 - F_c^2)^2/\sum wF_o^4]^{1/2}$. Goodness-of-fit $S = [\sum w(F_o^2 - F_o^2)^2/(n-p)]^{1/2}$, where *n* is the number of reflections and *p* the number of parameters.

meter, equipped with a Golden Gate ATR device, using the reflectance technique (4000–300 cm^{-1}).

2.3. Crystallographic analysis

2.3.1. Single crystal X-ray diffraction analysis for *1, 2 and 3*

The molecular structures of compounds **1**, **2** and **3** were determined by single-crystal X-ray diffraction methods. Crystallographic and experimental details for the different structures are summarized in Table 1. Intensity data and cell parameters were recorded at room temperature (293 K) on a Bruker AXS Smart 1000 single-crystal diffractometer (Mo Kα radiation) equipped with a CCD area detector. The data reductions were performed using the SAINT [27] and SADABS [28] programs. The structures were solved by direct methods using the SIR97 program [29] and refined on F_o^2 by full-matrix least-squares procedures, using the SHELXL-97 program [30]. The non-hydrogen atoms were refined with anisotropic atomic displacements, with the exception of the disordered acetonitrile molecule in compound **3**. The hydrogen atoms were included in the refinement at idealized geometries (C—H 0.95 Å) and refined "riding" on the corresponding parent atoms, with the exception of H1N in compounds **1** and **2** and H1N and H2N in compound **3**, which were located in the difference Fourier map. The weighting scheme used in the last cycle of refinement was $w = 1/[\sigma^2(F_o^2) + (0.1099P)^2]$ (**1**), $w = 1/[\sigma^2(F_o^2) + (0.0700P)^2]$ (**2**) and $w = 1/[\sigma^2(F_o^2) + (0.0747)^2]$ (**3**), where $P = (F_o^2 + 2F_c^2)/3$. Molecular geometry calculations were carried out using the PARST97 program [31]. All calculations were carried out on a DIGITAL Alpha Station 255 computer.

3. Results and discussion

3.1. General

The complexes **1**–**4** have been prepared by the reaction at 100 °C under autogenous pressure of the polydentate *N*,*N*′-{2,4-di-[(di-pyridin-2-yl)amine]-1,3,5-triazine}ethylenediamine ligand (L, Chart 1) with Zn(II) or Cd(II) nitrate. Interestingly, depending on the crystallisation solvent, mononuclear or trinuclear complexes have been obtained. **1** and **2** have been prepared in methanol and are formulated as $ZnL(NO_3)_2$ (**1**) and $CdL(NO_3)_2$ (**2**), according to X-ray single crystal analysis, while **3** and **4** have been isolated in acetonitrile. Complex **3** consists of a $Zn_3L(NO_3)_6 \cdot CH_3CN$ trinuclear species as elucidated by X-ray single crystal diffraction. Complex **4** crystallises as a poorly crystalline powder for which the X-ray powder diffraction pattern could not be interpreted. Elemental analyses of **4** are in agreement with a trinuclear stoichiometry and allow to state the formulation $Cd_3L(NO_3)_6 \cdot CH_3CN$ for this compound.

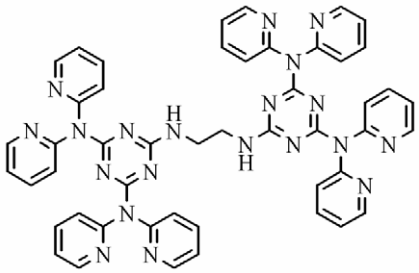

Chart 1. *N*,*N*′-{2,4-di-[(di-pyridin-2-yl)amine]-1,3,5-triazine}ethylene diamine (L).

3.2. Structures

3.2.1. Crystal structures of *1 and 2*

The complexes $ZnL(NO_3)_2$ (**1**) and $CdL(NO_3)_2$ (**2**) are isostructural and crystallise in the centric monoclinic *C*2/*c* space group, with the metal ions lying on the 2-fold rotation axis. Their ORTEP views are depicted in Figs. 1 and SI1, respectively. Selected bond distances and angles for both complexes are reported in Table 2. As can be seen in Fig. 1, only two of the four available dipyridylamine moieties of L are coordinated, and act as chelating ligands towards the same metal centre, resulting in the formation of a monometallic complex. The metal centre is in a distorted octahedral environment with a coordination sphere defined by four nitrogen atoms of two dipyridylamine units [Zn1—N6 = Zn1—N6′ = 2.127(3), Zn1—N7 = Zn1—N7′ = 2.148(3) Å for **1** and Cd1—N6 = Cd1—N6′ = 2.325(8), Cd1—N7 = Cd1—N7′ = 2.321(7) Å for **2**] and two oxygen atoms of the monodentate nitrate anions [Zn1—O1 = Zn1—O1′ = 2.146(5) Å for **1** and Cd1—O1 = Cd1—O1′ = 2.23(1) Å for **2**] (symmetry code ′: $1 - x$, y, $1/2 - z$ for **1** and $-x$, y, $1/2 - z$ for **2**).

The structures of **1** and **2** are additionally stabilised by π–π, C—H···O and C—H···N interactions (see Fig. 2 for compound **1**). The centroid-to-centroid distance between the triazine ring N1 C1 N2 C2 N3 C3 and the symmetry generated pyridine moiety N6′ C5′ C6′ C7′ C8′ C9′ is of 3.794(3) Å and the angle between the planes is of 28.74(3)°, indicating the presence of weak interactions

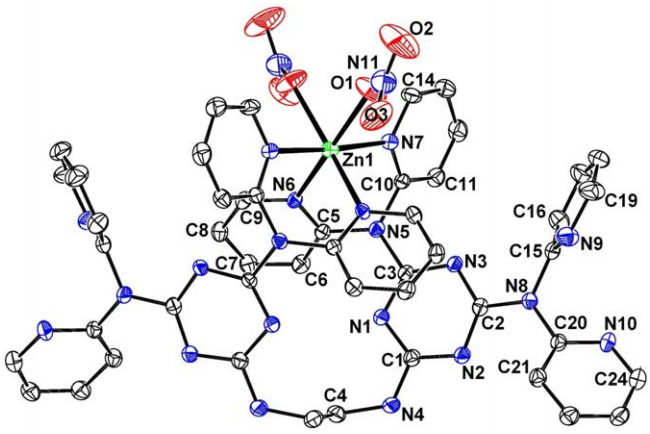

Fig. 1. ORTEP view of compound $ZnL(NO_3)_2$ (**1**) (thermal ellipsoids drawn at 20% probability level, hydrogen atoms omitted for clarity) (cf. Supporting Information for an ORTEP drawing of compound **2**).

Table 2
Selected bond lengths (Å) and angles (°) for $ZnL(NO_3)_2$ (**1**), $CdL(NO_3)_2$ (**2**) and $Zn_3L(NO_3)_6 \cdot CH_3CN$ (**3**)

1		**2**	
Zn1—N6	2.127(3)	Cd1—N6	2.325(8)
Zn1—N7	2.148(3)	Cd1—N7	2.321(7)
Zn1—O1	2.146(5)	Cd1—O1	2.23(1)
N6—Zn1—N7	85.3(1)	N6—Cd1—N7	81.0(3)
N6—Zn1—O1	167.4(2)	N6—Cd1—O1	111.4(4)
N7—Zn1—O1	84.3(2)	N7—Cd1—O1	96.6(5)
3			
Zn1—N6	2.065(4)	N6—Zn1—N7	92.0(2)
Zn1—N7	2.032(4)	O5—Zn1—O4	55.5(2)
Zn1—N11	2.493(3)	O2—Zn1—O1	59.7(2)
Zn1—O1	2.261(5)	O7—Zn2—N9A	98.3(1)
Zn1—O2	2.144(5)	O8—Zn2—N10	104.8(1)
Zn1—O4	2.086(4)	O7—Zn2—O8	58.2(1)
Zn1—O5	2.416(5)	N9A—Zn2—N10	99.1(1)
Zn2—N9	2.190(3)	O13—Zn3—N6A	116.0(2)
Zn2—N9A	2.101(3)	O13—Zn3—O16	117.1(2)
Zn2—N10	2.079(3)	O16—Zn3—N6A	126.9(2)
Zn2—N10A	2.195(3)		
Zn2—O7	2.230(3)		
Zn2—O8	2.191(3)		
Zn3—N6A	2.116(4)		
Zn3—N7A	2.155(4)		
Zn3—O10	2.088(3)		
Zn3—O13	2.067(4)		
Zn3—O16	2.088(5)		

[32]. Also intermolecular hydrogen bonds are present, namely those involving the hydrogens H1N and H1N′ of the ethylene diamine fragment and the O2 and O2′ atoms of nitrate groups from neighbouring complexes [N4···O2 2.87(1), H1N···O2 2.17(5) Å, N4—H1N···O2 154(5)°]. An analogous situation with similar distances and angles is observed for compound **2**.

3.2.2. Crystal structure of *3*

The ORTEP view of complex $Zn_3L(NO_3)_6 \cdot CH_3CN$ (**3**) is shown in Fig. 3 together with the atomic labelling scheme; selected bond distances and angles are listed in Table 2. As in **1** and **2**, the ligand L chelates a metal centre (Zn2) through two dipyridylamine moieties, but here also the four remaining pyridine rings are coordinated to two Zn ions (Zn1 and Zn3), giving rise to a trinuclear complex.

Zn1 and Zn2 are both hexacoordinated but show different environments. Zn1 presents a highly distorted octahedral coordination involving one dipyridylamine group [Zn1—N6 = 2.065(4), Zn1—N7 = 2.032(4) Å] and two asymmetrically chelating nitrate ions [Zn1—O1 = 2.261(4), Zn1—O2 = 2.144(5), Zn1—O4 = 2.086(5), Zn1—O5 = 2.416(5) Å]. On the contrary Zn2 is surrounded by two dipyridylamine groups and one chelating nitrate ion. The equatorial positions are occupied by the two oxygens of the nitrate [Zn2—O7 = 2.230(3), Zn2—O8 = 2.191(3) Å] and by two nitrogens which belong to different dipyridylamine units [Zn2—N9A = 2.101(3), Zn2—N10 = 2.079(3) Å]. The two remaining nitrogen atoms complete the octahedral coordination in axial position [Zn2—N9 = 2.190(3), Zn2—N10A = 2.195(3) Å].

Zn3 is pentacoordinated with one dipyridylamine group and three monodentate nitrate ions forming a trigonal bipyramidal environment ($\tau = 0.81$ [33]). Two oxygen atoms from the nitrate ions [Zn3—O13 = 2.067(4), Zn3—O16 = 2.088(5) Å] and one nitrogen atom from the dipyridylamine moiety [Zn3—N6A = 2.116(4) Å] constitute the equatorial plane, while the remaining nitrate anion and pyridine fragment occupy the axial positions [Zn3—N7A = 2.155(4), Zn3—O10 = 2.088(3) Å].

Also in **3** intramolecular π–π interactions are present (Fig. 4). The triazine ring N1 C1 N2 C2 N3 C3 interacts with the pyridine ring N9A C19A C18A C17A C16A C15A with a centroid-to-centroid distance of 3.794(3) Å and a dihedral angle between the least-square planes passing through the aromatic rings of 18.2(1)°. This centroid-to-centroid distance is at the upper limit for aromatic stacking interactions [32]. It can be highlighted that the second triazine moiety in the trinuclear unit is not involved in such non-covalent forces. Moreover the complex exhibits also C—H···N interactions involving the ethylene diamine fragment, the pyridine rings and the nitrate ions (Fig. 4).

Additionally, each trinuclear unit is connected to neighbouring trinuclear units via intermolecular forces, which gives rise to the formation of a three-dimensional network.

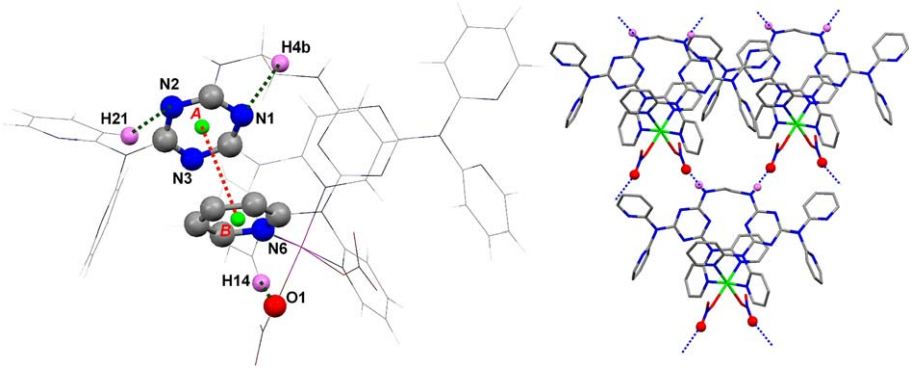

Fig. 2. Representation of the π–π, C—H···O, C—H···N interactions and intermolecular hydrogen bonds in **1**. *A*, centroid of the N1 C1 N2 C2 N3 C3 ring. *B*, centroid of the N6 C5 C6 C7 C8 C9 ring. Distance A···B = 3.794(3) Å. H4B···N1 2.395(4), H14···O1 2.481(5) and H21···N2 2.501(4) Å.

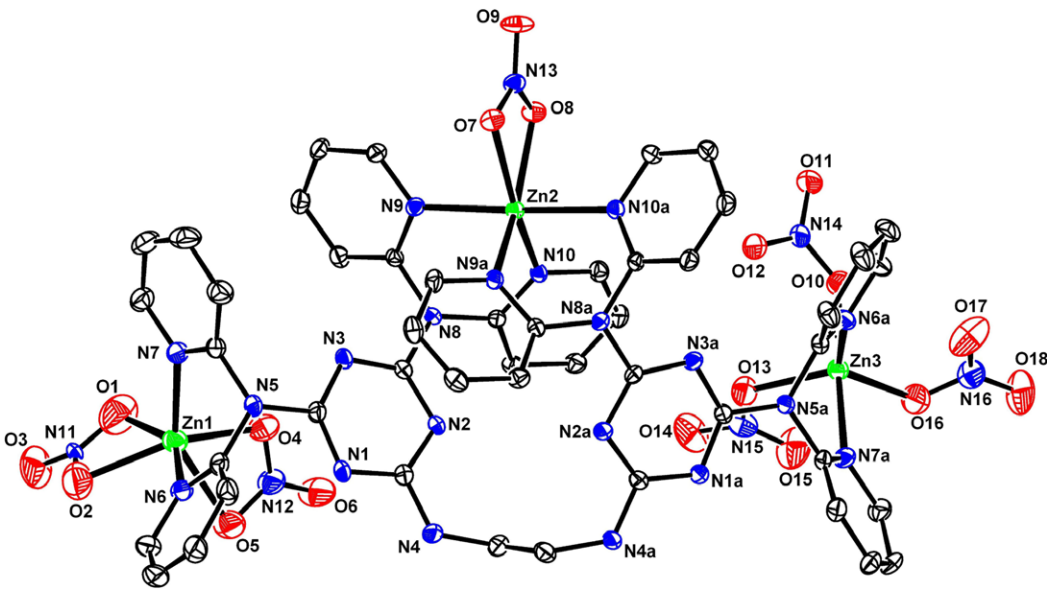

Fig. 3. ORTEP view of $Zn_3L(NO_3)_6 \cdot CH_3CN$ (**3**) (thermal ellipsoids drawn at 20% probability level, lattice solvent and hydrogen atoms are omitted for clarity).

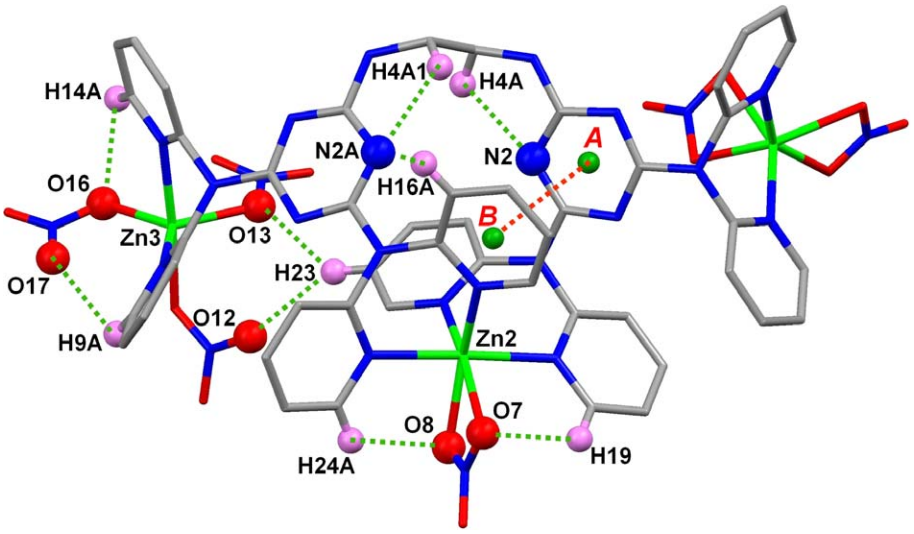

Fig. 4. Representation of the intramolecular non-covalent forces stabilising $Zn_3L(NO_3)_6 \cdot CH_3CN$ (**3**). π–π interactions: *A*, centroid of N1 C1 N2 C2 N3 C3 ring and *B*, centroid of N9A C15A C16A C17A C18A C19A ring. Distance A···B = 3.794(3) Å. C—H···N interactions: H4A1···N2A 2.412(3), H4A···N2 2.362(3), H16A···N2A 2.473(3) and H14a···O16 2.547(5) Å.

These forces are π–π stacking interactions and anion–π interactions (Fig. 5A and B, respectively). Through the π–π interactions a chain along the *c*-direction is formed; moreover the anion–π interactions involving the nitrate linked to Zn2 (N13 O7 O8 O9) favours the interchain interactions within the *ac*-plane, while the anion–π interactions involving the nitrate N15 O13 O14 O15 are responsible for the formation of an array along the *b*-direction.

3.3. Spectroscopy

First of all, it is important to highlight that only two distinct types of IR spectra were obtained for the four complexes. Indeed, the complexes **1** and **2** present similar spectra, and the compounds **3** and **4** exhibit also analogous spectra. For this reason, infrared spectroscopy appeared to be a powerful tool in the present study to discriminate between the mononuclear and trinuclear complexes. This is because some of the vibrations of the dipyridylamine pyridine ring are slightly, but clearly, affected upon coordination to a metal centre.

The vibration at 997 cm^{-1} observed in the free L ligand, associated with the pyridine ring breathing mode (ν_{CCN}), is known to shift to higher wave numbers when the pyridine is coordinated to a metal centre [23]. In our case, in the area 1050–950 cm^{-1}, the mononuclear complexes **1** and **2**

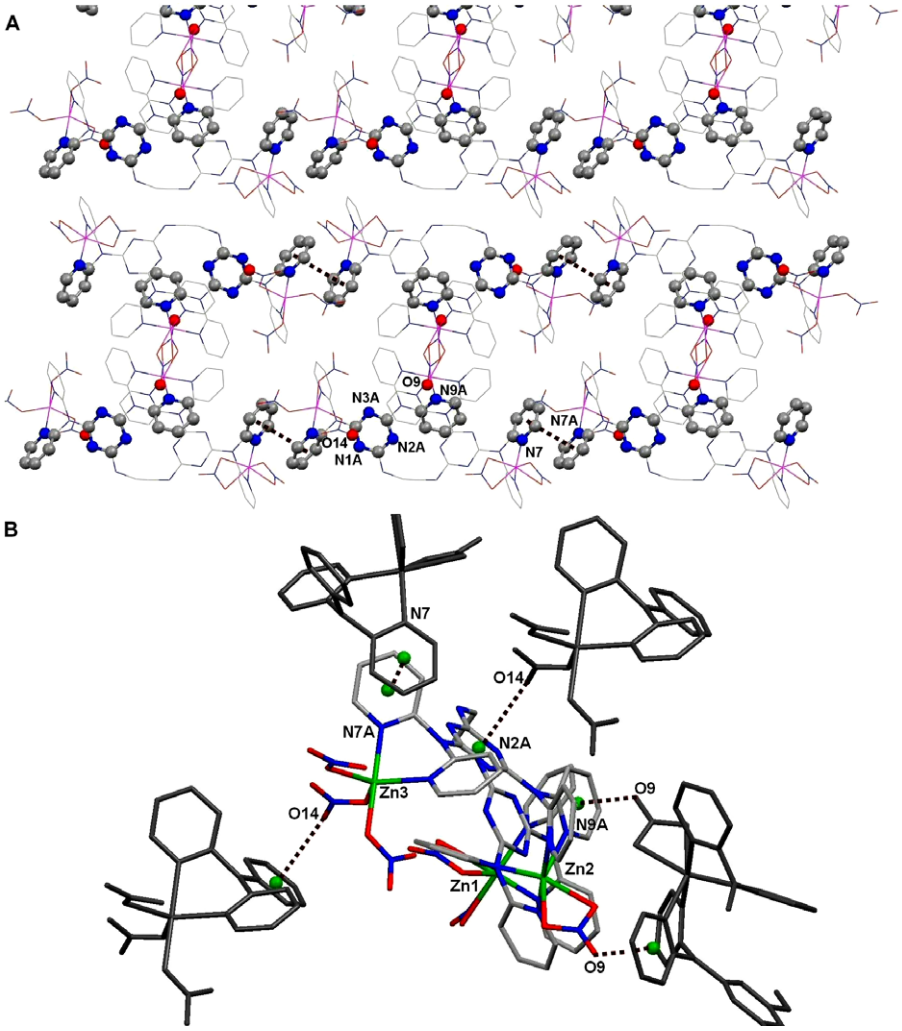

Fig. 5. (A) Schematic view of the packing of **3** along the *b*-direction, showing the intermolecular interactions between the pyridine rings (the atoms represented with balls are all involved in the interactions). (B) View of the asymmetric unit of **3** (represented in colour) involved in intermolecular interactions with fragments of four neighbouring complexes (represented in grey). π–π interactions between N7A C10A C11A C12A C13A C14A and N7i C10i C11i C12i C13i C14i. Centroid-to-centroid distance = 3.962(3) Å. Anion–π interactions (distance anion···ring centroid, Å): N13—O9...{N9A(ii) C15A(ii) C16A(ii) C17A(ii) C18A(ii) C19A(ii)} (3.067(4)); N15—O14...{N1A(iii) C1A(iii) N2A(iii) C2A(iii) N3A(iii) C3A(iii)} (3.28(6)). Symmetry codes: i: x, $1/2 - y$, $1/2 + z$; ii: $1 - x$, $1 - y$, $1 - z$; iii: x, $-1 + y$, z. (For interpretation of the references in colour in this figure legend, the reader is referred to the web version of this article.)

present two bands at ~1020 and 997 cm^{-1}, while the trinuclear complexes **3** and **4** show only one band at ~1020 cm^{-1} (Fig. 6). This clearly proves the partial coordination of L in **1**–**2** and its total coordination in **3**–**4**.

Important information is also provided by the bands present in the area 1610–1500 cm^{-1}. In this region, the pyridine ring stretching modes occur. For the free L ligand these $\nu_{C=C}$ modes are at 1579(s), 1550(s) and 1543(w) cm^{-1}. In **1**–**4** four bands are observed in this area at ~1605, ~1580, 1558 and 1540 cm^{-1}. The relative intensity of these bands allow to distinguish between mononuclear or trinuclear complexes: the mononuclear complexes show a very weak band at ~1600 cm^{-1} and an intense band at ~1580 cm^{-1}, while the trinuclear complexes present the inverse ratio (Fig. 6). The former band is assigned to the $\nu_{C=C-C=Csym}$ mode and the latter one to the $\nu_{C=C-C=Casym}$ mode [26].

At low frequency, below 800 cm^{-1}, the aromatic in-plane and out-of-plane deformation vibration modes (δ_{C-H}, γ_{C-H} and ρ_{C-H}) are found for the pyridine and triazine rings and the metal–nitrogen stretching vibrations (ν_{M-N}). Attempts to attribute these vibrations were unsuccessful due to the high numbers of bands in this area. The strong band observed at ~1370 cm^{-1} in all samples is assigned to the ring stretching of the triazine moiety. Characteristic aromatic stretching vibrations and N—H vibrations are found in the area 3300–3000 cm^{-1}.

Due to the large number of bands in the area characteristic for nitrate vibrations, it was rather difficult to assign the bands relative to nitrate anions. However, a band at ~1300 cm^{-1} could be clearly distinguished. In **1**–**2** this band appears at 1305 cm^{-1} and is assigned to the symmetric stretching vibration mode of monodentate nitrate anion. In **3** and **4** this band is observed at 1295 and

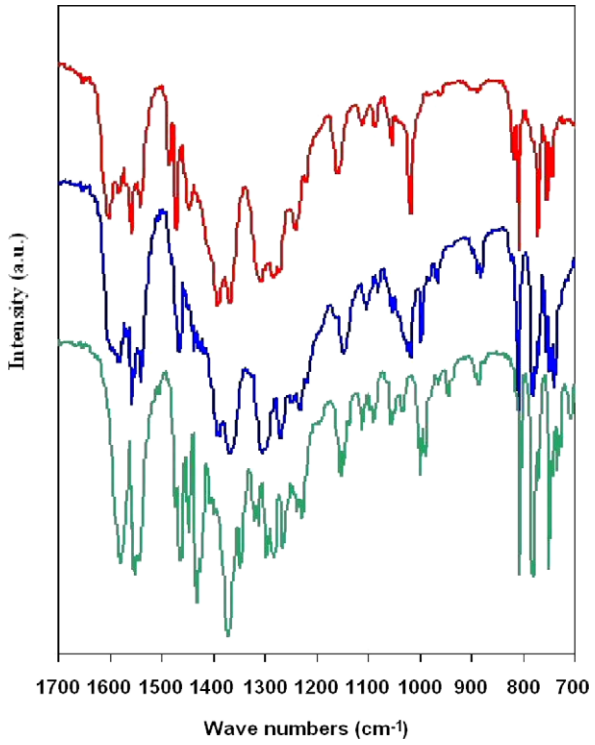

Fig. 6. IR spectra of the L ligand (red), the mononuclear $CdL(NO_3)_2$ (blue) and the trinuclear $Cd_3L(NO_3)_6 \cdot CH_3CN$ (green) complexes in the 1700–700 cm^{-1} area. (For interpretation of the references in colour in this figure legend, the reader is referred to the web version of this article.)

1300 cm^{-1}, respectively. It corresponds to the symmetric and asymmetric stretching vibration mode of monodentate and didentate nitrate anions.

From this analysis, it is clear that IR spectroscopy is a well suitable technique to distinguish between mononuclear and trinuclear complexes. As a consequence, this study gives an additional proof, if necessary, that the complex **4** can be stated as a trinuclear complex.

4. Conclusion

In conclusion, we have highlighted how the crystallisation solvent has a strong effect on the formation of three-dimensional supramolecular structures. Using the same synthetic procedure, i.e. self-assembly reaction at 100 °C under autogenous pressure, and changing only the nature of the solvent, we were able to tune the structure of Zn(II) and Cd(II) materials. In methanol, the mononuclear $ZnL(NO_3)_2$ (**1**) and $CdL(NO_3)_2$ (**2**) materials crystallised, whereas in acetonitrile, the trinuclear $Zn_3L(NO_3)_6 \cdot CH_3CN$ (**3**) and $Cd_3L(NO_3)_6 \cdot CH_3CN$ (**4**) compounds were obtained, as evidenced by single-crystal diffraction and infrared spectroscopy. The structures of these four materials are stabilised by an important network of non-coordinative forces: weak hydrogen bonding, aromatic stacking and anion–aromatic interactions.

It is worth mentioning that **1** and **2** represent the first examples of complexes where the L ligand is partially coordinated. As a perspective, these mononuclear species can be judiciously used as pre-constructed building blocks in further coordination reactions in order to prepare bimetallic supramolecular materials suitable for applications. Along this line, studies are in progress in the group to obtain heterometallic coordination compounds starting from **1** and **2**, which still have free coordination sites.

Acknowledgements

We thank the NRSC and especially Magmanet for Financial support. Coordination by the FP6 Network of Excellence "Magmanet"(Contract No. 515767) is also kindly acknowledged. This work has been supported financially by the National Graduate Research School Combination *NRSC-Catalysis*, a joint activity of the graduate research schools NIOK, HRSMC and PTN and by the italian MIUR.

Appendix A. Supplementary data

Supplementary data associated with this article can be found, in the online version, at doi:10.1016/j.poly.2006.04.030. Crystallographic data (excluding structure factors) for the structures reported have been deposited with the Cambridge Crystallographic Data Center as supplementary publication Nos. CCDC-299281 (**1**), -299282 (**2**) and -299283 (**3**) and can be obtained free of charge at www.ccdc.cam.ac.uk/conts/retrieving.html [or from the Cambridge Crystallographic Data Centre, 12, Union Road, Cambridge CB2 1EZ, UK; fax: (internat.) +44 1223/336 033; e-mail: deposit@ccdc.cam.ac.uk].

References

[1] J.M. Lehn, Polym. Int. 51 (2002) 825.
[2] B. Moulton, M.J. Zaworotko, Curr. Opin. Solid State Mater. Sci. 6 (2002) 117.
[3] B. Moulton, M.J. Zaworotko, Chem. Rev. 101 (2001) 1629.
[4] G. Leibeling, S. Demeshko, B. Bauer-Siebenlist, F. Meyer, H. Pritzkow, Eur. J. Inorg. Chem. (2004) 2413.
[5] B. Chand, U. Ray, G. Mostafa, T.H. Lu, C. Sinha, Polyhedron 23 (2004) 1669.
[6] D. Bose, J. Banerjee, S.H. Rahaman, G. Mostafa, H.K. Fun, R.D.B. Walsh, M.J. Zaworotko, B.K. Ghosh, Polyhedron 23 (2004) 2045.
[7] D.F. Sun, R. Cao, Y.Q. Sun, W.H. Bi, X.J. Li, Y.Q. Wang, Q. Shi, X. Li, Inorg. Chem. 42 (2003) 7512.
[8] P. Lin, R.A. Henderson, R.W. Harrington, W. Clegg, C.D. Wu, X.T. Wu, Inorg. Chem. 43 (2004) 181.
[9] M.A. Withersby, A.J. Blake, N.R. Champness, P.A. Cooke, P. Hubberstey, A.L. Realf, S.J. Teat, M. Schroder, J. Chem. Soc., Dalton Trans. (2000) 3261.
[10] O. Ohmori, M. Fujita, Chem. Commun. (2004) 1586.
[11] E.Y. Choi, Y.U. Kwon, Inorg. Chem. Commun. 7 (2004) 942.
[12] B.J. Holliday, C.A. Mirkin, Angew. Chem., Int. Ed. 40 (2001) 2022.
[13] P. Gamez, P. de Hoog, M. Lutz, W.L. Driessen, A.L. Spek, J. Reedijk, Polyhedron 22 (2003) 205.
[14] M.G. Barandika, M.L. Hernandez-Pino, M.K. Urtiaga, R. Cortes, L. Lezama, M.I. Arriortua, T. Rojo, J. Chem. Soc., Dalton Trans. 9 (2000) 1469.

[15] A.J. Blake, N.R. Champness, P.A. Cooke, J.E.B. Nicolson, C. Wilson, J. Chem. Soc., Dalton Trans. (2000) 3811.
[16] M.A. Withersby, A.J. Blake, N.R. Champness, P.A. Cooke, P. Hubberstey, W.S. Li, M. Schroder, Inorg. Chem. 38 (1999) 2259.
[17] J. Lu, T. Paliwala, S.C. Lim, C. Yu, T.Y. Niu, A.J. Jacobson, Inorg. Chem. 36 (1997) 923.
[18] S. Subramanian, M.J. Zaworotko, Angew. Chem., Int. Ed. 34 (1995) 2127.
[19] R.W. Gable, B.F. Hoskins, R. Robson, J. Chem. Soc., Chem. Commun. (1990) 1677.
[20] M.L. Taliaferro, T.D. Selby, J.S. Miller, Chem. Mater. 15 (2003) 3602.
[21] Y.B. Go, X.Q. Wang, E.V. Anokhina, A.J. Jacobson, Inorg. Chem. 44 (2005) 8265.
[22] P. Gamez, P. de Hoog, O. Roubeau, M. Lutz, W.L. Driessen, A.L. Spek, J. Reedijk, Chem. Commun. (2002) 1488.
[23] H. Casellas, C. Massera, P. Gamez, A.M. Manotti Lanfredi, J. Reedijk, Eur. J. Inorg. Chem. (2005) 2902.
[24] T.L. Hennigar, D.C. MacQuarrie, P. Losier, R.D. Rogers, M.J. Zaworotko, Angew. Chem., Int. Ed. 36 (1997) 972.
[25] P. Gamez, J. Reedijk, Eur. J. Inorg. Chem. (2006) 29.
[26] P. de Hoog, P. Gamez, W.L. Driessen, J. Reedijk, Tetrahedron Lett. 43 (2002) 6783.
[27] SAINT, Software Users Guide, Version 6.0, Bruker Analytical X-ray Systems, 1999.
[28] G.M. Sheldrick, SADABS v2.03: Area-Detector Absorption Correction, University of Göttingen, 1999.
[29] A. Altomare, M.C. Burla, M. Camalli, G.L. Cascarano, C. Giacovazzo, A. Guagliardi, A.G.G. Moliterni, G. Polidori, R. Spagna, J. Appl. Crystallogr. 32 (1999) 115.
[30] G.M. Sheldrick, SHELXL-97, Program for Crystal Structure Refinement, University of Göttingen, 1997.
[31] M. Nardelli, J. Appl. Crystallogr. 29 (1996) 296.
[32] C. Janiak, J. Chem. Soc., Dalton Trans. (2000) 3885.
[33] A.W. Addison, T.N. Rao, J. Reedijk, J. Van Rijn, G.C. Verschoor, J. Chem. Soc., Dalton Trans. (1984) 1349.

Pyrazine-derived ligands are important building-blocks in the design of extended structures because of the type and position of the donor atoms that allow linking metal ions together [17–37]. Particularly, 2-pyrazinecarboxylate has been demonstrated to be an extremely versatile ligand. It can act as a monodentate ligand through a carboxylate oxygen, as a bidentate chelating ligand through a pyrazine nitrogen and a carboxylate oxygen or as a tridentate bridging ligand [19,32–47]. Thus, its coordination versatility together with the nature of the central metal ion has led to a diversity of molecular architectures with different magnetic properties [19,32–47]. The coordination properties of 2-pyrazinecarboxylate can also be tuned by introducing various substituents into different positions of the pyrazine ring. The steric restrictions induced by these groups may allow for various molecular architectures and for the incorporation of interesting properties into the resulting coordination polymers. Our synthetic efforts are currently aimed towards synthesis of supramolecular architectures based on non-coordination intermolecular interactions and 5-methyl-2-pyrazinecarboxylate as ligand. Although 5-methyl-2-pyrazinecarboxylate has a great ability for the formation of coordinative bonds, as well as hydrogen-bonding and π–π stacking interactions, its coordination chemistry has hardly been explored [33,40,48–52]. In this paper, we report on the synthesis, spectroscopic and structural characterization, and magnetic properties of new complexes of 5-methyl-2-pyrazinecarboxylate (Hmpca) with cobalt(II), $[Co(mpca)_2(H_2O)_2]$ (**1**), nickel(II), $[Ni(mpca)_2(H_2O)_2]$ (**2**) and iron(III), $[Fe(mpca)_2(OH)]_2 \cdot 2H_2O$ (**3**). The use of the copper(II) ion leads to the mononuclear species $[Cu(mpca)_2(H_2O)] \cdot 3H_2O$ (**4**), which is in agreement with earlier reports [49,52]. However, we report herein the spectroscopic and magnetic properties of **4**, which had not been previously reported.

2. Experimental

2.1. General remarks

Starting materials were purchased from Aldrich and all manipulations were performed using materials as received.

2.2. Synthesis

2.2.1. $[Co(mpca)_2(H_2O)_2]$ (*1*)

A solution of $Co(ClO_4)_2 \cdot 6H_2O$ (0.5 mmol, 0.183 g) in 5 ml acetonitrile was slowly added to a solution of Hmpca (1 mmol, 0.138 g) in 5 ml water. Slow evaporation of the resulting orange solution led to orange crystals within two days. Yield: 68%. *Anal*. Calc. for $C_{12}H_{14}CoN_4O_6$: C, 39.04; H, 3.82; N, 15.18. Found: C, 38.54; H, 4.24; N, 15.46%. IR (ν_{max}/cm^{-1}): 3122 (br), 1652 (s), 1587 (m), 1540 (m), 1386 (s), 1328 (s) 1288 (s), 1186 (m), 1047 (s), 806 (s), 721 (m), 628 (m), 500 (m), 417 (s). UV/Vis/NIR (λ_{max}/nm): 379, 480, 1065, 1170.

2.2.2. $[Ni(mpca)_2(H_2O)_2]$ (*2*)

A solution of $Ni(ClO_4)_2 \cdot 6H_2O$ (0.5 mmol, 0.183 g) in 5 ml acetonitrile was slowly added to a solution of Hmpca (1 mmol, 0.138 g) in 5 ml water. Slow evaporation of the resulting blue solution led to blue crystals within two days. Yield: 56%. *Anal*. Calc. for $C_{12}H_{14}NiN_4O_6$: C, 39.06; H, 3.82; N, 15.18. Found: C, 38.50; H, 4.19; N, 15.35%. IR (ν_{max}/cm^{-1}): 3119 (br), 1652 (s), 1585 (m), 1543 (m), 1386 (s), 1331 (s) 1288 (s), 1187 (m), 1051 (s), 806 (s), 723 (m), 625 (m), 506 (m), 418 (s). UV/Vis/NIR (λ_{max}/nm): 390, 595, 920.

2.2.3. $[Fe(mpca)_2(OH)]_2 \cdot 2H_2O$ (*3*)

A solution of $Fe(ClO_4)_3 \cdot 10H_2O$ (2.5 mmol, 1.336 g) in 40 ml acetonitrile was slowly added to a solution of Hmpca (11.25 mmol, 1.554 g) and tetrabutyl ammonium hydroxide (11.25 mmol, 1 M solution in methanol) in 10 mL H_2O. After the mixture was stirred for 2 h the methanol was removed under reduced pressure. Orange cubic crystals of **3** were obtained by slow diffusion of diethyl ether into the acetonitrile–water solution. Yield: 48%. *Anal.* Calc. for $C_{24}H_{26}Fe_2N_8O_{12}$: C, 39.48; H, 3.59; N, 15.30. Found: C, 39.64; H, 3.08; N, 15.41%. IR (ν_{max}/cm^{-1}): 3066 (br), 1651 (s), 1588 (m), 1482 (m), 1373 (s), 1315 (s) 1281 (s), 1170 (m), 1010 (m), 874 (m), 800 (s), 720 (m), 671 (m), 631 (m), 500 (m), 416 (s). UV/Vis/NIR (λ_{max}/nm): 266, 350, 867.

2.2.4. $[Cu(mpca)_2(H_2O)] \cdot 3H_2O$ (*4*)

A solution of $Cu(ClO_4)_2 \cdot 6H_2O$ (0.5 mmol, 0.185 g) in 5 ml acetonitrile was slowly added to a solution of Hmpca (1 mmol, 0.138 g) in 5 ml water. Slow evaporation of the resulting blue solution led to blue crystals within one day. Yield: 72%. *Anal*. Calc. for $C_{12}H_{18}CuN_4O_8$: C, 35.17; H, 4.43; N, 13.67. Found: C, 35.50; H, 4.19; N, 13.35%. IR (ν_{max}/cm^{-1}): 3245 (br), 1636 (s), 1595 (m), 1560 (m), 1376 (s), 1329 (s) 11190 (s), 1168 (m), 1052 (s), 820 (m), 807 (s), 720 (m), 668 (m), 559 (m), 505 (m), 427 (s). UV/Vis/NIR (λ_{max}/nm): 365, 392, 623.

2.3. Physical measurements

C, H and N analyses were performed with a Perkin–Elmer 2400 series II analyzer. Infrared spectra (4000–300 cm^{-1}, resolution 4 cm^{-1}) were recorded on a Perkin–Elmer Paragon 1000 FTIR spectrometer equipped with a Golden Gate ATR device, using the reflectance technique. Diffuse reflectance spectra were obtained on a Perkin–Elmer Lambda 900 spectrophotometer with MgO as a reference. X-band powder EPR spectra were obtained on a Jeol RE2x electron spin resonance spectrometer using DPPH ($g = 2.0036$) as a standard. Magnetic susceptibility measurements (5–300 K) were carried out at 0.1 T using a Quantum Design MPMS-5 5T SQUID magnetometer. Data were corrected for the magnetization of the sample holder and for diamagnetic contributions, which were estimated from the Pascal constants.

Table 1
Crystal data and structure refinement for **1**–**3**

	1	**2**	**3**
Formula	$C_{12}H_{14}CoN_4O_6$	$C_{12}H_{14}NiN_4O_6$	$C_{24}H_{26}Fe_2N_8O_{12}$
Formula weight	369.20	368.96	730.23
Crystal system	triclinic	triclinic	triclinic
Space group	$P\bar{1}$	$P\bar{1}$	$P\bar{1}$
a (Å)	7.0480(6)	5.1156(1)	6.9694(2)
b (Å)	7.3825(9)	6.3992(1)	10.1796(4)
c (Å)	14.2921(11)	12.1082(2)	10.6417(2)
α (°)	89.402(7)	104.5790(15)	78.420(2)
β (°)	79.397(6)	90.6070(18)	89.577(2)
γ (°)	80.841(8)	110.1250(15)	77.469(2)
V (Å^3)	721.49(12)	358.12(1)	721.48(4)
Z	2	1	1
D_{calc} (mg m^{-3})	1.6995(3)	1.711	1.681
μ (Mo Kα) (mm^{-1})	1.228	1.393	1.084
Crystal size (mm)	$0.23 \times 0.14 \times 0.06$	$0.31 \times 0.14 \times 0.06$	$0.20 \times 0.14 \times 0.09$
T (K)	208(2)	208(2)	208(2)
Data collected	23372	11186	12537
Unique data	3310	1640	3283
R_{int}	0.069	0.030	0.030
Observed data [$I > 2\sigma(I)$]	2781	1561	2799
$R_w(F^2)$	0.0459	0.0246	0.0336
S	1.13	1.19	1.11
$\Delta\rho_{min}$, $\Delta\rho_{max}$ (e Å^{-3})	−0.37, 0.62	−0.22, 0.37	−0.32, 0.33

2.4. X-ray crystallographic analysis and data collection

Intensity data for single crystals of **1**–**4** were collected using Mo Kα radiation ($\lambda = 0.71073$ Å) on a Nonius KappaCCD diffractometer. The intensity data were corrected for Lorentz and polarization effects and for absorption (SADABS multiscan correction [53]). The structures were solved by Patterson methods. The programs EVALCCD [54], DIRDIF96 [55] and SHELXL-97 [56] were used for data reduction, structure solution and structure refinement, respectively. Refinement of F^2 was done against all reflections. The weighted R factor, wR, and goodness of fit S are based on F^2. Conventional R factors are based on F, with F set to zero for negative F^2. All non-hydrogen atoms were refined with anisotropic displacement parameters. The hydrogens of water molecules were taken from difference Fourier maps and were independently refined. All other hydrogens were initially placed at calculated positions and were freely refined subsequently. Geometric calculations and molecular graphics were performed with the PLATON package [57]. Crystal data and details of the structure refinement for **1**–**3** are given in Table 1.

3. Results and discussion

3.1. Synthesis and spectroscopic characterization

The neutral molecular complexes **1**–**4** were obtained through solution assemblies of equimolar amounts of 5-methyl-2-pyrazinecarboxylate (Hmpca) and the corresponding metal ions. Crystals suitable for X-ray crystallography have been obtained by slow evaporation of a water–acetonitrile solution. All complexes are stable under ambient conditions with poor solubility in most of the common organic solvents, but better solubility is observed in hot water; these characteristics are in agreement with their polymeric structure. It is worth noting that for the complexes **1** and **2**, the metal to ligand ratio does not affect the yield of the reaction and it does not determine the product. The mononuclear compound **4** is always obtained irrespective of the nature of the copper(II) salt used and the reaction conditions [49,52].

The infrared spectra of complexes **1** and **2** are very similar in the terms of the position, intensity and shape of the bands over the whole frequency range. The broad band centered at 3222 cm^{-1} in **1** and at 3119 cm^{-1} in **2** is characteristic of the ν(O–H) stretching vibration of the aqua molecules. The significant difference in the position of the ν(O–H) stretching vibration for **1** and **2** is in agreement with the presence of the *cis* isomer for **1** and the *trans* isomer for **2**. In both compounds, the band of the asymmetric stretching vibration $\nu_a(COO^-)$ is located at 1652 cm^{-1}, while that assigned to the symmetric stretching vibration $\nu_s(COO^-)$ is positioned at 1386 cm^{-1}. The difference $\Delta\nu = \nu_a(COO^-) - \nu_s(COO^-)$ is 266 cm^{-1}, suggesting a monodentate binding of the carboxylate group to the central metal ion [58]. The absorption bands resulting from the skeletal vibrations of the pyrazine rings appear at ca. 800 and 720 cm^{-1}.

The ligand field spectrum of **1** shows two principal regions of absorption: a broad band with maximum at 1170 nm (8.5×10^{-3} cm^{-1}) and a band at 480 nm (20.8×10^{-3} cm^{-1}) that together are indicative of a pseudo-octahedral cobalt(II) ion [59]. These two bands correspond to the $^4T_{1g}(F) \rightarrow {}^4T_{2g}(F)$ and $^4T_{1g}(F) \rightarrow {}^4T_{1g}(P)$ transitions [59]. For **2**,

the ligand field spectrum is typical of pseudo-octahedral nickel(II) complexes exhibiting a broad band with maximum at 920 nm (10.9×10^{-3} cm^{-1}) that is assigned to the $^4A_{2g} \rightarrow {}^4T_{2g}(F)$ transition. An absorption maxima is observed at 595 nm (16.8×10^{-3} cm^{-1}) due to the $^4A_{2g} \rightarrow {}^4T_{1g}(F)$ transition and the shoulder located at 390 nm (25.6×10^{-3} cm^{-1}) is attributed to the $^4A_{2g} \rightarrow {}^4T_{1g}(P)$ transition. On the basis of the octahedral symmetry, the value of the ligand field strength (*10Dq*) and the parameter *B* are 10.9×10^{-3} and 868 cm^{-1}. These values are in the range of those observed for nickel(II) complexes with a NiN_2O_4 chromophore group [59].

The reaction of the ligand Hmpca with $Fe(ClO_4)_3 \cdot 10H_2O$ (4.5:1) in the presence of 4.5 equiv. of Bu_4NOH leads to the formation of the complex **3**. The complex **3** shows good solubility only in methanol and it is very stable in the solid state. The IR spectrum displays peaks of the carboxylate group at 1651 and 1373 cm^{-1}. The peaks in the range of 500–850 cm^{-1} can be assigned to the bis-(μ-hydroxido)-bridged diiron(III) core. The ligand field spectrum of a polycrystalline sample of **3** displays the features typical of bis(μ-hydroxido)-bridged iron(III) complexes: an intense absorption band at 350 nm (28.5×10^{-3} cm^{-1}) with a lower energy shoulder in the region of 400–550 nm. These bands have been assigned to have an oxido-to-iron charge transfer character (LMCT) [60–64]. The absorption band with maximum at 867 nm (11.5×10^{-3} cm^{-1}) is often attributed to the d–d transitions involving forbidden states of the octahedral high-spin iron(III) complexes [59].

In the case of the complex **4**, the infrared spectrum displays the characteristic asymmetric and symmetric stretching vibrations of the carboxylate groups at 1636 and 1376 cm^{-1}, with $\Delta\nu$ equal to 260 cm^{-1}. The ν(O–H) stretching of the both ligand and lattice water is located at 3245 cm^{-1}. The ligand field spectrum shows a broad asymmetric band at 623 nm (16.1×10^{-3} cm^{-1}), a Cu–O charge transfer at 392 nm (25.5×10^{-3} cm^{-1}) and a Cu–N charge transfer at 350 nm (28.6×10^{-3} cm^{-1}), features that are characteristic for copper(II) complexes with a square-pyramidal coordination environment [59]. The complex shows an axial $S = 1/2$ EPR spectrum with $g_\perp = 2.05(7)$ and $g_\parallel = 2.25(3)$, values that are characteristic for a copper(II) ion in a square-pyramidal geometry [65,66].

3.2. Description of the crystal structures

The crystal structures of complexes **1**, **2** and **3** have been determined by X-ray crystallography; selected bond lengths and angles of the three structures are listed in Table 2.

Complex **1** crystallizes in space group $P\bar{1}$. The asymmetric unit of **1** consists of one $[Co(mpca)_2(H_2O)_2]$ neutral molecule (Fig. 1). The cobalt(II) ion is octahedrally coordinated to two nitrogens and two oxygens from two $mpca^-$ ligands and two oxygens of two water molecules in *cis* arrangement. The octahedral geometry is distorted, as the Co–N bond lengths (average 2.147(5) Å) are longer than the Co–O bond lengths (average 2.066(5) Å). The largest deviation from the octahedral geometry of the CoN_2O_4 chromophore is defined by the angles O1–Co1–O21 = 166.93(9)° and O11–Co1–N12 = 78.30(8)°. A similar coordination geometry has been observed in the complex of cobalt(II) with 6-methyl-2-pyridinecarboxylate [67]. In the cobalt(II) complex of the parent 2-pyrazinecarboxylate, $[Co(pca)_2(H_2O)_2]$,

Table 2
Selected bond lengths (Å) and angles (°) for **1**, **2** and **3**

Bond lengths		Bond angles	
1			
Co1–O1	2.058(2)	O1–Co1–O2	89.93(11)
Co1–O2	2.070(2)	O1–Co1–O11	88.91(10)
Co1–O11	2.071(2)	O1–Co1–O21	166.93(9)
Co1–O21	2.067(2)	O1–Co1–N12	93.59(9)
Co1–N12	2.154(2)	O1–Co1–N22	89.19(9)
Co1–N22	2.141(2)	O2–Co1–O11	173.09(9)
		O2–Co1–O21	92.27(10)
		O2–Co1–N12	94.98(9)
		O2–Co1–N22	87.34(9)
		O18–Co1–N12	78.30(8)
		O18–Co1–N22	99.45(8)
2			
Ni1–O1	2.0596(14)	O1–Ni1–O11	90.67(5)
Ni1–O11	2.0605(11)	O1–Ni1–N12	92.38(6)
Ni1–N12	2.0535(13)	O11–Ni1–N12	80.44(5)
		O1a–Ni1–O11a	89.34(5)
		O1–Ni1–O11a	89.33(5)
		O11–Ni1–N12a	99.56(5)
		O1–Ni1–N12a	87.62(5)
		O11–Ni1–O1a	89.34(5)
3			
Fe1–O1	1.9684(15)	O1–Fe1–O11	164.22(6)
Fe1–O11	1.9897(14)	O1–Fe1–O21	99.92(6)
Fe1–O21	1.9650(14)	O1–Fe1–N12	88.72(6)
Fe1–N12	2.1684(16)	O1–Fe1–N22	96.05(6)
Fe1–N22	2.1728(16)	O1–Fe1–O1a	80.29(6)
Fe1–O1a	1.9671(15)	O11–Fe1–O21	95.00(6)
		O11–Fe1–N12	77.25(6)
		O11–Fe1–N22	92.07(6)
		O21–Fe1–N12	168.44(6)
		O21–Fe1–N22	77.93(6)
		N22–Fe1–O1a	170.15(6)
		Fe1–O1–Fe1a	99.71(6)

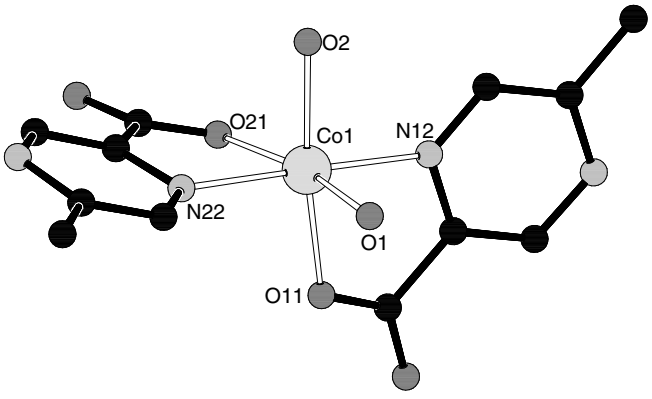

Fig. 1. Pluton projection of the molecular structure of *cis*-[Co(mpca)$_2$(H$_2$O)$_2$] (**1**). Hydrogens are omitted for clarity.

a *trans*-coordination of the two water molecules to cobalt(II) ion was observed [37].

The carbonyl oxygens and non-coordinated nitrogens of both mpca$^-$ ligands play an important role, as they are involved in an extended network of hydrogen bonds with the coordinated water molecules (Fig. 2 and Table 3). Through such hydrogen-bonding interactions, the cobalt(II) mononuclear units are linked together forming a two-dimensional architecture, with a Co···Co separation of 7.048 Å. The crystal lattice is further stabilized by face-to-face π–π stacking interactions involving the pyrazine rings. The shortest distance between the pyrazine planes is 3.59 Å, which is within the limit of common range for π–π interactions [68]. The pyrazine rings are nearly parallel with a deviation of 0.03°; the angle between the ring of the pyrazine and the centroid vector is 22.27°.

In the molecular structure of **2**, the nickel(II) ion is six-coordinated with a N_2O_4 donor set and a slightly distorted octahedral coordination geometry. In the equatorial plane, two mpca$^-$ ligands coordinate to nickel(II) ion in the bidentate N,O chelating manner, whilst the axial positions are occupied by two water molecules. A similar coordination geometry has been observed in the parent complex with 2-pyridinecarboxylate [69]. The complex **2** has an inversion center at the nickel(II) ion. The Ni–O bond lengths are slightly different (Ni–O1 = 2.0742(51) Å and Ni1–O11 = 2.0608(52) Å) and are somewhat shorter than the Ni–N bond lengths (Ni–N7 = 2.0488(48) Å). The largest distortion from the octahedral geometry is given by the angle O2–Ni1–N12 = 80.23(1)°. The pyrazine rings are coplanar with the equatorial chelate rings. This equatorial plane is stabilized by the weak C–H···O type intramolecular interactions (C16–H16···O1 = 3.310(2) Å). In **2**, the carbonyl oxygens of the mpca$^-$ ligands act as acceptors resulting in strong hydrogen bonds with the coordinated aqua molecules of adjacent mononuclear molecules (Table 3). Each $[Ni(mpca)_2(H_2O)_2]$ unit is hydrogen bonded to four neighboring molecules, thus forming a two-dimensional layer network (Fig. 3). The closest Ni···Ni separation is 6.339 Å.

The molecular structure of **3** consist of a centrosymmetric dinuclear bis(μ-hydroxido)iron(III) core that crystallizes

Table 3
Hydrogen bond details (distances (Å) and angles (°)) for the compounds **1**–**3**

Donor–H···acceptor	D–H	H···A	D···A	D–H···A
1				
O1–H1a···O22	0.74(4)	2.04(4)	2.738(3)	159(4)
O1–H1a···O21	0.74(4)	2.65(4)	3.153(3)	127(4)
O1–H1b···N15	0.81(4)	2.00(4)	2.797(3)	167(4)
O2–H2a···O12	0.83(4)	1.85(4)	2.675(3)	177(3)
O2–H2b···N25	0.79(4)	2.07(4)	2.842(3)	169(4)
2				
O1–H1a···O12	0.80(3)	1.90(3)	2.6695(19)	161(3)
O1–H1b···O11	0.77(3)	1.99(3)	2.7293(19)	160(3)
3				
O1–H1a···O30	0.80(3)	1.88(3)	2.672(3)	175(3)
O30–H30a···O1	0.76(4)	2.54(4)	3.257(3)	158(4)
O30–H30b···N25	0.78(4)	2.08(4)	2.851(3)	174(4)

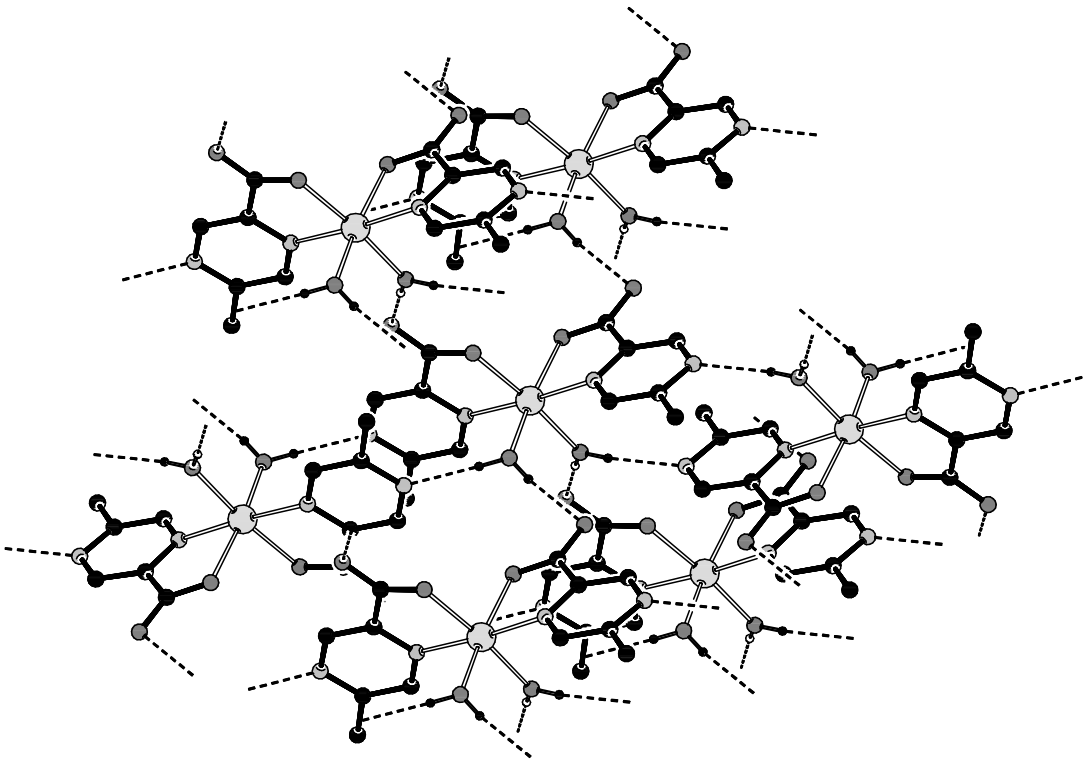

Fig. 2. View of the hydrogen-bonding and π–π stacking interactions in *cis*-$[Co(mpca)_2(H_2O)_2]$ (**1**).

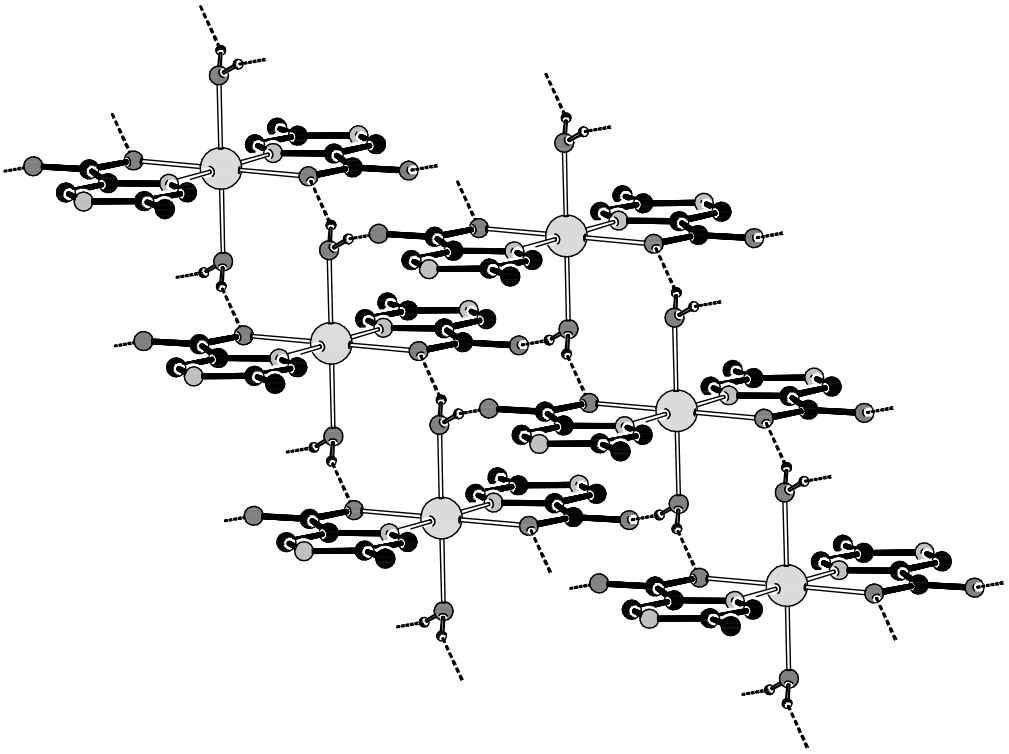

Fig. 3. View of the hydrogen-bonding and π–π stacking interactions in *trans*-[Ni(mpca)$_2$(H$_2$O)$_2$] (**2**).

with two water molecules in the lattice (Fig. 4). The two iron(III) ions of the dinuclear unit are equivalent and have pseudo-octahedral coordination geometry due to the bidentate chelating binding of two mpca$^-$ ions through one nitrogen atom of the pyrazine ring and one oxygen of the carboxylate group. The coordination geometry is completed by two bridging hydroxide ions coordinated *cis* to each other. The iron to nitrogen bond lengths are in the range 2.1684(16)–2.1728(16) Å, while the iron to oxygen bond lengths are in the range 1.9650(14)–1.9897(14) Å. The largest deviation from the octahedral geometry is indicated by the angle O1–Fe1–O11 = 164.22(6)°. The geometric features of the Fe$_2$(OH)$_2$ core, such as Fe···Fe = 3.008 Å and Fe1–O1–Fe1a = 99.71°, are in the range of those observed for other dinuclear bis(μ-hydroxido)iron(III) complexes [60–64].

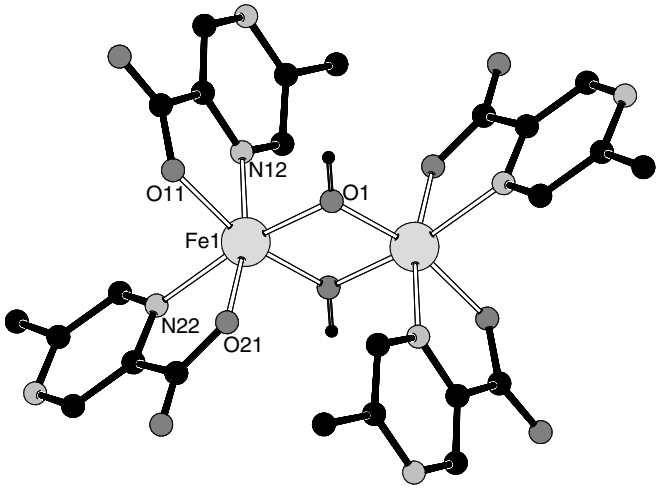

Fig. 4. Pluton projection of the molecular structure of [Fe(mpca)$_2$-(OH)]$_2$ · 2H$_2$O (**3**). Hydrogens are omitted for clarity.

In the crystal lattice of **3**, the dinuclear units Fe$_2$(OH)$_2$ are linked through π–π stacking and hydrogen-bonding interactions to form a three-dimensional network structure (Fig. 5). Each water molecule is involved in two O–H···O hydrogen bonding interactions with the hydroxido bridging groups of two neighboring Fe$_2$(OH)$_2$ cores and one O–H···N hydrogen bonding interaction with the pyrazine ring of a mpca$^-$ anion coordinated to a third Fe$_2$(OH)$_2$ unit (Table 3). The three-dimensional architecture is further stabilized by π–π stacking interactions between pyrazine rings of adjacent Fe$_2$(OH)$_2$ units, with a π–π stacking separation of 3.61 Å.

3.3. Magnetic properties

Temperature dependent magnetic susceptibility measurements for the complexes **1**–**4** were performed on polycrystalline samples in the range 5–300 K. In all cases the χ_M values have been corrected for diamagnetism.

The temperature dependence of $\chi_M T$ and χ_M for complex **1** is plotted in Fig. 6. The 2.582 cm^3 K mol^{-1} value of $\chi_M T$ observed in **1** at 300 K is significantly larger than the spin only value of 1.875 cm^3 K mol^{-1} expected for a total spin $S = 3/2$. Upon cooling, the $\chi_M T$ value decreases

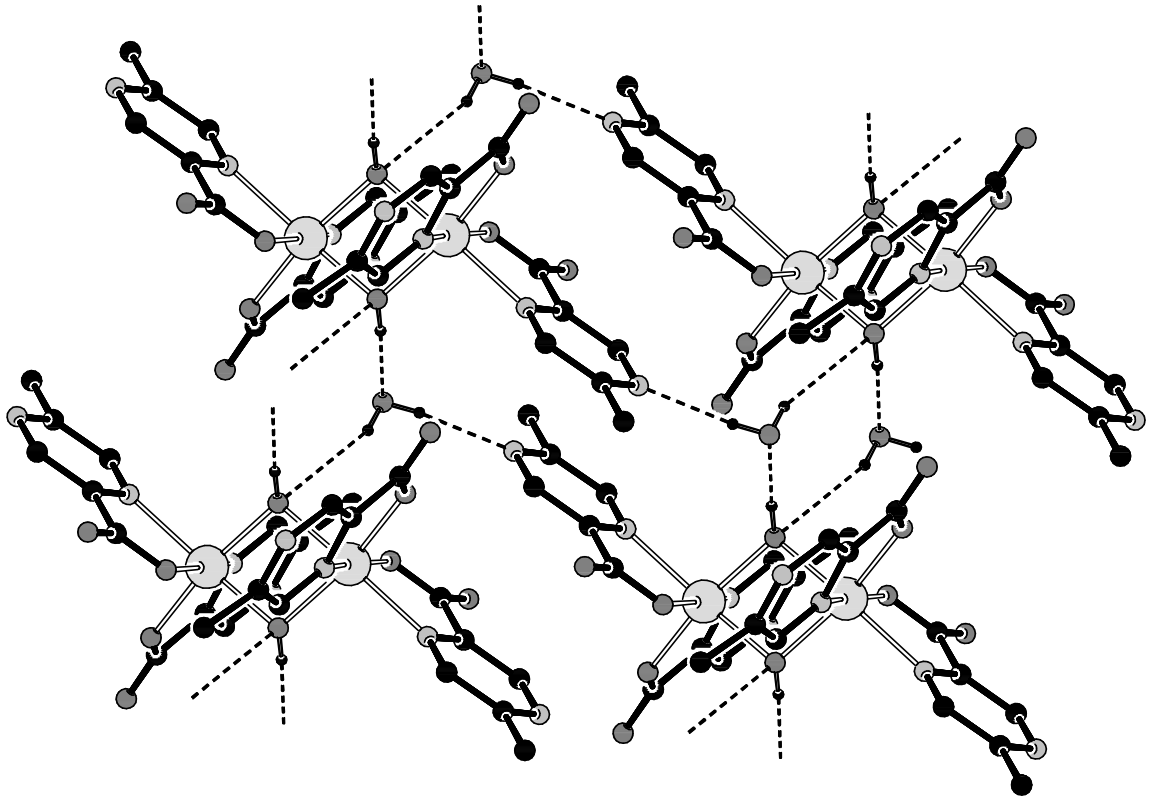

Fig. 5. View of the hydrogen-bonding and π–π stacking interactions in $[Fe(mpca)_2(OH)]_2 \cdot 2H_2O$ (**3**).

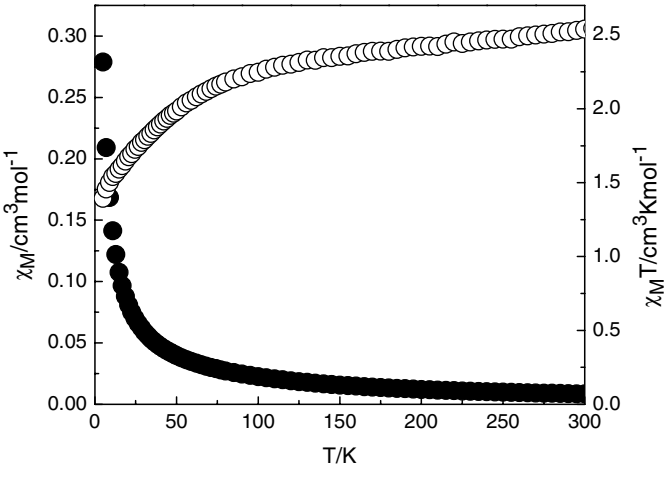

Fig. 6. Temperature dependence of $\chi_M T$ (○) and χ_M (●) at 0.1 T applied field for compound **1**.

to 1.394 cm^3 K mol^{-1} at 5 K. A plot of $1/\chi_M$ is linear between 40 and 300 K with a Curie constant of 2.698 cm^3 K mol^{-1} and a Weiss temperature of −20 K. From the fitted Curie constant, C, one can deduce the g value to be about 2.4. The high value of the Curie constant is a consequence of the spin–orbit coupling resulting from the $^4T_{2g}$ state of a cobalt(II) ion in an octahedral ligand field. Attempts to fit the magnetic data with the equation for the spin–orbital coupling [70] calculating the λ value (the spin–orbit coupling constant) and A parameter (A is a measure of the crystal field strength relative inter-electronic repulsions) have not been successful.

For **2**, the value of $\chi_M T$ observed at 300 K (1.215 cm^3 K mol^{-1}) is in the usual range for a non-interacting nickel(II) ion comprising a ^3A electronic state with $S = 1$. By lowering the temperature, the $\chi_M T$ value drops slightly to 1.092 cm^3 K mol^{-1} at 30 K, followed by a pronounced drop to 0.780 cm^3 K mol^{-1} at 5 K (Fig. 7). This behaviour is typical for a mononuclear nickel(II) complex with the low temperature drop associated to the zero-field splitting. The plot of $1/\chi_M$ is linear and obeys the Curie–Weiss law in the temperature range 30–300 K, giving a Curie constant of. 1.224 cm^3 K mol^{-1} and a Weiss temperature of −5.7 K. The calculated g value is found to be about 2.2, thus indicating the presence of magnetic anisotropy. The magnetic data were fitted to the model for isolated nickel(II) ions, in which the single-ion anisotropy was included [71]. With the consideration of a molecular field approximation (zJ'), the best fit was obtained with $g = 2.19$, $D = -2.5$ cm^{-1}, and $zJ' = -0.38$ ($R = 1.6 \times 10^{-4}$) in the temperature range 5–300 K. It is reasonable to assume that the intermolecular antiferromagnetic interactions occur via the hydrogen bonds [72]. The presence of magnetic anisotropy is also supported by the magnetization versus field measurements performed at different temperatures (results not shown).

The magnetic behaviour of **3** in the form $\chi_M T$ and χ_M versus T in the range 5–300 K at a 0.1 T applied field is

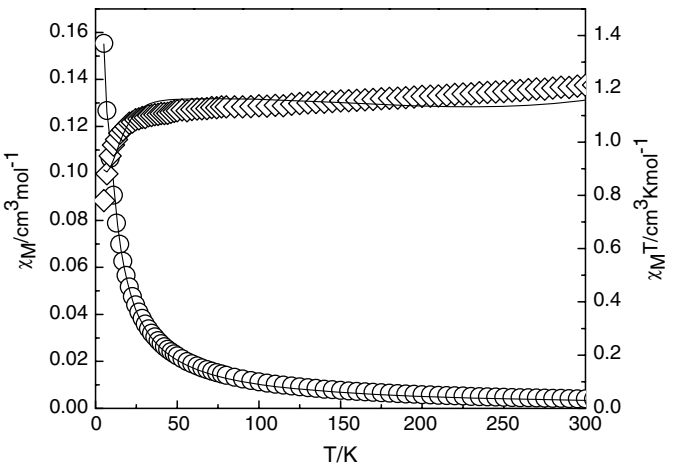

Fig. 7. Temperature dependence of $\chi_M T$ (◇) and χ_M (○) at 0.1 T applied field for compound **2**. Solid lines represents the calculated values for $g = 2.19$, $D = -2.5\ cm^{-1}$, and $zJ' = -0.38\ cm^{-1}$.

shown in Fig. 8. The value of the $\chi_M T$ product at room temperature ($8.68\ cm^3\ mol^{-1}\ K$) is close to the expected value for two non-interacting iron(III) ions with $S = 5/2$. The $\chi_M T$ product decreases gradually when lowering the temperature to 5 K, behaviour that suggests that antiferromagnetic interactions between the two iron(III) ions are operative in **3**. The magnetic experimental data were analyzed using the Van Vleck equation derived from the Heisenberg exchange Hamiltonian for two interacting spins $S_1 = S_2 = 5/2$ ($H = -JS_1S_2$) [73]. The temperature-independent paramagnetism ($TIP = 400 \times 10^{-6}\ cm^3\ K\ mol^{-1}$ for each iron ion) was taken into account. The best fit parameters were found to be $J = -21.2\ cm^{-1}$, $g = 2.01$ ($R = 2.5 \times 10^{-5}$). The exchange coupling parameter, J, is in the range of the values observed for other bis(μ-hydroxido)bridged iron(III) complexes, in which the low electron

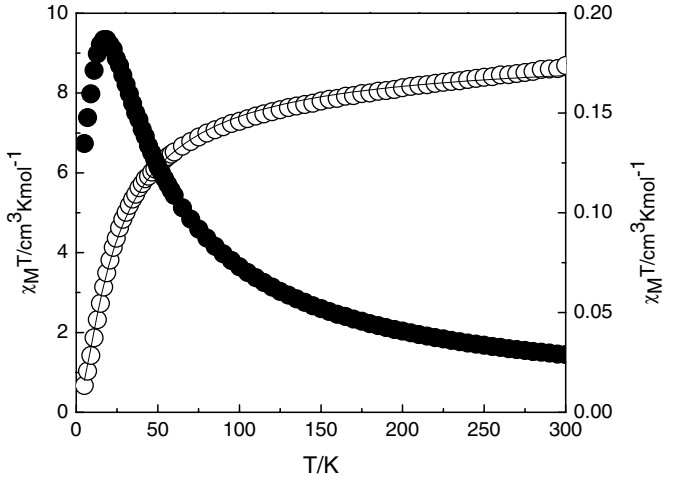

Fig. 8. Temperature dependence of $\chi_M T$ (○) and χ_M (●) at 0.1 T applied field for compound **3**. Solid line represents the calculated values for $J = -21.2\ cm^{-1}$ and $g = 2.01$.

density of the hydroxido-bridge is responsible for the observed weak antiferromagnetic coupling [60–64].

The $0.378\ cm^3\ K\ mol^{-1}$ value of $\chi_M T$ observed in **4** at 300 K corresponds to the expected value for non-interacting paramagnetic copper(II) ions ($S = 1/2$, $\chi_M T = 0.375\ cm^3\ K\ mol^{-1}$). The $\chi_M T$ value remains essentially constant as the temperature decreases to ca. 11 K, whereas below 11 K it decreases and at 5 K reaches the value of $0.316\ cm^3\ K\ mol^{-1}$. The magnetic data were fitted with the Curie–Weiss equation to give a Curie constant of $0.382\ cm^3\ K\ mol^{-1}$ and a Weiss temperature of −3 K.

4. Conclusions

Three new complexes of 5-methyl-2-pyrazinecarboxylate, i.e. *cis*-$[Co(mpca)_2(H_2O)_2]$ (**1**), *trans*-$[Ni(mpca)_2(H_2O)_2]$ (**2**) and $[Fe(mpca)_2(OH)]_2 \cdot 2H_2O$ (**3**), have been successfully synthesized and characterized. The mononuclear entities of **1** and **2** are linked through effective hydrogen-bonding and π–π stacking interactions to form extended network structures, in which the presence of antiferromagnetic interactions have been indicated by temperature dependent magnetic susceptibility measurements. The presence of the magnetic anisotropy in the complex $[Ni(mpca)_2(H_2O)_2]$ indicates that **2** might be a suitable building-block for the design of polynuclear complexes with single molecular magnet behaviour. The complex **3** has a bis(μ-hydroxido)diiron(III) core, in which the two iron(III) ions are antiferromagnetically coupled ($J = -21.2\ cm^{-1}$). In the crystal lattice, the adjacent dinuclear $Fe_2(OH)_2$ molecules are linked together via hydrogen-bonding and π–π stacking interactions to form a two-dimensional network.

5. Supplementary material

Crystallographic data (excluding structure factors) have been deposited with the Cambridge Crystallographic Data Centre as supplementary publication no. CCDC 296380–296383. Copies of the data can be obtained free of charge on application to The Director, CCDC, 12 Union Road, Cambridge CB2 1EZ, UK (fax: +44 1223 366 033, e-mail: deposit@ccdc.ac.uk or on the web www: http://www.ccdc.cam.ac.uk).

Acknowledgements

This work was financially supported by the Dutch Economy, Ecology, Technology programme (ECOX), a joint programme of the Ministry of Economic Affairs, the Ministry of Education, Culture and Science, the Ministry of Housing, Spatial Planning and the Environment and the Leiden University Study Group WFMO (Werkgroep Fundamenteel Materialen Onderzoek). S.T. acknowledges the Netherlands Organization for Scientific Research (NWO) for a Veni Grant.

References

[1] P.R. Andres, U.S. Schubert, Adv. Mater. 16 (2004) 1043.
[2] S. Vaucher, J. Fielden, M. Li, E. Dujardin, S. Mann, Nano Lett. 2 (2002) 225.
[3] J.S. Miller, J.L. Manson, Accounts Chem. Res. 34 (2001) 563.
[4] J.A. Real, A.B. Gaspar, V. Niel, M.C. Munoz, Coord. Chem. Rev. 236 (2003) 121.
[5] D. Maspoch, D. Ruiz-Molina, J. Veciana, J. Mater. Chem. 14 (2004) 2713.
[6] O. Kahn, C.J. Martinez, Science 279 (1998) 44.
[7] C. Janiak, Dalton Trans. (2003) 2781.
[8] H.W. Roesky, M. Andruh, Coord. Chem. Rev. 236 (2003) 91.
[9] L. Han, M. Hong, Inorg. Chem. Commun. 8 (2005) 406.
[10] D. Braga, L. Brammer, N.R. Champness, Crystengcomm. 7 (2005) 1.
[11] D. Braga, L. Maini, M. Polito, F. Grepioni, Struct. Bond. 111 (2004) 1.
[12] D. Bradshaw, J.B. Claridge, E.J. Cussen, T.J. Prior, M.J. Rosseinsky, Accounts Chem. Res. 38 (2005) 273.
[13] A.M. Beatty, Coord. Chem. Rev. 246 (2003) 131.
[14] S.R. Batten, K.S. Murray, Coord. Chem. Rev. 246 (2003) 103.
[15] S.A. Barnett, N.R. Champness, Coord. Chem. Rev. 246 (2003) 145.
[16] M.J. Hardie, Struct. Bond. 111 (2004) 139.
[17] S. Tanase, P.M. Gallego, E. Bouwman, R. de Gelder, J. Reedijk, Inorg. Chem. Commun. 8 (2005) 680.
[18] H.L. Sun, B.Q. Ma, S. Gao, S.R. Batten, Cryst. Growth Des. 5 (2005) 1331.
[19] X.M. Zhang, R.Q. Fang, Inorg. Chem. 44 (2005) 3955.
[20] R.J. Hill, D.L. Long, N.R. Champness, P. Hubberstey, M. Schroder, Accounts Chem. Res. 38 (2005) 335.
[21] H.L. Sun, Z.M. Wang, S. Gao, Inorg. Chem. 44 (2005) 2169.
[22] J. Carranza, H. Grove, J. Sletten, F. Lloret, M. Julve, P.E. Kruger, C. Eller, D.P. Rillema, Eur. J. Inorg. Chem. (2004) 4836.
[23] J. Carranza, J. Sletten, C. Brennan, F. Lloret, J. Cano, M. Julve, Dalton Trans. (2004) 3997.
[24] J.L. Manson, J.A. Schlueter, H.J. Koo, M.H. Whangbo, Inorg. Chem. 43 (2004) 4007.
[25] A.M. Kutasi, A.R. Harris, S.R. Batten, B. Moubaraki, K.S. Murray, Cryst. Growth Des. 4 (2004) 605.
[26] N. Schultheiss, D.R. Powell, E. Bosch, Inorg. Chem. 42 (2003) 8886.
[27] D. Armentano, G. de Munno, F. Guerra, J. Faus, F. Lloret, M. Julve, Dalton Trans. (2003) 4626.
[28] L.M. Baraldo, P. Forlano, A.R. Parise, L.D. Slep, J.A. Olabe, Coord. Chem. Rev. 219 (2001) 881.
[29] C. Hicks, G.Z. Ye, C. Levi, M. Gonzales, I. Rutenburg, J.W. Fan, R. Helmy, A. Kassis, H.D. Gafney, Coord. Chem. Rev. 211 (2001) 207.
[30] N.S. Persky, J.M. Chow, K.A. Poschmann, N.N. Lacuesta, S.L. Stoll, S.G. Bott, S. Obrey, Inorg. Chem. 40 (2001) 29.
[31] R. Hage, H.E.B. Lempers, J.G. Haasnoot, J. Reedijk, F.M. Weldon, J.G. Vos, Inorg. Chem. 36 (1997) 3139.
[32] M.G. Zhao, J.M. Shi, W.T. Yu, C.J. Wu, X. Zhang, J. Coord. Chem. 56 (2003) 1351.
[33] C.T. Chapman, D.M. Ciurtin, M.D. Smith, H.C. zur Loye, Solid State Sci. 4 (2002) 1187.
[34] R.P. Sharma, K.K. Bhasin, E.R.T. Tiekink, Acta Crystallogr. Sect. C-Cryst. Struct. Commun. 52 (1996) 2140.
[35] E.B. Shamuratov, A.S. Batsanov, K.T. Sharipov, Y.T. Struchkov, T. Azizov, Koord. Khim. 20 (1994) 616.
[36] C.L. Klein, C.J. O'connor, R.J. Majeste, L.M. Trefonas, Dalton Trans. (1982) 2419.
[37] C.J. Oconnor, E. Sinn, Inorg. Chem. 20 (1981) 545.
[38] B. Zheng, G. Liu, L. Gou, D.Y. Wang, H.M. Hu, Acta Crystallogr. Sect. E 61 (2005) M499.
[39] C.M. Liu, D.Q. Zhang, J.L. Luo, N.L. Wang, H.M. Hu, D.B. Zhu, Eur. J. Inorg. Chem. (2003) 3618.
[40] D.M. Ciurtin, M.D. Smith, H.C. zur Loye, Polyhedron 22 (2003) 3043.
[41] D.U. Huang, X.F. Zhang, C.N. Chen, F. Chen, Q.T. Liu, D.Z. Liao, L.C. Li, L.C. Sun, Inorg. Chim. Acta 353 (2003) 284.
[42] Y.C. Liang, M.C. Hong, J.C. Liu, R. Cao, Inorg. Chim. Acta 328 (2002) 152.
[43] L.M. Zheng, X.Q. Wang, Y.S. Wang, A.J. Jacobson, J. Mater. Chem. 11 (2001) 1100.
[44] L.M. Zheng, Y.S. Wang, X.Q. Wang, J.D. Korp, A.J. Jacobson, Inorg. Chem. 40 (2001) 1380.
[45] Y.B. Dong, M.D. Smith, H.C. zur Loye, Solid State Sci. 2 (2000) 861.
[46] L.M. Zheng, X.Q. Wang, A.J. Jacobson, J. Solid State Chem. 152 (2000) 174.
[47] S. Tanase, P. Marques Gallego, E. Bouwman, G.J. Long, L. Rebbouh, F. Grandjean, R. de Gelder, I. Mutikainen, U. Turpeinen, J. Reedijk, Dalton Trans. 13 (2006) 1675.
[48] D.M. Ciurtin, M.D. Smith, H.C. zur Loye, Inorg. Chim. Acta 324 (2001) 46.
[49] Y.B. Dong, M.D. Smith, H.C. zur Loye, Inorg. Chem. 39 (2000) 1943.
[50] C. Nather, M. Wriedt, I. Jess, Acta Crystallogr. Sect. C-Cryst. Struct. Commun. 57 (2001) 1395.
[51] H. Ptasiewicz-Bak, J. Leciejewicz, J. Coord. Chem. 49 (2000) 301.
[52] H. Ptasiewicz-Bak, J. Leciejewicz, Pol. J. Chem. 74 (2000) 877.
[53] SADABS: Area-Detector Absorption Correction, Siemens Industrial Automation, Inc., Madison, WI, 1996.
[54] A.J.M. Duisenberg, L.M.J. Kroon-Batenburg, A.M.M. Schreurs, J. Appl. Crystallogr. 36 (2003) 220.
[55] P.T. Beurskens, G. Beurskens, R. de Gelder, S. Garcica-Granda, R.O. Gould, R. Israel, J.M.M. Smits, The DIRDIF Programme, Technical Report on the Crystallography Laboratory, University of Nijmegen, Nijmegen, The Netherlands, 1996.
[56] G.M. Sheldrick, SHELXL97, Program for Crystal Structure refinement, University of Göttingen, Germany, 1997.
[57] A.L. Spek, PLATON, A Multipurpose Crystallographic Tool, Utrecht University, Utrecht, The Netherlands, 2003.
[58] K. Nakamoto, Infrared and Raman Spectra of Inorganic and Coordination Compounds, Wiley, New York, 1986.
[59] A.B.P. Lever, Inorganic Electronic Spectroscopy, Elsevier, Amsterdam, 1984.
[60] L. Borer, L. Thalken, C. Ceccarelli, M. Glick, J.H. Zhang, W.M. Reiff, Inorg. Chem. 22 (1983) 1719.
[61] E.J. Enemark, T.D.P. Stack, Inorg. Chem. 35 (1996) 2719.
[62] N. Kitajima, N. Tamura, M. Tanaka, Y. Moro-oka, Inorg. Chem. 31 (1992) 3342.
[63] S. Tanase, E. Bouwman, G.J. Long, A.M. Shahin, A.M. Mills, A.L. Spek, J. Reedijk, Eur. J. Inorg. Chem. (2004) 4572.
[64] J.A. Thich, C.C. Ou, D. Powers, B. Vasiliou, D. Mastropaolo, J.A. Potenza, H.J. Schugar, J. Am. Chem. Soc. 98 (1976) 1425.
[65] B.J. Hathaway, Comprehensive Coordination Chemistry, Pergamon Press, UK, 1987.
[66] A. Abragam, B. Bleaney, Electronic Paramagnetic Resonance of Transition Ions, Clarendon Press, London, 1970.
[67] R. March, W. Clegg, R.A. Coxall, L. Cucurull-Sanchez, L. Lezama, T. Rojo, P. Gonzales-Duarte, Inorg. Chim. Acta 353 (2003) 129.
[68] C. Janiak, Dalton Trans. 21 (2000) 3885.
[69] H. PtasiewiczBak, J. Leciejewicz, J. Zachara, J. Coord. Chem. 36 (1995) 317.
[70] J.W. Raebiger, J.L. Manson, R.D. Sommer, U. Geiser, A.L. Rheingold, J.S. Miller, Inorg. Chem. 40 (2001) 2578.
[71] R.L. Carlin, Magnetochemistry, Springer, Berlin, 1986.
[72] X. Ren, Y. Chen, C. He, S. Gao, J. Chem. Soc., Dalton Trans. (2002) 3915.
[73] O. Kahn, Molecular Magnetism, VCH Publishers., New York, 1993.

2. Experimental

2.1. Materials

Reagent grade chemicals and doubly distilled water were used throughout this work. QDC was prepared by the reported method [2–4] and was characterised by IR spectra and m.p. −160 °C. The QDC solution was prepared by dissolving QDC in water and determining its concentration iodometrically [4]. The mercury(I) solution was obtained by dissolving mercury(I) nitrate (Fluka) in 1 mol dm^{-3} perchloric acid (70%) and the solution was standardised against potassium iodate solution [15a]. The palladium(II) solution was obtained by dissolving palladium chloride (Johnson Matthey) in 0.20 mol dm^{-3} hydrochloric acid (AR) and assaying for palladium(II) by complexometric titration with EDTA [15b]. For some kinetic runs, chloride had to be absent and hence the chloride in the palladium(II) stock solution was removed by precipitation with silver nitrate, followed by repeated centrifugation. The resulting clear solution contained less than 1.0×10^{-6} mol dm^{-3} chloride and silver ions. Such extremely low concentrations of Ag^{+} and Cl^{-} were found to have no significant effect on the reaction. The required chloride concentration was maintained with sodium chloride. The chromium(III) solution was prepared by dissolving chromium(III) potassium sulfate (BDH, AR), $Cr_2(SO_4)_3 \cdot K_2SO_4 \cdot 24H_2O$ in water. The mercury(II) solution was obtained by dissolving mercuric oxide, HgO (BDH) in 0.50 mol dm^{-3} sulfuric acid. The ionic strength was kept constant with sodium sulfate. Use of sodium perchlorate was precluded since precipitation occurred under the reaction conditions.

2.2. Kinetic procedure

Since the reaction was too fast to be monitored by the usual method, kinetic measurements were performed on a Hitachi 150-20 spectrophotometer (Tokyo, Japan) connected to a rapid kinetic accessory (HITECH SFA-12 unit). Kinetics were followed at 25 ± 0.1°C and I = 1.60 mol dm^{-3}. The reaction was initiated by mixing the pre-equilibrated reactant solutions, which also contained known concentrations of sulfuric acid and sodium sulfate to give the required acidity and ionic strength. The reaction was followed under second order conditions by measuring the absorbance of QDC in the form of the monomer in the reaction mixture at 440 nm. Application of Beer's law under the reaction conditions had been verified earlier between 1.0×10^{-4} and 2.0×10^{-3} mol dm^{-3} of QDC at 440 nm with molar absorptivity, ε resulting as 395 ± 10 dm^3 mol^{-1} cm^{-1}. The second order plots were non-linear due to the autocatalytic effect of the one of the products, chromium(III). Hence the choice of initial rates at 5% completion of the reaction was made. The initial rates of the reaction were obtained from the slopes of concentrations versus time curves at the initial stages (5%) of the reaction by the plane mirror method. The initial rates were reproducible within ±5%.

3. Results and discussion

3.1. Stoichiometry

Different sets of concentrations of reactants and catalyst, palladium(II), in 0.50 mol dm^{-3} sulfuric acid at constant ionic strength, 1.60 mol dm^{-3}, were kept for over 8 h at 25 °C in a closed container. When [QDC] > [mercury(I)], the remaining QDC was assayed by measuring the absorbance at 440 nm, whereas under the conditions [mercury(I)] > [QDC], when QDC had fully reacted, the remaining mercury(I) concentration was determined by titration with potassium iodate [15a]. One of the products, the chromium(III) concentration, was determined by measuring the absorbance at 584 nm. The results showed that QDC reacted with mercury(I) in a 1:3 mole ratio. The catalyst concentration was unchanged at the end of the reaction as found by estimating it spectrophotometrically as the palladium(II) azide complex [16].

$$\mathrm{QDC} + 3\mathrm{Hg(I)} \overset{\mathrm{Pd(II)}}{\rightarrow} \mathrm{Cr(III)} + 3\mathrm{Hg(II)} \quad (1)$$

3.2. Order of reaction

The reaction order was found from log–log plots of initial rates versus concentrations at constant ionic strength, I = 1.60 mol dm^{-3} and at constant sulfuric acid concentration (0.50 mol dm^{-3}). At constant palladium(II) concentration, 8.0×10^{-6} mol dm^{-3}, the order with respect to QDC in the concentration range 5.0×10^{-5}–5.0×10^{-4} mol dm^{-3} was found to be unity. The order with respect to mercury(I), between 5.0×10^{-5} and 6.0×10^{-4} mol dm^{-3} was less than unity, ca. 0.42 (Table 1). At constant reactant concentrations (3[QDC] = [Hg(I)] = 6.0×10^{-4} mol dm^{-3}), constant acidity and ionic strength ([H_2SO_4] = 0.50 mol dm^{-3} and I = 1.60 mol dm^{-3}), the palladium(II) concentration was varied between 1.0×10^{-6} and 1.0×10^{-5} mol dm^{-3} and the order was found to be unity (Table 1).

3.3. Effect of added products

The initially added products, chromium(III) and mercury(II), were studied in the 5.0×10^{-5}–5.0×10^{-4} and 1.0×10^{-4}–5.0×10^{-4} mol dm^{-3} concentration ranges, respectively, while keeping the reactant concentrations and all other conditions constant. It was observed that added chromium(III) enhances the reaction rate with an order of less than unity (0.73), whereas, the added mercury(II), does not change the rate appreciably (Table 2). This result indicates the autocatalytic nature of the product, chromium(III), which is also evident from the concentration of chromium(III) values versus t plot (Fig. 1) and a linear plot of (Initial rate) versus $(\mathrm{rate})_{\mathrm{calc}}$ for chromium(III) variations (Fig. 1, inset). However, in the case of the palladium(II)

Table 1
Effect of QDC, Hg(I) and Pd(II) concentrations on Pd(II) catalysed oxidation of Hg(I) by QDC in acid medium: $[H_2SO_4] = 0.50$, $I = 1.60$ mol dm^{-3}, 25 °C

$[QDC] \times 10^4$ (mol dm^{-3})	$[Hg(I)] \times 10^4$ (mol dm^{-3})	$[Pd(II)] \times 10^6$ (mol dm^{-3})	Initial rate $\times 10^7$ (mol dm^{-3} s^{-1})
0.50	6.0	8.0	0.85
1.0	6.0	8.0	1.61
2.0	6.0	8.0	3.45
3.0	6.0	8.0	5.07
4.0	6.0	8.0	6.48
5.0	6.0	8.0	8.61
2.0	0.50	8.0	1.18
2.0	1.0	8.0	1.77
2.0	2.0	8.0	2.38
2.0	4.0	8.0	3.10
2.0	6.0	8.0	3.45
2.0	6.0	1.0	0.43
2.0	6.0	2.0	0.86
2.0	6.0	4.0	1.75
2.0	6.0	6.0	2.56
2.0	6.0	8.0	3.45
2.0	6.0	10.0	4.29

Table 2
Effect of initially added products, Cr(III) and Hg(II), on Pd(II) catalysed oxidation of Hg(I) in acid medium: $3[QDC] = [Hg(I)] = 6.0 \times 10^{-4}$; $[Pd(II)] = 8.0 \times 10^{-6}$; $[H_2SO_4] = 0.50$; $I = 1.60$ mol dm^{-3}, 25 °C

$[Cr(III)] \times 10^4$ (mol dm^{-3})	Initial rate $\times 10^6$ (mol dm^{-3} s^{-1})	$[Hg(II)] \times 10^4$ (mol dm^{-3})	Initial rate $\times 10^7$ (mol dm^{-3} s^{-1})
0.50	1.25	1.0	3.38
1.0	2.31	2.0	3.48
2.0	4.15	3.0	3.51
3.0	5.77	4.0	3.41
4.0	7.63	5.0	3.43
5.0	8.95		

catalysed chromium(VI) oxidation of mercury(I) reaction [14] such autocatalysis was not observed.

3.4. Effect of acid

At constant reactant concentrations and other constant conditions (Table 3) the sulfuric acid concentration was varied between 0.20 and 1.0 mol dm^{-3} and the rate was found to increase with an order of ca. 0.51 in $[H^+]$. The $[H^+]$ values calculated from the added sulfuric acid concentration and known equilibrium constant of the acid sulfate equilibrium [17] are shown in Table 3.

3.5. Effect of added chloride

For this purpose palladium(II) solutions, which did not contain chloride, were used. The initial rate increased with increase in $[Cl^-]$. This is ascribable to the formation of palladium(II) chloride complexes. The order in $[Cl^-]$ under the experimental conditions was close to unity (ca. 0.91). As with the dependence on mercury(I), the rate varies with

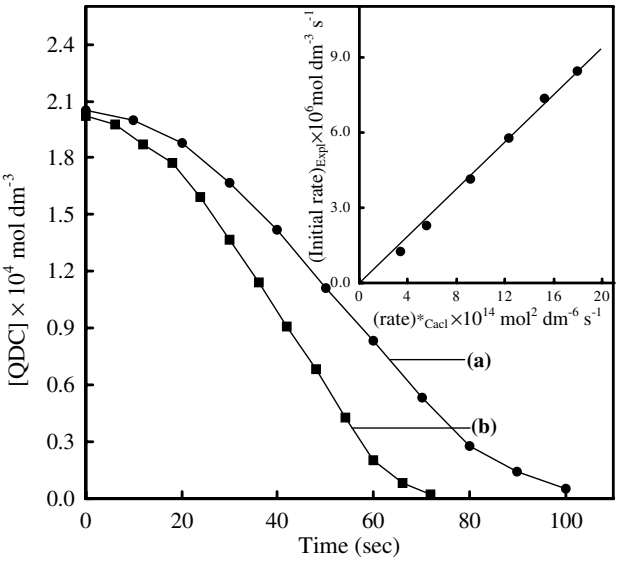

Fig. 1. Autocatalysis: [QDC] vs. t plots; $3[QDC] = [Hg(I)] = 6.0 \times 10^{-4}$, $[H_2SO_4] = 0.50$; $I = 1.60$ mol dm^{-3}. (a) $[Pd(II)] = 4.0 \times 10^{-6}$. (b) $[Pd(II)] = 8.0 \times 10^{-6}$ mol dm^{-3}. Inset: Plot of $(\text{Initial rate})_{\text{exptl}}$ vs. $(\text{rate})_{\text{calc}}$. $(\text{Rate})_{\text{calc}} = [QDC][Pd(II)][Hg(I)]^{0.42}[H^+]^{0.51}[Cr(III)]^{0.73}$ for variation of Cr(III) (Table 2).

Table 3
Effect of sulfuric acid concentration on Pd(II) catalysed oxidation of Hg(I) by QDC: $3[QDC] = [Hg(I)] = 6.0 \times 10^{-4}$; $[Pd(II)] = 8.0 \times 10^{-6}$; $I = 3.70$ mol dm^{-3}, 25 °C

$[H_2SO_4]$ (mol dm^{-3})	$[H^+]$ (mol dm^{-3})	Initial rate $\times 10^7$ (mol dm^{-3} s^{-1})
0.2	0.048	1.28
0.4	0.139	2.73
0.6	0.311	4.18
0.8	0.579	5.21
1.0	0.911	6.45

$[Cl^-]$. Palladium(II) is known to form chloride complexes [18] of the formula $Pd(Cl)_n^{+2-n}$, n having values 1–4, the cumulative stability constants β_1 to β_4 being 1.0×10^4, 3.1×10^7, 5.4×10^9 and 1.3×10^{11}, respectively, as shown in the following equilibrium:

$$Pd^{2+} + Cl^- \rightleftharpoons PdCl^+ \qquad K_1 \tag{2}$$

$$PdCl^+ + Cl^- \rightleftharpoons PdCl_2 \qquad K_2 \tag{3}$$

$$PdCl_2 + Cl^- \rightleftharpoons PdCl_3^- \qquad K_3 \tag{4}$$

$$PdCl_3^- + Cl^- \rightleftharpoons PdCl_4^{2-} \qquad K_4 \tag{5}$$

The approximate concentrations of such species may be calculated based on the following equation:

$$[Pd(II)]_T = [Pd(II)]_f \left\{1 + \beta_1[Cl^-] + \beta_2[Cl^-]^2 + \beta_3[Cl^-]^3 + \beta_4[Cl^-]^4\right\} \tag{6}$$

from the concentrations of the dissolved palladium(II) and chloride, with their competing equilibria [19,20]. Variation in the concentrations of such species with increase in $[Cl^-]$ is shown in Table 4, along with the rates of the respective

Table 4
Variation of different Pd(II) species[a] with [Cl^-] on Pd(II) catalysed oxidation of Hg(I) by QDC in acid medium: 3[QDC] = [Hg(I)] = 6.0×10^{-4}; [Pd(II)] = 8.0×10^{-6}; [H_2SO_4] = 0.50; I = 1.60 mol dm^{-3}, 25 °C

$[Cl^-] \times 10^5$ (mol dm^{-3})	α_0	$10^2\alpha_1$	$10^2\alpha_2$	$10^4\alpha_3$	$10^4\alpha_4$	Initial rate $\times 10^7$ (mol dm^{-3} s^{-1})
0	1.0					0.09
0.5	0.96	4.8	0.074	0.0064	0.0008	0.52
1.0	0.91	9.1	0.28	0.049	0.0126	1.17
1.5	0.86	13.0	0.60	0.158	0.0569	2.36
2.5	0.79	19.7	1.53	0.665	0.4003	3.82
4.0	0.69	26.5	3.42	2.38	2.300	5.75
5.0	0.63	31.7	4.91	4.28	5.148	6.50
6.0	0.58	35.0	6.52	6.81	9.837	7.98
8.0	0.50	40.0	9.91	13.8	26.61	9.83
10.0	0.43	43.2	13.4	23.3	56.15	11.2
15.0	0.31	46.7	21.7	56.7	204.7	12.5

[a] α_0, α_1, α_2, α_3 and α_4 are the fractions of total Pd(II) of the species Pd_f^{2+}, $PdCl^+$, $PdCl_2$, $PdCl_3^-$ and $PdCl_4^{2-}$, respectively. The stability constants of the different Pd(II) complexes are from Ref. [15].

catalysed reactions, and it is found that there is a parallelism only between rates and [$PdCl^+$] (Fig. 2).

Rates of reaction with 30 different sets of concentrations of QDC, mercury(I), palladium(II) and H^+ ion at constant ionic strength were found to obey the rate law (7) shown in Fig. 3.

$$\text{Rate} \propto [\text{QDC}][\text{Pd(II)}][\text{Hg(I)}]^{0.42}[\text{H}^+]^{0.51} \quad (7)$$

3.6. Effect of dielectric constant and ionic strength

When the acetic acid content (V/V) in the reaction medium was increased, keeping the reactant concentrations and other conditions constant, the reaction rate increases. Since the dielectric constants of aqueous acetic acid are not available in the literature, they were computed from the values for pure liquids [21]. No reaction of the solvent with the oxidant occurred under the experimental conditions employed. A plot of log(Initial rate) versus $1/D$ is linear with positive slope (Fig. 4, ($r \geqslant 0.999$, $\sigma \leqslant 0.015$)). Variation of ionic strength between 1.6 and 4.0 mol dm^{-3}, using sodium sulfate, caused a decrease in the rate of reaction. A plot of log(Initial rate) versus $I^{1/2}$ is linear with negative slope as shown in Fig. 4 ($r \geqslant 0.998$, $\sigma \leqslant 0.021$).

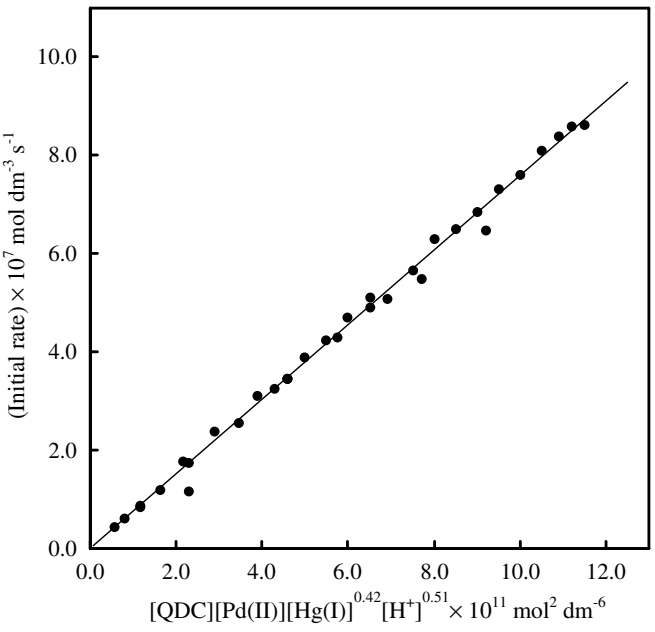

Fig. 3. Plot of the initial rate of the QDC–Hg(I) reaction vs. the product of reactant concentrations at 25 °C and I = 1.60 mol dm^{-3}.

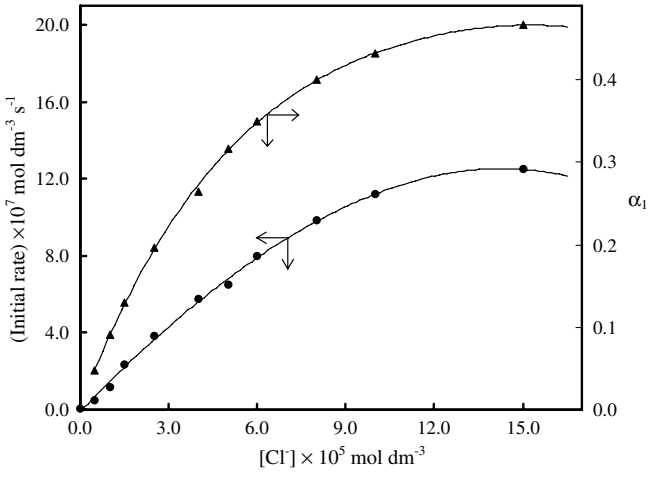

Fig. 2. Effect of chloride concentrations on different palladium(II) species and also on the rates of reaction (conditions as in Table 4).

3.7. Effect of added ions

In this case, the palladium(II) used contain chloride concentrations less than 1.0×10^{-6} mol dm^{-3} as stated in Section 2. When the reactant concentrations and other conditions were kept constant, ions such as Cu^{2+}, Na^+ and NO_3^- did not have any significant effect on the rate of the reaction, whereas added Mn^{2+} decreases the rate.

3.8. Effect of temperature

The rate constants (k_1) of the slow step of Scheme 1 were obtained from the intercepts of [QDC][Pd(II)]/(Initial rate) versus 1/[Hg(I)] plots at four different temperatures, by

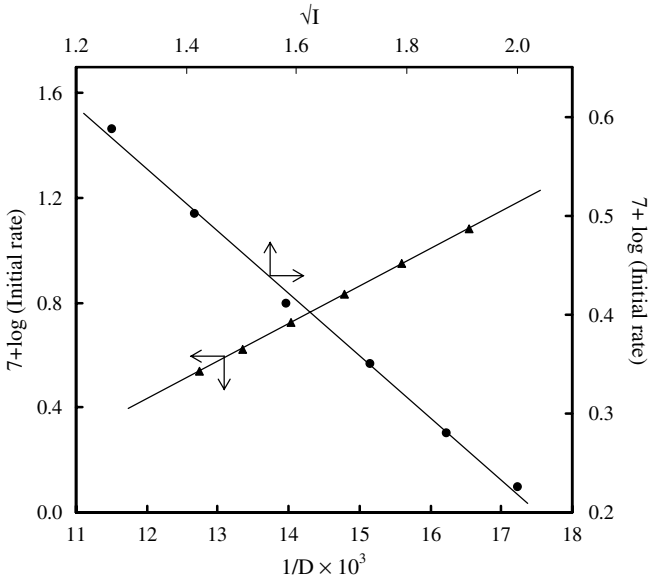

Fig. 4. Plot of log(Initial rate) vs. $I^{1/2}$ and log(Initial rate) vs. $1/D$.

employing the values of K_5. The activation parameters for the rate determining step were obtained by the least-square method and from a plot of $\log k_1$ versus $1/T$ ($r \geqslant 0.987$, $\sigma \leqslant 0.019$). The values of $k_1 \times 10^2$ ($dm^3\,mol^{-1}\,s^{-1}$) are 3.88, 5.02, 6.94 and 9.42 at 298, 303, 308 and 313 K, respectively, which lead to the activation parameters $E_a = 23 \pm 1$ kJ mol^{-1}, $\Delta H^{\#} = 21 \pm 1$ kJ mol^{-1}, $\log A = 6.7 \pm 0.5$, $\Delta S^{\#} = -126 \pm 10$ J K^{-1} mol^{-1} and $\Delta G^{\#} = 58 \pm 5$ kJ mol^{-1}.

Thermodynamic quantities of first step of Scheme 1 are evaluated from the slope of the plot of [QDC][Pd(II)]/(Initial rate) versus $1/[H^+]$ at different temperatures. The values of K_5 at 298, 303, 308 and 313 K are 4.24, 4.65, 4.91 and 5.28 $dm^3\,mol^{-1}$, respectively. The Van't Hoff plot was drawn for the variation of K_5 with temperature ($\log K_5$ versus $1/T$; $r \geqslant 0.996$, $\sigma \leqslant 0.023$). The values of the thermodynamic quantities are $\Delta H = 11.0 \pm 0.5$ kJ mol^{-1}, $\Delta S = 49. \pm 3$ J K^{-1} mol^{-1} and $\Delta G = -4.0 \pm 0.2$ kJ mol^{-1}. A comparison of these values with those values obtained for the slow step shows that the reaction before the rate-determining step is fairly rapid [22].

The oxidation of mercury(I) by QDC is not observed in the absence of palladium(II) and, in the presence of latter, occurs with measurable speed only in aqueous sulfuric acid. Furthermore, since QDC does not oxidise palladium(II), even at the higher temperature (ca. 90 °C) of the aqueous acid, it is unlikely that any higher oxidation states, such as palladium(III) or palladium(IV), are involved in the reaction. In the presence of perchloric acid and nitric acid, the palladium(II) catalyst is inefficient, possibly due to active species of palladium as palladium chloride complexes, which are not possible in such media. Hence the study was undertaken in sulfuric acid and chloride medium.

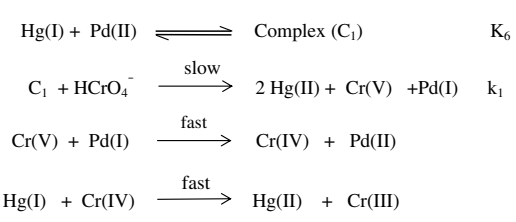

Scheme 1.

The reaction between mercury(I) and QDC in sulfuric acid in the presence of palladium(II) has a stoichiometry of 1:3 with an apparent less than unit order in mercury(I) and H^+ and first order dependence on QDC, palladium(II) and Cl^-. It was observed that one of the products, chromium(III), increases the reaction rate, whereas another product, mercury(II), does not affect the rate of the reaction. However, in the palladium(II) catalysed chromium(VI) oxidation of mercury(I) an apparent less than unit order in mercury(I) and Cl^-, and first order dependence on Cr(VI), palladium(II) and H^+ concentrations were obtained. In this study, the initially added products have no effect on the rate of the reaction. The different behaviour in the palladium(II) catalysed oxidation of mercury(I) by chromium(VI) and QDC might be due to the presence of the quinolinium moiety. There are reports [23] that the reactivities of substituted pyridine, quinoline and isoquinoline complexes of chromium(VI) resemble one another. Such complexes show no dimerisation or polymerisation in solutions [24a]. In aqueous solution, QDC and chromium(VI) behave in different manners. Quinoline acts as an electron donor. Due to this, considerable quantities of QDC are reduced to chromium(III) [24b]. The thus formed chromium(III) immediately forms a weak complex with QDC, which is responsible for autocatalysis.

It is well known that in aqueous acid solution, QDC exists mainly in the form of the acid chromate ion [25,26], $HCrO_4^-$. The results suggest that mercury(I) reacts with palladium(II) to give a complex, which then reacts with $HCrO_4^-$ in a rate determining step to give the mercury(II) product, the intermediates chromium(V) and palladium(I) being generated. The intermediate chromium(V) reacts in further fast steps to give the products, palladium(II) being regenerated. The results can be accommodated by Scheme 1.

The evidence for complex formation was obtained from UV–Vis spectra of both palladium(II) and mercury(I)–palladium(II) mixtures, in which a hypsochromic shift of palladium(II) from 320 to 300 nm and hyperchromicity at 300 nm, occurred (Fig. 5). This was also evident from the Michaelis–Menten plot and such complex formation between substrate and catalyst has also been observed in other studies [27,28]. Since oxidation of mercury(I) by QDC is a non-complementary reaction, it may occur by the intervention of reactive chromium(V) and chromium(IV) species. The intervention of chromium(V) is evident from the induction experiment with iodide [25,26]. The induced oxidation of iodide yields two equivalent of iodine for each equivalent of the inductor oxidised. In any induced oxidation the inductor factor is defined as the ratio of the number of equivalents of reducing agent oxidised to

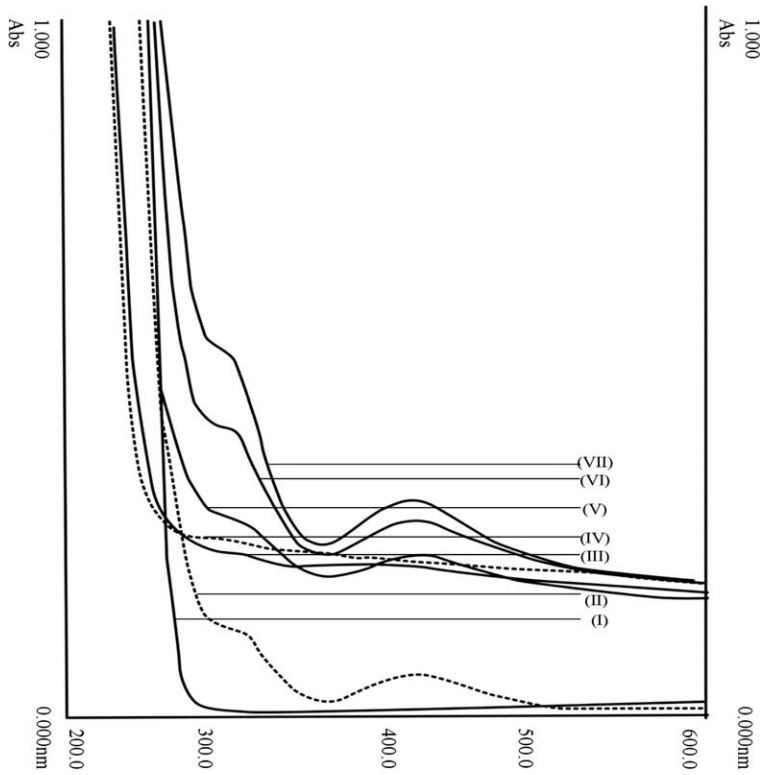

Fig. 5. UV–Vis spectra showing the formation of complex between Pd(II) and Hg(I) in the Pd(II) catalysed QDC oxidation of mercury(I) reaction in aqueous sulfuric acid at 25 °C. $[H_2SO_4] = 0.5$ mol dm^{-3} in all spectra. (I) Spectra of $[Hg(I)] = 2.0 \times 10^{-4}$ mol dm^{-3}. (II) Spectra of $[Pd(II)] = 2.0 \times 10^{-4}$ mol dm^{-3}. (III) Spectra of a mixture of $[Hg(I)] = 2.0 \times 10^{-4}$ and $[Pd(II)] = 0.5 \times 10^{-4}$/mol dm^{-3}. (IV) Spectra of a mixture of $[Hg(I)] = 2.0 \times 10^{-4}$ and $[Pd(II)] = 1.0 \times 10^{-4}$/mol dm^{-3}. (V) Spectra of a mixture of $[Hg(I)] = 2.0 \times 10^{-4}$ and $[Pd(II)] = 2.0 \times 10^{-4}$/mol dm^{-3}. (VI) Spectra of a mixture of $[Hg(I)] = 2.0 \times 10^{-4}$ and $[Pd(II)] = 3.0 \times 10^{-4}$/mol dm^{-3}. (VII) Spectra of a mixture of $[Hg(I)] = 2.0 \times 10^{-4}$ and $[Pd(II)] = 4.0 \times 10^{-4}$/mol dm^{-3}.

the number of equivalents of inductor oxidised. The induction factor for iodide oxidation is nearly two, which indicates that the active oxidising agent is pentavalent chromium. The intervention of chromium(IV) is evident from the progressive rate decrease in the presence of increasing amounts of added manganese(II), the decrease reaching a limit of about one half of the rate found in the absence of manganese(II). Such results have also been obtained for chromium(VI) oxidation of 2-propanol in aqueous acetic acid [29,30].

Scheme 1 leads to the rate law (8)

$$\text{Rate} = \frac{-\mathrm{d}[\text{QDC}]}{\mathrm{d}t} = \frac{k_1 K_5 K_6 [\text{QDC}][\text{Hg(I)}][\text{Pd(II)}][\text{H}^+]}{1 + K_5[\text{H}^+] + K_6[\text{Hg(I)}] + K_5 K_6 [\text{Hg(I)}][\text{H}^+]} \quad (8)$$

Rate law (8) accommodates all the experimental results except the autocatalytic effect of chromium(III). The rate law (8) may be rearranged to Eq. (9), which is suitable for verification.

$$\frac{[\text{QDC}][\text{Pd(II)}]}{\text{Rate}} = \frac{1}{k_1 K_5 [\text{H}^+]} + \frac{1}{k_1 K_6 [\text{Hg(I)}]} + \frac{1}{k_1 K_5 K_6 [\text{Hg(I)}][\text{H}^+]} + \frac{1}{k_1} \quad (9)$$

According to Eq. (9), a plot of the LHS versus $1/[\text{H}^+]$ and LHS versus $1/[\text{Hg(I)}]$ should be linear, and are found to be so (Fig. 6; $r \geqslant 0.999$, $\sigma \leqslant 0.018$ and $r \geqslant 0.998$, $\sigma \leqslant 0.018$). The slopes and the intercepts of such plots leads to values of k_1, K_5 and K_6 of $(3.88 \pm 0.15) \times 10^2$ dm^3 mol^{-1} s^{-1}, 4.24 ± 0.21 dm^3 mol^{-1} and $(8.23 \pm 0.38) \times 10^3$ dm^3 mol^{-1}, respectively. The modest activation energy and sizeable

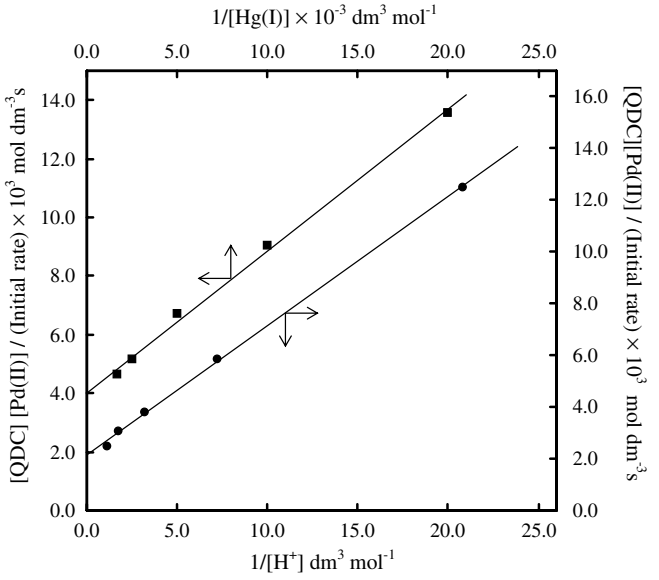

Fig. 6. Verification of rate law (8) in the form of (9) (conditions as in Tables 1 and 3).

$$QDC + H^+ \rightleftharpoons HCrO_4^- + Q\ (quinoline) \quad K_5$$
$$Hg_2^{2+} + SO_4^{2-} + HSO_4^- \rightleftharpoons [Hg_2(SO_4)HSO_4]^- \quad K_7$$
$$Pd^{2+} + Cl^- \rightleftharpoons PdCl^+ \quad K_1$$
$$[Hg_2(SO_4)HSO_4]^- + PdCl^+ \rightleftharpoons Complex\ (C_2) \quad K_6$$
$$C_2 + HCrO_4^- \xrightarrow{slow} 2\,HgSO_4 + PdCl + Cr(V) \quad k_1$$
$$PdCl + Cr(V) \xrightarrow{fast} PdCl^+ + Cr(IV)$$
$$Hg^+ + Cr(IV) \xrightarrow{fast} Hg^{2+} + Cr(III)$$

Scheme 2.

entropy of activation supports a complex transition state in the reaction.

The active species involved in the mechanism can be understood as follows. In aqueous acid media, QDC is known to exist mainly as $HCrO_4^-$. Mercury(I) has been shown to exist [31] as the complex $[Hg_2(SO_4)HSO_4]^-$. Oxidation of mercury(I) is greatly facilitated in sulfuric acid solution and the reason may be that mercury(I) sulfate complexes are actively involved. The variation of rate with chloride ion was shown in Section 3. Except $PdCl^+$ species, the remaining species of palladium(II) do not parallel the rate (Table 4 and Fig. 2). Hence $PdCl^+$ is considered as the active species of palladium(II) in acid medium. In the same way, $PdCl^+$ is considered as the active species of palladium(II) in aqueous alkaline medium, since $PdCl^+$ species parallel the rate [32]. In both cases, the role of the medium is not very significant compared to the complexation of the ligand, chloride ion, with palladium. The mechanism of Scheme 1 will therefore involve the species shown in Scheme 2.

The probable structure of the complex (C_2) is as follows:

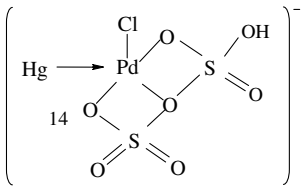

Therefore in terms of the active species, rate law (8) takes the following form:

$$Rate = \frac{k_1K_5K_6[HCrO_4^-][Hg_2(SO_4)HSO_4]^-[PdCl^+][H^+]}{1 + K_5[H^+] + K_6[Hg_2(SO_4)HSO_4]^- + K_5K_6[Hg_2(SO_4)HSO_4]^-[H^+]} \quad (10)$$

From the second equilibrium of Scheme 2

$$[Hg_2(SO_4)HSO_4]^- = K_7[Hg_2^{2+}][SO_4^{2-}][HSO_4^-] \quad (11)$$

But total [Hg(I)] is given by

$$[Hg(I)]_T = [Hg(I)]_f + [Hg_2(SO_4)HSO_4]^-$$
$$\therefore \quad [Hg(I)]_f = \frac{[Hg(I)]_T}{1 + K_7[SO_4^{2-}][HSO_4^-]} \quad (12)$$

Substituting Eq. (12) in Eq. (11), the following equation is obtained:

$$[Hg_2(SO_4)HSO_4]^- = \frac{K_7[Hg(I)]_T[SO_4^{2-}][HSO_4^-]}{1 + K_7[SO_4^{2-}][HSO_4^-]} \quad (13)$$

From the third step of Scheme 2

$$[PdCl^+] = K_1[Pd^{2+}][Cl^-] \quad (14)$$

Substituting Eq. (6) in Eq. (14)

$$\therefore \quad [PdCl^+] = \frac{K_1[Pd^{2+}]_T[Cl^-]}{1 + \beta_1[Cl^-] + \beta_2[Cl^-]^2 + \beta_3[Cl^-]^3 + \beta_4[Cl^-]^4} \quad (15)$$

Substituting Eqs. (13) and (15) in Eq. (10) and omitting subscripts, we obtain the following equation:

$$Rate = \left\{ \frac{k_1K_1K_5K_6K_7[Hg(I)][QDC][Pd(II)][Cl^-][SO_4^{2-}][HSO_4^-][H^+]}{(1 + K_7[SO_4^{2-}][HSO_4^-])\left(1 + \beta_1[Cl^-] + \beta_2[Cl^-]^2 + \beta_3[Cl^-]^3 + \beta_4[Cl^-]^4\right)} \right\} \times \left\{ 1 + K_5[H^+] + \frac{K_6K_7[Hg(I)][SO_4^{2-}][HSO_4^-]}{1 + K_7[SO_4^{2-}][HSO_4^-]} + \frac{K_5K_6K_7[Hg(I)][SO_4^{2-}][HSO_4^-][H^+]}{1 + K_7[SO_4^{2-}][HSO_4^-]} \right\}^{-1} \quad (16)$$

The reaction is accelerated in media of low polarity, which can be qualitatively explained by the involvement of oppositely charged ions, as in Scheme 1. However, the decrease in rate with increase in ionic strength is not easy to interpret. This might be due to the presence of various ionic reactions. The negative value of $\Delta S^{\#}$ (-126 ± 10 J K^{-1} mol^{-1}) suggests that the two ionic species combine in a rate determining step to give one intermediate complex which is more ordered than the reactants [33]. The negative value of $\Delta S^{\#}$ might be due to changes in vibrational frequencies and internal rotations of the reactants and complex [34]. The observed modest entropy of activation and higher rate constant of the slow step indicate that the oxidation presumably occurs by an inner-sphere mechanism. This conclusion is supported by the results of earlier work [35–37].

3.9. Autocatalysis

Autocatalysis by one of the products, chromium(III), is interesting. The apparent order of significantly less than

$$\text{QDC} + \text{Cr(III)} \rightleftharpoons \text{weak complex } (C_3) \quad K_8$$

$$C_3 + \text{Hg(I)} \xrightarrow{\text{slow}} \text{Products} \quad k_2$$

Scheme 3.

unity (0.73) in [Cr(III)], when [Cr(III)] is initially present, may be attributed to the weak complex formation between the product chromium(III) and oxidant, since chromium(III) is well known as a good complexing agent [38]. This is followed by the interaction of the weak complex with the reductant as in Scheme 3. The steps shown in Scheme 1 will form part of Scheme 1.

Evidence for the weak complex (C_3) was obtained by comparing UV–Vis spectra of chromium(III) with the mixture of QDC and chromium(III). There is a hypsochromic shift of chromium(III) from 584 to 580 nm, nearly 4 nm in the spectra of chromium(III) and the mixture of QDC and chromium(III). However, weak complex formation between chromium(III) and palladium(II) is disregarded due to our experimental rate law and lack of spectral evidence. Indeed such weak complex formation between QDC and chromium(III) has been observed in the literature [39–41].

Thus, when chromium(III) is initially present, a composite scheme involving all the steps of Schemes 1 and 3 operates and the rate law is given by the sum of the catalysed and autocatalysed rates.

$$\text{Rate}_{(\text{gross})} = \text{Rate}_{(\text{cat})} + \text{Rate}_{(\text{autocat})} \tag{17}$$

Thus, the rate law for the autocatalytic path can be obtained as:

$$\text{Rate}_{(\text{autocat})} = \text{Rate}_{(\text{gross})} - \text{Rate}_{(\text{cat})} = \frac{k_2 K_8 [\text{QDC}][\text{Hg(I)}][\text{Cr(III)}]}{1 + K_8[\text{Cr(III)}] + K_8[\text{QDC}] + K_8^2[\text{QDC}][\text{Cr(III)}]} \tag{18}$$

Eq. (18) can be rewritten as:

$$\frac{[\text{QDC}][\text{Hg(I)}]}{\text{Rate}_{(\text{autocat})}} = \frac{1 + K_8[\text{Cr(III)}] + K_8[\text{QDC}] + K_8^2[\text{QDC}][\text{Cr(III)}]}{k_2 K_8 [\text{Cr(III)}]} = \frac{1}{k_2 K_8 [\text{Cr(III)}]} + \frac{1}{k_2} + \frac{[\text{QDC}]}{k_2[\text{Cr(III)}]} + \frac{K_8[\text{QDC}]}{k_2} \tag{19}$$

Thus, Eq. (19) can be rearranged to the form (20) which is suitable for verification.

$$\frac{[\text{QDC}][\text{Hg(I)}]}{\text{Rate}_{(\text{autocat})}} = \frac{1}{k_2[\text{Cr(III)}]}\left\{\frac{1}{K_8} + [\text{QDC}]\right\} + \frac{1}{k_2}\{1 + K_8[\text{QDC}]\} \tag{20}$$

At constant concentrations of oxidant and reductant, a plot of LHS versus 1/[Cr(III)] of Eq. (20) should be linear and this was found to be so (Fig. 7; $r \geqslant 0.999$, $\sigma \leqslant 0.021$). Indeed it is to be noted that the plot shows an intercept which is in agreement with the complex formation, as in Scheme 3. The k_2 and K_8 values found from the intercepts and slope of such a plot were $(2.44 \pm 0.12) \times 10^2$ dm^3 mol^{-1} s^{-1} and $(1.10 \pm 0.04) \times 10^3$ dm^3 mol^{-1}, respectively. Using these values, the experimental rates for the added [Cr(III)] at constant concentrations of QDC and mercury(I) can be regenerated (Table 2).

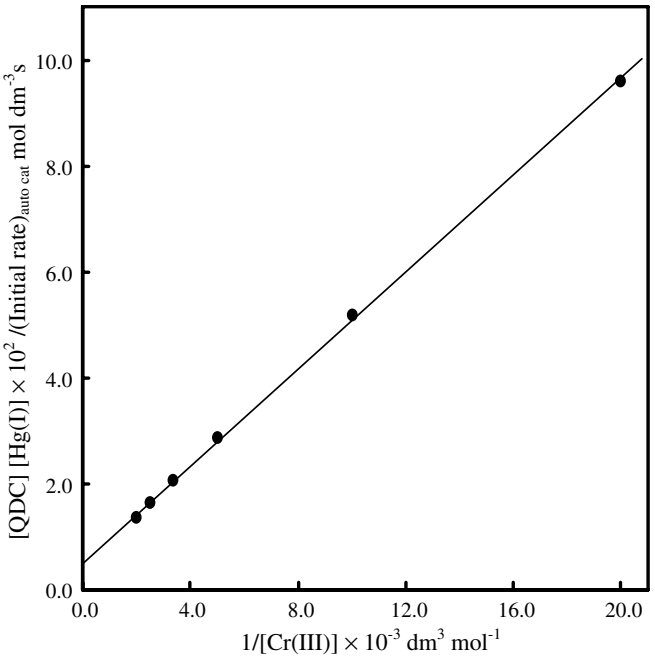

Fig. 7. Verification of rate law (19) in the form (20) (conditions as in Table 2).

4. Conclusion

The reaction between mercury(I) and QDC is very slow in sulfuric acid. Palladium(II) is known to catalyse the reaction with a measurable velocity at 10^{-6} mol dm^{-3}, especially in a sulfuric acid medium; which is not the case in perchloric acid and nitric acid media. The active species involved in the mechanism play an important role in the reaction. It is interesting to note that autocatalysis has taken place in the catalysed reaction, making a composite reaction scheme and rate law. The overall mechanistic sequence described here is consistent with the product, mechanistic and kinetic studies.

References

[1] E.J. Corey, M. Barette, P.A. Magriotis, Tetrahedron Lett. 26 (1985) 5855.
[2] G.G. Sarma, M.K. Mahanti, Bull. Soc. Chim. Fr. 128 (1991) 449.

[3] F. Ciminale, M. Camporeale, R. Mello, L. Troisi, R. Curci, J. Chem. Soc., Perkin Trans. 2 (1989) 417.
[4] K. Balasubramanian, V. Prathibha, Indian J. Chem. B 25 (1986) 326.
[5] S.A. Chimatadar, S.B. Koujalagi, S.T. Nandibewoor, Transition Met. Chem. 27 (2002) 704.
[6] D.R. Rosseinsky, J. Chem. Soc. (1963) 1181.
[7] S. Vincente-Perez, R. Perez-Perez, C. Rodriguez, Quim. Ind. (Madrid) 21 (1975) 712.
[8] R. Davis, B. Kipling, A.G. Sykyes, J. Am. Chem. Soc. 95 (1973) 7250.
[9] P.V. Subba Rao, M. Suryanarayana, K.V. Subbaiah, P.S.N. Murthy, J. Inorg. Nucl. Chem. 42 (1980) 1181.
[10] L.P. Tikhonova, S.N. Borkovets, Russ. J. Inorg. Chem. 23 (1978) 1687.
[11] R.J. Mureinik, E. Pross, J. Coord. Chem. 8 (1978) 127.
[12] G.C. Guilbault, W.H. McCurdy Jr., J. Phys. Chem. 70 (1966) 656.
[13] S.M. Tuwar, S.T. Nandibewoor, J.R. Raju, Indian J. Chem. A 29 (1990) 235.
[14] S.A. Chimatadar, S.B. Koujalagi, S.T. Nandibewoor, Transition Met. Chem. 26 (2001) 662.
[15] (a) G.H. Jeffery, J. Bassett, J. Mendham, R.C. Denney, Vogel's Text Book of Quantitative Chemical Analysis, 5th ed., ELBS: Longman, Essex, England, 1996, p. 403;
(b) G.H. Jeffery, J. Bassett, J. Mendham, R.C. Denney, Vogel's Text Book of Quantitative Chemical Analysis, 5th ed., ELBS: Longman, Essex, England, 1996, p. 329.
[16] G.C. Roy, E.H. Huffman, Anal. Chem. 37 (1965) 86.
[17] F.Ya. Kulba, Yu.B. Yokovlev, V.E. Mironov, Russ. J. Inorg. Chem. 10 (1965) 1113.
[18] V.I. Shlenskaya, A.A. Birykov, Russ. J. Inorg. Chem. 11 (1966) 28.
[19] T.R. Blackburn, Equilibrium, Rinehart–Winston, New York, 1969, p. 75.
[20] S.A. Chimatadar, J.R. Raju, J. Inorg. Nucl. Chem. 43 (1981) 1947.
[21] D.R. Lide (Ed.), CRC Hand Book of Chemistry and Physics, 73rd ed., Chemical Rubber Publishing Company, London, 1992, p. 8.
[22] C.V. Hiremath, T.S. Kiran, S.T. Nandibewoor, J. Mol. Catal. A 248 (2006) 163.
[23] H.H. Sisler, J.D. Bush, J. Accountius, J. Am. Chem. Soc. 70 (1948) 3827.
[24] (a) H.H. Sisler, W.C. Loh Ming, E. Metter, F.R. Hurley, J. Am. Chem. Soc. 75 (1952) 448;
(b) H.H. Sisler, W.C. Loh Ming, E. Metter, F.R. Hurley, J. Am. Chem. Soc. 75 (1952) 447.
[25] K.B. Wiberg, Oxidation in Organic Chemistry: Part A, Academic press, New York, 1965, p. 69.
[26] C.B. Lyngdoh, S. Das, M.K. Mahanty, Oxid. Commun. 24 (2001) 382.
[27] B.P. Sinha, H.P. Mathur, Z. Phys. Chem. (Leipzig) 246 (1971) 324.
[28] S.A. Chimatadar, S.B. Koujalagi, S.T. Nandibewoor, Transition Met. Chem. 26 (2001) 241.
[29] V. Watanabe, F.H. Westheimer, J. Chem. Phys. 17 (1949) 61.
[30] M. Rahaman, J. Rocek, J. Am. Chem. Soc. 93 (1971) 5462.
[31] S.A. Brown, J.E. Land, J. Am. Chem. Soc. 79 (1957) 3015.
[32] G.A. Hiremath, P.L. Timmanagoudar, S.T. Nandibewoor, J. Phys. Org. Chem. 11 (1998) 31.
[33] K.J. Laidler, Chemical Kinetics, 3rd ed., Pearson Education, Pvt. Ltd., New Delhi, 2004.
[34] H.E. O'Neal, S.W. Benson, J. Phys. Chem. 71 (1967) 2903.
[35] N. Sutin, Annu. Rev. Phys. Chem. 17 (1966) 119.
[36] M. Martinez, M. Pitaque, R.V. Eldik, J. Chem. Soc., Dalton Trans. (1996) 2665.
[37] G.A. Hiremath, P.L. Timmanagoudar, S.T. Nandibewoor, React. Kinet. Catal. Lett. 63 (1998) 403.
[38] J.C. Bailar Jr., H.J. Emeleus, R. Nyholm, A.F. Trotman-Dickenson, Comprehensive Inorganic Chemistry, Pergamon Press, New York, 1975, p. 675.
[39] J.O. Edwards, Inorganic Reaction Mechanisms, Benjamin, New York, 1964, p. 149.
[40] E.L. King, J.A. Neptune, J. Am. Chem. Soc. 77 (1955) 3186.
[41] C. Altman, E.L. King, J. Am. Chem. Soc. 83 (1961) 2825.

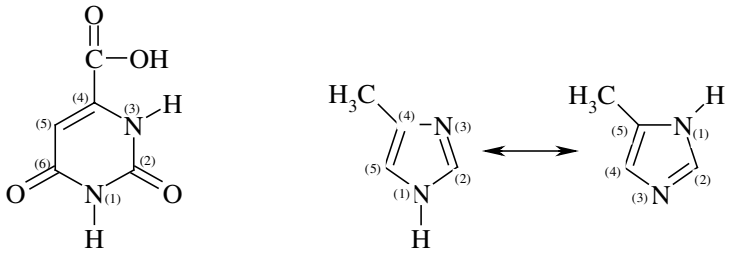

(a) (b)

Scheme 1. Structures of the ligands: (a) vitamin B13; (b) 4(5)-methylimidazole tautomers.

2. Experimental

2.1. Preparation of the complexes

A solution of 4-Meim (0.82 g, 10 mmol) in methanol (10 ml) was added dropwise with stirring to a solution of $[Co(HOr)(H_2O)_4]\cdot H_2O$ [24] (0.76 g, 2.5 mmol) or $[Ni(HOr)(H_2O)_4]\cdot H_2O$ [20] (0.76 g, 2.5 mmol) in distilled water (30 ml). The solution was heated to 60 °C in a temperature-controlled bath and then stirred for 5 h at 60 °C. The reaction mixture was then cooled to room temperature. The red and blue crystals formed for the Co(II) and Ni(II) complexes, respectively, were filtered and washed with 10 ml of cold distilled water and methanol, and dried in air. *Anal*. Calc. for $C_{17}H_{22}N_8O_5Co$: C, 42.78; H, 4.65; N, 23.47. Found: C, 43.02; H, 4.52; N, 23.24%. *Anal*. Calc. for $C_{34}H_{54}N_{16}O_{15}Ni_2$: C, 39.11; H, 5.21; N, 21.46. Found: C, 39.12; H, 5.28; N, 21.74%.

2.2. Materials and measurements

All chemicals used were analytical reagent products. The elemental and mass spectroscopic analysis was carried out in TÜBİTAK Marmara Research Centre of Turkey. Mass spectroscopic analysis was performed on a Fisons MD 800 mass spectrometer coupled to a Fisons 8000 GC and FAB ionisation source. Magnetic susceptibility measurements at room temperature were performed using a Sherwood Scientific MXI model Gouy magnetic balance. The UV–Vis spectra were obtained for an aqueous solution of the complexes (10^{-3} M) with a Unicam UV2 spectrometer in the range 900–190 nm. The IR spectra were recorded in the 4000–400 cm^{-1} region with a Mattson 1000 FT-IR spectrometer using KBr pellets. A TG8110 thermal analyzer was used to record simultaneous TG, DTG and DTA curves in static air atmosphere at a heating rate of 10 K min^{-1} in the temperature range 20–1000 °C using platinum crucibles. Highly sintered α-Al_2O_3 was used as a reference and the DTG sensitivity was 0.05 mg s^{-1}.

2.3. Crystallographic analysis

Data collection was performed on a STOE IPDS II image plate detector using Mo Kα radiation ($\lambda = 0.71073$ Å). Intensity data were collected in the θ range 1.87–28.08° at 100 K. Data collections: Stoe X-AREA [40]. Cell refinement: Stoe X-AREA [40]. Data reduction: Stoe X-RED [40]. The structure was solved by direct-methods using SIR97 [41] and anisotropic displacement parameters were applied to non-hydrogen atoms in a full-matrix least-squares refinement based on F^2 using SHELXL-97 [42]. Molecular drawings were obtained using ORTEP-III [43] and DIAMOND [44]. All H atoms except for water hydrogens were treated as riding. Restrain was applied to water hydrogens to idealized geometry.

3. Results and discussion

3.1. UV–Vis spectra and magnetic susceptibility

The λ_{max} values of the two absorption bands in the UV–Vis spectra of **1** are 384 ($\varepsilon = 22$ L mol^{-1} cm^{-1}) and 522 nm ($\varepsilon = 34$ L mol^{-1} cm^{-1}). These values were assigned to the following d–d transitions, ν_3: $^4T_{1g} \rightarrow {}^4T_{1g}(P)$ and ν_2: $^4T_{1g} \rightarrow {}^4A_{2g}$, respectively. ν_1: $^4T_{1g} \rightarrow {}^4T_{2g}$ transition was not observed which is of low energy and shifts to the IR region and the Δ_0 values for **1** could not be calculated. The electronic spectrum of **2** in H_2O exhibits two absorption bands at 540 and 884 nm and the corresponding ε values are 21 and 18 L mol^{-1} cm^{-1}, respectively. These values were assigned to ν_2: $^3A_{2g} \rightarrow {}^3T_{1g}$ and ν_1: $^3A_{2g} \rightarrow {}^3T_{2g}$ d–d transitions. The Δ_0 value for **2** was calculated as 11300 cm^{-1} since $\Delta_0 = \nu_1$ for d^8 complexes [45].

The complexes **1** and **2** exhibit magnetic moment values of 4.27 and 2.41 BM which corresponds to three and two unpaired electrons, respectively, which are consistent with

Table 1
IR spectra of the complexes[a] (cm^{-1})

Complexes	**1**	**2**
νOH	3544 s	3498 m
$\nu N_{(3)}H$; νNH^*_{Meim}	3255 m*	3222 m*
$\nu N_{(1)}H$	3207 m	3176 m
νCH	3087–2971 w	3012–2873 w
$\nu C{=}O_{acid} + \nu C_{(2)}{=}O$	1639 s	1614 vs, b
$\nu C_{(6)}{=}O + \nu C{=}C$	1620 s	
$\nu C{=}N_{HOr}$; $\nu C{=}N^*_{Meim}$	1483 m	1487 m
$\delta N_{(1)}H$; δNH^*_{Meim}	1427 w; 1373 m*	1398 m; 1371 m*
M–O; M–N	522 w; 466 w	576 w; 444 w

[a] Abbreviations: w – weak; m – medium; s – strong; vs – very strong, b – broad.

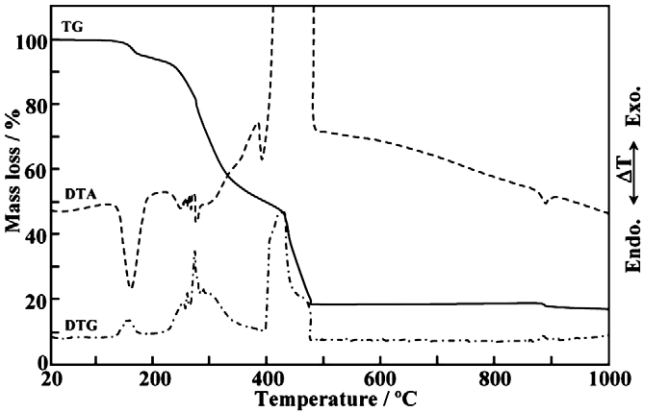

Fig. 1. TG, DTG and DTA curves of **1**.

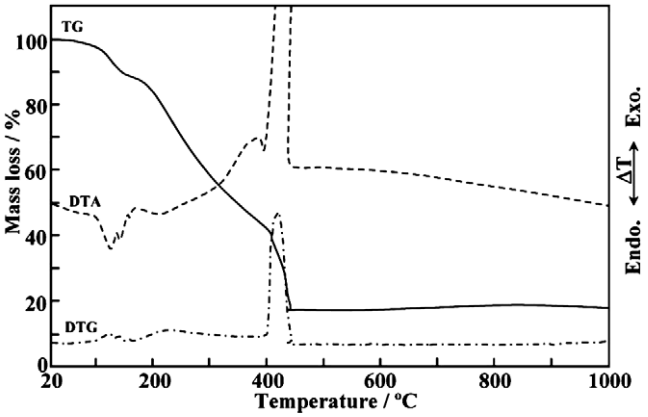

Fig. 2. TG, DTG and DTA curves of **2**.

a weak field octahedral geometry as expected. However, this magnetic moment value is lower than the spin only value for two unpaired electrons in the Ni(II) complex, indicative of some antiferromagnetic behavior [46].

3.2. IR spectra

The most significant frequencies in the IR spectra of both complexes are given in Table 1. The strong bands at 3544 and 3498 cm^{-1} are attributed to the ν(OH) vibration of water molecules in the IR spectra of **1** and **2**. The bands at 3255–3176 cm^{-1} are attributed to the NH stretching vibration in HOr and 4-Meim ligands. This data substantiates the suggestion that 4-Meim molecules coordinate to the central metal ion in their neutral form. The distinct weak bands in the 3012–2873 cm^{-1} region can be assigned to the CH stretching vibrations of the HOr and 4-Meim ligands in the complexes. The carbonyl groups appear as two main peaks at 1700 cm^{-1} [$\nu_{C=O(acid)} + \nu_{C(2)=O}$] and 1660 cm^{-1} [$\nu_{C(6)=O} + \nu_{C=C}$] in the free H_3Or [7]. These bands appear as strong bands at 1639 and 1620 cm^{-1} in the spectrum of the Co(II) complex, while the Ni(II) complex give a single and broad absorption band at 1614 cm^{-1}, probably due to overlapping of the two bands. The weak bands in the 450–500 and 500–600 cm^{-1} region are due to M–N and M–O stretching vibrations, respectively. In the Co(II) and Ni(II) complexes, the orotate ligand is coordinated as dianionic and bidentate through the carboxylic O and N(3) of the pyrimidine ring, while the 4-methylimidazole ligand is coordinated as neutral and monodentate through the N atom.

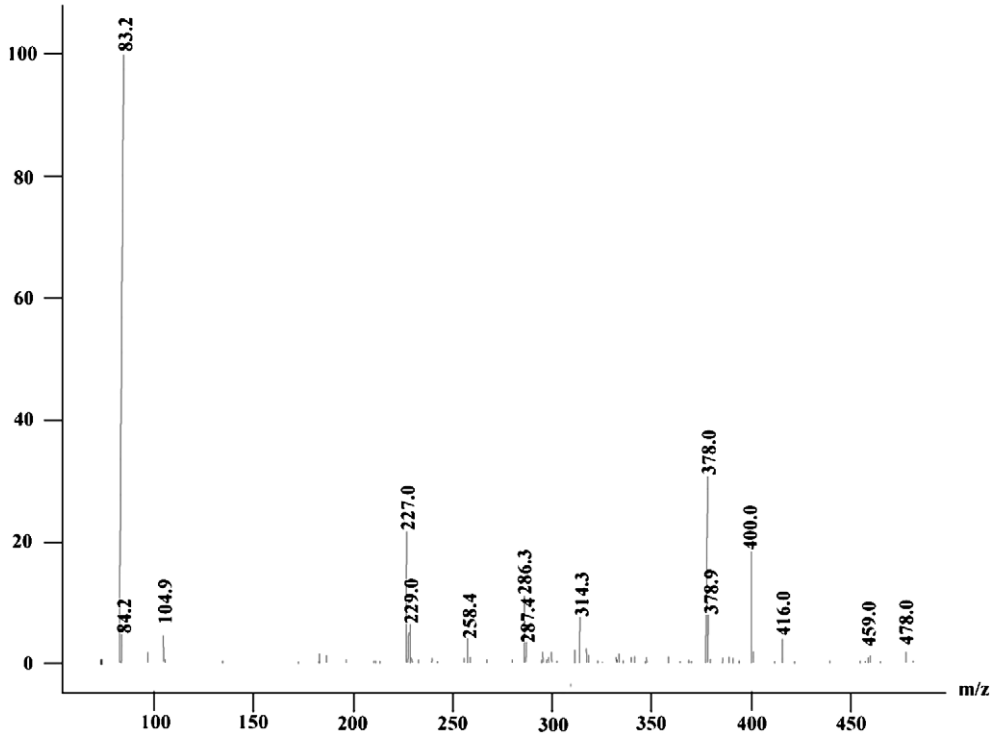

Fig. 3. The mass spectrum of **1**.

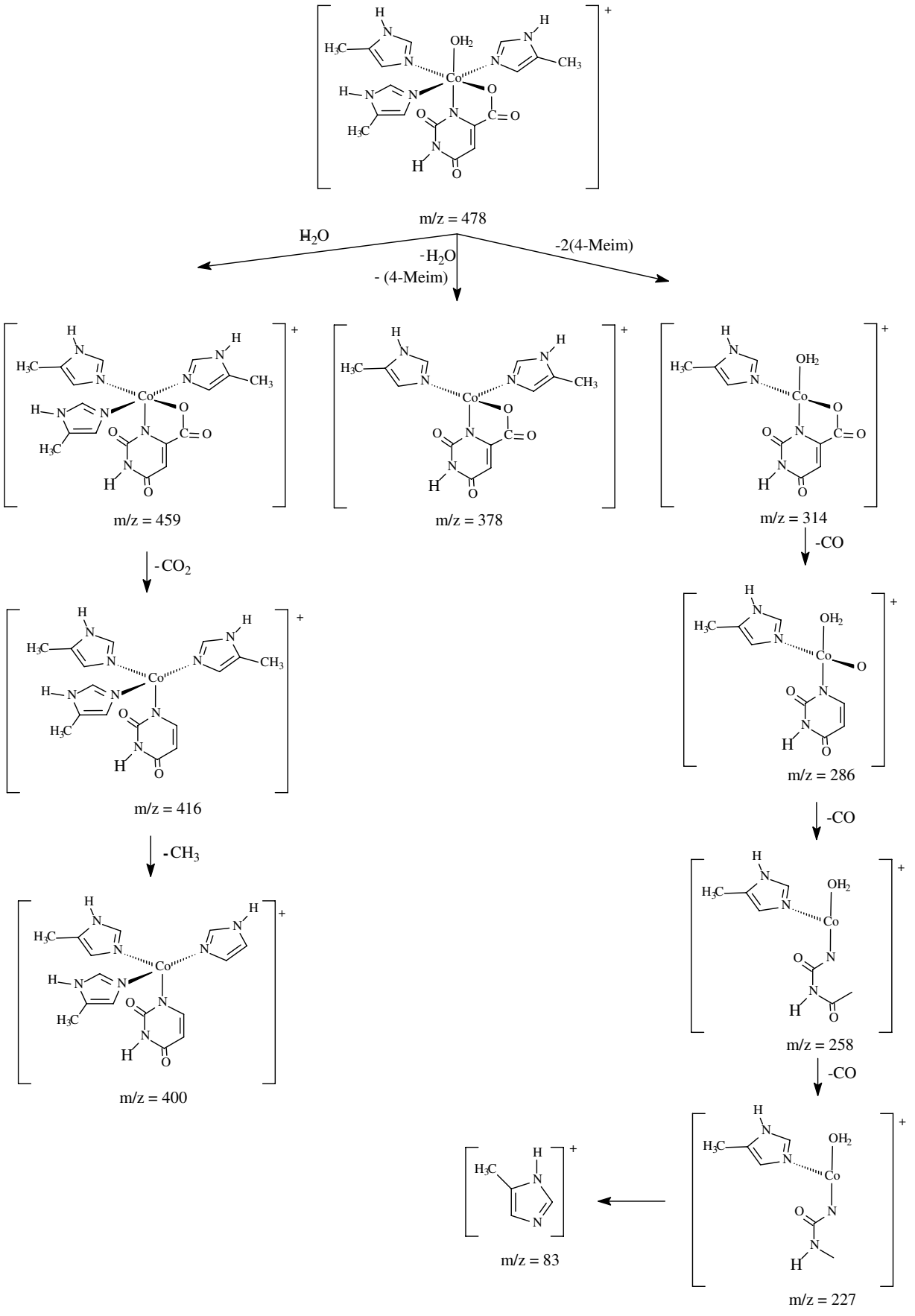

Fig. 4. Mass spectral fragmentation pattern of **1**.

3.3. Thermal analysis

3.3.1. [Co(HOr)(H$_2$O)(4-Meim)$_3$] (1)

Thermal decomposition of **1** proceeds in three stages (Fig. 1). The first stage, in the 122–190 °C temperature range, corresponds to the loss of one aqua ligand (found: 3.78; Calc. 4.35%), giving an endothermic effect (DTG_{max} = 161 °C). The originally red colour of the complex changes to blue-green on dehydration. The anhydrous complex reverts immediately to [Co(HOr)(H$_2$O)(4-Meim)$_3$] after cooling in the open atmosphere. The endothermic second stage of the Co(II) complex, observed as several consecutive steps, is related to the decomposition of the neutral 4-Meim ligans and decarboxylation of the orotato ligand, in the 191–380 °C temperature range (DTG_{max} = 241, 255, 276 and 300 °C). The mass spectrum of **1** also supports the decomposition of the orotate ligand with release of CO_2/CO (Fig. 3). In the last stage the strong exothermic peak of the DTA curve (DTG_{max} = 431 °C) is associated with the burning of the organic residue, leading finally to Co_3O_4. The endothermic peak at 889 °C (DTG_{max}) is related to the conversion of Co_3O_4 to CoO. The overall weight loss 82.19% (Calc. 84.30%) agrees with the propose structure well.

3.3.2. [Ni(HOr)(H$_2$O)(4-Meim)$_3$]$_2$ · 5H$_2$O (2)

The thermal decomposition of **2** (Fig. 2) is similar to **1**. In the first stage, dehydration of the complex occurs in the 49–173 °C range temperature, giving an endothermic effect. Initially 5 mol of crystal water are removed in the 49–138 °C range temperature (DTG_{max} = 128 °C, found: 8.51, Calc. 8.63%) and then two moles coordinated water molecules are released in the 139–173 °C range temperature (DTG_{max} = 147 and 163 °C, found: 3.33, Calc. 3.45%). The blue octahedral complex loses water molecules upon heating yielding a violet, probably square pyramidal dehydrated species. The second stage is related to the release of 4-Meim ligands and partial decomposition of the orotate ligand proceeds with release of CO_2/CO. In the following stage, the strong exothermic mass loss process occurs in a single step. During this stage, the remaining organic part is abruptly burnt (DTG_{max} = 431 °C). The final decomposition product, NiO, was identified by IR spectroscopy (found: 82.64, Calc. 85.70%).

3.4. Analysis of the mass spectrum

The volatile products observed in the thermal decomposition process were also observed in the mass spectrometer ionization process, except molecular peak, and it was concluded that the ionization and thermal decomposition pathway of the complex resemble each other.

The mass spectrum of **1** was recorded to establish a relation between the thermal and ionization process to predict a more appropriate thermal decomposition pathway. The mass spectrum recorded by the FAB technique is given in

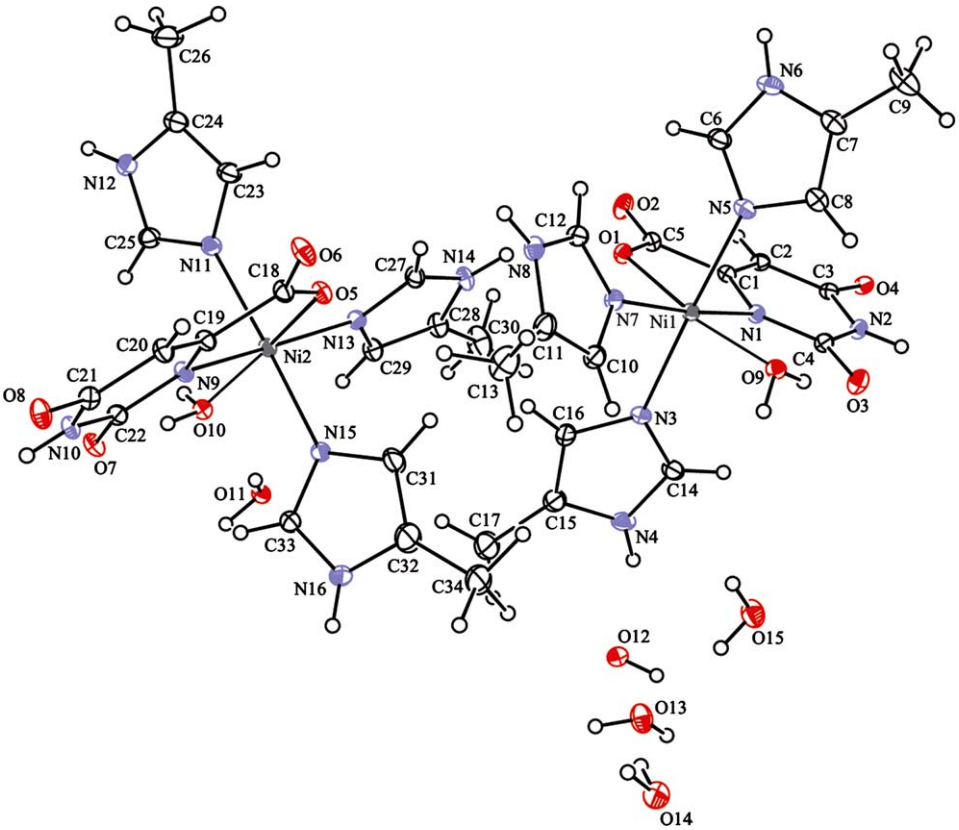

Fig. 5. ORTEP III view of **2** with the atom numbering scheme (30% probability ellipsoids).

Fig. 3. The mass spectrum of **1** is not very complicated and only the major peaks, which were produced in significant quantities, were apparent. In addition to this, the molecule ion peak (M^+) ($m/z = 478$) of **1** was visible in the mass spectrum. The peak observed at $m/z = 459$ possibly corresponds to the [Co(HOr)(4-Meim)$_3$] molecule produced by the loss of a water molecule from [Co(HOr)(H_2O)(4-Meim)$_3$] in the ionization process. The compound formed from [Co(HOr)(4-Meim)$_3$] by the release of CO_2 was observed in the mass spectrum at $m/z = 416$. In the literature, orotate and derivative complexes with similar structures are also reported to be decomposed by release of CO_2 [47–49]. The compound, [Co(uracil)(im)(4-Meim)$_2$], formed by the loss of the CH_3 ion was observed in the mass spectrum at $m/z = 400$. This type of ionization of the 4-Meim ligand in the [Zn(Han)$_2$(4-Meim)$_2$] (Han = *o*-aminobenzoate) complex has been reported earlier [50]. The peaks observed at $m/z = 378$ and $m/z = 314$ values may correspond to [Co(HOr)(4-Meim)$_2$] and [Co(HOr)(H_2O)(4-Meim)] complexes, respectively. Formation of these fragments in the thermal process may also be proved by the thermal analysis data. The possible decomposition products of the [Co(HOr)(H_2O)(4-Meim)$_3$] complex shows in the ionization process (Fig. 4).

3.5. Crystal structure of [Ni(HOr)(H_2O)-(4-Meim)$_3$]$_2$ · 5H_2O

The asymmetric unit of **2** is composed of two crystallographic independent [Ni(HOr)(H_2O)(4-Meim)$_3$]$_2$ molecules and five lattice water molecules, as shown in Fig. 5. The Ni(II) ion in [Ni(HOr)(H_2O)(4-Meim)$_3$]$_2$ is in a distorted octahedral configuration coordinated by a bidentate HOr ligand, a coordinated water molecule and three 4-Meim ligands (Fig. 6). The absolute configuration of the Ni(II) center is *Λ* and *Δ*, which is the highest energy conformation [51]. The distorted octahedral coordination geometry is comprised of a N atom and a carboxylate O atom from a doubly deprotonated bidentate orotate ligand, one aqua O atom and three N atoms from imidazole molecules. The N and O atoms of orotate are bonded to the metal to form a five-membered chelate ring [Ni(1)—N(1) = 2.0835(18) and Ni(1)—O(1) = 2.0783(15) Å in molecule A and Ni(2)—N(9) = 2.1184(18) and Ni(2)—O(5) = 2.0605(16) Å in molecule B]. All the N—Ni—N, N—Ni—O and O—Ni—O bond angles deviate significantly from 90° or 180°, which is presumably the result of the steric constraints arising from the shape of the ligands. The angles subtended at the Ni atom by the orotate ligand are 79.66(6)° in molecule A and 79.92(6)° in molecule B, which is in agreement with values previously reported for other orotate-containing Ni(II) complexes [20,52]. This 'bite' angle is far from the ideal value of 90° because of the constrained geometry of the orotate ligand.

The orotate ligand in **2** is essentially planar (r.m.s. deviations = 0.0600 and 0.0150 Å in molecules A and B, respectively), with a slight deviation from planarity arising from the non-zero torsion angle between the carboxylate group

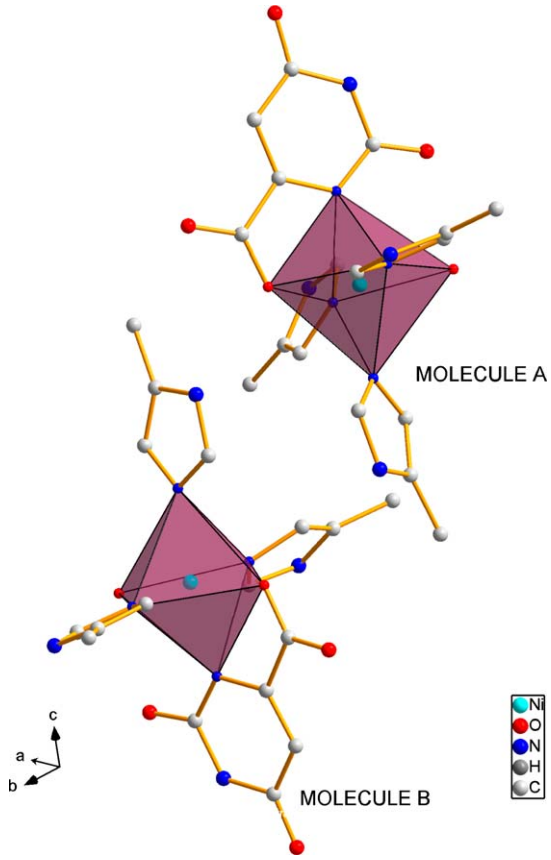

Fig. 6. Octahedral representation of **2**. Distorted octahedra are shaded dark. All H atoms and free water molecules have been omitted for clarity.

and the ring [N(1)—C(1)—C(5)—O(1) = 1.2(3)° and N(9)—C(19)—C(18)—O(5) = −7.5(3)°]. This torsion angle indicates distortion of the orotate ligand caused by coordination to the Ni(II) ion. While this torsion angle of molecule B is wider than the reported values in uncoordinated orotic acid ligands 5.9(4)° [37] and 5.0(2)° [38], the value for molecule A is even less. Of all the N—C bonds in the uracil ring of the orotate ligand, N(1)—C(1), N(1)—C(4), N(9)—C(19) and N(9)—C(12) are the shortest, with values in the range 1.340(2)–1.358(2) Å. This indicates a considerable π-electron delocalization within the C(2)—C(1)—N(1)—C(4) and C(20)—C(19)—N(9)—C(22) skeletons. The C=O bond lengths for exocyclic atoms are in the range 1.251(2)–1.260(2) Å. These values are slightly longer than those in typical orotate complexes and this can be attributed to the intermolecular hydrogen bonding (Table 2).

The orotate molecule seems to have a degree of elasticity with regard to its coordination to metal centers. In complexes of HOr with Ni(II) [37,52], Cu(II) [16] and Zn(II) [21], the C(4)—N(1)—C(1) and C(22)—N(9)—C(19) angles are smaller [119.16(16)° in molecule A and 118.12(16)° in molecule B, 118.25(15)°, 118.9(11)°, 117.9(2)° and 118.1(4)°, respectively] than that found in orotic acid 122.8(3)° [53], 123.07(14)° [38] and 122.8(3)° [37]. This shrinkage for this angle is due to the metal coordination at the N atom, which causes widening of the adjacent N—C—C and N—C—N angles (Table 2).

Table 2
Crystal data and structure refinement for **2**

Empirical formula	$[C_{17}H_{22}N_8NiO_5]_2 \cdot 5H_2O$
Formula weight	1044.35
Crystal dimensions (mm)	$0.35 \times 0.33 \times 0.12$
Crystal shape	plate
Colour	blue
Unit cell dimensions	
a (Å)	9.809(4)
b (Å)	16.444(5)
c (Å)	14.763(6)
β (°)	98.961(3)
Volume (Å^3)	2352.2(15)
Z	2
Crystal system, space group	monoclinic, $P2_1$
Density ρ_{calc} (Mg m^{-3})	1.475
Absorption coefficient (mm^{-1})	0.88
Data collection	STOE IPDS 2 diffractomer (ω-scan)
Temperature (K)	100
θ Range (°)	1.87–28.08
Index ranges	$-12 \leqslant h \leqslant 12$; $-21 \leqslant k \leqslant 21$; $-19 \leqslant l \leqslant 19$
Flack parameter [55]	0.001(6)
Reflections collected	40 583
Independent reflections	11 158, $R_{int} = 0.065$
Reflections with $I > 2\sigma(I)$	10 592
Absorption correction	integration
T_{min}, T_{max}	0.681, 0.890
Restraints; parameters	18, 665
Largest difference in peak and hole (e Å^3)	0.73, −0.61
Final R indices $I > 2\sigma(I)$	$R_1 = 0.0275$, $wR_2 = 0.0634$
R indices (all data)	$R_1 = 0.0312$, $wR_2 = 0.0644$
Goodness-of-fit on $\|F\|^2$	1.03

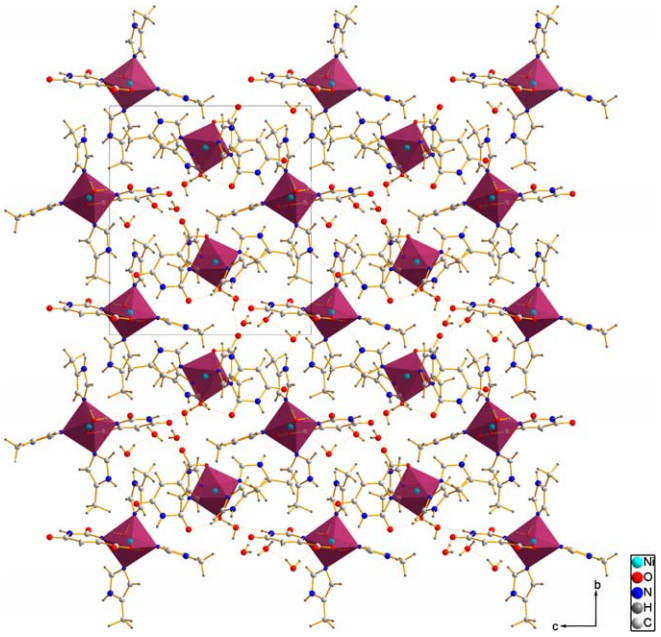

Fig. 7. Crystal packing and H bond interactions. Distorted octahedral are drawn as shaded dark.

The carboxylate C—O distances in the orotate anion also display some variability, depending on their environment. The C—O distances are practically equal in the uncoordinated HOr^{2-} anion and its Ni(II) and Li(I) complexes [54]. In **2**, the C—O bond lengths are in the range 1.244(2)–

Table 3
Geometric parameters (Å, °) for **2**

Ni(1)—N(7)	2.0602(17)	N(4)—C(14)	1.347(3)
Ni(1)—O(1)	2.0783(15)	N(4)—C(15)	1.373(3)
Ni(1)—N(1)	2.0835(18)	N(5)—C(6)	1.312(3)
Ni(1)—N(5)	2.0939(18)	N(5)—C(8)	1.386(3)
Ni(1)—N(3)	2.1055(18)	N(6)—C(6)	1.350(3)
Ni(1)—O(9)	2.1286(16)	N(6)—C(7)	1.371(3)
Ni(2)—O(5)	2.0605(16)	N(7)—C(12)	1.317(3)
Ni(2)—N(13)	2.0701(18)	N(7)—C(10)	1.374(3)
Ni(2)—N(11)	2.0702(19)	N(8)—C(12)	1.347(3)
Ni(2)—N(15)	2.0748(18)	N(8)—C(11)	1.369(3)
Ni(2)—N(9)	2.1184(18)	N(9)—C(22)	1.340(2)
Ni(2)—O(10)	2.1369(16)	N(9)—C(19)	1.358(2)
O(1)—C(5)	1.268(2)	N(10)—C(21)	1.372(3)
O(2)—C(5)	1.244(2)	N(10)—C(22)	1.385(3)
O(3)—C(4)	1.251(2)	N(11)—C(25)	1.307(3)
O(4)—C(3)	1.260(2)	N(11)—C(23)	1.379(3)
O(5)—C(18)	1.250(3)	N(12)—C(25)	1.345(3)
O(6)—C(18)	1.248(3)	N(12)—C(24)	1.362(3)
O(7)—C(22)	1.257(2)	N(13)—C(27)	1.318(3)
O(8)—C(21)	1.258(3)	N(13)—C(29)	1.382(3)
N(1)—C(4)	1.345(3)	N(14)—C(27)	1.347(3)
N(1)—C(1)	1.353(3)	N(14)—C(28)	1.377(3)
N(2)—C(3)	1.369(3)	N(15)—C(33)	1.311(3)
N(2)—C(4)	1.393(2)	N(15)—C(31)	1.368(3)
N(3)—C(14)	1.313(3)	N(16)—C(33)	1.344(3)
N(3)—C(16)	1.385(3)	N(16)—C(32)	1.361(4)
C(4)—N(1)—C(1)	119.16(16)	C(22)—N(9)—C(19)	118.12(16)
C(3)—N(2)—C(4)	124.90(17)	C(21)—N(10)—C(22)	124.54(17)
C(4)—N(1)—C(1)—C(2)	1.5(3)	C(22)—N(9)—C(19)—C(20)	0.6(3)

1.268(2) Å, which is comparable with those in similar Ni(II) complexes [37,52].

The 4-Meim rings in **2** are individually planar, with r.m.s. deviations in the range of 0.0017–0.0084 Å. The dihedral angles between the apical positioned 4-Meim rings are 44.1(8)° and 39.7(7)°. The internal geometries are as expected, with the bond lengths N—C [in the range of 1.307(3)–1.318(3) Å] and C—C [in the range of 1.347(3)–1.364 (3) Å] corresponding exactly to typical double-bond lengths.

As a result of the existence of five free crystallization waters, the crystal is mainly stabilized by many strong intermolecular H bonds O(W)—H...O(W), O(W)—H...O, O(W)—H...N, N—H...O(W), etc. There are also intramolecular H bonds between coordinated water molecules O9, O10 and exocyclic O atoms of orotate and also imidazole C(8) and C(27) atoms and coordinated water molecules. From all of these intermolecular interactions, a three-dimensional hydrogen-bonded network results (Table 3, Fig. 7).

4. Supplementary material

Crystallographic data for the structure reported here have been deposited at the CCDC as supplementary data, CCDC No. 603935. Copies of the data can be obtained on application to CCDC, 12 Union Road, Cambridge CB2 1EZ, UK (fax: +44 1223 336 033; e-mail: deposit@ccdc.cam.ac.uk or www.ccdc.cam.ac.uk).

References

[1] D.D. Genchev, Dokl. Bolg. Akad. Nauk. 23 (1970) 435.
[2] J. Leberman, A. Kornberg, E.S. Simms, J. Biol. Chem. 215 (1955) 403.
[3] N. Lalioti, C.P. Raptopoulou, A. Terzis, A. Panagiotopoulos, S.P. Perlepes, E. Manessi-Zoupa, J. Chem. Soc., Dalton Trans. 8 (1998) 1327.
[4] P. Castan, E. Colacio-Rodriguez, A.L. Beauchamp, S. Cros, S. Wimmer, J. Inorg. Biochem. 38 (1990) 225.
[5] H. Schmidbaur, H.G. Classen, J. Helbig, Angew. Chem. 102 (1990) 1122.
[6] H. Schmidbaur, H.G. Classen, J. Helbig, Angew. Chem., Int. Ed. Engl. 29 (1990) 1090.
[7] G. Maistralis, A. Koutsodimou, N. Katsaros, Trans. Met. Chem. 25 (2000) 166.
[8] D. Mentzafos, N. Katsaros, A. Terzis, Acta Crystallogr. C43 (1987) 1905.
[9] D.J. Darenbourg, D.L. Larkins, J.H. Reibenspies, Inorg. Chem. 37 (1998) 6125.
[10] X. Li, Q. Shi, D. Sun, W. Bi, R. Cao, Eur. J. Inorg. Chem. (2004) 2747.
[11] Karipides, B. Thomas, Acta Crystallogr. C42 (1986) 1705.
[12] D.A. Kose, B. Zümreoğlu-Karan, O. Şahin, O. Büyükgüngör, J. Mol. Struct. (in press).
[13] O. Kumberger, J. Riede, H. Schmidbaur, Chem. Ber. 124 (1991) 2739.
[14] D. Burrows, D.M.P. Mingos, A.J.P. White, D.J. Williams, J. Chem. Soc., Dalton Trans. (1996) 149.
[15] P. Castan, T. Ha, Inorg. Chim. Acta 221 (1994) 173.
[16] I. Mutikainen, P. Lumme, Acta Crystallogr. B36 (1980) 2233.
[17] I. Mutikainen, R. Hämäläinen, M. Klinga, U. Turpeinen, Z. Kristallogr. 212 (1997) 65.
[18] I. Mutikainen, R. Hämäläinen, M. Klinga, O. Orama, U. Turpeinen, Acta Crystallogr. C52 (1996) 2480.
[19] T. Solin, K. Matsumoto, K. Fuwa, Bull. Chem. Soc. Jpn. 54 (1981) 3731.
[20] M. Sabat, D. Zglinska, B. Jezowska-Trzebiatowska, Acta Crystallogr. B36 (1980) 1187.
[21] I. Mutikainen, Inorg. Chim. Acta 136 (1987) 155.
[22] X. Li, W. Bi, D. Yuan, R. Cao, Acta Crystallogr. E59 (2003) m470.
[23] X. Li, R. Cao, W. Bi, D. Sun, M. Hong, Acta Crystallogr. E59 (2003) m228.
[24] H. İçbudak, H. Ölmez, O.Z. Yeşilel, F. Arslan, P. Naumov, G. Jovanovski, A.R. Ibrahim, A. Usman, H.K. Fun, S. Chantrapromma, S.W. Ng, J. Mol. Struct. 657 (2003) 255.
[25] H. Olmez, H. Icbudak, O.Z. Yesilel, C. Arici, D. Ulku, Z. Kristallogr. 219 (2004) 300.
[26] I. Ucar, A. Bulut, O.Z. Yesilel, H. Olmez, O. Büyükgüngör, Acta Crystallogr. C60 (2004) m563.
[27] O.Z. Yeşilel, F. Tezcan, H. Ölmez, H. Paşaoğlu, O. Büyükgüngör, Z. Anorg. Allg. Chem. 631 (2005) 2497.
[28] O.Z. Yeşilel, H. Ölmez, I. Ucar, A. Bulut, C. Kazak, Z. Anorg. Allg. Chem. 631 (2005) 3100.
[29] O.Z. Yesilel, H. Olmez, H. Icbudak, O. Büyükgüngör, Z. Naturforsch. 60b (2005) 1138.
[30] M.J. Plater, M.R.J. Foreman, J.M.S. Skakle, R.A. Howie, Inorg. Chim. Acta 332 (2002) 135.
[31] I. Mutikainen, Finn. Chem. Lett. (1985) 193.
[32] X. Li, R. Cao, D. Sun, Q. Shi, M. Hong, Y. Ling, Inorg. Chem. Commun. 5 (2002) 589.
[33] T.T.B. Ha, A.M. Larsonneur-Galibert, P. Castan, J. Jaud, J. Chem. Crystallogr. 29 (1999) 565.
[34] D. Sun, R. Cao, Y. Liang, M. Hong, Y. Zhao, J. Weng, Aust. J. Chem. 55 (2002) 681.
[35] W. Brockner, R. Branscheid, M. Gjikaj, A. Adam, Z. Naturforsch. 60b (2005) 175.
[36] I. Bach, O. Kumberger, H. Schmidbaur, Chem. Ber. 123 (1990) 2267.
[37] L.R. Falvello, D. Ferrer, T. Soler, M. Tomás, Acta Crstallogr. C59 (2003) m149.
[38] A. Bulut, H. İçbudak, O.Z. Yeşilel, H. Ölmez, O. Büyükgüngör, Acta Crystallogr. E59 (2003) m736.
[39] O.Z. Yeşilel, I. Uçar, A. Bulut, H. Ölmez, O. Büyükgüngör, Z. Naturforsch. 61b (2006) 147.
[40] Stoe & Cie, X-AREA (Version 1.18), X-RED32 (Version 1.04), Stoe & Cie, Darmstadt, Germany, 2002.
[41] A. Altomare, M.C. Burla, M. Camalli, G.L. Cascarano, C. Giacovazzo, A. Guagliardi, A.G.G. Moliterni, G. Polidori, R. Spagna, J. Appl. Crystallogr. 32 (1999) 115.
[42] G.M. Sheldrick, SHELXS97, SHELXL97, University of Göttingen, Germany, 1997.
[43] L.J. Farrugia, J. Appl. Crystallogr. 30 (1997) 565.
[44] K. Brandenburg, DIAMOND, Demonstration Version 3.1, Crystal impact GbR, Bonn, Germany, 2005.
[45] D. Sutton, Electronic Spectra of Transition Metal Complexes, McGraw-Hill, London, 1968, p. 208.
[46] J.D. Ranford, P.J. Sadler, D.A. Tocher, J. Chem Soc., Dalton Trans. 3393 (1993).
[47] F. Hueso-Ureña, M.N. Moreno-Carretto, Thermochim. Acta 182 (1991) 9.
[48] F. Hueso-Ureña, M.N. Moreno-Carretto, J.M. Salas-Peregrín, Thermochim. Acta 170 (1990) 225.
[49] O.Z. Yeşilel, H. Ölmez, J. Ther. Anal. Calorim. (in press).
[50] M. Olczak-Kobza, Thermochim. Acta 419 (2004) 67.
[51] Y. Saito, Stereochemistry of Optically Active Transition Metal Complexes, American Chemical Society Symposium Series, 119, American Chemical Society, Washington, DC, 1985, p. 13.
[52] R. Wysokinski, B. Morzyk-Ocipea, T. Glowiak, D. Michalska, J. Mol. Struct. 606 (2002) 241.
[53] F. Takusagawa, A. Shimada, Bull. Chem. Soc. Jpn. 46 (1973) 2011.
[54] M. Lutz, Acta Crystallogr. E57 (2001) m103.
[55] H.D. Flack, Acta Crystallogr. A39 (1983) 876.

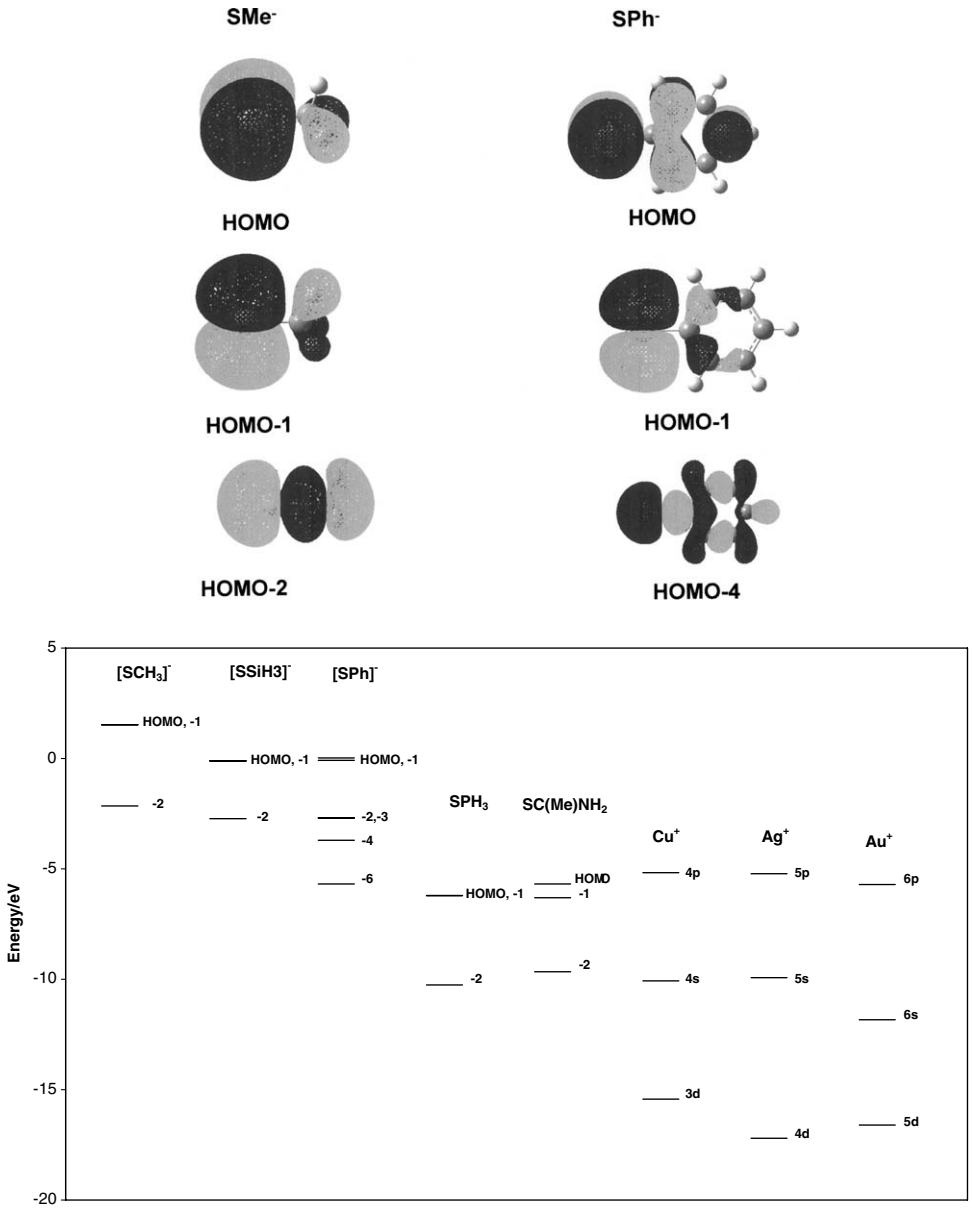

Fig. 1. Frontier molecular orbitals for 1–3 and energy level diagram for 1–5 and M^I.

3% and 10%, respectively [11]. Frequency calculations for energy minima showed no imaginary frequencies. Transition state structures exhibited one imaginary frequency. Calculated frequencies were scaled by a factor of 0.9613 [12]. Enthalpy values represent the sum of electronic and thermal enthalpies [13]. Molecular orbitals were generated using GaussView. All structures were minimised starting from a planar $M_n(SR)_n$ framework.

3. Results and discussion

3.1. $[SCH_3]^-$ as a model for $[SAr]^-$ and $[SSiR_3]^-$

For computational economy, all calculations have been performed using $[SCH_3]^-$ (**1**) as ligand. Most molecular $M_n(SR)_n$ complexes which have been structurally characterised in the solid state contain sterically demanding $[SAr]^-$ and $[SSiR_3]^-$ ligands to hinder aggregation. Using calculations on the free anions and on their CuSR complexes, an evaluation has been performed as to whether $[SCH_3]^-$ (**1**) serves as an adequate model electronically for $[SPh]^-$ (**2**) and $[SSiH_3]^-$ (**3**). All of **1**–**3** exhibit two filled orbitals perpendicular to the S–C axis and a third orbital at lower energy which is collinear with the S–C axis (Fig. 1) The HOMO/HOMO-1 pair of **2** are non-degenerate due to their differing interactions with the σ-framework of the ring. Also shown in Fig. 1 are the energies of the appropriate orbitals of SPH_3 (**4**) and thioacetamide **5**, sulfur ligands which are known to serve as neutral analogues of anionic thiolate (vide infra). The

donor orbitals for **1**–**3** are similar in energy, while those of the neutral sulfur donors **4** and **5** lie at slightly lower energy. No large differences are observed in the energies of the M^I valence orbitals.

The computed molecular structure of $CuSCH_3$ (**6a**) is non-linear with a Cu–S–C angle of 104°. Analysis of the molecular orbitals of **6a** (Fig. 2) shows that the HOMO-2 of $[SMe]^-$ (**1**) is used in formation of the HOMO-2/HOMO-7 pair whilst one of the degenerate HOMO/HOMO-1 pair is used to form the HOMO/HOMO-5 pair of π-symmetry. There is no net π-bond, and σ-bond formation provides the main stabilisation in the form of the bonding and weakly bonding HOMO-6/HOMO-1 pair. Two metal orbitals of δ-symmetry (HOMO-3/-4) remain non-bonding. The structures and energy level diagrams for $CuSSiH_3$ (**7**) and $MSCH_3$ (**6b**,**c**) (M = Ag, Au) are very similar. CuSPh (**8**) differs in that there is some mixing of one of the π-ring orbitals of **2** into the π-bonding molecular orbitals. The amount of stabilisation through delocalisation to the aryl ring is small, however, since the computed Cu–S bond rotational barriers in **6a** and **8** differ little (4.2 and 7.9 kJ mol^{-1}, respectively). It is therefore concluded that $[SMe]^-$ represents an adequate mimic in electronic terms for $[SAr]^-$ and $[SSiR_3]^-$ ligands.

Whilst no net π-bond exists in **6**–**8**, the HOMO in M(SMe) (M = Cu,Ag,Au) **6a**–**c** is a π-antibonding orbital. Removal of two electrons (either by oxidation or loss of a ligand) thus might be expected to turn on a net π-donor

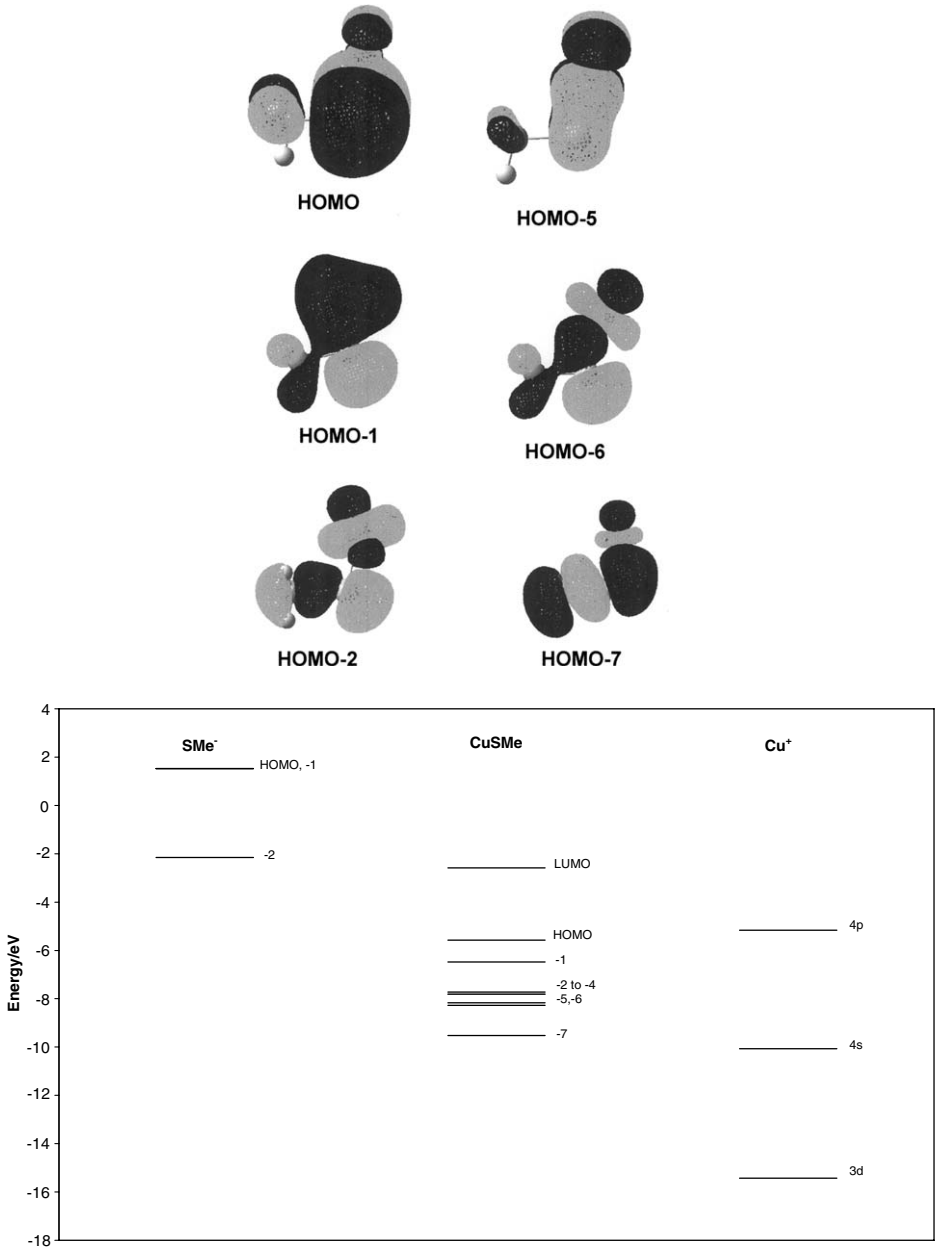

Fig. 2. Molecular orbitals and energy level diagram for CuSMe.

stabilisation. Hence, like Cl^-, thiolate may be viewed as a π-labilising ligand.

3.2. Ring formation in the $M_n(SMe)_n$ series ($n = 1$–6, M = Cu, Ag, Au)

The reader is referred to Table 1 for a full listing of experimental structures and their numbering.

Ring enlargement in this series corresponds to the formal reaction

$$M_n(SMe)_n + M(SMe) \rightarrow M_{n+1}(SMe)_{n+1}$$

A thermodynamic evaluation of the ring formation and enlargement process (Fig. 3) shows strongly exoenthalpic values for the $n = 2 \rightarrow 3$ and (to a lesser extent) the $n = 3 \rightarrow 4$ expansions, after which the enthalpy tends towards a more or less constant value. The energy value for $n = 1 \rightarrow 2$ corresponds to that for formation of the smallest possible $M_2(SMe)_2$ ring from M(SMe). No binary compounds containing only metal and thiolate exist for $n = 2$, though compounds supported by metal–ligand coordination are known. The driving force for ring expansion is an increase in the S–M–S angle towards the preferred linear coordination which is attained without substantial strain only for $n \geqslant 3$.

Table 1a
Structural data for $L_yM_n(SR)_n$ compounds: $n = 2$

	M–M (Å)	S–M–S (°)	M–S–M (°)	θ (°)[d]	L–C–L (°)	Reference
cis-**9a**	2.5	118	62	165		[a]
trans-**9a**	2.5	118	62	171		[a]
trans-**9b**	2.8	114	66	175		[a]
trans-**9c**	2.8	115	65	165		[a]
trans-**10a**	2.5	110[b], 125[c]	63	174		[a]
trans-**11a**	2.7	103	69	129		[a]
trans-**11b**	3.2	105	75	176		[a]
trans-**11c**	3.6	92	88	180		[16a]
trans-**11d**	2.9	111	69	180		[16b]
trans-**12a**	2.7	105[b], 112[c]	67	143	115	[a]
trans-**12b**	2.8	102, 114	72	164	118	[17a]
trans-**12c**	2.6	109, 117	67	163	116	[17b]
trans-**12d**	2.7	98, 107	70	131	121	[17c]
trans-**12e**	2.9	102, 110	74	174	123	[17c]
trans-**13a**	2.8	110	70	173	113	[a]
trans-**13b**		101	79	180	118	[18]
trans-**14a**	3.0	96	76	135	81	[a]
trans-**14b**	2.6	106	68	139	79	[19a]
trans-**14c**	3.0	97	81	171	80	[19b]

$M_2(SR)_2L_n$: **9a**,**b**,**c** M = Cu, Ag, Au, SR = methylthiolate, $n = 0$; **10a** M = Cu, *SR* = methylthiolate, $n = 1$, L = PH_3; **11a** M = Cu, SR = methylthiolate, $n = 2$, L = PH_3; **11b** M = Ag, SR = methylthiolate, $n = 2$, L = PH_3; **11c** M = Ag, SR = 2-methylphenylthiolate, $n = 2$, L = PPh_3; **11d** M = Ag, SR = 5-mercapto-2,2,6,6-tetramethyl-4-hepten-3-one, $n = 2$, L = PPh_3; **12a** M = Cu, SR = methylthiolate, $n = 3$, L = PH_3; **12b** M = Cu, SR = 1-naphthalenethiolate, $n = 3$, L = PPh_3; **12c** M = Cu, SR = phenylthiolate, $n = 3$, L = PPh_3; **12d**,**e** M = Cu, SR = (4-(4-*N*,*N*-diethylamido)phenyldiazenyl)phenylthiolate, $n = 3$, L = PEt_3, PPr_3; **13a** M = Cu, SR = methylthiolate, $n = 4$, L = PH_3; **13b** M = Cu, SR = phenylthiolate, $n = 4$, L = PPh_3; **14a** M = Cu, SR = methylthiolate, $n = 2$, L_2 = 1,4-diaza-1,3-butadiene; **14b** M = Cu, SR = 2-methylphenyl, $n = 2$, L_2 = 1,10-phenanthroline; **14c** M = Cu, SR = 2-methylphenyl, $n = 2$, L_2 = 2,9-dimethyl-1,10-phenanthroline.

[a] This work.

[b] More substituted metal atom.

[c] Less substituted metal atom.

[d] θ is defined as the angle between the copper atoms and the midpoint of the S–S axis.

3.2.1. $M_2(SR)_2$ rings

A molecular orbital analysis for the four-membered ring of $Cu_2(SMe)_2$ (**9a**) exhibits some features which are common to **9b**,**c** (M = Ag, Au) and to the higher analogues. Structural minima for **9a** can be located for both *cis* and *trans* isomers, with the *trans* isomer being more stable by only 2 kJ mol^{-1}. There is no torsional strain in this model example; the Me-Me separation in the *cis* isomer (5.6 Å) is still substantially greater than the sum of the covalent radii. *cis* → *trans* Isomerisation occurs through a transition state **9a*** with a barrier of only 28 kJ mol^{-1}. Even in the calculated structures of *cis*/*trans*-$Cu_2(SMe)_2(PH_3)_4$ (**14a**,**d**), the *trans* isomer is more stable by only 3 kJ mol^{-1}, with a barrier for *cis* → *trans* isomerisation of 23 kJ mol^{-1}.

Neglecting S–C and C–H orbitals, the MO diagram of *trans*-$Cu_2(SMe)_2$ (**9a**) exhibits 16 occupied molecular orbitals (Fig. 4). The lowest energy σ molecular orbitals (such as HOMO-15) use mainly the HOMO-2 of $[SMe]^-$ while higher energy σ orbitals (such as HOMO-13) use one of the HOMO/HOMO-1 orbitals of $[SMe]^-$. HOMO-12 can be viewed as a π molecular orbital utilising the second of the HOMO/HOMO-1 pair of $[SMe]^-$. Whilst the non-bonding and antibonding partners of HOMO-12 are filled, there is a net σ-stabilisation of the ring since two antibonding partners of σ-symmetry remain unoccupied. A nest of four metal-centred orbitals [HOMO-4 to -6, -8] derived from the non-bonding δ orbitals of CuSMe is also evident. There is an increase in the number of occupied molecular orbitals by eight for each increase of ring size from n to $n + 1$. As each MSMe fragment may be viewed as contributing nine fragment orbitals [three from SMe^- and six from M (one p + five d)], there is a net increase in one bonding electron pair with each insertion of MSMe.

The calculated M–M distances in $M_2(SMe)_2$ (**9a**–**c**) (2.45 Å, 2.84 Å and 2.79 Å; Table 1) are longer than twice the covalent radii for two coordinate Cu^I, Ag^I and Au^I (2.26 Å, 2.66 Å and 2.50 Å, respectively) [14], though the Au–Au distance in **9c** is much less than the Au–Au distance seen in the solid state for LAu(SR) dimers held together by aurophilic interactions (3.13–3.16 Å) [15].

To our knowledge, no binary $M_2(SR)_2$ cluster is known. The simplest structurally characterised examples are ligand supported complexes of formulae $M_2(SR)_2L_n$ ($n = 2, 3, 4$; L = phosphine) and $M_2(SR)_2(o\text{-phen})_2$, all having a *trans* conformation of the SR^- ligands. A thermodynamic evaluation of complexation of *trans*-$Cu_2(SMe)_2$ (**9a**) by PH_3 (**15**) (Fig. 5) illustrates that complexation is strongly favoured for $n = 1, 2$; no complexes of formula

Table 1b
Structural data for $L_yM_n(SR)_n$ compounds: $n = 3$

	M–M (Å)	S–M–S (°)	M–S–M (°)	Structure	L–Cu–L (°)	Reference
17a	2.8	165–167	73–74	planar		[a]
17b	3.1	164–165	75	planar		[a]
17c	3.1	162–164	76–78	planar		[a]
17d	2.6–2.7	150–163	75–76	planar		[22a]
17e	3.0–3.2	150–163	75–83	chair		[22b]
18a	3.1–4.1	95[b], 115[c]	86–124	twist boat	119	[23a]
18b	3.3–4.9	92[b], 114[c]	91–128	twist boat	120	[23b]
18c	2.7–2.8	116[b], 129–137[c]	71–76	twist boat	109	[a]
19a	2.7–3.7	114[b], 173[c]	73–112	twist boat	78	[24]
19b	2.7–3.9	107[b], 167[c]	68–108	twist boat	79	[a]
20a	2.9	113	74	chair		[a]
20b	4.0	111	126	chair		[25]
21a	2.9	136	76	chair		[a]
21b	3.5–3.6	110	104	chair		[26]

$M_3(SR)_3L_n$: **17a**,**b**,**c** M = Cu, Ag, Au, SR = methylthiolate, $n = 0$; **17d** M = Cu, SR = tris(trimethylsilyl)methylthiolate, $n = 0$; **17e** M = Ag, SR = tris(dimethylphenylsilyl)methylthiolate; **18a** M = Cu, SR = phenylthiolate, $n = 4$, L = PPh_3; **18b** M = Cu, SR = (4-(*N*,*N*-diethyamino)phenyldiazenyl)phenylthiolate, $n = 4$, L = PPh_3; **18c** M = Cu, SR = methylthiolate, $n = 4$, L = PH_3; **19a** M = Cu, SR = 2,4,6-trimethylphenylthiolate, $n = 4$, L_2 = 3,4,7,8-tetramethyl-1,10-phenanthroline; **19b** M = Cu, SR = methylthiolate, $n = 4$, L_2 = DAB; **20a**,**b** M = Cu, SR = thioacetamide, $n = 3$, L = Cl^-; **21a** M = Cu, SR = SPH_3, $n = 3$, L = Cl^-; 21b M = Cu, SR = $SPMe_3$, $n = 3$, L = Cl^-.

[a] This work.
[b] More substituted metal atom.
[c] Less substituted metal atom.

Table 1c
Structural data for $L_yM_n(SR)_n$ compounds: $n = 4$

	1,3-M–M (Å)	S–M–S (°)	M–S–M (°)	θ (°)[d]	α (°)[e,f]	β (°)[g]	γ (°)[h]	Reference
24a	4.2	175	80	116				[a]
24b	4.8	177	85	129				[a]
24c	4.8	177	87	131				[a]
25	3.8	176	77	107				[29]
26a	4.2	169–177	80–92	135				[30a]
26b	4.1–4.2	167–174	83–89	178				[30b]
27a	3.4–4.2	169–170	77	106				[31a]
27b	4.0	171–173	82	156				[31b]
27c	4.6	178–179	90–91	158				[31c]
27d	4.7	177–178	91–93	176				[31d]
28	4.0–4.1	165–173	78–86	142				[32]
29a	3.0–4.8	129[b], 171[c]	77–78		58			[a]
29b	3.4–6.4	116–119[b], 173–176[c]	74–130		18			[33]
30a	3.0–5.1	102[b], 167–175[c]	70–89		38			[a]
30b	4.0–5.5	113[b], 175[c]	72–131		0			[34]
31a	2.7–6.6	107–114	74–130		0	138	40	[a]
31b	3.4–6.4	106–110	74–130		0	123	25	[35a]
31c	3.8–6.0	104–109	73–127		0	119	26	[35b]

$M_4(SR)_4$: **24a**,**b**,**c** M = Cu, Ag, Au, SR = methylthiolate; **25** M = Cu, SR = bis(trimethylsilyl)methylthiolate; **26a** M = Cu, SR = (5-(diphenyl(hydroxyl)methyl)-2,2-dimethyl-1,3-dioxolan-4-yl)(diphenyl)methylthiolate; **26b** M = Cu, SR = triphenylsilylthiolate; **27a** M = Cu, SR = 2,4,6-tri-isopropylphenylthiolate; **27b** M = Cu, SR = tri-*t*-butoxysilanethiolate; **27c** M = Au, SR = tri-*t*-butoxysilanethiolate; **27d** M = Au, SR = trimethylsilylmethylthiolate; **28** M = Cu, SR = ^{t}Budimethylsilanethiolate.
$M_4(SR)_4L_y$: **29a** M = Cu, SR = methylthiolate, $y = 2$, L = PH_3; **29b** M = Cu, SR = ^{t}Butylthiolate, $y = 2$, L = PPh_3; **30a** M = Cu, SR = methylthiolate, $y = 2$, L_2 = DAB; **30b** M = Cu, SR = 2,4,6-tri-isopropylphenylthiolate, $y = 4$, L_2 = 2,2′-bipyridine. **31a** M = Cu, SR = methylthiolate, $y = 4$, L = PH_3; **31b** M = Cu, SR = phenylthiolate, $y = 4$, L = PPh_3; **31c** M = Cu, SR = thioacetate, $y = 4$, L = PPh_3.

[a] This work.
[b] More substituted metal.
[c] Least substituted metal.
[d] θ is defined as the angle between the two M_2S_3 planes.
[e] For **29a**,**b** and **30a**,**b**, α is defined as the dihedral S–S–S–S.
[f] For **31a**–**c**, α is defined as the dihedral S1–M2–S3–M4.
[g] For **31a**–**c**, β is defined as the average of the dihedrals S1–M2–S3–M3/M4–S3–M2–S2.
[h] For **31a**–**c**, γ is defined as the average of the dihedrals S1–M1–S4M4/M2–S2–M3–S3.

Table 1d
Structural data for $L_yM_n(SR)_n$ compounds: $n = 5,6$

	1,3-M—M (Å)	S–M–S (°)	M–S–M (°)	α (°)[b]	β (°)[c]	Reference
32	5.6–5.7	174–177	100–103	5	144	[21]
33a (*cis*)	4.7–4.9	174–179	76–94	5	86	[a]
33b (*trans*)	4.8–5.1	172–179	79–95	42	92	[a]
33c	5.7–5.8	177–179	86–98	30	113	[a]
33d	5.7–5.8	177–179	90–101	23	110	[a]
34	5.8–6.4	162–178	87–108	18	131	[21]
35a	5.2–5.3	178–179	83–84	0	83	[a]
35b	6.2–6.3	179–180	93–94	0	95	[a]
35c	6.1–6.2	178–179	94–95	0	85	[a]
35d	5.9–6.4	174–176	100–107	0	112	[36]

$M_5(SR)_5$: **32** M = Au, SR = 4-^{t}Butylphenylthiolate; **33a**,**b** M = Cu, SR = methylthiolate; **33c** M = Ag, SR = methylthiolate; **33d** M = Au, SR = methylthiolate.
$M_6(SR)_6$: **34** M = Au, SR = 2-^{t}Butylphenylthiolate; **35a**–**c**, M = Cu,Ag,Au, SR = methylthiolate; **35d** M = Au, SR = 2,4,6-tri-^{i}Propylphenylthiolate.
[a] This work.
[b] For $M_5(SR)_5$, α is defined as the dihedral S2–S3–S4–S5; for $M_6(SR)_6$, α is defined as the dihedral S2–S3–S5–S6.
[c] For $M_5(SR)_5$, β is defined as the average of the dihedrals S1–S2–S5–S4 and S1–S5–S2–S3; for $M_6(SR)_6$, β is defined as the average of the dihedrals S1–S2–S6–S5/S1–S6–S2–S3/S4–S3–S5–S6/S4–S3–S5–S2.

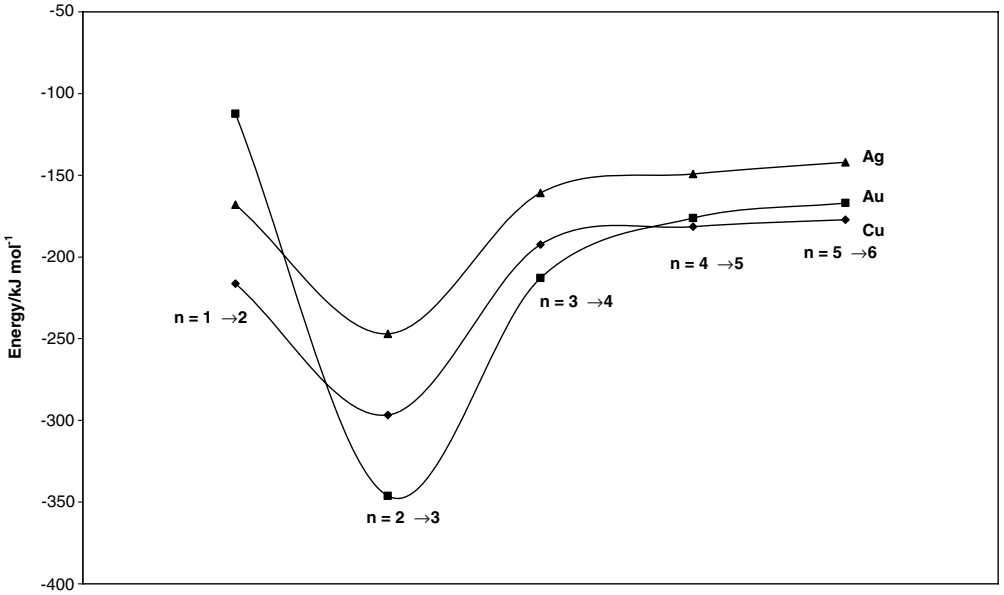

Fig. 3. Calculated enthalpy changes for the reaction $M_n(SMe)_n + M(SMe) \rightarrow M_{n+1}(SMe)_{n+1}$.

$M_2(SR)_2(PR_3)$ have been reported. The enthalpy of complexation for tri- and tetra-substitution by PH_3 is much less negative and relatively constant. For CuSMe (**6a**), the strong preference for a linear, two-coordinate structure can be seen in the very negative enthalpy for formation of $CuSMe(PH_3)$; additions of the second and third PH_3 ligands are much less exoenthalpic.

1,4-Diaza-1,3-butadiene (DAB) (**16**) has been used as a computationally less expensive analogue of 1,10-*o*-phenantholine [20]. The donor orbitals of PH_3 (**15**) and DAB (**16**) are incorporated mainly through mixing with the HOMO-2 of SMe^- to give low energy σ-bonding orbitals. The four molecular orbitals of π-symmetry observed for $Cu_2(SMe)_2$ (**9a**) remain essentially unperturbed and net non-contributory. Though decreasing symmetry means that mixing of the HOMO/-1/-2 orbitals of $[SMe]^-$ occurs in construction of the σ and π molecular orbitals for larger rings, $2n$ metal localised orbitals can be located for each $M_n(SMe)_n$ ring system. For planar ring systems ($n = 2,3$), the lowest energy ring-localised orbitals exhibit substantial M–M overlap, though there is no net M–M bond since the antibonding partner is also occupied. For non-planar rings ($n = 4$–6), direct M–M orbital overlap is substantially reduced or absent.

The calculated structures of $M_2(SMe)_2$ (**9a**–**c**) are planar with S–M–S and M–S–M angles expanded and contracted, respectively, from the ideal 90° internal angles (Table 1, Fig. 6). Calculated structures of $Cu_2(SMe)_2(PH_3)_3$ (**12a**)

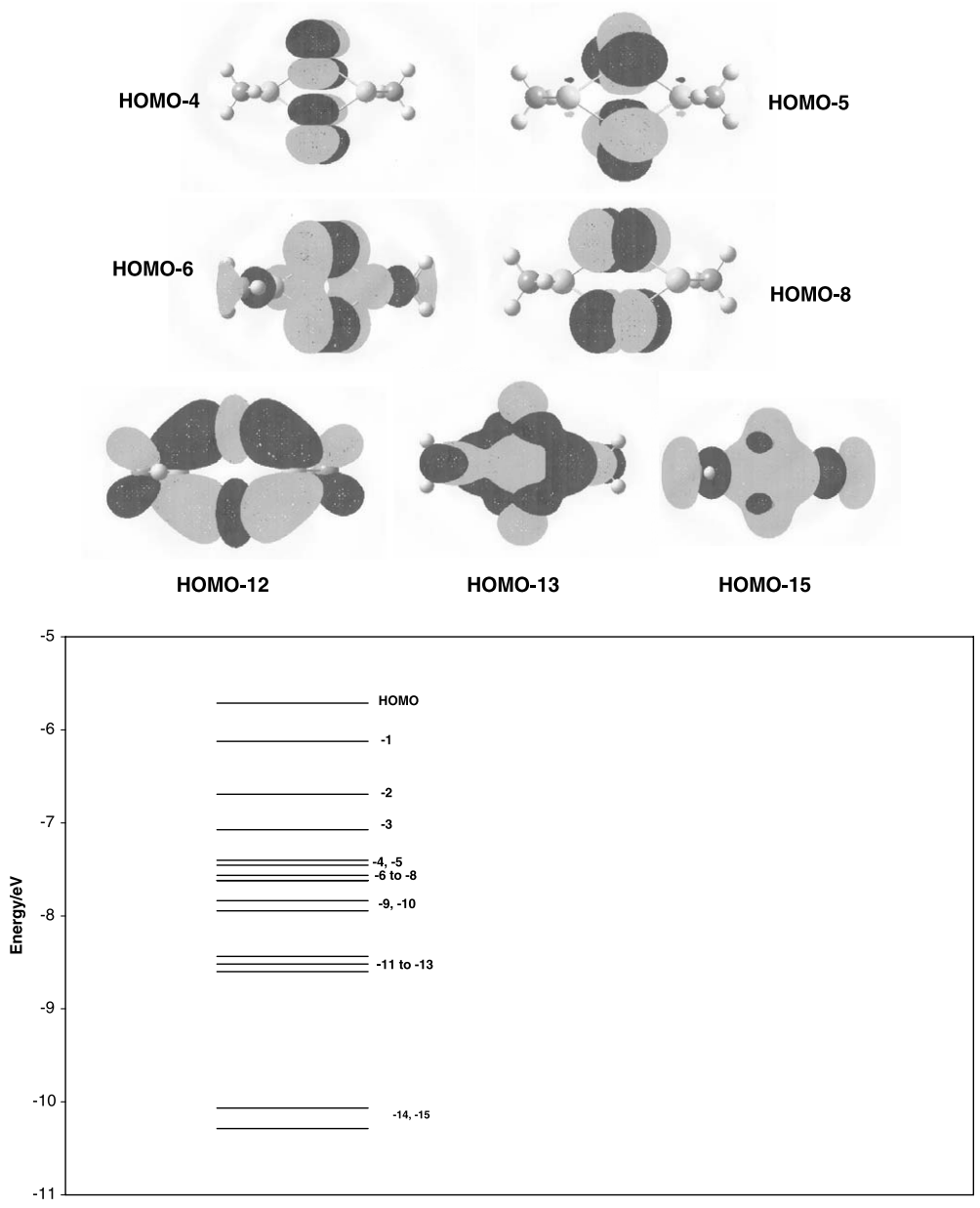

Fig. 4. Molecular orbitals and energy level diagram for *trans*-$Cu_2(SMe)_2$.

and $Cu_2(SMe)_2(DAB)_2$ (**14a**) show substantial deviations from ring planarity which are found experimentally in the $Cu_2(SR)_2(PR_3)_3$ complexes **12b–d** and the $Cu_2(SR)_2$-(*o*-phen) complex **14b**. Other things being equal, hinging along the S–S axis (as measured by the angle θ) results in a decrease in the S–M–S and M–S–M angles.[1] In **12b–d**, hinging may take place to accommodate a smaller S–M–S angle for the four-coordinate copper atom. In **14a**,**b** the bite angle of the DAB and *o*-phen ligands (about 80°) is much smaller than in the non-chelated $Cu_2(SR)_2(PR_3)_4$ derivative **13b** (118°), and hinging may take place to reduce an otherwise larger S–M–S angle. Nevertheless, these energy changes are subtle since the $Cu_2(SR)_2(PR_3)_3$ structure of **12e** and the $Cu_2(SR)_2$(*o*-phen) structure **14c** contain nearly planar rings.

It may be noted that no ligand-supported $L_yAu_n(SR)_n$ complexes have been reported. Computational attempts to minimise the structure of *trans*-$Au_2(SMe)_2(PH_3)_2$ result in decomposition to two molecules of $(PH_3)AuSMe$. In the case of $[Au_5(4\text{-}^tBuC_6H_4S)_5]_2$ (vide infra), reaction with PPh_3 is known to result in ring scission to give $(PPh_3)Au(4\text{-}^tBuC_6H_4S)$ [21].

3.2.2. $M_3(SR)_3$ rings

Unsupported rings are observed experimentally for the first time. The computed $M_3(SMe)_3$ structures **17a–c** and the experimental $M_3(SR)_3$ structures **17d**,**e** show only small deviations from planarity and compared to $M_2(SMe)_2$ (**9a–c**), the S–M–S angles (150–170°) are much

[1] The value of θ for cyclobutane is 166°.

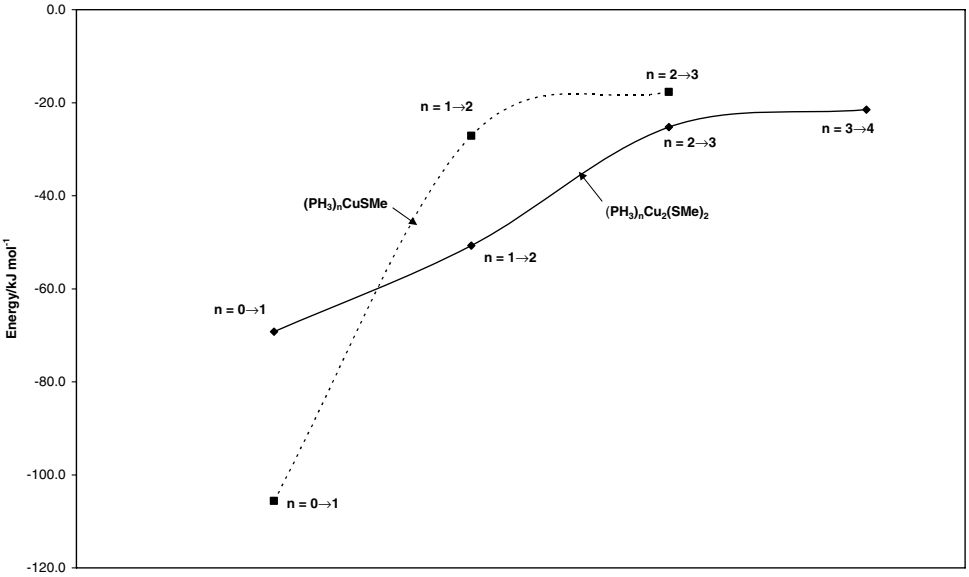

Fig. 5. Complexation enthalpies for reaction of CuSMe and *trans*-$Cu_2(SMe)_2$ with PH_3.

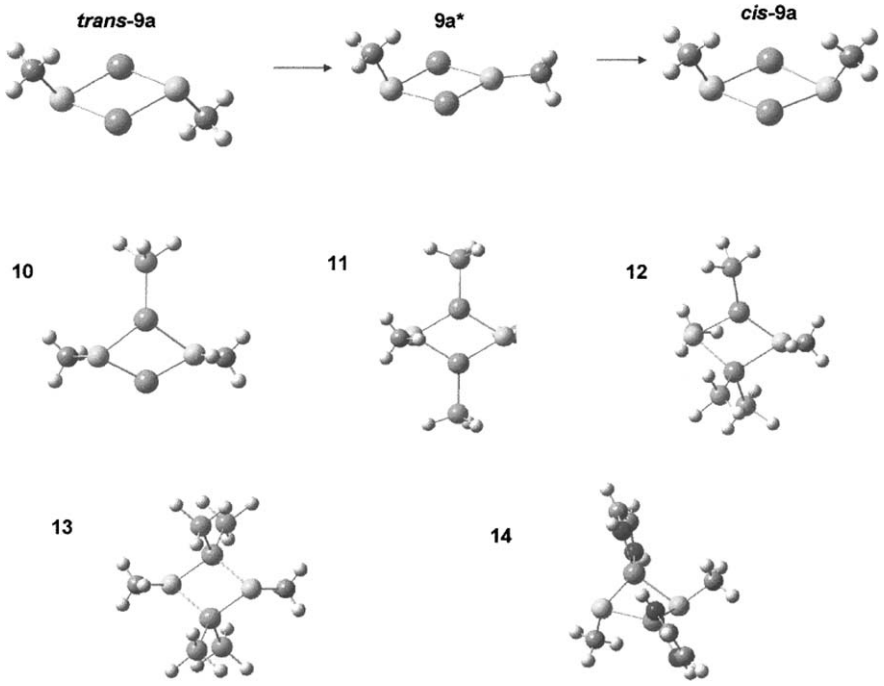

Fig. 6. Structures of $L_yM_2(SR)_2$ complexes.

expanded towards linearity (Table 1, Fig. 7). This is achieved by contraction of the M–S–M angle to about 75–85° from the natural angle of 120° for a planar six-membered ring. In relative terms, this is approximately the same degree of expansion/contraction of ideal ring angles observed in **9a**–**c**. The structures of three simple substituted derivatives $Cu_3(SR)_3(PR_3)_4$ (**18a**,**b**) and $Cu_2(SR)_2(o\text{-phen})_2$ (**19a**) have been reported. These complexes contain both trigonal planar and tetrahedral copper atoms; the calculated structures of $Cu_3(SMe)_3(PH_3)_4$ (**18c**) and $Cu_3(SMe)_4(DAB)_2$ (**19b**) are in good agreement and show that an approximate twist boat structure is the energy minimum and best satisfies a linear geometry for the single copper which remains uncoordinated by added ligand. For complexes where all metal atoms are ligand-substituted, the structures minimise to chair conformations. Complexes **20b** and **21b** contain *neutral* bridging sulfur ligands (thioacetamide and trimethylphosphine sulphide). Here, the trigonal planar coordination of the copper is completed by coordination of anionic Cl^-. The

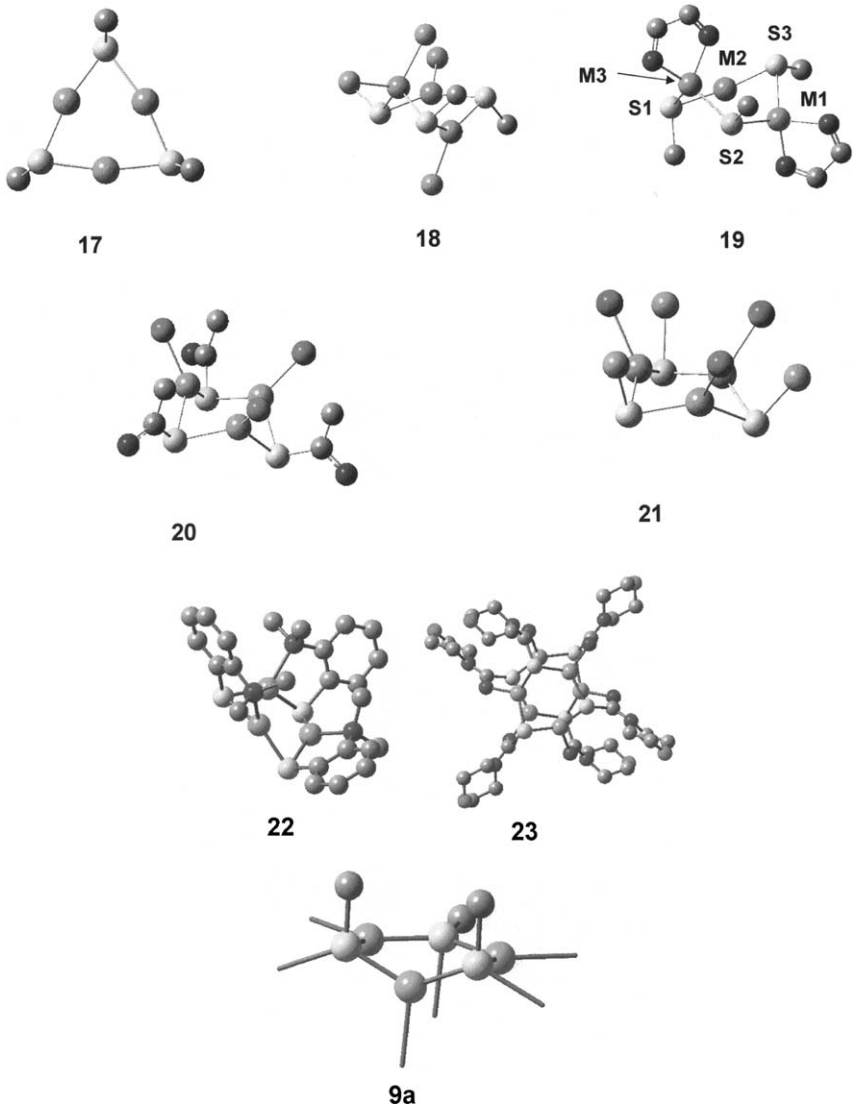

Fig. 7. Structures of $L_yM_3(SR)_3$ complexes.

calculated geometries of the model complexes **20a** and **21a** also show that a chair configuration best satisfies the requirements for trigonal planar coordination of copper.

Other related compounds containing trigonal planar copper and which also have a chair configuration include chelated derivatives such as **22** [26a–d] and **23** [27a–j]. A repeating chair motif is also seen in the structure of **9a** itself, determined by powder diffraction. Each copper atom is trigonally coordinated by three $[SMe]^-$ ligands and each thiolate bridges three copper atoms to form a distorted $MeSCu_3$ arrangement [28].

3.2.3. $M_4(SR)_4$ rings

For $M_n(SR)_n$ rings with $n \geqslant 4$, linearity of the S–M–S bonds can be achieved within a strain-free cycle, and the

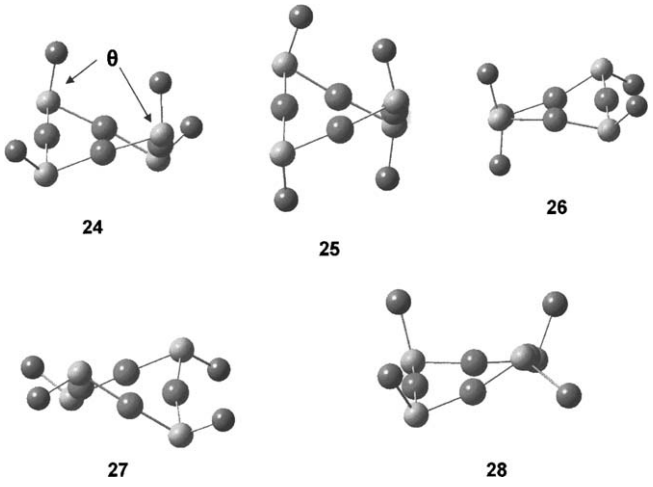

Fig. 8. Structures of $M_4(SR)_4$ complexes.

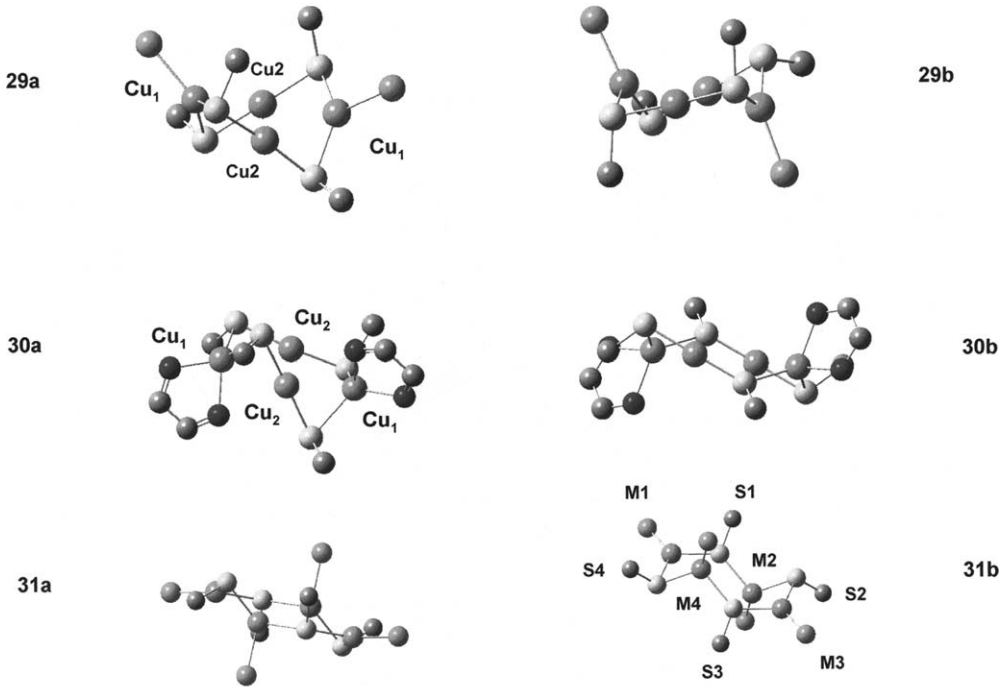

Fig. 9. Structures of $L_yM_4(SR)_4$ complexes.

structure is determined by the most efficient way of linking planar M_2S_3 units, with the sulfur atoms being placed at the vertices of the cycle.

The cyclobutane-like structures of several unsupported $M_4(SR)_4$ rings have been reported, and fall into one of four conformations **25** to **28** in terms of the arrangement of the sulfur substituents (Fig. 8). Energy minimisation of $M_4(SMe)_4$ (M = Cu, Ag, Au) from planar starting structures yields conformation **24** as the energy minimum. Geometrically, these structures differ mainly in the fold angle θ (Table 1). This angle is greatly dependent on the sulfur substituent; for example, the four compounds with conformation **27** have a θ range between 106° and 176°. The values of θ for the calculated $M_4(SMe)_4$ structures **24a–c** are thus reasonable.[1]

Supported complexes of formulae $M_4(SR)_4Ln$ ($n = 2$, $L = PPh_3$; $n = 4$, $L_2 = 2,2'$-bipyridine) exhibit non-planar M_2S_3 units, and are best regarded as six-membered cycles based on a $Cu_1S_4Cu_1$ framework with Cu_2 atoms inserted along the S–S edges (Fig. 9). The experimentally observed structures **29b** and **30b** exhibit a chair framework, whereas the model complexes **29a** and **30a** minimise to twist boat conformers. Where all the metal atoms are substituted, an eight-membered cyclooctane-type cycle is observed in **31a–c**.[2]

3.2.4. $M_5(SR)_5$ and $M_6(SR)_6$ rings

To our knowledge, the only compound reported which contains a $M_5(SR)_5$ ring is the catenated $Au_5(SR)_5$ compound **32** [21]. The configuration of the two rings is identical and has a cyclopentane-like structure containing an approximate M_3S_4 plane with the remaining planar M_2S fragment bent out of the plane (Fig. 10; Table 1).[3] The calculated geometry of the model complexes $M_5(SMe)_5$

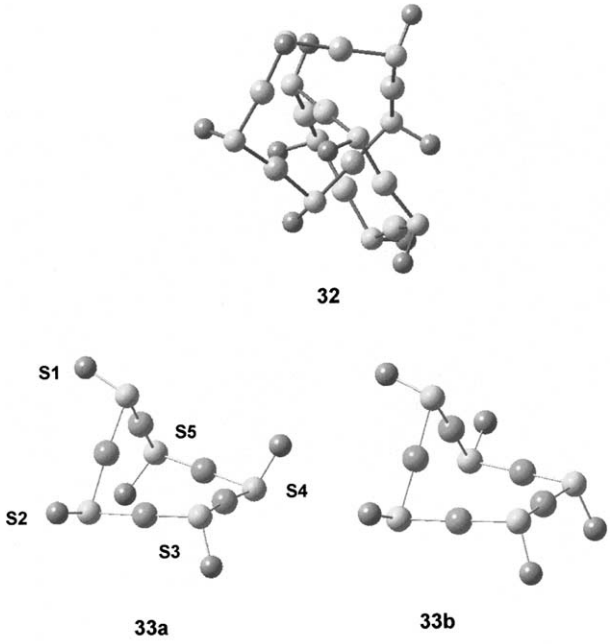

Fig. 10. Structures of $M_5(SR)_5$ complexes.

[2] The values of α, β and γ for cyclooctane are 0°, 122° and 38°.

[3] The values of α and β for cyclopentane are 10° and 141°.

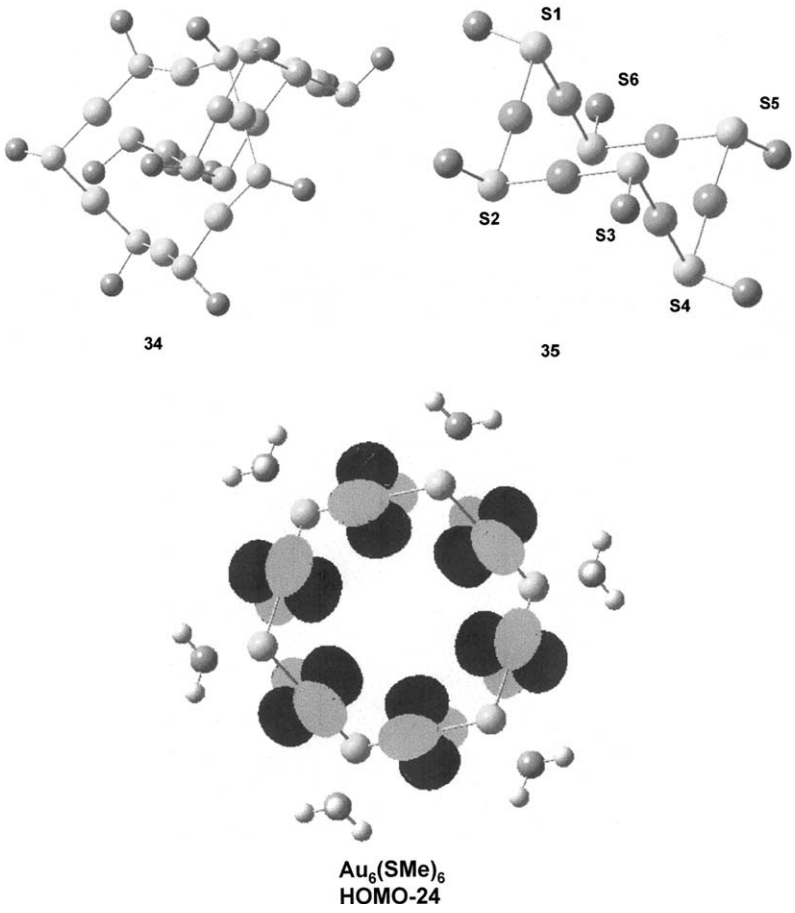

Fig. 11. Structures and non-bonding molecular orbital of $M_6(SR)_6$ complexes.

(**33a**–**c**) are similar. The degree of twist in the M_3S_4 plane is sensitive to the arrangement of the sulfur substituents, and in the case of copper, a structure **33b** having *cis* geometry about the S_3–S_4 axis lies only 3.1 kJ mol^{-1} higher in energy than the *trans* isomer **33a**, and has an almost perfectly planar M_3S_4 moiety.

Two $Au_6(SR)_6$ structures have been reported, one of which is the catenane **34**. The structure of **34**, and of the other calculated and observed $M_6(SR)_6$ complexes, may be described as a cyclohexane-like chair conformation defined by the sulfur atoms as ring vertices (Fig. 11; Table 1).[4] The catenated structures of **32** and **34** place mutual gold atoms at the centres of Au_5 and Au_6 pentagons and hexagons. This has been proposed to arise from delocalised aurophilic interactions [21], and Fig. 11 shows that the spatial extent of the Au_5 and Au_6 metal centred orbitals is sufficient to allow such overlap to occur.

Whilst monocyclic rings with $n > 6$ are known [37–39], we have not subjected them to computational examination. Nevertheless, their structures conform to the general principles of construction outlined above for rings with $n \leqslant 6$.

[4] The values of α and β for cyclohexane are 0° and 131° for a chair structure.

4. Conclusions

The bonding in cyclic $M_n(SR)_n$ complexes (M = Cu, Ag, Au) and their ligand substituted derivatives is primarily σ in nature. For each $M_n(SR)_n$ complex, there also exists a set of $2n$ metal-localised orbitals which in some cases have a spatial distribution suitable for M–M orbital overlap, though net M–M bonding is zero. The structures adopted are generally those which accommodate idealised linear, trigonal planar and tetrahedral metal coordination. In many case, the geometries resemble those of analogous cycloalkanes.

Acknowledgment

The use of the EPSRC's Chemical Database Service at Daresbury is acknowledged [40].

References

[1] (a) Y. Shichibu, Y. Negishi, T. Tsukuda, T. Teranishi, J. Am. Chem. Soc. 127 (2005) 13464;
(b) G.H. Woehrle, J.E. Hutchinson, Inorg. Chem. 44 (2005) 6149;
(c) W. Wang, R.W. Murray, Langmuir 21 (2005) 7015;
(d) R. Guo, A.J. Mills, R.W. Murray, J. Am. Chem. Soc. 127 (2005) 8126;

(e) G. Schmid, E. Emmerich, J.P. Majoral, A.M. Caminade, Small 1 (2005) 73;
(f) C.J. Ackerson, P.D. Jadzinsky, R.D. Kornberg, J. Am. Chem. Soc. 127 (2005) 6550;
(g) Y. Negishi, K. Nobusada, T. Tsukuda, J. Am. Chem. Soc. 127 (2005) 5261.

[2] (a) For recent reviews on templated nanoparticle synthesis, see C.M. Niemayer, U. Simon, Eur. J. Inorg. Chem. (2005) 3641;
(b) X.Y. Gao, H. Matsui, Adv. Mater. 17 (2005) 2037;
(c) M. Green, Chem. Commun. (2005) 3002;
(d) E. Katz, I. Willner, Angew. Chem., Int. Ed. Engl. 43 (2004) 6042;
(e) Z.Y. Tang, N.A. Kotov, Adv. Mater. 17 (2005) 951.

[3] (a) For recent reviews on self-assembled monolayers, see G. Grundmeier, M. Stratmann, Annu. Rev. Mater. Res. 35 (2005) 571;
(b) J.C. Love, L.A. Estroff, J.K. Kriebel, R.G. Nuzzo, G.M. Whitesides, Chem. Rev. 105 (2005) 1103;
(c) D. Witt, R. Klajn, P. Barski, B.A. Gryzbowski, Curr. Org. Chem. 8 (2004) 1763;
(d) V. Humblot, S.M. Barlow, R. Raval, Prog. Surf. Sci. 76 (2004) 1.

[4] (a) D.S. Moore, G.A. Baker, Anal. Bioanal. Chem. 382 (2005) 1751;
(b) N.L. Rosi, C.A. Mirkin, Chem. Rev. 105 (2005) 1547;
(c) J.R. Chen, Y.Q. Miao, N.H. He, X.H. Wu, S.J. Li, Biotechnol. Adv. 22 (2004) 505.

[5] (a) For overviews of the bioinorganic chemistry of copper, see W. Kaim, J. Rall, Angew. Chem., Int. Ed. Engl. 35 (1996) 43;
(b) K.D. Karlin, E. Tyeklar, The Bioinorganic Chemistry of Copper, Chapman & Hall, New York, 1993.

[6] (a) For reviews on bioaccumulation of silver and gold, respectively, see R.A. Bell, J.R. Kramer, Environ. Toxicol. Chem. 18 (1999) 9;
(b) I. Savvidis, V.I. Karamushka, H. Lee, J.T. Trevors, Biometals 11 (1998) 69.

[7] (a) For reviews of bioextraction of gold, see D.E. Rawlings, Annu. Rev. Microbiol. 56 (2002) 65;
(b) I. Suzuki, Biotechnol. Adv. 19 (2001) 119;
(c) G.J. Olson, FEMS Microbiol. Lett. 119 (1994) 1.

[8] (a) For reviews of chrysotherapy, see L. Messori, G. Marcon, Met. Ions Biol. Syst. 41 (2004) 279;
(b) R. Eisler, Inflamm. Res. 52 (2003) 487;
(c) G.R. Burmester, Z. Rheumatol. 60 (2001) 167.

[9] (a) R. Bau, J. Am. Chem. Soc. 120 (1998) 9380;
(b) M.C. Grootveld, P.J. Sadler, J. Inorg. Biochem. 19 (1983) 51, and references therein.

[10] M.J. Frisch, G.W. Trucks, H.B. Sclegel, G.E. Scuseria, M.A. Robb, J.R. Cheeseman, J.A. Montgomery Jr., T. Vreven, K.N. Kudin, J.C. Burant, J.M. Milam, S.S. Iyenar, J. Tomasi, V. Barone, B. Mennucci, M. Cossi, G. Scalmani, N. Rega, G.A. Petersson, H. Nakatsuji, M. Hada, M. Ehara, K. Toyota, R. Fukuda, J. Hasegawa, M. Ishida, T. Nakajima, Y. Honda, O. Kitao, H. Nakai, M. Klene, X. Li, J.E. Knox, H.P Hratchian, J.B. Cross, C. Adamo, J. Jaramillo, R. Gomperts, R.E. Stratmann, O. Yazyev, A.J. Austin, R. Cammi, C. Pomelli, J.W. Ochterski, P.Y. Ayala, K. Morokuma, G.A. Voth, P. Salvador, J.J. Dannenberg, V.G. Zakrzewski, S. Dapprich, A.D. Daniels, M.C. Strain, O. Farkas, D.K. Malick, A.D. Rabuck, K. Raghavachari, J.B. Foresman, J.V. Ortiz, Q. Cui, A.G. Baboul, S. Clifford, J. Cioslowski, B.B. Stefanov, G. Liu, A. Liashenko, P. Piskorz, I. Komaromi, R.L. Martin, D.J. Fox, T. Keith, M.A. Al-Laham, C.Y Peng, A. Nanayakkara, M. Challacombe, P.M.W. Gill, B. Johnson, W. Chen, M.W. Wong, C. Gonzalez, J.A. Pople, GAUSSIAN-03, Revision B.01, Gaussian Inc., Pittsburgh PA, 2003.

[11] G.S.M. Tong, A.S.C. Cheung, J. Phys. Chem. A 106 (2002) 11637.

[12] J.B. Foresman, A. Frisch, Exploring Chemistry with Electronic Structure Methods, 2nd ed., Gaussian Inc., Pittsburgh, PA, 1996, p. 64.

[13] J.B. Foresman, A. Frisch, Exploring Chemistry with Electronic Structure Methods, 2nd ed., Gaussian Inc., Pittsburgh, PA, 1996, p. 166.

[14] U.M. Tripathi, A. Bauer, H. Schmidbauer, J. Chem. Soc., Dalton Trans. (1997) 2865, and references therein.

[15] (a) J.P. Fackler, R.J. Staples, A. Eldeque, T. Grant, Acta Crystallogr., Sect. C 50 (1994) 520;
(b) A. Sladek, K. Angermeier, H. Schmidbauer, J. Chem. Soc., Chem. Commun. (1996) 1959.

[16] (a) J. Chojnacki, B. Becker, A. Konitz, M.J. Potrzebowski, W. Wojnowski, J. Chem. Soc., Dalton Trans. (1999) 3063;
(b) S.C. Ngo, K.K. Banger, P.J. Toscano, J.T. Welch, Polyhedron 21 (2002) 1289.

[17] (a) K.L. Tang, X.L. Jin, Y. Lu, Y.L. Long, P. Cui, Y.Q. Tang, Acta Chim. Sinica 58 (2000) 866;
(b) G. Speir, V. Fulop, G. Argay, Transition Met. Chem. 16 (1991) 576;
(c) O. Fuhr, D. Fenske, Z. Anorg. Allg. Chem. 630 (2004) 1607.

[18] I.G. Dance, P.J. Guerney, A.D. Rae, M.L. Scudder, Inorg. Chem. 22 (1983) 2883.

[19] (a) R.K. Chadha, R. Kumar, D.G. Tuck, Can. J. Chem. 65 (1987) 1336;
(b) A.F. Stange, E. Waldhor, M. Moscherosch, W. Kaim, Z. Naturforsch. B 50 (1995) 115.

[20] For another recent calculation using DAB as a model for 1,10-phenanthroline, see M. Bühl, F. Terstegen, F. Löffler, B. Meynhardt, S. Kierse, M. Müller, C. Näther, U. Lüning, Eur. J. Org. Chem. (2001) 2151.

[21] M.R. Wiseman, P.A. Marsh, P.T. Bishop, B.J. Brisdon, M.F. Mahon, J. Am. Chem. Soc. 122 (2000) 12598.

[22] (a) T. Kaluo, Y. Qingjan, Y. Jianping, T. Youqi, Beijing Daxue Xuebao Ziran Kexue Ban 24 (1988) 398;
(b) K. Tang, M. Islam, E. Block, T. Nicholson, J. Zubieta, Inorg. Chem. 26 (1987) 1488.

[23] (a) I.G. Dance, L.J. Fitzpatrick, M.L. Scudder, J. Chem. Soc., Chem. Commun. (1983) 546;
(b) O. Fuhr, D. Fenske, Z. Anorg. Allg. Chem. 630 (2004) 1607.

[24] A.F. Stange, A. Klein, K.W. Klinkhammer, W. Kaim, Inorg. Chim. Acta 324 (2001) 336.

[25] J.A. Tiethof, J.K. Stalick, D.W. Meek, Inorg. Chem. 12 (1973) 1170.

[26] (a) M.D. Janssen, J.G. Donkervoort, S.B. vanBerlekom, A.L. Spek, D.M. Grove, G. van Koten, Inorg. Chem. 35 (1996) 4752;
(b) D.M. Knotter, G. van Koten, H.L. van Maanen, D.M. Grove, A.L. Spek, Angew. Chem., Int. Ed. Engl. 29 (1989) 341;
(c) D.M. Knotter, H.L. van Maanen, D.M. Grove, A.L. Spek, G. van Koten, Inorg. Chem. 30 (1991) 3309;
(d) A. Togni, G. Rihs, R.E. Blumer, Organometallics 11 (1992) 613.

[27] (a) F.H. Herbstein, R.E. Marsh, Acta Crystallogr., Sect. B 54 (1998) 677;
(b) C. Wycliff, D.S. Barathi, A.G. Samuelson, M. Nethagi, Polyhedron 18 (1999) 949;
(c) H. Dietrich, W. Storek, G. Manecke, Makromol. Chem. 182 (1981) 2371;
(d) S. Ramaprabbu, E.A.C. Lucken, G. Bernardinelli, Z. Naturforsch. A 49 (1994) 193;
(e) N. Narasimhamurthy, A.G. Samuelson, H. Manohar, J. Chem. Soc., Chem. Commun. (1989) 1803;
(f) S. Kitagawa, M. Munakata, H. Shimono, S. Matsuyama, H. Matsuda, J. Chem. Soc., Dalton Trans. (1990) 2105;
(g) S. Kitagawa, Y. Nozaka, M. Munakata, S. Kawata, Inorg. Chim. Acta 187 (1992) 169;
(h) R. Castro, M.J. Duran, J.A. Garcia-Vazquez, J. Romero, A. Sousa, E.E. Castellano, J. Zukerman-Schpector, J. Chem. Soc., Dalton Trans. (1992) 2559;
(i) T. Chivers, A. Downard, M.N. Parvez, G. Schatte, Organometallics 20 (2001) 727;
(j) C. Wycliff, A.G. Samuelson, M. Nethaji, Inorg. Chem. 35 (1996) 5427.

[28] M. Baumgartner, H. Schmalle, C. Baerlocher, J. Solid State Chem. 107 (1993) 63.

[29] S.Z. Hu, Jiegon Huaxue 18 (1999) 476.

[30] (a) A. Pichota, P.S. Pregosin, M. Valentini, M. Worle, D. Seebach, Angew. Chem., Int. Ed. Engl. 39 (2000) 153;

(b) T. Komuro, H. Kawaguchi, K. Tatsumi, Inorg. Chem. 41 (2002) 5083.
[31] (a) I. Schroter-Schmid, J. Strahle, Z. Naturforsch. B 45 (1990) 1537;
(b) B. Becker, W. Wojnowski, K. Peters, E.M. Peters, H.G. von Schnering, Polyhedron 9 (1990) 1659;
(c) W. Wojnowski, B. Becker, J. Sassmannshausen, E.M. Peters, K. Peters, H.G. von Schnering, Z. Anorg. Allg. Chem. 620 (1994) 1417;
(d) P.J. Bonasia, D.E. Gindelberger, J. Arnold, Inorg. Chem. 32 (1993) 5126.
[32] T. Komuro, T. Matsuo, H. Kawaguchi, K. Tatsumi, J. Chem. Soc., Dalton Trans. (2004) 1618.
[33] I.G. Dance, L.J. Fitzpatrick, D.C. Craig, M.L. Scudder, Inorg. Chem. 28 (1989) 1853.
[34] D. Ohlmann, C.M. Marchand, H. Schonberg, H. Grutzmacher, H. Pritzkow, Z. Anorg. Allg. Chem. 622 (1996) 1349.
[35] (a) T.C. Deivaraj, G.X. Lai, J.J. Vittal, Inorg. Chem. 39 (2000) 1028;
(b) I.G. Dance, M.L. Scudder, L.J. Fitzpatrick, Inorg. Chem. 24 (1985) 2547.
[36] (a) D.J. LeBlanc, C.J.L. Lock, Acta Crystallogr., Sect. C 53 (1997) 1765;
(b) I. Schroter, J. Strahle, Chem. Ber. 124 (1991) 2161.
[37] (a) $M_8(SR)_8$: Q. Yang, K. Tang, H. Liao, Y. Han, Z. Chen, Y. Tang, J. Chem. Soc., Chem. Commun. (1987) 1076;
(b) I. Schroter-Schmid, J. Strahle, Z. Naturforsch. B 45 (1990) 1537.
[38] $M_{10}(SR)_{10}$: X.L. Jin, X.J. Xie, H. Qian, K.L. Tang, X. Wang, Q.H. Gong, Chem. Commun. (2002) 600.
[39] $M_{14}(SR)_{14}$: see Ref. [33].
[40] D.A. Fletcher, R.F. McMeeking, D. Parkin, J. Chem. Inf. Comput. Sci. 36 (1996) 746.

first row transition metals. Hmt, a spacer molecule which has been using to prepare different co-ordination polymers for decades can connect through two, three or all four of its tertiary nitrogen atoms to furnish a variety of polymers bearing interesting topologies [22]. Different co-ordination polymers are already reported in this area using it as a simple bidentate, tridentate or tetradentate spacer along with several bridging or non-bridging coligands as it seems to be quite efficient for the self-assembly of networks resulting in different topological motifs in the two or three-dimensional nets involving transition [12,23,24] and non-transition metal [25,26] centers. The self-assembly of these metallo-organic frameworks is vulnerable to many factors such as solvent system, template effect, pH of the solutions, steric parameters of the counter ions and above all the imposed reaction environment [24]. We have given our effort to study the combination effect of hmt, a polycyclic tertiary amine along with thiocyanate and azide as anionic ligands in two different cases with the same metal ion that ends in a construction of two new Co(II) metallo-organic clusters of high dimensionality containing hmt as a neutral organic spacer. In complex **1**, hexamine being attached terminally to the Co(II) center in one co-ordination group is acting as an efficient hydrogen bond carrier throughout the chain with its different donor sites. It helps to bind the adjacent metal centers to incorporate a high dimensionality inside the system by several inter-chain (O–H···N, O–H···S) and intra-chain (C–H···O, C–H···N, C–H···S) hydrogen bondings. In complex **2**, the same spacer ligand joins the adjacent Co(II) centers in a μ-*N*,*N*′ fashion by simple covalent bonds in a 1-D polymeric chain. Thiocyanate and azide are acting as terminal ligands in the respective complexes and efficiently involved in H-bondings with lattice water molecules to result in an infinite 2-D polymeric network finally.

We have reported herein the controlled hydrothermal synthesis of two extensively hydrogen bonded Co(II) L–M–L type polymeric co-ordination complexes. They have been systematically characterised by elemental analysis, FT-IR, UV–vis spectroscopy and thermal analyses. Structures have been established from X-ray single crystal diffraction data. Magneto-structural correlations have been drawn for both the complexes. Although there are plenty of interesting co-ordination complexes involving hmt as spacer, but their systematic characterisation, spectral and magneto-structural correlation studies especially for Co(II) is not a well explored field.

2. Experimental

2.1. Materials

All the chemicals and solvents used for this synthesis were of AR grade. Cobalt(II) chloride, hexahydrate; cobalt(II) acetate, tetrahydrate; potassium thiocyanate, sodium azide and hexamethylenetetramine were obtained from Aldrich Chemical Co. Inc. and used as received without further purification.

2.2. Physical measurements

The Fourier Transform infrared spectra (400–4000 cm^{-1}) of the complexes were recorded on a Perkin–Elmer Spectrum RX I FT-IR system with KBr disc. The electronic spectra were recorded on a Perkin–Elmer λ-40 UV/vis-spectrometer using HPLC grade methanol as solvent. C, H, N analyses were carried out using a Perkin–Elmer 2400 II elemental analyser. Thermal studies were done at a heating rate of 10 °C min^{-1} using a Schimadzu TGA-50 and DTA-50 thermal analyser system in a dynamic atmosphere of N_2 (flow rate 80 ml/min) in an alumina crucible.

Cryo-magnetic susceptibility measurements for the complexes were carried out at the Servei de Magnetoquímica of the Universitat de Barcelona, Spain with a Quantum Designed SQUID MPMS-XL susceptometer apparatus which works in the range 2–300 K under magnetic field of approximately 0.5 T. Diamagnetic corrections were estimated from Pascal's tables.

2.3. Synthesis of the complexes

2.3.1. $[\{Co(hmt)_2(NCS)_2(H_2O)_2\}\{Co(NCS)_2(H_2O)_4\}(2H_2O)]$ (**1**)

The complex was prepared under controlled hydrothermal condition. 0.299 g (1.03 mmol) $CoCl_2$, $6H_2O$, 0.217 g (2.237 mmol) KSCN, 0.067 g (0.484 mmol) hmt and 10 ml of water were loaded into a 23 cm^3 Teflon-lined stainless steel vessel, which was then sealed and placed in a computer programmable furnace. The resulting mixture was heated at the rate of 100 °C/h up to 160 °C, kept for 10 h, then cooled to 140 °C at the rate of 4 °C/h, held for 5 h, followed by further cooling at the same rate to room temperature to give an approximately 85.24% yield based on Co(II), as rosy pink colored prismatic single-crystals which were later collected by mechanical isolation and washed with water–ethanol (2:1 v/v) mixed solvent, then dried in an oven keeping them at 40 °C for 10 min.

Anal. Calc. for $[C_{16}H_{40}Co_2N_{12}O_8S_4]$: C, 24.80; H, 5.20; N, 21.70. Found: C, 24.79; H, 5.21; N, 21.69%.

2.3.2. $[Co(hmt)(N_3)_2(H_2O)_2]_n$ (**2**)

The complex was prepared following the same procedure as described above for the complex **1** except $Co(CH_3COO)_2 \cdot 4H_2O$, NaN_3 and hexamethylenetetramine were taken in the proportion of 0.262 g (1.05 mmol), 0.143 g (2.20 mmol) and 0.133 g (0.95 mmol), respectively. On slow cooling to ambient temperature purple prismatic single crystals were obtained with a yield of 80.04% based on Co(II). Suitable crystals were later collected by mechanical isolation and washed with water–ethanol (2:1 v/v) mixed solvent, dried in an oven keeping them at 40 °C for 10 min.

Anal. Calc. for $[C_6H_{16}CoN_{10}O_2]$: C, 22.57; H, 5.05; N, 43.87. Found: C, 22.56; H, 5.04; N, 43.85%.

2.4. Crystal structure determination

The X-ray diffraction experiment was carried out at 293 K on a rosy pink needle shaped single crystal block (0.09 mm × 0.08 mm × 0.07 mm) of complex **1** using graphite monochromatised Mo-K_α radiation ($\lambda = 0.71073$ Å). The data were collected on a CAD4 diffractometer with the ω-scan technique. Measuring standard reflections at fixed intervals during the data collection checked the stability of the crystal. However, no significant loss of intensity was noted for the crystals. The data were corrected for Lorentz and polarisation effects. The structures were solved by direct methods using the SHELXLTL-PLUS and SHELXS-97 system and refined to convergence by full-matrix least-squares techniques based on F^2 using SHELXL-97 [27]. The non-hydrogen atoms were refined with anisotropic thermal parameters in all the cases. The hydrogen atoms of the hexamethylenetetramine entity were positioned geometrically and allowed to ride on the parent C atoms; $U_{iso}(H) = 1.2U_{eq}(C)$.

The data for the complex **2** were collected at 293 K on a Rigaku AFC7R diffractometer using graphite monochromatised Mo-K_α radiation ($\lambda = 0.71073$ Å) and a rotating anode generator for a prismatic purple shaped single crystal block (0.50 mm × 0.20 mm × 0.10 mm). Cell constants and an orientation matrix for data collection were obtained from least-squares refinement using the setting angles of 12 carefully centered reflections in the range of $20° < 2\theta < 22°$. Structure was solved by direct methods with SHELXS-97 and refined to convergence on F^2 using SHELXL-97 [27]. Lorentz-polarisation corrections were applied. Hydrogen atoms attached to the oxygen atoms were located in the Fourier map and isotropically refined. All calculations were performed using SHELXS-97 and the structure was generated using TEXSAN crystallographic software package [27] from Molecular Structure Corporation. Other remaining measurement parameters are exactly the same as in the complex **1**. Selected crystallographic data, experimental conditions and some features of the structural refinements of both the complexes are summarised in Table 1.

Table 1
Crystal parameters of **1** and **2**

Parameters	**1**	**2**
Empirical formula	$C_{16}H_{40}Co_2N_{12}O_8S_4$	$C_6H_{16}CoN_{10}O_2$
Formula weight	774.74	319.22
Crystal system	triclinic	monoclinic
Space group	$P\bar{1}$ (No. 2)	$C2/c$ (No. 15)
a (Å)	7.916(16)	9.232(3)
b (Å)	9.024(18)	11.317(18)
c (Å)	12.880(3)	12.626(2)
α (°)	94.20(3)	90
β (°)	96.75(3)	108.19(17)
γ (°)	115.35(3)	90
V (Å^3)	817.9(4)	1253.3(5)
Z	1	4
T (K)	293	293
$\lambda_{Mo\ K\alpha}$ (Å)	0.71073	0.71073
D_c (g cm^{-3})	1.573	1.692
μ (mm^{-1})	1.327	1.388
$F(000)$	402	660
θ (°)	2.5–22.5	2.9–27.50
Total data	2253	1532
Unique data	2137	1445
Observed data [$I > 2\sigma(I)$]	1872	1198
N_{ref}, N_{par}	2137, 228	1445, 101
R[a]	0.0388	0.0418
R_w[b]	0.1081	0.1354
s	1.07	1.08
R_{int}	0.023	0.035
$\Delta\rho_{max}$ (e$^-$ Å^{-3})	0.49	0.76
$\Delta\rho_{min}$ (e$^-$ Å^{-3})	−0.86	−0.60

[a] $R = \sum(|F_o - F_c|)/\sum|F_o|$.
[b] $R_w = \{\sum[w(|F_o - F_c|)^2]/\sum[w|F_o|^2]\}^{1/2}$.

3. Results and discussion

Both the complexes have been synthesised under controlled hydrothermal condition by continuously varying the hmt concentration in different sets while keeping the concentration of other added reagents constant. Surprisingly, it was observed that the single crystal of the complex **1** was found as the sole product specifically in the concentration range of Co-salt:hmt:KSCN = 1:0.47:2.2, while single crystals were successfully obtained in case of complex **2** only when the relative concentrations were maintained at cobalt-salt:hmt:NaN_3 = 1:0.90:2.1.

3.1. FT-IR spectra

The solid state Fourier Transform infrared spectra of both the complexes, recorded on a FT-IR spectrophotometer for the range of 400–4000 cm^{-1} are fully consistent with their structures later confirmed from single crystal X-ray diffraction studies. The samples were studied as powder dispersed in KBr pellets. The spectral region for both the complexes are more or less similar due to their similar co-ordination modes except for the terminal ligands which is NCS^- in the first case and N_3^- in the later one. The whole spectrum region can be classified into three distinctive zones with the characteristic absorptions [28,29].

1. *Low energy range.* δ_{OH}: 1639 cm^{-1}; δ_{CH_2}: 1460 cm^{-1} and 1382 cm^{-1}. δ_{CN}: 1225 cm^{-1}, 1019 cm^{-1} and 1001 cm^{-1}; ν_{CS}: 1255 cm^{-1}.
2. *Mid energy range.* Shows characteristic absorption range for terminal NCS^- and N_3^- groups at 2110 cm^{-1} and 2117 cm^{-1}, respectively.
3. *High energy range.* ν_{CH_2}: at 2920 cm^{-1} reflects the frequency for methylene groups of hexamethylenetetramine molecules and ν_{OH_2}: >3400 cm^{-1} as a distinctive broad peak probably corresponding to different surroundings of methylene groups in hmt.

The peaks obtained in the different spectral regions correlate well with the observed values in the case of similar kind of systems found in the literature [25,26].

3.2. Electronic spectra

The UV–vis spectra of both the complexes were recorded in methanol HPLC grade solvent. They show a few strong and broad absorption bands at 8800, 12 000, 21 000 cm^{-1}, $\varepsilon = 6$ L mol^{-1} cm^{-1}, except ν_2 (very weak). Those absorption peaks can be tentatively assigned as typical d–d transitions of an octahedral Co(II) ion [30–32]. The speculated transitions may be due to the following: $^4T_{1g}(F) \rightarrow {}^4T_{2g} - \nu_1$, $^4T_{1g}(F) \rightarrow {}^4A_{2g} - \nu_2$, $^4T_{1g}(F) \rightarrow {}^4T_{1g}(P) - \nu_3$. The d–d transition energy levels for the octahedral Co(II) ion thus found experimentally are in well accordance with those found in the literature. The hydrogen bonding network structure in both the cases imparts apparently no effect on electronic absorption spectra.

3.3. Description of the crystal structures

3.3.1. $[\{Co(hmt)_2(NCS)_2(H_2O)_2\}\{Co(NCS)_2(H_2O)_4\}(2H_2O)]$ (1)

The X-ray structure of **1** reveals that it contains two independent neutral co-ordination groups: $[Co(hmt)_2(NCS)_2(H_2O)_2]$ and $[Co(NCS)_2(H_2O)_4]$ in the same asymmetric unit along with two lattice waters. In the first group Co(II) enjoys a perfectly octahedral environment with an equatorial base formed by two short distant Co(2)–N(2) bonds [2.043(4) Å] coming from NCS^- terminal ligands and two comparatively longer Co(2)–O(3W) bonds [2.095(3) Å] from co-ordinated water molecules while two hmt molecules occupying the apical positions with two Co(2)–N(3) bonds [2.325(3) Å]. An ORTEP drawing of the complex with atom labeling scheme has been provided in Fig. 1. Co(II) follows an ideal octahedral situation except a slight deviation in bond lengths between Co–N and Co–O, forming the equatorial base. Apical Co(2)–N(3) bonds are also a little bit longer by an amount of 0.265(3) Å than the average equatorial bonds. It may be due to the effect of slight distortion. The co-ordination group possesses an inversion center. The second co-ordination group contains one octahedral Co(II) center bearing a CoN_2O_4 chromophore where four oxygen atoms from four co-ordinated water molecules form an equatorial base while two terminal NCS^- groups occupy apical positions [Co(1)–O(1W) and Co(1)–O(2W): 2.065(3) Å and Co(1)–N(1): 2.096(4) Å, respectively]. The most interesting feature is that these independent co-ordination fragments are involved in extensive intra-chain hydrogen bondings [C(3)–H(3A)···O(3W), C(6)–H(6A)···N(2) and C(6)–H(6B)···O(3W)] among themselves or with lattice waters to shape it in an infinite 1-D polymeric chain that runs parallel to *bc*-plane. Such adjacent parallel 1-D chains lying on the same plane are further locked by several inter-chain hydrogen bonds [C(4)–H(4A)···S(2), C(9)–H(9A)···O(2W)] and many others involving the co-ordinated and lattice water molecules with the terminal NCS^- ligands to frame an infinite 2-D neutral polymeric sheet structure (Figs. 2 and 3) running along crystallographic *a*-axis. All the selected bond distances, bond angles and H-bonding parameters for complex **1** are listed in Tables 2 and 3, respectively.

3.3.2. $[Co(hmt)(N_3)_2(H_2O)_2]_n$ (2)

The X-ray analysis reveals that the complex **2** contains octahedral Co(II) center co-ordinated by two terminal N_3^- groups, two water molecules and two neutral hmt molecules (Fig. 4). The two nitrogen atoms N(1) and its

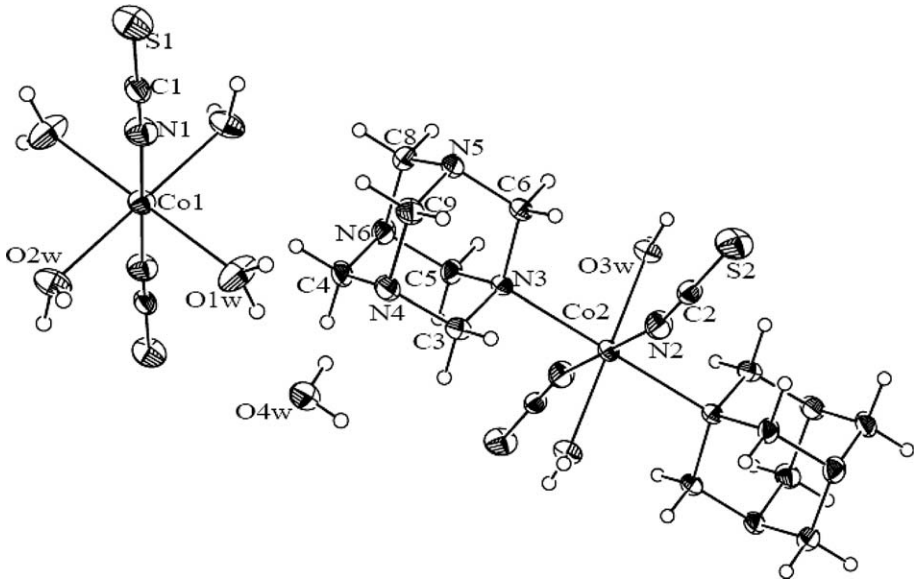

Fig. 1. ORTEP view of **1** with atom numbering scheme.

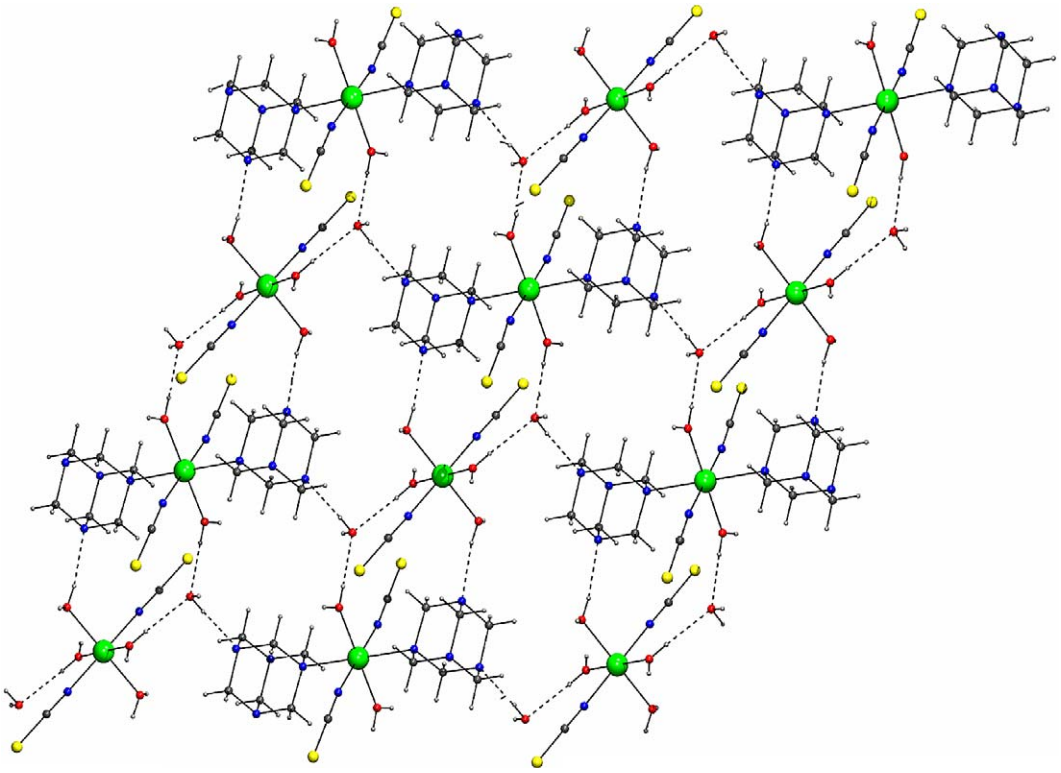

Fig. 2. 2D sheet view of **1**, showing the hydrogen-bonding interactions.

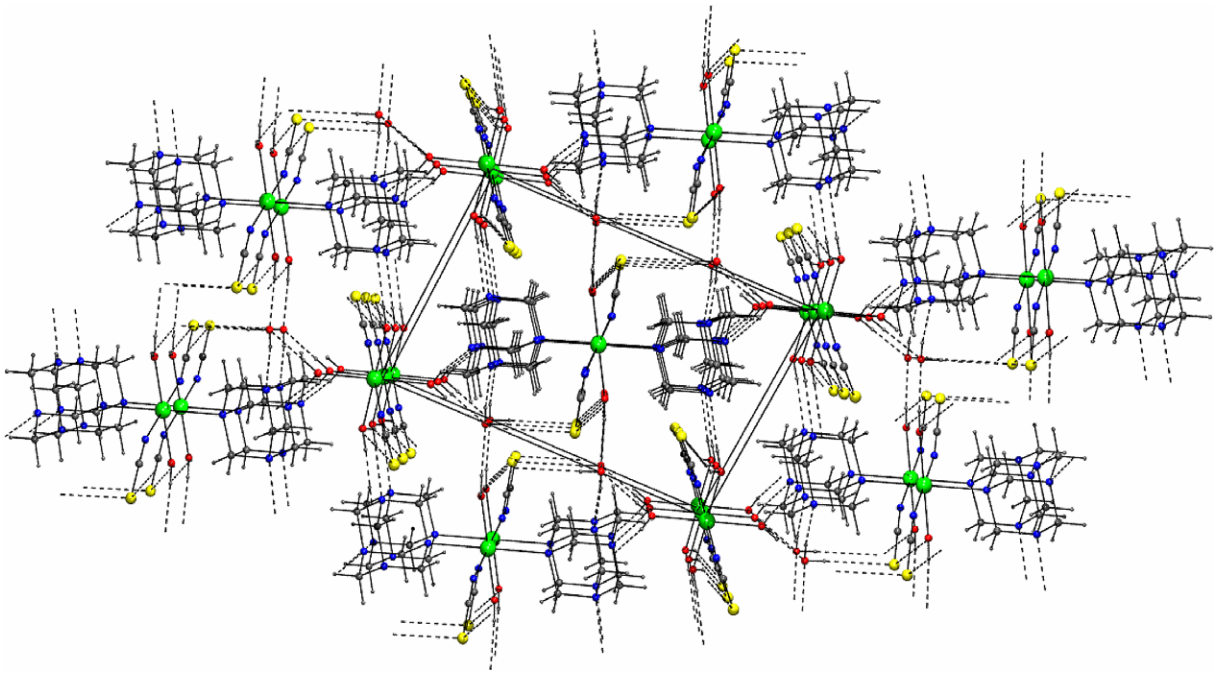

Fig. 3. Packing view along *a*-axis for **1**.

symmetry related counter part N(1**) of terminal azide groups [Co(1)−N(1) (azide): 2.044(3) Å] and the two oxygen atoms O(1) and O(1**) of coordinated water molecules [Co(1)–O(1)(H_2O): 2.099(2) Å], form the equatorial plane around each Co(II) and the *trans*-axial sites are occupied by the two nitrogen atoms N(4) and N(4**) from pendent bridging hmt molecules [Co(1)–N(4)(Hmt): 2.354(2) Å] to provide each Co(II) a $CoN_2(hmt)N_2(N_3^-)O_2(H_2O)$ chromophore (Fig. 4). The Co(II) atoms are bridged by neutral hmt molecule in a μ-*N*,*N*′ fashion with the occurrence of a

Table 2
Selected bond lengths and bond angles for **1** and **2**

Bond lengths (Å)		Bond angles (°)	
1			
Co(1)–O(1W)	2.065(3)	Co(1)–N(1)–C(1)	177.4(3)
Co(1)–O(2W)	2.102(3)	N(3)–Co(2)–N(3)	180(4)
Co(1)–N(1)	2.096(4)	Co(2)–N(2)–C(2)	168.52(13)
Co(2)–O(3W)	2.095(3)		
Co(2)–N(2)	2.043(4)		
Co(2)–N(3)	2.325(3)		
2			
Co(1)–O(1)	2.099(2)	O(1)–Co(1)–N(1)	89.56(5)
Co(1)–N(1)	2.044(3)	Co(1)–N(1)–N(2)	165.6(3)
Co(1)–N(4)	2.354(2)	N(4)–Co(1)–N(1)	90.15(12)
		O(1)–Co(1)–N(4)	88.12(9)

Table 3
Hydrogen bonding parameters for **1** and **2**

D–H···A	*d*(D–H) (Å)	*d*(H···A) (Å)	*d*(D···A) (Å)
1			
O4W–H4WB···N4	0.80(4)	2.03(4)	2.821(5)
O4W–H4WA···S2	0.79(5)	2.61(4)	3.341(4)
O3W–H3WA···S2	0.79(5)	2.85(5)	3.578(4)
O2W–H2WA···S1	0.79(5)	2.55(5)	3.300(4)
O1W–H1WB···N6	0.79(4)	2.07(4)	2.847(5)
O2W–H2WB···N5	0.79(3)	2.02(4)	2.800(4)
C3–H3A···O3W	0.97	2.60	3.040(5)
C4–H4A···S2	0.97	2.85	3.770(4)
C6–H6A···N2	0.97	2.61	3.179(5)
C6–H6B···O3W	0.97	2.60	3.155(5)
C9–H9A···O2W	0.97	2.60	3.557(5)
2			
O1–H1W···N5	0.90(5)	1.91(5)	2.782(4)
O1–H2W···N3	0.74(5)	2.09(5)	2.772(4)
C3–H3B···N1	0.97	2.55	3.175(5)
C3–H3A···O3W	0.93(2)	2.448(19)	2.901(2)

1-D infinite polymeric chain, further carrying into a 2-D net with the help of several weak inter-chain hydrogen bondings. ORTEP and PLATON [42] drawings of the chain with atom labeling scheme are shown in Figs. 5 and 6, respectively. The degrees of distortion from the ideal octahedral geometry are reflected in *cisoid* and *transoid* angles, all resembling the ideal values for an octahedral arrangement. The shortest Co–Co distance along the same chain is 6.313(3) Å. The N_3^- groups show almost linearity with N–N–N angle of 179.3(4)°. The azide ligand shows a slight deviation from linearity in connection with Co(II) [Co–N(1)–N(2): 165.6(3)°]. Each of the hmt molecule acts as a neutral organic bidentate spacer molecule joining the adjacent metal centers in μ-*N*,*N*′ fashion, while the Co(II) centers acting as a linear spacer to generate a 1-D zigzag polymeric chain. The hmt molecule bridges two consecutive metal centers using only two out of its four possible donor sites to link the adjacent units together. All the water molecules and uncoordinated N atoms are involved in intermolecular H-bondings (Fig. 5) making hmt a good tetrahedral template which is the ultimate requirement factor to establish an ordered supramolecular structure formed by self-assembly. Each of the infinite 1-D chains results in a 2-D polymeric network (Figs. 5 and 6) through pronounced inter-chain O–H···N hydrogen bonding between the co-ordinated water molecules to the Co(II) in one chain and N atom of the hmt in the other chain. Further inter-chain O–H···N hydrogen bonding is found between the co-ordinated water molecules of the Co(II) in one chain and the N atoms from terminal azide ligands present in an adjacent chain. Apart from this, there are also three different types of intra-chain hydrogen bonds present in the system (C–H···O, C–H···N, etc.). Another noteworthy point is that the water molecules co-ordinated to the alternative Co(II) centers along the same chain are not behaving identically in the hydrogen bonding mode to the acceptor sites present in the adjacent chain (Fig. 5). Such motif of H-bonding can be described in Etter's graph set notation as $R_2^2(12)$ [33]. As a result of these two types of hydrogen bonds the system has a high degree of thermal stability which is reflected through the thermal study. The co-ordinated water molecules are lost at a much higher temperature than what is

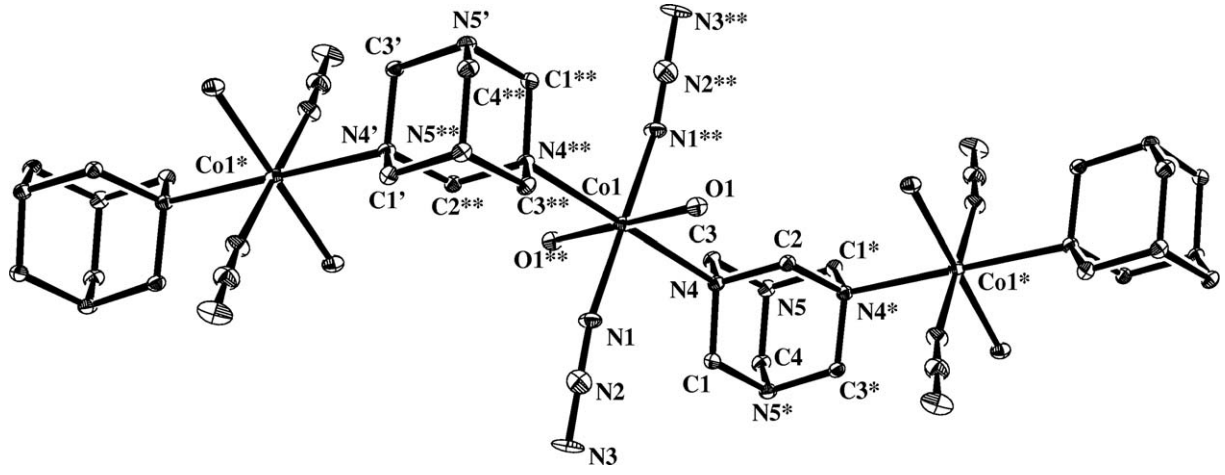

Fig. 4. ORTEP view of **2** with atom numbering scheme (symmetry code (′) = x, $-y$, $z+1/2$; (*) = $2-x$, y, $1/2-z$; (**) = $2-x$, $1-y$, $1-z$).

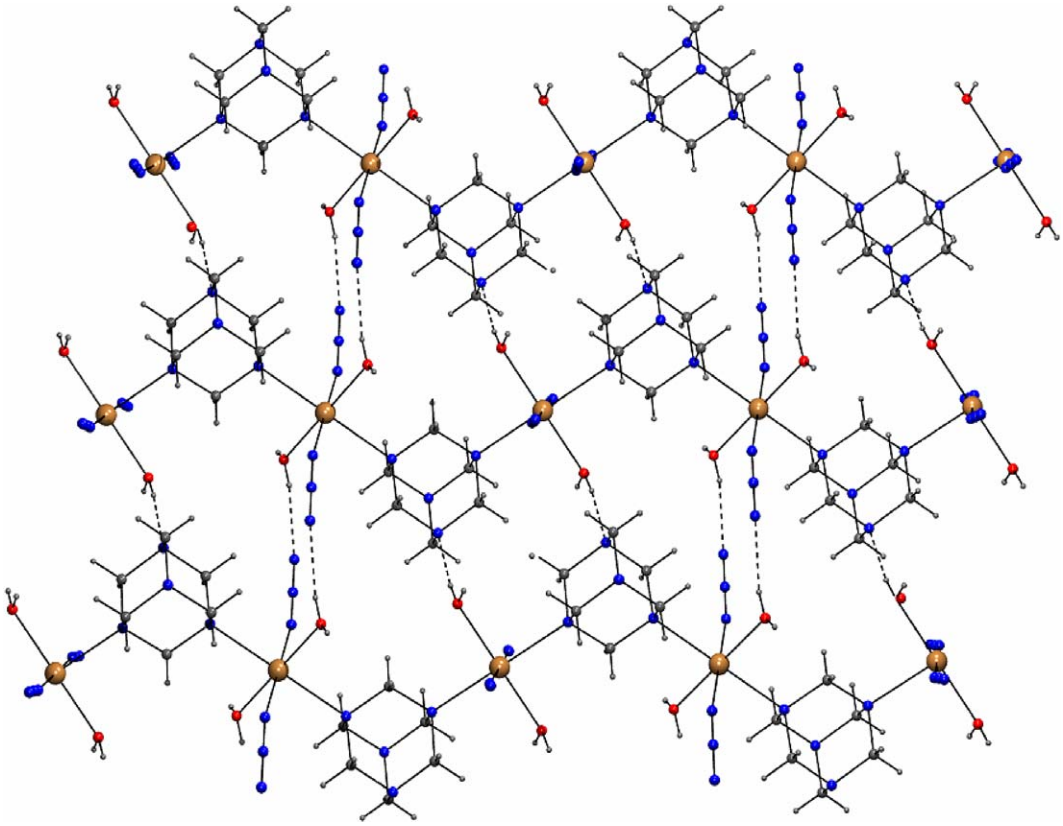

Fig. 5. 2D sheet view of **2**, showing the hydrogen-bonding interactions.

normally observed. All the selected bond distances, bond angles and H-bonding parameters for complex **2** are given in Tables 2 and 3, respectively.

3.4. Cryo-magnetic susceptibility studies

The magnetic properties of both the complexes are more or less same. So only a single plot of $\chi_M T$ versus T (χ_M is the molar magnetic susceptibility for one Co(II) ion), where T varies from 2 K to 300 K, has been provided for complex **2** (Fig. 7). An exactly similar curve corresponding to the first complex has been provided in Fig. 10 as Supplementary material. The value of $\chi_M T$ at 300 K is 2.685 cm^3 K mol^{-1}, which are larger than that expected for the spin-only case ($\chi_M T = 1.87$ cm^3 mol^{-1} K, $S = 3/2$) indicates that an important orbital contribution is involved. The $\chi_M T$ value continuously decreases from room temperature to 1.238 cm^3 K mol^{-1} at 1.99 K. The global feature is characteristic of weak antiferromagnetic interactions. The χ_M curve is less indicative at room temperature. It starts from 0.0089 cm^3 mol^{-1} and increases in a uniform way to 0.619 cm^3 mol^{-1} at 1.99 K. The absence of maxima in these χ_M curves may indicate that the possible antiferromagnetic coupling is very weak.

The analysis of magnetic data for cobalt complexes is usually complicated by the fact that single-ion effects, such as spin–orbit coupling, distortion from regular stereochemistry, electron delocalisation, crystal field mixing of excited states into the ground state, affect the magnetic properties in addition to possible magnetic exchange interactions [34a]. Considering the spin–orbit coupling due to the $^4T_{1g}$ ground state for octahedral Co(II) complexes [34b,34c,34d,34e,34f], exact calculations for deriving the J parameter from experimental data in all the temperature range is not possible unless for dinuclear complexes [35,36]. Other small polynuclear systems can also be fitted through sophisticated computer programs, based on full diagonalisation methods at low temperature region (where the effective spin $S' = 1/2$) [37]. One-dimensional systems of Co(II) are frequently associated with anisotropic Ising systems, and they can be fitted in the low temperature zone assuming again an effective spin $S' = 1/2$ [38]. More recently, Rueff et al. [38c,39] have proposed a phenomenological approach for some low-dimensional Co(II) systems that allows to gain an estimate of the strength of the antiferromagnetic exchange interactions. They postulate the phenomenological equation:

$$\chi_M T = A \exp(-E_1/kT) + B \exp(-E_2/kT) \quad (1)$$

in which, $A + B$ equals to the Curie constant (≈2.8–3.4 cm^3 mol^{-1} K for octahedral cobalt(II) ions), and E_1, E_2 represent the "activation energies" corresponding to the spin–orbit coupling and the antiferromagnetic exchange interaction, respectively. The E_1/k which is the effect of spin–orbit coupling and site distortion is of the

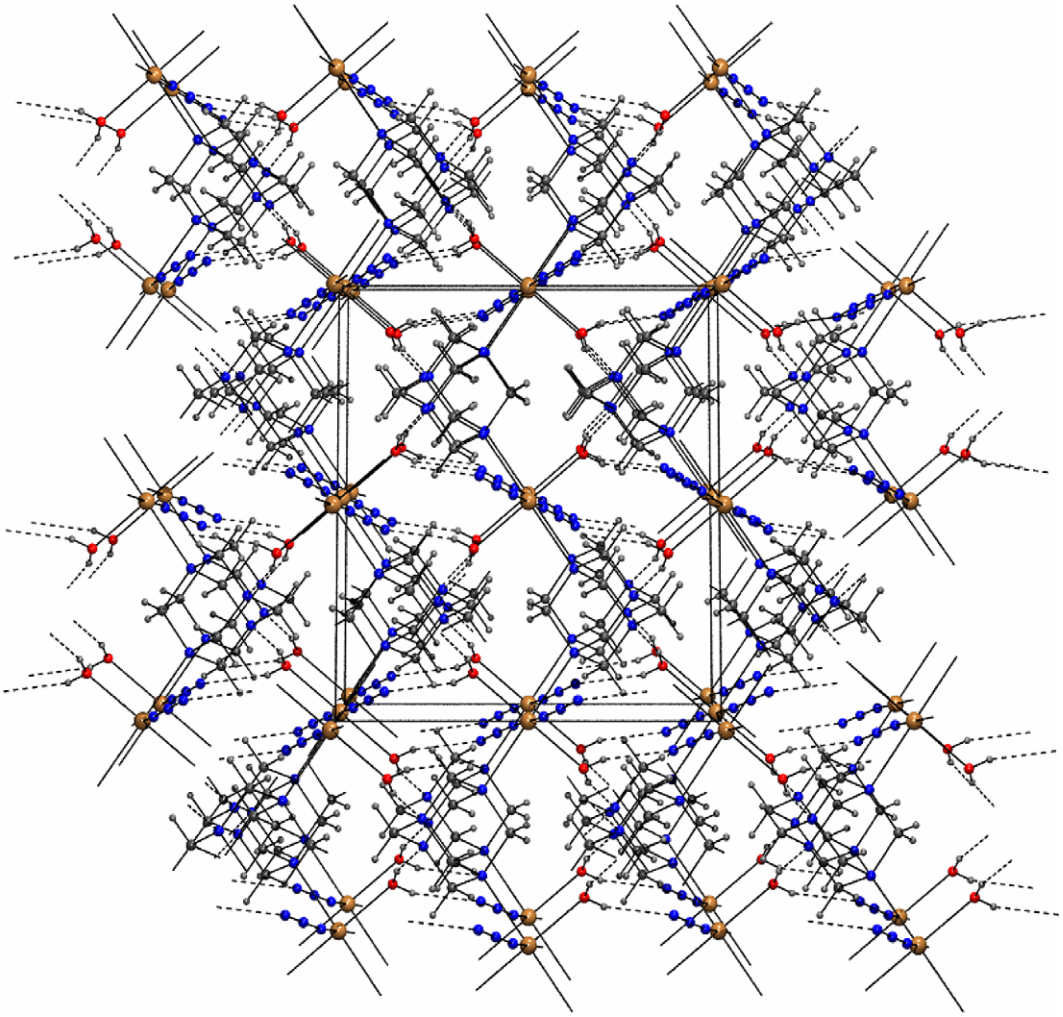

Fig. 6. Packing view along *a*-axis for **2**.

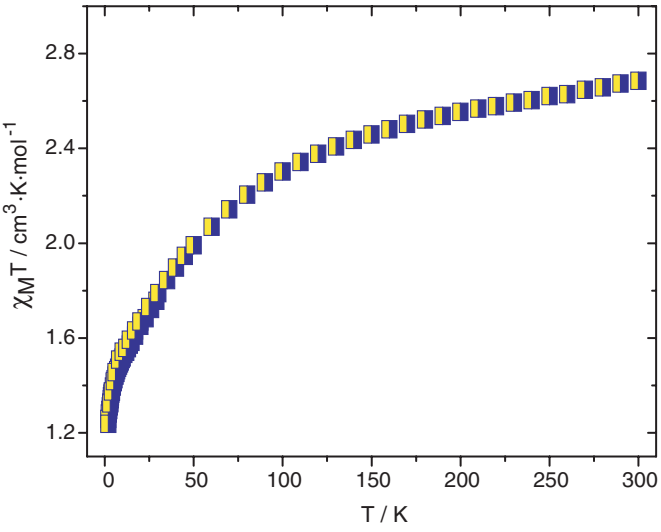

Fig. 7. Plot of $\chi_M T$ vs. T for **2**.

order of +100 K [38c–40]. Eq. (1) adequately describes the spin–orbit coupling, which results in a splitting between discrete levels, and the exponential low-temperature divergence of the susceptibility. Very good results have been reported in one- and two-dimensional Co(II) complexes [38c,39].

An important experimental feature obtained in these octahedral cobalt(II) complexes is that the $\chi_M T$ (or μ_{eff}) values at room temperature are greater than those expected for one isolated spin-only ion ($\chi_M T = 1.87\ cm^3\ mol^{-1}\ K$ for a $S = 3/2$ ion), indicating that an important orbital contribution is involved [34]. Typical values of $\chi_M T$ (or μ_{eff}) are 2.75–3.4 $cm^3\ mol^{-1}\ K$ (4.7–5.2 μ_β) [34,41]. Lower values at room temperature indicate perturbation from ideal octahedral geometry [41]. Based on Eq. (1), commented above, which is suitable for any temperature greater than the possible T_c [38c,39], an estimated J value for our complexes has been calculated. The fit values from this procedure are: $A + B = 2.87\ cm^3\ mol^{-1}\ K$, which perfectly agrees with those given in the literature for the Curie constant ($C \approx 2.8$–$3.4\ cm^3\ mol^{-1}\ K$), [38c,39] $E_1/k = 56.14\ K$ is of the same magnitude than those reported by Rueff et al. for several one- and two-dimensional cobalt(II) complexes [39]. As for the value found for the antiferromagnetic exchange interaction, it is very weak ($E_2/k = 0.55\ K$),

corresponding to $J = -1.1$ K ($=-0.77$ cm^{-1}), according to the Ising chain approximation, $\chi_M T \propto \exp(J/2kT)$.

These weak magnetic exchange couplings can be understood in both the cases considering the hexamethylenetetramine which is separating the Co(II) atoms with large distances (~6.313 Å) either through long distant covalent bondings or through weak hydrogen bondings, leading in this way to almost negligible coupling.

The attempts carried out to fit these complexes, assuming isolated Co(II) ions with perfect octahedral geometry [34] did not give good fit. Thus, we can conclude that these complexes are magnetically behaving as one-dimensional system, which are weakly coupled by hexamethylenetetramine in both the cases.

The reduced molar magnetisation ($M/N\beta$) per Co(II) attends to 1.88 (Fig. 8 for complex **2**, Fig. 11 corresponding to the first complex has been placed as Supplementary material). These values are less than that expected for an isolated Co(II) ion not coupled (2.5–3 $N\beta$). [39] This feature agrees to the weak antiferromagnetic coupling within the Co(II) ions reported in the literature [38c]. The shape of the curves at low fields (sigmoid shape) is also indicative that this antiferromagnetic coupling occurs in these complexes.

Experimental values of susceptibilities and other relevant magnetic parameters for the complexes **1** and **2** are listed in Tables 4 and 5.

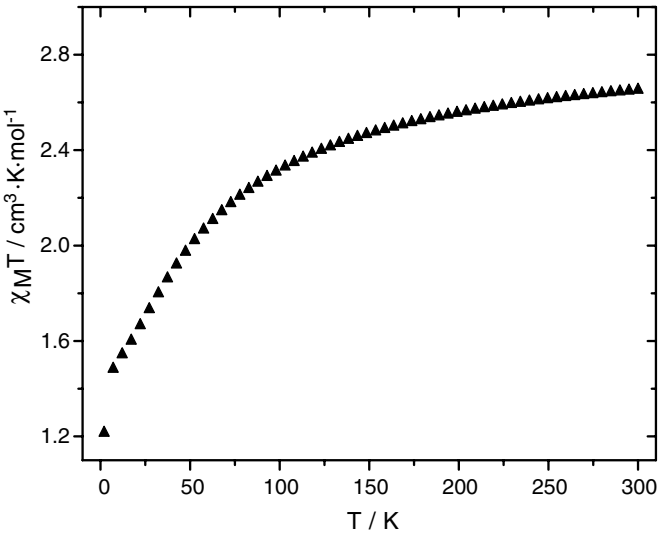

Fig. 10. Plot of $\chi_M T$ vs. T for **1**.

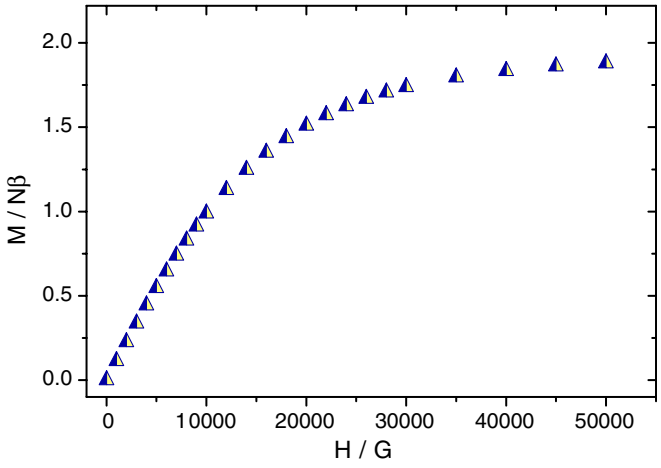

Fig. 8. Plot of the reduced magnetisation $M/N\beta$ vs. applied field H at 2 K for **2**.

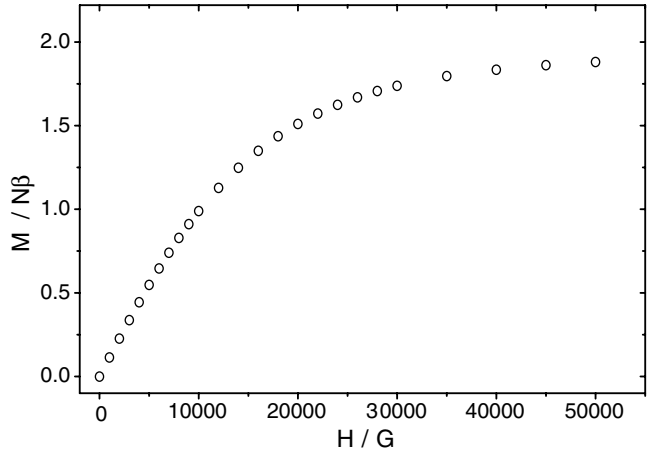

Fig. 11. Plot of the reduced magnetisation $M/N\beta$ vs. applied field H at 2 K for **1**.

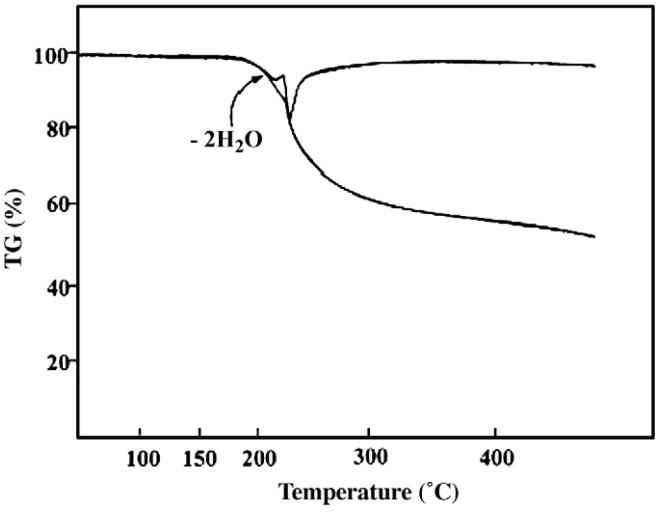

Fig. 9. Thermal stability curve for **1**.

Table 4
Experimental values of the susceptibility

Parameters	Complexes	
	1	**2**
$\chi_M T_{r.t.}$ (cm^3 K mol^{-1})	2.685 (at 300 K)	2.684 (at 300 K)
$\chi_M T_{low}$ (cm^3 K mol^{-1})	1.238 (at 1.99 K)	1.236 (at 1.99 K)
$\chi_{M\,r.t.}$ (cm^3 mol^{-1})	0.0089 (at 300 K)	0.0088 (at 300 K)
$\chi_{M\,low}$ (cm^3 mol^{-1})	0.619 (at 1.99 K)	0.617 (at 1.99 K)

Table 5
Different magnetic constants and parameters

Parameters	Complexes	
	1	**2**
A	1.26845	1.26843
B	1.60351	1.60351
$A + B$	2.87196	2.87194
E_1/k (K)	56.14565	56.14564
E_2/k (K)	0.55539	0.55540
Approximately $J = -E_2/k * 2 * 0.965$ (cm^{-1})	−0.772	−0.772

$\chi_M T = A\exp(-E_1/kT) + B\exp(-E_2/kT)$.

3.5. Thermal analyses

Thermal analysis was done only in the case of complex **1**. Complex **2** was avoided as it contains azide which may cause explosion under thermal treatment. The curve shown in Fig. 9 for thermal studies clearly depicts the decomposition of **1** in three consecutive steps. The weight losses are approximately 10.5% (205 °C); 15.0% (230 °C) and about 32% (234–345 °C) showing through three consecutive endothermal breaks. Weight loss at 205 °C is very close to the calculated water content for two co-ordinated H_2O molecules. So it can be regarded as an evidence of deaquation. This temperature is rather higher compared to the similar co-ordination polymers. It suggests the higher thermodynamic stability of the water molecules in the polymeric complex reported herein [43]. It may be due to the strong and extensive inter- and intra-chain hydrogen bonding network. The weight loss at 230 °C may be correlated to the decomposition of the SCN groups. The final step leads to the formation of a stable residue.

4. Conclusion

In this paper we have reported the controlled hydrothermal synthesis of two new hydrogen bonded metallo-organic co-ordination polymers $[\{Co(hmt)_2(NCS)_2(H_2O)_2\}\{Co(NCS)_2(H_2O)_4\}(2H_2O)]$ (**1**) and $[Co(hmt)(NNN)_2(H_2O)_2]_n$ (**2**) using hexamethylenetetramine as a neutral organic spacer or terminal ligand. Thiocyanate or azide is co-ordinated as terminal coligands in either case. Both the structures show an infinite robust 2-D network with several inter- and intra-chain hydrogen bondings which may be a probable cause for the stability of the system. The facts are well supported by several instrumental analyses and also firmly established from cryo-magnetic susceptibility studies.

Acknowledgements

We acknowledge the support to Joy Chakraborty from the University Grants Commission and also Defence Research and Development Organisation, Ministry of Defence, New Delhi, Government of India. M. Salah El Fallah acknowledges the financial support of the Ministerio de Educación y Ciencia (Programa Ramón y Cajal). Also the grant from Spanish Government (Grant BQU2003/00539) is acknowledged.

Appendix A. Supplementary data

X-ray crystallographic data in the 'CIF' format corresponding to the complexes reported in this paper have been deposited with the Cambridge Crystallographic Data Center and supplementary crystallographic data for this paper can be obtained free of charge on request at www.ccdc.cam.ac.uk/conts/retrieving.html [or from the Cambridge Crystallographic Data Centre (CCDC), 12 Union Road, Cambridge CB2 1EZ, UK; fax: +44 (0) 1223 336033; email: deposit@ccdc.cam.ac.uk], quoting the CCDC number 293386 and 293385 for complexes **1** and **2**, respectively. $\chi_M T$ versus T and $M/N\beta$ versus H curves corresponding to the complex **1** are also deposited as supplementary materials. Supplementary data associated with this article can be found, in the online version, at doi:10.1016/j.poly.2006.05.001.

References

[1] S.-L. Zheng, M.L. Tong, H.-L. Zhu, Yue Fang, X.-M. Chen, J. Chem. Soc., Dalton Trans. (2001) 2049.
[2] C.B. Aakeröy, K.R. Seddon, Chem. Soc. Rev. (1993) 397.
[3] R. Robson, B.F. Abrahms, S.R. Batten, R.W. Gable, B.F. Hoskins, J. Lieu, Supramolecular Architecture, ACS, Washington, DC, 1992.
[4] C.L. Bowes, G.A. Ozin, Adv. Mater. 8 (1996) 13.
[5] P. Feng, X. Bu, G.D. Stucky, Nature 388 (1997) 735.
[6] Y. Zhang, M. Nishiura, J. Li, W. Deng, T. Imamoto, Inorg. Chem. 38 (1999) 825.
[7] Y. Zhang, J. Li, M. Zhu, Q. Wang, X. Wu, Chem. Lett. (1998) 1803.
[8] M.L. Tong, S.-L. Zheng, X.-M. Chen, Chem. Commun. (1999) 561.
[9] G.R. Desiraju, Angew. Chem., Int. Ed. Engl. 34 (1995) 2311.
[10] O. Ermer, J. Am. Chem. Soc. 110 (1988) 3747.
[11] (a) M.L. Tong, X.-M. Chen, X.-L. Yu, T.C.W. Mak, J. Chem. Soc., Dalton Trans. (1998) 5;
(b) L.R. Macgillicray, R.H. Groeneman, J.L. Atwood, J. Am. Chem. Soc. 120 (1998) 2676;
(c) P. Lightfoot, A. Snedden, J. Chem. Soc., Dalton Trans. (1999) 3549.
[12] (a) X.-M. Chen, M.L. Tong, Y.-J. Luo, Z.-N. Chen, Aust. J. Chem. 49 (1996) 835;
(b) M.L. Tong, J.-W. Cai, X.-L. Yu, X.-M. Chen, S.W. Ng, T.C.W. Mak, Aust. J. Chem. 51 (1998) 637;
(c) M.L. Tong, S.-L. Zheng, X.-M. Chen, Polyhedron 19 (2002) 1809;
(d) M.L. Tong, X.-M. Chen, S.W. Ng, Inorg. Chem. Commun. 3 (2002) 436;
(e) M.L. Tong, X.-M. Chen, B.-H. Ye, L.-N. Ji, Angew. Chem., Int. Ed. Engl. 38 (1999) 2237;
(f) M.L. Tong, H.K. Lee, X.-M. Chen, R.B. Huang, T.C.W. Mak, J. Chem. Soc., Dalton Trans. (1999) 3657;
(g) M.L. Tong, B.-H. Ye, J.-W. Cai, X.-M. Chen, S.W. Ng, Inorg. Chem. 37 (1998) 2645.
[13] B.D. Wagner, G.J. Mc Manus, B. Moulton, M.J. Zaworotko, Chem. Commun. (2002) 2176.
[14] N. Mondal, M.K. Saha, S. Mitra, V. Gramlich, J. Chem. Soc., Dalton Trans. (2000) 3218.
[15] S.A. Barnett, A.J. Blake, N.R. Champness, C. Wilson, Chem. Commun. (2002) 1640.
[16] B. Zurowska, J. Mrozinske, M. Julve, F. Loret, A. Maslezova, W. Sawka-Dobrowolska, Inorg. Chem. 41 (2002) 1771.

[17] F. Wiesbrock, H. Schmidbaur, J. Chem. Soc., Dalton Trans. (2002) 3201.
[18] O.R. Evans, W. Lin, Inorg. Chem. 39 (2000) 2189.
[19] C. Livage, C. Egger, M. Nogues, G. Ferey, J. Mater. Chem. 8 (1998) 2743.
[20] S.O.H. Gutschke, M. Molinier, A.K. Powell, P.T. Wood, Angew. Chem., Int. Ed. Engl. 36 (1997) 991.
[21] D. Sun, R. Cao, Y. Liong, Q. Shi, W. Su, M. Hong, J. Chem. Soc., Dalton Trans. (2001) 2335.
[22] S. Wang, M.-L. Hu, S.W. Ng, Acta Crystallogr. E58 (2002) m242.
[23] S.L. Zheng, M.L. Tong, H. Zhu, Y. Fang, X.-M. Chen, J. Chem. Soc., Dalton Trans. (2001) 2049.
[24] S.L. Zheng, M.L. Tong, X.L. Yu, X.-M. Chen, J. Chem. Soc., Dalton Trans. (2001) 586.
[25] S. Banerjee, M.G.B. Drew, A. Ghosh, Polyhedron 22 (2003) 2933.
[26] Y. Zhang, J. Li, M. Nishiura, T. Imamoto, J. Mol. Struct. 523 (2000) 257.
[27] (a) G.M. Sheldrick, SHELXTL: Program for the Refinement of Crystal Structures, University of Göttingen, Germany, 1993;
(b) G.M. Sheldrick, SHELXS 97: Program for Crystal Structure Solution, University of Göttingen, Germany, 1997;
(c) G.M. Sheldrick, SHELXL 97: Program for Crystal Structure Refinement, University of Göttingen, Germany, 1997;
(d) Molecular Structure Corporation, TEXSAN, MSC, 3200, Research Forest Drive, the Woodlands, TX 77381, USA, 1992.
[28] R.T. Conley, Infrared Spectroscopy, Allyn & Bacon Inc., Boston, 1966.
[29] K. Nakamoto, Infrared and Raman Spectra of Inorganic and Coordination Compounds; Part A and B, 5th ed., Wiley, New York, 1997.
[30] A.B.P. Lever, Inorganic Electronic Spectroscopy, 2nd ed., Elsevier, New York, 1984.
[31] Y. Zhang, J. Li, Q. Su, G. Zhao, Spectrochim. Acta 48A (1992) 175.
[32] M. Linhard, M. Weigel, Z. Anorg. Allg. Chem. 64 (1951) 226.
[33] (a) M.C. Etter, Acc. Chem. Res. 23 (1990) 120;
(b) M.C. Etter, J. Phys. Chem. 95 (1991) 4601.
[34] (a) S. Emori, M. Inoue, M. Kubo, Coord. Chem. Rev. 21 (1976);
(b) F.E. Mabbs, D.J. Machin, Magnetism and Transition Metal Complexes, Chapman & Hall, London, 1973;
(c) J.W. Raebiger, J.L. Manson, R.D. Sommer, U. Geiser, A.L. Rheingold, J.S. Miller, Inorg. Chem. 40 (2001) 2578;
(d) E.W. Lee, Y.J. Kim, D.Y. Junag, Inorg. Chem. 41 (2002) 501;
(e) B.N. Figgis, M.A. Hitchman, Ligand Field Theory and its Applications, Wiley-VCH, New York, 2000;
(f) D. Armentano, G. de Munno, F. Lloret, M. Julve, Inorg. Chem. 38 (1999) 3744;
(g) S.J. Retting, R.C. Thompson, J. Trotter, S. Xia, Inorg. Chem. 38 (1999) 1360.
[35] G. de Munno, M. Julve, F. Lloret, J. Faus, A. Canneschi, J. Chem. Soc., Dalton Trans. (1994) 1175.
[36] M.E. Lines, J. Chem. Phys. 55 (1971) 2977.
[37] (a) MAGPACK Program: J.J. Borrás-Almenar, J.M. Clemente-Juan, E. Coronado, B.S. Tsukerblat, Inorg. Chem. 38 (1999) 6081;
(b) J.J. Borrás-Almenar, J.M. Clemente-Juan, E. Coronado, B.S. Tsukerblat, J. Comput. Chem. 22 (2001) 985.
[38] (a) M.E. Fisher, J. Math. Phys. 4 (1963) 124;
(b) S. Angelow, M. Drillon, E. Zhecheva, R. Stoyanova, M. Belaiche, A. Derory, A. Herr, Inorg. Chem. 31 (1992) 1514;
(c) J.-M. Rueff, N. Masciocchi, P. Rabu, A. Sironi, A. Skoulios, Eur. J. Inorg. Chem. (2001) 2843.
[39] J.-M. Rueff, N. Masciocchi, P. Rabu, A. Sironi, A. Skoulios, Chem. Eur. J. 8 (2002) 1813, and references therein.
[40] R.L. Carlin, Magnetochemistry, Springer, Berlin, 1986.
[41] (a) E.A. Boudreaux, L.N. Mulay (Eds.), Theory and Applications of Molecular Paramagnetism, Wiley, New York, 1976, p. 135 (Chapter 3);
(b) L.L. Lohr, J.C. Miller, R.R. Sharp, J. Chem. Phys. 111 (1999) 10148;
(c) S.G. Telfer, T. Sato, R. Kuroda, J. Lefebvre, D.B. Leznoff, Inorg. Chem. 43 (2004) 421.
[42] (a) L.J. Farrugia, J. Appl. Crystallogr. 30 (1997) 565;
(b) A.L. Spek, Acta Crystallogr. A46 (1990) C34.
[43] J. Xiang, J. He, Y. Yin, D. Li, Inorg. Chem. Commun. 9 (2006) 326.

of the complexes, we selected *p*-H_2CCA, *o*-H_2CCA, *p*-H_2BDC and *o*-H_2BDC, together with 1,2-bis(4-pyridyl)ethane (bpe) as linkers, to assemble coordination polymers. Under hydrothermal conditions, we obtained six coordination polymers, $[Co(o\text{-}CCA)(bpe)(H_2O)]_n \cdot 0.25nCH_3OH$ (**1**), $[Ni(o\text{-}CCA)(bpe)(H_2O)]_n \cdot 0.5nH_2O$ (**2**), $[M(p\text{-}CCA)(bpe)_{1.5}(H_2O)]_n \cdot nH_2O$ (M = Co, (**3**); Ni, (**4**)), $[Co(o\text{-}BDC)(bpe)(H_2O)]_n \cdot nH_2O$ (**5**) and $[Co(p\text{-}BDC)(bpe)]_n$ (**6**). Complex **6** is the same to that reported by Fu et al. [13], therefore, we report the syntheses and characterizations of five new complexes **1**–**5**.

2. Experimental

2.1. Materials and apparatus

All reagents were used as received without further purification. The C, H, N microanalyses were carried out with a Vario EL elemental analyzer. The IR spectra were recorded with a Nicolet Avatar 360 FT-IR spectrometer using the KBr pellet technique.

2.2. Synthesis

2.2.1. Synthesis of $[Co(o\text{-}CCA)(bpe)(H_2O)]_n \cdot 0.25nCH_3OH$ (*1*)

A mixture of *o*-H_2CCA (0.02 g, 0.1 mmol), $CoCl_2 \cdot 6H_2O$ (0.024 g, 0.1 mmol), bpe (0.018 g, 0.1 mmol), CH_3OH (5 mL) and deionized water (5 mL) was sealed in a Teflon-lined stainless vessel (25 mL), and heated at 140 °C for 72 h, then cooled slowly to room temperature. Yield: 0.037 g (80.4%). *Anal*. Calc. for $C_{22.25}H_{21}N_2O_{5.25}Co$: C, 58.13; H, 4.57; N, 6.10. Found: C, 58.31; H, 4.81; N, 6.14%. IR data (KBr pellet, cm^{-1}): 3442s, 3065m, 1637m, 1616s, 1571m, 1546s, 1419s, 1394s, 1285w, 1224w, 1071w, 1022w, 973w, 821w, 772m, 758m.

2.2.2. Synthesis of $[Ni(o\text{-}CCA)(bpe)(H_2O)]_n \cdot 0.5nH_2O$ (*2*)

A mixture of *o*-H_2CCA (0.02 g, 0.1 mmol), $NiCl_2 \cdot 6H_2O$ (0.024 g, 0.1 mmol), bpe (0.018 g, 0.1 mmol), NaOH aqueous solution (0.3 mL, 0.65 mol L^{-1}) and deionized water (5 mL) was sealed in a Teflon-lined stainless vessel (25 mL), and heated at 140 °C for 72 h, then cooled slowly to room temperature. Columnar crystals were obtained, washed with water and ethanol, and dried in air. Yield: 0.026 g (56.5%). *Anal*. Calc. for $C_{22}H_{21}N_2O_{5.5}Ni$: C, 57.38; H, 4.56; N, 6.09. Found: C, 57.52; H, 4.85; N, 5.94%. IR data (KBr pellet, cm^{-1}): 3454m, 3068m, 1637m, 1618s, 1571m, 1543s, 1411s, 1394s, 1285w, 1225w, 1071w, 973m, 821m, 772m, 759m.

2.2.3. Synthesis of $[Co(p\text{-}CCA)(bpe)_{1.5}(H_2O)]_n \cdot nH_2O$ (*3*)

The synthesis of complex **3** followed the similar procedure as for complex **2** except using *p*-H_2CCA instead of *o*-H_2CCA. Yield: 0.025 g (44.5%). *Anal*. Calc. for $C_{28}H_{28}N_3O_6Co$: C, 59.84; H, 4.99; N, 7.48. Found: C, 59.58; H, 5.17; N, 7.50%. IR data (KBr pellet, cm^{-1}): 3441s, 2930m, 1616s, 1559m, 1425m, 1376s, 1224m, 1070w, 1020m, 982w, 816m, 791m, 605w, 551m.

2.2.4. Synthesis of $[Ni(p\text{-}CCA)(bpe)_{1.5}(H_2O)]_n \cdot nH_2O$ (*4*)

The synthesis of complex **4** followed the similar procedure as for complex **3**. Yield: 0.026 g (46.3%). *Anal*. Calc. for $C_{28}H_{28}N_3O_6Ni$: C, 59.87; H, 5.35; N, 7.48. Found: C, 59.56; H, 5.06; N, 7.42%. IR data (KBr pellet, cm^{-1}):

Table 1
Crystal data and structure refinement parameters for **1**–**5**

	1	**2**	**3**	**4**	**5**
Chemical formula	$C_{22.25}H_{21}N_2O_{5.25}Co$	$C_{22}H_{21}N_2O_{5.50}Ni$	$C_{28}H_{28}N_3O_6Co$	$C_{28}H_{28}N_3O_6Ni$	$C_{20}H_{20}N_2O_6Co$
Crystal system	orthorhombic	orthorhombic	monoclinic	monoclinic	monoclinic
Space group	*Pccn*	*Pccn*	*C*2/*c*	*C*2/*c*	$P2_1/n$
a (Å)	19.511(3)	19.459(2)	21.397(5)	21.314(8)	13.627(2)
b (Å)	13.258(2)	13.166(1)	14.159(3)	14.144(5)	8.809(1)
c (Å)	16.241(3)	16.118(1)	20.368(5)	20.383(7)	15.457(2)
α (°)	90	90	90	90	90
β (°)	90	90	120.154(4)	120.298(5)	90.720(2)
γ (°)	90	90	90	90	90
V (Å^3)	4201.3(1)	4129.6(6)	5336(2)	5305(3)	1855.6(4)
Z	8	8	8	8	4
F(000)	1900	1912	2336	2344	916
D_{calc} (mg m^{-3})	1.452	1.480	1.398	1.405	1.587
Formula weight	459.34	460.12	561.46	561.24	443.31
T (°C)	293(2)	293(2)	293(2)	293(2)	293(2)
θ Range (°)	1.86–26.40	1.87–25.01	1.83–25.01	1.82–25.01	1.98–26.32
Absorption coefficient (mm^{-1})	0.855	0.979	0.690	0.779	0.967
Goodness-of-fit on F^2	0.995	1.093	1.029	1.146	1.026
Final *R* indices [$I > 2\sigma(I)$]	$R_1 = 0.0468$, $wR_2 = 0.1093$	$R_1 = 0.0413$, $wR_2 = 0.1052$	$R_1 = 0.0699$, $wR_2 = 0.1391$	$R_1 = 0.0644$, $wR_2 = 0.1564$	$R_1 = 0.0341$, $wR_2 = 0.0799$

3456s, 2972m, 1616s, 1560m, 1425m, 1377s, 1232m, 1070w, 1022m, 981w, 817m, 791m, 605w, 551m.

2.2.5. Synthesis of $[Co(o\text{-}BDC)(bpe)(H_2O)]_n \cdot nH_2O$ (5)

The synthesis of complex **5** followed the similar procedure as for complex **2** except using *o*-H_2BDC instead of *o*-H_2CCA. Yield: 0.023 g (51.9%). *Anal*. Calc. for $C_{20}H_{20}N_2O_6Co$: C, 54.14; H, 4.51; N, 6.32. Found: C, 54.12; H, 4.55; N, 6.37%. IR data (KBr pellet, cm^{-1}): 3406m, 3068w, 2926w, 2856w, 1640m, 1610m, 1578s, 1539s, 1438m, 1385s, 1227w, 1072w, 829m, 768m, 717m, 693m.

2.3. X-ray diffraction determination

Diffraction intensities for the six complexes were collected at 293 K on a Bruker SMART 1000 CCD diffractometer employing graphite monochromatized Mo Kα radiation ($\lambda = 0.71073$ Å). Semi-empirical absorption correction was applied using the SADABS program. The structures were solved by direct methods and refined by full-matrix least-squares on F^2 using SHELXTL 97 program [14]. Non-hydrogen atoms were refined anisotropically. All hydrogen atoms were initially located in a difference Fourier map. The O–H distances were then fixed at 0.85 Å and U_{iso}(H) of the hydrogen atoms of H_2O was 1.5 times of U_{eq}(O) in the next refinement. The crystallographic data for complexes **1**–**5** are listed in Table 1, and selected bond lengths (Å) and bond angles (°) in Tables 2 and 3.

Table 2
Selected bond lengths (Å) and angles (°) for complexes **1** and **2**

1			
Co(1)–O(1)	2.053(3)	Co(1)–O(5)	2.156(3)
Co(1)–O(3)#1	2.149(3)	Co(1)–N(1)	2.158(4)
Co(1)–O(4)#1	2.169(3)	Co(1)–N(2)	2.106(4)
O(1)–Co(1)–O(3)#1	103.6(1)	O(5)–Co(1)–O(4)#1	87.1(1)
O(1)–Co(1)–O(4)#1	164.1(1)	O(5)–Co(1)–N(1)	175.9(1)
O(1)–Co(1)–O(5)	89.6(1)	N(1)–Co(1)–O(4)#1	96.0(1)
O(1)–Co(1)–N(1)	88.2(1)	N(2)–Co(1)–O(3)#1	157.9(1)
O(1)–Co(1)–N(2)	98.9(1)	N(2)–Co(1)–O(4)#1	96.7(1)
O(3)#1–Co(1)–O(4)#1	61.0(1)	N(2)–Co(1)–O(5)	90.1(1)
O(3)#1–Co(1)–O(5)	91.1(1)	N(2)–Co(1)–N(1)	86.9(2)
O(3)#1–Co(1)–N(1)	92.7(1)		
2			
Ni(1)–O(1)	2.045(2)	Ni(1)–O(5)	2.100(2)
Ni(1)–O(3)#1	2.129(2)	Ni(1)–N(1)	2.109(3)
Ni(1)–O(4)#1	2.108(2)	Ni(1)–N(2)	2.061(3)
O(1)–Ni(1)–O(3)#1	101.3(1)	O(5)–Ni(1)–O(4)#1	87.1(1)
O(1)–Ni(1)–O(4)#1	163.3(1)	O(5)–Ni(1)–N(1)	177.3(1)
O(1)–Ni(1)–O(5)	90.5(1)	N(1)–Ni(1)–O(3)#1	92.8(1)
O(1)–Ni(1)–N(1)	87.4(1)	N(2)–Ni(1)–O(3)#1	160.9(1)
O(1)–Ni(1)–N(2)	97.9(1)	N(2)–Ni(1)–O(4)#1	98.7(1)
O(4)#1–Ni(1)–O(3)#1	62.2(1)	N(2)–Ni(1)–O(5)	90.8(1)
O(4)#1–Ni(1)–N(1)	95.4(1)	N(2)–Ni(1)–N(1)	87.7(1)
O(5)–Ni(1)–O(3)#1	89.3(1)		

Symmetry transformations used to generate equivalent atoms: #1 $-x+1$, $y+1/2$, $-z+1/2$.

Table 3
Selected bond lengths (Å) and angles (°) for complexes **3**, **4** and **5**

3			
Co(1)–O(1)	2.140(4)	Co(1)–N(1)	2.124(4)
Co(1)–O(3)	2.113(4)	Co(1)–N(2)#1	2.149(4)
Co(1)–O(5)	2.072(4)	Co(1)–N(3)	2.140(4)
O(1)–Co(1)–N(2)#1	84.6(2)	O(5)–Co(1)–N(2)#1	95.1(2)
O(3)–Co(1)–O(1)	175.9(2)	O(5)–Co(1)–N(3)	176.6(2)
O(3)–Co(1)–N(1)	88.8(2)	N(1)–Co(1)–N(3)	88.8(2)
O(3)–Co(1)–N(2)#1	97.4(2)	N(1)–Co(1)–O(1)	89.5(2)
O(3)–Co(1)–N(3)	89.2(2)	N(3)–Co(1)–O(1)	94.4(2)
O(5)–Co(1)–O(1)	88.9(2)	N(1)–Co(1)–N(2)#1	171.9(2)
O(5)–Co(1)–O(3)	87.4(1)	N(3)–Co(1)–N(2)#1	86.1(2)
O(5)–Co(1)–N(1)	90.4(2)		
4			
Ni(1)–O(1)	2.127(3)	Ni(1)–N(1)	2.089(4)
Ni(1)–O(3)	2.111(3)	Ni(1)–N(2)#1	2.116(4)
Ni(1)–O(5)	2.056(4)	Ni(1)–N(3)	2.111(4)
O(1)–Ni(1)–N(2)#1	85.1(1)	O(5)–Ni(1)–N(2)#1	95.0(2)
O(3)–Ni(1)–O(1)	176.3(1)	O(5)–Ni(1)–N(3)	176.4(1)
O(3)–Ni(1)–N(1)	88.0(2)	N(1)–Ni(1)–O(1)	89.9(2)
O(3)–Ni(1)–N(2)#1	97.2(2)	N(1)–Ni(1)–N(2)#1	173.0(2)
O(3)–Ni(1)–N(3)	89.2(2)	N(1)–Ni(1)–N(3)	89.1(2)
O(5)–Ni(1)–O(1)	89.6(1)	N(3)–Ni(1)–O(1)	93.8(2)
O(5)–Ni(1)–O(3)	87.4(1)	N(3)–Ni(1)–N(2)#1	86.4(2)
O(5)–Ni(1)–N(1)	89.8(2)		
5			
Co(1)–O(1)	2.055(2)	Co(1)–O(5)	2.156(2)
Co(1)–O(3)	2.152(2)	Co(1)–N(1)	2.161(2)
Co(1)–O(4)#1	2.066(2)	Co(1)–N(2)#2	2.151(2)
O(1)–Co(1)–O(3)	89.35(6)	O(4)#1–Co(1)–O(5)	97.06(7)
O(1)–Co(1)–O(4)#1	172.2(6)	O(4)#1–Co(1)–N(1)	89.90(7)
O(1)–Co(1)–O(5)	89.33(7)	O(4)#1–Co(1)–N(2)#2	86.71(7)
O(1)–Co(1)–N(1)	94.97(7)	O(5)–Co(1)–N(1)	87.11(7)
O(1)–Co(1)–N(2)#2	88.56(7)	N(2)#2–Co(1)–O(3)	90.18(7)
O(3)–Co(1)–O(5)	177.6(7)	N(2)#2–Co(1)–O(5)	91.82(7)
O(3)–Co(1)–N(1)	90.98(7)	N(2)#2–Co(1)–N(1)	176.3(8)
O(4)#1–Co(1)–O(3)	84.41(6)		

Symmetry transformations used to generate equivalent atoms: (#1) $-x+1/2$, $y+1/2$, $-z+1/2$ for **3** and **4**, (#1) $-x+5/2$, $y+1/2$,$-z+1/2$; (#2) $x+1$, y, z for **5**.

3. Results and discussion

3.1. Description of the structures

Complexes **1** and **2**, **3** and **4** are two isomorphous pairs except that in complexes **1** and **2**, the clathrated guest molecules are different (CH_3OH for complex **1** and H_2O for complex **2**). And because of the different radii of the Co(II) and Ni(II) ions, there are corresponding differences in the distances of M–O and M–N (M = Ni or Co) in the two paired complexes, however only the structures of **1**, **3** and **5** will be described in detail.

3.1.1. $[Co(o\text{-}CCA)(bpe)(H_2O)]_n \cdot 0.25nCH_3OH$ (1)

The coordination environment of Co(II) ion in complex **1** is shown in Fig. 1. Each Co(II) ion is six-coordinated by three oxygen atoms (O(1), O(3A), O(4A)) of two *o*-CCA anions, one oxygen atom (O(5)) of water molecule and two nitrogen atoms (N(1), N(2)) of two bpe ligands,

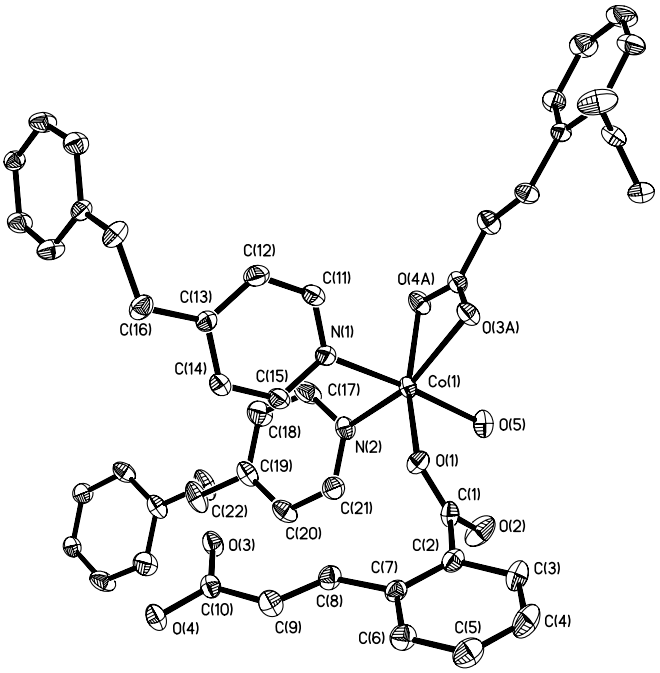

Fig. 1. Coordination environment of Co(II) ion in complex **1** with 30% thermal ellipsoids, all hydrogen atoms and crystal water molecules are omitted for clarity.

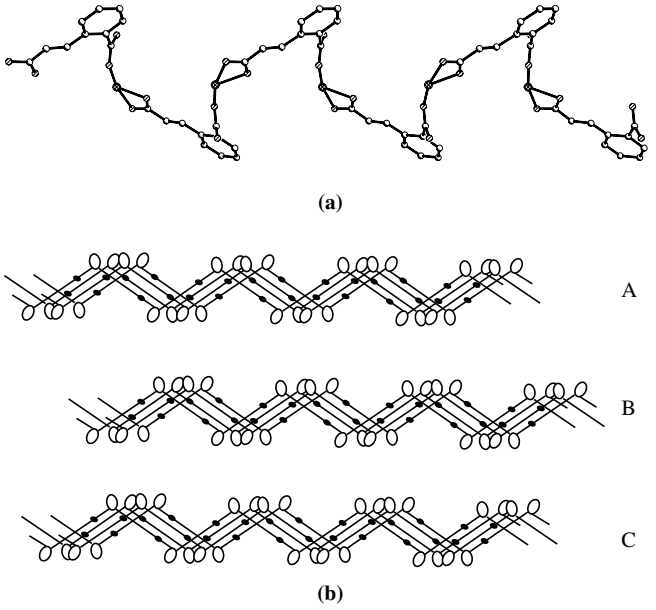

Fig. 2. (a) 1D zigzag chain constructed by *o*-CCA linking Co(II) ions and (b) the simplified representation of the 2D layers in complex **1** viewed along the *c* axis.

leading to a distorted octahedron. There is one kind of crystallographically independent *o*-CCA anion, acting as a tridentate ligand (see Scheme 1a). The formate group of the *o*-CCA anion adopts a monodentate mode, while the acrylate adopts a chelating-bidentate mode, and thus the *o*-CCA anion bridges two Co(II) ions, and the Co···Co distance is 7.181 Å (7.157 Å for Ni). All Co(II) ions are linked by *o*-CCA anions into 1D infinite zigzag chains, as shown in Fig. 2(a). Along the *c* axis, the chains are parallel to each other, forming 2D layers (see Fig. 2(b) A, B, C).

In complex **1**, bpe molecules adopt two conformations, anti and gauche forms (see Scheme 1f). They all act as bidentate ligands, bridging Co(II) ions into wave-like chains, as shown in Fig. 3. All these chains are parallel to

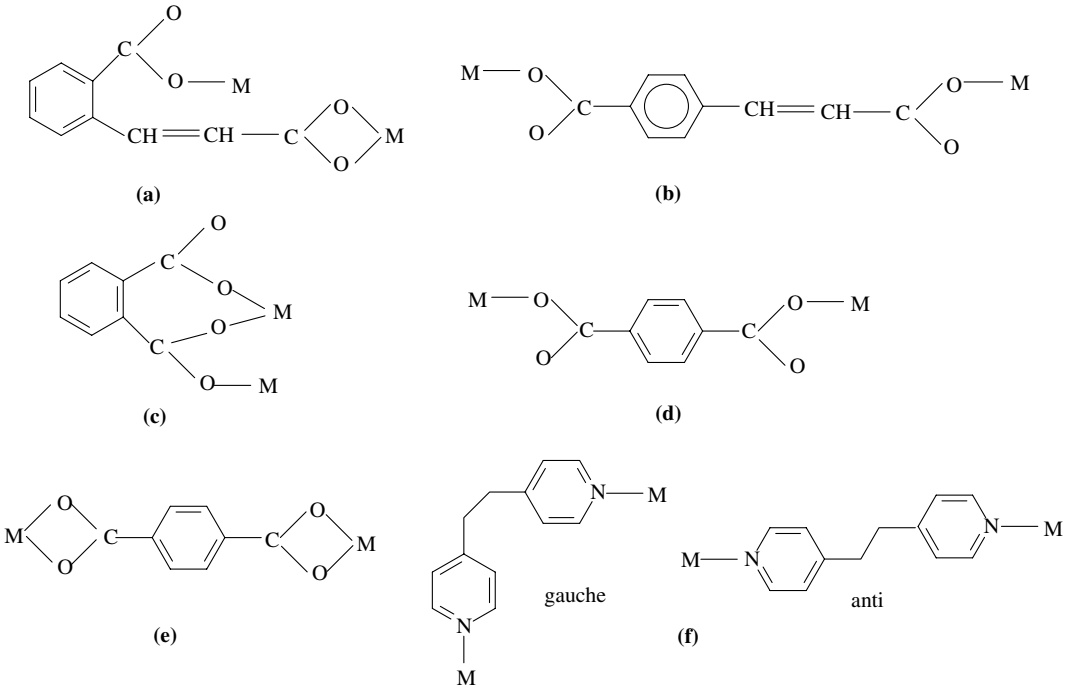

Scheme 1. The coordination modes of the ligands in complexes **1**–**6**.

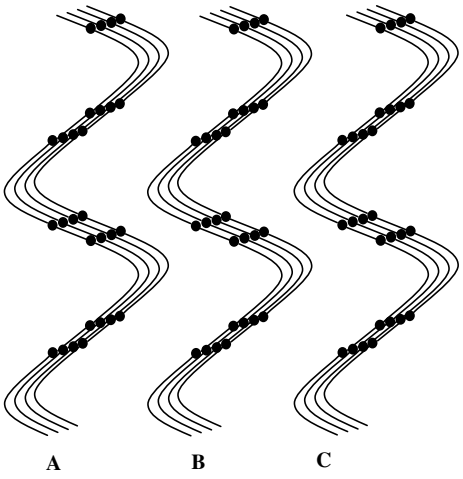

Fig. 3. The simplified representation of wave-like chains constructed by bpe linking Co(II) ions in complex **1** viewed along the *b* axis.

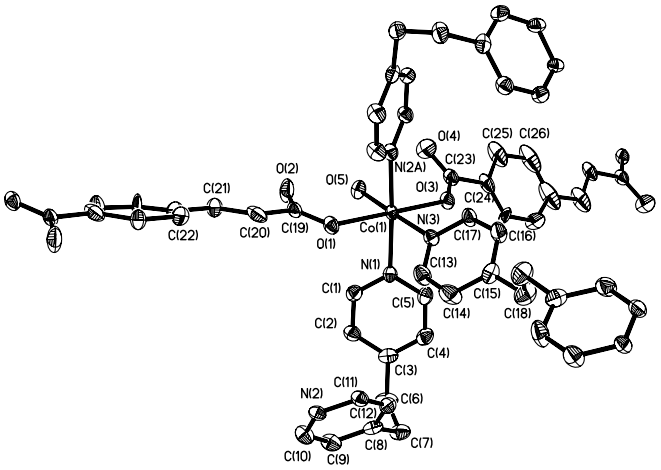

Fig. 5. Coordination environment of Co(II) ion in complex **3** with 30% thermal ellipsoids, all hydrogen atoms and crystal water molecule are omitted for clarity.

each other, forming 2D layers (see Fig. 3 A, B, C). The chains shown in Figs. 2 and 3 intersect at Co(II) ions and thus form a 3D metal-organic framework, in which free methanol molecules are clathrated (see Fig. 4, crystal water molecules in complex **2**). Hydrogen bonds are observed between the coordination water molecules and the uncoordinated carboxylate oxygen atoms (H···O = 1.831 Å, O···O = 2.662 Å, ∠OHO = 164.2°), and between the free methanol molecules and the uncoordinated carboxylate oxygen atoms (H···O = 1.895 Å, O···O = 2.738 Å, ∠OHO = 170.8°), which brings further stability for the structure.

3.1.2. $[Co(p\text{-}CCA)(bpe)_{1.5}(H_2O)]_n \cdot nH_2O$ (3)

Complex **3** possesses a 3D metal-organic framework with clathrated free water molecules. There is only one metal environment in complex **3**, as shown in Fig. 5. The coordination geometry around each Co(II) ion, comprising N_3O_3 from two *p*-CCA anions, one water molecule and three bpe molecules, can be described as a distorted octahedron. The oxygen atom (O5) of water molecule and the nitrogen atom (N3) of bpe ligand occupy the axial position. There is one kind of crystallographically independent *p*-CCA anion, acting as a bidentate ligand (see Scheme 1b). Both carboxylate groups of *p*-CCA anion adopt a monodentate mode, bridging two Co(II) ions, and the Co···Co distance is 7.657 Å (7.641 Å for Ni). In complex **3**, *p*-CCA anions are disordered and the occupancy is 0.5. All Co(II) ions are linked by *p*-CCA anions into 1D straight infinite chains, as shown in Fig. 6(a). The chains are parallel to each other, forming 2D layers, as shown in Fig. 6(b) A, B, C and D.

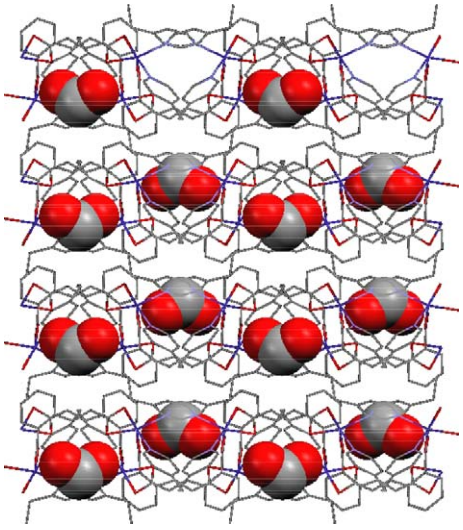

Fig. 4. The 3D network of complex **1** viewed along the *a* axis (the space filling diagram represents the clathrated methanol molecules).

In complex **3**, bpe ligands adopt two conformations, and act as bidentate ligands, too. All Co(II) ions are bridged by bpe ligands to form 2D brick-wall-like grids, as shown in Fig. 7. The chains shown in Fig. 6 and grids shown in Fig. 7 intersect at Co(II) ions, and thus form a 3D complicated metal-organic framework. And free water molecules are clathrated. There are hydrogen bonds between the coordinated/free water molecules and the uncoordinated carboxylate oxygen atoms (H···O = 1.887–2.767 Å, O···O = 2.583–2.892 Å, ∠OHO = 128.5°–138.0°), which stabilizes the structure.

3.1.3. $[Co(o\text{-}BDC)(bpe)(H_2O)]_n \cdot nH_2O$ (5)

There is only one kind of metal environment in complex **5** (see Fig. 8). Each Co(II) ion is coordinated by three oxygen atoms (O(1), O(3), O(4A)) of two *o*-BDC anions, one oxygen atom (O(5)) of coordinated water molecule and two nitrogen atoms (N(1), N(2A)) of two bpe ligands. The coordination geometry can be described as a distorted octahedron. In complex **5**, *o*-BDC anion adopts a tridentate mode, as shown in Scheme 1c. One carboxylate group adopts a bridging-bidentate mode, and the other adopts a monodentate mode, thus linking two Co(II) ions, in which the Co···Co distance is 5.290 Å. All bpe ligands are in

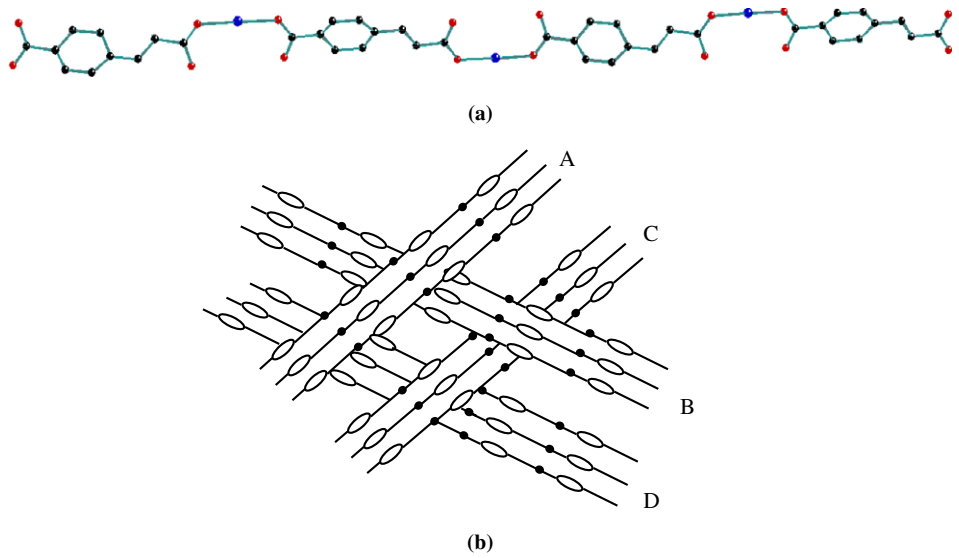

(a)

(b)

Fig. 6. (a) 1D chain constructed by *p*-CCA linking Co(II) ions and (b) the simplified representation of the 2D layers in complex **3**.

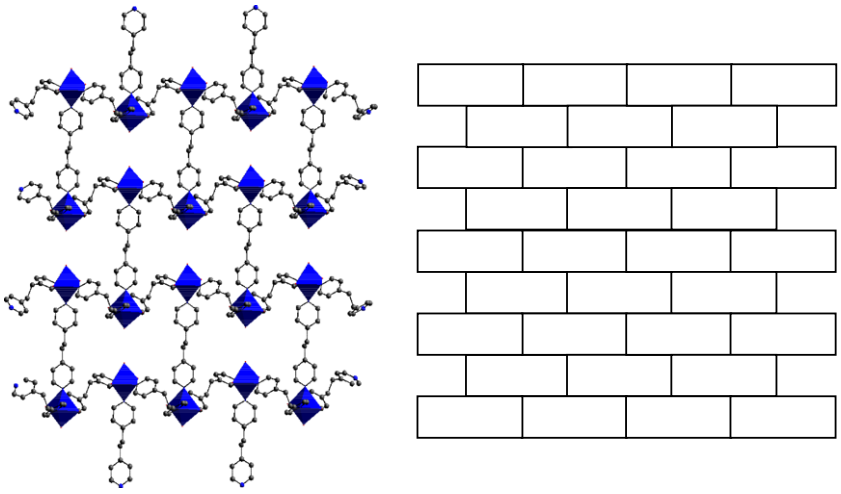

(a) (b)

Fig. 7. (a) The brick-wall-like grids constructed by bpe linking Co(II) ions in complex **3** and (b) the brick-wall scheme of Co(II)-bpe linking assembly in complex **3**.

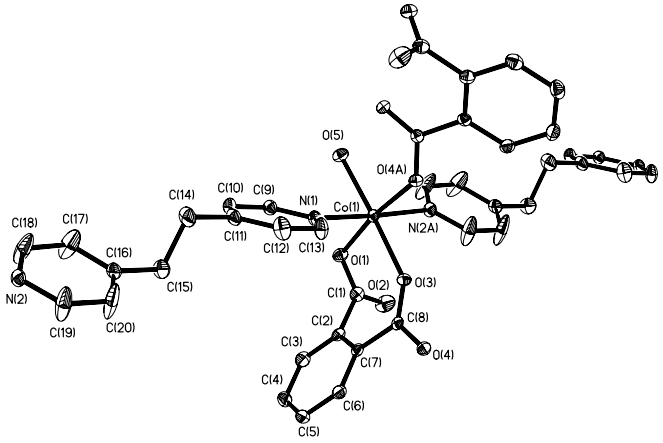

Fig. 8. The coordination environment of Co(II) ion in complex **5** with 30% thermal probability, all hydrogen atoms are omitted for clarity.

anti-form and act as bidentate ligands. Both *o*-BDC anions and bpe ligands link Co(II) ions into (4,4) 2D grid-like layers with cavity of 13.627×5.290 Å. These layers are stacked parallel along the *c* axis exhibiting the ABABAB sequence (see Fig. 9(a)). Crystal water molecules are located between the layers, as shown in Fig. 9(b). There are hydrogen bonds between the coordinated/crystal water molecules and carboxylate oxygen atoms (H···O = 2.110–2.311 Å, O···O = 2.880–2.972 Å, ∠OHO = 134.4°–163.2°), and between the coordinated water molecules and crystal water molecules (H···O = 2.121 Å, O···O = 2.924 Å, ∠OHO = 156.7°).

3.1.4. Comparison of the structures

From the above descriptions, it is obvious that the geometry of ligands has a significant effect on the formation and

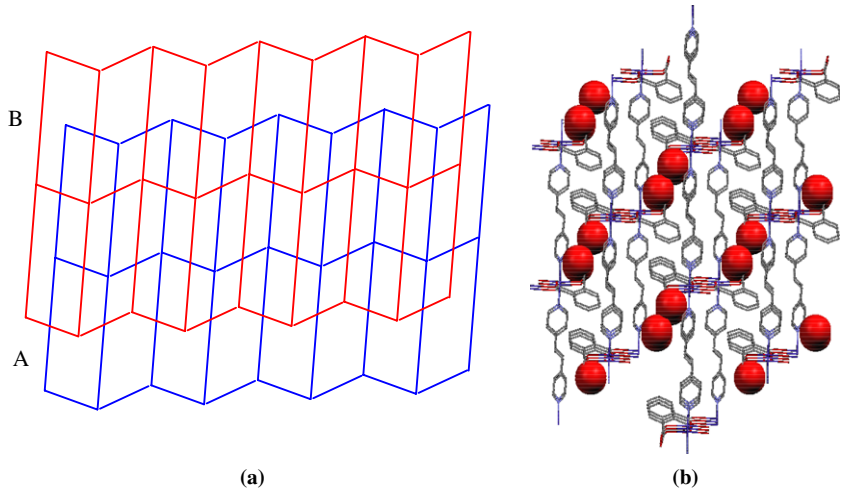

Fig. 9. (a) The simplified representation of 2D layers of complex **5** and (b) the 3D network of complex **5** viewed along the *b* axis (the red balls represent crystal water molecules). (For interpretation of the references to colour in this figure legend, the reader is referred to the Web version of this article.)

structure of the complexes. Complexes **1**–**4** all possess 3D metal-organic frameworks, while complexes **5** is of (4,4) 2D grid-like layers with cavities, and complex **6** is of 3D cuboidal box-like structure [13]. This may be attributed to flexible CCA ligands in complexes **1**–**4** and rigid BDC ligands in complexes **5** and **6**, respectively. The combination of mixed flexible ligands such as CCA and bpe in the construction of coordination polymers may result in complicated structure, while mixed rigid and flexible ligands such as BDC and bpe may result in regular geometry. Other examples can be found in literatures, such as 3,4-pyridinedicarboxylate and bpe [15], 5-nitro-1,3-benzenedicarboxylate and bpe [16], *o*-H_2CCA and 4,4′-bipyridine [11], nitrilotriacetic acid and 4,4′-bipyridine [17], 4,4′-oxybis(benzoic acid) and 4,4′-bipyridine [18]. In order to construct regular geometry for coordination polymers, it is feasible to use mixed rigid and flexible ligands, rather than mixed flexible ligands.

Comparing the structures of complexes **1** and **3**, it can be concluded that the position of functional groups takes an important role in formation and architecture of the complexes. In *o*-CCA anions, the two carboxylate groups are in the adjacent position and there is an angle of nearly 60° between the two carboxylate groups; while in *p*-CCA anions, the two carboxylate groups are in opposite position. So the two carboxylate groups in *o*-CCA anion are much nearer than those in *p*-CCA anion, which induces different steric effect. In complex **1**, there are two bpe and two *o*-CCA anions around each Co(II) ion, while in complex **3** there are three bpe and two *p*-CCA anions. In order to complete the six-coordination of the Co(II) ion, the acrylate group of *o*-CCA anion adopts a chelating-bidentate mode in complex **1** (see Scheme 1a). That is the reason why *p*-CCA and *o*-CCA anions adopt different coordination modes. Similar situation is observed in complexes **5** and **6**. In complex **5**, *o*-BDC anions act as tridentate ligands (see Scheme 1c), while in complex **6**, *p*-BDC anions adopt bis(monodentate) mode and bis(chelating-bidentate) mode (see Scheme 1d and e) [13], which induces distinctive structures for complexes **5** and **6.**

Table 4
Thermogravimetric analyses data of complexes **1**–**4**

	1	**2**	**3**	**4**
The first weight loss temperature [°C]	91–161	126–206	105–173	126–185
Loss of weight: Found (Calc.) [%]	5.9(5.7)	5.8(5.9)	6.1(6.4)	6.2(6.4)
Further decomposition temperature [°C]	196–685	263–712	185–600	223–610
The residue	CoO	NiO	CoO	NiO

3.2. Thermal analyses

Thermogravimetric analyses of the complexes **1**–**4** were carried out to examine their thermal stabilities. The data of the thermogravimetric analyses for **1**–**4** are listed in Table 4. All guest molecules (methanol for **1** and water for **2**–**4**) and coordinating water molecules were lost at the first weight loss, indicating that the clathrated molecules are correlated with the formation and architecture of metal-organic frameworks in complexes **1**–**4**. Taking complex **1** as an example, the TG curve shows that the first weight loss of 5.9% from 91 °C to 161 °C corresponds to the loss of free methanol molecules and coordinating water molecules (calcd. 5.7%). Increasing temperature led to the further decomposition of complex **1** at 196 °C. The final pyrolysis was completed at 685 °C, giving the powder of CoO.

4. Conclusion

In summary, using hydrothermal reactions, we obtained five new coordination polymers $[Co(o\text{-CCA})(bpe)(H_2O)]_n$

$\cdot 0.25n$$CH_3OH$ (**1**), $[Ni(o\text{-}CCA)(bpe)(H_2O)]_n \cdot 0.5n$$H_2O$ (**2**), $[M(p\text{-}CCA)(bpe)_{1.5}(H_2O)]_n \cdot n$$H_2O$ (M = Co, (**3**); Ni, (**4**) and $[Co(o\text{-}BDC)(bpe)(H_2O)]_n \cdot n$$H_2O$ (**5**)). In complex **1**, bpe ligands link Co(II) ions into wave-like chains, while in complex **3**, Co(II) ions are bridged by bpe into brick-wall-like grids, which is mainly attributed to coordination characteristics of *o*-CCA anion and *p*-CCA anion, respectively. The position of functional dicarboxylate groups takes an important role in the architectures of metal-organic frameworks. Complexes **1**–**4** all possess 3D complicated and different metal-organic frameworks, while complex **5** is of (4,4) 2D grid-like layers with cavities. These results show that in order to construct regular geometry, it is feasible to use mixed rigid and flexible ligands rather than mixed flexible ligands.

5. Supplementary data

Crystallographic data for the structural analysis have been deposited with the Cambridge Crystallographic Data Centre, CCDC Nos. 601065–601069 for **1**–**5**, respectively. Copies of this information may be obtained free of charge from the CCDC, 12 Union Road, Cambridge CB2 1EZ, UK (fax: +44 1223 336 033; e-mail:deposit@ccdc.cam.ac.uk or www:http://www.ccdc.cam.ac.uk).

Acknowledgements

This project is supported by National Nature Science Foundation of China (20331010, 20501003).

References

[1] (a) M. Fujita, Y.J. Kwon, S. Washizu, K. Ogura, J. Am. Chem. Soc. 116 (1994) 1151;
(b) T. Sawaki, Y. Aoyama, J. Am. Chem. Soc. 121 (1999) 4793;
(c) J.S. Seo, D. Whang, H. Lee, S.I. Jun, J. Oh, Y. Jeon, K. Kim, Nature 404 (2000) 982;
(d) L. Pan, H.M. Liu, X.G. Lei, X.Y. Huang, D.H. Olson, N.J. Turro, J. Li, Angew. Chem., Int. Ed. 42 (2003) 542.

[2] (a) K.S. Min, M.P. Suh, Chem. Eur. J. 7 (2001) 303;
(b) K. Uemura, S. Kitagawa, M. Kondo, K. Fukui, R. Kitaura, H.C. Chang, T. Mizutani, Chem. Eur. J. 8 (2002) 3587;
(c) D.N. Dybtsev, H. Chun, S.H. Yoon, D. Kim, K. Kim, J. Am. Chem. Soc. 126 (2004) 32.

[3] (a) S. Noro, S. Kitagawa, M. Kondo, K. Seki, Angew. Chem., Int. Ed. 39 (2000) 2081;
(b) M. Eddaoudi, J. Kim, N.L. Rosi, D.T. Vodak, J. Wachter, M. O'Keeffe, O.M. Yaghi, Science 295 (2002) 469;
(c) L. Pan, M.B. Sander, X.Y. Huang, J. Li, M. Smith, E. Bittner, B. Bochrath, J.K. Johnson, J. Am. Chem. Soc. 126 (2004) 1308.

[4] (a) M. Albrecht, M. Lutz, A.L. Spek, G. Koten, Nature 406 (2000) 970;
(b) L.G. Beauvais, M.P. Shores, J.R. Long, J. Am. Chem. Soc. 122 (2000) 2763.

[5] (a) M. Eddaoudi, D.B. Moler, H. Li, B. Chen, T.M. Reineke, M. O'Keeffe, O.M. Yaghi, Acc. Chem. Res. 34 (2001) 319;
(b) M.E. Braun, C.D. Steffek, J. Kim, P.G. Rasmussen, O.M. Yaghi, Chem. Commun. (2001) 2532;
(c) C. Ruiz-Pérez, P. Lorenzo-Luis, M. Hernández-Molina, M.M. Laz, F.S. Delgado, P. Gili, M. Julve, Eur. J. Inorg. Chem. (2004) 3873.

[6] (a) B.Q. Ma, P. Coppens, Chem. Commun. (2003) 2290;
(b) E. Coronado, J.R. Galán-Mascarós, C.J. Gómez-García, E. Martínez-Ferrero, S.V. Smaalen, Inorg. Chem. 43 (2004) 4808.

[7] (a) M. Oh, G.B. Carpenter, D.A. Sweigart, Angew. Chem., Int. Ed. 42 (2003) 2025;
(b) F.A.A. Paz, J. Klinowski, Inorg. Chem. 43 (2004) 3882.

[8] (a) J.F. Ma, J. Yang, G.L. Zheng, L. Li, J.F. Liu, Inorg. Chem. 42 (2003) 7531;
(b) D.N. Dybtsev, H. Chun, K. Kim, Angew. Chem., Int. Ed. 43 (2004) 5033.

[9] M.C. Hong, W.P. Su, R. Cao, M. Fujita, J.X. Lu, Chem. Eur. J. 6 (2000) 427.

[10] H. Kumagai, Y. Oka, K. Inoue, M. Kurmoo, J. Chem. Soc., Dalton Trans. (2002) 3442.

[11] F. Li, Z. Ma, Y.L. Wang, R. Cao, W.H. Bi, X. Li, CrystEngComm. 7 (2005) 569.

[12] (a) H.L. Li, M. Eddaoudi, M. Ókeeffe, O.M. Yaghi, Nature 402 (1999) 276;
(b) M. Eddaoudi, J. Kim, N. Rosi, D. Vodak, J. Wachter, M. Ókeeffe, O.M. Yaghi, Science 295 (2002) 469;
(c) K. Barthelet, J. Marrot, D. Riow, G. Férey, Angew. Chem., Int. Ed. 41 (2002) 281;
(d) S. Kitagawa, R. Kitaura, S. Noro, Angew. Chem., Int. Ed. 43 (2004) 2334.

[13] Z.Y. Fu, X.T. Wu, J.C. Dai, S.M. Hu, W.X. Du, H.H. Zhang, R.Q. Sun, Eur. J. Inorg. Chem. (2002) 2730.

[14] G.M. Sheldrick, SHELXTL 97, Program for the Refinement of Crystal Structures, University of Göttingen, Germany, 1997.

[15] Z.Y. Fu, S.M. Hu, J.C. Dai, J.J. Zhang, X.T. Wu, Eur. J. Inorg. Chem. (2003) 2670.

[16] J. Luo, M. Hong, R. Wang, R. Cao, L. Han, Z. Lin, Eur. J. Inorg. Chem. (2003) 2705.

[17] X.Q. Lu, J.J. Jiang, C.L. Chen, B.S. Kang, C.Y. Su, Inorg. Chem. 44 (2005) 4515.

[18] C.Y. Sun, X.J. Zheng, S. Gao, L.C. Li, L.P. Jin, Eur. J. Inorg. Chem. (2005) 4150.

C–H···Cl hydrogen bonding both in the solid and solution states.

2. Experimental

2.1. Carboxymethyl(ethoxycarbonylmethyl)aminoacetic acid (6)

To a suspension of glycine ethyl ester hydrochloride (9.0 g, 64.5 mmol) and NaI (1.93 g) in CH_3CN (120 mL) was added diisopropylethylamine (35.9 mL, 206 mmol) at room temperature. The mixture was cooled to 0 °C and treated with benzyl bromoacetate (20.5 mL, 129 mmol) dropwise, after which it was warmed to room temperature and stirred for 24 h. The mixture was extracted with ethyl acetate and purified by flash chromatography (gradient elution: 10% EtOAc/hexane, and then 30% EtOAc/hexane) to afford dibenzyl ester **5** (23.3 g, 90%): δ_H (300 MHz; $CDCl_3$; Me_4Si) 7.3 (10H, m), 5.2 (4H, s), 4.2 (2H, q, $J = 7.1$ Hz), 3.8 (4H, s), 3.7 (2H, s), 1.3 (3H, t, $J = 7.1$ Hz); δ_C (75 MHz; $CDCl_3$; Me_4Si) 171.14, 171.05, 136.0, 129.0, 128.7, 66.9, 61.1, 55.6, 14.6; *m/z* 400 (M^+, 15), 326 (33), 308 (75), 264 (100); ν_{max}/cm^{-1} 3064, 2980, 2895, 1747, 1498, 1455, 1262, 1187, 1147. Hydrogenolysis of dibenzyl ester **5** (10% Pd/C, 5 wt%) at room temperature afforded diacid **6** in quantitative yield, after filtration through Celite and concentration in vacuo: m.p. 100–102 °C; δ_H (300 MHz; $CDCl_3$; Me_4Si) 12.4 (2H, br s), 4.1 (2H, q, $J = 7.1$ Hz), 3.6 (2H, s), 3.5 (4H, s), 1.2 (3H, t, $J = 7.1$ Hz); δ_C (75 MHz; $CDCl_3$; Me_4Si) 173.1, 171.5, 60.8, 55.3, 14.9; *m/z* 219 (M^+, 3), 174 (30), 146 (100), 102 (94); *Anal.* Calc. for $C_8H_{13}NO_6$: C, 43.84; H, 5.98; N, 6.39. Found: C, 43.87; H, 5.91; N, 6.00%.

2.2. (S,S)-(Bis[{(1-hydroxymethyl-2-methyl)-propylcarbamoyl}methyl]amino)acetic acid ethyl ester (7)

To a solution of diacid **6** (4.0 g, 18.2 mmol) in THF (150 mL) at −20 °C was added Et_3N (5.3 mL, 38 mmol), followed by $ClCO_2Et$ (1.76 mL, 18.2 mmol) dropwise. The mixture was stirred for 30 min at −20 °C, after which it was warmed to 0 °C and treated with L-valinol (882 mg, 18.2 mmol). The mixture was stirred 45 min at 0 °C, and then it was recooled to −20 °C and treated with $ClCO_2Et$ (1.76 mL, 18.2 mmol). The mixture was stirred for 45 min at −20 °C, and then it was rewarmed to 0 °C and treated with L-valinol (882 mg, 18.2 mmol). The mixture was stirred for 1 h at 0 °C, and then it was treated with water and extracted with ethyl acetate. The combined extracts were dried and evaporated under reduced pressure to leave an oil, which was purified by column chromatography on silica using 5% MeOH in ethyl acetate as eluent to give diamide **7** (5.3 g, 74%): $[\alpha]_D^{23}$ − 9.0 (*c* 0.8 in $CHCl_3$); δ_H (300 MHz; $CDCl_3$; Me_4Si) 7.6 (2H, d, $J = 9.2$ Hz, N*H*), 4.2 (3H, q, $J = 7.1$ Hz), 4.16 (1H, br s), 3.5–3.8 (4H, m), 3.4 (2H, s), 2.9 (1H, br s), 1.8–1.9 (2H, m), 1.3 (3H, t, $J = 7.1$ Hz), 0.94 (6H, d, $J = 7.3$ Hz), 0.92 (6H, d, $J = 7.3$ Hz); δ_C (75 MHz; $CDCl_3$; Me_4Si) 172.13, 172.06, 63.5, 61.7, 59.5, 57.6, 57.2, 29.9, 20.1, 19.6, 14.8; ν_{max}/cm^{-1} 3408, 2962, 1734, 1647, 1541, 1207, 1156, 1025.

2.3. (S,S)-[Bis{(4-isopropyl-4,5-dihydrooxazol-2-yl)-methyl}amino]acetic acid ethyl ester (11)

To a solution of diamide **7** (5.3 g, 13.5 mmol) in CH_2Cl_2 (45 mL) was added DMAP (160 mg, 1.3 mmol), followed by mesyl chloride (2.2 mL, 28 mmol). The mixture was cooled to 0 °C and treated with Et_3N (8.0 mL, 57 mmol), after which it was warmed to room temperature and further stirred for 20 h. The mixture was treated with aqueous NH_4Cl and extracted with CH_2Cl_2. The combined extracts were dried and evaporated under reduced pressure to leave an oil, which was purified by column chromatography on silica (gradient elution: EtOAc followed by 10% MeOH in EtOAc) to give bis(oxazoline) **11** (4.2 g, 88%): δ_H (300 MHz; $CDCl_3$; Me_4Si) 4.2–4.3 (2H, m), 4.16 (2H, m), 3.8–4.0 (4H, m), 3.7 (4H, s), 3.6 (2H, s), 1.6–1.8 (2H, m), 1.2 (3H, t, $J = 7.1$ Hz), 1.0 (6H, d, $J = 6.8$ Hz), 0.9 (6H, d, $J = 6.8$ Hz); δ_C (75 MHz; $CDCl_3$; Me_4Si) 171.1, 164.3, 72.5, 70.5, 60.9, 55.1, 51.1, 50.3, 32.9, 19.3, 18.6, 14.6; *m/z* 353 (M^+, 9), 227 (50), 181 (24), 153 (71), 127 (100); ν_{max}/cm^{-1} 2961, 1738, 1662, 1531, 1467, 1388, 1199, 1155, 1028.

2.4. (S,S)-[Bis{(4-isopropyl-4,5-dihydrooxazol-2-yl)-methyl}amino]acetic acid sodium salt (1)

A solution of bis(oxazoline) **11** (1.5 g, 4.2 mmol) in THF–water (3:1, 15 mL) at room temperature was treated with NaOH (210 mg) for 1 h, which resulted in the complete hydrolysis of the ester group. The mixture was concentrated under reduced pressure, after which it was redissolved in CH_2Cl_2 and filtered through a short pad of Celite to remove NaCl. The filtered solution was concentrated under reduced pressure to give sodium carboxylate **1** as an white powder in a quantitative yield, and it can be further purified by recrystallization from CH_2Cl_2/EtOAc/Et_2O: $[\alpha]_D^{28}$ − 56 (*c* 1.0 in $CHCl_3$); δ_H (300 MHz; $CDCl_3$; Me_4Si) 4.4 (2H, m, Ox-CH_2), 4.1 (2H, m, Ox–CH_2), 4.0 (2H, m, Ox–C*H*), 3.5 (4H, N–CH_2–Ox), 3.3 (2H, s, N–CH_2–CO_2Na), 1.7 (2H, m, ^{i}Pr–C*H*), 0.9 (12H, m); δ_C (75 MHz; $CDCl_3$; Me_4Si) 178.2, 166.2, 71.1, 71.0, 58.0, 50.7, 32.0, 17.93, 17.88; *m/z* 390 (M+Na^+, 100), 348 (M+H^+, 44); *Anal.* Calc. for $C_{16}H_{26}N_3O_4Na$: C, 55.32; H, 7.54; N, 12.10. Found: C, 55.16; H, 7.50; N, 11.94%.

2.5. Zn(II) complex 12

A solution of flamed-dried $ZnCl_2$ (40 mg, 0.29 mmol) in THF (1.0 mL) was added to a suspension of sodium carboxylate **1** (102 mg, 0.29 mmol) in THF (2.0 mL) through a cannula at room temperature. The mixture was stirred for 24 h, and then it was filtered through a short pad of

Celite to give a white solid. This solid was dissolved in CH_2Cl_2 and filtered through Celite again to remove NaCl, and the filtered solution was concentrated under reduced pressure to give **12** as a white solid in quantitative yield. The crude product can be purified by recrystallization from diethyl ether–chloroform: $[\alpha]_D^{20}$ +91 (*c* 0.9 in CH_2Cl_2); δ_H (300 MHz; $CDCl_3$; Me_4Si) 4.8 (1H, m), 4.3–4.6 (5H, m), 3.7–4.1 (4H, m), 3.3 (1H, d, $J = 17$ Hz), 3.1 (1H, d, $J = 17$ Hz), 2.5 (2H, m, ^{i}Pr–C*H*), 0.9 (6H, d, $J = 7.0$ Hz), 0.7–0.8 (6H, m); δ_C (75 MHz; $CDCl_3$; Me_4Si) 174.7, 173.9, 173.5, 73.7, 73.4, 67.7, 67.4, 61.9, 54.5, 54.3, 30.4, 19.2, 15.7.

2.6. Crystal structure determination of complex *12*

Single crystals suitable for X-ray diffraction study were grown by slow diffusion of diethyl ether into a solution of **12** in chloroform.

2.7. Crystal data

$C_{17}H_{27}C_{14}N_3O_4Zn$, $M = 544.59$, monoclinic, $a = 6.4791(2)$, $b = 18.1976(4)$, $c = 10.2735(3)$ Å, $T = 223(2)$ K, space group $P2_1$, $Z = 2$, μ (Mo Kα) = 1.509 mm^{-1}, 4829 reflections measured, 2640 unique ($R_{int} = 0.0371$). The final $wR(F_2)$ was 0.0942 (all data).

3. Results and discussion

3.1. Synthesis of the ligand *1*

As a part of our program toward the synthesis of several N_3O-type chelates and their metal complexes, we designed bis(oxazoline)-based, C_2 symmetric carboxylate **1** as a N_3O type chelate. The carboxylate group in **1** can act as O-ligand, and such an N_3O-chelate may be useful for the synthesis of novel metal complexes for further applications [7]. The symmetric nature of the ligand **1** together with the carboxylate donor may be useful for the synthesis of structurally simple, homochiral metal complexes, compared to a linear N_4 type of ligand **2** [5,6].

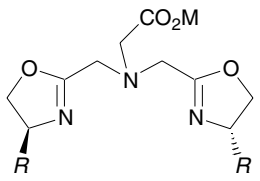

1 (M = Na; R = *i*-Pr)

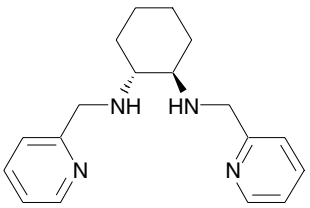

2

The synthesis of bis(oxazoline)-*N*-carboxylate **1** was started with glycine methyl ester (**3**). Our initial attempt at the di-alkylation of glycine methyl ester with benzyl bromoacetate in the presence of K_2CO_3 in DMF at room temperature, however, gave a cyclic compound **4** as the major product, through dimerization of a mono-substituted intermediate. However, by changing the base to triethylamine and the solvent to acetonitrile, we were able to get the desired product **5** in rather low yields (30–50%). Furthermore, by using a bulky base, diisopropylethylamine, we could dramatically increase the yield (90–95%). Then, hydrogenolysis of benzyl ester **5** provided diacid **6** in 97% yield. Next, an attempt to couple diacid **6** with L-valinol using DCC (*N*,*N*-dicyclohexylcarbodiimide) did not proceed at all. Therefore, the coupling method was changed to a mixed anhydride method, $ClCO_2Et$–Et_3N. Thus, treatment of diacid **6** with 2.0 molar equivalents of valinol under the mixed anhydride conditions (one-step coupling), however, gave diamide **7** in moderate yields (30–50%). There was little improvement in the coupling yield when *t*-butyl chloroformate was used instead of ethyl chloroformate. Also, this one-step coupling showed a problem in its reproducibility. We found that an ethyl carbamate of valinol (**8**) was a major side product along with monoamide **10**, which can be probably explained by the formation of anhydride **9** (Scheme 1).

To overcome this problem, we carried out the amide formation in a stepwise manner. Thus, diacid **6** was treated with an equimolar amount of ethyl chloroformate in the presence of triethylamine at −20 °C, and then an equimolar amount of valinol was added at 0 °C to generate a mono-amide intermediate **10**. This mono-amide **10** was treated in situ again with an equimolar amount of ethyl chloroformate at −20 °C, and then an equimolar amount of valinol was added at 0 °C. This stepwise procedure greatly reduced the side product **8** and afforded diamide **7** in 74% yield. Finally, mesylation of the hydroxyl groups in **7**, and then a prolonged treatment of the resulting mesylate with triethylamine afforded bis(oxazoline)-ethyl ester **11** in 90% isolated yield. Hydrolysis of the ester with an aqueous NaOH in THF gave the desired N_3O chelate **1** in a quantitative yield (Scheme 2). Acidification of this sodium salt gave the corresponding acid, which is soluble in water and thus cannot be extracted with an organic solvent. Fortunately, the sodium salt **1**, obtained by condensation of water in vacuo, was soluble in CH_2Cl_2 and thus the remaining NaOH can be removed by simple filtration. An analytically pure sample could be obtained by recrystallization from CH_2Cl_2/EtOAc/Et_2O.

3.2. Zinc complex formation from the N_3O chelate *1*

The C_2 symmetric, carboxylate-containing N_3O ligand **1** may be potentially useful for the synthesis of various metal complexes. Among possible metal complexes, we synthesized the corresponding Zn(II) complex, keeping in mind that some oxazoline-based Zn(II) complexes are known [19]. Treatment of the N_3O chelate **1** with dry $ZnCl_2$ in THF at room temperature overnight afforded the corresponding Zn(II) complex **12** as a white solid, which was

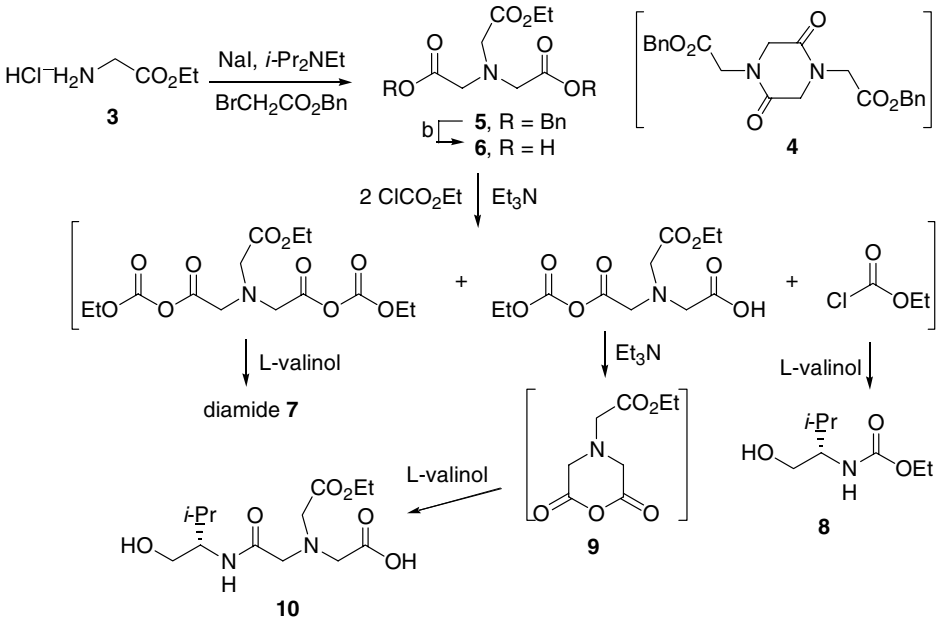

Scheme 1. Plausible reaction pathways in the one-step coupling route.

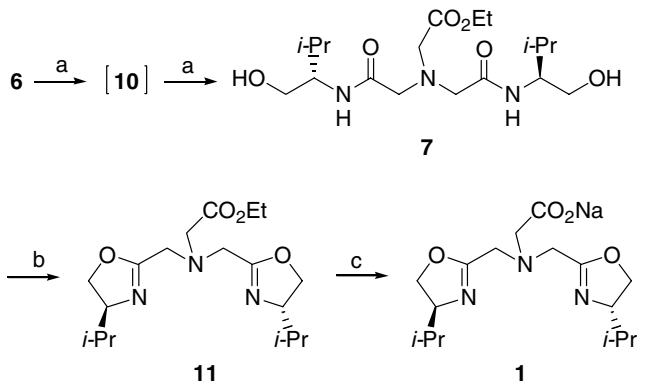

Scheme 2. Synthesis of sodium bis(oxazoline)-N-carboxylate **1** through a stepwise route: (a) $ClCO_2Et$, Et_3N, THF; (b) MsCl, Et_3N, cat. DMAP, CH_2Cl_2; (c) NaOH, THF-H_2O (3:1).

purified by recrystallization from $CHCl_3/Et_2O$. The formation of the Zn(II) complex **12** was supported by ^1H NMR analysis in comparison with the sodium salt **1**. The sodium carboxylate **1** showed a splitting pattern expected for a symmetric structure, exhibiting total seven groups of proton peaks. Whereas, its Zn(II) complex **12** exhibited a more split pattern with significant downfield shifts for most of the protons (Fig. 2). These results indicate that, in the case of the Zn(II) complex, the two oxazolines bind to the metal but do not or very weakly bind in the case of the sodium salt. Also, the ^{13}C NMR spectrum of sodium salt **1** exhibited nine carbon peaks, including three peaks for the isopropyl groups, of which methyl groups appeared as narrowly separated, two peaks ($\Delta\delta = 0.5$ ppm). Whereas, its Zn(II) complex showed 13 carbon peaks, including three peaks for the isopropyl groups, of which methyl groups appeared as widely separated, two peaks ($\Delta\delta = 3.5$ ppm). Thus, the Zn(II) complex is no longer C_2- or pseudo-C_2-symmetric, being judged from the splitting pattern of its ^1H and ^{13}C NMR spectra. These NMR data suggest a chelated structure in the case of the Zn(II) complex, depicted as **12**. Of particular note is that the methine proton of the isopropyl group shows an unusual downfield shift ($\Delta\delta = 0.7$ ppm) and appears at 2.5 ppm, compared to the sodium carboxylate **1**. Such a large downfield shift of the CH protons is not likely due to an inductive effect from the rather remote Zn(II) metal coordinated to the oxazoline nitrogens. Also, steric congestion around the methine proton, without evoking C–H···Cl–Zn hydrogen bonding, cannot rationalize the large downfield shift, because an upfield shift should be observed in the case of steric congestion. Under such a hydrogen bonding, the isopropyl methyl groups would also appear as widely separated peaks due to the conformational restriction, as indeed observed. A CPK model of the Zn(II) complex suggested that both the isopropyl CH hydrogens have van der Waals contacts with the chloride atom bound to the Zn(II) (Fig. 1). Although C–H···Cl hydrogen bonding has been suggested from X-ray crystal structures of many complexes, its existence in solution has been known very recently. Recently, Rivas et al. reported a Zn(II) complex of a tripodal N_4 ligand, in which a downfield shift of a CH proton ($\Delta\delta = 0.11$ ppm) near Zn–Cl was observed due to similar C–H···Cl–Zn hydrogen bonding [18]. Together with this precedent, our Zn(II) complex provides an additional example of the C–H···Cl–M hydrogen bonding in solution.

3.3. Crystal structure of **12** · ($CHCl_3$)

Single crystals of the complex **12** was obtained as a colorless plate form by the diffusion of ethyl ether into a solution of Zn(II) complex **12** in chloroform. From X-ray crystallographic analysis, Zn(II) complex **12** was found to

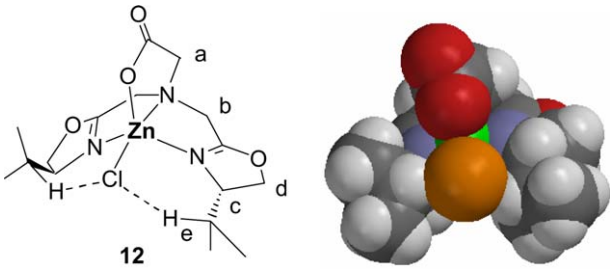

Fig. 1. A hydrogen bonded structure of Zn(II) complex **12** and its CPK model.

exist as a chiral monoclinic unit cell with space group $P2_1$ ($a = 6.480$, $b = 18.200$, $c = 10.274$ Å, $\beta = 100.943°$), wherein the bis(oxazoline)-*N*-carboxylate was chelated to the zinc atom in a tripodal fashion (see Fig. 3).

The zinc atom is trigonal bipyramidaly surrounded by two oxazoline nitrogen atoms (N2, N3) and one oxygen atom (O4) from the carboxylate in equatorial position, and central tertiary nitrogen (N1) and the chloride atom in the axial position. The triangle plane defined by N2, N3, O4, and central Zn atoms is slightly deviated from the flat plane, showing average in-plane bond angles of

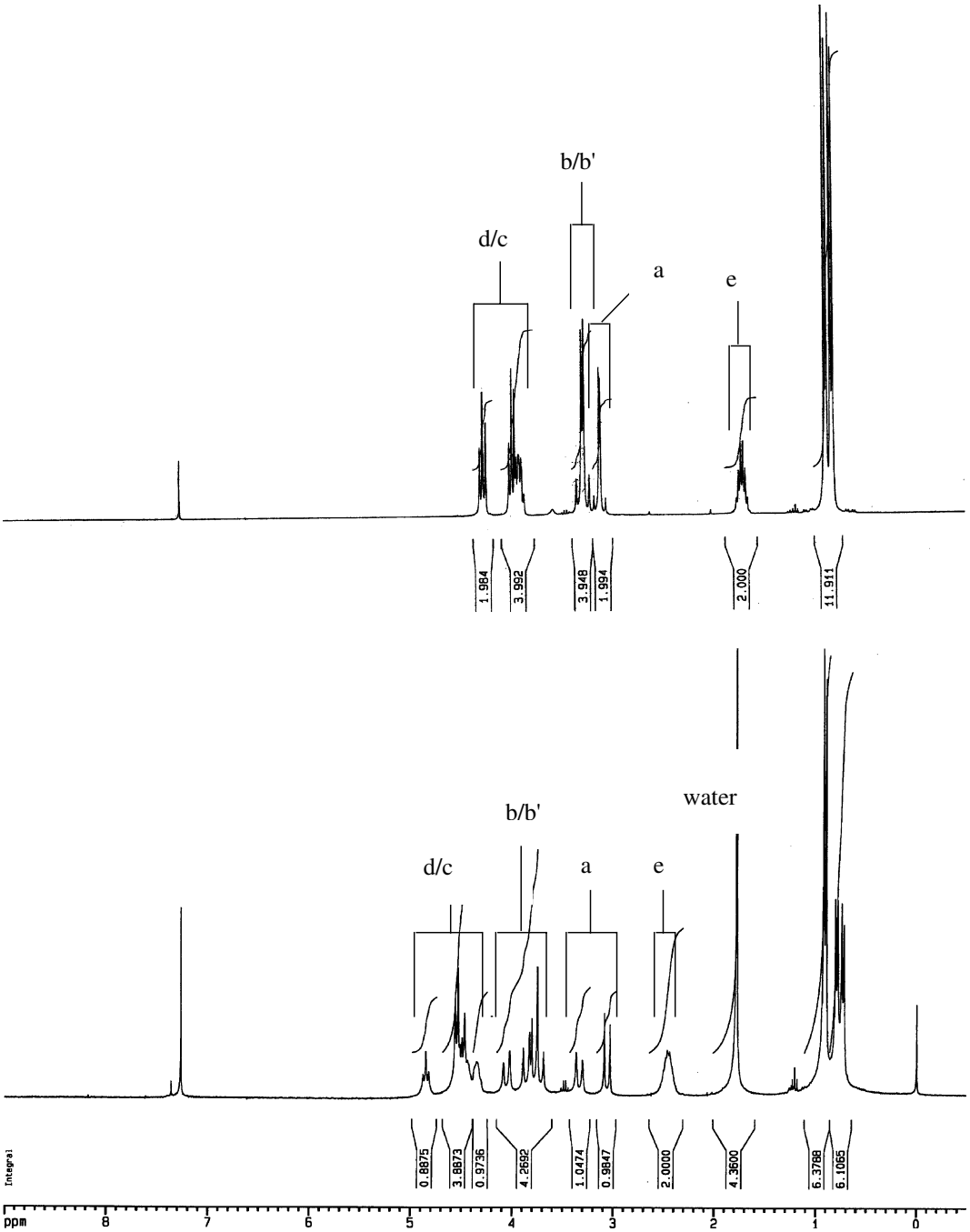

Fig. 2. NMR spectra of sodium carboxylate **1** (upper) and Zn(II) complex **12** (lower).

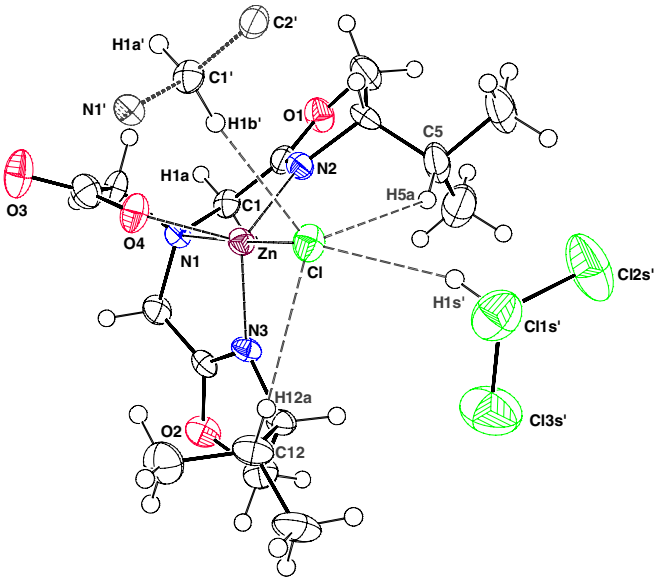

Fig. 3. Hydrogen bonding interactions surrounding the chloride in **12** · ($CHCl_3$) with displacement ellipsoids at the 50% probability level.

Table 1
Selected bond lengths and angles around the Zn in **12**

Bond lengths		Bond angles	
Zn–Cl	2.3026(18)	Cl–Zn–N(1)	177.61(15)
Zn–N(1)	2.386(5)	Cl–Zn–N(2)	103.00(15)
Zn–N(2)	2.057(5)	Cl–Zn–N(3)	105.40(16)
Zn–N(3)	2.041(5)	Cl–Zn–O(4)	102.29(14)
Zn–O(4)	1.993(4)	Zn–N(1)–C(1)	107.6(4)
		Zn–N(1)–C(8)	105.1(4)
		Zn–N(1)–C(15)	102.2(4)

115° (Table 1). The coordination distances involving the zinc atom are also given in Table 1.

Three types of hydrogen bonding interactions were observed in the lattice structure involving the C–H···Cl–Zn hydrogen bonding. One type is between the chloride atom and a few protons of the bis(oxazoline)-*N*-carboxylate ligand; and another is between the chloride and the proton of solvent chloroform, which are strong and asymmetric with the shortest intra- and inter-molecular hydrogen distances: Cl···H(5a), 2.911 Å; Cl···H(12a), 2.850 Å; Cl···H(1b′), 2.560 Å; Cl···H(1s′), 2.489 Å (Fig. 3). The bond lengths and angles related to the C–H···Cl hydrogen bonding conform to the distance and angle criteria proposed by Aakeröy et al. [10]. The other type is the intermolecular hydrogen bonding interactions between oxygen atoms of the carboxylate and H(1b) and H(8a) with O···H distances of 2.2–3.0 Å (Table 2). This intermolecular hydrogen bonding interactions are mainly contributed to an evolution of unique framework. The unique binding mode ultimately yields microchannels in the *a*-axis direction, encapsulating a linear array of chloroform molecules (Fig. 4).

Table 2
Structure data of hydrogen bonding interactions in **12** · ($CHCl_3$)

Interaction	C–H (Å)[a]	C···A (Å)	H···A (Å)	∠(C–H···A) (°)
[b]C1–H1b···Cl	0.980	3.493	2.560	159.08
C12–H12a···Cl	0.990	3.721	2.853	146.79
C5–H5ab···Cl	0.990	3.740	2.909	142.04
[c]C1s–H1s···Cl	0.990	3.385	2.491	150.08
[d]C10–H10b···O3	0.98	3.600	2.705	151.98
[d]C14–H14a···O3	0.97	3.904	2.935	176.70
[d]C3–H3b···O3	0.98	3.544	2.692	145.52
[d]C7–H7c···O3	0.97	3.483	2.515	174.98
[b]C1–H1b···O4	0.98	3.479	2.862	121.78
[b]C8–H8a···O4	0.98	3.860	2.277	170.72

Symmetry operation: [b]$x+1, y, z$; [c]$2-x, 0.5+y, 1-z$; [d]$x, y, 1-z$.
[a] Fixed distance and calculated position.

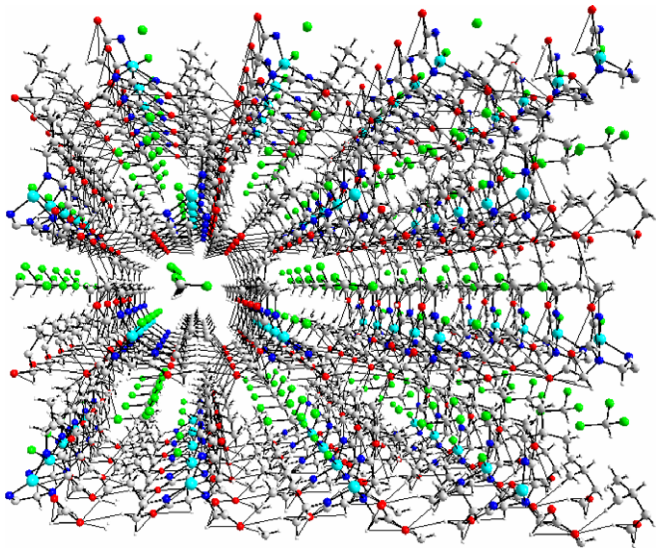

Fig. 4. A perspective view of the *bc*-plane showing the 3D-network structure by the intermolecular hydrogen bonding interactions with the carboxylate oxygen atoms, showing a porous structure along the *a*-axis: Zn, sky; Cl, green; O, red; N, blue; C, grey. (For interpretation of the references to colour in this figure legend, the reader is referred to the web version of this article.)

4. Conclusion

We have established an efficient route to a novel N_3O type chelate **1**. A key step of the synthesis involved a stepwise diamide formation, through which a detrimental side reaction was suppressed. A Zn(II) complex was formed from the N_3O ligand, which suggests C–H···Cl–Zn hydrogen bonding both in solid and solution states. This result provides a rare example of the C–H···Cl hydrogen bonding in solution. The X-ray crystal structure of the Zn(II) complex also shows unique microchannels, encapsulating a linear array of chloroform molecules.

Acknowledgments

This work was supported by Korea Research Foundation Grant (KRF-2001-C060400-DP0332) and Center for

Integrated Molecular Systems. K.H.A. thanks Dr. R. Ramesh for helpful discussion.

Appendix A. Supplementary data

CCDC 287963 contains the supplementary crystallographic data for the structure reported in this paper, which can be obtained free of charge from the Cambridge Crystallographic Data Centre via www.ccdc.cam.ac.uk/data_request/cif. Supplementary data associated with this article can be found, in the online version, at doi:10.1016/j.poly.2006.05.011.

References

[1] E.N. Jacobson, A. Pfaltz, H. Yamamoto (Eds.), Comprehensive Asymmetric Catalysis I–III, Spring-Verlag, Berlin, 1999.
[2] For a recent special issue on applications of catalysis in academia and industry, see: Tetrahedron 61 (2005) 6169.
[3] J. Seyden-Penne, Chiral Auxiliaries and Ligands in Asymmetric Synthesis, Wiley, New York, 1995.
[4] For a review on nitrogen-containing ligands in asymmetric catalysis, see F. Fache, E. Schulz, M.L. Tommasino, Chem. Rev. 100 (2000) 2159.
[5] R.R. Fenton, F.S. Stephens, R.S. Vagg, P.A. Williams, Inorg. Chim. Acta 236 (1995) 109.
[6] J.R. Aldrich-Wright, R.S. Vagg, P.A. Williams, Coord. Chem. Rev. 166 (1997) 361.
[7] U. Knof, A. von Zelewsky, Angew. Chem., Int. Ed. 38 (1999) 302.
[8] J. Chin, S.S. Lee, K.J. Lee, S. Park, D.H. Kim, Nature 401 (1999) 254.
[9] For a review on coordination chemistry of oxazoline ligands, see M. Gómez, G. Muller, M. Rocamora, Coord. Chem. Rev. 193–195 (1999) 769.
[10] C.B. Aakeröy, T.A. Evans, K.R. Seddon, I. Pálinkó, New J. Chem. (1999) 145–152.
[11] P.K. Thallapally, A. Nangia, CrystEngComm. 27 (2001) 1.
[12] G. Aullón, D. Bellamy, L. Brammer, E.A. Bruton, A.G. Orpen, Chem. Commun. (1998) 653.
[13] R. Taylor, O. Kennard, J. Am. Chem. Soc. 104 (1982) 5063.
[14] T. Spaniel, H. Görls, J. Scholz, Angew. Chem., Int. Ed. 37 (1998) 1862.
[15] M. Freytag, P.G. Jones, Chem. Commun. (2000) 277.
[16] P.G. Jones, B. Ahrens, Chem. Commun. (1998) 2307.
[17] D. Braga, S.M. Draper, E. Champeil, F. Grepioni, J. Organomet. Chem. 573 (1997) 73.
[18] J.C.M. Rivas, R.T.M. de Rosales, S. Parsons, Dalton Trans. (2003) 2156.
[19] C. Bolm, K. Weickhardt, M. Zehnder, T. Ranff, Chem. Ber. 124 (1991) 1173.

with solid-state oxide gas-sensors. Typically solid-state oxide gas-sensors are made by screen-printing and tend to be very porous.

Here we report the first instance of an antimony oxide film being made using APCVD and the first investigation of the gas sensing properties of such a film. Indeed we show that thin film CVD prepared antimony oxide can be a useful gas sensing material for reducing gases such as ethanol.

2. Experimental

Nitrogen (99.99%) was obtained from the British Oxygen Company (BOC) and used as supplied. Coatings were obtained on SiO_2 coated float glass. APCVD experiments were conducted on 150 mm × 45 mm × 3 mm pieces of glass using a flat-bed cold-walled APCVD reactor. The glass was cleaned prior to use by washing with petroleum ether (60–80 °C) and isopropanol and then dried in air. A graphite block containing a Whatman cartridge heater was used to heat the glass substrate. The temperature of the substrate was monitored by a Pt–Rh thermocouple. Independent thermocouple measurements indicated that temperature gradients of up to 50 °C cm^{-1} were observable at 600 °C across the surface of the glass. The rig was designed so that four independent gas lines could be used. All gas handling lines, regulators and flow valves were made of stainless steel and were 6.5 mm internal diameter except for the inlet to the mixing chamber and the exhaust line from the apparatus that were 13 mm in diameter. In these experiments three gas lines were used. Gases came directly from a cylinder and were preheated by passing along 2 m lengths of stainless steel tubing, which were curled and inserted inside a tube furnace. The temperatures of all the gas inlet lines were monitored by Pt–Rh thermocouples and Eurotherm heat controllers.

Antimony (V) chloride (99.99%) was obtained from Aldrich and used without further purification and was placed into a stainless steel bubbler. The bubbler was heated to 120 °C by a heating jacket and $SbCl_5$ introduced into the gas streams by passing hot nitrogen gas through the liquid. Anhydrous methanol was purchased from Aldrich and used without further treatment. This was preferred over water as the later gives rise to powdery films. The two components of the system were mixed by the use of two concentric pipes of 6.5 and 13 mm diameter, respectively, the inner pipe being 3 cm shorter than the outer pipe. The concentric pipes were attached directly to the mixing chamber of the coater. Gas flows were adjusted using suitable regulators and flow controllers. The exhaust from the reactor was vented directly into the extraction system of a fume cupboard. All of the apparatus was baked out with nitrogen at 150 °C for 30 min before use. Deposition experiments were conducted by heating the horizontal-bed reactor and the bubblers to the desired temperatures before diverting the nitrogen line through the bubbler and hence to the reactor. Deposition experiments were timed by use of a stopwatch and were conducted typically for 1 min. The maximum possible deposition temperature with this equipment was 600 °C. At the end of the deposition only nitrogen was allowed to flow over the glass substrate until the substrate was sufficiently cool to handle (~60 °C). Samples were handled and stored in air. Additional runs were conducted using iron, copper and silicon wafer substrates and subjected to the same analysis. Deposition temperatures varied from 350 to 600 °C. Nitrogen flow rates were varied between 0.3 and 1.0 L min^{-1}.

X-ray photoelectron spectra were recorded with a VG ESCALAB 220I XL instrument using a focused (300 μm spot) monochromatic Al Kα radiation at a pass energy of 20 eV. Scans were acquired with steps of 50 meV. A flood gun was used to control charging and the binding energies were referenced to an adventitious C 1s peak at 284.6 eV. Depth profiling measurements were obtained by using argon beam sputtering. Electron microprobe analysis was obtained on a JEOL EMA and referenced against gallium and oxygen standards. EDXA was conducted using a JEOL 35-CF instrument. SEM images were acquired on a Hitachi S570 instrument. X-ray powder diffraction patterns were measured on a Siemens D5000 diffractometer using filtered (Cu Kα1, $\lambda = 1.5406$ Å) radiation in the reflection mode using glancing angle incidence (1.5°). Reflectance and transmission spectra were recorded between 300 and 1150 nm on a Zeiss miniature spectrometer. Measurements were standardised relative to a rhodium mirror (reflectance) and air (transmission). UV–Vis spectra were obtained using a Helios double beam instrument. Raman spectra were acquired on a Renishaw Raman system 1000 using a helium–neon laser of wavelength 632.8 nm. The Raman system was calibrated against the emission lines of neon. Electrical properties were determined by using a 4-probe device. Contact angle experiments were determined by measuring the spread of a 1 μl droplet of water on the film surface, and applying a simple trigonometric program.

For gas response, films were deposited onto commercially produced sensor substrates. The sensors consist of a gold track printed on the top of an alumina tile and a platinum heater track printed on the reverse side of the tile. Gold electrodes were formed by laser trimming to produce an interdigitised section with gap and finger widths of 50 μm. Contacts to the devices were formed by spot welding 50 μm diameter platinum wire to pads of the track material in the corner of the sensor chip. The sensor heater was kept at constant resistance and hence constant temperature by incorporating it into a Wheatstone bridge. Electrical experiments were formed on a locally constructed test rig [22]. Test gasses were diluted from cylinders of synthetic air (79% nitrogen, 21% oxygen) containing ethanol (100 ppm). The devices were investigated over a variety of temperatures between 400 and 600 °C.

3. Results

3.1. Synthesis and characterisation

Atmospheric pressure chemical vapour deposition reaction of antimony (III) chloride and ethyl acetate led to the creation of antimony (III) oxide thin films on glass and gas sensor substrates. The process was studied across a range of different substrate temperatures and flow conditions (Table 1).

Films would not grow at substrate temperatures lower than 550 °C and uniform films were obtained at 600 °C. In all cases films appeared transparent, unreflective and colourless. Some birefringence was observed at the edges of the films – this indicates a slight variation in thickness. The films all passed the Scotch tape test and were resistant to marking by a wet towel or a brass stylus, but could be marked by a steel scalpel. None of the films showed any change in their appearance on storage in air for six months.

Compositional analysis was determined by electron probe microanalysis (EPMA) and energy dispersive X-ray analysis (EDXA) and indicated that the films had single composition Sb_2O_3. With EDXA some breakthrough to the underlying glass substrate was seen. This was corrected for based on a sample of the pure substrate. The EDXA results showed that the films were free from contaminants such as chlorine and carbon. A film thickness of 500 nm (±100 nm) was estimated based on EDXA breakthrough to the underlying substrate for a sample prepared at 600 °C for 1 min giving a nominal growth rate of 500 nm min^{-1}. Samples prepared at lower deposition temperatures had film thickness in the region of 300–500 nm.

Scanning electron microscopy analysis of the films (Fig. 1) indicated, that in all cases, deposition occurred through an island growth mechanism. Antimony oxide consisted of grains of material forming a coherent coating across the surface of the substrate. There was no change or even variation of film morphology with differing substrate.

The films were investigated using Raman microscopy however, no Raman pattern was observed, it is thought antimony (III) oxide is a poor Raman scatterer, however this could be due to thickness effects. Raman microscopy did however; indicate the absence of impurities such as graphitic carbon.

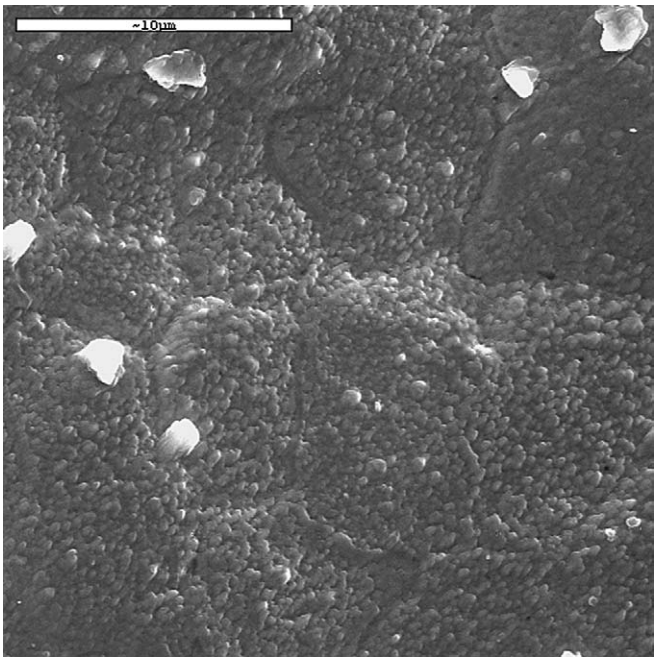

Fig. 1. A typical SEM picture for an antimony oxide sample produced by APCVD from antimony (V) chloride and ethyl acetate with a reactor temperature of 600 °C. Scale bar is 10 μm.

X-ray photoelectron spectroscopy of an Sb_2O_3 sample (Fig. 2) revealed binding energy shifts of 20.6 eV for O 2s and 35.4 eV for Sb 4d, respectively. The O 2s peak was investigated rather than the O 1s as this peak was obscured by the antimony Sb 3d5/2 peak. The XPS peak profiles are consistent with a single environment for antimony and oxygen. The binding energy shifts are in agreement with previous literature values [23].

The optical properties of the films were investigated using reflectance, transmission and UV–Vis measurements between 400 and 1100 nm. All samples showed a slight shift in the adsorption edge towards the visible relative to a plain glass substrate. The films displayed minimal reflectivity (5–15%) and high transmission (60–80%). All of the films were shown to have contact angles for water droplets in the

Table 1
Table of reaction conditions and micro-analytical results for the antimony oxide films formed from APCVD of $SbCl_5$ and ethylacetate

Substrate temperature (°C)	Nitrogen flow through SbX_5 bubbler l/min (bubbler set at 120 °C)	Nitrogen flow through ethyl acetate bubbler l/min (precursor) (bubbler set at 45 °C)	Nitrogen flow of make up gas l/min	EDAX and electron probe analysis of resultant film
550	0.5	0.5	1.0	Sb_2O_3
600	0.5	0.5	1.0	Sb_2O_3
600	0.5	0.3	1.0	No film
600	0.5	0.7	1.0	Sb_2O_3
600	0.7	0.5	1.0	No film
600	0.3	0.5	1.0	Sb_2O_3
600	0.7	0.3	1.0	No film
600	0.3	0.7	1.0	Sb_2O_3
600	0.5	0.5	1.5	Sb_2O_3

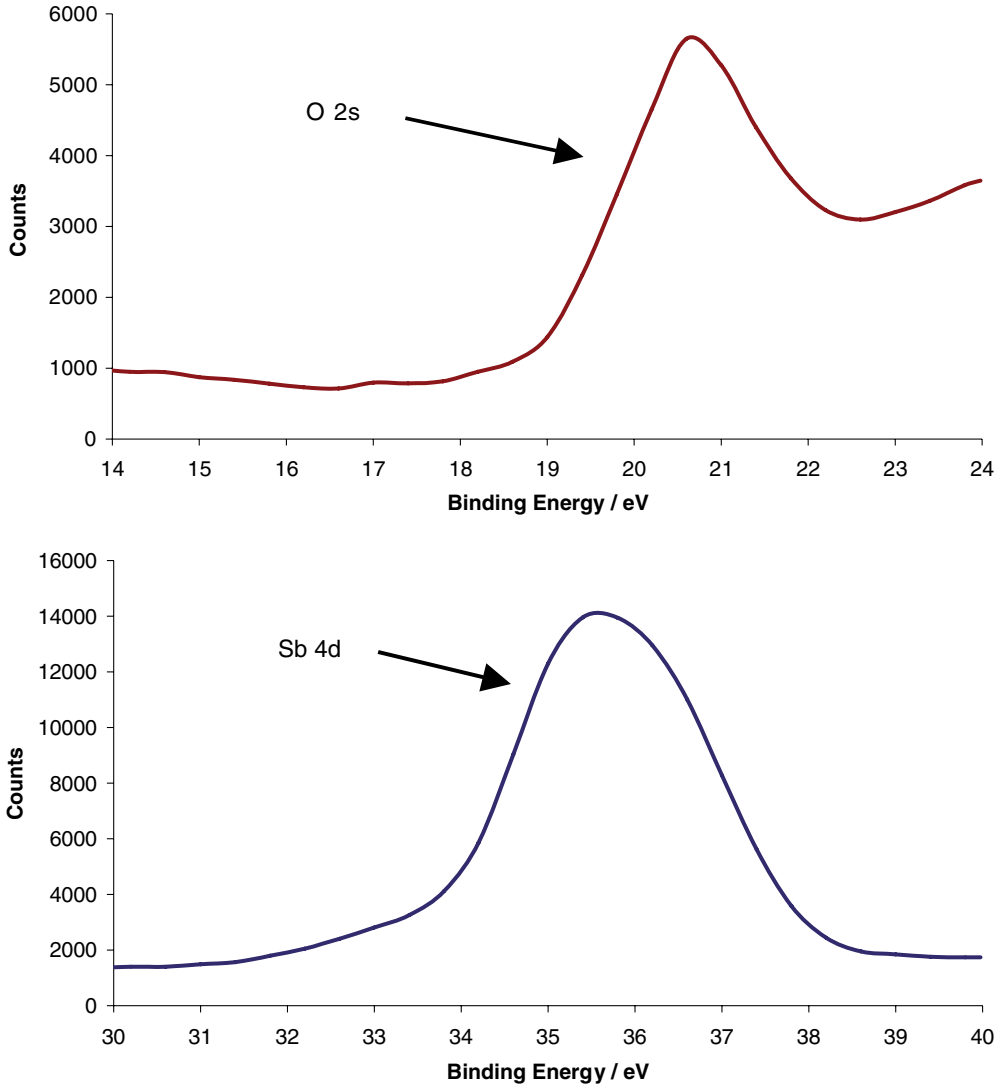

Fig. 2. XPS peaks produced from a sample of antimony oxide.

region of 65–85°, this is similar to that of plain glass 60–75°. Sheet resistance measurements using a four-point probe indicated that the antimony (III) oxide samples are insulators at room temperature.

3.2. Gas sensing properties

Gas response was measured as the ratio between R (the resistance when exposed to ethanol) and R_0 (the resistance at the point immediately preceding the introduction of ethanol). The resistance was measured between the two electrodes of an interdigitized gold electrode structure on an alumina tile. All samples were tested across a range of operation temperatures; from 400 to 600 °C, for their response to ethanol gas at concentrations ranging from 1 to 100 ppm. Additionally the sensors were evaluated for their response in dry air and humid air (50% humidity).

The antimony oxide sensors showed an n-type response to ethanol gas at a variety of operating temperatures. A typical example is indicated in Fig. 3.

In all cases response increased with ethanol concentration. The response is initially fast but tails off as a near plateau is reached after approximately 5 min. Once ethanol flow is stopped the response rapidly falls to near baseline levels then tails off more slowly. There is minimal baseline drift throughout the course of the experiment. The greatest response (R/R_0) was 1.47–100 ppm ethanol gas at an operating temperature of 400 °C (Table 2).

The gas response of the CVD produced antimony oxide sensor in the presence of 50% humidity was also evaluated (Fig. 4).

Addition of humidity into the chamber seems to have little effect on the resistance baseline, which is relatively flat. The magnitude of the resistance response is similar in dry and humid air.

4. Discussion

Reaction of antimony (V) chloride with ethyl acetate under APCVD conditions affords transparent films of

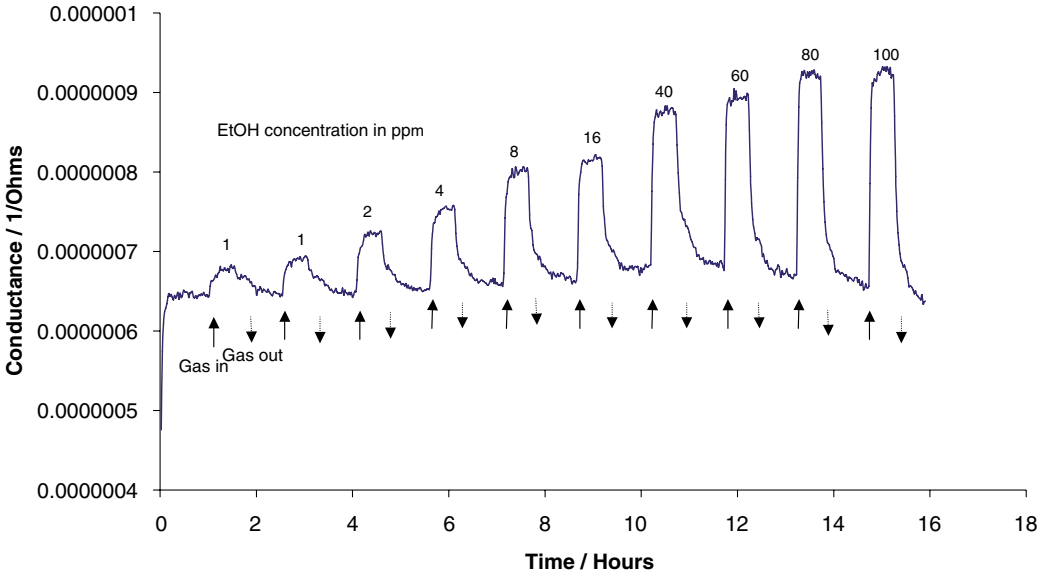

Fig. 3. The gas response of a CVD prepared antimony oxide sensor to varying concentrations of ethanol at an operational temperature of 400 °C.

Table 2
Gas-sensing response of antimony oxide sensors to various concentrations of ethanol gas

Ethanol concentration in ppm	Operating temperature 400 °C R/R_0	Operating temperature 450 °C R/R_0	Operating temperature 500 °C R/R_0	Operating temperature 550 °C R/R_0	Operating temperature 600 °C R/R_0
1	1.13	1.07	1.04	1.06	1.01
2	1.14	1.12	1.05	1.12	1.02
4	1.22	1.16	1.09	1.16	1.02
8	1.31	1.21	1.14	1.21	1.06
16	1.30	1.36	1.14	1.37	1.05
40	1.41	1.27	1.16	1.28	1.07
60	1.41	1.31	1.19	1.31	1.06
80	1.47	1.38	1.20	1.38	1.08
100	1.47	1.40	1.24	1.40	1.10

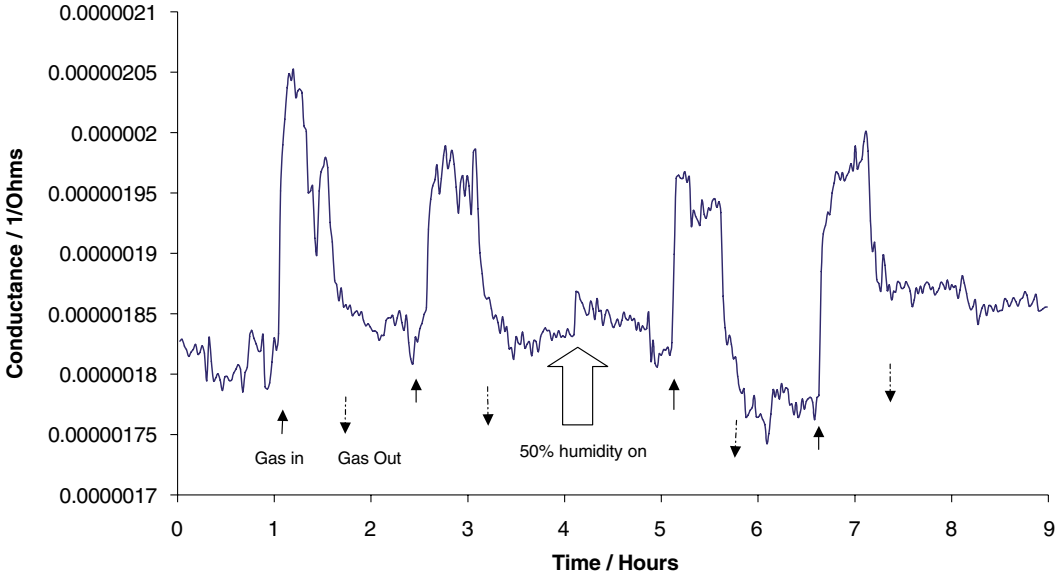

Fig. 4. The gas response of a CVD prepared antimony oxide sensor to 100 ppm ethanol at an operational temperature of 400 °C under dry and wet conditions.

antimony (III) oxide on glass or gas sensor substrates. The films show good surface coverage, adhesion and uniformity. Oxide films of a single phase were obtained. These were colourless in appearance and were electrical insulators at room temperature.

Faster film growth rates were observed with an increase in substrate temperature, indicating that the reaction is surface reaction rate limited. The choice of substrate (glass or gas sensor) appeared not to affect the films in any way. The same composition, morphology and reaction onset temperature was seen irrespective of substrate. This indicates that deposition is not substrate specific.

The mechanism in these reactions was not investigated, though it appears likely that HCl is produced along with C_2H_5Cl and CH_3Cl [24] as exhaust gas tested with universal indicator paper during the reaction turned red. It is unlikely that an adduct reaction occurs as no material other than product was recovered from the reactor [25].

The surface of the APCVD films investigated here is relatively uneven and rough. There is evidence of some gas phase nucleation in that the surface consists mainly of interlinking islands, however, there is an absence of ''pin holing'' normally associated with gas phase nucleation and seen in other work where the deposited film had a similar morphology [26]. Pin holing is indicative of gas phase nucleation where particles grow in the gas phase but do not strongly bond to the substrate surface and may be blown off or fall off during handling. Additionally no solid material was recovered from the reactor exhaust, as is usually the case where gas phase nucleation is observed [27]. It is perhaps the case that nucleation can occur in the gas phase but due to either precursor species concentration or short gas phase residence time particle growth is primarily surface limited.

APCVD produced films are highly adherent to the substrate surface; this may prove to be an advantage over thick film technologies used in the production of sensor materials.

Previous work [12,13] on the production of antimony oxide thin films by CVD and thermal evaporation show some similarities with the antimony oxide films produced here. Films of antimony oxide produced by thermal evaporation of Sb_2O_3 powder were made up of small grains of antimony oxide; these were typically in the range of 50–150 nm across in size. The films were shown to be crystalline by XRD. A strictly island growth mechanism was seen with particles typically around 2 μm in diameter. Multiple phases were observed in these reaction systems, some Sb_6O_{13} were observed amongst the Sb_2O_3 on the substrate, these were found to increase if oxygen was added to the reactant gas flow. This is in contrast to what is reported here as no mixed phases were observed only Sb_2O_3 was found. The Sb_2O_3 films were X-ray amorphous and an island growth mechanism prevailed.

The current widely held view of gas sensors [20] states that the conductivity of semi-conducting oxides in air is determined by the trapping of electrons in surface states associated with surface absorbed oxygen. If interstitials or oxygen vacancies are immobile in the lattice, then the behaviour is described in terms of electron distribution between bulk and surface states. The surface conductivity is sensitive to small amounts of reactive gas as catalytic surface processes result in a change in the surface coverage of the oxygen surface trap states. If oxygen defects are mobile within the lattice then the conductivity is determined by the equilibrium between bulk lattice defects and oxygen in the gas phase, and sensitivity to trace reactive gases is lost. A further case for gas sensing can arise where there is a time dependence on the equilibration of lattice and surface states. Conductivity time dependence can also be observed as a result of lattice defect migration, which alters the potential and thus the charge carrier distribution near the surface. Due to a micro-structural effect part of the conductivity is gas sensitive due to modification in surface reactions whilst the conductivity contributed by the bulk is not gas sensitive [21]. If the films are especially thin (100s of nm) then dense films such as those produced by CVD methodology may produce high quality gas sensors. Semiconductor gas sensors are either n-type or p-type; this affects the type of gas response they provide. In an n-type semi-conducting oxide, such as tin oxide, oxygen adsorption decreases the charge carrier density at the surface; this is balanced by the charge carried on the ionised donors. A p-type semi-conducting oxide in contrast has an increased charge carrier density at the surface due to adsorption; this increase in charge is balanced by holes in the valence band. The change in electrical resistance on exposure to ppm levels of ethanol gas in the antimony oxide materials reported here is due to changes in oxygen trap sites in response to the catalytic oxidation of ethanol. This is not due to absorption, as we would expect to see a marked change in gas response on the introduction of humidity into the chamber. It is therefore likely that for these materials that surface absorbed water is not associated with the same surface state as the surface absorbed ethanol. Indeed this is a current problem in sensor technology that makes SnO_2 (the most widely used) devices unsuitable for a range of applications [28,29]. For these materials surface states are non-specific towards absorbed species. Much work has been conducted to improve the surface selectivity of SnO_2 devices [16] to lessen the effect of variable humidity.

The response peak shape for the antimony (III) oxide samples is quite ''square''; this indicates that some of the resistivity change is a result of contributions from the bulk of the material [30]. As dense films, such as those produced by CVD, have relatively fewer absorption sites than porous films, such as those produced by screen printing, they will saturate more quickly. This is likely to be a key factor to the square nature of the response. This will also affect the extent of the response. Sensors that give rise to a lower response are also subject to noise, which limits their usefulness in devices. Although in previous work [30] CVD prepared sensors had an advantage over other methodologies in terms of energy usage.

5. Conclusion

Reaction of antimony (V) chloride and ethyl acetate under APCVD conditions affords clear films of antimony (III) oxide on glass and gas sensor substrates. The films show good surface coverage, adhesion and uniformity. Single-phase films of antimony (III) oxide were obtained. These films were colourless in appearance and insulating at room temperature. The response to reducing gas (ethanol) by APCVD prepared antimony (III) oxide sensors was evaluated. It was found that there was a significant gas response to ethanol that was most pronounced at an operating temperature of 400 °C.

References

[1] G. Centi, S. Perathoner, Appl. Catal. 124A (1995) 317.
[2] D.Z. Dzmitrowice, J.B. Goodenough, P.J. Wiseman, Mater. Res. Bull. 17 (1982) 971.
[3] S. Tanabe, Ceram. Trans. 163 (2005) 1.
[4] K. Kleveland, M.A. Einarsrud, T. Grande, J. Am. Ceram. Soc. 83 (2000) 315.
[5] Zhang, L. Feng, F. Qiu, B. Lin, Huaxue Jinzhan 16 (4) (2004) 508.
[6] Y. Zhang, G. Li, J. Zhang, L. Zhang, Nanotechnology 15 (7) (2004) 762.
[7] Y.F. Liu, Dianci Bileiqi 192 (2003) 36.
[8] N. Tigau, V. Ciupina, G. Prodan, J. Cryst. Growth 277 (2005) 529.
[9] N. Tigau, V. Ciupina, G. Prodan, G.L. Rusu, E. Vasile, J. Cryst. Growth 269 (2004) 392.
[10] M. Fang, Q. Li, F. Gan, Cailiao Yanjiu Xuebao 18 (1) (2004) 1.
[11] P.W. Haycock, G.A. Horley, K.C. Molloy, C.P. Myers, S.A. Rushworth, L.M. Smith, CVD 7 (5) (2001) 191.
[12] W.A. Badawy, E.A. El-Taher, Thin Solid Films 158 (1988) 277.
[13] W.A. Badawy, Thin Solid Films 186 (1990) 59.
[14] C.C. Wang, S.A. Akbar, M.J. Madou, J. Electroceram. 2 (4) (1998) 273.
[15] P.W. Haycock, G.A. Horley, K. Molloy, C.P. Myers, S.A. Rushworth, L.M. Smith, J. Phys. IV Proc. (2001) 11.
[16] J.S. Bae, D.H. Yun, C.O. Park, J.S. Hwang, Sens. Actuators B 75 (3) (2001) 160.
[17] F. Maury, CVD 2 (1996) 113.
[18] K.D. Sanderson, A. Simpson, S. Hurst, T. McKittrick, D. Rimmer, L. Ye, D. Strickler, M. Soubeyrand, in: Glass Processing Days, 2001, p. 762 (Session 32).
[19] D.W. Sheel, M.E. Pemble, CVD Coatings on Glass ICCG4 (2002).
[20] D. Niemeyer, D.E. Williams, P. Smith, K.F.E. Pratt, B. Slater, C.R.C.A. Catlow, A.M. Stoneham, J. Mater. Chem. 12 (2002) 667.
[21] D.E. Williams, K.F.E. Pratt, Sens. Actuators B 70 (2000) 214.
[22] G.S. Henshaw, D.H. Dawson, D.E. Williams, J. Mater. Chem. 5 (1995) 1791.
[23] D. Briggs, M.P. Seah (Eds.), Practical Surface Analysis, Auger and X-ray Photoelectron Spectroscopy, second ed., vol. 1, Wiley, 1990.
[24] J.T. Scheper, K.C. Jayaratne, L.M. Liable-Sands, G.P.A. Yap, A.L. Rheingold, C.H. Winter, Inorg. Chem. 38 (1999) 4354.
[25] C.S. Blackman, C.J. Carmalt, S.A. O'Neill, I.P. Parkin, L. Apostilco, K.C. Molloy, J. Mater. Chem. 11 (2001) 2408.
[26] R. Binions, C.J. Carmalt, I.P. Parkin, Polyhedron 22 (13) (2003) 1683.
[27] R. Binions, C.S. Blackman, C.J. Carmalt, S.A. O'Neill, I.P. Parkin, K. Molloy, L. Apostilco, Polyhedron 21 (19) (2002) 1943.
[28] D. Kohl, Sens. Actuators B 1 (1990) 158.
[29] J.F. McAleer, P.T. Moseley, J.O.W. Norris, D.E. Williams, J. Chem. Soc., Faraday Trans. 1 83 (1987) 1323.
[30] R. Binions, C.J. Carmalt, I.P. Parkin, K.F.E. Pratt, G.A. Shaw, Chem. Mater. 16 (2004) 2489.

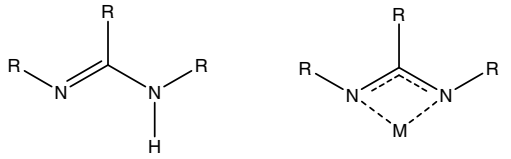

Fig. 1. Amidine pro-ligand (Am) and coordinated amidinato ligand (MAm) with charge delocalization.

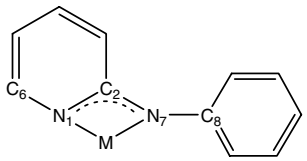

Fig. 2. The delocalized bonding mode of the phenylamidopyridine ligand, M = early transition metal and approximative non-linear angles of amidopyridine: M–N1–C2 = 90°; M–N1–C6 = 150°; M–N7–C2 = 100°; M–N7–C8 = 140° (*vide supra*).

aminopyridine moieties in the complex [18]. Reference to a situation in which delocalization does not occur can be found in 2,6-(amidomethyl)pyridine complexes with a methylene group between the amido nitrogen and pyridine ring [19].

The pentagonal bipyramid represents one of the seven-coordination geometries. It is known that seven-coordinated complexes are prone to stereochemical nonrigidity. In the case of tantalum amidopyridines the coordination isomerism around tantalum probably originates from delocalization of nitrogens or loosely coordinated pyridine nitrogen. We have previously isolated amidopyridine complexes with amido groups *cis* to each other. Now, we tried to use bulky aminopyridine ligands to isolate and characterize the still unknown isomer of tantalum amidopyridine complexes with amido groups *trans* to each other (*vide infra*).

2. Experimental

For the synthesis of complexes **1** and **2** it was first necessary to synthesize the precursor aminopyridine. This was achieved using a typical method of aminopyridine synthesis involving a melt reaction described earlier [20]. The aminopyridine ligand for the complex **3** was purchased from Aldrich. The ligand precursor was then treated with $TaCl_5$ according to a previously known procedure [8]. Recrystallization from toluene produced crystals suitable for X-ray measurements. All reaction steps were carried out under an argon atmosphere using standard Schenk techniques. In all cases a portion of air-sensitive crystals was transferred to perfluoropolyether. The crystal selected for the X-ray measurements was mounted on glass fibre using the oil-drop method [21].

2.1. Structure determination and refinement

Structures were solved with the SHELXTL-5.1 program package using direct methods that showed the positions of the non-hydrogen atoms. Further refinement with full-matrix least-squares on F^2 was carried out with SHELXL-97 using all collected reflections. Non-hydrogen atoms were refined anisotropically. Hydrogen atoms were introduced into calculated positions.

Compound	**1**	**2**	**3**
Empirical formula	$C_{34}H_{44}Cl_3N_4Ta$[a]	$C_{26}H_{26}Cl_3N_4Ta$	$C_{22}H_{18}Cl_3N_4Ta$
Formula mass (g/mol)	796.06[a]	681.81	625.70
Crystal system	triclinic	triclinic	monoclinic
Space group	$P\bar{1}$	$P\bar{1}$	$P2_1/n$
Crystal color	dark red	dark red	dark red
a (Å)	10.379(2)	8.861(2)	15.268(5)
b (Å)	19.727(4)	11.373(2)	9.108(4)
c (Å)	21.406(4)	13.419(3)	15.730(3)
α (°)	96.12(3)	95.94(3)	90
β (°)	103.61(3)	102.51(3)	99.87(4)
γ (°)	90.37(3)	98.53(3)	90
V (Å^3)	4233(2)	1292.7(5)	2155.1(13)
Z	4	2	4
D_{calc} (Mg/m^3)	1.427	1.486	1.929
Upper 2θ limit (°)	50	50	50
Independent reflections	13 568	4549	3796
Parameters	1011	307	271
Goodness-of-fit	1.075	1.045	1.029
R for $F^2 > 2\sigma(F^2)$	0.0419	0.0227	0.0568
wR_2 (all)	0.1117	0.0515	0.1606

[a] Solvate molecules excluded.

Complex **1**, trichlorobis{2-[2,6-di(2-propyl)phenylamido]-pyridine}tantalum(V): ^{1}H NMR (200 MHz, $CDCl_3$): $\delta = 1.07$ (dd, 24H), 3.08 (sept, 4H), 6.06 (d, 2H), 6.62 (t, 2H), 7.04–7.60 (m, 8H), 8.02 (br s, 2H). ^{13}C NMR (200 MHz, $CDCl_3$): $\delta = 23.76$, 28.39, 107.57, 113.10, 124.15, 128.15, 131.80, 140.23, 143.53, 147.48, 157.33.

Complex **2**, trichlorobis{2-[3,4-di(methyl)phenylamido]-pyridine}tantalum(V): ^{1}H NMR (200 MHz, $CDCl_3$): $\delta = 2.16$ (s, 12H), 6.64 (ddd, 2H), 6.80 (d, 2H), 6.92–7.17 (m, 6H), 7.46 (ddd, 2H), 7.97 (d, 2H). ^{13}C NMR (200 MHz, $CDCl_3$): $\delta = 19.13$, 19.81, 108.85, 113.88, 119.73, 123.67, 130.44, 133.06, 136.16, 137.85, 139.66, 144.08, 155.48.

Complex **3**, trichlorobis{[2-phenylamido]-pyridine}tantalum(V): ^{1}H NMR (200 MHz, $CDCl_3$): $\delta = 6.66$ (t, 2H), 6.84 (d, 2H), 6.95–7.26 (m, 10H), 7.44 (t, 2H), 8.07 (d, 2H).

^{13}C NMR (200 MHz, $CDCl_3$): $\delta = 108.84$, 114.64, 121.08, 123.56, 129.34, 138.87, 139.48, 145.97, 155.51.

3. Results and discussion

The coordination spheres of bis(amidopyridine) complexes presented in this work are pseudo-pentagonal bipyramids. In the polyhedron two chloro ligands occupy axial positions and the third together with four nitrogen atoms forms the pentagonal plane. The pentagonal bipyramidal coordination sphere seems to be quite typical of seven-coordinated niobium(V) and tantalum(V) complexes that contain two didentate ligands with a relatively small bite. Similar coordination polyhedra have been found for the amidinato [22], thioamidinato [23], thiocarbamato [24] and carboxylato [25] complexes.

Hence, amidopyridine ligands are unsymmetrical and three ligand arrangements with the described polyhedron can be found. In the two symmetric orientations either amido or pyridine nitrogen atoms are in *cis*-positions in the pentagonal plane. When one amido and one pyridine nitrogen atom are *cis* the complex adopts lower symmetry. If the axial ligands in the complex are different to each other two chiral isomers can exist. In the case of complexes presented here these isomers are equivalent because the pentagonal plane forms a mirror plane that gives C_s-symmetry to the complexes. All the complexes with 2-(benzyl-amido)pyridine ligands were found to crystallize in C_{2v}-symmetric orientations where amido groups are in *cis*-positions (Fig. 3B). In bis[2-(phenylamido)pyridine]

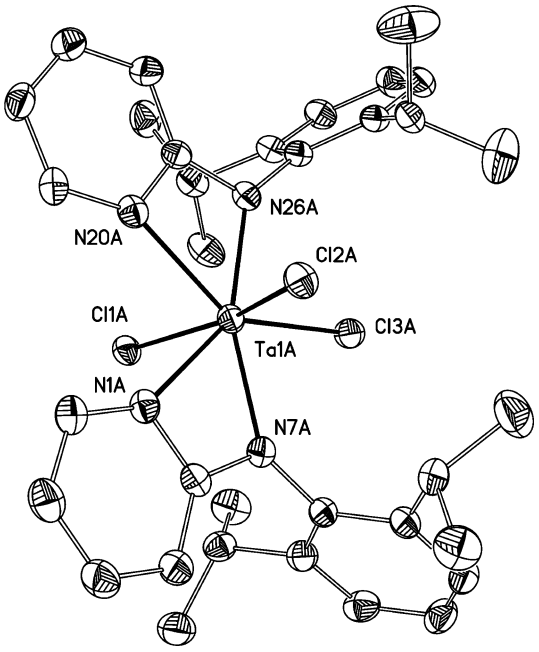

Fig. 4. The molecular structure of complex **1**, trichlorobis{2-[2,6-di(2-propyl)phenylamido]-pyridine}tantalum(V). Hydrogen atoms are omitted for clarity. The thermal ellipsoids correspond to 25% probability.

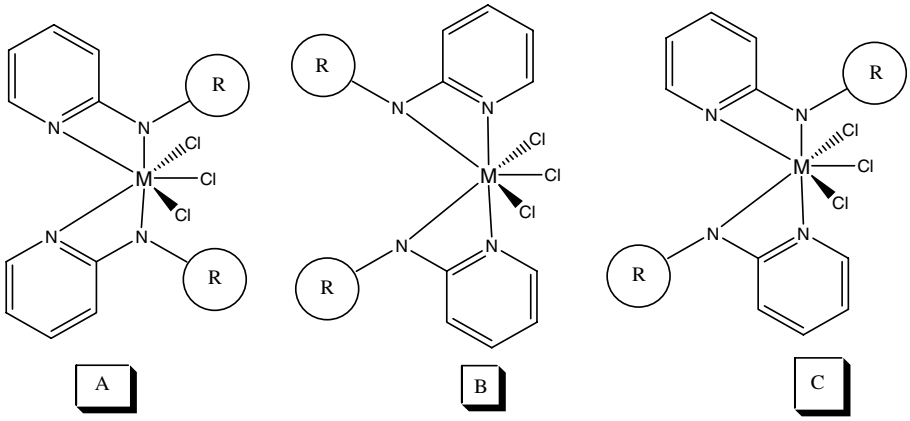

A		B		C	
R	M	R	M	R	M
2,6-(2-Pr)$_2$Ph (**1**)	Ta	3,4-(Me)$_2$Ph (**2**)	Ta	Ph (**3**)	Ta, Nb [8]
		Ph	Ta [8], Zr [8]		
		Bz	Ta [10], Nb [10]		
		PhNPyNHPh	Ta [9]		
		BzN-6-MePy	Ta [11]		
		BzN-4-MePy	Ta [11]		

Fig. 3. Configurational isomerism in bis(amidopyridine)chloro complexes.

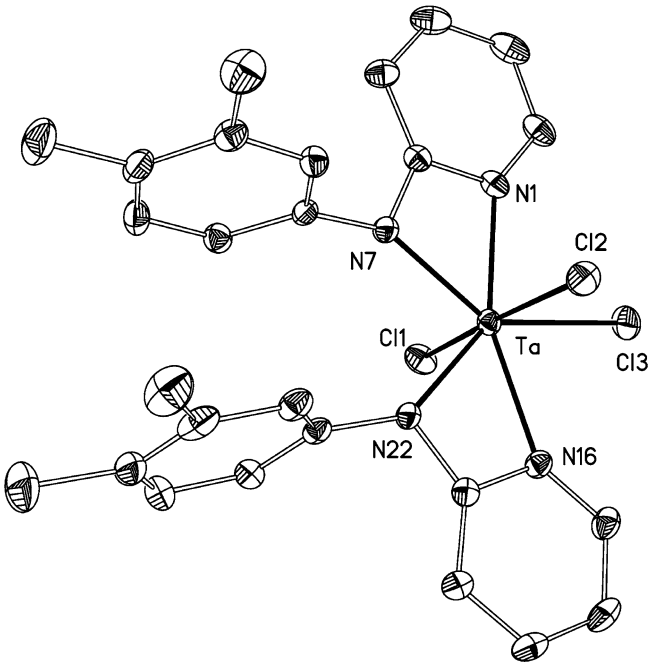

Fig. 5. The molecular structure of complex **2**, trichlorobis{2-[3,4-di(methyl)phenylamido]-pyridine}tantalum(V). Hydrogen atoms are omitted for clarity. The thermal ellipsoids correspond to 25% probability.

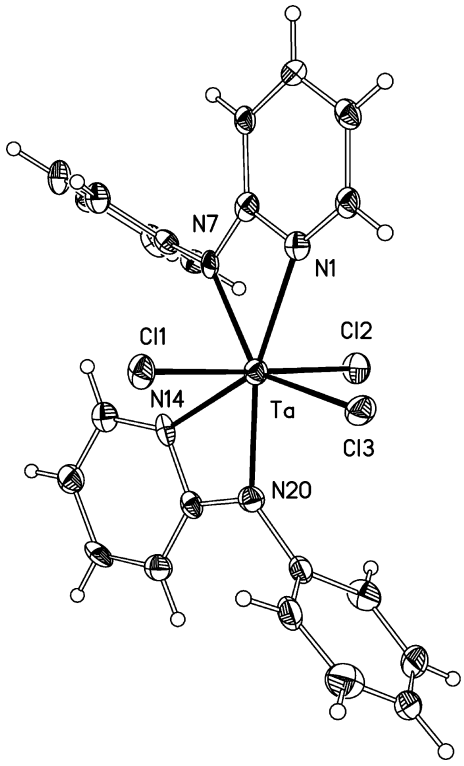

Fig. 6. The molecular structure of complex **3**, trichlorobis{[2-phenylamido]-pyridine}tantalum(V). Hydrogen atoms are omitted for clarity. The thermal ellipsoids correspond to 25% probability.

complexes of zirconium and tantalum the ligands adopt an orientation similar to that found in benzylamidopyridine complexes. Complex **3** was the only one that was found to crystallize in the C_s-symmetric configuration (Fig. 3C).

In order to obtain the other C_{2v}-symmetric orientation where the amido groups are in *trans*-positions, crowded 2,6-di(2-propyl)phenyl substituents were used at 2-amino-positions. Single crystal analysis of the trichlorobis{2-[2,6-di(2-propyl)phenylamido]-pyridine}tantalum(V) (Fig. 4) revealed that the third possible configuration (Fig. 3A) can be obtained when bulky ligands are used (vide supra). Furthermore, we assume that the other C_{2v}-symmetric orientation (Fig. 3B) is not possible because of steric reasons. It seems that configurational changes easily take place in seven-coordinated bis(amidopyridine) complexes (see Figs. 5 and 6).

Neglecting the ligand configuration, complex **1** is similar to our other studied tantalum complexes: it has very similar interatomic distances and angles (Table 1). The compound was found to crystallize with two complex molecules and three toluene solvate molecules in the asymmetric unit (see Tables 2 and 3).

Seven-coordinated bis(amidopyridine) complexes distort from ideal pentagonal bipyramids in various ways. Ideal *cis*-angles in pentagonal plane are 72° but the N–Ta–N

Table 1
Selected bond lengths (Å) and angles (°) in complex **1**, trichlorobis{2-[2,6-di(2-propyl)phenylamido]pyridine}tantalum(V)

	Molecule a	Molecule b		Molecule a	Molecule b
Ta1–Cl1	2.3769(12)	2.3757(13)	Cl1–Ta1–N26	92.54(10)	92.69(11)
Ta1–Cl2	2.3549(12)	2.3537(13)	Cl2–Ta1–N1	81.79(10)	82.77(10)
Ta1–Cl3	2.3512(13)	2.3711(13)	Cl2–Ta1–N7	91.95(11)	92.00(11)
Ta1–N1	2.267(4)	2.280(4)	Cl2–Ta1–N20	83.84(10)	82.90(10)
Ta1–N7	2.108(4)	2.087(4)	Cl2–Ta1–N26	92.19(10)	90.90(11)
Ta1–N20	2.276(4)	2.279(4)	N1–Ta1–N7	60.16(14)	60.87(14)
Ta1–N26	2.094(4)	2.101(4)	N1–Ta1–N20	83.83(14)	82.85(15)
			N1–Ta1–N26	143.96(14)	143.32(14)
			N7–Ta1–N20	143.95(14)	143.72(14)
Cl1–Ta1–Cl2	160.39(4)	159.84(4)	N7–Ta1–N26	155.87(14)	155.77(14)
Cl1–Ta1–Cl3	99.52(5)	97.97(5)	N20–Ta1–N26	60.16(14)	60.49(14)
Cl2–Ta1–Cl3	100.08(5)	102.18(5)	Cl3–Ta1–N1	138.02(10)	138.64(11)
Cl1–Ta1–N1	83.21(10)	82.52(10)	Cl3–Ta1–N7	77.87(10)	77.85(11)
Cl1–Ta1–N7	91.48(11)	92.81(11)	Cl3–Ta1–N20	138.15(10)	138.37(11)
Cl1–Ta1–N20	82.05(10)	81.65(10)	Cl3–Ta1–N26	78.01(10)	78.02(11)

Table 2
Selected bond lengths (Å) and angles (°) in complex **2**, trichlorobis{2-[3,4-di(methyl)phenylamido]-pyridine}tantalum(V)

Ta1–Cl1	2.3721(11)	Cl1–Ta1–N22	92.57(9)
Ta1–Cl2	2.3569(11)	Cl2–Ta1–N1	90.73(8)
Ta1–Cl3	2.4371(13)	Cl2–Ta1–N7	91.97(9)
Ta1–N1	2.223(3)	Cl2–Ta1–N16	87.96(9)
Ta1–N7	2.082(3)	Cl2–Ta1–N22	93.29(9)
Ta1–N16	2.214(3)	N1–Ta1–N7	60.49(12)
Ta1–N22	2.078(3)	N1–Ta1–N16	155.35(12)
		N1–Ta1–N22	143.97(12)
		N7–Ta1–N16	144.15(12)
Cl1–Ta1–Cl2	172.81(4)	N7–Ta1–N22	83.58(12)
Cl1–Ta1–Cl3	86.26(4)	N16–Ta1–N22	60.66(12)
Cl2–Ta1–Cl3	86.59(5)	Cl3–Ta1–N1	77.87(9)
Cl1–Ta1–N1	86.97(8)	Cl3–Ta1–N7	138.32(9)
Cl1–Ta1–N7	92.81(9)	Cl3–Ta1–N16	77.48(9)
Cl1–Ta1–N16	91.29(9)	Cl3–Ta1–N22	138.10(9)

Table 3
Selected bond lengths (Å) and angles (°) in complex **3**, trichlorobis-{[2-phenylamido]-pyridine}tantalum(V)

Ta1–Cl1	2.356(3)	Cl1–Ta1–N20	92.3(3)
Ta1–Cl2	2.383(3)	Cl2–Ta1–N1	90.5(3)
Ta1–Cl3	2.396(3)	Cl2–Ta1–N7	86.3(2)
Ta1–N1	2.231(10)	Cl2–Ta1–N14	92.5(3)
Ta1–N7	2.129(9)	Cl2–Ta1–N20	88.9(3)
Ta1–N14	2.285(10)	N1–Ta1–N7	60.0(4)
Ta1–N20	2.076(10)	N1–Ta1–N14	141.7(4)
		N1–Ta1–N20	158.8(4)
		N7–Ta1–N14	82.1(4)
Cl1–Ta1–Cl2	176.28(12)	N7–Ta1–N20	141.1(4)
Cl1–Ta1–Cl3	92.42(12)	N14–Ta1–N20	59.6(4)
Cl2–Ta1–Cl3	91.25(12)	Cl3–Ta1–N1	77.7(3)
Cl1–Ta1–N1	89.7(3)	Cl3–Ta1–N7	137.5(3)
Cl1–Ta1–N7	90.6(2)	Cl3–Ta1–N14	140.4(3)
Cl1–Ta1–N14	85.0(3)	Cl3–Ta1–N20	81.1(3)

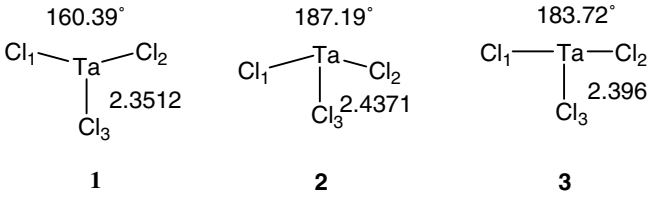

Fig. 7. The T-shape behavior of $TaCl_3$ of the complexes **1**–**3**; the Cl1–Ta–Cl2 angle decreases because of bulky isopropyl substituents occupy the space between the Cl1 and Cl3, and Cl2 and Cl3. Angle values for structures **2** and **3** are explementary values of tabulated values in order to be comparable with the structure **1**.

chelate angle is only about 60° due to the narrow bite of the rigid amidopyridine ligand. Regularity of the polyhedra can also be evaluated by how well the atoms fit to the pentagonal plane. This phenomenon was analyzed by calculating least-square mean planes through the M–N4–Cl equatorial-atoms. In all the bis[2-(phenylamido)pyridine] complexes, the plane forming atoms are located very close to the calculated planes, the average deviations are around 0.1 Å and all distances from the planes are less than 0.20 Å. In complex **1** deviations are smallest, even the maximum deviation is marginal, only 0.048(2) Å. Bis[2-(benzylamido)pyridine] complexes **7**–**10** seem to be more distorted in this sense, the average atom distances from the plane are typically around 0.2 Å. Maximum deviation, 0.418(5) Å, was found in complex **10**. All the maximal deviations were found for nitrogen atoms. In fact, distortion of the pentagonal plane can be seen as tilting of the chelate rings. One donor atom is located above the plane whereas the other nitrogen donor is tilted downwards. In most complexes the other ligand is tilted to the opposite direction (Table 4).

Axial chloro ligands fit quite well to their positions without significant distortions. In most bis(amidopyridine) complexes Cl–M–Cl *cis*-angles are typically between 85°

Table 4
Distortions in bis(amidopyridine) complexes according to calculated mean least-square planes through the atoms in M–N4–Cl equatorial and chelate rings

Complex	Deviations from the pentagonal planes (Å)			Interplanar angles between four-membered chelate ring (1) and their tilts from the pentagonal planes (2) (°)		
	Average	Maximum	Atom	1	2	
[Ta(2,6-PrPhNPy)$_2$Cl$_3$] (**1**)						
Molecule a	0.0178	0.026(2)	Namido	2.35(19)	0.97(17)	1.38(12)
Molecule b	0.0347	0.048(2)	Npyridine	1.42(19)	1.21(13)	2.13(17)
[Ta(3,4-Me$_2$PhNPyCl)$_3$] (**2**)	0.0283	0.041(1)	Npyridine	3.30(22)	1.75(17)	1.80(17)
[Ta(PhNPy)$_2$Cl$_3$] (**3**)	0.0678	0.101(5)	Namido	7.93(22)	3.64(18)	4.83(19)
[(Zr(PhNPy)$_2$Cl$_2$)$_2$] (**4**) [8]	0.12	0.170(2)	Npyridine	8.10(6)	1.53(7)	9.33(6)
[Nb(PhNPy)$_2$Cl$_3$] (**5**) [8]	0.07	0.106(2)	Namido	8.15(8)	3.45(6)	5.11(6)
[Ta(PhNPy)$_2$Cl$_3$] (**6**) [8]	0.057	0.089(2)	Namido	6.5(2)	2.04(14)	4.53(12)
[Nb(BzNPy)$_2$Cl$_3$] (**7**) [5]						
Molecule a	0.144	0.230(4)	Namido	18.1(5)	6.9(4)	11.4(4)
Molecule b	0.15	0.238(4)	Namido	19.6(5)	8.0(4)	11.7(4)
[Ta(BzNPy)$_2$Cl$_3$] (**8**) [5]	0.143	0.225(5)	Namido	18.3(5)	7.6(4)	10.8(4)
[Ta(BzN-4-MePy)$_2$Cl$_3$] (**9**) [11][a]	0.128	0.188(3)	Namido	15.96(4)	8.17(15)	8.17(15)
[Ta(BzN-6-MePy)$_2$Cl$_3$] (**10**) [11]	0.254	0.418(5)	Namido	33.9(4)	13.9(4)	20.9(4)
[Ta(PhNPyNHPh)$_2$Cl$_3$] (**11**) [9]	0.245	0.384(5)	Namido	31.2(6)	14.2(5)	17.4(5)

[a] Recalculated values differ from that given in Ref. [11].

and 90°. Tantalum complexes with bulky amidopyridine ligands show more distortion. In complex **1** the axial chloro ligands are bent away from the equatorial chloro ligands leading to Cl–Ta–Cl *cis*-angles between 99.52(5)° and 100.08(5)° (Fig. 7). In complex **11** the direction of bending is opposite, Cl–Ta–Cl angles are 81.86(8)° and 81.87(8)°.

Charge delocalization at donor nitrogens cannot be seen in the complexes **1**–**3**. The Ta–$N_{pyridine}$ bond lengths are approximately 0.1–0.2 Å longer than Ta–N_{amido} bond lengths. The bond lengths are in accordance with the literature data on amidopyridine complexes.

4. Conclusions

Tantalum(V) was found to form mononuclear bis(amidopyridine) complexes that have a pentagonal bipyramidal coordination sphere. This seven-coordination displays configurational isomerism that can be affected by substituents in the amidopyridine ligands. In contrast to our previous reports, we have successfully isolated the first C_{2v}-symmetric tantalum bis(amidopyridine) complex with the amido groups oriented in a *trans*-manner. This was caused by steric crowding of di-isopropyl substituents at the 2,6-positions of the phenyl part of the aminopyridine moiety. With the 3,4-dimethylaminopyridine ligand, the amido groups adopted a *cis*-orientation as they did in most of our earlier reported tantalum complexes. The tantalum bis[2-(phenylamido)pyridine] complex was found in two forms: one similar to its niobium congener and the other resembling the tantalum bis[3,4-dimethylamidopyridine] complex. All of the studied complexes indicate that the negative charge is localized on the amido nitrogen.

5. Supplementary data

Crystallographic data (excluding structure factors) for the structure reported in this paper have been deposited with the Cambridge Crystallographic Data Centre: CCDC 293089–CCDC 293091. Copies of the data can be obtained free of charge from The Director, CCDC, 12 Union Road, Cambridge CB2 1EZ, UK (fax: +44 1223 336 033; e-mail: deposit@ccdc.cam.ac.uk or www: http://www.ccdc.cam.ac.uk).

References

[1] M. Talja, M. Klinga, M. Polamo, E. Aitola, M. Leskelä, Inorg. Chim. Acta 358 (2005) 1061.
[2] C. Morton, P. O'Shaughnessy, P. Scott, Chem. Commun. 21 (2000) 2099.
[3] C. Jones, P.C. Junk, S.G. Leary, N.A. Smithies, Inorg. Chem. Commun. 6 (2003) 1126.
[4] H. Fuhrmann, S. Brenner, P. Arndt, R. Kempe, Inorg. Chem. 35 (1996) 6742.
[5] R. Kempe, A. Spannenberg, S. Brenner, Z. Kristallogr. 211 (1996) 497.
[6] R. Kempe, S. Brenner, P. Arndt, Organometallics 15 (1996) 1071.
[7] E.J. Crust, A.J. Clarke, R.J. Deeth, C. Morton, P. Scott, Dalton Trans. (2004) 4050.
[8] M. Polamo, M. Leskelä, J. Chem. Soc., Dalton Trans. (1996) 4345.
[9] M. Polamo, Acta Crystallogr., Sect. C 52 (1996) 2977.
[10] M. Polamo, M. Leskelä, Acta Chem. Scand. 51 (1997) 449.
[11] M. Polamo, M. Leskelä, Acta Chem. Scand. 51 (1997) 709.
[12] R. Fandos, C. Hernandez, A. Otero, A. Rodriguez, M.J. Ruiz, J. Organomet. Chem. 690 (2005) 4828.
[13] J.J.H. Edema, S. Gambarotta, A. Meetsma, A.L. Spek, N. Veldman, Inorg. Chem. 30 (1991) 2062.
[14] A. Spannenberg, A. Tillack, P. Arndt, R. Kirmse, R. Kempe, Polyhedron 17 (1998) 845.
[15] M. Polamo, M. Leskelä, Acta Chem. Scand. 51 (1997) 69.
[16] F.A. Cotton, L.M. Daniels, D.J. Maloney, C.A. Murillo, Inorg. Chim. Acta 242 (1996) 31.
[17] R. Kempe, P. Arndt, Inorg. Chem. 35 (1996) 2644.
[18] G. Hillebrand, A. Spannenberg, P. Arndt, R. Kempe, Organometallics 16 (1997) 5585.
[19] F. Guerin, D.H. McConville, J.J. Vittal, Organometallics 14 (1995) 3154.
[20] M. Polamo, M. Talja, A.J. Piironen, Z. Kristallogr. NCS 220 (2005) 41.
[21] T. Kottke, D. Stalke, J. Appl. Crystllogr. 26 (1993) 615.
[22] (a) M.G.B. Drew, J.D. Wilkins, J. Chem. Soc., Dalton Trans. (1975) 2611;
(b) S.M. Mullins, J.R. Hagadorn, R.G. Bergman, J. Arnold, J. Organomet. Chem. 607 (2000) 227.
[23] M.G.B. Drew, J.D. Wilkins, J. Chem. Soc., Dalton Trans. (1974) 198.
[24] R.A. Henderson, D.L. Hughes, A.N. Stephens, J. Chem. Soc., Dalton Trans. (1990) 1097.
[25] M.H. Chisholm, L.-S. Tan, J.C. Huffman, J. Am. Chem. Soc. 104 (1982) 4879.

2. Experimental

2.1. Materials and methods

All materials were commercially available and used without further purification. Elemental analyses were conducted using the Vario EL elemental analyzer. PXRD (Powder X-ray diffraction) was performed on a Rigaku D/Max-IIIA diffractometer operated using a 0.02° step scan from 3° to 70° in 2θ and 0.2 s preset time. Infrared spectra were obtained as KBr pellets on a Bruker EQUINOX 55 FTIR spectrometer. Thermogravimetry was carried out with a Netzsch TG-209 analyzer under flowing nitrogen.

2.2. Syntheses of compounds I, *II* and *III*

$[Cu(1,5\text{-nds})(H_2O)_4]_n$ (**I**) and $[Cu(H_2O)_6](1,5\text{-nds})$ (**II**) were obtained according to the reported procedure [7]. $[Cd(p\text{-}NH_2C_6H_4SO_3)_2]$ (**III**) was prepared by heating $[Cd(p\text{-}NH_2C_6H_4SO_3)_2(H_2O)_2]$ [3] at 200 °C for 2 h. $C_{10}H_{14}CuO_{10}S_2$ (**I**): *Anal.* Calc. C, 28.47; H, 3.34. Found:

Table 1
TGA and EA results of amine complexes formed by $[Cu(1,5\text{-nds})(H_2O)_4]$ (**I**)

Compound	TGA (%)		Releasing T (°C)	Elemental analyses	
	Calculated[a]	Observed		Calculated C, N, H (%)	Observed C, N, H (%)
$Cu(1,5\text{-nds})(H_2O)_2(CH_3NH_2)_4$	31.4	29.5	81–137, 176–320	32.97, 10.98, 5.93	33.06, 11.05, 5.72
$Cu(1,5\text{-nds})(H_2O)_2(C_2H_5NH_2)_4$	38.2	35.9	93–151, 241–316	38.18, 9.90, 6.76	38.18, 9.73, 6.49
$Cu(1,5\text{-nds})(H_2O)_2(n\text{-}C_3H_7NH_2)_4$	43.8	38.4	94–143, 252–306	42.46, 9.00, 7.45	41.86, 8.64, 7.15
$Cu(1,5\text{-nds})(H_2O)_2(n\text{-}C_4H_9NH_2)_3$	42.2	39.9	108–300	43.66, 6.94, 7.16	44.47, 7.16, 7.10
$Cu(1,5\text{-nds})(i\text{-}C_4H_9NH_2)_3$	38.5	38.7	90–320	46.42, 7.38, 6.91	47.15, 8.42, 7.27
$Cu(1,5\text{-nds})(H_2O)_2(t\text{-}C_4H_9NH_2)_3$	42.2	41.8	124–277	43.66, 6.94, 7.16	43.13, 7.06, 7.09

[a] Calculated weight loss includes water and amine molecules.

Table 2
TGA and EA results of amine complexes formed by $[Cd(p\text{-}H_2NC_6H_4SO_3)_2]$ (**III**)

Compound	TGA (%)		Releasing T (°C)	Elemental analyses	
	Calculated[a]	Observed		Calculated C, N, H (%)	Observed C, N, H (%)
$Cd(p\text{-}H_2NC_6H_4SO_3)_2(CH_3NH_2)_3$	16.9	15.7	102–314	32.76, 12.73, 4.95	32.63, 12.58, 5.14
$Cd(p\text{-}H_2NC_6H_4SO_3)_2(H_2O)_2(C_2H_5NH_2)_4$	32.1	30.9	57–90, 152–300	35.69, 12.48, 6.59	37.41, 13.02, 6.55
$Cd(p\text{-}H_2NC_6H_4SO_3)_2(n\text{-}C_3H_7NH_2)_4$	34.1	32.5	86–115, 141–310	41.58, 12.12, 6.98	40.68, 11.87, 7.11
$Cd(p\text{-}H_2NC_6H_4SO_3)_2(i\text{-}C_3H_7NH_2)$	11.5	12.4	134–175, 198–289	34.92, 8.15, 4.10	34.89, 8.01, 4.36
$Cd(p\text{-}H_2NC_6H_4SO_3)_2(n\text{-}C_4H_9NH_2)_4$	39.0	38.9	59–113, 150–321	44.88, 11.22, 7.53	44.77, 11.20, 7.27

[a] Calculated weight loss includes water and amine molecules.

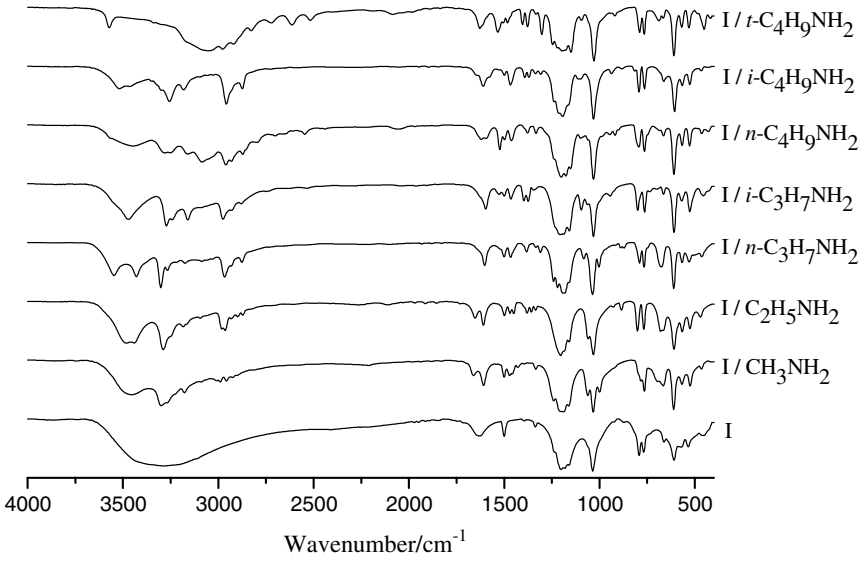

Fig. 1. IR spectra of amine complexes formed by $[Cu(1,5\text{-nds})(H_2O)_4]$ (**I**).

C, 28.31; H, 3.37%. $C_{12}H_{12}CdN_2O_6S_2$ (**III**): *Anal*. Calc. C, 31.55; N, 6.13; H 2.65. Found: C, 31.55; N, 6.15; H, 2.76%. $[Cu(H_2O)_6]$(1,5-nds) (**II**) was characterized by its PXRD which matched the simulated PXRD from its single crystal structure.

2.3. Solid–vapor reaction

Compounds **I**–**III** and the amine liquids were placed in two different but connected vessels and the reactions were carried out at room temperature. The reaction process was monitored via the net weight gain. It took a few days to 2 weeks for the reaction process to be complete. All reaction products were placed in an N_2 flow to remove the deposited amine and moisture on the crystalline surface before submission for characterization.

2.4. Characterization

The reaction products were characterized by EA, TGA, IR and PXRD. Since the final products formed by compounds **I** and **II** have the same PXRD patterns, only the results of **I** are presented. The EA and TGA results are showed in Tables 1 and 2. All complexes have similar IR patterns and only those obtained from **I** is shown in Fig. 1. The PXRD is shown in Fig. 2.

2.5. X-ray structure analysis

Diffraction data of $[Cd(n\text{-}C_3H_7NH_2)_4(H_2O)_2](p\text{-}H_2NC_6H_4SO_3)_2$ were collected on a Bruker Smart 1000 CCD area detector diffractometer with graphite monochromated Mo Kα radiation ($\lambda = 0.71073$ Å) at room temperature.

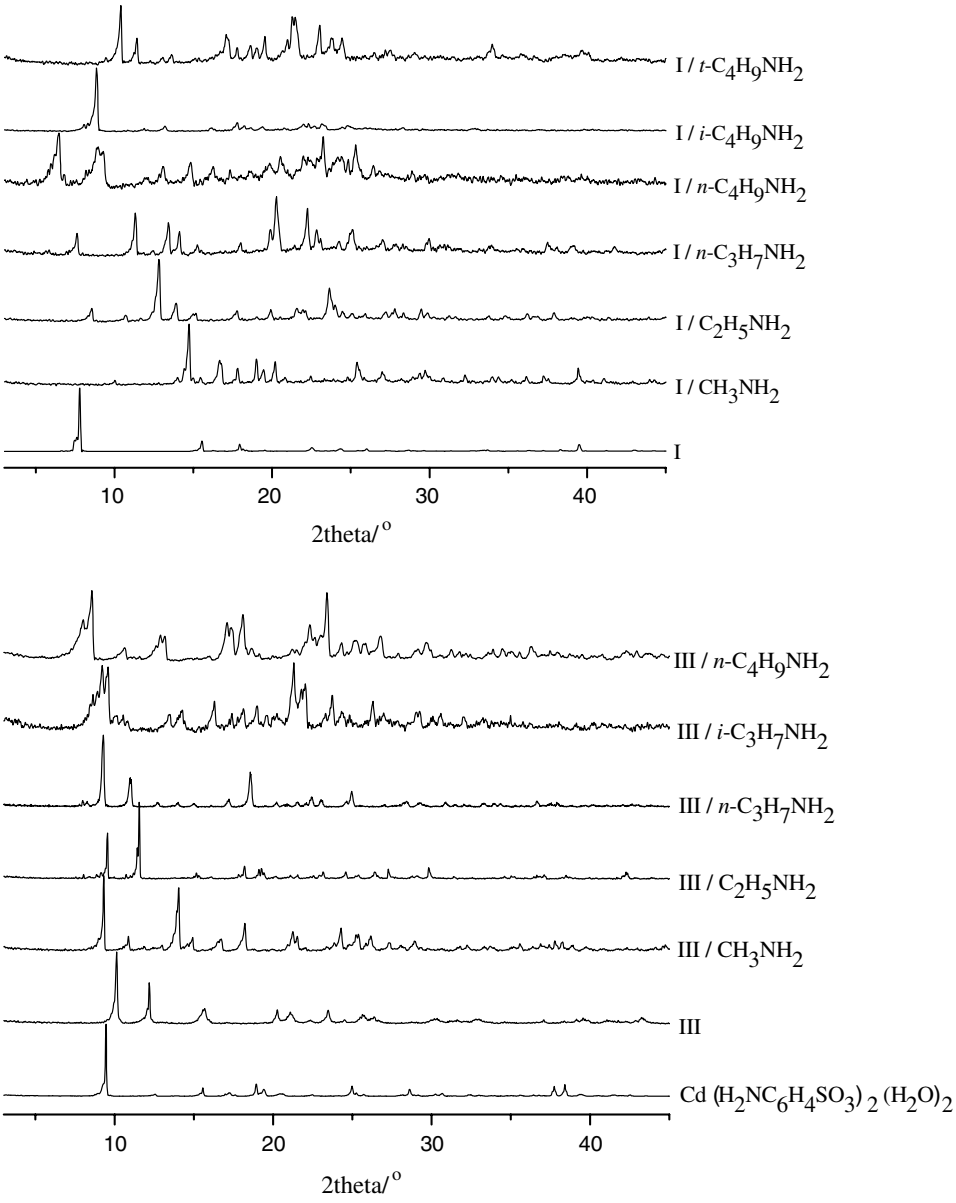

Fig. 2. PXRD of the amine complexes formed by $[Cu(1,5\text{-nds})(H_2O)_4]$ (**I**) and $[Cd(p\text{-}H_2NC_6H_4SO_3)_2]$ (**III**).

Table 3
Crystallographic data for $[Cd(n\text{-}C_3H_7NH_2)_4(H_2O)_2](p\text{-}H_2NC_6H_4SO_3)_2$

Empirical formula	$C_{24}H_{52}CdN_6O_8S_2$
Formula weight	729.24
Temperature (K)	293(2)
Wavelength (Å)	0.71073
Crystal system	triclinic
Space group	$P\bar{1}$
Unit cell dimensions	
a (Å)	8.093(3)
b (Å)	9.907(3)
c (Å)	11.212(4)
α (°)	76.573(5)
β (°)	78.813(5)
γ (°)	83.288(5)
Volume (Å^3)	855.4(5)
Z	1
D_{calc} (Mg/m^3)	1.416
Absorption coefficient (mm^{-1})	0.810
$F(000)$	382
Crystal size (mm)	$0.48 \times 0.45 \times 0.42$
θ Range for data collection (°)	2.12–27.00
Limiting indices	$-10 \leqslant h \leqslant 10$, $-12 \leqslant k \leqslant 12$, $-14 \leqslant l \leqslant 13$
Reflections collected/unique [R_{int}]	7288/3665 [0.0163]
Completeness to $\theta = 27.00$ (%)	97.8
Absorption correction	empirical
Maximum and minimum transmission	0.7272 and 0.6971
Refinement method	full-matrix least-squares on F^2
Data/restraints/parameters	3665/3/192
Goodness-of-fit on F^2	1.079
Final R indices [$I > 2\sigma(I)$]	$R_1 = 0.0222$, $wR_2 = 0.0591$
R indices (all data)	$R_1 = 0.0240$, $wR_2 = 0.0605$
Largest different peak and hole (e Å^{-3})	0.259 and −0.352

Absorption corrections were applied by SADABS [8]. The structure was solved by direct methods and refined using full-matrix least-squares/difference Fourier techniques by SHELXTL [9]. All non-hydrogen atoms were refined with anisotropic displacement parameters. After that, all hydrogen atoms of the ligands were placed in idealized positions and refined as riding atoms with the relative isotropic parameters. Crystal data are listed in Table 3.

3. Results and discussion

3.1. Syntheses and characterization

$[Cu(1,5\text{-nds})(H_2O)_4]_n$ (**I**) and $[Cu(H_2O)_6](1,5\text{-nds})$ (**II**) were obtained via the reaction between $CuCl_2$ and 1,5-naphthalenedisulfonate acid (1,5-nds) in aqueous media at different temperatures [7]. In **I**, Cu(II) is coordinated by the sulfonate group as well as by 4 water molecules, while one $-SO_3$ group coordinates as a $\eta^2\mu^2$ ligand to two different $[Cu(H_2O)_4]^+$ ions in *syn*/*anti* fashion, resulting in a one-dimensional structure, as shown in Fig. 3. In **II**, Cu(II) is coordinated by 6 water molecules and the sulfonate is the counter anion. They show different reactivity toward amine vapors, with **II** being more reactive than **I**. However, they produce the same final amine-coordinated complexes. Both complexes can quantitatively take up to 4 moles of CH_3NH_2, $C_2H_5NH_2$ and n-$C_3H_7NH_2$, 3 moles of i-$C_3H_7NH_2$, n-$C_4H_9NH_2$, i-$C_4H_9NH_2$ and t-$C_4H_9NH_2$, and form stable coordination compounds.

It is noted that the reaction process of $[Cu(1,5\text{-nds})(H_2O)_4]_n$ (**I**) with amine was accompanied by a color change, depending on the different amine molecules that the reactant was exposed to. With CH_3NH_2 and i-$C_3H_7NH_2$, the color changed from light blue to purple; with $C_2H_5NH_2$, n-$C_3H_7NH_2$, n-$C_4H_9NH_2$ and i-$C_4H_9NH_2$, the light blue deepened; with t-$C_4H_9NH_2$, the color became brown.

$[Cd(\mu_2\text{-N,O-}p\text{-}NH_2C_6H_4SO_3)_2(H_2O)_2]$ is a layered coordination compound with a 2D structure [3]. It can react with amine vapors and produce mono-amine coordinated complexes. $[Cd(p\text{-}NH_2C_6H_4SO_3)_2]$ (**III**) was obtained by dehydrating $[Cd(\mu_2\text{-N,O-}p\text{-}NH_2C_6H_4SO_3)_2(H_2O)_2]$ and is also a crystalline material. $[Cd(p\text{-}NH_2C_6H_4SO_3)_2]$ (**III**) can uptake 3 moles of CH_3NH_2, 4 moles of $C_2H_5NH_2$, n-$C_3H_7NH_2$ and n-$C_4H_9NH_2$, and 1 mole of i-$C_3H_7NH_2$. It is interesting to note that **III** has a much stronger amine-intercalation property for amines with a longer chain than that of $[Cd(\mu_2\text{-N,O-}p\text{-}NH_2C_6H_4SO_3)_2(H_2O)_2]$. $[Cd(p\text{-}NH_2\text{-}C_6H_4SO_3)_2]$ (**III**) can uptake 4 moles of n-$C_4H_9NH_2$, while its hydrated form can only uptake 1 mole of n-$C_4H_9NH_2$. This observation can be explained by the result that dehydration creates vacant reaction sites in Cd(II) that are more accessible for amines with longer carbon chains.

All complexes release amine molecules at temperatures higher than 50 °C, after the boiling points of the free amine molecules, indicating the coordinative nature of the amine ligands to the metal centers. Considering the compatible coordination strength of H_2O and $-SO_3$, whether the water molecules or the sulfonate groups occupy the spare coordination sites of the metal centers is not clear.

There are strong peaks around 3150–3350 cm^{-1} in the IR spectra of all the amine complexes, corresponding to the stretching bands of the coordinated N–H groups. There are alkyl C–H stretching bands observed around 2900–3000 cm^{-1} that are contributed by the alkyl amines, confirming the existence of the adducted amine molecules. The broad bands around 3500 cm^{-1} are contributed by the O–H stretching of the water molecules.

All the amine-coordinated complexes obtained via the solid–vapor reactions are crystalline materials, similar to that observed in the Cd(II) analogs [2,3]. The $C_2H_5NH_2$ and n-$C_3H_7NH_2$ products of $[Cd(p\text{-}NH_2C_6H_4SO_3)_2]$ (**III**) grow into single crystals in situ in the solid–vapor reaction, which makes direct structure characterization possible.

3.2. Reaction selectivity and preference

$[Cu(1,5\text{-nds})(H_2O)_4]$ (**I**) and $[Cu(H_2O)_6](1,5\text{-nds})$ (**II**) do not react with $(C_2H_5)_3N$ and $PhNH_2$. $[Cd(p\text{-}NH_2C_6H_4\text{-}SO_3)_2]$ (**III**) does not react with $NH_2CH_2CH_2NH_2$, $(C_2H_5)_2NH$ and $PhNH_2$.In order to reveal the reaction preferences toward different amines, the absorption exper-

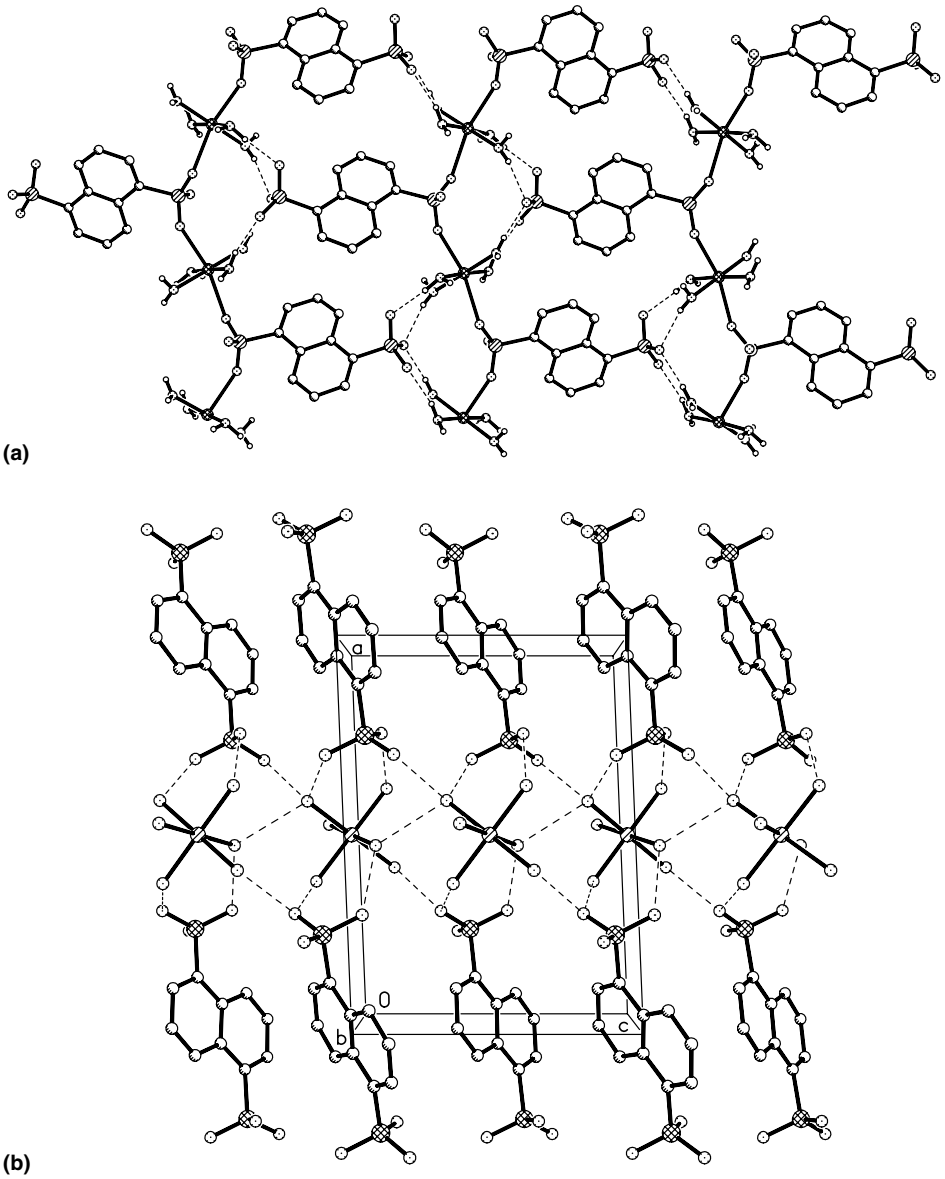

Fig. 3. Structures of $[Cu(1,5\text{-nds})(H_2O)_4]_n$ (**I**) (a) and $[Cu(H_2O)_6](1,5\text{-nds})$ (**II**) (b). The dashed lines represent the hydrogen bonds formed between the $-SO_3$ groups and H_2O.

iments of **I** and **II** with mixed amines $CH_3NH_2/C_2H_5NH_2$ and $C_2H_5NH_2/(C_2H_5)_2NH$ were conducted, and the results are shown in Fig. 4. The PXRD spectra of the resulting amine adduct is identical to that observed for Cu(1,5-nds)-$(H_2O)_2(C_2H_5NH_2)_4$, indicating that compound **I** has preferential reaction behavior, a similar observation made in its Cd(II) analogs [2,3].

3.3. Crystal structure of $[Cd(n\text{-}C_3H_7NH_2)_4(H_2O)_2](p\text{-}H_2NC_6H_4SO_3)_2$

When exposed to $C_2H_5NH_2$ and n-$C_3H_7NH_2$, the powder compound $[Cd(p\text{-}NH_2C_6H_4SO_3)_2]$ (**III**) became moisturized and single crystals were formed after 2–4 weeks which could be used directly for single crystal structure analysis, a phenomenon similar to that observed for $[Cd(\mu_2\text{-N,O-}p\text{-}NH_2\text{-}C_6H_4SO_3)_2(H_2O)_2]$ [3]. The crystal obtained in the case of $C_2H_5NH_2$ exposure has the cell parameters $a = 10.751(3)$, $b = 7.876(2)$, $c = 18.994(5)$ Å, $\alpha = 90$, $\beta = 100.432(5)$, $\gamma = 90°$, similar to that of $[Cd(C_2H_5NH_2)_4(H_2O)_2](p\text{-}H_2NC_6\text{-}H_4SO_3)_2$ [3], suggesting that water molecules were taken up from the $C_2H_5NH_2$ solution and the same complex as that from $[Cd(\mu_2\text{-N,O-}p\text{-}NH_2C_6H_4SO_3)_2(H_2O)_2]$ was formed.

It is noted that there are two forms of crystals produced in the case of n-$C_3H_7NH_2$ exposure. One of them has cell parameters $a = 8.016(2)$, $b = 15.422(4)$, $c = 15.680(4)$ Å, $\alpha = 89.097(3)$, $\beta = 88.123(3)$, $\gamma = 78.069(3)°$, similar to that recorded for $[Cd(n\text{-}C_3H_7NH_2)_4(p\text{-}H_2NC_6H_4SO_3)_2]\cdot C_3H_7\text{-}NH_2$ [3]. The other one is $[Cd(n\text{-}C_3H_7NH_2)_4(H_2O)_2]\text{-}(p\text{-}H_2NC_6H_4SO_3)_2$. The coordination structure of $[Cd\text{-}(n\text{-}C_3H_7NH_2)_4(H_2O)_2](p\text{-}H_2NC_6H_4SO_3)_2$, as well as that of $[Cd(n\text{-}C_3H_7NH_2)_4(p\text{-}H_2NC_6H_4SO_3)_2]\cdot C_3H_7NH_2$ [3] are

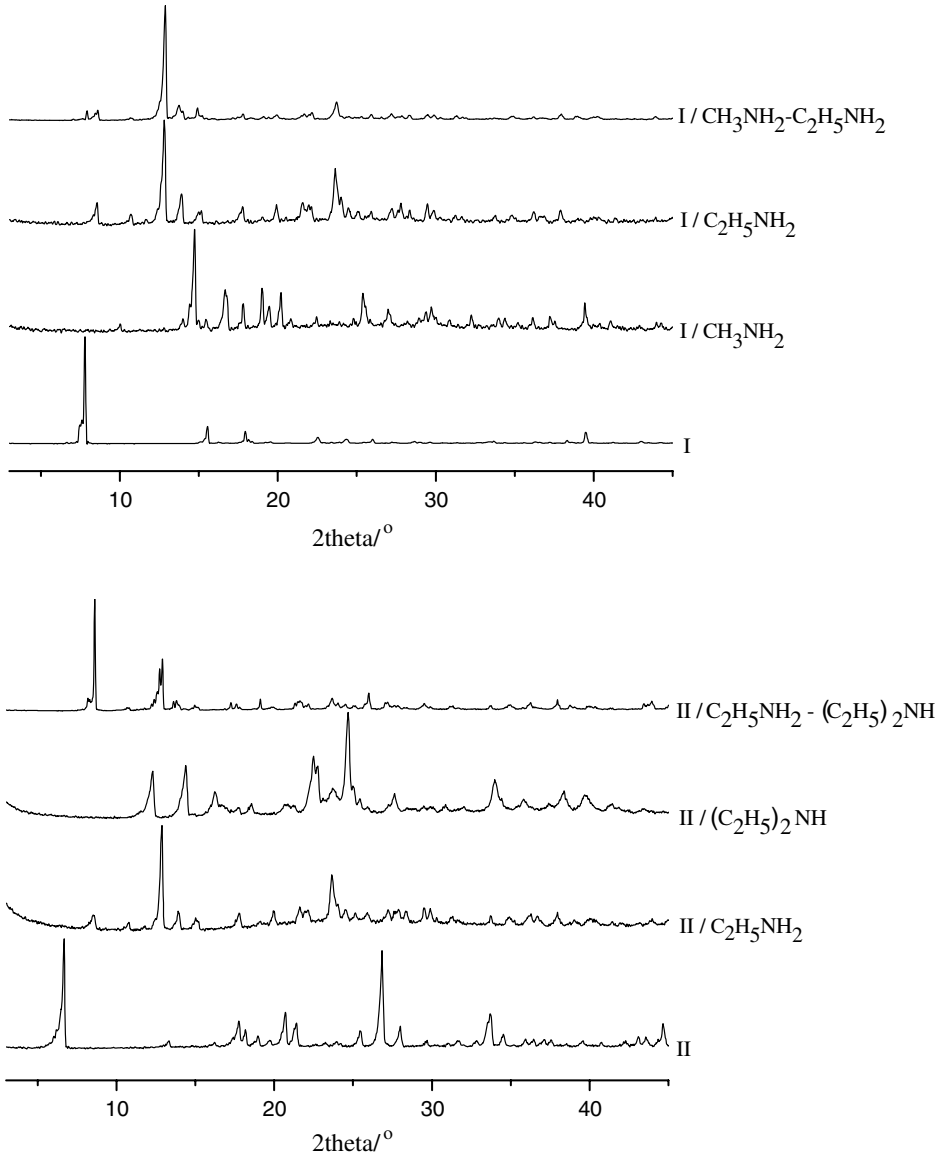

Fig. 4. PXRD of **I** and **II** with mixed amines.

shown in Fig. 5. In $[Cd(n\text{-}C_3H_7NH_2)_4(H_2O)_2](p\text{-}H_2NC_6H_4SO_3)_2$, four $C_3H_7NH_2$ molecules substitute the $p\text{-}H_2NC_6H_4SO_3^-$ ligands from the Cd(II) coordination sphere, and there are two water molecules coordinated to the metal center. The Cd–N distances are 2.3483(15) and 2.3231(16) Å, which are consistence with those observed in its analogs [3]. In $[Cd(n\text{-}C_3H_7NH_2)_4(p\text{-}H_2NC_6H_4SO_3)_2]\cdot C_3H_7NH_2$, four amines replace the two coordinated water molecules and $-NH_2$ groups of the two $p\text{-}H_2NC_6H_4SO_3^-$ ligands, and the two sulfonates remain coordinated to Cd(II).

The PXRD obtained for the final absorption powder is identical to that simulated for the single crystal structure of $[Cd(n\text{-}C_3H_7NH_2)_4(H_2O)_2](p\text{-}H_2NC_6H_4SO_3)_2$, as shown in Fig. 6, indicating that $[Cd(n\text{-}C_3H_7NH_2)_4(p\text{-}H_2NC_6H_4SO_3)_2]\cdot C_3H_7NH_2$ could be an intermediate product which is not stable and transforms into $[Cd(n\text{-}C_3H_7NH_2)_4(H_2O)_2](p\text{-}H_2NC_6H_4SO_3)_2$. This conclusion is also supported by the observation that $[Cd(n\text{-}C_3H_7NH_2)_4(p\text{-}H_2NC_6H_4SO_3)_2]\cdot C_3H_7NH_2$ crystals decayed and lost reflection power quickly when exposed to air [3], while $[Cd(n\text{-}C_3H_7NH_2)_4(H_2O)_2](p\text{-}H_2NC_6H_4SO_3)_2$ is much more stable.

The TGA behavior of the $n\text{-}C_4H_9NH_2$ complex of **III** is similar to that of $C_2H_5NH_2$ and $n\text{-}C_3H_7NH_2$, suggesting that the $n\text{-}C_4H_9NH_2$ complex could have a similar coordination structure as that of $[Cd(C_2H_5NH_2)_4(H_2O)_2](p\text{-}H_2NC_6H_4SO_3)_2$ and $[Cd(n\text{-}C_3H_7NH_2)_4(H_2O)_2](p\text{-}H_2NC_6H_4SO_3)_2$, with 4 $n\text{-}C_4H_9NH_2$ and 2 water molecules coordinated to Cd(II).

4. Summary

The solid–vapor reaction between metal sulfonates and amines has been extended from cadmium(II) to copper(II), and the properties of three transition metal compounds $[Cu(1,5\text{-nds})(H_2O)_4]_n$ (**I**), $[Cu(H_2O)_6](1,5\text{-nds})$ (**II**) and $[Cd(p\text{-}NH_2C_6H_4SO_3)_2]$ (**III**) with alkyl amines were

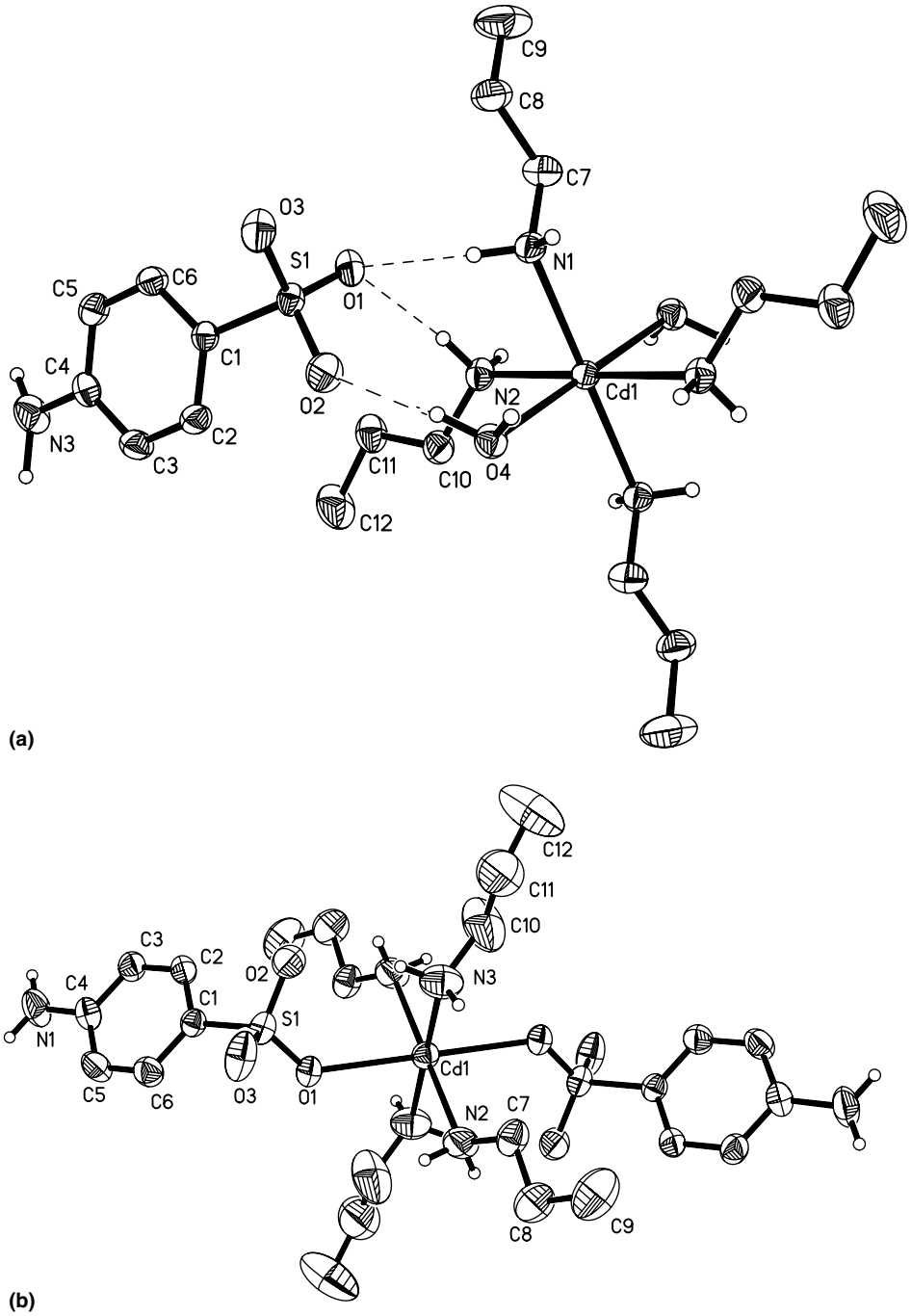

Fig. 5. The coordination structures of $[Cd(n\text{-}C_3H_7NH_2)_4(H_2O)_2](p\text{-}H_2NC_6H_4SO_3)_2$ (a) and $[Cd(n\text{-}C_3H_7NH_2)_4(p\text{-}H_2NC_6H_4SO_3)_2]\cdot C_3H_7NH_2$ (b). Hydrogen bonds are represented as dashed lines. Both Cd(II) centers locate on the symmetric centers and only the independent atoms are labelled. Hydrogen atoms bonded to carbon atoms are omitted for clarity.

investigated and the reaction products were characterized. The results show that the single phase monoamine-coordinated copper(II) and cadmium(II) complexes could be obtained without using any solvent or involving any purification process. The distinctive heterogeneous reaction can be employed as a solvent-free method to synthesize monoamine-coordinated Cu(II) and Cd(II) complexes. Furthermore, single crystals of the reaction products could be obtained in situ of the heterogeneous reaction process, which represents a unique method to obtain a single crystal via a green route [10].

5. Supplementary data

Crystallographic data for $[Cd(n\text{-}C_3H_7NH_2)_4(H_2O)_2](p\text{-}H_2NC_6H_4SO_3)_2$ has been deposited with the Cambridge Crystallographic Data Center as supplementary publication number CCDC 290252. Copies of the data can be

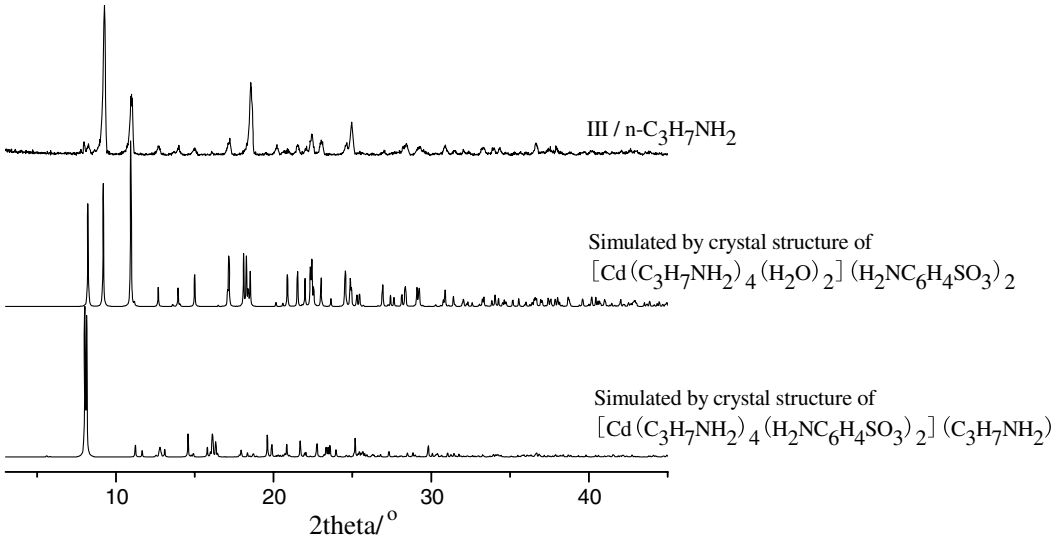

Fig. 6. PXRD of the n-$C_3H_7NH_2$ complex obtained from the reaction powder and the simulated PXRD from single crystal structures.

obtained, free of charge, on application to CCDC, 12 Union Road, Cambridge CB2 1EZ, UK (fax: +44(0) 1223 336033 or email: deposit@ccdc.cam.ac.uk).

Acknowledgements

We are thankful for the financial support from the National Natural Sciences Foundation of China (Grant No. 20271053).

References

[1] (a) D.M. Poojary, A. Clearfield, J. Am. Chem. Soc. 117 (1995) 11278;
(b) Y. Zhang, A. Clearfield, Inorg. Chem. 31 (1992) 2821;
(c) G. Cao, V.M. Lynch, L.N. Yacullo, Chem. Mater. 5 (1993) 1000;
(d) Y. Zhang, K.J. Scott, A. Clearfield, Chem. Mater. 5 (1993) 495;
(e) G. Cao, T.E. Mallouk, Inorg. Chem. 30 (1991) 1434;
(f) K.J. Frink, R.-C. Wang, J.L. Colon, A. Clearfield, Inorg. Chem. 30 (1991) 1438;
(g) F. Fredoueil, D. Massiot, P. Janvier, F. Gingl, M. Bujoli-Doeuff, M. Evain, A. Clearfield, B. Bujoli, Inorg. Chem. 38 (1999) 1831.
[2] J. Cai, J.-S. Zhou, M.-L. Lin, J. Mater. Chem. 13 (2003) 1806.
[3] J.-S. Zhou, J. Cai, L. Wang, S.W. Ng, J. Chem. Soc. Dalton Trans. 4 (2004) 1493.
[4] J. Cai, Coord. Chem. Rev. 248 (2004) 1061.
[5] (a) G.K.H. Shimizu, G.D. Enright, C.I. Ratcliffe, G.S. Rego, J.L. Reid, J.A. Ripmeester, Chem. Mater. 10 (1998) 3282;
(b) S.K. Mäkinen, N.J. Melcer, M. Parvez, G.K.H. Shimizu, Chem. Eur. J. 4 (2001) 5176;
(c) A.P. Côté, G.K.H. Shimizu, Coord. Chem. Rev. 245 (2003) 49.
[6] (a) S. Kitagawa, R. Kitaura, S. Noro, Angew. Chem. Int. Ed. 43 (2004) 2334;
(b) S. Kitagawa, K. Uemura, Chem. Soc. Rev. 34 (2005) 109.
[7] L. Wang, X.-L. Yu, J. Cai, J.-W. Huang, J. Chem. Crystallogr. 35 (2005) 481.
[8] G.M. Sheldrick, SADABS, Bruker Area Detector Absorption Corrections, Bruker AXS Inc., Madison, WI, USA, 1996.
[9] G.M. Sheldrick, SHELXL97, Program for X-ray Crystal Structure Solution and Refinement, Göttingen University, Göttingen, Germany, 1997.
[10] D. Braga, D. D'Addario, S.L. Giaffreda, L. Maini, M. Polito, F. Grepioni, Top. Curr. Chem. 254 (2005) 71.

pyridyl)-2,3-diaza-1,3-butadiene (**2**) and 3,6-di-(2-thienyl)-1,2,4,5-tetrazine (**3**), in which the ligand bridges the diiron (Fe—Fe) unit through pyrrolyl, pyridyl and thienyl imine groups, imine nitrogen groups, imine σ and π, and N—N diaza groups. The original ligand undergoes nitrogen—nitrogen bond cleavage, *endo* cyclometallation or diaza coordination during the course of the reaction with $Fe_2(CO)_9$. The choice of this series of ligands stems from our interest in the synthesis and finding the reactivity of new diiron complexes, as well as their biological aspects. The (μ-η^1:η^2-pyrrolyl/thienyl; η^1:$\eta^1(N)$)hexacarbonyldiiron complexes, imine-bridged (μ-σ;π-η^1:η^2-(C,N); $\eta^1(N_{py})$)hexacarbonyldiiron complex and imine-bridged (μ-π-η^1:η^1-(C, N); $\eta^1(N_{py})$; $\eta^1(N'_{py})$)hexacarbonyldiiron complex show unique binding modes to the diiron (Fe—Fe) unit.

2. Results and discussion

2.1. Synthesis of ligands

The pyrrolyl, pyridyl and thienyl Schiff bases 1,4-di-(*N*-methyl-2-pyrrolyl)-2,3-diaza-1,3-butadiene (**1**), 1,4-di-(6-methyl-2-pyridyl)-2,3-diaza-1,3-butadiene (**2**) and 3,6-di-(2-thienyl)-1,2,4,5-tetrazine (**3**) were prepared by condensation of *N*-methyl-2-formylpyrrol, 6-methyl-2-formylpyridine and 2-thiophenecarbonitrile with hydrazine in anhydrous ethanol. These compounds were fully characterized spectrally. Each pyrrolyl, pyridyl or thienyl proton in each ligand can be easily assigned from the ^{1}H NMR spectra according to its specific chemical shift and the characteristic coupling constant(s). All the ligands show a characteristic C═N stretching absorption around 1600 cm^{-1} in their IR spectra. The mass spectra of the ligands all show their own specific molecular ion peak (M^+). The structures of the ligands **1** and **3** were further confirmed by single crystal X-ray analysis. Crystal and data collection parameters are shown in Table 1. Their crystal structures are shown in Figs. 1 and 2, respectively. Selected bond distances and bond angles are tabulated in Table 2. The geometries of both **1** and **3** are well planar and all the π electrons are delocalized through the whole molecule.

2.2. Complex formation and characterization

2.2.1. Complexes derived from ligand *1*

The pyrrolyl Schiff base **1** reacts with $Fe_2(CO)_9$ in refluxing toluene to give two complexes, which we formulated as **1a** and **1b**, respectively (Scheme 1). Product **1a** is a diiron hexacarbonyl complex with two new chemically identical independent ligands, *N*-methyl-2-pyrrolylmethylideneamido, which were derived from the N—N bond cleavage of the original ligand **1**, and that bridge two $Fe(CO)_3$ units through azomethine nitrogen atoms. Product **1b** is a cyclometallated diiron hexacarbonyl complex, in which the C—H bond of the β-carbon on one of the pyrrolyl groups has been activated.

The ^{1}H NMR spectrum of **1a** shows five sets of signals with the same pattern as that of ligand **1**, indicating that two pyrrolyl rings as well as two imines in the complex are in the same chemical environment. Although three sets of pyrrolyl protons show a little upfield shift, the signal corresponding to the imine proton downfield shifts from δ

Table 1
Crystal and data collection parameters for compounds **2**, **3** and **5**

Compound	**1**	**3**	**1a**	**2a**	**3a**	**3c**
Formula	$C_{12}H_{14}N_4$	$C_{10}H_6N_4S_2$	$C_{19}H_{18}Fe_2N_4O_7$	$C_{20}H_{14}Fe_2N_4O_6$	$C_{16}H_6Fe_2N_4O_6S_2$	$C_{33}H_{21}Fe_2N_4O_5PS_2$
F_w	214.27	246.30	526.07	518.05	526.06	760.34
Crystal system	orthorhombic	monoclinic	triclinic	triclinic	triclinic	orthorhombic
Space group	*Pbcn*	$P2_1/n$	$P\bar{1}$	$P\bar{1}$	$P\bar{1}$	$P2_12_12_1$
a (Å)	24.737(4)	5.227(2)	7.9882(8)	8.351(1)	7.956(2)	15.281(3)
b (Å)	6.0359(9)	9.129(1)	11.6292(12)	8.444(1)	15.107(3)	18.193(2)
c (Å)	7.6523(11)	10.922(1)	12.9607(13)	15.943(2)	17.61(1)	12.444(3)
α (°)	90		99.674(2)	96.46(1)	75.61(1)	90
β (°)	90	92.84(2)	99.752(2)	93.89(1)	78.13(2)	90
γ (°)	90		96.104(2)	96.93(1)	87.25(2)	90
Volume (Å^3)	1142.6(3)	520.5(2)	1158.4(2)	1105.2(3)	2032.0(7)	3460(1)
Z	4	2	2	2	4	4
D_{calc} (g/cm^3)	1.246	1.571	1.494	1.557	1.719	1.460
Crystal size (mm)	0.38 × 0.36 × 0.13	0.52 × 0.42 × 0.20	0.37 × 0.14 × 0.10	0.36 × 0.24 × 0.22	0.78 × 0.30 × 0.20	0.96 × 0.42 × 0.40
Temperature (K)	150(2)	298.2	150(2)	298.2	298.2	298.2
θ Range (°)	1.65–27.52	2.23–25.00	1.62–27.49	2.45–26.00	2.05–24.99	2.11–25.99
Reflections measured	6436	1095	7296	4672	7461	4124
Number of data collected (R_{int})	1311 (0.0465)	986 (0.011)	5101 (0.0237)	4359 (0.030)	7162 (0.1222)	3820 (0.011)
Number of reflections	768 ($I > 2.00\sigma(I)$)	799 ($I > 3.00\sigma(I)$)	3523 ($I > 2.00\sigma(I)$)	3127 ($I > 3.00\sigma(I)$)	5077 ($I > 3.00\sigma(I)$)	3314 ($I > 3.00\sigma(I)$)
Number of parameters	74	73	304	289	541	424
F(000)	456	252	526	524	1048	1544
Goodness-of-fit	0.982	3.275	1.055	1.126	3.237	2.519
R_1	0.0453	0.032	0.0464	0.0277	0.0476	0.0351
wR_2	0.1163	0.040	0.1266	0.0396	0.0518	0.0470

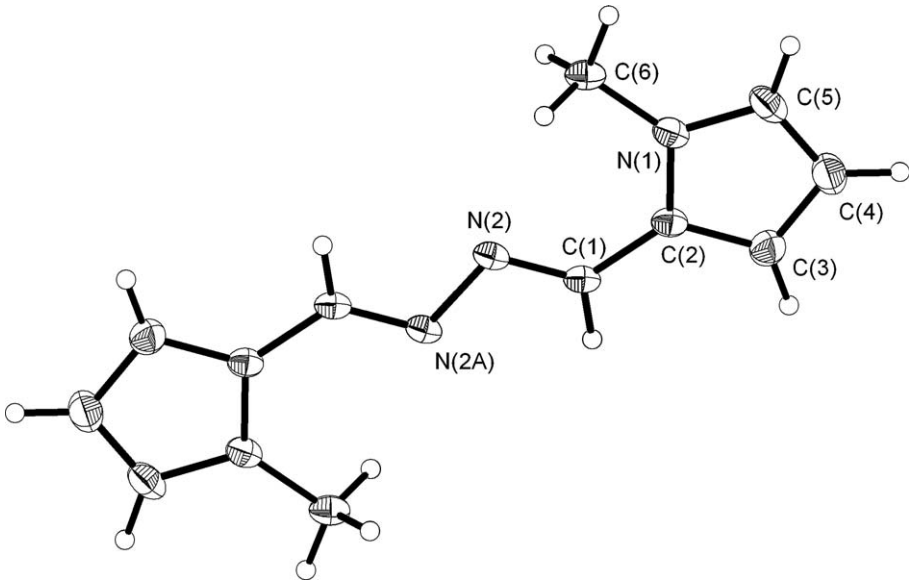

Fig. 1. ORTEP diagram of **1** at the 30% probability level.

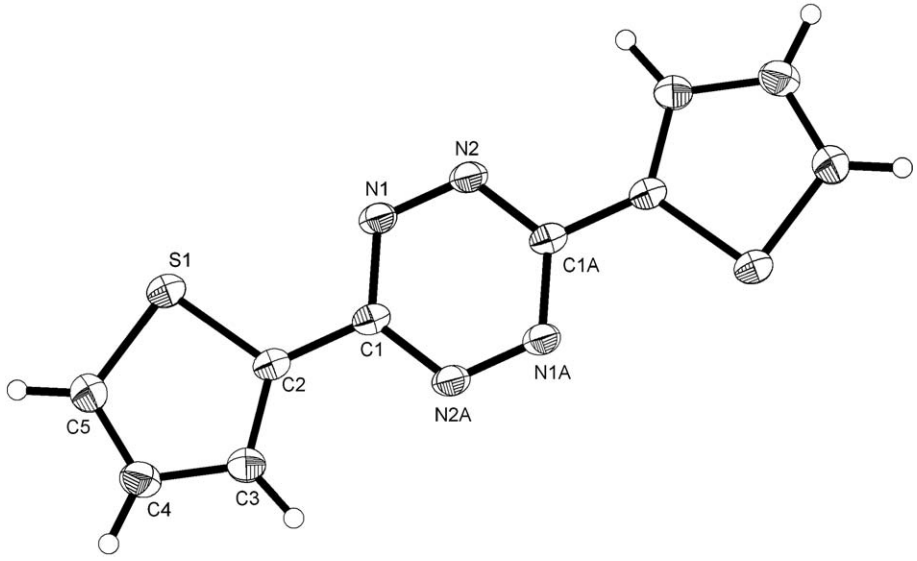

Fig. 2. ORTEP diagram of **3** at the 30% probability level.

Table 2
Selected bond lengths (Å) and bond angles (°) for ligands **1** and **3**

1			
N(2)—N(2A)	1.417(3)	N(2)—C(1)	1.284(2)
C(1)—C(2)	1.437(2)		
N(2A)—N(2)—C(1)	111.3(2)		
3			
N(1)—N(2)	1.317(3)	N(1)—C(1)	1.350(3)
N(2A)—C(1)	1.351(3)	C(1)—C(2)	1.444(3)
N(1)—N(2)—C(1A)	117.6(2)	C(1)—N(1)—N(2)	117.8(2)
N(1)—C(1)—N(2A)	124.5(2)	N(1)—C(1)—C(2)	117.8(2)

8.50 ppm (ligand **1**) to 9.00 ppm. In its IR spectrum, the C=N stretching shifts from 1625 cm^{-1} in **1** to 1638 cm^{-1}, and there are three sharp and intense C=O stretches appearing at 2061, 2021 and 1972 cm^{-1}. The fragmentation pattern of its mass spectrum shows no evidence of a peak with a m/z value of 214, corresponding to ligand **1**. However, peaks at m/z 107 and 108 were observed to accompany the presence of a molecular ion peak at m/z 495 and six peaks corresponding to sequential CO loss products, in accordance with the formulated structure.

The ^{1}H NMR spectrum of **1b** shows only one azomethine proton at δ 7.96 ppm, two methylene protons at δ 4.53 ppm, and six methyl protons at δ 3.84 ppm, in addition to the five sets of pyrrolyl protons in the range of δ 7.23–6.08 ppm. Among the five sets of pyrrolyl protons, three are doublets with a coupling constant $J_{H-H} = 2.7$ Hz, one is a doublet with a coupling constant $J_{H-H} = 3.6$ Hz, and another set

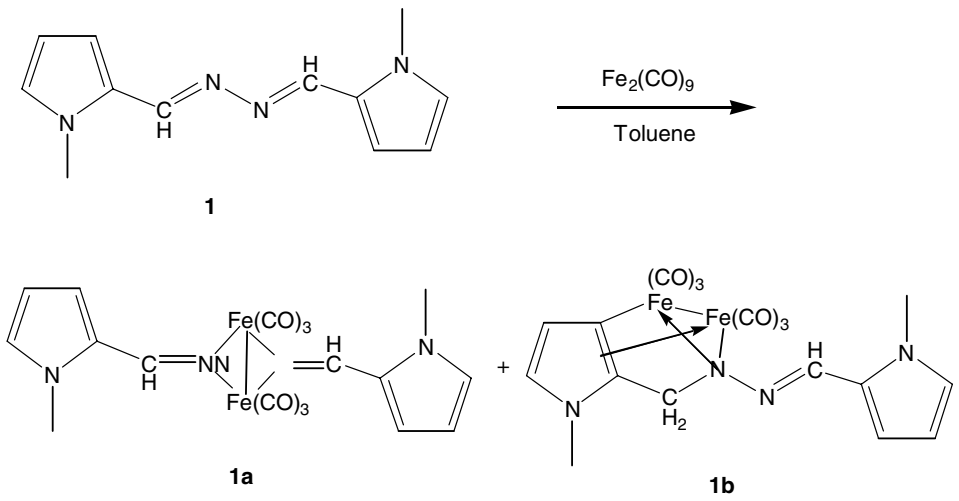

Scheme 1.

is a doublet of doublets with coupling constants $J_{H-H} = 3.6$ and 2.7 Hz, respectively. This result was interpreted as coordination of one of the azomethine nitrogens of the pyrrolyl azine ligand on one of the iron centers, C—H activation occurs at the β-carbon of the pyrrolyl ring, which is adjacent to the coordinated imine, to form a five-membered *endo* metallacycle, and the methine group becomes a methylene group by adopting the hydrogen originating from the β-carbon. This transformation follows the sequential route: coordination, *endo* cyclometallation and 1,3-hydrogen shift. The singlet signal of the methylene protons indicates that the two protons are equivalent. The lack of diastereotopicity of the methylene protons in the azametallacycle of the complex indicates that a fluxional process, the so-called 'windscreen-wiper type oscillation', of the ligand might occur in the complex [11]. The IR spectrum of the complex shows a characteristic C=N stretching at 1622 cm^{-1} and three sharp and intense C=O stretches at 2055, 2011 and 1963 cm^{-1}. The mass spectrum of **1b** shows the molecular ion peak and the complete loss of six CO ligands in a sequential manner, in accordance with the formulated structure.

2.2.2. Complexes derived from ligand 2

The pyridyl Schiff base **2** reacts with $Fe_2(CO)_9$ in refluxing THF to yield two hexacarbonyldiiron complexes **2a** and **2b** (Scheme 2) in moderate yield. Neither N—N bond cleavage of the molecule nor cyclometallation, as expected, was observed in this reaction. In both complexes, one of the imines of the original ligand is involved in coordination by using its π-electron system and bridges to two $Fe(CO)_3$ units. In complex **2a**, the azomethine nitrogen acts as the second bridging atom to the two $Fe(CO)_3$ units and one pyridyl nitrogen serves as a σ-donor atom to complete

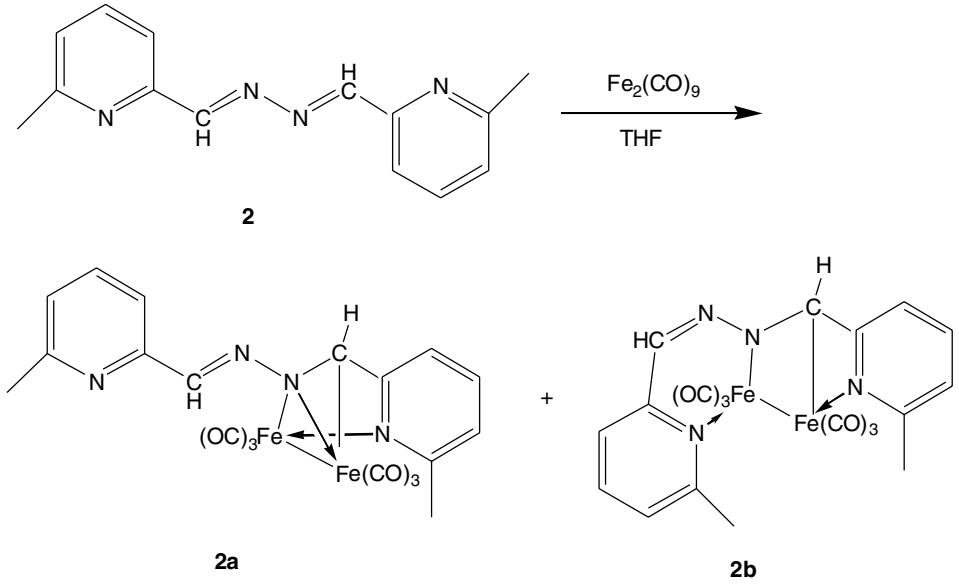

Scheme 2.

the 36-electron structure of the iron centers. In complex **2b**, in addition to the bridging imine, both pyridines are involved and coordinate to the two $Fe(CO)_3$ units, separately. When the reaction was conducted at room temperature, complex **2a** and a trace amount of **2b** were obtained. If the reaction was allowed to proceed under irradiation of UV light, a high yield of complex **2a** was obtained as the sole product.

The ^1H NMR spectrum of **2a** shows only one azomethine proton at δ 8.82 ppm, which is downfield shifted relative to that in the original ligand **2** (δ 8.58 ppm). There are six sets of signals in the aromatic region corresponding to two groups of three pyridyl protons indicating that the two pyridine rings are in different environments. One group of three pyridyl protons (δ 7.45(*t*), 7.21(*d*) and 6.79(*d*) ppm) are found to be substantially upfield shifted relative to that in the free ligand (δ 7.98(*d*), 7.81(*t*) and 7.37(*d*) ppm), due to the coordination of the pyridyl nitrogen, while another group of three pyridyl protons remain unchanged in their chemical shifts to that in the free ligand. There is a new singlet proton, appearing at δ 4.82 ppm, that is assigned to be the proton on the coordinated azomethine carbon, which has been turned from sp^2 into sp^3 hybridization causing a drastic upfield shift of the proton signal from δ 8.53 to 4.82 ppm. The IR spectrum of the complex shows a characteristic C=N stretching at 1583 cm^{-1} and three sharp and intense C=O stretches at 2054, 1083 and 1926 cm^{-1}. The mass spectrum of **2a** contains a signal for the molecular ion and six peaks corresponding to sequential CO loss products, in accordance with the formulated structure.

The ^1H NMR spectrum of **2b** is very similar in pattern to that of **2a**. Only one azomethine proton appears at δ 8.86 ppm. Six different pyridyl protons indicate that the two pyridine rings are in different chemical environments. However, different from that in complex **2a**, both two groups of pyridyl protons are found to be upfield shifted, indicating the coordination of both pyridine rings. The new singlet signal at δ 4.54 ppm is assigned to the proton on the coordinated azomethine carbon. The IR spectrum of the **2b** shows a characteristic C=N stretching at 1573 cm^{-1} and three sharp and intense C=O stretches at 2045, 1992 and 1967 cm^{-1}. The mass spectrum of **2b** shows the same result as that of **2a**.

2.2.3. Complexes derived from ligand 3

The thienyl ligand **3** reacts with $Fe_2(CO)_9$ in refluxing benzene to yield two hexacarbonyldiiron complexes **3a** and **3b** (Scheme 3). In complex **3a**, a diazo group acts as a 6-electron donor and bridges two $Fe(CO)_3$ units. Complex **3b** is a cyclometallated product, in which the C—H bond of the β-carbon on one of the thienyl groups has been activated. We attempted to prepare the doubly cyclometallated tetrairon complex and the N—N bond cleaved product under more vigorous reaction conditions in toluene, but in vain. In the presence of an excess

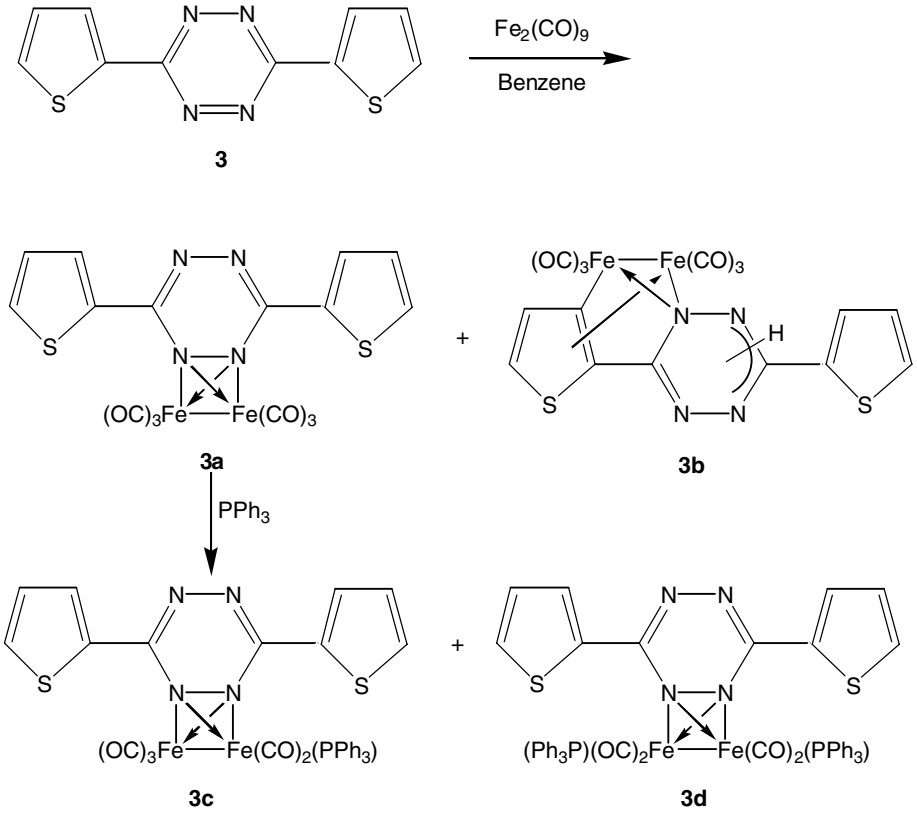

Scheme 3.

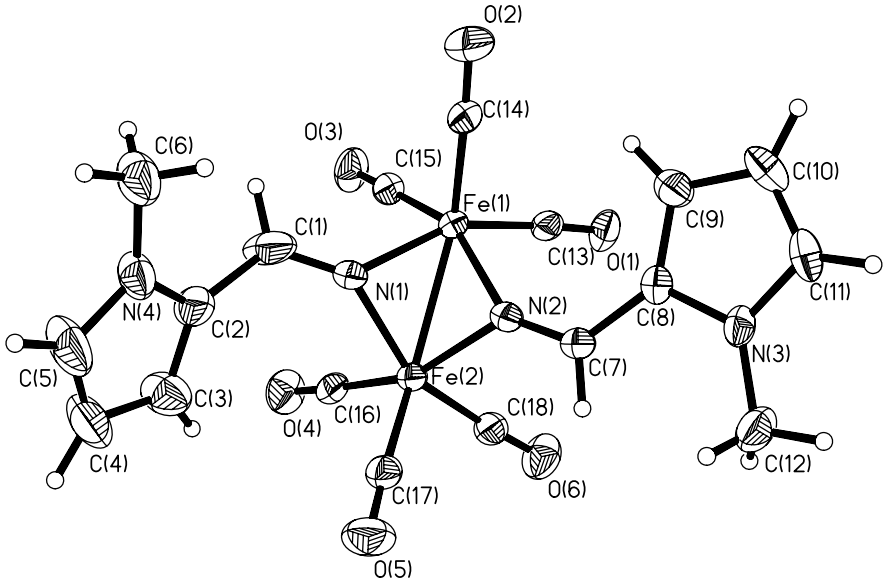

Fig. 3. ORTEP diagram of **1a** at the 30% probability level.

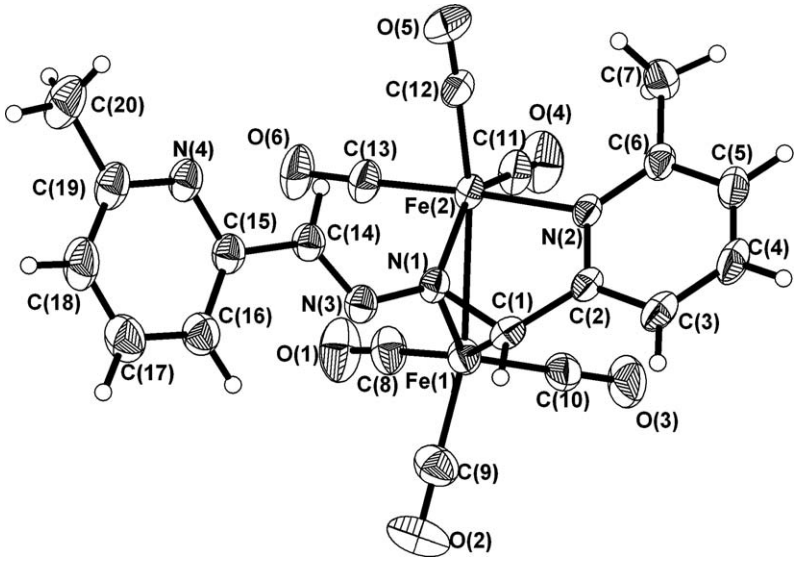

Fig. 4. ORTEP diagram of **2a** at the 30% probability level.

amount of triphenylphosphine, complex **3a** was converted into **3c** and **3d** in which one or two carbonyls were substituted by triphenylphosphine.

The ^{1}H NMR spectrum of **3a** shows three sets of thienyl proton signals similar to that of ligand **3**, indicating a symmetric geometry of the complex. In its IR spectrum, there is an imine stretching absorption at 1543 cm^{-1} and a number of terminal carbonyl stretches appearing in the range of 2076–1972 cm^{-1}. The mass spectrum of **3a** contains a signal for the molecular ion and six peaks corresponding to sequential CO loss products, in accordance with the formulated structure.

The ^{1}H NMR spectrum of **3b** shows five sets of signals with characteristic coupling constants ($J_{H-H} = 5.1$ and 3.6 Hz) corresponding to five specific thienyl protons, indicating an asymmetrical geometry of the complex, and a β-proton on one of the thienyl rings disappeared. There appears a new broad signal at δ 9.01 ppm, which is subjected to shift with different concentrations, and is assigned as an amine proton. In its IR spectrum, other than the imine (C═N) stretching absorptions at 1637 and 1573 cm^{-1} and terminal carbonyl (─CO) stretches at 2072–1952 cm^{-1}, there is a secondary amine N─H stretching absorption at 3352 cm^{-1} and a bending absorption at

1521 cm^{-1}. The mass spectrum of **3b** shows the same result as that of **3a**.

Complexes **3c** and **3d** are derived from **3a** through the substitution of carbonyl ligand(s) with triphenylphosphine. Their ^1H NMR spectra adopt the same pattern as that of **3a** except the additional signals of triphenylphosphine. However, the thienyl protons are upfield shifted from **3a** to **3c** to **3d** due to the inductive effect of the phosphine ligand. The inductive effect also drives the lower energy shift of the IR stretching frequencies of the terminal carbonyls in the same sequence. The mass spectra of **3c** and **3d** show their own specific molecular ion peak (M^+) at *m/z* 761 and 995, respectively, fragments corresponding to the sequential loss of CO ligands, phosphine and the ligand ion peak, in accordance with the formulated structures.

2.3. Molecular structure of complexes *1a, 2a, 3a* and *3c*

The molecular structures of **1a**, **2a**, **3a** and **3c**, as confirmed by the single crystal X-ray diffraction analysis, are shown in Figs. 3–6, respectively. Their crystal and data collection parameters are tabulated in Table 1 and selected bond distances and bond angles are summarized in Tables 3 and 4.

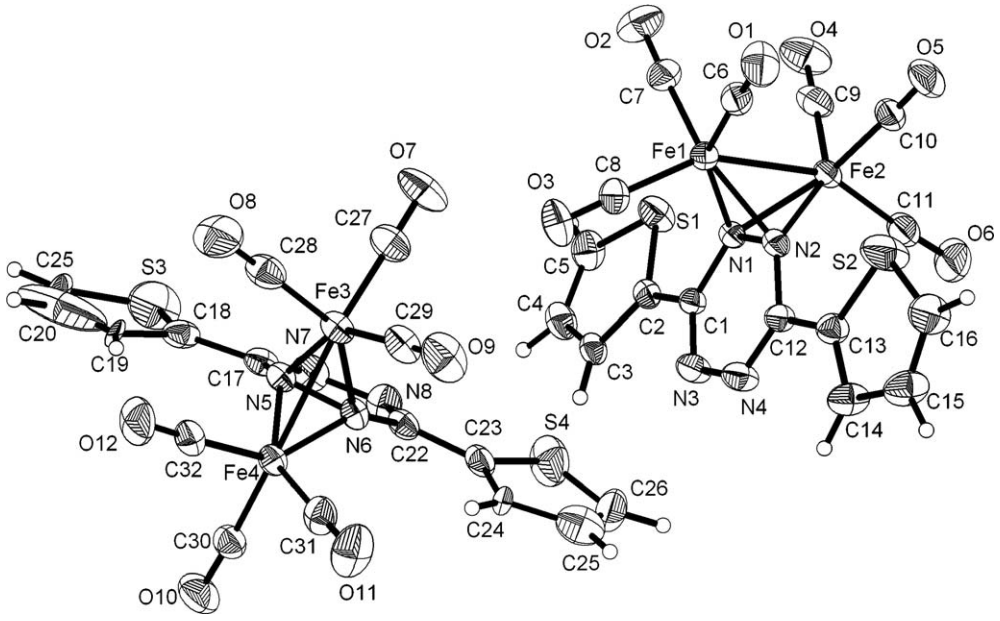

Fig. 5. ORTEP diagram of **3a** at the 30% probability level.

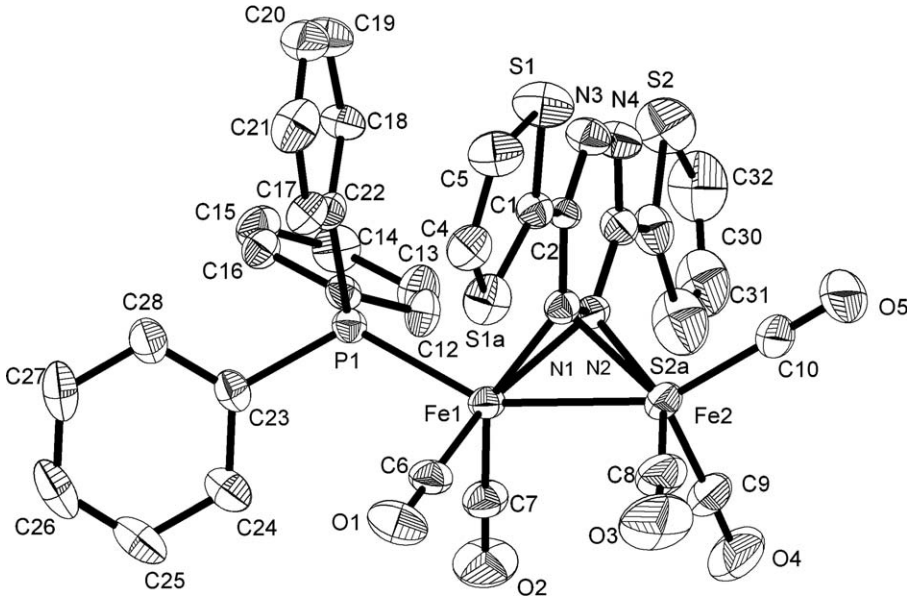

Fig. 6. ORTEP diagram of **3c** at the 30% probability level.

Table 3
Selected bond lengths (Å) and bond angles (°) for complexes **1a** and **2a**

1a			
N(2)—C(1)	1.274(6)	Fe(1)—Fe(2)	2.4084(7)
Fe(1)—N(1)	1.934(3)	Fe(1)—N(2)	1.922(3)
Fe(2)—N(1)	1.935(3)	Fe(2)—N(2)	1.922(3)
Fe(1)—N(1)—Fe(2)	77.0(1)	Fe(1)—N(2)—Fe(2)	77.42(11)
Fe(2)—Fe(1)—N(1)	51.52(10)	Fe(1)—Fe(2)—N(1)	51.50(9)
N(1)—Fe(1)—N(2)	76.77(13)	N(1)—Fe(2)—N(2)	76.93(13)
Fe(1)—N(1)—C(1)	136.2(3)	Fe(2)—N(1)—C(1)	140.7(3)
N(1)—C(1)—C(2)	125.1(4)		
2a			
Fe(1)—Fe(2)	2.5698(5)	Fe(1)—N(1)	1.930(2)
Fe(1)—C(1)	2.025(3)	Fe(2)—N(1)	1.948(2)
Fe(2)—N(2)	2.030(2)	C(1)—N(1)	1.401(3)
C(14)—N(3)	1.268(3)	N(1)—N(3)	1.419(3)
N(1)—Fe(1)—Fe(2)	48.48(6)	C(1)—Fe(1)—Fe(2)	72.19(7)
N(1)—Fe(1)—C(1)	41.40(9)	N(1)—Fe(2)—Fe(1)	48.20(6)
N(2)—Fe(2)—Fe(1)	86.64(6)	N(1)—Fe(2)—N(2)	83.35(8)
Fe(1)—N(1)—Fe(2)	82.99(8)	Fe(2)—N(1)—C(1)	108.8(2)
Fe(1)—N(1)—C(1)	72.9(1)	Fe(2)—N(1)—N(3)	135.9(2)
Fe(1)—N(1)—N(3)	120.8(1)	N(3)—N(1)—C(1)	113.4(2)
Fe(2)—N(2)—C(6)	130.3(2)	Fe(2)—N(2)—C(2)	110.3(2)
N(1)—C(1)—C(2)	114.8(2)	Fe(1)—C(1)—N(1)	65.7(1)
Fe(1)—C(1)—C(2)	113.6(2)	N(1)—N(3)—C(14)	115.9(2)

Table 4
Selected bond lengths (Å) and bond angles (°) for complexes **3a** and **3c**

3a			
Fe(1)—Fe(2)	2.502(1)	Fe(1)—N(1)	1.920(4)
Fe(1)—N(2)	1.918(4)	Fe(2)—N(1)	1.923(4)
Fe(2)—N(2)	1.921(4)	N(1)—N(2)	1.410(6)
N(1)—C(1)	1.395(6)	N(2)—C(12)	1.410(6)
C(1)—N(3)	1.300(7)	C(12)—N(4)	1.286(7)
N(4)—N(3)	1.396(6)	C(1)—C(2)	1.444(7)
Fe(2)—Fe(1)—N(1)	49.4(1)	Fe(2)—Fe(1)—N(2)	49.4(1)
N(1)—Fe(1)—N(2)	43.1(2)	Fe(1)—Fe(2)—N(1)	49.3(1)
Fe(1)—Fe(2)—N(2)	49.3(1)	N(1)—Fe(2)—N(2)	43.0(2)
Fe(1)—N(1)—Fe(2)	81.3(2)	Fe(1)—N(2)—Fe(2)	81.4(2)
Fe(1)—N(1)—N(2)	68.4(3)	Fe(1)—N(2)—N(1)	68.5(2)
Fe(2)—N(1)—N(2)	68.4(3)	Fe(2)—N(2)—N(1)	68.6(2)
N(2)—N(1)—C(1)	116.7(4)	N(1)—C(1)—N(3)	123.1(5)
N(1)—C(1)—C(2)	117.3(5)	C(1)—N(3)—N(4)	119.7(5)
3c			
Fe(1)—Fe(2)	2.512(1)	Fe(1)—N(1)	1.910(2)
Fe(1)—N(2)	1.947(4)	Fe(1)—P(1)	2.254(2)
Fe(2)—N(1)	1.904(2)	Fe(2)—N(2)	1.934(4)
N(1)—N(2)	1.419(5)	N(1)—C(1)	1.417(6)
N(2)—C(29)	1.384(7)	C(1)—N(3)	1.275(6)
C(29)—N(4)	1.322(7)	N(3)—N(4)	1.387(6)
Fe(2)—Fe(1)—N(1)	48.7(1)	Fe(2)—Fe(1)—N(2)	49.4(1)
N(1)—Fe(1)—N(2)	43.4(2)	P(1)—Fe(1)—N(1)	105.6(1)
P(1)—Fe(1)—N(2)	104.5(1)	P(1)—Fe(1)—Fe(2)	151.42(5)
Fe(1)—Fe(2)—N(1)	48.7(1)	Fe(1)—Fe(2)—N(2)	49.4(1)
N(1)—Fe(2)—N(2)	43.4(2)	Fe(1)—N(1)—Fe(2)	82.4(2)
Fe(1)—N(1)—N(2)	69.8(3)	Fe(1)—N(2)—Fe(2)	82.4(2)
Fe(2)—N(1)—N(2)	69.4(2)	Fe(1)—N(2)—N(1)	69.8(3)
N(2)—N(1)—C(1)	116.8(4)	Fe(2)—N(2)—N(1)	69.4(2)
N(1)—C(1)—N(3)	122.5(5)	N(1)—C(1)—C(2)	115.5(5)
C(1)—N(3)—N(4)	121.6(5)		

2.3.1. $[Fe(CO)_3(MeC_4H_3NCHN)]_2$ (**1a**)

The structure of **1a**, as shown in the Fig. 3, contains two 2-pyrrolylmethylideneamido moieties which bridge two $Fe(CO)_3$ units through amido nitrogen atoms. It is clear that the N—N bond in ligand **1** has been cleaved during the coordination reaction and the non-bonded N···N distance is 2.399 Å. The configuration of the individual molecule has idealized 2-fold symmetry. The tricarbonyl groups are eclipsed. The amido nitrogen and iron atoms form a tetrahedron. The central position of the molecule is thus similar in shape to that of $Co_2(CO)_8$. Plane calculations show that all pairs of atoms are equidistant from opposite sides to the C_2 axis, which is perpendicular to the mid-point of the Fe—Fe bond. Each iron center is coordinated by two nitrogen atoms and three carbonyls located at the corners of a distorted octahedron. The Fe—Fe distance is only 2.4084(7) Å, which is shorter than usual for diiron complexes (2.5–2.7 Å) [4f,4g,12], but can be compared with the value found in some nitrogen-bridged diiron complexes [4a,10g,13], and can be attributed to a distinct 'bent' iron—iron bond [14]. The bond distances between iron and bridging nitrogens are Fe(1)—N(1) 1.934(3) Å, Fe(1)—N(2) 1.922(3) Å, Fe(2)—N(1) 1.935(2) Å and Fe(2)—N(2) 1.922(2) Å, which are shorter than those in reported nitrogen bridged diiron complexes [4f,4g,10,12e,12f,13]. The significantly shorter averaged Fe—N bond distance of 1.928 Å in this complex can be ascribed to the structure possessing two three-coordinated trigonal-like bridging nitrogen atoms, instead of four-coordinated tetrahedral-like bridging nitrogen atoms, and the nitrogen atoms of the complex can be considered as sp^2 hybridized [15]. The bond distance between C(1) and N(1) (1.273(4) Å) is shorter than the C=N bond distance in ligand **1** (1.284(2) Å), and yet is still in the range of usual bond lengths of imine double bonds. In the central Fe_2N_2 system, the averaged Fe—N—Fe, N—Fe—Fe and N—Fe—N bond angles are 77.20°, 51.51° and 76.87°, respectively. The bond angles of Fe(1)—N(1)—C(1), Fe(2)—N(1)—C(1), Fe(1)—N(2)—C(7) and Fe(2)—N(2)—C(6) are 136.2(3)°, 140.7(3)°, 146.4(3)° and 134.1(3)°, respectively. These large angles are associated with the short Fe—Fe bond length and the sp^2 hybridization of the nitrogen atoms.

The cleavage of the N—N bond during the course of ligand coordination leads to a reduced degree of conjugation of the ligand and might increase the π-electron density on the imine group which explains why there is a 0.50 ppm downfield chemical shift of the azomethine protons in its ^{1}H NMR spectrum. On the other hand, relative to the highly conjugated ligand **1**, the bond order of the imine group in the complex might increase. The IR stretching absorption of the C=N group is higher energy shifted from 1625 cm^{-1} in ligand **1** to 1638 cm^{-1} in the iminato-bridged complex and is consistent with the shortening of the C=N bond length in **1a**.

2.3.2. $Fe_2(CO)_6(MeC_5H_3NCHNNCHC_5H_3NMe)$ (**2a**)

The molecular structure of compound **2a**, as shown in Fig. 4, shows that the iron atoms possess a distorted

octahedral coordination geometry. The Fe—Fe inter-metallic distance is 2.5689(5) Å (Table 3). The iron atoms are bridged by one of the imine fragments, C(1)=N(1), of the ligand in the η^2-C=N bonding mode. The azomethine N(1) atom and the pyridine N(2) atom, which is next to the coordinated azomethine, are σ-bonded to the Fe(1) and Fe(2) centers, respectively. Therefore, it can be inferred that the pyridyl azine is coordinated in the σ-N, μ^2-N′, η^2-C=N′ bonding mode to the iron atoms in which the ligand forms a 6e bridge between the two $Fe(CO)_3$ moieties. The Fe(1)—N(1) and Fe(2)—N(1) distances are 1.930(2) and 1.948(2) Å, respectively; the Fe(1)—C(1) distance is 2.025(3) Å, while the Fe(2)—N(2) distance is 2.030(2) Å. These are normal values for such bonds. The C(1)—N(1) distance of 1.401(3) Å is significantly elongated compared to the C(14)—N(3) bond distance (1.268(3) Å) in the uncoordinated C=N moiety, as expected for the η^2-bonding mode of this fragment [16]. The C(2)—N(2) distance of 1.353(3) Å in the σ-N-coordinated pyridine ring is comparable to the usual σ-N-coordinated azomethine group [17], which can be attributed to effective delocalization of electron density in the coordinated pyridine ring in the complex.

Around the central core, the N(1)—Fe(1)—Fe(2), N(1)—Fe(2)—Fe(1) and N(1)—Fe(1)—C(1) bond angles are 48.81(6)°, 48.20(6)° and 41.40(9)°, respectively, while the N(2)—Fe(2)—Fe(1) and N(2)—Fe(2)—N(1) angles are 86.64(6)° and 83.35(8)°. The Fe(1)—N(1)—Fe(2), Fe(1)—N(1)—C(1) and Fe(1)—C(1)—N(1) bond angles are 82.99°, 72.9(1)° and 65.7(1)°, respectively. The C(1)—N(1)—N(3) bond angle is squeezed to a value of 113.4(2)°. The Fe(2)—N(1)—C(1)—C(2)—N(2) atoms form a plane with a torsion angle of 21.44° between the C(1)—N(1) and C(2)—N(2) bonds. This implies that the planarity of the N=C—C=N system in the free ligand is not affected much by the σ-N, μ^2-N′, η^2-C=N′ type coordination [17b,18] and the dihedral angle defined by the mean plane of Fe(2)—N(1)—C(1)—C(2)—N(2) and the pyridine plane is 7.57°.

2.3.3. $Fe_2(CO)_6(C_4H_3SC_2N_4C_4H_3S)$ (**3a**)

The molecular structure of complex **3a**, as shown in Fig. 5, shows that the dithienyltetrazine ligand coordinates to the metal centers through one of its diazo moieties. The ligand has a σ-N, σ-N′, μ^2-η^2-N=N′ type of coordination mode in which the ligand forms a 6e bridge between the two $Fe(CO)_3$ units. The iron centers possess a distorted octahedral coordination geometry. The tricarbonyl groups are eclipsed. There are two geometries in the unit cell of **3a** with a difference in the orientation of the thienyl rings. The geometry of ligand **3**, as shown in Fig. 2, is planar with a C_{2h} symmetry. However, the two thienyl rings in complex **3a** are oriented in the same direction – with both of their thienyl S atoms pointing towards the iron centers in one geometry and backwards to the iron centers in the other geometry. In both cases the Fe—Fe bond is perpendicular to the N—N bond of the tertrazine ring. The dihedral angles between the central tetrazine ring and two thienyl rings, S(1)—C(2)—C(3)—C(4)—C(5) plane and S(2)—C(13)—C(14)—C(15)—C(16) plane, are 12.59° and 9.01°, respectively.

The Fe—Fe bond distance is 2.502(1) Å (Table 4). The bond distances Fe(1)—N(1), Fe(1)—N(2), Fe(2)—N(1) and Fe(2)—N(2) are 1.920(4), 1.918(4), 1.923(4) and 1.921(4) Å, respectively, which are shorter than usual nitrogen bridged diiron complexes. The Fe(1)—Fe(2)—N(1) and Fe(2)—Fe(1)—N(2) bond angles are 49.3(1)° and the Fe(2)—Fe(1)—N(1) and Fe(2)—Fe(1)—N(2) bond angles are 49.4(1)°. The bond angles of Fe(1)—N(1)—N(2), Fe(1)—N(2)—N(1), Fe(2)—N(1)—N(2) and Fe(2)—N(2)—N(1) are about the same and have an average value of 68.5(3)°. The N(1)—Fe(1)—N(2) and N(1)—Fe(2)—N(2) angles are also about the same (43.1(2)° versus 43.0(2)°), indicating that the Fe(1)Fe(2)N(2)N(1) core is quite symmetrical. The N(1)—N(2) bond of 1.410(6) Å is significantly elongated compared to the N(1)—N(2) bond distance (1.317(3) Å) in the highly conjugated ligand **3**, as expected for the σ-N and η^2-N=N bonding mode of this fragment. The elongation of N(3)=N(4), N(1)—C(1) and N(2)—C(12) bond distances (1.396(6), 1.395(6) and 1.410(6) Å) and the shortening of C(1)—N(3) and C(12)—N(4) distances (1.300(7) and 1.286(7) Å), relative to that in the uncoordinated ligand **3**, indicate that the aromaticity of the tetrazine ring has been destroyed and the ring has become the combination of a diaza (N—N) and a diimine (—C= N—N=C—).

2.3.4. $Fe_2(CO)_5PPh_3(C_4H_2SC_2N_4HC_4H_3S)$ (**3c**)

The molecular structure and bonding features of **3c**, as shown in Fig. 6 and Table 4, close resemble that of **3a** except one of carbonyl ligands on Fe(1) has been replaced by a triphenylphosphine ligand. The Fe(1)—P distance is 2.2542(2) Å. The P(1)—Fe(1)—N(1), P(1)—Fe(1)—N(2) and P(1)—Fe(1)—Fe(2) bond angles are 105.6(1)°, 104.5(1)° and 151.42(5)°, respectively. A disorder between S1 and S1a and between S2 and S2a on the two thiophene rings has been observed. The geometry of the molecule has ~70% with two thienyl sulfur atoms pointing toward the iron centers and ~30% with two sulfur atoms pointing backwards from the iron centers.

3. Conclusion

We have demonstrated that using different heterocyclic substituted azines **1**, **2** and **3** as ligands, hexacarbonyldiiron complexes with various coordination modes can be synthesized. In the reaction of iron carbonyls with azines, complexes with different coordination modes have been reported. In the reaction of $Fe_3(CO)_{12}$ with ketazines (R^1R^2C=N—N=C—R^1R^2, where $R^1 = R^2$ = Me; $R^1 = R^2 = p$-CH_3Ph; R^1 = Me, R^2 = Ph; R^1 = H, R^2 = thienyl), bis-(μ-ketoiminato)hexacarbonyldiiron complexes were produced, formed by cleavage of the N—N bond [10a,10f,19]. In contrast, in the similar benzaldazine system (R^1 = H, $R^2 = p$-substituted Ph), it led only to the *endo* cyclometallation of the phenyl ring [4a,20]. However, in

the reaction of *N*,*N*′-bis-(3-phenyl-allylidene)-hydrazine (RC=C–C=N–N=C–C=CR) with $Fe_2(CO)_9$, mono-, di- and tetrametallic iron carbonyl complexes were synthesized. In this case, no cleavage of the ligand was observed and only azomethine nitrogen atom(s) and allyl double bond(s) are bonded to the discrete $Fe(CO)_3$ center(s) [21]. Thus, the type of substituent on the azine system is critical for the way of complexation.

In this study, in the reaction with $Fe_2(CO)_9$, both N–N bond cleavage (η^2-N; η^2-N′ mode) and endo cyclometallation (μ-2,3-η^1:η^2-pyrrolyl; η^1:η^1(*N*) mode) are observed for ligand **1**, one pyridyl N and one imine-bridged (μ-σ;π-η^1:η^2-(*C*, *N*); η^1(N_{py}) mode), and two pyridyl N and one imine-bridged (μ-π-η^1:η^1-(*C*,*N*); η1(N_{py}); η^1(N'_{py}) mode) coordinations are found in the case of ligand **2**, whereas diaza-bridged (μ-η^2:η^2-(*N*,*N*′) mode) and endo cyclometallated (μ-2,3-η^1:η^2-thienyl; η^1:η^1(*N*) mode) coordinations are involved in the case of ligand **3**.

4. Experimental

4.1. General

Diiron nonacarbonyl was prepared through the photolysis of iron pentacarbonyl (Aldrich) in glacial acetic acid [22]. Solvents were dried (sodium/benzophenone, P_4O_{10}) and distilled under nitrogen prior to use. *N*-Methyl-2-pyrrolecarboxaldehyde (Acros) and 2-thiophenemethylamine (Aldrich) were distilled by a Kugelrohr distillation apparatus under reduced pressure (0.1 mmHg) prior to use. All other chemicals were reagent grade and used without further purification. The NMR spectra were recorded on a Bruker DX-300 NMR spectrometer (^{1}H, 299.95 MHz; ^{13}C, 75.43 MHz). Chemical shifts were referenced to TMS and deuterated acetone (Janssen) was used as a solvent and as a secondary reference. Mass spectra were obtained from a Micromass Platform II spectrometer. IR spectra were recorded employing a Mattson Genesis FTIR spectrophotometer. Elemental analyses were performed using a Perkin–Elmer 2400, 2400II elemental analyzer. Crystals for X-ray diffraction were obtained from ethyl acetate/dichloromethane (**1**), ethyl acetate/methanol (**1a**), ethyl acetate/ether (**2a**) and dichloromethane (**3**, **3a** and **3c**). A single crystal was mounted on a glass fiber and the X-ray diffraction intensity data were measured on a Bruker Smart 1000 CCD XRD (**1** and **1a**) or a Rigaku AFC7S diffractometer (**2a**, **3**, **3a**, and **3c**).

4.2. Synthesis of Schiff bases 1,4-di-(*N*-methyl-2′-pyrrolyl)-2,3-diaza-1,3-butadiene (*1*) and 1,4-di-(6-methyl-2′-pyridyl)-2,3-diaza-1,3-butadiene (*2*)

The synthesis of Schiff bases employed the usual approach of condensation in alcohol solution [23]. *N*-Methyl-2-formylpyrrol or 6-methyl-2-formylpyridine (40.0 mmol) and $N_2H_4 \cdot H_2O$ (Acros, 20.0 mmol) were heated at reflux in 95% ethanol (E. Merck, 100 mL) for 24 h. The solvent was removed by filtration. The precipitate was washed with several portions of ether and dried in vacuo to give pure yellow product **1** (18.8 mmol, 94% yield) or **2** (19.6 mmol, 98% yield).

*Compound **1**:* M.p. 114–115 °C. ^{1}H NMR: δ 8.50 (s, 2H), 6.93 (d, J_{H-H} = 2.6 Hz, 2H), 6.61 (d, J_{H-H} = 3.8 Hz, 2H), 6.15 (dd, J_{H-H} = 3.9, 2.7 Hz, 2H), 3.99 (s, 6H). ^{13}C NMR: δ 151.8, 128.8, 127.8, 117.0, 108.6, 36.1. IR (KBr film) $\nu_{C=N}$: 1625 cm^{-1}. MS (FAB): *m*/*z* 214 (M^+). *Anal.* Calc. for $C_{12}H_{14}N_4$: C, 67.28; H, 6.54; N, 26.16. Found: C, 67.01; H, 6.64; N, 26.30%.

*Compound **2**:* M.p. 175–176 °C. ^{1}H NMR (methanol-d_4): δ 8.58 (s, 2H), 7.98 (d, J_{H-H} = 7.8 Hz, 2H), 7.82 (t, J_{H-H} = 7.8 Hz, 2H), 7.37 (d, J_{H-H} = 7.8 Hz, 2H), 2.60 (s, 6H). ^{13}C NMR (methanol-d_4): δ 161.4, 158.8, 151.8, 137.4, 125.2, 119.4, 22.5. IR (KBr film) $\nu_{C=N}$: 1630 cm^{-1}. MS (FAB): *m*/*z* 239 (M^+). *Anal.* Calc. for $C_{14}H_{16}N_4$: C, 70.00; H, 5.87; N, 23.32. Found: C, 70.29; H, 5.79; N, 23.45%.

4.3. Synthesis of 3,6-bis(2′-thienyl)-1,2,4,5-tetrazine (*3*)

2-Thiophenecarbonitrile (4.36 g, 40.0 mmol) and hydrazine monohydrate (8.00 g, 160 mmol) were refluxed in ethanol (Merck, 50 ml) for 48 h. After the filtration, the filtrate was stirred at room temperature under air for 12 h. The red precipitate was collected and recrystallized using dichloromethane as a solvent to give pure product **3** (21.6 mmol, 54% yield). M.p. 191.5–192.5 °C. ^{1}H NMR: δ 8.28 (dd, *J* = 3.6, 1.2 Hz, 2H), 7.96 (dd, *J* = 3.6, 1.2 Hz, 2H), 7.38 (dd, *J* = 5.1, 3.6, 2H). ^{13}C NMR: δ 162.6, 137.3, 133.6, 131.6, 130.1. IR (KBr film) $\nu_{C=N}$: 1533 cm^{-1}. MS (FAB): *m*/*z* 247 (M^+). *Anal.* Calc. for $C_{10}H_6N_4S_2$: C, 48.78; H, 2.44; N, 22.76; S, 26.02. Found: C, 48.84; H, 2.56; N, 22.78; S, 26.62%.

4.4. Reaction of *1* with $Fe_2(CO)_9$ in refluxing toluene to yield complexes *1a* and *1b*

1.07 g (5.0 mmol) of compound **1** and 5.46 g (15.0 mmol) of $Fe_2(CO)_9$ were heated at reflux in 60 ml of toluene in the dark under nitrogen for 12 h. The reaction mixture was filtered through Celite 545 and the solvent was removed under reduced pressure. The residue was separated by a 3.5 cm diameter and 40 cm height column (230–400 mesh ASTM silica gel (Merck)) with ether/*n*-hexane (1:3) as eluent. The orange red band produced 0.97 g (2.0 mmol, 40% yield) of complex **1a**. The red band produced 0.69 g (1.4 mmol, 28% yield) of complex **1b**.

*Complex **1a**:* M.p. 148–149 °C. ^{1}H NMR: δ 9.00 (s, 2H), 6.93 (dd, J_{H-H} = 2.4, 2.1 Hz, 2H), 6.84 (dd, J_{H-H} = 3.6, 2.1 Hz, 2H), 6.20 (dd, J_{H-H} = 3.6, 2.7 Hz, 2H), 3.74 (s, 6H). ^{13}C NMR: δ 207.1, 155.7, 128.8, 126.1, 117.1, 108.6, 36.1. IR (CH_2Cl_2) $\nu_{C=N}$: 1638 cm^{-1}, $\nu_{C=O}$: 2061, 2021, 1972 cm^{-1}. MS (FAB): *m*/*z* 495 (M^+), 467 (M^+–CO), 439 (M^+–2CO), 411 (M^+–3CO), 383 (M^+–4CO), 355 (M^+–5CO), 327 (M^+–6CO), 271 (M^+–6CO–Fe). *Anal.*

Calc. for $C_{18}H_{14}Fe_2N_4O_6$: C, 43.76; H, 2.86; N, 11.34. Found: C, 43.65; H, 2.94; N, 11.24%.

Complex ***1b***: M.p. 129–130 °C. ^{1}H NMR: δ 7.96 (s, 1H), 7.23 (d, $J_{H-H} = 2.7$ Hz, 1H), 6.86 (d, $J_{H-H} = 2.7$, 1H), 6.55 (d, $J_{H-H} = 2.7$ Hz, 1H), 6.44 (dd, $J_{H-H} = 3.6$ Hz, 1H), 6.08 (dd, $J_{H-H} = 3.6$, 2.7 Hz, 1H), 4.53 (s, 2H), 4.21 (s, 6H). ^{13}C NMR: δ 211.9, 151.8, 144.7, 141.0, 131.9, 128.5, 126.7, 116.6, 117.6, 108.2, 61.8, 36.3, 34.7. IR (CH_2Cl_2) $\nu_{C\equiv N}$: 1638 cm^{-1}, $\nu_{C\equiv O}$: 2055, 2011, 1963 cm^{-1}. MS (FAB): *m/z* 495 (M^+), 466 (M^+-CO), 438 (M^+-2CO), 410 (M^+-3CO), 382 (M^+-4CO), 354 (M^+-5CO), 326 (M^+-6CO), 270 (M^+-6CO—Fe), 214 (L^+). *Anal.* Calc. for $C_{18}H_{14}Fe_2N_4O_6$: C, 43.76; H, 2.86; N, 11.34. Found: C, 43.85; H, 2.98; N, 11.17%.

4.5. Reaction of ***2*** *with $Fe_2(CO)_9$ in THF to yield complexes* ***2a*** *and* ***2b***

1.50 g (6.20 mmol) of compound **2** and 7.30 g (20.0 mmol) of $Fe_2(CO)_9$ were heated at reflux in 100 ml of anhydrous THF in the dark under nitrogen for 24 h. The reaction mixture was filtered through Celite 545 and the solvent was removed under reduced pressure. The residue was chromatographed on a silica gel column with ethyl acetate and then with ethanol as eluent to isolate dark red product **2a** (0.85 g, 1.6 mmol, 26% yield) and purple complex **2b** (1.30 g, 2.45 mmol, 40% yield), respectively.

If the reaction was carried on at room temperature, complex **2a** (3.3 mmol, 53% yield) and trace amount of complex **2b** were isolated. If the reaction was preceded under irradiation of UV light, only complex **2b** was produced in 94% yield.

Complex ***2a****:* M.p. 126–127 °C. ^{1}H NMR: δ 8.82 (s, 1H), 7.98 (d, $J_{H-H} = 7.8$ Hz, 1H), 7.81 (t $J_{H-H} = 7.8$ Hz, 1H), 7.45 (t, $J_{H-H} = 7.8$ Hz, 1H), 7.37 (d, $J_{H-H} = 7.8$ Hz, 1H), 7.21 (d, $J_{H-H} = 7.8$ Hz, 1H), 6.79 (d, $J_{H-H} = 7.5$ Hz, 1H), 4.82 (s, 1H), 2.64 (s, 3H), 2.62 (s, 3H). ^{13}C NMR: δ 212.8, 170.3, 160.7, 158.8, 155.7, 151.9, 137.8, 137.1, 124.3, 120.3, 118.6, 115.6, 67.9, 26.0, 23.4. IR (CH_2Cl_2) $\nu_{C\equiv N}$: 1562 cm^{-1}, $\nu_{C\equiv O}$: 2054, 2000, 1983, 1927 cm^{-1}. MS (FAB): *m/z* 518 (M^+), 490 (M^+-CO), 462 (M^+-2CO), 434 (M^+-3CO), 406 (M^+-4CO), 378 (M^+-5CO), 350 (M^+-6CO), 294 (M^+-6CO—Fe), 239 (L^+). *Anal.* Calc. for $C_{20}H_{14}Fe_2N_4O_6$: C, 46.37; H, 2.72; N, 10.81. Found: C, 46.55; H, 2.78; N, 10.88%.

Complex ***2b***: ^{1}H NMR: δ 8.86 (s, 1H), 7.58 (t, $J_{H-H} = 7.8$ Hz, 1H), 7.52 (t $J_{H-H} = 7.8$ Hz, 1H), 7.41 (d, $J_{H-H} = 7.8$ Hz, 1H), 7.32 (d, $J_{H-H} = 7.8$ Hz, 1H), 7.02 (t, $J_{H-H} = 7.8$ Hz, 1H), 6.88 (d, $J_{H-H} = 7.8$ Hz, 1H), 4.54 (s, 1H), 2.54 (s, 3H), 2.51 (s, 3H). IR (CH_2Cl_2) $\nu_{C\equiv N}$: 1573 cm^{-1}, $\nu_{C\equiv O}$: 2045, 1992, 1967 cm^{-1}. MS (FAB): *m/z* 518 (M^+), 490 (M^+-CO), 462 (M^+-2CO), 434 (M^+-3CO), 406 (M^+-4CO), 378 (M^+-5CO), 350 (M^+-6CO), 294 (M^+-6CO—Fe), 239 (L^+). *Anal.* Calc. for $C_{20}H_{14}Fe_2N_4O_6$: C, 46.37; H, 2.72; N, 10.81. Found: C, 46.21; H, 2.88; N, 11.10%.

4.6. Reaction of ***3*** *with $Fe_2(CO)_9$ in benzene to give complexes* ***3a*** *and* ***3b***

0.75 g (3.0 mmol) of compound **3** and 4.38 g (12.0 mmol) of $Fe_2(CO)_9$ were heated at reflux in 100 ml of anhydrous benzene in the dark under nitrogen for 24 h. The reaction mixture was filtered through Celite 545 and the solvent was removed under reduced pressure. The residue was separated by a 3.5 cm diameter and 40 cm height column (230–400 mesh ASTM silica gel (Merck)) with ethyl acetate/*n*-hexane (1:30) as eluent. The red band recovered 0.15 g of unreacted ligand **3** (20%). The orange red band produced 0.84 g (1.6 mmol, 53% yield) of complex **3a**. The orange yellow band produced 0.16 g (0.3 mmol, 10% yield) of complex **3b**.

Complex ***3a****:* M.p. 127.8–128.8 °C (decomp.). ^{1}H NMR: δ 8.00 (d, $J = 5.1$ Hz, 2H), 7.69 (d, $J = 3.6$ Hz, 1H), 7.38 (dd, $J = 4.8$, 3.6 Hz, 2H). IR (KBr film) ν_{CO}: 2076, 2035, 2001, 1987, 1972 cm^{-1}; ν_{CN}: 1543 cm^{-1}. MS(FAB): *m/z* 527 (M^+), 499 (M^+-CO), 471 (M^+-2CO), 443 (M^+-3CO), 415 (M^+-4CO), 378 (M^+-5CO), 359 (M^+-6CO), 331 (M^+-5CO—Fe), 247 (L^+). *Anal.* Calc. for $Fe_2C_{16}H_6N_4O_6S_2$: C, 36.50; H, 1.14; N, 10.65; S, 12.17. Found: C, 36.55; H, 1.22; N, 10.78; S, 12.45%.

Complex ***3b****:* M.p. 194.7 °C (decomp.). ^{1}H NMR: δ 9.01 (s, 1H), 7.95 (d, $J = 5.1$ Hz, 1H), 7.65 (d, $J = 5.1$ Hz, 1H), 7.55 (d, $J = 3.6$ Hz, 1H), 7.46 (d, $J = 5.1$ Hz, 1H), 7.11 (dd, $J = 5.1$, 3.6 Hz, 1H). IR (KBr film) ν_{NH}: 3355, 1521 cm^{-1}; ν_{CO}: 2073, 2033, 2012, 1995, 1977, 1952 cm^{-1}; ν_{CN}: 1638, 1574 cm^{-1}. MS(FAB): *m/z* 527 (M^+), 499 (M^+-CO), 471 (M^+-2CO), 443 (M^+-3CO), 415 (M^+-4CO), 387 (M^+-5CO), 359(M^+-6CO), 247 (L^+). *Anal.* Calc. for $Fe_2C_{16}H_6N_4O_6S_2$: C, 36.50; H, 1.14; N, 10.65; S, 12.17. Found: C, 36.62; H, 1.19; N, 10.54; S, 12.31%.

4.7. Reaction of complex ***3a*** *with triphenylphosphine in dichloromethane to give* ***3c*** *and* ***3d***

0.20 g (0.38 mmol) of complex **3a** in a 50 ml of anhydrous dichloromethane was stirred with 0.20 g (0.76 mmol) of PPh_3 at room temperature under N_2 atmosphere for 24 h. After the filtration, the solvent was removed under reduced pressure and the residue was separated by a 3.5 cm diameter and 40 cm height column (230–400 mesh) with ethyl acetate/*n*-hexane (1:5) as eluent to give 0.26 g (0.34 mmol, 89% yield) of complex **3c** and 40 mg (0.040 mmol, 10% yield) of complex **3d**.

Complex ***3c****:* M.p. 171.4–172.0 °C (decomp.). ^{1}H NMR: δ 7.89 (d, $J = 5.1$ Hz, 2H), 7.49 (d, $J = 3.6$ Hz, 1H), 7.32 (dd, $J = 5.1$, 3.6 Hz, 2H), 7.27 (m, 15 H). ^{13}C NMR: δ 211.4, 156.9, 135.3, 134.6, 134.0, 133.7, 133.5, 132.9, 131.5, 129.9, 129.6, 129.4, 129.3. IR (KBr film) ν_{CO}: 2046, 1978, 1926 cm^{-1}; ν_{CN}: 1541 cm^{-1}. MS(FAB): *m/z* 761 (M^+), 733 (M^+-CO), 705 (M^+-2CO), 677 (M^+-3CO), 649 (M^+-4CO), 621 (M^+-5CO), 565 (M^+-5CO—Fe), 263 ($PPh_3 + 1$), 247 (L^+). *Anal.* Calc. for $Fe_2C_{33}H_{21}$-

$N_4O_5PS_2$: C, 52.11; H, 2.76; N, 7.37; S, 8.42. Found: C, 52.24; H, 2.73; N, 7.27; S, 8.32%.

Complex ***3d****:* M.p. 217.3–217.8 °C. ^{1}H NMR: δ 7.71 (d, $J = 5.1$ Hz, 2H), 7.31 (d, $J = 3.6$ Hz, 1H), 7.22 (m, 20H), 7.27 (m, 12 H). IR (KBr film) ν_{CO}: 1994, 1947, 1926 cm^{-1}; ν_{CN}: 1537 cm^{-1}. MS(FAB): *m*/*z* 995 (M^+), 967 (M^+−CO), 939 (M^+−2CO), 911 (M^+−3CO), 883 (M^+−4CO), 636 (M^+−4CO-L), 318 ($FePPh_3^+$), 263 ($PPh_3 + 1$), 247 (L+).

Acknowledgements

Financial support from the National Science Council (Taiwan, ROC) and National Dong Hwa University are gratefully acknowledged.

Appendix A. Supplementary data

Crystallographic data for the structural analysis have been deposited with the Cambridge Crystallographic Data Center, CCDC No. 277567 for **1**, 277568 for **3**, 277569 for **1a**, 277570 for **2a**, 277571 for **3a** and 277572 for **3c**. Copies of this information may be obtained free of charge from The Director, CCDC, 12 Union Road, Cambridge CB2 1EZ, UK (fax: +44 1223 336033; e-mail: deposit@ccdc.com.ac.uk or http://www.ccde.cam.ac.uk). Supplementary data associated with this article can be found, in the online version, at doi:10.1016/j.poly.2006.04.031.

References

[1] (a) G.W. Parshall, Acc. Chem. Res. 3 (1970) 139;
(b) H. Alper, A.S.K. Chan, J. Am. Chem. Soc. 95 (1973) 4905;
(c) H. Alper, W.G. Root, J. Am. Chem. Soc. 97 (1975) 4251;
(d) M.I. Bruce, Angew. Chem., Int. Ed. Engl. 16 (1977) 73;
(e) G.R. Newkome, W.E. Puckett, W.K. Gupta, G.E. Kiefer, Chem. Rev. 86 (1986) 451;
(f) P.W. Clark, S.F. Dyke, G. Smit, C.H.L. Kennard, J. Organomet. Chem. 330 (1987) 427;
(g) I. Omae, Coord. Chem. Rev. 83 (1988) 137;
(h) A.D. Ryabov, Chem. Rev. 90 (1990) 403;
(i) J. Albert, J. Barro, J. Granell, J. Organomet. Chem. 408 (1991) 115;
(j) J. Alber, R.M. Ceder, M. Gómez, J. Granell, J. Sales, Organometallics 11 (1992) 1536;
(k) J. Alber, J. Granell, R. Moragas, J. Sales, M. Font-Bardía, X. Solans, J. Organomet. Chem. 494 (1995) 95;
(l) K.A. Azam, R. Dilshad, S.E. Kabir, M.A. Mottalib, M.B. Hursthouse, K.M.A. Malik, Polyhedron 19 (2000) 1081.
[2] A.C. Cope, E.C. Friedrich, J. Am. Chem. Soc. 90 (1968) 909.
[3] (a) J. Albert, J. Granell, J. Sales, J. Organomet. Chem. 273 (1984) 393;
(b) J. Albert, M. Gómez, J. Granell, J. Sales, X. Solans, Organometallics 9 (1990) 1405.
[4] (a) P.E. Baikei, O.S. Mill, J. Chem Soc., Chem. Commun. (1966) 707;
(b) M.M. Bagga, W.T. Flannigan, G.R. Knox, P.L. Pauson, F.J. Preston, R.I. Reed, J. Chem. Soc. C (1968) 36;
(c) D.L. Wang, W.S. Hwang, L.C. Liang, L.Y. Wang, L. Lee, M.Y. Chiang, Organometallics 16 (1997) 3109;
(d) W. Imhof, A. Göbel, D. Ohlmann, J. Flemming, H. Fritzsche, J. Organomet. Chem. 584 (1999) 33;
(e) D.L. Wang, W.S. Hwang, L. Lee, M.Y. Chiang, J. Organomet. Chem. 579 (1999) 211;
(f) W. Imhof, Organometallics 18 (1999) 4845;
(g) W.S. Hwang, T.S. Tzeng, D.L. Wang, M.Y. Chiang, Polyhedron 20 (2001) 353.
[5] A.I. Khodair, P. Bertrand, Tetrahedron 54 (1988) 4859.
[6] E.E. Schweizer, A.L. Rheingold, M. Bruch, J. Org. Chem. 58 (1993) 4339.
[7] (a) R. Centore, C. Garzillo, J. Chem. Soc., Perkin Trans. 2 2 (1997) 79;
(b) P. Espinet, J. Etxebarria, M. Marcos, J. Péres, A. Remón, J.L. Serrano, Angew. Chem., Int. Ed. Engl. 28 (1998) 1065.
[8] H.S. Nalwa, A. Kakatu, A. Mukoh, J. Appl. Phys. 73 (1993) 4743.
[9] (a) F. Mull, G. van Koten, K. Vrieze, K.A.A. Duineveld, D. Heijdenrijk, A.N.S. Mak, C.H. Stam, Organometallics 8 (1989) 1324;
(b) F. Mull, G. van Koten, K. Vrieze, D. Heijdenrijk, Organometallics 8 (1989) 33;
(c) F. Mull, G. van Koten, K. Vrieze, D. Heijdenrijk, B.B. Krijnen, C.H. Stam, Organometallics 8 (1989) 41;
(d) F. Mull, G. van Koten, M.J.A. Kraakman, K. Vrieze, D. Heijdenrijk, M.C. Zoutberg, Organometallics 8 (1989) 1331;
(e) F. Mull, G. van Koten, L.H. Polm, K. Vrieze, M.C. Zoutberg, D. Heijdenrijk, E. Kragten, C.H. Stam, Organometallics 8 (1989) 1340.
[10] (a) D. Bright, O.S. Mills, J. Chem Soc., Chem. Commun. (1967) 245;
(b) A. Albini, H. Kisch, J. Organomet. Chem. 94 (1975) 75;
(c) L.S. Hegedus, A. Krama, Organometallics 3 (1984) 1263;
(d) F.A. Cotton, S.A. Duraj, W.J. Roth, J. Am. Chem. Soc. 106 (1984) 4749;
(e) K. Weiss, P. Kindl, Angew. Chem., Int. Ed. Engl. 13 (1984) 629;
(f) A. Zimniak, J. Zachara, J. Organomet. Chem. 533 (1997) 45;
(g) C.J. Lin, W.S. Hwang, M.Y. Chiang, J. Organomet. Chem. 640 (2001) 85.
[11] W.P. Mull, C.J. Elsevier, M. van Leijen, K. Vrieze, A. Spek, Organometallics 10 (1991) 533.
[12] (a) A.E. Ogilva, M. Draganjic, T.B. Rauchfuss, S.R. Wilson, Organometallics 7 (1988) 1171;
(b) J.M. Cassidy, K.H. Whitmire, G.J. Long, J. Organomet. Chem. 427 (1992) 355;
(c) W. Petz, F.Z. Weller, Kristallografiya 212 (1997) 157;
(d) H.B. Chin, M.B. Smith, R.D. Wilson, R. Bau, J. Am. Chem. Soc. 96 (1974) 5285;
(e) H.-J. Knölker, E. Baum, P. Gonser, G. Rohde, H. Röttele, Organometallics 17 (1998) 3916;
(f) W.S. Hwang, D.L. Wang, M.Y. Chiang, J. Organomet. Chem. 613 (2000) 231;
(g) F. Ortega-Jiménez, C. Ortega-Alfaro, J.G. López-Cortés, R. Gutiérrez-Pérez, R.A. Toscano, L. Velasco-Ibarra, E. Peña-Cabrera, C. Alvarez-Toledano, Organometallics 19 (2000) 4127;
(h) B. Neumüller, W. Petz, Organometallics 20 (2001) 163;
(i) W.S. Hong, C.Y. Wu, C.S. Lee, W.S. Hwang, M.Y. Chiang, J. Organomet. Chem. 689 (2004) 277;
(j) C.Y. Wu, L.H. Chen, W.S. Hwang, H.S. Chen, C.H. Hung, J. Organomet. Chem. 689 (2004) 2192.
[13] (a) M.M. Bagga, P.E. Baikie, O.S. Mills, P.L. Pauson, J. Chem Soc., Chem. Commun. (1967) 1106;
(b) P.E. Baikie, O.S. Mills, Inorg. Chim. Acta 1 (1967) 55;
(c) L.F. Dahl, W.R. Costello, R.B. King, J. Am. Chem. Soc. 90 (1968) 5422;
(d) A. De Cain, R. Weiss, Y. Chauvin, D. Commereuc, D. Hugo, J. Chem. Soc., Chem. Commun. (1976) 249;
(e) H.-J. Knölker, Chem. Rev. 100 (2000) 2491;
(f) S.Y. Jing, C.Y. Wu, C.S. Lee, A. Datta, W.S. Hwang, J. Organomet. Chem. 687 (2004) 3173.
[14] L.F. Dahl, C. Martell, D.L. Wander, J. Am. Chem. Soc. 83 (1961) 1761.
[15] (a) L. Pauling, in: The Nature of the Chemical Bond, 3rd ed., Cornell University Press, Ithaca, NY, 1960 (Chapter 7);
(b) D.R. Lide, Tetrahedron 17 (1962) 125;
(c) O. Bastiansen, M. Traetteberg, Tetrahedron 17 (1962) 147.

[16] K. Vrieze, G. van Koten, Inorg. Chim. Acta 100 (1985) 79.
[17] (a) L.H. Staal, L.H. Polm, R.W. Balk, G. van Koten, K. Vrieze, A.F.M. Brouwers, Inorg. Chem. 19 (1980) 3343;
(b) L.H. Polm, C.J. Elsevier, G. van Koten, J.M. Ernsting, D.J. Stufkens, K. Vrieze, Organometallics 6 (1987) 1096;
(c) Y.F. Tzeng, C.Y. Wu, W.S. Hwang, C.H. Hung, J. Organomet. Chem. 687 (2003) 16.
[18] H.-W. Frühauf, A. Landers, R. Goddard, C. Krüger, Angew. Chem. 90 (1978) 56.
[19] A. Zimniak, G. Bakalarski, J. Mol. Struct. 597 (2001) 211.
[20] J. Zachara, A. Zimniak, Acta Crystallogr. C54 (1998) 353.
[21] S.U. Son, K.H. Park, I.G. Jung, Y.K. Chung, Organometallics 21 (2002) 5366.
[22] D.F. Shriver, K.H. Whitmire, in: G. Wilkinson, F.G.A. Stone, E.W. Abel (Eds.), Comprehensive Organometallic Chemistry, vol. 4, Pergamon, Oxford, 1982 (Chapter 31.1).
[23] P. Guerrieor, E. Bullita, P.A. Vigato, B. Pelli, P. Traldi, J. Heterocyclic Chem. 125 (1988) 145.

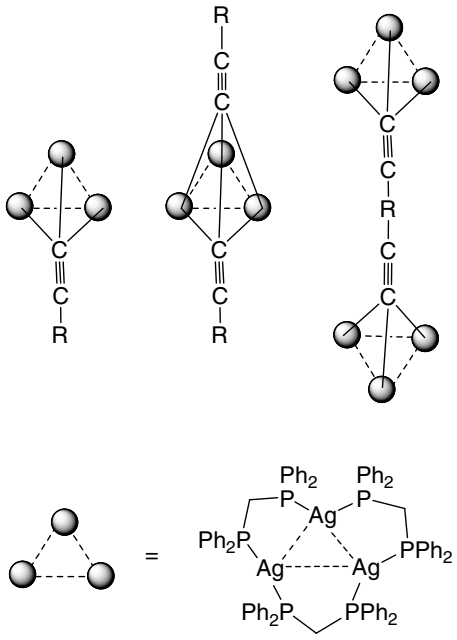

Fig. 1. Schematic examples of trinuclear silver(I) alkyne clusters.

have been studying binuclear phosphane gold(I) acetylide complexes [12] as well as complexes containing the readily available propargyl alcohol ligands HC≡CCRR′OH (R = R′ = H, Me; R = Me, R′ = Et) [13]. Sigma-bonded *C*-coordinated propargyl alcohols readily undergo dehydration reactions (often spontaneous) to form vinylidene or allenylidene complexes, particularly in the presence of metals such as Os, Ru and Pt [14]. There are, however, very few examples of metal complexes containing σ-bonded *C*-coordinated propargyl alcohol ligands that do not undergo any dehydration reactions. We therefore wished to extend our studies of metal complexes of propargyl alcohols by preparing some silver(I) derivatives. The results of our investigation are presented here.

2. Results and discussion

Initially we attempted to react the propargyl alcohols 3-methyl-1-pentyn-3-ol, 2-methyl-3-butyn-2-ol and propargyl alcohol with the dinuclear silver(I) complex $[Ag_2(\mu\text{-dppm})_2](NO_3)_2$ in the presence of KOH. Somewhat surprisingly, we found that under these conditions no reaction took place; only starting materials were recovered. We then attempted to prepare silver(I) acetylides of the propargyl alcohols and planned to react those with dppm. However, during isolation of one of the propargyl silver(I) acetylides a violent explosion occurred! This prompted us to develop a new and safer method for the preparation of trinuclear silver(I) clusters. The strategy we employed was to prepare the polymeric silver(I) acetylides in situ and then to immediately react those with dppm. Thus, treatment of a MeCN solution of $AgNO_3$ with 0.33 equivalents of propargyl alcohol derivative and Et_3N resulted in instantaneous precipitation of the silver(I) acetylide complexes. Upon addition of dppm a pale yellow solution formed out of which the trinuclear silver(I) clusters $[Ag_3(\mu_3\text{-}\eta^1\text{-}C{\equiv}CCRR'OH)(\mu\text{-dppm})_3](NO_3)_2$ (R = R′ = H (**1**), Me (**2**); R = Me, R′ = Et (**3**)) could be isolated as air- and light-stable colourless solids in good yields after removal of $[Et_3NH]NO_3$ and recrystallisation (Scheme 1).

During the course of optimising reaction conditions, we found that the reaction time between the alkyne, Et_3N and $AgNO_3$ is critical to obtain a pure product. Even though the silver(I) acetylides precipitate instantaneously, shorter reaction times lead to isolation of a mixture of the desired Ag_3 clusters and the binuclear silver(I) dppm complex $[Ag_2(\mu\text{-dppm})_2](NO_3)_2$; in extreme cases a 50:50 mixture of these two complexes was obtained. The $^{31}P\{^1H\}$ NMR spectra (Fig. 2) of all three complexes consist of a pair of multiplet resonances, the major lines of which are separated by ca. 391 Hz. This coupling pattern is due to superposition of all four possible ^{31}P, ^{107}Ag and ^{109}Ag isotopomers ($^{107}Ag_3{}^{31}P$, $^{107}Ag_2{}^{109}Ag{}^{31}P$, $^{107}Ag{}^{109}Ag_2{}^{31}P$ and $^{109}Ag_3{}^{31}P$) further complicated by the fact that the two phosphorus atoms on each dppm unit are non-equivalent. At low temperatures (−80 °C) this spectral pattern did not change significantly, thus preventing us from obtaining data useable to attempt a simulation of this rather complex spin system.

The ^1H NMR spectra of the three compounds show very broad resonances for the dppm CH_2 protons, as well as the expected signals for the propargyl alcohol ligands. In the case of complex **1**, the hydroxyl proton can be observed as a triplet with small coupling (ca. 4 Hz) with the propargyl alcohol methylene protons. The IR spectra of complexes **1**–**3** show a weak signal due to the C≡C stretch at ca. 1965 cm^{-1}, typical for metal acetylide compounds. In the FAB+ mass spectra weak peaks of the mono-nitrato cationic clusters as well as peaks due to loss of dppm ligands are observed. The trinuclear structure of these compounds was confirmed by an X-ray crystallographic study of complex **3**. The unit cell contains a total of four molecules, two *R* and two *S* enantiomers due to the chiral centre

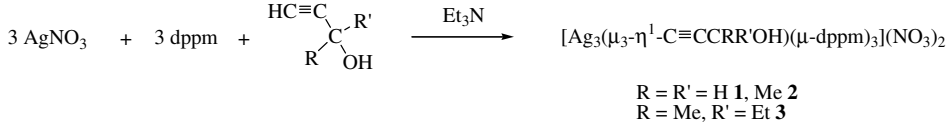

Scheme 1.

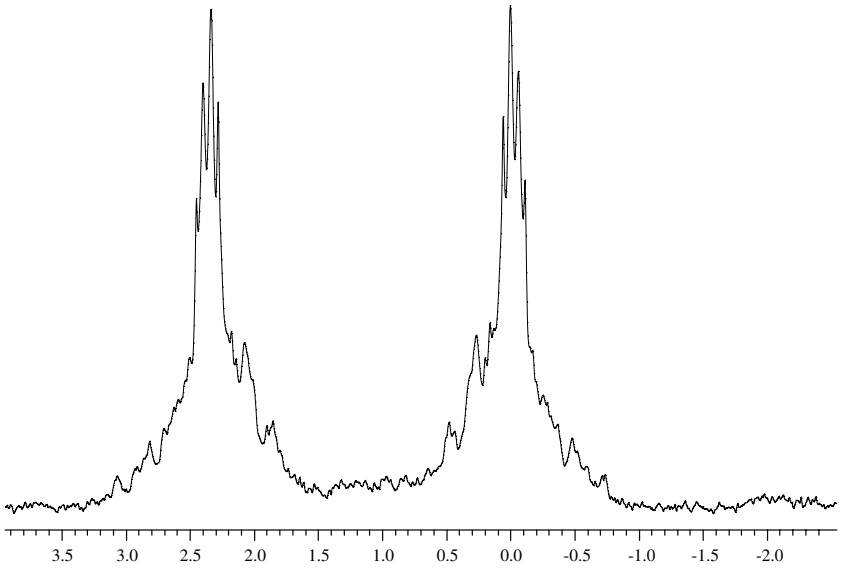

Fig. 2. Room temperature $^{31}P\{^{1}H\}$ NMR spectrum of complex **2**.

at C6. The molecular structure of one of these molecules is shown in Fig. 3. The complex consists of a planar triangle of silver atoms with Ag···Ag distances of 3.0046(7), 3.1876(7) and 3.3840(7) Å, bridged by three molecules of dppm. Although these distances represent only weak, if any, bonding interactions (van der Waals radius of silver 1.72 Å), they are examples of *argentophilicity*, i.e. weak closed-shell interactions between silver atoms [15,16]. The carbon atom of the alkynyl group, C(4), located above the centre of the Ag triangle, triply bridges the three silver atoms with the respective Ag–C distances being 2.265(5), 2.278(6) and 2.358(6) Å. On the other side of the Ag_3 triangle, a nitrato group acts as a weakly μ_3-bridging ligand via only two oxygen atoms so that the Ag(1)···O(2), Ag(2)···O(4) and Ag(3)···O(4) distances are 2.625(5), 2.700(5) and 2.783(5) Å, respectively. The other nitrate anion is located in the crystal space far away from the cluster but is associated via hydrogen bonding interactions to the O(1) atom of the acetylide group. In this case, and for the major component of the disordered acetylide, the O(1)–H atom lies between the O(5) and O(6) atoms and

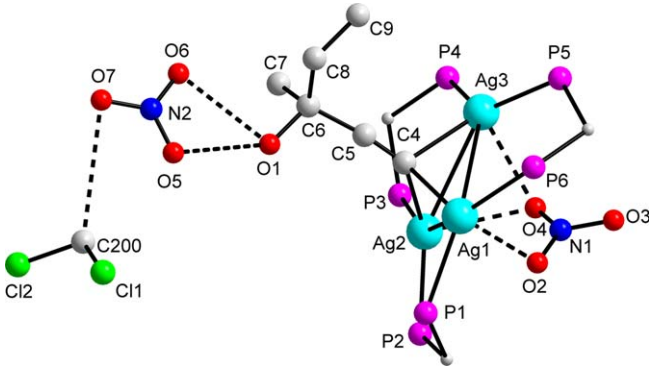

Fig. 3. Molecular structure of one of the enantiomers of *rac*-$[Ag_3\{\mu_3\text{-}\eta^1\text{-}C{\equiv}CC(Et)(Me)OH\}(\mu_2\text{-}O\text{-}NO_3)(\mu\text{-dppm})_3]NO_3 \cdot CH_2Cl_2$. Phenyl groups of the dppm ligands and hydrogen atoms have been omitted for clarity.

forms hydrogen bonds of O(1)–H···O(5) 2.28 Å [O(1)···O(5) = 2.940(12) Å] and an angle of 138°; the equivalent parameters for the O(1)–H···O(6) interaction are 2.10 Å, 2.859(12) Å and 154°. In turn, this nitrate anion is connected to the dichloromethane molecule of solvation with the most directional interaction involving the hitherto unused O(7) atom: C(200)–H···O(7) is 2.46 Å, C(200)···O(7) is 3.392(10) Å with an angle at H of 162°.

The three Ag···Ag distances in complex **3** are longer and more asymmetric than those in $[Ag_3(\mu_3\text{-}\eta^1\text{-}C{\equiv}CPh)_2(\mu\text{-dppm})_3]Cl$ [Ag···Ag = 2.983(1) and 2.866(2) Å] [6] but very similar to those in $[Ag_3(\mu_3\text{-}\eta^1\text{-}C{\equiv}CC_6H_4\text{-}4\text{-}NO_2)(\mu\text{-dppm})_3](BF_4)_2$ [Ag–Ag = 2.9850(6), 3.0877(6) and 3.4030(6) Å] [8]. It is worth noting the similarly in the asymmetry of the Ag···Ag distances: like in complex **3** two Ag–Ag distances are ca. 3 Å, while one is considerably longer with ca. 3.4 Å. Interestingly, in the ferrocenyl substituted alkyne cluster $[Ag_3(\mu_3\text{-}\eta^1\text{-}C{\equiv}CFc)(\mu\text{-dppm})_3](OTf)_2$ the Ag–Ag distances [Ag–Ag = 3.2416(6), 3.2451(6) and 3.2527(6) Å] are almost equal [9]. The angles within the Ag_3 triangle [54.32(1)°, 59.51(1)° and 66.18(2)°] as well as the Ag–C distances. are also very similar to those in $[Ag_3(\mu_3\text{-}\eta^1\text{-}C{\equiv}CC_6H_4\text{-}4\text{-}NO_2)(\mu\text{-dppm})_3](BF_4)_2$ [54.49°, 57.37° and 68.14° (no SUs given)] [Ag–C = 2.224(5), 2.269(5), 2.349(6) Å] [8]. All other bond distances and angles are unexceptional. Complexes **1**–**3** are luminescent in the solid state, both at room temperature and at 77 K. Photophysical data are shown in Table 1 and the emission spectrum (298 K) of complex **3** is shown in Fig. 4.

The emission maxima of complexes **1**–**3** are similar to those reported for other trinuclear silver(I) acetylide clusters [6,8]. At 298 K two maxima are observed for complexes **1** and **3**, whilst complex **2** displays a single broad band. Upon cooling to 77 K single, very broad bands are observed for all three complexes. The lowest energy transition is likely to be due to metal–metal $[d_{\sigma^*}(M\cdots M)]$ to ligand $[\pi^*(RC{\equiv}C^-)]$ charge transfer bands, consistent with

Table 1
Photophysical data of complexes **1**–**3**[a]

Complex	Emission λ_{max} (nm) at 298 K	Emission λ_{max} (nm) at 77 K
1	536, 565	550
2	540 (broad)	545
3	527, 545	530

[a] All the complexes excited at 265–275 nm.

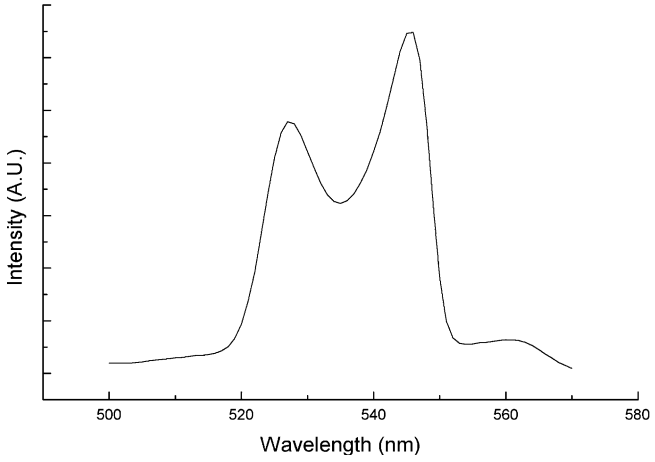

Fig. 4. The solid-state emission spectra of complex **3** at 298 K.

spectral and computational data reported by Che and co-workers [6].

We also attempted to prepare bicapped silver(I) clusters of the type $[Ag_3(\mu_3\text{-}\eta^1\text{-}C{\equiv}CR)_2(\mu\text{-dppm})_3]NO_3$, however, even with a large excess of alkyne only the monocapped cluster was formed. This result is in contrast to the work by Yam et al. who have successfully prepared and structurally characterised the bicapped cluster $[Ag_3(\mu_3\text{-}\eta^1\text{-}C{\equiv}CC_6H_4\text{-}4\text{-}NO_2)_2(\mu\text{-dppm})_3]OTf$ by simply increasing the ratio of alkyne:Ag [8]. A likely explanation for this behaviour in our case is the presence of the bridging nitro group. The Ag–O bonds may simply be too strong compared to the Ag–C bond so that addition of a second alkyne is disfavoured. We therefore attempted to prepare the bicapped cluster by using $AgBF_4$ as silver(I) precursor, however, during formation of the polymeric silver(I) acetylide significant decomposition to metallic Ag occurred and the only isolated product was the dinuclear $[Ag_2(\mu\text{-dppm})_2](OTf)_2$, as evident from the $^{31}P\{^1H\}$ NMR spectrum. Similarly, when AgOTf was used as precursor, we only obtained the monocapped clusters independent of the Ag:alkyne ratio. We also attempted to introduce the second alkyne by reacting the monocapped cluster **1** with a further equivalent of alkyne in the presence of Et_3N; however, after stirring for ca. 18 h only unreacted cluster **1** was isolated after work-up.

In conclusion, we present here a safe and simple one-pot self-assembly reaction that allows the high-yield synthesis of monocapped trinuclear silver(I) clusters with hydroxy-functionalised alkynes from simple, commercially available starting materials.

3. Experimental

3.1. General

^1H and $^{31}P\{^1H\}$ NMR spectra were recorded on a 400 MHz Bruker Avance spectrometer. Chemical shifts are quoted relative to external TMS (^1H) and 85% H_3PO_4 (^{31}P); coupling constants are reported in Hz. FAB mass spectra were measured on a VG Autospec spectrometer in positive ion mode using NBA as matrix. IR spectra were run as KBr pellets on a Perkin–Elmer Spectrum One instrument. Solid-state luminescence spectra were recorded at 275 and 77 K using a Fluorolog FL-11 spectrometer. All reagents and solvents were commercially available and used as received. All compounds gave satisfactory elemental analyses.

3.2. Preparation of $[Ag_3(\mu_3\text{-}\eta^1\text{-}C{\equiv}CRR'OH)(\mu\text{-dppm})_3](NO_3)_2$ complexes

To a solution of $AgNO_3$ (0.174 g, 1.02 mmol) in MeCN (10 mL) was added propargyl alcohol derivative (0.343 mmol) followed by Et_3N (0.4 mL, excess). After stirring the mixture protected from light for 3 h solid dppm (0.392 g, 1.02 mmol) was added. After a further 18 h of stirring the pale yellow solutions were passed through Celite and evaporated to dryness. The resulting solids were washed well with H_2O, Et_2O and dried. Recrystallisation from CH_2Cl_2/hexane afforded the complexes as colourless, crystalline solids.

Using this procedure the following compounds were prepared.

3.2.1. $[Ag_3(\mu_3\text{-}\eta^1\text{-}C{\equiv}CCH_2OH)(\mu\text{-dppm})_3](NO_3)_2$ (**1**)

Yield: 99% (no recrystallisation was necessary for this complex). ^1H NMR (400 MHz, $CDCl_3$, 25 °C): $\delta = 6.89$–7.20 (m, 60H, PPh_2), 6.25 (t, $J = 4.1$ Hz, 1H, O*H*), 4.66 (d, $J = 3.8$ Hz, 2H, CCH_2), 3.43 (br s, 6H, PCH_2P). $^{31}P\{^1H\}$ NMR (162 MHz, $CDCl_3$, 25 °C): $\delta = 1.16$ (centre of complex pattern; separation of main lines = 391 Hz). FAB MS *m*/*z* (%) = 1593 (5) $[M-NO_3]^+$, 1210 (25) $[M-NO_3-dppm]^+$. IR (KBr disk) 3289 cm^{-1} ν(OH), 1966 cm^{-1} ν(C≡C).

3.2.2. $[Ag_3(\mu_3\text{-}\eta^1\text{-}C{\equiv}CCMe_2OH)(\mu\text{-dppm})_3](NO_3)_2$ (**2**)

Yield: 57%. ^1H NMR (400 MHz, $CDCl_3$, 25 °C): $\delta = 6.90$–7.28 (m, 60H, PPh_2), 3.47 (br s, 6H, PCH_2P), 1.61 (s, 6H, Me). $^{31}P\{^1H\}$ NMR (162 MHz, $CDCl_3$, 25 °C): $\delta = 1.87$ (centre of complex pattern; separation of main lines = 390 Hz). FAB MS *m*/*z* (%) = 1621 (11) $[M-NO_3]^+$, 1236 (30) $[M-NO_3-dppm]^+$. IR (KBr disk) 3392 cm^{-1} ν(OH), 1965 cm^{-1} ν(C≡C).

3.2.3. rac-$[Ag_3\{\mu_3\text{-}\eta^1\text{-}C{\equiv}CC(Me)(Et)OH\}(\mu\text{-dppm})_3](NO_3)_2$ (**3**)

Yield: 80%. ^1H NMR (400 MHz, $CDCl_3$, 25 °C): $\delta =$ 6.89–7.28 (m, 60H, PPh_2), 3.47 (br s, 6H, PCH_2P), 1.85

Table 2
Crystal data and refinement details for complex **3**

Empirical formula	$C_{28}H_{77}Ag_3Cl_2N_2O_7P_6$
Formula weight	1782.79
Crystal system	monoclinic
Space group	$P2_1/c$
a (Å)	16.2742(1)
b (Å)	14.5722(10)
c (Å)	32.758(2)
β (°)	100.676(2)
V (Å^3)	7634.5(9)
Z	4
D_{calc} (g cm^{-3})	1.551
Absorption coefficient (mm^{-1})	1.014
$F(000)$	3616
Data/restraints/parameters	18247/10/407
Goodness-of-fit on F^2	0.90
Final R indices $[I > 2\sigma(I)]$	
R_1[a]	0.068
wR_2[b]	0.139

[a] $R_1(F) = \sum||F_o| - |F_c||/\sum|F_o|$.
[b] $wR_2(F^2) = [\sum w(F_o^2 - F_c^2)^2/\sum w(F_o^2)^2]^{1/2}$.

(m, 2H, CH_2CH$_3$), 1.54 (s, 3H, Me), 0.98 (t, $J = 7.3$ Hz, 3H, CH_3). ^{31}P{^{1}H} NMR (400 MHz, $CDCl_3$, 25 °C): $\delta = 1.68$ (centre of complex pattern; separation of main lines = 390 Hz). FAB MS m/z (%): 1637 (10) $[M-NO_3]^+$, 1250 (35) $[M-NO_3-dppm]^+$. IR (KBr disk) 3296 cm^{-1} ν(OH), 1964 cm^{-1} ν(C≡C).

3.3. X-ray crystallography

Crystals of complex **3** suitable for X-ray diffraction were obtained by slow diffusion of hexane into a CH_2Cl_2 solution of the compound. A colourless needle with the dimensions $0.04 \times 0.09 \times 0.16$ mm^3 was mounted in oil on a glass fibre. Data were collected at 100 K using a Bruker Apex CCD. Data reduction and empirical absorption corrections were applied using SADABS [17]. The structure was solved using direct-methods and refined on F^2 using a full-matrix least-squares procedure [18]. Despite the data having been collected at 100 K, considerable disorder was noted in the structure. Two positions were discerned for the acetylide residue disposed approximately 120° to each other with respect to the C4–C6 axis. From refinement, the site occupancies were 0.676(10):0.324(10); the atoms comprising the disordered residue were refined with isotropic thermal parameters. Soft restraints were introduced (i.e. C–O = 1.35 Å and C–C = 1.52 Å) so as to allow for a chemically sensible model and, finally, the aromatic rings were refined as rigid hexagonal C_6H_5 groups. The remaining atoms were refined with anisotropic displacement parameters and all hydrogen atoms included in their calculated positions, including for the disordered residue. With the above model, convergence was readily achieved and the final shift/error (Δ/σ) was <0.001. Crystallographic and refinement details are collected in Table 2.

4. Supplementary data

Full crystallographic details for complex **3** (CIF file format) are available from the CCDC, 12 Union Road, Cambridge, CB2 1EZ, UK by quoting the deposition code CCDC 600470.

Acknowledgements

We thank the Ministerio de Ciencia y Tecnología Spain for financial support (CTQ2005-08099-C03-01) and the Universidad de Burgos for a visiting fellowship to F.M. (Grant No. 112-541A-487.01).

References

[1] K.L. Cheung, S.K. Yip, V.W.W. Yam, J. Organomet. Chem. 689 (2004) 4451.
[2] V.W.W. Yam, K.K.W. Lo, K.M.C. Wong, J. Organomet. Chem. 578 (1999) 3.
[3] M.P. Cifuentes, M.A. Humphrey, J. Organomet. Chem. 689 (2004) 3968.
[4] C.P. McArdle, M.C. Irwin, M.C. Jennings, R.J. Puddephatt, Angew. Chem., Int. Ed. Engl. 38 (1999) 3376.
[5] N.C. Habermehl, M.C. Jennings, C.P. McArdle, F. Mohr, R.J. Puddephatt, Organometallics 24 (2005) 5004.
[6] C.F. Wang, S.M. Peng, C.K. Chan, C.M. Che, Polyhedron 15 (1996) 1853.
[7] V.W.W. Yam, W.K.M. Fung, K.K. Cheung, Chem. Commun. (1997) 963.
[8] V.W.W. Yam, W.K.M. Fung, K.K. Cheung, Organometallics 16 (1997) 2032.
[9] J.H.K. Yip, J. Wu, K.Y. Wong, K.W. Yeung, J.J. Vittal, Organometallics 21 (2002) 1612.
[10] Y.Y. Lin, S.W. Lai, C.M. Che, K.K. Cheung, Z.Y. Zhou, Organometallics 21 (2002) 2275.
[11] C. Brasse, P.R. Raithby, M.A. Rennie, C.A. Russel, A. Steiner, D.S. Wright, Organometallics 15 (1996) 639.
[12] L.A. Méndez, J. Jiménez, E. Cerrada, F. Mohr, M. Laguna, J. Am. Chem. Soc. 127 (2005) 852.
[13] F. Mohr, E. Cerrada, M. Laguna, Organometallics 25 (2006) 644.
[14] M.I. Bruce, Chem. Rev. 98 (1998) 2797.
[15] K. Singh, G.J. Long, P. Stavropoulos, J. Am. Chem. Soc. 119 (1997) 2942.
[16] P. Pyykkö, Chem. Rev. 97 (1997) 597.
[17] G.M. Sheldrick, SADABS version 2.03, Universiät Göttingen, Göttingen, Germany, 2002.
[18] G.M. Sheldrick, SHELXTL-NT 6.1, Universität Göttingen, Göttingen, Germany, 1998.

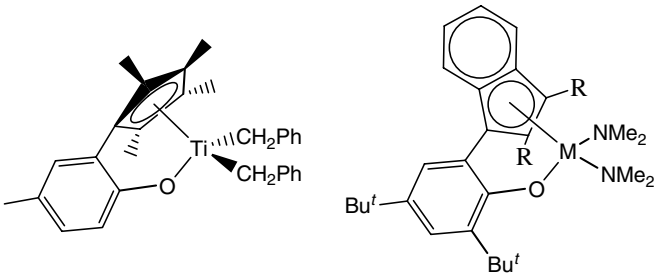

M=Ti, Zr; R=H, Me

I **II**

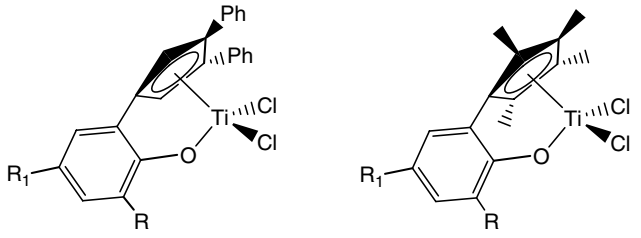

R = Ph (**a**), ^{t}Bu (**b**), ^{t}Bu (**c**), Me(**d**)
R_1=H(**a**, **b**,**d**), ^{t}Bu (**c**)

R = ^{t}Bu (**a**), ^{t}Bu (**b**), Ph (**c**), Me(**d**)
R_1= ^{t}Bu (**a**), H(**b**, **c**, **d**)

III **IV**

Chart 1.

higher than those of polymers produced by 2-tetramethylcyclopentadienyl-6-phenyl-phenoxytitanium dichloride [(TCPP)$TiCl_2$, **IVc**] and **IVd** under similar conditions.

2. Results and discussion

2.1. Synthesis of ligand *1*

The new bidentate ligand **1** was synthesized with anisole as starting material. Dry anisole was added at room temperature to *n*-BuLi in which *n*-hexane has been removed, and then the mixture was heated to 80 °C for 48 h to obtain the lithium salt of anisole. Reaction of the lithium salt with 2,3,4,5-tetramethyl-2-cyclopentenone in toluene at room temperature, followed by hydrolysis with saturated NH_4Cl (aq) and dehydration with concentrated HCl produced the ligand **1** (Scheme 1) in a moderate yield. The lithium salt of anisole could not be obtained when reactions were carried out in the presence of Et_2O or THF as solvent. The preparation of the lithium salt of anisole was reported in literature by reaction of 2-bromoanisole with *n*-BuLi [3a]. In comparison with the literature method, our method is simple and low cost. Ligand **1** was characterized by elemental analysis and NMR spectroscopy. ^{1}H NMR spectroscopic analysis indicates that freshly prepared sample of **1** is a mixture of three isomers, and the ratio of the isomers changes with time. When the sample was left at room temperature, one of the isomers was found to become the major product after several days. It has been reported by Marks et al. that a single isomer of the similar ligand for **I** was obtained after vacuum distillation [4]. Similar behavior has also been observed for the *N*,*N*-dimethylaminophenyl-tetramethylcyclopentadiene ligand system [10] and the substituted tetramethylcyclopentadienylphenol ligands [9].

2.2. Synthesis of (TCP)$TiCl_2$ (*2*)

Complex **2** was prepared by a convenient procedure (Scheme 2) from the reaction of $TiCl_4$ with the lithium salt of **1**. The ligand **1** was treated with one equivalent of *n*-BuLi, and then a solution of $TiCl_4$ in toluene was slowly added at −78 °C. The reaction mixture was allowed to warm to room temperature and then was heated to 65 °C overnight. After filtration and concentration of the reaction mixture, complex **2** was obtained as a yellowish crystalline solid in a moderate yield. The reaction was tried by One-Step Direct Synthesis strategy [11] while the yield of product was low. When the reaction was carried out at room temperature, some red oil was obtained. ^{1}H NMR analysis indicates that the red oil is a complicated mixture from which no pure compound could be isolated. Complex **2** should be formed by a CH_3Cl elimination reaction through a thermocyclization procedure (Scheme 3). It has been reported that the thermocyclization could take place between Ti–Cl and O–CH_3 in monocyclopentadienyltitanium trichloride complexes with a pendant methoxyphenyl group [3a,12]. The solid sample of complex **2** was found to be considerably stable to air and moisture and could be exposed to air for several days without obvious decomposition. Complex **2** also exhibits good thermostability and could be heated to 200 °C without decomposition.

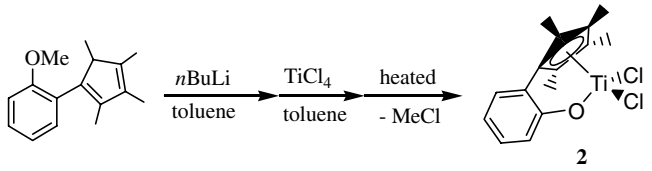

2

Scheme 2. Synthetic procedure of complex **2**.

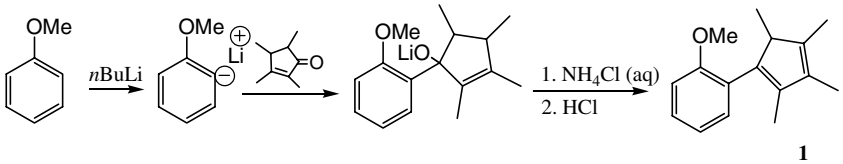

1

Scheme 1. Synthetic procedure of ligand **1**.

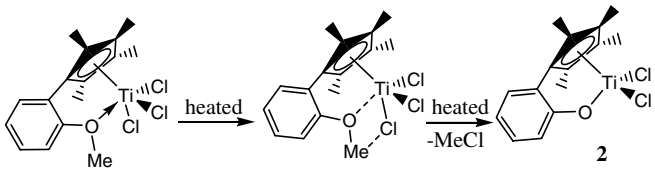

Scheme 3. Possible mechanism for the formation of complex **2**.

2.3. Crystal structures of 2 and IVd

The molecular structures of complexes **2** and **IVd** were determined by X-ray crystal structure analyses. The ORTEP drawings of the molecule structures are shown in Figs. 1 and 2. The selected bond lengths and angles are summarized in Table 1. There are two independent molecules (**IVd** and **IVd′**) with minor structural differences in one unit cell for **IVd**. Selected bond lengths and angles for **IVd** will be used in subsequent discussion. The general structure features of **2** and **IVd** are comparable to those previously reported for **III**, **IV** and **I**. All molecules adopt C_s-symmetry with pseudo-tetrahedral geometry. The Cp(cent)–Ti–O angles for **2** and **IVd** are 107.4° and 107.0°, which are in line with those of complexes **IIIa**–**IIIb** (107.4°, 106.7°) [8], **IVa**–**IVc** (106.8°, 107.1°, 107.3°) [9], and that in **I** (107.7°) [4], indicating similar sterically open features for **2** to complexes **III**, **IV** and **I** as catalyst precursors. The Ti–C(ring) (av.) distances of 2.016 Å for **2** and 2.012 Å for **IVd** are similar to those in **IIIa**–**IIIb** (2.031 Å, 2.032 Å) [8]and **IVa**–**IVc** (2.014 Å, 2.005 Å, 2.011 Å) [9], and shorter than that in **I** (2.36(1) Å) [4]. The distances of Ti–C3 and Ti–C4 in **2** and **IVd** are obviously longer than those of the rest Ti–C(ring) bonds and the Ti–Cp(cent)–C1 angles of **2** (87.6°) and **IVd** (88.6°) are less than 90°, which is characteristic of constrained geometry metallocene catalyst [2–4]. The phenolate plane–Cp plane dihedral angle is 89.8° for **2** and 85.5° for **IVd** and the (phenolate)C–C(ring) vector is bent 11.2° in **2** and 12.0° in **IVd** from the Cp ring plane, which are similar to those for complexes **IIIa**–**IIIb** (89.7° and 9.4°, 86.5° and 9.4°) [8], **IVa**–**IVc** (89.3° and 9.9°, 87.6° and 10.8°, 85.3° and 11.3°) [9]. The corresponding data in **I** are 81(1)° and 15(1)°, reflecting less steric strain in **2**, **III** and **IV** than that in **I** in the solid state. The Ti–O bond lengths of 1.846(2) Å in **2** and 1.823(2) Å in **IVd** are shorter than that in **I** (1.851(7) Å) but longer than those in **IIIa** (1.813(4) Å) and **IIIb** (1.818(4) Å), while the Ti–O–C angles of 127.3(2)° in **2** and 127.7(2)° in **IVd** are larger than the one in **I** (126.6(6)°) and smaller than those in **IIIa**–**IIIb** (129.1(4)°, 129.8(4)°) [8], **IVa**–**IVb** (128.9(3)°, 128.8(4)°, 128.31(18)°) [9]. These results indicate that the Ti–O double-bond character [4,13] in **2** and **IVd** are intermediate compared with that in **III**, **IV** and **I**. It should be pointed out that the differences in solid state structures of **2**, **III**, **IV** and **I** probably result from packing force since there is no other reasonable explanation for them [8,9].

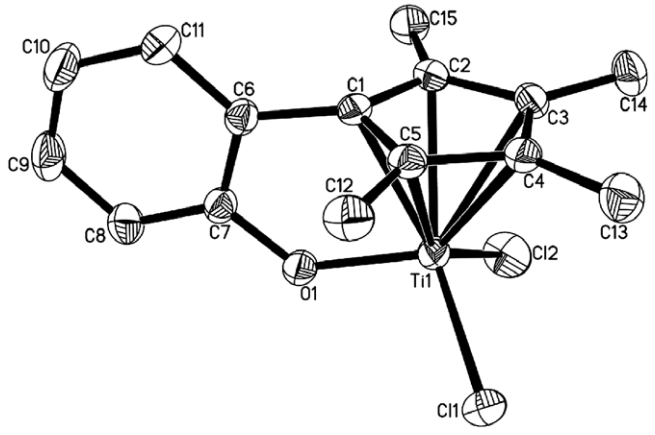

Fig. 1. Structure of complex **2** (thermal ellipsoids are drawn at the 30% probability level).

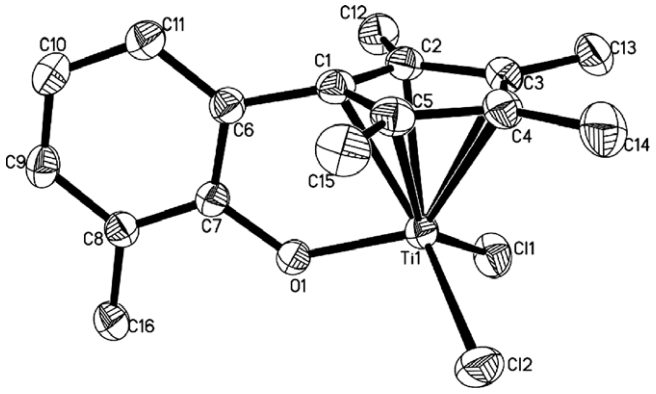

Fig. 2. Structure of complex **IVd** (thermal ellipsoids are drawn at the 30% probability level).

Table 1
Selected bond lengths and angles

Complex ***2***			
Ti(1)–O(1)	1.8458(19)	Ti(1)–C(1)	2.307(3)
Ti(1)–C(2)	2.334(3)	Ti(1)–C(3)	2.387(3)
Ti(1)–C(4)	2.389(3)	Ti(1)–C(5)	2.339(3)
Ti(1)–Cl(1)	2.2646(9)	Ti(1)–Cl(2)	2.2667(10)
O(1)–C(7)	1.374(3)	Cp(cent)–Ti(1)	2.016(2)
C(1)–C(6)	1.486(4)	O(1)–Ti(1)–Cl(1)	105.50(7)
O(1)–Ti(1)–Cl(2)	105.17(7)	Cl(1)–Ti(1)–Cl(2)	104.38(5)
Cp(cent)–Ti(1)–O(1)	107.4(3)	Ti(1)–Cp(cent)–C(1)	87.6(4)
C(6)–C(1)–Cp(cent)	168.8(2)	C(1)–C(6)–C(7)	113.1(2)
C(6)–C(7)–O(1)	115.8(2)	C(7)–O(1)–Ti(1)	127.28(17)
Complex ***IVd***			
Ti(1)–O(1)	1.823(2)	Ti(1)–C(1)	2.320(3)
Ti(1)–C(2)	2.321(3)	Ti(1)–C(3)	2.358(3)
Ti(1)–C(4)	2.376(3)	Ti(1)–C(5)	2.360(3)
Ti(1)–Cl(1)	2.2607(13)	Ti(1)–Cl(2)	2.2750(12)
O(1)–C(7)	1.374(3)	Cp(cent)–Ti(1)	2.012(3)
C(1)–C(6)	1.475(4)	O(1)–Ti(1)–Cl(1)	104.33(9)
O(1)–Ti(1)–Cl(2)	105.48(8)	Cl(1)–Ti(1)–Cl(2)	104.14(5)
Cp(cent)–Ti(1)–O(1)	107.0(2)	Ti(1)–Cp(cent)–C(1)	88.6(4)
C(6)–C(1)–Cp(cent)	168.0(3)	C(1)–C(6)–C(7)	112.7(3)
C(6)–C(7)–O(1)	116.0(3)	C(7)–O(1)–Ti(1)	127.68(19)

2.4. Ethylene polymerization studies

Complex **2** was studied briefly as ethylene polymerization catalyst together with other complexes **IVa–d** of this type and the results were summarized in Table 2. Upon alkylation and activation with Al^iBu_3 and $Ph_3C^+B(C_6F_5)_4^-$, complex **2** show moderate catalytic activity for ethylene polymerization, producing polyethylenes with moderate molecular weights and melting points, which are comparable to complexes **IVa–d**. The catalytic activity of complex **2** is slightly lower than those of complexes **IVc** and **IVd**, while obviously lower than those of **IVa** and **IVb**. These results further confirm the influence of the substituents on the phenolate on the catalytic property [9]. On the other hand, it was found that the M_η of the polyethylene produced by complex **2** is somewhat higher than those of polymers produced by **IVc** and **IVd** under similar conditions. It is possible that the O atom in **2** can coordinate to Al^iBu_3 due to the absence of a substituent at the *ortho* position of the phenolate, which should make the ligand bulkier and therefore affect the rates of chain propagation and termination reactions. Similar to complexes **IV**, the catalytic activity of **2** increases with the increase of Al/Ti ratio and reaches the highest catalytic activities with the Al/Ti ratio about 75. Further increase of the Al/Ti ratio results in a decrease in the catalytic activity. A possible explanation for this is that excessive Al^iBu_3 would consume so much $Ph_3C^+B(C_6F_5)_4^-$ that the catalyst could not be efficiently activated [14]. The catalytic activity of **2** was also found to increase with the B/Ti ratio increasing from 1.1 to 1.3. Further increase of the B/Ti ratio results in a decrease in the catalytic activity. It is understandable that excessive $Ph_3C^+B(C_6F_5)_4^-$ would further react with the already activated catalyst cation and deactivate the catalyst. The catalytic activity of complex **2** is also sensitive to temperature, which has been attributed to tight interaction between the catalyst cation and the cocatalyst anion in the constrained geometry catalyst systems [15]. The degree of ethyl branching is about 1 branch per 1000 C atoms for samples obtained with **2,** which is similar to the samples obtained with **IV**.

3. Experimental

3.1. General comments

Reactions with organometallic reagents were carried out under an argon atmosphere (ultra-high purity) using standard schlenk techniques [16]. Solvents were dried and distilled prior to use [17]. Polymerization grade ethylene was further purified by passage through columns of 10 A molecular sieves and MnO. $Al(^iBu)_3$, *n*-BuLi and $TiCl_4$ were purchased from Aldrich. 2,3,4,5-Tetramethyl-2-cyclopentenone [18], $Ph_3C^+B(C_6F_5)_4^-$ [19], and complex **IVd** [9] were prepared according to the literature procedures. NMR spectra were measured using a Varian Mercury-300 NMR spectrometer.

3.2. Preparation of 1-(2-methoxyphenyl)-2,3,4,5-tetramethyl cyclopentadiene (*1*)

8.3 mL of anisole (0.076 mol) was added dropwise to 76.0 mL (0.076 mol) of 1.0 M *n*-BuLi, in which the *n*-hexane has been evaporated, and then the mixture was heated to 80 °C for 48 h. The anisole lithium salt was washed with *n*-hexane and dissolved in toluene. At room temperature 11.5 mL (0.076 mol) of 2,3,4,5-tetramethyl-2-cyclopentenone was added. The reaction mixture was hydrolyzed with 20 mL of saturated NH_4Cl (aq) followed by dehydration with 20 mL of concentrated HCl. The organic layer was separated, dried over $MgSO_4$, filtered and concentrated by distillation under reduced pressure. Pure product (7.9 g, 45.6%) was obtained by column chromatography over silica (Hexanes/CH_2Cl_2, 3:2) as yellow oil. *Anal*. Calc. for $C_{16}H_{20}O$ (228.15): C, 84.16; H, 8.83. Found: C, 84.11; H, 8.80%. ^1H NMR ($CDCl_3$, 300 MHz, 298 K): δ 7.25 (m, 4H, Ph), 3.79 (s, 3H, OCH_3), 3.40 (q, 1H, CpH), 1.91

Table 2
Summary of ethylene polymerization catalyzed by complex **2** and complexes **IV** (activated by $Ph_3C^+[B(C_6F_5)_4]^-$)[a]

No.	Catalyst	Al:Ti	T (°C)	B:Ti	Yield (g)	Activity[b] $\times 10^{-6}$	M_η[c] $\times 10^{-4}$	T_m (°C)[d]
1	**2**	50	80	1.3	0.63	0.63	6.5	131.9
2	**2**	75	80	1.3	0.83	0.83	6.3	131.5
3	**2**	100	80	1.3	0.71	0.71	6.1	131.8
4	**2**	75	100	1.3	0.65	0.65	5.2	131.4
5	**2**	75	60	1.3	0.59	0.59	7.4	132.1
6	**2**	75	40	1.3	0.42	0.42	8.7	132.3
7	**2**	75	80	1.1	0.54	0.54	6.4	131.4
8	**2**	75	80	1.5	0.78	0.78	5.8	131.7
9	**IVd**	75	80	1.3	1.12	1.12	4.3	130.7
10	**IVa**	75	80	1.3	5.06	5.06	9.4	131.4
11	**IVb**	75	80	1.3	4.85	4.85	8.3	131.3
12	**IVc**	75	80	1.3	1.43	1.43	3.8	131.1

[a] Polymerization conditions: solvent 50 mL of toluene, catalyst 2 μmol, B/Ti ratio 1.3, time 30 min, ethylene pressure 5 bar.
[b] 10^6 g PE (mol Ti)$^{-1}$ h^{-1}.
[c] Measured in decahydro-naphthalene at 135 °C.
[d] Determined by DSC at a heating rate of 10 °C min^{-1}.

(s, 3H, C_5Me_4), 1.86 (s, 6H, C_5Me_4), 0.88 (d, 3H, C_5Me_4). ^{13}C NMR ($CDCl_3$, 75.4 MHz; 298 K): δ 157.26, 140.86, 140.31, 138.06, 134.54, 131.35, 127.35, 126.60, 120.17, 110.72, 55.39, 50.09, 14.29, 12.84, 12.01, 11.27.

3.3. Preparation of [η^5:η^1-(2,3,4,5-tetramethylcyclopentadienyl)-C_6H_4O]$TiCl_2$ (2)

A solution of *n*-BuLi (4.4 mmol) was added dropwise to a solution of 1-(2-methoxyphenyl)-2,3,4,5-tetramethylcyclopentadiene (1.0 g, 4.4 mmol) in Et_2O (100 mL) at −78 °C and the reaction mixture was warmed slowly to room temperature. After stirred overnight, the solvent was removed in vacuo and the residue was washed with hexane, and then dissolved in toluene (150 mL). A solution of $TiCl_4$ (4.4 mmol) in toluene (50 mL) was slowly added at −78 °C. The reaction mixture was allowed warm to room temperature and then was heated to 65 °C for 12 h. The precipitate was filtered off and the solvent was removed to leave a yellow residue. Recrystallization from CH_2Cl_2:hexane (1:4) gave pure **2** as yellow crystals (0.68 g, 46.7%). Calc. for $C_{15}H_{16}Cl_2OTi$ (331.06): C, 54.42; H, 4.87. Found: C, 54.32; H, 4.79%. ^1H NMR ($CDCl_3$, 300 MHz, 298 K): δ 7.30 (t, 1H, Ph), 7.27 (d, 1H, Ph), 7.16 (t, 1H, Ph), 6.65 (d, 1H, Ph), 2.44 (s, 6H, C_5Me_4), 2.08 (s, 6H, C_5Me_4). ^{13}C NMR ($CDCl_3$, 100.5 MHz, 298 K): δ 175.51, 146.34, 143.45, 131.09, 130.15, 129.04, 128.58, 123.86, 114.25, 13.75, 13.39.

3.4. X-ray structure determinations of 2 and IVd

Single crystals of **2** and **IVd** suitable for X-ray structural analysis were obtained from the mixture of CH_2Cl_2/hexane (V/V = 1/3). The data were collected at 293 K on the Bruker SMART-CCD diffractometer for **2** and **IVd** (graphite-monochromated Mo Kα-radiation: $\lambda = 0.71073$ Å). Details of the crystal data, data collections, and structure refinements are summarized in Table 3. All structures were solved by direct methods [20] and refined by full-matrix least-squares on F^2. All non-hydrogen atoms were refined anisotropically and the hydrogen atoms were included in idealized position. All calculations were performed using the SHELXTL [21] crystallographic software packages. CCDC-292295 (**2**), -292294 (**IVd**) contain the supplementary crystallographic data for this paper. These data can be obtained free of charge at www.ccdc.cam.ac.uk/conts/retrieving.html or from the Cambridge Crystallographic Data Centre, 12 Union Road, Cambridge CB2 1EZ, UK; fax: +44 1223 336 033; e-mail: deposit@ccdc.cam.ac.uk.

3.5. Ethylene polymerization

A dry 250 mL steel autoclave was charged with 60 mL of toluene, thermostated at desired temperature and saturated with ethylene (1.0 bar). The polymerization reaction was started by injection of a mixture of catalyst and $Al(^iBu)_3$ in toluene (5 mL) and a solution of $Ph_3C^+B(C_6F_5)_4^-$ in toluene (5 mL) at the same time. The vessel was repressurized to needed pressure with ethylene immediately and the pressure was kept by continuously feeding of ethylene. After 30 min, the polymerization was quenched by injecting acidified methanol [HCl (3 M)/methanol = 1:1]. The mixture was stirred overnight and the polymer was collected by filtration, washed with water, methanol, and dried at 60 °C in vacuo to a constant weight.

Table 3
Crystal data and structural refinement details for **2** and **IVd**

	2	**IVd**
Molecular formula	$C_{15}H_{16}Cl_2OTi$	$C_{16}H_{18}Cl_2OTi$
Molecular weight	331.08	345.10
Crystal system	triclinic	triclinic
Space group	$P\bar{1}$	$P\bar{1}$
a (Å)	6.6982(5)	7.4803(15)
b (Å)	10.3287(11)	15.188(3)
c (Å)	11.1713(9)	15.842(3)
α (°)	96.199(6)	109.20(3)
β (°)	93.802(6)	102.49(3)
γ (°)	90.388(6)	97.08(3)
V (Å^3)	766.59(12)	1622.3(6)
Z	2	4
D_{calc} (g cm^{-3})	1.434	1.413
$F(000)$	340	712
Absolute coefficient (mm^{-1})	0.895	0.849
Scan type	ω–2θ	ω–2θ
Collection range (°)	$1.84 \leqslant 2\theta \leqslant 24.99$	$1.45 \leqslant 2\theta \leqslant 27.48$
Number of reflections	4199	10063
Number of independent reflections	2645	6578
R_{int}	0.0628	0.0413
Number of data/restraints/parameters	2645/0/172	6578/0/361
R [$I > 2\sigma(I)$]	0.0376	0.0505
R_w [$I > 2\sigma(I)$]	0.0932	0.1500
Goodness-of-fit	1.024	1.032
Largest difference in peak and hole (e Å^{-3})	0.259 and −0.273	0.456 and −0.373

4. Supplementary material

Crystallographic data for the structural analysis has been deposited with the Cambridge Crystallographic Data Centre, CCDC reference number: 292295 (**2**), 292294 (**IVd**). Copies of this information may be obtained free of the charge from The Director, CCDC, 12 Union Road, Cambridge, CB2 1EZ, UK (fax: +44 1223 336033; e-mail: deposit@ccdc.cam.ac.uk or http://www.ccdc.cam.ac.uk).

Acknowledgement

This work was supported by the National Natural Science Foundation of China (No. 20374023).

References

[1] (a) A.L. McKnight, R.M. Waymouth, Chem. Rev. 96 (1998) 2587;
(b) U. Siemeling, Chem. Rev. 100 (2000) 1495;

(c) Y.L. Qian, J.L. Hung, D.B. Muhammad, B. Lian, H. Zhang, H. Zhang, Chem. Rev. 103 (2003) 2633.
[2] (a) A.K. Hughes, A. Meetsma, J.H. Teuben, Organometallics 12 (1993) 1936;
(b) K.E. du Plooy, U. Moll, S. Wocadol, W. Massa, J. Okuda, Organometallics 14 (1995) 3129;
(c) J. Okuda, S. Verch, T.P. Spaniol, R. Stuermer, Chem. Ber. 129 (1996) 1429;
(d) F. Amor, J. Okuda, J. Organomet. Chem. 520 (1996) 245;
(e) J. Okuda, T. Eberle, T.P. Spaniol, Chem. Ber. 130 (1997) 209;
(f) J.T. Park, S.C. Yoon, B.-J. Bae, W.S. Seo, I.-H. Suh, T.K. Han, J.R. Park, Organometallics 19 (2000) 1269;
(g) M. Dahlmann, J. Schottek, R. Fröhlich, D. Kunz, M. Nissinen, G. Erker, G. Fink, R. Kleinschmidt, J. Chem. Soc., Dalton Trans. (2000) 1881;
(h) J. Okuda, Chem. Ber. 123 (1990) 1649;
(i) Y.X. Chen, C.L. Stern, S. Yang, T.J. Marks, J. Am. Chem. Soc. 118 (1996) 12451;
(j) H.G. Alt, A. Reb, W. Milins, A. Weis, J. Organomet. Chem. 628 (2001) 169.
[3] (a) A. Rau, S. Schmitz, G. Luft, J. Organomet. Chem. 608 (2000) 71;
(b) S.D.R. Christie, K.W. Man, R.J. Whitby, A.M.Z. Slawin, Organometallics 18 (1999) 348;
(c) E.E.C.G. Gielens, J.Y. Tiesnitsch, B. Hessen, J.H. Teuben, Organometallics 17 (1998) 1652;
(d) A.A.H. van der Zeijden, C. Matteis, Organometallics 16 (1997) 2651;
(e) G. Trouve, D.A. Laske, A. Meetsma, J.H. Teuben, J. Organomet. Chem. 511 (1996) 255;
(f) J. Christoffers, R.G. Bergman, Angew. Chem., Int. Ed. Engl. 34 (1995) 2266;
(g) Q. Huang, Y. Qian, G. Li, Y. Tang, Trans. Met. Chem. 15 (1990) 483;
(h) K. Kunz, G. Erker, G. Kehr, R. Fröhlich, H. Jacobsen, H. Berke, O. Blacque, J. Am. Chem. Soc. 124 (2002) 3316;
(i) Y. L Qian, J.L. Huang, Polyhedron 13 (1994) 1105.
[4] Y.X. Chen, T.J. Marks, Organometallics 16 (1997) 5958.
[5] M.G. Thom, P.E. Fanwick, R.W. Chesnut, I.P. Rothwell, Chem. Commun. (1999) 2543.
[6] L.E. Turner, M.G. Thorn, P.E. Fanwick, I.P. Rothwell, Chem. Commun. (2003) 1034.
[7] L.E. Turner, M.G. Thorn, P.E. Fanwick, I.P. Rothwell, Organometallics 23 (2004) 1576.
[8] Y. Zhang, J. Wang, Y. Mu, Z. Shi, C. Lü, Y. Zhang, L. Qiao, S. Feng, Organometallics 22 (2003) 3877.
[9] Y. Zhang, Y. Mu, C. Lü, G. Li, J. Xu, Y. Zhang, D. Zhu, S. Feng, Organometallics 23 (2004) 540.
[10] M. Enders, G. Ludwig, H. Pritzkow, Organometallics 20 (2001) 827.
[11] Y. Zhang, Y. Mu, Organometallics 25 (2006) 631.
[12] Y. Qian, J. Hung, J. Yang, A.S.C. Chan, W. Chen, X. Chen, G. Li, X. Jin, Q. Yang, J. Organomet. Chem. 547 (1997) 263.
[13] (a) J.C. Huffman, K.G. Moloy, J.A. Marsella, K.G. Caulton, J. Am. Chem. Soc. 102 (1980) 3009;
(b) B. Cetinkaya, P.B. Hitchcock, M.F. Lappert, S. Torroni, J.L. Atwood, W.E. Hunter, M.J. Zaworotko, J. Organomet. Chem. 188 (1980) C31;
(c) R. Fandos, A. Meetsma, J.H. Teuben, Organometallics 10 (1991) 59.
[14] M. Bochmann, M. Sarsfield, J. Organomet. 17 (1998) 5908.
[15] Y.X. Chen, T.J. Marks, Organometallics 16 (1997) 3649.
[16] D.F. Shriver, The Manipulation of Air-Sensitive Compounds, McGraw-Hill, New York, 1969.
[17] D.D. Perrin, W.L.F. Armarego, D.R. Perrin, The Purification of Laboratory Chemicals, Pergamon, New York, 1980.
[18] F.X. Kohl, P. Jutzi, J. Organomet. Chem. 243 (1983) 119.
[19] (a) A.G. Massey, A.J. Park, J. Org. Chem. 2 (1962) 245;
(b) A.G. Massey, A.J. Park, J. Organomet. Chem. 5 (1966) 218;
(c) J.C.W. Chien, W.M. Tsai, M.D. Rasch, J. Am. Chem. Soc. 113 (1991) 8570.
[20] SHELXTL, PC Siemens Analytical X-ray Instruments, Madison, WI, 1993.
[21] G.M. Sheldrick, SHELXTL Structure Determination Programs, Version 5.0, PC Siemens Analytical Systems, Madison, WI, 1994.

confirmation has been carried out by single crystal X-ray diffraction studies in one case.

2. Experimental

2.1. Materials

$Co(OAc)_2 \cdot 4H_2O$ and NaN_3 were purchased from Loba Chemi, Bombay and 1-alkyl-2-(naphthyl-(α/β)-azo)imdazoles (α-/β-NaiR) were prepared following the literature procedures [9]. All other chemicals and solvents were of reagent grade. Solvents were used after drying.

2.2. Physical measurements

Microanalyses (C, H, N) were performed using a Perkin–Elmer 2400 CHNO/S elemental analyzer. Spectroscopic measurements were carried out using the following instruments: UV–Vis spectra, reflectance spectra, JASCO UV–Vis/NIR model V-570; IR spectra (KBr disk, 4000–200 cm^{-1}), JASCO FT-IR model 420. The room temperature magnetic moment was measured using a Vibrating sample 155 magnetometer at 298 K. Molar conductances (Λ_M) were measured in a Systronics conductivity meter 304 model using *ca.* 10^{-3} M solutions in MeOH. Electrochemical measurements were carried out with the use of computer controlled EG&G PARC VersaStat model 250 electrochemical instruments using a Pt-disk working electrode. The solution was IR compensated and the results were collected at 298 K. The reported results are referenced to SCE in acetonitrile and are uncorrected for junction potentials. Estimation of cobalt was carried out by the complexometric titration method [18].

CAUTION! Azide complexes of transition metal ions containing organic ligands are potentially explosive. Only a small amount of materials should be prepared, and it should be handled with care.

2.3. Preparation of bis-chelated azido complexes, $[Co(\alpha\text{-}NaiEt)_2(N_3)_2]$ (**3b**)

1-Ethyl-2-(naphthyl-α-azo)imidazole (α-NaiEt) (0.06 g, 0.50 mmol) in MeOH (10 ml) was added dropwise to a stirred solution of $Co(OAc)_2 \cdot 4H_2O$ (0.062 g, 0.25 mmol) in MeOH (10 ml) at 298 K. The brown solution was stirred for 15 min. Then NaN_3 (0.03 g, 0.50 mmol) in MeOH (10 ml) was added to the brown solution. The color changed from brown to deep brown. The solution was filtered and then left undisturbed for a week. Dark brown crystals were obtained, which were washed with water, methanol and ether. Finally, they was dried *in vacuo*. The yield was 0.12 g, (75%). The microanalytical data of the complexes are as follows: $[Co(\alpha\text{-}NaiMe)_2(N_3)_2]$ (**3a**): *Anal.* Calc. for $C_{28}H_{24}N_{14}Co$: C, 54.64; H, 3.90; N, 31.87; Co, 9.58. Found: C, 54.71; H, 4.01; N, 31.78; Co, 9.50%. $[Co(\alpha\text{-}NaiEt)_2(N_3)_2]$ (**3b**): *Anal.* Calc. for $C_{30}H_{28}N_{14}Co$: C, 55.99; H, 4.35; N, 30.48; Co, 9.16. Found: C, 55.71; H, 4.45; N, 30.28; Co, 9.12%. $[Co(\alpha\text{-}NaiBz)_2(N_3)_2]$ (**3c**): *Anal.* Calc. for $C_{36}H_{32}N_{14}Co$: C, 60.08; H, 4.45; N, 27.26; Co, 8.19. Found: C, 60.01; H, 4.40; N, 27.19; Co, 8.12%.

2.4. Preparation of $[Co(\beta\text{-}NaiEt)_2(N_3)_2]$ (**4b**)

1-Ethyl-2-(naphthyl-β-azo)imidazole (β-NaiEt) (0.06 g, 0.50 mmol) in MeOH (10 ml) was added dropwise to a stirred solution of $Co(OAc)_2 \cdot 4H_2O$ (0.062 g, 0.25 mmol) in MeOH (10 ml) at 298 K. The brown solution was stirred for 15 min. Then NaN_3 (0.03 g, 0.50 mmol) in MeOH (10 ml) was added to the brown solution. The color changed from brown to deep brown. The solution was filtered and then left undisturbed for a week. A dark brown crystal was obtained. It was washed with water, methanol and ether. Finally, it was dried *in vacuo*. Yield was 0.11 g, (70%). The microanalytical data of the complexes are as follows: $[Co(\beta\text{-}NaiMe)_2(N_3)_2]$ (**4a**): *Anal.* Calc. for $C_{28}H_{24}N_{14}Co$: C, 54.64; H, 3.90; N, 31.87; Co, 9.58. Found: C, 54.73; H, 4.06; N, 31.81; Co, 9.52%. $[Co(\beta\text{-}NaiEt)_2(N_3)_2]$ (**4b**): *Anal.* Calc. for $C_{30}H_{28}N_{14}Co$: C, 55.99; H, 4.35; N, 30.48; Co, 9.16. Found: C, 55.81; H, 4.41; N, 30.36; Co, 9.13%. $[Co(\beta\text{-}NaiBz)_2(N_3)_2]$ (**4c**): *Anal.* Calc. for $C_{36}H_{32}N_{14}Co$: C, 60.08; H, 4.45; N, 27.26; Co, 8.19. Found: C, 60.03; H, 4.41; N, 27.21; Co, 8.13%.

2.5. Preparation of tris-chelates, $[Co(\alpha\text{-}NaiMe)_3](ClO_4)_2 \cdot H_2O$ (**5a**)

To a degassed dry ethanol solution (15 ml) of $Co(ClO_4)_2 \cdot 6H_2O$ (0.25 g, 0.68 mmol), α-NaiMe (0.58 g, 2.46 mmol) in the same solvent (15 ml) was added under N_2 and stirred continuously. The solution colour turned to deep brown-violet. It was then refluxed for 8 h. Excess of $LiClO_4$ (5 mmol) in MeOH (5 ml) was added. Nitrogen gas was bubbled through this solution to reduce its volume to half of its original value and the flask was corked and kept at 10 °C for 18 h. Brown crystals deposited on the glass wall were collected by filtration, washed with ethanol and stored over $CaCl_2$. Yield: 0.25 g (37%). The purity of the compound was checked by microanalytical data. The compounds are sensitive to moisture and were kept under dry conditions. Microanalytical data of the complex is as follows: $[Co(\alpha\text{-}NaiMe)_3](ClO_4)_2 \cdot H_2O$ (**5a**) *Anal.* Calc. for $C_{42}H_{38}N_{12}Cl_2O_9Co$: C, 51.22; H, 3.66; N, 17.07. Found: C, 51.31; H, 3.71; N, 17.18%. All other complexes were prepared by the same procedure. The yield varied from 35% to 40% and microanalytical data of the complexes are as follows. $[Co(\alpha\text{-}NaiEt)_3](ClO_4)_2 \cdot H_2O$ (**5b**) *Anal.* Calc. for $C_{45}H_{44}N_{12}Cl_2O_9Co$: C, 52.64; H, 4.09; N, 16.38. Found: C, 52.59; H, 4.17; N, 16.29%. $[Co(\beta\text{-}NaiMe)_3](ClO_4)_2 \cdot H_2O$ (**6a**) *Anal.* Calc. for $C_{42}H_{38}N_{12}Cl_2O_9Co$: C, 51.22; H, 3.66; N, 17.07. Found: C, 51.30; H, 3.74; N, 17.16. $[Co(\alpha\text{-}NaiEt)_3](ClO_4)_2 \cdot H_2O$ (**6b**) *Anal.* Calc. for $C_{45}H_{44}N_{12}Cl_2O_9Co$: C, 52.64; H, 4.09; N, 16.38. Found: C, 52.58; H, 4.15; N, 16.27%.

2.6. X-ray crystal structure analysis of [Co(β-NaiEt)$_2$(N$_3$)$_2$] (**4b**)

The crystals were grown by slow evaporation of the reaction mixture over a week. Data were collected with a Bruker CCD area detector diffractometer [19] using fine-focus sealed graphite-monochromatized Mo Kα radiation ($\lambda = 0.71073$ Å) at 295(2) K for **4b**. Diffractions were recorded with 2θ in the range $3.84 \leqslant 2\theta \leqslant 56.62°$. A summary of the crystallographic data and structure refinement parameters are given in Table 1. Reflection data were recorded using the ψ and ω scan techniques. Data were corrected for Lp and an empirical absorption correction [20] in the hkl range: $-25 \leqslant h \leqslant 25$; $-17 \leqslant k \leqslant 18$; $-17 \leqslant l \leqslant 17$. Data reduction was carried out using the SAINT program [20]. In order to restrain the anisotropic displacements, we used several DELU and SIMU instructions in the refinement, so the number of restrained parameters is a little larger. The structure was solved by the direct method using SHELXS-97 [21] and successive difference Fourier syntheses. All non-hydrogen atoms were refined anisotropically. The hydrogen atoms were fixed geometrically and refined using the riding model. The molecular graphics were carried out using ORTEP-3 for Windows [21]. In the final difference Fourier map, the residual maxima and minima Δ_{max} (e Å^{-3}), 0.342 and Δ_{min} (e Å^{-3}), −0.264 for **4b** were carried out using SHELXL-97 [22], indicating that there is no solvent in the crystal.

3. Results and discussion

3.1. The complexes and their formulation

1-Alkyl-2-(naphthyl-(α/β)-azo)imidazoles, (α-/β-NaiR), are used in this work. The reaction of 1-alkyl-2-(naphthyl-(α/β)-azo)imidazoles (α/β-NaiR), $Co(OAc)_2 \cdot 4H_2O$ and NaN_3 in any mole ratio [1:1:2, 1:2:2; 1:1:excess (>4 mole)] in MeOH affords complexes of the formulae [Co(α/β-NaiR)$_2$(N$_3$)$_2$] (**3**, **4**).

$$Co(OAc)_2 + 2(\alpha/\beta) - NaiR + 2NaN_3 \xrightarrow[\text{Stir. 298 K}]{\text{MeOH}} \underset{\mathbf{3/4}}{[Co(N_3)_2(\alpha/\beta - NaiR)_2]} + 2NaOAc \quad (1)$$

The complexes are non-electrolytes in MeCN. The composition of the complexes was supported by microanalytical data. Room temperature (298 K) magnetic moment measurements show high spin data in the range 4.9–5.2 B.M.

3.2. Structure description of [Co(N$_3$)$_2$(β-NaiEt)$_2$] (**4b**)

The molecular structure of [Co(N$_3$)$_2$(β-NaiEt)$_2$] (**4b**) is shown in Fig. 1. The bond distances and angles are set out in Table 2. The structure is a severely distorted tetrahedron with C_{2v} symmetry. The cobalt(II) centre is surrounded by two N(imidazole) donor atoms from two β-NaiEt ligands and two azide-N atoms. β-NaiEt has two N-centres: N(imidazole) and N(azo). It could serve as a monodentate imidazole-N donor or N(azo), N(imidazole)

Table 1
Summarised crystallographic data for [Co(β-NaiEt)$_2$(N$_3$)$_2$] (**4b**)

	[Co(β-NaiEt)$_2$(N$_3$)$_2$] (**4b**)
Empirical formula	$C_{30}H_{28}N_{14}Co$
Formula weight	643.59
Temperature (K)	295(2)
Crystal system	monoclinic
Space group	*C*2/*c*
Crystal size (mm)^3	0.30 × 0.20 × 0.20
Unit cell dimensions	
a (Å)	19.2314(13)
b (Å)	14.0994(9)
c (Å)	13.4699(9)
β (°)	123.3860(10)
V (Å)^3	3049.7(3)
Z	4
λ (Å)	0.71073
μ (Mo Kα) (mm^{-1})	0.609
D_{calc} (g cm^{-3})	1.402
Refined parameters	204
Total reflection	3706
Unique data [$I > 2\sigma(I)$]	2647
R_1[a] [$I > 2\sigma(I)$]	0.0554
wR_2[b]	0.1198
Goodness-of-fit	0.938

[a] $R_1 = \sum|F_o - F_c|/\sum F_o$.
[b] $wR_2 = [\sum w(F_o^2 - F_c^2)/\sum wF_o^4]^{1/2}$, $w = 1/[\sigma^2(F_o^2) + (0.0800P)^2]$ for **4b** where $P = (F_o^2 + 2F_c^2)/3$.

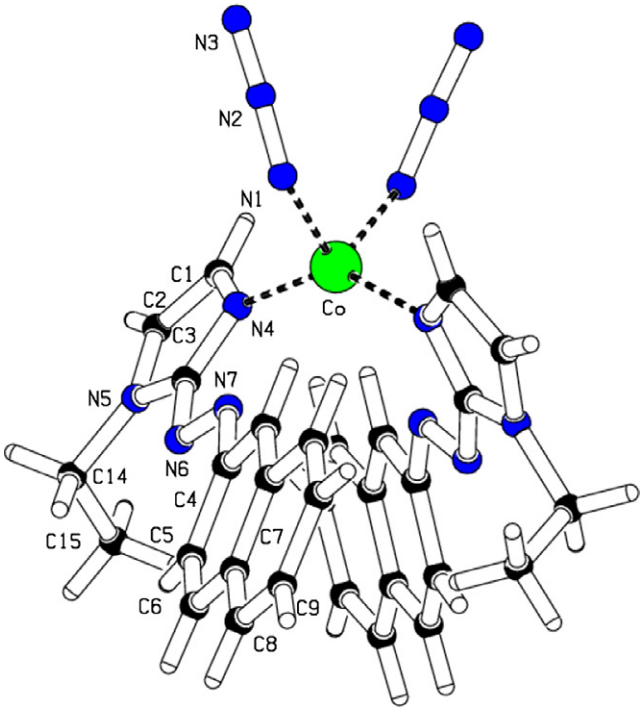

Fig. 1. ORTEP view of [Co(β-NaiEt)$_2$(N$_3$)$_2$] (**4b**) with 30% probability ellipsoids.

Table 2
Selected bond distance (Å) and angles (°) for $[Co(\beta\text{-NaiEt})_2(N_3)_2]$ (**4b**)

Bond distance (Å)		Bond angle (°)	
Co—N(4)	2.0428(16)	N(1)—Co—N(1*)[a]	102.79(14)
Co—N(1)	1.992(2)	N(1)—Co—N(4)	110.29(8)
N(1)—N(2)	1.195(3)	N(1)—Co—N(4*)[a]	92.99(8)
N(2)—N(3)	1.148(3)	N(4)—Co—N(4*)[a]	142.73(10)
N(6)—N(7)	1.252(2)	N(6)—N(7)—C(4)	113.84(17)
N(4)—C(3)	1.303(3)	N(7)—N(6)—C(3)	110.07(17)
N(5)—C(2)	1.357(3)	N(2)—N(1)—Co	134.66(16)
N(5)—C(3)	1.366(2)	N(1)—N(2)—N(3)	175.4(2)
N(6)—C(3)	1.407(3)	C(3)—N(4)—Co	123.62(13)
N(7)—C(4)	1.420(2)	C(1)—N(4)—Co	130.90(16)

[a] Symmetry: $1-x, 1+y, 1.5-z$.

bidentate chelating agent. Forced chelation with the azoimine (—N=N—C=N—) function gives a very long Co—N(azo) distance (2.6844(1) Å) and low chelate angle (N(azo)—Co—N(imidazole), 66.22(5)°). The Co—N(imidazole) (2.0428(16) Å) distances are of reasonable length and are comparable with reported data [13,23]. The distortion may arise from the long Co···N(azo) distance. So, the structure may be considered as a tetrahedron with two additional weak interactions. In 1-alkyl-2-(arylazo)imidazole (RaaiR′) complexes of Co(II) we have isolated octahedral complexes when azide N_3^- is present as the counter ion [13]. In the presence of ClO_4^- as a counter ion we have isolated tetrahedral $[Co(RaaiR')_4]^{2+}$ where the ligands bind through N(imidazole) only, [19] which upon reaction with N_3^- or NCS^- have isolated octahedral complexes $Co(RaaiR')_2(X)_2$ ($X = N_3^-$ or NCS^-). That means azoimidazole may bind Co(II) as a monodentate imidazole-N or bidentate N(imidazole), N(azo) ligand [13,23]. There is a small difference in CFSE between octahedral and tetrahedral symmetry of high-spin Co(II) complexes and hence the steric reason is the determining factor in the geometrical preference of the complex. The naphthyl group is sterically more crowded than the pendant aryl group in azoimidazoles, which may lead to the generation of the distorted tetrahedral Co(II) geometry in the present case. The Co—N(azido) bond length is comparable with the reported data [13]. The N=N bond length is 1.252(2) Å in **4b.** Although data are not available for this ligand system, its isomeric analogue 1-ethyl-2-(naphthyl-α-azo)imidazolium hexafluorophosphate shows 1.267(3) Å for the N=N length [11]. The N—N—N bond parameters lie within the reported range [13,24]. An intermolecular hydrogen bonded unit is constituted by interaction between the imidazole C(2)—H(2) of one molecule with the azide—N(3) of a neighbouring molecule: (C(2)—H(2)···N(3): C(2)—H(2), 0.93 Å, H(2)—N(7), 2.54 Å, C(2)···N(3), 3.370(1) Å and ∠C(2)—H(2)···N(3), 149.22°). The existence of C—H···π (Cg) (Fig. 2) (C(13)—H(13)...Cg(1), 2.796(8) Å; C(15)—H(15B)···Cg(2), 3.390(5) Å) and π···π interactions (face-to-face type) (Cg(1)—Cg(2), 4.305(4) Å; Cg(1)—Cg(3), 4.039(7) Å; Cg(2)—Cg(2), 4.389(6) Å) increases the robustness of the structure (Cg(1): N(4)—C(1)—N(5)—C(2)—C(3);

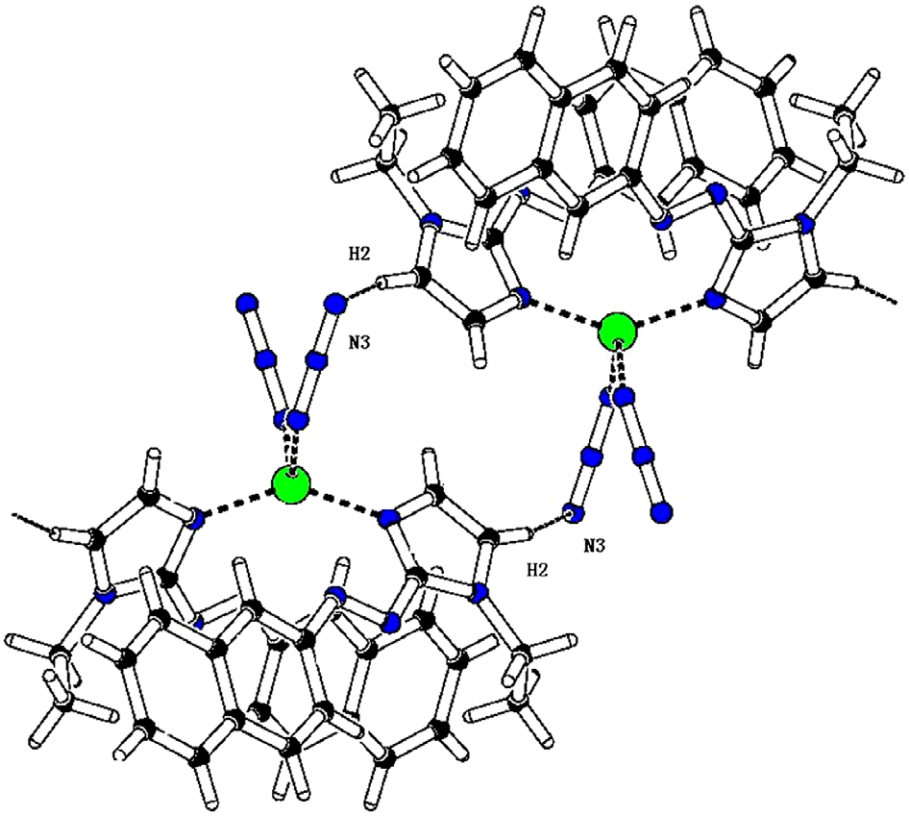

Fig. 2. Packing of two molecules.

Cg(2): C(4)—C(5)—C(6)—C(7)—C(12)—C(13); Cg(3): C(7)—C(8)—C(9)—C(10)—C(11)—C(12); symmetry, 1/2 − *x*, 1/2 − *y*, 1 − *z*).

3.3. Spectral studies

The IR bands were assigned by comparing with the free ligand data. The most significant observation is the appearance of a very strong sharp single band at 2035–2045 cm^{-1}. This corresponds to $\nu_{asym}(N_3)$. This supports the mononuclear monodentate N_3^- bonding in the complexes. The ligand α/β-NaiR shows characteristic vibrations at 1600–370 cm^{-1}. Moderately intense stretchings at 1570–1600 and 1435–1440 cm^{-1} are due to ν(C=N) and ν(N=N), respectively.

The solution electronic spectra of the complexes were recorded in acetonitrile solution in the UV/Vis region (250–900 nm). The data are listed in Table 3. In the visible region both types of complexes exhibit an intense band ⩽400 nm. These transitions are presumably due to intra-ligand π–π*/and n–π* transitions. The structural distortion undoubtedly effects the spectral transitions and intensity of the bands [25]. High-spin tetrahedral Co(II) complexes may exhibit two or three weak transitions at the visible to near-IR region. However, the intensity of these bands is very much dependent on the degree of distortion of the structures [26]. In the present example, the structural distortion from regular tetrahedron arises from weak Co···N(azo) (*vide supra*) interactions. There are three transitions in the range 415–640 nm for complexes **3**. The intensity patterns of the bands are different; the transitions 415–425 and 440–455 nm are highly intense ($\varepsilon \sim 10^4$ mol^{-1} cm^{-1}) and sharp, while the transition 630–640 nm is weak ($\varepsilon \sim 180$–450 mol^{-1} cm^{-1}) and very broad. Based on the low intensity and low energy, the band at 630–640 nm may be due to d–d transitions [26]. The high intense bands at 415–455 nm may be assigned to MLCT transitions. The complexes **4** also exhibit three transitions in the range 445–675 nm. The transition 440–445 nm is of high intensity ($\varepsilon \sim 10^4$ mol^{-1} cm^{-1}) and is sharp, while the other two transitions at 600–615 and 660–670 nm are weak and broad.

3.4. Cyclic voltammetry

Representative voltammograms are shown in Fig. 3 and data are collected in Table 4. The complexes display one oxidation couple at 1.3–1.5 V and I_{pa}/I_{pc} equals 0.9–1.0.

Table 3
UV–Vis spectra[a], IR and magnetic moment (μ) data of $[Co(\alpha/\beta\text{-NaiR})_2(N_3)_2]$ (**3**,**4**) and $[Co(\alpha/\beta\text{-NaiR})_3](ClO_4)_2 \cdot H_2O$ (**5**,**6**)[b]

Compound	UV–Vis spectral data (λ_{max}/nm) (10^{-3} ε M^{-1} cm^{-1})	IR data			
		νN_3^-	ν(C=N)	ν(N=N)	μ (B.M.)
$[Co(\alpha\text{-NaiMe})_2(N_3)_2]$ (**3a**)	632(0.24), 452(7.76), 422(8.71), 392(12.24)	2035	1598	1436	4.91
$[Co(\alpha\text{-NaiEt})_2(N_3)_2]$ (**3b**)	636(0.32), 444(7.44), 416(8.13), 396(14.21)	2034	1600	1438	5.06
$[Co(\alpha\text{-NaiBz})_2(N_3)_2]$ (**3c**)	634(0.27), 450(6.83), 417(7.91), 392(14.48)	2034	1598	1434	4.82
$[Co(\beta\text{-NaiMe})_2(N_3)_2]$ (**4a**)	668(0.18), 602(0.32), 451(9.80), 394(12.02)	2036	1598	1435	4.21
$[Co(\beta\text{-NaiEt})_2(N_3)_2]$ (**4b**)	672(0.29), 612(0.41), 448(10.05), 396(14.05)	2038	1597	1438	4.18
$[Co(\beta\text{-NaiBz})_2(N_3)_2]$ (**4c**)	665(0.21), 604(0.38), 448(9.98), 396(13.60)	2038	1598	1436	4.24
$[Co(\alpha\text{-NaiMe})_3](ClO_4)_2$ (**5a**)			1595	1398	1.65
$[Co(\alpha\text{-NaiEt})_3](ClO_4)_2$ (**5b**)			1597	1395	1.58
$[Co(\beta\text{-NaiMe})_3](ClO_4)_2$ (**6a**)			1598	1398	1.73
$[Co(\beta\text{-NaiEt})_3](ClO_4)_2$ (**6b**)			1596	1396	1.67

[a] Solvent: MeCN.
[b] Mixture of isomers, $\nu(ClO_4)$ at 1120–1100, 1090–1080 cm^{-1}.

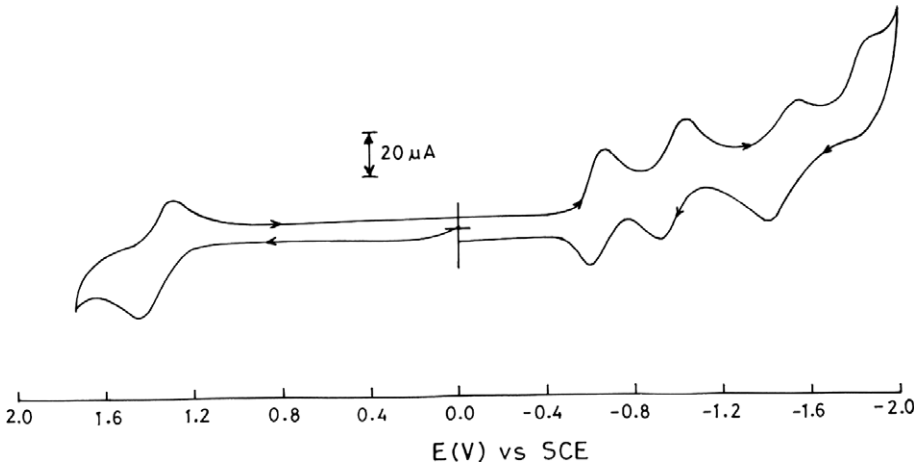

Fig. 3. Cyclic voltammogram of $Co(\alpha\text{-NaiMe})_2(N_3)_2$ (**3a**).

Table 4
Cyclic voltammetric data of $[Co(\alpha/\beta\text{-NaiR})_2(N_3)_2]$ (**3**, **4**)[a]

Compound	Co(III)/Co(II)	Ligand reductions			
$[Co(\alpha\text{-NaiMe})_2(N_3)_2]$ (**3a**)	1.46 (120)	−0.58 (120)	−0.98 (130)	−1.30 (160)	−1.59[b]
$[Co(\alpha\text{-NaiEt})_2(N_3)_2]$ (**3b**)	1.43 (130)	−0.62 (120)	−0.95 (120)	−1.43 (140)	−1.60[b]
$[Co(\alpha\text{-NaiBz})_2(N_3)_2]$ (**3c**)	1.47 (120)	−0.60 (130)	−0.90 (150)	−1.38 (150)	−1.60[b]
$[Co(\beta\text{-NaiMe})_2(N_3)_2]$ (**4a**)	1.37 (130)	−0.64 (140)	−0.98 (120)	−1.44 (160)	−1.62[b]
$[Co(\beta\text{-NaiEt})_2(N_3)_2]$ (**4b**)	1.33 (120)	−0.70 (130)	−1.02 (130)	−1.37 (160)	−1.60[b]
$[Co(\beta\text{-NaiBz})_2(N_3)_2]$ (**4c**)	1.39 (120)	−0.64 (120)	−0.94 (140)	−1.30 (180)	−1.60[b]

[a] Solvent, MeCN; working electrode, Pt-disk milli electrode, Pt-wire auxiliary, SCE reference; supporting electrolyte $[n\text{Bu}_4\text{N}][\text{ClO}_4]$; scan rate 0.05 V s^{-1}, potential $E_{1/2} = 0.5(E_{pa} + E_{pc})$, $\Delta E_p = |E_{pa} - E_{pc}|$, mV; E_{pa} = anodic peak potential, E_{pc} = cathodic peak potential.
[b] $E_{pc.}$

Although the peak heights are not equivalent for the various complexes, the areas under the peaks are comparable. The peak-to-peak separation is >120 mV. This supports the quasireversibility of the couple. The oxidation couple refers to the Co(III)/Co(II) response. Azo (—N=N—) is a good π-acidic function and can assist $d\pi \rightarrow \pi^*$(azo) charge transfer, which effectively stabilizes the lower oxidation state. The data in Table 4 suggest that Co(II) could be better stabilized in $Co(\alpha\text{-NaiR})_2(N_3)_2$ than in $Co(\beta\text{-NaiR})_2(N_3)_2$. There are three observable quasireversible to irreversible reduction couples appearing at −0.6 to −0.7 V, −1.3 to −1.4 V and <−1.6 V. Naphthylazoimidazole is an eligible reducing ligand. The azo (N=N) group is a potential electron receiving centre. Each ligand can accommodate two electrons corresponding to [—N=N—]/[—N⁻—N—]⁻ and [—N⁻—N]⁻/[—N⁻—N⁻—]²⁻ redox responses. In principle there will be four redox couples. However, we observed three reductive responses. α-NaiR is thermodynamically more stable than β-NaiR and this is supported by higher redox potential data of the respective cobalt complexes.

3.5. Tris-[{1-alkyl-2-(naphthyl-(α/β)-azo}imidazole]-cobalt(II) perchlorate monohydrate, $[Co(\alpha\text{-}/\beta\text{-})NaiR)_3](ClO_4)_2 \cdot H_2O$

The brown complexes of $[Co(NaiR)_3](ClO_4)_2 \cdot H_2O$ (**5**, **6**) have been prepared by stirring $Co(ClO_4)_2 \cdot 6H_2O$ and NaiR in the mole proportion 1:3.5 in dry ethanol under N_2 atmosphere and have been isolated as the monohydrate perchlorate salt by adding $NaClO_4$ under cold conditions. A very dry condition is absolutely necessary to get the pure product. On exposure to air the brown crystalline shining compound becomes moistened and results in an impure gummy compound. Because of its moisture sensitivity we could not crystallise this compound to get an X-ray quality crystal. In a dry inert atmosphere the compound is highly stable. In solution the complex is unstable and presumably dissociates to the solvato species $[Co(NaiR)_2(S)_2]^{2+}$. Upon addition of NaN_3 to an ethanolic solution of the complex, it immediately separates into $[Co(NaiR)_2(N_3)_2]$, which has been proved by spectral (IR, UV–Vis), magnetic, conductance data and on comparing with the previously prepared complex (*vide supra*). All our attempts to prepare $Co(NaiR)_2Cl_2$ using $CoCl_2$ and NaiR in different metal:ligand ratios, and even by addition of LiCl to an alcoholic solution of $Co(ClO_4)_2$ and NaiR, have failed.

$Co(NaiR)_3(ClO_4)_2$ is sufficiently stable in dry inert atmosphere. Solid state bulk magnetic moment measurements establish this conjecture. Initial measurement of the moment immediately after removal from a dessicator gives a magnetic moment corresponding to a low-spin electron configuration ($t_{2g}^6 e_g^1$, μ, ∼ 1.8B.M.). Exposure to air for a week in the same sample tube gives a moment much higher than the low-spin value, although it is lower than the spin-free ($t_{2g}^5 e_g^2$) value. This suggests the formation of a mixture of low-spin and high-spin complexes. The azido complexes, $Co(NaiEt)_2(N_3)_2$ are a high-spin system. Air oxidation of cobalt(II)-azoimine complexes has been ruled out from the literature report [13,23,26].

The complexes show a very strong and structured vibration at 1120–1110, 1100–1090 cm^{-1}, and a sharp, medium intense band at 630 cm^{-1}. This is assigned to the ClO_4^- vibration. The structured stretching may be due to reduction in Td symmetry of the ion by a hydrogen-bonding interaction with crystallized H_2O and/or C—H···O(ClO_3). A strong and sharp stretch at 1590–1600 cm^{-1} is due to ν(C=N) and ν(C=C) while another stretch at 1400–1390 cm^{-1} is referred to ν(N=N). The stretching vibration of the water of crystallization appears as a broad medium band centred at 3450 cm^{-1}.

Tris-chelates with unsymmetric *N*,*N*′ donor centre may, in principle, exist in two different isomeric forms: facial and meridional [27]. Additionally, tris-chelates undergo quick ligand dissociation to give bis-chelated solvento species. So we logically assume that the spectral transitions may be the combination of similar transitions from several isomers present in the solution. Similarly studies on the redox properties by solution electrochemistry of these complexes do not bring any definite conclusion. Thus, we are not interested in extending the solution studies of the tris-chelates.

4. Conclusion

This paper describes the mononuclear bis-azido Co(II) complexes of 1-alkyl-2-(naphthyl-(α/β)-azo)imidazoles. The complexes are characterized by different physicochemical

methods and single crystal X-ray structure determination in one case shows a distorted tetrahedral CoN_4 coordination arrangement. The complexes show high potential Co(III)/Co(II) redox couples along with azo reductions.

5. Supplementary material

Crystallographic data for the structure have been deposited with the Cambridge Crystallographic data center, CCDC No. 251235 for $[Co(\beta\text{-NaiEt})_2(N_3)_2]$ (**4b**). Copies of this information may be obtained free of charge from the Director, CCDC, 12 Union Road, Cambridge CB2 1EZ, UK (e-mail: deposit@ccdc.cam.ac.uk or www:http://www.ccdc.cam.ac.uk).

Acknowledgements

Financial support from the Council of Scientific and Industrial Research, New Delhi, are gratefully acknowledged. The authors thank Ms. Fen-Ling Liao of the National Science Council in Taiwan for the collection of X-ray diffraction data. The authors thank the National Science Council, Republic of China, for support under Grant No. 92-2112-M-046.

References

[1] H. Sigel (Ed.), Metal Ions in Biological System, vol. 13, Marcel Dekker, New York, 1981.
[2] T.K. Misra, D. Das, C. Sinha, P. Ghosh, C.K. Pal, Inorg. Chem. 37 (1998) 1672.
[3] B.K. Ghosh, A. Chakravorty, Coord. Chem. Rev. 95 (1989) 239.
[4] H. Hartmann, T. Scheiring, J. Fielder, W. Kaim, J. Organomet. Chem. 604 (2000) 267.
[5] K. Pramanik, M. Shivakumar, P. Ghosh, A. Chakravorty, Inorg. Chem. 39 (2000) 195.
[6] A.C.G. Holtze, H. Kooijman, A.L. Spek, J.G. Haasnoot, J. Reedijk, New J. Chem. 28 (2004) 565.
[7] U.S. Ray, D. Banerjee, C. Sinha, Proc. Indian Acad. Sci. (Chem. Sci) 115 (2003) 169.
[8] D. Datta, A. Chakravorty, Inorg. Chem. 22 (1983) 1085.
[9] S. Pal, D. Das, P. Chattopadhyay, C. Sinha, K. Pannerselvam, T.-H. Lu, Polyhedron 19 (2000) 1263.
[10] J. Dinda, U.S. Ray, G. Mostafa, T.-H. Lu, A. Usman, I.A. Razak, S. Chantrapromma, H.-K. Fun, C. Sinha, Polyhedron 22 (2003) 247.
[11] J. Dinda, K. Bag, C. Sinha, G. Mostafa, T.-H. Lu, Polyhedron 23 (2004) 1367.
[12] D. Banerjee, U.S. Ray, S. Chandrapromma, H.-K. Fun, J.-N. Lin, T.-H. Lu, C. Sinha, Polyhedron 24 (2005) 000.
[13] U.S. Ray, B.G. Chand, G. Mostafa, J. Chang, T.-H. Lu, C. Sinha, Polyhedron 22 (2003) 2587.
[14] U.S. Ray, D. Banerjee, G. Mostafa, T.-H. Lu, C. Sinha, New J. Chem. 28 (2004) 1432.
[15] D. Das, A.K. Das, C. Sinha, Talanta 48 (1999) 1013.
[16] E.C. Constable, Coord. Chem. Rev. 93 (1989) 205.
[17] I.L. Finar, Organic Chemistry, 6th ed., vol. 1, Longman, New York, 1971 (Chapter 29).
[18] A.I. Vogel, A Text-Book of Quantitative Inorganic Analysis, 3rd ed., ELBS, Longman, 1975, p. 433.
[19] Bruker, SMART (Version 5.054), Bruker AXS Inc., Madison, WI, 1998.
[20] Bruker, SADABS (Version 2.03) and SAINT (version 6.02a), Bruker AXS Inc., Madison, WI, 2000.
[21] L.J. Farrugia, J. Appl. Cryst. 30 (1997) 565.
[22] G.M. Sheldrick, SHELXL97 and SHELXS97, University of Göttingen, Germany, 1997.
[23] U.S. Ray, D. Banerjee, S. Chandtrapromma, H.-K. Fun, J.-N. Lin, T.-H. Lu, C. Sinha, Polyhedron 24 (2005) 1071.
[24] J. Ribas, A. Escuer, M. Monfort, R. Vicente, R. Cortés, L. Lezama, T. Rojo, Coord. Chem. Rev. 193–195 (1999) 1027.
[25] P.S. Zacharias, A. Chakravorty, Inorg. Chem. 10 (1971) 1961.
[26] A.B.P. Lever, Inorganic Electronic Spectroscopy, Elsevier Science Publishers B.V., Amsterdam, 1984.
[27] B.K. Santra, G.K. Lahiri, J. Chem. Soc., Dalton Trans. (1997) 1883.

The carbonyl functional group is generally considered as non-bridging, but the group of N,N,O donor tridentate Schiff base ligands, derived from 1:1 condensation of acetylacetone and various diamines, can readily be involved in *basal–apical* type peripheral oxo-bridging to result in the formation of trinuclear Cu(II) complexes with a $[Cu_3OH]$ core by self-assembly [10]. The magneto structural correlation of such complexes reported so far suggest that the greatest coplanarity of the lowest distance of the O(H) above the Cu_3 plane and the greatest Cu–O–Cu′ angles provide the strongest antiferromagnetic coupling. However, new complexes need to be prepared with this kind of ligand to be able to draw clearer magneto-structural conclusions.

The mono-condensation product of salicylaldehyde and diamines, on the other hand, can yield either similar trinuclear [10c] or phenoxo-bridged dinuclear [11] compounds on reaction with Cu(II) perchlorate. We would like to replace the acetylacetone part of the Schiff base with 1- benzoylacetone to investigate whether the resulting complexes are dinuclear or trinuclear. If the complexes are trinuclear, one may expect wider Cu–O–Cu′ angles because of the steric effect of the phenyl group compared to their acetylacetone analogue. With this expectation, we synthesized three new tridentate ligands by mono condensation of 1-benzoylacetone with 1,2-ethanediamine (HL^1), 1,2-propanediamine (HL^2) and 1,3-propanediamine (HL^3), adopting a similar procedure as for acetylacetone analogue. On reaction with Cu(II), the ligands HL^1 and HL^2 produce trinuclear μ_3-hydroxo bridged complexes whereas HL^3 undergoes hydrolysis and affords an interesting mononuclear ternary complex in which two different chelating ligands, 1,3-propanediamine and 1-benzoylacetonate are coordinated to Cu(II). In this paper we report the synthesis, spectroscopic study and X-ray structures of these three complexes. The variable temperature magnetic behavior of the two trinuclear complexes has also been described and the results have been compared with those of similar complexes reported in the literature.

2. Experimental

The diamines and 1-benzoylacetone were purchased from Lancaster and were of reagent grade. They were used without further purification. Three new monocondensed ligands HL^1, HL^2 and HL^3 (Scheme 1) have been synthesized in our laboratory by the methods described below.

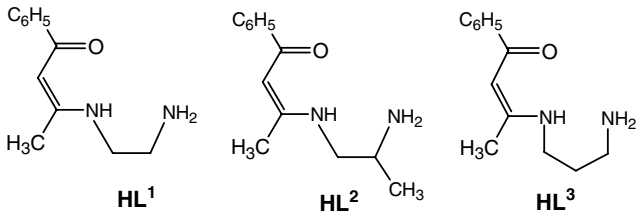

Scheme 1.

Caution! Although no problems were encountered in this work, perchlorate salts containing organic ligands are potentially explosive. They should be prepared in small quantities and handled with care.

2.1. Preparations

2.1.1. Preparation of HL^1 [6-amino-3-methyl-1-phenyl-4-azahex-2-en-1-one], HL^2 [6-amino-3,6-dimethyl-1-phenyl-4-azahex-2-en-1-one] and HL^3 [7-amino-3-methyl-1-phenyl-4-azahept-2-en-1-one]

The three ligands HL^1, HL^2 and HL^3 are the single condensation products of 1,2-ethanediamine, 1,2-propanediamine and 1,3-propanediamine, respectively, with 1-benzoylacetone. They were prepared by following a similar method to that adopted for the half condensation of 1,2-ethanediamine or 1,3-propanediamine with 2,4-pentanedione as reported earlier, i.e. by reacting the constituents in chloroform under high dilution [10,12–15].

A solution of 1-benzoylacetone (10 mmol, 1.62 g) in chloroform (50 cm^3) was added dropwise to a solution of 1,2-ethanediamine (10 mmol, 0.67 cm^3), 1,2-propanediamine (10 mmol, 0.85 cm^3) or 1,3-propanediamine (10 mmol, 0.83 cm^3) in chloroform (50 cm^3) at room temperature. After the addition, the solution was stirred for an additional 3 h and the chloroform was evaporated under reduced pressure. The resultant semi-solid product was collected as the ligand and dissolved in methanol (30 cm^3) for the synthesis of the respective complexes.

2.1.2. Synthesis of complexes $[(CuL^1)_3(\mu_3\text{-}OH)](ClO_4)_2$ (**1**), $\{[(CuL^2)_3(\mu_3\text{-}OH)]_2(ClO_4)_4\}_2 \cdot 0.75H_2O$ (**2**) and $[Cu(bn)(pn)ClO_4]$ (**3**) [bn = 1-benzoylacetonate and pn = 1,3-propanediamine]

A solution of $Cu(ClO_4)_2 \cdot 6H_2O$ (10 mmol, 3.7 g) in methanol (20 cm^3) was added to a stirred solution of each of the ligands, HL^1, HL^2 and HL^3 (10 mmol) in methanol (10 cm^3). Triethylamine (15 mmol, 2.1 cm^3) was then added dropwise to this solution with constant stirring. In the case of **1** and **2** an immediate separation of a small amount of green hydrolyzed product occurred during the addition of triethylamine, which was filtered off. The resulting green filtrate of **1** on keeping in a refrigerator for several days yielded single crystals as dark green hexagons, whereas the green microcrystalline product of **2** was obtained on keeping the filtrate overnight at room temperature. Single crystals of **2** suitable for X-ray diffraction analysis were obtained as green prisms by slow diffusion of *n*-hexane into a dichloromethane solution of the compound.

In the case of **3**, there was no immediate separation of a precipitate after addition of triethylamine. The resulting solution was set aside for several days at room temperature and deep blue single crystals of **3** suitable for X-ray analysis separated out.

Complex **1**: (Yield: 4.1 g; 67%). *Anal.* Calc. for $C_{36}H_{45}Cl_2Cu_3N_6O_{12}$ (1015.3): C, 42.59; H, 4.47; N, 8.28. Found: C, 42.71; H, 4.81; N, 8.12%. λ_{max}/nm (ε_{max}/

$dm^3\ mol^{-1}\ cm^{-1}$) (acetonitrile), 596 (49.36); IR: ν(N—H), 3279 and 3334 cm^{-1}, ν(C=N), 1517 cm^{-1}, ν(O—H), 3535 cm^{-1}.

Complex **2**: (Yield: 3.9 g; 62%). *Anal.* Calc. for $C_{39}H_{53.5}Cl_2Cu_3N_6O_{12.75}$ (1071.9): C, 43.70; H, 5.03; N, 7.84. Found: C, 43.60; H, 4.87; N, 7.76%. λ_{max}/nm (ε_{max}/$dm^3\ mol^{-1}\ cm^{-1}$) (acetonitrile), 594 (73.33); IR: ν(N—H), 3267 and 3322 cm^{-1}, ν(C=N), 1515 cm^{-1}, ν(O—H), 3508 cm^{-1}.

Complex **3**: (Yield: 4.2 g; 69%). *Anal.* Calc. for $C_{13}H_{19}ClCuN_2O_6$ (398.3): C, 39.20; H, 4.81; N, 7.03. Found: C, 39.12; H, 4.98; N, 6.91%. λ_{max}/nm (ε_{max}/$dm^3\ mol^{-1}\ cm^{-1}$) (acetonitrile), 576 (68.41); IR: ν(C=N), 1522 cm^{-1}, ν(N—H), 3263 and 3312 cm^{-1}.

2.2. Physical measurements

Elemental analyses (carbon, hydrogen and nitrogen) were performed using a Perkin–Elmer 240C elemental analyzer. IR spectra in KBr (4500–500 cm^{-1}) were recorded using a Perkin–Elmer RXI FT-IR spectrophotometer. Electronic spectra in methanol (1200–350 nm) were recorded in a Hitachi U-3501 spectrophotometer. The magnetic measurements were carried out in the "Servei de Magnetoquimica (Universitat de Barcelona)" on polycrystalline samples (20 mg) with a Quantum Design SQUID MPMSXL magnetometer in the temperature range of 2–300 K and the magnetic field was 0.1 T. The diamagnetic corrections were evaluated from Pascal's constants. EPR spectra were recorded on powder samples at X-band frequency with a Bruker 300 E automatic spectrometer, varying the temperature between 4 and 300 K.

2.3. Crystallographic studies

The independent reflections for complexes **1**–**3** were measured with Mo Kα radiation using the MAR research Image Plate System at 293 K. Suitable single crystals of all three complexes were positioned at 70 mm from the Image Plate. A total of 100 frames were measured at 2° intervals with a counting time of 2 min. Data analyses were carried out with the XDS program [16]. The structures were solved using direct methods with the SHELX-97 program [17]. The non-hydrogen atoms were refined with anisotropic thermal parameters. The hydrogen atoms bonded to carbon and nitrogen were included in geometric positions and given thermal parameters equivalent to 1.2 times those of the atom to which they were attached. In **2** there are two independent cations and four independent perchlorate anions, all of which are disordered, and two sets of four oxygen atoms were refined. Solvent water molecules with 50% occupancy were located but the hydrogen atoms could not be located. Empirical absorption correction was applied using DIFABS [18], an empirical method amended to be suitable for the Image Plate. The structures were refined on F^2 using SHELXL [17]. The crystal structure illustrations were generated using ORTEP-3 [19]. Significant crystallographic data are summarized in Table 1.

3. Results and discussion

The two tridentate ligands HL^1 and HL^2 (Scheme 1) on treatment with the methanol solution of copper perchlorate hexahydrate and triethylamine in a 2:2:3 ratio yielded the trinuclear complexes **1** and **2**, respectively (Scheme 2). The ligand HL^3 (Scheme 1), on the other hand, undergoes hydrolysis under similar conditions and yielded the ternary complex **3**. There are several reports in the literature where the monocondensation of diamine and carbonyl compounds was done in presence of a metal ion [20]. In fact, it was the usual procedure for the synthesis of such ligands and their complexes before the discovery of the high dilution method [21]. Therefore, the formation of **3** is very interesting as one diamine and one 1-benzoylacetone molecule, that are the products of the hydrolysis of the Schiff base, are coordinated to each Cu(II) and to our knowledge this is the first such example in Cu(II) complexes. It is to be noted that HL^3 on hydrolysis produces 1,3-propanediamine and 1-benzoylacetone which on reaction with Cu(II) perchlorate would have yielded Cu-benzoylacetonate as well as Cu-diamine complexes along with **3**. But on repeating the procedure several times, we observed that **3** is always the exclusive product. A probable explanation may be given as follows: on the reaction of the tridentate Schiff base ligand, L^3 and Cu-perchlorate, probably a trinuclear complex like **1** or **2** is produced initially. The trinuclear complex is expected to be under high steric strain [10b] as there are two six-membered rings in each unit that facilitates the hydrolysis of the ligand in the complex. The ternary complex (**3**) thus produced separated immediately from the methanolic solution owing to its very low solubility, excluding the formation of other rearranged products.

3.1. IR and electronic spectra

Complex **1** shows a well defined band at 3535 cm^{-1} due to O–H stretching. Compound **2** contains a non-coordinating water molecule, which makes the assignment of the O–H stretching somewhat ambiguous. However, the well-defined bands at 3508 cm^{-1} appear within the typical range for O–H stretching vibrations in monohydroxo-bridged copper complexes [10,22]. Considering the ClO_4^- anions, the ν_3 mode at 1097 and 1107 cm^{-1} for **1** and **2**, respectively, is somewhat broadened, but the ν_4 band at 619, 622 cm^{-1}, respectively, is devoid of any splitting and is consistent with the IR normal modes for a T_d symmetry, suggesting that these anions are not coordinated to the copper atoms. However, both ν_3 (1163, 1102 and 1009 cm^{-1}) and ν_4 (665 and 623 cm^{-1}) for complex **3** are split, indicating the presence of coordinating perchlorate as substantiated by the crystal structure.

The electronic spectra of these compounds were recorded in acetonitrile solution and in the solid state.

Table 1
Crystal data and refinement details of complexes **1**, **2** and **3**

Compound	**1**	**2**	**3**
Formula	$C_{36}H_{45}Cl_2Cu_3N_6O_{12}$	$C_{39}H_{53.5}Cl_2Cu_3N_6O_{12.75}$	$C_{13}H_{19}ClCuN_2O_6$
Molecular weight	1015.33	1071.90	398.30
Crystal system	triclinic	monoclinic	triclinic
Space group	$P\bar{1}$	$C2/c$	$P\bar{1}$
Unit cell dimensions			
a (Å)	13.298(15)	18.34(2)	9.158(11)
b (Å)	13.531(15)	22.68(2)	9.204(14)
c (Å)	13.970(17)	25.18(2)	10.404(14)
α (°)	93.76(1)	(90)	91.70(1)
β (°)	114.16(1)	106.74(1)	98.07(1)
γ (°)	102.24(1)	(90)	106.08(1)
V (Å^3)	2208(4)	10030(19)	832.1(20)
Z	2	8	2
D_{calc} (g cm^{-3})	1.532	1.422	1.594
Number of measured reflections	11986	43191	4800
Reflections/constraints/parameters	7031/0/535	13477/0/1102	2695/0/219
R_1, wR_2 [$I > 2\sigma(I)$]	0.0831, 0.1533	0.1199, 0.2811	0.0936, 0.2526
R_1, wR_2 (all data)	0.1157, 0.1655	0.1634, 0.3058	0.1065, 0.2616
Largest peak and hole (e Å^{-3})	0.477 and −0.468	1.318 and −1.163	0.792 and −0.866

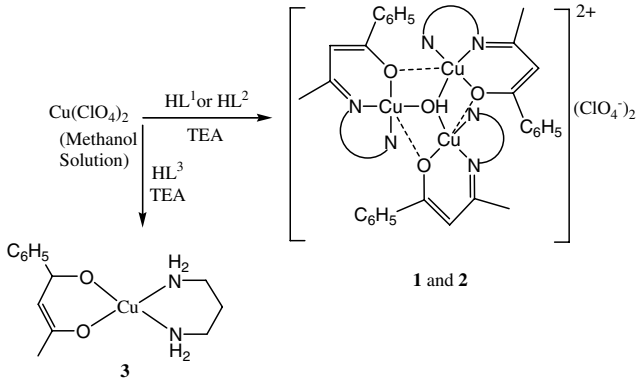

Scheme 2.

The observed ligand-field bands are in agreement with the fact that the trinuclear structures for **1** and **2** are retained in acetonitrile solution since similar visible absorption bands are observed in the solid state and in acetonitrile solution. The electronic spectra show a single absorption band at 596, 594 and 576 nm for **1**, **2** and **3**, respectively, in acetonitrile. The positions of these bands are consistent with the observed square based geometry around the copper center [10,23].

3.2. Description of the structures of complexes *1*, *2* and *3*

3.2.1. Complexes *1* and *2*

The structures of **1** and **2** are equivalent in essential detail and consist of a $[Cu_3L_3(OH)]^{2+}$ cationic fragment and two non-coordinated perchlorate anions per cation. In complex **2** there is lattice water molecule, which has partial occupancy. The molecular structure of **1** is shown in Fig. 1 together with the common atom-numbering scheme. There are two trimers (A and B) in the asymmetric unit of complex **2**, one of which is shown in Fig. S1. Selected bond distances and bond angles for the complexes are summarized in Table 2.

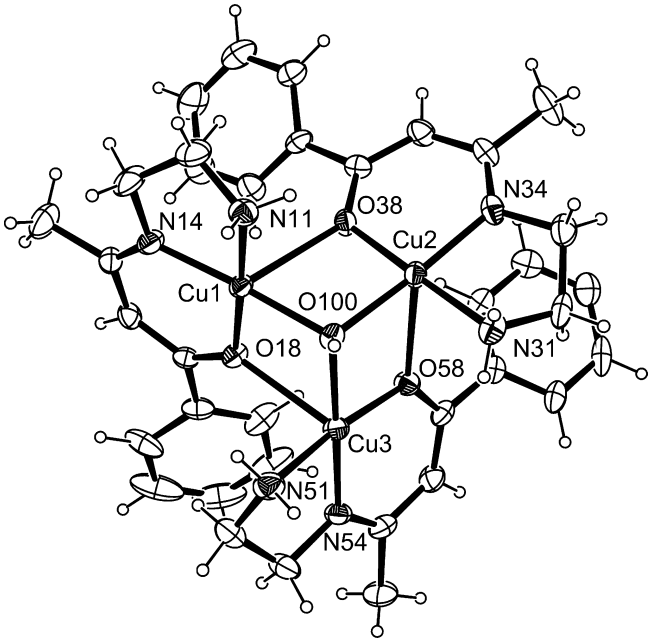

Fig. 1. The structure of **1** with ellipsoids at 25% probability.

In both complexes, each trinuclear cluster contains a triangular Cu_3 skeleton in which the copper atoms are held together by two bridging systems: (i) the oxygen atom (O100) of the central μ_3-hydroxo group and (ii) the three bridging carbonyl oxygen atoms, each of them from a different ligand molecule. The resulting trinuclear species do not contain any threefold symmetry axis. The three copper(II) ions and the bridging hydroxo group form a flattened trigonal pyramid with the copper atoms falling at

Table 2
Selected bond lengths (Å) and bond angles (°) for complexes **1**, **2** and **3**

Compound	1	2a	2b
Cu(1)–O(18)	1.918(6)	1.918(8)	1.910(9)
Cu(1)–N(14)	1.942(9)	1.949(11)	1.944(13)
Cu(1)–N(11)	2.005(7)	2.026(10)	2.018(13)
Cu(1)–O(100)	2.014(6)	2.003(8)	2.032(9)
Cu(1)–O(38)	2.542(6)	2.525(9)	2.494(9)
Cu(2)–O(38)	1.919(6)	1.932(9)	1.922(10)
Cu(2)–N(31)	2.008(9)	2.027(13)	1.986(12)
Cu(2)–N(34)	1.955(7)	1.960(15)	1.942(10)
Cu(2)–O(100)	2.036(6)	1.994(8)	2.047(8)
Cu(2)–O(58)	2.529(6)	2.471(9)	2.484(9)
Cu(3)–O(58)	1.915(6)	1.899(9)	1.891(9)
Cu(3)–N(51)	2.009(7)	1.992(11)	2.013(12)
Cu(3)–N(54)	1.943(7)	1.925(12)	1.940(13)
Cu(3)–O(100)	2.022(6)	2.031(8)	2.017(8)
Cu(3)–O(18)	2.535(7)	2.498(9)	2.452(10)
O(18)–Cu(1)–N(11)	176.5(3)	177.1(5)	175.5(6)
O(18)–Cu(1)–N(14)	94.4(3)	94.5(4)	94.4(5)
N(14)–Cu(1)–N(11)	84.9(3)	83.3(5)	85.6(6)
O(18)–Cu(1)–O(100)	86.1(2)	85.5(3)	85.0(4)
N(11)–Cu(1)–O(100)	94.3(3)	96.5(4)	94.3(5)
N(14)–Cu(1)–O(100)	175.4(3)	177.1(4)	171.8(4)
O(38)–Cu(2)–N(31)	178.0(3)	175.8(3)	175.4(5)
O(38)–Cu(2)–N(34)	94.6(3)	93.9(5)	95.2(5)
N(31)–Cu(2)–N(34)	84.6(3)	84.5(7)	83.7(5)
O(38)–Cu(2)–O(100)	86.1(2)	85.8(3)	86.0(4)
N(31)–Cu(2)–O(100)	94.4(3)	95.6(5)	94.8(4)
N(34)–Cu(2)–O(100)	172.6(3)	177.5(4)	175.9(4)
O(58)–Cu(3)–N(51)	172.3(3)	175.9(4)	179.2(5)
O(58)–Cu(3)–N(54)	94.7(3)	94.0(5)	94.4(5)
N(51)–Cu(3)–N(54)	83.8(3)	83.5(5)	84.9(6)
N(51)–Cu(3)–O(100)	95.9(3)	97.0(4)	94.9(4)
N(54)–Cu(3)–O(100)	179.2(2)	177.5(3)	169.0(5)
O(58)–Cu(3)–O(100)	85.7(2)	84.9(3)	85.8(4)
Cu(1)–O(100)–Cu(2)	107.6(3)	109.0(4)	106.1(4)
Cu(1)–O(100)–Cu(3)	108.0(2)	106.4(4)	105.9(4)
Cu(2)–O(100)–Cu(3)	108.1(3)	107.8(4)	106.7(4)

Compound **3**	
Cu(1)–O(41)	1.919(7)
Cu(1)–O(45)	1.945(7)
Cu(1)–N(11)	2.009(8)
Cu(1)–N(15)	2.016(9)
Cu(1)–O(13)	2.463(11)
O(41)–Cu(1)–O(45)	93.8(3)
O(41)–Cu(1)–N(15)	172.6(3)
O(41)–Cu(1)–N(11)	85.1(3)
O(45)–Cu(1)–N(11)	176.4(3)
O(45)–Cu(1)–N(15)	85.8(3)
N(11)–Cu(1)–N(15)	95.7(4)
O(41)–Cu(1)–O(13)	95.8(6)
O(45)–Cu(1)–O(13)	92.4(4)
N(15)–Cu(1)–O(13)	91.6(6)
N(11)–Cu(1)–O(13)	84.4(4)

the corners of an approximate equilateral triangle. In the pyramidal [Cu_3OH] group, the averaged Cu–O–Cu′ angle is 107.85° in complex **1**, 107.75° in trimer A and 106.29° in trimer B of **2**. The oxygen atom (O100) of central μ_3-hydroxo group is situated above the plane defined by the three copper atoms at 0.727 Å in complex **1**, 0.724 Å in trimer A and 0.777 Å in trimer B of complex **2**.

As for the copper environment, in all the three structures (**1**, **2**A and **2**B), the three copper atoms of the trinuclear entity are five-coordinated with a (4 + 1) square-pyramidal (NNOO and O) geometry. The four coordinating atoms consisting the basal plane are the carbonyl oxygen, one imine nitrogen and one amino nitrogen from the tridentate Schiff base ligand (L) and the hydroxo (OH^-), while the apical site is occupied by one oxygen of another tridentate Schiff base ligand, which, in turn, is basal to a second copper atom. As expected, the axial Cu–O bond is much longer than the equatorial one. The lengths of the bonds between the copper atoms and the donor sites (O, N, N) of the tridentate ligand are within the range of values normally found for such bonds [10]. The Addison parameter τ [24] values are 0.018, 0.09 and 0.112 for Cu1, Cu2 and Cu3 of complex **1** and 0.003, 0.028 and 0.025 for Cu1, Cu2 and Cu3 of trimer A of complex **2** and 0.062, 0.008 and 0.168 for Cu4, Cu5 and Cu6 of trimer B of complex **2**, respectively. The τ values of other reported complexes [10] are also shown in Table 3 for comparison.

These trimeric structures can be compared with those observed previously with same type of N,N,O donor Schiff base ligands (acetylacetone analogues) [10]. There are two significant differences, first the axial oxygen atoms are much more weakly bound in the present trimers with an average of ca 2.51 Å compared to 2.25 Å in those previous structures and second the Cu–O–Cu angles are significantly greater compared to those found previously (Table 3). It seems likely that the presence of the phenyl ring in the present compounds compared to methyl groups in the previous compounds [10] has increased the non-bonded interactions leading to these significant changes.

The perchlorate anions in both complexes show some disorder. In **2** all the perchlorate ions are disordered such that the oxygen atoms are distributed over two sets of tetrahedral sites around the same chlorine atom while complex **1** shows the complete anion distribution over two separate sites.

In both complexes hydrogen-bonding interactions are observed among the isolated trimeric units with the perchlorate anions (Table 4). In complex **1** two centrosymmetrically related trinuclear units are linked via a N–H···O hydrogen bond involving hydrogen, H51a(N51) and oxygen, O13 of the centrosymmetrically related ($-x$, $1-y$, $-z$) perchlorate ion (Fig. S2, Table 4). The hydrogen atom H11b (N11) is also involved in another N–H···O contact with O12 of one of two perchlorate anions. H31a (N31) and H100 of the μ_3-hydroxy group form strong hydrogen bonds with same oxygen atom O13 of the same perchlorate ion. In the asymmetric unit of complex **2** two trimers are linked via a N–H···O hydrogen bond through the perchlorate ions. A view of hydrogen-bonded structure of complex **2** is shown in Fig. S3.

3.2.2. Complex 3

The ORTEP-3 view of complex **3** with the atom numbering scheme is shown in Fig. 2. This complex is ternary

Table 3
Selected structural parameters for complexes **1** and **2** and seven reported complexes **3–9** related to their magnetic properties

Compounds	**1**	**2A**	**2B**	**3**	**4**	**5**	**6**	**7**	**8**	**9**
Cu(1)–O(H)–Cu(2) (°)	107.50	109.15	106.10	108.9(3)	107.3(2)	103.1(3)	103.9(3)	104.8(1)	105.4(2)	102.9(1)
Cu(1)–O(H)–Cu(3) (°)	108.02	107.71	106.04	108.4(2)	102.9(2)	105.2(3)	103.2(3)	104.9(1)	106.5(2)	102.9(1)
Cu(2)–O(H)–Cu(3) (°)	108.05	106.40	106.73	106.4(2)	105.8(2)	103.8(2)	102.5(3)	105.5(1)	108.3(2)	102.9(1)
Cu–O(H)–Cu′(av) (°)	107.85	107.75	106.29	107.9	105.3	104.0	103.2	105.1(1)	106.7(2)	102.9
O(H)·Cu3 plane (Å)[a]	0.727	0.724	0.777	0.728(5)	0.797(4)	0.836(6)	0.861(6)	0.804(2)	0.796(5)	0.881(6)
Cu/Cu′(av) (°)[b]	81.8	80.6	78.33	89.7	85.8	94.6	92.5	82.9(1)	83.7(3)	92.3
τ	0.02, 0.09, 0.11	0.00, 0.03, 0.03	0.06, 0.01, 0.17	0.19, 0.08, 0.39	0.19, 0.08, 0.10	0.13, 0.04, 0.17	0.09, 0.14, 0.03	0.01, 0.11, 0.09	0.26, 0.09, 0.20	0.04, 0.05, 0.03
$-J$ (cm^{-1})[c]	−25.6	−11.2 (average)		−66	−36	−24	−15	−24	−30	−2.4
Reference	this work	this work		[10d]	[10d]	[10d]	[10d]	[10a]	[10b]	[10c]

[a] Deviation of the oxygen atom of the triply bridging hydroxy group above the plane of the three copper atoms.
[b] Coplanarity between the least-squares planes defined by [O(H), N, N, O]; average value calculated from the Cu1/Cu2, Cu1/Cu3, Cu2/Cu3 dihedral angles.
[c] The J values from the literature have been modified according to the Hamiltonian used in this paper.

Table 4
Hydrogen bonding distances (Å) and bond angles (°) for the complexes **1**, **2** and **3**

D–H···A	D···A (Å)	H···A (Å)	∠D–H···A (°)
*Compound **1***			
N11–H11b···O12	3.11(1)	2.23	165
N31–H31a···O13	3.08(1)	2.40	133
O100–H1000···O13	3.18(1)	2.44	132
N51–H51a···O13[j]	3.27(1)	2.48	147
*Compound **2***			
N11–H11a···O92	3.36(2)	2.60	142
N11–H11b···O401	3.04(3)	2.15	174
N111–H11d···O92	3.06(2)	2.18	165
N31–H31b···O402	2.82(3)	1.92	177
N51–H51a···O103	3.13(4)	2.24	171
N51–H51b···O400	3.06(3)	2.16	178
N71–H71a···O73	3.29(3)	2.40	172
N91–H91a···O94	3.28(2)	2.45	153
N91–H91b···O72	3.20(3)	2.45	141
O200–H200···O93	3.05(2)	2.16	151
*Compound **3***			
N11–H11a···O13[k]	3.29(2)	2.56	139
N11–H11b···O41[k]	3.36(2)	2.54	152
N15–H15b···O14[l]	3.29(2)	2.39	176

Symmetry elements: (j) $-x$, $1-y$, $-z$; (k) $1-x$, $2-y$, $2-z$; (l) $1-x$, $2-y$, $1-z$.

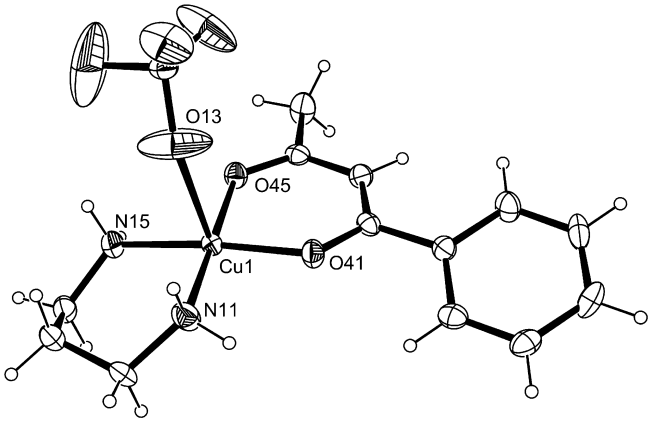

Fig. 2. The structure of **3** with ellipsoids at 25% probability.

in the sense that the copper atom is coordinated with two different ligands: a chelating diamine and a benzoylacetone moiety. This structure consists of a mononuclear cation together with a perchlorate anion.

The metal atom is in a five-coordinate square pyramidal environment with a disordered perchlorate oxygen atom O(13) weakly bound at 2.453(11) Å in an axial site. The four coordinating atoms consisting the equatorial plane are the two carbonyl oxygen atoms from the benzoylacetone moiety and two amine nitrogen atoms. The dimensions in the equatorial plane are as expected with Cu–O 1.919(7), 1.945(7) Å and Cu–N 2.009(8), 2.016(8) Å. The deviations of the coordinating atoms N11, N15, O45, O41 from the least square mean plane through them are 0.093(4), −0.093(4), 0.089(4), −0.088(4) Å. The deviations

of copper(II) from the same plane towards the axially coordinated site is 0.034(4) Å. The Addison parameter for the copper atom is 0.06 [24].

The perchlorate ions play a significant role in the H-bonding network (Table 4). A view of the supramolecular hydrogen-bonded array of complex **3** is shown in Fig. 3. Of the two hydrogen atoms on N11, H11a is engaged in hydrogen bond formation with O13 of the perchlorate ion and H11b is involved in a strong hydrogen bond with the oxygen atom O41 of a benzoylacetone moiety of a neighboring centrosymmetrically related unit $(1-x, 2-y, 2-z)$ forming a H-bonded dimeric entity. These dimeric entities are interconnected via H15b of N15 by hydrogen bond formation with the perchlorate oxygen atom O14 from another crystallographically related unit $(1-x, 2-y, 1-z)$, providing an one-dimensional array.

3.3. Magnetic properties of *1* and *2*

In complexes **1** and **2** the three copper(II) ions, the μ_3-hydroxy ion and three μ_2-carbonyl oxygen atoms of the ligand molecules form an incomplete cube, with one apex lacking from the cube (Scheme 3).

Magnetic susceptibilities were determined for complexes **1** and **2** over the temperature range 2–300 K in an applied field of 0.1 T. The temperature dependence of $\chi_M T$ (χ_M being the magnetic susceptibility per $[Cu_3O_4]$ entity) for complexes **1** and **2** is shown in Figs. 4 and 5, respectively. At room temperature, the $\chi_M T$ values (1.31 and 1.22 $cm^3\,mol^{-1}\,K$ for **1** and **2**, respectively) are as expected for three uncoupled $S = 1/2$ spins (ca. 1.2 $cm^3\,mol^{-1}\,K$) and they decrease steadily with decreasing temperature. These curves clearly indicate that an intra-trimer antiferromagnetic coupling is operating. The typical plateau, at low temperatures, corresponding to the isolated trinuclear Cu^{II} species with antiferromagnetic coupling between the metal ions (spin doublet state, $\chi_M T = 0.375$, $g = 2.00$) do not appear due to the existence of a noticeable inter-trimer exchange interaction.

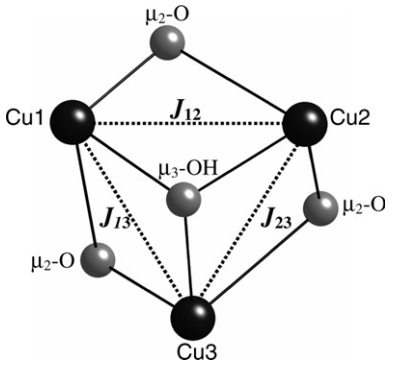

Scheme 3.

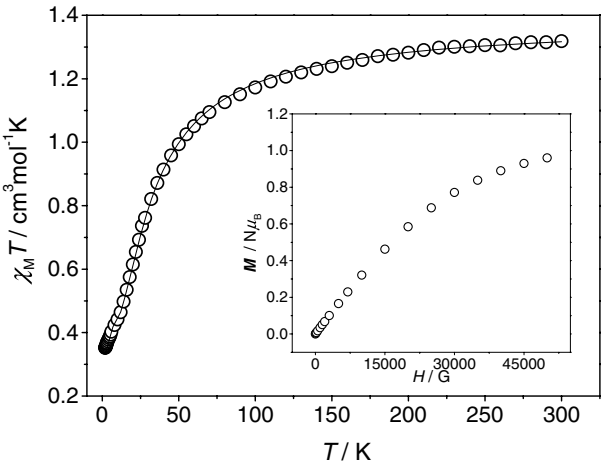

Fig. 4. Plot of the $\chi_M T$ vs. T in the range 2–300 K for **1**. Inset: magnetization vs. H at 2 K for **1**.

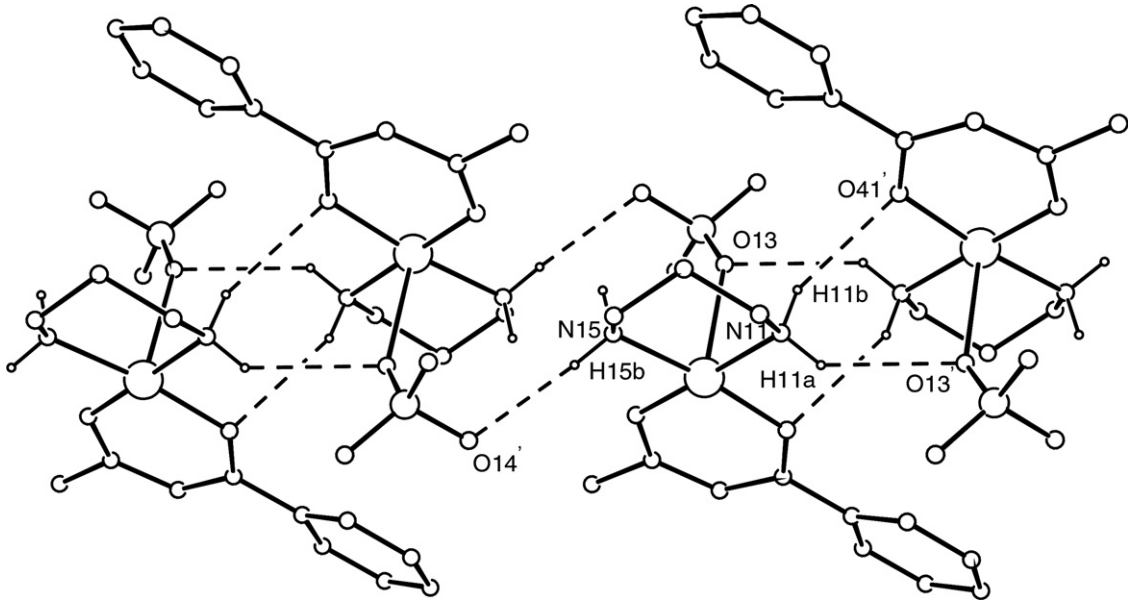

Fig. 3. Extended hydrogen-bonded network of complex **3**.

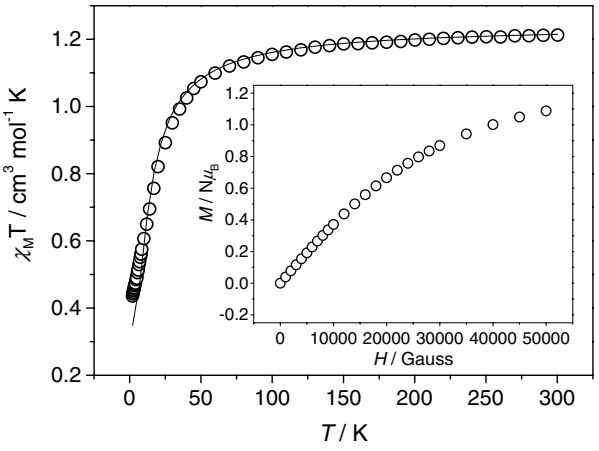

Fig. 5. Plot of the $\chi_M T$ vs. T in the range 2–300 K for **2**. Inset: magnetization vs. H at 2 K for **2**.

To determine the nature of the individual exchange interactions, we noted that the three copper(II) ions of the $[Cu_3O_4]$ system (complex **1** and trinuclear units A and B of complex **2**) occupy alternate partial cube corners. Thus there are three exchange interactions between the three magnetic ions in the molecule (Scheme 3). Each magnetic interaction involves the triple bridging hydroxo group and the bridging carbonyl oxygen atom of the ligand molecule. In order to investigate the magnetic behavior of these trinuclear complexes, an isotropic Heisenberg–Dirac–van Vleck (HDVV) Hamiltonian formalism (Eq. (1)) was used in the approach.

$$H = -J_{12}S_1S_2 - J_{13}S_1S_3 - J_{23}S_2S_3 \quad (1)$$

Since the three copper atoms of the $[Cu_3O_4]$ unit define a *quasi*-equilateral triangle, the three Cu^{II} ions can be considered equivalents and so $J_{12} = J_{13} = J_{23}$.

The magnetic susceptibility deduced from the Hamiltonian is given in Eq. (2), where N, g, β and k have their usual meanings [5e,25–27].

$$\chi_M = (N\beta^2 g^2/4kT)[1 + 5\exp(3J/2kT)]/[1 + \exp(3J/2kT)] \quad (2)$$

To take into account the interaction between the trinuclear entities, the susceptibility can be corrected by the molecular field approximation [28] (Eq. (3)) where zJ' denotes the intramolecular exchange parameter.

$$\chi'_M = \chi_M/[1 - 2zJ'\chi_M/Ng^2\beta^2] \quad (3)$$

The experimental data for **1** and **2**, corrected for diamagnetic contributions and TIP (0.3×10^{-3} cm^3 mol^{-1}), were analyzed by Eqs. (2) and (3) on $\chi_M T$. The best-fitted curves are plotted in Figs. 4 and 5 along with the experimental data. The best-fit parameters obtained are $J = -25.6$ cm^{-1}, $g = 2.21$ and $zJ' = -2.0$ with $R = 9 \times 10^{-5}$ for **1** and $J = -11.2$ cm^{-1}, $g = 2.10$ and $zJ' = -1.0$ with $R = 2 \times 10^{-4}$ for **2** (where R is the agreement factor defined as $\sum_i[(\chi_M T)_i^{exp} - (\chi_M T)_i^{calc}]^2/\sum_i[(\chi_M T)_i^{exp}]^2$). The J' values are consistent with the presence of inter-trimer interactions through hydrogen bonds. The copper(II) ions are in a square pyramidal environment, as is described in the structural part. The axial bonds of each copper(II), which involve the oxygen atom of the carbonyl group of the ligand, are elongated (above 2.5 Å) due to a pseudo-Jahn–Teller distortion. Hence a very weak or null contribution to the magnetic exchange between each pair of copper(II) ions through this oxygen atom is expected and the J value is due to the interaction through the OH group of the $[Cu_3OH]$ core. The reduced molar magnetization of complexes **1** and **2**, at 2 K, tends to $1N\beta$ when the field reaches 5 T (Figs. 4 and 5 inset) indicating that the ground state at this temperature is $S = 1/2$.

It is well known that in triangular complexes when the arrangement of the magnetic centers corresponds to equilateral triangles and they show antiferromagnetic coupling giving rise to spin frustration effects [7c,29], it is impossible for all possible pairings of spins to be simultaneously antiferromagnetic (Scheme 4a). The spin frustration requires two conditions: (a) a highly symmetrical triangle and (b) a degenerate ground state. Complexes **1** and **2** are not fully equilateral, thus, spin frustration behavior might not be expected.

In the case of three $S = 1/2$ spins sitting in the corners of an isosceles triangle, the scheme of the magnetic interactions is shown in Scheme 4b. The magnetic interaction between the two Cu1 atoms is labelled J' and the magnetic interaction between the Cu2 atom and the two Cu1 atoms is labelled J. Using the CLUMAG program [30], the relative energy values of the different states of the trinuclear Cu_3

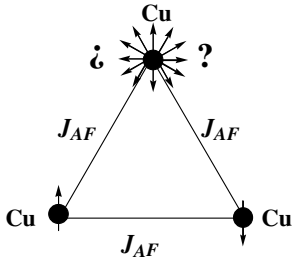

Scheme 4a.

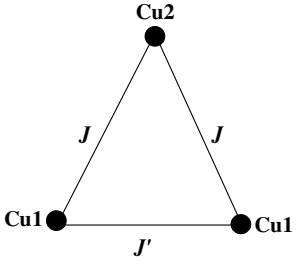

Scheme 4b.

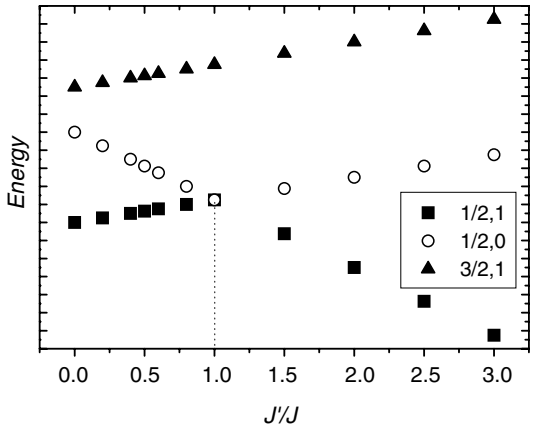

Fig. 6. Relative energies values for a trinuclear complex where the ions have a spin of 1/2 vs. J'/J (see text).

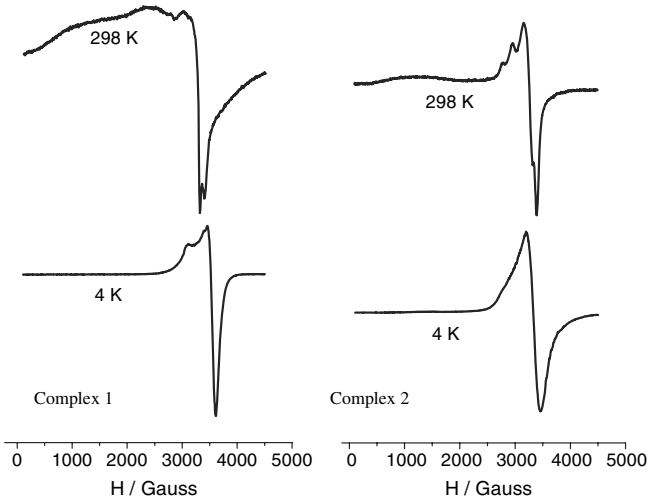

Fig. 7. Polycrystalline X-band EPR spectra for complexes **1** and **2** at room temperature and 4 K.

complex were calculated in the function of J'/J (Fig. 6). For the case of an equilateral triangle, $J'/J = 1$, the ground state is accidentally degenerated, ^2E ($|1/2, 0\rangle$, $|1/2, 1\rangle$) and the system is said to be frustrated. A small perturbation in the chemical surrounding of the metal ions may slightly change the J'/J ratio so that the degeneracy is lifted, leading to a well-defined ground state.

The necessity to introduce an antisymmetric exchange (G_{AB}) in the treatment of the magnetic data of highly symmetric spin clusters has long been known [25]. The presence of inter-trimeric exchange, due to the presence of hydrogen bonds, that is observable at low temperatures as the antisimetric exchange, preclude any calculation of the antisymmetric exchange term G_{AB}. From the literature data it seems more appropriate to study the possibility of the presence of spin frustration for this kind of complexes by means of EPR spectra at very low temperatures when only the degenerate $S = 1/2$ states are populated. One of the signatures of spin frustration is the appearance of g values lower than 2.00 [31,32].

3.4. EPR spectra

The X-band EPR spectra of complexes **1** and **2** were recorded on powder samples varying the temperature between 4 and 295 K (Fig. 7). The EPR spectra of trinuclear $S = 1/2$ compounds have been analyzed in terms of three active states (one quartet and two doublets), with a temperature dependent population [32–34]. In the light of the super-exchange parameter from the magnetic measurements, at low temperature only the doublets should be populated, whereas at room temperature signals due to the transitions inside the quartet may also be observed. This transition may show noticeable zero-field splitting (ZFS) ($S = 3/2$). Complex **2** shows a broad band at low fields at $g = 5.0$ due to the presence of ZFS of the $S = 3/2$ state, for complex **1** the spectra at low fields is not so clear (Fig. 7). At 4 K the spectra of complex **1** is anisotropic with $g_{\|} = 2.18$ and $g_{\perp} = 1.91$ and that corresponding to complex **2** shows a quasi-isotropic spectrum with a shoulder with $g = 2.23$, and a band centered at $g = 2.03$. The low value of $g_{\perp} = 1.91$, for complex **1**, could be indicative of a spin-frustrated system.

The EPR measurements in frozen methanol solution (Fig. S4) for complexes **1** and **2** clearly show the hyperfine splitting in $g_{\|}$ of approximately 190 G for the two complexes. In $g_{\perp}$ there is also a significant partial splitting.

3.5. Discussion

There are many examples in the literature of complexes with a cubane-like $[Cu_4O_4]$ core where the Cu^{II} ions and the oxygen atoms are located at alternating corners of a pseudo-cube [3d]. By contrast, complexes with a $[Cu_3O_4]$ core, with an incomplete cubane structure, are scarce [10]. From the magnetic point of view, complex **1** and **2** are trinuclear complexes in which the magnetic interaction takes place through the μ_3-OH group in the $[Cu_3OH]$ core. Previous work has established relationships for this kind of complexes between the magnetic coupling and structural features [27,35,36]. The electronic factors related to the nature of the ligands that afford the bridge are decisive in the magnetic behavior, so in Table 3 we correlate the magnitude of the magnetic coupling for trinuclear complexes of $[Cu_3O]$ core with analogous peripheral bridges. The general trends are: the shortest distance of the O(H) group above the plane formed by the three copper ions in the trinuclear Cu^{II} complexes and the greatest Cu–O–Cu′ angle provides the strong antiferromagnetic coupling.

In triangular arrangements of symmetric antiferromagnetically coupled metal ions, the magnetic properties at low temperatures can become complicated by the possible presence of spin frustration effects, because of the presence of the antisymmetric exchange interactions (ASE), described by the G_{AB} term [5e,25]. The experimental data for complex **1** indicate that this term is non-zero and the

phenomenon of spin frustration occurs. For complex **2** all data seem to indicate that there is no spin frustration.

4. Conclusion

The synthesis of the two new trinuclear complexes **1** and **2** suggests that the mono-condensation products of various diamines and benzoylacetone are also a group of tridentate ligands which can readily be involved in *basal–apical* type peripheral oxo-bridging to result in the formation of trinuclear Cu(II) complexes having a partial cubane structure with a $[Cu_3OH]$ core by self-assembly. However, replacing the acetyl acetone by benzoyl acetone make the ligands sterically more demanding. As a result, the Cu–O–Cu angles become significantly greater and the axial Cu–O bonds weaker. The effect is so much pronounced in the ligand derived from 1,3-propanediamine that the trinuclear complex does not exist and the ligand undergoes hydrolysis to produce the ternary complex **3**. Both complexes **1** and **2** show antiferromagnetic coupling, as was also found in other similar peripheral bridging complexes. The values of the coupling constants are in agreement with the hypothesis that the greatest coplanarity of the three principal ligand planes, the lowest distance of O(H) above the Cu_3 plane and the greatest Cu–O–Cu′ angles provide the strongest antiferromagnetic coupling.

Acknowledgments

This work was supported by CSIR, Government of India [Junior Research Fellowship to B.S., Sanction No. 9/28(620)/2003-EMR-I] and the Spanish Government (Grant BQU2003-00539). We also thank EPSRC and the University of Reading for funds for the Image Plate system.

Appendix A. Supporting information

The ORTEP diagram for complex **2**, diagrams for H-bonding interactions of **1** and **2**, and X-band EPR spectra for **1** and **2** in frozen methanolic solution at 4 K.

Significant crystallographic data are summarized in Table 1. CCDC Nos. 295907 (**1**), 295908 (**2**) and 295909 (**3**) contain the supplementary crystallographic data for this paper. These data can be obtained free of charge from The Cambridge Crystallographic Data Centre via www.ccdc.cam.ac.uk/data_request/cif. Supplementary data associated with this article can be found, in the online version, at doi:10.1016/j.poly.2006.05.032.

References

[1] (a) H. Borzel, P. Comba, H. Pritzkow, Chem. Commun. (2001) 97;
(b) S.S.Y. Chui, S.M.F. Lo, J.P.H. Charmant, A.G. Orpen, I.G. Williams, Science 283 (1999) 1148.
[2] (a) V.H. Crawford, H.W. Richardson, J.R. Wasson, D.J. Hodgson, W.E. Hatfield, Inorg. Chem. 15 (1976) 2107;
(b) L.K. Thompson, S.K. Mandal, S.S. Tandon, J.N. Bridson, M.K. Park, Inorg. Chem. 35 (1996) 3117;
(c) E. Ruiz, P. Alemany, S. Alvarez, J. Cano, Inorg. Chem. 36 (1997) 3683.
[3] (a) H. Oshio, N. Hoshino, T. Ito, J. Am. Chem. Soc. 122 (2000) 12602;
(b) N. Hoshino, T. Ito, M. Nihei, H. Oshio, Chem. Lett. (2002) 844;
(c) M. Nihei, N. Hoshino, T. Ito, H. Oshio, Chem. Lett. (2002) 1016;
(d) A. Mukherjee, R. Raghunathan, M.K. Saha, M. Nethaji, S. Ramasesha, A.R. Chakravarty, Chem. Eur. J. 11 (2005) 3087, and the references therein.
[4] (a) K.O. Karlin, Q.-F. Gan, A. Farooq, S. Liu, J. Zubieta, Inorg. Chem. 29 (1990) 2549;
(b) P. Chowdhury, I. Karpenstein, M. Winter, C. Butzlaff, E. Bill, A.X. Trautwein, U. Florke, H.-J. Haupt, J. Chem. Soc., Chem. Commun. (1992) 321;
(c) H. Adams, N.A. Bailey, M.J.S. Dwyer, D. Fenton, P.C. Hellier, P.D. Hempstead, J.M. Latour, J. Chem. Soc., Dalton Trans. (1993) 1207;
(d) S. Meenakumari, S.K. Tiwary, A.R. Chakravarty, Inorg. Chem. 33 (1994) 2085;
(e) J. Padilla, D. Gatteschi, P. Chaudhuri, Inorg. Chim. Acta 260 (1997) 217.
[5] (a) P. Chaudhuri, I. Karpenstein, M. Winter, B.P.C. Della Védova, E. Bill, A.X. Trautwein, S. Gehring, P. Fleischhauer, B. Nuber, J. Ewiss, Inorg. Chem. 30 (1991) 2148;
(b) E. Colacio, J.M. Dominguez-Vera, A. Escuer, M. Klinga, R. Kivekäs, A. Romerosa, J. Chem. Soc., Dalton Trans. (1995) 343;
(c) A.P. Cole, D.E. Root, P. Mukherjee, E.I. Solomon, T.D.P. Stack, Science 273 (1996) 1848;
(d) P.L. Jones, J.C. Jeffery, J.P. Maher, J.A. McCleverty, P.H. Rieger, M.D. Ward, Inorg. Chem. 36 (1997) 3088;
(e) S. Ferrer, J.G. Haasnoot, J. Reedijk, E. Müller, M. Biagini-Cingi, M. Lanfranchi, A.M. Lanfredi, J. Ribas, Inorg. Chem. 39 (2000) 1859.
[6] (a) S.T. Frey, H.H.J. Sun, N.N. Murthy, K.D. Karlin, Inorg. Chim. Acta 242 (1996) 329;
(b) L. Spiccia, B. Graham, M.T.W. Hearn, G. Lazarev, B. Moubaraki, K.S. Murray, E.D. Tiekink, J. Chem. Soc., Dalton Trans. (1997) 4089.
[7] (a) D. Gatteschi, O. Kahn, J.S. Miller, F. Palacio (Eds.), Magnetic Molecular Materials, Kluwer Academic Publishers, Dordrecht, 1991;
(b) O. Kahn, Y. Pei, Y. Yournaux, in: D.W. Bruce, O.O. Hare (Eds.), Inorganic Materials, Wiley, Chichester, 1992;
(c) O. Kahn, Molecular Magnetism, VCH, New York, 1993;
(d) Molecular-based Magnetic Materials: Theory, Techniques and Applications M.M. Turnbull, T. Sugimoto, L.K. Thompson (Eds.), ACS Symposium Series 644, American Chemical Society, Washington, DC, 1996.
[8] J.E. Greedan, J. Mater. Chem. 11 (2001) 37.
[9] (a) R.H. Holm, G.W. Everett Jr., A. Chakravarty, Prog. Inorg. Chem. 7 (1967) 83;
(b) Y.Y. Chen, D.E. Chu, B.D. McKinney, L.J. Willis, S.E. Cummings, Inorg. Chem. 20 (1981) 1885;
(c) W.M. Coleman, L.T. Taylor, J. Inorg. Nucl. Chem. 42 (1980) 683.
[10] (a) J.P. Costes, F. Dahan, J.P. Laurent, Inorg. Chem. 25 (1986) 413;
(b) M. Kwiatkowski, E. Kwiatkowski, A. Olechnowicz, D.M. Ho, E. Deutsch, Inorg. Chim. Acta 150 (1988) 65;
(c) H.-D. Bian, J.-Y. Xu, W. Gu, S.-P. Yan, P. Cheng, D.-Z. Liao, Z.-H. Jiang, Polyhedron 22 (2003) 2927;
(d) M.S. Ray, S. Chattopadhyay, M.G.B. Drew, A. Figuerola, J. Ribas, C. Diaz, A. Ghosh, Eur. J. Inorg. Chem. (2005) 4562.
[11] M.S. Ray, G. Mukhopadhyay, M.G.B. Drew, T.-H. Lu, S. Chaudhuri, A. Ghosh, Inorg. Chem. Commun. 6 (2003) 961.
[12] (a) J.-P. Costes, G. Cros, M.-H. Darbieu, J.-P. Laurent, Inorg. Chim. Acta 60 (1982) 111;
(b) G. Cros, J.-P. Costes, C.R. Acad Sci. II 294 (1982) 173.
[13] (a) M. Sinha Ray, R. Bhattacharya, S. Chaudhuri, L. Righi, G. Bocelli, G. Mukhopadhyay, A. Ghosh, Polyhedron 22 (2003) 617;
(b) M. Sinha Ray, A. Ghosh, G. Mukhopadhyay, M.G. B. Drew, J. Coord. Chem. 56 (2003) 1141;

(c) M. Sinha Ray, A. Ghosh, R. Bhattacharya, G. Mukhopadhyay, M. G.B. Drew, J. Ribas, J. Chem. Soc., Dalton Trans. (2004) 252.
[14] (a) J.-P. Costes, Inorg. Chim. Acta 130 (1987) 17;
(b) E. Kwiatkowski, M. Kwiatkowski, A. Olechnowiez, Inorg. Chim. Acta 90 (1984) 145;
(c) H. Adams, N. A Bailey, I.S. Bard, D.E. Fenton, J.-P. Costes, G. Cros, J.-P. Laurent, Inorg. Chim. Acta 101 (1985) 7;
(d) E. Kwiatkowski, M. Kwiatkowski, Inorg. Chim. Acta 117 (1986) 145;
(e) M. Kwiatkowski, G. Bandoli, J. Chem. Soc., Dalton Trans. (1992) 379;
(f) M. Kwiatkowski, E. Kwiatkowski, A. Olechnowiez, D.M. Ho, E. Deutsch, J. Chem. Soc., Dalton Trans. (1990) 2497;
(g) M. Kwiatkowski, E. Kwiatkowski, A. Olechnowiez, D.M. Ho, E. Deutsch, J. Chem. Soc., Dalton Trans. (1990) 3063;
(h) N. Matsumoto, S. Yamashita, A. Ohyoshi, S. Kohata, H. Okawa, J. Chem. Soc., Dalton Trans. (1988) 1943;
(i) N. Matsumoto, H. Murakami, T. Akui, J. Honto, H. Okawa, A. Ohyoshi, Bull. Chem. Soc. Jpn. 59 (1986) 1609;
(j) T. Nagahara, M. Suzuki, K. Kasuga, Inorg. Chim. Acta 149 (1988) 279;
(k) C.T. Brewer, G. Brewer, J. Chem. Soc., Chem. Commun. (1988) 85;
(l) E. Kwiatkowski, M. Kwiatkowski, Inorg. Chim. Acta 82 (1984) 101.
[15] (a) N. Matsumoto, T. Akui, H. Murakami, J. Kanesaka, A. Ohyoshi, H. Okawa, J. Chem. Soc., Dalton Trans. (1988) 1021;
(b) J.P. Costes, F. Dahan, A. Dupuis, J.P. Laurent, J. Chem. Soc., Dalton Trans. (1998) 1307.
[16] W. Kabsch, J. Appl. Crystallogr. 21 (1988) 916.
[17] G.M. Sheldrick, SHELXL: Program for Crystal Structure Refinement, University of Göttingen, Göttingen, Germany, 1997.
[18] DIFABS program N. Walker, D. Stuart, Acta Crystallogr., Sect. A 39 (1983) 158.
[19] M.N. Burnett, C.K. Johnson, ORTEP-3: Oak Ridge Thermal Ellipsoid Plot Program for Crystal Structure Illustrations, Report ORNL-6895, Oak Ridge National Laboratory, Oak Ridge, TN, USA, 1996.
[20] (a) R.C. Elder, Aust. J. Chem. 31 (1978) 35;
(b) A.P. Summerton, A.A. Diamantis, M.R. Snow, Inorg. Chim. Acta 27 (1978) 123;
(c) A.P. Gardner, B.M. Gatehouse, J.C.B. White, Acta Crystallogr., Sect. B 27 (1971) 1505;
(d) T.H. Benson, M.S. Bilton, N.S. Gill, Aust. J. Chem. 30 (1977) 261;
(e) P.J. Burke, D.R. McMillin, J. Chem. Soc., Dalton Trans. (1980) 1794.
[21] (a) J.-P. Costes, G. Cros, M.-H. Darbieu, J.-P. Laurent, Inorg. Chim. Acta 60 (1982) 111;
(b) G. Cros, J.-P. Costes, C.R. Acad. Sci. II 294 (1982) 173.
[22] J.R. Ferraro, W.R. Walker, Inorg. Chem. 4 (1965) 1382.
[23] B.J. Hathaway, A.A.G. Tomlinson, Coord. Chem. Rev. 5 (1970) 1.
[24] A.W. Addison, T.N. Rao, J. Reedijk, J. van Rijn, G.C. Verschoor, J. Chem. Soc., Dalton Trans. (1984) 1349.
[25] S. Ferrer, F. Lloret, I. Bertomeu, G. Alzuet, J. Borrás, S. García-Granada, M. Liu-González, J.G. Haasnoot, Inorg. Chem. 41 (2002) 5821, and the references therein.
[26] A.V. Virovets, N.V. Podberezskaya, L.G. Lavrenova, J. Struct. Chem. 38 (1997) 441.
[27] B.S. Tsukerblat, M.I. Belinskii, V.E. Fainzil'berg, Sov. Sci. Rev. B (Engl. Trans.) 9 (1987) 339.
[28] C.J. O'Connor, Prog. Inorg. Chem. 29 (1982) 203.
[29] J.K. McCusker, E.A. Schmitt, D.N. Hendrickson, in: D. Gatteschi, O. Khan, J.S. Miller, F. Palacio (Eds.), Magnetic Molecular Materials, Kluwer, Dordrecht, 1991, p. 297.
[30] D. Gatteschi, D. Pardi, Gazz. Chim. Ital. 123 (1993) 231.
[31] X. Liu, M.P. de Miranda, E.J.L. McInnes, C.A. Kilner, M.A. Halcrow, J. Chem. Soc., Dalton Trans. (2004) 59.
[32] J. Padilla, D. Gatteschi, P. Chaudhuri, Inorg. Chim. Acta 260 (1997) 217.
[33] H. López-Sandoval, R. Contreras, A. Escuer, R. Vicente, S. Bernès, H. Nöth, G.J. Leigh, N. Barba-Behrens, J. Chem. Soc., Dalton Trans. (2002) 2648.
[34] B. Cage, F.A. Cotton, N.S. Dalal, E.A. Hillard, B. Rakvin, C.M. Ramsey, J. Am. Chem. Soc. 125 (2003) 5270.
[35] R.J. Butcher, C.J.O. Connor, E. Sinn, Inorg. Chem. 20 (1981) 573.
[36] M. Angaroni, G.A. Ardizzoia, T. Berenghelli, G. La Monica, D. Gatteschi, N. Masciocchi, M. Moret, J. Chem. Soc., Dalton Trans. (1990) 3305.

synthetic sequences incorporate an oxidation step in one form or another [8]. Oxidation of primary and secondary alcohols to aldehydes and ketones respectively, is a very fundamental accomplishment in organic synthesis. The transition metal-catalyzed oxidation of alcohols is of current interest, and various metal compounds and oxidant systems have been reported [9]. Among the second row transition metal ions, ruthenium mediated oxidations are finding application due to the unique properties of this extremely versatile transition metal, whose oxidation state can vary from −II to +VIII [10]. Of mechanistic relevance is the fact that different oxygen activated species formed in the presence of iodosylbenzene, sodium hypochlorite, hydrogen peroxide, *t*-BuOOH and *N*-methylmorpholine-*N*-oxide as oxygen sources operate in the oxygen transfer by these catalytic oxidation systems [11]. High valent ruthenium-oxo complexes have proven to be very suitable in the design of redox catalysts for a variety of reasons [12]. Sharpless et al. [13] carried out a yield oriented study of oxidation of cholesterol, geranial, etc., catalyzed by ruthenium complexes in the presence of *N*-methylmorpholine-*N*-oxide and *N*,*N*-dimethylaniline-*N*-oxide. Furthermore, the catalytic activities of ruthenium complexes containing tertiary phosphine or arsine ligands are well established [14] and these ligands modify the oxidation chemistry of ruthenium-oxo complexes due to their variety of steric and electronic properties [15]. In addition, new kind of chemotherapeutic Schiff bases are now attracting the attention of biochemists [16]. Earlier work reported that some drugs showed increased activity when administered as metal complexes rather than as organic compounds [17]. Chen et al. [18] have proposed that intercalation, hydrogen bonding and π–π interactions are some of the features implicated in the mode of action of ruthenium complexes as antitumour and antimetastatic agents and some compounds are in advance stages of preclinical studies. Although the mechanism of the action of antitumour-active ruthenium compounds is not fully understood yet, it is thought that, similar to platinum drugs [19], the chloride complexes can hydrolyze in vivo, allowing the Ru to bind to the nucleobases of the DNA [20].

In continuation of our research interest [21] to understand the role of these simple and inexpensive N,O-donor ligands towards ruthenium, the reaction of Schiff bases derived from DHA with ruthenium(III) precursors containing PPh_3/$AsPh_3$ has been carried out. Thus, the present paper describes the results of the synthesis, characterization and redox properties of hexacoordinated Ru(III) complexes exhibiting a N,O ligating core with their catalytic activity towards oxidation of alcohols in the presence of NMO. Further, the antibacterial activity of the Schiff bases and their ruthenium complexes were examined. The following Schiff bases, derived from condensation of dehydroacetic acid (DHA) with methylamine, cyclohexylamine and 2-aminopyridine (Scheme 1), were used to prepare the new ruthenium(III) complexes.

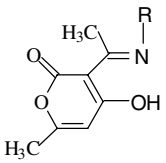

Where R = -CH_3; HL1 = DHA-met
= -C_6H_{11}; HL2 = DHA-chx
= -C_5H_4N; HL3 = DHA-ampy

Scheme 1. Structure of Schiff bases.

2. Experimental

2.1. Reagents and materials

All the reagents used were chemically pure and were of analytical reagent grade. The solvents were dried and distilled before use following the standard procedures [22]. $RuCl_3 \cdot 3H_2O$ was purchased from Loba-Chemie Pvt. Ltd., and was used without further purification. The reagent *N*-methylmorpholine-*N*-oxide was obtained from Aldrich. Dehydroacetic acid (DHA) was purchased from SRL. The supporting electrolyte tetrabutyl ammonium perchlorate (TBAP) was dried in vacuum prior to use.

2.2. Physical measurements

The carbon, hydrogen and nitrogen microanalysis content of each sample was determined at STIC, Cochin University of Science and Technology, Cochin, India by analytic function testing VarioEL III CHNS elemental analyzer. Infrared spectra were collected using KBr pellets on a Jasco 400 Plus, FT-IR spectrophotometer in the range 4000–400 cm^{-1}. Electronic spectra of the complexes in chloroform were recorded on a Cary 300 Bio UV–Vis Varian spectrophotometer. Room temperature solid-state magnetic susceptibilities were measured using an EG and G model 155 vibrating sample magnetometer at IIT, Chennai. Diamagnetic corrections calculated from Pascal's constants [23] were used to obtain the molar paramagnetic susceptibilities. The X-band EPR spectra of the powdered samples were recorded on JEOL JES-FA200 EPR spectrometer at 278 K, the field being calibrated with diphenylpicryl hydrazyl (DPPH, $g = 2.0037$) at Pondicherry University, India. Electrochemical studies were performed using a Princeton EG and G-PARC model potentiostat in 0.001 M acetonitrile solutions of $[(n\text{-}C_4H_9)_4N]ClO_4$ (TBAP) as supporting electrolyte under a nitrogen atmosphere. A three-electrode cell was employed with a platinum working electrode, a platinum wire auxiliary electrode and an Ag/AgCl reference electrode. Melting points were recorded with a Boetius micro-heating table and are uncorrected. The precursor ruthenium(III) complexes $[RuCl_3(PPh_3)_3]$ [24], $[RuCl_3(AsPh_3)_3]$ [25], $[RuBr_3(AsPh_3)_3]$ [26] and $[RuBr_3(PPh_3)_2(CH_3OH)]$ [27] were prepared according to the literature procedures.

2.3. Preparation of Schiff base ligands

The monobasic bidentate Schiff base ligands were prepared by the condensation of dehydroacetic acid (0.21 g, 0.125 mmol) with the primary amines methylamine, cyclohexylamine and 2-aminopyridine (0.038–0.124 g, 0.125 mmol) in a 1:1 molar ratio in methanol (20 cm^3). The solution was heated under reflux for 3 h and then concentrated to 5 cm^3. Slow evaporation of the solvent led to the formation of the Schiff base ligands. The product was recrystallized from methanol and the purity was checked by TLC.

2.4. Synthesis of ruthenium(III) complexes

All the reactions were performed under strictly anhydrous conditions and the complexes were prepared by the following general procedure. To a benzene (20 cm^3) solution of $[RuX_3(EPh_3)_3]$ (0.124–0.157 g, 0.125 mmol) (X = Cl, E = P; X = Cl or Br, E = As) or $[RuBr_3(PPh_3)_2(CH_3OH)]$ (0.112 g, 0.125 mmol) was added the appropriate Schiff bases (0.022–0.031 g, 0.125 mmol) (HL1–HL3). The solution was allowed to heat under reflux for 7 h. The colour of the reaction mixture gradually deepened and the resulting solution was concentrated to ca. 3 cm^3 and cooled. Light petroleum ether (60–80 °C) (5 cm^3) was then added whereupon the complex separated out. Thus obtained solid product was recrystallized from a CH_2Cl_2/light petroleum ether mixture and dried in vacuo. The purity of the complexes were checked by TLC (yield:55–65%).

2.5. Catalytic oxidation

The catalytic activity of one of the synthesized complexes $[RuCl_2(AsPh_3)_2(DHA\text{-}ampy)]$ (**10**) for the oxidation of primary and secondary alcohols to their corresponding aldehydes or ketones was determined in the presence of NMO as co-oxidant. A typical reaction using the complex as a catalyst and various activated and non-activated alcohols as substrates in 1:100 molar ratio is described as follows. A solution of ruthenium complex **10** (0.01 mmol) in 20 cm^3 CH_2Cl_2 was added to the solution of the substrate (1 mmol) and NMO (3 mmol). The solution mixture was refluxed for an appropriate period of time, as mentioned, and the solvent was then evaporated from the mother liquor under reduced pressure. The solid residue was then extracted with petroleum ether (60–80 °C) (20 cm^3) and the products were analyzed and quantified by GC. In case of benzhydrol and benzoin, the products benzophenone and benzil were isolated and confirmed by melting point, IR and ^1H NMR.

2.6. Antibacterial activity

The in vitro antibacterial screening effects of the investigated compounds were tested against the bacteria *Staphylococcus aureus* (209p) and *Escherichia coli* ESS (2231) by the well diffusion method using agar nutrient as the medium at 37 °C for 18 h. The stock solutions of the Schiff bases and the complexes were prepared in 10% DMSO in methanol and were stored dry at room temperature. In a typical procedure [28] a well was made on the agar medium inoculated with microorganisms. The well was then filled with the test solution using a micropipette and the plates were incubated at 35 °C for 24 h for bacteria. During this period, the test solutions diffused and the growth of the inoculated microorganisms was affected. The inhibition zone developed on the plate was measured and the data is summarized in Table 6. Ampicillin was used as the control.

3. Results and discussions

The reactions of $[RuX_3(EPh_3)_3]$ (X = Cl, E = P; X = Cl or Br, E = As) or $[RuBr_3(PPh_3)_2(CH_3OH)]$ with Schiff base ligands (HL1–HL3) in a 1:1 molar ratio in dry benzene afforded new hexacoordinated low spin ruthenium(III) Schiff base complexes. The reaction proceeds as shown in Scheme 2. The proposed molecular formulae for all the complexes are in good agreement with the stoichiometries concluded from their analytical data (Table 1). In all these reactions, the Schiff bases behave as monobasic bidentate ligands replacing one triphenylphosphine or triphenylarsine molecule, one chloride or bromide and one methanol ligand from the precursors. All the complexes are air-stable, non-hygroscopic in nature, insoluble in water and highly soluble in common solvents such as dichloromethane, acetonitrile, chloroform and DMSO, producing intense dark color solutions.

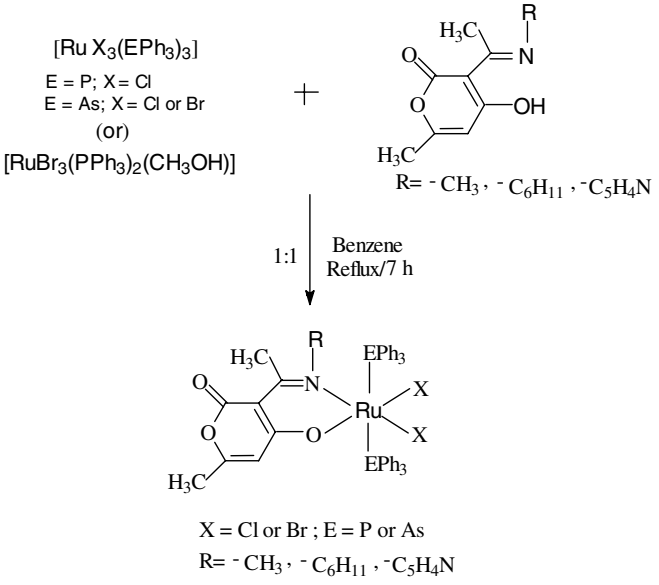

Scheme 2. Structure of Ru(III) Schiff base complexes.

Table 1
Analytical data of ruthenium(III) Schiff base complexes

S. No.	Complexes	Empirical formula	Colour	m.p. (°C)	Elemental analysis		
					Found(calculated) (%)		
					C	H	N
1	$[RuCl_2(PPh_3)_2(DHA\text{-}met)]$	$C_{45}H_{40}NO_3Cl_2P_2Ru$	brown	160	61.23(61.64)	4.43(4.56)	1.79(1.59)
2	$[RuCl_2(AsPh_3)_2(DHA\text{-}met)]$	$C_{45}H_{40}NO_3Cl_2As_2Ru$	brown	154	55.86(56.01)	3.98(4.15)	1.25(1.45)
3	$[RuBr_2(AsPh_3)_2(DHA\text{-}met)]$	$C_{45}H_{40}NO_3Br_2As_2Ru$	brown	176	50.98(51.28)	3.46(3.79)	1.19(1.33)
4	$[RuBr_2(PPh_3)_2(DHA\text{-}met)]$	$C_{45}H_{40}NO_3Br_2P_2Ru$	brown	172	55.65(55.95)	3.88(4.14)	1.20(1.45)
5	$[RuCl_2(PPh_3)_2(DHA\text{-}chx)]$	$C_{50}H_{48}NO_3Cl_2P_2Ru$	brown	160	63.19(63.55)	4.82(5.08)	1.24(1.48)
6	$[RuCl_2(AsPh_3)_2(DHA\text{-}chx)]$	$C_{50}H_{48}NO_3Cl_2As_2Ru$	brown	172	57.96(58.13)	4.35(4.65)	1.19(1.35)
7	$[RuBr_2(AsPh_3)_2(DHA\text{-}chx)]$	$C_{50}H_{48}NO_3Br_2As_2Ru$	brown	175	53.22(53.52)	4.02(4.28)	1.04(1.25)
8	$[RuBr_2(PPh_3)_2(DHA\text{-}chx)]$	$C_{50}H_{48}NO_3Br_2P_2Ru$	brown	193	57.89(58.08)	4.45(4.64)	1.08(1.35)
9	$[RuCl_2(PPh_3)_2(DHA\text{-}ampy)]$	$C_{49}H_{41}N_2O_3Cl_2P_2Ru$	brown	198	62.24(62.57)	4.16(4.36)	2.69(2.97)
10	$[RuCl_2(AsPh_3)_2(DHA\text{-}ampy)]$	$C_{49}H_{41}N_2O_3Cl_2As_2Ru$	brown	179	56.89(57.20)	3.72(3.99)	2.48(2.72)
11	$[RuBr_2(AsPh_3)_2(DHA\text{-}ampy)]$	$C_{49}H_{41}N_2O_3Br_2As_2Ru$	brown	178	52.26(52.66)	3.41(3.67)	2.22(2.50)
12	$[RuBr_2(PPh_3)_2(DHA\text{-}ampy)]$	$C_{49}H_{41}N_2O_3Br_2P_2Ru$	brown	168	56.94(57.16)	3.72(3.98)	2.34(2.72)

3.1. Spectroscopic characterization

The IR bands for the metal complexes derived from Schiff bases of DHA, which are most useful in attempting to determine the mode of coordination, are listed in Table 2. The IR spectra of the free Schiff base ligands show a strong band in the region 1640–1659 cm^{-1} that is characteristic of the azomethine group. Coordination of the Schiff bases to the metal through the nitrogen atom is expected to reduce the electron density in the azomethine frequency. The band due to azomethine nitrogen $\nu_{(C=N)}$ shows a modest decrease in the stretching frequency for the complexes and is shifted to lower frequencies, appearing around 1631–1651 cm^{-1}, which indicates the coordination of the azomethine nitrogen [21a,29]. Also, there is an upward shift in the stretching frequency of phenolic oxygen in the complexes $\nu_{(C-O)} = 1273–1276\ cm^{-1}$ [30]. This fact is further supported by the disappearance of the $\nu_{(OH)}$ band in the range 3415–3434 cm^{-1} for all the complexes, indicating the subsequent deprotonation of the phenolic proton prior to coordination. Bands in the 510–550 and 450–475 cm^{-1} regions are ascribed to the formation of M–O and M–N bonds, respectively [31] which further supports the coordination of the azomethine nitrogen and the phenolic oxygen. The bands observed in the range 1719–1728 cm^{-1} of the ligands are due to the lactone carbonyl group, which remain unchanged after complexation indicating that they do not participate in bond formation with the metal ion. Further, the ruthenium(III) Schiff base complexes show strong vibrations near 520, 695, 740, 1445 and 1532 cm^{-1}, which are attributable to the triphenylphosphine or triphenylarsine fragments [32].

Table 2
IR and electronic spectral data of ruthenium(III) Schiff base complexes[c]

Complexes	ν(C=N)	ν(C–O)	λ_{max} (ε)
1	1651	1270	790[a](557), 513[b](1695), 301(10391), 249(20326)
2	1649	1272	812[a](511), 515[b](2053), 303(12730), 247(21730)
3	1645	1270	563[b](1325), 310(19788), 265(22134)
4	1642	1274	520[b](2130), 243(32208)
5	1646	1272	794[a](640), 522[b](2166), 311(23238)
6	1649	1270	754[a](640), 562[b](2684), 394(12342), 252(18234)
7	1647	1275	554[b](1675), 341(12039), 318(19517)
8	1650	1272	535[b](1814), 315(12266), 245(21976)
9	1631	1273	738[a](658), 558[b](1974), 363(19181), 301(23257)
10	1635	1275	704[a](556), 568[b](1668), 364(18507)
11	1632	1276	739[a](479), 586[b](1639), 320(16765), 241(21345)
12	1633	1275	711[a](587), 573[b](2154), 367(14152), 308(19894)

[a] $^2T_{2g} \rightarrow {}^2A_{2g}$.
[b] Charge transfer (LMCT).
[c] Where ν is in cm^{-1}, λ_{max} is in nm, ε is in $dm^3\ mol^{-1}\ cm^{-1}$.

The electronic spectra of the ruthenium(III) complexes were recorded in chloroform in the range 800–200 nm. Most of the complexes showed two to three bands in the region 812–241 nm, and are listed in Table 2. The ground state of ruthenium(III) in an octahedral environment is $^2T_{2g}$, arising from the t_{2g}^5 configuration, and the first excited doublet levels in the order of increasing energy are $^2A_{2g}$ and $^2T_{1g}$, arising from the $t_{2g}^4e_g^1$ configuration. Hence, two bands corresponding to $^2T_{2g} \rightarrow {}^2A_{2g}$ and $^2T_{2g} \rightarrow {}^2T_{1g}$ are possible. The absorption bands around 812–704 and 586–513 nm are assigned to d–d ($\varepsilon = 511–556\ dm^3/mol/cm$) and charge transfer (LMCT) ($\varepsilon = 1639–1696\ dm^3/mol/cm$) transitions respectively. In most ruthenium(III) Schiff base chelates, charge transfer bands of the type $L_{\pi y} \rightarrow T_{2g}$ are prominent in the low energy region, which obscures the weaker bands due to d–d transitions [21a]. It is therefore difficult to assign conclusively the bands of the ruthenium(III) complexes that appear in the visible region. However, the extinction coefficients for the bands 812–704 nm are found to be low compared to that of the charge transfer bands. Hence, the bands around 812–704 nm have been assigned to the $^2T_{2g} \rightarrow {}^2A_{2g}$ transition, which is in conformity with the assignment made for similar octahedral

ruthenium(III) complexes [33]. The spectral profiles below 400 nm are very similar and are ligand centered transitions. These bands have been designated as π–π^* and n–π^* transitions of non-bonding electrons present on the nitrogen of the azomethine group in the Schiff base complexes [21a]. The pattern of the electronic spectra of all the ruthenium(III) Schiff base complexes indicates the presence of an octahedral environment around the ruthenium(III) ion.

3.2. Magnetic moments and EPR spectra

The room temperature magnetic susceptibility measurements for the complexes lie in the range 1.79–1.92 BM, which indicates that these complexes are one electron paramagnetic, suggesting a low spin t_{2g}^5 ($S = 1/2$) configuration around the ruthenium(III) ion in an octahedral environment.

The room temperature solid-state EPR spectra of all the complexes were recorded at X-band frequencies. The 'g' values are given in Table 3 and a representative spectrum is shown in Fig. 1. The low spin d^5 configuration is a good probe of the molecular structure and bonding since the observed 'g' values are very sensitive to small changes in the structure and to metal–ligand covalency. The EPR spectra of all the complexes exhibit two different 'g' values ($g_x = g_y \neq g_z$) with $g_\perp = 2.03$–2.39 and $g_\parallel = 1.99$–1.89, characteristic of an axially symmetric system. The presence of two different 'g' values indicate a tetragonal distortion in the complexes [21a,34]. Overall the positions of lines and nature of the EPR spectra of the complexes are characteristic of low spin ruthenium(III) octahedral complexes.

3.3. Electrochemistry of the complexes

The redox properties of all the complexes were investigated in dichloromethane solution with tetrabutyl ammonium perchlorate (TBAP) as the supporting electrolyte by cyclic voltammetry and the redox potentials are expressed with reference to Ag/AgCl. A representative cyclic voltammogram of complex **11** is shown in Fig. 2 and voltammetric

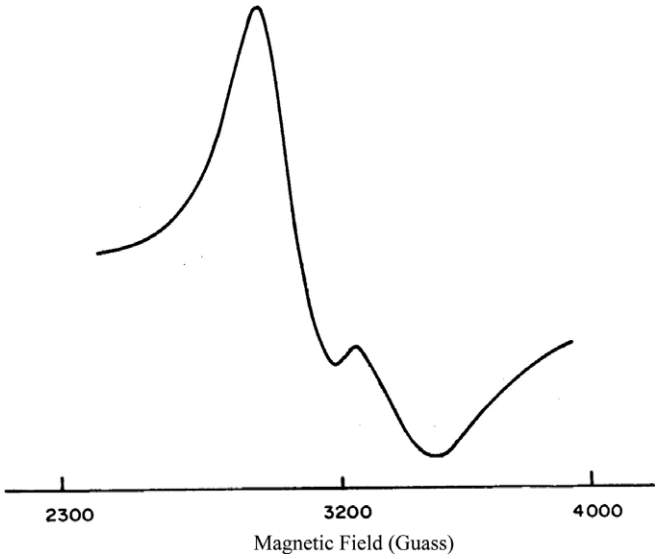

Fig. 1. EPR spectrum of $[RuCl_2(PPh_3)_2(DHA\text{-}met)]$.

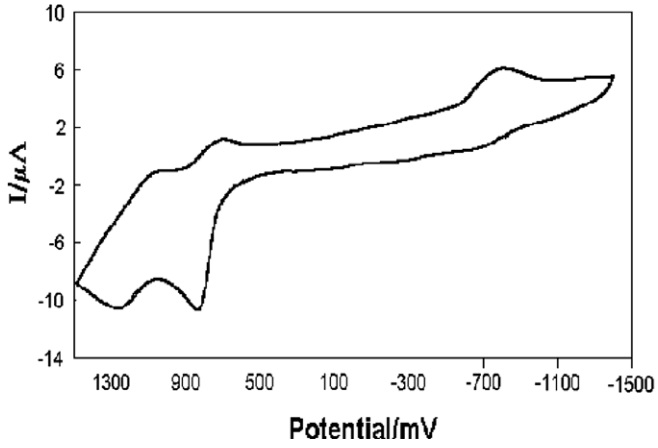

Fig. 2. Cyclic voltammogram of $[RuBr_2(AsPh_3)_2(DHA\text{-}ampy)]$.

data are presented in Table 4. All the complexes displayed two quasi-reversible oxidation couples Ru^{III}/Ru^{IV} at $E_{1/2} = 0.67$–0.82 V with a peak-to-peak separation $\Delta E_P =$ 100–150 mV and Ru^{IV}/Ru^{V} with $E_{1/2} = 1.00$–1.17 V with $\Delta E_P = 150$–210 mV, with respect to Ag/AgCl, which do not change with a change in scan rates, supporting reversibility [35]. The oxidations observed are quasi-reversible in nature, characterized by a rather large peak-to-peak separation (ΔE_p), and the cathodic peak current (i_{pc}) is less than the anodic peak current (i_{pa}). Further, all the complexes exhibit an irreversible reduction in the range -0.79 to -0.92 V. The reason for the irreversibility observed for the reductive response of all the complexes may be due to a short lived reduced state of the metal ion [36] or due to oxidative degradation of the ligands [37]. In these redox couples, electrons are gained or lost from the dπ levels orbital of the coordinated metal [38]. There is not much variation due to replacement of chlorides by bromides and triphenylphosphine by triphenylarsine. Hence, it is inferred

Table 3
EPR data of ruthenium(III) Schiff base complexes

Complexes	g_x	g_y	g_z	$\langle g \rangle^*$
1	2.25	2.25	1.99	2.16
2	2.23	2.23	1.98	2.14
3	2.34	2.34	1.89	2.19
4	2.33	2.33	1.94	2.20
5	2.14	2.14	1.96	2.08
6	2.24	2.24	1.95	2.14
7	2.32	2.32	1.93	2.19
8	2.39	2.39	1.95	2.24
9	2.03	2.03	1.98	2.01
10	2.27	2.27	1.94	2.16
11	2.28	2.28	1.94	2.16
12	2.26	2.26	1.94	2.16

$\langle g \rangle^* = [1/3g_x^2 + 1/3g_y^2 + 1/3g_z^2]^{1/2}$.

Table 4
Electrochemical data of ruthenium(III) Schiff base complexes

Complexes	Ru^{III}/Ru^{IV}				Ru^{IV}/Ru^{V}				Ru^{III}/Ru^{II}
	E_{pa}	E_{pc}	ΔE_P (mV)	$E_{1/2}$ (V)	E_{pa}	E_{pc}	ΔE_P (mV)	$E_{1/2}$ (V)	E_{pc}
1	0.87	0.73	140	0.80	1.23	1.05	180	1.14	−0.86
2	0.84	0.74	100	0.79	1.24	1.03	210	1.13	−0.87
3	0.85	0.70	150	0.77	1.23	1.03	200	1.13	−0.88
4	0.84	0.74	100	0.79	1.19	1.01	180	1.10	−0.79
5	0.86	0.74	120	0.80	1.23	1.07	160	1.15	−0.92
6	0.72	0.62	100	0.67	1.08	0.93	150	1.00	−0.89
7	0.83	0.72	110	0.77	1.23	1.04	190	1.13	−0.81
8	0.87	0.75	120	0.81	1.25	1.05	200	1.15	−0.85
9	0.90	0.75	150	0.82	1.13	0.97	160	1.05	−0.88
10	0.85	0.72	130	0.78	1.26	1.08	180	1.17	−0.80
11	0.84	0.73	110	0.79	1.22	1.05	170	1.13	−0.85
12	0.87	0.76	110	0.81	1.21	1.03	180	1.12	−0.87

Supporting electrolyte, NBu_4ClO_4 (0.005 M); complex, 0.001 M; solvent, CH_3CN; $\Delta E_p = E_{pa} - E_{pc}$ where E_{pa} and E_{pc} are anodic and cathodic potentials respectively; $E_{1/2} = 0.5(E_{pa} + E_{pc})$; scan rate: 100 mV s^{-1}.

from the electrochemical data that the present ligand system is ideally suitable for stabilizing the higher oxidation state of ruthenium.

3.4. Catalytic activity of the complexes

Catalytic oxidation of primary and secondary alcohols by one of the synthesized ruthenium(III) Schiff base complexes was carried out in CH_2Cl_2 in the presence of NMO and the by-product water was removed using molecular sieves. The results are summarized in Table 5. The catalytic reaction was carried out under a set of conditions (see experimental for reaction conditions) and a series of blank or control experiments suggest that none of $RuCl_3 \cdot 3H_2O$, Ru(III) precursors or DHA-ampy, NMO alone or as a mixture causes these transformations under identical reaction conditions. This ascertained the necessity of the ruthenium(III) complex to observe the ensuing catalytic organic transformations. Complex **10** oxidizes primary alcohols to the corresponding aldehydes and secondary alcohols to ketones with high yield.

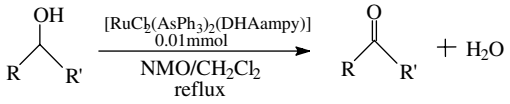

R, R' = alkyl (or) aryl

The aldehydes or ketones formed after reflux for the time mentioned was determined by GC with authentic samples. Results of the present investigation suggest that the complexes are able to react efficiently with NMO to yield a high valent ruthenium-oxo species [39,40], capable of oxygen transfer to alcohols. This was further supported by changes that occur on addition of NMO to a dichloromethane solution of the ruthenium(III) complexes. The appearance of the peak at 380 nm is attributed to the formation of $Ru^{V}{=}O$ species, which is in conformity with other ruthenium(V)-oxo complexes [40–42]. Further, support in favor of the formation of such species is identified from the IR spectrum of the solid mass (obtained by evaporation of the resultant solution to dryness), which shows a band at 860 cm^{-1}, characteristic of ruthenium(V)-oxo species [11d,40,41a] (see Scheme 3).

Table 5
Catalytic oxidation of alcohols by $[RuCl_2(AsPh_3)_2$(DHA-ampy)] /NMO

Entry	Substrates	Products	Time (h)	Yield[b] (%)
1			3	88
2			3	96
3	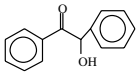	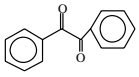	3	52[a]
4			7	99
5			7	90
6			8	99
7			8	98
8	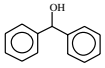		3	65[a]
9			4	63
10	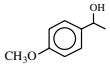	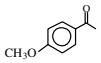	4	88
11			7	84
12			7	92

Substrate (1 mmol); NMO (3 mmol); complex (0.01 mmol); solvent – dichloromethane.

[a] Isolated yield, characterized by melting point, IR and ^1H NMR.

[b] Yield determined by GC and comparing with authentic samples.

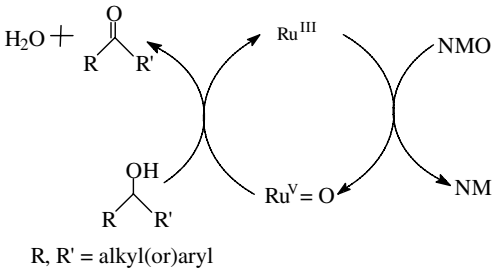

Scheme 3. Proposed catalytic cycle for the oxidation of alcohols by the Ru(III) Schiff base complex.

The oxidation of benzyl alcohol to benzaldehyde resulted in 89% conversion. An important characteristic of the ruthenium/NMO system results in the selective oxidation at the alcoholic group of unsaturated cinnamyl alcohol to cinnamaldehyde, tolerating the other reactive functional group (double bond). In case of benzoin and benzhydrol, the oxidized products, benzil and benzophenone respectively, were isolated and characterized by melting point, IR and ^{1}H NMR.

Allylic and benzylic alcohols are oxidized with maximum selectivity to aldehydes with, importantly, no further oxidation to the corresponding carboxylic acids. Unactivated secondary alcohols such as 2-butanol and 2-pentanol were also effectively oxidized into their corresponding ketones, ethyl methyl ketone and ethyl propyl ketone with 84% and 92% conversion respectively. Also, activated secondary alcohols such as 1-phenyl ethanol and 4-methoxy-1-phenyl ethanol undergo significant oxidation to give their corresponding ketones with high selectivities of 63% and 88% conversion respectively. The higher conversion in the case of 4-methoxy-1-phenyl ethanol, when compared to 1-phenyl ethanol, is due to the presence of the electron-withdrawing methoxy (OCH_3) group, which increases the reactivity by destabilizing the ruthenium-oxo intermediate making it a more reactive oxidant [8]. Interestingly, the complex efficiently catalyses the oxidation of five, six, seven and eight membered cyclic alcohols to the corresponding ketones with conversions >90% respectively.

It has been observed that these ruthenium(III) Schiff base complexes have better catalytic efficiency in the case of oxidation of benzyl alcohol, cinnamyl alcohol and cyclohexanol when compared to the earlier reports [11d,40–42], on similar ruthenium complexes as catalysts in the presence of NMO/*t*-BuOOH. Hence, it is relevant from the cyclic voltammetric data that the oxidation is likely to occur via higher ruthenium oxidation states, which are easily accessible through chemical oxidation with the co-oxidant NMO [39,42].

3.5. Antimicrobial studies

The Schiff base ligands and ruthenium(III) complexes were screened in vitro for their microbial activity against two human pathogenic bacterial species using the well diffusion method. These compounds were found to exhibit considerable activity against Gram +ve (*S. aureus* 209p) and Gram −ve (*E. coli* ESS 2231). The test solutions were prepared in dimethyl sulfoxide and the results are summarized in Table 6. Blank experiments with $RuCl_3 \cdot 3H_2O$ and the Ru(III) precursors were carried out under identical experimental conditions and show the inability of these complexes to inhibit the bacterial growth. The effectiveness of an antimicrobial agent in sensitivity is based on the zones of inhibition. The diameter of the zone is measured to the nearest millimeter (mm).

The obtained results indicate that the complexes (ruthenium chelates) are more toxic than the free ligands against same microbes under identical experimental conditions. This would suggest that the chelation could facilitate the ability of a complex to cross a cell membrane [43] and can be explained by Tweedy's chelation theory [44]. Chelation considerably reduces the polarity of the metal ion because of partial sharing of its positive charge with donor groups and possible π-electron delocalization over the whole chelate ring. Such a chelation could enhance the lipophilic character of the central metal atom, which subsequently favors its permeation through the lipid layers of the cell membrane [45] and blocking the metal binding sites on enzymes of microorganisms. The different compounds exhibit microbial activity with small variations against the bacterial species and this difference in activity could be attributed to the impermeability of the cell of the microbes which, in the case of Gram +ve is single layered and in the case of Gram −ve is a multilayered structure [46] or differences in the ribosomes of the microbial cells.

The observed results seem to conclude that the present ruthenium(III) chelates possess more cytotoxicity than the free Schiff base ligands. Further, it has been noted that these complexes show better antibacterial activity when compared to other metal complexes against the microbes *S. aureus* and *E. coli* [47]. Though complexes of this type

Table 6
Antibacterial activities of ruthenium(III) Schiff base complexes

Sl. No.	Complexes	Diameter of inhibition zone (mm)	
		S. aureus (209p) (100 μl)	*E. coli* ESS (2331) (100 μl)
1	DHA-met	–	–
2	$[RuCl_2(PPh_3)_2$(DHA-met)]	12	13
3	$[RuCl_2(AsPh_3)_2$(DHA-met)]	13	13
4	$[RuBr_2(AsPh_3)_2$(DHA-met)]	11	12
5	$[RuBr_2(PPh_3)_2$(DHA-met)]	10	10
6	DHA-chx	–	–
7	$[RuCl_2(PPh_3)_2$(DHA-chx)]	14	9
8	$[RuCl_2(AsPh_3)_2$(DHA-chx)]	11	11
9	$[RuBr_2(AsPh_3)_2$(DHA-chx)]	10	8
10	$[RuBr_2(PPh_3)_2$(DHA-chx)]	12	10
11	DHA-ampy	–	–
12	$[RuCl_2(PPh_3)_2$(DHA-ampy)]	11	10
13	$[RuCl_2(AsPh_3)_2$(DHA-ampy)]	16	15
14	$[RuBr_2(AsPh_3)_2$(DHA-ampy)]	15	11
15	$[RuBr_2(PPh_3)_2$(DHA-ampy)]	11	13

– No inhibition; standard; solvent, DMSO (no inhibitory against the microorganisms).

were found to have potential antibacterial activity against the bacterial microbes, they could not reach the effectiveness of the conventional bacterial control Ampicillin.

4. Conclusion

In summary, we have synthesized and characterized a series of new ruthenium(III) Schiff base complexes incorporating triphenylphosphine/triphenylarsine and chloride/bromide ligands. One of the complexes has been tested as a new and efficient catalyst for the oxidation of both primary and secondary alcohols to the corresponding carbonyl compounds with excellent yields in the presence of *N*-methylmorpholine-*N*-oxide. Further, the possible explanations for the mode of action of these complexes against two different microbes are described.

Acknowledgement

We express our sincere thanks to Professor P. Sambasiva Rao, Department of Chemistry, Pondicherry University for providing the EPR facility.

References

[1] A.C. Sullivan et al., J. Chem. Soc., Dalton Trans. (2000) 2661.
[2] Y.N. Ito, T. Katsuki, Bull. Chem. Soc. Jpn. 72 (1999) 603.
[3] N. Hoshimo, Coordn. Chem. Rev. 174 (1998) 77.
[4] T. Nishiya, S. Yamauchi, N. Hirota, M. Baba, I. Hamazaki, J. Phys. Chem. 90 (1986) 5730.
[5] W.J. Evans, Cy.H. Ziller, J.W. Ziller, Polyhedron 21 (2002) 1683.
[6] (a) M. Amirnasr, A.H. Mahmoud Khani, A. Gorji, S. Dehghanpour, H.R. Bijanzadeh, Polyhedron 21 (2002) 2733;
(b) S. Yamada, Coordn. Chem. Rev. 190–192 (1999) 537.
[7] (a) J.Y. Kim, M.J. Jun, W.Y. Lee, J. Organomet. Chem. 665 (2003) 87;
(b) L. Qiu, J. Qi, C.-C. Pai, S. Chan, Z. Zhou, M.C.K. Choi, A.S.C. Chan, Org. Lett. 4 (2002) 4599;
(c) Y.-G. Zhou, W. Tang, W.-B. Wang, W. Li, X. Zhang, J. Am. Chem. Soc. 124 (2002) 4952;
(d) P. Barbaro, C. Bianchini, A. Meli, M. Moreno, F. Vizza, Organometallics 21 (2002) 1430;
(e) M. Urbala, M. Antoszczyszyn, S. Krombiec, Technologia Chemiczna Przelomie Wiekow (2000) 383;
(f) J.G.De. Vries, G. Roelfes, R. Green, Tetrahedron Lett. 39 (1998) 8329;
(g) H. Dai, X. Hu, H. Chen, C. Bai, Z. Zheng, Tetrahedron Assym. 14 (2003) 1467;
(h) H. Imai, T. Nishiguchi, M. Kobayashi, K. Fukuzumi, Bull. Chem. Soc. Jpn. 48 (1975) 1585;
(i) S. Priya, M.S. Balakrishna, S.M. Mobin, R. Mc Donald, J. Organomet. Chem. 688 (2003) 227.
[8] N.S. Venkataramanan, G. Kuppuraj, S. Rajagopal, Coord. Chem. Rev. 249 (2005) 1249.
[9] R.A. Sheldon, J.K. Kochi, Metal-catalyzed Oxidations of Organic Compounds, Academic Press, New York, 1981.
[10] (a) M. Pagliaro, S. Campestrini, R. Ciriminna, Chem. Soc. Rev. 34 (2005) 837;
(b) R.A. Sheldon, I.W.C.E. Arends, G.-J.T. Brink, A. Dijksman, Acc. Chem. Res. 35 (2002) 774;
(c) K. Yamaguchi, N. Mizuno, Angew. Chem. Int. Ed. 41 (2002) 4538;
(d) T. Nao Ta, H. Takaya, S. Murahashi, Chem. Rev. 98 (1998) 2599.
[11] (a) D.M. Ziegler, Ann. Rev. Biochem. 54 (1984) 305;
(b) J.C. Dobson, W.K. Seok, T.J. Meyer, Inorg. Chem. 25 (1986) 1513;
(c) S. Das, T. Punniyamurthy, Tetrahedron Lett. 44 (2003) 6033;
(d) D. Chatterjeea, A. Mitra, B.C. Roy, J. Mol. Catal. A 161 (2000) 17;
(e) D. Chatterjeea, A. Mitra, Inorg. Chem. Commun. 3 (2000) 640.
[12] (a) A. Rossi, W.F. Giovani, J. Mol. Catal. A: Chem. 243 (2003) 40;
(b) A. Deronzier, J.-C. Moutet, in: A. Mc Cleverty, T.J. Meyer (Eds.), Comprehensive Coordination Chemistry II, vol. 9, Elsevier, Oxford, 2004, p. 471507.
[13] K.B. Sharpless, K. Akashi, K. Oshima, Tetrahedron Lett. 29 (1976) 2503.
[14] W.K. Wong, X.P. Chen, J.P. Gao, Y.G. Chi, W.X. Pan, W.Y. Pan, W.Y. Wang, J. Chem. Soc., Dalton Trans. (2002) 113.
[15] M.S. Thompson, T.J. Meyer, J. Am. Chem. Soc. 104 (1982) 4106.
[16] B. Katia, L. Simon, R. Anne, C. Gerad, D. Francoise, M. Bernard, Inorg. Chem. 35 (1996) 387.
[17] B.K. Kepler, Metal Complexes in Cancer Chemotheraphy, VCH, Weinheim, Germany, 1993.
[18] H. Chen, J.A. Parkinson, S. Parsons, R.A. Coxall, R.O. Gould, P.J. Sadler, J. Am. Chem. Soc. 124 (2002) 3064.
[19] (a) M.J. Clarke, F. Zhu, D.R. Frasca, Chem. Rev. 99 (1999) 2511;
(b) Z. Guo, P.J. Sadler, Angew. Chem., Int. Ed. Engl. 38 (1999) 1512.
[20] P.M.T. Piggot, L.A. Hall, A.J.P. White, D.J. Williams, Inorg. Chim. Acta 357 (2004) 207.
[21] (a) R. Ramesh, S. Maheswaran, J. Inorg. Biochem. 96 (2003) 457;
(b) K. Naresh Kumar, R. Ramesh, Spectrochim. Acta A 60 (2004) 2913;
(c) S. Kannan, R. Ramesh, J. Coordn. Chem. 58 (2005) 567.
[22] A.I. Vogel, Test Book of Practical Organic Chemistry, 5th ed., Longman, London, 1989.
[23] W.E. Hatfield, in: E.A. Boudreaux, L.N. Mulay (Eds.), Theory and Applications of Molecular Paramagnetism, Wiley, New York, 1976, p. 491.
[24] J. Chatt, G.J. Leigh, D.M.P. Mingos, R.J. Paske, J. Chem. Soc. A (1968) 2636.
[25] R.K. Poddar, I.P. Khullar, U. Agarwala, J. Inorg. Nucl. Chem. Lett. 10 (1974) 221.
[26] K. Natarajan, R.K. Poddar, U. Agarwala, J. Inorg. Nucl. Chem. 39 (1977) 431.
[27] T.A. Stephenson, G. Wilkinson, J. Inorg. Nucl. Chem. 28 (1966) 954.
[28] M.J. Pelezar, E.C.S. Chan, N.R. Krieg, Microbiology, 5th ed., McGraw-Hill, New York, 1998.
[29] S.N. Pal, S. Pal, J. Chem. Soc., Dalton Trans. (2002) 2102.
[30] B. Khera, A.K. Sharma, N.K. Kaushik, Polyhedron 2 (1983) 1177.
[31] K. Nakamato, Infrared and Raman Spectra of Inorganic and Coordination Compounds, Wiley Interscience, New York, 1971.
[32] A.K. Das, S.M. Peng, S. Bhattacharya, J. Chem. Soc., Dalton Trans. (2000) 181.
[33] (a) A.B.P. Lever, Inorganic Electronic Spectroscopy, 2nd ed., Elsevier, New York, 1984;
(b) S. Pal, S. Pal, Eur. J. Inorg. Chem. (2003) 4244.
[34] (a) M.M.T. Khan, D. Srinivas, R.I. Khureshy, N.H. Khan, Inorg. Chem. 29 (1990) 2320;
(b) O.K. Medhi, U. Agarwalla, Inorg. Chem. 19 (1980) 1381.
[35] J. Chakravarthy, S. Bhattacharya, Polyhedron 13 (1994) 2671.
[36] A.M. Bond, R. Colton, D.R. Mann, Inorg. Chem. 29 (1990) 4665.
[37] A. Basu, T.G. Kasan, N.Y. Sapre, Inorg. Chem. 27 (1988) 4639.
[38] T.J. Meyer, V. Huyng, Inorg. Chem. 42 (2003) 8140.
[39] (a) M.M.T. Khan, C. Sreelatha, S.A. Mirza, G. Ramachandriah, S.H.R. Abdi, Inorg. Chim. Acta 154 (1988) 102;
(b) A.S. Goldstein, R.S. Drago, J. Chem. Soc., Chem. Commun. (1991) 21.

[40] W.H. Leung, C.M. Chem, Inorg. Chem. 28 (1989) 4619.
[41] (a) M.S. El-Shahawi, A.F. Shoair, Spectrochim. Acta A 60 (2004) 121;
(b) R.S. Drago, Coordn. Chem. Rev. 117 (1992) 185.
[42] A.M. El-Hendawy, A.H. Alkubaisi, A.E. Kurashy, M.M. Shanab, Polyhedron 12 (1993) 2343.
[43] C.S. Allardyce, P.J. Dyson, D.J. Ellis, P.A. Salter, J. Organomet. Chem. 668 (2003) 35.
[44] B.G. Tweedy, Phytopathalogy 55 (1964) 910.
[45] S.C. Singh, N. Gupta, R.V. Singh, Ind. J. Chem. 34A (1995) 733.
[46] J. Mann, M.J.C. Crabbe, Bacteria and Antibacterial Agents, Spectrum Academic Publishers, Oxford, UK, 1990, 76.
[47] (a) A. Choudhary, N. Bansal, A. Gajraj, R.V. Singh, J. Inorg. Biochem. 96 (2003) 393;
(b) M. Joseph, V. Suni, M.R. Prathapachandra Kurup, M. Nethaji, A. Kishore, S.G. Bhat, Polyhedron 23 (2004) 3069;
(c) M. Nath, R. Jairath, G. Eng, X. Song, A. Kumar, J. Organomet. Chem. 690 (2005) 134.

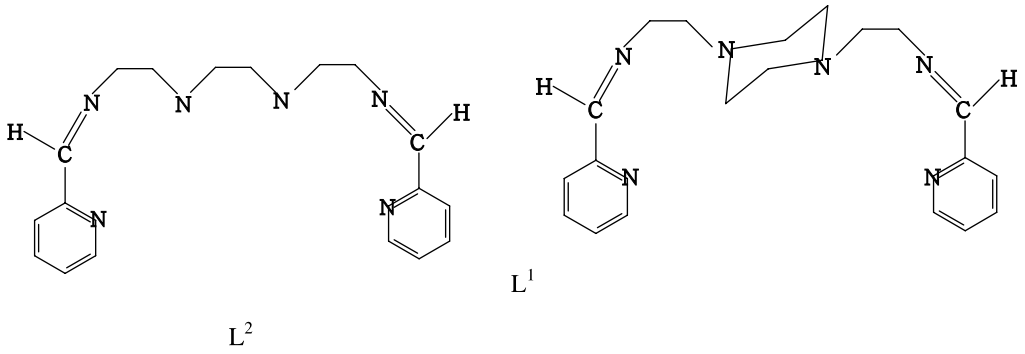

Scheme 1.

most important ones, which form various networks with different transition and non-transition metal ions in combination with organic spacers of varied denticities. In an effort to isolate and study new forms of such aggregates, we have been exploring the coordination behaviour of two different hexadentate Schiff base ligands (Scheme 1) towards zinc(II) in combination with pseudohalides. In this paper, we have reported the synthetic details, spectral characterization and different physicochemical properties of two series of zinc(II) pseudohalide complexes, along with the X-ray crystal structures of representative members, $[Zn_2(L^2)(N_3)_4]$ (**1c**) and $[Zn(L^1)][Zn(NCS)_4]$ (**2b**), where the azides and thiocyanates, established bridging ligands [16,17] in dimeric and polymeric systems, act as terminal ligands instead of adopting a bridging mode in the presence of a bis(tridentate) Schiff base.

2. Experimental

2.1. Materials and methods

High purity pyridine-2-carboxaldehyde (Lancaster, UK), triethylenetetramine (Lancaster, UK), 2-[4-(2-aminoethyl)-piperazin-1-yl]ethylamine (Aldrich, USA), sodium azide (Aldrich, USA), ammonium thiocyanate (Fluka, Germany) and zinc(II) nitrate tetrahydrate (E. Merck, India) were purchased from the respective concerns and used as received. Zinc(II) perchlorate hexahydrate was prepared by treatment of zinc carbonate (E. Merck, India) with perchloric acid (E. Merck, India) followed by slow evaporation on a steam-bath, then filtration through a fine glass-frit, and it was preserved in a desiccator containing concentrated sulfuric acid for subsequent use. All other chemicals and solvents were AR grade and were used as received.

Caution! Azido and perchlorate compounds of metal ions are potentially explosive especially in the presence of organic ligands. Only a small amount of the materials should be prepared and they should be handled with care.

2.2. Physical measurements

Elemental analyses (carbon, hydrogen and nitrogen) were performed on a Perkin–Elmer 2400 CHNS/O elemental analyzer. IR spectra (KBr discs, 4000–300 cm^{-1}) were recorded using a Perkin–Elmer FT-IR model RX1 spectrometer. Molar conductances were measured using a Systronics conductivity meter where the cell constant was calibrated with 0.01 M KCl solution and dry MeOH was used as the solvent. Ground state absorption and steady-state fluorescence measurements were made with a Jasco model V-530 UV–Vis spectrophotometer and Hitachi model F-4010 spectrofluorimeter, respectively. Time-resolved fluorescence measurements were carried out using a time-correlated single photon counting (TCSPC) spectrometer Edinburgh Instruments, model 199; a hydrogen filled coaxial flash lamp with a pulse width of 1.2 ns at FWHM and a Philips XP-2020Q Photopmultiplier tube were, respectively, used as the excitation source and the fluorescence detector.

2.3. Preparation of Schiff bases

The Schiff bases L^1 and L^2 were prepared following using reported method [15] with a little modification. Details are described below.

2.3.1. *N-(1-Pyridin-2-ylformylidene)-N′-[2-({2-[(1-pyridin-2-ylformylidene)amino]ethyl}amino)-ethyl]ethane-1,2-diamine (L^1)*

Pyridine-2-carboxaldehyde (0.214 g, 2 mmol) was refluxed with triethylenetetramine (0.146 g, 1 mmol) in dehydrated alcohol (15 cm^3). After 10 h the reaction solution was evaporated under reduced pressure to yield a gummy mass, which was dried and stored in vacuo over $CaCl_2$ for subsequent use. Yield: 0.212 g (80%). *Anal.* Calc. for $C_{18}H_{24}N_6$ (L^1): C, 66.63; H, 7.45; N, 25.91. Found: C, 66.58; H, 7.41; N, 25.86%. IR (KBr, cm^{-1}): 1590 ($\nu_{C=N}$). UV–Vis (λ_{max}, nm): 266, 280.

2.3.2. *N-(1-Pyridin-2-ylformylidene)-N′-[2-(4-{2-[(1-pyridin-2ylformylidene)amino]ethyl}-piperazin-1-yl)-ethyl]amine (L^2)*

L^2 was prepared similarly using 2-[4-(2-aminoethyl)-piperazin-1-yl]ethylamine [18] instead of triethylenetetramine. Yield: 0.212 g (80%). *Anal.* Calc. for $C_{20}H_{28}N_6$ (L^2): C, 68.14; H, 8.01; N, 23.84. Found: C, 68.09; H, 7.94; N, 23.79%. IR (KBr, cm^{-1}): 1592 ($\nu_{C=N}$). UV–Vis (λ_{max}, nm): 242, 290.

2.4. Preparation of the complexes

Complexes **1a**–**1d** were prepared from the perchlorate salt of zinc(II) using a 2:1:4 mole ratio of the metal, L^1/L^2 and azide/thiocyanate. Using a 1:1 mole ratio of metal–L^1/L^2 and a 1:4 mole ratio of metal-azide/thiocyanate **2a**–**2d** were isolated.

2.4.1. Synthesis of $[Zn_2(L^1)(N_3)_4]$ (**1a**) and $[Zn_2(L^1)(NCS)_4]$ (**1b**)

A methanolic solution (5 cm^3) of L^1 (0.32 g, 1 mmol) was added dropwise to a solution of $Zn(ClO_4)_2 \cdot 6H_2O$ (0.74 g, 2 mmol) in the same solvent (10 cm^3) then an aqueous solution (5 cm^3) of sodium azide (0.26 g, 4 mmol) was mixed slowly. The light yellow solution was filtered and the supernatant liquid was kept in air for slow evaporation. After a few days, the fine microcrystalline compound **1a** that separated out was washed with toluene and dried in vacuo over silica gel indicator. Compound **1b** was prepared by the same procedure using ammonium thiocyanate in place of sodium azide. Yield: 0.91 g (70%). *Anal.* Calc. for $C_{13}H_{24}N_{18}Zn_2$ (**1a**): C, 27.72; H, 4.29; N, 44.76. Found: C, 27.67; H, 4.23; N, 44.71%. IR (KBr, cm^{-1}): 1595 ($\nu_{C=N}$), 2042 (ν_{N_3}). UV–Vis (λ_{max}, nm): 330. Yield: 0.49 g (72%). *Anal.* Calc. for $C_{17}H_{24}N_{10}S_4Zn_2$ (**1b**): C, 32.55; H, 3.85; N, 22.33. Found: C, 32.48; H, 3.79; N, 22.281%. IR (KBr, cm^{-1}): 1595 ($\nu_{C=N}$), 2050, 2071 (ν_{NCS}). UV–Vis (λ_{max}, nm): 335.

2.4.2. $[Zn_2(L^2)(N_3)_4]$ (**1c**) and $[Zn_2(L^2)(NCS)_4]$ (**1d**)

To zinc(II) perchlorate tetrahydrate (0.74 g, 2 mmol) in methanol (10 cm^3), faint yellow L^2 (0.35 g, 1 mmol) was added dropwise. To this solution a methanolic solution of sodium azide (0.26 g, 4 mmol) was added with constant stirring. The final light brown solution was filtered and left for slow evaporation in air. After a few days fine whitish brown plate shaped single crystals of **1c**, suitable for X-ray measurements, separated out, and these were washed with toluene and dried in vacuo over silica gel indicator. The same route was followed to prepare **1d** only using ammonium thiocyanate instead of sodium azide. Yield: 0.91 g (70%). *Anal.* Calc. for $C_{20}H_{28}N_{18}Zn_2$ (**1c**): C, 36.88; H, 4.33; N, 38.71. Found: C, 36.80; H, 4.25; N, 38.67%. IR (KBr, cm^{-1}): 1595 ($\nu_{C=N}$), 2045 (ν_{N_3}). UV–Vis (λ_{max}, nm): 330. Yield: 0.50 g (70 %). *Anal.* Calc. for $C_{24}H_{28}N_{10}S_4Zn_2$ (**1d**): C, 40.29; H, 3.94; N, 19.58. Found: C, 40.20; H, 3.87; N, 19.51%. IR (KBr, cm^{-1}): 1595 ($\nu_{C=N}$), 2050, 2071 (ν_{NCS}). UV–Vis (λ_{max}, nm): 328.

2.4.3. Synthesis of $[Zn(L^1)][Zn(N_3)_4]$ (**2a**) and $[Zn(L^1)][Zn(NCS)_4]$ (**2b**)

2.4.3.1. Method A. An aqueous solution (5 cm^3) of NaN_3 (0.26 g, 4 mmol) was added to a solution of $Zn(NO_3)_2 \cdot 4H_2O$ (0.24 g, 1 mmol) in the same solvent (10 cm^3) with the formation of a colourless solution. In an another container $Zn(NO_3)_2 \cdot 4H_2O$ (0.24 g, 1 mmol) and L^1 (0.32 g, 1 mmol) were mixed together in MeOH (10 cm^3) producing a yellowish solution. This coloured solution was added dropwise to the above colourless solution. The final light brown mixture was filtered and left for slow evaporation in air. Light yellow compound **2a** separated out. X-ray quality cubic single crystals of **2b** were prepared by the same procedure using NH_4NCS in place of sodium azide. Yield: 0.51 g (75%). *Anal.* Calc. for $C_{13}H_{24}N_{18}Zn_2$ (**2a**): C, 27.72; H, 4.29; N, 44.76. Found: C, 27.67; H, 4.21; N, 44.71%. IR (KBr, cm^{-1}): 1601 ($\nu_{C=N}$), 2145 (ν_{N_3}). UV–Vis (λ_{max}, nm): 330. Yield: 0.49 g (72%). *Anal.* Calc. for $C_{17}H_{24}N_{10}S_4Zn_2$ (**2b**): C, 32.55; H, 3.85; N, 22.33. Found: C, 32.50; H, 3.84; N, 22.27%. IR (KBr, cm^{-1}): 1592 ($\nu_{C=N}$), 2065, 2071 (ν_{NCS}). UV–Vis (λ_{max}, nm): 330.

2.4.3.2. Method B. $Zn(NO_3)_2 \cdot 4H_2O$ (0.48 g, 2 mmol), L^1 (0.32 g, 1 mmol) and NaN_3 (0.26 g, 4 mmol) were mixed in a single container containing 20 cm^3 methanol, which resulted in a light brown solution. The mixture was filtered and kept for slow evaporation in air. Light yellow rectangular crystals of **2a** were formed after a week. NH_4NCS was used in place of NaN_3 to isolate **2b** by the same process. Yield: 0.51 g (75%). *Anal.* Calc. for $C_{13}H_{24}N_{18}Zn_2$ (**2a**): C, 27.72; H, 4.29; N, 44.76. Found: C, 27.67; H, 4.21; N, 44.71%. IR (KBr, cm^{-1}): 1595 ($\nu_{C=N}$), 2065, 2052 (ν_{N_3}). UV–Vis (λ_{max}, nm): 326. Yield: 0.49 g (72%). *Anal.* Calc. for $C_{17}H_{24}N_{10}S_4Zn_2$ (**2b**): C, 32.55; H, 3.85; N, 22.33. Found: C, 32.50; H, 3.84; N, 22.27%. IR (KBr, cm^{-1}): 1595 ($\nu_{C=N}$), 2065, 2071 (ν_{NCS}). UV–Vis (λ_{max}, nm): 330.

2.4.4. Synthesis of $[Zn(L^2)][Zn(N_3)_4]$ (**2c**) and $[Zn(L^2)][Zn(NCS)_4]$ (**2d**)

2.4.4.1. Method A. To a methanolic solution (10 cm^3) of L^2 (0.35, 1 mmol) a solution of $Zn(NO)_3 \cdot 4H_2O$ (0.24 g, 1 mmol) was added slowly in a glass beaker. In an another container, a solution of sodium azide (0.26 g, 4 mmol) was added to $Zn(NO)_3 \cdot 4H_2O$ (0.24 g, 1 mmol) in methanol (10 cm^3). The former yellow solution was transferred dropwise to the latter colourless solution yielding a whitish brown mixture. This was filtered and left for slow evaporation in air. Whitish brown rectangular crystals were found after a few days. A similar procedure was applied to yield **2d** except using NH_4NCS in place of NaN_3. Yield: 0.51 g (75%). *Anal.* Calc. for $C_{20}H_{28}N_{18}Zn_2$ (**2c**): C, 36.87; H, 4.33; N, 38.71. Found: C, 36.77; H, 4.28; N, 38.67%. IR (KBr, cm^{-1}): 1602 ($\nu_{C=N}$), 2040 (ν_{N_3}). UV–Vis (λ_{max}, nm): 328. Yield: 0.49 g (72%). *Anal.* Calc. for $C_{24}H_{28}N_{10}S_4Zn_2$ (**2d**): C, 40.29; H, 3.95; N, 19.58. Found: C, 40.21; H, 3.87; N, 19.50%. IR (KBr, cm^{-1}): 1595 ($\nu_{C=N}$), 2124, 2072 (ν_{NCS}). UV–Vis (λ_{max}, nm): 332.

2.4.4.2. Method B. $Zn(NO)_3 \cdot 4H_2O$ (0.48 g, 2 mmol), L^2 (0.35 g, 1 mmol) and sodium azide (0.26 g, 4 mmol) were mixed in a single pot giving a brownish solution which on slow evaporation in air yielded **2c**. When ammonium thiocyanate was used in place of sodium azide in the same reaction procedure, **2d** was separated out. Yield: 0.51 g (75%). *Anal.* Calc. for $C_{13}H_{24}N_{18}Zn_2$ (**2c**): C, 36.87; H, 4.33; N, 38.71. Found: C, 36.77; H, 4.28; N, 38.67%. IR

(KBr, cm^{-1}): 1602 ($\nu_{C=N}$), 2040 (ν_{N_3}). UV–Vis (λ_{max}, nm): 328. Yield: 0.49 g (72%). *Anal.* Calc. for $C_{24}H_{28}N_{10}S_4Zn_2$ (**2d**): C, 40.29; H, 3.95; N, 19.58. Found: C, 40.21; H, 3.87; N, 19.50%. IR (KBr, cm^{-1}): 1595 ($\nu_{C=N}$), 2124, 2072 (ν_{NCS}). UV–Vis (λ_{max}, nm): 332.

2.5. X-ray diffraction study

A plate-shaped single crystal ($0.10 \times 0.15 \times 0.20$ mm^3) of **1c** and a cube-shaped single crystal ($0.30 \times 0.30 \times 0.30$ mm^3) of **2b** were obtained by slow evaporation of MeOH solutions of the appropriate reaction mixtures. Colourless crystals, suitable for X-ray crystallographic analysis, were selected following examination under a microscope. Diffraction data at 297 K and 296 K for **1c** and **2b**, respectively, were collected on a Bruker-SMART CCD diffractometer using Mo Kα radiation ($\lambda = 0.71073$ Å). Systematically absent reflections led to the identification of space group $P2_1/n$ (No. 14) for **2b**. Of the 3159 and 6968 total reflections for the two respective complexes, 2349 and 4192 with $[I > 2\sigma(I)]$ were used for structure solutions. The structures were solved by direct methods, and the structure solution and refinement were based on $|F|^2$. All non-hydrogen atoms were refined with anisotropic displacement parameters whereas hydrogen atoms were placed in calculated positions when possible and given isotropic U values 1.2 times that of the atom to which they are bonded. At convergence the final residuals were $R_1 = 0.0360$; $wR_2 = 0.0884$ for **1c** and $R_1 = 0.0560$ and $wR_2 = 0.1070$ for **2b** with $[I > 2\sigma(I)]$, goodness-of-fit = 1.000 and 0.868 for **1c** and **2b**, respectively. The final differences Fourier map showed the minimum and maximum peak heights at −0.60 and 0.56 e $Å^{-3}$ for **1c** and −0.36 and 0.37 e $Å^{-3}$ for **2b** with no chemical significance. All calculations were carried out using SHELXL-97 [19] and ORTEP-32 [20]. The crystal data and data collection parameters are listed in Table 1.

Table 1
Crystallographic data for **1c** and **2b**

Compound	**1c**	**2b**
Formula	$C_{20}H_{28}N_{18}Zn_2$	$C_{22}H_{26}N_{10}S_4Zn_2$
Crystal system	triclinic	monoclinic
Space group	$P\bar{1}$	$P2_1/n$
a (Å)	7.9068(5)	9.7898(6)
b (Å)	9.1408(6)	15.6644(9)
c (Å)	9.6317(6)	19.1902(11)
α (°)	74.0710(10)	90
β (°)	83.5010(10)	90.8610(10)
γ (°)	87.3770(10)	90
V ($Å^3$)	665.02(7)	2942.5(3)
λ (Å)	0.71073	0.71073
ρ_{calc} (g cm^{-3})	1.627	1.557
Z	1	4
T (K)	297	296
μ (mm^{-1})	1.853	1.946
F(000)	334	1408
Crystal size (mm)	$0.10 \times 0.15 \times 0.20$	$0.30 \times 0.30 \times 0.30$
θ Ranges (°)	2.2–28.3	1.7–28.3
$h/k/l$	−10, 10/−11, 12/−12, 12	−12, 12/−19, 20/−22, 25
Reflections collected	7061	6968
Independent reflections (R_{int})	3159 (0.033)	4192 (0.033)
T_{max} and T_{min}	0.8309 and 0.6903	0.563 and 0.563
Data/restraints/parameters	3159/0/181	6968/0/343
Goodness-of-fit on F^2	1.000	0.868
Final R indices $[I > 2\sigma(I)]$	2349	4192
R indices (all data)	$R_1 = 0.0360$, $wR_2 = 0.0884$	$R_1 = 0.0560$, $wR_2 = 0.1070$
Largest peak and hole (e $Å^{-3}$)	−0.60 and 0.56	−0.36 and 0.37

Weighting scheme: Calculated $w = 1/[\sigma^2(F_o^2) + (0.0339P)^2 + 0.5866P]$ (**1c**); $w = 1/[\sigma^2(F_o^2) + (0.0520P)^2 + 2.2367P]$ (**2d**) where $P = (F_o^2 + 2F_c^2)/3$.

3. Results and discussion

3.1. Synthesis and formulation

The ligands (L^1 and L^2) were synthesized by refluxing triethylenetetramine with pyridine-2-carboxaldehyde and 2-[4-(2-aminoethyl)-piperazin-1-yl]ethylamine, respectively, in a 1:2 mole ratio in boiling alcohol (Scheme 2).

Colourless powders of the pentacoordinated dinuclear complexes $[Zn_2(L^1/L^2)(X)_4]$ (**1a**–**1d**) (L^1:X = N_3^-, **1a** and X = NCS^-, **1b**; L^2:X = N_3^-, **1c** and X = NCS^-, **1d**) were produced in good yield through the reaction of a 2:1:4 molar ratio of the metal salts, organic blockers and pseudohalides. The process is summarized in the following equation:

$$Zn(ClO_4)_2 \cdot 6H_2O + L^1/L^2 + 4NaN_3/NH_4NCS \xrightarrow[298\ K]{MeOH} [Zn_2(L^1/L^2)(NCS/N_3)_4]\ (\mathbf{1}) + 4NaClO_4 + 6H_2O \quad (1)$$

The homobimetallic complexes $[Zn(L^1/L^2)][Zn(X)_4]$ (**2a**–**2d**) (L^1:X = N_3^-, **2a** and X = NCS^-, **2b**; L^2:X = N_3^-, **2c** and X = NCS^-, **2d**) were initially synthesized by the reaction of 2:1:4 molar ratios of the metal salts, organic blockers and pseudohalides at room temperature (298 K) with the aim to obtain homopolymers $[Zn_2(L^1/L^2)(NCS)_4]_n$. However, to our surprise ion pair complexes were obtained in low yields. The molecular ion, $[Zn(NCS)_4]^{2-}$, was generated in solution by addition of four moles of ammonium thiocyanate to one mole of zinc nitrate tetrahydrate in methanol. The complementary unit $[Zn(L^1/L^2)]^{2+}$ was prepared by dropwise addition of one mole of L^1/L^2 to one molar zinc nitrate tetrahydrate in methanol in a separate container. Compound **2** resulted in good yield through union of the $[Zn(L^1/L^2)]^{2+}$ and $[Zn(NCS)_4]^{2-}$ building blocks. The details of the sequential reactions are summarized in the following equations:

$$Zn(NO_3)_2 \cdot 4H_2O + L^1/L^2 \xrightarrow[298\ K]{MeOH} [Zn(L^1/L^2)](NO_3)_2 + 4H_2O \quad (2)$$

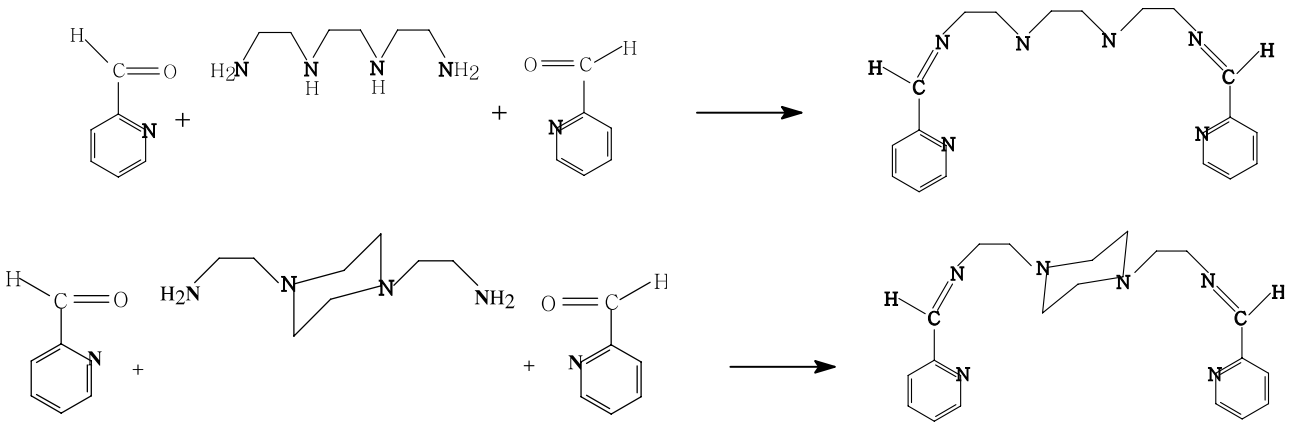

Scheme 2.

$$Zn(NO_3)_2 \cdot 4H_2O + 4NH_4NCS/NaN_3 \xrightarrow[298\ K]{MeOH} (NH_4)_2[Zn(NCS/N_3)_4] + 2NH_4NO_3 + 4H_2O \quad (3)$$

$$[Zn(L^1/L^2)](NO_3)_2 + (NH_4)_2[Zn(NCS/N_3)_4] \xrightarrow[298\ K]{MeOH} [Zn(L^1/L^2)][Zn(NCS/N_3)_4](\mathbf{2}) + NH_4NO_3 \quad (4)$$

The complexes were characterized using microanalytical, spectroscopic and physicochemical results. The air-stable moisture-insensitive complexes are soluble in common solvents like methanol, ethanol, acetonitrile, dimethylformamide and dimethylsulfoxide. In methanol solution complex **1** behaves as neutral and complex **2** shows a conductivity value of $\sim 140\ \Omega^{-1}\ cm^2\ mol^{-1}$ which reflects molecular association of the complex ions [21].

3.2. Spectral studies

In the IR spectra, the point of interest for **1a**, **1c**, **2a** and **2c** is the band due to the azide. The spectra exhibit a very strong and sharp absorption band at 2040–2060 cm^{-1} due to an asymmetric stretching vibration of the azide. Well resolved peaks attributed to ν(NCS) are observed for **1b**, **1d**, **2b** and **2d** at 2124, 2075, 2048 cm^{-1}. The presence of multiple bands in line with the different force constants of thiocyanates are observed. A band corresponding to the ν(CS) stretching frequency appears at 769 cm^{-1}. The bands belonging to the deformation frequency δ(NCS) are found as doublets at 468 and 472 cm^{-1}. The bimetallic assembly shows bands around 1590–1630 cm^{-1} due to the C=N stretching frequency of the Schiff base and weak bands in the range 2980–2900 cm^{-1} are assignable to the aliphatic C–H stretching frequency.

3.3. X-ray crystal structure

3.3.1. $[Zn_2(L^2)(N_3)_4]$ (**1c**)

In order to define the coordination sphere conspicuously, a single-crystal X-ray diffraction study was made. An ORTEP diagram with the atom numbering scheme of the dinuclear unit in **1c** is shown in Fig. 1. Selected bond distances and bond angles relevant to the Zn coordination sphere are given in Table 2. The crystal lattice of **1c** consists of neutral dinuclear $[Zn_2(L^2)(N_3)_4]$ units. The coordination polyhedron around zinc is best described as distorted trigonal bipyramidal, with a ZnN_5 chromophore. The distortion from ideal trigonal bipyramidal geometry is due to the asymmetric nature of the bound hexadentate Schiff base and the deviations of the angles formed at the metal center (Table 2). The metal ion is ligated by one pyridine nitrogen

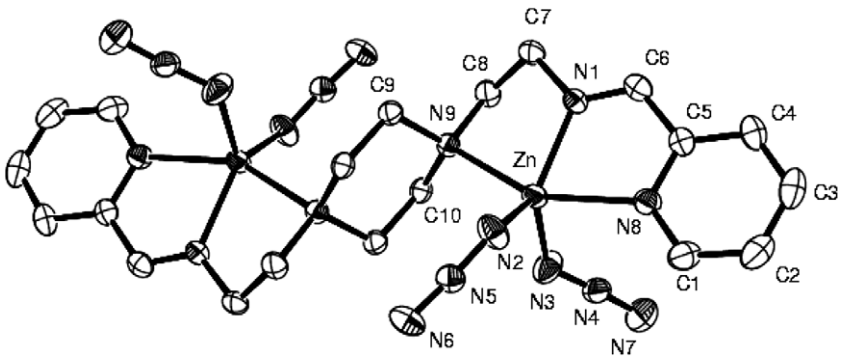

Fig. 1. ORTEP plot of $[Zn_2(L^2)(N_3)_4]$ (**1c**) with the atom numbering scheme and 20% probability ellipsoids for all non-hydrogen atoms.

Table 2
Selected bond distances (Å) and bond angles (°) for **1c**

Bond distances (Å)			
Zn–N(1)	2.0515(19)	N(2)–N(5)	1.191(3)
Zn–N(2)	1.960(3)	N(5)–N(6)	1.143(3)
Zn–N(3)	1.977(3)	N(3)–N(4)	1.175(4)
Zn–N(8)	2.289(2)	N(4)–N(7)	1.138(5)
Zn–N(9)	2.3645(18)		
Bond angles (°)			
N(1)–Zn–N(2)	127.60(10)	N(2)–Zn–N(8)	93.97(9)
N(1)–Zn–N(3)	118.76(12)	N(2)–Zn–N(9)	108.31(9)
N(1)–Zn–N(8)	74.68(8)	N(3)–Zn–N(8)	94.20(10)
N(1)–Zn–N(9)	78.57(8)	N(3)–Zn–N(9)	92.17(9)
N(2)–Zn–N(3)	112.90(13)	N(8)–Zn–N(9)	152.24(7)

(N8), one amine nitrogen (N9), one imine nitrogen (N1) and two terminal azide nitrogens (N2, N3). One imine nitrogen (N1) and two terminal azide nitrogens (N2, N3) occupy the equatorial positions of the distorted trigonal bipyramid, whereas the axial positions are occupied by the one pyridine nitrogen (N8) and the amine nitrogen (N9). Both the equatorial Zn–N distances [1.960(3)–2.3645(18) Å] and bond angles [112.90–127.60°] have some significant variation in that plane. The axial Zn–N distances are 2.289(2) and 2.3645 (18) Å. The axial bond angle N8–Zn–N9 [152.24(7)°] deviates from the ideal 180°. The sum (359.26°) of the equatorial angles N2–Zn1–N3 (112.90°), N1–Zn1–N3 (118.76°) and N1–Zn1–N2 (127.60°) are very close to 360.00°. So the atoms N1, N2, N3 and Zn1 are almost in a least-squares plane. In the terminal azide ligands, the N2–N5 [1.191(3) Å] and N3–N4 [1.175 (4) Å] distances are longer than N5–N6 [1.143(3) Å] and N4–N7 [1.138(5) Å], respectively, which indicates that the nitrogen atoms (N2 and N3) of the two terminal azides are coordinated to the zinc(II) centre.

In the crystal lattice the dinuclear units are packed with weak C–H···N hydrogen bonding. The nitrogen atoms (N3, N5, N6 and N7) from terminal azide ligands are hydrogen bond acceptors and C–H (H4, H6A, H7B, H10A and H10B) hydrogens of the organic ligand skeleton are donors (Table 3). An infinite 1D supramolecular chain (Fig. 2) results through C–H···N hydrogen bonding interactions [C(4)–H(4)···N(7), 2.5 Å, ∠C(4)–H(4)···N(7), 174°; ∠C(6)–H(6A)···N(6), 2.32 Å, 149°; ∠C(7)–H(7B)···N(7), 2.62 Å, 149°; C(10)–H(10A)···N(3), 2.58 Å, ∠C(10)–H(10A)···N(3), 116°; C(10)–H(10B)···N(5), 2.54 Å, ∠C(10)–H(10B)···N(5), 165°]. This chain is further stabilized by strong face-to-face π···π interactions from two terminal pyridine rings [ring(3)–ring(3): Cg(3)–Cg(3)^{i} separation: 4.5395(19) Å, vertical displacement of Cg: 3.471 Å; $^{i}1-x,\ 2-y,\ 1-z$. Ring3 = N(8)–C(1)–C(2)–C(3)–C(4)–C(5)] (Table 4).

Table 3
Hydrogen bond distances (Å) and angles (°) for **1c**

D–H···A	D–H (Å)	H···A (Å)	D···A (Å)	∠D–H···A (°)
C4–H4···N7^{a}	0.9300	2.5000	3.430(5)	174.00
C6–H6A···N6^{b}	0.9700	2.3500	3.216(4)	149.00
C7–H7B···N7^{c}	0.9700	2.6200	3.487(5)	149.00
C10–H10A···N3	0.9700	2.5800	3.134(4)	116.00
C10–H10B···N5^{d}	0.9700	2.5400	3.488(4)	165.00

Symmetry codes: (a) $1-x,\ 2-y,\ 1-z$; (b) $1-x,\ 1-y,\ 2-z$; (c) $x,\ -1+y,\ z$; (d) $2-x,\ 1-y,\ 2-z$.

3.3.2. $[Zn(L^1)][Zn(NCS)_4]$ (**2b**)

An ORTEP view with the atom numbering scheme of the ion-pair complex **2b** is shown in Fig. 3. Selected bond distances and bond angles relevant to the Zn coordination sphere are given in Table 5. In the solid state **2b** consists of $[Zn(L^1)]^{2+}$ cations and $[Zn(NCS)_4]^{2-}$ anions. The coordination polyhedron around zinc(II) is best described as a

Table 4
π···π Interaction for **1c**

Ring(*i*) → Ring(*j*)	Dihedral angle(*i*,*j*) (°)	Centroid separation Cg–Cg (Å)	Vertical displacement of Cg's (Å)
Ring3 → Ring3^{i}	0.00	4.5395(19)	3.471

Symmetry code: (i) $1-x,\ 2-y,\ 1-z$. Ring3 = N(8)–C(1)–C(2)–C(3)–C(4)–C(5).

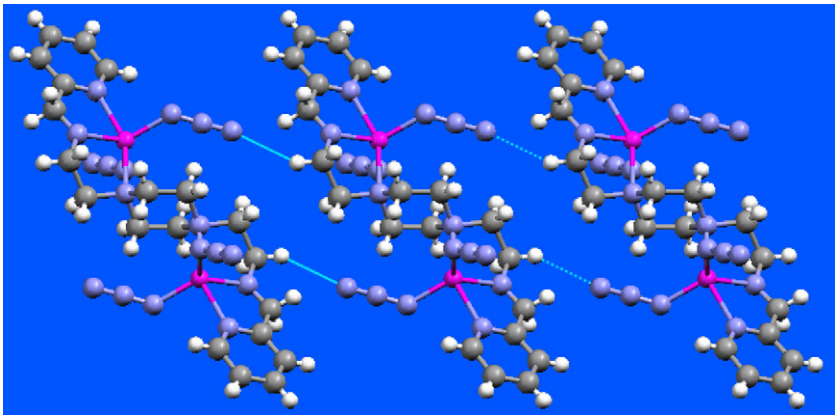

Fig. 2. C–H···N hydrogen bonded 1D chain of **1c** along the *ac*-plane.

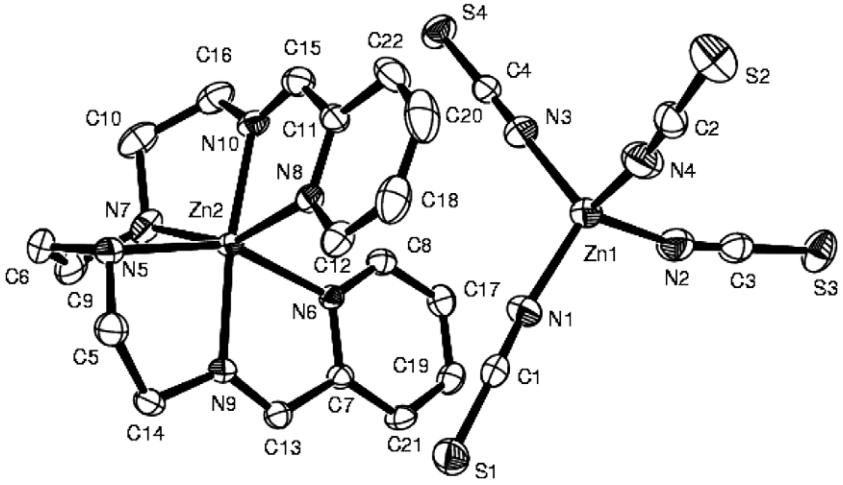

Fig. 3. Perspective view of $[Zn(L^1)][Zn(NCS)_4]$ (**2b**) with the atom numbering scheme and 20% probability ellipsoids for all non-hydrogen atoms.

Table 5
Selected bond distances (Å) and bond angles (°) for **2b**

Bond distances (Å)			
Zn(2)–N(5)	2.219(3)	N(1)–C(1)	1.149(5)
Zn(2)–N(6)	2.201(2)	N(2)–C(3)	1.136(6)
Zn(2)–N(7)	2.163(3)	N(3)–C(4)	1.137(5)
Zn(2)–N(8)	2.211(3)	N(4)–C(2)	1.136(6)
Zn(2)–N(9)	2.077(2)	S(1)–C(1)	1.614(4)
Zn(2)–N(10)	2.080(3)	S(2)–C(2)	1.609(5)
Zn(1)–N(3)	1.958(4)	S(3)–C(3)	1.589(4)
Zn(1)–N(4)	1.960(4)	S(4)–C(4)	1.610(4)
Zn(1)–N(1)	1.935(3)		
Zn(1)–N(2)	1.975(4)		
Bond angles (°)			
N(5)–Zn(2)–N(6)	153.74(9)	N(9)–Zn(2)–N(10)	172.70(11)
N(5)–Zn(2)–N(7)	80.55(11)	N(1)–Zn(1)–N(4)	108.35(16)
N(5)–Zn(2)–N(8)	96.05(10)	N(1)–Zn(1)–N(2)	110.61(15)
N(5)–Zn(2)–N(9)	78.24(10)	N(1)–Zn(1)–N(3)	115.12(15)
N(5)–Zn(2)–N(10)	108.36(11)	N(3)–Zn(1)–N(4)	109.54(17)
N(6)–Zn(2)–N(7)	100.67(10)	N(2)–Zn(1)–N(3)	107.37(18)
N(6)–Zn(2)–N(8)	94.22(9)	N(2)–Zn(1)–N(4)	105.41(17)
N(6)–Zn(2)–N(9)	76.14(9)	S(1)–C(1)–N(1)	178.8(3)
N(6)–Zn(2)–N(10)	97.57(10)	S(2)–C(2)–N(4)	179.2(5)
N(7)–Zn(2)–N(8)	152.60(11)	S(3)–C(3)–N(2)	179.2(4)
N(7)–Zn(2)–N(9)	105.14(11)	S(4)–C(4)–N(3)	179.3(4)
N(7)–Zn(2)–N(10)	79.45(12)		
N(8)–Zn(2)–N(9)	100.67(10)		
N(8)–Zn(2)–N(10)	75.86(11)		

Table 6
Hydrogen bond distances (Å) and angles (°) for **2b**

D–H···A	D–H (Å)	H···A (Å)	D···A (Å)	∠D–H···A (°)
N7–H7···S2[a]	0.9100	2.8100	3.596(3)	146.00
C13–H13B···S1	0.9700	2.6100	3.449(3)	144.00
C15–H15A···S3[b]	0.9700	2.8500	3.478(4)	123.00
C15–H15B···S4	0.9700	2.6300	3.582(4)	166.00

Symmetry codes: (a) $-1/2+x$, $1/2-y$, $-1/2+z$; (b) $1/2+x$, $1/2-y$, $-1/2+z$.

distorted octahedron with a ZnN_6 chromophore for the cationic part and a distorted tetrahedron with a ZnN_4 chromophore for the anionic part. In the octahedral part, the metal ion is ligated by two pyridine nitrogens (N6, N8), two amine nitrogens (N5, N7) and two imine nitrogens (N9, N10). The two amine nitrogens (N5, N7) and two pyridine nitrogens (N6, N8) occupy the equatorial positions of the distorted octahedron, whereas the axial positions are occupied by the two imine nitrogens (N9, N10). The equatorial Zn–N distances lie within a close range [2.163(3)–2.219(3) Å] but there is a significant variation in the bond angles [80.55(11)–153.74(9)°] in that plane. The axial Zn–N distances [2.077(2) and 2.080 (3) Å] are found to be smaller than the equatorial ones. The N–C [1.136(6)–1.149(5) Å] and C–S [1.589(4)–1.614(4) Å] distances are as expected for N-coordination [17c]. Here tetragonal compression of the octahedral geometry may be raised from the π-acceptance of imine nitrogen atoms. Four hydrogen bonds, two of N–H···S type

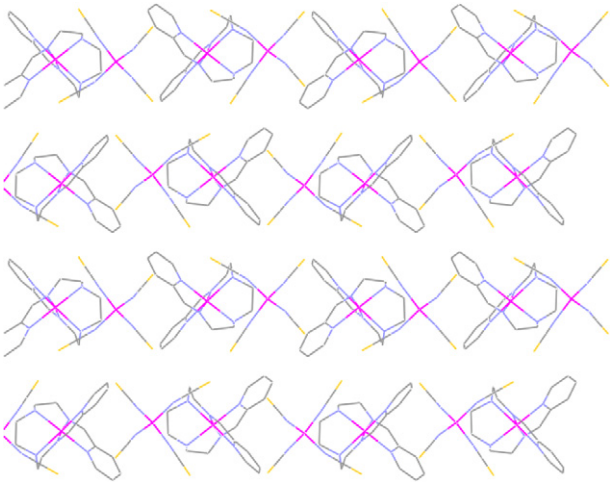

Fig. 4. Packing in **2b** viewed down the (100) plane.

Table 7
Photophysical data

Sample	Absorption (λ (nm))	Emission (λ (nm))		Life times (ns)
		Fluorescence	Phosphorescence	
1c	330	392	470	2.72
2b	330	390	482	2.43

[N(7)–H(7)···S(2), 2.81 Å; ∠N(7)–H(7)···S(2), 146°] and three of C–H···S type [C(13)–H(13B)···S(1), 2.61 Å, ∠C(13)–H(13B)···S(1), 144°; C(15)–H(15A)···S(3), 2.85 Å, ∠C(15)–H(15A)···S(3), 123°; C(15)–H(15B)···S(4), 2.63, ∠C(15)–H(15B)···S(4), 166°] link the components into an infinite line structure (Table 6, Fig. 4).

3.4. Luminescence properties

The spectroscopic data in methanol solutions and glasses of two representative compounds are listed in Table 7. Compound **1c** shows an emission spectrum at 392 nm while compound **2b** has a band at 390 nm at 298 K. These are assignable to intraligand $^1(\pi–\pi^*)$ fluorescence. Compound **2b** has very weak fluorescence; the lifetimes are 2.72 ns (**1c**) and 2.43 ns (**2b**), respectively. This higher lifetime in **1c** may be due to the presence of stronger π···π interactions, which are mainly responsible for fluorescence. In glassy solutions (77 K) a red shift is observable at ~470 nm which is presumably due to $^3(\pi–\pi^*)$ phosphorescence [22].

4. Conclusion

This work reports the synthesis, structure and photophysical behaviour of two different Zn(II) complexes with hexa- and pentacoordination environments of the metal centre. Tetracoordinated/pentacoordinated zinc(II) is well recognized [23] but hexacoordination of the metal ion is scarce. Under enforced conditions, the neutral N-donor hexacoordinated Schiff base directs such coordination of this 3d member of Group 12.

5. Supplementary data

Crystallographic data for the structural analysis have been deposited with the Cambridge Crystallographic Data Centre Nos. 267534 for **1c** and 267535 for **2b**. Copies of this information can be obtained free of charge from The Director, CCDC, 12 Union Road, Cambridge CB2 1EZ, UK (fax: +44 1223 336 033; e-mail: deposit@ccdc.cam.ac.uk or www: http://www.ccdc.cam.ac.uk).

Acknowledgements

Financial support from the Department of Science and Technology (DST), Council of Scientific and Industrial Research (CSIR), New Delhi, India is gratefully acknowledged. Ms. Fen-Ling Liao of National Science Council in Taiwan is acknowledged for her data collection of X-ray diffraction.

References

[1] (a) G.R. Desiraju, Angew. Chem., Int. Ed. Engl. 34 (1995) 2311;
(b) J.-M. Lehn, Supramolecular Chemistry, VCH, Weinheim, 1995;
(c) G.R. Desiraju, Chem. Commun. (1997) 1475.
[2] (a) G.A. Jerrey, An Introduction to Hydrogen Bonding, Oxford University Press, Oxford, 1997;
(b) G.R. Desiraju, Nature 412 (2001) 397;
(c) G.R. Desiraju, Acc. Chem. Res. 35 (2002) 565;
(d) T. Steiner, Angew. Chem., Int. Ed. 41 (2002) 48.
[3] (a) G.R. Desiraju, T. Steiner, The Weak Hydrogen Bond in Structural Chemistry and Biology, Oxford University Press, Oxford, 1999;
(b) G.R. Desiraju (Ed.), Crystal Design: Structure and Function, Perspectives in Supramolecular Chemistry, vol. 7, Wiley, Chichester, 2003.
[4] (a) D. Bose, S.H. Rahaman, G. Mostafa, R.D.B. Walsh, M.J. Zaworotko, B.K. Ghosh, Polyhedron 23 (2004) 545, and references therein;
(b) J. Pons, J. Rius, J. Ros, Inorg. Chim. Acta 359 (2006) 379;
(c) Z.-M. Hao, X.-M. Zhang, Inorg. Chem. Commun. 9 (2006) 57.
[5] (a) S.-Q. Bai, E.-Q. Gao, Z. He, C.-J. Fanga, C.-H. Yan, Cryst. Eng. Commun. 6 (2004) 606;
(b) F.J. Barros-Garcý, F. Luna-Giles, M.A. Maldonado-Rogado, E. Viñuelas-Zahý'nos, Polyhedron 25 (2006) 43.
[6] (a) J. Wang, X. Qian, Chem. Commun. (2006) 109;
(b) A.A. Mohamed, H.E. Abdou, J.P. Fackler Jr., Inorg. Chem. 45 (2006) 11;
(c) K.K. Sarker, B.G. Chand, A.D. Jana, G. Mostafa, C. Sinha, Inorg. Chim. Acta 359 (2006) 695.
[7] (a) B. Cornils, W.A. Herrmann, R. Schlogl (Eds.), Catalysis from A to Z: A Concise Encyclopedia, Wiley, New York, 2000;
(b) C. Janiak, Coord. Chem. Rev. 250 (2006) 66;
(c) Catalyst for Fine Chemical Synthesis, vol. 3, Wiley, New York, 2004.
[8] (a) D. Demus, J.W. Goodby, G.W. Gray, H.-W. Spiess, V. Vill (Eds.), Handbook of Liquid Crystals, Wiley–VCH, Weinheim, 1998;
(b) I.M. Saez, J.W. Goodby, J. Mater. Chem. 15 (2005) 26.
[9] (a) J.R. Farraro, J.M. Williams, Introduction to Synthetic Electrical Conductors, Academic Press, New York, 1987;
(b) S.R. Marder, in: D.W. Bruce, D. O'Hare (Eds.), Metal Containing Materials for Non-linear Optics in Inorganic Materials, Wiley, Chichester, 1996;
(c) S.R. Marder, Chem. Commun. (2006) 131.
[10] (a) O. Kahn, Molecular Magnetism, VCH, New York, 1993;
(b) J.S. Miller, M. Drillon (Eds.), Magnetism: Molecules to Materials V, Wiley–VCH, Weinheim, 2005;
(c) Special Issue on Chemical Sensors, Chem. Rev. 100 (2000) 7.
[11] (a) D. Bose, J. Banerjee, S.H. Rahaman, G. Mostafa, H.-K. Fun, R.D.B. Walsh, M.J. Zaworotko, B.K. Ghosh, Polyhedron 23 (2004) 2045;
(b) S.H. Rahaman, R. Ghosh, G. Mostafa, B.K. Ghosh, Inorg. Chem. Commun. 8 (2005) 700;
(c) D. Bose, G. Mostafa, H.-K. Fun, B.K. Ghosh, Polyhedron 24 (2005) 747.
[12] (a) S.H. Rahaman, D. Bose, H. Chowdhury, G. Mostafa, H.-K. Fun, B.K. Ghosh, Polyhedron 24 (2005) 1837;
(b) S.H. Rahaman, H. Chowdhury, D. Bose, G. Mostafa, H.-K. Fun, B.K. Ghosh, Inorg. Chem. Commun. 8 (2005) 1041;
(c) S.H. Rahaman, H. Chowdhury, H.L. Milton, A.M.Z. Slawin, J.D. Woollins, B.K. Ghosh, Inorg. Chem. Commun. 8 (2005) 1031.
[13] (a) S.H. Rahaman, H.-K. Fun, B.K. Ghosh, Polyhedron 24 (2005) 3091;
(b) D. Bose, S.H. Rahaman, R. Ghosh, G. Mostafa, J. Ribas, C.-H. Hung, B.K. Ghosh, Polyhedron 25 (2006) 645;

(c) D. Bose, G. Mostafa, R.D.B. Walsh, M.J. Zaworotko, B.K. Ghosh, Polyhedron 25 (2006) 663.
[14] T. Ceyhan, A. Altindal, A.R. Özkaya, M.K. Erbil, B. Salihd, Ö. Bekaroglu, Chem. Commun. (2006) 320.
[15] (a) T.K. Karmakar, B.K. Ghosh, A. Usman, H.-K. Fun, E. Riviere, T. Mallah, G. Aromi, S.K. Chandra, Inorg. Chem. 44 (2005) 2391;
(b) S.H. Rahaman, R. Ghosh, T.-H. Lu, B.K. Ghosh, Indian J. Chem. A 44 (2005) 2427;
(c) C.T. Zeyreka, A. Elmalib, Y. Elermanb, Z. Naturforsch. B 60 (2005) 520;
(d) S. Sarkar, A. Mondal, M.S.E. Fallah, J. Ribas, D. Chopra, H.S. Evans, K.K. Rajak, Polyhedron 25 (2006) 25.
[16] T.K. Karmakar, S.K. Chandra, J. Ribas, G. Mostafa, T.-H. Lu, B.K. Ghosh, Chem. Commun. (2002) 2364.
[17] (a) A.M. Golub, H. Kohler, V.V. Skopenko (Eds.), Chemistry of Pseudohalides, Elsevier, Amsterdam, 1986;
(b) J.-M. Shi, Y.-M. Sun, Z. Liu, L.D. Liu, W. Shi, P. Chen, J. Chem. Soc., Dalton Trans. (2006) 376;
(c) S.H. Rahaman, R. Ghosh, G. Mostafa, B.K. Ghosh, Inorg. Chem. Commun. 8 (2005) 1137.
[18] F. Chuburu, R. Tripier, M.L. Baccon, H. Handel, Eur. J. Org. Chem. (2003) 1050.
[19] ORTEP-32 G.M. Sheldrick, SHELXL-97: Program for Refinement of Crystal Structures, University of Göttingen, Göttingen, Germany, 1997.
[20] L.J. Farrugia ORTEP-3, J. Appl. Crystallogr. 30 (1997) 565.
[21] W.J. Geary, Coord. Chem. Rev. 7 (1971) 81.
[22] (a) K.-Y. Ho, W.-Y. Yu, K.-K. Cheung, C.-M. Che, Chem. Commun. (1998) 2101;
(b) K.-Y. Ho, W.-Y. Yu, K.-K. Cheung, C.-M. Che, J. Chem. Soc., Dalton Trans. (1999) 1581.
[23] F.A. Cotton, G. Wilkinson, C.A. Murrilo, M. Bochmann, Advanced Inorganic Chemistry, 6th ed., Wiley, New York, 1999, p. 598.

functional groups for subsequent introduction of ligands/chelating moieties which make them quite attractive. PEI is a cationic polymer exhibiting the highest positive charge density when fully protonated in aqueous solution [24–27]. These properties are useful for a variety of industrial applications, e.g., in the paper industry for flocculation of negatively charged fibers [28–30]. Meanwhile, new applications for PEI have emerged in biology and medicine. The branched form of PEI has yielded significantly greater success in terms of cell transfection and a possible alternative to viral and liposomal routes of gene delivery [31–34].

In this work, we present our results on the synthesis and studies on the interaction of DNA with a new polymer bound cobalt complex, which possesses both polyethyleneimine and bipyridyl ligands in the coordination sphere and some free amine groups of the polymer molecule. This polymer bound complex will provide a polymer with cationic metal complex moieties with high charges(+2) which will increase the electrostatic binding of the polymer to DNA. Thereby, our polymer-cobalt chelate may be a better candidate for viral and liposomal routes of gene delivery. The binding properties of this polymer-cobalt(III) complex to calf thymus DNA were studied using absorption and fluorescence spectroscopy. Electrophoresis experiments were also carried out using pBR322 DNA.

2. Experimental

2.1. Materials and methods

Cobaltous chloride hexahydrate and 2,2′-bipyridine were purchased from Merck, India. Calf thymus DNA and branched polyethyleneimine (BPEI) (M_w ca. 25000) were obtained from Sigma–Aldrich, Germany, and were used as such. The spectroscopic titration was carried out in the buffer (50 mM NaCl–5 mM Tris–HCl, pH 7.1) at room temperature. A solution of calf thymus DNA in the buffer gave a ratio of UV absorbance at 260 and 280 nm of ~1.8–1.9:1, indicating that the DNA was sufficiently free of protein [35]. Milli-Q water was used to prepare the solutions. The complex, *cis*-$[Co(bpy)_2Cl_2]Cl \cdot 3H_2O$, was prepared as reported earlier [36].

2.2. Synthesis of *cis*-$[Co(bpy)_2(BPEI)Cl]Cl_2 \cdot 4H_2O$

To 0.15 g of BPEI dissolved in 15 mL of ethanol was added a solution of 0.6 g of *cis*-$[Co(bpy)_2Cl_2]Cl \cdot 3H_2O$ in 15 mL of water. The mixture was heated to between 50 and 60 °C for 10 h in a water bath. The colour of the solution changed from violet to reddish brown. After being warmed, the mixture was filtered and the filtrate was dialyzed against cold water for several days. Afterwards the solvent was evaporated by a rotary evaporator under reduced pressure at room temperature. A dark reddish filmy substance was obtained. It was pulverized and dried. Yield: 0.2 g. *Anal.* Calc.: C, 36.99; H, 6.32; N, 16.08. Found: C, 36.99; H, 6.56; N, 16.73%.

2.3. Cobalt analysis

The cobalt content of the polymer-cobalt(III) complex was estimated by following Kitson's method [37]. A known weight of the complex was reduced with tin and concentrated hydrochloric acid. The reduced aqueous cobalt(II) ion was made up to 10 mL in a volumetric flask using 0.1 M perchloric acid. Two millilitres of this solution and 1 mL of 50% ammonium thiocyanate solution were pipetted into a 10 mL volumetric flask and made up to the 10 mL mark with acetone. The absorbance of this solution was measured at 625 nm against a blank reagent. From the absorbance, the concentration of the cobalt was calculated. Knowing the concentration of cobalt present in a given weight of the polymer-cobalt(III) complex, the ratio of the number of moles of amine groups coordinated to the cobalt chelate to the total number of moles of amine groups in the polymer chain was calculated. The percentage of cobalt thus obtained for our polymer-cobalt(III) complex, *cis*-$[Co(bpy)_2(BPEI)Cl]Cl_2 \cdot 4H_2O$, is 11.36%. *Anal.* Calc. 11.32%.

2.4. Determination of the degree of coordination

The structure of the polymer-cobalt complex is shown in Fig. 1. In this figure '*x*' represents the degree of coordination. The degree of coordination (x), means the number of moles of cobalt(III) chelate per mole of the repeating unit (amine group) of the polymeric ligand. If all the repeating units (amine groups) in the polymer are coordinated to cobalt, then the value of x is 1. The degree of coordination (x) of the cobalt chelate in the polymer-cobalt(III) complex could be calculated from the carbon content. Based on the x value thus calculated, the C, H and N contents were calculated [38]. The degree of coordination (x) thus obtained for our polymer-cobalt(III) complex, *cis*-$[Co(bpy)_2(BPEI)Cl]Cl_2 \cdot 4H_2O$, is 0.219.

2.5. Physical measurements

Absorption spectra were recorded on a UV–Vis–NIR Cary300 spectrophotomer using cuvettes of 1 cm path length, and emission spectra were recorded on a JASCO

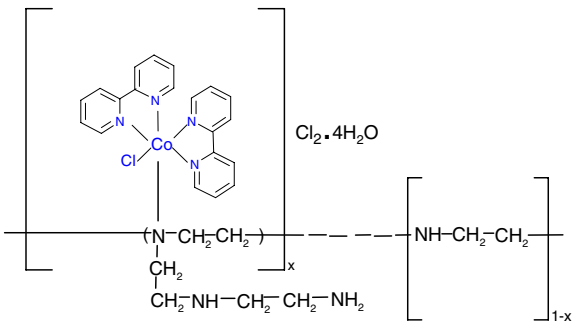

Fig. 1. Structure of *cis*-$[Co(bpy)_2(BPEI)Cl]Cl_2 \cdot 4H_2O$.

FP 770 spectrofluorimeter. FT-IR spectra were recorded on a FT-IR Perkin–Elmer spectrophotometer with samples prepared as KBr pellets. ^{1}H NMR spectra were recorded on a BRUKER 300 MHz spectrometer using D_2O as solvent.

2.6. DNA-binding experiments

The DNA concentration per nucleotide was determined by absorption spectroscopy using the known molar extinction coefficient value of 6600 M^{-1} cm^{-1} at 260 nm [39]. Absorption titrations were performed by using a fixed polymer-cobalt(III) complex concentration to which increments of the DNA stock solution were added. Polymer-cobalt(III) complex–DNA solutions were allowed to incubate for 10 min before the absorption spectra were recorded. Fluorescence quenching experiments were carried out with DNA pretreated with ethidium bromide (EB) for 30 min. To this pretreated DNA solution various amounts of polymer-cobalt complex were added and their effect on the emission intensity was measured. Samples were excited at 450 nm and the emission was observed between 500 and 700 nm.

For the gel electrophoresis experiments, supercoiled pBR322 DNA (0.1 μg) was treated with the polymer-coblat(III) complex in 50 mM Tris–HCl, 18 mM NaCl buffer, pH 7.2. The samples were electrophoresed for 3 h at 50 V on a 0.8% agarose gel in tris–acetic acid–EDTA buffer. The gel was stained with 0.5 μg/mL ethidium bromide and then photographed under UV light.

3. Results and discussion

3.1. Spectral characterization

3.1.1. IR spectrum

In the IR spectrum, there were some bands around 2853 cm^{-1} and 2924 cm^{-1} which might be assigned to C–C symmetric and asymmetric stretching vibrations of BPEI. The bands around 1018 cm^{-1} and 1629 cm^{-1} were due to the coordinated bipyridyl ligand, which were higher than the frequencies of free bipyridyl (990 cm^{-1} and 1670 cm^{-1}) [40–42]. This shift to higher frequency can be explained by the fact that the two nitrogen atoms of the bipyridyl ligands donate a pair of electrons each to the central metal forming a coordinate covalent bond.

3.1.2. UV–Visible spectrum

In the UV–Visible region, intense absorption bands appeared from 200 to 300 nm which are attributed to charge transfer transitions. Another band which appeared around 486 nm is assigned to ligand field transitions.

3.1.3. ^{1}H NMR spectrum

In the ^{1}H NMR spectrum, signals appeared between δ 2.3 and 3.6 ppm which correspond to N–CH_2–CH_2–N protons of BPEI [43]. The signals at δ 8.72, 8.42, 7.66 and 7.35 ppm might be assigned to bipyridyl protons [44].

3.2. DNA binding studies

3.2.1. Absorption spectral measurements

Electronic absorption spectra are initially employed to study the binding of the polymer-cobalt(III) complex with CT-DNA. Addition of increasing amounts of CT DNA results in the obvious tendency of hyperchromism and blue shift of the absorption bands (Fig. 2). An electrostatic interaction between the DNA and polymer-cobalt(III) complex can be predicted based on the hyperchromism exhibited and shift in absorbance of the polymer-cobalt complex. Since our complex contains the bipyridyl ligand, which is expected to be non-planar and possesses a smaller π system than phenanthroline, a classical intercalative interaction is precluded [45]. However, the high hyperchromism effects observed suggest that van der Waals contacts between the methylene groups of BPEI of the complex and the thymine methyl group (in DNA) are also very important. Also a coordination bond of DNA base with cobalt can occur through replacement of the chloride ligand in the complex, probably through aquation as has been observed with cisplatin [46]. It should be noted that a favorable hydrogen bond may be formed between NH in BPEI of the complex and N of adenine or O of thymine in the DNA. The intrinsic binding constant, K_b, was determined by using the following equation [47]:

$$[DNA]/(\varepsilon_a - \varepsilon_f) = [DNA]/(\varepsilon_o - \varepsilon_f) + 1/K_b(\varepsilon_o - \varepsilon_f)$$

where [DNA] is the concentration of DNA in base pairs, ε_a, ε_f and ε_o correspond to A_{obsd}/[Co], the extinction coefficient of the free cobalt complex and the extinction coefficient of the complex in the fully bound form, respectively, and K_b is the intrinsic binding constant. The ratio of the slope to intercept in the plot of [DNA]/($\varepsilon_a - \varepsilon_f$) versus [DNA] gives

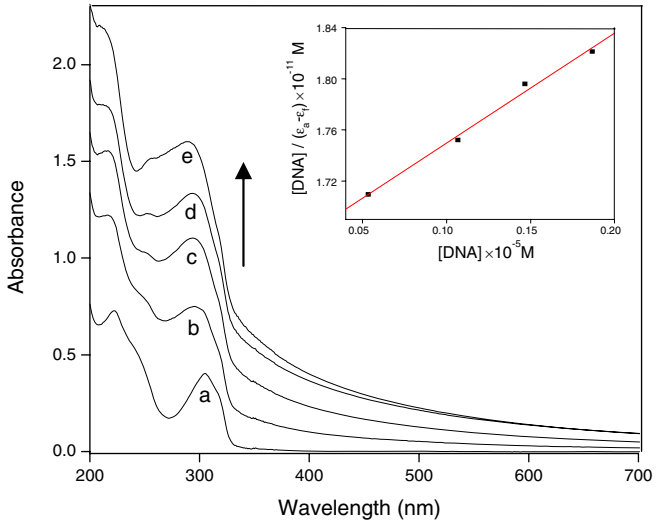

Fig. 2. Absorption spectra of *cis*-[Co(bpy)$_2$(BPEI)Cl]$Cl_2 \cdot 4H_2O$ in the absence (a) and in the presence of increasing amounts of DNA (b–e) [Complex] = 12 μM, [DNA] = 0.5–2 μM, Inset: plot of [DNA]/($\varepsilon_a - \varepsilon_f$) vs. [DNA]. Arrow shows the absorbance change upon increasing DNA concentrations.

the value of K_b and for our polymer-cobalt(III) complex it is 5.12×10^5 M^{-1}. Interestingly, this K_b value obtained for our polymer-cobalt(III) complex is very much higher than that for other ordinary complexes like $[Co(bpy)_3]^{3+}$ (K_b, 9.3×10^3 M^{-1}) [45], $[Co(bpy)_2(imp)]^{3+}$ (K_b, 1.1×10^4 M^{-1}) [48], $[Co(bpy)_3(BHBMe)]^{2+}$ (K_b, 1.23×10^4 M^{-1}), $[Co(bpy)_2(BHBNO_2)]^{2+}$ (K_b, 2.06×10^4 M^{-1}) [49]. This shows that our polymer-cobalt(III) complex binds very strongly with DNA compared to other ordinary cobalt(III)-bipyridyl complexes known in the literature [45,48,49].

3.2.2. Fluorescence studies

As the present polymer-cobalt(III) complex is non-emissive, ethidium bromide(EB) binding studies were undertaken to gain support for the extent of binding of the complex with DNA. Ethidium bromide (EB) was shown to emit intense fluorescence light in the presence of DNA, due to its strong intercalation between the adjacent DNA base pairs. It was previously reported that the fluorescent light could be quenched by the addition of a second molecule [50]. The quenching extent of the fluorescence of EB binding to DNA is used to determine the extent of binding between the second molecule and DNA. The addition of the complex to DNA pretreated with EB causes appreciable reduction in the emission intensity. This behaviour can be analysed through the Stern–Volmer equation [51], $I_o/I = 1 + K_{sv}r$, where I_o and I are the fluorescence intensities in the absence and the presence of complex, respectively. K_{sv} is a linear Stern–Volmer quenching constant, r is the ratio of the total concentration of complex to that of DNA. The quenching plot (Fig. 3) illustrates that the quenching of EB bound to DNA by the polymer-cobalt(III) complex is in good agreement with the linear Stern–Volmer equation, which also indicates that the complex binds to DNA. In the plot of I_o/I versus [Complex]/[DNA], K_{sv} is given by the ratio of the slope to intercept. The K_{sv} value for our polymer-cobalt(III) complex thus obtained is 0.2023, which is higher than that for ordinary transition metal terpyridine complexes [7]. This suggest that our polymer bound cobalt(III) complex binds strongly with DNA, which is also consistent with our absorption spectral results. It is generally agreed that strong fluorescence enhancement accompanies a strong interaction of the polymeric cobalt complex with calf thymus DNA. There is also evidence for additional non-intercalative fluorescence enhanced sites which are presumed to involve electrostatic binding [52].

3.2.3. Gel electrophoresis studies

Bronich et al. [53] and Tang and Szoka [54] have reported that DNA-polycation complexes are formed as a result of ionic interactions between cationic groups of the polycation and negatively charged phosphate groups of DNA. Branched polyethyleneimine is a cationic polymer exhibiting the highest positive charge density when fully protonated and it consists of primary, secondary and tertiary amines and about 25% of primary amines of PEI are reported to participate in forming complexes with

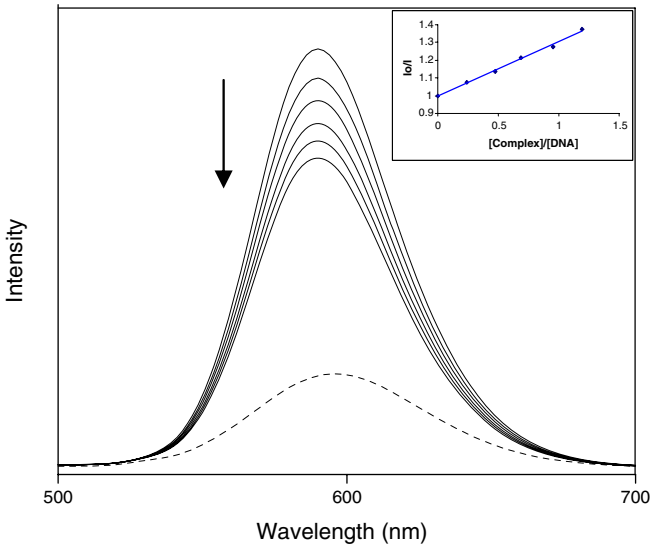

Fig. 3. Emission spectra of EB bound to DNA in the absence and in the presence of *cis*-$[Co(bpy)_2(BPEI)Cl]Cl_2 \cdot 4H_2O$ (—), [EB] = 4 μM, [DNA] = 4 μM, [Complex] = 0–6 μM. Inset: plot of I_o/I vs. [Complex]/[DNA]. Emission spectrum of EB alone (---).

DNA by an ionic interaction with the phosphate groups in the DNA [55,56]. Vinogradov et al. [57] also have reported that the binding between DNA and PEI is thought to occur mainly through electrostatic interactions among the participating species. That is the polymer-DNA complex is produced spontaneously resulting from the formation of ion pairs between ionized amino groups of PEI and the phosphate groups of DNA. In order to substantiate the binding of our polymer-cobalt complex to DNA, a gel retardation assay has been performed on pBR322 DNA (Fig. 4). Lane 1 is free polymer-cobalt(III) complex. Lane 2 is pure DNA not treated with any complex. Lanes 3–5 represent the DNA treated with the polymer-cobalt(III) complex. As reported by previous workers on the interaction of DNA–polyethyleneimine, in

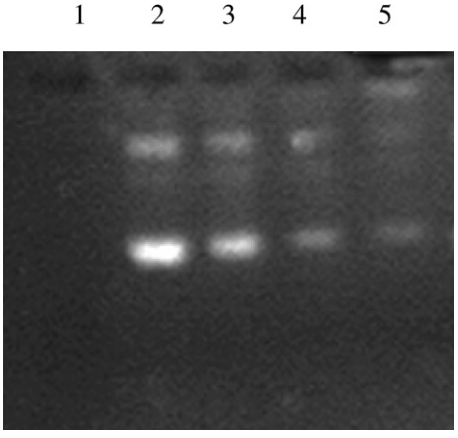

Fig. 4. Gel retardation assay of pBR322 DNA by *cis*-$[Co(bpy)_2(BPEI)Cl]Cl_2 \cdot 4H_2O$. Lane 1: polymer-cobalt complex alone, Lane 2: DNA (0.1 μg), Lanes 3–5: DNA + polymer-cobalt complex in the concentration of 20, 40, 60 μM.

our work the migration of the DNA band is also retarded as the amount of polymer-cobalt(III) complex is increased. This clearly demonstrates that the cationic segments of the polyethyleneimine are neutralizing the negative charges of DNA which could be facilitated further due to the increase of bpy groups of the cobalt(III) complex moieties [58].

4. Conclusion

The DNA binding of a polymer-cobalt complex containing the bipyridyl ligand has been examined by absorption spectroscopy, fluorescence spectroscopy and gel electrophoresis. The binding seems to be stronger than ordinary cobalt(III)-bipyridyl complexes. This may be due to the presence of multiple cobalt(III) complex molecular units and free amine groups in a single polymer molecule which between them cooperatively help in binding to DNA.

Acknowledgements

We are grateful to the UGC-SAP & COSIST and DST-FIST programs and University Research Fellowship sanctioned to one of the authors, R.S.K., by the Bharathidasan University, Tiruchirappalli, India. We thank Dr. L. Uma and Dr. D. Prabhakaran, National Centre for Marine Cyanobacteria, for providing the Gel documentation facility.

References

[1] A.M. Pyle, E.C. Long, J.K. Barton, J. Am. Chem. Soc. 111 (1989) 4520.
[2] A. Sitlani, E.C. Long, A.M. Pyle, J.K. Barton, J. Am. Chem. Soc. 114 (1992) 2303.
[3] L. Jin, P. Yang, Polyhedron 16 (1997) 3395.
[4] Y.-M. Song, X.-l. Lu, M.-l. Yang, X.-R. Zheng, Transition Met. Chem. 30 (2005) 499.
[5] Q.-L. Zhang, J.-G. Liu, H. Chao, G.-Q. Xue, L.-N. Ji, J. Inorg. Biochem. 83 (2001) 49.
[6] Q.-L. Zhang, J.-G. Liu, H. Xu, H. Li, J.-Z. Liu, H. Zhou, L.-H. Qu, L.-N. Ji, J. Inorg. Biochem. 20 (2001) 3049.
[7] C.-W. Jiang, H. Chao, H. Li, L.-N. Ji, J. Inorg. Biochem. 93 (2003) 247.
[8] V.G. Vaidyanathan, B.U. Nair, J. Chem. Soc., Dalton Trans. (2005) 2842.
[9] H. Chao, W.-J. Mei, Q.-W. Huang, L.-N. Ji, J. Inorg. Biochem. 92 (2002) 165.
[10] K. Jiao, Q.-X. Wang, W. Sun, F.F. Jian, J. Inorg. Biochem. 99 (2005) 1369.
[11] Q.-L. Zhang, J.-G. Liu, J. Liu, G.-Q. Xue, H. Li, J.-Z. Liu, H. Zhou, L.-H. Qu, L.-N. Ji, J. Inorg. Biochem. 85 (2001) 291.
[12] H.M. Torshizi, S. Ghadimy, N. Akbarzadeh, Chem. Pharm. Bull. 49 (2001) 1517.
[13] Z.-S. Yang, Y.-L. Wang, G.-C. Zhao, Anal. Sci. 20 (2004) 1127.
[14] H. Shimakoshi, T. Kaieda, T. Matsuo, H. Sato, Y. Hisaeda, Tetrahedron Lett. 44 (2003) 5197.
[15] D. Putnam, J. Kopecek, J. Adv. Polym. Sci. 122 (1995) 55.
[16] J.S. Roman, A. Gallardo, B. Levenfeld, Adv. Mater. 7 (1995) 203.
[17] H.J. Ringsdorf, J. Polym. Sci. 51 (1975) 135.
[18] J.G. Joseph, React. Funct. Polym. 39 (1999) 99.
[19] E. Dfaz, R. Valenciano, P. Landa, J.L. Arana, J. Gonzalez, Polym. Test 21 (2002) 247.
[20] I. Katime, J.R. Ochoa, J. Appl. Polym. Sci. 34 (1987) 1953.
[21] M. Kaneko, E.T. Tsuchida, J. Polym. Sci. Macromol. Rev. 16 (1987) 397.
[22] E.T. Tsuchida, H. Nishide, Adv. Polym. Sci. 24 (1977) 1.
[23] J.M. Clear, J.M. Kelly, J.G. Vos, Macromol. Chem. 184 (1983) 613.
[24] E.A. Bekturov, S.E. Kudaibergenov, G.M. Zhaimina, Y.P. Saltykov, Makromol. Chem. Rapid. Commun. 7 (1986) 339.
[25] K. Ito, N. Minoura, J. Polym. Sci., Part A. Polym. Chem. 30 (1992) 2071.
[26] S. Kobayashi, K.D. Suh, Y. Shirokura, Macromolecules 22 (1989) 2363.
[27] J.W. Gohdes, B.L. Duran, N.C. Clark, T.W. Robinson, B.F. Smith, N.N. Sauer, Separ. Sci. Technol. 36 (2001) 2647.
[28] D. Horn, F. Linhart, in: J.C. Roberts (Ed.), Paper Chemistry, Blackie, London, 1991, p. 44.
[29] Nippon Shokubai Kagaku Kogyo Co. Ltd., Chem. Abstract 103 (1983) 89266.
[30] K. Matsumoto, A. Suganuma, D. Kunui, Powder Technol. 25 (1980) 1.
[31] W.T. Godbey, K.K. Wu, A.G. Mikos, J. Control. Release 60 (1999) 149.
[32] B. Abdallah, A. Hassan, C. Benoist, D. Goula, J.P. Behr, B.A. Demeneix, Hum. Gene Ther. 7 (1996) 1947.
[33] W.T. Godbey, K.K. Wu, A.G. Mikos, Med. Sci. 96 (1999) 5177.
[34] A. Boletta, A. Benigni, J. Lutz, G. Remuzzi, M. Soria, L. Monaco, Hum. Gene Ther. 8 (1997) 1243.
[35] J. Marmur, J. Mol. Biol. 3 (1961) 208.
[36] A.A. Vlcek, Inorg. Chem. 6 (1967) 1425.
[37] R.E. Kitson, Anal. Chem. 22 (1950) 664.
[38] Y. Kurimura, E. Tsuchida, M. Kaneko, J. Polym. Sci., Part A-1 9 (1971) 3511.
[39] M.F. Reichmann, S.A. Rice, C.A. Thomas, P. Doty, J. Am. Chem. Soc. 76 (1954) 3047.
[40] S.P. Sinha, Spectrochim. Acta 20 (1964) 879.
[41] TI.A. Gerber, J. Coordin. Chem. 56 (2003) 1397.
[42] K. Nakamoto, Infrared and Raman Spectra of Inorganic and Coordination Compounds, Wiley InterScience, New York, 1978.
[43] D. Wang, A. Narang, M. Kotb, D.O. Gaber, D.D. Miller, S.W. Kim, R.I. Mahoto, Biomacromolecules 3 (2002) 1197.
[44] S. Ghosh, A.C. Barve, A.A. Kumbhar, A.S. Kumbhar, V.G. Puranik, P.A. Datar, U.B. Sonawane, R.R. Joshi, J. Inorg. Biochem. 100 (2006) 331.
[45] M.T. Carter, M. Rodriguez, A.J. Bard, J. Am. Chem. Soc. 111 (1989) 8901.
[46] S.E. Sherman, D. Gibson, A.H.J. Wang, S.J. Lippard, J. Am. Chem. Soc. 110 (1988) 7368.
[47] A.M. Pyle, J.P. Rehmann, R. Meshoyrer, C.V. Kumar, N.J. Turro, J.K. Barton, J. Am. Chem. Soc. 111 (1989) 3051.
[48] P. Tamil Selvi, M. Palaniandavar, Inorg. Chim. Acta 337 (2002) 420.
[49] S. Srinivasan, J. Annaraj, PR. Athappan, J. Inorg. Biochem. 99 (2005) 876.
[50] B.C. Baguley, M. Lebret, Biochemistry 23 (1984) 937.
[51] J.R. Lakowicz, G. Webber, Biochemistry 12 (1973) 4161.
[52] C.-L. Liu, J. Zhou, H. Xu, J. Inorg. Biochem. 71 (1998) 1.
[53] T.K. Bronich, H.K. Nguyen, A. Eisenberg, A.V. Kabanov, J. Am. Chem. Soc. 122 (2000) 8339.
[54] M.X. Tang, F.C. Szoka, Gene Ther. 4 (1997) 823.
[55] A.V. Harpe, H. Petersen, Y. Li, T. Kissel, J. Control. Release 69 (2000) 309.
[56] C.H. Ahn, S.Y. Chae, Y.H. Bae, S.W. Kim, J. Control. Release 80 (2002) 275.
[57] S.V. Vinogradov, T.K. Bronich, A.V. Kabonov, Bioconjugate Chem. 9 (1998) 805.
[58] J. Annaraj, S. Srinivasan, K.M. Ponvel, P.R. Athappan, J. Inorg. Biochem. 99 (2005) 669.

non-oxidative, hydrolytic pathway [5]. Recently, some lanthinide(III) complexes of amino acids have also been found to hydrolytically cleave bis(4-nitrophenyl)phosphate, a model DNA compound [6].

This report is part of a long term, systematic effort to investigate the factors affecting the nucleolytic efficiency of metal-chelated amino acids and peptides. Here, the potential nucleolytic property of different metal(II) complexes of *N*,*N*′-ethylenediaminediacetic acid (which is also called *N*,*N*′-ethylenediglycine, a *N*,*N*′-ethylene-bridged diaminoacid) seems interesting to us. *N*,*N*′-ethylene-bridged amino acids can act as tetradentate ligands, in contrast to bidentate simple amino acids such as glycine and L-alanine. The metal complexes of the former tetradentate ligands should also be more stable in aqueous solution than the latter bidentate ligands. In addition, the bridging excludes *cis–trans* isomerism as it fixes both the coordinated amino nitrogen atoms of these complexes into a *cis*-position, unlike the situation in the bis(aminoacidato)metal(II) complexes. Furthermore, copper(II) complexes of some *N*,*N*′-ethylene-bridged bidentate amino acids have been found to be SOD-mimetic, i.e. they have the ability to quench harmful superoxide anion radicals [7]. Another fascinating aspect of the M(edda) complexes is the position of the coordinated water molecules; the crystal structure of the octahedral Ni(edda) shows the two coordinated water molecules to be in a *cis*-position [8,9]. If the *cis*-coordinated water molecules of such a metal complex are labile and the Lewis acid strength of the metal is sufficiently strong, the complex is a potential phosphodiester hydrolytic agent [10].

Besides reporting the crystal structure of the Co(edda) complex, this paper details the solution properties of a series of metal complexes (M = Co, Ni, Cu, Zn) by UV–visible spectroscopy and electrospray ionization mass spectroscopy. For the reaction of the Cu(edda) complex with pBR322 in the presence of hydrogen peroxide, agarose gel electrophoresis has been used to study the effect of the concentration of the complex, pH, type of buffer and radical scavengers on the extent of DNA cleavage. An electrophoretic study has also been undertaken to compare the nucleolytic efficiency of Cu(edda) with (i) *cis*-aqua*bis*(glycinato)copper(II), *cis*-Cu(gly)$_2$; (ii) *trans*-aqua*bis*(*N*,*N*-dimethylglycinato)-copper(II) dihydrate, Cu(dmg)$_2$ and (iii) Fe(II)-EDTA. The reactions of Cu(edda), *cis*-Cu(gly)$_2$ and Cu(dmg)$_2$ with H_2O_2 have also been monitored with *p*-nitrosodimethyl-aniline (PNDA) which is one of two reagents used for determining the formation of hydroxyl radicals [11,12]. ROS scavengers have also been used to ascertain the reactive species responsible for DNA cleavage. In addition, electrospray ionization mass spectrometry and circular dichroism spectroscopy are used to investigate the binding and binding effect of Cu(edda) with a dodecanucleotide sequence d(CGCGAATTCGCG) which has been widely adopted as a general template for minor groove drugs [13].

2. Experimental

2.1. Reagents and materials

Most of the reagents were of analytical grade and were used as supplied. The pBR 322, gene ruler 1 kb DNA ladder, ethidium bromide, loading buffer, Tris and agarose were bought from BioSyn Tech (Fermentas). All solutions for DNA experiments were prepared with ultra-pure water from a Elga PURELAB ULTRA Bioscience water purification system with UV light accessory. The Tris–NaCl buffer (TN buffer) contains 0.1 M Tris and 0.15 M NaCl; TN buffer at lower pH was obtained by adding 1 M HCl acid. Phosphate buffer was prepared by adding 10 mM NaH_2PO_4 to 10 mM Na_2HPO_4 solution to adjust the pH to pH 7.5. TBE buffer (1×) contains Tris (0.09 M), boric acid (0.09 M) and Na_2H_2EDTA (0.002 M). The pH of the resulting TBE buffer was adjusted by adding 1 M HCl to pH 7.5. The Hepes buffer contain Hepes at 10 mM. All stock solutions of H_2O_2 in water and metal complexes in TN, TBE and Hepes buffers were freshly prepared daily.

2.2. Synthesis of the complexes

The Cu(dmg)$_2$, M(edda) and *cis*-Cu(gly)$_2$ complexes were synthesized by previously reported procedures [3,8,9,14].

Elemental analysis for Ni(edda): found C, 25.60; H, 5.52; N, 9.91% and calculated for $Ni(C_6H_{10}O_4N_2)\cdot 3H_2O$ C, 25.12; H, 5.62; N, 9.76. For Zn(edda): found C, 26.52; H, 4.94; N, 10.41% and calculated for $Zn(C_6H_{10}O_4N_2)\cdot 2H_2O$ C, 26.15; H, 5.12; N, 10.17%. For Cu(edda); found C, 30.13; H, 3.98; N, 11.57% and calculated for $Cu(C_6H_{10}O_4N_2)$ C, 30.32; H, 4.24; N, 11.79%. The FTIR of Cu(dmg)$_2$ and *cis*-Cu(gly)$_2$ were identical with those of aqua*bis*(*N*,*N*-dimethylglycinato)copper(II) [3] and *cis*-aqua*bis*(glycinato)copper(II) [14], respectively.

2.3. Synthesis of diaqua(*N*,*N*′-ethylenediaminediacetato)cobalt(II) monohydrate

NaOH solution was added to a mixture of $CoCl_2\cdot 6H_2O$ (4.07 g, 0.017 mol) and *N*,*N*-ethylenediaminediacetatic acid (3 g, 0.017 mol) until the pH value was 5.5. The deep wine red solution was filtered and the filtrate was heated in a water-bath at 45 °C for 2 days. The solution was allowed to cool at room temperature and slow evaporation of the solution yielded red crystals suitable for X-ray crystal structure analysis. Elemental analysis for Co(edda): found C, 25.46; H, 5.16; N, 9.32% and calculated for $Co(C_6H_{10}O_4N_2)\cdot 3H_2O$ C, 25.10; H, 5.62; N, 9.76%.

2.4. Physical measurements

The C, H and N microanalysis was carried out with a Perkin–Elmer 2400 CHN analyzer. Infrared spectra of all

compounds were recorded as KBr pellets using a Perkin–Elmer FT-IR spectrometer in the frequency range 4000–400 cm^{-1}. UV–visible spectroscopic measurement was carried out on a Perkin–Elmer Lambda 40 spectrophotometer; for studies on aqueous sample solutions, distilled water was filled into the reference cell while for those on buffered solutions, the corresponding buffer was the reference material. Positive ion electrospray ionization mass spectra of a 1:1 ultra pure water:methanol (v/v) solution of each M(edda) complex was obtained by using a MicroMass Quattro Micro LC-MS-MS triple quadrupole mass spectrometer. For a desolvation temperature (T_d) of 80 °C, the cone voltage (V_c) was 70 V, while for desolvation temperatures of 100 and 150 °C, the cone voltage was 60 V. A capillary voltage (V_s) of 4 kV was used for all measurements. Conformation studies of M(edda) complexes with the duplex oligonucleotide in phosphate buffer was carried out by the use of a Jasco J-810 spectropolarimeter.

2.5. X-ray crystallography

Room-temperature diffraction data were collected on a Bruker SMART APEX area-detector diffractometer (Mo Kα radiation, $\lambda = 0.71073$ Å) on a crystal of size $0.48 \times 0.28 \times 0.18$ mm over the range $2.0° < \theta < 26.0°$. The intensity data for Co(edda) was collected over the range $\theta = 2.0$–$26.0°$ for 4551 reflections. The structure was solved and refined by using the SHELX suite [15]. The final R ($I > 2\sigma(I)$) and R_w values were 0.025 and 0.075. All non-hydrogen atoms were refined anisotropically. The water and amino hydrogen atoms were located in a difference Fourier map and were refined. The perspective view of the molecule was obtained using ORTEP-3 for Windows [16]. Selected bond distances and angles together with hydrogen bonding data are listed in Table 1.

Table 1
Selected bond lengths (Å) and bond angles (°)

Co1–O1W	2.0700(13)	Co1–O2W	2.1200(12)
Co1–O1	2.0782(11)	Co1–N1	2.1609(15)
Co1–O3	2.0853(11)	Co1–N2	2.1632(13)
O1W–Co1–O1	92.31(5)	O3–Co1–N1	93.48(5)
O1W–Co1–O3	94.32(6)	O2W–Co1–N1	92.97(5)
O1–Co1–O3	173.07(4)	O1W–Co1–N2	94.31(5)
O1W–Co1–O2W	91.68(5)	O1–Co1–N2	97.04(5)
O1–Co1–O2W	93.88(5)	O3–Co1–N2	80.44(5)
O3–Co1–O2W	87.96(5)	O2W–Co1–N2	167.31(5)
O1W–Co1–N1	171.06(6)	N1–Co1–N2	82.67(5)
O1–Co1–N1	79.77(5)		

D–H···A	D–H	H···A	D···A	D–H···A
Hydrogen bonding (Å, °)				
O1w–H1w1···O2^{i}	0.85	1.95(1)	2.777(2)	163(2)
O1w–H1w2···O2^{ii}	0.85	1.84(1)	2.679(2)	169(2)
O2w–H2w1···O4^{iii}	0.85	1.87(1)	2.709(2)	169(2)
O2w–H2w2···O3w	0.85	1.87(1)	2.675(2)	158(2)
O3w–H3w1···O3	0.86(1)	2.03(1)	2.816(2)	151(2)
O3w–H3w2···O4^{iv}	0.85(1)	1.85(1)	2.693(2)	170(2)
N1–H1n···O2w^{v}	0.86(1)	2.61(1)	3.379(2)	150(2)
N2–H2n···O1^{ii}	0.85(1)	2.22(2)	2.990(2)	149(2)

Symmetry codes: (i) x, $1 - y$, $1/2 + z$; (ii) $1/2 - x$, $y - 1/2$, $1/2 - z$; (iii) x, $1 + y, z$; (iv) $1 - x$, $-y$, $1 - z$; (v) $1 - x$, y, $1/2 - z$.

2.6. DNA cleavage experiments

Agarose gel electrophoresis experiments were carried out on supercoiled plasmid DNA pBR322 (4.4 kb) using a horizontal gel system. Each 20 μL sample consisted of the complex dissolved in buffer, DNA, the required volume of additional buffer and finally H_2O_2. All samples were incubated in the dark in a water-bath at a temperature of 37 °C for 2 h. For the hydrolytic cleavage studies, incubation of the samples was similarly carried out. The DNA cleavage profile was analyzed using 1% agarose gel in a horizontal gel set with a running time of 2.5 h, at a constant voltage of 78 V. Unless otherwise mentioned, each reaction mixture consisted of 0.0125 μg/μL DNA, 2 mM H_2O_2 and TN buffer, pH 7.5. The resultant DNA bands after the electrophoresis step for each set of experiments were stained with ethidium bromide before being photographed under UV light using a Syngene Bio Imaging system, and the digital image was viewed with Gene Flash software.

Besides comparing the nucleolytic property of the M(edda) complexes, the effect of various factors (concentration of complex, pH of the TN buffer and type of buffer used) on the cleavage of the DNA by Cu(edda) in presence of hydrogen peroxide was similarly investigated. The effect of radical scavengers DMSO and sodium azide on the oxidative cleavage of Cu(edda) was also carried out. In addition, a comparative study of DNA cleavage by Cu(edda), *cis*-$Cu(gly)_2$, $Cu(dmg)_2$ and $[Fe(EDTA)]^{2-}$ in TN buffer, pH 7.5, in the presence of hydrogen peroxide was undertaken. In the above investigations as well as other factors affecting the nucleolytic efficiency, the chosen fixed concentration of the complexes was sometimes varied to obtain a satisfactory visual comparison of the DNA banding patterns which resulted from varying the factor under consideration. The production of ·OH radicals from the reactions of the copper(II) amino acid complexes (0.1 mM) in TN buffer, pH 7.5, with 200 mM hydrogen peroxide was assayed by the use of *p*-nitrodimethylaniline (PNDA) indicator (56 μM) according to a previous procedure [12]. The % bleaching of PNDA after time t (in minutes) was calculated by using the formula $(A_0 - A_t)/A_t \times 100$ where A_0 and A_t are the absorbance of PNDA in the reaction mixture at the initial time and at time t. The initial absorbance reading was measured within 30 s. Additionally, a study to compare the DNA cleavage by the M(edda) complexes in the presence of hydrogen peroxide to that of the respective MCl_2 complexes was undertaken.

2.7. Interaction of the complex with ds(12-mer)

The self-complimentary 12-*mer* (5′-CGCGAATTCGCG-3′) was bought from Biosyn Tech and this was first annealed according to a previously reported procedure using a 0.1 M ammonium acetate solution to

give a 100 μM ds(12-*mer*) for ESI-MS studies [17,18]. The reaction mixture was prepared by mixing the pre-prepared ds(12-*mer*) with Cu(edda) stock solution. This was diluted using 0.1 M ammonium acetate prior to analysis by ESI-MS. Negative ion ESI mass spectra of ds(12-*mer*) and Cu(edda)-ds(12-*mer*) were obtained using the above mentioned MicroMass Quattro Micro LC-MS-MS.

For the CD studies of M(edda) with ds(12-*mer*), the annealing of the oligonucleotide was performed by using the supplied annealing buffer. Freshly prepared complex solutions, mixtures of M(edda) and ds(12-*mer*), and dilution were performed using phosphate buffer, pH 7.5. The concentration of each component in each M(edda)-ds(12-*mer*) mixture was set at 3.425 μM and the total volume of solution for each CD scan was 300 μL. The scan range for the CD spectra was 340–220 nm.

3. Results and discussion

3.1. Crystal structure of Co(edda) and analysis of the aqueous solution of M(edda)

The general formula of the solid state M(edda) complexes is $M(C_6H_{10}N_2O_4)\cdot xH_2O$ (where the M(II) and x values are: Co, 3; Ni, 3; Cu, 0; Zn, 2), where $(C_6H_{10}N_2O_4)^{2-}$ represents the dianionic edda ligand. These complexes are abbreviated as **1** (Co), **2** (Ni), **3** (Cu) and **4** (Zn). The synthesis of Cu(edda) needs treatment with ethanol, acetone and drying in an oven to recover a dry solid from the aqueous solution; otherwise, a gel or paste is recovered upon evaporation of the aqueous solution. The dried blue powder of Cu(edda) is completely dehydrated and can then be characterized by FTIR and elemental analysis.

Fig. 1 shows the molecular structure of diaqua(*N*,*N*′-ethylenediamine-diacetato)cobalt(II) monohydrate (**1**). The dianionic edda ligand is tetradentate and its coordinates to the cobalt atom such that the two amino nitrogen atoms occupy *cis*-positions while the two carboxylate oxygen atoms occupy *trans*-positions. Two coordinated water molecules, *cis* with respect each other, complete the octahedron about the cobalt(II) atom, resulting in a α-*cis* configuration of the ligating atoms. Therefore, the Co(edda) complex is isostructural with Ni(edda) [8,9]. Not surprisingly, both complexes have very similar FTIR spectra. Hydrogen bonding, both the direct intermolecular type and that through interlinking with the lattice water molecule, connects the $[Co(edda)(H_2O)_2]$ units into a vast three-dimensional network. The hydrogen bonding linkage involves the amino nitrogen, carbonyl and carboxylate oxygen, coordinated water and lattice water molecules. Selected bond distances and bond angles are summarized in Table 1.

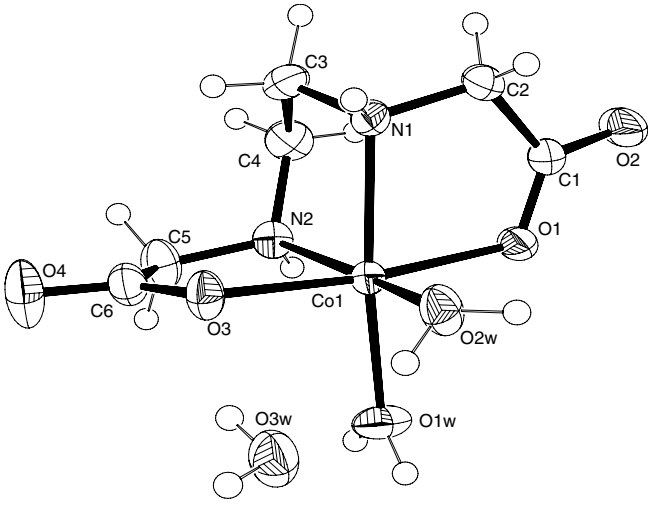

Fig. 1. 50% Probability ORTEP plot of the diaqua(*N*,*N*′-ethylenediglycinato)cobalt(II) molecule.

The electrospray ionization mass spectra (ESI-MS) of all the M(edda) complexes in 1:1 water-methanol solvent mixture (v/v) show the presence of molecule ion peaks ascribed to the various metal(II) complex species, each of which contains the $(C_6H_{10}N_2O_4)$ moiety ($C_6H_{10}N_2O_4$ = edda). This suggests that the edda ligand remains undissociated in aqueous solution (Table 2). Sufficiently high capillary

Table 2
ESI-MS of M(edda) complexes

M(II)	$T_d/V_c/V_s$	*m*/*z* (found)	*m*/*z* (calc.)	Assignment	I_r (%)
Co	80/70/4	233.7	233.09	$[Co(edda)]^+$	88
		251.1	251.10	$[Co(edda)(H_2O)]^+$	47
		268.8	269.12	$[Co(edda)(H_2O)_2]^+$	100
Ni		232.8	232.86	$[Ni(edda)]^+$	100
Cu		237.8	237.70	$[Cu(edda)]^+$	100
		255.7	255.72	$[Cu(edda)(H_2O)]^+$	27
Zn		239.8	239.55	$[Zn(edda)]^+$	41
		257.7	257.56	$[Zn(edda)(H_2O)]^+$	100
		275.7	275.57	$[Zn(edda)(H_2O)_2]^+$	33
Co	100/60/4	233.8	233.09	$[Co(edda)]^+$	72
		251.2	251.10	$[Co(edda)(H_2O)]^+$	85
		270.0	270.13	$[Co(edda)(H_2O)_2 + H]^+$	100
		268.6	269.12	$[Co(edda)(H_2O)_2]^+$	85
Ni		232.8	232.86	$[Ni(edda)]^+$	100
		269.0	268.89	$[Ni(edda)(H_2O)_2]^+$	7
		286.9	286.90	$[Ni(edda)(H_2O)_3]^+$	5
Cu		237.9	237.70	$[Cu(edda)]^+$	100
		255.7	255.72	$[Cu(edda)(H_2O)]^+$	16
		273.7	273.73	$[Cu(edda)(H_2O)_2]^+$	2
Zn		239.7	239.55	$[Zn(edda)]^+$	100
		257.2	257.56	$[Zn(edda)(H_2O)]^+$	55
		275.6	275.57	$[Zn(edda)(H_2O)_2]^+$	45
		293.0	293.59	$[Zn(edda)(H_2O)_3]^+$	13
Co	150/60/4	233.4	233.09	$[Co(edda)]^+$	57
		251.5	251.10	$[Co(edda)(H_2O)]^+$	75
		268.7	269.12	$[Co(edda)(H_2O)_2]^+$	100
Ni		232.8	232.86	$[Ni(edda)]^+$	100
		269.6	269.89	$[Ni(edda)(H_2O)_2 + H]^+$	8
		286.0	286.90	$[Ni(edda)(H_2O)_3]^+$	3
Cu		237.8	237.70	$[Cu(edda)]^+$	100
		255.7	255.72	$[Cu(edda)(H_2O)]^+$	16
Zn		239.7	239.55	$[Zn(edda)]^+$	33
		257.5	257.56	$[Zn(edda)(H_2O)]^+$	100

voltage (4 kV) and cone voltage (60–70 V) are needed to observe the above species. Depending on the desolvation temperature ($T_d = 80$, 100 and 150 °C), molecular ion peaks with T_d-dependent relative intensities corresponding to three metal(II) complex species, viz. $[M(edda)]^+$, $[M(edda)(H_2O)]^+$ and $[M(edda)(H_2O)_2]^+$, have been detected in the mass spectra. At $T_d = 80$ °C, the most abundant peaks (100%) in the ESI-MS for the M(edda) aqueous solutions are $[Co(edda)(H_2O)_2]^+$, $[Ni(edda)]^+$ (only this peak detected), $[Cu(edda)]^+$ and $[Zn(edda)(H_2O)]^+$. A very small amount (2–7%) of $[Ni(edda)(H_2O)_2]^+$ and $[Cu(edda)(H_2O)_2]^+$ can be observed at $T_d = 100$ °C while the most abundant species is $[M(edda)]^+$ (100%) for both metal complexes. With an increase of T_d to 150 °C, it is found that: (i) $[Co(edda)(H_2O)_2]^+$ still remains the most abundant of the three Co(II) complex species; (ii) $[Cu(edda)]^+$ and $[Ni(edda)]^+$ are most abundant among their respective species; and (iii) the relative abundance of $[Zn(edda)(H_2O)]^+$ is the highest among the Zn(II) species. It seems reasonable to assume that $[Co(edda)(H_2O)_2]$ is the octahedral diaqua(*N*,*N*′-ethylenediaminediacetato)-cobalt(II) complex and to conclude that it is the most stable and easily ionizable $[M(edda)(H_2O)_2]$ species.

The gaseous molecular ions $[Co(edda)(H_2O)_2]^+$, observed in the ESI-MS, suggest the structure of the solid octahedral complex **1** persists in aqueous solution. This is substantiated by the visible spectrum of **1** in water which has two bands at 503 nm (€, 11 M^{-1} cm^{-1}) and 1090 nm (€, 6 M^{-1} cm^{-1}) which are comparable with those of the aqueous solution of other octahedral complexes of 1-allylimidazole (495 nm) and of 4-methylimidazole-5-carbaldehyde (513 nm) [19,20]. The visible spectrum of an aqueous solution of **2** (Ni) shows two bands at 367 nm (€, 7 M^{-1} cm^{-1}) and 611 nm (€, 4 M^{-1} cm^{-1}) and this is consistent with a Ni(II) complex with an octahedral geometry [19]. The charge transfer band at 249 nm (€, 3847 M^{-1} cm^{-1}) and the visible d–d transition band centered at 672 nm (€, 100 M^{-1} cm^{-1}) for the aqueous solution of **3** (Cu) is consistent with a six-coordinate copper(II) complexes with octahedral geometry [19,21]. As for complex **4** (Zn), its ESI-MS at $T_d = 80$ °C shows an *m*/*z* molecular ion peak at 275.57 attributed to $[Zn(edda)(H_2O)_2]^+$ at 30% relative abundance. Thus, the M(edda) complexes (**1**–**4**) exist as octahedral species in aqueous solution.

3.2. Nucleolytic property. Electrophoresis study of M(edda) with pBR322 in the presence and absence of hydrogen peroxide

Agarose gel electrophoresis is a convenient method to assess the hydrolytic or oxidative cleavage of DNA by metal complexes, to assess the factors affecting the nucleolytic efficiency of a complex and to compare the nucleolytic property of different metal complexes. These have been done in the present study with the M(edda) complexes.

We have previously studied whether M(edda) complexes could hydrolytically cleave λDNA [22]. Incubation of the DNA with up to 6 mM of the complexes in Tris–NaCl buffer (abbreviated as TN buffer) at pH 7 overnight at 37 °C failed to induce any cleavage. Repetition of this experiment by incubating all the M(edda) complexes with pBR322 for 24 h in TN buffer at pH 7.5 also gave negative results. The M(edda) complexes are unable to effect hydrolytic cleavage due to some possible factors. The nucleolytic ability of lanthanide(III) complexes of α-amino acids (aa) has been attributed to the high Lewis acidity of the trivalent lanthanide ions and the active complex species have been identified as $[Ln(aa)_3(OH)]^{2+}$ and $[Ln(aa)_2(OH)_2]^+$ [6]. Various mononuclear metal-coordinated hydroxide containing species, such as $[(TACH)Cu(OH)(OH_2)_2]^+$, $[(cyclen)Co(OH)(OH_2)]^{2+}$ and $[(trpn)Co(OH)(OH_2)]^{2+}$, have been found to be capable of hydrolytic cleavage of DNA [23]. The insufficient Lewis acidity of the metal ion alone in $[M(edda)(H_2O)_2]$ or the absence of a overall positive charge may explain our negative results [23,24]. Thus, we have focused our studies on the cleavage of pBR322 by these complexes in the presence of hydrogen peroxide.

When 500 μM of the M(edda) complexes were incubated with pBR322 (0.0125 μg/μl) in TN buffer, pH 7.5, in the presence of 2 mM hydrogen peroxide, only **3** (Cu) showed appreciable cleavage of the DNA (Fig. 2; lanes **7**–**10**); there was complete conversion of supercoiled DNA to nicked and linear DNA. The complex **1** (Co) shows slight cleavage, nicking a small amount of the supercoiled pBR322. The complexes **2** (Ni) and **4** (Zn) are virtually inactive. A similar result has been obtained when 1 mM of these four complexes were incubated with λDNA (0.02 μg/μl) in TN buffer at pH 7 in the presence of 0.5 mM hydrogen peroxide [22].

The above shows that **3** (Cu(edda)) is more efficient than **1** (Co(edda)) as a nucleolytic agent. Both **2** and **4** are inactive. Similar results have been obtained when a comparison of the nucleolytic ability of different metal(II) complexes of *N*-(2-ethoxyethanol)-bis(2-picolyl)amine was made [25]. Due to its greater nucleolytic efficiency, the nucleolytic property of **3** in the presence of hydrogen peroxide has been more thoroughly investigated. This involves the use of radical scavengers to ascertain the type of radical species, the various factors affecting its nucleolytic efficiency and a comparison of its nucleolytic efficiency with

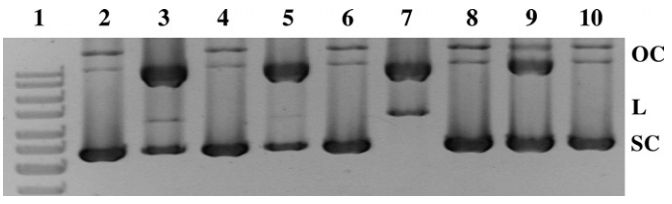

Fig. 2. Electrophoresis results of incubating different M(edda) complexes with pBR 322(0.0125 μg/μL) in the presence of 2 mM H_2O_2. Lane **1**, Gene Ruler 1 kb DNA ladder; lane **2**, DNA alone; lanes **3**–**6** refer to 100 μM of Cu(edda), Ni(edda), Co(edda) and Zn(edda), respectively; lanes **7**–**10** refer to 500 μM of Cu, Ni, Co and Zn complexes in the same sequence. DNA form: **SC**, supercoiled; **L**, linear; **OC**, open circular or nicked.

$[Fe(EDTA)]^{2-}$ and copper(II) complexes of glycine and *N*,*N*-dimethylglycine.

The effect of concentration of complex **3** (at various intervals, from 10 μM to 2 mM) is shown in Fig. 3. A low concentration of 10 μM can induce a single-strand break of the plasmid DNA in the presence of hydrogen peroxide as shown by the slightly more intense band of one of the nicked bands (Fig. 3, lane **6**). The extent of DNA cleavage is concentration dependent, and this is clearly shown in Fig. 3.

As the DNA in the presence of 2 mM hydrogen peroxide or the DNA in the presence of 2 mM of complex **3** shows no change in banding patterns compared to the control DNA alone, both **3** and hydrogen peroxide are needed for the DNA cleavage. This suggests oxidative cleavage. Both DMSO (a known $^{\cdot}OH$ radical scavenger) and sodium azide (a singlet oxygen scavenger) can inhibit DNA cleavage by **3**, suggesting involvement of both $^{\cdot}OH$ and $^1O_2$ (Fig. 4). The DNA cleavage can be totally quenched by 10 mM of EDTA (disodium salt; Fig. 4, lane **12**). Our investigation shows that quenching is due to displacement of edda from **3** by EDTA. Visible spectroscopic investigation of the titration of Cu(edda) with EDTA shows formation of $[Cu(EDTA)]^{2-}$ with a λ_{max} of 732 nm (**3** has λ_{max} of 672 nm); also, a white solid recovered from the reaction mixture is shown to be the edda ligand based on its FTIR spectrum. Complete quenching can thus be attributed to absence of the Cu(edda) species **3** and formation of the nucleolytically inactive $[Cu(EDTA)]^{2-}$. As such, the loading dye (6× loading dye solution containing 10 mM Tris–HCl (pH 7.6), 0.03% bromophenol blue, 0.03% xylene cyanol FF, 60% glycerol and 60 mM EDTA) used in our electrophoresis contains sufficient EDTA to quench the DNA reaction mixtures prior to the electrophoresis run on the horizontal gel set.

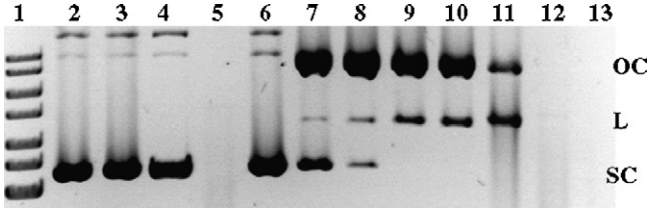

Fig. 3. Electrophoreis results of incubating pBR322 with varying concentration of Cu(edda) with 2 mM H_2O_2. Lane **1**, Gene Ruler 1 kb DNA ladder; lane **2**, DNA alone; lane **3**, DNA + 2 mM Cu(edda); lane **4**, DNA + 2 mM H_2O_2; lane **5**, DNA + 2 mM $CuCl_2$ + 2 mM H_2O_2. Lanes **6**–**13** involve DNA + H_2O_2 + different concentrations of Cu(edda): lane **6**, 10 μM; **7**, 50 μM; **8**, 100 μM; **9**, 200 μM; **10**, 250 μM; **11**, 500 μM; **12**, 1 mM; and lane **13**, 2 mM.

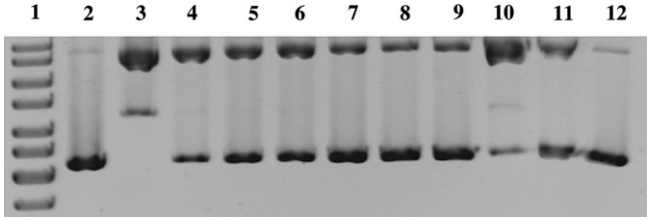

Fig. 4. Effect of radical scavengers on the reaction of DNA with 250 μM Cu(edda) and 2 mM H_2O_2. Lane **1**,Gene Ruler 1 kb DNA ladder; lane **2**, DNA alone; lane **3**, DNA + 250 μM Cu(edda) + 2 mM H_2O_2. Lanes **4**–**9** involve reaction mixtures with increasing concentrations of DMSO: lane **4**, 1 M; lane **5**, 2 M; lane **6**, 3 M; lane **7**, 4 M; lane **8**, 5 M; lane **8**, 7 M; lane **9**, 7 M DMSO. Lanes **10**–**11** involve reaction mixtures with different concentrations of NaN_3: lane **10**, 0.5 M; lane **11**, 2 M. Lane **12**: DNA + Cu(edda) + H_2O_2 + 10 mM EDTA.

The pH of the TN buffer was found to affect the extent of DNA cleavage by **3** in the presence of hydrogen peroxide (Fig. 5). Generally, more alkaline medium (pH 7.0–10.0) of the buffer brings about greater DNA cleavage compared to the acidic medium (pH 6.5). A recent study on the oxidation of quinaldine blue by copper(II)/amino acid/H_2O_2 system also obtained similar findings [12]. Here, the quinaldine blue indicator has been oxidized by hydroxyl radicals whose formation increases as the reaction medium becomes more alkaline.

Besides pH, we found that the type of buffer also affect the nucleolytic efficiency of complex **3**. At pH 7.5, a **3**/H_2O_2 mixture induces significantly more cleavage of DNA in Hepes and phosphate buffers than in TBE and TN buffers (Fig. 6). In a similar study on the interaction of Pd complexes with plasmid DNA in different buffer systems, it was found that the DNA binding efficiency capable of modifying the tertiary structure of pBR322 decreased from $NaClO_4$ to Hepes 2, Hepes 1 [Hepes = 4-(2-hydroxyethyl)-1-piperazineethanesulfonic acid] and Tris[tris(hydroxymethyl)aminomethane] buffers, in this order [26]. Cisplatin has also been found to cause more damage to DNA in Hepes buffer than in Tris buffer at the same concentration

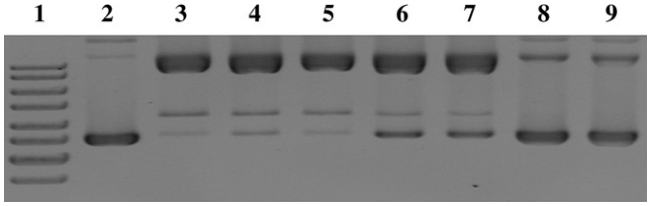

Fig. 5. Effect of pH on incubating pBR322 (0.0125 μg/μL) with 46 μM Cu(edda) and 2 mM H_2O_2 in TN buffers: lane **1**, Gene Ruler 1 kb DNA ladder; lane **2**, DNA alone; lanes **3**–**9** refers to pH 10.0, 9, 8.5, 8.0, 7.5, 7.0 and 6.5, respectively.

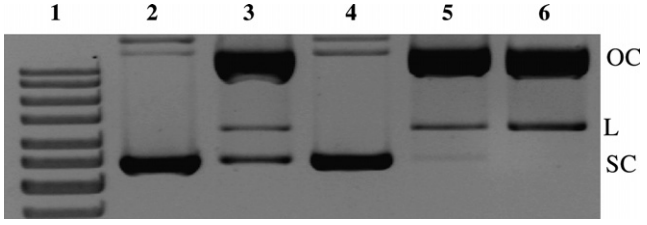

Fig. 6. Effect of type of buffer (at pH 7.5) on DNA cleavage by Cu(edda) (115 μM) in the presence of 2 mM H_2O_2: lane **1**, Gene Ruler 1 kb DNA ladder; lane 2, DNA alone (0.0125 μg/μL); for lanes **3**–**6**, the buffers are TN, 1× TBE, phosphate and Hepes, respectively.

[27]. The lower nucleolytic property of **3** in TBE and TN buffers may be due to the complexing agents in these buffers. TBE buffer contains EDTA, a well known strong chelating agent while both Hepes and TN buffers contains the hepes ligand and Tris, both of which can bind to the complex. The relative nucleolytic efficiency of **3** in TBE, TN and Hepes buffers may be due to the difference in the increasing potential of the buffer system components to bind transition metal complexes that compete with DNA for binding to the metal or hinders binding of the altered complex to the DNA. Nevertheless, the more bulky Hepes may not be able to bind to **3** as **3** has almost the same cleavage efficiency in both phosphate and Hepes buffers (Fig. 6).

In view of the above discussion, we have carried out further spectroscopic studies on complex **3** in TN buffer (which contain 0.1 M Tris component). In TN buffer in the pH range 5.0–7.5, λ_{max} remains quite stable (671–675 nm) and this suggests no change in the coordination sphere of **3**. At lower pH values, an increasing shift of λ_{max} to 728 nm suggests dissociation while at higher pH values, the significant decrease in λ_{max} suggests coordination of Tris (at pH 9, λ_{max} reaches 639 nm). Titration of an aqueous solution of **3** with increasing concentration of Tris (1 mM:0 mM to 1 mM:50 mM) shows initially an unchanged $\lambda_{max} \sim 672$ nm (up to 1:2 mole ratio of complex to Tris) and then a progressive decrease in λ_{max} to 629 nm. Thus, some complexation of Tris to Cu in complex **3** in our studies can occur in TN buffer above pH 7.5. Complex **3** is stable in TN buffer, pH 7.5, and there is no or minimal complexation of Tris. For the validity of the study on the dependence of the nucleolytic efficiency on the concentration of the complex, a plot of the absorbance at 672 nm against concentration (0.05–2 mM) in TN buffer, pH 7.5, gives a straight line with a good linearity factor of $R^2 = 0.9991$.

Additionally, we have compared the oxidative cleavage of DNA by **3** with two *bis*(aminoacidato)copper(II) complexes and $[Fe(EDTA)]^{2-}$ in TN buffer at pH 7.5 (Fig. 7). At complex concentrations of 100 and 500 μM, the *cis*-$Cu(gly)_2$ and $Cu(dmg)_2$ show distinctly superior nucleolytic ability than both **3** and $[Fe(EDTA)]^{2-}$. For example, 500 μM of the former two complexes totally degraded the DNA while the latter two at the same concentration merely converted the supercoiled DNA into nicked and linear DNA. In contrast to $[Cu(EDTA)]^{2-}$, $[Fe(EDTA)]^{2-}$ still can cleave DNA in the presence of hydrogen peroxide.

To elucidate the cause of the above differences in nucleolytic efficiency, a known hydroxyl radical assay has been used [12]. In *p*-nitrosodimethylaniline (PNDA) assay, it has been established that the production of ·OH radicals can be monitored by measuring the strong absorption peak of PNDA at 440 nm [12]. The percentage bleaching of PNDA corresponds to the formation of ·OH radicals as the molar ratio of PNDA: ·OH is 1:1. Our results show that the bleaching ability of both *cis*-$Cu(gly)_2$ and $Cu(dmg)_2$ is about twice that of **3**, and therefore their greater nucleolytic efficiency is the result of a higher production of ·OH (Fig. 8). As far as we know, this is the first instance whereby the oxidative-nucleolytic efficiency of such metal complexes has been correlated with the amount of hydroxyl radicals produced. An earlier study on the coordination-structural factors affecting similar oxidative damage of DNA by a series of copper(II) complexes does not show such a correlation as the trend of production of hydroxyl radical decreases in this order $Cu(HTCD)^{2+} \sim Cu(Im)_4Cl_2 > Cu(IDB)(NO_3)_2 > Cu(IDB)Cl_2 > Cu(IDBt)Cl_2$ while the order of decreasing DNA damage capacity is $Cu(Im)_4Cl_2 \sim Cu(IDB)(NO_3)_2 > Cu(HTCD)^{2+} > Cu(IDBt)Cl_2 > Cu(IDB)Cl_2$ [28].

Lastly, we have compared the nucleolytic property of the M(edda) complexes with their corresponding MCl_2 salts to elucidate the role of the edda anionic ligand. The results (Fig. 9) clearly show that edda upon complexation to the metal(II) ion inhibits DNA cleavage. How this inhibition comes about is now under investigation. Both the copper(II) ion and the Cu(edda) complex can cleave DNA better than the other metal(II) ions and their M(edda) complexes. The Cu(edda) complex may still undergo similar reactions as those proposed for the Cu(II) ion with hydrogen peroxide, as shown in the following equations, to yield the ROS responsible for the DNA cleavage [29,30].

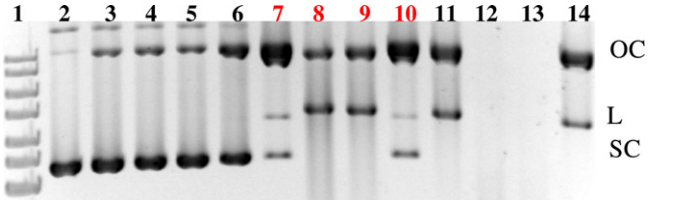

Fig. 7. Comparison of the nucleolytic properties of different copper(II) amino acid complexes and $[Fe(edta)]^{2-}$. Incubating pBR322 (0.0125 μg/μL) with the specified concentration of complexes with 2 mM H_2O_2: Lane **1**, Gene Ruler 1 kb DNA ladder; lane **2**, DNA alone; lanes **3**–**6** involve 10 μM of Cu(edda), *cis*-$Cu(gly)_2$, $Cu(dmg)_2$ and $[Fe(EDTA)]^{2-}$, respectively; lanes **7**–**10** involve 100 μM of Cu(edda), *cis*-$Cu(gly)_2$, $Cu(dmg)_2$ and $[Fe(EDTA)]^{2-}$, respectively; lanes **11**–**14** involve 500 μM of Cu(edda), *cis*-$Cu(gly)_2$, $Cu(dmg)_2$ and $[Fe(EDTA)]^{2-}$, respectively.

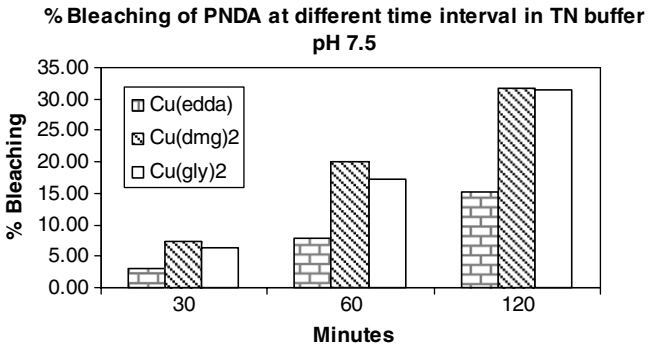

Fig. 8. The relative production of hydroxyl radicals by reaction of the copper(II) complexes with hydrogen peroxide in TN buffer at pH 7.5 as shown by the % bleaching of PNDA.

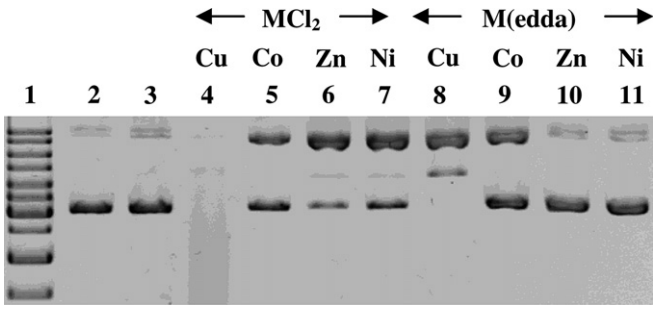

Fig. 9. Comparison of the nucleolytic properties of metal(II) ions with their corresponding M(edda) complexes. Incubating pBR322 with 500 μM of metal(II) salt or M(edda) complex with 2 mM H_2O_2. Lane **1**, Gene Ruler 1 kb DNA ladder; lane **2**, DNA alone; lane **3**, DNA + H_2O_2 alone; lanes **4**–**7** involve $CuCl_2$, $CoCl_2$, $ZnCl_2$ and $NiCl_2$; and lanes **8**–**11** involve Cu(edda), Co(edda), Zn(edda) and Ni(edda), respectively.

$$Cu^{II}(edda) + H_2O_2 \rightarrow [Cu^{I}(edda)]^- + O_2^{\cdot-} + 2H^+ \quad (1)$$

$$[Cu^{I}(edda)]^- + O_2 \rightarrow Cu^{II}(edda) + O_2^{\cdot-} \quad (2)$$

$$Cu^{II}(edda) + O_2^{\cdot-} \rightarrow [Cu^{I}(edda)]^- + O_2 \quad (3)$$

$$[Cu^{I}(edda)]^- + H_2O_2 \rightarrow Cu^{II}(edda) + {}^{\cdot}OH + OH^- \quad (4)$$

$$O_2^{\cdot-} + Cu^{II}(edda) \rightarrow {}^1O_2 + [Cu^{I}(edda)]^- \quad (5)$$

3.3. ESI-MS and CD studies on interaction of 3 with d(5′-CGCGAATTCGCG-3′)

Heating 200 μM of 12-*mer* oligonucleotide to 20 °C above its melting temperature and cooling it slowly to room temperature successfully converted it to ds(12-*mer*) which has a relative molecular mass, M_{ds}, of 3646.4. This is evidenced by a most intense negative ion ESI-MS peak of 1827.0 attributed to $[ds(DNA) + Na]^{4-}$ (calculated value, 1827.7). No *m*/*z* peak for the single strand 12-*mer* or its abducts with Na or K at negative charges of −1 to −11 can be found. An ESI-MS of a freshly prepared solution of 1:1 ratio of **3** and ds(12-*mer*) in 0.1 M ammonium acetate shows *m*/*z* peaks of 1828.3 (100%), 1887.8 (16%) and 1896.2 (33%) which are attributed to negative ions of $[ds(12\text{-}mer) + Na]^{4-}$ (calculated *m*/*z*, 1827.7), $[ds(12\text{-}mer) + Cu(edda) + Na]^{4-}$ (calculated *m*/*z*, 1887.1) and $[ds(12\text{-}mer) + [Cu(edda)(H_2O)_2] + Na]^{4-}$ (calculated *m*/*z* 1896.1), respectively.

The ds(12-*mer*) in phosphate buffer at pH 7.5 has B-form conformation, as shown by its CD spectrum which has a negative band at 247 nm and a positive band at 280 nm (Fig. 10). The CD spectrum of a freshly prepared mixture of 1:1 molar ratio of ds(12-*mer*) (3.425 μM) and Cu(edda) (3.425 μM) shows a decrease in the negative band of ds(12-*mer*) and an enhancement of the positive band of ds(12-*mer*). This change in the CD spectrum is similarly observed in the binding of antitumor trinuclear platinum complexes to B-DNA (Calf Thymus) at relatively low r_b values (<0.05) and it was ascribed to occurrence of short single-stranded segments containing unpaired bases (denatured regions) [31]. Thus, a similar non-denaturational conformational change may be induced by **3** on binding to ds(12-*mer*). Ni(edda), **2**, and Zn(edda), **4**, can induce a similar conformation change whereas Co(edda), **1**, has practically no effect on the CD of ds(12-*mer*).

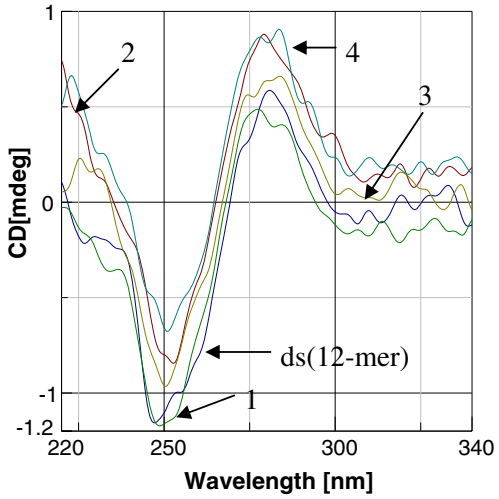

Fig. 10. CD spectra of ds(12-*mer*) alone and its modification by M(edda) complexes. The DNA and the complexes were dissolved in phosphate buffer at pH 7.5 (10 μM $Na_2HPO_4 \cdot 2H_2O$ and 10 μM $NaH_2PO_4 \cdot 2H_2O$). Ratio of DNA:complex is 1:1 with each species at a concentration of 3.425 μM. CD spectra of DNA modified by complexes: curve 1, Co(edda); curve 2, Ni(edda); curve 3, Cu(edda); curve 4, Zn(edda).

4. Conclusion

It seems that the copper(II) complex of *N*,*N*′-ethylene-bridged *bis*(amino acid), edda, is a poorer nucleolytic agent compared to the corresponding unbridged *bis*(aminoacidato)copper(II). This probably arises from the greater inhibitory effect of the tetradentate edda upon the nucleolytic property of the copper(II) ion compared to the unbridged bidentate amino acidate ligands. Comparison of nucleolytic efficiency of metal complexes should be made with care as various factors can affect it. For example, the component of the buffer system used can act as complexing agent and thus alter the property of the metal complex under investigation. The extent of DNA cleavage by the M(edda) and other metal(II) complexes in the presence of hydrogen peroxide can be predicted by or correlated with the total production of ·OH radicals produced. In this study, the binding of the some of the complexes to DNA seems to cause localized unwinding of the DNA at the binding sites.

5. Supplementary data

Detailed crystallographic data for the crystal structure analysis have been deposited with the Cambridge Crystallographic Data Center, CCDC 294380. Copies of this information can be obtained free of charge from The Director, CCDC, 12 Union Road, Cambridge, CB2 1EZ,

UK (fax: +44 1223 336 033; e-mail: deposit@ccdc.cam.ac.uk or www: http://www.ccdc.cam.ac.uk).

Acknowledgments

This project is funded by a SAGA research grant from the Malaysian Academy of Science and the Ministry of Science, Technology and Inovation of Malaysia (C/4/02). We also like to acknowledge and thank the Chemistry Department of Malaysia in Kuala Lumpur for the use of the ESI-MS, and our respective universities.

References

[1] J.A. McCleverty, T.J. Meyer (Eds.), Comprehensive Coordination Chemistry II, vol. 9, Elsevier, United Kingdom, 2003, ch. 18.
[2] M. Chikira, M. Inoue, R. Nagane, W. Harada, H. Shindo, J. Inorg. Biochem. 66 (1997) 131.
[3] C.H. Ng, H.K. Alan Ong, C.W. Kong, K.K. Su, S.W. Ng, J. Coord. Chem. (2006), advance article online.
[4] A. Barzilai, K.-I. Yamamoto, DNA Repair 3 (2004) 1109.
[5] R. Ren, P. Yang, W.-J. Zheng, Z.-C. Hua, Inorg. Chem. 39 (2000) 5454.
[6] J. Torres, M. Brusoni, F. Peluffo, C. Kremer, S. Dominguez, A. Mederos, E. Kremer, Inorg. Chim. Acta 358 (2005) 3320.
[7] B.M. Katz, V.I. Stenberg, Polyhedron 4 (1985) 2031.
[8] R. Wen, I. Bernal, F. Somoza, W.-J. Li, F.R. Fronczek, Inorg. Chim. Acta 282 (1998) 96.
[9] C.H. Ng, S.B. Teo, S.G. Teoh, H.K. Fun, J.-P. Declercq, Inorg. Chim. Acta 340 (2002) 81.
[10] K.A. Deal, J.N. Burstyn, Inorg. Chem. 35 (1996) 2792.
[11] H.H. Yu, X.G. Liu, R.E. Xing, S. Liu, Z.Y. Guo, P.B. Wang, C.P. Li, P.C. Li, Food Chemistry 95 (2006) 123.
[12] T.-Y. Lin, C.-H. Wu, J. Mol. Catal. 232 (2005) 117.
[13] S. Neidle, Nat. Prod. Rep. 18 (2001) 291.
[14] H.C. Freeman, M.R. Snow, I. Nitta, K. Tomita, Acta Crystallogr. 17 (1964) 1463.
[15] G.M. Sheldrick, SHELX-97, Programs for Crystal Structure Analysis (Release 97-2), Göttingen University, Germany, 1997.
[16] L.J. Farrugia, Ortep-3 for Windows, J. Appl. Cryst. 30 (1997) 565.
[17] J.L. Beck, R. Gupta, T. Urathamakul, N.L. Williamson, M.M. Sheil, J.R. Aldrich- Wright, S.F. Ralph, Chem. Commun. (2003) 626.
[18] S.F. Ralph, private communication.
[19] K. Kurdziel, T. Głowiak, Polyhedron 19 (2000) 2183.
[20] B. Barszcz, S.A. Hodorowicz, K. Stadnicka, A. Jabłońska-Wawrzycka, Polyhedron 24 (2005) 627.
[21] S. Sharma, F. Athar, M.R. Maurya, F. Naqvi, A. Azam, Eur. J. Med. Chem. 40 (2005) 557.
[22] C.H. Ng, M.L. Chia, Poon Hui, unpublished data.
[23] E.L. Hegg, J.N. Burstyn, Coord. Chem. Rev. 173 (1998) 133.
[24] J.A. Cowan, Curr. Opin. Chem. Biol. 5 (2001) 634.
[25] S.I. Kirin, C.M. Happel, S. Hrubanova, T. Weyhermuller, C. Klein, N. Metzler-Nolte, J. Chem. Soc., Dalton Trans. (2004) 1201.
[26] K. Akdi, R.A. Vilaplana, S. Kamah, F. González-Vílchez, J. Inorg. Biochem. 99 (2005) 1360.
[27] V. Murray, J. Whittaker, M.D. Temple, W.D. McFadye, Biochim. Biophys. Acta 1354 (1997) 261.
[28] C. Liu, J. Zhou, Q. Li, L. Wang, Z. Liao, H. Xu, J. Inorg. Biochem. 75 (1999) 233.
[29] Y. Kato, N. Kitamoto, Y. Kawai, T. Osawa, Free Radic. Biol. Med. 31 (2001) 624.
[30] J.-L. Yang, L.-C. Wang, C.-Y. Chang, T.-Y. Liu, Environ. Mol. Mutagen. 33 (1999) 194.
[31] J. Kasparkova, O. Vrana, N. Farrell, V. Brabec, J. Inorg. Biochem. 98 (2004) 1560.

We have determined the kinetic parameters and the reaction mechanism of the process to be:

$$[W_2S_4(\text{di-}i\text{-propyldtc})_2B_2]\ (\text{solid}) \rightarrow [W_2S_4((\text{di-}i\text{-propyldtc}))_2]\ (\text{solid}) + 2B\ (\text{gas})$$

and we have determined the activation energy and the pre-exponential Arrhenius factor for all the adducts synthesized, using a new non-isothermal kinetic method, reported previously by us.

The determination of kinetic parameters by non-isothermal methods offers interesting advantages over conventional isothermal studies [19–26]. Only a single sample and fewer data are required and the kinetics can be calculated over an entire temperature range in a continuous manner.

A disadvantage of the non-isothermal methods, when are compared with the isothermal techniques, is that the reaction mechanism cannot usually be determined, and hence the meaning of the kinetics parameters is uncertain. However, with the new proposed method, the reaction mechanism can be determined [27–29].

A comparison between activation energies (E_a), steric or inductive factors, infrared and electronic spectral data and pK_b values of the coordinated bases has also been explored.

2. Experimental

2.1. Synthesis

[W_2S_4(*di-i-propyldtc*)$_2$]: Prepared as previously reported [15].

[W_2S_4(*di-i-propyldtc*)$_2B_2$]: 0.01 mol of [W_2S_4(di-*i*-propyldtc)$_2$] was dissolved in 0.02 mol of the organic base (pyridine, 3-methyl, 4-methyl and 3,5-dimethylpyridine) or in an ethanolic solution of 0.02 mol of 3-amino and 4-aminopyridine and heated in a water bath for about 15 min. After cooling for 2 days, the adducts, obtained as brownish powders, were separated by filtration *in vacuo* and dried over P_4O_{10} in a nitrogen atmosphere.

[$W_2S_4(C_7H_{14}NS_2)_2(C_5H_5N)_2$]. Anal. Calc.: W, 36.58; C, 28.62; N, 5.56; H, 3.77; S, 25.44. Found: W, 36.92; C, 29.01; N, 5.66; H, 3.81; S, 25.39%. $\mu = 0.03$ B.M.

[$W_2S_4(C_7H_{14}NS_2)_2(C_5H_4N,3\text{-}CH_3)_2$]. Anal. Calc.: W, 35.58; C, 30.17; N, 5.41; H, 4.06; S, 24.75. Found: W, 35.61; C, 30.00; N, 5.92; H, 3.85; S, 24.64%. $\mu = 0.00$ B.M.

[$W_2S_4(C_7H_{14}NS_2)_2(C_5H_4N,4\text{-}CH_3)_2$]. Anal. Calc.: W, 35.58; C, 30.17; N, 5.41; H, 4.06; S, 24.75. Found: W, 35.44; C, 29.87; N, 5.32; H, 4.12; S, 24.52%. $\mu = 0.07$ B.M.

[$W_2S_4(C_7H_{14}NS_2)_2[C_5H_3N(CH_3)_2]_2$]. Anal. Calc.: W, 34.65; C, 31.63; N, 5.27; H, 4.33; S, 24.10. Found: W, 34.81; C, 31.27; N, 5.18; H, 4.51; S, 24.00%. $\mu = 0.10$ B.M.

[$W_2S_4(C_7H_{14}NS_2)_2(C_5H_4N,3\text{-}NH_2)_2$]. Anal. Calc.: W, 35.52; C, 27.79; N, 8.10; H, 3.86; S, 24.71. Found: W, 35.77; C, 27.80; N, 8.74; H, 3.91; S, 24.53%. $\mu = 0.05$ B.M.

[$W_2S_4(C_7H_{14}NS_2)_2(C_5H_4N,4\text{-}NH_2)_2$]. Anal. Calc.: W, 35.52; C, 27.79; N, 8.10; H, 3.86; S, 24.71. Found: W, 35.66; C, 27.50; N, 7.87; H, 3.74; S, 24.78%. $\mu = 0.03$ B.M.

3. Instrumentation

Elemental analyses were performed in a Perkin–Elmer 240 B elemental analyzer. Tungsten was determined by Atomic Absorption with a Perkin–Elmer 430 Atomic Absorption spectrophotometer, after decomposing the complexes with a 1:1 mixture of concentrated nitric and sulfuric acid. Magnetic susceptibility determinations were performed at room temperature on a Mettler H-51 AR balance and a type C Newport electromagnet. Reported magnetic moments are corrected for ligand diamagnetism. Infrared spectra were measured on a Perkin–Elmer 283 spectrophotometer. Visible–near UV spectra of the compounds were measured on a Beckman DU7 spectrophotometer, using complex solutions in DMSO. Thermogravimetric analysis and differential scanning calorimetry, were performed between 25 and 600 °C on a Mettler TA 3000 system fitted with a Mettler TG-50 thermobalance and a Mettler DSC-20 differential scanning calorimeter. The scanning rate used was 2 °C min^{-1} and samples of about 5 mg, as a very fine powder, were used, so as to render insignificant the temperature non-uniformity within the sample. An aluminium pan was used under a dynamic nitrogen atmosphere. The instrument calibration was checked periodically with standard samples of indium (99.99 % purity). Several runs were made.

3.1. Kinetic studies

The rate of a thermal decomposition reaction of a solid can be expressed by the Arrhenius equation:

$$d\alpha/dt = Ae^{-E_a/RT} f(\alpha) \quad (1)$$

In Eq. (1), α is the fraction of material which has reacted at time t, E_a is the activation energy, $f(\alpha)$ is a function which depends on the actual reaction mechanism and A is the pre-exponential Arrhenius factor.

We have collected in Table 1 the mathematical expressions of the functions $f(\alpha)$ corresponding to some of the thermal decomposition mechanisms found in the literature [19].

When the temperature of the sample is increased at a constant rate, we can write Eq. (2), where β is the heating rate, dT/dt:

$$d\alpha/dT = \alpha' = (A/\beta)e^{-E_a/RT} f(\alpha) \quad (2)$$

By differentiating the logarithmic form of Eq. (2) with respect to $d\ln(1-\alpha)$, we obtain the following equation:

$$\begin{aligned} d\ln\alpha'/d\ln(1-\alpha) &= -(E_a/R)[d(1/T)/d\ln(1-\alpha)] \\ &\quad + [d\ln f(\alpha)/d\ln(1-\alpha)] \quad \text{or} \\ \Delta\ln\alpha'/\Delta\ln(1-\alpha) &= -(E_a/R)[\Delta(1/T)/\Delta\ln(1-\alpha)] \\ &\quad + [\Delta\ln f(\alpha)/\Delta\ln(1-\alpha)] \quad \text{and} \\ [\Delta\ln\alpha' - \Delta\ln f(\alpha)]/\Delta\ln(1-\alpha) &= -(E_a/R)[\Delta(1/T)/\Delta\ln(1-\alpha)] \end{aligned} \quad (3)$$

Table 1
Kinetic equations

Mechanism (rate-controlling process)	$f(\alpha)$
D1 (one-dimensional diffusion)	$(1/2\alpha)$
D2 (two-dimensional diffusion)	$[-\ln(1-\alpha)]^{-1}$
D3 (three-dimensional diffusion: Jander equation)	$(3/2)(1-\alpha)^{2/3}[1-(1-\alpha)^{1/3}]^{-1}$
D4 (three-dimensional diffusion: Ginstling–Brounshtein equation)	$(3/2)[(1-\alpha)^{-1/3}-1]^{-1}$
F1 (random nucleation)	$(1-\alpha)$
R2 (phase-boundary reaction: cylindrical symmetry)	$2(1-\alpha)^{1/2}$
R3 (phase-boundary reaction: spherical symmetry)	$3(1-\alpha)^{2/3}$

Thus, the plots of $[\Delta\ln\alpha' - \Delta\ln f(\alpha)]/\Delta\ln(1-\alpha)$ versus $[\Delta(1/T)/\Delta\ln(1-\alpha)]$ should be a straight line with a slope $-E_a/R$, irrespective of the $f(\alpha)$ employed. However, we can select the $f(\alpha)$ that best fits the actual reaction mechanism studied, by means of the intercept value, which in an ideal agreement with Eq. (3) should be zero.

In order to test the validity of the above conclusions we have substituted the seven forms of $f(\alpha)$ into the Arrhenius equation in the logarithmic form (2), giving the following equation:

$$\ln\alpha' = \ln(A/\beta) - E_a/RT + \ln f(\alpha) \quad \text{or}$$
$$\ln\alpha' - \ln f(\alpha) = \ln(A/\beta) - E_a/RT \qquad (4)$$

The plot of $\ln\alpha' - \ln f(\alpha)$ versus $1/T$ should be a straight line with a slope $-E_a/R$ and intercept $\ln(A/\beta)$.

If the suggested mechanism is correct, the activation energy value should be the same as the value previously obtained.

4. Discussion

4.1. Magnetic susceptibility

All the complexes studied present very low values for the magnetic moments (0.10–0.00 B.M.), as occurs in similar W(V) complexes [12–18], which can be attributed to an interaction through the bridge atoms, or to the possible formation of a direct metal–metal bond, as has been proved for similar molybdenum(V) oxo-complexes [30–32].

4.2. Infrared spectra

The IR spectra show, in all cases, a band in the range 552–507 cm^{-1}, which we attribute to the vibration of the terminal W=S bond. If we compare the complex $[W_2S_4$(di-*i*-propyldtc$)_2]$ with the adducts $[W_2S_4$(di-*i*-propyldtc$)_2B_2]$, one observes that the adducts show the W=S band displaced to lower frequencies (539–507 cm^{-1}) than the complex (552–545 cm^{-1}). This displacement can be attributed to the different basicity of the pyridine or substituted pyridine employed [33,34]. The pK_b value reflects the basicity of the ligand towards the proton. It may be assumed that the pK_b of the ligand provides a measure of the ligand ability to form σ-bonds to metal ions. In general (see Table 2), the greater the basicity the lower the frequency of the W=S vibration.

The IR spectra of the adducts exhibit a band over 348–333 cm^{-1}, which is assigned to the stretching vibration of the W–N(base) bond [35–37]. The frequencies of this band listed in decreasing order are:

$[W_2S_4$(di-*i*-propyldtc$)_2$(4-AP$)_2]$
$> [W_2S_4$(di-*i*-propyldtc$)_2$(3-AP$)_2]$
$> [W_2S_4$(di-*i*-propyldtc$)_2$(3, 5-DMP$)_2]$
$> [W_2S_4$(di-*i*-propyldtc$)_2$(3-MP$)_2]$
$> [W_2S_4$(di-*i*-propyldtc$)_2$(4-MP$)_2]$
$> [W_2S_4$(di-*i*-propyldtc$)_2$Py$_2]$.

These differences can be attributed to the electronic donation of the pyridine or substituted pyridine to the tungsten (N → W) which increases the electron density on the metal d-orbitals and consequently the $p_\pi \rightarrow d_\pi$ donation from the sulfur atom to tungsten is expected to be reduced to an extent which depends of the base donor ability. As a result there will be a lowering of the W=S bond [hence ν(W=S)] and a greater frequency of the W–N bond.

We assign the bands corresponding to W–S–W bridge, which appear over 460 and 365 cm^{-1}, to the antisymmetric and symmetric stretching mode, respectively.

The IR spectra of these complexes show the C–N and C–S vibrations over 1515 and 1090 cm^{-1}. The displacement to greater frequencies for the C–N band and to lower frequencies for the C–S band, in comparison with the sodium dithiocarbamate, are indicative of bidentate ligands.

Table 2
Infrared absorption maxima, in cm^{-1}, of tungsten(V) thiocomplexes

Compound	νW=S	ν_aW–S$_b$	ν_sW–S$_b$	νC–N	νC–S	νW–N
$[W_2S_4$(di-*i*-propyldtc$)_2]$	552–545	461	363	1518	1090	
$[W_2S_4$(di-*i*-propyldtc$)_2$(Py$)_2]$	539	458	361	1515	1093	333
$[W_2S_4$(di-*i*-propyldtc$)_2$(3-MP$)_2]$	532	462	360	1513	1094	338
$[W_2S_4$(di-*i*-propyldtc$)_2$(4-MP$)_2]$	535	457	364	1517	1087	334
$[W_2S_4$(di-*i*-propyldtc$)_2$(3,5DMP$)_2]$	521	460	365	1514	1089	343
$[W_2S_4$(di-*i*-propyldtc$)_2$(3-AP$)_2]$	513	462	367	1513	1091	343
$[W_2S_4$(di-*i*-propyldtc$)_2$(4-AP$)_2]$	507	459	368	1512	1083	348

4.3. Visible and ultraviolet spectra

The electronic spectra of the compounds obtained is in accordance with the Ballhausen–Gray and Gray–Hare schemes [38,39] with a square pyramidal structure for the complex and a distorted octahedral structure for the adducts.

Table 3
Electronic absorption spectra of tungsten(V) thiocomplexes

Compound	ν (cm^{-1})	ε ($M^{-1}.cm^{-1}$)	Transition
$[W_2S_4(di\text{-}i\text{-}propyldtc)_2]$	16993	213	$^2B_2 \rightarrow {}^2B_1$
	20422	2840	charge transfer
	21775	4828	charge transfer
	26467	8853	charge transfer
	28990	13048	$n \rightarrow n^*$
	33658	20404	$\pi \rightarrow \pi^*$
	36088	31412	$n \rightarrow \sigma^*$
$[W_2S_4(di\text{-}i\text{-}propyldtc)_2(Py)_2]$	17547	117	$^2B_2 \rightarrow {}^2B_1$
	20658	2654	charge transfer
	22315	3672	charge transfer
	26587	8143	charge transfer
	30457	21125	$n \rightarrow n^*$
	31989	14995	$\pi \rightarrow \pi^*$
	34785	34114	$n \rightarrow \sigma^*$
$[W_2S_4(di\text{-}i\text{-}propyldtc)_2(3\text{-}MP)_2]$	17555	198	$^2B_2 \rightarrow {}^2B_1$
	20508	3204	charge transfer
	21825	4654	charge transfer
	26602	7601	charge transfer
	30132	14419	$n \rightarrow n^*$
	32256	22623	$\pi \rightarrow \pi^*$
	35598	47989	$n \rightarrow \sigma^*$
$[W_2S_4(di\text{-}i\text{-}propyldtc)_2(4\text{-}MP)_2]$	17325	131	$^2B_2 \rightarrow {}^2B_1$
	20232	3125	charge transfer
	21878	4125	charge transfer
	26119	6319	charge transfer
	30358	16985	$n \rightarrow n^*$
	31983	19657	$\pi \rightarrow \pi^*$
	36021	39568	$n \rightarrow \sigma^*$
$[W_2S_4(di\text{-}i\text{-}propyldtc)_2(3,5DMP)_2]$	17702	216	$^2B_2 \rightarrow {}^2B_1$
	21989	2154	charge transfer
	21358	3125	charge transfer
	26596	7893	charge transfer
	39930	16489	$n \rightarrow n^*$
	32301	22531	$\pi \rightarrow \pi^*$
	34995	35106	$n \rightarrow \sigma^*$
$[W_2S_4(di\text{-}i\text{-}propyldtc)_2(3\text{-}AP)_2]$	17959	229	$^2B_2 \rightarrow {}^2B_1$
	20186	2435	charge transfer
	21987	4023	charge transfer
	26668	7003	charge transfer
	30129	14206	$n \rightarrow n^*$
	31657	19293	$\pi \rightarrow \pi^*$
	35369	31136	$n \rightarrow \sigma^*$
$[W_2S_4(di\text{-}i\text{-}propyldtc)_2(4\text{-}AP)_2]$	18458	376	$^2B_2 \rightarrow {}^2B_1$
	19961	2023	charge transfer
	22153	3951	charge transfer
	26354	6302	charge transfer
	30096	13483	$n \rightarrow n^*$
	32627	21969	$\pi \rightarrow \pi^*$
	35250	33364	$n \rightarrow \sigma^*$

The electronic spectra for all the complexes present a band in the 18500–16900 cm^{-1} region, which can be assigned to a $^2B_2 \rightarrow {}^2B_1$ transition. This band shows the greater or lesser bonding force from the tungsten to the ligand. Therefore the band is displaced to higher frequencies in the adducts, because the introduction of the base in the six-coordination position and the "*trans*" effect strengthen the ligand–tungsten σ-bond, as we have observed in the IR spectra (see Table 3).

In the visible zone we can detect three other bands over 20000, 22000 and 26500 cm^{-1} that we attribute to charge transfer transitions. The band which appears over 22000 cm^{-1} can be attributed to a $S^{2-} \rightarrow W(V)$ charge transfer, as has been observed in others transition metal complexes with a sulfur bridge [40,41].

In the ultraviolet zone, three transitions are detected over 30000, 32000 and 35000 cm^{-1}, attributable to intraligand transitions like $n \rightarrow n^*$, $\pi \rightarrow \pi^*$ and $n \rightarrow \sigma^*$, respectively.

4.4. DSC, TGA and kinetic studies

On the DSC curves of all the compounds, a first endothermic peak can be appreciated. The mass loss accompanying this transition corresponds on the TG curves to the loss of two moles of coordinated base to tungsten atoms, the residue being $[W_2S_4(di\text{-}i\text{-}propyldtc)_2]$ in all cases.

Table 4
ΔH, α, T and α' obtained from the DSC curve for the complex $[W_2S_4(di\text{-}i\text{-}propyldtc)_2Py_2]$

ΔH (mJ)	α	T (°C)	α' (K^{-1})
144.91	0.08045	121.0	0.01111
205.28	0.11396	123.0	0.01398
257.84	0.14314	125.0	0.01758
319.89	0.17759	127.0	0.02260
399.19	0.22161	129.0	0.02641
494.20	0.27436	131.0	0.03194
604.32	0.33549	133.0	0.03733
737.04	0.40917	135.0	0.04344
887.00	0.49242	137.0	0.04918
1062.37	0.58978	139.0	0.05349
1252.43	0.69529	141.0	0.05206
1453.74	0.80705	143.0	0.04056
1628.18	0.90389	145.0	0.02174

Table 5
Results obtained by using the seven mechanisms for the plot of $[\Delta \ln \alpha' - \Delta \ln f(\alpha)]/\Delta \ln(1-\alpha)]$ vs. $[\Delta(1/T)/\Delta \ln(1-\alpha)]$ for the complex $[W_2S_4(di\text{-}i\text{-}propyldtc)_2Py_2]$

Mechanism	r	m	i	E_a (kJ mol^{-1})
D1	−0.99761	−36837.84	0.64519	294 ± 3
D2	−0.99762	−37014.92	0.34992	295 ± 4
D3	−0.99762	−36924.59	−0.16012	295 ± 4
D4	−0.99762	−36924.63	0.18125	295 ± 4
F1	−0.99984	−17323.45	−0.44752	137 ± 3
R2	−0.99999	−17323.45	0.00592	137 ± 2
R3	−0.99987	−17323.45	−0.16253	137 ± 3

Table 6
Thermal and kinetic parameters for the complexes W_2S_4(di-*i*-propyldtc)$_2B_2$

Compound	Mechanism	ΔH (kJ mol^{-1})	E_a (kJ mol^{-1})	A (s^{-1})	pK_b
[W_2S_4(di-*i*-propyldtc)$_2$(Py)$_2$]	R2	21.7 ± 0.3	137 ± 3	$(3.3 \pm 0.2) \times 10^{13}$	8.87
[W_2S_4(di-*i*-propyldtc)$_2$(3-MP)$_2$]	R2	26.5 ± 0.4	162 ± 2	$(3.4 \pm 0.1) \times 10^{20}$	8.32
[W_2S_4(di-*i*-propyldtc)$_2$(4-MP)$_2$]	R2	25.0 ± 0.3	154 ± 1	$(6.8 \pm 0.3) \times 10^{9}$	7.98
[W_2S_4(di-*i*-propyldtc)$_2$(3,5DMP)$_2$]	R2	34.6 ± 0.7	187 ± 2	$(1.2 \pm 0.1) \times 10^{27}$	7.85
[W_2S_4(di-*i*-propyldtc)$_2$(3-AP)$_2$]	R2	40.1 ± 0.3	203 ± 1	$(7.5 \pm 0.3) \times 10^{32}$	7.49
[W_2S_4(di-*i*-propyldtc)$_2$(4-AP)$_2$]	R2	31.3 ± 0.9	257 ± 3	$(2.5 \pm 0.2) \times 10^{27}$	4.88

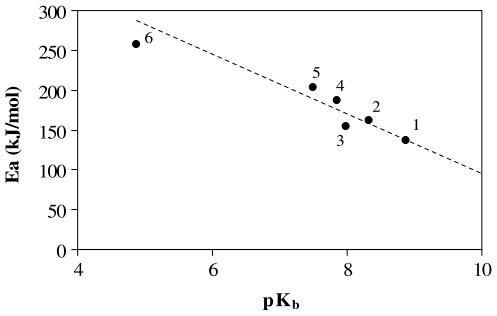

Fig. 1. Activation energy for decomposition of [W_2S_4(di-*i*-propyldtc)$_2B_2$] complexes vs. pK_b. Points 1–6 correspond to complexes with Py, 3-MP, 4-MP, 3,5-DMP, 3-AP and 4-AP, respectively.

Table 4 shows the data obtained from the DSC curve of the adduct [W_2S_4(di-*i*-propyldtc)$_2$Py$_2$], α being the reacted fraction at time t and $\alpha' = d\alpha/dT$.

We have plotted $[\Delta \ln \alpha' - \Delta \ln f(\alpha)]/\Delta \ln(1-\alpha)]$ versus $[\Delta(1/T)/\Delta \ln(1-\alpha)]$. From these representations, we can calculate the activation energy of the process. Table 5 shows the results for r (correlation coefficient), m (slope), i (intercept value) and E_a (activation energy) obtained for the seven mechanisms.

We can observe that in all cases the correlation coefficients (r) are very near to unity, consistent with the results of Criado [42]. Nevertheless, only when the analysis was performed with the mechanism R2 does the straight line present an intercept value (i) close to zero.

Therefore, according with our proposed method, we deduce that the thermal decomposition of the complex [W_2S_4(di-*i*-propyldtc)$_2$Py$_2$] and the loss of pyridine, is carry out by a R2 mechanism (Phase boundary reaction: cylindrical symmetry) with a function $f(\alpha) = 2(1-\alpha)^{1/2}$, an activation energy $E_a = 137 \pm 3$ kJ mol^{-1} and a pre-exponential Arrhenius factor $A = (3.3 \pm 0.2) \times 10^{13}$ s^{-1}.

The results obtained for the compounds studied, are listed in Table 6.

We can assume that the thermal decomposition and loss of coordinated base of the adducts with pyridine, 3-methylpyridine, 4-methylpyridine, 3,5-dimethylpyridine, 3-aminopyridine and 4-aminopyridine follows a R2 mechanism.

If we compare the results, in general, as can be seen from the data in Table 6, the greater the basicity of the base employed, the higher the activation energy and the pre-exponential Arrhenius factor for the process of the loss of the base. The outstanding exception is the 4-MP and 4-AP adducts, which can be attributed to the existence of resonance structures and a pronounced effect on the stability of the complex [29,33,34]. It can be seen that the steric impediment of 3,5-DMP, does not modify the kinetic parameters.

The plot of pK_b versus activation energy presented in Fig. 1, shows that, except for the 4-AP adduct, a very satisfactory correlation was obtained. It is obvious from this figure that the activation energy is linearly related to the basicity of the ligands.

References

[1] E.I. Stiefel, Prog. Inorg. Chem. 1 (1977) 22.
[2] B.K. Burgess, D.B. Jacobs, E.I. Stiefel, Biochim. Biophys. Acta Enzymol. 614 (1980) 196.
[3] R. Lozano, A.L. Doadrio, A. Doadrio, Polyhedron 1 (1982) 163.
[4] R. Lozano, J. Román, E. Alarcón, A.L. Doadrio, A. Doadrio, Rev. Chim. Miner. 20 (1983) 173.
[5] R. Lozano, J. Román, D. Armada, A. Doadrio, Polyhedron 4 (1985) 1563.
[6] R. Lozano, J. Román, F. De Jesús, E. Alarcón, Transit. Met. Chem. 15 (1990) 141.
[7] C. Sharp, A.G. Sykes, Inorg. Chem. 27 (1988) 501.
[8] M.R. Maurya, N. Bharti, Transit. Met. Chem. 24 (1999) 389.
[9] K. Umakoshi, E. Nishimoto, M. Sokolov, H. Kawano, Y. Sasaki, M. Onishi, J. Organomet. Chem. 611 (2000) 370.
[10] B. Keshavan, K. Gowda, Proc. Indian Acad. Sci. 3 (2001) 165.
[11] D. Miguel, V. Riera, M. Wang, Inorg. Chim. Acta 307 (2000) 82.
[12] R. Lozano, A.L. Doadrio, E. Alarcón, J. Román, A. Doadrio, Rev. Chim. Minér. 20 (1983) 109.
[13] R. Lozano, E. Alarcón, A.L. Doadrio, A. Doadrio, Polyhedron 2 (1983) 435.
[14] R. Lozano, E. Alarcón, A.L. Doadrio, A. Doadrio, Polyhedron 3 (1984) 25.
[15] R. Lozano, E. Alarcón, J. Román, A. Doadrio, Rev. Chim. Minér. 21 (1984) 177.
[16] R. Lozano, E. Alarcón, J. Román, A. Doadrio, Polyhedron 3 (1984) 1021.
[17] R. Lozano, J. Román, M.D. Armada, E. Parrondo, Eur. J. Solid State Inorg. Chem. 25 (1988) 191.
[18] R. Lozano, J. Román, F. de Jesús, Polyhedron 7 (1989) 947.
[19] W.W. Wendlant, Thermal Methods of Analysis, Wiley, New York, 1974.
[20] A.E. Nerwkirk, Anal. Chem. 32 (1960) 1558.
[21] E.S. Freeman, B. Carroll, J. Phys. Chem. 62 (1958) 394.
[22] H.H. Horowitz, G. Metzger, Anal. Chem. 35 (1963) 1464.
[23] A.W. Coats, J.P. Redfern, Nature 201 (1964) 68.
[24] C.D. Doyle, J. Appl. Polym. Sci. 5 (1961) 285.
[25] T.R. Ingraham, P. Marrier, Can. J. Chem. Eng. (1984) 161.
[26] J.M. Thomas, T.A. Clarke, J. Chem. Soc. (A) (1968) 457.

[27] R. Lozano, J. Román, F. de Jesús, A. Jerez, M. Gaitán, E. Ramos, Thermochim. Acta 141 (1989) 261.
[28] R. Lozano, J. Román, F. de Jesús, A. Jerez, M. Gaitán, E. Ramos, Thermochim. Acta 143 (1989) 93.
[29] R. Lozano, J. Martínez, A. Martínez, J. Román, F. de Jesús, Polyhedron 8 (1989) 2611.
[30] F.A. Cotton, S.M. Morehouse, J.S. Wood, Inorg. Chem. 3 (1964) 1063.
[31] L. Ricard, C. Martin, R. Wiest, R. Weiss, Inorg. Chem. 14 (1975) 2300.
[32] L. Ricard, J. Stienne, J. Karagiannidis, P. Toledano, J. Fisher, A. Mitschler, J. Coord. Chem. 3 (1974) 277.
[33] R. Lozano, J. Martínez, A. Martínez, A. Doadrio, Polyhedron 2 (1983) 997.
[34] R. Lozano, J. Román, J. Martínez, A. Martínez, A. Doadrio, Polyhedron 5 (1986) 1341.
[35] V.C. Gibson, T.P. Kee, A. Shaw, Polyhedron 7 (1988) 579.
[36] M.A. Ansari, J. Chandrasekaran, S. Sarkar, Polyhedron 7 (1988) 471.
[37] M.H. Chisholm, J.C. Huffman, J.W. Pasterczyk, Polyhedron 6 (1987) 551.
[38] C.J. Ballhausen, H.B. Gray, Molecular Orbital Theory, Benjamin, New York, 1965.
[39] H.B. Gray, C.R. Hare, Inorg. Chem. 1 (1962) 363.
[40] I.G. Dance, A.E. Landers, Inorg. Chem. 18 (1979) 3487.
[41] A. Kay, P.C.H. Mitchell, J. Chem. Soc. (A) (1970) 2421.
[42] J.M. Criado, D. Dollimore, G.R. Heal, Thermochim. Acta 54 (1982) 159.

also report, for the first time, the molecular structure of one of the products, tris(diphenyloxophosphino)ethylenediamine, elucidated by single crystal X-ray diffraction.

2. Experimental

2.1. General remarks

All reactions and manipulations were carried out under nitrogen unless otherwise stated and using nitrogen saturated solvents. Analytical grade and deuterated solvents were purchased from Merck (Darmstadt, Germany); ethylenediamine and diphenylchlorophosphine were purchased from Fluka (Buchs, Switzerland) and were used as received. Spectra were recorded on the following instruments: NMR, Bruker Avance DPX 400 (400.1 MHz for ^{1}H; and 100.6 MHz for ^{13}C); Elemental analyses, Fisons Model EA 1108; IR, Matson UNICAM-FTIR Model 1000 spectrophotometer; Melting points, Gallenkamp Model apparatus with open capilleries.

The reactions of diphenylchlorophosphine (PPh_2Cl) with ethylenediamine ($H_2NCH_2CH_2NH_2$) in different molar ratios 2:1, 3:1 and 4:1 were carried out for the synthesis of bis-, tris- and tetrakis(diphenyloxophosphino)ethylenediamine, respectively.

2.2. Bis(diphenyloxophosphino)ethylenediamine, $Ph_2P(O)NHCH_2CH_2NHP(O)Ph_2$

Diphenylchlorophosphine, Ph_2PCl (1.15 g, 5.2 mmol) was added slowly to a solution of ethylenediamine (0.16 g, 2.6 mmol) and Et_3N (0.53 g, 5.2 mmol) in dry diethyl ether (60 mL) at −10 °C under vigorous stirring. The resulting white suspension was stirred under argon at room temperature for 24 h. Solid triethylammonium chloride was removed by filtration under argon and the solvent removed in vacuo. The remaining solid was crystallised in ethylacetate in air. 0.80 g (67% yield): $C_{26}H_{26}O_2N_2P_2$; m.p.: 156–158 °C; *Anal.* Calc. for $C_{26}H_{26}O_2N_2P_2$: C, 67.88; H, 5.65. Found: C, 67.96; H, 5.52%. MS: *m*/*z* 460 (M^+). ^{1}H NMR (ppm rel. to TMS in $CDCl_3$): $\delta = 3.02$ (4H, N–CH_2–), 4.26 (2H, –NH–), 7.32 (m, 8H, *m*-hydrogens of phenyls), 7.38 (m, 4H, *p*-hydrogens of phenyls), and 7.76 (m, 8H, *o*-hydrogens of phenyls); ^{13}C NMR (ppm rel. to TMS in $CDCl_3$): $\delta = 43.26$ (N–CH_2–), 128.93 (d, $J(^{31}P\text{-}^{13}C) = 12$ Hz, *o*-carbons of phenyls), 132.18 (d, $J(^{31}P\text{-}^{13}C) = 2$ Hz, *p*-carbons of phenyls), 132.46 (d, $J(^{31}P\text{-}^{13}C) = 10$ Hz, *m*-carbons of phenyls), 132.79 (d, $J(^{31}P\text{-}^{13}C) = 122$ Hz, *i*-carbons of phenyls). ^{31}P NMR (ppm rel. to H_3PO_4 in $CDCl_3$): $\delta = 26.10$. Selected IR (KBr pellet, cm^{-1}): ν(P═O) = 1182, ν(N–H) = 3191.

2.3. Tris(diphenyloxophosphino)ethylenediamine, $(Ph_2P(O))_2NCH_2CH_2NHP(O)Ph_2$

Diphenylchlorophosphine, Ph_2PCl (9.80 g, 44.4 mmol) was added slowly to a solution of ethylenediamine (0.89 g, 14.8 mmol) and Et_3N (4.50 g, 44.5 mmol) in dry diethyl ether (80 mL) at −10 °C under vigorous stirring. The resulting white suspension was stirred under argon for 72 h at room temperature. Solid triethylammonium chloride was removed by filtration under argon and the solvent removed in vacuo. The remaining solid was crystallised in ethylacetate in air. 5.9 g (60% yield), $C_{38}H_{35}O_3N_2P_3$; m.p.: 178–180 °C. *Anal.* Calc. for $C_{38}H_{35}O_3N_2P_3$: C, 67.82; H, 5.62. Found: C, 67.94; H, 5.48%. MS: *m*/*z* 660 (M^+). ^{1}H NMR (ppm rel. to TMS in $CDCl_3$): $\delta = 2.86$ (m, 2H, N–CH_2–), 3.42 (m, 2H, N–CH_2–), 5.12 (broad, 1H, –NH–), 7.18, 7.32 and 7.72 (m, 30H, phenyl); ^{13}C NMR (ppm in $CDCl_3$): $\delta = 41.00$ (s, N–CH_2–), 48.50 (d, $J(^{31}P\text{-}^{13}C) = 8$ Hz, N–CH_2–), 128.54 (m, $J(^{31}P\text{-}^{13}C) = 10$ Hz, *o*-carbons of phenyls), 128.82 (d, $J(^{31}P\text{-}^{13}C) = 11$ Hz, *o*-carbons of phenyls), 130.87 (d, $J(^{31}P\text{-}^{13}C) = 126$ Hz, *i*-carbons of phenyls), 131.96 (s, *p*-carbons of phenyls), 132.22 (d, $J(^{31}P\text{-}^{13}C) = 10$ Hz, *m*-carbons of phenyls), 132.54 (s, *p*-carbons of phenyls), 132.87 (d, $J(^{31}P\text{-}^{13}C) = 185$ Hz, *i*-carbons of phenyls), 133.03 (m, $J(^{31}P\text{-}^{13}C) = 10$ Hz, *m*-carbons of phenyls); ^{31}P NMR (ppm rel. to H_3PO_4 in $CDCl_3$): $\delta = 24.82$, 32.92. Selected IR(KBr pellet, cm^{-1} ν(P–N–P) = 906, ν(P═O) = 1182, ν(N–H) = 3198.

2.4. Tetrakis(diphenylphosphino)ethylenediamine, $(Ph_2P)_2NCH_2CH_2N(PPh_2)_2$

Diphenylchlorophosphine, Ph_2PCl (2.62 g, 11.88 mmol) was added slowly to a solution of ethylenediamine (0.18 g, 2.99 mmol) and Et_3N (1.20 g, 11.86 mmol) in dry THF (75 mL) at −10 °C under vigorous stirring. The resulting white suspension was stirred under argon for 1 h. Solid triethylammonium chloride was removed by filtration under argon. The solution was evaporated to dryness. The residue was washed with diethylether and dried in vacuum. It was identified as $(Ph_2P)_2NCH_2CH_2N(PPh_2)_2$: 1.46 g (61% yield). m.p. 203–205 °C. *Anal.* Calc. for $C_{50}H_{44}N_2P_4$: C, 75.38; H, 5.53%. Found: C, 75.94; H, 5.80%, ^{1}H NMR (ppm in $CDCl_3$): $\delta = 3.10$ (s, 4H, N–CH_2–), 7.19–7. 31 (m, 40H, phenyls); ^{13}C NMR (ppm in $CDCl_3$): $\delta = 45.81$ (N–CH_2–), 128.00 (d, 6 Hz), 128.57, 132.71 (d, 21 Hz) 132.82, 139.23, 139.40; ^{31}P NMR (ppm rel. to H_3PO_4 in $CDCl_3$): $\delta = 61.29$. Selected IR (KBr, cm^{-1}): 889 ν(P–N–P).

2.5. Tetrakis(diphenyloxophosphino)ethylenediamine, $(Ph_2P(O))_2NCH_2CH_2N(P(O)Ph_2)_2$

H_2O_2 (0.28 mmol) was added slowly to a solution of $(Ph_2P)_2NCH_2CH_2N(PPh_2)_2$ (57 mg, 0.072 mmol) in 5 mL THF under stirring. The mixture was stirred for 2 h at room temperature. Then diethyl ether (5 mL) was added to the mixture and cooled to −10 °C. The white precipitate was separated from the supernatant solution and dried in vacuum. $(Ph_2P(O))_2NCH_2CH_2N(P(O)Ph_2)_2$ 42 mg (68% yield).; m.p.: 248–251 °C. *Anal.*, Calc. for $C_{50}H_{44}O_4N_2P_4$:

C, 69.76; H, 5.12. Found: C, 69.93; H, 5.28%, MS: *m*/*z* 860 (M^+). ^{1}H NMR (ppm rel. to TMS in $CDCl_3$): $\delta = 3.69$ (s, 4H, N–CH_2–), 7.18 (m, 16H, *m*-hydrogens of phenyls), 7.31 (m, 8H, *p*-hydrogens of phenyls), and 7.56 (m, 16H, *o*-hydrogens of phenyls);); ^{13}C NMR (ppm in $CDCl_3$): $\delta = 45.82$ (N–CH_2–), 127.90 (d, $J(^{31}P\text{-}^{13}C) = 14$ Hz, *o*-carbons of phenyls), 131.72 (s, *p*-carbons of phenyls), 131.38 (d, $J(^{31}P\text{-}^{13}C) = 124$ Hz, *i*-carbons of phenyls), 132.59 (d, $J(^{31}P\text{-}^{13}C) = 10$ Hz, *m*-C of phenyls), ^{31}P NMR (ppm rel. to H_3PO_4 in $CDCl_3$): $\delta = 31.53$).

Table 1
Crystal data and experimental details of the structural analysis of tris(diphenyloxophosphino)ethylenediamine

Empirical formula	$[PO(C_6H_5)_2]_3N_2H(CH_2)_2OH_2$
Formula weight	678.61
Crystal system	monoclinic
Crystal shape and color	Plate and colorless
Space group	$P2_1/n$
Unit cell dimensions	
a (Å)	16.415(13)
b (Å)	13.159(3)
c (Å)	17.213(3)
β (°)	109.189(12)
Volume (Å^3)	3512(3)
Z	4
D_{calc} (Mg/m^3)	1.283
Absorbtion coefficient (mm^{-1})	0.212
F(000)	1424
h, *k*, *l* Ranges	$-20 \rightarrow 0$, $0 \rightarrow 16$, $-20 \rightarrow 21$
Number of reflections collected/unique (R_{int})	7366–7113 (0.0326)
Number of reflections [$I > 2\sigma(I)$]	4184
Number of parameters/restrains	437/4
Goodness-of-fit on F^2	1.03
R indices [$I > 2\sigma(I)$]	$R_1 = 0.0497$, $wR_2 = 0.1161$
R indices [all data]	$R_1 = 0.01238$, $wR_2 = 0.1389$
$(\Delta/\sigma)_{max}$	0.000
Largest difference peak and hole (e/Å^3)	0.294 and −0.252

Additional material available from the Cambridge Crystallographic Data Center as deposition No: CCDC 296237 comprises H-atom coordinates, thermal parameters, and the remaining bond lengths and angles.

2.6. X-ray diffraction structure analysis

A colorless-plate crystal of $0.4 \times 0.4 \times 0.1$ mm was used for the X-ray diffraction study. X-ray diffraction data were collected on an Enraf-Nonius CAD4 (κ-geometry) diffractometer operating in $\omega/2\theta$ scan mode using graphite-monochromated Mo Kα radiation ($\lambda = 0.71073$ Å) at 20 ± 1 °C. The lattice parameters and their estimated standard deviations were determined from a least-squares refinement of 25 centered reflections in the range $9.90 \leqslant \theta \leqslant 18.01°$ by using CAD4 Express [12]. Three standard reflections were measured every 100 reflections and their intensities showed a good stability. A total of 7366 reflections were collected in the range $2.51 \leqslant \theta \leqslant 26.29°$, of which 7113 independent reflections were used for the structure determination. The intensity data were not corrected for absorption.

Data reduction was carried out using XCAD4 [13]. The structure was solved by direct methods and refined by full-matrix least-squares refinement on F^2 using the programs SHELXS97 and SHELXL97 [14], respectively, in the WinGX package [15]. Atomic scattering factors were taken from the International Tables for X-ray Crystallography [16]. Hydrogen atoms of the water molecule and the H atom on N1 were taken from a difference Fourier map, while the other hydrogen atoms were placed with

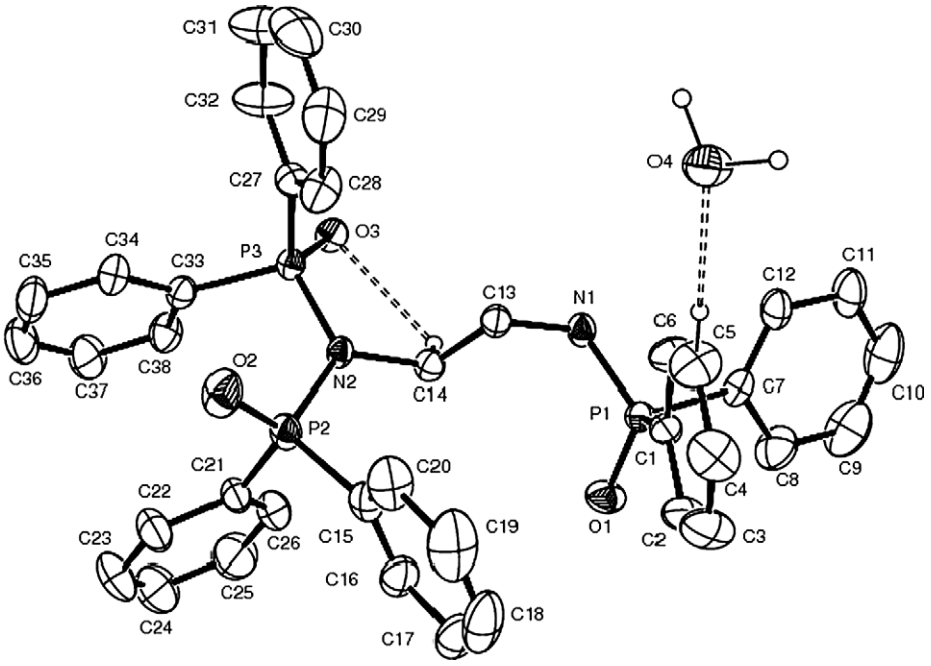

Fig. 1. ORTEP [17] drawing of the molecular structure of tris(diphenyloxophosphino)ethylenediamine with the atomic numbering scheme. Displacement ellipsoids are drawn at the 50% probability level and H atoms are shown as small circles of arbitrary radii.

Table 2
Selected bond lengths (Å) and bond angles (°)

C13–N1	1.458(3)	C13–N1–P1	123.3(2)
C14–C13	1.510(4)	C14–N2–P3	117.27(16)
N2–C14	1.493(3)	C14–N2–P2	121.48(17)
P1–O1	1.482(2)	C21–P2–C15	106.31(16)
P1–N1	1.631(3)	C27–P3–C33	107.35(14)
P1–C7	1.798(3)	C7–P1–C1	107.18(13)
P1–C1	1.803(3)	N1–P1–C7	104.04(13)
P2–O2	1.462(2)	N1–P1–C1	105.65(13)
P2–N2	1.692(2)	N1–C13–C14	112.8(2)
P2–C21	1.795(4)	N2–P3–C27	109.14(13)
P2–C15	1.799(3)	N2–P3–C33	106.56(12)
P3–O3	1.4808(19)	N2–P2–C21	107.00(13)
P3–N2	1.686(2)	N2–P2–C15	107.26(12)
P3–C27	1.798(3)	N2–C14–C13	111.9(2)
P3–C33	1.800(3)	O1–P1–N1	118.03(13)
		O2–P2–C15	111.54(15)
O1–P1–C7	111.45(14)	O3–P3–N2	109.99(11)
O1–P1–C1	109.79(13)	O3–P3–C27	111.34(13)
O2–P2–N2	110.84(13)	O3–P3–C33	112.29(12)
O2–P2–C21	113.54(15)	P3–N2–P2	120.90(12)

Table 3
Structural parameters of hydrogen bonds between donor (D), acceptor (A) and hydrogen (H)

D–H···A	D–H (Å)	A···H (Å)	D·····A (Å)	D–H···H (°)
O4–H1A···O1^{i}	0.97(3)	1.88(3)	2.831(4)	165(3)
O4–H1B···O1^{ii}	0.91(2)	1.94(2)	2.842(4)	174(3)
N1–H1N···O3^{iii}	0.79(3)	2.13(3)	2.891(4)	160(3)
C10–H10···O2^{iv}	0.93	2.49	3.199(6)	133
C5–H5···O4	0.93	2.50	3.431(5)	176
C14–H14A···O3	0.97	2.45	2.925(4)	110

Symmetry codes. i: $x-1/2$, $-y+1/2$, $z-1/2$; ii: $-x+1/2$, $y+1/2$, $-z+1/2$; iii: $-x+1$, $-y+1$, $-z+1$; iv: $x-1/2$, $-y+1/2$, $z+1/2$.

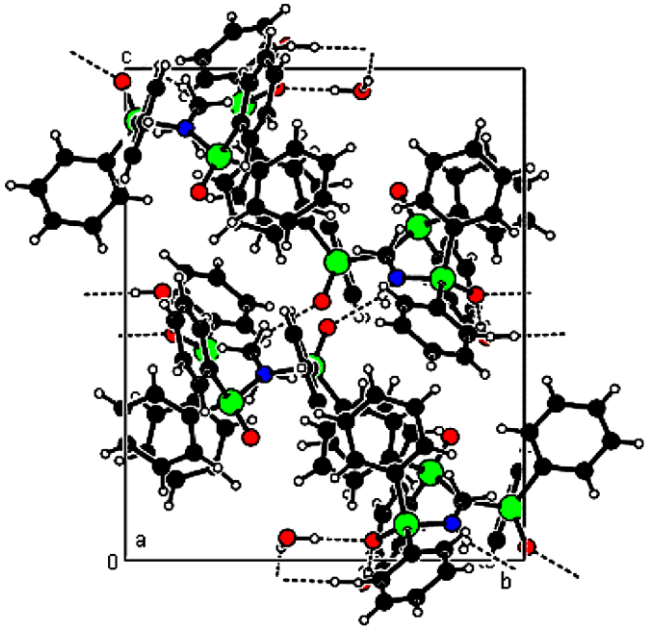

Fig. 2. Packing diagram of tris(diphenyloxophosphino)ethylenediamine.

$U_{iso}(H) = 1.2U_{eq}(C)$. For all non-hydrogen atoms anisotropic displacement parameters were refined. The data collection details, crystal data and refinement parameters are summarized in Table 1.

A perspective view of the molecule [17] is given in Fig. 1. Selected bond lengths and angles are given in Table 2. The hydrogen bonding and molecular packing geometry of the tris(diphenyloxophosphino)ethylenediamine molecule were calculated with PLATON [18] and the hydrogen bonding geometry is summarized in Table 3. There are two intra and four inter molecular hydrogen bonds occurring in the structure. Fig. 2 gives a perspective view of the crystal packing.

3. Results and discussion

The reaction of ethylenediamine with diphenylchlorophosphine in various stoichiometric ratios gives the respective phosphine oxides through the intermediate $(Ph_2P)_nNCH_2CH_2N(PPh_2)_m$ $(n,m = 1,2)$ at room temperature (Scheme 1).

Bis(diphenylphosphino)ethylenediamine and tris(diphenylphosphino)ethylenediamine are formed as intermediates and can be oxidized to the respective phosphine oxides by oxygen dissolved in the reaction solution, while terakis(diphenylphosphino)ethylenediamine is less liable to oxidation and its oxidation requires a stronger oxidizing agent such as hydrogen peroxide. Consequently, only tetrakis(diphenylphosphino)ethylenediamine could be isolated from the reaction mixture and characterized.

All the three phosphine oxides could be isolated as analytically pure solid materials and fully characterized by elemental analysis, MS and NMR spectroscopies. In the case of tris(diphenylphosphino)ethylenediamine, single crystals could be obtained, so that its molecular structure could be elucidated by X-ray diffraction.

The molecular structure of tris(diphenyloxophosphino)ethylenediamine given in Fig. 1 shows the presence of one H_2O molecule, which is involved in hydrogen bonding through both of its hydrogen atoms with the host molecule. As shown in Fig. 2 and Table 3 there are two intermolecular hydrogen bonding sets involving the water molecule: ([O4–H1A···O1]^{i} and [O4–H1B···O1]^{ii} H-bonds with symmetry codes: (i) $x-1/2$, $y+1/2$, $z-1/2$ and (ii) $-x+1/2$, $y+1/2$, $-z+1/2$, respectively). The oxygen atom of the water molecule is also involved in relatively weak hydrogen bonding with the one of the phenyl hydrogens, [C5–H5···O4]). A strong intramolecular hydrogen bond is seen between N1 and O3, ([N1–H1N···O3] with symmetry code: $-x+1$, $-y+1$, $-z+1$). There are two more hydrogen bonding sets involving hydrogen atoms attached to the carbon, [C10–H10···O2] and [C14–H14A···O3]. The former one is intramolecular and the latter one is an intermolecular hydrogen bonding between two molecules of tris(diphenyloxophosphino)ethylenediamine within the unit cell.

Inspection of bond lengths and bond angles given in Table 2 for the tris(diphenyloxophosphino)ethylenedia-

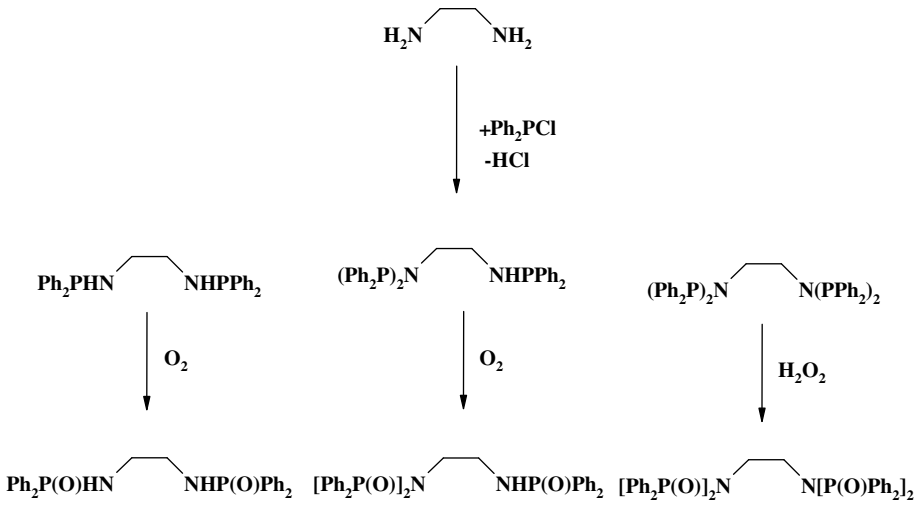

Scheme 1. The reaction of ethylenediamine with diphenylchlorophosphine in the presence of triethylamine at room temperature.

mine reveals that the C–C, C–N, P–N and P–O bonds are of usual length as compared to similar compounds [4,10,19].

The ^{31}P NMR signal shows a remarkable shift on passing from the phosphino to oxophosphino compound, as illustrated in the case tetrakis(diphenylphosphino)etheylenediamine ($\delta = 61.29$ ppm) and its oxidized form ($\delta = 31.53$ ppm). This shift, due to the formation of an oxo group, is useful in the sense that the transformation of diphosphine to its oxo derivative can be followed by taking the ^{31}P NMR spectra during the reaction.

Acknowledgements

Partial support of this work by the Council of Dicle University (DUAPK) for financial support under Project No. DUAPK-02-FF-32 and the Turkish Academy of Sciences (DPT-TUBİTAK 2003–K-120340) are gratefully acknowledged.

References

[1] (a) N. Biricik, Z. Fei, R. Scopelliti, P.J. Dyson, Helv. Chim. Acta 86 (2003) 3281;
(b) F. Agbossou, J.F. Carpentier, F. Hapiot, Coord. Chem. Rev. 178–180 (1998) 1615;
(c) A.M.Z. Slawin, M.B. Smith, J.D. Woollins, J. Chem. Soc., Dalton Trans. (1998) 1537;
(d) A.M.Z. Slawin, M.B. Smith, J.D. Woollins, Chem. Commun. (1996) 2095;
(e) K.V. Katti, V.S.R. Reddy, P.R. Singh, Chem. Soc. Rev. (1995) 97;
(f) P. Bhattacharyya, J.D. Woolins, Polyhedron 14 (1995) 3367.
[2] (a) F. Agbossou-Niedercorn, I. Suisse, Coord. Chem. Rev. 242 (2003) 145;
(b) D. Gleich, R. Schmid, W.A. Herrmann, Organometallics 17 (1998) 2141;
(c) H. Bricout, J.F. Carpentier, A. Mortreux, Tetrahedron Lett. 37 (1996) 6105;
(d) B. Cornils, E.G. Kuntz, J. Organomet. Chem. 502 (1995) 177;
(e) I. Suisse, H. Bricout, A. Mortreux, Tetrahedron Lett. 35 (1994) 413;
(f) S. Ganguly, R.M. Roundhill, Organometallics 12 (1993) 4825.
[3] (a) K.G. Gaw, M.B. Smith, J.W. Steed, J. Organomet. Chem. 664 (2002) 294;
(b) E. Lindner, M. Mohr, C. Nachtigal, R. Fawzi, G. Henkel, J. Organomet. Chem. 595 (2000) 166.
[4] M. Necas, M.R.J. Foreman, J. Marek, J.D. Woollins, J. Novosad, New J. Chem. 25 (2001) 1256.
[5] S. Priya, M.S. Balakrishna, J.T. Mague, S.M. Mobin, Inorg. Chem. 42 (2003) 1272.
[6] (a) S.J. Dossett, A. Gillon, A.G. Orpen, J.S. Fleming, P.G. Pringle, D.F. Wass, M.D. Jones, Chem. Commun. (2001) 699;
(b) M.R.I. Zubiri, M.L. Clarke, D.F. Foster, D.J. Cole-Hamilton, A.M.Z. Slawin, J.D. Woollins, J. Chem. Soc., Dalton Trans. (2001) 969;
(c) J. Liedtke, H. Rüegger, S. Loss, H. Grützmacher, Angew. Chem., Int. Ed. Engl. 39 (2000) 2478;
(d) S.C. van der Slot, P.C.J. Kamer, P.W.N.M. van Leeuwen, J. Fraanje, K. Goubitz, M. Lutz, A.L. Spek, Organometallics 19 (2000) 2504;
(e) J.M. Brunel, A. Heumann, G. Buono, Angew. Chem., Int. Ed. Eng. 39 (2000) 1946;
(f) A. Wegner, W. Leitner, Chem. Commun. (1999) 1583.
[7] P. Kafarski, P. Mastalerz, Aminophosphonates. Beitr. Wrikstofforsch. 21 (1984) 1.
[8] K.P. Kumar, C. Muthaiah, S. Kumaraswamy, K.C. Kumaraswamy, Tetrahedron Lett. 42 (2001) 3219.
[9] (a) D.R. Armstrong, D. Barr, M.G. Davidson, G. Hutton, P. O'Brien, R. Snaith, S. Warren, J. Organomet. Chem. 529 (1997) 29;
(b) J. Clayden, E.W. Collington, R.B. Ramonti, S. Warren, Tetrahedron Lett. 34 (1993) 2203.
[10] M.S. Balakrishna, M.N. Walawalker, J. Organomet. Chem. 628 (2001) 76.
[11] S. Priya, M.S. Balakrishna, J.T. Mague, Inorg. Chem. Commun. 4 (2001) 437.
[12] Enraf-Nonius, CAD-4, Express Software. Version 1.1, Enraf-Nonius, Delft, The Netherlands, 1993.
[13] K. Harms, S. Wocadlo, XCAD-4. Program for Processing CAD-4 Diffractometer Data, University of Marburg, Germany, 1995.
[14] G.M. Sheldrick, SHELXS97 and SHELXL97. Program for Crystal Structure Solution and Refinement, University of Göttingen, Germany, 1997.
[15] L.J. Farrugia, J. Appl. Cryst. 32 (1999) 837.
[16] A.J.C. Wilson, International Tables for Crystallography, vol. C, Kluwer Academic Publishers, Dordrecht, The Netherlands, 1992.
[17] L.J. Farrugia, J. Appl. Cryst. 30 (1997) 565.
[18] A.L. Spek, J. Appl. Cryst. 36 (2003) 7.
[19] S. Özkar, D. Ülkü, L. Tatar-Yıldırım, N. Biricik, B. Gümgüm, J. Mol. Struct. 688 (2004) 207.

bond donor) ligands bound to palladium centres [10]. These compounds have been used as starting materials to achieve organic-organometallic hydrogen bonded networks by reaction with carboxylic acids. A study on a Pd_2N_4 core incorporating a diazo ligand is also known [11]. We report herein a new complex $[(3,5\text{-Hdmpz})_2Pd_2(\mu\text{-}3,5\text{-dmpz})_2(2,6\text{-dipic})]$ (**1**) that affords an unsymmetrical 1D chain, and the binuclear units assemble in a zigzag way propagated through 3,5-Hdmpz-carboxylate (2,6-dipic^{2-}) hydrogen bonds. The asymmetric unit of this compound shows a central Pd_2N_4 six-member heterocycle that adopts a distorted boat-like conformation.

We considered it of further interest to use another substituted pyrazole, 3-methyl-1-phenylpyrazole (3-me-1-phpz). An earlier report has been made that 3-me-1-phpz displaces acetonitrile from $[PdCl_2(CH_3CN)_2]$ to form *trans*-$[Pd(N_3)_2(3\text{-me-1-phpz})_2]$ via $[PdCl_2(3\text{-me-1-phpz})_2]$ [12]. In addition, the unsymmetrical N-substituted pyrazoles offer the possibility of formation of cyclometallated products [13]. With the aim to generate a pyrazole based product, we carried out the reaction of $PdCl_2(CH_3CN)_2$, 3-me-1-phpz and NaH2,6-dipic. The compound $[Na_2(H_2O)_4Pd(2,6\text{-dipic})_2]$ (**2**) is formed without incorporation of the 3-me-1-phpz ligand. A couple of precedents of Pd-2,6-dipic^{2-} complexes are known in the literature [14,15]. The single crystal X-ray analysis shows that **2** is stabilized through cationic Na^+–H_2O and anionic Pd-2,6-dipic^{2-} units to form an extended two-dimensional coordination polymer. A detailed study of the molecular and electronic structures coupled with experimental results obtained from IR, UV–Vis, ^{1}H NMR and mass spectral studies have been made. Data on the luminescence property and antimicrobial activity of **1** are also presented.

2. Experimental

2.1. Materials

Palladium chloride ($PdCl_2$) used in the complex was obtained from Arora-Matthey Limited (India). $PdCl_2(CH_3CN)_2$ was prepared according to the literature procedure [16]. 3,5-Dimethylpyrazole was purchased from Fluka. Pyridine-2,6-dicarboxylic acid and 3-methyl-1-phenylpyrazole were obtained from Lancaster. Sodium hydroxide was a Merck product. All solvents were dried and kept over molecular sieves prior to use. Double distilled water was used throughout.

2.2. Physical measurements

Elemental analysis was carried out in a 2400 Series-II CHN analyzer, Perkin–Elmer, USA. IR spectra were recorded on a Nicolate Magna IR 750 Series-II IR spectrophotometer. The ^{1}H NMR spectra were recorded on a 300 MHz Bruker Avance DPX 300 machine, Switzerland in $(CD_3)_2SO$ and D_2O solvent with TMS as the internal standard at room temperature. The mass spectra were recorded on a Qtof Micro YA263 mass spectrometer. Absorption and luminescence spectra were studied on a Shimadzu UV2100 UV–VIS recording spectrophotometer and a Perkin–Elmer LS 55 Luminescence spectrometer, respectively.

2.3. Computational details

A detailed quantum-chemical calculation on the Na-chain as retrieved from the crystal geometry of **2** was made at the DFT-level of B3LYP/6-31G$^+$(d,p) [17]. These sets of calculations have been performed using the GAUSSIAN 03 program suite [18].

2.4. Synthesis of the complexes

2.4.1. Synthesis of $[(3,5\text{-Hdmpz})_2Pd_2(\mu\text{-}3,5\text{-dmpz})_2(2,6\text{-dipic})]$ (**1**)

0.026 g (0.1 mmol) of $PdCl_2(CH_3CN)_2$ was dissolved in 10 cm^3 of methanol. To this deep orange solution was added a 10 cm^3 methanolic solution of 3,5-Hdmpz (0.020 g, 0.2 mmol). The resulting mixture was stirred for 10 min at room temperature and filtered off to remove any suspended material. To the filtrate, 15 cm^3 aqueous solution of NaH2,6-dipic (0.040 g, 0.2 mmol) was added and the solution was warmed at 50 °C for 30 min. The light yellow solution was cooled to room temperature. Deep yellow crystals suitable for X-ray diffraction were obtained after 7 days in a 71% yield based on Pd. *Anal*. Calc. for **1**: C, 42.60; H, 4.34; N, 16.57. Found: C, 42.26; H, 4.23; N, 16.43%. IR spectrum (KBr disk, ν/cm^{-1}): 3123 (w), 3090 (w), 1683 (s), 1673 (s), 1621 (s), 1573 (m), 1414 (m), 1375 (s). ^{1}H NMR spectrum (300 MHz, d_6-DMSO) δ: 2.43 (CH_3, s), 1.66 (CH_3, s), 6.08 (H, s), 2.43 (CH_3, s), 1.86 (CH_3, s), 5.93 (H, s); 2.11 (CH_3, s), 2.30 (CH_3, s), 5.44 (H, s), 12.96 (N–H,s), 2.20 (CH_3, s), 2.23 (CH_3, s), 5.61 (H, s), 17.21 (N–H, s); 7.90, 7,92 (H, d), 8.21, 8.24, 8.27 (H, t), 7.77, 7.79 (H, d). Mass spectrum (CH_3CN/H_2O): 762.28.

2.4.2. Synthesis of $[Na_2(H_2O)_4Pd(2,6\text{-dipic})_2]$ (**2**)

$PdCl_2(CH_3CN)_2$ (0.052 g, 0.2 mmol) was dissolved in 5 cm^3 of DMF. To the deep orange solution was added a solution of 3-me-1-phpz (0.063 g, 0.4 mmol) in 5 cm^3 of DMF under stirring. After 10 min, an aqueous solution of NaH2,6-dipic (0.080 g, 0.4 mmol) was added to the mixture and the solution stirred for 1 h. The resulting yellow solution was filtered off to remove any suspended material. Yellow crystals suitable for X-ray diffraction were obtained after 5 days in a 40% yield based on Pd. *Anal*. Calc. for **2**: C, 30.73; H, 1.10; N, 5.12. Found: C, 30.81; H 1.16; N, 5.14%. IR spectrum (KBr disk, ν/cm^{-1}): 3528 (s), 3426 (w), 1683 (s), 1633 (s), 1411 (m), 1376 (s). ^{1}H NMR spectrum (300 MHz, d_6-DMSO) δ: 7.90, 7.92 (H, d), 8.18, 8.20, 8.23 (H, t), 7.75, 7.72 (H, d). Mass spectrum (H_2O): 546.28.

Table 1
Crystal data and details for structure refinement for **1** and **2**

Formula	$C_{27}H_{33}N_9O_4Pd_2$	$C_{14}H_6N_2Na_2O_{12}Pd$
Formula weight	760.42	546.59
Crystal system	monoclinic	triclinic
Space group	$C2/c$ (no. 15)	$P\bar{1}$ (no. 2)
a (Å)	29.848(6)	6.4521(13)
b (Å)	11.649(2)	6.5686(13)
c (Å)	17.713(4)	11.661(2)
α (°)	90.00	106.19(3)
β (°)	94.18(3)	93.57(3)
γ (°)	90.00	107.21(3)
V (Å^3)	6143(2)	447.68(19)
Z	8	1
D_{calc} (g/cm^3)	1.645	2.027
μ (mm^{-1})	1.219	1.158
$F(000)$	3056	268
Temperature (K)	293	294
λ (Å) (Mo Kα)	0.71073	0.71073
$\theta_{min-max}$ (°)	2.2–25.0	3.3–25.0
Reflections collected	5511	1631
Independent reflections [R_{int}]	5403 [0.055]	1541 [0.061]
Observed data [$I > 2\sigma(I)$]	3429	1522
Data/restraints/parameters	5403/0/372	1541/0/142
Goodness-of-fit on F^2	0.973	1.114
Final R indices [$I > 2\sigma(I)$]	$R_1 = 0.0602$	$R_1 = 0.0437$
	$wR_2 = 0.1289$	$wR_2 = 0.1197$
R indices (all data)	$R_1 = 0.1108$	$R_1 = 0.0442$
	$wR_2 = 0.1451$	$wR_2 = 0.1205$

2.5. Crystal structure determination and structural refinement of complexes *1* and *2*

Crystals of dimensions $0.19 \times 0.21 \times 0.49$ mm (**1**) and $0.19 \times 0.26 \times 0.55$ mm (**2**) were mounted on a Siemens P4 4-circle-diffractometer which was equipped with graphite monochromated Mo Kα radiation ($\lambda = 0.71073$ Å). Unit cell dimensions and intensity data were measured at 293 K for both **1** and **2**. All calculations for data reduction, structure solution and refinement were done by standard procedures (SHELXS-97) [19], (SHELXL-97) [20]. All non-hydrogen atoms were refined anisotropically by full-matrix least-squares techniques on F^2. All the hydrogen atoms of **1** and **2** were included at calculated positions and refined isotropically. Information concerning crystallographic data collection and refinement of the structures are summarized in Table 1.

3. Results and discussion

3.1. Synthesis and spectroscopic characterization of the complexes

The complexes reported here are formed by the process of slow crystallization. Sometimes it takes a long time to isolate the desired product. Moreover, the reported complexes are sparingly soluble in common organic solvents. We have tried to crystallize the products from an optimum dilution so that we could strike a balance between improved crystal quality and time of crystallization. Compound **1** [(3,5-Hdmpz)$_2$Pd$_2$(μ-3,5-dmpz)$_2$(2,6-dipic)] has been obtained as a deep-yellow crystalline solid by addition of 3,5-Hdmpz and NaH2,6-dipic to $PdCl_2(CH_3CN)_2$ in methanol at 50 °C without addition of the hydroxide ion or other bases. Compound **2** was obtained also as a well-formed deep-yellow crystalline solid by the addition of 3-me-1-phpz and an aqueous solution of NaH2,6-dipic to a DMF solution of $PdCl_2(CH_3CN)_2$. The formation of compound **2** instead of a substituted pyrazolate one is the result of a failed experiment. It clearly points out the relevance of the strength of the bidentate chelate (Hdipic$^-$) in determining the course of the reaction. In the absence of 3-me-1-phpz, no product is obtained. However, a similar compound, *trans*-$Na_2[Pd(2,6\text{-dipic})_2 \cdot 2H_2O$, was obtained earlier by the addition of K_2PdCl_4 to a warm aqueous solution of pyridine-2,6-dicarboxylic acid and maintaining the pH to 6 with 1 N NaOH solution. The yellow crystalline product was characterized by elemental analysis, ^{1}H NMR, IR and UV–Vis spectroscopy [14]. There is no report of the single crystal X-ray structural study of this compound. The IR spectrum of complex **1** displays all the characteristic bands of the coordinated 3,5-Hdmpz and 2,6-dipic^{2-} ions. These include a pair of strong bands at ca. 1683 and 1621 cm^{-1} corresponding to $\nu_{asym}(COO^-)$ vibrations of the bonded and free carboxylates, respectively, and another pair for $\nu_{sym}(COO^-)$ at 1414 and 1375 cm^{-1}, respectively for the bonded and free carboxylate groups. The ring-breathing mode for 3,5-Hdmpz is observed at 1573 cm^{-1}. The relatively low value of the ν(N–H) frequency at 3123 cm^{-1} indicates that the N–H $\cdots$ O hydrogen bonds observed in the X-ray structure of the compound must be quite strong. The IR spectrum of complex **2** is quite simple. The bands at 1683 and 1411 cm^{-1} correspond to the $\nu_{asym}(COO^-)$ and $\nu_{sym}(COO^-)$ vibrations, respectively, of the bonded carboxylates whilst that for the free carboxylates are observed at 1633 and 1376 cm^{-1}. A strong band at 3528 cm^{-1} is observed for the ν(O–H) frequency, which reveals the presence of the solvent water molecules. The ESIMS of compounds **1** and **2** corroborate well with their simulated spectra. The ^{1}H NMR spectrum of **1** at room temperature shows three sets of signals, one for the bridging 3,5-dmpz ($\delta = 2.43$ (CH_3, s), 1.66 (CH_3, s), 6.08 (H, s), 2.43 (CH_3, s), 1.86 (CH_3, s) 5.93 (H, s) ppm) and another one for the terminal 3,5-Hdmpz groups ($\delta = 2.11$ (CH_3, s), 2.30 (CH_3, s), 5.44 (H, s), 12.96 (N–H, s) 2.20 (CH_3, s), 2.23 (CH_3, s) 5.61 (H, s), 17.21 (N–H, s) ppm). The third set is for the 2,6-dipic^{2-} moiety ($\delta = 7.90$, 7.92 (H, d), 8.21, 8.24, 8.27 (H, t) and 7.77, 7.79 (H, d) ppm). The ^{1}H NMR spectrum of **2** at room temperature shows signals only for the 2,6-dipic^{2-} unit comparable to the signals observed in complex **1**.

3.2. Description of the crystal structures

As can be seen from the asymmetric unit (Fig. 1), **1** is a binuclear Pd(II) complex that contains two 3,5-Hdmpz,

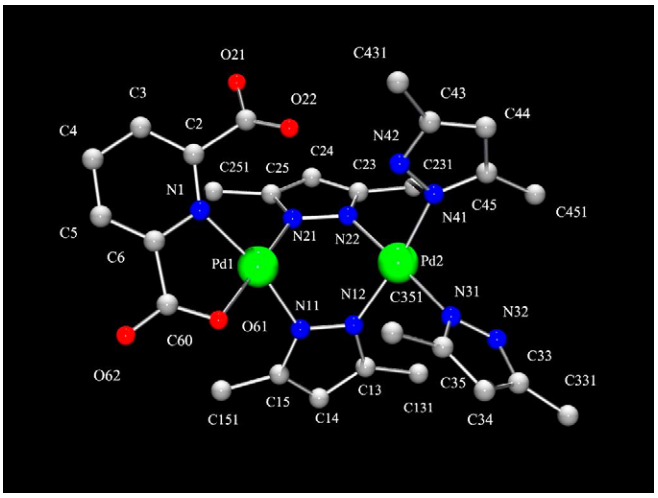

Fig. 1. Molecular structure of complex $[(3,5\text{-Hdmpz})_2Pd_2(\mu\text{-}3,5\text{-dmpz})_2(2,6\text{-dipic})]$ (**1**). All hydrogen atoms have been omitted for clarity.

two 3,5-dmpz and a 2,6-dipic unit. Pd2 contains two Hdmpz units as coordinating ligands whereas Pd1 contains only one 2,6-pyridinedicarboxylate unit. The two 3,5-dmpz units bridge the metal centres in a bidentate fashion. Table 2 lists selected bond distances and angles. Despite the presence of bridging 3,5-dmpz groups between the metal atoms, the intermetallic separation (3.397 Å) indicates no metal–metal bond. The intermetallic distance is comparable to $[\{Pd_2(\mu\text{-}3,5\text{-dmpz})(3,5\text{-dmpz})(3,5\text{-Hdmpz})\}_2]$ [9] (3.4020 Å) and $[Pd(\mu\text{-}3,5\text{-dmPz})(\eta^3\text{-}C_3H_4)]_2$ [21] (3.343 Å) but is longer than the corresponding distances in $[Pd_2Cl_2(\mu\text{-}3,5\text{-dmpz})_2(PMe_2Ph)_2]$ [22] (3.115(1) Å) and $[\{Pd_2(CH_2C_6H_4P\text{-}(o\text{-tolyl})_2\text{-}\kappa C,P)_2(\mu_3\text{-}3,5\text{-dmpz-}N,N',C^4)_2Ag(\mu\text{-}ClO_4)\}_2]$ [4] (3.2297(7) Å). Each palladium atom is in an almost square-planar coordination environment. The central six-member $[Pd(\mu\text{-}3,5\text{-dmpz})_2Pd]$ core is non-planar with Pd–$N_{3,5\text{-dmpz}}$ distances between 1.981(7) and 2.007(7) Å. These fall in the range found in other Pd and Pt complexes with this type of ligand [4,22–28]. The N–Pd–N angles are 87.8(3)° and 86.2(3)° between the 3,5-dimethylpyrazolate groups. The Pd_2N_4 six-member ring reveals a boat-like conformation; the dihedral angle formed by the best least-squares coordination planes of the metals being 89.7°. The metal atoms are positioned at the vertices of the boat and the angle between the planes containing the Pd–N–N–Pd fragments is 73.8° [29]. The boat folding of the Pd_2N_4 core has also been observed earlier for other pyrazolato bridged palladium complexes [9,30,31]. The mean deviation of the plane constructed by the four nitrogen atoms N11, N12, N21 and N22 is 0.0589 Å. The displacement of Pd1 towards N22 is 0.9391 Å while that for Pd2 towards N22 is 1.1145 Å. All of the 3,5-Hdmpz, 3,5-dmpz and 2,6-$dipic^{2-}$ ligands are planar, within experimental error. Comparable bond lengths within the 3,5-dimethylpyrazolate rings suggest substantial delocalization upon deprotonation. The bow angles between the planes N11–N12–N21–N22 and N12–Pd2–N22, N11–Pd1–N21 are 40.73°, 50.12°, respectively. This difference reflects the unsymmetrical environment around the metal centres. The dihedral angles between the monodentate 3,5-Hdmpz ligands N31–N32–C33–C34–C35 and N41–N42–C43–C44–C45, and bridging 3,5-dmpz ligands N11–N12–C13–C14–C15 and N21–N22–C23–C24–C25 are 91.1° and 90.3°, respectively. The ligand 2,6-$dipic^{2-}$ coordinates to Pd1 in a bidentate fashion through its pyridine nitrogen and one carboxylate oxygen atom while the other carboxylate remains free. To achieve internal charge balance, the non-coordinated oxygen atom O21 of the free carboxylate group must be deprotonated. The complex exhibits a zigzag chain configuration of the 1D network through intermolecular 3,5-Hdmpz-carboxylate hydrogen bonds. This arrangement results from the *trans* orientation of one protonated pyrazole and a free carboxylate group of 2,6-$dipic^{2-}$ moieties. This network is clearly affected by the intermolecular and intramolecular hydrogen bonding occurring between the atoms N32–H32 ··· O21 and N42–H42 ··· O22, respectively, which is responsible for the conformation and stability.

Table 2
Selected bond lengths (Å) and angles (°) in complex **1** with esds in parentheses

Bond lengths (Å)			
Pd1–O61	2.018(6)	Pd2–N41	2.053(6)
Pd1–N1	2.059(7)	N11–N12	1.368(10)
Pd1–N11	2.007(7)	N21–N22	1.375(10)
Pd1–N21	1.996(7)	N31–N32	1.364(10)
Pd2–N12	2.002(6)	N41–N42	1.360(10)
Pd2–N22	1.981(7)	N32–H32	0.8604
Pd2–N31	2.029(7)	N42–H42	0.8597
Bond angles (°)			
O61–Pd1–N1	81.1(2)	Pd1–O61–C60	111.9(6)
O61–Pd1–N11	91.1(3)	Pd1–N1–C2	132.2(6)
O61–Pd1–N21	177.1(2)	Pd1–N1–C6	107.7(5)
N1–Pd1–N11	169.1(3)	Pd1–N11–N12	123.0(5)
N1–Pd1–N21	99.5(3)	Pd1–N11–C15	127.4(6)
N11–Pd1–N21	87.8(3)	Pd2–N12–N11	116.6(5)
N12–Pd2–N22	86.2(3)	Pd2–N12–C13	134.4(6)
N12–Pd2–N31	91.0(3)	Pd1–N21–N22	120.6(5)
N12–Pd2–N41	170.5(3)	Pd1–N21–C25	131.5(5)
N22–Pd2–N31	176.9(3)	Pd2–N22–N21	120.4(5)
N22–Pd2–N41	91.2(3)	Pd2–N22–C23	127.7(6)
N31–Pd2–N41	91.7(3)		
Hydrogen bonds (Å, °)			
D–H–A	D–A	H–A	∠D–H–A
N32–H32–O21	2.740(10)	1.8800	173.00
N42–H42–O22	2.720(10)	2.0200	138.00

The X-ray structure and numbering scheme for complex **2** are shown in Fig. 2. Selected bond lengths and angles are listed in Table 3. The crystal is built up by centrosymmetric Pd-2, 6-$(dipic)_2^{2-}$ anions and Na^+ cations hexacoordinated by four water molecules and two carboxylate oxygens belonging to the $dipic^{2-}$ moiety. The 2,6-dipicolinate ion chelates in a bidentate fashion to the palladium atom and the resulting coordination around the palladium is square planar with Pd–N1 and Pd1–O1 bond distances of 2.028 and 2.004 Å, respectively. The arrangement of the oxygen atoms around the Na^+ ion is approximately octahedral

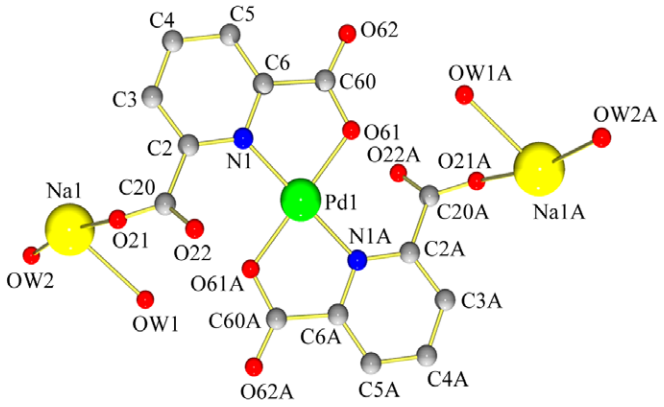

Fig. 2. Molecular structure of complex $[Na_2(H_2O)_4Pd(2,6\text{-dipic})_2]$ (**2**). All hydrogen atoms have been omitted for clarity.

Table 3
Selected bond lengths (Å) and angles (°) in complex **2** with esds in parentheses[a]

Bond lengths (Å)			
Pd1–O61	2.004(3)	Na1–O21	2.384(5)
Pd1–N1	2.028(4)	Na1–O2_a	2.410(4)
Na1–OW1	2.478(5)	Na1–OW1_b	2.541(5)
Na1–OW2	2.411(4)	Na1–OW2_d	2.509(5)
Bond angles (°)			
O61–Pd1–N1	81.43(16)	O61_c–Pd1–N1	98.57(16)
O61–Pd1–O61_c	180.00	N1–Pd1–N1_c	180.00
OW1–Na1–OW2	106.28(17)	OW1–Na1–O21	99.90(18)
OW1–Na1–O2_a	77.99(16)	OW1–Na1–OW1_b	89.99(16)
OW1–Na1–OW2_d	169.71(17)	OW2–Na1–O21	85.61(16)
O2_a–Na1–OW2	171.5(2)	OW1_b–Na1–OW2	90.51(16)
OW2–Na1–OW2_d	84.01(15)	O2_a–Na1–O21	101.00(16)
OW1_b–Na1–O21	170.04(18)	OW2_d–Na1–O21	80.63(17)
OW1_b–Na1–O2_a	82.11(16)	O2_a–Na1–OW2_d	91.80(15)
OW1_b–Na1–OW2_d	89.85(16)	Na1–OW1–Na1_b	90.01(17)
Na1–OW2–Na1_d	95.99(15)		

[a] Symmetry transformations used to generate equivalent atoms: $a = -x, 1-y, 1-z$; $b = -x, 2-y, 2-z$; $c = 1-x, 1-y, 1-z$; $d = 1-x, 2-y, 2-z$.

as shown in Fig. 2. The cation coordination can be rationalized in terms of bond valence [32,33], which assumes that the total charge of the cations has to be saturated by the summation of the separated bond valence s_i of each coordinated atom or ion. The quantity s can be calculated by the expression $s = \exp[(r_0 - r)/B]$, where r is the actual Na–O distance, and r_0, B are parameters empirically determined ($r_0 = 1.803$ and $B = 0.37$) [34]. In the present structure, the value of 1.04 for $\sum s_i$ obtained for the sodium cation is in good agreement with the expected charge value of 1.00. The packing arrangement of **2** consists of cationic Na^+-water and anionic Pd-2,6-dipic^{2-} units to form a two-dimensional coordination-polymeric network as shown in Fig. 3. In the cationic part, solvent water molecules OW1 and OW2 link the Na atoms to form a –Na1–H_2O–Na– zigzag chain where there are two types of Na–Na distances, 3.656 and 3.550 Å. The chains line up in the *ab*-plane and are parallel to the Pd-2,6-dipic^{2-} sheet. Finally, every Pd-2,6-dipic^{2-} layer links two adjacent parallel Na-layers through the oxygen atoms (O2 and O21) to form the two dimensional network. No short contacts between Pd(II) atoms exist, the minimum Pd–Pd distance being 6.569 Å.

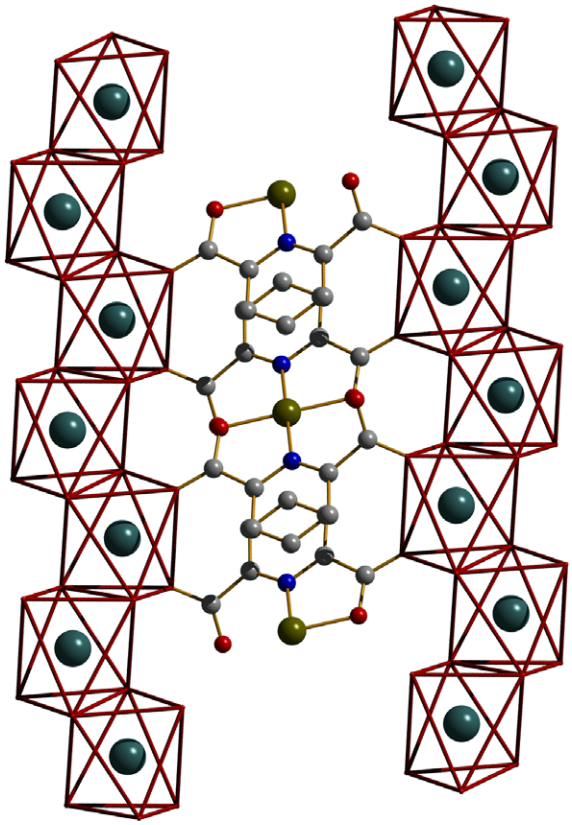

Fig. 3. The perspective view of the packing of $[Na_2(H_2O)_4Pd(2,6\text{-dipic})_2]$ (**2**) comprising of cationic Na^+–H_2O and anionic Pd-2,6-dipic^{2-} units.

A detailed analysis of the crystal geometries reveals an interesting phenomenon in compound **2**. The 1D Na-chain in the crystal shows a significant distortion with short and long alternating Na–Na distances [Na–Na (type 1) = 3.550 Å; Na–Na (type 2) = 3.655 Å]. Examples of Na–H_2O chains are known in the literature whereby alternating Na–Na distances in a particular system do not show any difference. The Na–Na distance in polyhedral $[Na_3(O)_4(H_2O)_{10}]^{3+}$ is 3.477(8) Å [35] and that in the cationic Na–H_2O-malonate chain is 3.786 Å [36]. A marginal difference in Na–Na distances (3.566(3) and 3.534(4) Å) has been reported in $[(L^3VO_2Na)_2(H_2O)_7]_\infty$ (L^3 = a schiff base ligand) [37]. Our observation is very similar to that known in the famous case of Peierls-distortion in *trans*-polyacetylene that leads formation of a gap near the Fermi-energy and leads to insulating behavior of polyacetylene [38,39]; for *trans*-polyacetylene, C=C (type 1) = 1.355 Å; C–C (type 2) = 1.54 Å. Thus, our system with a 1D Na-chain also exhibits a Peierls-distortion. To quantify the hypothesis, we performed a detailed quantum-chemical calculation on the Na-chain as retrieved from the crystal geometry at the DFT-level of B3LYP/6-31G$^+$(d,p). The calculations are performed on a finite sized

Fig. 4. Highest molecular orbital plot for the Na-chain: clearly seen electron localization over alternate Na–Na distances leading to alternate short and long distances supporting the Peierls-distortion in **2**.

(10 atoms) Na-atom chain. The Na atom, having one unpaired electron in the $3s^1$ orbital, shares a similarity to the polyacetylene chain which has one unpaired electron in the p_π orbital. The highest occupied molecular orbital (HOMO) indeed shows a localization of electrons on each alternating short bond and thereby supports the existence of alternating short and long Na–Na bonds with a Na–Na–Na angle of 127.11° (Fig. 4). It is true that the Na-chains do not have conventional bonding in terms of organic molecules. The Na–Na distance in the BCC Na-crystal is 3.72 Å. Of course, Na-crystal is bound through bonding interactions albeit weak in the solid state. One cannot argue that Na-atoms are packed with just hard-sphere packing with no Na–Na interactions. Anyway, in our system the Na–Na bonds are smaller than that in Na-crystal, rendering the possibility of weak interactions between the Na-atoms in the 1D-chains. Otherwise, one could see such localization on each atom and not on the bonds.

3.3. Absorption spectra and luminescence properties

Luminescent Pd(II) complexes are exceedingly rare if compared to the analogous Pt(II) luminophores [40]. With few notable exceptions [41,42], most systems emit only at low temperature and with low efficiency [43–46]. It has been also recognized that when incorporated in polynuclear complexes, Pd(II) centers may lead to partial quenching of luminescence. Nevertheless despite these unfavorable premises, several photoactive palladium(II) complexes recently have been the subject of accurate photophysical studies. The absorption spectrum of complex **1** in DMF solution is dominated by an intense band with the maxima at 267 nm in the ultraviolet region ($\varepsilon = 1.56 \times 10^4\ M^{-1}\ cm^{-1}$) which is assigned to a spin-allowed π–π^* transition. At longer wavelength in the range 320–400 nm, a shoulder is obtained which may be attributed to a metal-to-ligand charge transfer (MLCT) transition. Complex **2** also exhibits a strong band centered at 274 nm with a molar absorption coefficient of $7.19 \times 10^3\ M^{-1}\ cm^{-1}$. In addition, the lower energy band in the range 320–450 nm is assigned to the spin allowed MLCT transition. In the fluorescence emission spectrum of a solution of **1** in DMF (5.0×10^{-6} M) at room temperature, on excitation at 270 nm, the emission peaks are observed at 410 and 430 nm in the visible region and these are independent of the concentration of the solution. A value for quantum efficiency $\Phi_F = 0.04$ has been calculated using *p*-cresol in cyclohexane as a standard. The aqueous solution of compound **2** is very weakly emissive with a Φ_F value of 6.0×10^{-3} (measured against *p*-cresol in cyclohexane).

3.4. Antimicrobial activity

The antimicrobial activity of compound **1** was determined against *Bacillus subtilis*, *Escherichia coli* and *Aspergillus niger* in a medium of nutrient and Czapek-dox broth, respectively for bacteria and mold. 0.1 mL of cell suspension (5.0×10^5 cfu/mL) from 18 h cell culture of bacteria grown on nutrient agar at 37 °C was added per 5 ml of the medium. For *A. niger*, spore suspension was added instead of cell suspension. The compound was dissolved in a mixture of 1:1 DMF and absolute ethanol. The tubes were incubated at 37 °C for 24 h for the growth of the bacteria and at 30 °C for 48 h for mold. The lowest concentration of the compound that resulted in complete inhibition of the visible growth after incubation was recorded as the minimum inhibitory concentration (MIC). The MIC of the compound against *B. subtilis*, *E. coli* and *A. niger* has been found to be 100 μg/mL.

4. Conclusion

In conclusion, we have here shown two palladium derivatives, $[(3,5\text{-Hdmpz})_2Pd_2(\mu\text{-}3,5\text{-dmpz})_2(2,6\text{-dipic})]$ and $[Na_2(H_2O)_4Pd(2,6\text{-dipic})_2]$ which form hydrogen bonded 1D and 2D coordination networks, respectively. Compound **1** has been obtained as a homobimetallic complex bridged by two 3,5-dmpz units without addition of any external base. The central Pd_2N_4 core adopts a boat-like conformation. Compound **2** on the other hand, forms a 2D coordination polymeric network constructed of cationic Na^+–water and anionic Pd-2,6-dipic^{2-} units. Quantum-chemical calculation shows that alternate short and long Na–Na distances observed are due to Peierls-distortion in the Na-chains.

The binuclear compound **1** has been investigated as an inhibitory agent against microbial organisms and shows luminescence property with a Φ_F value of 0.04.

Acknowledgements

We thank Prof. A.K. Guha, Department of Biological Chemistry, IACS, Kolkata for his advice in the study of antimicrobial activity. We thank Mr. A. Datta of JNCASR, Bangalore for discussions on theoretical modelling.

Appendix A. Supplementary material

Full details of the crystal structure analyses of **1** and **2** have been deposited with the Cambridge Crystallographic Data Center, (CCDC Nos. 299284 and 299285). Copies may be obtained free of charge on application to the Director, CCDC, 12 Union Road, Cambridge CB2 1EZ, UK, fax: +44 1223 336 033, e-mail: deposit@ccdc.cam.ac.uk or on the www.ccdc.cam.ac.uk. Supplementary data associated with this article can be found, in the online version, at doi:10.1016/j.poly.2006.05.030.

References

[1] A.P. Sadimenko, S.S. Basson, Coord. Chem. Rev. 147 (1996) 247.
[2] G.L. Monica, G.A. Ardizzoia, Prog. Inorg. Chem. 46 (1997) 151.
[3] A.P. Sadimenko, Adv. Heterocycl. Chem. 80 (2001) 157.
[4] L. Falvello, J. Forniés, A. Martin, R. Navarro, V. Sicilia, P. Villarroya, Chem. Commun. (1998) 2429.
[5] C. Pettinari, F. Marchetti, A. Cingolani, S.I. Troyonov, A. Drozdov, J. Chem. Soc., Dalton Trans. (1998) 3335.
[6] S. Trofimenko, Prog. Inorg. Chem. 34 (1986) 115.
[7] F. Maury, J. Phys. IV 5 (1995) C5-449.
[8] R. Abul, M.B. Cleaver, J.S. Taylor, Inorg. Chem. 31 (1992) 3636.
[9] J. Forniés, A. Martín, V. Sicilia, L.F. Martín, Chem. Eur. J. 9 (2003) 3427.
[10] I. Ara, J. Forniés, R. Lasheras, A. Martín, V. Sicilia, Eur. J. Inorg. Chem. (2006) 948.
[11] A. Tiripicchio, F.J. Lahoz, L.A. Oro, M.T. Pinillos, C. Tejel, Inorg. Chim. Acta 100 (1985) L5.
[12] A.V. Godoy Netto, A.E. Mauro, R.C.G. Frem, A.M. Santana, R.H.A. Santos, J.R. Zoia, J. Coord. Chem. 54 (2001) 129.
[13] M.I. Bruce, B.L. Goodall, I. Masuda, Aust. J. Chem. 28 (1975) 1259.
[14] G. Chessa, G. Marangoni, B. Pitteri, V. Bertolasi, G. Gilli, V. Ferretti, Inorg. Chim. Acta 185 (1991) 201.
[15] P. Espinet, J.A. Miguel, S. García-Granda, D. Miguel, Inorg. Chem. 35 (1996) 2287.
[16] R.F. Heck, Palladium Reagents in Organic Synthesis: Best Synthetic Methods, Academic Press, New York, 1985.
[17] A.D. Becke, J. Chem. Phys. 98 (1993) 5648.
[18] M.J. Frisch, G.W. Trucks, H.B. Schlegel, G.E. Scuseria, M.A. Robb, J.R. Cheeseman, J.A. Montgomery Jr., T. Vreven, K.N. Kudin, J.C. Burant, J.M. Millam, S.S. Iyengar, J. Tomasi, V. Barone, B. Mennucci, M. Cossi, G. Scalmani, N. Rega, G.A. Petersson, H. Nakatsuji, M. Hada, M. Ehara, K. Toyota, R. Fukuda, J. Hasegawa, M. Ishida, T. Nakajima, Y. Honda, O. Kitao, H. Nakai, M. Klene, X. Li, J.E. Knox, H.P. Hratchian, J.B. Cross, C. Adamo, J. Jaramillo, R. Gomperts, R.E. Stratmann, O. Yazyev, A.J. Austin, R. Cammi, C. Pomelli, J.W. Ochterski, P.Y. Ayala, K. Morokuma, G.A. Voth, P. Salvador, J.J. Dannenberg, V.G. Zakrzewski, S. Dapprich, A.D. Daniels, M.C. Strain, O. Farkas, D.K. Malick, A.D. Rabuck, K. Raghavachari, J.B. Foresman, J.V. Ortiz, Q. Cui, A.G. Baboul, S. Clifford, J. Cioslowski, B.B. Stefanov, G. Liu, A. Liashenko, P. Piskorz, I. Komaromi, R.L. Martin, D.J. Fox, T. Keith, M.A. Al-Laham, C.Y. Peng, A. Nanayakkara, M. Challacombe, P.M.W. Gill, B. Johnson, W. Chen, M.W. Wong, C. Gonzalez, J.A. Pople, GAUSSIAN 03, Revision B.05, Gaussian, Inc., Pittsburgh, PA, 2003.
[19] G.M. Sheldrick, Acta Crystallogr., Sect. A 46 (1990) 467.
[20] G.M. Sheldrick, SHELXL-97, Program for Crystal Structure Refinement, University of Göttingen, 1997.
[21] G.W. Henslee, J.D. Oliver, J. Cryst. Mol. Struct. 7 (1977) 137.
[22] V.K. Jain, S. Kannan, E.R.T. Tiekink, J. Chem. Soc., Dalton Trans. (1992) 2231.
[23] C.H. Cheng, J.S. Lain, Y.J. Wu, S.L. Wang, Acta Crystallogr., Sect. C 46 (1990) 208.
[24] V.K. Jain, S. Kannan, E.R.T. Tiekink, J. Chem. Soc., Dalton Trans. (1993) 3625.
[25] V.Y. Kukushkin, E.A. Aleksandrova, V.M. Leovac, E.Z. Iveges, V.K. Belsky, V.E. Konovalov, Polyhedron 11 (1992) 2691.
[26] G.A. Ardizzoia, G. La Monica, S. Cenini, M. Moret, N. Masciocchi, J. Chem. Soc., Dalton Trans. (1996) 1351.
[27] A.B. Goel, S. Goel, D. Vanderveer, Inorg. Chim. Acta 82 (1984) L9.
[28] J. Ruiz, F. Florenciano, M.A. Sánchez, G. López, M.C. Ramírez de Arellano, J. Pérez, Eur. J. Inorg. Chem. (2000) 943.
[29] M. Nardelli, Comput. Chem. 7 (1983) 95.
[30] J. Pons, A. Chadghan, J. Casabo, A. Alvarez-Larena, J.F. Piniella, J. Ros, Inorg. Chem. Commun. 3 (2000) 296.
[31] A. Boixassa, J. Pons, X. Solans, M. Font-Bardia, J. Ros, Inorg. Chem. Commun. 6 (2003) 922.
[32] L. Pauling, J. Am. Chem. Soc. 51 (1929) 1010.
[33] I.D. Brown, Chem. Soc. Rev. 7 (1978) 359.
[34] I.D. Brown, D. Aldermatt, Acta Crystallogr., Sect. B 41 (1985) 244.
[35] G. Cao, R.C. Haushalter, K.G. Strohmaier, Inorg. Chem. 32 (1993) 127.
[36] D. Ghoshal, T.K. Maji, T. Mallah, T.-H. Lu, G. Mostafa, N. Ray Chaudhuri, Inorg. Chim. Acta 358 (2005) 1027.
[37] S. Samanta, S. Mukhopadhyay, D. Mandal, R.J. Butcher, M. Chaudhury, Inorg. Chem. 42 (2003) 6284.
[38] A.J. Heeger, Angew. Chem., Int. Ed. 40 (2001) 2591.
[39] A.J. Heeger, Rev. Mod. Phys. 60 (1988) 781.
[40] (a) M. Maestri, V. Balzani, C. Deuschel-Cornioley, A. von Zelewsky, Adv. Photochem. 17 (1992) 1;
(b) W. Paw, S.D. Cummings, M.A. Mansour, W.B. Connick, D.K. Geiger, R. Eisenberg, Coord. Chem. Rev. 171 (1998) 125.
[41] Y. Wakatsuki, H. Yamazaki, P.A. Grutsch, M. Santhaman, C. Kutal, J. Am. Chem. Soc. 107 (1985) 8153.
[42] M. Ghedini, D. Pucci, G. Calogero, F. Barigelletti, Chem. Phys. Lett. 267 (1997) 341.
[43] (a) C. Deuschel-Cornioley, T. Ward, A. von Zelewsky, Helv. Chim. Acta 71 (1988) 130;
(b) M. Maestri, D. Sandrini, V. Balzani, A. von Zelewsky, C. Deuschel-Cornioley, P. Jolliet, Helv. Chim. Acta 71 (1988) 1053;
(c) F. Barigelletti, D. Sandrini, M. Maestri, V. Balzani, A. von Zelewsky, L. Chassot, P. Jolliet, U. Maeder, Inorg. Chem. 27 (1988) 3644.
[44] C.A. Craig, R.J. Watts, Inorg. Chem. 28 (1989) 309.
[45] G. Guglielmo, V. Ricevuto, A. Giannetto, S. Campagna, Gazz. Chim. It. 119 (1989) 457.
[46] (a) V.W.-W. Yam, V.W.-M. Lee, K.-K. Cheung, Organometallics 16 (1997) 2833;
(b) E. Zahavy, M.A. Fox, Chem. Eur. J. 4 (1998) 1647;
(c) R.V. Slone, K.D. Benkstein, S. Belanger, J.T. Hupp, I.A. Guzei, A.L. Rheingold, Coord. Chem. Rev. 171 (1998) 221.

the metal–oxime interactions. The application of a previously developed theoretical model for $Ni(TRISOXH_3)Cl_2$ [7] to very similar complexes yields insight into the applicability and feasibility of using molecular modeling to explore the more complicated oxygen active complexes.

The series of complexes chosen for this study (Fig. 1) includes $Ni(TRISOXH_3)Cl_2$ (**1**), $Ni(TRISOXH_3)Br_2$ (**2**), $[Ni(TRISOXH_3)(CH_3OH)I]I$ (**3**), and $[Ni(TRISOXH_3)(H_2O)_2]F_2 \cdot 2H_2O$ (**4**). The complexes have been studied by a combined experimental and theoretical approach utilizing X-ray crystallography, vibrational spectroscopy and molecular modeling. X-ray crystallography has provided structural information for the series of complexes. Infrared and Raman spectroscopy reveal trends in the intraligand and metal ligand vibrations that result from the influences of the different halide or solvent ligands. As the molecules of interest are all relatively large transition metal complexes with two unpaired electrons, density functional theory is employed as the principal theoretical method; this approach has been successfully employed for studying electronic structure of transition metal systems [8–12].

We recently detailed the development of a theoretical model for $Ni(TRISOXH_3)Cl_2$ that compared the results of density functional theory (DFT) calculations with a variety of basis sets to structural and vibrational data [7]. This model, including theory level and basis set choice, has now been applied to the other complexes in the series. When using the functional B3LYP, the addition of polarization and diffuse functions to the metal center basis set has been shown to increase accuracy, notably in reproducing the metal–ligand bond lengths [7–12]. A theoretical model of the complex $Ni(TRISOXH_3)F_2$ (**5**), which has not yet been successfully isolated, is also presented and discussed. Electronic structure analysis is facilitated by performing a natural population analysis (npa) of the optimized theoretical models [13–15]. As a more useful alternative to the default Mulliken analysis, npa assists evaluation of the total and atomic spin densities as well as comparison of the natural charges of the metal, halide or solvent ligands, and the three oxime groups of the $TRISOXH_3$ ligand. This study highlights the utility of and caveats related to employing DFT theoretical models to a series of similar transition metal complexes notably in the pursuit of understanding the role of ligand variation in optimizing the unusual substrate oxidation chemistry of $Ni^{II}(TRISOX)$ derivatives. In addition, this work exploits an interesting wavenumber scaling approach to improve the correlation between experimental and theoretical vibrational modes previously developed and now applied to a series of similar complexes. The data suggest a single empirically derived linear scale function can be applied to other complexes, which are very similar in electronic structure to significantly improve the agreement between experimental and theoretical frequencies.

2. Experimental methods

2.1. Synthesis of complexes

All solvents and chemicals were obtained from Fisher/Acros or Sigma–Aldrich and were used as supplied, unless otherwise indicated. Syntheses of the ligand tris(1-propan-2-onyl oxime)-amine ($TRISOXH_3$) [5], $Ni(TRISOXH_3)Cl_2$ (**1**) [2], and $[Ni(TRISOXH_3)(NO_3)(H_2O)](NO_3)$ [1] have been previously reported.

2.1.1. $Ni(TRISOXH_3)Br_2$ (2)

0.46 mmol (0.21 g) of $[Ni(TRISOXH_3)(NO_3)(H_2O)](NO_3)$ was dissolved in 5 mL acetonitrile to form a purple solution; 1.02 mmol (0.33 g) of tetraethylammonium bromide was added and the mixture was stirred for approximately 5 min with gentle heating. The resulting blue-green solution was evaporated; the solid (75% yield) was dissolved in methanol and recrystallized by ethyl acetate vapor diffusion. Sapphire blue crystals were obtained. *Anal*. Calc. for $NiC_9N_4O_3H_{18}Br_2$: C, 24.09; H, 4.04; N, 12.48. Found: C, 24.35; H, 3.72; N, 12.52%.

2.1.2. $[Ni(TRISOXH_3)(CH_3OH)I]I$ (3)

After 30 mL methanol was purged with Ar for 30 min, 2.17 mmol (0.5 g) of $TRISOXH_3$ was combined with

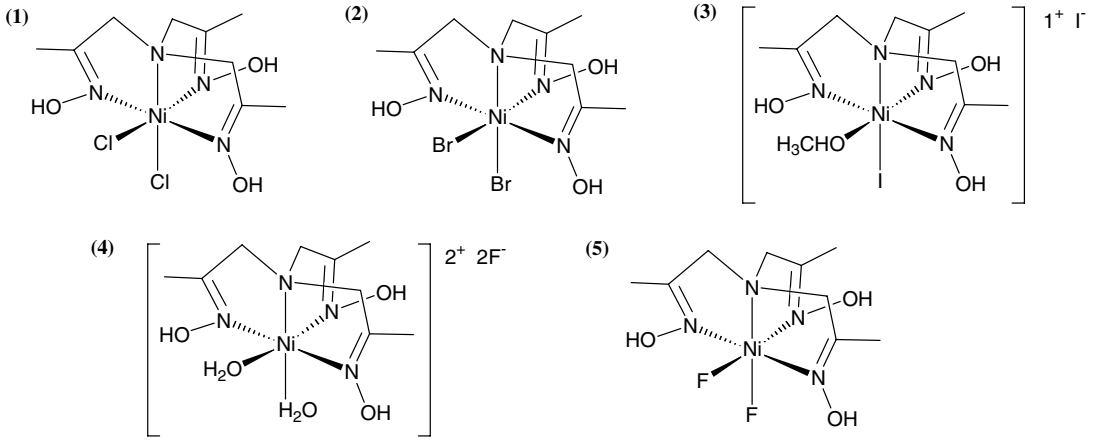

Fig. 1. Halide series of complexes $Ni(TRISOXH_3)Cl_2$ (**1**), $Ni(TRISOXH_3)Br_2$ (**2**), $[Ni(TRISOXH_3)(CH_3OH)I]I$ (**3**), $[Ni(TRISOXH_3)(H_2O)_2]F_2 \cdot 2H_2O$ (**4**), and $Ni(TRISOXH_3)F_2$ (**5**).

Table 1
Crystallographic data and structure refinement for **2**, **3**, and **4**

Complex	**2**	**3**	**4**
Empirical formula	$C_9H_{18}Br_2N_4NiO_3$	$[C_{10}H_{22}IN_4NiO_4]I$	$[C_9H_{22}N_4O_5Ni]F_2 \cdot 2H_2O$
Formula weight	448.80	574.83	399.05
Temperature (K)	295(2)	150(2)	150(2)
Crystal system	monoclinic	orthorhombic	monoclinic
Space group	$P2_1/n$	$Pbca$	$P2_1/n$
Unit cell dimensions			
a (Å)	9.2134(5)	8.0740(2)	8.2001(5)
b (Å)	18.0080(9)	15.3781(4)	14.0265(9)
c (Å)	9.3824(5)	28.4815(8)	14.8658(9)
α (°)	90	90	90
β (°)	94.5930(10)	90	96.9720(10)
γ (°)	90	90	90
V (Å^3)	1551.68(14)	3536.34(16)	1697.20(18)
Z	4	8	4
D_{calc} (Mg/m^3)	1.921	2.159	1.562
Absorption coefficient (mm^{-1})	6.409	4.608	1.202
Final R indices [$I > 2\sigma(I)$]	$R_1 = 0.0350$, $wR_2 = 0.0748$	$R_1 = 0.0198$, $wR_2 = 0.0457$	$R_1 = 0.0548$, $wR_2 = 0.1134$
R indices (all data)	$R_1 = 0.0476$, $wR_2 = 0.0784$	$R_1 = 0.0274$, $wR_2 = 0.0491$	$R_1 = 0.0566$, $wR_2 = 0.1141$

0.679 g nickel (II) iodide hydrate with stirring and low heat until dissolved, forming a green brown solution. The complex was crystallized by vapor diffusion of ethyl acetate into the reaction solution. Light blue-purple rods were obtained in a 40% yield. *Anal.* Calc. for $NiC_{10}N_4O_4H_{22}I_2$: C, 20.90; H, 3.86; N, 9.75. Found: C, 20.61; H, 3.46; N, 9.61%.

2.1.3. *[Ni(TRISOXH$_3$)(H$_2$O)$_2$]F$_2$ · 2H$_2$O (**4**)*

0.58 mmol (0.26 g) of [Ni(TRISOXH$_3$)(NO$_3$)(H$_2$O)](NO$_3$) was dissolved in 20 mL acetonitrile to form a purple solution; 1.2 mmol (0.40 g) of tetrabutylammonium fluoride trihydrate was added with gentle heating and stirring. After the salt dissolved, the solution turned green and a light purple powder precipitate formed. The purple powder (60% yield) was filtered, washed with acetonitrile, redissolved in methanol and recrystallized by ethyl acetate vapor diffusion. Lavender plates were obtained. *Anal.* Calc. for $NiC_9N_4O_7H_{26}F_2$: C, 27.28; H, 5.43; N, 13.88. Found: C, 27.09; H, 5.87; N, 14.04%.

3. X-ray crystallography: general procedures

Intensity data for **2** (150 K) and **4** (295 K) were collected on a Bruker SMART 1K CCD diffractometer while data for **3** (150 K) were collected on a Bruker SMART6000 CCD diffractometer. Both instruments used graphite-monochromated Mo Kα radiation, $\lambda = 0.71073$ Å, and a detector distance of 5 cm. A series of 10–30 s data frames measured at 0.3° increments of ω were collected to calculate a unit cell. For data collection, frames were measured for 10–25 s at 0.3° intervals of ω with a maximum θ value of 26° for **2** and 28° for **3** and **4**. All frames were processed using the program SAINT.[3] Absorption and beam corrections were applied using SADABS [16].

[3] SMART v5.622 & 5.628 and SAINT v6.02A & 6.28A programs were used for data collection and data processing, respectively.

All structures were solved by a combination of direct methods in SHELXTL [17] and the difference Fourier technique and refined by full-matrix least-squares on F^2. Non-hydrogen atoms were refined with anisotropic displacement parameters. For all complexes, the –OH hydrogens were located directly and the positions refined. All remaining hydrogen atoms were either located directly or calculated based on geometric criteria and treated with a riding model. The isotropic temperature factors for the hydrogen atoms were set as a^*U_{eq} of the adjacent atom ($a = 1.5$ for methyl and hydroxyl and 1.2 for all others). The refinements converged with crystallographic parameters as summarized in Table 1.

3.1. Vibrational spectroscopy

Raman spectra were collected using a SPEX 1404 0.85 m double spectrometer with a liquid N_2 cooled 13.6 mm back-thinned SPEX Spectrum-1 CCD chip detector. Raman scattering was excited by the 488.0 nm or 514.5 nm line of a Coherent 10 W Sabre Ar ion laser; the laser lines were chosen for intensity and the availability of holographic notch filters. The power used was typically 300 mW at the sample and no sample decomposition was observed. The scattered light was directed through a Kaiser Optical Systems holographic SuperNotch filter for each wavelength. Raman shifts were calibrated against the appropriate Raleigh line. Samples for Raman experiments were prepared by finely grinding the recrystallized complex with an agate mortar and pestle and filling a 1 mm i.d. melting point capillary tube. Samples were cooled to approximately −100 °C by a liquid nitrogen chilled stream of N_2 gas blown thru a quartz EPR-type cooling tube (Bruker Instruments). Resulting spectra were 4-point baseline corrected using GRAMS/32 (v5.22) and then multiple corrected spectra were averaged to improve the signal-to-noise ratios. Infrared spectra were collected using a Bio-Rad

Excalibur spectrometer and samples were dispersed in a KBr pellet.

3.2. Theoretical calculations

All calculations were performed with GAUSSIAN-98, Version A.11 [18] (G98) for **2**, **3**, and **5** and with GAUSSIAN-03, Revision B.05 [19] (G03) for **4** on a cluster of 16 Linux nodes, each with a 1.4 GHz processor. Modeling was performed on each molecule in its entirety, excluding solvents of crystallization and non-coordinated halides; gas-phase geometry optimizations and frequency calculations had neither symmetry constraints nor bond restrictions imposed. The theoretical models of **2** and **5** were neutral while **3** and **4** were given overall charges of 1^+ and 2^+, respectively. Spin unrestricted calculations on each triplet complex were first performed at Hartree–Fock levels with the 6-31G(d) basis set on all atoms; all further calculations used this UHF/6-31G(d) optimized geometry as a starting point. Density functional calculations facilitated the Becke three-parameter hybrid exchange functional [20] and the Lee, Yang, and Parr correlation functional [21], hereafter abbreviated B3LYP. Often, split basis sets were employed, via the *gen* keyword of G98, which applied a larger basis set such as 6-311+G(d) to the metal center and the smaller 6-31G(d) to

Table 2
Computational details for complexes **1**–**5**

Complex	Theory level	Basis set C, N, O, H	Basis set X	Basis set Ni
1	ub3lyp	6-31G(d)	6-311++G(d,p)	6-311++G(d,p)
2	ub3lyp	6-31G(d)	6-31G(d)	6-311+G(d)
3	ub3lyp	6-31G(d)	lanl2dz	lanl2dz
4	ub3lyp	6-31G(d)	6-31G(d)	6-311+G(d)
5	ub3lyp	6-31G(d)	6-311++G(d,p)	6-311++G(d,p)

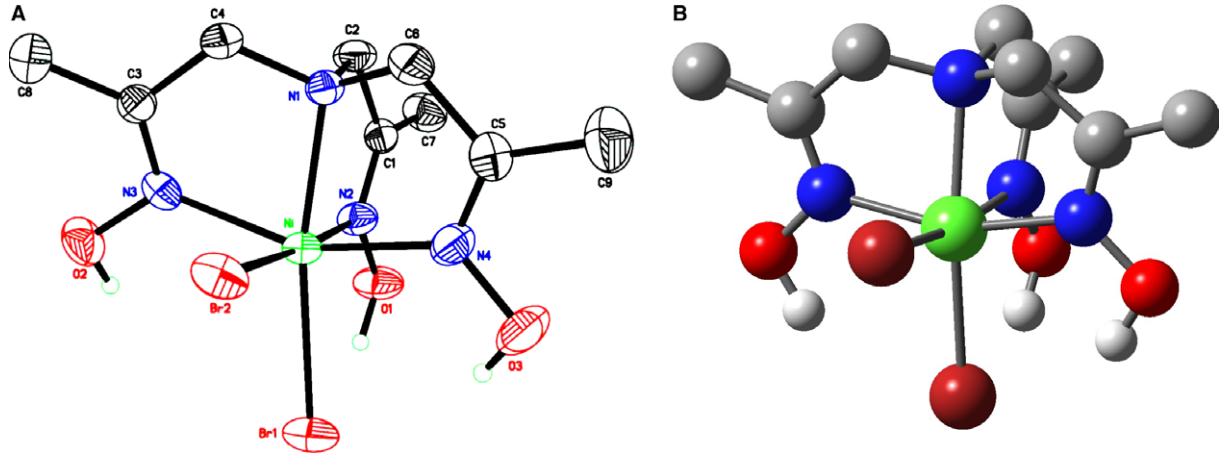

Fig. 2. Comparison of molecular geometries from X-ray crystallography (A, ORTEP view, 50% probability) and computationally optimized geometry (B) of $Ni(TRISOXH_3)Br_2$ (**5**), where the atoms correlate exactly to the arrangement shown in A. In both, methylene and methyl hydrogen atoms are omitted for clarity.

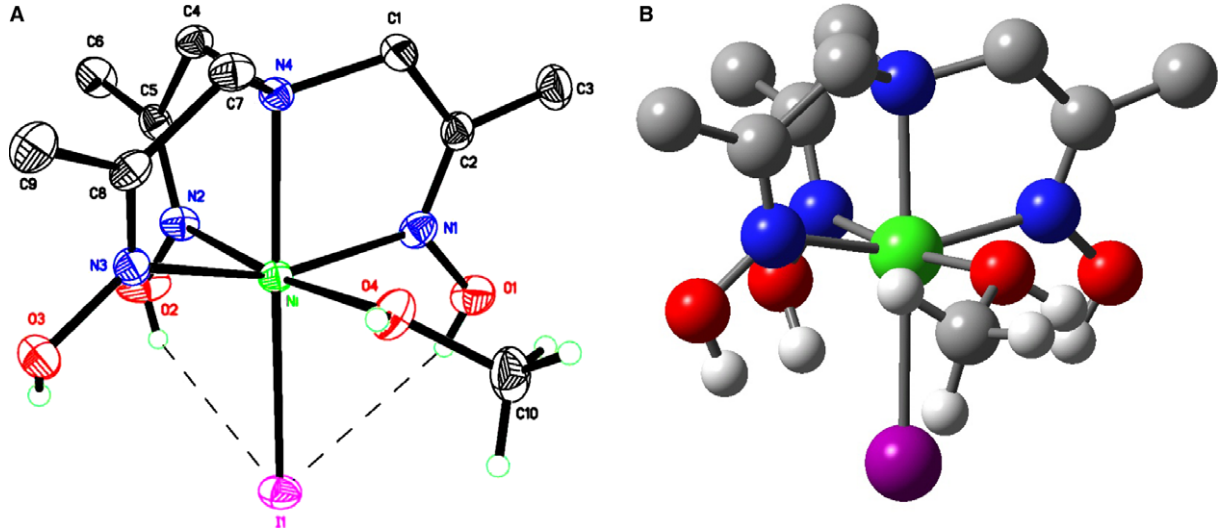

Fig. 3. Comparison of molecular geometries from X-ray crystallography (A, ORTEP view, 50% probability) and computationally optimized geometry (B) of $[Ni(TRISOXH_3)(CH_3OH)I]I$ (**3**), where the atoms correlate exactly to the arrangement shown in A. In both, methylene and methyl hydrogen atoms are omitted for clarity.

all other atoms. Except in the case of **3**, all-electron basis sets were chosen for accuracy. Due to the size of iodide, modeling complex **3** required additional considerations; the LANL2DZ basis set was applied to both the metal center and iodide in all calculations of **3**. Table 2 is a summary of the relevant theory and basis set details. Natural population analysis was preformed using the pop = npa keyword of Gaussian; GaussView was used to visualize molecular vibrations and spin density [22].

4. Results and analysis

Figs. 2–4 show the crystal structures and theoretically optimized geometry of **2**, **3**, and **4**, respectively; these data for **1** have been previously reported [7]. All complexes are characterized by a pseudo-octahedral geometry and intramolecular hydrogen bonding between the oxime protons and the axial halide. Intermolecular hydrogen bonds are also observed in the crystal structure; in **2**, the proton on O2 is intermolecularly H-bonded to Br2 of an adjacent molecule; in **3**, the proton on O3 is intermolecularly H-bonded to non-coordinated iodide in the crystal lattice; in **4**, the bound water molecules are intermolecularly H-bonded to non-coordinated fluoride ions in the crystal lattice. Selected bond distances are given in Tables 3–5 for the experimental crystal structures and best theoretical models.

Theoretical models for **2**, **3**, and **4** show good agreement with the experimental crystal structures, especially for important intraligand features, such as the carbon–nitrogen imine and nitrogen–oxygen oxime bonds, and the metal–ligand bonds. These data have similar average absolute deviations from experiment as observed for $Ni(TRISOXH_3)Cl_2$ (**1**): for the intraligand bonds noted, **1** (0.0141 Å), **2** (0.0196 Å), **3** (0.0175 Å), **4** (0.0128 Å); for the metal–ligand bonds, **1** (0.0320 Å), **2** (0.0495 Å), **3** (0.0452 Å), **4** (0.0476 Å). As an expected result of crystal-packing interactions, intermolecular hydrogen-bonds, and less accurate hydrogen atom determination based on X-ray rather than neutron data, bond angles and hydrogen-bonding distances in the crystal structures are not well reproduced in the theoretical models; these data are available in Tables 1S–4S. However, the observed deviations between the experiment and models for these features in **2**, **3**, and **4** are similar to those calculated for **1** [7].

Table 3
Geometry comparison of crystal structure and theoretical model for $Ni(TRISOXH_3)Br_2$ (**2**)

Feature	Crystal structure	ub3lyp/6-31G(d) and 6-311+G(d)
X(axial)	Br1	Br
X(equatorial)	Br2	Br
Ni–N(amine)	2.112(3)[a]	2.1546(0.0436)[b]
Ni–N(a)[c]	2.099(3)	2.0333(0.0657)
Ni–N(b)	2.049(3)	2.1253(0.0763)
Ni–N(c)	2.045(3)	2.0332(0.0108)
Ni–X(axial)	2.5513(5)	2.5219(0.0295)
Ni–X(eq)	2.5915(5)	2.5205(0.0710)
C=N(a)	1.274(4)	1.2817(0.0077)
C=N(b)	1.272(4)	1.2787(0.0067)
C=N(c)	1.265(4)	1.2818(0.0468)
N(a)–O	1.401(4)	1.3739(0.0271)
N(b)–O	1.396(3)	1.371(0.0260)
N(c)–O	1.390(4)	1.374(0.0030)
H(a)···X(axial)[d]	3.65(5)	2.652(0.968)
H(b)···X(axial)	2.48(5)	2.2496(0.1304)
H(c)···X(axial)	2.58(5)	2.6597(0.1497)

[a] All bond distances shown in Å, crystal structure e.s.d.'s are provided in parentheses when available.
[b] Absolute deviations of calculated values from experimental data are given in parentheses.
[c] Letter designations on atoms have the following meaning: N1 represents the amine, N(a) and N(c) are oxime bound nitrogen atoms coordinated *trans* to each other – equivalent in calculations with C_s symmetry, N(b) is the oxime bound N *trans* to the equatorial ligand (denoted X(eq)), X(axial) is *trans* to the amine, H(a) is the proton on the oxygen of oxime with N(a) and similarly for H(b) and H(c).
[d] ··· indicates hydrogen bonding and/or through space distances.

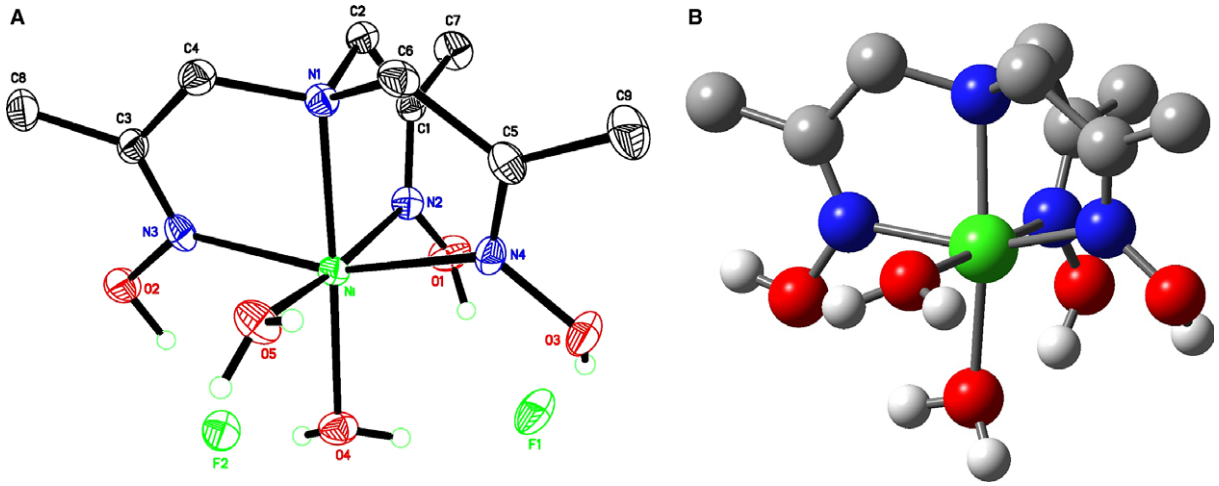

Fig. 4. Comparison of molecular geometries from X-ray crystallography (A, ORTEP view, 50% probability) and computationally optimized geometry (B) of $[Ni(TRISOXH_3)(H_2O)_2]F_2 \cdot 2H_2O$ (**4**), where the atoms correlate exactly to the arrangement shown in A. In both, methylene and methyl hydrogen atoms are omitted for clarity. In B, no fluorides were included in the optimization.

Table 4
Geometry comparison of crystal structure and theoretical model for $[Ni(TRISOXH_3)(CH_3OH)I]I$ (**3**)

Feature	Crystal structure	ub3lyp/6-31G(d) and LANL2DZ
X(axial)	I1	I
X(equatorial)	O4	O
Ni–N(amine)	2.096(2)[a]	2.1657(0.0697)[b]
Ni–N(a)[c]	2.053(2)	2.0780(0.0250)
Ni–N(b)	2.044(2)	2.0946(0.0456)
Ni–N(c)	2.044(2)	2.0857(0.0417)
Ni–X(axial)	2.7056(3)	2.7208(0.0152)
Ni–X(eq)	2.1195(19)	2.1937(0.0737)
C=N(a)	1.280(3)	1.2841(0.0041)
C=N(b)	1.272(3)	1.2803(0.0083)
C=N(c)	1.269(3)	1.2847(0.0157)
N(a)–O	1.400(3)	1.3739(0.0261)
N(b)–O	1.401(3)	1.3731(0.0279)
N(c)–O	1.398(3)	1.3753(0.0227)
H(a)···X(axial)[d]	3.47(4)	2.9446(0.5255)
H(b)···X(axial)	2.81(4)	2.6586(0.1614)
H(c)···X(axial)	2.83(4)	2.9176(0.0876)

[a–d] See footnotes for Table 3.

Table 5
Geometry comparison of crystal structure and theoretical model for $[Ni(TRISOXH_3)(H_2O)_2]F_2 \cdot 2H_2O$ (**4**)

Feature	Crystal structure	ub3lyp/6-31G(d) and 6-311+G(d)
X(axial)	O4	O
X(equatorial)	O5	O
Ni–N(amine)	2.088(3)[a]	2.1061(0.0181)[b]
Ni–N(a)[c]	2.073(3)	2.0400(0.0330)
Ni–N(b)	2.070(3)	2.0128(0.0562)
Ni–N(c)	2.056(3)	2.0668(0.0108)
Ni–X(axial)	2.041(3)	2.1609(0.1189)
Ni–X(eq)	2.089(3)	2.1374(0.0484)
C=N(a)	1.288(5)	1.2847(0.0034)
C=N(b)	1.267(5)	1.2825(0.0155)
C=N(c)	1.277(5)	1.2907(0.0127)
N(a)–O	1.391(4)	1.3811(0.0101)
N(b)–O	1.410(4)	1.3787(0.0323)
N(c)–O	1.391(4)	1.3927(0.0027)
H(a)···X(axial)[d]	2.88(5)	3.7982(1.0482)
H(b)···X(axial)	2.91(5)	2.1116(0.6785)
H(c)···X(axial)	3.05(5)	3.4871(0.3471)

[a–d] See footnotes for Table 3.

One exception to the generally excellent correlation between the theoretical models and experimental data is observed in the Ni–amine bond lengths. The expected lengthening of the bond due to the *trans* influence of the axial halide is observed in the theoretical geometries [Ni–amine bond length for axial ligands I^- (2.1657 Å) > Br^- (2.1546 Å) > Cl^- (2.1471 Å)], however, it is not observed in the crystallographic data [I^- (2.096(2) Å), Br^- (2.112(3) Å), Cl^- (2.1131(13) Å)].

Vibrational spectra for **1**–**4** are shown in Figs. 5–9 along with theoretical line spectra for five regions, which include important metal–ligand and intraligand vibrations. By comparison to the mode assignments empirically derived

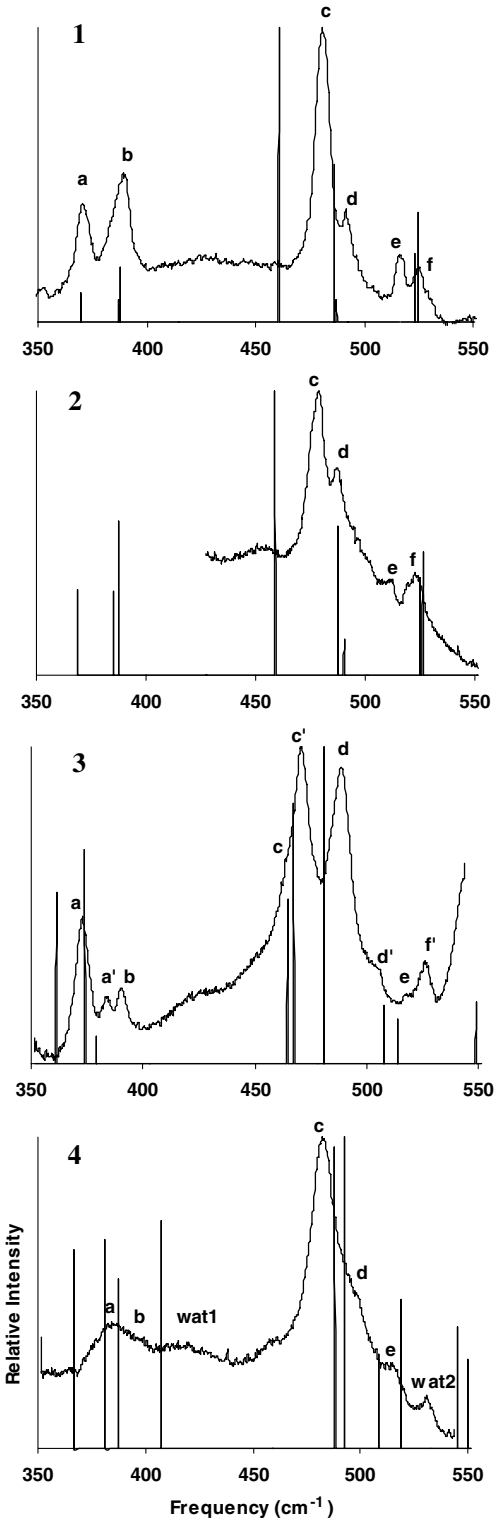

Fig. 5. Raman spectra and calculated vibrational positions and intensities for **1**–**4**, 350–550 cm^{-1}.

for **1**, via isotopic labeling [7], and the predicted theoretical modes, the vibrational modes for **2**, **3**, and **4** are assigned in Tables 6–8. Individual modes are assigned bold lower-case letters or phrases to aid in discussion. When the modes assigned for **2**, **3**, and **4** are very similar to those for **1**, the same lower case letter is used for each mode. Modes

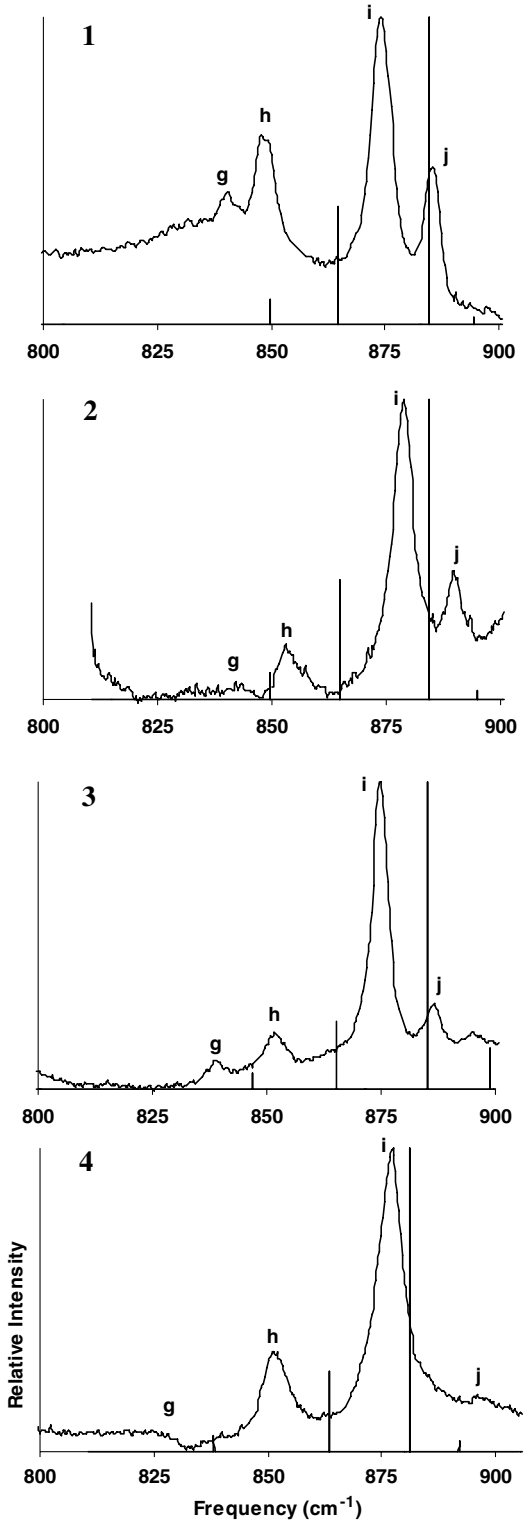

Fig. 6. Raman spectra and calculated vibrational positions and intensities for **1**–**4**, 800–900 cm^{-1}.

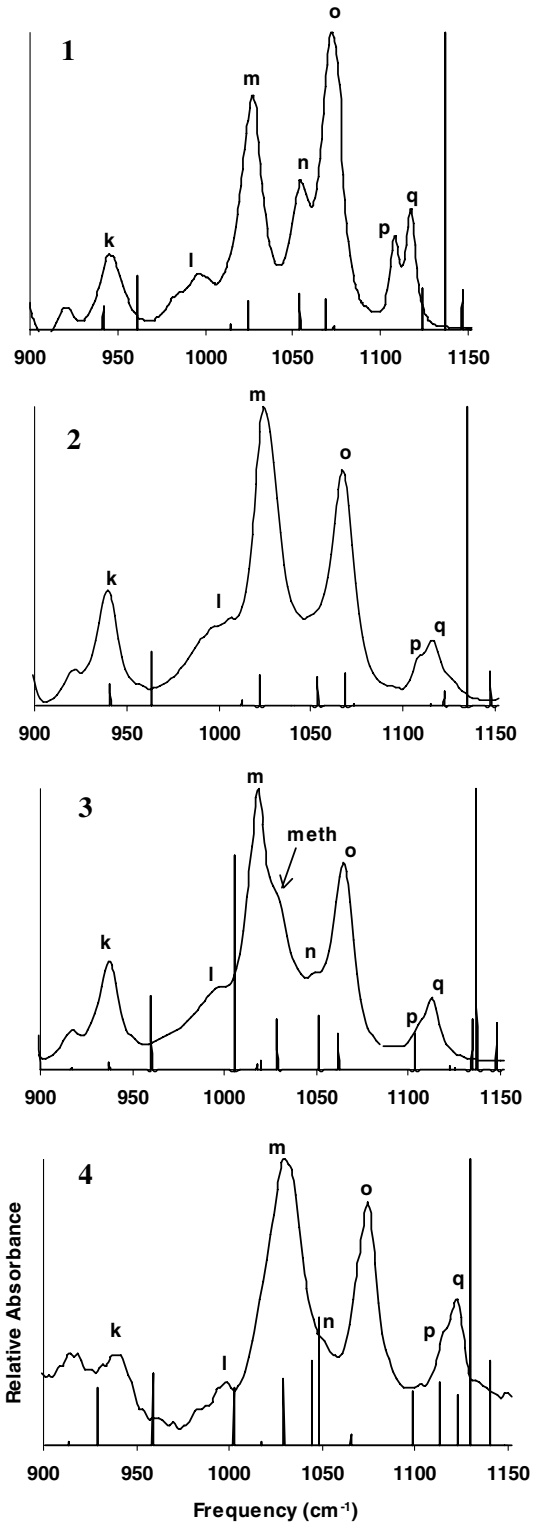

Fig. 7. Infrared spectra and calculated vibrational positions and intensities for **1**–**4**, 900–1150 cm^{-1}.

that are similar to those for **1**, but substantially influenced by the different X ligands of the halide series, are given the same descriptive letter as for **1** with a prime or double prime, for **3** and **4**, respectively. For example, upon substitution of methanol in the equatorial position in **3**, the symmetry is reduced to C_1 and two Ni–N(amine) stretching modes (labeled c and c′) are observed rather than the one mode observed (c) for **1**. Modes which exhibit bound solvent vibrations are given a phrase assignment, e.g. **meth** for the methanol centered vibration at 1030.0 cm^{-1} in **3**.

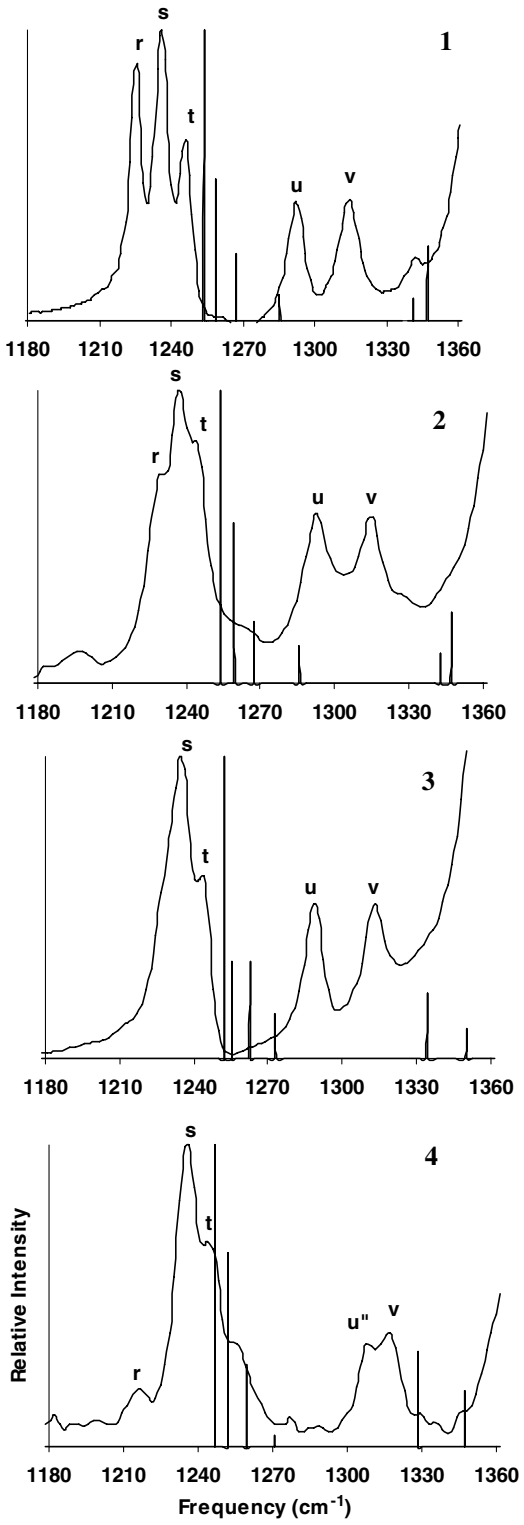

Fig. 8. Infrared spectra and calculated vibrational positions and intensities for **1**–**4**, 1180–1350 cm^{-1}.

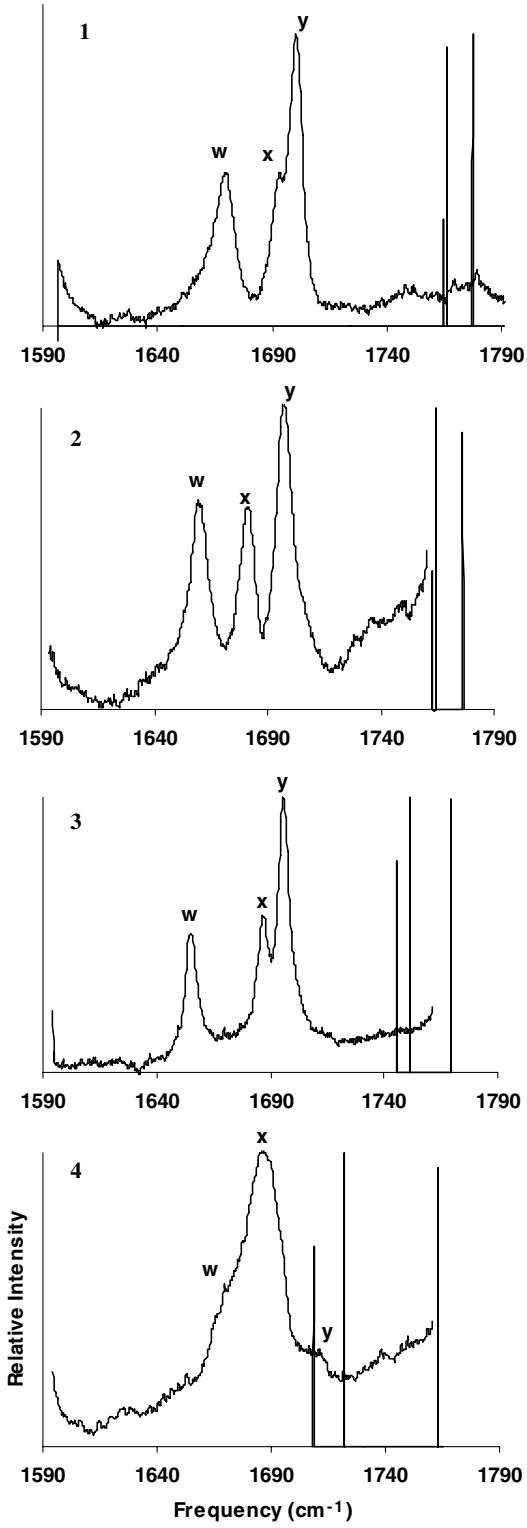

Fig. 9. Raman spectra and calculated vibrational positions and intensities for **1**–**4**, 1590–1790 cm^{-1}.

The complex closest to the benchmark $Ni(TRISOXH_3)Cl_2$ is **2** and very similar modes were observed experimentally and predicted theoretically. However, for complexes **3** and **4**, the loss of mirror symmetry leads to different mixing of the molecules' internal coordinates and thus different descriptions for the fundamental vibrational modes. For example, the two lowest energy imine stretches for **1** and **2** are clearly the asymmetric and symmetric combinations of the C=N(a) and C=N(c) stretches. However, for **3** and **4**, which do not have a mirror plane of symmetry, the two lowest energy imine stretches are dominated by either the C=N(a) or C=N(c) stretch. In addition,

Table 6
Vibrational mode assignment of Ni(TRISOXH$_3$)Br$_2$ (**2**)

Mode	Experiment[a]	Assigned wavenumber unscaled[b]	Assigned wavenumber scaled[c]	Symmetry[d] and mode description[e]	
c	478.6	458.8	471.9	A′	Ni–N1 stretch
d	487.2	487.5	498.7	A′	TRISOXH$_3$ torsion, sym CH$_2$ and CH$_3$ (a,c) rock
e	515.2	525.3	533.9	A′	TRISOXH$_3$ torsion, H(a,c) sym wagging
f	525.3	526.2	534.7	A″	CH$_2$(b) rock, H(a,c) wagging, arm b torsion
g	843.4	849.7	836.2	A″	arms a, c compression, some Ni–N(a,c) stretch
h	853.1	864.8	850.2	A′	arm b compression, some Ni–N(b) stretch
i	878.9	884.2	868.3	A′	arms a, b, c compression, some Ni–N(a,b,c) stretch
j	890.7	894.8	878.2	A′	N(amine)–CH$_2$(a,b,c) stretch, some Ni–N1 stretch and Ni–N(b) compression
k	941.3	963.1	941.8	A′	CH$_2$ and CH$_3$(a,c) rock
l	999.1	1022.1	996.8	A′	CH$_3$(b) rock, some Ni–N(b) stretch
m	1026.1	1053.8	1026.3	A″	CH$_3$(a,b,c) rock, some N1–CH$_2$(a,b,c)
o	1068.5	1134.7	1101.7	A′	N–O(a,b,c) stretch
p	1110.9	1147.6	1113.7	A′	N(amine)–CH$_2$(b) stretch, N(amine)–CH$_2$(a,c) compression
q	1116.8	1152.3	1118.1	A″	N(amine)–CH$_2$(a) stretch, N(amine)–CH$_2$(c) compression
r	1230.6	1253.9	1212.7	A″	CH$_2$(a,c) wag, ∠H(a,c)–O–N compression, H$_2$C–C(a,c) stretch
s	1238.3	1259.5	1217.9	A′	H$_2$C–C(b) stretch, ∠H(a,c)–O–N compression, ∠H(b)–O–N expansion
t	1244.0	1267.3	1225.2	A′	H$_2$C–C(a,c) stretch, ∠H(a,b,c)–O–N expansion
u	1292.3	1342.6	1295.4	A″	CH$_2$(a,b,c) rock
v	1315.5	1346.9	1299.4	A′	CH$_2$(a,c) rock, CH$_2$ (b) wag
w	1660.7	1762.6	1686.7	A″	C=N(a,c) stretch
x	1682.2	1764.7	1688.6	A′	C=N(a,c) stretch, small C=N(b) stretch
y	1698.2	1776.3	1699.4	A′	C=N(b) stretch, small C=N(a,c) stretch

[a] Natural abundance wavenumber data reported from both Raman and infrared experiments.
[b] Theoretical data assigned from calculation listed in Table 2.
[c] Assigned theoretical wavenumbers were scaled by applying Eq. (1).
[d] The optimized geometry for Ni(TRISOXH$_3$)Br$_2$ has C_s symmetry which places a mirror in the plane of arm b of the ligand and through each halide; mode symmetry was theoretically determined.
[e] Letter designations for atoms are the same as in Tables 3–5, utilizing a, b, and c to represent the three arms of the TRISOXH$_3$ ligand and atoms therein. Breathing modes for arms a, b, c involve all atoms. Twist and rock modes involve two or more atoms moving together, while wag modes are dominated by 1 atom motion. OOP indicates the modes are out-of-phase with respect to each other, and are not necessarily anti-symmetric with respect to the mirror plane.

complexes **3** and **4** exhibit modes specific to the bound solvents, methanol or water, respectively. In the regions studied, one methanol specific mode was observed for **3** and two water modes were observed for **4**.

The predicted theoretical frequencies for the halide series are generally higher than those observed experimentally; this is consistent with the literature precedent [23,24], including the trend observed for **1** [7]. A modified wavenumber-linear-scaling (WLS) approach [25,26] was employed after completing the vibrational mode assignment for **2**, **3**, and **4**; unique scale functions for each complex were derived by determining the best-fit linear function between the experimental and theoretical data. The resulting functions are very similar to the derived function for **1** and are shown in Eqs. (1)–(4), which correspond to complexes **1**–**4**. The scaled vibrational data were useful in clarifying previously ambiguous assignments of two vibrational modes in **4** and confirming assignments made principally by comparison to **1**.

$$(\mathbf{1})\ \nu_{\text{scaled}} = 0.919\nu_{\text{unscaled}} + 54.9\,\text{cm}^{-1}\ (R^2 = 0.999, 28\ \text{data}) \quad (1)$$

$$(\mathbf{2})\ \nu_{\text{scaled}} = 0.932\nu_{\text{unscaled}} + 44.5\,\text{cm}^{-1}\ (R^2 = 0.999, 22\ \text{data}) \quad (2)$$

$$(\mathbf{3})\ \nu_{\text{scaled}} = 0.939\nu_{\text{unscaled}} + 32.2\,\text{cm}^{-1}\ (R^2 = 0.999, 28\ \text{data}) \quad (3)$$

$$(\mathbf{4})\ \nu_{\text{scaled}} = 0.964\nu_{\text{unscaled}} + 19.6\,\text{cm}^{-1}\ (R^2 = 0.999, 27\ \text{data}) \quad (4)$$

As an alternative to Mulliken population analysis, the default charge distribution analysis protocol in Gaussian, natural population analysis offers more logical electron distributions for transition metal complexes [13–15]. The resulting natural charge data allow for a direct comparison of ligand influences on the metal center and the oximes and are summarized in Table 9.

For clarity, the equatorial plane is defined here as the plane that contains the oxime nitrogens, the nickel and the ligand X *cis* to the amine nitrogen; the axial positions are filled by the amine nitrogen and the ligand X *trans* to it. The natural charge on Ni predictably changes upon the ligand substitutions in the halide series; the value decreases (becomes less positive) along the series from 1.470 for the difluoride (**5**) to 1.194 for the methanol–iodide (**3**). The series trend in electron withdrawing strength follow the usual halide order, $F^- > Cl^- > Br^- > I^-$. The neutral aqua ligands result in a charge on nickel nearly as high as that of the fluoride complex. Throughout the halide series, oxime b, *trans* to the ligand X, generally shows larger (more negative) natural charge values than oxime a or c, which are *trans* to each other. The one exception to this trend is observed in **3**, where the charges on all three oximes are calculated to be essentially equal. In this complex,

Table 7
Vibrational mode assignment of [Ni(TRISOXH$_3$)(CH$_3$OH)I]I (**3**)

Mode[a]	Experiment[b]	Assigned wavenumber unscaled[c]	Assigned wavenumber scaled[d]	Mode description[e]
a	373.1	361.5	371.8	TRISOXH$_3$ breathing mode, CH$_2$(a,c) rock
a′	385.2	374.1	383.7	TRISOXH$_3$ breathing mode, arms a,c alternating with b
b	391.6	379.3	388.5	CH$_2$(a,b,c) rock
c′	464.5	464.6	468.6	Ni–N(amine) stretch, arm a twist and bend
c	471.6	467.6	471.4	Ni–N(amine) stretch, arm c twist and bend
d	489.7	480.9	484.0	TRISOXH$_3$ torsion, sym CH$_2$ and CH$_3$ (a,c) rock
d′	506.7	508.0	509.4	TRISOXH$_3$ torsion, arm b torsion
e	520.3	513.8	514.8	TRISOXH$_3$ torsion, H(a,c) sym wagging
f′	527.8	548.9	547.8	H(a,b,c) wag, O4-H wag
g	839.9	846.9	827.7	arms a, c compression, some Ni–N(a,c) stretch
h	852.4	865.3	845.0	arm b compression, some Ni–N(b) stretch
i	875	885.0	863.5	arms a, b, c compression, some Ni–N(a,b,c) stretch
j	887.6	899.0	876.7	N1–CH$_2$(a,b,c) stretch, some Ni–N1 stretch and Ni–N(b) compression
k	939.3	960.3	934.3	CH$_2$ and CH$_3$ (a,c) rock
l	999.1	1028.7	998.5	CH$_3$(b) rock, some Ni–N(b) stretch
m	1018.4	1051.2	1019.6	CH$_3$(a,b,c) rock, some N1–CH$_2$(a,b,c)
meth	1030.0	1103.5	1068.8	MeO–H stretch
n	1053.1	1122.3	1086.4	N–O(a,c) stretch
o	1064.7	1134.6	1097.9	N1–CH$_2$(b) stretch, N1–CH$_2$(a,c) compression
p	1107.1	1137.1	1100.3	N–O(a,b,c) stretch
q	1112.9	1147.8	1110.3	N1–CH$_2$(a) stretch, N1–CH$_2$(c) compression
s	1234.4	1255.2	1211.2	H$_2$C–C(b) stretch, ∠H(a,c)–O–N compression, ∠H(b)–O–N expansion
t	1244.0	1262.6	1218.2	H$_2$C–C(a,c) stretch, ∠H(a,b,c)–O–N expansion
u	1288.4	1334.3	1285.5	CH$_2$(a,c) rock, CH$_2$ (b) wag
v	1313.5	1349.9	1300.2	CH$_2$(a,b,c) rock
w	1655.0	1745.9	1672.1	C=N(c) stretch, small C=N(a) stretch
x	1686.7	1751.0	1677.0	C=N(a) stretch, small C=N(c) stretch
y	1695.5	1769.6	1694.5	C=N(b) stretch, small C=N(a,c) stretch

[a] Mode label assigned based upon comparison to those frequencies assigned for **1**; similar modes between **3** and **1** are given the same letter, modes affected by the different X ligands in **3** are given the same letter with a prime symbol, the one observed methanol mode is assigned **meth**.
[b] Frequency (wavenumber) data reported from both Raman and infrared experiments.
[c] Theoretical data assigned from calculation listed in Table 2.
[d] Assigned theoretical wavenumbers were scaled by applying Eq. (2).
[e] The optimized geometry for Ni(TRISOXH$_3$)(CH$_3$OH)I has C1 symmetry; all vibrational frequencies have A symmetry. Letter designations for atoms are the same as in Tables 3–5, utilizing a, b, and c to represent the three arms of the TRISOXH$_3$ ligand and atoms therein. Breathing modes for arms a, b, c involve all atoms. Twist and rock modes involve two or more atoms moving together, while wag modes are dominated by one atom motion.

oxime b is *trans* to methanol rather than a negatively charged halide and all three oximes are *trans* to neutral atoms.

The localized spin density for each of 13 atoms (including Ni, nine oxime atoms (C, N, O for arms a, b, and c), the amine N, and the two X ligands) is defined as the difference between the α and β electron spin densities on each atom and is summarized in Table 10. The sum of these local spin densities is 2.00 ± 0.01 and accounts for the predicted two unpaired electrons in each complex. The unpaired electron density is mainly on the nickel, but significant portions are also delocalized onto the atoms directly bonded to the metal. Very similar unpaired electron densities are calculated for nickel in **1**, **2**, **4**, and **5** (all between 1.63 and 1.67). In **3**, the spin density is somewhat smaller (1.53) as a result of delocalization onto the axial iodide. There is very little unpaired electron density on the oxime C's and O's; however, including these values gives the expected total unpaired electron density.

5. Discussion

Notable trends in molecular geometries are observed in the series of complexes presented in this work, where two coordination positions are varied and the tetradentate TRISOXH$_3$ ligand remains intact. The Ni–amine bond, *trans* to the axial ligand X, should weaken upon substitution of a better σ-donating ligand, such as iodide, in the axial position due to the *trans* influence. This trend is observed in the theoretical geometries, in which the Ni–amine bond length is longest for **3**, with an axial iodide, and shortest for **1**, with an axial chloride. However, the trend is not observed in the crystallographic data, where the Ni–amine bond lengths in **1**, **2**, and **3** are very similar [2.096(2) Å, 2.112(3) Å, 2.1131(13) Å, respectively].

The inconsistency between the experimental and calculated nickel–amine bond lengths may result from inaccurate relative weighting of two effects in the calculation; the amount of covalency present in the bonds and the influence of the chelate ring strain on the bond length.

Table 8
Vibrational mode assignment of $[Ni(TRISOXH_3)(H_2O)_2]F_2 \cdot 2H_2O$ (**4**)

Mode[a]	Experiment[b]	Assigned wavenumber unscaled[c]	Assigned wavenumber scaled[d]	Mode description[e]
a	387.4	366.8	373.1	sym $TRISOXH_3$ breathing mode, mainly arms a,c
b	400.6	379.7	385.6	CH_2(a,b,c) rock
wat1	423.6	407.6	412.5	H_2O(eq) wag, H(b,c) wag, H_2O(ax) rock
c	483.6	488.2	490.2	Ni–N(amine) stretch
d	499.5	508.4	509.6	$TRISOXH_3$ torsion, sym CH_2 and CH_3(a,c) rock
e	516.1	519.1	519.9	$TRISOXH_3$ torsion, H(a,c) sym wagging
wat2	531.9	550.0	549.7	H_2O(eq) + H_2O(ax) rock
g	828.3	838.2	827.5	asym arms a, c compression, some Ni–N(a,c) stretch
h	852.3	863.4	851.8	arm b compression, some arms a,c stretch
i	877.4	881.2	869.0	arms a, b, c compression, some Ni–N(a,b,c) stretch
j	898.9	891.9	879.3	N1–CH_2(a,b,c) stretch, some Ni–N1 stretch and Ni–N(b) compression
k	941.2	958.8	943.8	CH_2 and CH_3(a,c) rock
l	1001.1	1044.7	1026.6	CH_3(b) rock, some Ni–N(b) stretch
m	1031.9	1065.3	1046.4	CH_3(a,b,c) rock, some N1–CH_2(a,b,c)
n	1051.2	1098.7	1078.6	large N–O(c) stretch, small N–O(a,b)
o	1074.3	1113.1	1092.5	large N–O(a) stretch, small N–O(b,c)
p	1116.8	1129.5	1108.3	N–O(b) stretch
q	1122.6	1140.1	1118.5	N1–CH_2(a,c) asym stretch
r	1219.0	1246.8	1221.4	CH_2(a,c) wag, ∠H(a,c)–O–N compression, H_2C–C(a,c) stretch
s	1236.3	1251.9	1226.3	H_2C–C(b) stretch, ∠H(a,c)–O–N compression, ∠H(b)–O–N expansion
t	1244.0	1259.8	1233.9	H_2C–C(a,c) stretch, ∠H(a,b,c)–O–N expansion
u″	1309.6	1328.4	1300.0	CH_2(a,c) sym rock, CH_2 (b) wag
v	1317.3	1347.5	1318.4	CH_2(a,b) asym rock
w	1672.2	1708.5	1666.4	C=N(c) stretch, small C=N(a) stretch, ∠H–O–H(eq) bend
x	1688.2	1722.3	1679.7	C=N(a) stretch, small C=N(c) stretch
y	1713.3	1762.8	1718.7	C=N(b) stretch, very small C=N(a,c) stretch

[a] Mode label assigned based upon comparison to those frequencies assigned for **1**; similar modes between **3** and **1** are given the same letter, modes affected by the different X ligands in **3** are given the same letter with a double-prime symbol, the modes dominated by water ligands are assigned **wat1** or **wat2**.
[b] Frequency (wavenumber) data reported from both Raman and infrared experiments.
[c] Theoretical data assigned from calculation listed in Table 2.
[d] Assigned theoretical wavenumbers were scaled by applying Eq. (3).
[e] The optimized geometry for $Ni(TRISOXH_3)(H_2O)_2$ has C1 symmetry; all vibrational frequencies have A symmetry. Letter designations for atoms are the same as in Tables 3–5, utilizing a, b, and c to represent the three arms of the $TRISOXH_3$ ligand and atoms therein. Breathing modes for arms a, b, c involve all atoms. Twist and rock modes involve two or more atoms moving together, while wag modes are dominated by one atom motion.

Table 9
Summary of calculated natural charge distribution

Natural charge[a]	**1**	**2**	**3**	**4**	**5**
Ni	1.374	1.328	1.194	1.457	1.470
Oxime a[b]	−0.035	−0.019	0.002	−0.029	−0.014
Oxime b	−0.054	−0.059	0.000	−0.011	−0.057
Oxime c	−0.035	−0.019	−0.005	−0.032	−0.014

[a] Natural charge is the sum of the charge in the α and β orbitals obtained from a natural population analysis.
[b] Oxime a, b, and c correspond to the C, N, O, and H atoms in arms a, b, and c, respectively, of the $TRISOXH_3$ ligand; the natural charge for each oxime in the sum of all the α and β orbitals of each atom in the oxime.

DFT calculations using the B3LYP functional have been shown to overestimate the covalency of transition metal bonds [27]. As a result, the observed *trans* influence trend may be exaggerated in the model systems. In the crystal structures, the three five-membered chelate rings of $TRISOXH_3$ may exert considerable strain on the nickel–amine bond length and render the predicted *trans* influence trend imperceptible. As an indicator of the influence of these two effects, we examine the methylene bond angles present in the chelate rings; if the covalency has been overestimated relative to the ring strain in the theoretical models, we expect to see greater deviations from ideal bond angles. Three intraligand bond angles, between the oxime carbons, methylene carbons, and amine nitrogen, in the calculated models are larger, averaging 113.3°, than those observed in the experimental structures, averaging 112.5°; these larger angles (Table 5S) are consistent with a relative underestimate of the ring strain compared to the covalency of the nickel–amine bond. In the crystallographically determined structures, the strain present in each five-membered chelate ring is more dominant and results in the lack of an experimentally observed trend.

The Ni–oxime nitrogen bonds (Ni–N(a), Ni–N(b), Ni–N(c)) also illustrate an interesting trend in theoretical molecular geometries. For the complexes (**1**, **2**, **3**, and **5**) which have at least one halide in the X positions, the theoretical models reveal longer bond lengths for Ni–N(b) than for Ni–N(a) and Ni–N(c), consistent with the *trans* equatorial ligand X being a better σ-donating ligand than an oxime nitrogen. However, no significant trend is found in

Table 10
Localized unpaired electron densities

Atom	1	2	3	4	5
Ni	1.64[a]	1.63	1.53	1.67	1.67
N(amine)	0.06	0.06	0.08	0.09	0.05
N(a)[b]	0.06	0.05	0.07	0.06	0.04
N(b)	0.06	0.05	0.09	0.09	0.06
N(c)	0.06	0.04	0.07	0.05	0.04
X(eq)[c]	0.08	0.09	0.04	0.02	0.08
X(ax)	0.06	0.06	0.12	0.02	0.05
C(a)	−0.01	0.00	−0.01	−0.01	0.01
C(b)	−0.01	−0.01	−0.01	−0.01	−0.02
C(c)	−0.01	0.02	−0.01	−0.01	0.01
O(a)	0.00	0.00	0.00	0.00	0.00
O(b)	0.01	0.01	0.01	0.01	0.01
O(c)	0.00	0.00	0.00	0.01	0.00
Total[d]	2.00	2.00	1.99	1.99	2.00

[a] Unpaired electron density was determined by subtracting the total β spin density from the total α spin density for each atom.
[b] Atoms labels of a, b, or c are assigned to oxime arms a, b, or c, respectively.
[c] X(eq) is *trans* to N(b) and X(ax) is *trans* to the amine N.
[d] The sum unpaired electron density is the total of the densities on each of the 12 atoms listed; all other atoms in the molecule are neglected, due to very small unpaired electron densities.

the experimental bond lengths, where only very small or no differences in the collective Ni–N distances are observed. In the crystal structure of **1**, the longest Ni–oxime nitrogen bond is Ni–N(c), whereas for **2**, the longest Ni–oxime nitrogen bond is Ni–N(a). These longer experimental bond lengths are due to the intermolecular hydrogen-bonding observed in the crystal structure involving the hydrogen atoms of these oximes. In the crystal structures of **3** and **4**, all Ni–oxime nitrogen bonds are equivalent within the experimental range.

Vibrational spectroscopy serves as both a useful tool for considering the electronic differences between the complexes in the halide series and an evaluation of the theoretical models and derived scale functions. Due to their similarity and common $TRISOXH_3$ ligand, the complexes chosen in this study are not expected to have vastly different vibrational spectra. As described above, Ni($TRISOXH_3$)Cl_2 (**1**) and Ni($TRISOXH_3$)Br_2 (**2**) have very similar vibrational modes with no notable differences in the descriptions of the modes above 350 cm^{-1}; intensities and energies for the vibrations were different for some modes, specifically the symmetric imine stretching mode **x** which was 10 cm^{-1} lower in energy for **2** than **1**. The Ni–amine nitrogen stretch was very close in energy for both **2** (478.6 cm^{-1}) and **1** (481.1 cm^{-1}). In total, 22 normal modes were assigned for **2**.

The other two complexes in the series that were studied with vibrational spectroscopy, [Ni($TRISOXH_3$)(CH_3OH)I]I (**3**) and [Ni($TRISOXH_3$)(H_2O)$_2$]$F_2 \cdot 2H_2O$ (**4**), are expected to have somewhat different vibrational modes, due to the replacement of halides by solvent molecules and the C1 symmetry of their theoretical models (compared to C_s for **1** and **2**). The presence of a mirror plane in the optimized geometries of **1** and **2** simplifies the assignment and description of vibrational modes.[4] Without this symmetry element, the molecular vibrations become more complex and are more difficult to describe. For example, a Ni–amine stretch can be described by only one mode in both **1** and **2**, while two modes have significant Ni–amine character in **3** (**c′**, 464.5 and **c**, 471.6 cm^{-1}). The Ni–amine stretching frequencies consistently move to lower energy as the size of the X ligands is increased. In addition, vibrational modes for complexes **3** and **4** are influenced by the bound solvent molecules, methanol and water, respectively. Mode **f** was observed in **1** as being out-of-phase oxime H(a) and H(c) proton wagging; in **3**, this mode (denoted **f′**) also includes a proton wag from the metal-bound methanol molecule. In complex **4**, two modes (**wat1**, 423.6 cm^{-1} and **wat2**, 531.9 cm^{-1}) are observed in the lowest energy region studied, which can be solely attributed to the two bound water molecules.

The modified wavenumber-linear-scaling procedure is applied with success to partially correct for the anharmonicity of the true potential energy surfaces of the complexes [7,25,26]. Each unique empirically derived linear scale function has a very high correlation value. The resulting scaled theoretical wavenumbers (as listed in Tables 6–8) show a significant increase in agreement with experimental data, which is remarkably similar to the improvement in accuracy reported for **1**. For **2**, an average percent deviation of 2.59% (from 0.3 to 101.9 cm^{-1}, averaging 31.0 cm^{-1}) for the unscaled values is reduced to 1.13% (from 0.2 to 33.2 cm^{-1}, averaging 10.4 cm^{-1}) by applying the derived linear scale function (Eq. (2)). For **3**, an average percent deviation of 2.85% (from 0.1 to 90.8 cm^{-1}, averaging 29.7 cm^{-1}) for the unscaled values is reduced to 1.15% (from 0.2 to 38.8 cm^{-1}, averaging 10.7 cm^{-1}) by applying the derived linear scale function (Eq. (3)). Finally, for **4**, an average percent deviation of 2.30% (from 3.0 to 49.5 cm^{-1}, averaging 21.8 cm^{-1}) for the unscaled values is reduced to 1.29% (from 0.5 to 27.4 cm^{-1}, averaging 10.1 cm^{-1}) by applying the derived linear scale function (Eq. (4)). Application of the derived linear scale function for **4** aided assignment of two different modes associated with bound water (**wat1** and **wat2**). In summary, for **2** and **3**, the improvement in the agreement between experimental and theoretical absolute wavenumbers is 3-fold and for **4**, more than a 2-fold improvement is observed after scaling.

This series of complexes provides the opportunity to test the generality of the scale function derived from one complex for application to other similar complexes. The similarity between the unique scale functions (Eqs. (1)–(4)) for the halide series is striking. Might the function derived for **1** be applied to the series to yield improvement similar to the uniquely derived functions? The linear scale function derived for **1** yields close to a 3-fold improvement when

[4] Because of intermolecular hydrogen-bonding, the mirror plane predicted for **1**, **2**, and **5**, does not exist in the crystal structures; this symmetry element is used to facilitate mode assignment and identify the dominant vibrations associated with the experimentally observed peaks.

applied to the theoretical frequencies of **2** and **3**, the two other complexes which contain a metal-bound halide; the average deviation in **2** is improved from 31.0 to 12.2 cm^{-1} and in **3** from 29.6 to 13.1 cm^{-1}. However, applying the scale function derived for **1** to complex **4**, with two bound water molecules, yields no significant improvement; the average deviation changes from 21.8 to 20.1 cm^{-1}. The negligible improvement observed when applying the scale function derived for **1** to complex **4** indicates the interchange of the linear scale functions between complexes should be done with caution.

Evaluating the natural charge data facilitates a comparison of the ligand influences on the interactions between the metal center and oxime arms of $TRISOXH_3$. Through the series of theoretical model complexes, from $Ni(TRISOXH_3)F_2$ (**5**), $Ni(TRISOXH_3)Cl_2$ (**1**), $Ni(TRISOXH_3)Br_2$ (**2**), $[Ni(TRISOXH_3)(MeOH)I]^+$ (**3**), to $[Ni(TRISOXH_3)(H_2O)_2]^{2+}$ (**4**), we observe a decreasing (less positive) natural charge on Ni, consistent with the decreasing electronegativity of the ligands X. The complexes also show an interesting trend in the natural charge of the oxime arms; for **1**, **2**, and **5**, oxime b (*trans* to an equatorial Cl^-, Br^-, and F^-, respectively) has a more negative natural charge than oxime a or c (*trans* to each other), consistent with the halide ligands being better σ-donors than an oxime. For **4**, this trend is reversed, with oxime b having a smaller negative charge than either oxime a or c; intramolecular hydrogen-bonding and/or the neutrality of the aqua ligands in this complex may explain this observation. Despite the different *trans* ligand groups in **3**, there are very small differences between the three oxime arms (less than 0.005 Å), revealing a similarity in the σ-donation abilities of the equatorial methanol and oxime functional arms of $TRISOXH_3$.

For all of the complexes studied here, the unpaired electron density is not completely localized on the metal. The theoretical models of **1**–**5** show approximately 20% of the unpaired electron density is delocalized over ligand atoms. Recent EPR studies suggest that a ligand derived iminoxyl radical may be involved as an intermediate in the oxygen reaction with the Ni(TRISOX) complexes [6]. Thus, the computational evaluation of delocalization of the unpaired electron density will become more significant in future studies of the oxygen activating complexes.

This study of a series of nickel tris(oxime)amine complexes combines theoretical and experimental methods to evaluate trends in molecular geometry, vibrational spectra and electronic structure. The electronic structures of these complexes, which exhibit different natural charges on the metal center and delocalized unpaired electron density, are significantly influenced by the different halide and solvent ligands in the series. The subtle effect of changing the halide ligand, while maintaining the $TRISOXH_3$ ligand, yields small changes to the geometry and vibrational features; more significant differences are noted when solvent, such as water or methanol, replace one or both of the halide ligands. Experimentally observed trends are generally reproduced well in the computational models, however, the overestimation of bond covalency may exaggerate some electronic structure-based geometric features. In addition, the theoretical models of these complexes reveal inherent features and trends of the molecules that are masked in the solid state structure by intermolecular interactions. With this work as precedent, future research will apply these well developed molecular models to oxygen active complexes with different ligands from the bis(oxime)amine series [2]. By comparison to the detailed vibrational spectra for this series of complexes and facilitating the successful modified wavenumber-linear scaling procedure, spectra of the oxygen-active Ni(TRISOX) species will be elucidated in the pursuit of understanding their unique substrate oxidation chemistry.

Acknowledgments

The authors thank Professor Thomas Beck and Dr. Anping Liu of the University of Cincinnati for helpful discussions and computational support. The authors also thank Dr. James Hess and Douglas J. Fox from Gaussian, Inc. for software support. Data collection for **2** and **4** on the SMART 1K diffractometer was through the Ohio Crystallographic Consortium, funded by the Ohio Board of Regents 1995 Investment Fund (CAP-075) located at the University of Toledo, Instrumentation Center in A&S, Toledo, OH 43606. Funding for the SMART6000 diffractometer, which was used for **3**, was through NSF-MRI Grant CHE-0215950 located at the University of Cincinnati, Cincinnati, OH 45221-0172. Acknowledgment is made to the donors of the Petroleum Research Fund administered by the American Chemical Society (ACS-PRF 37653-AC3) and the Department of Chemistry at the University of Cincinnati who funded this research.

Appendix A. Supporting information

X-ray structural data and all pertinent crystallographic tables (excluding structure factors) are available in CIF format (CCDC-602155–602157). Information can be obtained free of charge at www.ccdc.cam.ac.uk/conts/retrieving.html or from the Cambridge Crystallographic Data Centre (CCDC), 12 Union Road, Cambridge CB2 1EZ, UK (fax: +44 1223 336 033; e-mail: deposit@ccdc.cam.ac.uk). Supplementary data associated with this article can be found, in the online version, at doi:10.1016/j.poly.2006.05.025.

References

[1] M.J. Goldcamp, S.E. Robison, J.A. KrauseBauer, M.J. Baldwin, Inorg. Chem. 41 (2002) 2307.
[2] M.J. Goldcamp, S.E. Edison, L.N. Squires, D.T. Rosa, N.K. Vowels, N.L. Coker, J.A. KrauseBauer, M.J. Baldwin, Inorg. Chem. 42 (2003) 717.
[3] S.E. Edison, R.P. Hotz, M.J. Baldwin, J. Chem. Commun. (2004) 1212.

[4] G. Matthaiopoulos, Chem. Ber. 31 (1898) 2396.
[5] M.J. Goldcamp, J.A. KrauseBauer, M.J. Baldwin, Acta Crystallogr., Sect. C 56 (2000) e602.
[6] S.E. Edison, Investigation of nickel (II)-oximate complexes that react with molecular oxygen, Ph.D. Dissertation, University of Cincinnati, 2004.
[7] R.M. Jones, M.J. Baldwin, J. Phys. Chem. A 108 (2004) 3537.
[8] F. Neese, E.I. Solomon, J. Am. Chem. Soc. 120 (1998) 12829.
[9] P. Chen, K. Fujisawa, E.I. Solomon, J. Am. Chem. Soc. 122 (2000) 10177.
[10] R.K. Szilagyi, M. Metz, E.I. Solomon, J. Phys. Chem. A 106 (2002) 2994.
[11] D.E. Wheeler, J.H. Rodriguez, J.K. McCusker, J. Phys. Chem. 103 (1999) 4101.
[12] S. Li, M.B. Hall, Inorg. Chem. 40 (2001) 18.
[13] A.E. Reed, R.B. Weinstock, F. Weinhold, J. Chem. Phys. 83 (1985) 735.
[14] A.E. Reed, L.A. Curtiss, F. Weinhold, Chem. Rev. 88 (1988) 899.
[15] A.E. Reed, F. Weinhold, J. Chem. Phys. 83 (1985) 1736.
[16] SADABS v2.03 was used for the application of semi-empirical absorption and beam corrections. G.M. Sheldrick, University of Göttingen, Göttingen, Germany.
[17] SHELXTL v6.1 & 6.14 was used for the structure solution and generation of figures and tables. Neutral-atom scattering factors were used as stored in this package. G.M. Sheldrick, University of Göttingen, Göttingen, Germany and Bruker Analytical X-ray Instruments, Inc., Madison, WI.
[18] M.J. Frisch, G.W. Trucks, H.B. Schlegel, G.E. Scuseria, M.A. Robb, J.R. Cheeseman, V.G. Zakrzewski, J.A. Montgomery, R.E. Stratmann, J.C. Burant, S. Dapprich, J.M. Millam, A.D. Daniels, K.N. Kudin, M.C. Strain, O. Farkas, J. Tomasi, V. Barone, M. Cossi, R. Cammi, B. Mennucci, C. Pomelli, C. Adamo, S. Clifford, J. Ochterski, G.A. Petersson, P.Y. Ayala, Q. Cui, K. Morokuma, D.K. Malick, A.D. Rabuck, K. Raghavachari, J.B. Foresman, J. Cioslowski, J.V. Ortiz, A.G. Baboul, B.B. Stefanov, G. Liu, A. Liashenko, P. Piskorz, I. Komaromi, R. Gomperts, R.L. Martin, D.J. Fox, T. Keith, M.A. Al-Laham, C.Y. Peng, A. Nanayakkara, C. Gonzalez, M. Challacombe, P.M.W. Gill, B. Johnson, W. Chen, M.W. Wong, J.L. Andres, C. Gonzalez, M. Head-Gordon, E.S. Replogle, J.A. Pople, GAUSSIAN-98, Revision A.11, Gaussian, Inc., Pittsburgh, PA, 1998.
[19] M.J. Frisch, G.W. Trucks, H.B. Schlegel, G.E. Scuseria, M.A. Robb, J.R. Cheeseman, J.A. Montgomery, T. Vreven, K.N. Kudin, J.C. Burant, J.M. Millam, S.S. Iyengar, J. Tomasi, V. Barone, B. Mennucci, M. Cossi, G. Scalmani, N. Rega, G.A. Petersson, H. Nakatsuji, M. Hada, M. Ehara, K. Toyota, R. Fukuda, J. Hasegawa, M. Ishida, T. Nakajima, Y. Honda, O. Kitao, H. Nakai, M. Klene, X. Li, J.E. Knox, H.P. Hratchian, J.B. Cross, V. Bakken, C. Adamo, J. Jaramillo, R. Gomperts, R.E. Stratmann, O. Yazyev, A.J. Austin, R. Cammi, C. Pomelli, J.W. Ochterski, P.Y. Ayala, K. Morokuma, G.A. Voth, P. Salvador, J.J. Dannenberg, V.G. Zakrzewski, S. Dapprich, A.D. Daniels, M.C. Strain, O. Farkas, D.K. Malick, A.D. Rabuck, K. Raghavachari, J.B. Foresman, J.V. Ortiz, Q. Cui, A.G. Baboul, S. Clifford, J. Cioslowski, B.B. Stefanov, G. Liu, A. Liashenko, P. Piskorz, I. Komaromi, R.L. Martin, D.J. Fox, T. Keith, M.A. Al-Laham, C.Y. Peng, A. Nanayakkara, M. Challacombe, P.M.W. Gill, B. Johnson, W. Chen, M.W. Wong, C. Gonzalez, J.A. Pople, GAUSSIAN-03, Revision B.05, Gaussian, Inc., Wallingford, CT, 2004.
[20] A.D. Becke, J. Chem. Phys. 98 (1993) 5648.
[21] C. Lee, W. Yang, R.G. Parr, Phys. Rev. B 37 (1988) 785.
[22] GaussView 3.0 and GaussViewW. Available from: <http://www.gaussian.com/gv_plat.htm>.
[23] J.B. Foresman, A. Frisch, Exploring Chemistry with Electronic Structure Methods, 2nd ed., Gaussian, Inc., Pittsburgh, PA, 1996.
[24] W. Koch, M.C. Holhausen, A Chemist's Guide to Density Funcitonal Theory, Wiley–VCH, Weinheim, 2000.
[25] H. Yoshida, A. Ehara, H. Matsuura, Chem. Phys. Lett. 325 (2000) 477.
[26] H. Yoshida, K. Takeda, J. Okamur, A. Ehara, H. Matsuura, J. Phys. Chem. A 106 (2002) 3580.
[27] R.J. Deeth, J. Chem. Soc., Dalton Trans. (2001) 664.

2. Experimental

2.1. Materials and methods

Palladium and platinum complexes, $MCl_2(P^{\frown}P)$ (M = Pd or Pt; $P^{\frown}P$ = dppm, dppe, dppp), *trans*-$MCl_2(P^nPr_3)_2$ [13,14] and $[M(SeCOC_6H_4Me\text{-}4)_2(P^{\frown}P)]$ [12] were prepared according to the literature methods. All reactions were carried out under an inert atmosphere (N_2 or Ar). Solvents were dried and distilled before use. All the newly reported complexes were crystallized from a CH_2Cl_2-hexane mixture. UV–Vis absorption spectra were recorded in CH_2Cl_2 on a Chemito Spectrascan UV double beam UV–Vis spectrophotometer. Microanalyses were carried out on a Carlo-Erba EA-1110 CHN-O instrument. ^1H, $^{31}P\{^1H\}$, $^{77}Se\{^1H\}$, $^{195}Pt\{^1H\}$ NMR spectra were recorded in CD_2Cl_2 on a Bruker DPX-300 NMR spectrometer operating at 300, 121.49, 57.24, 64.52 MHz, respectively and chemical shifts are relative to internal CH_2Cl_2 for ^1H, external 85% H_3PO_4 for $^{31}P\{^1H\}$, Me_2Se for ^{77}Se (secondary reference Ph_2Se_2 δ 463 ppm) and Na_2PtCl_6 in D_2O for $^{195}Pt\{^1H\}$.

2.2. Syntheses of complexes

2.2.1. Synthesis of $[Pd_3(\mu_3\text{-}Se)_2(dppm)_3][BPh_4]_2$ (**1a**)

A mixture of $[Pd(SeCOC_6H_4Me\text{-}4)_2(dppm)]$ (198 mg, 0.22 mmol) and $PdCl_2(dppm)$ (252 mg, 0.44 mmol) in dichloromethane (25 ml) containing few drops of methanol was stirred for 20 min. To the resulting orange solution, a methanolic solution (10 ml) of $NaBPh_4$ (307 mg, 0.90 mmol) was added and the reaction mixture was further stirred for 40 min. The solvents were removed *in vacuo* and the residue was extracted with dichloromethane. The extract was passed through a Florisil column (0.7 × 5 cm), concentrated and few drops of hexane were added which on cooling in a freezer gave orange microcrystals of the title compound (250 mg, 49%), m.p. 257–259 °C (decomp.) *Anal.* Calc. for $C_{123}H_{106}B_2P_6Pd_3Se_2$: C, 65.1; H, 4.7. Found: C, 64.7; H, 4.6%. UV–Vis(CH_2Cl_2): λ_{max}/nm (ε), 239 (1.3×10^5), 268 (sh, 6.5×10^4), 274 (sh, 6.0×10^4), 299 (5.6×10^4), 365 (3.7×10^4). $\delta_H(CD_2Cl_2)$: 4.29 (s, br, 6 H, PCH_2P); 6.85–7.63 (m, 100 H, Ph). $\delta_P(CD_2Cl_2)$: −46.6. $\delta_{Se}(CD_2Cl_2)$: −168.4.

2.2.2. Synthesis of $[Pd_3(\mu_3\text{-}Se)_2(dppe)_3][BPh_4]_2$ (**1b**)

Prepared analogously to **1a** from $[Pd(SeCOC_6H_4Me\text{-}4)_2(dppe)]$ (118 mg, 0.13 mmol), $PdCl_2(dppe)$ (152 mg, 0.26 mmol) and $NaBPh_4$ (184 mg, 0.54 mmol). Recrystallization from dichloromethane–hexane gave orange crystals of **1b** (192 mg, 63%), m.p. 292–295 °C (decomp.) *Anal.* Calc. for $C_{126}H_{112}B_2P_6Pd_3Se_2$: C, 65.5; H, 4.9. Found: C, 65.1; H, 4.6%. UV–Vis(CH_2Cl_2): λ_{max}/nm (ε), 239 (1.1×10^5), 266 (sh, 5.7×10^4), 275 (sh, 5.5×10^4), 302 (4.0×10^4), 357 (2.5×10^4). $\delta_H(CD_2Cl_2)$: 2.23 (d, 22 Hz, 12 H, PCH_2); 6.84–7.91 (m, 100 H, Ph). $\delta_P(CD_2Cl_2)$: 50.6. $\delta_{Se}(CD_2Cl_2)$: −131.7.

2.2.3. Synthesis of $[Pd_3(\mu_3\text{-}Se)_2(dppp)_3][BPh_4]_2$ (**1c**)

Prepared similar to **1a** by reacting $[Pd(SeCOC_6H_4Me\text{-}4)_2(dppp)]$ (132 mg, 0.14 mmol) with $PdCl_2(dppp)$ (170 mg, 0.29 mmol) and $NaBPh_4$ (228 mg, 0.67 mmol). Recrystallization from dichloromethane–hexane gave orange crystals of **1c** (260 mg, 76%), m.p. 277–280 °C (decomp.) *Anal.* Calc. for $C_{129}H_{118}B_2P_6Pd_3Se_2$: C, 65.8; H, 5.1. Found: C, 66.1; H, 5.2%. UV–Vis(CH_2Cl_2): λ_{max}/nm (ε), 239 (1.1×10^5), 266 (sh, 4.9×10^4), 273 (sh, 4.2×10^4), 291 (4.8×10^4), 356 (2.0×10^4). $\delta_H(CD_2Cl_2)$: 1.80 (br, 6H, CH_2); 2.41 (br, 12H, PCH_2); 6.86–7.44 (m, 100H, Ph). $\delta_P(CD_2Cl_2)$: −2.6. $\delta_{Se}(CD_2Cl_2)$ 48.8.

2.2.4. Synthesis of $[Pt_3(\mu_3\text{-}Se)_2(dppm)_3][BPh_4]_2$ (**2a**)

A dichloromethane solution (10 ml) of $[Pt(SeCOC_6H_4Me\text{-}4)_2(dppm)]$ (225 mg, 0.23 mmol) was added to a suspension (15 ml) of $PtCl_2(dppm)$ (285 mg, 0.45 mmol) in the same solvent containing few drops of methanol. Reaction mixture was stirred for 20 min and subsequent addition of methanolic solution (10 ml) of $NaBPh_4$ (308 mg, 0.90 mmol) gave orange solution. After further stirring for 1 h, solvent was removed under vacuum and contents were extracted with dichloromethane. The extract was passed through a Florisil column (0.7 × 5 cm) and concentrated to 2 ml. To this a few drops of hexane were added and the solution was cooled in freezer whereupon yellow microcrystals of **2a** were obtained (240 mg, 41%) m.p. 290–293 °C (decomp.) *Anal.* Calc. for $C_{123}H_{106}B_2P_6Pt_3Se_2$: C, 58.2; H, 4.2. Found: C, 57.7; H, 3.8%. UV–Vis(CH_2Cl_2): λ_{max}/nm(ε), 238 (1.1×10^5), 268 (sh, 7.7×10^4), 343 (3.9×10^3). $\delta_H(CD_2Cl_2)$: 4.60 (t, br, [$^2J_{P-H}$ = 10 Hz; $^3J_{Pt-H}$ = 63 Hz], 6H, PCH_2); 6.83–7.60 (m, 100H, Ph). $\delta_P(CD_2Cl_2)$: −57.1 [$^1J_{Pt-P}$ = 2817 Hz; $^2J_{Pt-Pt}$ = 795 Hz]. $\delta_{Se}(CD_2Cl_2)$: −292.7 [$^1J_{Pt-Se}$ = 482 Hz]. $\delta_{Pt}(CD_2Cl_2)$: −4242 [$^1J_{Pt-P}$ = 2820 Hz; $^2J_{Pt-Pt}$ = 796 Hz].

2.2.5. Synthesis of $[Pt_3(\mu_3\text{-}Se)_2(P^nPr_3)_6][BPh_4]_2$ (**2b**)

Prepared analogus to **2a** from $PtCl_2(P^nPr_3)_2$ (207 mg, 0.35 mmol), $[Pt(SeCOPh)_2(P^nPr_3)_2]$ (156 mg, 0.18 mmol) and $NaBPh_4$ (242 mg, 0.71 mmol). Recrystallization with dichloromethane–hexane gave orange microcrystals of title compound (163 mg, 51%) m.p. 271–273 °C (decomp.) *Anal.* Calc. for $C_{102}H_{166}B_2P_6Pt_3Se_2$: C, 52.3; H, 7.1. Found: C, 52.2; H, 7.2%. UV–Vis(CH_2Cl_2): λ_{max}/nm(ε), 240 (8.6×10^4), 309 (1.4×10^4). $\delta_H(CD_2Cl_2)$: 1.14 (t, 7 Hz, 18H, $PCH_2CH_2\mathbf{CH_3}$); 1.52 (br, 12H, PCH_2CH_2); 1.92 (br, 12H, PCH_2CH_2); 6.9 (t, 7 Hz); 7.06 (t, 7 Hz); 7.36 (br) (Ph). $\delta_P(CD_2Cl_2)$: −39.8, $^1J_{Pt-P}$ = 3122 Hz. $\delta_{Se}(CD_2Cl_2)$: −291.5 [$^1J_{Pt-Se}$ = 312 Hz]. $\delta_{Pt}(CD_2Cl_2)$: −4546, $^1J_{Pt-P}$ = 3122 Hz.

2.2.6. Synthesis of $[PdPt_2(\mu_3\text{-}Se)_2(dppm)_3][BPh_4]_2$ (**3**)

To a dichloromethane suspension (15 ml) of $PtCl_2(dppm)$ (289 mg, 0.44 mmol) a solution (10 ml) of $[Pd(SeCOC_6H_4Me\text{-}4)_2(dppm)]$ (197 mg, 0.22 mmol) in the same solvent was added with few drops of methanol and stirred for 20 min. To the resulting orange solution, a methanolic solution (10 ml) of $NaBPh_4$ (310 mg, 0.91 mmol) was

added and further stirred for 1 h. The solvents were removed *in vacuo* and the residue was extracted with dichloromethane which was passed through a Florisil column (0.7 × 5 cm) and concentrated (2 ml). To the concentrate few drops of hexane were added and cooled in freezer for one day to yield yellow microcrystals of the title compound (260 mg, 48%) m.p. 265 °C (decomp.). *Anal.* Calc. for $C_{123}H_{106}B_2P_6PdPt_2Se_2$: C, 60.4; H, 4.4. Found: C, 60.6; H, 4.4%. $\delta_H(CD_2Cl_2)$: 4.24 (m, CH_2, Pd bound dppm); 4.61 (m, Pt bound dppm, CH_2); 6.79–7.67 (m, 100H, Ph). $\delta_P(CD_2Cl_2)$: −55.4 (Pt bound dppm; $^1J_{Pt-P}$ = 2768 Hz); −49.1 (s, Pd bound dppm). $\delta_{Pt}(CD_2Cl_2)$: −4200 ($^1J_{Pt-P}$ = 2777 Hz).

2.2.7. Synthesis of $[Pd_2Pt(\mu_3\text{-}Se)_2(dppm)_3][BPh_4]_2$ (4)

Prepared from [Pt(SeCOC$_6$H$_4$Me-4)$_2$(dppm)] (260 mg, 0.27 mmol) and $PdCl_2$(dppm) (300 mg, 0.53 mmol) and $NaBPh_4$ (366 mg, 1.07 mmol). Recrystallization from dichloromethane–hexane yielded orange microcrystals of **4** (290 mg, 46%), m.p. 260 °C (decomp.). *Anal.* Calc. for $C_{123}H_{106}B_2P_6Pd_2PtSe_2$: C, 62.7; H, 4.5. Found: C, 61.3; H, 4.5%. $\delta_H(CD_2Cl_2)$: 4.24 (m, CH_2, Pd bound dppm); 4.62 (m, CH_2, Pt bound dppm); 6.79–7.67 (m, 100H, Ph). $\delta_P(CD_2Cl_2)$: −53.8 (Pt bound dppm, $^1J_{Pt-P}$ = 2745 Hz); −47.5 (s, Pd bound dppm). $\delta_{Pt}(CD_2Cl_2)$: −4160 ($^1J_{Pt-P}$ = 2774 Hz).

Table 1
Crystal data and structure refinement details for $[Pd_3(\mu\text{-}Se)_2(dppe)_3][BPh_4]_2$

Empirical formula	$C_{126}H_{112}B_2P_6Pd_3Se_2$
Formula weight	2310.72
Temperature (K)	93(2)
Crystal size (mm^3)	0.48 × 0.35 × 0.18
Wavelength (Å)	0.71073
Crystal system	triclinic
Space group	$P\bar{1}$
Unit cell dimensions	
a (Å)	14.018(3)
b (Å)	15.226(3)
c (Å)	29.585(5)
α (°)	90.877(3)
β (°)	99.711(3)
γ (°)	115.394(3)
Volume (Å^3)	5595.6(17)
Z	2
Density (calculated) (Mg/m^3)	1.371
Absorption coefficient (mm^{-1})	1.261
F(000)	2348
θ Range of data collection (°)	1.66 to 28.62
Index ranges	$-18 \leqslant h \leqslant 17$, $-20 \leqslant k \leqslant 19$, $-37 \leqslant l \leqslant 39$
Reflections collected	42916
Independent reflections [R_{int}]	26125 [0.0255]
Completeness to theta = 28.62°	91.1%
Absorption correction	semi-empirical from equivalents
Maximum and minimum transmission	1.000 and 0.736
Refinement method	full-matrix least-squares on F^2
Data/restraints/parameters	26125/0/1252
Goodness-of-fit on F^2	1.097
Final R indices [$I > 2\sigma(I)$]	$R_1 = 0.0384$, $wR_2 = 0.0797$
R indices (all data)	$R_1 = 0.0503$, $wR_2 = 0.0845$
Largest difference in Peak and hole (e Å^{-3})	0.851 and −1.202

2.3. Crystallography

X-ray data of a yellow-orange crystal of $[Pd_3(\mu_3\text{-}Se)_2(dppe)_3][BPh_4]_2$ (**1b**) were collected on a Bruker Smart CCD diffractometer (at 93 (2) K) using graphite monochromated Mo Kα radiation (λ = 0.71073 Å). The intensity data were corrected for Lorentz, polarization and absorption effects [15]. The structure was solved by direct methods and refined by full matrix least square on F^2. All calculations were performed using SHELXL-97 program [16]. Selected crystallographic data are given in Table 1.

3. Results and discussion

3.1. Synthesis and spectroscopy

Treatment of [M(SeCOC$_6$H$_4$Me-4)$_2$(P⌒P)] with two equivalents of MCl$_2$(P⌒P) in dichloromethane/methanol mixture in the presence of $NaBPh_4$ gave the cationic tri-nuclear selenido-bridged complexes, $[M_3(\mu_3\text{-}Se)_2(P⌒P)_3][BPh_4]_2$ in fairly good yields (Eq. 1). These complexes were formed via unprecedented cleavage of the C–Se bond of monoselenocarboxylate.

The $^{31}P\{^1H\}$ NMR spectra of **1** showed single resonances suggesting that all the six P ligands are magnetically equivalent. The $^{31}P\{^1H\}$ NMR chemical shifts of **1b** (50.6 ppm) and **1c** (−2.6 ppm) can be compared with $[Pd_3(\mu_3\text{-}Se)_2(P⌒P)_3][PF_6]_2$ (P⌒P = dppe (50.6 ppm), dppp (−3.8 ppm)) [4]. The selenido ligands are also equivalent as only one ^{77}Se resonance is observed in the $^{77}Se\{^1H\}$ NMR spectra. The shielding of the ^{77}Se resonance depends on the chelate ring size of the phosphines and the signal appears at δ −168 (dppm), −132 (dppe) and 48.8 (dppp) ppm.

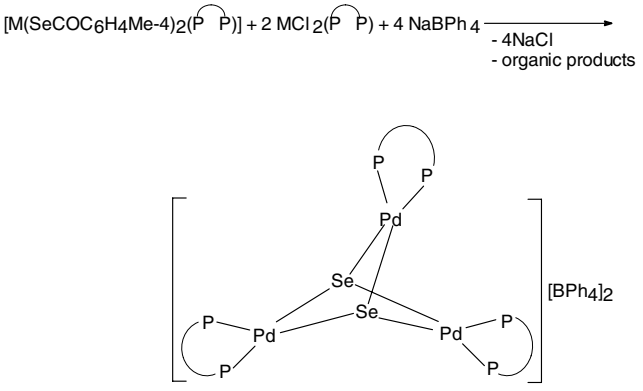

M	P⌒P	
Pd	dppm	**1a**
Pd	dppe	**1b**
Pd	dppp	**1c**
Pt	dppm	**2a**
Pt	$(P^nPr_3)_2$	**2b**

(1)

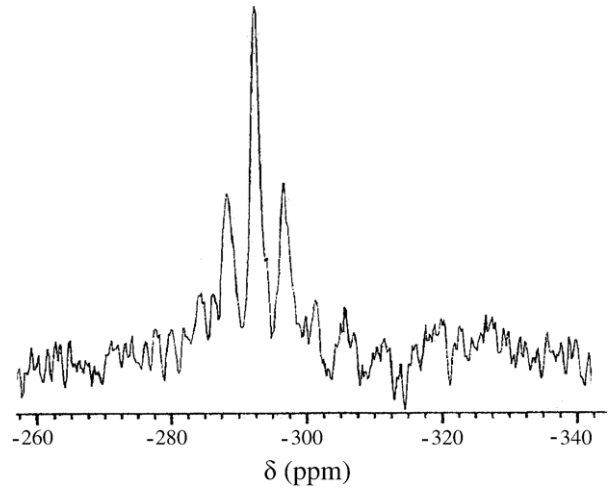

Fig. 1. $^{77}Se\{^{1}H\}$ NMR spectrum of $[Pt_3(\mu\text{-}Se)_2(dppm)_3][BPh_4]_2$ (**2a**) in CD_2Cl_2.

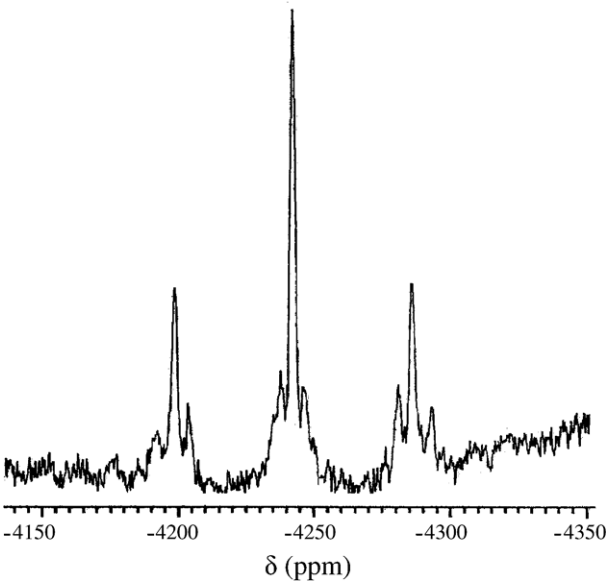

Fig. 2. $^{195}Pt\{^{1}H\}$ NMR spectrum of $[Pt_3(\mu\text{-}Se)_2(dppm)_3][BPh_4]_2$ in CD_2Cl_2.

The $^{31}P\{^{1}H\}$ NMR spectrum of **2a** showed a signal at δ −57.1 ppm with $^{1}J_{Pt-P}$ 2817 and $^{2}J_{Pt-Pt}$ 795 Hz. The magnitude of $^{1}J_{Pt-P}$ is in the range (∼3000 Hz) expected for phosphines *trans* to chalcogenido ligands [11,17,18]. However, for this complex $^{1}J_{Pt-P}$ of 4141 Hz has been reported earlier [4]. The $^{77}Se\{^{1}H\}$ NMR spectrum displayed a triplet at δ −292 ppm with $^{1}J_{Pt-Se}$ 482 Hz (Fig. 1). The ^{195}Pt NMR spectrum exhibited a triplet at −4242 ppm due to phosphorus coupling with $^{1}J_{Pt-P} = 2820$ Hz. Each peak of the triplet also showed $^{2}J_{Pt-Pt}$ of 796 Hz (Fig. 2). The ^{195}Pt resonance is progressively shielded by ∼40 ppm on replacing palladium by platinum atom in $[Pd_3(\mu_3\text{-}Se)_2(dppm)_3]^{2+}$ (Pd_2Pt (**4**) (−4160 ppm), $PdPt_2$ (**3**) (−4200 ppm) and Pt_3 (**2a**) (−4242 ppm)).

To assess whether the reaction **1** can be employed for the preparation of hetero-tri-nuclear Pd and Pt complexes, we carried out reactions of $[Pd(SeCOC_6H_4Me\text{-}4)_2(dppm)]$ with two equivalents of $PtCl_2(dppm)$ and $[Pt(SeCOC_6H_4Me\text{-}4)_2(dppm)]$ with two equivalents of $PdCl_2(dppm)$. These

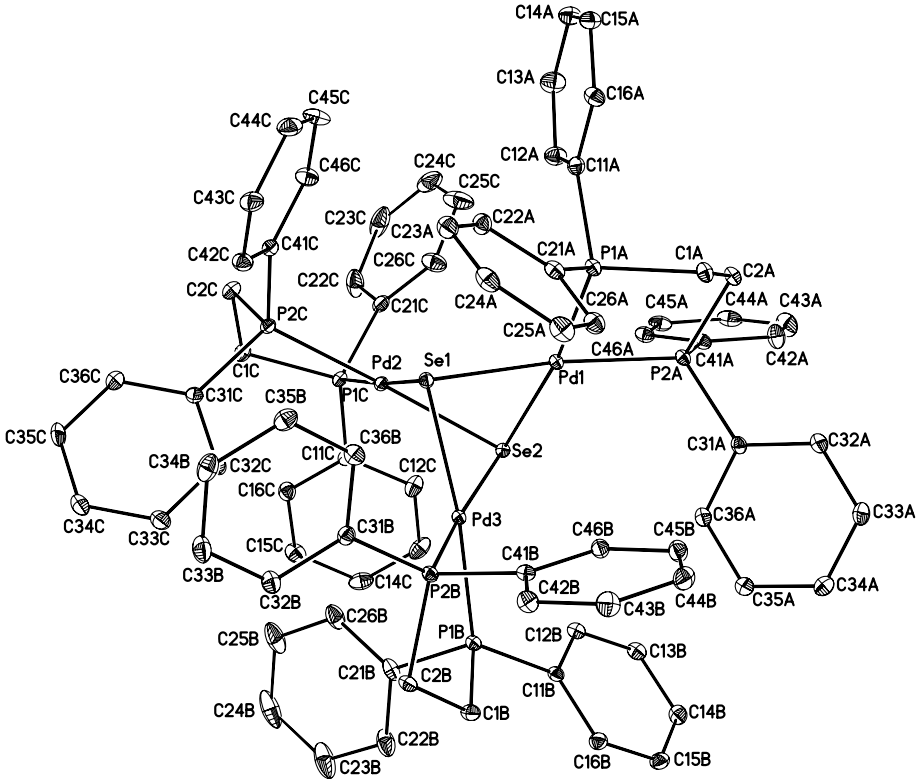

Fig. 3. ORTEP drawing of $[Pd_3(\mu\text{-}Se)_2(dppe)_3][BPh_4]_2$ (**1b**) with atomic number scheme (the two anion fragments, $[BPh_4]$, are omitted for clarity).

reactions gave $[PdPt_2(\mu_3\text{-}Se)_2(dppm)_3]^{2+}$ (**3**) and $[Pd_2Pt(\mu_3\text{-}Se)_2(dppm)_3]^{2+}$ (**4**), respectively, together with some redistribution products as established by ^{31}P NMR spectroscopy. The relative ratio of each species was calculated by integration of the ^{31}P NMR spectra. The former reaction gave a mixture of $[PdPt_2(\mu_3\text{-}Se)_2(dppm)_3]^{2+}$ (**3**) (65%); $[Pd_2Pt(\mu_3\text{-}Se)_2(dppm)_3]^{2+}$ (**4**) (20%); $[Pt_3(\mu_3\text{-}Se)_2(dppm)_3]^{2+}$ (**2a**) (13%) and $Pd_3(\mu_3\text{-}Se)_2(dppm)_3]^{2+}$ (**1a**) (2%) whereas from the latter reaction **4** (55%); **3** (36%) and **1a** (9%) were formed. These products seem to form during the course of the reaction. Attempts to separate individual tri-nuclear species by repeated crystallization were thwarted due to their similar solubility. No redistribution of the metal centers in the trinuclear species is observed when $CDCl_3$ solutions of **1a** and **2a** are mixed in 2:1 ratio. The $^{31}P\{^1H\}$ spectrum for this mixture showed signals for individual species even after a few days.

3.2. Structure of *1b*

The X-ray diffraction analysis of **1b** revealed the formation of a selenido-bridged tri-nuclear palladium complex (Fig. 3). The geometry around each palladium atom is approximately square planer with two P atoms of the chelating dppe and two Se atoms defining the coordination sphere. The two μ_3-Se ligands are shared by all the three palladium atoms.

Table 2
Selected bond lengths (Å) and bond angles (°) of $[Pd_3(\mu\text{-}Se)_2(dppe)_3][BPh_4]_2$

Pd(1)–Se(1)	2.4425(5)	Pd(1)–Pd(3)	3.1407(5)
Pd(1)–Se(2)	2.4785(5)	Pd(2)–Pd(3)	3.1366(5)
Pd(2)–Se(1)	2.4514(5)	Pd(1)–Pd(2)	3.3243(5)
Pd(2)–Se(2)	2.4774(5)	Pd(1)–P(1A)	2.2720(8)
Pd(3)–Se(1)	2.4646(5)	Pd(1)–P(2A)	2.2946(8)
Pd(3)–Se(2)	2.4773(6)	Pd(2)–P(1C)	2.2867(8)
P(1A)–C(1A)	1.837(3)	Pd(2)–P(2C)	2.2666(8)
P(1A)–C(11A)	1.821(3)	Pd(3)–P(1B)	2.2925(8)
P(1A)–C(21A)	1.816(3)	Pd(3)–P(2B)	2.2734(9)
P(2A)–C(2A)	1.839(3)	P(1B)–C(1B)	1.845(3)
P(2A)–C(31A)	1.829(3)	P(1B)–C(11B)	1.820(3)
P(2A)–C(41A)	1.813(3)	P(1B)–C(21B)	1.821(3)
P(1C)–C(1C)	1.844(3)	P(2B)–C(2B)	1.839(3)
P(1C)–C(11C)	1.812(3)	P(2B)–C(31B)	1.817(3)
P(1C)–C(21C)	1.819(3)	P(2B)–C(41B)	1.823(3)
C(1A)–C(2A)	1.528(4)	P(2C)–C(2C)	1.835(3)
C(1B)–C(2B)	1.531(4)	P(2C)–C(31C)	1.820(3)
C(1C)–C(2C)	1.536(4)	P(2C)–C(41C)	1.810(3)
Se(1)–Pd(1)–Se(2)	82.909(13)	Se(1)–Pd(3)–Se(2)	82.484(12)
P(1A)–Pd(1)–P(2A)	85.61(3)	P(1B)–Pd(3)–P(2B)	85.79(3)
Se(1)–Pd(1)–P(1A)	91.61(2)	Se(1)–Pd(3)–P(1B)	173.46(2)
Se(1)–Pd(1)–P(2A)	169.54(2)	Se(1)–Pd(3)–P(2B)	93.59(2)
Se(2)–Pd(1)–P(1A)	172.74(2)	Se(2)–Pd(3)–P(1B)	98.98(2)
Se(2)–Pd(1)–P(2A)	100.62(2)	Se(2)–Pd(3)–P(2B)	171.27(2)
Se(1)–Pd(2)–Se(2)	82.751(13)	Pd(1)–Se(1)–Pd(2)	85.573(16)
P(1C)–Pd(2)–P(2C)	84.89(3)	Pd(1)–Se(1)–Pd(3)	79.586(14)
Se(1)–Pd(2)–P(1C)	176.15(2)	Pd(2)–Se(1)–Pd(3)	79.290(15)
Se(1)–Pd(2)–P(2C)	92.10(2)	Pd(1)–Se(2)–Pd(2)	84.254(11)
Se(2)–Pd(2)–P(1C)	100.36(2)	Pd(1)–Se(2)–Pd(3)	78.654(11)
Se(2)–Pd(2)–P(2C)	174.24(2)	Pd(2)–Se(2)–Pd(3)	78.552(13)

All six Pd–Se distances manifest the strong *trans* influence of the phosphine ligand. These distances are in good agreement with the values reported for the compounds, $[Pd_2Cl_3(\mu\text{-}SeC_5H_4N)(PPr_3)_2]$ (2.5077 (8) Å) [19] and $[Pd(SeCH_2CH_2CH_2NMe_2)]_6$ (~2.43 Å) [20], where selenium is trans to a strong *trans* influencing ligand. The Pd–Se distances in **1b** are, however, longer than those observed (2.32–2.40 Å) for $[Pd_3Cl_3(\mu\text{-}SeCH_2CH_2NMe_2)_3]$ [21], $[Pd_2Cl_2(\mu\text{-}SeCH_2CH_2NMe_2)_2]$ [22] and $[PdCl(SeCH_2CH_2NMe_2)(PMePh_2)]$ [23]. As is evident from Table 2, the Pd–Se(1) distances are marginally shorter than the Pd–Se(2) bond lengths. All the six Pd–P distances are essentially similar and are well in agreement with the reported values [24].

4. Conclusion

It has been demonstrated that monoselenocarboxylate complexes provide a useful route for the one pot synthesis of selenido-bridged tri-nuclear complexes in fairly good yields. This reaction can also be utilized for the preparation of hetero-tri-nuclear complexes.

Acknowledgements

Authors are grateful to Dr. T. Mukherjee and Dr. S.K. Kulshreshtha for encouragement of this work. We also thank Head, Radiochemistry Division, BARC, for providing microanalyses.

Appendix A. Supplementary data

CCDC 298632 contains the supplementary crystallographic data for $[Pd_3(\mu_3\text{-}Se)_2(dppe)_3][BPh_4]_2$. These data can be obtained free of charge at www.ccdc.cam.ac.uk/conts/retrieving.html or from the Cambridge Crystallographic Data Center, 12 Union Road, Cambridge CB2 1EZ, UK. Supplementary data associated with this article can be found, in the online version, at doi:10.1016/j.poly.2006.05.026.

References

[1] V.K. Jain, L. Jain, Coord. Chem. Rev. 249 (2005) 3075.
[2] S.W.A. Fong, T.S.A. Hor, J. Chem. Soc., Dalton Trans. (1999) 639.
[3] K. Matsumoto, N. Kotoku, T. Shizuka, R. Tanaka, S. Okeya, Inorg. Chim. Acta 321 (2001) 167.
[4] K. Matsumoto, K. Takahashi, H. Ikuzawa, H. Kimoto, S. Okeya, Inorg. Chim. Acta 281 (1998) 174.
[5] K. Matsumoto, K. Takahashi, S. Hada, Y. Nakao, Polyhedron 18 (1999) 1811.
[6] K. Matsumoto, N. Saiga, S. Tanaka, S. Ooi, J. Chem. Soc., Dalton Trans. (1991) 1265.
[7] K. Matsumoto, M. Ikuzawa, M. Kamikubo, S. Ooi, Inorg. Chim. Acta 217 (1994) 129.
[8] M. Capdevila, W. Clegg, P. Gonzalez-Duarte, B. Harris, I. Mira, J. Sola, I.C. Taylor, J. Chem. Soc., Dalton Trans. (1992) 2817.
[9] V.K. Jain, S. Kannan, R.J. Butcher, J.P. Jasinski, J. Chem. Soc., Dalton Trans. (1993) 1509.
[10] A. Singhal, V.K. Jain, B. Varghese, E.R.T. Tiekink, Inorg. Chim. Acta 285 (1999) 190.

[11] A. Singhal, V.K. Jain, A. Klein, M. Niemeyer, W. Kaim, Inorg. Chim. Acta 357 (2004) 2134.
[12] L.B. Kumbhare, V.K. Jain, B. Varghese, Inorg. Chim. Acta 359 (2006) 409.
[13] T.G. Appleton, M.A. Bennett, I.B. Tomkins, J. Chem. Soc., Dalton Trans. (1976) 439.
[14] G.K. Anderson, J.A. Davies, D.J. Choeck, Inorg. Chim. Acta 76 (1983) L251.
[15] J.A. Ibers, W.C. Hamilton, Acta Crystallogr. 17 (1964) 781.
[16] G.M. Sheldrick, SHELX-97, A Computer Program for Crystal Structure Solution and Refinement, Universitat Gottingen, Gottingen, Germany, 1997.
[17] V.K. Jain, L. Jain, Coord. Chem. Rev. 249 (2005) 3075.
[18] G.W. Bushnell, K.R. Dixon, R. Ono, A. Pidcock, Can. J. Chem. 62 (1984) 696.
[19] S. Narayan, V.K. Jain, B. Varghese, J. Chem. Soc., Dalton Trans. (1998) 2359.
[20] S. Dey, V.K. Jain, A. Klein, W. Kaim, Inorg. Chem. Commun. 7 (2004) 601.
[21] S. Dey, V.K. Jain, S. Chaudhary, A. Knoedler, F. Lissner, W. Kaim, J.Chem. Soc., Dalton Trans. (2001) 723.
[22] S. Dey, V.K. Jain, A. Knoedler, W. Kaim, Inorg. Chim. Acta 349 (2003) 104.
[23] S. Dey, L.B. Kumbhare, V.K. Jain, T. Schurr, W. Kaim, A. Klein, F. Belaj, Eur. J. Inorg. Chem. (2004) 4510.
[24] S. Narayan, V.K. Jain, R.J. Butcher, Polyhedron 17 (1998) 2037.

certain biological systems and their potential to act as multielectron redox catalysts [11–14]. Some novel studies have been exploring a group of macrocyclic dioxime complexes of Co(III) in which the bridging protons of the bis-dioxime ligands have been replaced by BF_2^+ groups, an alteration that firms up the macrocyclic structure while removing acidic protons from the vicinity of the O_2 binding site [15–17].

In this work the synthesis and characterization of a (*E*,*E*)-dioxime containing bis(diazadioxa-12-crown-4 ethoxy) units and Ni(II), Cu(II) and Co(III) complexes of **H_2L** are reported. A cobalt(III) complex containing the BF_2^+ bridge macrocycle is synthesized as well. In addition, alkali and heavy metal extraction abilities of **1**, **3**, **6** and **10** are also examined.

2. Experimental

2.1. Materials

1,2-Bis(2-hydroxyethoxy)benzene [18], 1,2-bis(2-chloroethoxy)benzene [19], 1,2-bis(2-chloroethoxy)-4-nitrobenzene [20], 1,2-bis(2-iodoethoxy)-4-nitrobenzene [20], 6-[(4-methylphenyl)sulfonyl]-3,9-dioxa-6-aza-1,11-undecandiol-bis(methanesulfanate) [21], benzyl-4-[(4-methylphenyl)sulfonyl]-1,7-dioxa-4,10-diazacyclododecan [21], 4-[(4-methylphenyl)sulfonyl]-1,7-dioxa-4,10-diazacyclododecan [21] and cyanogen di-N-oxide [22] were prepared according to the literature procedures. Reagent grade chemicals were used as received. Solvents were purified according to standard methods [23] before use. Silica gel (70–230 mesh) was used for chromatographic separations.

2.2. Measurements

Melting points were determined using an electrothermal apparatus and were uncorrected. The ^{1}H and ^{13}C NMR spectra were recorded on a Varian XL-200 spectrometer and IR spectra were recorded on a Perkin–Elmer Spectrum One spectrometer with the samples in KBr pellets. The UV–Vis spectra were recorded on a model Schimadzu 1601 UV–Vis spectrometer using a 1 cm pathlength quartz UV-cell. Fast atom bombardment mass spectra were recorded on a Varian MAT 711 and VG Zap Spec spectrometers using *m*-nitrobenzyl alcohol as the matrix. The elemental analysis and the metal contents of the compounds were determined on a Hewlett-Packard 185 CHN analyzer and on a Unicam 929 AA spectrophotometer.

2.3. Synthesis

2.3.1. 4-[(4-Methlyphenyl)sulfonyl]-10-[2-((4-nitro-2-{2-[10-phenylsulfonyl)-1,7-dioxa-4,10-diazacyclododecan-4-yl]ethoxy}phenoxy)ethyl]-1,7-dioxa-4,10-diazacyclododecan (3)

Finely ground anhydrous Na_2CO_3 (4.0 g, 3.81 mmol), compound **1** (2.5 g, 7.62 mmol), anhydrous NaI (0.572 g, 3.81 mmol) and 70 mL dry acetonitrile were added to a three-necked flask fitted with a condenser which was evacuated, refilled three times with argon, and connected to a vacuum line. Under argon, the mixture was stirred at 45 °C for 30 min. Compound **2** (1.764 g, 3.81 mmol) was added to this mixture under argon and the reaction mixture was heated and stirred at 95 °C for 7 days. The reaction mixture was cooled to room temperature and filtered off and the precipitated salt was washed with 25 mL dichloromethane. The major liquor and washing solvents were combined and evaporated and a pale yellow solid-oily crude was obtained. The residue was purified in a silica gel column using chloroform:petroleum ether:methanol (7:2:1) as eluents. The second fraction was combined and evaporated, 10–15 mL methanol was added and the mixture was stirred at room temperature for 30 min. The precipitated pale yellow crystals were filtered off and dried in vacuo.

Compound ***3***: Yield: 2.92 g (89%); m.p. 190–192 °C. *Anal*. Calc. for $C_{40}H_{57}N_5O_{12}S_2$: C, 55.62; H, 6.60; N, 8.11. Found: C, 55.25; H, 6.47; N, 8.22%. IR (KBr): ν_{max} (cm^{-1}): 3087, 3027, 2919–2851, 1597, 1587–1338, 1514–1453, 1275–1229, 1160–1019. ^{1}H NMR ($CDCl_3$): δ 8.01 (d, 1H, Ar–H), 7.84 (s, 1H, Ar–H), 7.32 (d, 1H, Ar–H), 7.61 (d, 4H, Ar–H), 6.90 (d, 4H, Ar–H), 4.52–4.40 (m, 4H, Ar–O–CH_2), 4.13-3.95 (m, 4H, –CH_2N), 3.76–3.52 (m, 16H, $CH_2CH_2OCH_2CH_2$), 3.18–2.80 (m, 16H, CH_2N), 2.36 (s, 6H, Ar–CH_3). ^{13}C NMR ($CDCl_3$): δ 154.05 (ArCO), 148.12 (ArCS), 143.29 (ArCH), 141.25 (ArCN), 135.67, 129.68, 127.2, 117.93, 111.12, 107.72 (ArC), 70.25–69.75 (OCH_2), 56.08–55.06–60.63 (NCH_2), 21.5 (CH_3–Ar). MS (FAB positive): *m*/*z* 863 $[M]^+$.

2.3.2. 3,4-Bis(2-{10-[(4-methylphenyl)sulfonyl]-1,7-dioxa-4,10-diazacyclododecan-4-yl}ethoxy)aniline (4)

Compound **3** (2.92 g, 3.38 mmol) was dissolved in 120 mL *n*-butanol at 60 °C under an argon atmosphere and degassed in a vacuum line. 0.417 g Pd/C (10%) was added to the reaction mixture and heated at 125 °C. At reflux temperature, 5.96 mL hydrazinium hydrate (100%) was added to this mixture dropwise over 30 min. After 14 h, the reaction mixture was filtered off using Celite as the filtering agent and washed several times with *n*-butanol. The major liquor and washing solvents were combined and evaporated to dryness under reduced pressure. Diethyl ether was added to the residue under argon and the resulting solution was kept in darkness, otherwise the amino derivative can decompose. A little amount of the amino derivative **4** was kept to take its IR, ^{1}H NMR, ^{13}C NMR, elemental analysis and mass spectra. Compound **4** was used for the following reaction without any further purification.

Compound ***4***: Yield: 2.32 g (84%); m.p. 128–131 °C. *Anal*. Calc. for $C_{40}H_{59}N_5O_{10}S_2$: C, 57.62; H, 7.08; N, 8.40. Found: C, 57.40; H, 6.98; N, 8.57%. IR (KBr): ν_{max} (cm^{-1}): 3439–3362, 3060–3032, 2924–2856, 1621, 1597, 1511–1448, 1303–1225, 1159–1019. ^{1}H NMR ($CDCl_3$): δ

6.95 (d, 1H, Ar–CH–C–O), 6.72 (s, 1H, Ar–N–CH–C–O), 6.35 (d, 1H, Ar–NH_2–C–CH), 7.58 (d, 4H, Ar–SO_2–C–CH), 6.76 (d, 4H, H_3C–AR–CH), 4.57 (br, s, 2H, NH_2), 4.48–4.36 (m, 4H, Ar–O–CH_2), 4.01–3.87 (m, 16H, $CH_2CH_2OCH_2CH_2$), 3.72–3.46 (m, 4H, –CH_2N), 3.15–2.72 (m, 16H, CH_2N), 2.34 (s, 6H, Ar–CH_3). ^{13}C NMR ($CDCl_3$): δ 146.12 (ArCO), 143.36 (ArCS), 141.03 (ArCH), 138.11 (ArCN), 135.72, 129.65, 127.10, 108.22, 102.50 (ArC), 70.27–69.70–67.45 (OCH_2), 56.08–55.04–50.59 (NCH_2), 21.5. MS (FAB positive): m/z 833 $[M]^+$.

2.3.3. H_2L (6)

A cold solution, −10 °C, of cyanogen di-*N*-oxide (**5**) in 25 mL dichloromethane, which was prepared from (*E*,*E*)-dichloroglyoxime (0.785 g, 5 mmol), and 25 mL of an aqueous solution at −10 °C of 0.5 M Na_2CO_3 was added to a cold solution of 3,4-bis(2-{10-[(4-methylphenyl)sulfonyl]-1,7-dioxa-4,10-diazacyclododecan-4-yl}ethoxy)aniline **4** (2.36 g, 2.8 mmol) in 200 mL dichloromethane. The reaction was continued for 10–12 h at the same temperature and then evaporated to dryness. The crude product was crystallized from a dichloromethane:ethanol mixture (9:1) to yield champagne colored crystals.

Compound ***6***: Yield: 1.54 g (62%); mp 154–156 °C (dec). *Anal*. Calc. for $C_{82}H_{118}N_{12}O_{22}S_4$: C, 56.23; H, 6.74; N, 9.60. Found: C, 56.09; H, 6.52; N, 9.76%. IR (KBr): ν_{max} (cm^{-1}): 3350, 3230, 3082-3042, 2922-2868, 1640, 1611, 1596, 1514–1448, 1289–1228, 1160–1020, 942. ^1H NMR (DMSO-d_6): δ 10.20 (s, 2H, OH), 7.86 (s, 2H, NH), 7.60 (d, 8H, Ar–SO_2–C–CH), 6.78 (d, 8H, H_3C–Ar–CH), 6.92 (d, 2H, Ar–CH–C–O), 6.49 (s, 2H, Ar–N–CH–C–O), 6.25 (d, 2H, Ar–NH–C–CH), 4.45–4.34 (m, 8H, Ar–O–CH_2), 3.98-3.82 (m, 32H, $CH_2CH_2OCH_2CH_2$), 3.69–3.42 (m, 8H, –CH_2N), 3.14–2.71 (m, 32H, CH_2N), 2.35 (s, 12H, Ar–CH_3). ^{13}C NMR ($CDCl_3$): δ 154.09, 148.17, 145.02 (C=N–O–H), 143.25, 141.30, 135.69, 129.68, 127.15, 117.95, 111.12, 107.80, 70.29, 69.77, 67.53, 56.10, 55.04, 50.61, 21.5. MS (FAB positive): m/z 1750 $[M]^+$.

2.3.4. $[Ni(HL)_2]$ (7)

A solution of $NiCl_2 \cdot 6H_2O$ (12 mg, 0.05 mmol) in 5 mL ethanol was added to a solution of H_2L **6** (175 mg, 1 mmol) in 25 mL ethanol at 60 °C. A distinct change in color and a decrease in the pH of the solution (pH 2.42) was observed. While heating and stirring at the same temperature, an equivalent of ethanolic triethylamine (0.1 M) was added in order to increase the pH to 4.5–5.0. After heating the reaction mixture for 2 h in a water-bath, the precipitate was filtered off, washed several times with water, ethanol and diethyl ether and then dried in vacuo by P_2O_5.

Compound 7: Yield: 146 mg (82%); m.p. >300 °C. *Anal*. Calc. for $C_{164}H_{234}N_{24}O_{44}S_8Ni$: C, 55.34; H, 6.58; N, 9.45. Found: C, 55.13; H, 6.35; N, 9.54%. IR (KBr): ν_{max} (cm^{-1}): 3392, 3060–3018, 2923–2865, 1718, 1627, 1618, 1597, 1506–1449, 1286–1220, 1159–1020, 946. ^1H NMR (DMSO-d_6): δ 16.80 (s, 2H, O–H···O), 7.98 (br, s, 4H, NH), 7.58 (d, 16H, Ar–SO_2–C–CH), 6.73 (d, 16H, H_3C–Ar–CH), 6.88 (d, 4H, Ar–CH–C–O), 6.43 (s, 4H, Ar–N–CH–C–O), 6.21 (d, 4H, Ar–NH–C–CH), 4.40–4.32 (m,16H, Ar–O–CH_2), 3.92–3.78 (m, 64H, $CH_2CH_2OCH_2CH_2$), 3.67–3.39 (m, 16H, –CH_2N), 3.09–2.63 (m, 64H, CH_2N), 2.37 (s, 24H, Ar–CH_3). MS (FAB positive): m/z 3556 $[M+1]^+$.

2.3.5. $[Cu(HL)_2]$ (8)

A solution of $CuCl_2 \cdot 2H_2O$ (9 mg, 0.05 mmol) in 5 mL ethanol was added to a solution of H_2L **6** (175 mg, 1 mmol) in 25 mL ethanol at 60 °C. A distinct change in color and a decrease in the pH of the solution (pH 2.38) was observed. While heating and stirring at the same temperature, an equivalent of ethanolic triethylamine (0.1 M) was added in order to increase the pH to 5.0–6.0. After heating the reaction mixture for 2 h in a water-bath, the precipitate was filtered off, washed several times with water, ethanol and diethyl ether and then dried in vacuo by P_2O_5.

Compound ***8***: Yield: 136 mg (76%); m.p. >300 °C. *Anal*. Calc. for $C_{164}H_{234}N_{24}O_{44}S_8$: C, 55.26; H, 6.27; N, 9.43; Cu, 1.78. Found: C, 55.19; H, 6.13; N, 9.56; Cu, 1.63%. IR (KBr): ν_{max} (cm^{-1}): 3389, 3054–3021, 2920–2881, 1733, 1624, 1598, 1508–1446, 1303–1220, 1160–1020, 941. MS (FAB positive): m/z 3561 $[M+1]^+$.

2.3.6. $[Co(HL)_2L'Cl]$ (9)

A solution of $CoCl_2 \cdot 6H_2O$ (24 mg, 0.1 mmol) in 10 mL ethanol was added to a solution of H_2L **6** (350 mg, 2 mmol) in 75 mL ethanol at 60 °C whilst bubbling oxygen through the ligand solution. After 30 min, 0.01 mL pyridine (0.01 g, 0.1 mmol) in 5 mL ethanol was added to the mixture. The reaction mixture was heated and stirred for 4–5 h with oxygen passing through it. The total volume of the residue was decreased to 1/4 and then filtered off, washed several times with water, ethanol and diethyl ether and then dried in vacuo by P_2O_5.

Compound ***9***: Yield: 206 mg (56%); m.p. >300 °C. *Anal*. Calc. for $C_{169}H_{239}N_{25}O_{44}S_8CoClPy$: C, 55.24; H, 6.51; N, 9.53; Co, 1.59. Found: C, 55.17; H, 6.38; N, 9.47; Co, 1.50%. IR (KBr): ν_{max} (cm^{-1}): 3325, 3070, 3063–3025, 2924–2870, 1722, 1621, 1597, 1601, 1549–1510, 1286–1226, 1159–1020, 943. ^1H NMR (DMSO-d_6): δ 16.85 (s, 2H, O–H···O), 8.02 (br, s, 4H, NH), 7.71 (d, 2H, py-H), 7.50 (t, 2H, py-H), 6.84 (t, 1H, py-H), 7.60 (d, 16H, Ar–SO_2–C–CH), 6.79 (d, 16H, H_3C–Ar–CH), 6.84 (d, 4H, Ar–CH–C–O), 6.42 (s, 4H, Ar–N–CH–C–O), 6.21 (d, 4H, Ar–NH–C–CH), 4.42–4.31 (m, 16H, Ar–O–CH_2), 3.94–3.76 (m, 64H, $CH_2CH_2OCH_2CH_2$), 3.65–3.37 (m, 16H, –CH_2N), 3.11–2.65 (m, 64H, CH_2N), 2.35 (s, 24H, Ar–CH_3). MS (FAB positive): m/z 3671 $[M+1]^+$.

2.3.7. $[Co(LBF_2)_2L'Cl]$ (10)

A suspension of the diamagnetic cobalt (III) complex $[Co(HL)_2L'Cl]$ **9** (0.734 g, 0.2 mmol) in 100 mL of freshly distilled acetonitrile was brought to reflux temperature under an argon atmosphere. The equivalent amount of $BF_3 \cdot OEt_2$ (0.1 mL, 0.4 mmol) was added to the above

suspension and the reaction mixture became red immediately. The solution was boiled under reflux with stirring for 5 h and then allowed to cool to room temperature. The solvent was concentrated to 10 mL under reduced pressure; 20 mL of dry Et_2O was then added dropwise and the solution was allowed to stand at −18 °C overnight, whereupon the desired product precipitated. The claret red solid was collected by filtration, washed with cold acetonitrile and Et_2O and then dried in vacuo.

*Compound **10***: Yield: 512 mg (68%); m.p. >300 °C. *Anal.* Calc. for $C_{169}H_{237}N_{25}O_{44}S_8CoClB_2F_4$: C, 53.84; H, 6.29; N, 9.29; Co, 1.56. Found: C, 54.65; H, 6.78; N, 9.02, Co, 1.32%. IR (KBr): ν_{max} (cm^{-1}): 3336, 3068, 3060–3022, 2950–2863, 1649, 1590, 1605, 1545–1510, 1284–1223, 1156–1030, 948, 875–843. ^1H NMR (DMSO-d_6): δ 7.96 (br, s, 4H, NH), 7.68 (d, 2H, py-H), 7.47 (t, 2H, py-H), 6.80 (t, 1H, py-H), 7.59 (d, 16H, Ar–SO_2–C–CH), 6.75 (d, 16H, H_3C–Ar–CH), 6.81 (d, 4H, Ar–CH–C–O), 6.41 (s, 4H, Ar–N–CH–C–O), 6.19 (d, 4H, Ar–NH–C–CH), 4.39–4.27 (m, 16H, Ar–O–CH_2), 3.92–3.70 (m, 64H, $CH_2CH_2OCH_2CH_2$), 3.64–3.35 (m, 16H, –CH_2N), 3.13–2.64 (m, 64H, CH_2N), 2.38 (s, 24H, Ar–CH_3). MS (FAB positive): *m*/*z* 3768 $[M+1]^+$, 3785 $[M+H_2O]^+$ and 3686 $[M-pyr\text{-}2]^+$.

2.3.8. Measurement of alkali and heavy metal-binding properties of *1*, *3*, *6* and *10*

The extraction properties of **1**, **3**, **6** and **10** were investigated under liquid–liquid phase and neutral conditions using alkaline (Li^+, Na^+, K^+, Cs^+) and heavy metal picrates (Ag^+, Pb^{2+}, Cd^{2+}, Cu^{2+}, Zn^{2+}) as substrates and measuring by UV–Vis spectra the amounts of metal picrate in the aqueous phase before and after treatment with the compounds. Alkali metal picrates (3×10^{-5} M) were prepared from a mixture of the alkali metal hydroxides and picric acid in deionized water whereas the heavy metal picrates were prepared from a mixture of the metal nitrates and picric acid in deionized water. We also prepared 3×10^{-3} M solutions of the compounds (**1**, **3**, **6**, **10**) in 1,2-dichloroethane. Then equal volumes of both metal picrate solutions and compound solutions were added into plastic bottles and kept closed then shaken for 12 h by a shaker at 25 ± 1 °C. Finally we took the aqueous phase and measured the absorbance at maximum wavelength (~358 nm). For each combination of host and metal picrate, the picrate extraction was conducted on three different samples and the average value of percent picrate extracted, with a standard deviation, was calculated. The picrate extraction results are presented in Table 1. In the absence of host, a blank experiment, no metal ion picrate extraction was detected. The extractability was determined based on the absorbance of the picrate ion in the aqueous solutions. The extractability was calculated by using the equation below:

$$E(\%) = [(A_{before} - A_{after})/A_{before}] \times 100$$

where A_{before} is the absorbance in the absence of ligand. A_{after} denotes the absorbance in the aqueous solution phase after extraction.

3. Results and discussion

The synthesis of the nitro derivative **3** was performed by starting with 1,2-bis(2-iodoethoxy)-4-nitrobenzene (**2**) [20] and 4-[(4-methylphenyl)sulfonyl]-1,7-dioxa-4,10-diazacyclododecan (**1**) [21] in acetonitrile in the presence of anhydrous Na_2CO_3 and NaI for a period of 7 days, affording 4-[(4-methlyphenyl)sulfonyl]-10-[2-((4-nitro-2-{2-[10-phenylsulfonyl)-1,7-dioxa-4,10-diazacyclododecan-4-yl]ethoxy}phenoxy)ethyl]-1,7-dioxa-4,10-diazacyclododecan (**3**) (Scheme 1). The template effect of sodium cations accounts for the high yield obtained in the desired synthesis. Final purification of the nitro derivative **3** by chromatography [silica gel, chloroform:petroleum ether:methanol (7:2:1)] afforded **3** in 89% yield, for which elemental analysis and FAB mass spectral data were satisfactory: 863 $[M]^+$. In the ^1H NMR spectrum of **3**, the NH group of compound **1** disappeared as expected. It can also be observed in its IR spectrum, confirming the formation of compound **3**. The NO_2 functional group also can be seen at 1587–1338 cm^{-1} in the IR spectrum of compound **3**.

The transformation of the nitro derivative **3** into the amino derivative **4** was performed in the presence of *n*-butanol using hydrazinium hydrate (100%) and Pd/C (10%) for 14 h with a 84% yield. Since this method is more advantageous than the others, we preferred to use this one. No further purification was performed for compound **4** when it was obtained because of the characteristic property of so many amino derivatives that they decomposes very easily when exposed to light and heat. ^1H NMR spectrum of **4** showed a new signal due to NH_2 protons at $\delta = 4.52$, as expected. It is possible to see the NH_2 stretching vibra-

Table 1
Alkaline and heavy metal picrate extractions from aqueous solutions into 1,2-dichloroethane by using **1**, **3**, **6** and **10**[a]

Host molecule	Percent of metal picrate extracted (%)[b]								
	Li^+	Na^+	K^+	Cs^+	Ag^+	Zn^{2+}	Cd^{2+}	Cu^{2+}	Pb^{2+}
1	9.3 ± 0.1	42.3 ± 0.1	22.6 ± 0.1	0.4 ± 0.1	39.1 ± 0.1	27.5 ± 0.1	18.6 ± 0.1	36.7 ± 0.1	11.8 ± 0.1
3	15.2 ± 0.1	78.3 ± 0.1	48.7 ± 0.1	1.6 ± 0.1	69.3 ± 0.1	43.6 ± 0.1	30.2 ± 0.1	56.9 ± 0.1	29.8 ± 0.1
6	18.6 ± 0.1	82.1 ± 0.1	58.3 ± 0.1	2.8 ± 0.1	78.1 ± 0.1	46.3 ± 0.1	34.5 ± 0.1	60.4 ± 0.1	37.3 ± 0.1
10	23.4 ± 0.1	85.5 ± 0.1	62.9 ± 0.1	6.7 ± 0.1	81.6 ± 0.1	49.2 ± 0.1	37.8 ± 0.1	68.7 ± 0.1	45.6 ± 0.1

[a] Temperature 25 ± 1 °C; aqueous phase (10 ml), [picrate] = 3.0×10^{-3} M; organic phase (1,2-dichloroethane, 10 ml), [host molecule] = 3.0×10^{-3} M.
[b] Average and standard deviation for three independent measurements.

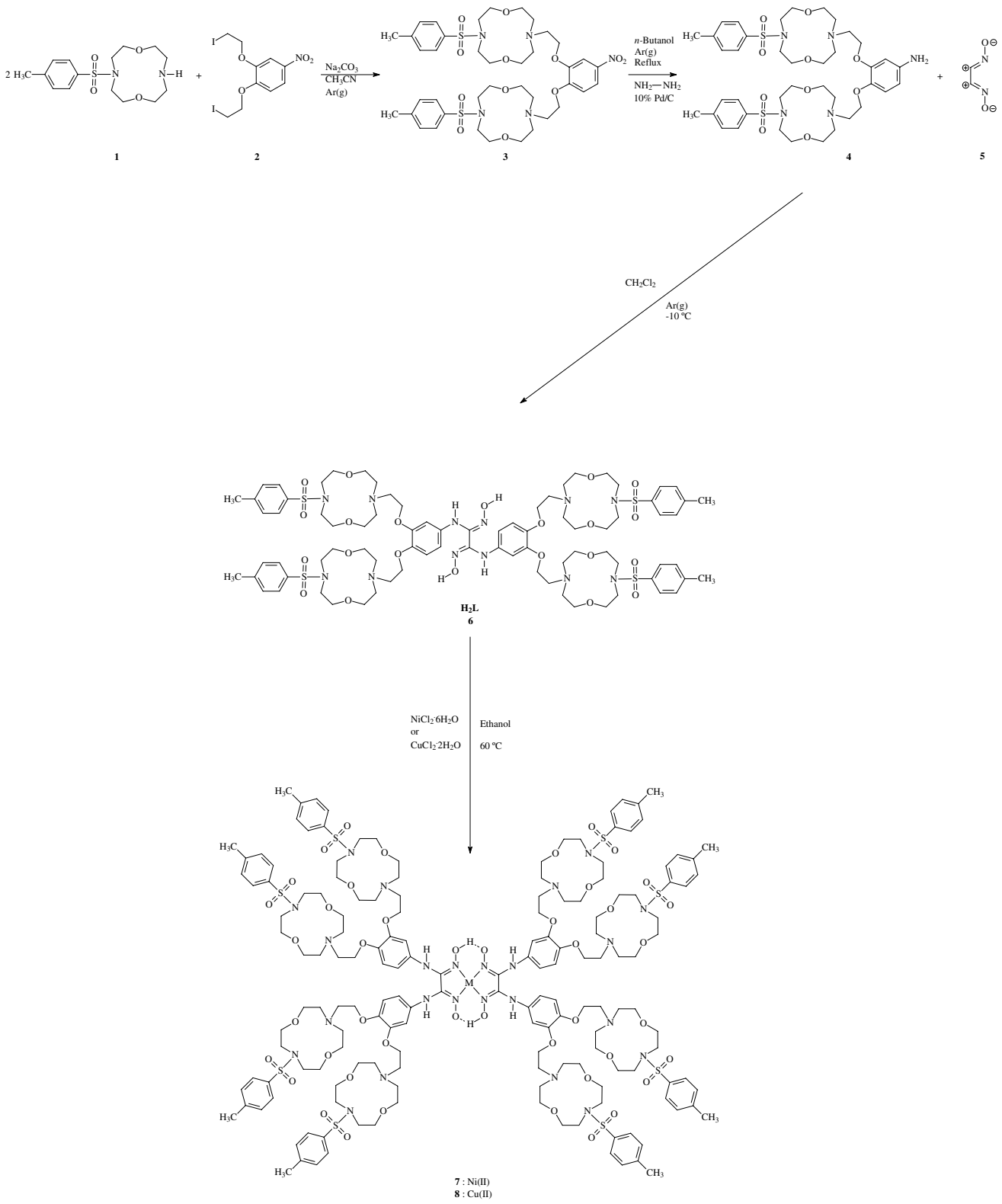

Scheme 1. Synthesis of $\mathbf{H_2L}$ and its complexes [Ni(II),Cu(II)].

tions at 3439 and 3362 cm^{-1} in the IR spectrum of compound **4**. In addition to this information, at 1621 cm^{-1} in the IR spectrum of compound **4** there is a peak belonging to NH_2 bending. Elemental analysis data was very satisfactory and FAB mass spectral data was: 833 $[M]^+$, as expected.

The novel *vic*-dioxime **6** was synthesized from the reaction of compound **4** and cyanogen di-*N*-oxide **5** at −10 °C

in dichloromethane in the presence of an aqueous solution of Na_2CO_3 (−10 °C) for a period of 10–12 h in 62% yield. In the ^1H NMR spectrum of **6** there are singlet signals at $\delta = 10.20$ and $\delta = 7.86$ due to the hydroxy imino groups and NH protons respectively which can be identified easily owing to deuterium-exchangeable characteristics of these protons. The singlet chemical shifts of the hydroxy imino groups indicate that the structure of this novel oxime derivative is (*E*,*E*). That the diamino glyoxime has the s-*trans* form was determined by ^1H NMR and X-ray structural analyses [24]. Therefore, the same structure can be proposed for this new oxime derivative **6**, too. A ^{13}C NMR spectrum is one of the most convenient ways to prove the true structure of *vic*-dioximes, and in the ^{13}C NMR spectrum of **6** a singlet peak at $\delta = 145.02$ belongs to hydroxy imino groups. That only one resonance is displayed relating to carbon atoms of oxime indicates that the structure of this novel oxime derivative **6** is of the (*E*,*E*)-dioxime formation [25]. In the IR spectrum of compound **6** there are NH, OH, C=N and NO stretching vibrations at 3350, 3230, 1640 and 942 cm^{-1}, respectively. Both C=N and OH stretching vibration data are harmonious with other oxime derivatives whose structures are of the s-formation [26]. Furthermore, FAB mass spectral data was 1750 $[M]^+$, proving that the structure is the same as the proposed structure. Elemental analysis data displays that the desired compound is synthesized as well.

The mononuclear Ni(II) and Cu(II) complexes $[Ni(HL)_2]$ and $[Cu(HL)_2]$, **7** and **8**, were prepared from the oxime derivative **6** and with a stoichiometric amount of $NiCl_2 \cdot 6H_2O$ and $CuCl_2.2H_2O$ respectively, in the presence of ethanol (Scheme 1). FAB mass spectral data for the compounds **7** and **8** were 3556 $[M+1]^+$ and 3561 $[M+1]^+$ respectively. Both elemental analysis and FAB mass spectral data showed that the metal:ligand ratio is 1:2 for compounds **7** and **8**. In the IR spectra of compounds **7** and **8**, C=N stretching vibrations are at 1624 and 1627 cm^{-1}, respectively. That the C=N stretching vibrations of compounds **7** and **8** are lower than the stretching vibration of the oxime derivative **6** (1640 cm^{-1}) proved that the oxime ligand coordinates with the Ni(II) and Cu(II) cations in the *N*,*N*′ style. In addition, the disappearance of functional groups relating to δ OH and ν OH for compound **6**, at 1427 and 3230 cm^{-1}, indicates that intramolecular hydrogen bonds form with a peak at 1733 cm^{-1} for each complex. That there is a singlet peak at $\delta = 16.80$ in place of the OH functional group in the ^1H NMR spectrum of the square planar complex **7** indicates the existence of intramolecular hydrogen bonds (O–H···O) which can be easily observed by the deuterium-exchange method.

The mononuclear Co(III) complex, $[Co(HL)_2PyCl]$ **9**, was prepared from ligand **6**, pyridine and an equivalent amount of $CoCl_2 \cdot 6H_2O$ in the presence of ethanol (Scheme 2). Whilst the reaction proceeded, oxygen gas was passed through the reaction mixture in order to oxidize Co(II) to Co(III). The FAB mass spectral data for compound **9** was 3671 $[M+1]^+$. The metal:ligand ratio is 1:2 for this complex too, with the pyridine and chlorine ligands in axial positions of the octahedral complex, according to elemental analysis data. That there is a singlet peak at $\delta = 10.20$ in place of the OH functional group in the ^1H NMR spectrum of complex **9** indicates the existence of intramolecular hydrogen bonds (O–H···O) which can be easily observed by the deuterium-exchange method. The chemical shifts for pyridine at $\delta = 7.71$, 7.50 and 6.84 indicates the existence of an octahedral complex **9**. The stretching vibrations of the OH functional group at 3230 cm^{-1} for compound **6** disappeared and a new peak was observed at 1722 cm^{-1} which indicates of the existence of intramolecular hydrogen bonds. A broad C=N stretching vibration of compound **9** at 1621 cm^{-1} is lower than the stretching vibration of the oxime derivative **6** (1640 cm^{-1}) which proves that the oxime ligand coordinates with Co(III). All these data show that all the relevant groups participate in the formation of the complex.

The BF_2-bridged cobalt(III) complex **10** was obtained in high yield, 68%, at moderate dilution (0.2 mmol) from the hydrogen-bridged cobalt(III) complex and boron trifluoride etherate (0.4 mmol) linking reagent (Scheme 2). This reagent readily reacts with the O–H···O bridge in the precursor molecule, yielding an extremely stable compound containing two O–BF_2–O bridges, and the single mole of the axial ligand pyridine was retained, according to ^1H NMR and IR spectra and elemental analysis data of $[Co(LBF_2)_2L'Cl]$. In the IR spectrum of the BF_2^+-capped cobalt(III) complex, the C=N stretching region can be used to distinguish between the dihydrogen-bridged compound and the diboron-bridged compound. This BF_2-macrocycle exhibits upward shifts of ca. 35 cm^{-1} due to the strong electron-withdrawing influence of the BF_2 groups incorporated in the macrocycle. The weak and broad band at 1722 cm^{-1}, concerning O–H···O in-plane deformation of the short hydrogen bond, disappeared upon encapsulation of the H-bonded complex, with the concomitant appearance of peaks around 1156–1030 and 875–843 cm^{-1} for the B–O and B–F groups, respectively [27]. In the ^1H NMR spectrum of the BF_2^+-capped macrocycle, the deuterium exchangeable hydrogen-bridged protons belonging to the H-bonded pseudomacrocylic precursor cobalt(III) complex are no longer present after the formation of the BF_2 bridge [28]. This BF_2-bridged cobalt(III) complex is also confirmed by its fast atom bombardment mass spectrum, which gives a molecular ion peak at $m/z = 3768$ $[M+1]^+$.

3.1. Solvent extraction of alkali and heavy metal cations

The alkali and heavy metal ion binding properties of the compounds having diaza-12-crown-4 units was estimated by solvent extraction of alkali- and heavy metal picrates from the aqueous to an organic phase (Table 1). For comparison, the values obtained under the same conditions for *N*-tosyl-diazadioxa-12-crown-4 (**1**) are included in Table 1. In addition to compounds **3** and **6**, since the introduction of BF_2 groups to complex **9** leads

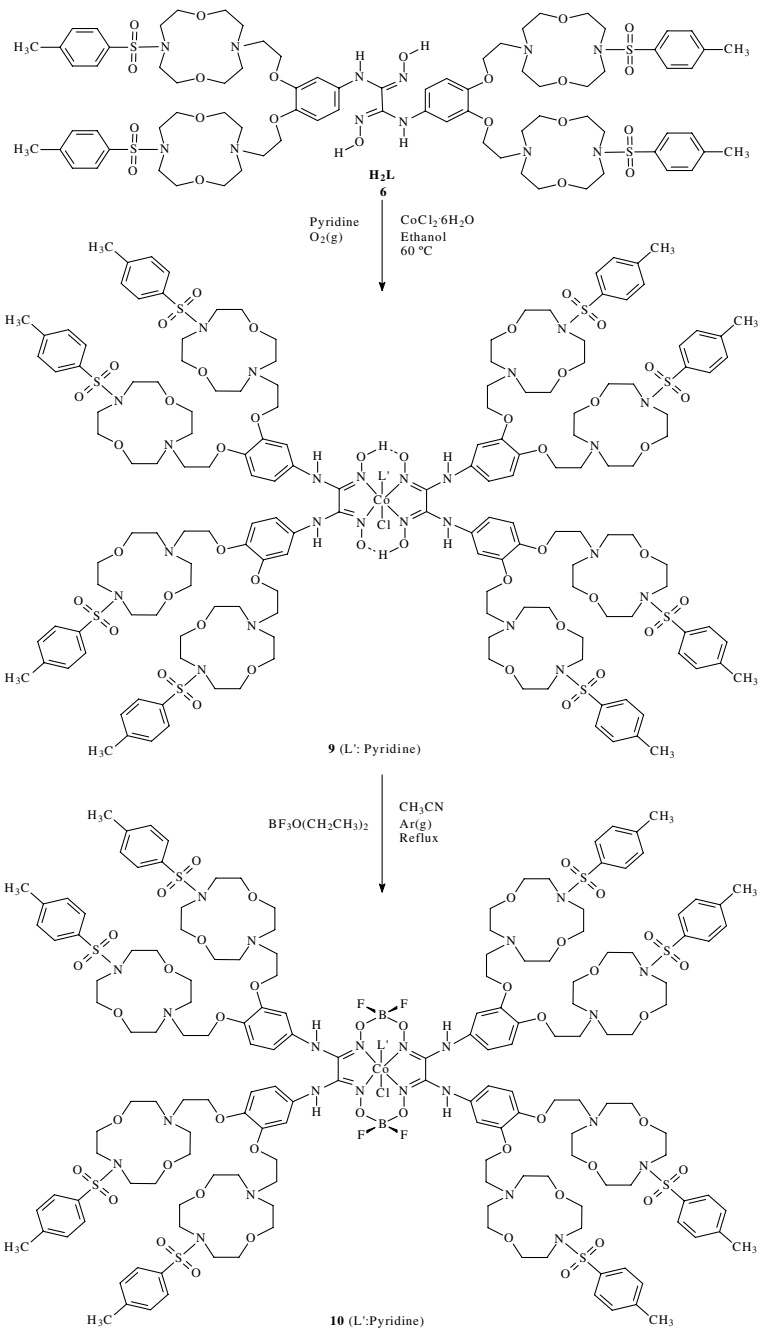

Scheme 2. Synthesis of complexes **9** and **10**.

to an increase in the solubility, in addition to the bulky diazacrown units just the BF_2-bridged cobalt(III) complex **10** among the other complexes was used as an extractant. In the case of all the host compounds, it might be expected that the capability of extraction of the lithium ion would be the highest among the alkali metal cations on comparing its size to the cavity size, as the diameter of the lithium ion is much more compatible with 12-membered macrocyclic units. Nevertheless the extraction was highest for the sodium ion due to the bis-crown effect. Therefore the sodium cation forms a sandwich type complex by binding between two diazacrown units with a metal:ligand ratio of 1:2. The capability of extraction for alkali metal cations increased with compounds **1**, **3**, **6** and **10**. However this increase was not so noteworthy as compared to the increase of the 12-membered macrocyclic units. This might be due to steric hindrance of the bulky diaza-12-crown-4 units.

We were not able to find extraction studies in the literature with heavy metal cations for compounds containing bis(diaza-12-crown-4) moieties. Therefore this work caused us to investigate and perform such a kind of study. However, there are some reports on the extracting properties of tricyclic compounds. According to these studies,

compounds having (diaza-12-crown-4) subunits can form dinuclear complexes with silver(I), zinc(II) and copper(II). They can also form mononuclear complexes with other cations such as mercury(II), lead(II) and cadmium(II) [29–31].

Aza-crown ethers form stable complexes with the Ag^+ cation by replacement of O atoms with N atoms in crown ether moieties [31]. As can be easily figured out from Table 1, Ag^+ has the highest extracting capability by forming M_2L type complexes since there are more diaza-12-crown-4 units which can coordinate with cations that have a small cation diameter. Also the compounds having diaza-12-crown-4 units form ML type complexes with cations having a bigger cation diameter. It means there are less diaza-12-crown-4 units per cation which is why their extracting capabilities are low. The other important fact obtained from the data in Table 1 is that the sodium and silver picrate capabilities of host molecules are closely parallel. It might be attributed the similarity of the cation diameters between Na^+ and Ag^+.

The cation binding properties of the ligands depend upon different factors such as macrocyclic effect, cavity size and the type and number of donor atoms. Also, it is known that *vic*-dioximes form stable complexes with transition metal cations. In the case of compound **6**, an increase concerning its extraction capability might be expected with the investigated metal cations having both oximes and macrocyclic groups for complexation. Since there is no noteworthy increase in its extraction capability, it is not remarkable in our work. This can be easily seen when it is compared to compound **3** or **10**. The number of macrocyclic groups from **3** to **6** increases. It is difficult to comment whether or not the increase in extraction capability is the result of oxime groups or the increase in the number of macrocyclic groups, but, according to these data, we can conclude that the macrocyclic effect and the number of donor atoms are much more effective than oxime groups.

4. Conclusions

In the course of this study, a new *vic*-dioxime ligand **H_2L** containing bis(diaza-12-crown-4) moieties and its complexes [Ni(II), Cu(II), Co(III) and BF_2-briged Co(III)] have been synthesized in good yields and characterized. Additionally, their cation-binding abilities were evaluated using a solvent extraction technique. Picrate was used as a counter anion for all compounds.

The results obtained by the extraction experiments of alkali and heavy metal picrates indicate that the extraction capability of **10** among the bis(diaza-12-crown-4) moieties studied has the highest value in all cases. The cation-binding abilities of **1**, **3**, **6** and **10** were found to be the highest for Na^+ among the alkali metals and Ag^+ among the heavy metals. The alkali and heavy metal ions extracting capabilities of bis(diaza-12-crown-4) moieties synthesized in this work follow the order **10** > **6** > **3** > **1**.

Acknowledgements

This study was supported by The Scientific and Technical Research Council of Turkey (TUBITAK), Project Number: TBAG-2453(104T065) (Ankara, Turkey) and the Research Fund of Karadeniz Technical University, Project Number: 2002.111.2.8 (Trabzon/Turkey). We are also indebted to Dr. Ayhan Çelik (University of Edinburgh/England) for assistance with some spectral data.

References

[1] H. Sakamoto, K. Kimura, Y. Koseki, M. Matsuo, T. Shono, J. Org. Chem. 51 (1986) 4974, and references cited therein.
[2] S. Sinkai, T. Ogawa, Y. Kusano, O. Manabe, K. Kikukawa, T. Goto, T. Matsuda, J. Am. Chem. Soc. 104 (1982) 1960.
[3] Y.H. Cho, S.G. Rha, S.K. Chang, T.D. Chung, K.C. Cho, H. Kim, J. Inclusion Phenom. Mol. Recognit. Chem. 31 (1998) 119.
[4] J.D. Lamb, J. J Christensen, J.L. Oscarson, B.L. Nielsen, B.W. Asay, R.M. Izatt, J. Am. Chem. Soc. 102 (1980) 6820.
[5] A.M. Costero, J. Sanchis, S. Peransi, S. Gil, V. Sanz, A. Domenech, Tetrahedron 60 (2004) 4683.
[6] R.C. Mehrotra, in: G. Wilkinson, R.D. Gillard, J.A. McCleverty (Eds.), Comprehensive Coordination Chemistry, vol. 2, Pergamon Press, New York, 1988, p. 269.
[7] A. Chakravorty, Coord. Chem. Rev. 13 (1974) 1.
[8] F.J. Welcher, Org. Anal. Reag. 3 (1947) 154.
[9] P.J. Toscano, L.G. Marzilli, Prog. Inorg. Chem. 31 (1983) 105.
[10] T.W. Thomas, A.E. Underhill, Chem. Soc. Rev. (1972) 99.
[11] F. Birkelbach, M. Winter, U. Florke, H.J. Haupt, C. Butzlaff, M. Zengen, E. Bill, X. Trautwein, F. Wieghand, P. Chaudhuri, Inorg. Chem. 33 (1994) 3390.
[12] S.A.S. Jurisson, J.D. Lydon, Chem. Rev. 99 (1999) 2205.
[13] P. Mitchell, Science 206 (1979) 1148.
[14] B. Cervara, R. Ruiz, F. Lloret, M. Julve, J. Faus, M.C. Munoz, Y. Journnaux, Inorg. Chim. Acta 288 (1999) 57.
[15] J.C. Stevens, D.H. Busch, J. Am. Chem. Soc. 102 (1980) 3285.
[16] N. Herron, D.H. Busch, J. Am. Chem. Soc. 103 (1981) 1236.
[17] N. Herron, J.E. Cameron, G.L. Neer, D.H. Busch, J. Am. Chem. Soc. 105 (1983) 298.
[18] D. Landini, F. Montanari, F. Rolla, Synthesis 3 (1978) 223.
[19] G. Topal, N. Demirel, M. Toğrul, Y. Turgut, H. Hoşgören, J. Heterocyclic Chem. 38 (2001) 281.
[20] D. Mendil, A. Bilgin, Y. Gök, H.B. Şentürk, J. Inclusion Phenomena Macrocyclic Chem. 43 (2002) 265.
[21] P.L. Anneli, F. Montanari, S. Quici, J. Org. Chem. 53 (1988) 5292.
[22] K.A. Lance, K.A. Goldsby, D.H. Busch, Inorg. Chem. 29 (1990) 4537.
[23] D.D. Perrin, W.L.F. Armarego, Purification of Laboratory Chemicals, 2nd ed., Pergamon, Oxford, 1989.
[24] H.E. Ungnade, L.W. Kissinger, A. Narath, D.C. Barham, J. Org. Chem. 28 (1963) 134.
[25] Y. Gök, New J. Chem. 20 (1996) 971.
[26] Y. Gök, H. Ertepınar, S.Z. Yıldız, Spect. Lett. 123 (1990) 713.
[27] M.S. Hussain, H.M. Al-Mohdhar, A.R. Al-Arfaj, J. Coord. Chem. 18 (1988) 339.
[28] S. Karabocek, A. Bilgin, Y. Gok, Transition Met. Chem. 22 (1997) 420.
[29] J. Cheney, J.-M. Lehn, J.P. Sauvage, M.E. Stubbs, J. Chem. Soc., Chem. Commun. (1972) 1100.
[30] F. Arnaud-Neu, M. Sanchez, R. Yahya, M.J. Schwing-Weill, J.-M. Lehn, Helv. Chim. Acta 68 (1985) 456.
[31] J.-M. Lehn, Pure Appl. Chem. 52 (1980) 2441.

[13–18] and solution [19–21] clearly indicate that the bis(imidazol-2-yl)methyl moiety can form especially stable complexes with 3d transition metal ions, resulting in six membered chelate rings.

The coordination chemistry of bis(imidazol-2-yl)methyl ligands is more versatile when the chelating nitrogen donors are linked to other chelating ligands creating multi- and/or ambi-dentate ligands. In the last ten years we have studied copper(II), nickel(II) and zinc(II) complexes of numerous compounds, in which the bis(imidazol-2-yl) methyl group is connected to the C-terminal end of an amino acid or peptide molecule [22–27]. It can be concluded from the results of these studies that, because of the presence of two chelatable moieties, the coordination properties of the molecules are significantly different from both the simplest bis(imidazol-2-yl)methyl compounds and amino acids or peptides. In all cases, the bis(imidazol-2-yl)methyl residue is the main binding site in strongly acidic medium, but the amino group on the N-termini behaves as an anchor group promoting the deprotonation and coordination of the amide nitrogen. It results in the formation of dinuclear species with ligand bridging [22,24–27] and trinuclear complexes with a negatively charged imidazolato bridge [24,25,27]. The structure of the latter complexes for some amino acid and dipeptide derivatives is reminiscent of the active site of Cu,Zn-superoxide dismutase.

The structures of the copper(II) and zinc(II) complexes of all the studied amino acid and peptide derivatives, however, unambiguously show that at least one imidazole-N donor atom of bis-(imidazol-2-yl)methyl moiety takes part in the metal binding in the whole pH range, which, together with the coordination of the amino acid or peptide chain, lead to the formation of polynuclear species.

The recently synthesized and studied three ligands are tripeptide derivatives of the bis(imidazol-2-yl)methyl group: AlaPheGly-BIMA, GlyIleGly-BIMA and GlyGlyHis-BIMA (BIMA = bis(imidazol-2-yl)methylamine) (Scheme 1).

The difference between recently and earlier studied ligands is the length of the peptide chain, and the number of potential donor atoms. The nitrogen donor atoms of the peptide backbone could saturate the coordination sphere of the metal ion, excluding the binding of the imidazole nitrogens of the bis(imidazol-2-yl)methyl group. In the case of GlyGlyHis-BIMA, the formation of the outstandingly stable "GlyGlyHis"-like (NH_2,N^-,N^-,N(His)) coordination mode [28,29] could compete with the "bis(imidazol-2-yl)methyl"-like and "peptide"-like binding modes.

In this paper, we report the results of combined potentiometric and spectroscopic (EPR, UV–Vis, MS, NMR) studies on copper(II) and zinc(II) complexes of three tripeptide derivatives (AlaPheGly-BIMA, GlyIleGly-BIMA, GlyGlyHis-BIMA).

2. Experimental

2.1. Synthesis

The synthetic procedure for the preparation of the free amino acids and dipeptides containing BIMA on their C-terminus has already been reported [22,30]. AlaPheGly-BIMA, GlyIleGly-BIMA and GlyGlyHis-BIMA were prepared accordingly. The purity of the above peptide derivatives was checked by thin layer chromatography (TLC) and high pressure liquid chromatography (HPLC) and their structures were proved by ^{1}H NMR.

2.2. Potentiometric measurements

The pH-potentiometric titrations in the pH range 2.0–11.0 were performed on 3–4 cm^3 samples in the concentration range 2×10^{-3}–8×10^{-3} mol dm^{-3} at metal ion to ligand ratios ranging between 1:3 and 2:1. Argon was bubbled through the samples to ensure the absence of oxygen and to stir the solutions. Measurements were carried out at 298 K and at a constant ionic strength of 0.2 mol dm^{-3} KCl with a MOLSPIN pH meter equipped with a 6.0234.100 combined glass electrode (Metrohm) and a MOL-ACS microburette controlled by computer.

The number of experimental points reached around 50–70 data (cm^3–pH) for each titration curve. The pH readings were converted into hydrogen ion concentration as described earlier [31].

Protonation constants of the ligands and the overall stability constants ($\log\beta_{pqr}$) of the systems were calculated by means of general computational programs, PSEQUAD [32] and SUPERQUAD [33] using:

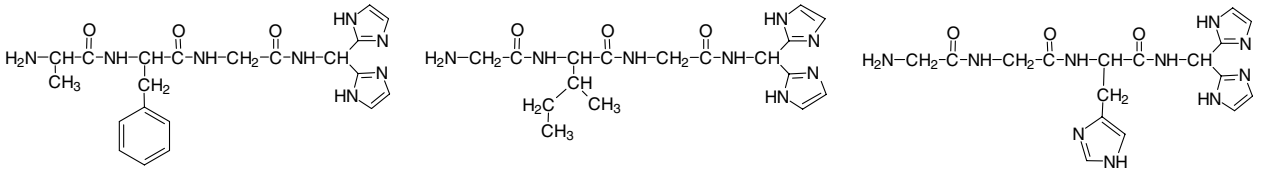

AlaPheGly-BIMA **GlyIleGly-BIMA** **GlyGlyHis-BIMA**

Scheme 1.

$$pM + qH + rL \rightleftharpoons M_pH_qL_r \quad (1)$$

$$\beta_{pqr} = \frac{[M_pH_qL_r]}{[M]^p \cdot [H]^q \cdot [L]^r} \quad (2)$$

2.3. Spectroscopic measurements

UV–Vis spectra of the copper(II) complexes were recorded on a Hewlett Packard HP 8453, Perkin–Elmer Lambda 35 or JASCO UVIDEC-610 spectrophotometer in the same concentration range as used for the potentiometry.

Anisotropic X-band EPR spectra (9.15 GHz) of frozen solutions were recorded at 120 K, using a Varian E-9 and a Bruker EMX spectrometer after addition of 10% ethylene glycol to ensure good glass formation in frozen solutions. Copper(II) stock solutions for EPR measurements were prepared from $CuSO_4 \cdot 5H_2O$ enriched with ^{63}Cu to get better resolution for the EPR spectra. For this purpose metallic copper (99.3% ^{63}Cu and 0.7% ^{65}Cu) was purchased from JV Isoflex, Moscow, Russia and converted to the sulfate.

2.4. Electrospray ionization time-of-flight mass spectrometry (ESI-TOF MS)

ESI-MS analysis for the copper(II)-GlyGlyHis-BIMA system was performed on a Bruker BIOTOF II ESI-TOF instrument using 1×10^{-4} mol dm^{-3} GlyGlyHis-BIMA concentration and 1:1 and also 3:2 copper(II) to ligand ratios. The pH was set to 6.96 and 7.64, respectively, by addition of the required amount of 0.2 mol dm^{-3} KOH solution and measured with a Radiometer pHM 84 instrument equipped with a Metrohm combined electrode (type 6.0234.110).

The solutions were introduced directly into the ESI source by a syringe pump (Cole-Parmer Ins. Comp. type 74900) at a flow rate of 2 μL/min. The temperature of the drying gas (N_2) was maintained at 100 °C. The pressure of the nebulizating gas (N_2) was 30 psi. The voltages applied on the capillary entrance and the first and the second skimmers were 4500 V, 40 V and 30 V, respectively. The voltage applied on the capillary exit was varied between 50 V and 120 V to get the best resolution of the spectrum. The spectra were accumulated and recorded by a digitizer at a sampling rate of 2 GHz. The spectrometer was operated at unit mass resolution and was calibrated to the sodium salt of trifluoroacetic acid. The data acquisition was carried out with BioTOF v 2.2 software, the processing was done with XmassBioTOF v 6.0.0.

2.5. NMR

A pH-dependent series of ^1H NMR spectra for GlyGlyHis-BIMA and for the copper(II)- and zinc(II)-GlyGlyHis-BIMA system was recorded on a Bruker 360 MHz instrument at 25 °C. D_2O was used as the solvent. The pH measurements in the pH range 1.5–12.2 were performed in 2 cm^3 vessels, not in the NMR tubes, at a ligand concentration of 0.01 mol dm^{-3}. Different concentrations (1, 0.1 and 0.01 mol dm^{-3}) of NaOD and DCl solutions in D_2O were used to adjust the pH. The pH readings were converted into pD values by adding 0.4 to the pH values read. Chemical shifts were referenced to sodium 3-(trimethylsilyl)-1-propanesulfonate (DSS). Microscopic protonation processes of GlyGlyHis-BIMA were calculated using a method described earlier [34].

3. Results and discussion

3.1. Protonation equilibria of the ligands

The protonation constants of the tripeptide derivatives containing bis(imidazol-2-yl)methyl groups are collected in Table 1 together with some literature data for comparison.

It is clear from Table 1 that the highest pK values belong to the deprotonation process of protonated terminal amino groups. These values are in good agreement with those of simple tri- and tetrapeptides [35–37] and aliphatic amino acid- and dipeptide-derivatives of the bis(imidazol-2-yl)methyl group [22,25]. It can be concluded that the bis(imidazol-2-yl)methyl moiety does not affect the deprotonation of the protonated amino group on the N-termini and its pK value is practically independent of the length of the peptide chain. For GlyGlyHis-BIMA an additional imidazole ring is present in the molecule, but it is far away from the N-terminal end of the ligand and does not influence the protonation equilibrium of the amino group, similarly to GlyGlyHis [29] and Gly_4His [38].

The pK values of the bis(imidazol-2-yl)methyl moiety of AlaPheGly-BIMA and GlyIleGly-BIMA are similar and close to those of the amino acid- [22], dipeptide- [25] and N-protected tripeptide-derivatives [23] reflecting that the deprotonation processes of the bis(imidazol-2-yl) group do not depend on the length of the peptide chain connected to the bis(imidazol-2-yl) residue, namely the presence of the N-terminal amino group. The deprotonation of the imidazole rings of the bis(imidazol-2-yl) and histidine moieties of GlyGlyHis-BIMA, however, takes place at slightly lower pH than that of other tripeptide derivatives and GlyGlyHis or Gly_4His, respectively. As a consequence, the presence of an additional imidazole ring close to the bis(imidazol-2-yl) residue decreases the pK values of all imidazole nitrogens. Similar effects were observed for PheHis-BIMA [26] and BOC-ProLeuHis-BIMA [23].

The macroconstants of the proton complexes, however, do not give detailed information about the overlapping protonation equilibria of the three imidazole groups. The exact assignment of protonation sites requires the determination of microscopic protonation constants, which was done for GlyGlyHis-BIMA by the ^1H NMR technique [34]. The calculation results (Table 1, Fig. 1.) show that the lowest pk (and p$k^{1/2}$) values belong to the

Table 1
Protonation constants, pK values and microscopic protonation constants for 50% degree of protonation (p$k^{1/2}$) [34] of the ligands investigated and some other peptides and bis(imidazol-2-yl)methyl derivatives

	HL	H_2L	H_3L	H_4L	pK (Im(1))	pK (Im(2))	pK (His)	pK(NH_3^+)	p$k^{1/2}$ (Im(1))	p$k^{1/2}$ (Im(1))	p$k^{1/2}$ (His)	p$k^{1/2}$ (NH_3^+)
AlaPheGly-BIMA	7.78(1)	13.38(1)	16.57(1)		3.19(1)	5.60(1)		7.78(1)				
GlyIleGly-BIMA	7.84(1)	13.25(2)	16.16(4)		2.91(4)	5.41(2)		7.84(1)				
GlyGlyHis-BIMA	7.86(1)	14.32(1)	19.55(1)	22.66(1)	3.11(1)	5.23(1)	6.46(1)	7.86(1)	3.1	5.2	6.4	7.9
GlyGlyGly [35]	7.93	11.25						7.93				
Gly_4 [35]	7.94	11.18						7.95				
AlaAlaAla [36]	8.08	11.44						8.08				
Ala_4 [37]	8.13	11.65						8.13				
GlyGlyHis [29]	8.06	14.88	17.68				6.82	8.06				
Gly_4His [38]	8.05	14.98	17.88				6.87	8.05				
Gly-BIMA [22,34]	7.95	13.46	16.68		3.22	5.51		7.95	3.2	5.6		7.8
LeuGly-BIMA [25]	7.76	13.35	16.53		3.18	5.59		7.76				
Ac-ProLeuGly-BIMA [23]	5.67	8.98			3.31	5.67						
His-BIMA [34]	7.28	13.09	17.62	20.23	2.61	4.53	5.81	7.28	2.8	5.2	5.3	7.2
PheHis-BIMA [26,34]	7.27	13.58	18.65	21.48	2.83	5.07	6.31	7.27	2.9	5.4	6.0	7.2
BOC-ProLeuHis-BIMA [23]	6.64	11.89	14.74		2.85	5.25	6.64					

first and second imidazole groups of the bis(imidazol-2-yl)methyl moiety. The actual values are in very good agreement with the bis(imidazol-2-yl)methyl pk and pK values of other derivatives. When the pH increases, histidine is the next group to be deprotonated. The p$k^{1/2}$ value for GlyGlyHis-BIMA is somewhat higher than that of His-BIMA or PheHis-BIMA, because both the protonated amino (in the case of His-BIMA) and the aromatic Phe (for PheHis-BIMA) group have electron-withdrawing effects. Furthermore, the amino p$k^{1/2}$ value is also higher for GlyGlyHis-BIMA than for the above mentioned other X-His-BIMA (X = H or Phe) derivatives, in agreement with several literature amino pK values measured for GlyGlyY (Y = His or GlyGlyHis) (see Table 1). Because of these effects, the overlap of four deprotonation steps (especially the pk values of the second imidazole of the bis(imidazol-2-yl)methyl moiety and the histidine imidazole) of GlyGlyHis-BIMA is much less than those found for His-BIMA and PheHis-BIMA.

3.2. Metal complexes of the ligands

It can be seen from the structures of the molecules (Scheme 1) that all three ligands have several different types of binding sites. In addition to the chelatable bis(imidazol-2-yl)methyl group, the tripeptide can coordinate to metal ions saturating its coordination sphere. In the case of histidine containing compounds, the very stable "GlyGlyHis"-like binding mode may form. These coordination modes alone and a mixture of them lead to very diverse complex formation processes. The stability constants of copper(II) and zinc(II) complexes and some selected equilibrium parameters are summarized in Table 2.

3.3. Copper(II) complexes of AlaPheGly-BIMA and GlyIleGly-BIMA

The bis(imidazol-2-yl)methyl residue is the main binding site in the acidic pH range. Protonated mono- and bis-

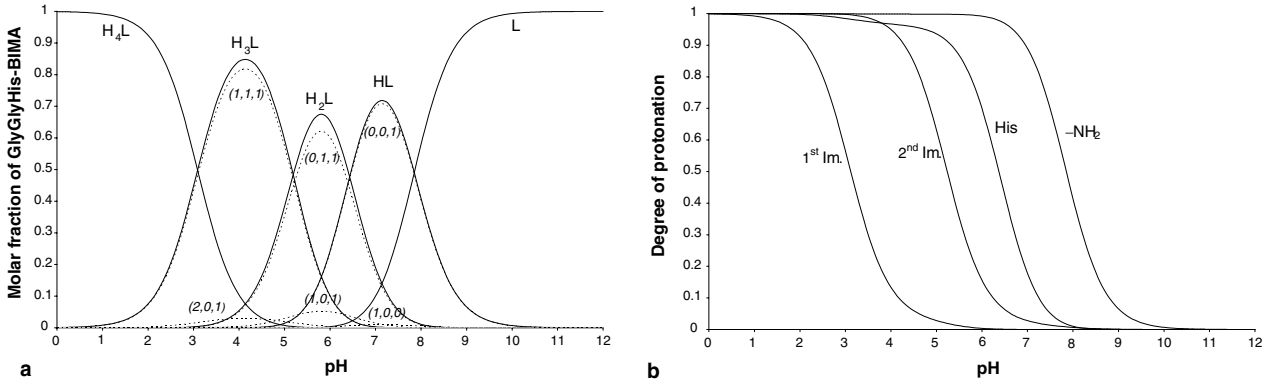

Fig. 1. Distribution of the macro- (solid lines) and microspecies (dashed lines) (a) and the degree of protonation as a function of pH for GlyGlyHis-BIMA (b).

Table 2
Stability constants ($\log\beta_{pqr}$) of copper(II) and zinc(II) complexes ($T = 298$ K, $I = 0.2$ mol dm^{-3}, SDs are in parentheses)

Complexes	AlaPheGly-BIMA	GlyIleGly-BIMA	GlyGlyHis-BIMA	
	Cu(II)	Cu(II)	Cu(II)	Zn(II)
$[MH_4L_2]^{6+}$			42.52(4)	
$[MH_3L_2]^{6+}$				32.09(7)
$[MH_2L_2]^{4+}$	30.47(2)	30.42(3)	31.11(7)	26.2(1)
$[MHL_2]^{3+}$	23.39(8)	24.54(8)		20.17(8)
$[ML_2]^{2+}$	15.81(5)	17.23(6)	17.09(14)	12.5(1)
$[MH_2L]^{4+}$			22.35(2)	18.81(2)
$[MHL]^{3+}$	16.19(1)	16.52(11)	18.23(3)	14.20(2)
$[ML]^{2+}$	11.69(2)	13.15(2)	12.88(5)	8.18(2)
$[MH_{-1}L]^{+}$		5.42(4)		−0.12(6)
$[MH_{-2}L]$	−4.10(5)	−3.68(4)	−0.97(4)	
$[M_2H_{-2}L]^{2+}$			8.17(3)	
$[M_3H_{-4}L_2]^{2+}$	5.03(5)	5.13(5)	13.89(7)	
$\log(K_1/K_2)^{H}$	1.91	2.62	2.18, 5.35	2.20
$\log(K_1/K_2)$	7.57	9.07	8.67	3.86
$pK(MH_3L_2/MH_2L_2)$				5.89
$pK(MH_4L_2/MH_2L_2)$			5.705	
$pK(MH_2L_2/MHL_2)$	7.08	5.88		6.03
$pK(MHL_2/ML_2)$	7.58	7.31	7.01	7.67
$pK(MH_2L/MHL)$			4.12	4.61
$pK(MHL/ML)$	4.50	3.37	5.35	6.02
$pK(ML/MH_{-1}L)$		7.73		8.30
$pK(MH_{-1}L/MH_{-2}L)$		9.10		
$pK(ML/MH_{-2}L)$	7.895		6.925	

$\log(K_1/K_2)^{H} = 2\log\beta([MH_2L]^{4+}) - \log\beta([MH_4L_2]^{6+})$ or $2\log\beta([MHL]^{3+}) - \log\beta([MH_2L_2]^{4+})$.
$\log(K_1/K_2) = 2\log\beta([ML]^{2+}) - \log\beta([ML_2]^{2+})$.

ligand complexes are formed with the coordination of two or four imidazole nitrogens, while the non-coordinated amino nitrogens are protonated ($[CuHL]^{3+}$, $[CuH_2L_2]^{4+}$). The EPR and UV–Vis spectroscopic parameters (Table 3) are very similar to each others and those of BIM [39] ($[CuL]^{2+}$: $\lambda_{max} = 680$ nm, $g_{\parallel} = 2.307$, $A_{\parallel} = 181 \times 10^{-4}$ cm^{-1}, $[CuL_2]^{2+}$: $\lambda_{max} = 578$ nm, $g_{\parallel} = 2.237$, $A_{\parallel} = 199 \times 10^{-4}$ cm^{-1}), Gly-BIMA [22] ($[CuHL]^{3+}$: $\lambda_{max} = 681$ nm, $g_{\parallel} = 2.299$, $A_{\parallel} = 175 \times 10^{-4}$ cm^{-1}, $[CuH_2L_2]^{4+}$: $\lambda_{max} = 590$ nm, $g_{\parallel} = 2.236$, $A_{\parallel} = 201 \times 10^{-4}$ cm^{-1}) and BOC-His-LeuGly-BIMA [23] (Table 3).

The ratio of stepwise stability constants for protonated species ($\log(K_1/K_2)^{H}$) corresponds to that of BIM [20] ($\log(K_1/K_2) = 2.78$), Gly-BIMA [22] ($\log(K_1/K_2)^{H} = 2.58$), LeuGly-BIMA [25] ($\log(K_1/K_2)^{H} = 1.52$) and Ac-ProLeu-Gly-BIMA [23] ($\log(K_1/K_2) = 2.06$), which also indicate that the ligands are coordinated via the bis(imidazol-2-yl)methyl nitrogens in these complexes. The deprotonation of $[CuHL]^{3+}$ and $[CuH_2L_2]^{4+}$ can be assigned to the deprotonation of the N-terminal amino group and $[CuL]^{2+}$ and $[CuL_2]^{2+}$ species are present above pH 4 (Fig. 2).

The characteristic pK values (pK(MHL/ML), pK(MH_2L_2/MHL_2), pK(MHL_2/ML_2)) are, however, much lower than those of the amino group in the free ligands. As a consequence, the deprotonation of the terminal amino group occurs parallel with its binding to the copper(II)

Table 3
UV–Vis and EPR spectral parameters of the copper(II) complexes (λ_{max} values in nm; ε values in M^{-1} cm^{-1}, $A_{\parallel}$ values in 10^{-4} cm^{-1})

Species	Coordination	AlaPheGly-BIMA		GlyIleGly-BIMA		GlyGlyHis-BIMA		BOC-HisLeuGly-BIMA [23]	
		$\lambda_{max}(\varepsilon)$	$g_{\parallel}$; $A_{\parallel}$	$\lambda_{max}(\varepsilon)$	$g_{\parallel}$; $A_{\parallel}$	$\lambda_{max}(\varepsilon)$	$g_{\parallel}$; $A_{\parallel}$	$\lambda_{max}(\varepsilon)$	$g_{\parallel}$; $A_{\parallel}$
$[CuH_2L]^{4+}$	N(Im),N(Im)					680(35)	2.293; 174		
$[CuHL]^{3+}$	N(Im),N(Im)	693(36)	2.298; 168	688(43)		639(63)		685(37)	2.30; 172
$[CuL]^{2+}$	N(Im),N(Im) + NH_2/N(His)	672(38)	2.282; 162	652(42)	2.270; 171	586(36)	2.241; 185	635(54)	2.27; 176
$[CuH_4L_2]^{6+}$	2 × (N(Im),N(Im))					592(57)	2.234; 195		
$[CuH_2L_2]^{4+}$	2 × (N(Im),N(Im))	595(40)	2.235; 192	~582(44)	2.230; 195			595(62)	2.24; 197
$[CuHL_2]^{3+}$, $[CuL_2]^{2+}$	2 × (N(Im),N(Im) + NH_2)	652(68)	2.263; 167	653(64)	2.256; 171	653(64)	2.257; 178	636(89)	2.24; 191
$[(CuH_{-1}L)_n]^{n+}$	(NH_2,N^-) + N(Im)			596(77)					
$[CuH_{-2}L]$	NH_2,N^-,N^-,N(Im)					516(104)	2.181; 206		
$[Cu_3H_{-4}L_2]^{2+}$	2 × (NH_2,N^-,N^-,N(His)) + 2 × (N(Im),N(Im))					531(68)			

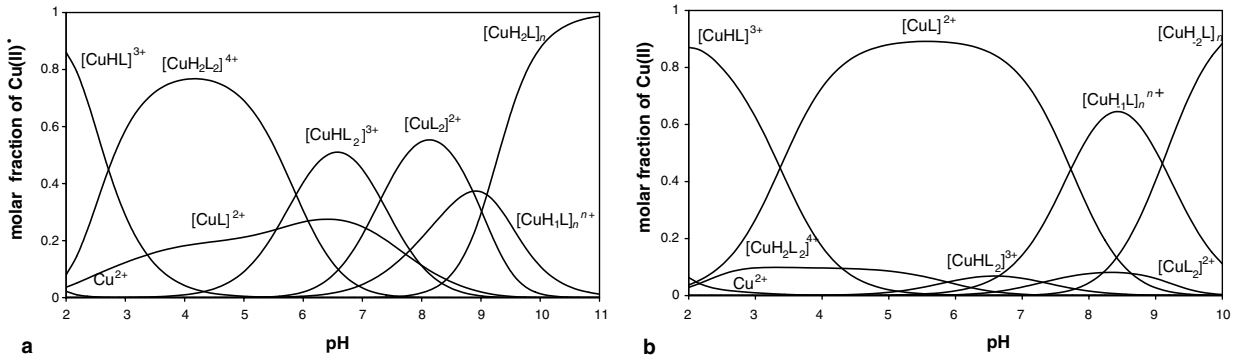

Fig. 2. Species distribution of the complexes formed in the copper(II)-GlyIleGly-BIMA system ($c_L = 4 \times 10^{-3}$ mol dm^{-3}, $c_M = 2 \times 10^{-3}$ mol dm^{-3} (a), $c_L = 5.5 \times 10^{-3}$ mol dm^{-3}, $c_M = 5 \times 10^{-3}$ mol dm^{-3} (b)).

ion. In contrast with dipeptide derivatives, it does not result in the formation of dimeric species, but mononuclear complexes are present in the physiological pH range, too. It means that both the bis(imidazol-2-yl)methyl residue and the terminal amino group are bound to the same metal ion forming macrochelated complexes. These structures are proved by EPR and UV–Vis spectra obtained in equimolar solution (Fig. 3) and with an excess of ligand. The deprotonation of $[CuHL]^{3+}$ and $[CuH_2L_2]^{4+}$ is accompanied by significant changes of EPR and UV–Vis parameters. The increase in $g_{\|}$ and decrease in $A_{\|}$ values indicate a strong axial interaction in the $[CuL_2]^{2+}$ complexes coordinated by four imidazole nitrogens in the equatorial plane. The strong axial binding of the amino group and the distorted octahedral structure of the complexes are also confirmed by the significant blue shift of the absorption maximum, accompanying the formation of $[CuL_2]^{2+}$. The spectral parameters of the $[CuL]^{2+}$ complexes are also different from those of the $[CuHL]^{3+}$ complexes of tripeptide derivatives and $[CuL]^{2+}$ of BIM, which suggests that a third nitrogen donor atom is bound in the coordination sphere of the metal ions. The length of the peptide chain makes the equatorial coordination of three nitrogen donor atoms possible, but the calculated absorption maximum for $(NH_2,CO) + (N(Im),N(Im))$ coordination is ~616 nm on the basis of an empirical formula [40]. So the equatorial–axial coordination of one end of the ligand is more probable in the $[CuL]^{2+}$ complex. Similar spectroscopic changes were observed in the case of $[CuL]^{2+}$ and $[CuL_2]^{2+}$ of BOC-HisLeuGly-BIMA[23] (Table 3), in which the axial coordination of histidine imidazole nitrogen was supposed.

Unfortunately, potentiometry is not an adequate method to distinguish between mononuclear and polynuclear complexes, which is why the stability constants for $[(CuH_{-1}L)]^{+}$ and $[(CuH_{-2}L)]$ species were calculated (Table 2). In the $[(CuH_{-1}L)_n]^{n+}$ and $[(CuH_{-2}L)_n]$ complexes, equatorial coordination of (NH_2,N^-) or (NH_2,N^-,N^-) donor sets can be supposed, respectively, while the one or two imidazole nitrogens of the other end of the ligand bind to another metal ion creating ligand bridged polynuclear structures. Above pH 10, it was not possible to observe the deprotonation of the third amide nitrogen because of the precipitation of the neutral polymeric species $[(CuH_{-2}L)_n]$.

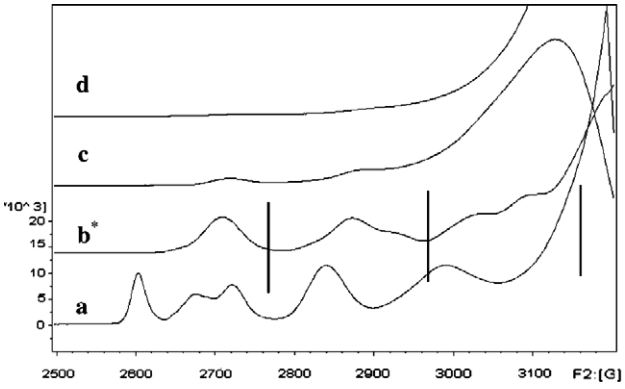

Fig. 3. EPR spectra obtained in the copper(II)-GlyIleGly-BIMA system at a 1:1.1 ratio at different pH values in frozen solution ($c_M = 5 \times 10^{-3}$ mol dm^{-3}) pH 2.17 (a), pH 5.66 (b), pH 8.48 (c), pH 10.37 (precipitation) (d). *At this pH in addition to $[CuL]^{2+}$ species bis chelated complexes with bis(imidazol-2-yl)methyl coordination are present (see Fig. 2b).

The two different coordination sites of the ligands make the binding of more than one copper(II) ion possible with a metal ion excess. The presence of $[Cu_3L_2H_{-4}]^{2+}$ complexes are proposed in slightly basic solution, in which two copper(II) ions are bound by an (NH_2,N^-,N^-) donor set, while the third metal ion is coordinated with four imidazole nitrogens. The EPR spectra measured at pH 8 in a solution at 3:2 copper(II) to ligand ratio is poorly resolved and this could be an indication of the formation of this trinuclear species.

3.4. Copper(II) complexes of GlyGlyHis-BIMA

The complex formation processes of GlyGlyHis-BIMA are very similar to the other two tripeptide derivatives in acidic medium. Mono- and bis-ligand complexes ($[CuH_4L_2]^{6+}$, $[CuH_2L]^{4+}$) are formed with the binding of four imidazole nitrogens; the amino and histidine residues

are protonated. The deprotonation of these groups results in the formation of $[CuHL]^{3+}$, $[CuL]^{2+}$ and $[CuH_nL_2]^{(2+n)+}$ ($n = 3$–0) species (Fig. 4).

The deprotonation steps of these complexes are cooperative and the averages of pK values are usually lower than those of the histidine imidazole and the amino groups of the free ligand. The ratio of characteristic stepwise stability constants are increased in comparison with that of fully protonated complexes. On the other hand, spectroscopic parameters assigned to the protonated and non-protonated species are different, and they are similar to those of $[CuL]^{2+}$ and $[CuL_2]^{2+}$ complexes of AlaPheGly-BIMA and GlyIleGly-BIMA, respectively. It can be concluded from these observations that the deprotonation of the amino and histidine imidazole nitrogen donor atoms occurs in parallel with their binding to the same metal ion forming macrochelates, similarly to the other two tripeptide derivatives. It means that the ligand is coordinated to the metal ion at least tridentately through the bis(imidazol-2-yl)methyl group and the amino or histidine imidazole nitrogens. This coordination mode could be supported by ^{1}H NMR measurements. The NMR spectra of the free ligand and the solution containing copper(II) and the ligand in a 1:10 ratio were detected at different pH values. A comparison of the spectra of the free ligand and the copper(II) containing system shows that the presence of copper(II) causes a broadening of the ^{1}H NMR signals of all three imidazole protons in the pH range 2–8, so it indicates that all three imidazole nitrogens take part in the coordination of copper(II) ion for $[CuH_nL_2]^{(n+2)+}$ ($n = 3$–0) complexes.

The deprotonation and coordination of amino and histidine imidazole groups are followed by extra base consuming processes, which correspond to the deprotonation and coordination of amide nitrogens. Both in equimolar solution and at ligand excess, $[CuH_{-2}L]$ complex predominates in basic solution (pH > 9). Its stoichiometry and spectroscopic parameters are in good agreement with that of $[CuH_{-2}L]^{2-}$ of GlyGlyHis [38] ($\lambda_{max} = 525$ nm, $g_{\|} = 2.178$, $A_{\|} = 209 \times 10^{-4}$ cm^{-1}), which indicates the ''GlyGlyHis''-like coordination mode. Although this binding mode is predominant above pH 5 for the Cu(II)-GlyGlyHis system [29], the coordination of the bis(imidazol-2-yl) residue of GlyGlyHis-BIMA suppresses the formation of (NH_2,N^-, N^-,N(His)) coordinated species. Fig. 5 is used to demonstrate the competition between the ''bis(imidazol-2-yl)methyl''- and ''GlyGlyHis''-like coordination modes. The theoretical distributions of the parent complexes formed in the Cu(II)-BIM(A)-GlyGlyHis(B) system are shown at 1:2:2 and 1:1:1 ratios (because of the high stability of both coordination modes, the formation of mixed complexes can be neglected).

It is clear from these figures that the ''bis(imidazol-2-yl)-methyl''-like coordination mode predominates in the pH range 4–8 at a 1:2:2 ratio, but above pH 9, the (NH_2,N^-,N^-,N(His)) coordinated species ($[CuH_{-2}B]^{2-}$) represents all the copper(II) in solution and, as a consequence, the binding of the bis(imidazol-2-yl)methyl group is replaced by the ''GlyGlyHis''-like coordination mode.

The coordination of the copper(II) ion to the peptide chain of the molecule, however, makes the binding of

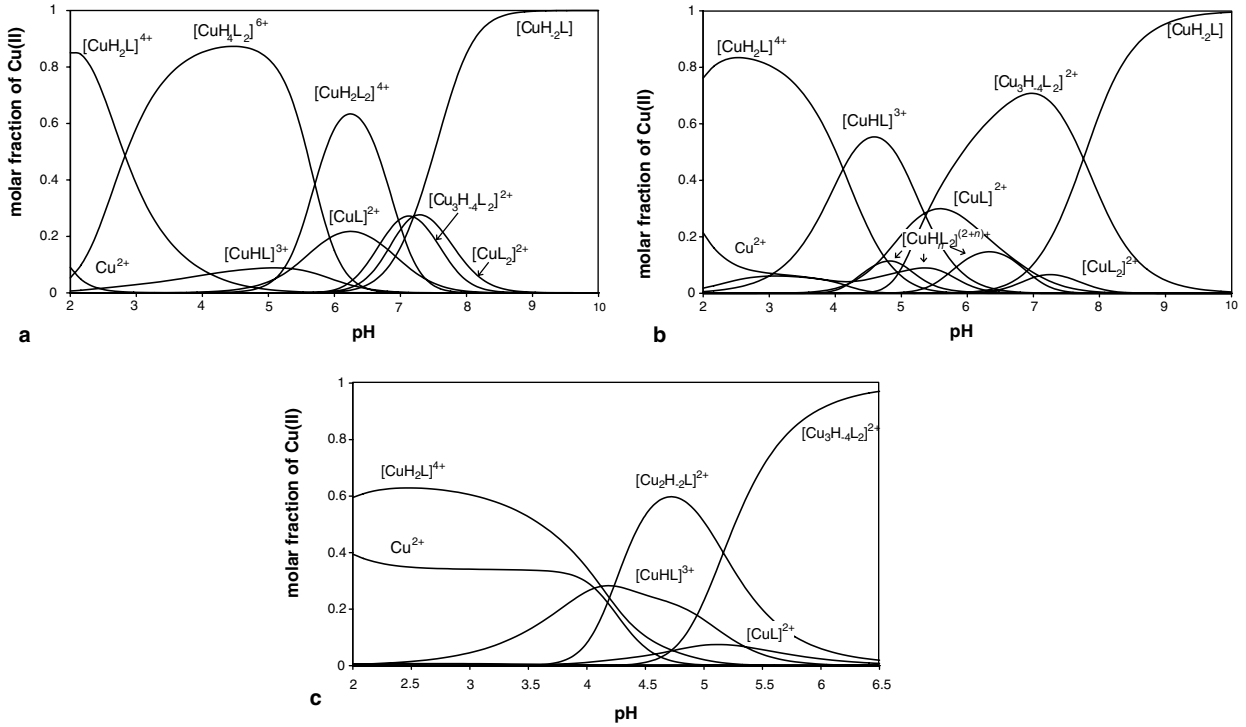

Fig. 4. Species distribution of the complexes formed in the copper(II)-GlyGlyHis-BIMA system ($c_L = 4 \times 10^{-3}$ mol dm^{-3}, $c_M = 2 \times 10^{-3}$ mol dm^{-3} (a), $c_L = 4 \times 10^{-3}$ mol dm^{-3}, $c_M = 4 \times 10^{-3}$ mol dm^{-3} (b), $c_L = 4 \times 10^{-3}$ mol dm^{-3}, $c_M = 6 \times 10^{-3}$ mol dm^{-3} (c)).

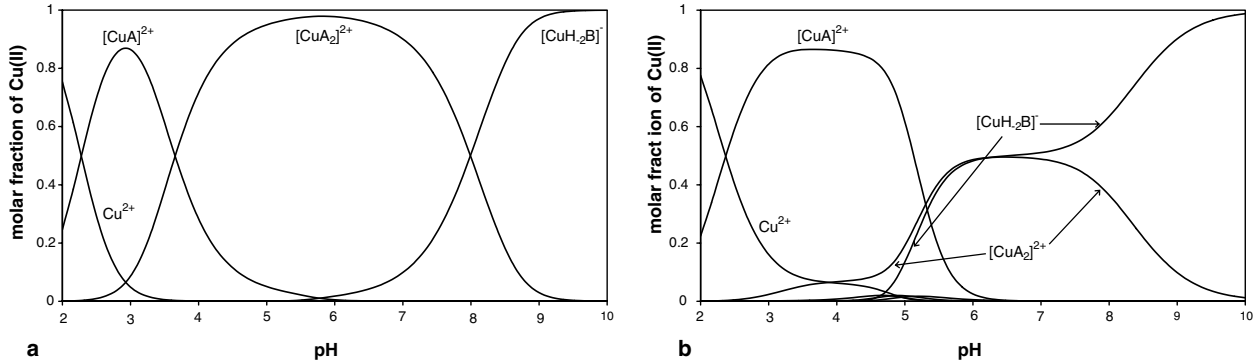

Fig. 5. Species distribution of the complexes formed in the copper(II)-BIM(*A*)-GlyGlyHis(*B*) system ($c_A = 4 \times 10^{-3}$ mol dm^{-3}, $c_B = 4 \times 10^{-3}$ mol dm^{-3}, $c_M = 2 \times 10^{-3}$ mol dm^{-3} (a), $c_A = 4 \times 10^{-3}$ mol dm^{-3}, $c_B = 4 \times 10^{-3}$ mol dm^{-3}, $c_M = 4 \times 10^{-3}$ mol dm^{-3} (b)).

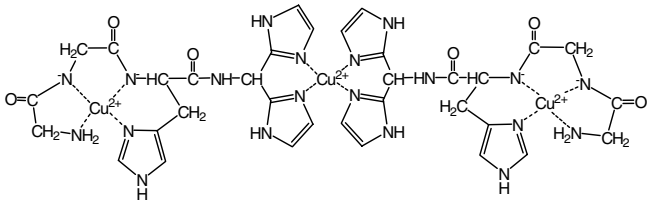

Scheme 2.

another metal ion to the ligand possible, resulting in the appearance of a trinuclear $[Cu_3H_{-4}L_2]^{2+}$ complex (Scheme 2).

This complex exists around pH 7 in an equimolar solution (Fig. 4b), whilst it is predominant above pH 6 with a metal ion excess (Fig. 4c). The speciation curves of the system Cu(II)-GlyGlyHis-BIM = 1:1:1 also support the distribution of the copper(II) ion between the bis(imidazol-2-yl)methyl group and the GlyGlyHis peptide chain. The existence of trinuclear species was proved by mass spectroscopic measurements carried out at 1:1 and 3:2 Cu(II)-GlyGlyHis-BIMA ratios at pH 7–8. Fig. 6 shows a small region of the spectra, and this region indicates the formation of a copper(II) complex with 3:2 stoichiometry both at 1:1 and 3:2 copper(II) to ligand ratios. The isotopic distribution patterns obtained for the complexes are in very good agreement with that calculated for the molecular ion $[Cu_3H_{-4}L_2]^{2+} = [Cu_3C_{34}H_{39}N_{30}O_6K]^{2+}$. (In the mass spectrum, one H of the ligand is replaced by K, which is present in the solution in relatively high concentration since KOH solution was used to adjust the pH.)

The two coordination sites of the ligand result in the formation of di- and trinuclear species in a solution of copper(II)–ligand with a ratio of 3:2 in almost the whole pH range, and both types of coordination mode (N(Im),N(Im) and NH_2,N^-,N^-,N(His)) are proposed in these complexes. The EPR spectra obtained at this ratio are poorly resolved, which also indicates the dipolar interaction between copper(II) ions (Fig. 7).

3.5. Zinc(II) complexes of GlyGlyHis-BIMA

The zinc(II) complexes of only GlyGlyHis-BIMA were studied and a comparison of data with those of BIM reveal that the presence of the GlyGlyHis residue does not influence the complex formation processes significantly. The stoichiometry and stability constants of complexes are collected in Table 2. In acidic medium, similarly to the copper(II) ion, protonated and non-protonated mono- and bis-ligand complexes are formed. The ratio of stepwise

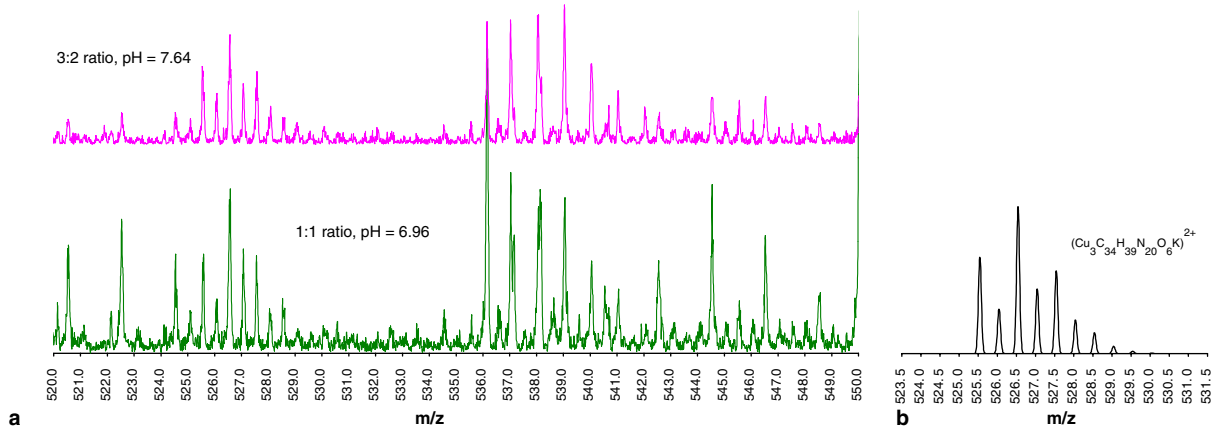

Fig. 6. ESI-MS spectra obtained in the copper(II)-GlyGlyHis-BIMA system at a 3:2 ratio and in equimolar solution (a) and the calculated isotopic distribution pattern for the molecule ion $[Cu_3H_{-4}L_2]K^{2+} = [Cu_3C_{34}H_{39}O_6N_{20}]K^{2+}$ (b).

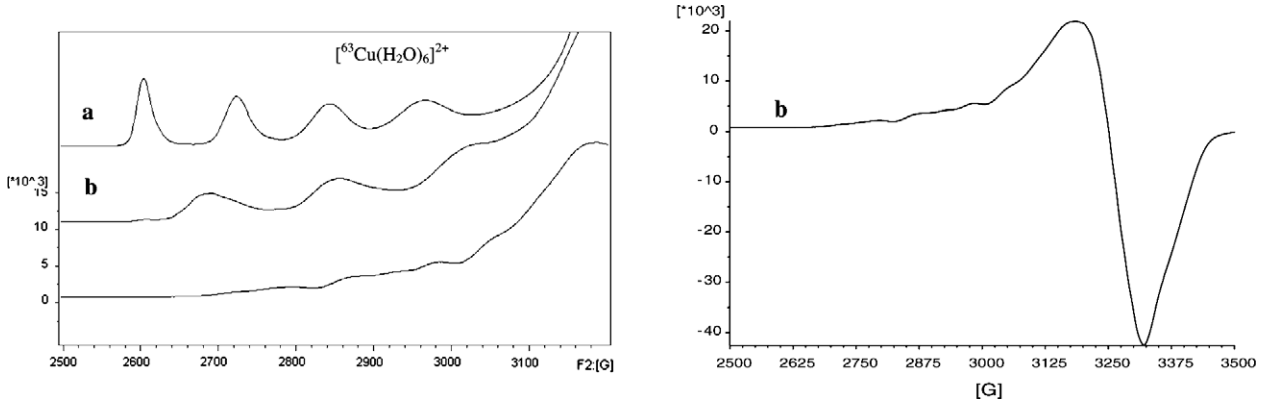

Fig. 7. EPR spectra obtained for the copper(II)-GlyGlyHis-BIMA system at a 3:2 ratio at different pH values in frozen solution ($c_M = 5 \times 10^{-3}$ mol dm^{-3}), pH 4.87 (a), pH 7.14 (b).

stability constants of protonated and non-protonated complexes, respectively, are higher than those of BOC-ProHis-Gly-BIMA [20] ($\log(K_1/K_2)^H = 0.56$, $\log(K_1/K_2) = 2.08$) and BIM [20] ($\log(K_1/K_2) = 0.84$), which indicates an additional weak interaction of one of the nitrogen donor atoms of the peptide chain. It is confirmed by the pK values characterizing the deprotonation processes of complexes too, which are slightly lower than those of the free ligand.

Fig. 8 shows the NMR spectra detected in a solution containing zinc(II) and ligand in 1:1 and 1:2 ratios, and also the difference of ^{1}H NMR shifts between the free ligand and the zinc(II) containing system ($\Delta\delta = \delta_{\text{zinc(II)–ligand system}} - \delta_{\text{free ligand}}$ at a given pH) together with the distribution of the complexes formed as a function of pH and at 1:2 zinc(II) to GlyGlyHis-BIMA ratio. It can be seen that the presence of the zinc(II) ion changes the signals of imidazole protons of the bis(imidazol-2-yl)methyl residue and the methylene protons of the N-terminal glycyl residue. On the basis of these data, it is probable that the terminal amino group takes part in the metal coordination forming macrochelates in addition to binding of the two imidazole rings of the bis(imidazol-2-yl)methyl residue. This coordination mode enhances the stability of $[ZnL]^{2+}$ and $[ZnL_2]^{2+}$ complexes and, in contrast to dipeptide derivatives [25], the hydrolysis of the complexes was not observed below pH 8. This coordination mode, however, is not able to promote the deprotonation of the amide nitrogen and precipitation occurs in basic solution both in equimolar solution and at ligand excess.

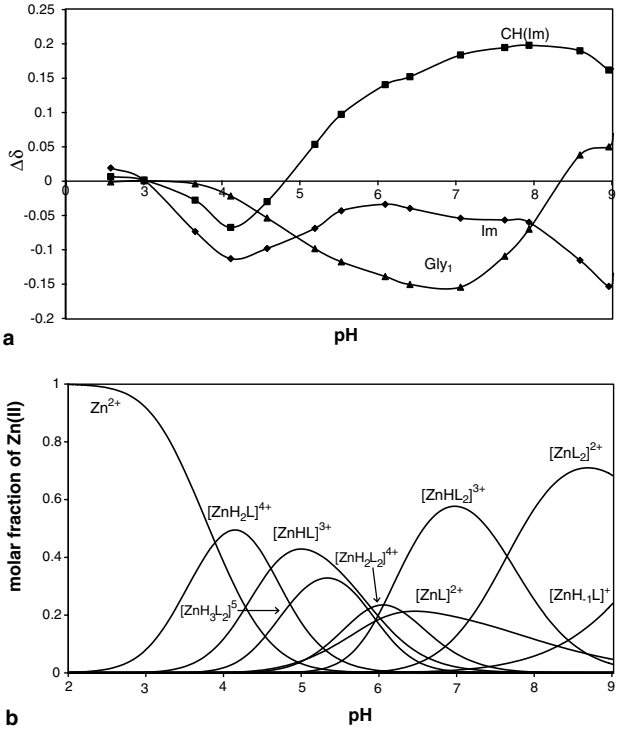

Fig. 8. Species distribution of the complexes formed in the zinc(II)-GlyGlyHis-BIMA system ($c_L = 4 \times 10^{-3}$ mol dm^{-3}, $c_M = 4 \times 10^{-3}$ mol dm^{-3}) (a) and the difference of ^{1}H NMR shifts between the free ligand and the zinc(II) containing system ($\Delta\delta = \delta_{\text{zinc(II)–ligand system}} - \delta_{\text{free ligand}}$) as a function of pH.

4. Conclusion

In our previous papers, copper(II) and zinc(II) complexes of a series of bis(imidazol-2-yl)methyl derivatives containing different amino acids and peptide chains were studied. We have continued our work with the studies on copper(II) and zinc(II) complexes of three tripeptide derivatives of the bis(imidazol-2-yl)methyl residue. The results of combined potentiometric, UV–Vis, EPR, ^{1}H NMR and mass spectroscopic measurements with these types of compounds provide further information about the coordination properties of this ligand family and allow the understanding of the effect of increased peptide chain connected to the bis(imidazol-2-yl)methyl moiety compared to amino acid and dipeptide derivatives.

The data reveal that the presence of two potential binding sites in the ligands makes their coordination chemistry versatile. Similarly to all the other studied ligands, the bis(imidazol-2-yl)methyl residue is the main binding site

in acidic medium in these cases. The presence of a terminal amino group modifies this coordination mode at higher pH. In contrast with amino acid and dipeptide derivatives, however, the coordination of the amino nitrogen donor atom does not lead to the formation of dimeric species in slightly acidic and neutral solution. Mononuclear complexes are present, in which the ligands are bound to the metal ions at least tridentately, resulting in macrochelates. This coordination mode increases the stability of $[ML]^{2+}$ and $[ML_2]^{2+}$ species resulting in a suppression of the deprotonation processes of the amide nitrogens for the copper(II) ion and the appearance of hydrolysis for the zinc(II) ion. In the case of copper(II) complexes, the deprotonation and coordination of the amide nitrogen take place at higher pH. For GlyIleGly-BIMA, polynuclear species exist in basic solution with participation of both binding sites of the molecules. The formation of a precipitate above pH 10, however, prevented the clarification whether the deprotonation and coordination of the third amide nitrogen or hydrolysis take place saturating the coordination sphere of the copper(II) ion. For GlyGlyHis-BIMA, the coordination of the (NH_2,N^-,N^-,N(His)) donor set was detected above pH 6 in equimolar solution together with the binding of the bis(imidazol-2-yl)methyl residue, leading to the formation of a trinuclear $[Cu_3H_{-4}L_2]^{2+}$ complex. Moreover, the ''GlyGlyHis''-like coordination was able to replace the bis(imidazol-2-yl)methyl residue in the coordination sphere of copper(II) ion at higher pH and the $[CuH_{-2}L]$ complex was predominant above pH 9 both with an excess of ligand and in equimolar solution.

To summarise, it can be stated that the presence of a longer peptide chain changes the coordination properties of the bis(imidazol-2-yl)methyl ligands compared to those of dipeptide or amino acid derivatives, because the long chain makes the formation of macrochelates sterically possible. The very effective binding ability of the bis(imidazol-2-yl)methyl group is reflected by the fact that the binding of at least one imidazole nitrogen of this group takes part in the metal ion coordination in all the cases in almost the whole pH range. Only the ''GlyGlyHis''-like coordination was detected, which is able to replace the binding of bis(imidazol-2-yl)methyl nitrogen donor atoms completely.

Acknowledgement

This work was supported by the Hungarian Scientific Research Fund (OTKA T042722).

References

[1] T. Gajda, R. Krämer, A. Jancsó, Eur. J. Inorg. Chem. (2000) 1635.
[2] M. Beretta, E. Bouwman, L. Casella, B. Douziech, W.L. Driessen, L. Gutierrez-Soto, E. Monzani, J. Reedijk, Inorg. Chim. Acta 310 (2000) 41.
[3] W.A. Alves, I.A. Bagatin, A.M. Da Costa Ferreira, Inorg. Chim. Acta 321 (2001) 11.
[4] S.-P. Yang, Y.-X. Tong, H.-L. Zhu, H. Cao, X.-M. Chen, L.-N. Ji, Polyhedron 20 (2001) 223.
[5] H. Ohtsu, S. Itoh, S. Nagatomo, T. Kitagawa, S. Ogo, Y. Watanabe, S. Fukuzumi, Inorg. Chem. 40 (2001) 3200.
[6] A. Jancsó, I. Török, L. Korecz, A. Rockenbauer, T. Gajda, J. Chem. Soc., Dalton Trans. (2002) 2601.
[7] R.N. Patel, N. Singh, K.K. Shukla, W.L.N. Gundla, Spectrochim. Acta A 61 (2005) 1893.
[8] R.N. Patel, N. Singh, K.K. Shukla, U.K. Chauhan, Spectrochim. Acta A 61 (2005) 287.
[9] W.L. Driessen, D. Rehorst, J. Reedijk, I. Mutikainen, U. Turpeinen, Inorg. Chim. Acta 358 (2005) 2167.
[10] P.C.A. Bruijnincx, M. Lutz, A.L. Spek, E.E. van Faassen, B.M. Weckhuysen, G. van Koten, R.J.M. Klein Gebbink, Eur. J. Inorg. Chem. (2005) 779.
[11] E. Fursova, G. Romanenko, V. Ikorskii, V. Ovcharenko, Polyhedron 22 (2003) 1957.
[12] J.-F. Ma, J. Yang, G.-L. Zheng, L. Li, Y.-M. Zhang, F.-F. Li, J.-F. Liu, Polyhedron 23 (2004) 553.
[13] B. Gimeno, L. Soto, A. Sancho, F. Dahan, J.-P. Legros, Acta Crystallogr. C48 (1992) 1671.
[14] G.J. Anthony, A. Koolhaas, P.M. van Berkel, S.C. van der Slot, G. Mendoza-Diaz, W.L. Driessen, J. Reedijk, Inorg. Chem. 35 (1996) 3525.
[15] S. Elgafi, L.D. Field, B.A. Messerle, T.W. Hambley, P. Turner, J. Chem. Soc., Dalton Trans. (1997) 2341.
[16] R. Bhalla, M. Helliwell, C.D. Garner, Inorg. Chem. 36 (1997) 2944.
[17] Y. Akhriff, J. Server-Carrio, A. Sancho, J. García-Lozano, E. Escrivá, J.V. Folgado, L. Soto, Inorg. Chem. 38 (1999) 1174.
[18] S. Abuskhuna, M. McCann, J. Briody, M. Devereux, V. McKee, Polyhedron 23 (2004) 1731.
[19] M.S. Mohan, Ind. J. Chem., Sect. A 20 (1981) 252.
[20] K. Várnagy, I. Sóvágó, K. Ágoston, Z. Likó, H. Süli-Vargha, D. Sanna, G. Micera, J. Chem. Soc., Dalton Trans. (1994) 2939.
[21] H. Sigel, A. Saha, N. Saha, P. Carloni, L.E. Kapinos, R. Griesser, J. Inorg. Biochem. 78 (2000) 129.
[22] K. Várnagy, I. Sóvágó, W. Goll, H. Süli-Vargha, G. Micera, D. Sanna, Inorg. Chim. Acta 283 (1998) 233.
[23] K. Várnagy, I. Sóvágó, H. Süli-Vargha, D. Sanna, G. Micera, J. Inorg. Biochem. 81 (2000) 35.
[24] K. Ősz, K. Várnagy, H. Süli-Vargha, D. Sanna, G. Micera, I. Sóvágó, Inorg. Chim. Acta 339 (2001) 373.
[25] K. Ősz, K. Várnagy, H. Süli-Vargha, D. Sanna, G. Micera, I. Sóvágó, Dalton Trans. (2003) 1.
[26] K. Ősz, K. Várnagy, H. Süli-Vargha, A. Csámpay, D. Sanna, G. Micera, I. Sóvágó, J. Inorg. Biochem. 98 (2004) 24.
[27] Cs. Kállay, M. Cattari, D. Sanna, K. Várnagy, H. Süli-Vargha, A. Csámpai, I. Sóvágó, G. Micera, New J. Chem. 28 (2004) 727.
[28] E. Farkas, I. Sóvágó, T. Kiss, A. Gergely, J. Chem. Soc., Dalton Trans. (1984) 611.
[29] R.W. Hay, M.M. Hassan, C. You-Quan, J. Inorg. Biochem. 52 (1993) 17.
[30] Z. Likó, H. Süli-Vargha, Tetrahedron Lett. 34 (1993) 1673.
[31] H. Irving, G. Miles, L.D. Pettit, Anal. Chim. Acta 38 (1967) 475.
[32] L. Zékány, I. Nagypál, in: D. Leggett (Ed.), Computational Methods for the Determination of Formation Constants, Plenum, New York, 1985, p. 291.
[33] P. Gans, A. Sabatini, A. Vacca, J. Chem. Soc., Dalton Trans. (1985) 1196.
[34] K. Ősz, G. Lente, Cs. Kállay, J. Phys. Chem. B 109 (2005) 1039.
[35] I. Sóvágó, D. Sanna, A. Dessí, K. Várnagy, G. Micera, J. Inorg. Biochem. 63 (1996) 99.
[36] G. Bryce, F. Gurd, J. Biol. Chem. 241 (1966) 1439.
[37] J.-F. Galey, B. Decock Le-Reverand, A. Lebkiri, L.D. Pettit, S.I. Pyburn, H. Kozlowski, J. Chem. Soc., Dalton Trans. (1988) 887.
[38] K. Várnagy, J. Szabó, I. Sóvágó, G. Malandrinos, N. Hadjiliadis, D. Sanna, G. Micera, J. Chem. Soc., Dalton Trans. (2000) 467.
[39] I. Sóvágó, K. Várnagy, K. Ősz, Comments Inorg. Chem. 23 (2002) 149.
[40] H. Sigel, R.B. Martin, Chem. Rev. 82 (1982) 385.

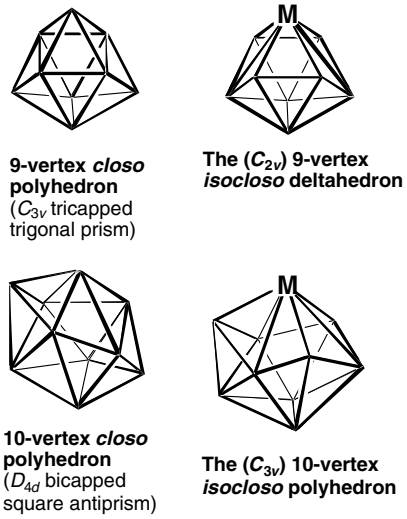

Fig. 1. A comparison between the *closo* and *isocloso* polyhedra with 9 and 10 vertices. The degree 6 vertices of the *isocloso* polyhedra occupied by transition metal atoms in the corresponding *isocloso* metallaboranes are indicated by **M**.

structures based on deltahedral topologically distinct from the deltahedra found in simple boranes and carboranes [5]. Of particular interest are the 9- and 10-vertex structures based on a deltahedron with a transition metal at a degree 6 vertex whereas the corresponding metal-free deltahedron has only degree 4 and 5 vertices (Fig. 1). What is even more interesting is the fact that such "anomalous" metallaborane structures are also "disobedient" in not having the expected $2v + 2$ skeletal electrons but only $2v$ skeletal electrons. Such disobedient deltahedral metallaborane skeletons with the anomalous $2v$ skeletal electrons have been called *isocloso* metallaboranes and this terminology will be used in this paper. These *isocloso* deltahedral metallaborane structures are derived from the corresponding *closo* deltahedron by diamond–square–diamond rearrangements, as has long been recognized [6]. A previous paper by one of us (RBK) [7] shows how removal of the transition metal vertex from an *isocloso* metallaborane having 9, 10, or 11 vertices and $2v$ skeletal electrons leads to a $B_nH_n^{2-}$ ligand or isoelectronic derivative thereof having one open hexagonal face for hexahapto bonding to the transition metal. This paper examines the roles of the formal oxidation state and valence electron count of the transition metal vertex in rationalizing the structures of metallaboranes.

2. Relationships between metal oxidation state, metal valence electron count, and metallaborane structure

The *closo*, *isocloso*, *nido*, and *isonido* structures for a metallaborane with v vertices have $2v + 2$, $2v$, $2v + 4$, and $2v + 2$ skeletal electrons, respectively. The relationships between the metal formal oxidation state (ω), the metal valence electron count (ε), and the structure type in such metallaboranes can be summarized as follows:

A. closo ($\omega = Y$, $\varepsilon = Z$) to isocloso ($\omega = Y + 2$, $\varepsilon = Z$)

This relationship arises from the following:

(a) The defining relationships for *closo* and *isocloso* metallaboranes can be summarized as follows:

$$\begin{aligned} &\textit{closo}\text{-M(borane)} \rightarrow [M^{x+} + \textit{nido}\text{-(borane)}^{x-}] \\ &\quad \leftrightarrow [M^{(x+2)+} + \textit{arachno}\text{-(borane)}^{(x+2)-}] \leftarrow \textit{isocloso}\text{-M(borane)} \end{aligned}$$

(b) Isolobal considerations relate to the equivalence of the metal fragment in an *isocloso* metallaborane to BH^{2+}, rather than BH in a *closo* metallaborane with the same number of vertices but two more skeletal electrons.

(c) Discrete oxidation reactions (Eqs. (1)–(3)) suggest a change in formal oxidation state (ω) without a change in the metal valence electron count (ε) [8]:

$$\begin{aligned} &\textit{closo}\text{-}(\eta^6\text{-}Me_6C_6)RuB_9H_9^{2-}\ (\mathbf{1}) \\ &\quad \rightarrow \textit{isocloso}\text{-}(\eta^6\text{-}Me_6C_6)RuB_9H_9\ (\mathbf{2}) + 2e^- \qquad (1) \\ &\textit{nido}\text{-}(CO)_3MnB_9H_{13}^-\ (\mathbf{3}) \\ &\quad \overset{UV}{\rightarrow} \textit{isocloso}\text{-}(CO)_3MnB_9H_9^-\ (\mathbf{4}) + 2H_2 \qquad (2) \\ &\textit{nido}\text{-}(\eta^6\text{-}Me_6C_6)CoB_9H_{13}\ (\mathbf{5}) + MeNC \\ &\quad \rightarrow \textit{isocloso}\text{-}(\eta^6\text{-}Me_6C_6)CoB_9H_9\ (\mathbf{6}) + Me_2NH \qquad (3) \end{aligned}$$

The diamond–square–diamond process converting a *closo* metallaborane to the corresponding *isocloso* metallaborane [7] with an increase of the degree of the metal vertex can be considered as an internal oxidative addition reaction at the metal atom.

(d) Experimental evidence for retention of the metal valence electron count ε arises from the observation that substitution of one PPh_3 ligand in *isocloso*-$(PPh_3)_2RuB_{10}H_8(OEt)_2$ (**7**) by the more strongly reducing PMe_3 gives *closo*-$(PMe_3)(PPh_3)RuB_{10}H_8(OEt)_2$ (**8**) with no apparent change in ε [9].

B. closo ($\omega = Y$, $\varepsilon = Z$) and isonido ($\omega = Y$, $\varepsilon = Z$)

This relationship arises from the following:

(a) The observed *closo–isonido* continua in 9-, 10- and 12-vertex structures indicate that *closo* and *isonido* cluster geometries are related by a smooth electronic continuum.

(b) The bonding topologies reported previously [7] suggest a close connection between *closo* and *isonido* structures.

C. closo ($\omega = Y$, $\varepsilon = Z$) and nido ($\omega = Y - 2$, $\varepsilon = Z$)

(a) Isolobal considerations relate to the equivalence of the metal vertex in the *nido* structure to BH^{2-} rather than BH.

(b) A unique pair of *closo* (Os(II)) and *nido* (Os(0)) isomers with $\varepsilon = 18$ exists as discussed below.

The two skeletal electrons added to a *closo* metallaborane deltahedron with $2v + 2$ skeletal electrons to open one of the (triangular) faces to give the corresponding *nido* metallaborane with $2v + 4$ skeletal electrons can be considered to reduce the metal formal oxidation state by two units.

The relationship between *nido* ($\omega = Y - 2$, $\varepsilon = Z$) and *isonido* ($\omega = Y$, $\varepsilon = Z$) structures follows directly from the relationships indicated above and takes precisely the same form as that relating *closo* to *isocloso* structures so that all of the interrelationships are self-consistent. Furthermore, in metallaboranes the *closo* → *isocloso* or *nido* → *isonido* conversion is seen to increase the metal formal oxidation state by two units whereas the *closo* → *nido* conversion is seen to reduce the metal formal oxidation state by two units.

3. Nature of the borane ligands in metallaboranes: capping regime descriptors

The previous study [7] on the bonding topology in *isocloso* metallaboranes removed the transition metal vertex to give a free borane ligand. The electron donor properties of the resulting free borane ligand are influenced by the position on the open face of the nodal planes of the two highest occupied molecular orbitals (HOMOs). A *closo* metallaborane is generated by symmetrical "centroid" capping of the open face with the metal atom. A *nido* metallaborane is generated by skew-symmetrical or offset capping of the open face with the metal atom so that the metal atom is part of a remaining non-triangular face. The former can be considered to be symmetric borane ligands and the latter as asymmetric borane ligands. Each of these types of borane ligands has an associated capping regime.

Capping regime descriptors, typically of the form {**420**}, can be used to describe the capping regimes of the metallaborane ligands of interest. The first number in the capping regime descriptor refers to the number of electrons donated by the borane ligand to the metal center in the primary bonding mode of the capping process. In this connection, symmetric borane ligands donate 6 electrons. However, asymmetric borane ligands donate only 4 electrons since one borane-to-metal orbital overlap is spatially unfavorable, i.e., the relevant orbitals are effectively out of phase. The second two numbers in the capping regime descriptor refer to the number of electrons donated to the metal center in the secondary bonding mode, which can be applied more than once so that the descriptor can be extended further if required. Each application of the secondary bonding mode invokes an additional 2-electron donation from borane to metal. The role of this secondary mode is to generate the *iso*-classes (see below).

The postulate that asymmetric borane ligands function as donors of only four rather than six electrons is provided by some observations on iron derivatives of pentaborane (Fig. 2) [10]. Thus, photolysis of the *nido*-pentaborane

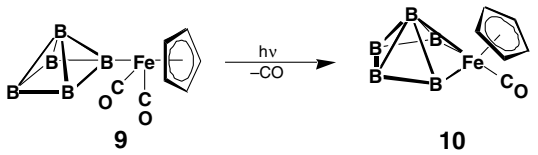

9 **10**

Fig. 2. Photolytic decarbonylation of 2-{(η^5-C_5H_5)Fe($CO)_2$}-*nido*-B_5H_8 (**9**) to give *nido*-2-(η^5-C_5H_5)Fe(CO)B_5H_8 (**10**). For clarity the hydrogen atoms and other monovalent groups are omitted from this and subsequent figures.

derivative 2-{(η^5-C_5H_5)$(OC)_2$Fe}-*nido*-B_5H_8 (**9**), with an iron atom external to the B_5 cluster, expels a single CO ligand to give directly a *nido*-FeB_5 cluster with an asymmetric borane ligand, namely *nido*-2-(η^5-C_5H_5)(OC)FeB_5H_8 (**10**). In this reaction, the metal formal oxidation state ($\omega = +2$) and metal valence electron count ($\varepsilon = 18$) are both preserved. If the asymmetric borane ligand in the metallaborane functioned as a 6-electron donor in (**10**), a second molecule of CO would need to be expelled in order to conserve the metal valence electron count.

The capacity of symmetric borane ligands to behave as 6-electron donor ligands becomes apparent upon comparison of the *nido*-ferrahexaborane (**10**) with other related ferraboranes (Fig. 3) including the 7-vertex *closo*-(η^6-arene)-$FeC_2B_4H_4R_2$ (**11**) [11] and even the less closely related 12-vertex *closo*-(η^6-C_6H_6)$FeC_2B_9H_{11}$ (**12**) [12]. Such comparisons indicate that when a symmetric borane ligand is present, there is no capacity for an additional two-electron donor ligand, such as CO, on the metal atom in the more symmetrical environment, in accord with a metal valence electron count of 18. Moreover, this cannot simply be attributed to steric hindrance as indicated by the 7-vertex *closo*-(η^5-C_5H_5)(H)$FeC_2B_4H_6$ (**13**) [10] closely related to **(11)**.

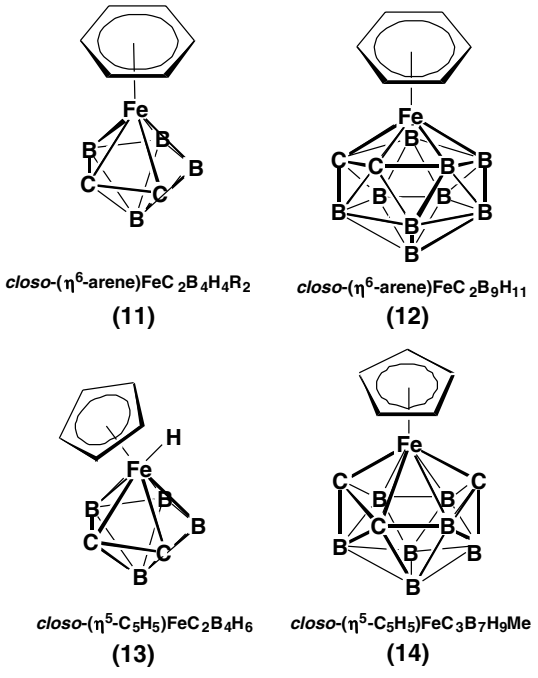

Fig. 3. Some ferracarborane derivatives.

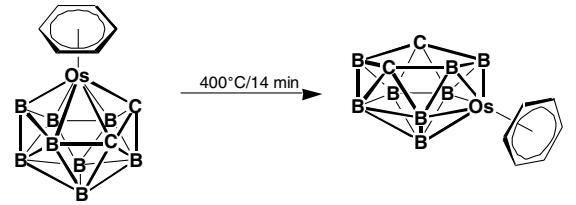

Fig. 4. A rearrangement in the 11-vertex osmacarborane series.

The fact that the "asymmetric" *arachno*-B_5H_8 ligand, acting as a 4-electron donor to the offset Fe center in (**10**), changes to a symmetric 6-electron donor in (**13**) is supported by comparing (**10**) with the 11-vertex Fe(II) species *closo*-(η^5-C_5H_5)$FeC_3B_7H_9Me$ (**14**) (Fig. 3) [13]. Here, the *nido*-$C_3B_7H_9Me$ ligand must be acting as a 6-electron donor by virtue of the loss of the CO ligand from the Fe center. The formulation of (**14**) as an authentic Fe(II) species, rather than an Fe(IV) species, is supported by the ease of oxidation of (**14**) to its Fe(III) analogue by Ag^+ ion.

A metallaborane obeying the Wade–Mingos rules [2] is not always the most stable possible isomer. For example, when *closo*-(η^6-Me_6C_6)$OsC_2B_8H_8Me_2$ (**15**), a cluster obeying the Wade–Mingos rules, is heated at 400 °C for 14 min, the *nido* isomer (**16**) is obtained in quantitative yield (Fig. 4) [14]. This product violates the Wade–Mingos rules and yet is clearly thermodynamically preferred. The abnormally long Os–B distances in (**16**) indicate that the osmium atom is in a lower formal oxidation state than is usually observed in osmaboranes, which are always assumed to contain Os(II) through isolobal considerations. The formal oxidation state in the *nido* isomer (**16**) is probably Os(0).

There are examples where an *isonido* structure is obtained when the *closo* isomer is predicted according to the Wade–Mingos rules [2]. Moreover, *nido*-2-(η^6-Me_6C_6)-RuB_9H_{13} (**17**) has been isolated with a hexagonal open face (Fig. 5) along with its *isoarachno*-1-(η^6-Me_6C_6)RuB_9H_{13} isomer (**18**) with a heptagonal open face [15]. In going from the *nido* isomer (**17**) to the corresponding *isoarachno* isomer

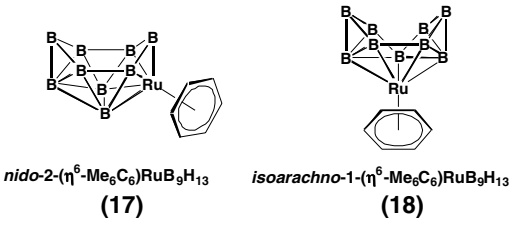

Fig. 5. Two isomers of (η^6-Me_6C_6)RuB_9H_{13}.

(**18**), one of the B–B edges is lengthened from ~2.00 Å in (**17**) to 2.50 Å in (**18**).

In some cases *closo* and *isonido* isomers have been found to lie on a structural continuum. Thus, metallaboranes with 9, 10 and 12 vertices have been isolated that exhibit structures intermediate between the two geometrical extremes [5c,16]. In addition, there is a case where a fluxional process has been observed to occur in solution, indicating that the two extreme geometries can possess very similar ground state energies, i.e., *trans*{*closo*-(η^6-$MeC_6H_4Pr^i$)$RuC_2B_9H_9Ph$}$_2$-(CH=CH) (**19**) versus an isomer in which one of the two (η^6-$MeC_6H_4Pr^i$)$RuC_2B_9H_9Ph$ units has changed from *closo* to *isonido* geometry by stretching the C···C distance in one of the RuC_2B_9 polyhedra from 1.77 to 2.36 Å [17]. The continuum can be explained in electronic terms by a smoothly progressive change in the capping regime from *closo* {**600**} to *isonido* {**420**} that, in turn, is permitted by the selection rules for rearrangement processes in polyhedra. Indeed, in support of this conjecture, an intrinsic mirror plane is retained throughout the "budding" open face in all of these cases. There are no known *closo–isonido* continua without this symmetry element being present.

The metallaboranes displaying structures between the *closo* and *isonido* isomers can be considered to be clusters in which the diamond–square component of a diamond–square–diamond (dsd) transformation [18] is "frozen". Although many examples of "frozen" dsd processes are known, no known metallaboranes exhibit structures lying along the square–diamond part of the dsd transformation. In terms of cluster geometry, this corresponds to the *isonido–isocloso* transformation. The lack of examples on this "discontinuum" is easily explicable from Table 1 by virtue of the fact that an *isonido–isocloso* transformation requires a discrete change in the metal formal oxidation state at the metal atom. This constitutes a "catastrophic flip" [19] so a continuum is not possible.

We can now use the capping regime to access previously unimagined cluster geometries. By ascribing to the *closo* form an arbitrary formal metal oxidation state, Y, and an arbitrary metal valence electron count, Z, the *closo/nido* electrostructural correlation table shown in Table 1 can be generated where Z remains constant, typically the favored 18-electron rare gas configuration for transition metals.

The "idealized" capping regimes specified in Table 1 depend upon the nodal plane-related symmetry characteristics of the borane ligand as well as the acceptor capability and the stereochemical preference of the metal center under consideration. The following aspects of the capping regimes indicated in Table 1 should be noted:

Table 1
The *closo/nido* electrostructural correlation table

Geometry (G)	*isoisocloso*	*isocloso*	*closo*	*isoisonido*	*isonido*	*nido*
Formal metal oxidation state (ω)	$Y+4$	$Y+2$	Y	$Y+2$	Y	$Y-2$
Capping regime	{622}	{620}	{600}	{422}	{420}	{400}
Metal valence electrons (ε)	Z	Z	Z	Z	Z	Z

Table 2
The *nido*/*arachno* electrostructural correlation table

G	*isoisonido*	*isonido*	*nido*	*isoisoarachno*	*isoarachno*	*arachno*
Formal metal oxidation state (ω)	$Y+2$	Y	$Y-2$	Y	$Y-2$	$Y-4$
Capping regime	{422}	{420}	{400}	{422}	{420}	{400}
Metal valence electrons (ε)	Z	Z	Z	$Z+2$	$Z+2$	$Z+2$

(1) A {**400**} capping regime would result in a complete, single capping of an open face that would normally be accorded a {**600**} capping regime, e.g., as in 11-vertex *closo*-PtC_2B_8 species derived from d^8 Pt(II) capping fragments ($\varepsilon = 12$), in "slipped *closo*" structures and also in *nido*-2,8,10-(η^6-Me_6C_6)-$OsC_2B_8H_8Me_2$ (**16**) with its unusual "canastide" type borane ligand (Fig. 4).

(2) A {**600**} capping regime, not {**400**}, is required to generate a *nido*, *arachno*, etc., structures with C_{nv} symmetry; as in the well-known C_{4v} *nido*-1-$CpCoB_4H_8$ (**20**) and its hypothetical homologue C_{5v} *nido*-1-$CpCoB_{10}H_{14}$ (**21**) (Fig. 6).

(3) A {**420**} capping regime, not {**620**}, results in an "unsymmetrical" *isocloso* structure.

(4) A {**422**} capping regime, not {**622**}, gives a less symmetrical *isoisocloso* structure, as in the putative Mo(IV) $[(\eta^3\text{-}C_3H_5)(OC)_2MoC_2B_9H_9Ph_2]^-$ ion (**22**) derived from an *arachno*-$C_2B_9H_9Ph_2^{4-}$ ligand and containing an irregular MoC_2B_9 icosahedron with two degree 6 vertices (the Mo vertex and a nearly antipodal B vertex), eight degree 5 vertices, and two degree 4 vertices (the two carbon vertices) (Fig. 7) [20].

An analogous *nido*/*arachno* electrostructural correlation table can be generated (Table 2).

The *isoiso* cluster geometries requiring more than one dsd transformation [18] from the most spherical deltahedron with the same number of vertices can be defined as "exotic". Such clusters exhibit highly oblate structures deviating considerably from a "spherical" geometry. Several examples of *isoiso* structures are known including not only the $[(\eta^3\text{-}C_3H_5)(OC)_2MoC_2B_9H_9Ph_2]^-$ ion discussed above (**22**: Fig. 7) but also the Re_2B_n ($n = 6$–9) and related W_2B_7 and W_3B_8 deltahedra [21] requiring two dsd transformations from the most spherical deltahedra (Fig. 8). A "supra-exotic" species, (η^5-Me_5C_5)$_2Re_2B_{10}H_{10}$ (**23**) [21c] (Fig. 8) is also known requiring four dsd transformations from the corresponding most spherical deltahedron. Since each "*iso*" dsd process requires an increase of two units in the formal metal oxidation state, such "exotic" metallaboranes are found with second and third row transition metals exhibiting relatively high oxidation states, notably molybdenum, tungsten, and rhenium. Furthermore, the two rhenium atoms in each of the oblate Re_2B_n deltahedra provide sites for the internal oxidative addition reactions required for the dsd processes to form the observed oblate deltahedra.

The "exotic" dirhenaboranes in Fig. 8 all have $2n - 4$ apparent skeletal electrons rather than the $2n + 2$ skeletal electrons required by the Wade–Mingos rules [2] for *closo*

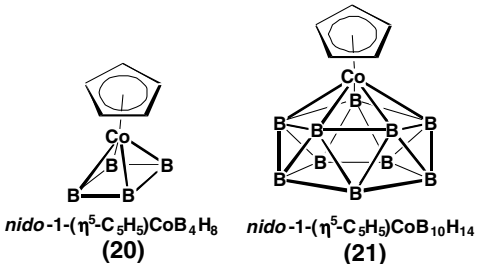

Fig. 6. Some *nido* cobaltaboranes with C_{nv} symmetry.

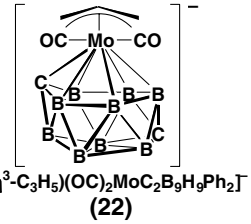

Fig. 7. An irregular icosahedral MoC_2B_9 molybdacarborane.

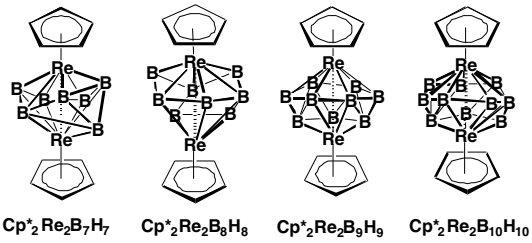

Fig. 8. Some "*isoisocloso*" and more "exotic" dirhenaboranes with oblate Re_2B_n deltahedra ($Cp^* = \eta^5$-Me_5C_5; methyl groups and hydrogen atoms omitted for clarity).

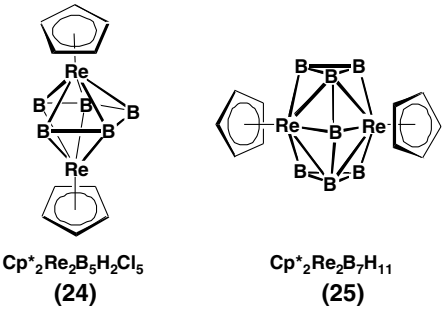

Fig. 9. The complexes $Cp^*_2Re_2B_5H_2Cl_5$ and $Cp^*_2Re_2B_7H_{11}$ ($Cp^* = \eta^5$-Me_5C_5; methyl groups, hydrogen atoms, and chlorine atoms omitted for clarity).

deltahedra assuming the Cp^*Re vertices and BH vertices to be donors of zero and two skeletal electrons, respectively. Related "exotic" *nido*- and *arachno*-type species (Fig. 9) are $Cp^*_2Re_2B_5H_2Cl_5$ (**24**) [21c] and $Cp^*_2Re_2B_7H_{11}$ (**25**) [22], respectively. Both of these species also have six fewer apparent skeletal electrons than required by the Wade–Mingos rules.

4. Summary

Relationships have been observed between the metal formal oxidation state and the metal valence electron counts in *closo*/*isocloso* and *nido*/*isonido* pairs of polyhedral metallaboranes. In general, the metal formal oxidation state increases by two units in a *closo* → *isocloso* or *nido* → *isonido* structural transformation, generally involving diamond–square–diamond processes. More exotic "*isoiso*" structures are found for metallaboranes containing metals exhibiting relatively high formal oxidation states such as molybdenum, tungsten, and rhenium.

The free borane ligand obtained by removal of the metal vertex from a metallaborane structure can be classified as symmetric or asymmetric depending upon the nature of the metal–ligand bond. In symmetric borane ligands found in *closo* metallaboranes, the metallaborane structure is generated by symmetrical "centroid" metal capping of the ligand open face. However, in asymmetric borane ligands found in *nido* metallaboranes, the metallaborane structure is generated by skew-symmetric or offset metal capping of the ligand open face. Capping regime descriptors are defined to describe these types of metal–borane bonding. In addition, electrostructural correlation tables are presented for *closo*/*nido* and *nido*/*arachno* pairs relating metal formal oxidation states, the numbers of metal valence electrons, and the capping regime descriptors.

Acknowledgement

One of us (R.B.K) is indebted to the US National Science Foundation for partial support of this work under Grant CHE-0209857.

References

[1] R.E. Williams, Inorg. Chem. 10 (1971) 210.
[2] (a) K. Wade, J. Chem. Soc., Chem. Commun. (1971) 792;
(b) K. Wade, Adv. Inorg. Chem. Radiochem. 18 (1976) 1;
(c) D.M.P. Mingos, Nature Phys. Sci. 99 (1972) 236;
(d) D.M.P. Mingos, Acc. Chem. Res. 17 (1984) 311.
[3] R.W. Rudolph, W.P. Pretzer, Inorg. Chem. 11 (1972) 1974.
[4] K.P. Callahan, M.F. Hawthorne, Adv. Organometal. Chem. 14 (1976) 145.
[5] (a) J. Bould, J.D. Kennedy, M. Thornton-Pett, J. Chem. Soc., Dalton Trans. (1992) 563;
(b) J.D. Kennedy, B. Štibr, in: G.W. Kabalka (Ed.), Current Topics in the Chemistry of Boron, Royal Society of Chemistry, Cambridge, 1994, p. 285;
(c) J.D. Kennedy, in: J. Casanova (Ed.), The Borane–Carborane–Carbocation Continuum, Wiley, New York, 1998, p. 85 (Chapter 3);
(d) B. Štibr, J.D. Kennedy, E. Drdáková, M. Thornton-Pett, J. Chem. Soc., Dalton Trans. (1994) 229.
[6] R.L. Johnston, D.M.P. Mingos, P. Sherwood, New J. Chem. 15 (1991) 831.
[7] (a) R.B. King, Inorg. Chem. 38 (1999) 5151;
(b) R.B. King, Inorg. Chim. Acta 300–302 (2000) 537.
[8] (a) R. Littger, U. Englich, K. Ruhlandt-Senge, J.T. Spencer, Angew. Chem., Int. Ed. Engl. 39 (2000) 1472;
(b) E.J. Ditzel, X.L.R. Fontaine, N.N. Greenwood, J.D. Kennedy, Z. Sisan, M. Thornton-Pett, J. Chem. Soc., Chem. Commun. (1989) 1762.
[9] M. Bown, X.L.R. Fontaine, N.N. Greenwood, J.D. Kennedy, M. Thornton-Pett, Z. Anorg. Allgem. Chem. 553 (1987) 24.
[10] B.H. Goodreau, L.R. Orlando, J.T. Spencer, J. Amer. Chem. Soc. 117 (1995) 11754, and references therein.
[11] R.G. Swisher, E. Sinn, R.N. Grimes, Organometallics 2 (1983) 506.
[12] S.S. Lee, C.B. Knobler, M.F. Hawthorne, J. Organomet. Chem. 394 (1990) 29.
[13] M.D. Wasczcak, C.C. Lee, I.H. Hall, P.J. Carroll, L.G. Sneddon, Angew. Chem., Int. Ed. Engl. 36 (1997) 2228.
[14] M. Bown, X.L.R. Fontaine, N.N. Greenwood, J.D. Kennedy, M. Thornton-Pett, J. Chem. Soc., Chem. Commun. (1987) 1650.
[15] M. Bown, X.L.R. Fontaine, N.N. Greenwood, J.D. Kennedy, P. MacKinnon, J. Chem. Soc., Chem. Commun. (1987) 817.
[16] (a) J. Bould, W. Clegg, T.R. Spalding, J.D. Kennedy, Inorg. Chem. Commun. 2 (1999) 315;
(b) R.Ll. Thomas, A.J. Welch, J. Chem. Soc., Dalton Trans. (1997) 631.
[17] (a) R.Ll. Thomas, G.M. Rosair, A.J. Welch, J. Chem. Soc., Chem. Commun. (1996) 1327;
(b) Fluxionality confirmed, in: R.Ll. Thomas, Talk presented at INTRABORON XVI, Durham, England, September 18–20, 1996.
[18] W.N. Lipscomb, Science 153 (1966) 373.
[19] J. Bould, J.D. Kennedy, M. Thornton-Pett, J. Chem. Soc., Dalton Trans. (1992) 563; see p. 571.
[20] S. Dunn, G.M. Rosair, R.Ll. Thomas, A.S. Weller, A. Welch, J. Angew Chem. Int. Ed. Engl. 36 (1997) 645.
[21] (a) A.S. Weller, M. Shang, T.P. Fehlner, J. Chem. Soc., Chem. Commun. (1998) 1787;
(b) A.S. Weller, M. Shang, T.P. Fehlner, Organometallics 18 (1999) 853;
(c) S. Ghosh, M. Shang, Y. Li, T.P. Fehlner, Angew. Chem., Int. Ed. Engl. 40 (2001) 1125;
(d) S. Ghosh, A.M. Beatty, T.P. Fehlner, J. Am. Chem. Soc. 123 (2001) 9188;
(e) B. Le Guennic, H. Jiao, S. Kahlal, J.-Y. Saillard, J.-F. Halet, S. Ghosh, M. Shang, A.M. Beatty, A.L. Rheingold, T.P. Fehlner, J. Am. Chem. Soc. 126 (2004) 3203.
[22] S. Ghosh, A.L. Rheingold, T.P. Fehlner, J. Chem. Soc., Chem. Commun. (2001) 895.

Nomenclature

dppa	bis(diphenylphosphino)amine	dpp^{n}pr	bis(diphenylphosphino)*n*-propylamine
dppm	bis(diphenylphosphino)methane	OTf	trifluoromethane sulfonate anion
dppi-Pr	bis(diphenylphosphino)isopropylamine		

method adopted by us is outlined in (Scheme 1), in which silver triflate was used as the halide scavenger. To our surprise, this method did not yield the targeted ruthenium bipyridyl diphosphazane complexes; instead, silver(I) complexes of diphosphazanes were obtained, thus providing an unexpected entry into the silver(I) chemistry of diphosphazane ligands. Subsequently, the silver(I) complexes of the diphosphazanes, $Ph_2PN(Pr^i)PPh(OC_6H_3Me_2\text{-}2,6)$ ($\mathbf{L}^1$), $Ph_2PN(Pr^i)PPh_2$ ($\mathbf{L}^2$) and $Ph_2PN(H)PPh_2$ ($\mathbf{L}^3$) have been synthesized by the reactions of appropriate silver salts with these ligands. The silver(I) complexes have been characterized by ^1H, and $^{31}P\{^1H\}$ NMR spectroscopy, and the structures of some representative complexes determined by single crystal X-ray diffraction studies. The results of these studies are reported in this paper. While the silver(I) complexes of diphosphinoalkanes have been explored extensively [8,9], similar studies on "P–N–P" based ligands are limited mainly to the three ligands, $Ph_2PN(R)PPh_2$ (R = H, Me or *n*-Pr) [10–15].

2. Experimental

All reactions were carried out under an atmosphere of dry nitrogen by using standard Schlenk-line techniques. The ligands $Ph_2PN(Pr^i)PPh_2$ ($\mathbf{L}^2$) and $Ph_2PN(H)PPh_2$ ($\mathbf{L}^3$) were prepared using published procedures [16]. The syntheses of the silver complexes were carried out under dark conditions owing to the sensitivity of these compounds to light. Solvents were purified by standard procedures and freshly distilled prior to use. The ^1H and $^{31}P\{^1H\}$ NMR spectra were recorded in $CDCl_3$ using a Bruker Avance-400 spectrometer with Me_4Si as an internal standard for ^1H NMR measurements and 85% H_3PO_4 as an external standard for ^{31}P NMR measurements. The variable temperature $^{31}P\{^1H\}$ NMR experiments were carried out in CD_2Cl_2 from 183 to 303 K. Chemical shifts downfield from the standard were assigned positive values. Infrared spectra were recorded using a Perkin–Elmer Model 457 spectrometer. Elemental analyses were carried out using a Perkin–Elmer 2400 CHN analyzer.

2.1. Synthesis of $Ph_2PN(Pr^i)PPh(OC_6H_3Me_2\text{-}2,6)$ (L^1)

A solution of PPh_2Cl (3.6 mL, 0.02 mol) in 20 mL benzene was added drop wise with stirring to a solution of isopropyl amine (5.12 mL, 0.06 mol) in 30 mL benzene at 0 °C. The reaction mixture was stirred at room temperature for 6 h and was filtered to remove the precipitated isopropyl amine hydrochloride. The filtrate was evaporated to dryness under vacuum to give the aminophosphane $Ph_2PNH(Pr^i)$ as a viscous oil. The oily residue was redissolved in benzene, and triethylamine (4.16 mL, 0.03 mol) added. The solution was cooled to 0 °C, and $PPhCl_2$ (2.71 mL, 0.02 mol) in benzene was added drop wise with stirring. The reaction mixture was stirred for 6 h at room temperature and filtered. The filtrate was evaporated to dryness and the residue dissolved in THF. This solution was added drop wise at room temperature to sodium 2,6-dimethylphenoxide, which was prepared by adding sodium hydride (60% dispersion in paraffin), (0.80 g, 0.016 mol) to a solution of 2,6-dimethylphenol (1.952 g, 0.016 mol) in dry THF. The reaction mixture was stirred at 30 °C for 5 h and evaporated to dryness. The residue was chromatographed on silica gel using benzene-petroleum ether (1:1 v/v) as the eluant. A concentrated solution of the ligand in $CHCl_3$ when cooled at 0 °C for 24 h gave colorless transparent crystals. Yield: 5.7 g, 60%. *Anal.* Calc. for $C_{29}H_{31}N_1O_1P_2$: C, 73.9; H, 6.6; N, 3.0. Found: C, 73.8; H, 6.6; N, 2.8%. ^1H NMR ($CDCl_3$, 293 K): δ 0.84, 1.38 (d, $CHMe_2$), 2.12 (s, $C_6H_3Me_2$), 3.99 (m, $CHMe_2$), 6.8–7.5 (m, aryl protons). $^{31}P\{^1H\}$ NMR ($CDCl_3$, 293 K): δ 36.5 (s), 121.8 (s). IR (KBr, cm^{-1}): 3443 w, 3202 w, 2960 s, 1600 s, 1260 s, 797 s, 695 s.

2.2. Synthesis of $[Ag_3(\mu\text{-}Cl)_2\{Ph_2PN(Pr^i)PPh_2\}_3]X$, ($X = NO_3$, PF_6) (**1a**, **1b**)

2.2.1. Method A

A solution of $Ru(bipy)_2Cl_2\cdot 2H_2O$ [7] (0.325 g, 6.25×10^{-4} mol) and $AgNO_3$ (0.138 g, 8.125×10^{-4} mol) in acetonitrile was stirred for 30 min after which Ph_2PN-

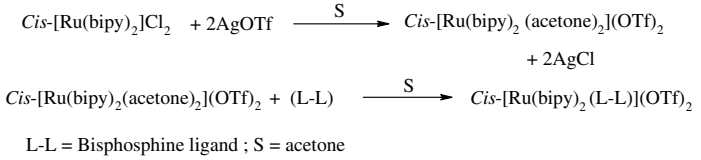

Scheme 1. Procedure adopted for the attempted synthesis of diphosphazane-bipyridyl complexes of ruthenium.

(Pr^i)PPh_2 (**L^2**) (0.267 g, 6.25×10^{-4} mol) was added. The reaction mixture was stirred for 3 h, and passed through a short plug (7 cm × 2 cm) of celite. The filtrate was concentrated under vacuum to ~5 mL. Colorless crystals of (**1a**) appeared over a period of 24 h. Yield: 0.85 g, 60%. *Anal.* Calc. for (**1a**): $C_{81}H_{81}Ag_3Cl_2N_4P_6O_3$: C, 55.8; H, 4.7; N, 3.2. Found: C, 55.7; H, 4.6; N, 3.2%. ^{1}H NMR ($CDCl_3$, 293 K): δ 0.32 (d, 18H, CHMe_2), 3.82 (s br, 3H, CHMe$_2$), 7–7.5 (m, 60H, C_6H_5). ^{31}P {^{1}H} NMR ($CDCl_3$, 293 K): δ 72.0 (s br). IR (Nujol, cm^{-1}): 3428 m, 3049 s, 2978 s, 1481 s, 1322 s, 1127 s, 1316 s, 967 s, 887 s, 855 s, 696 s, 424 m, 385 m, 342 m, 312 w.

The complex (**1b**) could be obtained from (**1a**) by a metathesis reaction, using a twofold excess of NH_4PF_6 in acetone. Yield (**1b**): 0.86 g, 58% (see below for characterization data).

2.2.2. Method B for (*1b*)

A solution of AgCl (0.117 g, 8.125×10^{-4} mol) and $Ph_2PN(Pr^i)PPh_2$ (0.521 g, 1.22×10^{-3} mol) in piperidine (20 mL) was stirred at room temperature for 12 h. Solvent was evaporated from the reaction mixture and freshly distilled acetone (20 mL) was added followed by the addition of a twofold excess of NH_4PF_6. The reaction mixture was stirred for a further period of 1 h; solvent was evaporated and the residue redissolved in the minimum quantity of dichloromethane (2 mL). The addition of diethyl ether gave a precipitate of the title complex (**1b**) in 40% yield (0.60 g). *Anal.* Calc. for (**1b**): $C_{81}H_{81}Ag_3Cl_2F_6N_3P_7$: C, 53.3; H, 4.4; N, 2.3. Found: C, 53.5; H, 4.5; N, 2.3%. ^{1}H NMR ($CDCl_3$, 293 K): δ 0.30 (d, 18H, CHMe_2), 3.76 (s br, 3H, CHMe$_2$), 7.0–7.7 (m, 60H, C_6H_5). ^{31}P{^{1}H} NMR ($CDCl_3$, 293 K): δ 73.5 (s, br). IR (Nujol, cm^{-1}): 3422 m, 3053 s, 2989 s, 1481 s,1127 s, 959 s, 887 s, 851 s, 695 s, 420 m, 382 m, 348 m, 322 w.

2.3. Synthesis of [$Ag_3(\mu$-$Cl)_2\{Ph_2PN(H)PPh_2\}_3$]X, (X = NO_3, PF_6) (*2a, 2b*)

Complexes (**2a**, **2b**) were prepared by the same procedures (method A for (**2a**), (**2b**); method B for (**2b**)) as described above for complexes (**1a**, **1b**) except that the ligand $Ph_2PN(H)PPh_2$ (**L^3**) was used instead of (**L^2**). Yield (**2a**): 0.56 g, 40% (method A). *Anal.* Calc. for (**2a**): $Ag_3C_{72}H_{63}N_4O_3P_6Cl_2$: C, 52.5; H, 3.9; N, 3.5. Found: C, 52.4; H, 4.0; N, 3.4%.

^{1}H NMR ($CDCl_3$, 293 K): δ 4.52 (s, 3H, NH), 6.9–7.4 (m, 60H, C_6H_5). ^{31}P {^{1}H} NMR ($CDCl_3$, 293 K): δ 53.0 (d, ^1J (^{31}P, Ag) = 452 Hz). IR (Nujol, cm^{-1}), (**2a**): 3289 s, 3160 s, 3058 m, 1574 m, 1312 s, 982 m, 897 m, 501 s, 432 s, 423 w, 385 w, 360 m, 330 m.

Yield (**2b**): 0.58 g, 40% (method A); 0.48 g, 33% (method B). *Anal.* Calc. for (**2b**) $C_{78}H_{75}Ag_3Cl_2F_6N_3O_2P_7$: C, 51.6; H, 4.1; N, 2.3. Found: C, 52.0; H, 4.0; N, 2.2%. ^{1}H NMR (**2b**) ($CDCl_3$, 293 K): δ 4.44 (s, 3H, NH), 7.0–7.6 (m, 60H, C_6H_5). ^{31}P {^{1}H} NMR (**2b**) ($CDCl_3$, 293 K): δ 52.5 (d, ^1J (^{31}P, Ag) = 450 Hz). IR (Nujol, cm^{-1}), (**2b**): 3286 s, 3168 s, 3050 m, 1584 m, 928 m, 900 m, 506 s, 437 s, 421 w, 380 w, 367 m, 319 m.

2.4. Synthesis of [$Ag(Ph_2PN(Pr^i)PPh_2)X]_2$ (X = NO_3, OTf) (*3a, 3b*)

The ligand $Ph_2PN(Pr^i)PPh_2$ (**L^2**) (0.267 g, 6.25×10^{-4} mol) was added to a solution of AgOTf (0.160 g, 6.25×10^{-4} mol) in acetonitrile at room temperature and the reaction mixture stirred for 4 h. Solvent was removed from the reaction mixture and the resulting colorless solid was redissolved in dichloromethane. The solution was passed through a short plug of celite (7 cm × 2 cm) and concentrated to ~5 mL. Colorless micro-crystals of (**3b**) appeared over a period of 24 h. Yield: 0.53 g, 62%. *Anal.* Calc. for (**3b**): $C_{56}H_{54}Ag_2F_6N_2O_6P_4S_2$: C, 49.0; H, 3.9; N, 2.0. Found: C, 49.2; H, 3.9; N, 2.2%. ^{1}H NMR ($CDCl_3$, 293 K): δ 0.59 (s br, 12H, CHMe_2), 3.94 (s br, 2H, CHMe$_2$), 7.2–7.6 (m, 40H, C_6H_5). ^{31}P{^{1}H}NMR ($CDCl_3$, 293 K): δ 81.8 (t, br). IR (Nujol, cm^{-1}), (**3b**): 3468 s, 3050 m, 2584 m, 1611 m, 1263 w, 1226 s, 1170 s, 968 m, 506 s, 421 w, 367 m, 305 m.

Complex (**3a)** was prepared by following the same procedure as above for (**3b)** using $AgNO_3$ in place of AgOTf. Yield (**3a**): 0.41 g, 55%. *Anal.* Calc. for (**3a**): $C_{54}H_{54}Ag_2N_4O_6P_4$: C, 54.2; H, 4.5; N, 4.7. Found: C, 54.0; H, 4.6; N, 4.7%. ^{1}H NMR ($CDCl_3$, 293 K): δ 0.61 (s br, 12H, CHMe_2), 3.90 (s br, 2H, CHMe$_2$), 7.1–7.6 (m, 40H, C_6H_5). ^{31}P{^{1}H}NMR ($CDCl_3$, 293 K): δ 82.0 (s, br). IR (Nujol, cm^{-1}), (**3a**): 3478 w, 3059 m, 2979 m, 1609 w, 1474 m, 1315 s, 1261 s, 964 m, 695 s, 570 s, 515 m, 411 s, 332 m, 307 w.

2.5. Synthesis of [$Ag\{Ph_2PN(Pr^i)PPh(OC_6H_3Me_2$-2,6)$\}_2$]-($PF_6$) (*4*)

The ligand $Ph_2PN(Pr^i)PPh(OC_6H_3Me_2$-2,6) (**$L^1$**) (0.589 g, 12.5×10^{-4} mol) was added to a solution of $AgNO_3$ (0.106 g, 6.25×10^{-4} mol) in acetonitrile at room temperature and the reaction mixture stirred for 24 h followed by the addition of a twofold excess of NH_4PF_6. The reaction mixture was stirred for a further period of 1 h; the colorless precipitate was filtered off using a Whatman No. 42 filter paper. The filtrate was concentrated to 5 mL, 5–6 drops of $CHCl_3$ were added, and the solution kept at 0 °C for 2 days to obtain colorless micro-crystals of the title compound. Yield: 0.52 g, 70%. *Anal.* Calc. for (**4**): $C_{58}H_{62}AgF_6N_2O_2P_5$: C, 58.2; H, 5.2; N, 2.3. Found: C, 58.4; H, 5.3; N, 2.2%. ^{1}H NMR ($CDCl_3$, 293 K): δ 1.41, (s br, 12H, CHMe_2), 2.19 (s, 12H, $C_6H_3Me_2$), 4.2 (m, 2H, CHMe$_2$), 7.5–6.8 (m, 36H, C_6H_5).

^{31}P {^{1}H} NMR ($CDCl_3$, 293 K): δP_A 136.0 ppm (s, br), δP_B 83.0 ppm (s, br). IR (Nujol, cm^{-1}): 3413 w, 3122 s, 2966 s, 1650 s, 1240 s, 798 s, 692 s, 615 m.

Table 1
Summary of X-ray diffraction data for the ligand (L^1) and complexes (**1b**), (**2b**), (**3b**) and (**4**)

Compound	Ligand (L^1)	Complex (**1b**)	Complex (**2b**)	Complex (**3b**)	Complex (**4**)
Formula	$C_{29}H_{31}N_1O_1P_2$	$C_{81}H_{81}Ag_3Cl_2N_3P_7F_6$	$C_{78}H_{75}Ag_3Cl_2F_6N_3O_2P_7$	$C_{56}H_{54}Ag_2F_6N_2O_6P_4S_2$	$C_{58}H_{62}Ag_1F_6N_2O_2P_5$
M	471.5	1821.79	1811.71	1368.75	1195.82
Crystal system	monoclinic	orthorhombic	monoclinic	monoclinic	orthorhombic
Space group	$P2(1)$	$P21\ 21\ 21$	$P2(1)/c$	$P2(1)/n$	$Pbca$
a (Å)	10.682(1)	10.760(2)	12.051(12)	10.739(7)	22.345(3)
b (Å)	8.233(9)	23.088(5)	29.39(3)	21.078(4)	22.025(3)
c (Å)	14.798(3)	32.684(6)	22.40(2)	12.679(2)	23.716(4)
α (°)	90.00	90.00	90.00	90.00	90.00
β (°)	91.56(5)	90.00	97.01(2)	93.940(3)	90.00
γ (°)	90.00	90.00	90.00	90.00	90.00
U (Å^3)	1301(4)	8120(3)	7877(14)	2863.4(9)	11672(3)
Z	2	4	4	2	8
M (Mo Kα) (mm^{-1})	0.188	0.978	1.010	0.939	0.543
Total reflections	11487	67055	47742	19964	90729
Unique reflections	5946	16612	11313	4879	11926
R_{int}	0.057	0.051	0.321	0.055	0.082
R_1 (all data)	0.145	0.066	0.151	0.041	0.108
R_1 ($I_0 > 2\sigma(I_0)$)	0.088	0.052	0.081	0.032	0.072
wR_2 ($I_0 > 2\sigma(I_0)$)	0.156	0.104	0.202	0.093	0.181
2θ max (°)	28.0	26.4	23.3	24.7	26.4
wR_2 (all data)	0.185	0.113	0.257	0.081	0.215

2.6. Synthesis of $[Ag\{Ph_2PN(Pr^i)PPh_2\}_2](PF_6)$ (**5**)

The ligand $Ph_2PN(Pr^i)PPh_2$ (L^2) (0.534 g, 12.5×10^{-4} mol) was added to a solution of $AgNO_3$ (0.160 g, 6.25×10^{-4} mol) in acetonitrile. The reaction mixture was stirred for 5 h at room temperature followed by the addition of a twofold excess of NH_4PF_6. The reaction mixture was stirred for a further period of 1 h; solvent was evaporated to dryness. The colorless solid residue was redissolved in CH_2Cl_2–$CHCl_3$ mixture (1:1 v/v), and the solution passed through a plug of celite and concentrated to ~15 mL. This solution was added drop wise to 30 mL of diethyl ether with rapid stirring. The colorless fluffy solid that precipitated was filtered, washed with diethyl ether (2×20 mL) and dried in air. Yield: 0.51 g, 73%. *Anal.* Calc. for $AgC_{54}H_{54}N_2P_5F_6$ (**5**): C, 58.5; H, 4.9; N, 2.5. Found: C, 58.1; H, 4.9; N, 2.6%. ^{1}H NMR ($CDCl_3$, 293 K): δ 0.60 (s br, 12H, CHMe_2), 3.78 (m, 2H, CHMe$_2$), 7.2–7.4 (m, 40H, C_6H_5). ^{31}P {^{1}H} NMR ($CDCl_3$, 293 K): δ 89.9 (s br). IR (Nujol, cm^{-1}): 3245 w, 3049 s, 2873 s, 1712 s, 1435 s, 965 s, 696 s, 516 s, 367 s, 319 s.

2.7. X-ray crystallography

Crystal data for the ligand (L^1) and the complexes (**1b**), (**2b**), (**3b**) and (**4**) were collected on a BRUKER SMART APEX CCD diffractometer with a D8 goniometer (graphite-monochromated Mo Kα radiation, $\lambda = 0.71073$ Å) using the SMART software [17a]. The data was integrated with SAINT [17b] and an empirical absorption correction was applied using SADABS [17c]. The structure was solved by SIR 92 [18a] or by Patterson method using SHELXS-97 [18b] and refined by full-matrix least-squares methods against F^2 (SHELXL-97) [18c]. All non-hydrogen atoms were refined with anisotropic displacement parameters and hydrogen atoms were placed in their calculated positions. Attempts to improve the data quality of (**2b**) were unsuccessful due to the poor stability of the compound when subjected to X-rays. The details of the structure solution and refinement are given in Table 1.

3. Results and discussion

3.1. Synthesis and NMR spectroscopic studies

When the reaction of $Ru(bipy)_2Cl_2 \cdot 2H_2O$ with the diphosphazane ligand $Ph_2PN(R)PPh_2$ ($R = Pr^i$, H) is carried out in the presence of a silver salt AgX ($X = NO_3$, OTf), a trinuclear silver species analogous to (**1a**) or (**2a**) is obtained in modest yield. The ruthenium precursor merely acts as a source of chloride ions in the formation of these trinuclear Ag(I) complexes, and no ruthenium bipyridyl complexes of diphosphazanes are formed.[2] Subsequently, the reactions of AgX salts with diphosphazane ligands (L^1–L^3) were carried out and the reaction conditions were optimized to obtain best yields of monuclear, binuclear and trinuclear silver complexes as outlined in Schemes 2–4 (see Section 2).

The reaction of the unsymmetrical ligand (L^1) with $AgNO_3$ in the presence of NH_4PF_6 gives the bischelate complex (**4**) in good yield (Scheme 2). The structure of (**4**) has been established by single crystal X-ray analysis

[2] A direct reaction of $[Ru(bipy)_2(MeCN)_2](PF_6)$ with the diphosphazane (L^2) in boiling MeCN was very sluggish and gave a P^{III} product with δ_P 79.0 (s) over a period of 48 h, along with a P^V species ($\delta_P \approx 30$); the two products could not be separated. Only a P^V species was formed if harsh conditions (DMSO, 120 °C) were employed.

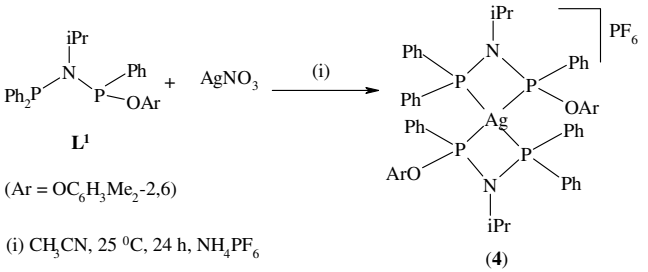

Scheme 2. Synthesis of mononuclear bischelate complex (**4**) using the unsymmetrical ligand ($\mathbf{L}^1$).

(see Section 3). The ^{31}P NMR spectrum of complex (**4**) at 293 K shows two broad peaks at 136.0 ppm and 83.0 ppm, which are assigned to the $-PPh_2(OAr)$ and the $-PPh_2$ phosphorus nuclei, respectively. These are shifted downfield compared to the ^{31}P chemical shifts for the free ligand. ($\delta_P = 121.8$ and 36.5 ppm, respectively). The ^{31}P NMR spectrum recorded at 183 K shows two symmetrical quartets, which constitute the AA′XX′ part of an AA′XX′M spin system. (A and X = P, M = Ag). Thus, complex (**4**) shows fluxional behavior in solution which is typical of the coordination chemistry of silver [8b,19]. The reaction of ligand ($\mathbf{L}^1$) with AgX (X = OTf, Cl) in a 1:1 or 1:2 molar ratio did not give products analogous to complex (**4**) when monitored by ^{31}P NMR spectroscopy, but instead formed a white intractable solid which could not be characterized any further.

The reaction of the symmetrical diphosphazane ($\mathbf{L}^2$) with $AgNO_3$ in a 1:1.3 ratio using $Ru(bipy)_2Cl_2 \cdot 2H_2O$ as the halide donor source gives the trinuclear complex (**1a**) (Scheme 3). Complex (**1b**) is prepared by the direct reaction of AgCl with ($\mathbf{L}^2$) in a 1:1.5 molar ratio in piperidine for 12 h, followed by counter ion metathesis using NH_4PF_6. The analogous complexes (**2a**, **2b**) of the ligand $Ph_2PNHPPh_2$ ($\mathbf{L}^3$) were obtained by following the same procedure (Scheme 4). Ellerman et al. have reported the synthesis of complex (**2b**) by the reaction of AgCl and ($\mathbf{L}^3$) in methanol [10a]. Structural assignment for this complex was based on analytical and spectroscopic data. The structures of (**1b**) and (**2b**) have been established by X-ray crystallography. The ^{31}P {^1H} NMR spectra of the trinuclear complexes $[Ag_3(\mu\text{-}Cl)_2\{Ph_2PN(Pr^i)PPh_2\}_3]X$ (X = NO_3, PF_6) (**1a**, **1b**) show a broad singlet (δ 72.0 ppm, br) at 293 K which is shifted downfield from the free ligand value ($\delta = 48.8$ ppm). The spectra of (**2a**) or (**2b**) show a doublet at 53.0 δ (δ free ligand = 43.1 ppm).

The silver salt AgX (X = NO_3, OTf) reacts with ($\mathbf{L}^2$) in a 1:1 molar ratio to form the binuclear complexes (**3a**) or (**3b**), respectively. The reaction of $AgNO_3$ with two molar equivalents of ($\mathbf{L}^2$) in acetonitrile in the presence of NH_4PF_6 gives the bischelate complex $[Ag\{Ph_2PN(Pr^i)\text{-}PPh_2\}_2](PF_6)$ (**5**) (Scheme 3). The molecular structure of (**3b**) has been established by X-ray crystallography (see Section 3). The ^{31}P NMR spectrum of $[Ag\{Ph_2PN(Pr^i)\text{-}PPh_2\}(NO_3)]_2$ (**3a**) shows a broad singlet at ~81.0 ppm, whereas that of $[Ag\{Ph_2PN(Pr^i)PPh_2\}(OTf)]_2$ (**3b**) displays a broad unresolved triplet at 81.8 ppm at 293 K with a $\Delta\delta$ value of ~33 ppm compared to the free ligand. This difference in the spectral pattern can be attributed to the effect of the counter ion on the Ag–P bond strength, which in turn would affect the Ag–P coupling constant [19b]. Complex (**3b**) contains a weakly coordinating anion such as triflate and probably exists essentially as an ionic species

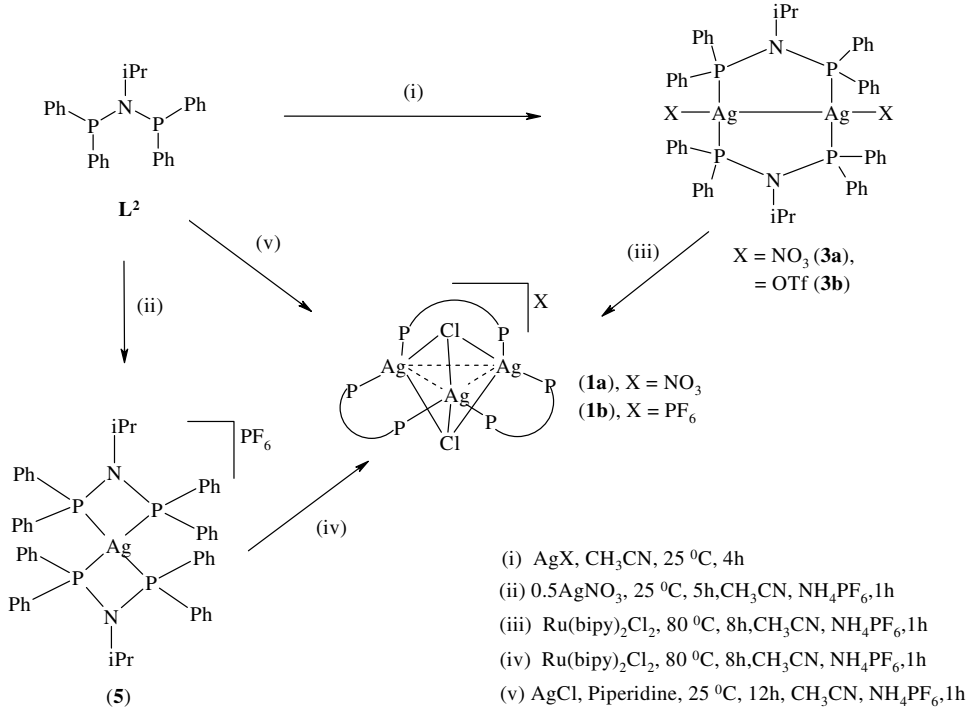

Scheme 3. Synthesis of Ag(I) diphosphazane complexes of ligand ($\mathbf{L}^2$).

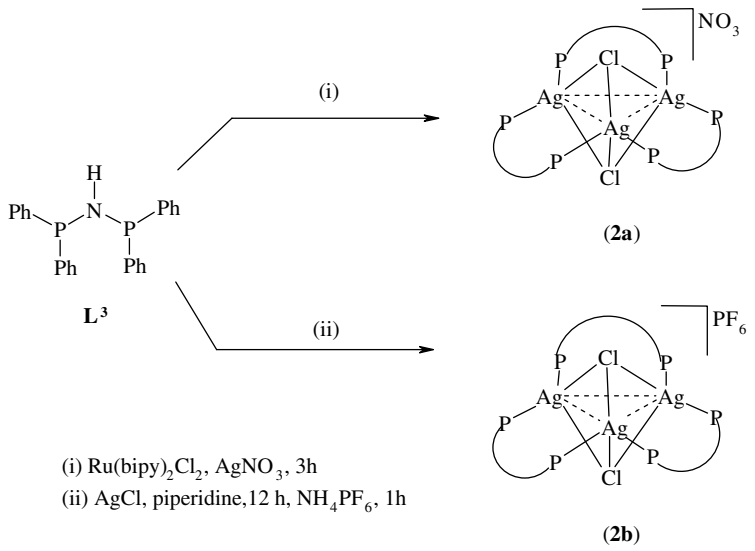

Scheme 4. Synthesis of trinuclear Ag(I) complexes (**2a**) and (**2b**) of the ligand ($\mathbf{L}^3$).

$[Ag_2(\mathbf{L}^2)_2]^{2+}[(OTf)_2]^{2-}$. By contrast, in complex (**3a**), the counter ion nitrate is strongly bound to the metal. The impact of the counter ion on the Ag–P bond has been well documented in the literature; larger ^1J (^{31}P, Ag) coupling constants are observed for silver(I) phosphine complexes containing the triflate ion [8d,19b]. The ^{31}P $\{^1$H$\}$ NMR spectrum of (**3b**) at 183 K appears as four distinct sets (1:1:1:1) centered at δ 98.4, 98.3, 71.7 and 68.1 ppm, respectively (Fig. 1). This result can be explained by assuming an exchange between two species (**3b**) and (**3b′**) at low temperature in CD_2Cl_2, as illustrated in (Scheme 5).

The isolation and X-ray crystallographic characterization of Ag(I) complexes $[Ag(CH_2Cl_2)(\eta^1\text{-}P_3N_3Cl_6)_2]X$ [20a] and $[Ag(CH_2Cl_2)_3]X$ [20b], in which dichloromethane is chelated to silver through its chlorine atoms lends credence to the above assumption. The ^{31}P $\{^1$H$\}$ NMR spectrum of (**5**) shows a broad resonance at 90.0 ppm at 293 K; the downfield shift compared to the free ligand value ($\Delta\delta = 41$ ppm) is maximum for this complex.

The reaction of AgOTf with ($\mathbf{L}^2$) in a 1:1 molar ratio was monitored by ^{31}P $\{^1$H$\}$ NMR spectroscopy (Fig. 2). The free-ligand resonance ($\delta = 48.8$ ppm, br) disappeared

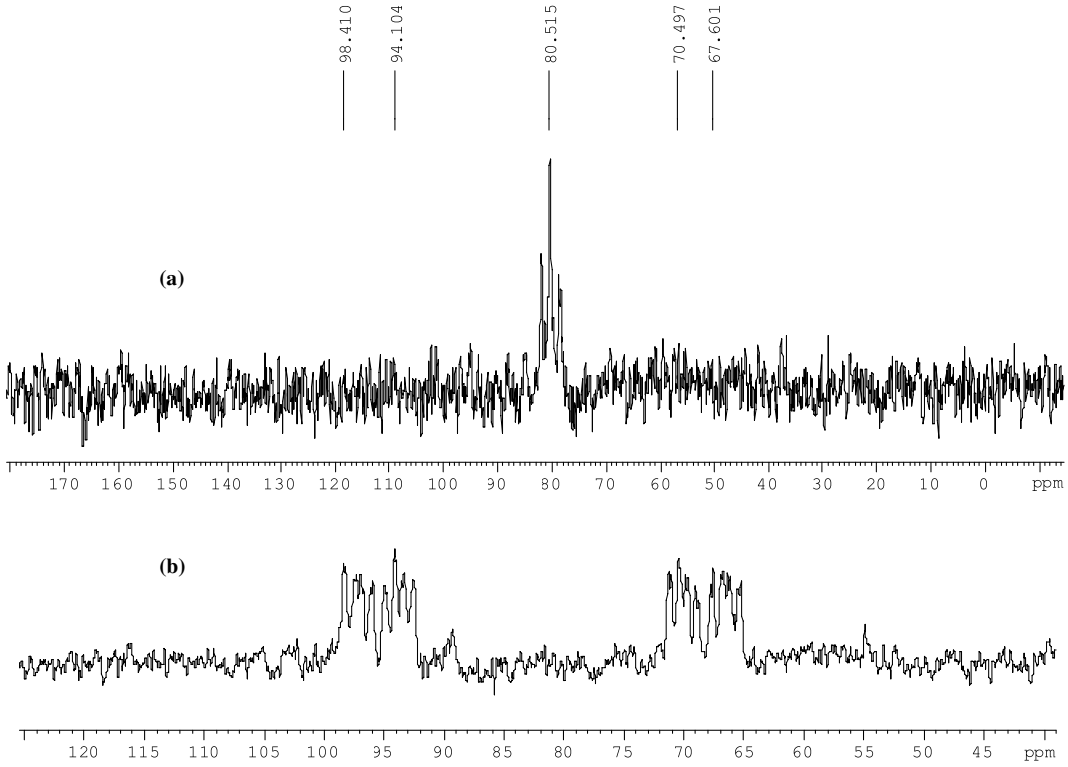

Fig. 1. The ^{31}P $\{^1$H$\}$ NMR spectrum of complex (**3b**) at 293 K (a) and 183 K (b) in CD_2Cl_2 solvent.

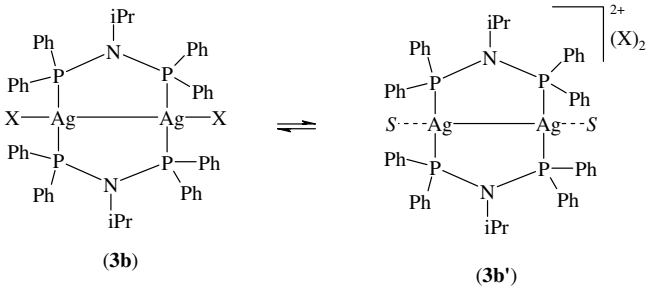

Scheme 5. Proposed structures for (**3b**) ⇋ (**3b**′) at 183 K.

completely within 15 min and two broad resonances at δ 52–55 ppm and 80 ppm appeared. The latter peak was assigned to complex (**3b**). The peak at δ 52–55 ppm which is attributed to an intermediate (**I**) disappeared over a period of 3 h at the expense of the resonance at 81 ppm (**3b**). When two more equivalents of the ligand $Ph_2PN(Pr^i)PPh_2$ ($\mathbf{L}^2$) were added to the reaction mixture of (**3b**) and (**I**) in the NMR tube, a single broad resonance at δ 90.0 ppm appeared immediately and the resonance at 80 ppm slowly disappeared. The resonance at δ 90.0 ppm was assigned to a mononuclear bischelate core as present in (**5**). Complex (**5**) could be isolated by adding NH_4PF_6 to the reaction mixture. Similarly, when an excess of ($\mathbf{L}^2$) was added to a mixture of the intermediate (**I**) (δ 52–55 ppm) and complex (**3b**), both the resonances disappeared completely and the resonances at δ 90 ppm due to (**5**) and the resonance at δ 48.8 ppm arising from unreacted ligand were observed (Fig. 2). This observation indicates that the intermediate species (**I**) is involved in the formation of both the complexes (**3b**) and (**5**). It is noteworthy that none of these complexes revert to the intermediate (**I**) under the given experimental conditions. It was further noted that, in the presence of a suitable chloride source in solution, the complexes (**3b**) and (**5**) transformed slowly to the trinuclear species at room temperature over a period of 20 h. The reaction occurred faster (within a period of 8 h) when the solution was heated under reflux. The ratio of free ligand to the silver salt appears to be the key factor that decides the nature of the complex formed, as noted previously [19,21]. The broad unresolved pattern at δ 52–55 ppm (293 K) attributed to intermediate species (**I**) splits into two doublets of equal intensity centered at δ 57.1 and 37.0 ppm at 183 K, with large Ag–P coupling constants of 812 Hz and 795 Hz (Fig. 3). The temperature dependence of the ^{31}P NMR spectra of the intermediate species (**I**) indicates that a dynamic chemical exchange process occurs in solution. We tentatively propose that the intermediate (**I**) consists of two species (**Ia**) and (**Ib**) in equilibrium (Scheme 6). Attempts to isolate and characterize the intermediate have been unsuccessful to date.

3.2. X-ray diffraction analyses

3.2.1. The crystal structure analysis of the ligand (L^1)

The solid-state structure of ligand ($\mathbf{L}^1$) has been determined by X-ray diffraction. A perspective view of the

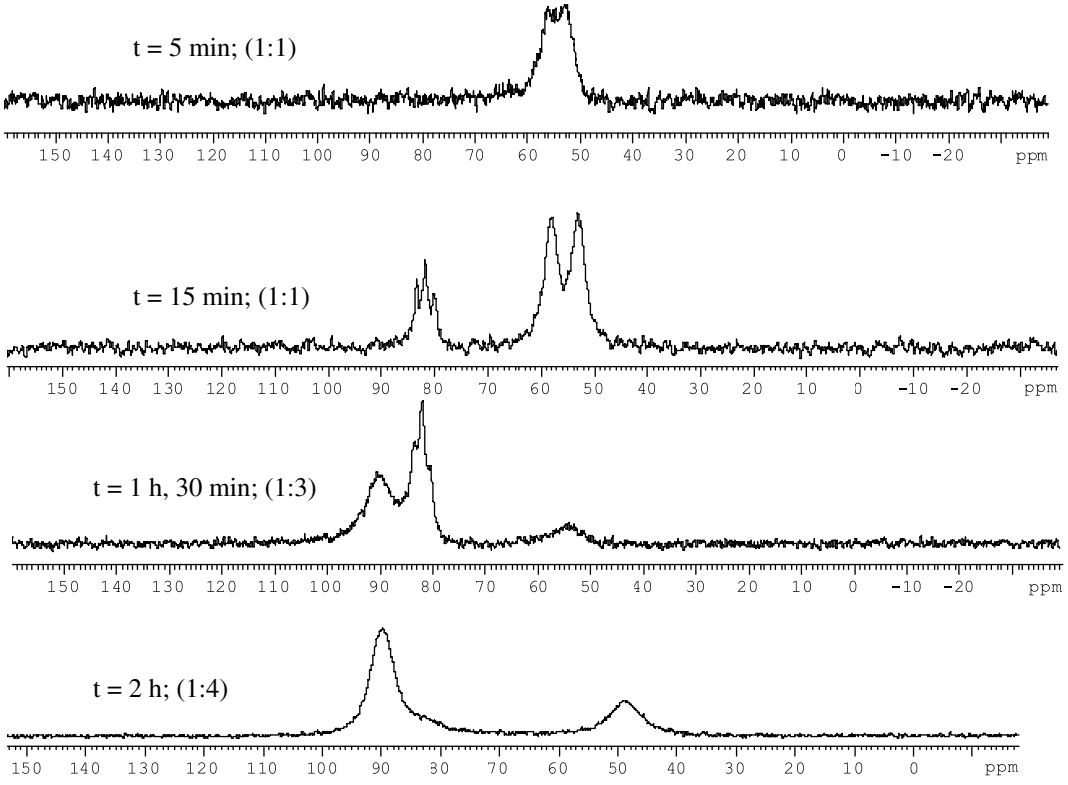

Fig. 2. ^{31}P NMR monitoring of the reaction of AgOTf with $Ph_2PN(Pr^i)PPh_2$ ($\mathbf{L}^2$) at 293 K in CD_2Cl_2 solvent. The ratios shown on each spectrum represents the relative proportions of AgOTf and ligand ($\mathbf{L}^2$).

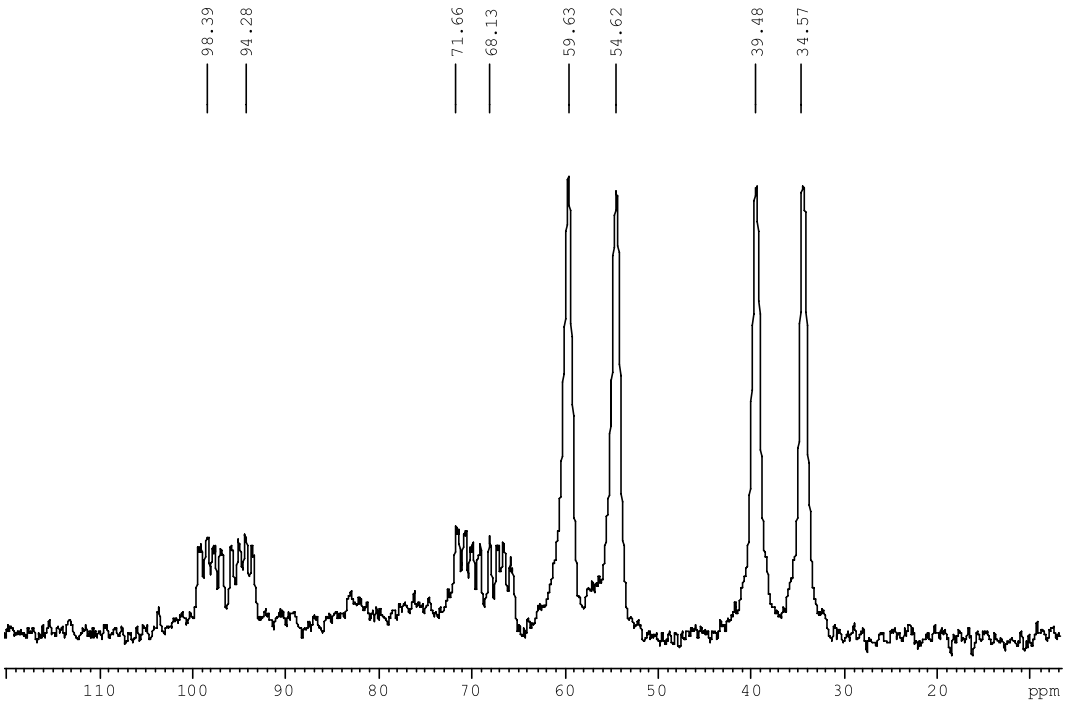

Fig. 3. The $^{31}P\{^{1}H\}$ NMR spectrum of complex (**3b**) and the intermediate (**I**) at 183 K in CD_2Cl_2 solvent.

molecule is shown in Fig. 4. Selected bond distances and bond angles are listed in Table 2. The geometry around the nitrogen atom is trigonal planar with a P–N–P angle of 122°. The ligand adopts a conformation wherein the lone pair on the PPh_2 phosphorus is oriented *trans* to the isopropyl group on the nitrogen atom whereas the lone pair on the PPh(OAr) fragment is *cis* to it. This is in contrast to the previous observation that the lone pair on the PPh_2 phosphorus in $Ph_2PN(Pr^i)P(O_2C_6H_4)$ [22a] and Ph_2PN-(CHMePh)PPh($N_2C_3HMe_2$-3,5) [22b] lies *cis* to the isopropyl group on nitrogen. The two phenyl rings subtend an angle of 101.5° at the PPh_2 phosphorus atom, but substituents on the PYY′ phosphorus subtend an angle of 94.7°. This could probably be due to the oxygen spacer, which relieves the steric strain arising from the 2,6- disubstituted aryl rings to some extent. Both the P–N bond lengths are nearly equal (1.71 Å) in the ligand ($\mathbf{L}^1$) and are close to the bond lengths observed for the diphosphazane ligands $Ph_2PN(Pr^i)PPh_2$ (1.71 Å) [23a] and $Ph_2PN((S)$-CHMePh)-PPh_2 (1.72 Å) [23b]. Two different P–N bond lengths are observed for the unsymmetrically substituted diphospha-

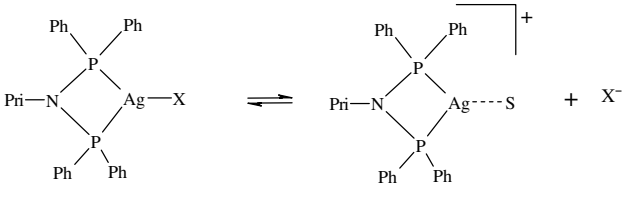

X = CF_3SO_3 , S = coordinating solvent

(**Ia**) (**Ib**)

Scheme 6. Tentative structures for (**Ia**) ⇋ (**Ib**) at 183 K.

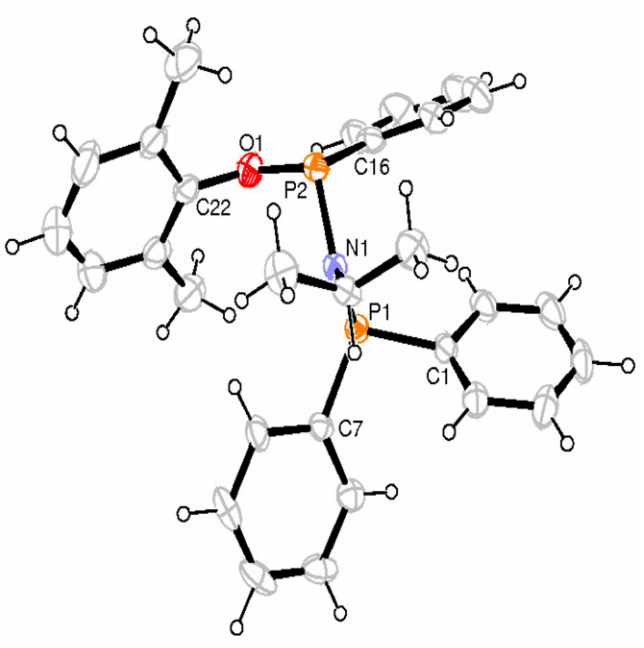

Fig. 4. ORTEP plot and atom labeling scheme for ligand [$Ph_2PN(Pr^i)$-$PPh(OC_6H_3Me_2$-2,6)] ($\mathbf{L}^1$).

zanes, $Ph_2PN(Pr^i)P(O_2C_6H_4)$ [22a] and $Ph_2PN((S)$-CH-MePh)PPh($N_2C_3HMe_2$-3,5) [22b]; the P–N bond connected to the $P(O_2C_6H_4)$ or PPh($N_2C_3HMe_2$-3,5) (1.65 Å, 1.69 Å, respectively) is shorter than the other P–N bond connected to the PPh_2 center (1.74 Å, 1.73 Å, respectively). These differences are best explained in terms of the negative hyperconjugative interaction between the nitrogen lone pair and the adjacent P-X σ^* orbitals [24]. The near equality of the

Table 2
Selected bond distances (Å) and angles (°) for (**1b**), (**2b**), (**3b**), (**4**) and ($\mathbf{L}^1$)

*$[Ag_3(dppi\text{-}Pr)_3(Cl)_2]PF_6$ (**1b**)*			
Ag–Cl–Ag (ave)	69.46(7)	Ag–P (ave)	2.460(3)
P(3)–N(2)–P(4)	117.8(3)	Cl–Ag (ave)	2.716 (5)
P(5)–N(3)–P(6)	117.2(2)	Ag(1)···Ag(2)	3.096(6)
P(1)–N(1)–P(2)	114.9(2)	Ag(1)···Ag(3)	2.968(9)
Cl–Ag–Cl (ave)	98.89(8)	Ag(2)···Ag(3)	3.102(1)
*$[Ag_3(dppa)_3(Cl)_2]PF_6$ (**2b**)*			
Ag–Cl–Ag (ave)	72.803(8)	Ag–P (ave)	2.450(2)
P(1)–N(1)–P(2)	126.0(6)	Cl–Ag (ave)	2.719(8)
P(3)–N (2)–P(4)	124.4(6)	Ag(1)···Ag(2)	3.153(3)
P(5)–N(3)–P(6)	126.9(6)	Ag(1)···Ag(3)	3.244(3)
Cl–Ag–Cl (ave)	93.80(3)	Ag(2)···Ag(3)	3.288(2)
*$[Ag_2(dppi\text{-}Pr)_2(OTf)_2]$ (**3b**)*			
O(1)–Ag(1)–Ag(1)′	114.56(9)	Ag(1)–O(1)	2.398(3)
O(1)–Ag(1)–P(2)	113.84(9)	Ag(1)–P(1)	2.442(9)
P(2)–Ag(1)–Ag(1)′	78.97(2)	Ag(1)–P(2)	2.417(9)
P(2)–Ag(1)–P(1)	143.37(3)	Ag(1)–Ag(1)′	2.868(6)
O(1)–Ag(1)–P(1)	102.18(9)		
P(2)–Ag(1)–Ag(1)′	91.48(2)		
*$Ag(Ph_2PN(Pr^i)PPhOC_6H_3Me_2\text{-}2,6)_2PF_6$ (**4**)*			
Ag–P (ave)	2.52(4)	P–N–P (ave)	109.9(2)
P(**1**)–Ag(**1**)–P(**2**)	66.93(5)	P(**2**)–Ag(**1**)–P(**4**)	118.27(5)
P(**3**)–Ag(**1**)–P(**4**)	66.97(5)	P(**2**)–Ag(**1**)–P(**3**)	141.54(5)
P(**1**)–Ag(**1**)–P(**4**)	131.76(5)	P(**1**)–Ag(**1**)–P(**3**)	141.26(5)
$Ph_2PN(Pr^i)PPh(OC_6H_3Me_2\text{-}2,6)$ ($\mathbf{L}^1$)			
P(2)–O (1)–C(22)	121.2(4)	P(2)–O(1)	1.662(4)
P(2)–N (1)–C(13)	114.9(4)	N(1)–C(13)	1.492(7)
P(1)–N (1)–P(2)	122.0(3)	P(1)···P(2)	2.986
P(1)–N (1)–C(13)	121.8(3)	O(1)–C(22)	1.405(7)
C(1)–P (1)–C(7)	101.5(2)	P–N (ave)	1.713(5)

two P–N bonds in ligand ($\mathbf{L}^1$) arises because the electron withdrawing effect of the oxygen spacer is compensated by the electron donating methyl substituents on the phenyl rings.

3.2.2. The crystal structure analyses of $[Ag_3(\mu\text{-}Cl)_2\{Ph_2PN(R)PPh_2\}_3]PF_6$ (R = Pr^i, (**1b**) and R = H (**2b**))

X-ray crystallographic studies reveal that the central core in both complexes (**1b**) and (**2b**) comprises a pair of halogen atoms, each of which is bonded to three Ag atoms which form an approximately equilateral triangular plane. The three metal atoms are bridged around the periphery of the triangle by three diphosphazane ligands in such a way that the coordination environments of the chlorine atoms are pyramidal three-coordinate $ClAg_3$, and the metal atoms are four coordinate $P_2Ag(\mu\text{-}Cl)_2$. The molecular structures of (**1b**) and (**2b**) are shown in Figs. 5 and 6, respectively. Selected bond lengths and bond angles for (**1b**) and (**2b**) are given in Table 2. The Ag–P distances of ~2.45 Å and Ag–Cl distances of ~2.72 Å in complexes (**1b**) and (**2b**) are comparable to those observed for $[Ag_3(\mu\text{-}Cl)_2(dppm)_3]$-X complexes reported recently in the literature [8b]. The Ag···Ag distances [2.97–3.10 Å in (**1b**) and 3.15–3.29 Å in (**2b**)] are shorter than that in the trinuclear Ag complex $[Ag_3(dppm)_3Cl_2]^+$(≈3.42 Å) [8b] and comparable to the bond distance in $[Ag_3(dppm)_3(\mu_3\text{-}\eta^1\text{-}C{\equiv}C\text{–}C_6H_4\text{-}NO_2\text{-}p)_2]^+$ (≈3.01 Å) [13b].

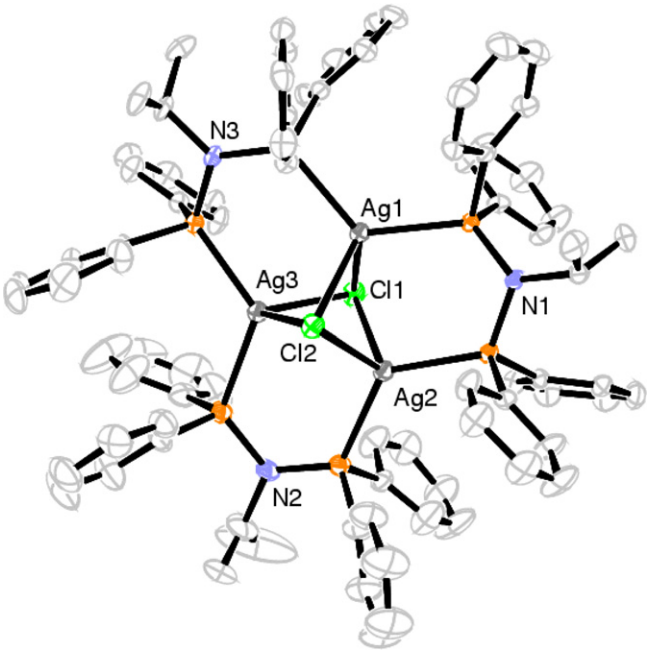

Fig. 5. ORTEP plot and atom labeling scheme for $[Ag_3(\mu\text{-}Cl)_2\{Ph_2PN(Pr^i)PPh_2\}_3](PF_6)$ (**1b**). (The hydrogen atoms and PF_6 ion have been omitted for clarity.)

3.2.3. The crystal structure analysis of $\{Ag(Ph_2PN(Pr^i)PPh_2)OTf\}_2$ (**3b**)

The molecular structure of $[Ag(\mathbf{L}^2)(OTf)]_2$ which has a crystallographic inversion symmetry is depicted in Fig. 7. The selected bond distances and angles are given in Table 2. The solid-state structure consists of a neutral dimeric molecular unit, in which the two silver atoms are bridged by a pair of diphosphazane ligands. In addition, each silver atom is bonded to a single triflate anion in a monodentate fashion. The Ag–P distances of 2.442 Å and 2.417 Å are in good agreement with those found for analogous dppm complexes reported earlier [25a]. The observed Ag–O distance of 2.398 Å is comparable to the bonding distance of 2.439 Å for the asymmetrically bound nitrate in $(PPh_3)AgNO_3$ [25b] and the reported value of 2.417 Å in case of the dppm analogue [25a]. The Ag–Ag distance (2.869 Å) is shorter than those observed in complexes (**1b**) and (**2b**), and also the corresponding dppa complex (2.961 Å) [14]. The P–Ag–P units are non-linear and eclipsed, resulting in a folding of the Ag_2P_4 core along the Ag–Ag axis to give rise to a staggered arrangement. The P (2)–Ag–P (1′) angle of 143.4° is significantly greater than the corresponding P (1)–Ag–P (2′) angle of 138.3 (1)° found in the related binuclear dppm complex with the formula $[Ag(dppm)(NO_3)]_2$ [25a] but less than that (148.4°) found for the dppa analogue [14].

3.2.4. The crystal structure analyses of complex (4)

The molecular structure of complex (**4**) as revealed by a single crystal X-ray study is shown in Fig. 8 and features a four coordinated tetrahedral silver ion. Selected bond lengths and bond angles are displayed in Table 2. The

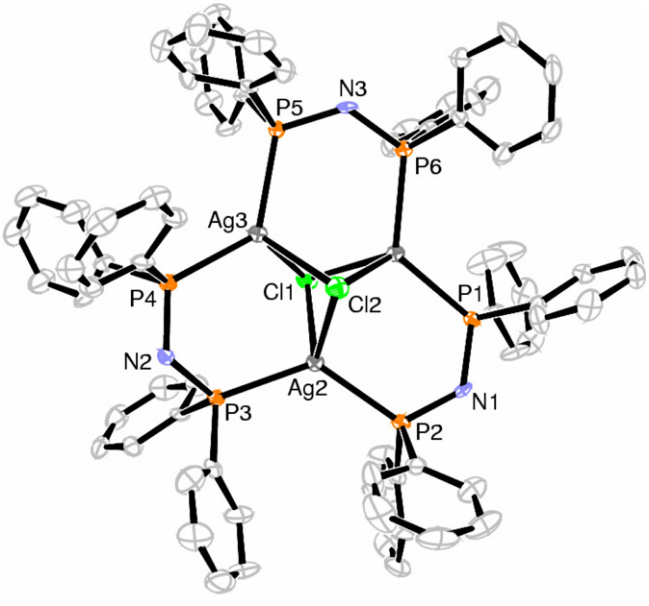

Fig. 6. ORTEP plot and atom labeling scheme for $[Ag_3(\mu\text{-}Cl)_2\{Ph_2PN(H)PPh_2\}_3](PF_6)$ (**2b**). (The hydrogen atoms and PF_6 ion have been omitted for clarity.)

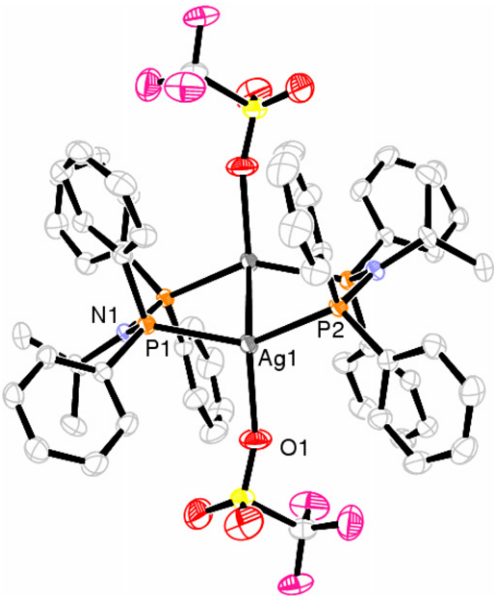

Fig. 7. ORTEP plot and atom labeling scheme for $[Ag\{Ph_2PN(Pr^i)PPh_2\}(OTf)]_2$ (**3b**). (The hydrogen atoms have been omitted for clarity.)

two "P–N–P" ligands are chelated to the metal center with a P–N–P angle of ~110° which is considerably less than that observed in case of the free ligand (122°). The bite angles of the two ligands are similar (~66.95°), while the interligand P–Ag–P angles vary approximately from 141.5° to 118.3° suggesting a highly distorted tetrahedral core. The Ag–P distances are in the range observed for the similar structures reported in the literature [21]. A comparison of the structural data for the complexes (**1b**), (**3b**) and (**4**) shows that the P–Ag–P angle subtended by the diphosphazane ligands on the metal center follows the

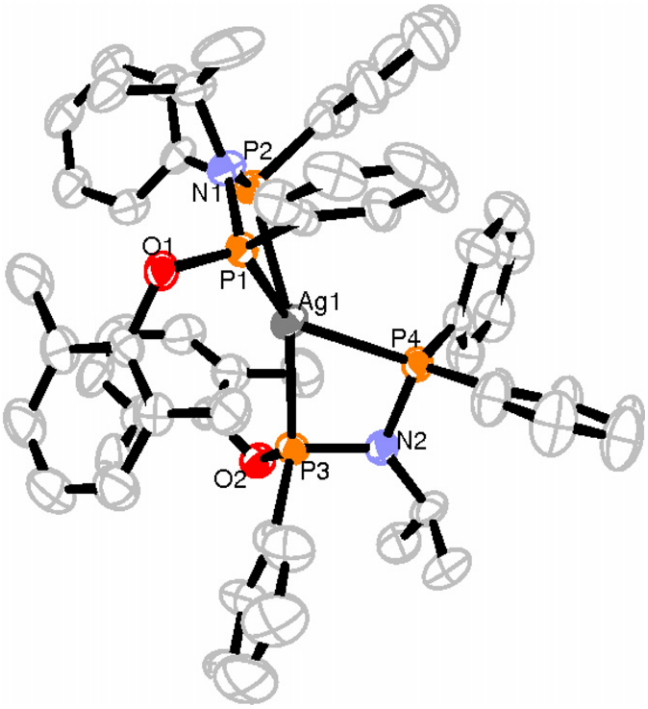

Fig. 8. ORTEP plot and atom labeling scheme for $[Ag\{Ph_2PN(Pr^i)PPh(OC_6H_3Me_2\text{-}2,6)\}_2](PF_6)$ (**4**). (The hydrogen atoms and PF_6 ion have been omitted for clarity.)

decreasing trend: (**3b**) > (**1b**) > (**4**). This observation is in accord with earlier findings that a change in the number of phosphine ligands around silver leads to difference in '*s*' contribution to the hybridization at the silver center, which in turn results in different P–Ag–P angles in the silver(I)-phosphine complexes [19].

4. Conclusions

Novel silver(I) complexes have been synthesized by the reaction of AgX (X = NO_3, OTf) with diphosphazane ligands $Ph_2PN(Pr^i)PPh(R)$ [R = Ph or $OC_6H_3Me_2$-2,6] by varying the stoichiometry and the reaction conditions. Symmetrically substituted diphosphazanes ($\mathbf{L}^2$ and $\mathbf{L}^3$) bearing a relatively weak π-acceptor phosphorus form stable Ag(I) complexes with different coordination numbers and geometries depending on the ratio of the reactants. On the other hand, the diphosphonite ligand, $(RO)_2PN(Me)P(OR)_2$ (R = C_6H_5) bearing a strong π-acceptor phosphorus does not form stable silver(I) complexes.[3] The unsymmetrical ligand ($\mathbf{L}^1$) which has similar π-acceptor ability as ligands ($\mathbf{L}^2$ and $\mathbf{L}^3$) forms only the mononuclear bischelate complex irrespective of the reaction stoichiometry, presumably due to steric reasons. It may also be noted that the sterically bulky [$(RO)_2PN(Me)P(OR)_2$, (R = OC_6-

[3] The diphosphonite ligands $(RO)_2PN(Me)P(OR)_2$ react with one equivalent of $AgNO_3$ in CH_3CN to give unstable Ag(I) complexes as shown by the ^{31}P NMR spectra of the reaction mixtures [δ_P 122.0 (d, br) and 126.0 (s, br) for R = C_6H_5; δ_P 126.0 (d, br) for R = C_6H_3 Me_2-2,6]; the complexes could not be isolated.

H_3Me_2-2,6] does not form stable silver(I) complexes.[3] NMR monitoring of the formation of silver(I) complexes of the diphosphazane ligand ($\mathbf{L}^2$) shows the involvement of an intermediate species in the transformation of bridged binuclear species to mononuclear bischelate species. In the presence of a chloride source, the mono and the binuclear species are converted into dichloro-bridged trinuclear complex. Further investigations are required to gain insights into the nature of the intermediate species and the mechanism of interconversions of Ag(I) complexes of varying nuclearity.

Acknowledgements

We thank the Department of Science and Technology, New Delhi, India for financial support and also for data collection using the CCD X-ray facility at IISc, Bangalore set up under IRHPA program.

Appendix A. Supplementary data

Tables of bond distances and angles, atomic anisotropic displacement parameters, hydrogen atoms positions, H-bond distances and angles have been deposited with the Cambridge Crystallographic Data Centre, CCDC Nos. 293534–293538. Copies of this information are available free of charge from The Director, CCDC, 12 Union Road, Cambridge, CB2 1EZ, UK (fax: +44 1223 336 033; e-mail: deposit@ccdc.cam.ac.uk or http://www.ccdc.cam.ac.uk). Supplementary data associated with this article can be found, in the online version, at doi:10.1016/j.poly.2006.05.017.

References

[1] (a) D. Mitra, N. Di Cesare, H.F. Sleiman, Angew. Chem., Int. Ed. 43 (2004) 5804;
(b) P. Mobian, J.-M. Kern, J.-P. Sauvage, Angew. Chem., Int. Ed. 43 (2004) 2392;
(c) K.M. Stewart, J. Rojo, L.W. McLaughlin, Angew. Chem., Int. Ed. 43 (2004) 5808.

[2] (a) E. Rüba, J.R. Hart, J.K. Barton, Inorg. Chem. 43 (2004) 4570;
(b) J.K. Barton, Science 233 (1986) 727;
(c) R. Hartshorn, J.K. Barton, J. Am. Chem. Soc. 114 (1992) 5919;
(d) F.R. Keene, Coord. Chem. Rev. 166 (1997) 121.

[3] (a) E.A.P. Armstrong, R.T. Brown, M.S. Sekwale, N.C. Fletcher, X.-Q. Gong, P. Hu, Inorg. Chem. 43 (2004) 1714;
(b) D. Hesek, Y. Inoue, S.R.L. Everitt, H. Ishida, M. Kunieda, M.G.B. Drew, Inorg. Chem. 39 (2000) 308;
(c) D. Hesek, Y. Inoue, S.R.L. Everitt, H. Ishida, M. Kunieda, M.G.B. Drew, Inorg. Chem. 39 (2000) 317.

[4] D. Hesek, G.A. Hembury, M.G.B. Drew, S. Taniguchi, Y. Inoue, J. Am. Chem. Soc. 12 (2000) 10236.

[5] (a) A. Shulman, F.P. Dwyer, in: F.P. Dwyer, D.P. Mellor (Eds.), Chelating Agents and Metal Chelates, Academic Press, New York, 1964, p. 383;
(b) A.K. -De Mesmaeker, J.-P. Lecomte, J.M. Kelly, Top. Curr. Chem. 177 (1996) 25;
(c) K. Warnmark, J.A. Thomas, O. Heyke, J.-M. Lehn, Chem. Commun. (1996) 701;
(d) R. Caspar, H. Amouri, M. Gruselle, C. Cordier, B. Malézieux, R. Duval, H. Leveque, Eur. J. Inorg. Chem. (2003) 499.

[6] (a) P.A. Anderson, G.B. Deacon, K.H. Haarmann, F.R. Keene, T.J. Meyer, D.A. Reitsma, B.W. Skelton, G.F. Strouse, N.C. Thomas, Inorg. Chem. 34 (1995) 6145;
(b) R. Haid, R. Gutmann, T. Stampfl, C. Langes, G. Czermak, H. Kopacka, K.-H. Ongania, P. Bruggeller, Inorg. Chem. 40 (2001) 7099;
(c) R. Gutmann, G. Czermak, A. Dumfort, W.E. Veer, B. Hong, H. Kopacka, K.-H. Ongania, T. Bechtold, P. Bruggeller, Inorg. Chem. Commun. 8 (2005) 319.

[7] B.P. Sullivan, D.J. Salmon, T.J. Meyer, Inorg. Chem. 17 (1978) 3334.

[8] (a) Effendy, C. di Nicola, M. Nitiatmodjo, C. Pettinari, B.W. Skelton, A.H. White, Inorg. Chim. Acta 358 (2005) 735;
(b) C. di Nicola, Effendy, F. Fazaroh, C. Pettinari, B.W. Skelton, N. Somers, A.H. White, Inorg. Chim. Acta 358 (2005) 720;
(c) A. Cingolani, C. di Nicola, Effendy, C. Pettinari, B.W. Skelton, N. Somers, A.H. White, Inorg. Chim. Acta 358 (2005) 748;
(d) Effendy, C di Nicola, M. Fianchini, C. Pettinari, B.W. Skelton, N. Somers, A.H. White, Inorg. Chim. Acta 358 (2005) 763;
(e) G.G. Lobbia, M. Pellei, C. Pettinari, C. Santini, B.W. Skelton, A.H. White, Polyhedron 24 (2005) 181;
(f) Effendy, J.V. Hanna, F. Marchetti, D. Martini, C. Pettinari, R. Pettinari, B.W. Skelton, A.H. White, Inorg. Chim. Acta 357 (2004) 1523;
(g) W.B. Zhou, Z.C. Dong, J.L. Song, H.Y. Zeng, R. Cao, J. Cluster Sci. 13 (2002) 119.

[9] C.J. Blake, V.C. Cook, M.A. Keniry, H.J. Kitto, D.A. Rae, G.F. Swiegers, A.C. Willis, J. Zank, B.S. Wild, Inorg. Chem. 42 (2003) 8709.

[10] (a) J. Ellermann, K.J. Meier, Z. Anorg. Allg. Chem. 603 (1991) 77;
(b) J. Ellermann, J. Utz, F.A. Knoch, M. Moll, Z. Anorg. Allg. Chem. 622 (1996) 1871.

[11] (a) D.E.T. James, W. Ely, A. Schier, H. Schmidbaur, J. Chem. Soc., Dalton Trans. 24 (2001) 3647;
(b) R.P. Feazell, C.E. Carson, K.K. Klausemeyer, Acta Cryst. C 60 (2004) m598.

[12] (a) M.L. Mckee, W.E. Hill, J. Phys. Chem. A. 106 (2002) 6201;
(b) E.J. Sekabunga, M.L. Smith, T.R. Webb, W.E. Hill, Inorg. Chem. 41 (2002) 1205.

[13] (a) C.S. Browning, D.H. Farrar, D.C. Frankel, Z. Kristallogr, New Cryst. Struct. 212 (1997) 201;
(b) V.W. Wah Yam, W.K. Mai Fung, K. Kai Cheung, Organometallics 16 (1997) 2032.

[14] H. Liu, M.J. Calhorda, M.G.B. Drew, V. Felix, J. Novosad, L.F. Veiros, F.F. de Biani, P. Zanello, J. Chem. Soc., Dalton Trans. (2002) 4365.

[15] (a) Q.-H. Wei, G.-Q. Yin, L.-Y. Zhang, L.-X. Shi, Z.-W. Mao, Z.-N. Chen, Inorg. Chem. 43 (2004) 3484;
(b) Q.-H. Wei, G.-Q. Yin, Z. Ma, L.-X. Shi, Z.-N. Chen, Chem. Commun. 17 (2003) 2188.

[16] (a) R.J. Cross, T.H. Green, R. Keat, J. Chem Soc. Dalton Trans. (1976) 1424;
(b) H. Noeth, L. Meinel, Z. Anorg. Allg. Chem. 349 (1967) 225.

[17] (a) Bruker SMART, V. 6.028, Bruker AXS Inc., Madison, WI, USA, 1998.;
(b) Bruker SAINT, V. 6.02, Bruker AXS Inc., Madison. WI, USA, 1998.;
(c) G.M. Sheldrick, SADABS, University of Göttingen, Göttingen, Germany, 1997.

[18] (a) A. Altomare, G. Cascarano, C. Giacovazzo, A. Gualardi, J. Appl. Crystallogr. 26 (1993) 343;
(b) G.M. Sheldrick, SHELXS-97, Program for Crystal Structure Solution, University of Göttingen, Göttingen, Germany, 1997;
(c) G.M. Sheldrick, SHELXL-97, Program for Refinement of Structure, University of Göttingen, Göttingen, Germany, 1997;
(d) G.M. Sheldrick, SHELXTL, version 5.10, Bruker Analytical X-ray Instruments, Inc., Madison, WI, 1997.

[19] (a) M. Bardaji, O. Crespo, A. Laguna, A.K. Fischer, Inorg. Chim. Acta 304 (2000) 7;
(b) E.L. Muetterties, C.W. Alegranti, J. Am. Chem. Soc. 94 (1972) 6386.
[20] (a) M. Gonsior, S. Antonijevic, I. Krossing, Chem. Eur. J. 12 (2006) 1997;
(b) A. Bihlmeier, M. Gonsior, I. Raabe, N. Trapp, I. Krossing, Chem. Eur. J. 10 (2004) 5041.
[21] D. Affandi, S.J. Berners Price, Effendy, P.J. Harvey, P.C. Healy, B.E. Ruch, A.H. White, J. Chem. Soc., Dalton Trans. (1997) 1411.
[22] (a) R.P.K. Babu, S.S. Krishnamurthy, M. Nethaji, Heteroatom Chem. 2 (1991) 477;
(b) R.P.K. Babu, S.S. Krishnamurthy, M. Nethaji, Tetrahedron: Asymmetry 6 (1995) 427.
[23] (a) R. Keat, L. Manojlovic-Muir, K.W. Muir, D.S. Rycroft, J. Chem. Soc., Dalton Trans. (1981) 2192;
(b) F. Robert, Y. Gimbert, M.-T. Averbuch-Pouchot, A. Greene, Z. Kristallogr, New Cryst. Struct. 215 (2000) 233.
[24] (a) A.E. Reed, P.v.R. Schleyer, J. Am. Chem. Soc. 112 (1990) 1434;
(b) S.S. Krishnamurthy, Phosphorus Sulfur and Silicon 87 (1994) 101;
(c) S.S. Krishnamurthy, Phosphorus Sulfur and Silicon 97 (1994) 271.
[25] (a) D.M. Ho, R. Bau, Inorg. Chem. 22 (1983) 4073;
(b) R.A. Stein, C. Knobler, Inorg. Chem. 16 (1977) 242.

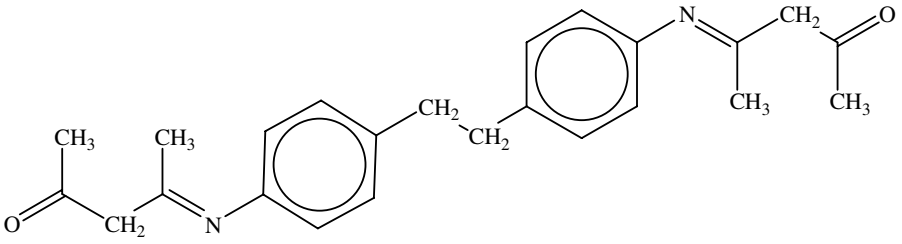

Fig. 1. Chemical structure of the ligand.

The keto-amine and enol-imine equilibrium of the Schiff base, 2-deoxy-2-(2-hydroxybenzaldimino)-D-glucopyranose was described in methanolic and dimethyl sulfoxide solutions. It reacts with nickel acetate to give a bidentate mononuclear Ni(II) complex [6].

Recently, Cerchiaro et al. reported some copper(II) complexes with isatin or imine ligands derived from isatin. In some derivatives, the metal ion is bound though the keto oxygen atom [7].

In our continuous work about symmetric Schiff bases built around 4,4′-diaminodiphenyl [8,9] we present here the crystal structure of a new symmetrical compound: 1,2-di[4-(2-imino 4-oxo pentane)phenyl]ethane (see Fig. 1) obtained by reacting 4,4′-diaminodiphenyl with acetylacetone. In addition, we discuss the structure and the electrochemical behaviour of its complexes with cobalt(II), nickel(II), copper(II) and cadmium(II).

2. Experimental

2.1. Reactants

All reactants and solvents were analytical grade. 4,4′-Diaminodiphenyl ethane and acetylacetone were purchased from Sigma–Aldrich, France. All the metals were used as hydrated chlorides and were used as received.

2.2. Preparation of the ligand

The ligand is obtained by reacting 4,4′-diaminodiphenyl ethane and acetylacetone in MeOH with a 1:2 ratio as previously described [10,11]. To a solution of diaminodiphenyl ethane (1 mmol, 0.21 g, 40 mL) was added a solution of acetylacetone (2 mmol, 0.2 g, 7 mL). The mixture was refluxed for 3 h and cooled. The yellow product was filtered, washed twice with EtOH (10 mL) and finally recrystallised from a mixture EtOH/$CHCl_3$ (30/70 v/v) and dried under vacuum. The single crystals for X-ray diffraction were obtained by slow evaporation from toluene.

2.3. Syntheses of the complexes

All the complexes were prepared by mixing in EtOH equimolar amounts of ligand (0.2 g, 4 mL) and hydrated chlorides (10 mL). After standing under reflux conditions for 8 h, the mixture was kept overnight at room temperature. After the addition of toluene (30 mL), the complex precipitated. It was removed by filtration, washed several times with hot EtOH, dried under vacuum.

Besides this operating mode we have obtained these complexes by template synthesis without isolating the ligand [12]. In a first step, we have mixed 4,4′-diaminodiphenyl ethane and acetylacetone as indicated above (see Section 2.2), after an 8-h reflux, the hydrated metal chloride (EtOH, 10 mL) in stoichiometric amount, was added. Finally, the complex species was obtained and purified, in the same way than previously described.

2.4. Measurements

All elemental analysis were carried out at the Service d'Analyse du C.N.R.S. de l'I.C.S.N., Gif sur Yvette (France). The melting points were determined with a Kofler bank and are uncorrected. The i.r. spectra were recorded with a Perkin–Elmer 1000 series FTIR spectrophotometer, using KBr disks. The UV–Vis spectra were obtained with a UNICAM UV300 spectrophotometer in DMF solutions. The ^1H NMR spectra were recorded on a Jeol GSX WB spectrometer at 270 MHz in $CDCl_3$ or DMSO-D_6, the chemical shifts are given in ppm, using TMS as internal reference. Electrochemical measurements were recorded on a Radiometer VOLTALAB 32 (DEA 332 type): the working electrode was a Pt rotating disk (2 mm diameter) and the auxiliary electrode a Pt wire. A saturated calomel electrode was used as the reference electrode and measurements were carried out at 25 ± 0.2 °C. DMF was used as solvent and the ionic strength was maintained at 0.1 mol L^{-1}, with Bu_4NPF_6 as supporting electrolyte. The concentration of all species was 2.5×10^{-3} mol L^{-1}.

2.5. Crystal data collection and processing

Crystals of H_2L are monoclinic with space group $P2_1/c$. The crystal and instrumental parameters used in the unit-cell determination and data collection are summarised in Table 1. X-ray single-crystal diffraction data were collected at 293 K on a STOE-IPDS diffractometer, equipped with a graphite monochromator utilising Mo Kα radiation ($\lambda = 0.71073$ Å) (CIMMA, UMR CNRS 6200, Angers). The structure was solved by direct methods using SIR92 [13] and the refinement was performed on F^2 by full matrix

Table 1
Crystallographic data for the ligand

Formula	$C_{12}H_{14}NO$
Formula weight	188.24
Crystal system	monoclinic
Space group	$P2_1/c$
a (Å)	10.632(2)
b (Å)	6.2615(6)
c (Å)	16.370(2)
α (°)	90
β (°)	98.09(2)
γ (°)	90
V (Å^3)	1078.9(3)
Z	4
Color	yellow
D_{calc} (g cm^{-3})	1.159
$F(000)$	404
μ (mm^{-1})	0.074
hkl limits	$-12 \leqslant h \leqslant 13$, $-7 \leqslant k \leqslant 7$, $-20 \leqslant l \leqslant 19$
θ_{min}, θ_{max} (°)	2, 26
Number of data with $I > 2\sigma(I)$	$1295F_o$
Weighting scheme	$w = 1/[\sigma^2(F_o^2) + (0.1714P)^2]$ with $P = (F_o^2 + 2F_c^2)/3$
Number of variables	127
R_1	0.0759
wR_2	0.2288

least-squares techniques using SHELX-97 package [14]. All non-H atoms were refined anisotropically and the H atoms were included in the calculation without refinement. Absorption was corrected by Gaussian technique.

3. Results and discussion

3.1. Crystal structure of the ligand

The main crystal parameters are reported in Table 1. The bond distances and their angles are given in Table 2.

Table 2
Bond lengths (Å) and angles (°)

Bond lengths (Å)		Bond angles (°)	
C01—C′01	1.500(6)	C′01—C01—C02	114.3(3)
C01—C02	1.516(3)	C07—C02—C03	117.0(2)
C02—C07	1.374(4)	C07—C02—C01	120.9(3)
C02—C03	1.403(4)	C03—C02—C01	122.2(3)
C03—C04	1.386(3)	C04—C03—C02	121.6(2)
C04—C05	1.379(4)	C05—C04—C03	120.4(2)
C05—C06	1.385(4)	C04—C05—C06	118.8(2)
C05—N01	1.436(3)	C04—C05—N01	118.5(2)
C06—C07	1.394(4)	C06—C05—N01	122.6(2)
C08—N01	1.346(3)	C05—C06—C07	120.3(2)
C08—C10	1.375(3)	C02—C07—C06	121.9(2)
C08—C09	1.500(4)	N01—C08—C10	120.9(2)
C10—C11	1.421(4)	N01—C08—C09	118.2(2)
C11—O01	1.244(3)	C10—C08—C09	120.8(2)
C11—C12	1.507(3)	C08—C10—C11	124.4(2)
		O01—C11—C10	122.0(2)
		O01—C11—C12	119.3(2)
		C10—C11—C12	118.6(2)
		C08—N01—C05	127.9(2)

The molecule presents a symmetrical structure with two identical independent half-molecules. The structure, with the atoms numbering scheme, is given in Fig. 2. The angles and the distances around C11 are typical of a keto functional group. The bond distances between C05 and N01 correspond to a double bond length as already observed in similar compounds [15]. The C08—C10 (1.375 Å) and C08—N01 (1.346 Å) bond distances are close to that published by Nathan and Traina (1.368 Å and 1.365 Å, respectively) [15] but in our ligand, we note a shorter bond distance for C10—C11 (1.421 instead of 1.502 Å). These results are in good agreement with keto-imine or keto-amine tautomers.

All angles are close to 120°, showing sp^2 hybridisation of all atoms without taking into account the methyl groups. The azomethine moiety presents an E configuration around the carbon–nitrogen double bond.

In a molecule, the two aromatic rings are in parallel planes and the two carbonyl oxygen atoms lie on the two sides of these planes. The packing along b-axis (Fig. 3) shows that the molecules lie in parallel planes. In a cell, there are four half-molecules giving two independent complete symmetrical ligands. The half-molecules lie in two planes with a 77° angle between them as presented in Fig. 4.

3.2. Complexes formulae

The analytical data are reported in Table 3. The purity of each species was verified using t.l.c. The complexes are formulated as $[CoL]\cdot(H_2O)_3$, $[(NiCl_2)_2(H_2L)]$, $[CuCl_2(H_2L)]$ and $[CdCl_2(H_2L)]$, respectively. The cobalt complex is the only complex obtained through the ionised hydroxyl enol-imino tautomer. The compounds **4** and **5** are slightly unstable as indicated by higher errors in elemental analysis. So, all spectroscopic and electrochemical determinations were performed using freshly prepared compounds.

3.3. Spectroscopic results

The main spectroscopic data are given in Table 4. We have to take into account the tautomeric equilibria giving three tautomers [15,16]:

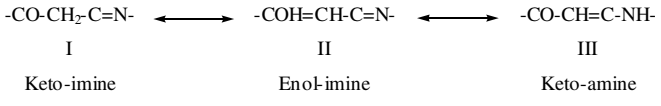

As indicated by crystallographic data, a keto tautomer was observed in the solid state in the case of the ligand. The hydroxyl stretching vibration band appearing in the infrared spectra of the complex with cobalt is due to coordination water molecules [17]. In the case of the nickel(II) complex, the band centred at 3380 cm^{-1} is due to ν(N—H) from keto-amine tautomer [18]. The aromatic cycle vibrations at ca. 1270, 1030 and 825 cm^{-1} [19] and

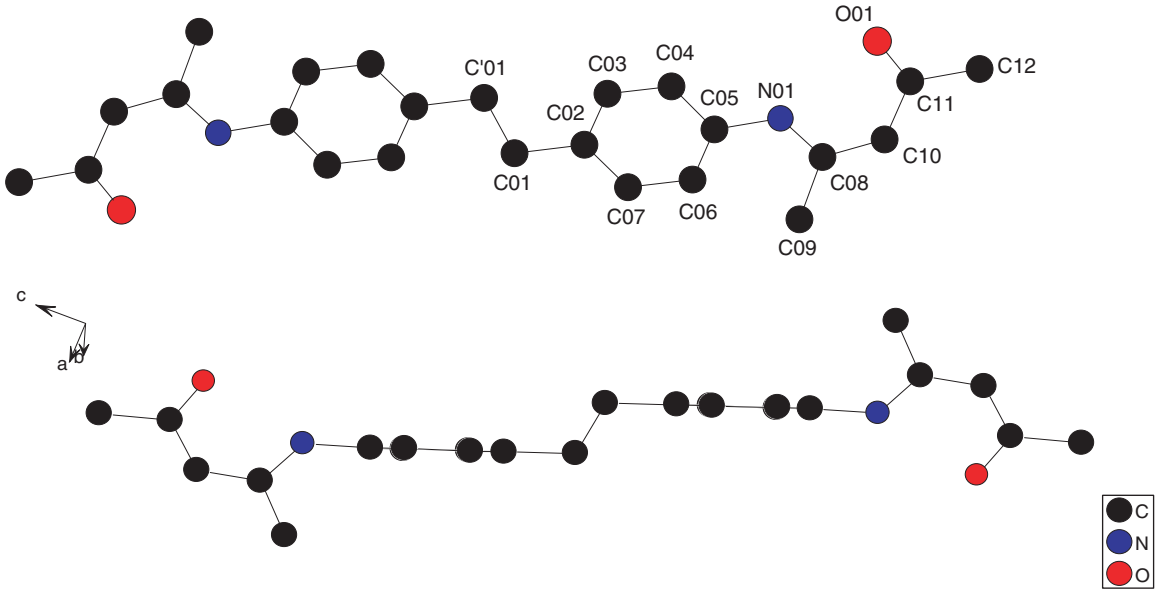

Fig. 2. Perspective view of the ligand with atom numbering (in the second identical part of the molecule, the atoms are noted C′, N′ and O′, respectively).

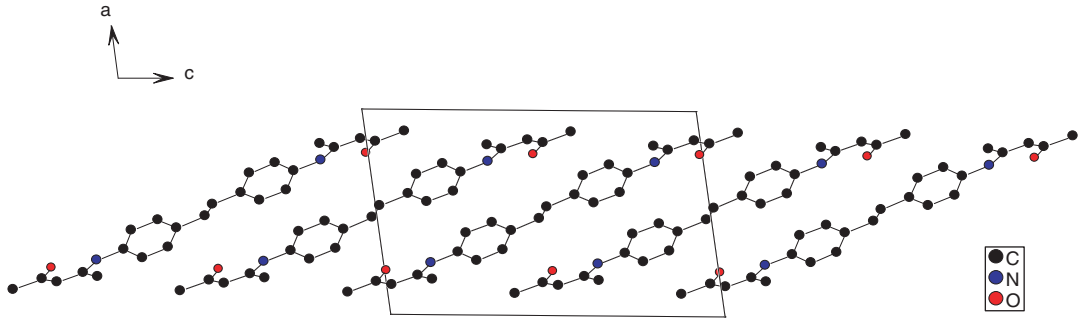

Fig. 3. Packing of the molecules along *b*-axis.

the CH_3 and CH_2 vibration band around 2925 cm^{-1} are not modified by coordination. The stretching vibration band ν(C=N) appearing at 1625 cm^{-1} is in good agreement with the values published for similar compounds [18]. In the complexes, this band is slightly shifted down as already observed by Losada et al. [20].

The electronic spectra in DMF solutions (see Table 4) show one absorption band at 332 nm in the case of the ligand. The Co^{II} compound absorbs at 315 nm and with a weak molar absorption coefficient. In Ni(II) complex, two bands are located at 305 and 270 nm while two shoulders are observed at 350 nm ($\varepsilon = 49\,000$ L mol^{-1} cm^{-1}) and 330 nm ($\varepsilon = 65\,000$ L mol^{-1} cm^{-1}). In the case of the cupric complex, a weak shoulder at 330 nm appears together with the absorption band at 300 nm. In the UV region three new bands are located at 265 ($\varepsilon = 14\,200$ L mol^{-1} cm^{-1}), 250 ($\varepsilon = 10\,600$ L mol^{-1} cm^{-1}) and 230 nm ($\varepsilon = 9000$ L mol^{-1} cm^{-1}). As expected, the spectra of the cadmium complex and of the free ligand are similar. These results agree with previous published results ([20–22] and references cited therein).

3.4. ^1H NMR

The ^1H NMR data for the ligand (in $CDCl_3$) and the cadmium complex (in DMSO–D_6) is given in Table 5. Though the ligand crystallises in keto-imine tautomer I, the solution NMR spectra of both compounds show signals corresponding to keto-amine tautomer III: the singlet at 12.3 ppm corresponds to the N—H proton [16] (the hydroxyl proton of the enol-imino tautomer leads to a singlet in the 8–9 ppm range [23]). This signal could be also observed in the spectrum of the cadmium complex with the same chemical shifts as it has been observed in similar compounds [24,25]. The signal of the aromatic protons, of the ethylene moiety and of the methyl groups are not modified by coordination. The only change is observed in the methyl groups signals: in the ligand, the terminal methyl groups give a singlet at 2.0 ppm and the methyl attached to C08 and C′08 a second signal at 2.1 ppm while the four methyl groups appear as a singlet corresponding to 12 hydrogen atoms in the cadmium complex.

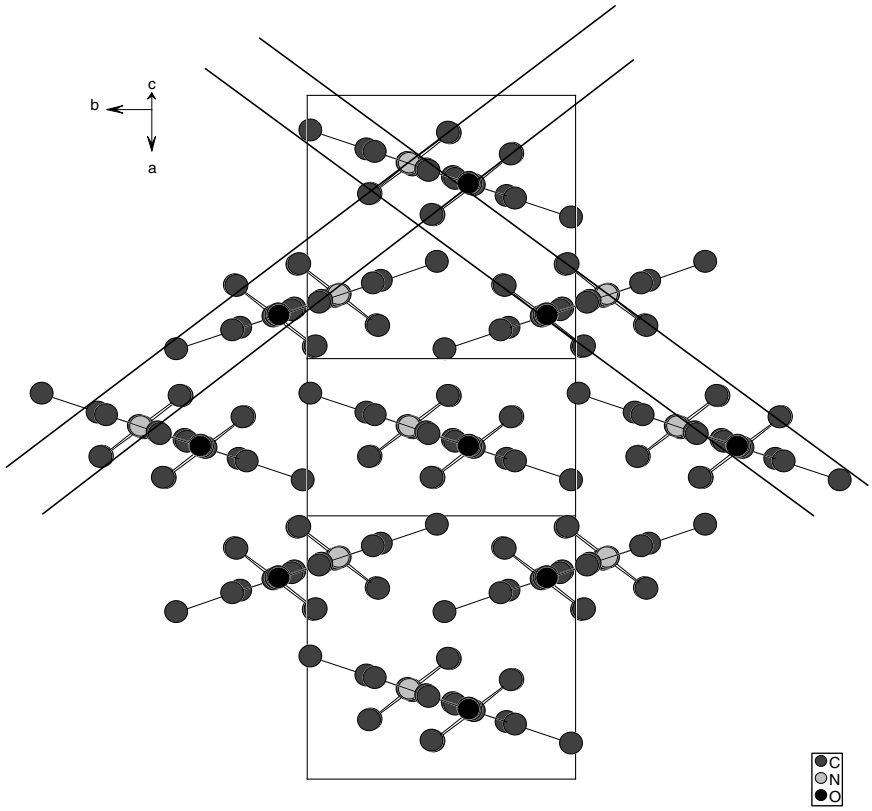

Fig. 4. Angles of 77° between the two types of aromatic planes.

Table 3
Analytical data

Compound	Color	Yield (%)	m.p. (°C)	Elemental analysis found (Calc.)		
				C (%)	H (%)	N (%)
Ligand H_2L (**1**)	yellow	65	152	76.0 (76.6)	7.4 (7.5)	7.4 (7.4)
$[CoL]\cdot(H_2O)_3$ (**2**)	green	42	183	58.1 (59.1)	6.6 (6.6)	6.1 (5.8)
$[(NiCl_2)_2(H_2L)]$ (**3**)	yellow	45	>260	45.5 (45.3)	5.5 (4.4)	5.5 (4.4)
$[CuCl_2(H_2L)]$ (**4**)	brown	51	>260	53.2 (56.4)	5.0 (5.5)	6.8 (5.5)
$[CdCl_2(H_2L)]$ (**5**)	tan	65	>260	50.8 (54.9)	6.0 (5.4)	5.8 (5.3)

3.5. Cyclic voltammetry

The main electrochemical data are given in Table 6 and some representative voltammograms are presented in Fig. 5.

For the ligand, a cyclic sweep in the −1.80 to +0.00 V range shows a cathodic peak at −1.05 V and an anodic peak at −1.15 V. The peak at −1.05 V is due to the reduction of the imino moiety of the molecule as suggested by Gilli et al. [26] and Andrieu and Savéant [27]:

$$R{-}CH{=}N{-}R' \overset{e^-}{\rightleftharpoons} [R{-}CH{=}N{-}R']^{-\cdot} \overset{H^+}{\rightarrow} [R{-}CH_2{-}N{-}R']^{\cdot}$$
$$\rightarrow \tfrac{1}{2}R{-}CH_2{-}N(R'){-}N(R'){-}CH_2{-}R$$

When the sweep is performed between 0.00 and +1.80 V, two anodic peaks are obtained at +0.91 and +1.37 V, respectively. The reoxidation of the last product in the above mechanism occurs at +1.37 V. In the range −1.80 to +1.80 V, a cathodic peak is located at −1.05 V together with a new anodic peak at −0.05 V. When performing a second sweep in the same range, a new cathodic peak is observed at −0.42 V and the peak at −1.05 V is shifted to higher potential values (−0.97 V).

In the case of the cobalt(II) complex, and in the −2.00 to +1.80 V, a cathodic peak appears at −0.98 V while three anodic peaks are observed at −0.17, +0.80 and +1.32 V, respectively. When the sweep is limited to the −1.00 to 0.00 V range, the peak at −0.17 V is lacking. This peak should be attributed to the reoxidation of the ligand previously reduced [26]. In addition, when performing a second sweep (−1.00 to 0.00 V), a new peak is observed at −0.36 V due to the reoxidation of cobalt reduced at −0.98 V [28]. The intensity of the anodic peak at +1.32 V is a linear function of the square root of sweep speed showing a slow electron transfer.

Table 4
Spectroscopic data

Compound	Infrared					UV–Vis	
	ν(O—H)	ν(N—H)	ν(C=O)	ν(C=N)	Aromatic ring	λ (nm)	[ε (L mol^{-1} cm^{-1})]
1			1625	1565	1275	330	[152000]
					1015	255	[55000]
					850	235	[95000]
2	3420		1615	1567	1280	315	[11000]
					1030		
					850		
3		3380	1615	1560	1245	350	[49000]
					1030	330	[65000]
					825	305	[120000]
						270	[160000]
4			1580	1522	1275	300	[13600]
					1015	265	[14200]
					820	255	[10600]
						230	[9000]
5		3460	1615	1550	1280	330	[200000]
					1020		
					820		

Table 5
^{1}H NMR data, chemical shifts in ppm (TMS); ligand in $CDCl_3$, complex in DMSO-D_6

	Ligand (**1**)	Cd(II) complex (**5**)
H (C10)	5.2	5.2
CH_3 (C12)	2.1	2.0
CH_3 (C9)	2.0	2.0
CH_2—CH_2 (C01—C′01)	2.8	2.9
Aromatic	7.1	7.1
NH (keto amine)	12.3	12.4

The cyclic voltammogram of nickel(II) species shows one cathodic peak located at −1.31 V when sweeping from −1.80 to +1.80 V. During the reverse sweep, we observe three anodic peaks at +0.04 V, +0.83 V and +1.35 V. When performing successive sweeps in the same range, the peak at −1.35 V and its corresponding reoxidation peak disappear (Fig. 5c) while a new one appears at −1.10 V. The peak at +0.83 V has been reported by Pereira et al. [29] for nickel(II) complexes of asymmetric tetradentate Schiff bases.

A sweep from −1.80 to +1.80 V for copper(II) complex shows three cathodic peaks (−1.60 V, −0.78 V, +0.15 V) and the back sweep (+1.80 to −1.80 V) shows five anodic peaks at −0.16, +0.10, +0.63, +0.88 and +1.38 V, respectively. The peak at −0.88 V has already been observed by Losada et al. [20] in similar compounds. A second sweep shows that the peak at −1.60 V disappears, the peak at +1.38 V is slightly shifted to +1.36 V while its intensity diminishes. In the −2.00 to +0.30 V range, a peak is observed at +0.10 V. If the studied range is limited from −0.10 to +0.80 V, we observed the oxidation of Cu^{II} into Cu^{III} at +0.55 V while the reduction peak is located at +0.37 V [30]. The variation of the scan rate from 200 to 10 mV s^{-1} shows that the curve E_{pc} as a function of log v, for this reduction peak, is a straight line (Fig. 5g) and it does not depend upon the sweep speed.

Table 6
Voltamperometric results at 25 °C in DMF, ionic strength 0.1 mol L^{-1} (Bu_4NPF_6), results in V vs. SCE, sweep speed: 100 mV s^{-1}, E_a: anodic; E_c: cathodic

Compound	E range (V)	E_{pa1}	E_{pa2}	E_{pa3}	E_{pa4}	E_{pa5}	E_{pc1}	E_{pc2}	E_{pc3}
1	−1.8/0	−1.15					−1.05		
	0/1.8				+0.91	+1.37			
	−1.8/+1.8	−0.05					−1.05		
2	−2.0/+1.8	−0.17			+0.80	+1.32	−0.98		
	−1.0/0				+0.80	+1.32	−0.98		
3	−1.8/+1.8	+0.43			+0.83	+1.35		−1.31	
4	−1.8/+1.8	−0.17	+0.10	+0.63	+0.88	+1.38	+0.15	−0.78	−1.6
	−2.0/+0.3		+0.10						
	−0.1/+0.8			+0.54					
5	−1.8/+1.8					+1.45	−0.92	−1.18	

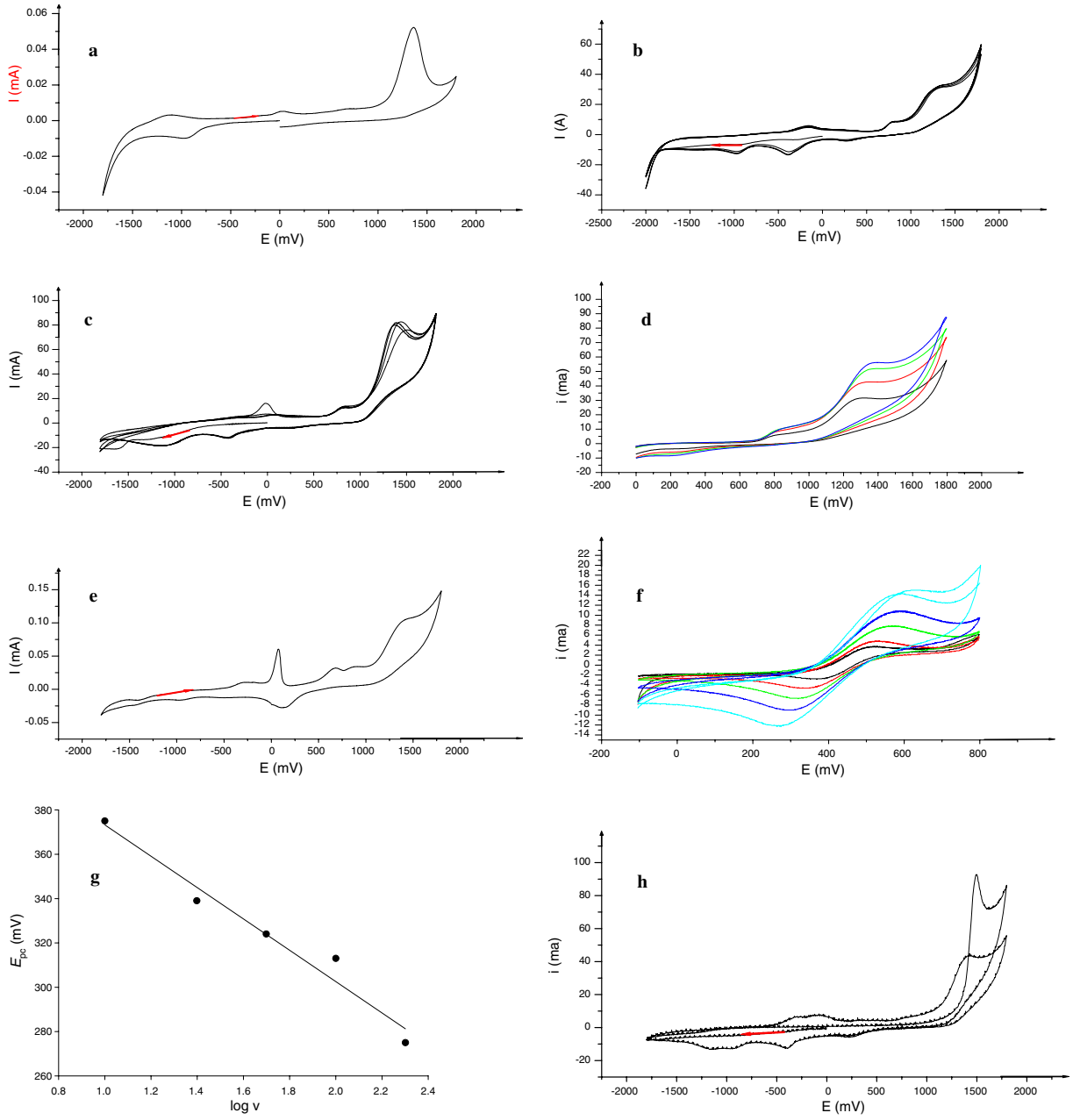

Fig. 5. Representative cyclic voltammograms in DMF (25 °C, ionic strength: 0.1 mol L^{-1}, Bu_4NPF_6, i in μA, $v = 100$ mV s^{-1}): (a) ligand; (b) Co(II) complex, successive sweeps; (c) Ni(II) complex, successive sweeps; (d) Co(II) with variable speed; (e) Cu(II) complex; (f) Cu(II) complex, variable speed; (g) Cu(II) complex $E_{pc} = f(\log v)$; (h) Cd(II) complex.

Finally, for the cadmium(II) compound, when sweeping from −180 to +1.80 V, two cathodic waves at −1.18 and −0.92 V and one anodic peak at +1.45 V are obtained (Fig. 5h). We note that, in this case, the reoxidation of the imino moiety occur at higher potential values in the other compounds (+1.45 V instead of +1.37 V). A second sweep leads to three oxidation peaks at −0.78 and −0.33 V together with two reduction ones located at −0.95 and −1.15 V.

3.6. Proposed structures for the complexes

The proposed structures for the complexes are given in Fig. 6. As indicated along the discussion, some differences have been noted between solid state and solution because of the tautomeric equilibria. The cobalt complex is obtained with ionised enol-imine tautomer. In this compound, two water molecules are bounded to Co(II). In addition this cation is linked to N (imino) and O^- (ionised

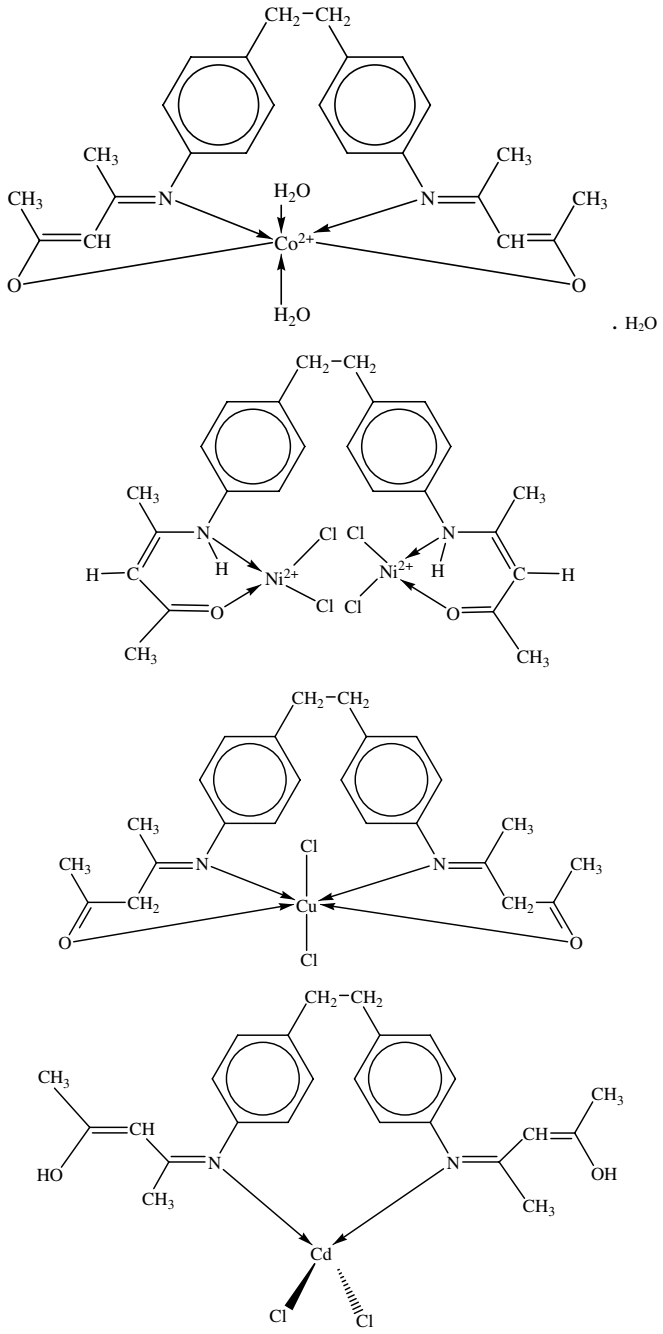

Fig. 6. Proposed structures for the complexes.

enol). So this metal ion shows an octahedral geometry. Finally, a third water molecule is in the outer coordination sphere.

The nickel(II) compound is a binuclear complex in which each nickel(II) ion presents a square planar arrangement and the Schiff base acts as a symmetrical tetradentate ligand through the keto-amine tautomer.

The copper(II) is the only compound obtained with the non-ionised keto-imine tautomer. The copper(II) ion shows a distorted octahedral geometry with O atoms (keto), N atoms (imine) in a plane and two chloride ions located on the orthogonal axis.

In the cadmium complex, the geometry around the metal cation is tetrahedral. It is linked to the keto-amine tautomer of the ligand through N (amine) atom.

4. Supplementary data

Crystallographic data have been deposited with the CCDC, 12 Union Road, Cambridge, CB2 1EZ, UK (fax: +44 1223 336033; e-mail: deposit@ccdc.cam.ac.uk or at http://www.ccdc.cam.ac.uk), and are available on request quoting the deposition number CCDC 287415.

References

[1] P. Pfeiffer, E. Breith, E. Lubbe, T. Tsumaki, Ann. (1933) 84.
[2] A. Anthonysamy, S. Balasubramanian, Inorg. Chem. Commun. 8 (2005) 908.
[3] N. Tidjani-Rahmouni, S. Djebbar-Sid, N. Chenah, O. Benali-Baïtich, Synth. React. Inorg. Met-Org. Chem. 29 (1999) 979.
[4] R. Karmakar, C.R. Choudhury, A.S. Batsanov, S.R. Batten, S. Mitra, Struct. Chem. 16 (2005) 535.
[5] A. Mukherjee, M. Nethaji, A.R. Chakravarty, Polyhedron 23 (2004) 3081.
[6] J. Costamagna, L.E. Lillo, B. Matsuhiro, M.D. Noseda, M. Villagrán, Carbohyd. Res. 338 (2003) 1535.
[7] G. Cerchiaro, K. Aquilano, G. Filomeni, G. Rotilio, M.R. Ciriolo, A.M. Da Costa Ferreira, J. Inorg. Biochem. 99 (2005) 1433.
[8] D. Haffar, T. Douadi, S. Chafaa, M.A. Khan, G. Bouet, Trans. Met. Chem. 29 (2004) 245.
[9] S. Issaadi, D. Haffar, T. Douadi, S. Chafaa, D. Séraphin, G. Bouet, M.A. Khan, Synth. React. Inorg. Nano-Met. Chem. 35 (2005) 875.
[10] M. Gullotti, A. Pasini, P. Fantucci, U. Renato, R.D. Gillard, Gazz. Chim. Ital. (1972) 855.
[11] Y. Sharma, H.N. Pandey, P. Mathur, Polyhedron 13 (1994) 3111.
[12] D.M. Boghaei, M. Lashanizadegan, Synt. React. Inorg. Met-Org. Chem. 30 (2000) 1393.
[13] Altomare et al., SIR92 – A Program for Crystal Structure Solution, 1993.
[14] G.M. Sheldrick, SHELX-97 – Programs for Crystal Structure Analysis (Release 97-2), University of Gottingen, Germany, 1998.
[15] L.C. Nathan, C.A. Traina, Polyhedron 22 (2003) 3213.
[16] G.O. Dudek, R.H. Holm, J. Am. Chem. Soc. 83 (1961) 2099.
[17] S.M. Ben-Saber, A.A. Maihub, S.S. Hudere, M.M. El-Ajaily, Microchem. J. 81 (2005) 191.
[18] K. Ueno, A.E. Martell, J. Phys. Chem. 59 (1955) 998.
[19] K. Nakanishi, Infrared Absorption Spectroscopy – Practical, Holden-Day, San Francisco, 1962, p. 26.
[20] J. Losada, I. del Peso, L. Beyer, Inorg. Chim. Acta 321 (2001) 107.
[21] V.T. Kasumov, Spectrochim. Acta A 57 (2001) 451.
[22] M.A. Khan, J. Meullemeestre, M.J. Schwing, F. Vierling, Inorg. Chem. 28 (1989) 3306.
[23] M. Lal, A. Langels, H.J. Deiseroth, J. Schlirf, M. Schmittel, J. Phys. Org. Chem. 16 (2003) 373.
[24] S. Claramunt, C. Lopez, S. Lott, M.D. Santa Maria, I. Alkorta, J. Elguero, Helv. Chim. Acta 88 (2005) 1931.
[25] V.I. Slesarev, A.S. Popov, Russ. J. Gen. Chem. 72 (2002) 949.
[26] P. Gili, M.G. Martin Reyes, P. Martin Zarza, I.L.F. Machado, M.F.C. Guedes da Silva, M.A.N.D.A. Lemos, A.J.L. Pombiero, Inorg. Chim. Acta 244 (1996) 25.
[27] C.P. Andrieu, J.M. Savéant, J. Electroanal. Chem. 33 (1971) 453.
[28] S.H. Rahaman, H. Chowdhury, D. Bose, R. Ghosh, C.H. Hung, B.K. Ghosh, Polyhedron 24 (2005) 1755.
[29] E. Pereira, L. Gomes, B. de Castro, Inorg. Chim. Acta 271 (1998) 83.
[30] N. Raman, A. Kulandaisamy, A. Shunmugasundaram, K. Jeyabramanian, Trans. Met. Chem. 26 (2001) 131.

$CH_2CCl(C_5H_5FeC_5H_3)C(CH_3)_2Fc'CClCH_2$, prepared by the reaction of $POCl_3$ and $CH_3CO(C_5H_5FeC_5H_3)C(CH_3)_2Fc'COCH_3$ in DMF. The other reactions carried out in this work are summarized in Scheme 1. Because of the reactivity between the C≡C triple bonds of **1** and the Co–Co bond, complexes **4** and **5** can be prepared from ligand **1** and $Co_2(CO)_8$. Only stable complex **5** was obtained even if the mole ratio of $Co_2(CO)_8$ to ligand **1** was fixed at 1:1. Complex **4** slowly decomposed during the process of purification because of its thermal instability, and its IR spectrum (2090s, 2049vs, 2020vs) supports that there is a coordinated $Co_2(CO)_6$ species with an alternate C≡C triple bond of **1**. Complex **5** is a dark-green and air-stable crystalline compound which is soluble in both non-polar solvents such as hexane, petroleum ether, benzene and polar solvents such as acetonitrile and chloroform. The molecular structure of complex **5** was determined by X-ray crystallography and is shown in Fig. 1.

Complex **3** is regarded as the starting compound for synthesizing complex **6** by the nuclear expansion reaction between the C_2Co_2 core of complex **3** and $Fe_2(CO)_9$. If the reactivity could be extended, complex **6** may also be regarded as the starting compound for further synthesis of other polynuclear mix-metal clusters by a metal exchange reaction [6]. The IR spectrum of **6** indicates the characteristic absorption bands of terminal carbonyl ligands coordinated to Co and Fe in the region 2097–1961 cm^{-1}. ^1H and ^{13}C NMR spectra reflect that there are Fc, CH=C, $C(CH_3)_2$ and CO groups in complex **6**. The component of complex **6** is further proved by its element analysis data and MS. Complex **6** is a dark-red crys-

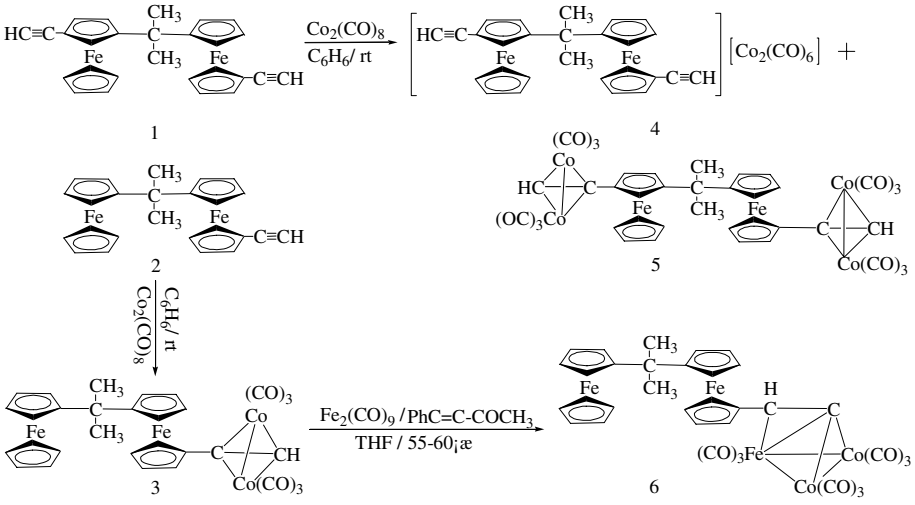

Scheme 1.

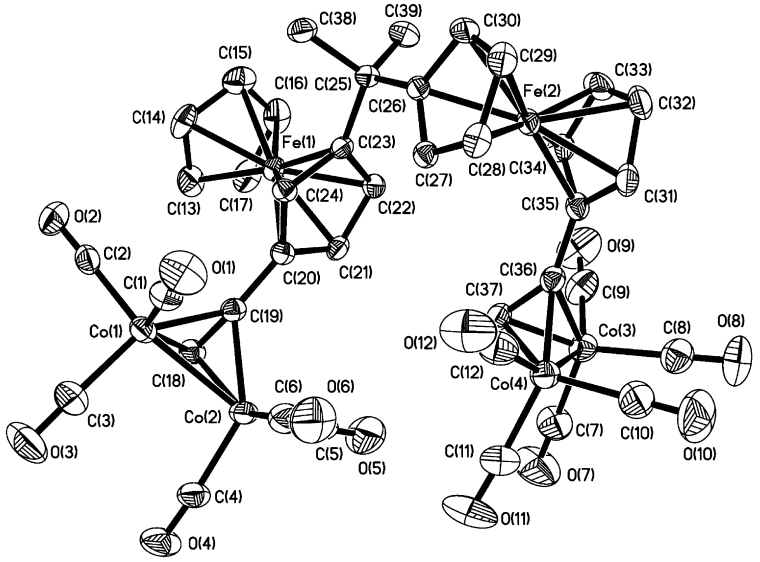

Fig. 1. Molecular structure of complex **5**.

talline solid and is soluble in common polar solvents and slightly soluble in non-polar solvents.

2.2. Electrochemical properties of compounds *1*, *2*, *3*, *5* and *6*

The electrochemical properties of compounds **1**, **2**, **3**, **5** and **6** have been studied by cyclic voltammetry at 298 K in a standard three-electrode system with NEt_4ClO_4 in CH_3CN solution as the supporting electrolyte. The results are given in Table 1.

For compounds **1**, **2**, **3** and **6** the usual electrochemically quasi-reversible ferrocene (0, 0/0, 1+; 0, 1+/1+, 1+) peak couples were observed (Table 1), but these did not appear for complex **5**. The two ferrocenyl units in **2**, **3** and **6** are non-equivalent and show two resolved one-electron redox processes at $E_1^0 = 0.52,\ 0.45,\ 0.50$ V and $E_2^0 = 0.85,\ 0.75,\ 0.77$ V, respectively. ΔE^0 data of **2**, **3** and **6** indicate that there is significant electronic communication between the two ferrocenyl units, though the alkyl $C(CH_3)_2$ spacer is interpolated and the electronic communication decreases with weakening of the conjugation between the ferrocenyl unit and the alkyne group, which is induced by the coordination of the terminal acetylene with the Co_2 or $FeCo_2$ core. Noteworthy is the decrease in separation between the two ferrocenyl redox centres from 0.34 V, 0.30 V to 0.27 V within the series $FcC(CH_3)_2Fc'C{\equiv}CH$ (**2**), $[FcC(CH_3)_2Fc'C{\equiv}CH]Co_2(CO)_6$ (**3**) to $[FcC(CH_3)_2Fc'CH{=}C]FeCo_2(CO)_9$ (**6**), which demonstrates that the σ–π coordination of the $FeCo_2(CO)_9$ or $Co_2(CO)_6$ moieties decreases the communication between the two ferrocenyl redox centres because of the strengthening of interaction between the cluster core and the alkyne group [11]. In **1** two resolved one-electron redox processes are observed at $E_1^0 = 0.64$ V and $E_2^0 = 0.85$ V. The separation of the "two-electron" oxidation process for **1** into individual E_1^0 (0, 0/0, 1+) and E_2^0 (0, 1+/1+, 1+) couples is easily seen at ambient temperature. The change of the electrochemical data in **5** shows that the $Co_2(CO)_6$ moieties participate in the reducing process, which affects the two ferrocenyl redox centres. The irreversible reduction peak at $E_{pc} = -1.00$ V in **6** is regarded as the result of the arising reduction process on the $FeCo_2(CO)_9$ moieties [16]. The redox processes of compounds **1** and **6** are shown in Scheme 2.

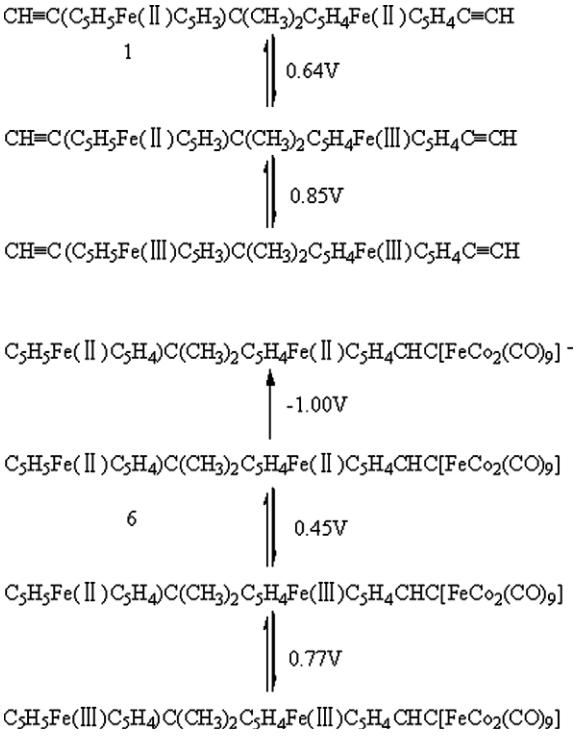

Scheme 2.

2.3. Molecular structure of complex *5*

The molecular structure of complex **5** was determined by X-ray single crystal analysis. The selected bond lengths and angles are listed in Table 2.

The molecule of complex **5** contain two ferrocenyl units with approximately tetrahedral (μ-alkyne)dicobalt moieties bound to a cyclopentadiene ring (see Fig. 1). The CO ligands coordinated to the Co atoms are terminal and the average Co–Co bond distance (2.475 Å) is typical for the Co–Co bond lengths of classical alkyne dicobalt complexes. The alkyne bond adopts a typical μ_2–η^2 coordination fashion with the alkyne bond lying essentially perpendicular to the Co–Co bond in the C_2Co_2 units. The C–C bond lengths of the C_2Co_2 fragments are 1.320 Å and 1.341 Å, respectively, which reflect a bond dis-

Table 1
Voltammetric data[a]

Complex	First oxidation–reduction					Second oxidation–reduction					
	E_{pa}	$i_{pa} \times 10^6$	E_{pc}	$i_{pc} \times 10^6$	i_{pa}/i_{pc}	E_{pa}	$i_{pa} \times 10^6$	E_{pc}	$i_{pc} \times 10^6$	i_{pa}/i_{pc}	ΔE^0
1	0.76	2.88	0.51	3.35	0.86	0.96	2.21	0.74	3.29	0.67	0.21
2	0.66	2.90	0.37	4.91	0.59	0.97	3.63	0.72	3.62	1.00	0.34
3	0.60	1.17	0.29	2.63	0.44	0.90	0.99	0.59	1.17	0.85	0.30
5	0.22	0.74	−0.80	3.12	0.24	1.24	1.67	0.87	10.28	0.16	1.35
6	0.62	3.57	0.37	4.18	0.85	0.89	2.92	0.65	2.68	1.09	0.27
								−1.00	6.46		

E_{pc} is the cathodic peak potential (V); E_{pa} is the anodic peak potential (V); $E^0 = 1/2(E_{pc} + E_{pa})$ (V); $\Delta E^0 = E_2^0 - E_1^0$ (mV); i_{pc} is the cathodic peak current (A); i_{pa} is the anodic peak current (A).

[a] Platinum electrode (Ag/Ag^+ standard) with 0.001 M TEAP at 20 °C in 100 mV scan rate.

Table 2
Selected bond lengths (Å) and angles (°) for **5**

Co(1)–Co(2)	2.474(1)	Co(3)–Co(4)	2.476(1)
Co(1)–C(18)	1.965(5)	Co(3)–C(37)	1.942(5)
Co(1)–C(19)	1.964(4)	Co(3)–C(36)	1.996(4)
Co(1)–C(1)	1.964(4)	Co(4)–C(37)	1.957(5)
Co(2)–C(18)	1.930(5)	Co(4)–C(36)	1.963(5)
Co(2)–C(19)	2.000(4)	C(37)–C(36)	1.320(7)
C(18)–C(19)	1.341(6)	C(36)–C(35)	1.448(6)
C(19)–C(20)	1.437(6)	C(35)–C(31)	1.414(7)
C(20)–C(21)	1.435(6)	C(26)–C(25)	1.520(6)
C(23)–C(25)	1.520(6)	C(25)–C(39)	1.543(6)
Co(1)–Co(2)–C(18)	51.2(1)	Co(3)–Co(4)–C(37)	50.3(1)
Co(2)–Co(1)–C(18)	50.0(1)	Co(4)–Co(3)–C(37)	50.8(1)
Co(1)–Co(2)–C(19)	50.7(1)	Co(3)–Co(4)–C(36)	51.9(1)
Co(2)–Co(1)–C(19)	52.0(1)	Co(4)–Co(3)–C(36)	50.7(1)
C(1)–Co(1)–Co(2)	101.1(2)	C(7)–Co(3)–Co(4)	102.4(2)
C(18)–C(19)–C(20)	145.2(5)	C(37)–C(36)–C(35)	143.1(5)
C(19)–C(20)–C(21)	126.4(4)	C(36)–C(35)–C(31)	127.3(5)
C(22)–C(23)–C(25)	127.0(4)	C(27)–C(26)–C(25)	127.6(4)
C(23)–C(25)–C(26)	109.9(3)	C(26)–C(25)–C(39)	111.1(4)
C(23)–C(25)–C(38)	110.5(4)	C(26)–C(25)–C(38)	106.4(4)

tance of the coordinated C≡C bond in the scope of a C–C double bond. The Fe–C distances of the ferrocenyl moieties in complex **5** vary from 2.018 to 2.065 Å, comparable with those found in compounds with a ferrocenylalkynyl unit [9].

The bond distance figures of C(23)–C(25) (1.520 Å) and C(25)–C(26) (1.520 Å) indicate two ferrocenyl units in complex **5** are linked by two single bonds to the C atom in the $C(CH_3)_2$ group. The C atom of the $C(CH_3)_2$ group carries two ferrocenyl units orientated *trans* to each other and two C_2Co_2 units adopt a *cis*-bent configuration relative to the two cyclopentadiene rings. The molecular structure of complex **5** is asymmetric, which is similar to ligand **1**. One C_2Co_2 unit is linked to the unsubstituted cyclopentadiene ring of Fc′ by a short single bond (1.448 Å) between C(35) and C(36), and another C_2Co_2 unit is bonded to the substituted cyclopentadiene ring by a short single bond (1.437 Å) between C(19) and C(20), which suggests some degree of electron delocalization between the alkyne and the cyclopentadiene ring. The distortion of the quasi tetrahedral C_2Co_2 core is evidenced by the non-equivalence of the Co–C bond lengths and bond angles (see Table 2). The bond angle [C(18)–C(19)–C(20) 145.2° or C(35)–C(36)–C(37) 143.1°] is much smaller than 180° of sp-hybridized C(19) or C(36), which is attributed to the steric requirement between the (μ-alkyne)dicobalt and ferrocenyl moieties. The angle C(23)–C(25)–C(26), 109.9°, is nearly the angle of sp^3-hybridized C(25) and other angles around C(25) deviate from 109° as a result of steric influences.

The distances of the Fe atom to the plane of the cyclopentadiene rings [Fe(1) to the plane(1) C(13)C(14)C(15)C(16)C(17), 1.66 Å; Fe(1) to the plane(2) C(20)C(21)C(22)C(23)C(24), 1.64 Å; Fe(2) to the plane(3) C(26)C(27)C(28)C(29)C(30), 1.65 Å; Fe(2) to the plane(4) C(31)C(32)C(33)C(34)C(35), 1.65 Å] are nearly equal. The dihedral angle data between plane(1) and plane(2) (3.74°) and between plane(3) and plane(4) (4.86°) show that the two Cp planes in each ferrocenyl unit deviate from parallel because of the different substituted Cp rings. The dihedral angle between plane(2) and plane(3) is 74.07° as a result of the steric interaction between the $C_5H_5FeC_5H_3$ and $C(CH_3)_2Fc'$ groups.

3. Experimental

Published procedures or extensions thereof were used to synthesize initial intermediates $FcC(CH_3)_2Fc$, $CH_3CO(C_5H_5FeC_5H_3)C(CH_3)_2Fc'COCH_3$, ligand **2** $FcC(CH_3)_2Fc'$-C≡CH and complex **3** $[FcC(CH_3)_2Fc'C{\equiv}CH]Co_2(CO)_6$ [15,17,18]. Other chemicals were purchased and used as received.

Unless it is stated otherwise, all reactions and manipulations were carried out using standard Schlenk techniques under an atmosphere of pure nitrogen. Solvents were purified, dried and distilled under a nitrogen atmosphere prior to use. The reactions were monitored by TLC. Chromatographic separations and purification were performed on 200–300 mesh silica gel.

IR spectra were recorded on a Nicolet FT-IR spectrometer as KBr disks. Elemental analyses were carried out on an Elementar var III-type analyzer. $^1H(^{13}C)$ NMR spectra in $CDCl_3$ were recorded on an Inova 500FT-MHz spectrometer. Mass spectra were determined by using a Polaris Q MS and a Micromass Autospec ultima-TOF instrument. Electrochemical properties were determined by a BAS 100A-type analyzer. Melting points were determined using XT-4 melting point apparatus.

3.1. Synthesis of ligand $HC{\equiv}C(C_5H_5FeC_5H_3)C(CH_3)_2Fc'C{\equiv}CH$ (**1**)

$POCl_3$ (0.7 ml, 7.7 mmol) was dissolved in a 5 ml solution of *N*,*N*-dimethylformamide (DMF), which was dropped into a 6 ml DMF solution of $CH_3CO(C_5H_5FeC_5H_3)C(CH_3)_2Fc'COCH_3$ (0.2 g, 0.4 mmol) at 0 °C. The solution was stirred for 1.5 h at 0 °C and then 2 h at room temperature. The reaction mixture was transferred to a 30 ml solution of NaAc (20%) and stirred for 1.5 h. The resulting red mixture was extracted with CH_2Cl_2 and the organic phase was incorporated, and then dried using dehydrated $MgSO_4$ and filtered. The filtrate was concentrated and the residue was subjected to chromatographic separation on a neutral alumina column (1.5 × 30 cm). Elution with ether afforded a purplish red band. A red oil was obtained by concentrating the solution. The red oil was dissolved in 8 ml 1,4-dioxane, heated to reflux temperature, and then NaOH (4.5 ml, 0.5 M) was added. After refluxing for 15 min the reaction mixture was cooled to room temperature. The mixture was poured into 50 g water at 0 °C, and then the solution was neutralized to pH 6–8 using HCl (0.5 M). The mixture was extracted with ether and the ether layer was washed with water, dried over dehydrated $MgSO_4$, and the solvent was removed under reduced pres-

sure. The residue was purified by neutral alumina column chromatography using hexane–ether (4:1, v/v) as eluant. Ligand **1** was obtained as a yellow oil. Yield: 35%. *Anal.* Calc. for $C_{27}H_{24}Fe_2$: C, 70.47; H, 5.26. Found: C, 71.61; H, 6.04%. IR (KBr disk) *v* 823s, 1000w, 1107m, 2106s, 2868w, 2926w, 2970m, 3093w, 3289s cm^{-1}. ^1H NMR ($CDCl_3$, δ): 3.98–4.42 (m, 16H, Fc-H), 2.69 (s, 1H, C≡C–H), 2.72 (s, 1H, C≡C–H), 1.50–1.66 [m, 6H, $C(CH_3)_2$]. ^{13}C NMR ($CDCl_3$, δ): 30.28 (s, CH_3), 33.20 [s, $C(CH_3)_2$], 73.30–73.74 and 82.55–82.84 (m, C≡CH), 62.51–72.20 and 101.50–102.38 (m, Fc). MS (EI) 460 (M^+).

3.2. Syntheses of complexes $[HC{\equiv}C(C_5H_5FeC_5H_3)C(CH_3)_2Fc'C{\equiv}CH][Co_2(CO)_6]$ (4) and $[HC{\equiv}C(C_5H_5FeC_5H_3)C(CH_3)_2Fc'C{\equiv}CH][Co_2(CO)_6]_2$ (5)

A benzene solution of $Co_2(CO)_8$ (90 mg, 0.26 mmol) and ligand **1** (120 mg, 0.26 mmol) was stirred for 11 h at room temperature. The solvent of the resulting dark-green mixture was removed in vacuum. The residue was dissolved in a minimal amount of benzene and subjected to chromatographic separation on a silica gel column (1.5 × 30 cm). Elution with hexane–benzene (5:1 for **5**, 3:1 for **4**, v/v) afforded a first dark-green band (**5**) and then a second dark-green band (**4**). The pure product of complex **4** was too difficult to obtain because of its instability. A trace of complex **4** was only checked by IR (KBr disk, cm^{-1}) 3309 (w, $\nu_{\equiv C-H}$), 2109 (w, $\nu_{C\equiv C}$), 2925 (m, ν_{CH3}), 2966 (m, ν_{CH3}), 2090 (s, ν_{CO}), 2049 (s, ν_{CO}), 2020 (vs, ν_{CO}), 809 (s, δ_{Cp}), 1019 (s, γ_{Cp}), 1096 (s, γ_{Cp}). Crystals of complex **5** were obtained by recrystallizing solid **5** from hexane at −20 °C. Complex **5**: Yield: 74%. m.p., 123 °C (dec.). *Anal.* Calc. for $C_{39}H_{24}Co_4Fe_2O_{12}$: C, 45.39; H, 2.34. Found: C, 45.62; H, 2.37%. IR (KBr disk) *v*(CO) 2090s, 2044s, 2023vs cm^{-1}. ^1H NMR ($CDCl_3$, δ): 6.23 (s, 1H, C≡C–H), 6.27 (s, 1H, C≡C–H), 3.89–4.32 (m, 16H, Cp), 1.62, 1.63 [d, 6H, $C(CH_3)_2$]. ^{13}C NMR ($CDCl_3$, δ): 199.62 (CO), 83.17, 84.12, 101.90, 102.13 (–C≡CH), 67.8–73.87 (Cp), 33.46 [$C(CH_3)_2$], 30.15, 30.95 (CH_3). MS (FAB, relative abundance): 864 (M^+−6CO, 51%), 836 (M^+−7CO, 63%), 808 (M^+−8CO, 32%), 696 (M^+−12CO, 49%), 578 (M^+−12CO–2Co, 31%).

3.3. Synthesis of complex $[FcC(CH_3)_2Fc'CH{=}C][FeCo_2(CO)_9]$ (6)

A THF solution of complex **3** [$FcC(CH_3)_2Fc'C{\equiv}CH]Co_2(CO)_6$ (200 g, 0.28 mmol), $Fe_2(CO)_9$ (311 mg, 0.86 mmol) and $C_6H_5CH{=}CHCOCH_3$(83 mg, 0.57 mmol) was stirred for 39 h at 55–60 °C. The solvent of the resulting red mixture was removed in vacuum. The residue was dissolved in a minimal amount of benzene and subjected to chromatographic separation on a silica gel column (1.5 × 30 cm). Elution with hexane–benzene (7:1) afforded a red band (**6**). Crystals of **6** were obtained by recrystallizing the red solid **6** from hexane at −20 °C. Yield: 42%. m.p., 133 °C (dec.). *Anal.* Calc. for $C_{34}H_{24}Co_2Fe_3O_9$: C, 47.38; H, 2.81. Found: C, 47.59; H, 2.73%. IR(KBr disk) *v*(CO) 2097s, 2066s, 2034vs, 2004s, 1977s, 1961s cm^{-1}. ^1H NMR ($CDCl_3$, δ): 6.69 (s, 1H, HC), 3.87–4.48 (m, 17H, Cp), 1.50 [s, 6H, $C(CH_3)_2$]. ^{13}C NMR ($CDCl_3$, δ): 204.10 (CO), 103.12, 107.02 (CH=C), 66.19–69.95 (Cp), 30.63 (CH_3), 33.23 (C). MS (FAB, relative abundance): 862 (M^+, 24%), 750 (M^+−4CO, 75%), 694 (M^+−6CO, 96%), 610 (M^+−9CO, 18%), 227 ($C_5H_5FeC_5H_4C_3H_6^+$, 87%).

3.4. X-ray crystallography of complex 5

A dark-green crystal of **5** was mounted on a glass fiber. All measurements were made on a Bruker SMART APEX CCD diffractometer with graphite monochromated Mo Kα ($\lambda = 0.71073$ Å) radiation. All data were collected at 20 °C using the π and ω scan techniques. The structure was solved by direct methods and expanded using Fourier techniques [19]. An absorption correction based on SADABS was applied [20]. All non-hydrogen atoms were refined by full matrix least-squares on $F\langle 2\rangle$. Hydrogen atoms were located and refined geometrically. Data collection, data reduction and cell refinement were performed by Bruker SMART and SAINT software [21]. The structure solution and refinement were performed by SHELXL97 [22]. The crystal data and details of measurements are shown in Table 3.

Table 3
Crystal data and structure refinement of complex **5**

Empirical formula	$C_{39}H_{24}Co_4Fe_2O_{12}$
Formula weight	1032.00
Temperature (K)	293(2)
Wavelength (Å)	0.71073
Crystal system, space group	triclinic, $P\bar{1}$
Unit cell dimensions	
a (Å)	8.355(3)
b (Å)	11.048(4)
c (Å)	22.740(7)
α (°)	91.128(5)
β (°)	97.480(5)
γ (°)	107.381(5)
Volume (Å^3)	1982.5(11)
Z, calculated density (Mg/m^3)	2, 1.729
Absorption coefficient (mm^{-1})	2.408
F(000)	1028
Crystal size (mm)	0.25 × 0.10 × 0.10
θ Range for data collection (°)	0.90–26.01
Limiting indices	$-10 \leqslant h \leqslant 10$, $-12 \leqslant k \leqslant 13$, $-28 \leqslant l \leqslant 21$
Reflections collected/unique [R_{int}]	9177/7613 [0.0257]
Completeness to $\theta = 26.01$ (%)	97.6
Maximum and minimum transmission	0.7947 and 0.5843
Refinement method	full-matrix least-squares on F^2
Data/restraints/parameters	7613/0/516
Goodness-of-fit on F^2	0.999
Final *R* indices [$I > \sigma(I)$]	$R_1 = 0.0518$, $wR_2 = 0.0943$
R indices (all data)	$R_1 = 0.0876$, $wR_2 = 0.1095$
Largest difference in peak and hole (e Å^{-3})	0.510 and −0.396
Weighing scheme	$w = 1/[\sigma^2(F_o^2) + (0.0420P)^2 + 0.1703P]$ where $P = (F_o^2 + 2F_c^2)/3$

Acknowledgements

We are grateful to the Startup Foundation of China Scholar Abroad, the Inner Mongolia Talent Foundation and the Inner Mongolia Science Foundation for financial support of this work.

Appendix A. Supplementary data

Crystallographic data for structural analysis have been deposited at the Cambridge Crystallographic Data Centre, CCDC No. 297323 for **5**. Copies of this information may be obtained free of charge from the Director, CCDC, 12 Union Road, Cambridge CB2 1EZ, UK, fax: +44 1223 336 033, e-mail: deposit@ccdc.cam.ac.uk. Supplementary data associated with this article can be found, in the online version, at doi:10.1016/j.poly.2006.05.022.

References

[1] G. Gervasio, P.J. King, D. Marabello, E. Sappa, Inorg. Chim. Acta 350 (2003) 215.
[2] C.U. Pittman, J. Organomet. Chem. 90 (1975) 203.
[3] M. Akita, A. Sakurai, M.C. Chung, Y. Moro-oka, B.H. Robinson, J. Organomet. Chem. 670 (2003) 2.
[4] M.I. Bruce, F.D. Montigny, M. Jevric, C. Lapinte, B.W. Skelton, M.E. Smith, A.H. White, J. Organomet. Chem. 689 (2004) 2860.
[5] P. Butler, J.F. Gallagher, A.R. Manning, H. Mueller-Bunz, C.J. McAdam, J. Simpson, B.H. Robinson, J. Organomet. Chem. 690 (2005) 4545.
[6] S.L. Wu, E.R. Ding, Y.Q. Yin, J. Sun, J. Organomet. Chem. 570 (1998) 71.
[7] M.C. Chung, A. Sakurai, M. Akita, Y. Moro-oka, Organometallics 18 (1999) 4684.
[8] D. Osella, L. Milone, C. Nervi, M. Ravera, Eur. J. Inorg. Chem. (1998) 1473.
[9] L.A. Hore, C.J. McAdam, J.L. Kerr, N.W. Duffy, B.H. Robinson, J. Simpson, Organometallics 19 (2000) 5039.
[10] J.F. Gallagher, P. Butler, R.D.A. Hudson, A.R. Manning, J. Chem. Soc., Dalton Trans. (2002) 75.
[11] L.B. Gao, L.Y. Zhang, L.X. Shi, Z.N. Chen, Organometallics 24 (2005) 1678.
[12] L. Cuffe, R.D.A. Hudson, J.F. Gallagher, S. Jennings, C.J. McAdam, A.R. Manning, B.H. Robinson, J. Simpson, Organometallics 24 (2005) 2051.
[13] R.D. Adams, B. Qu, M.D. Smith, T.A. Albright, Organometallics 21 (2002) 2970.
[14] A. Tarraga, P. Molina, D. Curiel, V.M. Desamparados, Organometallics 20 (2001) 2145.
[15] L.M. Han, Q.L. Suo, N. Zhu, J. Inner Mongolia Univ. Tech. 23 (2004) 113.
[16] Q.L. Suo, H. Zhang, Y.B. Wang, L. Wang, L.H. Weng, X.B. Leng, J. Organomet. Chem. 631 (2001) 87.
[17] M. Rosenblum, N. Brawn, J. Papenmeier, M. Applebaum, J. Organomet. Chem. 6 (1966) 173.
[18] Q.L. Suo, L.M. Han, Y.B. Wang, J.H. Ye, N. Zhu, X.B. Leng, J. Sun, J. Coord. Chem. 57 (2004) 1591.
[19] G.M. Sheldrick, Acta Crystallogr., Sect. A 46 (1990) 467.
[20] G.M. Sheldrick, SADABS. Siemens Area Detector Absorption, Correction Software, University of Göttingen, Germany, 1997.
[21] Bruker, SMART and SAINT. Area Detector Control and Integration Software, Bruker Analytical X-ray Instruments Inc., Madison, WI, USA, 1998.
[22] G.M. Sheldrick, SHELXL-97. Program for Crystal Structure Analysis, University of Göttingen, Germany, 1997.

2. Results and discussion

The reactions of two equivalents of morpholine or *N*-methylpiperazine with diphenylchlorophosphine in diethyl ether at room temperature afford the corresponding derivatives *N*-diphenylphosphinoamines $Ph_2PNC_4H_8O$ (**1**) and $Ph_2PNC_4H_8NMe$ (**2**) in good yield. Similarly, the reaction of four equivalents of morpholine with $PhPCl_2$ afforded bis(morpholino)phenylphosphine $PhP(NC_4H_8O)_2$ (**3**). Both the morpholine and *N*-methylpiperazine derivatives (**1**–**3**) react smoothly with elemental sulfur or selenium in toluene under reflux conditions to give the corresponding sulfide or selenide derivatives **4**–**9** as air stable solids. The preparation of some of these chalcogen derivatives have been reported previously but without all the details [12]

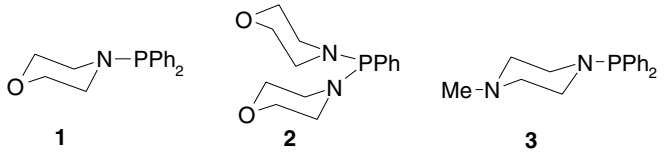

The $^{31}P\{^1H\}$ NMR spectra of compounds **1**–**3** show single resonances at 61.7, 63.3 and 95.8 ppm, respectively, whereas their chalcogenides **4**–**9** show single resonance in the range of 65–79 ppm. The mono-morpholine and *N*-methylpiperazine derivatives **7** and **8** show $^1J_{PSe}$ coupling around 760 Hz whereas the bis(morpholine) derivative **9** shows a $^1J_{PSe}$ coupling of 788 Hz. The ^1H NMR spectral data of **1**–**9** are consistent with the structures proposed. The structural composition of all compounds has been confirmed by elemental analysis.

The reaction of *N*-diphenylphosphinomorpholine **1** with paraformaldehyde in toluene under reflux conditions lead to methylene inserted product **10** in good yield. The methylene insertion reaction proceeds in accordance with our reports on similar aminophosphines [10e,13]. The ^{31}P NMR spectrum of **10** shows a singlet at 28.4 ppm. The ^1H NMR spectrum of compound **10** exhibits two types of resonances for the alkyl (NC_4H_8O and CH_2) protons apart from aryl protons. The NC_4H_8O protons appear at 3.80 ppm and CH_2 protons appear at 3.42 ppm. In the mass spectrum (MS), the most intense fragment ion appears at *m*/*e* 302 [$M^+ + 1$] which is the expected molecular ion.

The reactions of **2** with either $M(CO)_6$ or *cis*-$W(CO)_4(piperidine)_2$ under refluxing conditions produce the *trans*-tetracarbonyl complexes of the type *trans*-$[M(CO)_4(PPh_2NC_4H_8NMe)_2]$ (**11**, M = Mo; **12**, M = W). The ^{31}P NMR spectra of **11** and **12** exhibit single resonances at 106.2 and 80.8 ppm with tungsten complex showing tungsten satellites with a $^1J_{WP}$ coupling of 304.4 Hz which confirms the mutual *trans* dispositions of two phosphine ligands [10f]. Further confirmation for the *trans* geometry of complexes **11** and **12** comes from IR spectra which show single absorption for *ν*CO at 1888 and 1895 cm^{-1}, respectively, characteristic of complexes containing *trans*-$M(CO)_4$ moieties [14].

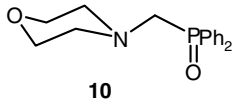

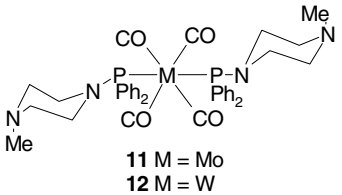

The ruthenium-arene dimer, $[(p\text{-cymene})RuCl_2]_2$ reacts with two equivalents of **2** in dichloromethane at room temperature to produce an orange-red complex $[(\eta^6\text{-}C_{10}H_{14})RuCl_2\{PPh_2NC_4H_8NMe\}]$ (**13**) in quantitative yield. The ^{31}P NMR spectrum of **13** shows a single resonance at 73.5 ppm with a coordination shift of 12 ppm. The mass spectrum of **13** exhibits parent ion peak (M + 1) at 591.3. The structure of complex **13** was further confirmed by single crystal X-ray diffraction study.

2.1. Structure of $[(\eta^6\text{-}C_{10}H_{14})RuCl_2\{PPh_2NC_4H_8NMe\}]$ (13)

Perspective view of the molecular structure of the compound **13** with the atomic numbering scheme is shown in Fig. 1 along with selected bond lengths and bond angles. The details of the structure determination are given in Table 1.

The coordination geometry around the ruthenium center in **13** can be best described as pseudo octahedral three-legged piano stool, typically of half-sandwich complexes. The P–N (1.680(2) Å) bond is shorter than the

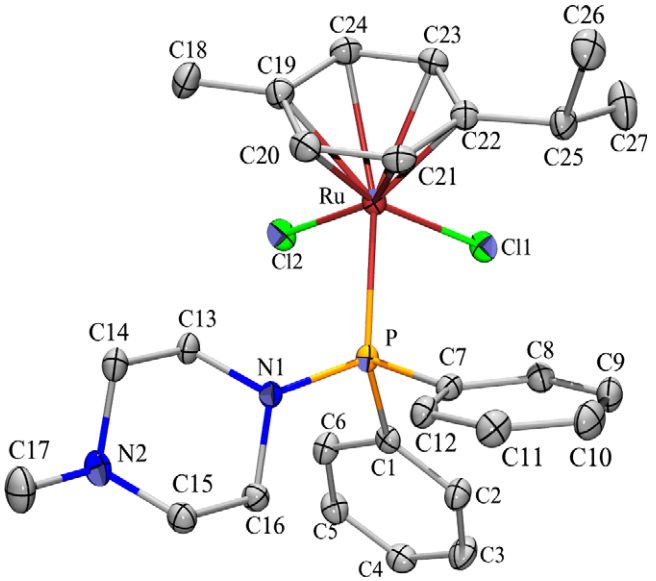

Fig. 1. Molecular structure of **13**. For clarity, solvent and all hydrogen atoms have been omitted. Thermal ellipsoids are drawn at 50% probability. Selected bond distances (Å): Ru–Cl(1), 2.4031(7); Ru–Cl(2), 2.4095(6); Ru–P, 2.3356(6); P–N(1), 1.680(2); N(1)–C(13), 1.471(3); N(2)–C(17), 1.448(3). Selected bond angles (°): Cl(1)–Ru–Cl(2), 86.83(2); Cl(1)–Ru–P, 84.78(2); Cl(1)–Ru–C(19), 150.28(6); Cl(2)–Ru–P, 87.25(2).

Table 1
Crystallographic data for complexes **14** and **13**

Formula	$C_{32}H_{36}Cl_4N_2O_2P_2Pd_2$	$C_{27}H_{35}Cl_2N_2PRu \cdot CH_2Cl_2$
M	897.2	675.44
Crystal size (mm)	$0.08 \times 0.09 \times 0.13$	$0.09 \times 0.12 \times 0.19$
Crystal system	monoclinic	triclinic
Space group	$C2_1/c$	$P\bar{1}$ (No. 2)
a (Å)	17.3015(9)	11.7680(10)
b (Å)	8.3673(4)	11.8570(10)
c (Å)	23.6400(1)	11.9230(10)
α (°)	90	67.78(1)
β (°)	95.91(1)	76.59(1)
γ (°)	90	72.59(1)
V (Å^3)	3404.1(3)	1456.3(2)
Z	4	2
D_{calc} (g cm^{-3})	1.751	1.540
μ (mm^{-1})	1.498	0.981
T (K)	293	100
$\theta_{min,max}$ (°)	1.7, 28.3	2.2, 28.4
Total number of reflections	14700	25781
Number of unique reflections	4106	7177
R_{int}	0.031	0.025
R	0.0373	0.0315
R'	0.0833	0.0747

normally accepted value for a single bond (1.77 Å), but it compares well with those found in a variety of phosphorus(III)–nitrogen compounds suggesting a degree of P–N multiple bonding. Similarly, the Ru–P bond distance is (2.336(1) Å) comparable with those observed in ruthenium complexes containing a variety of tertiary phosphines. The average Ru–Cl bond distance is 2.403(1) Å.

Treatment of $Pd(COD)Cl_2$ with one equivalent of ligand **1** in dichloromethane, afforded a chloro-bridged dinuclear complex, $[Pd_2Cl_2(\mu\text{-}Cl_2)\{Ph_2P(NC_4H_8O)\}_2]$ (**14**). The reaction of two equivalents of **1** with $Pd(COD)Cl_2$ in dichloromethane afforded mononuclear complex, *cis*-$[PdCl_2\{Ph_2PNC_4H_8O\}_2]$ (**15**) as a major product containing small quantities of dinuclear complex, **14** [15] which are separated by fractional crystallization. Surprisingly, $Pd(COD)Cl_2$ on treatment with **2** produced exclusively the *cis*-$[PdCl_2\{PPh_2NC_4H_8NMe\}_2]$ (**16**) as a major product irrespective of the stoichiometry of the reactants and the reaction conditions

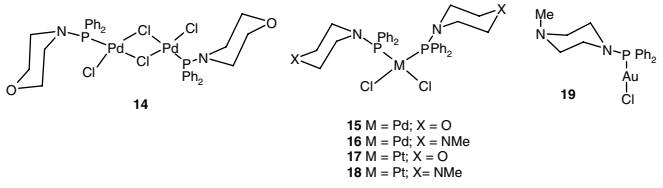

In contrast, the reaction of either one or two equivalents of ligand **1** or **2** with $Pt(COD)Cl_2$ afforded only the mononuclear complexes, *cis*-$[PtCl_2\{Ph_2PNC_4H_8X\}_2]$ (**17**, X = O; **18**, X = NMe) in good yield. Further attempts to synthesize a dinuclear platinum complex analogues to the dipalladium complex **14** have been unsuccessful.

The $^{31}P\{^1H\}$ NMR spectra of **14** show a single resonance at 75.4 ppm. In the mass spectrum (MS) the expected molecular ion appears at m/e 862 [M − Cl]. The structure of **14** was confirmed by a single crystal X-ray diffraction study. The $^{31}P\{^1H\}$ NMR spectra of **15** and **16** exhibit single resonances at 67.3 and 68.5 ppm, respectively. The phosphorus-31 chemical shifts due to the corresponding platinum derivatives (**17** and **18**) are relatively shielded and appear at 50.7 and 50.2 ppm, respectively. Both the complexes show large $^1J_{PtP}$ coupling (**17**, 3968 Hz; **18**, 3965 Hz) which is characteristic of phosphines having mutually *cis*-dispositions [16].

The gold(I) complex, $[ClAu(PPh_2NC_4H_8NMe)]$ (**19**) was produced in the reaction between **2** and $AuCl(SMe_2)$ as colorless light sensitive solid soluble in most of the organic solvents. The ^{31}P NMR spectrum of **19** shows a single resonance at 77.9 ppm with a coordination shift of 16.5 ppm.

2.2. Structure of $[Pd_2Cl_2(\mu\text{-}Cl_2)\{Ph_2P(NC_4H_8O)\}_2]$ (**14**)

Perspective view of the molecular structure of the compound **14** with the atomic numbering scheme is shown in Fig. 2 along with selected bond lengths and bond angles. The Pd_2Cl_2 plane is perpendicular to morpholine rings. The Cl(1)–Pd–P angle is 93.35(3)° where as Cl(1_a)–Pd–Cl(2) angle is 89.61(3)° which clearly indicates some distortion at the metal center. The Cl(1)–Pd–P angle (93.35(3)°) appears to have increased from the squareplanar value of 90° to an extent limited by the development of phosphine–chloride interactions. The Pd–Cl(1) (2.32 Å) bond distance is slightly longer than Pd–Cl(2) (2.27 Å) bond distance. That there is only a single ^{31}P NMR resonance in solution suggests that the observed difference may result from packing (or) other solid state effects.

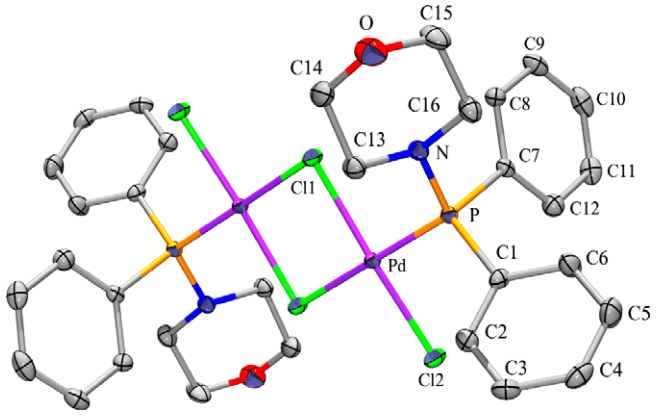

Fig. 2. Molecular structure of **14**. For clarity, solvent and all hydrogen atoms have been omitted. Thermal ellipsoids are drawn at 50% probability. Selected bond distances (Å): Pd–Cl(1), 2.325(8); Pd–Cl(2), 2.271(1); Pd–P, 2.215(1); Pd–Cl(1a), 2.437(1); P–N, 1.676(3); P–Cl, 1.808(3); P–C(7), 1.804(3). Selected bond angles (°): Cl(1)–Pd–Cl(2), 171.39(3); Cl(1)–Pd–P, 93.35(3); Cl(1)–Pd–C(11a), 86.80(3); Cl(2)–Pd–P, 89.73(5); Pd–P–N, 113.46(9).

3. Experimental

All experimental manipulations were carried out under an atmosphere of dry nitrogen or argon using Schlenk techniques. All the solvents were purified by conventional procedures and distilled prior to use. The metal precursors $[W(CO)_4(pip)_2]$ [17], $[(p\text{-cymene})RuCl_2]_2$ [18], $[AuCl(SMe_2)]$ [19], $[(COD)PdCl_2]$, $[(COD)PtCl_2]$ [20] are prepared according to the literature methods and $[Mo(CO)_6]$ was obtained from Aldrich chemicals.

The ^1H and ^{31}P NMR (δ in ppm) spectra were obtained on a VXR300S spectrometer operating at frequencies of 300 and 121 MHz, respectively. The spectra were recorded in $CDCl_3$ solutions with $CDCl_3$ as an internal lock; TMS and 85% H_3PO_4 were used as external standards for ^1H and $^{31}P\{^1H\}$ NMR, respectively. Positive shifts lie downfield of the standard in all cases. Melting points of all compounds were determined on Veego melting point apparatus and were uncorrected. Mass spectra were recorded on MASPEC (msco/9849) system. Microanalyses were carried out on a Carlo Erba model EA 1112 elemental analyzer.

3.1. Preparation of $Ph_2P(NC_4H_8O)$ (1)

A solution of HNC_4H_8O (1.73 g, 19.93 mmol) in dry diethyl ether (20 mL) was added drop wise to a chlorodiphenylphosphine (2 g, 9.06 mmol) also in diethyl ether (70 mL) at 0 °C with vigorous stirring. Then the solution was allowed to room temperature and stirring was continued for 24 h. The morpholine hydrochloride was removed by filtration. The solvent was removed under vacuum to give a white solid of the crude product, which was crystallized from dichloromethane/petroleum ether (b.p. 60–80 °C) (2:1). Yield: 89% (2.20 g); m.p. 84–85 °C. *Anal.* Calc. for $C_{16}H_{18}NOP$: C, 70.83; H, 6.68; N, 5.16. Found: C, 70.02; H, 6.32; N, 5.06%. ^1H NMR (300 MHz, $CDCl_3$): δ 7.23–7.59 (m, 10H, Ph), δ 3.71 (t, 4H, OC_2H_4), δ 3.07 (tt, 4H, NC_2H_4). $^{31}P\{^1H\}$ NMR (300 MHz, $CDCl_3$): δ 63.7 (s).

3.2. Preparation of $[Ph_2PNC_4H_8NMe]$ (2)

To an ice cooled solution of *N*-methylpiperazine (2.26 g, 22.5 mmol) in diethyl ether (50 mL), a solution of chlorodiphenylphosphine (2.48 g, 11.25 mmol) in diethyl ether (30 mL) was added dropwise over a period of 15 min with constant stirring. The reaction mixture was allowed to warm to room temperature and stirring was continued for 16 h. The piperazinehydrochloride was filtered off and the filtrate was dried under vacuum. The residue obtained was dissolved in 20 mL of acetonitrile and the solution was cooled to −25 °C for 10 h to give analytically pure product of **1** as colorless blocks. Yield: 70% (2.24 g); m.p. 58–60 °C. *Anal.* Calc. for $C_{17}H_{21}N_2P$: C, 71.81; H, 7.44; N, 9.85. Found: C, 71.31; H, 7.22; N, 9.91%. ^1H NMR (400 MHz, $CDCl_3$): δ 2.98 (s, 4H, CH_2), 2.38 (s, 4H, CH_2), 2.20 (s, 3H, *NMe*), 7.30–7.55 (m, 10H, *phenyl*). $^{31}P\{^1H\}$ NMR (400 MHz, $CDCl_3$): δ 61.3 (s).

3.3. Preparation of $PhP(NC_4H_8O)_2$ (3)

A solution of HNC_4H_8O (1.73 g, 19.93 mmol) in dry diethyl ether (20 mL) was added drop wise to chlorodiphenylphosphine (2 g, 9.06 mmol) also in diethyl ether (70 mL) at 0 °C with vigorous stirring. Then the solution was allowed to warm to room temperature and stirring was continued for 24 h. The morpholine hydrochloride was removed by filtration. The solvent was removed under vacuum to give a white solid of the crude product, which was crystallized from dichloromethane/petroleum ether (2:1). Yield: 91.0% (2.95 g); m.p. 98–100 °C. *Anal.* Calc. for $C_{14}H_{21}N_2O_2P$: C, 59.98; H, 7.51; N, 9.94. Found: C, 59.02; H, 7.24; N, 9.27%. $^{31}P\{^1H\}$ NMR (300 MHz, $CDCl_3$): δ 95.8 (s).

3.4. Preparation of $Ph_2P(S)(NC_4H_8O)$ (4)

A mixture of compound **1** (0.5 g, 1.8 mmol) and sulfur (0.06 g, 1.8 mmol) in toluene (10 mL) was heated under reflux for 12 h to give a clear solution. Solvent was removed under reduced pressure to give a white residue. The residue was dissolved in CH_2Cl_2 (5 mL), layered with 1 mL of petroleum ether and kept at room temperature to give colorless crystals of **3**. Yield: 90% (0.49 g); m.p. 116–118 °C (decomp.). *Anal.* Calc. for $C_{16}H_{18}NOPS$: C, 63.32; H, 5.98; N, 4.61; S, 10.57. Found: C, 63.61; H, 5.99; N, 4.92; S, 8.74%. $^{31}P\{^1H\}$ NMR (300 MHz, $CDCl_3$): δ 65.9 (s).

3.5. Synthesis of $[P(S)Ph_2NC_4H_8NMe]$ (5)

As for **4**, using $Ph_2PNC_4H_8NMe$ (0.19 mg, 67.5 mmol) and elemental sulfur (0.022 mg, 67.6 mmol). Yield: 95% (0.202 g); m.p. 106–108 °C. *Anal.* Calc. for $C_{17}H_{21}N_2PS$: C, 64.53; H, 6.69; N, 8.85; S, 10.13. Found: C, 63.92; H, 6.45; N, 8.31; S, 9.6%. ^1H NMR (400 MHz, $CDCl_3$): δ 2.98 (s, 4H, CH_2), 2.38 (s, 4H, CH_2), 2.2 (s, 3H, *NMe*), 8.1 (m, 5H, *phenyl*), 7.25 (m, 5H, *phenyl*). $^{31}P\{^1H\}$ NMR (400 MHz, $CDCl_3$): δ 65.8 (s).

3.6. Preparation of $PhP(S)(NC_4H_8O)_2$ (6)

As for **4**, using $PhP(NC_4H_8O)_2$ (1 g, 3.56 mmol) and selenium powder (0.15 g, 3.56 mmol). Yield: 92% (1 g); m.p. 120–122 °C. *Anal.* Calc. for $C_{14}H_{21}N_2O_2PS$: C, 53.83; H, 6.77; N, 8.99; S, 10.26. Found: C, 53.70; H, 6.68; N, 9.18; S, 8.85%. $^{31}P\{^1H\}$ NMR (300 MHz, $CDCl_3$): δ 74.8 (s).

3.7. Preparation of $Ph_2P(Se)(NC_4H_8O)$ (7)

A mixture of **1** (1 g, 3.68 mmol) and selenium powder (0.29 g, 3.68 mmol) in toluene (25 mL) was heated under reflux for 12 h. The solution was then cooled to 25 °C and filtered to remove any undissolved selenium. The solvent was removed under reduced pressure to give a sticky residue. The residue was dissolved in 3 mL of CH_2Cl_2, layered with 1 mL of petroleum ether and kept at room temperature to afford crystals of **5**. Yield: 92% (0.12 g); m.p.

120–122 °C. *Anal.* Calc. for $C_{16}H_{18}NOPSe$: C, 54.86; H, 5.17; N, 3.99. Found: C, 55.3; H, 5.2; N, 4.4%. ^{1}H NMR (300 MHz, $CDCl_3$): δ 8.12–7.2.1 (m, 21H, Ph), δ 3.77 (tt, 4H, OC_2H_4), δ 2.82 (tt, 4H, NC_2H_4). $^{31}P\{^1H\}$ NMR (300 MHz, $CDCl_3$): δ 66.9 (s), $^1J_{PSe} = 760$ Hz.

3.8. Preparation of *[P(Se)Ph$_2$NC$_4$H$_8$NMe] (**8**)*

As for **7** using $Ph_2PNC_4H_8NMe$ (0.230 g, 80.9 mmol) and grey selenium (0.064 g, 80.9 mmol). Yield: 90% (261 mg); m.p. 114–116 °C. *Anal.* Calc. for $C_{17}H_{21}N_2PSe$: C, 56.20; H, 5.83; N, 7.71. Found: C, 56.37; H, 5.46; N, 7.29%. ^{1}H NMR (400 MHz, $CDCl_3$): δ 2.9 (s, 4H, *CH*$_2$), 2.5 (s, 4H, *CH*$_2$), 2.3 (s, 3H, *NMe*), 8.2 (m, 5H, *phenyl*), 7.5 (m, 5H, *phenyl*). $^{31}P\{^1H\}$ NMR (400 MHz, $CDCl_3$): δ 66.28 (s), $^1J_{PSe} = 758.4$ Hz.

3.9. Preparation of *PhP(Se)(NC$_4$H$_8$O)$_2$ (**9**)*

As for **7** using $PhP(NC_4H_8O)_2$ (1 g, 3.68 mmol) and selenium powder (0.29 g, 3.68 mmol). Yield: 78% (1 g); m.p. 120–122 °C. *Anal.* Calc. for $C_{14}H_{21}N_2O_2PSe$: C, 46.86; H, 5.58; N, 7.79. Found: C, 46.8; H, 5.34; N, 8.04%. ^{1}H NMR (300 MHz, $CDCl_3$): δ 7.98–7.26 (m, 5H, Ph), δ 3.66 (tt, 4H, OC_2H_4), δ 3.07 (tt, 4H, NC_2H_4). $^{31}P\{^1H\}$ NMR (300 MHz, $CDCl_3$): δ 78.2 (s), $^1J_{PSe} = 788$ Hz.

3.10. Preparation of *Ph$_2$(O)PCH$_2$NC$_4$H$_8$O (**10**)*

A mixture of **1** (0.2 g, 0.73 mmol) and paraformaldehyde (0.02 g, 0.81 mmol) in toluene (6 mL) was heated at 100 °C with stirring for 12 h. The solution was then cooled to 25 °C and filtered to remove any undissolved impurities. The compound was crystallized from CH_2Cl_2–*n*-hexane (4:1). Yield: 81% (0.18 g); m.p. 136–138 °C. *Anal.* Calc. for $C_{17}H_{20}N0_2P$: C, 67.76; H, 6.69; N, 4.64. Found: C, 66.78; H, 6.79; N, 4.62%. ^{1}H NMR (300 MHz, $CDCl_3$): δ 7.85–7.26 (m, 10H, Ph), δ 3.72 (t, 4H, OC_2H_4), δ 3.42 (d, 2H, CH_2, $^2J_{PH} = 6$ Hz), δ 2.85 (s, 4H, NC_2H_4). $^{31}P\{^1H\}$ NMR (300 MHz, $CDCl_3$): δ 28.4 (s). MS (FAB): 302 ($M^+ + 1$).

3.11. Preparation of *trans-[Mo(CO)$_4${(Ph$_2$PNC$_4$H$_8$NMe)-κP}$_2$] (**11**)*

A mixture of **2** (0.044 g, 0.153 mmol) and $[Mo(CO)_6]$ (20.22 mg, 0.076 mmol) in toluene (15 mL) was heated at 90 °C for 10 h. The yellow solution obtained was cooled to room temperature and passed through a column containing celite and the solvent was removed under *vacuo*. The pale yellow micro crystalline residue obtained was washed twice with diethyl ether (3 mL) to afford analytically pure product of **11**. Yield: 70% (41 mg); m.p. 186–188 °C (dec). *Anal.* Calc. for $C_{38}H_{42}O_4N_4P_2Mo$: C, 58.77; H, 5.45; N, 7.21. Found: C, 57.69; H, 5.42; N, 6.38%. FT IR (KBr disc) cm^{-1}: ν_{CO} at 1888 s. ^{1}H NMR (400 MHz, $CDCl_3$): δ 3.2 (s, 4H, *CH*$_2$), 2.4 (s, 4H, *CH*$_2$), 2.2 (s, 3H, *NMe*), 7.4 (m, 5H, *phenyl*), 7.1 (m, 5H, *phenyl*). $^{31}P\{^1H\}$ NMR (400 MHz, $CDCl_3$): δ 106.2 (s).

3.12. Preparation of *trans-[W(CO)$_4${(Ph$_2$PNC$_4$H$_8$NMe)-κP}$_2$] (**12**)*

As for **11** using $[Ph_2PNC_4H_8NMe]$ (0.053 mg, 188 mmol) and $[W(CO)_4(pip)_2]$ (0.044 g, 94 μmol). Yield: 68% (0.055 g); m.p. 178–180 °C (dec). *Anal.* Calc. for $C_{38}H_{42}O_4N_4P_2W$: C, 52.79; H, 4.89; N, 6.48. Found: C, 53.23; H, 5.09; N, 6.65%. ^{1}H NMR (400 MHz, $CDCl_3$): δ 2.82 (s, 4H, *CH*$_2$), 2.43 (s, 4H, *CH*$_2$), 2.10 (s, 3H, *NMe*), 7.61–7.24 (m, 10H, *phenyl*). IR (KBr disc) cm^{-1}: ν_{CO} at 1890 s. $^{31}P\{^1H\}$ NMR (300 MHz, $CDCl_3$): δ 80.8 (s), $^1J_{PW} = 304.4$ Hz.

3.13. Preparation of *[Ru(η^6-C$_{10}$H$_{14}$)Cl$_2${(PPh$_2$NC$_4$H$_8$-NMe)-κP}] (**13**)*

A solution of [(*p*-cymene)$RuCl_2]_2$ (0.033 mg, 54.5 μmol) in dichloromethane (5 mL) was added dropwise to a solution of **2** (0.031 mg, 109 μmol) in the same solvent (5 mL) at room temperature. After the completion of the addition, the reaction mixture was stirred for 4 h and the solvent was removed under reduced pressure. The residue obtained was washed with diethyl ether to give analytically pure product of **13** as red micro crystalline solid. Yield: 85% (55 mg); m.p. 168–170 °C (dec). *Anal.* Calc. for $C_{27}H_{35}N_2PRuCl_2$: C, 54.91; H, 5.97; N, 4.74. Found: C, 54.63; H, 5.74; N, 4.07. ^{1}H NMR (400 MHz, $CDCl_3$): δ 7.70–7.43 (m, 10H, *phenyl*), 5.15 (d, $J_{HH} = 6.4$ Hz, 2H, *Cymene phenyl*), 4.95 (d, $J_{HH} = 6.4$ Hz, 2H, *Cymene phenyl*), 3.1 (s, 3H, *NMe*), 2.75 (septet, 1H, *CH*), 2.5 (s, 4H, *CH*$_2$) 2.4 (s, 4H, *CH*$_2$), 1.95 (s, 3H, *CH*$_3$). $^{31}P\{^1H\}$ NMR (300 MHz, $CDCl_3$): δ 73.5 (s).

3.14. Preparation of *[Pd$_2$(μ-Cl)$_2$Cl$_2${(Ph$_2$PNC$_4$H$_8$O)-κP}$_2$] (**14**)*

To a mixture of $Pd(COD)Cl_2$ (0.05 g, 0.17 mmol) and compound **1** (0.05 g, 0.17 mmol) a CH_2Cl_2 solution (8 mL) was added and the resultant reaction mixture was stirred at room temperature for 48 h. The solution was concentrated to 3 mL and 1 mL of petroleum ether was added. Cooling this solution to 0 °C gave **8** as red crystals. Yield: 77% (0.06 g); m.p. 160–162 °C. *Anal.* Calc. for $C_{32}H_{36}Cl_4N_2O_2P_2Pd_2$: C, 42.83; H, 4.04; N, 3.12. Found: C, 42.6; H, 3.7; N, 3.5%. ^{1}H NMR (300 MHz, $CDCl_3$): δ 7.26–8.05 (m, 10H, Ph), δ 3.68 (t, 4H, OC_2H_4), δ 3.13 (tt, 4H, NC_2H_4). $^{31}P\{^1H\}$ NMR (300 MHz, $CDCl_3$): δ 75.4 (s). MS (FAB): 862 (M − Cl).

3.15. Preparation of *cis-[PdCl$_2${(PPh$_2$NC$_4$H$_8$O)-κP}$_2$] (**15**)*

To a mixture of $Pd(COD)Cl_2$ (0.05 g, 0.17 mmol) and compound **1** (0.11 g, 0.35 mmol) a CH_2Cl_2 solution

(8 mL) was added and the resultant reaction mixture was stirred at room temperature for 48 h. The solution was concentrated to 3 mL and 1 mL of petroleum ether was added. Cooling this solution to 0 °C gave **9** as red crystalline material. Further cooling the remaining solution gave **9** as yellow crystals. Yield: 61% (0.08 g); m.p. 180–185 °C. *Anal.* Calc. for $C_{32}H_{36}Cl_2N_2O_2P_2Pd$: C, 53.38; H, 5.04; N, 3.91. Found: C, 52.82; H, 5.36; N, 3.72%. ^{1}H NMR (300 MHz, $CDCl_3$): δ 7.71–7.27 (m, 10H, Ph), δ 3.64 (t, 4H, OC_2H_4), δ 3.01 (tt, 4H, NC_2H_4). $^{31}P\{^1H\}$ NMR (300 MHz, $CDCl_3$): δ 67.3 (s).

3.16. Preparation of cis-[$PdCl_2\{(PPh_2NC_4H_8NMe)$-κP$\}_2$] (16)

As for **15**, using [Pd(COD)Cl_2] (25 mg, 88 μmol) and **2** (50 mg, 175 μmol). Yield: 95% (62 mg); m.p. 150–152 °C (dec). *Anal.* Calc. for $C_{34}H_{42}Cl_2N_4P_2Pd$: C, 54.74; H, 5.67; N, 7.51. Found: C, 53.68; H, 5.38; N, 7.32%. ^{1}H NMR (400 MHz, $CDCl_3$): δ 3.1 (s, 4H, CH_2), 2.5 (s, 4H, CH_2), 2.2 (s, 3H, CH_2), 7.71–7.42 (m, 10H, *phenyl*). $^{31}P\{^1H\}$ NMR (400 MHz, $CDCl_3$): δ 68.5 (s).

3.17. Preparation of cis-[$PtCl_2\{(Ph_2PNC_4H_8O)$-κP$\}_2$] (17)

To a solution of [Pt(COD)Cl_2] (0.03 g, 0.08 mmol) in CH_2Cl_2 (4 mL) was added a solution of **1** (0.04 g, 0.16 mmol) also in CH_2Cl_2 (5 mL) and the reaction mixture was stirred at room temperature for 48 h. The solution was concentrated to 2 mL and 1 mL of petroleum ether was added. Cooling this solution to 0 °C gave **10** as white crystalline material. Yield: 92% (0.06 g); m.p. 216–218 °C. *Anal.* Calc. for $C_{32}H_{36}Cl_2N_2O_2P_2Pt \cdot 0.5CH_2Cl_2$: C, 45.86; H, 4.38; N, 3.29. Found: C, 45.71; H, 4.30; N, 3.46%. ^{1}H NMR (300 MHz, $CDCl_3$): δ 7.89–6.91 (m, 10H, Ph), δ 3.53 (t, 4H, OC_2H_4), δ 3.22 (t, 4H, NC_2H_4). $^{31}P\{^1H\}$ NMR (300 MHz, $CDCl_3$): δ 50.7 (s), $^1J_{PPt} = 3968$ Hz. MS (FAB): 772 (M − Cl).

3.18. Preparation of cis-[$PtCl_2\{(Ph_2PNC_4H_8NMe)$-κP$\}_2$] (18)

As for **17**, using [Pt(COD)Cl_2] (0.02 g, 53 μmol) and **2** (0.03 g, 106 μmol). Yield: 95% (43 mg); m.p. 164–166 °C (dec). *Anal.* Calc. for $C_{34}H_{42}Cl_2N_4P_2Pt$: C, 48.93; H, 5.07; N, 6.71. Found: C, 48.26; H, 5.09; N, 6.17%. ^{1}H NMR (400 MHz, $CDCl_3$): δ 3.2 (s, 4H, CH_2), 2.4 (s, 4H, CH_2), 2.2 (s, 3H, CH_2), 7.43–7.16 (m, 10H, *phenyl*). $^{31}P\{^1H\}$ NMR (400 MHz, $CDCl_3$): δ 50.2 (s), $^1J_{PPt} = 3965$ Hz.

3.19. Preparation of [$AuCl\{(PPh_2NC_4H_8NMe)$-κP$\}$] (19)

A solution of [ClAu(SMe_2)] (0.026 g, 88.8 μmol) in dichloromethane (10 mL) was added dropwise to a solution of **2** (0.030 g, 88.8 μmol) also in dichloromethane (8 mL) at room temperature and the reaction mixture was stirred for 4 h. The solvent was removed under reduced pressure and the residue was washed with diethyl ether to give analytically pure product of **19** as white micro crystalline solid. Yield: 96% (41 mg); m.p. 150–152 °C (dec). *Anal.* Calc. for $C_{17}H_{21}N_2PAuCl$: C, 39.51; H, 4.09; N, 5.42. Found: C, 38.96; H, 3.85; N, 4.92%. ^{1}H NMR (400 MHz, $CDCl_3$): 3.24 (s, 4H, CH_2), 2.43 (s, 4H, CH_2), 2.21 (s, 3H, *NMe*), 7.71–7.50 (m, 10H, *phenyl*). $^{31}P\{^1H\}$ NMR (400 MHz, $CDCl_3$): δ 77.9 (s).

4. X-ray crystallography

Crystals of compounds **13** and **14** suitable for X-ray crystal analysis were mounted on Cryoloops™ with Paratone oil and placed in the cold nitrogen stream of the Bruker Kryoflex™ attachment of the Bruker APEX CCD diffractometer. Full spheres of data were collected using 606 scans in ω (0.3° per scan) at 0°, 120° and 240° and graphite-monochromated Mo Kα radiation ($\lambda = 0.71073$ Å). The raw data were reduced to F^2 values at a resolution of 0.75 Å using the SAINT+ software (SAINT+, V. 6.35A, Bruker-AXS, Madison, WI, 2002) and global refinements of unit cell parameters using 5000–9000 reflections chosen from the full sets of data were performed. Multiple measurements of equivalent reflections provided the basis for empirical absorption corrections as well as corrections for any crystal deterioration during the data collection (SADABS, V. 2.05, Bruker-AXS, Madison, WI, 2000). The structures were solved by direct methods (SHELX-97) and refined by full-matrix least-squares based on F^2 using the SHELXTL-PLUS program package (SHELXTL-PLUS, V. 6.10, Bruker-AXS, Madison, WI, 2000). Hydrogen atoms were placed in calculated positions provided by a difference map. All were included as riding contributions (C–H = 0.95–0.98 Å) with isotropic displacement parameters 1.2–1.5 times those of the attached carbon atoms. Two orientations were deduced from difference maps and were constrained to be regular hexagons in the final refinement. Other details of the data collections and refinements specific to these compounds are summarized in Table 1.

Acknowledgements

We thank the Department of Science and Technology (DST), New Delhi, for financial support of the work done at the Indian Institution of Technology, Bombay. J.T.M. acknowledges the support of the Louisiana Board of Regents through the Louisiana Educational Quality Support Fund (Grant: LEQSF (2002-2003)-ENH-TR-67) for purchase of the Bruker APEX diffractometer and Tulane University, New Orleans, LA, USA for the support of the Crystallography Laboratory. We thank the regional Sophisticated Center (RSIC), IIT Bombay for recording NMR spectra.

Appendix A. Supplementary material

Full details of data collection and structure refinement for compounds **8** and **14** have been deposited with the Cambridge Crystallography Data Centre, CCDC Nos. 606036 and 265737. Copies of this information may be obtained free of charge from the Director, CCDC, 12 Union Road, Cambridge CB2 1EZ, UK (fax: +44 1223 336033; e-mail: deposit@ccdc.cam.ac.uk or www://http.ccdc.cam.ac.uk). Supplementary data associated with this article can be found, in the online version, at doi:10.1016/j.poly.2006.05.041.

References

[1] (a) N. Oberbeckmann-Winter, X. Morise, P. Braunstein, R. Welter, Inorg. Chem. 44 (2005) 1391;
(b) C. Muller, L.J. Ackerman, J.N.H. Reek, P.C.J. Kamer, P.W.N.M. van Leeuwen, J. Am. Chem. Soc. 126 (2004) 14960;
(c) F. Goettmann, D. Grosso, F. Mercier, F. Mathey, C. Sanchez, Chem. Commun. (2004) 1240;
(d) W.M. Dai, Y. Li, Y. Zhang, K. Wah-Lai, J. Wu, Tetrahedron Lett. 45 (2004) 1999;
(e) P. Braunstein, B.T. Heaton, C. Jacob, L. Manzi, X. Morise, Dalton Trans. (2003) 1396.

[2] (a) O. Piechaczyk, M. Doux, L. Ricard, P. le Floch, Organometallics 24 (2005) 1204;
(b) H. Liang, S. Ito, M. Yoshifuji, Org. Lett. 6 (2004) 425;
(c) J.W. Faller, J.C. Wilt, J. Parr, Org. Lett. 6 (2004) 1301;
(d) A. Dervisi, R.L. Jenkins, K.M.A. Malik, M.B. Hursthouse, S. Coles, Dalton Trans. (2003) 1133.

[3] (a) R.J. Kloetzing, P. Knochel, Tetrahedron Asymmetr. 17 (2006) 116;
(b) F. Speiser, P. Braunstein, L. Saussine, Dalton Trans. (2004) 1539;
(c) W. Tang, W. Wang, X. Zhang, Angew. Chem., Int. Ed. 42 (2003) 943;
(d) G. Chelucci, G. Orru, G.A. Pinna, Tetrahedron 59 (2003) 9471;
(e) P. Braunstein, J. Zhang, R. Welter, Dalton Trans. (2003) 507.

[4] (a) O.M. Ni-Dhubhghaill, J. Lennon, M.G.B. Drew, Dalton Trans. (2005) 3213;
(b) M.R. Zubiri, A.M.Z. Slawin, M. Wainwright, J.D. Woollins, Polyhedron 21 (2002) 1729;
(c) M.R. Zubiri, M.L. Clarke, D.F. Foster, D.J. Cole-Hamilton, A M.Z. Slawin, J.D. Woollins, J. Chem. Soc., Dalton Trans. (2001) 969;
(d) M.R. Zubiri, J.D. Woollins, Comment Inorg. Chem. 24 (2003) 189.

[5] (a) S. Priya, M.S. Balakrishna, S.M. Mobin, R. McDonald, J. Organomet. Chem. 688 (2003) 227;
(b) M.L. Clarke, D.J. Cole-Hamilton, J.D. Woollins, J. Chem. Soc., Dalton Trans. (2001) 2721.

[6] (a) J. Cheng, F. Wang, J. Xu, Y. Pan, Z. Zhang, Tetrahedron Lett. 44 (2003) 7095;
(b) A. Caballero, F.A. Jalo'n, B.R. Manzano, G. Espino, M. Pe'rez-Manrique, A. Mucientes, F.J. Poblete, M. Maestro, Organometallics 23 (2004) 5694.

[7] O. Kühl, T. Koch, F.B. Somoza, P.C. Junk, E. Hey-Hawkins, D. Plat, M.S. Eisen, J. Organomet. Chem. 604 (2000) 116.

[8] (a) K. Maartmann-Moe, C. Roemming, J. Songstad, Acta Chem. Scand. Ser. A 36 (1982) 757;
(b) C.J. Thomas, M.N.S. Rao, J. Chem. Soc., Dalton Trans. (1988) 1445;
(c) C.J. Thomas, M.N.S. Rao, Heteroatom Chem. 3 (1992) 321;
(d) T. Mohan, M.N.S. Rao, Heteroatom Chem. 8 (1997) 225.

[9] Y. Chevallier, R. Stern, L. Sajus, Tetrahedron Lett. 15 (1969) 1197.

[10] (a) M.S. Balakrishna, R.M. Abhyankar, J.T. Mague, J. Chem. Soc., Dalton Trans. (1999) 1407;
(b) M.S. Balakrishna, R. Panda, J.T. Mague, Inorg. Chem. 40 (2001) 5620;
(c) M.S. Balakrishna, R. Panda, J.T. Mague, J. Chem. Soc., Dalton Trans. (2002) 4617;
(d) M.S. Balakrishna, R. Panda, J.T. Mague, Polyhedron 22 (2003) 587;
(e) S. Priya, M.S. Balakrishna, J.T. Mague, S.M. Mobin, Inorg. Chem. 42 (2003) 1272;
(f) S. Priya, M.S. Balakrishna, J.T. Mague, J. Organomet. Chem. 689 (2004) 3335;
(g) M.S. Balakrishna, S. Priya, W. Sommer, S.P. Nolan, Inorg. Chim. Acta 358 (2005) 2817;
(h) P. Chandrasekaran, J.T. Mague, M.S. Balakrishna, Organometallics 24 (2005) 3780;
(i) P. Chandrasekaran, J.T. Mague, M.S. Balakrishna, Inorg. Chem. 44 (2005) 7925.

[11] (a) B. Punji, J.T. Mague, M.S. Balakrishna, Dalton Trans. (2006) 1322;
(b) S. Mohanty, B. Punji, M.S. Balakrishna, Polyhedron 25 (2006) 815.

[12] (a) K. Bergesen, B. Pedersen, J. Songstad, Acta Chem. Scand. Ser. A 35 (1981) 147;
(b) A.J. Elias, C.J. Thomas, M.N.S. Rao, Phosphorus, Sulfur, Silicon, Relat. Elem. 30 (1987) 253;
(c) N.L. Smith, H.H. Sisler, J. Org. Chem. 26 (1961) 5145.

[13] (a) S. Priya, M.S. Balakrishna, J.T. Mague, Inorg. Chem. Commun. 4 (2001) 437;
(b) S. Priya, M.S. Balakrishna, S.M. Mobin, Polyhedron 24 (2005) 1641.

[14] M.S. Balakrishna, T.K. Prakasha, S.S. Krishnamurthy, U. Siriwardane, N.S. Hosmane, J. Organomet. Chem. 390 (1990) 203.

[15] R.B. Bedford, S.L. Hazelwood, P.N. Horton, M.B. Hursthouse, Dalton Trans. (2003) 4164.

[16] M.S. Balakrishna, S.S. Krishnamurthy, R. Murugavel, M. Netaji, I.I. Mathews, J. Chem. Soc., Dalton Trans. (1993) 477.

[17] D.J. Darensbourgh, R.L. Kump, Inorg. Chem. 17 (1978) 2680.

[18] M.A. Bennett, T.N. Huang, T.W. Matheson, A.K. Smith, Inorg. Synth. 21 (1982) 74.

[19] C.M. Brandys, C.M. Jennings, R.J. Puddephatt, J. Chem. Soc., Dalton Trans. (2000) 4601.

[20] D. Drew, J.R. Doyle, Inorg. Synth. 28 (1990) 346.

$Tp^{Th,Me}$. We have also synthesized the heteroscorpionate complexes of hydrogen bis(5-methyl-3-phenylpyrazol-1-yl)(3-methyl-5-phenylpyrazol-1-yl)borate ([HB(3-Me-5-Phpz)(5-Me-3-Phpz)$_2$]$^-$) with molybdenum and studied their fluxional behavior and reactivity along with the known hydrogen tris(3,5-dimethylpyrazol-1-yl)borate (Tp^*) analogues [4–6]. The oxidation of synthesized complexes of the type [Et_4N][Tp′Mo(CO)$_3$] and Tp′Mo(CO)$_2$(η^3-allyl) with iodine, *tert*-butylhydrogenperoxide, and dioxygen was studied here in order to detect high-valent molybdenum complexes with Tp′ ligands. We have isolated and structurally characterized the product of aerial oxidation of Tp^*Mo(CO)$_2$I.

2. Experimental

2.1. Syntheses

2.1.1. Syntheses of substituted pyrazoles and sodium hydrogen trispyrazolylborates (NaTp′)

3,5-Dimethylpyrazole and 3(5)-methyl-5(3)-phenylpyrazole were obtained by condensation of appropriate diketones with hydrazine as described by Trofimenko et al. [7]. 3(5)-Methyl-5(3)-(2-thienyl)pyrazole was obtained as follows.

In a three-necked round-bottomed flask 11.08 g of sodium was placed in a 250 cm^3 of dry toluene under nitrogen atmosphere, to which 200 cm^3 anhydrous methanol was added in portions until all sodium was converted into sodium methanolate. The excess of methanol was distilled off under reduced pressure. To the slurry of NaOMe 50 cm^3 of acetylthiophene was added (58.4 g, 0.463 mol). The color of the mixture changed to violet. To this mixture ethyl acetate (150 cm^3, 135 g, 1.53 mol) was added dropwise and the mixture was gradually heated up to reflux and kept as such for 1 h. The sodium diketonate precipitated upon cooling, which was filtered off, washed thoroughly with petroleum ether, dried and dissolved in 150 cm^3 methanol. Hydrazine monohydrate was added (30 cm^3, 0.506 mol), the mixture was heated under reflux for 1 h and then poured onto ice water (1 dm^3), neutralized with 36% aqueous HCl (ca. 25 cm^3), and left for 40 min for precipitation of 3(5)-methyl-5(3)-(2-thienyl)pyrazole. The crude product was dried on air, and three times dissolved in benzene, which was distilled off, then the dry product was boiled twice with petroleum ether and filtered off. Final yield: 8.89 g, 11.7%.

The sodium hydrogen tris(3-R^1-5-R^2-pyrazol-1-yl)-borates ($NaTp^{R1,R2}$) were obtained by condensation of sodium borohydride with three equivalents of substituted pyrazoles dispersed in high-boiling hydrocarbons. The progress of reaction was monitored by measuring the volume of hydrogen evolved. The heteroscorpionate Na[HB(3-Me-5-Phpz)(5-Me-3-Phpz)$_2$] [8] was obtained according to the optimized protocol [9]. In case of $NaTp^{Th,Me}$ the octadecane reflux (b.p. 317 °C) was used.

2.1.2. [Et_4N][$Tp^*Mo(CO)_3$] (**1**), $Tp^*Mo(CO)_2$(allyl) (**2**), and $Tp^*MoI(CO)_2$ (**3**)

Complex **1** was obtained from Mo(CO)$_6$ by heating with equimolar amount of $NaTp^*$ in refluxing acetonitrile for 2 h, followed by addition of excess aqueous [Et_4N]Cl into cold mixture and purified as described in [4]. **2** was synthesized according to published protocol [10]. From **1** the $Tp^*MoI(CO)_2$ (**3**) was prepared by oxidation with I_2 [11].

2.1.3. [Et_4N][HB(5-Me-3-Phpz)$_2$(3-Me-5-Phpz)Mo(CO)$_3$] (**4**)

Molybdenum hexacarbonyl (Mo(CO)$_6$ (0.496 g, 1.84 mmol) was dissolved in 15 cm^3 degassed acetonitrile and refluxed for 2 h under nitrogen atmosphere. Then 0.948 g of Na[HB(5-Me-3-Phpz)$_2$(3-Me-5-Phpz)] (1.87 mmol) was added in one portion and the mixture was stirred for 2 h at room temperature, later the volume of mixture was reduced twice and poured into 50 cm^3 of 1 M aqueous [Et_4N]Br. The yellow precipitate of crude **4** was filtered off and dried under reduced pressure. Yield: 1.213 g, 81.7%.

Elemental analysis: Calc. for $C_{41}H_{48}N_7O_3BMo$ (MW 793.63): C, 62.05; H, 6.10; N, 12.35. Found: C, 62.25; H, 6.16; N, 12.48%.

^{1}H NMR (chloroform-*d*, 298 K): 7.88–7.29 (15H, overlapping multiplets, aromatic (3,5-Ph)); 6.42 (1H, s, 4-H(3-Me-5-Phpz)); 6.33 (2H, s, (5-Me-3-Phpz)); 3.42 (8H, q, $CH_2(Et_4N^+)$; 2.20 (6H, s, 5-CH_3(5-Me-3-Phpz)); 2.11 (3H, s, CH_3(3-Ph-5-Mepz)); 1.34 (12H, t, $CH_3(Et_4N^+)$).

IR (KBr): $\nu_{(BH)}$ 2536 (w); $\nu_{(CO)}$ 1994, 1937, 1885 (all s) cm^{-1}.

Electrochemical properties throughout the paper the potentials are quoted versus Fc^+/Fc): one-electron reversible oxidation at $E_{1/2} = -662$ mV ($\Delta E = 70$ mV, in MeCN) and one-electron irreversible oxidation wave (no corresponding reduction wave) at $E_a = 225$ mV.

2.1.4. [HB(5-Me-3-Phpz)$_2$(3-Me-5-Phpz)]Mo(CO)$_2$(allyl) (**5**)

Molybdenum hexacarbonyl (Mo(CO)$_6$ (0.797 g, 3.02 mmol) was dissolved in degassed acetonitrile (20 cm^3) and 15 cm^3 of allyl bromide was added. The mixture was refluxed under nitrogen for 2 h, Na[HB(5-Me-3-Phpz)$_2$(3-Me-5-Phpz)] (1.528 g, 3.02 mmol) was added in one portion into the cold mixture and stirred for 2 h. Then the solvent was removed on rotary evaporator, the residue was dissolved in benzene and the solution was passed through short bed of alumina. The benzene was distilled off under reduced pressure and solid yellow product was collected. Yield: 0.763 g, 37.3%.

Elemental analysis: Calc. for $C_{35}H_{33}N_6O_2BMo$ (MW 676.44): C, 62.15; H, 4.92; N, 12.42. Found: C, 62.59; H, 4.86; N, 12.24%.

^{1}H NMR (chloroform-*d*, 298 K): 8.03–7.15 (15H, overlapping multiplets, aromatic (3,5-Ph)); 6.22 (1H, s, 4-H(3-Me-5-Phpz)); 5.95 (2H, 4-H(5-Me-3-Phpz)); 3.53 (1H, br m, 2′-H(allyl)); 3.09 (3H, s, 5-CH_3(5-Me-3-Phpz)); 2.49 (6H,

s, 3-CH_3(3-Me-5-Phpz)); 1.56 (2H, br m, 1′,3′-H_{exo}(allyl)); 0.69 (2H, br m, 1′,3′-H_{endo}(allyl)).

IR (KBr): $\nu_{(BH)}$ 2475 (w); $\nu_{(CO)}$ 1918, 1834 (both s) cm^{-1}.

Electrochemical properties: two-electron oxidation at $E_{1/2} = 201$ mV (at 100 mV s^{-1} irreversible with no corresponding reduction wave, at higher scan rates becomes quasi-reversible, ΔE=110 mV, in THF).

2.1.5. $[Et_4N][Tp^{Th,Me}Mo(CO)_3]$ (6)

Complex **6** was synthesized according to the same protocol as **4** starting from 0.428 g $NaTp^{Th,Me}$ and 0.218 g $Mo(CO)_6$ (0.82 mmol scale). 0.390 g of yellow crystals of **6** (59.0% yield) was collected upon twice crystallization from acetonitrile.

Elemental analysis: Calc. for $C_{35}H_{42}N_7O_3S_3BMo$ (MW 811.69): C, 51.79; H, 5.22; N, 12.08. Found: C, 51.55; H, 5.16; N, 12.43%.

^{1}H NMR (DMSO-d_6, 298 K): 7.37–6.93 (9H, overlapping multiplets, thienyl (3-(2-thienyl)-5-Mepz)); 6.25 (3H, s, 4-H(pz)); 3.10 (8H, q, $CH_2(Et_4N^+)$; 2.18 (9H, s, 3-CH_3); 1.10 (12H, t, $CH_3(Et_4N^+)$).

IR (KBr): $\nu_{(BH)}$ 2556 (w); $\nu_{(CO)}$ 1994, 1937, 1886 (all s) cm^{-1}.

Electrochemical properties: one-electron irreversible oxidation at $E_a = -890$ mV (in MeCN) and a second irreversible oxidation wave at $E_a = 18$ mV.

2.1.6. $Tp^{Th,Me}Mo(CO)_2(allyl)$ (7)

Complex **7** was synthesized by the same procedure as **5** starting from 0.694 g $NaTp^{Th,Me}$ and 0.350 g $Mo(CO)_6$ (1.32 mmol scale) and isolated as yellow crystals upon twice crystallization from tetrahydrofuran. Yield: 0.630 g, 68.6%.

Elemental analysis: Calc. for $C_{29}H_{27}N_6O_2S_3BMo$ (MW 694.50): C, 50.15; H, 3.92; N, 12.10. Found: C, 50.55; H, 3.86; N, 12.40%.

^{1}H NMR (chloroform-*d*, 298 K): 7.74 (1H, dd ($J_{3'4'} = 3.6$ Hz, $J_{3'5'} = 1.1$ Hz), 3-H(3-(2-thienyl-pz_b)); 7.49 (1H, dd ($J_{4'5'} = 5.0$ Hz), 4-H(3-(2-thienyl-pz_b)); 7.34 (2H, dd ($J_{4'5'} = 5.1$ Hz, $J_{3'5'} = 1.1$ Hz), 5-H(3-(2-thienyl-pz_a)); 7.30 (2H, dd ($J_{3'4'} = 3.6$ Hz), 3-H(3-(2-thienyl-pz_a)); 7.22 (1H, dd, 4-H(3-(2-thienyl-pz_b)); 7.06 (2H, dd, 4-H(3-(2-thienyl-pz_a)); 6.18 (1H, s, 4-H(pz_b)); 6.05 (2H, s, 4-H(pz_a)); 2.71 (2H, d ($J_{1',3'\text{-}exo,2'} = 6.6$Hz, 1′,3′-$H_{exo}$(allyl)); 3.59 (1H, m, 2′-H(allyl)); 2.43 (6H, s, 5-CH_3(pz_a)); 2.32 (3H, s, 5-CH_3(pz_b)); 0.76 (2H, d ($J_{1'3'\text{-}endo,2'} = 10.4$ Hz, 1′,3′-H_{endo}(allyl)).

IR (KBr): $\nu_{(BH)}$ 2552 (w); $\nu_{(CO)}$ 1937, 1844 (both s) cm^{-1}.

Electrochemical properties: one-electron oxidation at $E_a = 216$ mV (at 100 mV s^{-1} irreversible with no corresponding reduction wave but at high scan rates (5 V s^{-1}) $\Delta E = 190$ mV, in THF) and a second irreversible oxidation process at $E_a = 746$ mV.

2.1.7. $[Tp^*Mo(O)(\mu\text{-}O)_2Mo(O)]_2(\mu\text{-}OH)_2$ (8)

50.0 mg of **3** was dissolved in 5 cm^3 acetonitrile and the solution was left on air for partial evaporation of the solvent. The red crystals of **8** suitable for X-ray analysis were collected after four days, yield 19.8 mg, 62.0%.

Elemental analysis: Calc. for $C_{46}H_{70}N_{20}O_{10}B_2Mo_4$ (MW 1468.60): C, 37.62; H, 4.80; N, 19.08. Found: C, 37.85; H, 4.91; N, 19.39%.

2.2. Methods

2.2.1. Spectroscopic and electrochemical measurements

The ^{1}H NMR spectra were recorded with Bruker AMX 300 spectrometer. Standard COSY and NOESY experiments were performed with repetition time 1.0 and mixing time 0.3 s (NOESY). IR spectra were recorded in KBr pellets on PARAGON 1000 FT-IR instrument (Perkin–Elmer). The cyclovoltametric (CV) measurements were performed with a BAS 100B/W instrument (Bioanalytical Systems, USA). CV runs were recorded using $[Bu_4N][BF_4]$ as the supporting electrolyte, platinum disc as the working and Ag/AgCl as the reference electrode at 100 mV s^{-1} standard sweep rate for 1 mM samples in MeCN and/or in THF. Throughout the paper, the potentials are quoted versus ferrocenium/ferrocene pair used as an internal standard (added to the solution for final measurements).

2.2.2. X-ray crystallography

Crystal data are given in Table 1, together with refinement details. All measurements of crystal were performed at low temperature using an Oxford Cryosystem device on a Kuma KM4CCD κ-axis diffractometer with graphite-monochromated Mo Kα radiation. The crystal was positioned 65 mm from the CCD camera. 612 frames were measured at 0.75° intervals with a counting time of 20 s. Accurate cell parameters were determined and refined by least-squares fit of 7200 of the strongest reflections. The data were corrected for Lorentz and polarization effects. No absorption correction was applied. Data reduction and analysis were carried out with the Oxford Diffraction (Poland) Sp. z o.o (formerly Kuma Diffraction Wrocław, Poland) programs. The structure was solved by direct methods (program SHELXS97 [12]) and refined by the full-matrix least-squares method on all F^2 data using the SHELXL97 [13] programs. Non-hydrogen atoms were refined with anisotropic displacement parameters; hydrogen atoms were included from geometry of molecules and $\Delta\rho$ maps. During refinement they were fixed.

3. Results and discussion

3.1. X-ray structures

The low-valence molybdenum complexes are suitable precursors for oxygen transfer catalyst [14]. Our systematic studies on transition metal ion complexes with polypyrazolylborates of low-symmetry prompted us to synthesize series of complexes of molybdenum(0) and (II) of the general formula $[Et_4N][Tp'Mo(CO)_3]$ and $Tp'Mo(CO)_2(\eta^3\text{-allyl})$ and attempted to oxidize them under spectroscopic

Table 1
Crystal data and structure refinement

Compound	**6**	**7**	**8**
Empirical formula	$C_{35}H_{42}BN_7O_3S_3Mo$	$C_{29}H_{27}BN_6O_2S_3Mo$	$C_{46}H_{70}B_2N_{20}O_{10}Mo_4$
Formula weight	811.69	694.50	1468.60
T (K)	100(2)	100(2)	100(2)
λ (Å)	0.71073	0.71073	0.71073
Crystal system	monoclinic	monoclinic	triclinic
Space group	$P2_1/n$	$P2_1/c$	$P\bar{1}$
a (Å)	10.7376(4)	13.4742(5)	10.3185(4)
b (Å)	19.7384(6)	10.3510(3)	10.4885(4)
c (Å)	16.9659(5)	21.7855(7)	16.0242(6)
α (°)	90	90	72.798(4)
β (°)	92.842(3)	101.810(3)	86.647(3)
γ (°)	90	90	74.739(4)
V (Å^3)	3591.4(2)	2974.14(17)	1597.88(11)
Z	4	4	1
D_c (Mg m^{-3})	1.501	1.551	1.526
μ (mm^{-1})	0.587	0.691	0.833
$F(000)$	1680	1416	744
Crystal size (mm)	$0.18 \times 0.16 \times 0.14$	$0.26 \times 0.26 \times 0.24$	$0.24 \times 0.18 \times 0.16$
θ Range for data collection (°)	3.09–27.00	3.28–35.18	3.11–26.99
Ranges of h, k, l	$-13 \rightarrow 10$, $-25 \rightarrow 25$, $-21 \rightarrow 21$	$-18 \rightarrow 21$, $-16 \rightarrow 16$, $-35 \rightarrow 34$	$-13 \rightarrow 13$, $-13 \rightarrow 13$, $-20 \rightarrow 20$
Reflections collected	27009	53032	20784
Independent reflections (R_{int})	7815 (0.0428)	12595 (0.0297)	6976 (0.0533)
Data/parameters	7815/458	12595/401	6976/380
Goodness-fo-fit (F^2)	1.064	1.069	1.032
Final R_1/wR_2 indices ($I > 2\sigma_I$)	0.0468/0.1156	0.0371/0.1005	0.0318/0.0667
Largest difference in peak/hole (e Å^{-3})	1.190/−0.851	1.994/−1.146	0.639/−0.565

control. Thus, we have obtained a pair of compounds with relatively unexplored ligand $Tp^{Th,Me}$: the Mo(0) species **6** and Mo(II) derivative **7**. These complexes were characterized crystallographically. We have found that in both of them the Tp′ ligand was coordinated in η^3 mode via nitrogen donors only (Figs. 1 and 2). The averaged Mo–N(pz) bond length in **7** (2.305 Å) remain almost unchanged in comparison with that in **6** (2.313 Å). However upon increase of the coordination number from 6 to 8, i.e. the increase of steric crowding in **7** the $Tp^{Th,Me}$ is bound less tight than in **6** if consider the boron-centered angle α, which is considerably larger in **7** (92.3°) in comparison with 81.8° in **6**. This has been observed before for Tp^* ligand (compare entries 2 and/or 3 with 9 and 10) but obviously not for unhindered Tp ligand (compare entries 1 with 6 and 7 in Table 2). Within the Tp′Mo(CO)$_2$(allyl) series the growth of steric hindrance imposed by 3-substituents at pyrazolyl residues as measured by decreasing bite angle

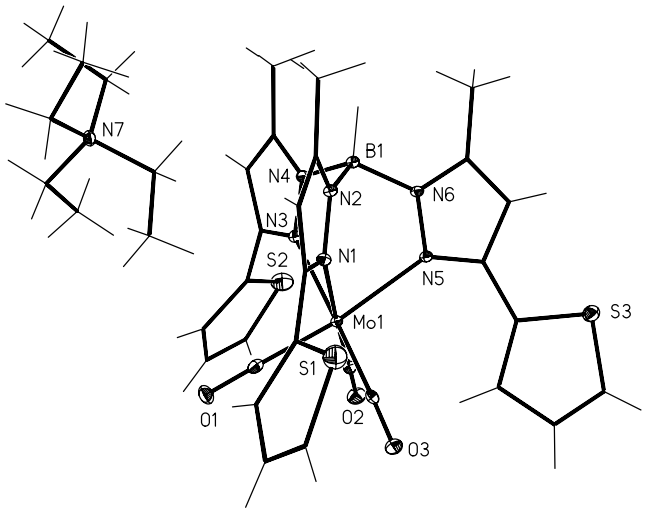

Fig. 1. View of molecule of **6**. Selected bond lengths (Å): Mo(1)–C(31), 1.929(3); Mo(1)–C(33), 1.940(3); Mo(1)–C(32), 1.946(3); Mo(1)–N(3), 2.303(3); Mo(1)–N(1), 2.310(3); Mo(1)–N(5), 2.325(3).

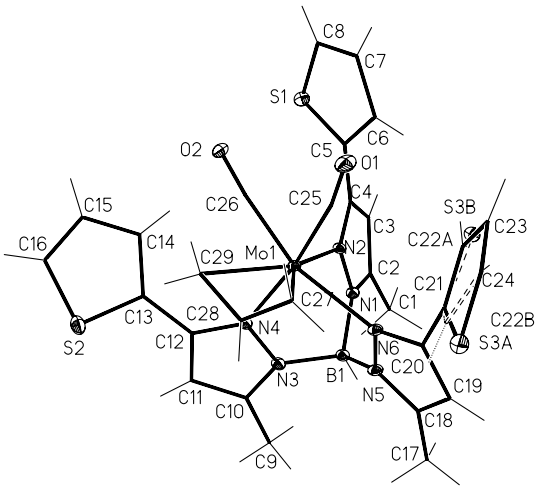

Fig. 2. View of molecule of **7**. Selected bond lengths (Å): Mo(1)–N(2), 2.2213(13); Mo(1)–N(4), 2.3732(14); Mo(1)–N(6), 2.3198(13); Mo(1)–C(25), 1.9456(17); Mo(1)–C(26), 1.9618(16); Mo(1)–C(28), 2.2273(16); Mo(1)–C(29), 2.3352(16); Mo(1)–C(27), 2.3543(17).

Table 2
Metric parameters for the $[X]^+[Tp'Mo(CO)_3]^-$ and $Tp'Mo(CO)_3$(allyl) complexes (X = cation)

Entry	Compound; reference	[Mo–N(pz)] ([Mo–N(pz)]$_{av}$) (Å)[a]	α (°)[b]
1	$[Et_4N][TpMo(CO)_3]$; [15]	2.264; 2.273; 2.262 (2.266)	112.8
2	$[Et_4N][Tp^*Mo(CO)_3]$; [5]	2.259; 2.260; 2.269 (2.263)	95.5
3	[4-CN-N-Mepy][$Tp^*Mo(CO)_3$]; [16]	2.288; 2.273; 2.288 (2.283)	95.9
4	$[Et_4N][Tp^{Me}Mo(CO)_3]$; [17]	2.285; 2.281; 2.289 (2.285)	96.2
5	**6**	2.303; 2.310; 2.325 (2.313)	81.8
6	$TpMo(CO)_2(\eta^3$-allyl); [18]	2.198; 2.270; 2.318 (2.262)	113.1
7	$TpMo(CO)_2(\eta^3$-2-methallyl); [19]	2.209; 2.282; 2.312 (2.268)	112.8
8	$[PhB(pz)_3]Mo(CO)_2(\eta^3$-allyl); [20]	2.256; 2.251; 2.204 (2.237)	109.9
9	$Tp^*Mo(CO)_2(\eta^3$-allyl); [6]	2.339; 2.289; 2.215 (2.281)	100.6
10	$Tp^*Mo(CO)_2(\eta^3$-2-methallyl); [21]	2.301; 2.218; 2.308 (2.276)	101.4
11	$Tp^{CH_2Ph,Me}Mo(CO)_2(\eta^3$-2-methallyl); [22]	2.306; 2.220; 2.319 (2.282)	101.7
12	$Tp^{Mes}Mo(CO)_2(\eta^3$-2-methallyl); [23]	2.280; 2.409; 2.409 (2.366)	106.4
		2.415; 2.415; 2.242 (2.357)	106.3
13	$Tp^{Br,Br,Br}Mo(\eta^3$-2-methallyl); [21]	2.334; 2.236; 2.325 (2.298)	100.4
14	$Tp^{Chex}Mo(CO)_2(\eta^3$-2-methallyl); [24]	2.347; 2.299; 2.225 (2.290)	
15	$[HB(indazolyl)_3]Mo(CO)_2(\eta^3$-2-methallyl)[c]; [25]	2.232; 2.257; 2.277 (2.255)	112.2
		2.299; 2.206; 2.286 (2.264)	112.8
16	$[HB(2H\text{-benz(g)indazol-2yl})_3]Mo(CO)_2(\eta^3$-2-methallyl)[c]; [26]	2.213; 2.305 (2.259)	[d]
		2.226; 2.298 (2.262)	
17	**7**	2.221; 2.373; 2.320 (2.305)	92.3

[a] ±0.004 Å or less.
[b] Measured as defined in [9].
[c] Two independent molecules
[d] η^2 coordination mode, α not measured.

(column 4 in Table 2) increases in the raw of ligands: $Tp \approx [HB(indazolyl)_3]^- < Tp^{Mes} < Tp^{CH_2Ph,Me} \approx Tp^* \approx Tp^{Br,Br,Br} < Tp^{Th,Me}$. Surprisingly the $Tp^{Th,Me}$ ligand has remarkably smallest bite while the averaged Mo–N(pz) distance is longer than in other $Tp'Mo(CO)^2$(allyl) complexes except Tp^{Mes}. At the limit of high steric hindrance there is the $[HB(2H\text{-benz(g)indazol-2yl})_3]^-$ ligand which coordinates in η^2 fashion to molybdenum(II) (entry 16 in Table 2).

During recrystallization of $Tp^*Mo(CO)_2I$ complex **3** from acetonitrile we have noticed the formation of another species, which crystallized well to give X-ray quality, red crystals of the tetranuclear Mo(V) complex **8** (Fig. 3). The Tp^* ligand was partially lost and two inner molybdenum(V)

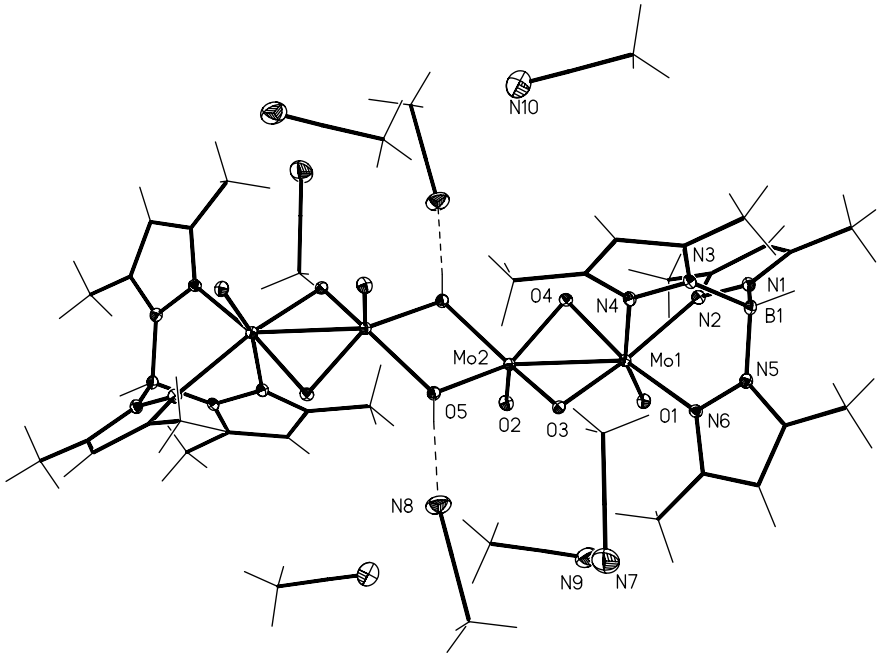

Fig. 3. View of molecule of **8**. Selected bond lengths (Å): Mo(1)–O(1), 1.6879(18); Mo(1)–O(3), 1.9634(18); Mo(1)–O(4), 1.9675(17); Mo(1)–N(2), 2.177(2); Mo(1)–N(6), 2.187(2); Mo(1)–N(4), 2.377(2); Mo(1)–Mo(2), 2.5588(3); Mo(2)–O(2), 1.6855(18); Mo(2)–O(3), 1.9046(17); Mo(2)–O(4), 1.9133(18); Mo(2)–O(5)′, 2.0587(18); Mo(2)–O(5), 2.0648(18).

centers of linear **8** are surrounded exclusively by oxygen donors. Generally, there are three tetranuclear complexes of Mo(V) with Tp-type ligands (Tp′) which were obtained from equimolar mixture of KTp and $MoCl_5$ [27] or by oxidation of $[Tp'Mo(CO)_3]^-$ salt with dimethyldioxirane [28] or **3** with dioxygen (**8**) in non-aqueous solvents (Table 3, Chart 1). In the former case the tetranuclear side-product **T**[9] was spontaneously formed, in which two terminal Mo(V) centers coordinated with Tp ligand and two inner Mo(V) centers were bound to oxygen donors. The cyclic tetramer **T**[10] is also composed of four Mo(V) centers, all bearing Tp anions coordinated in η^3 fashion. The structure of linear framework in **8** is similar to that in **T**[9]; the Mo(V)–Mo(V) distances between terminal and inner metal ion are 2.559 and 2.553 Å, respectively, while the distance between inner molybdenum(V) centers, connected together via two μ-(OR) are around 3.4 Å, considerably shorter than those between molybdenum centers in Tp′Mo–O–MoTp′ fragments in **T**[10] or in any dinuclear complex **D**[11]–**D**[16], where it was ca. 3.7 Å. The Tp′ ligands are bound slightly weaker in tetranuclear complexes than Tp* in dinuclear or mononuclear molybdenum(V) compounds if consider the mean Mo–N(pz) distance, which equals: 2.25, 2.23, and 2.22 Å, respectively. Thus the Mo–N(pz) bond length for tetranuclear complexes of molybdenum (V) is rather close to that for mononuclear oxomolybdenum(VI) complexes (ca. 2.26 Å). Throughout all the oxo-molybdenum complexes of Tp* or Tp ligands the Mo=O bond length is almost invariable (column 2 in Table 3) and equals 1.68 (±0.02) Å with two exceptions.

Table 3
Metric parameters for oxo-molybdenum complexes with Tp and Tp* ligands

Compound	Mo=O[a] (Å)	$(N–Mo)_{av}$[a] (Å)	Mo–Mo[a] (Å)
Tetranuclear complexes			
T[9], [27]	1.682	2.247	2.553 (T/I) 3.454 (I/I)
T[10], [28]	1.674 1.665	2.262 2.250	3.625; 3.717; 3.636; 3.717
8	1.688 (T) 1.686 (I)	2.247	2.559 (T/I) 3.361 (I/I)
Dinuclear complexes			
D[11], (C_2), [27]	1.670 1.671	2.216	3.710
D[12], (C_i), [27]	1.779	2.211	3.722
D[13], *cis* Mo=O, [29]	1.651	2.246	3.771
D[14], *trans* Mo=O, [30]	1.664	2.238	3.773
D[15], [31]	1.695 (VI) 1.701 (VI)	2.422 2.220	3.755
D[16b], [32]	1.699 (V,VI)	2.263	3.793
Mononuclear molybdenum(V) complexes[c]			
M[17], [33]	1.680	2.225	
M[18], [34]	1.677	2.222	
M[19], [35]	1.693	2.221	
M[20], [36]	1.676	2.202	
M[21], [37]	1.682	2.234	
M[22], [38]	1.848	2.212	
Mononuclear molybdenum(VI) complexes[c]			
M[23], [39]	1.692; 1.697	2.263	
M[24], [40]	1.704; 1.694	2.249	

Abbreviations: T, terminal; I, inner.
[a] ±0.004 (Å) or less.
[b] Disordered structure with pseudo-C_2 symmetry.
[c] Only complexes with Tp* ligand.

3.2. The ^{1}H NMR spectroscopy of 4–7

The symmetry of the ^{1}H NMR spectra of complexes **4** and **6** corresponded to the anionic ligand symmetry, i.e. two set of 4-H(pz) resonances of 1:2 integral intensity ratio were observed for **4**, while only one 4-H(pz) resonance was found in case of **6**.

The ^{1}H NMR spectrum of **5** taken at ambient temperature consists of one set of broad resonances both from Tp′ and allyl ligands. Mutual rotation of those ligands becomes slow in the ^{1}H NMR timescale at lower temperatures (Fig. 4). Thus, two 4-H(pz) resonances of 1:2 intensity ratio are observed at 298 K, which split into two sets due to the presence of two rotational isomers ***I*** (of effective C_S symmetry) and ***II*** (Fig. 5). The spectral assignments for ***I*** and ***II*** were done on the basis of COSY and NOESY measurements. Series of EXSY peaks were observed within the 3-CH_3 and 5-CH_3 resonances between ***I*** and ***II***, which enabled to assign 3-CH_3 resonance at 2.10 ppm to isomer ***II***. Additionally, the NOE peak between 1′,3′-H_{endo} and 3-CH_3(3-Me-5-Phpz) in isomer ***I*** was observed.

Surprisingly, the ^{1}H NMR spectrum of **7** indicates that in this molecule mutual rotation of Tp′ and allyl ligands is already slow on a timescale of the method at 298 K in $CDCl_3$ solvent. Accordingly, two sets of pyrazolyl, 3-(2-thienyl) and 3-CH_3 resonances of 1:2 intensity ratio are observed.

3.3. The infrared spectroscopy of 4–7

The infrared spectra were obtained for solid complexes **4**–**7** in KBr pellets. The single ν(B–H) stretching vibration was observed in all cases confirming the one kind of complex molecules were present in solid state. While two ν(C–O) stretching vibrations attributed to carbonyl ligands were observed for **1** in acetonitrile [4,5] in case of **4** and **6** complexes three ν(C–O) bands were observed. This was attributed to low symmetry of complexes in solid state (cf. structural data, previous section). For allyl complexes **5** and **7** only two ν(C–O) bands were found, similarly to simple analogue **2** as could be anticipated.

3.4. Oxidation of molybdenum complexes

Electrochemical studies demonstrated that the first one-electron oxidation of $[Tp^*Mo(CO)_3]^-$ (**1**) in MeCN at −587 mV is reversible, while in THF it is shifted cathodically to −808 mV and only partially reversible, which suggests the involvement of the solvent molecule as a ligand in

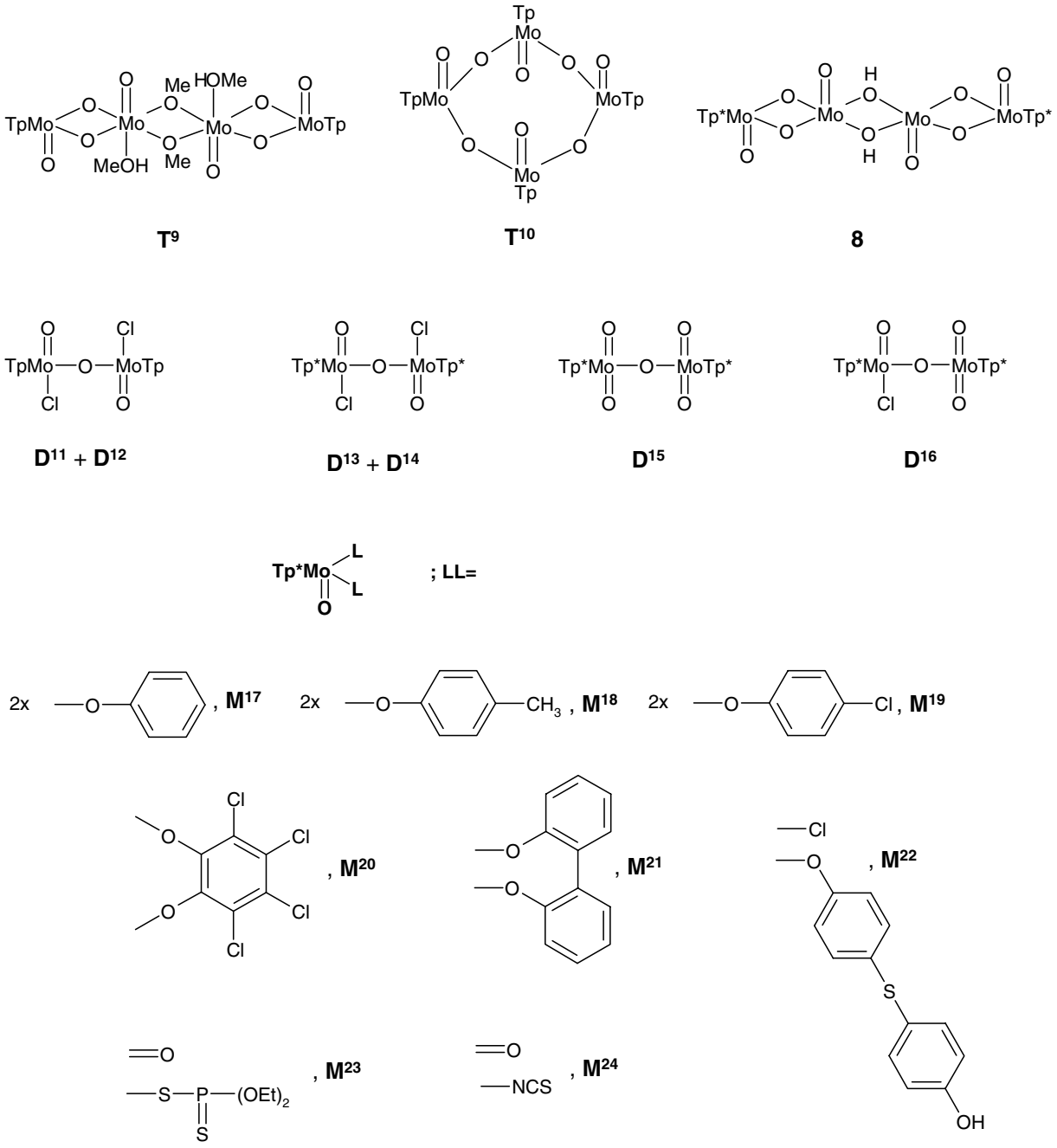

Chart 1. Schematic formulae of oxo-molybdenum complexes with Tp and Tp* ligands.

the process. The second oxidation is irreversible with no corresponding reduction wave, probably due to the loss of CO ligand from the two-electron oxidized species, which is characteristic of various $LMo(CO)_3$ type complexes. Surprisingly, the first oxidation of **4** occurs at a lower potential (−662 mV in MeCN) than that for **1** (−587 mV), which is counter to the expected electron-withdrawing effect of the phenyl substituents on pyrazolyl arms in **4**. This kind of such a reverse relationship has been previously observed for $Tp^{p\text{-}MeOPh}Mo(Cl)_2(NO)$ [41] and rationalized in terms of a weaker interaction between the $Tp^{p\text{-}MeOPh}$ ligand and Mo than that between Tp* and Mo in these compounds. The Mo–N(pz) bond distances in the former complex are longer. And indeed, in the case of our compounds, the Mo–N(pz) distances in **4** are longer than in **1** (cf. Table 2).

Within the $Tp'Mo(CO)_2(\eta^3\text{-allyl})$ complexes (**2**, **5**, and **7**) the oxidation of the molybdenum(II) complex was a two-electron process for **2** and **5**. It was virtually irreversible in the case of **5**, the corresponding reduction wave could be seen only at high scan rates. For **7**, however, two sluggish one-electron irreversible oxidation processes were observed with no corresponding reduction waves.

Chemical oxidation of reference complex **1** with iodine in $CDCl_3$ led to **3** as described in [11]. The complex **3** has characteristic spectrum, in which 3- and 5-methyl proton resonances are doubled due to effective C_S symmetry of

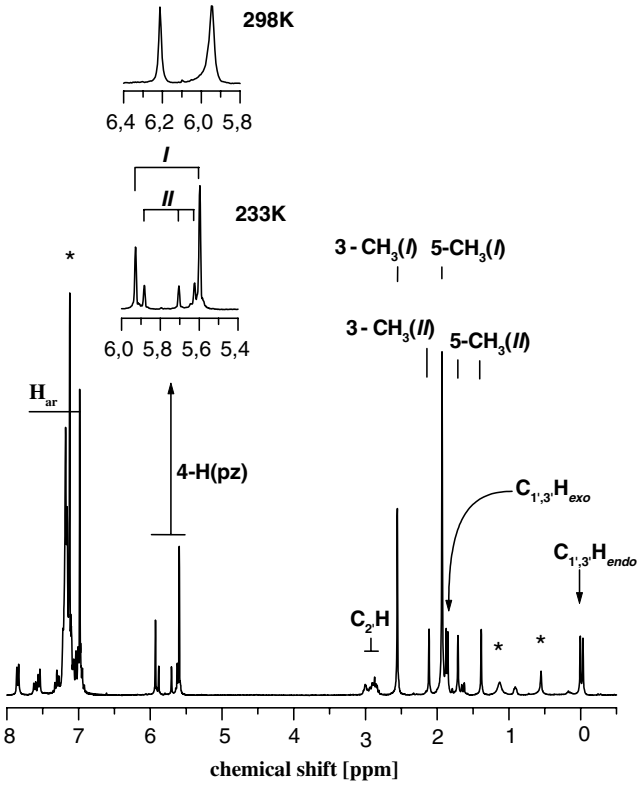

Fig. 4. The ^{1}H NMR spectrum of **5** in $CDCl_3$. The spectrum taken at 233 K (full spectrum presented) is composed of two set of resonances from isomers ***I*** and ***II***. Upper inset presents only the region of 4-H(pz) resonances at 298 K, which split into two sets at 233 K as presented in lower inset. The residual solvent and impurity resonances are labeled with asterisks.

$Tp^*Mo(CO)_2I$ complex and are observed at: 87.3 (3H); 70.1 (3H); 46.9 (6H); 34.7 (6H) ppm in $CDCl_3$ at 298 K. However, before this spectrum is produced, another species at early stage of titration of **1** with I_2 was observed; three low-intensity resonances at 18.7, 34.7, and 35.8 ppm are visible outside the diamagnetic region. That species is unstable and converts into the $Tp^*Mo(CO)_2Cl$ complex (**3′**) [11] identified on the basis of comparison with original sample (the 3- and 5-methyl proton resonances for the latter are observed at: 96.7 (3H); 71.4 (3H); 41.8 (6H); 31.7 (6H) ppm in $CDCl_3$ at 298 K). Upon addition of I_2, **3′** was further converted into **3**. Thus, the initial spectrum in undertitrated solution originate from $Tp^*Mo(CO)_3I$ or from other active form, like for instance $[Tp^*Mo(CO)_3]I$ or $Tp^*Mo(CO)_3I_2$, which is able to abstract the chloride anion from chloroform. This and the final conversion of **3′** into **3** mechanisms were unexplored. Oxidation of **2** with one equivalent I_2 or TBHP led cleanly to **3′** in $CDCl_3$ but not in acetone-d_6. Further addition of I_2 caused almost quantitative conversion of **3′** into the green species of the C_3 effective symmetry, for which only two methyl resonances were observed at 50.4 and 55.0 ppm.

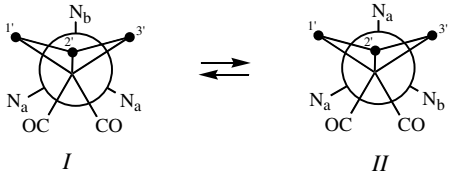

Fig. 5. Schematic presentation of two rotational isomers ***I*** and ***II*** of 5. N_a and N_b represent nitrogen donors from 3-Ph-5-Mepz and 3-Me-5-Phpz residues, respectively, the allyl carbon atoms (1′, 2′, and 3′) are depicted by dark circles.

A pair of molybdenum(0) and (II) complexes with $[HB(5\text{-Me-3-Phpz})_2(3\text{-Me-5-Phpz})]^-$ heteroscorpionate ligand, i.e. **4** and **5** were oxidized with I_2 under spectral control. Already at the very early stage of titration of **4** with I_2 the formation of many paramagnetic species was observed, among them the $[HB(5\text{-Me-3-Phpz})_2(3\text{-Me-5-Phpz})]Mo(CO)_2X$ (X = I or Cl) with characteristic methyl resonances at about 85 and 70 ppm. However, the major species was different. The attempts to isolate it were unsuccessful. The oxidation of **5** was monitored by the ^{1}H NMR spectroscopy. No paramagnetic spectra of intermediates were found in that experiment. Eventually, upon addition of two equivalents of I_2 two 4-H(pz) resonances of the 2:1 intensity ratio were found at about 6 ppm of the spectrum of diamagnetic product, which were tentatively assigned to $[Tp'MoO_3]^-$ species.

Generally, the molybdenum(II) complexes, either those obtained upon two-electron oxidation of $[Tp'Mo(CO)_3]^-$ or $Tp'Mo(CO)_2$(allyl) were easily oxidizable and no intermediates could be isolated or detected by the ^{1}H NMR method before final oxidation to Mo(V) or Mo(VI). Even simple and relatively stable ligand Tp^* was partially decomposed upon aerial oxidation of $Tp^*Mo(CO)_2I$ in mild conditions to produce complex **8**.

4. Supplementary data

Crystallographic data for the structures reported in this paper (excluding structure factors) have been deposited with the Cambridge Crystallographic Data Centre, CCDC no. 605472 (compound **6**), no. 605473 (compound **7**), and no. 605474 (compound **8**). Copies of this information may be obtained free of charge from the Director, CCDC, 12 Union Road, Cambridge CB2 1EZ, UK (fax: +44 1223 336 033; e-mail: deposit@ccdc.cam.ac.uk or http://www.ccdc.cam.ac.uk).

Acknowledgments

Authors thank to Ministry of Education and Science (Poland) for the Grant No. 3 T09A 06928.

References

[1] S. Trofimenko, Scorpionates: The Coordination Chemistry of Polypyrazolylborate Ligands, Imperial College Press, London, UK, 1999.
[2] T. Ruman, Z. Ciunik, S. Wołowiec, Polyhedron 23 (2004) 219, Part XII and Refs. [2–9] cited therein.
[3] Sheng-Ling Guo, Sheng-Ming Liu, Yuan-Qi Yin, Kai-Bei Yu, Chem. J. Chin. Univ. 19 (1998) 741.

[4] S. Trofimenko, J. Am. Chem. Soc. 91 (1969) 588.
[5] C.P. Marabella, J.H. Enemark, J. Organomet. Chem. 226 (1982) 57.
[6] D.S. Frohnapfel, P.S. White, J.L. Templeton, H. Ruegger, P.S. Pregosin, Organometallics 16 (1997) 3737.
[7] S. Trofimenko, J.C. Calabrese, J.S. Thompson, Inorg. Chem. 26 (1987) 1507.
[8] M. Łukasiewicz, Z. Ciunik, T. Ruman, M. Skóra, S. Wołowiec, Polyhedron 20 (2001) 237.
[9] T. Ruman, M. Łukasiewicz, Z. Ciunik, S. Wołowiec, Polyhedron 20 (2001) 2551.
[10] S. Trofimenko, J. Am. Chem. Soc. 91 (1969) 3183.
[11] A.A. Saleh, B. Pleune, J.C. Fettinger, R. Poli, Polyhedron 16 (1997) 1391.
[12] G.M. Sheldrick, Acta Crystallogr., Sect. A 46 (1990) 467.
[13] G.M. Sheldrick, SHELXL97, Program for Crystal Structure Refinement, University of Göttingen, Germany, 1997.
[14] H. Arzoumanian, Coord. Chem. Rev. 180 (1998) 191.
[15] Kom-Bei Shiu, J.Y. Lee, Yu. Wang, Ming-Chu Cheng, Sue-Lein Wang, Fen-Ling Liao, J. Organomet. Chem. 453 (1993) 211.
[16] T.M. Bockman, J.K. Kochi, New J. Chem. 16 (1992) 39.
[17] T.J. Desmond, F.J. Lalor, M. Parvez, J. Organomet. Chem. 277 (1984) 91.
[18] Y.D. Ward, L.A. Villanueva, D.G. Allred, S.C. Payne, M.A. Semones, L.S. Liebeskind, Organometallics 14 (1995) 4132.
[19] E.M. Holt, S.L. Holt, K.J. Watson, J. Chem. Soc., Dalton Trans. (1973) 2444.
[20] F.A. Cotton, C.A. Murillo, B.R. Slutts, Inorg. Chim. Acta 22 (1977) 75.
[21] A.L. Rheingold, L.M. Liable-Sands, C.L. Incarvito, S. Trofimenko, J. Chem. Soc., Dalton Trans. (2002) 2297.
[22] A.L. Rheingold, L.N. Zakharov, S. Trofimenko, Inorg. Chem. 42 (2003) 827.
[23] A.L. Rheingold, C.B. White, S. Trofimenko, Inorg. Chem. 32 (1993) 3471.
[24] S. Trofimenko, A.L. Rheingold, L.M. Liable-Sands, Inorg. Chem. 41 (2002) 1889.
[25] A.L. Rheingold, G. Yap, S. Trofimenko, Inorg. Chem. 34 (1995) 759.
[26] A.L. Rheingold, B.S. Haggerty, S. Trofimenko, Chem. Commun. (1994) 1973.
[27] S. Lincoln, A. Koch, Inorg. Chem. 25 (1986) 1594.
[28] S. Wołowiec, J.K. Kochi, Inorg. Chem. 30 (1991) 1215.
[29] M.B. Kassim, R.L. Paul, J.C. Jeffery, J.A. McCleverty, M.D. Ward, Inorg. Chim. Acta 327 (2002) 160.
[30] A.J. Millar, C.J. Doonan, L.J. Laughlin, E.R.T. Tiekink, C.G. Young, Inorg. Chim. Acta 337 (2002) 393.
[31] K.M. Bamhart, J.H. Enemark, Acta Crystallogr., Sect C: Cryst. Struct. Commun. 40 (1984) 1362.
[32] A.A. Eagle, M.F. Mackay, C.G. Young, Inorg. Chem. 30 (1991) 1425.
[33] C.A. Kipke, W.E. Cleland Jr., S.A. Roberts, J.H. Enemark, Acta Crystallogr., Sect C: Cryst. Struct. Commun. 45 (1989) 870.
[34] Chaung-Sheng J. Chang, T.J. Pecci, M.D. Carduzzi, J.H. Enemark, Inorg. Chem. 32 (1993) 4106.
[35] Chaung-Sheng J. Chang, T.J. Pecci, M.D. Carduzzi, J.H. Enemark, Acta Crystallogr., Sect. C: Cryst. Struct. Commun. 48 (1992) 1096.
[36] P. Basu, M.A. Bruck, Zheng Li, I.K. Dhawan, J.H. Enemark, Inorg. Chem. 34 (1995) 405.
[37] R.H. Laye, Z.R. Bell, M.D. Ward, New J. Chem. 27 (2003) 684.
[38] N.C. Hardern, E.R. Humphrey, J.C. Jeffery, Siu-Ming Lee, M. Marcaccio, J.A. McCleverty, L.H. Rees, M.D. Ward, J. Chem. Soc., Dalton Trans. (1999) 2417.
[39] S.A. Roberts, C.G. Young, W.E. Cleland Jr., R.B. Ortega, J.H. Enemark, Inorg. Chem. 27 (1988) 3044.
[40] S.A. Roberts, C.G. Young, C.A. Kipke, W.E. Cleland Jr., K. Yamanouchi, M.D. Carduzii, J.H. Enemark, Inorg. Chem. 279 (1990) 3650.
[41] M. Cano, J.V. Heras, A. Monge, E. Gutierrez, C.J. Jones, S.L.W. McWinnie, J.A. McCleverty, J. Chem. Soc., Dalton Trans. (1992) 2435.

cost ink-jet printing techniques [22,23]. However, because of the complicated and multi-step synthetic strategy for the preparation of polymer-supported AlQ_3, commercialization by this route is doubtful. Alternatively, reactive AlQ_3 derivatives such as $Al(Et)_2Q$ [24], $Al(Et)Q_2$ [25] and $Al(Q)_2(OH)$ [26] can be incorporated into polymers containing OH side groups by condensation reactions. High reactivity of the former and low solubility of the latter mentioned compounds can be overcome by replacing the ethyl or hydroxide group with long alkoxy groups. Furthermore, it has recently been proposed that the aluminium–nitrogen bond strength can be used as a parameter for tuning the complex emission wavelength [27], alternatively it may be possible to alter the emission wavelength to some extent using various alkoxy groups. As a contribution to the latest development of this interesting field, we would like to report the synthesis and characterization of the first examples of two highly soluble and stable alkoxy derivatives of AlQ_3, $[Al(Q_2)(OCH_2CH_2OR)]_2$ [R = CH_3 (**1**) and C_2H_5 (**2**)]. In addition, their photoluminescence behaviour was investigated and the molecular structure of complex **2** was determined by X-ray analysis.

2. Experimental

All manipulations were carried out under nitrogen, using standard Schlenk techniques. All chemicals were purchased from Merck and were used as received, except solvents which were dried and distilled under nitrogen prior to use. Both $Al(OCH_2CH_2OCH_3)_3$ and $Al(OCH_2CH_2OCH_2CH_3)_3$ were prepared by the alcohol exchange method from $Al(OCH(CH_3)CH_2CH_3)$ according to a previous report [28].

Infrared spectra were recorded on a Shimadzu 470 instrument, using KBr pellets. ^1H and ^{13}CNMR spectra were recorded in C_6D_6 on a Bruker AVANCE 300-MHz instrument using TMS as an internal reference. ^{27}Al NMR spectra were obtained on a Bruker AVANCE 500-MHz spectrophotometer in C_6D_6 using aluminium nitrate as an external reference in aqueous solution. The mass spectroscopy was performed on a Varian Matt 44 instrument (electron impact, 20 eV). Absorption spectra of solutions (10^{-6} M) were obtained in CH_2Cl_2 on a Shimadzu 2100 UV–Vis spectrophotometer. Emission spectra were recorded at room temperature on a Perkin–Elmer MPF-43A spectrofluorimeter from 440 to 550 nm by excitation with UV light using 30 μM solutions of **1** and **2** in dichloromethane.

2.1. Synthesis of *1*

Compound **1** was prepared by the reaction of 8-hydroxyquinoline (0.73 g, 5 mmol) with $Al(OCH_2CH_2OCH_3)_3$ (1.26 g, 5 mmol) in benzene (30 ml). The mixture was refluxed for 3 h and the solvent was removed under reduced pressure to leave a yellow solid. The solid was crystallized from dichloromethane–hexane; single crystals of the complex were isolated from the solution after several days at −5° C, m.p. decomposes at 280 °C. *Anal*. Calc. for $C_{21}H_{19}N_2O_4Al$: C, 64.62; H, 4.87; N, 7.18. Found: C, 64.22; H, 4.80; N, 6.62%. UV (CH_2Cl_2, nm): 318 (MLCT), 335 (π–π*) and 382 (n–π*). IR (cm^{-1}): 3035 (C–H, aromatic), 2968 (C–H, aliphatic), 1605 (C═N), 1575 (C═C), 1078 (C–O), 639 (Al–O), 752 (Al–O–Al). ^1H NMR (C_6D_6, ppm): 2.5 (3H, s, –OC*H*$_3$), 2.9–3.8 (4H, m, AlOC*H*$_2$C*H*$_2$–). C_9H_6NO ligand protons: 6.4 (1H, q), 6.9 (1H, d), 7.0 (1H, d), 7.1 (1H, d), 7.3 (2H, m), 7.4 (1H, t), 7.5 (1H, d) 7.6 (1H, t), 7.9 (1H, d), 8.6 (1H, d), 9.5 (1H, d). ^{13}C NMR (ppm): 57.15, 61.11, 73.63, 110.48, 110.79, 111.59, 120.67, 121.04, 129.25, 129.68, 130.44, 130.77, 138.33, 138.42, 140.31, 140.49, 144.21, 144.85, 147.25, 160.72, 160.87. ^{27}Al NMR (ppm): 26.8, 71.4. Mass spectral data, aluminium-bearing fragments (*m*/*e*): 390 $[Al(OCH_2CH_2OCH_3)(C_9H_6NO)_2]^{+\cdot}$, 315 $[Al(C_9H_6NO)_2]^+$, 246 $[Al(OCH_2CH_2OCH_3)(C_9H_6NO)]^{+\cdot}$, 201 $[Al(OCH_2)(C_9H_6NO)]^+$, 188 $[Al(C_9H_6NO)(OH)]^{+\cdot}$, 171 $[Al(C_9H_6NO)]^+$. Mass numbers are based upon ^1H, ^{12}C, ^{14}N, ^{16}O and ^{27}Al.

2.2. Synthesis of *2*

Compound **2** was prepared by the reaction of 8-hydroxyquinoline (0.73 g, 5 mmol) with $Al(OCH_2CH_2OCH_2CH_3)_3$ (1.47 g, 5 mmol) in benzene (30 ml). The mixture was refluxed for 3 h and the solvent was removed under reduced pressure to leave a yellow solid. The solid was crystallized from dichloromethane–hexane at −5 °C, m.p., decomposes at 240 °C. *Anal*. Calc. for $C_{22}H_{21}N_2O_4Al$: C, 65.34; H, 5.20; N, 6.93. Found: C, 64.75; H, 5.12; N, 7.1%. UV (CH_2Cl_2, nm): 317 (LMCT), 334 (π–π*), 382 (n–π*). IR (cm^{-1}): 3035 (C–H, aromatic), 2967 (C–H, aliphatic), 1603 (C═N), 1578 (C═C), 1081 (C–O), 644 (Al–O), 750 (Al–O–Al). ^1H NMR (C_6D_6, ppm): 0.6 (3H, t, –OCH$_2$C*H*$_3$), 2.7–3.7 (4H, m, –C*H*$_2$OC*H*$_2$CH$_3$), 3.8–4.0 (2H, m, AlOC*H*$_2$). C_9H_6NO ligand protons: 6.4 (1H, q), 6.9 (1H, d), 7.0 (1H, d), 7.0 (1H, d), 7.3 (2H, m), 7.4 (1H, t), 7.5 (1H, d) 7.6 (1H, t), 7.9 (1H, d), 8.6 (1H, d), 9.5 (1H, d). ^{13}C NMR (C_6D_6, ppm): 14.48, 61.60, 65.14, 71.93, 110.46, 110.89, 110.98, 111.52, 120.57, 121.8, 129.25, 129.89, 130.44, 130.79, 138.25, 138.44, 140.82, 141.15, 144.25, 147.19, 160.67, 160.90. ^{27}Al NMR (C_6D_6, ppm): 26.9 and 69.5. Mass spectral data, aluminium-bearing fragments (*m*/*e*): 404 $[Al(OCH_2CH_2OCH_2CH_3)(C_9H_6NO)_2]^{+\cdot}$, 315 $[Al(C_9H_6NO)_2]^+$, 260 $[Al(OCH_2CH_2OCH_2CH_3)(C_9H_6NO)]^{+\cdot}$, 201 $[Al(OCH_2)(C_9H_6NO)]^+$, 188 $[Al(C_9H_6NO)(OH)]^{+\cdot}$, 171 $[Al(C_9H_6NO)]^+$. Mass numbers are based upon ^1H, ^{12}C, ^{14}N, ^{16}O and ^{27}Al.

3. X-ray crystallography

A yellow prism-shaped crystal of **2**, air stable at room temperature, was used for the crystallographic measurements. The data were collected at 193 K on a Siemens P3 four-circle diffractometer. Crystal data and details of structure determination for compound **2** are presented in

Table 1
Crystal data and structure refinement for compound **2**

Empirical formula	$C_{44}H_{42}Al_2N_4O_8 \cdot 2(CH_2Cl_2) \cdot 3(H_2O)$
Formula weight	1032.68
Temperature (K)	193(2)
Wavelength (Å)	0.71073
Crystal system	triclinic
Space group	$P\bar{1}$
Unit cell dimensions	
a (Å)	13.771(3)
b (Å)	14.264(3)
c (Å)	14.685(3)
α (°)	74.41(3)
β (°)	72.31(3)
γ (°)	69.39(3)
Volume (Å^3)	2529.7(9)
Z	2
D_{calc} (Mg/m^3)	1.356
Absorption coefficient (mm^{-1})	0.329
$F(000)$	1076
Crystal size (mm)	$0.35 \times 0.25 \times 0.15$
Θ Range for data collection (°)	2.78–23.98
Index ranges	$0 \leqslant h \leqslant 13$, $-15 \leqslant k \leqslant 16$, $-16 \leqslant l \leqslant 16$
Reflections collected [R_{int}]	7763/7401 [0.0667]
Completeness to theta = 23.98°	93.3%
Refinement method	full-matrix least-squares on F^2
Data/restraints/parameters	7401/4/631
Goodness-of-fit on F^2	0.987
Final R indices for 2978 reflections with $[I > 2\sigma(I)]$	$R_1 = 0.0761$, $wR_2 = 0.1379$
R indices (all data)	$R_1 = 0.2157$, $wR_2 = 0.1521$
Larger difference in peak and hole (e A^{-3})	0.814 and −0.414

Table 1. Unit cell parameters were determined using Siemens P3/PC software [29]. The structure was solved by a direct method and refined with full matrix least-squares on F^2 to a final R value of 0.0761, $wR_2 = 0.1379$ with the SHELXL program [30]. The hydrogen atoms of CH_2Cl_2 and water molecules were found in difference Fourier synthesis; the H(C) atom positions were calculated. All hydrogen atoms were refined in isotropic approximation using the riding model with the U_{iso}(H) parameters equal to 1.2 U_{eq}(Ci), for methyl groups equal to 1.5 U_{eq}(Cii), where U(Ci) and U(Cii) are the equivalent thermal parameters of the atoms to which the corresponding H atoms are bonded.

4. Results and discussion

4.1. Preparation

Bis[μ-2-methoxy-ethanalato-di-(8-quinolinato)aluminium(III)] and bis[μ-2-ethoxy-ethanalato-di-(8-quinolinato)aluminium(III)] were obtained by the reaction of $Al(OCH_2CH_2OCH_3)_3$ and $Al(OCH_2CH_2OCH_2CH_3)_3$ with 8-hydroxyquinoline in a 1:1 ratio in refluxing benzene. These reactions are fast and their progress was followed by the appearance of a very intense yellow fluorescence colour. Due to the lability of metalloorganic and organometallic compounds, their reactions with 8-hydroxyquinoline and imine is facile and quantitative [31]. Both compounds are yellow solids and are soluble in common organic solvents and were purified by recrystallization from a mixture of dichloromethane and *n*-hexane. In contrast to the parent aluminium alkoxides, the 8-hydroxyquinoline derivatives are not sensitive to air and moisture, but they lose crystallinity when exposed to air. Our early attempt for the preparation of isopropoxide and ethoxide derivatives resulted in the formation of AlQ_3 in spite of using extra aluminium alkoxides. Apparently the long chain alkoxy ligands, 2-methoxyethoxide and 2-ethoxyethoxide, have a significant role in the stabilization of compounds **1** and **2**. Interestingly, the recent DFT optimization of the model pentacoordinated species $AlQ_2(OCH_3)$ shows that one of the pyridyl units of 8-hydroxyquinoline dissociates from aluminium [32].

4.2. Spectroscopic studies

The ready formation of compounds was established by the observation of $[Al(C_9H_6ON)_2(OCH_2CH_2OR)]^+$ and $[Al(C_9H_6ON)_2]^+$ (R = –CH_3 and –C_2H_5) fragments in the mass spectra. However, parent ions or dimeric species were not observed in the electron impact mass spectra. Furthermore, coordination of oxygen and nitrogen atoms of quinoline to aluminium was pursued by IR spectra by means of comparing the spectra with that of the free ligand. Absence of a band at 3300 cm^{-1} due to υ(OH) of free 8-hydroxyquinoline in the IR spectra of the complexes, and the appearance of new bands at 645 and 590 cm^{-1}, assigned to υ(Al–O) and υ(Al–N), respectively [33], confirmed coordination of the ligand to aluminium through oxygen and nitrogen. As previously noticed, by coordination of the 8-hydroxyquinoline nitrogen to various ions, υ(C=N) reduces in comparison with the free ligand value [34]. The absorption frequency of the phenolic C–O in the free ligand shifts from 1260 cm^{-1} to 1280 cm^{-1} on coordination to aluminium. The Al–O–Al vibrations appear at 755 cm^{-1} [31]. The ^{1}H NMR spectra of **1** and **2** exhibit the expected aromatic and aliphatic protons. However, there is

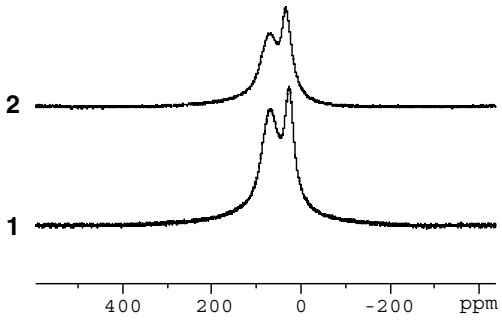

Fig. 1. ^{27}Al NMR spectra of **1** and **2**.

considerable deshielding of the proton bonded to the carbon atom adjacent to the nitrogen and shielding of the proton bonded to the carbon atom adjacent to the oxygen (phenolic ring) in comparison to the free ligand. Such a shift has been observed in the 8-quinolinolate vanadium complex [35]. The ^{27}Al NMR spectra of **1** and **2** (Fig. 1) with two signals at 26.9, 69.5 ppm (half width $w_{1/2}$, 2820 and 4812 Hz) and 26.6, 70.1 ppm (half width $w_{1/2}$, 2825 and 4832 Hz) indicate that the 6- and 4-coordinated aluminium atoms, respectively, exist in solution [36,37].

4.3. Crystal of **2** as the trihydrated bis(dichloromethane) solvate

Selected bond lengths and angles for **2** are given in Table 2. Compound **2**, as shown in Fig. 2, is an unsymmetrical dimer. Two 8-quinolinolato anions are chelated to Al and the coordination number is raised to six as the 2-ethoxymethoxy group is bridging, despite of the steric bulk of alkoxy ligand. The two bridging Al–O distances, Al(1)–O(5), 1.899(4) Å; Al(1)–O(7), 1.886(4) Å, are nearly identical and are somewhat longer than the other two Al–O distances, but they are somewhat shorter than those found in the six coordinated aluminium moiety in $\{C_6H_4O[CH{=}N(C_6H_5)]\}_2Al(\mu\text{-}OPr^i)_2Al(OPr^i)_2$ [37] and longer than those of in the centrosymmetric dimer $[Cp_2Al\text{-}\mu\text{-}OR]_2$ [38]. Interestingly, in the absence of an alkoxy group in a complex such as the centrosymmetric compound $[Al(Et)_2(Q)]_2$, for the formation of a dimeric complex, the quinoline oxygen atoms are bridged [24]. As noticed by several authors, oxygen bridging is more favourable in aluminium complexes with bidentate Schiff base ligands [31].

Table 2
Selected bond angles (°) and bond lengths (Å) for **2**

Bond distances			
Al(1)–O(3)	1.875(5)	Al(2)–O(4)	1.859(5)
Al(1)–O(2)	1.883(4)	Al(2)–O(1)	1.876(5)
Al(1)–O(7)	1.886(4)	Al(2)–O(7)	1.881(4)
Al(1)–O(5)	1.899(4)	Al(2)–O(5)	1.881(4)
Al(1)–N(2)	2.003(6)	Al(2)–N(1)	2.046(6)
Al(1)–N(3)	2.029(6)	Al(2)–N(4)	2.062(6)
Bond angles			
O(3)–Al(1)–O(2)	95.20(19)	O(4)–Al(2)–O(1)	167.7(2)
O(3)–Al(1)–O(7)	170.09(19)	O(4)–Al(2)–O(7)	90.1(2)
O(2)–Al(1)–O(7)	93.34(19)	O(1)–Al(2)–O(7)	98.8(2)
O(3)–Al(1)–O(5)	94.18(19)	O(4)–Al(2)–O(5)	99.2(2)
O(2)–Al(1)–O(5)	169.4(2)	O(1)–Al(2)–O(5)	90.9(2)
O(7)–Al(1)–O(5)	77.78(18)	O(7)–Al(2)–O(5)	78.34(18)
O(3)–Al(1)–N(2)	87.9(2)	O(4)–Al(2)–N(1)	88.7(2)
O(2)–Al(1)–N(2)	82.9(2)	O(1)–Al(2)–N(1)	81.9(2)
O(7)–Al(1)–N(2)	98.1(2)	O(7)–Al(2)–N(1)	97.1(2)
O(5)–Al(1)–N(2)	92.7(2)	O(5)–Al(2)–N(1)	170.8(3)
O(3)–Al(1)–N(3)	82.2(2)	O(4)–Al(2)–N(4)	82.2(2)
O(2)–Al(1)–N(3)	89.4(2)	O(1)–Al(2)–N(4)	89.9(2)
O(7)–Al(1)–N(3)	92.9(2)	O(7)–Al(2)–N(4)	169.5(2)
O(5)–Al(1)–N(3)	96.7(2)	O(5)–Al(2)–N(4)	95.8(2)
N(2)–Al(1)–N(3)	166.9(2)	N(1)–Al(2)–N(4)	89.9(2)

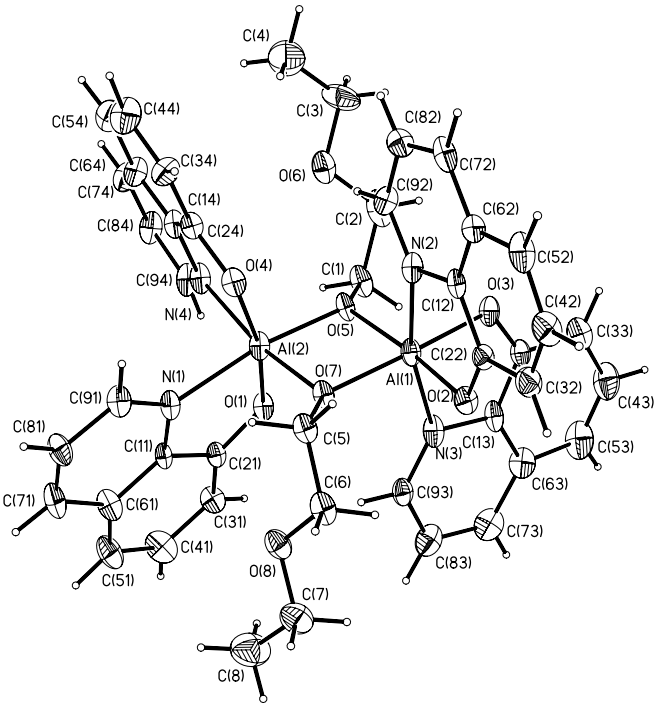

Fig. 2. ORTEP plot of **2**, with displacement ellipsoids at the 50% probability level. H atoms are drawn as spheres of arbitrary radii and solvent molecules are omitted for clarity.

Probably the most interesting feature of this structure is the geometries around the aluminium atoms. Al(1) and Al(2) are six-coordinated in distorted octahedral geometries by two phenolate oxygen, two nitrogen and two bridging 2-ethoxyethoxy group oxygen atoms; and their bond angles range from 77.78(18)° to 99.2(2)°. Two nitrogen atoms on Al(1), with bond distances of 2.003(6) and 2.029(6) Å, are *trans* to each other. The N(2)–Al(1)–N(3), O(2)–Al(1)–O(5) and O(3)–Al(1)–O(7) angles of 166.9(2)°, 169.4(2)° and 170.09(19)°, respectively, are severely bent. The quinolines bite angles of 82.9(2)° and 82.2(2)° on Al(1) are almost identical and are comparable with those in AlQ_3 [39]. Interestingly, the coordination geometry of Al(2) differs from Al(1), the two nitrogen atoms on Al(2), with bond distances of 2.046(6), 2.062(6) Å and a N(1)–Al(2)–N(4) angle of 89.9(2)°, are *cis* to each other. The discrete unsymmetrical dimer contains *cis* and *trans* isomers and they are linked to each other by two bridging alkoxy groups. To illustrate the difference in coordination geometries more clearly, we have drawn the structure in Scheme 1. To our knowledge, dinuclear aluminium alkoxides or dinuclear organoaluminium derivatives where two aluminium atoms have different geometries in same ligand environment is very rare. In principle, for compound **2**, which has C_2 symmetry, a large number of stereoisomers are possible, therefore a number of pairs of enantiomers is expected. Notably, there is no disorder in the structure, which indicates only one isomer is present in the crystal.

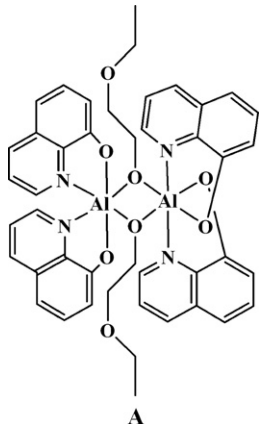

A

Scheme 1.

4.4. Solution behaviour of compounds *1* and *2*

Although the single crystal structure determination of compound **2** shows that the aluminium atoms are six coordinate, solution studies reveal that in solution six and four coordinated species are present. By taking into consideration that the molecule is severely distorted in the solid state, and also the steric hindrance caused by the two quinolines moieties around the aluminium atoms, it is not surprising to see that the solid structure is not retained in solution. Apparently, both nitrogen atoms around the aluminium atom dissociated and resulted in the formation of four-coordinated aluminium (Scheme 2). Dissociation of Al–N bonds and formation of a four-coordinate aluminium atom has also been observed for an unsymmetrical dimer of $[(CH_3COCHCOCH_3)Al(\mu\text{-}OPr^i)(C_9H_6NO)]_2$ [34]. Indeed, conversion of *fac*/*mer* isomers of AlQ_3 *via* dissociation of Al–N is well established [16]. Furthermore, 11 well resolved peaks in the ^1H and 18 in the ^{13}C NMR spectra of both compounds show that the C_2 symmetry after dissociation of the Al–N bond (Scheme 2) remains intact. We have not seen any evidence supporting the existence of other isomers.

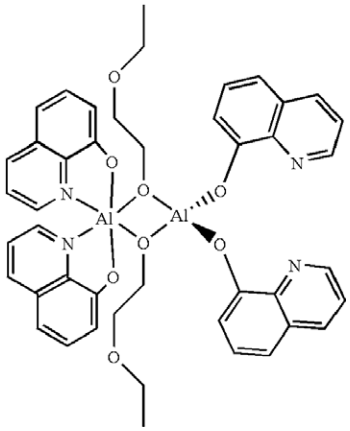

Scheme 2.

Interestingly, compound **2** shows a specific rotation of $[\alpha]^{25} = 1.87°$ in dichloromethane, which indicates that an excess of enantiomer (**ee**) exists in solution. However, in accordance with the ^{27}Al NMR data, the solid state structure is not retained in solution, therefore one can conclude that a C_2 symmetry or lower also is the case for compound **2** in solution. The excess of enantiomer may be attributed to the highly crowded environments of the aluminium atoms and a preference for one enantiomer.

Despite several attempts to determine the molecular structure of compound **1** by X-ray diffraction for a comparison with the structure of **2**, due to crystal twining, we have not succeeded. However, a somewhat similar behaviour has been found for compound **1**. In fact the ^{27}Al NMR spectrum of compound **1** almost is identical to that of compound **2**. Furthermore, a specific rotation of $[\alpha]^{25} = -2.97°$ indicates that there is no inversion centre, neither mirror plane nor improper rotation axis (S_n) for **1**. Therefore, it may be concluded that for compound **1** a C_2 symmetry or lower also is the case in solution. Consistently, the ^{13}C NMR spectrum of **1** contains 18 peaks for the carbons of the quinoline ligands, which corresponds to two non-equivalent quinoline ligands. However, there is a difference in the specific rotation of **1** in comparison to **2**, which can be attributed to the difference in concentration of **ee** that may exist in solution. The difference in **ee** can be explained by taking into consideration the steric hindrance that may be imposed by the 2-ethoxyethoxide ligands which alters the amount of **ee**.

4.5. Luminescence measurements

In order to demonstrate that the luminescence properties of the new derivatives of AlQ_3 are preserved, we have measured emission spectra of both compounds in dichloromethane from 400 to 700 nm upon excitation by UV light. The UV–Vis absorption spectra of **1** and **2** in dichloromethane show peaks at 320, 338 and 382 nm, and 317, 334 and 382 nm, respectively. Two absorptions are comparable with the 312 and 389 nm peaks of AlQ_3 [39]. The origin of the new peaks, 334 and 338 nm, which appeared in spectra of **1** and **2**, respectively, is not understood at this time, however, it could be associated with the involvement of the 2-methoxyethoxide/2-ethoxyethoxide groups and a $n \rightarrow \pi^*$ transition.

As shown in Fig. 3, both complexes have identical emission spectra and are fluorescence at a wavelength of 502 nm, which is lower than AlQ_3 (526 nm). Similar to azaindole complexes of aluminium, luminescence can be attributed to the π–π transition of the deprotonated 8-hydroxyquinoline which is stabilized by coordination to the aluminium ion [40]. The blue shift of **1** and **2** with respect to AlQ_3 can be attributed to the presence of electron withdrawing alkoxy groups. This conclusion is consistent with the recent study on AlQ_3 complexes which show electron withdrawing substituents on the quinoline results in a shift of emission to a lower wavelength [27,39], and

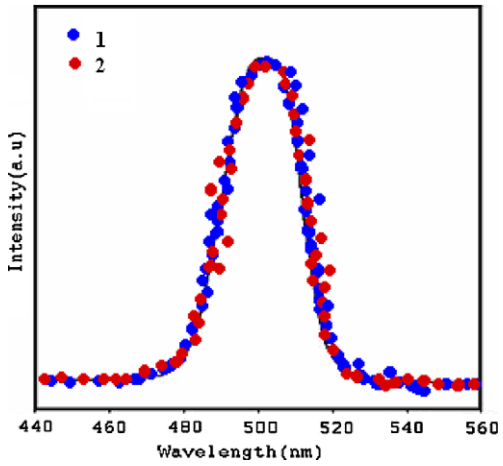

Fig. 3. Emission spectra of **1** and **2** in CH_2Cl_2.

also is consistent with the emission of AlQ_2OH at 485 nm [26]. Extensive studies on the photoluminescence properties of AlQ_3 show that the *fac*-AlQ_3 and *mer*-AlQ_3 spectral emission differ and each one has a distinctive fingerprint [16]. Therefore, a mixture of two isomers is expected to show a broad emission. Interestingly, a half width ($w_{1/2}$) of 60 nm has been observed for the emission spectrum of AlQ_3 [21,39], in comparison with a half width of 40 nm for the emission spectra of **1** and **2**. The smaller half width ($w_{1/2}$) may be attributed to the **ee** of compounds **1** and **2**, however additional work is required for new and deeper understanding.

In conclusion, we have prepared and characterized two derivatives of AlQ_3 containing long chain alkoxy groups. The derivatives have high solubility and suitable thermal stability and most importantly they have similar absorption and emission properties to AlQ_3. Further studies are underway to elucidate the correlation of the solution-state structure to electroluminescence performance.

Acknowledgments

The authors thank the Vice-President's Office for Research Affairs of Shahid Beheshti University for supporting this work and Professor Alexander Yanovsky and Dr. Zoya Starikov of the Russia Academy of Science for the crystallographic measurements.

Appendix A. Supplementary material

Crystallographic data for the structural analysis have been deposited with the Cambridge Crystallographic Data Centre, CCDC No. 296848. Copy of this information may be obtained free of charge from The Director, CCDC, 12 Union Road, Cambridge CB2 1EZ, UK, fax: +44 1223 336 033, e-mail: deposit@ccdc.cam.ac.uk or www:http://www.ccdc.cam.ac.uk. Supplementary data associated with this article can be found, in the online version, at doi:10.1016/j.poly.2006.05.031.

References

[1] S.M. Kelly, in: J.A. Connor (Ed.), Flat Panel Displays: Advanced Organic Materials, The Royal Society of Chemistry, Cambridge, 2000.
[2] M.M. Richlter, Chem. Rev. 104 (2004) 3003.
[3] S. Wang, Coord. Chem. Rev. 215 (2001) 215.
[4] C.W. Tangs, S.A. Van Slyke, Appl. Phys. Lett. 51 (1987) 913.
[5] R. Pohl, P. Anzenbacher Jr., Org. Lett. 5 (2003) 2769.
[6] M. Brinkmann, G. Gadret, M. Muccini, C. Taliani, N. Masciocchi, A. Sironi, J. Am. Chem. Soc. 122 (2000) 5147.
[7] Y. Yamada, T. Sano, K. Shibata, K. Kuroki, Jpn. J. Appl. Phys. 34 (1995) L824.
[8] W.F. Zeng, Y.S. Chen, M.Y. Chiang, S.S. Chern, C.P. Cheng, Polyhedron 21 (2002) 1081.
[9] Y. Qin, C. Pagba, P. Piotrowiak, F. Jakle, J. Am. Chem. Soc. 126 (2004) 7015.
[10] M. Brinkmann, B. Fite, S. Pratontep, C. Chaumont, Chem. Mater. 16 (2004) 4627.
[11] P.E. Burrows, L.S. Sapochak, D.M. McCarty, S.R. Forrest, M.E. Thompson, Appl. Phys. Lett. 64 (1994) 2718.
[12] P.E. Burrows, Z. Shen, V. Bulovic, D.M. McCarty, S.R. Forrest, J.A. Cronin, M.E. Thompson, J. Appl. Phys. 79 (1996) 7991.
[13] L.S. Sapochak, F.E. Benincasa, R.S. Schofield, J.L. Baker, K.K.C. Riccio, D. Fogarty, H. Kohlmann, K.F. Ferris, P.E. Burrows, J. Am. Chem. Soc. 124 (2002) 6119.
[14] Y.A. Bankovakii, V.K. Bel'skii, L.Y. Pech, T.V. Ashaks, Russ. J. Inorg. Chem. 38 (1993) 1862.
[15] A. Kolb, P. Bissinger, H. Schmidbaur, Inorg. Chem. 32 (1993) 5132.
[16] M. Muccini, M.A. Loi, K. Kenevey, R. Zamboni, Adv. Mater. 16 (2004) 861.
[17] S. Meloni, A. Palma, J. Schwatz, A. Kahn, R. Car, J. Am. Chem. Soc. 125 (2003) 7808.
[18] H.D. Burrows, M. Femandes, J.S. De Melo, A.P. Monkman, S. Navaratnam, J. Am. Chem. Soc. 125 (2003) 15310.
[19] X.T.H. Suzuki, T. Wada, S. Miyata, H. Sasabe, J. Am. Chem. Soc. 121 (1999) 9447.
[20] R.H. Friend, R.W. Gymer, A.B. Holmes, J.H. Burroughes, R.N. Marks, C. Taliani, D.A. Dos Santos, J.-L. Bre'das, M. Logdlund, W.R. Salaneck, Nature (London) 397 (1999) 121.
[21] A. Meyers, M. Weck, Macromolecule 36 (2003) 1766.
[22] Z. Bao, J.A. Rogers, H.E. Katz, J. Mater. Chem. 9 (1999) 1895.
[23] P. Calvert, Chem. Mater. 13 (2001) 3299.
[24] I. Yamaguchi, T. Iijima, T. Yamamoto, J. Organomet. Chem. 654 (2002) 229.
[25] T. Yamamoto, T. Iijima, J. Organomet. Chem. 689 (2004) 2421.
[26] L.M. Leung, W.Y. Lo, S.K. So, K.M. Lee, W.K. Choi, J. Am. Chem. Soc. 122 (2000) 5640.
[27] C.H. Chen, J. Shi, Coord. Chem. Rev. 171 (1998) 161.
[28] M.M. Amini, M. Mirzaee, J. Sol-Gel Sci. Technol. 36 (2005) 19.
[29] P3 and XDISK. Release 4.1. Siemens AXS, Madison, WI, USA, 1989.
[30] G.M. Sheldrick, SHELXTL, Version 5.10, Bruker AXS, Madison, WI, USA, 1998.
[31] A.K. Jain, A. Gupta, R. Bohra, I.-P. Lorenz, P. Mayer, Polyhedron 25 (2006) 654.
[32] C. Bae, S. Lee, S.-Y. Choi, G. Kwag, Inorg. Chem. 44 (2005) 7911.
[33] A. Singh, A.K. Rai, R.C. Mehrotra, Indian J. Chem. 11 (1973) 478.
[34] A. Dhammani, R. Bohra, R.C. Mehrotra, Polyhedron 17 (1998) 163.
[35] M. Bhattachargee, M.K. Chaudhuri, P.C. Paul, Can. J. Chem. 70 (1992) 2245.
[36] G.J. Gainsford, T. Kemmit, N.B. Milestone, Inorg. Chem. 34 (1995) 5244.

[37] N. Sharma, R.K. Sharma, R. Bohra, J.E. Drake, M.B. Hursthouse, M.E. Light, J. Chem. Soc., Dalton Trans. (2002) 1631.
[38] S. Szumacher, I. Madura, J. Zachara, A.R. Kunicki, A. Cebulski, L. Jerzykiewicz, J. Organomet. Chem. 669 (2003) 64.
[39] F. Papadimitrakopoulos, X.M. Zhang, D.L. Thomsen III, K.A. Higginson, Chem. Mater. 8 (1996) 1363.
[40] J. Ashenhurst, G. Wu, S. Wang, J. Am. Chem. Soc. 122 (2000) 2541.

2. Experimental

$Na_2MoO_4 \cdot 2H_2O$, dimethylsulfoxide and 1,10-phenanthroline were used as purchased from E. Merck. All solvents (methanol, ethanol, isopropanol, dichloromethane, and benzene) were dried by standard methods before use. Stringent precautions were taken to exclude moisture during experimental manipulations. Literature methods were used for the preparation of sodium or potassium salts of *N*,*N*-dialkyl dithiocarbamate [18] and *O*-alkyl dithiocarbonate [19].

2.1. Synthesis of $MoO_2Br(S_2CNEt_2)(OSMe_2)$ (1), $MoO_2Br(S_2CNPr^n_2)(OSMe_2)$ (2), $MoO_2Br(S_2CNPr^i_2)(OSMe_2)$ (3)

Typically, a suspension of NaS_2CNEt_2 in dichloromethane was added to a solution of $MoO_2Br_2(OSMe_2)_2$ (0.51 g, 1.14 mmol) in dichloromethane in equimolar ratio with constant stirring. The pale yellow solution immediately turned bright yellow. After stirring for 3 h, the precipitated NaBr was filtered and washed with CH_2Cl_2. Excess solvent was removed, then the product was dried in vacuo and purified by repeated washing with dried benzene to give $MoO_2Br(S_2CNEt_2)(OSMe_2)$ (**1**). Yellow powdery solid. Yield: 0.39 g, 80%; m.p. 92 °C. *Anal*. Calc. for $C_7H_{16}NO_3S_3BrMo$: Mo, 22.09; S, 22.15; Br, 18.40. Found: Mo, 22.56; S, 22.43; Br, 18.25%.

Method as above gave $MoO_2Br(S_2CNPr^n_2)(OSMe_2)$ (**2**). Pale yellow powdery solid. Yield: 84%; m.p. 82 °C. *Anal*. Calc. for $C_9H_{20}N_1O_3S_3BrMo$: Mo, 20.73; S, 20.81; Br, 17.28. Found: Mo, 20.73; S, 20.71; Br, 17.30%. *Anal*. Calc. for $C_9H_{20}N_1O_3S_3BrMo$: Mo, 20.73; S, 20.81; Br, 17.28%. Method as above gave $MoO_2Br(S_2CNPr^i_2)(OSMe_2)$ (**3**). Pale yellow powdery solid. Yield: 86%; m.p. 84 °C. *Anal*. Calc. for $C_9H_{20}N_1O_3S_3BrMo$: Mo, 20.73; S, 20.81; Br, 17.28. Found: Mo, 20.78; S, 20.71; Br, 17.29%.

2.2. Synthesis of $MoO_2Br(S_2COEt)(OSMe_2)$ (4), $MoO_2Br(S_2COPr^n)(OSMe_2)$ (5), $MoO_2Br(S_2COPr^i)(OSMe_2)$ (6)

A suspension of NaS_2COEt (0.15 g, 1.08 mmol) in dichloromethane was added to a solution of $MoO_2Br_2(OSMe_2)_2$ (0.48 g, 1.08 mmol) in dichloromethane, in equimolar ratio with constant stirring. The pale yellow solution immediately turned bright yellow. After stirring for 3 h, the precipitated NaBr was filtered and washed with dichloromethane. Excess solvent was removed and the product was dried in vacuo, and then purified by repeated washing with dried benzene to give $MoO_2Br(S_2COEt)(OSMe_2)$ (**4**). Yellow solid. Yield: 0.39 g, 89%; m.p. 96 °C. *Anal*. Calc. for $C_5H_{11}O_4S_3BrMo$: Mo, 23.56; S, 23.63; Br, 19.62. Found: Mo, 23.55; S, 23.51; Br 19.64%.

Method as above gave $MoO_2Br(S_2COPr^n)(OSMe_2)$ (**5**). Pale yellow solid. Yield: 81%; m.p. 89 °C. *Anal*. Calc. for $C_6H_{13}O_4S_3BrMo$: Mo, 22.78; S, 22.84; Br, 18.97. Found: Mo, 22.83; S, 22.80; Br, 18.97%. Method as above gave $MoO_2Br(S_2COPr^i)(OSMe_2)$ (**6**). Pale yellow solid. Yield: 85%; m.p. 91 °C. *Anal*. Calc. for $C_6H_{13}O_4S_3BrMo$: Mo, 22.78; S, 22.84; Br 18.97. Found: Mo, 22.79; S, 22.71; Br, 19.11%.

2.3. Synthesis of $MoO_2Br_2(OSMe_2)_2$ (7)

A solution of $Na_2MoO_4 \cdot 2H_2O$ (4.84 g, 20 mmol) in concentrated HBr (25 ml) was extracted with three 50 ml portions of diethyl ether. The combined extracts were concentrated under vacuum to approx. 25 ml and an ether solution of dimethylsulfoxide (3.11 g, 40 mmol) was added dropwise. A yellow precipitate was observed and the mixture was stirred for 30 min before the precipitate was filtered, washed with ether and dried over $P_2O_5 \cdot MoO_2Br_2(OSMe_2)_2$ (**7**). Yellow solid. Yield: 71%; m.p. 45 °C. *Anal*. Calc. for $C_4H_{12}O_4S_2Br_2Mo$: Mo, 21.61; S, 14.44; Br, 35.99. Found: Mo, 22.03; S, 14.58; Br, 36.57%.

2.4. Synthesis of $MoO_2Br_2(C_{12}H_8N_2)$ (8)

Concentrated HBr (5 ml) was added to a solution of $Na_2MoO_4 \cdot 2H_2O$ (0.51 g, 2.11 mmol) in distilled water (5 ml). A pale yellow solution along with a significant amount of crystallized NaBr was formed on stirring the mixture for 25–30 min. Diethyl ether (10 ml) was added, the solution was shaken vigorously, and the upper layer was collected. The extraction process was repeated twice more. The combined ether extract was stirred with anhydrous magnesium sulfate for 2 h and then filtered and washed with ether. A white precipitate was immediately observed when an ethanolic solution of $C_{12}H_8N_2$ (0.38 g, 2.11 mmol) was added dropwise to a stirred solution of the ether extract. The mixture was stirred for 30 min and filtered, washed with ether and dried under vacuum to give $MoO_2Br_2(C_{12}H_8N_2)$ (**8**). White solid. Yield: 86%; m.p. 88 °C. *Anal*. Calc. for $C_{12}H_8O_2N_2Br_2Mo$: Mo, 20.50; Br, 34.15%. Found: Mo, 20.13; Br, 34.72%.

2.5. Physical measurements

Molybdenum was estimated by precipitation as molybdenum oxinate, $MoO_2(C_9H_6ON)_2$. Sulfur was estimated gravimetrically as barium sulfate [Messenger's method] and bromide volumetrically by Volhard's method. IR spectra were recorded in the range 4000–400 cm^{-1} on a Shimadzu 8201 PC spectrophotometer as KBr pellets. Electronic spectra in the range 200–800 mm were recorded on a Systronic 2201 double beam UV–Vis spectrophotometer in CH_2Cl_2. ^1H NMR spectra were recorded on a Bruker DRX-300 spectrometer in $CDCl_3$ using TMS as an internal standard.

2.6. X-ray diffraction analysis

A green block crystal of $MoO_2Br_2(OSMe_2)_2$ and a colourless slab crystal of $MoO_2Br_2(C_{12}H_8N_2) \cdot CH_2Cl_2$ were

Table 1
Crystal data and structure refinement for $MoO_2Br_2(OSMe_2)_2$ (**7**) and $MoO_2Br_2(C_{12}H_8N_2)\cdot CH_2Cl_2$ (**8**)

Empirical formula	$C_4H_{12}O_4S_2Br_2Mo$	$C_{13}H_{10}O_2N_2Cl_2Br_2Mo$
Formula weight	444.02	552.89
Temperature (K)	120(2)	120(2)
Wavelength (Å)	0.71073	0.71073
Crystal system	$P2_1/n$	$P2_1/c$
Space group	monoclinic	monoclinic
a (Å)	7.9937(3)	9.028(2)
b (Å)	12.6343(4)	13.456(3)
c (Å)	12.6068(4)	13.484(3)
β (°)	92.285(3)	94.90(3)
Volume (Å^3)	1272.21(7)	1632.1(6)
Z	4	4
D_{calc} (g/cm^3)	2.318	2.250
Absorption coefficient (mm^{-1})	7.624	6.033
$F(000)$	848	1056
Crystal size (mm^3)	$0.10\times0.10\times0.09$	$0.40\times0.16\times0.08$
θ Range for data collection (°)	3.61–27.53	3.02–27.55
Index ranges	$-10\leqslant h\leqslant 10$, $-16\leqslant k\leqslant 16$, $-15\leqslant l\leqslant 16$	$-11\leqslant h\leqslant 11$, $-17\leqslant k\leqslant 17$, $-17\leqslant l\leqslant 17$
Reflections collected	15692	24438
Independent reflections (R_{int})	2917 (0.0364)	3759 (0.1745)
Maximum and minimum transmission	0.5470 and 0.5161	0.6439 and 0.1964
Refinement method	full-matrix least-squares on F^2	full-matrix least-squares on F^2
Data/restraints/parameters	2917/0/122	3759/0/199
Goodness-of-fit on F^2	1.061	1.019
Final R indices [$F^2>4\sigma(F^2)$]	$R_1=0.0306$, $wR_2=0.0680$	$R_1=0.0463$, $wR_2=0.1082$
R indices (all data)	$R_1=0.0394$, $wR_2=0.0717$	$R_1=0.0595$, $wR_2=0.1159$
Largest difference peak and hole (e Å^{-3})	0.502 and −1.143	1.143 and −1.474

mounted on a glass fibre. Data were collected on an Enraf Nonius KappaCCD area detector diffractometer, with ϕ and ω scans chosen to give a complete asymmetric unit. Data collection and cell refinement [20] gave cell constants corresponding to a monoclinic cell for both crystals, whose dimensions are given in Table 1 along with other experimental parameters. An absorption correction was applied [21,22].

The structures were solved by direct methods [23] and were refined using the WINGX version [24] of SHELX-97 [25]. All of the non-hydrogen atoms were treated anisotropically. Hydrogen atoms were included in idealized positions with isotropic thermal parameters set at 1.2 times that of the carbon atom to which they were attached. The final cycle of full-matrix least-squares refinement was based on 2917 (for **7**) and 3759 (for **8**), observed reflections (2506 (for **7**) and 3117 (for **8**) for $F^2>4s(F^2)$) and 122 (for **7**) and 199 (for **8**) variable parameters and converged (largest parameter shift was 0.001 times its esd).

Distances and bond angles are given in Tables 2 and 3 for molecules **7** and **8**, respectively and ORTEP diagrams are displayed in Figs. 1 and 2.

Table 2
Bond distances (Å) and angles (°) for $MoO_2Br_2(OSMe_2)_2$ (**7**)

Mo(1)–Br(1)	2.5432(5)	Mo(1)–Br(2)	2.5148(5)
Mo(1)–O(1)	1.687(3)	Mo(1)–O(2)	1.696(2)
Mo(1)–O(3)	2.180(2)	Mo(1)–O(4)	2.204(2)
S(1)–O(3)	1.538(2)	S(2)–O(4)	1.531(2)
S(1)–C(1)	1.775(4)	S(2)–C(3)	1.773(4)
S(1)–C(2)	1.777(4)	S(2)–C(4)	1.768(5)
O(1)–Mo(1)–O(2)	103.9(1)	Br(1)–Mo(1)–Br(2)	161.90(2)
O(1)–Mo(1)–Br(1)	95.6(1)	O(2)–Mo(1)–Br(1)	93.59(9)
O(1)–Mo(1)–Br(2)	96.3(1)	O(2)–Mo(1)–Br(2)	96.66(9)
O(1)–Mo(1)–O(3)	89.5(1)	O(2)–Mo(1)–O(3)	166.4(1)
O(1)–Mo(1)–O(4)	166.0(1)	O(2)–Mo(1)–O(4)	90.0(1)
O(3)–Mo(1)–Br(1)	83.25(6)	O(4)–Mo(1)–Br(1)	82.91(7)
O(3)–Mo(1)–Br(2)	83.31(7)	O(4)–Mo(1)–Br(2)	82.20(7)
Mo(1)–O(3)–S(1)	127.6(1)	Mo(1)–O(4)–S(2)	124.7(1)
O(3)–S(1)–C(1)	102.5(2)	O(4)–S(2)–C(3)	102.9(2)
O(3)–S(1)–C(2)	104.6(2)	O(4)–S(2)–C(4)	103.9(2)
C(1)–S(1)–C(2)	98.8(2)	C(3)–S(2)–C(4)	99.5(2)
O(3)–Mo(1)–O(4)	76.49(9)		

3. Results and discussion

Reactions of dibromodioxobis(dimethylsulfoxide)-molybdenum(VI) complexes with sodium/potassium salts of *N*,*N*′-dialkyl dithiocarbamates or *O*-alkyl dithiocarbonates in a 1:1 molar ratio in dichloromethane yield dioxomolybdenum(VI) complexes of the type, $MoO_2Br(S_2CNR_2)$-$(OSMe_2)$ or $MoO_2Br(S_2COR)(OSMe_2)$, respectively (see Fig. 3)

$$MoO_2Br_2(OSMe_2)_2 + NaS_2CNR_2 \rightarrow MoO_2Br(S_2CNR_2)(OSMe_2) + OSMe_2\ (\text{Free}) + NaBr$$

where R = Et, Pr^n, Pr^i

$$MoO_2Br_2(OSMe_2)_2 + NaS_2COR \rightarrow MoO_2Br(S_2COR)(OSMe_2) + OSMe_2\ (\text{Free}) + NaBr$$

where R = Et, Pr^n, Pr^i.

Table 3
Bond lengths (Å) and angles (°) for $MoO_2Br_2(C_{12}H_8N_2) \cdot CH_2Cl_2$ (**8**)

Mo(1)–O(1)	1.692(4)	Mo(1)–O(2)	1.688(4)
Mo(1)–N(1)	2.317(4)	Mo(1)–N(2)	2.322(4)
Mo(1)–Br(1)	2.522(1)	Mo(1)–Br(2)	2.5075(9)
N(1)–C(1)	1.354(6)	N(2)–C(6)	1.355(6)
C(1)–C(2)	1.402(7)	C(6)–C(7)	1.406(7)
C(2)–C(3)	1.402(7)	C(7)–C(10)	1.395(7)
C(3)–C(4)	1.373(8)	C(10)–C(11)	1.370(8)
C(4)–C(5)	1.389(8)	C(11)–C(12)	1.391(7)
N(1)–C(5)	1.325(6)	N(2)–C(12)	1.335(6)
C(1)–C(6)	1.434(7)	C(2)–C(9)	1.436(7)
C(7)–C(8)	1.430(7)	C(8)–C(9)	1.346(8)
Cl(1)–C(13)	1.765(6)	Cl(2)–C(13)	1.741(6)
Br(1)–Mo(1)–Br(2)	158.02(3)		
O(1)–Mo(1)–O(2)	106.9(2)	N(1)–Mo(1)–N(2)	70.4(1)
O(1)–Mo(1)–N(1)	90.4(2)	O(2)–Mo(1)–N(1)	162.7(2)
O(1)–Mo(1)–N(2)	160.7(2)	O(2)–Mo(1)–N(2)	92.3(2)
O(1)–Mo(1)–Br(1)	96.4(1)	O(2)–Mo(1)–Br(1)	96.7(1)
O(1)–Mo(1)–Br(2)	97.2(1)	O(2)–Mo(1)–Br(2)	95.8(1)
N(1)–Mo(1)–Br(1)	81.4(1)	N(2)–Mo(1)–Br(1)	80.1(1)
N(1)–Mo(1)–Br(2)	81.3(1)	N(2)–Mo(1)–Br(2)	81.4(1)
C(1)–N(1)–Mo(1)	117.3(3)	C(6)–N(2)–Mo(1)	117.6(3)
C(5)–N(1)–Mo(1)	123.8(3)	C(12)–N(2)–Mo(1)	124.3(3)
C(1)–N(1)–C(5)	118.9(4)	C(6)–N(2)–C(12)	118.1(4)
N(1)–C(1)–C(6)	117.7(4)	N(2)–C(6)–C(1)	116.8(4)
N(1)–C(1)–C(2)	122.2(4)	N(2)–C(6)–C(7)	123.2(4)
C(1)–C(2)–C(3)	117.6(5)	C(6)–C(7)–C(10)	116.8(5)
C(2)–C(3)–C(4)	119.4(5)	C(7)–C(10)–C(11)	119.9(5)
C(3)–C(4)–C(5)	119.3(5)	C(10)–C(11)–C(12)	119.7(5)
N(1)–C(5)–C(4)	122.6(5)	N(2)–C(12)–C(11)	122.1(5)
C(2)–C(1)–C(6)	120.1(4)	C(1)–C(6)–C(7)	119.9(4)
C(1)–C(2)–C(9)	118.5(4)	C(6)–C(7)–C(8)	118.7(5)
C(3)–C(2)–C(9)	123.8(5)	C(10)–C(7)–C(8)	124.4(5)
C(2)–C(9)–C(8)	121.3(5)	C(7)–C(8)–C(9)	121.4(5)
Cl(1)–C(13)–Cl(2)	111.3(3)		

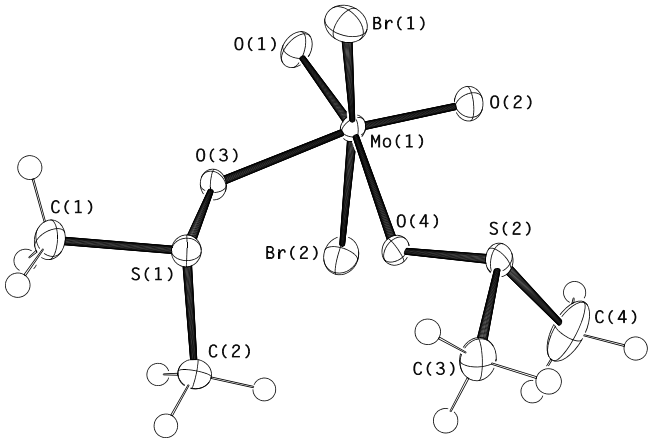

Fig. 1. ORTEP plot of the molecule $MoO_2Br_2(OSMe_2)_2$. The non-hydrogen atoms are drawn with 50% probability ellipsoids.

All of these molybdenum(VI) complexes are yellow powdery solids that are soluble in chloroform and dichloromethane and are characterized by elemental analysis and IR, UV–Vis and ^1H NMR spectroscopy.

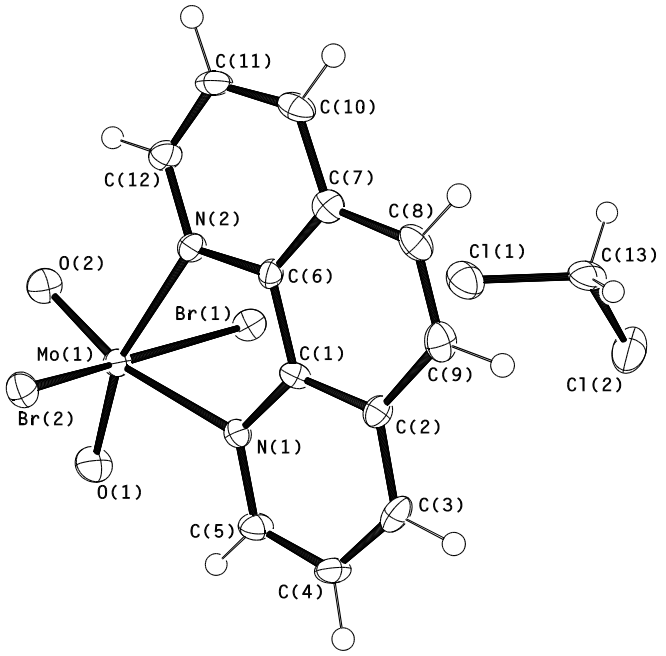

Fig. 2. ORTEP plot of the molecule MoO_2Br_2(1,10-phenanthroline) $\cdot CH_2Cl_2$. The non-hydrogen atoms are drawn with 50% probability ellipsoids.

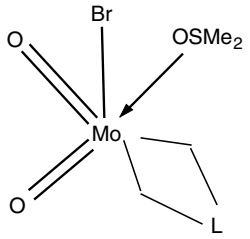

Fig. 3. Proposed structure of $MoO_2Br(L)(OSMe_2)$ [$L = S_2CNEt_2$, $S_2CNPr^n_2$, $S_2CNPr^i_2$, S_2COEt, S_2COPr^n, S_2COPr^i].

3.1. IR spectra

The assignments of the IR bands for bromodioxodimethylsulfoxide (*N*,*N*′-dialkyl dithiocarbamates)molybdenum(VI) and bromodioxodimethylsulfoxide(*O*-alkyl dithiocarbonate)molybdenum(VI) complexes (Table 4) were made by comparison with the spectra of the precursors, the complexes, dibromodioxobis(dimethyl sulfoxide)molybdenum(VI) and the sodium/potassium salts of *N*,*N*′-dialkyldithiocarbamates [18] and *O*-alkyl dithiocarbonates [19]. The bands arising from the C–N stretching mode in the dithiocarbamate derivatives are seen in the range 1520–1540 cm^{-1}, typical of analogous complexes [26]. Similarly, the presence of a band around 1250–1261 cm^{-1} in the xanthate derivatives can be attributed to ν(C–O–C) [26,27]. Complexes with both dithio ligand systems show CS_2^- group stretching vibration bands in the range 996–1100 cm^{-1} suggesting that the dithio ligands act as bidentate ligands [28].

Table 4
Some relevant IR spectral data (cm^{-1}) of the complexes[a]

S. no.	Compound	ν(C=N) or (C–O–C)	ν (C=S)	ν (S=O)	ν (Mo=O)
1	$MoO_2Br(S_2CNEt_2)(Me_2SO)$	1520(s)	1005(s)	1041(s)	910(s) 960(m)
2	$MoO_2Br(S_2CNPr^n_2)(Me_2SO)$	1530(s)	996(s)	1032(s)	924(s) 954(s)
3	$MoO_2Br(S_2CNPr^i_2)(Me_2SO)$	1540(s)	1020(w)	1043(s)	910(m) 978(s)
4	$MoO_2Br(S_2COEt)(Me_2SO)$	1261(s)	1100(s)	1043(s)	930(s) 969(s)
5	$MoO_2Br(S_2COPr^n)(Me_2SO)$	1250(br)	1050(s)	1045(s)	904(sbr)
6	$MoO_2Br(S_2COPr^i_2)(Me_2SO)$	1260(br)	1032(m)	1032(s)	906(sbr)

[a] *Key*. s, strong; m, medium; w, weak; br, broad.

A strong band due to ν(S=O) in the complexes is observed in the range 1033–1045 cm^{-1}, at slightly lower wave number than in the free ligands (1050 cm^{-1}), which is indicative of coordination through the oxygen atom [29]. Two characteristic strong bands in the range of 904–978 cm^{-1} can be assigned to the (Mo=O) symmetric and antisymmetric stretching modes in dioxomolybednum(VI) complexes [26].

3.2. Electronic absorption spectra

The electronic spectra of the dioxomolybdenum(VI) complexes recorded in CH_2Cl_2, are listed in Table 5. The bands in the region 329–332 and 203–212 nm may be ascribed to intra-ligand transitions of $n \rightarrow \pi^*$ and $\pi \rightarrow \pi^*$, respectively. The bands at 287–308 nm can be assigned to $O_T \rightarrow$ Mo(VI) charge transfer transitions. The intense bands at 347–369 nm can be attributed to S → Mo(VI) charge transfer [29].

3.3. ^1H NMR spectra

The chemical shifts and integrated intensity ratios of the protons in the dioxomolybdenum(VI) complexes are given in Table 6. These spectra were recorded in $CDCl_3$ solutions at room temperature. The ^1H NMR data of dioxomolybdenum(VI) complexes are remarkably similar to those of the salts of dithiocarbamates and dithiocarbonates [51], proba-

Table 5
Some relevant electronic absorption spectral data [$\lambda_{max.}$, nm (A)] for the complexes in CH_2Cl_2

S. no.	Compound	$\lambda_{max.}$ (nm)	Absorbance	Assignment
1	$MoO_2Br(S_2CNEt_2)$-(Me_2SO)	347	1.00	S → Mo^{VI}
		332	1.13	$n \rightarrow \pi^*$
		302	1.47	$O_t \rightarrow Mo^{VI}$
		203	0.08	$\pi \rightarrow \pi^*$
2	$MoO_2Br(S_2CNPr^n_2)$-(Me_2SO)	368	0.51	S → Mo^{IV}
		332	0.69	$n \rightarrow \pi^*$
		287	1.30	$O_t \rightarrow Mo^{VI}$
		203	0.06	$\pi \rightarrow \pi^*$
3	$MoO_2Br(S_2CNPr^i_2)$-(Me_2SO)	369	0.65	S → Mo^{VI}
		332	4.00	$n \rightarrow \pi^*$
		302	1.52	$O_t \rightarrow Mo^{VI}$
		209	0.07	$\pi \rightarrow \pi^*$
4	$MoO_2Br(S_2COEt)$-(Me_2SO)	359	0.35	S → Mo^{VI}
		332	0.46	$n \rightarrow \pi^*$
		308	0.52	$O_t \rightarrow Mo^{VI}$
		210	0.13	$\pi \rightarrow \pi^*$
5	$MoO_2Br(S_2COPr^n)$-(Me_2SO)	368	1.12	S → Mo^{VI}
		329	1.21	$n \rightarrow \pi^*$
		302	1.49	$O_t \rightarrow Mo^{VI}$
		212	0.10	$\pi \rightarrow \pi^*$
6	$MoO_2Br(S_2COPr^i)$-(Me_2SO)	362	1.04	S → Mo^{VI}
		332	1.15	$n \rightarrow \pi^*$
		299	1.47	$O_t \rightarrow Mo^{VI}$
		212	0.10	$\pi \rightarrow \pi^*$

Table 6
^1H NMR spectral data of the complexes[a,b,c]

S. no.	Compound	$NCH_2/OCH_2/NCH/OCH$	$NCCH_3/OCCH_3$	SCH_3
1	$MoO_2Br[S_2CN(CH_2CH_3)_2](Me_2SO)$	3.40 (4H, q, $J = 7$ Hz)	1.15 (6H, t, $J = 7$ Hz)	2.17 (6H, s)
2	$MoO_2Br[S_2CN(CH_2CH_2CH_3)_2](Me_2SO)$	3.73 (4H, m, $J = 7$ Hz)	1.57 (4H, m, $J = 6$ Hz)	2.17 (6H, s)
3	$MoO_2Br[S_2CN\{CH(CH_3)_2\}(Me_2SO)$	3.50 (2H, m, $J = 7$ Hz)	0.85 (12H, d, $J = 7$ Hz)	2.18 (6H, s)
4	$MoO_2Br[S_2COCH_2CH_3](Me_2SO)$	3.63 (4H, q, $J = 7$ Hz)	1.19 (6H, t, $J = 7$ Hz)	2.17 (6H, s)
5	$MoO_2Br[S_2COCH_2CH_2CH_3](Me_2SO)$	3.73 (4H, m, $J = 7$ Hz)	1.56 (4H, m, $J = 6$ Hz)	2.18 (6H, s)
6	$MoO_2Br[S_2COCH(CH_3)_2](Me_2SO)$	3.63 (4H, m, $J = 7$ Hz)	1.21 (12H, d, $J = 7$ Hz)	2.17 (6H, s)

[a] The spectra were recorded in $CDCl_3$ and reported in δ ppm from MeSi.
[b] Number of protons and multiplicities are in parentheses (s, singlet; d, doublet; t, triplet; m, multiplet).
[c] Coupling constants in Hz indicated by J(HH).

bly due to the large separation between the molybdenum and protons. The methyl protons of $OSMe_2$ show a downfield shift compared to the singlet observed in the precursor $MoO_2Br_2(OSMe_2)_2$ (δ 2.95 ppm) consistent with the coordination mode of these dithio ligands [15].

3.4. Molecular structures of trans-dibromodioxbis-(dimethylsulfoxide)molybdenum(VI), $MoO_2Br_2(OSMe_2)_2$ (7) and $MoO_2Br_2(C_{12}H_8N_2)\cdot CH_2Cl_2$ (8)

$MoO_2Br_2(OSMe_2)_2$ (**7**) and $MoO_2Br_2(C_{12}H_8N_2)\cdot CH_2Cl_2$ (**8**) both crystallize as monoclinic in the space groups $P2_1/n$ and $P2_1/c$, respectively. The asymmetric units of **7** and **8** are displayed as ORTEP diagrams in Figs. 1 and 2, respectively. The distorted octahedral environment around molybdenum in both molecules consists of *cis* terminal oxygen atoms (O_T) and *trans* bromine atoms with *cis* dimethylsulfoxide moieties in **7** and bidentate 1,10-phenanthroline in **8**. Comparable crystal structures of the complexes $MoO_2X_2L_2$ (X = Cl, Br and L = $OPPh_3$) [14] and $MoO_2Cl_2(OSMe_2)_2$ [15,16], have been reported. The average Mo–O_T bond distance of 1.691(4) Å in **7** and **8** is typical of a molybdenum–oxygen terminal double bond and is similar to those observed in the structurally similar complexes containing triphenylphosphine oxide {$MoO_2Cl_2(OPPh_3)_2$ (1.68(2) Å, ave.) and $MoO_2Br_2(OPPh_2)_2$ (1.71 (1) Å, ave.)} [14] as well as in several other dioxomolybdenum(VI) complexes such as $MoO_2Cl_2(OSMe_2)_2$ [15,16], $MoO_2(S_2CNEt_2)_2$ [30], $MoO_2(S_2CNPr^n_2)_2$ [31] and $MoO_2[S_2P(OEt)_2]\{HB(Me_2Pz)_3\}$ [32]. The Mo–O(dimethylsulfoxide) bond distances of 2.180(2) and 2.204(2) Å in **7** are in the range expected for unidentate oxygen donors and are comparable to the average length of 2.199(1) Å in $MoO_2Cl_2(OSMe_2)_2$ [15,16] and 2.214(9) Å in MoO_4 (Φ–O)$(OSMe_2)_2(SCN)_2$ [33]. These Mo–O_L bonds appear to be significantly stronger than the coordinated Mo–O(dimethylsulfoxide) bonds in $Mo_2O_2(\Phi\text{–}S_2)[S_2P(OEt)_2](OSMe_2)$ (2.462(2) Å) [34] and $Mo_2O_2(\phi\text{–}S_2)[S_2P(OPr^i)]_2(OSMe_2)$ (2.467(3) Å) [34]. The Mo–N bond distances of 2.317(4) and 2.322(4) Å in **8** are between the two Mo–N values (2.449(19) and 2.259(18) Å) obtained for MoO_2Br_2(2,2′-bipyridyl) [35]. The Mo–Br bond distances are slightly shorter, 2.5432(5) and 2.5148(5) Å in **7** and 2.522(1) and 2.5075(9) Å in **8** than those observed in $MoO_2Br_2(OPPh_3)_2$ (2.556(3) and 2.540(3) Å) [36], suggesting strong Mo–Br bonds in both **7** and **8**. There is no evidence of intermolecular interactions involving bromine or the ligands.

The four oxygen atoms and molybdenum in **7** are essentially coplanar, with bromine atoms "bent away" from the terminal oxygen atoms so that the Br–Mo–O_T angles range from 93.59(9)° to 96.66(9)° compared with 82.20(7)–83.31(7)° for those of Br–Mo–O_L. Similarly, two terminal oxygen, two nitrogen and the Mo atom are coplanar in **8**, with two bromine atoms also bent away from the terminal oxygen atoms and also from two nitrogen atoms. The Br–Mo–O_T angles range from 95.8(1)° to 97.2(1)° and those of Br–Mo–N_L from 80.1(1)° to 81.4(1)°. The Br–Mo–Br angles are 161.90(2)° and 158.02(3)° in **7** and **8**, respectively emphasizing that the distortion from octahedral is not limited to the presence of Mo–O/Mo–N bonding. As in the triphenylphosphine oxide analogues, the angle involving the terminal Mo=O double bonds [O_T–Mo–O_T, 103.9(1)° in **7** and 106.9(2)° in **8**] is considerably wider than 90°. The correspondingly compressed O_L–Mo–O_L angle of 76.49(9)° in **7** is as seen in $MoO_2Cl_2(OSMe_2)_2$ (77.68(5)°) [15], and also is unaltered when dimethylsulfoxide is replaced by triphenylphosphine oxide [$MoO_2Cl_2(OPPh_3)_2$ (77.81(5)°) and $MoO_2Br_2(OPPh_3)_2$ (77.0(4)°)] [14]. However, the N–Mo–N angle of 70.4(1)° in **8** is slightly larger than that found in MoO_2Br_2(2,2′-bipyridyl) (66.90(6)°) [35]. Therefore, the environment about the Mo atom is relatively unchanged whether unidentate dimethylsulfoxide, triphenylphosphine oxide or bidentated 1,10-phenanthroline is coordinated. Finally the bond lengths and angles within Me_2SO and 1,10-phenanthroline are similar to those obtained in other molybdenum complexes of these ligands [34,37].

4. Concluding comments

We have successfully prepared and characterized the following bromodioxodimethylsulfoxide(*N*,*N*′-dialkyldithiocarbamate/*O*-alkyldithiocarbonate)molybdenum(VI) complexes, $MoO_2Br(S_2CNR_2)(OSMe_2)$ (R = Et, Pr^n, Pr^i) and $MoO_2Br(S_2COR)(OSMe_2)$ (R = Et, Pr^n, Pr^i). The IR, UV–Vis and ^1H NMR spectra of all of these dioxomolybdenum(VI) complexes are consistent with the proposal of the following tentative structure.

The molecular structures of $MoO_2Br_2(OSMe_2)_2$ and $MoO_2Br_2(C_{12}H_8N_2)\cdot CH_2Cl_2$ have been determined. They have distorted octahedral environments around molybdenum which are similar to the structure reported for the complex $MoO_2Cl_2(OSMe_2)_2$ with *cis* terminal oxygen atoms, *cis* ligands and *trans* bromine atoms.

Acknowledgements

Two of us (R.K. and R.R.) are grateful to UGC, New Delhi for financial support. M.B. Hursthouse thanks the UK Engineering and Physical Sciences Council for support of the X-ray facilities at Southampton University. J.E.D. wishes to thank the University of Windsor for financial support. We are also thankful to RSIC, CDRI, Lucknow for the spectral analyses.

Appendix A. Supplementary material

Additional material is available from the Cambridge Crystallographic Data Centre, CCDC Nos. 600006 and 600007 for $MoO_2Br_2(OSMe_2)_2$ and $MoO_2Br_2(C_{12}H_8N_2)\cdot CH_2Cl_2$, respectively, and comprises the final atomic coordinates for all atoms, thermal parameters and a complete listing of bond distances and angles. Copies

of this information may be obtained free of charge on application to The Director, 12 Union Road, Cambridge CB2 1EZ, UK, fax: +44 1223 336 033, email: deposit @ccdc.cam.ac.uk or www: http://www.ccdc.cam.ac.uk. Supplementary data associated with this article can be found, in the online version, at doi:10.1016/j.poly.2006.05.034.

References

[1] R. Colton, Coord. Chem. Rev. 90 (1988) 29.
[2] D. Collison, C.D. Garner, J.A . Joule, Chem. Soc. Rev. (1996) 25.
[3] R. Hille, Chem. Rev. 96 (1996) 2757.
[4] E.I. Stiefel, J. Chem. Soc., Dalton Trans. (1997) 3915.
[5] R. Ratnani, P. Nag, B.S. Joshi, R. Bohra, in: R. Bohra (Ed.), Advances in Metallo-Organic Chemistry, RBSA Publishers, Jaipur, 1999, p. 253.
[6] A. Thapper, R.J. Deeth, E. Nordlander, Inorg. Chem. 38 (1999) 1015.
[7] B.J. Hamstra, B. Cheng, M.K. Ellison, W.R. Schiedt, Inorg. Chem. 38 (1999) 3554.
[8] A. Thapper, J.P. Conathue, K.B. Musgrave, M.W. Willer, E. Nordlunder, B. Hedman, K.O. Hodgson, R.H. Holm, Inorg. Chem. 38 (1999) 4104.
[9] M.L. Mader, M.D. Carducci, J.H. Enemark, Inorg. Chem. 39 (2000) 525.
[10] L.S. Villata, M.R. Feliz, A.L. Capparelli, Coord. Chem. Rev. 196 (2000) 65.
[11] J.M. Tunney, J. McMaster, C.D. Garner, in: J.A. McCleverty, T.J. Meyer (Eds.), Comprehensive Coordination Chemistry II, vol. 8, Elsevier, Amsterdam, 2003, p. 459.
[12] R.H. Holm, Chem. Rev. 87 (1987) 1401.
[13] F.E. Kuhn, M. Groarke, E. Bencze, E. Herdtweck, A. Prazeres, A.M. Santos, M.J. Calhorda, C.C. Romao, I.S. Goncalves, A.D. Lopes, M. Pillinger, Chem. Eur. J. 8 (2002) 2370.
[14] R.J. Butcher, B.R. Penfold, E. Slim, J.Chem. Soc., Dalton Trans. (1979) 668.
[15] N. Manwani, M.C. Gupta, R. Ratnani, J.E. Drake, M.B. Hursthouse, M.E. Light, Inorg. Chim. Acta 357 (2004) 939.
[16] F.J. Arnaiz, R. Aguado, M.R. Pedrosa, A. De Cian, Inorg. Chim. Acta 347 (2003) 33.
[17] F.J. Arnaiz, R. Aguado, J.M. Martinez Harduya, Polyhedron 13 (1994) 3257.
[18] H.L. Klopping, G.J.M. Van der Kerk, Res. Trav. Chim. 70 (1951) 919.
[19] R.J. Magee, M.J. O'Connor, Inorg. Chim. Acta 5 (1971) 554.
[20] Z. Otwinowski, W. Minor, in: C.W. Carter, Jr., R.M. Sweet (Eds.), Methods in Enzymology vol. 276, Macromolecular Crystallography, Part A, 1997, Academic Press, pp. 307.
[21] SORTAV R.H. Blessing, Acta Crystallogr., Sect. A 51 (1995) 33.
[22] R.H. Blessing, J. Appl. Cryst. 30 (1997) 421.
[23] G.M. Sheldrick, Acta Crystallogr., Sect. A 46 (1990) 467.
[24] L.J. Farrugia, J. Appl. Cryst. 32 (1999) 837.
[25] G.M. Sheldrick, SHELXL, 97, University of Gottingen, Gottingen, Germany, 1997.
[26] P. Nag, R. Bohra, R.C. Mehrotra, R. Ratnani, Synth. React. in Inorg. and Met.-Org. Chem. 32 (2002) 1549.
[27] R.N. Jowitt, P.C.H. Mitchell, J. Chem. Soc. (A) (1970) 1702.
[28] G.S. Bhat, A.D. Sawant, Thermochim. Acta 222 (1993) 231.
[29] F.J. Arnaiz, R. Aguado, M.R. Pedroso, A. De Cian, J. Fischer, Polyhedron 19 (2000) 2141.
[30] A. Kopwillen, Acta Chem. Scand. 26 (1972) 2941.
[31] L. Ricard, J. Estienne, P. Karagiannidis, P. Toledano, A. Mitchell, R. Weiss, J. Coord. Chem. 3 (1974) 277.
[32] S.A. Roberts, C.G. Young, W.E. Cleland, R.B. Ortega, J.H. Enermark, Inorg. Chem. 27 (1988) 3044.
[33] T. Shibahara, H. Kuroya, S. Ooi, Y. Mori, Inorg. Chim. Acta 76 (1983) L315.
[34] N. Manwani, R.N. Prasad, R. Ratnani, J.E. Drake, M.B. Hursthouse, M.E. Light, Inorg. Chim. Acta 351 (2003) 49.
[35] R.H. Fenn, J. Chem. Soc. (A) (1969) 1764.
[36] R. Ratnani, M.B. Hursthouse, W. Levason, G. Reid, Polyhedron 23 (11) (2004) 1915.
[37] Q. Hao, H.K. Fun, S. Chantrapromma, I.A. Razak, F. Jian, X. Yang, L. Lu, X. Wang, Acta Crystallog., Sect. C: Cryst. Struct. Commun. 57 (6) (2001) 717.

and characterization of new copper(II) and nickel(II) complexes of Hqaldsme, together with the X-ray crystallographic structures of two five-coordinate copper(II) and a six-coordinate nickel(II) complexes of this ligand.

2. Experimental

2.1. Materials and instrumentation

2-Quinoline carboxaldehyde and other chemicals employed in the present work were purchased from Aldrich Chemical Company and used as received. The solvents used were of analytical reagent grade. *S*-methyldithiocarbazate was prepared by following a published method [10]. The electronic spectra were recorded both in the solid state (as Nujol mull) on a Shimadzu UV-3100 spectrophotometer. The IR spectra were recorded as KBr discs on either a Perkin–Elmer 1600 FT IR spectrometer or a Perkin–Elmer 2000 spectrometer. Conductance measurements were made by means of a CMD 400 conductivity meter. Magnetic susceptibilities were measured with a Sherwood Scientific magnetic susceptibility balance calibrated with $HgCo(NCS)_4$. Diamagnetic corrections were applied using Pascal's constants.

2.2. Preparation of the Schiff base

The synthesis and characterization of the Schiff base has been reported previously [24].

2.3. General method of preparation of the complexes

A solution of hydrated metal(II) nitrate salt (0.001 mol) in hot methanol (20 ml) was added to a boiling solution of the Schiff base (0.001 mol for the copper complexes and 0.002 mol for the nickel complex) in methanol (100 ml). The mixture was gently heated on a water bath for 2 min and then left to stand overnight. The complexes that crystallized out of the reaction mixture were filtered off, washed with methanol and dried in a desiccator over anhydrous silica gel. The thiocyanato (**1**) and iodo (**3**) complexes of copper(II) were prepared by adding a solution of LiNCS or LiI (0.004 mol) to a boiling mixture containing copper(II) nitrate (0.001 mol) and ligand (0.001 mol) in methanol and letting the reaction mixture to stand overnight. Crystals of the copper(II)-nitrato complex (**1**) suitable for X-ray analysis were obtained during the preparation of the complex whereas those of the thiocyanato-copper complex (**2**) and nickel(II) complex (**4**) were obtained by recrystallizing the crude complexes from acetonitrile.

2.3.1. *[Cu(qaldsme)(NO$_3$)(MeOH)] (**1**)*

Dark green colour. Yield: 60%. *Anal.* Calc. for $C_{13}H_{14}N_4O_4S_2Cu$: C, 37.36; H, 3.38; N, 13.41. Found: C, 37.60; H, 3.31; N, 13.79%. Dec. temp. 173–175 °C; μ_{eff} (293 K) = 2.0 μ_B; Λ(ohm^{-1} cm^2 mol^{-1}) (DMSO) = 32.1.

2.3.2. *[Cu(qaldsme)(NCS)]$_2$ (**2**)*

Green colour. Yield: 48%. *Anal.* Calc. for $C_{13}H_{10}N_4S_3Cu$: C, 40.87; H, 2.63; N, 14.67. Found: C, 41.05; H,

Table 1
Crystal data and refinement data

	Cu(qaldsme)(NO_3)(CH_3OH)	[Cu(qaldsme)(NCS)]$_2$	Ni(qaldsme)$_2 \cdot 0.5CH_3CN$
Formula	$C_{13}H_{14}N_4O_4S_2Cu$	$C_{26}H_{20}Cu_2N_8S_6$	$C_{25}H_{21.5}N_{6.5}NiS_4$
Formula weight	417.94	763.94	599.94
Temperature (K)	293	293	293
Wavelength (Å)	0.71073	0.71073	0.71073
Crystal system	monoclinic	triclinic	triclinic
Space group	$P2_1/n$	$P\bar{1}$	$P\bar{1}$
Unit cell dimensions			
a (Å)	9.560(8)	7.207(1)	10.258(5)
b (Å)	17.938(5)	10.429(4)	10.446(2)
c (Å)	10.367(4)	11.173(2)	14.516(5)
α (°)		105.34(2)	109.01(2)
β (°)	110.03(4)	95.90(2)	108.69(4)
γ (°)		106.18(2)	90.59(3)
Volume (Å^3)	1670(2)	763.5(3)	1381.6(9)
Z	4	1	2
D_{calc} (g cm^{-3})	1.662	1.661	1.442
Absorption coefficient (mm^{-1})	1.583	1.836	1.032
F(000)	852	386	618
Reflections collected	3121	2916	5158
Independent reflections	2939	2682	4857
R_{int}	0.0951	0.0476	0.0632
Observed reflections [$I > 2\sigma(I)$]	1241	1605	2152
Parameters	217	191	328
Goodness-of-fit on F^2	1.009	1.010	0.986
R_1 [$I > 2\sigma(I)$]	0.0734	0.0549	0.0874
wR_2 (all data)	0.2530	0.1693	0.2811

2.70; N, 13.79%. μ_{eff} (293 K) = 1.85 μ_B; Λ(ohm^{-1} cm^2 mol^{-1}) (DMSO) = 17.1.

*2.3.3. [Cu(qaldsme)I] (**3**)*

Brownish-black colour. Yield: 60%. *Anal.* Calc. for $C_{12}H_{10}N_3SCuI$: C, 32.00; H, 2.20; N, 9.30. Found: C, 31.90; H, 2.30; N, 9.90%. μ_{eff} (293 K) = 1.75 μ_B; Λ(ohm^{-1} cm^2 mol^{-1}) (DMSO) = 31.9.

*2.3.4. [Ni(qaldsme)$_2$] · 0.5CH$_3$CN (**4**)*

Yield: 85%. *Anal.* Calc. for $C_{25}H_{21.5}N_{6.5}S_4Ni$: C, 50.05; H, 3.61; N, 15.18. Found: C, 49.90; H, 3.70; N, 14.90%. μ_{eff} (293 K) = 2.87 μ_B; Λ(ohm^{-1} cm^2 mol^{-1}) (DMSO) = 2.0.

2.4. Crystallography

Cell constants were determined by a least-squares fit to the setting parameters of 25 independent reflections, measured on an Enraf-Nonius CAD4 four-circle diffractometer using graphite monochromated Mo Kα radiation (0.71073 Å) and operating in the ω–2θ mode within the range $3° < 2\theta < 50°$. Empirical absorption correction (ψ scans) [25] and data reduction [26] were performed within the WINGX [27] suite of programmes. The structures were solved by direct methods with SHELX86 [28] and refined by full-matrix least-squares analysis with SHELXL97 [29]. Non-hydrogen atoms were refined with anisotropic thermal parameters whereas H-atoms were included at estimated positions. Drawings of the molecules were produced with ORTEP3 [30] and PLUTON [31]. A summary of the crystal data, structure solution and refinement parameters are given in Table 1.

3. Results and discussion

Compounds containing the thioamide functional group, –NH–C(S), are capable of exhibiting thione–thiol tautomerism. However, we have previously shown that, in the solid state as well as in solution, the Schiff base, Hqaldsme exists only as the thione (**1a**) tautomer [24] (see Fig. 1).

In addition to the possibility of thione and thiol tautomers, the Schiff base is also capable of existing as *E* and *Z* isomeric forms (Fig. 2) or as a mixture of *E* and *Z* isomers since it also contains the –C=N– moiety.

Although, both in the solid state as well as in solution, the Schiff base remains in its thioketo tautomeric form, in ethanol and in the presence of copper(II) salts, it rapidly

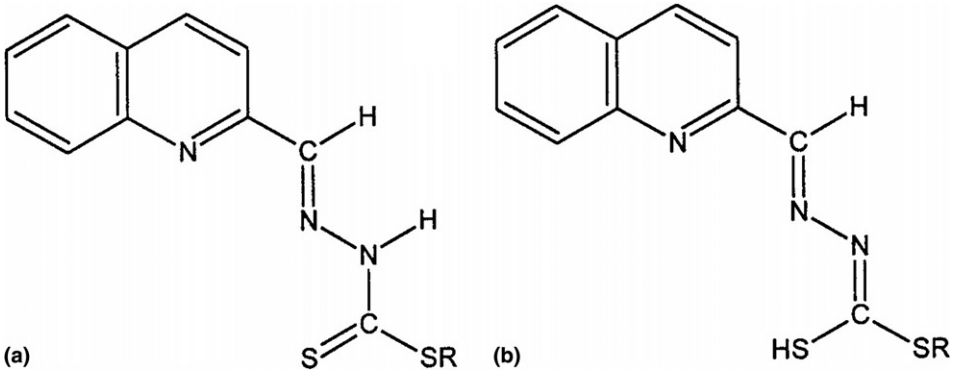

Fig. 1. The thione (**a**) and thiol (**b**) tautomeric forms of the Schiff bases.

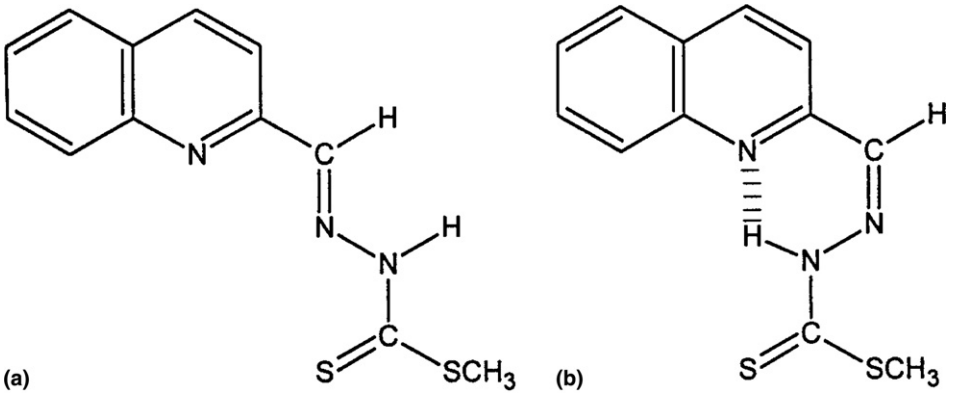

Fig. 2. The *E* and *Z* isomeric forms of the Schiff bases (**a**; the *E* form) (**b**; the *Z* form).

changes its configuration from the thione to the thiol form with the concomitant formation of complexes of empirical formula, $Cu(qaldsme)X(CH_3OH)_n$ (qaldsme = deprotonated form of the Schiff base; X = NCS, I, NO_3; $n = 0$, 1). The related tridentate NNS thiosemicarbazones derived from α-*N*-heterocyclic carboxaldehydes have been shown to coordinate to metal ions in both the protonated thione [32–37] and deprotonated thiolate [34] forms. In some metal–thiosemicarbazone complexes, the protonated thione and deprotonated thiolate forms of a thiosemicarbazone ligand have also been found to be present in the same complex [35–37]. In contrast with thiosemicarbazones, Schiff bases derived from *S*-alkyldithiocarbazates, however, almost always deprotonate upon coordination to give complexes of the ligands in their thiolate form. Our attempts to prepare copper(II) complexes of the protonated form of Hqaldsme have also not been successful.

The complexes are stable at room temperature and they do not show any sign of decomposition if kept in a desiccator over a long period of time. They are moderately soluble in organic solvents such as chloroform, dichloromethane, methyl cyanide, etc., but dissolve readily in donor solvents like DMSO, DMF, etc.

The molar conductances of the copper complexes in $(CH_3)_2SO$ fall in the 17.7–32.1 $ohm^{-1}\,cm^2\,mol^{-1}$ which are much lower than that expected for 1:1 electrolytes (50–70 $ohm^{-1}\,cm^2\,mol^{-1}$) in this solvent [38]. The conductivity of the nickel(II) complex is 2.0 $ohm^{-1}\,cm^2\,mol^{-1}$ indicating that it is essentially a non-electrolyte in this solvent. The conductivity data, therefore, indicate that the Schiff base is coordinated to the metal ions in its deprotonated thiolate form and that the anions in the copper complexes are also coordinated to the copper(II) ion. The IR spectrum of $[Cu(qaldsme)(NCS)]_2$ exhibits a strong band at 2095 cm^{-1} with a shoulder at ca. 2000 cm^{-1} indicating the presence of a monodentate N-bonded thiocyanate group [39] and that of $[Cu(qaldsme)(NO_3)(CH_3OH)]$ shows the ν_{sym} and ν_{asym} modes of the nitrate ligand at 1477 and 1298 cm^{-1}, respectively, indicating that the nitrate ion is coordinated to the copper(II) ion as monodentate ligand [40]. The IR spectra of the complexes also do not contain the *ν*NH band of the free ligand lending further support to the conductance evidence that the proton on the imine nitrogen atom of the ligand is lost during coordination with the copper(II) ion.

The IR spectral data containing relevant vibrational bands of the ligand and its nickel(II) and copper(II) complexes are given in Table 2. The data support coordination of the ligand via the quinoline nitrogen atom, azomethine nitrogen atom via the sulfur atom [41]. A similar tridentate NNS mode of coordination has already been established for the tin(IV) complex of this ligand [24].

The electronic spectral data of the complexes (Table 2), in addition to showing the intra-ligand bands in the 374–350 nm and 341–338 nm ranges corresponding to the $n \Rightarrow \pi^*$ and $\pi \Rightarrow \pi^*$ transitions, respectively, exhibit a d–d band in the 603–730 nm range for the copper complexes and two d–d bands at 815 and 515 nm for the nickel(II) complex. A strong $S \Rightarrow M$ charge-transfer band in the 406–448 nm range is also observed. The presence of a $S \Rightarrow M^{II}$ (LMCT) band in the electronic spectra of these complexes further supports bonding of the ligands to the metal ion via one of the sulfur atoms. The occurrence of a $S \Rightarrow M$ LMCT band is quite common in metal complexes of both thiosemicarbazones [42,43] and dithiocarbazates [23,44]. The appearance of a single d–d band at 645 nm for **1** and 724 nm for **2** is consistent with a square-pyramidal geometry similar to that found for the related $[Cu(bpsbz)NO_3]$ complex (bpsbz = anionic form of the tridentate dithiocarbazate ligand, 2-benzoylpyridine Schiff base of *S*-benzyldithiocarbazate), whose distorted square-pyramidal N_2SO_2 geometry has been established by X-ray diffraction [23].

The room temperature magnetic moments of the copper(II) complexes fall in the 1.75–2.1 B.M. range indicating that these complexes are magnetically dilute in nature. The room-temperature magnetic moment of the bis-ligand nickel(II) complex (2.83 B.M.) is consistent with a six-coordinate distorted octahedral nickel(II) complex. Six-coordinate nickel(II) complexes are expected to exhibit three bands in their electronic spectra corresponding to the $^3A_{2g} \rightarrow {}^3T_{2g}$, $^3A_{2g} \rightarrow {}^3T_{1g}(F)$ and $^3A_{2g} \rightarrow {}^3T_{1g}(P)$ transitions. In the electronic spectrum of the present nickel(II) complex, two d–d bands at 815 and 510 nm corresponding to the $^3A_{2g} \rightarrow {}^3T_{2g}(F)$ and $^3A_{2g} \rightarrow {}^3T_{1g}(F)$ transitions, respectively, are observed consistent with its six-coordinate octahedral geometry. The third band corresponding to the transition $^3A_{2g} \rightarrow {}^3T_{1g}(P)$ could not be observed because of the intrusion of the tail of the strong $S \rightarrow Ni^{II}$ charge transfer band in the visible region of the spectrum.

Table 2
IR and electronic spectral data for Hqaldsme and its copper(II) and nickel(II) complexes

Compound[a]	IR bands				Solid state (Nujol) electronic spectra
	ν(NH)	*ν*(CN)	*ν*(NN)	*ν*(CSS)	λ_{max} (nm)
Hqaldsme	3092m [3095m][b]	1605m [1610m][b]	1060s [1062s][b]	991m	ca. 400sh, 366, 349, 281
1		1591s	1099s	1008s, 1012sh	645, 479, ca. 360sh, 313
2		1585s	1073vs	1003s, 963sh	724, 423, 340, 267
3		1600sh	1086vs	1003s, 963sh	690, ca. 462, 360, 329, 279
4		1582s	1074s	980s, 989s	815, 565sh, 510, ca. 343, 253

[a] qaldsme = anionic form of Hqaldsme.
[b] Data taken from Ref. [24].

3.1. The crystal structure of [Cu(qaldsme)(NO_3)(CH_3OH)]

The structure of the nitrato complex is depicted in Fig. 3 and important bond lengths and angles are compiled in Table 3. The structure shows that the complex is a monomer in which the copper atom adopts a five-coordinate geometry with the Schiff base being coordinated to it as a uninegatively charged tridentate chelating agent via the quinoline nitrogen atom, the azomethine nitrogen atom and the thiolate sulfur atom. An oxygen atom of the monodentate nitrate ligand is coordinated to the copper atom at the equatorial coordination position whereas an oxygen atom of the methanol molecule occupies the axial site. While coordinating with the copper(II) ion, deprotonation of the ligand generates a negative charge on the thiolate sulfur atom which is delocalized over the N(1)–C(1)–S(1) group [N(1)–C(1) 1.28(1) Å and C(1)–S(1) 1.72(1) Å]. The corresponding C(1)–S(1) and N(1)–C(1) bonds of the free ligand Hqaldsme are 1.643(4) and 1.346(8) Å, respectively [24]. It is notable that the N(1)–N(2) and C(3)–N(2) bond lengths (genuine single and double bonds, respectively) do not differ significantly going from the protonated free ligand to the deprotonated coordinated anion [24].

The two five-membered chelate rings S(1)–C(1)–N(1)–N(2)–Cu and N(3)–C(3)–C(4)–N(2)–Cu are virtually coplanar, with all atoms comprising the two rings lying within 0.06 Å of their least-squares plane. The conformation of the ligand also changes upon coordination, e.g., in the free state the ligand remains in an *E*,*E*, conformation but upon coordination, it adopts an *E*,*Z* configuration.

A comparison of the metal–donor atom distances in [Cu(qaldsme)(NO_3)(H_2O)] (Table 3) with those in the analogous five-coordinate copper(II) complex of an analogous dithiocarbazate ligand, [Cu(bpysbz)(NO_3)] (bpysbz = anionic form of the 2-benzoylpyridine Schiff base of *S*-benzyldithiocarbazate) which also has a similar N_2SO_2 coordination kernel [23] indicates that the Cu–S [2.291(4) Å], Cu–$N_{azomethine}$ [1.95(1) Å] and Cu–$N_{heterocyclic\ ring}$ [2.107(9) Å] bond lengths agree well with each other except that the Cu–S bond in the present complex is weaker than that in the Cu-bpysbz complex. As is usually the case, the Cu–$N_{heterocycle}$ distance in the present nitrato complex is longer than the Cu–$N_{azomethine}$ distance. The Cu–$O_{nitrate}$ and Cu–$O_{methanol}$ distances are 1.963(8) Å and 2.275(8) Å,

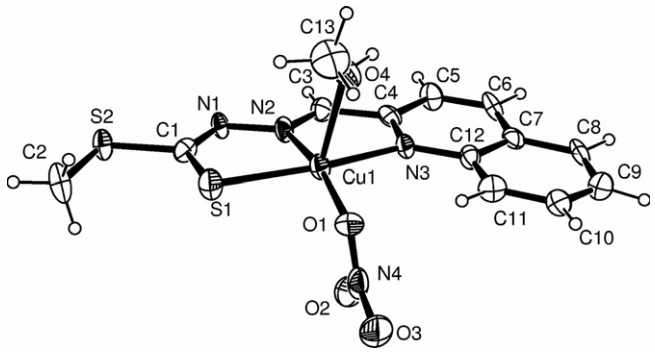

Fig. 3. The crystal structure of [Cu(qaldsme)(NO_3)(CH_3OH)] (30% ellipsoids).

Table 3
Bond lengths (Å) and bond angles (°) for [Cu(qaldsme)(NO_3)(CH_3OH)] and [Cu(qaldsme)(NCS)]$_2$

(a) [Cu(qaldsme)(NO_3)(CH_3OH)]	
Bond lengths	
N(2)–Cu(1)	1.95(1)
N(3)–Cu(1)	2.107(9)
O(1)–Cu(1)	1.963(8)
O(4)–Cu(1)	2.275(8)
S(1)–Cu(1)	2.291(4)
C(1)–N(1)	1.28(1)
C(1)–S(1)	1.72(1)
C(12)–N(3)	1.38(1)
C(1)–S(2)	1.76(1)
C(2)–S(92)	1.76(1)
C(3)–N(2)	1.25(1)
C(3)–C(4)	1.49(2)
C(4)–N(3)	1.34(1)
N(1)–N(2)	1.38(1)
Bond angles	
N(2)–Cu(1)–O(1)	168.5(4)
N(2)–Cu(1)–N(3)	80.5(4)
O(1)–Cu(1)–N(3)	104.6(4)
N(3)–Cu(1)–O(4)	84.6(3)
N(2)–Cu(1)–O(4)	100.4(4)
N(2)–Cu(1)–S(1)	83.8(3)
O(1)–Cu(1)–S(1)	90.2(3)
N(3)–Cu(1)–S(1)	163.8(3)
O(4)–Cu(1)–S(1)	101.9(2)
O(91)–Cu(1)–O(4)	90.5(3)
(b) [Cu(qaldsme)(NCS)]$_2$	
Bond lengths	
Cu(1)–N(2)	1.945(6)
Cu(1)–N(4)	1.897(6)
Cu–S(1)#1	2.783(2)
Cu(1)–S(1)	2.314(2)
Cu(1)–N(3)	2.139(5)
C(1)–S(1)	1.739(7)
C(1)–S(2)	1.724(7)
C(1)–N(1)	1.306(8)
N(1)–N(2)	1.367(7)
C(3)–N(2)	1.296(7)
N(2)–C(6)	1.272(6)
C(3)–C(4)	1.45(1)
C(4)–N(3)	1.341(8)
C(12)–N(3)	1.356(8)
C(13)–N(4)	1.155(8)
C(13)–S(3)	1.623(7)
Bond angles	
N(4)–Cu(1)–N(2)	163.9(2)
N(4)–Cu(1)–N(3)	104.9(2)
N(4)–Cu(1)–S(1)	90.6(2)
N(2)–Cu(1)–S(1)	82.5(2)
N(3)–Cu(1)–S(1)	162.2(2)
N(4)–Cu(1)–S(1)#1	96.6(2)
N(2)–Cu(1)–N(3)	80.3(2)
N(3)–Cu(1)–S(1)#1	96.3(1)
S(1)–Cu(1)–S(1)#1	90.47(6)

Symmetry operation: #1 $-x$, $-y$, $-z+2$.

respectively, which compare well with those found in other five-coordinate copper(II) complexes of dithiocarbazate ligands [2,44].

The coordination geometry of copper(II) ion in $[Cu(qaldsme)(NO_3)(CH_3OH)]$ is close to square-pyramidal. Addison et al. [45] have used an angular structural parameter τ (index of trigonality) for distinguishing between a trigonal-bipyramidal (TBPY) and square-pyramidal (SPY) geometry in five-coordinate complexes, $\tau = \beta - \alpha/60°$ where α and β are the two largest angles. $\tau = 0$ for an ideal square-pyramid (α and $\beta = 180°$) and $\tau = 1$ for an ideal trigonal-bipyramid ($\alpha = 120°$ and $\beta = 180°$). Using this criterion, the τ value is found to be 0.08 indicating that the complex has a near square-pyramidal geometry

3.2. The crystal structure of $[Cu(qaldsme)(NCS)]_2$

In contrast to the monomeric square-pyramidal complex defined in the nitrate salt $[Cu(qaldsme)(NO_3)(CH_3OH)]$, the thiocyanate analogue crystallized as a dimer. A view of the asymmetric (monomeric) unit of the structure is shown in Fig. 4, while the centrosymmetric dimer is depicted in Fig. 5. The two monomeric units are linked by a four-membered ring that includes both symmetry related Cu atoms and coordinated S-donors. The local coordination environment of each copper atom comprises a square-pyramidal N_3S_2 essential part. As expected, the deprotonated Schiff base again binds the copper atom via the quinoline nitrogen atom, the azomethine nitrogen atom and the thiolate sulfur atom. The quinoline nitrogen, the azomethine nitrogen atom and the thiolate sulfur atom of the Schiff base together with the nitrogen atom of the monodentate thiocyanate ligand comprise the basal plane whereas the apical position is occupied by a bridging sulfur atom, formally replacing the methanol ligand seen in $[Cu(qaldsme)(NO_3)(CH_3OH)]$.

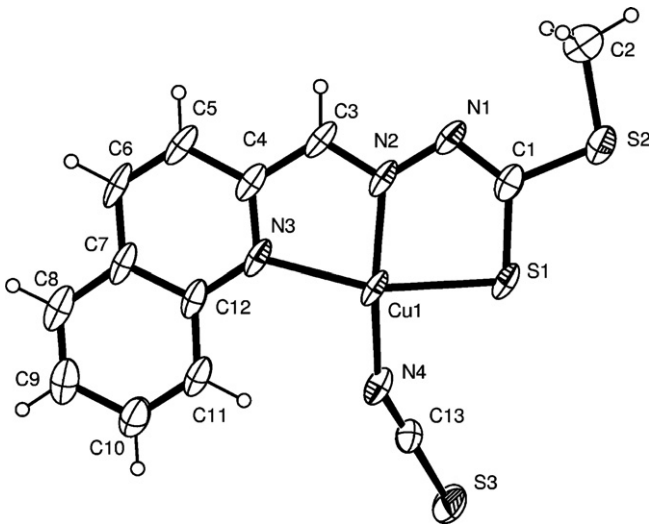

Fig. 4. ORTEP of the monomeric unit of $[Cu(qaldsme)(NCS)]_2$ (30% ellipsoids).

There are several structurally characterized dimeric copper(II) bearing a similar four-membered metallocyclic thiolate-bridging motif [46–51]. Most of these are 2-pyridine carboxaldehyde thiosemicarbazone complexes of Cu(II). For example $[Cu(fptsc)X]_2$ ($X = Cl^-$, Br^-, $HCOO^-$ and NO_3^-) (fptsc = anionic form of the 2-pyridinecarboxaldehyde thiosemicarbazone) whose structures have been confirmed by X-ray diffraction [46,49]. The Cu(1)–S(1), Cu(1)–N(2) and Cu(1)–N(4) bond distances, 2.314(2) Å, 1.945(6) Å and 1.897(6) Å, respectively, in $[Cu(qaldsme)(NCS)]_2$ compare favourably with those in $[Cu(fptsc)X]_2$. The coordination geometry around each copper(II) ion can be considered as approximately square-pyramidal since the geometrical parameter, τ, i.e., $\tau = (\beta - \alpha)/60°$ where α and β are N(4)–Cu(1)–N(3) and N(3)–Cu(1)–S(1) angles, respectively, has a value of 0.03.

The bond distances in the dithiocarbazate chain are the same within experimental uncertainty to those found in the monomeric analogue above. An examination of the bond angle data in Table 3 indicates that the complex does not have a perfect square-pyramidal geometry. The coordinate angles deviate significantly from 90° or 180° due to restraint imposed by the five-membered chelate rings; N(3)–Cu(1)–S(1) [162.2(2) versus 180°], N(4)–Cu(1)–N(2) [163.9(2) versus 180°], N(4)–Cu(1)–N(3) [104.9(2) versus 90°] and N(2)–Cu(1)–N(3) [80.3(2) versus 90°].

3.3. The crystal structure of $[Ni(qaldsme)_2] \cdot 0.5CH_3CN$

The structure of the complex with the atom numbering is depicted in Fig. 6. The bond lengths and bond angles are shown in Table 4. The nickel(II) ion in the complex, $[Ni(qaldsme)_2]$ is in a six-coordinate environment with both deprotonated ligands coordinated to the nickel(II) ion as NNS tridentates in an identical fashion to that seen in the Cu complexes above.

Although one would anticipate a shortening of the N(1)–C(1) and C(1)–S(1) bond lengths going from the free ligand to the coordinated anion (as seen in the Cu(II) complexes), the precision of the structure does not resolve these differences in the present case. The Schiff bases are coordinated to the nickel(II) ion in their meridional configurations the

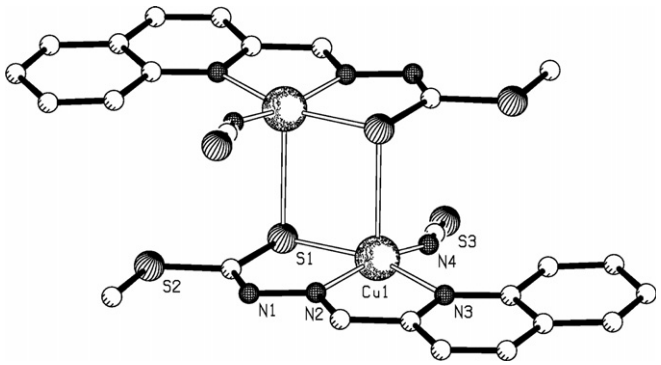

Fig. 5. PLUTON drawing of $[Cu(qaldsme)(NCS)]_2$ (H-atoms omitted).

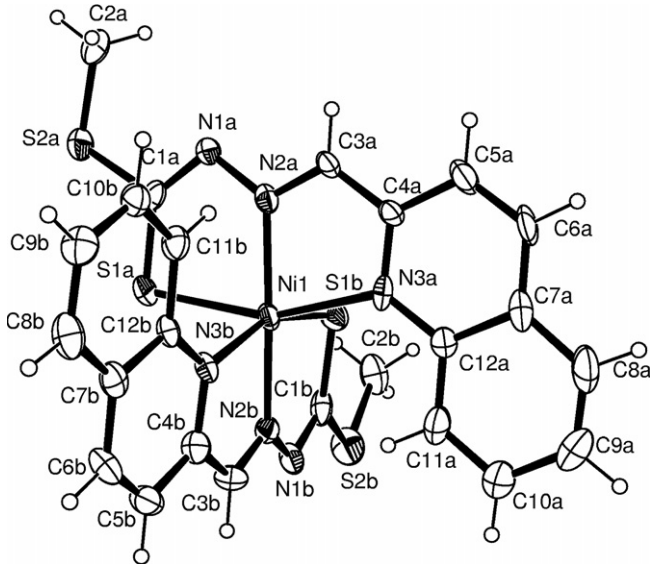

Fig. 6. An ORTEP3 view of Ni(qaldsme)$_2$ (MeCN solvent molecule omitted, 30% ellipsoids).

Table 4
Bond lengths and bond angles of [Ni(qaldsme)$_2$] · 0.5CH_3CN

Bond lengths (Å)	
Ni(1)–N(2A)	2.014(9)
Ni(1)–N(3B)	2.210(8)
NI(1)–S(1A)	2.412(3)
Ni(1)–N(2B)	2.006(8)
Ni(1)–S(1B)	2.415(3)
Ni(1)–N(3A)	2.213(8)
C(3A)–N(2A)	1.29(1)
C(1A)–N(1A)	1.32(1)
C(1B)–N(1B)	1.31(1)
C(1A)–S(1A)	1.68(1)
C(1B)–S(1B)	1.71(1)
N(1A)–N(2A)	1.39(1)
N(1B)–N(2B)	1.36(1)
C(3B)–N(2B)	1.29(1)
Bond angles (°)	
N(2B)–Ni(1)–N(2A)	173.2(4)
N(2B)–Ni(1)–N(3B)	78.3(3)
N(2A)–Ni(1)–N(3B)	106.5(3)
N(2B)–Ni(1)–N(3A)	106.8(3)
N(2A)–Ni(1)–N(3A)	77.8(3)
N(3B)–Ni(1)–N(3A)	94.1(3)
N(2B)–Ni(1)–S(1A)	94.9(3)
N(2A)–Ni(1)–S(1A)	80.6(3)
N(3B)–Ni(1)–S(1A)	89.2(2)
N(3A)–Ni(1)–S(1B)	80.3(3)
N(3A)–Ni(1)–S(1A)	158.3(3)
N(2A)–Ni(1)–S(1B)	94.9(2)
N(2B)–Ni(1)–S(1B)	80.3(3)
N(3B)–Ni(1)–S(1B)	158.6(2)

quinoline nitrogen and thiolate sulfur atoms *cis* to each other and the two azomethine nitrogen atoms *trans*. Similar meridional configurations of tridentate NNS ligands around nickel(II) have also been observed in other bis-chelated nickel(II) complexes of NNS thiosemicarbazones [52,53] and dithiocarbazates [53]. The Ni–S [2.412(3) and 2.415(3) Å], Ni–N_{imine} [2.014(9) and 2.006(8) Å] and Ni–$N_{heterocycle}$ [2.213(8) and 2.210(8) Å] bond lengths are similar to those of other six-coordinate distorted octahedral nickel(II) complexes of tridentate sulfur–nitrogen chelating agents. The two Ni–$N_{quinoline}$ bond distances are close but they are significantly different from the Ni–N_{imine} bond distances. Similar differences between the Ni–N_{imine} and Ni–$N_{pyridine}$ bonds have also been observed in other related six-coordinated nickel(II) complexes [21,54,55]. For the purpose of comparison, nickel-donor atom distances in some six-coordinated nickel(II) complexes of closely related ligands, whose structures have been determined by X-ray diffraction, are shown in Table 5. The data show that the Ni–N_{imine} and Ni–$N_{heterocyclic}$, distances are always different the former being consistently shorter than the latter. The coordination sphere of the present nickel(II) complex is a distorted octahedron. Except for the angles, N(3A)–NI(1)–S(1B) [90.4(2)°] and N(3B)–NI(1)–S(1A) [89.2(2)°], all other angles deviate, some of them substantially, from that of an ideal octahedral geometry. The distortion is due to the restricted bite angles imposed by planar tridenate qaldsme ligands.

Table 5
Comparison of nickel–donor atom distances (Å) in some six-coordinate nickel(II) complexes of tridentate N_2S ligands

	Ni–S	Ni–$N_{azomethione}$	Ni–$N_{heterocyclic}$	Ref.
[Ni(pytsc)$_2$][a]	2.440(2) 2.409(2)	2.004(6) 2.056(6)	2.215(7) 2.106(7)	[52]
[Ni(isoqtsc)$_2$][b]	2.424(2) 2.412(2)	2.013(5) 2.026(5)	2.110(6) 2.114(6)	[53]
[Ni(NNSMe)$_2$][c]	2.420(13) 2.412(3)	2.056(6) 2.016(6)	2.224(7) 2.166(7)	[21]
[Ni(dpksme)$_2$][d]	2.3961(13) 2.4253(12)	2.024(3) 2.013(3)	2.106(3) 2.104(3)	[54]
[Ni(aptsc)$_2$][e]	2.380(1) 2.409(2)	2.014(3) 2.017(4)	2.110(6) 2.096(4)	[55]
[Ni(qaldsme)$_2$]·0.5CH_3CN	2.412(3) 2.415(3)	2.014(9) 2.006(8)	2.213(8) 2.210(8)	this work

[a] pytsc = deprotonated form of pyridine-2-aldehydethiosemicarbazone.
[b] isoqtsc = deprotonated form of 2-fromylisoquinolinethiosemicarbazone.
[c] NNSMe = deprotonated form of the 6-methyl-2-pyridine Schiff base of *S*-methyldithiocarbazate.
[d] dpksme = deprotonated form of the di-2-pyridylketone Schiff base of *S*-methyldithiocarbazate.
[e] aptsc = deprotonated form of 2-acetylpyridine-^{4}*N*-methylthiosemicarbazone.

4. Supplementary materials

Crystallographic data in CIF format have been deposited at the Cambridge Crystallographic Data Centre with CCDC deposition numbers 249079, 249080 and 600758. Copies of this information may be obtained free of charge from The Director, CCDC, 12 Union Road, Cambridge, CB2 1EZ, UK (fax: +44 1223 336033; e-mail: deposit@ccdc.ac.uk or http://www.ccdc.cam.ac.uk).

Acknowledgement

M.A.A., A.H.M. and M.H.S.A.H. thank the Department of Chemistry, Universiti Brunei Darussalam for support.

References

[1] M. Akbar Ali, A.H. Mirza, L.K. Wei, A.-L. Tan, P.V. Bernnhardt, Polyhedron 23 (2004) 2037.
[2] M. Akbar Ali, A.H. Mirza, Thahira B.S.A. Ravoof, P.V. Bernhardt, Polyhedron 23 (2004) 2031.
[3] M. Akbar Ali, A.H. Mirza, C.W. Voo, Ai Ling Tan, P.V. Bernhardt, Polyhedron 22 (2003) 3433.
[4] M. Akbar Ali, A.H. Mirza, M. Nazimuddin, R. Ahmed, L.H. Gahan, P.V. Bernhardt, Polyhedron 22 (2003) 1471.
[5] M. Akbar Ali, A.H. Mirza, S.T.W. Keng, R.J. Butcher, Trans. Met. Chem. 28 (2003) 241.
[6] M. Akbar Ali, A.H. Mirza, R.J. Butcher, M.T.H. Tarafder, Tan Boon Keat, A. Manaf Ali, J. Inorg. Biochem. 92 (2002) 141.
[7] M. Akbar Ali, A.H. Mirza, M. Nazimuddin, H. Rahman, R.J. Butcher, Trans. Met. Chem. 27 (2002) 268.
[8] M. Akbar Ali, A.H. Mirza, M. Nazimuddin, P.K. Dhar, R.J. Butcher, Trans. Met. Chem. 27 (2002) 27.
[9] P. Bera, R.J. Butcher, S. Chaudhuri, N. Saha, Polyhedron 21 (2002) 1.
[10] M. Das, S.E. Livingstone, Inorg. Chim. Acta 19 (1976) 5.
[11] Karen A. Crouse, Kar-Benng Chew, M.T.H. Tarafder, A. Kasbollah, A.M. Ali, B.M. Yamin, H.-K. Fun, Polyhedron 23 (2004) 161.
[12] K.A. Crouse, Kar-Beng Chew, Bohari M. Yamin, Seik-Weng Ng, M.T.H. Tarafder, Acta Crystallogr. E59 (2003) 148.
[13] Yu-peng Tian, Chun-ying Duan, Cun-yuan Zhao, Xiao-zeng You, T.C.W. Mak, Zeying Zhang, Inorg. Chem. 36 (1997) 1247.
[14] Yu-Peng Tian, Chung-Ying Duan, Xiao-Zeng You, T.C.W. Mak, Q. Luo, Jian-Ying Zhou, Trans. Met. Chem. 23 (1998) 17.
[15] A. Abu-Raqabah, G. Davies, M.A. El-Sayed, A. El-Toukhy, S.N. Shaikh, J. Zubieta, Inorg. Chim. Acta 193 (1992) 43, and references therein.
[16] M. Akbar Ali, S.E. Livingstone, Coord. Chem. Rev. 13 (1974) 101.
[17] D.X. West, S.B. Padhye, P.B. Sonawane, Struct. Bond. (Berl.) 76 (1991) 1.
[18] S.E. Livingstone, Br. J. Cancer 37 (1978) 466.
[19] M. Akbar Ali, S.E. Livingstone, D.J. Phillips, Inorg. Chim. Acta 5 (1971) 493.
[20] M. Akbar Ali, M.T.H. Tarafder, J. Inorg. Nucl. Chem. 39 (1977) 1785.
[21] M. Akbar Ali, S.M.M.H. Majumder, R.J. Butcher, J.P. Jasinski, J.M. Jasinski, Polyhedron 16 (1997) 2749.
[22] M.E. Hossain, M.N. Alam, M. Akbar Ali, M. Nazimuddin, F.E. Smith, R.C. Hynes, Polyhedron 15 (1996) 973.
[23] M.E. Hossain, M.N. Alam, J. Begum, M. Akbar Ali, M. Nazimuddin, F.E. Smith, R.C. Hynes, Inorg. Chim. Acta 249 (1996) 207.
[24] M. Akbar Ali, A.H. Mirza, Fatriah Hj Bujang, Malai Haniti S.A. Hamid, P.V. Bernhardt, Polyhedron 23 (2004) 2405.
[25] A.C.T. North, D.C. Phillips, F.S. Mathews, Acta. Crystallogr. Sect. A 24 (1968) 351.
[26] K. Harms, S. Wocadlo, CAD4 Data Reduction, University of Marburg, Marburg, Germany, 1995.
[27] L. Farrugia, J. Appl. Crystallogr. 32 (1999) 837.
[28] G.M. Sheldrick, SHELXS86 – Programme for Crystal Structure Solution, Institute für Anorganisch Chemie der Universität, Göttingen, Germany, 1986.
[29] G.M. Sheldrick, SHELXL97, Institüt für Anorganisch Chemie der Universität, Göttingen, Germany, 1998.
[30] L. Farrugia, J. Appl. Crystallogr. 30 (1997) 565.
[31] A.L. Spek, Acta Crystallogr. Sect. A 46 (1990) C34.
[32] T. Siang-Guan, A. Show-Hing, T. Soon-Beng, F. Hoong-Kun, K. Khing -Ling, O. Chi-Wi, J. Chem. Soc., Dalton Trans. (1997) 465.
[33] A. Mohan, P. Sharma, N.K. Jha, Inorg. Chim. Acta 106 (1985) 197.
[34] M.B. Ferrari, S. Capacchi, F. Bisceglie, G. Pelosi, P. Tarasconi, Inorg. Chim. Acta 312 (2001) 81.
[35] D.K. Sau, R.J. Butcher, S. Chaudhuri, N. Saha, Polyhedron 23 (2004) 5.
[36] M.B. Ferrari, G.G. Fava, G. Pelosi, M.C. Rodriguez-Arguelles, P. Tarasconi, J. Chem. Soc., Dalton Trans. (1995) 3035.
[37] P. Souza, A.I. Matesanz, V. Fernandez, J. Chem. Soc., Dalton Trans. (1996) 3011.
[38] W.J. Geary, Coord. Chem. Rev. 7 (1971) 81.
[39] R.A. Bailey, S.L. Kojak, T.W. Michelson, W.N. Mills, Coord. Chem. Rev. 6 (1971) 407.
[40] K. Nakamoto, Infrared and Raman Spectra of Inorganic and Coordination Compounds, 5th ed., Wiley, New York, 1997.
[41] S. Bonati, S. Cenini, R. Ugo, J. Organomet. Chem. 9 (1967) 395.
[42] A.G. Bingham, H. Bogge, H. Muller, A. Ainscough, A.M. Brodie, J. Chem. Soc., Dalton Trans. (1987) 493.
[43] E.W. Ainscough, E.N. Baker, A.M. Brodie, R.J. Cresswell, J.D. Ranford, J.M. Waters, Inorg. Chim. Acta 172 (1990) 185.
[44] M. Akbar Ali, R.J. Butcher, J.C. Bryan, Inorg. Chim. Acta 287 (1999) 8.
[45] A. Addison, T. Rae, J. Reedjik, J. Van Rijn, G. Verschoor, J. Chem. Soc., Dalton Trans. (1984) 1349.
[46] J. Garcia-Tojal, M.K. Urtiaga, R. Cortes, L. Lezama, M.I. Arriortua, T. Rojo, J. Chem. Soc., Dalton Trans. (1994) 2233.
[47] J. Garcia-Tojal, L. Lezama, J.L. Pizarro, M. Insausti, M.I. Arriortua, Polyhedron 18 (1999) 3703.
[48] E.W. Ainscough, A.M. Brodie, J.D. Ranford, J.M. Waters, K.S. Murray, Inorg. Chim. Acta 197 (1992) 107.
[49] P. Gomez-Saiz, J. Garcia-Tojal, A. Mendina, B. Donadieu, L. Lezama, J.L. Pizarro, M.I. Arriortua, Eur. J. Inorg. Chem. (2003) 518.
[50] E. Bermejo, A. Castineiras, M. Gil, E. Labisbal, A. Sousa, H. Beraldo, D.X. West, Z. Anorg. Allg. Chem. 627 (2001) 827.
[51] P. Gomez-Saiz, J. Garcia-Tojal, M.A. Maestro, F.J. Arnaiz, T. Rojo, Inorg. Chem. 41 (2002) 1345.
[52] G.R. Clark, G.J. Palenik, Crystal. Struct. Commun. 9 (1980) 449.
[53] M. Mathew, G.J. Palenik, J. Am. Chem. Soc. 91 (1969) 6300.
[54] M. Akbar Ali, A.H. Mirza, M. Nazimuddin, H. Rahman, R.J. Butcher, Polyhedron 20 (2001) 2431.
[55] D.X. West, M.A. Lockwood, G. Gebremedhin, A. Castineiras, Polyhedron 12 (1993) 2489.

of these structures with salts, alcohols, proteins and other compounds [18]. Surface active materials are major building blocks of many physical, chemical and biological systems. They have been introduced into several commercial products such as antiseptic agents in cosmetics and as germicides [5], and also have found a wide range of applications because of their unique solution properties such as detergency, solubilization and surface wetting capabilities, in diverse areas such as mining, petroleum and pharmaceutical industries. It has been observed that several redox reactions in micellar media were influenced by the hydrophobic and electrostatic forces and for a given set of reactions the observed rate depends on the extent of association between the reactants and micellar aggregates [19–23]. A growing number of applications have been developed to study metallosurfactants in this content. They are a good enzymatic model for the catalytic hydrolysis of carboxylic acid esters, since they mimic not only the active center of the metalloenzyme but also the microenvironment of the metalloenzyme. In the course of studies on the effects of metallosurfactants on chemical reactions, catalytic effects were observed above a critical micelle concentration (CMC). Such systems offered the possibility to investigate the effects of the local reactant concentrations in the micellar subphase, as well as the local microenvironment on the reactivity [24–28].

Cobalt(III) complexes, by virtue of their abundance and diversity, have played a fundamental role in our understanding of the structural, spectroscopic and electrochemical properties of coordination compounds. We have been interested in the synthesis and micelle forming properties of Co^{III} complexes containing lipophilic ligands for a long time [29–31]. As in biology, such compounds may exhibit novel physical and chemical properties with interesting and useful associated applications. Studies on the chemistry of Co^{III} metallosurfactants have received a sustained high level of attention due to their relevance in various redox processes in biological systems and act as promising agents for antitumor [32], anthelmintic [33], antiparasitic [34], antibiotics [35] and antimicrobial activities [17], and a boost of interest because of their multiple applications in fields such as medicine [36], magnetic resonance imaging [37] and drug delivery [38].

A characteristic feature of transition metals is their ability to form complexes with a variety of neutral molecules such as bpy and phen. These are widely used as a classical *N*,*N*′-bidentate ligand to prepare mixed-ligand complexes in coordination chemistry. A common feature of these ligands is the presence of a vacant π orbital that can accept electron density from the metal ion to form a type of π bonding that supplements the σ bonding arising from the donation of a lone pair of electrons. Most of the metal complexes containing bpy and phen chelators can act as potential anti-tumor agents. Intensive investigations of the coordination chemistry of metallosurfactants with chelating ligands continue to be stimulated by interest for metallobiomolecules, the search for appropriate systems for binding and activating simple molecules, catalysis, and magnetic interactions [39,40]. In spite of the greatest effort and success in the study of metallosurfactants of cobalt(III) complexes, such complexes still attract much attention due to their interesting properties and the relative simplicity of their synthesis (Scheme 1). Recently, there has been increasing interest in the use of these organized media to study the fundamental photochemical reactions of metal complexes in relevance to the conversion of solar energy into other useful forms of energy through photochemical reactions [41,42]. As a part of our studies on transition metal-based surfactants [29–31] in this paper we report the synthesis, characterization and determination of critical micelle concentration values of some more novel Co^{III} metallosurfactants.

2. Experimental

2.1. Materials

All the reagents were of analytical grade (Aldrich and Merck). Ultra pure water, obtained by deionising distilled water (conductivity $<10^{-6}$ S m^{-1}) using a Milli-Q Reagent

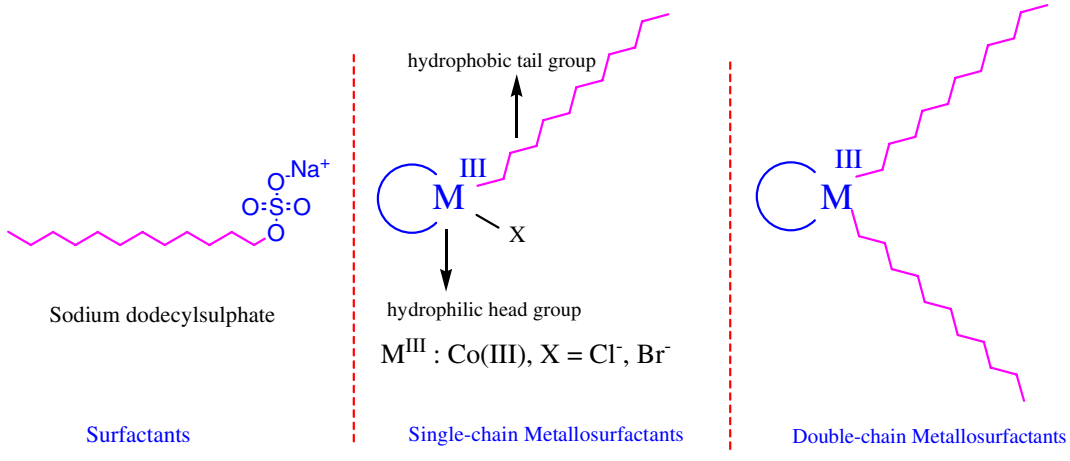

Scheme 1.

Grade water system, was used for preparative work and to make up solutions for all physical measurements.

2.2. Physical measurements and methods

^{1}H NMR spectra were recorded in appropriate deuteriated solvents using a Bruker AC 300F (300 MHz) spectrometer with TMS as internal reference. Infrared (IR) spectra were recorded on a Jasco 460 plus spectrometer using the potassium bromide discs method. Electronic absorption spectra were taken in 10^{-3} M perchloric acid medium recorded in a Varian Cary 500 Scan UV–Vis–NIR spectrophotometer. C, H and N were estimated using a Perkin–Elmer 2400 CHN instrument. Conductance measurements were carried out in aqueous solutions of the complexes with a Metrohm 712 conductivity meter and a dip-type cell with a cell constant of 1.0.

2.3. Synthesis of single chain metallosurfactants of cobalt(III) complexes

2.3.1. *cis*-$[Co(bpy)_2(C_{12}H_{25}NH_2)Cl](ClO_4)_2 \cdot 2H_2O$ and *cis*-$[Co(bpy)_2(C_{16}H_{33}NH_2)Cl](ClO_4)_2 \cdot 2H_2O$

Cis-$[Co(bpy)_2Cl_2]Cl \cdot 2H_2O$ [43] (3 g) was dissolved in water (10 mL). To this solution dodecylamine (1 mL), where the amine used was not sufficiently miscible with (soluble in) water, was first mixed with ethanol (2 mL) and then added drop by drop over a period of 30 min. The dark violet colour solution gradually became brown during the reaction. The mixture was set aside at 313 K for 2 days until no further change was observed. Afterwards a saturated solution of sodium perchlorate in very dilute perchloric acid was added. Slowly a pasty solid mass separated out and it was filtered off, washed with small amounts of alcohol followed by acetone, and then it was dried over air. The semi-dried solid was further dried in a drying pistol over fused calcium chloride and stored in a vacuum desiccator. For the complex *cis*-$[Co(bpy)_2(C_{16}H_{33}NH_2)Cl](ClO_4)_2 \cdot 2H_2O$, cetylamine was used in the place of dodecylamine.

2.3.2. *cis*-$[Co(bpy)_2(C_{12}H_{25}NH_2)Br](ClO_4)_2 \cdot 2H_2O$ and *cis*-$[Co(bpy)_2(C_{16}H_{33}NH_2)Br](ClO_4)_2 \cdot 2H_2O$

This complex was synthesized by adopting the same method as described for the synthesis of the complex *cis*-$[Co(bpy)_2(C_{12}H_{25}NH_2)Cl](ClO_4)_2 \cdot 2H_2O$ except that in place of *cis*-$[Co(bpy)_2Cl_2]Cl$, *cis*-$[Co(bpy)_2Br_2]Br$ [43] was used.

2.3.3. *cis*-$[Co(phen)_2(C_{12}H_{25}NH_2)Cl](ClO_4)_2 \cdot 2H_2O$, *cis*-$[Co(phen)_2(C_{16}H_{33}NH_2)Cl](ClO_4)_2 \cdot 2H_2O$, *cis*-$[Co(phen)_2(C_{12}H_{25}NH_2)Br](ClO_4)_2 \cdot 2H_2O$ and *cis*-$[Co(phen)_2(C_{16}H_{33}NH_2)Br](ClO_4)_2 \cdot 2H_2O$

The procedure for synthesizing these complexes is similar to that described above, but in the place of bipyridyl complexes, phenanthroline complexes *cis*-$[Co(phen)_2Cl_2]Cl$ and *cis*-$[Co(phen)_2Br_2]Br$ were used [44].

2.4. Synthesis of double-chain metallosurfactants of cobalt(III) complexes

2.4.1. *cis*-$[Co(en)_2(C_{12}H_{25}NH_2)_2](ClO_4)_3 \cdot 2H_2O$ and *cis*-$[Co(en)_2(C_{16}H_{33}NH_2)_2](ClO_4)_3 \cdot 2H_2O$

Trans-$[Co(en)_2Cl_2]Cl$ [45] (3.0 g) was dissolved in water (20 mL). To this solution a slightly more than the calculated amount of dodecylamine (4.3 mL) in ethanol (3 mL) was added drop by drop over a period of 30 min. The green solution gradually became red during the reaction and the mixture was set aside for 2 days at 313 K. Afterwards a saturated solution of sodium perchlorate in very dilute perchloric acid was added. The solid that formed filtered off and washed with alcohol followed by acetone and dried.

The complexes *cis*-$[Co(en)_2(C_{16}H_{33}NH_2)_2](ClO_4)_3 \cdot 2H_2O$, *cis*-α-$[Co(trien)(C_{12}H_{25}NH_2)_2](ClO_4)_3 \cdot 2H_2O$, *cis*-α-$[Co(trien)(C_{16}H_{33}NH_2)_2](ClO_4)_3 \cdot 2H_2O$, *cis*-$[Co(bpy)_2(C_{12}H_{25}NH_2)_2](ClO_4)_3 \cdot 2H_2O$, *cis*-$[Co(bpy)_2(C_{16}H_{33}NH_2)_2](ClO_4)_3 \cdot 2H_2O$, *cis*-$[Co(phen)_2(C_{12}H_{25}NH_2)_2](ClO_4)_3 \cdot 2H_2O$ and *cis*-$[Co(phen)_2(C_{16}H_{33}NH_2)_2](ClO_4)_3 \cdot 2H_2O$ were prepared by the ligand substitution method, replacing the chloride ion with dodecylamine/cetylamine from their corresponding parent complexes [29,43–45].

Safety note. Caution: Perchlorate salts of Co^{III} complexes containing organic ligands are potentially explosive! Although we have experienced no problems with the compounds reported in this work, they should only be handled in small quantities and never scraped from sintered glass frits nor heated in the solid state.

2.5. Determination of CMC

CMC values of the complexes were calculated using electrical conductance data measured using a digital conductivity meter (Metrohm 712). The conductivity cell (dip-type with a cell constant of 1.0) was calibrated with KCl solutions in the appropriate concentration range. The cell constant was calculated using molar conductivity data for KCl published by Barthel et al. [46]. Various concentrations of Co^{III}–surfactant complexes were prepared in the range 10^{-6}–10^{-2} mol dm^{-3}. All measurements were performed in a double-walled glass container, which was maintained at the desired temperature (±0.1 °C) using a circulating water bath. The conductivity of these solutions was measured at 303–313 K. The conductance was measured after thorough mixing and temperature equilibrating at each dilution. The measurement was started with a dilute solution and the subsequent concentrated solutions were prepared by adding a previously prepared stock solution. The establishment of equilibrium was checked by taking a series of reading after 15-min intervals until no significant change occurred.

3. Results and discussion

The cobalt(III)–surfactant complexes synthesized in the present study were characterized by UV–visible, IR and

NMR spectra and checked by comparing the spectra with those for the corresponding ordinary complexes where one of the ligands is butylamine instead of dodecylamine/cetylamine, which have been reported earlier [29]. The purity of the complexes was checked by cobalt [47], elemental, halide analyses, which were found to be in good agreement with that of calculated values (Table 1).

3.1. Spectroscopic characterization

3.1.1. Infrared spectra

For the assignment of a geometrical configuration to these complexes, infrared spectroscopy was used. Several attempts have been made to relate differences in infrared spectra to geometrical configuration of complexes. Various workers have employed [48–50] the NH_2 deformation mode in the 1700–1500 cm^{-1} region, CH_2 rocking mode in the 900–850 cm^{-1} and Co–N stretching mode in the 610–500 cm^{-1} region to distinguish between the *cis* and *trans* isomers of cobalt(III)–ethylenediamine complexes. Baldwin [48] suggested that the most consistent variations between the spectra of *cis*- and *trans*-isomers were found in the CH_2 rocking region (900–850 cm^{-1}). The *cis*-isomers always show two peaks, whereas the *trans*-isomers usually have only one. Hughes and Mcwhinnie [49] studied the infrared absorption spectra of several bis(ethylenediamine)cobalt(III) complexes and obtained a satisfactory correlation in the 610–500 cm^{-1} region, where Co–N stretching modes of the chelate ring occur. Here, no *trans*-isomers had more than three strong bands, while all *cis*-isomers had at least four, sometimes occurring as shoulders. The bands for the *trans* isomers were generally evenly distributed, while those for *cis*-complexes occurred in two groups with a wide separation between them. Because of the lower symmetry in the present study (Fig. 1), the *cis* isomers show two bands for the NH_2 deformation, two bands for the NH_2 wagging modes, two bands for CH_2 rocking mode and four bands occurring as groups of two with a

Table 1
Microanalysis and visible spectra of some cobalt(III) metallosurfactants

Surfactants · $2H_2O$	λ_{max} (nm)	Yield (%)	% Found (calculated)				
			Co	C	H	N	Cl/Br
cis-$[Co(en)_2(C_{12}H_{25}NH_2)_2](ClO_4)_2$	504	69	6.6 (6.7)	37.6 (38.0)	7.6 (7.8)	9.4 (9.5)	
cis-$[Co(en)_2(C_{16}H_{33}NH_2)_2](ClO_4)_2$	499	72	6.0 (5.9)	43.1 (43.4)	8.6 (8.5)	8.3 (8.4)	
cis-α-$[Co(trien)(C_{12}H_{25}NH_2)_2](ClO_4)_2$	475	66	6.4 (6.5)	42.0 (42.2)	8.0 (8.0)	9.1 (9.2)	
cis-α-$[Co(trien)(C_{16}H_{33}NH_2)_2](ClO_4)_2$	471	64	5.7 (5.8)	46.8 (47.0)	8.7 (8.7)	8.3 (8.2)	
cis-$[Co(bpy)_2(C_{12}H_{25}NH_2)Cl](ClO_4)_2$	524	54	7.0 (7.1)	46.4 (46.5)	5.5 (5.6)	8.4 (8.5)	4.2 (4.3)
cis-$[Co(bpy)_2(C_{12}H_{25}NH_2)Br](ClO_4)_2$	528	58	6.7 (6.7)	44.1 (44.1)	5.4 (5.3)	8.0 (8.0)	9.2 (9.1)
cis-$[Co(bpy)_2(C_{12}H_{25}NH_2)_2](ClO_4)_2$	510	60	5.4 (5.5)	49.0 (49.1)	6.6 (6.7)	7.7 (7.8)	
cis-$[Co(bpy)_2(C_{16}H_{33}NH_2)Cl](ClO_4)_2$	516	53	6.6 (6.7)	48.7 (49.0)	5.7 (5.7)	8.1 (8.0)	3.9 (4.0)
cis-$[Co(bpy)_2(C_{16}H_{33}NH_2)Br](ClO_4)_2$	520	50	6.4 (6.3)	46.4 (46.6)	5.3 (5.4)	7.4 (7.5)	8.3 (8.6)
cis-$[Co(bpy)_2(C_{16}H_{33}NH_2)_2](ClO_4)_2$	506	66	4.8 (4.9)	52.7 (52.5)	7.2 (7.4)	6.9 (7.1)	
cis-$[Co(phen)_2(C_{12}H_{25}NH_2)Cl](ClO_4)_2$	514	57	6.6 (6.7)	49.1 (49.1)	5.1 (5.3)	7.9 (8.0)	4.0 (4.0)
cis-$[Co(phen)_2(C_{12}H_{25}NH_2)Br](ClO_4)_2$	519	62	6.3 (6.4)	47.2 (47.0)	4.9 (5.0)	7.4 (7.6)	8.5 (8.7)
cis-$[Co(phen)_2(C_{12}H_{25}NH_2)_2](ClO_4)_2$	506	53	5.2 (5.2)	51.1 (51.3)	6.2 (6.4)	7.5 (7.5)	
cis-$[Co(phen)_2(C_{16}H_{33}NH_2)Cl](ClO_4)_2$	510	60	6.3 (6.3)	51.4 (51.6)	5.7 (5.8)	7.4 (7.5)	3.5 (3.8)
cis-$[Co(phen)_2(C_{16}H_{33}NH_2)Br](ClO_4)_2$	515	63	6.0 (6.0)	49.2 (49.2)	5.6 (5.6)	7.0 (7.1)	3.4 (3.6)
cis-$[Co(phen)_2(C_{16}H_{33}NH_2)_2](ClO_4)_2$	502	67	4.7 (4.8)	54.2 (54.4)	7.1 (7.2)	6.7 (6.8)	

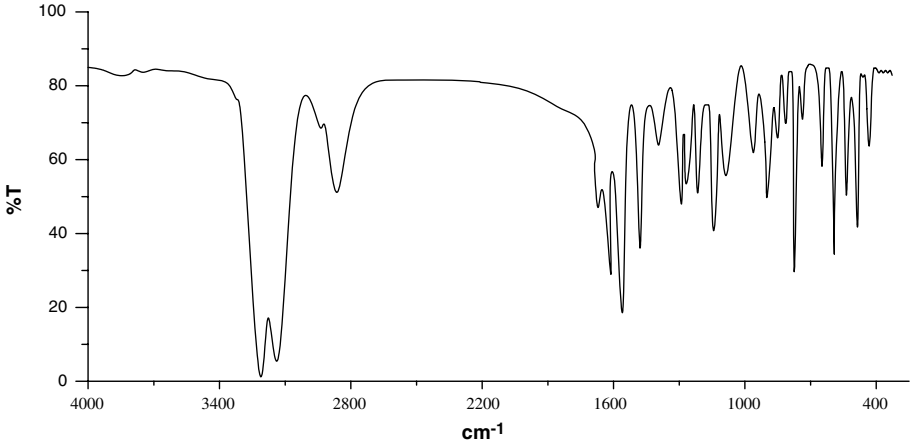

Fig. 1. Infrared spectra of *cis*-α-$[Co(trien)(C_{16}H_{33}NH_2)_2](ClO_4)_2$.

wide separation for the Co–N stretching mode. Complexes of the type *cis*-α-$[Co(trien)X_2]^{n+}$ in the present study show two bands for the NH_2 deformation in the region 1630–1580 cm^{-1}, two bands for the CH_2 or NH_2 twist mode in the region 1150–980 cm^{-1}, and the CH_2 rock mode in the region 940–860 cm^{-1} appearing as two bands [50]. Strukl and Walter [51] and Schilt and Taylor [52] studied the infrared spectra of several bipyridyl and phenanthroline complexes. They observed that the spectral shape of the bpy and phen complexes were quite similar, taking into account the similarity of both ligands. In the spectra of the phenanthroline complexes, strong bands were observed in three frequency regions namely between 700 and 900 cm^{-1}, between 1100 and 1250 cm^{-1} and between 1400 and 1650 cm^{-1}. Strong bands in the 700–900 cm^{-1} region were attributed to the aromatic hydrocarbons of the phenanthroline ring. The band near 720 cm^{-1} was assigned to the out of the plane motion of hydrogen atoms on the heterocyclic rings and the band near 840 cm^{-1} to the hydrogens on the centre ring. The multiple splitting which these bands exhibit in most of the spectra probably arise from out-of-plane hydrogen motion other than the one in which all atoms move in phase, and also possibly from overtones of low lying fundamentals in resonance. In the bipyridyl spectra, only one strong band was observed in this region as expected for two identical groups of four hydrogen atoms each. Not much can be said about the bands in the 1100–1250 cm^{-1} region expect that they may arise from in-plane hydrogen deformation motions or possibly ring vibrations. The spectra of the bpy complexes in general are less complicated than those of the phen complexes. Only three strong bands are present, one near 750 ascribed to out of plane bending of ring hydrogens, and one near 1450 cm^{-1} which is probably a ring frequency, and a ring frequency near 1600 cm^{-1}. Numerous weak bands were observed between 900 and 1350 cm^{-1}. The C=C and C=N stretching vibrations of the heterocyclic ring stem exhibit in the region at 1410, 1450, 1545 and 1570 cm^{-1}. Perchlorate bonds at ca. 1100, 925, 620 and 450 cm^{-1} belong to an ionic species; this means that this counter-ion is not involved in the cobalt-ligand coordination [53]. The IR spectroscopic data therefore clearly indicate a *cis* configuration for the cobalt(III) surfactant complexes.

3.1.2. ^1H NMR spectra

The ^1H NMR spectra offer a conclusive proof of the configuration of the isomers in solution. The *cis* and *trans* isomers of $[Co(en)_2X_2]^+$ ions have different symmetry properties, and this factor appears to govern the difference in their NMR spectra. The *cis* isomers possess C_2-symmetry with the twofold axis in the plane of cobalt and the two X groups and this makes $–CH_2CH_2–$ groups equivalent provided that the cobalt–ethylenediamine rings have the same conformation. In the present study (Fig. 2), for the *cis* complexes, due to the lower symmetry, the methylene protons of ethylenediamine show a more complex absorption around 2.5–2.8 ppm. The methylene protons of the long chain moieties (dodecylamine/cetylamine) give rise to a multiplet usually at 1.2–1.8 ppm, whereas the terminal methyl group of the hydrocarbon chain substituent gives a triplet at 0.84 ppm. The ^1H NMR spectral data for the cobalt(III)–triethylenetetramine complexes exhibit signals in the region 2.6–3.0 ppm attributable to the $–CH_2$ group of the triethylenetetramine chelate ring, thus confirming the *cis* structure of the complex. It is well established that bis-type cobalt(III) complexes of 2,2′-bipyridine or 1,10-phenanthroline take only the *cis*-configuration because of the repulsion between the ligands. The *cis* configuration of all the present complexes was confirmed by the ^1H NMR. The spectra of the 1,10 phenanthroline complexes exhibit patterns similar to those of the bipyridine complexes. The assignment of the 1,10 phenanthroline and bipyridine complexes were made in a manner similar to the case of their respective parent complexes [54,55].

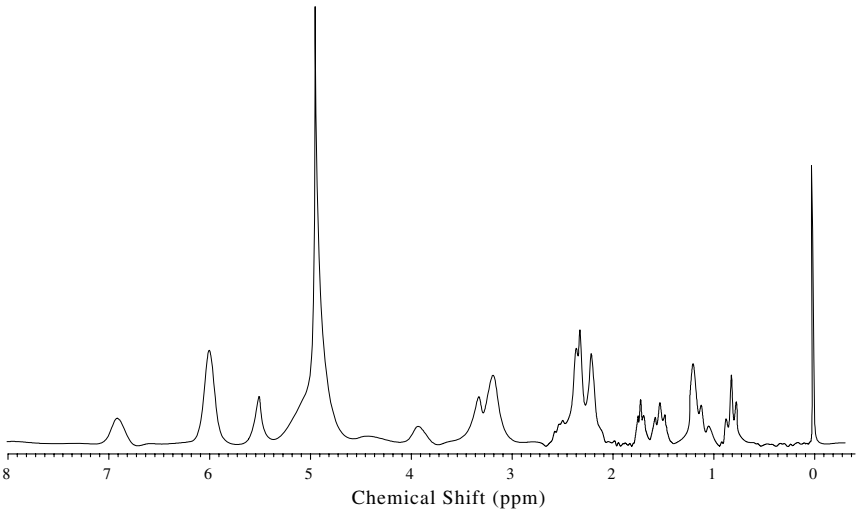

Fig. 2. ^1H NMR spectrum of *cis*-α-$[Co(trien)(C_{16}H_{33}NH_2)_2](ClO_4)_2$.

3.1.3. Electronic absorption spectra

The wavelength of the first absorption maximum in aqueous perchlorate medium for each complex is given in Table 1. It has been observed that the absorption spectra [56,57] of the *cis* and *trans* forms of $[Co(en)_2(NH_3)Y]^{n+}$ cations (Y = Cl or H_2O) showed some differences in the longest wavelength absorption band (d–d transition). The *trans* form showed a lower intensity ($\varepsilon < 50\ M^{-1}\ cm^{-1}$) whereas the *cis* form showed a higher intensity ($\varepsilon > 70\ M^{-1}\ cm^{-1}$). This observation can be used to determine the geometrical configuration of the present cations, whose longest wavelength absorption maxima are shown in Table 1. Similarly, the position of λ_{max} suggests that the strength of the bidentate ligands follows the order bpy < phen. The lower λ_{max} values for the complexes containing the phen ligand indicate that in these complexes the basal planes are comparatively more distorted than in the bpy containing complexes. By comparing the spectra of the corresponding butylamine complexes it reveals that both the ordinary and the surfactant complexes have the same structure and the replacement of lower aliphatic amine ligands by long chain aliphatic amine ligands does not affect the symmetry of the surfactant complexes. Consequently, it does not seem that micellization greatly influences the structure of the polar head.

3.2. Critical micelle concentration values (CMC)

The CMC values were computed from the slope of [Co(III)] versus specific conductance data. The complex concentration at which the micellization starts was evident from the change in the slope of the plot and that particular concentration is the CMC under the experimental conditions. The CMC values were determined at three different temperatures (303, 308 and 313 K). At all temperatures a break in the conductance versus concentration plots, characteristic of micelle formation, was observed. The CMC values were determined by fitting the data points above and below the break to two equation of the form $y = mx + c$ and solving the two equations simultaneously to obtain the point of intersection. Least-squares analysis was employed and correlation coefficients were greater than 0.98 in all the cases. The conductivity measurements at three different temperatures were repeated three times and the accuracy of the CMC values (Table 2) was found to be within ±3% error. Fig. 3 illustrates the plot for the complex *cis*-$[Co(en)_2(C_{12}H_{25}NH_2)_2](ClO_4)_2$; similar plots (not shown) were obtained for all the remaining complexes. It is observed that by changing the ion from Cl^- to Br^-, the CMC decreases. It may be due to the increase in the size of the ion in the coordination sphere, which makes it more weakly hydrated. Weakly hydrated ions can be adsorbed more readily in the micellar surface and that decreases the charge repulsion between the polar groups and thus facilitates the micellization. Further with the increase in the alkyl chain on polar head group, the CMC again shows a decrease. This may be due to an increase in hydrophobic character of the molecule in the coordination sphere with that of dodecyl/cetylamine.

3.3. Thermodynamics of micellization

The study of CMC versus temperature is often undertaken to obtain information on hydrophobic and head group interactions. This involves deriving various thermodynamic parameters of micelle formation. Two models are generally used, the mass-action or equilibrium model and the phase separation or pseudo-phase model. The mass-action model assumes that an equilibrium exists between the monomeric surfactant and the micelles. The phase separation model assumes that the aggregates have their counterions in the surrounding atmosphere in a separate phase [58–60]. According to these models, the standard Gibbs

Table 2
CMC values of some cobalt(III) metallosurfactants in aqueous solution

Surfactants · $2H_2O$	CMC (mol dm^{-3})			ΔG_m^0 (kJ mol^{-1})	ΔH_m^0 (kJ mol^{-1})	$T\Delta S_m^0$ (kJ mol^{-1})
	303 K	308 K	313 K			
cis-$[Co(en)_2(C_{12}H_{25}NH_2)_2](ClO_4)_2$	2.7×10^{-4}	4.0×10^{-4}	5.3×10^{-4}	-33.8 ± 0.2	-22.1 ± 0.1	11.7 ± 0.3
cis-$[Co(en)_2(C_{16}H_{33}NH_2)_2](ClO_4)_2$	3.3×10^{-5}	4.7×10^{-5}	6.1×10^{-5}	-46.0 ± 0.1	-33.6 ± 0.2	12.4 ± 0.1
cis-α-$[Co(trien)(C_{12}H_{25}NH_2)_2](ClO_4)_2$	0.9×10^{-4}	1.9×10^{-4}	2.6×10^{-4}	-44.4 ± 0.3	-16.4 ± 0.1	28.1 ± 0.2
cis-α-$[Co(trien)(C_{16}H_{33}NH_2)_2](ClO_4)_2$	2.1×10^{-5}	2.7×10^{-5}	3.3×10^{-5}	-48.7 ± 0.2	-30.2 ± 0.1	18.5 ± 0.2
cis-$[Co(bpy)_2(C_{12}H_{25}NH_2)Cl](ClO_4)_2$	7.4×10^{-4}	7.9×10^{-4}	8.3×10^{-4}	-34.4 ± 0.1	-11.6 ± 0.3	22.8 ± 0.1
cis-$[Co(bpy)_2(C_{12}H_{25}NH_2)Br](ClO_4)_2$	6.1×10^{-4}	6.6×10^{-4}	7.1×10^{-4}	-37.2 ± 0.3	-13.7 ± 0.2	23.5 ± 0.1
cis-$[Co(bpy)_2(C_{12}H_{25}NH_2)_2](ClO_4)_2$	9.4×10^{-5}	1.1×10^{-4}	1.8×10^{-4}	-45.6 ± 0.4	-14.3 ± 0.1	31.3 ± 0.1
cis-$[Co(bpy)_2(C_{16}H_{33}NH_2)Cl](ClO_4)_2$	6.7×10^{-5}	7.3×10^{-5}	7.9×10^{-5}	-45.2 ± 0.1	-24.6 ± 0.1	20.6 ± 0.2
cis-$[Co(bpy)_2(C_{16}H_{33}NH_2)Br](ClO_4)_2$	5.2×10^{-5}	6.0×10^{-5}	6.8×10^{-5}	-45.6 ± 0.2	-29.4 ± 0.1	16.2 ± 0.3
cis-$[Co(bpy)_2(C_{16}H_{33}NH_2)_2](ClO_4)_2$	1.7×10^{-5}	2.3×10^{-5}	2.9×10^{-5}	-49.3 ± 0.2	-27.4 ± 0.2	21.9 ± 0.1
cis-$[Co(phen)_2(C_{12}H_{25}NH_2)Cl](ClO_4)_2$	6.2×10^{-4}	7.0×10^{-4}	7.8×10^{-4}	-36.0 ± 0.2	-9.7 ± 0.2	26.3 ± 0.2
cis-$[Co(phen)_2(C_{12}H_{25}NH_2)Br](ClO_4)_2$	4.8×10^{-4}	5.4×10^{-4}	6.5×10^{-4}	-39.9 ± 0.1	-12.4 ± 0.1	27.5 ± 0.1
cis-$[Co(phen)_2(C_{12}H_{25}NH_2)_2](ClO_4)_2$	8.1×10^{-5}	8.8×10^{-5}	9.2×10^{-5}	-46.4 ± 0.2	-11.6 ± 0.1	34.8 ± 0.2
cis-$[Co(phen)_2(C_{16}H_{33}NH_2)Cl](ClO_4)_2$	5.3×10^{-5}	5.9×10^{-5}	6.4×10^{-5}	-47.1 ± 0.3	-20.3 ± 0.2	26.7 ± 0.3
cis-$[Co(phen)_2(C_{16}H_{33}NH_2)Br](ClO_4)_2$	3.0×10^{-5}	3.7×10^{-5}	4.5×10^{-5}	-47.4 ± 0.1	-23.8 ± 0.2	23.6 ± 0.3
cis-$[Co(phen)_2(C_{16}H_{33}NH_2)_2](ClO_4)_2$	0.5×10^{-5}	0.9×10^{-5}	1.6×10^{-5}	-55.3 ± 0.1	-23.5 ± 0.1	31.8 ± 0.2

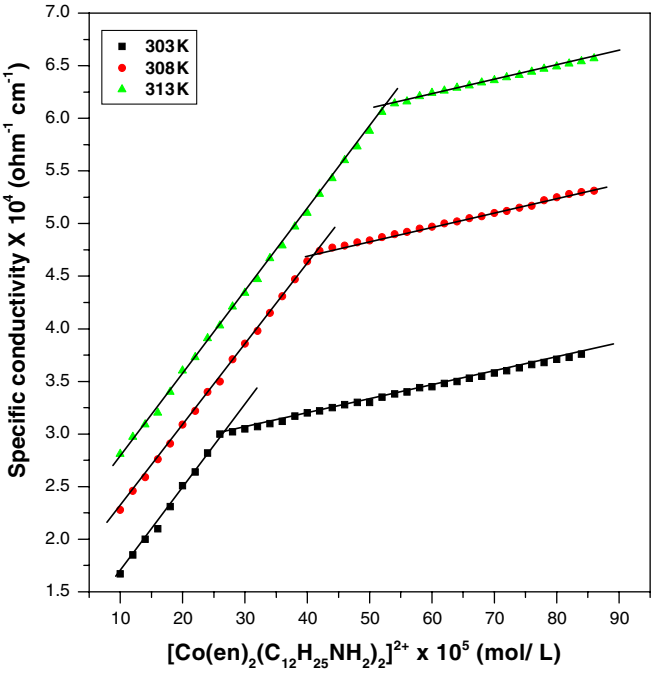

Fig. 3. Electrical conductivity vs. [Co(III)] in aqueous solution.

free energy of micelle formation per mole of monomer, ΔG^0_m, is given by

$$\Delta G^0_m = RT(2-\alpha_{ave})\ln \mathrm{CMC}, \quad (1)$$

where R, T and α_{ave} are gas constant, absolute temperature and average degree of micellar ionization, respectively.

The enthalpy of micelle formation can be obtained by applying the Gibbs–Helmholtz equation to Eq. (1)

$$\Delta H^0_m = -RT^2(2-\alpha_{ave})\mathrm{d}\ln \mathrm{CMC}/\mathrm{d}T. \quad (2)$$

Once the Gibbs free energy and the enthalpy of micelle formation are obtained, obviously the entropy of micelle formation can be determined by

$$\Delta S^0_m = (\Delta H^0_m - \Delta G^0_m)/T. \quad (3)$$

The thermodynamic parameters of micellization for the cationic surfactant are compiled in Table 2. The observed more negative Gibbs free energy of micellization indicates more favored micellization for the system under study when compared to hexadecyltrimethylammonium bromide ($\mathrm{CMC} = 9.0\times10^{-4}\,\mathrm{mol\,dm^{-3}}$). Moreover, since the changes of CMC with temperature are small, the value of ΔH^0_m and ΔS^0_m must be rather inaccurate and should be considered as only approximate. Nusselder and Engberts [61] have suggested that for negative ΔH^0_m values, London-dispersion forces play a major role in the micelle formation. Positive values of ΔS^0_m clearly indicate that the micellization of the studied surfactants in aqueous solution is governed mainly by hydrophobic interactions between the surfactant cations, resulting in the breakdown of the structured water surrounding the hydrophobic groups, and indicates that the cationic surfactant formation is an entropy driven process. The observed increase in the entropy values indicates that increasing head group polarity favors the micellization process. As mentioned in our previous reports [29–31], the CMC values for Co^{III} metallosurfactants in the present study are also very low compared to that of simple organic surfactants. Thus it is suggested that these metal surfactant complexes have more capacity to associate themselves forming aggregates compared to those of ordinary synthetic organic surfactants. Moreover, introduction of a metal complex to the hydrophilic part of the amphiphile can remarkably enhance the ability of aggregation.

References

[1] L. He, A.F. Dexter, A.P.J. Middelberg, Chem. Eng. Sci. 61 (2006) 989.
[2] J.F. Galisteo, F.G. Santamaria, D. Golmayo, B.H. Juarez, C. Lopez, E. Palacios, J. Opt. A 7 (2005) S244.
[3] C.L. Hill, X. Zhang, Nature 373 (1995) 324.
[4] A. Corma, Catal. Rev. Sci. Eng. 46 (2004) 3.
[5] T.F. Tadros, Applied Surfactants, first ed., Wiley-VCH, Germany, 2005.
[6] J.H. Fendler, E.J. Fendler, Catalysis in Micellar and Macromolecular Systems, Academic Press, New York, 1975.
[7] C. Mavroidis, A. Dubey, M.L. Yarmush, Ann. Biomed. Eng. 6 (2004) 363.
[8] V.V. Zhirnov, R.K. Cavin, Nat. Mater. 5 (2006) 11.
[9] M. Schonhoff, Curr. Opin. Colloid Interface Sci. 8 (2003) 86.
[10] M. Pisani, P. Bruni, C. Conti, E. Giorgini, O. Francescangeli, Mol. Cryst. Liq. Cryst. 434 (2005) 643.
[11] K. Bernauer, S. Ghizdavu, L. Verardo, Coord. Chem. Rev. 190 (1999) 357.
[12] M. Wolak, G. Stochel, R. Van Eldik, J. Am. Chem. Soc. 125 (2003) 1334.
[13] V.O. Saik, A.A. Goun, J. Nanda, K. Shirota, H.L. Tavernier, M.D. Fayer, J. Phys. Chem. A 108 (2004) 6696.
[14] L. Burel, M. Mostafavi, S. Murata, M. Tachiya, J. Phys. Chem. A 103 (1999) 5882.
[15] H.L. Tavernier, A.V. Barzykin, M. Tachiya, M.D. Fayer, J. Phys. Chem. B 102 (1998) 6078.
[16] L. Hammarström, T. Norrby, G. Stenhagen, J. Martensson, B. Akermark, M. Almgren, J. Phys. Chem. B 101 (1997) 7494.
[17] S. Srinivasan, J. Annaraj, PR. Athappan, J. Inorg. Biochem. 99 (2005) 876.
[18] M.J. Rosen, Surfactants and Interfacial Phenomena, second ed., Wiley, New York, 1989.
[19] M. Islam, B. Saha, A.K. Das, J. Mol. Catal. A 236 (2005) 260.
[20] R. de la Vega, P. Perez-Tejeda, P. Lopez-Cornejo, F. Sanchez, Langmuir 20 (2004) 1558.
[21] P. Lopez-Cornejo, P. Perez, F. Garcia, R. de la Vega, F. Sanchez, J. Am. Chem. Soc. 124 (2002) 5154.
[22] R. Prado-Gotor, R. Jimenez, P. Perez-Tejeda, M. Lopez-Lopez, F. Sanchez, Chem. Phys. 236 (2001) 139.
[23] R. Prado-Gotor, R. Jimenez, P. Lopez, P. Perez, C. Gomez-Herrera, F. Sanchez, Langmuir 14 (1998) 1539.
[24] L. Qiu, J. Xie, Y.H. Shen, J. Mol. Catal. A 244 (2006) 58.
[25] M. Ying, F. Jiang, H. Wei, X. Meng, X. Yu, X. Zeng, J. Dispersion Sci. Technol. 27 (2006) 15.
[26] J. Xie, S. Cheng, B. Jiang, D. Juan, C. Hu, X. Zeng, Colloids Surf. A 235 (2004) 137.
[27] X. Yan, B. Jiang, X. Zeng, J. Xie, J. Colloid Interface Sci. 247 (2002) 366.
[28] K. Santhakumar, N. Kumaraguru, S. Arunachalam, M.N. Arumugham, Int. J. Chem. Kinet. 38 (2006) 98.

[29] M.N. Arumugam, S. Arunachalam, Indian J. Chem. A 36 (1997) 84, and 315.
[30] K. Santhakumar, N. Kumaraguru, S. Arunachalam, M.N. Arumugham, Polyhedron 25 (2006) 1507.
[31] N. Kumaraguru, S. Arunachalam, M.N. Arumugham, K. Santhakumar, Transition Met. Chem. 31 (2006) 250.
[32] S. Osinsky, I. Levitin, L. Bubnovskaya, A. Sigan, I. Ganusevich, A. Kovelskaya, N. Valkovaskaya, L. Campanella, P. Wardman, Exp. Oncol. 26 (2004) 140.
[33] C.A. Behm, I. Creaser, B. Daszkiewicz, R.J. Geue, A.M. Sargeson, G.W. Walker, J. Chem. Soc., Chem. Commun. 24 (1993) 1844.
[34] C.A. Behm, P.F.L. Boreham, I.I. Creaser, B. Daszkiewicz, D.J. Maddalena, A.M. Sargeson, M. Snowdown, Aust. J. Chem. 48 (1995) 1009.
[35] G. Ghirlanda, P. Scrimin, P. Tecillam, A. Toffoletti, Langmuir 14 (1998) 1646.
[36] G.W. Walker, R.J. Geue, A.M. Sargeson, C.A. Behm, J. Chem. Soc., Dalton Trans. 15 (2003) 2992.
[37] R.W. Storrs, F.D. Tropper, H.Y. Li, C.K. Song, J.K. Kunjyoshi, D.A. Sipkins, K.C.P. Li, M.D. Bednarski, J. Am. Chem. Soc. 117 (1995) 7301.
[38] J.T. Kunjappu, V.K. Kelkar, C. Manohar, Langmuir 9 (1993) 352.
[39] D.D. Gutierrez, M. Surtchev, E. Eiser, C.J. Elsevier, Nanoletters 6 (2006) 145.
[40] P. Wang, C. Klein, J.E. Moser, R.H. Baker, N.C. Ha, R. Charvet, P. Comte, S.M. Zakeeruddin, M. Gratzel, J. Phys. Chem. B 108 (2004) 17553.
[41] S.A. Sapp, C.M. Eillott, C. Contado, S. Caramori, C.A. Bignozzi, J. Am. Chem. Soc. 124 (2002) 11215.
[42] P.J. Cameron, L.M. Peter, S.M. Zakeeruddin, M. Gratzel, Coord. Chem. Rev. 248 (2004) 1447.
[43] D.M. Palade, A.V. Ablov, V.N. Zubarev, Russian J. Inorg. Chem. 14 (1969) 227.
[44] A.V. Ablov, Russian J. Inorg. Chem. 6 (1961) 157.
[45] M. Krishnamurthy, J. Inorg. Nucl. Chem. 34 (1972) 3915.
[46] J. Barthel, F. Feuerlein, R. Neueder, R. Wachter, J. Sol. Chem. 9 (1980) 209.
[47] R.G. Linck, Inorg. Chem. 9 (1970) 2529.
[48] M.E. Baldwin, J. Chem. Soc. (1960) 4369.
[49] M.N. Hughes, W.R. Mcwhinnie, J. Inorg. Nucl. Chem. 28 (1966) 1659.
[50] D.A. Buckingham, D. Jones, Inorg. Chem. 4 (1965) 1387.
[51] J.S. Strukl, J.L. Walter, Spectrochim. Acta, Part A 27 (1971) 223.
[52] A.A. Schilt, R.C. Taylor, J. Inorg. Nucl. Chem. 9 (1959) 211.
[53] M.R. Rosenthal, J. Chem. Educ. 50 (1973) 331.
[54] J.D. Miller, R.H. Prince, J. Chem. Soc. A (1969) 519.
[55] S. Castellano, H. Gunther, S. Ebersole, J. Phys. Chem. 69 (1965) 4166.
[56] Y. Yasui, Y. Shimura, Bull. Chem. Soc. Jpn. 36 (1963) 1286.
[57] R.S. Nyholm, M.L. Tobe, J. Chem. Soc. (1956) 1707.
[58] P. Mukerjee, J. Phys. Chem. 66 (1962) 1375.
[59] J.J. Galan, A. Gonzalez-Perez, J.R. Rodriguez, J. Therm. Anal. Calorim. 72 (2003) 465.
[60] A. Gonzalez-Perez, J.C. Del Castillo, T. Czapkiewicz, J.R. Rodrigue, Colloid Polym. Sci. 280 (2002) 503.
[61] J.J.H. Nusselder, J.B.F.N. Engberts, J. Colloid Interface Sci. 148 (1992) 353.

eventually g_y), and zero-field splitting parameters D and E. This set can be enriched by the temperature-independent paramagnetism χ_{TIP}. The above parameters are frequently understood as internal characteristics of the complex under study (molecular constants). However, all of them originate in the electronic structure of the complex and they can be reconstructed with the help of the more principal electronic-structure parameters: the Racah parameters B and C (electron repulsion), the crystal-field strengths Dq, Ds, $\cdots$ (or more exactly the crystal-field poles for each ligand $F_2(L)$ and $F_4(L)$), the spin–orbit coupling constant ξ and the orbital reduction factors κ (which could be anisotropic, κ_z, κ_x) [9]. Such a target is far from being only of an academic interest, since just the sign and magnitude of the zero-field splitting parameter influence the key properties of the single-molecule magnets [10–12]. The tuning of the single-molecule magnets is, nowadays, an ultimate requirement for their possible technical exploitation.

Nickel(II) complexes are good candidates for studying the sign and magnitude of the zero-field splitting parameter D for several reasons. First, the ground-state of the octahedral and quasi-octahedral hexacoordinate complexes is $^3A_{2g}$ and $^3B_{1g}$, respectively so that the D-values can be studied over a wide range of geometries of the chromophore. Second, the D-values are enhanced by the spin–orbit splitting parameter $\lambda = -\xi/2S$ which adopts the highest value over the first-transition metal series. Moreover, the spin-Hamiltonian formalism offers a simple formula for the magnetic parameters in the form

$$D = \lambda^2[4\kappa_x^2/\Delta_{xy}(^3B_{1g} \rightarrow {}^3E_g) - 4\kappa_z^2/\Delta_z(^3B_{1g} \rightarrow {}^3B_{2g})], \quad (1)$$

$$g_z = g_e - 2\lambda[4\kappa_z^2/\Delta_z(^3B_{1g} \rightarrow {}^3B_{2g})] > g_e, \quad (2)$$

$$g_x = g_e - 2\lambda[4\kappa_x^2/\Delta_{xy}(^3B_{1g} \rightarrow {}^3E_g)] > g_e, \quad (3)$$

$$\chi_{TIP} = N_A\mu_0\mu_B^2(2/3)[2\cdot 4\kappa_x^2/\Delta_{xy}(^3B_{1g} \rightarrow {}^3E_g) + 4\kappa_z^2/\Delta_z(^3B_{1g} \rightarrow {}^3B_{2g})], \quad (4)$$

where the first excitation energy (split due to the tetragonality) occurs. Therefore, it is a natural demand to understand the impact of the quality of the ligands involved in the coordination sphere to the set of magnetic parameters.

In our preceding publications we correlated the zero-field splitting parameter D with analogous structural characteristics D_{str} that characterizes the degree of the tetragonality. Both these quantities measure the anisotropy (magnetic and/or structural). These parameters clearly show a mutual dependence (approximately along a straight line) [13,14]. However, the complexes involved in such a correlation were either homoleptic (imidazole and its derivative) or N-donor only of the $[Ni(base)_4(NCS)_2]$ type. In the present communication, we want to extend such a correlation to heteroleptic complexes possessing the $\{NiO_2O'_2N_2\}$ chromophore. Therefore, a series of complexes of the type $[Ni(base)_2(carboxylate)_2(H_2O)_2]$ have been prepared, structurally characterized and subjected to magnetochemical studies.

2. Experimental

2.1. Reagents

2-Methylimidazole, 1,2-dimethylimidazole, *iso*-quinoline, formic acid, $NiCl_2\cdot 6H_2O$ and CH_3COOK were purchased from commercial sources and used as received. Synthesis of the furo[3,2-*c*]pyridine has been conducted in accordance with published recipes [15–17].

Nickel(II) formate, as a hydrate, was synthesized by slowly adding a stoichiometric amount of nickel(II) carbonate to an aqueous-ethanol solution of formic acid in excess. Nickel(II) acetate was synthesized by adding potassium acetate to nickel(II) chloride ethanol solution. Elemental analysis (C, H, N) was performed on elemental analyzer Eager 300 (Carlo Erba). The nickel content was determined chelatometrically using murexide as an indicator.

2.2. Synthesis

The complexes $[Ni(2\text{-}Meiz)_2(HCOO)_2(H_2O)_2]$ (**1**) and $[Ni(1,2\text{-}Me_2iz)_2(HCOO)_2(H_2O)_2]$ (**2**) were prepared in warm dried ethanol over several hours under reflux. After several months green crystals were collected. The other two complexes $[Ni(iqu)_2(ac)_2(H_2O)_2]$ (**3**) and $[Ni(fupy)_2(ac)_2(H_2O)_2]$ (**4**) were prepared from nickel acetate: into a solution of nickel acetate a stoichiometric amount of ligand was added and stirred for half an hour. After two days the solid complexes were collected. Single crystals of **4** were grown from the ethanol solution. *Anal.* Calc. for (**1**) $C_{10}H_{18}N_4NiO_6$: C, 34.4; H, 5.21; N, 16.1; Ni, 15.9. Found: C, 35.0; H, 5.48; N, 15.9; Ni, 16.8%. Calc. for (**2**) $C_{12}H_{22}N_4NiO_6$: C, 38.2; H, 5.88; N, 14.9; Ni, 15.6. Found: C, 38.9; H, 6.01; N, 15.1; Ni, 15.6%. Calc. for (**3**) $C_{22}H_{24}N_2NiO_6$: C, 56.1; H, 5.13; N, 5.95; Ni, 12.5. Found: C, 56.1; H, 5.13; N, 5.95; Ni, 12.5%. Calc. for (**4**) $C_{18}H_{20}N_2NiO_8$: C, 47.9; H, 4.02; N, 6.21; Ni, 13.0. Found: C, 47.9; H, 4.47; N, 6.21; Ni, 13.0%.

2.3. Physical measurements

IR spectra were measured on Magna FTIR 750 spectrometer (Nicolet) in KBr pellets in the 4000–400 cm^{-1} region and in PE pellets in 400–200 cm^{-1} region.

Electronic spectra were measured using the DRIFT method on a Magna FTIR 750 spectrometer (Nicolet) in the region 5000–11 000 cm^{-1} and in Nujol mull on a Specord 200 (Analytical Jena) in the range 50 000–10 000 cm^{-1}.

Magnetic susceptibility and magnetization measurements were done using a SQUID magnetometer (Quantum Design) from 2 K at $B = 0.1$ T. The magnetization data were taken at $T = 2.0$ and 4.6 K, respectively. Raw susceptibility data were corrected for underlying diamagnetism using a set of Pascal constants. The effective magnetic moment has been calculated as usual: $\mu_{eff}/\mu_B = 798(\chi' T)^{1/2}$ where SI units are employed.

Single-crystal X-ray diffraction experiments for all complexes have been performed using Xcalibur CCD apparatus (Oxford Diffraction). Data reduction and empirical absorption correction were performed by SHELXS-97.

3. Results and discussion

3.1. Molecular and crystal structure

Crystal data for compounds **1**–**4** are collected in Table 1. The molecular structures are viewed in Fig. 1.

The structure of complex **1** consists of $[Ni(2\text{-}Meiz)_2(HCOO)_2(H_2O)_2]$ monomeric units in which the central Ni(II) atom has a distorted octahedral configuration. The coordination around Ni(II) atom is defined by two aqua ligands (w), two formato ligands (f) and two neutral 2-methylimidazole ligands (b). The distances Ni–O(f) are 2.081 Å, the distances Ni–O(w) are 2.075 and 2.136 Å and the distances Ni–N(b) are 2.082 Å (see Table 2). Two oxygen atoms from water molecules and two oxygen atoms from formato groups form the equatorial plane and two nitrogen atoms from 2–methylimidazole rings are situated in axial sites. The angle between the oxygen atoms from the formato groups is 169.61° and that feature points at deformation of the structure.

The registered intermolecular contacts for **1** are O–H···O [H···O = 1.94 and 1.97 Å, O···O = 2.714(5) and 2.827(5) Å, O–H···O = 172 and 167°] and N–H···O hydrogen bonds [H···O = 2.02 Å, N···O = 2.853(3) Å, N–H···O = 163°]. They are formed: (i) by aqua-ligand OH groups to the uncoordinated O atom from formato ligands in the equatorial plane; and (ii) through the secondary 2-methylimidazole N-atom to the coordinated formato O atom from another molecule of a neighboring layer. Thus, these hydrogen bonds form a three dimensional network. The N–H···O hydrogen bonds, present in **1**, are absent in the remaining complexes **2**, **3** and **4** (Fig. 2). The hydrogen-bond contacts are contained in the Supplementary material.

The molecular structure of complex **2** consists of discrete $[Ni(1,2\text{-}Me_2iz)_2(HCOO)_2(H_2O)_2]$ monomeric units with the Ni(II) atom in a distorted octahedral configuration defined by two formato ligands, two aqua ligands and two neutral 1,2-dimethylimidazole ligands. The distances Ni–O(f) are 2.071(2) Å, the distances Ni–O(w) are 2.11(2) Å and the distances Ni–N(1,2-dimethylimidazole) are 2.118(3) Å.

The intermolecular O–H···O hydrogen bonds for **2** [H···O = 1.898 and 1.939 Å, O···O = 2.737(3) and 2.776(4) Å and O–H···O = 168 and 165°] are formed from the aqua-ligand OH groups to the uncoordinated formato ligand O atoms from a neighboring molecule, and they are situated in the equatorial plane. In the crystal structure of this complex, the secondary N-atoms are not involved in the hydrogen bonds; consequently only a two-dimensional network is formed.

The $[Ni(iqu)_2(ac)_2(H_2O)_2]$ monomeric units represent the structure of compound **3**. The central Ni(II) atom possesses a distorted octahedral configuration formed by two acetato ligands (abbr. ac), two aqua ligands and two neutral *iso*-quinoline ligands (iqu). The distances inside the chromophore are Ni–O(w) 2.089 Å, Ni–O(ac) 2.061 Å and Ni–N(iqu) 2.115 Å. The deformation of the coordination polyhedron is caused by intramolecular and intermolecular hydrogen bonds. The intramolecular O–H···O hydrogen bonds [H···O = 1.828 Å, O···O = 2.657(2) Å, O–H···O = 166°] are in the equatorial plane between the oxygen atom from an aqua-ligand and an uncoordinated O atom from the acetato-ligand. Intermolecular O–H···O hydrogen bonds [H···O = 1.929 Å, O···O = 2.765 Å,

Table 1
Summary of X-ray crystallographic data

Compound	**1**	**2**	**3**	**4**
Formula	$C_{10}H_{18}N_4NiO_6$	$C_{12}H_{22}N_4NiO_6$	$C_{22}H_{24}N_2NiO_6$	$C_{18}H_{20}N_2NiO_8$
Formula weight	348.99	377.05	471.14	451.07
Crystal system	orthorhombic	triclinic	orthorhombic	monoclinic
Space group	*Fdd2*	$P\bar{1}$	*Pbca*	*P*21/*c*
Cell parameters				
a (Å)	12.280(2)	6.949(1)	13.1349(8)	10.075(1)
b (Å)	28.723(5)	7.294(1)	8.3912(5)	7.812(1)
c (Å)	7.993(1)	8.844(1)	19.403(1)	12.418(1)
α (°)	90	79.30(1)	90	90
β (°)	90	82.48(1)	90	99.767(8)
γ (°)	90	65.46(1)	90	90
V (Å^3)	2819.3(8)	399.96(9)	2138.6(2)	963.20(17)
Z	8	1	4	2
D_{calc} (g cm^{-3})	1.644	1.565	1.463	1.555
Absorption coefficient (mm^{-1})	1.410	1.249	0.949	1.057
F(000)	1456	198	984	468
Reflections collected	4464	2566	12872	5892
Refinement method	full matrix least squares on F^2			
Data/restraints/parameters	1003/3/103	1577/3/115	2187/3/169	1935/3/139
Final *R* indices	$R_1 = 0.0243$, $wR_2 = 0.0733$	$R_1 = 0.0503$, $wR_2 = 0.1499$	$R_1 = 0.0369$, $wR_2 = 0.0943$	$R_1 = 0.0356$, $wR_2 = 0.0763$
CCDC deposit number	297162	297165	297164	297163

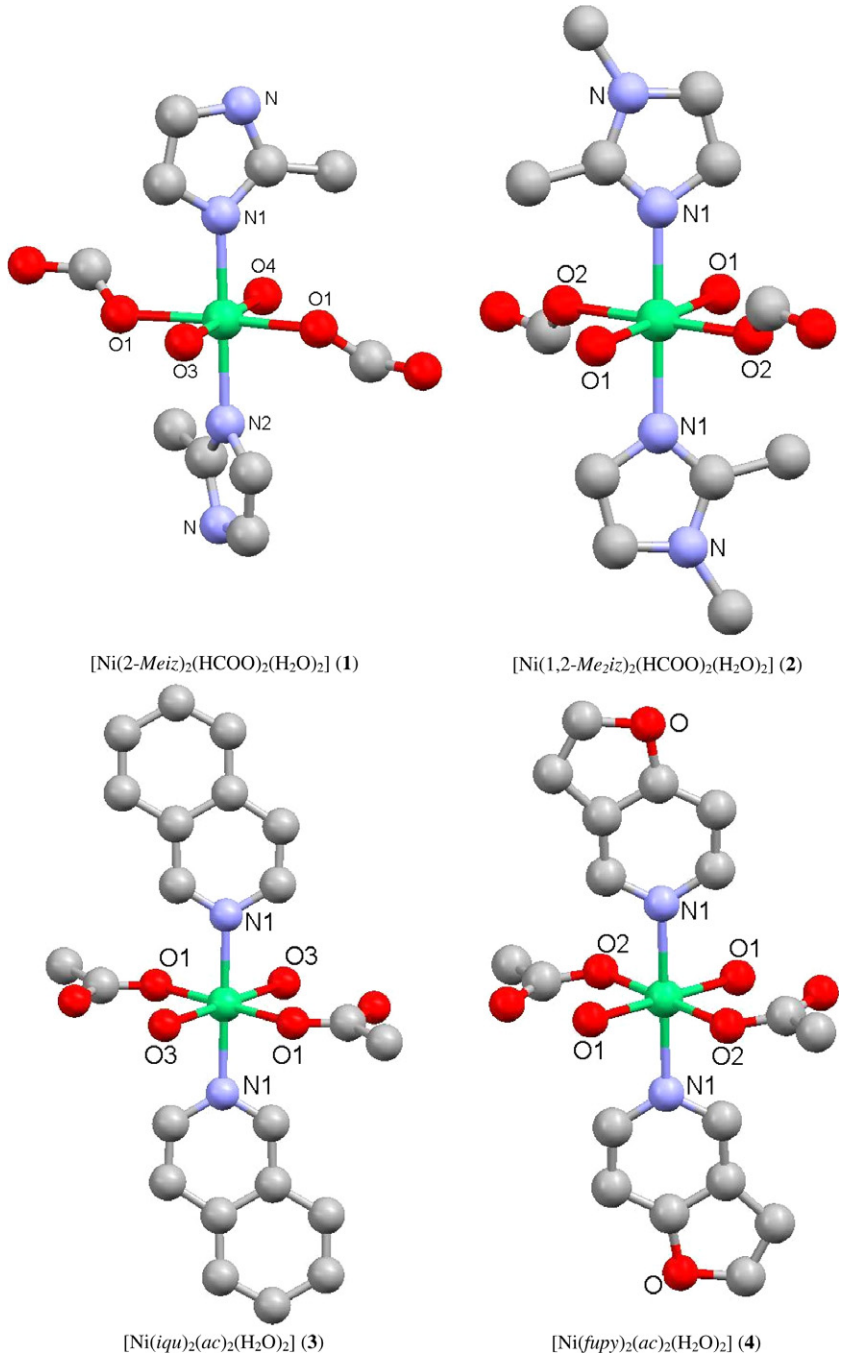

Fig. 1. Molecular structures of complexes **1**–**4** (hydrogen atoms are omitted for clarity).

O–H···O = 171°] from the aqua O atom to the uncoordinated acetato O atom join the molecules together to form a two-dimensional network.

The structure of **4** is formed by $[Ni(fupy)_2(ac)_2(H_2O)_2]$ monomeric units with a distorted octahedral configuration of the central Ni(II) atom. The distances inside the chromophore are Ni–O(w) 2.073 Å, Ni–O(ac) 2.052 Å and Ni–N(fupy) 2.130 Å. The intramolecular O–H···O hydrogen bonds [H···O = 1.849 Å, O···O = 2.652(3) Å, O–H..O = 160°] are formed in the equatorial plane between the oxygen atom from an aqua-ligand and an uncoordinated O atom from the acetato-ligand. The intermolecular O–H···O hydrogen bonds [H···O = 1.919 Å, O···O = 2.744 Å, O–H···O = 167°] are formed from the uncoordinated oxygen atom of the acetato-ligand to an aqua-ligand of a neighboring molecule, and the two-dimensional network is thus formed.

3.2. Infrared and electron spectra

The infrared spectra of the studied complexes show absorption bands of antisymmetric and symmetric vibrations of COO^- groups in the region 1548–1594 and 1353–1420 cm^{-1}. The bands assigned to the symmetric

Table 2
Selected bond lengths (Å) and angles (°)[a]

	1	2	3	4
Ni1–N1	2.084(2)	2.118(3)	2.1153 (17)	2.1295(19)
Ni1–O1	2.0819(19)	2.110(2), w	2.0614(15)	2.0735(17), w
Ni1–O3(O2)	2.074(6), w	2.071(2)	2.0886(16), w	2.0519(16)
Ni1–O4	2.136(6), w			
N1–Ni1–O1	90.49(8)	86.95(10)	90.63(7)	92.43(7)
N1–Ni1–O3(O2)	90.19(9)	88.62(10)	91.58(7)	88.62(7)
O1–Ni1–O3(O2)	84.91(7)	90.75(10)	90.48(6)	91.34(7)
O1–Ni1–O1	169.82(14)	180.0	180.00(8)	180.00(1)

[a] w – the aqua ligand.

stretching vibration are split into two sub-bands in all the complexes under study. The band assigned to the antisymmetric stretching vibration in compounds **3** and **4** is split into two sub-bands, too. The separation between antisymmetric and symmetric vibrations, $\Delta(COO^-)$, brings information about the carboxylate coordination mode. In the spectra of all four compounds the band of bending vibration of water spans the region 1630–1675 cm^{-1} and this value gives the information that the water molecule is coordinated to the central atom.

The electron spectra of the studied complexes show three principal d–d bands ($^3T_{2g} \leftarrow {}^3A_{2g}$, $^3T_{1g}(F) \leftarrow {}^3A_{2g}$ and $^3T_{1g}(P) \leftarrow {}^3A_{2g}$, characteristic for the octahedral geometry) in the region 9400–10 893, 15 300–16 207 and 26 000–26 870 cm^{-1}, which are split due to the symmetry lowering of the crystal field (Table 3, Fig. 3). The splitting is evidenced as an arm and is well visible for the second principal transition; this refers to the transition $^3B_{2g} \leftarrow {}^3B_{1g}$ within the point-group D_{4h}.

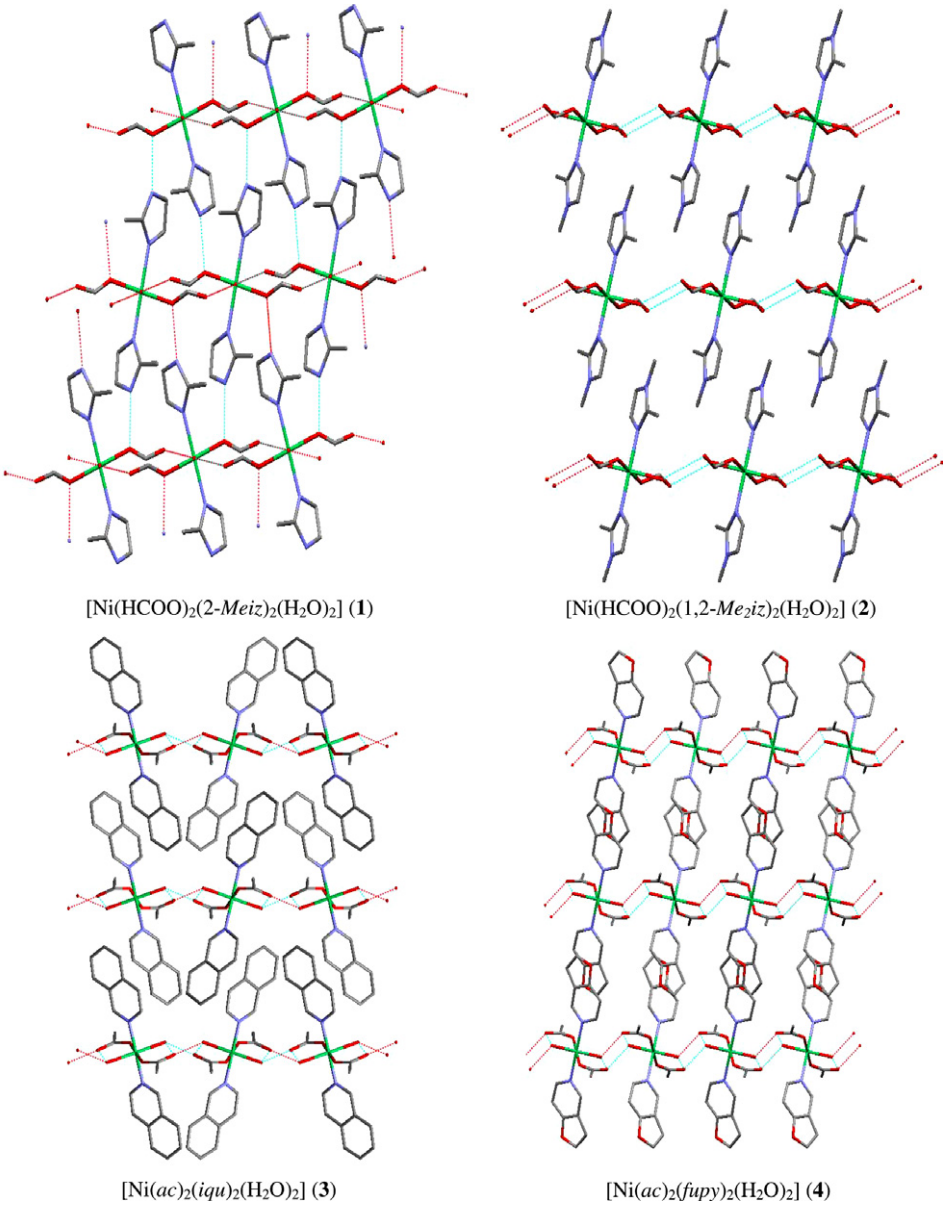

Fig. 2. The hydrogen bonds in complexes **1**–**4**.

Table 3
IR and ligand-field data (cm^{-1})

	1	2	3	4
$\nu_s(COO^-)$	1353, 1384	1358, 1383	1384, 1420	1412, 1467
$\nu_{as}(COO^-)$	1589	1594	1548, 1594	1560, 1592
$\Delta\nu(COO^-)$	236, 205	236, 211	164, 174	148, 125
$E_1(^3T_{2g} \leftarrow {}^3A_{2g})/hc = 10Dq$	9400	10893	9611	9945
$E_2(^3T_{1g}(F) \leftarrow {}^3A_{2g})/hc$[a]	15300 (13531)	16207 (13642)	15764 (13740)	15968 (13800)
$E_3(^3T_{1g}(P) \leftarrow {}^3A_{2g})/hc$	26000	26525	26000	26870

[a] Values in parentheses are the positions of the band-arms.

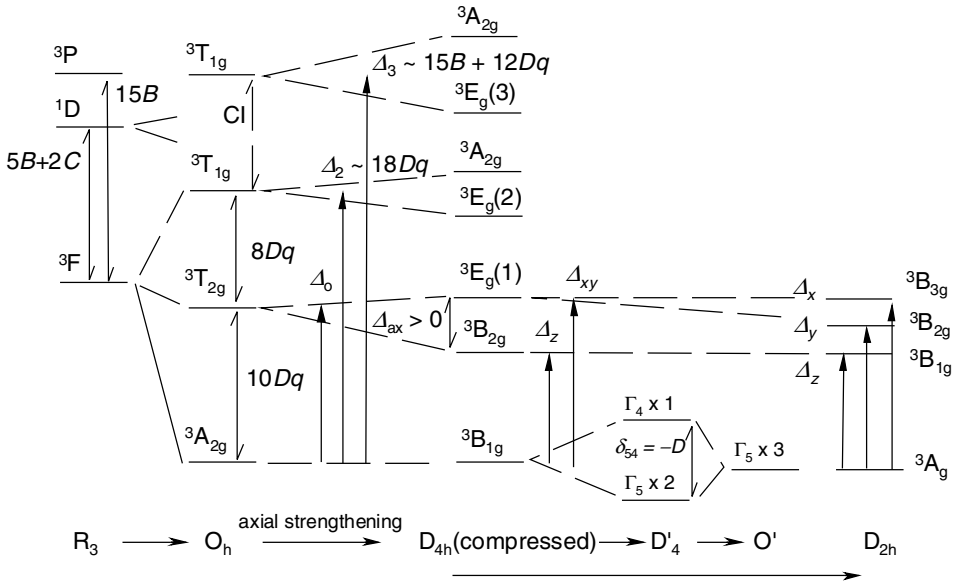

Fig. 3. Energy level diagram for tetragonally distorted octahedral d^8 complexes.

3.3. Magnetic data

The temperature dependence of the effective magnetic moment for complexes **1**–**4** is shown in Fig. 4. It can be seen that on cooling from room temperature μ_{eff} is almost constant down to low temperature (ca. 10 K); then it drops in value. These features are typical for zero-field splitting systems. It can be estimated that the axial zero-field splitting parameter will adopt moderate values of about $|D/hc| \sim 5\ cm^{-1}$.

The "susceptibility data-set" (in fact, M versus T at $B = 0.1$ T) and the magnetization data-set (M versus B at $T = 2.0$ and 4.6 K) have been treated simultaneously. They were used in constructing a common functional to be optimized by the same set of magnetic parameters: g_x, g_y, g_z and α_{TIP}. (The last quantity compensates uncertainties in determining the underlying diamagnetism and it accounts for the temperature-independent paramagnetism.) The zero-field splitting parameters entering the spin-Hamiltonian were calculated from the constraints $D = (\lambda/2)[g_z - (g_x + g_y)/2]$ and $E = (\lambda/4)(g_x - g_y)$, where $\lambda/hc = -315\ cm^{-1}$ is the spin–orbit splitting parameter for the Ni(II) ion [8,9]. The calculated data-points are also contained in Fig. 4 and the final set of magnetic parameters is presented in Table 4. Since the powder-sample data could bring an ambiguity in determining the sign of the D-parameter, both alternatives have been tested. In all cases the negative D-value results in a lower discrepancy R-factor (calculated from the susceptibility data). The magnetization data have been calculated as a correct powder average using a random spherical distribution of the magnetic-field vector [18,19].

The fitting procedure results in moderate and negative values of the axial zero-field splitting parameter D. They were used in a correlation with the structural D-values subtracted from the X-ray structure data. The latter, in the case of homoleptic complexes, has been defined using the bond-lengths within the chromophore as follows:

$$D_{str} = d_z - (d_x + d_y)/2, \quad (5)$$

$$E_{str} = (d_x - d_y)/2. \quad (6)$$

In the case of heteroleptic complexes this needs a modification

$$D_{str} = \Delta_z - (\Delta_y + \Delta_x)/2, \quad (7)$$

where $\Delta_a = (d_i - \bar{d}_i)$ for $a = x, y, z$ is a shift relative to the mean distance $\bar{d}_i$ for a given bond ($i = N, O$). For the N- and O-donor ligands these values have been taken from

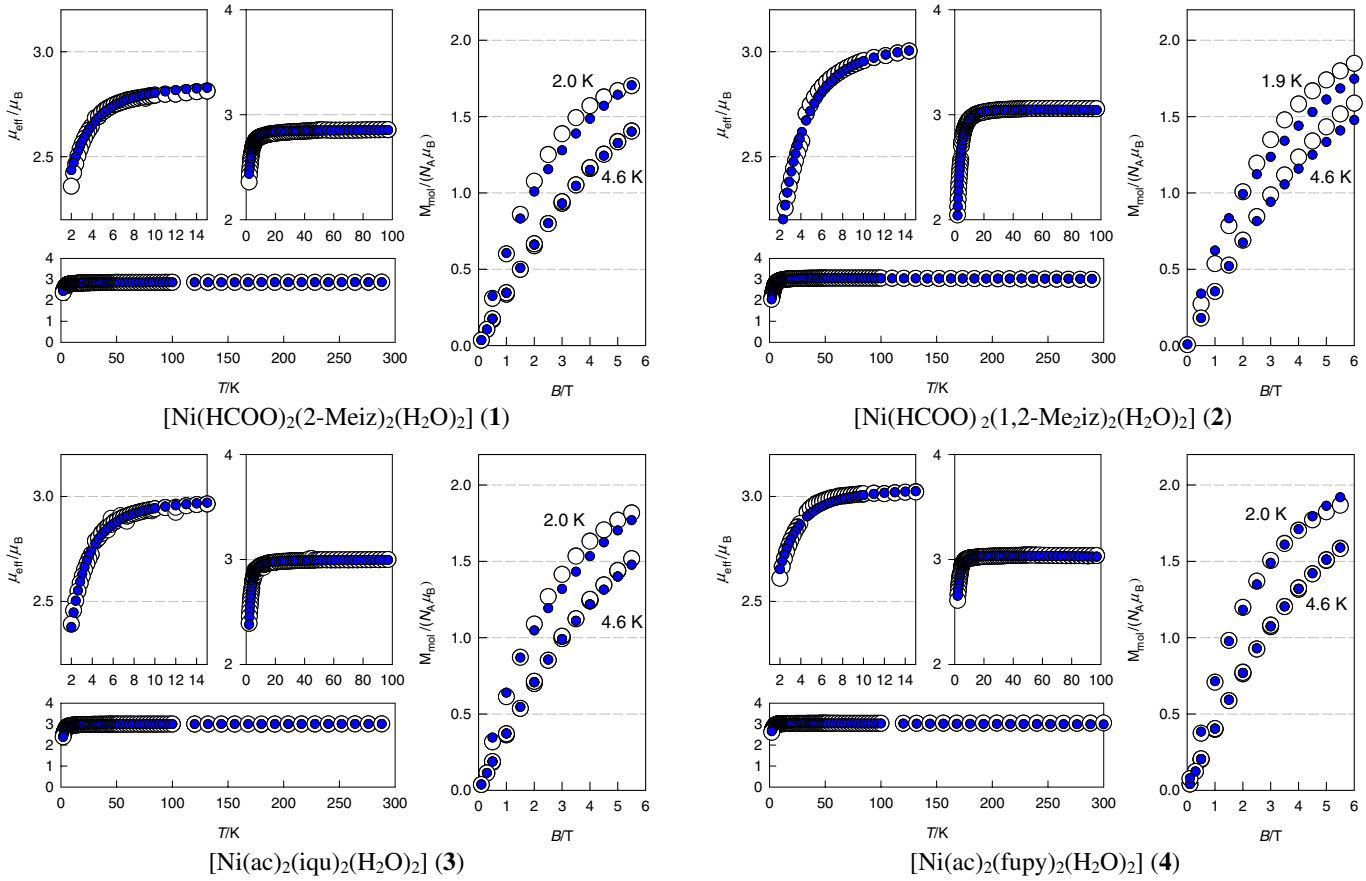

Fig. 4. Temperature dependence of the effective magnetic moment and field dependence of the magnetization (right panel) for **1**–**4**. Filled circles – fitted data assuming negative D.

Table 4
Fitted magnetic data with negative D-values

Compound[a]	g_x	g_y	g_z	D/hc (cm^{-1})	E/hc (cm^{-1})	α_{TIP} (10^9 m^3 mol^{-1})	R (%)	D_{str} (pm)	E_{str} (pm)
1	2.000	2.000	2.038	−6.0	0.7	+0.49	2.4	−9.9	1.1
2	2.140	2.139	2.190	−7.7	2.0	−1.12	1.8	−6.2	1.9
3	2.094	2.104	2.139	−5.3	1.2	+0.61	0.7	−5.0	1.4
4	2.147	2.149	2.179	−5.0	0.5	−2.25	0.5	−2.2	1.0

Estimated errors: 0.01 for g-factors, 0.1 for ZFS parameters.
[a] Compounds: **1** = $[Ni(2\text{-}Meiz)_2(HCOO)_2(H_2O)_2]$; **2** = $[Ni(1,2\text{-}Me_2iz)_2(HCOO)_2(H_2O)_2]$; **3** = $[Ni(iqu)_2(ac)_2(H_2O)_2]$; **4** = $[Ni(fupy)_2(ac)_2(H_2O)_2]$.

complexes containing the $[Ni(NH_3)_6]^{2+}$ and $[Ni(H_2O)_6]^{2+}$ units, respectively; $\bar{d}(Ni\text{–}N) = 2.145$ Å and $\bar{d}(Ni\text{–}O) = 2.055$ Å [20]. As seen from Fig. 5, the correlation of the magnetic D_{mag} values versus the structural distortion parameters D_{str} is fairly good. However, two notes need be added: (i) the magnetic as well as structural data bring evidence also for the rhombic anisotropy, which has not been accounted for in the correlation; (ii) the correlation curve cannot be linear, since the compressed bipyramid cannot be extrapolated to zero metal–ligand distances. Returning to Eq. (1) it needs to be pointed out that also the covalency (orbital reduction factor) enters the magnetic D-values and this is capable of altering its sign.

It is recapitulated that in free homoleptic Ni(II) complexes, like octahedral $[Ni(H_2O)_6]^{2+}$ in solution, the magnetic anisotropy vanishes [19]. In the solid state, however, the crystal packing along with the system of hydrogen bonds causes a symmetry-lowering of the chromophore and consequently the magnetic anisotropy appears: D/hc adopts values between −3.5 and +2.0 cm^{-1} for $[Ni(iz)_6](car)_2$ type complexes [14] (car – carboxylate). In heteroleptic complexes of the $[Ni(N\text{-}base)_4(NCS)_2]\cdot nH_2O$ type the registered magnetic anisotropy is not enhanced significantly: $D/hc = -3$ to -1.5 cm^{-1} [13]. This is due to analogous crystal-field strength of the N-donor heterocycle and thiocyanate groups, supported by an octahedral pattern of the electron spectra (no visible tetragonal splitting). This paper confirms the theoretical expectations that on passing to heteroleptic complexes of the $[Ni(N\text{-}base)_2(H_2O)_2(car)_2]$ type the magnetic anisotropy is enhanced: $D/hc = -8$ to -5 cm^{-1}. Such an enhancement could be in both negative and positive directions [21]; it originates in the electronic

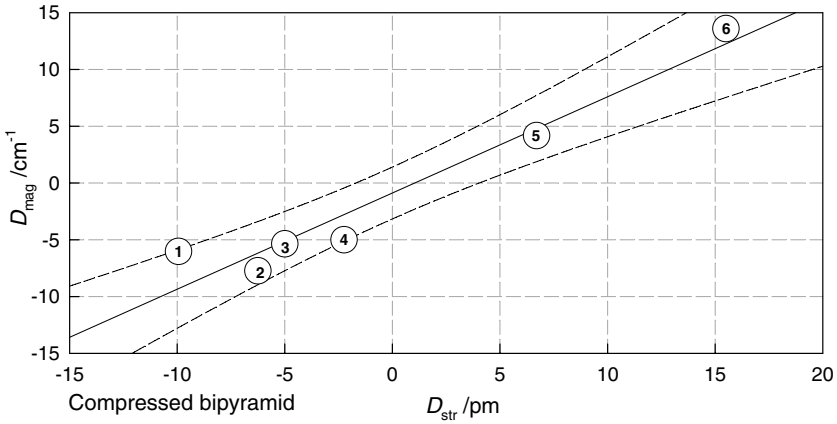

Fig. 5. Correlation of the magnetic vs. structural *D*-parameters. (Two compounds with the $\{NiN_4O_2\}$ chromophore, **5** = $[Ni(pz)_4(ac)_2]$ and **6** = $[Ni(chelate)_2(H_2O)_2]$, possessing positive *D*-values have been included into the correlation [21]; [**5**: +4.18 vs. +6.70, **6**: +13.60 vs. +15.50].) Broken lines – confidence intervals.

structure of the complex and it is supported by the splitting of the d–d bands in the electronic spectra. The crystal-packing effects, the hydrogen-bond networks and possible antiferromagnetic coupling among Ni(II) entities at low temperature, however, superimpose the electronic-structure driven magnetic anisotropy.

4. Supplementary material

Crystallographic data (excluding structure factors) for the structural analysis have been deposited with the Cambridge Crystallographic Data Centre, CCDC Nos. 297162, 297165, 297164 and 297163 for **1**, **2**, **3** and **4**. Copies of this information may be obtained free of charge from The Director, CCDC, 12 Union Road, Cambridge, CB2 1EZ, UK (fax: +44 1223 336 033; e-mail: deposit @ccdc.cam.ac.uk or www: http://www.ccdc.cam.ac.uk). Hydrogen-bond contacts (Table S1) and calculated magnetic data for two sets of magnetic parameters with an opposite sign of the *D*-parameter (Table S2, Fig. S1) are deposited.

Acknowledgments

Grant Agencies (Slovakia: VEGA 1/2453/05, APVT 20-005204, VEGA 1/3584/06; Germany: DAAD) are acknowledged for the financial support.

Appendix A. Supplementary data

Supplementary data associated with this article can be found, in the online version, at doi:10.1016/j.poly.2006.05.040.

References

[1] G.B. Deacon, R.J. Philips, Coord. Chem. Rev. 33 (1980) 227.
[2] D.M. Grove, G. van Koten, H.J.C. Ubbles, R. Zoet, Organometallics 3 (1984) 1003.
[3] D.V. Soldatov, J. Lipkowski, Zh. Strukt. Khim. 36 (1995) 1070.
[4] A.G. Leyva, G. Polla, D. Vega, R. Baggio, P.K. Parazzo, M.A.R. de Benyacar, M.T. Garland, J. Solid State Chem. 157 (2001) 23.
[5] K. Krogmann, R. Mattes, Z. Krystalogr. 118 (1963) 291.
[6] R. Baggio, D. Stoilova, G. Polla, G. Leyva, M.T. Garland, J. Mol. Struct. 697 (2004) 173.
[7] A. Mašlejová, R. Ivaniková, I. Svoboda, Advances in Coordination, Bioinorganic and Inorganic Chemistry, Slovak Technical University Press, Bratislava, 2003, p. 133.
[8] R. Boča, Coord. Chem. Rev. 248 (2004) 757.
[9] E. König, S. Kremer, Magnetism Diagrams for Transition Metal Ions, Plenum Press, New York, 1979.
[10] E.-C. Yang, W. Wernsdorfer, L.N. Zakharov, Y. Karaki, A. Yamaguchi, R.M. Isidro, G.-D. Lu, S.A. Wilson, A.L. Rheingold, H. Ishimoto, D.N. Hendrickson, Inorg. Chem. 45 (2006) 529.
[11] M. Soler, W. Wernsdorfer, K. Folting, M. Pink, G. Christou, J. Am. Chem. Soc. 126 (2004) 2156.
[12] A.L. Barra, A. Caneschi, A. Cornia, F. Fabrizi de Biani, D. Gatteschi, C. Sangregorio, R. Sessoli, L. Sorace, J. Am. Chem. Soc. 121 (1999) 5302.
[13] P. Baran, M. Boča, R. Boča, A. Krutošíková, J. Miklovič, J. Pelikán, J. Titiš, Polyhedron 24 (2005) 1510.
[14] A. Mašlejová, R. Ivaniková, I. Svoboda, B. Papánková, L. Dlháň, D. Mikloš, H. Fuess, R. Boča, Polyhedron 25 (2006) 1823.
[15] A. Krutošíková, M. Dandárová, Heterocycles 37 (1994) 1695.
[16] M. Bencková, A. Krutošíková, Monatsh. Chem. 126 (1995) 753.
[17] A. Krutošíková, R. Sleziak, Collect. Czech. Chem. Commun. 61 (1996) 1627.
[18] R. Boča, Theoretical Foundations of Molecular Magnetism, Elsevier, Amsterdam, 1999.
[19] R. Boča, Struct. Bonding 117 (2006) 1.
[20] Inorganic Crystal Structure Database, Fachinformationszentrum Karlsruhe, Germany. Available from: <http://www.fiz-informationsdienste.de/en/DB/icsd/index.html>.
[21] R. Boča, B. Papánková, I. Svoboda, J. Titiš, to be published.

choice of cation. The WS_4 tetrahedron is flexible and can exist in a variety of structural environments as evidenced by the structural characterization of several $[WS_4]^{2-}$ complexes with different counter ions [10–18]. In many of these compounds, the WS_4 tetrahedron is slightly distorted with one or two of the W–S bonds elongated, which has been attributed to S···H interactions between $[WS_4]^{2-}$ and the organic ammonium cation. Our work with $[WS_4]^{2-}$ has shown that organic amines can be used as cationic handles to distort the WS_4 tetrahedron [17]. In order to understand the importance of H-bonding interactions in the structural chemistry of tetrathiotungstates, we are investigating the reactions of $[WS_4]^{2-}$ with several amines, which differ in terms of their steric bulk and the number of potential donor H atoms. In the present work, we wish to describe the spectroscopic and structural characterization of three new tetrathiotungstates obtained by the reaction of $(NH_4)_2[WS_4]$ with the cyclic diamine (±)*trans*-1,2-diaminocyclohexane (*trans*-1,2-cn) and the acyclic triamines bis-(2-aminoethyl)amine (dien) and bis(3-aminopropyl)amine (dipn). The title compounds constitute three additions to the growing list of structurally characterized tetrathiotungstates. The availability of structural information for several tetrathiotungstates permits us to make a comparative study of the structural features, the details of which are described in this paper.

2. Experimental

2.1. Materials and methods

The organic amines *trans*-1,2-cn, dien, dipn and the solvents were used as obtained from commercial sources with analytical purity. $(NH_4)_2[WS_4]$ was prepared by a literature method [19]. The details of the instrumentation used for the elemental analysis, IR, Raman and UV–Vis spectroscopy are the same as described in our previous reports [16,17].

2.2. Synthesis of organic ammonium tetrathiotungstates *1*–*3*

$(NH_4)_2[WS_4]$ (348 mg, 1 mmol) was dissolved in 15 mL of distilled water containing a few drops of aqueous ammonia, and filtered. To the clear yellow filtrate *trans*-1,2-cn (0.3 mL) was added in drops at room temperature and the reaction mixture was kept for crystallization. After a day, yellow blocks of compound **1** slowly crystallized. The crystals were isolated by filtration, washed well with ice-cold water (5 ml), isopropanol (10 mL) and ether (10 mL) and dried under vacuum. The yield of the product was 400 mg. The use of dipn and dien instead of (*trans*-1,2-cn) in the above procedure afforded complexes **2** and **3** in 60% yield. All the complexes are quite stable in air.

(*trans*-1,2-cnH)$_2$[WS$_4$] **1**: *Anal*. Calc. for $C_{12}H_{30}N_4WS_4$: C, 26.57; H, 5.58; N, 10.33; S, 23.64. Found: C, 26.38; H, 5.49; N, 10.08; S, 22.65%.

IR data: 3309, 3239, 3095, 2939, 2856, 1581, 1498, 1443, 1398, 1229, 1126, 1002, 965, 847, 583, 521, 482 (ν_1), 465 (ν_3), 429, 409, 329, 286, 214, 136, 102 cm^{-1}; Raman data: 481 (ν_1), 464 (ν_3), 193 (ν_4), 178, 168 cm^{-1}.

UV–Vis data in nm (ε in mol^{-1} 1 cm^{-1}) 393 (18437), 277 (23802), 219 (24375).

(dienH$_2$)[WS4] **2**: *Anal*. Calc. for ($C_4H_{15}N_3WS_4$): C, 11.51; H, 3.60; N, 10.07; S, 30.74. Found: C, 11.63; H, 3.52; N, 9.94; S, 28.15%.

IR data: 3243, 3054 (br), 1563, 1547, 1513, 1458, 1365, 1297, 1279, 1257, 1203, 1162, 1122, 1107, 1094, 1026, 980, 959, 933, 866, 824, 797, 789, 770, 750, 627, 479 (ν_1) , 464 (ν_3), 443, 357, 324, 243, 185 (ν_4), 99 cm^{-1}; Raman data: 481 (ν_1), 460 (ν_3), 359, 188 (ν_4) cm^{-1}.

UV–Vis data in nm (ε in mol^{-1} 1 cm^{-1}) 393 (15858), 280 (17459), 220 (19244).

(dipnH$_2$)[WS$_4$] **3**: *Anal*. Calc. for ($C_6H_{19}N_3WS_4$): C, 16.18; H, 4.30; N, 9.44; S, 28.80. Found: C, 16.36; H, 4.26; N, 9.933; S, 29.12%.

IR data: 3275, 3235, 2993, 1573, 1518, 1460, 1420, 1380, 1284, 1208, 1083, 1040, 989, 922, 868, 823, 755, 478 (ν_1), 461 (ν_3), 292, 258, 233, 188 (ν_4) cm^{-1}; Raman data: 477 (ν_1), 458 (ν_3), 188 (ν_4) cm^{-1}.

UV–Vis data in nm (ε in mol^{-1} 1 cm^{-1}) 393 (12441), 277 (18114), 217 (21122).

2.3. Crystal structure determination

Intensity data were collected on a STOE Imaging Plate Diffraction System for compound **1** and on an AED-II four-circle diffractometer for compounds **2** and **3**, using graphite monochromated Mo Kα radiation (λ = 0.7107 Å). The raw intensities were corrected for Lorentz, polarization effects. All structures were solved with direct methods using SHELXS-97 [20] and refinement was done against F^2 using SHELXL-97 [21]. All non-hydrogen atoms were refined using anisotropic displacement parameters. The hydrogen atoms were located in the difference map but were positioned with idealized geometry and refined isotropically using a riding model. In compound **2** the N atom of dien is disordered due to symmetry. The structure can also be solved and refined in the non-centrosymmetric space group $Pmn2_1$. In this case no disorder is present but the absolute structure cannot be determined (Flack *x*-parameter 0.5) and strong correlation of the atomic coordinates of the symmetry related atoms occur. When the structure was checked for higher symmetry using Platon, the space group *Pmmn* was selected. Therefore this space group was chosen. Intensity data were additionally collected at low temperature (170 K) using a different crystal to check whether the disorder is dynamic or static in nature. However the disorder persists even at low temperature and no indications were found for a symmetry change. In the present contribution we describe only the room temperature data because the quality of the structure model was much better than that of the low temperature data set. The technical details of data acquisition and some selected refinement results are summarized in Table 1.

Table 1
Technical details of data acquisition and selected refinement results for **1**–**3**

Compound	**1**	**2**	**3**
Formula	$C_{12}H_{30}N_4S_4W$	$C_4H_{15}N_3WS_4$	$C_6H_{19}N_3WS_4$
Temperature (K)	293	293	293
Wavelength (pm)	71.073	71.073	71.073
Space group	*C*2/*c*	*Pmmn*	$Pca2_1$
a (Å)	19.3669(13)	11.559(1)	13.8110(8)
b (Å)	9.4959(5)	7.2424(6)	7.5327(6)
c (Å)	11.3836(7)	7.4956(5)	13.4999(7)
β (°)	107.713(7)		
Volume (Å^3)	1994.3(2)	627.50(9)	1404.45(16)
Z	4	2	4
μ (mm^{-1})	6.210	11.48	8.791
F(000)	1072	396	856
Molecular weight (g/mol)	542.49	417.28	445.33
D_{calc} (g cm^{-3})	1.807	2.402	2.106
Crystal size (in mm)	0.13, 0.09, 0.07	0.11, 0.09, 0.08	0.1, 0.09, 0.08
hkl Range	−27/27;−13/13;−16/16	−15/15;−9/8;−9/1	−19/3;−10/4;−18/3
2θ Range	3°–60°	3°–56°	3°–60°
Reflections collected	11868	3620	4895
Reflections unique	2978	859	2582
Data ($F_o > 4\sigma(F_o)$)	2675	812	2019
R_{int}	0.0369	0.0257	0.0350
Minimum/maximum transmission	0.3399/0.4861	0.2088/0.3116	0.1431/0.4355
$\Delta\rho$ (e/Å^3)	−1.336/1.191	−0.66/0.40	−1.051/1.200
Parameters	98	42	130
R_1 [$F_o > 4\sigma(F_o)$][a]	0.0305	0.0131	0.0218
WR_2 for all unique data	0.0740	0.0323	0.0531
Goodness-of-fit	1.102	1.128	1.006

[a] $R_1 = \sum\|\|F_o| - F_c\|\|/\sum|F_o|$.

3. Results and discussion

3.1. Synthesis and reactivity studies

The title compounds **1**–**3** were synthesized by a base promoted cation exchange method wherein the stronger organic bases *trans*-1,2-cn and the acyclic triamines dien and dipn replace the weak ammonia from the ammonium cation of $(NH_4)_2[WS_4]$. The complexes analyzed satisfactorily for the proposed formula containing the well-known $[WS_4]^{2-}$ anion in association with the monoprotonated cation of *trans*-1,2-cn in **1** and the diprotonated cations of dien and dipn in **2** and **3**. In an earlier report we have shown that the use of the polyamine tren (tren is tris(2-aminoethylamine)) results in the formation of $(trenH_2)^{2+}[WS_4]^{2-}$ [16]. In the present work, it is interesting to note that the terminal primary amine groups are protonated in **2** unlike in the related triamine dipropylenetriamine (dipn) in **3** where the protonation of the central secondary amine functionality and one of the terminal N atoms is observed. It has been reported that WO_3 dissolves in aqueous dien leading to the formation of the hexacoordinated neutral complex $[WO_3(dien)]$ where dien functions as a neutral tridentate ligand [22]. The neutral compound is highly water soluble and forms $(dienH_2)[WO_4]$ in solution. While $(dienH_2)[WO_4]$ exists only in solution, the corresponding tetrathio analogue **2** can be crystallized as a stable solid indicating the difference in the chemistry of oxo- and thiotungstates. The formation of **2** can be attributed to the weak H-bonding interactions (see the structure description) between the organic cation and $[WS_4]^{2-}$. Our efforts to prepare the neutral trithio complex $[WS_3(dien)]$ by the reaction of WS_3 with dien were not successful as WS_3 does not dissolve in aqueous dien unlike WO_3. Furthermore, our attempts to obtain a 1:1 $[WS_4]^{2-}$ complex containing the diprotonated cation of *trans*-1,2-cn or a 2:3 $[WS_4]^{2-}$ complex of the fully protonated dipn and dien by changing the reaction stoichiometries were not successful. It is well documented that $[WS_4]^{2-}$ can function as a bidentate ligand and bis(tetrathiotungstato) complexes of the type $[Ni(WS_4)_2]^{2-}$ are well known [3]. The availability of $[WS_4]^{2-}$ together with a N-donor ligand like dien suggested that the title complexes can be used to form S-bridged mixed ligand heterobimetallic complexes. Accordingly the reaction of the title complexes with $[Ni(H_2O)_6]Cl_2$ in aqueous ammonia were investigated. The use of ammonia was to facilitate the deprotonation of the organic cations. These reactions did not afford any mixed ligand complexes. However the reaction of the title complexes **1**–**3** under identical conditions with $[Ni(en)_3]^{2+}$ resulted in the formation of the highly insoluble complex $[Ni(en)_3][WS_4]$ in high yields. The complex $[Ni(en)_3][WS_4]$ has earlier been isolated under solvothermal conditions [12] and its facile formation indicates that $[WS_4]^{2-}$ is a weaker ligand as compared to en.

3.2. Description of crystal structures

Compound **1** crystallizes in the monoclinic space group $C2/c$ and is isostructural with the corresponding Mo analogue [23]. The substitution of Mo by W in **1** yields slightly larger unit cell parameters, which can be explained by the larger size of W. The asymmetric unit of **1** consists of the monoprotonated cation of *trans*-1,2-cn, which adopts a chair confirmation, and the $[WS_4]^{2-}$ anion (Fig. 1). The organic cation is located in a general position while the anion is situated on a twofold axis. The WS_4 tetrahedron is moderately distorted (S–W–S angles: 108.04(6)–110.89(5)°; average: 109.47°). The W–S bond lengths (2.1874(11)–2.1978(10) Å) have a mean value of 2.1926 Å (Table 2). The geometric parameters of **1** are in good agreement with those reported for other materials like $(enH_2)[WS_4]$ (en = ethylenediamine) [13] and $(1,3\text{-}pnH_2)[WS_4]$ (1,3-pn = 1,3-propanediamine) [14]. Two of the bond lengths are shorter while the other two are longer than the average W–S bond length of 2.1926 Å. As a result of the H-bonding interactions, the cations and anions in **1** are organized in a rod-like manner along [1 0 0] with the ammonium groups of *trans*-1,2-cn always pointing towards the S atoms of the anion. Hence, the sequence along this direction is $\cdots[WS_4]^{2-}$-*trans*-1,2-cnH-*trans*-1,2-cnH-$[WS_4]^{2-}\cdots$. The special arrangement of the constituents may be viewed as layers within the (0 0 1) plane. Along [0 1 0] and [0 0 1] the anions and cations each form individual stacks. Each anion is surrounded by six cations and five short S···H contacts ranging from 2.675 to 2.969 Å (Table 3) are observed, which are shorter than the sum of the van der Waals radii of S and H [24]. The shortest S···H contact of 2.675 Å and another at 2.769 Å observed for S1 can probably explain the elongation of the W–S1 bond. Although three S···H contacts are observed for S2, the W–S2 bond is slightly shorter at 2.1874(11) Å, which may be due to the longer S···H distances as well as the smaller values of the N–H···S angles. In addition, a very short N–H···N contact at 2.029 Å is observed which joins the cations to form pairs. The crystal packing diagram of the resulting hydrogen bonding network in **1** is shown in Fig. 2. The difference between the longest and shortest W–S bond Δ in **1** is 0.0104 Å and is indicative of little distortion. This value is much less compared to the Δ value of 0.0385 Å observed earlier for $(pipH_2)[WS_4]$ (pip is piperazine) [16].

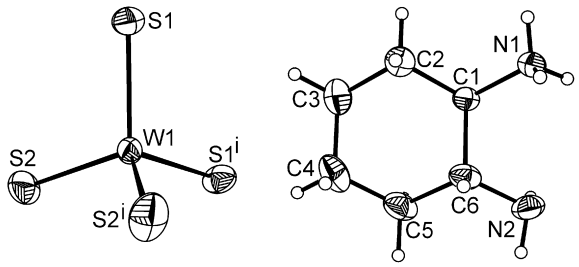

Fig. 1. Crystal structure of the anion (left) and cation (right) in $(trans\text{-}1,2\text{-}cnH)_2(WS_4]$ (**1**) with labelling and displacement ellipsoids drawn at the 50% probability level. [Symmetry code: (i) $-x+1$, y, $-z+1/2$].

Table 2
Selected geometric parameters (Å, °) for $(trans\text{-}1,2\text{-}cnH)_2[WS_4]$ (**1**)

W(1)–S(2)	2.1874(11)	W(1)–S(1)^{i}	2.1978(10)
W(1)–S(2)^{i}	2.1874(11)	W(1)–S(1)	2.1978(10)
S(2)–W(1)–S(2)^{i}	108.33(7)	S(2)–W(1)–S(1)	109.35(4)
S(2)–W(1)–S(1)^{i}	110.89(5)	S(2)^{i}–W(1)–S(1)	110.89(5)
S(2)^{i}–W(1)–S(1)^{i}	109.35(4)	S(1)^{i}–W(1)–S(1)	108.04 (6)

Symmetry transformations used to generate equivalent atoms: $^{i}-x+1$, y, $-z+1/2$.

Compound **2** crystallizes in the orthorhombic space group *Pmmn* and its structure consists of the $[WS_4]^{2-}$ anion and the $(dienH_2)^{2+}$ cation, both of which are located in special positions (Fig. 3). Four of the S–W–S angles are 109.4(1)°, the other two being 109.2(1)° and 110.1(1)°, indicating very little distortion. The W–S bond lengths vary from 2.172(1) to 2.189(1) Å (mean W–S bond length: 2.1805 Å) (Table 4). The geometric parameters are in good agreement with those for other organic ammonium tetrathiotungstates like **1** or $(enH_2)[WS_4]$. The W–S bonds show a pattern with two short (2.172(1) Å) and two longer (2.189(1) Å) values. In all, three short S···H contacts ranging from 2.531 to 2.968 Å are observed (Table 5). Interestingly the central secondary N atom is not involved in H-bonding. The single short contact of 2.765 Å is accompanied by a N–H···S angle of 140.76°, which may account for the shorter W–S2 bond, while the shortest contact of 2.531 Å accompanied by the largest N–H···S bond angle can explain the elongation of the W–S1 bond. The S···H interactions join adjacent WS_4 tetrahedra into layers extending in the (0 0 1) plane (Fig. 4). The difference between the longest and the shortest W–S bond Δ is 0.0170 Å and is slightly larger than that observed for **1**

Table 3
Hydrogen-bonding geometry (Å, °) for $(trans\text{-}1,2\text{-}cnH)_2[WS_4]$ (**1**)

D–H...A	d(D–H)	d(H...A)	d(D...A)	∠DHA	Symmetry code
N1–H1...S1	0.890	2.769	3.596	155.19	$-x+1$, $-y+1$, $-z$
N1–H1...S2	0.890	2.872	3.472	126.10	$-x+1$, $-y+1$, $-z$
N1–H2...N2	0.890	2.029	2.911	171.02	$-x+1$, y, $-z+1/2$
N1–H3...S1	0.890	2.675	3.538	163.69	$-x+1$, $y-1$, $-z+1/2$
N2–H1...S2	0.890	2.969	3.786	153.47	
N2–H2...S2	0.890	2.741	3.433	135.58	x, $-y+1$, $z+1/2$

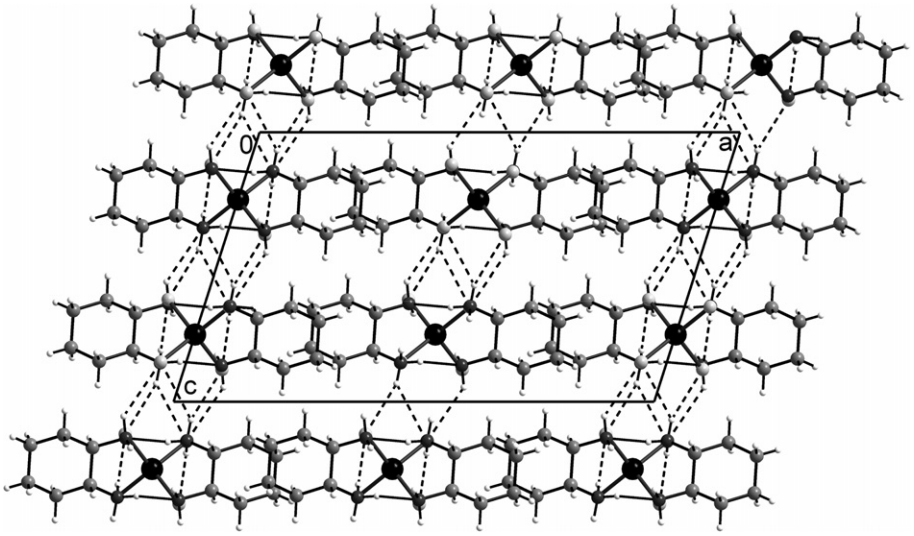

Fig. 2. Crystal packing diagram of **1** with a view along the *b* axis showing the H-bonding network running along the *c* axis (hydrogen bonding is shown as dashed lines).

but is quite less compared to the Δ value of 0.0385 Å observed earlier for $(pipH_2)[WS_4]$ [16].

Compound **3** crystallizes in the orthorhombic non-centrosymmetric space group $Pca2_1$ and its structure consists of discrete diprotonated dipn cations $(dipnH_2)^{2+}$ and $[WS_4]^{2-}$ anions (Fig. 5), with all atoms being located in general positions. One of the primary N atoms and the central secondary N atom are protonated, unlike in **2**. Again, the WS_4 tetrahedron is slightly distorted (S–W–S angles: 108.90(6)–110.23(5)°; average: 109.47°) with W–S bond lengths from 2.188(2) to 2.2053(12) Å (mean value: 2.195 Å) (Table 6). The geometric parameters are in close agreement with those for other organic ammonium tetrathiotungstates like **2** or $(tmenH_2)[WS_4]$ (tmen = *N*,*N*,*N*′,*N*′-tetramethylethylenediamine) [14]. Extended H-bonding interactions produce a three-dimensional network (Fig. 6). The cations and $[WS_4]^{2-}$ anions are stacked in rods along [0 0 1] to form a pseudo-hexagonal array. Along [1 0 0] and [0 1 0] cations and anions alternate. In the (0 1 0) plane a layer like arrangement is found with the anions being located in the pockets formed by three neighboring cations. A very short N3–H···N1 contact of 1.896 Å links the cations into a chain running along the *c* axis. Every anion is surrounded by four different cations and eight short S···H distances ranging from 2.532 to 2.958 Å (Table 7) indicate weak S···H bonding, with all H atoms attached to the N atoms being involved in H-bonding unlike in **2**. The difference between the longest and shortest W–S bond Δ is 0.0173 Å and is quite small compared to the Δ value (0.0385) observed earlier for $(pipH_2)[WS_4]$. In general the W–S bond lengths tend to be longer when the S···H contacts are shorter and the N–H···S angles are less acute [14–17]. In the present compound the shortest S···H

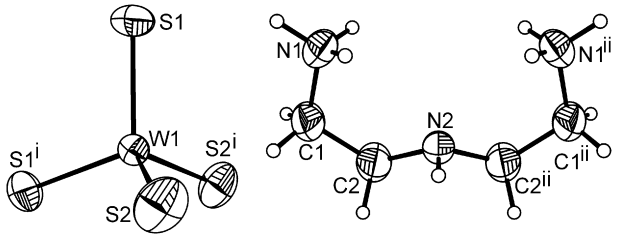

Fig. 3. Crystal structure of the anion (left) and cation (right) in $(dienH_2)[WS_4]$ (**2**) with labelling and displacement ellipsoids drawn at the 50% probability level [symmetry codes: (i) $-x+3/2$, $-y+1/2$, z (ii) $-x+1/2$, $-y+1/2$, z].

Table 4
Selected geometric parameters (Å, °) for $(dienH_2)[WS_4]$ (**2**)

W(1)–S(2)^{i}	2.172(1)	W(1)–S(1)	2.189(1)
W(1)–S(2)	2.172(1)	W(1)–S(1)^{i}	2.189(1)
S(2)^{i}–W(1)–S(2)	109.2(1)	S(1)–W(1)–S(1)^{i}	110.1(1)
S(2)^{i}–W(1)–S(1)	109.4(1)	S(2)^{i}–W(1)–S(1)^{i}	109.4(1)
S(2)–W(1)–S(1)	109.4(1)	S(2)–W(1)–S(1)^{i}	109.4(1)

Symmetry transformations used to generate equivalent atoms: $^{i}-x+3/2$, $-y+1/2$, z.

Table 5
Hydrogen-bonding geometry (Å, °) for $(dienH_2)[WS_4]$ (**2**)

D–H...A	*d*(D–H)	*d*(H...A)	*d*(D...A)	∠D–HA	Symmetry code
N1–H1...S1	0.890	2.531	3.344	152.13	
N1–H2...S2	0.890	2.765	3.500	140.74	$x-1/2$, $y+1/2$, $-z+1$
N1–H2 ...S1	0.890	2.968	3.657	135.61	$-x+1$, $-y+1$, $-z+1$

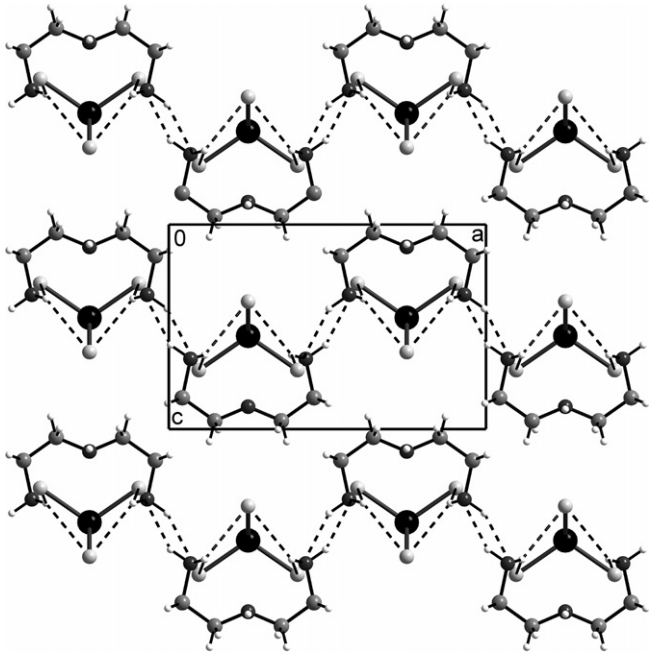

Fig. 4. Crystal packing diagram of **2** with a view along the *b* axis showing the H-bonding network (hydrogen bonding is shown as dashed lines).

contact of 2.532 Å is accompanied by the shortest W–S3 bond. The reason for this is not clear. It is to be noted that no structurally characterized $[WS_4]^{2-}$ compound containing a protonated primary amine (N3), a protonated secondary amine (N2) and a free primary amine (N1) has so far been reported. Hence a possible explanation may be the type of N–H···S interactions are probably different in view of the differing nature of the amine groups. In addition, the very strong N3–H···N1 interaction may weaken the S···H interaction. For a better understanding more examples with the above-mentioned situation are needed and synthesis and characterization of such tetrathiotungstates are under way in our laboratories.

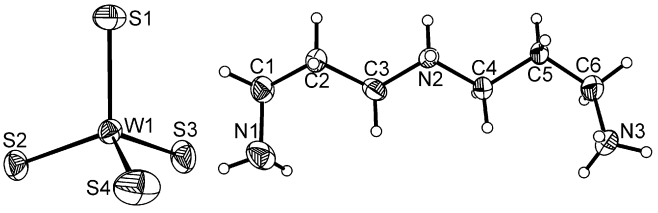

Fig. 5. Crystal structure of the anion (left) and cation (right) in $(dipnH_2)[WS_4]$ (**3**) with labelling and displacement ellipsoids drawn at the 50% probability level.

Table 6
Selected geometric parameters (Å, °) for $(dipnH_2)[WS_4]$ (**3**)

W(1)–S(3)	2.1882(22)	W(1)–S(4)	2.1950(21)
W(1)–S(2)	2.1935(13)	W(1)–S(1)	2.2053(12)
S(3)–W(1)–S(2)	108.90(7)	S(3)–W(1)–S(1)	109.40(8)
S(3)–W(1)–S(4)	109.21(8)	S(2)–W(1)–S(1)	110.23(5)
S(2)–W(1)–S(4)	109.83(9)	S(4)–W(1)–S(1)	109.25(7)

3.3. Spectral studies

A combination of UV–Vis, infrared and Raman spectroscopic techniques has been employed to characterize the compounds. The electronic spectra recorded in water exhibit bands at around 393, 280 and 220 nm. These peak positions are almost identical within experimental error to the corresponding ammonium or organic ammonium salts [3,16] and can be assigned to the charge transfer transitions of the $[WS_4]^{2-}$ moiety [3]. The mid IR up to 500 cm^{-1} exhibit several signals which can be attributed to the absorptions of the organic cations. Unlike the IR spectra of the previously reported compounds $(pipH_2)[WS_4]$, $(enH_2)[WS_4]$ etc., which exhibit a broad signal at around 3000 cm^{-1} for the N–H vibrations, more signals are observed in the N–H region (3300–3000 cm^{-1}) in **1**–**3**. This can be attributed to the presence of both free and protonated amine functionalities. For **1** the ν_{N-H} absorptions occur at around 3309 (s), 3239 (s) and 3054 (br) cm^{-1}. Similarly the bands at 3243 (s) and 3054 (br) cm^{-1} in **2** and the signals at 3309 (s), 3239 (s) and 3094 (br) cm^{-1} in **3** can be assigned to the N–H vibrations. The free tetrahedral $[WS_4]^{2-}$ anion is expected to show four normal modes of vibrations viz. $\nu_1(A_1)$, $\nu_2(E)$, $\nu_3(F_2)$ and $\nu_4(F_2)$ [25]. All four vibrations are Raman active while only ν_3 and ν_4 are infrared active. The usefulness of IR spectra for the characterization of the tetrathiotungstates is well documented in the literature as the metal–sulfur vibrations appear as characteristic signals below 500 cm^{-1} [26]. When the T_d symmetry of WS_4 is lowered to C_{2v}, as in $[Ni(WS_4)_2]^{2-}$ where $[WS_4]^{2-}$ functions as a bidentate ligand, it has been shown that this leads to a splitting of the triply degenerate $\nu_3(F_2)$ vibration of the W–S bond [25,26]. In $[Ni(WS_4)_2]^{2-}$ the W–S bond to the bridging S atom is long (W–S–Ni) and the W–S bond to terminal S atom is short (2.151 Å). In our compounds the longer W–S distances are always observed when strong S···H bonding interactions are present, and the W–S bond length distribution indicates a slight distortion of the tetrahedra. A splitting of the W–S vibration (Fig. 7) was observed in $(pipH_2)[WS_4]$ [16] which shows a difference of $\Delta = 0.0385$ Å between the longest and the shortest W–S bonds. However for **1**–**3** no such splitting is observed in the IR spectra. The symmetric stretching vibration ν_1 is observed as a shoulder along with the strong absorption due to the asymmetric mode of ν_3. In the Raman spectra of all the three compounds an intense signal is observed around 480 cm^{-1} indicating that the weak signal around the same frequency in the IR spectra should be due to the symmetric stretching mode. The asymmetric stretching vibration ν_3 in **1**–**3** occurs as a sharp signal at around 460 cm^{-1} along with a very weak band at about 480 cm^{-1} and these spectra do not show the characteristic splitting pattern observed in $(pipH_2)[WS_4]$ whose Δ value is more than twice that of the title complexes. The

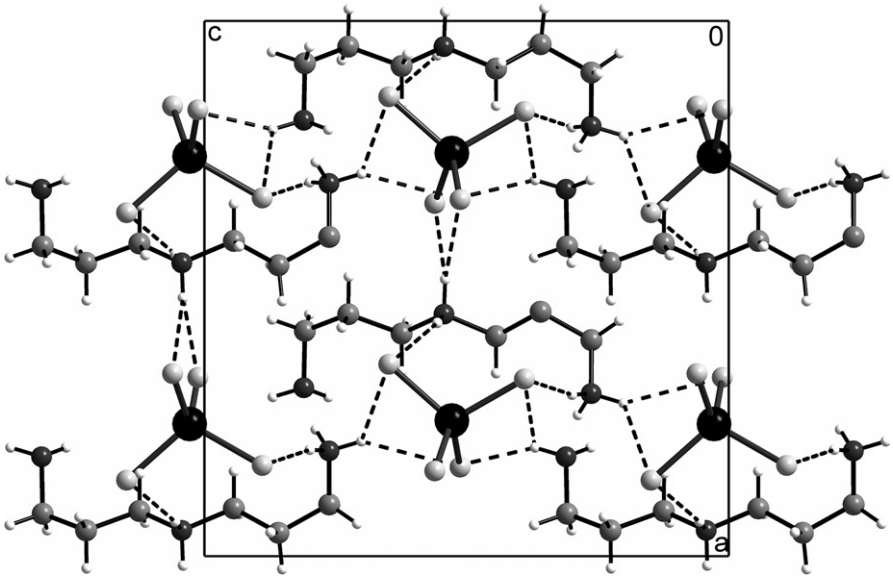

Fig. 6. Crystal packing diagram of **3** with a view along the *b* axis showing the extended H-bonding network (hydrogen bonding is shown as dashed lines).

Table 7
Hydrogen-bonding geometry (Å, °) for $(dipnH_2)[WS_4]$ (**3**)

D–H...A	*d*(D–H)	*d*(H...A)	*d*(D...A)	∠DHA	Symmetry code
N1–H2...S2	0.890	2.779	3.587	151.73	$-x+3/2, y-1, z+1/2$
N1–H2...S3	0.890	2.806	3.361	121.76	$-x+3/2, y-1, z+1/2$
N2–H1...S4	0.900	2.639	3.494	159.08	
N2–H2...S2	0.900	2.660	3.401	140.20	$x-1/2, -y+1, z$
N2–H2...S1	0.900	2.741	3.446	135.98	$x-1/2, -y+1, z$
N3–H1...S3	0.890	2.532	3.408	167.95	
N3–H2...S1	0.890	2.675	3.470	149.35	$-x+3/2, y, z-1/2$
N3–H2...S4	0.890	2.958	3.534	124.07	$-x+3/2, y, z-1/2$
N3–H3...N1	0.890	1.899	2.768	165.06	$-x+3/2, y, z-1/2$

signals due to the degenerate v_2 and v_4 vibrations occur at around 190 cm^{-1} in **1**–**3**.

3.4. Comparative study of the structural features of tetrathiotungstates

Tetrathiotungstates containing different cations like the fully inorganic $(NH_4)^+$, Rb^+, cationic metal complexes like $[Ni(tren)_2]^{2+}$, $[Ni(en)_3]^{2+}$ and $[Mn(en)_3]^{2+}$ and a variety of organic ammonium cations like $(enH_2)^{2+}$, $(dienH_2)^{2+}$ are known. The isolation and structural characterization of $[WS_4]^{2-}$ with these different cations indicates the flexibility of the tetrathiotungstate ion to exist in different structural environments. It is to be noted that of the 20 tetrathiotungstates listed in Table 8 only the $[WS_4]^{2-}$ complexes derived from $[Ni(en)_3]^{2+}$, en, N-Me-en and dipn crystallize in non-centrosymmetric space groups. In addition to $Rb_2[WS_4]$, where the mean Rb···S distance has been reported to be 3.5466 Å, the compounds $[(Et)_4N]_2[WS_4]$ and $[(Pr)_4N]_2[WS_4]$, which contain the fully alkylated organic ammonium cations, do not show any H-bonding interactions between the anion and cation [27]. All the other complexes exhibit weak H-bonding interactions between the cation and $[WS_4]^{2-}$. A comparative study of the structural parameters of 20 different tetrathiotungstates is presented here to explain the importance of the S···H bonding interactions in the structural chemistry of tetrathiotungstates. In all compounds the average S–W–S angles are very close to the ideal tetrahedral value. The average value of the W–S distance ranges from 2.1788 Å in $[Mn(en)_3][WS_4]$ to 2.195 Å in **3**. It is also noted that the difference Δ between the longest and the shortest W–S bond ranges from 0.0092 Å in $(enH_2)[WS_4]$ to 0.0542 in $[Ni(tren)_2][WS_4]$. The compound $[Ni(tren)_2][WS_4]$ is different compared with the organic ammonium tetrathiotungstates because it shows the shortest W–S distance of 2.1580 Å and also the maximum $\Delta = 0.0542$, even though the shortest S···H contact is observed for this complex at a distance of 2.73 Å. We note that in $[Ni(tren)_2][WS_4]$ the N atom of tren is not protonated, unlike in the organic ammonium compounds, but is linked to Ni(II). This indicates that the nature of the N–H···S contacts in $[Ni(tren)_2][WS_4]$ are probably different from those in the organic ammonium tetrathiotungstates. The same argument is applicable for the N–H···S contacts in the other two cationic complexes, namely $[Ni(en)_3][WS_4]$ and $[Mn(en)_3][WS_4]$.

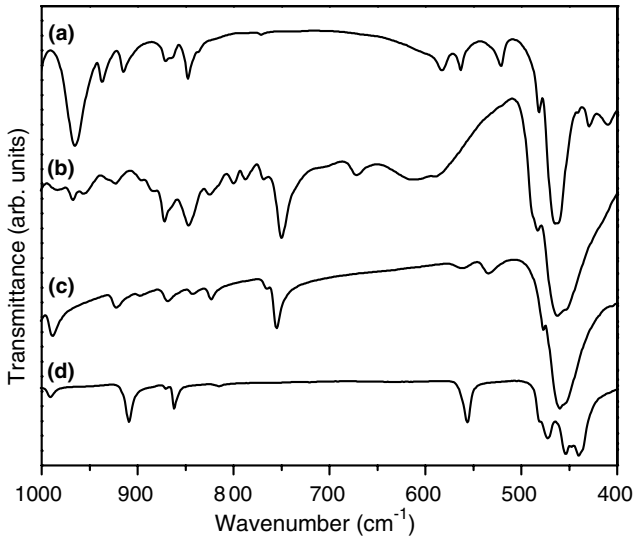

Fig. 7. Infrared spectra of (a) (*trans*-1,2-cnH)$_2$[WS$_4$], (b) (dienH$_2$)[WS$_4$], (c) (dipnH$_2$)[WS$_4$] and (d) (pipH$_2$)[WS$_4$].

In the organic ammonium $[WS_4]^{2-}$ complexes, including the fully protonated $(NH_4)_2[WS_4]$, the longest W–S bonds range from 2.2147 in (pipH$_2$)[WS$_4$] to 2.189 Å in (dienH$_2$)[WS$_4$] **2**. Furthermore, the shortest S···H contacts in all organic ammonium tetrathiotungstates are in a very narrow range of 2.31 Å for (N-Me-enH$_2$)[WS$_4$] (N-Me-en is *N*-methylethylenediamine) to 2.68 Å in **1** and **3**. The difference between the longest and shortest W–S bonds can probably be taken as a measure of the distortion of the $[WS_4]^{2-}$ tetrahedron. In an earlier report [17] we have shown that when the Δ value is larger than 0.033 Å a splitting of the W–S vibration is seen in the IR spectra. From the analysis of the structural features certain trends emerge. The substitution of one H by a methyl group in en to N-Me-en results in the increase of Δ, indicating the role of methyl groups in enhancing distortion. The same effect is also observed for the pair of cations 1,3-pn and (*N*,*N*′-dm-1,3-pn). It is of interest that when all H atoms in en are replaced by methyl groups, as in tmen, the experimental value for Δ is larger than that for en but smaller than that for N-Me-en by 0.01 Å. In all compounds listed in Table 8 (pipH$_2$)[WS$_4$] is unique as the cation is derived from a cyclic amine in which the N atoms are part of the ring. In the present work, the Δ value for compound **1** is 0.0104 Å and the cation in **1** is derived from the amine *trans*-1,2-cn where the –NH$_2$ functional groups are attached to a six membered ring.

The Δ values of the two organic ammonium tetrathiotungstates $[(Et)_4N]_2[WS_4]$ (Et is ethyl) and $[(Pr)_4N]_2[WS_4]$ (Pr is propyl) without N–H···S bonds are nearly identical (0.0184 and 0.0175 Å, respectively) [27] and the average is about 0.0180 Å. The usefulness of this value is that the observed difference Δ in the W–S bond lengths in these compounds is due to effects other than H-bonding interactions, i.e., they are probably of electrostatic nature. Interestingly, in the title compounds the values for Δ are 0.0104, 0.0170 and 0.0173 Å for **1**, **2** and **3**, respectively, and these values are smaller than or equal to that found for the fully alkylated organic ammonium tetrathiotungstates indicating that the H-bonding interactions do not show a pronounced influence in the title compounds to cause distortion in terms of the observed W–S bond

Table 8
Comparative structural parameters of tetrathiotungstates

Compound	Space group	W–S (long) in Å	W–S (short) in Å	Difference Δ in Å	W–S average in Å	S…H short in Å	References
$(NH_4)_2[WS_4]$	*Pnma*	2.2090	2.1856	0.0234	2.1905	2.57	[18]
$Rb_2[WS_4]$	*Pnma*	2.2053	2.1710	0.0343	2.1878		[10]
$[Ni(tren)_2][WS_4]$	$P2_1/c$	2.2122	2.1580	0.0542	2.1872	2.73	[11]
$[Ni(en)_3][WS_4]$	$Pna2_1$	2.190	2.162	0.028	2.1808	2.587	[12]
$[Mn(en)_3][WS_4]$	*Pbca*	2.189	2.168	0.021	2.1788	2.503	[12]
(enH$_2$)[WS$_4$]	$P2_12_12_1$	2.1943	2.1851	0.0092	2.1893	2.43	[13]
(N-Me-enH$_2$)[WS$_4$]	$P2_12_12_1$	2.2064	2.1727	0.0337	2.1919	2.31	[17]
(tmenH$_2$)[WS$_4$]	$P2_1/n$	2.1995	2.1772	0.0223	2.1891	2.56	[14]
(1,3-pnH$_2$)[WS$_4$]	$P2_1/c$	2.1946	2.1798	0.0148	2.1903	2.43	[14]
(*N*,*N*′-dm-1,3-pnH$_2$)[WS$_4$]	$P2_1/n$	2.1992	2.1771	0.0221	2.1931	2.42	[17]
(1,4-bnH$_2$)[WS$_4$]	$P\bar{1}$	2.2030	2.1799	0.0231	2.1918	2.39	[17]
(trenH$_2$)[WS$_4$] · H$_2$O	$P2_1/c$	2.1997	2.1739	0.0258	2.1904	2.46	[16]
(mipaH)$_2$[WS$_4$]	$C2/c$	2.2126	2.1792	0.0334	2.1940	2.47	[17]
(pipH$_2$)[WS$_4$]	$P2_1/c$	2.2147	2.1762	0.0385	2.1937	2.39	[16]
(1,4-dmpH$_2$)[WS$_4$]	*Pbca*	2.2136	2.1781	0.0355	2.1943	2.64	[15]
$[(Et)_4N]_2[WS_4]$	$P2_1/n$	2.2030	2.1846	0.0184	2.1919		[27]
$[(Pr)_4N]_2[WS_4]$	$C2/c$	2.2009	2.1834	0.0175	2.1935		[27]
(*trans*-1,2-cnH)$_2$[WS$_4$]	$C2/c$	2.1978	2.1874	0.0104	2.1926	2.68	this work
(dienH$_2$)[WS$_4$]	*Pmmn*	2.189	2.172	0.0170	2.1805	2.54	this work
(dipnH$_2$)[WS$_4$]	$Pca2_1$	2.2053	2.188	0.0173	2.195	2.68	this work

Abbreviations. tren, tris(2-aminoethyl)amine; en, ethylenediamine; N-Me-en, *N*-methylethylenediamine; tmen, *N*,*N*,*N*′,*N*′-tetramethylethylenediamine; 1,3-pn, 1,3-propanediamine; *N*,*N*′-dm-1,3-pn, *N*,*N*′-dimethyl-1,3-propanediamine; 1,4-bn, 1,4-butanediamine; mipa, monoisopropylamine; pip, piperazine; 1,4-dmp, 1,4-dimethylpiperazine; Et, ethyl; Pr, *n*-propyl.

distances. The infrared spectral observations are also indicative of a similar behavior. Hence the cation–anion interactions in the title compounds can be classified as weak interactions.

4. Conclusions

The reaction of $(NH_4)_2[WS_4]$ with the cyclic diamine *trans*-1,2-cn and the acyclic triamines bis(2-aminoethyl)amine (dien), bis(3-aminopropyl)amine (dipn) results in the formation of organic ammonium tetrathiotungstates **1**–**3**. The title complexes react with $[Ni(en)_3]^{2+}$ to form the highly insoluble complex $[Ni(en)_3][WS_4]$. The structures of **1**–**3** consist of tetrahedral $[WS_4]^{2-}$ anions which are linked to partially protonated organic ammonium cations with the aid of weak N–H···S interactions. The importance of these weak interactions can be evidenced especially in the case of compound **2** as the corresponding oxo analogue has been reported to exist only in solution [22]. Unlike WO_3, which dissolves in aqueous dien, WS_3 does not dissolve in dien indicating the differing nature of oxo and thio analogues of W. The complexes exhibit distinct W–S bond lengths and the observed Δ values are comparable to those observed in tetralkylammonium tetrathiotungstates. A comparative study of the structural features of 20 tetrathiotungstates indicates that tetrathiotungstates are less prone to pack in non-centrosymmetric space groups.

5. Supplementary material

Crystallographic data (excluding structure factors) for the structures reported in this paper have been deposited with the Cambridge Crystallographic Data Centre as Supplementary Publication No. CCDC 601986 (**1**), CCDC 601987 (**2**) and CCDC 601988 (**3**). Copies of the data can be obtained, free of charge, on application to CCDC, 12 Union Road, Cambridge CB2 1EZ, UK, fax: +44 122 3336 033 or email: deposit@ccdc.cam.ac.uk.

Acknowledgements

B.R.S. thanks the Department of Science and Technology (DST), New Delhi for financial support under Grant No. SR/S1/IC-41/2003. W.B. acknowledges the financial support by the State of Schleswig-Holstein and the Deutsche Forschungsgemeinschaft (DFG). The authors thank Frau Uschi Cornelissen for the vibrational spectra. The Department of Chemistry, Goa University is supported by the University Grants Commission, New Delhi under the Special Assistance Program (SAP). W.B. and B.R.S. thank the DST, New Delhi and Deutscher Akademischer Austauschdienst (DAAD) Bonn, for the sanction of a DST-DAAD (PPP) project.

References

[1] S.E. Skrabalak, K.E. Suslick, J. Am. Chem. Soc. 127 (2005) 9990.
[2] R. Tenne, M. Homyonfer, Y. Feldman, Chem. Mater. 10 (1998) 3225.
[3] A. Müller, E. Diemann, R. Jostes, H. Bögge, Angew. Chem., Int. Ed. Engl. 20 (1981) 934.
[4] T. Shibhahara, Coord. Chem. Rev. 123 (1993) 73.
[5] D. Coucouvanis, Adv. Inorg. Chem. 45 (1998) 1.
[6] M. Nath, A. Govindaraj, C.N.R. Rao, Adv. Mater. 13 (2001) 283.
[7] J. Chen, S.L. Li, F. Gao, Z.L. Tao, Chem. Mater. 15 (2003) 1012.
[8] Y.D. Li, X.L. Li, R.R. He, J. Zhu, Z.X. Deng, J. Am. Chem. Soc. 124 (2002) 1411.
[9] J.J. Berzelius, Poggendorffs Ann. Phys. Lpz. 8 (1826) 277.
[10] J. Yao, J.A. Ibers, Acta Crystallogr., Sect. E 60 (2004) i10.
[11] J. Ellermeier, R. Stähler, W. Bensch, Acta Crystallogr., Sect. C 58 (2002) m70.
[12] J. Ellermeier, Ph.D. Dissertation, University of Kiel, Germany, 2002.
[13] B.R. Srinivasan, S.N. Dhuri, C. Näther, W. Bensch, Acta Crystallogr., Sect. E 58 (2002) m622.
[14] B.R. Srinivasan, S.N. Dhuri, C. Näther, W. Bensch, Acta Crystallogr., Sect. C 59 (2003) m124.
[15] B.R. Srinivasan, S.N. Dhuri, C. Näther, W. Bensch, Acta Crystallogr., Sect. E 59 (2003) m681.
[16] B.R. Srinivasan, S.N. Dhuri, M. Poisot, C. Näther, W. Bensch, Z. Anorg. Allg. Chem. 631 (2005) 1087.
[17] B.R. Srinivasan, C. Näther, S.N. Dhuri, W. Bensch, Monats. Chem. 137 (2006) 397.
[18] B.R. Srinivasan, M. Poisot, C. Näther, W. Bensch, Acta Crystallogr., Sect. E 60 (2004) i136.
[19] J.W. McDonald, G.D. Friesen, L.D. Rosenhein, W.E. Newton, Inorg. Chim. Acta 72 (1983) 205.
[20] G.M. Sheldrick, SHELXS-97: Program for the Solution of Crystal Structures, University of Göttingen, Germany, 1994.
[21] G.M. Sheldrick, SHELXL-97: Program for the Refinement of Crystal Structures, University of Göttingen, 1997.
[22] R.S. Taylor, P. Gans, P.F. Knowles, A.G. Sykes, J. Chem. Soc., Dalton 24 (1972).
[23] B.R. Srinivasan, C. Näther, W. Bensch, Acta Crystallogr., Sect. C 62 (2006) m98.
[24] A. Bondi, J. Phys. Chem. 68 (1964) 441.
[25] K. Nakamoto, Infrared and Raman Spectra of Inorganic and Coordination Compounds, 5th ed., John Wiley, New York, 1997.
[26] K.H. Schmidt, A. Müller, Coord Chem. Rev. 14 (1974) 115.
[27] M. Poisot, C. Näther, W. Bensch, Z. Naturforsch (in press).

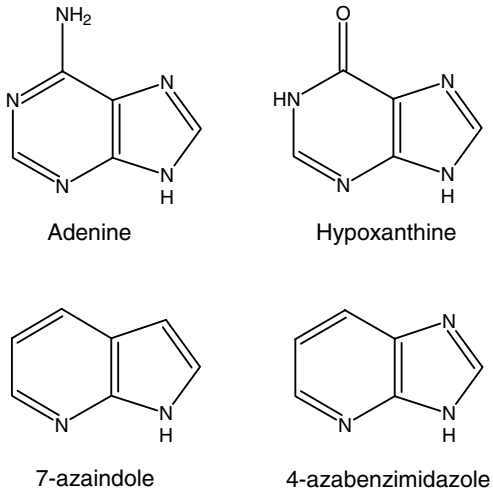

Scheme 1.

0.23 cm^{-1}. More recently the same structural type of compounds with the same structural, EPR and magnetically features as the above-mentioned compounds has been reported for some other ligands. In fact these ligands differ only slightly as they contain only one six-membered ring [14–16] in stead of two condensed rings, and they display a weaker antiferromagnetic interaction between the Cu(II) ions. An interesting application of $[Cu_2(7\text{-azaindole})_4(dmso)_2]$ has been reported to use this compound as a catalyst in the catalytic oxidation of aliphatic ethers and of some amines [29].

We have now extended the research on this type of compounds by using the ligand 4-azabenzimidazole (abbreviated as azab, see Scheme 1). Already in 1971 Cu(II) chloride and bromide compounds with azab have been synthesized [17], but X-ray structure analysis and magnetic susceptibility investigations lacked so far. A search in the CSD shows that only two X-ray structures with the ligand azab have been published before, i.e. with Fe(II) and Co(II) as metal ions [18].

We now report two related compounds with the general formula $[Cu_2(azab)_4X_2]X_2(S)$ (in which X = Cl (**1**), Br (**2**) and S = lattice solvent), together with their spectroscopic and magnetic properties and discuss them together with some related compounds. Also from both compounds $[Cu_2(azab)_4Cl_2]Cl_2(CH_3OH)_3$ (**1**) and $[Cu_2(azab)_4Br_2]Br_2(H_2O)_{1/2}$ (**2**), the X-ray structural analysis is presented in this study; they comprise the first 3D structures of dinuclear compounds with azab as a bridge.

2. Experimental

2.1. General

C, H, N determinations were performed on a Perkin–Elmer 2400 Series II analyzer. Ligand field spectra were obtained on a Perkin–Elmer Lambda900 spectrophotometer using the diffuse reflectance technique, with MgO as a reference. X-band powder EPR spectra were obtained on a Jeol RE2x electron spin resonance spectrometer using DPPH ($g = 2.0036$) as a standard. FT-IR spectra were obtained on a Perkin–Elmer Paragon 1000 FT-IR spectrophotometer equipped with a Golden Gate ATR device, using the reflectance technique (4000–300 cm^{-1}, res. 4 cm^{-1}). Magnetic susceptibility measurement (5–300 K) were carried out (at 0.1 T) using a Quantum Design MPMS-5S SQUID magnetometer. Data were corrected for the magnetization of the sample holder and for diamagnetic contributions, which were estimated from Pascal constants.

2.2. Synthesis

2.2.1. General synthesis of the compounds

The ligand azab and the metal salt were commercially available and used without purification. 0.2 mmol $CuCl_2$, or $CuBr_2$ and 0.4 mmol azab were each dissolved in methanol and put carefully together. The solution was filtered to remove any solid particles and was left to evaporate at room temperature. Within a few days blue crystals separated and were collected by filtration.

Yield about 75%. Elemental *Anal.* Calc. for $C_{27}H_{32}Cl_4Cu_2N_{12}O_3$ (**1**): C, 38.5; H, 3.8; N, 20.0. Found: C, 38.1; H, 3.8; N, 20.3%. IR: 3379 cm^{-1} (br, OH); strongest peaks: 1623, 1490, 1405, 1312, 1280, 1034, 971, 916, 801, 774, 736, 476 cm^{-1}.

Elemental *Anal.* Calc. for $C_{24}H_{21}Br_4Cu_2N_{12}O_{1/2}$ (**2**): C, 30.9; H, 2.3; N, 18.0%. Found: C, 31.0; H, 2.4; N, 18.2%. IR: 3485 cm^{-1} (br, OH); strongest peaks: 1628, 1490, 1408, 1309, 1274, 1030, 971, 922, 802, 774, 610, 478 cm^{-1}.

2.3. X-ray crystallography

A crystal was selected and mounted to the glass fiber using the oil-drop method; data were collected on a Nonius KappaCCD diffractometer (graphite-monochromated Mo Kα radiation). The intensity data were corrected for Lorentz and polarization effects, for absorption and extinction. The structures were solved by direct methods. The programs COLLECT [19], SHELXS-97 [20], SHELXL-97 [21] were used for data reduction, structure solution and structure refinement, respectively. Refinement of F^2 was done against all reflections. In compound **1**, one methanol molecule was found to be disordered and this molecule was refined isotropically at 3 positions with population parameters 0.5, 0.25 and 0.25.

In compound **2**, the lattice water molecule was found to be disordered and was refined at 2 positions with population parameter 0.5. The water hydrogen atoms could neither be located, nor introduced at calculated positions. All other non-hydrogen atoms were refined anisotropically. The H atoms (except from the water molecule in **2**) were introduced in calculated positions and refined with fixed geometry with respect to their carrier atoms. Crystallographic data are presented in Table 1.

Table 1
Crystallographic data for $[Cu_2(azab)_4Cl_2]Cl_2(CH_3OH)_3$ (**1**) and $[Cu_2(azab)_4Br_2]Br_2(H_2O)_{1/2}$ (**2**)

Compound	**1**	**2**
Formula	$C_{27}H_{32}Cl_4Cu_2N_{12}O_3$	$C_{24}H_{21}Br_4Cu_2N_{12}O_{1/2}$
Molecular weight	841.53	932.25
Crystal system	orthorhombic	monoclinic
T (K)	173(2)	173(2)
Space group	*Pnnm*	*C2/m*
a (Å)	10.665(2)	15.970(3)
b (Å)	15.503(3)	10.470(2)
c (Å)	20.966(4)	11.108(2)
β (°)	90	96.38(3)
V (Å^3)	3466.5(11)	1845.8(6)
Z	4	2
D_{calc} (g cm^{-3})	1.612	1.677
$F(000)$	1712	902
μ (mm^{-1})	1.585	5.515
Crystal size (mm)	$0.11 \times 0.10 \times 0.04$	$0.25 \times 0.15 \times 0.08$
Colour, shape	blue, block	blue, prismatic
Minimum to maximum θ range (°)	2.51–27.61	2.57–27.52
Total reflections	44705	13944
Total unique reflections (R_{int})	4110 (0.2298)	2222 (0.0726)
Number of refined parameters	228	104
R^a, $wR_2{}^b$, S	0.0638, 0.1445, 1.049	0.0587, 0.1651, 1.039
Minimum and maximum residual density (e/Å^3)	−0.705 and 0.893	−1.232 and 3.512

[a] $R_1 = \sum\|F_o| - |F_c\|/\sum|F_o|$.
[b] $wR_2 = [\sum[w(F_o^2 - F_c^2)^2]/\sum[w(F_o^2)^2]]^{1/2}$.

3. Results and discussion

3.1. Description of the crystal structures

3.1.1. Crystal structure of $[Cu_2(azab)_4Cl_2]Cl_2(CH_3OH)_3$ (*1*)

A plot of the projection of the structure of compound **1** is depicted in Fig. 1, with relevant bond length and bond angle information given in Table 2. The unit cell contains two chemically identical, but crystallographically independent dinuclear $[Cu_2(azab)_4Cl_2]$ units, four uncoordinating chloride anions and six molecules of methanol of which two are disordered over three positions. The basal plane of each Cu(II) ion is surrounded by four nitrogen atoms

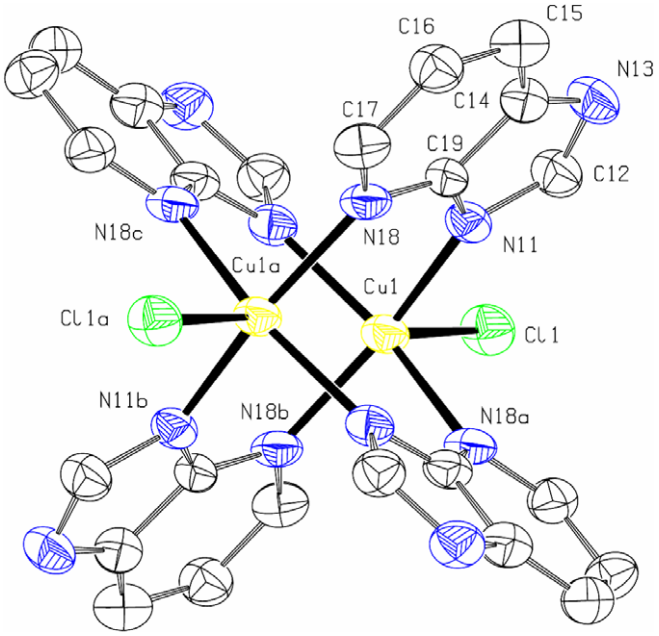

Fig. 1. Atomic displacement plot (50% probability level) of the molecular structure of one of the two crystallographic independent $[Cu_2(azab)_4Cl_2]Cl_2(CH_3OH)_3$ units. The uncoordinating chloride atoms and the uncoordinating methanol molecules are omitted for clarity.

of four bischelating azab molecules with Cu–N distances which vary from 2.033(5) to 2.056(5) Å in a paddlewheel-like fashion. The apical position is occupied by a chloride anion with Cu–Cl distances of 2.457(2) and 2.414(2) Å, while the Cu–Cu distances are 3.0611(14) and 3.0498(18) Å. The N–Cu–N angles in both dinuclear units are 162.38(18)° and 162.68(18)°.

The crystal lattice appears to be further stabilized by commonly found hydrogen bonding between the uncoordinating N atom and the uncoordinating Cl anion with N···Cl distances of 3.118(5)–3.257(5) Å and between the oxygen atom of a methanol molecule to an uncoordinating Cl atom with a distance of 3.135(6) Å.

3.1.2. Crystal structure of $[Cu_2(azab)_4Br_2]Br_2(H_2O)_{1/2}$ (*2*)

A plot of the projection of the structure of compound **2** is depicted in Fig. 2, with relevant bond length and bond angle

Table 2
Selected bond lengths (Å) and angles (°) for $[Cu_2(azab)_4Cl_2]Cl_2(CH_3OH)_3$ (**1**)

Cu(1)–N(11)	2.042(4)	Cu(1)–N(18)A	2.056(5)
Cu(1)–Cl(1)	2.457(2)	Cu(2)–N(21)	2.033(5)
Cu(2)–N(28)D	2.056(5)	Cu(2)–Cl(2)	2.414(2)
Cu(1)–Cu(1)A	3.0611(14)	Cu(2)–Cu(2)A	3.0498(18)
N(11)–Cu(1)–N(11)A	90.9(2)	N(11)–Cu(1)–N(18)B	162.38(18)
N(11)A–Cu(1)–N(18)B	87.42(17)	N(18)B–Cu(1)–Cl(1)	99.36(13)
N(18)B–Cu(1)–N(18)C	88.9(2)	N(11)–Cu(1)–Cl(1)	98.25(13)
N(21)A–Cu(2)–N(21)	88.4(3)	N(21)A–Cu(2)–N(28)D	89.27(18)
N(21)–Cu(2)–N(28)D	162.68(18)	N(28)D–Cu(2)–N(28)E	87.8(3)
N(21)–Cu(2)–Cl(2)	97.92(13)	N(28)D–Cu(2)–Cl(2)	99.39(13)

Symmetry codes: (A) $x, y, -z$; (B) $-x+1, -y, -z$; (C) $-x+1, -y, z$; (D) $-x, -y+1, -z$; (E) $-x, -y+1, z$.

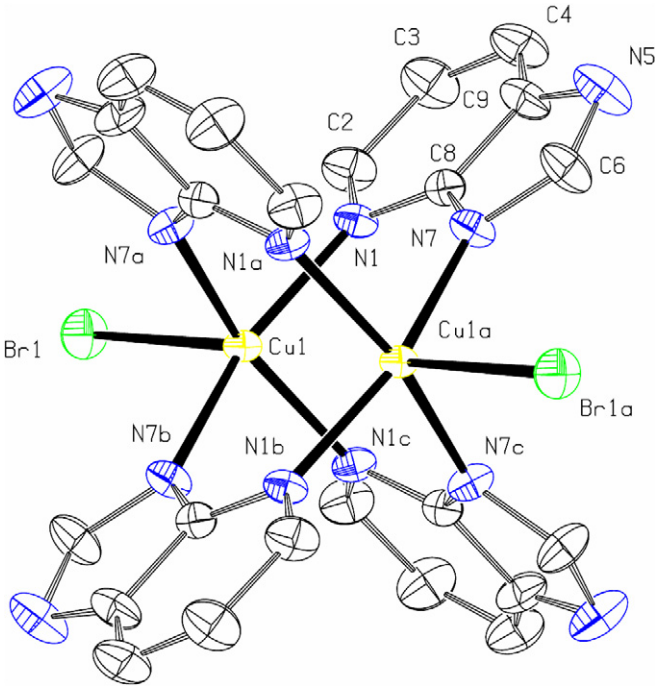

Fig. 2. Atomic displacement plot (50% probability level) of the molecular structure of $[Cu_2(azab)_4Br_2]Br_2(H_2O)_{1/2}$ unit. The uncoordinating bromide atoms and the uncoordinating water molecule are omitted for clarity.

information given in Table 3. Unlike the chloro compound **1**, this compound contains one dinuclear $[Cu_2(azab)_4Br_2]$ unit in the lattice unit, two uncoordinating bromide anions and one disordered water molecule per two dinuclear units. The basal plane of each Cu(II) ion is surrounded by four nitrogen atoms of four bischelating azab molecules with Cu–N distances of 2.036(5) and 2.039(5) Å in a paddle-wheel-like fashion. The apical position is occupied by a bromide anion with Cu–Br distance of 2.5922(14) Å, while the Cu–Cu distance is 3.038(2) Å. The N–Cu–N angles is 162.4(2)° and as the structure is very similar to the chlorido compound **1**, the Cu(II) ions have also a square-pyramidal geometry.

Table 3
Selected bond lengths (Å) and angles (°) for $[Cu_2(azab)_4Br_2]Br_2(H_2O)_{1/2}$ (**2**)

Cu(1)–N(1)	2.036(5)	Cu(1)–N(7)A	2.039(5)
Cu(1)–Br(1)	2.5922(14)	Cu(1)–Cu(1)A	3.038(2)
N(1)–Cu(1)–N(1)C	86.1(3)	N(1)A–Cu(1)–N(7)B	162.4(2)
N(1)–Cu(1)–N(7)A	89.1(2)	N(7)A–Cu(1)–N(7)B	90.3(3)
N(1)–Cu(1)–Br(1)	100.19(15)	N(7)B–Cu(1)–Br(1)	97.36(15)

Symmetry codes: (A) $x, -y-1, z$; (B) $-x, y, -z+1$; (C) $-x, -y-1, -z+1$.

The crystal lattice appears to be further stabilized by commonly found hydrogen bonding between the uncoordinating N atom and the uncoordinating Br anion with N···Br distance of 3.257(5) Å. As the water molecule is disordered over two positions its hydrogen bonds could not be located. Due to the difference in solvent the crystal lattice packing differs in both compounds (see Fig. 3).

3.2. Ligand field spectroscopy and EPR

The ligand-field transitions measured as a solid with the diffuse reflectance technique are observed as a very broad band with a maximum at $15.6\times10^3\ cm^{-1}$ and a shoulder at about $9.8\times10^3\ cm^{-1}$ for compound **1** and at $15.5\times10^3\ cm^{-1}$ with a broad shoulder at about $10.1\times10^3\ cm^{-1}$ for compound **2**. These are normal ligand-field transitions for (distorted) square pyramidal geometries [23].

The EPR spectra of compounds **1** and **2** were recorded as a polycrystalline powder at RT and 77 K from 0 to 800 mT at X-band frequency ($h\nu = 0.325\ cm^{-1}$).

For two antiferromagnetically coupled Cu(II) ions with a singlet ground state and an excited triplet state (with x, y and z as the principal axes) and in the case of an axial symmetry (axial zero-field splitting parameter $D < h\nu$ and rhombic zero-field splitting parameter $E = 0$) four $\Delta M_s = \pm1$ transitions along with a half-field ($\Delta M_s = \pm2$) transition are allowed [25]. The observed EPR spectrum of compound **1** measured at 77 K, which is almost identical as for compound **2**, is shown in Fig. 4. Transitions are

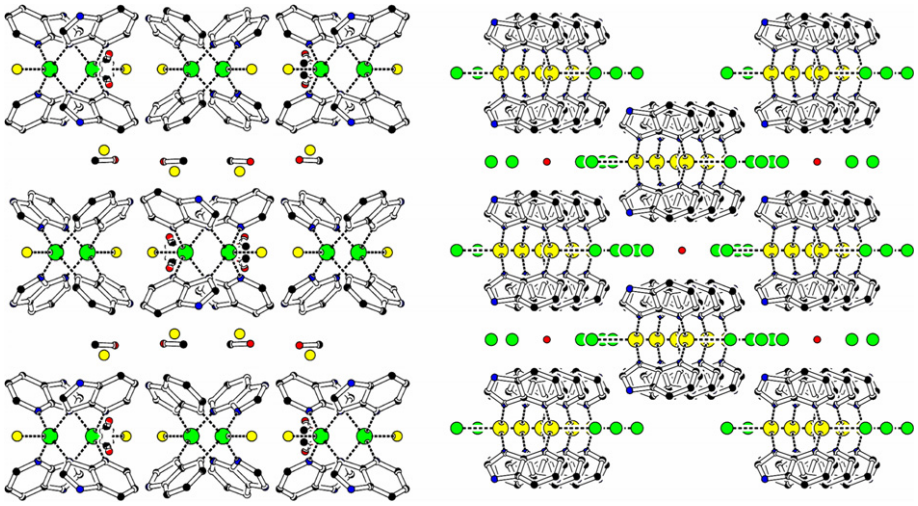

Fig. 3. Packing of both structures along the x-axis; left: compound **1**, right: compound **2**.

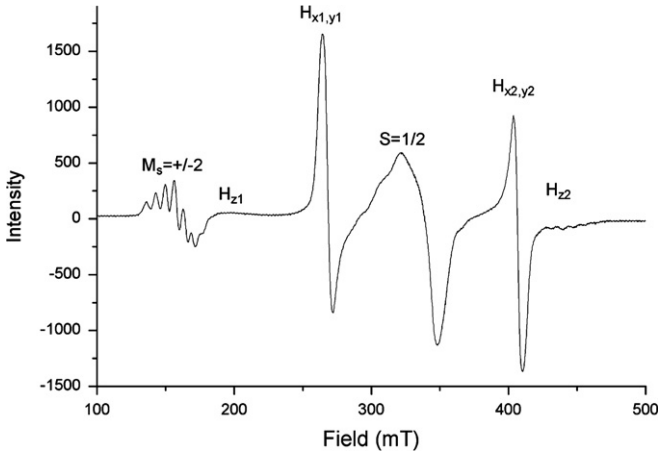

Fig. 4. EPR spectrum of compound **1** at 77 K.

observed at 190 (very weak), 260, 400 and 430 mT, which are assigned to the resonance fields H_{z1}, H_{x1y1}, H_{x2y2} and H_{z2}. The forbidden half-field signal ($\Delta M_s = \pm 2$) is observed at 155 mT and a typical copper hyperfine structure of seven lines is observed at 77 K, while at RT this splitting is not resolved. A copper hyperfine splitting is even observed at the (weak) resonances of the H_z components of $\Delta M_s = \pm 1$. The band at 320 mT is the $S = 1/2$ resonance from a mononuclear impurity, which in many cases is present in dinuclear compounds.

The observed spectra with the same features are in accordance with the earlier observed spectra with azab and a calculated D of 0.124 cm^{-1} [17]. In the related compounds, which are shown in Table 4, the EPR spectra, when published, are almost all similar to each other and the zero-field splitting parameter D was for these compounds calculated as being 0.11 cm^{-1} [10], 0.125 cm^{-1} [6], 0.11 cm^{-1} [24], 0.16 cm^{-1} [14] and 0.23 cm^{-1} [15,16]. The same type of EPR spectra were obtained from related Cu(7-methylazabenzimidazole) compounds (although no X-ray structures from these compounds were obtained) with a D of 0.135–0.140 cm^{-1} [22].

Table 4
Relevant $[Cu_2L_4]$ paddlewheel-like compounds, with X-ray structure and magnetism

Compound[a]	Geometry/chromophore	Cu–Cu distance (Å)	N–Cu–N angle (°)	J (cm^{-1})[d]	Reference[c]
$[Cu_2(ad)_4(H_2O)_2](H_2O)_2$	sq.pl./CuN_4	2.949	175.9	−257	[5] (S)[e] [13] (M)[e]
$[Cu_2(adH)_4Cl_2]Cl_2(H_2O)_6$	sq.pyr./$CuN_4(Cl)$	3.066	161.27	−285	[7] (S) [11] (M)[f]
$[Cu_2(hpH)_4Cl_2]_2Cl_2(H_2O)_6$	sq.pyr./$CuN_4(Cl)$	3.024	177.5 180.1	−139	[9] (S) [8] (M)[g]
$[Cu_2(azaind)_4(DMF)_2]$	sq.pyr./$CuN_4(O_{dmf})$	2.782	167.6 167.8	−361	[12] (S) [13] (M)[h]
$[Cu_2(5tpO)_4(H_2O)_2](H_2O)_2$	sq.pyr./$CuN_4(O_w)$	2.891(2)	165.5 165.4	−105	[14] (S + M)
$[Cu_2(tz\text{-}tol)_4]$	sq.pl. (dist)/CuN_4	2.7224(13)	178.04 155.71	−121	[15] (S + M)
$[Cu_2(tz\text{-}naf)_4]$	sq.pl. (dist)/CuN_4	2.626(1)	173.89 164.78	−104	[15] (S + M)
$[Cu_2(stz)_4]$	sq.pl. (dist)/CuN_4	2.671(2)	176.0(3) 157.1(2) 178.7(3) 159.5(2)	−62	[16] (S + M)
$[Cu_2(azab)_4Cl_2]Cl_2(CH_3OH)_3$	sq.pyr./$CuN_4(Cl)$	3.061(1) 3.050(2)[b]	162.38 162.68	−329	this work
$[Cu_2(azab)_4Br_2]_2Br_2(H_2O)_{1/2}$	sq.pyr./$CuN_4(Br)$	3.038(2)	162.4	−349	this work

[a] *Abbreviations:* sq.pyr., square pyramidal; sq.pl. (dist), square planar (distorted); adH, adenine (6-aminopurine); hpH, 6-hydroxypurine (Hypoxanthine); Hazaind, 7-azaindole; 5tpO, 4,5-dihydro-5-oxo[1,2,4]triazolo[1,5-α]pyrimidine; tz-tol, *N*-(thiazol-2-yl)toluenesulfonamide; tz-naf, *N*-(thiazol-2yl)naphthalenesulfonamide; azab, 4-azabenzimidazole; Hstz, sulfathiazole.

[b] The structure contains two crystallographic independent dinuclear units.

[c] (S), structure solved; (M), magnetic susceptibility measured.

[d] J is the exchange coupling parameter, which is also sometimes defined as $-2J$ (cm^{-1}) or $-J/k$ (K).

[e] Structure of the same compound with different lattice water, $[Cu_2(ad)_4(H_2O)_2](H_2O)_5$ was also solved [28]. Magnetic susceptibility was also measured of compounds with different lattice water, i.e. $[Cu_2(ad)_4(H_2O)_2](H_2O)$ with $J = -108$ cm^{-1} [8], $J = -210$ cm^{-1} [6] and $[Cu_2(ad)_4(H_2O)_2](H_2O)_6$ with $J = -179$ cm^{-1} [11].

[f] Magnetic susceptibility was also measured of a compound with different lattice water, i.e. $[Cu_2(adH)_4Cl_2]Cl_2(H_2O)$ with $J = -143$ cm^{-1} [8] and from the bromide adduct $[Cu_2(adH)_4Br_2]Br_2(H_2O)_4$ with $J = -145$ cm^{-1} [8].

[g] Magnetic susceptibility was measured from a sample with formula, $[Cu_2(hpH)_4Cl_2]Cl_2(H_2O)_2$, also the magnetism of the bromide adduct was measured, i.e. $[Cu_2(hpH)_4Br_2]Br_2(H_2O)$ with $J = -143$ cm^{-1} [8].

[h] Magnetic susceptibility was also measured from a DMSO adduct, $[Cu_2(azaind)_4(DMSO)_2]$ with $J = -389$ cm^{-1}.

3.3. Magnetic properties

The magnetic susceptibility of powdered samples were measured from 5 to 300 K. The magnetic behaviour of compounds **1** and **2** are depicted in Figs. 5 and 6 in the form of μ_{eff} versus T for two Cu(II) ions. At 300 K the μ_{eff} has a value of about 1.90 μ_B for both compounds (much below the spin only value for two Cu ions of 2.83 μ_B) and the μ_{eff} gradually decreases at 50 K to about 0.10 μ_B and stays then constant till 5 K. This behaviour agrees with a strong antiferromagnetic interaction. In compound **2** the value decreases somewhat more, due to the fact that some more paramagnetic impurity is present (vide infra).

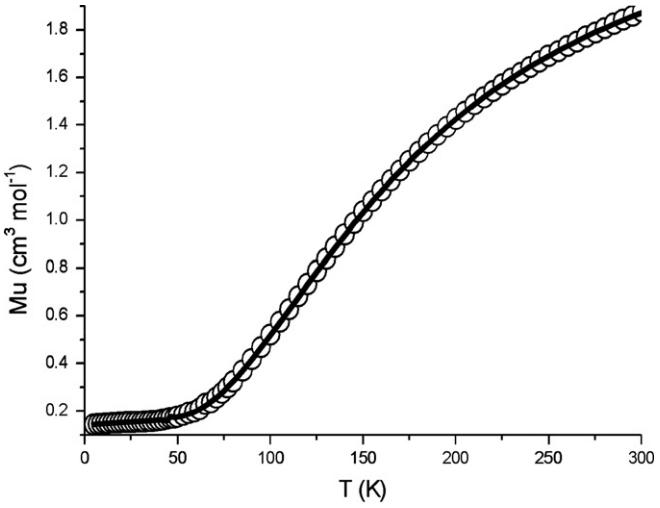

Fig. 5. A plot of the temperature dependence of μ vs. T for $[Cu_2(azab)_4Cl_2]Cl_2(CH_3OH)_3$ (**1**). The solid line represents the calculated curve for the parameters $J = -329\ cm^{-1}$, $g = 2.12$, $zJ' = 0.02.\ cm^{-1}$ (see text).

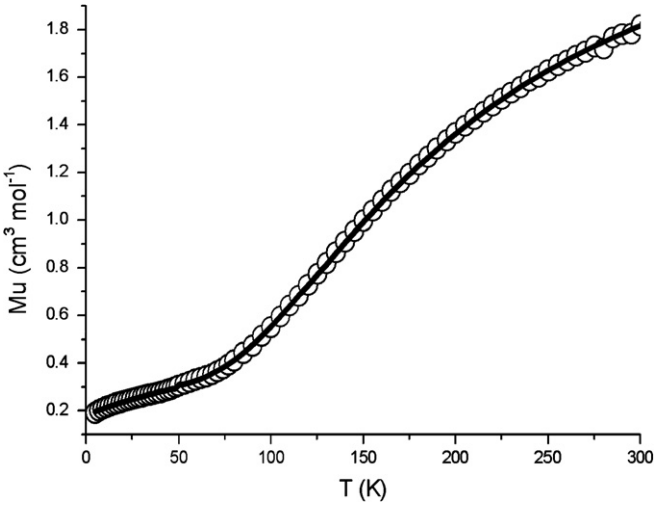

Fig. 6. A plot of the temperature dependence of μ vs. T for $[Cu_2(azab)_4Br_2]Br_2(H_2O)_{1/2}$ (**2**). The solid line represents the calculated curve for the parameters $J = -349\ cm^{-1}$, $g = 2.02$, $zJ' = -0.03\ cm^{-1}$ (see text).

The theoretical expression for the magnetic susceptibility for two interacting $S = 1/2$ centres, which is based on the general Hamiltonian [3] is: $H_{ex} = -JS_1S_2$, in which the exchange parameter J, is negative for antiferromagnetic and positive for ferromagnetic interaction. The magnetic data were fitted to the equation given in the literature [3] for dinuclear copper compounds:

$$\chi_m = (2Ng^2\beta^2)[kT - (2zJ'/(3 + \exp(-J/kT)))]^{-1} \times [3 + \exp(-J/kT)]^{-1}(1 - p) + \chi_p p,$$

in which N, g, β, k and T have their usual meanings [3]. The parameter p denotes the fraction of paramagnetic impurity in the sample and zJ' the interaction between neighbouring dinuclear identities. The fit was accomplished by minimization of $R = (\chi_m \cdot T_{calc} - \chi_m \cdot T_{obs})^2/(\chi_m \cdot T_{obs})^2$ by a least-squares procedure. The best fit for compound **1**, depicted in Fig. 5 as a solid line, was obtained for $J = -329\ cm^{-1}$, $g = 2.12$, $zJ' = 0.02\ cm^{-1}$, $p = 0.003$, with a final R of 3.5×10^{-3}. The best fit for compound **2**, depicted in Fig. 6 as a solid line, was obtained for $J = -349\ cm^{-1}$, $g = 2.02$, $zJ' = 0.03\ cm^{-1}$, $p = 0.005$, with a final R of 1.6×10^{-3}.

4. Concluding remarks

In this paper two novel dinuclear compounds with the chromophore $[Cu_2(azab)_4X_2]^{2+}$ (with X = Cl, Br) has been synthesized, characterized by infrared spectroscopy, EPR and also the X-ray structure of both compounds and the magnetic susceptibility have been investigated. As can be seen in Table 4, where related compounds are tabulated of which the X-ray structure has been performed as well as the magnetic susceptibility measured, the J values vary from -104 to $-361\ cm^{-1}$, while the Cu–Cu distances are between 2.7224(13) and 3.066 Å. All these compounds are structurally related with four ligands in a paddlewheel-like fashion and with (distorted) square pyramidal or square planar geometry and with the unpaired spin of the Cu(II) ion in the $d_{x^2-y^2}$ orbital.

The compounds investigated in this study have a very strong antiferromagnetic interaction (-328 and $-348\ cm^{-1}$). Only the Cu(II) compounds with 7-azaindole ($J = -361\ cm^{-1}$) and with the methylated 7-azaindole compounds, $[Cu(7\text{-methylazaindole})_4(H_2O)_2]^{4+}$, [20] ($J$ about $-350\ cm^{-1}$) have a related strong interaction, although from these last compounds no X-ray structure has been reported. The magnetic exchange interaction is due to the overlap of the unpaired Cu(II) electron in the $d_{x^2-y^2}$ orbital to the electrons of the N–C–N group. Some small geometric differences can influence the strength of the interaction. As can be seen from Table 4 the Cu–Cu distances or bond angles also vary and a correlation between such parameters could not be established so far. Casanova et al. [16] and Gutiérrez et al. [26] provided molecular orbital calculations to understand the differences between $[Cu_2(stz)_4]$ compounds (with one single ring) and

$[Cu_2(adenine)_4]$ compounds (with two condensed rings). They also calculated the influence of the axial atoms and observed indeed energy differences between the two types of compounds. However, they observed also still a great difference between the calculated (J_{calc}) and the experimental (J_{obs}) exchange coupling for the adenine compounds [26], so no pertinent conclusions can be drawn. Our further efforts are to obtain variations of this type of compounds with other ligands.

Acknowledgments

The work described in this paper was supported by the Leiden University Study group WFMO (Werkgroep Fundamenteel MaterialenOnderzoek). Part of the research was supported financially by the Graduate Research School Combination NRSC "Catalysis". Financial support and coordination by the FP6 Network of Excellence "Magmanet" (contract number 515767) is kindly acknowledged. Mr. Sharmarke Nur is thanked for his assistance in preparing some of the complexes.

Appendix A. Supplementary material

An ORTEP of the two units of compound **1** and the EPR spectra of compound **1** at RT and of compound **2** at RT and 77 K are given as Supplementary material.

Crystallographic data (excluding structure factors) for the structure reported in this paper have been deposited with the Cambridge Crystallographic Data Centre as supplementary publication numbers CCDC-607116 and -607117 for compounds **1** and **2**, respectively. Copies of available material can be obtained, free of charge, on application to the Director, CCDC, 12 Union Road, Cambridge CB2 1EZ, UK (fax: +44 1223 336 033 or e-mail: deposit@ccdc.cam.ac.uk). Supplementary data associated with this article can be found, in the online version, at doi:10.1016/j.poly.2006.06.009.

References

[1] J. Reedijk, in: G. Wilkinson, R.D. Gillard, J.A. McCleverty (Eds.), Comprehensive Coordination Chemistry, vol. 2, Pergamon Press, New York, 1987, p. 73.
[2] (a) E. Bouwman, W.L. Driessen, J. Reedijk, Coord. Chem. Rev. 104 (1990) 143;
(b) P. O'Brien, Coord. Chem. Rev. 58 (1984) 169.
[3] O. Kahn, Molecular Magnetism, VCH Publishers, New York, 1993.
[4] J.N. van Niekerk, F.R.L. Schoenig, Acta Crystallogr. 6 (1953) 227.
[5] (a) E. Sletten, Chem. Commun. (1967) 1119;
(b) E. Sletten, Acta Crystallogr., Sect. B 25 (1969) 1480;
(c) A. Terzis, A.L. Beauchamp, R. Rivest, Inorg. Chem. 12 (1973) 1166.
[6] D.M.L. Goodgame, K.A. Price, Nature 220 (1968) 783.
[7] (a) P. de Meester, A.C. Skapski, J. Chem. Soc. A (1971) 2167;
(b) P. de Meester, D.M.L. Goodgame, K.A. Price, A.C. Skapski, Nature 229 (1971) 191.
[8] T. Asakawa, M. Inoue, K.-i. Hara, M. Kubo, Bull. Chem. Soc. Jpn. 45 (1972) 1054.
[9] E. Sletten, Acta Crystallogr., Sect. B 26 (1970) 1609.
[10] R.W. Duerst, S.J. Baum, G.F. Kokoszka, Nature 222 (1969) 665.
[11] D. Sonnenfroh, R.W. Kreilick, Inorg. Chem. 19 (1980) 1259.
[12] S.-M. Peng, Y.-N. Lin, Acta Crystallogr., Sect. C 42 (1986) 1725.
[13] R.W. Brookes, R.L. Martin, Inorg. Chem. 14 (1975) 528.
[14] M. Abdul Haj, M. Quirós, J.M. Salas, J.A. Dobado, J.M. Molina, M.G. Basallote, M.A. Máñez, Eur. J. Inorg. Chem. (2002) 811.
[15] R. Cejudo-Marín, G. Alzuet, S. Ferrer, J. Borrás, A. Castiñeiras, E. Monzani, L. Casella, Inorg. Chem. 43 (2004) 6805.
[16] J. Casanova, G. Alzuet, J. Latorre, J. Borrás, Inorg. Chem. 36 (1997) 2052.
[17] D.M.L. Goodgame, S.V. Waggett, Biochem. Biophys. Res. Commun. 42 (1971) 63.
[18] S.J. Rettig, V. Sánchez, A. Storr, R.C. Thompson, J. Trotter, J. Chem. Soc., Dalton Trans. (2000) 3931.
[19] Nonius, COLLECT, Nonius BV, Delft, The Netherlands, 2002.
[20] G.M. Sheldrick, SHELXS-97: Program for Crystal Structure Determination, University of Göttingen, Göttingen, Germany, 1997.
[21] G.M. Sheldrick, SHELXL-97: Program for the Refinement of Crystal Structures, University of Göttingen, Göttingen, Germany, 1997.
[22] M. Rzepka, W. Surga, M. Korabik, J. Mroziński, Pol. J. Chem. 70 (1996) 19.
[23] B.J. Hathaway, in: G. Wilkinson, R.D. Gill, J.A. McCleverty (Eds.), Comprehensive Coordination Chemistry, vol. 5, Pergamon Press, Oxford, 1987, 1995 (Chapter 53).
[24] R. Acevedo-Chávez, M.E. Costas, R. Escudero, Inorg. Chem. 35 (1996) 7430.
[25] J.R. Wasson, C.-I. Shyr, C. Trapp, Inorg. Chem. 7 (1968) 469.
[26] L. Gutiérrez, G. Alzuet, J. Borrás, A. Castiñeiras, A. Rodríguez-Fortea, E. Ruiz, Inorg. Chem. 40 (2001) 3089.
[27] J.P. García-Terán, O. Castillo, A. Luque, U. García-Couceiro, P. Román, L. Lezama, Inorg. Chem. 43 (2004) 4549.
[28] J.F. González-Pérez, C. Alarcón-Payer, A. Castiñeiras, T. Pivetta, L. Lezama, D. Choquesillo-Lazarte, G. Crisponi, J. Niclós-Gutiérrez, Inorg. Chem. 45 (2006) 877.
[29] (a) S. Minakata, E. Imai, Y. Ohshima, K. Inaki, I. Ryu, M. Komatsu, Y. Ohshiro, Chem. Lett. (1996) 19;
(b) S. Minakata, Y. Ohshima, A. Takemiya, I. Ryu, M. Komatsu, Y. Ohshiro, Chem. Lett. (1997) 311.

the amino acid histidine of living systems. Therefore, these scorpionate ligands were selected as a second group to construct an N_2S_2 or NS_2 coordination around copper atoms.

As has been pointed in our previous publications, this type of cluster can exhibit nonlinear optical activity. Here we report the NLO properties and crystal structure of $(NEt_4)_2[MoS_4(CuBp)_4]$; the synthesis of the complex has been reported previously [21].

2. X-ray crystallography experimental

Suitable crystals for X-ray crystallography were obtained by diffusing Et_2O into a saturated acetone solution of the title complex and leaving it for 3 days in a refrigerator. Diffraction studies of the title complex were performed on a Nonius KappaCCD diffractometer. Mo Kα radiation ($\lambda = 0.71073$ Å) was employed for data collection at 150 K. Crystal data: $(C_8H_{20}N^+)_2$-$[C_{28}H_{32}Cu_4MoN_{16}S_4]^{2-}$, $M = 1331.5$, tetragonal, space group $I4_1/a$, $a = 13.341(2)$ Å, $c = 32.490(7)$ Å, $V = 5782.6(17)$ Å^3, $Z = 4$, $\mu = 1.85$ mm^{-1}, crystal size $0.24 \times 0.20 \times 0.18$ mm^3; 51 790 reflections measured ($2\theta < 27.5°$), 3311 unique ($R_{int} = 0.0521$); R [$F^2 > 2\sigma(F^2)$] = 0.0277, R_w (all F^2 values) = 0.0649, goodness of fit 1.067, final difference map extremes +0.34 and −0.62 e Å^{-3}. Absorption corrections were semi-empirical from symmetry-equivalent and repeated reflections. The structure was solved by direct methods and refined by full-matrix least-squares on all unique F^2. Non-hydrogen atoms were refined with anisotropic displacement parameters. Hydrogen atoms were included in calculated positions and refined with isotropic displacement parameters riding on those of the parent atoms. Programs were standard Bruker AXS control and integration software, and SHELXTL [28].

3. Description of crystal structure of $(NEt_4)_2[MoS_4(CuBp)_4]$ (1)

The Mo atom lies on a special position of S_4 symmetry, and the cation lies on a C_2 axis. The anion is constructed of one MoS_4 and four symmetry-equivalent CuBp fragments linked through the bridging sulfur atoms, completely comparable to the analogous and isostructural tungsten complex [21] (unlike the tungsten complex, no twinning was detected in the molybdenum complex **1**). There is no significant interaction between the dianion $[MS_4(CuBp)_4]^{2-}$ and the two Et_4N^+ counter-cations other than normal coulombic and van der Waals forces. A projection of the dianion of complex **1**, with the atomic labelling scheme, is shown in Fig. 1 and selected bonding parameters are presented in Table 1. As in the precursor compounds $[MS_4(CuX)_4]^{2-}$ (M = Mo, W; X = Cl, Br) [29,30], the MoS_4 core has retained its tetrahedral symmetry. Apparently, the symmetrical coordination of four CuL groups does not lower the symmetry of the MoS_4 core significantly and the two unique S–Mo–S angles are very similar [108.65(2)° and 111.13(3)°]. All of the

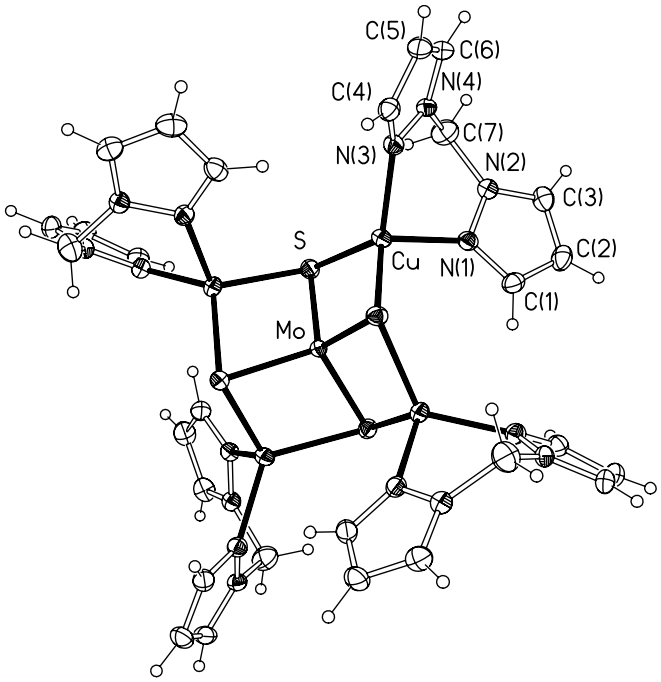

Fig. 1. Structure of the $[MoS_4(CuBp)_4]^{2-}$ anion, showing the numbering scheme for the asymmetric unit. The view is inclined to the S_4 axis.

Table 1
Selected bond lengths (Å) and bond angles (°) for $(NEt_4)_2[MoS_4(CuBp)_4]$

Mo–S	2.2472(6)	Cu–S	2.3097(7)
Cu–S(c)	2.2824(7)	Mo···Cu	2.6801(5)
Cu–N(1)	2.110(2)	Cu(1)–N(3)	2.020(2)
S–Mo–S(a)	108.65(2)	S–Mo–S(b)	111.13(3)
S–Cu–S(c)	105.31(3)	S–Cu–N(1)	105.27(6)
S–Cu–N(3)	122.09(6)	S(c)–Cu–N(1)	111.13(6)
S(c)–Cu–N(3)	119.11(6)	N(1)–Cu–N(3)	92.02(8)
Mo–S–Cu	72.04(2)	Mo–S–Cu(a)	72.55(2)
Cu–S–Cu(a)	111.97(3)		

Symmetry operations for equivalent atoms: (a) $-y + 5/4$, $x + 1/4$, $-z + 1/4$; (b) $-x + 1$, $-y + 3/2$, z; (c) $y - 1/4$, $-x + 5/4$, $-z + 1/4$.

Mo–S distances are 2.2472(6) Å, slightly longer than those of the similar bis-coordinated $(NEt_4)_2[MoS_4(CuBp')_2]$ (2.2103 Å) [$Bp' = H_2B(Pz^{Me2})_2$] [20] and rather longer than in the uncomplexed $[MoS_4]^{2-}$ anion (2.178 Å in the ammonium salt) [31]. This elongation of Mo–S and reduction of its double bond character as a result of coordination is in agreement with the decrease of the ν(Mo–S) stretching frequency in the IR spectrum. The very acute angles at the sulfur atoms bridging Cu and Mo [72.04(2)° and 72.55(2)°], together with the short Mo···Cu distances (2.680 Å) are suggestive of direct molybdenum–copper bonding interactions within the $Cu(S_b)_2Mo$ rings [Cu(I) (d^{10})–Mo(VI) (d^0) charge delocalization]. Although no definitive statement can be made about the existence of a metal–metal bond, the observed distances are consistent with a strong attractive interaction between Cu and Mo

atoms, as expected when placing two metals with greatly different formal oxidation states in close proximity, as they are in this pentanuclear cluster.

The coordination environment of all of the copper atoms is highly distorted tetrahedral, with angles ranging from 92.02(8)° (the bite angle of the chelating Bp ligand) to 122.09(6)°, and each Cu atom is coordinated by two sulfur atoms from MoS_4 and two nitrogen atoms of a Bp ligand. The bond distances in the CuS_2N_2 coordination are 2.3097(7) and 2.2824(7) Å for Cu–S, and 2.020(2) and 2.110(2) Å for Cu–N. These values are in agreement with reported ones for previous compounds of this type [21,32] or for similar compounds {e.g. 2.290(5) Å for Cu–S and 2.02(1) Å for Cu–N in $[WS_4Cu_3Cl(bpy)_2]$ [33]}.

In addition to the similarity between pyrazole (as N-donor in **1** and **2**) and imidazole in histidine, the arrangement and coordination environment of the Cu atoms in **1** are comparable to those found in active sites of some copper proteins such as poplar plastocyanin, cuperedoxin, cytochrome *c* oxides, etc. [22,34,35], indicating that the synthesized complex **1** can serve as a model for some copper proteins.

4. Nonlinear optical properties

Early investigations of planar-skeleton clusters revealed that the optical nonlinearity performance can be definitively attributed to the reverse saturable absorption under nanosecond pulsed radiation [36,37]. The *Z*-scan technique was applied to investigate the nonlinear optical refraction of $(NEt_4)_2[MoS_4(CuBp)_4]$. The output laser characteristics were as follows: pulse duration 8 ns; wavelength 532 nm; $E = 0.1$ mJ; 2 Hz repetition rate. The *Z*-scan scheme of complex **1** was calibrated using carbon disulfide (CS_2), which is often used as a standard reference nonlinear material. The nonlinear refractive index of CS_2 was measured as 2.5×10^{-10} esu (13.9×10^{-13} cm^2 W^{-1}) at 532 nm, which is in good agreement with previously reported data measured in the nanosecond range [18,38]. In Fig. 2, the normalized transmittance dependence of the sample of **1** is presented for the closed-aperture *Z*-scan scheme; it shows that the cluster possesses strong reverse saturable absorption, and it could be considered as a promising candidate for optical limiting. The closed-aperture scheme allowed us to determine the sign and magnitude of $n2$ and Re X(3). The normalized transmittance has a pair of sharp peaks and a valley. The peak-valley configuration is characteristic of self-defocusing and indicates that the sample possesses negative nonlinear refraction. Both the width and amplitude of the valley are smaller than those of the peak. The asymmetry of the peak and valley is caused by the strong reverse saturable absorption. From the measured value of the difference of normalized transmittance at the peak and valley positions, $\Delta T = 0.18$, the nonlinear optical refractive index $n2$ and Re X(3) were calculated to be -4.2×10^{-11} esu and -1.069×10^{-12} esu, respectively. The two-photon absorption coefficient β is 2.2×10^{-10} m W^{-1}. These results are comparable with those for ZnO and suitable for optical limiting applications.

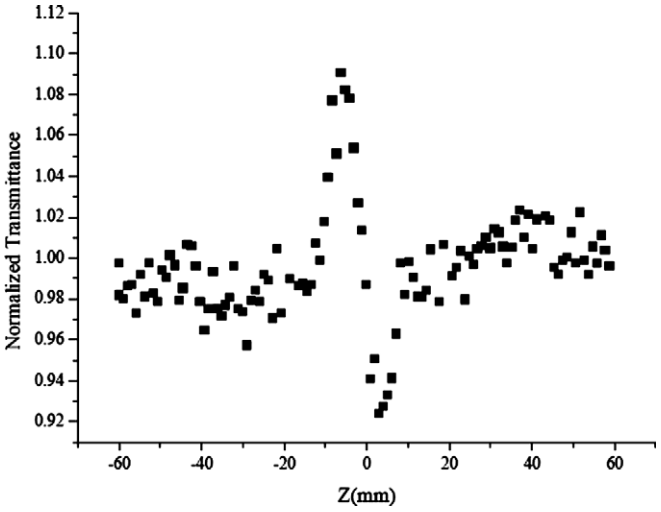

Fig. 2. The normalized transmittance dependence of $(NEt_4)_2[MoS_4(CuBp)_4]$ in the case of the closed-aperture scheme.

Acknowledgements

We thank the Research Institute for Fundamental Sciences (Tabriz, Iran) for financial support, EPSRC (UK) for equipment funding, and the Harbin Institute of Technology (China) for NLO measurements.

Appendix A. Supplementary material

Crystallographic data, excluding structure factors, have been deposited at the Cambridge Crystallographic Data Centre, CCDC No. 600512. Copies of this information may be obtained free of charge from the Director, CCDC, 12 Union Road, Cambridge CB2 1EZ, UK (fax: +44 1223 336 033; e-mail: deposit@ccdc.cam.ac.uk or www: http://www.ccdc.cam.ac.uk). Supplementary data associated with this article can be found, in the online version, at doi:10.1016/j.poly.2006.06.001.

References

[1] (a) A. Müller, E. Diemann, R. Jostes, H. Bögge, Angew. Chem., Int. Ed. Engl. 20 (1981) 934;
(b) E. Diemann, A. Müller, Coord. Chem. Rev. 10 (1973) 79.
[2] (a) R.H. Holm, Chem. Soc. Rev. 10 (1981) 455, and references therein;
(b) J. Sola, Y. Do, J.M. Berg, R.H. Holm, J. Am. Chem. Soc. 105 (1983) 105;
(c) Y. Do, E.D. Simhon, R.H. Holm, Inorg. Chem. 24 (1985) 4635.
[3] (a) D. Coucouvanis, Acc. Chem. Res. 14 (1981) 201;
(b) D. Diaz, J. Robles, T. Ni, S.E. Castillo-Blum, D. Nagesha, O.J.A. Fergoso, N.A. Kotov, J. Phys. Chem. B 103 (1999) 9859;
(c) G. Alonso, V. Petranovskii, M. Del Valle, J. Cruz-Reyes, A. Licea-Claverie, S. Fuentes, Appl. Catal. A 197 (2000) 87;
(d) C. Zhang, Y. Song, M. Fung, Z. Xued, X. Xin, Chem. Commun. (2001) 843.

[4] (a) I. Bezverkhyy, P. Afanasiev, M. Lacriox, Mater. Res. Bull. 37 (2002) 161;
(b) S. Shi, Z. Lin, Y. Mo, X.Q. Xin, J. Phys. Chem. 100 (1996) 10696;
(c) Y. Liu, J. Chen, M.D. Ryan, Inorg. Chem. 37 (1998) 425.
[5] S.H. Laurie, Eur. J. Inorg. Chem. (2000) 2443.
[6] (a) J.P. Lang, K. Tatsumi, Inorg. Chem. 37 (1998) 6308, and Refs. [2–8] therein;
(b) T. Ecclestone, I. Harvy, S.H. Laurie, M.C.R. Symons, F.A. Taiwo, Inorg. Chem. Commun. 1 (1998) 460;
(c) R. Dessapt, C. Simonnet-Jegat, J. Marroy, F. Secheresse, Inorg. Chem. 40 (2001) 4072.
[7] (a) K.E. Howard, J.R. Lockemeyer, M.A. Massa, T.B. Rauchfuss, S.R. Wilson, X. Yahg, Inorg. Chem. 29 (1990) 4385;
(b) H.G. Zheng, W. Tan, C. Jin, W. Ji, Q. Jin, X. Huang, X.Q. Xin, Inorg. Chim. Acta 305 (2000) 14.
[8] (a) D. Shaow, Z. Nianyong, C. Pengcheng, W. Xintao, L. Jiaxi, Polyhedron 11 (1992) 109;
(b) D.L. Long, J.T. Chen, J.S. Huang, Inorg. Chim. Acta 285 (1999) 241;
(c) M. Hong, D. Wu, R. Cao, X. Lei, H. Liu, J. Lu, Inorg. Chim. Acta 258 (1997) 25;
(d) Y. Jeannin, F. Secheresse, S. Bernesa, F. Robert, Inorg. Chim. Acta 198–200 (1992) 493.
[9] (a) C. Zhang, G.C. Jin, J.X. Chen, X.Q. Xin, K.P. Qian, Coord. Chem. Rev. 213 (2001) 51;
(b) H.W. Hou, X.Q. Xin, S. Shi, Coord. Chem. Rev. 153 (1996) 25;
(c) R. Colton, Coord. Chem. Rev. 62 (1985) 145.
[10] (a) Q. Liu, Y. Yang, L. Huang, D. Wu, B. Kang, C. Chen, Y. Lu, Inorg. Chem. 34 (1995) 1884;
(b) R.J. Salm, A. Misetic, J.A. Ibers, Inorg. Chim. Acta 240 (1995) 239.
[11] H.G. Zheng, W. Ji, M.L.K. Low, G. Sakane, T. Shibahara, X.Q. Xin, J. Chem. Soc., Dalton Trans. (1997) 2537.
[12] (a) H. Hou, D. Long, X. Xin, X. Huang, B. Kang, P. Ge, W. Ji, S. Shi, Inorg. Chem. 35 (1996) 5363;
(b) J.M. Manoli, C. Potvin, Inorg. Chim. Acta 150 (1988) 257.
[13] (a) W. Clegg, A. Beheshti, M. Hosaini Sadr, Acta Crystallogr. Sect. E (2002) m349;
(b) A. Beheshti, W. Clegg, H. Fallah, Inorg. Chim. Acta 322 (2001) 1.
[14] (a) W. Kaim, B. Schwederski, Bioinorganic Chemistry: Inorganic Elements in the Chemistry of Life, Wiley, New York, 1996 (Chapters 10 and 11);
(b) E.K. Quagraine, R.S. Reid, J. Inorg. Biochem. 85 (2001) 53.
[15] Q. Pan, C.G. Kleer, L.V. Golden, J. Irani, M. Bottema, C. Bias, M.D. Carvalho, E.A. Mesri, D.M. Robin, R.D. Dick, J. Brewer, S.D. Merajver, Cancer Res. 62 (2002) 4854, and Refs. [5–7] therein.
[16] K.D. Bissig, T.C. Voegelin, M. Solioz, FEBS Lett. 507 (2001) 367.
[17] (a) C. Zhang, Y. Song, Y. Xu, H. Fun, G. Fang, Y. Wang, X. Xin, J. Chem. Soc., Dalton Trans. (2000) 2823;
(b) H. Zheng, W. Leung, W. Tan, D. Long, W. Ji, J. Chen, F. Xin, X. Xin, J. Chem. Soc., Dalton Trans. (2000) 2145;
(c) S.J. Hibble, M.R. Feaviour, J. Mater. Chem. 11 (2001) 2607;
(d) A. Leist, S. Stauf, S.a. Loken, E.W. Finckh, S. Ludtke, K.K. Unger, W. Assenmacher, W. Mader, W. Tremel, J. Mater. Chem. 8 (1998) 241.
[18] (a) C. Zhang, Y. Song, X. Wang, F.E. Kuhn, Y. Wang, H. Fun, X. Xin, J. Mater. Chem. 12 (2002) 239;
(b) C. Zhang, Y. Song, X. Wang, F.E. Kuhn, Y. Wang, Y. Xue, X. Xin, J. Mater. Chem. 13 (2003) 571;
(c) G. Fang, Y. Song, Y. Wang, X. Zhang, C. Li, C. Zhang, X. Xin, Opt. Commun. 181 (2000) 97;
(d) Y. Song, C. Zhang, Y. Wang, G. Fang, G. Jin, C. Chang, S. Liu, X. Xin, H. Ye, Chem. Phys. Lett. 326 (2000) 341;
(e) Y. Song, C. Zhang, Y. Wang, G. Fang, C. Duan, S. Liu, X. Xin, H. Ye, Opt. Commun. 168 (1999) 131;
(f) Y. Song, C. Zhang, X. Wang, Y. Wang, G. Fang, G. Gin, X. Zhan, S. Liu, L. Chen, X. Xin, Mater. Lett. 46 (2000) 49.
[19] A. Beheshti, W. Clegg, M. Hosaini Sadr, Polyhedron 20 (2001) 179.
[20] A. Beheshti, W. Clegg, M. Hosaini Sadr, Inorg. Chim. Acta 335 (2002) 21.
[21] M. Hossaini Sadr, W. Clegg, H.R. Bijhanzade, Polyhedron 23 (2004) 637.
[22] (a) A.G. Sykes, Adv. Inorg. Chem. 36 (1991) 377;
(b) E.I. Solomon, K.W. Penfield, D.E.W. Cox, Struct. Bond. 53 (1983) 1.
[23] S. Trofimenko, Scorpionates: The Coordination Chemistry of Polypyrazolylborate Ligands, Imperial College Press, London, 1999.
[24] (a) S. Trofimenko, Chem. Rev. 93 (1993) 943;
(b) S. Trofimenko, Prog. Inorg. Chem. 34 (1986) 115;
(c) S. Trofimenko, Acc. Chem. Res. 4 (1971) 17;
(d) S. Trofimenko, Inorg. Chem. 1 (1970) 99;
(e) S. Trofimenko, J. Am. Chem. Soc. 88 (1966) 1842;
(f) S. Trofimenko, J. Am. Chem. Soc. 89 (1967) 3170.
[25] (a) C. Slugovc, I.P. Martinez, S. Sirol, E. Carmona, Coord. Chem. Rev. 213 (2001) 129;
(b) M.D. Ward, J.A. McCleverty, J.C. Jeffery, Coord. Chem. Rev. 222 (2001) 251;
(c) D. Reger, Coord. Chem. Rev. 147 (1996) 571;
(d) C. Slugovc, R. Schmid, K. Krichner, Coord. Chem. Rev. 185–186 (1999) 109;
(e) S. Hikichi, A. Munetaka, Y. Moro-oka, Coord. Chem. Rev. 198 (2000) 61;
(f) N. Marques, A. Sella, J. Takats, Chem. Rev. 102 (2002) 2159.
[26] (a) N. Kitajima, W.B. Tolman, Prog. Inorg. Chem. 43 (1995) 419;
(b) R.E. Davis, T.A. Dodds, T.H. Hseu, J.C. Wagnon, T. Devon, J. Tancrede, J.S. McKennis, R. Pettit, J. Am. Chem. Soc. 96 (1974) 7565;
(c) T.C. Higgs, D.J. Roman, S. Czernuscewicz, C.J. Carrano, Inorg. Chem. Acta 273 (1998) 14;
(d) N. Kitajima, K. Fujisawa, C. Fujimoto, Y. Moro-oka, S. Hashimoto, T. Kitagawa, K. Toriumi, K. Tatsumi, A. Nakamura, J. Am. Chem. Soc. 114 (1992) 1277;
(e) N. Kitajima, K. Fujisawa, Y. Moro-oka, J. Am. Chem. Soc. 111 (1989) 8975;
(f) N. Kitajima, T. Koda, S. Hashimoto, T. Kitagawa, Y. Moro-oka, J. Am. Chem. Soc. 113 (1991) 5664;
(g) R. Osterberg, Coord. Chem. Rev. 12 (1974) 309.
[27] S. Dhar, P.A.N. Reddy, M. Nethaji, S. Mahadevan, M.K. Saha, A.R. Chakravarty, Inorg. Chem. 41 (2002) 3469.
[28] G.M. Sheldrick, SHELXTL: User Manual, Bruker AXS Inc., Madison, WI, USA, 1997.
[29] (a) N.R. Brooks, W. Clegg, M. Hossaini Sadr, M. Esm-Hosseini, R. Yavari, Acta Crystallogr., Sect. E 60 (2004) m204;
(b) F. Secheresse, S. Bernes, F. Robert, Y. Jeannin, J. Chem. Soc., Dalton Trans. (1991) 2875.
[30] (a) M. Hossaini Sadr, S.M. Seyed Ahmadian, N.R. Brooks, W. Clegg, Acta Crystallogr., Sect. E 60 (2004) m1952;
(b) J.R. Nicholson, A.C. Flood, C.D. Garner, W. Clegg, J. Chem. Soc., Chem. Commun. (1983) 1179.
[31] J. Lapasset, N. Chezeau, P. Belougne, Acat Crystallogr., Sect. B 32 (1976) 3087.
[32] G. Alonso, G. Berhault, R.R. Chianlli, Inorg. Chim. Acta 316 (2001) 105.
[33] S. Bernes, F. Secheresse, Y. Jeannin, Inorg. Chim. Acta 194 (1992) 105.
[34] S. Mandal, G. Das, R. Singh, R. Shukla, P.K. Bharadwaj, Coord. Chem. Rev. 160 (1997) 191.
[35] (a) N. Kitajima, Adv. Inorg. Chem. 39 (1992) 18;
(b) N. Kitajima, K. Fujisawa, C. Fujimoto, Y. Moro-oka, Chem. Lett. (1989) 421.
[36] C. Zhang, Y.L. Song, B.M. Fung, Z.L. Xue, X.Q. Xin, Chem. Commun. (2000) 843.
[37] C. Zhang, Y.L. Song, F.E. Kühn, Y.X. Wang, X.Q. Xin, W.A. Herrmann, Adv. Mater. 14 (2002) 818.
[38] T. Kawazoe, H. Kawaguchi, J. Inoue, O. Haba, M. Ueda, Opt. Commun. 160 (1999) 125.

groups. In this paper, we introduce a series of new monoiminopyridyl ligands and their transition metal complexes. This monoiminopyridyl-transition metal catalyst system should be an interesting contrast to the previous system of iron and cobalt catalysts containing the 2,6-bis(imino)pyridine ligand [8–15]. We have explored the ethylene polymerization and oligomerization activity of these monoiminopyridyl-transition metal complexes in the presence of the cocatalyst methylaluminoxane (MAO) to clarify the reasons for this difference. We have also studied the influences of the metal center, the ligand architecture and the reaction conditions on the catalyst activity.

2. Results and discussion

2.1. Synthesis aspects

2.1.1. Synthesis of the precursor *4*

2-Carbethoxy-6-acetylpyridine (**4**) was prepared from 2,6-dimethylpyridine (**1**) (Scheme 1). Initially 2,6-dimethylpyridine (**1**) was converted to pyridine-2,6-dicarboxylic acid (**2**) according to the method reported in the literature [28,29]. Esterification of **2** was done by a modified procedure with a better yield (83%) than that of the reported method [30], resulting in 2,6-dicarbethoxypyridine (**3**), which was purified by a simplified method. **3** was dissolved in freshly distilled EtOAc, then treated with dry EtONa powder and an excess of concentrated HCl to afford compound 2-acetyl-6-carbethoxypyridine (**4**). The structure of the new compound **4** was proven by element analysis, ^{1}H NMR, IR and MS.

2.1.2. Synthesis of the ligands *5–7*

2-Carbethoxy-6-{1-[(2,6-dimethylphenyl)imino]ethyl}-pyridine (**5**), 2-carbethoxy-6-{1-[(2,4,6-trimethylphenyl)-imino]ethyl}pyridine (**6**), 2-carbethoxy-6-{1-[(2,6-diethylphenyl)-imino]ethyl}pyridine (**7**) were synthesized by condensation of 2-carbethoxy-6-acetylpyridine (**4**) and an excess of the corresponding substituted anilines using microwave irradiation (Scheme 2). After purification by column chromatography, the highly pure products were obtained in moderate yields (17.0–62.5%). Attempts to prepare **5–7** by catalytic condensation of **4** with the corresponding aryl aniline in refluxing ethanol and in the presence of acetic acid [31] were unsuccessful. We also found that the use of toluene as solvent, *p*-toluenesulfonic acid as catalyst and a Dean–Stark apparatus to remove the water formed in the reaction [32] afforded **5–7** in very low yields (about 10–15%), even after a long refluxing period (up to 3 days), and led to many byproducts. Compared with the two pathways mentioned above, microwave-assisted condensation seems to be much better in terms of improved reaction rate, simple work-up procedure and formation of cleaner products in preparing **5–7**, and moreover, it is a green method for chemical synthesis. The ligands **5–7** were characterized by element analysis, ^{1}H NMR and IR.

2.1.3. Synthesis of the complexes *8–19*

The transition metal complexes **8–13** (Schemes 3 and 4) were prepared by the reactions of ligand **5** with stoichiometric amounts of Mn(II), Fe(II), Co(II), Cu(II), Zn(II) and Ni(II) chlorides in ethanol at room temperature. The

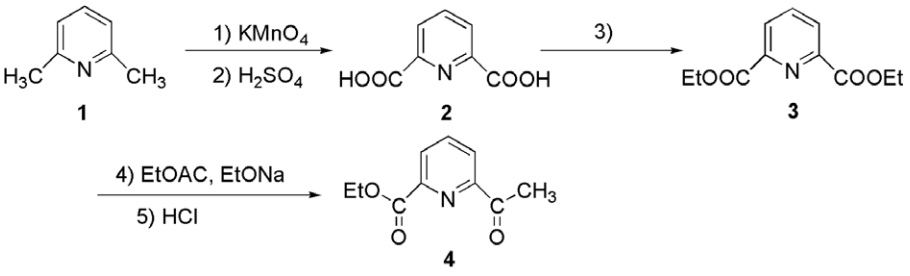

Scheme 1.

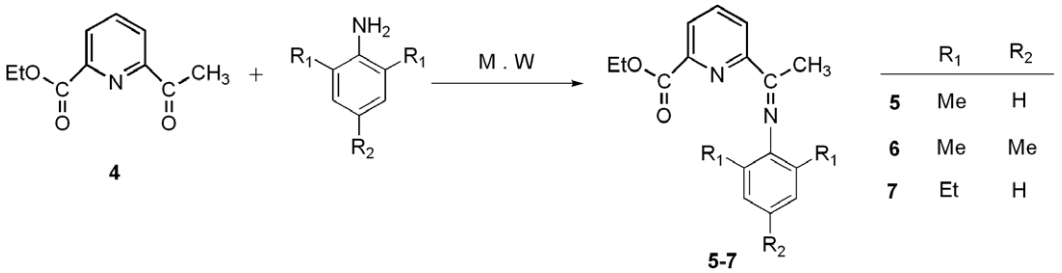

Scheme 2.

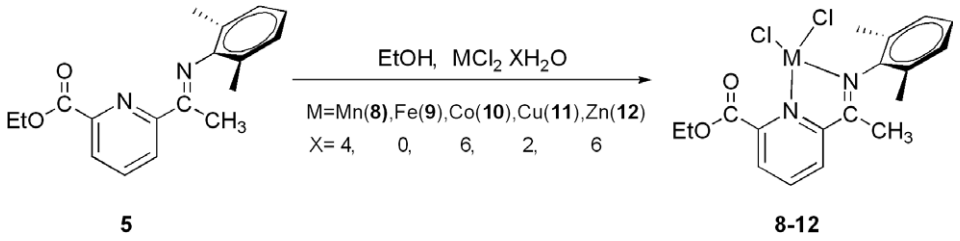

Scheme 3.

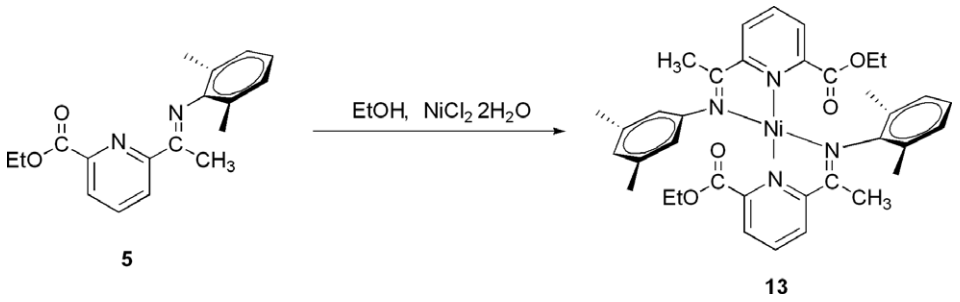

Scheme 4.

complexes **14**–**19** (Scheme 5) were synthesized by the selected metal Fe(II), Co(II), Ni(II) chlorides and the corresponding ligands **6** and **7** under the same experimental conditions as above. All the complexes were isolated as air-stable solids in high purity and in different yields. They were characterized by elemental analysis and IR spectroscopy. The elemental analysis results suggested that the components of complexes **8**–**12** and **14**–**19** were consistent with the formula $MLCl_2$, and complex **13** with the formula $ML_2Cl_2 \cdot H_2O$. The IR spectra of the free ligands **5**, **6** and **7** showed that the C=N stretching frequencies appeared at 1644, 1643 and 1640 cm^{-1}, respectively, and C=O vibrations at 1741, 1716 and 1742 cm^{-1}, respectively. In complexes **8**–**19**, the C=N stretching vibrations shifted toward lower frequencies ranging from 1621 to 1636 cm^{-1}, and were greatly reduced in intensity, which indicated coordination between the imino nitrogen atom and the metal ion. The C=O stretching vibrations also shifted toward lower frequencies ranging from 1665 to 1725 cm^{-1}, and were reduced in intensity, which suggested weak coordination between the carbonyl oxygen of the ester group and the metal ions.

2.2. The molecular structures of complexes *12* and *18*

Complexes **12** and **18** were further characterized by X-ray crystallography. Yellow crystals of **12** suitable for X-ray diffraction analysis were grown from a THF solution at room temperature, while green single crystals of complex **18** were obtained from a solution of $CoCl_2 \cdot 6H_2O$ in EtOH top layered with a solution of ligand **7** in Et_2O. The crystal structures of **12** and **18** are shown in Figs. 1 and 2, respectively, whereas selected bond lengths and angles are listed in Table 1. Fig. 1 indicates that in complex **12** the center Zn atom is coordinated in a distorted-tetrahedral environment by the pyridyl nitrogen atom, imino nitrogen atom and two chlorine atoms. The dimethyl-substituted phenyl ring is oriented nearly perpendicular to the coordination plane, and the dihedral angle is 89.50°. One THF molecule is observed in the crystal lattice of **12**. It should be pointed out that the oxygen atom in the carbonyl group is orientated toward the Zn center in **12**, and the distance between oxygen and Zn is 2.581 Å, which is longer than the normal Zn–O coordination bond length. The imino linkage N(1)–C(10) and linkage O(1)–C(16) have distinctive double-bond

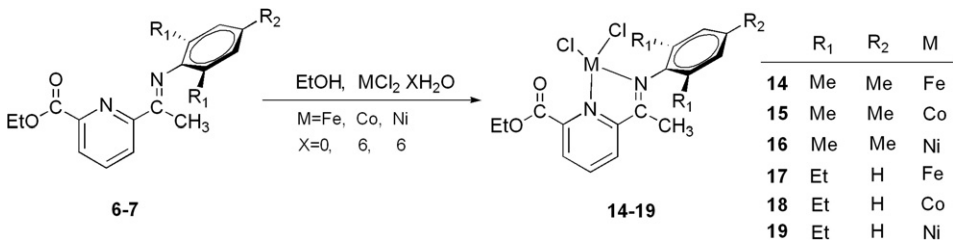

Scheme 5.

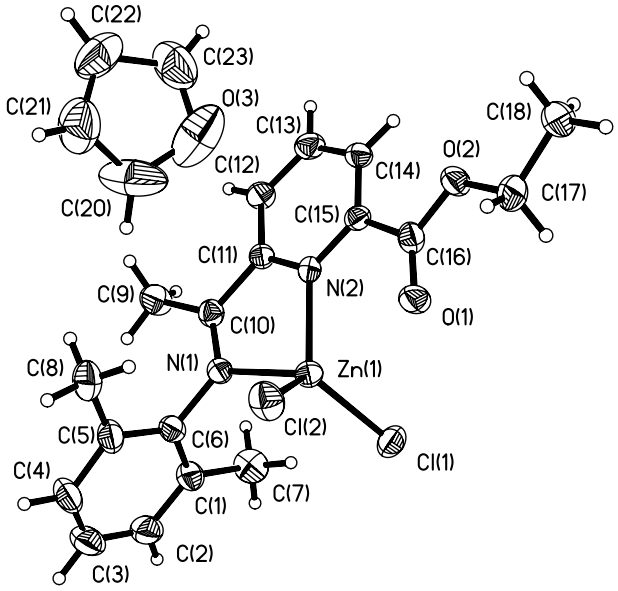

Fig. 1. Molecular diagram of {2-carbethoxy-6-[1-[(2,6-dimethylphenyl)-imino]ethyl]pyridine}-$ZnCl_2 \cdot THF$ (**12**).

character, with C–N and C–O distances of 1.275(7) and 1.206(7) Å, respectively. A perusal of the bond angles around the metal center of **12** shows that its coordination geometry is greatly distorted from an idealized tetrahedron, which may be attributed to the effect of the carbonyl oxygen atom on the coordination environment.

Fig. 2 shows that the carbonyl oxygen atom in **18** coordinates with Co(II). The coordination geometry around the central cobalt can be best described as distorted trigonal bipyramid, with the pyridyl nitrogen atom and the two chlorine atoms forming the equatorial plane. The deviation of the cobalt atom from the equatorial plane is 0.173 Å. The phenyl ring is oriented essentially orthogonal (88.11°) to the coordination plane containing the ligand backbone and the cobalt atom. It is noticeable that the Co–O(1) bond length (2.374(2) Å) is shorter than reported Co–O distances (2.460, 2.610 Å) [33], which indicates a strong coordination between the cobalt and carbonyl oxygen atom in **18**. As previously observed [12,13], the Co–N(pyridyl) bond (2.036(3) Å) is shorter than the Co–N(imino) bond (2.156(3) Å) in **18**.

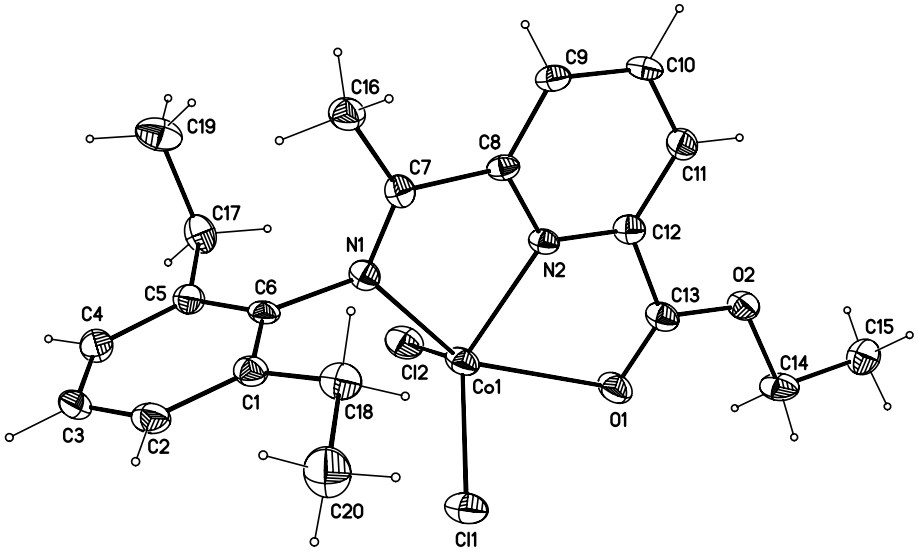

Fig. 2. Molecular diagram of {2-carbethoxy-6-[1-[(2,6-diethylphenyl)imino]ethyl]pyridine}-$CoCl_2$ (**18**).

Table 1
Selected bond lengths (Å) and angles (°) for complexes **12** and **18**

Complex **12**				Complex **18**			
Zn–N(2)	2.084(5)	N(1)–C(10)	1.275(7)	Co–N(1)	2.156(3)	Co–O(1)	2.374(2)
Zn–N(1)	2.157(5)	O(1)–C(16)	1.206(7)	Co–N(2)	2.036(3)	O(1)–C(13)	1.214(3)
Zn–Cl(2)	2.194(2)	C(10)–C(11)	1.496(8)	Co–Cl(1)	2.234(1)	O(2)–C(13)	1.308(4)
Zn–Cl(1)	2.226(2)	C(15)–C(16)	1.493(8)	Co–Cl(2)	2.242(1)	N(1)–C(7)	1.275(4)
N(2)–Zn–N(1)	76.7(2)	Cl(2)–Zn–Cl(1)	120.3(8)	N(2)–Co–N(1)	76.6(1)	Cl(1)–Co–Cl(2)	123.5(4)
N(2)–Zn–Cl(2)	120.8 (1)	C(10)–N(1)–Zn	115.1(4)	N(2)–Co–Cl(1)	125.9(9)	N(2)–Co–O(1)	73.3(1)
N(1)–Zn–Cl(2)	107.8(1)	C(6)–N(1)–Zn	124.1(4)	N(1)–Co–Cl(1)	101.7(8)	N(1)–Co–O(1)	149.2(9)
N(2)–Zn–Cl(1)	113.0(1)	C(11)–N(2)–Zn	116.4(4)	N(2)–Co–Cl(2)	108.6(8)	Cl(1)–Co–O(1)	90.8(7)
N(1)–Zn–Cl(1)	107.8(1)	C(15)–N(2)–Zn	124.7(4)	N(1)–Co–Cl(2)	104.5(8)	Cl(2)–Co–O(1)	91.2(7)

2.3. Application of complexes 8–19 in the polymerization/oligomerization of ethylene

To probe the catalytic nature of these complexes for the ethylene polymerization/oligomerization, we carried out series of experiments over a range of active metal centers, ligand modifications, as well as a variety of polymerization/oligomerization reaction conditions in which the reaction temperature, time and Al/Metal ratio were systematically altered. The results are indicated in Table 2, Figs. 3–6, respectively.

2.3.1. Effect of the active metal center on the polymerization and oligomerization of ethylene

The nature of the center metal greatly influences the catalyst activity. The activities of the transition metal Mn(II), Fe(II), Co(II), Cu(II), Zn(II), Ni(II) complexes **8**–**13** bearing the same ligand **5** were tested at 1.0 atm of ethylene at 15.0–23.5 °C for 1 h, employing 1000 equiv. of MAO as cocatalyst (Table 2). Fe complex **9** shows considerable activity for the ethylene polymerization and moderate activity for ethylene oligomerization (Run 2), which implies that in this system the rate of chain propagation is in excess of the rate of chain transfer. While the ethylene oligomerization activities indicated by Co complex **10** and Ni complex **13** (Runs 3, 6) imply the reverse rate order, mainly producing butenes and hexenes and small amounts of higher oligomers. From Table 2, it can be concluded that the Mn, Cu, Zn complexes **8**, **11**, **12** are inactive for the ethylene polymerization/oligomerization (Runs 1, 4, 5), which is in agreement with the results observed from the bis(imino)pyridine-based transition metal analogues. The above results show that the different inherent electronic properties of the transition metals play a significant role in the catalyst activity, possibly leading to differences in the catalytic activity and product distribution.

2.3.2. Aryl ring ligand modification

A variety of substituted aryl-ring-containing ligands, including those with steric bulk and *ortho*- and *para*-substituted position modifications in the aryl ring, were employed to study their influence on the catalytic activity and product distribution of ethyl polymerization and oligomerization. The effect of these modifications on the oligomer distribution is not as remarkable as the effect on the catalytic activity, and no precise conclusion can be reached. Herein we mainly give the results on the catalytic activity. In Fig. 3, the curve 1 (■) was obtained from the activity of Fe, Co, Ni-based catalysts bearing ligand **5**, the curve 2 (◆)

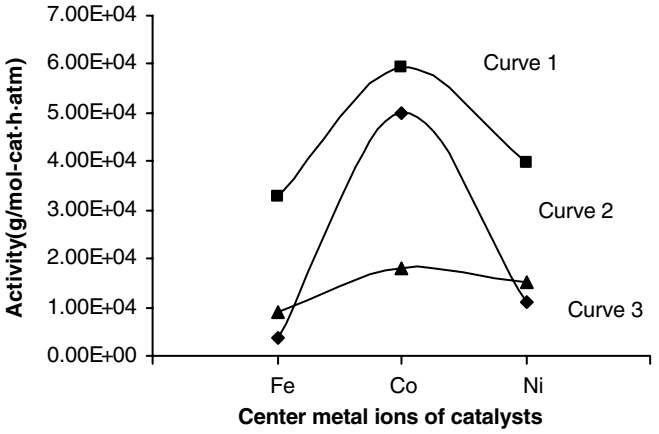

Fig. 3. Dependence of the activity on ligands **5** (curve 1 ■), **6** (curve 2 ◆), **7** (curve 3 ▲) for the Fe, Co, Ni-based catalysts.

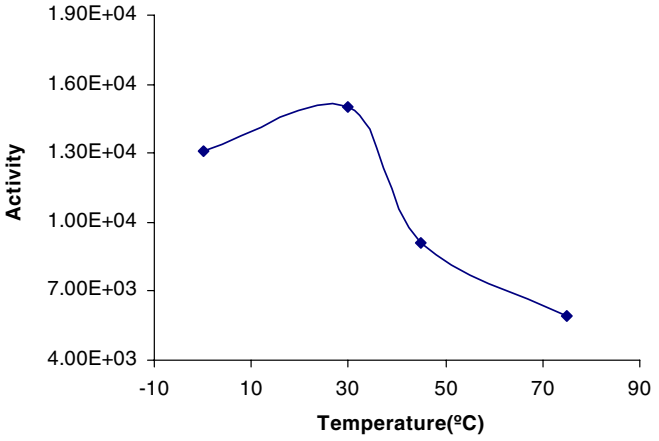

Fig. 4. Dependence of the activity on the reaction temperature for the catalyst **10**.

Table 2
Ethylene polymerization and oligomerization by the ML_nCl_2-MAO system [L = **5**, M = Mn (**8**), Fe (**9**), Co (**10**), Cu (**11**), Zn (**12**), Ni (**13**)][a]

Run	Complex	Temperature (°C)	Time (h)	Oligomer distribution[c] (%)				Activity (10^4g/mol-cat h atm)	
				$C_4/\sum C$	$C_6/\sum C$	$C_{\geqslant 8}/\sum C$	Linear α-olefin	Oligomer[c]	Polymer
1	**8**	23.5	1.0					no	no
2	**9**	15.0	1.0	91.50	4.33	4.17	>99.0	0.15	3.13
3	**10**[b]	15.5	0.5	82.10	15.46	2.44	96.3	5.93	trace
4	**11**	15.5	1.0					no	no
5	**12**	20.5	1.0	96.80	2.11	1.09	>99.0	0.16	no
6	**13**[b]	15.0	1.0	98.20	1.20	0.60	97.6	3.97	trace

[a] Reaction conditions: Complex 10 μmol, M/Al = 1/1000, P = 1 atm, solvent: toluene 30 mL, 100 mL autoclave, MAO in toluene (14%).
[b] Solvent: toluene 50 mL.
[c] Determined by GC. $\sum C$ means the total amounts of oligomers.

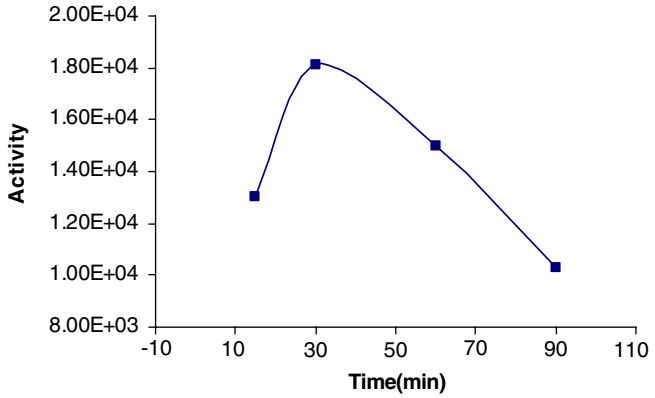

Fig. 5. Dependence of the activity on the reaction time for the catalyst **10**.

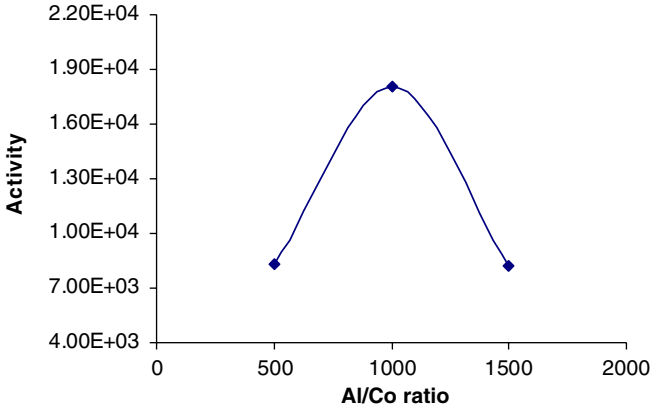

Fig. 6. Dependence of the activity on Al/Co ratio for the catalyst **10**.

and 3 (▲) were obtained from the activity of Fe, Co, Ni-based catalysts bearing ligands **6** and **7**, respectively. As shown in this figure, curve 1 is above both curve 2 and curve 3, which indicates that the activity of Fe, Co, Ni-based catalysts with a methyl group in the 2- and 6-position of the aryl ring are generally higher than those with a methyl group in the 2, 4, 6-position and those with an ethyl group in the 2- and 6-position. It suggests that replacing the *para*-aryl proton with a methyl group may result in a decrease in rate of propagation or β-H transfer (the major chain-transfer process), thus leading to a lower productivity in polymer or oligomer production (compare curve 1 with curve 2). On the other hand, bulky *ortho*-substituted aryl groups attached to the imine nitrogen also render less active catalysts (compare curve 1 with curve 3).

The influence of the metal center on catalytic activity also can be seen from Fig. 3. Comparison of the Fe, Co, Ni catalysts bearing different ligands indicates the same trend in activity changes. In general, Co catalysts are more active than the corresponding Ni catalysts, and Fe catalysts show the lowest activity in every set of Fe, Co, Ni catalysts. This result is slightly different from the trend observed for the bis(imino)pyridine ligand analogues [8,9]. The reason probably relates to the difference of the structure and electronic properties between the two types of ligands.

A study reported by Bianchini and co-workers [34,35] suggested that steric groups directly linked to the 2-position of pyridine were considered irrelevant in accounting for the superior activity of thiophenyl-substituted catalysts, but the chain length of the oligomers had been found to increase with the size of the sulfur-containing group in the catalyst 2-imino-6-(organyl)pyridine Co(II) dichloride. Compared with the other heteroatoms, the sulfur atom was suggested to have a great role in increasing both the activity and the Schulz–Flory parameter α (mol C_{n+2}/mol C_n). So the lesser activity indicated by the carbonyl group substituted in the 2-position of the pyridine ligand based Co(II) catalyst can be mainly attributed to the oxygen atom, but the great difference between the carbonyl group and the thiophenyl ring is also a reason for the catalytic performance. As yet no conclusion can be forwarded in the absence of further studies.

2.3.3. Effect of reaction conditions

To study the influence of the catalytic reaction conditions on the productivity of the catalyst system employed, we performed a series of experiments by employing Co catalyst **10** under different reaction temperatures, reaction times, as well as the ratio of Al/Metal. The results are shown in Figs. 4–6.

2.3.3.1. Effect of temperature on catalyst performance. To examine the role of the temperature variation on catalyst performance, four experiments were carried out at different temperatures (0, 30, 45 and 75 °C, respectively) for 60 min with an Al/Co ratio of 1000. As shown in Fig. 4, the activity increases slightly when the temperature rises from 0 to 30 °C (from 1.312×10^4 g/mol-Co h atm at 0 °C to 1.50×10^4 g/mol-Co h atm at 30 °C), and then it decreases as the temperature is increased continually up to 75 °C (0.593×10^4 g/mol-Co h atm at 75 °C). The lower temperature is unfavorable probably because it hinders the formation of the active species, but too high a temperature may also lead to a decrease of the activity due to a decrease of ethylene solubility [36,37] in toluene, and the deactivation of the catalyst.

2.3.3.2. Effect of reaction time. The reaction time can have a great effect on productivity as exemplified for catalyst **10**. At 30 °C and when Al/Co ratio was 1000, four ethylene polymerization experiments were performed for 15, 30, 60 and 90 min. From Fig. 5 we can see that as the reaction time increases from 15 to 30 min, the activity increases from 1.30×10^4 to 1.81×10^4 g/mol-Co h atm. Typically, 30 min later the activity slows down gradually and when the reaction has been performed for 90 min the activity reduces to 1.30×10^4 g/mol-Co h atm. These observations imply that a deactivation of the catalyst occurred about 30 min after initiating. The employed catalyst system has a relatively longer lifetime compared to other catalyst systems [38].

2.3.3.3. Effect of cocatalyst MAO. The cocatalyst is also a significant factor for the oligomerization of ethylene. To study this effect, three tests were performed for 30 min at 30 °C, in which the ratios of [MAO]/[Co] were systematically varied from 500 to 1500. As indicated in Fig. 6, the activity shows a maximum (1.81×10^4 g/mol-Co h atm) around a [MAO]/[Co] ratio of 1000. The possible reason is that an optimal amount of MAO as cocatalyst is needed to effectively activate the catalyst, while an excess amount of MAO will create too many trialkylaluminum impurities and may cause the degradation of the catalyst system.

3. Conclusion

A new compound 2-carbethoxy-6-acetylpyridine (**4**) was synthesized, from which a series of aryl substituted 2-carbethoxy-6-iminopyridine ligands (**5**, **6** and **7**) were prepared by microwave irradiation. Reactions of these ligands **5**, **6** and **7** with group 4B translation metal salts in ethanol provided the corresponding transition metal complexes (**8**–**19**). When MAO was employed as a cocatalyst, the Fe, Co, Ni complexes exhibited moderate catalytic activity and the Mn, Cu, Zn complexes were inactive for ethylene polymerization and oligomerization, which parallel the results observed for catalysts containing the 2,6-bis(imino)pyridine ligand. For the complexes of Fe, Co, Ni, the catalytic activities depend greatly on the structure and electronic properties of the ligand. In contrast to the bis(imino)pyridine analogue, the complexes bearing mono(imino)pyridine with two substituents in the *ortho*-position of the parent aniline are more active than those with substituents in both *ortho*- and *para*-positions as well as those with larger steric hindrance in the *ortho*-positions. Research on the influence of the carbethoxy group on catalytic activity is underway. The catalytic activity of the complexes is also influenced by the amount of cocatalyst employed and other factors such as reaction temperature and time. The optimum conditions have been chosen through a series of experiments to exhibit high activity. Comparing the activity of the catalyst bearing the asymmetrical mono(imino)-pyridine ligand **5** with the analogous catalyst [8,11] bearing the symmetrical bis(imino)pyridine ligand, we assume at this stage that the lesser activity of the former is due to the influence of the carbethoxy group in the ligand.

4. Experimental

4.1. General procedure

All experiments of air- and/or moisture-sensitive compounds were carried out under a nitrogen atmosphere using standard Schlenk techniques. Solvents were refluxed over an appropriate drying agent and distilled prior to use. C, H and N analyses were performed on a HP-MOD 1106 microanalyzer. IR spectra were measured with a Perkin–Elemer FTIR 2000 spectrometer. ^{1}H NMR spectra were recorded on a Bruker spectrometer DMX-300. Mass spectral analyses were performed with a Kratos AEI MS-50 instrument using the electron impact (EI) method. The microwave-assisted reactions were carried out in a domestic oven Midea PJ 21B-A 800w (21 L). The oligomerization products obtained were analyzed on a BF 3400 GC instrument which was equipped with a SE-54 capillary column (25 m × 0.32 mm) using a temperature program from 40 to 280 °C. 2,6-Dimethylpyridine, 2,6-dimethylaniline, 2,4,6-trimethylaniline and 2,6-diethylaniline were purchased from Acros and used as received. MAO in toluene (14 wt%) was from the Albemarle Co. (USA). Polymerization grade ethylene monomer, produced by Beijing Yanshan Petrochemical Co., was used without further purification.

4.2. Synthesis of complexes

4.2.1. 2-Carbethoxy-6-acetylpyridine (*4*)

Sodium (2.10 g, 91 mmol) was dissolved in 60 mL of pure, dry ethanol, then the excess ethanol was removed and the obtained white powder was dried in vacuum for 6 h. 11.17 g (50 mmol) of 2,6-dicarbethoxypyridine (**3**) in 40 mL of freshly distilled EtOAc was added dropwise to the dry EtONa powder with stirring to afford a yellow mixture, which was refluxed for 12 h, then allowed to stand overnight. An excess (33 mL) of concentrated HCl was added dropwise with stirring to the resulting mixture and refluxed for a period of 7–8 h to complete the reaction. After water was added to dissolve the NaCl formed in the reaction, the mixture turned into an orange solution (100 mL). The aqueous phase was shaken with $CHCl_3$ (4×25 mL). The combined extracts were washed with 5% aqueous Na_2CO_3 and the aqueous phase was extracted with $CHCl_3$ (3×10 mL) again. The combined organic phase was dried over anhydrous Na_2SO_4, filtered and the solvent was evaporated under reduced pressure. The obtained mixture was separated by column chromatography (silica-gel, petroleum ether:EtOAc = 4:1). First 2,6-diacetylpyridine was eluted, followed by 2-acetyl-6-carbethoxypyridine (yield: 2.71 g, 28.0%). M.p. 50.0–51.5 °C. ^{1}H NMR (400 MHz, $CDCl_3$): δ 8.27 (d, 1H, Py-Hm), 8.20 (d, 1H, Py-Hm), 7.99 (t, 1H, Py-Hp), 4.49 (m, 2H, CH_2), 2.81 (s, 3H, O–C(CH_3)), 1.47 (t, 3H, CH_2(CH_3)). IR (KBr): ν_{C-O} 1726, 1706, ν_{C-O-C} 1156 cm^{-1}. MS (EI): *m*/*z* 193 (M^+). *Anal.* Calc. for $C_{10}H_{11}NO_3$: C, 62.17; H, 5.74; N, 7.25. Found: C, 62.51; H, 5.76; N, 7.30%.

4.2.2. 2-Carbethoxy-6-{1-[(2,6-dimethylphenyl)imino]-ethyl}pyridine (*5*)

2-Carbethoxy-6-acetylpyridine (**4**) (0.580 g, 3.0 mmol) and an excess of 2,6-dimethylaniline (0.7272 g, 6.0 mmol) were mixed together in an opened Erlenmeyer flask (25 mL). The mixture was subjected to microwave for 30 min on the ''High'' setting (800 W). The crude product was purified by column chromatography (60 × 2.5 cm silica-gel, petroleum ether:EtOAc = 3:2). Ligand **5** was obtained as a highly pure yellow solid in 62.5% yield. M.p. 58.0–59.5 °C. ^{1}H NMR (400 MHz, $CDCl_3$): δ 8.57

(d, 1H, Py-Hm), 8.19 (d, 1H, Py-Hm), 7.94 (t, 1H, Py-Hp), 7.06 (d, 2H, Ar-Hm), 6.95 (t, 1H, Ar-Hp), 4.50 (m, 2H, CH_2), 2.26 (s, 3H, N-C(Me)), 2.02 (s, 6H, Ar-Me), 1.46 (t, 3H, $CH_2(CH_3)$). IR (KBr): ν_{C-O} 1741, ν_{C-N} 1644, ν_{C-O-C} 1141 cm^{-1}. *Anal.* Calc. for $C_{18}H_{20}N_2O_2$: C, 72.95; H, 6.80; N, 9.45. Found: C, 73.04; H, 6.81; N, 9.26%.

4.2.3. 2-Carbethoxy-6-{1-[(2,4,6-trimethylphenyl)imino]-ethyl}pyridine (6)

2,4,6-Trimethylaniline (1.08 g, 8.0 mmol) was mixed with **4** (0.772 g, 4.0 mmol) in a 25 mL Erlenmeyer flask. The mixture was subjected to microwave for 20 min on the "High" setting (800 W). The crude product was purified by column chromatography (60 × 2.5 cm silica-gel, petroleum ether:EtOAc = 2:1). Ligand **6** was obtained as yellow solid in 74.1% yield. M.p. 75.0–76.0 °C. ^1H NMR (400 MHz, $CDCl_3$): δ 8.56 (d, 1H, Py-Hm), 8.19 (d, 1H, Py-Hm), 7.94 (t, 1H, Py-Hp), 6.90 (s, 2H, Ar-Hm), 4.88 (m, 2H, CH_2), 2.26 (d, 3H, N-C(Me)), 2.06 (s, 6H, Ar-Me), 1.47 (t, 3H, $CH_2(CH_3)$). IR (KBr): ν_{C-O} 1715, ν_{C-N} 1643, ν_{C-O-C} 1137 cm^{-1}. *Anal.* Calc. for $C_{19}H_{22}N_2O_2$: C, 73.52; H, 7.14; N, 9.03. Found: C, 73.31; H, 7.12; N, 8.94%.

4.2.4. 2-Carbethoxy-6-{1-[(2,6-diethylphenyl)imino]-ethyl}pyridine (7)

2,6-Diethylaniline (1.07 g, 7.2 mmol) was mixed with **4** (0.67 g, 3.5 mmol) in a 25 mL Erlenmeyer flask. The mixture was subjected to microwave for 35 min on the "High" setting (800 W). The crude product was purified by column chromatography (30 × 1.5 cm silica-gel, *n*-hexane:dichloromethane = 1:2, 40 × 1.5 cm silica-gel, diethyl ether:petroleum ether = 2:3). Ligand **7** was obtained as yellow solid in 17.6% yield. M.p. 84.0–86.0 °C. ^1H NMR (400 MHz, $CDCl_3$): δ 8.48 (d, 1H, Py-Hm), 8.11 (d, 1H, Py-Hm), 7.87 (t, 1H, Py-Hp), 7.30 (d, 2H, Ar-Hm), 6.99 (t, 1H, Ar-Hp), 4.43 (m, 2H, $COOCH_2$), 2.28 (m, 4H, $(CH_2)CH_3$), 2.20 (s, 3H, N-C(Me)), 1.39 (t, 3H, $COOCH_2(CH_3)$), 1.05 (t, 6H, $CH_2(CH_3)$). IR (KBr): ν_{C-O} 1742, ν_{C-N} 1640, ν_{C-O-C} 1166 cm^{-1}. *Anal.* Calc. for $C_{20}H_{24}N_2O_2$: C, 74.04; H, 7.46; N, 8.64. Found: C, 74.18; H, 7.70; N, 8.17%.

4.2.5. {2-Carbethoxy-6-[1-[(2,6-dimethylphenyl)imino]-ethyl]pyridine}$MnCl_2$ (8)

A solution of $MnCl_2 \cdot 4H_2O$ (29.7 mg, 0.15 mmol) and **5** (44.4 mg, 0.15 mmol) in ethanol (8 mL) was stirred at room temperature for 6 h. During this period a yellow solid was obtained, which was washed repeatedly with diethyl ether and dried in vacuo. Yield: 26.3 mg (41.5%). M.p. >300 °C. IR (KBr): ν_{C-O} 1697, ν_{C-N} 1627 cm^{-1}. *Anal.* Calc. for $C_{18}H_{20}Cl_2MnN_2O_2$: C, 51.21; H, 4.77; N, 6.63. Found: C, 51.33; H, 4.80; N, 6.45%.

4.2.6. {2-Carbethoxy-6-[1-[(2,6-dimethylphenyl)imino]-ethyl]pyridine}$FeCl_2$ (9)

Using an analogous procedure as above, under a nitrogen atmosphere, **9** was obtained as a blue solid in 30.0% yield. M.p. >300 °C. IR (KBr): ν_{C-O} 1712, ν_{C-N} 1624 cm^{-1}. *Anal.* Calc. for $C_{18}H_{20}Cl_2FeN_2O_2$: C, 51.10; H, 4.76; N, 6.62. Found: C, 51.10; H, 4.83; N, 6.53%.

4.2.7. {2-Carbethoxy-6-[1-[(2,6-dimethylphenyl)imino]-ethyl]pyridine}$CoCl_2$ (10)

Using an analogous procedure as above, **10** was obtained as a green solid in 70.7% yield. M.p. >300 °C. IR (KBr): ν_{C-O} 1714, ν_{C-N} 1625 cm^{-1}. *Anal.* Calc. for $C_{18}H_{20}Cl_2CoN_2O_2$: C, 50.73; H, 4.73; N, 6.57. Found: C, 50.38; H, 4.85; N, 6.27%.

4.2.8. {2-Carbethoxy-6-[1-[(2,6-dimethylphenyl)imino]-ethyl]pyridine}$CuCl_2$ (11)

Using an analogous procedure as above, **11** was obtained as a yellow solid in 88.6% yield. M.p. >300 °C. IR (KBr): ν_{C-O} 1725, ν_{C-N} 1628 cm^{-1}. *Anal.* Calc. for $C_{18}H_{20}Cl_2CuN_2O_2$: C, 50.18; H, 4.68; N, 6.50. Found: C, 50.26; H, 4.77; N, 6.35%.

4.2.9. {2-Carbethoxy-6-[1-[(2,6-dimethylphenyl)imino]-ethyl]pyridine}$ZnCl_2$ (12)

Using an analogous procedure as above, **12** was obtained as a yellow solid in 88.3% yield. M.p. >300 °C. IR (KBr): ν_{C-O} 1723, ν_{C-N} 1636 cm^{-1}. *Anal.* Calc. for $C_{18}H_{20}Cl_2N_2O_2Zn$: C, 49.97; H, 4.66; N, 6.47. Found: C, 49.68; H, 4.68; N, 6.21%.

4.2.10. {2-Carbethoxy-6-[1-[(2,6-dimethylphenyl)imino]-ethyl]pyridine}$_2NiCl_2$ (13)

Using an analogous procedure as above, **13** was obtained as a red solid in 42.1% yield. M.p. >300 °C. IR (KBr): ν_{C-N} 1624 cm^{-1}. *Anal.* Calc. for $C_{36}H_{42}Cl_2N_4NiO_5$: C, 58.40; H, 5.72; N, 7.57. Found: C, 58.72; H, 5.46; N, 7.89%.

4.2.11. {2-Carbethoxy-6-[1-[(2,4,6-trimethylphenyl)-imino]ethyl]pyridine}$FeCl_2$ (14)

Using an analogous procedure as above, under a nitrogen atmosphere, **14** was obtained as a blue solid in 40.1% yield. M.p. >300 °C. IR (KBr): ν_{C-O} 1719, ν_{C-N} 1589 cm^{-1}. *Anal.* Calc. for $C_{19}H_{22}Cl_2FeN_2O_2$: C, 52.20; H, 5.07; N, 6.41. Found: C, 52.17; H, 5.01; N, 6.34%.

4.2.12. {2-Carbethoxy-6-[1-[(2,4,6-trimethylphenyl)-imino]ethyl]pyridine}$CoCl_2$ (15)

Using an analogous procedure as above, **15** was obtained as a green solid in 48.5% yield. M.p. > 300 °C. IR (KBr): ν_{C-O} 1717, ν_{C-N} 1592 cm^{-1}. *Anal.* Calc. for $C_{19}H_{22}Cl_2CoN_2O_2$: C, 51.84; H, 5.04; N, 6.36. Found: C, 51.88; H, 5.07; N, 6.20%.

4.2.13. {2-Carbethoxy-6-[1-[(2,4,6-trimethylphenyl)-imino]ethyl]pyridine}$NiCl_2$ (16)

Using an analogous procedure as above, **16** was obtained as a yellow solid in 50.7% yield. M.p. >300 °C. IR (KBr): ν_{C-O} 1720, ν_{C-N} 1592 cm^{-1}. *Anal.* Calc. for $C_{19}H_{22}Cl_2N_2NiO_2$: C, 51.87; H, 5.04; N, 6.37. Found: C, 52.09; H, 5.22; N, 6.11%.

4.2.14. {2-Carbethoxy-6-[1-[(2,6-diethylphenyl)imino]-ethyl]pyridine}$FeCl_2$ (**17**)

Using an analogous procedure as above, under a nitrogen atmosphere, **17** was obtained as a blue solid in 23.3% yield. M.p. >300 °C. IR (KBr): ν_{C-O} 1665, ν_{C-N} 1620 cm^{-1}. *Anal.* Calc. for $C_{20}H_{24}Cl_2FeN_2O_2 \cdot 0.5H_2O$: C, 52.20; H, 5.48; N, 6.09. Found: C, 52.39; H, 5.22; N, 5.99%.

4.2.15. {2-Carbethoxy-6-[1-[(2,6-diethylphenyl)imino]-ethyl]pyridine}$CoCl_2$ (**18**)

Using an analogous procedure as above, **18** was obtained as a green solid in 64.8% yield. M.p. >300 °C. IR (KBr): ν_{C-O} 1701, ν_{C-N} 1625 cm^{-1}. *Anal.* Calc. for $C_{20}H_{24}Cl_2CoN_2O_2$: C, 52.88; H, 5.33; N, 6.17. Found: C, 53.31; H, 5.38; N, 6.11%.

4.2.16. {2-Carbethoxy-6-[1-[(2,6-diethylphenyl)imino]-ethyl]pyridine}$NiCl_2$ (**19**)

Using an analogous procedure as above, **19** was obtained as a pale red solid in 61.0% yield. M.p. >300 °C. IR (KBr): ν_{C-O} 1691, ν_{C-N} 1623 cm^{-1}. *Anal.* Calc. for $C_{20}H_{26}Cl_2N_2NiO_3$: C, 50.89; H, 5.55; N, 5.93. Found: C, 50.71; H, 5.21; N, 5.78%.

4.3. General procedure for polymerization and oligomerization of ethylene

10 μmol of the transition metal complex was charged into a Schlenk tube. Air was eliminated from the Schlenk tube by three vacuum/nitrogen steps. Then the desired volume of MAO/toluene solution (14%) was added. Immediately the color of the solution changed. The solution was then stirred at 600 rpm for the time set and the active catalytic species in toluene solution was available.

The polymerization and oligomerization reactions were carried out in a 100 mL three-neck flask. After evacuation and flushing with nitrogen three times, then with ethylene two times, the flask was charged with 50 mL of toluene and magnetically stirred under ambient ethylene atmosphere. When the desired reaction temperature was established, the solution of the catalyst species was injected into the reactor. Stirring was carried out at 1200 rpm. After the times set for the experiment, the reaction solution was quickly cooled down to −20 °C and the reaction quenched with acidic ethanol solution. The precipitated polymer was collected and washed for several times with ethanol and then dried under vacuum at 50 °C for 24 h. The oligomer solution was dried over anhydrous Na_2SO_4, an aliquot of this solution was analyzed by GC (Gas Chromatograph).

4.4. X-ray analysis of **12** and **18**

Data collection for complexes **12** and **18** was performed at 293(2) and 296(2) K, respectively, on a Bruker SMART 1000 diffractometer with graphite-monochromated Mo Kα radiation ($\lambda = 0.71073$ Å). The Smart program package was used to determine the unit-cell parameters. A SADABS absorption correction was applied. The structure was solved by direct methods and refined by full-matrix least-squares techniques with anisotropic thermal parameters for non-hydrogen atoms. Hydrogen atoms were placed at calculation positions and were included in the structure calculation without further refinement of the parameters. All calculations were performed using the SHELXS-97 program. Crystal data and structure refinement for complexes **12** and **18** are summarized in Table 3.

Table 3
Crystal data, data collection and structure refinement for complexes **12** · THF and **18**

Complex	**12**	**18**
Empirical formula	$C_{22}H_{24}Cl_2N_2O_3Zn$	$C_{20}H_{24}Cl_2CoN_2O_2$
Formula weight	500.70	454.24
Temperature (K)	296(2)	293(2)
Wavelength (Å)	0.7107(3)	0.7107(3)
Crystal system	triclinic	monoclinic
Space group	$P\bar{1}$	$P2/m$
a (Å)	8.148(2)	18.500(4)
b (Å)	9.076(2)	8.093(2)
c (Å)	17.039(4)	14.563(3)
β (°)	99.08(4)	107.49(3)
Volume (Å^3)	1190.4(4)	2079.6(7)
Z	2	4
D_{calc} (g cm^{-3})	1.397	1.451
Absorption coefficient (mm^{-1})	1.280	1.099
$F(000)$	516	940
Crystal color, habit	yellow, block	green, irregular block
θ Range for data collection (°)	2.35–25.10	2.77–27.46
Index ranges	$-9 \leqslant h \leqslant 8$, $-10 \leqslant k \leqslant 9$, $-18 \leqslant l \leqslant 20$	$-23 \leqslant h \leqslant 22$, $-10 \leqslant k \leqslant 0$, $0 \leqslant l \leqslant 18$
Reflections collected/unique (R_{int})	6169/4182 (0.0468)	4592/4592 (0.0000)
Completeness (%)	98.5 (to $\theta = 25.10°$)	96.1 (to $\theta = 27.46°$)
Maximum and minimum transmission	0.9352 and 0.7229	1.1848 and 0.8675
Refinement method	full-matrix least-squares on F^2	full-matrix least-squares on F^2
Data/restraints/parameters	4182/0/276	4592/0/248
Goodness-of-fit on F^2	1.065	0.674
Final R indices [$I > 2\sigma(I)$]	$R_1 = 0.0650$, $wR_2 = 0.1451$	$R_1 = 0.0431$, $wR_2 = 0.0771$
R indices (all data)	$R_1 = 0.1229$, $wR_2 = 0.1683$	$R_1 = 0.1097$, $wR_2 = 0.0865$
Largest difference in peak and hole (e A^{-3})	0.430 and −0.389	0.537 and −0.568

Acknowledgments

We are grateful to the Program for Changjiang Scholars and Innovative Research Team in University, PCSIRT (IRT0559), the Natural Science Foundation of China (No. 20371039), National Basic Research Program (973 Program) (2003CB214600), the Key Laboratory Research and Establishment Program of Department of Education

of Shaanxi Province (No. 03JS006) and the Nature Science Foundation of Department of Education of Shaanxi Province (No. 04JK143) for financial support. We also thank for the Institute of Chemistry, Chinese Academy of Science for providing the visiting scholarship to J.-S. Zhao.

Appendix A. Supplementary material

Crystallographic data for the structural analysis have been deposited with the Cambridge Crystallographic Data Centre, CCDC No. 298285 for complex **12**, CCDC No. 250904 for complex **18**. Copies of these information may be obtained free of charge from: The Director, CCDC, 12 Union Road, Cambridge CB2 1EZ, UK (fax: +44 1223 336 033; e-mail: depodit@ccdc.cam.ac.uk or http://www.ccdc.cam.ac.uk). Supplementary data associated with this article can be found, in the online version, at doi:10.1016/j.poly.2006.06.015.

References

[1] K.H. Brintzinger, D. Fischer, R. Mülhaupt, B. Rieger, R.M. Waymouth, Angew. Chem., Int. Ed. Engl. 34 (1995) 1143.
[2] A.L. Mcknight, R.M. Waymouth, Chem. Rev. 98 (1998) 2587.
[3] D.W. Stephan, J.C. Stewart, F. Guérin, R.E.V.H. Spence, W. Wu, D.G. Harrison, Organometallics 18 (1999) 116.
[4] K. Nomura, N. Naga, M. Miki, K. Yanagi, A. Imai, Organometallics 17 (1998) 2152.
[5] K. Nomura, N. Naga, M. Miki, K. Yanagi, Macromolecules 31 (1998) 7588.
[6] G.J.P. Britoovsek, V.C. Gibson, G.F. Wass, Angew. Chem., Int. Ed. Engl. 38 (1999) 429.
[7] R. Vollmerhaus, P. Shao, N.J. Taylor, S. Collins, Organometallics 18 (1999) 2731.
[8] B.L. Small, M. Brookhart, A.M.A. Bennett, J. Am. Chem. Soc. 120 (1998) 4049.
[9] B.L. Small, M. Brookhart, J. Am. Chem. Soc. 120 (1998) 7143.
[10] A.M.A. Bennett, Chemtech 29 (1999) 24.
[11] G.J.P. Britovsek, V.C. Gibson, B.S. Kimberley, P.J. Maddox, S.J. McTavish, G.A. Solan, A.J.P. White, D.J. Williams, Chem. Commun. 849 (1998) 256.
[12] G.J.P. Britovsek, M. Bruce, V.C. Gibson, B.S. Kimberley, P.J. Maddox, S. Mastroianni, S.J. McTavish, C. Redshaw, G.A. Solan, S. Strömberg, A.J.P. White, D.J. Williams, J. Am. Chem. Soc. 121 (1999) 8728.
[13] G.J.P. Britovsek, S. Mastroianni, G.A. Solar, S.P.D. Baugh, C. Redshaw, V.C. Gibson, A.J.P. White, D.J. Williams, M.R.J. Elsegood, Chem. Eur. J. 6 (2000) 2221.
[14] G.J.P. Britovsek, V.C. Gibson, B.S. Kimberley, S. Mastroianni, C. Redshaw, G.A. Solar, A.J.P. White, D.J. Williams, J. Chem. Soc., Dalton Trans. (2001) 1639.
[15] G.J.P. Britovsek, V.C. Gibson, S. Mastroianni, D.C.H. Oakes, C. Redshaw, G.A. Solar, A.J.P. White, D.J. Williams, Eur. J. Inorg. Chem. (2001) 431.
[16] E.A.H. Griffiths, G.J.P. Britovsek, V.C. Gibson, I.R. Gould, Chem. Commun. (1999) 1333.
[17] E.L. Dias, M. Brookhart, P.S. White, Organometallics 19 (2000) 4995.
[18] V.C. Gibson, M.J. Humpries, K.P. Tellmann, D.F. Wass, A.J.P. White, D.J. Williams, Chem. Commun. (2001) 2252.
[19] B. Çetinkaya, E. Çetinkaya, M. Brookhart, P.S. White, J. Mol. Catal. A 142 (1999) 101.
[20] B. de Bruin, E. Bill, E. Bothe, T. Weyhermüller, K. Weighardt, Inorg. Chem. 39 (2000) 2936.
[21] E.L. Dias, M. Brookhart, P.S. White, J. Am. Chem. Soc. 123 (2001) 2442.
[22] E.L. Dias, M. Brookhart, P.S. White, Chem. Commun. (2001) 423.
[23] B.L. Small, A.J. Marcucci, Organometallics 20 (2001) 5738.
[24] F.A.R. Kaul, G.T. Puchta, H. Schneider, F. Bielert, D. Mihalios, W.A. Herrmann, Organometallics 21 (2002) 74.
[25] A.S. Abu-Surrah, K. Lappalainen, U. Piironen, P. Lehmus, T. Repo, M. Leskela, J. Organomet. Chem. 648 (2002) 55.
[26] M.A. Esteruelas, A.M. López, L. Méndez, M. Oliván, E. Oñate, Organometallics 22 (2003) 395.
[27] J.F. Plante, P.D. Jones, D.R. Powell, T.E. Glass, Chem. Commun. (2003) 336.
[28] A.W. Singer, S.M. McElvain, J. Am. Chem. Soc. 57 (1935) 1135.
[29] Beilstein Handbook of Organic Chemistry, fifth Supplementary Series, Springer, Berlin, vol. 22, 1990, part 4, p. 128.
[30] R.A. Barnes, H.M. Fales, J. Am. Chem. Soc. 75 (1953) 3830.
[31] E.C. Alyea, P.H. Merrell, Synth. React. Inorg. Met. Org. Chem. 4 (1974) 535.
[32] Y.-F. Chen, C.-T. Qian, J. Sun, Organometallics 22 (2003) 1231.
[33] W.-H. Sun, X.-B. Tang, T.-L. Gao, B. Wu, W.-J. Zhang, H.-W. Ma, Organometallics 23 (2004) 5037.
[34] C. Bianchini, G. Mantovani, A. Meli, F. Migliacci, F. Laschi, Organometallics 22 (2003) 2545.
[35] C. Bianchini, G. Giambastiani, G. Mantovani, A. Meli, D. Mimeau, J. Organomet. Chem. 689 (2004) 1356.
[36] M. Atiqullah, H. Hammawa, H. Hamid, Eur. Polym. J. 34 (1998) 1511.
[37] P.G.T. Fogg, W. Gerrard, Solubility of Gases in Liquids, Wiley, West Sussex, England, 1991.
[38] L.-Y. Chen, J.-X. Hou, W.-H. Sun, Appl. Catal. A 8494 (2003) 1.

Here we report the synthesis of two new complexes of tin tetrachloride with the ligands $R_2NP(O)F_2$ (R = Me or Et) in which two fluorine atoms have substituted two dialkylamino groups in the ligand $(R_2N)_3P(O)$. The new compounds were characterised by elemental analysis, IR and multinuclear (^{119}Sn, ^{31}P, ^{19}F and ^{1}H) NMR spectroscopy. On the basis of NMR data, we show that these ligands, once freed from the inductive and π-bonding (and/or steric) effects of the two dialkylamino groups, are unique in that they form almost exclusively the cis complex with $SnCl_4$ in solution. We have also carried out DFT/B3LYP calculations on the *cis* and *trans* isomers of complex **1** and its ligand in order to support and help the analysis of NMR data.

2. Experimental

2.1. General experimental procedures

All preparations were carried out under a nitrogen atmosphere in solvents dried by standard techniques [13] and stored over molecular sieves. NMR spectra were recorded on a Bruker AC-300 instrument in CD_2Cl_2 as solvent; ^{31}P at 121 MHz (85% H_3PO_4), ^{19}F at 282 MHz ($CFCl_3$), ^{1}H at 300 MHz (TMS) and ^{119}Sn at 111.8 MHz ($SnCl_4$). IR spectra: Perkin Elmer Paragon 1000 PC.

Tin tetrachloride was distilled under vacuum before use. The ligands $R_2NP(O)F_2$ were prepared according to methods described in literature (R = Me [14]; R = Et [15]).

2.2. Preparation of complexes

In a typical reaction $R_2NP(O)F_2$ (8 mmol) in dry $CHCl_3$ (10 cm^3) was slowly added to $SnCl_4$ (1.04 g, 4 mmol) in $CHCl_3$ (20 cm^3) over a 30 min period. The resulting solution, on continual stirring, began to precipitate the white solid complex $SnCl_4 \cdot 2(O)PF_2NR_2$. The precipitation was complete when the product was left 24 h at −15 °C. This was collected, washed with *n*-hexane/CCl_4 and obtained as a white powder (Yields: R = Me: 1.24 g, 60%; R = Et: 1.21 g, 53%). *Anal.* Calc. for $C_4H_{12}N_2O_2P_2F_4SnCl_4$: C, 9.26; H, 2.33; N, 5.40. Found: C, 9.00; H, 2.62; N, 5.68%. *Anal.* Calcd. for $C_8H_{20}N_2O_2P_2F_4SnCl_4$: C, 16.72; H, 3.51; N, 4.87. Found: C, 16.66; H, 3.52; N, 5.04%. IR (KBr): $\nu_{P=O}$ (1280–1310 cm^{-1}); ν_{Sn-O} (560–570 cm^{-1}).

2.3. Computational details

Density functional theory (DFT) calculations were carried out on the *cis* and *trans* isomers of complex **1** and its ligand using the suite of programs Gaussian 98W [16], with the non-local hybrid functional denoted as B3LYP [17]. Basis sets used were 6-31G* [18] for C, H, N, F, P, O and Cl and Steven, Bach and Krauss (SBK) [19] with ECP with polarisation for Sn. The geometries of both the *cis* and *trans* isomers of complex **1** and its ligand were optimised using analytical gradient. The harmonic vibrational frequencies of the different stationary points of the PES have been calculated at the same level of theory in order to identify the local minima as well as to estimate the corresponding zero-point vibrational energy (ZPE).

3. Results and discussion

3.1. Synthesis

Treatment of $SnCl_4$ in a chloroform solution with $R_2NP(O)F_2$ (R = Me or Et) gives white solids with the composition $SnCl_4 \cdot 2L$ ($L = R_2NP(O)F_2$). These complexes are soluble in dichloromethane and chloroform. They were characterised by elemental analysis and particularly by their NMR data and comparison with the corresponding data for the free ligands (see Table 1).

3.2. Spectroscopic studies

The infrared spectra show strong bands within the range 1285–1310 cm^{-1} attributed to $\nu_{P=O}$. The P=O stretching vibration is shifted towards lower wave numbers on coordination to the tin atom compared with its value for the free ligands. The coordination shift is about 35 cm^{-1} and is consistent with phosphoryl coordination to the tin atom. This shift is 30 cm^{-1} for $Me_2NP(O)F_2$ against 138 cm^{-1} for HMPA [5], explaining the difference in the basicity strength between these two ligands which is most probably due to the substitution of two dimethylamino groups by two fluorine atoms. The absorption band at 560–570 cm^{-1} corresponds to a stretching vibration of the Sn–O group.

The NMR spectra of the two complexes prepared are quite similar and the data obtained from these spectra are summarised in Table 1.

The ^{31}P NMR resonances of the bound ligands are shifted to lower frequency compared with those of the free ligand, whereas the ^{19}F and ^{1}H NMR resonances show a higher frequency shift on complexation. The difference in the ^{31}P chemical shift between free and bound ligands is more important than that observed in ^{19}F and ^{1}H NMR spectra, confirming coordination of the fluorophosphoramide ligand through the oxygen atom. The coupling constant $^{1}J_{P-F}$ is larger for the complexed ligand than for the free one (Table 1).

The ^{31}P NMR spectra of each of the complexes prepared showed a triplet pattern (the triplet being due to phosphorus–fluorine coupling) with splitting due to ^{31}P–Sn

Table 1
NMR data (δ/ppm and J/Hz) for the complexes $SnCl_4 \cdot 2L$ and the ligands $R_2NP(O)F_2$ in CD_2Cl_2 at −75 °C

Compound	$\delta_{^{31}P}$	$\delta_{^{19}F}$	$\delta_{^{1}H}$	$\delta_{^{119}Sn}$	$^{1}J_{P-F}$	$^{2}J_{P-Sn}$
$Me_2NP(O)F_2$	−2.50	81.50	2.78	–	997	–
$Et_2NP(O)F_2$	−5.00	83.50	–	–	1003	–
$SnCl_4 \cdot 2(O)PF_2NMe_2$ (**1**)	−7.63	83.16	2.93	−507	1015	145
$SnCl_4 \cdot 2(O)PF_2NEt_2$ (**2**)	−10.40	84.87	–	−510	1023	150

coupling. The latter splitting can be clearly seen only at low temperature (Fig. 1).

In addition, the spectra also contain a triplet of low intensity indicating the existence of a small amount of another species. This minor triplet also showed ^{31}P–Sn splitting at low temperature.

The ^{119}Sn NMR spectrum of each complex displayed at room temperature one broad signal in the region of hexacoordinated species [20]. This broad signal was converted at low temperature into the expected triplet. At −75 °C, the spectrum showed a triplet due to ^{119}Sn–^{31}P coupling. Clearly one species was present at this temperature and in which the tin atom is coupled to two phosphorus atoms, showing a stoichiometry of $SnCl_4 \cdot 2L$ (Fig. 2). This is in agreement with the ^{31}P NMR spectra where a triplet displaying Sn satellites with the corresponding coupling constants was present (Fig. 1).

At lower temperatures, the ^{119}Sn spectrum (Fig. 3) showed, in addition to the major triplet, two doublets in the region of pentacoordinated tin [20]. This indicates that these different tin species are presumably in rapid equilibrium with each other and with the free ligand, consistent with ^{31}P and ^{19}F NMR spectra where ligand exchange reactions are fast at room temperature. The rates of these reactions were decreased by lowering the temperature and separate signals corresponding to the free and bound ligands present in solution were observed. Cooling to −85 °C revealed the presence in the ^{31}P NMR spectrum (and also in the ^{19}F NMR spectrum) of a new signal at −9.41 ppm (Fig. 1), in addition to $SnCl_4 \cdot 2L$ and to the

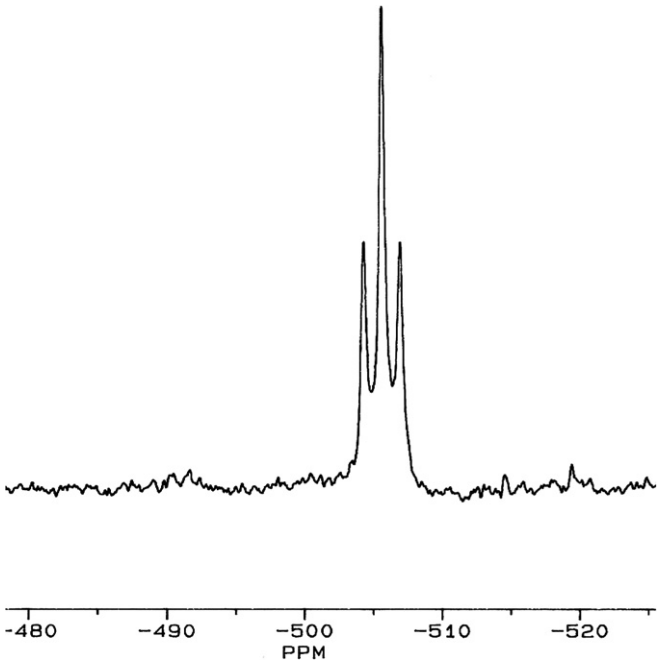

Fig. 2. ^{119}Sn NMR spectrum of the complex $SnCl_4 \cdot 2(O)PF_2NMe_2$ in CD_2Cl_2 at −75 °C.

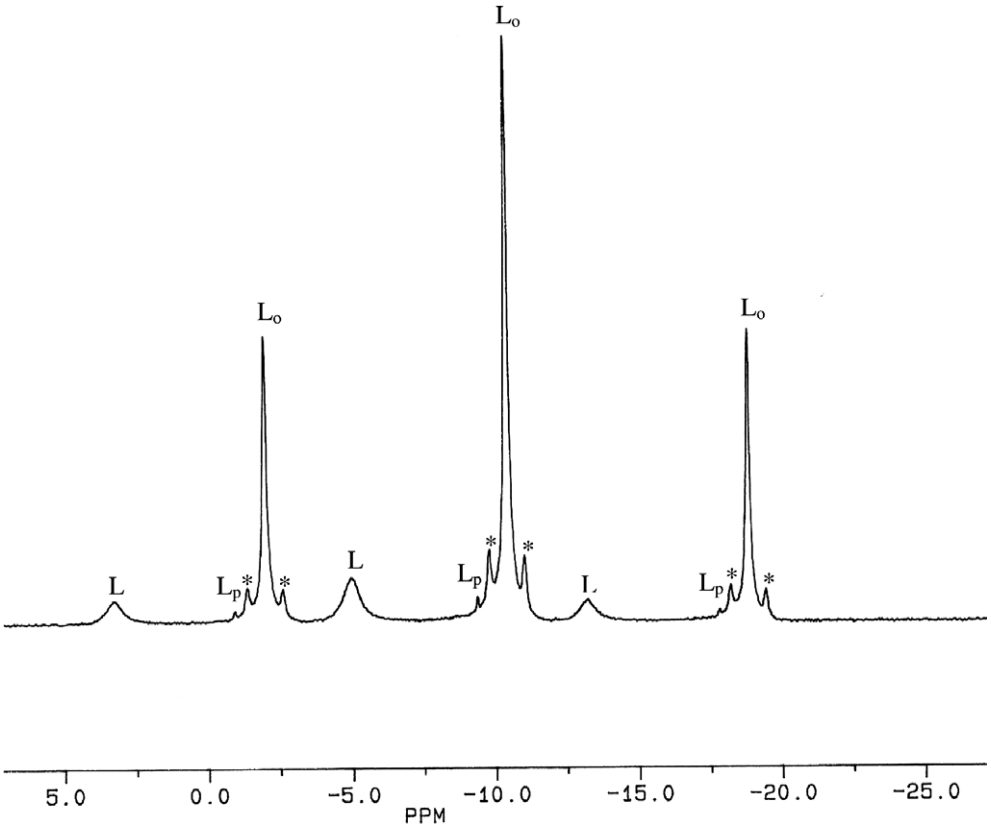

Fig. 1. ^{31}P-{^{1}H} NMR spectrum of the complex $SnCl_4 \cdot 2(O)PF_2NEt_2$ in CD_2Cl_2 at −85 °C (*: Sn satellites, L_o: octahedral tin complex, L_p: pentacoordinated tin complex, L: free ligand).

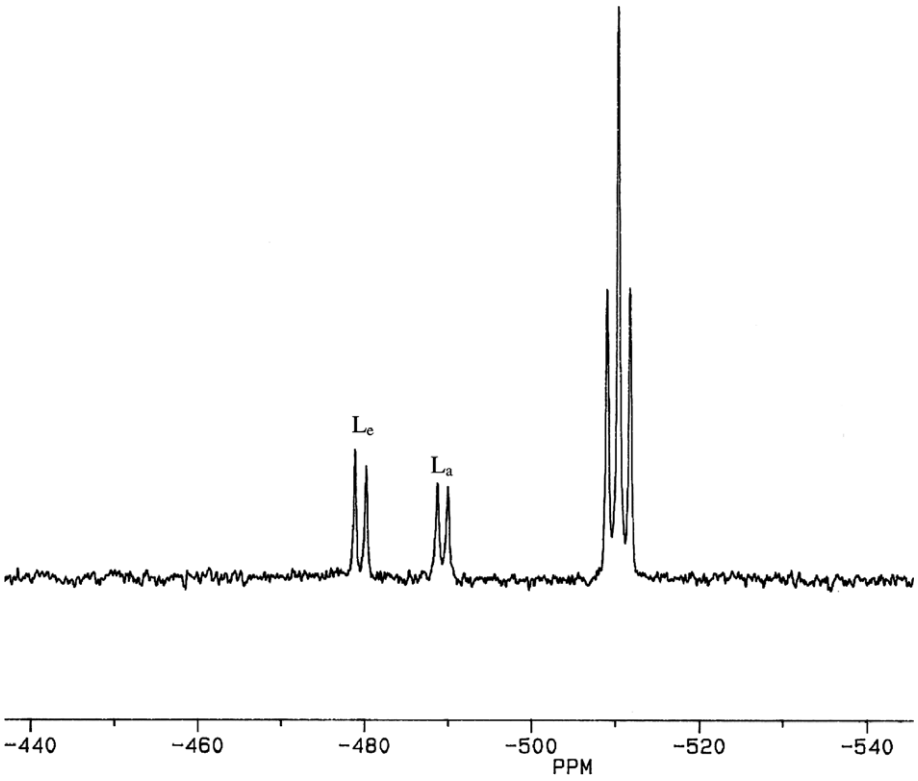

Fig. 3. ^{119}Sn NMR spectrum of the complex $SnCl_4 \cdot 2(O)PF_2NEt_2$in CD_2Cl_2 at −85 °C (L_a and L_e: ligands in axial and equatorial positions respectively).

free ligand, which we assign to $SnCl_4 \cdot L$. This assignment is supported by the presence of a doublet pattern in the ^{119}Sn NMR spectrum (10% relative intensity) (see Fig. 3).

This result suggests that the 1:1 complex is in equilibrium with the 1:2 complex and is detectable at −85 °C in significant concentration. Such an equilibrium was observed by Denmark et al. [21], sometimes referred to as partial dissociation of the type:

$$SnCl_4 \cdot 2L \rightleftharpoons SnCl_4 \cdot L + L$$

In solution, complexes of the general formula $SnCl_4 \cdot 2L$ exist as a mixture of both *cis* and *trans* isomers [22]. By correlating the IR and Raman data of the complex $SnCl_4 \cdot 2(HMPA)$ with ^{1}H and ^{31}P NMR studies, Ruzicka and Merbach [8] have shown that the coupling constants $^2J_{31P-119Sn}$ were different for *cis* and *trans* isomers in the complexes of $SnCl_4$ with $(MeO)_3PO$ (TMPA) and $Me_2N(MeO)_2PO$. At 203 K, the cis isomers of the two complexes had $^2J(^{31}P-^{119}Sn)$ of 146 and 141 Hz respectively, and those for the *trans* isomers were 195 and 194 Hz respectively, whereas coupling constants of 102 and 168 Hz at 183 K were observed for the *cis* and *trans* complexes of $SnCl_4 \cdot 2HMPA$ [9], respectively. These results are in agreement with the coupling constants of 126 and 192 Hz observed for $SnCl_4 \cdot 2(O)PF(NMe_2)_2$ at 268 K in our previous work [12] (see Table 2).

By comparing the coupling constants, the isomers of the complexes in Table 2 could be assigned by analogy, i.e., all of the complexes which have smaller $^2J(^{31}P-^{119}Sn)$ coupling constants could be assigned to the *cis* isomers and those with larger $^2J(^{31}P-^{119}Sn)$ coupling constants could be assigned to the *trans* ones. It is therefore possible to assign the only triplet observed in the ^{119}Sn NMR spectra of the complexes $SnCl_4 \cdot 2(O)PF_2NR_2$ at 198 K to the *cis* isomer ($^2J(^{31}P-^{119}Sn) = 145$ Hz for R = Me and 150 Hz for R = Et).

Table 2
^{119}Sn NMR data[a] of the complexes $SnCl_4 \cdot 2L$ in dichloromethane

Ligand (L)	$\delta_{^{119}Sn}$		$^2J_{P-Sn}$		% *Cis*[e]
	Cis	*Trans*	*Cis*	*Trans*	
$(Me_2N)_3P(O)$[b]	−569	−580	120	191	50
$(Me_2N)_2P(O)F$[c]	−548	−567	126	192	80
$Me_2NP(O)F_2$[d]	−507	–	145	–	100

[a] Measured at slow exchange where triplets are observed.
[b] At 25 °C.
[c] −5 °C.
[d] −75 °C.
[e] The approximate percentage of the cis isomer measured from ^{119}Sn NMR signals.

The two doublets observed in the five coordinate adduct region of the ^{119}Sn NMR spectrum at −85 °C (Fig. 3) presumably correspond to the two possible trigonal bipyramidal isomers. The chemical shifts and the magnitude of the couplings suggest that the downfield doublet at −479 ppm ($^2J(^{31}P-^{119}Sn) = 148$ Hz) is due to the equatorial isomer while the upfield doublet at −489 ppm ($^2J(^{31}P-^{119}Sn) = 140$ Hz) is due to axial phosphorus [23,24].

3.3. Theoretical calculations

Due to difficulties in obtaining crystals suitable for X-ray analysis, the geometries of the *cis* and *trans* isomers of **1** were optimised by means of the DFT/B3LYP method in order to confirm the NMR data obtained for the two complexes prepared. The optimised structure of the *cis* isomer is shown in Fig. 4. The *cis* and *trans* isomers of complex **1** and its ligand have been identified as local minima on the singlet potential energy surfaces (PES). Optimised values of selected geometrical parameters are listed in Table 3. The potential energy difference between the two isomers of **1** was 2 kcal mol^{-1}. This difference indicates that the Boltzmann population of the *cis* adduct corresponds to practically 100%. This is in good agreement with the experimental NMR data.

The value of the Sn–O distance, 2.228 Å, as well as the other bond distances and angles are in good agreement with the values reported for similar molecules using X-ray diffraction [7,9,25]. Interestingly, the P–O distance of 1.491 Å is identical to that of 1.49 obtained by the crystal structure for the HMPA complex [7].

In complex **1**, the coordination mode is confirmed by a lengthening of the P=O bond compared to that of the free ligand (1.467 Å) calculated at the same level of theory. This lengthening is consistent with the low stretching frequency observed in the IR spectra and may also explain the differences observed in the ^{31}P NMR chemical shifts between the free and bound ligands in solution. On forming complex **1** the ligand also shows a shortening of both the P–F and P–N bond distances by about 0.02 Å. This is accompanied by an increase in the bond angles at the phosphorus atom, i.e., the F–P–F and F–P–N angles are increased by 1.3° and 2.6° respectively compared to those of the free ligand (see Table 3).

The changes in bond distances are supported, in solution, by an observed increase in the $^{1}J_{P-F}$ coupling constant

Table 3
Selected B3LYP-optimized geometrical parameters[a] for complex **1** and its ligand

	Ligand	*Cis*	*Trans*
Sn–Cl1	–	2.421	2.424
Sn–Cl2	–	2.402	2.429
Sn–Cl3	–	2.410	2.424
Sn–Cl4	–	2.410	2.429
Sn–O1	–	2.254	2.204
Sn–O2	–	2.254	2.204
P1–O1	1.467	1.491	1.494
P2–O2	–	1.491	1.494
P1–F1	1.580	1.570	1.567
P1–F2	1.585	1.565	1.564
P2–F3	–	1.569	1.564
P2–F4	–	1.565	1.567
P1–N1	1.640	1.619	1.616
P2–N2	–	1.619	1.616
Sn–O1–P1	–	138.7	139.0
Sn–O2–P2	–	138.6	139.0
O1–Sn–O2	–	79.6	180.0
Cl1–Sn–Cl2	–	162.5	89.9
Cl3–Sn–Cl4	–	103.3	89.9
F1–P1–F2	96.5	097.8	097.9
F3–P2–F4	–	97.9	97.9
F1–P1–N1	103.7	106.3	107.0
F2–P1–N1	106.2	108.9	109.2

[a] See Fig. 4 for labelling of the atoms. Distances are in Å and angles in °.

value found in the complex compared with that in the free ligand. Comparable changes in geometry, i.e., shortened bonds and increased angles at the phosphorus atom, have been observed in related complexes [26,27].

It is worth noting that the longer Sn–O distance (2.25 versus 2.13 Å in the HMPA complex) and sharper Sn–O–P bond angles (139 versus 165° in the HMPA complex) in complex **1** probably reflect the effect of the substitution of two dimethylamino groups in HMPA by two fluorine atoms. The substantially longer Sn–O distance in complex **1** strongly suggests a weaker coordination of $Me_2NP(O)F_2$

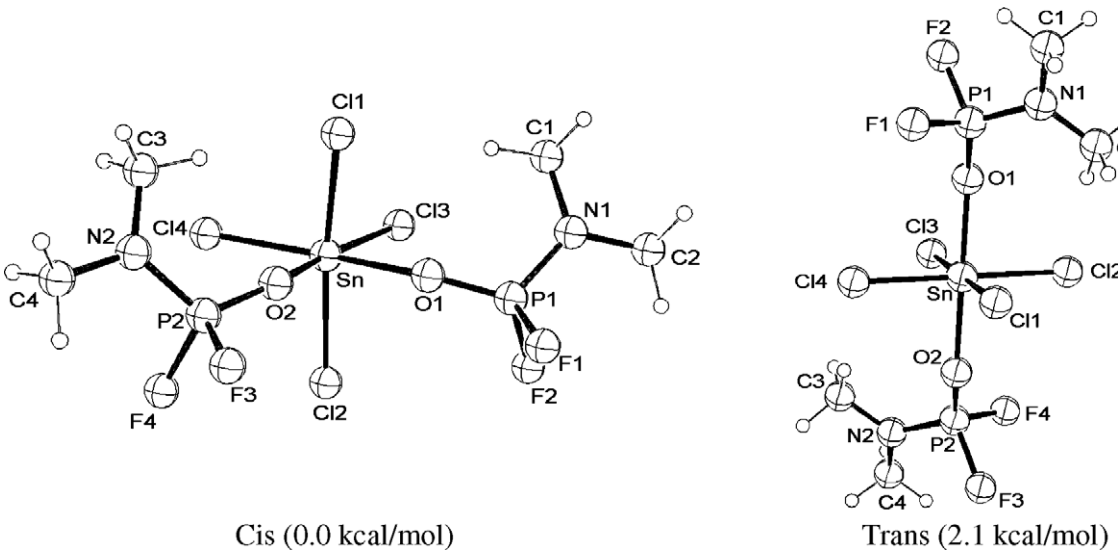

Fig. 4. DFT/B3LYP optimised structures and relative energies of *cis* and *trans* isomers of complex **1**.

compared to HMPA with $SnCl_4$, consistent with the experimental NMR data (see Table 2).

4. Conclusion

On the basis of the above results, the NMR data suggest the presence of only the *cis* geometry for the complexes $SnCl_4 \cdot 2(O)PF_2NR_2$ in dichloromethane solution within the temperature range studied. This could be explained in terms of a decrease both in the Lewis base character of the P=O group of the ligand $(O)PF_2NR_2$ and in its bulkiness compared with HMPA as a result of the substitution of two dialkylamino groups in the ligand $(R_2N)_3P(O)$ by two fluorine atoms. Our results are in good agreement with those reported by Smith and Wilkins [28] and Drago [29] who showed that in $SnX_4 \cdot 2L$ octahedral adducts the overlap of tin(IV) 5s, 5p and 5d orbitals depends on the positive charge on tin(IV). In our case, the presence of two fluorine atoms in the ligands renders the electronegativity of the donor atom of the ligand comparable to that of each of the four chlorine atoms on tin. This leads to a possible sp^3d^2 hybridisation and the molecule adopts the configuration which minimises the splitting between the $d_{x^2-y^2}$ and d_{z^2} orbitals, namely the *cis* one. The results further confirm the fact that the less bulky the ligand the more important the ratio of the *cis* isomer [30] (see Table 2). The NMR data also indicate that steric effects and/or the Lewis basicity of the ligand contribute to the equilibrium between hexacoordinate and pentacoordinate complexes. We have also shown that DFT calculations are a useful supporting tool for such a study since a combination of empirical and theoretical studies can, in favourable cases, overcome the limitations of each.

Acknowledgement

We are indebted to Professor A. Baklouti of the Department of Chemistry, Faculty of Sciences of Tunis, University of Tunis El Manar for his valuable help and discussions of this work.

References

[1] D. Fàrsaiu, R. Leu, P.J. Ream, J. Chem. Soc., Perkin Trans. 2 (2001) 427.
[2] S.E. Dann, A.R.J. Genge, W. Levason, G. Reid, J. Chem. Soc., Dalton Trans. (1997) 2207.
[3] C.H. Yoder, L.A. Margolis, J.M. Horne, J. Organomet. Chem. 633 (2001) 33, and references therein.
[4] H.R. Hays, D.J. Peterson, in: G.M. Kosolopoff, L. Mair (Eds.), Organic Phosphorus Compounds, Vol. 3, Wiley, New York, 1972.
[5] E. Le Coz, J.E. Guerchais, Bull. Soc. Chim. Fr. 1 (1971) 80.
[6] S.J. Ruzicka, A.E. Merbach, Inorg. Chim. Acta 20 (1976) 223.
[7] L.A. Aslanov, V.M. Ionov, V.M. Attiya, A.B. Permin, V.S. Petrosyan, Zhur. Strukt. Khim. 18 (1977) 1103.
[8] S.J. Ruzicka, A.E. Merbach, Inorg. Chim. Acta 22 (1977) 191.
[9] S.E. Denmark, X. Su, Tetrahedron 55 (1999) 8727.
[10] D. Tudela, V. Fernàndez, J.D. Tornero, J. Chem. Soc., Dalton Trans. (1985) 1281.
[11] J. Rupp-Bensadon, E.A.C. Lucken, J. Chem. Soc., Dalton Trans. (1983) 495.
[12] M.A.M. Khouna, M.T. Ben Dhia, M.R. Khaddar, Phosphorus, Sulfur and Silicon 180 (2005) 1673.
[13] D.D. Perrin, W.L.F. Armarego, D.R. Perrin, Purification of Laboratory Chemicals, Pergamon Press, Oxford, 1966.
[14] G. Schrader, B.I.O.S. Report No. 1103, London 1945.
[15] A. Kovache, H. Jean, G. Garnier, Chim et Industr. 64 (1950) 287.
[16] M.J. Frisch, Trucks, G.W., Schlegel, G.E. Scuseria, Robb, M.A., Cheeseman, J.R., Zakrzewski, V.G., Montgomery, J.R.E. Stratmann, J.C. Burant, S. Dapprich, J.M. Millam, A.D. Daniels, K.N. Kudin, M.C. Strain, O. Farkas, J. Tomasi, V. Barone, M. Cossi, R. Cammi, B. Menucci, C. Pomelli, C. Adamo, S. Clifford, J. Ochterski, G.A. Petersson, P.Y. Ayala, Q. Cui, K. Morokuma, D.K. Malick, A.D. Rabuck, K. Raghavachari, J.B. Foresman, J. Cioslowski, J.V. Ortiz, B.B.J.Stefanov, G. liu, A. Liashenko, P. Piskorz, I. Koaromi, R. Gomperts, R.L. Martin, D.J. Fox, T. Keith, M.A. Al-Laham, C.Y. Peng, A. Nanayakkara, C. Gonzalez, M. Challcombe, P.M.W. Gill, B.G. Johnson, W. Chen, M.W. Wong, J.L. Andres, M. Head-Gordon, E.S. Replogle, J.A. Pople, GAUSSIAN 98 Revision A.7, Gaussian Inc., Pittsburgh PA. 1998.
[17] (a) A.D. Becke, J. Chem. Phys. 98 (1993) 5648;
(b) C. Lee, W. Yang, R.G. Parr, Phys. Rev. B. 37 (1988) 785.
[18] (a) W.J. Hehre, R. Ditchfield, J.A. Pople, J. Chem. Phys. 56 (1972) 2257;
(b) G.A. Petersson, A. Bennett, T.G. Tensfeldt, M.A. Al-Laham, W.A. Shirley, J. Mantzaris, J. Chem. Phys. 89 (1988) 2193;
(c) G.A. Petersson, M.A. Al-Laham, J. Chem. Phys. 94 (1991) 6081;
(d) P.C. Hariharan, J.A. Pople, Theoret. Chimica Acta 28 (1973) 213;
(e) V.A. Rassolov, M.A. Ratner, J.A. Pople, P.C. Redfern, L.A. Curtiss, J. Comp. Chem. 22 (2001) 976.
[19] (a) W.J. Stevens, H. Basch, M. Krauss, J. Chem. Phys. 81 (1984) 6026;
(b) W.J. Stevens, H. Basch, M. Krauss, P. Jasien, Can. J. Chem. 70 (1992) 612;
(c) T.R. Cundari, W.J. Stevens, J. Chem. Phys. 98 (1993) 5555.
[20] M.S. Holt, W.L. Wilson, J.H. Nelson, Chem. Rev. 89 (1989) 11.
[21] S.E. Denmark, B.R. Henke, E. Weber, J. Am. Chem. Soc. 109 (1987) 2512.
[22] R. Selvaraju, K. Panchanatheswaran, Polyhedron 16 (1997) 2621.
[23] J. Holecek, M. Nadvornik, K. Handlir, A. Lycka, J. Organomet. Chem. 241 (1983) 177.
[24] C.J. Jameson, in: J. Mason (Ed.), Multinuclear NMR, Plenum Press, New York, 1987, p. 89.
[25] C.I. Bränden, Acta Chem. Scand. 17 (1963) 759.
[26] M.D. La Prade, C.E. Nordman, Inorg. Chem. 8 (1969) 1669.
[27] L.E. Sutton (Ed.), Tables of Interatomic Distances and Configuration in Molecules and Ions, The Chemical Society, London, 1958, supplement, 1965.
[28] J.A.S. Smith, E.J. Wilkins, Chem. Commun. (1965) 381.
[29] J.C. Hill, R.S. Drago, R.H. Herber, J. Am. Chem. Soc. 91 (1969) 1644.
[30] D.S. Dyer, R.O. Ragsdale, Inorg. Chem. 8 (1969) 1116.

molecules. Very recently, we described the synthesis of *tertiary* aromatic ferrocenylamines **4** by methylation of ferrocenylimines [9a] or secondary ferrocenylamines [9b]. In this paper, we wish to report the synthesis and characterization of their *ortho*-mercurated complexes ($R' = H$). In addition, their transpalladation and the influence of the structural factors of substrates on the product distributions and aggregations will also be discussed. As far as we know it is the first reported example of *ortho*-mercurated aromatic ferrocenylamines.

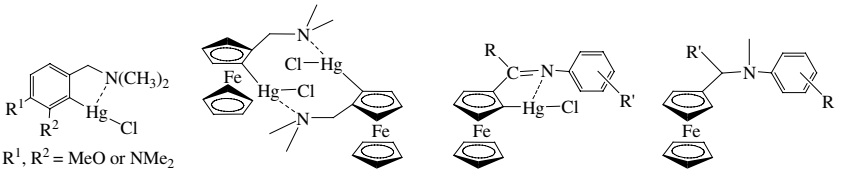

2. Results and discussion

2.1. Ortho-mercuration of ferrocenylamines *4*

The reactions of ferrocenylamines **4** ($R' = H$) and an equivalent amount of mercury (II) acetate were carried out in methanol at room temperature (Scheme 1) and the reactions progress were monitored by TLC. After the reactions were completed, 1.5 equivalent of lithium chloride was added and the mixtures were stirred for 30 min. Removal of solvent yielded residues which were purified by column chromatography (silica gel, ethyl acetate/hexane = 1:1, v/v) to afford *ortho*-mercurated ferrocenylamines **6** and the 1,1′-disubstituted ferrocene derivative **7**. Complexes **6** and **7** are stable in air, and are soluble in most of organic solvents, but poorly soluble in hexane.

Experimental results show that the character of the substituents on the phenyl ring will play an important role in governing product distributions. For example, mercuration of ferrocenylamines bearing electron-donating groups (**4a**, **b**) normally give **6a** (**b**) in higher yields ($\geqslant$62%), whereas for mercuration of ferrocenylamines bearing electron-withdrawing groups (**4d**, **f**), the yields of **6d** (**f**) are lower ($\leqslant$ 58%). When ([*N*-methyl-*N*-4-nitrophenylamino]methyl)ferrocene is treated with mercury (II) acetate, the expected *ortho*-mercurated product is not isolated.

2.2. Spectra characterization of *6a–f, 7*

Complexes **6** and **7** were characterized by elemental analysis, IR and ^{1}H NMR. Elemental analyses for **6** and **7** are in good agreement with the proposed formula. In the IR spectra of **6**, the presence of two medium absorption bands, ν 1100 and 1000 cm^{-1}, confirms that they all have an unsubstituted cyclopentadienyl (Cp) ring [10]. On the contrary, such absorptions in **7** are absent. In the ^{1}H NMR spectra of **6**, a singlet appearing at δ 4.20 ppm corresponds to the unsubstituted Cp ring, two doublets approximately at δ 4.10 ppm are assigned to H3 and H5, respectively, and a multiplet appearing at δ 4.40 ppm is attributed to H4. In all cases the chemical shifts of H11 are overlapped with those of H4. In addition, the protons in the phenyl rings also give their corresponding splitting patterns.

2.3. N–Hg intermolecular vs intramolecular coordination

The crystal structure of **6a** (Fig. 1) demonstrates that the crystal consists of two unsymmetric molecular units. The distance Hg1–N2 2.927(1) Å is shorter than the sum of their van der Waals radii (3.00–3.23 Å) [11a], indicating that an intermolecular N–Hg coordination is present in this molecule. However, such coordination between Hg2 and N1 is absent. In the crystal structure of **6e** (Fig. 2), although the crystal consists of a monomer, the intermolecular N–Hg coordination (N1B–Hg1A 3.863(1) Å) is still present (Fig. 3). In addition, in these two crystals, a 10 membered ring, like in **2**, is not formed. All these results are partially consistence with Jacob's observation [1f]. The intermolecular N–Hg distance in **6a** is slightly longer than that in **6e**, but the intramolecular N–Hg distances in **6a**, **e** (4.125(1) Å, 4.100(1) Å, respectively) are nearly same and they all are significantly longer than the sum of their

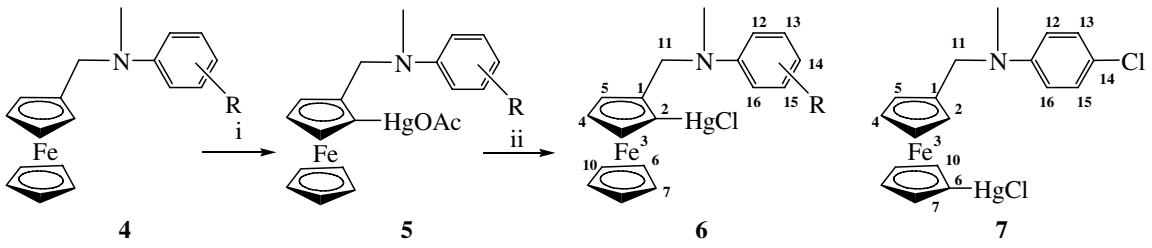

Scheme 1. (i) $Hg(CH_3CO_2)_2$, methanol and (ii) LiCl, methanol. R = 4-MeO (a), 4-Me (b), H (c), 4-Cl (d), 3-Cl (e), and 3-NO_2 (f).

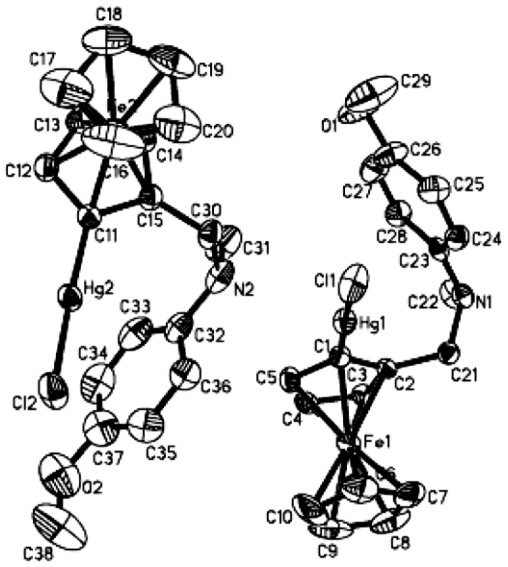

Fig. 1. Molecular structure of **6a** with the numbering scheme (H atoms are omitted for clarity).

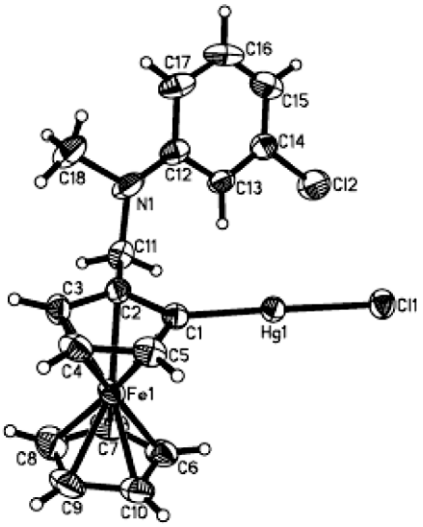

Fig. 2. Molecular structure of **6e** with the numbering scheme.

van der Waals radii [11a], suggesting that an N–Hg intramolecular coordination pattern is absent in these crystals. Therefore, we believe that the character of the substituents

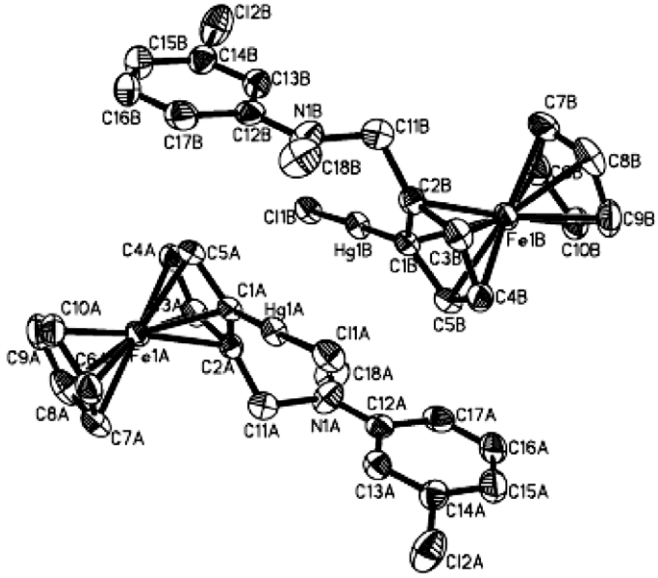

Fig. 3. Intermolecular N(1B)···Hg(1A) interaction pattern for compound **6e** (H atoms are omitted for clarity).

on the phenyl rings only increases or reduces the coordination ability of the N atom with Hg, but does not alter the type of N–Hg coordination (intermolecular *vs* intramolecular). Structurally, **4a**–**f** are more like FcN than ferrocenylimines, therefore, the possible mechanism for the formation of **6** is depicted as in Scheme 2.

According to the principle of *ortho*-metallation, initial coordination of the metal with the hetero atom is necessary, and then following is activation of its adjacent C–H bonds. As shown in Scheme 2, the coordinated N–Hg moiety can activate C–H bonds not only through path i (N–Hg intramolecular coordination) but also through path ii (N–Hg intermolecular coordination). However, the preference of intermolecular over intramolecular N–Hg coordination in our case is always observed. This is probably because (1) the N–Hg coordination is a non-covalent weak interaction, which is not sufficient to keep the rigid five member ring (path i) more stable than the corresponding palladocycles [12], and this weak coordination is supported by the molecular structure of **7** (Fig. 4), which is formed by the attack of free mercury (*i.e.*, without coordination with an N atom) on the unsubstituted Cp ring; (2) unlike the ferrocenylimines, their

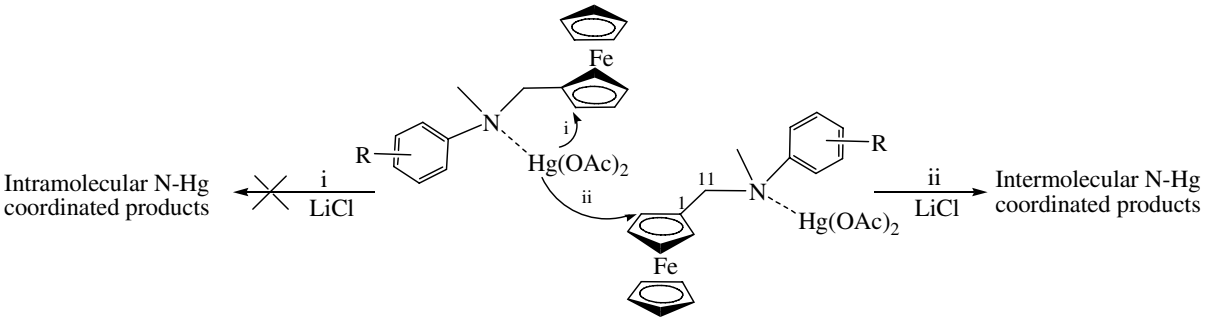

Scheme 2. Possible mechanism for the formation of **6**, path i, intramolecular activation; path ii, intermolecular activation.

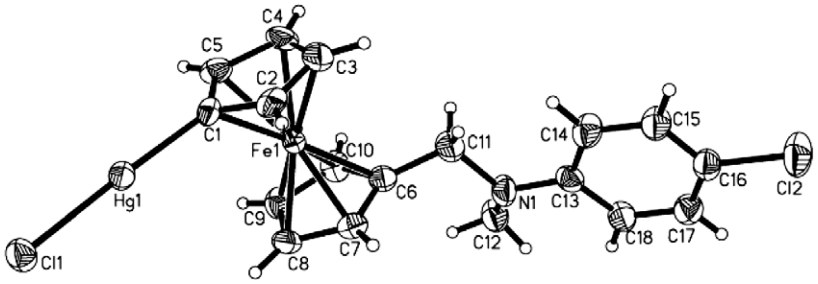

Fig. 4. Molecular structure of **7** with the numbering scheme.

imino groups are coplanar with the substituted Cp rings [8], the (*N*-methyl-*N*-phenyl)amino groups in **4** lie above the substituted Cp rings [9], thus the N–Hg coordinated intermediates adapting a similar conformation will disfavor the activation of the intramolecular C–H bond (path i). However, this conformation will enable the intermediates (Scheme 2) to activate the intermolecular C–H bonds with a minimum energy and hence produce a flexible zigzag link (path ii). This hypothesis is supported by the fact that both **6** and **4** keep a similar conformation (the torsion angle C2–C21–N1–C23 (69.5(5)°) in **6a** is the same as that in **4a** (70.0(3)°) [9b]. In addition, dimer complexes with a 10 membered ring are also excluded because their formation needs the N–Hg moiety in one intermediate to rotate around the axis of the C1–C11 bond and subsequently activate the intermolecular *ortho* C–H bond in another intermediate, and this rotation is probably retarded due to steric hindrance between the phenyl and the hydrogen in the Cp ring [12].

2.4. Crystal structures of *6a, e, and 7*

The molecular structures of **6a**, **e**, and **7** were determined by X-ray single crystal diffraction (Figs. 1, 2, and 4). The intermolecular N–Hg coordination pattern in **6e** is presented in Fig. 3. Crystal parameters and data collection for **6a**, **e** and **7** are summarized in Table 1. Their selected bond lengths and angles are listed in Tables 2 and 3, respectively.

Figs. 1 and 2 demonstrate that chloromercurio units in **6a** and **e** are connected directly to the *ortho* position of the amino group, whereas in **7** it is connected to the second Cp ring (Fig. 4). The Hg1–Cl bond lengths in **6a**, **e**, and **7** (2.043(4), 2.044(2), and 2.045(4) Å, respectively) are nearly the same and are in the normal range. The distance Fe–Hg 3.607(1) Å in **7** is nearly equal to the sum of the constituent van der Waals radii (3.55 Å) [11a], indicating that a weak Fe–Hg interaction is present. However, such an interaction in **6a** and **e** is absent. The Cl1–Hg1–C1 bond angles in **6a**, **e**, and **7** (176.2(2), 177.9(2), and 178.0(3)°, respectively) are closer to the ideal value of 180° in organic derivatives of mercury. The dihedral angle Cl1–Hg1–C1–C2 (−180(6)°) in **6e** means that the chloromercurio unit is coplanar with the substituted Cp ring. However, the Cl1 atom in **7** is pocketed between two paralleled Cp rings. The angle between the chloromercurio unit and the substituted Cp ring is 75.9(1)°, implying that they are nearly perpendicular to each other. In Fig. 1, the dihedral angle between the substituted Cp ring and the intramolecular phenyl

Table 1
Crystallographic data for **6a**, **e**, and **7**

Compound	**6a**	**6e**	**7**
Empirical formula	$C_{38}H_{40}Cl_2Fe_2Hg_2N_2O_2$	$C_{18}H_{17}Cl_2FeHgN$	$C_{18}H_{17}Cl_2FeHgN$
M	1140.50	574.67	574.67
Crystal dimensions (mm)	0.26 × 0.20 × 0.12	0.14 × 0.12 × 0.10	0.22 × 0.20 × 0.18
Crystal system, space group	triclinic, $P\bar{1}$	triclinic, $P\bar{1}$	triclinic, $P\bar{1}$
a (Å)	12.546(5)	7.9393(1)	6.1781(1)
b (Å)	12.750(3)	10.4298(2)	7.0755(2)
c (Å)	14.135(3)	12.268(2)	20.662(5)
α (°)	114.409(2)	68.447(2)	91.197(6)
β (°)	100.633(3)	72.426(2)	98.268(5)
γ (°)	103.511(3)	71.852(2)	103.698(5)
V (Å^3)	1898.4(9)	877.4(3)	867.0(3)
Z	2	2	2
ρ_{calcd} (Mg m^{-3})	1.995	2.175	2.201
μ (mm^{-1})	8.987	9.866	9.985
F(000)	1088	544	544
Reflections collected/unique [R_{int}]	10428/6628 [0.0186]	4945/3494 [0.0221]	6076/3476 [0.0331]
Data/restraints/parameters	6628/0/437	3494/0/209	3476/0/209
Final R_1, wR_2	0.0255, 0.0555	0.0307, 0.0733	0.0674, 0.1675
Largest difference in peak and hole (e Å^{-3})	0.677, −0.825	1.575, −1.384	5.181, −3.237

Table 2
Selected bond lengths (Å) for **6a**, **e**, and **7**

6a	(Å)	**6e**	(Å)	**7**	(Å)
Hg(1)–N(2)	2.927(1)	Hg(1)–C(1)	2.044(6)	Hg(1)–C(1)	2.045(1)
Hg(1)–C(1)	2.043(4)	Hg(1)–Cl(1)	2.324(2)	Hg(1)–Cl(1)	2.324(4)
Hg(1)–Cl(1)	2.318(1)	Fe(1)–C(1)	2.055(5)	Fe(1)–C(1)	2.033(1)
Fe(1)–C(1)	2.047(5)	Fe(1)–C(2)	2.057(6)	Fe(1)–C(2)	2.065(1)
Fe(1)–C(2)	2.028(4)	C(1)–C(2)	1.445(8)	Fe(1)–C(6)	2.043(1)
C(1)–C(2)	1.435(6)	C(2)–C(11)	1.477(8)	C(6)–C(11)	1.494(2)
C(2)–C(21)	1.500(6)	N(1)–C(11)	1.470(9)	N(1)–C(11)	1.471(2)
N(1)–C(21)	1.487(6)	N(1)–C(12)	1.375(9)	N(1)–C(12)	1.440(2)
N(1)–C(23)	1.423(6)	N(1)–C(18)	1.469(8)	N(1)–C(13)	1.403(2)
N(1)–C(22)	1.458(6)	C(12)–C(13)	1.413(9)	C(13)–C(14)	1.410(2)
C(23)–C(24)	1.386(7)	C(13)–C(14)	1.375(9)	C(14)–C(15)	1.370(2)
C(24)–C(25)	1.387(7)	C(14)–C(15)	1.357(1)	C(15)–C(16)	1.390(2)
C(25)–C(26)	1.393(8)	C(12)–C(17)	1.405(9)	Cl(2)–C(16)	1.759(1)
O(1)–C(26)	1.374(7)	Cl(2)–C(14)	1.757(7)		

ring is 56.8(1)°, the dihedral angle between the intermolecular two phenyl rings is 72.0(1)°. In addition, the two pentagonal rings of the ferrocenyl moiety in **6a**, **e**, and **7** are planar and nearly parallel (interplanar angles 1.1, 2.2, and 0.9°, respectively). In addition, the Cp rings are also nearly eclipsed.

*2.5. Transpalladation via **6** and disodium tetrachloropalladate (II)*

In order to assess the properties of **6a**–**f**, their transpalladation reactions *via* disodium tetrachloropalladate (II) were carried out in methanol at room temperature. However, most of the palladium (II) was reduced to palladium (0) black by **6a**–**f**, and the yields of the isolated cyclopalladated complexes **8** were much lower (⩽20%) than that of the cyclopalladated ({*N*-methyl-*N*-benzylamino}methyl)ferrocenes. Direct cyclopalladation of **4a**–**f** gave similar results [12]. It is believe that intermolecular N–Hg coordination may account for such low yields of the cyclopalladated complexes see Scheme 3.

3. Experimental

3.1. Materials and instruments

Ferrocenylamines were prepared according to the literature procedure [9b], disodium tetrachloropalladate (II) was prepared in our laboratory. Mercury (II) acetate, lithium chloride and triphenylphosphine were obtained commercially and used without further purification. All of the solvents were purified with standard methods prior to use. Melting points were obtained from Yanaco micro melting point apparatus and were uncorrected. Elemental analyses were measured on a Carlo Erba 1106 Elemental analyzer. ^{1}H NMR spectra were obtained with a Bruker AV-400 spectrometer using $CDCl_3$ as the solvent and TMS as internal standard. IR spectra were taken on a BIO-RAD 3000 spectrophotometer.

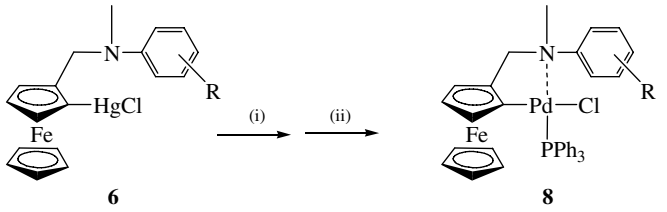

6 **8**

Scheme 3. (i) Na_2PdCl_4, methanol, room temperature and (ii) PPh_3, methanol. R = 4-MeO (a), 4-Me (b), H (c), 4-Cl (d), 3-Cl (e), and 3-NO_2 (f).

*3.2. Preparation of [(η^5-C_5H_5)Fe(η^5-C_5H_3(HgCl)CH_2N-(CH_3)C_6H_4-R)] (**6**) and [(η^5-C_5H_4HgCl)Fe-(η^5-$C_5H_4CH_2N(CH_3)$-C_6H_4–Cl-4)] (**7**)*

General procedure. To a stirred solution of the ferrocenylamines (**4**) (5 mmol) in methanol (20 ml) and dichloromethane (5 ml), was added dropwise a solution of mercury (II) acetate (5 mmol) in sufficient methanol. The reactions were monitored by TLC until they were complete. A solution of lithium chloride (7.5 mmol) in methanol was then added and the mixtures were stirred for 30 min. The solvent was removed and the residues were extracted with dichloromethane (3 × 30 ml), the organic layer was dried over anhydrous sodium sulfate and evaporated under reduce pressure to give the crude products which were purified by chromatography (silica gel, ethyl acetate/hexane = 1:1, v/v), the second band eluted was collected, the solvent was removed *in vacuo* to give **6** as yellow powders.

Table 3
Selected bond angles (°) for **6a**, **e**, and **7**

6a	(°)	**6e**	(°)	**7**	(°)
C(1)–Hg(1)–Cl(1)	176.2(1)	C(1)–Hg(1)–Cl(1)	177.9(2)	C(1)–Hg(1)–Cl(1)	178.0(3)
C(11)–Hg(2)–Cl(2)	174.3(1)	C(2)–C(1)–Hg(1)	127.4(4)	C(2)–C(1)–Hg(1)	125.8(1)
N(2)–Hg(1)–Cl(1)	87.8(2)	C(5)–C(1)–Hg(1)	125.1(4)	Fe(1)–C(1)–Hg(1)	124.4(6)
N(2)–Hg(1)–C(1)	94.5(2)	Hg(1)–C(1)–Fe(1)	125.0(3)	C(10)–C(6)–C(11)	127.6(2)
C(2)–C(1)–Hg(1)	126.8(3)	C(1)–C(2)–C(11)	126.6(5)	C(11)–C(6)–Fe(1)	124.3(1)
C(15)–C(11)–Hg(2)	124.8(4)	N(1)–C(11)–C(2)	112.7(5)	N(1)–C(11)–C(6)	112.3(1)
C(1)–C(2)–C(21)	126.8(4)	C(12)–N(1)–C(11)	123.8(5)	C(13)–N(1)–C(11)	118.4(1)
C(11)–C(15)–C(30)	126.2(4)	N(1)–C(12)–C(13)	122.3(6)	N(1)–C(13)–C(14)	122.5(1)
N(1)–C(21)–C(2)	113.9(4)	C(13)–C(14)–Cl(2)	117.4(5)	C(15)–C(16)–Cl(2)	118.5(1)
N(2)–C(30)–C(15)	114.0(4)				

*3.2.1. [(η^5-C_5H_4)Fe(η^5-C_5H_3(HgCl)N(CH_3)C_6H_4–OCH_3-4)] (**6a**)*

Yellow solid. Yield 67%; m.p. 142 °C (dec.). *Anal.* Calc. for $C_{19}H_{20}ClFeHgNO$: C, 40.02; H, 3.54; N, 2.46. Found: C, 39.87; H, 3.58; N, 2.50%. IR (KBr): 3085, 2934, 2832, 1511, 1455, 1244, 1037, 818, 480 cm^{-1}. ^1H NMR: δ 2.78 (s, 3H, *N*-CH_3), 3.76 (s, 3H, OCH_3), 3.98 (d, 1H, H3), 4.08 (d, 1H, H5), 4.17 (s, 5H, η-C_5H_5), 4.33 (m, 3H, H4, H11), 6.78–6.85 (q, 4H, H12, H13, H15, H16) ppm.

*3.2.2. [(η^5-C_5H_5)Fe(η^5-C_5H_3(HgCl)N(CH_3)C_6H_4–CH_3-4)] (**6b**)*

Yellow solid. Yield 62%; m.p. 140 °C (dec.). *Anal.* Calc. for $C_{19}H_{20}ClFeHgN$: C, 41.17; H, 3.64; N, 2.53. Found: C, 41.00; H, 3.70; N, 2.48%. IR (KBr): 3087, 2957, 2860, 1520, 1457, 1104, 803, 483 cm^{-1}. ^1H NMR: δ 2.16 (s, 3H, Ar-CH_3), 2.78 (s, 3H, N-CH_3), 4.02 (d, 1H, H3), 4.15 (s, 5H, η-C_5H_5), 4.16 (d, 1H, H5), 4.28 (m, 3H, H4, H11), 6.76–6.83 (q, 4H, H12, H13, H15, H16) ppm.

*3.2.3. [(η^5-C_5H_5)Fe(η^5-C_5H_3(HgCl)N(CH_3)C_6H_5)] (**6c**)*

Yellow solid. Yield 65%; m.p. 180 °C (dec.). *Anal.* Calc. for $C_{18}H_{18}ClFeHgN$: C, 40.02; H, 3.36; N, 2.59. Found: C, 39.97; H, 3.40; N, 2.51%. IR (KBr): 3092, 2927, 2857, 2812, 1598, 1505, 1449, 1343, 1105, 819, 748, 691, 480 cm^{-1}. ^1H NMR: δ 2.90 (s, 3H, N-CH_3), 4.04 (d, 1H, H3), 4.11 (d, 1H, H5), 4.19 (s, 5H, η-C_5H_5), 4.34 (m, 3H, H4, H11), 6.75–6.80 (m, 5H, H12–H16) ppm.

*3.2.4. [(η^5-C_5H_5)Fe(η^5-C_5H_3(HgCl)CH_2N(CH_3)-C_6H_4–Cl-4)] (**6d**)*

Yellow solid. Yield 60%; m.p. 138 °C (dec.). *Anal.* Calc. for $C_{18}H_{17}Cl_2FeHgN$: C, 37.62; H, 2.98; N, 2.44. Found: C, 37.36; H, 3.06; N, 2.36%. IR (KBr): 3088, 2937, 1593, 1497, 1244, 1101, 999, 809, 731, 486 cm^{-1}. ^1H NMR: δ 2.90 (s, 3H, *N*-CH_3), 4.03 (d, 1H, H3), 4.10 (d, 1H, H5), 4.22 (s, 5H, η-C_5H_5), 4.38 (m, 3H, H4, H11), 6.70 (d, 2H, H12, H16), 7.20 (d, 2H, H13, H15) ppm.

*3.2.5. [(η^5-C_5H_5)Fe(η^5-C_5H_3(HgCl)N(CH_3)C_6H_4–Cl-3)] (**6e**)*

Yellow solid. Yield 64%; m.p. 188 °C (dec.). *Anal.* Calc. for $C_{18}H_{17}Cl_2FeHgN$: C, 37.62; H, 2.98; N, 2.44. Found: C, 37.40; H, 3.00; N, 2.30%. IR (KBr): 3091, 2933, 2890, 1594, 1495, 1251, 1188, 1102, 987, 820, 795, 483 cm^{-1}. ^1H NMR: δ 2.90 (s, 3H, N-CH_3), 4.07 (d, 1H, H3), 4.11 (d, 1H, H5), 4.25 (s, 5H, η-C_5H_5), 4.40 (m, 3H, H4, H11), 6.78 (m, 3H, H12, H13, H14), 7.18 (t, 1H, H16) ppm.

*3.2.6. [(η^5-C_5H_5)Fe(η^5-C_5H_3(HgCl)CH_2N(CH_3)C_6H_4–NO_2-3)] (**6f**)*

Yellow solid. Yield 58%; m.p. 176 °C (dec.). *Anal.* Calc. for $C_{18}H_{17}ClFeHgN_2O_2$: C, 36.94; H, 2.93; N, 4.79. Found: C, 36.70, H, 3.02, N, 4.70%. IR (KBr): 3087, 2922, 1524, 1454, 1343, 1252, 1103, 734, 483 cm^{-1}. ^1H NMR: δ 2.92 (s, 3H, N-CH_3), 4.10 (d, 1H, H3), 4.12 (d, 1H, H5), 4.24 (s, 5H, η-C_5H_5), 4.41 (m, 3H, H4, 11), 6.97–7.57 (m, 4H, H12, H13, H14, H16) ppm.

*3.2.7. [(η^5-C_5H_4HgCl)Fe(η^5-$C_5H_4CH_2N(CH_3)$-C_6H_4–Cl-4)] (**7**)*

In the reaction of **4d** with mercury (II) acetate, the third band eluted was also collected and **7** was isolated as yellow powder. Yield 15%; m.p. 146 °C (dec.). *Anal.* Calc. for $C_{18}H_{17}Cl_2FeHgN$: C, 37.62; H, 2.98; N, 2.44. Found: C, 37.50; H, 2.84; N, 2.42%. IR (KBr): 3087, 2937, 1595, 1496, 1245, 809, 730, 486 cm^{-1}. ^1H NMR: ^1H–NMR: δ 2.70 (s, 3H, *N*-CH_3), 3.92 (d, 2H, H7, H10), 4.04 (m, 4H, H2, H5, H8, H9), 4.16 (d, 2H, H3, H4), 4.23 (s, 2H, H11), 6.58–7.00 (q, 4H, H12, H13, H15, H16) ppm.

3.3. Transpalladation of **6a–f** via disodium tetrachloropalladate (II)

To stirred solutions of **6** (2 mmol) in methanol (20 ml), was added dropwise a methanol solution (30 ml) of disodium tetrachloropalladate (II) (2 mmol) at room temperature over 1 h. The reactions progress were monitored by TLC until they were complete, then triphenylphosphine was added. The mixtures were filtered and the solvent was removed *in vacuo*. The residues were purified by column chromatography (silica gel, ethyl acetate/hexane = 3:1, v/v) to give **8** as red–purple solids. The yields of **8a–f** were 20%, 20%, 17%, 14%, 18%, and 10%, respectively. Their IR and NMR spectra were the same as the authentic samples [12].

3.4. Crystal structure determination for **6a, e, and 7**

Prismatic single crystals of **6a**, **e**, and **7** suitable for X-ray analysis were obtained by slow evaporation of a mixture of ethyl acetate and hexane at room temperature over a period of one week. The single crystals of **6a**, **e**, and **7** were mounted on a Bruker SMART CCD diffractometer equipped with graphite monochromated Mo Kα (λ = 0.71073 Å) radiation at ambient temperature (T = 294 K) using the ω-2θ multi-scans technique with the ranges $1.76° \leqslant \theta \leqslant 26.03°$ (**6a**), $1.83° \leqslant \theta \leqslant 26.32°$ (**6e**), and $1.00° \leqslant \theta \leqslant 26.59°$ (**7**) for data collection. Semi-empirical absorption corrections were applied using the SABABS program [13]. The structures were solved by direct methods and refined by full-matrix least-squares procedures on F^2 using the SHELX suite of programs [14]. The values of R_1 were given based on F_o with a typical threshold of $F^2 \geqslant 2\sigma(F^2)$. The weighted R-factors wR were based on F^2 with $w = 1/[\sigma^2(F_o^2) + (0.0265P)^2 + 0.0000P]$ where $P = (F_o^2 + 2F_c^2)/3$ for **6a**, $w = 1/[\sigma^2(F_o^2) + (0.0265P)^2 + 0.0000P]$ where $P = (F_o^2 + 2F_c^2)/3$ for **7**. Crystallographic data for **6a**, **e**, and **7** are summarized in Table 1. Selected bond lengths and angles for **6e**, **7** are presented in Tables 2 and 3, respectively.

4. Supplementary materials

Crystallographic data (excluding structure factors) for the structures of **6a**, **e**, and **7** in this paper have been deposited with the Cambridge Crystallographic Data Centre as supplementary publication numbers CCDC 290135, 275037, and 275036. Copies of the data can be obtained, free of charge, on application to CCDC, 12 Union Road, Cambridge CB2 1EZ, UK (fax: +44 1223 336033 or e-mail: deposit@ccdc.cam.ac.uk).

Acknowledgements

We are grateful to the Natural Scientific Foundation of Tianjin Metropolitan, People's Republic of China for their generous support for this project (Project No. 033609011), the Opening Fund from The State Key Laboratory of Elemento-organic Chemistry, Nankai University, People's Republic of China is also acknowledged.

References

[1] (a) L.G. Kuz'mina, Yu.T. Struchkov, L.L. Troitskaya, V.I. Sokolov, J. Strukt. Chem. (USSR) 26 (1985) 428;
(b) P.A. Bonnardel, R.V. Parish, J. Organomet. Chem. 515 (1996) 221;
(c) D.W. Slocum, T.R. Engelmann, J. Organomet. Chem. 24 (1970) 753;
(d) C. Kruger, K.H. Thiele, M. Dargatz, T. Bartik, J. Organomet. Chem. 362 (1989) 147;
(e) G. Phillips, P.J. Steel, J. Organomet. Chem. 410 (1991) 247;
(f) N. Seidel, K. Jacob, A.K. Fischer, K. Merzweiler, C. Wagner, M. Fontani, P. Zanello, J. Organomet. Chem. 630 (2001) 149.

[2] J. Vicente, J.A. Abad, B. Rink, F.S. Hernandez, M.C.R. de Arellano, Organometallics 16 (1997) 5269.

[3] R.C. Larock, D.J. Leuck, L.W. Harrison, Tetrahedron Lett. 28 (1987) 4977.

[4] (a) R.C. Larock, Comprehensive Organic Transformations: A Guide to Functional Group Preparations, 2nd ed., John Wiley/VCH, New York, 1999;
(b) R.C. Larock, Organomercury Compounds in Organic Synthesis, Springer-Verlag, Berlin–Heidelberg–New York–Tokyo, 1985.

[5] (a) K. Cheng, S.J. Lippard, Tetrahedron 61 (2005) 1587;
(b) R.C. Larock, M.S. Chow, Organometallics 5 (1986) 603.

[6] (a) J. Vicente, J.A. Abad, F.S. Herna'ndez-Mata, B. Rink, Organometallics 23 (2004) 1292;
(b) E.C. Constable, T.A. Leese, J. Organomet. Chem. 335 (1987) 293;
(c) E. Wehman, G. van Koten, J.T.B.H. Jastrzebski, H. Ossor, M. Pfeffer, J. Chem. Soc., Dalton Trans. (1988) 2975;
(d) Y.J. Wu, Y.H. Liu, K.L. Ding, H.Z. Yuan, X.A. Mao, J. Organomet. Chem. 505 (1995) 37;
(e) E.C. Constable, T.A. Leese, J. Organomet. Chem. 363 (1989) 419.

[7] R.C. Larock, D.R. Leach, Organometallics 1 (1982) 74.

[8] (a) Z.D. Chen, Y.J. Wu, X.P. Zhang, R.F. Chen, H.W. Hu, Acta Chimica Sinica 42 (1984) 792;
(b) K.L. Ding, Y.J. Wu, Y. Wang, Y. Zhu, L. Yang, J. Organomet. Chem. 463 (1993) 77;
(c) S.Q. Huo, Y.J. Wu, Y. Wang, X.A. Mao, H.Z. Yuan, Tetrahedron 50 (1994) 10467;
(d) S.Q. Huo, Y.J. Wu, Y. Zhu, L. Yang, J. Organomet. Chem. 70 (1994) 17;
(e) Y.J. Wu, S.Q. Huo, Y. Zhu, L. Yang, J. Organomet. Chem. 481 (1994) 235;
(f) Y.H. Liu, Y.J. Wu, S.Q. Huo, H.Z. Yuan, J. Organomet. Chem. 534 (1997) 7;
(g) Y.J. Wu, X.L. Cui, Y.H. Liu, H.Z. Yuan, X.A. Mao, J. Organomet. Chem. 543 (1997) 63;
(h) Y.J. Wu, X.L. Cui, C.X. Du, W.L. Wang, R.Y. Guo, R.F. Chen, J. Chem. Soc., Dalton Trans. (1998) 3727.

[9] (a) H.X. Wang, L. Ding, Y.J. Wu, J. Organomet. Chem. 679 (2003) 130;
(b) H.X. Wang, Y.J. Li, R. Jin, H.F. Wu, J.R. Niu, H.C. Zhou, J. Xu, R.Q. Gao, F.Y. Geng, J. Organomet. Chem. 691 (2006) 987.

[10] M. Rosenblum, R.B. Woodward, J. Am. Chem. Soc. 80 (1958) 5443.

[11] (a) A. Bondi, J. Phys. Chem. 68 (1964) 441;
(b) J. Canty, G.B. Deacon, Inorg. Chim. Acta. 45 (1980) L225.

[12] H.X. Wang, Y.J. Li, R.Q. Gao, H.F. Wu, F.Y. Geng, R. Jin, Inorg. Chem. Commun. 9 (2006) 658.

[13] G.M. Sheldrick, SADABS, University of Göttingen, 1996.

[14] G.M. Sheldrick, SHELXS-97 and SHELXL-97, programs for crystal structure solution and refinement, University of Göttingen, 1997.

containing a tridentate Schiff base (SAA) and a monodentate ligand (ImH)/bidentate ligands (bipy, phen). The single crystal X-ray analysis of complex **1** has revealed the presence of a distorted square planar geometry and complex **2** has a distorted square pyramidal geometry.

2. Experimental

2.1. Materials and methods

$CuCl_2 \cdot 2H_2O$, $CuSO_4 \cdot 5H_2O$, KOH, 1,10-phenanthroline, 2,2′-bipyridine, imidazole, MeOH, MeCN (S.D. Fine Chemicals) were used as purchased. The Schiff base was synthesized by reacting salicylaldehyde and anthranilic acid in an equimolar ratio at room temperature in methanol. Elemental analyses were performed on an elemental analyzer. FAB mass spectra were recorded on JEOL SX 102/DA 6000 mass spectrometer using xenon (6 kV, 10 mA) as the FAB gas. The magnetic susceptibility data were recorded on a Gouy balance at room temperature using mercury(II) tetrathiocyanato cobaltate(II) ($\chi_g = 16.44 \times 10^{-6}$ cgs unit) as the calibrant. The e.p.r. spectra were recorded at RT and also at LNT (77 K) on a Varian E-line Century Series EPR spectrometer operating at 9.4 GHz with TCNE as a calibrant. The e.p.r. parameters were measured using a reported method [21]. UV–Vis spectra were recorded on a Shimadzu UV–Vis 160 spectrophotometer in quartz cells. A BAS-100 Epsilon electrochemical analyzer was used for cyclic voltammetric experiments in a DMSO solution of the complex containing tetrabutylammonium perchlorate (TBAP) as the supporting electrolyte. The three electrode measurement was carried out at 298 K under a nitrogen atmosphere with a platinum working electrode, a platinum wire auxiliary electrode and a silver/silver chloride reference electrode (Ag/AgCl). The SOD activities were evaluated using alkaline DMSO as a source of superoxide radicals (O_2^-) and nitrobluetetrazolium chloride (NBT) as scavenger [18].

2.2. Synthesis of the complexes

2.2.1. Synthesis of [Cu(SAA)(ImH)] (1), [Cu(SAA)(bipy)]CH_3CN (2) and [Cu(SAA)(phen)] (3)

All the present complexes were synthesized following the same general procedure. To a MeOH solution (10 ml) of $CuCl_2 \cdot 2H_2O$ (1.0 mmol, 0.170 g) a solution of the potassium salt of the Schiff base (1 mmol, 0.240 g) was added and the reaction mixture was stirred for 30 min at 25 °C. To the above reaction mixture, a MeOH solution (10 ml) of ImH (1 mmol, 0.078 g) was added and the stirring was continued for 30 min more. The precipitate was separated by filtration and was dissolved in MeOH:MeCN (1:2 V/V) for recrystallization. After 2–3 days of slow evaporation of the reaction mixture, dark green prismatic crystals were

Table 1
Crystal data and structure refinement for complexes [Cu(SAA)(ImH)] (**1**) and [Cu(SAA)(bipy)]CH_3CN (**2**)

Empirical formula	$C_{17}H_{13}CuN_3O_3$	$C_{26}H_{20}CuN_4O_3$
Formula weight	370.84	500.00
Temperature (K)	293(2)	293(2)
Wavelength (Å)	0.71073	0.71073 A
Crystal system, space group	orthorhombic, $Pna2_1$	triclinic, $P\bar{1}$
Unit cell dimensions		
a (Å)	9.3805(9)	9.165(3)
b (Å)	11.546(4)	10.0261(19)
c (Å)	14.5258(14)	13.1393(18)
α (°)	90	76.469(14)
β (°)	90	79.100(19)
γ (°)	90	76.13(2)
V (Å^3)	1573.2(6)	1128.2(5)
D_{calc} (Mg/m^3)	1.566	1.472
Z	4	2
Absorption coefficient (mm^{-1})	1.409	1.005
$F(000)$	756	514
Crystal size (mm)	$0.18 \times 0.15 \times 0.13$	$0.35 \times 0.30 \times 0.30$
θ Range for data collection (°)	3.13–32.00	3.00–30.16
Limiting indices	$-13 \leqslant h \leqslant 13$, $-16 \leqslant k \leqslant 16$, $-21 \leqslant l \leqslant 21$	$-12 \leqslant h \leqslant 12$, $-14 \leqslant k \leqslant 14$, $-17 \leqslant l \leqslant 18$
Reflections collected/unique [R_{int}]	21 681/4649 [0.0245]	15 730/6571 [0.0186]
Completeness to θ	25.00, 99.8%	25.00, 99.5%
Absorption correction	semi-empirical from equivalents	
Maximum and minimum transmission	0.8381 and 0.7856	
Refinement method	full-matrix least-squares on F^2	full-matrix least-squares on F^2
Data/restraints/parameters	4649/1/217	6571/0/308
Goodness-of-fit on F^2	0.956	1.045
Final R indices [$I > 2\sigma(I)$]	$R_1 = 0.0249$, $wR_2 = 0.0570$	$R_1 = 0.0327$, $wR_2 = 0.0905$
R indices (all data)	$R_1 = 0.0361$, $wR_2 = 0.0595$	$R_1 = 0.0537$, $wR_2 = 0.0945$
Absolute structure parameter	−0.008(8)	
Largest difference in peak and hole (e Å^{-3})	0.247 and −0.267	0.402 and −0.234

collected and washed with a little amount of MeOH and then with diethyl ether successively. These were dried in air at room temperature and stored in a $CaCl_2$ desiccator. Yield, 70%. *Anal*. Calc. for $C_{17}H_{13}O_3N_3Cu$ (**1**) C, 55.05; H, 3.50; N, 11.33. Found: C, 55.38; H, 3.43; N, 11.70%. FAB Mass found: 371 Calc.: 370.54. Complexes **2** and **3** were synthesized as described above by employing bipy (1 mmol, 0.156 g), phen (1 mmol, 0.198 g) respectively in place of ImH. *Anal*. Calc. for $C_{26}H_{20}N_4O_3Cu$ (**2**) C, 62.45; H, 4.00; N, 11.21. Found: C, 62.58; H, 3.35; N, 11.85% FAB Mass found: 459, Calc.: 458.54. *Anal*. Calc. for $C_{26}H_{17}O_3N_3Cu$ (**3**): C, 64.65; H, 3.52; N, 8.70. Found: C, 64.02; H, 3.92; N, 9.07%. FAB Mass found: 482. Calc.: 482.54.

2.3. Crystal structure determination

Crystals suitable for single crystal X-ray analysis for complexes [Cu(SAA)(ImH)] (**1**) and [Cu(SAA)(bipy)]-CH_3CN (**2**) were grown by slow evaporation of the reaction mixture at room temperature. Single crystals suitable for single crystal X-ray of **1** and **2** were mounted on a glass fiber and used for data collection (Table 1). Crystal data were collected on an Enraf-Nonius $MACH_3$ diffractometer using graphite monochromatized Mo Kα radiation ($\lambda = 0.71073$Å). The crystal orientation, cell refinement and intensity measurements were made using the program CAD-4PC performing psi-scan measurements. The structure was solved by the direct method using the program SHELXS-97 [22] and refined by full-matrix least-squares techniques against F^2 using SHELXL-97 [23]. All non-hydrogen atoms were refined anisotropically. All the hydrogen atoms were geometrically fixed and allowed to refine using a riding model.

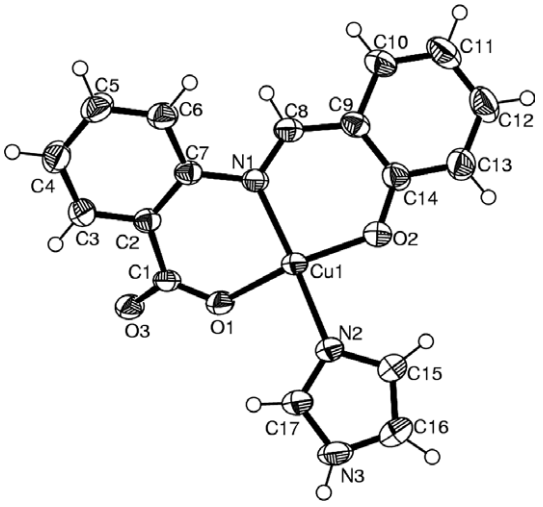

Fig. 1. ORTEP diagram of the complex [Cu(SAA)(ImH)] (**1**).

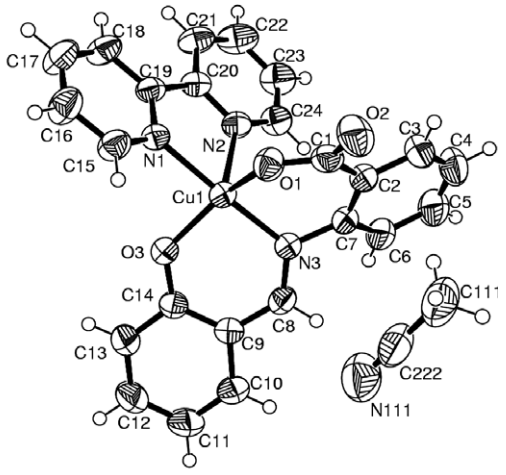

Fig. 2. ORTEP diagram of the complex [Cu(SAA)(bipy)]CH_3CN (**2**).

3. Results and discussion

All the reported complexes were synthesized by the following sequential routes:

$$L' + [Cu(H_2O)_6]^{2+} \xrightarrow{\text{Basic medium}} [Cu(L')H_2O] \quad (1)$$

$$[Cu(L')H_2O] + L'' \rightarrow [Cu(L')(L'')] + H_2O \quad (2)$$

where $L' = SAA$, $L'' = ImH/bipy/phen$.

The synthesized complexes were characterized by using different physio-chemical techniques.

3.1. Crystal structure

Complexes **1** and **2** have been characterized by the single crystal X-ray diffraction technique. The ORTEP views of the complexes are shown in Figs. 1 and 2. Crystallographic data, selected bond angles and distances are given in Tables 1–3. The crystal structures of the complexes reveals the presence of ternary copper(II) structures consisting of a tridentate ONO- donor Schiff base, a monodentate ligand (N-donor) or a bidentate ligand (NN-donor) and a copper (II) center in the discrete monomeric species. Complex **1** crystallizes in the orthorhombic system. The structure of complex **1** was solved in $Pna2_1$ space group, whereas **2** crystallizes in the triclinic $P\bar{1}$ space group. Complex **1** has a distorted square-planar geometry. The coordination geometry is distorted from square planar, as ascertained by the observed τ value of 0.13 (the structure index is defined as $\tau = (\beta - \alpha)/60$, where α and β are the largest coordination angles), such a square planar geometry was observed in a similar copper(II) complexes [24,25]. In these complexes the values of τ lie in the range 0.05–0.17. Complex **2** has a distorted square pyramidal (4 + 1) geometry, the distortion ($\tau = 0.59$) from square-pyramidal geometry was again ascertained by τ values; for a perfect square pyramidal geometry the τ value should be 0 [26]. The largest distortions from the square pyramidal geometry are indicated by the O(3)–Cu(1)–O(1) = 142.59(6)° and C(1)–O(1)–Cu(1) = 127.18(12)° angles. Similar copper(II) complexes, having distorted square planar geometries, have also been reported by Reddy et al. [2]. In both structures

Table 2
Selected bond lengths (Å) and angles (°) for [Cu(SAA)(ImH)] (**1**)

Cu(1)–O(2)	1.8879(13)	O(1)–C(1)	1.272(2)
Cu(1)–O(1)	1.9167(12)	O(2)–C(14)	1.304(2)
Cu(1)–N(1)	1.9834(14)	C(1)–C(2)	1.515(2)
Cu(1)–N(2)	2.0033(13)	C(2)–C(7)	1.408(2)
N(1)–C(8)	1.306(2)	C(8)–C(9)	1.431(2)
N(1)–C(7)	1.442(2)	C(9)–C(14)	1.428(3)
O(2)–Cu(1)–O(1)	159.18(7)	C(8)–N(1)–Cu(1)	120.99(11)
O(2)–Cu(1)–N(1)	95.58(6)	C(17)–N(2)–Cu(1)	127.00(15)
O(2)–Cu(1)–N(2)	87.86(8)	C(15)–N(2)–Cu(1)	127.79(16)
O(1)–Cu(1)–N(2)	87.55(6)	C(1)–O(1)–Cu(1)	129.96(10)
O(1)–Cu(1)–N(1)	93.47(5)	C(14)–O(2)–Cu(1)	127.85(12)
N(1)–Cu(1)–N(2)	166.85(9)	C(7)–N(1)–Cu(1)	121.74(10)

Table 3
Selected bond lengths (Å) and angles (°) for [Cu(SAA)(bipy)]CH_3CN (**2**)

Cu(1)–O(3)	1.9215(13)	N(2)–C(20)	1.342(2)
Cu(1)–N(3)	1.9460(14)	N(3)–C(8)	1.296(2)
Cu(1)–O(1)	1.9678(12)	N(3)–C(7)	1.428(2)
Cu(1)–N(1)	2.0162(14)	C(1)–C(2)	1.505(3)
Cu(1)–N(2)	2.2259(16)	C(2)–C(7)	1.405(3)
O(1)–C(1)	1.276(2)	C(8)–C(9)	1.421(3)
O(3)–C(14)	1.302(2)	C(9)–C(14)	1.414(2)
N(1)–C(19)	1.348(2)	C(19)–C(20)	1.478(3)
O(3)–Cu(1)–N(3)	93.46(6)	N(1)–Cu(1)–N(2)	77.40(6)
O(3)–Cu(1)–O(1)	142.59(6)	C(1)–O(1)–Cu(1)	127.18(12)
N(3)–Cu(1)–O(1)	89.58(6)	C(14)–O(3)–Cu(1)	127.12(11)
O(3)–Cu(1)–N(1)	88.46(6)	C(15)–N(1)–Cu(1)	122.49(12)
N(3)–Cu(1)–N(1)	177.49(6)	C(19)–N(1)–Cu(1)	118.43(12)
O(1)–Cu(1)–N(1)	89.87(5)	C(24)–N(2)–Cu(1)	129.71(12)
O(3)–Cu(1)–N(2)	114.01(6)	C(20)–N(2)–Cu(1)	112.06(12)
N(3)–Cu(1)–N(2)	100.33(6)	C(8)–N(3)–Cu(1)	124.35(12)
O(1)–Cu(1)–N(2)	102.01(6)	C(7)–N(3)–Cu(1)	116.83(11)

the Schiff base ligand occupies the basal plane. The ONO donor Schiff base forms a three membered chelate ring and it occupies the basal plane with a bond length of ~1.9 Å which is close to ~1.9 Å [2]. In complex **2**, the NN-donor atoms of bipy display an axial-equatorial binding mode with bond distances Cu(1)–N(2) = 2.2259(16), Cu(1)–N(1) = 2.0162(14) Å which is again close to ~2 Å [2].

3.2. Magnetic measurements

The magnetic susceptibility measurements in the solid state show that the present complexes are paramagnetic at ambient temperature. The observed magnetic moment values (1.79 ± 0.01 BM) are quite close to the values expected for copper(II) complexes and is in fair agreement with the spin system $S = 1/2$. The magnetic moment (μ_{eff}) lies within the range normally found for other copper(II) complexes [27,28].

3.3. E.p.r. investigation

X-band e.p.r. spectra of the complexes were recorded in the polycrystalline state and also in 100% DMSO solution.

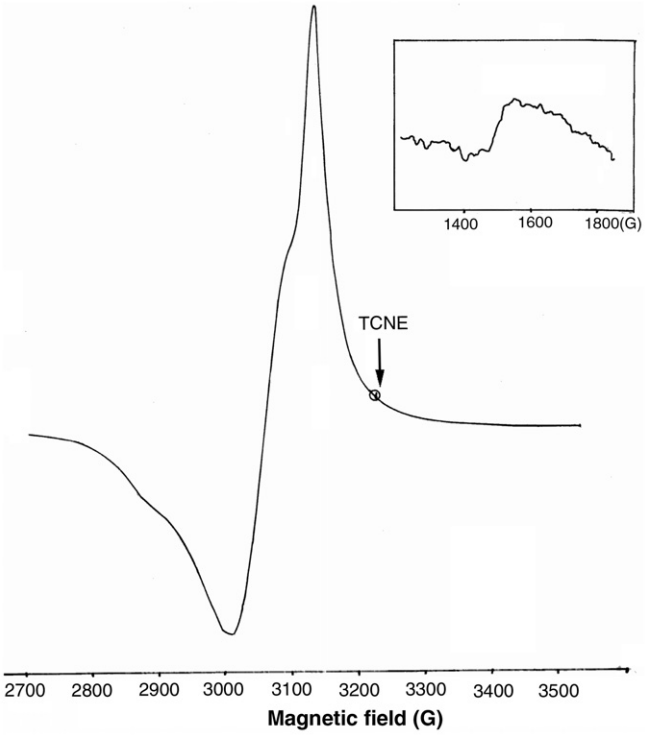

Fig. 3. Polycrystalline e.p.r. spectrum (room temperature) of [Cu(SAA)(phen)] (**3**).

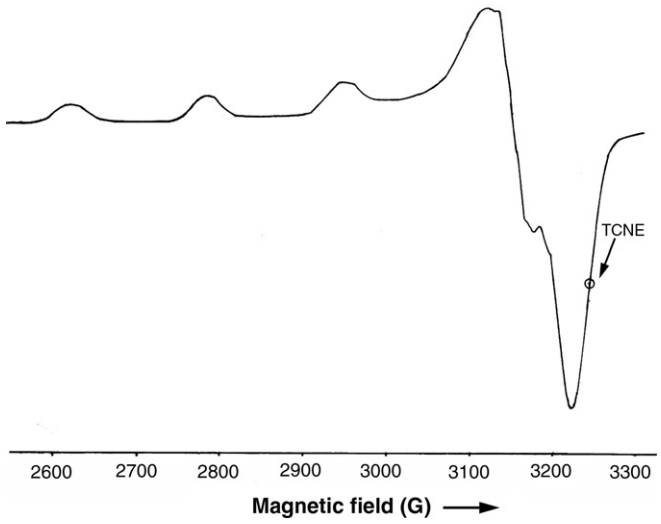

Fig. 4. E.p.r. spectrum (liquid nitrogen temperature) in 100% DMSO of [Cu(SAA)(ImH)] (**1**).

Some representative figures are shown in Figs. 3 and 4. The e.p.r. spectral parameters derived from their respective spectra are presented in Tables 4 and 5.

3.3.1. Solid state e.p.r. spectra

The e.p.r. spectra of polycrystalline samples show similar features at room temperature (RT) and at liquid nitrogen temperature (LNT). Basic spectral features at both

Table 4
E.p.r. parameters of polycrystalline samples (RT)

Complex	g_1	g_2	g_3	g_{av}
[Cu(SAA)(ImH)] (**1**)	2.049	2.110	2.237	2.132
[Cu(SAA)(bipy)] CH_3CN (**2**)	2.059	2.116	2.250	2.141
[Cu(SAA)(phen)] (**3**)	2.063	2.111	2.246	2.140

Table 5
E.p.r. parameters of frozen solution (77 K)

Complex	$g_\parallel$	$g_\perp$	$A_\parallel$ (G)	g_{av}
[Cu(SAA)(ImH)] (**1**)	2.224	2.057	165	2.140
[Cu(SAA)(bipy)] CH_3CN (**2**)	2.224	2.060	171	2.142
[Cu(SAA)(phen)] (**3**)	2.231	2.074	185	2.152

temperatures are the same with slightly better resolution at LNT. The e.p.r. spectra of the present complexes are indicative of a $S = 1/2$ system. $\Delta M_s = \pm 2$ signal (half-field signal) is observed in the e.p.r. spectra of the polycrystalline samples. The half field signal is due to interactions between the complexes in the pure solid. However, the nature of the interaction is intermolecular, which is confirmed by e.p.r. observations in solutions where the interaction is lost. The spectra of the present complexes at room temperature in the polycrystalline state show rhombic features with three g-tensor values viz. g_1, g_2 and g_3 where $g_3 > g_2 > g_1$. It is observed that the g_3 values for complexes are higher than 2.3 and assign covalent character to the M–L bonds [29].

In the spectra with $g_3 > g_2 > g_1$, the rhombic spectral values $R = (g_2 - g_1)/(g_3 - g_2)$ may be significant, if $R > 1$, a predominant d_{z^2} ground state is present. If $R < 1$, a predominant $d_{x^2-y^2}$ ground state is present and when $R = 1$, then the ground state is approximately an equal mixture of d_{z^2} and $d_{x^2-y^2}$, and the structure is intermediate between square planar and trigonal bipyramidal geometries. All the present complexes have values $R < 1$ (0.484 for **1**, 0.423 for **2** and 0.351 for **3**) suggesting a distorted square planar or square based pyramidal geometry with a $d_{x^2-y^2}$ ground state. These observations are consistent with the g values viz. g_1, g_2 and g_3 of the corresponding complexes in the polycrystalline state at room temperature and further supports the geometries, as observed by X-ray diffraction, around the copper(II) ion in these complexes.

3.3.2. Solution e.p.r. spectra

The g-tensor values of the copper(II) complexes can be used to derive the ground state. The one electron paramagnetic mononuclear copper(II) complexes display X-band e.p.r. spectra in 100% DMSO at 77 K giving $g_\parallel > g_\perp > 2.0023$, indicating a $d_{x^2-y^2}$ ground state, and spectral features are characteristic of axial symmetry [30–32]. Similar spectra have been observed by many workers for copper(II) mononuclear complexes [10,33]. α^2 (0.712–777), evaluated using the expression $\alpha^2 = A_\parallel/0.036 + (g_\parallel - 2.0023) + 3/7(g_\perp - 2.0023) + 0.04$ [34], indicate that there is substantial in-plane σ-bonding in these complexes. It has been observed [35] that the contribution of the 4s orbital to σ-bonding between the metal and the ligand donor atom orbitals is predominant in those complexes with α^2 values greater than 0.70. The values of the exchange-coupling parameters G of 3.18–4.03, estimated from low temperature e.p.r. spectra of the complexes, were ≈4.0, suggesting the presence of exchange interactions in these complexes in solution at LNT [36]. All complexes with $g_\parallel > g_\perp > 2.0023$, and G values falling within the range 2–4 are consistent with a $d_{x^2-y^2}$ ground state in a square planar or square pyramidal geometry. The same geometries have already been proved by single crystal X-ray analysis.

3.4. UV–Vis spectroscopy

The electronic spectra for complexes **1**–**3** show a prominent broad band (Fig. 5) in the range 680–700 nm, ascribed to the *d-d* transition ($d_{xz}, d_{yz} \rightarrow d_{x^2-y^2}$). These results are typical of square-planar and square pyramidal geometries [37], which in general exhibit a single band between 588–750 nm ($d_{xz}, d_{yz} \rightarrow d_{x^2-y^2}$). These geometries were further confirmed by e.p.r. and single crystal X-ray data.

3.5. Cyclic voltammetry

Cyclic voltammograms of the present complexes were recorded in DMSO with tetra butyl ammonium perchlorate (TBAP) as the supporting electrolyte in the potential range + 0.8 to −1.3 ± 1 V versus SCE. A typical voltammogram is displayed in Fig. 6. [Cu(SAA)(ImH)] (**1**) shows an irreversible redox wave ($E_{pc} = -0.767$ V, $E_{pa1} = -0.495$ V) with an additional oxidation wave ($E_{pa2} = 0.495$ V). We tentatively attribute the reduction wave as being the two electron reduction ($Cu^{2+} \rightarrow Cu^0$) $E_{pc} = -0.767$ V and two oxidation waves as being two step oxidation ($Cu^0 \rightarrow Cu^+$,

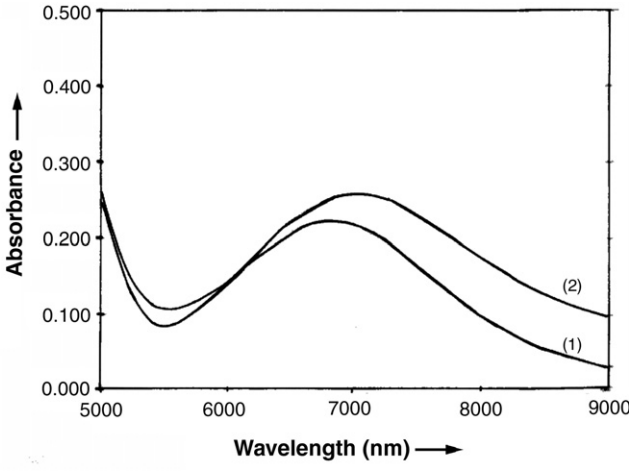

Fig. 5. The UV–Vis spectra (0.003 mol^{-1} dm^{-3}) of complexes: [Cu(SAA)(ImH)] (**1**) and [Cu(SAA)(bipy)]CH_3CN (**2**).

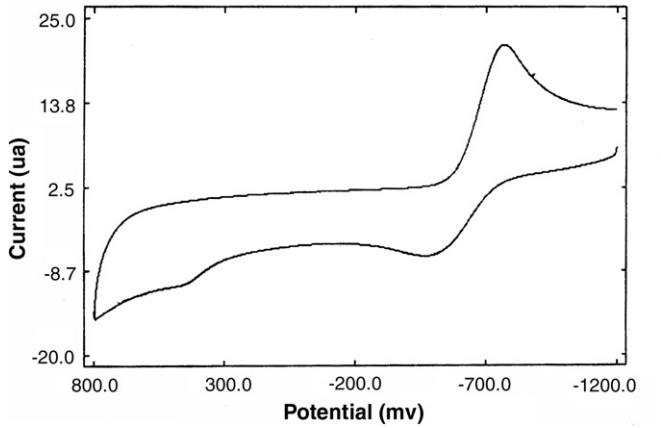

Fig. 6. Cyclic voltammogram of [Cu(SAA)(ImH)] (**1**) in 0.1 M TBAP [scan rate: 500 (mV/s)].

$Cu^{+} \rightarrow Cu^{2+}$) $E_{pa1} = -0.495$ V and $E_{pa2} = 0.495$ V. The electrochemical behaviour of the remaining two complexes are different to that observed for **1**. These two complexes exhibit two step reduction waves (peaks) ($Cu^{2+} \rightarrow Cu^{+}$ $E_{pc1} = -0.541$ V, $Cu^{+} \rightarrow Cu^{0}$ $E_{pc2} = -0.987$ V) and two oxidation waves ($E_{pa1} = -0.486$ for $Cu^{0} \rightarrow Cu^{+}$, $E_{pa2} =$ 0.113 V for $Cu^{+} \rightarrow Cu^{2+}$, for **2**). Similar observations were made by Kasumov et. al. [38] for copper(II) mononuclear complexes containing substituted salicylaldimines.

3.6. Superoxide dismutase activity

The superoxide dismutase activity of the present complexes were assayed by the use of alkaline dimethyl sulfoxide as a superoxide anion generating system in association with nitrobluetetrazolium chloride as a scavenger of superoxide [39]. Alkaline DMSO as a O_2^- generating system has the advantage that there is a marked decrease in the spontaneous dismutation rate of O_2^- due to the use of a relatively high pH combined with the low temperature and that a large amount of O_2^- is generated in solution as compared to SOD concentration. The SOD activity is related to the equatorial field experienced by the copper(II) complexes [40]. A strong equatorial field opposes the interaction of the complexed copper with superoxide radical, disfavouring the probable formation of the intermediate copper superoxide adduct [41]. Moreover, a strong field is a factor which disfavors the reduction process from copper(II) to copper(I). Another important factor in the catalytic process is the ability of the ligand to accommodate the reduced copper(I) in a tetrahedral-like or linear environment [42].

The complexes in the present study exhibit catalytic activity towards the dismutation of superoxide anions. The SOD activity data for complexes have been compiled in Table 6 along with the SOD activity values of some other ternary copper(II) complexes [10,19,43]. A representative plot of inhibition with increasing concentration of the complex **1** is given in Fig. 7 Complexes **1**–**3** are 750, 1400 and 1250 times less active than the native enzyme

Table 6
Superoxide dismutase activity of some copper(II) complexes

S. no.	Complex	IC_{50} (μmol dm^{-3})	Reference
1	$[Cu(PMDT)(bipy)](ClO_4)_2$	105	[10]
2	$[Cu(PMDT)(phen)](ClO_4)_2$	111	[10]
3	$[Cu(dien)(bipy)](BF_4)_2$	95	[19]
4	$[Cu(dien)(phen)](ClO_4)_2$	97	[19]
5	$[Cu(glygly)] \cdot 3H_2O$	132	[43]
6	$[Cu(glygly)(bipy)] \cdot 3H_2O$	22	[43]
7	$[Cu(glygly)(phen)] \cdot 3H_2O$	26	[43]
8	[Cu(SAA)(ImH)]	30	present work
9	$[Cu(SAA)(bipy)]CH_3CN$	56	present work
10	[Cu(SAA)(phen)]	50	present work

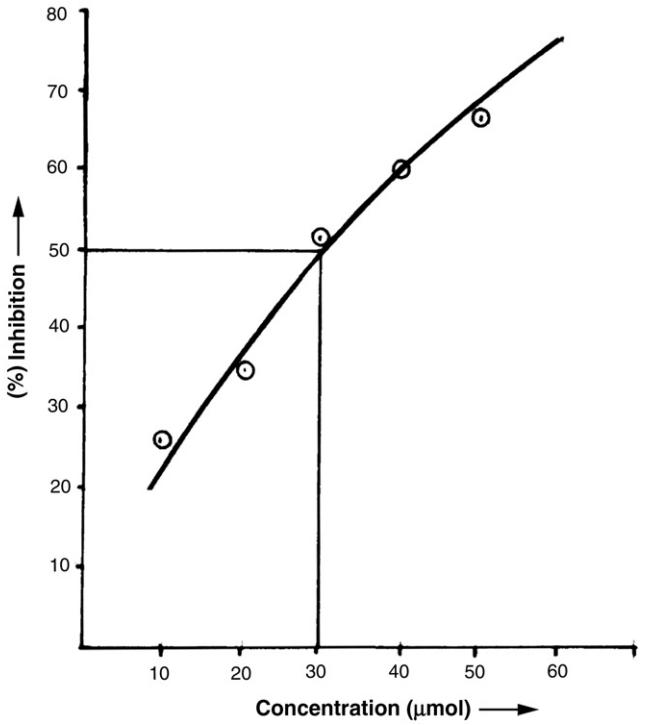

Fig. 7. Superoxide dismutase activity of [Cu(SAA)(ImH)] (**1**).

($IC_{50} = 0.04$ μmol dm^{-3}) on a molar base. This reduced activity may be due to the strong ligand field created by the SAA which opposes the interaction of the complexed copper with superoxide radical. In **1**, copper(II) is coordinated with two nitrogen atoms and two oxygen atoms to give a distorted square planar geometry whereas in complexes **2** and **3**, copper(II) is coordinated with three nitrogen atoms and two oxygen atoms to give a distorted square pyramidal geometry. The distortion of these complexes may favour the geometrical change, which is essential for the catalysis as the geometry of copper in the SOD enzyme also changes from distorted square pyramidal [44,45].

4. Conclusions

Copper(II) complexes of the general composition [Cu(SAA)(ImH)] (**1**) $[Cu(SAA)(bipy)]CH_3CN$ (**2**) and

[Cu(SAA)(phen)] (**3**) have been synthesized and characterized by using different physiochemical techniques. Molecular structures for complexes **1** and **2** have been revealed by single crystal X-ray analysis. The copper(II) complexes of **1**–**3** with Schiff base and mono/bidentate ligands are all neutral and found to have a distorted square planar geometry for (**1**) and distorted square pyramidal geometries for **2** and **3**. All complexes show $g_{\|} > g_{\perp} > 2.0023$, and G values falling within the range 2–4 are consistent with a $d_{x^2-y^2}$ ground state in a square planar geometry N_2O_2 **1** or a distorted square pyramidal geometry **2** and **3**. The complexes also exhibit catalytic activity towards the dismutation of superoxide anions. These complexes found to be less active than the native enzyme (SOD).

5. Supplementary material

Crystallographic data for the structural analysis have been deposited with the Cambridge Crystallographic Data Centre, CCDC No. 298983 for complex [Cu(SAA)(ImH)] (**1**) and CCDC No. 298982 for complex [Cu(SAA)(bipy)]-CH_3CN (**2**). Copies of this information may be obtained free of charge from The Director, CCDC, 12 Union Road, Cambridge, CB2 1EZ, UK, fax: +44 1223 336 033, e-mail: deposit@ccdc-cam.ac.uk or http://www.ccdc.cam. ac.uk).

Acknowledgements

Our grateful thanks are due to National Diffraction Facility, X-ray Division and RSIC (SAIF), IIT Mumbai for single crystal data collection and e.p.r. measurements respectively. The Head RSIC, Central Drug Research Institute, Lucknow is also thankfully acknowledged for providing analytical and spectral facilities. Financial assistance from UGC [Scheme No. F.30-76/2004(SR)] New Delhi is also thankfully acknowledged.

References

[1] P.A.N. Reddy, R. Datta, A.R. Chakravarty, Inrog. Chem. Commun. 3 (2000) 322.
[2] P.A.N. Reddy, M. Nethaji, A.R. Chakravarty, Inorg. Chim. Acta. 337 (2002) 450.
[3] R. Pradhan, A.M. Thomas, A. Mukherjee, S. Dhar, M. Nethaji, A.R. Chakravarty, Indian J. Chem. A 44 (2005) 18.
[4] A.M. Thomas, A.D. Naik, M. Nethaji, A.R. Chakravarty, Indian J. Chem. A 43 (2004) 691.
[5] A.D. Garnovskii, A.P. Sadimenko, M.I. Sadimenko, D.A. Garnovskii, Coord. Chem. Rev. 173 (1998) 31.
[6] S. Yamada, Coord. Chem. Rev. 190 (1999) 537.
[7] L. Que Jr., A.E. True, Prog. Inorg. Chem. 38 (1990) 97.
[8] V.L. Pecoraro (Ed.), Manganese Redox Enzymes, VCH, New York, 1992.
[9] A.L. Iglesias, G. Aguirre, R. Somanathan, M. Parra-Hake, Polyhedron 23 (2004) 3051, and references therein.
[10] R.N. Patel, Nripendra Singh, K.K. Shukla, U.K. Chauhan, J. Niclós-Gutiérrez, A. Castiñeiras, Inorg. Chim. Acta 357 (2004) 2469, and references therein.
[11] J.D. Ranford, P.J. Sadler, J. Chem. Soc., Dalton Trans (1993) 3393.
[12] G. Majella, S. Vivienne, M. Malachy, D. Michael, M. Vickie, Polyhedron 18 (1999) 2931.
[13] D.K. Saha, U. Sandbhor, K. Shirisha, S. Paddye, D. Deobagkar, C.E. Ansond, A.K. Powell, Bioorg. Med. Chem. Lett. 14 (2004) 3027.
[14] M.A. Zoroddu, S. Zanetti, R. Pogni, R. Basosi, J. Inorg. Biochem. 63 (1996) 291.
[15] R.N. Patel, Nripendra Singh, K.K. Shukla, V.L.N. Gundla, U.K. Chauhan, Spectrochim. Acta A 63 (2006) 21.
[16] R.N. Patel, Nripendra Singh, K.K. Shukla, U.K. Chauhan, Spectrochim. Acta A 61 (2005) 287.
[17] K. Skorda, S.P. Perlepes, C.P. Raptopoulou, R. Keuleers, A. Terzis, J.C. Plakatouras, Transition Met. Chem. 24 (1999) 541, and references therein.
[18] R.N. Patel, Nripendra Singh, K.K. Shukla, V.L.N. Gundla, U.K. Chauhan, J. Inorg. Biochem. 99 (2005) 651, and references therein.
[19] R.N. Patel, Nripendra Singh, K.K. Shukla, U.K. Chauhan, J. Niclós-Gutiérrez, A. Castiñeiras, V.G. Vaidyanathan, B.U. Nair, Spectrochim. Acta A 62 (2005) 261.
[20] R.N. Patel, Nripendra Singh, K.K. Shukla, V.L.N. Gundla, U.K. Chauhan, Spectrochim. Acta A 61 (2005) 1893.
[21] B.G. Malmstrom, T. Vanngard, J. Mol. Biol. 2 (1960) 118.
[22] G.M. Sheldrick, Acta Crystallogr., Sect. A 46 (1990) 467.
[23] G.M. Sheldrick, SHELXL-97. Program for the Refinement of Crystal Structures, University of Goettingen, Germany, 1997.
[24] J.A. Lewis, B.L. Iran, D.T. Puerta, E.M. Rumberger, D.N. Hendrickson, S.M. Cohen, J. Chem. Soc., Dalton Trans (2005) 2588.
[25] S. Gupta, A. Mukherjee, M. Nethaji, A.R. Chakravarty, Polyhedron 24 (2005) 1922.
[26] A.W. Addison, T.N. Rao, J. Rudijk, J. Van Rijn, G.C. Verschoor, J. Chem. Soc., Dalton Trans (1984) 1349.
[27] R.N. Patel, Nripendra Singh, V.L.N. Gundla, Indian J. Chem. A 45 (2006) 614.
[28] K. Skorda, S.P. Perlepes, C.P. Raptopoulou, Transition Met. Chem. 24 (1999) 541.
[29] D. Kivelson, R. Neimon, J. Chem. Phys. 35 (1961) 149.
[30] J.P. Klinman, Chem. Rev. 96 (1996) 2541.
[31] N.D. Chasteen, R.L. Belford, Inorg. Chem. 9 (1970) 169.
[32] B.J. Hathaway, F.F.G. Tomlinson, Chem. Rev. 5 (1970) 1.
[33] S. Chandra, H. Sangeetika, Shalini Thakur, Transition Met. Chem. 29 (2004) 925.
[34] A.H. Maki, B.R. McGarvey, J. Chem. Phys. 29 (1958) 35.
[35] B.J. Hathaway, Struct. Bond. 14 (1973) 60.
[36] I.M. Procter, B.J. Hathaway, P. Nicholls, J. Chem. Soc. (A) 1678 (1968).
[37] K. Matsumoto, N. Sekine, K. Arimura, M. Ohba, H. Ohba, H. Sakiyama, H. Okawa, Bull. Chem. Soc. Jpn. 77 (2004) 1343.
[38] V.T. Kasumov, F. Koksal, A. Sezer, Polyhedron 24 (2005) 1203.
[39] K. Hylond, I. Voisin, H. Bamoun, C. Auclair, Anal. Biochem. 135 (1983) 280.
[40] R.P. Bonomo, R. Marchelli, G. Tabbi, J. Inorg. Biochem. 60 (1995) 205.
[41] R.P. Bonomo, E. Conte, R. Marcelli, A.M. Sontoro, G.J. Tabi, J. Inorg. Biochem. 53 (1994) 127.
[42] R.P. Bonomo, E. Conte, G. Impellizzeri, G. Pappalardo, R. Purrello, E. Rizzarelli, J. Chem. Soc., Dalton. Trans (1996) 100.
[43] R.G. Bhirud, T.S. Shrivastava, Inorg. Chim. Acta 179 (1999) 125.
[44] S.J. Lipard, A.R. Burger, K. Ugurbil, J.S. Valentine, W. Pantaliano, in: K.N. Raymond (Ed.), Bioinorganic Chemistry, American Chemical Society, Washington, DC, 1977, p. 251.
[45] J.S. Richardson, D.C. Richardson, J.A. Trainer, E.D. Galtzoff, Nature (London) 306 (1986) 284.

the knowledge of the 'ionicity', i.e. degree of the partial oxidation. Resonance Raman and ^{129}I Mössbauer spectroscopies as well as diffuse X-ray scattering techniques are simple means of characterising the anionic polyiodine species and determine the 'ionicity' [19–23]. On the other hand, EPR spectroscopy is useful for characterising the materials, if both parts of the complex, i.e. the central metal (for example Mn, Fe, Co) and the π-electron macrocyclic ligand, are redox active since both oxidized forms $M^{2+}(Pc^{(1-)})I$ and $M^{3+}(Pc^{(2-)})I$ exhibit different EPR spectra. Additionally, EPR spectroscopy provides clear evidence for exchange coupling between the localised unpaired electron on the central metal ion and the π-carriers of the macrocycle within the stacks, as observed for CoPcI [24] and CuPcI [25], both linear-chain metal-spine conductors.

Although a few partially oxidized metallodiphthalocyaninato complexes are known [26], the correlation between the structure, π-orbital overlap and conductivity has not been systematically examined for such a system. In the course of our studies on metallodiphthalocyaninato complexes, the partially oxidized sandwich-type metallodiphthalocyanines are divided into two categories: (1) undoped metal(III) diphthalocyanines [27–32] and (2) iodine-doped partially oxidized metal(III) and metal(IV) diphthalocyanines [33–39]. In the first category M(III)Pc_2, exhibiting semiconducting properties, the central metal M(III) is sandwiched between the Pc^{2-} and one-electron oxidized $Pc^{-\cdot}$ radical ligand, however, the X-ray single crystal analysis shows that both halves of these sandwich complexes are equivalent structurally, thus a non-integral oxidation state should be assigned to both of them ($\rho = -1.5$). In the second category, iodine-doped metal(III) and metal(IV) diphthalocyanines, the conductivity depends strongly on the amount of iodine-doped atoms, which is closely correlated with the formal oxidation state of Pc macrocyclic ring.

Similar to iodine-doped metallomonophthalocyanines, the iodine-doped metallodiphthalocyaninato complexes also crystallise in the tetragonal system, in which the central metal ion is disordered over two symmetrically equivalent positions [33–39]. Quite recently we have stated that iodine-doped zirconium diphthalocyanine, depending on the crystallisation process and the amount of the iodine, can crystallise also in the monoclinic system [39]. Using a slightly modified method [40] we have obtained a new partially oxidized zirconium diphthalocyanine $[ZrPc_2]IBr_2$. Although, this complex contains the trihalide ions IBr_2^-, similar to the tetragonal iodine doped zirconium diphthalocyanine $[ZrPc_2](I_3)_{2/3}$ that contains the I_3^- ion [38], the complexes are not isostructural. Therefore for understanding the charge transport properties of $[ZrPc_2]IBr_2$ complex a knowledge of its crystal structure is needed. Additionally, the correlation between the crystal structures and charge transport properties of the two iodine-doped different zirconium diphthalocyaninato complexes $[ZrPc_2](I_3)_{2/3}$, $[ZrPc_2]I_3 \cdot I_2$, described earlier [38,39], with the third complex $[ZrPc_2]IBr_2$, described here, are reported. The crystal structures and properties of the partially oxidized zirconium diphthalocyanine complexes are discussed and compared with the undoped $ZrPc_2$ complex [41].

2. Experimental

2.1. Synthesis

All reagents were of the highest grade commercially available and were used as received. The crystals of $[ZrPc_2]IBr_2$ were obtained directly by the reaction of pure powdered zirconium and phthalonitrile under a stream of IBr. The powdered zirconium (0.182 g), phthalonitrile (2.050 g) and IBr (0.450 g) in a molar proportion of 1:8:2, with about 5% excess of IBr, were mixed together and pressed into pellets. The pellets were inserted into an evacuated glass ampoule (ca. 25 cm long) and sealed. The part of ampoule with the pellets was heated at about 220 °C for one day. At this temperature the liquid phthalonitrile undergoes catalytic tetramerization forming the phthalocyaninato rings, which accepts the electron from the zirconium and forms sandwich $ZrPc_2$ molecules. Simultaneously IBr partially oxidized the $ZrPc_2$ molecules and transforms into IBr_2^- ions and neutral diiodine molecules, yielding good quality single crystals with the composition $[ZrPc_2]IBr_2$. The major part of the iodine formed during formation of the $[ZrPc_2]IBr_2$ crystals resublimed at the cooler part of the ampoule. After opening the ampoule, the iodine that formed from IBr during the preparation procedure as an impurity is easily lost after expose to air at room temperature (3–4 days) or by slowly heating to about 40–45 °C. The elemental analysis has been performed on an energy dispersive spectrometer. Calc. for $C_{64}H_{32}N_{16}ZrIBr_2$: Zr, 6.50; I, 9.04; Br, 11.38; C, 54.78; N, 15.96; H, 2.34. Found: Zr, 6.45; I, 9.15; Br, 11.33; C, 54.84; N, 15.98; H, 2.29%.

2.2. X-ray diffraction study of $[ZrPc_2]IBr_2$

The X-ray single crystal data were collected on a KUMA KM-4 diffractometer equipped with a two-dimensional area CCD detector from a single crystal (black-violet) with dimensions of $0.22 \times 0.18 \times 0.14$ mm. The graphite-monochromatized Mo Kα radiation ($\lambda = 0.71073$ Å) and ω-scan technique with $\Delta\omega = 0.75°$ for one image were used. 960 images for six different runs covering over 95% of the Ewald sphere were performed. The exposure times were 20 s/image. Accurate cell parameters were refined by least-squares methods on the basis of 2577 of the strongest reflections. One image was monitored as a standard after every 40 images for a control of the stability of the crystal. Integration of the intensities, corrections for Lorentz and polarisation effects were carried out using KUMA KM-4 CCD software [42]. Face-indexed analytical absorption was calculated using the SHELXTL program [43]. The minimum and maximum transmission factors are 0.641 and 0.744, respectively. A total of 25 532 (6899 independent, $R_{int} = 0.0306$) reflections were integrated and used for the crystal

structure determination. The structure was solved by the Patterson heavy atom method and refined by full-matrix least-squares method using the SHELXL97 program [44] with anisotropic thermal parameters for all non-hydrogen atoms. The hydrogen atoms of the benzene rings were introduced in their geometrical positions (HFIX 43) with isotropic thermal parameters $U_{iso}(H) = 1.2U_{iso}(C)$, i.e. 20% higher than the thermal parameters of the carbon atom directly bonded to the H atom. The final difference Fourier maps showed no peaks of chemically significance (+0.335 e Å^{-3} and −0.926 e Å^{-3}). More details of data collection and final refinement parameters are listed in Table 1 and in the Supporting Information. Selected geometrical parameters are collected in Table 2.

2.3. Raman spectroscopy

The resonance Raman spectrum was recorded at room temperature on a Jobin-Yvon Ramanor U-1000 spectrometer equipped with a photomultiplier-type detector and phonon-counting hardware. 90° geometry was used. An argon-ion laser line at 514.5 nm at 100 mW power was used as the exciting radiation. The resolution was set at 3 cm^{-1}.

Table 1
Crystallographic data and final refinement parameters for $[ZrPc_2]IBr_2$

Chemical formula	$C_{64}H_{32}N_{16}ZrIBr_2$
Molecular weight	1403.00
Temperature (°C)	295(2)
Crystal system	monoclinic
Space group	$P2_1/m$ (No. 11)
Unit cell dimensions	
a (Å)	6.697(1)
b (Å)	25.483(5)
c (Å)	16.918(3)
β (°)	100.03(3)
V (Å^3)	2843.1(9)
Z	2
D_{obs} (measured by flotation) (g cm^{-3})	1.635
D_{calc} (g cm^{-3})	1.639
Radiation, Mo Kα (Å)	0.71073
Absorption coefficient, μ (mm^{-1})	2.200
Refinement on F^2	
R [$F^2 > 2\sigma(F^2)$][a]	0.0514
wR (F^2 all reflections)[b]	0.0669
Goodness-of-fit, S	0.994
Residual electron density, $\Delta\rho_{max,min}$ (e Å^{-3})	+0.335, −0.926

[a] $R = \sum||F_o| - |F_c||/\sum F_o$.
[b] $wR = \{\sum[w(F_o^2 - F_c^2)^2]/\sum wF_o^4\}^{1/2}$; $w^{-1} = \sigma^2(F_o^2) + (0.009P)^2$, where $P = (F_o^2 + 2F_c^2)/3$.

Table 2
Selected bond distances (Å) and angles (°) for $[ZrPc_2]IBr_2$

I1–Br1	2.694(1)	Zr–N2	2.377(4)
Zr–N4	2.311(4)	Zr–N6	2.287(6)
Zr–N8	2.280(5)	Zr–N10	2.283(6)
N2–Zr–N4	74.8(2)	N2–Zr–N6	76.7(2)
N2–Zr–N8	75.8(2)	N2–Zr–N2^{ii}	74.4(2)
N4–Zr–N2^{ii}	116.0(2)	N4–Zr–N6	143.6(2)
N4–Zr–N8	79.2(2)	N4–Zr–N10	77.9(2)
N6–Zr–N10	114.0(2)	N8–Zr–N10	73.8(2)
N2–Zr–N10	142.3(2)	N6–Zr–N8	72.3(2)
N4–Zr–N8^{ii}	142.2(2)	N2–Zr–N8^{ii}	140.9(2)
N4–Zr–N4^{ii}	70.8(2)	N8–Zr–N8^{ii}	115.3(3)

Symmetry code: $^{i}1 - x, 1 - y, 1 - z$; $^{ii}x, 1/2 - y, z$.

2.4. UV–Vis spectroscopy

Measurements of the electronic spectra of $[ZrPc_2]IBr_2$ and $ZrPc_2$ were carried out at room temperature using a Cary-Varian 2300 spectrometer. The UV–Vis spectra were recorded on a thin solid film between quartz glass prepared from a nujol mull, since a thin solid film of the $[ZrPc_2]IBr_2$ complex could not be obtained by sublimation in vacuum due to decomposition to $ZrPc_2$ and I_2 and Br_2.

2.5. Magnetic susceptibility measurement

Magnetic susceptibility measurement of $[ZrPc_2]IBr_2$ was carried out on a solid sample of 100 mg in the temperature range 300–2 K with a Quantum Design SQUID magnetometer (San Diego, CA). The susceptometer was calibrated with $(NH_4)_2Mn(SO_4)_2 \cdot 12H_2O$. Data were recorded at a magnetic field of 0.5 T.

2.6. Electron paramagnetic resonance measurements

EPR measurements were made on SE-Radiopan and ESR 300 E – Bruker X-band spectrometers at room temperature and variable temperature (300–90 K) using cold N_2 gas. The studies were carried out on solid samples of 4–10 mg. The concentrations of the free radicals in the samples of $[ZrPc_2]IBr_2$ were calculated using standard integration of the derivative signal and comparing the area with the area determined with the free radical standards. DPPH, TEMPO and TEMPOL were used as standards.

2.7. Single-crystal electrical conductivity measurements

Single crystals of $[ZrPc_2]IBr_2$ were mounted on silvered graphite fibers and electrical contacts were made with a palladium paste. Conductivity measurements were carried out along the a and c crystallographic axis (see Fig. 3a and b), i.e. along the stacks of one-electron oxidized $[ZrPc_2]^+$ units and perpendicular to the stacks using a standard four-point probe technique [45] with a sampling current of 20 μA. Variation of the temperature was archived by placing the samples in a cold-gas stream of N_2 or He. The conductivity of the material was calculated from the relationship $\sigma = L/RA$, where σ is the conductivity (in Ω^{-1} cm^{-1}), R is the measured resistance (in Ω) of the material between two inner contacts (in cm) and A is the cross-sectional area of the sample (in cm^2). For the conductivity measurement a crystal was selected with the greatest dimension of 0.834 mm (along the a axis), 0.456 mm (along the c axis) and 0.246 mm (along the b axis). The estimated uncertainty in these measurements is about 0.001 mm. The area A was estimated from the cross-sectional distance as

observed with a microscope. An empirical analysis of the measurement errors indicates that the area is uncertain by $\delta A/A \approx \pm 0.1$, leading to an uncertainty $\Delta\sigma/\sigma \approx 0.2$. The measurements were repeated on four single crystals with different dimensions (0.504–0.834, 0.322–0.456 and 0.186–0224 mm along the *a*, *c* and *b* axes, respectively). The differences in the measured conductivities on these single crystals are less than 5%. The conductivity measured on a single crystal perpendicular to the stacks of $[ZrPc_2]^+$ units (i.e. along the *c* axis) is smaller by a factor of $\sim 10^3$ than the conductivity along the stacks (*a* axis).

3. Results and discussion

3.1. Synthesis

Our preparation method leads directly to good-quality single crystals. The oxidation of the phthalocyaninato ring Pc(2−) → Pc(1−) by iodine is well known [46] and has been widely used to obtain partially oxidized metallophthalocyaninato and diphthalocyaninato complexes. IBr is a stronger oxidant than I_2 [47]. The synthesis of $[ZrPc_2]IBr_2$ from phthalonitrile and pure powdered zirconium under a stream of IBr requires the formation of the heterotrihalide IBr_2^- ions, i.e. electron-rich three center bonding mixed trihalide ions [48]. The formation of the IBr_2^- ion by the reaction of I^- with Br_2 is well known [49]. However, under the used reaction conditions the IBr_2^- ion is the result of heterolitic thermal dissociation of IBr: $3IBr \leftrightarrow I_2Br^+ + IBr_2^-$ or by the series of reactions: $2IBr + 2e \rightarrow I_2 + 2Br^-$ and $IBr + Br^- \rightarrow IBr_2^-$. Thus the formation of the $[ZrPc_2]IBr_2$ complex can be write as shown in Scheme 1, where $Pc = C_{32}H_{16}N_8$. During synthesis the $[ZrPc_2]IBr_2$, crystals grew in the hot part (∼220 °C) of the ampoule, and the I_2 resublimed in the cooler part. The crystals of $[ZrPc_2]IBr_2$ are air and light stable. Iodine as an impurity is easily lost by cooling up to ∼45 °C (10–15 min) or by exposure to air at room temperature (3–4 days).

The obtained $[ZrPc_2]IBr_2$ crystals are insoluble in water, ethanol and methanol and are slightly soluble in pyridine, DMF, DMSO, chloronaphthalene and other high boiling aromatic solvents. However, after several days a black powder material from the solution was obtained. Elemental analysis of this powder material is consistent with a $ZrPc_2$ complex that has been characterised earlier [41,50]. Thus it was found that a decomposition process takes place in solution. This process depends strongly on the temperature and is several times quicker in hot solvents. Contact of $[ZrPc_2]IBr_2$ with dilute inorganic acids (H_2SO_4, HNO_3 and their mixture or mixture with concentrated HCl) leads to demetallation, yielding the α-form of metal-free phthalocyanine (α-H_2Pc) [51] and the appropriate salts.

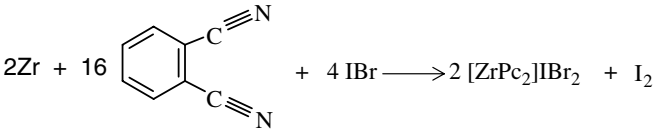

Scheme 1. Formation of the $[ZrPc_2]IBr_2$ complex; $Pc = C_{32}H_{16}N_8$.

3.2. Raman spectroscopy

In order to relate the charge transport properties the 'ionicity', i.e. the degree of oxidation of the $[ZrPc_2]$ unit, must be determined. Resonance Raman spectroscopy is useful for identification of the anionic part of the complex. The resonance Raman spectrum measured on a polycrystalline sample at room temperature (Fig. 1) exhibits only one strong fundamental band at 169 cm^{-1} (the expected value for IBr_2^- is 168 cm^{-1} [52]). The absence of a band at ∼110 cm^{-1} eliminates I_3^- ions and the absence of a peak at ∼160 cm^{-1} eliminates Br_3^- ions [19,20]. Free Br_2 ($\nu \approx 306$ cm^{-1}) [53,54] and free I_2 ($\nu \approx 210$ cm^{-1}) [55] are not present in detectable quantities in the crystals.

3.3. Description of the structure

The crystals of $[ZrPc_2]IBr_2$ are built up from one-electron oxidized $[ZrPc_2]^+$ sandwich units and mixed trihalide IBr_2^- counter ions. The $[ZrPc_2]^+$ unit is located on a special position and has crystallographic *m* symmetry, while the I atom of the IBr_2^- ion occupies the inversion center, so the IBr_2^- ion is linear and symmetrical. The central closed shell Zr^{4+} cation (d^0 configuration) is eight coordinated by two saucer shaped phthalocyaninato units (Fig. 2): Pc^{2-} and one-electron oxidized $Pc^{-\bullet}$ π-radical ligands (identified by EPR spectroscopy). This may be the reason for the slightly asymmetric location of the Zr^{4+} cation between the phthalocyaninato rings. The average Zr–N distance to one Pc ring is equal to 2.283 Å and is slightly longer (2.344 Å) than to the other Pc ring. On the other hand the slightly asymmetric location of the Zr^{4+} cation between the phthalocyaninato rings (1.233(3) Å from the N_4 plane of one Pc ring and 1.244(3) Å from the N_4 plane of the second ring) is due to the different interaction of the phthalocyaninato rings with the IBr_2^- ion that is located closely to the one of them. In conclusion, most probably the Zr^{4+} cation is sandwiched between the two phthalocyaninato macrocyclic rings with a non-integral formal oxidation state of −1.5.

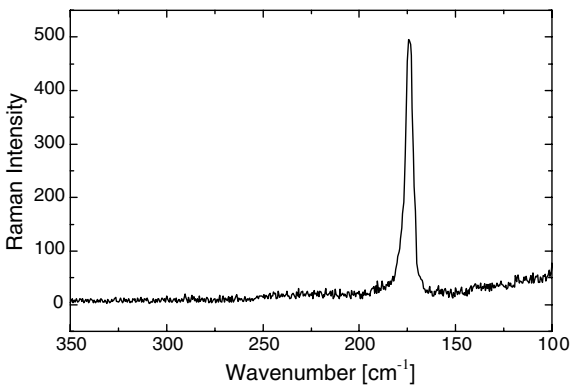

Fig. 1. Resonance Raman spectrum of $[ZrPc_2]IBr_2$ at room temperature.

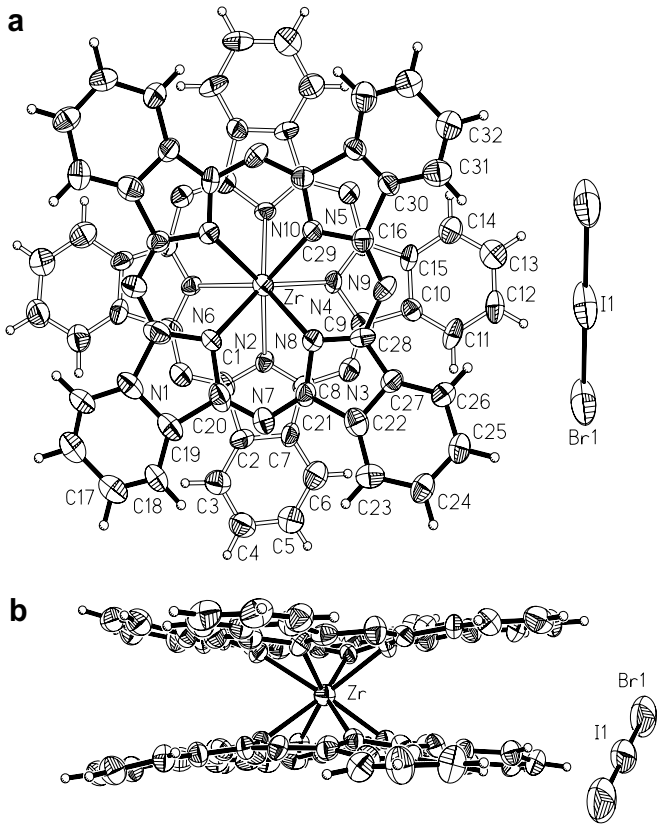

Fig. 2. Molecular structure of $[ZrPc_2]IBr_2$, top view (a) and side view (b). Displacement ellipsoids are shown at the 50% probability level.

Similarly a non-integral oxidation state of the Pc ring is observed in the class of partially oxidized $MPc(I_3)_{2/3}$, $[MPc_2](I_3)_{2/3}$ or $[MPc_2](I_3)_{5/9}$ complexes, in which the formal oxidation state of Pc ring equals −1.667 or −1.772 [35,37]. Both phthalocyaninato macrocyclic rings of the $[ZrPc_2]^+$ unit are significantly deviated from the weighted least-squares plane defined by four N-isoindole atoms. The largest deviations from the N_4-isoindole planes are observed for C5 (1.109 Å) for one Pc ring and C24 (0.762 Å) for the second Pc ring. The distortion of the phthalocyaninato rings from planarity is comparable to that found in the crystal of $[ZrPc_2](I_3 \cdot I_2)$ [39], but is smaller than that in the crystal of unoxidized $ZrPc_2$, in which the greatest deviation equals 1.47 Å [41]. The distortion of the phthalocyaninato macrocyclic rings of the zirconium diphthalocyaninato complexes, that can be estimated by the bending of the isoindole units with respect to the N_4-core and by the "twisting" of the peripheral carbon atoms of benzene rings, is collected in Table 3. The displacements of the carbon atoms of the benzene rings for some metallodiphthalocyaninato structures [55–61] are listed in Table 4, for a comparison. As can be seen from Tables 3 and 4, both one-electron oxidized zirconium diphthalocyanines, $[ZrPc_2]IBr_2$ and $[ZrPc_2]I_3 \cdot I_2$, and unoxidized $ZrPc_2$ contain the most deviated phthalocyaninato rings. The Zr–N distances in $[ZrPc_2]IBr_2$ range from 2.280(5) to 2.377(4) Å, and are compared with the distances in the $[ZrPc_2]I_3 \cdot I_2$ complex [39], but they are slightly shorter than those observed in the crystal structure of the unoxidized $ZrPc_2$ complex [41]. This is likely due to the weaker repulsive interaction between Pc^{2-} and the one-electron oxidized $Pc^{-\cdot}$ π-radical ligand in relation to the unoxidized $ZrPc_2$, in which the Pc···Pc interaction is undoubtedly greater, since both Pc rings are 2−. The M–N distances in zirconium diphthalocyaninato complexes are shorter than those of the other sandwich-type metallodiphthalocyaninato structures due to the relatively small radius of the Zr^{4+} cation [62]. The effect of the small radius of Zr^{4+} and its great formal oxidation state are the reasons for the more closely located phthalocyaninato macrocyclic rings around the Zr^{4+} cation, and the distance between the N_4-isoindole planes is the shortest within the sandwich-type metallodiphthalocyanines (see Table 5). The Pc rings in $[ZrPc_2]IBr_2$, similarly to $[ZrPc_2]I_3 \cdot I_2$, are staggered at an angle of 45.0(3)° and this is an additional reason for the closer location of the Pc rings in relation to the unoxidized $ZrPc_2$ complex in which the rotation angle of the Pc rings is equal to 42° [41]. The close proximity of the N_4-planes of the Pc rings indicates the strong interaction of the π-clouds and adds to the distortion of the rest of Pc rings from the N_4-planes. The π–π interaction is a common feature in the field of phthalocyanine chemistry, and it leads phthalocyanine and its metal complexes to form supramolecular aggregates [63–66]. The staggered orientation of the Pc rings give the square antiprismatic coordination of the central Zr^{4+} cation and, as can be seen from the Fig. 2a, indicates that the outermost carbon atoms of the benzene rings are apart, as for non-interpenetrating π-clouds. In the third crystal of

Table 3
Distortion of the phthalocyaninato rings in partially oxidized zirconium diphthalocyaninato complexes

Compound	Bending of the isoindole[a] with respect to the N_4 plane (°), e.s.d.'s = 0.02					"Twisting" of the external phenyl ring given by the displacement of the outermost carbon atoms of the phenyl ring (Å), e.s.d.'s = 0.01								Ref.
	N2	N4	N6	N8	N10	C4	C5	C12	C13	C24	C25	C17	C32	
$[ZrPc_2]IBr_2$	12.7	4.3	4.5	9.5	9.1	0.93	1.11	0.40	0.37	0.76	0.70	0.44	0.70	this work
$[ZrPc_2]I_3 \cdot I_2$	15.8	4.7	14.3	7.6	7.5	0.39	0.46	1.31	1.10	0.54	0.65	1.07	0.68	[39]
$[ZrPc_2](I_3)_{2/3}$	Both Pc-rings are closely planar, due to crystal symmetry of *P4/mcc*													[38]
$ZrPc_2$[b]	18.6	11.8	6.6	11.4		1.49	1.35	0.77	0.93	0.54	0.44	0.87	0.93	[41]
	14.9	12.3	14.8	8.0		1.22	1.21	0.99	0.99		1.22	0.70	0.66	

[a] Isoindole rings: N2, C1–C8; N4, C9–C16; N6, C17–C20, $C17^{ii}$–$C20^{ii}$; and N8, C21–C28; N10, C29–C32, $C29^{ii}$–$C32^{ii}$ (see Fig. 2 for labelling).
[b] First line related the one Pc ring, the second line related the other Pc ring in $ZrPc_2$.

Table 4
Comparison of the displacements of the outermost carbon atoms of phenyl rings from the N_4-isoindole plane in some metallodiphthalocyaninato (MPc_2) structures

Compound	Displacement of the phenyl ring C atoms from the N_4-isoindole plane		Ref.
	Least displaced (Å)	Most displaced (Å)	
$[ZrPc_2]IBr_2$	0.37(1)	1.11(1)	this work
$[ZrPc_2]I_3 \cdot I_2$	0.37	1.31	[39]
$ZrPc_2$	0.49	1.47	[41]
$[ZrPc_2](I_3)_{2/3}$[a]	0	0	[38]
α-$SnPc_2$	0.18	1.01	[56]
β-$SnPc_2$	0.25	1.21	[57]
$Ln^{(III)}Pc_2$	0.25	1.10	[58]
$TiPc_2$[b]	1.06	1.94	[59]
$[Nb^{(V)}Pc_2]IBr_2$[b]	0.91	1.53	[60]
$[Nb^{(V)}Pc_2]IBr_2 \cdot I_2$[b]	0.73	1.85	[60]
$[TiPc_2](I_3)_{2/3}$	0.61	0.67	[33]
UPc_2	0.48	1.10	[61]
$[UPc_2](I_3)_{5/9}$[a]	0	0	[35]
$[UPc_2](I_3)_{2/3}$	0.083	0.335	[37]
$In^{(III)}Pc_2$	0.12	0.88	[32]
$[In^{(III)}Pc_2](I_3)_{2/3}$[a]	0	0	[38]

[a] Pc rings are closely planar.
[b] 'Stapled' by two C–C σ bonds.

partially oxidized zirconium diphthalocyanine, $[ZrPc_2](I_3)_{2/3}$, the relatively long N_4–N_4 interplanar distance is due to the symmetry of the crystal (tetragonal system), and the space group of *P*4/*mcc* requires the location of the Pc rings on the special position in the crystal (the Pc rings are located on the crystallographic *m* plane) [38]. As can be seen from Tables 4 and 5, the greatest distortion of the Pc rings from planarity and the shortest N_4–N_4 interplanar distances are observed for $[NbPc_2]IBr_2 \cdot I_2$ and $[NbPc_2]IBr_2$ [60], as well as for $TiPc_2$ [59]. However, these three complexes belong to the new family of sandwiched metallodiphthalocyaninato complexes in which the close proximity of the Pc rings is due to two interligand C–C σ-bonds that have stapled both phthalocyaninato rings [59,60]. In this family of sandwiched MPc_2 complexes the delocalisation of the π-electrons in the inner 16-membered rings breaks down due to two C atoms with sp^3 hybridisation and the formation of the interligand σ-bonds. Additionally, it should be added that oxidation of the stapled $TiPc_2$ complex by iodine leads to the breaking of the interligand C–C σ-bonds [33].

The one-electron oxidized $[ZrPc_2]^+$ units of $[ZrPc_2]IBr_2$ in the crystal, similarly as in $[ZrPc_2]I_3 \cdot I_2$, form pseudo-mono-dimensional columnar stacks that are aligned along the *a* axis of the crystal (see Fig. 3a), and the mean planes of the phthalocyaninato rings are parallel to the *bc* plane (Fig. 3b). However, the anionic parts of these complexes are different (IBr_2^- in one and $I_3^- \cdot I_2$ in the second) and also are located differently in relation to the stacking columns of the $[ZrPc_2]^+$ units. In the crystal of $[ZrPc_2]I_3 \cdot I_2$ the slight bending of I_3^- ions due to the interaction with neutral I_2 molecules are parallel to the *b* crystallographic axis and together with I_2 neutral molecules form zigzag chains that are perpendicular to the columnar stacks of the $[ZrPc_2]^+$ units [39]. In this $[ZrPc_2]IBr_2$ crystal structure, the symmetrical mixed trihalide IBr_2^- that is located in the inversion center forms angles of 104.7(3)°, 47.3(3)° and 129.4(3)° with the *a*, *b* and *c* axes of the crystal, respectively. This structure ($[ZrPc_2]IBr_2$) is also different from the third zirconium diphthalocyaninato complex $[ZrPc_2](I_3)_{2/3}$ [38] in several aspects. The Pc rings of $[ZrPc_2](I_3)_{2/3}$ are crystallographically constrained to lie in the (0 0 1) plane of its tetragonal unit cell, so they are planar and strictly perpendicular to the stacking axis that is also the unique axis. Two Pc rings of $[ZrPc_2](I_3)_{2/3}$ are rotated by 42°, and are separated by a distance of 3.244(3) Å, which is significantly longer than the N_4–N_4 interplanar distance in the $[ZrPc_2]IBr_2$ crystal. The anionic part of the $[ZrPc_2](I_3)_{2/3}$ complex, i.e. the iodine doped atoms, form linear and symmetrical triiodide ions that in the crystal are disordered and located in the channels between the columnar stacks of $[ZrPc_2]^{2/3+}$ units, thus both mono-dimensional aggregates are parallel [38]. In the crystal of $[ZrPc_2]IBr_2$, the mono-dimensional columns of $[ZrPc_2]^+$ units are not parallel to the linear IBr_2^- ions. Additionally, due to the crystal symmetry and the space group of *P*4/*mcc*, the central

Table 5
Comparison of the coordination of the central metal ion of some MPc_2 structures

Compound	Formal oxidation state of Pc ring	Average M–N bond distance (Å)	Distance between N_4–N_4 plane (Å)	Staggering angle (°)	Ref.
$[ZrPc_2]IBr_2$	−1.5	2.314	2.434(3)	45.0(3)	this work
$[ZrPc_2]I_3 \cdot I_2$	−1.5	2.297	2.494(3)	45.0(2)	[39]
$[ZrPc_2](I_3)_{2/3}$	−1.667	2.527	3.244(3)	40.6(2)	[38]
$ZrPc_2$	−2	2.30	2.52	42	[41]
UPc_2	−2	2.43	2.81	37	[61]
$[UPc_2](I_3)_{5/9}$	−1.667	2.448	2.903(5)	40.2(6)	[37]
$[UPc_2](I_3)_{2/3}$	−1.772	2.549	3.250(1)	40.7(6)	[35]
$In^{(III)}Pc_2$	−1.5	2.333	2.741(9)	42.2(4)	[32]
$[In^{(III)}Pc_2](I_3)_{2/3}$	−1.167	2.523	3.196(1)	40.0(4)	[38]
$[Nb^{(V)}Pc_2]IBr_2$[a]	−2	2.21	2.331(5)	45.0	[60]
$[Nb^{(V)}Pc_2]IBr_2 \cdot I_2$[a]	−2	2.21	2.148(6)	45.0	[60]
$TiPc_2$[a]	−2	2.22	2.32	45	[59]
$[TiPc_2](I_3)_{2/3}$	−1.667	2.246	2.42	41.1	[33]

[a] 'Stapled' by two C–C σ bonds.

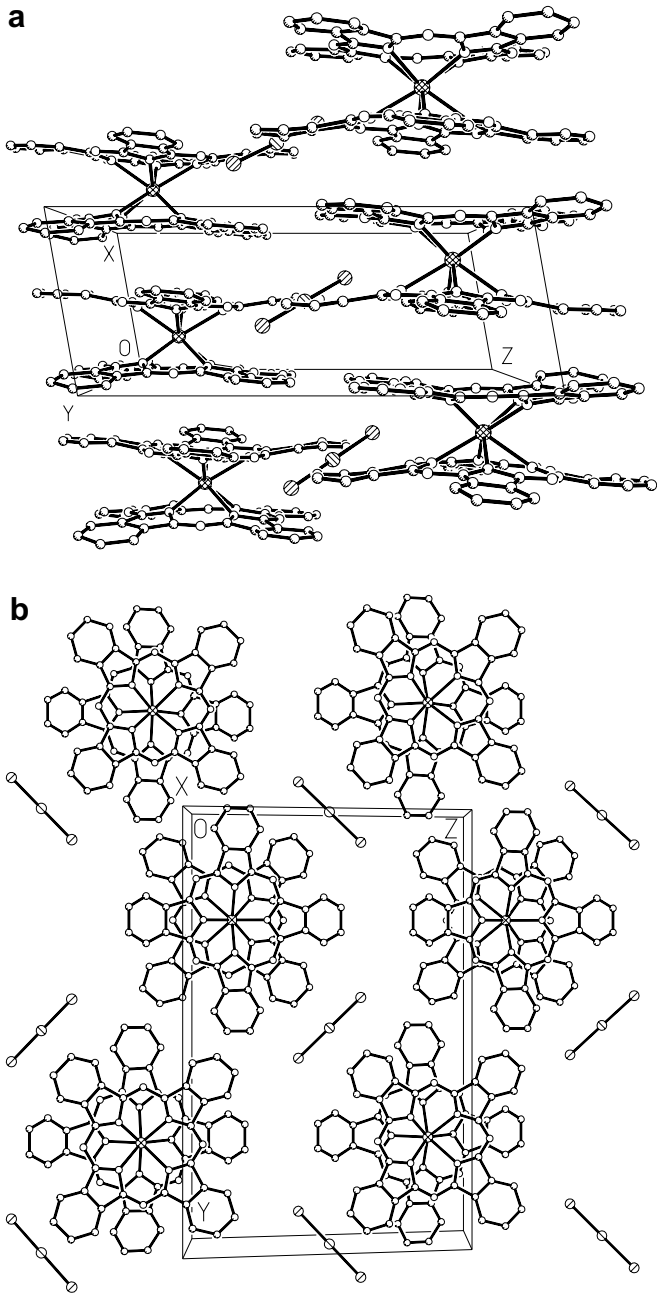

Fig. 3. View of the crystal structure of $[ZrPc_2]IBr_2$ perpendicular to the stacks of $[ZrPc_2]^+$ units (a) and along the stacks (b).

Zr^{4+} cation in the crystal of $[ZrPc_2](I_3)_{2/3}$ is statistically distributed over two symmetrically equivalent positions, in the $[ZrPc_2]IBr_2$ crystal the Zr^{4+} cation is ordered. One more difference between the $[ZrPc_2]IBr_2$ and $[ZrPc_2](I_3)_{2/3}$ complexes should be noted, the difference in the formal oxidation state of the cationic sandwich $[ZrPc_2]$ unit, +1 and +2/3 in $[ZrPc_2]IBr_2$ and $[ZrPc_2](I_3)_{2/3}$, respectively. The formal oxidation state of the $[ZrPc_2]$ units correlate with the holes of the electrons on the Pc rings that are strictly connected with the charge transport properties. The intermolecular back-to-back Pc ⋯ Pc distances in the crystal of $[ZrPc_2]IBr_2$, with an average value of ~3.35 Å between two neighbouring $[ZrPc_2]^+$ units, indicates a π–π interaction between the Pc rings within the columns, since this value is slightly shorter than the van der Waals distance of 3.4 Å for aromatic carbon atoms [67]. This π–π intermolecular interaction plays an important role in the charge transport.

The I–Br distances in the symmetrical IBr_2^- [(Br–I–Br)$^-$] ion are equal to 2.694(1) Å. This value is compared to those found in the other metallophthalocyaninato complexes containing the IBr_2^- ion [60,68]. The I–Br distances in the I_2Br^- ion [(I–Br–I)$^-$] are significantly longer as molecular orbital calculations show (the I–Br distance in the (I–Br–I)$^-$ ion is equal to ~2.91 Å) [48] and compared with those obtained by X-ray experimental results [69,70].

3.4. UV–Vis spectroscopy

The solid-state electronic absorption spectra recorded at room temperature on a thin-film made from nujol mulls between quartz plates of one-electron oxidized $[ZrPc_2]IBr_2$ and unoxidized $ZrPc_2$ are very similar (see Fig. 4). This indicates that the interaction between the $[ZrPc_2]^+$ and IBr_2^- units is insignificant in the positions of the phthalocyanine's HOMO and LUMO levels. The Q band arises from the excitation from HOMO (a_{1u}) to LUMO (e_g), while the B-Soret band is mostly an $a_{2u} \rightarrow e_g$ transition and the N band (at ~297 nm in both complexes) resulting mainly from a transition $b_{2u}(\pi) \rightarrow e_g(\pi^*)$. The Q band in the spectra of both complexes splits into two (Q_1 and Q_2) bands: 696 and 635 nm in unoxidized $ZrPc_2$ and 694 and 628 nm in one-electron oxidized $[ZrPc_2]IBr_2$. The splitting values of 61 nm in $ZrPc_2$ and 66 nm in $[ZrPc_2]IBr_2$ result from the vibronic coupling in the excited state [71–73]. Several authors reported that the splitting value of the Q band depends on the interplanar Pc–Pc distance, and decreases as the interplanar Pc–Pc distance increases [74,75]. Additionally, Takahashi et al. [74,76]. reported that if the interplanar Pc–Pc distance increases the intensity of the Q_1 band increases and the Q_2 band decreases. The inversion

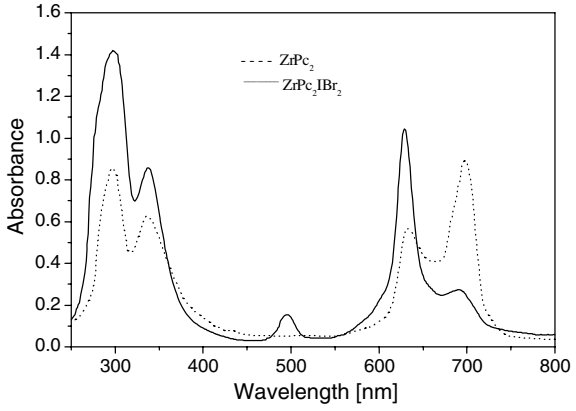

Fig. 4. Electronic absorption spectra of the one-electron oxidized $[ZrPc_2]IBr_2$ (solid line) and the non-oxidized $ZrPc_2$ complexes (dashed line).

of the intensities of the Q_1 and Q_2 bands and the splitting values in the spectra of $ZrPc_2$ and $[ZrPc_2]IBr_2$ are fully consistent with the X-ray single crystal analysis (the interplanar Pc–Pc distance of 2.434(3) Å in one-electron oxidized $[ZrPc_2]IBr_2$ is shorter than in $ZrPc_2$ (2.52 Å) [41]).

In the spectrum of $[ZrPc_2]IBr_2$, besides the characteristic bands (N, B and Q) also observed in the spectrum of unoxidized $ZrPc_2$, one additional band at ~496 nm is observed. Several authors that studied iodine-doped metallophthalocyaninato complexes containing the triiodide I_3^- ions suggested that the optical transition at ~500 nm may arise from a transition in the I_3^- ions, probably $\sigma_g \rightarrow \sigma_u^*$ split by spin–orbit coupling [54]. Gabes and Stufkens [77] studied the electronic absorption spectra of symmetrical and asymmetrical trihalide ions (I_3^-, IBr_2^-, ICl_2^-, Br_3^- and $BrCl_2^-$) observed in the spectrum of IBr_2^- ($CsIBr_2$) three bands at 248, 313 and 407 nm with decreasing intensities and one shoulder at about 493 nm. The intensity of the band at 493 nm in relation to the bands at 248, 313 and 407 nm is much lower [77] as well as lower than the intensities of the bands assigned to the transitions in the phthalocyaninato complexes. Therefore, the band observed at 496 nm in the spectrum of $[ZrPc_2]IBr_2$ complex is assigned to the electronic transition from a deeper level to the half-occupied HOMO level and is an evidence for the existence of the one-electron oxidized phthalocyaninato(1−) π-radical ligand . This assignment is supported by the fact that a similar band at ~500 nm has been observed in the spectra of other one-electron oxidized metallodiphthalocyaninato complexes such as $Ln^{(III)}Pc_2$ and $In^{(III)}Pc_2$ that not contain the trihalide ions [78,79].

3.5. Magnetic properties

The magnetic susceptibility of the $[ZrPc_2]IBr_2$ complex was measured between 300 and 1.8 K. The paramagnetic susceptibility was obtained by subtracting the temperature-independent diamagnetic contribution of the phthalocyaninato rings and the diamagnetic contribution of the closed shell (d^0) Zr^{4+} cation. Both contributions were obtained by the measurement of the diamagnetic susceptibility of the unoxidized $ZrPc_2$ complex, which is equal to -5.76×10^{-4} emu mol^{-1}. The value of the diamagnetic contribution of the mixed trihalide IBr_2^- ion was calculated from Pascal's constants as a sum of twice that for Br (42.4×10^{-6} emu mol^{-1}) and that for I^- (-50.6×10^{-6} emu mol^{-1}) [80–82]. The corrected paramagnetic susceptibility of one-electron oxidized $[ZrPc_2]IBr_2$ at 300 K is $\approx 1.162 \times 10^{-3}$ emu mol^{-1}. This value corresponds to ~0.96 spins per molecule ($S = 1/2$, $g \cong 2$). The temperature dependence of the corrected magnetic susceptibility of $[ZrPc_2]IBr_2$ can be fit approximately by the Curie–Weiss law, $\chi_M = C/(T - \Theta)$ with a Weiss constant Θ (K) of ≈−3.7 (see Fig. 5). The negative Weiss constant represents the antiferromagnetic coupling among unpaired electrons. The effective temperature-independent magnetic moment, calculated from the relationship $\mu_{eff} = 2.828(\chi_M T)^{1/2}$, is

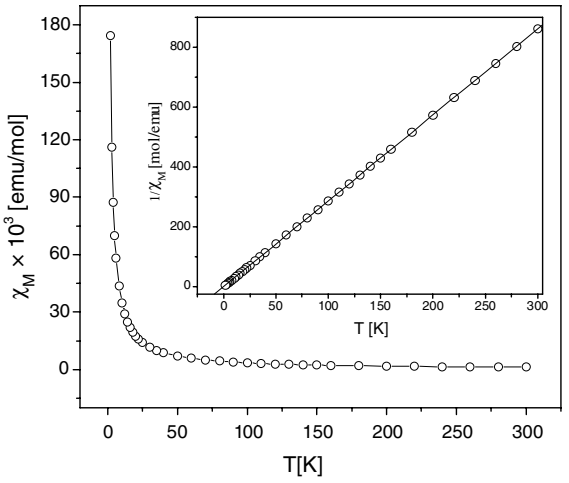

Fig. 5. Plots of the magnetic susceptibility (χ_M) of the $[ZrPc_2]IBr_2$ solid sample vs. temperature. Inset: $1/\chi_M$ vs. temperature.

equal to ≈1.67 μ_B. This value is slightly lower than the spin-only magnetic moment ($\mu_{spin\text{-}only} = 1.73\ \mu_B$).

The EPR spectrum, measured on a solid polycrystalline sample of $[ZrPc_2]IBr_2$ at room temperature (295 °C), exhibits one narrow signal in the proximity of the free electron g value. The g value of 2.0025 and a line width $\Gamma =$ 6.5 G indicate the formation of a ligand-centered π-radical. Integration of this signal results in 3.98×10^{20} spins/g, i.e. 0.927 spins per $[ZrPc_2]IBr_2$ molecule. The spin concentration obtained from the EPR measurements is in good agreement with that from magnetic susceptibility measurements. The EPR parameters, g, Γ and spins concentration per molecule obtained for the $[ZrPc_2]IBr_2$ complex are quite similar to that observed for one-electron oxidized $[ZrPc_2]I_3 \cdot I_2$ [39]. Although the g and Γ parameters observed in the spectrum of the third partially oxidized zirconium diphthalocyaninato complex $[ZrPc_2](I_3)_{2/3}$ are comparable, the spin concentration is significantly lower [38]. The difference in the spin concentrations between $[ZrPc_2]IBr_2$ and $[ZrPc_2]\ I_3 \cdot I_2$ – both one-electron oxidized and monoclinic and $[ZrPc_2](I_3)_{2/3}$ (tetragonal) results from the difference in their crystal structures. In the tetragonal crystal of $[ZrPc_2](I_3)_{2/3}$ the Pc ligands are closely planar and the interactions between $Pc^{-\cdot}$ radicals are more effective and decreases the spins concentration in relation to both monoclinic $[ZrPc_2]IBr_2$ and $[ZrPc_2]\ I_3 \cdot I_2$ crystals in which, due to the saucer shaped Pc rings, the interactions are less effective.

For $[ZrPc_2]IBr_2$ the g value remains constant with decreasing temperature, but the line width decreases only slightly to a value of 5.4 G at 80 K, the lowest measurement temperature. The narrow line width of the EPR signal within the temperature range is typical for one-dimensional conductors because the direction of spin–lattice relaxation is restricted and slower [83]. The decrease of the line width can be explained in term of enhanced motional narrowing from a reduction in carrier mobility with decreasing temperature.

3.6. Single-crystal electrical conductivity of $[ZrPc_2]IBr_2$

The single-crystal electrical conductivity along the stacking axis of one-electron oxidized $[ZrPc_2]^+$ units (*a* axis, see Fig. 3a) at room temperature is equal to $4.6\,\Omega^{-1}\,cm^{-1}$, while the conductivity measured along the *c* and *b* axes of the crystal is in the range $3.2–3.7\times10^{-3}\,\Omega^{-1}\,cm^{-1}$. The electrical conductivity of $[ZrPc_2]IBr_2$ is comparable to the conductivity of the second one-electron oxidized zirconium diphthalocyaninato complex $[ZrPc_2]I_3\cdot I_2$ [39]. The conductivity data of the third known, partially oxidized by iodine, zirconium diphthalocyanine $[ZrPc_2](I_3)_{2/3}$ are available only for the polycrystalline compacted sample [38]. Therefore, the electrical conductivity of this $[ZrPc_2]IBr_2$ complex was also performed on a polycrystalline sample, for comparison. The conductivity measured on the polycrystalline sample of $[ZrPc_2]IBr_2$ pressed into pellets ($\sim10^5$ kPa) is equal to $6.5–7.2\times10^{-2}\,\Omega^{-1}\,cm^{-1}$, and is slightly greater than for the complex of $[ZrPc_2](I_3)_{2/3}$ (see Table 6) [38]. The electrical conductivity measured on a polycrystalline sample of unoxidized $ZrPc_2$ at room temperature shows typical values for isolators ($\sigma_{RT}<10^{-9}\,\Omega^{-1}\,cm^{-1}$).

The single-crystal conductivity of $[ZrPc_2]IBr_2$ along the stacks of $[ZrPc_2]^+$ units decreases with decreasing temperature (Fig. 6), thus the crystal exhibits non-metallic character in conductivity ($d\sigma/dT>0$). Generally, non-metallic molecular conductors exhibit exponential temperature dependence of $\sigma_{(T)}$, because of the carrier density or mobility or both are activated. The temperature dependence of conductivity may be fitted to the expression $\sigma_{(T)}=\sigma_0\exp(-E_a/kT)$, where E_a is the activation energy and k is the Boltzman's constant. A least-squares fit to the data shows linear character of $\ln(\sigma_{(T)}/\sigma_{(RT)})$ versus $1/T$ (Fig. 6) and yields an activation energy of 0.025(2) eV. The relatively high room temperature conductivity of $[ZrPc_2]IBr_2$ along the stacking axis, but significantly lower in comparison to the conductivity of the best molecular conductor, i.e. iodine-doped nickel phthalocyanine $NiPcI_x$ ($\sigma_{(RT)}\approx600\,\Omega^{-1}\,cm^{-1}$)[3], can be explained by a significant overlap of the π-orbitals resulting from the staggered orientation of the Pc rings (rotation angle of the Pc rings equals 45.0(3)°) in the sandwich as well as between the sandwich within the stacks. This rotation of Pc rings makes eight short inter-ring contacts between the pyrrole α-carbon atoms (the inter-ring C_α–C_α contacts

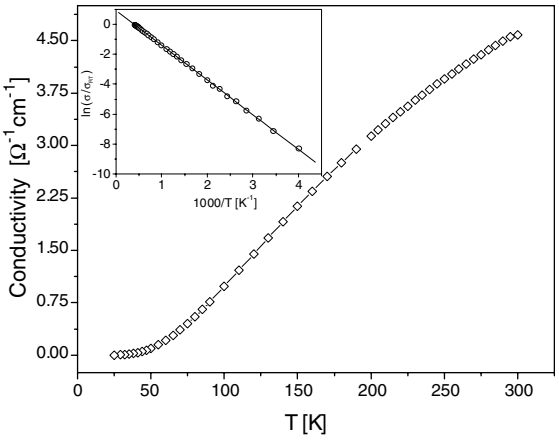

Fig. 6. Temperature dependence of the conductivity of $[ZrPc_2]IBr_2$ (single crystal) measured along the stacks of $[ZrPc_2]^+$ units. Inset: plot of $\ln(\sigma/\sigma_{RT})$ vs. $1000/T$.

range from 2.858(3) (C9–C28) to 3.017(3) Å (C8–C21)). The theoretical calculation shows that these carbon atoms make appreciable contributions to the partially occupied HOMO π-molecular orbital of the phthalocyaninato macrocycle and due to the relatively short contacts provide the greatest overlap of the HOMO π-molecular orbital of Pc that forms the conduction band of the partially oxidized molecular crystals [84,85]. These data clearly show that charge propagation mainly proceeds along the one-dimensional stacks of $[ZrPc_2]^+$ moieties. Each $[ZrPc_2]^+$ unit with the closed shell (d^0) Zr^{4+} cation contains the Pc^{2-} and one-electron oxidized $Pc^{-\cdot}$ π-radical ligands. During the charge transport there is no need for a change of the population distribution among the sites because the jumping of the electron from one side to another with the pre-formed hole takes place between isoenergetic configurations (see Scheme 2a). This is consistent with the relatively small activation energy of 0.025(2) eV, obtained by a fit of the conductivity data, compared with the activation energy of other one-dimensional iodine-doped molecular conductors [54]. The charge transport in the non-oxidized $ZrPc_2$ sample requires a large activation energy for carrier creation, since this involves high energy of states creating and separating the positive and negative (oxidized and reduced) $[ZrPc_2]^+$ and $[ZrPc_2]^-$ ions along the chains (see Scheme 2b). Thus the activation energy is compared to the sum of the energies

Table 6
EPR and electrical conductivity data (room temperature) of zirconium diphthalocyaninato complexes

Compound	*g*	*Γ*	Unpaired electron per molecule		Conductivity, σ_{RT} ($\Omega^{-1}\,cm^{-1}$)		Ref.
			From EPR	Theoretical value	Single crystal[a]	Powder[b]	
$[ZrPc_2]IBr_2$	2.0025	6.5	0.927	1	4.6	$6.5–7.4\times10^{-2}$	this work
$[ZrPc_2]I_3\cdot I_2$	2.0026	6.2	0.920	1	3.8	$5.5–6.2\times10^{-2}$	[39]
$[ZrPc_2](I_3)_{2/3}$	2.0026	6.6	0.185	0.3333	~3.5–3.8[c]	$5.2–5.5\times10^{-2}$	[38]
$ZrPc_2$[d]						$<10^{-9}$	this work

[a] Along the stacks.
[b] On the polycrystalline compacted sample.
[c] From correlation between conductivity on single crystal and pressed powder.
[d] EPR not active.

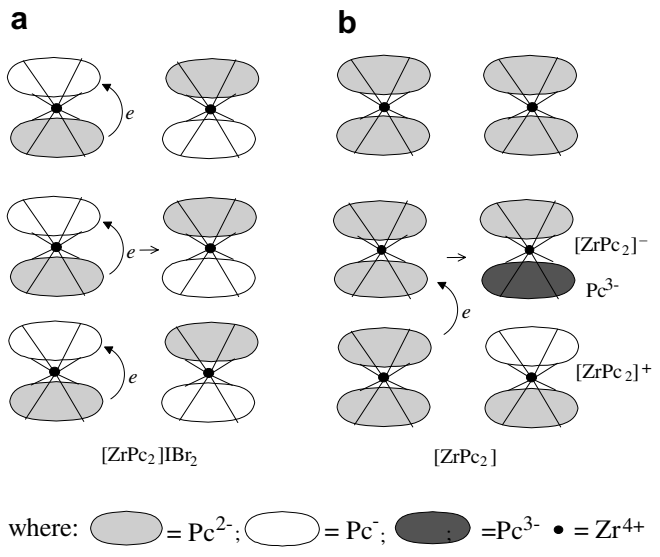

Scheme 2. Schematic representation of the charge propagation along the $\{[ZrPc_2]^+\}_n$ stacks.

that are related to the one-electron oxidation and the one-electron reduction of the $ZrPc_2$ complex, i.e. the formation of $[ZrPc_2]^+$ and $[ZrPc_2]^-$ ions. The first oxidation and first reduction peaks obtained by cyclic voltammetry for $ZrPc_2$ are observed at +1.2 V and −1.4 V, respectively [50]. The charge transport in the tetragonal complex $[ZrPc_2](I_3)_{2/3}$, in which the formal oxidation state of the $[ZrPc_2]$ units is equal to +2/3, is less effective, since statistically one $[ZrPc_2]$ unit per three contains two Pc^{2-} ligands ($[ZrPc^{2-}Pc^{2-}]$-$[ZrPc^{2-}Pc^{-\cdot}][ZrPc^{2-}Pc^{-\cdot}](I_3)_2$), so the charge transport, i.e. the jumping of the electron with a pre-formed hole, is broken.

4. Conclusions

The investigation of doped metallodiphthalocyaninato complexes was undertaken with the dual goals of developing new controls over the structures of mono-dimensional electrically conductive molecular materials as well as investigating the dependence of the conductivity on the formal partial oxidation state of the phthalocyaninato rings in the sandwich MPc_2 system and on the nature of the anionic part of the sandwich complexes $[MPc_2]X$, where $X = I_3^-$, IBr_2^- or $(I_3^- \cdot I_2)$. The present study of $[ZrPc_2]IBr_2$ and our earlier results related to two other iodine-doped zirconium diphthalocyaninato complexes, partially oxidized $[ZrPc_2](I_3)_{2/3}$ and one-electron oxidized $[ZrPc_2]I_3 \cdot I_2$, shed new light on the properties of both types of doped materials. Upon one electron oxidation the $ZrPc_2$ complex is converted to an architecture with staggered rings (rotation angle of 45° in both one-electron oxidized complexes: $[ZrPc_2]IBr_2$ and $[ZrPc_2]I_3 \cdot I_2$), regardless of the interplanar Pc–Pc spacing. The driving force for this conformation change are the net "bonding" overlaps between the π-electron macrocyclic rings. Concerning the relationship between the interplanar spacing in the one-electron oxidized $[ZrPc_2]^+$ units and charge transfer properties, the following can be concluded: decreasing interplanar separation results in increasing charge transfer. Although the electrical conductivities in the stacking direction of the third complex of $[ZrPc_2](I_3)_{2/3}$ with a non-integral oxidation state of sandwiched $[ZrPc_2]^{2/3+}$ units are not available, established empirical correlation between single crystal and pressed powder data (Table 6) afford a reasonable estimation of the value and allow a qualitative comparison with both one-electron oxidized zirconium diphthalocyaninato complexes.

The EPR measurement shows significantly lower 'unpaired' spins in the tetragonal partially oxidized complex of $[ZrPc_2](I_3)_{2/3}$, in which both Pc rings are closely planar, resulting in increased π-orbital overlap. In both one-electron oxidized zirconium diphthalocyaninato complexes the concentration of the 'unpaired' spins are comparable, however, on looking at these results it can be told that in $[ZrPc_2]IBr_2$ the 'unpaired' electrons as well as the conductivity are slightly greater than for $[ZrPc_2]I_3 \cdot I_2$ (see Table 6), which correlate well with the interplanar Pc–Pc distance (2.434(3) Å in $[ZrPc_2]IBr_2$ and 2.493(3) Å in $[ZrPc_2]\ I_3 \cdot I_2$). The decreasing of the EPR line width (Γ) in $[ZrPc_2]IBr_2$ was interpreted in the terms of reduction in carrier mobility with decreasing temperature which correlates well with the temperature dependence of single-crystal conductivity.

Acknowledgment

G.J. Perpétuo thanks the CNPq foundation (Brazil) for the scholarship.

Appendix A. Supplementary data

Crystallographic data for the structure reported in this paper have been deposited with the Cambridge Crystallographic Database as Supplementary Publication No. CCDC-606662. Copies of the data can be obtained free of charge on application to The Director, CCDC, 12 Union Road, Cambridge CB2 1EZ, UK (fax: +44 1223 336033; email: deposit@ccdc.cam.ac.uk or http://www.ccdc.cam.ac.uk). Supplementary data associated with this article can be found, in the online version, at doi:10.1016/j.poly.2006.06.020.

References

[1] J.L. Petersen, C.J. Schramm, D.R. Stojakovic, B.M. Hoffman, T.J. Marks, J. Am. Chem. Soc. 99 (1977) 286.
[2] C.J. Schramm, D.R. Stojakovic, B.M. Hoffman, T.J. Marks, Science 200 (1978) 47.
[3] C.J. Schramm, R.P. Scaringe, D.R. Stojakovic, B.M. Hoffman, J.A. Ibers, T.J. Marks, J. Am. Chem. Soc. 102 (1980) 6702.
[4] J.A. Ibers, L.J. Pace, J. Martinsen, B.M. Hoffman, Struct. Bond. (Berlin) 50 (1982) 1.
[5] J. Martinsen, R.L. Greene, S.M. Palmer, B.M. Hoffman, J. Am. Chem. Soc. 105 (1983) 677.
[6] B.M. Hoffman, J.A. Ibers, Acc. Chem. Res. 16 (1983) 15.

[7] T.E. Phillips, R.P. Scaringe, B.M. Hoffman, J.A. Ibers, J. Am. Chem. Soc. 102 (1980) 3435.
[8] J. Martinsen, L.J. Pace, T.E. Phillips, B.M. Hoffman, J.A. Ibers, J. Am. Chem. Soc. 104 (1982) 83.
[9] J. Martinsen, J. Tanaka, R.L. Greene, B.M. Hoffman, Phys. Rev. B: Condens. Matter 30 (1984) 6296.
[10] S.M. Palmer, M.Y. Ogawa, J. Martinsen, J.L. Stanton, B.M. Hoffman, J.A. Ibers, R.L. Greene, Mol. Cryst. Liq. Cryst. 120 (1985) 427.
[11] T.J. Marks, Science 227 (1985) 881.
[12] T.J. Marks, Angew. Chem., Int. Ed. Engl. 29 (1990) 857.
[13] K. Liou, M.Y. Ogawa, T.P. Newcomb, G. Quirion, M. Lec, M. Poirier, W.P. Halperin, B.M. Hoffman, J.A. Ibers, Inorg. Chem. 28 (1989) 3889.
[14] D.C. Miller, J.C. Bollinger, B.M. Hoffman, J.A. Ibers, Inorg. Chem. 33 (1994) 3354.
[15] H. Hasegawa, T. Naito, T. Inabe, T. Akutangawa, T. Nakamura, J. Mater. Chem. 8 (1998) 1567.
[16] J.M. Williams, J.A. Schultz, A.E. Underhill, K. Carneiro, in: J.S. Miller (Ed.), Extended Linear Chain Compounds, vol. 3, Plenum Press, New York, 1983, pp. 73–118.
[17] M.C. Bohm, One Dimensional Organometallic Materials, Lecture Notes in Chemistry, vol. 48, Springer, Berlin, 1987.
[18] B.M. Hoffman, J. Martinsen, L.J. Pace, J.A. Ibers, in: J.S. Miller (Ed.), Extended Linear Chain Compounds, vol. 3, Plenum Press, New York, 1983, pp. 459–549.
[19] R.C. Teitelbaum, S.L. Ruby, T.J. Marks, J. Am. Chem. Soc. 100 (1978) 3215.
[20] R.C. Teitelbaum, S.L. Ruby, T.J. Marks, J. Am. Chem. Soc. 102 (1980) 3222.
[21] R.P. Scaringe, J.A. Ibers, Acta Crystallogr. A35 (1979) 803.
[22] M. Cowie, A. Gleizes, G.W. Grynkiewich, D.W. Kalina, M.S. McClure, R.P. Scaringe, R.C. Teitebaum, S.L. Ruby, J.A. Ibers, C.R. Kannewurf, J. Am. Chem. Soc. 101 (1979) 2921.
[23] M. Mizuno, J. Tanaka, I. Harada, J. Phys. Chem. 85 (1981) 1789.
[24] J. Martinsen, J.L. Stanton, R.L. Greene, J. Tanaka, B.M. Hoffman, J.A. Ibers, J. Am. Chem. Soc. 107 (1985) 6915.
[25] M.Y. Ogawa, J. Martinsen, S.M. Palmer, J.L. Stanton, J. Tanaka, R.L. Greene, B.M. Hoffman, J.A. Ibers, J. Am. Chem. Soc. 109 (1987) 1115.
[26] R. Kubiak, J. Janczak, Cryst. Res. Technol. 36 (2001) 1095.
[27] M. Moussavi, A. DeCian, J. Fischer, R. Weiss, Inorg. Chem. 27 (1988) 1287.
[28] A. Darovsky, L.Y. Wu, P. Lee, H.S. Shen, Acta Crystallogr. C47 (1991) 1836.
[29] D. Chabach, M. Lachbar, A. DeCian, J. Fischer, R. Weiss, New J. Chem. 16 (1992) 431.
[30] A. Darovsky, V. Keserashvili, R. Harlow, I. Mutikainen, Acta Crystallogr. B50 (1994) 582.
[31] G. Ostendorph, J.P. Werner, H. Homborg, Acta Crystallogr. C51 (1995) 1125.
[32] J. Janczak, R. Kubiak, A. Jezierski, Inorg. Chem. 34 (1995) 3505.
[33] A. Copabianchi, C. Ercolani, A.M. Paoletti, G. Pennesi, G. Rossi, A. Chiesi-Villa, C. Rizzoli, Inorg. Chem. 32 (1993) 4605.
[34] J. Janczak, R. Kubiak, F. Hahn, Inorg. Chim. Acta 281 (1998) 195.
[35] J. Janczak, R. Kubiak, Polyhedron 18 (1999) 1621.
[36] J. Janczak, R. Kubiak, A. Jezierski, Inorg. Chem. 38 (1999) 2043.
[37] J. Janczak, R. Kubiak, I. Svoboda, A. Jezierski, H. Fuess, Inorg. Chim. Acta 304 (2000) 150.
[38] J. Janczak, Y.M. Idemori, Inorg. Chim. Acta 325 (2001) 85.
[39] J. Janczak, Inorg. Chem. 42 (2003) 3549.
[40] R. Kubiak, J. Janczak, J. Alloys Compd. 200 (1993) L7.
[41] J. Silver, J.P. Lukes, S.D. Howe, B. Howlin, J. Mater. Chem. 1 (1991) 29.
[42] KUMA Diffraction, KUMA KM-4 CCD Program Package, Ver. 163, Wrocław, Poland, 2000.
[43] G.M. Sheldrick, SHELXTL Program, Siemens Analytical X-ray Instrument Inc., Madison, WI, 1991.
[44] G.M. Sheldrick, SHELXL-97, Program for the Solution and Refinement of Crystal Structures, University of Göttingen, Göttingen, Germany, 1997.
[45] T.E. Phillips, J.R. Anderson, C.J. Schramm, B.M. Hoffman, Rev. Sci. Instrum. 50 (1979) 263.
[46] T. Inabe, T.J. Marks, R.L. Burton, J.W. Lyding, W.J. McCarthy, C.R. Kannewurf, G.M. Reisner, F.H. Herbstein, Solid State Commun. 54 (1985) 501.
[47] N.N. Greenwood, A. Earnshaw, Chemistry of the Elements, Pergamon Press, New York, 1989.
[48] G.A. Landrum, N. Goldberg, R. Hoffmann, J. Chem. Soc., Dalton Trans. (1997) 3605.
[49] A.I. Popov, R.E. Buckles, in: T. Moeller (Ed.), Inorganic Syntheses, vol. V, McGraw-Hill Book Co. Inc., New York, 1957, pp. 167–175.
[50] J. Silver, P.J. Lukes, P.K. Hey, J.M. O'Connor, Polyhedron 8 (1989) 1631.
[51] J. Janczak, Polish J. Chem. 74 (2000) 157.
[52] J.R. Ferraro, M.A. Beno, R.J. Thorn, H.H. Wang, K.S. Webb, J.M. Williams, J. Phys. Chem. Solids 47 (1986) 301.
[53] D.W. Kalina, J.W. Lyding, M.T. Ratajack, C.R. Kannewurf, T.J. Marks, J. Am. Chem. Soc. 102 (1983) 7854.
[54] B.N. Diel, T. Inabe, J.W. Lyding, K.F. Schoch Jr., C.R. Kannewurf, T.J. Marks, J. Am. Chem. Soc. 105 (1985) 1551.
[55] W. Kiefer, Appl. Spectrosc. 28 (1974) 115.
[56] W.E. Bennett, D.E. Broberg, N.C. Baenziger, Inorg. Chem. 12 (1973) 930.
[57] J. Janczak, R. Kubiak, J. Alloys Compd. 204 (1994) 5.
[58] A. DeCian, M. Moussavi, J. Fischer, R. Weiss, Inorg. Chem. 24 (1985) 3162.
[59] C. Ercolani, A.M. Paoletti, G. Pennesi, G. Rossi, A. Chiesi-Villa, C. Rizzoli, J. Chem. Soc., Dalton Trans. (1990) 1971.
[60] J. Janczak, R. Kubiak, Polyhedron 22 (2003) 313.
[61] A. Gieren, W. Hoppe, J. Chem. Soc., Chem. Commun. (1971) 413.
[62] R.D. Shannon, Acta Crystallogr. A32 (1967) 751.
[63] W.A. Nevin, W. Liu, A.B.P. Lever, Can. J. Chem. 65 (1987) 855.
[64] D.S. Terekhov, K.J.M. Noaln, C.R. MaArthur, C.C. Leznoff, J. Org. Chem. 61 (1996) 3034.
[65] H. Isago, D.S. Terekhov, C.C. Leznoff, J. Porphyr. Phthalocya. 1 (1997) 135.
[66] H. Isago, C.C. Leznoff, M.F. Ryan, R.A. Metcalfe, R. Davis, A.B.P. Lever, Bull. Chem. Soc. Jpn. 71 (1998) 1039.
[67] L. Pauling, The Nature of the Chemical Bond, 3rd ed., Cornell University Press, Ithaca, 1960, p. 262.
[68] A.S. Gardberg, S. Yang, B.M. Hoffman, J.A. Ibers, Inorg. Chem. 41 (2002) 1778.
[69] T. Naito, A. Tateno, T. Udagawa, H. Kobayashi, R. Kato, A. Kobayashi, T. Nagami, J. Chem. Soc., Faraday Trans. 90 (1994) 763.
[70] F.H. Allen, O. Kennard, Chem. Des. Autom. News 27 (1993) 303.
[71] A. Henrikson, B. Roos, R. Sundon, Theor. Chim. Acta 27 (1972) 303.
[72] L.K. Lee, N.H. Sabelli, P.R. Leberton, J. Phys. Chem. 86 (1982) 3926.
[73] H. Shiari, H. Tsuiki, E. Masuda, T. Koyama, K. Hanabusa, N. Kobayashi, J. Phys. Chem. 95 (1991) 417.
[74] K. Takahashi, Y. Tomita, Y. Harada, K. Tsubota, M. Honda, K. Kasuga, K. Sogabe, T. Tokii, Chem. Lett. (1992) 759.
[75] N. Ishikawa, Y. Kaizu, J. Phys. Chem. 100 (1996) 8722.
[76] K. Takahashi, Y. Tomita, Y. Harada, K. Tsubota, M. Honda, K. Kasuga, K. Sogabe, T. Tokii, Chem. Lett. (1998) 173.
[77] W. Gabes, D.J. Stufkens, Spectrochim. Acta Part A 30 (1974) 1835.
[78] E. Orti, J.E. Bredas, C. Clarisse, J. Chem. Phys. 92 (1990) 1228.
[79] J. Janczak, Polish J. Chem. 72 (1998) 1871.
[80] L.N. Mulay, in: L.N. Mulay, E.A. Brodeaux (Eds.), Theory and Applications of Molecular Diamagnetism, Wiley Interscience, New York, 1976 (Chapter 5.3).
[81] J.C. Bonner, M.E. Fischer, Phys. Rev. A 135 (1964) 640.
[82] A.J. Epstein, H. Rommelmann, M.A. Druy, A.J. Heegaer, A.G. MacDiarmid, Solid State Commun. 38 (1981) 683.
[83] K. Murata, K. Liou, J.A. Thompson, E.M. McGhee, D.E. Rende, D.E. Ellis, R.L. Musselman, B.M. Hoffman, J.A. Ibers, Inorg. Chem. 36 (1997) 3363.
[84] L.J. Pace, J. Martinsen, A. Ulman, B.M. Hoffman, J.A. Ibers, J. Am. Chem. Soc. 105 (1983) 2612.
[85] W.J. Pietro, T.J. Marks, M.A. Ratner, J. Am. Chem. Soc. 107 (1985) 5387.

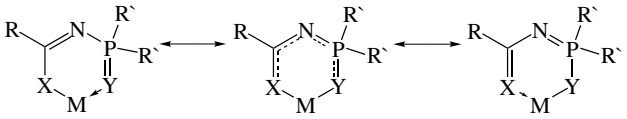

A B

Scheme 1.

the X-enolic form (A) (Scheme 1) with the negative charge delocalization in *N*-thioacylamidophosphate-anions [6] pulls them together with ligands **1**.

On the other hand, the presence in coordination sphere of the central ion "hard" donor atom of oxygen of the phosphoric group makes it coordinatively unsaturated. Because of this, it can lead to complex formation, in which the central ion has a coordination number of 6. A similar coordination environment for *N*-thioacylamidophosphates **3** has been shown by us previously as an example of phosphorylated thiobenzamide PhC(S)NHP(O)(OPr*i*)$_2$ (HQ) complexes with Co(II) [14], Ni(II) [15] and Cd(II) [16] cations. The X-ray data confirms that they have the M(HQ)$_2$Q$_2$ type structure. Central atoms having a tetragonal-bipyramidal environment $(O^{ax})_2(O^{eq})_2(S^{eq})_2$ is obtained in these compounds. Axial positions are occupied by two neutral molecules HQ. They are coordinated through the oxygen atoms of P=O-groups. Thus, *N*-thioacylamidophosphates **3** can undergo significant changes of coordination properties both in comparison with oxygen-containing **2** and with dithioanalogues **1**.

In the present study, new data about the structure and properties of *N*-thioacylamidophosphate chelate complexes **3** with the Co(II) cation are reported.

2. Experimental

2.1. Synthesis of [RC(S)NHP(O)(OPr*i*)$_2$] (3a–j)

N-Diisopropoxyphosphorylthiobenzamide (**3a**) (R = Ph) and *N*-phosphorylated thioureas (**3b**–**j**) (R = PhNH, *p*-MeOPhNH, *p*-BrPhNH, *i*PrNH, *t*BuNH, Et$_2$N, *c*-C$_5$H$_{10}$N, *c*-OC$_4$H$_8$N, *c*-C$_6$H$_{11}$NH), were prepared according to the previously described techniques [17] and [18].

2.2. Synthesis of [CoL$_2$] (4a–j and 5a)

A suspension of **3a**–**j** (5 mmol) in aqueous ethanol (20 ml) was mixed with an ethanol solution of potassium hydroxide (6 mmol). To the resulting potassium salt, a water (20 ml) solution of Co(NO$_3$)$_2$ · 6H$_2$O (2.8 mmol) was added dropwise whilst stirring. The mixture was stirred at room temperature for a further 3 h and left overnight. The resulting complexes **4a**–**j** were extracted with methylene chloride, washed with water and dried over anhydrous MgSO$_4$. The solvent was then removed under vacuum. Dark blue precipitates were obtained from a methylene chloride–*n*-hexane mixture, 1:5 v/v.

2.2.1. Co[PhC(S)NP(O)(OPri)$_2$]$_2$ (4a)

This complex was prepared according to the previously described technique [14]. UV–Vis spectra (CH_2Cl_2) [λ_{max}, nm (ε, 1 mol^{-1} cm^{-1})]: 569 (394), 614 (386), 666 (173).

2.2.2. Co[PhNHC(S)NP(O)(OPri)$_2$]$_2$ (4b)

This complex was prepared according to the previously described technique [19]. UV–Vis spectra (CH_2Cl_2) [λ_{max}, nm (ε, 1 mol^{-1} cm^{-1})]: 560 (342), 610 (360), 657 (187). EIMS, *m*/*z* (rel. int. %): 690 (0.1) [M]$^+$, 316 (32) [HL]$^+$.

2.2.3. Co[p-MeOPhNHC(S)NP(O)(OPri)$_2$]$_2$ (4c)

Yield: ~68%, m.p. 156 °C. *Anal.* Calc. for $C_{28}H_{44}CoN_4O_8P_2S_2$: C, 44.86; H, 5.92; N, 7.47; S, 8.55. Found: C, 44.96; H, 6.01; N, 7.39; S, 8.58%. IR (cm^{-1}): 1508(s) (SCN), 1008(b, vs) (POC), 1128(s) (P=O), 3296(b) (NH). UV–Vis spectra (CH_2Cl_2) [λ_{max}, nm (ε, 1 mol^{-1} cm^{-1})]: 560 (326), 611 (340), 662 (173). EIMS, *m*/*z* (rel. int. %): 750 (0.1) [M]$^+$, 346 (19) [HL]$^+$.

2.2.4. Co[p-BrPhNHC(S)NP(O)(OPri)$_2$]$_2$ (4d)

Yield: ~79%, m.p. 170 °C. *Anal.* Calc. for $C_{26}H_{38}Br_2CoN_4O_6P_2S_2$: C, 36.85; H, 4.52; Br, 18.86; N, 6.61; S, 7.57. Found: C, 36.81; H, 4.57; Br, 18.94; N, 6.63; S, 7.62%. IR (cm^{-1}): 1512(s) (SCN), 1008(b, vs) (POC), 1116(s) (P=O), 3288(b) (NH). UV–Vis spectra (CH_2Cl_2) [λ_{max}, nm (ε, 1 mol^{-1} cm^{-1})]: 559 (332), 610 (340), 662 (166). EIMS, *m*/*z* (rel. int. %): 848 (0.2) [M]$^+$, 395 (5) [HL]$^+$.

2.2.5. Co[iPrNHC(S)NP(O)(OPri)$_2$]$_2$ (4e)

Yield: ~48%, m.p. 166 °C. *Anal.* Calc. for $C_{20}H_{44}CoN_4O_6P_2S_2$: C, 38.64; H, 7.13; N, 9.01; S, 10.32. Found: C, 38.93; H, 7.11; N, 9.09; S, 10.34%. IR (cm^{-1}): 1512(s) (SCN), 1000(b, vs) (POC), 1128(s) (P=O), 3312(b) (NH). UV–Vis spectra (CH_2Cl_2), [λ_{max}, nm (ε, 1 mol^{-1} cm^{-1})]: 561 (251), 611 (289), 660 (161). EIMS, *m*/*z* (rel. int. %): 622 (74) [M]$^+$, 282 (89) [HL]$^+$.

2.2.6. Co[tBuNHC(S)NP(O)(OPri)$_2$]$_2$ (4f)

Yield: ~74%, m.p. 164 °C. *Anal.* Calc. for $C_{22}H_{48}CoN_4O_6P_2S_2$: C, 40.67; H, 7.45; N, 8.62; S, 9.87. Found: C, 40.63; H, 7.42; N, 8.74; S, 9.91%. IR (cm^{-1}): 1522(s) (SCN), 1000(b, vs) (POC), 1120(s) (P=O), 3320(b) (NH). UV–Vis spectra (CH_2Cl_2), [λ_{max}, nm (ε, 1 mol^{-1} cm^{-1})]: 561 (246), 611 (279), 661 (154). EIMS, *m*/*z* (rel. int. %): 650 (4) [M]$^+$, 296 (10) [HL]$^+$.

2.2.7. Co[Et$_2$NC(S)NP(O)(OPri)$_2$]$_2$ (4g)

Yield: ~80%, m.p. 64 °C. *Anal.* Calc. for $C_{22}H_{48}CoN_4O_6P_2S_2$: C, 40.67; H, 7.45; N, 8.62; S, 9.87. Found: C, 39.93; H, 7.51; N, 8.94; S, 9.77%. IR (cm^{-1}): 1512(s) (SCN), 1000(b, vs) (POC), 1135(s) (P=O). UV–Vis spectra (CH_2Cl_2) [λ_{max}, nm (ε, 1 mol^{-1} cm^{-1})]: 558 (275), 610 (302), 663 (169). EIMS, *m*/*z* (rel. int. %): 650 (51) [M]$^+$, 296 (5) [HL]$^+$.

*2.2.8. Co[$C_5H_{10}NC(S)NP(O)(OPri)_2]_2$ (**4h**)*

Yield: ~71%, m.p. 62 °C. *Anal.* Calc. for $C_{24}H_{48}CoN_4O_6P_2S_2$: C, 42.79; H, 7.18; N, 8.32; S, 9.52. Found: C, 42.66; H, 7.23; N, 8.54; S, 9.61%. IR (cm^{-1}): 1510(s) (SCN), 1010(b, vs) (POC), 1140(s) (P=O). UV–Vis spectra (CH_2Cl_2) [λ_{max}, nm (ε, 1 mol^{-1} cm^{-1})]: 559 (263), 610 (281), 662 (167). EIMS, *m/z* (rel. int. %): 674 (15) $[M]^+$, 308 (3) $[HL]^+$.

*2.2.9. Co[$OC_4H_8NC(S)NP(O)(OPri)_2]_2$ (**4i**)*

Yield: ~67%, m.p. 58 °C. *Anal.* Calc. for $C_{22}H_{44}CoN_4O_8P_2S_2$: C, 38.99; H, 6.54; N, 8.27; S, 9.46. Found: C, 39.05; H, 6.49; N, 8.22; S, 9.50%. IR (cm^{-1}): 1504(s) (SCN), 1010(b, vs) (POC), 1120(s) (P=O). UV–Vis spectra (CH_2Cl_2) [λ_{max}, nm (ε, 1 mol^{-1} cm^{-1})]: 560 (257), 612 (287), 659 (163). EIMS, *m/z* (rel. int. %): 678 (12) $[M]^+$, 310 (9) $[HL]^+$.

*2.2.10. Co[$C_6H_{11}NHC(S)NP(O)(OPri)_2]_2$ (**4j**)*

Yield: ~77%, m.p. 144 °C. *Anal.* Calc. for $C_{26}H_{52}CoN_4O_6P_2S_2$: C, 44.50; H, 7.47; N, 7.98; S, 9.34. Found: C, 44.26; H, 7.34; N, 7.63; S, 8.97%. IR (cm^{-1}): 1524(s) (SCN), 1010(b, vs) (POC), 1130(s) (P=O), 3312(b) (NH). UV–Vis spectra (CH_2Cl_2), [λ_{max}, nm (ε, 1 mol^{-1} cm^{-1})]: 562 (259), 611 (294), 663 (160). EIMS, *m/z* (rel. int. %): 702 (1) $[M]^+$, 322 (35) $[HL]^+$.

*2.2.11. Co[$PhC(S)NP(S)(OPri)_2]_2$ (**5a**)*

This complex was prepared according to the previously described technique [20].

*2.3. Synthesis of [Co(B)L_2] (**6a–d**)*

A solution of complexes **4a** or **4b** (0.45 mmol) in benzene (10 ml) was added dropwise whilst stirring to a solution of 2,2′-bipyridine (bpy) or 1,10-phenanthroline (phen) in benzene (10 ml). After complete addition, the solution was stirred for an hour. The solvent was then removed under vacuum. The residue was recrystallized from a methylene chloride–*n*-hexane mixture and the complexes **6a–d** have been isolated as red powders.

*2.3.1. Co[$PhC(S)NP(O)(OPri)_2]_2$(bpy) (**6a**)*

Yield: ~86%, m.p. 133 °C. *Anal.* Calc. for $C_{36}H_{46}CoN_4O_6P_2S_2$: C, 53.00; H, 5.68; N, 6.87; S, 7.86. Found: C, 52.96; H, 5.74; N, 7.17; S, 7.62%. IR (cm^{-1}): 1488(s) (SCN), 1016(b, vs) (POC), 1172(s) (P=O). UV–Vis spectra (CH_2Cl_2) [λ_{max}, nm (ε, 1 mol^{-1} cm^{-1})]: 546 (62). EIMS, *m/z* (rel. int. %): 659 (100) $[M]^+$, 301 (49) $[HL]^+$, 156 (18) $[bpy]^+$.

*2.3.2. Co[$PhC(S)NP(O)(OPri)_2]_2$(phen) (**6b**)*

Yield: ~94%, m.p. 148 °C. *Anal.* Calc. for $C_{38}H_{46}CoN_4O_6P_2S_2$: C, 54.35; H, 5.52; N, 6.67; S, 7.64. Found: C, 54.29; H, 5.57; N, 6.72; S, 7.68%. IR (cm^{-1}): 1490(s) (SCN), 996(b, vs) (POC), 1172(s) (P=O). UV–Vis spectra (CH_2Cl_2) [λ_{max}, nm (ε, 1 mol^{-1} cm^{-1})]: 549 (58). EIMS, *m/z* (rel. int. %): 659 (94) $[M]^+$, 301 (54) $[HL]^+$, 180 (20) $[phen]^+$.

*2.3.3. Co[$PhNHC(S)NP(O)(OPri)_2]_2$(bpy) (**6c**)*

Yield: ~91%, m.p. 142 °C. *Anal.* Calc. for $C_{36}H_{48}CoN_6O_6P_2S_2$: C, 51.12; H, 5.72; N, 9.94; S, 7.58. Found: C, 51.16; H, 5.69; N, 9.98; S, 7.53%. IR (cm^{-1}): 1522(s) (SCN), 1000(b, vs) (POC), 1172(s) (P=O), 3272(b) (NH). UV–Vis spectra (CH_2Cl_2), [λ_{max}, nm (ε, 1 mol^{-1} cm^{-1})]: 551 (56). EIMS, *m/z* (rel. int. %): 690 (0.8) $[M]^+$, 316 (27) $[HL]^+$, 156 (15) $[bpy]^+$.

*2.3.4. Co[$PhNhC(S)NP(O)(OPri)_2]_2$(phen) (**6d**)*

Yield: ~97%, m.p. 156 °C. *Anal.* Calc. for $C_{38}H_{48}CoN_6O_6P_2S_2$: C, 52.47; H, 5.56; N, 9.66; S, 7.37. Found: C, 52.51; H, 5.60; N, 9.61; S, 7.42%. IR (cm^{-1}): 1538(s) (SCN), 992(b, vs) (POC), 1172(s) (P=O), 3240(b) (NH). UV–Vis spectra (CH_2Cl_2), [λ_{max}, nm (ε, 1 mol^{-1} cm^{-1})]: 560 (60). EIMS, *m/z* (rel. int. %): 690 (0.5) $[M]^+$, 316 (22) $[HL]^+$, 180 (23) $[phen]^+$.

2.4. Physical measurements

Infrared spectra (Nujol) were recorded on a Specord M-80 spectrometer in the range 400–3600 cm^{-1}. Electron ionization mass-spectra were measured on the TRACE MS Finnigan MAT instrument. Ionization energy was 70 eV. The substance was injected directly into the ion source at 150 °C. Heating was carried out in a programmed mode from 35 to 200 °C at a rate of 35 °C/min. Electronic spectra of absorption in 0.001 M solution of CH_2Cl_2 were measured on a Lambda-35 spectrometer in the range 200–1000 nm.

2.5. Crystal structure determination and refinement

The crystals of **5a** were obtained from the mixture of dichloromethane and *n*-hexane by the method of slow evaporation. The X-ray diffraction data for the crystal of **5a** were collected on a CAD4 Enraf-Nonius automatic diffractometer using graphite monochromated Cu Kα (1.54158 Å) radiation. The molecule of **5a** in the crystals occur in a special position. The details of the crystal data, data collection and the refinement are given in Table 1. The stability of the crystal and experimental conditions were checked every 2 h using three control reflections, while the orientation was monitored every 200 reflections by centralising two standards. The decay of three control reflections was not observed. An empirical absorption correction based on ψ-scans was applied. Cell parameters, data collection and data reduction were performed on an Alpha Station 200 computer using the MOLEN [21] program. The structures were solved by direct methods using the SIR 92 [22] program, and refined using the SHELXL-97 program [23]. The positions of the hydrogen atoms were idealised. All figures were made using the program PLATON [24].

Table 1
Crystal data, data collection and refinement details for **5a**

	5a
Chemical formula	$C_{26}H_{38}N_2O_4P_2S_4Co$
Crystal type	green prism
Crystal size (mm^3)	$0.8 \times 0.6 \times 0.4$
Formula weight	691.73
Crystal system	monoclinic
Space group	$P2_1/c$
a (Å)	10.016(9)
b (Å)	17.960(8)
c (Å)	19.15(2)
α (°)	90.00
β (°)	100.88(7)
γ (°)	90.00
V (Å^3)	3383(5)
Z	4
D_{calc} (mg m^{-3})	1.36
$F(000)$	1444
Radiation (Å)	Cu Kα (1.54158)
Temperature (K)	293
Scan mode	ω
Recording range θ_{max} (°)	57.20
Absorption correction	ψ-scans
μ (cm^{-1})	74.45
Scan speed (deg min^{-1})	variable, 1–16.4
Reflections measured	4002
Number of independent reflections with $F^2 \geqslant 2\sigma(F^2)$	3098
R (%)	0.053
R_w (%)	0.134
S	1.031

3. Results and discussion

3.1. Synthesis

The ligand **3a** was prepared by reaction of thiobenzamide $PhC(S)NH_2$ with diisopropoxychlorphosphate $(iPrO)_2P(O)Cl$. Ligands **3b**–**j** were prepared by reaction of the corresponding amine with $(iPrO)_2P(O)NCS$.

Complexes of **3a**–**j** with Co(II) **4a**–**j** were prepared by the following procedure: the ligand was converted to the potassium salt, followed by interaction with $Co(NO_3)_2 \cdot 6H_2O$. The compounds obtained are crystalline solids soluble in most polar solvents.

Unsaturation of the CoO_2S_2 coordination environment opens up possibilities of a wide number of heteroligand complex syntheses. This can be obtained by interaction of such complexes with various donor agents [25]. As donors, both monodentate ligands and chelating agents might be used. A variety of donor structures opens up prospects for supramolecular units within the realm of advanced synthesis. We used bpy and phen in our work as donor ligands (Scheme 2).

Complexes **6a**–**d** were prepared by the following procedure: a benzene solution of bpy or phen was added dropwise to a benzene solution of the complex **4a** or **4b**. The compounds obtained **6a**–**d** are crystalline solids which are soluble in most polar solvents.

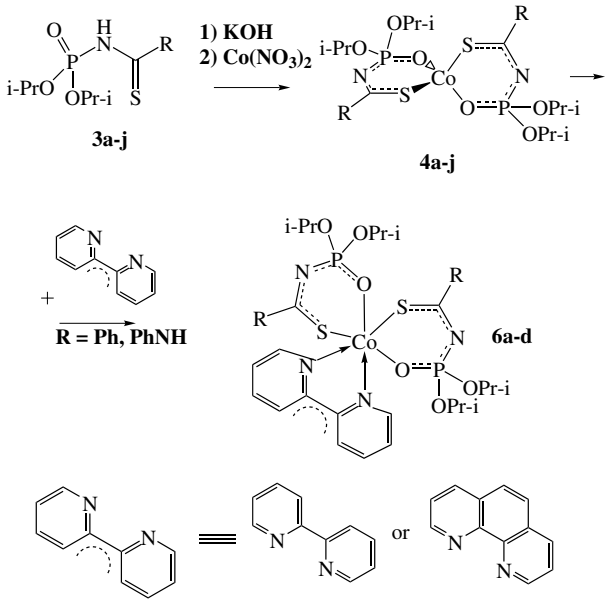

Scheme 2.

The research has shown that all listed complexes **4a**–**j** have the same coordination environment at the Co(II) atom. The UV–Vis spectroscopic data confirm that in a CH_2Cl_2 solution only ML_2 chelates with a tetrahedral MO_2S_2 core exist. In the case of complexes **6a**–**d** the coordination environment of the central atom differs from complexes **4a**–**j**. According to UV–Vis spectroscopy data obtained in a CH_2Cl_2 solution, complexes **6a**–**d** have an octahedral $MO_2S_2N_2$ core.

3.2. IR and UV–Vis spectroscopy

According to the IR spectroscopy, the absorption bands of the P═O group of anionic forms **3a**–**j** in complexes **4a**–**j** are shifted by approximately 76–116 cm^{-1} at low frequencies with respect to the parent ligand bands. It confirms their participation in chelate formation. In the spectra of the suspension of complexes **4a**–**j** in Nujol, there are intense absorption bands at 1504–1524 cm^{-1}, these are assigned to vibrations of the SCN fragment in the *N*-thioacylamidophosphate-anion [7]. The signal of the NH proton is absent in the IR spectra of the complexes **4a**,**g**–**i** and in the spectra of **4b**–**f** and **sj**, there is only a signal in the 3288–3320 cm^{-1} interval, corresponding to the NH-group vibrations of the R substituent.

The comparative analysis of IR spectra of **3a** and **3b** thioureas, their complexes with Co(II) cation formulas **4a** and **4b**, and adducts **6a**–**d** confirms the preservation of the CoL_2 core in compounds **6a**–**d**. The absorption band of the P═O group in complexes **6a**–**d** is shifted by approximately 72–80 cm^{-1} at low frequencies with respect to the free ligand bands **3a** and **3b**, and there is also an intense absorption band of the SCN fragment. All this confirms 1,5-S,O-coordination of the ligand anions. However, the shift of the P═O groups absorption bands in adducts **6a**–**d** is less than

32–36 cm^{-1}, compared to the initial Co(II) complexes **4a** and **4b**.

The structure of the chelate unit in Co(II) complexes in the CH_2Cl_2 solution is established by UV-spectroscopy. In complexes **4a–j** there is an absorption band with peaks in the ranges 558–562, 610–614 and 657–666 nm and with molar extinction coefficient (ε) 246–394, 279–386 and 154–187, respectively. Values of ε for complexes **4a–d**, containing arylamine substituents at thiocarbonic groups, are greater than 80–119 nm, compared to complexes **4e–j**. Absorption is observed in the red region of the spectrum, which explains the dark blue color of the complexes of Co(II) **4a–j**. The specified absorption band corresponds to a transition from the basic state $^4A_2$ to a $^4T_1(P)$ state. The thin structure is caused by spin–orbital interaction as a result of which, first, there is a splitting of the state $^4T_1(P)$ and, secondly, there are resolved transitions in the next doublet states with the same intensity. Other possible transitions: $^4A_2 \rightarrow {}^4T_2$ and $^4A_2 \rightarrow {}^4T_1(F)$ – are outside of the visible area. Data of UV-spectroscopy unequivocally confirm the tetrahedral environment of the Co(II) cation in complexes **4a–j**.

In the UV-spectra of complexes **6a–d** there is a shoulder with a peak of absorption in the region of 546–560 nm. Values of ε for **6a–d** are less, compered to the initial complexes **4a** and **4b**, which are in the 56–62 nm range. It is important to note that the absorption is weak enough and shifted to the violet part of a spectrum that causes the red color of complexes **6a–d**. The observable absorption band is caused by a $^4T_{1g}(F) \rightarrow {}^4T_{1g}(P)$ transition. It is easy to establish that the $^4T_{1g}(F) \rightarrow {}^4T_{2g}$ transition should correspond to the value of energy which is slightly lower in comparison with the energy of the $^4T_{1g}(F) \rightarrow {}^4T_{1g}(P)$ transition. But as the state $^4A_{2g}$ arises from a configuration $t_{2g}^3e_g^4$ and a state $^4T_{1g}(F)$ mainly from $t_{2g}^5e_g^2$, transition $^4T_{1g}(F) \rightarrow {}^4A_{2g}$ is in essence a two-electron transfer, and for this reason the band should be less intense (approximately by two orders), than the bands of other transitions. The specified two circumstances for $^4T_{1g}(F) \rightarrow {}^4A_{2g}$ transition: small intensity and affinity to the band $^4T_{1g}(F) \rightarrow {}^4T_{1g}(P)$ lead to fact that this transition is not observed in a spectrum. Data from UV-spectroscopy confirm a change of a Co(II) cation geometrical environment in compounds **4a** and **4b** after reaction with bpy and phen with the formation of adducts **6a–d**.

3.3. EI mass spectrometry

The electron impact (EIMS) mass spectra of **4b–j** contains the $[CoL_2]^+$ structure molecular ion peaks. The isotope bearing peaks of a molecular ion cluster correspond to the data calculated on the basis of gross-formulas of the CoL_2 structure. Stability of $[M]^+$ falls at complexes **4b** and **4c**, containing arylamine substituents at the carbon atom of the thiocarbonic groups. So, the peak of a molecular ion in the mass-spectrum of the complex **4b** has a very

Table 2
Selected bond distances (Å), bond and torsion angles (°) for six-membered cycles M–S–C–N–P–Y in the complexes ML_2-S,Y [Y = O, S; M = Co(II), Ni(II), Pd(II)]

	Co[L-S,O]$_2$ (**4a**) [19]	Co[L-S,O]$_2$ (**4b**) [14]	Co[L-S,S′]$_2$ (**5a**)	Ni[L-S,S′]$_2$ [26]	Ni[L-S,S′]$_2$ [27]	Pd[L-S,S′]$_2$ [28]
L	PhNHC(S)-NP(O)(OPr-*i*)$_2$	PhC(S)NP(O)-(OPr-*i*)$_2$	PhC(S)NP(S)-(OPr-*i*)$_2$	*n*-Pr$_2$NC(S)-NP(S)(OPh)$_2$	MeNHC(S)-NP(S)Ph$_2$	PhC(S)NP(S)-(OPr-*i*)$_2$
M–S(C)	2.306 2.319	2.289	2.301 2.292	2.2050	2.214	2.310
M–Y	1.974 1.959	1.940	2.311 2.320	2.226	2.217	2.341
C–S	1.789 1.779	1.731	1.735 1.733	1.745	1.760	1.712
C–N	1.305 1.305	1.297	1.283 1.300	1.321	1.294	1.299
C–N (exocyclic)	1.358 1.370			1.337	1.347	
P–N	1.614 1.625	1.610	1.612 1.613	1.574	1.610	1.613
P–Y	1.513 1.526	1.488	1.987 1.983	1.978	2.016	1.994
S–M–Y (endocyclic)	99.6 100.0	101.27	108.26 106.67	97.62	98.17	96.76
S–C–N–P	0.9 0.5	−3.11	−7.10 −1.12	±11.56	0.00	±2.15
C–N–P–Y	12.0 12.7	15.72	61.78 60.14	±27.43	±41.30	±40.92

small intensity equal to 0.1%, and in mass-spectrum of the complex **4c** – 0.2%. In EI mass-spectra of the **6a–d** adducts there are no peaks of molecular ions. Molecular ions of complexes **6a–d** are unstable under the conditions of measurement, and the heaviest molecular ion, observed in the spectra of **6a–d**, corresponds to the neutral CoL_2 complex core. In the EI-spectra there are also peaks of ligands **3a**, **3b**, bpy and phen, respectively.

3.4. The comparative analysis of molecular structure of CoL_2 complexes

The structure of complexes **4a** [14] and **4b** [19] have been investigated earlier by X-ray studies. It is of interest to compare their structure with the dithioanalogue **5a**.

According to the X-ray data complexes **4a**, **4b** and **5a** are spirocycling chelates in the crystal with a distorted-tetrahedral CoO_2S_2 core for **4a** and **4b** or CoS_4 for **5a**. The selected bond lengths and torsion angles are given in Table 2.

Distribution of bond lengths in a fragment S–C–N–P–Y for all compounds considered confirms the existence of two tautomeric forms: S-enolic (A) and Y-enolic (B) (Scheme 1). Bond lengths C–N and P–N in complexes of phosphorylated (Y = O) and thiophosphorylated (Y = S) derivatives differ slightly (Table 2). In order to make sense of this, one sees that the character of the negative charge delocalization in the coordinated *N*-thioacylamido(thio)phosphate-anion and the resonant forms (A) and (B) (Scheme 1) practically does not change at the transition from thiophosphoric derivatives to phosphoric derivatives.

In *N*-thioacylamidophospate complexes **1** the six-membered M–S1–P–N–C–S2 cycle, usually, has the conformation of a distorted boat. So, for example, in the complex **5a**, the cycles conformation is an asymmetrical boat with a planar PNCS fragment and with a deviation of metal and thiophosphoryl sulfur atoms (the fragment S2A–C1A–N1A–P1A is flat within the limits of 0.003(4) Å, a deviation of atoms S1A and Co1 −1.527(1) and −0.8364(7), respectively; similarly, the fragment S2B–C1B–N1B–P1B is flat within the limits of 0.029(4) Å, with a deviation of atoms Co1 and S1B of 1.1306(7) and 1.473(1) Å, respectively (Fig. 1)). Six-membered chelate cycles in molecules **4a** and **4b**, on the contrary, are appreciably flattened (Table 2).

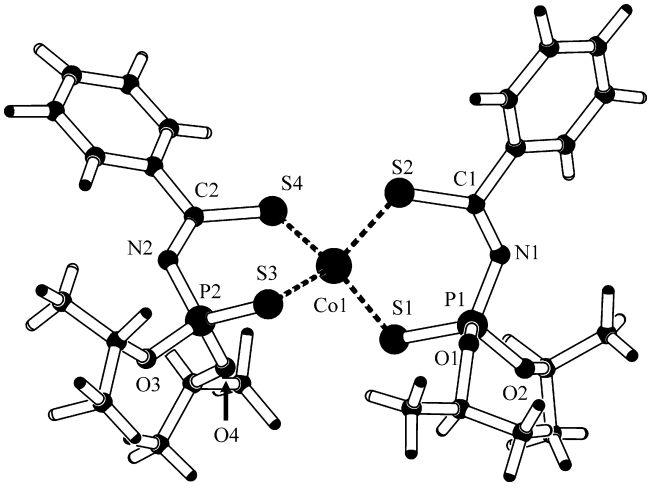

Fig. 1. Molecular structure of complex **5a**.

4. Conclusion

This research has shown that the structure and properties of *N*-thioacylamidophosphate complexes with the CoO_2S_2 core essentially differ from that investigated by us previously with the same cation. The Co(II) cation in such complexes shows coordination unsaturation. A consequence of this is the ability to increase the coordination number of the central atom with neutral donor ligands, with the formation of $Cd(B)L_2$ adducts. Ligands like the *N*-thioacylamidophosphate, as has been shown by us earlier [12], and also molecules of bpy and phen can act in this manner. Thus, complexes with CoO_2S_2 core can be used as electrophilic binding centers in organometallic receptor molecules, e.g. in polynuclear macrocyclic chelates of bifunctional *N*-thioacylamidophosphates [3].

Acknowledgements

This work was supported by the Russian Foundation for Basic Research (# 03-03-32372-a, 03-03-96225-r2003tatarstan_a) and the joint program of CRDF and the Russian Ministry of Education (BRHE 2004 Y2-C-07-02).

Appendix A. Supplementary data

Atomic coordinates, bond lengths, bond angles and thermal parameters have been deposited at the Cambridge Crystallographic Data Centre (CCDC). Data can be obtained free of charge via www.ccdc.cam.uk/conts/retrieving.html (or from the CCDC, 12 Union Road, Cambridge CB2 1EZ, UK; fax: +44 1223 336 033; or deposit@ccdc.cam.ac.uk). Any requests to the CCDC for data should quote the full literature citation and CCDC reference number 291905. Supplementary data associated with this article can be found, in the online version, at doi:10.1016/j.poly.2006.06.005.

References

[1] (a) V.V. Skopenko, V.M. Amirkhanov, T. Yu. Sliva, I.S. Vasilchenko, E.L. Anpilova, A.D. Garnovskii, Russ. Chem. Rev. 73 (2004) 737;
(b) D.J. Birdsall, J. Green, T.Q. Ly, J. Novosad, M. Necas, A.M.Z. Slawin, J.D. Woollins, Z. Zak, Eur. J. Inorg. Chem. 9 (1999) 1445.
[2] (a) O. Navratil, E. Herrmann, N.T.T. Chau, Ch. Tea, J. Smola, Collect. Czech. Chem. Commun. 58 (1993) 798;
(b) L.G. Shaidarova, A.V. Gedmina, V.V. Brusko, N.G. Zabirov, N.A. Ulakhovich, H.K. Budnikov, Anal. Sci. 17 (2001) 957;

(c) M.P. Kutyreva, N.G. Zabirov, V.V. Brusko, N.A. Ulakhovich, Anal. Sci. 17 (2001) 1049.
[3] (a) N.G. Zabirov, V.V. Brusko, A.Yu. Verat, D.B. Krivolapov, I.A. Litvinov, R.A. Cherkasov, Polyhedron 23 (2004) 2243;
(b) N.G. Zabirov, V.V. Brusko, A.Yu. Verat, D.B. Krivolapov, I.A. Litvinov, R.A. Cherkasov, Phosphorus Sulfur Silicon 177 (2002) 1869.
[4] (a) F.D. Sokolov, N.G. Zabirov, V.V. Brusko, D.B. Krivolapov, I.A. Litvinov, Mendeleev Commun. 13 (2003) 72;
(b) N.G. Zabirov, F.D. Sokolov, V.V. Brusko, A.K. Tashmukhamedova, N.I. Saifullina, R.A. Cherkasov, Mendeleev Commun. 12 (2002) 154.
[5] T.Q. Li, J.D. Woollins, Coord. Chem. Rev. 176 (1998) 451.
[6] (a) N.G. Zabirov, F.M. Shamsevaleev, R.A. Cherkasov, Usp. Khim. 60 (1991) 2189;
(b) F.D. Sokolov, V.V. Brusko, N.G. Zabirov, R.A. Cherkasov, Curr. Org. Chem. 10 (2006) 27.
[7] V.V. Brusko, A.I. Rakhmatullin, N.G. Zabirov, Russ. J. Gen. Chem. 70 (2000) 1705.
[8] V.V. Brusko, A.I. Rakhmatullin, V.G. Shtyrlin, D.B. Krivolapov, I.A. Litvinov, N.G. Zabirov, Polyhedron 25 (2006) 1433.
[9] I. Haiduc, Dichalcogenoimidodiphosph(in)ate Ligands Comprehensive Coordination Chemistry II. From Biology to Nanotechnology, in: A.B.P. Lever (Ed.), Fundamentals, Elsevier, 2003, pp. 323–347 (Chapter 1.14).
[10] (a) C. Silvestru, R. Rösler, I. Haiduc, R. Cea-Olivares, G. Espinosa-Perez, Inorg. Chem. 34 (1995) 3352;
(b) L.M. Gilby, B. Piggott, Polyhedron 18 (1999) 1077;
(c) J. Ellermann, J. Sutter, F.A. Knoch, M. Moll, Chem. Ber. 127 (1994) 1015;
(d) M.C. Aragoni, M. Arca, A. Garau, F. Isaia, V. Lippolis, G.L. Abbati, A.C. Fabretti, Z. Anorg. Allg. Chem. 626 (2000) 1454.
[11] E.A. Bundya, V.M. Amirkhanov, V.A. Ovchynnikov, V.A. Trush, K.V. Domasevitch, J. Sieler, V.V. Skopenko, Z. Naturforsch. B 54 (1999) 1033.
[12] E.A. Trush, V.M. Amirkhanov, V.A. Ovchynnikov, J. Swiatek-Kozlowska, K.A. Lanikina, K.V. Domasevitch, Polyhedron 22 (2003) 1221.
[13] J. Novosad, M. Necas, J. Marek, P. Veltsistas, C. Papadimitriou, I. Haiduc, M. Watanabe, J.D. Woollins, Inorg. Chim. Acta 290 (1999) 256.
[14] F.D. Sokolov, D.A. Safin, N.G. Zabirov, L.N. Yamalieva, D.B. Krivolapov, I.A. Litvinov, Mendeleev Commun. 14 (2004) 51.
[15] B.I. Khairutdinov, V.G. Shtyrlin, A.Yu. Verat, F.D. Sokolov, N.G. Zabirov, L.N. Yamalieva, V.V. Klochkov, in: Xth All-Russia Conference, Structure and dynamics of molecular systems, Kazan, Russia, 2003, p. 269 (Abstracts, Part 3).
[16] F.D. Sokolov, D.A. Safin, N.G. Zabirov, V.V. Brusko, B.I. Khairutdinov, D.B. Krivolapov, I.A. Litvinov, Eur. J. Inorg. Chem. 10 (2006) 2027.
[17] M.G. Zimin, N.G. Zabirov, R.M. Kamalov, A.N. Pudovik, Russ. J. Gen. Chem. 56 (1986) 2352.
[18] F.D. Sokolov, D.A. Safin, N.G. Zabirov, P.V. Zotov, R.A. Cherkasov, Russ. J. Gen. Chem. 75 (2005) 2009.
[19] F.D. Sokolov, N.G. Zabirov, L.N. Yamalieva, V.G. Shtyrlin, R.R. Garipov, V.V. Brusko, A.Yu. Verat, S.V. Baranov, P. Mlynarz, T. Glowiak, H. Kozlowski, Inorg. Chim. Acta 359 (2006) 2087.
[20] T.B. Tatarintseva, E.N. Cherezova, V.V. Brusko, O.V. Mikhailov, N.A. Mukmeneva, Russ. J. Gen. Chem. 69 (1999) 2000.
[21] L.H. Straver, A.J. Schierbeek, MOLEN. Structure Determination System, vols. 1 and 2, Nonius B.V., Delft, Netherlands, 1994.
[22] A. Altomare, G. Cascarano, C. Giacovazzo, D. Viterbo, Acta Crystallogr., Sect. A 47 (1991) 744.
[23] G.M. Sheldrick, SHELXL 97 – A Computer Program for Crystal Structure Determination, University of Göttingen, Göttingen, Germany, 1997.
[24] A.L. Spek, Acta Crystallogr., Sect. A 46 (1990) 3440.
[25] A.L. Konkin, V.G. Shtyrlin, A.V. Aganov, N.G. Zabirov, R.R. Garipov, A.V. Zakharov, Russ. J. Gen. Chem. 68 (1998) 1562.
[26] Z. Zak, T. Gloviak, N.T.T. Chau, E. Herrmann, Z. Anorg. Allg. Chem. 586 (1990) 136.
[27] T. Iwamoto, F. Ebina, H. Nakazawa, C. Nakatsuka, Bull. Chem. Soc. Jpn. 52 (1979) 1857.
[28] N.G. Zabirov, I.A. Litvinov, O.N. Kataev, S.V. Kashevarov, F.D. Sokolov, R.A. Cherkasov, Russ. J. Gen. Chem. 68 (1998) 1476.

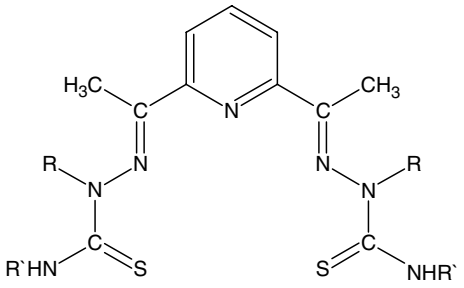

Fig. 1. 2,6-Diacetylpyridine bis(thiosemicarbazones).

characterized [14–18]. The related, 2,6-diacetylpyridine bis(^{4}N-methylthiosemicarbazone) (Fig. 1; R = H, R′ = CH_3) has also demonstrated its ability to act as a versatile chelating agent yielding a seven-coordinate manganese(II) complex [19], a five-coordinate lead(II) complex [20], a helical dimeric zinc(II) complex [20] and a seven-coordinate tin(II) complex [21].

Although pentagonal-bipyramidal complexes of zinc(II) [12], indium(III) [22], tin(IV) [14–18], tin(II) [21], iron(II) [22], bismuth(III) [23] of pentadentate N_3S_2 thiosemicarbazones have been well characterized, there does not seem to be a single report on seven-coordinate cadmium(II) complexes of a pentadentate thiosemicarbazone ligand. The only seven-coordinate cadmium(II) complex of a thiosemicarbazone that has been structurally characterized is $[Cd(HL^2)(Cl)_2(H_2O)_2]$ in which the HL^2 ligand is the 1:1 condensation product of 2,6-diacetylpyridine with thiosemicarbazide which behaves as an NNS tridentate chelating agent [24].

In view of limited structural and spectroscopic data available on seven-coordinate cadmium(II) complexes of pentadentate thiosemicarbazones and as part of our ongoing work on metal complexes of multidentate thiosemicarbazones, we report here the synthesis and characterization of new zinc(II) and cadmium(II) complexes of a neutral petadentate N_3S_2 thiosemicarbazone ligand, together with the X-ray crystal and molecular structures of the free ligand and its seven-coordinate cadmium(II) complex.

2. Experimental

2.1. Materials and instrumentation

All chemicals were of analytical reagent grades and used without any further purification. ^{2}N-Methylthiosemicarbazide was purchased from the Aldrich Chemical Company. The electronic spectra were recorded in solution on a Shimadzu UV-3100 spectrophotometer. The IR spectra were recorded as KBr discs on either a Perkin–Elmer 1600 FT IR spectrometer or a Perkin–Elmer 2000 spectrometer. Conductance measurements were made by means of a CMD 400 conductivity meter. The ^{1}H and ^{13}C NMR spectra were run in DMSO-d_6 on a Bruker Avance DPX 300 K FT NMR spectrometer using TMS as an internal standard.

2.2. Preparation of dap-^{2}NMetsc

2,6-Diacetylpyridine (1.63 g; 0.01 mol) was dissolved in boiling methanol (130 ml). Two drops of glacial acetic acid were added to the solution followed by the addition of a solution of ^{2}N-methylthiosemicarbazide (2.10 g; 0.02 mol) in methanol (100 ml). The reaction mixture was refluxed for three hours and then left to stand overnight. The yellow product that formed was filtered off, washed with cold methanol and dried in air. The crude compound was recrystallized from acetonitrile to afford crystals suitable for X-ray work. Yield: 2.30 g; 70%. *Anal.* Calc. for $C_{13}H_{19}N_7S_2$: C, 46.27; H, 5.67; N, 29.06. Found: C, 46.3; H, 5.66; N, 29.44%. NMR: δ_H(DMSO-d_6) 2.45 (6H, s, C–CH_3), 3.50 (6H, s, N–CH_3); 7.40 (s, br, NH_2); 8.34 (2H, d, pyH); 7.97 (1H, t, pyH), δ_C: (DMSO-d_6): 180.9 (C=S), 169.4 (pyC), 154.5 (pyC), 148.6 (C=N), 137.4 (pyC), 121.3 (pyC), 11.7 (CH_3), 41.9 (N–CH_3).

2.3. General method of preparation of $[M(dap\text{-}^2NMetsc)](NO_3)_2$ ($M = Zn^{2+}$, Cd^{2+})

The hydrated metal(II) nitrate salt (1 mmol) dissolved in boiling methanol (30 ml) was mixed with a boiling solution of the ligand (1 mmol) in a mixture of methanol (150 ml) and dichloromethane (20 ml). The reaction mixture was heated under reflux for 1 h and then left to stand overnight. The complexes generally crystallized out of the reaction mixture as diffraction quality crystals. Yield: 70–80%. *Anal.* Calc. for $[Zn(dap\text{-}^2NMetsc)(NO_3)_2]$ $C_{13}H_{19}N_9O_6S_2Zn$: C, 29.63; H, 3.63; N, 23.93. Found: C, 29.25; H, 3.73; N, 23.63%. δ_H(DMSO-d_6) 2.45 (6H, s, C–CH_3), 3.49 (6H, s, N–CH_3); 7.40 (s, br, NH_2); 8.30 (2H, d, pyH); 8.00 (1H, t, pyH), δ_C: (DMSO-d_6): 180.9 (C=S), 153.3 (C=N), 169.5, 168.3 (PyC), 126.4, 124.3, 123.5 (pyC); 138.9, 137.2 (pyC), 16.9, 16.8 (–CH_3), 41.9 (N–CH_3); Λ ($ohm^{-1}\,cm^2\,mol^{-1}$) in DMF: 90.7.

Anal. Calc. for $[Cd(dap\text{-}^2NMetsc)(NO_3)_2]$ ($C_{13}H_{19}N_9O_6Cd$): C, 27.20; H, 3.34; N, 21.96. Found: C, 27.11; H, 3.76; N, 21.39%. δ_H(DMSO-d_6): 2.63 (6H, s, C–CH_3), 8.60 (s, br, NH_2), 3.43 (6H, N–CH_3); 8.37 (2H, d, pyH);8.47 (1H, t, pyH); δ_C: (DMSO-d_6): 180.9 (C=S), 163.3 (pyC), 148.9 (C=N), 127.9 (pyC), 143.1 (pyC), 18.7 (CH_3); 43.77 (N–CH_3); Λ ($ohm^{-1}\,cm^2\,mol^{-1}$) in DMF: 47.7.

2.4. Crystallography

Cell constants were determined by a least-squares fit to the setting parameters of 25 independent reflections, measured on an Enraf-Nonius CAD 4 four-circle diffractometer using graphite monochromated Mo Kα radiation (0.71073 Å) and operating in the ω–2θ mode within the range $2° < 2\theta < 50°$. An empirical absorption correction (ψ scans) [25] and data reduction [26] were performed within the WINGX [27] suite programmes. The structures were solved by direct methods with SHELX86 [28] and

Table 1
Crystal and refinement data for dap-^{2}NMe and Cd(dap-^{2}NMe)$(NO_3)_2$

Formula	$C_{13}H_{19}N_7S_2$	$C_{13}H_{19}N_9O_6S_2Cd$
Formula weight	337.47	573.89
Temperature (K)	293	293
Wavelength (Å)	0.71073	0.71073
Crystal system	monoclinic	triclinic
Space group	$P2_1/n$	$P\bar{1}$
Unit cell dimensions		
a (Å)	11.996(2)	8.013(3)
b (Å)	7.7091(7)	9.400(2)
c (Å)	17.529(3)	14.567(2)
α (°)		103.74(2)
β (°)	91.36(1)	92.39(3)
γ (°)		100.65(2)
Volume (Å^3)	1620.6(4)	1043.2(5)
Z	4	2
D_{calc} (g cm^{-3})	1.383	1.827
Absorption coefficient (mm^{-1})	0.336	1.299
$F(000)$	712	576
Reflections collected	2982	3948
Independent reflections	2837	3664
R_{int}	0.0091	0.0368
Observed reflections [$I > 2\sigma(I)$]	2153	2910
Parameters	203	284
Goodness-of-fit on F^2	1.027	1.031
R_1 [$I > 2\sigma(I)$]	0.0328	0.0345
wR_2 (all data)	0.0952	0.0910

refined by full-matrix least-squares analysis with SHELXL97 [29]. Non-hydrogen atoms were refined with anisotropic thermal parameters whereas H-atoms were included at estimated positions. Drawings of the molecules were produced with ORTEP3 [30]. A summary of the crystal data, structure solution and refinement parameters are given in Table 1.

3. Results and discussion

Reaction of dap-^{2}NMetsc with zinc(II) and cadmium(II) nitrate in a boiling mixture of methanol and dichloromethane afforded crystalline complexes of empirical formula, [M(dap-^{2}NMetsc)$(NO_3)_2$] ($M = Zn^{II}$, Cd^{II}). These compounds are quite stable in air and could be kept in a desiccator for a long period of time without any sign of decomposition. The molar conductivities of the zinc and cadmium complexes in DMF are 90.7 and 47.7 ohm^{-1} cm^2 mol^{-1}, respectively indicating that the former behaves as a 1:1 electrolyte in DMF and the latter is extensively dissociated in this solvent. However, the IR spectrum of the zinc(II) complex exhibits the νN–O bands of the nitrato ligands at 1498 and 1308 cm^{-1} whereas that of the cadmium(II) complex shows the NO stretching bands at 1493 and 1298 cm^{-1} indicating that the nitrate anions are coordinated to the metal ions as monodentate ligands [31,32].

Reaction of dap-^{2}NMetsc with nickel(II) nitrate did not lead to the formation of a nickel(II) complex of dap-^{2}NMetsc but a green crystalline nickel(II) complex of formula, $[Ni(^2N\text{-Metsc})_2](NO_3)_2$ (^{2}N-Metsc = ^{2}N-methylthiosemicarbazide) was obtained due to complete hydrolysis of the bis(thiosemicarbazone) ligand to the precursors ^{2}N-methylthiosemicarbazide and 2,6-diacetylpyridine. The crystal structure of $[Ni(^2N\text{-Metsc})_2](NO_3)_2$ has previously been reported by Valdez-Martinez et al. [33]. The reluctance of the nickel(II) ion to form a seven-coordinate pentagonal bipyramidal nickel(II) complex with a planar pentadentate ligand is probably the driving force for the hydrolysis of the thiosemicarbazone ligand to its constituent thiosemicarbazide. Unlike Zn(II) and Cd(II) (both with d^{10} electronic configurations) there is an electronic (ligand field stabilization) driving force that favours for octahedral or square planar Ni(II) geometries of this d^8 ion. The planar pentadentate array of donor atoms offered by dap-^{2}NMetsc is thus incommensurate with the geometric preferences of the metal.

The IR spectrum of the ligand exhibits bands at 1646, 1072 and 894 cm^{-1} which can be assigned mainly to the νC=N, νN–N and νC=S vibrations, respectively. The νC=N and the νC=S bands of the free ligand are lowered in the spectra of the complexes consistent with coordination of the ligand to the metal ions *via* the azomethine and thione sulfur atoms.

The electronic spectrum of the free ligand shows a band at 340 nm attributable to the $n \rightarrow \pi^*$ transition of the azomethine group. In addition to this intra-ligand band, a new band at ca. 450 nm is observed in the spectra of the zinc and cadmium complexes. This band can safely be assigned to a $S \rightarrow M$ charge-transfer band. The appearance of an $S \rightarrow M$ charge transfer band in the electronic spectra of the zinc(II) and cadmium(II) complexes is strong evidence that the thione sulfur atoms of the ligand are coordinated to the zinc(II) and cadmium(II) ions (see Table 2).

The ^{1}H NMR spectrum of the free ligand when compared with those of the metal complexes indicates that the signals due to the protons on the C4, C11, N1, N7, C6 and C8 atoms are unaffected by complexation but the protons on C2, C12 and C7 are deshielded. The ^{13}C NMR spectra of the ligand and its complexes are more

Table 2
IR and electronic spectral data for dap-^{2}NMetsc and its zinc(II) and cadmium(II) complexes

Compound	ν(NH)	ν(CN)	ν(NN)	ν(CS)	State	λ_{max} (nm)
dap-^{2}NMetsc	3000br	1646m, br	1072s	894m	DMF	337(4.31)
[Zn(dap-^{2}NMetsc)$(NO_3)_2$]	3166m, br, 3310m	1628s	1054s	882m	DMF	407(2.81), 329(3.55), 275(3.99)
[Cd(dap-^{2}NMetsc)$(NO_3)_2$]	3390s, br, 3165s, br	1636s	1054m	882m	DMF	ca. 425sh, ca. 340sh

or less similar. A similar observation was also made with seven-coordinate cadmium(II) complex of the mono-condensed thiosemicarbazone of 2,6-diacetylpyridine [24].

3.1. The crystal structure of dap-^{2}NMetsc

The structure of the free ligand, dap-^{2}Metsc, together with the atom labelling scheme adopted, is shown in Fig. 2. The bond lengths and bond angles are given in Table 3. The ligand adopts an *E* configuration about the C3–N3 and C10–N5 bonds with both the azomethine nitrogen atoms and the pyridine nitrogen atom *trans* to the thione sulfur atoms. The conformation of the ligand as observed in the solid state, therefore, is ill-suited for it to act as a pentadentate N_3S_2 chelating agent. In order to coordinate through all of its donor atoms, 180° rotations about the C3–C5, C9–C10, C1–N2 and C13–N6 bonds must occur. The C1–S1 [1.688(2) Å], C1–N2 [1.368(3) Å], N2–N3 [1.419(2) Å], N3–C3 [1.283(2) Å] and C3–C5 [1.491(3) Å] bond lengths are comparable with those of the related ligands, 2,6-diacetylpyridine bis(3-hexamethyleneiminylthiosemicarbazone) monohydrate [16] and 2,6-diacetylpyridine bis(^{4}N-ethylthiosemicarbazone) [34]. The above bond lengths also indicate that there is some electron delocalization in the thiosemicarbazide side chain. The acetylpyridine moiety retains its expected planarity but the two terminal thiosemicarbazide residues are twisted about their N—N bonds well away from the plane of the pyridyl ring [C1–N2–N3–C3 150.1(2)° and C10–N5–N6–C13 148.7(2)°]. This twisting avoids 1,3-methyl-methyl interactions on each 'arm' of the ligand.

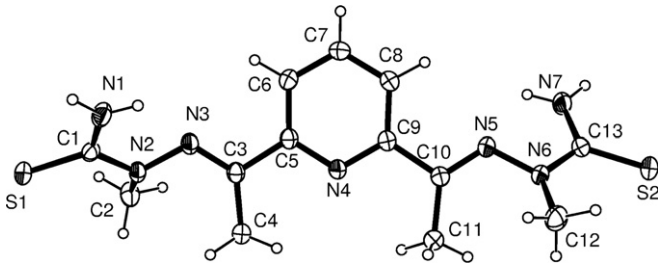

Fig. 2. ORTEP3 drawing of dap-^{2}NMetsc (30% ellipsoids).

Table 3
Selected bond lengths and bond angles for dap-^{2}NMetsc (L) and Cd(dap-^{2}NMetsc)$(NO_3)_2$

Bond	L	Cd		L	Cd		L	Cd
Bond lengths (Å)								
C(1)–S(1)	1.688(2)	1.697(5)	N(5)–N(6)	1.401(2)	1.412(5)	C(1)–N(1)	1.324(3)	1.315(6)
C(13)–S(2)	1.676(2)	1.700(5)	N(2)–N(3)	1.419(2)	1.394(3)	C(13)–N(7)	1.332(3)	1.320(6)
C(1)–N(2)	1.368(3)	1.368(6)	C(10)–N(5)	1.281(2)	1.268(6)	C(3)–C(5)	1.491(3)	1.498(6)
C(13)–N(6)	1.363(3)	1.354(6)	C(3)–N(3)	1.283(2)	1.285(6)	C(9)–C(10)	1.494(3)	1.501(6)
Cd(1)–N(4)		2.300(4)	Cd(1)–N(3)		2.496(3)	Cd(1)–N(5)		2.482(4)
Cd(1)–O(1a)		2.394(5)	Cd(1)–O(1b)		2.545(3)	Cd(1)–S(1)		2.589(1)
Cd(1)–S(2)		2.5869(16)						
Bond angles (°)								
N(2)–C(1)–S(1)	121.06(16)	124.7(3)						
N(6)–C(13)–S(2)	122.71(15)	123.8(3)						
C(1)–N(2)–N(3)	113.67(16)	117.1(4)						
C(13)–N(6)–N(5)	113.99(16)	116.4(4)						
C(3)–N(3)–N(2)	117.74(16)	120.5(4)						
C(10)–N(5)–N(6)	119.90(17)	117.4(4)						
N(3)–C(3)–C(5)	114.24(17)	114.7(4)						
N(5)–C(10)–C(9)	113.62(17)	115.0(4)						
C(6)–C(5)–C(3)	121.52(17)	121.5(4)						
C(8)–C(9)–C(10)	121.34(17)	121.3(4)						
C(4)–C(3)–C(5)	118.09(16)	116.9(4)						
C(11)–C(10)–C(9)	118.08(16)	117.2(4)						
Coordinate Bond angles in Cd(dap-^{2}NMetsc)$(NO_3)_2$								
O(1a)–Cd(1)–O(1b)	175.1(2)	O(1a)–Cd(1)–S(1)	98.43(16)					
O(1a)–Cd(1)–S(2)	96.9(2)	O(1a)–Cd(1)–N(5)	78.43(15)					
O(1a)–Cd(1)–N(4)	94.8(2)	O(1a)–Cd(1)–N(3)	96.55(19)					
O(1b)–Cd(1)–S(1)	83.81(8)	O(1b)–Cd(1)–N(3)	80.04(12)					
O(1b)–Cd(1)–N(4)	80.78(12)	O(1b)–Cd(1)–N(5)	101.50(11)					
O(1b)–Cd(1)–S(2)	87.61(9)	S(2)–Cd(1)–N(3)	153.03(9)					
S(2)–Cd(1)–N(5)	70.74(9)	S(2)–Cd(1)–N(4)	133.70(9)					
S(2)–Cd(1)–N(3)	153.03(9)	S(2)–Cd(1)–S(1)	83.40(5)					
N(5)–Cd(1)–N(4)	68.08(12)	N(5)–Cd(1)–N(3)	135.11(12)					
N(5)–Cd(1)–S(1)	153.20(9)	N(4)–Cd(1)–N(3)	67.96(12)					
N(4)–Cd(1)–S(1)	135.53(10)	N(3)–Cd(1)–S(1)	71.57(9)					
N(4)–Cd(1)–S(2)	133.70(9)							

The thiosemicarbazide moieties are also distinctly non-planar [S1–C1–N2–C2 22.5(3)° and S2–C13–N6–C12 14.4(3)°]. The distortion from planarity relieves $-CH_3\cdots S$ non-bonded repulsions. In the absence of this methyl group the S1–C1–N2–N3 residue would be ideally planar.

3.2. The crystal structure of Cd(dap-^{2}NMetsc)$(NO_3)_2$

The structure of the complex, Cd(dap-^{2}NMetsc)$(NO_3)_2$ is shown in Fig. 3 and selected bond lengths and bond angles are given in Table 3. The coordination environment of the cadmium atom may be considered as a distorted pentagonal bipyramid with the thiosemicarbazone ligand coordinated to the cadmium(II) ion as a pentadentate N_3S_2 chelate *via* the pyridine nitrogen atom, the two azomethine nitrogen atoms and the two thione sulfur atoms. The two axially coordinated monodentate nitrato ligands complete the seven-coordinate geometry.

The structure resembles that of the seven-coordinate pentagonal bipyramidal zinc(II) complex, [Zn(dap-tsc)$(H_2O)_2$]$(NO_3)_2\cdot H_2O$ [dap-tsc = the 2,6-diacetylpyridine-bis(thiosemicarbazone)] in which the two apical positions are occupied by aqua ligands [12]. The Cd–S bond distances [2.589(1) and 2.587(2) Å] are close to each other as are the two Cd–N_{imine} distances [2.496(3) and 2.482(5) Å]. These bond distances compare well with those of the seven-coordinate cadmium(II) complex $[Cd(HL^2)Cl_2(H_2O)]\cdot H_2O$ (HL^2 = the mono-condensed 2,6-diacetylpyridine thiosemicarbazone) whose structure has been reported by Casas et al. [24]. Although the azomethine nitrogen atoms are typically stronger donors than pyridine, the two Cd–N_{imine} bond distances in the present complex are longer than the Cd–N_{py} distance [2.300(4) Å]. While M–N_{imine} bond distances in complexes of tridentate NNS thiosemicarbazone derived from heterocyclic aldehydes and ketones are invariably shorter than the M–$N_{pyridine}$ distances, the reverse appears to be true for metal complexes of pentadentate thiosemicarbazone ligands. This is probably due to the geometric requirements of the pentadentate N_3S_2 ligand and the fact that the pyridine N-donor occupies the central position of the pentadentate ligand and is forced into a shorter than normal interaction with the metal due to the restraints of the two chelating arms either side of the coordinating atom. The two Cd–O distances [2.394(5) and 2.545(3) Å] in the [Cd(dap-^{2}NMetsc)$(NO_3)_2$] complex differ substantially, one being short and the other long. The Cd–O1b bond length is much longer that that observed in other seven-coordinate cadmium(II) complexes.

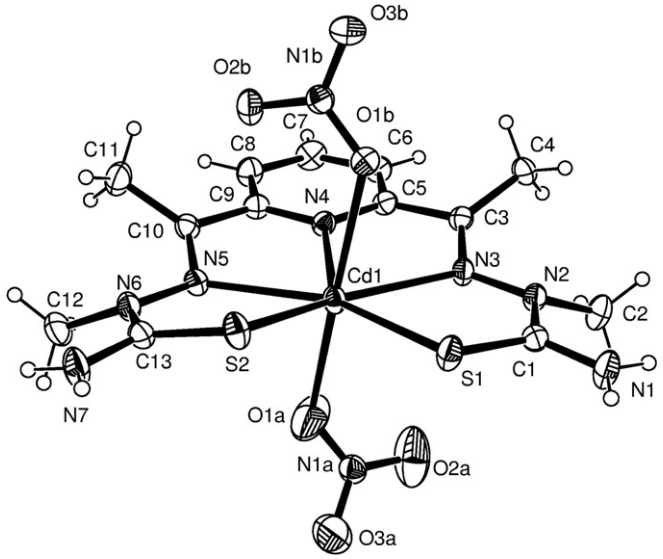

Fig. 3. ORTEP3 view of Cd(dap-^{2}NMetsc)$(NO_3)_2$ (30% ellipsoids).

As foreshadowed, the conformation of the coordinated ligand is very different to that seen in the metal free structure. However, similar steric influences are at work in the Cd complex that result in distortions from the normal planar conformation of a coordinated thiosemicarbazone. The ligand is still distinctly non-planar and a similar twisting distortion about both N–N bonds [C1–N2–N3–C3 159.1(4)° and C10–N5–N6–C13 –145.2(4)°] is seen in the complex in order to avoid methyl$\cdots$methyl non-bonded repulsions. Similarly the terminal thiosemicarbazide moieties are twisted about their C–N bonds by a similar degree as seen in the structure of the free ligand [N1–C1–N2–C2 19.5(7)° and N7–C13–N6–C12 –16.4(7)°]. Overall the ligand adopts a 'saddle' conformation with the methyl and terminal NH_2 groups alternating in their orientation above or below the approximate pentagonal coordination plane.

In most thiosemicarbazones, deprotonation of the N-atom at position 2 accompanies coordination and leads to significant alteration of electron density within the ligand backbone. In dap-^{2}NMetsc methylation of this N-atom blocks deprotonation and the intraligand bond lengths are basically unchanged upon coordination. The C–S bond length still has an intermediate value between a single bond (1.82 Å) and for a C=S double bond [1.56 Å]. The C1–N2 [1.368(6) Å], C13–N6 [1.354(6) Å], C–N1 [1.315(6) Å] and C13–N7 [1.320(6) Å] bond distances indicate that these bonds also have partial double bond characters. This is an indication that there is some electron delocalization in the hydrazine chain, but that it is independent of coordination.

For an ideal pentagonal bi-pyramidal complex, each of the five angles subtended at the equatorial plane should be 72°. Most of the coordinate angles within the equatorial plane are within 4° of this value; the S1–Cd–S1 angle (unrestrained by a chelate ring) shows the greatest deviation from the ideal value. It should be pointed out that for an ideal pentagonal array of donor atoms, a cyclic ligand with identical donor atoms and bond lengths is required.

4. Conclusions

The 2,6-diacetylpyridine bis(^{2}N-methylthiosemicarbazone) obtained by condensation of ^{2}N-methylthiosemicarbazide with 2,6-diacetylpyridine readily yields a

pentadentate N_3S_2 chelating agent forming pentagonal-bipyramidal zinc(II) and cadmium(II) complexes. Methylation at N2 blocks deprotonation of the ligand at each arm and the ligand binds as a neutral molecule in contrast to most other thiosemicarbazones which typically coordinate as anions. Notwithstanding the variations of bond lengths around the chelate rings within the coordinated ligand, the N_3S_2 donor set approaches that of an ideal pentagonal array and this ligand may be useful in enforcing this unusual geometry on other metal ions.

5. Supplementary material

Crystallographic data in CIF format (CCDC Deposition Nos. 604849 (dap-^{2}NMe) and 604850 (Cd(dap-^{2}NMe)$(NO_3)_2$)) have been deposited at the Cambridge Crystallographic Data Centre and are available on request from the Director, CCDC, 12 Union Road, Cambridge, CB2 1EZ, UK (fax: +44 1223 336 033; e-mail: deposit@ccdc.cam.ac.uk or http://www.ccdc.cam.ac.uk).

Acknowledgements

M. Akbar Ali and A.H. Mirza thank the University of Brunei Darussalam for supporting this work.

References

[1] M. Akbar Ali, S.E. Livingstone, Coord. Chem. Rev. 13 (1974) 101.
[2] M.J.M. Campbell, Coord. Chem. Rev. 15 (1975) 279.
[3] S.B. Padhye, G.B. Kauffman, Coord. Chem. Rev. 63 (1985) 127.
[4] D.X. West, S.B. Padhye, P.B. Sonawane, Struct. Bond. (Berlin) 76 (1991) 1.
[5] D.X. West, A.E. Liberta, S.B. Padhye, R.C. Chkate, P.B. Sonawane, A.S. Kumbhar, R.G. Yerande, Coord. Chem. Rev. 123 (1993) 49.
[6] J.S. Casas, M.S. García-Tasende, J. Sordo, Coord. Chem. Rev. 209 (2000) 197.
[7] J.K. Swearingen, D.X. West, Transit. Met. Chem. 26 (2001) 252, and references therein.
[8] A. Castineiras, M. Gil, E. Bermejo, D.X. West, Polyhedron 200 (2000) 449, and references therein.
[9] E. Bermejo, M. Gil, A. Castineiras, E. Labisbal, A. Sousa, H. Beraldo, D.X. West, Z. Naturforsch. B55 (2000) 863.
[10] M. Gil, E. Bermejo, A. Castineiras, H. Beraldo, D.X. West, Z. Anorg. Allg. Chem. 626 (2000) 2353.
[11] P.J. Blower, T.C. Castle, A.R. Cowley, J.R. Dilworth, P.S. Donnely, E. Labisbal, F.E. Sowrey, S.J. Teat, M.J. Went, J. Chem. Soc., Dalton Trans. (2003) 4416.
[12] A. Bino, N. Cohen, Inorg. Chim. Acta 210 (1993) 11.
[13] A.I. Matesanz, I. Cuadrado, C. Pastor, P. Souza, Z. Anorg. Allg. Chem. 631 (2005) 780.
[14] P.C. Moreno, R.H.P. Francisco, M.T. Do, P. Gambardella, G.F. De Sousa, A. Abras, Acta Crystallogr., Sect. C 53 (1997) 1411.
[15] J.S. Casas, A. Castiñeiras, A. Sánchez, J. Sordo, A. Vazquez-Lopez, M.C. Rodriguez-Arguelles, U. Russo, Inorg. Chim. Acta 221 (1994) 61.
[16] G.F. de Sousa, D.X. West, C.A. Brown, J.K. Swearingen, J. Valdéz-Martinez, R.A. Toscano, S. Hernández-Ortega, M. Hörner, R.J. Bortuluzzi, Polyhedron 19 (2000) 841.
[17] S.O. Sommerer, G.J. Palenik, Inorg. Chim. Acta 183 (1991) 217.
[18] G.F. de Sousa, C.A.L. Filgueiras, A. Abras, S.S. Al-Juaid, P.B. Hitchcock, J.F. Nixon, Inorg. Chim. Acta 218 (1994) 139.
[19] A.H. Othman, S.W. Ng, Acta Crystallogr., Sect. C 51 (1995) 1059.
[20] M.R. Bermejo, R. Pedrido, M.I. Fernandez, A.M. Gonzalez-Noya, M. Maneiro, M.J. Rodríguez, M.J. Romero, M. Vázquez, Inorg. Chem. Commun. 7 (2004) 4.
[21] R. Pedrido, M.R. Bermejo, M.J. Romero, M. Vazquez, A.M. González-Noya, M. Maneiro, M.J. Rodriguez, M.I. Fernandez, J. Chem. Soc., Dalton Trans. (2005) 572.
[22] S. Abram, C. Maichle-Mössmer, U. Abram, Polyhedron 17 (1998) 131.
[23] G. Dessy, V. Fares, Cryst. Struct. Commun. 10 (1981) 1025.
[24] J.S. Casas, A.E. Castellano, M.S. García-Tasende, A. Sánchez, J. Sordo, J. Zukerman-Schpector, Z. Anorg. Allg. Chem. 623 (1997) 825.
[25] A.C.T. North, D.C. Phillips, F.S. Mathews, Acta Crystallogr., Sect. A 24 (1968) 351.
[26] K. Harms, S. Wocadlo, CAD4 Data Reduction, University of Marburg, Marburg, Germany, 1995.
[27] L. Farrugia, J. Appl. Crystallogr. 32 (1999) 837.
[28] G.M. Sheldrick, SHEXS86 – Programme for Crystal Structure Solution, Institute für Anorganisch Chemie der Universität, Göttingen, Germany, 1986.
[29] G.M. Sheldrick, SHELXL97, Institüt für Anorganisch Chemie der Universität, Göttingen, Germany, 1998.
[30] L. Farrugia, J. Appl. Crystallogr. 30 (1997) 565.
[31] K. Nakamoto, Infrared Spectra of Inorganic and Coordination Compounds, 2nd ed., Wiley Interscience, 1970, pp. 171–172.
[32] B.M. Gatehouse, S.E. Livingstone, R.S. Nyholm, J. Chem. Soc. (1957) 4222.
[33] J. Valdez-Martinez, R.A. Toscano, R.C. Olivares, Acta Crystallogr., Sect. C 47 (1991) 2666.
[34] M. Vázquez, L. Fabrizzi, A. Taglietti, R.M. Pedrido, A.M. González-Noya, M.R. Bermejo, Angew. Chem. Int. Ed. 43 (2004) 1962.

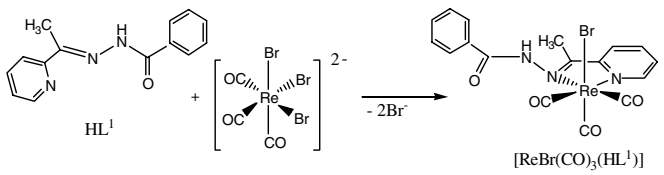

Scheme 1.

hydrazide, which was previously synthesized by Lu et al. [6], as well as the isolation and characterization of the rhenium(I) complex. The substitution of the acetylpyridine fragment of HL^1 by ferrocenyl carbaldehyde must give rise to a different coordination mode of the ligand. Furthermore, the incorporation of the ferrocenyl group into the complex will enable the exploration of potentially improved bioinorganic (antitumor and antivirus activities [7]) and catalytic applications. The latter possibility results from the modulation of the binding affinity of the ligand for the rhenium fragment by the redox state of the ferrocenyl group [8].

2. Results and discussion

2.1. Synthesis and spectroscopic characterization

Ligand $H(Fe)L^1$ was obtained by treatment of ferrocenylcarbaldehyde with benzoylhydrazine in dry methanol. Single crystals of this compound were obtained from the mother liquor. The compound is air stable and soluble in common organic solvents (see Scheme 2).

Reaction of the ligand with the adduct *fac*-$[ReBr(CO)_3(NCCH_3)_2]$ afforded a red solid that is stable in air, moderately soluble in chloroform and highly soluble in acetone. Elemental analysis and mass spectrometry confirmed the stoichiometry $[ReBr(CO)_3\{H(Fe)L^1\}]\cdot\frac{1}{2}CHCl_3$ the mass spectrum contains a signal corresponding to the molecular ion, although the peak due to the species $[M-Br]^+$ is slightly more intense, as observed in the thiosemicarbazone derivatives described in Ref. [9]. Facial geometry around the rhenium atom is suggested by the three strong ν(C≡O) IR bands in the range 2027–1891 cm^{-1}. Furthermore, the band corresponding to the ν(C=O) mode is shifted from 1646 cm^{-1} in $H(Fe)L^1$ to 1594 cm^{-1} in the rhenium complex. This effect is contrary to that observed in the complex $[ReBr(CO)_3(HL^1)]$ (1677 cm^{-1}) in comparison to HL^1 (1657 cm^{-1}) [5], suggesting a different coordination mode in which the amide C=O group is, as one would expect, directly involved in the coordination. Both of these aspects – configuration around the metal atom and coordination mode of the ligand – were confirmed by an X-ray diffraction study (vide infra).

The ^1H NMR spectra of both compounds display signals corresponding to the ferrocenyl group (with clear differences between the linked and free cyclopentadienyl groups), the phenyl group and N–H protons. In general, all proton signals in the complex are shifted at low field respect to the free ligand, as in $[ReBr(CO)_3(HL^1)]$. However, the hydrazinic proton singlet at 10.70 ppm in $H(Fe)L^1$ is strongly shifted (12.80 ppm) in the spectrum of the rhenium complex. This effect of rhenium coordination has also been observed in other hydrazine-based ligands such as thiosemicarbazones [9,10] when the N–H group is a member of the chelate ring. In cases where the coordination mode of the ligand excludes the N–H group of the chelate ring, the singlet is only shifted by around 1 ppm (see for instance Refs. [11,5] for thiosemicarbazone and hydrazone systems, respectively). Both title compounds show signals corresponding to the ferrocenyl group and these are distributed in two sets: a singlet at 4.20 and 4.40 ppm, respectively, due to the free cyclopentadienyl ring and two doublets between 4.40 and 5.30 corresponding to the ring linked to the hydrazone moiety.

The UV–Vis solution spectra of the ligand and complex were also recorded (Fig. 1) and the main data are included in Table 1. The data for HL^1 and $[ReBr(CO)_3(HL^1)]$ [5] are also included for the sake of comparison. The spectra of the title compounds are strongly dominated by the ferrocene bands, which have been discussed by John et al. [12]. The spectra of the compounds were obtained in two solvents of different polarities, such as MeOH and chloroform, and suggest a slight positive hyperchromic effect in the $H(Fe)L^1$ derivatives but a hypsochromic shift with polarity in the HL^1 derivatives.

The absorptions in the range 320–360 nm and the bands centered at 265 nm in the ferrocene derivatives are due to π–π^* transitions, the latter probably those of the cyclopentadienyl rings [6]. The band centered at 295 nm, which is present in all uncoordinated ligands included in Table 1, is attributed to the IL π–π^* transitions arising probably from the aroylhydrazone moiety [6]. The shoulder between 430–495 nm is attributed to MLCT from Fe to either the non-bonding or the antibonding orbitals of the cyclopentadienyl rings.

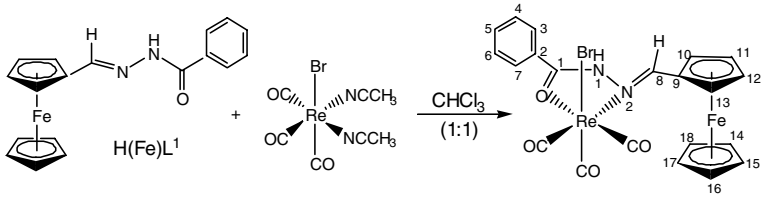

Scheme 2.

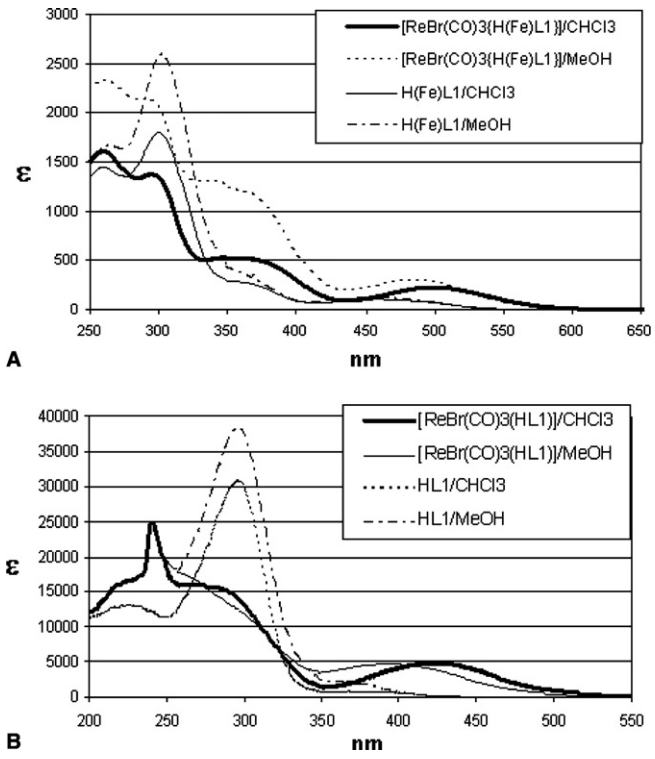

Fig. 1. UV–Vis spectra of $H(Fe)L^1$ (A) and HL^1 (B) and their rhenium(I) complexes.

The absorption patterns in the spectra of the complexes *fac*-[$ReBr(CO)_3(HL^1)$] and *fac*-[$ReBr(CO)_3\{H(Fe)L^1\}$] are quite similar to each other. The broad bands in the range 400–530 nm could be assigned to MLCT d –> π^* transitions, which are very similar to analogous absorptions in other rheniumtricarbonyl complexes [13]. The intense absorption at 294 nm is due to a ligand centered π–π^* transition, while the other IL transitions would be expected to appear in the range 200–210 nm. Surprisingly, the band due to the hydrazone group, in both kinds of complex, is strongly shifted when compared with that in the uncoordinated ligands – in spite of the very different chelation mode of the ligand with the rhenium centre observed in the solid state.

2.2. The molecular structures of the compounds

The molecular structures of the ligand $H(Fe)L^1$ and the rhenium(I) derivative are shown in Fig. 2 along with the atomic numbering scheme used. Selected bond lengths and angles are listed in Table 2.

Single crystals of the ligand were obtained from the mother liquor (methanol). Its structure is a rare example of the presence of four crystallographically independent molecules per asymmetric unit, together two methanol solvent molecules. All searches for missing symmetry were unsuccessful [14]. The differences between distances and angles in the $H(Fe)L^1$ molecules are statistically insignificant and, consequently, mean values are included in Table 2.

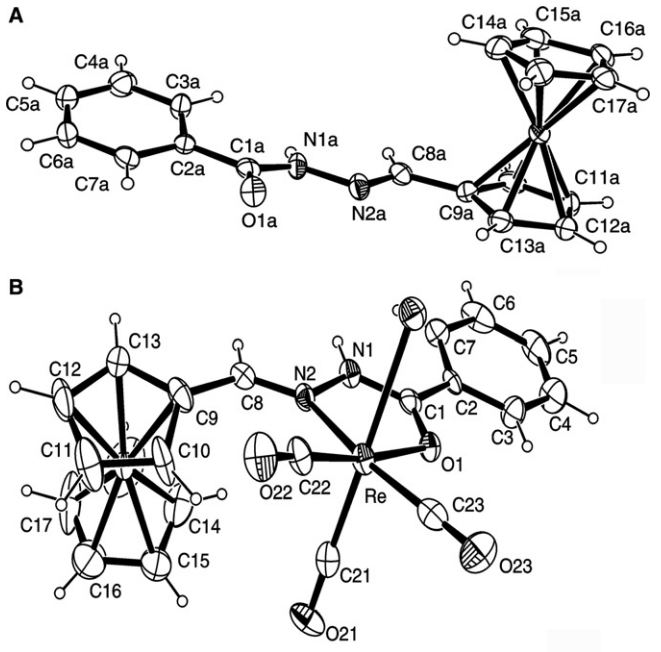

Fig. 2. Molecular structures of $H(Fe)L^1$ (A) and [$ReBr(CO)_3\{H(Fe)L^1\}$] (B) (the thermal ellipsoids represent 30% occupancy).

Table 1
Relevant UV data in nm ($\varepsilon \times 10^{-3}$) for the compounds

Compound	Solvent				
HL^1	MeOH		368(2.4)	296(38.5)	
	$CHCl_3$		380(0.9)	296(31.0)	227(13.0)
[$ReBr(CO)_3(HL^1)$]	MeOH	393(4.8)		299(12.0)	262(17.5)
	$CHCl_3$	422(5.0)		241(24.6)	216(15.6)
$H(Fe)L^1$	DMF[a]	430(2.8)	328(9.3)	295(12.0)	265(14.0)
	MeOH	453(1.3)	357(3.9)	302(26.1)	263(16.8)
	$CHCl_3$	459(0.1)	359(0.3)	299(1.8)	260(1.4)
[$ReBr(CO)_3\{H(Fe)L^1\}$]	MeOH	485(3.0)	351(12.4)	290(21.4)	261(23.3)
	$CHCl_3$	500(2.2)	353(5.2)	294(13.7)	259(16.1)

[a] Data in DMF obtained from Ref. [6].

Table 2
Interatomic distances (Å) and angles (°) for $[H(Fe)L^1]$ and $[ReBr(CO)_3\{H(Fe)L^1\}]$ molecules

	$[H(Fe)L^1]\cdot\frac{1}{2}CH_3OH$	$[ReBr(CO)_3\{H(Fe)L^1\}]\cdot\frac{1}{2}CHCl_3$
O(1)–C(1)	1.223(4)[a]	1.276(13)
N(1)–C(1)	1.341(4)[a]	1.321(12)
N(1)–N(2)	1.399(3)[a]	1.436(11)
N(2)–C(8)	1.277(4)[a]	1.301(12)
C(1)–C(2)	1.498(5)[a]	1.460(15)
C(8)–C(9)	1.451(4)[a]	1.453(16)
Re–O(1)		2.144(7)
Re–N(2)		2.194(9)
Re–Br		2.6435(15)
C(1)–N(1)–N(2)	118.3(3)[a]	117.8(9)
C(8)–N(2)–N(1)	115.0(3)[a]	113.0(9)
O(1)–C(1)–N(1)	122.4(3)[a]	119.4(11)
O(1)–C(1)–C(2)	121.2(3)[a]	121.3(11)
N(1)–C(1)–C(2)	116.2(3)[a]	119.2(11)
N(2)–C(8)–C(9)	120.9(3)[a]	127.8(12)
C(22)–Re–O(1)		172.6(5)
C(21)–Re–O(1)		96.2(4)
C(23)–Re–N(2)		169.3(4)
C(22)–Re–N(2)		102.7(4)
C(21)–Re–N(2)		94.7(4)
O(1)–Re–N(2)		74.5(3)
C(23)–Re–Br		94.4(4)
C(22)–Re–Br		89.9(4)
C(21)–Re–Br		178.2(4)
O(1)–Re–Br		83.0(2)
N(2)–Re–Br		83.5(2)
O(1)–Re–N(2)		74.5(3)
C(8)–N(2)–Re		137.7(8)
N(1)–N(2)–Re		109.2(6)
C(1)–O(1)–Re		116.4(7)

[a] Average values and standard deviations are estimated with the expressions: $x = (\sum x_j/\sigma_j^2)/\sum 1/\sigma_j^2$; $\sigma^2(x) = 1/\sum 1/\sigma_j^2$.

In the molecule of $H(Fe)L^1$, the hydrazone group and the cyclopentadienyl ring are almost coplanar, although the phenyl group deviates slightly from the idealized plane. The C–N and N–N bond distances suggest mainly a double-bond character for the C8–N2 link although some π delocalization around the hydrazone chain occurs is also possible. As in ferrocenylcarbaldehyde isonicotinylhydrazone [15], the configurations of the bonds in the fragment C1–N1–N2–C8 is, in all cases, *Z*,*E*,*E*, respectively.

Single crystals of the complex $[ReBr(CO)_3\{H(Fe)L^1\}]$ containing half chloroform molecule per asymmetric unit were obtained by slow evaporation of chloroform solutions. Since we were unable to find a statistical model for the disorder of the solvent molecule, the program SQUEEZE [16] was used to correct its diffuse scattering data. The rhenium atom is coordinated by the N2 and O1 hydrazone atoms, forming a five-membered chelate ring, as well as three carbonyl carbon atoms and bromine atoms. The resulting coordination polyhedron can be described as a distorted octahedron [the main distortion being C(22)–Re–N(2) and O(1)–Re–N(2)]. This coordination mode does not cause changes in the configuration of the hydrazone chain with respect to that observed in $H(Fe)L^1$. The C1–O1 distance is clearly longer than that in the free ligand as a consequence of Re–O1 coordination. However, this change does not appear to have any consequence on the hydrazone chain (only a slight shortening of the C1–C8 distance is observed).

2.3. Supramolecular structures

The supramolecular structure of $H(Fe)L^1\cdot\frac{1}{2}(CH_3OH)$ is shown in Figs. 3A and B and the main interactions are listed in Table 3. The association of the molecules in the crystal is strongly dominated by hydrogen bonding, either between

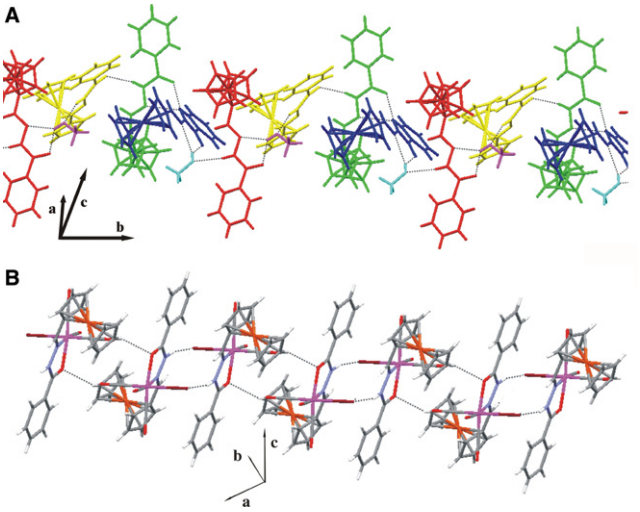

Fig. 3. Mercury [22] plots showing the hydrogen bonds in crystals of $[H(Fe)L^1]\cdot\frac{1}{2}CH_3OH$ (A) and $[ReBr(CO)_3\{H(Fe)L^1\}]\cdot\frac{1}{2}CHCl_3$ (B).

Table 3
Relevant intermolecular interactions

D–H...A	*d*(D–H)	*d*(H...A)	*d*(D...A)	∠(DHA)
$[H(Fe)L^1]\cdot\frac{1}{2}CH_3OH$				
Strong hydrogen bond				
N(1B)–H(1B)...O(1A)	0.86	2.12	2.940(6)	159.1
N(1C)–H(1C)...O(2M)[a]	0.86	2.22	3.055(7)	163.6
N(1D)–H(1D)...O(1M)	0.86	2.02	2.842(6)	159.0
N(1A)–H(1A)...O(1D)	0.86	2.04	2.856(6)	157.6
O(1M)–H(1M)...O(1C)	0.82	2.17	2.771(6)	130.1
O(2M)–H(2M)...O(1B)	0.82	2.08	2.791(7)	144.6
O(2M)–H(2M)...N(2B)	0.82	2.38	3.074(7)	142.3
Weak hydrogen bond				
N(1B)–H(1B)...N(2A)	0.86	2.67	3.229(6)	124.0
O(1M)–H(1M)...N(2C)	0.82	2.65	3.269(6)	133.3
$[ReBr(CO)_3\{H(Fe)L^1\}]\cdot\frac{1}{2}CHCl_3$				
Strong hydrogen bond				
C(15)–H(15)...O(1)[b]	0.95	2.49	3.27	139.3
Weak hydrogen bond				
N(1)–H(1)...Br[c]	0.88	2.64	3.487(9)	162.5
C(16)–H(16)...O(23)[d]	0.95	2.66	3.51(3)	149.3

[a] #1 = x, $y-1$, z.
[b] #3 = $-x$, $-y$, $-z$.
[c] #1 = $-x+1/2$, $-y+1/2$, $-z$.
[d] #2 = $x-1/2$, $y+1/2$, z.

ligand molecules or involving the methanol molecules. These aspects are depicted in Fig. 3A, in which the asymmetric unit is represented. Three molecules of $H(Fe)L^1$ are associated by interactions between N1–H groups and N2 or O1 atoms of crystallographically independent neighbouring molecules. This virtual trimer is associated with another crystallographically independent molecule of $H(Fe)L^1$ by a methanol molecule. The resulting unit is associated through a second methanol molecule of other units to form chains running along the *b* axis (Fig. 3B).

The coordination of the tricarbonylrhenium(I) fragment hinders the hydrogen-bonding interactions involving the O1 atom and, consequently, the association of the complex $[ReBr(CO)_3\{H(Fe)L^1\}]$. Indeed, these complex molecules are associated in dimers by weak hydrogen-bonding interactions between the N1–H and the Br atom of a neighbouring molecule. Similar dimeric structures based on rhenium(I) thiosemicarbazones have been observed previously [9] and, in the present case, form chains oriented by weak C(Fc)H···O interactions [17] along the *a* axis.

3. Experimental

3.1. Materials and methods

All operations performed in the synthesis and isolation of the compounds were carried out under an atmosphere of dry argon. All solvents were dried over appropriate drying agents, degassed using a vacuum line and distilled under an Ar atmosphere [18a]. $[ReX(CO)_5]$ [18b], $[ReX(CO)_3(CH_3CN)_2]$ [18c], HL^1 and $[ReBr(CO)_3(HL^1)]$ [5] were synthesized by published methods.

Elemental analyses were carried out on a Fisons EA-1108. Melting points (m.p.) were determined on a Gallenkamp MFB-595 and are uncorrected. Mass spectra were recorded on a VG Autospec Micromass spectrometer operating under FAB conditions (nitrobenzyl alcohol matrix). Infrared spectra were recorded from KBr pellets on a Bruker Vector 22FT. UV–Vis spectra were performed on a CARY 100 (Varian) spectrophotometer from $CHCl_3$ or acetone solutions. ^1H NMR spectra were obtained on a Bruker AMX 400 spectrometer from acetone-d_6 solutions.

3.2. Synthesis of the ligand $H(Fe)L^1$

Ferrocenyl carbaldehyde (1003.0 mg, 4.69 mmol) and benzoylhydrazine (638.0 mg, 4.69 mmol) were dissolved in methanol (13 mL) and the mixture was refluxed for 2 h. The reaction mixture was allowed to cool down to r.t. and methanol (15 mL) was added. The resulting brown solid was filtered off and dried under vacuum over KOH. Single crystals were obtained from slow evaporation of the mother liquor.

Yield: 987 mg (63%). M.p.: 171–172 °C. *Anal.* Calc. for $C_{18}H_{16}FeN_2O$ requires: C, 65.1; H, 4.8; N, 8.4. Found: C, 65.1; H, 4.8; N, 8.5%. Mass spectrum [*m*/*z* (%)]: 332(57.1) $[M]^+$. IR data (KBr, cm^{-1}): 3230 w, 3085 w ν(NH); 1646 vs ν(C=O); 1606 s, 1556 s, 1492 w, 1465 w ν(C=N) + ν(C=C). ^1H NMR data (acetone-d_6, ppm): 10.70s (1) δ(N1–H); 4.65s (2) δ(C13–H/C10–H); 4.40s (2) δ(C12–H/C11–H); 7.95d (2) δ(C7–H/C3–H); 7.55t (1) δ(C5–H); 7.50t (2) δ(C6–H/C4–H); 8.40s (1) δ(C8–H); 4.20s (5) δ(Cp–H).

Table 4
Crystal data and data collection for $[H(Fe)L^1]\cdot\frac{1}{2}CH_3OH$ and $[ReBr(CO)_3\{H(Fe)L^1\}]\cdot\frac{1}{2}CHCl_3$

	$[H(Fe)L^1]\cdot\frac{1}{2}CH_3OH$	$[ReBr(CO)_3\{H(Fe)L^1\}]\cdot\frac{1}{2}CHCl_3$
Empirical formula	$C_{18.50}H_{18}FeN_2O_{1.50}$	$C_{20.5}H_{15.5}BrCl_{1.5}FeN_2O_4Re$
Molecular weight	348.20	728.98
Space group	$P\bar{1}$	$C2/c$
Unit cell dimensions		
a (Å)	11.0331(9)	17.2073(15)
b (Å)	15.8682(12)	13.8648(12)
c (Å)	20.5606(15)	19.9923(17)
α (°)	85.113(2)	90
β (°)	76.029(2)	90.417(2)
γ (°)	72.806(2)	90
V (Å^3)	3336.7(4)	4769.6(7)
Z	8	8
D_{calc} (Mg/m^3)	1.386	2.030
Absorption coefficient (mm^{-1})	0.912	7.552
θ (°)	1.34–28.03	1.89–28.03
Reflections collected	18906	13110
Independent reflections [R_{int}]	13300 [0.0762]	5369 [0.0760]
Observed reflections [$I > 2\sigma(I)$]	5402	2105
Maximum and minimum transmission	0.830/0.631	0.339/0.250
Goodness-of-fit on F^2	0.805	0.813
Final R indices [$I > 2\sigma(I)$]	$R_1 = 0.0645$, $wR_2 = 0.1361$	$R_1 = 0.0499$, $wR_2 = 0.1076$
R indices (all data)	$R_1 = 0.1583$, $wR_2 = 0.1699$	$R_1 = 0.1622$, $wR_2 = 0.1242$

3.3. Synthesis of the complex $[ReBr(CO)_3\{H(Fe)L^1\}]\cdot CHCl_3$

H(Fe)L^1 (39.6 mg, 0.12 mmol) and *fac*-bis(acetonitrile)bromotricarbonylrhenium(I) (53.1 mg, 0.12 mmol) were dissolved in freshly distilled chloroform (10 mL) and the mixture was heated under reflux for 2 h. The resulting red solid was filtered off and dried under vacuum. Single crystals were obtained by slow evaporation of a chloroform solution.

Yield: 36.7 mg (45%). M.p.: 200–202 °C. *Anal*. Calc. for $C_{22}H_{17}N_2O_4Cl_3BrFeRe$ requires: C, 33.0; H, 2.1; N, 3.5. Found: C, 32.9; H, 1.9; N, 3.7%. Mass spectrum [*m*/*z* (%)]: 682(3.3) $[M]^+$, 603(3.7) $[M-Br]^+$, 332(57.1) $[H(Fe)L^1]^+$. IR data (KBr, cm^{-1}): 3204 w, 3093 w *ν*(OH)/*ν*(NH); 2027 s, 1924 vs, 1891 vs; *ν*(*C*═*O*); 1594 w *ν*(C═O); 1555 m, 1452 w, 1412 w *ν*(C═N) + *ν*(C═C). ^{1}H NMR data (acetone-d_6, ppm): 12.80s (1) *δ*(N1–H); 5.30d (2) *δ*(C13–H/C10–H); 4.90d (2) *δ*(C12–H/C11–H); 8.10d (2) *δ*(C7–H/C3–H); 7.80t (1) *δ*(C5–H); 7.60t (2) *δ*(C6–H/C4–H); 8.90s (1) *δ*(C8-H); 4.40s (5) *δ*(C(Cp)–H).

3.4. X-ray data collection, structure determination and refinement

Crystallographic data collection and refinement parameters are listed in Table 4. All crystallographic measurements were performed on a Bruker Smart CCD apparatus at CACTI (Universidade de Vigo). The data were corrected for absorption effects using the program SADABS [19]. Structure analyses were carried out by direct methods [20]. Least-squares full-matrix refinements on F^2 were performed using the program SHELXL 97. Atomic scattering factors and anomalous dispersion corrections for all atoms were taken from International Tables for Crystallography [21]. For $[ReBr(CO)_3\{H(Fe)L^1\}]\cdot\frac{1}{2}CHCl_3$ contributions from disordered solvent molecule were removed by the SQUEEZE [16] routine of PLATON [14], and the number of chloroform molecules was estimated from the number of electrons so excluded per unit cell. All non-hydrogen atoms were refined anisotropically. Hydrogen atoms were refined as riders except N2–H, which was refined isotropically at a position previously identified in the corresponding Fourier map. Graphics were produced with PLATON [14] and MERCURY [22].

Acknowledgements

This research was supported by the European Rural Development Fund and the Directorate General for Research of the Spanish Ministry of Science and Technology through project BQU200203543.

Appendix A. Supplementary data

Crystallographic data for the structural analysis have been deposited with the Cambridge Crystallographic Data Centre, CCDC Nos. 601647 and 601648 for compounds $H(Fe)L^1\cdot\frac{1}{2}CH_3OH$ and $[ReBr(CO)_3\{H(Fe)L^1\}]\cdot\frac{1}{2}CHCl_3$, respectively. Copies of this information may be obtained free of charge from The Director, CCDC, 12 Union Road, Cambridge CB2 1EZ, UK, fax: +44 1223 336 033, e-mail: deposit@ccdc.cam.ac.uk or http://www.ccdc.cam.ac.uk. Supplementary data associated with this article can be found, in the online version, at doi:10.1016/j.poly.2006.06.007.

References

[1] M.A. Al-Nuri, M. Abu-Eid, N.A. Zatar, S. Khalaf, M. Hannoun, Anal. Chim. Acta 259 (1992) 175, and references therein.
[2] M.A. Ali, R.N. Bose, Polyhedron 3 (1984) 517.
[3] (a) F. Zobi, B. Spingler, T. Fox, R. Alberto, Inorg. Chem. 42 (2003) 2818;
(b) F. Zobi, O. Blacque, H.W. Schmalle, B. Spingler, R. Alberto, Inorg. Chem. 43 (2004) 2087.
[4] F. Zobi, B. Spingler, R. Alberto, ChemBioChem 6 (2005) 1397.
[5] J. Grewe, A. Hagenbach, B. Stromburg, R. Alberto, E. Vázquez-López, U. Abram, Z. Anorg. Allg. Chem. 629 (2003) 303.
[6] Z.-L. Lu, W. Xiao, B.-S. Kang, C.-Y. Su, J. Liu, J. Mol. Struc. 523 (2000) 133.
[7] (a) M.A. Ali, S.E. Livingstone, D.J. Phillips, Inorg. Chim. Acta 7 (1973) 79;
(b) J.-X. Fang, Z. Jin, Z.-M. Li, W. Liu, Appl. Organomet. Chem. 17 (2003) 145.
[8] A.A. Allgeier, C.S. Slonre, C.A. Mirkin, L.M. Liable-Sands, G.P.A. Yap, A.L. Rheingold, J. Am. Chem. Soc. 119 (1997) 550.
[9] R. Carballo, J.S. Casas, E. García-Martínez, G. Pereiras-Gabián, A. Sánchez, J. Sordo, E.M. Vázquez-López, J.C. García-Monteagudo, U. Abram, J. Organomet. Chem. 656 (2002) 1.
[10] R. Carballo, J.S. Casas, E. García-Martínez, G. Pereiras-Gabián, A. Sánchez, J. Sordo, E.M. Vázquez-López, Inorg. Chem. 42 (2003) 6395.
[11] R. Carballo, J.S. Casas, E. García-Martínez, G. Pereiras-Gabián, A. Sánchez, J. Sordo, U. Abram, E.M. Vázquez-López, CrystEngComm 7 (2005) 113.
[12] Y.S. John, D.N. Hendrickson, H.B. Gray, J. Am. Chem. Soc. 93 (1971) 427.
[13] A. Vogler, H. Kunkely, Coord. Chem. Rev. 200–202 (2000) 991.
[14] A.L. Spek, PLATON v.21.08.03., University of Utrecht, The Netherlands, 2002.
[15] Z.-F. Chen, H.-L. Zou, H. Liang, R.-X. Yuan, Y. Zhang, Appl. Organomet. Chem. 18 (2004) 438.
[16] A.L. Spek, Acta Crystallogr., Sect. A 34 (1990) 46.
[17] G.R. Desiraju, T. Steiner, The Weak Hydrogen Bond, IUCr Monographs on Crystallography, vol. 9, Oxford University Press, Oxford, 1999.
[18] (a) D.D. Perrin, W.L.F. Armarego, Purification of Laboratory Chemicals, 3rd ed., Butterworth and Heinemann, Oxford, 1988;
(b) S.P. Schmidt, W.C. Trogler, F. Basolo, Inorg. Synth. 28 (1990) 160;
(c) M.F. Farona, K.F. Kraus, Inorg. Chem. 9 (1970) 1700.
[19] G.M. Sheldrick, SADABS, University of Göttingen, Germany, 1996.
[20] G.M. Sheldrick, SHELX-97, Program for the Solution and Refinement of Crystal Structures, University of Göttingen, Germany, 1997.
[21] International Tables for Crystallography. vol. C, Kluwer, Dordrecht, The Netherlands, 1992.
[22] I.J. Bruno, J.C. Cole, P.R. Edgington, M.K. Kessler, C.F. Macrae, P. McCabe, J. Pearson, R. Taylor, Acta Crystallogr., Sect. B 58 (2002) 389.

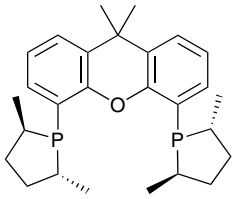

(*R*,*R*)-Duxantphos

Chart 1.

catalysis. Indeed, wide bite-angle bidentate diphospholane chiral ligands such as Duxantphos (Chart 1) are very efficient and selective in palladium-catalyzed asymmetric allylic alkylation, even with small allylic substrates [4,5]. Given their success, we planned to expand the family of chelate, chiral, xanthene-based ligands towards air-stable and easy-to-synthesize P,N or N,N chelate ligands.

We report hereafter the synthesis and analysis of chiral ligands with a rigid xanthene scaffold bearing air-stable imine functions, and their applications in coordination chemistry of palladium, silver and rhodium, and in homogeneous catalysis. We used cheap (1*R*)-camphor and (1*S*)-fenchone as chiral sources, in analogy with reported diimine [6] and iminophosphine [7] ligands. Some of the ligand syntheses have been described in a preliminary communication [8].

2. Experimental

2.1. General details

Experiments were carried out under a nitrogen or argon atmosphere, using a vacuum line or Vacuum Atmospheres glovebox equipped with Dri-Train HE-493 inert gas purifier, except the syntheses of **3**, **4**, **7**, **8**, **12** and **13** which were not air-sensitive. Diethyl ether, THF and pentane were distilled over sodium and benzophenone, toluene over sodium, dichloromethane and acetonitrile over calcium hydride under nitrogen immediately before use. Column chromatography was carried out on Merck silica gel 60, 70-230 mesh ASTM, and thin layer chromatography on Macherey–Nagel 0.25 mm Polygram® Sil G/UV_{254} precoated silica gel plates. The following commercial reagents were used as received; Aldrich: 9,9-dimethyl-9*H*-xanthene (**1**), 2,7-di-*tert*butyl-4,5-dibromo-9,9-dimethyl-9*H*-xanthene (**10**), *n*-BuLi solution in hexanes (1.6 M), PhLi solution in cyclohexane–Et_2O (1.7 M), diphenylphosphoryl azide (DPPA), (1*R*)-(−)-fenchone, dimethyl malonate, allyltriethoxysilane, diphenylsilane; Sigma: (1*R*)-(+)-camphor; Lancaster: (1*S*)-(+)-fenchone; Fluka: benzyl alcohol, triethylamine; Acros: acetophenone; Prolabo: KOH; Strem: $TiCl_4$, $AgBF_4$, AgOTf, AgF; Johnson Matthey: $RhCl_3 \cdot 3H_2O$. The concentration of organolithium reagents was checked before use following a reported method [9]. Diphenylchlorophosphine (95% min., Strem) was distilled at 170 °C under reduced pressure and stored under argon. NaH (60% in mineral oil, Fluka) was washed three times with pentane, dried in vacuo and stored in the glovebox. Benzaldehyde (Aldrich) was purified by filtration through silica gel. Gaseous CO_2 (obtained by sublimation of dry ice) was dried by bubbling in H_2SO_4. The compounds listed hereafter were synthesized following reported procedures: (*rac*)-(*E*)-1-acetoxy-1,3-diphenylprop-2-ene (**16a**) [10], (*rac*)-(*E*)-2-acetoxypent-3-ene (**16b**) [11], (*rac*)-1-acetoxycyclohex-2-ene (**16c**) [12], bis[(η^3-allyl)chloropalladium] [13], tris(acetonitrile)trichlororhodium [14], bis[(η^4-1,5-cyclooctadiene)chlororhodium] [15]. The NMR spectra were obtained at room temperature (unless otherwise indicated) on Bruker spectrometers. ^{1}H NMR spectra were recorded at 200.13 MHz (AC-200 instrument), 300.16 MHz (AC-300) or 500.13 MHz (ARX-500) and referenced to $SiMe_4$. $^{13}C\{^1H\}$ NMR spectra (broadband decoupled) were recorded at 50.32 MHz (AC-200), 75.48 MHz (AC-300), 100.62 MHz (AM-400) or 125.76 MHz (ARX-500) and referenced to $SiMe_4$. $^{31}P\{^1H\}$ NMR spectra (broadband decoupled) were recorded at 121.51 MHz (AC-300) or 202.46 MHz (ARX-500) and referenced to 85% aqueous H_3PO_4. For variable-temperature spectra, the probe temperature was controlled (±1 K) by a B-VT 2000 unit calibrated with a methanol NMR tube. The NMR signals were assigned in agreement with Refs. [6,16]; the assignments were supported by COSY, NOESY or ROESY spectra or irradiations for ^{1}H NMR, and DEPT-135° and/or HSQC spectra for $^{13}C\{^1H\}$ NMR. FT-IR spectra were recorded on a Perkin–Elmer 1600 Series spectrometer on KBr pellets; the IR signals of silver complexes were assigned in agreement with published data [17]. ES-MS spectra and elemental analyses were carried out by the corresponding facilities at the Institut de Chimie, Université Louis Pasteur, Strasbourg. Melting points were determined with a Reichert WME Kofler block and are uncorrected. Optical rotations ($[\alpha]_D^{20}$) were measured on a Perkin–Elmer Otopol III polarimeter ($\lambda = 589$ nm); specific rotations are reported in degrees per decimeter at 20 °C, and the concentration (*c*) is given in grams per 100 mL. GC analyses were performed on a Hewlett Packard 5890 series II apparatus equipped with a capillary column (Pd- and Ag-catalyzed reactions: 30 m × 0.25 mm Restek Rt-βDEXse™; Rh-catalyzed hydrosilylation: 50 m × 0.25 mm Chiraldex β-PM™). HPLC analyses were done on a Hewlett Packard series 1100 apparatus equipped with 250 mm × 4.6 mm Daicel Chiralpak™ AD analytical columns, flow rate 1 mL min^{-1}, eluant *n*-hexane–*i*PrOH (95:5).

2.2. Syntheses

2.2.1. 9,9-Dimethyl-9H-xanthene-4,5-dicarboxylic acid (2) [18]

To a yellow solution of 9,9-dimethyl-9*H*-xanthene (3.00 g, 14.28 mmol) in 60 mL Et_2O was added *n*-BuLi (22.5 mL solution, 36 mmol) at 0 °C. The solution rapidly turns brown. The reaction mixture was brought to RT

and appeared as a beige suspension after 16 h stirring. CO_2 was bubbled until the mixture was converted to a pale green solution. 70 mL of an aqueous HCl solution (2 M) was added. The organic phase was extracted and the product isolated (2.04 g, 6.83 mmol, 49% yield) as reported in Ref. [18]. *Anal.* Calc. for $C_{17}H_{14}O_5$: C, 68.45; H, 4.73. Found: C, 68.31; H, 5.00%.

2.2.2. *N,N′-bis(benzyloxycarbonyl)-9,9-dimethyl-9H-xanthene-4,5-diamine (**3**)*

A mixture of **2** (1.76 g, 5.90 mmol), DPPA (3.25 g, 11.82 mmol), benzylic alcohol (1.27 g, 11.76 mmol) and triethylamine (1.21 g, 11.83 mmol) dissolved in 50 mL toluene was heated at 100 °C for 18 h. The yellow solution was allowed to cool to room temperature and treated with 20 mL aqueous HCl (0.5 M). The organic phase was neutralized with saturated aqueous $NaHCO_3$ and dried over $MgSO_4$. After evaporation of the solvent under reduced pressure, the resulting pale yellow oil was purified by column chromatography over silica gel eluting with CH_2Cl_2 (TLC: $R_f = 0.40$). Crystallization of the colorless oil in a CH_2Cl_2–pentane mixture led to **3** as colorless crystals (1.89 g, 3.71 mmol, 64% yield). Mp 135–137 °C. *Anal.* Calc. for $C_{31}H_{28}N_2O_5$: C, 73.21; H, 5.55; N, 5.51. Found: C, 73.38; H, 5.51; N, 5.45%. IR (KBr): ν (cm^{-1}) 1732 (C═O), 3299 (N–H). ^1H NMR (300 MHz, $CDCl_3$): δ 1.62 (s, 6H, CH_3), 5.15 (s, 4H, CH_2), 7.09 (t, 2H, $^3J_{HH} = 7.8$ Hz, $H_{ar\ xanthene}$), 7.17 (dd, 2H, $^3J_{HH} = 7.8$ Hz, $^4J_{HH} = 1.5$ Hz, $H_{ar\ xanthene}$), 7.20–7.35 (m, 10H, 10 H_{phenyl}), 7.46 (broad s, 2H, NH), 7.75 (broad d, 2H, $^3J_{HH} = 6.3$ Hz, $H_{ar\ xanthene}$). $^{13}C\{^1H\}$ NMR (50 MHz, $CDCl_3$): δ 31.7 (s, CH_3), 34.4 (s, $C(CH_3)_2$), 67.2 (s, CH_2), 119.4 (s, CH_{ar}), 120.7 (s, CH_{ar}), 123.3 (CH_{ar}), 125.6 (s, C_{ar}), 128.1 (s, CH_{ar}), 128.4 (s, CH_{ar}), 129.7 (s, CH_{ar}), 130.6 (s, C_{ar}), 136.0 (s, C_{ar}), 140.5 (s, C_{ar}), 154.0 (s, C═O).

2.2.3. *9,9-Dimethyl-9H-xanthene-4,5-diamine (**4**)*

A solution of **3** (1.88 g, 3.70 mmol) in 100 mL KOH-saturated ethanol was refluxed for 20 h. The brown solution was allowed to cool to room temperature. 100 mL water was added and the product extracted with 3×150 mL CH_2Cl_2. The organic phase was washed with water until the pH of the water phase was 7 and dried with $MgSO_4$. After evaporation of the solvent under reduced pressure, the crude product was purified by column chromatography over silica gel eluting with Et_2O (TLC: $R_f = 0.23$) and the pure product recovered as a beige powder (0.470 g, 1.96 mmol, 53% yield). Mp 150–152 °C. *Anal.* Calc. for $C_{15}H_{16}N_2O$: C, 74.97; H, 6.71; N, 11.66. Found: C, 75.14; H, 6.95; N, 11.93%. IR (KBr): ν (cm^{-1}) 3386, 3450 (N–H). ^1H NMR (200 MHz, $CDCl_3$): δ 1.60 (s, 6H, CH_3), 3.87 (broad s, 4H, NH_2), 6.66 (dd, 2H, $^3J_{HH} = 7.2$ Hz, $^4J_{HH} = 2.0$ Hz, H_{ar}), 6.84 (dd, 2H, $^3J_{HH} = 7.9$ Hz, $^4J_{HH} = 2.0$ Hz, H_{ar}), 6.91 (t, 2H, $^3J_{HH} = 7.8$ Hz, H_{ar}). $^{13}C\{^1H\}$ NMR (50 MHz, $CDCl_3$): δ 31.9 (s, CH_3), 34.3 (s, $C(CH_3)_2$), 113.6 (s, CH_{ar}), 115.7 (s, CH_{ar}), 123.1 (s, CH_{ar}), 130.6 (s, C_{ar}), 134.5 (s, C_{ar}), 138.6 (s, C_{ar}).

2.2.4. *(1′R)-N,N′-bis(1′,7′,7′-trimethylbicyclo[2.2.1]hept-2-ylidene)-9,9-dimethyl-9H-xanthene-4,5-diamine (**5**)*

To a solution of **4** (0.6 g, 2.48 mmol) and (1*R*)-camphor (1.14 g, 7.49 mmol) in 50 mL toluene was added triethylamine (6.94 mL, 49.8 mmol) at room temperature. The solution was cooled to 0 °C and a solution of $TiCl_4$(2.37 g, 12.5 mmol) in 5 mL toluene was added. The resulting brown suspension was refluxed for 16 h, then the mixture was cooled to room temperature and filtered. The pasty solid remaining on the frit was extracted with 4×50 mL Et_2O. After evaporation of the solvent under reduced pressure, the crude product was purified by column chromatography over silica gel eluting with pentane–Et_2O (9:1) (TLC: $R_f = 0.25$). The resulting white powder was recrystallized in an ethanol–water mixture and dried under high vacuum (10^{-9} bar) for 24 h (0.54 g, 1.06 mmol, 43% yield). Mp 210–212 °C. $[\alpha]_D^{20}$ −305° ($c = 1$, EtOH). *Anal.* Calc. for $C_{35}H_{44}N_2O$: C, 82.63; H, 8.72; N, 5.51. Found: C, 82.65; H, 8.97; N, 5.30%. IR (KBr): ν (cm^{-1}) 1690 (C═N). ^1H NMR (500 MHz, CD_2Cl_2): δ 0.85 (s, 6H, H_9), 0.96 (s, 6H, H_{10}), 1.11 (s, 6H, H_8), 1.26 (ddd, 2H, $^2J_{HH} = 12.1$ Hz, $^3J_{HH} = 8.3$ Hz, $^3J_{HH} = 2.6$ Hz, H_{5endo}), 1.49 (d, 2H, $^2J_{HH} = 17.6$ Hz, H_{3endo}), 1.61 (s, 6H, $CH_{3xanthene}$), 1.73–1.96 (m, 8H, H_4+ H_{5exo} + H_6), 2.14 (ddd, 2H, $^2J_{HH} = 17.5$ Hz, $^3J_{HH} = 5$ Hz, $^4J_{HH} = 3$ Hz, H_{3exo}), 6.49 (dd, 2H, $^3J_{HH} = 7.6$ Hz, $^4J_{HH} = 1.5$ Hz, H_{11}), 6.97 (t, 2H, $^3J_{HH} = 7.6$ Hz, H_{12}), 7.11 (dd, 2H, $^3J_{HH} = 7.8$ Hz, $^4J_{HH} = 1.6$ Hz, H_{13}). $^{13}C\{^1H\}$ NMR (50 MHz, $CDCl_3$): δ 11.3 (s, C_8), 19.1 (s, C_9/C_{10}), 19.6 (s, C_{10}/C_9), 27.4 (s, C_5), 32.1 (s, C_6), 32.2 (s, $CH_{3xanthene}$), 34.2 (s, $C(CH_3)_{2xanthene}$), 36.9 (s, C_3), 43.6 (s, C_4), 47.8 (s, C_7), 54.0 (s, C_1), 118.5 (s, CH_{ar}), 120.2 (s, CH_{ar}), 122.6 (s, CH_{ar}), 131.0 (s, C_{ar}), 140.7 (s, C_{ar}), 141.3 (s, C_{ar}), 186.8 (s, C_2).

2.2.5. *9,9-Dimethyl-9H-xanthene-4-carboxylic acid (**6**)*

To a solution of 9,9-dimethyl-9*H*-xanthene (1.14 g, 5.42 mmol) in 35 mL THF was slowly added PhLi (8.0 mL solution, 13.6 mmol) at −78 °C. The solution rapidly turned brown. The reaction mixture was brought to RT and stirred for 18 h. The temperature was lowered to −78 °C and CO_2 was bubbled into the mixture for 15 min while raising the temperature again to RT. 20 mL of an aqueous HCl solution (2 M) was added and the product extracted with 4×60 mL Et_2O. The organic phase was dried with $MgSO_4$ and evaporated to dryness. The green crude product was heated at 70 °C under vacuum in order to eliminate the by-product benzoic acid by sublimation, and the residual solid was purified by column chromatography over silica gel eluting with CH_2Cl_2–MeOH (98:2) (TLC: $R_f = 0.20$). The pure product was recovered as a white powder (0.617 g, 2.44 mmol, 47% yield). Mp 192–194 °C. *Anal.* Calc. for $C_{16}H_{14}O_3$: C, 75.58; H, 5.55. Found: C, 75.43; H, 5.65%. IR (KBr): ν (cm^{-1}) 1695 (C═O). ^1H NMR (200 MHz, DMSO-d_6): δ 1.59 (s, 6H, CH_3), 7.02 (dd, 1H, $^3J_{HH} = 7.8$ Hz, $^4J_{HH} = 1.4$ Hz, H_{ar}), 7.15 (td, 1H, $^3J_{HH} = 7.4$ Hz, $^4J_{HH} = 1.4$ Hz, H_{ar}), 7.17 (t, 1H, $^3J_{HH} = 7.7$ Hz, H_{ar}), 7.26 (td, 1H, $^3J_{HH} = 7.6$ Hz,

$^4J_{HH} = 1.7$ Hz, H_{ar}), 7.57 (2dd, 2H, $^3J_{HH} = 7.6$ Hz, $^4J_{HH} = 1.7$ Hz, H_{ar}), 7.73 (dd, 1H, $^3J_{HH} = 7.8$ Hz, $^4J_{HH} = 1.7$ Hz, H_{ar}), 12.91 (broad s, 1H, OH). $^{13}C\{^1H\}$ NMR (50 MHz, $CDCl_3$): δ 31.9 (s, CH_3), 33.7 (s, $C(CH_3)_2$), 116.1 (s, CH_{ar}), 122.0 (s, C_{ar}), 122.5 (s, CH_{ar}), 123.6 (s, CH_{ar}), 126.2 (s, CH_{ar}), 127.5 (s, CH_{ar}), 128.3 (s, CH_{ar}), 129.1 (s, CH_{ar}), 129.6 (s, C_{ar}), 130.9 (s, C_{ar}), 148.0 (s, C_{ar}), 149.3 (s, C_{ar}), 167.5 (s, C=O).

2.2.6. N-benzyloxycarbonyl-9,9-dimethyl-9H-xanthen-4-amine (7)

A mixture of **6** (0.590 g, 2.32 mmol), DPPA (0.642 g, 2.33 mmol), benzylic alcohol (0.251 g, 2.33 mmol) and triethylamine (0.240 g, 2.35 mmol) dissolved in 25 mL toluene was heated at 100 °C for 18 h. The orange solution was allowed to cool to RT, treated with 20 mL aqueous HCl (0.5 M) and extracted with 3×80 mL CH_2Cl_2. The organic phase was neutralized with saturated aqueous $NaHCO_3$ and dried over $MgSO_4$. After evaporation of the solvent under reduced pressure, the resulting yellow oil was purified by column chromatography over silica gel eluting with CH_2Cl_2–pentane (1:1) (TLC: $R_f = 0.25$), leading to a colorless oil (0.726 g, 2.02 mmol, 86% yield). IR (KBr): ν (cm^{-1}) 1737 (C=O), 3433 (N–H). ^1H NMR (200 MHz, $CDCl_3$): δ 1.62 (s, 6H, CH_3), 5.26 (s, 2H, OCH_2), 7.0–7.25 (m, 5H, H_{ar}), 7.35–7.5 (m, 7H, H_{ar} + NH), 8.04 (broad dd, 1H, $^3J_{HH} = 6.4$ Hz, $^4J_{HH} = 2.8$ Hz, H_{ar}). $^{13}C\{^1H\}$ NMR (50 MHz, $CDCl_3$): δ 32.1 (s, CH_3), 34.1 (s, $C(CH_3)_2$), 67.1 (s, CH_2), 116.2 (s, CH_{ar}), 116.6 (s, CH_{ar}), 119.7 (s, CH_{ar}), 123.0 (s, CH_{ar}), 123.6 (s, CH_{ar}), 126.0 (s, C_{ar}), 126.2 (s, CH_{ar}), 127.4 (s, CH_{ar}), 128.4 (s, $2CH_{ar}$), 128.6 (s, CH_{ar}), 129.8 (s, C_{ar}), 130.0 (s, C_{ar}), 136.1 (s, C_{ar}), 138.9 (s, C_{ar}), 149.6 (s, C_{ar}), 153.3 (s, C=O).

2.2.7. 9,9-Dimethyl-9H-xanthen-4-amine (8)

A solution of **7** (0.652 g, 1.81 mmol) in 150 mL KOH-saturated ethanol was refluxed for 18 h. The brown solution was allowed to cool to RT. 150 mL water was added and the product extracted with 3×100 mL CH_2Cl_2. The organic phase was washed with water until the pH of the water phase was 7 and dried with $MgSO_4$. After evaporation of the solvent under reduced pressure, the resulting brown oil was purified by column chromatography over silica gel eluting with CH_2Cl_2 (TLC: $R_f = 0.42$). Product **8** was recovered as an orange powder after recrystallization in toluene–pentane (0.352 g, 1.56 mmol, 86% yield). *Anal.* Calc. for $C_{15}H_{15}NO$: C, 79.97; H, 6.71; N, 6.22. Found: C, 79.07; H, 6.73; N, 6.34%. IR (KBr): ν (cm^{-1}) 3382, 3472 (N–H). ^1H NMR (200 MHz, $CDCl_3$): δ 1.53 (s, 6H, CH_3), 5.04 (broad s, 2H, NH_2), 6.59 (dd, 1H, $^3J_{HH} = 7.6$ Hz, $^4J_{HH} = 1.7$ Hz, H_{ar}), 6.68 (dd, 1H, $^3J_{HH} = 7.8$ Hz, $^4J_{HH} = 1.6$ Hz, H_{ar}), 6.81 (t, 1H, $^3J_{HH} = 7.7$ Hz, H_{ar}), 7.06–7.17 (m, 2H, H_{ar}), 7.23 (ddd, 1H, $^3J_{HH} = 6.9$ Hz, $^3J_{HH} = 8.3$ Hz, $^4J_{HH} = 1.6$ Hz, H_{ar}), 7.50 (dd, 1H, $^3J_{HH} = 7.7$ Hz, $^4J_{HH} = 1.5$ Hz, H_{ar}). $^{13}C\{^1H\}$ NMR (50 MHz, $CDCl_3$): δ 31.8 (s, CH_3), 33.5 (s, $C(CH_3)_2$), 112.1 (s, CH_{ar}), 112.7 (s, CH_{ar}), 116.0 (s, CH_{ar}), 122.9 (s, $2CH_{ar}$), 126.2 (s, CH_{ar}), 127.1 (s, CH_{ar}), 129.3 (s, C_{ar}), 129.9 (s, C_{ar}), 136.1 (s, C_{ar}), 136.8 (s, C_{ar}), 149.7 (s, C_{ar}).

2.2.8. (1′R)-N-(1′,7′,7′-trimethylbicyclo[2.2.1]hept-2-ylidene)-9,9-dimethyl-9H-xanthen-4-amine (9)

To a solution of **8** (0.415 g, 1.85 mmol) and (1*R*)-camphor (0.420 g, 2.78 mmol) in 40 mL toluene was added triethylamine (2.58 mL, 18.5 mmol) at RT. The solution was cooled to 0 °C and a solution of $TiCl_4$ (0.880 g, 4.62 mmol) in 8 mL toluene was added dropwise. The resulting brown mixture was refluxed for 18 h, then the mixture was cooled to room temperature and filtered. The pasty solid remaining on the frit was extracted with 4×50 mL Et_2O. After evaporation of the solvent under reduced pressure, the crude product was purified by column chromatography over silica gel eluting with pentane–Et_2O (9:1) (TLC: $R_f = 0.22$). The resulting pale yellow powder was recrystallized in an ethanol–water mixture and dried under high vacuum (10^{-9} bar) for 24 h (0.44 g, 1.22 mmol, 66% yield). Mp 88–90 °C. *Anal.* Calc. for $C_{25}H_{29}NO$: C, 83.52; H, 8.13; N, 3.90. Found: C, 83.49; H, 8.18; N, 3.84%. IR (KBr): ν (cm^{-1}) 1686 (C=N). ^1H NMR (200 MHz, $CDCl_3$): δ 0.98 (s, 3H, H_9/H_{10}), 1.01 (s, 3H, H_{10}/H_9), 1.20 (s, 3H, H_8), 1.20–1.35 (m, 1H, H_{5endo}), 1.61 (s, 3H, $CH_{3xanthene}$), 1.65 (s, 3H, $CH_{3xanthene}$), 1.70–2.00 (m, 5H, $H_{3endo} + H_4 + H_{5exo} + H_6$), 2.17 (d, 1H, $^2J_{HH} = 17.6$ Hz, H_{3exo}), 6.66 (dd, 1H, $^3J_{HH} = 7.5$ Hz, $^4J_{HH} = 1.7$ Hz, H_{ar}), 6.94 (dd, 1H, $^3J_{HH} = 7.9$ Hz, $^4J_{HH} = 1.5$ Hz, H_{ar}), 7.00 (t, 1H, $^3J_{HH} = 7.4$ Hz, H_{ar}), 7.06 (td, 1H, $^3J_{HH} = 7.5$ Hz, $^4J_{HH} = 1.5$ Hz, H_{ar}), 7.12 (dd, 1H, $^3J_{HH} = 7.9$ Hz, $^4J_{HH} = 1.7$ Hz, H_{ar}), 7.17 (td, 1H, $^3J_{HH} = 7.5$ Hz, $^4J_{HH} = 1.8$ Hz, H_{ar}), 7.41 (dd, 1H, $^3J_{HH} = 7.6$ Hz, $^4J_{HH} = 1.6$ Hz, H_{ar}). $^{13}C\{^1H\}$ NMR (50 MHz, $CDCl_3$): δ 11.2 (s, C_8), 19.0 (s, C_9/C_{10}), 19.7 (s, C_{10}/C_9), 27.4 (s, C_5), 31.8 (s, C_6), 32.3 (s, $CH_{3xanthene}$), 32.6 (s, $CH_{3xanthene}$), 34.2 (s, $C(CH_3)_{2xanthene}$), 37.1 (s, C_3), 43.9 (s, C_4), 47.5 (s, C_7), 54.4 (s, C_1), 116.3 (s, CH_{ar}), 118.6 (s, CH_{ar}), 120.3 (s, CH_{ar}), 122.8 (s, CH_{ar}), 122.9 (s, CH_{ar}), 125.9 (s, CH_{ar}), 127.1 (s, CH_{ar}), 130.1 (s, C_{ar}), 130.7 (s, C_{ar}), 139.7 (s, C_{ar}), 139.9 (s, C_{ar}), 150.4 (s, C_{ar}), 186.9 (s, C_2).

2.2.9. 2,7-Ditertbutyl-5-bromo-9,9-dimethyl-9H-xanthene-4-carboxylic acid (11)

To a solution of **10** (0.48 g, 1.00 mmol) in 25 mL THF was added *n*-BuLi (0.650 mL solution, 1.04 mmol) at −78 °C. After stirring at this temperature for 1 h, CO_2 was bubbled into the solution for 15 min, then the reaction temperature was slowly raised to RT. 20 mL of an aqueous HCl solution (2 M) was added. The organic phase was extracted with 5×50 mL CH_2Cl_2, dried with $MgSO_4$ and evaporated to dryness. Column chromatography over silica gel eluting with a CH_2Cl_2–MeOH (99:1) mixture (TLC: $R_f = 0.40$), followed by recrystallization in a CH_2Cl_2–pentane mixture led to **11** as a white powder (0.378 g, 0.85 mmol, 85% yield). Mp 228–230 °C. *Anal.* Calc. for $C_{24}H_{29}BrO_3$: C, 64.72; H, 6.56. Found: C, 63.74; H, 6.55%. IR (KBr): ν (cm^{-1}) 1696 (C=O), 3412 (O–H). ^1H

NMR (200 MHz, $CDCl_3$): δ 1.34 (s, 9H, $C(CH_3)_3$), 1.36 (s, 9H, $C(CH_3)_3$), 1.67 (s, 6H, $C(CH_3)_2$), 7.41 (d, 1H, $^4J_{HH} = 2.2$ Hz, H_{ar}), 7.51 (d, 1H, $^4J_{HH} = 2.2$ Hz, H_{ar}), 7.67 (d, 1H, $^4J_{HH} = 2.5$ Hz, H_{ar}), 8.19 (d, 1H, $^4J_{HH} = 2.5$ Hz, H_{ar}), 10.87 (broad s, 1H, COOH). $^{13}C\{^1H\}$ NMR (50 MHz, $CDCl_3$): δ 31.3 (s, 2 $C(CH_3)_3$), 32.0 (s, $C(CH_3)_2$), 34.7 (s, 2$C(CH_3)_3$), 35.2 (s, $C(CH_3)_2$), 109.6 (s, C_{ar}), 116.3 (s, C_{ar}), 122.0 (s, CH_{ar}), 128.3 (s, CH_{ar}), 128.5 (s, CH_{ar}), 129.1 (s, CH_{ar}), 130.5 (s, C_{ar}), 131.1 (s, C_{ar}), 143.7 (s, C_{ar}), 147.1 (s, C_{ar}), 147.3 (s, C_{ar}), 148.7 (s, C_{ar}), 165.1 (s, COOH).

2.2.10. N-benzyloxycarbonyl-2,7-ditertbutyl-5-bromo-9,9-dimethyl-9H-xanthen-4-amine (**12**)

A mixture of **11** (4.77 g, 10.7 mmol), DPPA (3.30 g, 12.0 mmol), benzylic alcohol (1.30 g, 12.0 mmol) and triethylamine (1.29 g, 12.7 mmol) dissolved in 180 mL toluene was heated at 100 °C for 18 h. The yellow solution was allowed to cool to RT, treated with 100 mL aqueous HCl (0.2 M) and extracted with 4×80 mL Et_2O. The organic phase was neutralized with saturated aqueous $NaHCO_3$ and dried over $MgSO_4$. After evaporation of the solvent under reduced pressure, the resulting yellow oil was purified by column chromatography over silica gel eluting with CH_2Cl_2–pentane (1:1) (TLC: $R_f = 0.54$). Recrystallization of **12** in EtOH at −20 °C led to a beige powder (4.84 g, 8.80 mmol, 82% yield). Mp 136–138 °C. *Anal*. Calc. for $C_{31}H_{36}BrNO_3$: C, 67.63; H, 6.59; N, 2.54. Found: C, 67.71; H, 6.81; N, 2.57%. IR (KBr): ν (cm^{-1}) 1739 (C=O), 3420, 3437 (N–H). ^1H NMR (200 MHz, $CDCl_3$): δ 1.32 (s, 9H, $C(CH_3)_3$), 1.34 (s, 9H, $C(CH_3)_3$), 1.62 (s, 6H, $C(CH_3)_2$), 5.28 (s, 2H, CH_2), 7.08 (d, 1H, $^4J_{HH} = 2.2$ Hz, H_{ar}), 7.30–7.48 (m, 7H, H_{ar}), 7.56 (broad s, 1H, N–H), 8.12 (broad s, 1H, H_{ar}). $^{13}C\{^1H\}$ NMR (50 MHz, $CDCl_3$): δ 31.4 (s, $C(CH_3)_2$), 31.5 (s, 2$C(CH_3)_3$), 34.6 (s, $C(CH_3)_3$), 34.9 (s, $C(CH_3)_3$), 35.4 (s, $C(CH_3)_2$), 66.7 (s, CH_2), 110.2 (s, C_{ar}), 114.3 (s, CH_{ar}), 115.7 (s, CH_{ar}), 121.9 (s, CH_{ar}), 125.9 (s, C_{ar}), 127.9 (s, CH_{ar}), 128.1 (s, 2CH_{ar}), 128.5 (s, CH_{ar}), 129.1 (s, C_{ar}), 131.6 (s, C_{ar}), 136.4 (s, C_{ar}), 137.1 (s, C_{ar}), 144.6 (s, C_{ar}), 146.5 (s, C_{ar}), 147.3 (s, C_{ar}), 153.5 (s, C=O).

2.2.11. 2,7-Ditertbutyl-5-bromo-9,9-dimethyl-9H-xanthen-4-amine (**13**)

A solution of **12** (4.83 g, 8.80 mmol) in 130 mL KOH-saturated ethanol was refluxed for 18 h. The brown solution was allowed to cool to RT, 200 mL water was added and the product extracted with 4×100 mL CH_2Cl_2. The organic phase was washed with water until the pH of the water phase was 7 and dried with $MgSO_4$. After evaporation of the solvent under reduced pressure, the resulting brown oil was purified by column chromatography over silica gel eluting with pentane–Et_2O (4:1) (TLC: $R_f = 0.50$). Product **13** was recovered as a pale yellow powder (3.37 g, 8.10 mmol, 92% yield). Mp 178–180 °C. *Anal*. Calc. for $C_{23}H_{30}BrNO$: C, 66.34; H, 7.26; N, 3.36. Found: C, 66.08; H, 7.31; N, 3.18%. IR (KBr): ν (cm^{-1}) 3384, 3470 (N–H). ^1H NMR (200 MHz, $CDCl_3$): δ 1.31 (s, 9H, $C(CH_3)_3$), 1.33 (s, 9H, $C(CH_3)_3$), 1.63 (s, 6H, $C(CH_3)_2$), 4.00 (broad s, 2H, NH_2), 6.72 (d, 1H, $^4J_{HH} = 2.2$ Hz, H_{ar}), 6.80 (d, 1H, $^4J_{HH} = 2.2$ Hz, H_{ar}), 7.35 (d, 1H, $^4J_{HH} = 2.2$ Hz, H_{ar}), 7.44 (d, 1H, $^4J_{HH} = 2.2$ Hz, H_{ar}). $^{13}C\{^1H\}$ NMR (50 MHz, $CDCl_3$): δ 31.4, 31.5, 31.6 (s, $C(CH_3)_2 + 2C(CH_3)_3$), 34.6 (s, 2$C(CH_3)_3$), 35.4 (s, $C(CH_3)_2$), 110.2 (s, C_{ar}), 110.9 (s, CH_{ar}), 111.4 (s, CH_{ar}), 121.4 (s, C_{ar}), 121.9 (s, CH_{ar}), 127.8 (s, CH_{ar}), 129.5 (s, C_{ar}), 131.7 (s, C_{ar}), 134.1 (s, 2C_{ar}), 146.4 (s, C_{ar}), 146.6 (s, C_{ar}).

2.2.12. (1′R)-N-(1′,7′,7′-trimethylbicyclo[2.2.1]hept-2-ylidene)-2,7-ditertbutyl-5-bromo-9,9-dimethyl-9H-xanthen-4-amine (**14a**)

To a solution of **13** (1.20 g, 2.88 mmol) and (1*R*)-camphor (0.660 g, 4.34 mmol) in 50 mL toluene was added triethylamine (4.05 mL, 28.8 mmol) at room temperature. The solution was cooled to 0 °C and a solution of $TiCl_4$ (1.37 g, 7.21 mmol) in 5 mL toluene was added dropwise. The resulting brown mixture was refluxed for 18 h, then the mixture was cooled to room temperature and filtered. The pasty solid remaining on the frit was extracted with 4×50 mL Et_2O. After evaporation of the solvent under reduced pressure, the crude product was purified by column chromatography over silica gel eluting with pentane–Et_2O (9:1) (TLC: $R_f = 0.61$). Product **14a** was recovered as a pale yellow powder and dried by heating at 50 °C under high vacuum (10^{-9} bar) for 18 h (1.48 g, 2.68 mmol, 93% yield). Mp 180–182 °C. $[\alpha]_D^{20}$ +18° ($c = 1$, CH_2Cl_2). *Anal*. Calc. for $C_{33}H_{44}BrNO$: C, 71.98; H, 8.05; N, 2.54. Found: C, 72.01; H, 8.28; N, 2.46%. IR (KBr): ν (cm^{-1}) 1691 (C=N). ^1H NMR (300 MHz, $CDCl_3$): δ 0.93 (s, 3H, H_9/H_{10}), 0.99 (s, 3H, H_{10}/H_9), 1.20 (s, 3H, H_8), 1.30 (s, 9H, $C(CH_3)_3$), 1.31 (s, 9H, $C(CH_3)_3$), 1.22–1.40 (m, 1H, H_{5endo}), 1.60 (s, 3H, $CH_{3xanthene}$), 1.64 (s, 3H, $CH_{3xanthene}$), 1.76 (d, 1H, $^2J_{HH} = 17.5$ Hz, H_{3endo}), 1.76–1.94 (m, 4H, $H_4 + H_{5exo} + H_6$), 2.16 (d, 1H, $^2J_{HH} = 17.4$ Hz, H_{3exo}), 6.59 (d, 1H, $^4J_{HH} = 2.2$ Hz, H_{11}), 7.05 (d, 1H, $^4J_{HH} = 2.2$ Hz, H_{12}), 7.33 (d, 1H, $^4J_{HH} = 2.2$ Hz, H_{13}), 7.41 (d, 1H, $^4J_{HH} = 2.2$ Hz, H_{14}). $^{13}C\{^1H\}$ NMR (50 MHz, $CDCl_3$): δ 11.4 (s, C_8), 19.1 (s, C_9/C_{10}), 20.0 (s, C_{10}/C_9), 27.4 (s, C_5), 29.7 (s, C_6), 31.4 (s, $C(CH_3)_3$), 31.5 (s, $C(CH_3)_3$), 31.8 (s, $CH_{3xanthene}$), 32.6 (s, $CH_{3xanthene}$), 34.4 (s, 2$C(CH_3)_3$), 35.2 (s, $C(CH_3)_2$), 36.8 (s, C_3), 43.8 (s, C_4), 47.7 (s, C_7), 54.1 (s, C_1), 110.2 (s, C_{ar}), 115.9 (s, CH_{ar}), 116.5 (s, CH_{ar}), 121.7 (s, CH_{ar}), 128.1 (s, CH_{ar}), 129.5 (s, C_{ar}), 131.3 (s, C_{ar}), 138.4 (s, C_{ar}), 139.2 (s, C_{ar}), 145.3 (s, C_{ar}), 145.8 (s, C_{ar}), 146.2 (s, C_{ar}), 185.8 (s, C_2).

2.2.13. (1′R)-N-(1′,3′,3′-trimethylbicyclo[2.2.1]hept-2-ylidene)-2,7-ditertbutyl-5-bromo-9,9-dimethyl-9H-xanthen-4-amine (**14b**)

To a solution of **13** (1.20 g, 2.88 mmol) and (1*S*)-fenchone (0.660 g, 4.34 mmol) in 30 mL toluene was added triethylamine (3.97 mL, 28.5 mmol) at RT. The solution

was cooled to 0 °C and a solution of $TiCl_4$ (1.42 g, 7.48 mmol) in 5 mL toluene was added dropwise. The resulting brown suspension was refluxed for 24 h, then the mixture was cooled to 0 °C. The same amounts of triethylamine and (1*S*)-fenchone were sequentially added again while stirring at this temperature, and the reaction mixture was refluxed for 48 h. This operation was repeated and the mixture refluxed again for 48 h. The pasty solid obtained upon cooling was extracted with 5×50 mL Et_2O by trituration on a frit. After evaporation of the filtrate under reduced pressure, the resulting brown oil was purified by column chromatography over silica gel eluting with pentane–Et_2O (9:1) (TLC: $R_f = 0.70$). Recrystallization of **14b** in EtOH at −20 °C led to a white powder which was dried under high vacuum (10^{-9} bar) for 18 h (1.10 g, 2.00 mmol, 70% yield). Mp 170–172 °C. $[\alpha]_D^{20} + 40°$ ($c = 1$, CH_2Cl_2). *Anal.* Calc. for $C_{33}H_{44}BrNO \cdot 0.5EtOH$: C, 71.19; H, 8.26; N, 2.44. Found: C, 71.20; H, 8.44; N, 2.77%. IR (KBr): ν (cm^{-1}) 1691 (C=N). ^1H NMR (500 MHz, $CDCl_3$), major isomer: δ 0.93 (s, 3H, H_9/H_{10}), 0.98 (s, 3H, H_{10}/H_9), 1.28 (s, 9H, $C(CH_3)_3$), 1.31 (s, 9H, $C(CH_3)_3$), 1.40 (s, 3H, H_8), 1.59 (s, 3H, $CH_{3xanthene}$), 1.63 (s, 3H, $CH_{3xanthene}$), 1.2–2.1 (m, 7H, $H_4 + H_5 + H_6 + H_7$), 6.62 (d, 1H, $^4J_{HH} = 2.2$ Hz, H_{11}), 6.98 (d, 1H, $^4J_{HH} = 2.1$ Hz, H_{12}), 7.32 (d, 1H, $^4J_{HH} = 2.2$ Hz, H_{13}), 7.40 (d, 1H, $^4J_{HH} = 2.2$ Hz, H_{14}). $^{13}C\{^1H\}$ NMR (50 MHz, $CDCl_3$), major isomer: δ 17.6 (s, C_8), 23.8 (s, C_9/C_{10}), 25.1 (s, C_5), 25.3 (s, C_{10}/C_9), 31.4 (s, $2C(CH_3)_3$), 32.4 (s, $CH_{3xanthene}$), 33.0 (s, $CH_{3xanthene}$), 33.7 (s, C_6), 34.3 (s, $C(CH_3)_3$), 34.5 (s, $C(CH_3)_3$), 35.1 (s, $C(CH_3)_2$), 42.6 (s, C_7), 46.5 (s, C_3), 49.4 (s, C_4), 53.2 (s, C_1), 110.1 (s, C_{ar}), 115.7 (s, CH_{ar}), 116.7 (s, CH_{ar}), 122.0 (s, CH_{ar}), 128.1 (CH_{ar}), 128.6 (s, C_{ar}), 130.9 (s, C_{ar}), 137.1 (s, C_{ar}), 138.3 (s, C_{ar}), 144.8 (s, C_{ar}), 145.3 (s, C_{ar}), 146.0 (s, C_{ar}), 187.5 (s, C_2).

*2.2.14. (1′R)-N-(1′,7′,7′-trimethylbicyclo[2.2.1]hept-2-ylidene)-2,7-ditertbutyl-5-diphenylphosphanyl-9,9-dimethyl-9H-xanthen-4-amine (**15a**)*

To a solution of **14a** (1.38 g, 2.51 mmol) in 30 mL THF was added *n*-BuLi (2.00 mL solution, 3.20 mmol) at −78 °C. After stirring at this temperature for 1 h, a solution of PPh_2Cl (0.700 g, 3.18 mmol) in 4 mL pentane was added dropwise. The temperature was slowly raised to RT, and the solution was stirred for 18 h. After evaporation to dryness, the off-white solid was extracted with 4×50 mL Et_2O–pentane (1:1). Column chromatography over silica gel eluting with pentane–Et_2O (95:5) (TLC: $R_f = 0.15$), followed by drying under high vacuum (10^{-9} bar) for 18 h led to **15a** as a white powder (1.31 g, 1.99 mmol, 80% yield). Mp 90–92 °C. $[\alpha]_D^{20}$ −49° ($c = 1$, EtOH). *Anal.* Calc. for $C_{45}H_{54}NOP$: C, 82.40; H, 8.30; N, 2.14; P, 4.72. Found: C, 82.39; H, 8.42; N, 2.21; P, 4.77%. IR (KBr): ν (cm^{-1}) 1686 (C=N). $^{31}P\{^1H\}$ NMR (121.5 MHz, CD_2Cl_2): −17.2 (s). ^1H NMR (500 MHz, CD_2Cl_2): δ 0.84 (s, 3H, H_9), 0.95 (s, 3H, H_{10}), 0.99 (s, 3H, H_8), 1.09 (s, 9H, $C(CH_3)_3$), 1.16 (m, 1H, H_{5endo}), 1.28 (s, 9H, $C(CH_3)_3$), 1.62 (d, 1H, $^2J_{HH} = 17.4$ Hz, H_{3endo}), 1.63 (s, 3H, $CH_{3xanthene}$), 1.65 (s, 3H, $CH_{3xanthene}$), 1.66–1.74 (m, 1H, H_{6exo}), 1.76–1.85 (m, 2H, $H_4 + H_{5exo}$), 2.08 (m, 1H, H_{6endo}), 2.14 (dt, 1H, $^2J_{HH} = 17.4$ Hz, $^3J_{HH} = {}^4J_{HH} = 3.8$ Hz, H_{3exo}), 6.47 (d, 1H, $^4J_{HH} = 2.3$ Hz, H_{11}), 6.52 (dd, 1H, $^4J_{HH} = 2.3$ Hz, $^3J_{HP} = 4.5$ Hz, H_{14}), 7.08 (d, 1H, $^4J_{HH} = 2.3$ Hz, H_{12}), 7.19–7.35 (m, 10H, H_{phenyl}), 7.42 (dd, 1H, $^4J_{HH} = 2.3$ Hz, $^5J_{HP} = 0.7$ Hz, H_{13}). $^{13}C\{^1H\}$ NMR (50 MHz, CD_2Cl_2): δ 11.8 (s, C_8), 19.5 (s, C_{10}), 20.2 (s, C_9), 27.9 (s, C_5), 31.6 (s, $C(CH_3)_3$), 31.9 (s, $C(CH_3)_3$), 32.2 (s, $CH_{3xanthene}$), 32.5 (s, C_6), 32.8 (s, $CH_{3xanthene}$), 35.0 (s, $2C(CH_3)_3$), 35.4 (s, $C(CH_3)_2$), 37.0 (s, C_3), 44.5 (s, C_4), 48.3 (s, C_7), 54.5 (s, C_1), 116.1 (s, H_{11}), 117.0 (s, H_{12}), 124.1 (s, H_{13}), 124.3 (d, $J_{CP} = 17$ Hz, C_{ar}), 128.8 (s, $2CH_{ar}$), 128.9 (s, $2CH_{ar}$), 129.7 (s, H_{14}), 129.9 (s, C_{ar}), 130.7 (s, C_{ar}), 134.3 (d, $J_{CP} = 20$ Hz, CH_{ar}), 134.5 (d, $J_{CP} = 20$ Hz, CH_{ar}), 138.1 (d, $J_{CP} = 13$ Hz, C_{ar}), 138.5 (d, $J_{CP} = 14$ Hz, C_{ar}), 139.4 (s, C_{ar}), 140.2 (s, C_{ar}), 145.8 (s, C_{ar}), 146.2 (s, C_{ar}), 151.3 (d, $J_{CP} = 16$ Hz, C_{ar}), 185.5 (s, C_2).

*2.2.15. (1′R)-N-(1′,3′,3′-trimethylbicyclo[2.2.1]hept-2-ylidene)-2,7-ditertbutyl-5-diphenylphosphanyl-9,9-dimethyl-9H-xanthen-4-amine (**15b**)*

To a solution of **14b** (0.428 g, 0.777 mmol) in 10 mL THF was added *n*-BuLi (0.600 mL solution, 0.960 mmol) at −78 °C. After stirring at this temperature for 1 h, a solution of PPh_2Cl (0.230 g, 1.04 mmol) in 1.5 mL pentane was added dropwise. The temperature was slowly raised to RT, and the solution was stirred for 18 h. After evaporation to dryness, the off-white solid was extracted with 4×50 mL pentane. Column chromatography over silica gel eluting with pentane–Et_2O (95:5) (TLC: $R_f = 0.15$) , followed by drying under high vacuum (10^{-9} bar) for 18 h led to **15b** as a white powder (0.400 g, 0.610 mmol, 78% yield). Mp 90–92 °C. $[\alpha]_D^{20} + 42°$ ($c = 1$, EtOH). *Anal.* Calc. for $C_{45}H_{54}NOP$: C, 82.40; H, 8.30; N, 2.14; P, 4.72. Found: C, 82.62; H, 8.33; N, 2.23; P, 4.79%. IR (KBr): ν (cm^{-1}) 1689 (C=N). $^{31}P\{^1H\}$ NMR (121.5 MHz, CD_2Cl_2): δ −17.2 (s, major isomer), −16.5 (s, minor isomer). ^1H NMR (300 MHz, $CDCl_3$), major isomer: δ 0.83 (s, 3H, H_9/H_{10}), 0.87 (s, 3H, H_{10}/H_9), 1.08 (s, 9H, $C(CH_3)_3$), 1.22 (s, 3H, H_8), 1.27 (s, 9H, $C(CH_3)_3$), 1.40–2.00 (m, 7H, $H_4 + H_5 + H_6 + H_7$), 1.63 (s, 3H, $CH_{3xanthene}$), 1.64 (s, 3H, $CH_{3xanthene}$), 6.48 (dd, 1H, $^3J_{HP} = 4.6$ Hz, $^4J_{HH} = 2.2$ Hz, H_{14}), 6.52 (d, 1H, $^4J_{HH} = 2.2$ Hz, H_{11}), 6.99 (d, 1H, $^4J_{HH} = 2.2$ Hz, H_{12}), 7.10–7.38 (m, 10H, H_{phenyl}), 7.37 (d, 1H, $^4J_{HH} = 2.2$ Hz, H_{13}). $^{13}C\{^1H\}$ NMR (50 MHz, $CDCl_3$), major isomer: δ 17.4 (s, C_8), 24.1 (s, C_9/C_{10}), 25.2 (s, C_{10}/C_9), 25.3 (s, C_5), 31.3 (s, $C(CH_3)_3$), 31.4 (s, $C(CH_3)_3$), 32.2 (s, $CH_{3xanthene}$), 32.3 (s, $CH_{3xanthene}$), 33.7 (s, C_6), 34.3 (s, $C(CH_3)_3$), 34.4 (s, $C(CH_3)_3$), 34.7 (s, $C(CH_3)_2$), 42.4 (s, C_7), 46.2 (s, C_3), 49.4 (s, C_4), 53.0 (s, C_1), 115.3 (s, CH_{ar}), 116.9 (s, CH_{ar}), 123.3 (s, CH_{ar}), 123.4 (d, $J_{CP} = 17$ Hz, C_{ar}), 128.1 (s, $2CH_{ar}$), 128.2 (s, $2CH_{ar}$), 129.1 (s, C_{ar}), 129.3 (s, C_{ar}), 129.4 (s, CH_{ar}), 133.3 (s, C_{ar}), 133.6 (d, $J_{CP} = 20$ Hz, CH_{ar}), 134.0 (d,

$J_{CP} = 20$ Hz, CH_{ar}), 137.9 (d, $J_{CP} = 15$ Hz, C_{ar}), 138.0 (d, $J_{CP} = 13$ Hz, C_{ar}), 138.1 (s, C_{ar}), 144.1 (s, C_{ar}), 144.8 (s, C_{ar}), 150.8 (d, $J_{CP} = 16$ Hz, C_{ar}), 186.9 (s, C_2).

2.2.16. [Ag(**5**)(OTf)] (**18**)

In a Schlenk tube wrapped with aluminium foil, a solution of **5** (31 mg, 61 μmol) in 1 mL CH_2Cl_2 was added to a suspension of AgOTf (15 mg, 58 μmol) in 1.5 mL CH_2Cl_2. After stirring for 3 h at RT, the mixture was filtered through Celite. The solvent was reduced to 0.3 mL under reduced pressure and the solution was overlaid with pentane. Colorless crystals of **18** were obtained after 5 days, which were washed with Et_2O and dried *in vacuo* (40 mg, 52 μmol, 89% yield). *Anal.* Calc. for $C_{36}H_{44}AgF_3N_2O_4S \cdot CH_2Cl_2$: C, 52.25; H, 5.45; N, 3.29. Found: C, 51.98; H, 5.58; N, 3.26%. IR (KBr): *v* (cm^{-1}) 636 (OSO), 1024 (OSO), 1032, 1158 (C–F), 1238 (OSO), 1648 (C=N). ^1H NMR (300 MHz, CD_2Cl_2): 0.87 (s, 6H, H_9), 1.01 (s, 6H, H_{10}), 1.25–1.40, 1.50–1.65 and 1.75–1.92 (m, 8H, H_5+ H_6), 1.40 (s, 6H, H_8), 1.65 (s, 6H, $CH_{3xanthene}$), 2.00 (t, 2H, $^3J_{HH} = 4.2$ Hz, H_4), 2.15 (d, 2H, $^2J_{HH} = 18.3$ Hz, H_{3endo}), 2.56 (d, 2H, $^2J_{HH} = 18$ Hz, H_{3exo}), 6.82 (dd, 2H, $^3J_{HH} = 7.8$ Hz, $^4J_{HH} = 1.5$ Hz, H_{11}), 7.14 (t, 2H, $^3J_{HH} = 7.8$ Hz, H_{12}), 7.31 (dd, 2H, $^3J_{HH} = 7.8$ Hz, $^4J_{HH} = 1.5$ Hz, H_{13}). $^{13}C\{^1H\}$ NMR (75.5 MHz, CD_2Cl_2): δ 11.7 (s, C_8), 19.2 (s, C_9/C_{10}), 20.2 (s, C_{10}/C_9), 27.5 (s, C_5), 28.6 (s, $CH_{3xanthene}$), 32.8 (s, C_6), 36.3 (s, $C(CH_3)_2$), 38.9 (s, C_3), 44.0 (s, C_4), 48.6 (s, C_7), 55.2 (s, C_1), 120.6 (s, CH_{ar}), 122.0 (s, CH_{ar}), 124.3 (s, CH_{ar}), 135.1 (s, C_{ar}), 137.6 (s, C_{ar}), 145.2 (s, C_{ar}), 193.5 (s, C_2).

2.2.17. [Ag(**15a**)(BF_4)] (**19**)

In a Schlenk tube wrapped with aluminium foil, a solution of **15a** (37 mg, 56 μmol) in 1 mL CH_2Cl_2 was added to a suspension of $AgBF_4$ (11 mg, 56 μmol) in 1 mL CH_2Cl_2. After stirring for 16 h at RT, the mixture was filtered through Celite. The solvent was reduced to 0.3 mL under reduced pressure and the solution was overlaid with pentane. Colorless crystals of **19** were obtained after 5 days, which were washed with pentane and dried *in vacuo* (35 mg, 41 μmol, 73% yield). *Anal.* Calc. for $C_{45}H_{54}AgBF_4NOP \cdot 2.3CH_2Cl_2$: C, 54.32; H, 5.65; N, 1.34. Found: C, 54.33; H, 5.72; N, 1.36%. IR (KBr): *v* (cm^{-1}) 1099 (B–F), 1655 (C=N). ^1H NMR (300 MHz, CD_2Cl_2): δ 0.62 (s, 3H, CH_{3camph}), 0.97 (s, 3H, CH_{3camph}), 1.12–1.35 and 1.68–1.95 (m, 4H, $H_5 + H_6$), 1.14 (s, 9H, $C(CH_3)_3$), 1.33 (s, 9H, $C(CH_3)_3$), 1.53 (s, 3H, CH_{3camph}), 1.69 (s, 3H, $CH_{3xanthene}$), 1.70 (s, 3H, $CH_{3xanthene}$), 1.95 (d, 1H, $^2J_{HH} = 18.8$ Hz, H_{3endo}), 1.96 (t, 1H, $^3J_{HH} = 4.2$ Hz, H_4), 2.43 (d, 1H, $^2J_{HH} = 18$ Hz, H_{3exo}), 6.69 (dd, 1H, $^3J_{HP} = 10.0$ Hz, $^4J_{HH} = 2.2$ Hz, H_{14}), 6.85 (d, 1H, $^4J_{HH} = 2.0$ Hz, H_{11}), 7.38 (d, 1H, $^4J_{HH} = 2.2$ Hz, H_{12}), 7.40–7.63 (m, 10H, H_{phenyl}), 7.66 (d, 1H, $^4J_{HH} = 2.2$ Hz, H_{13}). $^{13}C\{^1H\}$ NMR (100.6 MHz, CD_2Cl_2): δ 11.6 (s, C_8), 19.0 (s, C_9/C_{10}), 19.3 (s, C_{10}/C_9), 27.2 (s, C_5), 28.5 (s, $CH_{3xanthene}$), 29.0 (s, $CH_{3xanthene}$), 31.2 (s, $C(CH_3)_3$), 31.5 (s, $C(CH_3)_3$), 32.5 (s, C_6), 35.0 (s, $C(CH_3)_3$), 35.1 (s, $C(CH_3)_3$), 36.7 (s, $C(CH_3)_2$), 39.0 (s, C_3), 43.9 (s, C_4), 48.6 (s, C_7), 55.3 (s, C_1), 118.1 (s, CH_{ar}), 119.2 (s, CH_{ar}), 125.7 (s, CH_{ar}), 129.1 (s, CH_{ar}), 129.3 (d, $J_{CP} = 10$ Hz, CH_{ar}), 129.5 (d, $J_{CP} = 10$ Hz, CH_{ar}), 129.9 (d, $J_{CP} = 9$ Hz, C_{ar}), 130.2 (s, C_{ar}), 131.3 (d, $J_{CP} = 2$ Hz, CH_{ar}), 131.6 (d, $J_{CP} = 2$ Hz, CH_{ar}), 133.8 (d, $J_{CP} = 15$ Hz, CH_{ar}), 134.2 (d, $J_{CP} = 16$ Hz, CH_{ar}), 135.7 (s, C_{ar}), 142.2 (s, C_{ar}), 148.1 (s, C_{ar}), 148.2 (s, C_{ar}), 148.3 (s, C_{ar}), 152.8 (d, $J_{CP} = 11$ Hz, C_{ar}), 196.3 (s, C_2). ES-MS: *m*/*z* 764.2 ($[M-BF_4]^+$, 100%).

2.2.18. [Ag(**15a**)(OTf)] (**20**)

In a Schlenk tube wrapped with aluminium foil, a solution of **15a** (34 mg, 52 μmol) in 0.5 mL CH_2Cl_2 was added to a suspension of AgOTf (13 mg, 51 μmol) in 2.5 mL CH_2Cl_2. After stirring for 1.5 h at RT, the mixture was evaporated to dryness and washed with pentane, which led to 45 mg crude **20** (49 μmol, 97% yield). *Anal.* Calc. for $C_{46}H_{54}AgF_3NO_4PS \cdot 0.5CH_2Cl_2$: C, 58.46; H, 5.80; N, 1.47. Found: C, 58.71; H, 5.84; N, 1.51%. IR (KBr): *v* (cm^{-1}) 636 (OSO), 1023 (OSO), 1032, 1156 (C–F), 1235 (OSO), 1656 (C=N). ^1H NMR (300 MHz, CD_2Cl_2): δ 0.48 (s, 3H, CH_{3camph}), 0.89 (s, 3H, CH_{3camph}), 1.0–1.2 and 1.4–2.0 (m, 5H, $H_{3endo} + H_5 + H_6$), 1.11 (s, 9H, $C(CH_3)_3$), 1.32 (s, 9H, $C(CH_3)_3$), 1.48 (s, 3H, CH_{3camph}), 1.67 (s, 3H, $CH_{3xanthene}$), 1.70 (s, 3H, $CH_{3xanthene}$), 1.85 (t, 1H, $^3J_{HH} = 4.2$ Hz, H_4), 2.27 (d, 1H, $^2J_{HH} = 17$ Hz, H_{3exo}), 6.59 (dd, 1H, $^3J_{HP} = 9.5$ Hz, $^4J_{HH} = 2.2$ Hz, H_{14}), 6.82 (d, 1H, $^4J_{HH} = 2.1$ Hz, H_{11}), 7.31 (d, 1H, $^4J_{HH} = 2.1$ Hz, H_{12}), 7.40–7.55 (m, 10H, H_{phenyl}), 7.61 (d, 1H, $^4J_{HH} = 2.2$ Hz, H_{13}). ES-MS: *m*/*z* 764.3 ($[M-BF_4]^+$, 100%).

2.2.19. [Rh(**15a**)Cl_3] (**21**)

To a solution of **15a** (16.4 mg, 25.0 μmol) in 0.7 mL CH_3CN was added a solution of $RhCl_3(H_2O)_3$ (6.6 mg, 25.0 μmol) in 0.3 mL CH_3CN at RT. The mixture was refluxed for 3h. Upon cooling to RT, the complex precipitated as an orange powder. After the solvent was removed under reduced pressure, the residue was purified by column chromatography over silica gel eluting with CH_2Cl_2 (TLC : $R_f = 0.34$), and then CH_2Cl_2–Et_2O (95:5) to give **21** as an orange solid (11.3 mg, 13.1 μmol, 52% yield). *Anal.* Calc. for $C_{45}H_{54}Cl_3NOPRh$: C, 62.47; H, 6.29; N, 1.62. Found: C, 62.35; H, 6.47; N, 1.49%. IR (KBr): *v* (cm^{-1}) 344, 358 (Rh–Cl), 1613 (C=N). $^{31}P\{^1H\}$ NMR (121.5 MHz, $CDCl_3$): δ 37.3 (d, $^1J_{PRh} = 105$ Hz). ^1H RMN (300 MHz, $CDCl_3$): δ 0.85 (s, 3H, H_8), 0.93 (s, 3H, H_{10}), 1.13 (s, 3H, H_9), 1.32 (s, 9H, $C(CH_3)_3$), 1.34 (s, 9H, $C(CH_3)_3$), 1.43 (s, 3H, $CH_{3xanthene}$), 1.58 (m, 1H, H_{5endo}), 1.90 (s, 3H, $CH_{3xanthene}$), 1.99–2.04 (m, 2H, H_{5exo}/H_{6exo}), 2.07 (m, 1H, H_4), 2.18 (m, 1H, H_{6endo}), 3.17 (d, 1H, $^2J_{HH} = 20.1$ Hz, H_{3endo}), 4.18 (d, 1H, $^2J_{HH} = 21$ Hz, H_{3exo}), 7.23 (d, 1H, $^4J_{HH} = 2.0$ Hz, H_{12}), 7.28 (d, 1H, $^4J_{HH} = 2.0$ Hz, H_{11}), 7.32 (m, 2H, H_{ar}), 7.40–7.55 (m, 4H, H_{ar}), 7.61 (dd, 1H, $^3J_{HP} = 10.2$ Hz, $^4J_{HH} = 2.1$ Hz, H_{14}), 7.69 (d, 1H, $^4J_{HH} = 1.9$ Hz, H_{13}), 7.87–7.96 (m, 4H, H_{ar}). $^{13}C\{^1H\}$

NMR (125.7 MHz, $CDCl_3$): 13.9 (broad s, C_8), 20.3 (s, C_9), 20.6 (s, C_{10}), 24.7 (broad s, $CH_{3xanthene}$), 27.3 (s, C_5), 31.4 (s, $2C(CH_3)_3$), 33.1 (s, C_6), 34.9 (s, $C(CH_3)_3$), 35.0 (s, $C(CH_3)_3$), 35.4 (broad s, $CH_{3xanthene}$), 35.5 (s, $C(CH_3)_2$), 43.2 (s, C_4), 47.1 (s, C_3), 53.6 (s, C_7), 58.8 (s, C_1), 117.8 (d, $J_{CP} = 53$ Hz, C_{ar}), 119.2 (s, C_{12}), 122.4 (s, C_{11}), 126.4 (s, C_{13}), 127.3 (s, C_{ar}), 127.8 (d, $J_{CP} = 12$ Hz, CH_{ar}), 128.3 (d, $J_{CP} = 11$ Hz, CH_{ar}), 128.9 (s, C_{ar}), 130.0 (s, C_{ar}), 130.4 (s, C_{14}), 131.1 (s, CH_{ar}), 131.4 (s, CH_{ar}), 133.4 (d, $J_{CP} = 7$ Hz, CH_{ar}), 133.9 (d, $J_{CP} = 7$ Hz, C_{ar}), 136.0 (d, $J_{CP} = 8$ Hz, CH_{ar}), 136.5 (s, C_{ar}), 145.8 (s, C_{ar}), 146.3 (s, C_{ar}), 149.2 (d, $J_{CP} = 6$ Hz, C_{ar}), 155.8 (d, $J_{CP} = 10$ Hz, C_{ar}), 201.5 (s, C_2).

2.3. Catalytic procedures

2.3.1. General procedure for palladium-catalyzed allylic alkylation with dimethyl malonate

A solution of $[Pd(\eta^3\text{-}C_3H_5)Cl]_2$ (0.9 mg, 2.5 μmol) and of ligand (4 or 6 μmol) in 1 mL THF was stirred for 20 min at RT. Alternatively, the catalyst solution was prepared by mixing together $AgBF_4$ (1 mg, 5 μmol) with $[Pd(\eta^3\text{-}C_3H_5)Cl]_2$ (0.9 mg, 2.5 μmol) for 15 min, filtering on Celite and adding the ligand (4 μmol) to the filtrate. A solution of dimethyl sodiomalonate was prepared by allowing a solution of dimethyl malonate (132 mg, 1 mmol) in THF (1.5 mL) to react with a suspension of NaH (24 mg, 1 mmol). A solution of the substrate **16a–c** (0.5 mmol) in THF (1 mL) was added to the catalyst solution, followed by the nucleophile solution. The conversion was periodically monitored by GC. When the reaction was over, water (10 mL) was added and the organic phase was extracted with Et_2O (3×15 mL). The extract was dried over $MgSO_4$, and the solvent was removed under reduced pressure. The crude product was purified by column chromatography on silica gel with pentane–Et_2O (4:1 v/v). The alkylation products were identified by comparison with literature data: dimethyl (*E*)-(1,3-diphenylprop-2-en-1-yl)malonate (**17a**) [19], dimethyl (*E*)-(pent-3-en-2-yl)malonate (**17b**) [20], dimethyl (cyclohex-2-en-1-yl)malonate (**17c**) [21]. The ee values were measured by analytical chromatography; **17a**: HPLC, $t(R) = 9.75$ min, $t(S) = 13.40$ min; **17b**: GC, temperature 40 °C (1 min), then 40 → 95 °C (1 °C min^{-1}), then 95 °C (30 min), $t(S) = 71.2$ min, $t(R) = 71.7$ min; **17c**: GC, temperature 40 °C (1 min), then 40 → 130 °C (1 °C min^{-1}), then 0.1 °C min^{-1}, $t(S) = 97.6$ min, $t(R) = 98.0$ min.

2.3.2. General procedure for silver-catalyzed allylation of benzaldehyde

In a Schlenk tube wrapped with aluminium foil, a solution of AgF (9 mg, 71 μmol) and of ligand (43 μmol) in 4 mL CH_3OH was stirred for 20 min at RT. The temperature was lowered to −20 °C, and benzaldehyde (75 μL, 707 μmol) and allyltrimethoxysilane (120 μL, 707 μmol) were successively added with a syringe. The solution was stirred at −20 °C for 4 h, then the temperature was raised to room temperature. The mixture was stirred at this temperature for 20 h, and was then worked up following a reported procedure [22]. The crude 1-phenylbut-3-en-1-ol was purified by column chromatography on silica gel with pentane–Et_2O (4:1). The ee values were measured by GC: temperature 40 °C, 5 min, then 40 → 180 °C, 2 °C min^{-1}, $t(S) = 52.47$ min, $t(R) = 52.75$ min. The retention times had been determined with an authentic sample [91% ee, (*S*) configuration] synthesized following the silver-catalyzed procedure using (*S*)-Binap as chiral ligand [22].

2.3.3. General procedure for rhodium-catalyzed hydrosilylation of acetophenone

To a solution of **21** (9 mg, 10 μmol) in 1 mL $CDCl_3$ was added $AgBF_4$ (4 mg, 20 μmol). The mixture was stirred for 20 h at room temperature and filtered through Celite. After NMR analysis, the solvent was evaporated to dryness and the catalyst redissolved in 1 mL CH_2Cl_2. Alternatively, the catalyst solution was prepared by mixing together $[Rh(cyclooctadiene)Cl]_2$ (2.5 mg, 5 μmol) and ligand **15a** or **15b** (6.5 mg, 10 μmol) in 1 mL CH_2Cl_2 and stirring for 18 h at room temperature. To the catalyst solution was added acetophenone (117 μL, 1 mmol). The temperature was lowered to 0 °C and diphenylsilane (297 μL, 1.6 mmol) was slowly added. The solution was stirred for 1 h at 0 °C, and then for 30 h at RT. The conversion was monitored by TLC and ^1H NMR. The reaction was quenched by adding 1 mL CH_3OH. Hydrolysis of the silyl ether was performed by adding a methanolic solution of K_2CO_3 (1% w/w, 10 mL) and stirring for 4 h. The product was extracted with Et_2O (3×10 mL). The combined organic layers were washed with brine (3 mL), dried over anhydrous $MgSO_4$ and evaporated to dryness. The resulting oil was purified by column chromatography over silica gel eluting with *n*-hexane–Et_2O (95:5 → 80:20 v/v). The ee values were measured by GC: temperature 120 °C, $t(R) = 24.7$ min, $t(S) = 25.9$ min, using (*S*)-(−)-1-phenylethanol (Acros) as a reference.

2.4. X-ray crystallography

Single crystals suitable for X-ray diffraction analysis were obtained by cooling a saturated CH_3CN solution to −23 °C (***ent*-15b**), slow diffusion of pentane into a saturated solution in CH_2Cl_2 (**18**), slow diffusion of pentane into a saturated solution in toluene (**19**), or slow diffusion of *n*-hexane into a saturated CH_2Cl_2 solution (**21**). The X-ray data were collected on a KappaCCD diffractometer with Mo Kα graphite-monochromated radiation ($\lambda = 0.71073$ Å). Details of data collection parameters and refinements results are listed in Table 1. The structures were solved using direct methods. Hydrogen atoms were introduced as fixed contributors at calculated positions (C–H = 0.95 Å, B(H) = 1.3 Beqv). Final difference maps revealed no significant maxima. All calculations were done using the Nonius OpenMoleN package [23]. Neutral atom scattering factor coefficients and anomalous dispersion coefficients were taken from a standard source [24].

Table 1
Crystal and refinement data

Compound	**18**	**19**	**21**
Chemical formula	$C_{36}H_{44}AgF_3N_2O_4S \cdot CH_2Cl_2$	$C_{45}H_{54}AgBF_4NOP$	$C_{45}H_{54}Cl_3NOPRh$
Color	colorless	colorless	orange
Formula weight	850.63	850.59	865.18
Crystal system	orthorhombic	monoclinic	orthorhombic
a (Å)	10.4265(1)	11.8287(2)	10.9681(1)
b (Å)	14.8480(2)	16.4340(3)	18.4672(2)
c (Å)	23.8250(4)	22.9519(5)	20.7059(3)
β (°)		99.976(5)	
V (Å^3)	3688.41(9)	4394.2(1)	4193.98(8)
T (K)	173	173	173
Space group	$P2_12_12_1$	$P12_11$	$P2_12_12_1$
Z	4	4	4
μ (mm^{-1})	0.805	0.545	0.671
Number of data measured	8455	16545	11950
Number of data with $I > 3\sigma(I)$	3301	6769	4891
R_{int}	0.040	0.040	0.040
R[a]	0.055	0.070	0.055
R_w[a]	0.140	0.152	0.140

[a] Values based on all data; $R = \sum||F_o| - |F_c||/\sum|F_o|$; $R_w = [\sum w(F_o - F_c)^2/\sum w(F_o)^2]^{1/2}$.

3. Results and discussion

3.1. Synthesis and analysis of the ligands

The diimine **5** was synthesized in four steps starting from 9,9-dimethyl-9*H*-xanthene **1** (Scheme 1). The first part of the synthetic scheme consisted in (i) double deprotonation of **1** in *ortho* position with an excess of *n*-butyllithium, followed by a nucleophilic attack of the dilithiated species onto CO_2; (ii) Curtius rearrangement using diphenylphosphorylazide; and (iii) basic hydrolysis leading to the diamine **4**. The final key step was the condensation of the amine functions of **4** with (1*R*)-camphor. It had been reported that the cheap and available titanium tetrachloride is an efficient catalyst for the synthesis of camphimines, when classical methods are unsuccessful because of steric hindrance on the ketone [25]. Indeed it has been used with success for the preparation of **5**, as well as that of other reported iminophosphines derived from camphor [7]. We optimized the condensation yield by employing an excess of camphor, and a large amount of $TiCl_4$ and triethylamine.

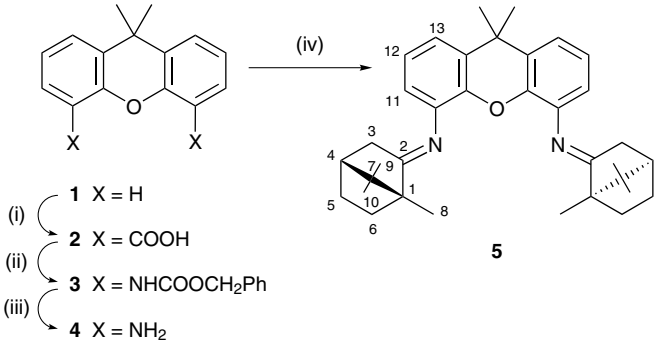

Scheme 1. Synthesis of the camphor-derived diimine ligand **5**. Reagents and conditions: (i) (a) *n*BuLi (2.5 equiv.), THF, −78 °C → RT; (b) CO_2, −78 °C → RT; (ii) diphenylphosphorylazide (2 equiv.), $PhCH_2OH$ (2 equiv.), NEt_3 (2 equiv.), $PhCH_3$, 100 °C; (iii) KOH, EtOH, reflux; (iv) (1*R*)-camphor (3 equiv.), $TiCl_4$ (5 equiv.), NEt_3 (20 equiv.), $PhCH_3$, reflux.

We have previously reported the X-ray structure of compound **5** [8]. The essential informations that it provided were (i) that the configuration of the imines is *E*, which is easily explained on steric grounds; and (ii) that the tricyclic 9,9-dimethylxanthene unit is planar in the unit cell. The question of whether 9,9-dimethylxanthene itself is also planar or not in solution has been addressed by Aizenshtat et al. [26]. They observed no influence of the temperature on its ^{1}H NMR spectrum; similarly, a variable-temperature analysis of **5** in the range −90 to 27 °C showed no major alteration of the NMR spectrum. The interpretation they proposed, i.e. that the tricycle is either planar or non-planar but rapidly inverting (butterfly motion) with a very low energy barrier, is suitable for **5**.

We expected to synthesize the iminophosphine ligand **15a** following a similar pathway, starting from the monocarboxylated derivative **6** (Scheme 2). The monofunctionalization of **1** proved to be a delicate step, because of the competitive formation of the *ortho*-dilithiated species that led to **2** upon reaction with CO_2. Indeed, using 1 equiv. *n*BuLi as a base gave **2** as the major product, whereas PhLi was found to be a better reagent, leading to **6** with an optimal yield (47%) when used in excess (2.5 equiv.). The three following steps were conducted in the same conditions as those depicted in Scheme 1, with better yields however, this being likely due to the conversion of only one chemical function instead of two (Curtius, **7**: 86%; basic hydrolysis, **8**: 86%; condensation with camphor, **9**: 66%). As mentioned previously [8], we were unsuccessful in transforming **9** into the iminophosphine shown Scheme 2: abstracting the

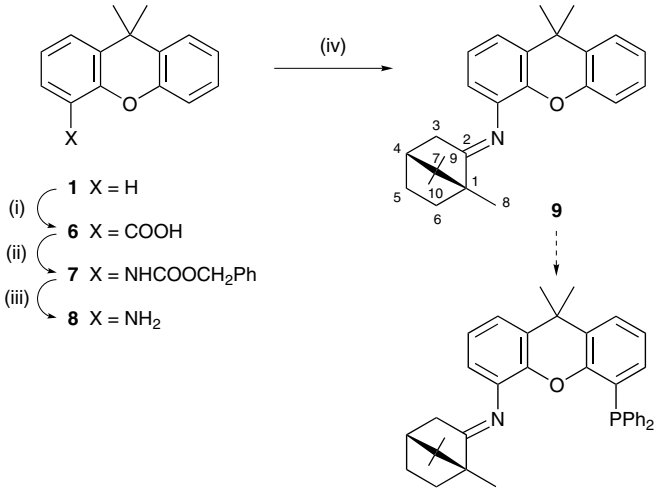

Scheme 2. Attempted synthesis of a camphor-derived iminophosphine from 9,9-dimethyl-9*H*-xanthene (**1**). (i) (a) PhLi (2.5 equiv.), THF, −78 °C → RT; (b) CO_2, −78 °C → RT; (ii) diphenylphosphorylazide (1 equiv.), $PhCH_2OH$ (1 equiv.), NEt_3 (1 equiv.), $PhCH_3$, 100 °C; (iii) KOH, EtOH, reflux; (iv) (1*R*)-camphor (1.5 equiv.), $TiCl_4$ (2.5 equiv.), NEt_3 (10 equiv.), $PhCH_3$, reflux.

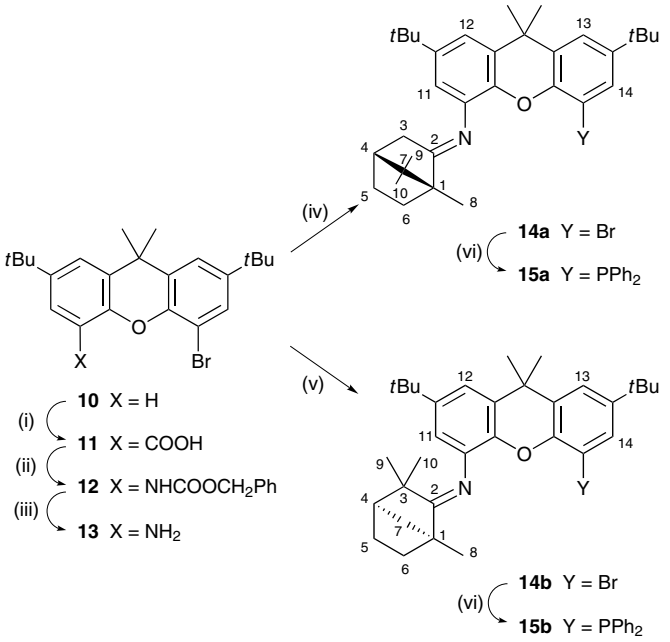

Scheme 3. Synthesis of the iminophosphine ligands **15a** from 2,7-di-*tert*butyl-4,5-dibromo-9,9-dimethyl-9*H*-xanthene (**10**). Reagents and conditions: (i) (a) *n*BuLi (1 equiv.), THF, −78 °C; (b) CO_2, −78 °C → RT; (ii) diphenylphosphorylazide (1.1 equiv.), $PhCH_2OH$ (1.1 equiv.), NEt_3 (1.1 equiv.), $PhCH_3$, 100 °C; (iii) KOH, EtOH, reflux; (iv) (1*R*)-camphor (1.5 equiv.), $TiCl_4$ (2.5 equiv.), NEt_3 (10 equiv.), $PhCH_3$, reflux; (v) (1*S*)-fenchone (1.5 equiv.), $TiCl_4$ (7.5 equiv.), NEt_3 (30 equiv.), $PhCH_3$, reflux; (vi) (a) *n*BuLi (1.3 equiv.), THF, −78 °C; (b) PPh_2Cl (1.3 equiv.), −78 °C → RT.

proton in *ortho* position of xanthene necessitates to use *n*BuLi and the temperature to be raised to ca. 20 °C, these conditions leading to complete decomposition of **9**. Replacement of *n*BuLi by other deprotonating agents (*s*BuLi, *t*BuLi, PhLi) did not lead to any improvements.

Instead, the air-stable iminophosphine ligands **15a** and **15b** were synthesized in five steps starting from 2,7-di-*tert*-butyl-4,5-dibromo-9,9-dimethyl-9*H*-xanthene **10** (Scheme 3) [8]. The major change with regard to the synthetic schemes described above was that the organolithium reactive species involved in the first and in the last steps of the synthetic pathways were not obtained by abstraction of the *ortho* xanthene protons, but by bromide–lithium exchange that was run with *n*BuLi under milder conditions [27] (lower temperature). Several attempts to synthesize similar chiral iminophosphine derived from (+)-menthone, (+)-nopinone or (−)-myrtenal, using either $TiCl_4$ or other Lewis acids, were unsuccessful.

Our NMR data indicate that only the *E* stereoisomers of the camphor-derived imines **14a** and **15a** are present in solution, as in the X-ray structure of the diimine **5**. This statement is notably supported by the ^1H–^1H ROESY spectrum of **15a** recorded in CD_2Cl_2 at room temperature. It exhibits strong NOE cross-peaks between the signal of H_{11}, belonging to the xanthene backbone, and those of H_{3exo} and H_9 that belong to the chiral bicycle, whereas no NOE effect was observed between the signals of H_{11} and H_8.

By contrast, in fenchone or its derivatives, the steric hindrance generated by Me_8 on one side of the carbon-heteroatom double bond, and by Me_9 and Me_{10} on the other side, are of the same order of magnitude; for instance, the energy difference between the *E* and *Z* isomers of oximes derived from fenchone is less than 4 kJ mol^{-1} [28]. Indeed, both *E* and *Z* isomers of the fenchone-derived imines **14b** and **15b** are observed in solution, according to their NMR spectra recorded at room temperature. Several of the protons of each stereoisomer have accidentally identical chemical shifts, such as the aromatic protons H_{12}–H_{14}, and the *t*Bu protons. By contrast, the signal of H_{11} is split in two non-equivalent signals, a major, narrow doublet and a minor, broad signal which is shifted upfield by ca. 0.1 ppm (respectively at 6.62 and 6.55 ppm in compound **14b**, see Fig. 1). In general, the aliphatic protons belonging to the chiral bicycle exhibit large overlapping signals that cannot be easily distinguished, with the exception of the methyl signals of the major isomer. However, on the spectrum of **14b**, we could identify both H_8 signals as a singlet at 1.40 ppm (major isomer) and a broad, shielded singlet at 0.68 ppm. The $^{31}P\{^1H\}$ NMR spectrum of **15b** recorded at room temperature also displays a narrow major signal and a broad minor one (Fig. 2), corresponding also to both stereoisomers.

The analysis of **14b** by ^1H–^1H NOESY spectroscopy allows us to assign the signals of the major isomer to the *Z* configuration (drawn Scheme 3). Indeed, strong NOE cross-peaks are displayed Fig. 1 that indicate spatial proximity between H_{11} and the dimethylmethylene unit of the bicycle (H_9 and H_{10}). The (*Z*)/(*E*) ratio was calculated from the integration of the proton signals; it reached a value of 4 for compound **14b** and 9 for compound **15b**.

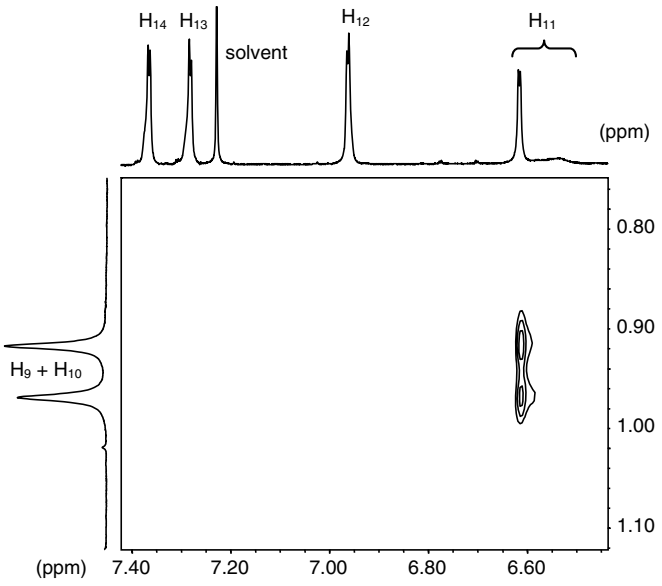

Fig. 1. Section of the ^{1}H–^{1}H NOESY spectrum of compound **14b** recorded in $CDCl_3$ at 298 K (500 MHz, $\tau_m = 450$ ms).

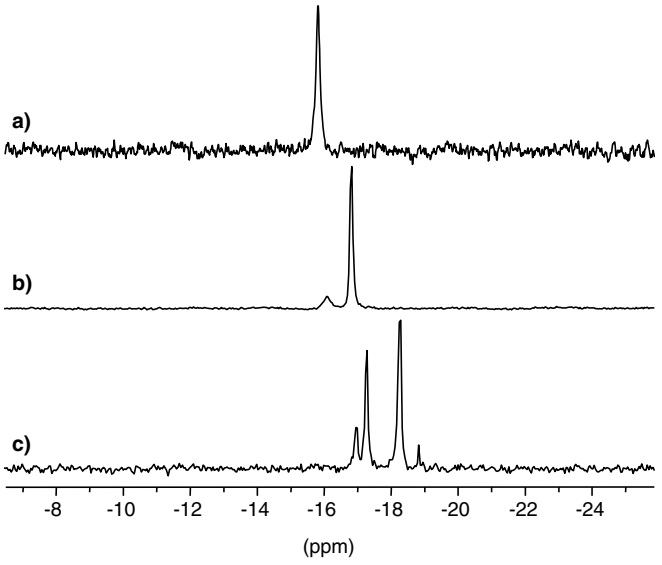

Fig. 2. $^{31}P\{^{1}H\}$ NMR spectra (121.5 MHz) of compound **15b** recorded (a) in CD_3CN at 333 K; (b) in $CDCl_3$ at 298 K; (c) in $CDCl_3$ at 243 K.

The broadness of some of the signals suggests that a chemical exchange process takes place in solution, and this assertion is supported by several elements. Various exchange cross-peaks between signals of the *Z* and *E* isomers are observed on the NOESY spectrum of **14b**, notably for H_8, H_9, H_{10}, H_{11} and for the xanthene methyl groups. Besides, the $^{31}P\{^{1}H\}$ NMR spectrum of **15b** in CD_3CN shows that the major and minor signals have coalesced into one singlet upon heating to 333 K (see Fig. 2; the spectra of **15b** at room temperature are practically identical in $CDCl_3$ and in CD_3CN). On the ^{1}H NMR spectrum recorded at 333 K in CD_3CN, the H_{11} signal also appears as a narrow, single averaged doublet. Those data can be interpreted as

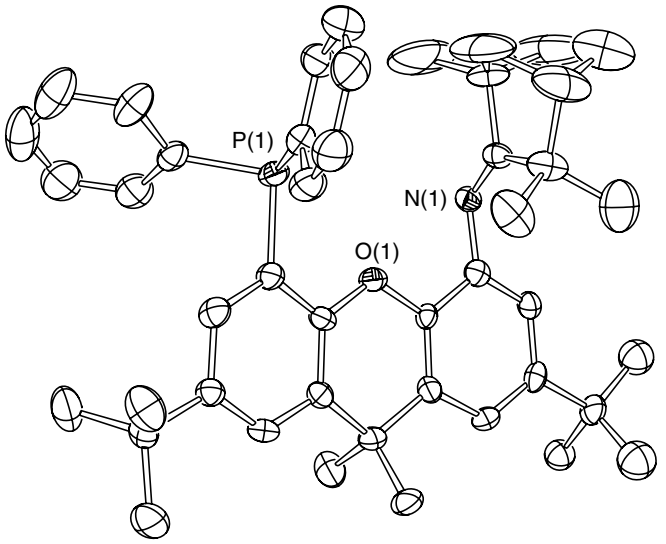

Fig. 3. ORTEP drawing of ligand ***ent*-15b** showing 50% probability thermal ellipsoids. Hydrogen atoms are omitted for clarity.

the result of a fast equilibrium between both isomers. Such isomerizations of imines have low energy barriers in comparison with alkenes [29]; this is in good agreement with our NMR observations at ambient and high temperature.

A decrease of the temperature also leads to important modifications of the phosphorus and proton NMR spectra of **15b**. Most of the ^{1}H NMR signals in CD_2Cl_2 broaden when the temperature is lowered, but even at 192 K those signals are still broad and overlapping. However, we can distinguish four large H_{11} signals of unequal intensity at 192 K between 6.3 and 6.6 ppm. Similarly, the $^{31}P\{^{1}H\}$ NMR spectrum recorded at 253 K in $CDCl_3$ exhibits four signals (Fig. 2), that result from a split of the two signals detected at room temperature. These observations can be interpreted as the result of a second, lower-energy fluxional process. It seems unlikely that it would be related to a butterfly motion of the xanthene backbone (supposing it would be non-planar in solution); if it were so, then we should probably observe similar modifications upon cooling of the NMR features of other compounds like **5**, and it is not the case (vide supra). We rather consider the low-temperature NMR spectra of **15b** as the result of a restricted rotation about the carbon-nitrogen single bond, because the xanthene backbone interacts sterically with Me_9 and Me_{10} in isomer *Z*, and with Me_8 in isomer *E*. Therefore, for each configuration of the imine, two atropoisomers are frozen at low temperature.

Single crystals of ***ent*-15b**, i.e. the enantiomer **15b** derived from (1*R*)-(−)-fenchone, were analyzed by X-ray diffraction. The quality of the structure was poor; however preliminary data X-ray were collected.[1] The solid state structure of ***ent*-15b** is represented Fig. 3.

[1] Crystallographic data: crystal system triclinic, space group $P\bar{1}$, $V = 3811.6(4)$ Å^3, $a = 14.3556(7)$ Å, $b = 16.330(1)$ Å, $c = 16.9783(9)$ Å, $\alpha = 77.536(5)°$, $\beta = 81.951(5)°$, $\gamma = 80.606(5)°$, $Z = 4$.

3.2. Applications in metal coordination and metal-catalyzed organic reactions

In analogy with our previous studies with diphospholanes [5], we attempted to isolate palladium complexes from our ligands. [Pd(cyclooctadiene)Cl_2] did not react with ligand **5**, whereas a reaction with **15a** led to a mixture of several complexes that could not be separated. We also tried to isolate palladium π-allyl and π-cyclohexenyl complexes following the classical synthetic pathway that we had used with other xanthene-based ligands (withdrawal of chloro bridges of palladium π-allyl dimers with $AgBF_4$, followed by addition of ligand **5** or **15a**) [5]. Unfortunately, NMR monitoring of the coordination reactions revealed that all attempts had led to mixtures. Obviously the xanthene-based diimine and iminophosphine ligands do not fit the square-planar geometry of palladium (II), probably because of their very large bite angle; therefore they lead to mixtures of ill-defined complexes (e.g. coordination polymers) and to unsatisfactory catalytic results. Similar difficulties to generate bidentate Rh or Pt complexes with xanthene-derived P,N or N,N ligands were previously experienced by van Leeuwen et al. [30]. Hence, we chose other metal ions, whose electronic or geometric characteristics would be more adapted to our ligands.

Indeed, the synthesis of the silver (I) complexes [Ag(**5**)(OTf)] (**18**), [Ag(**15a**)(BF_4)] (**19**) and [Ag(**15a**)(OTf)] (**20**) was straighforward (Scheme 4). They were prepared by mixing a silver salt (AgX, X = OTf or BF_4) with 1 equiv. of the proper ligand in methylene chloride at room temperature, with good-to-excellent yields (**18**: 89%; **19**: 73%; **20**: 97%).

We undertook an X-ray diffraction analysis of complexes **18** and **19**; their ORTEP representations are shown on Figs. 4 and 5 respectively, and a selection of their bond distances and angles are given in Tables 2 and 3. For **18**, the unit cell contains one molecule, whereas for **19** two of them are present, which correspond to two conformers of the complex (vide infra). In all cases, the geometry of the complex is trigonal planar, which is not the most common

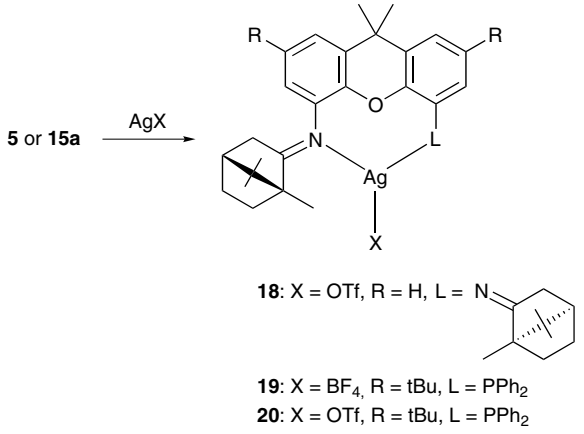

Scheme 4.

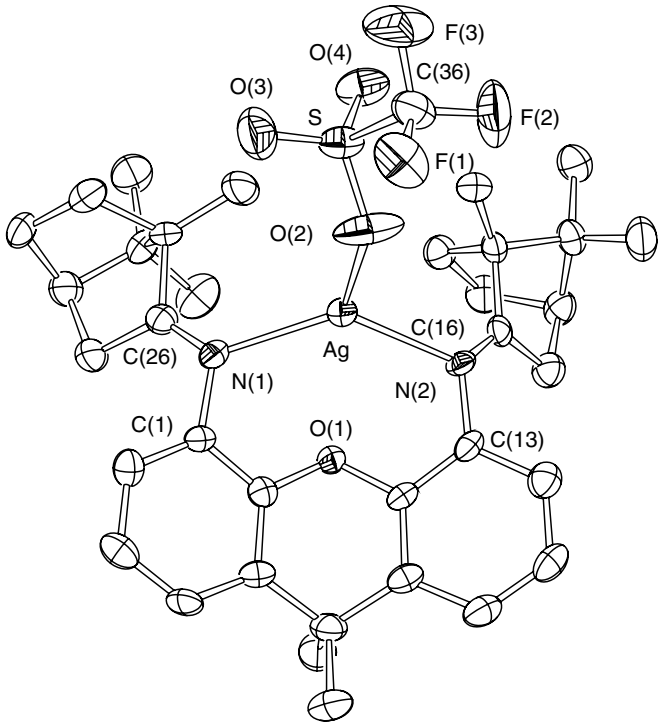

Fig. 4. ORTEP drawing of [Ag(**5**)(OTf)] (**18**) showing 50% probability thermal ellipsoids and the atom-numbering scheme. Hydrogen atoms and CH_2Cl_2 are omitted for clarity.

one among silver (I) complexes [31a]. The chiral ligands chelate the metal ion *via* their nitrogen or phosphorus donor atoms, but not *via* the xanthene oxygen atom; the third position is occupied by the triflate or tetrafluoroborate anion. As expected, the bite angle of the chiral ligand reaches higher values [**18**: 126.3(1)°; **19**: 123.6(1)° and 122.4(1)°] than in homologous diphospholane palladium complexes [5]. The xanthene backbone is tilted with regard to the coordination plane; as a consequence, in complex **18**, the diimine ligand **5** has lost its C_2 symmetry axis. The backbone is also folded along the O···CMe_2 axis, which results in a boat conformation of the central heterocycle. In all structures, the camphimines have retained their (*E*) configuration after coordination to the metal (assuming we do not consider Ag as a substituent for the determination of the absolute configuration). The Ag–N bond lengths (2.287(6)–2.351(4) Å) are within the lower range for silver complexes coordinated by Schiff bases [32], which suggests strong metal–ligand bonds.

In complex **18**, the small increase of the C=N bond lengths remains within the esd with regard to the free ligand (1.288(7) and 1.276(6) Å versus 1.258(4) and 1.268(4) Å). Similarly, coordination of an isothiazole to Ag^I only leads to a very slight increase of the nitrogen-carbon bond [33a]. In connection with this elongation, we observe a significant decrease of the C=N vibration wavenumber on the IR spectrum, from 1690 (**5**) to 1648 cm^{-1} (**18**). The Ag–O(2) bond length is also short (2.3415(4) Å) by comparison with other reported structures of η^1-OSO_2CF_3 silver (I) complexes (range 3.39–3.58 Å) [33].

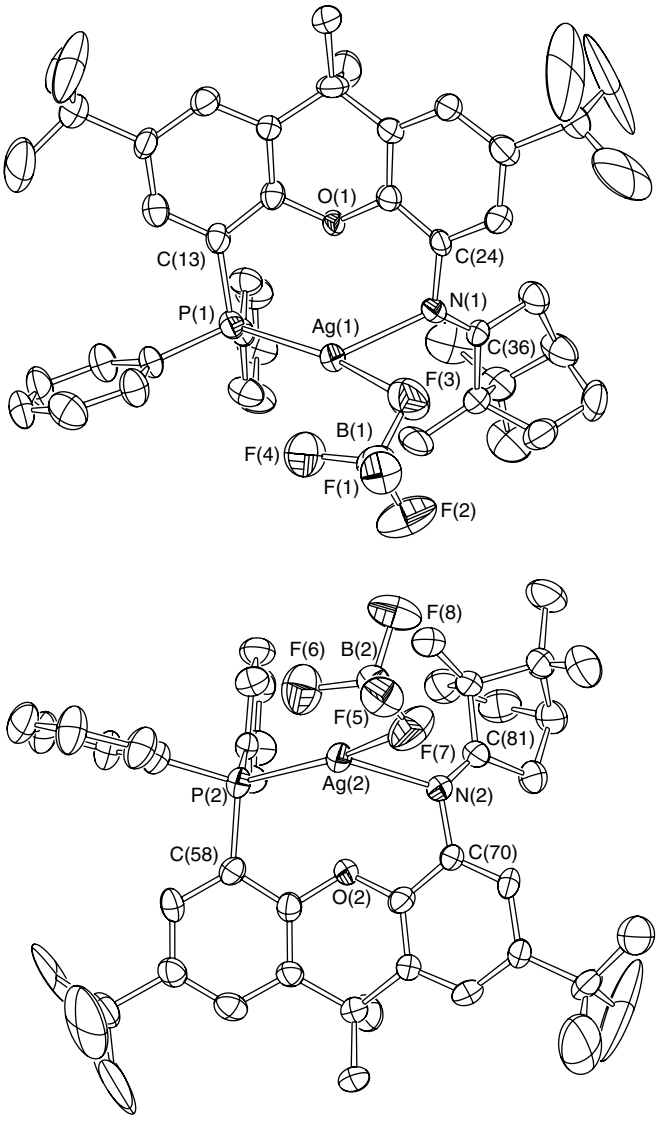

Fig. 5. ORTEP drawings of [Ag(**15a**)(BF_4)] (**19**) showing 50% probability thermal ellipsoids and the atom–numbering scheme. Both molecules present in the unit cell are represented.

Table 2
Selected bond lengths (Å) and angles (°) for [Ag(**5**)(OTf)] (**18**)

Ag–N(1)	2.310(4)	C(1)–N(1)	1.457(6)
Ag–N(2)	2.351(4)	C(26)–N(1)	1.288(7)
Ag–O(2)	2.341(4)	C(13)–N(2)	1.416(6)
S–O(2)	1.450(4)	C(16)–N(2)	1.276(6)
N(1)–Ag–N(2)	126.3(1)	N(2)–Ag–O(2)	111.1(2)
N(1)–Ag–O(2)	121.0(2)	Ag–O(2)–S	128.4(2)
Ag–N(1)–C(1)	112.2(2)	Ag–N(2)–C(13)	111.1(2)
Ag–N(1)–C(26)	129.6(3)	Ag–N(2)–C(16)	126.0(3)
C(1)–N(1)–C(26)	117.4(4)	C(13)–N(2)–C(16)	120.1(4)

The triflate anion is almost positioned symmetrically with regard to the nitrogen atoms, with close values for both N–Ag–O(2) bond angles (121.0(2)° and 111.1(2)°).

One of the X-ray structures of complex **19** corresponds to the conformer where the CMe_2 fragment of the bicycle

Table 3
Selected bond lengths (Å) and angles (deg) for [Ag(**15a**)(BF_4)] (**19**)

Ag(1)–N(1)	2.296(5)	Ag(2)–N(2)	2.287(6)
Ag(1)–P(1)	2.384(2)	Ag(2)–P(2)	2.386(2)
Ag(1)–F(3)	2.547(4)	Ag(2)–F(7)	2.450(4)
C(36)–N(1)	1.282(7)	C(81)–N(2)	1.279(8)
C(13)–P(1)	1.797(6)	C(58)–P(2)	1.831(7)
P(1)–Ag(1)–N(1)	123.6(1)	P(2)–Ag(2)–N(2)	122.4(1)
P(1)–Ag(1)–F(3)	153.9(1)	P(2)–Ag(2)–F(7)	153.8(1)
N(1)–Ag(1)–F(3)	78.0(2)	N(2)–Ag(2)–F(7)	82.0(2)
Ag(1)–N(1)–C(24)	112.3(3)	Ag(2)–N(2)–C(70)	112.5(3)
Ag(1)–N(1)–C(36)	129.0(3)	Ag(2)–N(2)–C(81)	127.7(4)
C(24)–N(1)–C(36)	118.3(6)	C(70)–N(2)–C(81)	118.9(6)
Ag(1)–P(1)–C(13)	107.9(2)	Ag(2)–P(2)–C(58)	109.1(2)

and the BF_4^- ligand are positioned *anti* with regard to the plane defined by Ag and C═N, whereas in the second one they are *syn* (Fig. 5). The trigonal planar geometry of the complexes is highly distorted, the η^1-BF_4 anion being located in pseudo-trans position with regard to the phosphorus donor atom. This tendency towards linearity is commonly observed in phosphine-coordinated silver complexes [34]. Comparison of the Ag–P (2.384(2) and 2.386(2) Å) and Ag–F bond distances (2.547(4) and 2.450(4) Å) with literature data [32,35] indicates that they are markedly short.

The ^1H and $^{13}C\{^1H\}$ NMR spectra of complex **18** in CD_2Cl_2 recorded at room temperature exhibit the narrow signals of an apparently C_2-symmetric diimine ligand. All the ^1H signals broaden upon cooling, and even at 178 K they are still broad and unresolved. This indicates that the complex is fluxional. A straightforward interpretation of this fluxionality is that the complex adopts in solution a conformation similar to the one observed in the solid state by crystallography, and that it undergoes a rapid conformational equilibrium (flip-flop interconversion [5], see Scheme 5). In this process, the metal-anion fragment rocks back and forth, which results here in apparent C_2-symmetry of the ligand. Besides, NOE cross-peaks detected on the ^1H–^1H ROESY spectrum between the aromatic H_{11} signal at 6.82 ppm, and the signals at 6.56 and 6.82 ppm of H_{3exo} and H_{3endo} that belong to the chiral bicycle, confirm the *E* configuration of the imines that was observed on the X-ray structure.

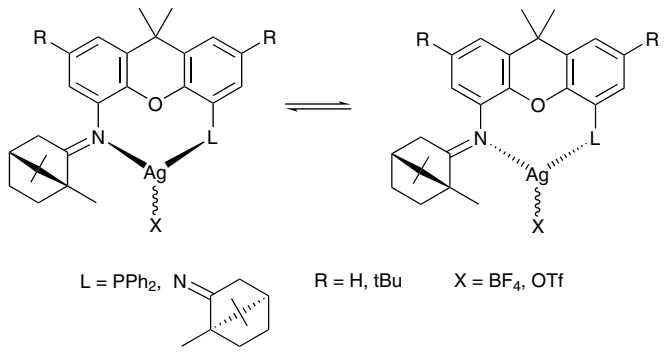

Scheme 5. Conformational equilibrium of the fluxional complexes **18**–**20**.

Analysis of the iminophosphine complexes **19** and **20** by variable-temperature ^{1}H NMR spectroscopy leads to similar conclusions. The room-temperature spectra exhibit narrow, averaged signals, and lowering the temperature leads to their broadening and splitting. In general the signals at low temperature are still broad and overlap; however, they could be identified for the H_{11} and H_{14} signals of **20** (Fig. 6), which are split into two signals of nearly equal intensity (integration ratio 53/47).

At 298 K, the $^{31}P\{^1H\}$ NMR signal of **19** in CD_2Cl_2 is a broad singlet at −5.8 ppm, whereas for **20** it appears as two doublets centered at −5.2 ppm, resulting from the coupling with both silver isotopes (^{107}Ag: $^1J_{PAg} = 642$ Hz; ^{109}Ag: $^1J_{PAg} = 741$ Hz). Cooling the solution of **19** gives rise to a broadening of the singlet and a splitting into two new singlets at 183 K (Fig. 7). Unlike other reported silver-phosphine complexes [36], no coupling with the silver nucleus appears at low temperature. Concerning **20**, its $^{31}P\{^1H\}$ NMR spectrum at 203 K consists of two pairs of doublets of equal intensity, one centered at −4.8 ppm ($^1J_{PAg} = 647$ and 747 Hz) and the other at −5.1 (2d, $^1J_{PAg} = 644$ and 744 Hz).

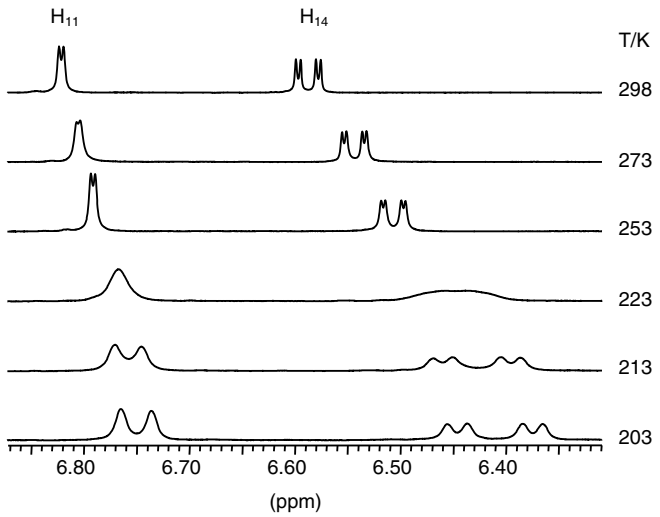

Fig. 6. Variable-temperature ^{1}H NMR spectra (500 MHz) of complex **20** in CD_2Cl_2: section of the aromatic region.

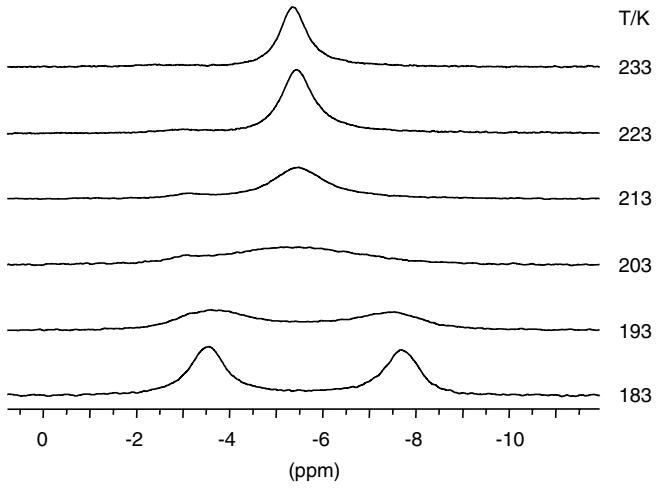

Fig. 7. Variable-temperature $^{31}P\{^1H\}$ NMR spectra (121.5 MHz) of complex **19** in CD_2Cl_2.

This fluxionality of complexes **19** and **20** is again reasonably explained by a conformational equilibrium between two conformers (Scheme 5). Each of the low-temperature signals of **19** or **20** shown in Figs. 6 and 7 corresponds to one of them, whereas at room temperature the equilibrium is fast and the signals are averaged. Indeed, in the solid state, both conformers of **19** were observed in the unit cell (vide supra). It is not surprising that they are in roughly equal proportion in solution, as long as in the X-ray structure there appeared to be no major differences in intramolecular steric interactions between the bicycle and the coordinating anion.

The rhodium (III) complex [Rh(**15a**)Cl_3] (**21**) was synthesized by refluxing $RhCl_3 \cdot 3H_2O$ with 1 equiv. of ligand **15a** in acetonitrile (Scheme 6). Partial hydrolysis of the imine function occurred upon coordination to Rh^{III}: some key NMR signals of an aminophosphine-coordinated complex were found on the ^{1}H NMR spectrum, such as an NH_2 signal that resonates at 6.36 ppm as a broad doublet ($^2J_{HRh} = 5$ Hz). This probably results from the enhancement of the electrophilicity of the coordinated imine; similarly, hydrolysis of an imine coordinated to Rh^I has been reported [37]. Nevertheless, complex **21** could be isolated in a pure form, although with moderate yield (52%), after purification by column chromatography over silica gel. By contrast, mixing ligand **5** with various rhodium sources ([Rh(cyclooctadiene)Cl]$_2$, $RhCl_3 \cdot 3H_2O$, $RhCl_3(CH_3CN)_3$) at room temperature did not lead to new Rh^I or Rh^{III} complexes.

Single crystals of complex **21** suitable for X-ray analysis were obtained. The X-ray structure is represented in Fig. 8, and a selection of its bond distances and angles is shown in Table 4. By contrast with the silver complexes, the chiral ligand is tridentate and meridional, coordinating the rhodium (III) cation by its oxygen atom in addition with its phosphorus and nitrogen donor atoms. Few examples of this coordination mode for xanthene-based or related ligands are reported in the literature [38]. The complex presents an expected distorted octahedral geometry [31b], with a large deviation from linearity of the N–Rh–P angle (163.16(8)°) due to the chelate effect. The fourth equatorial position and both axial positions are occupied by chloro ligands.

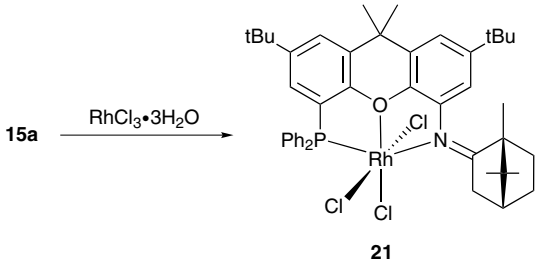

Scheme 6.

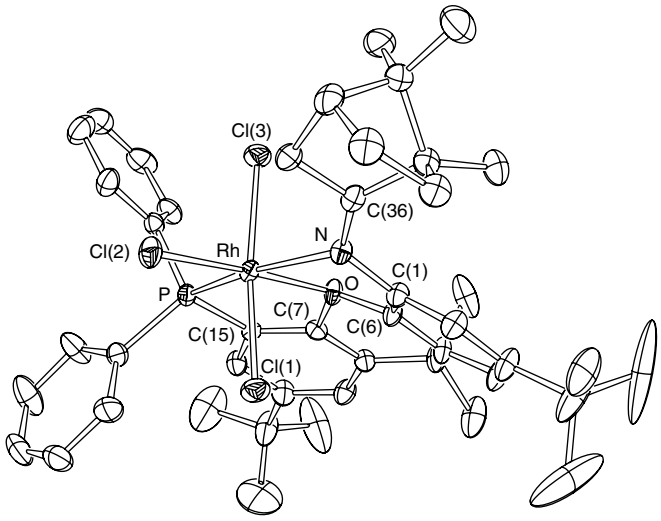

Fig. 8. ORTEP drawing of [Rh(**15a**)Cl_3] (**21**) showing 50% probability thermal ellipsoids and the atom-numbering scheme.

The X-ray structure reveals that the imine has isomerized upon coordination to Rh^{III}, the bridgehead methyl being now in *cis* position with regard to the aromatic xanthene cycle. We suppose that this isomerization is due to unfavorable steric interactions between the chloro ligand and this bridgehead methyl. However, steric repulsion also occurs between this methyl substituent and the backbone, so that the chiral bicycle lies above the equatorial plane and the backbone is bent below. As in the structures of the silver complexes, the xanthene tricycle is folded and the central cycle is in a boat conformation.

The oxygen atom is pyramidalized, as indicated by the sum of the Rh–O–C(6), Rh–O–C(7) and C(6)–O–C(7) bond angles (342°). The Rh–O bond length (2.128(2) Å) is very close to the value reported by van Leeuwen et al. for a Rh^{I}–xantphos complex (2.126(3) Å) [38b]. By comparison with tabulated data [32], the Rh–N bond length (2.178(3) Å) is rather long and the Rh–P (2.237(1) Å) and Rh–Cl (2.2922(9)–2.3322(9) Å) bond lengths are short; this is easily explained by the strong *trans* influence of $–PPh_2$ with regard to the other coordinating substituents [39]. The oxygen donor atom has a remarkably low *trans* influence, as indicated by the lower value of the Rh–Cl(2) bond distance (2.2922(9) Å) in comparison with the other rhodium–chloro distances. As in the silver complexes, the C=N bond undergoes an elongation upon coordination to rhodium (III) (1.298(5) Å versus 1.258(4) and 1.268(4) Å for the free ligand), in connection with a major shift ($-77\ cm^{-1}$) of the IR $\nu_{C=N}$ wavenumber.

It is remarkable that the ^1H NMR signals of the methyl groups borne by the xanthene tricycle in **21** have very different chemical shifts (1.43 and 1.90 ppm). This large $\Delta\delta$ value (0.47 ppm) is owed to the fact that one is frozen in axial position and the other in equatorial position. In comparison, $\Delta\delta$ is much lower in the fluxional silver complexes, where both positions exchange. The ^1H–^1H ROESY spectrum allows us to assign them, because the aromatic protons H_{12} and H_{13} display stronger NOE cross-peaks with the equatorial methyl that resonates at 1.90 ppm, than with the axial one that resonates at 1.43 ppm. The ROESY spectrum confirms also that the configuration of the imine is *Z* as in the X-ray structure: a close contact revealed by a NOE effect is found between H_8 (bridgehead methyl) and the aromatic proton H_{11}. In addition, no major modifications of the $^{31}P\{^1H\}$ or the ^1H NMR spectra were found when the solution was cooled to 213 K, indicating that complex **21** is not fluxional.

Catalytic tests were carried out either with preformed or with in situ-synthesized metal complexes. They consisted of asymmetric silver-catalyzed allylation of benzaldehyde (Scheme 7), rhodium-catalyzed hydrosilylation of acetophenone (Scheme 8), and palladium-catalyzed allylic alkylation (Scheme 9).

Yamamoto et al. have reported the catalytic addition of allyl silanes onto benzaldehyde [22]; their catalysts were prepared in situ by mixing silver fluoride with a chiral diphosphine. We first attempted to isolate a presumably active catalytic species from AgF and our ligand **15a**, and indeed the reaction run in methanol at room temperature yielded cleanly a new silver complex presumably formulated [AgF(**15a**)] which exhibited a $^{31}P\{^1H\}$ NMR signal centered at −3.8 ppm ($^1J_{PAg} = 641$ Hz and 737 Hz). Unfortunately, this species was far less stable than complexes **18**–**20**; it rapidly decomposed to a silver mirror even when the

Table 4
Selected bond lengths (Å) and angles (°) for [Rh(**15a**)Cl_3] (**21**)

Rh–N	2.178(3)	Rh–Cl(1)	2.3332(9)
Rh–P	2.237(1)	Rh–Cl(2)	2.2922(9)
Rh–O	2.128(2)	Rh–Cl(3)	2.3322(9)
C(1)–N	1.434(5)	C(36)–N	1.298(5)
N–Rh–P	163.16(8)	P–Rh–O	85.28(7)
N–Rh–O	77.9(1)	O–Rh–Cl(2)	177.18(7)
N–Rh–Cl(2)	103.82(8)	P–Rh–Cl(2)	93.02(4)
Cl(1)–Rh–Cl(2)	91.28(4)	Cl(1)–Rh–Cl(3)	173.56(4)
Rh–N–C(1)	106.8(2)	Rh–N–C(36)	129.3(2)
Rh–O–C(6)	110.3(2)	Rh–O–C(7)	115.4(2)
Rh–P–C(15)	98.6(1)	C(1)–N–C(36)	122.2(3)
C(6)–O–C(7)	116.1(3)		

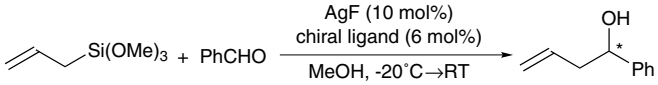

Scheme 7. Silver-catalyzed allylation of benzaldehyde.

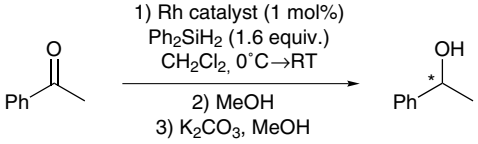

Scheme 8. Rhodium-catalyzed hydrosilylation of acetophenone.

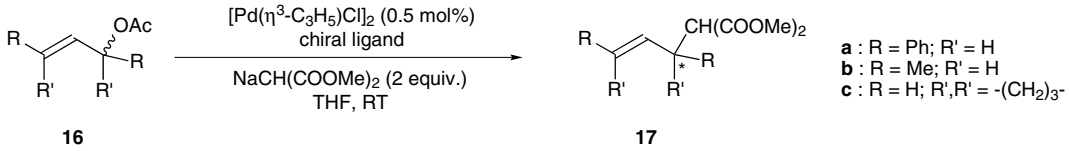

Scheme 9. Palladium-catalyzed allylic alkylation.

solution was protected from air and light, and could not be analyzed further. Therefore, we ran the allylation reaction with catalysts prepared in situ following the procedure of Yamamoto et al., replacing the diphosphines with our ligands. The reaction was conducted in methanol at −20 °C for 4 h, then at room temperature for 20 h. The diimine ligand **5** led to a low ee (18%, *S* enantiomer) with a conversion of 68%, whereas the homoallylic alcohol was racemic with the iminophosphines **15a,b** (conversions 62% and 68%, respectively).

For complex **21**, we applied the hydrosilylation procedure described for trichloro rhodium precursors by Nishiyama et al., who first converted them into cationic species with silver tetrafluoroborate [40]. This step was slow (20 h reaction time); it led cleanly to a single species that exhibited a doublet at 38.3 ppm in $CDCl_3$ on a $^{31}P\{^1H\}$ NMR spectrum ($^1J_{PRh} = 95$ Hz). The catalytic reaction run afterwards was almost quantitative but sluggish (95% conversion within 30 h at RT), and very poorly selective (5% ee). We also prepared hydrosilylation rhodium catalysts in situ from **15a** or **15b** and from [Rh(cyclooctadiene)Cl]$_2$[41]; the 1-phenylethanol yield reached then 76% and 72% respectively after 30 h at RT, but the product was racemic.

Palladium-catalyzed allylic alkylations were conducted with catalysts synthesized in situ from $[PdCl(\eta^3\text{-}C_3H_5)]_2$ and a chiral ligand. With substrates **16a** and **16c**, no reaction was observed when we used the diimine ligand **5**. By contrast, the iminophosphine ligands **15a,b** led to good conversions and moderate enantioselectivities as shown in previously reported preliminary results (up to 36% ee) [8]. Catalytic tests run with substrate **16c** confirmed this trend (ligand **15a**: 77% yield, 16% ee (*S*); ligand **15b**: 27% yield, 19% ee (*R*) after 20 h reaction time). Burgess et al. have emphasized the importance of the ligand/palladium ratio in asymmetric catalysis with P,N ligands [42]. A L/Pd ratio superior to 1 can be detrimental to the ee, probably because of the presence of reactive intermediates where the Pd-allyl moiety is coordinated by the phosphorus atoms of two ligands with dangling nitrogen atoms. To avoid this drawback, we ran some catalytic tests on substrates **16a** and **16b** using a default of ligand **15b** (L/Pd = 0.8), but this did not alter the conversion or the ee. Addition of 1 mol% $AgBF_4$ as chloride scavenger was also attempted, in case the chloride ions present in solution would prevent the hemilabile imine functions to coordinate the metal. However, this led to a dramatic decrease of the reactivity without any improvement of the ee.

4. Conclusion

The chiral P,N and N,N ligands with a rigid xanthene backbone have been synthesized; they display a marked specificity towards the chelate coordination of some metal ions and not to others. Our ligands are not well adapted to the coordination of palladium (II), leading only to mixtures. In Pd-catalyzed allylic alkylation, the enantioselectivities obtained are unfortunately lower than those obtained with Duxantphos [4,5]. We note that in general the iminophosphine derived from the sterically encumbered fenchone is slightly more selective than the one derived from camphor. Incidentally, this steric congestion is also the cause of a dynamic coexistence in solution of both configurations of the free ligand **15b**.

By contrast with palladium (II), silver (I) is coordinated by our ligands in a N,N or P,N bidentate fashion with a wide bite angle; the ligands obviously fit the usual geometries of this metal ion. Those are to our knowledge the first reported silver complexes with wide bite-angle chelate ligands. A P,O,N tridentate coordination mode is observed in a rhodium (III) complex with the iminophosphine **15a**. This difference with the silver complexes is related to the octahedral geometry of the Rh complex, and also to the hard character (according to the Pearson theory) of Rh^{III} compared to Ag^I (d^6 versus d^{10} electronic configuration). Besides, a feature characteristic of the bidentate mode by opposition with the tridentate mode is the fluxionality of the complexes, the latter displaying more rigidity than the former. Although the catalytic performances of the Ag and Rh complexes were poor, the Ag complexes may find application in other processes involving similar chiral species, like the resolution of racemic alkenes [43].

Acknowledgements

We thank Roland Graff, Jean-Daniel Sauer and Michelle Martigneaux for NMR analysis, and Vincent César for technical help with the determination of enantioselectivities. Financial support of the Centre National de la Recherche Scientifique, and a grant allowed to GM from the Ministère de l'Education Nationale are gratefully acknowledged.

Appendix A. Supplementary material

Crystallographic data for the structures reported on this paper have been deposited with the Cambridge Crystallographic Data Centre as supplementary publication nos.

CCDC-299536 (**18**), CCDC-299537 (**19**) and CCDC-299538 (**21**). Copies of the data can be obtained free of charge on application to the CCDC, 12 Union Road, Cambridge CB2 1EZ, UK [fax: (internat.) +44 1223 366 033; e-mail: deposit@ccdc.cam.ac.uk; Internet: http://www.ccdc.cam.ac.uk]. Supplementary data associated with this article can be found, in the online version, at doi:10.1016/j.poly.2006.06.006.

References

[1] (a) R. Noyori, Asymmetric Catalysis in Organic Synthesis, Wiley, New York, 1994;
(b) J. Seyden-Penne, Chiral Auxiliaries and Ligands in Asymmetric Synthesis, Wiley, New York, 1995;
(c) E.N. Jacobsen, A. Pfaltz, H. Yamamoto (Eds.), Comprehensive Asymmetric Catalysis I–III, Springer, Berlin, 1999;
(d) C. Bolm, J.A. Gladysz, Chem. Rev. 103 (2003) 2761;
(e) B.R. James, Coord. Chem. Rev. 248 (2004) 2129.

[2] (a) B.M. Trost, D.L. Van Vranken, Chem. Rev. 96 (1996) 395;
(b) P.W.N.M. van Leeuwen, P.C.J. Kamer, J.N.H. Reek, P. Dierkes, Chem. Rev. 100 (2000) 2741;
(c) P.C.J. Kamer, P.W.N.M. van Leeuwen, J.N.H. Reek, Acc. Chem. Res. 34 (2001) 895;
(d) Z. Freixa, P.W.N.M. van Leeuwen, Dalton Trans. (2003) 1890.

[3] (a) G. Helmchen, A. Pfaltz, Acc. Chem. Res. 33 (2000) 336;
(b) K.N. Gavrilov, A.I. Polosukhin, Russ. Chem. Rev. 69 (2000) 661;
(c) G. Chelucci, G. Orrù, G.A. Pinna, Tetrahedron 59 (2003) 9471;
(d) P.J. Guiry, C.P. Saunders, Adv. Synth. Catal. 346 (2004) 497.

[4] P. Dierkes, S. Ramdeehul, L. Barloy, A. De Cian, J. Fischer, P.C.J. Kamer, P.W.N.M. van Leeuwen, J.A. Osborn, Angew. Chem. Int. Ed. 37 (1998) 3116.

[5] G. Malaisé, S. Ramdeehul, J.A. Osborn, L. Barloy, N. Kyritsakas, R. Graff, Eur. J. Inorg. Chem. (2004) 3987.

[6] Z. Raza, S. Dakovic, V. Vinkovic, V. Sunjic, Croat. Chim. Acta 4 (1996) 1545.

[7] Y. Suzuki, Y. Ogata, K. Hiroi, Tetrahedron: Asymmetry 10 (1999) 1219.

[8] G. Malaisé, L. Barloy, J.A. Osborn, Tetrahedron Lett. 42 (2001) 7417.

[9] J. Suffert, J. Org. Chem. 54 (1989) 509.

[10] P.R. Auburn, P.B. Mackenzie, B. Bosnich, J. Am. Chem. Soc. 107 (1985) 2033.

[11] J.C. McKew, M.J. Kurth, J. Org. Chem. 58 (1993) 4589.

[12] A. Heumann, B. Åkermark, S. Hansson, T. Rein, Org. Synth. Coll. VIII (1993) 137.

[13] F.R. Hartley, S.R. Jones, J. Organomet. Chem. 66 (1974) 465.

[14] O. Renn, H. Rüegger, L.M. Venanzi, J. Gallus, V. Gramlich, A. Martelletti, Inorg. Chim. Acta 240 (1995) 575.

[15] G. Giordano, R.H. Crabtree, Inorg. Synth. 28 (1990) 88.

[16] R.M. Silverstein, F.X. Webster, Spectrometric Identification of Organic Compounds, sixth ed., Wiley, New-York, 1998.

[17] (a) J.O. Edwards, G.C. Morrison, V.F. Ross, J.W. Schultz, J. Am. Chem. Soc. 77 (1955) 266;
(b) P.L. Dedert, J.S. Thompson, J.A. Ibers, T.J. Marks, Inorg. Chem. 21 (1982) 969;
(c) N.E. Dixon, G.A. Lawrance, P.A. Lay, A.M. Sargeson, Inorg. Chem. 23 (1984) 2940.

[18] Y.M. Dunayevskiy, P. Vouros, E.A. Wintner, G.W. Shipps, T. Carell, J. Rebek Jr., Proc. Natl. Acad. Sci. USA 93 (1996) 6152.

[19] P. von Matt, A. Pfaltz, Angew. Chem., Int. Ed. Engl. 32 (1993) 566.

[20] P.A. Evans, J.D. Nelson, J. Am. Chem. Soc. 120 (1998) 5581.

[21] P. Sennhenn, B. Gabler, G. Helmchen, Tetrahedron Lett. 35 (1994) 8595.

[22] A. Yanagisawa, H. Kameyama, Y. Nakatsuka, K. Asakawa, Y. Matsumoto, H. Yamamoto, Angew. Chem. Int. Ed. 38 (1999) 3701.

[23] OpenMoleN, Interactive Structure Solution, Nonius B.V., Delft, The Netherlands, 1997.

[24] D.T. Cromer, J.T. Waber, International Tables for X-ray Crystallography, vol. IV, The Kynoch Press, Birmingham, 1974 (a) Table 2.2b; (b) Table 2.3.1.

[25] H. Weingarten, J.P. Chupp, W.A. White, J. Org. Chem. 32 (1967) 3246.

[26] Z. Aizenshtat, E. Klein, H. Weiler-Feilchenfeld, E.D. Bergmann, Isr. J. Chem. 10 (1972) 753.

[27] L.A. van der Veen, P.K. Keeven, P.C.J. Kamer, P.W.N.M. van Leeuwen, Chem. Commun. (2000) 333.

[28] K. Rissanen, K. Lahia, J. Korvola, E. Kolehmainen, Acta Chem. Scand. 45 (1991) 751.

[29] H.-O. Kanilowski, H. Kessler, in: N.L. Allinger, E.L. Eliel (Eds.), Topics in Stereochemistry, vol. 7, Wiley, New York, 1973, pp. 296–374.

[30] L.A. van der Veen, P.K. Keeven, P.C.J. Kamer, P.W.N.M. van Leeuwen, J. Chem. Soc., Dalton Trans. (2000) 2105.

[31] (a) F.A. Cotton, G. Wilkinson, Advanced Inorganic Chemistry, Wiley, New York, 1988, p. 941;
(b) F.A. Cotton, G. Wilkinson, Advanced Inorganic Chemistry, Wiley, New York, 1988, p. 908.

[32] A.G. Orpen, L. Brammer, F.H. Allen, O. Kennard, D.G. Watson, R. Taylor, J. Chem. Soc., Dalton Trans. (1989) S1.

[33] (a) M. Konrad, F. Meyer, M. Büchner, K. Heinze, L. Zsolnai, Chem. Ber./Recueil 130 (1997) 95;
(b) D.I. Arnold, F.A. Cotton, J.H. Matonic, C.A. Murillo, Polyhedron 16 (1997) 1837.

[34] (a) M.I. Bruce, J.D. Walsh, B.W. Skelton, A.H. White, J. Chem. Soc., Dalton Trans. (1981) 956;
(b) A. Codina, O. Crespo, E.J. Fernández, P.G. Jones, A. Laguna, J.M. López-de-Luzuriaga, M.E. Olmos, Inorg. Chim. Acta 347 (2003) 9.

[35] M. Camalli, F. Caruso, Inorg. Chim. Acta 127 (1987) 209.

[36] L. Lettko, J.S. Wood, M.D. Rausch, Inorg. Chim. Acta 308 (2000) 37.

[37] P. Marcazzan, C. Abu-Gnim, K.N. Seneviratne, B.R. James, Inorg. Chem. 43 (2004) 4820.

[38] (a) E.M. Vogl, J. Bruckmann, M. Kessler, K. Krüger, M.W. Haenel, Chem. Ber./Recueil 130 (1997) 1315;
(b) A. Sandee, L. van der Veen, J.N.H. Reek, P.C.J. Kamer, M. Lutz, A.L. Spek, P.W.N.M. van Leeuwen, Angew. Chem. Int. Ed. 38 (1999) 3231;
(c) P. Nieczypor, P.W.N.M. van Leeuwen, J.C. Mol, M. Lutz, A.L. Spek, J. Organomet. Chem. 625 (2001) 58;
(d) M.A. Zuideveld, B.H.G. Swennenhuis, M.D.K. Boele, Y. Guari, G.P.F. van Strijdonck, J.N.H. Reek, P.C.J. Kamer, K. Goubitz, J. Fraanje, M. Lutz, A.L. Spek, P.W.N.M. van Leeuwen, J. Chem. Soc., Dalton Trans. (2002) 2308.

[39] T.G. Appleton, H.C. Clark, L.E. Manzer, Coord. Chem. Rev. 10 (1973) 335.

[40] H. Nishiyama, M. Kondo, T. Nakamura, K. Itoh, Organometallics 10 (1991) 500.

[41] I. Ojima, T. Kogure, M. Kumagai, J. Org. Chem. 42 (1977) 1671.

[42] A.M. Porte, J. Reibenspies, K. Burgess, J. Am. Chem. Soc. 120 (1998) 9180.

[43] M.A. Cucciolito, G. Flores, A. Vitagliano, Organometallics 23 (2004) 15.

addition to regulate smooth muscle relaxation, neurotransmission, and immune response alterations in NO production and metabolism. The NO participates in multiple pathological circumstances such as hypertension, cardiomyopathy, pulmonary disorders, arteriosclerosis and endotoxemia [4–6]. Three different heme-containing NO-synthases (NOS) encoded by different genes mediate a common reaction, which converts L-arginine and molecular oxygen to citrulline and NO. Nevertheless, while two NOS proteins are constitutive enzymes first characterized in neurons (nNOS or Type I NOS) and vascular endothelium (eNOS or Type III NOS) in macrophages and other cell types the NO generation occurs through a normally absent inducible (iNOS or Type II NOS) isoform [4–6]. Under normal physiological conditions the widely distributed nNOS and eNOS isoforms release low levels of NO required for neural transmission, regulation of the vascular tone and normal tissue homeostasis. In contrast, the expression of the iNOS enzyme in macrophages and other cell types exposed to bacterial lipopolysaccharide (LPS), interferon-γ (IFNγ) and other agents generates large and sustained quantities of NO, a hallmark of such critical situations as septic shock [7], renal damage, adult respiratory distress syndrome, diabetes, neurodegeneration and chronic inflammatory disease [5]. In this context while NO donor drugs are currently used to compensate the reduced L-arginine–NO pathway of patients suffering from hypotension and angina, two different therapeutical strategies have been used to counteract the damaging effect of NO overproduction [7,8]. While the first approach is based on aminoacid and non-amino acid NOS inhibitors with pharmacologically useful isoform selectivity (particularly for iNOS), the second alternative method involves the use of other molecules endowed with the ability to scavenge or remove the excess of NO generated during the septic shock or chronic inflammatory diseases [7,8]. Despite the fact that some selective NOS inhibitors are useful in animal models of septic shock, treatment with these agents is frequently accompanied by adverse side effects such as pulmonary hypertension and mortality [8]. Therefore the search for NO scavenger molecules with demonstrated pharmacological activity represents a true alternative to the use of NOS inhibitors in a broad spectrum of disease models [4–6].

Among these scavenger molecules are some metal-dithiocarbamates. Recent reviews have focused on novel aspects of the chemistry of dithiocarbamates including topics as diverse as electrochemistry, photoelectron spectroscopy and analytical applications (e.g., for the determination of metals in foodstuff, water and environmental samples) and highlighted the potential value of these compounds as useful NO trapping agents [9].

In this respect kinetic studies of the interaction of iron dithiocarbamate complexes with NO have been reported and a mechanism for the reaction proposed [10–13]. Nevertheless, the studies of thermodynamic equilibria between iron dithiocarbamate complexes with NO in aqueous solution are still scarce.

Reported data [9,14,15] have shown the stability of the bonds between copper(II) dithiocarbamates and nitric oxide. We have carried out for first time the thermodynamic studies in aqueous solution [16,17]. In a previous work [16], we have published the first report on the stable coordination in aqueous solution of NO to copper(II)–bis(dithiocarbamates). Coordinated NO in complexes such as $CuL_2(NO)$ and $CuL_2(NO)_2$ is not removed by purging the solution with Ar or air. Only when the solution containing both complexes is heated up to 333 K, the $CuL_2(NO)_2$ complex is dissociated to $CuL_2(NO)$, which is stable. NO coordinates instantaneously to copper(II) in $CuL_2(NO)$ and then a slow electron transfer of the unpaired electron of the NO reduces the Cu(II) to Cu(I). The thermodynamic stability of the complexes $CuL_2(NO)$ and $CuL_2(NO)_2$ (L = (dihydroxyethyl)dithiocarbamate), in aqueous solution was confirmed in the following work [17]. In this last work [17], the theoretical studies by means of SPARTAN'02 programs were carried out also to take into account the possibility of the direct attack of NO on S atom of the dithiocarbamate. However, the isomer with S–NO bond was found to be by 12.29 kcal/mol less exotermic than the Cu–NO bonded isomer in complex $CuL_2(NO)$ thus confirming the experimental data in the first work [16].

This paper deals with the thermodynamic study of copper(II) dithiocarbamates complexes with NO. These studies allowed us to determine the stability constants of the complex species presented in our system. From the speciation diagrams we can deduce that copper(II) dithiocarbamates is more effective to trap NO.

In this work, we have prepared new copper(II) dithiocarbamates: bis(4-piperidonedithiocarbamato)copper(II) $[Cu(Pdtc)_2]_2$ (**1**), bis(piperidinedithiocarbamato)copper(II) $[Cu(Ppdtc)_2]_2$ (**2**) and bis[(2-piperidinecarboxy)dithiocarbamato]copper(II) $Cu(Ppidtc)_2$ (**3**), which have been characterized. The X-ray structure of **1** and **2** were determined. Complexes **1** and **2** are not soluble in water so their interaction with nitric oxide has been carried by theoretical methods. Complex **3** is soluble in water, which allowed us to study their interaction with nitric oxide in aqueous solution and analyse the chemical speciation of the complexes formed.

Furthermore, in this work we have also studied spectrophotometrically the interaction of the previously prepared but not characterized, bis[*N*-(dithiocarboxy)sarcosine]-copper(II), $Cu(Sdtc)_2$ (**4**) [18] and bis[(dicarboxymethyl)dithiocarbamato]copper(II), $Cu(Idadtc)_2$ (**5**) [19] with nitric oxide in aqueous solution. The analyses of the experimental data were carried out by means of the LETAGROP-SPEFO and HYPERQUAD programs [20–22] and the stability constants of the complexes CuL_2NO and $CuL_2(NO)_2$ were determined.

In addition and based on the above-mentioned results, we have also carried out studies on the biological effects of these dithiocarbamates. We report herein the ability of **3**, **4**, **5** and the previously studied [17] bis[(dihydroxyethyl)dithiocarbamato]copper(II), $Cu(Deadtc)_2$ (**6**) to trap NO released in vitro either by the model donor agent

sodium nitroprusside (NPS) or produced by murine macrophages J774 cells activated by the simultaneous treatment with lipopolysaccharide(LPS) and interferon IFNγ.

2. Experimental

2.1. General remarks

Elemental analyses for carbon, hydrogen, nitrogen and sulfur were performed on Fisons EA 1108 CHNS-O instrument. The IR spectra were recorded in the 4000–450 cm^{-1} region using KBr Pellets on Bruker IF S55 spectrophotometer. The electronic spectra were recorded on a Cary 50 Varian and Shimadzu UV-2101PC spectrophotometer (spectrophotometric studies). The electrospray ionization (ESI) mass spectral measurement of the complex was carried out on a Micromass QUATTRO LC spectrometer. A solution of the complex (0.606 mM) was prepared in dimethylsulfoxide–acetonitrile 50:50 v/v. The FAB-MS were recorded using VGAutoSpec Micromass spectrophotometer.

Magnetic susceptibility measurements on polycrystalline samples were carried out in the temperature range 5–300 K with Quantum Design SQUID magnetometer. Diamagnetic corrections of the constituent atoms were estimated from Pascal's constants. Experimental susceptibilities were also corrected for the temperature-independent paramagnetism and the magnetization of the sample holder.

2.2. Materials

4-Piperidone monohydrate hydrochloride, piperidine, 2-piperidinecarboxylic acid, sarcosine, iminodiacetic acid, *N*,*N*-dihydroxyethylamine, carbon disulfide and copper metal were purchased from Sigma–Aldrich. Cupric acetate monohydrate was purchased from Fluka. Cupric chloride dehydrate, ammonia solution, nitric acid and sodium hydroxide were obtained from Merck. Potassium hydroxide was obtained from Panreac.

For the preparation of all aqueous solution bidistilled water was used.

Lipopolysaccharide (LPS) was obtained from Boehringer. The NO donnor sodium nitroprusside (NPS), Interferon γ (IFNγ), L-glutamine, sodium nitrite, sulfanilamide and *N*-(1-naphtyl)ethylendiamine were purchased from Sigma–Aldrich (Barcelona, Spain). Fetal bovine serum (FBS), Dulbeco's modified Eagle's medium (DMEM), antibiotics (penicillin, streptomycin), phosphate-buffered saline (PBS) and other tissue culture reagents were obtained from Gibco (Grand Island, NY).

2.3. Preparation of the bis(dithiocarbamato)copper(II) complexes

2.3.1. $[Cu(Pdtc)_2]_2$ (**1**)

An ammonia solution (20%, 4 ml, 0.04 mol) of 4-piperidone monohydrate hydrochloride (3 g, 0.02 mol) was prepared. To this solution cooled down to 0 °C, 3 ml (0.05 mol) of carbon disulfide dissolves in 10 ml of ethanol was added dropwise under stirring. Then, an aqueous solution of 7 g of $Cu(NO_3)_2 \cdot 3H_2O$ (0.03 mol) was added and a brown precipitate appeared. After collection by filtration, the precipitate was washed with water and dried by repeater washing with ether. The complex was crystallized by slow evaporation at room temperature from acetonitrile as solvent. Yield: 60%.

2.3.2. $[Cu(Ppdtc)_2]_2$ (**2**)

To an aqueous solution of piperidine (7.3 mmol), potassium hydroxide (0.8 g) and carbon disulfide (0.4 ml) were added. A yellow solution appeared to which an aqueous solution of cupric acetate monohydrate was added. The resulting brown precipitate was filtered off and washed with water and dried with ether. Single crystals were obtained by slow evaporation at room temperature using a mixture of ethanol and ether (50:50) as solvent. Yield: 54%.

2.3.3. $Cu(Ppidtc)_2$, probably $[Cu(Ppidtc)_2]_2$ (**3**)

In an aqueous solution of 6.46 g (0.05 mol) of 2-piperidinecarboxylic acid and 5.6 g (0.1 mol) of potassium hydroxide (1:2), 3 ml (0.05 mol) of CS_2 was added dropwise. To this solution an aqueous solution of 6.25 g (0.025 mol) of $CuSO_4 \cdot 5H_2O$ (2:1) was added dropwise and a brown precipitate appeared. The resulting brown precipitate was filtered off and washed with water and dried in a dessicator. Yield: 60%.

Elemental analyses for $[Cu(Pdtc)_2]_2$, $[Cu(Ppdtc)_2]$ and $Cu(Ppidtc)_2$ complexes are presented in Table 1.

The compound $Cu(Sdtc)_2$ was reported by Sakay [18], $Cu(Idadtc)_2$ by Hulanicki and Minczewska [19] and $Cu(Deadtc)_2$ was synthesized according to Radha et al. [23].

2.4. X-ray structure determination

X-ray data for single crystal of **1** and **2** complexes were collected with a Bruker Smart CCD and Bruker Nonius KAPPA CCD diffractometers, respectively, using monochromatic Mo Kα radiation ($\lambda = 0.71073$ Å). For **1**, the data were processed with SAINT [24] and corrected for absorption using SADABS [25]. The structure was solved by direct methods and refined by full-matrix least-squares techniques against F^2 using SHELXTL-NT 5.10 [26]. Data

Table 1
Elemental analyses of the copper(II) complexes

Complex	Elemental analysis: found (calculated %)			
	C	H	N	S
$[Cu(Pdtc)_2]_2$	34.99 (34.99)	3.89 (3.89)	6.80 (7.24)	31.11 (30.11)
$[Cu(ppdtc)_2]_2$	37.62 (37.55)	5.33 (5.22)	7.75 (7.30)	33.83 (33.37)
$Cu(Ppidtc)_2$	40.24 (40.88)	4.62 (4.90)	5.94 (5.75)	27.15 (27.37)

$[Cu(Pdtc)_2]_2 = C_{24}H_{32}O_4N_4S_8Cu_2$.
$[Cu(ppdtc)_2]_2 = C_{24}H_{40}N_4S_8Cu_2$.
$Cu(Ppidtc)_2 = C_{14}H_{20}O_4N_2S_4Cu$.

reduction and cell parameters refinements for **2** were carried out with the programs COLLECT [27] and DENSO [28]. The structure was solved using SIR-97 [29] and refined with SHELXL-97 [30] using full-matrix least-squares with anisotropic thermal parameters for all non-H atoms. Hydrogen atoms were placed at idealized positions. The PLATON [31] package of programs was used for absorption corrections (MultiScan option) and for molecular graphics generation. Both crystals **1** and **2** are laminar dark brown.

For **1** and **2**, a summary of the key crystallographic information is given in Table 2. For **1**, selected bond distances and angles are listed in Table 3. For **2**, due to the high value of *R*, the bond distances and angles are shown in Table S1.

2.5. Molecular modeling

In order to obtain the most stable conformation, calculations of molecular modeling for different compounds were carried out using molecular mechanics force field MM^+, which is an extension of MM2 developed by Allinger and Burker [32]. The geometries were optimized using the UFF force field [33]. Both MM^+ and UFF provide qualitative accounts of molecular geometry conformation and strain energy. The MM^+ calculations were made with the HYPERCHEM program [34] and conformations of all compounds were generated using molecular dynamics for each one with the following options: starting 0 K, simulation temperature 300 K, heat time 0.1 ps, run time 1 ps. These conformations are optimized using a Fletcher–Reeves (conjugate gradient) protocol with the standard tight converge criterion (RMS gradient = 0.01 kcal $Å^{-1}$ in vacuo).

Molecular mechanics calculations were made also using the UFF force field implemented in GAUSSIAN-03 W package [35].

Table 2
Summary of the crystallographic results for the complexes **1** and **2**

Complex	$[Cu(Pdtc)_2]_2$ (**1**)	$[Cu(ppdtc)_2]_2$ (**2**)
Empirical formula	$C_{24}H_{32}Cu_2N_4O_4S_8$	$C_{24}H_{40}Cu_2N_4S_8$
Formula weight	824.20	768.26
Temperature (K)	297(2)	293(2)
Wavelength (Å)	0.71073	0.71069
Crystal system	triclinic	triclinic
Space group	$P\bar{1}$	$P\bar{1}$
a (Å)	8.658(3)	9.036(5)
b (Å)	10.319(3)	9.973(5)
c (Å)	11.064(4)	13.465(5)
α (°)	62.811(1)	91.630(5)
β (°)	77.880(7)	109.210(5)
γ (°)	65.953(7)	114.340(9)
V ($Å^3$)	802.6(5)	1024.8(9)
Z	1	1
D_{calc} (Mg m^{-3})	1.705	1.244
Absorption coefficient (mm^{-1})	1.884	1.461
F(000)	422	398
Crystal size (mm)	$0.36 \times 0.27 \times 0.26$	$0.15 \times 0.15 \times 0.20$
θ Range (°)	2.07–30.51	5.00–26.12
Limiting indices	$-7 \leqslant h \leqslant 12$, $-14 \leqslant k \leqslant 14$, $-15 \leqslant l \leqslant 15$	$-9 \leqslant h \leqslant 11$, $-12 \leqslant k \leqslant 12$, $-16 \leqslant k \leqslant 15$
Reflections collected/ unique (R_{int})	6532/4604 (0.0209)	8106/3913 (0.108)
Observed data [$I > 2.0\sigma(I)$]	3891	1672
Number of reflections and parameters	4606 and 191	3840 and 172
R, wR_2, *S*	0.0296, 0.0820, 1.02	0.1012, 0.2808, 0.85
Maximum and average shift/error	0.01/0.00	0.77/0.12
Minimum and maximum residual density (e $Å^{-3}$)	−0.54 and 1.03	−0.35 and 0.46

Table 3
Selected bond distances (Å) and bond angles (°) of $[Cu(Pdtc)_2]_2$

Bond lengths (Å)	
Cu(1)–S(4)	2.3067(9)
Cu(1)–S(3)	2.3080(8)
Cu(1)–S(5)	2.3352(8)
Cu(1)–S(2)	2.3732(9)
Cu(1)–S(2)#1	2.7036(10)
S(2)–C(1)	1.7347(17)
S(2)–Cu(1)#1	2.7036(10)
S(3)–C(7)	1.7177(18)
S(4)–C(1)	1.7108(18)
S(5)–C(7)	1.7168(18)
N(2)–C(7)	1.328(2)
N(2)–C(8)	1.463(2)
N(2)–C(9)	1.465(2)
N(1)–C(1)	1.327(2)
N(1)–C(2)	1.459(2)
N(1)–C(3)	1.464(2)
Bond angles (°)	
S(4)–Cu(1)–S(3)	153.82(3)
S(4)–Cu(1)–S(5)	99.51(2)
S(3)–Cu(1)–S(5)	76.52(2)
S(4)–Cu(1)–S(2)	76.260(19)
S(3)–Cu(1)–S(2)	100.963(18)
S(5)–Cu(1)–S(2)	165.37(2)
S(4)–Cu(1)–S(2)#1	99.42(2)
S(3)–Cu(1)–S(2)#1	106.72(3)
S(5)–Cu(1)–S(2)#1	102.36(3)
S(2)–Cu(1)–S(2)#1	92.20(2)
C(1)–S(2)–Cu(1)	83.43(6)
C(1)–S(2)–Cu(1)#1	102.04(6)
Cu(1)–S(2)–Cu(1)#1	87.80(2)
C(7)–S(3)–Cu(1)	85.01(6)
C(1)–S(4)–Cu(1)	86.02(6)
C(7)–S(5)–Cu(1)	84.18(6)
C(7)–N(2)–C(8)	122.67(16)
C(7)–N(2)–C(9)	123.62(15)
C(8)–N(2)–C(9)	113.55(15)
N(2)–C(7)–S(5)	123.48(13)
N(2)–C(7)–S(3)	122.84(13)
S(5)–C(7)–S(3)	113.68(10)
N(2)–C(9)–C(10)	111.71(18)
N(2)–C(8)–C(11)	109.45(18)
C(1)–N(1)–C(2)	124.71(15)
C(1)–N(1)–C(3)	122.53(15)
C(2)–N(1)–C(3)	112.57(14)
N(1)–C(1)–S(4)	123.27(13)
N(1)–C(1)–S(2)	122.70(13)
S(4)–C(1)–S(2)	114.02(9)
N(1)–C(3)–C(4)	108.96(16)
N(1)–C(2)–C(6)	109.94(16)

2.6. Equilibrium studies by electronic spectroscopy

The electronic spectra were recorded on a Shimadzu UV-2101 PC spectrophotometer.

A solution of copper(II) dithiocarbamate complexes and NO saturated aqueous solution were prepared by generating the gas from the reaction of metallic copper with 5 M nitric acid [2] using Schlenk techniques:

$$8HNO_3 + 3Cu \rightarrow 3Cu(NO_3)_2 + 4H_2O + 2NO$$

The gas was purified by passing it through five traps containing 50% NaOH solutions. The purified gas was bubbled in a Schlenk flask containing 20 ml of cold water. A thin Teflon hose was connected into the NO aqueous solution through the side arm of the flask. Teflon stopcocks were used to isolate each part of the Schlenk system when necessary. The whole system, tightly isolated from air, was previously deoxygenated by passing pure Ar for approximately 1 h [16,17]. Once the NO aqueous solution was obtained, the Schlenk flask was disconnected and then installed in a thermostated bath at 20 °C and the Teflon hose was connected to an Orion automatic microburet and purged with pure Ar. The concentrations of NO used for the calculations were made considering the reported concentration for saturated aqueous solution of NO (2.057 mM) at 20 °C [36]. The solutions of the bis(dithiocarbamato)copper(II) complexes **3**, **4** and **5**, respectively, were prepared in a 7.4 phosphate buffer solution (0.06 M). A number of 6–10 μl aliquots of the NO saturated aqueous solution thermostated at 20 °C were administered to the air tight flask containing the Cu(II) complex solution (**3**, **4** and **5**, respectively) using an Orion automatic microburette. The temperature of the cell was held at 20 °C with a Peltier controller system attached to the spectrophotometer. The same apparatus was used to administer the studied solution to the optical cell.

For a solution of $Cu(Ppidtc)_2$ (**3**) (48.5 μM) the electronic spectral data (19 absorbance values for each addition of NO solution within the range 420–476 nm at 20 °C) were processed using HYPERQUAD software [22].

For a solution of $Cu(Sdtc)_2$ (**4**) (76 μM) the electronic spectral data (16th absorbance values for each addition of NO solution within the range 348–436 nm at 20 °C) were processed using SPEFO version [20] of LETAGROP software [21].

For a solution of $Cu(Idadtc)_2$ (**5**) (52.1 μM) the electronic spectral data (33 absorbance values for each addition of NO solution within the range 348–436 nm at 20 °C) were processed using HYPERQUAD software [22].

2.7. Effect of dithiocarbamates on NO release in cell-free experiments

Stock solutions (30 mM) of copper(II) dithiocarbamates **3**, **4**, **5** and **6**, respectively, were prepared in PBS (pH 7.4) and sterilized using 0.2 μm Millipore filters. Sterile solutions of the NO donor SNP were prepared in DMEM (final concentration 30 mM) just before use. Aliquots of the SNP stock solution were dispensed into 96 well tissue culture plates containing either DMEM alone (to yield final concentrations of the donor in the range of 30–100 μM) or medium supplemented with copper(II) dithiocarbamates at final concentrations 10 μM. Culture plates containing the appropriate concentrations of SNP alone or in combination with copper(II) dithiocarbamates were placed (24 h) in a Haereus tissue culture incubator (5% CO_2 and 37 °C) and thereafter media were aspirated and used for nitrite determination (see below).

2.8. Effect of copper(II) dithiocarbamates on NO released by J774 murine macrophages stimulated with LPS and IFNγ

The J774 murine macrophage cell line characterized by the ability to express iNOS and generate large quantities of NO in response to the simultaneous stimulation with LPS and IFNγ [7,8,37,38] was donated by Dr. M. Fresno (CBM, Universidad Autónoma de Madrid). Cells were grown in 100 mm Falcon's tissue culture plates containing DMEM/10% fetal bovine serum (FBS) supplemented with L-glutamine (2 mM) and antibiotics (100 U/ml penicillin and 100 μg/ml streptomycin) and maintained at 37 °C in a 5% CO_2 incubator (Haerus). Cells from confluent cultures (65–75%) were detached form the plates, resuspended in serum depleted medium (DMEM/2% FBS) and aliquots (200 μl) containing equal number of cells ($\sim 25 \times 10^4$ cells) inoculated into 96-well tissue culture plates (Falcon). Cells were left untreated (controls) or stimulated (24 h) with a combination of LPS and IFNγ (final concentration 1 μg/ml and 100 U/ml, respectively) alone or in the presence of the indicated concentrations of the different copper(II) dithiocarbamates. After this period of time media were aspirated and used to measure total nitrite levels (see below) and the lack of cell toxicity determined by previously described methods (Mosman) [39].

2.9. Nitrite determinations

The ability of copper(II) dithiocarbamates to trap NO generated by chemical donors (NPS) or cytomix (LPS + IFNγ)-stimulated macrophages was evaluated by changes in the concentration of stable NO metabolites (nitrite + nitrate) in culture medium as determined by the Griess reaction [40]. Suitable aliquots (100 μl) of culture medium were mixed with an equal volume of Griess reagent (a 1:1 mixture of 1% sulfanilamide and 0.1% naphthylethylenediamine dihydrochloride in 2.5% H_3PO_4), incubated for 10 min at room temperature [40] and concentrations were determined at 550 nm in an EL-312 Microplate reader (Biotek Instruments, Winooski, VT). Sterile-filtered standard solutions of sodium nitrite (0–50 μM) were freshly prepared in culture medium and incubated in parallel with each experiment and comparable results were obtained using a nitrate reductase assay kit provided by Alexis Biochemicals (Laufelfingen, Switzerland).

2.10. Statistical methods

Results for nitrite concentrations are expressed as the means ± SEM from triplicate or quadruplicate cultures, and each experiment was repeated at least three times. The minimal effective doses and ED50 were determined with a software program based on a four-parameter logistic equation as previously described [40]. Statistical differences were examined using ANOVA and, as indicated, Student's *t*-test for comparison of the means. $P < 0.5$ was considered significant.

3. Results and discussion

3.1. Description of the structures of the complexes *1* and *2*

The crystallographic data of the complexes **1** and **2** are given in Table 2.

The structure of **1** is built up by centre-symmetric dimeric entities. Fig. 1 shows a perspective view of the dimeric unit showing the atomic numbering scheme of the complex.

For this compound, the distances Cu–S and Cu–S′ are 2.373 Å and 2.704 Å, respectively, in good agreement with the values found for the dimeric dithiocarbamates: $[CuS_2CN(Et)_2]_2$ [41] (Cu–S and Cu–S′: 2.327 Å and 2.844 Å, respectively) and $[CuS_2CN(CH_2Et)_2]_2$ [41] (Cu–S and Cu–S′: 2.322 Å and 2.740 Å, respectively).

The coordination sphere of copper(II) ions is described as a distorted square-pyramid. The basal coordination positions are occupied by four sulfur atoms belonging to two dithiocarbamate ligands.

Each bridging sulfur atom simultaneously occupies an equatorial coordination site on one copper(II) ion and an apical site on the other copper(II).

The axial Cu–S bond distance (2.7036(10) Å) is longer than the equatorial Cu–S ones. The Cu–S(2) bond length in [(2.373(10) Å] are longer in the Cu–S equatorial bond lengths because S(2) is a bridging atom. The bond angles S(2)–Cu(1)–S(4), S(3)–Cu(1)–S(5), 76.26(2)°, 76.52(2)°, respectively, are nearly the same.

The bridging network S(2)–Cu(1)–S(2)a is strictly planar owing to the inversion centre. These results are in good agreement with earlier determinations [41–43].

The overall geometry of the complex **2** (Fig. 2) is similar to complex **1**. However, because of the high values of *R* ($R = 0.1012$), the bond parameters (Table S1) are not accurate and should be treated with caution.

3.2. IR spectra

The most significant bands for the **1**, **2** and **3** complexes are given in Table 4. The bands in the range 1480–1510 cm^{-1} are attributed to the ν(C–N) (partial double bond) stretching vibration [17,41,44]. This position corresponds to a partial double bond character, and is recorded in the range previously reported for similar compounds [45–47]. The band in the range 940–1050 cm^{-1}, belonging to the ν(S–C) (partial double bond) stretching is considered indicative of dithiocarbamate acting as a bidentate ligand [44,48]. The band at 1588 cm^{-1} corresponds to antisymmetric carboxyl stretching frequencies of the non-complexed ionic COO^- in the ligand of the complex **3** [49]. The band at 1716 cm^{-1} in the complex **1** is assigned to

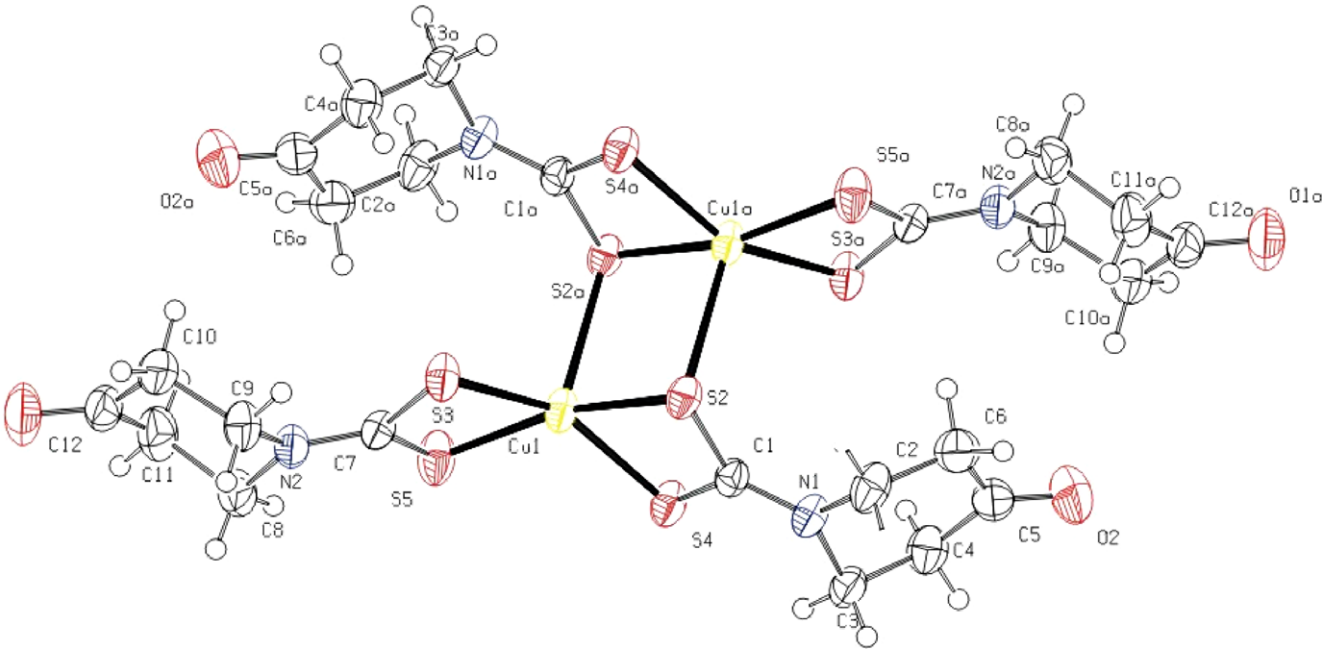

Fig. 1. Perspective view of **1** with thermal ellipsoids at the 50% probability level and showing the selective atom numbering scheme.

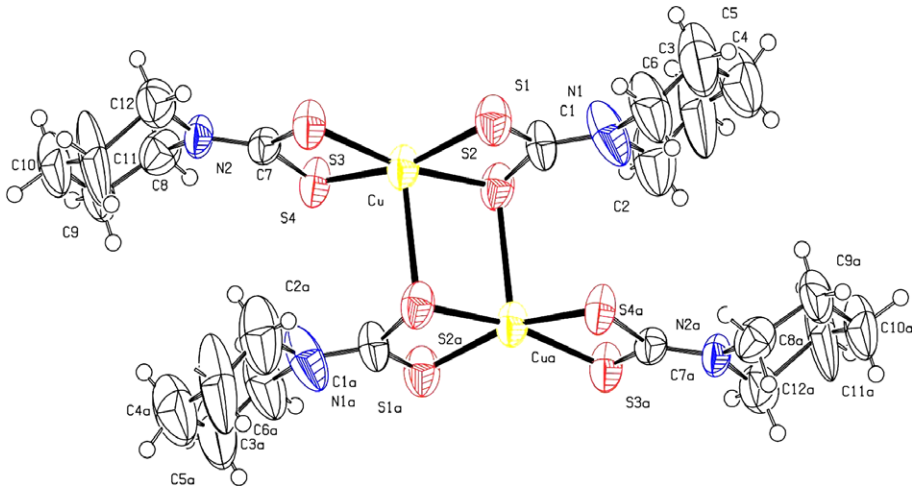

Fig. 2. Perspective view of **2** with thermal ellipsoids at the 50% probability level and showing the selective atom numbering scheme.

Table 4
Most significant IR bands (cm^{-1}) of $[Cu(Rdtc)_2]_2$

Compound	$[Cu(Pdtc)_2]_2$	$[Cu(ppdtc)_2]_2$	$Cu(Ppidtc)_2$
ν(C–N)	1508.84 s	1508.65 s	1474 s
ν(C–S)	1005.16 s[a]	1000.9 s[a]	970 m
ν(C=O)	1716.12 s		
$\nu(COO^-)$			1588 s
ν(OH)			3414 s

[a] Singlet.

C=O stretching vibration of the no complexed ketonic group $–CH_2–CO–CH_2–$ of the ligand [47,50].

3.3. Electronic spectra

The most significant bands of the copper(II) complexes **1** and **3** are presented in Table 5. For complex **2** in DMSO, the values are similar to complex **1**. The most intense band at 273 nm is probably a band of the ligand; the band at 438 nm is a $\sigma(S) \rightarrow Cu(II)$ ligand to metal charge transfer in a planar CuS_4 (CuS_5 in pyc geometry) chromophore, and the band at 630–650 nm (shoulder) is a d–d band [51–54], in agreement with a planar CuS_4 geometry (monomers) or pyc CuS_5 geometry (dimers).

3.4. Magnetic properties

The magnetic behaviour of complexes **1** and **3** is shown in Figs. S1 and S2 by means of a $\chi_M T$ versus T plot (χ_M being the molar magnetic susceptibility). At room temperature both compounds give a value for $\chi_M T$ that is slightly lower then expected for two non-interacting Cu(II) ions (0.9 $cm^3\,mol^{-1}\,K$), and upon cooling $\chi_M T$ continuously decreases also for both compounds. This behaviour is indicative of the occurrence of weak antiferromagnetic interactions in **1** and **3**. The pattern of the curve for both compounds is very similar, thus although the structure of **3** is not known in solid state it must be very similar to that of **1**. Other polymerizations also are possible: $[Cu(Et_2dtc)]_4$ is tetramer [55]. The structure of **1**, Fig. 1, consist of dinuclear copper(II) entities bridged by μ-S atoms. The antiferromagnetic coupling for these complexes is due to spin cancellation through the S bridge atoms [56]. However, we have not been able to fit the magnetic data to the numerical expression for copper(II) dinuclear complexes. May be some paramagnetic impurities or intermolecular interactions are present in the polycrystalline samples which were measured, that make the data to deviate from the ideal model.

Table 5
Electronic data of the complexes **1** and **3**

Complex	λ/nm ($\varepsilon/M^{-1}\,cm^{-1}$)			Solvent
1	273 (50.000)	438 (24.450)	650 (2.400)	DMSO
3	273 (505)	433 (184)	630 (13.4)	water

3.5. Mass spectrometry

Complex **1** was further characterized by electrospray ionization (ESI) mass spectrometry. The ESI spectrum of the monomeric complex $[Cu(Pdtc)_2]_2$ obtained at $\Delta V = 20$ V is presented in Fig. 3. The main peak observed at m/z 411.5 is corresponding to $[Cu(Pdtc)_2]^+$. The presence of three ions is not in good agreement with the isotropic distribution of the Cu: Cu^{63} (69.2%); Cu^{65} (30.8%) [57]. Probably the other two peaks can be assigned to protonated ions, Table 6.

This result implies that the dimer in dimethylsulfoxide–acetonitrile solution is broken showing only the monomeric complex.

3.6. Molecular modeling

In Ref. [17], we have studied the interaction between NO and the bis[1-(2-hydroxyethyl)piperazinedithiocarbamato]-copper(II) by means of molecular mechanics and semi-empirical methods.

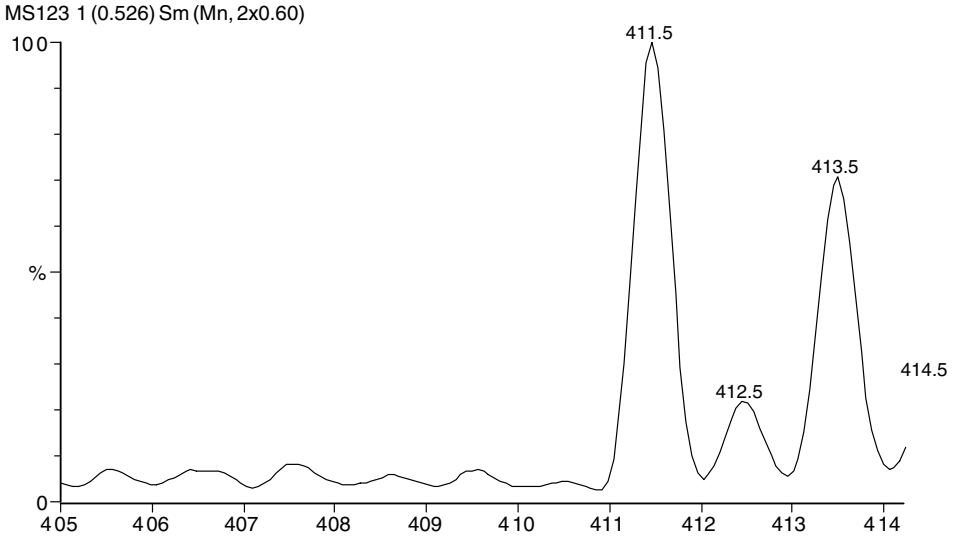

Fig. 3. ESI mass spectra of the monomeric complex of $[Cu(Pdtc)_2]_2$ obtained in 50:50 acetonitrile–dimethylsulfoxide; $\Delta V = 20$ V.

Table 6
Principal ions in the ESI spectra of the monomeric complex of $[Cu(Pdtc)_2]_2$

Complex	*m*/*z*	Relative abundance (%)	Assignment
$Cu(Pdtc)_2$	411.5	100	$[Cu(Pdtc)_2]^+$
	412.5	20	$[Cu(Pdtc)_2 + H]^{2+}$
	413.5	70	$[Cu(Pdtc)_2 + 2H]^{3+}$

Analogously, in this work we have studied in gaseous phase the interaction between NO and the monomeric complex $Cu(Pdtc)_2$, **M**, and the dimeric complex $[Cu(Pdtc)_2]_2$, **D**. Figs. 4 and 5 show the most stable confor-

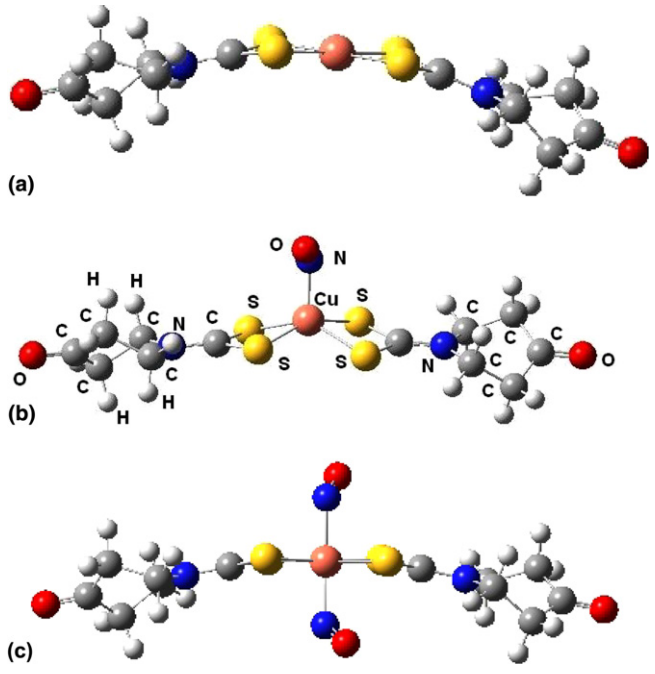

Fig. 4. Most stable conformations in gaseous phase for: (a) monomer **M**; (b) **M**(NO); and (c) **M**$(NO)_2$.

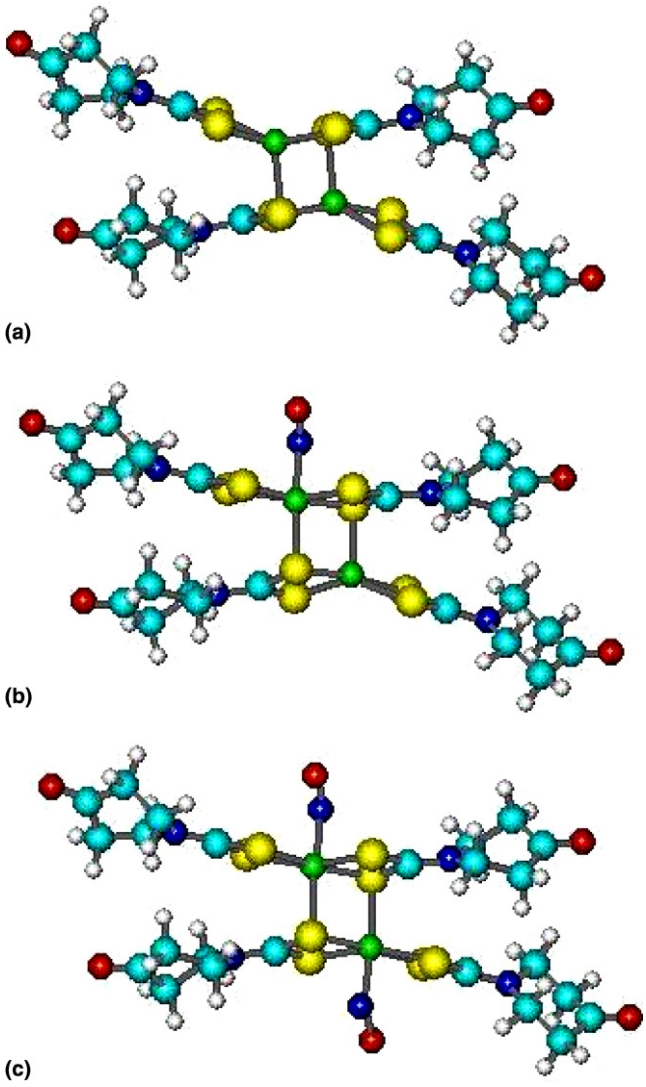

Fig. 5. Most stable conformations in gaseous phase for: (a) dimeric **D**; (b) **D**(NO); and (c) **D**$(NO)_2$.

mations in gaseous phase for the compounds **M** (4a), **M**(NO) (4b), **M**$(NO)_2$ (4c), **D** (5a), **D**(NO) (5b) and **D**$(NO)_2$ (5c), respectively, obtained by theoretical calculations. The most symmetrical conformations correspond to **M**$(NO)_2$ and **D**$(NO)_2$. It was found that in the dithiocarbamate complexes, the $[CuS_4]$ groups become more planar and they are coordinated to two molecules of nitric oxide.

A possibility of direct NO attack on S atom of the dithiocarbamate was also taken into account. For the monomeric complex **M**, the isomer with S–NO bond was found to be 12.29 kcal/mol less exothermic than the Cu–NO bond isomer M(NO). Also the complexes with S–NO bond are more distorted than the complexes containing Cu–NO bond. It was found in all cases, both for monomer and dimer that the bond angle Cu–NO is 120°, which indirectly shows that the charge transfer is metal to ligand which agree well with the previous experimental information [16].

3.7. Solution studies

A $Cu(Sdtc)_2$ (**4**) solution presents a maximum at 432 nm ($\log\varepsilon = 3.92$). With addition of a NO solution the maximum decreased in intensity and blue-shifted to 425 nm. At the same time a new band appears at 356 nm. Both bands correspond to LMCT transitions between the copper ion and dithiocarbamate and NO, respectively [16,51]. An isosbestic point is observed at 388 nm (Fig. 6), indicating that the reversible process is taking place. The blue shift variation of the absorbance from 432 nm (ratio Cu:NO = 1:0) to 425 nm (ratio Cu:NO = 1:2, curve 3, Fig. 6) and the red shift of the band at 356–360 nm (curve 3, Fig. 6) give two inflection points at 1:1 and 1:2 Cu:NO molar ratios, 388 and 390 nm, with formation of the complexes $Cu(Sdtc)_2(NO)$ and $Cu(Sdtc)_2(NO)_2$, respectively (Fig. 7). The experimental data were analysed by means of the SPEFO version [20] of the LETAGROP program [21]. The calculations indicate that **4** reacts stepwise with two moles of NO (Scheme 1, Table 7). The values of the stability constants and the species distribution diagram (Fig. 7) indicate that the complex corresponding to equilibrium (1) is thermodynamically more stable than the complex corresponding to equilibrium (2). The diagram also indicates that the complex 1:2 is formed from complex 1:1 (Fig. 7, Scheme 1 and Table 7). With excess of nitric oxide the complex $Cu(Sdtc)_2(NO)_2$ forms quantitatively (Fig. 7). The dithiocarbamate complex $Cu(Sdtc)_2$ is a versatile agent to capture the NO under physiological conditions (pH 7.4).

A $Cu(Ppidtc)_2$ (**3**) solution presents a maximum at 432 nm ($\log\varepsilon = 4.01$). With addition of a NO solution the maximum decreased in intensity and it is blue-shifted. At the same time a new band appears at 356 nm. An isosbestic point is observed at ≈382 nm, indicating that a reversible process is taking place. The experimental data were analysed using the HYPERQUAD program [22]. The stability constants for $Cu(Ppidtc)_2NO$ and $Cu(Ppidtc)_2(NO)_2$ complexes

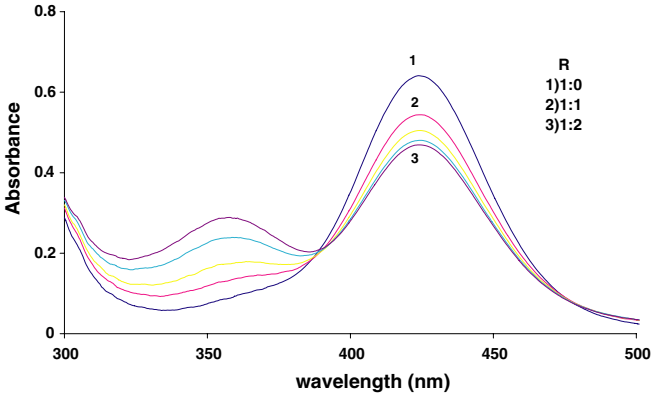

Fig. 6. UV spectra at 293 K for $Cu(Sdtc)_2$ (76 μM) with different additions of NO saturated aqueous solution: (1) $Cu(Sdtc)_2$:NO = 1:0. (2) $Cu(Sdtc)_2$:NO = 1:1. (3) $Cu(Sdtc)_2$:NO = 1:2.

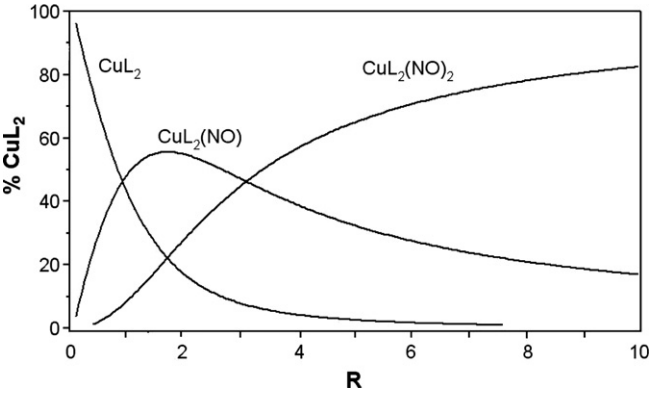

Fig. 7. Species distribution for **3**–NO system at pH 7.4 and 293 K. Concentration of complex **3**: 76 μM.

$$Cu(Dtc)_2 + NO \overset{K_1}{\rightleftharpoons} Cu(Dtc)_2NO \quad A$$

$$Cu(Dtc)_2NO + NO \overset{K_2}{\rightleftharpoons} Cu(Dtc)_2(NO)_2 \quad B$$

Scheme 1. A: equilibrium (1); B: equilibrium (2).

Table 7
Stability constants of the $Cu(Dtc)_2NO$ and $Cu(Dtc)_2(NO)_2$ complexes

Complex	$\log K_1$	$\log K_2$	Reference
$Cu(Ppidtc)_2$	3.16(1)	2.61(1)	this work
$Cu(Sdtc)_2$	4.7(5)	3.9(6)	this work
$Cu(Idadtc)_2$	8.5(1)	2.4(1)	this work
$Cu(Deadtc)_2$	10.3(1)	2.2(1)	[17]

are given in Table 7. That values for $\log K_1$ indicate that the complex $Cu(Ppidtc)_2NO_2$ is weaker than the $Cu(Sdtc)_2NO$ complex.

Complex **5** presents a maximum at 432 nm ($\log\varepsilon = 4.09$) which decreased in intensity with the addition of a NO solution and is blue-shifted (curve 3, Fig. 8). This decrease was accompanied by the simultaneous appearance of a new

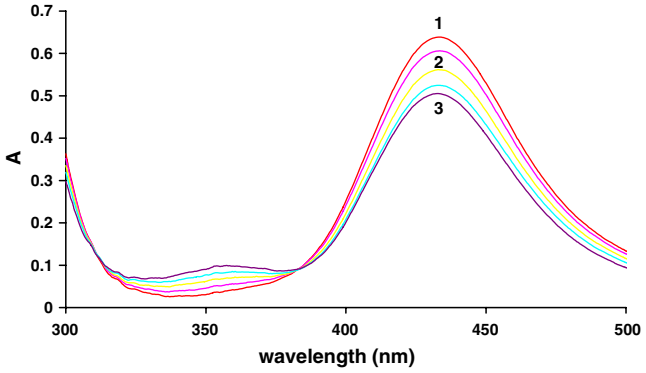

Fig. 8. Experimental UV–Vis spectrophotometric data for the Cu(Idadtc)$_2$/NO system at pH 7.4 and 20 °C. Concentration of the Cu(Idadtc)$_2$ complex (5.21 μM) and different ratios R = Cu(Idadtc)$_2$:NO (1), Cu(Idadtc)$_2$:NO 1:0; (2), Cu(Idadtc)$_2$:NO 1:1 (3); and Cu(Idadtc)$_2$:NO 1:2.

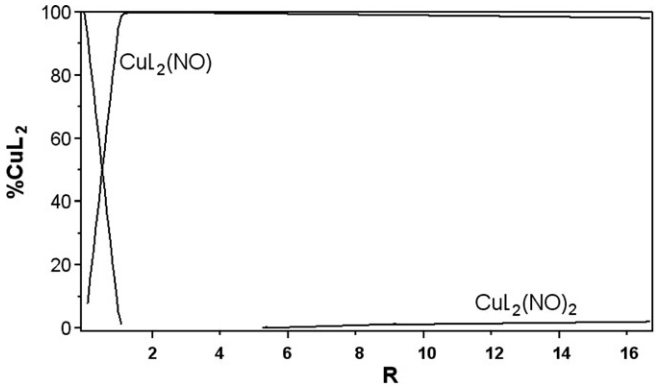

Fig. 9. Species distribution diagram for Cu(Idadtc)$_2$–NO system at pH 7.4 and 20 °C. Concentration of the Cu(Idadtc)$_2$ complex: 5.21 μM.

band at 352 nm which corresponds to a charge transfer transition between the copper ion of the dithiocarbamate complex and NO [16]. An isosbestic point is observed at ≈383 nm, batochromically shifted, by successive additions of NO to the Cu(Idadtc)$_2$ solution indicating that reversible processes are taking place. The experimental data analysed using the HYPERQUAD program [22] indicated that **5** reacts stepwise with two moles of NO (Scheme 1 and Table 7). Calculation of the stability constants for Cu(Idadtc)$_2$NO and Cu(Idadtc)$_2$(NO)$_2$ complexes allowed to obtain the values for logK_1, complex 1:1, equilibrium A in Scheme

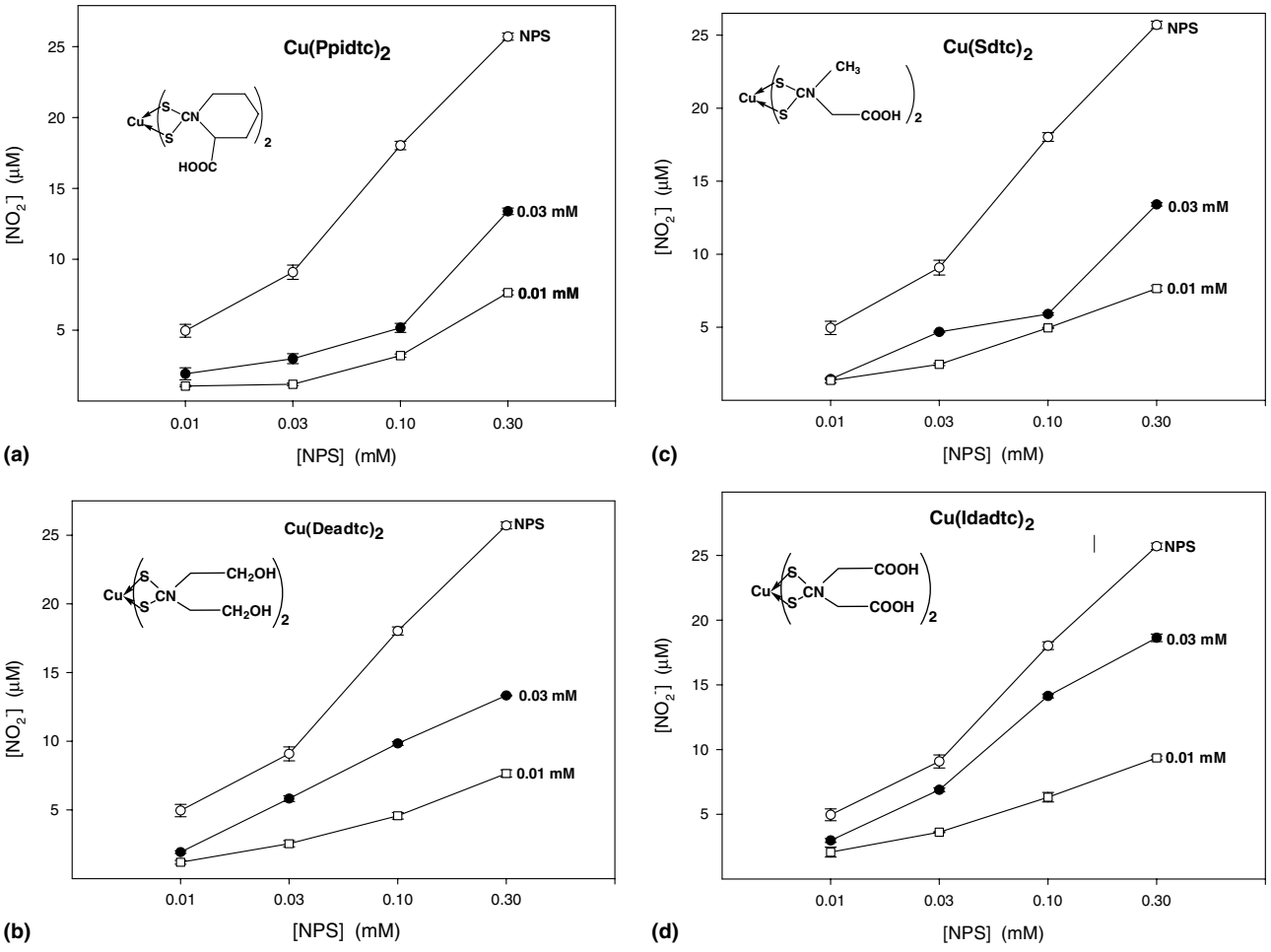

Fig. 10. Effect of copper(II) dithiocarbamates (at final concentrations of 10 and 30 μM) on nitrite levels present in culture media containing the NO-donnor NPS (final concentration). Each data point represents nitrite concentrations (means ± SEM) three different experiments using triplicate or quadruplicate wells per data point.

1, and $\log K_2$, complex 1:2, equilibrium B in Scheme 1 indicating that the complex 1:1 is much stronger than the complex 1:2. These data, together with the species distribution diagram (Fig. 9) indicate a stepwise process in which formation of the 1:2 complex requires that the complex 1:1 is practically formed in accordance with previous studies of our laboratory [16,17]. Similar behaviour with NO has the $Cu(Deadtc)_2$ complexes, with a higher value for $\log K_1$ [17] (Table 7).

3.8. The copper(II) dithiocarbamates reduce nitrite concentrations derived from the nitric oxide producing agent NPS

Since the complexes **3**, **4**, **5** (this work) and **6** [17] trap NO in aqueous solution, in the next set of experiments we explored their ability to trap NO generated by increasing concentrations (10–300 μM) of the specific NO-donor compound NPS (Fig. 10). Total nitrite levels were extremely low in wells containing DMEM alone, augmented in a concentration-dependent manner in cultures supplemented with NPS and significantly decreased in the presence of two different doses (10 μM or 30 μM) of the different copper(II) dithiocarbamates.

3.9. Effect of the copper(II) dithiocarbamates on the concentration of NO generated by cultured macrophages stimulated with LPS and IFNγ

Since the above-mentioned data demonstrate that copper(II) dithiocarbamate derivatives trap NO under cell-free conditions we performed additional experiments to test whether a similar activity was exerted in cytomix (LPS + IFNγ)-stimulated murine macrophages (Fig. 11). As expected nitrite concentrations were negligible in unstimulated cells (see control in Fig. 11) or cultures exposed only to the highest dose (300 μM) of copper(II) dithiocarbamate derivatives. In contrast, activation of

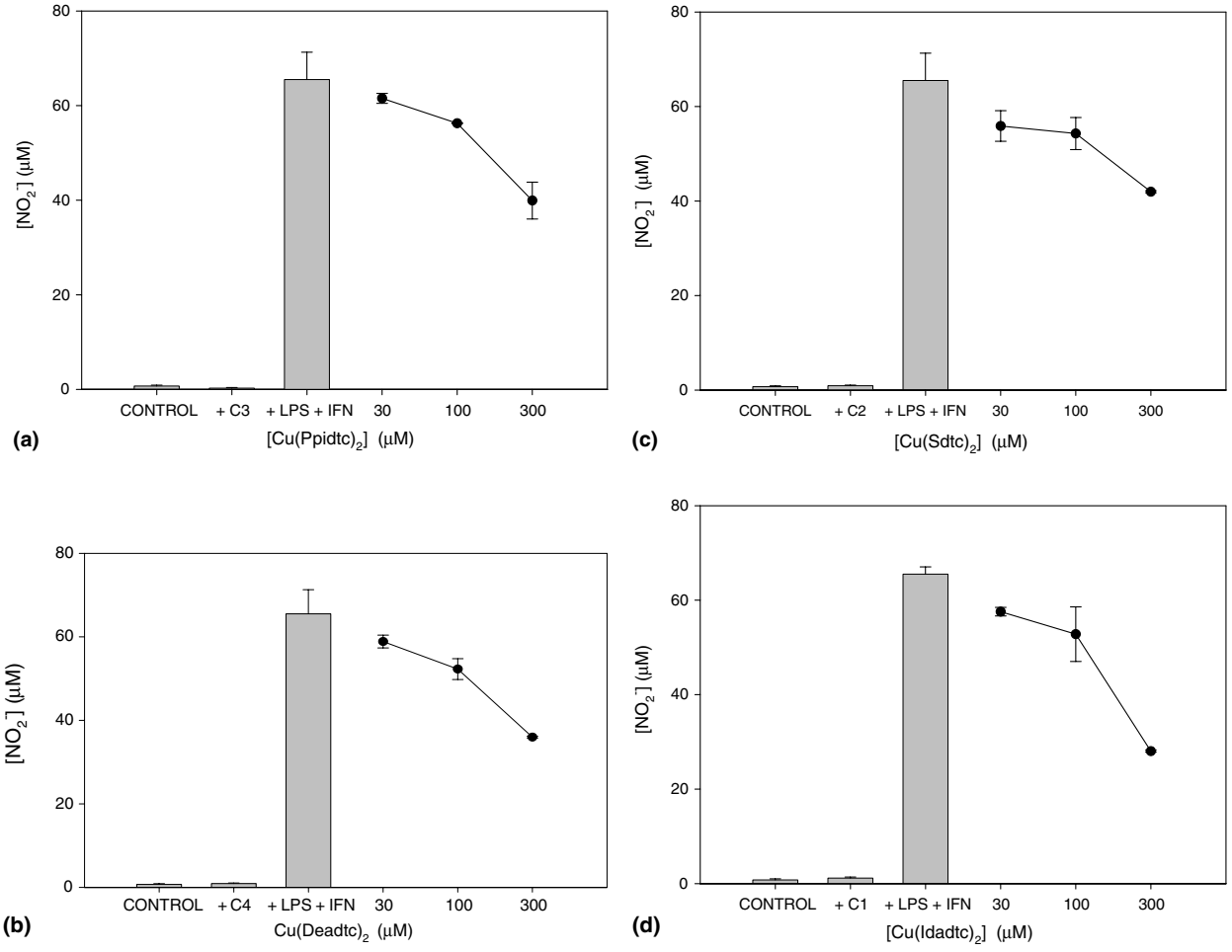

Fig. 11. Effect of increasing concentrations of copper(II) dithiocarbamates on NO production in control or cytomix (LPS and IFNγ) stimulated J774 murine macrophages. Macrophages were cultured (24 h) in the absence or presence of medium alone (controls), with citomix (LPS + IFNγ) alone or in the presence of three different concentrations (30–300 μM) of each Cu(II)dithiocarbamate. Each data point represents nitrite concentrations (means ± SEM) of three different experiments using triplicate or quadruplicate wells per data point. Additional groups of cells were treated with the highest dose (300 μM) of copper(II) dithiocarbamates alone.

macrophage iNOS by the simultaneous treatment (24 h) with cytomix (LPS and IFNγ) dramatically increased NO_2^- concentration (up to 65 μM) being these reaction dose-dependently reduced by the addition of cultures significantly reduced in the presence of graded doses of these copper(II) dithiocarbamates.

When considered together the data derived from experiments using chemical donors (SNP) or cytomix (LPS + IFNγ)-activated macrophages demonstrate that the different copper(II) dithiocarbamates studied are effective NO scavengers, which rapidly react with NO and prevent the formation of its stable oxidation product (NO_2^-) in aqueous solution.

This results confirm previous studies with Cu(ProDTC)$_2 \cdot 3H_2O$ [16].

4. Conclusions

Single crystals of **1** and **2** were prepared for the first time and characterized by X-ray diffraction. They are dimeric. For complex **2**, selected bond distance and bond angles are given in Supplementary material because of the high value of *R* (Table S1).

Complex **3** was also prepared for the first time.

The stability constants and speciation diagrams in aqueous solution of the Cu(Deadtc)$_2$–NO [17] and Cu(Idadtc)$_2$–NO systems indicate that these copper(II) dithiocarbamates have a great ability to trap NO under in physiologic conditions. The formation of the complexes $CuL_2(NO)$ and $CuL_2(NO)_2$ is successive.

The results for the Cu(Sdtc)–NO and Cu(Ppidtc)$_2$–NO systems indicate that the formation of the complexes $CuL_2(NO)$ and $CuL_2(NO)_2$ is simultaneous and therefore this dithiocarbamate copper(II) complex is more versatile to uptake and release NO in physiological conditions.

The species distribution diagrams in aqueous solution at physiological pH (7.4) also indicate that these copper(II) dithiocarbamates help to know the chemistry to regulate the NO in the tissues and to control its biological function.

Since NO yields stable oxidation products (mainly NO_2^- and lower levels of NO_3^-) in aqueous solution we also demonstrate that the copper(II) dithiocarbamates studied are able to decrease total nitrite concentrations produced by the model NO-donor NPS. Of further interest a similar decrease in the total nitrite concentrations was observed when the copper(II) dithiocarbamates were added to murine macrophages challenged with LPS and IFNγ to induce iNOS expression. These data support the potential application of copper(II) dithiocarbamates as therapeutic agents in animal models of septic shock. Verification of this possibility is currently under investigation in our laboratories.

5. Abbreviations

DMEM Dulbeco's modified eagle medium
IFNγ interferon gamma
iNOS inducible nitric oxide sinthase
LPS lypopolyssacaride
NOS nitric oxide sinthase
SNP sodium nitroprusside
PGE_2 prostaglandin type E_2
FBS fetal bovine serum

Acknowledgements

Agostinho Francisco Cachapa is very grateful to the Agencia Española de Cooperación Internacional (AECI) and University of La Laguna for a predoctoral fellowship at Departamento de Química Inorgánica, Universidad de La Laguna, Spain. Also thanks are due to the Departamento de Ciencias Experimentales, Universitat Jaume I, Spain where he carried out some of the experimental work of the present paper.

Financial support from MEC-Spain (research projects PM98-0148 and BQU2002-02794) is gratefully acknowledged.

We thank the Servicio General de Medidas Magneticas of La Laguna University for the magnetic measurements.

Appendix A. Supplementary material

Supplementary crystallographic data for complex **1** have been deposited with the CCDC No. 256287. These data can be obtained free of charge via www.ccdc.cam.ac.uk/data_request/cif, by e-mailing data_request@ccdc.cam.ac.uk, or by contacting The Cambridge Crystallographic Data Centre, 12, Union Road, Cambridge CB2 1EZ, UK (fax: +44 1223 336 033).

For complex **2**, Table S1 and supplementary crystallographic data (Tables S2–S10) are includes as Supplementary material in this paper.

Figs. S1 and S2 corresponding to the magnetic behaviour of **1** and **3** complexes are also included as Supplementary material. Supplementary data associated with this article can be found, in the online version, at doi:10.1016/j.poly.2006.06.008.

References

[1] J. LancasterJr. (Ed.), Nitric Oxide: Principles and Actions, Academic Press, New York, 1996.
[2] F.A. Cotton, G. Wilkinson, C.A. Murillo, M. Bochmann, Advanced Inorganic Chemistry, 6th ed., Wiley, New York, 1999, p. 325.
[3] G.M. Rosen, G. Tsai, S. Pou, Chem. Rev. 102 (2002) 191.
[4] P.C. Ford, I. Lorkovic, Chem. Rev. 102 (2002) 993.
[5] P. Kuppusamy, Antioxid. Redox Signal. 6 (2004) 583.
[6] T.B. Cai, P.G. Wang, A.A. Holder, in: P.G. Wang, T.B. Cai, N.T. Taniguchi (Eds.), Nitric Oxide Donors: For Pharmaceutical and Biological Applications, Wiley–VCH, GmbH, Germany, 2005, pp. 3–31 (Part 1).
[7] J.P. Cobb, Crit. Care Med. 27 (1999) 855.
[8] M.A. Marletta, J. Med. Chem. 37 (1994) 1899.
[9] I. Haiduc, Dithiocarbamates, in: J.A. McCleverty, T.J. Meyer, Editors-in-Chief, Comprehensive Coordination Chemistry II. From

Biology to Nanotechnology, vol. 1, Elsevier, Oxford, 2004, p. 367 (Chapter 1.15).
[10] S. Fujii, K. Kobayashi, S. Tagawa, T. Yoshimura, J. Chem. Soc., Dalton Trans. (2000) 3310.
[11] S. Fujii, T. Yoshimura, Coord. Chem. Rev. 89 (2000) 89.
[12] S. Fujii, T. Yoshimura, H. Kamada, Chem. Lett. (1996) 785.
[13] S. Porasuphatana, J. Weaver, T.A. Budzichowski, P. Tsai, G.M. Rosen, Anal. Biochem. 298 (2001) 50.
[14] R. Dash, D.V.R. Rao, Indian J. Chem. 52 (1975) 1009.
[15] N.D. Yordanov, V. Terziev, Inorg. Chim. Acta 58 (1982) 213.
[16] A. Díaz, M. Ortiz, I. Sánchez, R. Cao, A. Mederos, J. Sanchiz, F. Brito, J. Inorg. Biochem. 95 (2003) 283.
[17] A. Mederos, A. Cachapa, R. Hernández-Molina, M.T. Armas, P. Gili, M. Sokolov, J. González-Platas, F. Brito, Inorg. Chem. Commun. 6 (2003) 498.
[18] Y. Sakay, Talanta 27 (1980) 1073.
[19] A. Hulanicki, M. Minczewska, Talanta 14 (1967) 677.
[20] (a) L.G. Sillén, B. Warnqvist, Ark. Kemi 31 (1969) 377;
(b) J. Sánchis, S. Dominguez, A. Mederos, F. Brito, J.M. Arrieta, Inorg. Chem. 36 (1997) 4108.
[21] L.G. Sillén, R. Whiteker, Ark. Kemi 31 (1969) 365.
[22] P. Gans, A. Sabatinni, A. Vacca, Talanta 43 (1996) 1739.
[23] A. Radha, M. Sesha, K. Radha, Acta Crystallogr., Sect. C 41 (1985) 1166.
[24] Bruker, SMART, SAINT: Area Detector Control and Integration Software, Bruker Analytical X-ray Instruments Inc., Madison, WI, USA, 1997.
[25] G.M. Sheldrick, SADABS: Program for Empirical Absorption Correction of Area Detector Data, University of Göttingen, Göttingen, Germany, 1997.
[26] SHELXTL-NT version 5.10: Integrated System for Solving, Refining and Displaying Crystal Structures from Diffraction Data, Bruker-AXS, Madison, WI, USA, 1997.
[27] Nonius Kappa CCD Server Software, Nonius, R.V., Delft, The Netherlands, 1998.
[28] Z. Otwinowsky, W. Minor, in: C.E. Carter, R.M. Sweet (Eds.), Methods in Enzymology, Macromolecular Crystallography Part A, Academic Press; University of Texas, Southwestern Medical Centre at Dallas, 1997, p. 276, 307.
[29] A. Altomare, M.C. Burla, M. Camalli, G. Cascarazo, C. Giacovazzo, A.R.J. Guagliardi, Appl. Crystallogr. 32 (1999) 115.
[30] G.M. Sheldrick, SHELXL: Program of the Refinement of Crystal Structures, University of Göttingen, Göttingen, Germany, 1997.
[31] A.L. Spek, PLATON: A Multipurpose Crystollographic Tool, Utrech University, Utrech, Netherlands, 1992.
[32] N.L. Allinger, U. Burker, Molecular Mechanics, American Chemical Society, Washington, DC, 1982.
[33] A.K. Rappe, C.J. Casewit, K.S. Colwell, W.A. Goddard III, M. Skiff, J. Am. Chem. Soc. 114 (1992) 10024.
[34] HYPERCHEM, Release 7.0 for Windows, Molecular Modelling System, HYPERCUBE Inc., 2002.
[35] M.J. Frisch, G.W. Trucks, H.B. Schlegel, C.G. Scuseria, M.A. Robb, J.R. Cheeseman, J.A. Montgomery Jr., T. Vreven, K.N. Kudin, J.C. Burant, J.M. Millam, S.S. Iyengar, J. Tomasi, V. Barone, B. Mennucci, M. Cossi, G. Scalmani, N. Rega, G.A. Petersson, H. Nakatsuji, M. Hada, M. Ehara, K. Toyota, R. Fukuda, J. Hasegawa, M. Ishida, T. Nakajima, Y. Honda, O. Kitao, H. Nakai, M. Klene, X. Li, J.E. Knox, H.P. Hratchian, J.B. Cross, C. Adamo, J. Jaramillo, R. Gomperts, R.E. Stratmann, O. Yazyev, A.J. Austin, R. Cammi, C. Pomelli, J.W. Ochterski, P.Y. Ayala, K. Morokuma, G.A. Voth, P. Salvador, J.J. Dannenberg, V.G. Zakrzewski, S. Dapprich, A.D. Daniels, M.C. Strain, O. Farkas, D.K. Malick, A.D. Rabuck, K. Raghavachari, J.B. Foresman, J.V. Ortiz, Q. Cui, A.G. Baboul, S. Clifford, J. Cioslowski, B.B. Stefanov, G. Liu, A. Liashenko, P. Piskorz, I. Komaromi, R.L. Martin, D.J. Fox, T. Keith, M.A. Al-Laham, C.Y. Peng, A. Nanayakkara, M. Challacombe, P.M.W. Gill, B. Johnson, W. Chen, M.W. Wong, C. Gonzalez, J.A. Pople, GAUSSIAN-03, Revision B.04, Gaussian, Inc., Pittsburgh, PA, 2003.
[36] J.A. Dean (Ed.), Lange's Handbook of Chemistry, 15th ed., McGraw-Hill, New York, 1999, pp. 3–40.
[37] F. D'Acquisto, L. Sautebin, T. Iuvon, M. Di Rosa, R. Carnuccio, FEBS Lett. 444 (1998) 76.
[38] P. Marotta, L. Sautebin, M. Di Rosa, Brit. J. Pharmacol. 107 (1992) 640.
[39] T. Mosmam, J. Immunol. Methods 65 (1983) 55.
[40] Z.H. Taha, Talanta 61 (2003) 3.
[41] F. Jian, Z. Wang, Z. Bai, X. You, H.-K. Fun, K. Chinnakali, I. Razak, Polyhedron 18 (1999) 3401.
[42] M. Bonamico, G. Dessy, A. Mugnoli, A. Vaciago, L. Zambonelli, Acta Crystallogr. 19 (1965) 886.
[43] G. Peyronel, A. Pignedoli, L. Antonili, Acta Crystallogr., Sect. B 28 (1972) 3596.
[44] K. Nakamoto, Infrared and Raman Spectra of Inorganic and Coordination Compounds, 5th ed., Wiley, New York, 1997, p. 207.
[45] H.S. Sangari, G.S. Sodhi, J. Kaur, Chem. Papers 51 (1997) 280.
[46] M. Laila-Kantouri, M. Uddin, C.C. Hadjikostas, H. Papanokas, G. Palios, S. Anagnostis, V.Z. Anesti, Z. Anorg. Allg. Chem. 623 (1997) 1983.
[47] B. Macias, M.V. Villa, E. Chicote, S. Martin-Velasco, A. Castineiras, J. Borrás, Polyhedron 21 (2002) 1899.
[48] S.T. Breviglieri, E.T.G. Cavalheiro, G.O. Chierice, Thermochim. Acta 356 (2000) 79.
[49] L.J. Bellamy, The Infrared Spectra of Complex Molecules, 3rd ed., Chapman & Hall, London, 1975 (Table 9).
[50] K. Nakamoto, The Infrared Spectra of Complex Molecules, 3rd ed., Chapman & Hall, London, 1975, p. 60 (Table III-19).
[51] A.B.F. Lever, Inorganic Electronic Spectroscopy, 2nd ed., Elsevier, Amsterdam, 1984, pp. 306–308 (Tables 5–17).
[52] I. Isildack, A. Asan, M. Anadaç, Talanta 48 (1999) 219.
[53] G. Marcotriagiano, G. Pellaciani, C. Preti, J. Inorg. Nucl. Chem. 36 (1974) 3709.
[54] M.J. Weeks, J.P. Fackler, Inorg. Chem. 7 (1968) 2548.
[55] L.I. Victoriano, Polyhedron 19 (2000) 2269.
[56] O. Kahn, Molecular Magnetism, VCH, New York, 1993.
[57] C.E. Housecroft, A.G. Sharpe, Inorganic Chemistry, Pearson Education Limited, England, 2001, p. 742.

the water molecules. Ross also lists the infrared spectra of the pseudo-alums formed from one divalent and one trivalent cation. Halotrichite has infrared bands at v_1, 1000 cm^{-1}; v_2, 480 cm^{-1}; v_3, 1121, 1085, 1068 cm^{-1}; v_4, 645, 600 cm^{-1}. Pickeringite the Mg end member of the halotrichite–pickeringite series has infrared bands at v_1, 1000 cm^{-1}; v_2, 435 cm^{-1}; v_3, 1085, 1025 cm^{-1}; v_4, 638, 600 cm^{-1} [11]. These minerals display infrared water bands in the OH stretching, 3400 and 3000 cm^{-1} region; OH deformation, 1650 cm^{-1} region; OH libration, 725 cm^{-1} region. Ross also reports a weak band at ~960 cm^{-1} which is assigned to a second OH librational vibration [11]. As with the infrared spectra, Raman spectra of alums are based on the combination of the spectra of the sulphate and water. Sulphate typically is a tetrahedral oxyanion with Raman bands at 981 (v_1), 451 (v_2), 1104 (v_3) and 613 (v_4) cm^{-1} [13]. Some sulphates have their symmetry reduced through acting as monodentate and bidentate ligands [13]. In the case of bidentate behaviour both bridging and chelating ligands are known. This reduction in symmetry is observed by the splitting of the v_3 and v_4 into two components under C_{3v} symmetry and three components under C_{2v} symmetry.

In this work we report the Raman and infrared spectra of two synthetic halotrichites and compare the spectra with that of the natural minerals.

2. Experimental

2.1. Synthesis of halotrichites

The synthetic halotrichites type minerals Pickeringite and Apjohnite were prepared from an ultra pure water solution. Saturated solutions of both components were shaken together with the solid sulphates contained in filter bag sacks and were placed on either side of a beaker, which contained the saturated solution. In the synthesis of pickeringite, 9.824 g of $Al_2(SO_4)_3 \cdot 18H_2O$ and 2.491 g of $MnSO_4 \cdot H_2O$ were contained in the two sacks, while in the synthesis of apjohnite, 13.027 g of $Al_2(SO_4)_3 \cdot 18H_2O$ and 4.818 g of $MgSO_4 \cdot 7H_2O$ were used. The double salt was left over a period of a week to crystallise out. The crystals were dried and collected by vacuum filtration and washed with ethanol and diethyl ether. The minerals were analysed by X-ray diffraction for phase purity and by electron probe using energy dispersive techniques for quantitative chemical composition.

2.2. Raman spectroscopy

The crystals of halotrichite were placed and oriented on the stage of an Olympus BHSM microscope, equipped with 10× and 50× objectives and part of a Renishaw 1000 Raman microscope system, which also includes a monochromator, a filter system and a Charge Coupled Device (CCD). Raman spectra were excited by a HeNe laser (633 nm) at a resolution of 2 cm^{-1} in the range between 100 and 4000 cm^{-1}. Repeated acquisition using the highest magnification was accumulated to improve the signal to noise ratio. Spectra were calibrated using the 520.5 cm^{-1} line of a silicon wafer. In order to ensure that the correct spectra are obtained, the incident excitation radiation was scrambled. Previous studies by the authors provide more details of the experimental technique [14–17]. Spectra at elevated temperatures were obtained using a Linkam thermal stage (Scientific Instruments Ltd., Waterfield, Surrey, England). Spectral manipulation such as baseline adjustment, smoothing and normalisation was performed using the GRAMS® software package (Galactic Industries Corporation, Salem, NH, USA).

2.3. Infrared spectroscopy

Infrared spectra were obtained using a Nicolet Nexus 870 FTIR spectrometer with a smart endurance single bounce diamond ATR cell. Spectra over the 4000–525 cm^{-1} range were obtained by the co-addition of 64 scans with a resolution of 4 cm^{-1} and a mirror velocity of 0.6329 cm/s. Spectra were co-added to improve the signal to noise ratio.

Band component analysis was undertaken using the Jandel 'PEAKFIT' software package, which enabled the type of fitting function to be selected and allows specific parameters to be fixed or varied accordingly. Band fitting was done using a Lorentz–Gauss cross-product function with the minimum number of component bands used for the fitting process. The Lorentz–Gauss ratio was maintained at values greater than 0.7 and fitting was undertaken until reproducible results were obtained with squared regression coefficient of R^2 greater than 0.995.

3. Results and discussion

The Raman spectra of synthetic apjohnite and pickingerite in the 950–1050 cm^{-1} region are shown in Fig. 1; the infrared spectra in the 525–1225 cm^{-1} region in Fig. 2; the Raman spectra in the 100–700 cm^{-1} region in Fig. 3; the Raman spectra in the 2700–3700 cm^{-1} region in Fig. 4 and the infrared spectra in the 2100–3700 cm^{-1} region in Fig. 5. The results of the analyses of the Raman and infrared spectra of synthetic apjohnite and pickingerite together with the results of the Raman spectra of natural halotrichite, wupatkiite and apjohnite are reported in Table 1.

The Raman spectrum of pickingerite displays an intense symmetric band at 984 cm^{-1} assigned to the v_1 $(SO_4)^{2-}$ symmetric stretching mode. A second very low intensity band is observed at 971 cm^{-1}. According to Ross, this band is a water librational mode. A comparison may be made with the Raman spectrum of halotrichite where a single Raman band at 995 cm^{-1} is observed with a low intensity band at 975 cm^{-1}. The Raman spectrum of synthetic apjohnite shows two resolved bands at 995 and 990 cm^{-1} with a third band at 975 cm^{-1}. The first two bands are

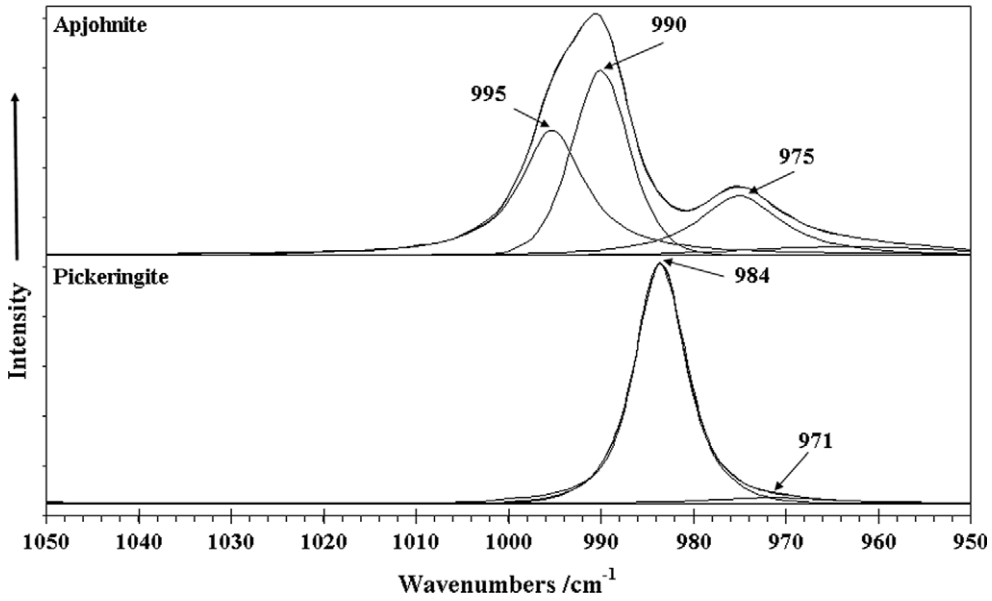

Fig. 1. Raman spectra of synthetic apjohnite and pickingerite in the 950–1050 cm^{-1} region.

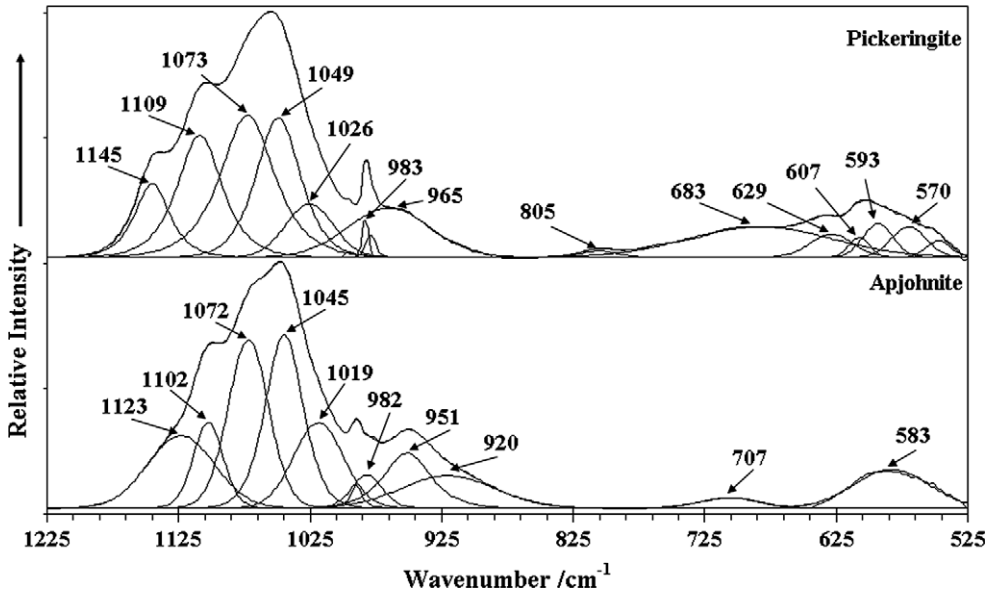

Fig. 2. Infrared spectra of synthetic apjohnite and pickingerite in the 525–1225 cm^{-1} region.

assigned to the v_1 $(SO_4)^{2-}$ symmetric stretching modes, whilst the latter band is assigned to the water librational mode. In comparison the Raman spectrum of the natural mineral apjohnite displays two bands at 997 and 991 cm^{-1}. A further comparison is made with the Raman spectrum of the cobalt alum wupatkiite where two bands are observed at 996 and 990 cm^{-1}. Both Ross and Griffith reported a single Raman band at 1006 cm^{-1}.

The infrared spectra of synthetic apjohnite and pickingerite are shown in Fig. 2. The spectra are complex with many overlapping bands. The band at 983 cm^{-1} (pickingerite) and 982 cm^{-1} (apjohnite) are assigned to the IR forbidden v_1 $(SO_4)^{2-}$ symmetric stretching mode. The bands at 965 and 951 cm^{-1} for pickeringite and apjohnite are ascribed to the water librational modes. The series of bands of pickingerite at 1145, 1109, 1073, 1049 and 1026 cm^{-1} and for apjohnite at 1123, 1102, 1072, 1045 and 1019 cm^{-1} for apjohnite are attributed to the v_3 $(SO_4)^{2-}$ antisymmetric stretching modes. The observation of multiple bands is in line with the concept of non equivalent sulphate anions in the pseudo-alum structure.

Alunogen ($Al_2(SO_4)_3 \cdot 18H_2O$) has an infrared band at 993 cm^{-1} and coquimbite ($Fe_2(SO_4)_3 \cdot 9H_2O$) a band at 1014 cm^{-1}. It is concluded that the higher wavenumber band at 995 cm^{-1} is attributable to the divalent cation (either Fe, Mg or Mn) and the second band at 990 cm^{-1} to the trivalent cation (Al) (see Fig. 1). However the relative intensities of apjohnite bands suggest otherwise. The

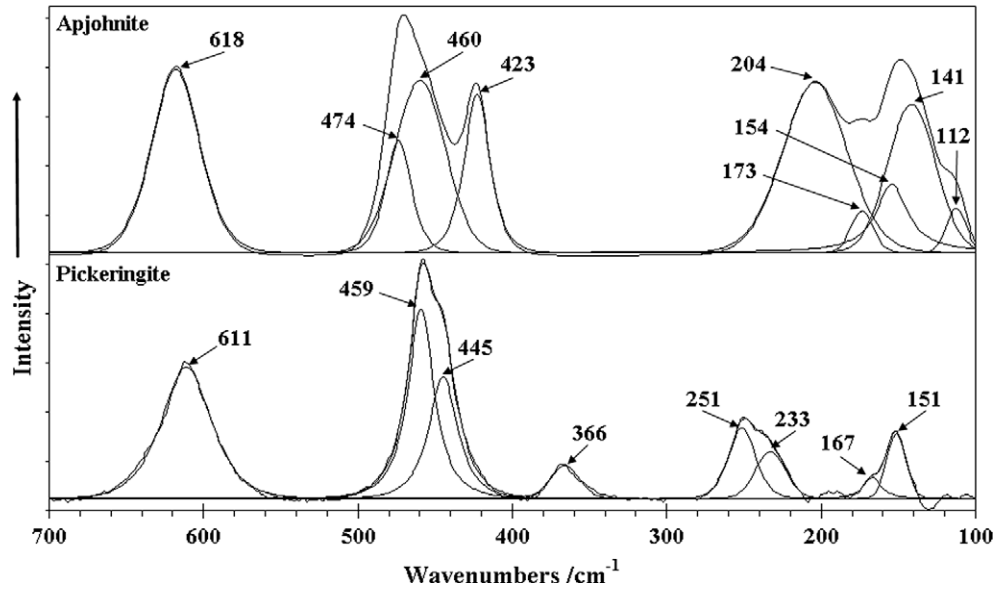

Fig. 3. Raman spectra of synthetic apjohnite and pickingerite in the 100–700 cm^{-1} region.

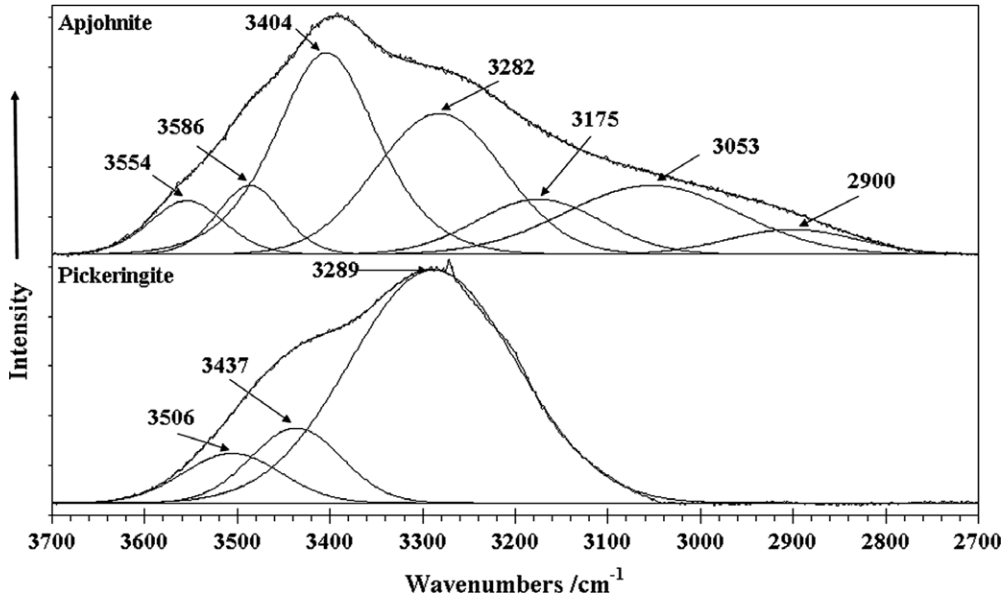

Fig. 4. Raman spectra of synthetic apjohnite and pickingerite in the 2700–3700 cm^{-1} region.

crystallographic data shows that there are four distinct sulphate groups with one of the sulphate groups coordinating the divalent cation. The relative intensity of the two bands at 995 and 990 cm^{-1} is ~3:1. Thus the lower wavenumber band is assigned to the sulphate coordinating to the divalent cation and the higher wavenumber band to the sulphates in the water hydration sphere of the aluminium. The infrared spectra of synthesised pickeringite and apjohnite show two weak bands at 983 and 965 cm^{-1} and at 982 and 951 cm^{-1}, respectively. The observation of two bands in both the Raman and infrared spectra supports the concept of two different sulphates associated with the hydration sphere of each cation. The bandwidths of the two bands at 996 and 990 cm^{-1} for natural halotrichite are 8.2 and 6.4 cm^{-1}. Similarly for wupatkiite the bandwidths of the two bands at 996 and 992 cm^{-1} in the 298 K spectrum are 7.8 and 6.4 cm^{-1}.

From a spectroscopic point of view, the situation of the Raman spectra of the v_1 $(SO_4)^{2-}$ symmetric stretching region is complex, since all these isomorphous minerals crystallise in a monoclinic space group $P2_1/c$ and four independently sulphate ions are present. In the unit cell, there are 16 anions in the primitive cell each located in the C_1 position. So additional numerous bands due to crystal effects are expected. There are four crystallographically independent sulphate ions. This will result in numerous band splittings, which may be more readily observed at 77 K. Hence it would be expected that each independent

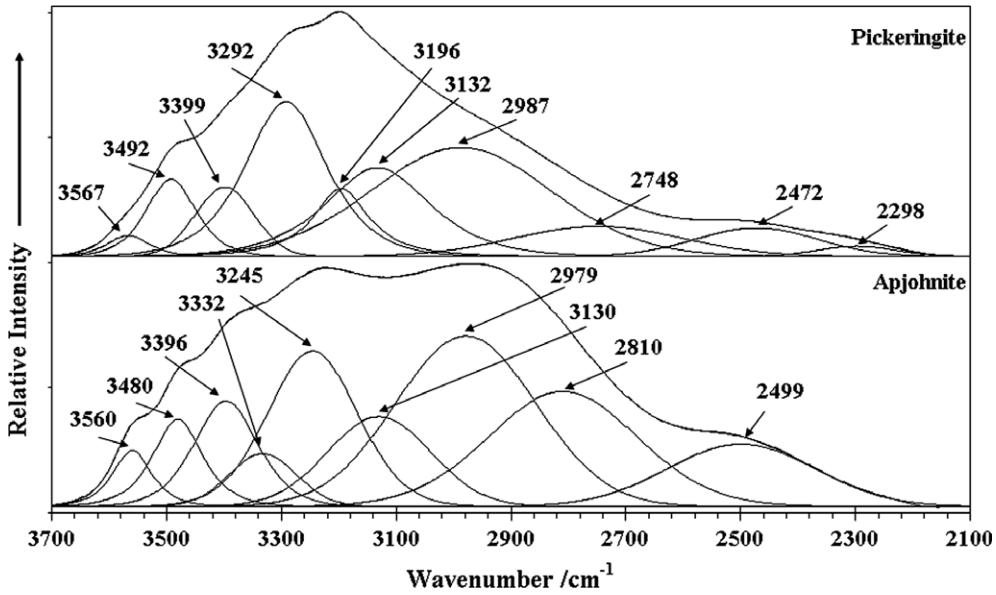

Fig. 5. Infrared spectra of synthetic apjohnite and pickingerite in the 2100–3700 cm^{-1} region.

sulphate anion would have its individual Raman spectrum. However accidental coincidence of the bands can occur, resulting in fewer bands than might be predicted. The Raman spectra of synthetic apjohnite and pickingerite show two very low intensity bands at 1141 and 1080 cm^{-1} and 1096 and 1058 cm^{-1}, respectively.

The antisymmetric stretching region of natural pseudo-alums is complex and is of low intensity in the Raman spectra. For halotrichite Raman bands are observed at 1148, 1112, 1091, 1070 and 1053 cm^{-1}. Raman bands are observed in similar positions for both wupatkiite and apjohnite. The number of bands observed in this region should reflect the number of sulphate anions in the primitive cell. Ross reported two infrared bands for pickeringite at 1085 and 1025 cm^{-1} and three bands for halotrichite at 1121, 1085 and 1068 cm^{-1} [18]. In obtaining the Raman spectra of the v_3 region for these pseudo-alums, some difficulty was experienced in obtaining high quality spectra because of low intensity throughput and high background, nevertheless some spectra were obtained.

The low frequency regions of synthetic pickingerite and apjohnite at 298 are shown in Fig. 3. For pickingerite two bands are observed at 459 and 445 cm^{-1} and for apjohnite three bands are observed at 474, 460 and 423 cm^{-1}. These bands are assigned to the v_2 bending modes. The Raman spectrum of the v_2 region of natural halotrichite shows two bands at 468, 424 and 390 cm^{-1}. The pickingerite spectrum has bands at 466, 427 and 396 cm^{-1}. Natural apjohnite shows two bands at 466 and 427 cm^{-1}. These two bands are well separated for halotrichite but overlap for the other two minerals. Infrared spectra of the minerals show two weak bands at 470 and 428 cm^{-1}. Ross reported one infrared band for halotrichite at 480 cm^{-1} and a band for pickeringite at 435 cm^{-1} [18]. There is good agreement between the infrared spectra reported by Ross and the Raman data reported here. Good band separation was obtained. Sodium sulphate shows three v_2 Raman bands at 435, 449 and 470 cm^{-1}. Basic aluminium sulphate (Al_{13} sulphate) shows three bands at 446, 459 and 496 cm^{-1}. The observation of three bands for synthetic halotrichites spectra supports the concept that (a) sulphate is of reduced site symmetry and (b) different sulphates exist around the water molecules coordinated to the two hydrated cations.

The v_4 mode is observed for natural halotrichite in the Raman spectrum at 298 K as a single band at 622 cm^{-1}. For wupatkiite, the band is observed at 619 cm^{-1} with a shoulder at 605 cm^{-1}. Apjohnite has a single Raman band at 617 cm^{-1}. Ross reports two v_4 modes in the infrared spectra at 645 and 600 cm^{-1} for halotrichite and 638 and 600 cm^{-1} for pickeringite [18]. The infrared spectrum of synthetic pickingerite shows low intensity bands at 683 (broad), 629, 607, 593 and 570 cm^{-1} and for apjohnite at 707 and 583 cm^{-1}. These bands are attributed to the v_4 bending modes. The infrared spectrum of natural halotrichite shows two bands at 632 and 595 cm^{-1}. A Wupatkiite Raman spectrum of this region is more complex with bands observed at 652, 626, 618, 606 and 589 cm^{-1}. The Raman spectrum of natural apjohnite shows good band separation in the v_4 region with bands at 650, 620, 605 and 590 cm^{-1} [13]. Sulphate typically is a tetrahedral oxyanion with bands at 981 (v_1), 451 (v_2), 1104 (v_3) and 613 (v_4) cm^{-1}. Some sulphates have their symmetry reduced through the formation of monodentate and bidentate ligands. In the case of bidentate formation both bridging and chelating ligands are known. This reduction in symmetry is observed by the splitting of the v_3 and v_4 into two components under C_{3v} symmetry and three components under C_{2v} symmetry. The observation that three or four bands are observed in the v_4 region of these halotrichites is attributed to the reduction of symmetry to C_{2v} or less, and the fact that four

Table 1
Raman and infrared spectral results of synthetic apjohnite, pickingerite and the Raman spectra of the natural minerals Wupatkiite, Apjohnite and Halotrichite and their assignments

Apjohnite (cm^{-1})		Pickingerite (cm^{-1})		Halotrichite (cm^{-1})	Wupatkiite (cm^{-1})	Apjohnite (cm^{-1})	Halotrichite (cm^{-1})	Halotrichite (cm^{-1})	Suggested assignment
Manganese alum		Magnesium alum		Ferrous alum	Cobalt alum	2Manganese alum	Ross (cm^{-1})	Griffith (cm^{-1})	
Raman	Infrared	Raman	Infrared	Raman	Raman	Raman			
3554	3560	3506	3567	3452	3452	3490			OH stretch $v_3(B_g)$ H_2O
3486	3480	3437	3492						
3404	3396	3289	3399	3369	3369	3394		3500	OH stretch $v_3(A_g)$ H_2O
3282	3332		3292	3452		3490			
3175	3245		3196	3255	3255	3281		3405	OH stretch v_1 H_2O
3053	3130		3132	3166	3166	3281			
2900	2979		2987	2944	2944	2925			
	2810		2748						
	2499		2472						
			2298						
	1679		1676			1620			$v_2(A_g)$ H_2O
	1654		1669						
			1648						
	1616					1658			$v_2(B_g)$ H_2O
1141	1123	1096	1145	1112	1115	1113	1144		$v_3(A_g)$ SO_4
	1102		1109	1148	1134	1148			
				1091	1085	1088	1138	1132	$v_3(B_g)$ SO_4
1080	1072	1058	1073	1053	1065	1051	1118		$v_3(B_g)$ SO_4
				1070		1070			
			1049	995	996	997	1006	1006	$v_1(A_g)$ SO_4
			1026						
995	1045	984	995		990	991			$v_1(A_g)$ SO_4
990	1019	971	983		975				
975	990		979	975		975			$v_1(A_g)$ SO_4
963	982		965						
	951		805						
	920								
	707		683		696		674/669	671	$v_4(B_g)$ SO_4
618		611	629	622	619	617	624	621/623	$v_4(B_g)$ SO_4
			607						
			593				604		$v_4(A_u)$ SO_4 or v_T (A_g) H_2O
		459	570					572	
	583	445	547	529	520	530			$v_2(A_g)$ SO_4
474		366		468	466	466	492	495	$v_2(A_g)$ SO_4
460				424	427	427	413	415	$v_2(A_g)$ SO_4
423				390	396				
		251		347	344	336		318	$v_g(A_g)$ H_2O
				314	318	313			
				267	266	264			
204		233							lattice modes
173		167							
154		151							
141									
112									

crystallographically distinct sulphate groups are present in the structure, one acts as a unidentate towards the M^{2+} ion.

The Raman and infrared spectra of synthetic pickingerite and apjohnite in the OH stretching region are shown in Figs. 4 and 5, respectively. The Raman spectrum of pickingerite displays bands at 3506, 3437 and 3289 cm^{-1}. The Raman spectrum of synthetic apjohnite is more complex. Raman bands are observed at 3554, 3586, 3404 and 3282 cm^{-1}. Additional bands are observed at 3175, 3053 and 2900 cm^{-1}. The infrared spectrum as shown in Fig. 5 is complex with many overlapping broad bands. The bands show greater intensity when compared with the intensity of the Raman bands. Raman spectroscopy is not very sensitive to the measurement of water in gels, crystals and minerals. Nevertheless, the OH stretching region of water in these pseudo-alums can be determined. The OH stretching region of natural halotrichite is complex and shows five bands at 3452, 3369, 3255, 3166 and 2944 cm^{-1}. Similar spectra are observed for apjohnite and wupatkiite. A Wupatkiite Raman spectrum shows bands at 3499, 3414, 3234, 3111, 2989 and 2852 cm^{-1}. The absence of bands in both the infrared and Raman spectra for natural halotrichites around 3550 cm^{-1} suggests that no adsorbed water is present. The v_2 water-bending mode is extremely weak in Raman spectra of alums but is readily observed in the infrared spectra (Fig. 6). Infrared spectra of the halotrichites show a broad profile centred upon 1650 cm^{-1}. Bands for apjohnite may be resolved at 1679, 1654, 1616 and 1582 cm^{-1}. Bands for pickingerite may be resolved at 1676, 1669 and 1648 cm^{-1}. The observation of the high frequency v_2 mode of water is indicative of coordinated water which is strongly hydrogen bonded. The observation of the second IR band suggests a second type of water molecule is present. This water is involved with hydrogen bonding to the sulphate and hence is another cause of the reduction in symmetry of the sulphate ion, as supported by the single crystal X-ray structure of apjohnite.

4. Conclusions

Halotrichites are a pseudo-alums which can form a continuous series of solid solutions with pickingerite by the substitution of Mg for Fe^{2+}. Raman spectroscopy is a very powerful tool for the study of these types of minerals and because of the compositional variation differences in the Raman spectrum of halotrichites of different origins are observed. In situ Raman spectroscopy at 298 enabled the spectra of synthetic pseudo-alums: pickingerite and apjohnite to be obtained. Multiple antisymmetric stretching bands are observed as well as multiple bending modes suggesting a reduction in symmetry of the sulphate in the halotrichite structure. The symmetry of the sulphate as observed by the number of bands in the v_2, v_3 and v_4 modes, is essentially reduced to C_{2v}. Two types of sulphate are identified and are associated with the two principal kinds of sites in the structure, as expected from the X-ray diffraction study. The crystal structure of halotrichites shows four non-equivalent sulphate units, three of which are bonded to water molecules and one to the divalent cation. Raman spectroscopy identifies two sulphate symmetric stretching vibrations in line with the crystal structure.

Acknowledgments

The financial and infra-structure support of the Queensland University of Technology, Inorganic Materials Research Program of the School of Physical and Chemical Sciences is gratefully acknowledged. The Australian Research Council (ARC) is thanked for funding the infrastructure.

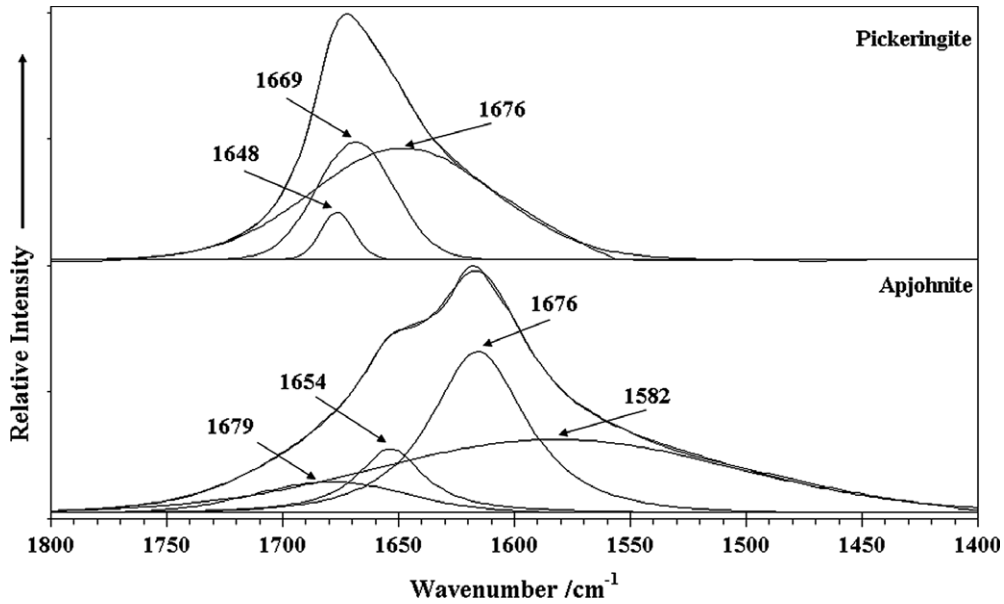

Fig. 6. Infrared spectra of synthetic apjohnite and pickingerite in the 1400–1800 cm^{-1} region.

References

[1] J. Uhlig, Centr. Min. (1912) 723.
[2] F. Wirth, Angew. Chem. 26 (1913) 81.
[3] Y.N. Neradovskii, A.N. Bogdanova, G.M. Neradovskaya, R.A. Popova, Zapiski Vsesoyuznogo Mineralogicheskogo Obshchestva 108 (1979) 343.
[4] J.L. Jambor, D.K. Nordstrom, C.N. Alpers, Rev. Miner. Geochem. 40 (2000) 303.
[5] R.G. Corbett, E.B. Nuhfer, H.W. Phillips, Proc. West VA Acad. Sci. 39 (1967) 311.
[6] R. Martin, K.A. Rodgers, P.R.L. Browne, Miner. Mag. 63 (1999) 413.
[7] A.D. Cody, T.R. Grammer, New Zeal. J. Geol. Geophys. 22 (1979) 495.
[8] M.C. Brandy, Am. Mineral. 23 (1938) 669.
[9] C. Palache, H. Berman, C. Frondel (Eds.), Dana's System of Mineralogy, vol. II, 7th ed., 1951.
[10] S. Menchetti, C. Sabelli, Mineral. Mag. 40 (1976) 599.
[11] S.D. Ross, The Infrared Spectra of Minerals, The Mineralogical Society, London, 1974, p. 423 (Chapter 18).
[12] S.D. Ross, Inorganic Infrared and Raman Spectra (European Chemistry Series), 1972.
[13] R.L. Frost, J.T. Kloprogge, P.A. Williams, P. Leverett, J. Raman Spectrosc. 31 (2000) 1083.
[14] R.L. Frost, Anal. Chim. Acta 517 (2004) 207.
[15] R.L. Frost, J.T. Kloprogge, W.N. Martens, J. Raman Spectrosc. 35 (2004) 28.
[16] R.L. Frost, M.L. Weier, J. Raman Spectrosc. 35 (2004) 299.
[17] R.L. Frost, P.A. Williams, W. Martens, P. Leverett, J.T. Kloprogge, Am. Mineral. 89 (2004) 1130.
[18] S.D. Ross, Inorganic Infrared and Raman Spectra, McGraw-Hill Book Company Ltd., London, 1972.

bifunctional 2-(methylphosphonic acid) pyridine *N*-oxides **1**-H_2 [16], **1′**-H_2 [16] and **2**-H_2 [17] and their coordination chemistry toward selected lanthanide ions. For example, **1**-H_2 and **1′**-H_2 form complexes $Er(\mathbf{1}\text{-}H^-)_3(\mathbf{1}\text{-}H_2)\cdot 8H_2O$ in which all four ligands act as bidentate chelates producing an eight-coordinate metal center [16]. The P–O and N–O groups also participate in the formation of an extensive 3D hydrogen bonding network. The ligand **2**-H_2, with its longer *exo*-ethyl phosphonic acid arm, forms a complex $Nd(\mathbf{2}\text{-}H^{-1})_3$. The solid-state structure contains chains along the *c*-axis in which the *N*-oxide does not participate in chelate formation on Er(III), but is involved in hydrogen bond interactions with phosphonic acid hydrogen atoms [17]. The differences between these ligands and their coordination properties has led us to explore the directed synthesis of the trifunctional ligand, 2,6-bis(methylphosphonic acid)pyridine *N*-oxide **3**-H_4, and its coordination chemistry with Nd(III). The results of that study are reported here.

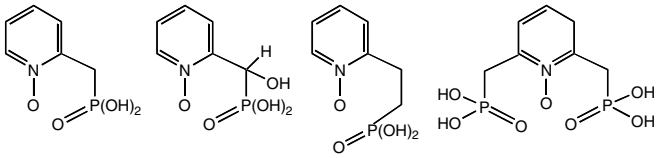

1-H_2 **1'-H_2** **2-H_2** **3-H_4**

2. Results and discussion

2.1. Synthesis and characterization of ligand

The target ligand, 2,6-bis(methylphosphonic acid)pyridine *N*-oxide, **3**-H_4, was prepared in good to fair overall yields by two related approaches that differ in the method of oxidation of the intermediate, 2,6-bis(diethylphosphonomethyl)pyridine (**4**) (Scheme 1). We have previously reported the synthesis of **4** from an Arbusov reaction between $P(OEt)_3$ and 2,6-bis(chloromethyl)pyridine [6] and under the conditions described there (140–150 °C, 4 h), **4** was obtained in 88% yield. We note here that performing the reaction at 150 °C for 7 h results in essentially quantitative formation of **4** with a single ^{31}P NMR resonance at δ 25.6. This ^{31}P NMR shift appears in the region expected for alkyl phosphonates, $RP(O)(OR)_2$ [18]. The direct oxidative hydrolysis of the ester **4** to the acid **3**-H_4 (Method 1) was examined by use of mixtures of glacial acetic acid and hydrogen peroxide. By this route, the oxidative conversion is only partially effective. Under the conditions described, about 65% of **4** remains unconverted after a typical reaction. Following extractive work up, the solid product is a mixture that contains ~93% **3**-H_4 and ~7% of the pyridine compound $[(HO)_2P(O)CH_2]_2C_5H_3N$, that is identified by its ^{31}P NMR resonance, δ 14. This mixture is difficult to separate, and this fact together with the unsatisfactory overall conversion led us to seek an alternate synthesis approach.

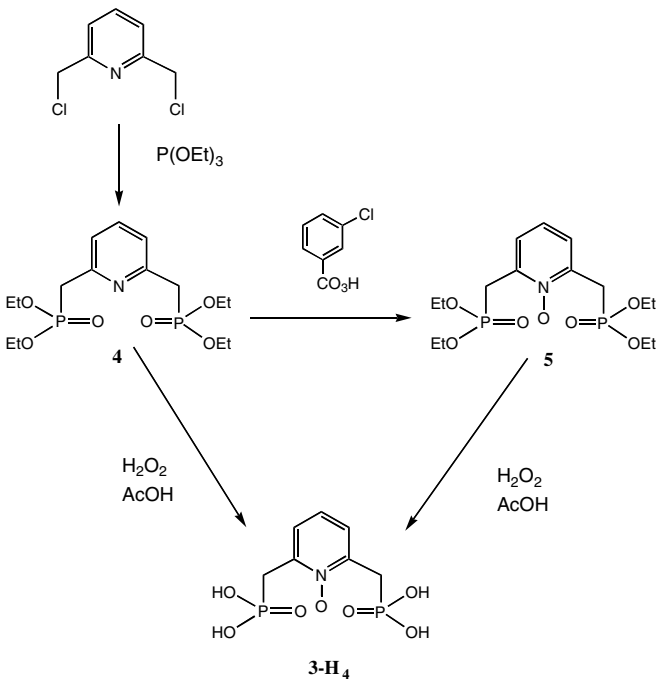

Scheme 1.

In our previous report [6], in which a synthesis for compound **5** was sought, we noted that when the oxidation of **4** with 3-chloroperbenzoic acid (70 °C, 16 h) was not carefully controlled, variable quantities of **3**-H_4 would also appear in samples of **5**. With the temperature sensitivity in mind, we performed here the N-oxidation of **4** with 3-chloroperbenzoic acid in $CHCl_3$ solution at 23 °C for 18 h (Method 2). This results in formation of **5** in 91% yield, which is a much improved yield compared to 47% obtained when the reaction is performed at elevated temperature. Characterization data obtained here for **5** are consistent with the data reported earlier. The subsequent hydrolysis of **5** with acetic acid/H_2O_2 solution is completed at 70 °C after ~17 h. The hydrogen peroxide is added to assist in the N-oxidation of any small quantities of **4** that remain in **5**. Simple work up normally provides pure **3**-H_4 in 90% yield. However, if small amounts of **4** or **5** are carried through, recrystallization from acetone/water or Et_2O/pentane solutions removes these impurities. The product is an analytically pure, white, crystalline solid obtained as a monohydrate. The NMR spectra are solvent dependent and ^{31}P and spectral data are provided for D_2O and d_6-DMSO solutions.

2.2. Synthesis of the complex

The 2:1 combinations of **3**-H_4 and $Nd(NO_3)_3$ in MeOH or $Nd(OH)_3$ in water produce clear solutions that deposit amorphous solids upon evaporation of the volatiles or addition of $CHCl_3$ to the reaction mixtures. Elemental analyses suggest formation of 2:1 ligand:metal complexes with varying degrees of solvation. However, when 2:1

combinations of **3-H**$_4$ and Nd(NO$_3$)$_3$ or Nd(OH)$_3$ in a minimum of water are heated in sealed glass tubes at 85 °C, blue-purple crystals of a complex Nd(**3-H**$_2^{2-}$)(**3-H**$_3^{1-}$)-(H$_2$O)$_{4/3}$ form and this complex has been characterized by single crystal X-ray diffraction analysis.

2.3. Crystallographic analysis of the complex

A diffraction quality crystal of the complex, obtained from the hydrothermal synthesis described above, was selected and its structure determined by single crystal X-ray diffraction techniques. One view of the asymmetric unit is shown in Fig. 1 and selected bond lengths are listed in Table 1. The formula for the asymmetric unit is Nd(**3-H**$_2^{2-}$)(**3-H**$_3^{1-}$)(H$_2$O)$_{4/3}$. The view of the asymmetric unit shown in Fig. 1 suggests that the Nd(III) ion is six coordinate; however, it is seven coordinate with the inner sphere coordination polyhedron best approximated as a mono-capped trigonal prism as shown in Fig. 2. The seventh oxygen atom position, O4A, not shown in the view of the asymmetric unit, results from bridge bonding with another asymmetric unit (see below). Both anionic ligands

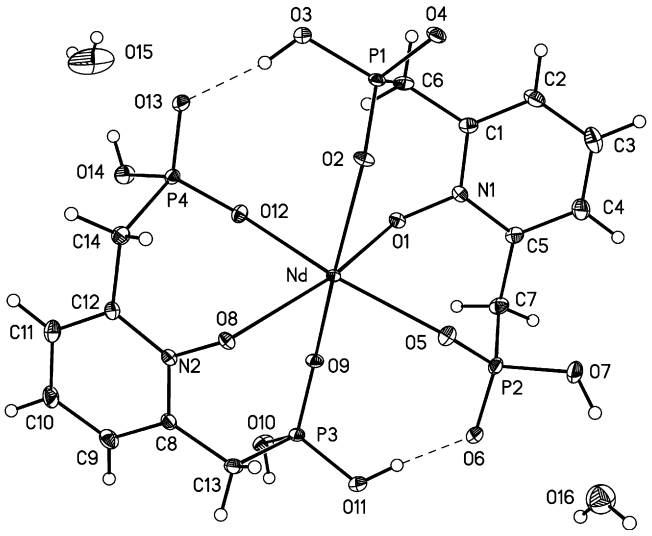

Fig. 1. Molecular structure and atom labeling scheme for the asymmetric unit Nd(**3-H**$_2^{2-}$)(**3-H**$_3^{1-}$)(H$_2$O)$_{4/3}$ (20% probability ellipsoids).

Table 1
Selected bond lengths (Å)

Nd–O1	2.526(4)	Nd–O8	2.369(3)
Nd–O2	2.338(3)	Nd–O9	2.427(3)
Nd–O5	2.375(4)	Nd–O12	2.378(4)
Nd–O4(#1)	2.340(4)		
N1–O1	1.332(5)	N2–O8	1.323(5)
P1–O2	1.511(4)	P3–O9	1.494(4)
P1–O3	1.571(4)	P3–O10	1.559(4)
P1–O4	1.500(4)	P3–O11	1.527(4)
P2–O5	1.495(4)	P4–O12	1.504(4)
P2–O6	1.516(4)	P4–O13	1.494(4)
P2–O7	1.551(4)	P4–O14	1.567(4)

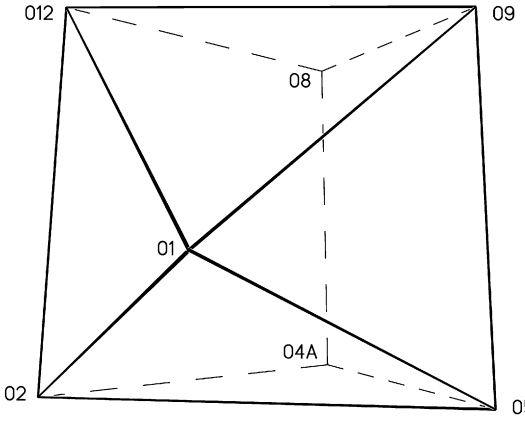

Fig. 2. Inner sphere coordination polyhedron for Nd(**3-H**$_2^{2-}$)(**3-H**$_3^{1-}$)-(H$_2$O)$_{4/3}$.

derived from the tetra-acid, **3-H**$_4$, are bonded to Nd(III) as tridentate chelates. One of the ligands exists as a symmetrical doubly deprotonated anion **3-H**$_2^{2-}$ while the second is a monoanion, **3-H**$_3^{1-}$. The **3-H**$_3^{1-}$ ligand symmetrically chelates to the Nd(III): Nd–O8N2 2.369(3) Å, Nd–O9P3 2.427(3) Å, Nd–O12P4 2.378(4) Å. The **3-H**$_2^{2-}$ ligand, on the other hand, displays more asymmetric binding in part because one phosphonate oxygen atom, O4, bridge bonds to a Nd(III) in a second asymmetric unit: Nd–O1N1 2.526(4) Å, Nd–O2P1 2.338(3) Å, Nd–O5P2 2.375(4) Å, Nd–O4(4/3 − x + y, 2/3 − x, z − 1/3) 2.340(4). The connectivity between asymmetric units is illustrated in Fig. 3. The resulting ···O4(4/3 − x + y, 2/3 − x, z − 1/3) Nd–O4–Nd(2/3 − y, −2/3 + x − y, 1/3 + z)··· and related interactions produce chains that spiral along the c direction of the unit cell and a view of the unit cell looking down the c-axis is shown in Fig. 4. The pyridine N–O bond lengths are equivalent as are the P–O bond lengths involving oxygen atoms coordinated to Nd(III): N1–O1 1.332(5) Å, N2–O8 1.323(5) Å; P–ONd avg. 1.501 ± 0.010 Å. The formally anionic oxygen atoms, O6 and O13, involved in hydrogen bonding to adjacent asymmetric units also display short P–O bond lengths: P2–O6 1.516(4) Å, P4–O13 1.494(4) Å. The unionized P–OH groups display longer P–O bond lengths: P1–O3 1.571(4) Å, P2–O7 1.551(4) Å, P3–O11 1.527(4) Å, P3–O10 1.559(4) Å, P4–O14 1.567(4) Å. There are two hydrogen-bond interactions within the asymmetric unit, O3H3···O13 1.73 Å (170°), O11H11···O6 1.62 Å (175°), that appear to help order the ligand chelation mode as indicated in Fig. 2. There is also an inter-asymmetric unit hydrogen bond between a phosphonic acid proton and the Nd coordinated pyridine *N*-oxide, O10H10···O1:1:77 Å (168°).

Finally, there is extensive hydrogen bonding involving phosphonic acid protons and lattice water molecules. The water molecules occupy columnar space generated by the spiral chains as depicted in Fig. 4. In that figure, the Nd(III) coordination polyhedra are shown in green, the phosphorus atom tetrahedral are shown in magenta, carbon atoms in the ligand backbone are shown as grey

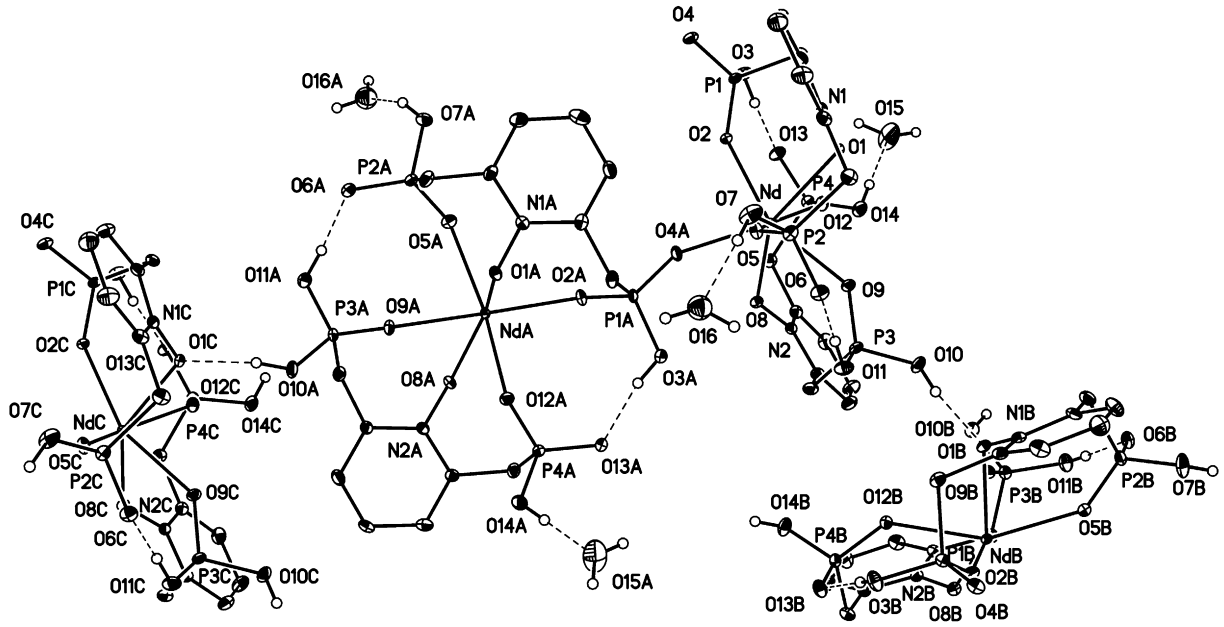

Fig. 3. View of the 1-D Chain structure for Nd(**3**-H_2^{2-})(**3**-H_3^{1-})$(H_2O)_{4/3}$: molecule A at $4/3 - x + y$, $2/3 - x$, $z - 1/3$; molecule B at $1/3 - y$, $x - y - 1/3$, $z - 1/3$; molecule C at $2/3 + x$, $1/3 + y$, $z - 1/3$.

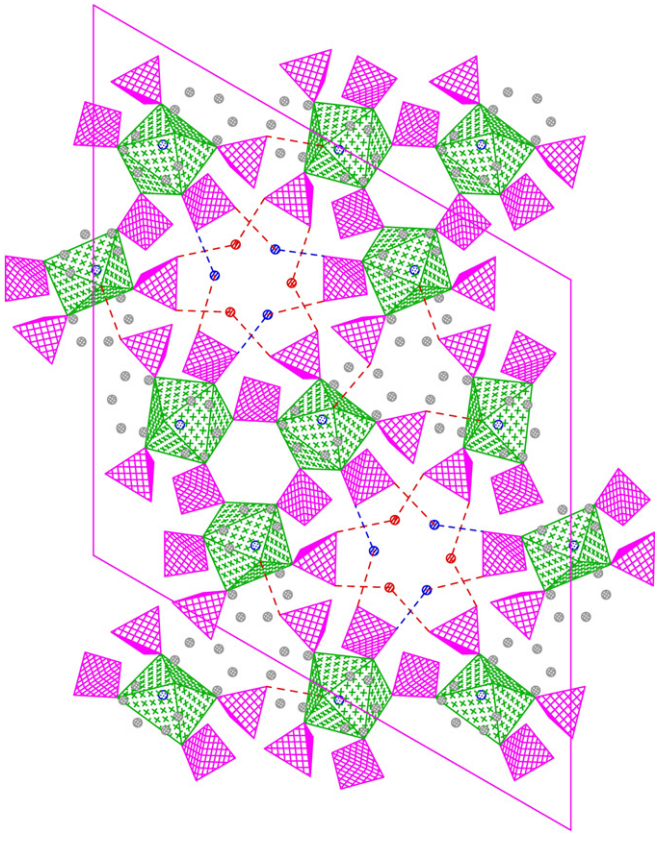

Fig. 4. View of the unit cell for Nd(**3**-H_2^{2-})(**3**-H_3^{1-})$(H_2O)_{4/3}$ looking down the *c*-axis. Seven coordinate Nd(III) polyhedra shown in green, four coordinate phosphate tetrahedra shown in magenta, ligand carbon backbone atoms shown in grey and water sites shown in red and blue. (For interpretation of the references to color in this figure legend, the reader is referred to the web version of this article.)

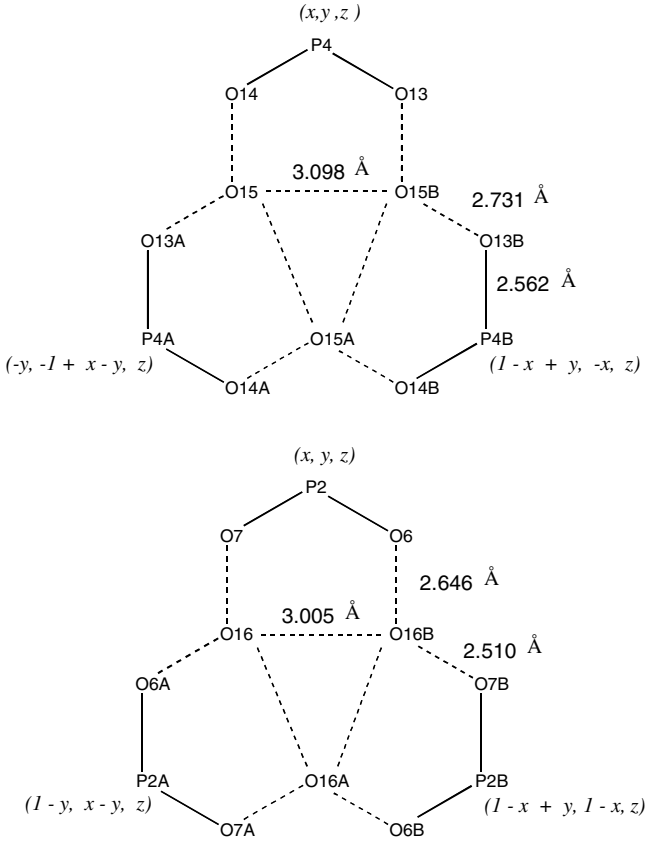

Fig. 5. Representation of the non-bonded oxygen atom distances between phosphonic acid hydrogen atoms and water molecules occupying the columnar space.

dots and the water oxygen atom positions O15, O15A, O15B are depicted in red and the disordered (three sites) O16 in blue. The resulting O···O non-bonded distances involved in the PO–H···OH_2 hydrogen bonds are shown in Fig. 5.

3. Conclusion

A high yield synthesis for the trifunctional phosphonic acid ligand **3-H$_4$** has been developed and this allows for the study of the coordination chemistry of the tetra-acid toward lanthanide ions without interference from competing chelation interactions with the impurity ligands **4**, **5** and $[(HO)_2P(O)CH_2]_2C_5H_3N$. The target ligand readily dissolves lanthanide hydroxides at 23 °C and forms amorphous 2:1 ligand/Ln(III) complexes that have variable elemental compositions due to easily lost lattice solvent molecules. However, hydrothermal synthesis conditions produce well-behaved crystalline solids and one of these complexes with Nd(III) has been structurally characterized. Single crystal X-ray diffraction analysis reveals formation of a bis-ligand complex in which both ligands act as tridentate chelates. A single P–O–Nd chain interaction and hydrogen bonding interactions link the asymmetric units in the unit cell. The strong chelation produced by anionic forms of **3-H$_4$** suggests utility as an acidic separations agent and such studies with uranium are in progress.

4. Experimental

4.1. General

The organic reagents were purchased from Aldrich Chemical Co. and organic solvents were obtained from VWR. The $Nd(NO_3)_3 \cdot 6H_2O$ was purchased from Ventron. All reactions were performed under dry conditions unless noted otherwise. Infrared spectra were recorded on a Mattson 2020 FT-IR and NMR spectra were obtained from Bruker FX-250 and JEOL-GSX400 instruments using Me_4Si (^1H and ^{13}C) and H_3PO_4 (^{31}P) as external shift standards. Downfield shifts are reported with $+\delta$. Elemental analyses were obtained from Galbraith Laboratories.

4.2. 4.2.1. Ligand synthesis Method 1

A sample of 2,6-bis[(diethylphosphono)methyl]pyridine (**4**) (8.0 g, 0.02 mole) *vide infra* in glacial acetic acid (40 mL) was combined with H_2O_2 (3.5 mL, 30%) and heated (70 °C, 8 h). The mixture was cooled, another portion of H_2O_2 (3.5 mL, 30%) was added and the mixture heated (70 °C, 18 h). Over this time, the solution becomes milky in appearance. The resulting mixture was then vacuum evaporated leaving a white powder that was vacuum dried (70 °C, 24 h) to remove traces of acetic acid residue. The dry powder was dissolved in water (40 mL) and poured into well-stirred acetone (500 mL). A precipitate formed immediately and the mixture was stored (−20 °C, 18 h). The solid was recovered by filtration in air, washed with acetone and vacuum dried. The solid was recrystallized twice from H_2O (min)/acetone mixtures: yield 1.8 g (28%).

4.2.2. Method 2

A sample of 2,6-bis(chloromethyl)pyridine [5,6] (8.0 g, 46 mmol) was added to $P(OEt)_3$ (80 mL) at once under a dry nitrogen atmosphere. The reaction mixture was heated (bath temp. 150 °C, 7 h) in a fashion so that the volatile EtCl that formed could escape through the top of a reflux condenser protected by a mercury bubbler. The reaction was cooled to 23 °C and excess $P(OEt)_3$ removed under vacuum leaving 2,6-bis[(diethylphosphono)-methyl]pyridine (**4**) as an orange oil (17.4 g). NMR ($CDCl_3$): $^{31}P\{^1H\}$ δ 25.6; ^1H δ 1.17 (t, $J = 7.0$ Hz, **C**$\mathbf{H}_3$), 3.26 (d, $J = 26.2$ Hz, **C**$\mathbf{H}_2$P), 3.95 (m, O**C**$\mathbf{H}_2$), 7.15 (d, $J = 3.8$ Hz), 7.47 (t, $J = 4.6$ Hz). A sample of **4** (17.0 g, 0.045 mol) and 3-chloroperbenzoic acid (9.0 g, 70–75%) were combined in $CHCl_3$ (80 mL) at 23 °C and stirred (18 h). A saturated solution of $NaHCO_3$ (300 mL) was added, stirred and the phases separated. The aqueous phase was washed with $CHCl_3$ (75 mL × 3) and the combined organic phases dried over anhyd. Na_2SO_4. Evaporation of the volatiles gave 2,6-bis[(diethylphosphono)methyl]pyridine *N*-oxide (**5**) as a colorless oil: yield, 16.2 g (91%). The oil slowly crystallized over several days (m.p. = 50–52 °C). NMR ($CDCl_3$): $^{31}P\{^1H\}$ δ 23.9; ^1H δ 0.86 (t, $J = 6.8$ Hz, **C**$\mathbf{H}_3$), 3.32 (d, $J = 21.8$ Hz, **C**$\mathbf{H}_2$P), 3.71 (m, O**C**$\mathbf{H}_2$), 6.88 (t, $J = 6.5$ Hz), 7.1 (d, $J = 7.1$ Hz); $^{13}C\{^1H\}$ δ 16.5 (d, $J = 6$ Hz, **C**H_3), 28.3 (d, $J = 140$ Hz; **C**H_2P), 63.2 (d, $J = 6.5$ Hz, O**C**H_2), 124.3, 125.8, 144.0. A sample of **5** (8.0 g, 0.02 mol) was dissolved in glacial acetic acid (20 mL) and H_2O_2 (3.6 mL, 30%) added. The mixture was stirred and heated (70 °C, 17 h). A milky solution formed during heating. The mixture was cooled, vacuum evaporated and a white powder collected that was further dried under vacuum (70 °C, 24 h). The dry powder was dissolved in water (40 mL) and the solution poured into well stirred acetone (500 mL). The combination produces a white precipitate and the mixture was cooled (−20 °C, 18 h). The solid was collected by filtration, washed with acetone and dried (70 °C, 24 h). 2,6-Bis(methylphosphonic acid)pyridine *N*-oxide (**3**) was recovered as a white solid: yield 5.1 g (90%), m.p. = 202–204 °C. NMR: ^{31}P $\{^1H\}$ (D_2O) δ 17.9, (d_6-DMSO) δ 19.3; ^1H (D_2O) δ 3.69 (d, 21.2 Hz, **C**$\mathbf{H}_2$), 7.72 (d, $J = 7.3$ Hz), 7.95 (t, $J = 7.6$ Hz); ^{13}C $\{^1H\}$ (d_6-DMSO) δ 35.2 (d, $J = 26.7$ Hz, **C**H_2), 130.2, 134.4, 150.3 (d, $J = 8.7$ Hz). *Anal.* Calc. for $C_7H_{11}NO_7P_2H_2O$ (301.128): C, 27.92; H, 4.35; N 4.65. Found: C, 27.79; H, 4.61; N 4.59%.

4.3. Coordination complexes

A sample of **3-H$_4$** (113 mg, 0.38 mmol) and $Nd(NO_3) \cdot 6H_2O$ (87.6 mg, 0.2 mmol) were dissolved in water (10 mL) and sealed in a pyrex tube. The tube was heated (85 °C, 24 h) and during this time frame blue-purple crystals began to deposit and continued to deposit on

Table 2
Crystal data and refinement details for Nd(**3**-H_2)(**3**-H_3) · 4/3H_2O

Formula	$C_{14}H_{21.67}N_2NdO_{15.33}P_4$
Formula weight (g mol^{-1})	731.45
Crystal system	rhombohedral
Space group	*R*3
Unit cell dimensions	
a (Å)	25.1227(18)
b (Å)	25.1227(18)
c (Å)	10.6173(12)
$\alpha = \beta$ (°)	90
γ (°)	120
V (Å^3)	5803.3(9)
Z	9
D_{calc} (g cm^{-3})	1.884
μ (mm^{-1})	2.334
hkl Range	$-31 \leqslant h \geqslant 31$
	$-32 \leqslant k \geqslant 32$
	$-13 \leqslant l \geqslant 13$
Reflections measured	6227
Unique (R_{int}) with $I > 2\sigma(I)$	5650 (0.0206)
Number of parameters	328
R(*F*)	0.0268
wR(F^2)	0.0832
Goodness-of-fit	1.068
Max./min. $\Delta\rho$ (e Å^{-3})	1.435/−0.534

standing at 23 °C. The crystals were collected, washed with a minimum of water and dried: yield 110 mg (80%). IR (KBr (cm^{-1})): $v = 3364$, 3084, 2989, 1577, 1491, 1402, 1284, 1221, 1155, 1057, 939, 868, 808, 748, 688, 520, 470. *Anal.* Calc. for $C_{14}H_{21.67}N_2NdO_{15.33}P_4$ (731.45): C, 22.99; H, 2.99; N, 3.83. Found: C, 20.87; H, 3.23; N, 3.43%.

4.4. Crystallography

Crystal data and refinement details for the structure determination are presented in Table 2. Data were collected in the ω scan mode in the θ range 1.62–27.49° on a crystal $0.46 \times 0.22 \times 0.22$ mm in size by using a Siemens R3m/V diffractometer equipped with a graphite monochromator using Mo Kα radiation ($\lambda = 0.71073$ Å). Crystal data parameters are summarized in Table 1. Calculations were performed with SHELXTL (VMS version) and the structure solved by direct methods. Full-matrix least-squares refinements were completed using appropriate neutral atom scattering factors and anomalous dispersion terms including anisotropic thermal parameters on the heavy atoms. Data were corrected for adsorption using semi-empirical psi-scans. The data collected included Friedel pairs and the model was refined in *R*3 (Flack parameter = 0.66 (2)). After all of the non-hydrogen atoms were included, the program suggests to provide for racemic twinning and this significantly improves the *R*-factors. The asymmetric unit is $NdP_4O_{14}N_2H_{19}C_{14}$ with 1 1/3 waters of crystallization. There are nine asymmetric units in the unit cell. The water molecule of 015 is in a fully occupied site but that of 016 has an occupation factor of 1/3. The arrangement of atoms about Nd is nearly centric but the intensities do not fit the *R*-3 space group.

5. Supplementary material

Supplementary crystallographic data are available free of charge from the Cambridge Crystallographic Data Centre, CCDC, 12 Union Road, Cambridge, CB2 1EZ, UK, fax: +44 1223 336033, email: deposit@ccdc.cam.ac.uk on request, quoting the deposit number 601867.

Acknowledgements

This work was supported by a Grant No. DE-FG02-03ER15419 from Chemical Sciences, Geosciences and Biosciences Office, Office of Basic Energy Sciences, US Department of Energy.

Appendix A. Supplementary data

Supplementary data associated with this article can be found, in the online version, at doi:10.1016/j.poly.2006.06.011.

References

[1] A. Clearfield, Prog. Inorg. Chem. 47 (1998) 371.
[2] P. Ayyappan, O.R. Evans, B.M. Foxman, K.A. Wheeler, T.H. Warren, W. Lin, Inorg. Chem. 40 (2001) 5954.
[3] P. Ayyappan, O.R. Evans, Y. Cui, K.A. Wheeler, W. Lin, Inorg. Chem. 41 (2002) 4978.
[4] D. Kong, A. Clearfield, Cryst. Growth Des. 5 (2005) 1263.
[5] B.M. Rapko, E.N. Duesler, P.H. Smith, R.T. Paine, R.R. Ryan, Inorg. Chem. 32 (1993) 2164.
[6] U. Engelhardt, B.M. Rapko, E.N. Duesler, D. Frutos, R.T. Paine, Polyhedron 14 (1995) 2361.
[7] X. Gan, E.N. Duesler, R.T. Paine, Inorg. Chem. 40 (2001) 4420.
[8] Y.-C. Tan, X. Gan, J.L. Stanchfield, E.N. Duesler, R.T. Paine, Inorg. Chem. 40 (2001) 2910.
[9] X. Gan, B.M. Rapko, E.N. Duesler, I. Binyamin, R.T. Paine, B.P. Hay, Polyhedron 24 (2005) 469.
[10] J.H. Matonic, M.P. Neu, A.E. Enriquez, R.T. Paine, B.L. Scott, J. Chem. Soc., Dalton Trans. (2002) 2328.
[11] E.M. Bond, E.N. Duesler, R.T. Paine, M.P. Neu, J.H. Matonic, B.L. Scott, Inorg. Chem. 39 (2000) 4152.
[12] E.M. Bond, U. Engelhardt, T.P. Deere, B.M. Rapko, R.T. Paine, Solvent Extr. Ion Exc. 15 (1997) 381.
[13] E.M. Bond, U. Engelhardt, T.P. Deere, B.M. Rapko, R.T. Paine, Solvent Extr. Ion Exc. 16 (1998) 967.
[14] K.L. Nash, C. Lavallette, M. Borkowski, R.T. Paine, X. Gan, Inorg. Chem. 41 (2002) 5849.
[15] L.D. Quin, A Guide to Organophosphorus Chemistry, Wiley, New York, 2000.
[16] X. Gan, I. Binyamin, B.M. Rapko, J. Fox, E.N. Duesler, R.T. Paine, Inorg. Chem. 43 (2004) 2443.
[17] X. Gan, B.M. Rapko, J. Fox, I. Binyamin, S. Pailloux, E.N. Duesler, R.T. Paine, Inorg. Chem. 45 (2006) 3741.
[18] M.M. Crutchfield, C.H. Dungen, J.H. Letcher, V. Mark, J.R. VanWazer, Top. Phosphorus Chem. 5 (1967) 1.

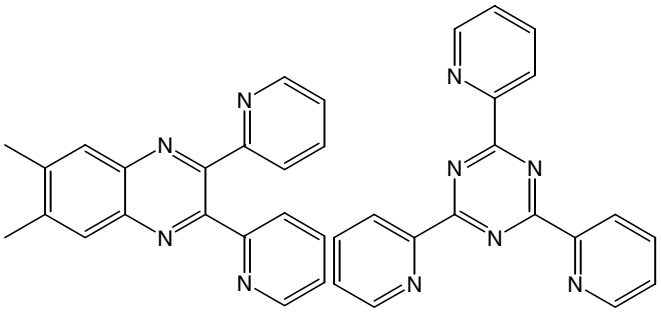

DMeDPQ TPT

Chart 1. Chemical structures of DMeDPQ and TPT.

of structurally characterized dicyanamide bridged discrete dinuclear compounds [2,13a,13b].

Although dicyanamide can mediate only weak interactions between paramagnetic metal centers [2–14], a few multidimensional dicyanamide-bridged compounds exhibit long range magnetic ordering [1]. Evidently, dicyanamide is also a promising building unit to derive magnetic materials.

It may be noted that the utilization of a new organic ligand may result in new types of topologies in the heteroleptic metal–dicyanamide family. As the blocking or bridging organic counterpart, although several ligands from polypyridine family has been used previously [1d], 6,7-dimethyl-2,3-di(2-pyridyl)quinoxaline (DMeDPQ) and 2,4,6-tri(2-pyridyl)-1,3,5-triazine (TPT) have still not been utilized. Herein, we report the syntheses, structures, and variable-temperature magnetic studies of a one-dimensional double chain compound, $[Mn^{II}(DMeDPQ)(\mu_{1,5}\text{-dca})_2]_n$ (**1**), and a discrete dinuclear compound, $[Mn_2^{II}(TPT)_2(\mu_{1,5}\text{-dca})_2(H_2O)_2](ClO_4)_2$ (**2**), derived from DMeDPQ and TPT, respectively (see Chart 1).

2. Experimental

2.1. Materials and physical methods

All the reagents and solvents were purchased from the commercial sources and used as received. Elemental (C, H, and N) analyses were performed on a Perkin–Elmer 2400 II analyzer. IR spectra were recorded in the region 400–4000 cm^{-1} on a Bio-Rad FTS40 spectrophotometer with samples as KBr disks. Variable-temperature (5–300 K) magnetic susceptibility measurements under fixed field strength of 1 T were carried out with a Quantum Design MPMS SQUID magnetometer.

2.2. Syntheses of $[Mn^{II}(DMeDPQ)(\mu_{1,5}\text{-dca})_2]_n$ (1) and $[Mn_2^{II}(TPT)_2(\mu_{1,5}\text{-dca})_2(H_2O)_2](ClO_4)_2$ (2)

The two complexes were synthesized in the same way and mixing the reactants in the same stoichiometric ratio as illustrated below for **1**, except using TPT instead of DMeDPQ for **2**.

To a stirred methanol solution (25 ml) containing DMeDPQ (0.156 g, 0.5 mmol) and $Mn(ClO_4)_2 \cdot 6H_2O$ (0.362 g, 1 mmol) was added an aqueous solution (5 ml) of sodium dicyanamide (0.178 g, 2 mmol). After stirring for 4 h, the yellow solution was filtered to remove any suspended particles and the filtrate was kept at room temperature for slow evaporation. After a few days, a yellow crystalline compound containing diffractable single crystals was deposited, collected by filtration and washed with methanol. Yield: 0.18 g (72%, in terms of DMeDPQ). *Anal.* Calc. for $C_{24}H_{16}MnN_{10}$: C, 57.7; H, 3.2; N, 28.0. Found: C, 57.6; H, 3.2; N, 27.9%. IR (KBr/cm^{-1}): dicyanamide: 2313, 2239, 2181. Data for **2**: color: yellow. Yield: 80% (in terms of TPT). *Anal.* Calc. for $C_{40}H_{28}Cl_2Mn_2N_{18}O_{10}$: C, 43.6; H, 2.6; N, 22.9. Found: C, 43.5; H, 2.6; N, 23.1%. IR (KBr/cm^{-1}): dicyanamide: 2329, 2235, 2192.

2.3. Crystal structure determination of $[Mn^{II}(DMeDPQ)(\mu_{1,5}\text{-dca})_2]_n$ (1) and $[Mn_2^{II}(TPT)_2(\mu_{1,5}\text{-dca})_2(H_2O)_2](ClO_4)_2$ (2)

Pertinent crystallographic data of these two complexes are summarized in Table 1. Diffraction data were collected on a NONIUS Kappa CCD (for **1**) and a Bruker SMART CCD (for **2**) diffractometer in the ω–2ϑ scan mode at 295 K using graphite monochomated Mo Kα radiation, having $\lambda = 0.71073$ Å. The structures were solved by direct and Fourier methods and refined by full-matrix least-squares methods based on F^2 using the programs SHELXS-97 and SHELXL-97 [15]. All non-hydrogen atoms were readily located and refined by anisotropic thermal parameters.

Table 1
Crystallographic data for **1** and **2**

Compound	**1**	**2**
Empirical formula	$C_{24}H_{16}MnN_{10}$	$C_{40}H_{28}Cl_2Mn_2N_{18}O_{10}$
Formula weight	499.41	1101.58
Crystal system	monoclinic	triclinic
Space group	$P2_1/c$	$P\bar{1}$
a (Å)	9.6835(1)	7.9394(1)
b (Å)	8.6890(1)	10.6920(1)
c (Å)	28.5043(5)	14.0373(2)
α (°)	90.00	71.4922(6)
β (°)	98.8178(6)	79.6184(6)
γ (°)	90.00	82.6036(6)
V (Å^3)	2370.00(6)	1108.20(2)
Z	4	1
T (K)	295(2)	295(2)
λ (Mo Kα) (Å)	0.71073	0.71073
D_{calc} (g cm^{-3})	1.400	1.651
μ (mm^{-1})	0.591	0.772
F(000)	1020	558
2θ Range (°)	4.26–55	3.10–55
Total reflections	26602	28495
Unique reflections (R_{int})	5398 (0.0658)	5083 (0.0467)
R_1[a]/wR_2[b] ($I > 2\sigma(I)$ data)	0.0482/0.1108	0.0488/0.1373
R_1[a]/wR_2[b] (all data)	0.0934/0.1355	0.0737/0.1618

[a] $R_1 = [\sum\|F_o| - |F_c\|/\sum|F_o|]$.
[b] $wR_2 = [\sum w(F_o^2 - F_c^2)^2 / \sum w(F_o^2)^2]^{1/2}$.

The final least-squares refinements (R_1) based on [$I > 2\sigma(I)$] converged to 0.0482 for **1** and 0.0488 for **2**.

3. Results and discussion

3.1. Description of the structure of $[Mn^{II}(DMeDPQ)(\mu_{1,5}\text{-}dca)_2]_n$ (1)

An ORTEP representation of the asymmetric unit of **1** is shown in Fig. 1, while the coordination environment and the construction of one-dimensional double chain is shown in Fig. 2. Selected bond lengths and bond angles are listed in Table 2. The metal ion is hexacoordinated by DMeDPQ and dicyanamide anions. DMeDPQ behaves as bidentate chelating ligand through one quinoxaline nitrogen and one pyridyl nitrogen, while the other two nitrogen atoms remain uncoordinated. The remaining four positions are occupied by the nitrile nitrogens of four dicyanamide ligands. The other ends of two dicyanamides, bonded to a metal ion in *trans* positions, coordinate to two different manganese(II) centers to result in a one-dimensional chain propagated along the crystallographic *b* axis. The remaining two dca, which are in *cis* positions, make bridges to the adjacent metal ion of neighboring one-dimensional chain. As a result, an infinite one-dimensional double chain is generated by two single EE and two double EE dicyanamides. The geometry around the manganese(II) ion is distorted octahedral. The best equatorial plane is defined by the pyridyl nitrogen (N(7)) and three dicyanamide nitrogens (N(1C), N(6B), and N(4)) with the deviations of the ligand atoms and the metal center being, respectively, 0.023 Å (average) and 0.028 Å. The axial positions are occupied by the quinoxaline nitrogen (N(8)) and nitrile nitrogen (N(3)) of one double EE dca. The four Mn–N(dca) bond lengths [Mn–N(1C) = 2.187(2) Å, Mn–N(3) = 2.209(2) Å, Mn–N(4) = 2.214(3) Å, and Mn–N(6B) = 2.167(3) Å] are shorter than the metal–polypyridyl bond distances (Mn–N(7) = 2.2799(19) Å, Mn–N(8) = 2.3421(19) Å). These differences in bond lengths are in the range as observed for other Mn^{II}–dca systems [2a–c,4a,5a,5b]. Again, the *transoid* and *cisoid* angles vary, respectively, from 163.49(8)° to 176.32(19)° and from 71.67(6)° to 106.64(8)° indicative of distortion from O_h geometry.

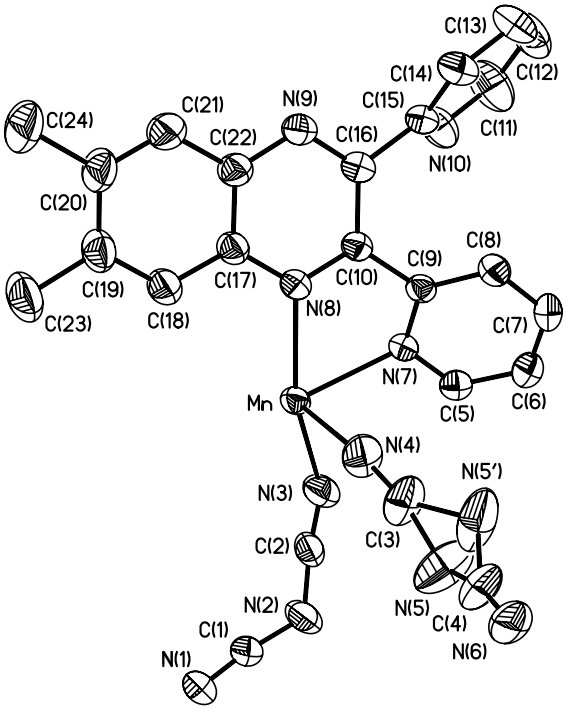

Fig. 1. ORTEP representation (40% thermal ellipsoids) of the asymmetric unit of **1**.

One single EE dca and one double EE dca link the metal ion in a nearly linear fashion with Mn–N–C angles of

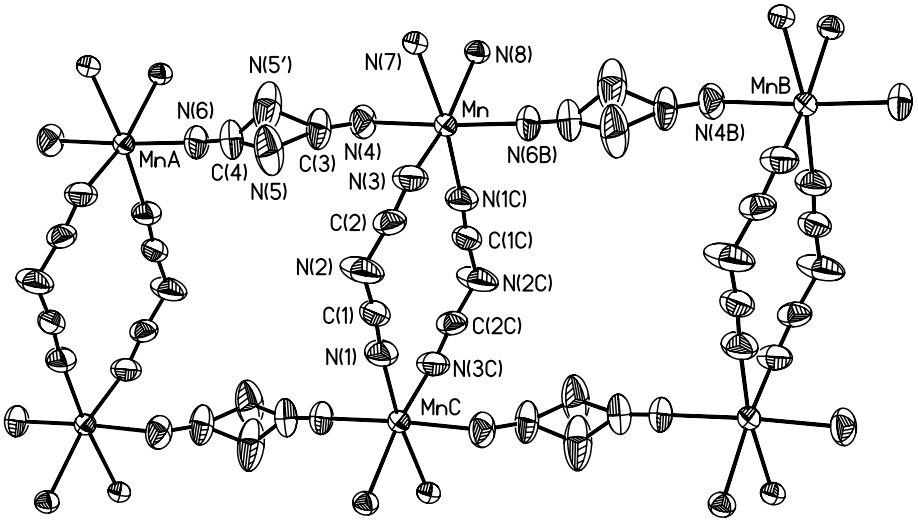

Fig. 2. Perspective view (40% thermal ellipsoids) of **1** demonstrating the coordination environment and construction of one-dimensional double chain. Except the donor centers, other atoms of the organic ligand (DMeDPQ) are omitted for clarity. Symmetry codes: Mn: x, y, z; MnA: x, $y-1$, z; MnB: x, $1+y$, z; MnC: $1-x$, $1-y$, $-z$.

Table 2
Selected bond lengths (Å) and angles (°) for **1**

M–N(1C)	2.187(2)
M–N(3)	2.209(2)
M–N(4)	2.214(3)
M–N(6B)	2.167(3)
M–N(7)	2.279(2)
M–N(8)	2.342(2)
C(1)–N(1)	1.129(3)
C(2)–N(3)	1.138(3)
C(3)–N(4)	1.105(4)
C(4)–N(6)	1.100(4)
C(1)–N(2)	1.293(4)
C(2)–N(2)	1.294(4)
C(3)–N(5)	1.347(7)
C(4)–N(5)	1.332(6)
N(1C)–M–N(7)	170.15(9)
N(3)–M–N(8)	163.49(8)
N(4)–M–N(6B)	176.32(19)
N(1C)–M–N(3)	89.79(9)
N(1C)–M–N(4)	89.50(9)
N(1C)–M–N(6B)	94.16(9)
N(1C)–M–N(8)	106.64(8)
N(3)–M–N(4)	87.77(10)
N(3)–M–N(6B)	92.62(10)
N(3)–M–N(7)	92.40(8)
N(4)–M–N(7)	80.99(7)
N(4)–M–N(8)	93.79(8)
N(6B)–M–N(7)	95.33(8)
N(6B)–M–N(8)	84.80(8)
N(7)–M–N(8)	71.67(6)
C(1)–N(2)–C(2)	121.7(3)
C(3)–N(5)–C(4)	116.4(5)
N(3)–C(2)–N(2)	172.8(3)
N(1)–C(1)–N(2)	172.6(3)
N(4)–C(3)–N(5)	164.0(7)
N(6)–C(4)–N(5)	162.9(7)
M–N(3)–C(2)	135.5(2)
M–N(1C)–C(1C)	173.3(2)
M–N(6B)–C(4B)	172.9(2)
M–N(4)–C(3)	149.1(3)

Symmetry code: as in Fig. 2.

172.9(2)° and 173.3(2)°. The other two dca coordinate in a significantly bent way having Mn–N–C angles of 135.5(2)° and 149.1(3)°. Due to the disorder of the amide nitrogen (N(5); N(5)···N(5′) = 1.07(3) Å) of the single EE dca, its C–N distances are larger than that in the double EE dca. However, the C≡N and C–N distances in either of the two crystallographically different dca anions are very similar (Table 2). In addition, the C–N–C angles (121.7(3)° and 116.4(5)°) indicate the pseudo C_{2v} symmetry of the dicyanamides.

3.2. Description of the structure of $[Mn^{II}_2(TPT)_2(\mu_{1,5}\text{-dca})_2(H_2O)_2](ClO_4)_2$ (**2**)

The structure of **2** (Fig. 3 and Table 3) shows that this is a discrete dinuclear complex where the metal centers are doubly bridged by two double EE dicyanamides. One triazine and two pyridine nitrogens of the multidentate heterocyclic ligand, TPT, coordinate to each of the two metal centers and hence block three coordination positions. Between the Mn–N(TPT) and Mn–N(dca) bond distances (2.235(2)–2.316(2) Å and 2.134(3)–2.181(2) Å, respectively), the former is significantly larger. Such differences in bond lengths have been observed previously in related compounds of manganese(II) [2a–c,4a,5a,5b]. The stereochemistry of the metal ion, due to the rigidity of the donor environment of TPT, deviates appreciably from ideal octahedron. In addition to the differences in the metal–ligand bond distances, the *transoid* angles (140.27(7)°, 167.17(10)°, and 172.97(9)°) and the wide range of *cisoid* angles (70.04(7)–118.29(11)°) are indicative of significant distortion of the coordination environment. While the deviations of the metal ion and the donor centers from the least-squares planes N(2)N(7)N(9)O(1) and N(1)N(2)N(3)N(9), the latter of which is a better square plane, are not very high (<0.08 Å), practically no plane is defined by N(1), N(3), N(7), and O(1) (deviations > 0.4 Å) which is indicative of significant distortion. All the bond distances and bond angles (Table 3) of the dicyanamide are within the usual ranges and are indicative of the pseudo C_{2v} symmetry. One end of the crystallographically equivalent dicyanamide is bonded almost linearly (Mn–N(9)–C(20) = 170.8(3)°), while the other end coordinates in a significantly bent way (Mn–N(7)–C(19) = 142.5(2)°).

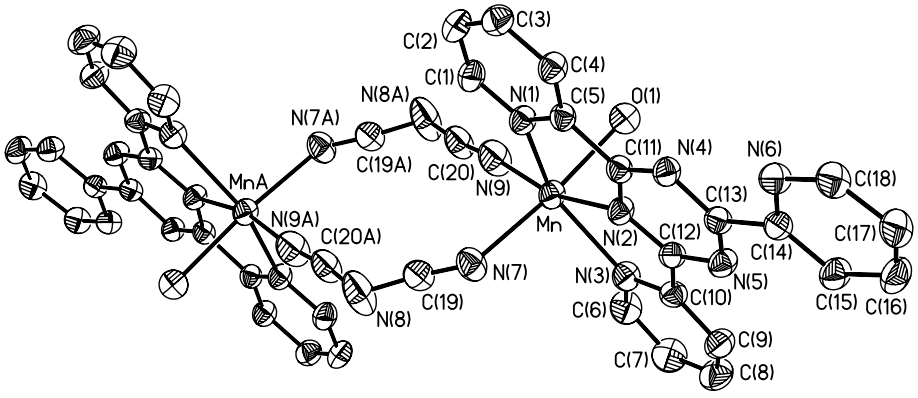

Fig. 3. ORTEP (40% thermal ellipsoids) representation of the dication in **2**. Symmetry codes: Mn, x, y, z; MnA, $2-x$, $1-y$, $1-z$.

Table 3
Selected bond lengths (Å) and angles (°) for **2**

M–N(1)	2.316(2)
M–N(2)	2.235(2)
M–N(3)	2.299(2)
M–N(7)	2.181(2)
M–N(9)	2.134(3)
M–O(1)	2.233(2)
C(19)–N(7)	1.139(4)
C(20)–N(9)	1.132(4)
C(19)–N(8)	1.296(4)
C(20A)–N(8)	1.289(4)
N(1)–M–N(3)	140.27(7)
N(2)–M–N(9)	167.17(10)
N(7)–M–O(1)	172.97(9)
N(1)–M–N(2)	70.04(7)
N(1)–M–N(7)	94.58(9)
N(1)–M–N(9)	100.87(11)
N(1)–M–O(1)	85.88(8)
N(2)–M–N(3)	70.24(8)
N(2)–M–N(7)	102.20(9)
N(2)–M–O(1)	84.56(8)
N(3)–M–N(7)	93.77(9)
N(3)–M–N(9)	118.29(11)
N(3)–M–O(1)	90.31(8)
N(7)–M–N(9)	87.24(10)
N(9)–M–O(1)	85.79(10)
C(19)–N(8)–C(20A)	123.1(3)
N(7)–C(19)–N(8)	173.3(3)
N(9)–C(20)–N(8A)	171.4(3)
M–N(7)–C(19)	142.5(2)
M–N(9)–C(20)	170.8(3)

Symmetry code: as in Fig. 3.

3.3. Magnetic properties

Variable-temperature (5–300 K) magnetic behaviors at fixed field strength of 1 T of the two complexes are shown in Fig. 4 in the form of $\chi_M T$ versus T plots. For **1**, the $\chi_M T$ value at 300 K is 4.37 $cm^3\ mol^{-1}$ K, which is equal to the spin-only $\chi_M T$ value of high spin Mn^{II}. The $\chi_M T$ value (8.67 $cm^3\ mol^{-1}$ K) of **2** at 300 K is also practically equal to the theoretical value (8.75 $cm^3\ mol^{-1}$ K) for two non-correlated spins of $S_1 = 5/2$ and $S_2 = 5/2$. On lowering the temperatures, $\chi_M T$ values of both the complexes remain almost constant to ~50 K and then decrease rapidly to 5 K where the $\chi_M T$ values are 2.51 and 4.63 $cm^3\ mol^{-1}$ K for **1** and **2**, respectively. The profiles indicate the existence of a very weak antiferromagnetic interaction in both complexes. It may be mentioned that consistent data of magnetic susceptibilities of **1** and **2** are obtained with the samples from different preparations using the same method as described in Section 2.

Currently, no theoretical model exists to analyze the magnetic data of one-dimensional ladder compounds containing $S = 5/2$ ions. However, the system can be modelled as single EE dca bridged infinite chains that are subjected to interchain interactions through the double EE dicyanamides. In that case, the compound can be analyzed with Eq. (1), where $\chi_{1\text{-D}}$ represents the susceptibilities of infinite chain compounds [16] and zJ' implies, in molecular field approximation, the exchange interaction mediated through the double EE dicyanamides.

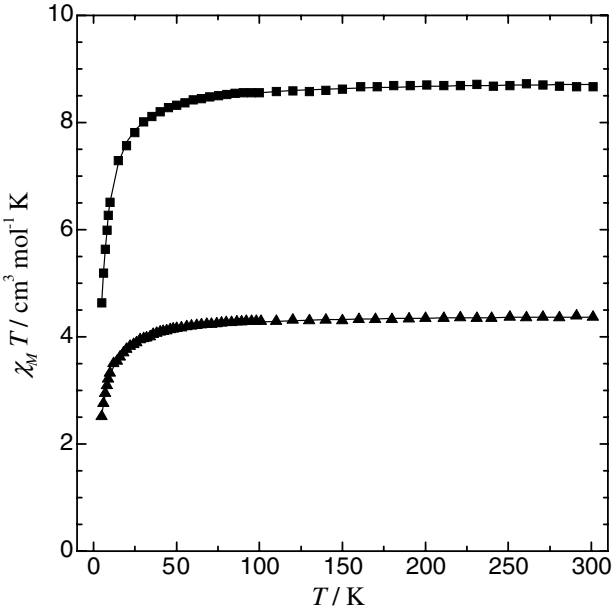

Fig. 4. Experimental (▲ for **1** and ■ for **2**) and calculated (——) $\chi_M T$ vs. T plots for **1** and **2**.

$$\chi_M = \frac{\chi_{1\text{-D}}}{1 - 2zJ'\chi_{1\text{-D}}/N\beta^2 g^2}, \tag{1}$$

where

$$\chi_{1\text{-D}} = \frac{N\beta^2 g^2 S(S+1)}{3kT}\,\frac{1+u}{1-u}$$

with

$$u = \coth\frac{2JS(S+1)}{kT} - \frac{kT}{2JS(S+1)}.$$

Taking the g value fixed at 2.0, least-squares fitting of the susceptibility data with Eq. (1) leads to an excellent simulation (Fig. 4) with $J = -0.12$ cm^{-1} and $zJ' = -0.13$ cm^{-1}; the agreement factor (R), defined as $[\sum\{(\chi_M T)_{obs} - (\chi_M T)_{calc}\}^2/\sum\{(\chi_M T)_{obs}\}^2]$, being 4.23×10^{-3}. Now, excluding single EE bridged centers, the number (z) of neighboring metal ions around a manganese(II) center is 1. Therefore, the value of J' becomes -0.13 cm^{-1}. Hence, the magnitudes (-0.12 and -0.13 cm^{-1}) of antiferromagnetic coupling through the single EE dca and double EE dca can be considered as almost equal. For the dinuclear complex **2**, the susceptibility data are well fitted (Fig. 4) with the theoretical equation derived from the Hamiltonian $\mathbf{H} = -2J\mathbf{S}_1 \cdot \mathbf{S}_2$. In this case, global minimization takes place with $J = -0.31$ cm^{-1}, $g = 2.0$ (fixed), and $R = 2.91 \times 10^{-3}$.

The susceptibility data of the double chain compound **1** can also be well fitted with the dinuclear model ($\mathbf{H} = -2J\mathbf{S}_1 \cdot \mathbf{S}_2$) converging with $J = -0.3$ cm^{-1}, $g = 2.0$ (fixed), and $R = 8.43 \times 10^{-3}$. Evidently, average J values for the two routes have been considered here. Again, consideration of the dinuclear model with molecular field

approximation results in global minimization with $J = -0.24\ \mathrm{cm}^{-1}$, $zJ' = -0.05\ \mathrm{cm}^{-1}$, $g = 2.0$ (fixed), and $R = 6.84 \times 10^{-3}$. Simulation of the experimental data of **1** with the three models mentioned above reveals that the J value of the double chain compound lies in the range -0.05 to $-0.24\ \mathrm{cm}^{-1}$. It may be noted that the observation of only a weak antiferromagnetic interaction in both compounds **1** and **2** is consistent with the magnetic properties of the previously reported examples of dicyanamide bridged manganese(II) compounds [2a–c,4a,5a,5b].

Acknowledgements

Financial support from the National Science Council, Taiwan (Grant NSC-93-2113-M-032-002) and Department of Science and Technology, Government of India (Grant SR/S1/IC-27/2002) is gratefully acknowledged.

Appendix A. Supporting information

Crystallographic information is available (CCDC reference numbers: 195435 (**1**) and 201878 (**2**)) from the Cambridge Crystallographic Data Center, 12 Union Road, Cambridge CB2 1EZ, UK (fax: +44 1223 336 033; e-mail: deposit@ccdc.cam.ac.uk). Supplementary data associated with this article can be found, in the online version, at doi:10.1016/j.poly.2006.06.019.

References

[1] (a) S.R. Batten, P. Jensen, B. Moubaraki, K.S. Murray, R. Robson, Chem. Commun. (1998) 439;
(b) J.L. Manson, C.R. Kmety, Q.-z. Huang, J.W. Lynn, G.M. Bendele, S. Pagola, P.W. Stephens, L.M. Liable-Sands, A.L. Rheingold, A.J. Epstein, J.S. Miller, Chem. Mater. 10 (1998) 2552;
(c) M. Kurmoo, C.J. Kepert, New J. Chem. (1998) 1515;
(d) S.R. Batten, K.S. Murray, Coord. Chem. Rev. 246 (2003) 103.

[2] (a) B. Vangdal, J. Carranza, F. Lloret, M. Julve, J. Sletten, J. Chem. Soc., Dalton Trans. (2002) 566;
(b) L.-Y. Zhang, L.-X. Shi, Z.-N. Chen, Inorg. Chem. 42 (2003) 633;
(c) V. Jacob, S. Mann, G. Huttner, O. Walter, L. Zsolnai, E. Kaifer, P. Rutsch, P. Kircher, E. Bill, Eur. J. Inorg. Chem. (2001) 2625.

[3] (a) G.A. van Albada, M.E. Quiroz-Castro, I. Mutikainen, U. Turpeinen, J. Reedijk, Inorg. Chim. Acta 298 (2000) 221;
(b) A. Escuer, F.A. Mautner, N. Sanz, R. Vicente, Inorg. Chem. 39 (2000) 1668;
(c) A. Claramunt, A. Escuer, F.A. Mautner, N. Sanz, R. Vicente, J. Chem. Soc., Dalton Trans. (2000) 2627;
(d) S. Martin, M.G. Barandika, J.I.R. de Larramendi, R. Cortés, M. Font-Bardia, L. Lezama, Z.E. Serna, S. Solans, T. Rojo, Inorg. Chem. 40 (2001) 3687;
(e) S.R. Batten, P. Jenson, C.J. Kepert, M. Kurmoo, B. Moubaraki, K.S. Murray, D. Price, J. Chem. Soc., Dalton Trans. (1999) 2987;
(f) J.L. Manson, A.M. Arif, J.S. Miller, J. Mater. Chem. 9 (1999) 979.

[4] (a) I. Riggio, G.A. van Albada, D.D. Ellis, A.L. Spek, J. Reedijk, Inorg. Chim. Acta 313 (2001) 120;
(b) S.R. Batten, A.R. Harris, P. Jensen, K.S. Murray, A. Ziebell, J. Chem. Soc., Dalton Trans. (2000) 3829;
(c) B.-W. Sun, S. Gao, B.-Q. Ma, Z.-M. Wang, New J. Chem. 24 (2000) 953;
(d) A. Claramunt, A. Escuer, F.A. Mautner, N. Sanz, R. Vicente, J. Chem. Soc., Dalton Trans. (2000) 2627;
(e) S.R. Marshall, C.D. Incarvito, J.L. Manson, A.L. Rheingold, J.S. Miller, Inorg. Chem. 39 (2000) 1969;
(f) S.R. Batten, P. Jenson, C.J. Kepert, M. Kurmoo, B. Moubaraki, K.S. Murray, D. Price, J. Chem. Soc., Dalton Trans. (1999) 2987;
(g) J.L. Manson, D.W. Lee, A.L. Rheingold, J.S. Miller, Inorg. Chem. 37 (1998) 5966;
(h) I. Dasna, S. Golhen, L. Ouahab, M. Fettouhi, O. Peña, N. Daro, J.-P. Sutter, Inorg. Chim. Acta 326 (2001) 37.

[5] (a) H.-H. Lin, S. Mohanta, C.-J. Lee, H.-H. Wei, Inorg. Chem. 42 (2003) 1584;
(b) B.-W. Sun, S. Gao, B.-Q. Ma, D.-Z. Niu, Z.-M. Wang, J. Chem. Soc., Dalton Trans. (2000) 4187;
(c) C. Paraschiv, J.-P. Sutter, M. Schmidtmann, A. Müller, M. Andruh, Polyhedron 22 (2003) 1611;
(d) G.A. van Albada, S. Tanase, A. Mohamadou, I. Mutikainen, U. Turpeinen, J. Reedijk, Polyhedron (2006) in press.

[6] (a) J.W. Raebiger, J.L. Manson, R.D. Sommer, U. Geiser, A.L. Rheingold, J.S. Miller, Inorg. Chem. 40 (2001) 2578;
(b) P.M. van der Werff, S.R. Batten, P. Jensen, B. Moubaraki, K.S. Murray, Inorg. Chem. 40 (2001) 1718;
(c) S. Triki, F. Thétiot, J.-R. Galán-Mascaros, J. Sala Pala, K. Dunbar, New J. Chem. 25 (2001) 954;
(d) S.R. Marshall, C.D. Incarvito, J.L. Manson, A.L. Rheingold, J.S. Miller, Inorg. Chem. 39 (2000) 1969;
(e) S. Martin, M.G. Barandika, R. Cortès, J.I. Ruiz de Larramendi, M.K. Urtiaga, L. Lezama, M.I. Arriortua, T. Rojo, Eur. J. Inorg. Chem. (2001) 2107;
(f) D. Armentano, G. de Munno, F. Guerra, J. Faus, F. Lloret, M. Julve, J. Chem. Soc., Dalton Trans. (2003) 4626.

[7] J.L. Manson, J.A. Schlueter, U. Geiser, M.B. Stone, D.H. Reich, Polyhedron 20 (2001) 1423.

[8] A.M. Kutasi, S.R. Batten, B. Moubaraki, K.S. Murray, J. Chem. Soc., Dalton Trans. (2002) 819.

[9] S.R. Batten, P. Jensen, B. Moubaraki, K.S. Murray, R. Robson, Chem. Commun. (2000) 793.

[10] (a) Y.-J. Shi, L.-H. Li, Y.-Z. Li, X.-T. Chen, Z. Xue, X.-Z. You, Polyhedron 22 (2003) 917;
(b) H.-L. Sun, S. Gao, B.-Q. Ma, G. Su, Inorg. Chem. 42 (2003) 5399.

[11] Y.M. Chow, D. Britton, Acta Crystallogr., Sect. B 31 (1975) 1934.

[12] Y.-J. Shi, X.-T. Chen, Y.-Z. Li, Z. Xue, X.-Z. You, New J. Chem. 26 (2002) 1711.

[13] (a) I. Potocnák, M. Burcák, W. Massa, L. Jäger, Acta Crystallogr., Sect. C 58 (2002) m523;
(b) R. Boča, M. Boča, M. Gembický, L. Jäger, C. Wagner, H. Fuess, Polyhedron 23 (2004) 2337;
(c) I. Potocnak, M. Dunaj-Jurco, D. Miklos, J. Jager, Acta Crystallogr., Sect. C 52 (1996) 1653.

[14] S.R. Marshall, C.D. Incarvito, W.W. Shum, A.L. Rheingold, J.S. Miller, Chem. Commun. (2002) 3006.

[15] (a) G.M. Sheldrick, SHELXL-97: A Program for Crystal Structure Solution, University of Göttingen, Göttingen, Germany, 1990;
(b) G.M. Sheldrick, SHELXL-97: A Program for Crystal Structure Refinement, University of Göttingen, Göttingen, Germany, 1997.

[16] M.E. Fisher, Am. J. Phys. 32 (1964) 343.

involve a room temperature dehydroxylation of the HAS_A form. We proposed that further substitution of $Si(OH)_4$ into HAS_A was driving the dehydroxylation [8] and it is this proposition that is tested further in the current research. We have used a combination of solution and solid-state structural techniques to provide evidence that the formation HAS_A is a prerequisite to the formation of HAS_B.

2. Experimental

2.1. Preparation of solutions

All reagents used were of the highest purity available. Solutions which included a wide range of concentrations of $Si(OH)_4$ (25–2000 μmol/L) applied across three molar ratios (0.5, 1.0, 2.0) of $Si(OH)_4$ to Al were prepared in PTFE phials and containers (Cowie Technology Ltd., UK) using ultrapure water (conductivity < 0.067 μS/cm, Elga UK) which included 100 mmol/L KNO_3 as background electrolyte and which were buffered at pH 6.0 with 25 mmol/L PIPES (piperazine-*N*,*N*′-bis-2-ethanesulphonic acid). Stock solutions of $Si(OH)_4$, up to a maximum concentration of 2.0 mmol/L, were prepared by cation exchange of Na_4SiO_4 and either diluted as required or used in the place of ultrapure water. Al was added from a freshly prepared 1 mol/L stock of $Al(NO_3)_3 \cdot 9H_2O$ in 1% HNO_3. An established method was used for the preparation of all HAS solutions [5] and all solutions were incubated at 20 °C for the requisite time period prior to sampling.

The precipitation experiments (see Fig. 1) involved the preparation of 20 mL volumes of 5 replicates of 21 different combinations of $Si(OH)_4$ and Al. These were aged for 24 h and then filtered through 0.1 μm polyvinylidene fluoride membrane filters (Durapore). For the ageing study (see Fig. 2) 100 mL volumes of 5 replicates of 4 preparations which included 800 μmol/L Al and either 800, 1100, 1500 or 2000 μmol/L $Si(OH)_4$ were aged for up to 500 h. These solutions were periodically sampled and filtered using syringe filters (Millipore) which incorporated the same 0.1 μm polyvinylidene fluoride membrane filters (Durapore). Analagous solutions of larger volume, 500 mL, were run in parallel and, following ageing for typically, 12, 72, 168 or 336 h, were filtered (0.1 μm membrane filtration) to collect significant quantities (>200 mg) of precipitate for subsequent solid-state analyses. For all studies, post-filtration [$Si(OH)_4$] were measured spectrophotometrically (λ_{max} 810 nm) as the reduced blue-molybdosilicic acid complex [9] and post-filtration [Al] by graphite furnace atomic absorption spectrometry (GFAAS) using a method developed in our laboratory [10].

2.2. Solid-state analyses

Solid phases collected by membrane filtration were dried to a constant weight at 37 °C and thereafter gently ground to a fine powder using an agate mortar and pestle. The elemental composition, structural identity and thermal chemistry of each of the solid phases were determined by electron microprobe analysis, solid-state NMR and thermogravimetric analysis, respectively, using methods which have been described in detail in recent publications [8,11].

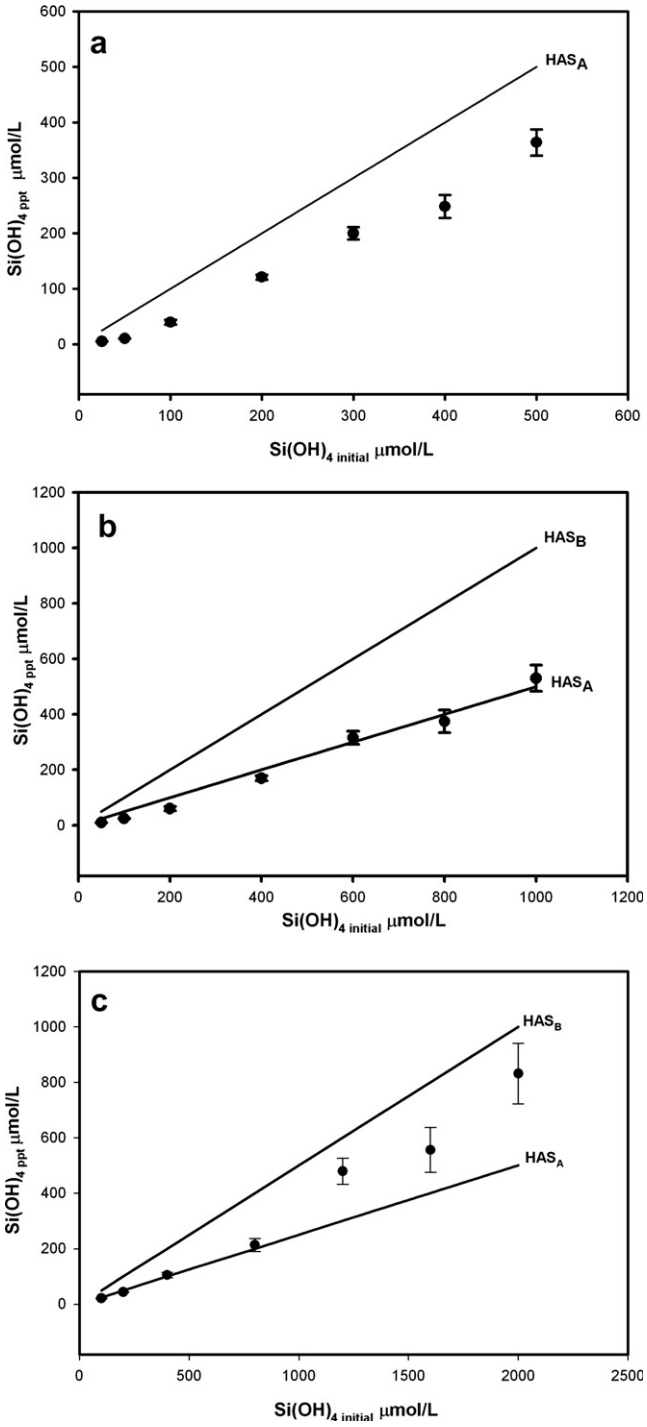

Fig. 1. The precipitation of $Si(OH)_4$ from solutions ($Si(OH)_{4\ ppt}$) in which the initial ratio of $Si(OH)_4$ to Al was (a) 1:2; (b) 1:1; (c) 2:1. Mean and SD are plotted, $n = 5$. Solid lines indicate the theoretical precipitation of $Si(OH)_4$ if all of the available Al were precipitated by the formation of HAS_A (a) and HAS_A or HAS_B (b,c).

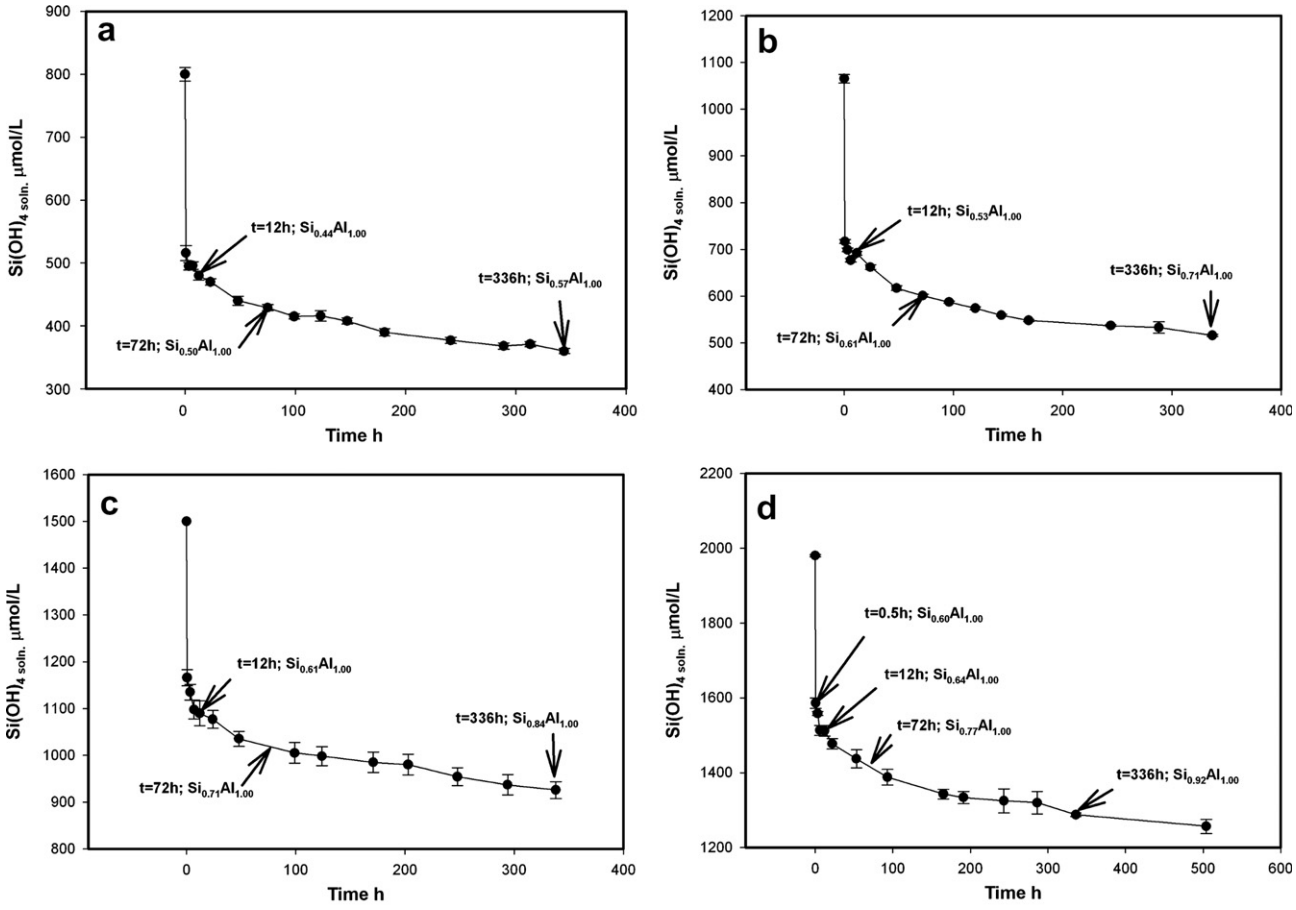

Fig. 2. The concentration of $Si(OH)_4$ remaining in solution ($Si(OH)_{4soln.}$) following the reaction of (a) 800; (b) 1100; (c) 1500; (d) 2000 μmol/L $Si(OH)_4$ with 800 μmol/L Al and ageing of the solutions at 20 °C for up to 500 h. Mean and SD are plotted, $n = 5$. The arrows indicate the times at which solid phases were collected and their relative contents of Si and Al determined by electron probe microanalysis.

3. Results

3.1. Precipitation of $Si(OH)_4$ by Al

$Si(OH)_4$ was precipitated within the 24 h period of ageing under each of the solution conditions which ranged from ca 25 μmol/L $Si(OH)_4$/50 μmol/L Al to ca 2000 μmol/L $Si(OH)_4$/1000 μmol/L Al. The proportion of available $Si(OH)_4$ precipitated in the former was ca 20% whereas this increased up to ca 100% in the latter. There was no Al post-filtration for any of the initial combinations of $Si(OH)_4$ and Al. When these filtration data were expressed according to the theoretical composition of the solid phase formed (i.e. either HAS_A or HAS_B) it was clear that the probable composition of precipitate depended upon the initial solution concentrations of $Si(OH)_4$ and Al and their ratio (Fig. 1). Thus for $Si(OH)_4$:Al ratios of 0.5 and 1.0 the filtration data predicted the formation of HAS_A whereas for a ratio of 2.0 the data predicted the formation of HAS_A at lower total concentrations (<1000 μmol/L $Si(OH)_4$) and HAS_B, or a mixture of HAS_A and HAS_B, at higher total concentrations (1000–2000 μmol/L $Si(OH)_4$) (Fig. 1).

3.2. Influence of ageing on the precipitation of $Si(OH)_4$ and the nature of the solid phase formed

Four different solution compositions were investigated over an ageing period up to 500 h (Fig. 2). The compositions were chosen to reflect a range of $Si(OH)_4$ to Al ratios over which the formation of either HAS_A or HAS_B was predicted [7].

3.2.1. 800 μmol/L $Si(OH)_4$:800 μmol/L Al

The $[Si(OH)_4]$ was rapidly reduced to ca 500 μmol/L within only 0.5 h ageing and thereafter continued to fall steadily before approaching a plateau $[Si(OH)_4]$ of ca 370 μmol/L after approximately 300 h ageing (Fig. 2a). There was no Al post-filtration and so ca 800 μmol/L Al resulted in the co-precipitation of ca 400 μmol/L $Si(OH)_4$ within 300–336 h. The Si:Al ratio of solid phases collected after 12 ($Si_{0.44}Al_{1.00}$), 72 ($Si_{0.50}Al_{1.00}$) and 336 h ($Si_{0.57}Al_{1.00}$) increased with ageing of solutions and mirrored the slow reductions in $[Si(OH)_4]_{soln.}$. Investigation of these three solid phases by TGA revealed a sharp exotherm at 191 °C at 12 h (Fig. 3) which was absent at 72 and 336 h. Each of

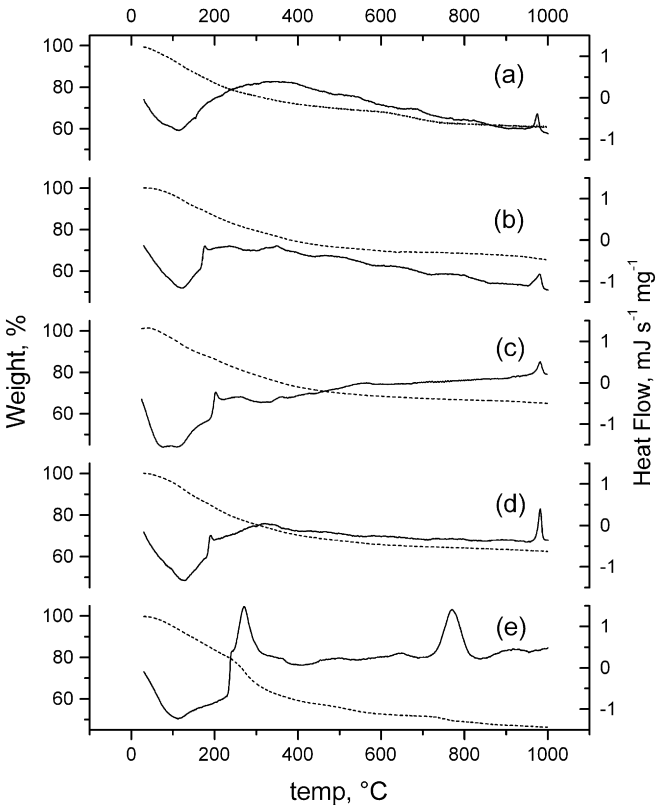

Fig. 3. Representative TGA–DSC plots of solid phases collected after 12 h ageing at 20 °C from PIPES-buffered solutions containing (a) 2000 μmol/L $Si(OH)_4$ and 800 μmol/L Al; (b) 1500 μmol/L $Si(OH)_4$ and 800 μmol/L Al; (c) 1100 μmol/L $Si(OH)_4$ and 800 μmol/L Al; (d) 800 μmol/L $Si(OH)_4$ and 800 μmol/L Al; (e) 800 μmol/L Al. Heat flows are indicated by solid lines and weight losses by dashed lines.

the solid phases revealed an endotherm at 115–120 °C and a sharp exotherm at ca 980 °C.

3.2.2. 1100 μmol/L $Si(OH)_4$:800 μmol/L Al

The initial $[Si(OH)_4]$ was rapidly reduced to ca 700 μmol/L within 0.5 h and continued to fall to ca 500 μmol/L after ageing for 336 h (Fig. 2b). There was no Al post-filtration and ca 800 μmol/L Al co-precipitated ca 400 μmol/L $Si(OH)_4$ within 0.5 h and 600 μmol/L $Si(OH)_4$ after 336 h. The Si:Al ratios of solid phases collected after 12 ($Si_{0.53}Al_{1.00}$), 72 ($Si_{0.61}Al_{1.00}$) and 336 h ($Si_{0.71}Al_{1.00}$) increased with ageing and again mirrored the reductions in $[Si(OH)_4]_{soln.}$. TGA of solid phases revealed a sharp exothermic peak at 204 °C in the precipitate collected after 12 h ageing (Fig. 3) which was not present in precipitates collected after 24, 72, 168 and 336 h. Each of the solid phases revealed an endotherm at 115–120 °C and a sharp exotherm at ca 980 °C.

3.2.3. 1500 μmol/L $Si(OH)_4$:800 μmol/L Al

The initial $[Si(OH)_4]$ was rapidly reduced to ca 1100 μmol/L within 0.5 h and thereafter fell less quickly and reached a plateau $[Si(OH)_4]$ of ca 930 μmol/L after 336 h (Fig. 2c). There was no Al post-filtration and ca 800 μmol/L Al co-precipitated ca 400 μmol/L $Si(OH)_4$ within 0.5 h and 600 μmol/L $Si(OH)_4$ after 336 h. The Si:Al ratios of solid phases collected after 12 ($Si_{0.61}Al_{1.00}$), 72 ($Si_{0.71}Al_{1.00}$) and 336 h ($Si_{0.84}Al_{1.00}$) increased with ageing and reflected the continued precipitation of $Si(OH)_4$ from the solutions. TGA of solid phases showed a small exotherm at 176 °C for the solid collected after 12 h (Fig. 3) which was not evident after 72 or 336 h. All three solid phases indicated endotherms at 115–120 °C and sharp exotherms at ca 980 °C.

3.2.4. 2000 μmol/L $Si(OH)_4$:800 μmol/L Al

The initial $[Si(OH)_4]$ was rapidly reduced to ca 1600 μmol/L within 0.5 h and continued to fall to ca 1300 μmol/L after more than 500 h ageing (Fig. 2d). There was no Al post-filtration and ca 800 μmol/L Al co-precipitated ca 400 μmol/L $Si(OH)_4$ within 0.5 h and ca 700 μmol/L $Si(OH)_4$ after 500 h. These changes in $[Si(OH)_4]_{soln.}$ were mirrored by increased Si:Al ratios of solid phases collected after 0.5 ($Si_{0.60}Al_{1.00}$), 12 ($Si_{0.64}Al_{1.00}$), 72 ($Si_{0.77}Al_{1.00}$) and 336 h ($Si_{0.92}Al_{1.00}$). TGA spectra for solid phases collected after 12, (Fig. 3) 72 and 336 h were identical and showed an endotherm at 115–120 °C and a sharp exotherm at ca 980 °C. Solid-state ^{27}Al MAS NMR of solid phases collected after 0.5, 72 and 336 h revealed two discrete shifts at 1.25 (Al^{VI}) and 55 (Al^{IV}) ppm and that the proportion of Al^{IV} to Al^{VI} increased with the age of the solid phase (Fig. 4a). Solid-state ^{29}Si MAS NMR (Fig. 4b) indicated a single shift, the peak of which increased from −83 to −89 ppm with increased age of the solid phase, which was generally indicative of Si in the vicinity of 1-2Al (Q^3(1-2Al)).

4. Discussion

The formation of HAS and their subsequent nucleation and growth towards aggregates which could be collected by 0.1 μm membrane filtration occurred in all combinations of concentrations of $Si(OH)_4$ and Al. For some of the combinations the precipitation cascade was sufficiently rapid to enable solid phases to be collected within only 0.5 h ageing. The experiments in which different combinations of initial concentration of $Si(OH)_4$ and ratio's of $Si(OH)_4$ to Al were aged for only 24 h appeared to demonstrate that within this time period the nature of the precipitate formed was finely balanced between three possible idealised forms;

$$Al(OH)_{3(s)} \leftrightarrow HAS_A \leftrightarrow HAS_B$$

In solutions in which the initial ratio of $Si(OH)_4$ to Al was 0.5 (the stoichiometry of HAS_A) the amount of $Si(OH)_4$ which was precipitated from solution was always less than would be expected if HAS_A was the only product (Fig. 1a). Post-filtration analyses of [Al] in each combination of initial $[Si(OH)_4]$ and $Si(OH)_4$ to Al ratio indicated that ca 100% of the available Al was co-precipitated and thus the solid phases formed for $Si(OH)_4$ to Al ratios of 0.5 must have included both $Al(OH)_{3(s)}$ and HAS_A. This indicated

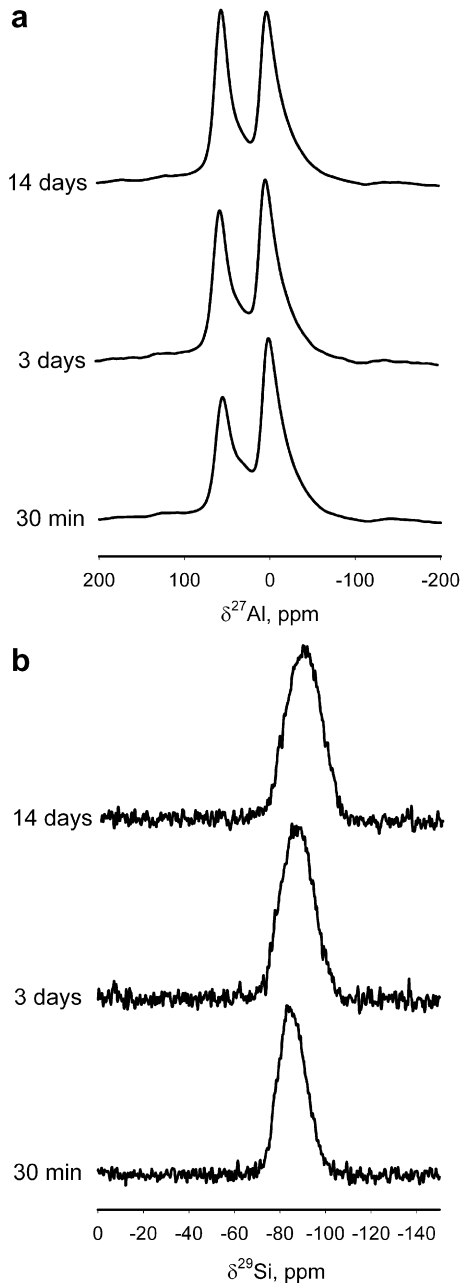

Fig. 4. Representative (a) ^{27}Al and (b) ^{29}Si NMR spectra of solid phases collected after 0.5, 72 and 336 h ageing at 20 °C from PIPES-buffered solutions containing 2000 μmol/L $Si(OH)_4$ and 800 μmol/L Al.

that while HAS_A was rapidly formed something prevented all of the theoretically possible $Si(OH)_4$ being incorporated into this phase within the 24 h period of ageing. The results of the precipitation experiments in which the initial ratio of $Si(OH)_4$ to Al was 1.0 (the stoichiometry of HAS_B) suggested that the 'something' was the residual $[Si(OH)_4]$ which followed the initial rapid formation of HAS_A (Fig. 1b). In these experiments the amount of $Si(OH)_4$ which was co-precipitated was in each case equivalent to what would have been expected from the formation of HAS_A (Fig. 1b). Thus HAS_A was the dominant solid phase formed under these conditions and the higher residual $[Si(OH)_4]$ which was due to the initial $Si(OH)_4$ to Al ratio of 1.0 was critical in ensuring that all of the available Al was incorporated into HAS_A. For example, if we compare the efficacy with which 800 μmol/L Al precipitated $Si(OH)_4$ in solutions in which the initial $Si(OH)_4$ to Al ratio was either 0.5 (Fig. 1a) or 1.0 (Fig. 1b) we find that 248.4 ± 20.9 μmol/L of $Si(OH)_4$ were precipitated in the former (ca 150 μmol/L $Si(OH)_4$ remained in solution) whereas 374.7 ± 40.8 μmol/L $Si(OH)_4$ were precipitated in the latter (ca 425 μmol/L $Si(OH)_4$ remained in solution). These results have demonstrated that for initial solution conditions of 800 μmol/L Al and 400 μmol/L $Si(OH)_4$ while HAS_A was the predominant solid phase formed the reaction was prevented from reaching completion (i.e. all $Al(OH)_{3(s)}$/$Si(OH)_4$ precipitated as HAS_A) by a limiting residual $[Si(OH)_4]$. However, when the initial $[Si(OH)_4]$ was 800 μmol/L the additional residual $Si(OH)_4$ ensured that all available $Al(OH)_{3(s)}$ reacted with $Si(OH)_4$ to give a solid phase consisting of ca pure HAS_A. By logical extension, an initial $Si(OH)_4$ to Al ratio of 1.0 should, theoretically, have been sufficient to allow the formation of HAS_B and yet there was little evidence that HAS_B was formed in these solutions during 24 h ageing (Fig. 1b). Thus while the residual $[Si(OH)_4]$ promoted the formation of HAS_A it was not sufficient to support the subsequent formation of HAS_B through the reaction of $Si(OH)_4$ with HAS_A. In these 24 h ageing experiments evidence for the formation of HAS_B was only obtained from those solutions in which the initial $Si(OH)_4$ to Al ratio was 2.0 (Fig. 1c). However, it was not simply the ratio of $Si(OH)_4$ to Al that was important since the evidence for the formation of HAS_B only became clear at initial $[Si(OH)_4] \geqslant 1200$ μmol/L (Fig. 1c). The results of the 24 h precipitation experiments appeared to suggest that the formation of HAS was dependent upon the combination of both the initial $[Si(OH)_4]$ and the $Si(OH)_4$ to Al ratio. In addition they afforded strong evidence that the formation of HAS_A was a prerequisite to the formation of HAS_B.

When the formation of HAS in solutions including 800 μmol/L Al and 800, 1100, 1500 or 2000 μmol/L $Si(OH)_4$ were investigated over time we found further evidence that HAS_A was a prerequisite to the formation of HAS_B. It was remarkable that in each of these conditions the initial $[Si(OH)_4]$ was reduced by ca 400 μmol/L within the first 0.5 h (Fig. 2a–d). This strongly suggested that regardless of the initial solution conditions the first step in the precipitation of HAS (or the co-precipitation of $Si(OH)_4$ by Al) was the formation of HAS_A. Electron microprobe analyses of the stoichiometries of the solid phases confirmed that HAS_A was the predominant solid phase formed during the first 12 h in solutions which included 800 μmol/L Al and 800, 1100 or 1500 μmol/L $Si(OH)_4$. Thereafter, ageing of solutions resulted in the further precipitation of $Si(OH)_4$ and its concomitant incorporation into solid phases such that after 336 h there was clear evidence of the formation of HAS_B in those solutions in which $Si(OH)_4$ had initially been present to excess

(Fig. 2b–d). The formation of HAS_B appeared to be most rapid in the presence of the greatest excess of $Si(OH)_4$ (Fig. 2d) and analyses of solid phases collected after only 0.5 h confirmed its presence in these rapidly formed precipitates. Solid-state ^{27}Al NMR indicated the presence of Al^{VI} and a significant component of Al^{IV} the latter only being found in HAS_B [7]. In addition solid-state ^{29}Si NMR did not indicate a significant shift at −78 ppm ($Q^3(3Al)$) which would normally be indicative of HAS_A [7]. The results of the NMR did not tally well with those of filtration (only 400 μmol/L $Si(OH)_4$ was co-precipitated at this time) or the electron microprobe as the Si:Al ratio of the solid phase collected after only 0.5 h was 0.60 and would normally be indicative of a phase composed primarily of HAS_A with, perhaps, some HAS_B. TGA of solid phases collected at 12h included exotherms in the region ca 175–200 °C for all conditions except that with the highest excess of $Si(OH)_4$ (Fig. 3). Exotherms in this temperature region have not hitherto been observed for solid phases collected from solutions with initial $Si(OH)_4$ to Al ratio's of $\geqslant 1.0$ [11]. However, the exotherms were not evident in solid phases collected from solutions after more than 12 h ageing. The initial presence and thereafter absence of exotherms in aged precipitates, including those collected from solutions which contained equimolar [$Si(OH)_4$] and [Al] and were likely to be composed of almost exclusively HAS_A, strongly suggested that the exothermic peaks were not characteristic of HAS_A but indicative of contaminating amounts of $Al(OH)_{3(s)}$. The latter being absent in precipitates collected from solutions with the highest excess of $Si(OH)_4$ and in precipitates collected from solutions after more than 12 h ageing.

We have investigated the mechanism of formation of HAS and provided further evidence of equilibria between $Al(OH)_{3(s)}$, HAS_A and HAS_B and, in particular, the role of $Si(OH)_4$ in determining which of these solid phases will predominate for any given solution conditions. We have shown that HAS_A is formed rapidly in solutions which include stoichiometric concentrations of $Si(OH)_4$ and Al (i.e. 1:2) though the reaction does not approach completion (i.e. Si:Al ratio of 0.5 in solid phase) in the absence of an excess of $Si(OH)_4$ in the 'equilibrated' solution (i.e. initial solution conditions of 1:1). We have observed that HAS_A was the likely initial product of the reaction of $Al(OH)_{3(s)}$ with $Si(OH)_4$ even in solutions in which $Si(OH)_4$ was present to significant excess and this supported the contention that HAS_A was the necessary precursor to HAS_B. The latter was not fully supported by the ^{29}Si NMR of the precipitate collected after only 0.5 h from solutions containing 2000 μmol/L $Si(OH)_4$ and 800 μmol/L Al since we did not observe a significant HAS_A-characteristic shift at −78 ppm. Future research on similar freshly precipitated solid phases should help to resolve this conundrum.

Finally TGA of the solid phases confirmed what we had believed to be true in our earlier study [11] that exotherms in the temperature region ca 175–300 °C were not characteristic of HAS_A but were actually indicative of the presence of residual $Al(OH)_{3(s)}$. In relation to the latter, we have investigated the thermal chemistry of $Al(OH)_{3(s)}$ prepared in the presence of PIPES and collected after only 12 h ageing. This solid phase was prepared as a control for the HAS phases. We observed two significant exotherms (Fig. 3e) one at ca 271 °C, similar to that seen previously [11] and a second at ca 771 °C which has not hitherto been observed. Remnants of the former were observed in several of the other solid phases collected after only 12 h (Fig. 3b–d) whereas the latter exotherm was absent from these precipitates. The significance of these exothermic peaks to the structure of $Al(OH)_{3(s)}$ formed in the presence of a pH buffer remain to be determined.

Acknowledgements

This research was funded by NERC. D.C. Apperley is thanked for all his help with the solid-state NMR which were obtained through the EPSRC solid-state NMR service at Durham. D. Plant is thanked for electron microprobe analyses which were carried out at the Electron Microprobe Facility at Manchester.

References

[1] C. Exley, J. Inorg. Biochem. 69 (1998) 139.
[2] J.D. Birchall, C. Exley, J.S. Chappell, M.J. Phillips, Nature 338 (1989) 146.
[3] C. Exley, J.D. Birchall, Polyhedron 11 (1992) 1901.
[4] C. Exley, J. K Pinnegar, H. Taylor, J. Theor. Biol. 189 (1997) 133.
[5] C. Exley, J.D. Birchall, Polyhedron 12 (1993) 1007.
[6] C. Exley, C. Schneider, F.J. Doucet, Coord. Chem. Rev. 228 (2002) 127.
[7] F.J. Doucet, C. Schneider, S.J. Bones, A. Kretchmer, I. Moss, P. Tekely, C. Exley, Geochim. Cosmochim. Acta 65 (2001) 2461.
[8] S. Strekopytov, C. Exley, Polyhedron 24 (2005) 1585.
[9] Department of the Environment, Silicon in Waters and Effluents, HMSO, London, 1980.
[10] C. Schneider, C. Exley, J. Inorg. Biochem. 87 (2001) 45.
[11] S. Strekopytov, C. Exley, Polyhedron 25 (2006) 1707.

(**7**); *n*-Bu (**8**))] were obtained by reaction of di- and trialkyltin with 2,4,5-trifluoro-3-methoxybenzoic acid. All the complexes were characterized by elemental, IR, ^{1}H and ^{13}C NMR spectra analyses. Among them, complexes **1**, **3**, **7** and **8** are also characterized by X-ray crystallography diffraction analyses.

2. Experimental

2.1. Materials and measurements

Triphenyltin chloride, trimethyltin chloride, tri-*n*-butyltin chloride, dimethyltin dichloride, di-*n*-butyltin dichloride, diphenyltin dichloride and 2,4,5-trifluoro-3-methoxybenzoic acid were commercially available, and they were used without further purification. Dibenzyltin dichloride and tribenzyltin chloride were prepared by a standard method reported in the literature [12]. The melting points were obtained on a Kofler micro melting point apparatus and are uncorrected. Infrared-spectra were recorded on a Nicolet-460 spectrophotometer using KBr discs and sodium chloride optics. ^{1}H and ^{13}C NMR spectra were obtained on a Varian Mercury Plus 400 MHz NMR spectrometer. The chemical shifts are reported in ppm with respect to the references and are stated relative to external tetramethylsilane (TMS) for ^{1}H and ^{13}C NMR. Elemental analyses were performed with a PE-2400 II elemental apparatus.

2.2. Syntheses of the complex *1*–*8*

2.2.1. $[Ph_3SnO_2CC_6HF_3OCH_3]$ (*1*)

Under a dry nitrogen atmosphere, 2,4,5-trifluoro-3-methoxybenzoic acid (0.206 g, 1.0 mmol) and sodium ethoxide (0.068 g, 1.0 mmol) were added in benzene (20 ml) to a Schlenk flask and stirred for about 10 min, then triphenyltin chloride (0.385 g, 1.0 mmol) was added to the mixture. The stirring was continued for 12 h at 40 °C and then the solution was filtered. The filtrate was gradually evaporated until a solid product was obtained. The solid was recrystallized from ether–petroleum and a transparent colorless crystal of complex **1** was formed. Yield: 88%; m.p. 109–110. °C. *Anal.* Calc. for $C_{26}H_{19}F_3O_3Sn$: C, 56.25; H, 3.45. Found: C, 56.49; H, 3.34%. IR (KBr, cm^{-1}): ν_{as}(C=O) 1582, ν_s(C–O)1380, ν_{as}(Sn–C) 564, ν_s(Sn–C) 523, ν(Sn–O) 484. ^{1}H NMR ($CDCl_3$, ppm): δ 7.26–7.52 (m, 1H, $C_6HF_3OCH_3$), 7.49–7.80 (m, 15H, Sn–C_6H_5), 4.02 (s, 3H, OCH_3). ^{13}C NMR ($CDCl_3$, ppm): δ 168.24 (COO), 113.45, 129.00, 129.32, 129.64, 129.62, 130.61, 130.68, 130.75, 136.92, 137.16, 137.40, 137.80 (Ar–C), 62.36 (OCH_3).

2.2.2. $[(PhCH_2)_3SnO_2CC_6HF_3OCH_3]$ (*2*)

The procedure is similar to that of complex **1**. 2,4,5-Trifluoro-3-methoxybenzoic acid (0.206 g, 1.0 mmol), sodium ethoxide (0.068 g, 1.0 mmol) and tribenzyltin chloride (0.427 g, 1.0 mmol) were reacted for 12 h at 40 °C. Recrystallized from ether–petroleum, a transparent colorless crystal was formed. Yield: 77%; m.p. 123–125 °C. *Anal.* Calc. for $C_{29}H_{25}F_3O_3Sn$: C, 58.32; H, 4.22. Found: C, 58.72; H, 4.31%. IR (KBr, cm^{-1}): ν_{as}(C=O), 1590 ν_s(C–O) 1381, ν_{as}(Sn–C) 560, ν_s(Sn–C) 518, ν(Sn–O) 479. ^{1}H NMR ($CDCl_3$, ppm): δ 7.31–7.81 (m, 1H, $C_6HF_3OCH_3$), 7.23–7.52 (m, 15H, Sn–$CH_2C_6H_5$), 3.16 (s, 6H, Sn–$CH_2C_6H_5$), 4.03 (s, 3H, OCH_3). ^{13}C NMR ($CDCl_3$, ppm): δ 32.5 ($ArCH_2$), 112.85, 112.92, 129.76, 128.88, 129.15, 129.37, 130.29, 130.35, 136.74, 136.90, 137.20, 137.32 (Ar–C), 168.25(COO), 62.35 (OCH_3).

2.2.3. $[Me_3SnO_2CC_6HF_3OCH_3]$ (*3*)

The procedure is similar to that of complex **1**. 2,4,5-Trifluoro-3-methoxybenzoic acid (0.206 g, 1.0 mmol), sodium ethoxide (0.068 g, 1.0 mmol) and trimethyltin chloride (0.199 g, 1.0 mmol) were reacted for 12 h at 40 °C. Recrystallized from ether–petroleum, a transparent colorless crystal was formed. Yield: 87%; m.p. 104–106 °C. *Anal.* Calc. for $C_{11}H_{13}F_3O_3Sn$: C, 35.81; H, 3.55. Found: C, 35.80; H, 3.73. IR (KBr, cm^{-1}): ν_{as}(C=O) 1589, ν_s(C–O) 1372, ν_{as}(Sn–C) 555, ν_s(Sn–C) 530, ν(Sn–O) 488. ^{1}H NMR ($CDCl_3$, ppm): δ 7.25–7.80 (m, 1H, $C_6HF_3OCH_3$), 0.60–0.87 (m, 9H), 4.03 (s, 3H, OCH_3) ppm. ^{13}C NMR ($CDCl_3$, ppm): δ 167.46 (COO), 114.87, 138.75, 145.65, 148.02, 148.34, 152.35 (Ar–C), 62.36 (OCH_3), 14.27 (–CH_3).

2.2.4. $[n\text{-}Bu_3SnO_2CC_6HF_3OCH_3]$ (*4*)

The procedure is similar to that of complex **1**. 2,4,5-Trifluoro-3-methoxybenzoic acid (0.206 g, 1.0 mmol), sodium ethoxide (0.068 g, 1.0 mmol) and tri-*n*-butyltin (0.325 g, 1.0 mmol) were reacted for 12 h at 40 °C. Recrystallized from ether–petroleum, a transparent colorless crystal was formed. Yield: 78%. m.p. 163–165 °C; *Anal.* Calc. for $C_{20}H_{31}F_3O_3Sn$: C, 48.51; H, 6.31. Found: C, 48.71; H, 6.18%. IR (KBr, cm^{-1}): ν_{as}(C=O) 1586, ν_s(C–O) 1380, ν_{as}(Sn–C) 561, ν_s(Sn–C) 527, ν(Sn–O) 482. ^{1}H NMR ($CDCl_3$, ppm): δ 7.26–7.75 (m, 1H, $C_6HF_3OCH_3$), 0.83–1.54 (m, 27H, Sn–C_4H_9), 4.04 (s, 3H, OCH_3). ^{13}C NMR ($CDCl_3$, ppm): δ 167.46 (COO), 113.00, 138.68, 145.46, 145.85, 147.91, 148.02, 153.67 (Ar–C), 62.36 (OCH_3), 22.83, 31.773, 45.57 (–CH_2–), 14.27 (CH_3).

2.2.5. $[Ph_2Sn(O_2CC_6HF_3OCH_3)_2]$ (*5*)

The procedure is similar to that of complex **1**. 2,4,5-Trifluoro-3-methoxybenzoic acid (0.412 g, 2.0 mmol), sodium ethoxide (0.136 g, 2.0 mmol) and dimethyltin dichloride (0.219 g, 1.0 mmol) were reacted for 12 h at 40 °C. Recrystallized from ether–petroleum, a transparent colorless crystal was formed. Yield: 83%; m.p. 187–189 °C. *Anal.* Calc. for $C_{28}H_{18}F_6O_6Sn$: C, 49.23; H, 2.66. Found: C, 49.31; H, 2.86%. IR (KBr, cm^{-1}): ν_{as}(C=O) 1586, ν_s(C–O) 1378, ν_{as}(Sn–C) 559, ν_s(Sn–C) 525, ν(Sn–O) 488. ^{1}H NMR ($CDCl_3$, ppm): δ 7.15–7.72 (m, 12H, Sn–C_6H_5 and $C_6HF_3OCH_3$), 4.04 (s, 3H, OCH_3). ^{13}C NMR ($CDCl_3$, ppm): δ168.65 (COO), 112.42, 112.51, 129.56, 128.78, 129.35, 129.47, 130.49, 130.45, 136.64, 136.77, 137.40, 137.68 (Ar–C), 62.36 (OCH_3).

*2.2.6. [$(PhCH_2)_2Sn(O_2CC_6HF_3OCH_3)_2$] (**6**)*

The procedure is similar to that of complex **1**. 2,4,5-Trifluoro-3-methoxybenzoic acid (0.412 g, 2.0 mmol), sodium ethoxide (0.136 g, 2.0 mmol) and dibenzyltin dichloride (0.371 g, 1.0 mmol) were reacted for 12 h at 40 °C. Recrystallized from ether–petroleum, a transparent colorless crystal was formed. Yield: 85%; m.p. 192–194 °C. *Anal.* Calc. for $C_{30}H_{22}F_6O_6Sn$: C, 50.66; H, 3.12. Found: C, 50.45; H, 3.24%. IR (KBr, cm^{-1}): ν_{as}(C=O) 1589, ν_s(C–O) 1381, ν_{as}(Sn–C) 588, ν_s(Sn–C) 533, ν(Sn–O) 460. ^{1}H NMR ($CDCl_3$, ppm): δ 7.84–7.36 (m, 12H, $C_6HF_3OCH_3$ and $Sn–CH_2C_6H_5$), 3.29 (s, 4H, $Sn–CH_2C_6H_5$), 4.06 (s, 3H, OCH_3). ^{13}C NMR ($CDCl_3$, ppm): δ 168.05 (COO), 112.65, 112.32, 129.46, 128.58, 129.05, 129.17, 130.19, 130.15, 136.54, 136.70, 137.10, 137.22 (Ar–C), 32.6 ($ArCH_2$), 62.52 (OCH_3).

2.2.7. [$Me_2Sn(O_2CC_6HF_3OCH_3)_2$] (7)

The procedure is similar to that of complex **1**. 2,4,5-Trifluoro-3-methoxybenzoic acid (0.412 g, 2.0 mmol), sodium ethoxide (0.136 g, 2.0 mmol) and dibenzyltin dichloride (0.371 g, 1.0 mmol) were reacted for 12 h at 40 °C. Recrystallized from ether–petroleum, a transparent colorless crystal was formed. Yield: 85%; m.p. 192–194 °C. *Anal.* Calc. for $C_{18}H_{14}F_6O_6Sn$: C, 38.67; H, 2.52. Found: C, 38.65; H, 2.33%. IR (KBr, cm^{-1}): ν_{as}(C=O) 1587, ν_s(C–O)1379, ν_{as}(Sn–C) 586, ν_s(Sn–C) 532, ν(Sn–O) 461. ^{1}H NMR ($CDCl_3$, ppm): δ 7.26–7.60 (m, 2H, $C_6HF_3OCH_3$), 4.06 (s, 3H, OCH_3), 0.85–1.28 (m, 6H, $Sn–CH_3$). ^{13}C NMR ($CDCl_3$, ppm): δ 170.80 (COO), 113.29, 145.72, 147.10, 148.18, 149.53, 151.83 (Ar–C), 62.49 (OCH_3), 8.87 ($–CH_3$).

*2.2.8. [$n\text{-}Bu_2Sn(O_2CC_6HF_3OCH_3)_2$] (**8**)*

The procedure is similar to that of complex **1**. 2,4,5-Trifluoro-3-methoxybenzoic acid (0.412 g, 2.0 mmol), sodium ethoxide (0.136 g, 2.0 mmol) and di-*n*-butyltin dichloride (0.303 g, 1.0 mmol) were reacted for 12 h at 40 °C. Recrystallized from ether–petroleum, a transparent colorless crystal was formed. Yield: 80%; m.p. 117–119 °C. *Anal.* Calc. for $C_{24}H_{26}F_6O_6Sn$: C, 44.82; H, 4.07. Found: C, 45.0; H, 4.10%. IR (KBr, cm^{-1}): ν_{as}(C=O) 1579, ν_s(C–O)1373, ν_{as}(Sn–C) 586, ν_s(Sn–C) 537, ν(Sn–O) 462. ^{1}H NMR (CDCl, ppm): δ 7.27–7.62 (m, 2H, $Sn–C_6HF_3OCH_3$), 0.88–1.81 (m, 12H, $Sn–C_4H_9$), 4.06 (s, 3H, OCH_3). ^{13}C NMR ($CDCl_3$, ppm): δ 170.10 (COO), 113.19, 145.62, 146.87, 148.08, 149.33, 151.63 (Ar–C), 62.50 (OCH_3), 22.83, 31.75, 45.36 ($–CH_2–$), 14.28 (CH_3).

3. Results and discussion

3.1. Syntheses

The syntheses procedure is given in Scheme 1.

3.2. IR spectra

Comparing the IR spectra of the free ligand with complexes **1**–**8**, the explicit feature is the absence of a band in the region 3200–3500 cm^{-1}, which appears in the free ligand as the –OH stretching vibration, thus indicating metal-ligand bond formation through this site. The absorption in the region 460–488 cm^{-1}, which is absent in the spectrum of the free ligand, is assigned to the Sn–O stretching mode. All these values are consistent with those detected in a

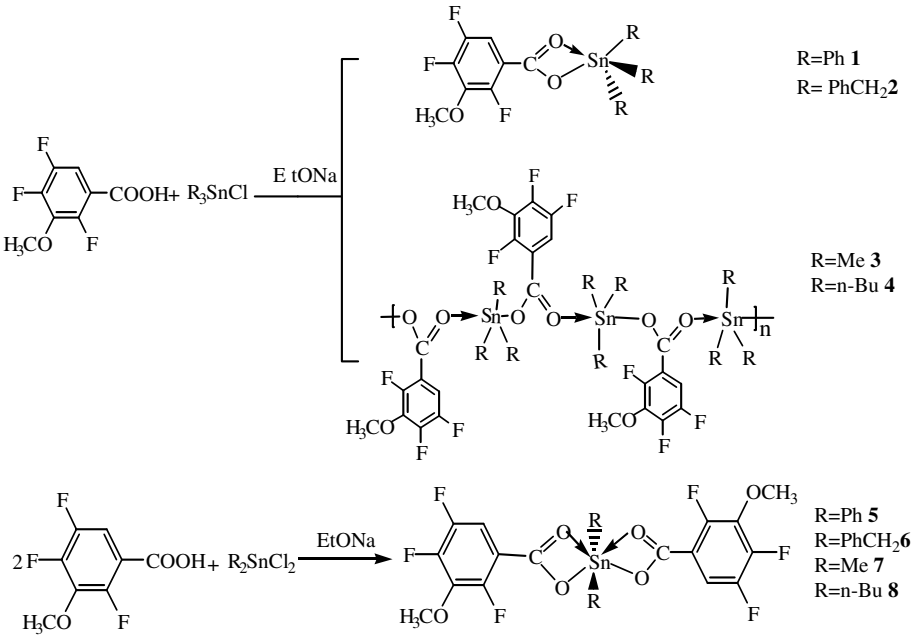

Scheme 1.

number of organotin-oxygen derivatives [13,14]. In the organotin carboxylate complexes, IR spectroscopy can provide useful information concerning the coordinate formation of the carboxylate [15]. $\Delta v(v_{as}(COO)–v_s(COO))$, 202–217 cm^{-1}, are smaller than that of the free ligand, 341 cm^{-1}, but near to that in the sodium salt of the ligand, 200 cm^{-1}, which suggest the presence of bidentate chelating carboxylate groups [16]. This information is consistent with the analysis of related X-ray crystallography data.

3.3. NMR spectra

The ^1H NMR spectra show that the signal for the OH proton (10.89 ppm) in the spectrum of the ligand is absent in the spectra of the complexes, thus indicating the removal of the OH proton and the formation of Sn–O bonds. This is consistent with the IR data. Signals for the other groups appear in the same positions as in the ligand.

The ^{13}C NMR spectra of all the complexes shown a significant downfield shift of all carbon resonances compared with the free ligand. The shift is a consequence of electron density transfer from the ligand to the acceptor.

3.4. X-ray crystallographic studies

3.4.1. Crystal structure of $[Ph_3SnO_2CC_6HF_3OCH_3]$ (1)

The molecular structure of complex **1** is shown in Fig. 1 and selected bond lengths and angles are given in Table 1. As can be seen from Fig. 1, the complex possesses a monomeric structure, the Sn(1)–O(1) [2.076(3) Å] bond length lies in the range that has been reported as the Sn–O covalent bond length [2.054(3)–2.083(2) Å for Sn(1)–O(1)] [17a], which proves that the oxygen atoms are coordinated to the tin atoms by a strong chemical bond. The intramolecular distance [Sn(1)···O(2)] is 2.743(4) Å. Although the distance is considerably longer than the normal Sn–O covalent bond length, they lie in the range of Sn···O distances of (2.61–3.02 Å), which have been confidently reported for intramolecular bonds [17b,17c]. As the oxygen atom is involved in a weak coordinative interaction with tin along one of the tetrahedral faces, the structure distortion for the tin atom in complex **1** is best described as a capped tetrahedron.

Table 1
Selected bond lengths (Å) and angles (°) for **1**

Bond lengths			
Sn(1)–C(9)	2.130(4)	Sn(1)–O(1)	2.076(3)
Sn(1)–C(15)	2.123(5)	Sn(1)–O(2)	2.743(4)
Sn(1)–C(21)	2.133(5)		
Bond angles			
O(1)–Sn(1)–C(15)	108.19(16)	C(15)–Sn(1)–C(9)	112.57(19)
O(1)–Sn(1)–C(9)	97.24(16)	C(15)–Sn(1)–C(21)	116.14(19)
O(1)–Sn(1)–C(21)	112.47(15)	C(9)–Sn(1)–C(21)	108.69(18)
O(1)–Sn(1)–O(2)	52.18 (12)	C(9)–Sn(1)–O(2)	149.13(15)

As shown in Fig. 2, a pair of intermolecular C–H···F hydrogen bonds are recognized, which associate the discrete molecule into a dimer. The C–H···F distance is 2.557 Å, which is shorter than the sum of van der waals radii of H and F (2.67 Å) [18]. The C···F distance and the C–H···F angle are 3.343 Å and 142.5°, respectively.

The dimers of complex **1** are further linked by intermolecular C–H···F hydrogen bonds. As shown in Fig. 3, the C(13A) atom acts as a hydrogen-bond donor via the

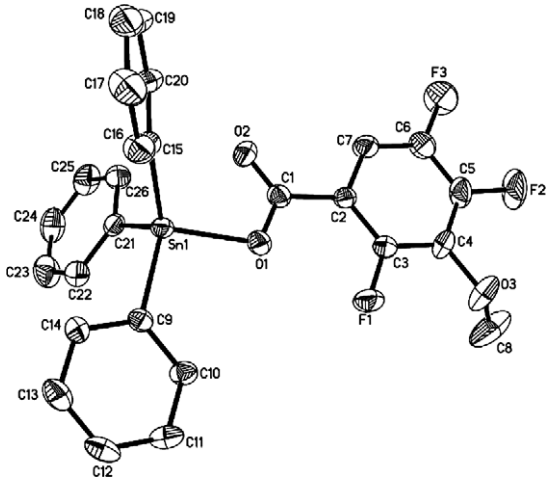

Fig. 1. Molecular structure of complex **1**.

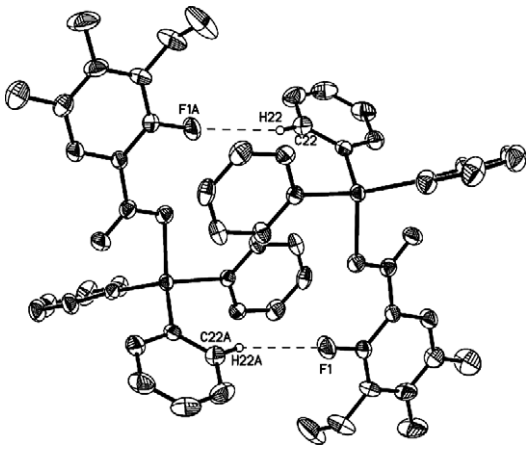

Fig. 2. Dimer structure of complex **1**.

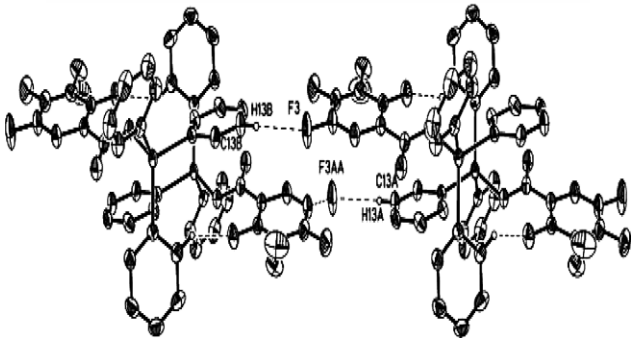

Fig. 3. 1D chain structure of complex **1**, propagation by weak C–H···F interactions.

H(13A) atom to the fluorine F(3AA) atom, and the C(13B) atom acts the same as C(13A), so the dimers form a 1D chain with a head-to-tail arrangement. The C···F and H···F distances and the C–H···F angle are 3.239 Å, 2.556 Å and 130.62°, respectively. The observed C–H···F distances are consistent with phenyl C–H···F interactions reported for various fluorobenzene complexes (2.36–2.86 Å) [19].

3.4.2. Crystal structure of $[Me_3SnO_2CC_6HF_3OCH_3]$ (3)

The molecular structure of complex **3** is shown in Fig. 4 and selected bond lengths and angles are given in Table 2. As can be seen from Fig. 4, the geometry of the tin center is a distorted trigonal bipyramid and the structure adopted in the solid state is *trans*-R_3SnO_2. The central tin atom is five-coordinated with the two O atoms [O(1) and O(2A)] occupying the axial sites, the angle of the axial ligands [O(1)–Sn(1)–O(2A)] is 174.93(9)°. Three methyl groups define the equatorial plane and the sum of the trigonal C–Sn–C angles is 356.7°. The carboxylate ligand bridges two symmetry-related Sn atoms and gives rise to the unequal Sn–O bond distances. This inequality is reflected in the C(1)–O bond distance, and the longer C(1)–O(1) [1.282(4) Å] is associated with the shorter Sn(1)–O(1) [2.120(3) Å] bond, which is shorter than other reported trimethylorganotin(IV) polymeric structures [2.14(1)–2.208(2) Å] [20a,21] and approaches the covalent radii of Sn and O (2.13 Å) [18]. The Sn(1)–O(2A) distance [2.668(3) Å] is longer than other reported complexes [21], but is far shorter than the sum of the van der Waals radii of Sn and O (3.68 Å) [18]. All these information indicate that Sn(1)–O(2) is a weak coordinate bond. The Sn-C distances [2.103(4)–2.114(4) Å] are consistent with those reported in other triorganotin(IV) carboxylates [17d,20a].

The intermolecular C=O → Sn coordination in **3** leads to infinite zigzag chains containing the tin centers and carboxyl groups [Fig. 5], which is consistent with another organotin(IV) complex that has been reported [20a]. Furthermore, the F(2) atom of the ligand in one chain and the F(2E) atom in another chain form an intermolecular non-bonding F···F interaction [Fig. 6], which is similar to that of the Cl···Cl interaction reported in the literature [21]. The F···F distance (2.820 Å) is a little longer than that has been reported (2.80 Å) [22], but is considerably shorter than the sum of the van der waals radii of two fluorine atoms (2.94 Å)[18]. The C(5)···F(2A) distance and C(5)–F(2)···F(2A) angle is 3.399 Å and 103.98° respectively. These 1D chains are further linked by intermolecular C–H···F hydrogen bonds, as shown in Fig. 7, the C(9) and C(9B) atoms act as a hydrogen-bond donors via H(9C) and H(9CB) atoms to phenyl F(2C) and F(2BA) atoms [Fig. 7] The C···F, F···H distance and the C–H···F angle are 3.522 Å, 2.631 Å and 148.2° respectively. The F···H distance (2.631 Å) and the C–H···F angle are bigger than the same type of measurements that are found in complex **1** (2.557 Å and 142.5°, 2.556 Å and 130.62°), but shorter than the sum of van der waals radii of H and F (2.67 Å) [18]. These intermolecular F···F and C–H···F interactions

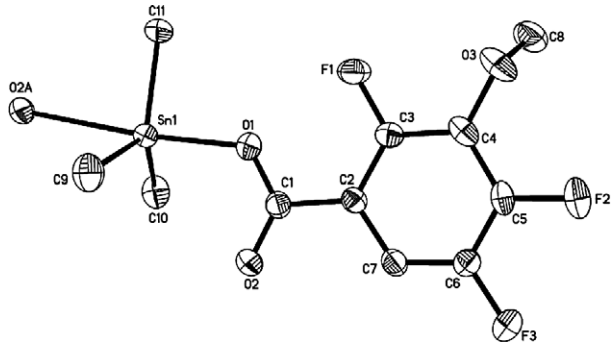

Fig. 4. The molecular structure of complex **3**.

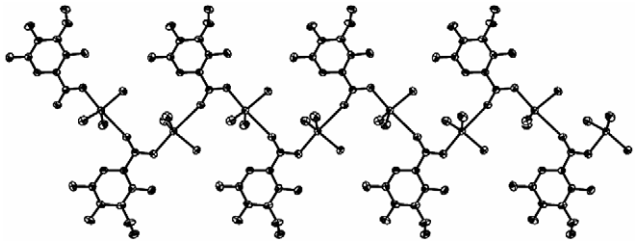

Fig. 5. The 1D chain structure of complex **3**, propagation via O → Sn coordination.

Table 2
Selected bond lengths (Å) and angles (°) for **3**

Bond lengths			
Sn(1)1–C(9)	2.109(4)	Sn(1)–O(1)	2.120(3)
Sn(1)–C(10)	2.114(4)	Sn(1)–O(2A)	2.668(3)
Sn(1)–C(11)	2.103(4)	C(1)–O(1)	1.282(4)
C(2)–O(2)	1.227(4)		
Bond angles			
C(11)–Sn(1)–C(9)	118.8(2)	C(11)–Sn(1)–O(1)	91.15(15)
C(11)–Sn(1)–C(10)	115.4(2)	C(9)–Sn(1)–O(1)	99.16(15)
C(9)–Sn(1)–C(10)	122.50(19)	C(10)–Sn(1)–O(1)	97.56(15)
O(1)–Sn(1)–O(2A)	174.93(9)	C(9)–Sn(1)–O(2A)	82.21(14)
C(10)–Sn(1)–O(2A)	85.71(15)	C(11)–Sn(1)–O(2A)	83.94(15)
O(1)–Sn(1)–O(2A)	174.93(9)		

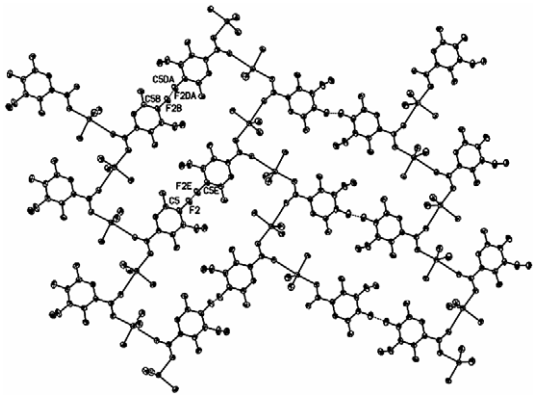

Fig. 6. The 2D network structure of complex **3**.

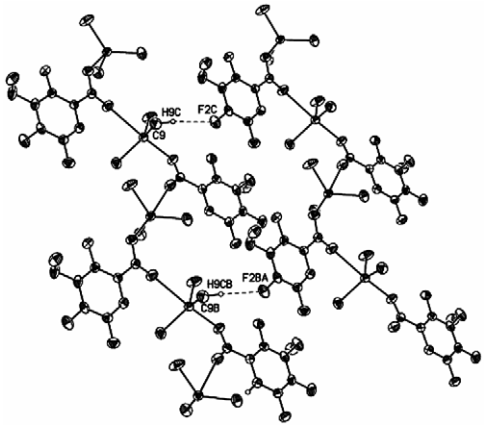

Fig. 7. The 2D network structure of complex **3**.

lead to an expansion of the supramolecular structure of **3** and make it form a 2D network.

3.4.3. Crystal structures of $[Me_2Sn(O_2CC_6HF_3OCH_3)_2]$ (7) and $[n\text{-}Bu_2Sn(O_2CC_6HF_3OCH_3)_2]$ (8)

The molecular structures of complexes **7** and **8** are shown in Figs. 8 and 10, and selected bond lengths and angles are given in Tables 3 and 4. The geometry at the central Sn atoms in both complexes of **7** and **8** is a skew-trapezoidal bipyramidal geometry. The four O atoms, which derive from two chelate carboxylate ligands, define the basal plane. The C–Sn–C angle [142.4(4)° for **7**, 147.5(2)° for **8**] lies in the range of C–Sn–C angles of 122.6–156.9° found for diorganotin derivatives in which the organo substituents do not adopt *cis*- or *trans*-geometries about the tin atom [23]. The carboxylate ligands chelate the Sn center with asymmetric Sn–O bond distances and this asymmetry is related to the shorter Sn–O bonds. The degree of asymmetry in the Sn–O bond distances is not equal to the difference between the Sn–O bond distances for two carboxylate

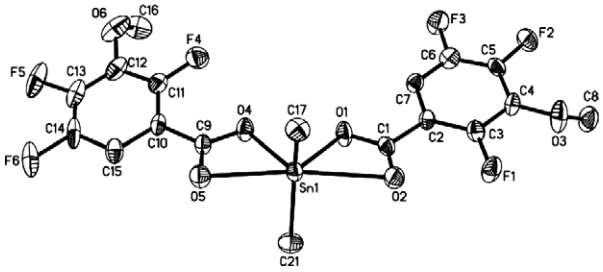

Fig. 8. The molecular structure of complex **7**.

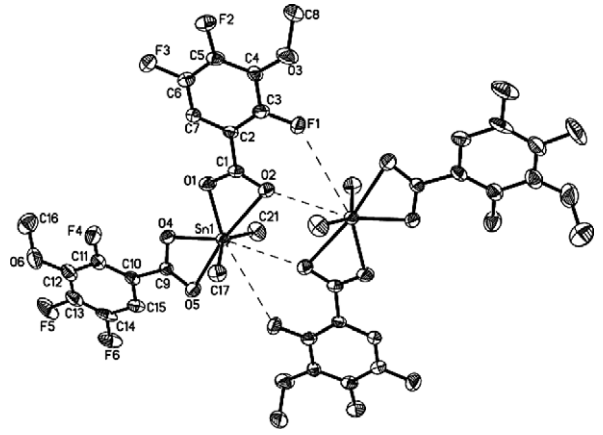

Fig. 9. The dimer structure of complex **7**.

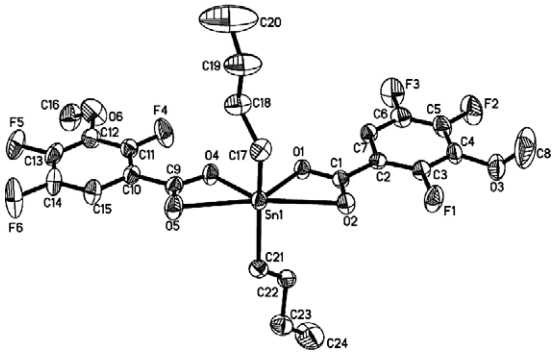

Fig. 10. The molecular structure of complex **8**.

Table 3
Selected bond lengths (Å) and angles (°) for **7**

Bond lengths			
Sn(1)–C(21)	2.090(9)	Sn(1)–O(4)	2.118(5)
Sn(1)–C(17)	2.091(8)	Sn(1)–O(5)	2.506(6)
Sn(1)–O(1)	2.115(6)	Sn(1)–O(2)	2.656(6)
C(1)–O(1)	1.262(9)	C(1)–O(2)	1.234(10)
C(9)–O(4)	1.288(10)	C(9)–O(5)	1.229(10)
Bond angles			
C(21)–Sn(1)–C(17)	142.2(4)	C(17)–Sn(1)–O(4)	103.1(3)
C(21)–Sn(1)–O(1)	105.2(4)	O(1)–Sn(1)–O(4)	80.3(2)
C(17)–Sn(1)–O(1)	103.9(3)	C(21)–Sn(1)–O(5)	86.3(3)
C(21)–Sn(1)–O(4)	105.1(3)	C(17)–Sn(1)–O(5)	89.4(3)
O(1)–Sn(1)–O(5)	135.8(2)	O(4)–Sn(1)–O(5)	55.6(2)
C(21)–Sn(1)–O(4)	105.1(3)	C(17)–Sn(1)–O(2)	88.4(3)
O(1)–Sn(1)–O(2)	53.0(2)	O(4)–Sn(1)–O(2)	133.3(2)
O(5)–Sn(1)–O(2)	171.17(18)		

Table 4
Selected bond lengths (Å) and angles (°) for **8**

Bond lengths			
Sn(1)–C(21)	2.109(5)	Sn(1)–O(4)	2.141(3)
Sn(1)–C(17)	2.107(5)	Sn(1)–O(5)	2.531(4)
Sn(1)–O(1)	2.128(3)	Sn(1)–O(2)	2.562(3)
C(1)–O(1)	1.287(6)	C(1)–O(2)	1.226(6)
C(9)–O(4)	1.281(6)	C(9)–O(5)	1.245(6)
Bond angles			
C(17)–Sn(1)–C(21)	147.5(2)	C(17)–Sn(1)–O(4)	102.97(19)
C(17)–Sn(1)–O(1)	99.8(2)	O(1)–Sn(1)–O(4)	82.60 (13)
C(21)–Sn(1)–O(1)	105.04(17)	C(17)–Sn(1)–O(5)	88.02(19)
C(21)–Sn(1)–O(4)	100.69(17)	C(21)–Sn(1)–O(5)	87.41(18)
O(1)–Sn(1)–O(5)	137.80(12)	O(4)–Sn(1)–O(5)	55.31(12)
C(17)–Sn(1)–O(2)	88.60(19)	C(21)–Sn(1)–O(2)	89.06(17)
O(1)–Sn(1)–O(2)	54.58(12)	O(4)–Sn(1)–O(2)	137.08(12)
O(5)–Sn(1)–O(2)	167.61(12)		

ligands (0.541 Å and 0.388 Å for **7**, 0.434 Å and 0.390 Å for **8**). The anisobidente mode of coordination of the carboxylate is also reflected in the disparity of the associated carbon–oxygen bonds. Although the Sn(1)–O(2) (2.656 Å for **7** and 2.562(3) Å for **8**) and Sn(1)–O(5) (2.506 Å for **7** and 2.531(4) Å for **8**) bonds are longer than the sum of the covalent radii of Sn and O (2.13 Å), they are nevertheless significantly below the sum of the van der waals radii of these atoms (3.68Å) [18].

The most interesting aspect of the structure concerns the intermolecular weak Sn···O and Sn···F interactions, which help in the construction of the dimer as shown in Figs. 9 and 11. The two weak Sn···O bond lengths are equal (3.121 Å for **7** and 3.097 Å for **8**), which is less than the sum of the van der Walls radii of Sn and O (3.68 Å) [18] and between those that have been reported in $[Et_2Sn(O_2CC_4H_3S)]$ (2.891 Å) and $Ph_2Sn(O_2CCH_2Cl)_2$ (3.552 Å) [24,25]. The interaction of Sn···F is similar to the Sn···Cl interaction that has been reported [26] and the distance is 3.635 Å for **7** and 3.638Å for **8**.

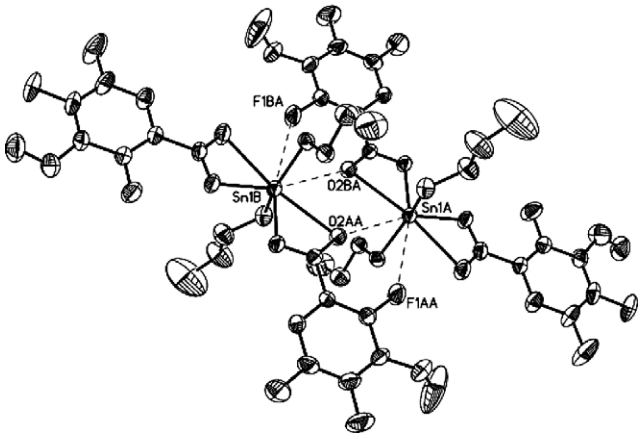

Fig. 11. The dimer structure of complex **8**.

Moreover, for complex **7** the dimers are connected into a 1 D chain through C–H···F hydrogen bonding. The C···F and H···F distances and the C–H···F angle are 3.312 Å, 2.612 Å and 130.01° respectively, these data are consistent with those found in the literature [19]. For complex **8**, we can find two types of shorter distances that are formed by the phenyl F and the methyl H. One is a little longer than the other. For the longer one, its C···F and H···F distances and the C–H···F angle are 3.511 Å, 2.607 Å and 157.06° respectively; and for the shorter one, its C···F and H···F distances and the C–H···F angle are 3.297 Å, 2.517 Å and 138.34° respectively. So a 1D chain structure in the solid state is propagated by two types of C–H···F weak interactions. Further, the C–H···F distance (2.517 Å) is the shortest among the above mentioned in this article.

4. X-ray crystallography

Crystals were mounted in Lindemann capillaries under nitrogen. All X-ray crystallographic data were collected on a Bruker SMART CCD 1000 diffractometer with graphite monochromated Mo Kα radiation ($\lambda = 0.71073$ Å) at

Table 5
Crystal data collection and structure refinement parameters for **1**, **3**, **7** and **8**

Complex	**1**	**3**	**7**	**8**
Empirical formula	$C_{26}H_{19}F_3O_3Sn$	$C_{11}H_{13}F_3O_3Sn$	$C_{18}H_{14}F_6O_6Sn$	$C_{24}H_{26}F_6O_6Sn$
Formula weight	555.10	368.90	558.98	643.14
Crystal system	monoclinic	monoclinic	triclinic	monoclinic
Space group	*P*2 (1)/c	P2 (1)/c	$P\bar{1}$	*P*2 (1)/c
Unit cell dimensions				
a (Å)	11.805(4)	10.970(8)	7.684(4)	9.3711(15)
b (Å)	8.705(3)	10.132(7)	9.530(6)	19.609(3)
c (Å)	22.985(8)	13.235(9)	14.285(8)	14.772(2)
α (°)	90	90	84.725(8)	90
β (°)	98.804(5)	113.691(9)	75.599(8)	103.894(2)
γ (°)	90	90	77.605(5)	90
Z	4	4	2	4
D_{calc} (Mg m^{-3})	1.580	1.819	1.878	1.621
Absorption coefficient (mm^{-1})	1.143	1.929	1.382	1.048
F (000)	1104	720	548	1288
Crystal size (mm)	0.52 × 0.48 × 0.43	0.53 × 0.48 × 0.43	0.45 × 0.38 × 0.29	0.58 × 0.43 × 0.41
θ Range for data collection (°)	1.75–25.00	2.62–25.00	2.19–25.01	2.08–25.01
Index ranges	$-14 \leqslant h \leqslant 11$	$-12 \leqslant h \leqslant 13$	$-9 \leqslant h \leqslant 9$	$-10 \leqslant h \leqslant 11$
	$-10 \leqslant k \leqslant 10$	$-12 \leqslant k \leqslant 11$	$-11 \leqslant k \leqslant 11$	$-23 \leqslant k \leqslant 23$
	$-18 \leqslant l \leqslant 27$	$-15 \leqslant l \leqslant 15$	$-14 \leqslant l \leqslant 16$	$-15 \leqslant l \leqslant 17$
Reflections collected	11816	6664	5047	13586
Unique reflections (R_{int})	4111 (0.0459)	2361 (0.0327)	3382 (0.0304)	4644 (0.0367)
Data/restraints/parameters	4111/0/299	2361/0/163	3382/0/282	4644/290/334
Goodness-of-fit on F^2	1.000	1.006	1.001	1.006
Final *R* indices [$I > 2\sigma(I)$]	$R_1 = 0.0469$, $wR_2 = 0.1135$	$R_1 = 0.0296$, $wR_2 = 0.0760$	$R_1 = 0.0625$, $wR_2 = 0.1626$	$R_1 = 0.0402$, $wR_2 = 0.1011$
R indices (all data)	$R_1 = 0.0631$, $wR_2 = 0.1304$	$R_1 = 0.0366$, $wR_2 = 0.0825$	$R_1 = 0.0754$, $wR_2 = 0.1736$	$R_1 = 0.0644$, $wR_2 = 0.1188$

298(2) K. A semi-empirical absorption correction was applied to the data. The structure was solved by direct methods using SHELXS–97 and refined against F^2 by full-matrix least squares using SHELXL–97. Hydrogen atoms were placed in calculated positions. Crystal data and experimental details of the structure determinations are list in Table 5.

5. Supplementary material

Crystallographic data (excluding structure factors) for the structure analysis of the compounds have been deposited with the Cambridge Crystallographic Data Center, CCDC No. 600461 **1**, 600462 **3**, 600459 **7**, 600460 **8**. Copies of these information may be obtained free of charge from The Director, CCDC, 12 Union Road, Cambridge, CB2 1EZ, UK (fax: +44-1223-336033; e-mail: deposit@ccdc.cam.ac.uk or www: http://www.ccdc.cam.ac.uk).

Acknowledgement

We thank the National Natural Science Foundation of China (20271025) for financial support.

References

[1] L. Pellerito, L. Nagy, Coord. Chem. Rev. 224 (2002) 111, and the reference of therein.
[2] P. Quevauviller, R. Ritsema, R. Morabit, W.M.R. Dirkx, Appl. Organomet. Chem. 8 (1994) 541.
[3] A.J. Crowe, Appl. Organomet. Chem. 1 (1987) 143.
[4] M. Gielen, Appl. Organomet. Chem. 16 (2002) 481.
[5] J.F. Liebman, A. Greenberg, W.R. DolbierJr. (Eds.), Fluorine-Containing Molecules, VCH Publishers., New York, 1988.
[6] J.T. Welch, S. Eswarakrishnan, Fluorine in Bioorganic Chemistry, Wiley, New York, 1991.
[7] T. Hiyama, Organofluorine Compounds, Chemistry and Applications, Springer, Berlin, 2000.
[8] (a) J.A.K. Howard, V.J. Hoy, D. O'Hagan, G.T. Smith, Tetrahedron 52 (1996) 12613;
(b) M.A. Bramonte, A. Vasella, Helv, Chim. Acta 81 (1998) 695;
(c) V.R. Thalladi, H-C. Weiss, D. Bläser, R. Bose, A. Nangia, G.R. Desiraju, J. Am. Chem. Soc. 120 (1998) 8702.
[9] (a) A.R. Choudhury, U.K. Urs, N.T. Guru Row, K. Nagarajan, J. Mol. Struct. 605 (2002) 71;
(b) A.R. Choudhury, U.K. Urs, P.S. Smith, R. Goddard, A.J.K. Howard, N.T. Guru Row, J. Mol. Struct. 641 (2002) 225;
(c) A.R. Choudhury, N.T. Guru Row, Cryst. Growth Des. 4 (2004) 47;
(d) A. Sun, D.C. Lankin, K. Hardcastle, J.P. Snyder, Chem. Eur. J. 11 (2005) 1579.
[10] (a) C.L. Ma, Y.F. Han, R.F. Zhang, D.Q. Wang, J. Chem. Soc. Dalton Trans. (2004) 1832;
(b) C.L. Ma, J.F. Sun, J. Chem. Soc. Dalton Trans. (2004) 1785;
(c) C.L. Ma, Q. Jiang, R.F. Zhang, D.Q. Wang, J. Chem. Soc. Dalton Trans. (2003) 2975;
(d) C.L. Ma, Y.F. Han, R.F. Zhang, D.Q. Wang, Eur. J. Inorg. Chem. (2005) 1649;
(e) C.L. Ma, Q.F. Zhang, R.F. Zhang, D.Q. Wang, Chem. Eur. J. 12 (2006) 420;
(f) C.L. Ma, J.K. Li, R.F. Zhang, D.Q. Wang, Inorg. Chim. Acta. 358 (2005) 4575.
[11] (a) R. Willem, A. Bouhdid, M. Biesemans, J.C. Martins, D. de Vos, E.R.T. Tiekink, M. Gielen, J. Organomet. Chem. 514 (1996) 203;
(b) M. Gielen, A.E. Khloufi, M. Biesemans, F. Kayser, R. Willem, B. Mahieu, D. Maes, J.N. Lisgarten, L. Wyns, A. Moreira, T.K. Chattoadhay, R.A. Palmer, Organometallics 13 (1994) 2849.
[12] K. Sisido, Y. Takeda, Z. Kinugawa, J. Am. Chem. Soc. 83 (1961) 538.
[13] R.R. Holmes, C.G. Schmid, V. Chandrasekhar, R.O. Day, J.M. Homels, J. Am.Chem. Soc. 122 (2000) 5158.
[14] G.K. Sandhu, R. Hundal, J. Organomet. Chem. 412 (1991) 31.
[15] K. Chandra, R.K. Sharma, B.S. Garg, R.P. Singh, J. Inorg. Nucl. Chem. 42 (1980) 187.
[16] G.K. Sandhu, S.P. Verma, Polyhedron 6 (1987) 587.
[17] (a) J.F. Vollano, R.O. Day, D.N. Rau, V. Chandrasekhar, R.R. Holmes, Inorg.Chem. 23 (1984) 3153;
(b) K.C. Molloy, T.G. Purcell, K. Quill, I.W. Nowell, J. Organomet. Chem. 267 (1984) 237;
(c) A.R. Forrester, S.J. Garden, R.A. Howie, J.L. Wardell, J. Chem. Soc. Dalton Trans. (1992) 2165.
[18] A. Bondi, J. Phys. Chem. 68 (1964) 441.
[19] V.R. Thalladi, H.-C. Weiss, D. Blaser, R. Boese, A. Nangia, G.R. Desiraju, J. Am. Chem. Soc. 120 (1998) 8702.
[20] (a) C.L. Ma, Q.F. Zhang, R.F. Zhang, L.L. Qiu, J. Organomet. Chem. 690 (2005) 3033;
(b) P.J. Smith, R.O. Day, V. Chandrasekhar, J.M. Holmes, R.R. Holmes, Inorg. Chem. 25 (1986) 2495;
(c) M.J. Begley, D.B. Sowerby, P. Kapoor, R. Kapoor, Polyhedron 14 (1995) 1937.
[21] H.D. Yin, M. Hong, Chin. Inorg. Chem. 20 (2004) 297.
[22] V.R. Vangala, A. Nangia, V.M. Lynch, Chem. Comm. (2002) 1304.
[23] (a) S.W. Ng, C. Wei, V.G. Kumar Das, T.C.W. Mak, J. Organomet. Chem. 334 (1987) 295;
(b) S.G. Eoh, S.H. Ang, J.P.D. Declercq, Polyhedron 16 (1997) 3729.
[24] N.W. Alcock, J. Culver, S.M. Roe, J. Chem. Soc. Dalton Trans. (1992) 1477.
[25] C. Vatsa, V.K. Jain, T. Kesavadas, J. Organomet. Chem. 410 (1991) 135.
[26] H.D. Yin, C.H. Wang, C.L. Ma, Y. Wang, Chin. J. Inorg. Chem. 19 (2003) 617.

complexes to include molybdenum. The reaction between $CpMo(CO)_3SH$ and acid chlorides which gives the expected thiocarboxylate complexes $CpMo(CO)_3SCOR$ is discussed in this report.

2. Results and discussion

2.1. Synthesis and characterization

Treatment of the molybdenum hydrosulfido complex $CpMo(CO)_3SH$ with acid chlorides gave the thiocarboxylate complexes $CpMo(CO)_3SCOR$, **1**–**5** as shown in the following equation:

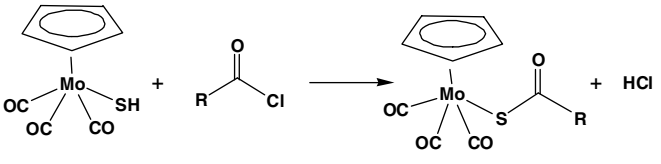

1 - 5

R= Me (**1**), CH_2Cl (**2**), Ph (**3**), 4-$C_6H_4NO_2$ (**4**), 3,5-$C_6H_3(NO_2)_2$ (**5**)

(1)

The resulting dark-red thiocarboxylate complexes, **1**–**5**, are air stable as solids. In solution, these complexes are quite unstable and they decompose to brown insoluble materials. In some experiments small amounts of the chloride complex $CpMo(CO)_3Cl$ were also obtained. Complexes **1**–**5** have been fully characterized by IR, ^1H NMR spectra, elemental analysis and by the single crystal X-ray structure determination of **3**. The IR spectra of **1**–**5** display three absorption bands in the range of 2048–2042, 1980–1971, and 1936–1942 cm^{-1}, respectively, for the terminal carbonyl ligands. These bands are lower than those observed for $CpMo(CO)_3SH$ (2039, 1963 cm^{-1}) [33,34], but similar to those observed for $CpMo(CO)_3S_2CSR$ (2050–2046, 1976, and 1951–1952 cm^{-1}) [35]. An additional distinctive absorption appears between 1644 and 1736 cm^{-1}, corresponding to the ketonic carbonyl group of the thiocarboxylate ligand. This value is higher than those observed for the analogous iron thiocarboxylates $CpFe(CO)_2SCOR$ (1590–1630 cm^{-1}), suggesting less electron density around the Mo center compared to that of Fe.

The ^1H NMR spectra of **1**–**5** show the expected signals of the Cp protons in the range 5.55–5.66 ppm. These resonances are found at lower field than the peak for $CpMo(CO)_3SH$ (4.55 ppm) and $CpMo(CO)_3(S_2CSR)$ (4.32 ppm), suggesting that the thiocarboxylate group is a stronger π-acceptor (or weaker σ-donor) ligand compared to the thioxanthate unit [35]. The peaks for the R-group of the thiocarboxylate ligands are shown in the expected ranges with the expected multiplicities.

2.2. Crystal structure

The molecular structure of **3** with the atom numbering scheme is shown in Fig. 1. Selected bond distances (Å) and angles (°) of **3** are presented in Table 1. The crystal lattice of **3** contains two crystallographically independent molecules. The Cp-ring is bonded to the molybdenum atom in a η^5-fashion with Mo–C bond distances ranging from 2.295(4) Å to 2.355(4) Å. The Mo–S bond distance 2.5191(10) Å is similar to that reported for $Mo(\kappa^2C,S\text{-}SCOPr^i)(\kappa S\text{-}SCOMe)(CO)_2(PMe_3)_2$, 2.511(4) Å [28]. The $Mo–C_{CO}$ bond distances (average of 1.986 Å) are in agreement with those found in $CpMo(CO)_3$-containing complexes. The C=O bond distance of the thiocarboxylate ligand of 1.214(5) Å is similar to that reported for $Mo(\kappa^2C,S\text{-}SCOPr^i)(\kappa S\text{-}SCOMe)(CO)_2(PMe_3)_2$ of 1.19(2) Å [28] and to that found in other complexes containing thiocarboxylate groups [22,26].

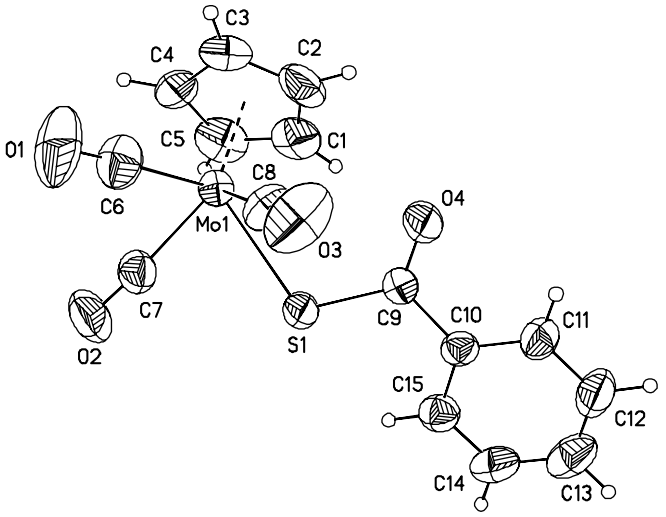

Fig. 1. ORTEP drawing of $CpMo(CO)_3SCOC_6H_5$ (**3**).

Table 1
Selected bond lengths (Å) and angles (°) of $CpMo(CO)_3SCOC_6H_5$ (**3**)

Mo1–S1	2.5191(10)
Mo1–C1	2.355(4)
Mo1–C2	2.345(4)
Mo1–C3	2.304(4)
Mo1–C4	2.295(4)
Mo1–C5	2.312(4)
Mo1–C6	1.973(5)
Mo1–C7	1.989(4)
Mo1–C8	1.995(4)
S1–C9	1.753(3)
C9–O4	1.214(5)
C6–O1	1.153(5)
C7–O2	1.143(5)
C8–O3	1.128(5)
C6–Mo1–C7	76.71(17)
C7–Mo1–C8	77.96(17)
C6–Mo1–C8	111.39(18)
C6–Mo1–S1	133.10(14)
C7–Mo1–S1	76.57(12)
C8–Mo1–S1	76.93(11)
Mo1–S1–C9	107.45(12)
O4–C9–S1	123.8(3)

3. Experimental

3.1. General

Synthetic work was carried out under a dinitrogen atmosphere using Schlenk techniques. Tetrahydrofuran, diethyl ether, hexane, and dichloromethane were dried, distilled and stored under nitrogen. The reagent $CpMo(CO)_3SH$ was prepared as described previously [34,35]. Acid chlorides, molybdenum hexacarbonyl and sulfur were obtained commercially and were used as received.

Nuclear magnetic resonance (NMR) spectra were obtained on a Bruker spectrometer operating at 200 MHz with chemical shifts reported in ppm downfield from TMS, using the solvent residual peak as an internal reference. Infrared (IR) spectra were recorded on a Nicolet-Impact 410 FT-IR spectrometer in CH_2Cl_2 solutions. Elemental analyses were done at Laboratoire D'Analyse Élementaire, Universite de Montréal, Montréal, Québec, Canada. Melting points were reported on a Staurt Melting point apparatus (SMP3) and are uncorrected.

3.2. General procedure for the preparation of $CpMo(CO)_3SCOR$, 1–5

A diethyl ether solution of $CpMo(CO)_3SH$ (0.28 g, 1.00 mmol) was cooled to −78 °C. The respective acid chloride (1.10 mmol) was added as one portion. The cooling bath was removed and the solution was stirred for 2 h at room temperature. The volatiles were removed under vacuum and the resulting solid was redissolved in a minimum amount of dichloromethane and introduced onto a silica gel column made up with hexane. Elution with hexane removes the excess acid chlorides and with a 1:1 v:v ratio of diethyl ether:hexane gives an orange band. This band was collected and the volatiles were removed under vacuum. The resulting red solid was recrystallized from dichloromethane/hexane at 0 °C.

3.2.1. $CpMo(CO)_3SCOMe$ (1)

Yield: 70%. M.p.: 193–194 °C. IR (CH_2Cl_2, cm^{-1}): 2044 (s), 1971 (s), 1936 (s) (ν(C≡O)), 1644 (m) (ν(C=O)). ^{1}H-NMR ($CDCl_3$): δ 2.49 (s, 3H, CH_3), 5.55 (s, 5H, C_5H_5). *Anal.* Calc. for $C_{10}H_8MoO_4S$: C, 37.51; H, 2.52; S, 10.01. Found: C, 37.08; H, 2.32; S, 9.74%.

3.2.2. $CpMo(CO)_3SCOCH_2Cl$ (2)

Yield: 75%. M.p.: 150–151 °C. IR (CH_2Cl_2, cm^{-1}): 2048 (s), 1980 (s), 1957 (ν(C≡O)), 1736 (m) (ν(C=O)). ^{1}H-NMR ($CDCl_3$): δ 4.15 (s, 2H, CH_2Cl), 5.59 (s, 5H, C_5H_5). *Anal.* Calc. for $C_{10}H_7ClMoO_4S$: C, 33.87; H, 1.99; S, 9.04. Found: C, 33.17; H, 1.89; S, 8.33%.

3.2.3. $CpMo(CO)_3SCOPh$ (3)

Yield: 65%. M.p.: 108–110 °C. IR (CH_2Cl_2, cm^{-1}): 2042 (s), 1976 (s), 1941 (s) (ν(C≡O)), 1685 (m) (ν(C=O)). ^{1}H-NMR ($CDCl_3$): 5.63 (s, 5H, C_5H_5), 7.40 (m, 3H, C_6H_5), 8.30 (m, 2H, C_6H_5). *Anal.* Calc. for $C_{15}H_{10}MoO_4S$: C, 47.13; H, 2.64; S, 8.39. Found: C, 46.83; H, 2.28; S, 7.98%.

3.2.4. $CpMo(CO)_3SCO\text{-}4\text{-}C_6H_4NO_2$ (4)

Yield: 87%. M.p.: 134–135 °C. IR (CH_2Cl_2, cm^{-1}): 2045 (s), 1977 (s), 1942 (s) (ν(C≡O)), 1707 (m) (ν(C=O)). ^{1}H-NMR ($CDCl_3$): 5.64 (s, 5H, C_5H_5), 8.32 (2d, 4H, $C_6H_4NO_2$, $J_o = 9.1$ Hz). *Anal.* Calc. for $C_{15}H_9MoNO_6S$: C, 42.17; H, 2.12; N, 3.29; S, 7.50. Found: C, 41.86; H, 1.87; N, 2.95; S, 7.02%.

3.2.5. $CpMo(CO)_3SCO\text{-}4\text{-}C_6H_3(NO_2)_2$ (5)

Yield: 87%. M.p.: 162–163 °C. IR (CH_2Cl_2, cm^{-1}): 2046 (s), 1977 (s), 1941 (s) (ν(C≡O)), 1710 (m) (ν(C=O)). ^{1}H-NMR ($CDCl_3$): 5.66 (s, 5H, C_5H_5), 8.33 (d, 2H, $C_6H_3(NO_2)_2$, $J_m = 3.1$ Hz), 8.67 (t, 1H, $C_6H_3(NO_2)_2$, $J_m = 3.1$ Hz). *Anal.* Calc. for $C_{15}H_9MoN_2O_8S$: C, 38.23; H, 1.50; N, 5.94; S, 6.80. Found: C, 37.75; H, 1.37; N, 5.45; S, 6.38%.

3.3. X-ray structure analysis

X-ray data of a dark red crystal of $CpMo(CO)_3SCOPh$ (**3**) were collected with an Oxford Gemini S diffractomer with a graphite monochromator λ(Mo Kα) = 0.71073 Å. The crystallographic data are presented in Table 2. The structure was solved by direct methods using SHELXS-97 [36] and refined by full-matrix least-square procedures on

Table 2
Selected crystal data and refinement parameters for $CpMo(CO)_3SCOC_6H_5$ (**3**)

Empirical formula	$C_{15}H_{10}MoO_4S$
Formula weight	382.23
Crystal size (mm)	0.3 × 0.3 × 0.2
Crystal system	Orthorhombic
Space group	*Pca2(1)*
Unit cell dimension	
a (Å)	33.833 (3)
b (Å)	7.6070 (5)
c (Å)	11.7042 (9)
α (°)	90
β (°)	90
γ (°)	90
V (Å^3)	3012.3 (4)
Z	8
Index ranges	$-40 \leqslant h \leqslant 40$
	$-9 \leqslant k \leqslant 9$
	$-13 \leqslant l \leqslant 14$
Refections collected/unique [R_{int}]	19510/5385 [0.0321]
Data/restrains/parameters	5385/1/379
GooF	1.062
D_{calc} (Mg m^{-3})	1.686
μ (mm^{-1})	1.020
θ Range (°)	2.94–25.20
$R[F^2 > 2\sigma(F^2)]$	0.0279
$\omega R(F^2)$[a]	0.0501
Flack x parameter[b]	0.02(3)

[a] $\omega = 1/[\sigma^2(F_o^2) + (0.0186P)^2 + 1.5711P]$ where $P = (F_o^2 + 2F_c^2)/3$.
[b] H.D. Flack, Acta Crystallogr., Sect. A (39) (1983) 876.

F^2, using SHELXTL-97 [37]. All non-hydrogen atoms are refined anisotropically and the hydrogen atom positions have been refined using the riding model. The absolute structure was determined by the refinement of the Flack x parameter. The asymmetric unit comprises two independent molecules.

Acknowledgements

The authors thank the Deanship of Research, Jordan University of Science and Technology and Shoman Foundation for financial support.

Appendix A. Supplementary data

Crystallographic data for the structural analysis have been deposited with the Cambridge Crystallographic Data Centre, CCDC No. 600973 for compound **3**. Copies of this information may be obtained free of charge from The Director, CCDC, 12 Union Road, Cambridge CB2 1EZ, UK (fax: +44 1233 336 033; e-mail: deposit@ccdc.cam.ac.uk or www: http://www.ccdc.cam.ac.uk). Supplementary data associated with this article can be found, in the online version, at doi:10.1016/j.poly.2006.06.021.

References

[1] H.J. Gysling, Coord. Chem. Rev. 42 (1982) 133.
[2] P.J. Blower, J.R. Dilworth, Coord. Chem. Rev. 76 (1987) 121.
[3] R. Oilunkaniemi, R.S. Laitinen, M. Ahlgren, J. Organomet. Chem. 587 (1999) 200.
[4] I.G. Dance, Polyhedron 5 (1986) 1037.
[5] V.G. Albano, M. Monari, I. Orabona, A. Panunzi, G. Roviello, F. Rufo, Organometallics 22 (2003) 1223.
[6] A.J. Canty, M.C. Denney, J. Patel, H. Sun, B.W. Skelton, A.H. White, J. Organomet. Chem. 689 (2004) 672.
[7] C.N. Satterfield, in: Heterogeneous Catalysis in Industrial Practice, 2nd ed., McGraw-Hill, New York, 1991, pp. 378–384.
[8] J.R. Dilworth, N. Wheatley, Coord. Chem. Rev. 199 (2000) 89.
[9] D.V. Vivic, W.D. Jones, Organometallics 18 (1999) 134.
[10] A. Shaver, H. Boily, A.-M. Lebuis, Inorg. Chem. 35 (1996) 6356.
[11] A. Shaver, M. El-khateeb, A.-M. Lebuis, Angew. Chem., Int. Ed. Engl. 35 (1996) 2362.
[12] S. Dey, V.K. Jain, S. Chaudhury, A. Knoedler, F. Lissner, W. Kaim, J. Chem. Soc., Dalton Trans. (2001) 723.
[13] Q. Liu, J. Lin, P. Jiang, J. Zhang, L. Zhu, Z. Guo, Eur. J. Inorg. Chem. (2002) 2170.
[14] E.R. Jamieson, S.J. Lippard, Chem. Rev. 99 (1999) 2467.
[15] K.M. Williams, C. Rowan, J. Mitchell, Inorg. Chem. 43 (2004) 1190.
[16] J.T. Saponthar, J.J. Vittal, P.A.W. Dean, J. Chem. Soc., Dalton Trans. (1999) 3135.
[17] Y.C. Neo, J.J. Vittal, T.S.A. Hor, J. Organomet. Chem. 637–639 (2001) 575.
[18] J.M. Lisy, E.D. Dobrzynski, R.J. Angelici, J. Clardy, J. Am. Chem. Soc. 97 (1975) 656.
[19] T.C. Deivaraj, G.X. Lai, J.J. Vittal, Inorg. Chem. 39 (2000) 1028.
[20] V. Riera, F.J. Arnaiz, G.G. Herbosa, J. Organomet. Chem. 315 (1986) 51.
[21] F.A. Cotton, P.E. Fanwick, R.H. Niswander, J.C. Sekutowski, Acta Chem. Scan. A 32A (1978) 663.
[22] M.A. El-Hinnawi, A. Ajlouni, J. Abu-Nasser, K. Powell, H. Vahrenkamp, J. Organomet. Chem. 359 (1989) 79.
[23] M.A. El-Hinnawi, A. Ajlouni, J. Organomet. Chem. 332 (1987) 321.
[24] M.A. El-Hinnawi, M. El-khateeb, I. Jibril, S.T. Abu-Orabi, Synth. React. Inorg. Met. Org. Chem. 19 (1989) 309.
[25] M.A. El-Hinnawi, F.T. Smadi, M. Esmadi, J. Organomet. Chem. 377 (1989) 373.
[26] W.A. Schenk, N. Sonnhalter, N. Burzlaff, Z. Naturforsch. 52b (1997) 117.
[27] R. Devy, J.J. Vittal, Inorg. Chem. 37 (1998) 6939.
[28] L. Contreras, F.R. Lainez, A. Pizzano, L. Sanchez, E. Carmona, A. Monge, C. Ruiz, Organometallics 19 (2000) 261.
[29] M. Cindric, D. Matkovic-Calogovic, V. Vrdoljak, B. Kamenar, Inorg. Chim. Acta 284 (1999) 223.
[30] I. Jibril, M.A. El-Hinnawi, M. El-khateeb, Polyhedron 10 (1991) 2095.
[31] A. Matthies, K.V. Rajagopalan, R.R. Mendel, S. Leimkuehler, Proc. Natl. Acad. Sci. USA 101 (2004) 5946.
[32] M.M. Wuebbens, K.V. Rajagopalan, J. Biol. Chem. 278 (2003) 14523.
[33] U. Behrens, F. Edelmann, J. Organomet. Chem. 263 (1984) 179.
[34] A. Bauer, K.B. Capps, B. Wixmerten, K.A. Abboud, C.D. Hoff, Inorg. Chem. 28 (1999) 2136.
[35] W. Dean, B. Heyl, J. Organomet. Chem. 159 (1978) 171.
[36] G.M. Sheldrick, Acta Crystallogr., Sec. A: Fund. Crystallogr. 46 (1990) 467.
[37] G.M. Sheldrick, SHELXS-97 (Release 97-2), University of Göttingen, Germany, 1997.

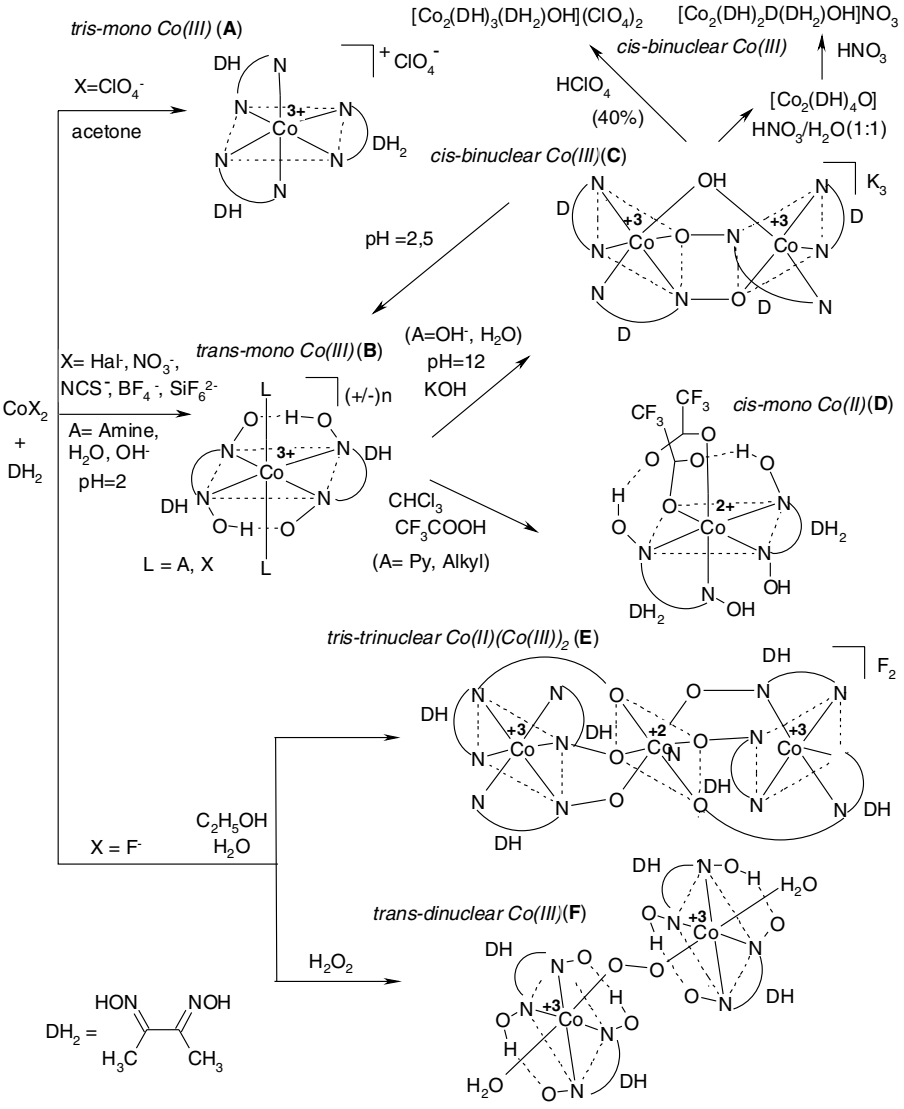

Scheme 1. Synthetic and structural flexibility of the Co/DH_2 system.

Taking into account that no examples with cobalt dimethylglyoxymate containing directly coordinated fluorine ion to the cobalt center were known, our previous investigations were focused in this direction. Our attempt to prepare such compounds was unsuccessful, instead non-trivial binuclear Co(III)-*trans* with a μ-peroxo bridge [11] (type F Scheme 1), and tris-trinuclear mixed-valence Co(II)-$(Co(III))_2$ [12] (type E Scheme 1) compounds were obtained using CoF_2 or HF as the fluorine sources. Exploiting these reagents directly in the synthesis has proven to have some serious drawbacks related to their toxic and corrosive properties. That is why our attention has now turned to the $Co(OTf)_2 \cdot 6H_2O$ ($CF_3SO_3^-$ or OTf^- – triflate) salt which is less toxic, chemically inert and contains a weakly coordinating anion with a fluorocarbon functionality. Within this context, we report hereafter on the synthesis and crystal X-ray structural characterization of three new complexes, one trinuclear tris-Co(II) and two *trans*-cobaloxime type Co(III) complexes prepared from a Co(II) triflate precursor.

2. Experimental

2.1. Materials

All chemicals were of reagent grade and used as purchased without further purification. $Co(CF_3SO_3)_2 \cdot 6H_2O$ was prepared according to [21], by dropwise treating of a water suspension of basic cobalt carbonate with a small excess of CF_3SO_3H (98%).

2.2. Synthesis

2.2.1. $[Co_3(\mu\text{-}DH)_6] \cdot 24H_2O$ (*I*)

Dimethylglyoxime (0.23 g, 0.002 mol) and $Co(CF_3SO_3)_2 \cdot 6H_2O$ (0.47 g, 0.001 mol) were dissolved in 10 ml of an ethanol/water (1:1) mixture and heated in a graphite crucible for 10 min at 70 °C. After cooling a brown solid was filtered out, washed with ethanol and dried in air. The yield was 43%. Single crystals suitable for X-ray

diffraction studies were obtained by recrystallization from water/ethanol (1:1) mixture.

Found: C, 22.63; H, 6.48; N, 12.82. Calc. for $C_{24}H_{90}Co_3N_{12}O_{36}$ (fw = 1299.87) C, 22.18; H, 6.98; N, 12.93.

UV–Vis, $\lambda_{max}(\varepsilon)$, $C = 1.2 \times 10^{-4}$ M, DMF: 432 nm (sh, 13 192), 268 nm (42 032) ($dm^3\ mol^{-1}\ cm^{-1}$).

IR (KBr, cm^{-1}): 500(s), 637(w), 733(w), 804(w), 973(m), 1071(s), 1130(w), 1214(s), 1383(w), 1495(w), 1558(w), 1627(m), 1742(w), 2852(w), 2923(m), 3435(s).

MS FAB(−), *m/z*: 864.5 (I, 100%) $[Co_3(DH)_6 - 3H]^-$, 749.3 (I, 22%) $[Co_3(DH)_5 - 3H]^-$, 403.7 (I, 8%) $[Co(DH)_3]^-$, 597.7 (I, 8%), 633.3 (I, 5%) $[Co_3(DH)_4 - 4H]^-$, 523.3 (I, 5%) $[Co_3(DH)_3]^-$, 461.5 (I; 4%) $[Co_2(DH)_3 - H]^-$, 287.5 (I; 3%) $[Co(DH)_2 - H]^-$.

2.2.2. $[Co(DH)_2Tu_2]CF_3SO_3$ (*II*)

Dimethylglyoxime (0.23 g, 0.002 mol) and $Co(CF_3SO_3)_2 \cdot 6H_2O$ (0.47 g. 0.001 mol) were dissolved in 10 ml of a methanol/water (1:1) mixture and heated in a graphite crucible for 10 min at 70 °C. The solution was then filtered to remove unreacted dimethylglyoxime. Thiourea (Tu) (0.15 g, 0.002 mol) solubilized in 5 ml methanol was finally added and the mixture was heated for an additional 10 min. After cooling a brown solid was filtered out, washed with ethanol and dried in air. The yield was 71%.

Found: C, 22.17; H, 3.59; N, 18.81. Calc. for $C_{11}H_{22}CoF_3N_8O_7S_3$ (fw = 590.48) C, 22.36; H, 3.73; N, 18.97.

UV–Vis, $\lambda_{max}(\varepsilon)$, $C = 1.2 \times 10^{-4}$ M, CH_3OH: 281 nm (12 868), 263 nm (18 823) ($dm^3\ mol^{-1}\ cm^{-1}$).

IR (KBr, cm^{-1}): 604(m), 686(w), 824(s), 875 (m), 1050 (s), 1076(w), 1107(w), 1204(w), 1262 (w), 1339(w), 1402(m), 1449(m), 1494(s), 1550.1(w), 1608(m), 1731(w), 2330(br,w), 2857(m), 2926(m), 3017(w), 3462(br,w).

MS FAB(−), *m/z*: 149.1 (I, 100%) $[CF_3SO_3]^-$, MS FAB (+), *m/z*: 610.8 (I, 100%) $[2(Co(DH)_2) + 2O]^+$, 728.8 (I, 70%) $[2(Co(DH)_2) + 2Tu]^+$, 289.0 (I, 46%) $[Co(DH)_2]^+$, 652.7 (I, 41%) $[2(Co(DH)_2) + Tu]^+$, 804.7 (I, 36%) $[2(Co(DH)_2) + 3Tu]^+$, 537.9 (I, 23%) $[Co_2(DH)_3{+}Tu]^+$, 464.9 (I, 17%) $[2Co_2(DH)_3]^+$, 363.9 (I, 15%) $[Co(DH)_2 + Tu]^+$.

^1H NMR, 400 MHz (DMSO, ppm): δ 2.37 (12H, CH_3(DH)), 7.92 (8H, NH_2(Tu)), 17.55 (2H, bs, O...HO).

^{13}C NMR, 100.6 MHz (DMSO), 13.79 (Me, DH), 121.53 (q, $^1J_{CF} = 321.48$ Hz, CF_3), 154.37 (C=N, DH), 176.49 (C=S (Tu)).

2.2.3. $[Co(DH)_2Py_2]CF_3SO_3$ (*III*)

Dimethylglyoxime (0.23 g, 0.002 mol) and $Co(CF_3SO_3)_2 \cdot 6H_2O$ (0.47 g, 0.001 mol) were dissolved in 10 ml of a methanol/water (1:1) mixture and heated in a graphite crucible for 10 min at 70 °C. After filtration of unreacted dimethylglyoxime, pyridine (0.20 ml, 0.0024 mol) was added dropwise. The reaction mixture was heated in a graphite crucible for 10 min at 80 °C. After cooling a brown solid was filtered out, washed with ethanol and dried on air. The yield was 67%.

Found: C, 38.57; H, 4.29; N, 13.83. Calc. for $C_{19}H_{24}CoF_3N_6O_7S$ (fw = 596.43) C, 38.26; H, 4.06; N, 14.09.

UV–Vis, $\lambda_{max}(\varepsilon)$, $C = 1.2 \times 10^{-4}$ M, CH_3OH: 250 (10 406), 222 (12 606) nm ($dm^3\ mol^{-1}\ cm^{-1}$).

IR (KBr, cm^{-1}): 515(m), 571 (w), 635(s), 651(w), 688,6(w), 701–738(d,w), 773(w), 985(w), 1032.1(s), 1069–1092(d,m), 1136–1149(d,m), 1238(s), 1269–1281(d,s), 1372(w), 1454(m), 1497(w), 1560(m), 1611(w), 22982(w), 2929(w), 3062(w), 3124(w), 3437(br, m).

MS FAB(−), *m/z*: 149.1 (I, 100%) $[CF_3SO_3]^-$, MS FAB (+), *m/z*: 289.0 (I, 100%) $[Co(DH)_2]^+$, 446.8 (I, 50%) $[Co(DH)_2Py_2]^+$, 258.8 (I, 16%) $[Co(DH)_2 - 2CH_3]^+$, 204.9 (I, 13%), 367.8 (I, 11%) $[Co(DH)_2Py]^+$.

^1H NMR, 400 MHz (DMSO, ppm): δ 2.31 (12 H, s, CH_3 (DH)), 7.59 (4H, tr, Py-*meta*), 8.02 (2H, tr, Py-*para*) 8.17 (4H, d, Py-*ortho*), 18.16 (2H, bs, O...HO).

^{13}C NMR, 100.6 MHz (DMSO), 14.13 (Me, DH), 121.50 (q, $^1J_{CF} = 321.50$ Hz, CF_3), 127.9, (CH, Py-*meta*), 141.6 (CH, Py-*para*), 151.47 (CH, Py-*ortho*), 153.90 (C=N, DH).

2.3. Analyses and physical measurements

Elemental analyses were made by standard micromethods. Mass-spectrometric analyses were performed on an Analytical VG 7070 EQ instrument using the FAB method. UV–Vis spectra were obtained with Lambda 6 Perkin–Elmer spectrophotometer. IR spectra were recorded with KBr discs in the range 4000–400 cm^{-1} on a Perkin–Elmer spectrometer. UV–Vis spectra were obtained with Lambda 6 Perkin–Elmer spectrophotometer. Both ^1H (400 MHz) and ^{13}C NMR (100.6 MHz) measurements were carried out on a Bruker Avance 400 spectrometer, using DMSO as the solvent. Chloroform solution ESR spectra were obtained with a Bruker spectrometer, type ER100D, using DPPH as the reference. All spectra were recorded at 298 and 170 K, using a standard low temperature apparatus Bruker ER 4111VT. Magnetic susceptibility of powdered samples was obtained at 290 K using Oxford Instruments with a CF200 cryo-system and microbalance Cahn 2000. The equipment was previously calibrated with $HgCo(NCS)_4$ standard [22]. The magnetic measurement was corrected for cell and sample diamagnetic contributions [23].

2.3.1. X-ray crystallography

Diffraction data were collected at 130 K for **I** and **II** and at 293 K for **III** with a KM4CCD diffractometer using Mo Kα graphite-monochromated radiation. Crystallographic data and details of the refinement process are summarized in Table 1. The structures were solved by direct methods using the program SHELXS-97 [24]. Refinement and all further calculations were carried out using SHELXL-97 [25]. In the case of structure **I** refinement of the structure presented some problems. We localized quite straightforwardly two cobalt atoms at special positions, the DH ligand, four

Table 1
Crystallographic data for **I**, **II** and **III**

Identification code	**I**	**II**	**III**
Empirical formula	$C_{24}H_{90}Co_3N_{12}O_{36}$	$C_{11}H_{22}CoF_3N_8O_7S_3$	$C_{19}H_{24}CoF_3N_6O_7S$
Formula weight	1299.87	590.48	596.43
Temperature	130 K	130 K	293 K
Crystal system, space group	trigonal, $R\bar{3}$	triclinic, $P\bar{1}$	monoclinic, $P2_1/n$
a, b, c (Å)	19.858(1), 19.858(1), 12.588(1)	8.114(2), 11.887(2), 13.197(3)	12.278(2), 7.430(1), 14.443(3)
α, β, γ (°)	90, 90, 120	116.00(3), 101.35(3), 94.82(3)	90, 110.243(3), 90
V (Å^3)	4298.9(5)	1100.5(4)	1236.2(4)
Z	3	2	2
D_c (g cm^{-3})	1.506	1.782	1.602
Absorption coefficient (mm^{-1})	0.961	1.142	0.853
$F(000)$	2061	604	612
Range θ (°)	3.45–26.33	3.52–29.91	3.33–26.36
Reflections collected/unique [R_{int}]	16008/1954 [0.0327]	10462/5513 [0.0230]	6858/2490 [0.0230]
Data/restraints/parameters	1954/0/144	5513/0/386	2490/0/215
Goodness-of-fit on F^2	1.078	1.048	1.263
Final R indices [$I > 2\sigma(I)$]	$R_1 = 0.0540$, $wR_2 = 0.1451$	$R_1 = 0.0329$, $wR_2 = 0.0814$	$R_1 = 0.0537$, $wR_2 = 0.1118$
R indices (all data)	$R_1 = 0.0550$, $wR_2 = 0.1462$	$R_1 = 0.0359$, $wR_2 = 0.0838$	$R_1 = 0.0597$, $wR_2 = 0.1143$

water molecules (one is disordered over two positions) and all hydrogen atoms. However, the refinement converged poorly and there were two high residual peaks of ca. 6 and 4 e Å^{-3} on difference electron density maps which were initially difficult to explain. The highest peak was located at the Wyckoff position 1b of C_{3i} symmetry at a distance of 2.4 Å from six DH oxygen atoms. The second peak was located very close to the Co1 atom. Additionally, the displacement parameters of the Co2 atom were relatively high whereas the displacement ellipsoid of Co1 was strongly elongated in the z direction. To explain these features we assumed a disorder of the trinuclear complex molecules in the crystal lattice which can be described as follows. Trinuclear complex molecules in **I** are arranged into columns running along the [0 0 1] direction and only every second site of the C_{3i} symmetry along this direction is occupied by a Co2 atom. The 'unoccupied' C_{3i} sites are surrounded by six hydrogen bonded OH groups of the DH ligand. However, shifting the complex molecule along the z direction by 0.5c so that the Co2 atom is placed in the nearest unoccupied Wyckoff 1b site, does not substantially influence the intermolecular interactions of the complex molecules with the surrounding water molecules because after this transformation atoms of the DH and DH$_x$ ligand closely overlap (Fig. 1a) and the Co1′ atom is placed only 0.5 Å apart from Co1. We noticed that whereas [0 0 1] columns of the complex molecules should be ordered, there might be some faults in their distribution (i.e. their arrangement does not always obey the space group symmetry) giving rise to the observed crystal disorder. Therefore, the complex molecule was generated in this second alternative position, and introduced as a rigid group for further refinement. The sum of the occupancy factors of the minor and major positions of the complex molecule was kept equal to 1. The molecule in the minor position was refined isotropically and its final occupancy factor refined at 0.18. With these considerations, the structure refinement of **I** proceeded smoothly giving the results presented in Table 1. The triflate ion in **III** is disordered. This non-centrosymmetric ion is located at a crystallographic inversion center

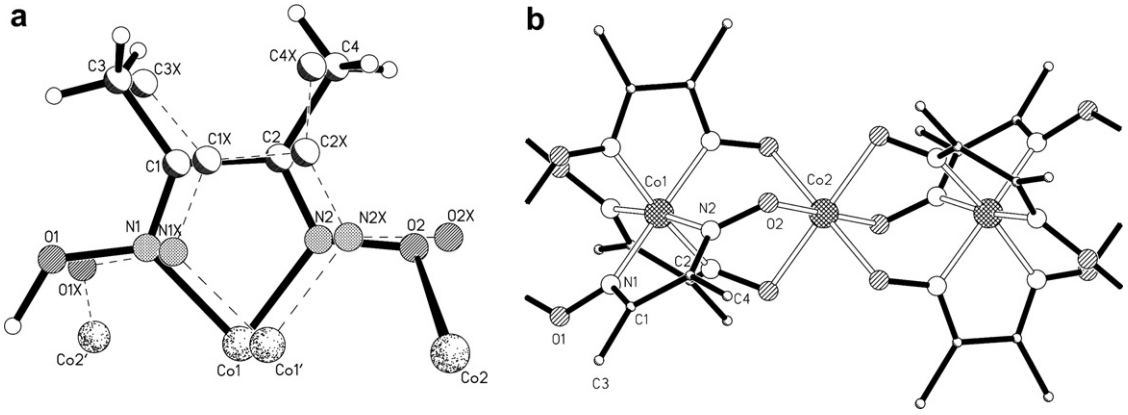

Fig. 1. (a) Drawing of the asymmetric part of the complex molecule in **I** showing disorder encountered in this crystal structure (the molecule with lower occupancy is presented with dashed lines) and (b) the complex molecule in **I** shown without disorder.

Table 2
Selected bond lengths (d, Å) and bond angles (°) for compounds **I**–**III**

Bond length	d (Å)	Bond angles	∠ (°)
Compound **I**			
Co1–N1	1.926(4)	N1–Co1–N2	80.6(2)
Co1–N2	1.886(4)	N1–Co1–N2^{ii}	92.3(1)
Co2–O2	2.082(3)	N1–Co1–N1^{iii}	95.4(2)
Compound **II**			
Co1–N1	1.885(2)	N1–Co1–N2	81.2(1)
Co1–N2	1.902(2)	N1–Co1–N3	178.6(1)
Co1–N3	1.898(2)	N1–Co1–N4	98.7(1)
Co1–N4	1.901(2)	N2–Co1–N3	99.1(1)
Co1–S1	2.279(1)	N2–Co1–N4	179.1(1)
Co1–S2	2.298(1)	N3–Co1–N4	81.0(1)
Compound **III**			
Co1–N1	1.895(3)	N1–Co1–N2	81.1(1)
Co1–N2	1.893(3)	N1–Co1–N2^{i}	98.9(1)
Co1–N3	1.965(3)	N2–Co1–N2^{i}	180.0(1)

Symmetry code: (i) $-x, -y, -z$; (ii) $-y, x-y, z$; (iii) $-x+y, -x, z$.

where it adopts two distinct orientations with O atoms overlapping with F atoms and C atoms overlapping with S atoms.

H-atoms were located from Fourier difference maps and refined isotropically. H-atoms from water molecules were also located from difference maps but their positions were kept fixed with $U_{iso} = 1.5U_{eq}$ of their carrier O atom. The non-H atoms were refined anisotropically, using weighted full-matrix least-squares on F^2. Selected bond lengths and angles for **II** and **III** are listed in Table 2.

3. Results and discussion

3.1. Mass-, IR and UV–Vis data

The complexes **I**–**III** have been prepared in good yields and characterized from analytical and physicochemical data (Sections 2.2.1–2.2.3). The elemental analysis data of **1** suggest a 1:2 stoichiometric ratio between cobalt and the DH-ligand, and a formula $[Co(DH)_2X_2]CF_3SO_3$ where X = Tu and Py for **II** and **III**, respectively. Their brick red or brown color suggests an octahedral stereochemistry. In the FAB(+) mass spectrum of **I** the highest mass species detected is the trinuclear dimethylglyoximate core $[Co_3(DH)_6 - 3H]^-$. An insignificant fragmentation with subsequent loss of the DH residue $[Co_3(DH)_5 - 3H]^-$, $[Co_3(DH)_4 - 4H]^-$, $[Co_3(DH)_3]^-$, and generation of bi- and mononuclear species $[Co_2(DH)_3 - H]^-$, $[Co(DH)_3]^-$, $[Co(DH)_2 - H]^-$ were also observed. No signal corresponding to the triflate anion was detected in FAB(−). In the case of **II** and **III**, the 100% intensive and the single signal in FAB(−) corresponds to the counter anion OTf^-. In the positive FAB spectra in both cases the signal corresponding to the $[Co(DH)_2]^+$ unit is present as well as its combination with one or two molecules of axial ligands.

Their UV–Vis spectra are also different, **II**–**III** have a relatively weak and featureless visible spectrum as do other octahedral *trans* Co(III) dimethylglyoximates, with an intensity that rises into the UV toward the general cobaloxime-type absorption at ca 263 and 222 nm for **II** and **III**, respectively (due to the intraligand (DH) π–π* transition). The second band at 281 and 250 nm (for **II** and **III**) is assigned to the corresponding apical ligands Tu or Py, molecules which are located in *trans* positions related to each other, and is due to the charge transfer from the axial ligands to the cobalt ion. No d–d transition bands of the metal are observed for **II**–**III**, which in most Co(III) complexes are assigned as $^1A_{1g} \rightarrow {}^1T_{1g}$ at between 476 and 625 nm [26]. In contrast the UV/visible spectrum of **I** contains a weak absorption at 432–614 nm (sh, broad band) characteristic of Co(II) d–d transitions and a maximum band at 268 nm, attributed to the intraligand DH π–π* transitions. Generally, the electronic spectra of octahedral Co(II) complexes show as a rule two main bands, one transition occurring in the 950–1540 nm range and the other in the 460–660 nm range [27] identified with $^4T_{1g}(F) \rightarrow {}^4T_{2g}(F)$ and $^4T_{1g}(F) \rightarrow {}^4T_{1g}(P)$ transitions, respectively. No near IR measurements were made on our compounds.

In the IR spectrum of **I** the presence of water molecule are reflected by a strong absorption at 3434 nm. The C=N frequencies of coordinated dimethylglyoxime molecules are also present at 1627 nm. Two strong absorption bands at 1213 and 1070 nm are attributed to NO groups. The signal at 500 nm corresponds to Co–N bonds. No Co–O absorption bands were detected, probably due their presence in the field lower than 450 nm. The IR spectrum of **II** is more complicated and represents a combination of contributions from the cation and anion. In the solid state IR spectrum of **III** the triflate group causes absorption bands at 1269 cm^{-1}, 1032 ($\nu s(SO_2)$) and 635 cm^{-1} ($\delta s(SO_3)$) and which can be assigned to the uncoordinated counterion. The band at 515 cm^{-1} is assignable to the Co–N stretching frequency between cobalt and nitrogen atoms of dimethylglyoxime [28].

Taking into account the data of mass-, UV–Vis and IR data, the synthesized compounds were proposed to have an octahedral structure, as in simple cobaloxime type species. The different behavior of **I**, the missing bands in the IR spectra of characteristic OTf^- stretching bands, the absence of a triflate peak in the FAB(−) as well as the presence in the FAB(+) of the highest peak corresponding to a trinuclear dimethylglyoximate core indicate its non electrolytic and polynuclear nature, which was confirmed by its X-ray structure analysis.

3.2. NMR spectra

The ^1H NMR spectra of diamagnetic compounds **II** and **III** indicate their *trans*-configuration. The signals of methyl groups of DH residues in the ^1H NMR spectra are 2.37 and 2.31 ppm for **I** and **II**, respectively, which are shifted downfield compared to the "free" DH_2 molecule (1.48 ppm, D_2O). The presence of a large downfield singlet 17.55 (for **II**) and 18.16 ppm (for **III**) in the ^1H NMR is due to the two symmetrical intramolecular hydrogen bonds, and is

an indirect proof of the *trans*-type configuration. The coordination of apical ligands (Tu and Py) is well illustrated in the ^{1}H and ^{13}C NMR spectra (Sections 2.2.2 and 2.2.3). In the ^{1}H NMR, a downfield shift of about 0.87 ppm (for free Tu in DMSO, ^{1}H NMR, δNH 7.05 ppm; $\delta^{13}C$ (C=S) 183.81 ppm [29] and for studied compound **II** these values are 7.92 and 176.49 ppm, respectively) was observed for the N–H proton of Tu in **II** on its complexation with the cobaloxime core. An upfield shift of about 7.32 ppm is observed in the C=S resonance (^{13}C NMR $\delta^{13}C_{(C=S)}$ 176.49 ppm) of Tu (**II**) on its complexation. This is due to the lowering of the C=S bond order upon coordination and a shift of N → C electron density producing a partial double bond character in the C–N bond, as observed in other metal complexes of thiourea [30]. The presence of an aromatic proton in the region 7.59 –8.17 ppm (^{1}H NMR) is due to the coordinated pyridine molecule in **III**. The uncoordinated triflate anions give rise to a quartet system, 121.53 (q, $^{1}J_{CF} = 321.48$ Hz, CF_3), in the ^{13}C NMR spectra of both compounds.

3.3. Magnetic measurements and ESR spectra

Most cobalt(II) complexes of non-macrocyclic tetradentate ligands with nitrogen and/or oxygen donors are high-spin, five or six coordinate complexes [31].

The studied compound **I** $[Co_3(DH)_6]$ falls into the same category, its magnetic moment of $\mu_B = 4.3$ MB is quite comparable to the values expected (spin-only, 3.88 MB) and found (typically 4.3–5.2 MB) for high spin Co(II), but distinctly different from the value 1.73 MB characteristic to Co(II) with a low spin configuration [32]. The slight decrease in the value compared with literature data for high spin octahedral complexes of Co (II) could be due to the interaction with the other nuclei of cobalt, or with the bridging ligand.

No ESR signal for **I** in both the solid or in solution were observed at room temperature. The lack of a signal can be the result of fast spin-lattice relaxation times and strongly suggests the presence of a high-spin Co(II) complex [33–35].

3.4. Crystal structures

3.4.1. Compound *I*

The trigonal R-3 crystals of **I** are built from neutral, C_{3i} symmetrical trinuclear $[Co^{II}(DH)_3]_2Co^{II}$ molecules and water of crystallization (24 H_2O molecules per one complex molecule). Two $\{Co^{2+}(\mu\text{-}DH)_3\}$ units with cis-oriented DH^- groups are connected to the central Co^{II} ion via bridging oxygen atoms (Fig. 1b). Thus, both types of Co^{II} atoms have octahedral coordination, however their environment in the molecule is different. Co(2) is surrounded by six O atoms from six deprotonated oxime groups whereas Co(1) is coordinated by six N atoms from three DH^- units. the structure of this neutral molecule is very similar to that reported in [11] for the $[Co_2^{III}Co^{II}(DH)_6]^{2+}$ cation. The $(Co1–N)_{DH}$ distances are 1.892(4) and 1.919(4) Å and the $(Co2–O)_{DH}$ bond is 2.083(3) Å (Table 2). However the difference from [11] consists in that all three atoms of cobalt are Co(II).

In the crystal the $[Co^{II}(DH)_3]_2Co^{II}$ molecules are connected end-to-end by hydrogen bonds between their oxime OH groups into a polymeric structure running along the *z* axis (Fig. 2). Six hydrogen-bonded OH groups belonging to two molecules form a cyclic motif with the graph symbol $R_6^6(12)$ [36]. These hydrogen-bonded columns of $[Co^{II}(DH)_3]_2Co^{II}$ are immersed in the 3D hydrogen-bond network formed by four symmetry-independent water molecules. They join to this network by hydrogen bonds O3W–H···O2 and O4WB–H···O1 (Fig. 3). Molecules of crystal-water are joined among themselves by an elaborate system of hydrogen bonds, forming their own supramolecular system. Disorder of the water molecule OW4B can, to some extend, be related to the disorder of the complex molecules (see Section 2). The hydrogen-bond parameters are listed in Table 3.

3.4.2. Compound *II*

The crystals of **II** consist of non-centrosymmetric $[Co(DH)_2Tu_2]^+$ cations and $[CF_3SO_3]^-$ anions (Fig. 4). The complex cation shows an usual *trans*-octahedral configuration (4N2S) around the metal ion with the two

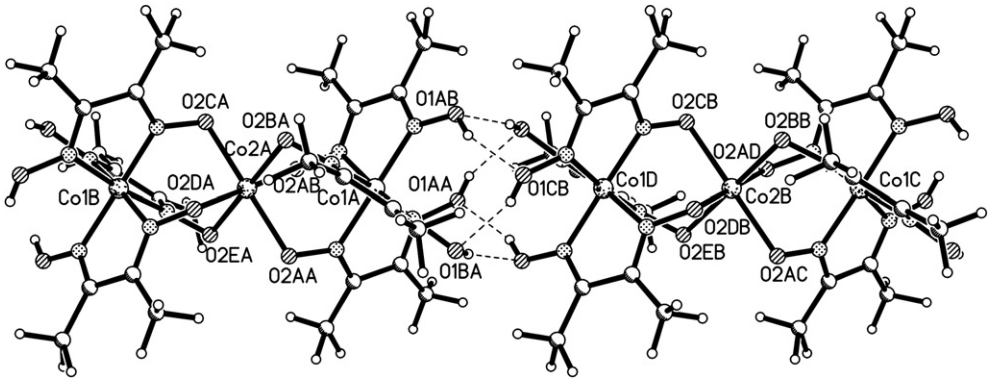

Fig. 2. Polymeric structure formed from hydrogen-bonded trinuclear complex molecules in **I**. Hydrogen bonds between OH groups are shown as dashed lines.

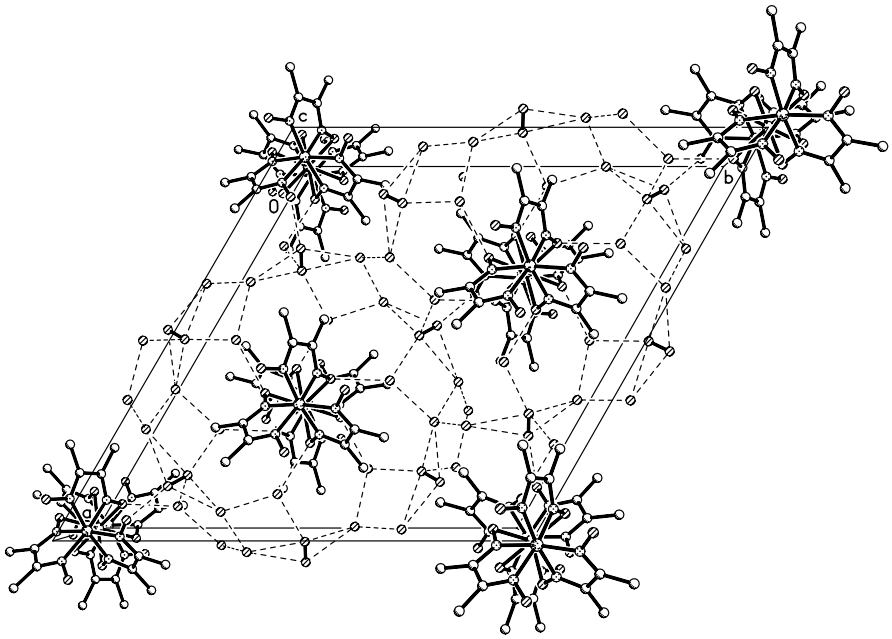

Fig. 3. Crystal packing in **I** viewed along [0 0 1].

Table 3
Hydrogen-bond geometry (Å, °) for **I**

D–H...A	D–H	H...A	D...A	D–H–A
O1–H1...O1$^{\$1}$	1.19	1.91	2.825(8)	130.2
O1W–H1WB...O2W	0.85	1.97	2.819(3)	176.1
O1W–H1WA...O4WA	0.85	2.11	2.890(4)	152.9
O1W–H1WA...O4WB	0.85	1.91	2.761(5)	174.6
O1W–H1WC...O2W$^{\$2}$	0.85	1.92	2.750(3)	167.0
O2W–H2WB...O1W$^{\$3}$	0.85	1.91	2.750(3)	169.2
O2W–H2WA...O4WA$^{\$4}$	0.85	1.94	2.771(4)	167.5
O2W–H2WA...O4WB$^{\$4}$	0.85	2.05	2.858(5)	157.4
OW3–H3WA...O2$^{\$5}$	0.85	1.91	2.758(3)	171.1
O3W–H3WB...O2W	1.08	1.71	2.768(3)	166.7
O3W–H3WD...O4WA$^{\$5}$	0.85	2.11	2.666(4)	122.3
O4WA–H4WA...O3W	0.85	2.06	2.880(5)	162.6
O4WB–H4WB...O1$^{\$6}$	0.85	1.63	2.478(7)	175.8
O4WB–H4WC...O3W$^{\$5}$	0.85	2.10	2.930(5)	163.7

Symmetry code: (\$1) $-x+1/3, -y+2/3, -z-1/3$; (\$2) $-x+y, -x+1, z$; (\$3) $-y+1/3, x-y+2/3, z-1/3$; (\$4) $x-y+2/3, x+1/3, -z-2/3$; (\$5) $-x+y+1/3, -x+2/3, z-1/3$; (\$6) $-x+y-1/3, -x+1/3, z+1/3$.

DH-chelating units in the equatorial plane of the Co^{III} ion and the apical coordination sites occupied by two thiourea molecules. The coordination geometry for compound **II** is given in Table 2. The DH^- ligands in the cation are connected via two strong intramolecular hydrogen bonds O1–H1...O4 2.508(3) Å and O3–H3...O2 2.529(3) Å. The two thiourea moieties are differently situated relative to the complex equatorial plane: the S(2)C(9)N(5)N(6) unit is approximately perpendicular to this plane [dihedral angle equal to 87.6(1)°] whereas the S(1)C(10)N(7)N(8) unit shows a nearly parallel orientation [dihedral angle equal to 22.3(1)°]. The perpendicular orientation of the thiourea molecule in the complex cation is stabilized by the "bifurcated" intramolecular N6–H6...O1 and N6–H6...O4 hydrogen bonds with N...O distances of 3.180(3) and

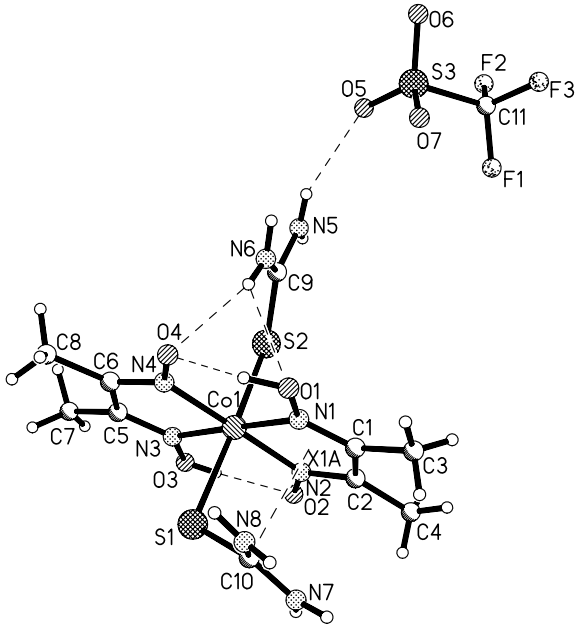

Fig. 4. Ortep drawing and atom labelling in **II**.

3.049(3) Å, respectively. In turn, the thiourea molecule in the parallel arrangement relative to the complex cation equatorial plane can be involved in an intramolecular π–π interaction with the π-delocalized chelate ring Co1 N1 N2 C1 C2, distance C10...X1A 3.001(3) Å (where X1A is the centre of the chelate ring). Similar orientations of the thiourea fragments in the $[Co(DH)_2Tu_2]$ units have already been noticed in some earlier reported structures of similar complexes [37–39].

The $[Co(DH)_2Tu_2]^+$ cations and $[CF_3SO_3]^-$ anions are connected in the crystal via numerous hydrogen bonds. Interaction of the amino groups from the S(1)C(11)N(7)-

Table 4
Hydrogen-bond geometry (Å, °) for **II**

D–H...A	D–H	H...A	D...A	D–H–A
O1–H1...O4	0.90(5)	1.61(5)	2.506(2)	172(5)
O3–H3...O2	0.72(4)	1.81(4)	2.528(2)	175(5)
N5–H5A...O5	0.82(4)	2.22(4)	2.918(3)	144(4)
N6–H6A...O6$^{\#1}$	0.82(3)	2.04(3)	2.809(3)	155(3)
N6–H6B...O4	0.82(4)	2.27(4)	3.049(3)	158(4)
N6–H6B...O1	0.82(4)	2.55(4)	3.180(3)	135(3)
N7–H7B...O2$^{\#2}$	0.84(3)	2.12(3)	2.844(3)	145(3)
N7–H7A...O5$^{\#3}$	0.88(3)	2.09(3)	2.895(3)	152(2)
N8–H8A...O7$^{\#4}$	0.85(3)	1.97(3)	2.815(3)	175(3)
N8–H8B...O4$^{\#5}$	0.83(4)	2.17(4)	2.956(3)	158(3)
C7–H7D...F1$^{\#6}$	0.87(4)	2.54(4)	3.396(3)	170(3)

Symmetry code: (#1) $-x+1, -y-2, -z$; (#2) $-x+1, -y, -z+1$; (#3) $x, y+1, z$; (#4) $-x+1, -y-1, -z$; (#5) $-x, -y-1, -z$; (#6) $-x+1, -y-1, -z+1$.

N(8) moiety with the oxygen atoms of the DH-units leads to the formation of an infinite centrosymmetric 1D network N7–H7B...O2$^{\#2}$ 2.844(3) Å, N8–H8B...O4$^{\#5}$ 2.956(3) Å. Hydrogen-bond interactions of thiourea molecules with the triflate anions generate a 3D hydrogen-bond network in the crystal. The hydrogen-bond geometry is given in Table 4.

3.4.3. Compound *III*

The crystals of **III** consist of centrosymmetric $[Co(DH)_2Py_2]^+$ cations and $[CF_3SO_3]^-$ anions (Fig. 5). The triflate ion is disordered around the inversion center located in the middle of the C–S bond. The complex cation shows a *trans*-octahedral configuration (6N) around the metal ion with the two DH-chelating units in the equatorial plane of the Co^{III} ion and apical sites occupied by the two pyridine ligands. The coordination geometry, which for compound **III** shows no unusual features, is given in Table 2. The pyridine molecule is nearly perpendicular to the equatorial plane of the complex cation with a dihedral angle equal to 88.6(1)°. The OH groups from two DH^- units are involved in typical strong O–H...O intramolecular hydrogen bonds and there are no other classical hydrogen-bond donors in **III**.

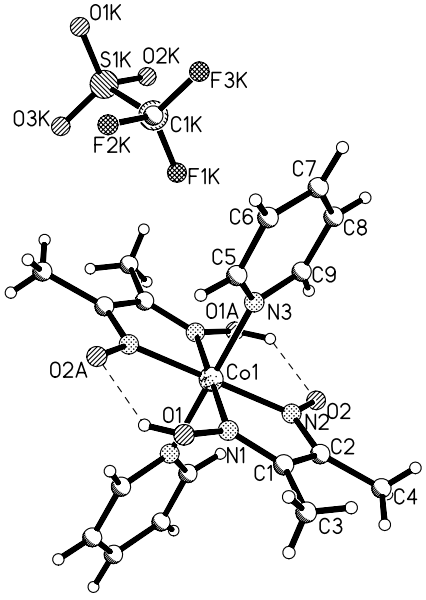

Fig. 5. Ortep drawing and atom labelling in **III**.

The crystal structures in **II** and **III** are different. In the first Tu fragments have an essential role in crystal formation. The $[Co(DH)_2Tu_2]^+$ cations and $[CF_3SO_3]^-$ anions are connected in the crystal via numerous hydrogen bonds. Interaction of the amino groups from the S(1)C(11)N(7)N(8) moiety with the oxygen atoms of the DH-units leads to the formation of the infinite centrosymmetric 1D network N7–H7B...O2$^{\#2}$ 2.844(3) Å, N8–H8B...O4$^{\#5}$ 2.956(3) Å. The last leads to the formation of infinite chains with various centre-symmetrical dimers motifs. Hydrogen-bond interactions of thiourea molecules with the triflate anions generate a 3D hydrogen-bond network in the crystal. The hydrogen-bond geometry is given in Table 4.

Only one type of dimer motive takes part in the formation of infinite centre-symmetrical dimer chains in**III**. The several short intermolecular C–H...O contacts with H...O distances less than 2.6 Å can be found. The shortest of them is between C5–H of the pyridine ring and O1 from the DH^- ligand C5...O1 3.171(5), C5–H5 0.91(4), H5...O1 2.45(5) Å and C5–H5...O1 136(4)°. This interaction generates (on principle different from **II**) centrosymmetric dimer-chains.

The X-ray structural analysis confirmed the identity of two types of complexes: trinuclear tris Co(II) and mononuclear *trans* cobaloxime compounds, obtained by using Co(II) trifluoromethanesulfonate as the starting material in the synthesis of dimethylglyoximate complexes (Scheme 2).

The assembling of the first system is due to the synthetic behavior of the TfO-anion, especially its leaving group ability and non-coordinating properties which provoke the coordination unsaturation of the central atom and evidently the tris-type structure. The formation of *cis*-cobaloxime seems to be a general feature of weakly coordinated and less strong anions like perchlorate, trifluoroacetate and triflate, and can be considered as an alternative way for the synthesis of *cis*-cobaloxime. If the *cis*-formation via the "rearrangement of *trans*-precursors" is governed by the destruction of the hydrogen-bonded system: by proton abstraction (compound **C** from Scheme 1) [5] or opposite their addition (compound **D** from Scheme 1) [8,9], in our case (**I**) as well as in [10 and 12] (compound **A** and **E**, respectively, from Scheme 1), this process occurs during the one pot reaction of the starting reagents (DH_2 and CoX_2, where $X^- = CF_3SO_3^-, ClO_4^-, F^-$). To the best of our knowledge this is the first report on structurally characterized Co(II) tris-cobaloxime.

When additional donor ligands (Py, Tu) are present during the reaction under similar conditions, exclusively mononuclear Co(III) *trans*-mixed-ligand cobaloxime

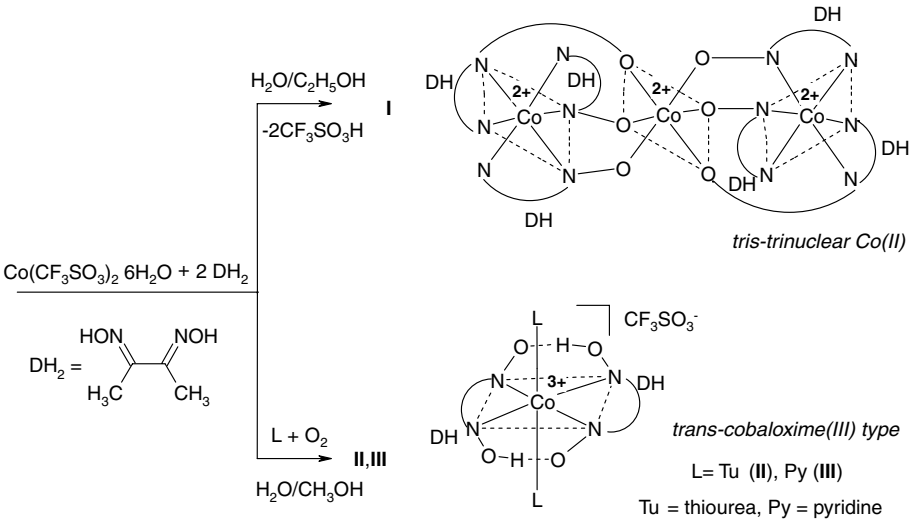

Scheme 2. Synthesis of compounds **I**–**III**.

complexes were obtained (**II**–**III**). The preference for a *trans*-conformation is probably due to the coordination saturation of the central atom with additional apical donors and the steric demand of bulky DH^- chelating ligands which are located in-plane and tailored with two intramolecular hydrogen bonds in a stable quasi-macrocyclic system. Although these complexes form from Co(II) salts, the central atom in **II** and **III** is oxidized to Co(III) by air oxygen during the reaction.

Generally, dimethylglyoxime can act not only as a "classical" bidentate ligand (via two nitrogen atoms), but also in a tridentate bridging manner (μ-ONN) or a double bridging tetradentate mode (μ^2-ONNO), giving rise to linear polynuclear (multimetal) systems. In complex **I** the DH_2 group exhibits a tridentate bridging behavior whereas in complexes **II** and**III** it acts as a typical bidentate chelating ligand.

4. Conclusions

Cobalt triflate has been found to be a useful starting material for the formation of two types of dimethylglyoximate species trinuclear tris- Co(II) and "classical" Co(III) octahedral *trans*-mononuclear structures. The identity of the compounds was confirmed by X-ray crystallography, elemental analysis, FAB mass spectrometry, ^1H and ^{13}C NMR, UV–Vis, IR and magnetochemistry. No oxidation of Co(II) starting precursors occurs during the assembling of non-trivial trinuclear tris-dimethylglyoximate species. This is the first report on structurally characterized Co(II) tris-cobaloxime.

References

[1] G.N. Schrauzer, R.J. Windgassen, J. Am. Chem. Soc. 89 (1967) 1999.
[2] D. Dolphin (Ed.), B12, Wiley, New York, 1982.
[3] P.J. Toscano, L.G. Marzilli, Prog. Inorg. Chem. 31 (1984) 105.
[4] K.M. McCauley, S.R. Wilson, W.A. van der Donk, Inorg. Chem. 41 (2002) 393.
[5] A.V. Ablov, Y.A. Simonov, S.T. Malinovskii, O.A. Bologa, T.I. Malinovskii, Dokl. Acad. Nauk. SSSR (Russ.) 221 (1975) 605.
[6] S.T. Malinovskii, Y.A. Simonov, A.V. Ablov, T.I. Malinovskii, I.D. Samusi, O.A. Bologa, Dokl. Acad. Nauk. SSSR (Russ.) 232 (1977) 326.
[7] Y.A. Simonov, S.T. Malinovskii, O.A. Bologa, V.E. Zavodnik, V.I. Andrianov, T.A. Shibanova, Kristallografiya (Russ.) 28 (1983) 682.
[8] N.W. Alcock, M.P. Atkins, E.H. Curzon, B.T. Golding, P.J. Sellars, J. Chem. Soc., Chem. Commun. (1980) 1238.
[9] N.W. Alcock, M.P. Atkins, B.T. Golding, P.J. Sellars, J. Chem. Soc., Dalton Trans. (1982) 337.
[10] A.T.H. Lenstra, J.F.J. Van Loock, S.K. Tyrlik, Bull. Pol. Acad. Sci., Chem. 31 (1983) 23.
[11] Yu.A. Simonov, A.A. Dvorkin, A.P. Gulea, A.N. Sobolev, O.A. Bologa, N.V. Gerbeleu, J.I. Gradinaru, T.I. Malinovskii, Dokl. Acad. Nauk. SSSR (Russ.) 305 (1989) 635.
[12] Yu.A. Simonov, O.A. Bologa, A.A. Dvorkin, A.P. Gulea, J.I. Gradinaru, N.V. Gerbeleu, T.I. Malinovskii, Koord. Khim. (Russ.) 20 (1994) 106.
[13] U. Englert, J. Straehle, Gazz. Chim. Ital. 118 (1988) 845.
[14] M. Megnamisi-Belombe, R.P.M. Bokanjo, B. Nuber, Z. Naturforsch. B: Chem. Sci. 46 (1991) 165.
[15] W.R. Cullen, D. Dolphin, F.W.B. Einstein, L.M. Mihichuk, A.C. Willis, J. Am. Chem. Soc. 101 (1979) 6898.
[16] R.S. Drago, J.H. Elias, J. Am. Chem. Soc. 99 (1977) 6570.
[17] S.V. Lindeman, Y.T. Struchkov, Y.Z. Voloshin, J. Coord. Chem. 34 (1995) 203.
[18] Y.Z. Voloshin, V.K. Belsky, V.V. Trachevskii, Polyhedron 11 (1992) 1939.
[19] D. Burdinski, F. Birkelbach, T. Weyhermueller, U. Floerke, H.-J. Haupt, M. Lengen, A.X. Trautwein, E. Bill, K. Wieghardt, P. Chaudhuri, Inorg. Chem. 37 (1998) 1009.
[20] P. Chaudhuri, M. Winter, P. Fleischhauer, W. Haase, U. Floerke, H.-J. Haupt, Chem. Commun. (1990) 1728.
[21] P. Leoni, E. Vichi, S. Lencion, M. Pasquali, E. Chiarentin, A. Albinati, Organometallics 19 (2000) 3062.
[22] V. McKee, J. Nelson, D.J. Speed, R.M. Town, J. Chem. Soc., Dalton Trans. (2001) 3641.
[23] Ch.J. O'Connor, in: S.J. Lippard (Ed.), Progress in Inorganic Chemistry, vol. 29, John Wiley & Sons, New York, 1982, p. 208.
[24] G.M. Sheldrick, Acta Crystallogr. A 46 (1998) 467.
[25] G.M. Sheldrick, SHELXS-97, Univesity of Göttingen, Germany, 1999.
[26] J. Lewis, R.G. Wilkins (Eds.), Modern Coordination Chemistry: Principles and Methods, London, 1960, p. 291.
[27] L. Banci, A. Bencini, C. Benelli, D. Gatteschi, C. Zanchini, Struct. Bonding (Berlin) 52 (1982) 37.

[28] R. Blinc, D. Hadzi, J. Chem. Soc. (1958) 4536.
[29] S. Amad, A.A. Isab, W. Ashraf, Inorg. Chem. Commun. 5 (2002) 816.
[30] S. Ahmad, A. Anvarhusein, H.P. Perzanowski, Transition Met. Chem. 27 (2002) 782.
[31] G.W. Roberts, S.C. Cummings, J.A. Cunningham, Inorg. Chem. 15 (1976) 2503.
[32] K. Burger, Coordination Chemistry: Experimental Methods, Butterworths, London, 1973, p. 223.
[33] J. Zarembowitch, O. Kahn, Inorg. Chem. 23 (1984) 589.
[34] A. Louati, A. Kuncaka, M. Gross, C. Haubtmann, M. Bernard, J.-J. Andre, J.-P. Brunette, J. Organomet. Chem. 486 (1995) 95.
[35] F.E. Mabbs, D. Collison, Electron Paramagnetic Resonance of d Transition Metal Compounds, Elsevier, Amsterdam, 1992.
[36] J. Bernstein, R.E. Davis, L. Shimoni, N.L. Chang, Angew. Int. Ed. Engl. 34 (1995) 1555.
[37] Yu.A. Simonov, V.Kh. Kravtsov, N.V. Gerbeleu, O.A. Bologa, E.B. Koropchanu, Zh. Neorg. Khim. (Russ.) 44 (1999) 1468.
[38] P.N. Bourosh, E.V. Koropchanu, Yu.A. Simonov, M. Gdaniec, O.A. Bologa, N.V. Gerbeleu, Zh. Neorg. Khim. (Russ.) 47 (2002) 1604.
[39] P.N. Bourosh, E.V. Koropchanu, Yu. A Simonov, M. Gdaniec, O.A. Bologa, N.V. Gerbeleu, Russ. J. Coord. Chem. (Translation of Koord. Khim.) 28 (2002) 647.

environmental changes, which could be easily followed, for instance by optical spectroscopy [7b].

Oxomolybdenum(V) complexes were among the porphyrins studied in the past for both catalytic and analytical purposes [1–3,17–27]. One point of interest in these compounds is that they present ligand exchange behaviour similar to that encountered in the biochemical function of iron porphyrins. The main difference between the iron and molybdenum porphyrins is that in the molybdenum case the oxo ligand is placed in one of the two axial positions and that ligand exchange reactions are based on the ease of removal of the ligand placed at the *trans* position to this oxo ligand [1,28–31]. These reactions are usually redox ones, accompanied by oxidation or reduction of the metal, and sometimes can be photoassisted. In the last case the oxomolybdenum(V) porphyrins function as photoreducing agents [32,33].

In this context, we are interested in investigating the photoassisted ligand exchange reactions of oxomolybdenum(V) porphyrins, mainly in view of possible sensing applications, but also for the dechlorination of chlorinated pollutants. Herein, we study the photochemical behaviour of oxomolybdenum(V) porphyrins in different chemical environments and under different conditions. More specifically, we report on the photochemically-induced ligand exchange reactions of the ethoxy-oxo(TPP)Mo(V) complex mainly in chlorinated solvents and secondarily in non-chlorinated solvents.

2. Experimental

2.1. Materials

The starting chemicals were reagent grade and were used without further purification, except as noted. The basic type I alumina column was activated at 150 °C for a minimum of 24 h. H_2(TPP) and $Mo(CO)_6$ were the starting materials used for the synthesis of the dimer μ-oxo(TPP)-Mo(V) according to a slightly modified (dichloromethane was used instead of chloroform as eluant) Srivastava method [34,35]. The synthesis was performed under an argon stream atmosphere using Schlenk-tube techniques. The dimer was identified with FTIR and UV–visible spectroscopy and the spectra obtained were compared with the corresponding ones in the literature [28] (Fig. S1). Elution of the reaction mixture from the basic activated alumina column with dichloromethane, containing a small quantity of ethanol for stabilization, resulted in the formation of the ethoxy-oxo(TPP)Mo(V) complex, as was identified by UV–visible spectroscopy.

2.2. Instrumentation and physicochemical measurements

Absorption spectra were collected on a Perkin–Elmer Lambda 6 grating spectrophotometer and ε ($M^{-1}\,cm^{-1}$) measurements were performed in $CHCl_3$ solutions of 0.05×10^{-3} M. FTIR spectra were recorded on a Perkin–Elmer FT series 1760 spectrophotometer in KBr pellets. ESR spectra were obtained with a X-band Buker 220 SE spectrometer. GC analyses were conducted with a DANI 8521 gas chromatograph equipped with a flame ionization detector, using columns packed with Carbowax, 20 M, 5% on Chromosorb W-AW.

Solutions of the ethoxy-oxo complex with concentration 2.4×10^{-4} M in various solvents were initially prepared. More concentrated solutions of $\sim10^{-3}$ M of this complex were prepared only for detection reasons and it is explicitly stated when used. The solutions of the ethoxy-oxo complex were irradiated with a 500 W high-pressure Hg lamp (usually operated at 300 W) and the desired wavelength range (450–455 nm) has been selected with an ORIEL monochromator.

For the measurement of the quantum yield, e.g. of the photochemical conversion of the ethoxy-oxo complex to the chloro-oxo complex during the exposure at ~450 nm, the number of moles of photons absorbed was measured with radiometry at this wavelength and the number of moles of the ethoxy-oxo complex reacted was calculated from the corresponding UV spectra: initially (absorbance A_o at 450 nm) and after the irradiation (absorbance A at 450 nm), where A_o and A differ less than 10%. Repeated experiments indicated that this method for the determination of the quantum yield had an error of up to 20%.

3. Results and discussion

3.1. Photochemically-induced ligand exchange reactions

The first experimental evidence of photochemically-induced ligand exchange reactions of ethoxy-oxo(TPP)-Mo(V) porphyrin has been obtained during its elution with dichloromethane in a chromatographic column. The green solution of this porphyrin was unstable under laboratory light and it was converted to a brown species, which was identified with UV–visible spectroscopy as the chloro-oxo derivative. More specifically, it was noticed that the characteristic 452 nm peak of the ethoxy-oxo complex was significantly reduced under laboratory light and the characteristic 497 nm peak of the chloro-oxo complex was formed, along with all the other peaks of that complex mentioned in the literature [1,28] (see Fig. 1 and Table 1).

This photochemical reaction was further investigated under controlled conditions. It was found that photoexcitation of a dichloromethane solution of the ethoxy-oxo complex (concentration 2.4×10^{-4} M) in the Soret band region (450–455 nm) induced a ligand exchange reaction: the ethoxy ligand was replaced by the chloride one. UV–visible spectroscopy indicated that the ethoxy-oxo complex was completely (100%) converted to the chloro-oxo complex (after 340 s of illumination under the experimental conditions used), as shown in Fig. 1. The quantum yield of this photochemical reaction at 450 nm was $\sim38\times10^{-4}$ (Table 1). The reaction progress shown in this figure is similar to the one obtained through chloride anion addition to a

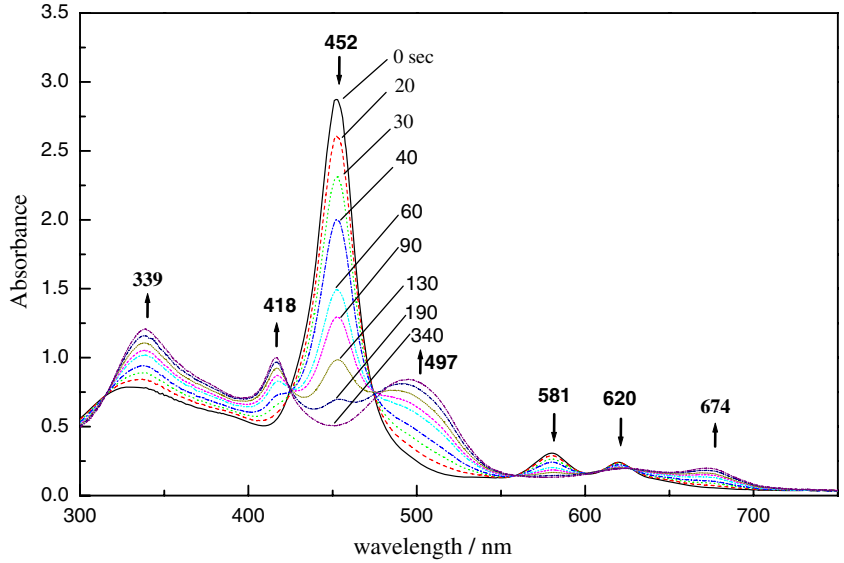

Fig. 1. UV–vis spectra evolution during Soret band irradiation of the ethoxy-oxo complex in dichloromethane. The ethoxy-oxo complex is completely converted to the chloro-oxo complex. (The exposure time is written on each spectrum.)

Table 1
(a) UV–vis absorption data and (b) quantum yields of photochemical reactions of molybdenum porphyrins[a]

(a)

Complex	Solvent	Wavelength (nm) ($\varepsilon \times 10^{-3}$ M^{-1} cm^{-1})	Ref.
Ethoxy-oxo Mo(V)	dichloromethane	453(182), 540(3.5), 581(15.9), 620(10.9)	[1,28]
Chloro-oxo Mo(V)	dichloromethane	343(60), 417(3.3), 498(43), 628(8.6), 674(9.3)	[1,28]
Hydroxy-oxo Mo(V)	dichloromethane	464(90), 593(10.8), 635(8.4)	[1,28]
μ-Oxo Mo(V)	benzene	410(36), 444(59), 583(3.5), 617(4.2), 667(3.3)	[1,28]
Oxo Mo(IV)	dichloromethane	429(295), 480(2.43), 511(3.79), 553(17.2), 590(3.4), 640(1.2)	[1,23]

(b)

Initial complex	Solvent	Additive-concentration (%v/v)	Photochemically formed complex	Quantum yield ($\Phi \times 10^4$)
Ethoxy-oxo Mo(V)	dichloromethane		chloro-oxo Mo(V)	38 ± 8
Ethoxy-oxo Mo(V)	acetone		oxo Mo(IV)	13 ± 3
Ethoxy-oxo Mo(V)	tetrachloroethylene		chloro-oxo Mo(V)	2.5 ± 0.5
Ethoxy-oxo Mo(V)	acetone	CH_2Cl_2 (2.5%)	chloro-oxo Mo(V)	2.5 ± 0.5

[a] The concentration of the initial ethoxy-oxo complex was 2.4×10^{-4} M.

methoxy-oxo(TPP)Mo(V) solution, as has been reported before [23].

The observed photoassisted ligand exchange process may be explained on the basis of reactions (1)–(4). According to the literature [32,33], photolysis of the ethoxy-oxo(TPP)Mo(V) porphyrin is expected to induce primarily the reduction of the metalloporphyrin and the formation of ethoxy radicals according to the following equation:

$$Mo^{V}O(TPP)OEt + h\nu \rightarrow Mo^{IV}O(TPP) + CH_3CH_2O^{\cdot} \quad (1)$$

In agreement with this statement, irradiation of an acetone solution of the ethoxy-oxo complex (concentration 2.4×10^{-4} M) in the Soret band provided evidence that some amounts of the oxo(TPP)Mo(IV) complex are accumulated. In fact, Fig. 2 shows a decrease of the ethoxy-oxo complex absorption at 450 nm and the growth of a new band at 420 nm, which can be ascribed to the formation of the oxo-complex [1,23,28]. The quantum yield of this photochemical reaction at 450 nm was $\sim 13 \times 10^{-4}$ (Table 1).

Evidence for the formation of ethoxy radicals was obtained by irradiating ethoxy-oxo porphyrin solutions containing phenyl-*tert*-butylnitrone (PBN) as a spin trap [36a] in the cavity of an ESR spectrometer. This experiment was carried out in the presence of an excess of ethanol (2.5% v/v). The obtained spectrum reported in Fig. 3 consists of a triplet of doublets with the following values of the hyperfine splitting constants: $a_N = 14.2$ and $a_H = 2.5$ G. This spectrum is consistent with the formation of a paramagnetic adduct between PBN and the photogenerated ethoxy radical [36b].

Ethoxy radicals are powerful reducing agents [37] and they are expected to react with dichloromethane resulting in the ejection of Cl^-, in accordance with Eq. (2) [38–41]:

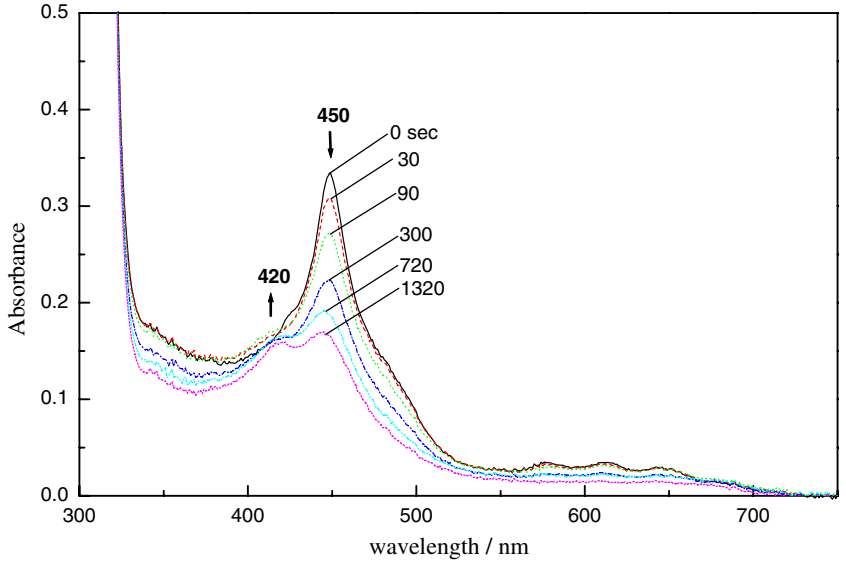

Fig. 2. UV–vis spectra progression during Soret band irradiation of the ethoxy-oxo complex in acetone. The ethoxy-oxo complex is converted to the oxo Mo(IV) complex. (The exposure times are shown.)

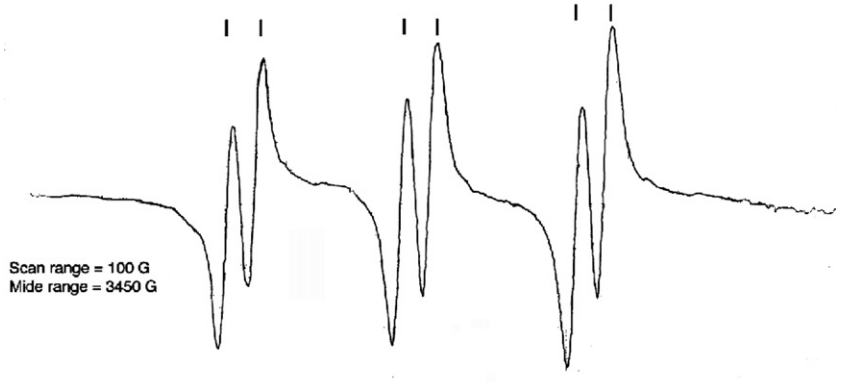

Fig. 3. ESR spectrum of the ethoxy-oxo complex ($\sim 10^{-3}$ M) in dichloromethane containing ethanol (2.5% v/v) and PBN that indicates the formation of a paramagnetic adduct between PBN and the photogenerated ethoxy radical.

$$CH_3CH_2O^{\cdot} + CH_2Cl_2 \rightarrow {}^{\cdot}CH_2Cl + Cl^- + H^+ + CH_3CHO \quad (2)$$

The formation of acetaldehyde through Eq. (2) was demonstrated by gas chromatographic analysis of irradiated dichloromethane solutions of the ethoxy-oxo complex (2.4×10^{-4} M) containing ethanol and water (2.5% v/v each). In fact, we were able to detect with GC analysis the acetal derivative of acetaldehyde, formed through its reaction with EtOH under acidic conditions. Chain propagation reactions that lead to further dechlorination of the ${}^{\cdot}CH_2Cl$ radical are also possible, as has been reported with other dechlorination photocatalysts [42]. The formation of chloride ions through Eq. 2 was verified indirectly by the formation of the chloro-oxo complex during reaction (3).

Thus, the dechlorination reaction (2) is likely to be followed by the equilibrium reaction (3), where Cl^- ions replace the ethoxy ligand of the porphyrin:

$$Cl^- + Mo^{V}O(TPP)OEt + H^+ \rightleftharpoons Mo^{V}O(TPP)Cl + EtOH \quad (3)$$

Reaction (3) has already been reported [23,43] but we also verified it: addition of HCl to the solution of the ethoxy-oxo complex resulted in ligand exchange and the formation of the chloro-oxo complex with the characteristic optical spectrum. We also noticed that the photochemically formed chloro-oxo complex was stable in the absence of light and it did not reconvert to the initial ethoxy-oxo complex, as observed from its optical spectrum.

The reduced complex formed by Eq. (1) is also able to react with dichloromethane, leading to the dechlorination of this solvent and to the formation of the chloro-oxo(TPP)Mo(V) complex according to the following equation:

$$Mo^{IV}O(TPP) + CH_2Cl_2 \rightarrow Mo^{V}O(TPP)Cl + {}^{\cdot}CH_2Cl \quad (4)$$

A similar behaviour has been previously reported for iron *meso*-tetraarylporphyrins and other iron porphyrins dissolved in CCl_4 or $CHCl_3$ [38–40,44].

In an alternative route, it is possible that the photoreduced complex is oxidized by oxygen forming the superoxide ion, O_2^-, which, in turn, has been reported to lead to dechlorination reactions [25,45–48]. This dechlorination pathway is expected to occur with lower efficiency, because the opposite redox reaction, the reduction of oxo(TPP)-molybdenum(V) porphyrins by the superoxide ion, has been reported to take place in similar systems [20].

As it has been already reported [1,33] for analogous compounds, the chloro-oxo complex did not undergo photochemically-induced ligand exchange reactions, a behaviour attributed to the high polarity of the axial coordination bond. It is generally known that the more ionic the axial coordination bond of an oxomolybdenum(V) complex the less readily the complex is photoreduced, because this bond is cleaved homolitically upon photoirradiation [1,33].

3.2. Effects of the reaction medium on the photoproduct formation

3.2.1. Homogeneous systems

The photoassisted ligand exchange reaction of the ethoxy-oxo metalloporphyrin was also investigated in tetrachloroethylene, in the presence of oxygen. Thus, a tetrachloroethylene solution of the ethoxy-oxo complex (concentration 2.4×10^{-4} M) was irradiated at the Soret band. The ethoxy-oxo complex was completely (100%) converted to the chloro-oxo complex after ~72 min exposure via the same photochemical ligand exchange reaction, as shown in Fig. 4. In this figure, two isosbestic points appear again, but these points are red shifted (at 384 and 467 nm) in comparison with the spectra obtained before in dichloromethane. On the other hand, the disappearance of the characteristic 450 nm peak of the ethoxy-oxo complex and the appearance of the characteristic 492 nm peak of the chloro-oxo complex shows an almost identical behaviour with the one observed in dichloromethane. Additionally, the photochemical reaction in tetrachloroethylene is significantly slower than in dichloromethane, since the quantum yield of the ligand exchange reaction in tetrachloroethylene ($\sim 2.5 \times 10^{-4}$) is almost one order of magnitude smaller than the one in dichloromethane (Table 1). Similar photochemical behaviour of the ethoxy-oxo complex was also observed in experiments with other chlorinated solvents, such as 1,2-dichloroethane and 1,2,4-trichlorobenzene.

The photoinduced ligand exchange process was also investigated in acetone containing a low percentage of a chlorinated solvent, to be compared with results obtained in pure acetone. Thus, an acetone solution of the ethoxy-oxo complex (2.4×10^{-4} M) containing dichloromethane (2.5% v/v) was irradiated at the Soret band. The ethoxy-oxo complex was converted to the chloro-oxo complex, but with lower efficiency than in pure dichloromethane. Indeed, the quantum yield was $\sim 2.5 \times 10^{-4}$, which is almost one order of magnitude smaller than the one in dichloromethane only (Table 1).

Spectral evidence indicates that the described photoassisted formation of the chloro-oxo metalloporphyrin occurs also when irradiation is carried out in the presence of a large excess of ethanol (molar ratio EtOH/complex ~220:1) in dichloromethane solution. This is a clear indication that equilibrium (3) remains shifted to the right despite the high concentration of the ethanol added. The high stability of the chloro-oxo complex in the presence of ethanol was confirmed by the finding that addition of ethanol

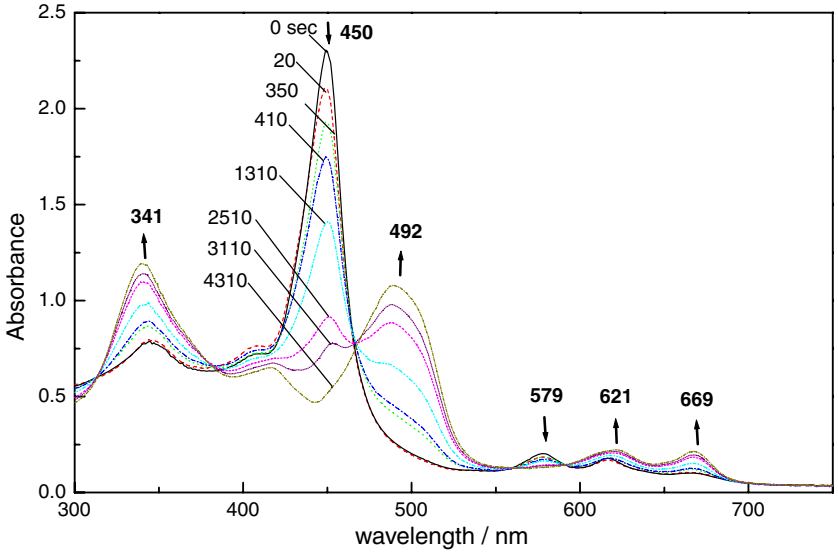

Fig. 4. UV–vis spectra evolution during Soret band exposure of the ethoxy-oxo complex in tetrachloroethylene. The ethoxy-oxo complex is completely converted to the chloro-oxo complex. (The exposure times are given; compare with data of Fig. 2.)

(0.5% v/v) to a dichloromethane solution of the photochemically obtained chloro-oxo complex (2.4×10^{-4} M) did not induce any spectral changes. An undesired consequence of these results is that the restoration of the initial ethoxy-oxo complex for initiating a new photocatalytic cycle is not possible by simple addition of ethanol in excess.

3.2.2. Biphasic systems

The results discussed so far indicate that the photochemical conversion of the ethoxy-oxo complex to its chloro-oxo derivative puts an end to the desired photoassisted ligand exchange process, due to the high stability of the chloro complex, also in the presence of an excess of ethanol. In the following, we demonstrate that the use of biphasic systems enables us to regenerate the starting ethoxy-oxo porphyrin, so inducing the photoassisted ligand exchange process in a cyclic manner.

Addition of ethanol and water (2.5% v/v each) to a dichloromethane solution of the photogenerated chloro-oxo complex (2.4×10^{-4} M) resulted in its quantitative conversion to the ethoxy-oxo derivative, as was observed with UV–visible spectroscopy (Fig. 5a). Under these conditions, water removes high amounts of Cl^- ions from the organic phase, where the metalloporphyrin complex is dissolved, favouring in this way the detachment of Cl^- from its axial position and the coordination of ethanol. Subsequently, Soret band irradiation for 170 min of the last solution resulted in the complete formation of the chloro-oxo

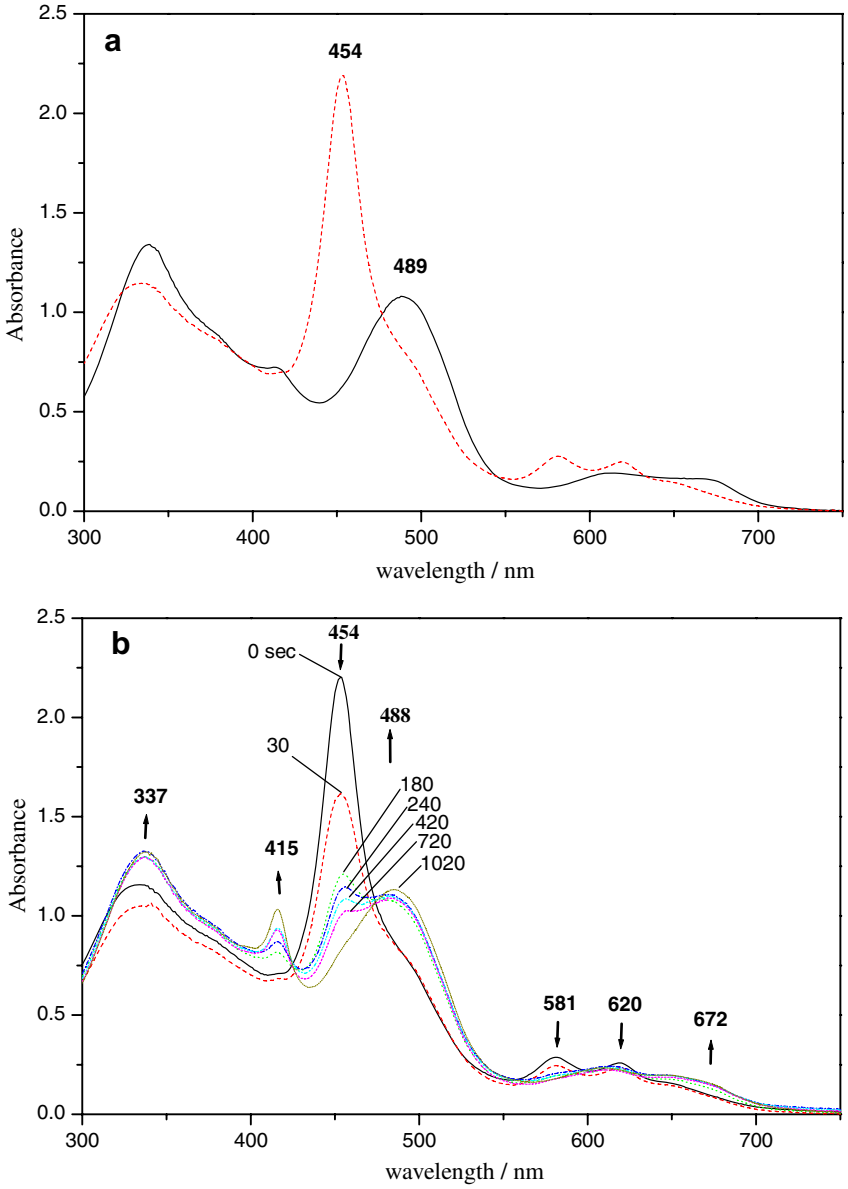

Fig. 5. UV–vis spectra progression during: (a) addition of ethanol and water (2.5% v/v each) to the photochemically converted chloro-oxo complex (2.4×10^{-4} M in dichloromethane), which resulted in the formation of the initial ethoxy-oxo complex; (b) Soret band irradiation (for 170 min) of the ethoxy-oxo complex formed in case (a), which resulted in the formation of the chloro-oxo complex.

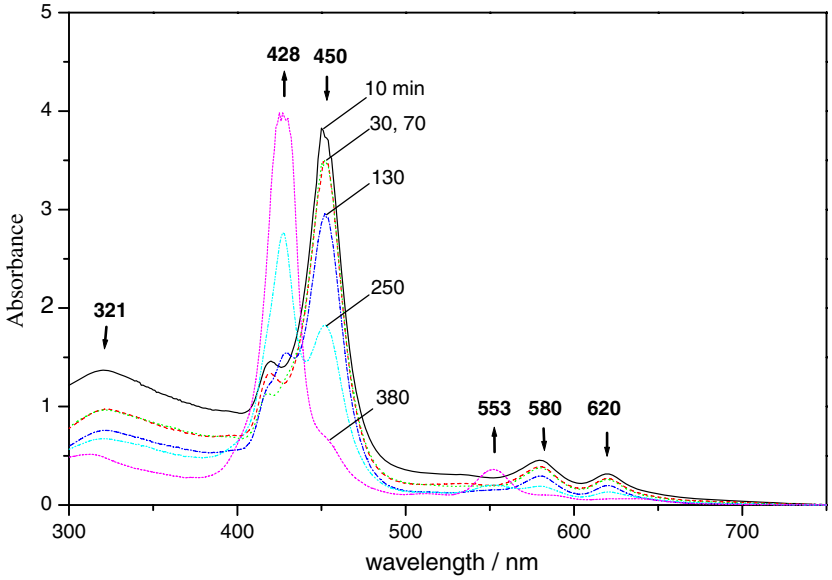

Fig. 6. UV–vis spectra evolution during Soret band exposure of a dichloromethane solution of the ethoxy-oxo complex (2.4×10^{-4} M) containing EtOH, H_2O and aqueous NaOH solution 1 M (2.5% v/v each). The ethoxy-oxo complex is completely converted to the oxo(TPP)Mo(IV) complex.

complex through the same photochemical ligand exchange route (Fig. 5b). In this case, the whole heterogeneous solution was irradiated, but in fact the organic phase was exposed and the UV–visible spectrum of this phase was obtained, as the small quantity of the added water occupied the bottom of the cell. In Fig. 5b, the complete disappearance of the characteristic 454 nm peak of the ethoxy-oxo complex and the appearance of the characteristic 488 nm peak of the chloro-oxo complex are presented.

Consequently, the formation of the biphasic system (dichloromethane/water with a major concentration of ethanol) of the ethoxy-oxo complex favours the photocatalytic inducement of the previous ligand exchange route. The photocatalytic cycles are terminated as soon as the whole quantity of ethanol in the organic phase is photooxidised. New catalytic cycles can be achieved by the biphasic system with addition of a further quantity of ethanol. Thus, the studied photoassisted ligand exchange process could be used for the dechlorination of pollutants upon addition of ethanol and water forming a biphasic system.

In order to increase the photocatalytic cycles of the photoassisted ligand exchange process, ethanol, water and NaOH were added to a dichloromethane solution of the ethoxy-oxo porphyrin. More specifically, ethanol, water and aqueous NaOH solution 1 M (2.5% v/v each) were added to a dichloromethane solution of the ethoxy-oxo complex (2.4×10^{-4} M). Subsequently, Soret band irradiation of the solution for 380 min led to the complete formation of the oxoMo(IV) complex, as was observed by UV–vis spectroscopy (Fig. 6). The formation of the hydroxy-oxo(TPP)Mo(V) complex, which could be expected in this case, was not observed (i.e. the major 464 nm peak of the hydroxy-oxo complex along with the other peaks of that complex were not observed, see Fig. 6 and Table 1). On the other hand, both the characteristic peaks at 428 and 553 nm of the oxoMo(IV) complex were obtained. Furthermore, detection of the acetal derivative in this irradiated biphasic system with GC analysis was not feasible, due to the predominant basic conditions. Therefore, in this last, quite complicated biphasic system, the photoassisted ligand exchange route was changed, as no chloro-oxo complex was observed. A possible explanation is that NaOH removes more effectively the Cl^- ions from the organic phase than water does. Nevertheless, further investigation on this system is necessary in order to clarify the picture.

4. Conclusions

In this contribution, the photoassisted ligand exchange reactions of ethoxy-oxo(TPP)Mo(V) porphyrin were studied. In this first investigation specific attention has been given to the formation of the photochemically inert chloro-oxo complex, which results in a net overall photoassisted ligand exchange reaction. This reaction is easily followed due to the characteristic UV–visible spectra evolution in different chlorinated solvents. Regeneration of the starting ethoxy-oxo complex and, thus, photocatalytic inducement of the ligand exchange route was not possible by simple addition of ethanol in excess, but only with the addition of water and ethanol in the reaction medium, where a biphasic system is formed. Further addition of NaOH changed the photoassisted ligand exchange route, and led to the formation of the oxoMo(IV) complex, instead of the chloro-oxo complex. The mechanistic details and the possible practical value of the described chemistry in bonded chlorine detection and dechlorination of pollutants appear worthy of further investigation.

Appendix A. Supplementary data

Supplementary data associated with this article can be found, in the online version, at doi:10.1016/j.poly.2006.06.027.

References

[1] Y. Matsuda, Y. Murakami, Coordin. Chem. Rev. 92 (1988) 157–192.
[2] H. Brand, J. Arnold, Coordin. Chem. Rev. 140 (1995) 137–168.
[3] B. Meunier, Chem. Rev. 92 (1992) 1411–1456.
[4] M.R. Wasielewski, Chem. Rev. 92 (1992) 435–461.
[5] A.K. Burrell, M.R.J. Wasielewski, Porphyrins Phthalocyanines 4 (2000) 401–406.
[6] Q. Li, S. Surthi, G. Mathur, S. Gowda, Q. Zhao, T.A. Sorenson, R.C. Tenent, K. Muthukumaran, J.S. Lindsey, V. Misra, Appl. Phys. Lett. 85 (2004) 1829–1831.
[7] (a) C. Di Natale, R. Paolesse, A. Macagnano, V.I. Troitsky, T.S. Berzina, A. D'Amico, Anal. Chim. Acta 384 (1999) 249–259;
(b) C. Di Natale, D. Salimbeni, R. Paolesse, A. Macagnano, A. D'Amico, Sensor. Actuator. B 65 (2000) 220–226.
[8] M. Andersson, M. Holmberg, I. Lundström, A. Lloyd-Spetz, P. Mårtensson, R. Paolesse, C. Falconi, E. Proietti, C. Di Natale, A. D'Amico, Sensor. Actuator. B 77 (2001) 567–571.
[9] R. Purrello, S. Gurrieri, R. Lauceri, Coordin. Chem. Rev. 190 (1999) 683–706.
[10] M.A. Awawdeh, J.A. Legako, H.J. Harmon, Sensor. Actuator. B 91 (2003) 227–230.
[11] C.M. Drain, F. Nifiatis, A. Vasenko, J.D. Batteas, Angew. Chem., Int. Ed. 37 (1998) 2344–2347.
[12] C.V.K. Sharma, G.A. Broker, J.G. Huddleston, J.W. Baldwin, R.M. Metzger, R.D.J. Rogers, Am. Chem. Soc. 121 (1999) 1137–1144.
[13] Y. Shen, J. Liu, J. Jiang, B. Liu, S. Dong, Electroanalysis 14 (2002) 1557–1563.
[14] M.S. Boeckl, A.L. Bramblett, K.D. Hauch, T. Sasaki, B.D. Ratner, J.W. Rogers, Langmuir 16 (2000) 5644–5653.
[15] C.V.K. Sharma, G.A. Broker, G.J. Szulczewski, R.D. Rogers, Chem. Commun. (2000) 1023–1024.
[16] I. Prieto, M.T. Martin, D. Möbius, L. Camacho, J. Phys. Chem. B 102 (1998) 2523–2529.
[17] B. Chevrier, T. Diebold, R. Weiss, Inorg. Chim. Acta 19 (1976) L57–L59.
[18] H. Ledon, M. Bonnet, J.-Y. Lallemand, J. Chem. Soc., Chem. Commun. (1979) 702–704.
[19] B.F. Mentzen, M.C. Bonnet, H. Ledon, Inorg. Chem. 19 (1980) 2061–2066.
[20] K. Hasegawa, T. Imamura, M. Fujimoto, Inorg. Chem. 25 (1986) 2154–2160.
[21] J.-H. Fuhrhop, K.M. Kadish, D.G. Davis, J. Am. Chem. Soc. 95 (1973) 5140–5147.
[22] T. Malinski, P.M. Hanley, K.M. Kadish, Inorg. Chem. 25 (1986) 3229–3235.
[23] Y. Matsuda, S. Yamada, Y. Murakami, Inorg. Chem. 20 (1981) 2239–2246.
[24] H. Ledon, B. Mentzen, Inorg. Chim. Acta 31 (1978) L393–L394.
[25] T. Imamura, K. Hasegawa, M. Fujimoto, Chem. Lett. (1983) 705–708.
[26] J. Tachibana, T. Imamura, Y. Sasaki, J. Chem. Soc., Chem. Commun. (1993) 1436–1438.
[27] (a) T. Fujihara, K. Hoshiba, Y. Sasaki, T. Imamura, Bull. Chem. Soc. Jpn. 73 (2000) 383–390;
(b) T. Fujihara, K. Myougan, A. Ichimura, Y. Sasaki, T. Imamura, Chem. Lett. (2001) 178–179.
[28] H. Ledon, M.C. Bonnet, Y. Brigandat, F. Vareson, Inorg. Chem. 19 (1980) 3488–3491.
[29] H.C.R. Ledon, Acad. Sci. Paris 287 (1978) C59–C61.
[30] T. Imamura, T. Numatatsu, M. Terui, M. Fujimoto, Bull. Chem. Soc. Jpn. 54 (1981) 170–174.
[31] T. Imamura, T. Tanaka, M. Fujimoto, Inorg. Chem. 24 (1985) 1038–1041.
[32] H. Ledon, M. Bonnet, J. Am. Chem. Soc. 103 (1981) 6209–6211.
[33] Y. Matsuda, T. Takaki, Y. Murakami, Bull. Chem. Soc. Jpn. 59 (1986) 1839–1844.
[34] T.S. Srivastava, E.B. Fleischer, J. Am. Chem. Soc. 92 (1970) 3518–3519.
[35] E.B. Fleischer, T.S. Srivastava, Inorg. Chim. Acta 5 (1971) 151–154.
[36] (a) E.G. Janzen, Acc. Chem. Res. 4 (1971) 31;
(b) G.R. Buettner, Free Radical Biol. Med. 3 (1987) 259.
[37] E. Papaconstantinou, J. Chem. Soc., Faraday Trans. I 78 (1982) 2769–2772.
[38] A. Maldotti, C. Bartocci, R. Amadeli, V. Carassiti, J. Chem. Soc., Dalton Trans. (1989) 1197–1201.
[39] C. Bartocci, A. Maldotti, G. Varani, P. Battioni, V. Carassiti, D. Mansuy, Inorg. Chem. 30 (1991) 1255–1259.
[40] C. Bartocci, A. Maldotti, G. Varani, V. Carassiti, P. Battioni, D. Mansuy, J. Chem. Soc., Chem. Commun. (1989) 964–965.
[41] D. Brault, C. Bizet, P. Morliere, M. Rougee, E.J. Land, R. Santus, A.J. Swallow, J. Am. Chem. Soc. 102 (1980) 1015–1020.
[42] (a) D. Sattari, C.L. Hill, J. Chem. Soc., Chem. Commun. (1990) 634–635;
(b) D. Sattari, C.L. Hill, J. Am. Chem. Soc. 115 (1993) 4649–4657.
[43] M.S. Bains, D.G. Davis, Inorg. Chim. Acta 37 (1979) 53–60.
[44] D. Brault, M. Rougee, M. Momentau, J. Chim. Phys. 68 (1971) 1621–1629.
[45] T. Imamura, K. Hasegawa, T. Tanaka, W. Nakajima, M. Fujimoto, Bull. Chem. Soc. Jpn. (1984) 194–197.
[46] (a) J.L. Roberts Jr., D.T. Sawyer, J. Am. Chem. Soc. 103 (1981) 712–714;
(b) J.L. Roberts Jr., T.S. Calderwood, D.T. Sawyer, J. Am. Chem. Soc. 105 (1983) 7691–7696.
[47] H. Sugimoto, S. Matsumoto, D.T. Sawyer, J. Am. Chem. Soc. 109 (1987) 8081–8082.
[48] J.R. Kanofsky, H. Sugimoto, D.T. Sawyer, J. Am. Chem. Soc. 110 (1988) 3698–3699.

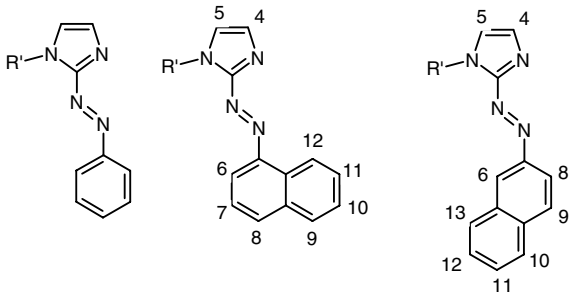

RaaiR′ **1** α-NaiR′, **2** β-NaiR′ **3**

R′ = CH_3 (**a**), CH_2-CH_3 (**b**)

2. Experimental

2.1. Materials and methods

1-Alkyl-2-(naphthyl-α/β-azo)imidazoles (α-NaiR′, **2** and β-NaiR′ **3**; R′ = CH_3 (**a**), CH_2-CH_3 (**b**)) were prepared by the reported procedure [18]. $M(CO)_6$ (M = Cr, Mo) and $Me_3NO \cdot 2H_2O$ were Sigma–Aldrich reagents. Reactions were carried out under an extremely dry oxygen free atmosphere under Atmos bags (Sigma–Aldrich). THF and *n*-heptane were dried before use [21]. For the solution spectral studies spectroscopic grade solvents were used from Lancester, UK. Microanalyses (C, H, N) were performed using a Perkin–Elmer 2400 CHN elemental analyzer. Spectroscopic measurements were carried out using the following instruments: UV–VIS spectra, Lambda 25 Perkin–Elmer; IR spectra (KBr disk, 4000–450 cm^{-1}), RX-1 Perkin–Elmer; ^1H NMR and ^{13}C NMR spectra in $CDCl_3$ Bruker 300 MHz FT-NMR spectrometers in the presence of TMS as an internal standard. Emission was examined by a LS 55 Perkin–Elmer spectrofluorimeter at room temperature (298 K) in MeCN under degassed conditions. FAB-MS was collected from JEOL-AX 500. Electrochemical measurements were carried out with the use of a computer controlled EG&G PARC VersaStat model 250 Electrochemical instrument using a Pt-disk working electrode and Pt-wire auxiliary electrode under an inert (dry N_2) environment. The solution was IR compensated and the results were collected at 298 K. The reported results were referenced to Ag/AgCl in CH_2Cl_2 and were uncorrected for junction potential. [*n*-Bu_4N][ClO_4] was used as the supporting electrolyte.

2.2. Preparation of $Cr(CO)_4$(NaiR′) (**4**, **5** (Cr); **6**, **7** (Mo))

A representative case of [$Cr(CO)_4$(α-NaiMe)] (**4a**) is detailed below. To $Cr(CO)_6$ (60 mg, 0.27 mmol) dissolved in dry CH_2Cl_2 (10 cm^3) was added $Me_3NO \cdot 2H_2O$ (62 mg, 0.56 mmol) and the solution was stirred for 45 min. To the resulting yellow solution α-NaiMe (65 mg, 0.28 mmol) was added and the solution was stirred for 4 h. The colour of the solution changed from brown red to dark blue. Then the solvent was evaporated under low pressure and the crude product was passed down a neutral Al_2O_3 column. A blue portion was eluted with benzene:pet-ether (60–80°) (1:1 v/v). Removal of the solvent afforded the analytically pure product (**4a**) in 22% yield.

In analogous reactions treatment of $Cr(CO)_6$ with two molar equivalents of $Me_3NO \cdot 2H_2O$ and an equimolar quantity of α-NaiEt, β-NaiMe and β-NaiEt afforded the complexes [$Cr(CO)_4$(α-NaiEt)] (**4b**) (yield, 29%; blue), [$Cr(CO)_4$(β-NaiMe)] (**5a**) (yield, 35%; green) and [$Cr(CO)_4$(β-NaiEt)] (**5b**) (yield, 30%; green). Microanalytical data are as follows: *Anal.* Calc. for [$Cr(CO)_4$(α-NaiMe)] (**4a**), $C_{18}H_{12}N_4O_4Cr$, C, 54.00; H, 3.00; N, 14.00. Found: C, 53.88; H, 3.04; N, 14.08%. *Anal.* Calc. for [$Cr(CO)_4$-(α-NaiEt)] (**4b**): $C_{19}H_{14}N_4O_4Cr$, C, 55.07; H, 3.38; N, 13.53. Found: C, 55.00; H, 3.30; N, 13.64%. *Anal.* Calc. for [$Cr(CO)_4$(β-NaiMe)] (**5a**): $C_{18}H_{12}N_4O_4Cr$, C, 54.00; H, 3.00; N, 14.00. Found: C, 54.08; H, 3.08; N, 14.05%. *Anal.* Calc. for [$Cr(CO)_4$(β-NaiEt)] (**5b**): $C_{19}H_{14}N_4O_4Cr$, C, 55.07; H, 3.38; N, 13.53. Found: C, 55.02; H, 3.34; N, 13.46%.

2.3. Preparation of [$Mo(CO)_4$(α-NaiMe)] (**6a**)

To $Mo(CO)_6$ (60 mg, 0.23 mmol) dissolved in dry CH_2Cl_2 (10 cm^3) was added $Me_3NO \cdot 2H_2O$ (52 mg, 0.47 mmol), and the solution was stirred for 45 min. To the resulting solution α-NaiMe (54 mg, 0.23 mmol) was added and the solution was stirred for a further 5 h. The colour of the solution changed from brown red to dark blue. Then the solvent was evaporated under reduced pressure and the crude product was passed down a neutral Al_2O_3 column. A blue portion was eluted with benzene: pet-ether (1:1, v/v). Removal of the solvent afforded the analytically pure dark blue product [$Mo(CO)_4$(α-NaiMe)] (**6a**) in 43% yield.

In analogous reactions treatment of $Mo(CO)_6$ with two molar equivalents of $Me_3NO \cdot 2H_2O$ and an equimolar quantity of α-NaiEt, β-NaiMe and β-NaiEt afforded the complexes [$Mo(CO)_4$(α-NaiEt)] (**6b**) (yield, 30%; blue), [$Mo(CO)_4$(β-NaiMe)] (**7a**) (yield, 44%, green) and [$Mo(CO)_4$(β-NaiEt)] (**7b**) (yield, 40%, green). Microanalytical data are as follows: *Anal.* Calc. for [$Mo(CO)_4$-(α-NaiMe)] (**6a**), $C_{18}H_{12}N_4O_4Mo$, C, 48.65; H, 2.70; N, 12.61. Found: C, 48.60; H, 2.64; N, 12.68%. *Anal.* Calc. for [$Mo(CO)_4$(α-NaiEt)] (**6b**): $C_{19}H_{14}N_4O_4Mo$, C, 49.78; H, 3.06; N, 12.23. Found: C, 49.84; H, 3.11; N, 12.14%. *Anal.* Calc. for [$Mo(CO)_4$(β-NaiMe)] (**7a**): $C_{18}H_{12}N_4O_4$ Mo, C, 48.65; H, 2.70; N, 12.61. Found: C, 48.62; H, 2.74; N, 12.56%. *Anal.* Calc. for [$Mo(CO)_4$(β-NaiEt)] (**7b**): $C_{19}H_{14}N_4O_4Mo$, C, 49.78; H, 3.06; N, 12.23. Found: C, 49.72; H, 3.10; N, 12.28%.

3. Results and discussion

3.1. Synthesis

The equimolar reaction of α/β-NaiR′ and $M(CO)_6$ (M = Cr, Mo) under stirring conditions in dry CH_2Cl_2 in the presence of two equivalents of Me_3NO under a nitrogen environment for a period of 4–6 h has synthesized blue or green complexes in 25–45% yield. The ligands, 1-alkyl-2-(naphthyl-α/β-azo)imidazoles (α-NaiR′, **1**; β-NaiR′, **2** and R′ = -CH_3 (**a**), CH_2-CH_3 (**b**)), are N, N′ chelating systems where N and N′ refer to N(imidazole) and N(azo) donor centres, respectively. Use of Me_3NO has reduced the reaction time to one-tenth of the reaction time in its absence and also increases the yield of the product from <5% to >20%. The composition of the complexes, *cis*-[$M(CO)_4$(NaiR′)] (M = Cr (**4** for α-NaiR′ and **5** for β-NaiR′); Mo (**6** for α-NaiR′ and **7** for β-NaiR′)), has been supported by microanalytical and spectroscopic data. We have attempted to crystallize these complexes but failed to get a good quality diffracting crystals. We have attempted to synthesize the complexes *cis*-[$M(CO)_2$(NaiR′)$_2$] and [M(NaiR′)$_3$] using an excess of the ligands and Me_3NO, but in each experiment (at varied temperature and solvent) we get only an intractable brown solid

$$M(CO)_6 + 2Me_3NO + \alpha/\beta\text{-NaiR}' \rightarrow [M(CO)_4(\alpha/\beta\text{-NaiR}')] + 2CO_2 + 2Me_3N \quad (1)$$

The complexes are soluble in solvents of different polarity, from benzene to acetonitrile, chloroform, dichloromethane. Solutions of *cis*-[$M(CO)_4$(α-NaiR′)] (**4** and **6**) are blue while those of *cis*-[$M(CO)_4$(β-NaiR′)] (**5** and **7**) are green. They are non-electrolytes and are diamagnetic.

3.2. Spectroscopic characterization

3.2.1. FT-IR and mass spectra

FT-IR spectra were taken in KBr discs and in CH_2Cl_2 solution. The carbonyl stretching frequencies of the complexes are presented in Table 1. The spectra show three or four bands (three bands appear in the intensity ratio 1:2:1, where intensity is compared from the area measurement using the ORIGIN 6.0 program). The spectra in solution (CH_2Cl_2) show ν(CO) at 2–15 cm^{-1} higher frequency than that of KBr-phase data. The mean value of the three or four ν(CO) in these cases is lower ($\Delta\nu$(CO) = 15–25 cm^{-1}) than that of $M(CO)_4$(2-PAP) (2-PAP = 2-(phenylazo)pyridine) [4]. This supports weaker π-acidity of naphthylazoimidazoles than that of phenylazopyridine. On comparing with the spectral pattern and frequency of CO stretching of [$M(CO)_4$(2-PAP)] [4] and [$M(CO)_4$(RaaiR′)] [12] (RaaiR′ = 1-alkyl-2-(arylazo)imidazole), the present complexes are assigned to *cis*-tetracarbonyl complexes with octahedral coordination where the ligand NaiR′ binds as a bidentate chelating agent. The ν(N=N) and ν(C=N) bands appear at 1390–1400 and 1590–1600 cm^{-1} respectively. The mass fragmentation by FAB-MS of the complexes supports the expected fragmentation pattern of M^+, $(M-CO)^+$, $(M-2CO)^+$, $(M-3CO)^+$, $(M-4CO)^+$ (Table 1). This information also helps us to identify the tetracarbonyl complexes of NaiR′.

3.2.2. UV–Vis spectra and emission properties

Benzene solutions of the complexes are either blue (α-NaiR′ complexes, [$M(CO)_4$(α-NaiR′)] (**4**, **6**)) or green (β-NaiR′ complexes, [$M(CO)_4$(β-NaiR′)] (**5**, **7**)). The spectra show three or four high intense ($\varepsilon \sim 10^4$) bands within 350–625 nm (Figs. 1 and 2). The main band around 600 nm shifts to shorter wavelength on going from the less polar CH_2Cl_2 to a more polar solvent (MeCN). In d^6-

Table 1
FT-IR and mass spectral data of *cis*-[$M(CO)_4$(α/β-NaiR′)] (**4**–**7**)

Compound	ν_{CO} Value	*m/z* Value (% conversion)				
		M^+	$(M-CO)^+$	$(M-2CO)^+$	$(M-3CO)^+$	$(M-4CO)^+$
4a	2011, 1918, 1865	400	372	344	316	288
	(2014, 1979, 1933, 1875)	(14)	(5)	(9)	(64)	(95)
5a	2006, 1914, 1839	400	372	344	316	288
	(2011, 1930, 1862)	(21)	(3)	(6)	(66)	(92)
4b	2001, 1922, 1901, 1860	414	386	358	330	302
	(2014, 1932, 1874)	(18)	(3)	(5)	(70)	(98)
5b	2006, 1927, 1839	414	386	358	330	302
	(2011, 1928, 1863)	(22)	(6)	(8)	(70)	(94)
6a	2017, 1911, 1854	446	418	390	362	334
	(2021, 1931, 1870)	(22)	(32)	(52)	(10)	(30)
7a	2008, 1915, 1853	446	418	390	362	334
	(2018, 1979, 1927, 1858)	(24)	(27)	(60)	(10)	(33)
6b	2013, 1923, 1903, 1856	460	432	404	376	348
	(2020, 1929, 1868)	(23)	(28)	(57)	(12)	(35)
7b	2012, 1937, 1897, 1834	460	432	404	376	348
	(2017, 1926, 1857)	(25)	(32)	(60)	(11)	(32)

In KBr discs (values in parentheses are from CH_2Cl_2 solution).

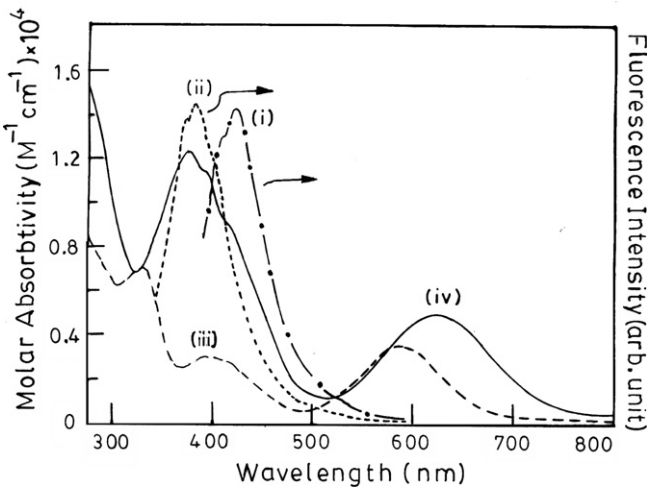

Fig. 1. UV–Vis spectra of *cis*-[$Cr(CO)_4$(α-NaiMe)] (– – –), *cis*-[$Cr(CO)_4$-(β-NaiMe)] (—); fluorescence spectra of *cis*-[$Cr(CO)_4$(α-NaiMe)] (. . .), *cis*-[$Cr(CO)_4$(β-NaiMe)] (–•–•–) in benzene at 298 K.

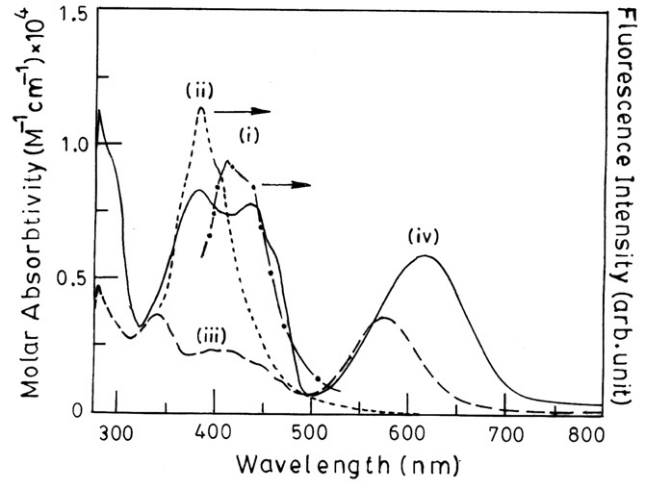

Fig. 2. UV–Vis spectra of *cis*-[$Mo(CO)_4$(α-NaiMe)] (– – –), *cis*-[$Mo(CO)_4$(β-NaiMe)] (—); fluorescence spectra of *cis*-[$Mo(CO)_4$-(α-NaiMe)] (. . .), *cis*-[$Mo(CO)_4$(β-NaiMe)] (–•–•–) in benzene at 298 K.

octahedral complexes of the M(0)-state, the lowest energy electronic transition is from a filled metal d orbital to the unoccupied lowest energy π^* orbital of the ligand, and the transition in this case is rightly defined as a MLCT transition. Other transitions <400 nm are intraligand (n–π^*/π–π^*) transitions (ILCT) and have been verified with free ligand data [22]. [$M(CO)_4$(β-NaiR′)] show ILCT at longer wavelength (370–385 nm) compared to [$M(CO)_4$(α-NaiR′)] (330–340 nm). This suggests that [$M(CO)_4$(α-NaiR′)] has a better ground state stability than [$M(CO)_4$(β-NaiR′)] while the excited state energy is more or less same as these complexes.

The photoluminescence properties of the complexes (**4**–**7**) were studied at room temperature (298 K) in benzene (Figs. 1 and 2). The ligands are photo-inactive both at room temperature and low temperature. The emission is observed upon excitation at shorter wavelength 330–380 nm (Table 2). The absorptions <400 nm are assigned to n–π^*/π–π^* transitions. Thus, the emission observed in the complexes is tentatively assigned to (π–π^*) intraligand fluorescence. In the absence of metal ions, fluorescence of the ligand is probably quenched by the occurrence of a photoinduced electron transfer (PET) process due to presence of a lone pair of nitrogen atoms. Such a PET process is prevented by the complexation of ligand with metal ions; thus the fluorescence intensity may be enhanced by the coordination to a metal ion. However, naphthylazoimidazole complexes of Ru(II) (d^6), Os(II) (d^6) or Pt(II) (d^8) [23–25] do not exhibit emission properties. Fluorescence activity of [$M(CO)_4$-(NaiR′)] may be due to the presence of CO. The high π-acidity of CO may be important to maintain a population at an excited state and hence the emission property.

3.2.3. ^1H and ^{13}C NMR spectra

The ^1H NMR spectra (Table 3) were assigned on comparing with free ligand values [22]. An important observation is the downfield shifting of the imidazole protons, 4- and 5-H, by 0.4–0.7 ppm. 4-H is shifted by 0.6–0.7 ppm compared to the shift of 5-H of 0.4–0.5 ppm. This supports the coordination of the imidazole-N (N(3)) to the metal centre. Naphthyl protons (6-H to 13-H) experience small perturbations and the chemical shift data are comparable with free ligand data [22]. The 1-alkyl group shows the usual splitting pattern: 1-Me is a singlet (4.00–4.1 ppm); 1-CH_2-CH_3 shows quartet for the –CH_2– group (4.6–4.7 ppm, $J = 10.0$ Hz) and triplet for the –CH_3 group (1.6–1.7 ppm, $J = 8.0$ Hz). [$M(CO)_4$(β-NaiR′)] show a downfield singlet at 8.4 (for M = Cr) and 8.8 ppm (for M = Mo) which corresponds to the 6-H signal. While the other protons show reverse information, i.e., protons in [$Mo(CO)_4$(NaiR′)] (**6**, **7**) show a marginal upfield shifting by 0.02–0.1 ppm with reference to [$Cr(CO)_4$(NaiR′)] (**4**, **5**).

The ^{13}C NMR spectra are complicated due to a large number of C centres (data are collected in the Supplementary material, Table 4). The assignment has been done by comparing with the spectra of the free ligands [22]. The DEFT study has also distinguished the primary, secondary, tertiary and quaternary C centres. The most downfield signals, observed between 190 and 220 ppm, are due to C in CO. Mo(CO) complexes show higher chemical shift data than the Cr(CO) system. The lowest δ is observed at 42–45 ppm and is assigned to N(1)–CH_3 or N(1)–CH_2–C-centres.

3.2.4. Electrochemistry

The electrochemical properties of the complexes were investigated by cyclic voltammograms (CV) in 0.1 M [*n*-Bu_4N][ClO_4] in CH_2Cl_2 solution at a scan rate of 50 mV S^{-1}. All CV data were collected under a nitrogen environment and potentials are expressed with reference to Ag/AgCl. The results are collected in Table 2. All of the compounds show two oxidations and two reductions. By analogy with similar types of α-diimine complexes [1]

Table 2
UV–Vis,[a] fluorescence[b] spectral and cyclic voltammetric[c] data

Compound	UV–Vis data, λ_{max}/nm ($10^{-3}\,\varepsilon/M^{-1}\,cm^{-1}$)	λ_{ex} (nm)	λ_{em} (nm)	Cyclic voltammetric data			
				Metal oxidation		Ligand reduction	
				$1^+/0$	$2^+/1^+$	azo/azo$^-$	azo$^-$/azo$^=$
[Cr(CO)$_4$(α-NaiMe)] (**4a**)	590 (3.48), 416 (2.74), 397 (2.92), 332 (7.06), 281 (7.71)	332	382	0.677 (140)	1.425[d]	−1.09 (125)	−1.40[e]
[Cr(CO)$_4$(β-NaiMe)] (**5a**)	624 (4.91), 393 (11.41), 378 (12.30), 273(17.37)	378	422	0.663 (150)	1.427[d]	−1.20 (150)	−1.42[e]
[Cr(CO)$_4$(α-NaiEt)] (**4b**)	591 (8.62), 416 (5.88), 395 (6.24), 334 (9.82), 283 (13.56)	334	381	0.578 (100)	1.151 (120)	−0.945 (150)	−1.328[e]
[Cr(CO)$_4$(β-NaiEt)] (**5b**)	624 (3.43), 396 (8.84), 376 (9.63), 279 (9.90)	376	423	0.541 (120)	1.152 (160)	−0.988 (120)	−1.304 (128)
[Mo(CO)$_4$(α-NaiMe)] (**6a**)	576 (3.59), 418 (2.33), 397 (2.36), 341 (3.61), 279 (4.72)	341	383	0.626 (120)	1.214[d]	−0.854 (170)	−1.425[e]
[Mo(CO)$_4$(β-NaiMe)] (**7a**)	614 (5.87), 437 (7.84), 381 (8.27), 281 (10.60)	381	433, 408	0.618 (170)	1.130[d]	−1.129[e]	−1.340 (180)
[Mo(CO)$_4$(α-NaiEt)] (**6b**)	577 (3.76), 434 (1.50), 335 (3.95), 279 (5.01)	335	385	0.709 (100)	0.997 (170)	−0.928 (125)	−1.255 (200)
[Mo(CO)$_4$(β-NaiEt)] (**7b**)	614 (2.44), 436 (3.33), 381 (3.93), 276 (4.47)	381	432	0.622 (130)	1.304[d]	−0.975 (200)	−1.244 (170)

[a] In C_6H_6.
[b] In C_6H_6 at 298 K.
[c] Solvent, CH_2Cl_2; Pt-working electrode, Ag/AgCl, Cl^- reference, Pt-auxiliary electrode; [*n*-Bu_4N](ClO_4) supporting electrolyte, scan rate 50 mV/s; metal oxidation $E^1_M = 0.5(E_{pa} + E_{pc})$, V for M(I)/M(0) couple, E^2_M for M(II)/M(I) couple in unit of V, $\Delta E_p = |E_{pa} - E_{pc}|$, mV.
[d] E_{pa} (anodic-peak-potential).
[e] E_{pc} (cathodic-peak-potential).

Table 3
^{1}H NMR spectral data of [M(CO)$_4$(NaiR)] (**4**–**7**) in $CDCl_3$

Compound	δ/ppm (*J*/Hz)									
	4-H[a]	5-H[a]	6-H[a]	7-H[b]	8-H[c]	9-H[c]	10-12-H[c]	13-H[b]	N(1)-Me	1-CH_2-
4a	7.60	7.39		7.90 (8.0)	7.75	7.75	7.51	7.70 (8.0)	4.08[a]	
5a	7.56	7.31	8.45		8.06	8.06	7.55	7.91 (8.0)	4.00[a]	
4b	7.58	7.37		7.90 (8.0)	7.70	7.70	7.48	7.65 (8.0)	1.66[d] (7.5)	4.55[e] (10.0)
5b	7.58	7.33	8.41		8.03	7.96	7.58	7.96 (8.0)	1.60[d] (7.5)	4.46[e] (10.0)
6a	7.57	7.36		7.93 (8.0)	7.73	7.73	7.48	7.64 (8.0)	4.04	
7a	7.55	7.35	8.83		8.11	8.11	7.58	7.89 (8.0)	4.11	
6b	7.58	7.37		7.90 (8.0)	7.70	7.70	7.48	7.65 (8.0)	1.66[d] (7.5)	4.55[e] (9.0)
7b	7.58	7.36	8.82		8.13	8.13	7.58	7.90 (8.0)	1.65[d] (7.5)	4.53[e] (9.0)

[a] Broad singlet.
[b] Doublet.
[c] Multiplet.
[d] Triplet.
[e] Quartet.

and [M(CO)$_4$(2-PAP)] (2-PAP = 2-(phenylazo)pyridine) [4] we suggest that the oxidation is primarily a metal-centred electron extraction. In every case the first oxidation on scan reversal shows a cathodic peak at a potential difference >100 mV to that of the anodic peak and supports quasireversibility (Fig. 3) of the voltammogram. The second oxidation ($M^+ \rightarrow M^{2+}$) in most of the complexes is irreversible in nature and the cathodic peak does not appear at all on scan reversal. [M(CO)$_4$(α-NaiR′)] shows a higher M^+/M^0 redox potential than that of [M(CO)$_4$(β-NaiR′)]. The reduction is referred to electron accommodation to the π^* MO of the chelated NaiR′. The first reduction in each case appears at a more positive potential than that of the free ligand [22], reflecting the stabilization

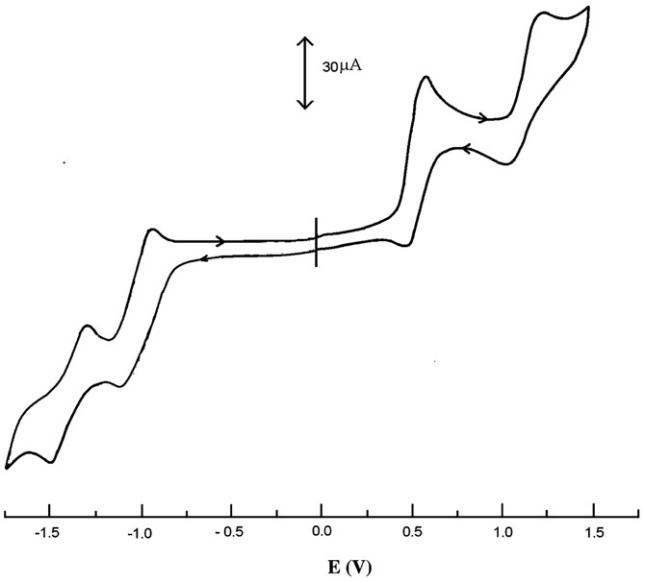

Fig. 3. Cyclic voltammogram of *cis*-[Cr(CO)$_4$(β-NaiEt)] in CH_2Cl_2 using a Pt-disk working electrode, Pt-auxiliary electrode, Ag/AgCl reference and [*n*-Bu_4N][ClO_4] supporting electrolyte.

of the π^* MO upon coordination. The reduction potential follows α-NaiR′ > β-NaiR′ and Mo > Cr. On considering the literature data of NaiR′ complexes [22–25], the reduction is referred to azo/azo$^-$ and azo$^-$/azo$^=$, which appear at a more negative potential than that of analogous 2-(phenylazo)pyridine complexes. This is due to higher π-acidity of pyridine compared to imidazole [13] and higher electronic susceptibility of the naphthyl group compared to the phenyl group [26].

4. Conclusion

Cis-[M(CO)$_4$(α/β-NaiR′)] (M = Cr(0), Mo(0); α/β-NaiR′ = 1-alkyl-2-(naphthyl-α/β-azo)imidazole) are characterized by different spectroscopic tools (FT-IR, UV–Vis, Mass, ^{1}H and ^{13}C NMR). The mass fragmentation pattern shows successive removal of CO. The ligands belong to the π-acidic azoimine family and stabilize efficiently Cr(0) and Mo(0) oxidation states. The cyclic voltammogram gives two metal centred oxidations, M^+/M^0 and M^{2+}/M^+, and two ligand centred reductions, azo/azo$^-$ and azo$^-$/azo$^=$. The complexes exhibit π–π^* emission; *cis*-[M(CO)$_4$(α-NaiR′)] emits at a higher energy than *cis*-[M(CO)$_4$(β-NaiR′)].

Acknowledgements

Financial support from Department of Science & Technology, New Delhi is gratefully acknowledged. One of us (P.D.) thanks the Council of Scientific and Industrial Research, New Delhi for a fellowship.

Appendix A. Supplementary data

Supplementary data associated with this article can be found, in the online version, at doi:10.1016/j.poly.2006.06.025.

References

[1] (a) M.H.B. Stiddard, J. Chem. Soc. (1962) 4712;
(b) I. Veroni, C. Makedonas, A. Rontoyianns, C.A. Mitsopoulou, J. Organomet. Chem. 691 (2006) 267;
(c) I.G. Virrels, M.W. George, J.J. Turner, J. Peters, A. Vlcek Jr., Organometallics 15 (1996) 4089;
(d) B. Bildstein, M. Malau, H. Kopaeka, M. Fontani, P. Zanello, Inorg. Chim. Acta 300–302 (2000) 16;
(e) P.S. Hadded, A.E. Mauro, V.M. Nogueira, S.I. Klein, Transition Met. Chem. 28 (2003) 899;
(f) S.A. Ali, A.A. Solimon, M.M. Aboaly, R.M. Ramadan, J. Coord. Chem. 55 (2002) 1161;
(g) H.T. Macholdt, H. Elian, Inorg. Chem. 23 (1984) 4315.
[2] A. Vleck Jr., Coord. Chem. Rev. 230 (2002) 225.
[3] M.N. Ackermann, K.B. Moore, A.S. Colligan, J.A. Thomas Wohlver, K.J. Warren, J. Organomet. Chem. 667 (2003) 81.
[4] M.N. Ackermann, C.R. Barton, C.J. Deodene, E.M. Specht, S.C. Keill, W.E. Schreiber, Hiodong Kim, Inorg. Chem. 28 (1989) 397.
[5] F. Alper, C. Kayram, S. Ozkar, J. Organomet. Chem. 691 (2006) 2734.
[6] W. Kaim, S. Ernst, S. Kohlmann, Polyhedron 5 (1986) 295.
[7] W. Kaim, S. Kohlmann, Inorg. Chem. 25 (1986) 3442.
[8] W. Kaim, S. Kohlmann, Inorg. Chem. 26 (1987) 68.
[9] M.N. Ackermann, W.G. Fairbrother, N.S. Amin, C.J. Deodene, C.M. Lamborg, P.T. Martin, J. Organomet. Chem. 523 (1996) 145.
[10] M.J. Alder, W.I. Cross, K.R. Flower, R.G. Pritchard, J. Organomet. Chem. 568 (1998) 279.
[11] M.N. Ackermann, S.R. Kiihne, P.A. Saunders, C.E. Barnes, S.C. Stalling, H. Kim, C. Woods, M. Lagunoff, Inorg. Chim. Acta 334 (2002) 193.
[12] M.N. Ackermann, M.P. Robinson, I.A. Maher, E.B. LeBlane, R.V. Raz, J. Organomet. Chem. 682 (2003) 248.
[13] E.C. Constable, Coord. Chem. Rev. 93 (1989) 205.
[14] R.H. Crabtree, The Organometallic Chemistry of the Transition Metal, third ed., Wiley, New York, 2001.
[15] V.N. Nemyken, P. Basu, Inorg. Chim. Acta 358 (2005) 2876.
[16] L.F. Tang, Z.H. wang, J.F. Chai, X.B. Leng, J.T. Wang, H.G. Wang, J. Organomet. Chem. 642 (2002) 179.
[17] S.R. Marder, in: D.W. Bruce, D. O'Hare (Eds.), Inorganic Materials, Wiley, New York, 1992, p. 78.
[18] J. Dinda, D. Das, P.K. Santra, C. Sinha, L.R. Falvello, J. Organomet. Chem. 629 (2001) 28.
[19] S. Senapoti, Sk. Jasimuddin, C. Sinha, Indian J. Chem. 45A (2006) 1153.
[20] S. Senapoti, Sk. Jasimuddin, G. Mostafa, T.H. Lu, C. Sinha, Polyhedron 25 (2006) 1571.
[21] A.I. Vogel, A Text Book of Practical Organic Chemistry, Longmann, London, 1959.
[22] J. Dinda, K. Bag, C. Sinha, G. Mostafa, T.-H. Lu, Polyhedron 22 (2003) 1367.
[23] P. Byabartta, P.K. Santra, T.K. Misra, C. Sinha, C.H.L. Kennard, Polyhedron 20 (2001) 905.
[24] J. Dinda, S. Pal, B.K. Ghosh, J. Cheng, F.-L. Liao, T.-H. Lu, C. Sinha, J. Coord. Chem. 55 (2002) 1271.
[25] S. Pal, D. Das, P. Chattopadhyay, C. Sinha, K. Panneerselvam, T.-H. Lu, Polyhedron 19 (2000) 1263.
[26] I.L. Finar, Organic Chemistry, sixth ed., vol. 1, Springer, New York, 1971.

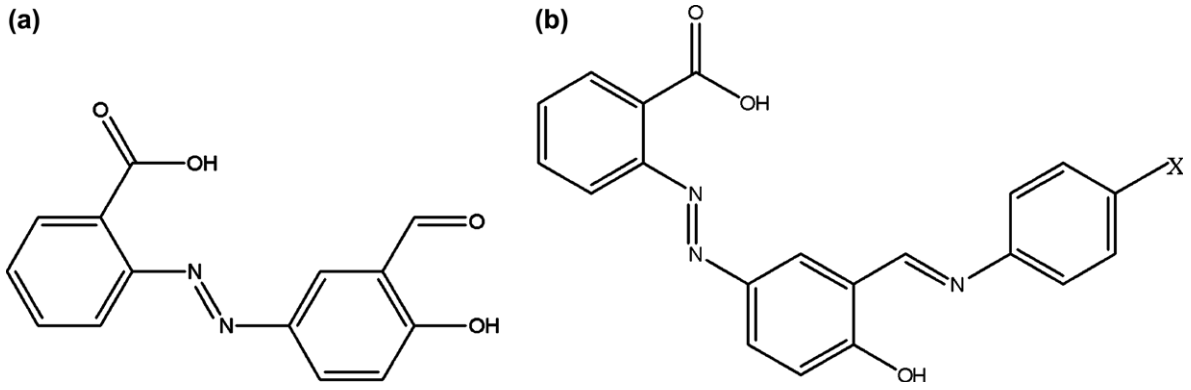

Fig. 1. Generic structure of the ligand. *Abbreviations*. (a) LHH′ (pre-ligand) (b) L^1HH': X = –CH_3; L^2HH': X = –Br, L^3HH': X = –Cl, L^4HH': X = –OCH_3, where H and H′ represent hydroxy and carboxylic acid H atoms, respectively.

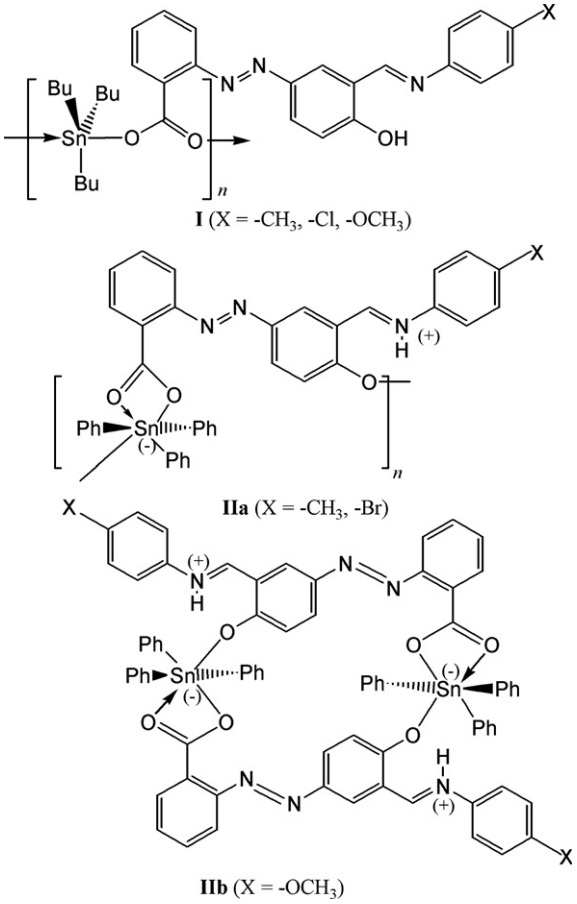

Scheme 1. Structural motifs in $R_3Sn[O_2CC_6H_4\{N{=}N(C_6H_3\text{-}4\text{-}OH\text{-}(C(H){=}NC_6H_4X\text{-}4))\}\text{-}o]$ complexes.

solid state, the three investigated tri-*n*-butyltin(IV) complexes (X = –Cl [4], –OCH_3 [5] or –CH_3 [6]) have the motif **I** structure. The complexes are one-dimensional polymers in which the two carboxylate O atoms of a single benzoate ligand bridge the adjacent $SnBu_3$ groups. The Sn atom has a slightly distorted *trans*-Bu_3SnO_2 trigonal-bipyramidal coordination geometry with O atoms from two different carboxylate ligands occupying the axial positions. In contrast to the tri-*n*-butyltin(IV) analogues, the carboxylate ligands in the triphenyltin(IV) complexes (X = –Br or –CH_3 [1]) were found to exist in a zwitterionic form as a result of the coordination of the phenoxide O atom to a Sn atom. Two structural motifs, **IIa** and **IIb**, were found. In motif **IIa**, a polymeric *trans*-Ph_3SnO_2 configuration was observed where the adjacent $SnPh_3$ moieties are bridged by a single carboxylate ligand through a carboxylate O atom and the phenoxide O atom. The pattern then continues indefinitely. Each Sn atom has a slightly distorted trigonal-bipyramidal coordination geometry with the carboxylate and phenoxide O atoms from two different carboxylate ligands occupying the axial positions. On the other hand, a subtle modification of the X-substituent in the ligand framework (from –CH_3 or –Br to –OCH_3) results in discrete cyclic centrosymmetric dimers where two $SnPh_3$ entities are bridged by two carboxylate anions through their carboxylate and phenoxide O atoms (motif **IIb**) [1]. Despite the dimerization instead of polymerization, the coordination geometry about the Sn atom is virtually the same as that found in motif **IIa**. The triorganotin(IV) complexes of the type $R_3Sn[O_2CC_6H_4\{N{=}N(C_6H_3\text{-}4\text{-}OH(C(H){=}NC_6H_4X\text{-}4))\}\text{-}o]$, particularly the tri-*n*-butyltin(IV) complexes, were screened for larvicidal activity against the second larval instar of the *Aedes aegypti* and *Anopheles stephensi* mosquito [4,5] as well as for embryo toxicity against the sea urchin (*Paracentrotus lividus* and *Sphaerechinus granularis*) early developmental stages [7]. These compounds have shown promise as larvicides but were found to be toxic against the sea urchin.

Given the synthetic and structural importance and the potential biological activity of the $R_3Sn[O_2CC_6H_4\{N{=}N(C_6H_3\text{-}4\text{-}OH(C(H){=}NC_6H_4X\text{-}4))\}\text{-}o]$ class of complexes, it is of interest to explore the chemistry of the analogous complexes of these ligands with Bz_3Sn(IV). The present contribution details the preparation and spectroscopic characterization of four complexes of this type, viz. $Bz_3Sn[O_2CC_6H_4\{N{=}N(C_6H_3\text{-}4\text{-}OH(C(H){=}NC_6H_4X\text{-}4))\}\text{-}o](OH_2)$ (X = –CH_3, –Br, –Cl, –OCH_3). The crystal structures of two aqua complexes, $Bz_3Sn[O_2CC_6H_4\{N{=}N(C_6H_3\text{-}4\text{-}OH(C(H){=}NC_6H_4X\text{-}4))\}\text{-}o](OH_2)$ (X = –Cl, –OCH_3), are also reported.

2. Experimental

2.1. Materials

Bz_3SnOH was prepared as described by Sisido et al. [8]. The solvents used in the reactions were of AR grade and were dried using standard procedures. Toluene was distilled from sodium benzophenone ketyl. The ligands, 2-{(*E*)-4-hydroxy-3-[(*E*)-4-(aryl)iminomethyl] phenyldiazenyl}benzoic acids, $L^{1-4}HH'$, were prepared and characterized as described in our earlier report [4]. The compound $Bz_3SnLH \cdot OH_2$ (where $LH = O_2CC_6H_4(N{=}N(C_6H_3\text{-}4\text{-}OH\text{-}5\text{-}CHO)\text{-}o)$ [9]) has been included for the convenience of the discussion.

2.2. Physical measurements

Carbon, hydrogen and nitrogen analyses were performed with a Perkin–Elmer 2400 series II instrument. IR spectra in the range 4000–400 cm^{-1} were obtained on a BOMEM DA-8 FT-IR spectrophotometer with samples investigated as KBr discs. The ^1H, ^{13}C and ^{119}Sn NMR spectra were recorded on a Bruker AMX 400 spectrometer and measured at 400.13, 100.62 and 149.18 MHz, respectively. The ^1H, ^{13}C and ^{119}Sn chemical shifts were referred to Me_4Si set at 0.00 ppm, $CDCl_3$ set at 77.0 ppm and Me_4Sn set at 0.00 ppm, respectively. The Mössbauer spectra of the complexes in the solid state were recorded using a Model MS-900 spectrometer in the acceleration mode with a moving source geometry. A 10 mCi $Ca^{119m}SnO_3$ source was used and counts of 30,000 or more were accumulated for each spectrum. The spectra were measured at 80 K using a liquid-nitrogen cryostat. The velocity was calibrated at ambient temperature using a composition of $BaSnO_3$ and tin foil (splitting 2.52 mm s^{-1}). The resultant spectra were analyzed using the Web Research software package.

2.3. Synthesis of the tribenzyltin(IV) complexes

A typical method is described below.

2.3.1. Synthesis of $Bz_3SnLH \cdot OH_2$ (1)

Compound **1** was synthesized by reacting LHH′ (0.38 g, 1.40 mmol) and Bz_3SnOH (0.58 g, 1.41 mmol) in 50 ml of anhydrous toluene in a 100 ml flask equipped with a Dean-Stark moisture trap and water-cooled condenser. The reaction mixture was refluxed for 8 h and filtered while hot. The filtrate was collected and the volatiles were removed using a rotary evaporator. The residue was dried in vacuo, washed with hexane thoroughly, extracted into benzene and filtered. The crude product was obtained after evaporation and this was then recrystallized from benzene to yield dark-red crystals of the desired product. Yield: (0.36 g, 39%); m.p.: 73–75 °C. *Anal.* Calc. for $C_{35}H_{32}N_2O_5Sn$: C, 61.85; H, 4.70; N, 4.12. Found: C, 61.48; H, 4.53; N, 4.29%. IR (cm^{-1}): 1659 $\nu(OCO)_{asym}$. ^1H NMR ($CDCl_3$): 11.3 (brs, 1H, OH, D_2O exchangeable), 9.78 (s, 1H, C(H)=O), 2.68 (s, 6H, CH_2: Bz_3Sn), 6.72–7.60 (complex multiplets, 22H, remaining ligand and Bz_3Sn protons) ppm. ^{13}C NMR ($CDCl_3$): 196.5 (C(H)=O), 174.9 (CO_2), not detected (C–OH), 24.2 (CH_2: Bz_3Sn), 116.3–161.2 (complex nature of the remaining ligand and Bz_3Sn carbon signals which could not be identified with certainty owing to poor signal to noise ratio) ppm. ^{119}Sn Mössbauer: $\delta = 1.04$, $\Delta = 2.51$ mm s^{-1}, $\rho = 2.4$.

The other tribenzyltin(IV) complexes (**2**–**5**) were prepared by reacting Bz_3SnOH with the appropriate ligand (L^1HH'–L^4HH') following an analogous procedure. The characterization and spectroscopic data of the complexes are given below.

2.3.2. $Bz_3SnL^1H \cdot OH_2$ (2)

Orange-red crystals of compound **2** was obtained from a benzene–hexane mixture (1:3 v/v). Yield: 79%; m.p.: 96–98 °C. *Anal.* Calc. for $C_{42}H_{39}N_3O_4Sn$: C, 65.62; H, 5.11; N, 5.46. Found: C, 65.42; H, 4.83; N, 5.49%. IR (cm^{-1}): 1619 $\nu\ (OCO)_{asym}$. ^1H NMR ($CDCl_3$): 13.1 (brs, 1H, OH, D_2O exchangeable), 8.45 (s, 1H, C(H)=N), 2.69 (s, 6H, CH_2: Bz_3Sn), 2.42 (s, 3H, CH_3), 6.70–8.10 (26H, remaining ligand and Bz_3Sn protons) ppm. ^{13}C NMR ($CDCl_3$): 174.9 (CO_2), 164.5 (C–OH), 160.8 (C(H)=N), 24.3 (CH_2: Bz_3Sn), 20.9 (CH_3), 151.9, 145.7, 144.9, 138.6, 137.3, 131.3, 129.9, 129.1, 128.6, 128.3, 127.8, 127.2, 124.5, 120.9, 118.9, 118.1, 117.8 (remaining ligand and Bz_3Sn carbon signals) ppm. ^{119}Sn NMR (δ, ppm): −10.5. ^{119}Sn Mössbauer: $\delta = 1.39$, $\Delta = 3.07$ mm s^{-1}, $\rho = 2.2$.

2.3.3. $Bz_3SnL^2H \cdot OH_2$ (3)

Red crystals of compound **3** were obtained from a benzene–hexane mixture (1:3 v/v). Yield: 64%; m.p.: 72–74 °C. *Anal.* Calc. for $C_{41}H_{36}BrN_3O_4Sn$: C, 59.09; H, 4.35; N, 5.04. Found: C, 60.19; H, 4.26; N, 5.18%. IR (cm^{-1}): 1619 $\nu\ (OCO)_{asym}$. ^1H NMR ($CDCl_3$): 13.5 (brs, 1H, OH, D_2O exchangeable), 8.43 (s, 1H, C(H)=N), 2.63 (s, 6H, CH_2: Bz_3Sn), 6.70–7.99 (26H, remaining ligand and Bz_3Sn protons) ppm. ^{13}C NMR ($CDCl_3$): 173.4 (CO_2), 164.1 (C–OH), 162.3 (C(H)=N), 24.3 (CH_2: Bz_3Sn), 151.9, 146.6, 145.8, 138.5, 132.5, 131.4, 129.9, 129.5, 129.3, 128.8, 127.9, 127.0, 124.6, 122.8, 120.8, 118.8, 118.2, 117.6 (remaining ligand and Bz_3Sn carbon signals) ppm. ^{119}Sn NMR (δ, ppm): −9.82. ^{119}Sn Mössbauer: $\delta = 1.27$, $\Delta = 2.76$ mm s^{-1}, $\rho = 2.2$.

2.3.4. $Bz_3SnL^3H \cdot OH_2$ (4)

Red crystals of compound **4** were obtained from a toluene–hexane mixture (1:3 v/v). Yield: 49%; m.p.: 71–73 °C. *Anal.* Calc. for $C_{41}H_{36}ClN_3O_4Sn$: C, 62.43; H, 4.59; N, 5.33. Found: C, 62.01; H, 4.49; N, 5.40%. IR (cm^{-1}): 1617 $\nu(OCO)_{asym}$. ^1H NMR ($CDCl_3$): 13.6 (brs, 1H, OH, D_2O exchangeable), 8.49 (s, 1H, C(H)=N), 2.69 (s, 6H, CH_2: Bz_3Sn), 6.70–8.05 (26 H, remaining ligand and Bz_3Sn protons) ppm. ^{13}C NMR ($CDCl_3$): 173.2 (CO_2), 163.9 (C–OH), 162.2 (C(H)=N), 24.3 (CH_2: Bz_3Sn), 151.7, 146.1,

145.8, 139.8, 138.4, 132.8, 131.2, 129.9, 129.4, 129.2, 128.6, 127.8, 126.8, 124.5, 122.2, 118.7, 117.9, 117.5 (remaining ligand and Bz_3Sn carbon signals) ppm. ^{119}Sn NMR (δ, ppm): −10.2. ^{119}Sn Mössbauer: $\delta = 1.14$, $\Delta = 2.99$ mm s^{-1}, $\rho = 2.6$.

2.3.5. $Bz_3SnL^4H \cdot OH_2$ (5)

Red crystals of compound **5** were obtained from a benzene–hexane mixture (1:3 v/v). Yield: 75%; m.p.: 74–76 °C. *Anal.* Calc. for $C_{42}H_{39}N_3O_5Sn$: C, 64.30; H, 5.01; N, 5.36. Found: C, 64.50; H, 4.89; N, 5.28%. IR (cm^{-1}): 1617 $\nu(OCO)_{asym}$. ^1H NMR ($CDCl_3$): 14.1 (brs, 1H, OH, D_2O exchangeable), 8.53 (s, 1H, C(H)=N), 3.84 (s, 3H, OCH_3), 2.69 (s, 6H, CH_2: Bz_3Sn), 6.70–8.03 (26 H, remaining ligand and Bz_3Sn protons) ppm. ^{13}C NMR ($CDCl_3$): 173.2 (CO_2), 164.3 (C–OH), 159.5 (C(H)=N), 55.5 (OCH_3), 24.3 (CH_2: Bz_3Sn), 151.9, 145.8, 140.5, 138.6, 131.3, 130.3, 129.9, 129.2, 128.6, 128.4, 126.8, 124.5, 122.3, 119.1, 117.9, 117.7, 114.7 (remaining ligand and Bz_3Sn carbon signals) ppm. ^{119}Sn NMR (δ, ppm): −10.48. ^{119}Sn Mössbauer: $\delta = 1.39$, $\Delta = 3.13$ mm s^{-1}, $\rho = 2.3$.

2.4. X-ray crystallography

Crystals of compounds **4** and **5** suitable for an X-ray crystal-structure determination were obtained from a toluene–hexane and a benzene–hexane solution, respectively, by slow evaporation of the solvent at room temperature. All measurements were made at low temperature on a Nonius KappaCCD diffractometer [10] with graphite-monochromated Mo Kα radiation ($\lambda = 0.71073$ Å) and an Oxford Cryosystems Cryostream 700 cooler. Data reduction were performed with HKL DENZO and SCALEPACK [11]. The intensities were corrected for Lorentz and polarization effects, and an empirical absorption correction based on the multi-scan method [12] was applied. Equivalent reflections were merged. The data collection and refinement parameters are given in Table 1. Views of the molecular structures are shown in Figs. 3 and 4. The structures were solved by direct methods by using SIR-92 [13]. For each structure, the non-hydrogen atoms were refined anisotropically. The water ligand and phenoxy H atoms were placed in positions indicated by the difference electron density map and their positions were allowed to refine together with individual isotropic displacement parameters. All remaining H atoms in each structure were placed in geometrically calculated positions and refined using a riding model where each H atom was assigned a fixed isotropic displacement parameter with a value equal to $1.2U_{eq}$ of its parent atom ($1.5U_{eq}$ for the methyl group in **5**). The refinement of each structure was carried out on F^2 using full-matrix least-squares procedures, which minimized the function $\sum w(F_o^2 - F_c^2)^2$. A correction for secondary extinction was applied in the case of complex **5**. One reflection, whose intensity was considered to be an extreme outlier, was omitted from the final refinement of **4**. All calculations were performed using the SHELXL-97 [14] program.

Table 1
Crystallographic data and structure refinement parameters for the tribenzyltin(IV) complexes **4** and **5**

	4	**5**
Empirical formula	$C_{41}H_{36}ClN_3O_4Sn$	$C_{42}H_{39}N_3O_5Sn$
Formula weight	788.80	784.39
Crystal size (mm)	0.10 × 0.17 × 0.32	0.12 × 0.17 × 0.28
Crystal shape	tablet	prism
Temperature (K)	160(1)	160(1)
Crystal system	monoclinic	monoclinic
Space group	$P2_1/n$	$P2_1/n$
a (Å)	12.5388(1)	13.1825(2)
b (Å)	22.6661(2)	21.9417(4)
c (Å)	14.1787(2)	14.3594(2)
β (°)	114.8089(5)	115.9489(8)
V (Å^3)	3657.78(7)	3734.7(1)
Z	4	4
D_x (g cm^{-3})	1.432	1.395
μ (mm^{-1})	0.817	0.732
Transmission factors (minimum; maximum)	0.804; 0.925	0.759; 0.916
$2\theta_{max}$ (°)	60	55
Reflections measured	88 212	82 555
Independent reflections (R_{int})	10 662 (0.068)	8548 (0.091)
Reflections with $I > 2\sigma(I)$	8172	6020
Number of parameters	463	474
$R(F)$ ($I > 2\sigma(I)$ reflections)	0.037	0.039
$wR(F^2)$ (all data)	0.090	0.091
Goodness-of-fit (F^2)	1.05	1.05
Maximum, minimum $\Delta\rho$ (e Å^3)	1.61, −0.92	1.52, 0.67

3. Results and discussion

3.1. Synthetic aspect

Recently, we have investigated the reaction of Bz_3SnCl with sodium 2-[(*E*)-2-(3-formyl-4-hydroxyphenyl)-1-diazenyl]benzoate, LHNa (Fig. 1a) in anhydrous methanol. The reaction proceeded via debenzylation and oxidative decarbonylation [15]. This reaction afforded a cyclic dinuclear dibenzyltin(IV) complex, $[Bz_2\{O_2CC_6H_4\{N(H)=N=(C_6H_3\text{-}4(=O)\text{-}5\text{-}O)\}\text{-}o\}Sn]_2$ (Fig. 2) instead of the polymeric Me_3Sn(IV) [16] and Bu_3Sn(IV) [4] as well as the monomeric Ph_3Sn(IV) [9] analogues. In a similar way, the reactions of Bz_3SnCl with sodium 2-{(*E*)-4-hydroxy-3-[(*E*)-4-(aryl)iminomethyl]phenyldiazenyl}benzoates, L^1H-Na–L^4HNa (Fig. 1b) were attempted under identical

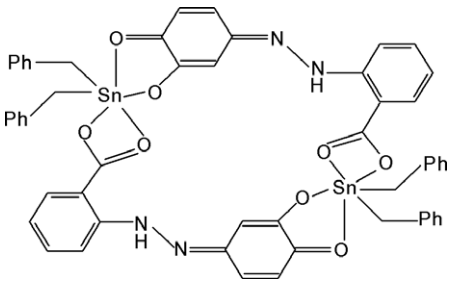

Fig. 2. Cyclic dibenzyltin(IV) complex: $[Bz_2\{O_2CC_6H_4\{N(H)\text{–}N=(C_6H_3\text{-}4(=O)\text{-}5\text{–}O)\}\text{-}o\}Sn]_2$.

reaction conditions, in the expectation of obtaining the corresponding $Bz_3Sn(IV)$ derivatives. Instead, the work-up of the reaction mixture yielded crystals of the same cyclic dibenzyltin(IV) dimer, i.e. $[Bz_2\{O_2CC_6H_4\{N(H)\text{—}N{=}(C_6H_3\text{-}4(=O)\text{-}5\text{-}O)\}\text{-}o\}Sn]_2$. The melting point, microanalytical, spectroscopic and crystallographic data of the two products were identical. In the latter reactions, cleavage of the H–C=N–Ar part from the ligand molecule and simultaneous debenzylation was noticed. At present, however, the exact mechanism of the cleavage/rearrangement is not clearly understood. On the other hand, attempted reactions of the free acids (LHH′ (pre-ligand) and L^1HH'–L^4HH') with Bz_3SnOH in anhydrous toluene afforded the desired products $Bz_3SnLH \cdot OH_2$ and $Bz_3SnL^{1-4}H \cdot OH_2$ in moderate to good yields, respectively. Attempted crystallization of these $Bz_3Sn(IV)$ complexes from an anhydrous benzene-methanol mixture again afforded crystals of the dimeric dibenzyltin complex (Fig. 2). Hence, the crystallization attempts were made using anhydrous benzene, benzene–hexane or toluene–hexane.

3.2. Spectroscopy

The diagnostically important infrared absorption frequencies for the carboxylate antisymmetric [ν_{asym}(OCO)] stretching vibration of the complexes are given in Section 2. The assignment of the symmetric [ν_{sym}(OCO)] stretching vibration band could not be made owing to the complex pattern of the spectra. The assignment of the band is based on comparison with the spectra of the free ligands. The antisymmetric [ν_{asym}(OCO)] stretching vibrations for the uncomplexed ligands have been detected at 1733 cm^{-1} in LHH′ [9] and around the 1725 cm^{-1} region for $L^{1-4}HH'$ [4]. In the complexes, the carbonyl stretching frequencies are found to be shifted to lower wavenumber, which is ascribed to carboxylate coordination in accordance with earlier reports [1,4,17,18].

The ^1H and ^{13}C NMR data of LHH′ and $L^{1-4}HH'$ have been reported earlier [4,9] and the conclusions drawn from the ligand assignments were then subsequently extrapolated to the complexes owing to the data similarity for at least a few signals. The ^1H NMR integration values were completely consistent with the formulation of the products. Individual assignments of the ^1H and ^{13}C signals of the tribenzyltin(IV) moiety and most parts of the ligand skeleton could not be made owing to serious signal overlap resulting in complex patterns. The ^{119}Sn NMR chemical shifts of the tribenzyltin(IV) complexes (**2**–**5**) in $CDCl_3$ solution are listed in Section 2.3. The complexes exhibit a single sharp resonance at around −10.0 ppm, suggesting that the complexes are isostructural in solution. The ^{119}Sn NMR resonances fall within the range from +55.0 to −25.0 ppm, which is usually indicative of four-coordinate tribenzyltin(IV) species in solution [19]. This indicates that the five-coordinate structure of the solid (see X-ray discussion, vide infra) breaks up in solution [20], presumably by loss of the water ligand.

The Mössbauer results from the complexes are listed in Section 2.3. The ratio of the quadrupole splitting (Δ) value to the isomer shift (δ) value ($\rho = \Delta/\delta$) can be used to distinguish between the different coordination states of the central tin atom [21]. Tin compounds which are four coordinate have ρ values less than 1.8 while ρ values larger than 2.1 would indicate compounds with greater than four coordination. Complexes **2**–**5** (slightly lower in the case of **1**) have similar δ and Δ parameters, and the ρ values are greater than 2.1 suggesting that the complexes are isostructural with a coordination number greater than four. Trigonal-bipyramidal triorganotin(IV) complexes with organic groups in the equatorial plane [22] have been reported to have Δ values between 3.00 and 4.00 mm s^{-1}. This value has also been found to change as a function of the axial bond distances [22]. The tribenzyltin(IV) complexes in the present investigation exhibited Δ values of ~3.00 mm s^{-1} which correspond with a trigonal-bipyramidal geometry around the tin atom with equatorial benzyl groups, [20,23–25] and is in agreement with the structures determined by X-ray crystallography (see Section 3.3).

3.3. X-ray crystallography

The crystal structures of complexes **4** and **5** are very similar and the principal geometric parameters do not differ significantly (Table 2). In contrast to the polymeric tri-*n*-butyltin(IV) [4–6] and polymeric and dimeric triphenyltin(IV) [1] analogues (Scheme 1), both of the tribenzyltin(IV)

Table 2
Selected bond lengths (Å) and angles (°) for **4** and **5**

	4	**5**
Sn–O(1)	2.150(1)	2.164(2)
Sn–O(4)	2.399(2)	2.396(2)
Sn···O(2)	3.056(2)	3.008(2)
Sn–C(21)	2.150(2)	2.151(3)
Sn–C(28)	2.148(2)	2.147(3)
Sn–C(35)	2.143(2)	2.139(3)
O(1)–C(1)	1.278(3)	1.288(3)
O(2)–C(1)	1.238(3)	1.234(3)
N(1)–N(2)	1.252(3)	1.254(3)
N(1)–C(3)	1.425(3)	1.421(4)
N(2)–C(8)	1.429(3)	1.429(4)
O(1)–Sn–O(4)	173.58(6)	172.64(8)
O(1)–Sn–C(21)	89.12(8)	89.05(9)
O(1)–Sn–C(28)	96.40(8)	96.4(1)
O(1)–Sn–C(35)	99.12(7)	98.98(9)
O(4)–Sn–C(21)	85.22(8)	84.1(1)
O(4)–Sn–C(28)	83.66(8)	84.2(1)
O(4)–Sn–C(35)	86.13(7)	86.58(9)
C(21)–Sn–C(28)	118.19(9)	114.9(1)
C(21)–Sn–C(35)	116.35(9)	117.9(1)
C(28)–Sn–C(35)	123.18(9)	124.9(1)
Sn–O(1)–C(1)	116.4(1)	114.1(2)
N(2)–N(1)–C(3)	114.3(2)	115.3(2)
N(1)–N(2)–C(8)	113.2(2)	113.2(2)
O(1)–C(1)–O(2)	123.6(2)	123.5(2)
O(1)–C(1)–C(2)	117.0(2)	116.7(2)
O(2)–C(1)–C(2)	119.4(2)	119.8(2)

complexes, **4** and **5**, exhibit the same monomeric *trans*-R_3SnO_2 structural motif, as illustrated in Figs. 3 and 4. The structures are also shown in Scheme 2 for clarity. The Sn atom has a slightly distorted trigonal-bipyramidal coordination geometry with equatorial benzyl groups and the axial positions occupied by an O atom from the carboxylate ligand and the O atom from the water ligand. A monomeric structure with a similar mode of coordination and geometry about the Sn atom was observed in the triphenyltin(IV) complex of the pre-ligand i.e. $Ph_3Sn[O_2CC_6H_4(N{=}N(C_6H_3$-4-OH-5-CHO))-*o*$](OH_2)$ [9]. The carbonyl O atom of the carboxylate ligand in **4** and **5** also coordinates very weakly to the Sn atom with long Sn···O(2) distances of 3.056(2) and 3.008(2) Å, respectively. Although the Sn···O(2) distances are well inside the sum of the van der Waals radii of the Sn and O atoms (ca. 3.6 Å), there does not appear to be any major distortion of the principal trigonal bipyramidal Sn-coordination geometry as a result of this contact. A similar additional weak Sn···O coordination was also observed in the structures of related polymeric $[R_3SnLH]_n$ (R = ^{n}Bu, Ph) derivatives [1,4–6]. The Sn atom coordination geometry found for complexes **4** and **5** is in good agreement with that

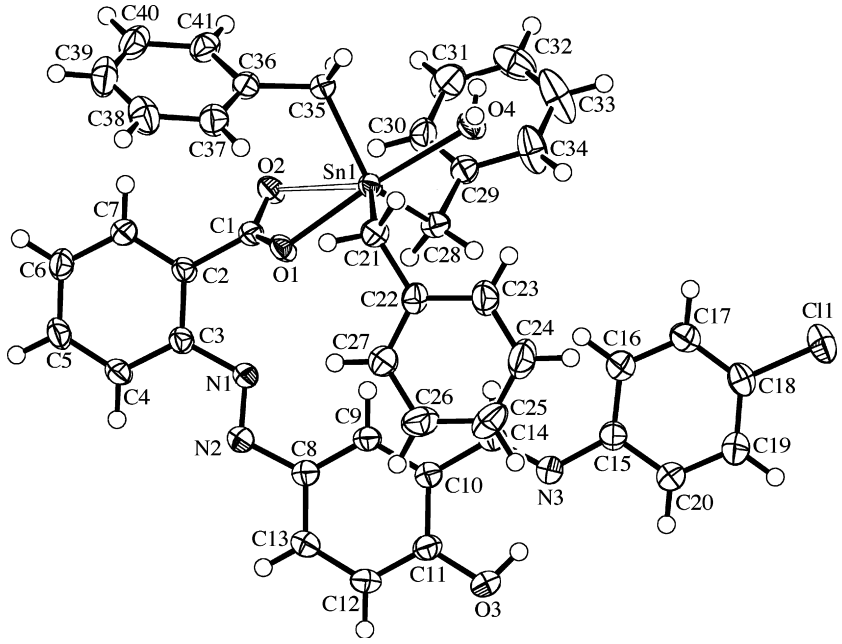

Fig. 3. The molecular structure of $Bz_3SnL^3H \cdot OH_2$ (**4**) showing the atom-labelling scheme (50% probability ellipsoids).

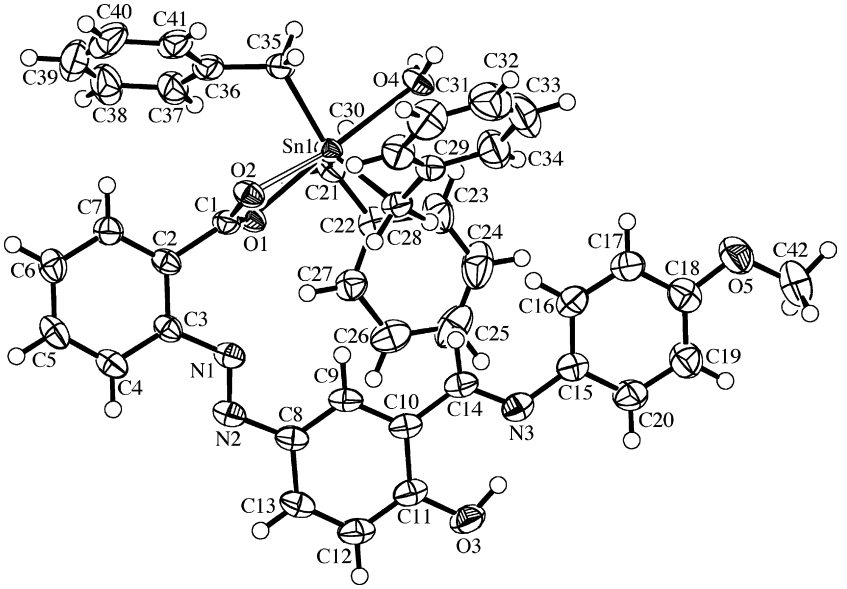

Fig. 4. The molecular structure of $Bz_3SnL^4H \cdot OH_2$ (**5**) showing the atom-labelling scheme (50% probability ellipsoids).

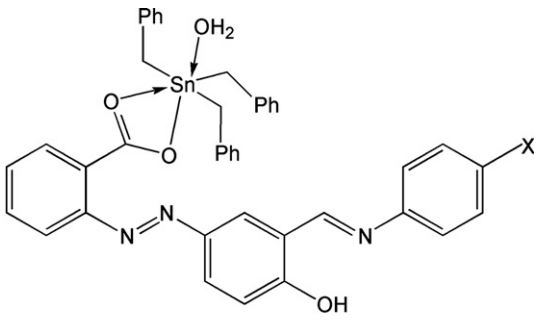

III (X = -Cl, -OCH_3)

Scheme 2. Structures of the complexes **4** and **5**.

inferred from ^{119m}Sn Mössbauer spectroscopy (see Section 3.2).

In complexes **4** and **5**, the phenoxy H atom forms an intramolecular hydrogen bond with the imine N atom, thereby creating a loop with a graph set motif [26,27] of S(6). The H atoms of the water ligand form intermolecular hydrogen bonds with the phenoxy O atom of one neighbouring molecule and with the weakly coordinating carboxylate O atom of a different neighbouring molecule (Table 3). The former interaction links the molecules into extended chains which run parallel to the [0 1 0] direction and can be described by a graph set motif of C(14). The

Table 3
Hydrogen bonding geometry (Å, °) for **4**[a] and **5**[b]

D–H···A	D–H	H···A	D···A	D–H···A
O(3)–H(3)···N(3)	0.90(3) [0.95(5)]	1.72(3) [1.69(5)]	2.562(3) [2.572(4)]	155(3) [151(4)]
O(4)–H(41)···O(3′)	0.80(4) [0.79(3)]	1.98(4) [1.89(3)]	2.783(3) [2.678(3)]	172(4) [171(3)]
O(4)–H(42)···O(2″)	0.83(4) [0.84(4)]	1.85(4) [1.97(4)]	2.668(3) [2.779(3)]	174(3) [162(4)]

Primed atoms refer to the molecule in the following symmetry related positions.
The H-bonding geometrical parameters for complex **5** are in parentheses.
[a] For **4**: ′ $\frac{1}{2}-x, \frac{1}{2}+y, \frac{1}{2}-z$ and ″ $x-\frac{1}{2}, \frac{1}{2}-y, z-\frac{1}{2}$.
[b] For **5**: ′ $x, \frac{1}{2}-y, z-\frac{1}{2}$ and ″ $1-x, \frac{1}{2}+y, \frac{1}{2}-z$.

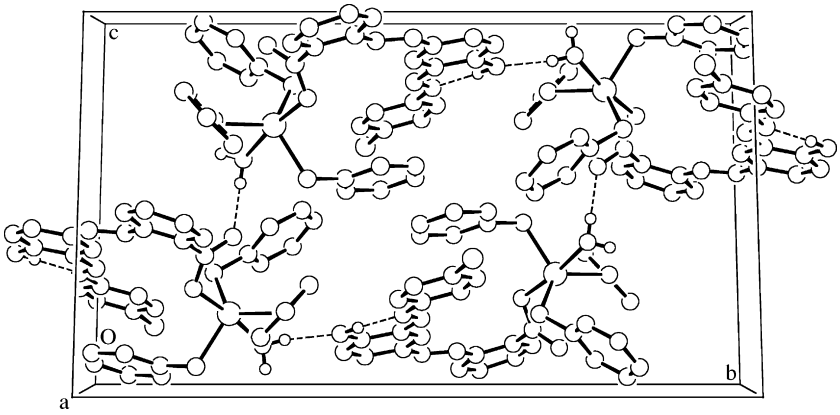

Fig. 5. The molecular packing of $Bz_3SnL^3H \cdot OH_2$ (**4**) showing the intra- and inter-molecular hydrogen bonding. The hydrogen bonding interactions are shown as dashed lines.

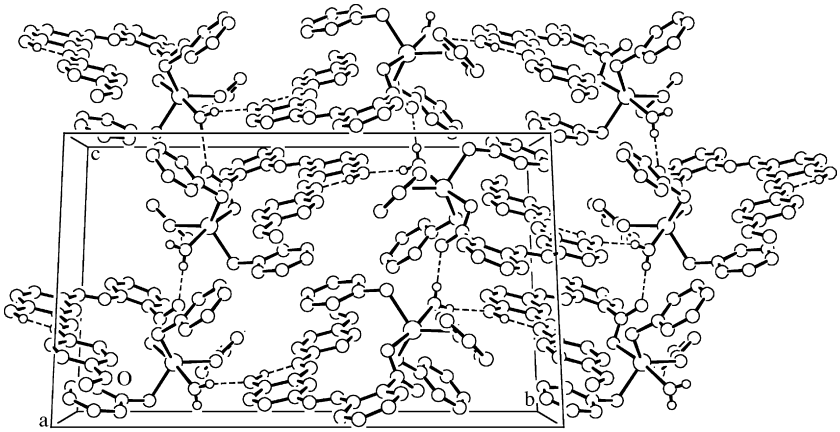

Fig. 6. The molecular packing of $Bz_3SnL^4H \cdot OH_2$ (**5**) showing the intra- and inter-molecular hydrogen bonding. The hydrogen bonding interactions are shown as dashed lines.

latter interaction links the molecules into extended chains which can be described by a graph set motif of C(4) and which run parallel to the [1 0 1] direction in **4** and the [0 0 1] direction in **5**. Together, the intermolecular interactions link the molecules into two-dimensional networks. In the case of **4**, these networks lie parallel to the $(10\bar{1})$ plane (Fig. 5), while in **5**, they lie parallel to the (1 0 0) plane (Fig. 6).

Acknowledgements

The financial support of the Department of Science & Technology, New Delhi, India (Grant No. SP/S1/IC-03/2005, T.S.B.B.) and National Institutes of Health Minority Biomedical Research Support Program, USA (Grant No. GM08005, G.E.) is gratefully acknowledged.

Appendix A. Supplementary material

CCDC-604414–CCDC-604415 contain the supplementary crystallographic data for complexes **4** and **5**, respectively. These data can be obtained free of charge from The Cambridge Crystallographic Data Centre via www.ccdc.cam.ac.uk/data_request/cif. Supplementary data associated with this article can be found, in the online version, at doi:10.1016/j.poly.2006.06.026.

References

[1] T.S. Basu Baul, K.S. Singh, M. Holčapek, R. Jirásko, E. Rivarola, A. Linden, J. Organomet. Chem. 690 (2005) 4232.
[2] A. Linden, T.S. Basu Baul, K.S. Singh, Acta Crystallogr., Sect. E 62 (2006) o2566.
[3] R.J. Butcher, T.S. Basu Baul, K.S. Singh, F.E. Smith, Acta Crystallogr., Sect. E 61 (2005) o1007.
[4] T.S. Basu Baul, K.S. Singh, X. Song, A. Zapata, G. Eng, A. Lyčka, A. Linden, J. Organomet. Chem. 689 (2004) 4702.
[5] T.S. Basu Baul, K.S. Singh, M. Holčapek, R. Jirásko, A. Linden, X. Song, A. Zapata, G. Eng, Appl. Organomet. Chem. 19 (2005) 935.
[6] A. Linden, T.S. Basu Baul, K.S. Singh, Acta Crystallogr., Sect. E 61 (2005) m2711.
[7] T.S. Basu Baul, W. Rynjah, K.S. Singh, C. Pellerito, P. D'Agati, L. Pellerito, Appl. Organomet. Chem. 19 (2005) 1189.
[8] K. Sisido, T. Takeda, J. Kinigawa, J. Am. Chem. Soc. 83 (1961) 538.
[9] T.S. Basu Baul, S.M. Pyke, K.K. Sarma, E.R.T. Tiekink, Main Group Met. Chem. 19 (1996) 807.
[10] R. Hooft, KappaCCD Collect Software, Nonius BV, Delft, The Netherlands, 1999.
[11] Z. Otwinowski, W. Minor, in: C.W. Carter, Jr., R.M. Sweet (Eds.), Methods in Enzymology, Macromolecular Crystallography, Part A, vol. 276, Academic Press, New York, 1997, pp. 307–326.
[12] R.H. Blessing, Acta Crystallogr., Sect A 51 (1995) 33.
[13] A. Altomare, G. Cascarano, C. Giacovazzo, A. Guagliardi, M.C. Burla, G. Polidori, M. Camalli, J. Appl. Crystallogr. 27 (1994) 435.
[14] G.M. Sheldrick, SHELXL 97, Program for the Refinement of Crystal Structures, University of Göttingen, Germany, 1997.
[15] T.S. Basu Baul, K.S. Singh, A. Lyčka, M. Holčapek, A. Linden, J. Organomet. Chem. 690 (2005) 1581.
[16] T.S. Basu Baul, E.R.T. Tiekink, Z. Kristallogr. NCS 212 (1997) 363.
[17] T.S. Basu Baul, S. Dhar, N. Kharbani, S.M. Pyke, R. Butcher, F.E. Smith, Main Group Met. Chem. 22 (1999) 413.
[18] T.S. Basu Baul, S. Dhar, S.M. Pyke, E.R.T. Tiekink, E. Rivarola, R. Butcher, F.E. Smith, J. Organomet. Chem. 633 (2001) 7.
[19] A. Lyčka, J. Jirman, A. Kolonicny, J. Holeček, J. Organomet. Chem. 333 (1987) 305.
[20] T.S. Basu Baul, C. Masharing, E. Rivarola, F.E. Smith, R. Butcher, Str. Chem. (in press).
[21] J.J. Zuckerman, in: F.G.A. Stone, R. West (Eds.), Advances in Organometallic Chemistry, vol. 9, Academic Press, New York, 1970, p. 21.
[22] A.G. Davies, P.J. Smith, in: G. Wilkinson, F.G.A. Stone, E.W. Abel (Eds.), Comprehensive Organometallic Chemistry, vol. 2, Pergamon Press, New York, NY, 1982, p. 519.
[23] R. Barbieri, F. Huber, L. Pellerito, G. Ruisi, A. Silvestri, in: P.J. Smith (Ed.), Chemistry of Tin: ^{119}Sn Mössbauer Studies on Tin Compounds, Blackie, London, 1998, pp. 496–540.
[24] T.S. Basu Baul, S. Dutta, E. Rivarola, R. Butcher, F.E. Smith, J. Organomet. Chem. 654 (2002) 100.
[25] G.M. Bancroft, R.H. Platt, Adv. Inorg. Chem. Radiochem. 15 (1972) 59.
[26] J. Bernstein, R.E. Davis, L. Shimoni, N.-L. Chang, Angew. Chem. 107 (1995) 1689.
[27] J. Bernstein, R.E. Davis, L. Shimoni, N.-L. Chang, Angew. Chem. Int. Ed. Engl. 34 (1995) 1555.

ligands (L) of the general formula Ln(β-diketonate)$_3$L, for which impressive photoluminescence properties have been demonstrated [18]. For the diketonate ligand, we have chosen 1,1,1,5,5,5-hexafluoro-2,4-pentanedionate (hfac) because of its low vibrational coupling with Eu(III) emission [9,19–21], enhanced thermal stability and volatility of the resulting lanthanide complexes when compared with its non-fluorinated analogs [22]. Our choice of ligand L is 2,4,6-tri(2-pyridyl)-1,3,5-triazine (tptz), a bulky aromatic compound featuring three 2-pyridyl rings fixed on a central 1,3,5-triazine platform [23]. Lanthanide complexes with tptz ligand have first been introduced by Durham et al. [24]. Recently a number of structurally characterized lanthanide complexes were reported [16,25–28], including the very first tptz adduct of a lanthanide β-diketonate reported by us [16]; tptz acts as a terdentate ligand in these structurally characterized complexes, coordinating the lanthanide ion with one of the three pyrazine N atoms and the N atoms on the *ortho*-substituted pyridyl groups. The remaining N atoms allow for further coordination to other metals, transition metals in particular [29]. Thus, structurally sophisticated multinuclear heterometallic complexes may be envisioned, whose magnetic and photophysical properties are of fundamental interest and practical significance.

By adopting a procedure used previously for the synthesis of Eu(dbm)$_3$(tptz) (dbm = dibenzoylmethanate) [16], in which a tptz complex with the starting $EuCl_3$ hydrate was prepared followed by the substitution of Cl^- for the diketonate ligands, an unexpected complex formulated as [Eu(hfac)$_2$(H_2O)(EtOH)(tptz)][$CF_3CO_2^-$] (**1**) was obtained. The complex planned for, Eu(hfac)$_3$(tptz) (**2**), was subsequently produced by using the more traditional route of making the hydrated lanthanide diketonate first, followed by the replacement of the aqua ligands by tptz. Here the synthesis, structural characterization by single-crystal X-ray diffraction, and photoluminescence studies of these two new Eu(III) complexes are reported (Scheme 1).

2. Experimental

$EuCl_3 \cdot 6H_2O$ (99.9%), 2,4,6-tri(2-pyridyl)-1,3,5-triazine (98%), 1,1,1,5,5,5-hexafluoro-2,4-pentanedione (98%), and potassium *tert*-butoxide (95%) were purchased from Aldrich and used without further purification. A slightly modified procedure for the recently reported Eu(dbm)$_3$(tptz) was adopted [16]. Elemental analysis (CHN) was performed by Numega Resonance Laboratory, San Diego, California.

2.1. Synthesis of [Eu(hfac)$_2$(H_2O)(EtOH)(tptz)][$CF_3CO_2^-$] (1)

A mixture of tptz (0.312 g, 1.00 mmol) and $EuCl_3 \cdot 6H_2O$ (0.366 g, 1.00 mmol) in 20 mL of absolute ethanol was stirred at 60 °C for 10 min to afford a clear solution. To this solution was added over 10 min a solution of $KOBu^t$ (0.336 g, 3.00 mmol) and Hhfac (0.624 g, 3.00 mmol) in 10 mL of absolute ethanol, and the resulting mixture was stirred at 60 °C for 1 h under nitrogen, and then at room temperature for 3 h. The mixture thus obtained was filtered, and the solid was washed with copious de-ionized water to remove KCl. The crude product was dissolved in acetone, and the solution was dried over anhydrous $MgSO_4$. The filtrate was collected, from which a pale yellow solid was obtained upon removal of the solvent. Recrystallization from ethanol:acetone (v/v 1:1) produced a crystalline solid as the analytically pure product (0.64 g, 61%). *Anal.* Calc.

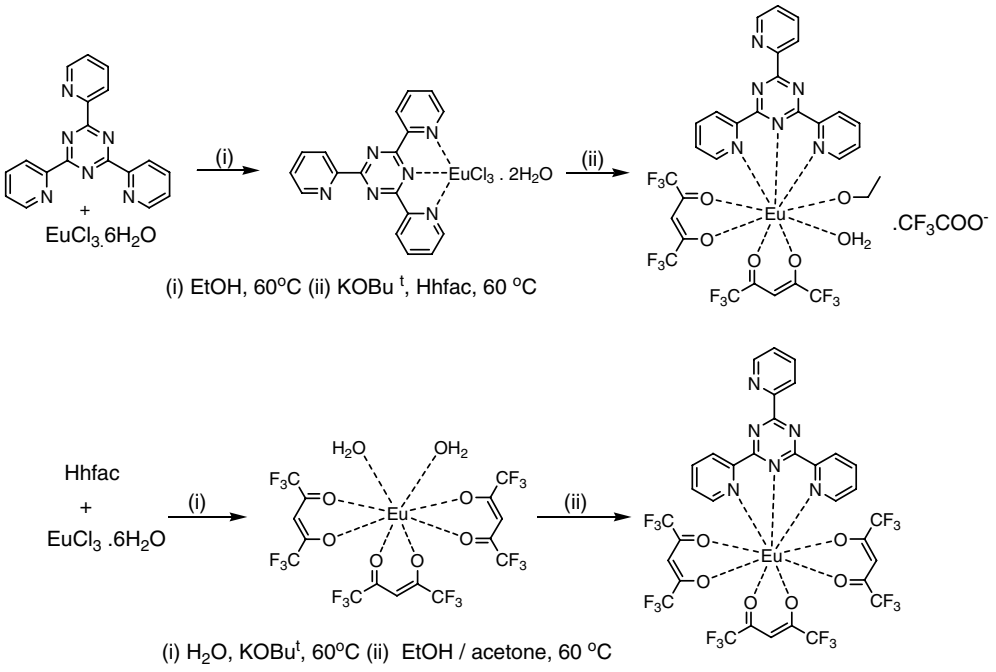

Scheme 1. Synthesis of [Eu(hfac)$_2$(H_2O)(EtOH)(tptz)][$CF_3CO_2^-$] (**1**) and Eu(hfac)$_3$(tptz) (**2**).

for $C_{32}H_{22}N_6O_8F_{15}Eu$: C, 36.41; H, 2.10; N, 7.96. Found: C, 36.33; H, 2.06; N, 8.09%.

2.2. Synthesis of Eu(hfac)$_3$(tptz) (2)

Using a modified literature [11], $Eu(hfac)_3(H_2O)_2$ was first prepared. Briefly, Hhfac (0.624 g, 3.0 mmol) was added to a solution of $KOBu^t$ (0.336 g, 3.0 mmol) in H_2O (10 mL). The resulting clear solution was stirred for 10 min at room temperature and then added to an aqueous solution of $EuCl_3 \cdot 6H_2O$ (0.366 g 1.0 mmol in 10 mL H_2O). The mixture was stirred at 60 °C for 30 min under nitrogen and then for 2.5 h at room temperature. The mixture was filtered, and the precipitate was washed with cold de-ionized water (2 × 100 mL) and dried under vacuum at room temperature for 12 hr. If necessary, the product can be recrystallized from acetone:ethanol (v/v 1:1).

To a solution of $Eu(hfac)_3(H_2O)_2$ (0.808 g, 1.0 mmol) in acetone (15 mL) was added tptz (0.312 g, 1.00 mmol) in ethanol (15 mL). The mixture was stirred at 60 °C for 0.5 h and then overnight at room temperature. The mixture was filtered, and the filtrate was allowed to evaporate at room temperature to afford analytically pure product (0.73 g, 67%). *Anal.* Calc. for $C_{33}H_{15}N_6O_6F_{18}Eu$: C, 36.52; H, 1.39; N, 7.74. Found: C, 36.65; H, 1.36; N, 7.80%.

2.3. X-ray structure determinations

Single crystals of both compounds suitable for X-ray diffraction studies were obtained by slow evaporation of their saturated solutions in ethanol:acetone (v/v 1:1) at room temperature over several days.

The crystals were mounted on a glass fiber in a random orientation and cooled to −93 °C in a stream of nitrogen gas controlled with Cryostream Controller 700. Data collection was performed on a Bruker SMART CCD 1000 X-ray diffractometer with graphite-monochromated Mo Kα radiation ($\lambda = 0.71073$ Å), operating at 50 kV and 30 mA over 2θ ranges of 2.58–50.00°. No significant decay was observed during the data collection.

Data were processed on a Pentium PC using the Bruker AXS Crystal Structure Analysis Package, Version 5.10 [30]. Neutral atom scattering factors were taken from Cromer and Waber [31]. The raw intensity data were integrated using the program SAINT-Plus and absorption corrections were applied using program SADABS. The structure was solved by direct methods. Full-matrix least-square refinements minimizing the function $\sum W(F_o^2 - F_c^2)$ were applied to the compound. All non-hydrogen atoms were refined anisotropically. All of the water hydrogen atoms and the hydroxyl hydrogen atoms were located gradually

Table 1
Crystal data and structure refinement for $[Eu(hfac)_2(H_2O)(EtOH)(tptz)][CF_3CO_2^-]$ (**1**) and $Eu(hfac)_3(tptz) \cdot EtOH$ (**2** · EtOH)

Crystal data	$[Eu(hfac)_2(H_2O)(EtOH)(tptz)][CF_3CO_2^-]$	$[Eu(hfac)_3(tptz)] \cdot EtOH$
Empirical formula	$C_{34}H_{30}EuF_{15}N_6O_{10}$	$C_{35}H_{21}EuF_{18}N_6O_7$
Formula weight	1119.60	1131.54
Temperature (K)	180(2)	180(2)
Crystal system	triclinic	triclinic
Space group	$P\bar{1}$	$P\bar{1}$
a (Å)	10.3854(15)	10.7819(14)
b (Å)	13.3089(18)	13.4118(17)
c (Å)	16.452(2)	14.8428(19)
α (°)	93.673(3)	98.559(2)
β (°)	104.942(2)	95.931(2)
γ (°)	103.719(2)	97.830(2)
Volume (Å^3)	2115.3(5)	2085.8(5)
Z	2	2
Density (calculated) (mg/m^3)	1.758	1.802
Absorption coefficient (mm^{-1})	1.610	1.638
$F(000)$	1108	1108
θ Range for data collection (°)	1.29–25.00	1.40–25.00
Index ranges	$-12 \leqslant h \leqslant 12$, $-15 \leqslant k \leqslant 15$, $-19 \leqslant l \leqslant 18$	$-12 \leqslant h \leqslant 12$, $-15 \leqslant k \leqslant 15$, $-17 \leqslant l \leqslant 17$
Reflections collected	12 200	12 328
Independent reflections [R_{int}]	7389 [0.0473]	7309 [0.0156]
Completeness to $\theta = 25.00°$ (%)	99.1	99.6
Maximum and minimum transmission	0.4642 and 0.3449	1.0000 and 0.8472
Refinement method	full-matrix least-squares on F^2	full-matrix least-squares on F^2
Data/restraints/parameters	7389/6/668	7309/0/664
Goodness-of-fit on F^2	1.052	1.034
Final R indices [$I > 2\sigma(I)$]	$R_1 = 0.0414$, $wR_2 = 0.1118$	$R_1 = 0.0298$, $wR_2 = 0.0829$
R indices (all data)	$R_1 = 0.0446$, $wR_2 = 0.1145$	$R_1 = 0.0325$, $wR_2 = 0.0850$
Largest difference peak and hole (e Å^{-3})	2.803 and −1.652	0.873 and −0.702

in difference Fourier map, while the rest hydrogen atoms were calculated, and their contributions were included in the structure factor calculations. Details on data collection and structure refinements are given in Table 1.

2.4. Photophysical studies

Electronic absorption spectra in dichloromethane solutions were recorded on a Perkin Elmer Lambda 10 spectrophotometer. Photoluminescence studies were carried out using a Fluorolog-3 fluorometer. The measured fluorescence in the visible range was excited by the light from a Xe-Arc lamp and detected with a photo multiplier tube at an angle of 90° to the incident beam. Photoluminescent quantum yields were measured and calculated using cresyl violet perchlorate ($\Phi = 0.54$ in methanol) [32] or rhodamin 6G (95% in ethanol) [33] as the standards. Corrections were made for the instrumental parameters and differing refractive indices of the solvents used [34,35]. The experimental uncertainty for the quantum efficiency calculations is 10%.

3. Results and discussion

Most of the lanthanide β-diketonates reported were synthesized either by an one-pot synthesis in which the lanthanide starting material, a β-diketone, and a selected neutral ligand are reacted in the presence of a suitable base or by first making the electrically neutral β-diketonate hydrates, followed by substitution of the aqua ligand(s) for neutral ligands of a different type [8,36]. However, adventitious hydrolysis producing unexpected lanthanide oxo/hydroxo complexes has been observed in both syntheses [37]. We noted recently that introducing the neutral Lewis base ligand prior to the introduction of the β-diketonate ligand is an effective approach to suppressing the formation of the hydrolysis products [16]. Subsequently, this procedure was utilized for the successful production of a number of tptz adducts with various lanthanide β-diketonates [17].

Surprisingly, when the same procedure was applied for the synthesis of $Eu(hfac)_3(tptz)$, a complex formulated as $[Eu(hfac)_2(H_2O)(EtOH)(tptz)][CF_3CO_2^-]$ (**1**) was instead isolated in good yield. Only two diketonate ligands are incorporated into the coordination sphere, although the initial molar ratios of Eu(III) to HFA is 1:3. Charge balancing is provided by $CF_3CO_2^-$ whose formation is also worth noting since it was not present in the starting materials. This *in situ* formation of $CF_3CO_2^-$ is not unprecedented; it has been observed by other researchers as the result of hfac decomposition via the reverse reaction of Claissen condensation, a process facilitated by a base in the presence of trace amount of water [38,39]. In the present case, the uncoordinated N atoms of tptz may serve as the base catalyst for the decomposition of the third HFA that is used for Eu(III) coordination.

The tptz adduct initially planned for, $Eu(hfac)_3(tptz)$ (**2**), was subsequently synthesized by using the more traditional approach. $EuCl_3 \cdot 6H_2O$ was reacted with three equivalents of Hhfac/base to form $Eu(hfac)_3(H_2O)_2$, whose aqua ligands were then substituted for tptz under mild conditions.

Both **1** and **2** are air-stable and readily soluble in solvents such as acetone, chloroform, and dichloromethane, but sparingly soluble in alcohols. Product purification was facile by recrystallization from a mixture of acetone and ethanol. Satisfactory microanalysis results (CHN) were obtained for both compounds.

The molecular structures of **1** and **2** · EtOH were established by single crystal X-ray diffraction, and are shown in Figs. 1 and 2, respectively. The Eu(III) of **1** is coordinated by two hfac, one tptz, one H_2O, and one EtOH, whereas the coordination of **2** features three hfac and one tptz ligands. In both cases, the coordination polyhedron may be best described as a distorted square antiprism monocapped by the middle coordinating N atom [N(1)]. For complex **1**, the charge-balancing $CF_3CO_2^-$ is hydrogen-

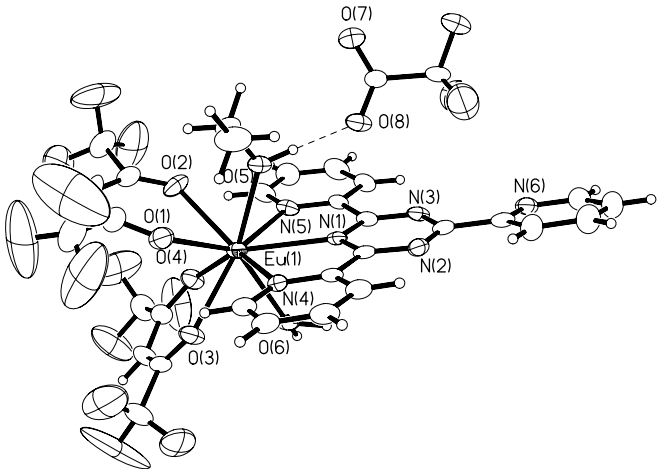

Fig. 1. An ORTEP view of the crystal structure of $[Eu(hfac)_2(H_2O)(EtOH)(tptz)][CF_3CO_2^-]$ (**1**). Thermal ellipsoids are drawn at the 50% probability level.

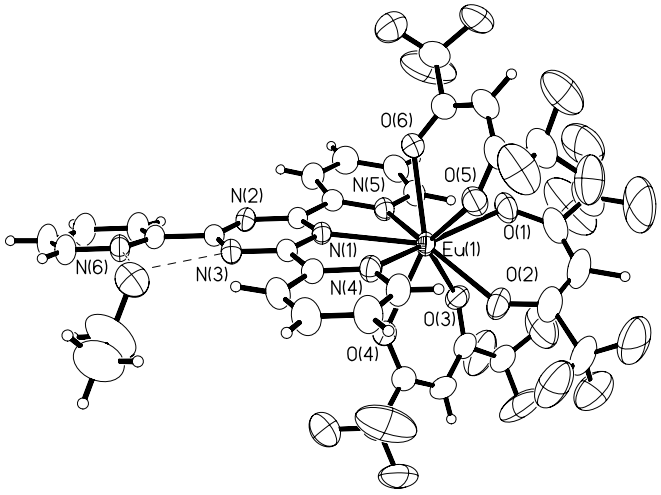

Fig. 2. An ORTEP view of the crystal structure of $Eu(hfac)_3(tptz) \cdot EtOH$ (**2**). Thermal ellipsoids are drawn at the 50% probability level.

bonded with the OH group of the Eu(III)-bound EtOH. For **2** · EtOH, there is a molecule of EtOH, hydrogen-bonded to the metal free N3 and N6 of the tptz ligand. The Eu–O(hfac) distances of **1** range from 2.390(3) Å to 2.450(3) Å, with an average of 2.420(8) Å. For **2** · EtOH, the corresponding values are from 2.354(2) Å to 2.503(2) Å, with an average of 2.411(4) Å. These distances are within the range reported for similar complexes [9,13,40,41]. The tptz ligand is nearly coplanar in both complexes. The Eu–N(1) bond distance is 2.534(3) Å and 2.539(2) Å for **1** and **2**, respectively. These values, indicated in bold face in Table 2, are the shortest of the three, consistent with the findings made with previously reported lanthanide-tptz complexes [16,25,28].

As compared with previously reported tptz adducts of europium β-diketonates, a number of structural features of **1** and **2** merit further discussions. The Eu–N1 distances [2.534(3) Å for **1** and 2.539(2) Å for **2**] are noticeably shorter than those of Eu(β-diketonate)$_3$(tptz). The corresponding values are 2.580(7) Å (tta, thinoyltrifluoroacetone), 2.607(3) Å (btfa, 4,4,4-trifluoro-1-phenyl-1,3-butanedione), 2.618(11) Å (ba, 1-benzoylacetone), and 2.676(2) Å (dbm, dibenzoylmethane) [16,17]. They are even shorter than those of Eu(tptz)Cl_3(MeOH)$_2$ [2.555(4) Å] and Eu(tptz)-$(NO_3)_3(H_2O)$ [2.576(2) Å] whose Eu(III) ions are situated in a less sterically congested environment [25,28]. This observation may be rationalized in terms of the electron withdrawing power of the fluorinated ligands; hfac is less reactive toward the Eu(III) center due to the relatively low electron density on its O atoms. As a result, the net positive charge of the lanthanide ion with hfac coordination is probably more than when non-fluorinate ligands are utilized. A corollary is that tptz ligand is more strongly bound to Eu(III) in the case of hfac coordination, resulting in a shorter Eu–N distance.

The preoccupation of part of the coordination sphere by the bulky tptz ligand in the synthesis of **1** may have prevented the coordination of three hfac ligands, particularly so if the relatively weak coordinating ability of the hfac ligand is considered. A similar observation was made in the synthesis of Yb(hfac)$_2$(NO_3)(terpy) (terpy = 2,2′:6′,2″-terpyridine) where Yb(III) ion is coordinated to two hfac ligands instead of three due to the preoccupation of the metal center by terpy, which has a similar steric bulk of coordination to that of tptz [42].

Table 2
Selected bond distances (Å) and angles (°) of [Eu(hfac)$_2$(H_2O)(EtOH)-(tptz)][$CF_3CO_2^-$] (**1**) and Eu(hfac)$_3$(tptz) · EtOH (**2** · EtOH)

[Eu(hfac)$_2$(H_2O)(EtOH)(tptz)][$CF_3CO_2^-$]		Eu(hfac)$_3$(tptz) · EtOH	
Eu(1)–O(1)	2.390(3)	Eu(1)–O(1)	2.354(2)
Eu(1)–O(2)	2.435(3)	Eu(1)–O(2)	2.374(2)
Eu(1)–O(3)	2.437(3)	Eu(1)–O(3)	2.503(2)
Eu(1)–O(4)	2.411(3)	Eu(1)–O(4)	2.392(2)
Eu(1)–O(5)	2.450(3)	Eu(1)–O(5)	2.438(2)
Eu(1)–O(6)	2.400(3)	Eu(1)–O(6)	2.406(2)
Eu(1)–N(1)	**2.534(3)**	**Eu(1)–N(1)**	**2.539(2)**
Eu(1)–N(4)	2.570(3)	Eu(1)–N(4)	2.581(3)
Eu(1)–N(5)	2.581(3)	Eu(1)–N(5)	2.576(3)
O(1)–Eu(1)–O(2)	69.92(11)	O(1)–Eu(1)–O(2)	74.83(9)
O(1)–Eu(1)–O(4)	101.00(11)	O(2)–Eu(1)–O(3)	72.57(8)
O(4)–Eu(1)–O(3)	69.96(10)	O(3)–Eu(1)–O(4)	67.79(8)
O(6)–Eu(1)–O(3)	69.85(10)	O(1)–Eu(1)–O(5)	75.57(8)
O(2)–Eu(1)–O(5)	73.56(11)	O(5)–Eu(1)–O(6)	69.00(8)
O(6)–Eu(1)–N(4)	82.63(10)	O(6)–Eu(1)–N(5)	67.84(8)
O(5)–Eu(1)–N(5)	81.34(11)	O(4)–Eu(1)–N(4)	67.41(8)
N(1)–Eu(1)–N(4)	63.64(10)	N(1)–Eu(1)–N(4)	62.87(8)
N(1)–Eu(1)–N(5)	62.73(10)	N(1)–Eu(1)–N(5)	63.20(8)
N(4)–Eu(1)–N(5)	126.34(10)	N(4)–Eu(1)–N(5)	126.03(8)

3.1. Electronic spectroscopic and photoluminescence studies

The electronic absorption spectra obtained for **2** and its ligands (Hhfac and tptz) in dichloromethane are shown in Fig. 3. Tptz shows absorption bands at 247 nm and 282 nm, whereas a strong absorption is shown at 275 nm for Hhfac. The spectrum of **2** (λ_{max} = 295 nm) contains essentially the combined ligand absorptions, but with slight red shifts due to metal complexation. Complex **1** displays almost identical ligand-based absorption in the range of 225–350 nm.

The electronic excitation and photoluminescence of **1** and **2** were studied in dichloromethane solution at room temperature, and they exhibit very similar properties. Only the spectra of **2** are shown in Fig. 4. The excitation spectrum resembles its absorption spectrum, confirming that the energy transfer occurs from the ligands to the Eu(III) ion. Five narrow emission peaks are observed in the range 570–715 nm, characteristic of Eu(III)-originated luminescence.

The photoluminescence quantum yields of **1** and **2** were determined to be 52% and 60%, respectively. The maximum excitation wavelength of the title complexes (295 nm) is very close to the maximum absorption wave-

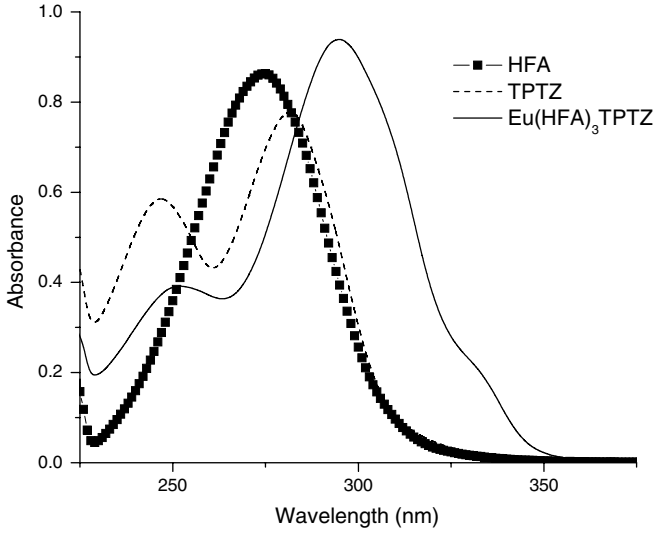

Fig. 3. Absorption spectra of Hhfac, tptz, and **2** in dichloromethane solution.

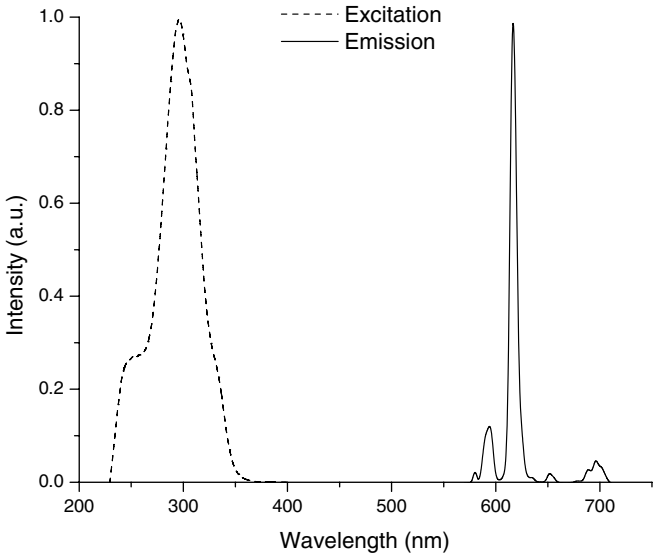

Fig. 4. Excitation (—) and emission (–) spectra of **2** in dichloromethane solution.

lengths of both Hhfac (275 nm) and tptz (282 nm). As such, both ligands are presumably responsible for the ligand-mediated energy transfer, resulting in effective population of the Eu(III) $^5D_0$ emissive state and high quantum yields of light emission. Thus, tptz ligand not only saturates the coordination sphere but also enhances the ligand-mediated energy transfer. This may be the reason why the quantum yield observed for **1** is still high despite the presence of luminescence–quenching water and ethanol ligands. In fact, the two complexes reported here possess the highest quantum yields among all the reported Eu(III)-hfac complexes, lending further support to the significant role(s) of tptz. In comparison, the photoluminescence quantum yields for $Eu(dbm)_3(tptz)$, $Eu(ba)_3(tptz)$, $Eu(tta)_3(tptz)$, and $Eu(btfa)_3(tptz)$ were found to be 17.4, 15.5, 40.2, and 69.7%, respectively [17]. In these cases, the energy transfer was believed to be mainly mediated by the β-diketonate ligands as the excitation wavelengths match the absorption spectra of the corresponding β-diketonate ligands. The comparably high values for $Eu(tta)_3(tptz)$ and $Eu(btfa)_3$-(tptz) may be the result of a better energy match between the ligand singlet and triplet excited states and/or a better energy match between the ligand triple excited state and the metal ion's resonance levels [7,14], with the tptz ligand providing additional advantages of site-protection.

4. Summary

Two new europium β-diketonates featuring 1,1,1,5,5,5-hexafluoro-2,4-pentanedionate and 2,4,6-tri(2-pyridyl)-1,3,5-triazine, a rigid neutral ligand were synthesized. These two complexes, formulated as $[Eu(hfac)_2(H_2O)(EtOH)(tptz)][CF_3CO_2^-]$ (**1**) and $Eu(hfac)_3(tptz)$ (**2**), were structurally characterized using single crystal X-ray diffraction. The difference in the composition and structure between these two complexes is caused by simply reversing the order of ligand (Hhfac and tptz) addition during the complex synthesis. Both complexes display bright photoluminescence characteristic of Eu(III) ion. Both ligands are believed to be responsible for the high quantum yields observed.

Acknowledgements

This work was supported by NSF CAREER Grant No. CHE-0238790. Acknowledgment is also made to the Donors of The Petroleum Research Fund, administered by the American Chemical Society, for partial support of this research. We thank Professor K. Miranda for the use of fluorometer. The CCD-based X-ray diffractometer was purchased through an NSF Grant (CHE-96103474, USA).

Appendix A. Supporting information available

Crystallographic data of $[Eu(hfac)_2(H_2O)(EtOH)(tptz)][CF_3CO_2^-]$ and $Eu(hfac)_3$ (tptz) · EtOH(CIF) have been deposited with the Cambridge Crystallographic Data Centre, CCDC 603042 and 603043. This material is available free of charge from the Director, CCDC, 12 Union Road, Cambridge CB2 1EZ, UK (fax: +44 1223 336033; email: deposit@ccdc.cam.ac.uk or http://www.ccdc.cam.ac.uk/deposit). Supplementary data associated with this article can be found, in the online version, at doi:10.1016/j.poly.2006.06.032.

References

[1] N. Sabbatini, M. Guardogi, J.M. Lehn, Coord. Chem. Rev. 123 (1993) 201.
[2] J.G. Bunzli, C. Piguet, Chem. Soc. Rev. 34 (2005) 1048.
[3] J. Kido, Y. Okamoto, Chem. Rev. 102 (2002) 2357.
[4] M.L. Bhaumik, M.A. EI-Sayed, J. Chem. Phys. 42 (1965) 787.
[5] S. Quici, M. Cavazzini, G. Marzanni, G. Accorsi, N. Armaroli, B. Ventura, F. Barigelletti, Inorg. Chem. 44 (2005) 529.
[6] F.S. Richardson, Chem. Rev. 82 (1982) 541.
[7] K. Binnemans, Rare-earth β-diketonates, in: K.A. GschneidnerJr., J.-C.G. Bünzli, V.K. Pecharsky (Eds.), Handbook on the Physics and Chemistry of Rare Earths, vol. 35, Elsevier B.V., 2005.
[8] L.R. Melby, N.J. Rose, E. Abramson, J.C. Caris, J. Am. Chem. Soc. 86 (1964) 5117.
[9] S. Kang, Y.S. Jung, Y.S. Sohn, Bull. Korean Chem. Soc. 18 (1997) 75.
[10] H.J. Batista, A.V.M. de Andrade, R.L. Longo, A.M. Simas, G.F. de Sa, N.K. Ito, L.C. Thompson, Inorg. Chem. 37 (1998) 3542.
[11] P.C. Christidis, I.O. Tossidis, D.G. Paschalidis, L.C. Tzavellas, Acta Crystallogr. Sect. C54 (1998) 1233.
[12] Z. Zheng, J. Wang, H. Liu, M.D. Carducci, N. Peyghambarian, G.E. Jabbourb, Acta Crystallogr. Sect. C58 (2002) m50.
[13] Y. Hasegawa, M. Yamamuro, Y. Wada, N. Kanehisa, Y. Kai, S. Yanagida, J. Phys. Chem. A 107 (2003) 1697.
[14] C.H. Huang, F.Y. Li, W. Huang, Introduction to Organic Light-Emitting Materials and Devices, Fudan Press, Shanghai, China, 2005 (chapter 8).
[15] R. Wang, R. Wang, J. Yang, Z. Zheng, M.D. Carducci, T. Cayou, N. Peyghambarian, G.E. Jabbour, J. Am. Chem. Soc. 123 (2001) 6179.

[16] C.R. De Silva, J. Wang, M.D. Carducci, S.A. Rajapakshe, Z. Zheng, Inorg. Chim. Acta 357 (2004) 630.
[17] C.R. De Silva, J.R. Maeyer, A. Dawson, Z. Zheng, Inorg. Chem. submitted to publication.
[18] Y. Hasegawa, H. Kawai, K. Nakamura, N. Yasuda, Y. Wada, S. Yanagida, J. Alloy Compd. 408 (2006) 669.
[19] L.J. Nugent, J.L. Burnett, R.D. Baybarz, G.K. Werner, S.P. Tanner, J.R. Tarrant, O.L. Keller, J. Phys. Chem. 73 (1969) 1540.
[20] G. Malandrino, M. Bettinelli, A. Speghini, I.L. Fragala, Eur. J. Inorg. Chem. (2001) 1039.
[21] S. Kang, Y.S. Jung, Y.S. Sohn, Bull. Korean Chem. Soc. 18 (1997) 266.
[22] J. Yu, L. Zhou, H. Zhang, Y. Zheng, H. Li, R. Deng, Z. Peng, Z. Li, Inorg. Chem. 44 (2005) 1611.
[23] G. Ionova, C. Raber, R. Guillaumont, S. Ionov, C. Madic, J.C. Krupa, D. Guillaneux, New J. Chem. 26 (2002) 234.
[24] D.A. Durham, G.H. Frost, F.A. Hart, J. Inorg. Nucl. Chem. 31 (1969) 571.
[25] R. Wietzke, M. Mazzanti, J. Latour, J. Pecaut, Inorg. Chem. 38 (1999) 3581.
[26] M.G.B. Drew, M.J. Hudson, P.B. Iverson, C. Madic, Acta Crystallogr. Sect. C 56 (2000) 434.
[27] G.Y.S. Chan, M.G.B. Drew, M.J. Hudson, N.S. Isaacs, P. Byers, Polyhedron 15 (1996) 3385.
[28] S.A. Cotton, V. Franckevicius, M.F. Mahon, L.L. Ooi, P.R. Raithby, S.J. Teat, Polyhedron 25 (2006) 1057.
[29] R. Zibaseresht, R.M. Hartshorn, Aust. J. Chem. 58 (2005) 345.
[30] Bruker AXS Crystal Structure Analysis Package, Version 5.10 (SMARTNT (Version 5.053), SAINT-Plus (Version 6.01), SHELXTL (Version 5.1)); Bruker AXS Inc., Madison, WI, 1999.
[31] D.T. Cromer, J.T. Waber, International Tables for Xray Crystallography, vol. 4, Kynoch Press, Birmingham, UK, 1974, Table 2.2 A.
[32] F.R.G. Silva, O.L. Malta, C. Reinhard, H. Gudel, C. Piguet, J.E. Moser, J. Bunzli, J. Phys. Chem. A 106 (2002) 1670.
[33] R.F. Kubin, A.N. Fletcher, J. Lumin. 27 (1982) 455.
[34] J.N. Demas, G.A. Crosby, J. Phys. Chem. 75 (1971) 991.
[35] J.V. Caspar, T.J. Meyer, J. Am. Chem. Soc. 105 (1983) 5583.
[36] J.A. Fernandes, R.A. Sa Fereira, M. Pillinger, L.D. Carlos, J. Jepsen, A. Hazell, P. Ribeiro-Claro, I.S. Goncalves, J. Lumin. 113 (2005) 50.
[37] R. Wang, D. Song, S. Wang, Chem. Commun. (2002) 368.
[38] S.R. Drake, A. Lyons, D.J. Otway, D.J. Williams, Inorg. Chem. 33 (1994) 1230.
[39] S. Wang, Z. Pang, K.D.L. Smith, Y. Hua, C. Deslippe, M.J. Wagner, Inorg. Chem. 34 (1995) 908.
[40] C. Benelli, A. Caneschi, A.C. Fabretti, D. Gatteschi, L. Pardi, Inorg. Chem. 29 (1990) 4153.
[41] W.J. Evans, D.G. Giarikos, M.A. Johnston, M.A. Greci, J.W. Ziller, J. Chem. Soc., Dalton Trans. (2002) 520.
[42] K. Hayashi, N. Nagao, K. Harada, M. Haga, Y. Fukuda, Chem. Lett. (1998) 1173.

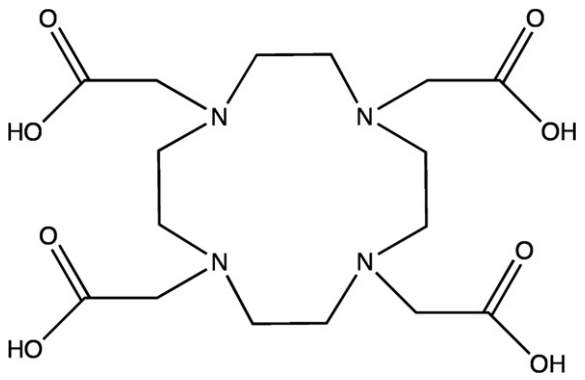

Fig. 1. 1,4,7,10-tetraazacyclo-dodecane-*N*,*N*′,*N*″,*N*‴-tetraacetic acid (DOTA). Note the pendant acetic acid 'arms'.

Innovative Technology Labmaster 100 Dry Box and standard Schlenk techniques. Gallium trichloride (99.9%), ammonium acetate and ethanol (chromatography grade) were purchased from Sigma. DOTA was purchased from Strem Chemicals (Toronto, Canada). Water was distilled and deionized to 18.6 MΩ using a Barnstead Diamond RO Reverse Osmosis machine coupled to a Barnstead Nano Diamond ultrapurification machine. An Agilent 1100 HPLC with manual injection and automated fraction collector was fitted with a Zorbax C_{18} analytical column for purification. Inductively Coupled Plasma (ICP) was conducted on a Perkin–Elmer ELAN 6100. Nuclear magnetic resonance was carried out on a Bruker 300 MHz machine. Electrospray mass spectrometry was performed on a Schimadzu LCMS-2010 A system at a cone voltage of 4.5 kV. Infrared spectra were recorded on a Nicolet Magna-IR 850 Series II spectrophotometer as KBr pellets.

2.1. Synthesis and characterization

0.12 g (0.68 mmol) of $GaCl_3$ was dissolved in 66.5 ml of 0.2 M ammonium acetate buffer (pH 5.0). To this solution was added a 55 ml solution of DOTA (0.68 mmol, (5 mg/ml)) in 0.2 M ammonium acetate buffer (pH 5.0). The resulting mixture was heated at 95 °C for 25 min. The volume was reduced in vacuo to approximately 10–15 ml. The solution was filtered (0.45 μM, Fisher) and then purified using reverse phase HPLC: (A) 100% for 5 min then (B) 100% for 10 min. (A) 0.2 M ammonium acetate (pH 5.0); (B) 100% ethanol. Complex **1** eluted with a retention time of $T_r = 7.81$ min. The retention time for uncomplexed DOTA under these conditions was noted as $T_r = 7.21$ min. A fivefold excess of ice-cold acetone was added to the combined Gallium-DOTA fractions and the solution filtered and allowed to stand at 4 °C. Colorless rod shaped crystals formed after ~24 h. ES-MS *m*/*z*: 470.85 ($M + H^+$), calculated 470.7 for $GaC_{16}H_{25}N_4O_8$. ^1H NMR (300 MHz, D_2O): δ 3.73–3.65(d), δ 3.44–3.31(d), δ 2.7(t), δ 2.24(s), δ 2.0(m). FTIR (KBr) 1734(s), 1700(s), 1684(m), 1653(s), 1636(s), 1559(s), 1540(s), 1521(m), 1506(s), 1457(m), 667(m), 564(w).

2.2. Determination of crystal structure

Structural measurements were performed on a Bruker-AXS SMART-CCD diffractometer at low temperature (90 K) using graphite-monochromated Mo Kα radiation ($\lambda_{Mo\ K\alpha} = 0.71073$Å). The structures were solved by direct methods. All non-hydrogen atoms were refined anistropically. After all of the non-hydrogen atoms were located, the model was refined against F^2, initially using isotropic and later anisotropic thermal displacement parameters.

Table 1
Selected bond lengths (Å) and angles (°) for **1**

Ga1–N1	2.112(4)	O5–Ga1–O1	85.29(13)
Ga1–N2	2.136(4)	O5–Ga1–N3	83.57(14)
Ga1–N3	2.111(4)	O1–Ga1–N3	168.01(13)
Ga1–N4	2.133(4)	O5–Ga1–N1	168.21(14)
Ga1–O5	1.929(3)	O1–Ga1–N1	83.70(14)
Ga1–O1	1.940(3)	O5–Ga1–N4	102.11(13)
O1–C10	1.297(5)	*Torsional angles*:	
O2–C10	1.223(6)	N1–N3–O2–O5	5.38
N1–C1	1.475(6)	O2–O6–N1–N3	2.37
N1–C9	1.491(5)	O7–O8–O1–O5	96.03

Table 2
Crystal data and structure refinement for *C*2*c*

Identification code	*C*2*c*
Empirical formula	$C_{16}H_{36}GaN_4O_{13.50}$
Formula weight	570.21
Temperature (K)	273(2)
Wavelength (Å)	0.71073
Crystal system	monoclinic
Space group	*c*2/*c*
Unit cell dimensions	
a (Å)	22.732(3)
b (Å)	16.015(2)
c (Å)	12.9708(19)
α (°)	90
β (°)	96.275(3)
γ (°)	90
Volume (Å^3)	4693.8(12)
Z	8
Density (calculated) (Mg/m^3)	1.614
Absorption coefficient (mm^{-1})	1.248
F(000)	2392
Crystal size (mm^3)	0.60 × 0.32 × 0.04
θ Range for data collection (°)	2.15–28.28
Index ranges	$-30 \leqslant h \leqslant 30$; $-21 \leqslant k \leqslant 21$; $-17 \leqslant l \leqslant 17$
Reflections collected	22375
Independent reflections (R_{int})	5806 (0.0781)
Completeness to θ = 28.28° (%)	99.3
Maximum and minimum transmission	0.9518 and 0.5213
Refinement method	full-matrix least-squares on F^2
Data/restraints/parameters	5806/0/323
Goodness-of-fit on F^2	1.053
Final *R* indices [$I > 2\sigma(I)$]	$R_1 = 0.0682$, $wR_2 = 0.1790$
R indices (all data)	$R_1 = 0.0759$, $wR_2 = 0.1829$
Largest difference in peak and hole (e Å^{-3})	1.425 and −0.599

Hydrogen atoms were introduced in calculated positions and refined isotropically. Lattice water hydrogens were not observed in the difference Fourier maps. Neutral atom scattering coefficients and anomalous dispersion corrections were taken from the *International Tables*, volume C. All calculations were performed using SHELXTL crystallographic software packages [8]. Selected bond lengths and angles are given in Table 1. Crystallographic details have been summarized in Table 2.

2.3. Thermogravimetric analysis (TGA)

Thermal analysis was performed on a TA instruments TGA Q500 using 5–11 mg samples placed on platinum pans and run under a nitrogen atmosphere (50 mL/min). The temperature was ramped from ~25 to 400 °C at a rate of 5 °C/min. Analysis was performed using the TA instruments Universal Analysis 2000 software program.

3. Results and discussion

3.1. Synthesis of 1

Complex **1** was obtained by reaction of stoichiometric equivalents of gallium chloride with the DOTA ligand in aqueous solution at acidic pH (pH 5) to prevent the formation and precipitation of $Ga(OH)_3$. Separation of the targeted compound from unreacted material or gallium impurities was achieved by HPLC with the new complex exhibiting a retention time of $T_r = 7.81$ min. Single crystals suitable for X-ray crystallography were obtained after purification by concentrating an aqueous solution of **1** in vacuo until initial precipitation was observed. Water was then added drop-wise with vigorous stirring until complete redissolution was observed. The solution was then filtered and ~five equivalents of ice-cold acetone, by volume, was added. Upon addition of the acetone, the borosilicate glass flask was sealed and placed at 4 °C. Suitable crystals, as colorless rods, were obtained after approximately 24 h. The presence of gallium in the crystals was determined prior to X-ray structure determination by removing and dissolving some of the crystals in water and performing ICP (data not shown) and electrospray mass spectrometry (Section 3.3; Figs. 4 and 5).

3.2. Structural characterization

The structure of **1** displaying an asymmetric unit and numbering scheme is shown in Fig. 2. It was solved in space group *C*2*c* with monoclinic symmetry. Selected bond lengths and angles are given in Table 1.

The gallium coordination sphere consists of a N_2O_4 donor set. The equatorial plane is composed of two DOTA nitrogens from the ring and two oxygens from the pendant carboxylate arms. The plane formed by the coordinated N_2O_2 set is slightly distorted with a torsional angle of 5.38°.

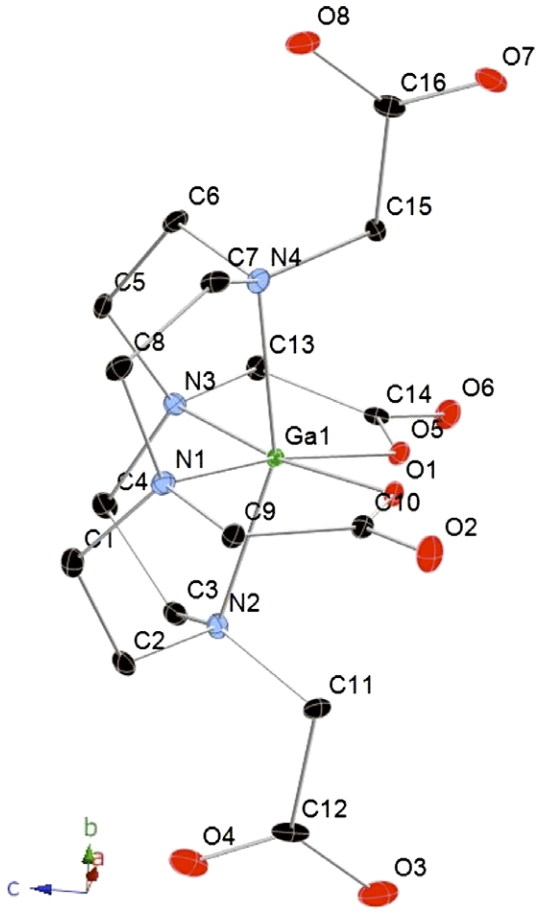

Fig. 2. ORTEP structure of **1** looking down the *a* axis. Hydrogen atoms and waters of crystallization have been omitted for clarity.

DOTA ring nitrogens complete the distorted octahedral geometry about the metal centre by occupying the axial positions. The distortion from perfect linearity predicted by a perfect octahedral geometry is best demonstrated by the angle created by the two axial nitrogens and gallium [N2–Ga1–N4] noted as 156.48°. Equatorial Ga–N bond lengths are also slightly shorter than those observed for the *trans* Ga–N bonds (Table 1). The gallium–oxygen bond lengths are shorter again at 1.940 Å [Ga1–O1] and 1.929 Å [Ga1–O5]. While two of the four-carboxylate 'arms' of the DOTA ligand are directly involved in metal coordination, the two remaining 'arms' are uncoordinated. One of the uncoordinated arms remains a carboxylic acid moiety and the hydrogen was assigned in the crystal structure [O3–H3 0.819 Å]. The angle produced by C12–O3–H3 is 109.4° consistent with the tetrahedral nature of a C–OH moiety. For the remaining carboxylic 'arm' a hydrogen atom could not be found and a deprotonated conjugate base is predicted. This serves to balance the charge of the trivalent gallium to leave an overall neutral complex and is consistent with a peptide modified DOTA structure described by Mäcke et al., where they also predicted the uncoordinated carboxylate to be deprotonated [9]. This arrangement is further corroborated by electrospray mass spectrometry conducted and described herein (Section 3.3).

Complex **1** packs to produce alternating ABAB layers of asymmetric units along the crystallographic *b* axis. The units align to optimize the arrangement of the 'dangling' carboxylate/carboxylic acid arms (see Fig. 3). Within each individual layer the pendant carboxylate moieties of each individual asymmetric unit are connected through intermolecular hydrogen bonding between the uncoordinated carboxylate groups to lattice water molecules to give a one-dimensional chain structure. In addition H-bonding between each AB layer is facilitated through intermolecular H-bonding with lattice water molecules producing an overall 2D supramolecular system such as we have described before for copper systems [10]. While lattice water hydrogen atoms were not found, oxygen–oxygen bond distances and angles characteristic of such contacts can infer H-bonding e.g. [O(4)···O(91w) 2.789 Å, O(8′)···O(91w) 2.720 Å, O(4)···O(91w)···O(8′) 130.76°] (Fig. 4) [11].

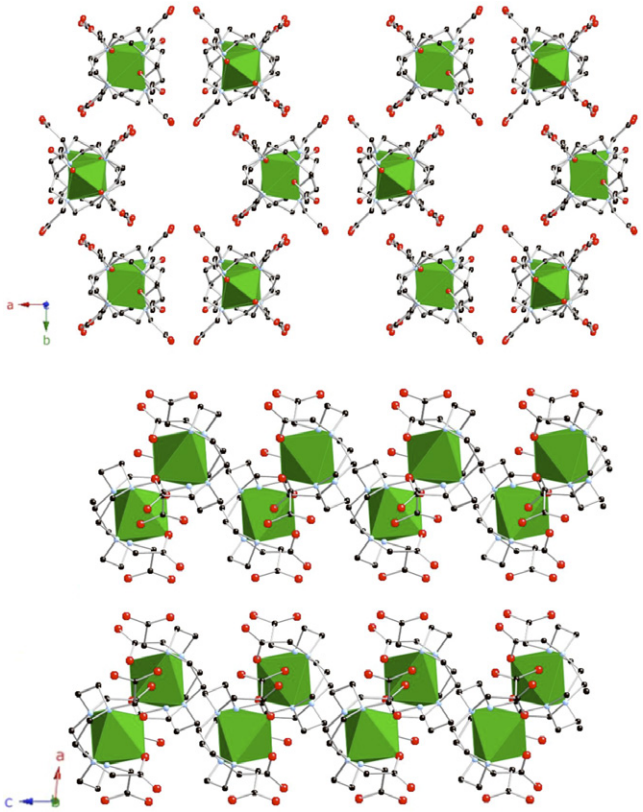

Fig. 3. (a) Packing of **1** looking down the *c* axis and (b) longing down the *b* axis. Lattice waters and hydrogen atoms removed for clarity.

3.3. Electrospray mass spectrometry

Electrospray mass spectrometry was conducted on an aqueous solution of redissolved crystals of **1** (Fig. 5). Briefly, crystals were removed using a Pasteur pipette and dried on filter paper. The crystals become powdered on standing and were then retrieved and redissolved in 18.6 MΩ water.

The data illustrates the presence of complex **1** in an aqueous environment and demonstrates that complex **1** can be isolated and redissolved without ionization. It also corroborates what is noted from the X-ray analysis, namely the formation of a resonance stabilized carboxylate species forming to balance charge and produce a neutral complex, as indicated by the fact that the electrospray indicates a formula containing 25 hydrogen atoms [$C_{16}H_{25}N_4O_8Ga$], consistent with the loss of three hydrogens from the DOTA ligand. This is as expected for a complex with DOTA given the predicted kinetic and thermodynamic stability of similar metal-DOTA complexes [4]. This stability is important if gallium is to be incorporated into anti-cancer or diagnostic bioconjugates to work in an aqueous environment.

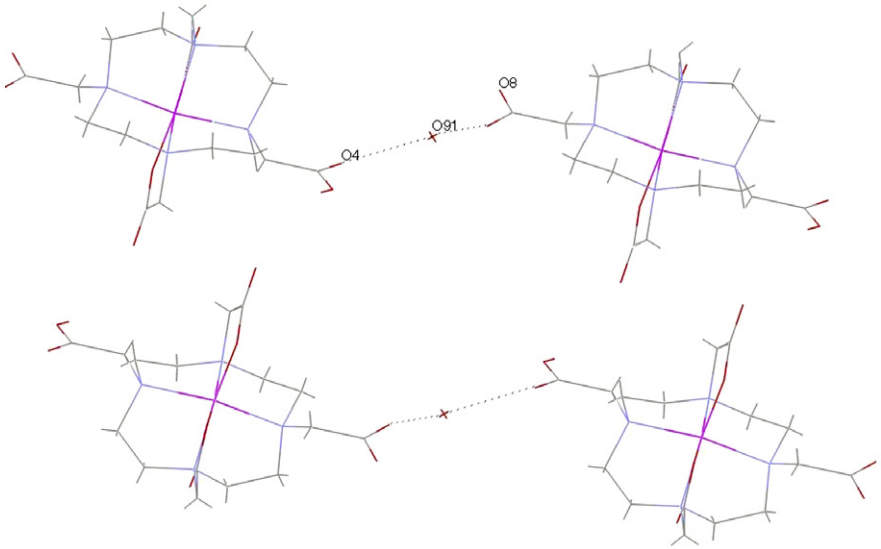

Fig. 4. Packing of **1** looking down the *c* axis indicating H-bonding between asymmetric units facilitated through lattice water molecules. Additional lattice waters omitted for clarity.

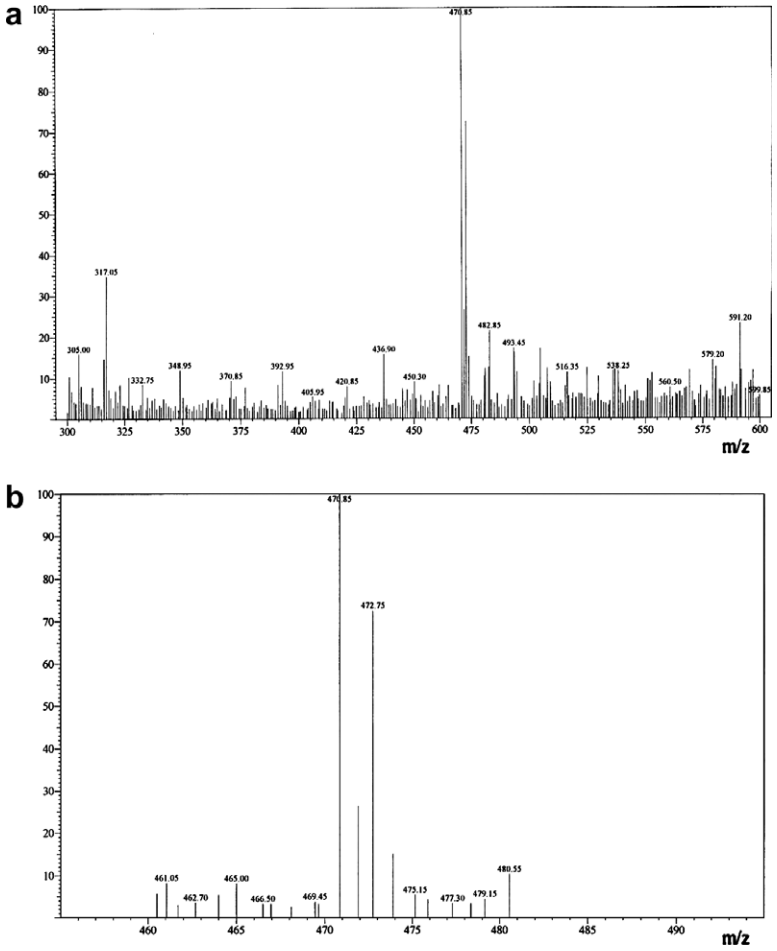

Fig. 5. Electrospray mass spectrum for **1**. (a) 300–600 m/z range and (b) 460–480 m/z range to show isotopic pattern. The theoretical isotopic pattern of 470 (100%): 471 (29.4 %): 472 (69.8): 473 (13.3 %) for **1** can be clearly observed.

3.4. Thermal properties of *1*

Complex **1** is stable in air at ambient temperature. TGA was carried out to examine the thermal stability of **1**. The samples were ramped from ~25 to 400 °C at a rate of 5 °C/min. The TGA curve can be seen in Fig. 6.

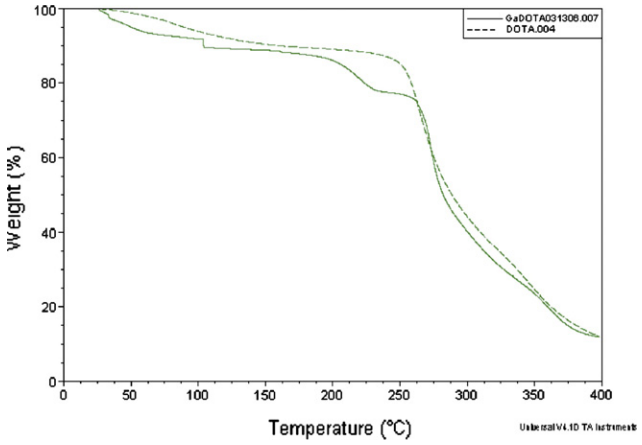

Fig. 6. TGA curve for **1** (solid line) and uncomplexed DOTA (dotted line). ICP was performed on a sample of **1** used to conduct TGA studies to confirm gallium prior to run.

There is no indication of there being any appreciably stable intermediate between the temperatures investigated. However, a slight inflection point at ca. 200 °C is evident and occurs after a mass loss of ~12.5% consistent with the departure of 7 waters of crystallization. The remainder of the trace is consistent with the loss of the remaining water molecules (presumably more extensively involved in hydrogen bonding within **1** consistent with the crystallography) and subsequent complex decomposition beginning at ~270 °C. This can be rationalized as the 'break-up' of the organic DOTA moiety. This is consistent with a TGA trace obtained for the uncomplexed DOTA ligand and indicates that complexation of the metal cation does not confer any greater thermal stability to DOTA.

4. Conclusions

We have successfully synthesized and characterized, both in solution and in the solid state, the Ga(III) chelate complex **1**. The species crystallizes with a high degree of hydration, which plays a role in H-bond interactions producing an ornate 2D supramolecular structure. Most importantly for our work is the fact that the complex is

stable in aqueous solution as indicated by electrospray mass spectrometry. This is vital if these systems are to be conjugated to delivery vectors and transported in vivo. We are currently extending our synthetic approach to look at ruthenium and rhenium complexes with DOTA and incorporation of these complexes into thiamin and folic acid based bioconjugates.

Acknowledgements

This work was supported by funds from Syracuse University. The authors wish to thank Colin Fuss at the Centre for Environmental Science and Engineering at Syracuse University for conducting the ICP experiments and Professor Karin Ruhlandt-Senge for use of a Innovative Technology Labmaster 100 Dry Box for weighing of the $GaCl_3$.

Appendix A. Supplementary material

Crystallographic data (CIF file) for complex **1** has been deposited with the Cambridge Crystallographic Data Centre, CCDC No. 606649. Copies of this information may be obtained free of charge from The Director, CCDC, 12 Union Road, Cambridge, CB2 1EZ, UK (fax + 44 1223 336 033; e-mail: deposit@ccdc.cam.ac.uk or via the internet www.ccdc.cam.ac.uk. Supplementary data associated with this article can be found, in the online version, at doi:10.1016/j.poly.2006.06.039.

References

[1] M.M. Hart, C.F. Smith, S.T. Yancey, R.H. Adamson, J. Natl. Cancer Inst. 47 (1971) 1121.
[2] (a) S.V. Govindan, R.B. Michel, G.L. Griffiths, D.M. Goldberg, M.J. Mattes, Nucl. Med. Biol. 32 (2005) 513;
(b) B. Desoize, Anticancer Res. 24 (2004) 1529;
(c) S. Jurisson, D. Berning, W. Jia, M. Da, Chem. Rev. 93 (1993) 1137;
(d) L.R. Bernstein, T. Tanner, C. Godfrey, B. Noll, Metal-Based Drugs 7 (2000) 33.
[3] M.A. Jakupec, B.K. Kepplar, Curr. Top. Med. Chem. 4 (2004) 1575.
[4] (a) Y.H. Jang, M. Blanco, S. Dasgupta, D.A. Keire, J.E. Shively, W.A. Goddard III, J. Am. Chem. Soc. 121 (1999) 6142;
(b) C. Waldherr, M. Pless, H.R. Maecke, T. Scumacher, A. Crazzolara, E.U. Nitzsche, A. Halsemann, J. Mueller-Brand, J. Nucl. Med. 43 (2002) 610;
(c) A. Otte, J. Mueller-Brand, S. Dellas, E.U. Nitzsche, R. Hermann, H.R. Maecke, Lancet 351 (1998) 417.
[5] C. Chapon, L. Lemaire, F. Franconi, L. Marescaux, P. Legras, B. Denizot, J-J. Le Jeune, Magn. Reson. Med. 52 (2004) 932.
[6] J. Chen, Z. Cheng, Y. Miao, S.S. Jurisson, T.P. Quinn, Cancer 94 (2002) 1196.
[7] H. Gari, G.L. Sieckman, T.J. Hoffman, N.K. Owen, D.G. Mazuru, L.R. Forte, W.A. Volkert, Bioconj. Chem. 13 (2002) 224.
[8] SHELXTL PC, version 6.1; Bruker-AXS Inc.: Madison, WI, 2002.
[9] A. Heppeler, S. Froidevauz, H.R. Mäcke, E. Jermann, M. Béhé, P. Powell, M. Hennig, Chem. Eur. J. 5 (1999) 1974.
[10] (a) R.P. Doyle, P.E. Kruger, B. Moubaraki, K.S. Murray, M. Nieuwenhuyzen, Dalton Trans. 22 (2003) 4230;
(b) R.P. Doyle, P.E. Kruger, M. Nieuwenhuyzen, Dalton Trans. 23 (2005) 3745.
[11] R.P. Doyle, M. Julve, F. Lloret, M. Nieuwenhuyzen, P.E. Kruger, Dalton Trans. 17 (2006) 2071.

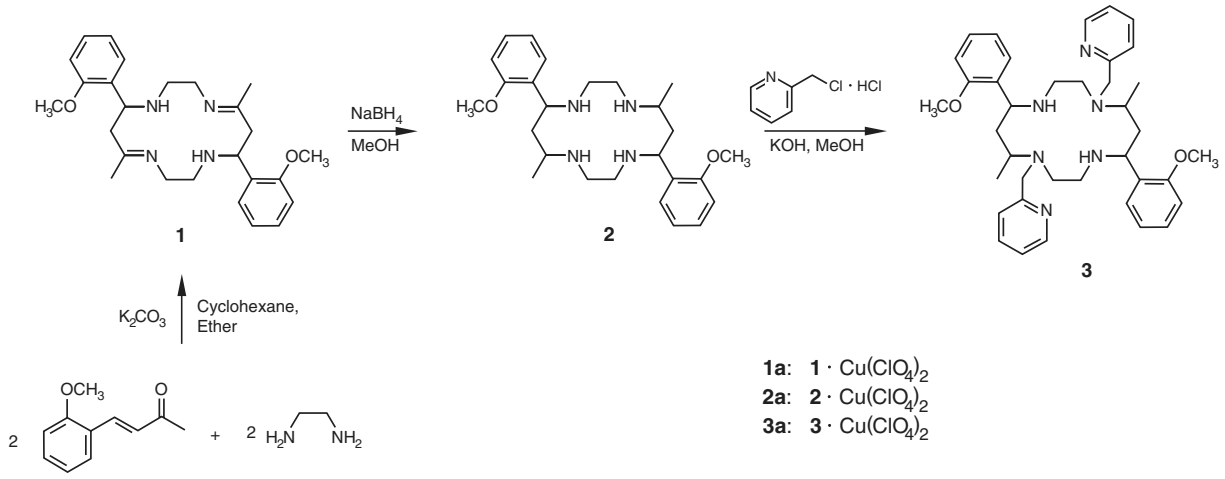

Scheme 1. Synthesis of the tetraaza macrocycles and specification of complexes studied.

N-linked 2-picolyl groups. Both, the crystal structures of all the uncomplexed macrocycles **1**–**3** and the respective Cu(II) complexes have been solved and comparatively discussed to reveal structural consequences on the coordination behavior. Thus, the present study will serve as a useful example of cyclam-type co-ordination chemistry being supplement to the known structures of related cyclams and cyclam complexes that differ in the absence of the methoxy substituents, respectively, anisyl pendants, or show other structural modifications [21–29].

2. Experimental

Caution: Although we did not encounter any problems, perchlorate salts of metal complexes containing organic ligands and solvents are potentially explosive and should be handled only in small quantities and with great caution!

2.1. General methods and materials

Melting points (uncorrected) were taken on a heating stage microscope (Rapido, Dresden). The IR spectrum (ν in cm^{-1}) was recorded on a Perkin–Elmer 1600 FT-IR instrument. NMR spectra (δ in ppm, J in Hz, Me_4Si as internal standard) were obtained with Bruker Avance DPX 400 (^1H: 400 MHz, ^{13}C: 100.6 MHz). The mass spectrum (ESI) was determined on a Hewlett–Packard HP 59987 A instrument.

Reactions were monitored by thin-layer chromatography (TLC) carried out on Merck silica gel 60 F254 coated plates. All reagents were commercial products and were utilized without further purification. The solvents used were purified or dried by common literature procedures [30].

2.2. Synthesis of the macrocycles

2-Methoxybenzylideneacetone was obtained from 2-methoxybenzaldehyde and acetone according to the literature [31].

2.2.1. 7,14-Bis(2-methoxyphenyl)-5,12-dimethyl-1,4,8,11-tetraazacyclotetradeca-5,12-diene (*1*)

Prepared from 2-methoxybenzylideneacetone and ethylenediamine with anhydrous potassium carbonate in cyclohexane–diethyl ether (1:2) following the literature procedure [27]. Recrystallization form chloroform–diethyl ether yielded 80% yellowish crystals; m.p. 144–145 °C (literature [32] m.p. 143–145 °C).

2.2.2. 7,14-Bis(2-methoxyphenyl)-5,12-dimethyl-1,4,8,11-tetraazacyclotetradecane (*2*)

Synthesized by treatment of **1** with $NaBH_4$ in dry ethanol and workup according to the literature [32] which yielded 92% colourless crystals; m.p. 197–198 °C (literature [32] m.p. 198–199 °C).

2.2.3. 4,11-Bis(2-pyridylmethyl)-7,14-bis(2-methoxyphenyl)-5,12-dimethyl-1,4,8,11-tetraazacyclotetradecane (*3*)

To a stirred solution of **2** (1.0 g, 2.43 mmol) and sodium hydroxide (0.44 g, 11.0 mmol) in water (20 cm^3) was added dropwise a solution of picolyl chloride hydrochloride in methylene chloride (20 cm^3). The mixture was stirred for 10 h at 25 °C. The organic phase was separated and the aqueous phase extracted with three 50 cm^3 portions of methylene chloride. The combined organic phases were evaporated under reduced pressure and the remaining oil crystallized from ethanol to give a colorless solid with m.p. 236–238 °C (yield: 82%). *Anal.* Calc. for $C_{38}H_{50}N_6O_2$ (FW = 622.85): C, 73.28; H, 8.09; N, 13.49. Found: C, 73.03; H, 8.19; N, 13.41%. IR (KBr): 3252, 2966, 2934, 2895, 2834, 2817, 1597 (s), 1588 (s), 1491 (s), 1472 (s), 1434 (s), 1364, 1274, 1237, 1135, 1084, 1050, 1029, 786, 766 (s), 756 (s) cm^{-1}. ^1H NMR ($CDCl_3$): $\delta = 0.96$ (s, 3H, CH_3), 0.98 (s, 3H, CH_3), 1.60–1.66 (m, 2H, C*H*–CH_3), 1.93 (b, 2H, NH), 2.29–2.90 (m, 12H, CH_2), 3.81 (s, 6H, OCH_3), 3.83 (m, 2H, NC*H*-Ar), 4.05 (s, 4H, CH_2-Ar), 6.86 (d, $J = 8.4$, 2H, Ar-H), 6.93 (m, 4H, Ar-H), 7.11 (d, $J = 6.8$, 2H, Ar-H), 7.20 (m, 2H, Ar-H), 7.59 (t,

$J = 3.6$, 2H, Ar-H),7.71 (d, $J = 7.2$, 2H, Ar-H), 8.47 (d, $J = 3.6$, 2H, Ar-H). ^{13}C NMR ($CDCl_3$): $\delta = 13.8$ (CH_3), 40.5, 44.6 (CH*C*H$_2$CH, N*C*H$_2$*C*H$_2$N), 54.0, 54.6 (*C*HCH$_3$, *C*HAr), 55.3 (OCH_3), 56.1 (N*C*H$_2$Ar), 110.4, 120.7, 121.6, 123.2, 127.2, 127.4, 132.6, 157.1, 161.4 (Ar). MS (ESI): $m/z = 622$ (M^+).

2.3. Preparation of the $Cu(ClO_4)_2$ complexes

To a stirred solution of the corresponding macrocycle (0.7 mmol) in methanol (20 cm^3) was added $Cu(ClO_4)_2 \cdot 6H_2O$ (0.26 g, 0.7 mmol). The precipitate which had formed during 4 h was collected, washed with methanol and dried under vacuum.

1 $\cdot$ *Cu(ClO$_4$)$_2$ (**1a**)*: violet crystals (yield: 91%). *Anal.* Calc. for $C_{26}H_{36}Cl_2CuN_4O_{10}$ (FW = 699.04): C, 44.67; H, 5.19; N, 8.01. Found: C, 44.41; H, 5.21; N 7.94%. MS(ESI): $m/z = 598$ [M − ClO$_4^-$].

2 $\cdot$ *Cu(ClO$_4$)$_2$ (**2a**)*: dark-pink crystals (yield: 93%). *Anal.* Calc. for $C_{26}H_{40}Cl_2CuN_4O_{10}$ (FW = 703.07): C, 44.42; H, 5.37; N, 7.97. Found: C, 44.22; H, 5.78; N 7.91%. MS(ESI): $m/z = 601$ [M − ClO$_4^-$].

3 $\cdot$ *Cu(ClO$_4$)$_2$ (**3a**)*: blue crystals (yield: 95%). *Anal.* Calc. for $C_{38}H_{50}Cl_2CuN_6O_{10}$ (FW = 885.03): calcd. C, 51.56; H, 5.69; N, 9.49. Found: C, 51.45; H, 5.72; N, 9.38%. MS(ESI): $m/z = 783$ [M − ClO$_4^-$].

2.4. X-ray crystallography

In a general procedure, the addition of $Cu(ClO_4)_2 \cdot 6H_2O$ to an equimolar solution of the respective ligand (**1**–**3**) in methanol yielded the complexes **1a**–**3a** as amorphous powders. Further crystallization from selected solvents produced crystals suitable for X-ray crystallographic analysis. Crystallographic data of the complexes and those of the free ligands are summarized in Table 1.

X-ray diffraction studies of **1**, **2**, **2a**, **3** $\cdot$ 2CHCl$_3$ and **3a** were carried out on a Bruker-AXS APEX2 diffractometer with a CCD area detector (Mo Kα; $\lambda = 0.71073$ Å, graphite monochromator): frames were collected at $T = 93$ K or 103 K with ω and ϕ rotation at 5 or 10 s per frame. The measured intensities were reduced to F^2 and corrected for absorption with SADABS (SAINT-NT [33]). Structure solution, refinement and data output were carried out with the SHELXTL program package [34]. All non-hydrogen atoms were refined anisotropically. With the exception of the amino hydrogens in the structures **3a**, **2** and **3** all other hydrogens were included in the models in calculated positions and were refined as constrained to bonding atoms. The X-ray diffraction data collection of **1a** were collected on a CAD4 diffractometer in the ω–2θ scan mode (Cu Kα; $\lambda = 1.5418$ Å, graphite monochromator). The SHELXS-97 program was applied for structure solution, while the SHELXL-97 was used for structure refinement [35]. All data were corrected for Lorentz and polarization effects.

3. Results and discussion

3.1. Synthesis

The macrocyclic **1** (Scheme 1) was synthesized via the cyclocondensation route [36] starting form 2-methoxybenzylideneacetone and ethylenediamine [32]. Subjection of **1** to a sodium borohydride reduction yielding the substituted cyclam **2** [32]. Reaction of **2** with picolyl chloride hydrochloride and sodium hydroxide gave the cyclam derivative **3**. The complexes **1a**, **2a** and **3a** were prepared from the respective macrocycles (**1**–**3**) with $Cu(ClO_4)_2 \cdot 6H_2O$ in methanolic solution.

3.2. X-ray structural study

In order to investigate, how complex formation mutually affects molecular conformations, we performed both crystal structure determination of the free macrocyclic ligands and their complexes with Cu(II) perchlorate.

Crystal data and selected experimental details are summarized in Table 1. Perspective views of the structures including the numbering schemes of relevant atoms are shown in Figs. 1, 3, 5, 7, 9 and 11. Packing illustrations are presented in Figs. 2, 4, 6, 8, 10 and 12. Geometric parameters of the co-ordinative interactions are given in Table 2.

3.2.1. Crystal structure of *1* and *1a* [*1* $\cdot$ *Cu(ClO$_4$)$_2$*]

The X-ray crystallographic analysis of the macrocyclic diimine **1** yields the orthorhombic space group $P2_12_12_1$. Obviously, under the chosen conditions of crystal growing spontaneous optical resolution occurs, so that a given crystal consists of molecules of the same absolute configuration, which is *R*,*R* or *S*,*S* at the chiral centers C(1) and C(6) (Fig. 1a). The mean planes of the two C-N=C–C ring fragments are oriented at an angle of nearly 50° to each other inducing a boat-like conformation which forces the two exocyclic methyl groups into a *syn*-diequatorial arrangement. The aromatic rings are inclined with an angle of 40.9° towards each other. Moreover, as illustrated by the space filling model (Fig. 1b), partial collapsing of the intramolecular cavity leaves only a small 'hole' of approximately 2.6×2.8 Å being defined by the four nitrogen atoms. The fact, that neither significant conventional hydrogen bonds [37] nor weak directional contacts like C–H$\cdots\pi$ [38,39] and $\pi\cdots\pi$ interactions [40,41] are found in the crystal structure suggests that the strongly bent and compact shape of the molecule follows close-packing requirements. Thus, the crystal packing of **1** (Fig. 2) is characterized by an intensive nesting of molecules with the methoxy substituents and the voids of adjacent molecules gearing together.

Crystallization of the complex **1a** from acetonitrile/H_2O yields violet crystals of the non-centrosymmetric space group *Pn*. Due to the presence of a glide plane, the crystal

Table 1
Crystallographic and structure refinement data of the compounds studied

Compound	**1**	**1a**	**2**	**2a**	**3**	**3a**
Empirical formula	$C_{26}H_{36}N_4O_2$	$C_{26}H_{36}N_4O_{10}CuCl_2$	$C_{26}H_{40}N_4O_2$	$C_{26}H_{40}N_4O_{10}CuCl_2$	$C_{26}H_{36}N_4O_2 \cdot 2CHCl_3$	$C_{38}H_{50}N_6O_{10}CuCl_2$
Formula weight	436.60	699.04	440.62	703.06	861.58	885.28
Crystal system	orthorhombic	monoclinic	monoclinic	monoclinic	triclinic	monoclinic
Space group	$P2_12_12_1$	Pn	$P2_1/n$	$P2_1/n$	$P\bar{1}$	$P2_1/n$
a (Å)	8.0569(3)	9.455(2)	7.5373(2)	17.8549(6)	8.6908(2)	8.9596(2)
b (Å)	13.2765(7)	13.833(2)	14.8712(5)	9.1070(3)	9.1665(3)	12.8072(2)
c (Å)	22.5701(8)	11.765(2)	11.1425(4)	19.5525(8)	13.6417(4)	16.7692(2)
α (°)	90.0	90.0	90.0	90.0	89.295(2)	90.0
β (°)	90.0	93.18(3)	99.931(2)	107.507(1)	75.642(1)	95.322(1)
γ (°)	90.0	90.0	90.0	90.0	87.870(1)	90.0
V (Å^3)	2414.27(18)	1536.4(5)	1230.23(7)	3032.06(19)	1052.08(5)	1915.93(8)
Z	4	2	2	4	1	2
F(000)	952	726	480	1468	452	926
D_c (Mg m^{-3})	1.201	1.511	1.189	1.540	1.360	1.535
μ (mm^{-1})	0.077	0.945	0.076	0.958	0.451	0.777
Data collection						
Temperature (K)	93(2)	298(2)	103(2)	103(29)	93(2)	93(2)
Number of collected reflections	18134	3539	14433	36331	61353	40344
Within the θ-limit (°)	2.4–29.8	2.3–27.0	2.7–28.5	1.4–29.5	2.2–40.5	2.4–31.9
Index ranges $\pm h$, $\pm k$, $\pm l$	−11/9, −16/17, −31/31	0/12, 0/17, −15/14	−5/10, −19/19, −14/13	−24/13, −11/12, −25/27	−15/15, −16/16, −24/24	−13/13, −19/18, −23/24
Number of unique reflections	6480	3539	3076	8367	13414	6544
R_{int}	0.0738	0.0000	0.0439	0.0450	0.0263	0.0342
Refinement calculations	full-matrix least-squares on F^2 values	full-matrix least-squares on F^2 values	full-matrix least-squares on F^2 values	full-matrix least-squares on F^2 values	full-matrix least-squares on F^2 values	full-matrix least-squares on F^2 values
Weighting expression w[a]	$[\sigma^2(F_o^2) + (0.0490P)^2 + (0.0000P)^{-1}]$	$[\sigma^2(F_o^2) + (0.0967P)^2 + (0.0000P)^{-1}]$	$[\sigma^2(F_o^2) + (0.1000P)^2 + (0.0000P)^{-1}]$	$[\sigma^2(F_o^2) + (0.1131P)^2 + (12.8379P)^{-1}]$	$[\sigma^2(F_o^2) + (0.0524P)^2 + (0.3052P)^{-1}]$	$[\sigma^2(F_o^2) + (0.0000P)^2 + (0.0000P)^{-1}]$
Number of refined parameters	293	401	163	443	252	265
Number of F values used [$I > 2\sigma(I)$]	4016	2003	2022	5302	10123	5529
Final R-indices						
$R(=\sum\|\Delta F\|/\sum\|F_o\|)$	0.0598	0.0617	0.0530	0.0785	0.0408	0.0419
wR on F^2	0.1308	0.1708	0.1676	0.2299	0.1128	0.0739
S(=Goodness of fit on F^2)	1.014	0.984	1.031	0.992	0.984	0.956
Final $\Delta\rho_{max}/\Delta\rho_{min}$ (e Å^{-3})	0.23/−0.46	0.84/−0.53	0.45/−0.21	0.87/−0.96	1.282/−0.986	1.09/−0.94

[a] $P = (F_o^2 + 2F_c^2)/3$.

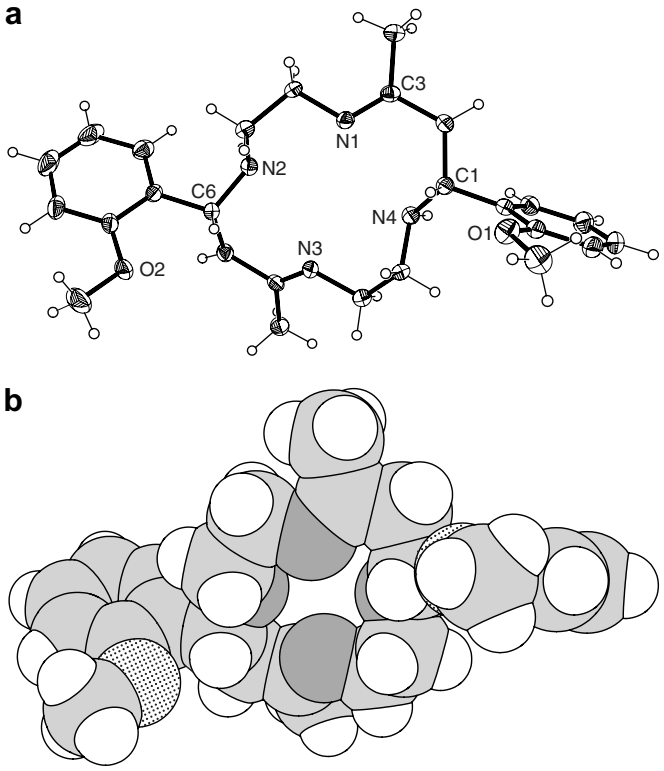

Fig. 1. (a) Molecular structure with atom labelling of relevant atoms and displacement ellipsoids at the 40% probability level and (b) space filling model of **1**.

Table 2
Structural parameters (distances/Å, angles/°) involving co-ordinative interactions of complexes **1a**, **2a** and **3a**

Atoms involved	**1a**	**2a**	**3a**
Cu(1)–N(1)	1.966(12)	2.015(4)	2.036(1)
Cu(1)–N(2)	1.975(11)	2.038(3)	2.106(1)
Cu(1)–N(3)	2.032(10)		2.517(1)
Cu(1)–N(4)	1.979(11)		
Cu(1)–O(1)	2.574(10)	2.562(3)	
Cu(1)–O(5)	2.976(11)		
Cu(2)–N(1A)		2.022(3)	
Cu(2)–N(2A)		2.029(3)	
Cu(2)–O(1A)		2.363(4)	
N(1)–Cu(1)–N(2)	94.7(5)	93.2(1)	86.5(1)
N(1)–Cu(1)–N(3)	175.8(6)		91.3(1)
N(2)–Cu(1)–N(4)	177.7(5)		
N(1)–Cu(1)–N(4)	85.7(4)		
N(2)–Cu(1)–N(3)	87.8(5)		78.5(1)
N(3)–Cu(1)–N(4)	91.7(4)		
O(1)–Cu(1)–O(5)	163.6(5)		
O(1)–Cu(1)–N(1)	88.2(5)		
O(1)–Cu(1)–N(2)	90.4(5)		
O(1)–Cu(1)–N(3)	95.2(4)		
O(1)–Cu(1)–N(4)	91.8(5)		
O(5)–Cu(1)–N(1)	71.5(5)		
O(5)–Cu(1)–N(2)	91.0(6)		
O(5)–Cu(1)–N(3)	105.1(4)		
O(5)–Cu(1)–N(4)	86.9(5)		
N(1A)–Cu(2)–N(2A)		88.5(1)	
O(1A)–Cu(2)–N(1A)		101.9(1)	
O(1A)–Cu(2)–N(2A)		89.8(1)	

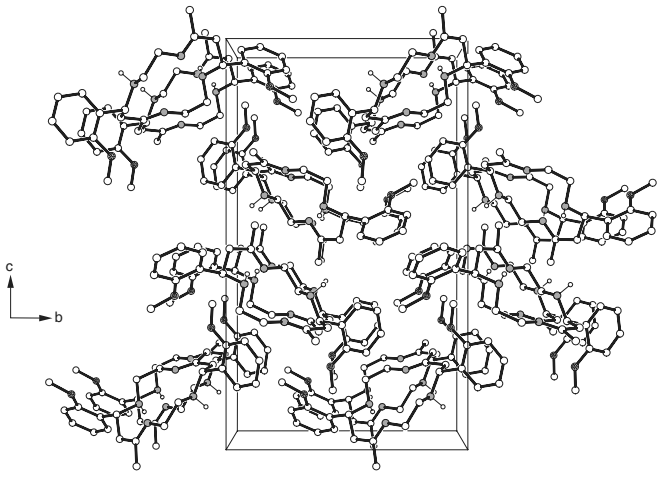

Fig. 2. Packing structure of **1** with carbon-bonded hydrogen atoms omitted.

consists of a racemic mixture of stereoisomers of the configuration *R*,*R* and *S*,*S* while the meso *R*,*S*-stereoisomer has not been found in the crystalline form. The amino hydrogens H(1′) and H(3′) of **1a** are located on one side of the macrocycle. Since they contact to the ether oxygens of the anisyl residues, their methoxy groups exhibit a *syn*-arrangement (Fig. 3). Another interesting structural feature of **1a** can be seen in the highly distorted coordination sphere of the copper ion, which is reflected by unequal Cu–O bond lengths and the O–Cu–O angle that deviates significantly from linearity (163.6°). The Cu–O distances of 2.574(10) and 2.976(11) Å also indicate rather weak coordination of the anions to the copper center. The Cu–N(sp^2) distances [1.975(11), 1.979(11) Å] and the Cu–N(sp^3) bond lengths [1.966(12), 2.032(10) Å] are in the same order of magnitude. The high degree of conformational distortion can be attributed to the different binding behavior of the two perchlorate anions. One of them is

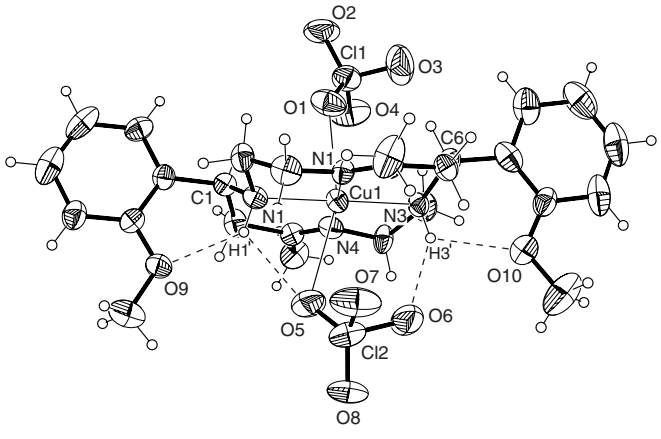

Fig. 3. Molecular structure of **1** · $Cu(ClO_4)_2$ with atom labelling of relevant atoms and displacement ellipsoids at the 40% probability level. Only one site of the disordered perchlorate ions is displayed. Broken lines represent hydrogen bond type contacts.

primarily associated to the ligand via intramolecular N–H···O contacts (O···H 2.243, 2.302 Å), while the other one is involved in intermolecular C–H···O hydrogen bonding (O···H 2.495, 2.664 Å) [42,43]. The crystal packing of **1a** is composed of molecular layers running parallel to the crystallographic B-plane (Fig. 4). They are held together by weak C–H···O hydrogen bond type contacts (O···H 2.49 Å) and π···π stacking interactions between the aromatic groups. The interlayer association is accomplished by the perchlorate ions that form weak interactions to arene and methylene hydrogens.

Previous papers have been published on metal complexes formed by the unsubstituted diphenyl analogue of **1** [21,29]. The crystal structure of the $Ni(ClO_4)_2$ complex [29], in which the diimine ligand has the same chirality as in **1a**, shows that the absence of the methoxy groups does not much effect the molecular conformation. On the other hand, the Ni(II) cation induces significant changes in coordination behavior compared to the Cu(II) in **1a**. Only one of the perchlorate ions occupies an axial position with both N–H groups oriented towards the opposite side of the NiN_4 plane, forming N–H···O hydrogen bonds to oxygen atoms of different perchlorate ions. Thus, a totally different molecular assembly within the crystal results.

3.2.2. Crystal structure of **2** and **2a** [**2** · $Cu(ClO_4)_2$]

The macrocyclic tetraamine **2** yields colorless crystals of the monoclinic space group $P2_1/n$ with two molecules within the unit cell. The torsion angles along the macroring are all ±*gauche* and *anti*. Although not all of them adopt idealized values (−66.0°, 175.4°, −175.2°, 69.6°, 168.3°, −168.8°, 72.8°), the macrocycle shows a regular, less strained conformation (Fig. 5). With the exception of the axial amino hydrogens H(2′), which for sterical reasons are not associated, all other strong donors and acceptors are involved in intramolecular hydrogen bonding. Two of the N–H bonds are directed towards the ring center, which opens the possibility of forming asymmetrical bifurcated hydrogen bonds [37] of the N–H···N type [N(1)–H(1′)···N(2) 2.32 Å, 135.0°; N(1)–H(1′)···N(2A) 2.57 Å, 110.7°], thus giving a cyclic four-membered hydrogen bond motif inside the macroring. As a consequence, van der Waals type interactions primarily contribute to the stabilization of the columnar packing mode of compound **2** (Fig. 6). Former investigations have shown that reduction of the unsubstituted diphenyl analogue of the diimine **1** yields the three possible stereo isomeric tetraazacyclotetradecanes in ca. 85:15:1 ratio [44,45]. The major product,

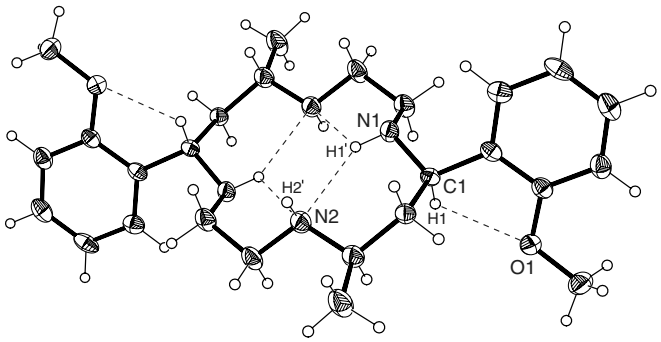

Fig. 5. Perspective view of **2** with numbering of relevant atoms and displacement ellipsoids at the 40% probability level. Broken lines represent hydrogen bond type contacts.

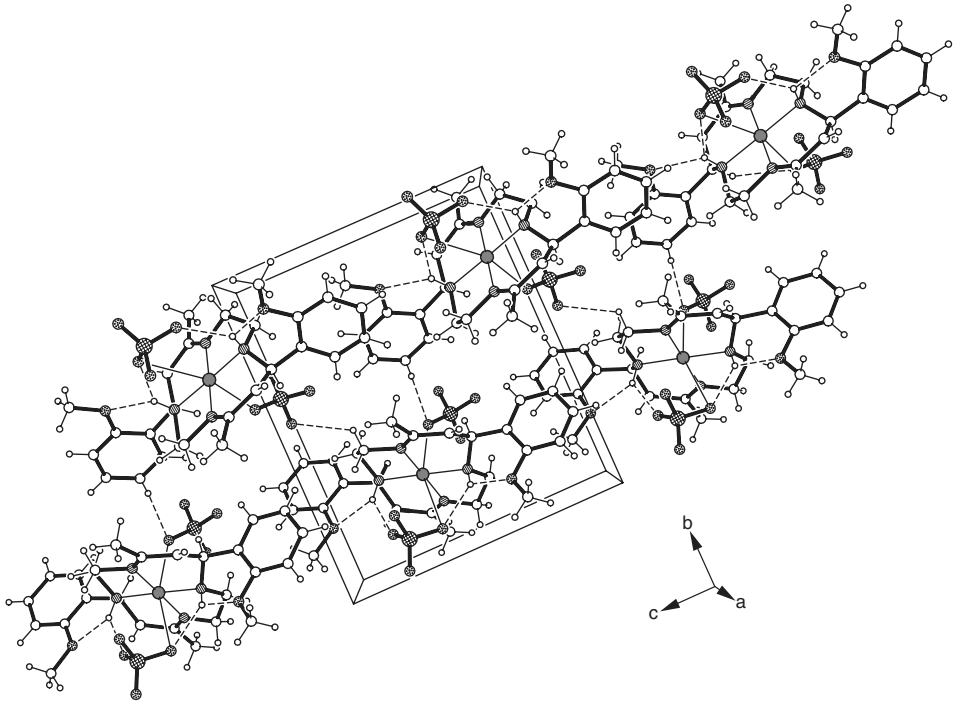

Fig. 4. Packing illustration of **1** · $Cu(ClO_4)_2$. Non-relevant hydrogen atoms are omitted for clarity.

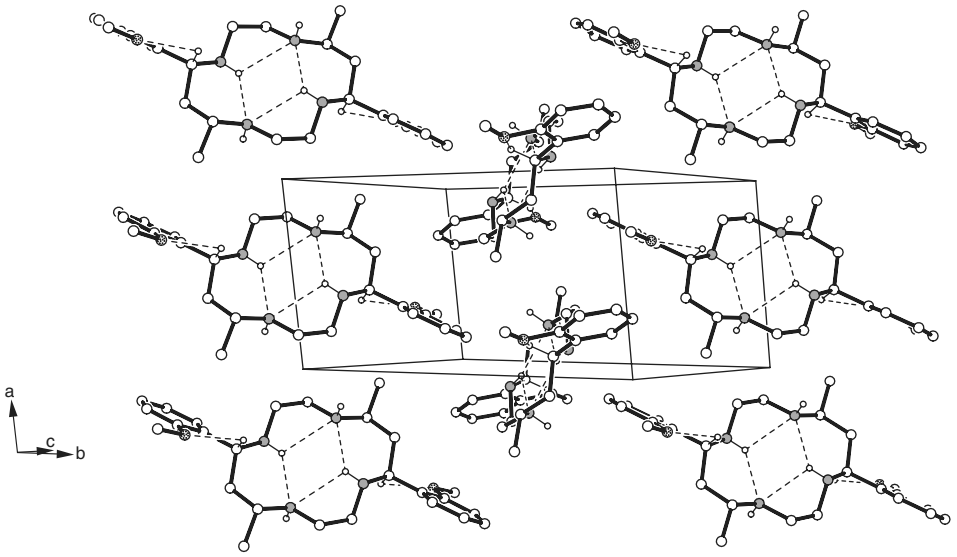

Fig. 6. Packing structure of **2**. Non-relevant hydrogen atoms are omitted for clarity.

which has been characterized by X-ray analysis [46] agrees with the configuration found for **2**.

Crystallization of complex **2a** from acetonitrile/H_2O yields crystals of the monoclinic space group $P2_1/c$ with two crystallographically independent halves of molecules in the asymmetric unit of the cell (Fig. 7), i.e. the copper atoms are located on crystallographic inversion centers (1/2, 1/2, 0 and 1, 0, 0). In both molecules, the anions are disordered over two sites. The Cu(II) exhibits an elongated octahedral coordination environment with the axial positions being occupied by one oxygen atom of each perchlorate ion. In one of the complexes, the Cu–O distance is rather long [2.562(3) Å] indicating only a weak binding, while in the second complex the respective bond is 2.363(4) Å. The Cu–N bond lengths [2.015(4)–2.038(3) Å] are within the expected range [7]. The six-membered chelate rings of the complex molecules adopt a distorted chair-like conformation with the anisyl and methyl substituents in equatorial positions, whereas the five-membered chelate rings are twisted. The aromatic units are arranged nearly perpendicular (88.4°, 86.7°) with respect to the CuN_4-plane. Although the independent molecules have similar conformations, they deviate in their mode of interactions. In molecule 1, the atom H(1′) forms an intramolecular bifurcated hydrogen bond [37] to the oxygens O(2) (2.245 Å) of the perchlorate anion and O(5) (2.225 Å) of

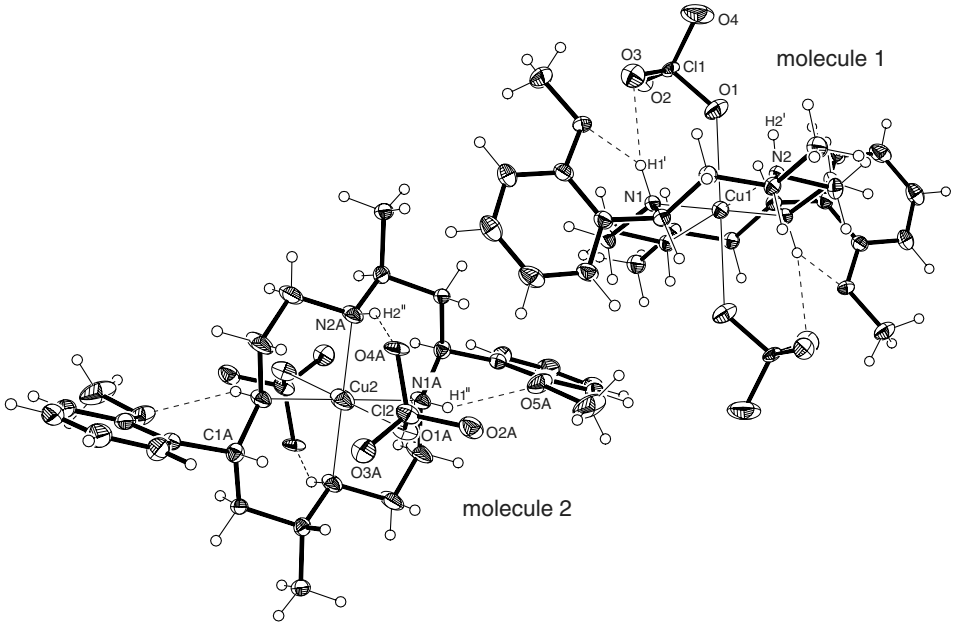

Fig. 7. Molecular structure of **2** · $Cu(ClO_4)_2$ with numbering of relevant atoms and displacement ellipsoids at the 40% probability level. Only one site of the disordered perchlorate ions is displayed. Broken lines represent hydrogen bond type contacts.

the anisyl group, while H(2′) remains free. In molecule 2, all amino hydrogens participate in intramolecular hydrogen bonding [H(1″)···O(1A) 2.284 Å, H(2″)···O(4A) 2.196 Å]. The packing of the crystals consists of infinite molecular chains extending in direction of the crystallographic *c*-axis (Fig. 8). Within these chains, the basal planes of consecutive molecules are titled to each other with an angle of 52.5° thus allowing formation of intermolecular C–H···O hydrogen bonds (O···H 2.200, 2.562 Å) between the anions and methyl groups of the ligands.

3.2.3. Crystal structure of $\mathbf{3}\cdot 2CHCl_3$ and **3a** [$\mathbf{3}\cdot Cu(ClO_4)_2$]

Crystals of compound **3**, suitable for diffraction experiments, could only be obtained as 1:2 (host:guest) solvent complex with chloroform (space group $P\bar{1}$). The unit cell of the crystal contains one complex entity (Fig. 9) with the solvent molecules associated via C–H···N hydrogen bond type interactions [42,43] with the pyridyl nitrogen [N(3)···H(1G) 2.37 Å]. Also in the present case, intramolecular contacts contribute to the molecular conformation. The hydrogen atom attached to N(2), the position of which could be gained from the difference electron density map, is directed towards the interior of the ring, and its well-defined N–H···N geometry suggests the existence of a weak hydrogen bridge to N(1) [N(2)–H(2′)···N(1) 2.25 Å, 137.7°]. The packing structure of the solvent complex of

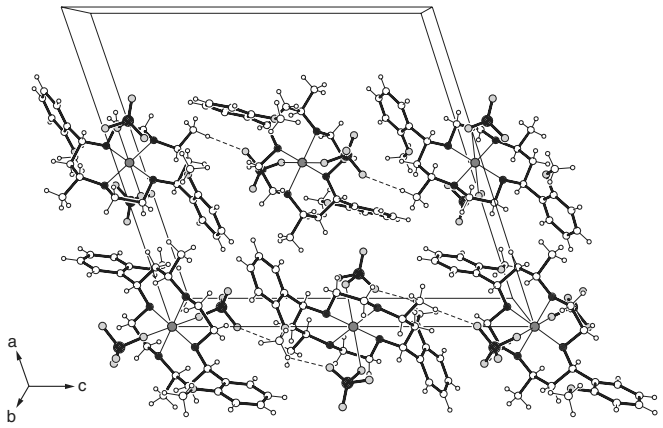

Fig. 8. Packing illustration of $\mathbf{2}\cdot(ClO_4)_2$.

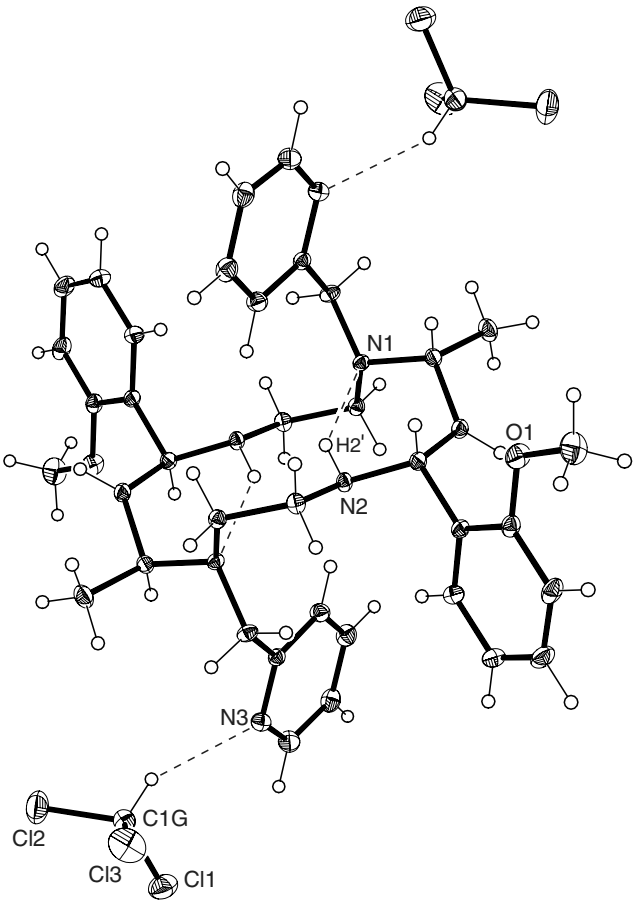

Fig. 9. Perspective view of the host–guest unit $\mathbf{3}\cdot CHCl_3$ (1:2) with numbering of relevant atoms and displacement ellipsoids at the 40% probability level. Hydrogen bond type contacts are displayed as broken lines.

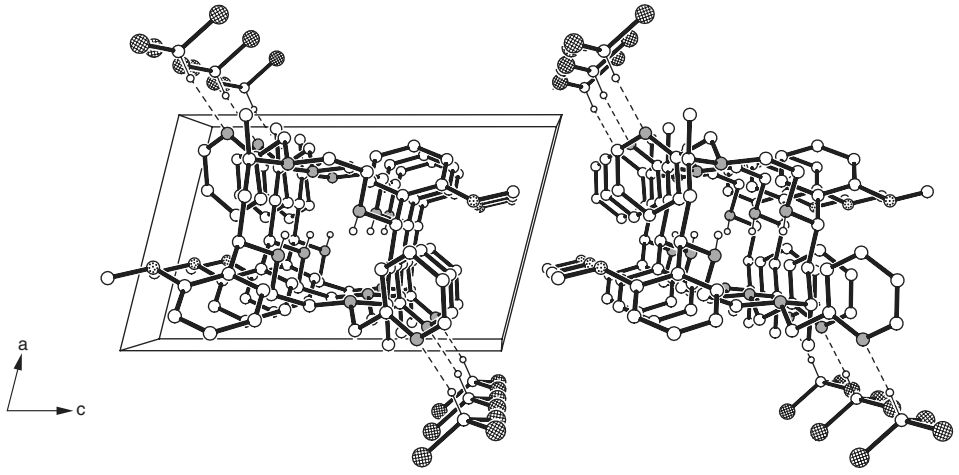

Fig. 10. Packing diagram of $\mathbf{3}\cdot CHCl_3$ (1:2). Non-relevant hydrogen atoms are omitted for clarity.

3 is composed of discrete **3** · $CHCl_3$ 1:2 aggregates stacked in a columnar array along the crystallographic *b*-axis (Fig. 10). Within the stacks, the host molecules are associated by aromatic edge-to-face (C–H···π) contacts [38,39] with the electron deficient pyridyl residues acting as donors and the electron-rich anisyl groups as hydrogen bond acceptors. The distance between the *para* C–H hydrogen of the pyridine and the ring centroid of the anisyl is 2.53 Å, while the C–H···centroid angle is 152.2°.

The Cu(II) complex **3a** yields blue crystals of the monoclinic space group $P2_1/n$ when crystallized from methanol. The asymmetric unit of the cell contains one half of the molecule with the copper atom located on the symmetry center 1/2, 1, 0. Different from structures **1a** and **2a**, the perchlorate ions of **3a** are not involved in complexation (Fig. 11). Instead, the nitrogen atoms of the two pyridylmethyl substituents occupy the apical sites of the octahedral coordination polyhedron. The axial Cu–N distances are 2.517(1) Å, whereas the equatorial Cu–N bonds are 2.036(1) and 2.106(1) Å. For steric reasons, the planes of the pyridyl residues are inclined at an angle of 54.3° with respect to the CuN_4 basal plane. Although rich in strong hydrogen bond acceptors, the anions show only poor association. Obviously, shielding of the amino hydrogens by the 2-picolyl units prevents effective hydrogen bonding to the counter ions. The same co-ordination behavior is also found in reported structures of copper(II) complexes having a similar pyridyl-substituted cyclam framework but differ in the mode of substitution [25–28]. It is also interesting to compare the structure of **3a** with the crystal structure of the copper(II) complex of the *N*-acetyl diphenyl substituted cyclam derivative reported previously [24]. In this structure, the charged carboxylate oxygens act as apical coordination sites of the *trans*-octahedral coordination environment of Cu(II). In addition, two ethanol molecules are hydrogen bonded to the two coordinated carboxyl oxygens thus preventing further intermolecular contacts.

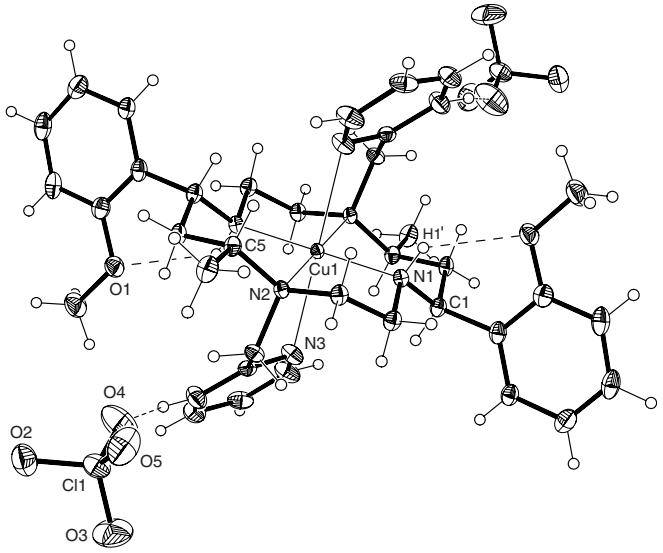

Fig. 11. Molecular structure of **3** · $Cu(ClO_4)_2$ with numbering of relevant atoms and displacement ellipsoids at the 40% probability level. Broken lines represent hydrogen bond type interactions.

The packing structure of **3a** is characterized by two-dimensional layers of complex cations which are stacked along the crystallographic *c*-axis (Fig. 12). The arrangement is stabilized by perchlorate ions, which fill the interstitial spaces between the layers and bridge the cations by weak C–H···O contacts (O···H 2.34–2.58 Å) [42,43]. Aromatic π···π interactions [40,41] are formed within the layers. The interacting aryl groups are displaced relative to each other, showing centroid–centroid distances of 4.50 Å for the phenyl rings and 4.30 Å for coordinated pyridyl

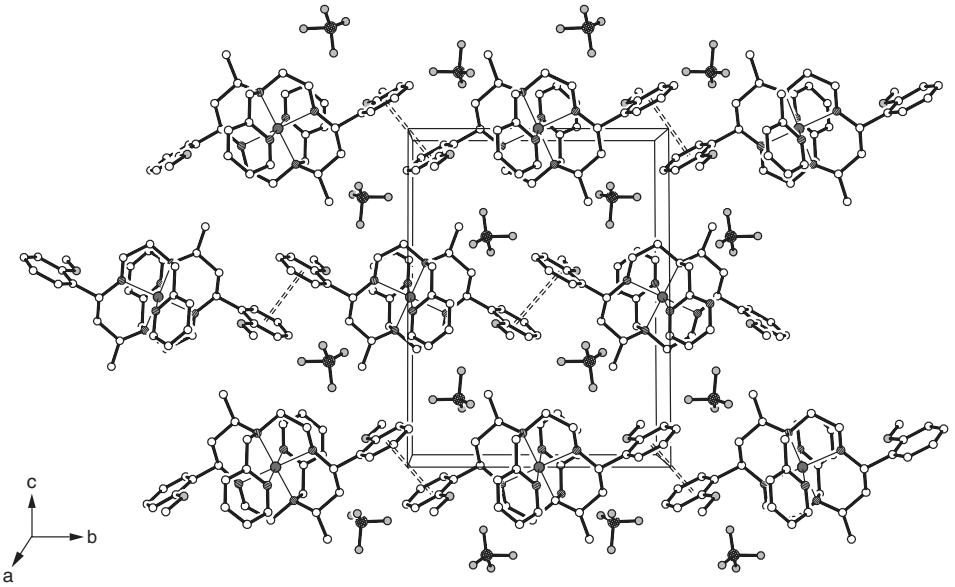

Fig. 12. Packing illustration of **3** · $Cu(ClO_4)_2$ with aromatic π–π interactions depicted as broken double lines. All hydrogen atoms are omitted for clarity.

fragments. Other types of non-covalent cation–cation interactions are not observed in the crystal.

4. Conclusion

A comparative structural study involving a designed series of cyclam type derivatives **1**–**3** that feature a different degree of saturation, and thus flexibility of the macroring, different number of functional appendages, and thus power of coordination, including their respective complexes with Cu(II) perchlorate has been reported.

X-ray crystal structures of the uncomplexed macrocycles **1**–**3** reveal that steric shielding caused by the ring substituents prevents the amino hydrogens from forming effective non-covalent bonding between molecules. Instead, these donors are either free or are used for intramolecular hydrogen bonding. The unsaturated diimine macrocycle **1** crystallizes in a non-centrosymmetric crystal structure. According to the given space group, a selected crystal contains molecules of the same absolute configuration and therefore is optically active. The strongly distorted geometry with a nearly complete collapsing of the macrocyclic cavity means that no intramolecular hydrogen bonds are present. In the case of **2**, two of the amino hydrogens are directed to the interior of the macrocycle giving a four-membered system of bifurcated hydrogen bonds, which is also found in crystal structures of related cyclam derivatives [22,23]. Intramolecular hydrogen bonding of the *N*-substituted macrocyclic ring is also found in the 1:2 inclusion compound of **3** with chloroform. However, only two bent N–H···N hydrogen bonds are present giving the molecule a pseudo-tricyclic structure.

In the complexes **1a**–**3a**, the metal center exhibits a more or less distorted octahedral coordination environment in which the four macroring nitrogens define the equatorial coordination sites of the polyhedron. Nevertheless, the ligand molecules show marked differences in their complexing behavior. The cyclam-based copper(II) complexes **2a** and **3a** show centrosymmetric molecular structures in the solid state. As expected, the apical coordination sites in **2a** are occupied by the oxygen atoms of two perchlorate anions [47]. A second oxygen of each anion forms an intramolecular N–H···O hydrogen bond to the complexed macroring. The presence of two *N*-substituted chelating pyridine containing pendants in the macrocycle **3** affects a different mode of coordination of the complex **3a** which is now of the CuN_6 type. As a result, its crystal structure consists of discrete complex cations and perchlorate anions which are cross-linked by weak C–H···O hydrogen bonds. The fact that the gross structure of **3a** corresponds to reported copper(II) complexes of related pyridyl-substituted cyclams [25–28] suggests rather robust conformational behavior of the macroring, including the pyridyl side arms, even in the presence of other potentially co-ordinating pendants such as the anisyl residues in **3a**, indicating particular co-ordinative interaction of this system. Similar to the uncomplexed diimine macroring **1**, the crystal structure of the respective complex **1a** has also an enantiomorphous configuration attributed to the *R*,*R* or *S*,*S* configuration at the chiral C atoms. Obviously, the reduced number of strong hydrogen bond donors, which is only half of those found in the complexes **2a** and **3a** and which determine the degree of cation–anion interactions, results in a less symmetric boat-like geometry of the complexed macrocycle.

Thus, only the pyridine containing pendants in **3a** proved effective in coordination of the metal ion while the uncomplexed macrocycle **3** yielded an inclusion compound with chloroform, also indicating a special ability relating to this series of compounds.

5. Supplementary data

Full details of the crystal structure analyses of **1**, **2**, **3**, **1a, 2a** and **3a** have been deposited with the Cambridge Crystallographic Data Centre (CCDC Nos. 288907–288909 and 288904–288906, respectively). Copies may be obtained free of charge on application to the Director, CCDC, 12 Union Road, Cambridge CB2 1EZ, UK [fax (int. code): +44 1223 336 033, e-mail: deposit@ccdc.cam.ac.uk].

Acknowledgements

We gratefully acknowledge financial support by the firms of Hoechst and Clariant, as well as the Fonds der Chemischen Industrie.

References

[1] J.L. Atwood, J.E.D. Davies, D.D. MacNicol, F. Vögtle (Eds.), Comprehensive Supramolecular Chemistry, vol. 1, Elsevier, Oxford, 1996.
[2] L.F. Lindoy, The Chemistry of Macrocyclic Ligand Complexes, Cambridge University Press, Cambridge, 1989.
[3] P.G. Potvin, J.M. Lehn, in: R.M. Izatt, J.J. Christensen (Eds.), Synthesis of Macrocycles – The Design of Selective Complexing Agents, Progress in Macrocyclic Chemistry, vol. 3, Wiley, New York, 1987, p. 167.
[4] A. Bianchi, K. Bowman-James, E. Garcia-Espana (Eds.), Supramolecular Chemistry of Anions, Wiley–VCH, Weinheim, 1997.
[5] K. Gloe (Ed.), Macrocyclic Chemistry, Springer, Dordrecht, 2005.
[6] W. Niu, E.H. Wong, G.R. Weisman, Y. Peng, C.J. Anderson, L.N. Zakharov, J.A. Golen, A.I. Rheingold, Eur. J. Inorg. Chem. (2004) 3310.
[7] T. Schönherr, E. Weber, W. Seichter, Z. Anorg. Allg. Chem. 627 (2001) 2420.
[8] R.I. Haines, Rev. Inorg. Chem. 21 (2002) 165.
[9] K.P. Wainwright, Coord. Chem. Rev. 166 (1997) 35.
[10] J. Costamagna, G. Ferraudi, B. Matsuhiro, M. Campos-Vallette, J. Canals, M. Villagráu, J. Vargas, M.J. Aguirre, Coord. Chem. Rev. 196 (2000) 125.
[11] B. Korybut-Daszkiewicz, J. Taraszewska, K. Zieba, A. Makal, K. Wozniak, Eur. J. Inorg. Chem. (2004) 3335.
[12] K.S. Miu, M.P. Suh, Chem. Eur. J. 7 (2001) 303.
[13] T. Schönherr, E. Weber, W. Seichter, J. Incl. Phenom. 50 (2004) 187.
[14] J.S. Bradshaw, K.E. Krakowiak, R.M. Izatt, Aza-Crown Macrocycles, Wiley, New York, 1993.
[15] E. Weber, in: J.L. Atwood, J.W. Steed (Eds.), Encyclopedia of Supramolecular Chemistry, Marcel Dekker, New York, 2004, p. 261.

[16] J.W. Steed, J.L. Atwood, Supramolecular Chemistry, Wiley, Chichester, 2000.
[17] E. Brucher, A.D. Sherry, in: A.E. Merbach, E. Toth (Eds.), The Chemistry of Contrast Agents in Medical Magnetic Resonance Imaging, Wiley, New York, 2001 (Chapter 6).
[18] J.W. Siebert, A.H. Cory, J.G. Cory, Chem. Commun. (2002) 154.
[19] X. Liang, J.A. Parkinson, M. Weishäupl, R.O. Gould, S.J. Paisey, H.-S. Park, T.M. Hunter, C.A. Blindauer, S. Parsons, P.J. Sadler, J. Am. Chem. Soc. 124 (2002) 9105.
[20] C. Saudan, V. Balzani, M. Gorka, S.-K. Lee, J. van Heyst, M. Maestri, P. Ceroni, V. Vicinelli, F. Vögtle, Chem. Eur. J. 10 (2004) 899.
[21] D.F. Cook, N.F. Curtis, R.W. Hay, J. Chem. Soc., Dalton Trans. (1973) 1160.
[22] P.W.R. Caulkett, D. Greatbanks, R.W. Turner, Heterocycles 9 (1978) 1003.
[23] Z. Urbanczyk-Lipkowska, J.W. Krajewski, P. Gluzinski, G.D. Andretti, G. Bocelli, Acta Crystallogr., Sect. B 37 (1981) 470.
[24] L. Chen, L.K. Thompson, J.N. Bridson, J. Xu, S. Ni, R. Guo, Can. J. Chem. 71 (1993) 1805.
[25] S.-G. Kang, S.-J. Kim, J.H. Jeong, Polyhedron 17 (1998) 3227.
[26] K.-Y. Choi, K.-M. Chun, I.-H. Suh, Polyhedron 18 (1999) 2811.
[27] K.-Y. Choi, H.-O. Lee, Y.-S. Kim, K.-M. Chun, K.-C. Lee, S.-N. Choi, C.-P. Hong, Y.-Y. Kim, Inorg. Chem. Commun. 5 (2000) 496.
[28] A.E. Goeta, J.A.K. Howard, D. Maffeo, H. Puschmann, J.A.G. Williams, D.S. Yufit, J. Chem. Soc., Dalton Trans. (2000) 1873.
[29] N.F. Curtis, D.C. Weatherburn, Acta Crystallogr., Sect. E 58 (2002) m423.
[30] J. Leonard, B. Lygo, G. Procter, Praxis der Organischen Chemie, Wiley–VCH, New York, 1996.
[31] I.M. Heilbron, J.S. Buck, J. Chem. Soc. (1921) 1509.
[32] K. Hideg, D. Lloydt, J. Chem. Soc., Sect. C (1971) 3441.
[33] Bruker Analytical X-ray Systems, SAINT-NT Version 6.0, 2003.
[34] Bruker Analytical X-ray Systems, SHELXTL-NT Version 6.10, 2000.
[35] G.M. Sheldrick, SHELX-97: Program for Crystal Structure Solution and Refinement, University of Göttingen, Göttingen, Germany, 1997.
[36] N.F. Curtis, Coord. Chem. Rev. 3 (1968) 3.
[37] G.A. Jeffrey, An Introduction to Hydrogen Bonding, Oxford University Press, Oxford, 1997.
[38] M. Nishio, M. Hirota, Y. Umezawa, The CH/π Interaction, Evidence, Nature, and Consequences, Wiley–VCH, New York, 1998.
[39] M. Nishio, CrystEngComm 6 (2004) 130.
[40] E.A. Meyer, R.K. Castellano, F. Diederich, Angew. Chem. 115 (2003) 1244.
[41] E.A. Meyer, R.K. Castellano, F. Diederich, Angew. Chem., Int. Ed. 42 (2001) 1210.
[42] G.R. Desiraju, T. Steiner, The Weak Hydrogen Bond, IUCr Monographs on Crystallography, vol. 9, Oxford University Press, Oxford, 1999.
[43] M. Nishio, in: J.L. Atwood, J.W. Steed (Eds.), Encyclopedia of Supramolecular Chemistry, Marcel Dekker, New York, 2004, p. 1576.
[44] D.F. Cook, Ph.D. Thesis, Victoria University of Wellington, Wellington, New Zealand, 1972.
[45] G. Ferguson, P. Roberts, D. Lloyd, K. Hideg, J. Chem. Soc., Chem. Commun. (1977) 149.
[46] G. Ferguson, P.J. Roberts, R.W. Hay, D.P. Liplani, J. Chem. Res. 314 (1978) 3734.
[47] M. Melnik, M. Kabesova, L. Macaskova, C.E. Holloway, J. Coord. Chem. 45 (1998) 31.

hydrophobic core have been shown to promote binding in aqueous environments.

Herein, we describe the synthesis and structure of mononuclear, octahedral zinc(II) complexes of the tetradentate DAHC derivative *cis*-3,5-*bis*[(2-pyridinyleneamin]-*trans*-hydroxycyclohexane (DDOP) [13], with both nitrate and triflate as anions. Complexation of a series of amino acid substrates with these complexes was examined using isothermal titration calorimetry, revealing that the nature of the counterion has an important influence not only upon the solid state supramolecular architecture, but also upon interactions with other molecules in solution.

2. Results and discussion

2.1. Ligand/complex design overview

DDOP is synthesised from DAHC by a simple Schiff base derivatisation using 2-pyridinecarbaldehyde [13], yielding a more highly pre-organised ligand with a tetradentate (or *bis*-bidentate) donor set. The aromatic rings increase the system's rigidity, strengthening the hand of the ligand and reducing the influence of anions, solvent and metal centres on the outcome of the complexation. Furthermore, they provide a hydrophobic surface capable of participating in π-stacking or other van der Waals interactions.

Despite the rigidity of the donor set, the conformational flexibility of the cyclohexane backbone gives this derivative two possible coordination modes depending upon the preferences of the metal centre (Scheme 1); either a dinucleating, *bis*-bidentate chelator with tetrahedral metal centres, or a tetradentate mononucleating coordination pocket for octahedral, square pyramidal or square planar centres. In the mononuclear case, coordination of an octahedral metal centre leaves two vacant coordination sites which may be filled by solvent molecules, counterions or other co-ligands. In this way, the use of various anions and solvents may influence the shape, hydrogen bonding and packing properties of the complex, or allow bridging to form multinuclear aggregates; while the hydrophobic environment around the zinc centre may encourage substrate binding in aqueous environments.

2.2. Synthesis and crystal structure

Complexes **1** and **2** were synthesised in high yields by simply mixing the ligand with a small excess of the appropriate zinc(II) salt in methanol, and crystallising by slow diffusion of diethyl ether into the methanolic solution. Predictably, the highly preorganised nature of the tetradentate coordination pocket resulted in similar mononuclear complex cations. Interestingly, however, there is one significant difference between the two complexes. In **1**, the water ligand is arranged *anti* to the DDOP alcohol group, whereas in **2** it is arranged *syn* (Fig. 1).

In most other respects, the geometries of the two complexes are highly similar. Both show a slight opening of the ligand "arms" away from a parallel orientation, as demonstrated by a large N–Zn–N angle between the pyridyl nitrogens, and a smaller angle between the imine nitrogens (Table 1). Significantly shorter bond lengths show that axial ligation is stronger to the softer water O-donor than to the harder anions, with this effect being more pronounced in the triflate complex, **2**, and both complexes have an O–Zn–O angle that deviates from the ideal 180°. However, in **2** the equatorial Zn–N bond lengths are slightly longer than in 1, while Zn–O distances are shorter.

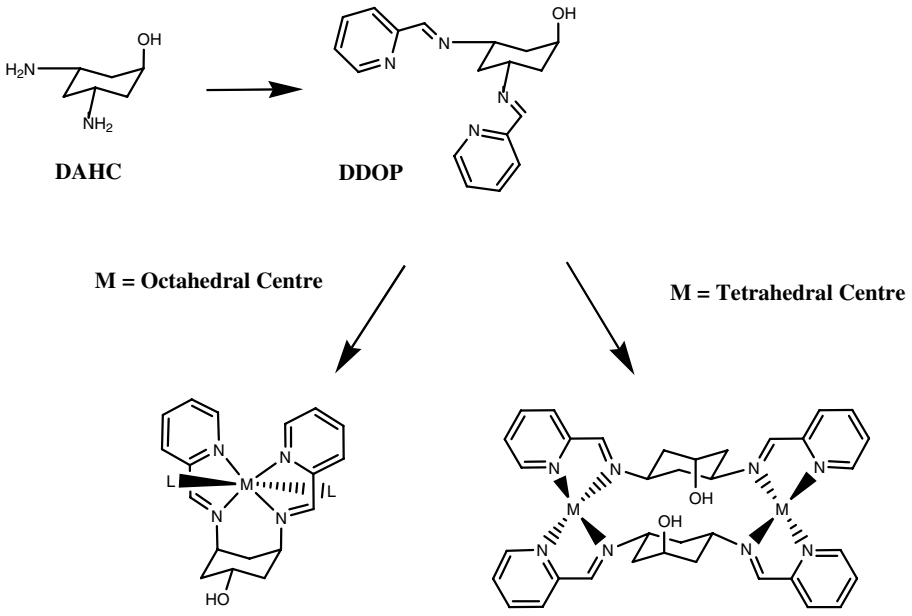

Scheme 1. The parent amine DAHC, Schiff base ligand DDOP, and its two coordination modes.

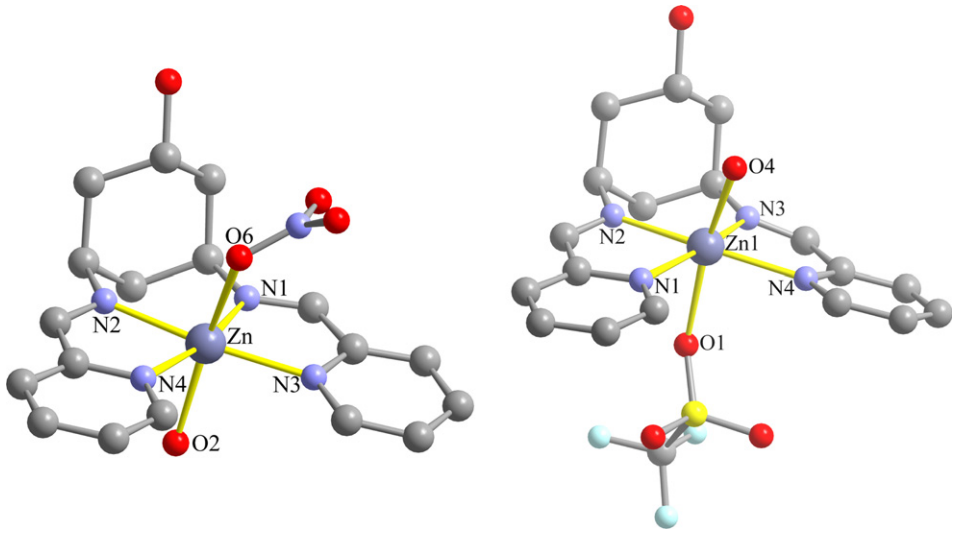

Fig. 1. The complex cations in $[Zn(DDOP)(NO_3)(H_2O)](NO_3)$ (**1**, left), and $[Zn(DDOP)(OTf)(H_2O)](OTf)$ (**2**, right), showing the *anti* and *syn* arrangements of the water ligand respectively. C is grey; F, pale blue; N, blue; O, red; S, yellow; Zn, blue grey. Hydrogen atoms are omitted for clarity. This colour scheme is retained in all figures. (For interpretation of references in colour in this figure legend, the reader is referred to the web version of this article.)

Table 1
Selected bond lengths and angles in $[Zn(DDOP)(H_2O)(NO_3)](NO_3)$ (**1**) and $[Zn(DDOP)(H_2O)(OTf)](OTf)$ (**2**)

		Compound **1**		Compound **2**	
Bond distances (Å)	DDOP	N(1)–Zn	2.110(2)	N(1)–Zn	2.133(2)
		N(2)–Zn	2.136(2)	N(2)–Zn	2.123(2)
		N(3)–Zn	2.136(2)	N(3)–Zn	2.145(2)
		N(4)–Zn	2.125(2)	N(4)–Zn	2.140(2)
	Water ligand	O(2)–Zn	2.173(2)	O(4)–Zn	2.107(2)
	Coordinated anion	O(6)–Zn	2.280(2)	O(1)–Zn	2.240(2)
Bond angles (°)	Pyridyl-N	N(4)–Zn–N(3)	113.77(8)	N(1)–Zn–N(4)	114.81(6)
	Imine-N	N(1)–Zn–N(2)	88.77(8)	N(2)–Zn–N(3)	88.05(6)
	Oxygen	O(2)–Zn–O(6)	164.67(8)	O(4)–Zn–O(1)	166.66(6)

Furthermore, the Zn atom is substantially displaced (0.131 Å) from the N4 plane in **2**, while in **1** it is almost perfectly coplanar (0.006 Å displacement).

The change in position of the water ligand observed in **2** has a significant impact on the long range ordering of the crystal structure, with a change from a 2-dimensional hydrogen bonded network in **1** to isolated hydrogen bonded dimers in **2**. In **1**, hydrogen bonded layers of complex cations and nitrate counterions run parallel to the crystallographic *ab* plane (Fig. 2). These layers are constructed by hydrogen bonds between the water ligand of one cation and the nitrato ligand of the next, and further interactions between nitrate counterions, DDOP alcohol groups and water ligands (for distances and angles see Table 2). Association of the layers to form the crystal may occur through π-stacking interactions, with aromatic systems from alternate layers taking an alignment close to that of a classic slipped π–π stack [14], with a long centroid–centroid distance (3.97 Å) and shorter atom to atom contacts (3.52 Å).

In **2**, the hydrogen bonded dimers consist of two complex cations and two triflate counterions, while the shorter D . . . A distances and near-ideal (180°) D–H . . . A angles imply that the hydrogen bonds are stronger in this system (Table 2). Each cation has its water ligand and DDOP alcohol group bridged by hydrogen bonding interactions with two oxygens from a triflate anion to form a "half-dimer"; these halves are connected by hydrogen bonds between the water ligands and DDOP alcohol groups of the two complex cations. The participation of the water ligand in two strong hydrogen bonding interactions explains the relatively large displacement of the zinc atom from the N_4 plane, with the hydrogen bonds and strong Zn–O coordinate bond acting to pull the metal centre out of position in the absence of any counteracting hydrogen bonds to the coordinated triflate anion. This apparent influence of hydrogen bonding over the metal coordination environment suggests that it may be a factor in the positioning of the water ligand. For example, the wider separation of the oxygens in the triflate anion (≈2.4 Å compared with 2.1 Å) may allow it to form a strong hydrogen bonded bridge between the alcohol group and water ligand in **2**, making the *syn* arrangement more favourable. Another factor may be the larger size of the triflate anion, which

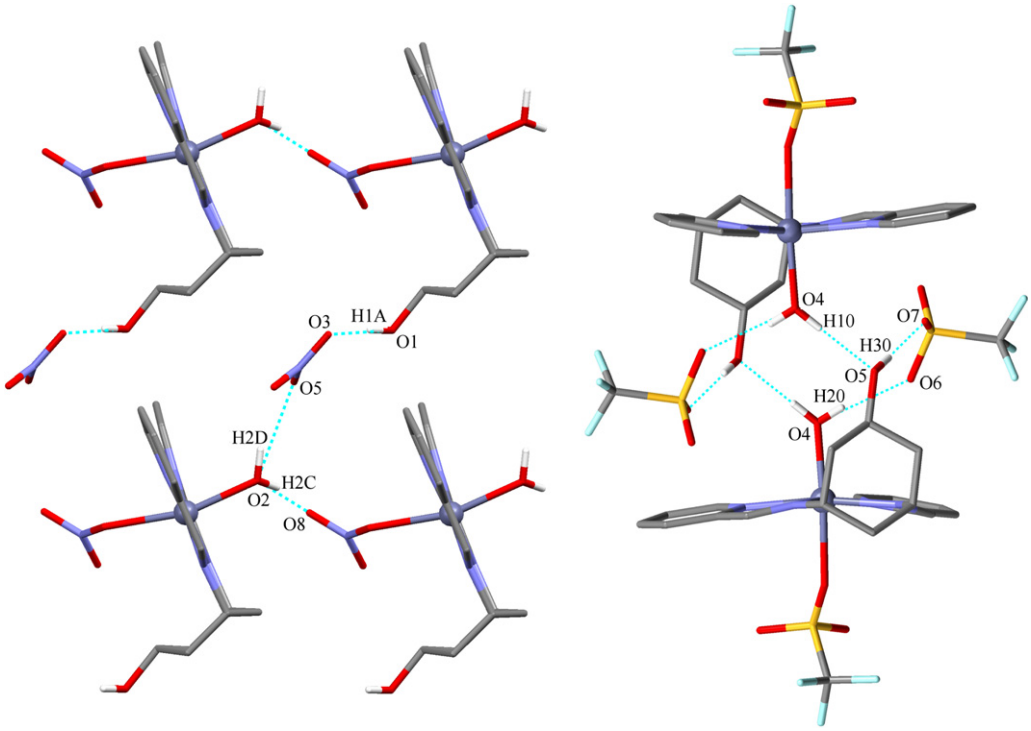

Fig. 2. Assembly of a hydrogen bonded layer in [Zn(DDOP)(NO_3)(H_2O)](NO_3) (**1**, left), and a hydrogen bonded dimer in [Zn(DDOP)(H_2O)(OTf)](OTf) (**2**, right). Hydrogen bonds are shown heavy atom to heavy atom as bright blue dotted lines, selected hydrogens are shown in white. (For interpretation of references in colour in this figure legend the reader is referred to the web version of this article.)

Table 2
Hydrogen bond lengths and angles in [Zn(DDOP)(H_2O)(NO_3)](NO_3) (**1**) and [Zn(DDOP)(H_2O)(OTf)](OTf) (**2**), calculated using PLATON [15]

	H-bonding atoms	D–H (Å)	H···A (Å)	D···A (Å)	D–H···A (°)
Compound **1**	O(1)–H(1A)···O(3)	0.87(4)	2.07(4)	2.919(4)	169(4)
	O(2)–H(2C)···O(8)	0.81(3)	1.94(3)	2.737(3)	166(3)
	O(2)–H(2D)···O(5)	0.86(2)	2.12(2)	2.911(4)	153(3)
Compound **2**	O(4)–H(10)···O(5)	0.83(3)	1.88(3)	2.697(2)	171(3)
	O(4)–H(20)···O(6)	0.74(3)	2.00	2.728(3)	171(3)
	O(5)–H(30)···O(7)	0.76(3)	1.97	2.730(3)	177(4)

in the *anti* arrangement could make an unfavourable steric clash with the DDOP cyclohexane backbone.

2.3. Solution chemistry

The overall structure of **1** and **2**, with four equatorial N-donors and an axial water ligand, is reminiscent of the zinc cyclams. ^{1}H NMR measurements in deuterated methanol indicated that the basic mononuclear, tetradentate chelated structure of the cations was retained upon dissolution, as revealed by the cyclohexane protons which provide an excellent conformational probe. This, coupled with the hydrophobic surface offered by the aromatic system, suggested that these molecules had potential as molecular recognition agents. Using isothermal titration calorimetry (ITC) [16] we analyzed the binding properties of the two metal complexes against a series of amino acids. Serine, tyrosine and histidine offered an interesting spectrum of coordinating amino acids to gauge the effect of the nitrate and triflate on the metal centre's ability to bind the substrates. In all cases it was shown that binding constants to the triflate complex **2** were considerably higher than the corresponding nitrate complex **1**. In the both the serine and tyrosine binding experiments the interactions were highly endothermic. This phenomenon is characteristic of hydrophobic interactions through the expulsion of solvent/counter anions from the receptor surface and substrate environs. For example, serine, when complexed with **2** afforded an endothermic interaction, $\Delta H \approx +2.71$ kcal mol^{-1}. The nitrate species **1**, gives a smaller positive ΔH of $\sim$0.85 kcal mol^{-1}. The substantially lower endothermic interaction observed could be assigned to the ineffective expulsion of the strongly coordinating nitrate anion.

However, for both complex **1** and **2**, the ITC traces (Fig. 3) indicate the coordination of two histidine amino acids to the zinc metal centre. While binding of the first histidine is endothermic (for complex **2**, $\Delta H \approx +0.94$ kcal

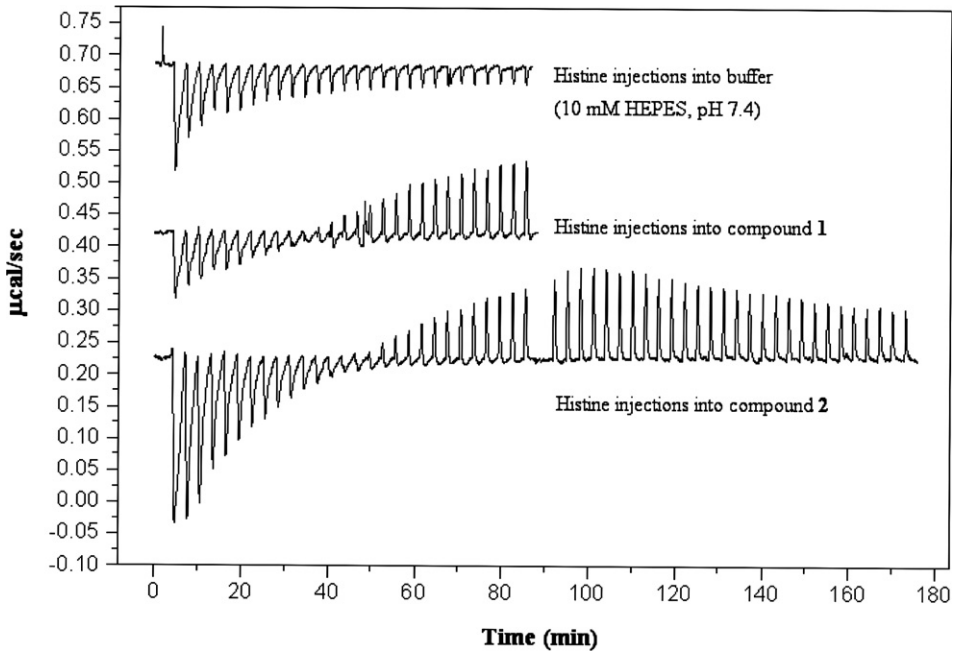

Fig. 3. ITC traces showing the binding of histidine to compounds **1** and **2**, indicating a two centre binding mode with endothermic followed by exothermic binding.

mol^{-1}), binding of the second is an exothermic process (for complex **2**, $\Delta H \approx -5.1$ kcal mol^{-1}). It appears that binding must occur above and below the planar platform via the imidazole moiety, giving an octahedral species reminiscent of the 6-coordinate iron centre observed in some haemoglobins [17]. This is because: (i) zinc has previously been shown to form 6-coordinate imidazole complexes in aqueous solution [18]; while (ii) any 5-coordinate possibilities would first require hydrolysis of one arm of the DDOP ligand to free a donor site, or, improbably, dissociation of this tetradentate chelating ligand. It should be noted that Schiff bases are generally considered relatively stable to hydrolysis [19], and furthermore such a transformation would be endothermic [20]. The two centre binding observed with histidine is probably due to the higher affinity for zinc of the softer imidazole N-donor, which unlike the carboxylic acid O-donors of the other amino acids is capable of displacing water as well as the counterions.

The two complexes were also tested against a series of phosphates, but the binding constants were negligible. The large solvent exposed areas around the metal centre probably contribute to the poor affinity of these polar substrates. Improved hydrophobic shielding would potentially increase the binding affinity for more hydrophilic substrates.

3. Conclusions

A change of anion from nitrate to triflate induces a change in the positioning of the coordinated anion in an octahedral zinc(II) complex. This change appears to result from the triflate anion's larger size and contrasting hydrogen bonding properties, which in the solid state favour formation of a *syn* complex, with a corresponding change from a 2D hydrogen bonded network to isolated hydrogen bonded dimers. In addition, the non-coordinating nature of the triflate anion in solution increases the ability of the zinc complex to bind amino acid substrates, giving it the potential for further development as a molecular recognition agent.

4. Experimental

4.1. Materials, methods and instrumentation

The ligand DDOP was synthesised by reaction of *cis*-3,5-diamino-*trans*-hydroxycyclohexane with 2-pyridinecarbaldehyde [13]. All other reagents and solvents were purchased (Fisher/Lancaster/Riedel-de Haën/Aldrich) as AR grade and used without further purification. Deuterated solvents were obtained from Aldrich. All complexations were performed in the ambient atmosphere. Infra-red spectra were measured with Jasco FTIR-410 and Bruker TENSOR 27 spectrometers and ^{1}H NMR measurements were performed using Bruker DPX-400 and Avance-400 spectrometers. X-ray diffraction data were collected using Nonius Kappa-CCD and Bruker CCD-1000 diffractometers with Mo Kα radiation and a graphite monochromator. Isothermal titration calorimetry was performed using Microcal MCS and VP-ITC titration microcalorimeters.

4.2. Preparation of $[Zn(DDOP)(H_2O)(NO_3)](NO_3)$ (**1**)

$Zn(NO_3)_2 \cdot 6H_2O$ (0.0675 g, 0.227 mmol) in methanol (5 mL) was added to a solution of DDOP (0.070 g, 0.226 mmol) in methanol (20 mL) and the resulting clear, colourless solution was stirred for 2 h at room temperature.

Evaporation of solvent *in vacuo* to a volume of ≈4 mL, followed by diffusion of ether into the methanolic solution yielded **1** as large colourless crystals in around 24 h (0.0714 g, 0.138 mmol, 61%). ^{1}H NMR (400 MHz, CD_3OD): δ 9.09 (d, 2H), 8.78 (s, 2H), 8.32 (*p*td, 2H), 8.06 (d, 2H), 7.93 (m, 2H), 4.51 (m, 2H), 4.26 (tt, 1H), 2.16 (m, 4H), 1.92 (*p*td, 2H). IR (KBr disc) cm^{-1}: 3415 s, 2922 w, 1641 m, 1603 m, 1385 s, 1329 s, 1068 m, 781 m. Elemental analysis for $C_{18}H_{22}N_6O_8Zn$, actual (expected) %: C, 42.00 (41.92); H, 4.25 (4.30); N, 15.89 (16.29).

4.3. Preparation of [Zn(DDOP)(H$_2$O)(OTf)](OTf) (2)

$Zn(CF_3SO_3)_2 \cdot 6H_2O$ (0.103 g, 0.283 mmol) in methanol (≈1 mL) was added to a solution of DDOP (0.073 g, 0.234 mmol) in methanol (2.5 mL). After stirring for around 1 h at room temperature, diffusion of ether into the methanolic solution yielded colourless crystals of **2** in less than 24 h (0.138 g, 0.20 mmol, 85%). ^{1}H NMR (400 MHz, CD_3OD): δ 9.09 (d, 2H), 8.80 (s, 2H), 8.23 (*p*td, 2H), 8.08 (d, 2H), 7.97 (m, 2H), 4.50 (m, 2H), 4.22 (tt, 1H), 2.16 (m, 4H), 1.93 (*p*td, 2H). IR (KBr disc) cm^{-1}. Elemental analysis for $C_{20}H_{22}F_6N_4O_8S_2Zn$, actual (expected) %: C, 34.75 (34.82); H, 3.11 (3.21); N, 7.96 (8.12).

4.4. Single-crystal structure determination

Suitable single crystals of **1** and **2** were mounted on the end of a thin glass fiber using Fomblin oil or epoxy glue. X-ray diffraction intensity data were measured at 150 K on a Nonius Kappa-CCD diffractometer, **1**, and at 193 K on a Bruker CCD-1000 diffractometer, **2**, in both cases using molybdenum radiation [λ(Mo Kα) = 0.7107 Å]. Structure solution and refinement for **1** was carried out with SHELXS-97 [21] and SHELXL-97 [22] via WinGX [23], and for **2** with SHELXTL [24]. Corrections for incident and diffracted beam absorption effects were applied using empirical methods [25]. Both compounds crystallized in the space group $P2_1/n$, as determined by systematic absences in the intensity data, intensity statistics and the successful solution and refinement of the structures. Both structures were solved by a combination of the Patterson method and difference Fourier syntheses and refined against F^2 by the full-matrix least-squares technique, with all non-hydrogen atoms refined anisotropically. Hydrogen atoms of alcohol groups and water ligands were found objectively on a Fourier difference map and were refined in the isotropic approximation, while other hydrogen atoms were calculated using the riding model. Crystal data, data collection parameters and refinement statistics for **1** and **2** are listed in Table 3.

4.5. Isothermal titration calorimetry

Isothermal titration calorimetry (ITC) experiments were used to measure the binding of the two complexes to various substrates, and were performed at 25 °C (298 K) using Microcal MCS and VP-ITC titration microcalorimeters. In order to minimize mixing heat effects caused by differences in solution composition, the substrates and zinc complexes were both dissolved in freshly prepared HEPES buffer (pH = 7.4) before each titration experiment. All solutions prior to experiments were degassed before being added to the calorimeter cell. The substrates, at a concentration of 5.0 mM, were injected in 10 μL increments into the reaction cell (cell volume 1.31–1.41 mL) containing **1** or **2** at a concentration of ≈0.25 mM, until there occurred a saturation of the macrocyclic cavity. A 250 μL injection syringe with 310–400 rpm stirring was used to give a series of 10 μL injections at 3-min intervals. Control experiments for heats of mixing and dilution were performed under identical conditions and used for data correction in subsequent analysis. Data acquisition and subsequent non-linear regression analysis were done in terms of a simple binding model using the Microcal ORIGIN software package.

Table 3
Crystallographic data for compounds **1** and **2**

	1	**2**
Empirical formula	$C_{18}H_{22}N_6O_8Zn$	$C_{20}H_{22}F_6N_4O_8S_2Zn$
Formula weight	515.79	689.91
Crystal system	monoclinic	monoclinic
Space group	$P2_1/n$	$P2_1/n$
a (Å)	9.9335(3)	10.963(3)
b (Å)	7.3304(2)	9.554(3)
c (Å)	28.4068(9)	26.170(7)
α (°)	90	90
β (°)	91.277(2)	97.753(4)
γ (°)	90	90
V (Å^3)	2067.97(11)	2716.1(13)
Z	4	4
Temperature (K)	150(2)	193(2)
ρ_{calc} (g cm^{-3})	1.657	1.687
μ (mm^{-1})	1.249	1.151
Reflections collected	15290	15958
Unique reflections (R_{int})	4654 (0.0464)	6333 (0.0392)
Number of parameters	306	382
Goodness-of-fit on F^2	1.040	0.986
Final R indices [$R > 2\sigma(I)$][a]	$R_1 = 0.0406$, $wR_2 = 0.0871$	$R_1 = 0.0343$, $wR_2 = 0.0882$
R-indices (all data)	$R_1 = 0.0557$, $wR_2 = 0.0938$	$R_1 = 0.0418$, $wR_2 = 0.0929$
Maximum, minimum $\Delta\rho$ (e Å^{-3})	0.876, −0.652	0.501, −0.455

[a] $R_1 = \sum\|F_o| - |F_c\|/\sum|F_o|$, $wR_2 = \{\sum[w(F_o^2 - F_c^2)^2]/\sum[w(F_o^2)^2]\}^{1/2}$.

Acknowledgements

J.F. would like to thank the EPSRC, and D.-L. the Leverhulme Trust, for funding. Ames Laboratory is operated for the U.S. Department of Energy by Iowa State University under Contract No. W-7405-Eng-82. We would also like to thank Prof. A. Cooper for allowing us access to the ITC equipment in Glasgow for the binding measurements.

Appendix A. Supplementary data

Crystallographic data (excluding structure factors) for the structure reported in this paper has been deposited with

the Cambridge Crystallographic Data Centre as supplementary publication nos. CCDC 606809 (compound 2) -606810 (compound 1). Copies of the data can be obtained free of charge on application to CCDC, 12 Union Road, Cambridge CB2 1EZ, UK [fax: int. code +44 1223 336 033; E-mail: deposit@ccdc.cam.ac.uk; http://www.ccdc.cam.ac.uk]. Supplementary data associated with this article can be found, in the online version, at doi:10.1016/j.poly.2006.06.044.

References

[1] S.R. Seidel, P.J. Stang, Acc. Chem. Res. 35 (2002) 972.
[2] M. Fujita, K. Umemoto, M. Yoshizawa, N. Fujita, T. Kusukawa, K. Biradha, Chem. Commun. (2001) 509.
[3] D.L. Caulder, K.N. Raymond, J. Chem. Soc., Dalton Trans. (1999) 1185.
[4] L. Applegarth, A.E. Goeta, J.W. Steed, Chem. Commun. (2005) 2405.
[5] D.R. Turner, M.B. Hursthouse, M.E. Light, J.W. Steed, Chem. Commun. (2004) 1354.
[6] D.R. Turner, E.C. Spencer, J.A.K. Howard, D.A. Tocher, J.W. Steed, Chem. Commun. (2004) 1352.
[7] M.J. Hannon, C.L. Painting, E.A. Plummer, L.J. Childs, N.W. Alcock, Chem. Eur. J. 8 (2002) 2226.
[8] J. Fielden, J. Sprott, D.-L. Long, P. Kögerler, L. Cronin, Inorg. Chem. 45 (2006) 2886.
[9] J. Fielden, D.-L. Long, L. Cronin, Chem. Commun. (2004) 2156.
[10] S. Aoki, E. Kimura, Chem. Rev. 104 (2004) 769.
[11] (a) J.L. Sessler, S. Camiolo, P.A. Gale, Coord. Chem. Rev. 240 (2003) 17;
(b) P.T. Gunning, A.C. Benniston, R.D. Peacock, Chem. Commun. (2004) 2226;
(c) P.T. Gunning, Org. Biomol. Chem. (2005) 3877.
[12] K.H. Lee, S.S. Yoon, Bull. Kor. Chem. Soc. 27 (2006) 127.
[13] J. Fielden, J. Sprott, L. Cronin, New J. Chem. 29 (2005) 1152.
[14] C. Janiak, J. Chem. Soc., Dalton Trans. (2000) 3885.
[15] A.L. Spek, PLATON, A Multipurpose Crystallographic Tool, Utrecht University, Utrecht, The Netherlands, 2005.
[16] I. Jelesarov, H.R. Bosshard, J. Mol. Recogn. 12 (1999) 3.
[17] A.J. Gow, A.P. Payson, J. Bonaventura, J. Inorg. Biochem. 99 (2005) 903.
[18] M. Alei Jr., L.O. Morgan, W.E. Wageman, Inorg. Chem. 17 (1978) 2288.
[19] M.B. Smith, J. March, March's Advanced Organic Chemistry, fifth ed., John Wiley & Sons, New York, 2001, p. 1177.
[20] For hydrolysis of a Schiff base, $\Delta H \approx +5$ kcal mol^{-1}, based on the mean bond enthalpies for O–H, N–H, C=O and C=N bonds found in: P. Atkins, J. de Paula, Physical Chemistry, seventh ed., W.H. Freeman & Company, New York, 2002, p. 1096.
[21] G.M. Sheldrick, Acta Crystallogr., Sect. A 46 (1990) 467.
[22] G.M. Sheldrick, Programs for Crystal Structure Analysis (Release 97-2), University of Göttingen, Germany, 1998.
[23] L.J. Farrugia, J. Appl. Crystallogr. 32 (1999) 837.
[24] G.M. Sheldrick, SHELXTL version 5.1, Bruker Analytical X-Ray Systems, Inc., Madison, WI, USA, 1997.
[25] R.H. Blessing, Acta Crystallogr., Sect. A 51 (1995) 33.

Waal's radii. The mercury complex $[HgCl_2(\mathbf{L})]$ decomposes on crystallization resulting in Th_2TeCl_2 (Th = 2-thienyl), which has been characterized by single crystal X-ray diffraction. The results of these investigations are reported in this paper.

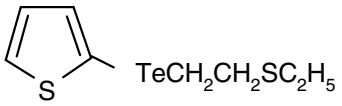

L

2. Experimental

The C and H analyses were carried out with a Perkin–Elmer elemental analyzer 240 C. Tellurium was estimated using a flame atomic absorption spectrometer (Perkin–Elmer, Analyst 100). Mercury was determined by the cold vapour AAS method. The ^1H and $^{13}C\{^1H\}$ NMR spectra were recorded on a Bruker Spectrospin DPX-300 NMR spectrometer at 300.13 and 75.47 MHz, respectively. IR spectra, in the range 4000–250 cm^{-1}, were recorded on a Nicolet Protége 460 FT-IR spectrometer as KBr pellets. The conductance measurements were made in acetonitrile (concentration ~1 mM) using an ORION conductivity meter model 162. The molecular weights (concentration ~5 mM) in chloroform were determined with a Knauer vapour pressure osmometer model A0280. The melting points determined in open capillary are reported as such.

2.1. X-ray crystallography

The data for **1** and **5** were collected (at 120 K) on an Enraf Nonius Kappa CCD area detector diffractometer, with ϕ and ω scans chosen to give a complete asymmetric unit. Cell refinement [12,13a] corresponds to a monoclinic cell for both **1** and **5**. The dimensions of both are given in Table 1 along with other experimental parameters. Absorption correction was applied [12,13]. The structures of both **1** and **5** were solved by direct methods [14] and refined using the WINGX version [15] of SHELX-97 [16]. Hydrogen atoms were included in idealized positions with isotropic thermal parameters set at 1.2 times that of the carbon atom to which they were attached. Non-hydrogen atoms were treated anisotropically. In **1**, the 64/36 disorder in the (C_4H_3S) group was successfully modelled by placing restraints on distances and thermal parameters within the group. The final cycle of full-matrix least-squares refinement for **1** was based on 16484 observed (3034 independent) reflections (2550 for $F^2 > 4\sigma(F^2)$) and 126 variable parameters, and converged (largest parameter shift was 0.001 times its esd). The molecular structure of **1** is displayed as an ORTEP diagram in Fig. 1. Its selected bond lengths and angles are given in Table 2. The final cycle of full-matrix least-squares refinement for **5** was based on 945 observed reflections (918 for $F^2 > 4\sigma(F^2)$) and 54 variable parameters, and converged (largest parameter shift was 0.001 times its esd). The disorder in the (C_4H_3S) group was also successfully modelled by placing restraints on distances and thermal parameters. The crystal and structure refinement data for **5** are given in Table 1. Selected bond lengths and bond angles are given in Table 3. The molecular structure of **5** is displayed as an ORTEP diagram in Fig. 2.

Table 1
Crystal data and structure refinement for **1** and **5**

Compound	**1**	**5**
Empirical formula	$C_8H_{12}S_2Cl_2PdTe$	$C_8H_6S_2Cl_2Te$
Formula weight	477.20	364.75
Temperature (K)	120(2)	120(2)
Wavelength (Å)	0.71073	0.71073
Crystal system	monoclinic	monoclinic
Space group	$P2_1/n$	$C2/c$
Unit cell dimensions		
a (Å)	13.3463(9)	18.006(4)
b (Å)	8.3277(6)	4.858(1)
c (Å)	13.395(1)	15.043(3)
β (°)	117.188(6)	124.68(3)
Volume (Å^3)	1324.3(2)	1082.2(4)
Z	4	4
D_{calc} (g/cm^3)	2.393	2.239
Absorption coefficient (mm^{-1})	4.241	3.576
$F(000)$	896	688
Crystal size (mm)	$0.35 \times 0.10 \times 0.03$	$0.18 \times 0.08 \times 0.03$
θ Range for data collection (°)	3.42–27.53	4.42–25.01
Index ranges	$-17 \leqslant h \leqslant 15$, $-10 \leqslant k \leqslant 10$, $-17 \leqslant l \leqslant 17$	$-21 \leqslant h \leqslant 21$, $-5 \leqslant k \leqslant 5$, $-17 \leqslant l \leqslant 17$
Reflections collected	16484	7966
Independent reflections (R_{int})	3034 (0.0487)	945 (0.0559)
Maximum and minimum transmission	0.8833 and 0.3184	0.9003 and 0.5653
Refinement method	full-matrix least-squares on F^2	full-matrix least-squares on F^2
Data/restraints/parameters	3034/14/126	945/14/54
Goodness-of-fit on F^2	1.041	1.069
Final R indices ($F^2 > 4\sigma(F^2)$)	$R_1 = 0.0308$, $wR_2 = 0.0724$	$R_1 = 0.0295$, $wR_2 = 0.0695$
R indices (all data)	$R_1 = 0.0402$, $wR_2 = 0.0772$	$R_1 = 0.0303$, $wR_2 = 0.0701$
Largest difference in peak and hole (e Å)	1.116 and −1.128	1.482 and −0.692

2.2. Synthesis of 1-ethylthio-2-[2-thienyltelluro]ethane (*L*)

A 2-thienyl lithium solution (5.0 cm^3 of 1.0 M solution in THF) was added to elemental tellurium (0.63 g, 5.0 mmol) taken in dry THF (25 cm^3) at 0 °C in a Schlenk tube. The mixture was stirred at this temperature for 1.5 h (tellurium was dissolved) after which it was cooled to −78 °C. 2-Chloroethyl ethyl sulfide (0.62 g, 5.0 mmol) was added with constant stirring at −78 °C. The mixture was allowed to come to room temperature slowly over ~12 h, after which it was poured into 100 cm^3 of ice cold

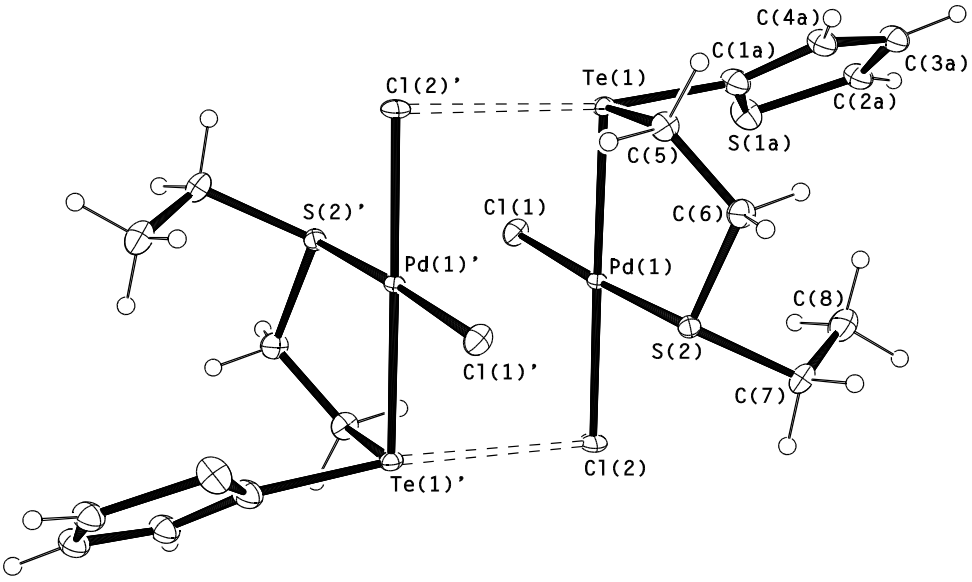

Fig. 1. Molecular structure of $[PdCl_2(\mathbf{L})]$ (**1**).

water. The ligand **L** was extracted into chloroform ($3 \times 50\ cm^3$) from the aqueous mixture. The combined chloroform extract was washed with brine (saturated solution of NaCl) ($2 \times 10\ cm^3$), dried over Na_2SO_4 and evaporated under reduced pressure on a rotary evaporator to give **L** as a red oil. Yield, 70%. ^1H NMR (δ versus TMS, $CDCl_3$, 25 °C): 1.19 (t, 3H, H_1), 2.52 (t, 2H, H_4), 2.92–2.99 (m, 4H, H_3 and H_2), 6.90–6.93 (bm, 1H, H_7), 7.37–7.38 (bd,1H, H_6), 7.42–7.44 (bd, 1H, H_8). $^{13}C\{^1H\}$ NMR (δ versus TMS, $CDCl_3$, 25 °C): 10.5 (C_4), 14.5 (C_1), 25.2 (C_2), 33.1 (C_3), 128.7 (C_6), 134.2 (C_7), 141.3 (C_8), 142.7(C_5). IR (KBr, cm^{-1}): 3455mb, 2958m, 2924w, 1580s, 1483s, 1386w, 1324w, 1281m, 1256s, 1170m, 1046m, 872m, 816w, 706s, 622m, 512m, 463w.

Table 2
Bond distances [Å] and angles [°] for $[PdCl_2(\mathbf{L})]$ (**1**)[a]

Pd(1)–Cl(1)	2.322(1)	Pd(1)–Cl(2)	2.380(1)
Pd(1)–Te(1)	2.5040(4)	Pd(1)–S(1)	2.273(1)
Te(1)–C(5)	2.147(4)	C(1)–C(2)	1.520(6)
S(2)–C(6)	1.822(4)	S(2)–C(7)	1.820(5)
C(5)–C(6)	1.521(6)	C(7)–C(8)	1.483(7)
Te(1)–C(1a)	2.10(2)	S(1a)–C(1a)	1.69(1)
S(1a)–C(2a)	1.713(8)	Te(1)–Cl(2)	3.401(1)
Pd(1)–Pd(1)	3.4156(6)	Cl(1)–S(2)	3.488(2)
Cl(1)–Pd(1)–Cl(2)	94.46(4)	S(2)–Pd(1)–Te(1)	91.25(3)
Cl(1)–Pd(1)–Te(1)	86.83(3)	Cl(1)–Pd(1)–S(2)	177.27(4)
Cl(2)–Pd(1)–Te(1)	178.71(3)	Cl(2)–Pd(1)–S(2)	87.46(4)
C(1a)–Te(1)–Pd(1)	95.3(3)	C(1a)–Te(1)–C(5)	95.9(3)
C(1a)–S(1a)–C(2a)	90.7(5)	S(1a)–C(2a)–C(3a)	115.5(7)
C(4a)–C(1a)–S(1a)	109(1)	S(1a)–C(1a)–Te(1)	120.2(6)
C(3A)–C(4A)–C(1A)	118(1)	Pd(1)–Te(1)–C(5)	95.4(1)
C(5)–C(6)–S(2)	113.1(3)	Te(1)–C(5)–C(6)	110.8(3)
C(6)–S(2)–Pd(1)	108.9(1)	C(6)–S(2)–C(7)	99.8(2)
C(7)–S(2)–Pd(1)	107.0(2)	C(8)–C(7)–S(2)	116.5(3)

[a] Symmetry equivalent position $(-x+2, -y+1, -z)$ given by a prime.

Table 3
Bond lengths [Å] and angles [°] for $TeCl_2(C_4H_5S)_2$ (**5**)

Te(1)–Cl(1)	2.480(2)	Te(1)–Cl(1)	2.480(2)
Te(1)–C(1a)	2.151(3)	S(1a)–C(1a)	1.654(3)
S(1a)–C(4a)	1.651(9)	C(1a)–C(2a)	1.400(5)
C(2a)–C(3a)	1.40(1)	C(3a)–C(4a)	1.40(1)
Cl(1)–Te(1)–Cl(1)	178.06(6)	C(1A)–Te(1)–C(1a)	94.6(2)
C(1a)–Te(1)–Cl(1)	88.58(6)	Te(1)–C(1a)–S(1a)	120.4(2)
C(1a)–Te(1)–Cl(1)	90.10(6)	S(1a)–C(1a)–C(2a)	112.8(3)
Te(1)–C(1a)–C(2a)	126.7(3)	C(1a)–C(2a)–C(3a)	113.6(6)
C(2a)–C(3a)–C(4a)	105.7(9)	C(3a)–C(4a)–S(1a)	117.7(8)
C(1a)–S(1a)–C(4a)	90.2(4)		

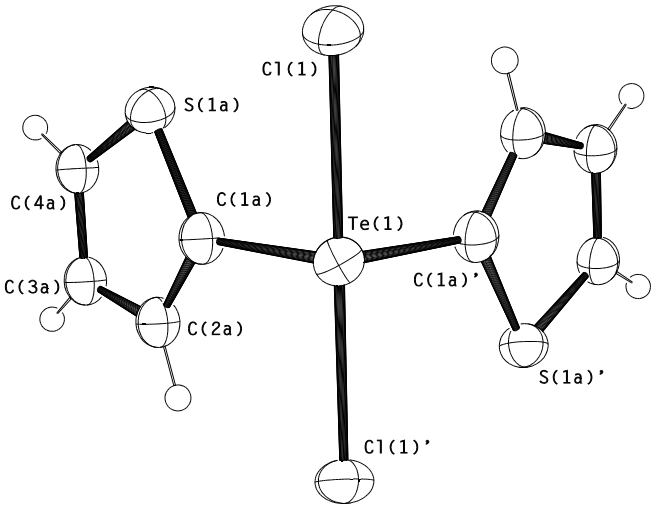

Fig. 2. Molecular structure of $[Th_2TeCl_2]$ (**5**).

2.3. Synthesis of $[PdCl_2(\mathbf{L})]$ (**1**)

To a solution of **L** (0.08 g, 0.25 mmol) made in 10 cm^3 of acetone was added $Na_2[PdCl_4]$ (0.07 g, 0.25 mmol) dissolved in 10 cm^3 of water. The resulting mixture was stirred

for 2 h at room temperature and poured into 100 cm^3 of water. The complex was extracted into chloroform (4×25 cm^3). The extract was dried over anhydrous sodium sulfate, concentrated to ~10 cm^3 on a rotary evaporator and mixed with hexane (20 cm^3). The resulting yellow solid (**1**) was filtered, washed with hexane and dried *in vacuo*. It was recrystallized from a chloroform–hexane mixture (1:1). Yield, 80%; m.p. 94 °C (d). *Anal.* Calc.: C, 20.12; H, 2.51; Te, 26.75. Found: C, 20.10; H, 2.65; Te, 26.05%. Λ_m: 4.80 Ω^{-1} cm^2 mol^{-1}. Mol. wt.: 611.0 (477.00). ^{1}H NMR (δ versus TMS, $CDCl_3$, 25 °C): 1.36 (t, 3H, H_1), 3.09–3.63 (bm, 6H, H_4, H_3 and H_2), 7.16 (m, 1H, H_7), 7.63–7.71 (m, 2H, H_6 and H_8). $^{13}C\{^1H\}$ NMR (δ versus TMS, $CDCl_3$, 25 °C): 20.2 (C_4), 13.3 (C_1), 30.0 (C_2), 42.0(C_3), 129.3 (C_6), 135.2 (C_7), 139.7(C_8), 142.7(C_5). IR (KBr, cm^{-1}): 3435 mb, 3067w, 2960m, 2924s, 1623w, 1448m, 1406m, 1390m, 1260m, 1212s, 1102m, 1048m, 970w, 887w, 842m, 792vw, 715s, 464w, 326sh, 303sh, 292sh, 279sh, 246sh, 234vs.

2.4. Synthesis of [$PtCl_2$(**L**)] (**2**)

$K_2[PtCl_4]$ (0.10 g, 0.25 mmol) was dissolved in 10 cm^3 of water and mixed with a solution of **L** (0.08 g, 0.25 mmol) in 10 cm^3 of acetone. The resulting mixture was stirred for 3 h at room temperature and poured into 100 cm^3 of water. The complex was extracted into chloroform (4×25 cm^3). The extract was dried over anhydrous sodium sulfate, concentrated to ~10 cm^3 on a rotary evaporator and mixed with hexane (20 cm^3). The resulting light yellow colored compound (**2**) was filtered, washed with hexane and recrystallized from a chloroform–hexane (2:1) mixture. Yield, 78%; m.p. 84 °C (d). *Anal.* Calc.: C, 16.92; H, 2.12; Te, 22.54. Found: C, 16.17; H, 2.26; Te, 23.01%. Λ_m: 5.30 Ω^{-1} cm^2 mol^{-1}. Mol. wt.: 602.0 (565.68). ^{1}H NMR (δ versus TMS, $CDCl_3$, 25 °C): 1.43 (t, 3H, H_1), 3.00–3.48 (bm, 6H, H_4, H_3 and H_2), 7.14–7.19 (m, 1H, H_7), 7.60–7.65 (m, 2H, H_6 and H_8). $^{13}C\{^1H\}$ NMR (δ versus TMS, $CDCl_3$, 25 °C): 17.1, 18.9 (C_4), 11.1, 11.5 (C_1), 29.9, 30.5 (C_2), 39.9, 40.4 (C_3), 127.3 (C_6), 132.9 (C_7), 137.1 (C_8), 142.7 (C_5). IR (KBr, cm^{-1}): 3436mb, 3072w, 2961m, 2923m, 2853w, 2360vs, 2338vs, 1620w, 1448w, 1390m, 1214m, 1048w, 951w, 892w, 842m, 717s, 463w, 320mb, 299mb, 245sh, 232vs.

2.5. Synthesis of [$Ag(L)_2][ClO_4]$ (**3**)

A solution of $AgClO_4$ (0.1 g, 0.58 mmol) in 15 cm^3 of dry methanol was stirred under a dry nitrogen atmosphere in the absence of light. It was mixed with a solution of **L** (0.34 g, 1.16 mmol) in 10 cm^3 of chloroform. The mixture was stirred at room temperature for 1 h. A pink colored complex precipitated, which was filtered, washed well with acetone (3×10 cm^3) followed by cold chloroform (3×10 cm^3) and dried *in vacuo*. It was recrystallized with acetonitrile. Yield, 72%; m.p. 108 °C (d). *Anal.* Calc.: C, 23.80; H, 2.97; Te, 31.64. Found: C, 24.13; H, 3.01; Te, 32.06%. Λ_m: 35.90 Ω^{-1} cm^2 mol^{-1}. ^{1}H NMR (δ versus TMS, $CDCl_3$, 25 °C): 1.34 (t, 3H, H_1), 2.81 (m, 3H, $2H_2 + 1H_3$), 2.96 (m, 1H, $1H_3$), 3.24–3.25 (m, 2H. H_4), 6.99–7.00 (m, 1H, H_7), 7.43–7.48 (m, 2H, H_6 and H_8). IR (KBr, cm^{-1}): 3460mb, 2958m, 2923w, 1630w, 1584s, 1487s, 1460m, 1391w, 1285m, 1249s, 1178m, 1092vs, 816m, 622s, 512w, 463w.

2.6. Synthesis of [$CuBr(L)]_2$ (**4**)

To a solution of **L** (0.14 g, 0.50 mmol) in 10 cm^3 of chloroform was added Cu_2Br_2 (0.07 g, 0.50 mmol) dissolved in 10 cm^3 of nitromethane. The resulting mixture was stirred under an inert atmosphere for 2 h at room temperature, after which the solution was filtered through celite. The clear filtrate was concentrated to ~10 cm^3 on a rotary evaporator and mixed with hexane (20 cm^3). The resulting white solid was filtered, washed with hexane, dried *in vacuo* and stored under inert conditions. Complex **4** was recrystallized from a chloroform–hexane mixture (1:1). Yield, 62%; m.p. 82 °C (d). *Anal.* Calc.: C, 21.66; H, 2.70; Te, 28.79. Found: C, 22.26; H, 2.01; Te, 28.92%. Λ_m: 6.80 Ω^{-1} cm^2 mol^{-1}. Mol. wt.: 857 (887) ^{1}H NMR (δ versus TMS, $CDCl_3$, 25 °C): 1.32–1.39 (t, 3H, H_1), 2.92–2.96 (m, 2H, H_4), 2.67–2.77 (m, 4H, H_3 and H_2), 6.95–6.98 (m, 1H, H_7), 7.45–7.47 (m, 1H, H_6), 7.68–7.70 (m, 1H, H_8). $^{13}C\{^1H\}$ NMR (δ versus TMS, 25 °C): 19.9 (C_4), 13.9 (C_1), 29.0 (C_2), 33.8 (C_3), 129.0 (C_6), 134.6 (C_7), 141.9 (C_8), 141.0(C_5). IR (KBr, cm^{-1}): 3430mb, 3062m, 2960m, 2920s, 1447m, 1386s, 1324w, 1256m, 1213vs, 1078w, 1046w, 943w, 872vw, 840s, 793m, 706vs, 464s, 336s.

2.7. Reaction of $HgCl_2$ with **L**

$HgCl_2$ (0.15 g, 0.55 mmol) dissolved in acetone (20 cm^3) was mixed with a solution of **L** (0.16 g, 0.55 mmol) made in chloroform (20 cm^3). The resulting mixture was stirred at room temperature until the ligand **L** was consumed (as monitored by TLC). The solvent was removed from the mixture on a rotary evaporator. The resulting residue was dissolved in 20 cm^3 of chloroform and filtered through celite. The filtrate was concentrated to 10 cm^3 on a rotary evaporator and mixed with 20 cm^3 of hexane. A white complex was separated, filtered, dried *in vacuo* and kept at 0 °C for recrystallization from a chloroform–hexane (1:1) mixture. White crystals of bis(thienyl) tellurium(IV) chloride (**5**) resulted which were characterized by single crystal X-ray diffraction. Yield, 23 %. *Anal.* Calc.: C, 26.33; H, 1.64; Te, 33.59. Found: C, 26.19; H, 1.57; Te, 32.75%. ^{1}H NMR (δ versus TMS, DMSO-d_6, 25 °C): 6.91–6.94 (m, 1H, H_2), 7.78–7.79 (d, 1H, H_3), 8.14–8.15 (d, 1H, H_1).

3. Results and discussion

Ligand **L** has been synthesized according to Eq. (1), given below, as red brown oil, which is stable under ambient conditions but starts decomposing after three weeks

with the precipitation of a white insoluble powder (tellurium dioxide). It is soluble in common organic solvents such as chloroform, dichloromethane and acetone, but insoluble in hexane. Its complexes are also soluble in common organic solvents such as chloroform and dichloromethane and are stable under ambient conditions, except **4** which disproportionates easily into Cu(II) species:

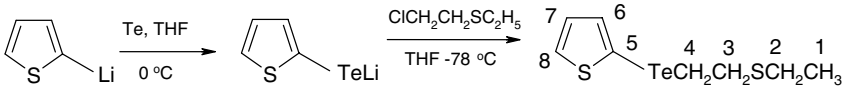

(1)

The mercury complex of **L** decomposes on crystallization resulting in Th_2TeCl_2 (Th = 2-thienyl), probably by mechanism shown in Scheme 1, which is supported by the decomposition of $[HgBr_2L]$ reported earlier [17]. Complex **5** was characterized by X-ray diffraction studies on its single needle shaped transparent crystals, which are sparingly soluble in chloroform but easily dissolve in dimethylsulfoxide. The free radical $C_2H_5SCH_2^{\cdot}$ combines to give the semi-solid $C_2H_5SCH_2CH_2SC_2H_5$ [^{1}H NMR (δ versus TMS, $CDCl_3$, 25 °C): 1.34 (t, 3 H, CH_3 of Et), 2.56–2.64 (q, 2H, CH_2 of Et), 2.73–2.96 (m, 2H, CH_2); $^{13}C\{^1H\}$ NMR (δ versus TMS, $CDCl_3$, 25 °C): 14.5 (CH_3 of Et), 23.5 (CH_2 of Et), 30.0 (CH_2)]. HgTe (0.1 g) was digested with 20 cm^3 of $HCl + HNO_3$ (3:1). The solution, after suitable dilution, was subjected to the appropriate AAS measurement. *Anal*. Calc.: Hg, 61.12; Te 38.87. Found: Hg, 60.23; Te, 39.90%.

The molar conductance values, Λ_M of the complexes **1**–**4** in acetonitrile at ~1 mM concentration level have been determined. The found values for all the complexes except **3** are much lower than the values expected for a 1:1 electrolyte. This suggests that they all are non-electrolytes except **3**, which is found to be 1:1 electrolyte. The molecular weight of **2** determined in chloroform by the vapour pressure osmometric method was found to be very close to the value calculated from its molecular formula, whereas in the case of **1** the difference between found and calculated values of molecular weight was found to be of the order which does not rule out some kind of molecular association. Thus, no appreciable molecular dissociation or association of **2** in solution is indicated by molecular weight measurements. The molecular weight of **4** was found to be nearly double the value calculated from the formula [CuBrL], supporting its dimeric nature.

In the IR spectrum of **1** the bands observed at 326 and 303 cm^{-1} may be assigned to a *cis* Cl–Pd–Cl system. This is supported by the single crystal structure of **1**. In the IR spectrum of **2** the bands at 320 cm^{-1} may be assigned to *cis* Cl–Pt–Cl of a square planar complex. The Te–C (aliphatic) stretching vibrations in the IR spectra of **1** and **2** are observed around 463 cm^{-1}. In the IR spectrum of **3** two bands appear at 1092 and 622 cm^{-1}, which show the presence of ionic ClO_4^-, i.e. outside the coordination sphere. In the IR spectrum of **4**, there is no band around 300 cm^{-1}, which indicates the absence of terminal Cu–Br, therefore it may have a bromo bridged structure if **L** is presumed to be in a bidentate mode.

3.1. NMR spectra

In the ^{1}H NMR spectrum of **L**, signals for the protons of the two $-CH_2$ groups attached to sulfur are merged together and give a multiplet at 2.92–2.99 ppm. The CH_2 protons attached to Te appear as a triplet at 2.52 ppm. The protons of the thienyl group viz. H_7, H_6 and H_8 appear separately, the first one as a broad multiplet and the other two as broad doublets. In the ^{1}H NMR spectrum of **1** the signals of H_1 appear as a multiplet and are deshielded by ~0.18 ppm as compared to free **L**. The signals due to H_2 and H_3 also merge with that of H_4. The broad multiplet between 3.09 and 3.63 is due to six protons of three $-CH_2$ groups. All the

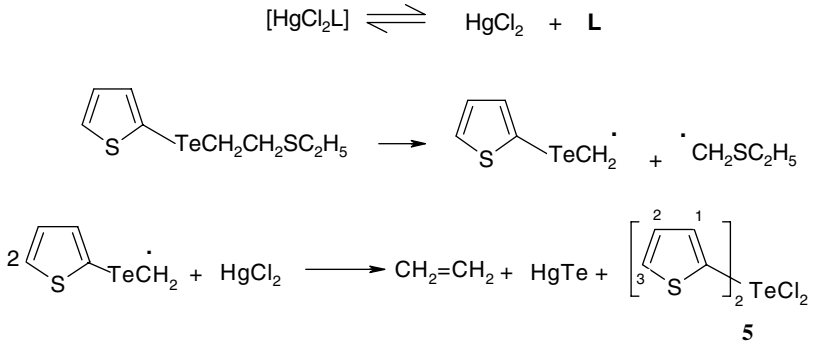

Scheme 1.

CH_2 protons, therefore, appear deshielded by at least 0.6 ppm as compared to those of free ligand **L**. The protons of the thienyl group viz. H_6 and H_8 merge together and appear as a multiplet at 7.63–7.71 ppm. The H_7 proton also appears as a multiplet but is upfield compared to H_6 and H_8. The ^{1}H NMR spectrum of **2** is essentially the same as that of **1**. All CH_2 protons merge together and appear deshielded by up to ~0.52 ppm as compared to those of free **L**. The Te–CH_2 signal in the ^{1}H NMR spectrum of **3** shows a downfield shift of ~0.7 ppm (with respect to that of **L**), whereas an upfield shift (~0.1 ppm) is noticed in the signal of protons attached to sulfur, suggesting that the binding of **L** with metal takes place at least through Te. In the case of d^{10} metal ions, deshielding of protons associated with the donor site on coordination is not always observed, therefore the involvement of sulfur in coordination in **3** cannot be ruled out on this basis. Also in the ^{1}H NMR spectrum of **4** the Te–CH_2 signal appears deshielded by ~0.4 ppm as compared to that of free **L**. The two signals due to CH_2–S–CH_2 merge together and show an upfield shift of ~0.25 ppm with respect to those of **L**. The shifts observed in the proton signals of the thienyl group are virtually insignificant in the spectra of both **3** and **4**, indicating that the thienyl sulfur is not involved in any type of bonding. A conclusion similar to that of **3** may also be drawn about the coordination mode of **L** in **4**. Thus, the overall picture emerging from the proton NMR is that **L** coordinates through its Te with all four metals and in the case of **1** and **2** coordination via S also appears to exist but it cannot be predicted on the basis of ^{1}H NMR unequivocally in the case of **3** and **4** as CH_2 protons linked to S are found to be shielded, which may be because metal ions in both the complexes are d^{10} systems, and with them such an observation is not uncommon.

In the carbon-13 NMR spectra of **1** and **2**, the CH_2–Te signal exhibits a deshielding of ~8–9 ppm as compared to that of free ligand **L**, thereby supporting the ligation of **L** through Te. The downfield shifts (with respect to **L**) in the signals of C_2 and C_3 in the spectra of both the complexes are ~4 and 7–8 ppm, respectively, indicating ligation through sulfur also along with Te, as evidenced by the single crystal structure of **1**. In the carbon-13 NMR spectrum of **2**, two signals for each carbon atom appear, which may be due to the ^{13}C–^{195}Pt coupling. The shifts observed on complexation in the signals of the thienyl ring carbon atoms of **L** are almost insignificant. In the carbon-13 NMR spectrum of **4** the CH_2–Te signal also appears with a deshielding (~9.5 ppm) as compared to that of free **L**. Signal of C_2 also gets deshielded by ~3.8 ppm on the formation of **4**. These observations indicate that **L** coordinates in a bidentate mode with Cu in **4**. The shifts observed in the signals of all other carbon atoms are insignificant, which implies that the ligation of **L** is not through the thienyl sulfur. The carbon-13 NMR spectrum of **3** could not be recorded due to inadequate solubility.

3.2. Crystal structure

The molecular structure of **1** is shown in Fig. 1. Pd has a square planar geometry with **L** ligating in a bidentate mode. The Pd(1)–Cl(1) bond (2.322(1) Å) is shorter than Pd(1)–Cl(2) (2.38(1) Å) due to the *trans* influence of Te, but both are consistent with the values of 2.287(3) and 2.352(3) Å reported for a Pd-complex of (4-MeC_6H_4 $TeCH_2CH_2$-2-(C_5H_4N)) [18] and the values of 2.3160(7) and 2.3915(7) Å for a Pd-complex of N-{2-(4-methoxyphenyltelluro)ethyl} pyrrolidine [19]. The square planar geometry around palladium is supported by Cl(1)–Pd(1)–Cl(2), S(2)–Pd(1)–Cl(2) and Te(1)–Pd(1)–Cl(1) bond angles (94.46(4)°, 177.27(4)° and 86.83(3)°, respectively). The Pd–Te bond length of 2.504 Å observed for **1** is shorter than the sum of the respective covalent radii of 2.63 Å [1.31 Å (Pd(II)) and 1.32 Å (Te)] [20]. Similarly, the Pd–S bond length of 2.273(1) Å is also comparable with the sum of the respective covalent radii, 2.33 Å [1.31 Å (Pd(II)) and 1.02 Å (S)] and consistent with the earlier literature reports of 2.38 Å [21]. The single crystal structure of a Pd(II) complex of (Te, S) ligand 4-$MeOC_6H_4TeCH_2CH_2$ SEt has been reported earlier [8]. The various bond lengths of this Pd–(Te, S) ligand complex [Pd–Cl, 2.316(4)/2.344(3); Pd–Te, 2.492(13); Pd–S, 2.268(4) Å] are consistent with those of **1** and suggest that the donor ability of Te is little affected by replacing the substituted phenyl group with the thienyl group. The interesting feature of the crystal structure of **1** is the intermolecular interactions between Te (coordinated to Pd) and Cl and sulfur and Cl. The Te–Cl distance (3.401 Å) is shorter than sum of van der Waal's radii (3.81 Å). The S–Cl distance 3.488 Å is also shorter than sum of van der Waal's radii (3.55 Å). The Pd–Pd distance between the two molecules is 3.4156(6) Å, greater than the sum of van der Waal's radii (3.26 Å). Thus, these interactions result in the formation of dimeric units in the crystal, which dissociate in solution as the molecular weight of **1** is not found to correspond to a dimeric moiety. However, when all secondary interactions are of the Te–Cl type, the Pd–Pd distance between the molecules in the crystal is lowered below the sum of van der Waal's radii [23]. The C–C bond lengths and bond angles of the thiophene rings are found to be normal. The Te–C(1a) bond length, 2.10(2) Å, is shorter than the Te–C(5) bond length, 2.147(4) Å, but both are consistent with the earlier reported values [22] of 2.116(20) and 2.158(30) Å, respectively. Fig. 2 shows an ORTEP diagram of **5**. The structure of **5** is typical of that of a tellurium(IV) compound (saw-horse type). The geometry around Te, with a Cl(1)–Te(1)–Cl(1) angle of 178.06° and a C(1)–Te(1)–Cl(1) angle of 88.58°, can be best described as pseudo tetrahedral (trigonal bipyramidal with a stereochemically active lone pair on one corner of the triangle). The two Te–Cl bond lengths are same, 2.480(1) Å and are longer than the sum of the covalent radii, 2.36 Å. However they are somewhat shorter than the axial Te–Cl bond lengths, 2.499(3) and 2.525(4) Å reported earlier in the case of a $RR'TeCl_2$ type compound [24]. Thus, the

bonding in the Cl–Te–Cl system may be described in terms of a 3c–4e bond. The Te–C bond length in **5**, 2.151(3) Å, is longer than Te–C(aryl) of **1** but closer to its Te–C(alkyl) value, in spite of the fact that Te is in the +IV oxidation state in **5**.

Acknowledgements

A.K.S. and G.S. thank the Council of Scientific & Industrial Research (India) and the Department of Science and Technology (India) for their financial support in the form of research projects and a fellowship to G.S.

Appendix A. Supplementary material

CCDC numbers 607848 and 607849 contain the supplementary crystallographic data for **1** and **5**, respectively. These data can be obtained free of charge at www.ccdc.cam.ac.uk/conts/retrieving.html [or from the Cambridge Crystallographic Data Centre, 12, Union Road, Cambridge CB2 1EZ, UK; fax: (internet) +44 1223/336 033; e-mail: deposit@ccdc.cam.ac.uk]. Supplementary data associated with this article can be found, in the online version, at doi:10.1016/j.poly.2006.06.042.

References

[1] A.K. Singh, V. Srivastava, J. Coordin. Chem. 27 (1992) 237.
[2] A.K. Singh, S. Sharma, Coordin. Chem. Rev. 209 (2000) 49.
[3] A.K. Singh, Proc. Indian Acad. Sci., Chem. Sci. 114 (2002) 357.
[4] (a) E.G. Hope, W. Levason, Coordin. Chem. Rev. 12 (1993) 109; (b) W. Levason, D. Orchard, G. Reid, Coordin. Chem. Rev. 225 (2002) 159; (c) J.A. Barton, A.R.J. Genge, N.J. Hill, W. Levason, S.D. Orchard, B. Patel, G. Reid, A.J. Ward, Heteroatom Chem. 13 (2002) 550.
[5] R. Kumar, P.G. Singh, S. Bali, A.K. Singh, Phosphorus Sulfur Silicon 180 (2005) 903.
[6] A.K. Singh, V. Srivastava, J. Coordin. Chem. 21 (1990) 269.
[7] A.K. Singh, V. Srivastava, S.K. Dhingra, J.E. Drake, J.H.E. Bailey, Acta Crystallogr. C48 (1992) 655.
[8] A.K. Singh, C.V. Amburose, M. Misra, R.J. Butcher, J. Chem. Res. S (1999) 716.
[9] M. Misra, A.K. Singh, J. Coordin. Chem. 48 (1999) 43.
[10] M. Misra, A.K. Singh, Phosphorus Sulfur Silicon 134/135 (1998) 537.
[11] M. Hesford, W. Levason, S.D. Orchard, G. Reid, J. Organomet. Chem. 649 (2002) 214.
[12] A.J.M. Duisenberg, J. Appl. Cryst. 25 (1992) 92.
[13] (a) DENZO data collection and processing software Z. Otwinowski, W. Minor, Methods in enzymology, in: C.W. CarterJr., R.M. Sweet (Eds.), Macromolecular Crystallography, Part A, vol. 276, Academic Press, 1997, pp. 307–326; (b) G.M. Sheldrick, SADABS V2.10, 2003.
[14] G.M. Sheldrick, Acta Crystallogr. A46 (1990) 467.
[15] L.J. Farrugia, J. Appl. Cryst. 32 (1999) 837.
[16] G.M. Sheldrick, SHELXL97, University of Gottingen, Germany.
[17] G. Singh, S. Bali, A.K. Singh, J.E. Drake, C.L.B. Macdonald, M.B. Hursthouse, M.E. Little, Inorg. Chim. Acta 358 (2005) 912.
[18] A. Khalid, A.K. Singh, Polyhedron 16 (1997) 33.
[19] G. Singh, A.K. Singh, P. Sharma, J.E. Drake, M.B. Hursthouse, M.E. Light, J. Organomet. Chem. 688 (2003) 20.
[20] L. Pauling, The Nature of the Chemical Bond, 3rd ed., Cornell University Press, Ithaca, New York, 1960.
[21] D.A. Evans, K.R. Campos, J.S. Tedrow, F.E. Michael, M.R. Gagne, J. Am. Chem. Soc. 122 (2000) 7905.
[22] F.H. Allen, O. Kennard, D.G. Watson, L. Brammer, A.G. Orpen, R. Taylor, J. Chem. Soc., Perkin Trans. II. (1987) SI.
[23] S. Bali, A.K. Singh, P. Sharma, R.A. Toscano, J.E. Drake, M.B. Hursthouse, M.E. Light, J. Organomet. Chem. 689 (2004) 2345.
[24] S. Husebye, E.A. Meyers, R.A. Zingaro, J.V. Comasseto, N. Petragnani, Acta Crystallogr. C43 (1987) 1147.

emission quantum efficiency (η) by protecting the metal ion from the luminescence quencher such as O–H and N–H oscillators [5].

The spectroscopic properties of the 2-acyl-1,3-indandione complexes have been only moderately studied. Up to now, the main investigation about rare earth complexes with 2-acyl-1,3-indandiones have been concerned with complexation investigation and luminescence properties of these systems in solution [6–9]. They made a correlation between the intensity parameter η for the Eu^{3+}-complexes, which was defined as the ratio between the intensity of the $^5D_0 \rightarrow {}^7F_2$ and $^5D_0 \rightarrow {}^7F_1$ transitions, and dielectric constant of the solvents and the average polarizability of the ligand molecules. However, to the best of our knowledge, so far, no detailed studies of luminescence, including intensity parameters and ligand-to-metal energy transfer processes in solid state and X-rays structural information on these kinds of complexes have been reported yet.

The present work is devoted to the synthesis, characterization and study of the photoluminescence behavior of seven trivalent Eu^{3+}-complexes $[Eu(ACIND)_3(H_2O)_2]$ and $[Eu(ACIND)_3(TPPO)_2]$ (where ACIND is stands for the ligands 2-acetyl-1,3-indandionate (AIND), 2-isovaleryl-1,3-indandionate (ISOVIND) or 2-benzyl-1,3-indandionate (BIND) in solid state with 2-acyl-1,3-indandionates (Fig. 1). X-ray crystal structure of the $[Eu(ISOVIND)_3 \cdot (H_2O)\text{-}(EtOH)]$ complex is also presented, which, to our knowledge, it is the first report on structural analysis of a complex with the 2-acyl-1,3-indandione ligand. An analysis of the intramolecular energy transfer processes for these compounds was also performed by theoretical methods.

2. Experimental

2.1. Materials and methods

Carbon and hydrogen contents were determined by usual microanalytical procedures using an elemental analyzer model CHN 2400 (Perkin–Elmer). Infrared spectra were recorded in the range from 4000 to 400 cm^{-1} in KBr pellets by using a Bomem model MB102 FTIR spectrophotometer. TG analysis were performed with a TG-50 thermobalance (Shimadzu) by using platinum crucibles with 2 mg of sample, under a dynamic nitrogen atmosphere (50 mL min^{-1}) and a heating rate of 10 °C min^{-1}. Excitation and emission spectra at room (~298 K) and liquid nitrogen temperatures were collected at an angle of 22.5° (front face) in a spectrofluorimeter (SPEX-Fluorolog 2) with double grating 0.22 m monochromator (SPEX 1680), and a 450 W Xenon lamp as excitation source. Luminescence decay curves were measured using a phosphorimeter SPEX 1934D accessory coupled to the spectrofluorimeter.

All reagents diethyl phthalate, acetone, methyl isobutyl ketone, acetophenone and Eu_2O_3 were purchased from Aldrich Chemical Co., $EuCl_3 \cdot 6H_2O$ were prepared according to Ref. [10] by reaction between europium oxide and hydrochloric acid.

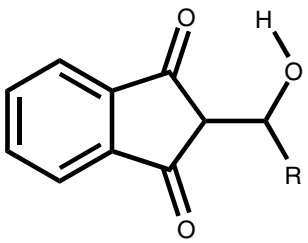

R= CH_3, $CH_2CH(CH_3)_2$, C_6H_5

Fig. 1. Structural formula of the 2-acyl-1,3-indandione ligands.

2.2. Synthesis of the ligands

2-Acetyl-1,3-indandione (AIND), 2-isovaleryl-1,3-indandione (ISOVIND) and 2-benzoyl-1,3-indandione (BIND) ligands were synthesized using a method reported by Kilgore and co-workers [11]. Firstly, sodium ethoxide was formed by reacting 5.7 g (0.25 mol) of sodium with 12 mL (0.25 mol) of dried ethanol in benzene (200 mL), under stirring. A mixture of 55.5 g (0.25 mmol) of diethyl phthalate and the appropriate methyl ketone (acetone, isopropyl methyl ketone or acetophenone) was added, and refluxed at 80 °C for 6 h. After that, the solvent was evaporated under reduced pressure to give a yellow precipitate, which was diluted in 1 L of water and it was allowed to stand overnight. After acidifying with hydrochloric acid a yellow oil was produced, which after 24 h yield a solid product. This product was filtered, dried and recrystallized in methanol to give compound in 40% yield.

Anal. Calc. for AIND, $C_{11}H_8O_3$: C, 70.20; H, 4.30. Found: C, 69.48; H, 4,35%. IR (KBr, cm^{-1}): 3416br, 1762w, 1712s, 1660s, 1627s, 1593s, 1424s, 1390s, 1367s, 1209s, 1147m, 876s, 740s, 695m, 543m. For ISOVIND, $C_{14}H_{14}O_3$: C, 73.02; H, 6.13. Found: C, 72.48; H, 5.67%. IR (KBr, cm^{-1}): 3440br, 2962m, 1713s, 1651s, 1584s, 1465w, 1398w, 1330m, 1286w, 1218m, 1139m, 886s, 745s, 650w. For BIND, $C_{16}H_{10}O_3$: C, 76.80; H, 4.03. Found: C, 77.04; H, 4.16%. IR (KBr, cm^{-1}): 3439br, 3055w, 1711s, 1649s, 1599s, 1559s, 1497m, 1441m, 1401m, 1333s, 1293m, 1169m, 927m, 740s, 684m, 622m, 531w.

2.3. Synthesis of the hydrated Eu^{3+}-complexes

The preparation method of europium indandionate complexes were similar to those used in Ref. [12]. Sodium 2-acetyl-1,3-indandionate was prepared by neutralizing 1.0 g (5.3 mmol) of the ligand 2-acetyl-1,3-indandione with NaOH (1 mol L^{-1}) using deionized water and pH adjusted to 7. To the resulting solution was added dropwise an aqueous solution of $EuCl_3 \cdot 6H_2O$ (0.5 g, 1.4 mmol), forming immediately a yellow precipitated that was filtered, washed with water and dried under vacuum to give the desired product (yields ~90%). The same procedure, was

used to synthesize hydrated Eu^{3+}-complex with 2-isovaleril-1,3-indandionate and 2-benzoyl-1,3-indandionate ligands. In the case of the hydrated Eu^{3+}-complex with ISOVIND, a single crystal suitable for X-ray structure analysis was obtained by slow evaporation from an ethanol solution. The compositions of the complexes were confirmed by elemental analysis:

Anal. Calc. for $[Eu(AIND)_3(H_2O)_2]$, $C_{33}H_{25}EuO_{11}$: C, 52.88; H, 3.36. Found: C, 52.58; H, 3.83%. IR (KBr, cm^{-1}): 3452m, 1676s, 1624s, 1582s, 1510s, 1565s, 1357s, 1211m, 1155m, 1082w, 987m, 885m, 736s, 662m, 534s. For $[Eu(ISOVIND)_3(H_2O)_2]$, $C_{42}H_{43}EuO_{11}$: C, 57.60; H, 4.95. Found: C, 58.30; H, 4.69%. IR (KBr, cm^{-1}): 3415m, 3068m, 2956m, 2870m, 1680s, 1620s, 1579s, 1465s, 1355s, 1284m, 1207m, 1155m, 1072m, 894m, 734s, 667m, 670w, 530m. For $[Eu(ISOVIND)_3\ (H_2O)(EtOH)]$. $C_{44}H_{47}EuO_{11}$: C, 58.47; H, 5.24. Found: C, 58.33; H, 5.20%. IR (KBr, cm^{-1}): 3367m, 3078m, 2952m, 2867m, 1677s, 1629s, 1585s, 1510s, 1470s, 1650s, 1282m, 1205m, 1153m, 1072m, 896m, 733m, 654m, 532m. For $[Eu(BIND)_3(H_2O)_2]$. Calc. for $C_{48}H_{31}EuO_{11}$: C, 61.61; H, 3.34. Found: C, 61.68; H, 3.27%. IR (KBr, cm^{-1}): 3427m, 3062m, 1620s, 1585s, 1490s, 1454s, 1425s, 1363m, 1153w, 885m, 800w, 742m, 702m, 640m, 534m.

2.4. Synthesis of the Eu^{3+}-complexes with TPPO

Europium complexes with TPPO as a second kind of ligand were synthesized using the correspondent hydrated $[Eu(ACIND)_3(H_2O)_2]$ complexes as precursors. A solution of TPPO (0.37 g, 1.3 mmol) in acetone (10 mL) was added to a solution of $[Eu(ACIND)_3(H_2O)_2]$ (0.5 g, ~0.6 mmol) in acetone (20 mL), and the mixture was stirred for 2 h at room temperature. After solvent evaporation, a precipitated was produced, which was filtered, washed with ethanol and dried in vacumm. Yield: ~80%. The compositions of the complex systems were confirmed by elemental analysis and IR data: *Anal.* Calc. for $[Eu(AIND)_3(TPPO)_2]$, $C_{69}H_{51}EuO_{11}P_2$: C, 65.25; H, 4.05. Found: C, 64.93; H, 4.11%.IR (KBr, cm^{-1}): 3107m, 1558s, 1531s, 14317s, 1396s, 1342m, 1227m, 1120m, 1080w, 1037m, 862m, 820s, 777s, 725s, 659m, 430m. For $[Eu(ISOVIND)_3(TPPO)_2]$, $C_{78}H_{69}EuO_{11}P_2$: C, 67.09; H, 4.98. Found: C, 67.04; H, 5.27%. IR (KBr, cm^{-1}): 3056m, 1689m, 1589s, 1491m, 1452s, 1425s, 1362m, 1340m, 1340m, 1167m, 1118m, 1018w, 881m, 798w, 742m, 694m, 636m, 540s. For $[Eu(BIND)_3(TPPO)_2]$, $C_{84}H_{57}EuO_{11}P_2$: C, 69.28; H, 3.95. Found: C, 69.06; H, 3.83%. IR (KBr, cm^{-1}): 3055w, 1687m, 1620s, 1589s, 1490m, 1452s, 1425s, 1340m, 1164m, 1121m, 1020w, 743m, 696m, 636m, 540s.

2.5. X-ray structure determination of $Eu(ISOVIND)_3(H_2O)(EtOH)$

A suitable crystal of the $Eu(ISOVIND)_3(H_2O)(EtOH)$ complex for X-ray diffraction was obtained dissolving the complex in a mixture of ethanol and water in a ratio 3/1 (v/v). The resulting solution was kept in stand by for a week, resulting in yellow hexagonal crystals. A crystal of this compound was mounted in a Enraf-Nonius CAD4 diffractometer with graphite-monochromated Mo Kα ($\lambda = 0.71073$ Å), at 293 K. The structure was solved by direct methods using the SIR92 program [13] and refined by full-matrix least-squares methods on F^2 by the SHELX97 program package [14]. The hydrogen atoms for the water molecule was found in the Fourier difference map, and refined with U equal to 1.3 times the U_{eq} of the Ow. All others non-hydrogen atoms were refined anisotropically and the hydrogen atoms position were calculated in ideal geometry with thermal parameters equal to 1.5 times the U_{eq} of the attached C atom for the methyl groups and 1.2 for the others. Crystallographic data for the $Eu(ISOVIND)_3(H_2O)(EtOH)$ complex are shown in Table 1.

3. Results and discussion

IR spectra of the complexes as compared to the free indandione ligands show a displacement of the C=O stretching to lower frequencies (about 70 cm^{-1}), suggesting that the indandionate ligands are coordinated through oxygen atoms. In the case of the complexes $Eu(ACIND)_3(TPPO)_2$, the displacement of the P=O stretching from 1190 cm^{-1} in the free TPPO ligand to 1170 cm^{-1} in the compounds provides good evidence that the coordination of the TPPO to europium ion is also occurring through oxygen atom.

Table 1
Crystal data and structure refinement for the $[Eu(ISOVIND)_3(H_2O)(EtOH)]$ complex

Formula	$C_{44}H_{47}Eu_1O_{11}$
Formula weight	903.78
Crystal system	monoclinic
Space group	$P2_1/n$ (no. 14)
a (Å)	15.361(1)
b (Å)	18.364(2)
c (Å)	15.705(2)
β (°)	106.373(8)
V (Å^3)	4250.6(8)
Z	4
D_{calc} (g/cm^3)	1.412
μ(Mo Kα) (/mm)	1.533
$F(000)$	1848
Crystal size (mm)	$0.08 \times 0.10 \times 0.15$
Temperature (K)	293
Radiation (Å) Mo Kα	0.71069
θ(Min.–Max.) (°)	2.6, 28.5
Data set hkl, min:max	−19:20; 0:24; −21:0
Total, unique data, R_{int}	11178, 10809, 0.054
Observed data [$I > 2\sigma(I)$]	4859
N_{ref}, N_{par}	10809, 518
R, wR_2, S	0.0516, 0.1360, 0.94
Maximum and average shift/error	0.22, 0.01
Minimum and maximum residual density [e/Å^3]	−0.89, 0.78

$w = 1/\sigma^2(F_o^2) + 0.0517P)^2$ where $P = (F_o^2 + 2F_c^2)/3$.

Thermogravimetric curves for the $[Eu(ACIND)_3(H_2O)_2]$ complexes exhibited similar profiles (figure not shown). The curves show a first weight loss in the range from 120 to 190 °C, which is assigned to the release of two water molecules coordinated to the Eu(III) ion. For [Eu(ISOVIND)$_3$(H_2O)(EtOH)] complex the first weight loss corresponds to 6.8%, which agrees to the release of one water and one ethanol molecule. The complexes with the TPPO ligand present no weight loss until 230 °C, confirming the anhydrous character of these complexes.

3.1. Structure of [Eu(ISOVIND)$_3$(H_2O)(EtOH)]

X-ray analysis reveals that eight oxygen atoms are coordinated to the central europium ion (six from the bidentate ISOVIND ligand, one from the water molecule and another from the ethanol). A key feature of the structure described herein is that, to the best of our knowledge, it is the first example of a rare earth coordination compound with a 2-acyl-1,3-indandionate ligand to be reported. The carbon atoms –CH_2 and –CH_3 from the ligands (2-acyl-1,

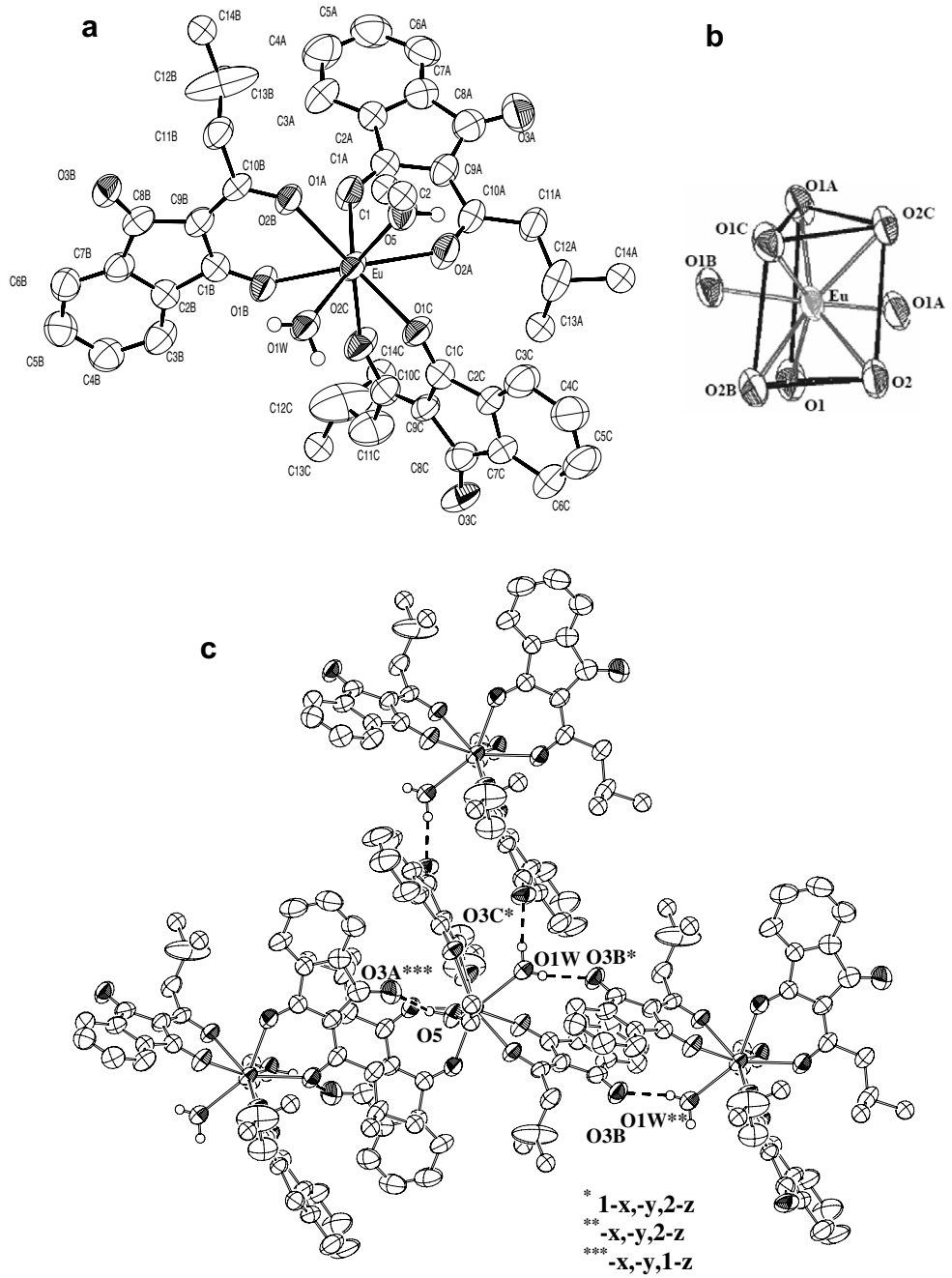

Fig. 2. (a) ORTEP drawing (50% of probability) displaying the X-ray structure of [Eu(ISOVIND)$_3$(H_2O)(EtOH)] complex; the thermal disordered methyl carbon atoms are arbitrary taken with Ueq equal to 0.05. (b) Coordination polyhedron of Eu^{3+} ion and (c) Molecules of [Eu(ISOVIND)$_3$(H_2O)(EtOH)] complex showing intermolecular H-bonding connections as dashed lines.

3-indandionate and ethanol) presents disorder by the thermal vibration. An ORTEP drawing displaying the molecular structure, with the methyl carbon atoms assuming an isotropical displacement supposition, the coordination polyhedron of the Eu(III) ion, and representation of the intermolecular hydrogen bonds in $[Eu(ISOVIND)_3(H_2O)(EtOH)]$, are presented in Fig. 2.

The geometrical arrangement of the oxygen atoms in the first coordination sphere can be described as a bicapped trigonal prism presenting a site symmetry close to C_{2v} (Fig. 2b). The Eu–O distances fall into two distinct ranges where those including O atoms from ISOVIND are shorter (Eu–O ~ 2.40 Å) than those from neutral aqua and ethanol ligands, which present Eu–O distances of 2.422(5) and 2.447(4) Å, respectively (Table 2). It is also important to observe in the crystal structure of $Eu(ISOVIND)_3(H_2O)(EtOH)$ that the hydrogen bond scheme (Table 2) gives rise to a supermolecular polymer (Fig. 2c). The water molecule coordinated to the Eu^{3+} ion is simultaneously hydrogen-bonded to two uncoordinated carbonyl oxygen atom of ISOVIND of two adjacent molecules (symmetry operation $\bar{1}$), and the OH from ethanol is connected to the third CO group of ISOVIND through O–H···O hydrogen bonds. The O_{water}–H···$O_{carbonyl}$ hydrogen bonds are similar to those found for rare earth complexes with aliphatic β-diketonate ligands reported in the literature [15].

Excitation spectra of the europium complexes with 2-acyl-1,3-indandione ligands, recorded at 77 K in the spectral range 250–590 nm (Fig. 3) were obtained with emission monitored at $^5D_0 \rightarrow {}^7F_2$ hypersensitive transition around

Table 2
Selected bond distances (Å), angles (°) and hydrogen bonds in the $[Eu(ISOVIND)_3(H_2O)(EtOH)]$ complex

Distance (Å)			
Eu–O1a	2.400(4)	Eu–O2a	2.401(5)
Eu–O1b	2.403(4)	Eu–O2b	2.382(3)
Eu–O1c	2.410(5)	Eu–O2c	2.348(4)
Eu–O1w	2.420(5)	Eu–O5	2.448(4)
Angles (°)			
O1a–Eu–O1b	78.5(2)	O1c–Eu–O2a	69.8(2)
O1a–Eu–O1c	140.9(2)	O1c–Eu–O2b	132.7 (1)
O1a–Eu–O1w	149.5(2)	O1c–Eu–O2c	73.0(1)
O1a–Eu–O2a	71.2(2)	O1c–Eu–O5	74.0(2)
O1a–Eu–O2b	76.2(2)	O1w–Eu–O2a	139.3(2)
O1a–Eu–O2c	98.2(1)	O1w–Eu–O2b	80.1(2)
O1a–Eu–O5	97.2(1)	O1w–Eu–O2c	89.6(2)
O1b–Eu–O1c	129.9(2)	O1w–Eu–O5	93.8(2)
O1b–Eu–O1w	76.3(2)	O2a–Eu–O2b	129.2(2)
O1b–Eu–O2a	134.0(1)	O2a–Eu–O2c	79.8(2)
O1b–Eu–O2b	72.5(2)	O2a–Eu–O5	74.0(1)
O1b–Eu–O2c	71.17(2)	O2b–Eu–O2c	143.6(2)
O1b–Eu–O5	145.0(2)	O2b–Eu–O5	72.7(2)
O1c–Eu–O1w	69.6(2)	O2c–Eu–O5	143.3(2)

A	H	B	*d* (A–H) (Å)	*d* (H...B) (Å)	*d* (A...B) (Å)	Angle (°)	Symmetry operation
Hydrogen bonds for the [Eu(ISOVIND)$_3$(H$_2$O)(EtOH)] complex							
O1w	H1Ow	O3b	0.76(8)	1.98(8)	2.717(7)	166(8)	$1-x, -y, 2-z$
O1w	H2Ow	O3c	0.87(8)	1.93(8)	2.793(7)	168(5)	$-x, -y, 2-z$
O5	H1O5	O3a	0.93	2.12	2.770(7)	125	$-x, -y, 1-z$

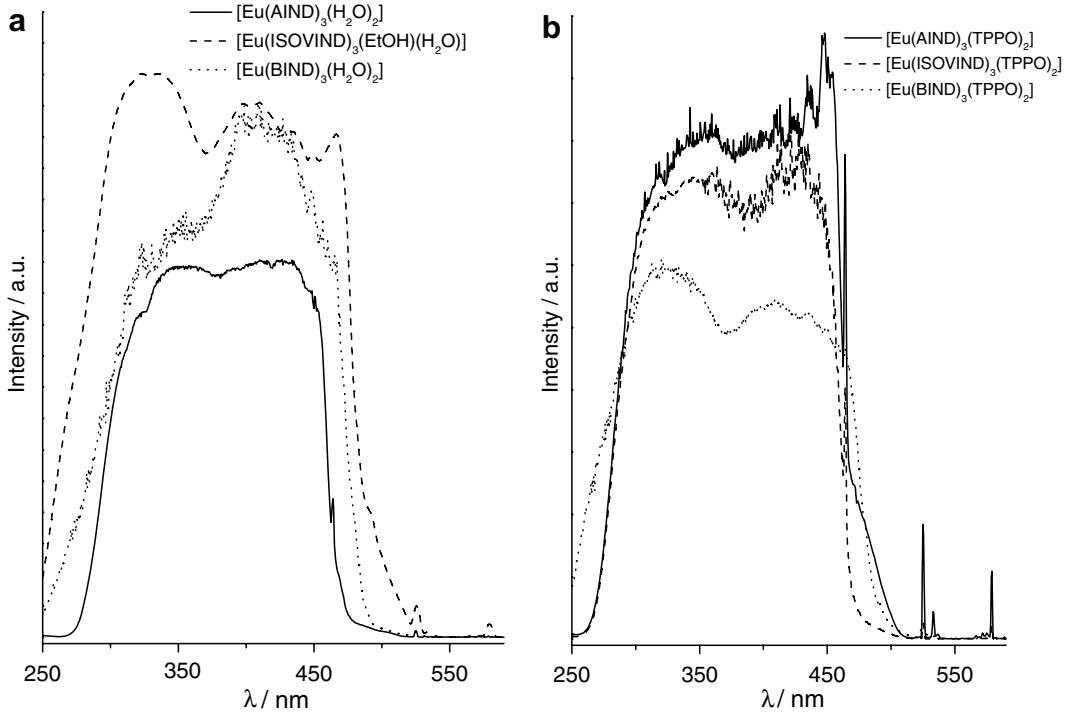

Fig. 3. Excitation spectra of (a) $[Eu(ACIND)_3 \cdot (H_2O)_2]$ and (b) $[Eu(ACIND)_3 \cdot (TPPO)_2]$ complexes in solid state, at 77 K. The spectra were recorded with emission monitored at 612 nm.

612 nm. These spectra present a strong broad band between 270 and 470 nm assigned to the photoexcitation process of the Eu(III) ion via the $S_0 \rightarrow S_1$ transition. The excitation spectra also exhibit narrow bands assigned to the 4f–4f transitions from the $^7F_0$ ground level to the excited states. However, these bands are less intense than those bands corresponding to the $S_0 \rightarrow S_1$ transition. This result gives evidence of europium luminescence sensitization through intramolecular energy transfer from the 2-acyl-1,3-indandione ligands.

Photoluminescence spectra of the hydrated complexes and those with the TPPO ligand, at 77 K, are displayed in Fig. 4. The emission spectra show characteristic $^5D_0 \rightarrow {}^7F_J$ ($J = 0$–4) transitions of Eu(III), with the hypersensitive $^5D_0 \rightarrow {}^7F_2$ transition (at 612 nm) as the most prominent one. The local-ligand field splitting is particularly evident for $^5D_0 \rightarrow {}^7F_{1-4}$ transitions, presenting Stark $(2J + 1)$-components, indicating that the Eu^{3+} ion occupies a site with low symmetry [16,17]. It is observed that, in general, emission spectra of complexes with TPPO present different profiles from the respective hydrated compounds, reflecting changes in the chemical environment around the Eu^{3+} ion. It is also important to mention that the emission spectra of all europium complexes do not exhibit ligand centered transitions, indicating that there is an efficient intramolecular energy transfer from the indandionate ligands to the Eu^{3+} ion.

In order to get further information on the chemical environment of the Eu^{3+} ions in these complexes, experimental intensity parameters Ω_λ ($\lambda = 2$ and 4), radiative rates (A_{0J}) for the $^5D_0 \rightarrow {}^7F_2$ and $^5D_0 \rightarrow {}^7F_4$ transitions and emission quantum efficiency (η) were determined (Table 3) according to Refs. [16,18].

Experimental intensity parameter Ω_2 exhibits values around 40×10^{-20} cm^2 for the hydrated complexes, suggesting the presence of a highly polarizable chemical environment around the Eu^{3+} ion [5]. These values are as high as those presented for europium complexes containing aliphatic β-diketonate, such as TTA and DBM-europium complexes [3]. It is also observed a decrease in Ω_2 for complexes with TPPO as compared to the hydrated ones. This result may be a consequence of steric hindrance due to phenyl groups that belong to the TPPO ligand.

Comparing the values of η for the complexes containing the TPPO ligand with their respective hydrated compounds, it is concluded that indeed a substitution of water

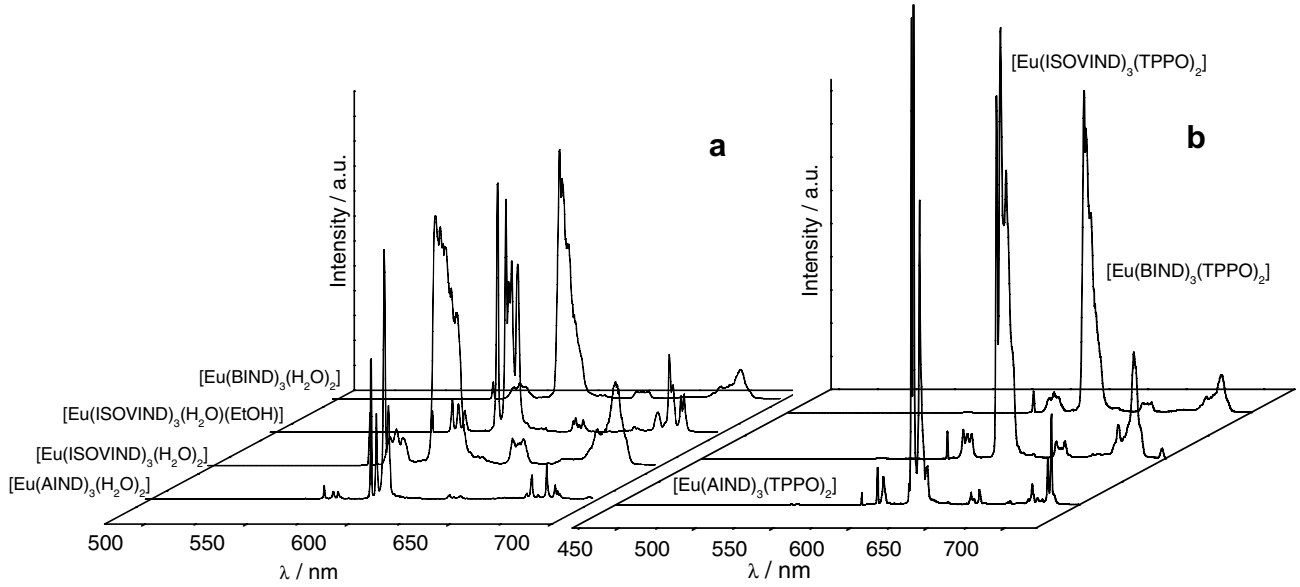

Fig. 4. Emission spectra of (a) $[Eu(ACIND)_3 \cdot (H_2O)_2]$ and (b) $[Eu(ACIND)_3 \cdot (TPPO)_2]$ complexes in solid state, at 77 K, recorded under excitation at 350 nm.

Table 3
Intensity parameters (Ω_λ), radiative (A_{rad}), non-radiative (A_{nrad}) rates and emission quantum efficiency of the $^5D_0$ emitting level determined for the 2-acyl-1,3-indandionate complexes

Compound	Ω_2 (10^{-20} cm^2)	Ω_4 (10^{-20} cm^2)	τ (ms)	A_{rad} (s^{-1})	A_{nrad} (s^{-1})	A_{tot} (s^{-1})	η (%)
$[Eu(AIND)_3 \cdot (H_2O)_2]$	42.1	14.8	0.1079	1532	7739	9261	16.5
$[Eu(AIND)_3 \cdot (TPPO)_2]$	35.5	8.9	0.5309	1255	628	1883	66.7
$[Eu(ISOVIND)_3 \cdot (H_2O)_2]$	40.4	15.8	0.0387	1499	24330	25830	5.8
$[Eu(ISOVIND)_3 \cdot (H_2O)(EtOH)]$	40.9	17.5	0.056	1537	16320	17860	8.6
$[Eu(ISOVIND)_3 \cdot (TPPO)_2]$	35.3	11.4	0.5071	1283	688	1972	65.1
$[Eu(BIND)_3 \cdot (H_2O)_2]$	40.5	14.2	0.0539	1482	17080	18560	8.0
$[Eu(BIND)_3 \cdot (TPPO)_2]$	29.4	15.9	0.3181	1165	1978	3143	37.1

molecules in the first coordination sphere of the Eu^{3+} ion by the TPPO ligand occurs. This result reflects a decrease in the non-radiative rates (A_{nrad}) that is a consequence of the absence of O–H oscillators present in coordinated water molecules, which causes multiphonon deactivation process in the Eu^{3+} ion [5].

Theoretical structure for the [Eu(ISOVIND)$_3$(H_2O)-(EtOH)] complex was calculated using the Sparkle/AM1 model [16]. The result obtained agrees with those determined by X-rays diffraction (Fig. 2), indicating that the Sparkle/AM1 model has also proved to be very useful in predicting coordination geometries of the Eu-indandionate complexes.

Theoretical quantum yield, q, for [Eu(ISOVIND)$_3$-(H_2O)(EtOH)] was calculated according to the procedure described in Refs. [4,19]. The calculated values of transfer (W_{ET}) and back-transfer (W_{BT}) rates between ligand and Eu^{3+} ion levels are the following: $S_1 \rightarrow {}^5D_2$, $W_{ET} = 4.42 \times 10^6\ s^{-1}$; $S_1 \rightarrow {}^5D_1$, $W_{ET} = 1.30 \times 10^{10}\ s^{-1}$; $S_1 \rightarrow {}^5D_0$, $W_{ET} = 9.5 \times 10^9\ s^{-1}$; $T \rightarrow {}^5D_1$, $W_{ET} = 5.45 \times 10^9\ s^{-1}$ ($W_{BT} = 4.95 \times 10^9\ s^{-1}$); $T \rightarrow {}^5D_0$, $W_{ET} = 6.16 \times 10^9\ s^{-1}$ ($W_{BT} = 1.37 \times 10^6\ s^{-1}$). The back-transfer ($W_{BT}$) rates ${}^5D_J \rightarrow S_1$ are negligible. Consequently, there are two probable intramolecular energy transfer processes as operative channels from ISOVIND to the Eu^{3+} ion in [Eu(ISOVIND)$_3$-(H_2O)(EtOH)]: (**1**) $S_0 \rightarrow S_1 \rightarrow T \rightarrow ({}^5D_1, {}^5D_0) \rightarrow {}^7F_J$ and (**2**) $S_0 \rightarrow S_1 \rightarrow ({}^5D_1, {}^5D_0) \rightarrow {}^7F_J$. Besides, the value of q (8.0%) is close to $\eta = 8.6\%$, indicating that an efficient energy transfer from indandionate ligands to the Eu^{3+} ion in fact occurs.

4. Conclusions

It has been demonstrated that the first structurally characterized Eu^{3+}–(2-acyl-1,3-indandione) complex indicated that their coordination to the metal ion occurs in similar form as for aliphatic β-diketonates. Our results indicate that an efficient ligand-metal ion energy transfer process occurs for the Eu–(2-acyl-1,3-indandione) complexes, and that the channels (**1**) and (**2**) are the most probable ones involved in photoluminescent mechanism for [Eu(ISOVIND)$_3$(H_2O)-(EtOH)] complex.

Acknowledgments

The authors acknowledge FAPESP, CNPq, RENAMI and IMMC for financial support.

Appendix A. Supplementary data

Crystallographic data (excluding structure factors) for the structure have been with the Cambridge Crystallographic Data Centre as supplementary publication no. CCDC 296851. Copies of the data can be obtained free of charge on application to CCDC, 12 Union Road, Cambridge CB2 1EZ, UK [fax: int. code + 44 1223 336 033; e-mail:deposit@ccdc.cam.ac.uk]. Supplementary data associated with this article can be found, in the online version, at doi:10.1016/j.poly.2006.06.035.

References

[1] P.R. Selvin, Ann. Rev. Biophys. Biomol. Struct. 31 (2002) 275.
[2] I. Hemmila, V.W. Mukkala, Crit. Rev. Clin. Lab. Sci. 38 (2001) 441.
[3] J. Kido, Y. Okamoto, Chem. Rev. 102 (2002) 2357.
[4] R. Reyes, M. Cremona, E.E.S. Teotonio, H.F. Brito, O.L. Malta, Chem. Phys. Lett. 396 (2004) 54.
[5] G.F. de Sá, O.L. Malta, C.D. Donega, A.M. Simas, R.L. Longo, P.A. Santa-Cruz, E.F. Silva, Coord. Chem. Rev. 196 (2000) 165.
[6] G.I. Gerasimenko, N.S. Poluektov, Dokl. Akad. Nauk SSSR 278 (1984) 117.
[7] N.S. Poluektov, G.I. Gerasimenko, T.M. Ulyanova, M.A. Tishchenko, R.A. Vitkun, Zh. Neorg. Khim. 27 (1982) 2242.
[8] S. Zhinkun, W. Jiang, Y. Ding, J. Hu, Fresen. J. Anal. Chem. 360 (1998) 731.
[9] T.B. Kravchenko, S.V. Beltiukova, N.A. Nazarenko, L.I. Kononenko, N.S. Poluektov, Dokl. Akad. Nauk SSSR 259 (1981) 151.
[10] M.P. Bemquerer, C. Bloch, H.F. Brito, E.E.S. Teotonio, M.T.M. Miranda, J. Inorg. Biochem. 91 (2002) 363.
[11] L.B. Kilgore, J.H. Ford, W.C. Wolfe, Ind. Eng. Chem. 34 (1942) 494.
[12] H.F. Brito, O.L. Malta, M.C.F.C. Felinto, E.E.S. Teotonio, J.F.S. Menezes, C.F.B. Silva, C.S. Tomiyama, C.A.A. Carvalho, J. Alloy Comp. 344 (2002) 293.
[13] SIR92 – A. Altomare, G. Cascarano, C. Giacovazzo, A. Guagliardi, J. Appl. Crystallogr. 26 (1993) 343.
[14] G.M. Sheldrick, SHELX-97, Program for Crystal Structure Refinement, Göttingen University, Germany, 1997.
[15] C. Pettinari, F. Marchetti, R. Pettinari, A. Drozdov, S. Troyanov, A.I. Voloshin, N.M. Shavaleev, J. Chem. Soc., Dalton Trans. 10 (2002) 1409.
[16] W.M. Faustino, S.A. Junior, L.C. Thompson, G.F. de Sá, O.L. Malta, A.M. Simas, Inter. J. Quantum Chem. 103 (2005) 572.
[17] J.A. Fernandes, S.S. Braga, M. Pillinger, R.A. Sá Ferreira, L.D. Carlos, A. Hazell, P. Ribeiro-Claro, I.S. Gonçalves, Polyhedron 25 (2006) 1471.
[18] E.E.S. Teotonio, J.G.P. Espínola, H.F. Brito, O.L. Malta, S.F. Oliveira, D.L.A. de Faria, C.M.S. Izumi, Polyhedron 21 (2002) 1837.
[19] W.M. Faustino, G.B. Rocha, F.R.G.E. Silva, O.L. Malta, G.F. Sa, A.M. Simas, J. Mol. Struct.-Theochem. 527 (2000) 245.

ucts (from Alfa and Aldrich) and were used without further purification. Solvents were of reagent grade and were purified by the usual methods. *Caution*: Although no problems were encountered during the course of this work, attention is drawn to the potentially explosive nature of the perchlorate salts.

2.2. Synthesis of the macrocycle L

The synthesis of L was achieved following the literature method [5]. To a refluxing suspension of Ba(II) chloride dihydrate (1.22 g, 5 mmol) and 2,6-diformylpyridine (1.35 g, 10 mmol) in methanol (200 ml), a solution of diethylenetriamine (1.08 ml, 10 mmol) was added dropwise. The mixture was refluxed for 3 h and cooled to 0 °C. Sodium tetrahydroborate (1.52 g, 40 mmol) was added, and after 30 min a second portion (0.76 g, 20 mmol) was added. The mixture was stirred for 10 h at room temperature, and after that it was concentrated to dryness under reduced pressure. The crude solid was extracted with chloroform (3 × 100 ml) and a brown oil was obtained. It was dissolved in methanol and hydrobromic acid was added dropwise until acid pH. The tetrahydrobromide salt of the ligand L^1 was isolated.

Anal. Calc. for $C_{22}H_{36}N_8$ (molecular weight: 412.58): C, 64.1; H, 8.8; N, 27.2. Found: C, 64.2; H, 8.7; N, 27.1%. Yield: 65%. IR (KBr cm^{-1}): 1454, 1575, 1592 [ν(C=C) and $\nu(C{=}N)_{py}$]. MS (FAB, *m*/*z*) 413. ^1H NMR ($CDCl_3$): 7.74 (t, 2H, $H_{py(p)}$), 7.30, (d, 4H, $H_{py(m)}$), 3.8 (s, 8H, CH_2), 2.67 (s, 16H, $CH_{2ethylene}$).

2.3. Synthesis of the metal complexes: general procedure

The appropriate metal salt (0.25 mmol in a 1:1 or 0.5 mmol in a 2:1 M:L molar ratio) was dissolved in acetonitrile (10 mL) and added to a stirred solution of the ligand L (0.1031 g, 0.25 mmol) in acetonitrile (20 mL). The solution was stirred for 2 h and concentrated in a rotary evaporator until ca. 5–6 mL remained. The product obtained was filtered off and dried. In both cases the same dinuclear complexes were obtained and the data gathered here belong to the 2:1 procedure.

2.3.1. $[Co_2L](NO_3)_4 \cdot H_2O$

Anal. Calc. for $C_{22}H_{38}N_{12}O_{13}Co_2$: C, 33.2; H, 4.8; N, 21.1. Found: C, 33.3; H, 4.8; N, 21.0%. Yield: 49%. IR (KBr, cm^{-1}): 1607, 1579, 1443 [ν(C=C) and $\nu(C{=}N)_{py}$], 1495, 1383, 1279, 1074, 830, 798, 791 [$\nu(NO_3^-)$]. MS (FAB, *m*/*z*): 533 $[CoL(NO_3)]^+$, 716 $[Co_2L(NO_3)_3]^+$. $\Lambda_M/\Omega^{-1}\,cm^2\,mol^{-1}$ (in CH_3CN): 284 (2:1). Colour: pink.

2.3.2. $[Ni_2L(NO_3)_2](NO_3)_2 \cdot H_2O$

Anal. Calc. for $C_{22}H_{38}N_{12}O_{13}Ni_2$: C, 33.2; H, 4.8; N, 21.1. Found: C, 33.0; H, 4.7; N, 21.3%. Yield: 55%. IR (KBr, cm^{-1}): 1608, 1582, 1444 [ν(C=C) and $\nu(C{=}N)_{py}$], 1498, 1383, 1277, 1072, 830, 798, 791 [$\nu(NO_3^-)$]. MS (FAB, *m*/*z*): 469 $[NiL]^+$, 717 $[Ni_2L(NO_3)_3]^+$. $\Lambda_M/\Omega^{-1}\,cm^2\,mol^{-1}$ (in CH_3CN): 233 (2:1). Colour: blue.

2.3.3. $[Cu_2L(NO_3)_4] \cdot 4H_2O$

Anal. Calc. for $C_{22}H_{44}N_{12}O_{16}Cu_2$: C, 30.84; H, 5.2; N, 19.6. Found: C, 30.8; H, 5.2; N, 19.6%. Yield: 35%. IR (KBr, cm^{-1}): 1604, 1584, 1444 [ν(C=C) and $\nu(C{=}N)_{py}$], 1470, 1384, 1091, 831, 804 [$\nu(NO_3^-)$]. MS (FAB, *m*/*z*): 663 $[Cu_2L(NO_3)_2]^+$, 726 $[Cu_2L(NO_3)_3]^+$. $\Lambda_M/\Omega^{-1}\,cm^2\,mol^{-1}$ (in CH_3CN): 246 (2:1). Colour: blue.

2.3.4. $[Co_2L](ClO_4)_4 \cdot 4H_2O$

Anal. Calc. for $C_{22}H_{44}N_8O_{20}Cl_4Co_2$: C, 26.4; H, 4.4; N, 11.2. Found: C, 26.3; H, 4.2; N, 11.3%. Yield: 47%. IR (KBr, cm^{-1}): 1609, 1583, 1456 [ν(C=C) and $\nu(C{=}N)_{py}$], 1142, 1120, 1108, 1087, 636, 627 [$\nu(ClO_4^-)$]. MS (FAB, *m*/*z*): 468 $[CoL]^+$, 827 $[Co_2L(ClO_4)_3]^+$. $\Lambda_M/\Omega^{-1}\,cm^2\,mol^{-1}$ (in CH_3CN): 363 (3:1). Colour: brown.

2.3.5. $[Ni_2L](ClO_4)_4 \cdot CH_3CN$

Anal. Calc. for $C_{24}H_{39}N_9O_{16}Cl_4Ni_2$: C, 29.8; H, 4.1; N, 13.0. Found: C, 30.0; H, 4.2; N, 13.3%. Yield: 55%. IR (KBr, cm^{-1}): 1603, 1583, 1469 [ν(C=C) and $\nu(C{=}N)_{py}$], 1144, 1116, 1089, 636, 628 [$\nu(ClO_4^-)$]. MS (FAB, *m*/*z*): 571 $[NiL(ClO_4)]^+$, 827 $[Ni_2L(ClO_4)_3]^+$. $\Lambda_M/\Omega^{-1}\,cm^2\,mol^{-1}$ (in CH_3CN): 351 (3:1). Colour: blue.

2.3.6. $[Cu_2L(ClO_4)_4] \cdot 5H_2O$

Anal. Calc. for $C_{22}H_{46}N_8O_{21}Cl_4Cu_2$: C, 25.7; H, 4.5; N, 10.9. Found: C, 25.9; H, 4.0; N, 10.9%. Yield: 51%. IR (KBr, cm^{-1}): 1604, 1584, 1444 [ν(C=C) and $\nu(C{=}N)_{py}$], 1145, 1119, 1087, 636, 627 [$\nu(ClO_4^-)$]. MS (FAB, *m*/*z*): 537 $[Cu_2(ClO_4)]^+$, 837 $[Cu_2L(ClO_4)_3]^+$. $\Lambda_M/\Omega^{-1}\,cm^2\,mol^{-1}$ (in CH_3CN): 383 (3:1). Colour: blue.

2.4. Physical measurements

Elemental analyses were performed in a Carlo-Erba EA microanalyser. Infra-red spectra were recorded as KBr discs on a Bruker IFS-66V spectrophotometer. The L-SIMS mass spectra were recorded using a Micromass Autospec spectrometer using 3-nitrobenzyl alcohol as the matrix. Conductivity measurements were carried out in 10^{-3} mol dm^{-3} acetonitrile solutions at 20 °C using a WTW LF3 conductivitymeter. The ^1H NMR spectra were recorded on a Bruker 500 MHz, and $CDCl_3$ was used as the solvent. Solid state electronic spectra were recorded on a Hitachi 4–3200 spectrophotometer using $MgCO_3$ as the reference. Magnetic studies were determined at room temperature on a vibration sample magnetometer (VSM) Digital Measurement System 1660 with a magnetic field of 5000 G.

2.5. Crystal structure determination

By slow recrystallisation from acetonitrile, crystals of the compounds $[Ni_2L(NO_3)_2](NO_3)_2$, $[Cu_2L(NO_3)_4]$ and

Table 1
Crystal data and structure refinement for $[Ni_2L(NO_3)_2](NO_3)_2$, $[Cu_2L(NO_3)_4]$ and $[Cu_2L(ClO_4)_4]$

	$[Ni_2L(NO_3)_2](NO_3)_2$	$[Cu_2L(NO_3)_4]$	$[Cu_2L(ClO_4)_4]$
Empirical formula	$C_{11}H_{18}N_6O_6Ni$	$C_{22}H_{36}N_{12}O_{12}Cu_2$	$C_{22}H_{36}N_8O_{16}Cl_4Cu_2$
Formula weight	389.02	787.71	937.47
Temperature (K)	298(2)	293(2)	293(2)
Wavelength (Å)	0.71073	0.71073	0.71073
Crystal system	monoclinic	triclinic	triclinic
Space group	$P21/n$	$P\bar{1}$	$P\bar{1}$
Unit cell dimensions			
a (Å)	9.2363(16)	7.897(2)	8.3346 (10)
b (Å)	14.084(2)	8.807(3)	9.1615(11)
c (Å)	12.289(2)	12.011(3)	12.1615(14)
α (°)		98.402(9)	98.590(2)
β (°)	96.270(3)	91.877(7)	91.782(2)
γ (°)		111.178(7)	110.675(2)
Volume (Å^3)	1589.0(5)	767.3(4)	855.54(18)
Z	4	1	1
Density (calculated) (Mg/m^3)	1.626	1.705	1.820
Absorption coefficient (mm^{-1})	1.264	1.468	1.639
$F(000)$	808	406	478
Crystal size (mm^3)	$0.40 \times 0.16 \times 0.15$	$0.23 \times 0.11 \times 0.07$	$0.27 \times 0.20 \times 0.18$
Theta range for data collection	2.21–26.38°	2.52–28.04°	1.70–28.05°
Index ranges	$-11 \leqslant h \leqslant 11$, $0 \leqslant k \leqslant 17$, $0 \leqslant l \leqslant 15$	$-10 \leqslant h \leqslant 10$, $-11 \leqslant k \leqslant 11$, $-15 \leqslant l \leqslant 13$	$-10 \leqslant h \leqslant 11$, $-12 \leqslant k \leqslant 10$, $-16 \leqslant l \leqslant 13$
Reflections collected	18041	4503	5258
Independent reflections (R_{int})	3251 (0.0240)	3127 (0.0543)	3649 (0.0327)
Completeness to θ (%)	99.8 (26.38°)	84.0 (28.04°)	88.2 (28.05°)
Absorption correction	SADABS	SADABS	SADABS
Maximum and minimum transmission	0.8331 and 0.6319	0.9042 and 0.7289	0.7568 and 0.6659
Refinement method	full-matrix least-squares on F^2	full-matrix least-squares on F^2	full-matrix least-squares on F^2
Data/restraints/parameters	3251/0/217	3127/0/217	3649/0/235
Goodness-of-fit on F^2	1.042	0.794	0.870
Final R indices $[I > 2\sigma(I)]$	$R_1 = 0.0239$, $wR_2 = 0.0613$	$R_1 = 0.0676$, $wR_2 = 0.1201$	$R_1 = 0.0516$, $wR_2 = 0.1002$
R indices (all data)	$R_1 = 0.0291$, $wR_2 = 0.0648$	$R_1 = 0.1682$, $wR_2 = 0.1453$	$R_1 = 0.0975$, $wR_2 = 0.1114$
Largest difference in peak and hole (e Å^{-3})	0.299 and −0.244	1.039 and −0.968	0.560 and −0.606

$[Cu_2L(ClO_4)_4]$, suitable for X-ray diffraction, were obtained. The details of the X-ray crystal data and the structure solution and refinement are given in Table 1. Measurements were made on a Bruker SMART CCD 1000 area diffractometer. All data were corrected for Lorentz and polarization effects. Empirical absorption corrections were also applied for all the crystal structures obtained [6]. Complex scattering factors were taken from the program package SHELXTL [7]. The structures were solved by direct methods, which revealed the position of all non-hydrogen atoms. All the structures were refined on F^2 by a full-matrix least-squares procedure using anisotropic displacement parameters for all non-hydrogen atoms. The hydrogen atoms were located in their calculated positions and refined using a riding model (see Scheme 1).

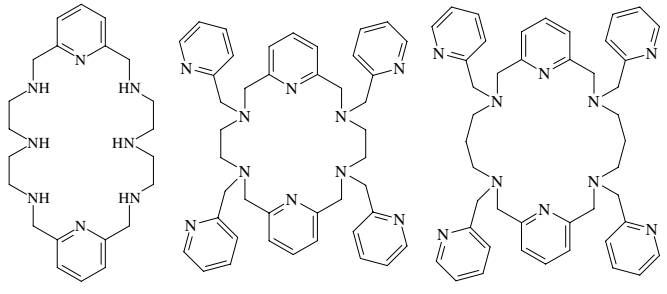
NH
HN
NH
HN
NH
HN
N
N
N

investigated, and the complexation was performed by mixing acetonitrile solutions of both ligand and metal salt. In all cases, the products isolated were the dinuclear complexes, $[Co_2L](NO_3)_4 \cdot H_2O$, $[Ni_2L(NO_3)_2](NO_3)_2 \cdot H_2O$, $[Cu_2L(NO_3)_4] \cdot 4H_2O$, $[Co_2L](ClO_4)_4 \cdot 4H_2O$, $[Ni_2L](ClO_4)_4 \cdot CH_3CN$ and $[Cu_2L(ClO_4)_4] \cdot 5H_2O$. Crystalline products were obtained upon evaporation of the solutions.

The complexes appear to be air stable; they are soluble in acetonitrile, dimethylformamide and dimethylsulfoxide and insoluble in water, methanol, ethanol and chloroform. They were characterized by elemental analysis (C, N, H), molar conductivity, mass spectrometry, IR spectroscopy, magnetic measurements, UV–Vis spectroscopy and X-ray diffraction for $[Ni_2L(NO_3)_2](NO_3)_2$, $[Cu_2L(NO_3)_4]$ and $[Cu_2L(ClO_4)_4]$ complexes.

3.1. Crystal structures

Blue prisms of $[Ni_2L(NO_3)_2](NO_3)_2$, $[Cu_2L(NO_3)_4]$ and $[Cu_2L(ClO_4)_4]$, were obtained by slow recrystallization of the complexes in acetonitrile. The details of the X-ray crystal structure solution and refinement for all complexes are given in Table 1. The molecular structure and selected bond lengths relating to the coordination environment of the metals are given in Figs. 1–3 for $[Ni_2L(NO_3)_2](NO_3)_2$, $[Cu_2L(NO_3)_4]$ and $[Cu_2L(ClO_4)_4]$, respectively.

The $[Ni_2L(NO_3)_2](NO_3)_2$ crystal structure is consistent with the cationic complex $[Ni_2L(NO_3)_2]^{2+}$ and two non-coordinated nitrate anions. In $[Ni_2L(NO_3)_2]^{2+}$, the structure shows two metal atoms endocyclically coordinated into the macrocyclic cavity, each one situated in opposite sides of the ligand hole in a N_4O_2 environment. The metal ions are bonded to one pyridine group, three secondary amine nitrogen atoms – two adjacent from one side of the macrocyclic framework and the third from the other side – and two oxygen atoms from one asymmetric bidentate nitrate group. As is usual in this kind of structure, the distortion from octahedral geometry is due to the small bite of the bidentate nitrate ligand O(1N)–Ni(1)–O(2N), 60.06(5)°. The other two nitrate ions are positioned outside the primary metal coordination sphere, showing a hydrogen bond contact with N(2)–H(2A), where the N(2)–H(2A)···O(4N) distance is 2.298 Å. The shorter bond length corresponds to the pyridine nitrogen atom, Ni–N1, 1.995(1) Å, the average value for the Ni–N_{amine} bond lengths being 2.134 Å, similar to that found in other similar octahedral Ni(II) complexes [8].

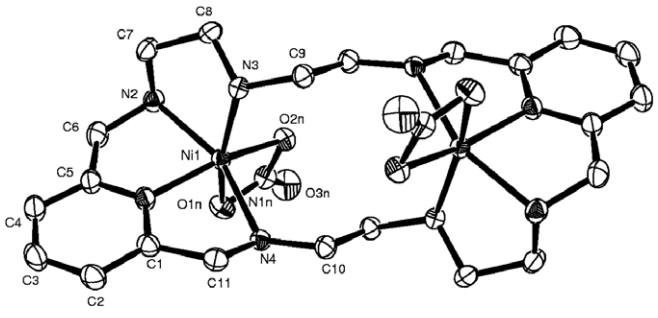

Fig. 1. Crystal structure of $[Ni_2L(NO_3)_2](NO_3)_2$; Selected bond lengths (Å) and angles (°): N(1)–Ni(1) 1.9949(14), N(2)–Ni(1) 2.1138(14), N(3)–Ni(1) 2.0967(14), N(4)–Ni(1) 2.1904(13), O(1N)–Ni(1) 2.1794(14), O(2N)–Ni(1) 2.1136(12), N(1)–Ni(1)–N(3) 101.89(6), N(1)–Ni(1)–N(2) 79.06(6), N(3)–Ni(1)–N(2) 83.97(5), N(1)–Ni(1)–O(2N) 156.89(5), N(3)–Ni(1)–O(2N) 100.23(5), N(2)–Ni(1)–O(2N) 96.75(5), N(1)–Ni(1)–O(1N) 97.15(6), N(3)–Ni(1)–O(1N) 159.36(5), N(2)–Ni(1)–O(1N) 91.96(6), O(2N)–Ni(1)–O(1N) 60.06(5), N(1)–Ni(1)–N(4) 78.54(6), N(3)–Ni(1)–N(4) 101.21(5), N(2)–Ni(1)–N(4) 157.59(5), O(2N)–Ni(1)–N(4) 103.63(5), O(1N)–Ni(1)–N(4) 90.25(5).

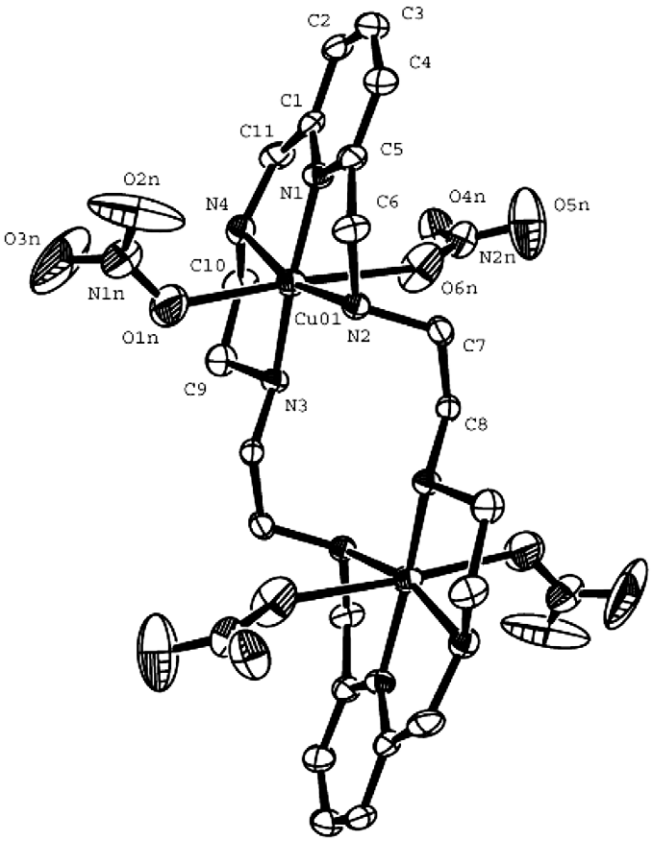

Fig. 2. Crystal structure of $[Cu_2L(NO_3)_4]$; Selected bond lengths (Å) and angles (°): N(1)–Cu(01) 1.914(6), N(2)–Cu(01) 2.072(5), N(3)–Cu(01)#1 2.024(5), N(4)–Cu(01)#1 2.018(5), O(1N)–Cu(01) 2.339(7), O(6N)–Cu(01) 2.626(7), Cu(01)–N(4)#1 2.018(5), Cu(01)–N(3)#1 2.024(5), N(1)–Cu(01)–N(4)#1 81.2(3), N(1)–Cu(01)–N(3)#1 161.3(2), N(4)#1–Cu(01)–N(3)#1 86.5(2), N(1)–Cu(01)–N(2) 82.6(2), N(4)#1–Cu(01)–N(2) 163.8(2), N(3)#1–Cu(01)–N(2) 109.3(2), N(1)–Cu(01)–O(1N) 105.2(3), N(4)#1–Cu(01)–O(1N) 91.9(3), N(3)#1–Cu(01)–O(1N) 89.2(3), N(2)–Cu(01)–O(1N) 91.8(3), N(1)–Cu(01)–O(6N) 79.2(3), N(4)–Cu(01)–O(6N) 87.1(3), N(3)–Cu(01)–O(6N) 87.4(3), N(2)–Cu(01)–O(6N) 38.63(3).

The copper(II) crystal structures show the neutral compound $[Cu_2LX_4]$ ($X = NO_3^-$ or ClO_4^-) with similar gross features for both cases. The crystal structures confirm the presence of dinuclear endomacrocyclic complexes, where the metal atoms are six coordinated by four donor nitrogen atoms from the macrocyclic backbone, similar to that described above for the nickel complex, and two oxygen atoms from two monodentate anions, nitrate for

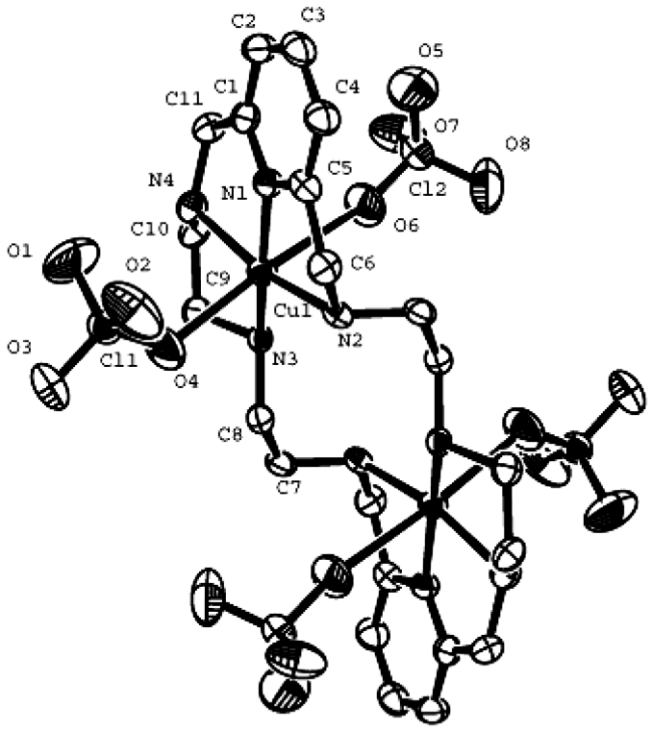

Fig. 3. Crystal structure of $[\mathbf{Cu_2L(ClO_4)_4}]$; Selected bond lengths (Å) and angles (°). Cu(1)–N(1) 1.921(4), Cu(1)–N(3) 2.016(4), Cu(1)–N(4) 2.018(4), Cu(1)–N(2) 2.090(4), Cu(1)–O(4) 2.414(4), Cu(1)–O(6) 2.617(4), N(1)–Cu(1)–N(3) 162.24(16), N(1)–Cu(1)–N(4) 81.73(17), N(3)–Cu(1)–N(4) 86.44(15), N(1)–Cu(1)–N(2) 82.51(16), N(3)–Cu(1)–N(2) 109.33(15), N(4)–Cu(1)–N(2) 164.12(16), N(1)–Cu(1)–O(4) 104.30(15), N(3)–Cu(1)–O(4) 89.78(15), N(4)–Cu(1)–O(4) 94.74(16), N(2)–Cu(1)–O(4) 87.33(16), N(1)–Cu(1)–O(6) 83.76(14), N(3)–Cu(1)–O(6) 82.79(14), N(4)–Cu(1)–O(6) 55.70(14), N(2)–Cu(1)–O(6) 94.16(14).

$[Cu_2L(NO_3)_4]$ and perchlorate for $[Cu_2L(ClO_4)_4]$. A tetragonally distorted octahedral geometry is observed in both complexes where the oxygen atoms are situated in axial positions giving rise to two different and longest distances to the metal atoms, O(1N)–Cu(1) 2.339(7) and O(6N)–Cu(1) 2.626(7) Å, for the nitrate complex and Cu(1)–O(4) 2.414(4) and Cu(1)–O(6) 2.617(4) Å for perchlorate derivative. The basal plane is provided by the four nitrogen amino atoms from the ligand, the deviation from planarity of the square base for these structures being 0.1079 for $[Cu_2L(NO_3)_4]$ and 0.1117 Å for the $[Cu_2L(ClO_4)_4]$ complex. The pyridine ring again provides the strongest bond to the copper metal, Cu–N1, 1.914(6) and 1.921(4) Å for $[Cu_2L(NO_3)_4]$ and $[Cu_2L(ClO_4)_4]$, respectively, shorter than the Cu–N_{amine} bond lengths, which have average values of 2.038 and 2.041 Å for the nitrate and perchlorate complexes, respectively. Both sorts of distances are shorter than that found for other similar octahedral Cu(II) complexes [8].

The three complexes described have a markedly step conformation, and in all cases the dihedral angle between the pyridine groups from the macrocyclic backbone is 0°, showing that there is no twisting in the ligand molecules; nevertheless the planes containing the pyridinic rings are 1.54, 3.28 and 3.66 Å apart for $[Ni_2L(NO_3)_2](NO_3)_2$, $[Cu_2L(NO_3)_4]$ and $[Cu_2L(ClO_4)_4]$, respectively.

The crystal structures show that there is no significant interaction between the metal ions, they are 5.58, 5.48 and 5.44 Å away from each other, for $[Ni_2L(NO_3)_2](NO_3)_2$, $[Cu_2L(NO_3)_4]$ and $[Cu_2L(ClO_4)_4]$, respectively.

3.2. Spectroscopic and magnetic studies

The presence of water molecules was confirmed by the appearance in the IR spectra of an intense broad band centered at ca. 3400 cm^{-1}. The ν(C=N) and ν(C=C) bands from the pyridine ring appear at 1592, 1575 and 1454 cm^{-1} in the free ligand, and they undergo a shift toward higher frequencies on complexation, appearing at 1610, 1580 and 1450 cm^{-1} in the IR spectra of the complexes, suggesting an interaction between the metal and the pyridine nitrogen atoms [9,10]. The secondary amine stretches in the region 3100–3300 cm^{-1} are split and/or shifted relative to that in the free macrocycle, suggesting coordination to the metal ion.

The IR spectra of all the complexes show the presence of several bands in the region associated with nitrate and perchlorate vibrations, suggesting coordination to the metal ion [11–13]. However, the spectra of the nitrate complexes show also an intense band at 1380 cm^{-1} due to the presence of ionic nitrate, and in some perchlorate complexes a band at 1100 cm^{-1}, attributable to the asymmetric Cl–O stretching mode of the perchlorate anions, is observed. This result is supported by the X-ray crystallographic studies, which show the presence of coordinated and ionic counterions in $[Ni_2L(NO_3)_2](NO_3)_2$. The X-ray crystal studies of $[Cu_2L(NO_3)_4]$ and $[Cu_2L(ClO_4)_4]$ show all counterions coordinated to the metals, but some of them can probably be displaced by the Br^- ion of the KBr disc.

Molar conductivity data, measured at room temperature using acetonitrile as the solvent, showed the presence of ionic and coordinated counterions, since they are in the range reported in that solvent for 2:1 and 3:1 electrolytes for nitrate and perchlorate complexes, respectively [14]. It seems that two nitrate ions remain in the inner coordination sphere in the nitrate complexes whilst only one perchlorate ion is coordinated to the metal ions in solution, in accordance with the different coordinative capacity between nitrate and perchlorate anions. This is in agreement with the results obtained from the IR and X-ray studies.

The L-SIMS mass spectra of the complexes confirm in most cases the dinuclear nature of the complexes, as they feature peaks attributable to the dinuclear species $[M_2L(X)]$, $[M_2L(X)_2]$ or $[M_2L(X)_3]$, ($X = NO_3^-$ or ClO_4^-).

The diffuse reflectance spectra were measured at room temperature for all complexes. The solid state electronic spectra of the Co(II) complexes $[Co_2L](ClO_4)_4 \cdot 4H_2O$ and $[Co_2L](NO_3)_4 \cdot H_2O$ are very similar and they show five bands at 8636, 15300, 18000, 19685 and 21552 cm^{-1} for $[Co_2L](NO_3)_4 \cdot H_2O$ and 8803, 11000, 16200, 18100 and

21 786 cm^{-1} for $[Co_2L](ClO_4)_4 \cdot 4H_2O$, indicative of a high spin distorted trigonal bipyramidal arrangement for the metal ions [15]. The electronic spectra of $[Ni_2L](ClO_4)_4 \cdot CH_3CN$ and $[Ni_2L(NO_3)_2](NO_3)_2 \cdot H_2O$ show bands at 10 460 cm^{-1} (ν_1), 17 420 cm^{-1} (ν_2) and 28 328 cm^{-1} (ν_3) and 10 850 (ν_1), 17 130 (ν_2) and 27 430 cm^{-1} (ν_3), respectively. These values are typical of octahedral Ni(II) complexes and they can accordingly be attributed to $^3T_{2g} \leftarrow {}^3A_{2g}$, $^3T_{1g}(F) \leftarrow {}^3A_{2g}$ and $^3T_{1g}(P) \leftarrow {}^3A_{2g}$, transitions [16]. This result is in agreement with the X-ray crystal structure of the $[Ni_2L(NO_3)_2](NO_3)_2 \cdot H_2O$ complex, which presents the metal ion in a distorted octahedral environment.

For $[Cu_2L(ClO_4)_4] \cdot 5H_2O$ and $[Cu_2L(NO_3)_4] \cdot 4H_2O$ the electronic reflectance spectra show one broad band at 17 241 and 16 639 cm^{-1}, respectively, as expected for octahedrally coordinated Cu^{II} complexes [17,18].

The value of the room temperature magnetic moments of the compounds $[Ni_2L](ClO_4)_4 \cdot CH_3CN$ (5.1 BM), $[Ni_2L(NO_3)_2](NO_3)_2 \cdot H_2O$ (5.6 BM), $[Cu_2L(ClO_4)_4] \cdot 5H_2O$ (2.8 BM) and $[Cu_2L(NO_3)_4] \cdot 4H_2O$ (3.0 BM) lie within the range usually observed for octahedral Ni(II) and Cu(II) complexes [19]. The magnetic moment values obtained for $[Co_2L](ClO_4)_4 \cdot 4H_2O$ and $[Co_2L](NO_3)_4 \cdot H_2O$ are indicative of the presence of dinuclear five coordinated Co(II) complexes, with values of 5.9 and 6.2 BM, respectively [20].

The magnetic susceptibility results support the evidence of the reflectance spectra obtained for all the transitional metal complexes and are compatible with the crystal structures obtained for the complexes $[Ni_2L(NO_3)_2](NO_3)_2$, $[Cu_2L(NO_3)_4]$ and $[Cu_2L(ClO_4)_4]$.

4. Conclusions

The complexation capacity of the 24-membered octaazamacrocyclic ligand L in a 1:1 and 2:1 metal:ligand molar ratio towards the transitional metal ions Co(II), Ni(II) and Cu(II) has been investigated. Probably, because the ligand L has a large enough cavity to give rise to dinuclear endomacrocyclic complexes with these ions, the attempts to obtain mononuclear complexes were unsuccessful and dinuclear complexes were always obtained. The nitrate and perchlorate metal complexes of Ni(II) and Cu(II) present a distorted N_4O_2 octahedral environment, the metal being coordinated by a pyridine group, three secondary amine nitrogen atoms from the macrocyclic ligand and oxygen atoms from the nitrate or perchlorate anions. The spectroscopic studies reveal that the Co(II) complexes exhibit a five coordinated environment.

Acknowledgements

We thank Xunta de Galicia (PGIDT01PXI20901PR) for financial support. Intensity measurements were performed at the Unidade de Raios X. RIAIDT. University of Santiago de Compostela. SPAIN.

Appendix A. Supplementary data

Crystallographic data for the structural analysis have been deposited with the Cambridge Crystallographic Data Centre, CCDC Nos. 608103 for $[Ni_2L(NO_3)_2](NO_3)_2$, 608104 for $[Cu_2L(NO_3)_4]$ and 608105 for $[Cu_2L(ClO_4)$. Copies of this information may be obtained free of charge from The Director, CCDC, 12 Union Road, Cambridge, CB2 1EZ, UK (fax: +44 1233 336033; e-mail: deposit@ccdc.cam.ac.uk or http://www.ccdc.ac.uk). Supplementary data associated with this article can be found, in the online version, at doi:10.1016/j.poly.2006.06.038.

References

[1] (a) R.M. Izatt, J.S. Bradshaw, S.A. Nielsen, J.D. Lamb, J.J. Christensen, D. Sen, Chem. Rev. 85 (1985) 271;
(b) K.E. Krakowiak, J.S. Bradshaw, D.J. Zamecka-Krakowiak, Chem. Rev. 89 (1989) 929.
[2] (a) G.A. Melson (Ed.), Coordination Chemistry of Macrocyclic Compounds, Plenum Press, New York, 1979;
(b) D.E. Fenton, Pure Appl. Chem. 58 (1986) 1437.
[3] (a) L. Valencia, R. Bastida, M. Lopez-Deber, A. Macias, A. Rodríguez, M. Vicente, Z. Anorg. Allg. Chem. 629 (2) (2002) 268;
(b) L. Valencia, J. Martínez, A. Macías, R. Bastida, R.A. Carvalho, C.F.G.C. Geraldes, Inorg. Chem. 41 (20) (2002) 5300.
[4] R. Bastida, D.E. Fenton, M. López-Deber, A. Macías, L. Valencia, M. Vicente, Inorg. Chim. Acta 355 (2003) 292.
[5] G.L. Rothermel Jr., L. Miao, A.L. Hill, S.C. Jackels, Inorg. Chem. 31 (1992) 4854.
[6] G.M. Sheldrick, SADABS, Program for Empirical Absorption Correction of Area Detector Data, University of Göttingen, Germany, 1996.
[7] SHELXTL version, An integrated system for solving and refining crystal structures from diffraction data, Revision 5.1, Bruker AXS LTD.
[8] (a) L. Valencia, R. Bastida, Ma. del Carmen Fernández-Fernández, A. Macias, M. Vicente, Inorg. Chim. Acta 358 (2005) 2618;
(b) J. Martínez, R. Bastida, A. Macias, L. Valencia, M. Vicente, Z. Anorg. Allg. Chem. 631 (2005) 2046.
[9] N.S. Gill, R.H. Nuttall, D.E. Scaife, J. Inorg. Nucl. Chem. 18 (1981) 79.
[10] S. Aime, M. Botta, U. Casellato, S. Tamburini, P.A. Vigato, Inorg. Chem. 34 (1995) 5825.
[11] N.A. Bailey, D.E. Febton, S.J. Kitchen, T.H. Lilley, M.G. Williams, P.A. Tasker, A.J. Leong, L.F. Lindoy, J. Chem. Soc., Dalton Trans. (1991) 627.
[12] A.J. Hataway, A.E. Underhill, J. Chem. Soc. (1961) 3091.
[13] M.F. Rosenthal, J. Chem. Educ. 50 (1973) 331.
[14] W.J. Geary, Coord. Chem. Rev. 7 (1971) 81.
[15] A. Bencini, C. Benelli, D. Gatteschi, Inorg. Chem. 11 (1978) 3313.
[16] W.J. Eilbeck, F. Holmes, A.E. Underhill, J. Chem. Soc. (A) (1967) 757.
[17] B.J. Hataway, R.J. Dudley, P. Nicholls, J. Chem. Soc. (A) (1969) 1845.
[18] B.J. Hataway, I.N. Proctor, R.C. Slade, A. Thompson, J. Chem. Soc. (A) (1969) 2219.
[19] B.N. Figgis, J. Lewis, Prog. Inorg. Chem. 6 (1964) 37.
[20] B.N. Figgis, Introduction to Ligand Fields, Interscience, New York, 1967.

of peroxo-bridged compounds with amino acids and peptides serving as co-ligands, synthesized by us, proved to be powerful oxidant of bromide at near neutral pH [21–23].

Bromination of organic substrates, particularly aromatics, has been attracting considerable contemporary interest [24–31] mainly due to the commercial importance of such compounds [32]. Since the traditional bromination methods require the use of elemental bromine and solvents which are environmentally hazardous [33], there has been a continued search for alternative benign catalytic systems which can mimic the biological bromoperoxidase in the synthesis of brominated organics. Bromoperoxidases (VBPO), involved in the biosynthesis of brominated marine natural products, catalyze bromination by using H_2O_2 and bromide salts instead of Br_2 [34,35]. A large number of model systems mimicking the enzymatic activity have been developed [35–41], focusing mainly on vanadium and peroxovanadium compounds, particularly to elucidate the mechanistic details of the enzyme function which is yet to be fully understood. Contrary to natural V-BPO which is most efficient at pH 5.5–7 several model complexes were found to be catalytically active in acid medium [35–38, 40–42] which limits their utility as effective catalyst. By itself, H_2O_2 is capable of oxidizing bromide in highly acidic medium (pH < 3) but is ineffective in solution at pH > 5.0. Oxidation of bromide by hydrogen peroxide has been reported to be catalyzed by tungstate(VI) systems in acidic medium [42]. A tungstate-exchanged layered double hydroxide has also been studied as a heterogeneous catalyst in oxidative bromination of olefines by H_2O_2system [31,32]. However, examples of well-defined synthetic heteroligand peroxotungstate compounds displaying activity in oxidative bromination is scanty in literature [43] despite the number of such compounds known.

In view of the above observations in the present work we endeavored to establish rational synthetic routes to new oxo-bridged peroxotungsten complexes containing dipeptide as co-ligand, with appropriate characteristics of solubility and stability. We were particularly interested to examine whether such dinuclear compounds could act as oxidant of bromide with good activity at physiological pH, an essential requirement of a biomimetic model. Reported in this paper are the first synthesis, characterization of oxo bridged dinuclear complexes, $Na_2[W_2O_3(O_2)_4(gly\text{-}gly)_2]\cdot 3H_2O$ (**1**) and $Na_2[W_2O_3(O_2)_4(gly\text{-}leu)_2]\cdot 3H_2O$ (**2**), and studies on their stability and bromination activity. We have also investigated the bromination activity of the complex, $Na_2[W_2O_3(O_2)_4(cystine)]\cdot 4H_2O$ (**3**), synthesized previously by us.

2. Materials and methods

The chemicals used were all reagent grade products. The sources of chemicals are given below: sodium tungstate, cysteine (CDH, New Delhi, India); tungstic acid, (Himedia Laboratories, Mumbai, India); glyclyl-peptides (Sigma–Aldrich Chemical Company); hydrogen peroxide (30%) (Ranbaxy, New Delhi, India); phenol red (from *Aspergillus niger*); potassium bromide, potassium dihydrogen phosphates, sodium and potassium hydroxides (SD fine chemicals, Mumbai, India). The complex, $Na_2[W_2O_3(O_2)_4(cystine)]\cdot 4H_2O$ (**3**) was prepared by methods reported earlier [20]. The water used for solution preparation was deionised and distilled.

2.1. Synthesis of peroxotungsten complexes, $Na_2[W_2O_3(O_2)_4(gly\text{-}gly)_2]\cdot 3H_2O$ (*1*) and $Na_2[W_2O_3(O_2)_4(gly\text{-}leu)_2]\cdot 3H_2O$ (*2*)

In a typical reaction H_2WO_4 (0.25 g, 1.0 mmol) was added to 10 ml of 30% H_2O_2 (88.2 mmol) contained in a 250 ml beaker. The mixture was kept in an ice bath and stirred slowly until all the solids dissolved and a clear solution was obtained. To this solution dipeptide (1.0 mmol) was added. The pH of the clear solution was recorded to be 1.6. The pH of the reaction mixture was adjusted to ca. 2.5 by adding sodium hydroxide (46.0 mmol). On adding pre-cooled acetone (ca. 50 ml) to the above solution under continuous stirring, a white pasty mass separated out. After allowing it to stand for about 15 min in the ice bath, the supernatant liquid was decanted and the residue was treated repeatedly with acetone under scratching until it became a microcrystalline solid. The product was separated by centrifugation, washed with cold acetone and dried in vacuo over concentrated sulfuric acid. In the solid state these complexes were found to be stable for several weeks stored dry at <20 °C but tended to be hygroscopic at ambient conditions and decomposed in a few days.

Anal. Calc. for $Na_2[W_2O_3(O_2)_4(gly\text{-}gly)_2]\cdot 3H_2O$ (**1**): Na, 5.06; W, 40.52; O_2^{2-}, 14.09; C, 10.57; N, 6.16; H, 2.20. Found: Na, 4.98; W, 40.13; O_2^{2-}, 13.86; C, 10.35; N, 5.90; H, 2.23%. Yield: approximately 38%.

Anal. Calc. for $Na_2[W_2O_3(O_2)_4(gly\text{-}Leu)_2]\cdot 3H_2O$ (**2**): Na, 4.50; W, 36.07; O_2^{2-}, 12.54; C, 18.82; N, 5.49; H, 3.52. Found: Na, 4.42; W, 35.88; O_2^{2-}, 12.32; C, 18.76; N, 5.40; H, 3.20%. Yield: approximately 37%.

2.2. Elemental analysis

The compounds were analyzed for C, H, and N at the Regional Sophisticated Instrumentation Centre (RSIC), North Eastern Hill University, Shillong, India. The total peroxide content was determined by adding a weighed amount of the compound to a cold solution of 1.5% boric acid (W/V) in 0.7 M sulfuric acid (100 ml) and titration with standard Cerium(IV) solution [44]. Tungsten was determined gravimetrically [45] as $BaWO_4$. The values are given as % by weight of the compounds from which the ratios of W:peroxide are derived.

2.3. Physical and spectroscopic measurements

Spectra in the visible and ultraviolet region were recorded in a Cary Model Bio 100 spectrophotometer,

equipped with a peltier controlled constant temperature cell. The absorbance values are denoted as A_{592} at the wavelength indicated. The infrared (IR) spectra were recorded with samples as KBr pellets in a Nicolet Model Impact 410 FT-IR spectrophotometer and also in a Perkin–Elmer Model 983 spectrophotometer. The spectra were recorded at ambient temperatures by making pressed pellets of the compounds. The ^{1}H NMR spectra were recorded in deuterated chloroform in a Varian EM-390 90 MHz spectrophotometer using TMS as the internal standard. HPLC analyses were performed using a Waters Tm 2487 dual λ detector and assayed at fixed wavelengths using a C_{18} column (Nova-Pak C_{18}, 3.9 × 150 mm, Waters). Magnetic susceptibilities of the complexes were measured by the Gouy method, using Hg[Co(NCS)] as the calibrant. Molar conductance measurements were made at ambient temperature using Systronics Conductivity meter 306. Thermo gravimetric analysis was done in Mettler Toledo Star system at a heating rate of 5 °C/min under the atmosphere of nitrogen using aluminum pan.

2.4. Measurements of bromination activity in solution

The method of de Boer et al. [46] of introducing four bromine atoms into the molecule of phenol red (ε^{433} mmol = 19.7) to form bromophenol blue (ε^{592} mmol = 67.4) was used to measure bromination activity. Phenol red acts as an efficient trap of active bromine species without influencing the rate of reaction until it is exhausted. The reaction mixture contained phosphate buffer (50 mM, pH 5.5), KBr (0.5 M) and phenol red (0.1 mM). The redox activity was tested by adding a measured amount of aliquot from solution of the synthesized compound (1 mM), and by monitoring the possible change in absorbance at 592 nm at 30 °C. The volume of the reaction mixture was kept at 25 ml. Aliquots were transferred to the spectrophotometer immediately after mixing.

2.5. Bromination of organic substrates and product analysis

In a representative procedure, organic substrate (0.5 mmol) was added to a solution of acetonitrile: water (1:1) (3 ml) containing KBr (1.5 mmol). A weighed amount of solid peroxotungstate complex **1** (0.25 mmol) was then added to the reaction mixture at room temperature under continuous stirring. The stirring was continued for ca. 1 h. Reaction products as well as unreacted organic substrates were then extracted with diethyl ether and dried over anhydrous Na_2SO_4. Products were then separated by TLC and HPLC. ^{1}H NMR spectroscopy and melting point determinations were made to interpret the products.

In order to isolate the tungsten species remaining after the completion of the reaction, the following method has been adopted. After extraction of the organic reaction product, the aqueous part of the reaction mixture was transferred to a 250 ml beaker. Keeping the solution in an ice bath, pre cooled acetone was added with constant stirring until a colorless pasty mass separated out. After allowing it to stand for 10 min in an ice bath, the supernatant liquid was decanted off and the residue was treated repeatedly with acetone under scratching until it became white microcrystalline solid. The product was separated by centrifugation, washed with cold acetone and dried in vacuo over concentrated sulfuric acid.

3. Results and discussion

3.1. Synthesis and characterization

The reaction of tungsten with H_2O_2 is highly sensitive to pH and it is known that a number of peroxotungsten species are formed in solution with slight variation of pH of the reaction medium [12,15]. The methodology for the successful synthesis of the white microcrystalline dinuclear peroxotungstate compounds **1** and **2** was based on the reaction of H_2WO_4 with 30% H_2O_2 and the respective ligand in an aqueous acidic medium. Since one of our primary aims was to isolate complexes with a $[WO(O_2)_2]_2O$ moiety which has been reported to exist in an acidic solution [15], the pH of the reaction medium was strategically maintained at <3. Thus the use of acidic pH and choice of the ancillary ligand appeared to be essential parameters for achieving success of the synthesis of the dimeric title compounds. The factors such as maintenance of required time and temperature at ⩽4 °C were found to be equally important for achieving the desired syntheses. We have earlier synthesized such oxo-bridged dimeric compounds, $A_2[W_2O_3(O_2)_4(\text{cystine})]\cdot 4H_2O$ (A = Na and K) by adopting a similar synthetic strategy [20]. Our attempts to isolate analogous dinuclear compounds in the presence of some other ligand systems such as proline, glutamic acid, asparatic acid, thioglycolic acid etc. were unsuccessful. At a relatively higher pH of ca. 5.5 and using Na_2WO_4 as source of tungsten(VI), monomeric diperoxotungsten complexes were obtained in each of these cases. This suggests that the chosen dipeptide ligands may have a role in stabilizing the products.

The title compounds were diamagnetic in nature as was evident from the magnetic susceptibility measurement in conformity with the presence of tungsten(VI) in each case. From the elemental analysis data, the ratio of 1:2 was obtained for W:peroxide, while W:co-ligand ratio was ascertained to be 1:1 in each of the complexes. The elemental analysis results and molar conductance values obtained from measurement at ambient temperature were in complete agreement with the formulation of the complex species as $Na_2[W_2O_3(O_2)_4(\text{gly-gly})_2]\cdot 3H_2O$ (**1**) and $Na_2[W_2O_3(O_2)_4(\text{gly-Leu})_2]\cdot 3H_2O$ (**2**), respectively.

Each of the title compounds displayed characteristic spectral patterns in the infra-red region involving absorptions due to co-ordinated peroxide, amino acid or dipeptide ligand and lattice water (Table 1). The strong absorption at ca. 960 cm^{-1} was consistent with the presence of a terminally bonded W=O group in each case [15,16]. For the dinuclear W–O–W unit the antisymmetric

Table 1
The structurally significant IR bands of the compounds **1** and **2**

S. no.	Compound	IR bands					
		ν(W=O)	ν(O–O)	ν(W_2O)	ν_{as}(W–O_2)	ν_s(W–O_2)	ν_{sym}(W_2O)
1	$Na_2[W_2O_3(O_2)_4(gly\text{-}gly)_2]\cdot 3H_2O$ (**1**)	952	843	770	612	531	410
2	$Na_2[W_2O_3(O_2)_4(gly\text{-}leu)_2]\cdot 3H_2O$ (**2**)	949	845	767	613	534	415

and symmetric stretchings were expected in the 750–770 and 500 cm^{-1} regions [15,16], respectively. In the spectra of the complexes **1** and **2**, a prominent band at ca. 770 cm^{-1} and another weak intensity band appearing at ca. 410 cm^{-1} attributable to $\nu_{asym}(W_2O)$ and $\nu_{sym}(W_2O)$ modes gave clear indication of the presence of a bridging oxo group in each of them. The presence of side-on bound peroxo ligand in the compounds, was evident from the observance of the expected ν(O–O), ν_2 and ν_3 modes which involve metal-oxygen stretches of W–O_2 vibrations in the range of ca. 850, ca. 610 and ca. 530 cm^{-1}, respectively.

IR spectroscopy is immensely useful and informative for the characterization of heteroligand peroxometal complexes since it provides information not only about co-ordination of peroxo but also ligand groups when compared with the spectra of the free ligands. The characteristic shifts of heteroligand bands that occur upon co-ordination compared to the spectra of the free ligand reveal the bonding sites in the co-ordinated ligands. The spectra of the complexes **1** and **2** exhibited two distinct bands in the range of 1680–1660 cm^{-1} and 1630–1590 cm^{-1} which have been assigned to ν(C=O) (amide) and ν_{as}(COO) of the co-ordinated peptide ligands [47–49]. The position of ν(C=O) band in the complexes almost remained unaltered compared to its position in free ligand which indicated that the amide group was not taking part in co-ordination. The broadening of the band was probably owing to their participation in hydrogen bonding. Co-ordination through N-atom of the amide group was unlikely as evident from the spectra because such co-ordination is known to cause considerable decrease in the peptide carbonyl stretching frequency which was not observed in case of these compounds [50,51]. The ν_s(COO) vibration of the free ligands were observed in the range of 1410–1400 cm^{-1} in the IR spectra [47]. A medium intensity band with some broadening observed in the range of 1395–1405 cm^{-1} region was assigned to ν_s(COO) of the unidentate carboxylate group (ν_{as}–$\nu_s \approx 300$ cm^{-1}) [47]. The broadening of the band was probably caused by its mixing with the C–N stretching of amide group expected to occur in this region [49]. The spectra showed N–H stretching bands of coordinated peptide residue at 3300–3100 cm^{-1} region as expected from the –N^+H_3 group. N–H deformation modes (1520–1600 cm^{-1}) in their position and pattern in the spectra of the complexes significantly remained unaltered compared to the free ligand. Based on these observations it may be inferred that the dipeptide ligands, occurring as zwitterions in the complexes, co-ordinate to tungsten(VI) through carboxylate group. The presence of lattice water in each of the complexes **1** and **2** was indicated by the strong ν(OH) absorptions displayed at 3500–3400 cm^{-1}. However, the bending mode of water could not be assigned with certainty as it occurred in the carbonyl frequency region.

Depending on the pH of the reaction solution and the nature of the metal, a ligand like an amino acid or a simple peptide can act as mono, bi or tridentate ligand with different combinations of donor sites, viz., terminal amino and carboxylate groups [52] as well as amide groups in peptides and can occur in complexes in either neutral zwitterionic form or anionic form. In addition, they are known to form bridges between metal atoms leading to the formation of dinuclear or polynuclear structures. In the present study, the low pH apparently favored the co-ordination of dipeptides in their neutral zwitterionic form to the two W(VI) centers through carboxylate groups thereby stabilizing the $[WO(O_2)_2]_2O$ moiety and leading to the synthesis of the desired complexes **1**and **2**. Hydrogen bonding between the side chains is likely to stabilize the complex species in the solid state. Based on these observations a structure of the type shown in Fig. 1 has been proposed for complexes **1** and **2**, which is shown for the glycyl-glycine complex as a representative.

3.2. Stability of the complexes in solution

The stability of the compounds in an aqueous solution of pH 3.5, which is the pH attained by the solution on dissolution of the compounds, has been studied by estimating the peroxide content and molar conductances at different time intervals for any possible change. The investigations revealed that their peroxide content and molar conductance values (261 Ω^{-1} cm^2 mol^{-1} for **1** and 257 Ω^{-1} cm^2 mol^{-1} for **2**) remained unaltered for over a period of 12 h and oxygen was not released on dissolution of the complexes in

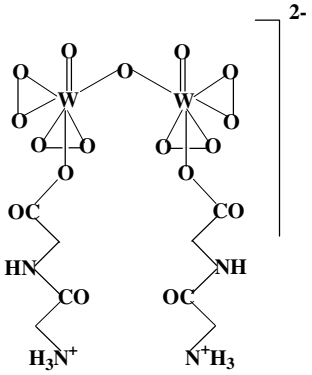

Fig. 1. Proposed structure of the dinuclear peroxotungstate compounds shown with $Na_2[W_2O_3(O_2)_4(gly\text{-}gly)_2]\cdot 3H_2O$ as representative.

water. The compounds were also found to be stable at pH 7.0 as well as at pH 8.0. The high stability of the compounds in solution at acidic as well as physiological pH is likely to be a consequence of the additional stability imparted by the heteroligands.

3.3. Thermal analysis

Thermo gravimetric analysis data of the compounds provided crucial information regarding composition of the compounds and their thermal stability. It has been evident from the TG and DTG curves (Fig. 2) that after the initial dehydration, the compounds **1** and **2** undergo multistage decomposition up to a final decomposition temperature of 550 °C.

The first stage of decomposition occurs at 40–100 °C with the liberation of the outer sphere water molecules from the complexes (Table 2). The observed weight loss of 5.4% and 5.0% for the complexes **1** and **2**, respectively are in good agreement with the calculated values (Table 2). Another decomposition stage observed in the temperature region of 110–200 °C for complex **1** and 90–160 °C for complex **2** with a corresponding weight loss of 13.2% and 11.5%, respectively is characteristic of complete loss of co-ordinated peroxo groups from the complexes [17]. It seems likely that the nature of the heteroligand has a specific effect on the thermal stability of the complexes, though not a large one, as reflected in the variation in their decomposition temperatures with respect to the loss of peroxide. Absence of peroxo group in the decomposition product was confirmed from the infrared spectral analysis. Mention must be made that some peroxotungstate and peroxomolybdate compounds containing amino acids as co-ligands were reported to behave in a similar manner losing their peroxide completely on heating [17].

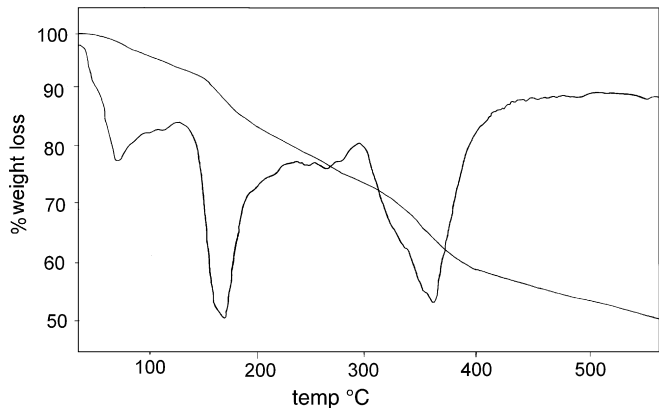

Fig. 2. TG and DTG plot of $Na_2[W_2O_3(O_2)_4(gly\text{-}gly)_2]\cdot 3H_2O$ (**1**).

The total weight loss which occurred during the course of the overall decomposition process on heating the compounds up to a final temperature of 550 °C was recorded to be 48.08% for complex **1**, which is in good agreement with the theoretically calculated value of 49.15% for the complete loss of the components viz, lattice water, co-ordinated peroxide, and the glycyl-glycine ligands. The remaining dark brown sticky residue after heating up to 550 °C was found to be a hydrated oxotungstate species as indicated by the IR spectrum which displayed the characteristic ν(W=O) and ν(OH) absorptions and was devoid of bands attributable to peroxo and the dipeptide ligands of the original compounds.

3.4. Redox activity of the complexes in bromination reaction

The bromination of phenol red to its tetra brominated product, bromophenol blue was used to measure the bromination activity of the complexes **1**–**3** in solution. Addition of freshly prepared aqueous solution of each of the compounds **1**–**3**, at concentrations indicated (Table 3), to the standard reaction of bromide in phosphate buffer with phenol red as trap for oxidized bromine resulted in gradual color change of the solution from yellow to blue. The spectrum recorded showed a peak at A_{592} characteristic of the product bromophenol blue and a decrease in absorbance of the peak at A_{433} due to loss of phenol red (Fig. 3). The data in Table 3 show that the dinuclear complexes **1**–**3** possess bromination activity.

A similar reaction when carried out in absence of phenol red displayed a peak at 262 nm with a shoulder at 237 nm on addition of solutions of compounds. Addition of phenol red to this solution resulted in the decrease in A_{262} nm and a peak at 592 nm appeared indicating the formation of bromophenol blue. The 262 nm peak, therefore, represents a bromination competent oxidized species of bromide, probably an equilibrium mixture of BrOH, Br_2 and Br_3^- as proposed earlier [34].

It was of significance to note that the bromination activity of each of the dimeric tetraperoxo complexes with two oxo-bridged diperoxotungsten units were recorded to be limited

Table 2
Thermal decomposition of peroxotungstate(VI) complexes **1** and **2**

Compound	Temperature range (°C)	Weight loss			
		H_2O (%)		O_2^{2-} (%)	
		Found	Calc.	Found	Calc.
$Na_2[W_2O_3(O_2)_4(gly\text{-}gly)_2]\cdot 3H_2O$ (**1**)	40–100	5.4	5.9		
	110–200			13.2	14.1
$Na_2[W_2O_3(O_2)_4(gly\text{-}leu)_2]\cdot 3H_2O$ (**2**)	40–90	5.0	5.2		
	100–160			11.5	12.5

Table 3
Bromination of phenol red with peroxotungstate complexes **1**–**3**

Compounds	Conc. (mM)	Rate of bromine transfer		Total bromine transfer (extrapolated to 1 mM compound)
		ΔA_{592}/min	μM Br/min	mM Br/mM compound
1. $Na_2[W_2O_3(O_2)_4(gly\text{-}gly)_2]\cdot 3H_2O$ (**1**)	0.1	0.16	9.5	2.01
2. $Na_2[W_2O_3(O_2)_4(gly\text{-}leu)_2]\cdot 3H_2O$ (**2**)	0.1	0.18	10.9	1.88
3. $Na_2[W_2O_3(O_2)_4(cystine)]\cdot 4H_2O$ (**3**)	0.1	0.19	11.2	1.94

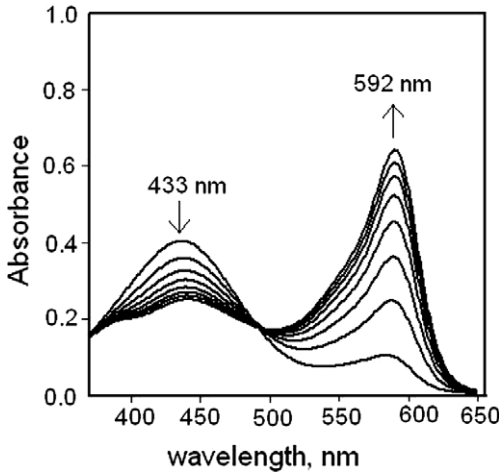

Fig. 3. Bromination activity with dinuclear peroxotungstate compound **1**. The spectrum recorded immediately after adding the compound solution to the reaction mixture. Spectral changes at 2 min interval. The reaction mixture contained phosphate buffer (0.05 M, pH 5.5), KBr (0.5 M), phenol red (0.1 mM) and compound **1** (0.05 mM).

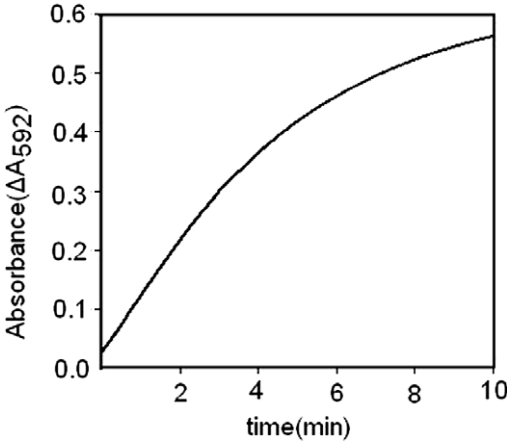

Fig. 4. The increase of absorbance at 592 nm indicating the rate of bromination with compound **1**. The reaction mixture contained phosphate buffer (0.05 M, pH 5.5), KBr (0.5 M), phenol red (0.1 mM) and compound **1** (0.05 mM).

to ca. 50% of that expected on the basis of the total number of peroxo groups present in the complexes (Table 3). Decrease or increase in concentrations of the compound, substrate or KBr in the reaction solution had no effect on this feature. The consistently observed stoichiometry of 2:1 for bromine transferred: peroxotungsten compound cause us to infer that only one of the peroxo groups of a diperoxotungsten moiety of the tetraperoxotungsten complex would be active in bromide oxidation.

The effect of H_2O_2 on the bromination reaction under standard assay conditions was tested. While the initial addition of H_2O_2 (0.5 mM) to the reaction solution had no observable effect on the initial rate of bromination (Fig. 4), it was quite intriguing to note a revival of the bromination activity on addition of H_2O_2 (0.5 mM), after bromination to a spent reaction mixture which contained excess bromide and substrate. It is thus plausible that an inactive tungsten intermediate formed after completion of the bromination process probably combines with peroxide in presence of excess H_2O_2 to regenerate the respective starting dimeric tetraperoxo tungstate complex giving rise to a catalytic cycle. Exogenous hydrogen peroxide is therefore required to maintain the tungsten complexes in their tetraperoxo forms in order to obtain a catalytic cycle.

The bromination activity of the compounds was surprisingly, found to be maximum at pH 7.5, unlike in the case of peroxovanadate catalyzed oxidative bromination where the rate was reported to increase monotonously with increasing acidity of the reaction medium [53]. We have obtained the data in Table 3 at pH 5.5 since the use of this method is limited to pH range near 5.0 in order to achieve conversion from phenol red (pK_a 7.9) to bromophenol blue (pK_a 4.0). Omission of phosphate buffer from the reaction medium did not alter the bromination activity of the complexes. This indicated that the presence of phosphate was not essential for such activity of the peroxotungsten compounds.

Efficacy of the complexes in mediating bromination of organic substrates in presence of bromide in aqueous-organic media has been explored. Bromination of several activated aromatics into their corresponding bromo-organics took place in moderate yields in presence of the dinuclear pW complexes (Table 4) at ambient temperature. Reactions were carried out in the absence of buffer. Preferential bromination at either *ortho* or *para* positions of the aromatic ring leading to mono substitution indicate an electrophilic bromination mechanism. That the brominating species was 'Br^+' and not a '$Br^{\bullet}$' in these reactions was further evident from the ring substituted products obtained from the substrate, 2-methoxy toluene (Table 4). Bromination through radical reaction would have produced benzyl bromide instead of bromo-methoxy toluene.

In order to ascertain the nature of the inactive intermediate formed in solution and to rationalize the reaction sequence the product isolated from the aqueous extract

Table 4
Bromination of organic substrates mediated by compound **1**

Substrate	Product	% Yield
Aniline	4-bromoaniline	52
	2-bromoaniline	35
o-Nitroaniline	4-bromo-2-nitroaniline	61
	2-bromo-6-nitroaniline	30
m-Nitroaniline	2-bromo-5-nitroaniline	56
	4-bromo-3-nitroaniline	30
p-Nitroaniline	2-bromo-4-nitroaniline	85
o-Aminophenol	2-amino-5-bromophenol	79
m-Aminophenol	3-amino-6-bromophenol	60
	3-amino-4-bromophenol	30
p-Aminophenol	4-amino-3-bromophenol	76
Quinol	2-bromo-4-hydroxyphenol	72
o-Methoxytoluene	3-bromo-6-methoxytoluene	58
	3-bromo-2-methoxytoluene	34

of the reaction mixture, after completion of the reaction, was subjected to IR and elemental analysis. IR spectrum of the compound resembled closely the spectrum of the original starting complex showing the presence of peroxo group, bridging as well as terminal oxo groups and co-ordinated dipeptide. Elemental analysis results suggested the presence of one peroxo group per W(VI) indicating the formation of a monoperoxotungsten species. It thus appears that the dimeric complex remains intact throughout the course of the bromination process where two of its peroxo groups participate, leading to the formation of a dimeric peroxotungsten compound with two heteroligand monoperoxo moieties bonded through an oxo group. It is interesting to note that we could also isolate an analogous dimeric mono peroxotungsten species from a separate experiment involving complex **1** (0.5 mM) and KBr (2.0 mM) under standard assay condition with phenol red omitted from the reaction medium. This observation is consistent with the proposal which implicates formation of a monoperoxotungsten intermediate which is inactive in bromination.

A scheme of reactions, shown in Fig. 5, is proposed which satisfactorily describes the principal features of our results. The dimeric compounds react with bromide to yield oxidized bromine species, proposed to be an equilibrium mixture of BrOH, Br_2 and Br_3^-, with concomitant formation of dinuclear intermediate which is likely to possess two monoperoxotungsten units with the oxo-bridge retained (reaction a). Transfer of the bromine atom to the substrate AH from the bromination competent oxidised bromine intermediate takes place (reaction b). In the presence of excess H_2O_2 the diperoxo intermediate combines with peroxide to regenerate the starting tetraperoxo ditungstate complex giving rise to a catalytic cycle (reaction c). To us it appears that bromide would attack an edge-bound peroxo group in preference to a hepta co-ordinated tungsten centre as observed in some other redox processes involving peroxo compounds of W(VI) and Mo(VI) [13,14,43].

Formation of an inactive monoperoxo intermediate from a catalytically active diperoxotungsten or molybdenum complex during oxygen-atom transfer reactions mediated by such complexes is not unprecedented [13,14]. A monoperoxo Mo(VI) has been implicated as an intermediate in the mechanisms proposed by Reynolds et al. [43] as well as by Butler and co-workers for the Mo(VI) and W(VI) catalyzed bromide oxidations [42]. It is also relevant in this context that during one of our previous studies involving redox activity of the complex **3** with respect to reduced glutathione (GSH), only two of the peroxo groups out of four peroxides present per molecule of the complex were found to be involved in oxidation [20]. These considerations fortify our proposed mechanism.

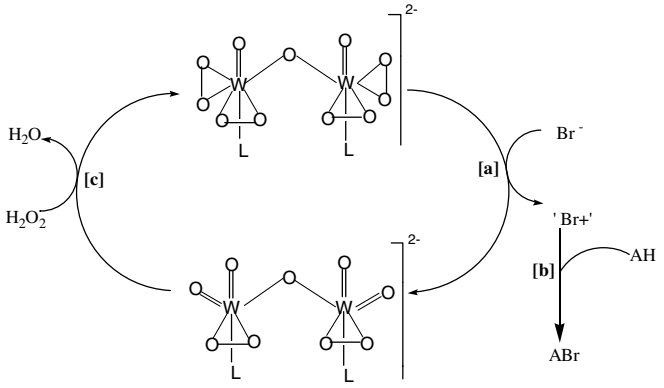

Fig. 5. Schematic representation of reactions occurring with dinuclear tetraperoxotungsten(VI) compounds (L = cystine, gly-gly or gly-leu). (a) reaction of the complex with bromide to yield oxidized bromine and an intermediate postulated as a diperoxotungsten species having two monoperoxotungsten units with the oxo-bridge retained; (b) transfer of bromine from the active species to acceptor AH; (c) in presence of excess H_2O_2 the diperoxo intermediate combines with peroxide to regenerate the starting tetraperoxo tungstate complex giving rise to a catalytic cycle. No attempt is made to show the exact stoichiometry of the reaction.

The observed reaction pattern is in accord with the earlier suggestions that for a peroxotungsten complex to be active in oxidation an oxo-diperoxo configuration may be a prerequisite [13]. This feature is however, in contrast to the findings that diperoxo-vanadate compounds with only η^2-peroxo groups in its co-ordination sphere were catalytically incompetent in bromide oxidation at neutral pH [23,53]. A dinuclear peroxovanadate with a μ-peroxo group, on the other hand was highly active in bromination at physiological pH [21–23,53]. The proposed reaction pathway conferred the status of a bromide oxidant, at physiological pH, on the VOOV group [21–23,53]. The mechanisms of bromide oxidation mediated by pW and pV compounds, tested by us, thus appear to be distinctly different. It is not completely clear however, as to why a η^2-peroxo group of diperoxotungsten(VI) species is highly reactive in oxidative bromination while a diperoxovanadate species with similar edge-bound peroxo groups is ineffective in bromination at near neutral pH.

4. Conclusion

In summary, with the examples of the newly synthesized dinuclear complexes the present investigation has

established that it is possible to isolate the oxo-bridged tetraperoxotungstate(VI) species formed in solution into solid state, through complexation with specific ligands under appropriate experimental conditions. A noteworthy observation of the present investigation, which may also be of biochemical importance, is the high stability of the compounds in solution at a wide range of pH values particularly at acidic pH. Undoubtedly, the most notable aspect of the present study is the finding that the newly synthesized complexes besides being stoichiometric reagents for bromide oxidation in aqueous medium, also acted as a catalyst for the same reaction when used in conjunction with H_2O_2 at neutral pH. Isolation of the diperoxoditungsten(VI) species as reaction intermediate lends support to the proposed mechanism. Information generated from the present investigation may find relevance in the context of designing safer biomimetic redox catalysts for organic bromination.

Acknowledgements

Financial support from the Department of Science and Technology, New Delhi is gratefully acknowledged. We are thankful to Prof. T. Ramasarma, Hon. Distinguished Chair, Centre for DNA Fingerprinting and Diagnostics, Hyderabad, for valuable discussion.

References

[1] M.K. Johnson, D.C. Rees, M.W.W. Adams, Chem. Rev. 96 (1996) 2817.
[2] J.H. Enemark, J.J.A. Cooney, J.J. Wang, R.H. Holm, Chem. Rev. 104 (2004) 1175.
[3] J. Li, G. Elberg, D. Gefel, Y. Shechter, Biochemistry 34 (1995) 6218.
[4] P.J. Stankiewiez, M.J. Gresser, Biochemistry 27 (1988) 206.
[5] R.L. Van-Etten, P.P. Waymack, D.M. Rehkop, J. Am. Chem. Soc. 96 (1974) 6782.
[6] G. Soman, Y.C. Chang, D.J. Graves, Biochemistry 22 (1983) 4994.
[7] Y.S. Heo, J.M. Ryu, S.M. Park, J.H. Park, H.C. Lee, K.Y. Hwang, J. Kim, Exp. Mol. Med. 34 (2002) 211.
[8] A.Y. Louie, T.J. Meade, Chem. Rev. 99 (1999) 2711.
[9] S. Kenneth, K.S. Krishenbaum, K.B. Sharpless, J. Org. Chem. 50 (1985) 1979.
[10] O. Bortolini, F.D. Furia, G. Modena, R. Seraglia, J. Org. Chem. 50 (1985) 2688.
[11] N.M. Gresley, W.P. Griffith, A.C. Laemmel, H.I.S. Nogueira, B.C. Parkin, J. Mol. Catal. A 117 (1997) 185.
[12] M.H. Dickman, M.T. Pope, Chem. Rev. 94 (1994) 569.
[13] A.F. Ghiron, R.C. Thompson, Inorg. Chem. 28 (1989) 3647.
[14] S.E. Jacobson, D.A. Mccigrosso, F. Mares, J. Org. Chem. 44 (1979) 921.
[15] N.J. Campbell, A.C. Dengal, C.J. Edwards, W.P. Griffith, J. Chem. Soc., Dalton Trans. (1989) 1203.
[16] A.C. Dengal, W.P. Griffith, R.D. Powell, A.C. Skapski, J. Chem. Soc., Dalton Trans. (1987) 991.
[17] T.T. Bhengu, D.K. Sanyal, Thermochim. Acta 397 (2003) 181.
[18] J.Y. Piquemal, S. Halut, J.M. Bregault, Angew. Chem., Int. Ed. 37 (1998) 1146.
[19] M.C. Chakravorti, S. Ganguly, M. Bhattacharjee, Polyhedron 12 (1993) 55.
[20] P. Hazarika, D. Kalita, S. Sarmah, N.S. Islam, Mol. Cell. Biochem. 287 (2006) 39.
[21] S. Sarmah, N.S. Islam, J. Chem. Res. (S) (2001) 172.
[22] S. Sarmah, P. Hazarika, N.S. Islam, A.V.S. Rao, T. Ramasarma, Mol. Cell. Biochem. 236 (2002) 95.
[23] S. Sarmah, D. Kalita, P. Hazarika, R. Bora, N.S. Islam, Polyhedron 23 (2004) 1097.
[24] H.A. Muathen, J. Org. Chem. 57 (1992) 2740.
[25] V. Conte, F. DiFuria, S. Moro, Tetrahedron Lett. 35 (1994) 7429.
[26] C.U. Dinesh, R. Kumar, B. Pandey, P. Kumar, J. Chem. Soc., Chem. Commun. (1995) 611.
[27] K. Smith, D. Bahzad, Chem. Commun. (1996) 467.
[28] J.H. Clark, J.C. Ross, D.J. Macquarrie, S.J. Barlow, T.W. Bastock, Chem. Commun. (1997) 1203.
[29] M.K. Chaudhuri, A.T. Khan, B.K. Patel, Tetrahedron Lett. 39 (1998) 8163.
[30] B.F. Sels, D.E. De Vos, P.A. Jacobs, J. Am. Chem. Soc. 123 (2001) 8350.
[31] B.F. Sels, D.E. De Vos, M. Buntinx, P.A. Jacobs, J. Catal. 216 (2003) 288.
[32] A. Butler, J.V. Walker, Chem. Rev. 93 (1993) 1937.
[33] J.H. Clark (Ed.), Chemistry of Waste Minimisation, Chapman and Hall, London, 1995.
[34] E. de Boer, Y. Van Kooyk, M.G.M. Tromp, R. Wever, Biochem. Biophys. Acta 869 (1986) 48.
[35] A. Butler, M.J. Clague, G.E. Meister, Chem. Rev. 94 (1994) 625.
[36] D. Rehder, M. Bashirpoor, S. Jantzen, H. Schmidt, M. Farahbakhsh, H. Nekola, in: A.S. Tracey, D.C. Crans (Eds.), Vanadium Compounds, Chemistry, Biochemistry and Therapeutic Applications, Oxford University Press, New York, 1998, pp. 60–70.
[37] A. Butler, Coord. Chem. Rev. 187 (1999) 17.
[38] M.J. Clague, A. Butler, J. Am. Chem. Soc. 117 (1995) 3475.
[39] M. Bhattacharjee, Polyhedron (1992) 2817.
[40] G.J. Colpas, B.J. Hamstra, J.W. Kampf, V.L. Pecoraro, J. Am. Chem. Soc. 118 (1996) 3469.
[41] V. Conte, O. Bortolini, M. Carrano, S. Moro, J. Inorg. Biochem. 80 (2000) 41.
[42] G.E. Meister, A. Butler, Inorg. Chem. 33 (1994) 3269.
[43] M.S. Reynolds, S.J. Morandi, J.W. Raebiger, S.P. Melican, S.P.E. Smith, Inorg. Chem. 33 (1994) 4977.
[44] M.K. Chaudhuri, S.K. Ghosh, N.S. Islam, Inorg. Chem. 24 (1985) 2706.
[45] G.H. Jeffery, J. Basset, J. Mendham, R.C. Denny, Vogel's Textbook of Quantitative Inorganic Analysis Including Elementary Instrumental Analysis, 4th ed., Longman, London, 1978, pp. 486–487.
[46] E. de Boer, H. Plat, M.G.M. Tromp, R. Wever, M.C.R. Franssen, H.C. van der Plas, H.C. Meijer, H.E. Schoemaker, Biotech. Bioeng. 30 (1987) 607.
[47] K. Nakamoto, Infrared and Raman Spectra of Inorganic and Coordination Compounds, 5th ed., Wiley, New York, 1997, p. 60.
[48] T. Miyazawa, E.R. Blout, J. Am. Chem. Soc. 83 (1961) 712.
[49] R.A. Meyers (Ed.), Encyclopedia of Analytical Chemistry, vol. 2, Wiley, New York, 2000, p. 546.
[50] K. Nakamoto, Infrared and Raman Spectra of Inorganic and Coordination Compounds, 5th ed., Wiley and Sons, New York, 1997, p. 71.
[51] H. Seigel, R.B. Martin, Chem. Rev. 82 (1982) 385.
[52] S.T. Chow, C.A. McAuliffe, in: S. Lippared (Ed.), Progress in Inorganic Chemistry, vol. 19, Wiley Interscience, New York, 1975, pp. 15–104.
[53] A.V.S. Rao, H.N. Ravishankar, T. Ramasarma, Arch. Biochem. Biophys. 334 (1996) 121.

no inert μ-OH polymer complexes [19–22] must be present in order to avoid dramatic decreases in reaction rate. The existence of an important degree of outer-sphere hydrogen-bonding in the previous steps to the substitution reactions is clear in all cases [21,23,24], and the play of the anionic phosphate groups is considered crucial [25–28].

The use of inert octahedral d^6 complexes has been initiated by the use of Pt(IV) complexes. Nevertheless, their reactivity has always been associated with a Pt(II) reduced form, followed by the coordination to nitrogen donors of the purine bases [29–31]. The use of much more classical inert t_{2g}^6-type complexes, such as those derived from Co(III), has been explored in very few cases [21,32–37]. The problems arising from the charge of the initial dichloro complexes, as well as the extraordinary inertness of their t_{2g}^6 octahedral coordination sphere are crucial in the scarcity of their use. Furthermore, the stability of the complexes at physiological pH is drastically reduced, and the formation of inert μ-OH polymer species dominant [38]. The behaviour of *cis*-tetraamine Co(III) complexes is fundamentally different from the platinum or palladium complexes in a crucial fact: coordination of the oxo groups of the phosphate groups is highly favoured instead of the purine base nitrogens. As a consequence, the kinetic reactivity of this complexes has been generally associated with the enhancement of the hydrolytic cleavage of the phosphate esters by an extra hydroxo ligand attached to the Co(III) centre at pH $\geqslant$ 8 [38–42]. The interest in the initial substitution processes leading to this reactivity is great, but the difficulties encountered have not allowed what, in principle, represents an easy study. The careful choice of a proper and wide pH range for the study of the substitution processes is not trivial either, although it has been used in some relevant cases [43]. One has to accept that the *quality* of the data obtained is bound to be lower in these cases than for the typical situation where only a margin of one unit in pH is used.

The use of *cyclam*-type ligands represents an important way to sort some of the inherent problems arising from the use of the above mentioned inert Co(III) complexes. Functionalization of the amine groups by carboxylates can induce important changes in the overall charge of the complex [44,45], and the possibility of outer-sphere interactions between the added groups and the polynucleotide chains cannot be neglected [46]. The *cis* geometry of the tetraamine ligand can be forced by the use of the smaller *cyclen* analog. In these three circumstances, the existence of already immense number of substituted DOTA type ligands has to be taken into account [44,47]. Finally, conjugate-base catalyses has been observed for the substitution processes of this type of complexes. This is a favourable aspect in view of the extraordinary inertness of the centre and the kinetic stability of the possible μ-OH polymers formed at physiological pH [48–52].

In view of these facts we present in this paper the study of the substitution processes of the water bound to the *cis*-$[Co(H_2O)_2(cyclen)]^{3+}$ complex by 5′AMP and 5′IMP at different pH values. The study of the process is accompanied by a parallel monitoring of the substitution by chloride and inosine (INO), in order to obtain information about the specific factors influencing phosphate substitution. ^{31}P NMR monitoring of the reactions indicate that the process is clean, and that no hydrolysis of the phosphate esters is observed at pH $\leqslant$ 7.0. The stability of the final phosphatosubstituted cobaltocomplex is demonstrated and a further intramolecular process leading to the partial chelate formation of a *O*(phosphato)-*N*(nucleoside) species proved. The importance of these facts can be envisaged in view of the interactions of these type of complexes with polynucleotide chains.

2. Results and discussion

2.1. Aqua and chloro complexes

cis-$[Co(H_2O)_2(tren)]^{3+}$ and *cis*-$[Co(H_2O)_2(cyclen)]^{3+}$ complexes have been prepared *via* triflate solvolysis [53,54] from the corresponding dichloro precursors [51,55]. The partially substituted chloroaqua derivatives are obtained from the dichloro complexes *via* the spontaneous hydrolysis of one of the chloride ions in aqueous medium [49]. Table 1 collects the electronic spectral relevant data used for their characterization. The values are in good agreement with the published above mentioned data, despite the difficulties encountered given their high conjugate-base hydrolytic reactivity. Potentiometric and UV–vis titrations, using SPECFIT [56], were carried out for the determination of the pK_a values corresponding to the two cobalt-bound aquo ligands. Both set of independently obtained data produced reasonable agreement between them and the values given in the literature for these systems [57,58].

Given the fact that the reactivity involved in the studies to be carried out comprehends the $[Co(H_2O)_2(N)_4]^{3+}$/$[CoCl(H_2O)(N)_4]^{2+}$/$[Co(OH)(H_2O)(N)_4]^{2+}$/$[CoCl(OH)(N)_4]^{+}$-{$(N)_4$ = tetraamine ligand} mixtures, the determination of the pK_a value of the *cis*-$[CoCl(H_2O)(cyclen)]^{2+}$ species was also pursued. Unfortunately, the fast hydrolysis of

Table 1
UV–Vis spectral data for the series of complexes prepared as a function of the pH of the medium used (perchlorate or triflate salts unless stated) for the substitution kinetic measures

Species	pH	$\lambda(\varepsilon)$/nm (M^{-1} cm^{-1})	
cis-$[CoCl(H_2O)(tren)]^{2+}$	0	535 (138)	375 (155)
cis-$[Co(H_2O)_2(tren)]^{3+}$	1	505 (107)	350 (99)
cis-$[Co(OH)(H_2O)(tren)]^{2+}$	6.5[a]	510 (100)	356 (105)
cis-$[Co(OH)_2(tren)]^{+}$	8.5[a]	517 (105)	366 (115)
cis-$[CoCl(H_2O)(cyclen)]^{2+}$	0.3 (HCl)	534 (205)	374 (171)
cis-$[CoCl(OH)(cyclen)]^{+}$	12.5 (1.0 M NaCl)	544 (207)	360 (201)
cis-$[Co(H_2O)_2(cyclen)]^{3+}$	1	502 (177)	358 (134)
cis-$[Co(OH)(H_2O)(cyclen)]^{2+}$	7.1[b]	526 (179)	358 (124)
cis-$[Co(OH)_2(cyclen)]^{+}$	12.5[b]	548 (164)	360 (150)

[a] pK_{a1} = 5.44, pK_{a2} = 7.70.
[b] pK_{a1} = 5.66, pK_{a2} = 8.14.

the cobalt-bound chloro ligand cannot be avoided under the titration conditions (see appropriate entry in Table 1), as for the simple tetraamminocobalt(III) complexes [59]. The process results in the formation of the dihydroxo complex in major quantities, even in the presence of 1.0 M of chloride ions. An apparent value of about 6.4 was estimated from a non-rigorous SPECFIT fitting of the UV–vis titration data to an equilibrium involving the four relevant species, indicated above, in 1.0 M NaCl.

UV–vis monitoring substitution of H_2O by Cl^- on the complexes containing *tren* and *cyclen* tetraamines showed a good retention of isosbestic points at high acidity. These correspond solely to the process of formation of the monochloro cobaltocomplex, as expected from the data available in the literature [50,51]. Furthermore, treatment of the dichloro complexes in 1 M chloride solution at higher pH (up to 5.0) produced solely mixtures of diaquo and monochloro complexes, which indicates that under the conditions of the studies, only the formation of the mono-substituted chloro complex has to be considered [49]. In *cis*-$[Co(H_2O)_2(tren)]^{3+}$ the two water molecules occupy geometrically distinct positions, while nitrogen-based isomerism leads the two aqua ligands in *cis*-$[Co(H_2O)_2(cyclen)]^{3+}$ also inequivalent in the isolated *syn*,*anti* complexes [48]. The relative lability of the two non-chelated ligands in these complexes has already been established, and a base-catalysed mechanism, even at relatively low pH found to be operative for both *tren* and *cyclen* derivatives [48]. In view of these facts the kinetic experiments were designed to study only the $[Co(H_2O)_2(tren)]^{3+}/[CoCl(H_2O)(tren)]^{2+}$ and $[Co(H_2O)_2(cyclen)]^{3+}/[Co(OH)(H_2O)(cyclen)]^{2+}/[CoCl(H_2O)(cyclen)]^{2+}$ product systems, where the different acidity of the aqua ligands has been established [50,60]. For these systems the operation of the internal alternative base-catalysed substitution mechanism from the hydroxo complexes has to be considered [61,62].

2.2. Nucleoside and nucleotide complexes

The complexation of these biologically relevant ligands to the Co(III) complexes has only been studied for the *cis*-$[Co(H_2O)_2(cyclen)]^{3+}$ system, given the simpler characteristics of its substitution processes [50]. In view of the possible hydrolysis of nucleotides by this complex at physiological pH [38–40,63], the stability of the diaquacomplex at pH 7 was monitored. In all cases only the mono and dihydroxo derivatives were detected, the formation of other type of polymers were not observed by UV–vis, except for experiments carried out at high complex concentrations and/or more alkaline conditions. Even in these conditions, decreasing pH back to 7 produced the immediate and quantitative reappearance of the aquahydroxo complex, *cis*-$[Co(OH)(H_2O)(cyclen)]^{2+}$. This allowed us to study the substitution reactions without the problems derived from the existence of very stable and inert μ-OH polymeric forms that have been detected for some Pd(II) and Pt(II) model systems at physiological pH [11,64]. The values of the pK_a for the different ligands used in the study (Chart 1) have also to be considered. Literature values for the $H(INO)^+/INO/(INO–H)^-$ system are 1.1 and 8.8, while they are 3.8 and 6.2 for the $H_2(5'AMP)/H(5'AMP)^-/(5'AMP)^{2-}$ system, and 2.4 and 6.4 for the $H_2(5'IMP)/H(5'IMP)^-/(5'IMP)^{2-}$ equilibria [65,66]. Given the fact that for the nucleotide systems the mono/deprotonated equilibrium lies in the margin of pH used in this study, the values of the pK_a for these ligands were determined potentiometrically at the relevant ionic strength (1.0 M), Table 2 collects the determined data.

The nature of the nucleotide-substituted complexes has been studied *via* ^{31}P NMR spectroscopy; Table 2 collects the data obtained for the experiments carried out at different $[H^+]$ and in conditions of excess of ligand or cobaltocomplex. The data for the blank experiment carried out with phosphate as entering ligand is revealing, and agree with a cobalt-bound varying mixture of $H_2PO_4^-$ and HPO_4^{2-} [5,67,68]. At acidic pH, and with 25-fold excess phosphate, the formation of both the mono and bisphosphato complexes has to be considered. The set of data collected, with two ^{31}P NMR signals in the monodentate phosphate zone agree with this fact only if the two positions have become equivalent. Although, the signals could also be associated to two inequivalent monophosphato complexes, due to the initial *syn*/*anti* isomerism of the equatorial amines, the absence of two more signals corresponding to the bisphosphato derivative does not agree with this supposition, unless only this derivative has been formed. In this respect it is important to note that only a signal is observed when the experiment is carried out with cobalt complex in excess (Table 2 third entry), and at the same position that one of the signals observed in the systems with excess phosphate. As a whole, these observations seem to indicate that under the conditions of the experiment the two inequivalent *syn*/*anti* aqua ligand positions in *cis*-$[Co(H_2O)_2(cyclen)]^{3+}$ become equivalent when both are substituted by phosphate. Intramolecular hydrogen bonding between the phosphato ligand and the equatorial amine protons probably forces a symmetrical

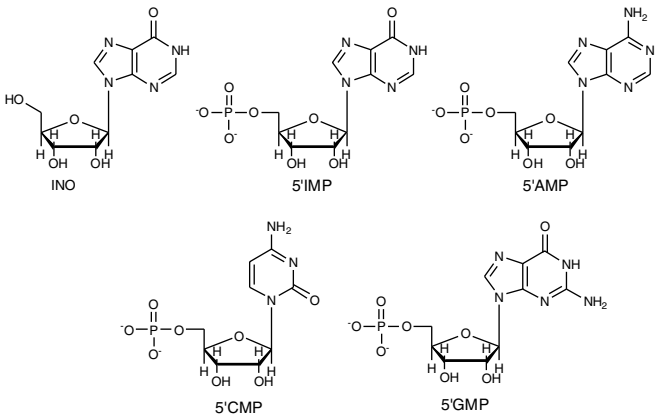

Chart 1.

Table 2
^{31}P NMR data for the reaction mixtures of *cis*-$[Co(H_2O)_2(cyclen)]^{2+}$ with 5′AMP and 5′IMP at different pH and concentration ratio conditions. Data for the blank reaction with phosphate has also been included for comparative purposes, n.c. indicates that no changes are observed

cis-$[Co(H_2O)_2(cyclen)]^{3+}$ *plus*	pH	[Co]:[ligand]	δ (ppm) *after mixing*	δ (ppm) *stabilized*
$H_2PO_4^-/HPO_4^{2-}$	2	0.04	8, 9	n.c.
	4	0.04	10, 11	10, 20
	5.3	5	11	28, 29
	9	0.04	26	n.c.
$H_2(5'AMP)/H(5'AMP)^-/(5'AMP)^{2-}$ [a]	5	0.04	14, 15	14, 15, 19
	5.2	7	14	14, 15, 19
	7	0.04	14, 15	14, 15
$H_2(5'IMP)/H(5'IMP)^-/(5'IMP)^{2-}$ [b]	5.2	7	14	14, 15, 19
	7	7	14	14, 15, 19

[a] $pK_{a1} = 3.3$, $pK_{a2} = 5.2$ at $I = 1.0$ M $NaClO_4$.
[b] $pK_{a1} = 2.0$, $pK_{a2} = 5.0$ at $I = 1.0$ M $NaClO_4$.

syn/*syn* isomerism of the bisphosphato complex and a preferential phosphate substitution of the aqua ligand *cis* to the equatorial amine with *syn* arrangement in the initial *syn*/*anti* complex (Fig. 1) [52,60,61]. The signal at 11 ppm at pH 4.0 is associated to the monophosphato complex and its disappearance with time to give a new signal at 20 ppm is assigned to a bridged Co^{III}-*O*(HPO_2)*O*-Co^{III} species [68]. For the experiment at pH 5.3 the same signal disappears by formation of phosphato bridged species, favoured by the excess of cobalt complex, that includes some chelate-bridging, μ-κ^2-PO_4, geometries (30 ppm zone) given the higher pH [39,43]. Finally, the spectrum at pH 9.0 shows only a signal at 26 ppm attributable to the simple chelate [Co(κ^2-PO_4)(cyclen)] complex [65].

For the nucleotide derivatives the set of ^{31}P NMR signals at pH 5.0 and 7.0 do not have any resemblance with the blank reactivity pattern seen for the phosphato derivatives. Hydrolysis of the ligand is evidently not taking place, despite that found for similar systems described [38,39]. For the experiments carried out with excess 5′AMP ligand, the formation of the mono and bis derivatives might be envisaged from the data collected in Table 2. On standing, a further wide signal in the 19 ppm region appears that we associate to some sort of bridged complex as indicated before. For the experiments run for 5′AMP and 5′IMP with excess cobalt only a signal (monosubstituted complex) at 14 ppm appears just after mixing, and a further signal, much less intense at 15 ppm, is made evident as time increases (Figure S1); thus, this signal cannot be due to bis-

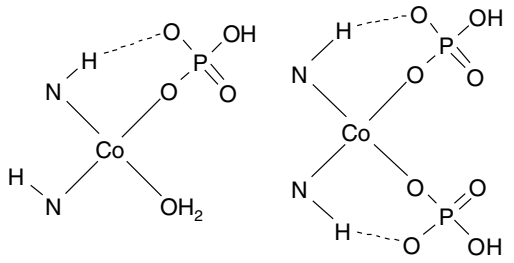

Fig. 1.

complexes. Possible phosphato bridged complexes cannot be considered either, given the fact that the chemical shift is expected at lower fields [68]. An equilibrium mixture with a chelate, or bridged, complex involving both one of the phosphate oxo groups and some other donors of the nucleotide can be held responsible for this fact [69]. The chemical shift of the phosphato group is not expected to be greatly affected and the formation process is expected to be concentration independent (*vide infra*). Some control experiments carried out with 5′CMP and 5′GMP also show this set of two signals in the monophosphato complex region, in good agreement with the above mentioned assumption.

As a whole, the studies indicate that the chemistry of the substitution processes on *cis*-$[Co(H_2O)_2(cyclen)]^{3+}$ by nucleotides at physiological pH does not involve hydrolysis of the ligands on coordination. No signals in the 30 ppm zone of the ^{31}P NMR spectrum are detected, a clear indication of the lack of the μ-κ^2-PO_4 complexes expected from hydrolysed phosphate at this pH [43]. The complexes, though, evolve to the formation of *O*(phosphato)-*N*(nucleoside) species.

2.3. Substitution kinetics

Once the nature of the complexes has been established, the full sequence of the kinetics of the reactions at physiological pH has to be considered. In principle the careful determination of the pK_a values of the diaquacobalt complexes and the entering ligands should enable an easy study. Nevertheless, these systems are surprising labile for a Co(III)–amine complex, expected to react fairly slowly at the pH range used [38,70]. The study of the substitution reactions of H_2O by chloride in *cis*-$[Co(H_2O)_2(tren)]^{3+}$ or *cis*-$[Co(H_2O)_2(cyclen)]^{3+}$ is acidity-dependent even at fairly high $[H^+]$ values, implying that an internal conjugate-base reaction mechanism is operative on the aqua-complexes even at acidic pH [48,50,52,61,62]. Scheme 1 (left side) corresponds to the set of possible reaction paths operating for the substitution process by a ligand (**L**) on the substrates

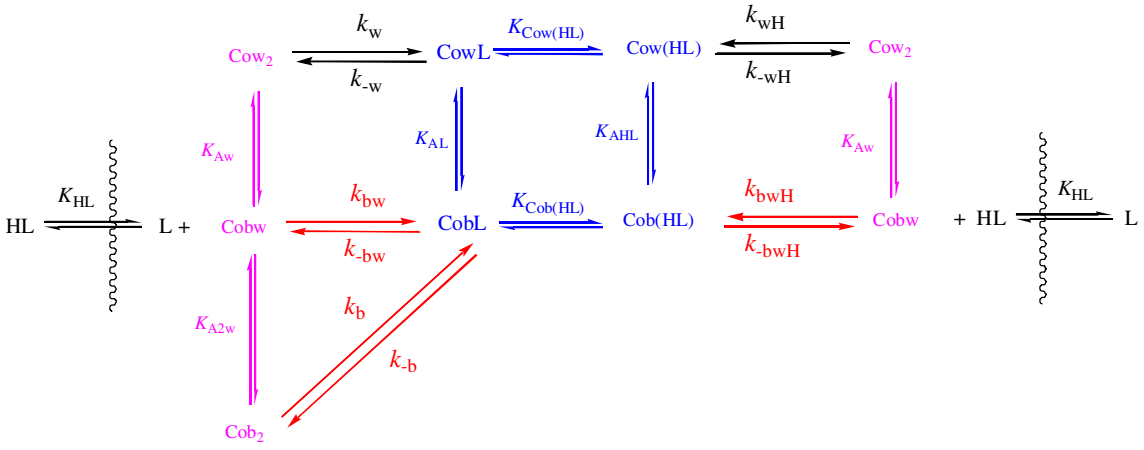

Scheme 1.

derived from the complex *cis*-$[Co(H_2O)_2(tetraamine)]^{3+}$, **Cow**$_2$, at different acidities. That is, in the fully protonated form of the tetraamine *tren* or *cyclen* ligands (**Co**≡{Co(tren)}$^{3+}$ or {Co(cyclen)}$^{3+}$) or in the form containing a reactive internal base-conjugated tetraamine (**Co**$^-$≡{Co(tren-H)}$^{2+}$ or {Co(cyclen-H)}$^{2+}$) produced from proton transfer to coordinated hydroxo ligands of the inert complexes [61,62]. The acid–base equilibria to be considered in the range of pH in which the experiments were carried out are the following:

$$k_{on} = \frac{\{k_{wH}\}[H^+]^2 + \{k_w k_{HL} + k_{bwH} k_{Aw}\}[H^+] + \{k_{bw} K_{Aw} K_{HL}\} + \{k_b K_{Aw} K_{A2w} K_{HL}\}(1/[H^+])}{\{[H^+] + K_{HL}\}\{[H^+] + K_{Aw}\}} \quad (1)$$

$$k_{off} = \frac{\{k_{-wH}/K_{Cow(HL)})\}[H^+]^2 + \{k_{-w} + k_{-bwH} K_{AHL}/K_{CowHL}\}[H^+] + \{k_{-bw} K_{AL}\} + \{k_{-b} K_{AL}\}(1/[H^+])}{([H^+] + K_{AL})} \quad (2)$$

$$k_{on}\{[H^+]K_{HL}^{-1} + 1\}\{[H^+] + K_{Aw}\} = \{k_{wH}K_{HL}^{-1}\}[H^+]^2 + \{k_w + k_{bwH}K_{Aw}K_{HL}^{-1}\}[H^+] + \{k_{bw}K_{Aw}\} + \{k_b K_{Aw} K_{A2w}\}(1/[H^+]) \quad (3)$$

$$k_{off}([H^+] + K_{AL}) = \{k_{-wH}/K_{Cow(HL)})\}[H^+]^2 + \{k_{-w}k_{-bwH}K_{AHL}/K_{CowHL}\}[H^+] + \{k_{-bw}K_{AL}\} + \{k_{-b}K_{AL}\}(1/[H^+]) \quad (4)$$

Co$(H_2O)_2$/**Co**$(OH)(H_2O)$ ≡ **Cow**$_2$/**Cobw**;
K_{Aw} producing reactive **Co**$^-$**w**$_2$

Co$(OH)(H_2O)$/**Co**$(OH)_2$ ≡ **Cobw**/**Cob**$_2$;
K_{A2w} producing reactive **Co**$^-$**bw**

Co(H_2O)L;/**Co**(OH)L ≡ **CowL**/**CobL**;
K_{AL} producing reactive **Co**$^-$**wL**

Whenever the ligand **L** can further be involved in an acid–base equilibrium, at the pH used for the experiments (as is the case for the 5′IMP and 5′AMP ligands) species **HL** has also to be considered. The parallel reaction scheme showed on the right of Scheme 1 applies, related through the corresponding deprotonation equilibria.

Only the k_w/k_{-w} and k_{wH}/k_{-wH} paths corresponds to a spontaneous process, while the k_{bw}/k_{-bw}, k_{bwH}/k_{-bwH} and k_b/k_{-b} reactions correspond to internal base catalysed processes, as indicated for equivalent systems [50,52,61]. The possible k_{bH}/k_{-bH} term, derived from **Cob**$_2$ plus **HL** reactivity, should not be considered given the fact that pH requirements for **Cob**$_2$ do not allow for the existence of **HL**. For the full reaction scheme the rate law can be written as $k_{obs} = k_{on} \times [L]_{total} + k_{off}$. The expression for k_{on} can be derived as in Eq. (1), taking into account that the amount of **Cob**$_2$ in negligible under the pH conditions used. For k_{off} Eq. (2) applies, if the concentrations of **Cow(HL)** and **Cob(HL)** are considered negligible, given the increased acidity of the coordinated HL ligand.

Fig. 2 represents typical plots of k_{obs} *versus* $[L]_{total}$ for the systems studied. From the plots of $k_{on}\{([H^+]K_{HL}^{-1} + 1)([H^+] + K_{Aw})\}$ (Eq. (3)) or $k_{off}\{[H^+] + K_{AL}\}$ (Eq. (4)) *versus* $[H^+]$ (or $[H^+]^{-1}$), shown in Figs. 3 and S2, the values of the specific combinations of rate and equilibrium constants involved in the different reaction $[H^+]$-dependent paths can be derived [14]. It is clear that data have errors much larger than those derived from the mathematical treatment, only the relative weight of the acidity-dependent contributions can be considered. The choice of the plot *versus* $[H^+]$ or $[H^+]^{-1}$ has been done according to the range of acidity values used, as indicated in Tables 3 and 4 that collect the relevant data calculated using the pK_{Aw} and pK_{HL} values in Tables 1 and 2. A value of pK_{AL} of 6.4 has been estimated (see Section 2.1) for $[CoCl(H_2O)(cyclen)]^{2+}$/$[CoCl(OH)(cyclen)]^+$, and the value has been used for all the rest of the $[CoL(H_2O)(tetraamine)]^{n+}$/$[CoL(OH)(tetraamine)]^{(n-1)+}$ equilibria.

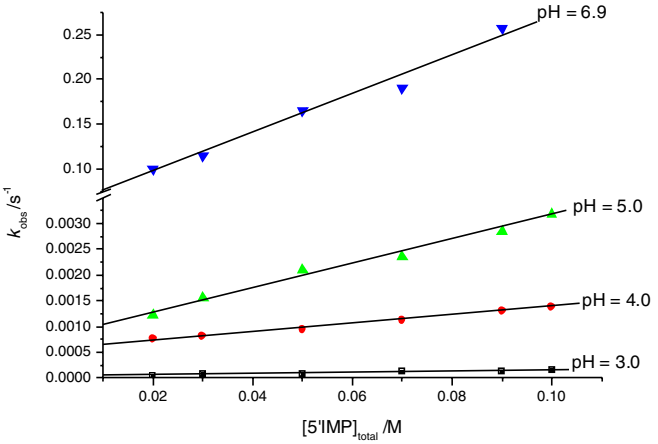

Fig. 2. Plot of k_{obs} *vs.* $[5'IMP]_{total}$ for the substitution on *cis*-$[Co(H_2O)_2(cyclen)]^{3+}$ at 21 °C, $I = 1.0$ M ($NaClO_4$) and different acidities.

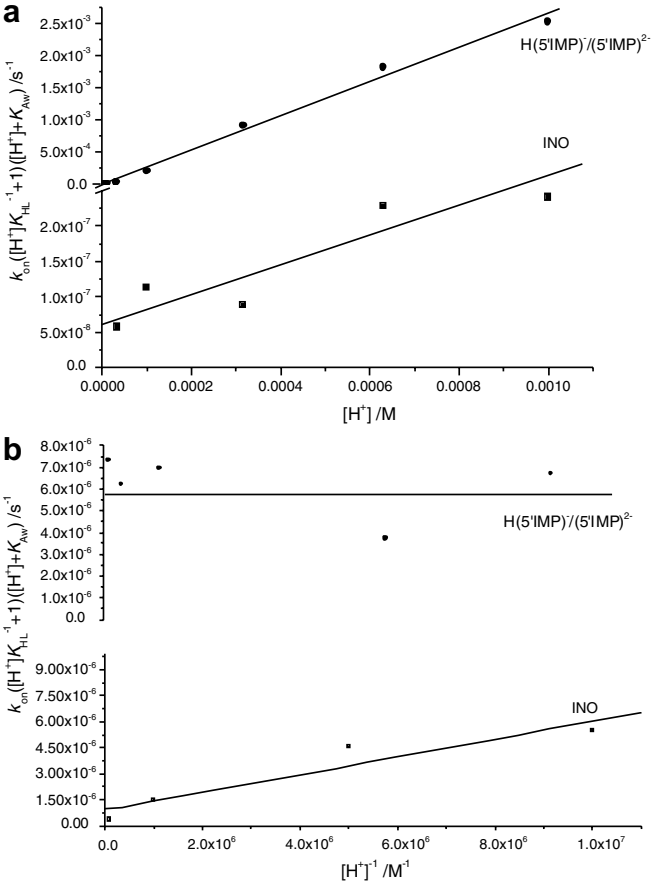

Fig. 3. Plots of $k_{on}\{([H^+]K_{HL}^{-1}+1)([H^+]+K_{Aw})\}$, for the *cis*-$[Co(H_2O)_2$-(cyclen)$]^{3+}$ plus the hypoxanthine nucleoside and nucleotide derivatives, *vs.* $[H^+]$ (a) or $[H^+]^{-1}$ (b) according to Eq. (3), at the pH range indicated in Table 3 ($T = 21$ °C, $I = 1.0$ M ($NaClO_4$)).

The chloride substitution reaction on the *tren* cobalt complexes has only contribution from the spontaneous path down to pH 4. For the complex having the more acidic *cyclen* ligand the path derived from the first internal base-catalysed is active in the same pH range. Despite the fact that the concentration of the **Cob**$_2$ species is very low ($K_{A2w} = 10^{-8.14}$) under the conditions used the k_b/k_{-b} internal base-catalysed path is also active for this complex at the pH range used. Nevertheless, its contribution to the process is ca. 5 orders of magnitude lower, which could be considered an indicative of the concerted internal conjugate-base process that necessarily forces a hydroxo ligand (a much better Lewis-base ligand) out of the coordination sphere of the cobalt.

On moving to the similar substitution process on *cis*-$[Co(H_2O)_2(cyclen)]^{3+}$ by inosine, the nucleoside is found active in the same reaction paths detected for the chloride anion at the working pH. The values calculated for the rate constants show, however, surprising differences with respect to the chloride substitution process. Spontaneous substitution is 1–2 orders of magnitude larger, while the contribution to substitution of the two conjugate-base paths are reduced by the same degree. Given the neutral charge of the INO entering ligand at the working pH, a variety of factors on these dissociatively activated substitutions, such as the existence of hydrogen-bonded outer-sphere complexes involving the cyclic amines and the biologically relevant ligands [2,71–73], have to be held responsible of the unexpected trend. Equilibrium constants are definitively larger than for the chloride ligands, in good agreement with the nature of the nitrogen donor groups [16,23,74,75].

As for the substitution processes by 5′AMP and 5′IMP on *cis*-$[Co(H_2O)_2(cyclen)]^{3+}$, the main contribution corresponds to the spontaneous process on **Cow**$_2$, k_w, and/or the internal conjugate-base generated for the k_{bwH} path, both being kinetically undistinguishable by proton ambiguity. The reaction rate of the path related to the internal conjugate-base generated from **Cobw** is five orders of magnitude lower. The reverse reaction is only active *via* the latter producing a *partial* equilibrium constant of ca. 200, in good agreement with the preference of phosphate to water of the cobalt(III) centre [76,77]. The values found for the substitution rate constants are practically the same for the two systems, indicating the fairly equivalent nature of the phosphate entering groups.

Given the dissociatively activated character of the process studied, the difference on the values corresponding to the rate constants for the nucleoside and nucleotide substitution processes in the second column of Table 3 has to be related to a large value of k_{bwH}. The non-innocent outer-sphere hydrogen bonded complex between the **Cobw** and **HL** species, can be held responsible for this large increase, as in many of the reactivity associated with biologically relevant ligands [45]. In this case {**Cobw**;**HL**} and {**Cow**$_2$;**L**} would be undistinguishable, but the former will enable a very active internal conjugate-base pathway that can explain the enormous acceleration observed.

Finally the mentioned slow appearance of a second ^{31}P NMR signal at ca. 15 ppm, related to the presence of a system where both the phosphate and the purine base are attached to a Co(III) centre, has to be considered. The

Table 3
Values of the rate constants derived from k_{on} obtained for the different systems studied, according to the reaction Scheme 1a and b and using Eq. (3) ($T = 21$ °C, [**Co**] = (2–3) × 10^{-3} M, $I = 1.0$ M $NaClO_4$)

System	pH	$k_{wH}K_{HL}^{-1}$ (s^{-1} M^{-2})	$k_w + k_{bwH}K_{Aw}K_{HL}^{-1}$ (s^{-1} M^{-1})	$k_{bw}K_{Aw}$ (s^{-1})	$k_bK_{Aw}K_{A2w}$ (s^{-1} M)	Plots *vs.*
$[Co(H_2O)_2(tren)]^{3+} + Cl^{-}$[a]	1.0, 2.0, 3.0, 4.0	[b]	$(1.2 \pm 0.1) \times 10^{-5}$	[c]	[c]	$[H^+]$
$[Co(H_2O)_2(cyclen)]^{3+} + Cl^{-}$	0, 0.3, 1.0, 2.0, 2.5, 3.0, 3.5	[b]	$(3.4 \pm 0.3) \times 10^{-6}$	$(1.7 \pm 0.1) \times 10^{-5}$	[c]	$[H^+]$
	2.5, 3.0, 3.5, 3.9, 4.7, 5.0	[b]	[c]	$(3.0 \pm 0.5) \times 10^{-6}$	$(9 \pm 1) \times 10^{-11}$	$[H^+]^{-1}$
$[Co(H_2O)_2(cyclen)]^{3+} + INO$	3.0, 3.2, 3.5, 4.0, 4.5	[b]	$(1.9 \pm 0.5) \times 10^{-4}$	$(7 \pm 3) \times 10^{-8}$	[c]	$[H^+]$
	5.0, 6.0, 6.7, 7.0	[b]	[c]	$(9 \pm 7) \times 10^{-7}$	$(5 \pm 1) \times 10^{-13}$	$[H^+]^{-1}$
$[Co(H_2O)_2(cyclen)]^{3+} + 5'IMP$	3.0, 3.2, 3.5, 4.0, 4.5, 5.0, 5.5, 6.0, 6.6, 6.9		$(1.1 \pm 0.1) \times 10^{-1}$		[c]	$[H^+]$
	4.5, 5.0, 5.5, 6.0, 6.6, 6.9		[c]	$(8 \pm 2) \times 10^{-7}$		$[H^+]^{-1}$
$[Co(H_2O)_2(cyclen)]^{3+} + 5'AMP$	3.5, 4.0, 4.3, 4.5, 5.0 6.0, 6.9		$(2.4 \pm 0.1) \times 10^{-1}$	$(9 \pm 4) \times 10^{-6}$	[c]	$[H^+]$
	5.0, 6.0, 6.6, 6.9		[c]	$(5 \pm 2) \times 10^{-6}$		$[H^+]^{-1}$

[a] At 25 °C.
[b] Non-applicable for chloride and inosine substitution at this pH range.
[c] The pH range used for the measures does not allow for the determination of these values.

Table 4
Values of the rate constants derived from k_{off} obtained for the different systems studied, according to the reaction Scheme 1a and b and using Eq. (4) ([**Co**] = (2–3) × 10^{-3} M, $I = 1.0$ M $NaClO_4$)[a]

System	pH	$k_{-w}/K_{Cow(HL)}$ (s^{-1} M^{-2})	$k_{-w} + k_{-bwH}K_{AHL}/K_{Cob(HL)}$ (s^{-1} M^{-1})	$k_{-bw}K_{AL}$ (s^{-1})	$k_{-b}K_{AL}$ (s^{-1} M)	Plots *vs.*
$[Co(H_2O)_2(tren)]^{3+} + Cl^{-}$[b]	1.0, 2.0, 3.0, 4.0	[c]	$(1.8 \pm 0.1) \times 10^{-5}$	[d]	[d]	$[H^+]$
$[Co(H_2O)_2(cyclen)]^{3+} + Cl^{-}$	0, 0.3, 1.0, 2.5, 2.0, 3.0, 3.5	[c]	$(4.6 \pm 0.6) \times 10^{-6}$	$(7 \pm 3) \times 10^{-6}$	[d]	$[H^+]$
	2.5, 3.0, 3.5, 3.9, 4.7, 5.0	[c]	[d]		$(1.1 \pm 0.4) \times 10^{-11}$	$[H^+]^{-1}$
$[Co(H_2O)_2(cyclen)]^{3+} + INO$	3.0, 3.2, 3.5, 4.0, 4.5	[c]	$(2.8 \pm 0.1) \times 10^{-5}$	$(1.5 \pm 0.6) \times 10^{-9}$	[d]	$[H^+]$
	5.0, 6.0, 6.7, 7.0	[c]	[d]	$(6 \pm 1) \times 10^{-10}$		$[H^+]^{-1}$
$[Co(H_2O)_2(cyclen)]^{3+} + 5'IMP$	3.0, 3.2, 3.5, 4.0, 4.5, 5.0, 5.5, 6.0, 6.6			$(3.6 \pm 0.8) \times 10^{-8}$	[d]	$[H^+]$
	5.0, 5.5, 6.0, 6.6, 6.9		[d]	$(3 \pm 1) \times 10^{-8}$		$[H^+]^{-1}$
$[Co(H_2O)_2(cyclen)]^{3+} + 5'AMP$	3.5, 4.0, 4.3, 4.5, 5.0, 6.0, 6.9			$(2.6 \pm 0.4) \times 10^{-8}$	[d]	$[H^+]$
	5.0, 6.0, 6.6, 6.9		[d]	$(3.3 \pm 0.5) \times 10^{-8}$		$[H^+]^{-1}$

[a] K_{AL} is approximated to 6.4 as indicated in the text.
[b] At 25 °C.
[c] Non-applicable for chloride and inosine substitution at this pH range.
[d] The pH range used for the measures does not allow for the determination of these values.

UV–vis monitored experiments showed irregular small drifts in the final absorbance readings, which were independent of the concentration of the nucleotides, and were associated to an intramolecular process. As expected from the small intensity of this ^{31}P NMR signal, the amplitude of these changes are very small making difficult its proper quantification. This observation is of great importance, and further studies are underway. Substitution of the last available ligand in the coordination sphere of the cobalt should render the complex unreactive towards hydrolysis of the phosphate group [15].

3. Conclusions

The study of the substitution of water by chloride and biologically relevant ligands has been carried out with cobaltocomplexes containing *cyclen* and *tren* tetraamine ligands. These ligands enable both the stability of the metal complex and the actuation of fast conjugate-base pathways even at physiological pH. The lability and stability of the inert skeleton of the complex permit the rapid dissociation of any polymeric μ-OH species appearing in the medium, the substitution reactivity becoming much simpler. The kinetic processes for the substitution of water by nucleotides are seen to be dominated by a concerted conjugate-base path on the hydrogen bonded outer-sphere complexes formed between *cis*-$[Co(OH)(H_2O)(cyclen)]^{2+}$ and the monoprotonated nucleotide. As a whole, comparison of the data for the full set of ligands used in this study indicates that the reaction paths are common to all processes, as expected for a dissociatively activated process.

^{31}P NMR monitoring of the experiments indicates that the substitution processes are clean and that no phosphate hydrolysis is observed at pH $\leqslant$ 7.0, which represents a

striking difference with most of the studies carried out on Co(III) complexes with this type of ligands. The formation of a phosphate-purine base chelated complex is observed in the experiments, after the initial formation of the phosphato monosubstituted *cis*-[Co(*O*PO$_2$Onucleoside)-(H$_2$O)(cyclen)]$^{2+}$ complex. This represents a promising way into the reactivity of this type of complexes, given the absence of any other hydroxo ligand attached to the cobalt centre capable of promoting the expected phosphate hydrolysis.

4. Experimental

4.1. Compounds

The chlorides of dichlorotetraaminecobalt complexes, *cis*-[Co(Cl)$_2$(tetraamine)]Cl, have been prepared according to the published procedures [51,55]. The perchlorate salts of the aquachlorocomplexes, *cis*-[CoCl(H$_2$O)(tetraamine)]$^{2+}$, were also prepared following literature procedures, except that an excess of NaClO$_4$ was used instead of ammonium sulfate [49]. The diaquacomplexes, *cis*-[Co(H$_2$O)$_2$(tetraamine)]$^{3+}$, were prepared *via* triflate solvolysis [53,54] from the corresponding dichloro precursors. The resulting solid from the triflate solvolysis (3 g) was dissolved in 20 cm^3 of water and after 1–2 h the solution was cooled at 0 °C and NaClO$_4$ or triflic acid were added. On standing the corresponding perchlorates or triflates of the diaquacomplexes crystallize; the complexes were characterized by their UV–vis spectra (Table 1) and elemental analyses. *Anal.* Calc. for [Co(H$_2$O)$_2$(tren)](CF$_3$SO$_3$)$_3$: C, 15.7; N, 8.14. Found: C, 16.0; N, 8.32%. *Anal.* Calc. for [Co(H$_2$O)$_2$-(cyclen)](CF$_3$SO$_3$)$_3$ · H$_2$O: C, 18.0, N, 7.65. Found: C, 18.0; N, 7.47%. ^{13}C NMR (D$_2$O, 0.1 M HClO$_4$) indicated that the complexes have the expected *syn*/*anti* form as derived from the number of spectral signals [52], 60.20, 56.82, 52.72, 50.70 and 122.6 (q) ($^1J_{CF} = 315$ Hz).

Controlled pH solutions were achieved by addition of HClO$_4$ (pH 0–3), NaOH (pH 11–13) or using MES and HEPES buffers (pH 4–7) [78]. As a general rule the buffer (pH 4–7) concentration was 0.05 M, and the final pH was adjusted *via* de addition of HClO$_4$ or NaOH solutions until the desired reading in the pH metre (4–7 range). Ionic strength was fixed to 1.0 M by the addition of the calculated volume of NaClO$_4$ solutions.

4.2. Instruments

All the ^{31}P NMR spectra were recorded in H$_2$O on a Bruker DRX 250 instrument (101.25 MHz) of the Serveis Científico-Tècnics de la Universitat de Barcelona or on a Bruker Avance 500 instrument (202.46 MHz) of the Institut Català d'Investigació Química; using capilar tubes or coaxial insets containing H$_3$PO$_4$ (D$_2$O) or trimethylphosphite (CD$_3$COCD$_3$) as references. UV–vis spectra were carried out on HP8452A or Cary50 instruments.

4.3. pK_a titrations

Potentiometric titrations of the different diaquacomplexes, *cis*-[Co(H$_2$O)$_2$(tetraamine)]$^{3+}$, and the relevant ligands, 5′AMP and 5′IMP, were carried out in order to determine their acidity constants under the conditions of the study, i.e. $I = 1.0$ M (NaClO$_4$). For the cobalt complexes, their solutions in water (ca. 1×10^{-2} M) were transferred to a 50 cm^3 cell and thermostated at 25 °C; addition of small amounts of standard 0.1 M NaOH produced successive e.m.f. readings on a Metrohm 713 pH meter (glass and Ag/AgCl reference electrodes). For nucleotides the solutions (ca. 1×10^{-2} M) were prepared in aqueous 0.01 M NaOH and transferred to a 50 cm^3 cell thermostated at 25 °C; addition of small amounts of standard 0.01 M HClO$_4$ produced successive e.m.f. readings on the same instrument. Argon was bubbled through the solution during the experiment to avoid the presence of CO$_2$. The general technique is the same as that described in the literature [79].

Spectrophotometric titrations [80] of the cobalt tetraamine complexes produced changes in the UV–vis spectrum with pH which indicated also the presence of two distinct processes. Samples were titrated on a thermostated (25 °C) vessel and circulated to a UV–vis cell inside the spectrophotometer, basically with the same procedure indicated for the potentiometric titrations. The pK_a values were derived by the use of the SPECFIT program [56].

4.4. Kinetics

The reactions were followed by UV–vis spectroscopy in the full 250–700 nm range. Runs with $t_{1/2} > 170$ s were recorded on an HP8452A or a Cary 50 instrument equipped with a thermostated multicell transport; for runs with $t_{1/2} < 7$ s an Applied-Photophysics stopped-flow instrument connected to a J&M TIDAS spectrophotometer was used. Kinetics with intermediate $t_{1/2}$ were measured on a Hi-Tech SFA rapid mixing accessory connected to the HP8452A or J&M TIDAS instruments. Observed rate constants were derived from absorbance *versus* time traces at the wavelengths where a maximum increase and/or decrease of absorbance was observed. No dependence of the observed rate constant values on the selected wavelengths was detected, as expected for reactions where a good retention of isosbestic points is observed. The general kinetic technique is that previously described [11,81], in all cases the cobaltocomplex concentration was maintained at $(2–3) \times 10^{-3}$ M. In most of the experiments the observed absorbance *versus* time traces behaved as first-order producing reproducible rate constants within a 5% error. In some of the kinetic experiments with nucleotides a secondary change in the final absorbance was observed. Its quantification indicated its independence of the entering ligand concentration, although no definite values could be extracted (see Section 2.3). Table S1 (supporting information) collects all the obtained k_{obs} values for all the

complexes studied as a function of the starting complex, entering ligand, entering ligand concentration, pH and temperature.

Acknowledgements

We wish to thank the Ministerio de Educación y Ciencia (CTQ2006-14909-C02-02/BQU) and the AECI (ICI) for financial support. The valuable help of Fabian Benzo Moreira during the first stages of this work is also acknowledged.

Appendix A. Supplementary data

Supplementary data associated with this article can be found, in the online version, at doi:10.1016/j.poly.2006.06.041.

References

[1] B. Rosenberg, L. van Camp, J.E. Trosko, V.H. Mansour, Nature 222 (1969) 385.
[2] J.A. Cowan, Inorganic Biochemistry. An Introduction, Wiley-VCH, 1997.
[3] U. Felk, K.I. Goldberg, J. Am. Chem. Soc. 124 (2002) 6804.
[4] M.S. Davies, Berners, T.W. Hambley, J. Am. Chem. Soc. 120 (1998) 11380.
[5] J.E. Huheey, L.A. Keiter, R.L. Keiter, Inorganic Chemistry: Principles of Structure and Reactivity, Harper and Collins, New York, 1993.
[6] F. Reeder, F. Gonnet, J. Kozelka, J.C. Chottard, Chem. Eur. J. 2 (1996) 1068.
[7] S.E. Sherman, D. Gibson, A.H. Wang, S.J. Lippard, Science 230 (1985) 412.
[8] F. Gonnet, J. Kozelka, J. Chottard, Angew. Chem. Int. Ed. 31 (1992) 1483.
[9] F. Gonnet, F. Reeder, J. Kozelka, J.C. Chottard, Inorg. Chem. 35 (1996) 1653.
[10] C.A. Leppre, K.G. Strothkamp, S.J. Lippard, Biochemistry 26 (1987) 5651.
[11] N. de Barrios, G. González, A. Grandas, M. Martínez, V. Moreno, Inorg. React. Mech. 1 (1999) 205.
[12] S. Suvachittanont, H. Hohmann, R. van Eldik, J. Reedijk, Inorg. Chem. 32 (1993) 4544.
[13] M. Mikola, K.D. Klika, A. Hakala, J. Arpalahti, Inorg. Chem. 38 (1999) 571.
[14] M.L. Tobe, J. Burgess, Inorganic Reaction Mechanisms, Longman, 1999.
[15] R.G. Wilkins, Kinetics and Mechanisms of Reactions of Transition Metal Complexes, VCH, Wheinheim, 1991.
[16] T. Rau, R. van Eldik, Metal Ions in Biological Systems 32 (1996) 339.
[17] M.-H. Baik, R.A. Friesnes, S.J. Lippard, J. Am. Chem. Soc. 125 (2003) 14082.
[18] J. Kozelka, F. Legendre, F. Reeder, J.C. Chottard, Coord. Chem. Rev. 190-2 (1999) 61.
[19] M.S. Davies, S.J. Berners-Price, T.W. Hambley, Inorg. Chem. 39 (2000) 5603.
[20] M.L. Gonzalez, J.M. Tercero, A.N. Matilla, M.T. Fernandez, C. Alonso, S. Gonzalez, Inorg. Chem. 36 (1997) 1806.
[21] H.T. Chifotides, K.M. Koshlap, L.M. Pérez, K.R. Dunbar, J. Am. Chem. Soc. 125 (2003) 10714.
[22] J. Arpalahti, M. Mikola, S. Mauristo, Inorg. Chem. 32 (1993) 3327.
[23] T. Rau, R. van Eldik, Chem. Ber./Recueil 130 (1997) 1551.
[24] T. Suzuki, Y. Hirai, H. Monjushiro, S. Kaizaki, Inorg.Chem. 43 (2004) 6435.
[25] H. Hohman, B. Hellquist, R. van Eldik, Inorg. Chem. 31 (1992) 1090.
[26] R. Jacobs, F. Prinsloo, E. Breet, J. Chem. Soc., Chem. Commun. (1992) 212.
[27] V. Monjardet-Bas, M.-A. Elizondo-Riojas, J.C. Chottard, J. Kozelka, Angew. Chem. Int. Ed. 41 (2002) 2998.
[28] J. Kozelka, G. Barre, Chem. Eur. J. 3 (1997) 1405.
[29] M. Galanski, B.K. Keppler, Inorg. Chim. Acta 300 (2000) 783.
[30] K. Lemma, T. Shi, L.I. Elding, Inorg. Chem. 39 (2000) 1728.
[31] S. Choi, S. Mahalingaiah, S. Delaney, N.R. Neale, S. Masood, Inorg. Chem. 38 (1999) 1800.
[32] S. Moghaddas, P. Hendry, R.J. Geue, C. Qin, A.M.T. Bygott, A.M. Sargeson, N.E. Dixon, J. Chem. Soc., Dalton Trans. (2000) 2085.
[33] A. Rodger, A. Parkinson, S. Best, Eur. J. Inorg. Chem. (2001) 2311.
[34] D. Chatterjee, A. Mitra, M.S.A. Hamza, R. van Eldik, J. Chem. Soc., Dalton Trans. (2002) 962.
[35] M.J. Clarke, Coord. Chem. Rev. 232 (2002) 69.
[36] C. Metcalfe, J.A. Thomas, Chem. Soc. Rev. 32 (2003) 215.
[37] H.T. Chifotides, K.M. Koshlap, L.M. Pérez, K.R. Dunbar, J. Am. Chem. Soc. 125 (2003) 10703.
[38] T. Humphry, M. Forconi, N.H. Williams, A.C. Hengge, J. Am. Chem. Soc. 126 (2004) 11864.
[39] G.P. Haight, Coord. Chem. Rev. 79 (1987) 293.
[40] D.R. Jones, L.F. Lindoy, A.M. Sargeson, J. Am. Chem. Soc. 105 (1983) 7327.
[41] P. Hendry, A.M. Sargeson, J. Am. Chem. Soc. 111 (1989) 2521.
[42] J. Chin, X. Zou, J. Am. Chem. Soc. 110 (1988) 223.
[43] R.L. Fanshawe, A.G. Blackman, C.R. Clark, Inorg. Chim. Acta 342 (2003) 114.
[44] D.A. Knight, J.B. Delchanty, E.R. Goldman, J. Bongard, F. Streich, L.W. Edwards, E.L. Chang, Dalton Trans. (2004) 2006.
[45] R. Hettich, H.-J. Schneider, J. Am. Chem. Soc. 119 (1997) 5638.
[46] Md. Abdus Salam, K. Aoki, Inorg. Chim. Acta 314 (2001) 71.
[47] A. Bianchi, L. Calabi, C. Giorgi, P. Losi, P. Mariani, D. Palano, P. Paoli, P. Rossi, B. Valtancoli, J. Chem. Soc., Dalton Trans. (2001) 917.
[48] A.J. Clarkson, D.A. Buckingham, A.G. Blackman, C.R. Clark, Inorg. Chem. 39 (2000) 4769.
[49] W.V. Miller, S.K. Madan, Inorg. Chem. 10 (1971) 1250.
[50] N.J. Curtis, P. Hendry, G.A. Lawrance, J. Chem. Soc., Dalton Trans. (1988) 47.
[51] N.J. Curtis, G.A. Lawrance, J. Chem. Soc., Dalton Trans. (1985) 1923.
[52] A.J. Clarkson, A.G. Blackman, C.R. Clark, J. Chem. Soc., Dalton Trans. (2001) 758.
[53] N.E. Dixon, M.J. Lancaster, G.A. Lawrance, A.M. Sargeson, Inorg. Chem. 20 (1981) 470.
[54] N.E. Dixon, G.A. Lawrance, P.A. Lay, A.M. Sargeson, Inorg. Chem. 23 (1984) 2940.
[55] J.P. Collman, P.W. Schneider, Inorg. Chem. 5 (1966) 1380.
[56] R.A. Binstead, A.D. Zuberbuhler, B. Jung, SPECFIT32. [3.0.34]. 2005. Spectrum Software Associates.
[57] A.A. El- Awady, G.M. Harris, Inorg. Chem. 20 (1981) 1660.
[58] N.E. Brasch, D.A. Buckingham, C.R. Clark, A. Rogers, Inorg. Chem. 37 (1998) 4865.
[59] A.B. Lamb, E.B. Damon, J. Am. Chem. Soc. 59 (1937) 383.
[60] D.A. Buckingham, C.R. Clark, A.J. Rogers, J. Simpson, Inorg. Chem. 37 (1998) 3497.
[61] C.K. Poon, M.L. Tobe, Inorg. Chem. 7 (1968) 2398.
[62] W.G. Jackson, Inorg. Chim. Acta 10 (1974) 51.
[63] J. Cin, M. Banaszczyk, V. Jubian, X. Zou, J. Am. Chem. Soc. 111 (1989) 186.
[64] M. Vicens, A. Caubet, V. Moreno, Metal Based Drugs 4 (1997) 43.
[65] H. Sigel, S.S. Massoud, N.A. Corfu, J. Am. Chem. Soc. 116 (1994) 2958.
[66] R.M. Smith, A.E. Martell, Y. Chen, Pure & Appl. Chem. 63 (1991) 1015.

[67] W. Schmidt, H. Taube, Inorg. Chem. 2 (1963) 698.
[68] F. von Seel, G. Bohnstedt, Z. Anorg. Allg. Chem. 435 (1977) 257.
[69] L. Lomozik, A. Gasowska, R. Bregier-Jarzenbowska, R. Jastrzab, Coord. Chem. Rev. 249 (2005) 2335.
[70] R.D. Cornelius, W.W. Cleland, Biochemistry 17 (1978) 3279.
[71] P.V. Bernhardt, F. Bozoglián, B.P. Macpherson, M. Martínez, G. González, B. Sienra, Eur. J. Inorg. Chem. (2003) 2512.
[72] G. González, M. Martínez, E. Rodríguez, Eur. J. Inorg. Chem. (2000) 1333.
[73] M. Martínez, M.A. Pitarque, R. van Eldik, J. Chem. Soc., Dalton Trans. (1996) 2665.
[74] V. Marchan, V. Moreno, E. Pedroso, A. Grandas, Chem. Eur. J. 7 (2001) 808.
[75] F.A. Cotton, E.C. Wilkinson, P.L. Gauss, Basic Inorganic Chemistry, Wiley, New York, 1987.
[76] M. Ferrer, J. Llorca, M. Martínez, J. Chem. Soc., Dalton Trans. (1992) 229.
[77] M. Ferrer, G. González, M. Martínez, J. Chem. Soc., Dalton Trans. (1990) 2597.
[78] N.E. Good, G.D. Winget, W. Winter, T.N. Connoly, S. Izawa, R.M.M. Singh, Biochemistry 5 (1966) 467.
[79] J. Torres, C. Kremer, E. Kremer, H. Pardo, L. Suescun, A. Mombru, S. Domingo, A. Mederos, J. Alloys Comp. 323–324 (2001) 119.
[80] H.H. Perkampus, UV–Vis Spectroscopy and its Applications, Springer, Berlin, 1992.
[81] F. Benzo, P.V. Bernhardt, G. González, M. Martínez, B. Sienra, J. Chem. Soc., Dalton Trans. (1999) 3973.

phase [14–18]. The results showed that most of these complexes still undergo photochromism upon complexation. In some cases the complexes could show reversible photoreactions even with the S atoms of the thiophene rings from the ligand being coordinated to the metal center, which is generally considered to suppress the free movement of the thiophene groups during photocyclization. As a continuous work, we reported herein the syntheses and photochromism of two novel copper(II) polymers with BM-2-PTP or closed-BM-2-PTP. [Cu(closed-BM-2-PTP)Cl_2] (**2**) was found to be a mixture containing two conformers with a ratio of 1:1 by X-ray crystallographic analysis, and showed effective photoreaction in the crystalline state upon irradiation.

2. Experimental

2.1. General methods

Unless otherwise indicated, all starting materials were obtained from commercial suppliers (Aldrich, Tokyo Kasei Chemicals and Wako Chemicals) and were used without further purification. Infrared spectra were recorded as KBr disks on JASCO FT-IR 8000 and FT/IR-430 spectrometers. Absorption spectra in the crystalline state were measured by diffuse reflection using the Kubelka–Munk method on a SHIMADZU UV-2450 spectrometer, and barium sulfate was used as a reference. Photoirradiation was carried out using a 150 W Xe lamp, and monochromatic light was obtained by passing the light through a monochromator.

2.2. Syntheses

2.2.1. Closed-BM-2-PTP

BM-2-PTP was synthesized as reported elsewhere [18]. A CH_2Cl_2 solution of BM-2-PTP was irradiated with 340 nm light which resulted in a blue solution, chromatography over silica gel (1% NMe_3/CH_2Cl_2) afforded closed-BM-2-PTP as a deep blue powder. *Anal.* Calc. for $C_{25}H_{16}F_6N_2S_2$: C, 57.46; H, 3.09; N, 5.36. Found: C, 57.56; H, 3.12; N, 5.24%. IR (KBr pellet): 3056 (w), 2857 (w), 1624 (m), 1581 (m), 1566 (m), 1552 (m), 1458 (m), 1433 (m), 1341 (s). UV–Vis (solid state) $\lambda_{max} = 350$ nm, $\lambda_2 = 610$ nm: after irradiation with 610 nm light (solid state) $\lambda_{max} = 350$ nm, after irradiation with 350 nm light (solid state) $\lambda_{max} = 530$ nm.

2.2.2. [Cu(BM-2-PTP)Cl_2] (**1**)

A solution of BM-2-PTP (15.9 mg, 30 μmol) in benzene (3 mL) was layered with a solution of $CuCl_2$ (3.9 mg, 30 μmol) in THF (3 mL). After standing at room temperature for 1 week, purple block crystals were obtained at the interface between the two solutions. *Anal.* Calc. for $C_{25}H_{16}Cl_2CuF_6N_2S_2$: C, 45.70; H, 2.45; N, 4.26. Found: C, 45.36; H, 2.50; N, 4.28%. IR (KBr pellet): 3058 (w), 2919 (w), 1600 (m), 1566 (m), 1495 (m), 1468 (m), 1430 (m), 1273 (s), 1060 (m), 1028 (m), 637 (m). UV–Vis (solid state) $\lambda_{max} = 340$ nm: after irradiation with 340 nm light (solid state) $\lambda_{max} = 620$ nm. Complex **1** is insoluble in common solvents due to its polymeric structure.

2.2.3. [Cu(closed-BM-2-PTP)Cl_2] (**2**)

Closed-BM-2-PTP (10.4 mg, 20 μmol) and $CuCl_2$ (2.7 mg, 20 μmol) were dissolved in 4 mL acetone. The mixture was introduced into a narrow-diameter glass tube and layered with a hexane solution. After standing at room temperature for 1 week, dark blue block crystals were obtained at the interface between the two solutions. *Anal.* Calc. for $C_{25}H_{16}Cl_2CuF_6N_2S_2$: C, 45.70; H, 2.45; N, 4.26. Found: C, 45.39; H, 2.49; N, 4.16%. IR (KBr pellet): 3056 (w), 2857 (w), 1626 (m), 1599 (m), 1566 (m), 1498 (w), 1474 (w), 1430 (s), 1341 (s). UV–Vis (solid state) $\lambda_{max} = 535$ nm, $\lambda_2 = 630$ nm: after irradiation with 535 nm light (solid state) $\lambda_{max} = 335$ nm. Complex **2** is insoluble in common solvents due to its polymeric structure.

2.3. X-ray data collection and structure solutions and refinements

Diffraction data for complexes **1** and **2** were collected on a Quantum CCD area detector coupled with a Rigaku MSC Mercury CCD diffractometer with graphite-monochromated Mo Kα radiation ($\lambda = 0.71070$ Å). The intensity data were collected at 150 K and 220 K for complexes **1** and **2**, respectively, using the multi-scan technique, and a total of 2994 and 2951 reflections were collected for complexes **1** and **2**, respectively. The linear absorption coefficient μ for Mo Kα radiation was 12.57 and 8.22 cm^{-1}, respectively.

Table 1
Crystallographic data for complexes **1** and **2**

Compound	**1**	**2**
Formula	$C_{25}H_{16}Cl_2CuF_6N_2S_2$	$C_{25}H_{16}Cl_2CuF_6N_2S_2$
Formula weight	656.98	656.98
Crystal system	monoclinic	orthorhombic
Space group	*C*2/*c* (#15)	*Pnma* (#62)
a (Å)	14.079(3)	6.927(3)
b (Å)	18.884(1)	20.812(8)
c (Å)	23.287(4)	17.401(7)
β (°)	115.758(8)	
V (Å^3)	2623.2(8)	2508(1)
Z	4	4
D_{calc} (g cm^{-3})	1.663	1.740
μ (cm^{-1})	12.57	8.22
Observed reflections [$I > 2\sigma(I)$]	2404	2712
R^a	0.060	0.069
$R_w{}^b$	0.121	0.142
Goodness-of-fit	1.09	1.41

[a] $R = \sum\|F_o| - |F_c\|/\sum|F_o|$.
[b] $R_w = [\sum w(F_o^2 - F_c^2)^2/\sum w(F_o^2)^2]^{1/2}$.

Table 2
Selected bond length (Å) and bond angles (°) for complexes **1** and **2**

Complex ***1***			
Cu(1)–N(1)	1.992(3)	Cu(1)–Cl(1)	2.2378(9)
Cu(1)–N(1*)	1.992(3)	Cu(1)–Cl(1*)	2.2378(9)
Cl(1)–Cu(1)–Cl(1*)	180.0	Cl(1)–Cu(1)–N(1*)	90.80(8)
N(1)–Cu(1)–N(1*)	180.0	Cl(1*)–Cu(1)–N(1*)	89.20(8)
Cl(1)–Cu(1)–N(1)	89.20(8)	Cl(1*)–Cu(1)–N(1)	90.80(8)
Complex ***2***			
Cu(1)–N(1)	2.010(3)	Cu(1)–Cl(1)	2.250(1)
Cu(1)–N(1*)	2.010(3)	Cu(1)–Cl(1*)	2.250(1)
Cl(1)–Cu(1)–Cl(1*)	180.0	Cl(1)–Cu(1)–N(1*)	90.65(9)
N(1)–Cu(1)–N(1*)	180.0	Cl(1*)–Cu(1)–N(1*)	89.35(9)
Cl(1)–Cu(1)–N(1)	89.35(9)	Cl(1*)–Cu(1)–N(1)	90.65(9)

Symmetric codes: complex **1**, * $-x$, $1-y$, $-z$; complex **2**, * $1-x$, $-y$, $1-z$.

The structures were solved by direct methods followed by subsequent Fourier calculations [20]. The non-hydrogen atoms were refined anisotropically. The final cycle of the full-matrix least-squares refinement was based on 2404 and 2712 observed reflections and 174 and 190 variable parameters for complexes **1** and **2**, respectively, converged with the unweighted and weighted agreement factors of $R = \sum\|F_o| - |F_c\|/\sum|F_o|$ and $R_w = [\sum w(F_o^2 - F_c^2)^2/\sum w(F_o^2)^2]^{1/2}$. The atomic scattering factors and anomalous dispersion terms were taken from the International Tables for X-ray Crystallography, vol. IV [21]. All calculations were performed using the teXsan crystallographic software package [22]. Details of the X-ray experiments and crystal data are summarized in Table 1. Selected bond lengths and bond angles are given in Table 2.

3. Results and discussion

3.1. Structural characterizations

The crystal structures of complexes **1** and **2** were determined by X-ray crystallographic analyses. Each Cu(II) of complex **1** is coordinated linearly by two N atoms from different ligands and two chloride anions, showing a slightly distorted square planar geometry (Fig. 1). The Cu atom lies

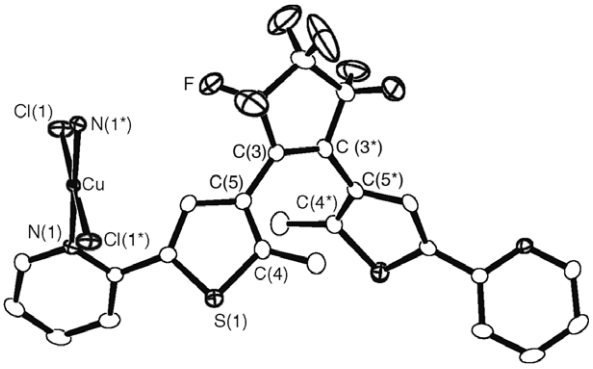

Fig. 1. Crystal structure of **1**, ORTEP view with an atomic labelling scheme, showing 50% thermal ellipsoids. Symmetric code: * $-x$, $1-y$, $-z$.

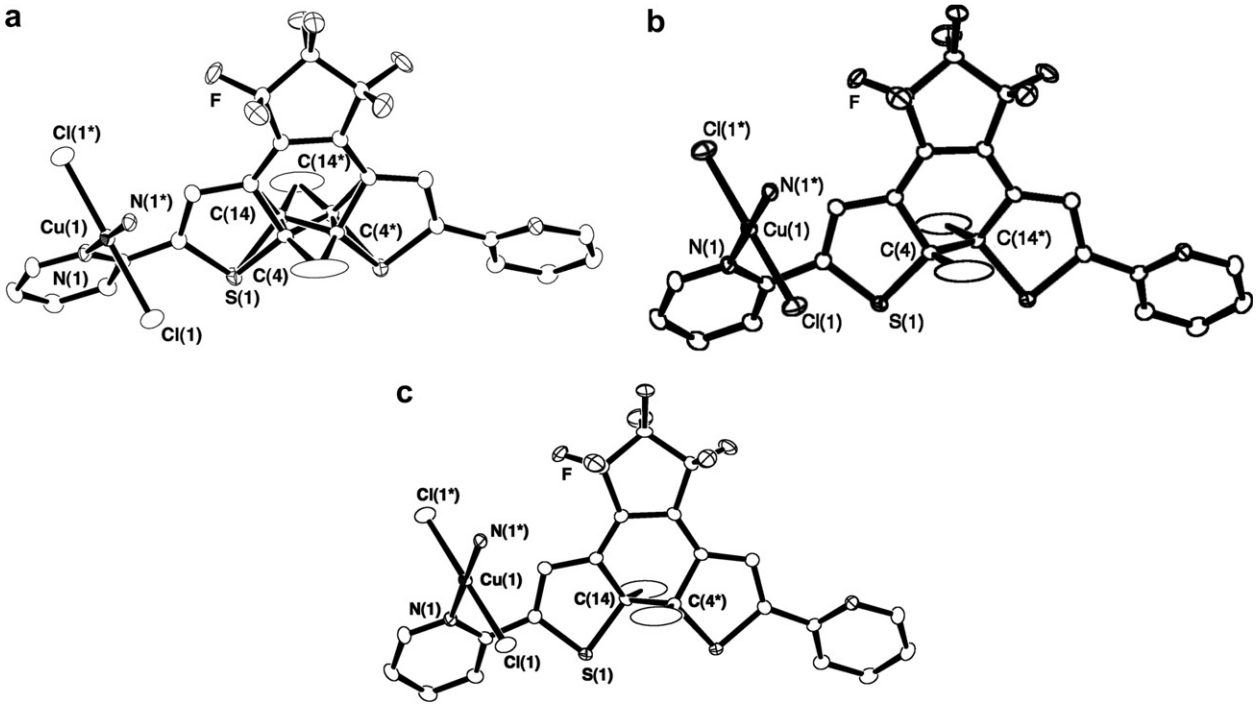

Fig. 2. Crystal structure of **2**, ORTEP view with an atomic labelling scheme, showing 50% thermal ellipsoids. (a) Complex **2** showing two conformers; (b) conformer A; (c) conformer B; symmetric code: * $1-x$, $-y$, $1-z$.

inside the plane constructed by N(1), N(1*), Cl(1) and Cl(1*), and the two pyridyl rings of the ligands are essentially perpendicular [N(1*)–Cu(1)–Cl(1) = 89.20(8)° and N(1*)–Cu(1)–Cl(1*) = 90.80(8)°] to the equatorial plane [Cl(1)Cu(1)Cl(1*)]. The bond lengths of Cu–N and Cu–Cl are 1.992(3) Å and 2.2378(9) Å, respectively, and fall within the normal range of $[Cu(py)_xCl_2]$ complexes [23–28]. Moreover, the two thienyl rings in complex **1** adopt an antiparallel configuration and the distance between the two reactive carbons C(4) and C(4*) is 3.394(6) Å, which is shorter than those of the metal free ligand [3.486(4) Å] and Ag(I) complexes with same ligand [3.548(1)–3.632(5) Å] [18], suggesting possible photoreactivity in the solid state. On the other hand, the mean torsion angle between the thiophene and perfluorocyclopentene rings [C(3*)–C(3)–C(5)–C(4) and C(3)–C(3*)–C(5*)–C(4*)] is 55.36°, larger than those of the Ag(I) complexes [48.43–53.35°].

The structures of complexes **2** and **1** are essentially the same except the dihedral angels between the pyridyl rings and the N(1)N(1*)Cl(1)Cl(1*) plane differ. It is noted that complex **2** has either a *R*,*R* or *S*,*S* asymmetric structure, with the ratio of two conformers A/B = 1/1 (Fig. 2). The bond distances between reactive carbons C(4) and C(14*)/C(14) and C(4*) in the two conformers are the same, 1.53(1) Å, a value which is usual for a single bond.

Both complexes **1** and **2** form 1-D infinite polymeric chains where two adjacent BM-2-PTP or closed-BM-2-PTP molecules are bridged by Cu(II) via two N atoms from pyridyl rings. The nearest distance between adjacent 1-D chains is ca. 8.32 Å and ca. 6.90 Å for complexes **1** and **2**, respectively, indicating no interaction between neighboring chains (Fig. 3).

3.2. Photochromism in the crystalline phase

The photoirradiation process of closed-BM-2-PTP and Cu(II) complexes were followed by electronic spectroscopy. The absorption spectra in the crystalline state were measured by diffuse reflection using barium sulfate as the reference and are illustrated in Figs. 4–6.

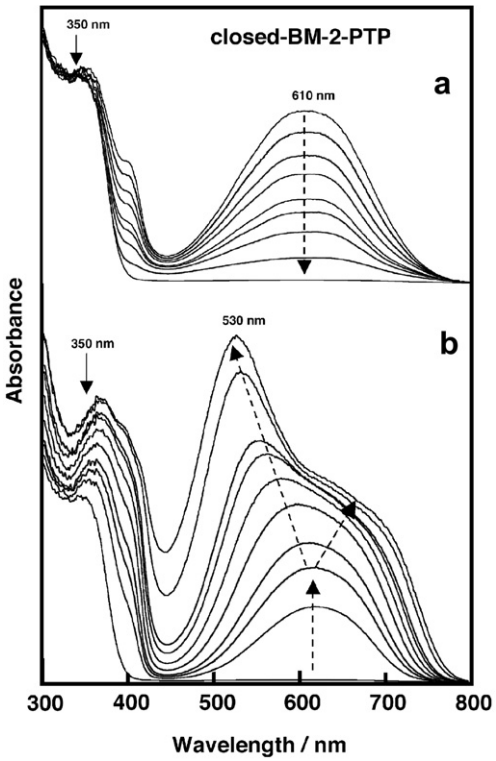

Fig. 4. Absorption spectral changes of closed-BM-2-PTP: (a) irradiated with 610 nm light; (b) irradiated with 350 nm light.

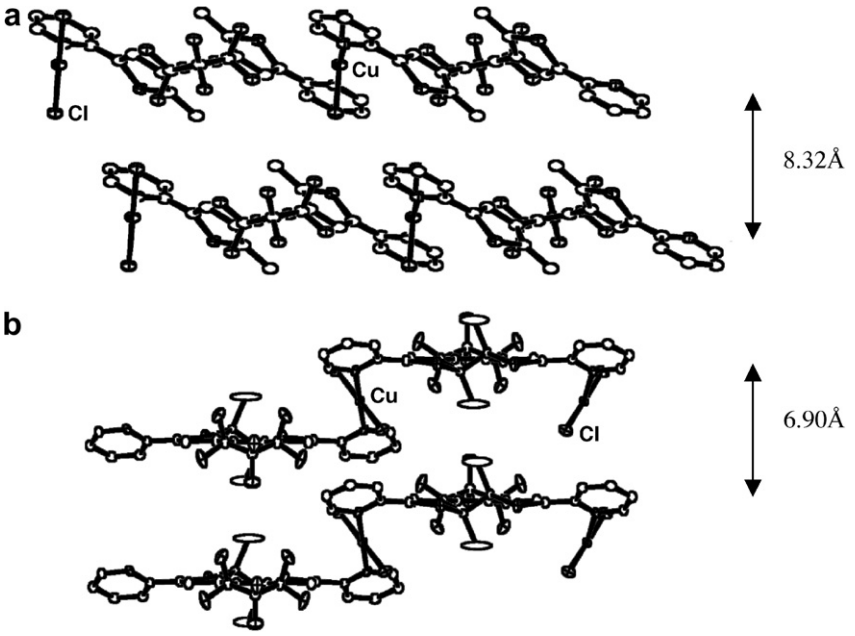

Fig. 3. Packing structures of complexes **1** and **2**.

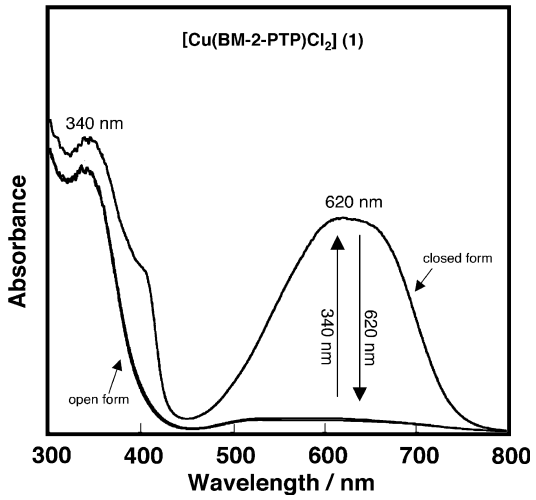

Fig. 5. Absorption spectral changes of complex **1**.

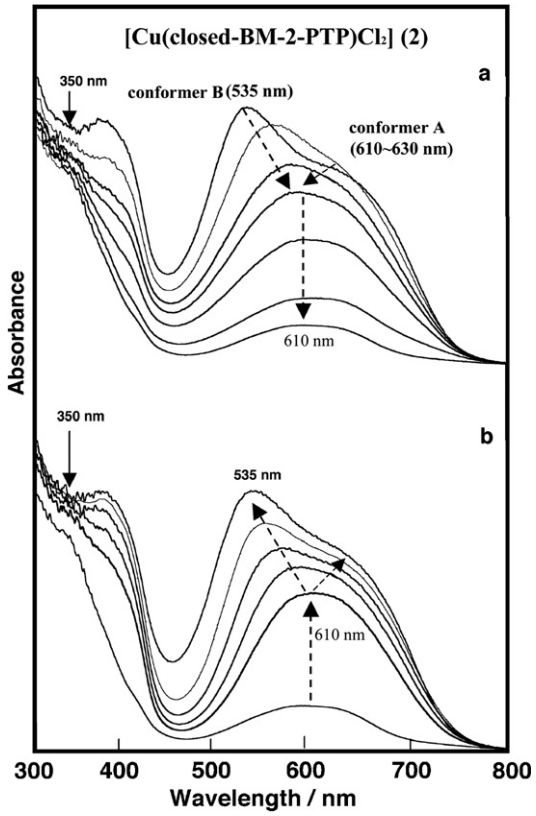

Fig. 6. Absorption spectral changes of complex **2**: (a) irradiated with 535 nm light; (b) irradiated with 335 nm light.

3.2.1. Photochromism of closed-BM-2-PTP

Photochromism of closed-BM-2-PTP was observed in the solid state, as shown in Fig. 4. Before irradiation the blue powder of closed-BM-2-PTP has λ_{max} values of 610 nm and ca. 350 nm. The 610 nm peak is characteristic of the closed-ring conformer but it is much longer than the λ_{max} value (580 nm, [18]) of the closed-ring form obtained by irradiation of BM-2-PTP. Upon irradiation with 610 nm light the λ_{max} value of 610 nm gradually flattened accompanying the pale blue color being bleached completely, which is attributed to a change to the corresponding open form. However, upon irradiation with 350 nm light the regenerated absorption peak of 610 nm shifted to shorter wavelength to give a broad absorption spectrum with a peak at 530 nm and a shoulder at 610–630 nm. Also, the color changed to purple, distinctive from the initial blue of closed-BM-2-PTP. These unexpected spectral changes indicated that the structure of closed-BM-2-PTP is changed after one cycle of coloration/decoloration. Before irradiation only one conformer was detected in closed-BM-2-PTP, which showed a 610 nm peak in the visible region, but during photocyclization it is possible for the ligand to form two conformers because the diarylethene undergoes a photochemical conrotatory cyclization [29]. The cyclization might contain two steps according to the changes of the absorptions: (1) the open-ring form was first converted to the corresponding closed-ring form which has an absorption peak at 610 nm; (2) with prolonged irradiation part of the conformer was gradually changed to another conformer and finally forms a mixture of two species which resulted in the different absorption peaks observed at 530 nm and 610–630 nm, respectively. This assumption is consistent with the previous work reported by Yamaguchi et al., who separated the two conformers by means of HPLC and found one isolated isomer was changed to the mixture of two diastereomers after irradiation [29].

3.2.2. Photochromism of complex *1*

Complex **1** displays normal photochromism in the crystalline state as expected. Fig. 5 shows its spectral changes. Similarly to the free ligand (BM-2-PTP) and Ag(I) complexes with BM-2-PTP, complex **1** has a maximum absorption at 340 nm before irradiation. After photoirradiation with 340 nm light, the purple color turned blue, accompanying a new strong absorption at 620 nm which appeared due to the formation of the closed form. The blue species reverted to their initial color by irradiation with 620 nm light, indicative of reversible photochromic behavior in the crystalline phase. Compared with the free ligand, the λ_{max} value of complex **1** increased as much as 40 nm and the maximum absorption is also longer than those of the Ag(I) complexes with BM-2-PTP [18].

3.2.3. Photochromism of complex *2*

Fig. 6 shows the quite different photochromism of complex **2** from that of complex **1**. Before irradiation the blue complex **2** shows a broad absorption spectrum with a λ_{max} value of 535 nm (conformer B) and a shoulder at 610–630 nm (conformer A). Irradiation with visible light of 535 nm leads to the disappearance of the 535 nm peak and the formation of an new absorption peak at 610 nm. With prolonged irradiation of visible light the intensity of the 610 nm peak gradually flattened, accompanying the

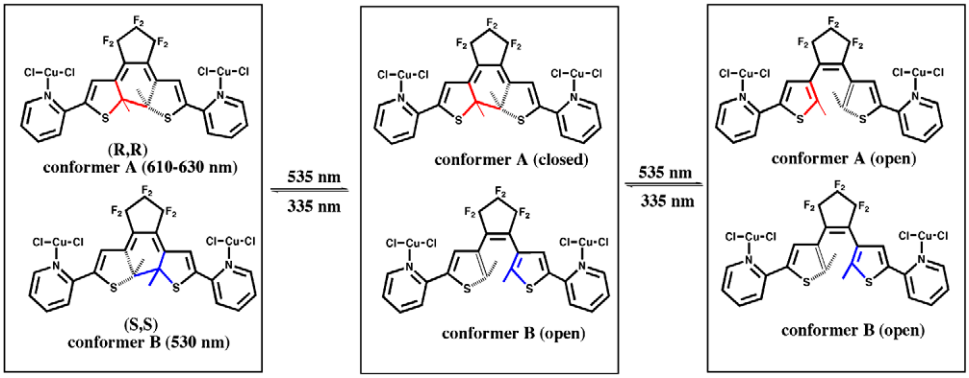

Scheme 1. Photochromism of complex **2** in the crystalline phase.

color fading completely due to the transformation of the closed to open isomer. When the open isomer was exposed to UV (335 nm) light, the intensity of the 610 nm peak increased and then this absorption peak gradually shifted to 535 nm and 610–630 nm, with the color turning from blue to purple. These spectral changes show clearly that complex **2** displays reversible photochromism in the crystalline state. The spectral changes during the photocyclization of complex **2** are very similar to those of the cyclizative transformation of the ligand.

As noted before, X-ray crystallographic analyses revealed complex **2** to be a racemic mixture of *R*,*R* and *S*,*S* enantiomer pairs. This is due to closed-BM-2-PTP because diarylethene undergoes a photochemical conrotatory cyclization producing two enantiomers originating from two asymmetric carbon atoms. Yamaguchi and Kodani once reported such mixtures and investigated their photoreactions in solution by introducing a chiral substituent into the diarylethene [29,30]. It was found that one isolated enantiomer shows normal cycloreversion, while during cyclization it is easily transferred to a mixture of two enantomers in solution. Yamaguchi et al. also examined a diarylethene system containing two conformers wherein two open isomers transformed into closed-ring isomers independently upon irradiation to give two absorptions in the visible region [31,32]. We could not separate the two enantiomers because of the insolubility of complex **2** in common solvents, so no direct evidence was obtained to prove the absorption features of complex **2**. However, the above-mentioned previous works are agreeable with our assumptions. It is tentatively considered that conformers A and B in complex **2** display photochromism independently in the crystalline phase. The original absorption of 535 nm and 610–630 nm of complex **2** should be assigned to the coexistence of two conformers. In cycloreversion the two conformers convert to the corresponding open isomers separately. The disappearance of the 530 nm absorption indicated conformer B (535 nm) changed to the corresponding open form first. While with irradiation of 335 nm light, conformer A (610–630 nm) was reverted to the closed-form which regenerated the absorption of 610 nm, as shown in Scheme 1.

Further investigation on the crystal structure of the open form of complex **2** was not successful due to the poor quality of the single crystal after irradiation. In spite of the limited evidence it is indicated clearly that the two types of ring-closed forms in complex **2** are photoreactive and both isomers display photocycloreversion reactions in the crystalline phase. The photogenerated ring-open form of complex **2** is packed in an antiparallel conformation [33]. We reported Rh(II) complexes with *cis*-dbe showed photocyclization in the crystalline state where three conformations coexisted in one crystal [16], and Irie and co-worker's group also proved a mixture of dithienylethene in the open form could undergo reversible photochromism in the solid state [34,35]. The findings obtained here evidence that two ring-closed photoactive isomers coexist in one crystal and the mixture undergoes photochromic reactions effectively in the crystalline phase.

4. Conclusions

Two novel Cu(II) single crystals were prepared by the reaction of $CuCl_2$ with BM-2-PTP in the open or closed form. Their structures were characterized by X-ray crystallographic analyses and their photoreactivities were investigated in the crystalline phase. It has been demonstrated that both complexes possess a similar coordination environment but display quite different photoreactions, which are attributed to the distinct photoresponsive patterns of BM-2-PTP and closed-BM-2-PTP. It was proved by X-ray crystallographic analyses that a mixture of closed-ring conformers could undergo photochromic reactions in the crystalline phase. It is suggested that two closed-ring conformers in complex **2** are both photoactive and the photogenerated ring-opening form adopts an antiparallel conformation. The mechanism of the photochromism of complex **2** is tentatively concluded as two conformers displaying photoreactions independently. It is hoped that this work will be helpful for accumulating evidence to clarify the rule of photocycloreversion reactions in the crystalline phase.

Acknowledgments

This work was partially supported by a Grant-in-Aid for Science Research (Nos. 14340211 and 16350037) from the Ministry of Education, Science, Sports and Culture in Japan.

Appendix A. Supplementary data

Crystallographic data for the X-ray crystal structural analysis have been deposited with the Cambridge Crystallographic Data Center, Nos. (0580) 608983 and 608984 for complexes **1** and **2**, respectively. Copies of this information may be obtained free of charge from The Director, CCDC, 12 Union Road, Cambridge CB2 1EZ, UK (fax: +44 1233 336 033; e-mail: deposit@ccdc.cam.ac.uk or www: http://www.ccdc.cam.ac.uk). Supplementary data associated with this article can be found, in the online version, at doi:10.1016/j.poly.2006.06.045.

References

[1] M. Irie, M. Mohri, J. Org. Chem. 53 (1988) 803.
[2] M. Irie, K. Sayo, J. Phys. Chem. 96 (1992) 7671.
[3] S. Kobatake, T. Yamada, K. Uchida, N. Kato, M. Irie, J. Am. Chem. Soc. 121 (1999) 2380.
[4] S. Yamamoto, K. Matsuda, M. Irie, Chem. Eur. J. 9 (2003) 4878.
[5] H.K.K. Hirschberg, L. Brunsveld, A. Ramzi, J.A. Vekemans, R.P. Sijbesma, E.W. Meijer, Nature 167 (2000) 407.
[6] S.H. Kawasi, S.L. Gilat, R. Ponsinet, Chem. Eur. J. 1 (1995) 285.
[7] H. Tian, S.J. Yang, Chem. Soc. Rev. 33 (2004) 85.
[8] D.V. Kozlov, F.N. Castellano, J. Phys. Chem. A 108 (2004) 10619.
[9] K. Higashiguchi, K. Matsuda, M. Irie, Angew. Chem., Int. Ed. 42 (2003) 3537.
[10] S. Fraysse, C. Coudret, J.-P. Launay, Eur. J. Inorg. Chem. 39 (2000) 1581.
[11] M. Frigoli, G.H. Mehl, Chem. Commun. (2004) 818.
[12] B. Qin, R.X. Yao, X.L. Zhao, H. Tian, Org. Biomol. Chem. 12 (2003) 2187.
[13] S. Kobatake, M. Irie, Bull. Chem. Soc. Jpn. 77 (2004) 195.
[14] M. Munakata, L.P. Wu, T. Kuroda-Sowa, M. Maekawa, Y. Suenaga, K. Furuichi, J. Am. Chem. Soc. 118 (1996) 3305.
[15] H. Konaka, L.P. Wu, M. Munakata, T. Kuroda-Sowa, M. Maekawa, Y. Suenaga, Inorg. Chem. 42 (2003) 1928.
[16] J. Han, H. Konaka, T. Kuroda-Sowa, M. Maekawa, Y. Suenaga, H. Isihara, M. Munakata, Inorg. Chim. Acta 359 (2006) 99.
[17] J. Han, A. Nabei, Y. Suenaga, M. Maekawa, H. Isihara, T. Kuroda-Sowa, M. Munakata, Polyhedron 252 (2006) 2483.
[18] M. Munakata, J. Han, A. Nabei, T. Kuroda-Sowa, M. Maekawa, Y. Suenaga, N. Gujima, Inorg. Chim. Acta 359 (2006) 4281.
[19] S. Kobatake, K. Uchida, E. Tsuchida, M. Irie, Chem. Commun. (2002) 2804.
[20] P.T. Beurskens, G. Admiraal, G. Beurskens, W.P. Bosman, R. de Gelder, R. Israel, J.M.M. Smits, The DIRDIF-94 Program System, Technical Report of the Crystallography Laboratory, University of Nijmegen, The Netherlands, 1994.
[21] D.T. Cromer, J.T. Waer, International Tables for X-ray Crystallography, vol. IV, The Kynoch Press, Birmingham, England, 1974.
[22] Crystal Structure Analysis Package, Molecular Structure Corporation, 1985 and 1992..
[23] J.A. Campbell, C.L. Raston, A.H. White, Aust. J. Chem. 30 (1977) 1937.
[24] B. Morosin, Acta Crystallogr., Sect. B 31 (1975) 632.
[25] P.C. Healy, J.D. Kildea, B.W. Skelton, A.H. White, Aust. J. Chem. 42 (1989) 93.
[26] M. Maekawa, M. Munakata, S. Kitagawa, M. Nakamura, Anal. Sci. 7 (1991) 827.
[27] Y. Agnus, M. Labarelle, R. Louis, B. Metz, Acta Crystallogr., Sect. C 50 (1994) 536.
[28] J.B. Gary, J.A. Kautz, K.K. Klausmeyer, C.W. Wong, Acta Crystallogr., Sect. E 60 (2004) m328.
[29] T. Yamaguchi, K. Uchida, M. Irie, J. Am. Chem. Soc. 119 (1997) 6066.
[30] T. Kodani, K. Matsuda, T. Yamada, S. Kobatake, M. Irie, J. Am. Chem. Soc. 122 (2000) 9631.
[31] T. Yamaguchi, T. Inagawa, H. Nakazumi, S. Irie, M. Irie, J. Mater. Chem. 11 (2001) 2453.
[32] T. Yamaguchi, H. Nakazumi, K. Uchida, M. Irie, Chem. Lett. 7 (1999) 653.
[33] T. Yamada, S. Kobatake, K. Muto, M. Irie, J. Am. Chem. Soc. 122 (2000) 1589.
[34] T. Yamada, K. Muto, S. Kobatake, M. Irie, J. Org. Chem. 66 (2001) 6164.
[35] T. Yamada, S. Kobatake, M. Irie, Bull. Chem. Soc. Jpn. 75 (2002) 167.

with azodicarboxylic and acetylenic esters [32], oxime-phosphazene derivatives with alkyl and acyl substituents [33,34], polymers from 4-formylphenoxy [35,36], maleic [37] and 3,4-methylenedioxyphenoxy substituents [38].

In this paper, we have prepared oxime-cyclophosphazenes from hexakis(4-formylphenoxy)cyclotriphosphazene and hexakis(4-acetylphenoxy)cyclotriphosphazene, and have studied their reactions with benzyl and benzoyl halides such as benzyl chloride, benzenesulfanoyl chloride, benzoyl chloride, 4-methoxybenzoyl chloride and 2-chlorobenzoyl chloride. We hope that this original work is potentially an useful addition to the literature and can lead to some high polymer works.

2. Experimental

2.1. General remarks

Solvents and other liquids used in the experimental works were dried by conventional methods. Hexachlorocyclotriphosphazene [$N_3P_3Cl_6$] (**1**) was recrystallized from hexane. Other chemicals were used as purchased. Hexakis(4-formylphenoxy)cyclotriphosphazene (**2**) and hexakis(4-acetylphenoxy)cyclotriphosphazene (**8**) were prepared as described by Carriedo and et al. [25]. The reactions of [$N_3P_3Cl_6$] with the phenols were carried out under the dry nitrogen.

The IR spectra were recorded on an ATI Unicam Mattson 1000 FTIR spectrometer. ^1H, ^{13}C and ^{31}P NMR spectra were recorded using a Bruker DPX-300 spectrometer operating at 300.13, 75.46 and 121.49 MHz, respectively. The ^1H and ^{13}C NMR chemical shifts were measured using $SiMe_4$ as an internal standard and the ^{31}P chemical shifts were measured using 85% H_3PO_4 as an external standard. Chemical shifts downfield from the standard were assigned positive δ values. Microanalysis was carried out by a LECO 932 CHNS-O apparatus.

2.2. Synthesis of compound 2

A mixture of **1** (10.34 g, 29.74 mmol), 4-hydroxybenzaldehyde (22.05 g, 180.56 mmol) and K_2CO_3 (50.00 g, 361.76 mmol) was stirred in THF (250 mL) at 0 °C and then reacted at ambient temperature for 48 h. The solvent was removed under vacuum. The residue was extracted with CH_2Cl_2 (4 × 75 mL). After the solvent was removed, a white solid **2** formed in 92% (23.57 g) yield. IR (cm^{-1}): 1706 $\nu_{C=O}$, 1184 $\nu_{P=N}$, 962 ν_{P-O-C}. ^1H NMR (in $CDCl_3$-d, for numbering see Scheme 2, coupling constants J (Hz), is.: isomer, s: singlet, w: weak): 7.10 (d) H^2 ($^4J_{POCCH}$: 8.50), 7.60 (d) H^3 ($^5J_{POCCCH}$: 8.56), 9.90 (s) H^5; H^2:H3:H^5 = 2:2:1. ^{13}C NMR: 121.60 C^2, 131.40 C^3, 134.14 C^4, 154.80 C^1, 190.83 C^5.

2.3. Synthesis of compound 3

A mixture of **2** (20.00 g, 23.21 mmol) and hydroxylaminehydrochloride (10.00 g, 143.90 mmol) was refluxed in pyridine (15 mL) for 3 h. After the reaction was complete, the mixture was allowed to cool and was slowly poured into water (100 mL) and reprecipitated twice from water. The white solid **3** was washed with alcohol and dried at 50 °C in a vacuum. Yield: 83% (18.33 g). IR (cm^{-1}): 3340 ν_{OH}, 1187 $\nu_{P=N}$, 949 ν_{P-O-C}. ^1H NMR (in acetone-d): 6.86 (d) H^2 ($^4J_{POCCH}$: 8.45), 7.28 (d) H^3 ($^5J_{POCCCH}$: 8.50), 7.96 (s) H^5, 10.17 (s) H^6, 7.20 (w) H^2 (is.), 7.77 (w) H^3 (is.); H^2:H^3:H^5:H^6 = 2:2:1:1. ^{13}C NMR: 121.50 C^2, 121.33 C^2 (is.), 129.00 C^3, 129.37 C^3 (is.), 131.00 C^4, 131.00 C^4 (is.), 148.19 C_5, 151.70 C^1.

2.4. Reaction of 3 with benzyl chloride

A solution of 0.70 mL (0.77 g, 6.08 mmol) benzyl chloride in acetone (10 mL) was slowly added dropwise to a stirred and cooled (0–5 °C) mixture of **3** (0.80 g, 0.84 mmol) and K_2CO_3 (2.00 g, 14.47 mmol) in acetone (30 mL). The reaction was carried out at room temperature for 1 h and then was refluxed for 48 h. After the reaction was complete, the precipitate was filtered off and the solvent was removed. An oily product was obtained. It was dissolved in a very small amount of acetone and was precipitated with hexane. The solvent was removed under vacuum over 96 h. A white solid **4** formed. Yield: 66% (0.83 g). IR (cm^{-1}): 1183 $\nu_{P=N}$, 1024 ν_{N-O-C}, 952 ν_{P-O-C}. ^1H NMR (in DMSO-d): 6.95 (d) H^2, 7.2–7.6 (m) H^3, H^8, H^9, H^{10}, 8.30 (s) H^5, 5.20 (s) H^6. ^{13}C NMR: 150.95 C^1, 148.49 C^5, 147.60 C^5 (is.), 137.79 C^7, 137.85 C^7 (is.), 129.64 C^4, 129.28 C^4 (is.), 128.78 C^9, 128.69 C^{10}, 128.63 C^8, 128.32 C^3, 121.31 C^2, 121.00 C^2 (is.), 76.04 C^6. (The solvents could not be removed completely, so there are very very weak peaks at 0.8 and 1.3 ppm.)

2.5. Reaction of 3 with benzenesulfanoyl chloride

A solution of 0.55 mL (0.76 g, 4.29 mmol) benzenesulfanoyl chloride in acetone (10 mL), **3** (0.60 g, 0.63 mmol) and Et_3N (2 mL) in acetone (30 mL) was used for **4**. The reaction was carried out at room temperature for 12 h and then was refluxed for 48 h. Compound **5** was obtained. The orange colour solid **5** was washed with alcohol and dried at 50 °C in a vacuum for 48 h. Yield: 68% (0.36 g). IR (cm^{-1}): 2230 ν_{CN}, 1188 $\nu_{P=N}$, 950 ν_{P-O-C}. ^1H NMR (in DMSO-d): 7.15 (d) H^2, 7.85 (d) H^3. ^{13}C NMR: 152.88 C^1, 135.07 C^3, 121.99 C^2, 118.85 C^4, 109.37 C^5.

2.6. Reaction of 3 with 1-napthalenesulfanoyl chloride

A solution of 1.00 g (4.41 mmol) 1-napthalenesulfanoyl chloride in acetone (10 mL), **3** (0.60 g, 0.63 mmol) and Et_3N (2 mL) in acetone (30 mL) was used for **4**. The reaction was carried out at room temperature for 12 h and then was refluxed for 60 h. Compound **5** was obtained. The orange colour solid **5** was washed with alcohol and dried at 50 °C in a vacuum for 48 h. Yield: 85% (0.45 g).

2.7. Reaction of **3** with benzoyl chloride

A solution of 0.55 mL (0.66 g, 4.73 mmol) benzoyl chloride in acetone (10 mL), **3** (0.60 g, 0.63 mmol) in acetone (30 mL) and Et_3N (2 mL) was used for the preparation of **6** for **4**. The reaction was carried out at room temperature for 12 h. After the reaction was complete, the precipitate was filtered off, the liquid mixture was slowly poured into water (100 mL) and the solid product was obtained. It was reprecipitated twice from water, then it was dissolved in hot alcohol and any impurities were filtered off. The white solid **6** was crystallized from alcohol and dried at 50 °C in a vacuum for 48 h. Yield: 27% (0.25 g). IR (cm^{-1}): 3410 ν_{OH}, 1746 $\nu_{C=O}$, 1181 $\nu_{P=N}$, 1082 ν_{N-O-C}, 955 ν_{P-O-C}. ^1H NMR (in DMSO-d): 6.90–8.30 (m) H^2, H^3, H^8, H^9, H^{10}, H^{12}, H^{13}, 8.90 (s) H^5, H^{15}, 11.30 (s) H^{16}. ^{13}C NMR: 167.80 C^6, 163.55 C^5, 157.32 C^{15}, 153.28 C^1, 152.27 C^{11}, 135.00 C^{10}, 134.00 C^4, 132.00 C^{14}, 128.08–129.7 C^3, C^7, C^8, C^9, C^{13}, 121.95 C^2, 121.67 C^{12}.

2.8. Synthesis of compound **7**

A mixture of **1** (7.00 g, 20.13 mmol), 4-hydroxyacetophenone (16.72 g, 122.80 mmol) and K_2CO_3 (34.00 g, 245.99 mmol) was refluxed in acetone (250 mL) for 3 h. The solvent was evaporated in a vacuum and the residue was extracted with CH_2Cl_2 (4 × 75 mL). After the evaporation of the solvent in a vacuum, a white solid **7** formed in 87% (16.50 g) yield. IR (cm^{-1}): 1685 $\nu_{C=O}$, 1188 $\nu_{P=N}$, 949 ν_{P-O-C}. ^1H NMR (in DMSO-d): 7.05 (d) H^2, 7.85 (d) H^3, 2.45 (s) H^6, H^2:H^3:H^6 = 2:2:3. ^{13}C NMR: 27.04 C^6, 120.96 C^2,131.20 C^3, 134.54 C^4, 153.27 C^1, 197.00 C^5.

2.9. Synthesis of compound **8**

Hydroxylaminehydrochloride (4.50 g, 64.75 mmol) and **7** (10.00 g, 10.57 mmol) were used for the preparation of **8**, as for **3**. After the reaction was complete, the mixture was allowed to cool and the mixture was slowly poured into water (100 mL) and reprecipitated twice from water. The white solid **8** was obtained in 99% (10.89 g) yield. IR (cm^{-1}): 3460 ν_{OH}, 1208 $\nu_{P=N}$, 960 ν_{P-O-C}. ^1H NMR (in DMSO-d): 6.85 (d) H^2, 7.50 (d) H^3, 2.10 (s) H^6, 11.25 (s) H^7, H^2:H^3:H^6:H^7 = 2:2:3:1. ^{13}C NMR: 11.90 C^6, 120.93 C^2, 127.36 C^3, 134.64 C^4, 150.39 C^1, 152.51 C^5.

2.10. Reaction of **8** with benzyl chloride

A solution of 0.50 mL (0.55 g, 4.34 mmol) benzyl chloride in acetone (10 mL), **8** (0.60 g, 0.58 mmol) and K_2CO_3 (2.00 g, 14.47 mmol) in acetone (30 mL) was used for the preparation of **9**, as for **4**. The oily product **9** was obtained and dried under vacuum for 48 h. Yield: 80% (0.60 g). IR (cm^{-1}): 3295 ν_{OH}, 1183 $\nu_{P=N}$, 1014 ν_{N-O-C}, 955 ν_{P-O-C}. ^1H NMR (in DMSO-d): 11.30 (s) H^{18}, 6.85 H^2, 7.70 (m) (H^3, H^9, H^{10}, H^{11}, H^{13}, H^{14}), 5.20(s) H^7, 2.10 (s) H^{17}, 2.15 (s) H^6. ^{13}C NMR: 153.97 C^{16}, 152.48 C^5, 150.76 C^{12}, 150.31 C^1, 138.25 C^8, 134.66 C^{15}, 133.44 C^4, 128.79 C^{10}, 128.48 C^{11}, 128.22 C^9, 127.73 C^{14}, 127.37 C^3, 120.95 C^2, C^{13}, 75.94 C^7, 12.82 and 11.88 C^{17}, C^6.

2.11. Reaction of **8** with benzoyl chloride

A solution of 0.70 mL (0.74 g, 5.22 mmol) benzoyl chloride in acetone (10 mL), **8** (0.60 g, 0.58 mmol) and Et_3N (2 mL) in acetone (30 mL) was used for the preparation of **10**, as for **4**. The reaction was carried out at room temperature for 12 h and then was refluxed for 24 h. After the reaction was complete, the mixture was allowed to cool and the mixture was slowly poured into water (100 mL) and reprecipitated twice from water. The white solid **10** was crystallized from alcohol. Yield: 88% (0.85 g). IR (cm^{-1}): 1747 $\nu_{C=O}$, 1173 $\nu_{P=N}$, 1063 ν_{N-O-C}, 962 ν_{P-O-C}. ^1H NMR (in DMSO-d): 7.10 (d) H^2, 7.75 (d) H^3, 8.01 (d) H^9, 7.70 (t) H^{11}, 7.50 (t) H^{10}. ^{13}C NMR: 163.40 C^7, 163.19 C^5, 151.75 C^1, 151.78 C^1 (is.), 134.12 C^{11}, 132.6 C^4, 132.40 C^4 (is.), 129.60 C^9, 129.35 C^{10}, 129.18 C^3, 128.87 C^8, 121.32 C^2, 14.64 C^6.

2.12. Reaction of **8** with 4-methoxybenzoyl chloride

A solution of 0.70 g (4.10 mmol) 4-methoxybenzoyl chloride in acetone (10 mL), **8** (0.60 g, 0.58 mmol) and Et_3N (2 mL) in acetone (30 mL) was used for the preparation of **11**, as for **4**. The reaction was carried out at room temperature for 24 h. The white solid **11** was washed with hot alcohol and acetone. Yield: 80% (0.85 g). IR (cm^{-1}): 1741 $\nu_{C=O}$, 1210 $\nu_{P=N}$, 1023 ν_{N-O-C}, 951 ν_{P-O-C}. ^1H NMR (in DMSO-d): 6.87 (d) H^{10}, 7.12 (d) H^2, 7.70 (d) H^3, 7.90 (d) H^9, 2.43 (s) H^6, 3.85 (s) H^{12}. ^{13}C NMR: 163.79 C^7, 162.83 C^5, C^{11}, 151.72 C^1, 151.78 C^1 (is.), 132.22 C^4, 132.40 C^4 (is.), 131.73 C^9, 129.07 C^3, 121.25 C^2, 120.88 C^8, 114.58 C^{10}, 55.93 C^{12}, 14.52 C^6.

2.13. Reaction of **8** with 2-chlorobenzoyl chloride

A solution of 0.60 mL (0.82 g, 4.73 mmol) 2-chlorobenzoyl chloride in acetone (10 mL), **8** (0.60 g, 0.58 mmol) and Et_3N (2 mL) in acetone (30 mL) was used for the preparation of **12**, as for **4**. The reaction was carried out at room temperature for 12 h and then was refluxed for 8 h. The white solid **12** was washed with hot alcohol. Yield: 76% (0.82 g). IR (cm^{-1}): 1741 $\nu_{C=O}$, 1210 $\nu_{P=N}$, 1032 ν_{N-O-C}, 953 ν_{P-O-C}. ^1H NMR (in DMSO-d): 7.10–7.88 H^{Ar}, 2.42 (s) H^6. ^{13}C NMR: 14.99 C^6, 121.33 C^2, 151.77 C^1, 162.75 C^5, 163.83 C^7, 133.95 C^9, 132.38 C^4, 131.92 C^{11}, 131.53 C^8, 131.28 C^{13}, 129.33 C^{10}, 129.22 C^3, 127.87 C^{12}.

3. Results and discussion

The reaction of **1** with 6 equivalent of 4-hydroxybenzaldehyde and 4-hydroxyacetophenone in the presence of K_2CO_3 in THF gave hexakis(4-formylphenoxy)cyclotriphosphazene (**2**) and hexakis(4-acetylphenoxy)cyclo-

triphosphazene (**7**). Oxime compounds hexakis(4-[(hydroxyimino)methyl]phenoxy)cyclotriphosphazene (**3**) and hexakis(4-[(1)-*N*-hydroxyethaneimidoyl]phenoxy)cyclotriphosphazene (**8**) were synthesized from the reactions of **2** and **7** with hydroxlaminehydrochloride in pyridine, respectively.

Hexa and pentasubstituted compounds were obtained from the reaction of hexakis(4-[(hydroxyimino)methyl] phenoxy)cyclotriphosphazene (**3**) with benzyl chloride and benzoyl chloride in acetone (in the presence of K_2CO_3 for benzyl chloride, and Et_3N for benzoyl chloride) via replacement of all the oxime protons with benzyl and benzoyl groups, respectively. However, the oxime groups on **3** rearranged to nitrile (**5**) in the reaction of **3** with benzenesulfanoyl chloride and 1-napthalenesulfanoyl chloride via dehydration of the oximes [39,40]. Compound **5** was previously synthesized by Carriedo. $N_3P_3(OC_6H_4\text{-}CN)_6$ was directly obtained from the reaction of $N_3P_3Cl_6$ with 4-cyanophenol and characterized by elemental analysis and ^1H, ^{13}C and ^{31}P NMR spectra (25). The analysis results of **5** are in good accordance with the literature values (25). Similar compounds, $N_3P_3(OPh)_5(OC_6H_4\text{–}CN\text{–}p)$ and $N_3P_3(OC_6H_4\text{–}R\text{–}4)_5(OC_6H_4\text{–}CN\text{–}4)$ (R=H or ^{t}Bu), were synthesized by Allcock et al. [41] and Carriedo et al. [42], respectively. Hexasubstituted compounds were obtained from the reactions of **8** with benzoyl chloride, 4-methoxybenzoyl chloride and 2-chlorobenzoyl chloride. A trisubstituted compound was obtained from the reaction of **8** with benzyl chloride in acetone (in the presence of K_2CO_3 for benzyl chloride, and triethylamine for benzoyl chloride, 4-methoxybenzoyl chloride and 2-chlorobenzoyl chloride). The reactions are shown in Scheme 1. All the products were generally obtained in high yields. Pure and defined products could not be obtained from the reaction of **3** with 4-methoxybenzoyl chloride and 2-chlorobenzoyl chloride.

The structures of the compounds were defined by elemental analysis, IR and ^1H, ^{13}C and ^{31}P NMR spectroscopy (structures **2**–**12** are shown in Scheme 2). Physical properties and analytical data for **2**–**12** are shown in Table 1. Compounds **2**–**12** were synthesized in high yields except for **4** and **6**. The solvents used for the purification of compounds **4**, **5**, **6** and **9** could not be removed completely, so weak peaks of trace amounts of solvents were observed at 0.8 and 1.3 ppm for **4**, 1.3 and 2.4 ppm for **5**, 0.8, 1.3 and 4.4 ppm for **6** and **9** in the ^1H NMR spectra. Similarly, solvent peaks were observed at 18 and 25 ppm for **4**, 20 and 29 ppm for **5**, 19 and 57 ppm for **6** and 8 and 30 ppm for **9** in the ^{13}C NMR spectra. Thus the presence of these trace amounts of solvent affect the elemental analysis, in particular the carbon value.

The characteristic stretching peaks in the IR spectra of the phosphazenes have been assigned in the experimental section. The P=N stretching vibrations, which are observed between 1173 and 1210 cm^{-1}, are characteristic of cyclophosphazenes. Compared to **1**, which appeared at 1218 cm^{-1}, these peaks are shifted to longer wavelengths for **2**–**12**. The OH stretching vibrations in the IR spectra of **3**, **6**, **8** and **9** indicate oxime compounds. While **3** and **8** are initial oximes, all hydrogen atoms of the OH groups of **6** and **9** could not be replaced by the benzoyl and benzyl substituents, respectively.

The NMR data for **2**–**12** are presented in the experimental section. The ^{31}P NMR shifts of **2**–**12** change between 7.51 and 17.21 ppm. Although there is only one peak in the ^{31}P NMR spectra of **1**, **2**, **5**, **6**, **7**, **9**, **10** and **12** at 20.12, 8.33, 7.51, 8.36, 8.05, 9.00, 8.88 and 8.84 ppm, respectively, two peaks, with very weak second signals, are observed at $\delta = 17.21$, 17.26, $\delta = 8.67$, 8.57, $\delta = 9.04$, 9.01 and $\delta = 8.89$, 8.79 ppm for **3**, **4**, **8** and **11**, respectively. It is assumed that the weak peaks are due to the *cyn* and *anti* isomerism of the –C=N– groups. The effects of the *cyn* and *anti* isomerism are also observed in the ^{13}C NMR spectra of **3**, **4** and **11**. This data demonstrates that compounds **3**, **4**, **8** and **11** consist of a mixture of two isomers, but the others have one isomer. Although there are different phosphorus environments in the molecule of **6**, the main peak is observed as a singlet. It is understood that the phosphorus peaks are not affected by these changes because the substituted groups are far away from the phosphorus atoms.

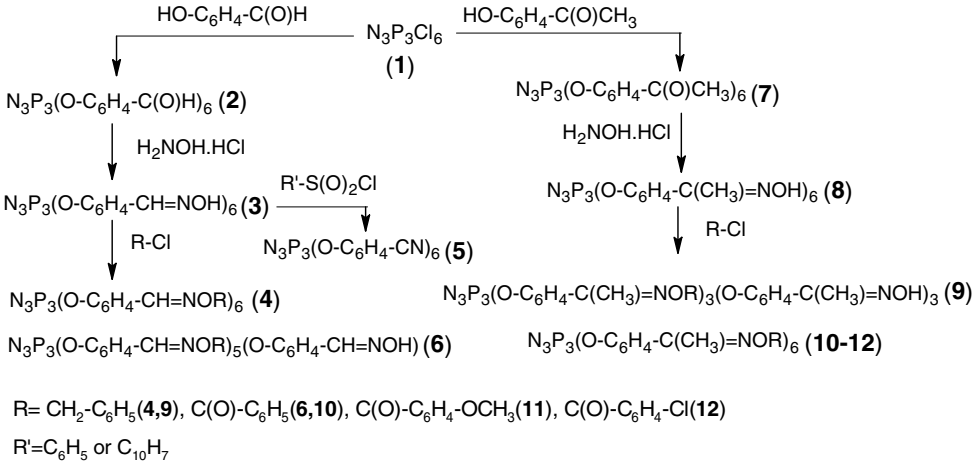

Scheme 1. General pathway of the reactions.

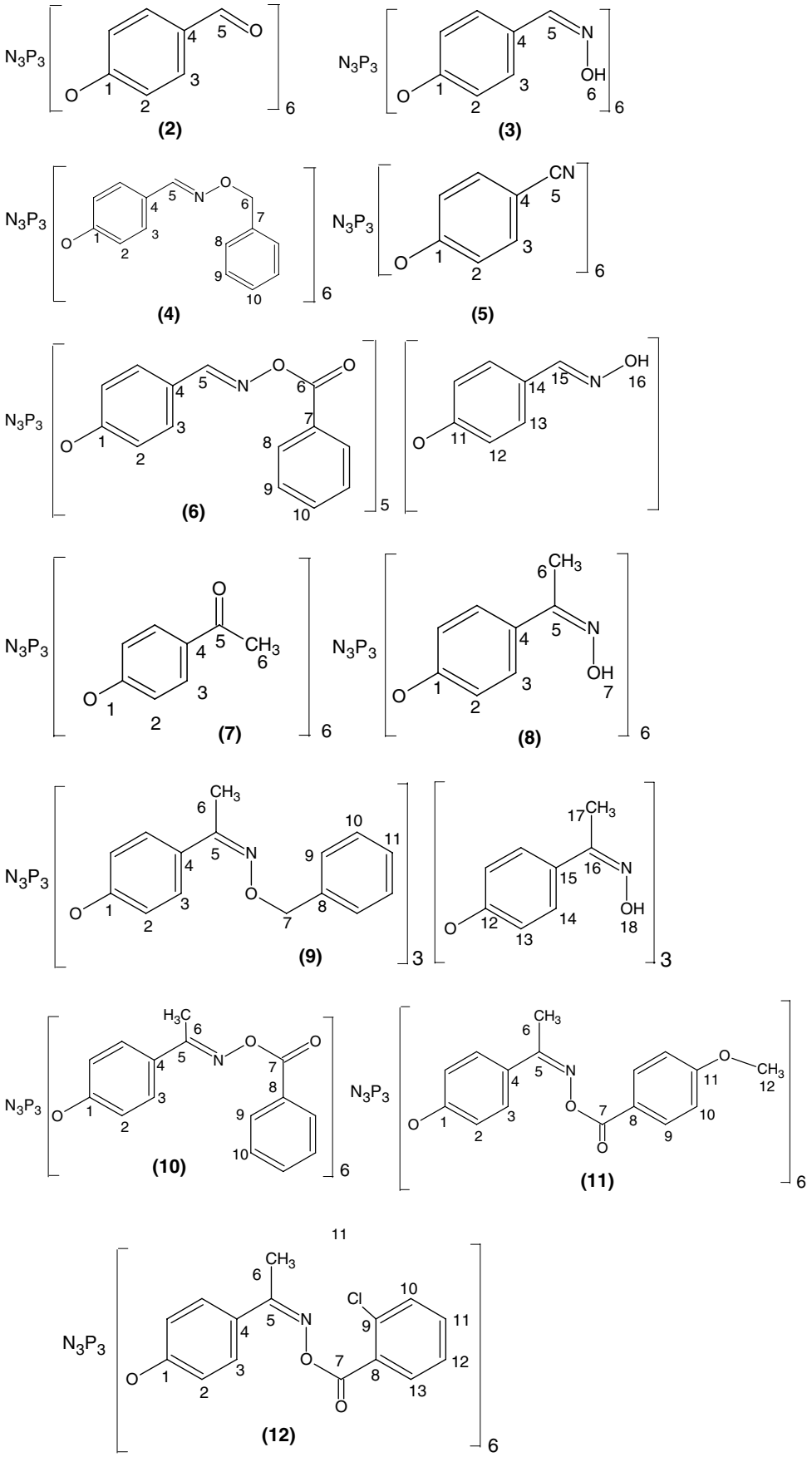

Scheme 2. The structures of the compounds **2**–**12**.

Table 1
Physical properties and analytical data of **2**–**12**

	Yield (%)		Found	Calcd.
2	92	C	58.52	58.55
		H	3.39	3.514
		N	4.51	4.88
3	83	C	53.43	53.00
		H	3.75	3.81
		N	12.98	13.25
4	66	C	66.56	67.60
		H	4.78	4.86
		N	7.70	8.45
5	94	C	58.29	59.80
		H	2.96	2.87
		N	13.33	14.94
6	27	C	61.70	62.80
		H	3.87	3.83
		N	8.07	8.56
7	87	C	60.93	60.96
		H	4.50	4.48
		N	4.40	4.44
8	99	C	55.67	55.66
		H	4.69	4.67
		N	11.98	12.17
9	80	C	62.23	63.44
		H	5.01	5.09
		N	8.60	9.65
10	88	C	61.43	62.10
		H	4.34	4.37
		N	6.76	7.59
11	80	C	59.81	60.64
		H	4.36	4.60
		N	5.79	6.85
12	76	C	57.38	57.89
		H	3.41	3.56
		N	5.58	6.75

The ^{1}H and ^{13}C NMR data also confirm the structures of **2**–**12** (Scheme 2). In the ^{1}H NMR spectra (Table 1), the OH protons are observed at 10.17, 11.30, 11.25 and 11.30 ppm for **3**, **6**, **8** and **9**, respectively. It is understood from the integral intensities that there are six OH protons in **3** and **8**, which are the original oxime-phosphazenes, one OH proton in **6** and three OH protons in **9**. This observation for **6** and **9** indicates that benzoyl or benzyl groups have not replaced all the OH protons in **3** and **8**. The aldehyde proton for **2** appears at 9.90 ppm. The azomethine protons for **3**, **4** and **6** are observed at 7.96 (H^5), 8.30 (H^5) and 8.90 (H^5, H^{15}) ppm, respectively. The aromatic protons for all the compounds appear between 6.85 and 8.30 ppm.

Table 2
The ^{31}P NMR data of **1**–**12**

	Major isomer		Minor isomer	
	ppm	Rel. intensity (%)	ppm	Rel. intensity (%)
1	20.12			
2	8.33			
3	17.21	82	17.26	18
4	8.67	62	8.57	38
5	7.51			
6	8.36			
7	8.05			
8	9.04	79	9.01	21
9	9.00			
10	8.88			
11	8.89	79	8.79	21
12	8.84			

Detailed ^{13}P NMR spectral data are shown in Table 2. The aldehyde carbon atom for **2** and the ketone carbon atom for **7** are observed at 190.83 and 197.00 ppm, at the lowest downfield position of the carbon atoms. Compared to **3** and **8**, the azomethine carbon atoms in the substituted moiety of the molecules are shifted to lower downfield for compounds **6**, **10**, **11** and **12**, except for **4** and **9** in which the benzyl group releases an electron to the molecule. The azomethine resonances do not change or show very little change in the non-substituted moiety of **9**.

4. Conclusion

Hexa and pentasubstituted compounds were obtained from the reaction of hexakis(4-[(hydroxyimino)methyl]-phenoxy)cyclotriphosphazene (**3**) with benzyl chloride and benzoyl chloride via replacement of all the oxime protons with benzyl and benzoyl groups, respectively. However, the oxime groups in **3** rearranged to nitrile (**5**) in the reaction of **3** with benzenesulfanoyl chloride and 1-napthalenesulfanoyl chloride via dehydration of the oxime groups. Hexasubstituted compounds were obtained from the reactions of **8** with benzoyl chloride, 4-methoxybenzoyl chloride and 2-chlorobenzoyl chloride. A trisubstituted compound was obtained from the reaction of **8** with benzyl chloride. Pure and defined products could not be obtained from the reaction of **3** with 4-methoxybenzoyl chloride and 2-chlorobenzoyl chloride.

Acknowledgement

We thank the Firat University Research Fund for support (Project No: FUBAP 923).

References

[1] H.R. Allcock, Phosphorus–Nitrogen Compounds, Academic Press, New York, 1972.
[2] C. Diaz, I. Izquierdo, F. Mendizabal, N. Yutronic, Inorg. Chim. Acta 294 (1999) 20.
[3] A. Kılıç, S. Begeç, B. Çetinkaya, T. Hökelek, Z. Kılıç, N. Gündüz, M. Yıldız, Heteroatom Chem. 7 (1996) 249.
[4] G.A. Carriedo, F.J.G. Alonso, P.G. Elipe, E. Brillas, L. Julia, Org. Lett. 3 (2001) 1625.
[5] H.R. Allcock, C.T. Morrissey, W.K. Way, N. Winograd, Chem. Mater. 8 (1996) 2730.
[6] H.R. Allcock, In: H.R. Allcock, M. Zeldin, K.J. Wynne (Eds.), Inorganic and Organometallic Polymers, 360, Chap. 19, ACS Symposium Series, Washington, DC, 1988.
[7] C.T. Laurencin, H.J. Koh, T.X. Neenan, H.R. Allcock, R. Langer, J. Biomed. Mater. Res. 21 (1987) 1231.
[8] H.R. Allcock, S.R. Pucher, R.J. Fitzpatrick, K. Rashid, Biomaterials 13 (1992) 857.

[9] G. Giavaresi, M. Tschon, V. Borsari, J.H. Daly, J.J. Liggat, M. Fini, V. Bonazzi, A. Nicolini, A. Carpi, M. Morra, C. Cassinelli, R. Giardino, Biomed. Pharmacother. 58 (2004) 411.
[10] Y.J. Jun, J.I. Kim, M.J. Jun, Y.S. Sohn, J. Inorg. Biochem. 99 (2005) 1593.
[11] K. Brandt, R. Kruszynski, T.J. Bartczak, I.P. Czomperlik, Inorg. Chim. Acta. 322 (2001) 138.
[12] A.I. Ozturk, O. Yılmaz, S. Kırbag, M. Arslan, Cell. Biochem. Funct. 18 (2000) 117.
[13] V. Konar, O. Yılmaz, A.I. Ozturk, S. Kırbag, M. Arslan, Bioorg. Chem. 28 (2000) 214.
[14] O. Yılmaz, F. Aslan, A.I. Ozturk, N. Vanlı, S. Kırbag, M. Arslan, Bioorg. Chem. 30 (2002) 303.
[15] C.W. Allen, J. Fire Sci. 11 (1993) 320.
[16] M. Gleria, R.D. Jaeger, J. Inorg. Organomet. Polym. 11 (2001) 1.
[17] M.T.R. Laguna, M.P. Tarazona, G.A. Carriedo, F.J.G. Alonso, J.I. Fidalgo, E. Saiz, Macromolecules 35 (2002) 7505.
[18] E. Cil, M. Arslan, F. Aslan, A.I. Ozturk, Phosphorus Sulfur Silicon Relat. Elem. 178 (2003) 1037.
[19] A.I. Ozturk, F. Aslan, E. Cil, M. Arslan, A. Kılıç, Phosphorus Sulfur Silicon Relat. Elem. 178 (2003) 2097.
[20] M. Arslan, F. Aslan, A.I. Ozturk, Heteroatom Chem. 14 (2003) 138.
[21] F. Aslan, A.I. Ozturk, M. Arslan, Heteroatom Chem. 14 (2003) 413.
[22] C.V. Diaz, I.G. Izquierdo, Polyhedron 18 (1999) 1479.
[23] R. Bertani, G. Facchin, M. Gleria, Inorg. Chim. Acta 165 (1989) 73.
[24] A. Kılıç, S. Beğeç, Z. Kılıç, T. Hokelek, J. Mol. Struct. 516 (2000) 255.
[25] G.A. Carriedo, L.F. Catuxo, F.J.G. Alonso, P.G. Elipe, P.A. Gonzalez, G. Sanchez, J. Appl. Polym. Sci. 59 (1996) 1879.
[26] H.R. Allcock, M.L. Turner, Macromolecules 26 (1993) 3.
[27] G.A. Carriedo, L.F. Catuxo, F.J.G. Alonso, P.G. Elipe, P.A. Gonzalez, Macromolecules 29 (1996) 5320.
[28] S. Bilge, Z. Kılıç, N. Çaylak, T. Hökelek, J. Mol. Struct. 707 (2004) 139.
[29] S. Begeç, A. Kılıç, Heteroatom Chem. 16 (2005) 308.
[30] U. Belluco, R. Bertani, R.A. Michelin, M. Mozzan, F. Zingales, M. Gleria, Inorg. Chim. Acta 229 (1995) 13.
[31] M.B. McIntosh, T.J. Hartle, H.R. Allcock, J. Am. Chem. Soc. 121 (1999) 884.
[32] F. Palacios, C. Alonso, G.G. Rubialesa, J.M. Ezpeleta, Tetrahedron 60 (2004) 2469.
[33] E. Çil, M. Arslan, A.O. Görgülü, Heteroatom Chem. 17 (2006) 112.
[34] E. Çil, M. Arslan, A.O. Görgülü, Can. J. Chem. 83 (2005) 2039.
[35] W. Yuan, L. Zhu, X. Huang, S. Theng, X. Tang, Eur. Polym. J. 41 (2005) 1867.
[36] W. Yuan, X. Tang, X. Huang, S. Zheng, Polymer 46 (2005) 1701.
[37] G. Fontana, F. Minto, M. Gleria, G. Facchin, R. Bertani, G. Favero, Eur. Polym. J. 32 (1996) 1273.
[38] T. Muraki, M. Ueta, E. Ihara, K. Inoue, Poly. Degrad. Stab. 84 (2004) 87.
[39] N. Coşkun, N. Arıkan, Tetrahedron 55 (1999) 11943.
[40] H.J.P. Lijser, F.H. Fardoun, J.R. Sawyer, M. Quant, Org. Lett. 4 (2002) 2325.
[41] H.R. Allcock, T.X. Neenan, W.C. Kosa, Macromolecules 15 (1982) 693.
[42] G.A. Carriedo, L.F. Catuxo, F.J.G. Alonso, P.G. Elipe, J. Organomet. Chem. 503 (1995) 59.

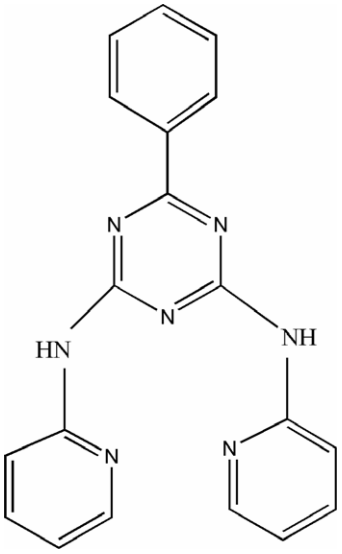

Chart 1. *N*,*N*′-di(2-pyridyl)-2,4-diamino-6-phenyl-1,3,5-triazine(dp dapt).

association running along the 1D open channels. A recent report described a discrete ice-like hexameric water cluster stabilized by a cyano-bridged trimetallic complex [16,17]. Here, the hexameric water cluster is unique and unlike the previously published hexamer water clusters [16–22]. There is mounting evidence of the presence of ordered water clusters in the active clefts of proteins such as dimeric haemoglobin, crambin, actinidin and carbonic anhydrase, however, positional information for the waters and their nature is still preliminary [16,17]. As water molecules play an important role in contributing to conformation, stability, function and dynamics of biomacromolecules, the new 1D water clusters arrays may provide insight into the hydrogen-bonding motif of the aqueous environment in living systems and enhance understanding of the 1D water morphologies.

2. Experimental

2.1. Materials and physical measurements

The new ligand *N*,*N*′-di(2-pyridyl)-2,4-diamino-6-phenyl-1,3,5-triazine was synthesized according to the literature method [15]. All other reagents and solvents employed were commercially available and used as received without further purification. Infrared spectra on KBr pellets were recorded on a Nicolet 170SX FT-IR spectrophotometer in the range 4000–400 cm^{-1}. Electronic spectra were taken on a Cary 300 Bio UV–Vis spectrophotometer in the range 200–800 nm at ambient temperature. Elemental analysis was conducted with a Perkin–Elmer model 240C instrument. Fluorescence experiments used a HITACHI F-4500 Fluorescence spectrophotometer and were measured in methanol. Thermal analysis was performed on a NETZSCH STA 449C microanalyzer in a nitrogen atmosphere at a heating rate of 10 °C min^{-1}.

2.2. Synthesis of $\{[Cu(dpdapt)(Hhbd)]\cdot 6H_2O\}_n$ (1)

A methanol suspension (15 mL) of dpdapt (68.2 mg, 0.2 mmol) was added slowly dropwise to methanol (15 mL) dissolved Cu(Hhbd) (42.3 mg, 0.22 mmol). The resulting mixture was stirred for 30 min and then filtered. The aqua filtrate solution was transferred a tube and evaporated at room temperature. After two months, deep blue crystals were obtained. Yield: 65%. *Anal.* Calc. for $C_{23}H_{31}CuN_7O_{11}$ (645.09): C, 41.78; H, 4.74; N, 14.83. Found: C, 41.91; H, 4.70; N, 14.72%. IR spectrum (cm^{-1}): 3425(w), 2923(w), 1640(s), 1592(m), 1502(w), 1469(s), 1429(s), 1381(s), 1242(w), 1195(w), 1157(w), 1023(w), 891(w), 821(w), 773(m), 703(w), 633(w), 525(w).

2.3. Synthesis of $[Cu(dpdapt)(SO_4)]\cdot 2H_2O$ (2)

$CuSO_4\cdot 5H_2O$ (50.0 mg, 0.2 mmol) was dissolved in methanol (15 mL) and mixed with a methanol suspension (15 mL) of dpdapt (68.2 mg, 0.2 mmol) and then stirred for 1 h. Diffused in Et_2O after filtration, finally blue crystals were produced. Yield: 59%. *Anal.* Calc. for $C_{19}H_{19}CuN_7O_6S$ (537.01): C, 42.50; H, 3.57; N, 18.26. Found: C, 42.32; H, 3.43; N, 18.38%. IR spectrum (cm^{-1}): 3493(w), 2925(w), 1636(s), 1587(s), 1502(m), 1469(s), 1434(s), 1242(w), 1195(w), 1162(w), 977(w), 867(w), 832(w), 770(m), 696(w), 634(w), 517(w), 432(w).

2.4. Synthesis of $[Cu(dpdapt)(oxa)]\cdot H_2O$ (3)

Cu(oxa) (30.3 mg, 0.2 mmol) was dissolved in methanol (15 mL) and mixed with a methanol suspension (15 mL) of dpdapt (68.2 mg, 0.2 mmol) and then stirred for 2 h. Green crystals **3** were obtained after the mixture was allowed to stand at room temperature for a month. Yield: 60%. *Anal.* Calc. for $C_{21}H_{17}CuN_7O_5$ (510.96): C, 51.16; H, 3.07; N, 19.89. Found: C, 51.33; H, 2.94; N, 19.73%. IR spectrum (cm^{-1}): 3411(w), 2913(w), 1665(s), 1573(m), 1510(w), 1466(s), 1385(s), 1269(w), 1240(w), 1202(w), 1157(w), 1115(w), 1059(w), 1023(w), 779(m), 706(w), 627(w), 524(w).

2.5. Crystallographic data collection and structure determination

Single-crystal X-ray diffraction of complexes **1**, **2** and **3** were performed on a BRUKER SMART 1000 CCD diffractometer equipped with a graphite crystal monochromator situated in the incident beam for data collection. Crystallographic data were collected with Mo Kα radiation ($\lambda = 0.71073$ Å) for the three complexes at 296(2) K. The structures were solved by direct methods and refined by full-matrix least-squares method on F^2 values using SHELXL 97 and SHELXL 97 programs, respectively [23,24]. Single crystal X-ray structural analysis shows the hydroxyl group might lie on one of the two adjacent methylenes, which would present the hydroxyl group disordered in a half-occupied position in complex **1**. All non-hydrogen atoms

were refined with anisotropic displacement parameters. Hydrogen atoms of all water molecules in complex **1** were not visible in the difference Fourier map. In complexes **2** and **3**, the hydrogen atoms of the lattice water molecules could be trustfully inferred from analysis of the difference Fourier map. Crystal data, data collection and refinement parameters for three complexes are shown in Table 1, and selected bond lengths and bond angles are listed in Table 2.

3. Results and discussion

3.1. Description of the crystal structures

A single crystal X-ray structural analysis shows **1** crystallizes in monoclinic space group C_2/c. Each copper atom has a slightly distorted [CuN_3O_2] trigonal bipyramid geometry. Owing to the symmetry of the ligand, each copper atom lies on a two-fold axis in the subunit (Fig. 1). The

Table 1
Crystallographic data and structure refinement for **1**, **2** and **3**

Complex	1	2	3
Empirical formula	$C_{23}H_{31}CuN_7O_{11}$	$C_{19}H_{19}CuN_7O_6S$	$C_{21}H_{17}CuN_7O_5$
Formula weight	645.09	537.01	510.96
Temperature (K)	296(2)	296(2)	296(2)
Crystal system	monoclinic	orthorhombic	monoclinic
Space group	*C*2/*c*	*Pnnm*	$P2_1/n$
a (Å)	16.372(3)	15.911(2)	9.7005(16)
b (Å)	17.534(4)	11.4246(15)	17.487(3)
c (Å)	10.867(2)	12.2370(16)	13.373(2)
β (°)	116.330(3)	90	110.366(3)
V (Å^3)	2796.1(10)	2224.5(5)	2126.7(6)
Z	4	4	4
D_{calc} (Mg m^{-3})	1.532	1.603	1.596
Absorption coefficient (mm^{-1})	0.852	1.128	1.078
F(000)	1340	1100	1044
Crystal size (mm)	0.35 × 0.08 × 0.04	0.29 × 0.20 × 0.10	0.20 × 0.14 × 0.06
λ (Å)	0.71073	0.71073	0.71073
θ Range (°)	1.81–25.04	2.10–25.09	2.00–25.10
Reflections collected	7046	10914	10792
Limiting indices	$-16 \leqslant h \leqslant 19$, $-19 \leqslant k \leqslant 20$, $-12 \leqslant l \leqslant 12$	$-18 \leqslant h \leqslant 18$, $-13 \leqslant k \leqslant 10$, $-14 \leqslant l \leqslant 14$	$-11 \leqslant h \leqslant 8$, $-19 \leqslant k \leqslant 20$, $-15 \leqslant l \leqslant 15$
R_{int}	0.0503	0.0377	0.0483
Goodness-of-fit on F^2	1.044	1.038	1.016
R_1[a], wR_2[b] [$I > 2\sigma(I)$]	0.0548, 0.1419	0.0372, 0.0934	0.0483, 0.1148
R_1, wR_2 (all data)	0.0756, 0.1561	0.0478, 0.1002	0.0854, 0.1352

[a] $R = \sum\|F_o| - |F_c\|/\sum|F_o|$.
[b] $wR_2 = [\sum[w(F_o^2 - F_c^2)^2]/\sum[(F_o^2)^2]]^{1/2}$.

Table 2
Selected bond lengths (Å) and angles (°) of complexes **1**, **2** and **3**

1		2		3	
Bond lengths					
Cu1–N1#1	1.978(3)	Cu1–N1	1.979(2)	Cu1–N1	2.013(3)
Cu1–N1	1.978(3)	Cu1–N1#2	1.979(2)	Cu1–N3	1.954(3)
Cu1–N3	2.032(4)	Cu1–N4	1.949(3)	Cu1–N7	2.068(3)
Cu1–O1#1	2.096(3)	Cu1–O2	2.208(3)	Cu1–O1	1.912(3)
Cu1–O1	2.096(3)	Cu1–O3	1.961(2)	Cu1–O2	2.064(3)
Bond angles					
N3–Cu1–O1	134.3(9)	N1–Cu1–N1#2	130.4(5)	N1–Cu1–N7	122.6(1)
N3–Cu1–O1#1	134.3(9)	O2–Cu1–N1#2	114.5(8)	N1–Cu1–O2	133.4(1)
O1–Cu1–O1#1	91.6(2)	N1–Cu1–O2	114.5(8)	N7–Cu1–O2	103.9(2)
N1–Cu1–N1#1	174.2(2)	N4–Cu1–O3	163.2(9)	N3–Cu1–O1	170.9(1)
Hydrogen bonds					
N2–H···O2[a]	2.832(4)	N2–H···O4[b]	2.794(5)	O9–H···O3[d]	2.687(5)
O3–H···O4	2.729(2)	O4–H···O1[c]	2.738(4)	O9–H···O4[e]	2.855(5)
O3–H···O6	2.819(3)	O4–H···O4	2.763(5)	N2–H···O9[f]	2.730(5)

Symmetry codes: #1: $-x+1$, y, $-z+1/2$; #2: x, y, $-z+1$; (a) $-x+1$, $-y+2$, $-z+1$; (b) x, y, $-z+1$; (c) $x+1/2$, $-y+1/2$, $z+1/2$; (d) x, y, $z-1$; (e) $x+1/2$, $-y+1/2$, $z-1/2$; (f) $x-1$, y, $z+1$.

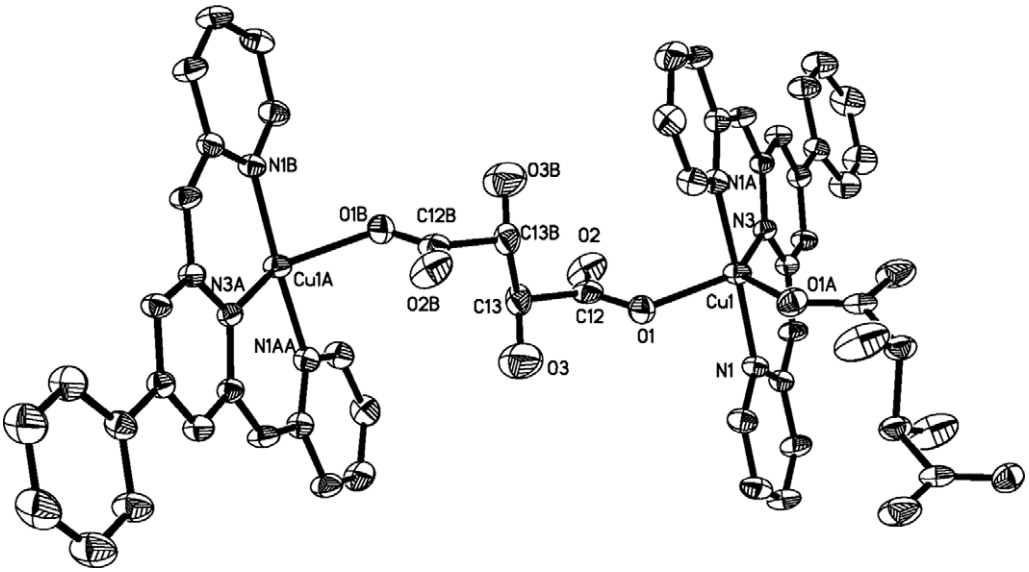

Fig. 1. Repeat unit of the infinite coordination polymer of **1**. Thermal ellipsoids are drawn at the 30% probability level. Hydrogen atoms and water molecules are omitted for clarity.

copper (II) ion is coordinated to three nitrogen atoms from the dpdapt ligand, and two oxygen atoms from two different Hhbd dianions. The two pyridyl rings of the dpdapt ligand are nearly coplanar with a dihedral angle of ca. 4.5°. It is worthwhile to note that the Hhbd dianions bridge copper centers to create a 1D polymeric chain running along the *a* axis with an adjacent Cu···Cu distance of 8.957(2) Å. The dpdapt ligands lie on both sides of this 1D chain in an antiparallel fashion. Interestingly, these 1D polymeric chains self-assemble to generate a 2D

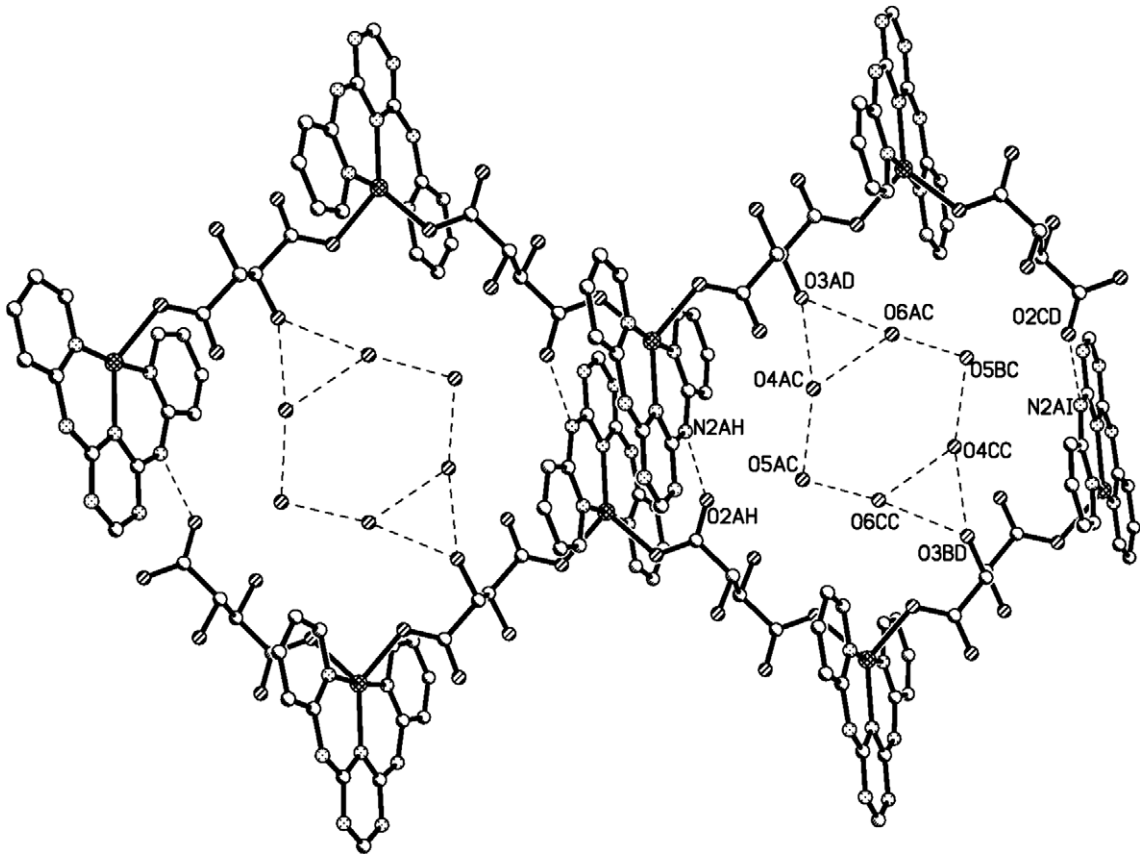

Fig. 2. View of the 2D supramolecular structure of complex **1** self-assembled by hydrogen bonds and π–π stacking interactions.

supramolecular architecture under the direction of hydrogen bonding (N_{amido}–H···$O_{carbonyl}$, 2.832(4) Å) and π–π stacking interactions between the pyridyl and triazine ring with a center-to-center distance of 3.55 Å and with a dihedral angle of ca. 2.7° (Symmetry code: $-x$, $-y$, $-z$) (Fig. 2). There are also significant hydrogen bonds involving hydroxyl oxygen atoms (O3AD, O3BD) of the dicarboxylate ligands and aqua oxygen atoms (O4AC, O6AC, O4CC, O5AC, O5BC, O6CC) from lattice water molecules. These observed hydrogen bonding interactions, with the donor–acceptor distances, are shown in Tables 2 and 3. These interactions generate the final 3D framework that feature 1D open channels (14.626 × 15.110 Å) when viewed along the *c* axis (Fig. 3).

The most remarkable feature in **1** is that these 1D channels are occupied by six water molecules, which are associated by strong O–H···O hydrogen bonds into cyclic centrosymmetric hexamers that adopt a hexagon configuration (Fig. 4(a)). The geometric parameters of the hexamers are summarized in Table 3. The average distance between the oxygen atoms is 2.838(6) Å, which is very similar to the O···O distance of 2.85 Å in liquid water [25]. Unlike the previously reported hexamer clusters [16–22], here it is noteworthy that the water hexamer clusters are self-assembled along the channels by interhexamer O6···O6 hydrogen bonds to give extended 1D arrays consisting of six-membered rings of water (Fig. 4(a)). When viewed down the crystallographic *c* axis, more interestingly, an adjacent hexameric water cluster is not complete superposition but is in a slipped stacking mode (Fig. 4(b)).

Additionally, the hydrogen bonding between water molecules and the hydroxyl oxygen atoms of dicarboxylate ligands plays an important role in contributing to the stability of the 1D hexameric water cluster arrays. This supramolecular association of water molecules in arrays is presumably enforced by the shape and the condition of the interior of the host's channel. These results further illustrate the structural diversity possible for water clusters and the sensitive dependence of their structures on the nature of their environment.

Table 3
Geometrical parameters [Å, °] for the cyclic water hexamers in complex **1**

O–H···O	O···O	O···O···O	
O4–H···O5[a]	2.783(9)	O4···O5···O6	107.44(2)
O4–H···O6	2.844(5)	O5···O6···O4	128.73(2)
O5–H···O6	2.887(5)	O6···O4···O5	123.72(2)
O6–H···O6	2.633(1)		

Symmetry codes: (a) $-x + 3/2$, $y - 1/2$, $-z + 3/2$.

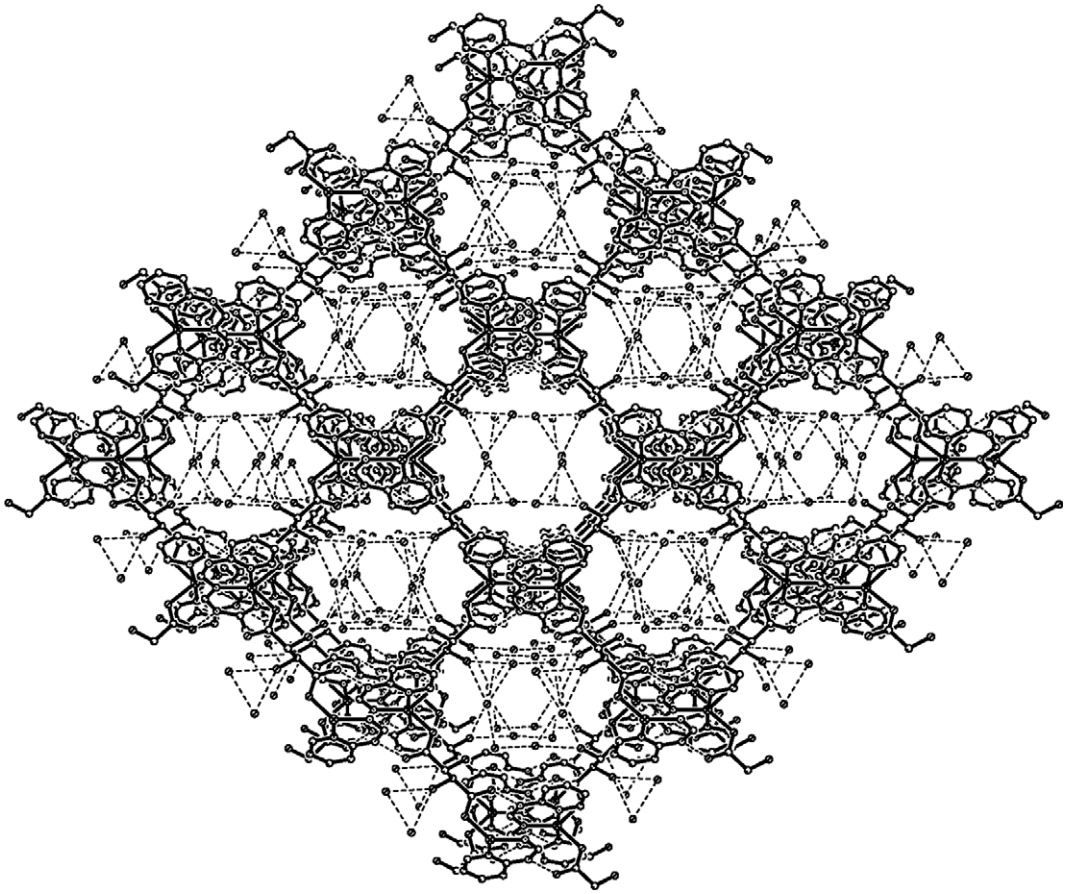

Fig. 3. View of the 3D supramolecular framework of complex **1** that contains 1D open channels encapsulating arrays of cyclic $(H_2O)_6$ clusters.

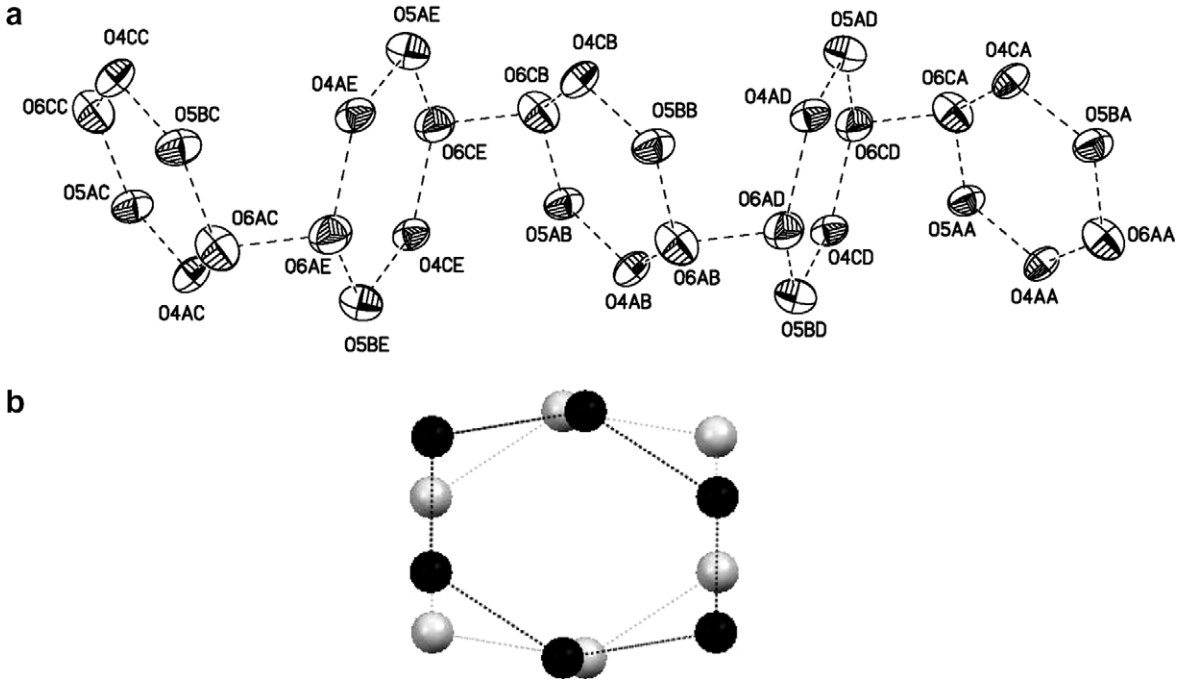

Fig. 4. (a) Extended 1D array consisting of six-membered rings of water molecules in the 3D framework of complex **1**. The hydrogen bond O···O distances [Å]: O5AB···O4AB, 2.783(9); O4AB···O6AB, 2.844(5); O6AB···O5BB, 2.887(5). (b) View of hexameric water cluster array in the 1D open channels of complex **1**. Black and grey represent the different array of an adjacent cyclic $(H_2O)_6$ cluster. Dotted lines show the hydrogen bonding between water molecules.

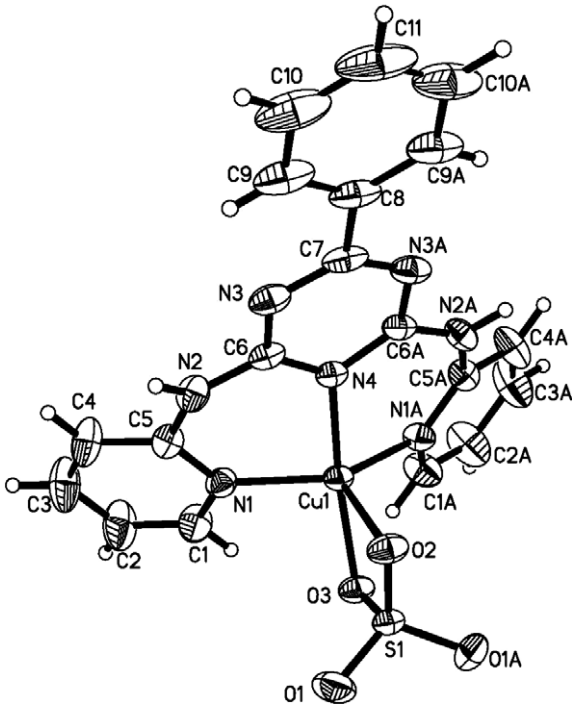

Fig. 5. ORTEP view of $[Cu(dpdapt)(SO_4)]\cdot 2H_2O$ (**2**) with 30% probability ellipsoids. The water molecules are omitted here.

The molecular structure of **2** is shown in Fig. 5. The complex crystallizes in the orthorhombic space group *Pnnm*. The Cu1 is five-coordinate being bonded in a bidentate fashion to two oxygen atoms (O2, O3) of the sulfate dianion and in a tridentate fashion to one triazine-N atom (N4) and two pyridine-N atoms (N1, N1A). The two pyridyl rings of the dpdapt ligand are non-coplanar with a dihedral angle of ca. 52.2°. In mononuclear $[Cu(dpdapt)(SO_4)]\cdot 2H_2O$, the bond angles N1–Cu1–N1A (130.4(5)°), N1A–Cu1–O2 (114.5(8)°) and O2–Cu1–N1 (114.5(8)°) add up to approximately to 360° and the angle N4–Cu1–O3 is close to 180°, so the coordinated geometry of the central copper can be described as a distorted trigonal bipyramid configuration, Cu1, N1, N1A, O2 forming the equatorial plane and N4, O3 occupying the axial positions. The lattice water molecules act as a hydrogen bond donor/acceptor, forming hydrogen bonds with the oxygen atoms of the sulfate anion and the amido nitrogen atoms (as shown in Table 2), to give rise to a 2D network structure in the *ac* plane as shown in Fig. 6.

Complexes **3** and **1** have the same crystal system and different space group, and complex **3** displays a $P2_1/n$ space group. The central copper(II) is five-coordinate being bonded in a bidentate fashion to two oxygen atoms (O1, O2) of an oxalate dianion and in a tridentate fashion to one triazine-N atom (N3) and two pyridine-N atoms (N1, N7) (Fig. 7). The dihedral angle between the two pyridyl ring planes of the dpdapt ligand is 38.9°. The bonds distance to the terminal triazine N3 (Cu1–N3) is 1.954(3) Å and the distance with the pyridyl donors N1 and N7 are 2.013(3) and 2.068(3) Å, respectively. The average Cu–N bond length is observed to be 2.011(9) Å, which is longer than that of **1**. Both Cu–N bond lengths are typical of those found for five-coordinate Cu(II)-μ-

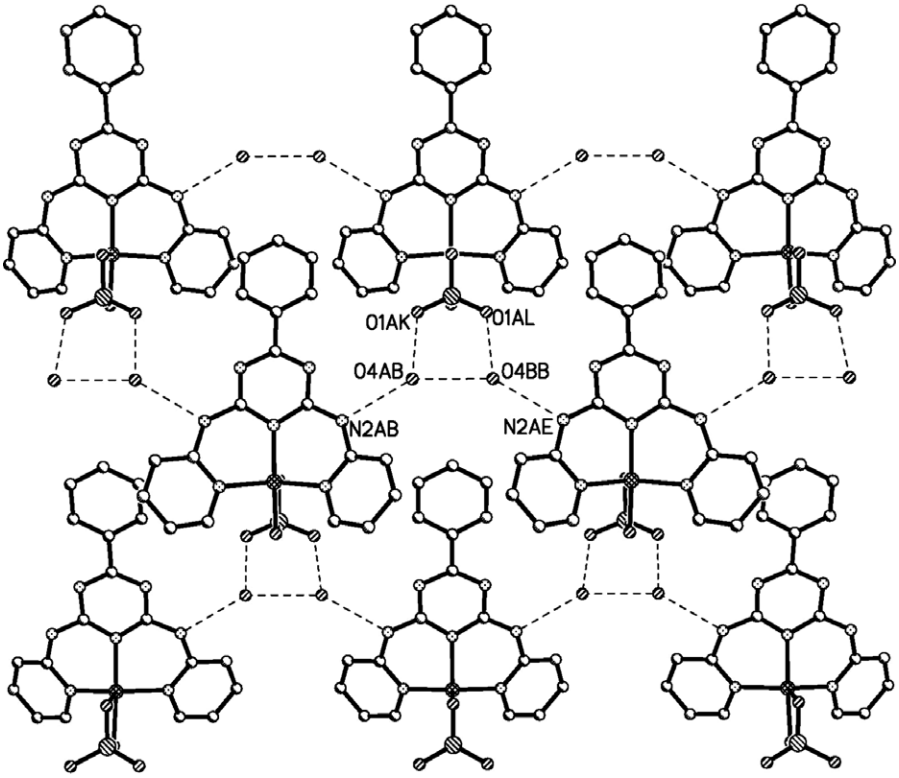

Fig. 6. View of the 2D network of $[Cu(dpdapt)(SO_4)] \cdot 2H_2O$ (**2**) constructed through two kinds of hydrogen bonds (O–H···O, N–H···O) in the *ac* plane.

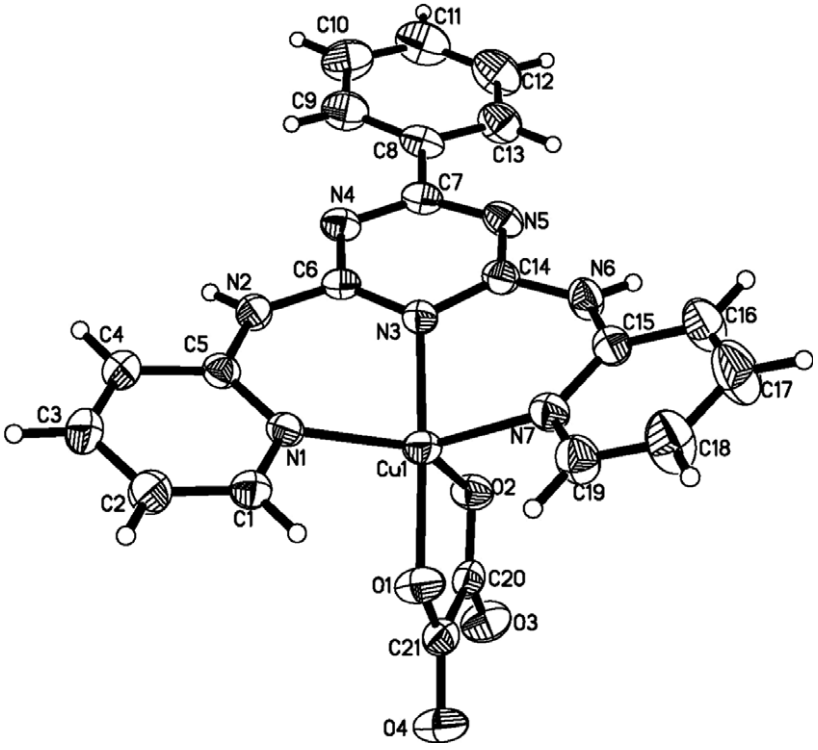

Fig. 7. Perspective view of the coordination environment of the copper atom in the complex $[Cu(dpdapt)(oxa)] \cdot H_2O$ (**3**). Thermal ellipsoids are drawn at the 30% probability level. One water molecule is omitted here.

pmea analogues [26]. The adjacent monomeric entity is interconnected through hydrogen bonding interactions involving the oxygen atoms of the lattice water molecule and the oxalate dianion and the amido nitrogen atoms (Table 2), to generate a 2D wavelike network in the *ac* plane (Fig. 8).

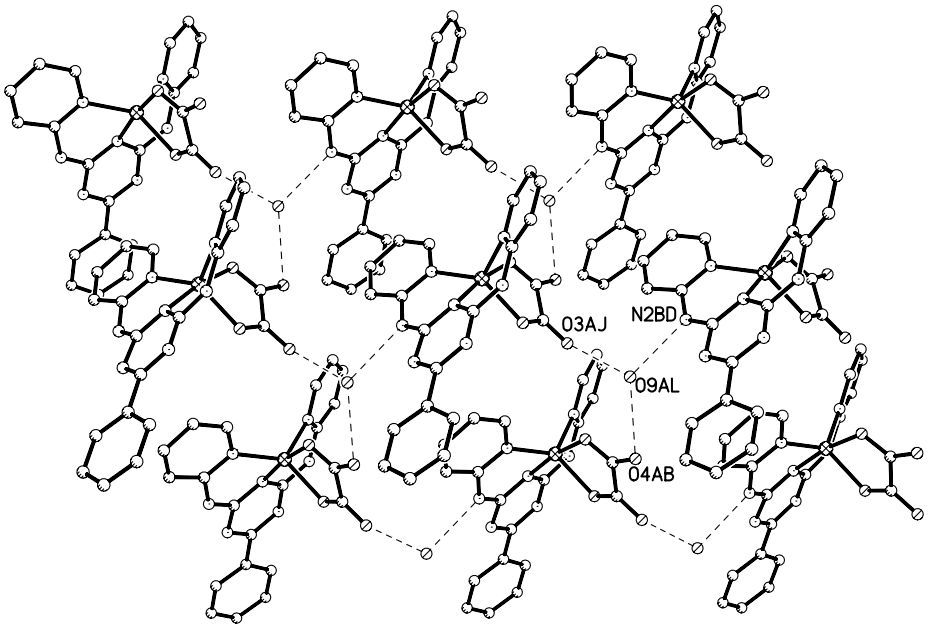

Fig. 8. View of the 2D supramolecular network of [Cu(dpdapt)(oxa)]·H_2O (**3**) formed by hydrogen bonds (O9AL–H···O3AJ, 2.687(5) Å, O9AL–H···O4AB, 2.855(5) Å; N2BD–H···O9AL, 2.730(5) Å). The hydrogen atoms of the lattice water molecules and the organic ligand are omitted for clarity here.

Although the structures of **1**, **2** and **3** exhibit the coordination character of the dpdapt ligand in part, the framework structures of the three complexes are rare for inorganic triazine compounds. To the best of our knowledge only one dimeric unit of a transition-metal complex based on 1,3,5-tris(2-pyridyl)triazine (tpt) has been reported [27], but no solvent molecules effect and π–π interactions were discussed. Additionally, in our previous works, two complexes have been reported [15], which show ladder and layer frameworks via intermolecular and intramolecular hydrogen bonds, respectively. However, we discuss here the action of guest solvent molecules in constructing the three complexes. There are hexameric, dimeric and one water molecule located in the lattices of complexes **1**, **2** and **3**, respectively. It is the water molecules that extend complexes **2** and **3** into 2D supramolecular networks. While in **1**, water molecules form a hexagon configuration in the adjacent 1D polymeric chains, Furthermore, the individual water hexamer self-assembles 1D chains by interhexamer hydrogen bonds, which exert a great influence on extending the architecture of complex **1**.

3.2. Spectroscopic properties

The IR spectra of the three complexes were performed as KBr pellets in the range 4000–400 cm^{-1}. In complex **1**, the bands around 1425 and 1496 cm^{-1} for the ligand dpdapt, attributed to the C=N groups, are shifted to 1469 and 1592 cm^{-1}. In complex **2**, the corresponding bands for the C=N groups are shifted to 1469 and 1587 cm^{-1}, the bands corresponding to SO_4^{2-} are at 634 cm^{-1}. The corresponding bands for the C=N groups for **3** are shifted to 1466 and 1573 cm^{-1}, respectively. Furthermore, the spectra exhibit ν_{as}(OCO) and ν_s(OCO) vibrations of the carboxylate groups that occur at 1640 and 1381 cm^{-1} for **1** and 1665 and 1385 cm^{-1} for **3**. $\Delta[\nu_{as}(OCO)-\nu_s(OCO)] > 200$ cm^{-1} for complexes **1** and **3**, and the value reveals that the carboxylate is coordinated in a monodentate fashion, which is consistent with the results of the X-ray analysis. These data confirm the involvement of acid radical ligands and ligand dpdapt in the copper complexation. The UV–Vis spectra of the complexes are recorded in methanol and are characterized by several spectral regions. The absorption bands in the range 260–285 nm for the dpdapt ligand are ligand-centered (LC) due to π–π^* transitions. The peak at 300 nm for complexes **1**, **2** and **3** is due to the d–d transition and the low-energy bands at 300, 302 and 297 nm are assigned to metal-to-ligand charge transfer transitions (MLCT) [28,29]. This slight shift of absorption bands of the complexes relative to that of dpdapt is caused by the effect of metal-to-ligand charge transfer transitions.

The luminescence data were obtained in methanol at room temperature. It was reported that the dpdapt ligand showed a strongest emission peak at 375.4 nm with an excitation peak at 330.0 nm [15]. The emission bands for complexes **1**, **2** and **3** can be attributed to intraligand fluorescent emission of the coordinated dpdapt ligand. The emission peak for complex **1** is at 310.8 nm, for complex **2** at 330.6 nm and for complex **3** at 320.2 nm, and their emission spectra show strong peaks at 448.6, 414.2 and 423.6 nm, respectively. Compared with the excitation–emission spectrum of the ligand, obvious enhancement of the fluoroscence intensities is realized in complexes **1**, **2** and **3**; the emission bands for three complexes are red-shifted. This drastic shift can be attributed to the strong hydrogen-bonding interactions between the water

molecules and the nearby O atoms of acid radical ligands that change the donor–acceptor character of the dpdapt moieties. These peaks of the emission spectra are probably assigned to intramolecular charge transfer (ICT) transitions [30].

3.3. Thermogravimetric analysis

Thermogravimetric analysis (TGA) for complexes **1**, **2** and **3** were recorded under a nitrogen atmosphere. The TGA result for complex **1** shows an initial weight loss of 16.07% at about 200 °C, corresponding to the removal of six water molecules per formula unit (16.35% calculated). Heating above 500 °C results in complete collapse of complex **1** accompanied by a rapid mass change as the organic component burns off. The two water molecules in complex **2** are lost at about 115 °C with mass loss of 5.39% (5.72%, calculated). Heating above 450 °C leads complete collapse of complex **2**. Complex **3** loses its one water molecule at about 118 °C, leading to a 3.32% loss of the formula unit (3.53%, calculated). The complete collapse of **3** is showed above 470 °C.

4. Conclusion

In summary, we have successfully synthesized three copper (II) complexes by the combination of coordination bonds, hydrogen bonds and π–π interactions. Importantly, this type of ligand contains functional groups capable of O–H···X (X = N, O) hydrogen bonds and supporting π–π interactions that sustain supramolecular architectures. Complex **1** self-assembles a 1D polymeric chain by dicarboxylate bridges and exhibits a 3D framework with 1D open channels, while complexes **2** and **3** show 2D wavelike networks constructed through two kinds of hydrogen bonding (O–H···O, N–H···O) interactions. We anticipate SO_4^{2-} and $C_2O_4^{2-}$ could play the same role as in the complexes $[C_4N_2H_{12}][Ni_3F_2(SO_4)_3(H_2O)_2]$ [31] and $\{Zn(ox)(py)_2H_2O\}_n$ [32], in which acid radical ligands link adjacent metal ions, acting as bridges. However, in complexes **2** and **3**, two kinds of acid radical ligands display a chelate coordination mode. Interestingly, in **1** the host framework encapsulates cyclic $(H_2O)_6$ clusters that are connected into 1D arrays along the 1D open channels. These unique water cluster arrays may be important in understanding the hydrogen-bonding motifs responsible for the anomalous character of water in living systems, as well as in the study of synthetic models, useful in theoretical and computational studies.

Acknowledgements

This work was supported by the National Natural Science Foundation of China (No. 20471048) and TRAPOYT, and Specialized Research Found for the Doctoral Program of Higher Education (No. 20050697005).

Appendix A. Supplementary material

Crystallographic data for the structural analysis have been deposited with the Cambridge Crystallographic Data Centre, CCDC No. 294,845 for **1**, 294,843 for **2** and 294,844 for **3**. Copies of this information may be obtained free of charge on application to CCDC, 12 Union Road, Cambridge CB2 1EZ, UK (fax: +44 1223 336 033; e-mail: deposit@ccdc.cam.ac.uk or http://www.ccdc.cam.ac.uk). Supplementary data associated with this article can be found, in the online version, at doi:10.1016/j.poly.2006.07.012.

References

[1] S.R. Batten, R. Robson, Angew. Chem., Int. Ed. 37 (1998) 1461.
[2] J.M. Lehn, Supramolecular Chemistry: Concepts and Perspectives, VHC, Weinheim, 1995.
[3] M. Munakata, L.P. Wu, T. Kuroda-Sowa, M. Maekawa, K. Moriwaki, S. Kitagawa, Inorg. Chem. 36 (1997) 5416.
[4] C. Juan, R. Mareque, B. Lee, Coord. Chem. Rev. 183 (1999) 43.
[5] S.A. Bourne, A. Mondal, M.J. Zaworotko, Cryst. Eng. 4 (2001) 25.
[6] A.S. Batsanov, M.J. Begley, P. Hubberstey, J. Stroud, J. Chem. Soc., Dalton Trans. (1996) 1947.
[7] M. Kondo, M. Shimaura, S. Noro, T. Yoshitomi, S. Minakoshi, S. Kitagawa, Chem. Lett. (1999) 285.
[8] L. Carlucci, G. Ciani, D.M. Proserpio, J. Chem. Soc., Dalton Trans. (1999) 1799.
[9] Y.J. Kang, S.S. Lee, K.M. Park, S.H. Lee, S.O. Kang, J.J. Ko, Inorg. Chem. 40 (2001) 7027.
[10] H.-J. Choi, M.P. Suh, J. Am. Chem. Soc. 120 (1998) 10622.
[11] K.S. Min, M.P. Suh, J. Am. Chem. Soc. 122 (2000) 6834.
[12] A.J. Blake, N.R. Champness, P.A. Cooke, J.E.B. Nicolson, C. Wilson, J. Chem. Soc., Dalton Trans. (2000) 3811.
[13] J. Fan, M.-H. Shu, T. Okamura, Y.-Z. Li, W.-Y. Sun, W.-X. Tang, N. Ueyama, New J. Chem. 27 (2003) 1307.
[14] M.G. Barandika, M.L. Hernandez-Pino, M.K. Urtiaga, R. Cortes, L. Lezama, M.I. Arriortua, T. Rojo, J. Chem. Soc., Dalton Trans. (2000) 1469.
[15] C.-J. Wang, Y.-Y. Wang, H.-R. Ma, H. Wang, Q.-Z. Shi, S.-M. Peng, Polyhedron 25 (2006) 195.
[16] U. Mukhopadhyay, I. Bernal, Cryst. Growth Des. 5 (2005) 1687.
[17] U. Mukhopadhyay, I. Bernal, Cryst. Growth Des. 6 (2006) 363.
[18] R. Custelcean, C. Afloroaei, M. Vlassa, M. Polverejan, Angew. Chem., Int. Ed. 39 (2000) 3094.
[19] R. Custelcean, C. Afloroaei, M. Vlassa, M. Polverejan, Angew. Chem., Int. Ed. 112 (2000) 3224.
[20] C. Foces-Foses, F.H. Cano, M. Martinez-Ripoll, R. Faure, C. Roussel, R.M. Claramunt, C. Lopez, D. Sanz, Elguero, J. Tetrahedron Asymmetry 1 (1990) 65.
[21] K.-M. Park, R. Kuroda, T. Iwamoto, Angew. Chem. 105 (1993) 939.
[22] K.-M. Park, R. Kuroda, T. Iwamoto, Angew. Chem., Int. Ed. Engl. 32 (1993) 884.
[23] G.M. Sheldrick, SADABS: Siemens Area Detector Absorption Correction Software, University of Göttingen, Göttingen, 1996.
[24] G.M. Sheldrick, SHELXL-97: Program for Structure Refinement, University of Göttingen, Göttingen, 1997.
[25] A.H. Narten, W.E. Thiessen, L. Blum, Science 217 (1982) 1033.
[26] K.-Y. Choi, Y.- M. Jeon, H. Ryu, J.-J. Oh, H.-H. Lim, M.-W. Kim, Polyhedron 23 (2004) 903.

[27] G. Thomas, L. Thomas, F. Roland, Eur. J. Inorg. Chem. (2004) 394.
[28] A. Volger, H. Kunkely, Coord. Chem. Rev. 177 (1998) 81.
[29] R.M. Berger, D.D. Ellis, Inorg. Chim. Acta 241 (1996) 1.
[30] S. Das, P.K. Bharadwaj, Cryst. Growth Des. 6 (2006) 187.
[31] J.N. Behera, K.V. Gopalkrishnan, C.N.R. Rao, Inorg. Chem. 43 (2004) 2636.
[32] S.K. Ghosh, G. Savitha, P.K. Bharadwaj, Inorg. Chem. 43 (2004) 5495.

area-detector diffractometer. Intensity data sets were collected using Mo Kα radiation ($\lambda = 0.71073$ Å) through the program COLLECT [22]. Correction for Lorentz-polarization effects, peak integration and background determination was carried out with the program DENZO [23]. Frame scaling and unit cell parameters refinement were performed with the program SCALEPACK [23]. Numerical absorption correction was performed by modelling the crystal faces [24]. Crystallographic data at 293 and 100 K are listed in Table 1.

Both structures were solved in the monoclinic symmetry, space group $P2_1/n$ at 293 K and $P2_1/a$ at 100 K, according to the automated search for space groups available in Wingx [25]. Copper and sulfur atoms were located using direct methods with the program SHELXS-97 [26]. The oxygen atoms and the organic moieties were found from successive difference Fourier calculations using SHELXL-97 [27]. For the room temperature phase, all H atoms were located by difference Fourier syntheses after several cycles of least-squares refinements. H–O and H–H distances, within water molecules, were restrained to 0.96(2) and 1.48(2) Å, respectively. C–H and H–H distances within the disordered organic moiety were also constrained to 0.97(2) and 1.58(4) Å, respectively, so that the H–C–H angles fitted the ideal value of a tetrahedral angle. In the low temperature phase, the aqua H atoms and H atoms bonded to N atoms were located in a difference Fourier map and their positions and isotropic displacement parameters were refined. H–O and H–H distances, within water molecules, were restrained to 0.96(2) and 1.48(2) Å, respectively. H atoms bonded to C atoms were positioned geometrically (the C–H bonds were fixed at 0.97 Å) and allowed to ride on their parent atoms. Atomic scattering factors were taken from the International Tables for Crystallography [28]. The atomic coordinates and isotropic displacement parameters appear in Table 2. Bond distances and angles calculated from the final atomic coordinates, as well as probable hydrogen bonds, are given in Tables 3 and 4.

2.3. Thermal behaviour

Differential scanning calorimetry at low temperature was performed with a SETARAM DSC131 instrument for temperatures ranging from 133 to 315 K at a rate of 5 K min^{-1}. A polycrystalline sample of 22.23 mg was placed in a hermetic aluminium cell in nitrogen atmosphere.

The measurements of the complex's electric permittivity, ε^*, were performed with an impedance analyzer Hewlett–Packard 4192 A LF in the frequency range from 100 Hz to 1 MHz. Crystals of the title compound were crushed and pressed to dense and translucent pellets (8 mm in diameter; 0.75 mm in thickness) at a pressure of 200 MPa. Both planar faces of these pellets were coated with silver paint and the pellets were then sandwiched between metal electrodes, which were also coated with silver paint. The measurements were carried out in a vacuum between 120 and 360 K.

Table 1
Crystallographic data for $(C_6H_{14}N_2)[Cu(H_2O)_6](SO_4)_2$

Empirical formula	$C_6CuH_{26}N_2O_{14}S_2$	$C_6CuH_{26}N_2O_{14}S_2$
Formula weight	477.95	477.95
Temperature (K)	293(2)	100(2)
Crystal system	monoclinic	monoclinic
Space group	$P2_1/n$	$P2_1/a$
a (Å)	6.9533(2)	11.9443(1)
b (Å)	12.5568(2)	12.5926(2)
c (Å)	9.9434(2)	12.1347(2)
β (°)	90.526(1)	110.120(1)
V (Å^3)	868.13(3)	1713.79(4)
Z	2	4
ρ_{cal} (g cm^{-1})	1.828	1.852
Crystal size (mm^3)	$0.179 \times 0.264 \times 0.349$	$0.174 \times 0.233 \times 0.309$
Habit-colour	prism-blue	prism-blue
λ (Mo Kα) (Å)	0.71073	0.71073
μ (mm^{-1})	1.572	1.593
θ Range (°)	3.24–30.00	3.24–27.00
Index ranges	$-9 \leqslant h \leqslant 9$, $-17 \leqslant k \leqslant 17$, $-13 \leqslant l \leqslant 13$	$-15 \leqslant h \leqslant 15$, $-16 \leqslant k \leqslant 16$, $-15 \leqslant l \leqslant 15$
Unique data	2493	3736
Observed data [$I > 2\sigma(I)$]	2264	3535
$F(000)$	498	996
Extinction coefficient	0.052(5)	0.0037(7)
Refinement method	full-matrix least-squares on $\|F^2\|$	full-matrix least-squares on $\|F^2\|$
R_1	0.0456	0.0511
wR_2	0.1205	0.1175
Goodness-of-fit	1.096	1.260
Number of parameters	207	283
Transmission factors	0.67520 and 0.80872	0.97188 and 0.98225
Largest difference map hole and peak (e Å^{-3})	−0.773 and 1.149	−0.759 and 0.917

Table 2
Fractional atomic coordinates and equivalent isotropic temperature factor (Å^2) with e.s.d.'s in parentheses

Atom	x	y	z	$U_{éq}$[a]
$(C_6H_{14}N_2)[Cu(H_2O)_6](SO_4)_2$ (293 K)				
Cu	0.0000	0.0000	0.0000	0.0239(2)
S	−0.01190(9)	−0.25093(4)	0.35884(6)	0.0277(2)
OW1	0.2076(3)	0.0844(2)	−0.0820(2)	0.0312(4)
OW2	0.2078(3)	−0.0833(2)	0.0879(2)	0.0313(4)
OW3	−0.0020(3)	−0.1212(2)	−0.1860(2)	0.0457(5)
O1	−0.0393(4)	−0.1715(2)	0.4647(3)	0.0616(7)
O2	−0.1766(3)	−0.2444(2)	0.2655(3)	0.0490(6)
O3	−0.0064(3)	−0.3584(2)	0.4188(2)	0.0337(4)
O4	0.1699(3)	−0.2315(2)	0.2869(2)	0.0398(5)
N	0.6418(4)	−0.0549(2)	−0.5285(3)	0.0415(6)
C1	0.479(1)	−0.1113(2)	−0.549(1)	0.050(2)
C2	0.6942(9)	0.0399(5)	−0.4714(8)	0.048(2)
C3	0.6589(8)	0.0475(5)	−0.6053(6)	0.041(1)
C4	0.500(1)	−0.1231(5)	−0.4469(7)	0.042(1)
C5	0.663(1)	−0.0218(7)	−0.3754(8)	0.041(1)
C6	0.519(1)	−0.0355(6)	−0.6632(6)	0.042(1)
$(C_6H_{14}N_2)[Cu(H_2O)_6](SO_4)_2$ (100 K)				
Cu	0.25898(4)	0.50579(3)	0.25262(3)	0.0085(2)
S1	0.42844(7)	0.75876(6)	0.56509(7)	0.0085(2)
S2	0.41763(7)	0.76449(7)	0.06577(7)	0.0093(2)
OW1	0.3190(2)	0.4234(2)	0.3990(2)	0.0122(5)
OW2	0.1937(2)	0.5894(2)	0.1067(2)	0.0114(5)
OW3	0.1096(2)	0.4217(2)	0.1920(2)	0.0115(5)
OW4	0.4107(2)	0.5870(2)	0.3115(2)	0.0125(5)
OW5	0.1686(2)	0.6276(2)	0.3426(2)	0.0139(5)
OW6	0.3574(2)	0.3868(2)	0.1597(2)	0.0162(5)
O1	0.4744(2)	0.8383(2)	0.5015(2)	0.0151(5)
O2	0.2972(2)	0.7695(2)	0.5279(2)	0.0124(5)
O3	0.4572(2)	0.6499(2)	0.5365(2)	0.0123(5)
O4	0.4832(2)	0.7764(2)	0.6937(2)	0.0125(5)
O5	0.4488(2)	0.6828(2)	−0.0053(2)	0.0178(6)
O6	0.4778(2)	0.7428(2)	0.1926(2)	0.0145(5)
O7	0.2866(2)	0.7655(2)	0.0388(2)	0.0171(6)
O8	0.4560(2)	0.8704(2)	0.0376(2)	0.0113(5)
N1	0.1852(3)	0.4525(3)	−0.3366(3)	0.0131(6)
N2	0.2963(3)	0.5640(3)	−0.1649(3)	0.0129(6)
C1	0.1043(3)	0.4821(3)	−0.2716(3)	0.0145(7)
C2	0.2892(3)	0.3904(3)	−0.2590(3)	0.0173(8)
C3	0.2293(3)	0.5491(3)	−0.3801(3)	0.0152(7)
C4	0.2768(3)	0.6256(3)	−0.2754(3)	0.0144(7)
C5	0.1783(3)	0.5357(3)	−0.1559(3)	0.0144(7)
C6	0.3667(3)	0.4653(3)	−0.1643(3)	0.0173(8)

[a] U_{eq} is defined as one-third of the trace of the orthogonalized U_{ij} tensor.

Thermogravimetric (TG) measurement was performed with a Rigaku Thermoflex instrument under flowing air, with a heating rate of 15 °C h^{-1} from ambient temperature to 900 °C. A powdered sample, 96.01 mg, was spread evenly in a large platinum crucible to avoid mass effects.

Temperature-dependent X-ray powder diffraction (TDXD) was performed with a powder diffractometer combining the curved-position-sensitive detector (CPS120) from INEL and a high temperature attachment from Rigaku. The detector was used in a semi-focusing arrangement by reflection (Cu Kα_1 radiation, $\lambda = 1.5406$ Å) as described elsewhere [29]. The thermal decomposition of the title compound was carried out in flowing air with a heating rate of 7 °C h^{-1} from ambient temperature to 610 °C.

3. Results and discussion

3.1. Crystal structures

3.1.1. Structure at room temperature

A projection of the structure of the title compound is presented in Fig. 1. The structure consists of a hydrogen-bonded network involving $Cu(H_2O)_6$ octahedra, SO_4 tetrahedra and the disordered protonated diamine. The Cu atoms, lying in a special position on a centre of inversion, are coordinated by four water oxygens forming a slightly distorted square plane. The Cu–OW1 and Cu–OW2 distances are 1.974(2) and 1.980(2) Å, respectively (Table 3). The coordination sphere of the Cu^{2+} cation is completed by two symmetry-equivalent water-molecule oxygen atoms located above and below the square plane. The Cu–OW3 distance of 2.395(2) Å is strongly elongated so that the coordination polyhedron around the copper cation can be described as a strongly distorted octahedron. The Cu ions in this compound display the so-called (4 + 2) type of coordination that has often been observed, which is consistent with a Jahn–Teller distortion. The distances within the $[Cu(H_2O)_6]^{2+}$ octahedron are comparable to those observed in other compounds [30–32]. As it can be seen in Figs. 1 and 2, these octahedra are isolated from one another with a shortest Cu–Cu distance value of 6.953 Å. They are stacked along the *a* and *c* axes while they alternate along the *b* axis.

The dabco groups are located around inversion centres at (1/2 0 1/2) and (0 1/2 0), while all their atoms are located in general positions. Thus, the molecule adopts two possible orientations. The C atoms are distributed between two positions related by the symmetry centre, with a refined site occupancy factor equal to 0.5. It is the consequence of the fact that the internal symmetry of the protonated diamine does not contain any inversion centre. The organic moieties are stacked along the *a* and *c* axes (as for the $Cu(H_2O)_6$ octahedra). The organic and inorganic cations alternate along the [1 0 1] direction so that they form mixed cationic layers parallel to *a*–*c* plane. There is no hydrogen bond between the cationic entities. Within the dabcodiium cations, the N–C distances and the C–N–C angles range from 1.353(7) to 1.602(7) Å and from 100.7(4) to 116.2(4)°, respectively (Table 3).

As it is seen in other organically templated metal sulfates, the sulfur atom has four oxygen atoms coordinating to form a slightly distorted tetrahedron. In fact, the S–O distances range from 1.464(3) to 1.478(2) Å and the O–S–O angles vary from 108.1(2) to 110.7(2)° (Table 3). These tetrahedra are isolated and they are stacked in the *a*–*c* plane to form anionic layers alternating with the cationic layers previously described. These anions are connected to the cations via N–H···O and OW–H···O hydrogen bonds. Three oxygen atoms belonging to the SO_4

Table 3
Selected bond distances (Å) and angles (°)

Octahedron around Cu		Tetrahedron around S		Within the organic moiety	
$(C_6H_{14}N_2)[Cu(H_2O)_6](SO_4)_2$ (293 K)					
Cu–OW1	1.974(2)	S–O1	1.464(3)	N–C1	1.353(7)
Cu–OW2	1.980(2)	S–O2	1.470(2)	N–C2	1.367(7)
Cu–OW3	2.395(2)	S–O3	1.475(2)	N–C3	1.501(7)
OW1–Cu–OW2	86.14(8)	S–O4	1.478(2)	N–C4	1.541(7)
OW1–Cu–$OW2^{I}$	93.86(8)	O1–S–O2	108.1(2)	N–C5	1.584(9)
OW1–Cu–OW3	91.21(8)	O1–S–O3	109.6(2)	N–C6	1.602(7)
OW1–Cu–$OW3^{I}$	88.79(8)	O1–S–O4	110.7(2)	C1–$C2^{II}$	1.51(1)
OW2–Cu–OW3	90.25(8)	O2–S–O3	108.9(1)	C4–$C3^{II}$	1.551(9)
OW2–Cu–$OW3^{I}$	89.75(8)	O2–S–O4	110.5(1)	C6–$C5^{II}$	1.51(1)
		O3–S–O4	109.1(1)	C1–N–C3	116.2(5)
				C1–N–C5	110.8(5)
				C3–N–C5	105.0(4)
				C2–N–C4	115.8(5)
				C2–N–C6	110.7(5)
				C4–N–C6	100.7(4)
				N–C1–$C2^{II}$	109.5(4)
				N–C4–$C3^{II}$	107.3(4)
				N–C6–$C5^{II}$	107.6(5)

Symmetry codes: $^{I}-x, -y, -z$; $^{II}-x+1, -y, -z-1$

Octahedron around Cu		Tetrahedron around S(1)		Within the organic moiety	
$(C_6H_{14}N_2)[Cu(H_2O)_6](SO_4)_2$ (100 K)					
Cu–OW1	1.967(3)	S1–O1	1.480(3)	N1–C1	1.490(5)
Cu–OW2	1.975(2)	S1–O2	1.480(2)	N1–C2	1.495(5)
Cu–OW3	1.986(2)	S1–O3	1.483(3)	N1–C3	1.493(5)
Cu–OW4	1.987(3)	S1–O4	1.487(2)	N2–C4	1.496(5)
Cu–OW5	2.350(3)	O1–S1–O2	108.8(2)	N2–C5	1.494(4)
Cu–OW6	2.411(3)	O1–S1–O3	110.3(2)	N2–C6	1.499(5)
OW1–Cu–OW2	178.1(1)	O1–S1–O4	109.8(2)	C1–C5	1.534(5)
OW1–Cu–OW3	93.2(1)	O2–S1–O3	108.6(2)	C2–C6	1.529(5)
OW1–Cu–OW4	86.7(1)	O2–S1–O4	110.1(2)	C3–C4	1.539(5)
OW1–Cu–OW5	90.4(1)	O3–S1–O4	109.3(2)	C1–N1–C2	110.3(3)
OW1–Cu–OW6	90.6(1)	Tetrahedron around S(2)		C1–N1–C3	110.8(3)
OW2–Cu–OW3	85.7(1)	S2–O5	1.470(3)	C2–N1–C3	109.3(3)
OW2–Cu–OW4	94.5(1)	S2–O6	1.473(3)	C4–N2–C5	109.2(3)
OW2–Cu–OW5	88.0(1)	S2–O7	1.484(3)	C4–N2–C6	110.4(3)
OW2–Cu–OW6	91.0(1)	S2–O8	1.488(3)	C5–N2–C6	110.1(3)
OW3–Cu–OW4	178.4(1)	O5–S2–O6	110.5(2)	N1–C1–C5	108.7(3)
OW3–Cu–OW5	91.3(1)	O5–S2–O7	109.7(2)	N1–C2–C6	108.0(3)
OW3–Cu–OW6	90.9(1)	O5–S2–O8	109.4(2)	N1–C3–C4	107.0(3)
OW4–Cu–OW5	90.3(1)	O6–S2–O7	109.2(2)	N2–C4–C3	108.4(3)
OW4–Cu–OW6	87.5(1)	O6–S2–O8	109.0(2)	N2–C5–C1	107.4(3)
OW5–Cu–OW6	177.5(1)	O7–S2–O8	109.1(2)	N2–C6–C2	108.3(3)

tetrahedra are involved in two hydrogen bonds accepting two water hydrogen atoms, while the O1 atom is involved in the N–H···O bond accepting only one hydrogen atom from the organic moiety (Fig. 3). The intermolecular N–H···O bond has a value equal to 2.659(3) Å and the OW–H···O hydrogen bond lengths vary from 2.716(3) to 2.947(3) Å with a mean D···O distance value of 2.766 Å (Table 4). A similar crystal structure is observed in the nickel related phase [21].

3.1.2. Structure at low temperature (100 K)

In the low temperature phase, which crystallizes in the $P2_1/a$ space group, the crystal structure consists of isolated $[Cu(H_2O)_6]^{2+}$, SO_4^{2-} and fully ordered $(C_6H_{14}N_2)^{2+}$ ions linked together by a hydrogen-bonding network (Fig. 4).

At 100 K, the copper ion is coordinated by six water molecule oxygen atoms and also displays the so-called (4 + 2) type of coordination due to the Jahn–Teller effect. In fact, four Cu–OW distances are almost equal while the two others are substantially longer (Table 3). The $Cu(OW)_6$ polyhedra are not connected and they are separated with a shortest Cu–Cu distance of 6.741 Å, which is shorter than that found in the room temperature phase (Cu–Cu = 6.953 Å). This result can be due to the dabco ordering which probably leads to a decrease of the mean volume of the amino group. The Cu^{2+} octahedron is surrounded by six sulfate tetrahedra connected via hydrogen bonds in a bidentate fashion to the octahedron (Fig. 5).

The $[dabcoH_2]^{2+}$ cations are staked along the [1 0 1] direction and they alternate with the inorganic cations

Table 4
Hydrogen-bonding geometry (Å, °)

D–H···A	*d*(D–H) (Å)	*d*(H···A) (Å)	*d*(D···A) (Å)	∠D–H···A (°)
$(C_6H_{14}N_2)[Cu(H_2O)_6](SO_4)_2$ (293 K)				
N–HN···O1^{V}	0.96(5)	1.73(5)	2.659(3)	164(5)
OW1–H11···O3^{IV}	0.95(1)	1.78(1)	2.721(3)	173(4)
OW1–H12···O2^{I}	0.95(1)	1.80(2)	2.721(3)	164(4)
OW2–H21···O4	0.96(1)	1.79(1)	2.731(3)	169(5)
OW2–H22···O3^{II}	0.95(1)	1.77(1)	2.716(3)	174(3)
OW3–H31···O4^{III}	0.95(1)	2.00(1)	2.947(3)	176(4)
OW3–H32···O2^{II}	0.96(1)	1.91(1)	2.867(3)	180(3)
Symmetry codes: $^{I}-x, -y, -z$; $^{II}x+1/2, -y-1/2, z-1/2$; $^{III}x-1/2, -y-1/2, z-1/2$; $^{IV}-x+1/2, y+1/2, -z+1/2$; $^{V}x+1, y, z-1$.				
$(C_6H_{14}N_2)[Cu(H_2O)_6](SO_4)_2$ (100 K)				
N1–HN1···O1^{III}	0.93(6)	1.74(6)	2.661(4)	168(5)
N2–HN2···O5	0.95(5)	1.71(5)	2.623(4)	162(5)
OW1–H11···O2^{I}	0.94(2)	1.77(2)	2.705(4)	171(5)
OW1–H12···O3^{II}	0.94(2)	1.74(2)	2.678(3)	179(6)
OW2–H21···O8^{IV}	0.95(2)	1.77(2)	2.716(3)	174(6)
OW2–H22···O7	0.95(2)	1.79(2)	2.731(4)	169(6)
OW3–H31···O8^{III}	0.95(2)	1.76(2)	2.700(3)	172(4)
OW3–H32···O4^{I}	0.95(2)	1.81(2)	2.748(4)	169(5)
OW4–H41···O3	0.95(2)	1.77(2)	2.711(4)	171(4)
OW4–H42···O6	0.94(2)	1.79(2)	2.714(4)	168(5)
OW5–H51···O2	0.94(2)	1.93(2)	2.869(4)	174(5)
OW5–H52···O6^{IV}	0.94(2)	1.94(2)	2.884(4)	176(4)
OW6–H61···O7^{III}	0.94(2)	1.94(2)	2.871(4)	177(6)
OW6–H62...O4^{II}	0.94(2)	2.01(2)	2.947(4)	175(5)
Symmetry codes: $^{I}-x+1/2, y-1/2, -z+1$; $^{II}-x+1, -y+1, -z+1$; $^{III}-x+1/2, y-1/2, -z$; $^{IV}x-1/2, -y+3/2, z$.				

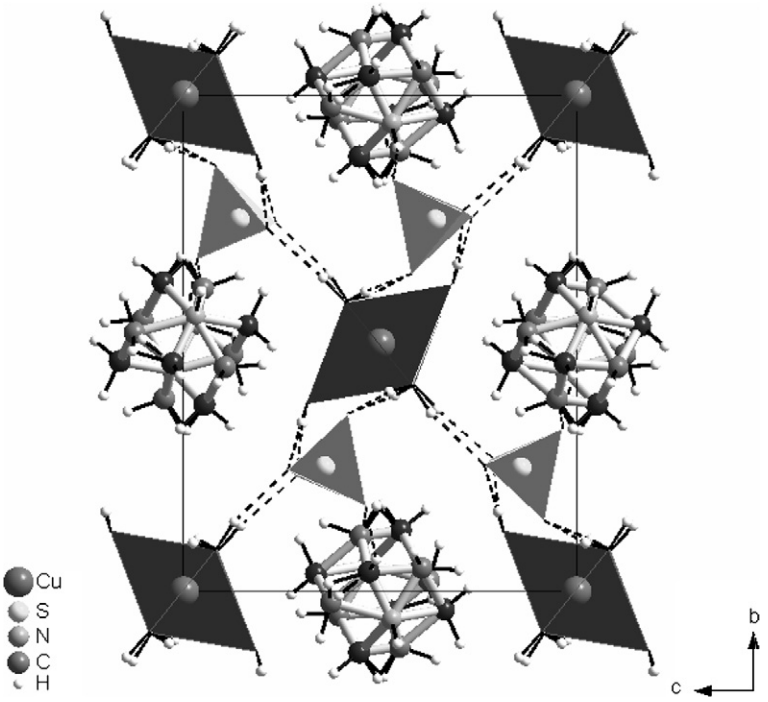

Fig. 1. A projection of the crystal structure of $(C_6H_{14}N_2)[Cu^{II}(H_2O)_6](SO_4)_2$ at 293 K. The minor part of the disordered ($dabcoH_2$) group is in dark grey. Hydrogen bonds are shown as dashed lines.

along the *a*, *b* and *c* axes, leading to mixed cationic layers perpendicular to the *b* axis (Fig. 6). Within the protonated diamine molecules, the C–C and N–C distances and the C–N–C angles range, respectively from 1.529(5) to 1.539(5) Å, 1.490(5) to 1.499(5) Å and 109.2(3) to 110.8(3)° (Table 3). There are two crystallography distinct S atoms with tetrahedral geometries located in general positions. The sulfate ions are quite regular with mean tetrahedral angles of

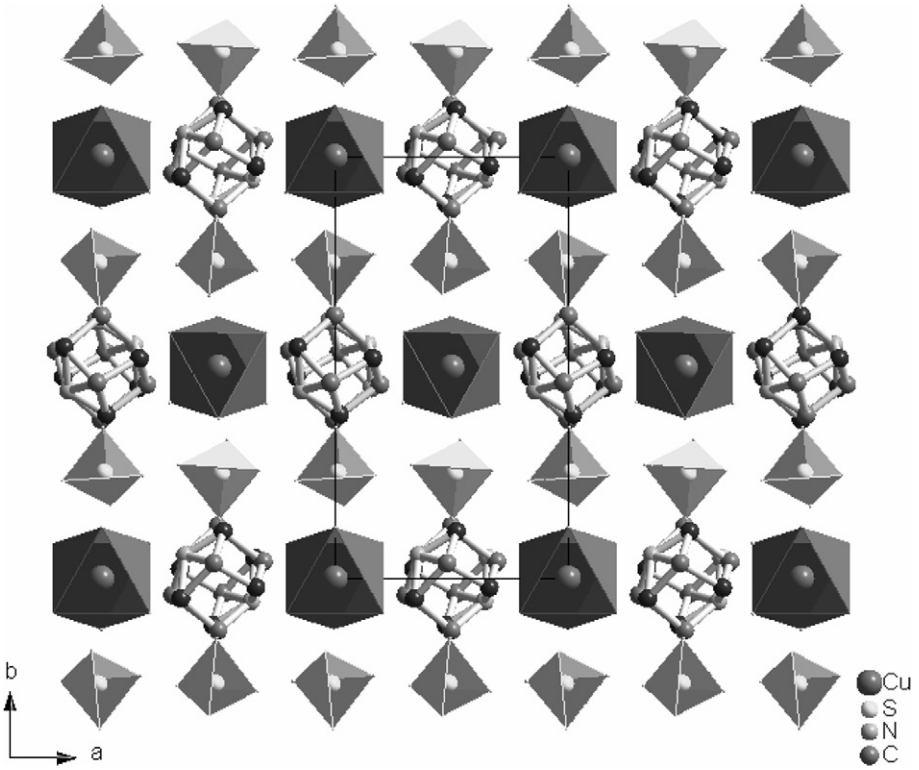

Fig. 2. A projection of the structure of the title compound at room temperature along the *c* axis. The minor part of the disordered ($dabcoH_2$) group is dark grey. H atoms are omitted for clarity.

109.47° and mean S–O bond lengths of 1.482 Å for the low temperature phase (Table 3). The SO_4 tetrahedra are staked in a manner such that they form anionic layers parallel to the *a*–*c* plane. The anionic and cationic layers alternate along the *b* axis and connect themselves by N–H···O and OW–H···O hydrogen bonds only. The asymmetric

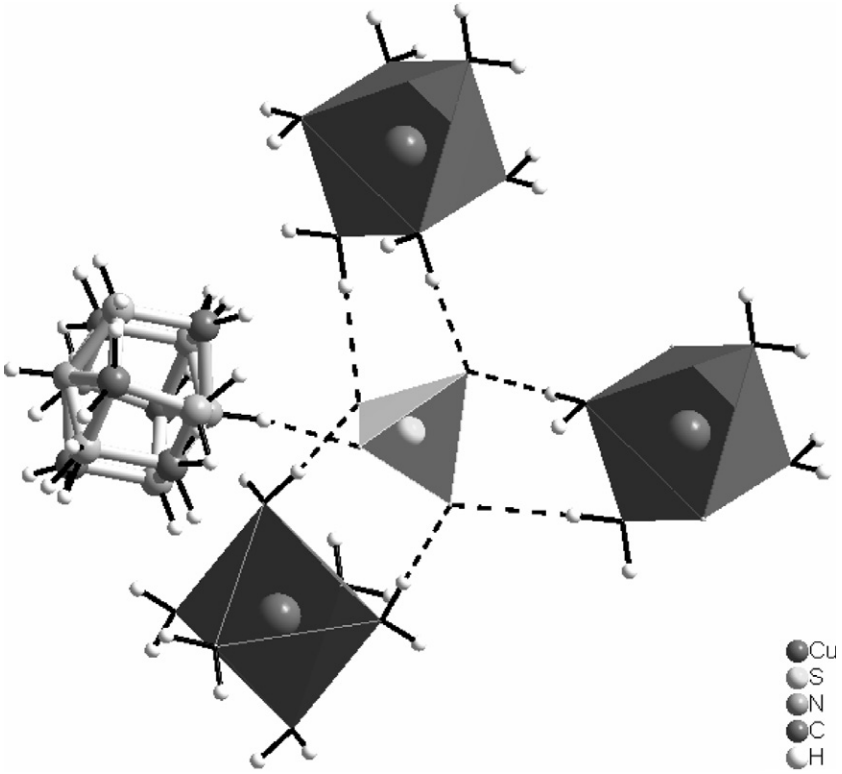

Fig. 3. The hydrogen bonds formed with the sulfate tetrahedra.

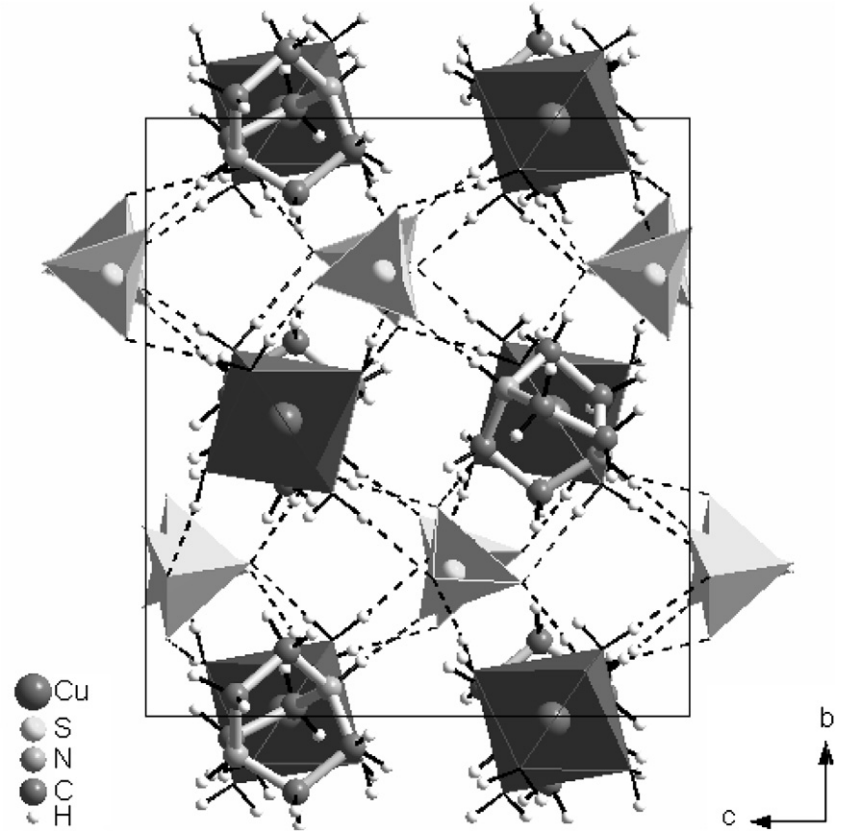

Fig. 4. A projection of the low temperature structure of the title compound along the *a* axis, showing the hydrogen-bond network formed by the $[Cu(H_2O)_6]^{2+}$, SO_4^{2-} and $C_6H_{14}N_2^{2+}$ ions. Hydrogen bonds are shown as dashed lines.

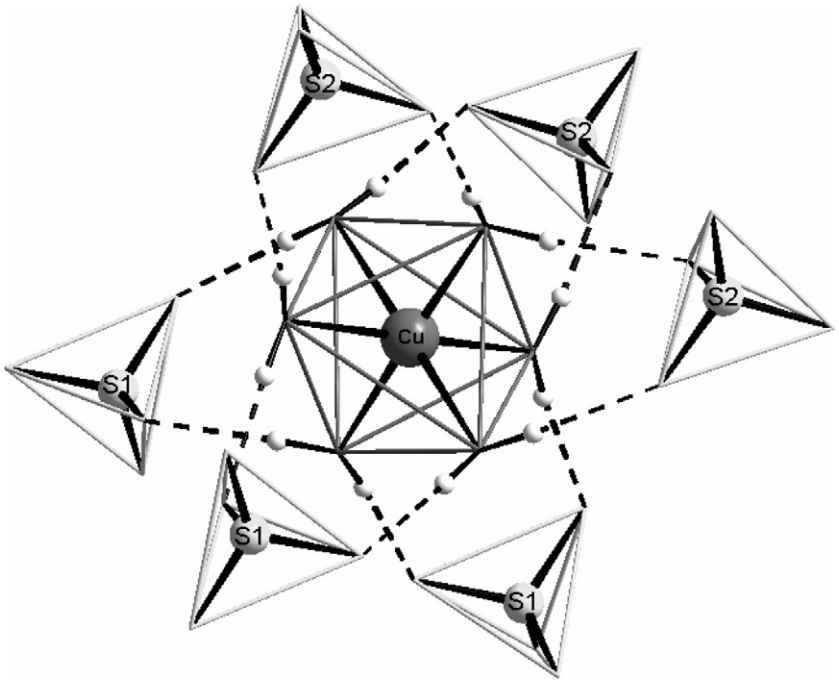

Fig. 5. The environment around the Cu atom and the hydrogen bonds formed with $Cu(H_2O)_6$ octahedra at 100 K.

unit of the low temperature phase (Fig. 7) reveals that the oxygen atoms of each sulfate anion participate as acceptors in hydrogen bonds, through H atoms bonded to N atoms and water-molecule hydrogen atoms. The donor···acceptor bond distances range from 2.623(4) to 2.947(4) Å ($\langle D\cdots O\rangle = 2.754$ Å) and the D–H···O angles vary between

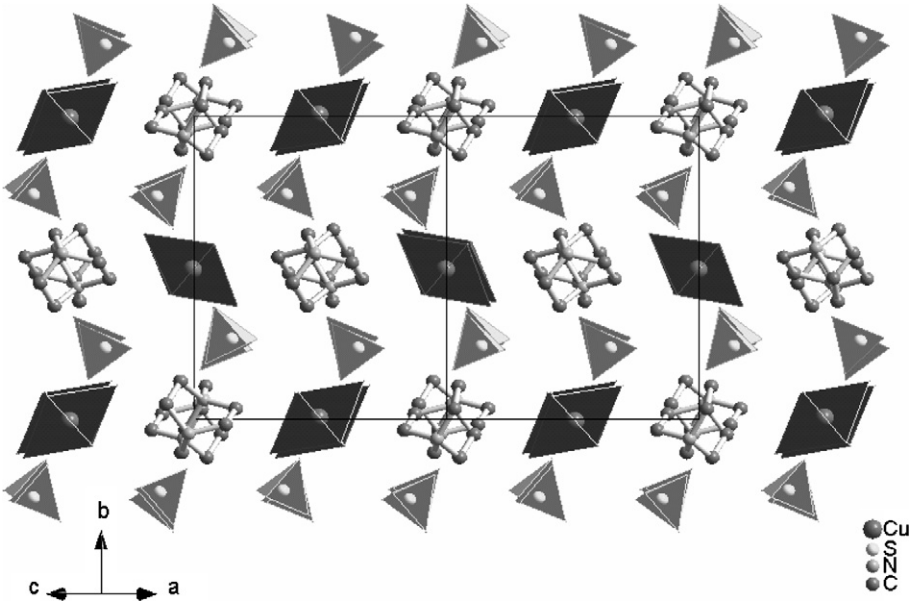

Fig. 6. A projection of the structure of the title compound at 100 K along the [1 0 1] direction. H atoms are omitted for clarity.

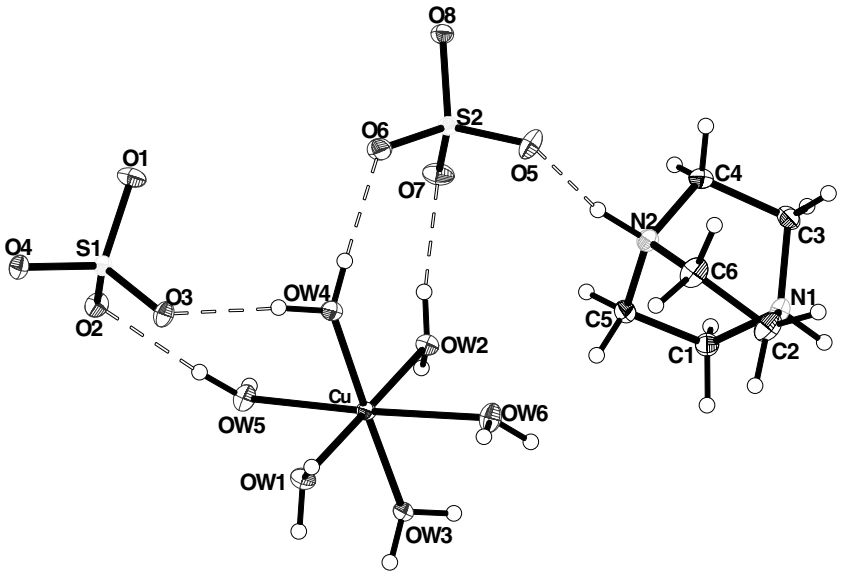

Fig. 7. A part of the crystal structure at 100 K showing the asymmetric unit and atom numbering. Displacement ellipsoids are drawn at the 50% probability level. Hydrogen bonds are represented by dashed lines.

162(5) and 179(6)°, with a mean value 173.07° (Table 4). It should be noted that the hydrogen bonds at low temperature are slightly stronger than those at 293 K ($\langle D\cdots O\rangle =$ 2.766 Å). At 100 K, O1 and O5 accept only one dabcodium hydrogen atom while all the other oxygen atoms belonging to the SO_4 tetrahedra are involved in two hydrogen bonds accepting two water hydrogen atoms, as in the structure solved at 293 K.

3.2. Thermal behaviour

3.2.1. Differential scanning calorimetry

Differential scanning calorimetry (DSC) curves of a powdered sample of the title compound, between 133 and 315 K, including heating and cooling processes are shown in Fig. 8. The thermal changes of $(C_6H_{14}N_2)[Cu(H_2O)_6](SO_4)_2$ are reversible in the measured temperature range. Only one observed heat anomaly at 265.7/281.8 K (heating–cooling) clearly indicates a first order phase transition. The characteristic thermodynamic values have been determined as follows:

Increasing temperature	Decreasing temperature
T_o (onset) $= 265.7 \pm 0.3$ K	T_o (onset) $= 281.8 \pm 0.3$ K
T_s (peak) $= 268.9 \pm 0.3$ K	T_s (peak) $= 276.0 \pm 0.3$ K
$\Delta H = 4.50$ kJ mol^{-1}	$\Delta H = -4.30$ kJ mol^{-1}
$\Delta S = 16.72$ J mol^{-1} K^{-1}	$\Delta S = 15.59$ J mol^{-1} K^{-1}

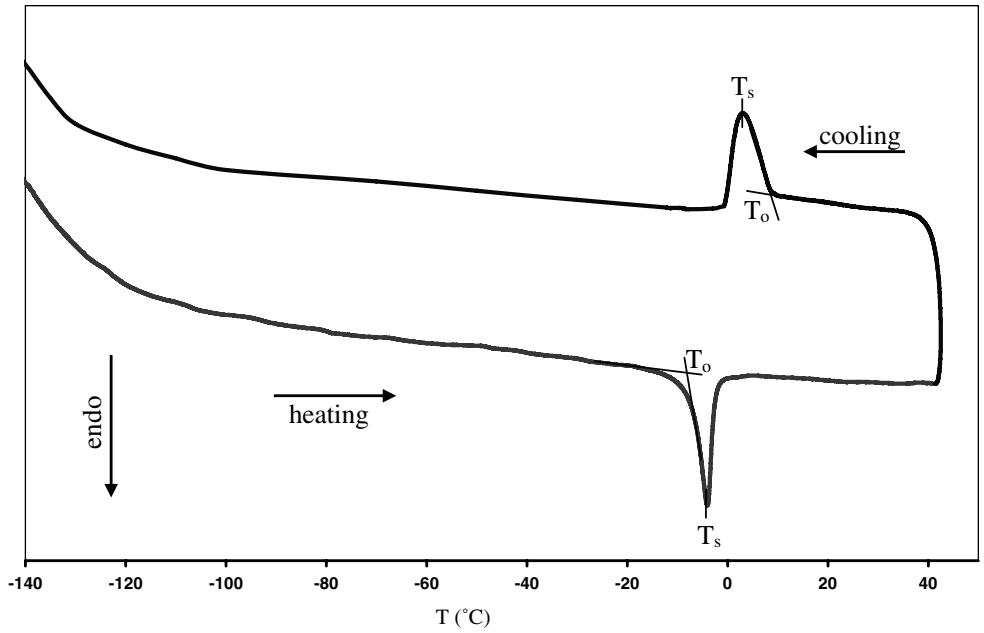

Fig. 8. DSC curves obtained upon heating and cooling $(C_6H_{14}N_2)[Cu(H_2O)_6](SO_4)_2$.

The entropy change (ΔS) accompanying the first order transition is equal to 16.72 J mol^{-1} K^{-1} which suggests an order–disorder mechanism for this transition, as expected from the crystal structure analyses.

3.2.2. Dielectric properties

The electrical data measured as an impedance Z^* have been converted into permittivity ε^* using the relation, $\varepsilon^* = 1/iwC_0Z^*$ where C_0 is the vacuum capacitance [33]. The temperature dependence of the real part of the complex permittivity, ε', at several frequencies is presented in Fig. 9. A transition is characterized by a weak increase of ε' from 5.8 to 7 (for all frequencies). The observed dielectric anomaly at about 262 K confirms the transition observed by differential scanning calorimetry at about the same temperature. The behaviour of the real part of the dielectric permittivity is similar to that reported by Bednarska-Bolek et al. for the $(C_5H_{10}NH_2)SbCl_6 \cdot (C_5H_{10}NH_2)Cl$ crystal [34] so that the phase transition is expected to be of the prototype-ferroelastic nature. In order to make clear whether the

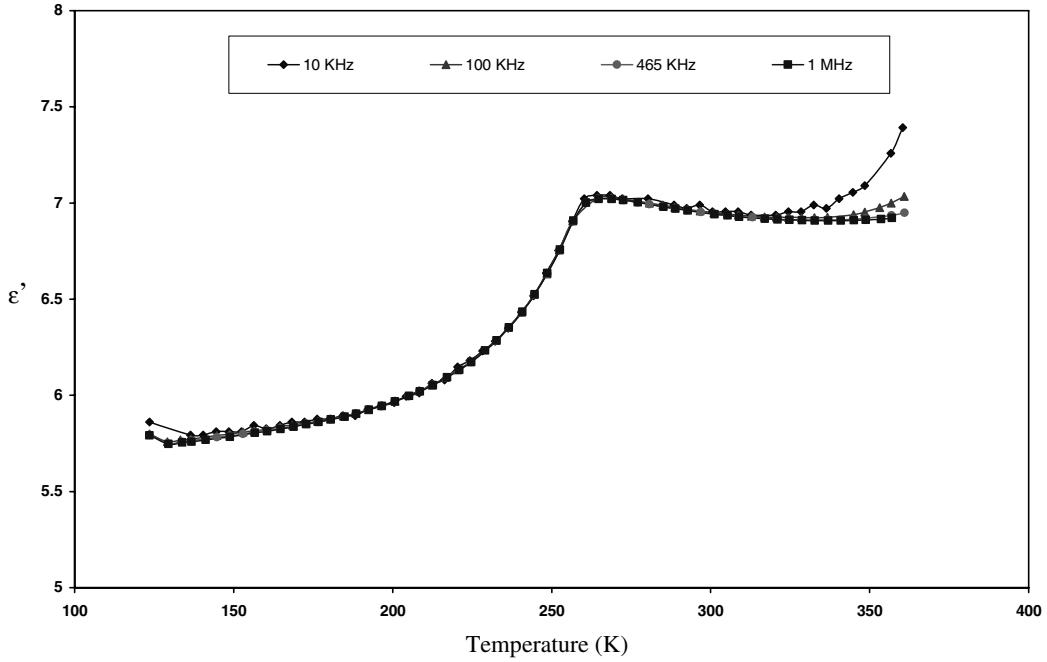

Fig. 9. Temperature dependence of ε' at different frequencies.

265 K transition is a ferroelastic transition or not, some photographs using an optical polarization microscope have been made below and above the phase transition temperature.

3.2.3. Polarizing microscope observations

The optical observations of $(C_6H_{14}N_2)[Cu(H_2O)_6](SO_4)_2$ were carried out over a wide temperature range by means of the Leitz optical polarization microscope (ortholux2-pol type). Fig. 10 shows photographs of a title compound crystal upon heating from 233 to 293 K. No ferroelastic domain structure is observed below and above the transition temperature. These results evidence that the material undergoes only an order–disorder phase transition.

3.2.4. Thermal decomposition

The thermogravimetry curve and the three-dimensional representation of the powder diffraction patterns obtained during the decomposition of $(C_6H_{14}N_2)[Cu(H_2O)_6](SO_4)_2$ under flowing air are shown in Figs. 11 and 12, respectively. The thermal decomposition of the title compound takes place in several steps. In the first stage, the compound loses 4.5 water molecules in the temperature range 66–100 °C (observed weight loss, 17.01%; calculated weight loss, 16.95%). In the second step of decomposition (temperature range 122–150 °C) the compound loses the remaining 1.5 water molecules. The TDXD plot shows that the anhydrous phase, obtained after the complete dehydration of the title compound, is amorphous to X-rays until 200 °C. At this temperature some diffraction lines emerge from the background. A few lines disappear at about 250 °C while the remaining ones are observed up to 300 °C. Analysis of the last peaks reveals that it is the pattern of $Cu(NH_4)_2(SO_4)_2$ [ICDD No., 18-090]. Then $Cu(NH_4)_2(SO_4)_2$ is formed together with a second phase at the beginning of the decomposition of the anhydrous phase $(dabcoH_2)Cu(SO_4)_2$. It is supposed that the unknown phase corresponds to a crystallized variety of the anhydrous dabcodiium copper sulfate. Indeed, a similar thermal behaviour has already been observed for anhydrous lanthanum potassium oxalate [35], anhydrous potassium yttrium squarate [36] and piperazinediium copper sulfate [20]. Unfortunately, the low quality of the powder data of the

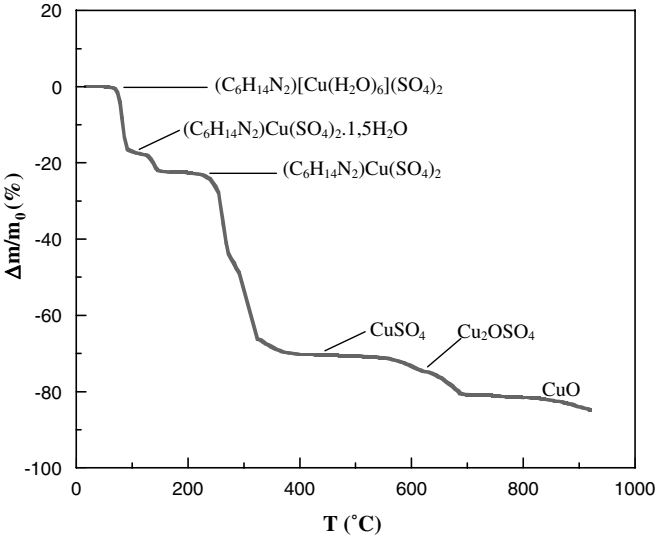

Fig. 11. TG curve for the decomposition of $(C_6H_{14}N_2)[Cu(H_2O)_6](SO_4)_2$ in air (15 °C h^{-1}).

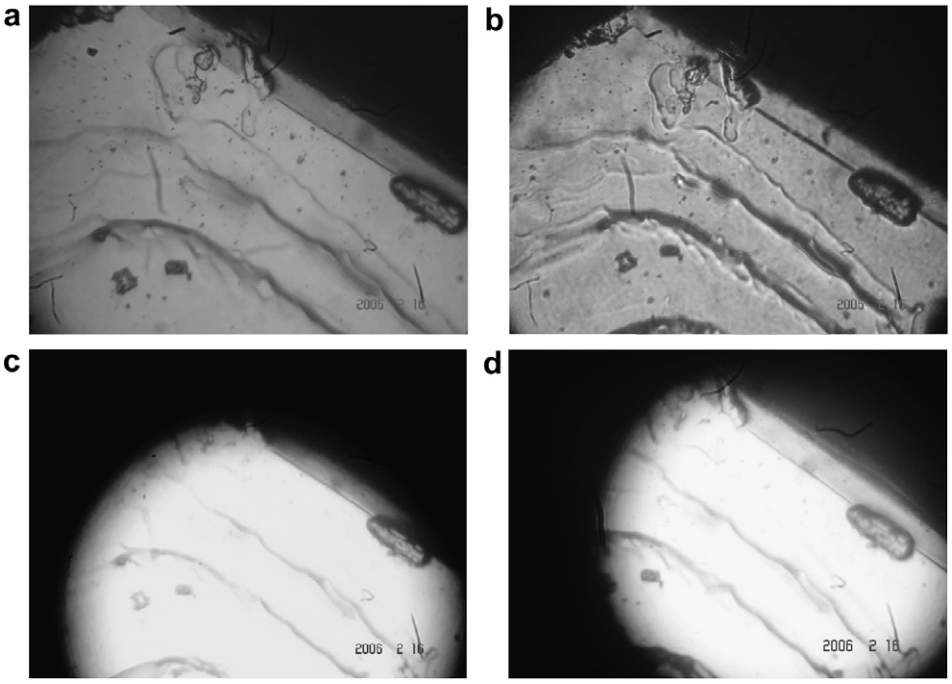

Fig. 10. Photographs of a $(C_6H_{14}N_2)[Cu(H_2O)_6](SO_4)_2$ crystal upon heating: (a) 233, (b) 253, (c) 273 and (d) 293 K.

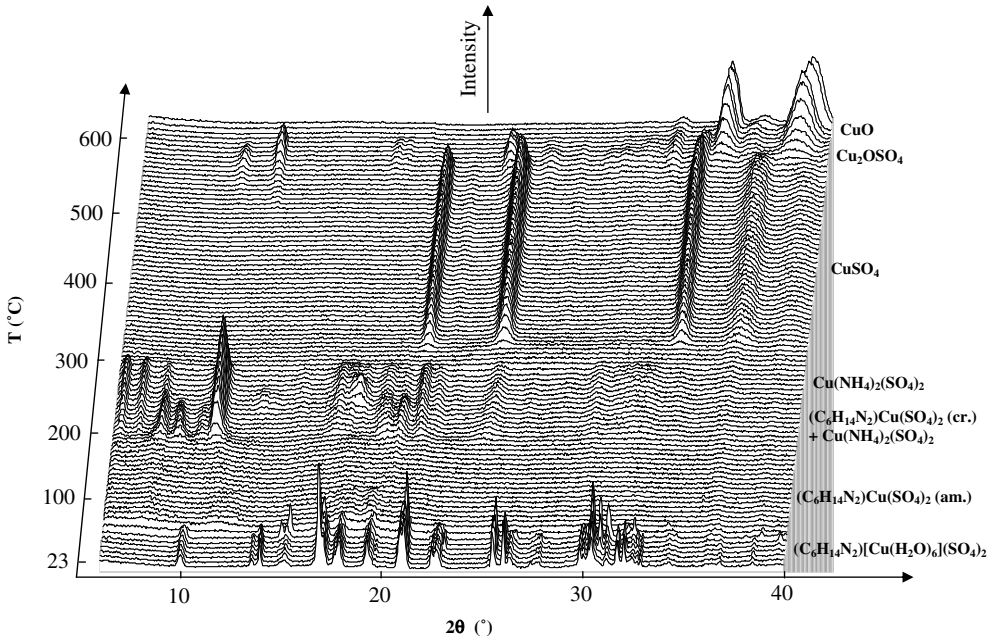

Fig. 12. TDXD plot for the decomposition of $(C_6H_{14}N_2)[Cu(H_2O)_6](SO_4)_2$ in air (7 °C h^{-1} from 18 to 610 °C; counting time of 3600 s per pattern).

anhydrous phase did not allow further structural investigations on the compound. The end of the decomposition of $Cu(NH_4)_2(SO_4)_2$ leads to anhydrous copper sulfate. It decomposes, at 560 °C, into Cu_2OSO_4 as evidenced on the TDXD plot and by the weight loss of 74.96% (calculated weight loss, 74.99%) observed on the TG curve at the inflection. The last transformation corresponds to the formation of copper oxide, CuO, which crystallise immediately after the beginning of the decomposition of Cu_2OSO_4.

4. Concluding remarks

The first copper(II) sulfate templated by 1,4-diazabicyclo[2.2.2]octane, $(C_6H_{14}N_2)[Cu(H_2O)_6](SO_4)_2$, has been prepared and characterized. The crystal structures at 293 and 100 K have been resolved by X-ray single-crystal diffraction data. Crystallographic studies show that it crystallizes with monoclinic symmetry (space group $P2_1/n$ and $P2_1/a$ at room temperature and 100 K, respectively). Both phases exhibit similar crystal structures consisting of Cu^{2+} cations octahedrally coordinated to six water molecules, sulfate tetrahedra and dabcodiium cations (disordered at room temperature) linked by hydrogen bonds only. A structural phase transition, due to the ordering of the dabcodiium cation, is detected by differential scanning calorimetry and confirmed by dielectric studies. The dabcodiium templated copper sulfate undergoes an order–disorder phase transition of the first order at about 265.7/281.8 K on heating cooling runs. Optical observations show that no domain structures are distinguished in both phases. The thermal decomposition of the precursor, studied by TG and TDXD, proceeds through several stages giving rise to copper oxide.

Acknowledgements

Grateful thanks are expressed to Dr. T. Roisnel (Centre de Diffractométrie X, Université de Rennes I) for the assistance in single-crystal X-ray diffraction data collection and Professor Régnault Von der Mühll (ICMCB-CNRS Université Bordeaux 1) for the optical observations.

Appendix A. Supplementary data

Further details of the crystal structure investigations at 293 and 100 K can be obtained from the Cambridge Crystallographic Data Center. The deposition numbers are respectively CCDC Nos. 607328 and 607329. Supplementary data associated with this article can be found, in the online version, at doi:10.1016/j.poly.2006.07.010.

References

[1] L.F. Kirpichnikova, E.F. Andreev, N.R. Ivanov, et al., Kristallografiya 33 (1988) 1437.
[2] A.N. Holden, B.V. Matthias, W.J. Merz, et al., Phys. Rev. 98 (1955) 546.
[3] N. Galesic, V.B. Jordanovska, Acta Crystallogr., Sect. C 48 (1992) 256.
[4] L.F. Kirpichnikova, L.A. Shuvalov, N.R. Ivanov, B.N. Prasolov, E.F. Andreyev, Ferroelectrics 96 (1989) 313.
[5] A. Pietraszko, K. Lukaszewicz, L.F. Kirpichnikova, Pol. J. Chem. (1993) 1877.
[6] W. Rekik, H. Naïli, T. Mhiri, T. Bataille, Acta Cryst. E 61 (2005) m629.
[7] J.-X. Pan, G.-Y. Yang, Y.-Q. Sun, Acta Cryst. E 59 (2003) m286.
[8] M. Fleck, L. Bohaty, E. Tillmanns, Solid State Sci. 6 (2004) 469.
[9] M.H. Ben Ghozlen, A. Daoud, Z. Kristallogr. 209 (1994) 383.

[10] A. Rujiwatra, J. Limtrakul, Acta Crystallogr., Sect. E 61 (2005) m1403.
[11] S. Chaabouni, S. Kamoun, A. Daoud, T. Mhiri, Acta Crystallogr., Sect. C 52 (1996) 505.
[12] P.C. Healy, J.M. Patrick, A.H. White, Aust. J. Chem. 37 (1984) 1105.
[13] C.N. Morimoto, E.C. Lingafelter, Acta Crystallogr., Sect. B 26 (1970) 335.
[14] V. Jordanovska, S. Aleksovska, J. Siftar, J. Thermal Anal. 38 (1992) 1563.
[15] Y.-J. Zhao, X.-H. Li, S. Wang, Acta Crystallogr., Sect. E 61 (2005) m671.
[16] I. Turel, I. Leban, M. Zupancic, P. Bukovec, K. Gruber, Acta Crystallogr., Sect. C 52 (1996) 2443.
[17] M. Rademeyer, Acta Crystallogr., Sect. E 60 (2004) m993.
[18] X.-H. Li, Q. Miao, H.-P. Xiao, M.-L. Hu, Acta Crystallogr., Sect. E 60 (2004) m1784.
[19] Y.-L. Fu, Z.-W. Xu, J.-L. Ren, S.W. Ng, Acta Crystallogr., Sect. E 61 (2005) m1639.
[20] W. Rekik, H. Naïli, T. Bataille, T. Roisnel, T. Mhiri, Inorg. Chim. Acta 359 (2006) 3954.
[21] W. Rekik, H. Naïli, T. Bataille, T. Mhiri, J. Organomet. Chem., in press.
[22] Nonius, KappaCCD Program Software, Nonius BV, Delft, The Netherlands, 1998.
[23] Z. Otwinowski, W. Minor, C.W. Carter, R.M. Sweet (Eds.), Methods in Enzymology, vol. 276, Academic Press, New York, 1997, p. 307.
[24] J. de Meulenaer, H. Tompa, Acta Crystallogr. 19 (1965) 1014.
[25] L.J. Farrugia, J. Appl. Cystallogr. 32 (1999) 837.
[26] G.M. Sheldrick, Acta Crystallogr., Sect. A 46 (1990) 467.
[27] G.M. Sheldrick, SHELXL-97: Program for Crystal Structure Refinement, University of Göttingen, Germany, 1997.
[28] International Tables for Crystallography, vol. C, Kluwer, Dordrecht, 1992.
[29] J. Plévert, J.-P. Auffrédic, M. Louër, D. Louër, J. Mater. Sci. 24 (1989) 1913.
[30] A. Monge, E. Gutierrez-Puebla, Acta Crystallogr., Sect. B 37 (1981) 427.
[31] I. Persson, P. Persson, M. Sandström, A. Ullström, J. Chem. Soc., Dalton Trans. (2002) 1256.
[32] Q.-H. Zhao, L. Du, R.-B. Fang, Acta Crystallogr., Sect. E 62 (2006) m360.
[33] I.M. Hodge, M.D. Ingram, A.R. West, J. Electroanal. Chem. 74 (1976) 125.
[34] B. Bednarska-Bolek, A. Pietraszko, R. Jakubas, G. Bator, B. Kosturek, J. Phys.: Condens. Matter 12 (2000) 1143.
[35] T. Bataille, M. Louër, J. -P Auffrédic, D. Louër, J. Solid State Chem. 150 (2000) 81.
[36] N. Mahé, T. Bataille, Inorg. Chem. 43 (2004) 8379.

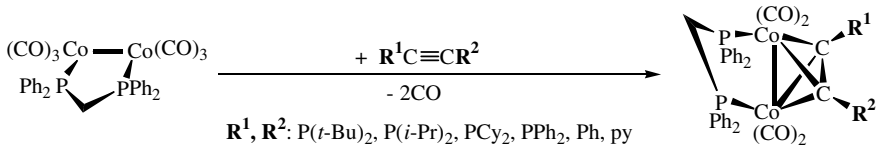

Scheme 1.

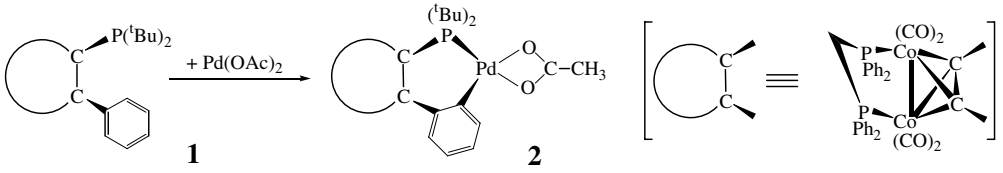

Scheme 2.

prepared **1**/$Pd(OAc)_2$ and **2** were carried out. In general, complex **2** results in lower efficiency compared with that of in situ prepared **1**/$Pd(OAc)_2$.

It is well-known that halide-coordinated palladium complexes such as $[(\eta^4\text{-}C_4Ph_4)PdBr_2]_2$ are always present in dimeric form with two bridging halides [6]. The bonding of the chelating acetate toward palladium atom in **2** is seemingly weak resulting in replacement by a stronger ligand such as halide. It leads naturally to an energetically favorable form, a dimeric complex. Herein, we report the preparation of a new unusually large sized palladium dimeric compound and its catalytic activity in Suzuki reactions.

2. Results and discussion

2.1. Preparation and characterization of a palladium dimer 3

A new and unusually large-sized palladium dimeric compound, $\{(\mu\text{-}PPh_2CH_2PPh_2)Co_2(CO)_4(\mu,\eta\text{-}(t\text{Bu})_2PC{\equiv}CC_6H_4\text{-}\kappa C^1)Pd(\mu\text{-}Cl)\}_2$ (**3**), was obtained in good yield from the treatment of **2** with LiCl in toluene at 25 °C for 72 h (Scheme 3).

The identity of **3** was confirmed by spectroscopic means as well as X-ray diffraction methods (Table 1). Interestingly, the spectroscopic data of **3** exhibit two distinct sets of signals for its constructed units, $(\mu\text{-}PPh_2CH_2PPh_2)Co_2(CO)_4(\mu,\eta\text{-}(t\text{Bu})_2PC{\equiv}CC_6H_4\text{-}\kappa C^1)$. These two components are not magnetically equivalent. In ^{1}H NMR, two sets of doublets appear at 8.52 and 8.69 ppm, which correspond to the adjacent protons of the orthomatallated arene. Another two sets of multiplets signals observed at 3.34 and 3.50 ppm are assigned to two distinct sets of methylene protons of **3**. The ^{31}P NMR spectrum displays two sets of singlets at 82.87 and 84.40 ppm assigned to two phosphorous atoms coordinated to Pd. In addition, two sets of multiplets at 38.00 and 41.43 ppm correspond to the coordinated dppm ligand. The ^{13}C NMR data also support the account that the two constructed components of **3** are not in the same magnetical environment. The ORTEP diagram for **3** is depicted in Fig. 1. As shown, it is a doubly chloride-bridged palladium dimer. The original chelating acetate ligand was removed from **2**. The four atoms, Pd_2Cl_2, are arranged in a diamond shape and almost coplanar. The conformation of the rest of the dimer is almost unaltered from its counterpart in **2**. Two isomeric forms of **3** might

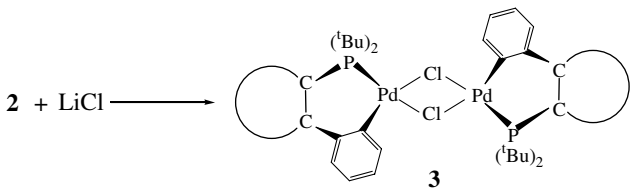

Scheme 3.

Table 1
Crystal data of **3**

Compound	**3**
Formula	$C_{45}H_{44}ClCo_2O_4P_3Pd$
Formula weight	1001.42
Crystal system	monoclinic
Space group	*C*2/*c*
a (Å)	28.1956(18)
b (Å)	26.0181(16)
c (Å)	18.2245(11)
α (°)	
β (°)	128.0030(10)
γ (°)	
V (Å^3)	10534.8(11)
Z	8
D_c (Mg/m^3)	1.263
λ (Mo Kα, Å)	0.71073
μ (mm^{-1})	1.136
θ Range (°)	1.36–26.05
Observed reflections ($F > 4\sigma(F)$)	10370
Number of refined parameters	485
R_1[a] for significant reflections	0.0526
wR_2[b] for significant reflections	0.1624
Goodness-of-fit[c]	0.997

[a] $R_1 = \|\sum(|F_o| - |F_c|)/|\sum F_o\|$.

[b] $wR_2 = \{\sum[w(F_o^2 - F_c^2)^2/\sum[w(F_o^2)^2]\}^{1/2}$; $w = 0.1015$ for **3**.

[c] Goodness-of-fit $= [\sum w(F_o^2 - F_c^2)^2/(N_{\text{reflections}} - N_{\text{parameters}})]^{1/2}$.

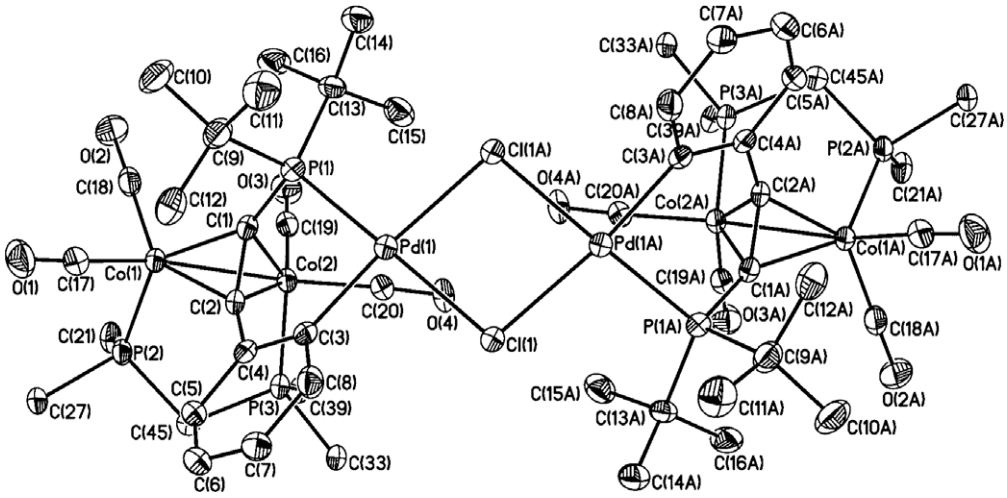

Fig. 1. ORTEP drawing of **3**. Hydrogen atoms are omitted for clarity. Selected bond lengths (Å) and angles (°): Pd(1)–C(3) 2.013(7); Pd(1)–P(1) 2.2690(19); Pd(1)–Cl(1) 2.4329(18); Pd(1)–Cl(1)#1 2.4512(19); Co(1)–C(2) 1.960(6); Co(1)–C(1) 1.998(7); Co(1)–P(2) 2.239(2); Co(1)–Co(2) 2.4770(13); Co(2)–C(2) 1.956(7); Co(2)–C(1) 1.959(7); Co(2)–P(3) 2.208(2); P(1)–C(1) 1.793(8); P(2)–C(45) 1.827(7); P(3)–C(45) 1.831(7); Cl(1)–Pd(1)#1 2.4512(19); C(1)–C(2) 1.362(9); C(2)–C(4) 1.461(10); C(3)–Pd(1)–P(1) 89.41(19); C(3)–Pd(1)–Cl(1) 90.42(19); P(1)–Pd(1)–Cl(1) 170.10(8); C(3)–Pd(1)–Cl(1)#1 164.9(2); P(1)–Pd(1)–Cl(1)#1 100.45(7); Cl(1)–Pd(1)–Cl(1)#1 81.83(7) and C(2)–Co(1)–C(1) 40.3(3); C(2)–Co(2)–C(1) 40.7(3); C(1)–P(1)–Pd(1) 104.3(2); Pd(1)–Cl(1)–Pd(1)#1 96.60(7); C(2)–C(1)–P(1) 123.2(5); C(2)–C(1)–Co(2) 69.5(4); C(2)–C(1)–Co(1) 68.4(4); Co(2)–C(1)–Co(1) 77.5(3); C(1)–C(2)–C(4) 128.8(7); Co(2)–C(2)–Co(1) 78.5(3); P(2)–C(45)–P(3) 110.8(4).

be presented in solution. Crystal structure of **3** only represents one of the two isomeric forms.

The authors have previously reported the preparation of a novel palladium complex *cis*-dichloride(1,2-bis(diphenylphosphino)vinyl-P,P′,C)palladium(II)–(bis(diphenyl phosphino)methane-P,P′)cobaltacarbonyl (**5**). It was obtained from the treatment of $(\mu\text{-}Ph_2PCH_2PPh_2)Co_2(CO)_4$-$((\mu,\eta\text{-}Ph_2PC{\equiv}CPPh_2)\text{-}\kappa^2P,P')PdCl_2$ (**4**) with hydrochloric acid (Scheme 4) [7]. This complex can be regarded as an unique derivative of the well known compound, $PdCl_2$(dppe) [8]. Nevertheless, there was no sign of forming a doubly chloride-bridged palladium dimer **6** from the reaction of **4** with LiCl.

2.2. Suzuki reactions using 2

Palladium-catalyzed Suzuki reactions of bromobenzenes with phenylboronic acid were carried out by employing **2** as a catalyst precursor (Scheme 5). The general procedures for the catalytic reactions under investigation are described as follows. A suitable Schlenk tube was charged with 1.0 mmol of bromobenzene, 1.5 mmol of phenylboronic acid, 1.0 ml THF, 3.0 mmol KF and 1.0 mol% of **2**. The reaction mixture was stirred at 60 °C for 3–19 h followed by a work-up (Diagram 1). A satisfactory result was obtained only when the reaction time was 19 h.

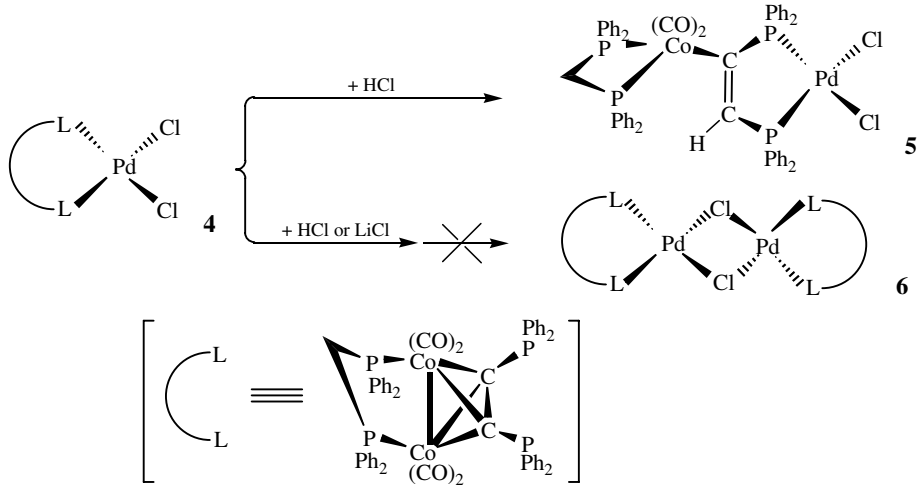

Scheme 4.

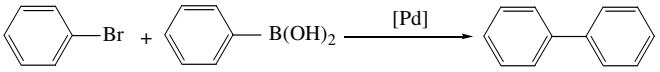

Scheme 5.

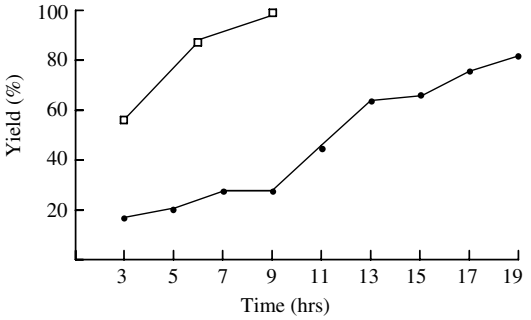

Diagram 1. The dependence of yield of the Suzuki coupling reactions employing **2** (in ●) and **3** (in □) on reaction hours.

Subsequently, the impact of various solvents used in the reaction was evaluated. As shown, the reaction rate is greatly affected by the kind of solvent used (Table 2). For instance, the coupling reaction was ineffective when DMF was used (entry 4). However, the yield was greatly improved when 1,4-dioxane was employed as solvent (entry 5).

It is well-known that the choice of a base is crucial to the success of a palladium-catalyzed Suzuki reaction [9]. Therefore, the influences of the bases used on the reactions were examined (Table 3). As shown, excellent yields were observed when alkaline metal fluorides such as KF and CsF (entries 1and 2) as well as NaO^{t}Bu and K_3PO_4 (entries 4 and 6) were used as bases. The yields were lower when NaOH and K_2CO_3 were employed as bases under the same reaction condition (entries 3 and 5). Amine derived bases such as morpholine, NEt_3 and piperidine failed to promote the reactions resulting in very low yields (entries 7–9).

Table 2
Suzuki coupling reactions employing **2** in various solvents[a]

Entry	Solvent	Yield (%)[d]
1	THF	82.7[c]
2	toluene	43.1[b]
3	DME	78.2[b]
4	DMF	25.9[b]
5	1,4-dioxane	93.7[b]
6	CH_3CN	68.4[b]
7	H_2O	48.3[b,e]

[a] *Condition*: 1.0 mmol bromobenzene, 1.5 mmol phenylboronic acid, 1.0 mol% **2**, 1.0 ml solvent, 3.0 mmol KF, 60 °C, 19 h.
[b] Isolated yield.
[c] Determined by GC.
[d] Average of two runs.
[e] 0.2 mmol TBAB added.

Table 3
Suzuki coupling reactions employing **2** with various bases[a]

Entry	Base	Yield (%)[b]
1	KF	93.7
2	CsF	99.7
3	NaOH	75.9
4	NaO^{t}Bu	99.2
5	K_2CO_3	82.7
6	K_3PO_4	96.7
7	morpholine	3.1
8	NEt_3	31.5
9	piperidine	7.2

[a] *Condition*: 1.0 mmol bromobenzene, 1.5 mmol phenylboronic acid, 1.0 mol% **2**, 1.0 ml 1,4-dioxane, 3.0 mmol base, 60 °C, 19 h.
[b] Isolated yield; average of two runs.

2.3. Suzuki reactions using 3

For comparison, the same Suzuki reactions were carried out by employing **3** as the catalyst precursor. The general procedures for the catalytic reactions under investigation are described as follows. A suitable Schlenk tube was charged with 1.0 mmol of bromobenzene, 1.5 mmol of phenylboronic acid, 1.0 ml THF, 3.0 mmol KF and 0.5 mol% of **3**. The reaction mixture was stirred at 60 °C for 3–9 h followed by a work-up. As shown in Diagram 1, the catalytic efficiencies were much better than in the

Table 4
Suzuki coupling reactions employing **3** in various solvents[a]

Entry	Solvent	Yield (%)[d]
1	THF	85.1[b]
2	toluene	62.5[c]
3	DME	16.2[c]
4	DMF	31.0[c]
5	1,4-dioxane	94.8[c]
6	CH_3CN	38.9[c]
7	H_2O	52.9[c,e]

[a] *Condition*: 1.0 mmol bromobenzene, 1.5 mmol phenylboronic acid, 0.5 mol% **3**, 3.0 mmol KF, 60 °C, 1.0 ml solvent, 6 h.
[b] Determined by GC.
[c] Isolated yield.
[d] Average of two runs.
[e] 0.2 mmol TBAB added.

Table 5
Suzuki coupling reaction employing **3** with various bases[a]

Entry	Base	Yield[b]
1	KF	94.8
2	CsF	99.1
3	K_3PO_4	25.9
4	K_2CO_3	30.1
5	NaOH	36.6
6	NaO*t*-Bu	55.9
7	morpholine	23.3
8	NEt_3	19.8
9	piperidine	4.1

[a] *Condition*: 1.0 mmol bromobenzene, 1.5 mmol phenylboronic acid, 0.5 mol% **3**, 3.0 mmol base, 60 °C, 1.0 ml 1,4-dioxane, 6 h.
[b] Isolated yield; average of two runs.

Table 6
Suzuki coupling reactions under various substrate/**3** ratios[a]

Entry	**3** (mmol%)	Yield (%)[b]
1	0.5	99.1
2	0.25	97.3
3	0.1	91.2
4	0.05	85.9

[a] *Condition*: 1.0 mmol bromobenzene, 1.5 mmol phenylboronic acid, 3.0 mmol CsF, 60 °C, 1.0 ml 1,4-dioxane, 6 h.
[b] Isolated yield; average of two runs.

previous case when **2** was employed. With **3** it takes a shorter reaction time to reach the same conversion. As known, the halide bridging bond is intrinsically weak in dimer. It is ready to break and form an unsaturated palladium monomer. The latter is presumably an active species that promptly accepts the oncoming substrate(s) for further catalytic reaction.

The effect of the solvent used was evaluated as well (Table 4). The procedures for Suzuki reactions were the same as previously mentioned. Again, the best yield was observed using 1,4-dioxane as a solvent (entry 5). It is in accord with the previous case (Table 2).

The influences of the bases used on the reactions were examined next (Table 5). As shown, excellent yields were observed when alkaline metal fluorides KF and CsF were used as bases (entries 1 and 2). Other bases, especially amines, were much less effective (entries 3–9).

The Suzuki coupling reactions with various substrate/catalyst loading ratios (0.5–0.05 mol% **3**) were also examined (Table 6). A reasonable yield was achieved even when 0.05 mol% **3** was employed.

The following table shows the results from the **3**-assisted Suzuki cross-coupling reactions (Table 7). The catalytic performance was good for the substrate with electron-withdrawing group (entries 6–8). Nevertheless, the efficiency was low for the substrate with electron-donating group (entries 2 and 3). It is consistent with the general observation for the palladium-catalyzed Suzuki reaction.

Table 7
Suzuki coupling reactions employing **3** under various substrate[a]

Entry	Subtract	Temperatue (°C)	Yield (%)[b]
1	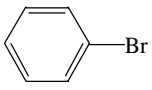	50 60	83.9 89.7
2	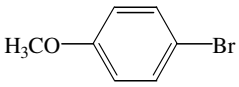	50 60	14.7 62.8
3	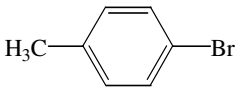	50 60	17.7 71.5
4	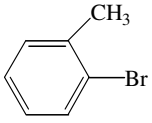	50 60	2.5 50.3
5	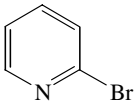	50 60	4.4 40.1
6	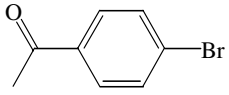	50 60	83.1 91.2
7	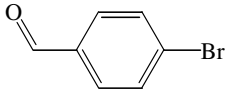	50 60	87.3 95.1
8	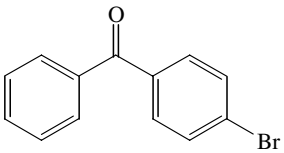	50 60	87.9 96.8

[a] *Conditions*: 1.00 mmol phenylbromide, 1.50 mmol phenylboronic acid, 3.00 equiv. CsF, 0.05 mol% **3**, 1.0 mL 1,4-dioxane, 5 h, 50 °C.
[b] Averaged by two runs; isolated yield.

3. Concluding remarks

We have demonstrated that the Suzuki reactions of aryl bromides with phenylboronic acid could be carried out catalytically with two novel palladium complexes **2** and **3**. The catalytic performance is better with **3** probably due to its readiness to form the unsaturated active monomer.

4. Experimental

4.1. General

All manipulations were carried out under a dry nitrogen atmosphere. All solvents including deuterated solvents were purified before use. All separations of the products were performed by Centrifugal Thin Layer Chromatography (CTLC, Chromatotron, Harrison model 8924). ^{1}H NMR spectra were recorded (Varian VXR-300S spectrometer) at 300.00 MHz; chemical shifts are reported in ppm relative to internal $CHCl_3$ or CH_2Cl_2. ^{31}P and ^{13}C NMR spectra were recorded at 121.44 and 75.46 MHz, respectively. Some other routine ^{1}H NMR spectra were recorded on Gemini-200 spectrometer at 200.00 MHz or Varian-400 spectrometer at 400.00 MHz. Mass spectra were recorded on JOEL JMS-SX/SX 102A GC/MS/MS spectrometer. Elemental analyses were obtained on Heraeus CHN-O-S-Rapid.

4.2. Synthesis of 3

A 100 cm^3 round-bottomed flask was charged with 1.00 mmol (1.025 g) (μ-$PPh_2CH_2PPh_2$)$Co_2(CO)_4$(μ,η-(tBu)$_2$PC$\equiv$CC_6H_4-κC^1)Pd(μ-OAc) **2** and one molar equivalent of LiCl (0.0424 g) as well as 15 ml of toluene. The mixture was stirred at 25 °C for 72 h. Subsequently, purification of products using centrifugal thin-layer chromatography (CTLC) was carried out. The first band, brown in color, was eluted out by a mixture solvent of

CH_2Cl_2/ethyl acetate (10/1). It was identified as the title compound $\{(\mu\text{-}PPh_2CH_2PPh_2)Co_2(CO)_4(\mu,\eta\text{-}(t\text{Bu})_2PC{\equiv}CC_6H_4\text{-}\kappa C^1)Pd(\mu\text{-}Cl)\}_2$ (**3**). The yield of **3** is 75% (0.1503 g, 0.750 mmol).

3: ^{1}H NMR (C_6D_6, δ/ppm): 1.37 (t, $J_{P-H} = 30.0$, 36H, $-C(CH_3)_3$), 3.34, 3.50 (m, 2H, dppm), 6.71–7.46 (m, 46H, arene), 8.52 (d, $J_{H-H} = 6.8$, 1H, *o*-hydrogen of the orthometallated arene), 8.69 (d, $J_{H-H} = 7.2$, 1H, *o*-hydrogen of the orthometallated arene); ^{13}C NMR (C_6D_6, δ/ppm): 30.5 (d, 12C, $C(CH_3)_3$), 39.0 (d, 4C, $C(CH_3)_3$), 40.8 (s, 2C, CH_2), 73.8 (d, 4C, $PhC{\equiv}CP(t\text{-}Bu)_2$), 124.6–146.9 (m, 56C, arene), 146.0 (s, 2C, *ipso* of arene), 158.4 (d, 2C, *ipso* of arene), 202.8–207.0 (m, 8C, CO); ^{31}P NMR (C_6D_6, δ/ppm): 38.0 (dd, $J_{P-P} = 109.9$, 2P, dppm), 41.4 (t, $J_{P-P} = 86.1$, 2P, dppm), 82.9 (s, 1P, $P(t\text{-}Bu)_2$), 84.4 (s, 1P, $P(t\text{-}Bu)_2$). *Anal.* Calc. for **3**: C, 41.60; H, 4.07. Found: C, 41.59; H, 4.04%. M.S.: *m*/*z* 696 (M^+).

4.3. General procedures for the Suzuki cross-coupling reactions

Suzuki cross-coupling reactions were performed according to the following procedures. Complex **3** (10.02 mg, 0.005 mmol), boronic acid (0.183 g, 1.500 mmol) and potassium fluoride (0.174 g, 3.0 mmol) were placed into a 20 ml Schlenk flask. The flask was evacuated and backfilled with nitrogen before adding THF (1 ml) and bromobenzene (0.11 ml, 1.000 mmol). The solution was stirred at 60 °C for 6 h. Subsequently, excess amount of water was added and the product was extracted with ether (2×30 ml). The combined organic extracts were dried over anhydrous $MgSO_4$ and concentrated under vacuum. The crude residue was purified by flash chromatography on silica gel or gas chromatography.

4.4. X-ray crystallographic studies

Suitable crystals of **3** were sealed in thin-walled glass capillaries under nitrogen atmosphere and mounted on a Bruker AXS SMART 1000 diffractometer. Intensity data were collected in 1350 frames with increasing ω (width of 0.3° per frame). The absorption correction was based on the symmetry equivalent reflections using SADABS program. The space group determination was based on a check of the Laue symmetry and systematic absences, and was confirmed using the structure solution. The structure was solved by direct methods using a SHELXTL package [10]. All non-H atoms were located from successive Fourier maps and the hydrogen atoms were refined using a riding model. Anisotropic thermal parameters were used for all non-H atoms and fixed isotropic parameters were used for H atoms.[1] Crystallographic data of **3** are summarized in Table 1.

[1] The hydrogen atoms were ride on carbons or oxygen atoms in their idealized positions and held fixed with the C–H distances of 0.96 Å.

Acknowledgement

We thank the National Science Council of the ROC (Grant NSC-94-2113-M-005-011) for the financial support.

Appendix A. Supplementary data

Crystallographic data for the structural analysis of compound **3** have been deposited with the Cambridge Crystallographic Data Center, CCDC no. 293127. Copies of this information may be obtained free of charge from the Director, CCDC, 12 Union Road, Cambridge CB2 1EZ, UK, fax: +44 1223 336 033, e-mail: deposit@ccdc.cam.ac.uk or www:http://www.ccdc.cam.ac.uk. Supplementary data associated with this article can be found, in the online version, at doi:10.1016/j.poly.2006.07.005.

References

[1] (a) T.E. Barder, S.D. Walker, J.R. Martinelli, S.L. Buchwald, J. Am. Chem. Soc. 127 (2005) 4685;
(b) S.D. Walker, T.E. Barder, J.R. Martinelli, S.L. Buchwald, Angew. Chem., Int. Ed. 43 (2004) 1871;
(c) W. Tang, X. Zhang, Chem. Rev. 103 (2003) 3029;
(d) Q.-S. Hu, Y. Lu, Z.-Y. Tang, H.-B. Yu, J. Am. Chem. Soc. 125 (2003) 2856;
(e) T.E. Pickett, F.X. Roca, C.J. Richards, J. Org. Chem. 68 (2003) 2592;
(f) Z.-Y. Tang, Y. Lu, Q.-S. Hu, Org. Lett. 5 (2003) 297;
(g) J. Hassan, M. Sévingnon, C. Gozzi, E. Schulz, M. Lemaire, Chem. Rev. 102 (2002) 1359;
(h) N. Kataoka, Q. Shelby, J.P. Stambuli, J.F. Hartwig, J. Org. Chem. 67 (2002) 5553;
(i) J.G. Planas, J.A. Gladysz, Inorg. Chem. 41 (2002) 6947;
(j) N.G. Andersen, B.A. Keay, Chem. Rev. 101 (2001) 997;
(k) C.A. Bessel, P. Aggarwal, A.C. Marschilok, K.J. Takeuchi, Chem. Rev. 101 (2001) 1031;
(l) A.F. Littke, C. Dai, G.C. Fu, J. Am. Chem. Soc. 122 (2000) 4020;
(m) J.F. Hartwig, Angew. Chem., Int. Ed. 37 (1998) 2046;
(n) G. Mann, J.F. Hartwig, J. Am. Chem. Soc. 118 (1996) 13109.
[2] (a) S. Eichenseher, O. Delacroix, K. Kromm, F. Hampel, J.A. Gladysz, Organometallics 24 (2005) 245;
(b) O. Delacroix, J.A. Gladysz, Chem. Commun. (2003) 665;
(c) K. Kromm, F. Hampel, J.A. Gladysz, Organometallics 21 (2002) 4264.
[3] (a) R.C.J. Atkinson, V.C. Gibson, N.J. Long, Chem. Soc. Rev. 33 (2004) 313;
(b) T.J. Colacot, Chem. Rev. 103 (2003) 3101.
[4] (a) F.-E. Hong, Y.-J. Ho, Y.-C. Chang, Y.-L. Huang, J. Organomet. Chem. 690 (2005) 1249;
(b) C.-P. Chang, Y.-L. Huang, F.-E. Hong, Tetrahedron 61 (2005) 3835;
(c) Y.-C. Chang, F.-E. Hong, Organometallics 24 (2005) 5686;
(d) F.-E. Hong, Y.-C. Chang, C.-P. Chang, Y.-L. Huang, Dalton Trans. (2004) 157;
(e) F.-E. Hong, Y.-J. Ho, Y.-C. Chang, Y.-C. Lai, Tetrahedron 60 (2004) 2639;
(f) F.-E. Hong, C.-P. Chang, Y.-C. Chang, Dalton Trans. (2003) 3892;
(g) F.-E. Hong, Y.-C. Lai, Y.-J. Ho, Y.-C. Chang, J. Organomet. Chem. 688 (2003) 161;
(h) F.-E. Hong, Y.-C. Chang, R.-E. Chang, S.-C. Chen, B.-T. Ko, Organometallics 21 (2002) 961.
[5] J.-C. Lee, M.-G. Wang, F.-E. Hong, Eur. J. Inorg. Chem. (2005) 5011.

[6] (a) A.T. Blomquist, P.M. Maitlis, J. Am. Chem. Soc. 84 (1962) 2329;
(b) P.M. Maitlis, M.L. Games, Can. J. Chem. 42 (1964) 183;
(c) J. Dupont, C.S. Consorti, J. Spencer, J. Chem. Rev. 105 (2005) 2527;
(d) M. Prashad, X.Y. Mak, Y. Liu, O. Repic, J. Org. Chem. 68 (2003) 1163;
(e) K. Yuan, T.K. Zhang, X.L. Hou, J. Org. Chem. 70 (2005) 6085.
[7] C.-P. Chang, F.-E. Hong, J. Chin. Chem. Soc. 52 (2005) 1105.
[8] (a) P. Collman, L.S. Hegedus, J.R. Norton, R.G. Finke, Principles and Applications of Organotransition Metal Chemistry, University Science Books, Mill Valley, CA, 1987 (Chapter 3);
(b) R.J. Puddephatt, Chem. Soc. Rev. 12 (1983) 99.
[9] (a) N. Miyaura, K. Yamada, H. Suginome, A. Suzuki, J. Am. Chem. Soc. 107 (1985) 972;
(b) G.A. Grasa, A.C. Hillier, S.P. Nolan, Org. Lett. 3 (2001) 1077;
(c) S.R. Dubbaka, P. Vogel, Org. Lett. 6 (2004) 95.
[10] G.M. Sheldrick, SHELXTL PLUS User's Manual. Revision 4.1 Nicolet XRD Corporation, Madison, WI, USA, 1991.

[11] and hexacatenar 4,4′-disubstituted 2,2′-bipyridines [12] as ligands.

In this paper we report on the structural features of bis-dithiocarboxylate complexes of zinc. The focus of this study is on the role of 2,5-disubstituted thiophene as a chain-director being part of a dithiocarboxylate ligand and whether this can have an effect on the liquid-crystalline properties of zinc complexes. Unlike *p*-substituted dithiobenzoate ligands that afford linear rods, the presence of thiophene results in the formation of small kinks in the chains. An interesting field of recent research deals with bent-shaped molecules that can exhibit either columnar or lamellar mesophases [13]. The 2,5-disubstituted thiophene derivatives reported by Swager [14] displayed an antiparallel bent-rod structure resulting from the disubstituted thiophene and alkyl chains. However, a hexagonal columnar phase was observed because of the symmetrically substituted benzene molecules at the end of the chains. There is some controversy over claims that 2,5-disubstituted 5-membered heterocycles display bent-core and not conventional calamitic liquid crystal behaviour.

In this study, thiophene-containing ligands is used in four coordinated complexes of zinc and the structural features resulting from the five-membered thiophene rings should display a ''step-rod'' type of structure. In addition, the thiophene unit can electronically affect the coordination properties of dithiocarboxylato ligands by π-delocalization in a similar fashion as observed in thienyl carbene complexes [15].

2. Experimental

2.1. General

All commercially available chemicals were used as received. Solvents were dried and distilled under nitrogen prior to use. Diethyl ether, tetrahydrofuran and hexane were distilled from sodium metal, with benzophenone as indicator in the case of the etheral solvents. Dichloromethane was distilled from phosphorus pentoxide. Thiophene was purified as described by Spies and Angelici [16]. Reactions were performed in an inert atmosphere of either nitrogen or argon using standard Schlenk and vacuum-line techniques. Column chromatography was carried out under a nitrogen atmosphere using silica gel (particle size 0.063–0.200 nm) as stationary phase. All other reagents were purchased from commercial suppliers and used without further purification. All NMR spectra were recorded in degassed deuterated chloroform on a Bruker ARX-300 spectrometer. Chemical shifts were referenced to chloroform. ^{1}H and ^{13}C NMR spectra were measured at 300.133 and 75.469 MHz, respectively. Infrared spectra were recorded on a Perkin–Elmer Spectrum RX1 FT-IR spectrophotometer with a NaCl cell using hexane as solvent. Melting points were recorded on a hot stage Gallenkamp melting point apparatus and are uncorrected. Liquid-crystalline properties were examined on a differential scanning calorimeter (DSC) Q 100 V8.2 Build 268 and Hot-stage Polarising Optical Microscope (POM) Olympus BX60 equipped with a Linkam THMS600 hot stage and a Linkam TMS93 programmable temperature controller.

2.2. Synthesis

2.2.1. Synthesis of the 5-alkyl-2-thiophenedithiocarboxylate ligands ($RTCS_2^-$)

(a) Preparation of 2-alkylthiophene (RT). The procedure used was similar to the one described by Brandsma [17]. *n*-Butyl lithium (15.6 ml, 25.0 mmol) was added to a mixture of THF (50.0 ml) and hexane (30.0 ml), which was cooled to −20 °C. Thiophene (1.68 g, 20.0 mmol) was introduced over 10 min with cooling between 0 °C and 10 °C. The cooling bath was removed and the mixture allowed to warm to room temperature. The alkyl bromide (2.74 g for butyl bromide, 20.0 mmol) was added in one portion without external cooling. The temperature of the solution was raised to 50 °C and kept at this temperature for a further 30 min. The rest of the procedure was carried out in air. Ice water (100 ml) was added with vigorous stirring. Two separate layers formed and were separated. Two further extractions of the aqueous phase with 20 ml diethyl ether gave a combined organic solution that was dried over anhydrous $MgSO_4$. The mixture was concentrated in a rotary evaporator to afford the crude product. Yield = 2.38 g; 85% for R = butyl and in the range 78–89% for the other R groups.

(b) Preparation of 5-alkyl-2-thiophenedithiocarboxylic acid ($RTCS_2H$). *n*-Butyl lithium (12.5 ml, 20.0 mmol) was added to a solution of THF (50.0 ml) and hexane (30.0 ml), which was cooled to −20 °C. 2-Alkyl thiophene (R = butyl, 2.38 g, 17.0 mmol) was introduced over 10 min with cooling between 0 °C and 10 °C. The cooling bath was removed and the mixture warmed to room temperature while being stirred for a further 10 min. The solution was cooled to 0 °C and copper(I) bromide (0.1 g) added. Carbon disulfide (1.29 g, 17.0 mmol) was added drop-wise to the stirred mixture. The colour of the reaction mixture changed to deep-red. The cooling bath was removed and the mixture was allowed to reach room temperature while stirring was continued for a further 1 h. Ice water (100.0 ml) was added followed by dilute hydrochloric acid (20.0 ml, 1 mol/dm^3). The organic layer was separated in air and the product extracted into diethyl ether (70.0 ml) and washed with 2 × 50.0 ml of water. The product was dried over $MgSO_4$ and the solvent removed *in vacuo*. Yield = 3.30 g; 89.8% for R = butyl and in the range of 69–90% for the other R groups.

(c) Preparation of sodium 5-alkyl-2-thiophenedithiocarboxylate ($RTCS_2Na$). Sodium metal (0.35 g, 15.28 mmol) was added over 10 min to vigorously stirred methanol (50.0 ml). When all the sodium had dissolved, additional (20.0 ml) methanol was added. 5-Alkyl-2-thiophenedithiocarboxylic acid (for R = butyl, 3.30 g, 15.28 mmol) was added over 5 min to the mixture and left stirring for

30 min. The solvent was removed under reduced pressure, affording the sodium 5-alkyl-2-thiophenedithiocarboxylate as an orange-brown solid. Yield = 3.09 g (85%) for R = butyl and in the range 72–88% for the other R groups.

2.2.2. Synthesis of the bis-5-alkyl-2-thiophenedithiocarboxylato complexes $[Zn_2(S_2CTR)_4]$

The procedure was similar to that of Adams et al. [9], who prepared dithiobenzoate complexes. A colourless solution of $ZnCl_2$ (0.41 g, 3.0 mmol) in water (10.0 ml) was added to a stirred solution of sodium 5-alkyl-2-thiophenedithiocarboxylate (for R = butyl, 1.55 g, 6.5 mmol) in water (25.0 ml) at room temperature. The colour of the solution turned orange-brown and the mixture was left to stir for 3 h. The mixture was concentrated to 25.0 ml on a rotary evaporator and 20.0 ml of methanol was added. The precipitate was separated by filtration and dried. The product, an oily solid, was purified on a silica gel column with hexane as the initial eluent. The first fraction, on evaporation, afforded an oily red liquid that consisted of a mixture of organic products containing carbon disulfides. The desired product was eluted from the column with a solvent mixture hexane:CH_2Cl_2 (1:1). Orange powder was obtained on evaporation of the solvent. Yield = 0.49 g, 33% for R = butyl and in the range 29–37% for the other R groups.

Five complexes, tetra(5-alkyl-2-thiophenedithiocarboxylato)dizinc(II), $[Zn_2(S_2CTR)_4]$, were synthesized by using different alkyl bromide derivatives as precursors, C_4H_9 (**1**), C_6H_{13} (**2**), C_8H_{17} (**3**), $C_{12}H_{25}$ (**4**) and $C_{16}H_{33}$ (**5**). The atomic numbering scheme used for the NMR data is shown below

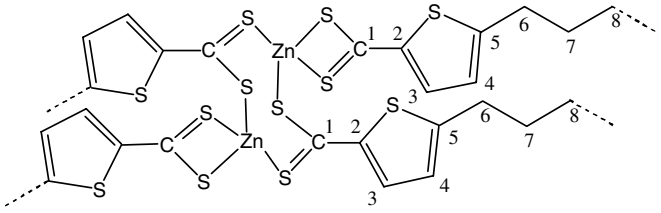

*Complex **1**:* Orange solid; m.p. 132 °C; Yield: 33%. ^{1}H NMR (δ/ppm in $CDCl_3$; J/Hz): 7.87 (d, 2H, H3, $J = 3.9$), 6.83 (d, 2H, H4, $J = 3.6$), 2.82 (t, 4H, H6, $J = 7.5$), 1.66 (m, 4H, H7), 1.42 (m, 4H, H8), 0.92 (t, 6H, H9, $J = 7.2/7.5$). ^{13}C NMR (δ/ppm in $CDCl_3$): 208.0 (C1), 161.8 (C2), 153.9 (C5), 134.6 (C3), 127.5 (C4), 33.2, 29.8, 22.1, 13.7 (C6–C9).

*Complex **2**:* Orange solid; m.p. 119 °C; Yield: 46%. ^{1}H NMR (δ/ppm in $CDCl_3$; J/Hz): 7.87 (d, 2H, H3, $J = 3.9$), 6.83 (d, 2H, H4, $J = 3.9$), 2.81 (t, 4H, H6, $J = 7.5$), 1.69 (m, 4H, H7), 1.30 (m, 12H, H8–H10), 0.87 (t, 6H, H11, $J = 6.7$). ^{13}C NMR (δ/ppm in $CDCl_3$): 207.0 (C1), 162.5 (C2), 148.7 (C5), 135.2 (C3), 128.0 (C4), 31.8, 31.5, 31.4, 29.0, 22.9, 14.4 (C6–C11).

*Complex **3**:* Orange solid; m.p. 102 °C; Yield: 52%. ^{1}H NMR (δ/ppm in $CDCl_3$): 7.87 (d, 2H, H3, $J = 3.9$), 6.82 (d, 2H, H4, $J = 3.9$), 2.80 (t, 4H, H6, $J = 7.5/7.8$), 1.69 (m, 4H, H7), 1.26 (m, 20H, H8–H12), 0.87 (t, 6H, H13, $J = 6.7/7.0$). ^{13}C NMR (δ/ppm in $CDCl_3$; J/Hz): 207.5 (C1), 162.1 (C2), 148.3 (C5), 134.8 (C3), 127.6 (C4), 31.8, 31.1, 30.6, 29.2, 29.1, 29.0, 22.6, 14.0 (C6–C13).

*Complex **4**:* Orange solid; m.p. 84 °C; Yield: 38%. ^{1}H NMR (δ/ppm in $CDCl_3$): 7.85 (d, 2H, H3, $J = 3.9$), 6.81 (d, 2H, H4, $J = 3.9$), 2.79 (t, 4H, H6, $J = 7.5$), 1.68 (m, 4H, H7), 1.23 (m, 36H, H8–H16), 0.85 (t, 6H, H17, $J = 6.2/7.0$). ^{13}C NMR (δ/ppm in $CDCl_3$; J/Hz): 206.8 (C1), 161.6 (C2), 134.3 (C5), 128.8 (C3), 127.5 (C4), 35.7, 31.9, 31.1, 30.9, 29.7, 29.6, 29.4, 29.2, 29.0, 26.4, 22.7, 14.1 (C6–C17).

*Complex **5**:* Orange solid; m.p. 52 °C; Yield: 32%. ^{1}H NMR (δ/ppm in $CDCl_3$; J/Hz): 7.86 (d, 2H, H3, $J = 3.9$), 6.82 (d, 2H, H4, $J = 4.1$), 2.80 (t, 4H, H6, $J = 7.5$), 1.67 (m, 4H, H7), 1.24 (m, 52H, H8–H20), 0.86 (t, 6H, H21, $J = 6.5/6.7$). ^{13}C NMR (δ/ppm in $CDCl_3$): 207.4 (C1), 161.5 (C2), 153.9 (C5), 134.2 (C3), 127.5 (C4), 31.9, 31.3, 31.1, 30.8, 30.7, 30.5, 29.8, 29.7, 29.6, 29.5, 29.3, 29.2, 29.0, 26.4, 22.7, 14.1 (C6–C21).

2.3. Crystallography

Re-crystallization from a saturated dichloromethane solution layered by hexane gave red needles of **2** suitable for X-ray diffraction studies. Data were collected at 20 °C by means of a combination of ϕ and ω scans on a Bruker (Siemans) P4 diffractometer, fitted with a SMART [18] 1K CCD detector, using graphite-monochromated, Mo Kα radiation. Semi-empirical absorption corrections, derived from multiple scanning of equivalent reflections, were applied using SADABS [18]. All hydrogen atom positions were obtained from a difference Fourier map and were refined. All non-hydrogen atoms were refined with anisotropic displacement parameters, all hydrogen atoms were refined with isotropic displacement parameters. Cell refinement and data reduction were performed using SAINT [18]. The structure was solved using SHELXTL [18] and refined using SHELXTL and SHELXL97 [19]. Structure graphics were prepared using ORTEP-3 [20], POV-RAY [21] and Mercury [22] software. Crystal data and other experimental procedures and refinement parameters are given in Table 1.

3. Results and discussion

Five complexes of the type $[Zn_2(S_2CTR)_4]$ (where T = 2,5-disubstituted thiophene, R = alkyl group; C_4H_9 (**1**), C_6H_{13} (**2**), C_8H_{17} (**3**), $C_{12}H_{25}$ (**4**), $C_{16}H_{33}$ (**5**)) were synthesized via a four-step reaction route as shown in Scheme 1.

The sodium 5-alkyl-2-thiophenedithiocarboxylate precursors were synthesized according to the literature procedures [17]. The final step was similar to that used by Adams

Table 1
Crystal data and structure refinement data for $[Zn_2(S_2CTC_6H_{13})_4]$ (**2**)

Empirical formula	$C_{44}H_{60}S_{12}Zn_2$
Formula weight	1104.54
Temperature (K)	293(2)
Wavelength (Å)	0.71073
Crystal system	monoclinic
Space group	*C*2/*c*
Unit cell dimensions	
a (Å)	29.1118(19)
b (Å)	6.4571(4)
c (Å)	28.8391(19)
α (°)	90
β (°)	112.5790(10)
γ (°)	90
Volume (Å^3)	5005.6(6)
Z	4
D_{calc} (Mg/m^3)	1.465
Absorption coefficient (mm^{-1})	1.490
F(000)	2304
Crystal size (mm^3)	$0.34 \times 0.14 \times 0.05$
θ Range for data collection (°)	2.53–26.50
Index ranges	$-36 \leqslant h \leqslant 14$, $-7 \leqslant k \leqslant 7$, $-35 \leqslant l \leqslant 35$
Reflections collected	12744
Independent reflections (R_{int})	4712 (0.0354)
Completeness to $\theta = 25.00°$ (%)	99.5
Absorption correction	semi-empirical from equivalents
Maximum and minimum transmission	0.928 and 0.734
Refinement method	full-matrix least-squares on F^2
Data/restraints/parameters	4712/0/382
Goodness-of-fit on F^2	1.082
Final *R* indices [$I > 2\sigma(I)$]	$R_1 = 0.0324$, $wR_2 = 0.0718$
R indices (all data)	$R_1 = 0.0582$, $wR_2 = 0.0838$
Extinction coefficient	0
Largest difference in peak and hole (e Å^{-3})	0.272 and −0.401

et al. for the preparation of the corresponding dithiobenzoate complexes [9]. It was also possible to obtain the products in a one-pot procedure by executing the first two steps at low temperature in THF and without the acidification. Solid zinc chloride was added in small portions to a −50 °C solution of the *in situ* prepared 5-alkyl-2-thiophenedithiocarboxylate. On removing the reaction mixture from a cold bath, the colour of the solution changed to red-brown. The solvent was removed under reduced pressure and purification was accomplished as previously described. The products **1**–**5** were obtained as orange powders and afforded red needles on re-crystallization. The complexes were characterized by NMR spectroscopy.

The chemical shifts recorded in the ^{1}H NMR spectra of **1**–**5** are all comparable, as one would expect from the very similar ligands in these complexes. Compared to thiophene, the signals assigned to H3 are 0.90 ppm (av.) more downfield than the corresponding protons in thiophene. The chemical shifts of the ^{1}H and ^{13}C NMR resonances in the spectra of thiophene are found for C2/C5 at 7.20 and 124.9 ppm and for C3/C4 at 6.96 and 126.7 ppm [23]. This demonstrates the electronic involvement of the thiophene ring in the complexes and reflects strong electron withdrawing effects of the coordinated and chelating carbon disulfide moieties. By contrast, the alkyl substituents in the 5-position display an inductive effect on the thiophene ring and the signal for H4 is shifted slightly upfield compared to the corresponding value in thiophene. Support for these results are found in the ^{13}C NMR spectra of the complexes with the coordinating-CS_2 (C1) carbon at 207 ppm and the thiophene *ipso*-carbon (C2) at 162 ppm, respectively. The infrared spectra of all the complexes are very similar and display peaks at 1046 and 980 cm^{-1} that were assigned to the C–S stretching frequencies of the dithiocarboxylate groups. Usually, the stretching frequencies of dithiocarboxylate complexes of Ni(II) and Zn(II) are observed between 900 and 1100 cm^{-1} [24].

3.1. Crystal structure of $[Zn_2(S_2CTC_6H_{13})_4]$ (2)

Crystals of **2** were grown from refrigerated solutions of **2** in dichloromethane and hexane using the solvent layering technique. The structure of **2** was confirmed by single crystal X-ray crystallography. An ORTEP + POV-Ray plot of the geometry of **2** with displacement ellipsoids set at 50% probability, is presented in Fig. 1. Computer generated

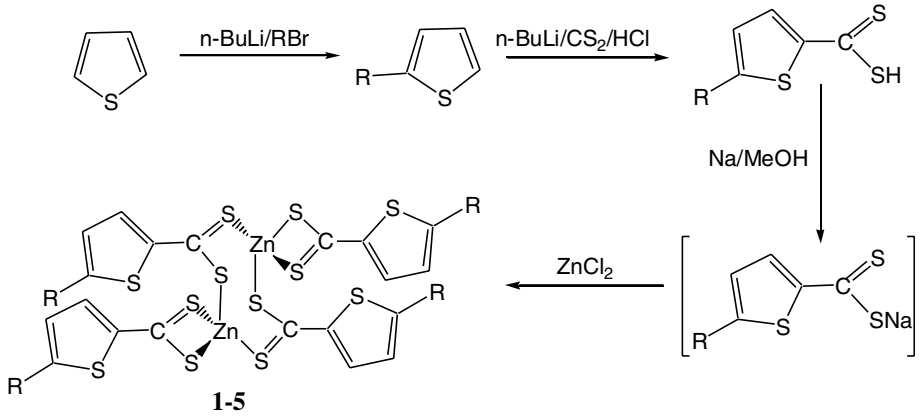

Scheme 1.

models [22] of two views of the structure of **2** are shown in Fig. 2 and a packing diagram in Fig. 3. Selected bond lengths and bond angles are listed in Table 2. Unlike the monomeric structure of $[Zn(S_2CPh)_2]$ [4] which displays a distorted tetrahedral geometry around the zinc, the structure for **2** is similar to those observed for 4-butyloxy and 4-octyloxy dithiobenzoates [9] and the dithio- [11] and diselenocarbamates [25]. Two zinc ions and four ligands form the structural unit. Each zinc ion has one bidentate dithiocarboxylate ligand, while the other two ligands bridge between the two zinc ions to form an eight membered ring.

One sulfur atom of one of the two chelate rings of two $[Zn(S_2CTC_6H_{13})_2]$ molecules is also coordinated through a lone electron pair to the second zinc centre. This represents a significantly longer Zn–S bond length of

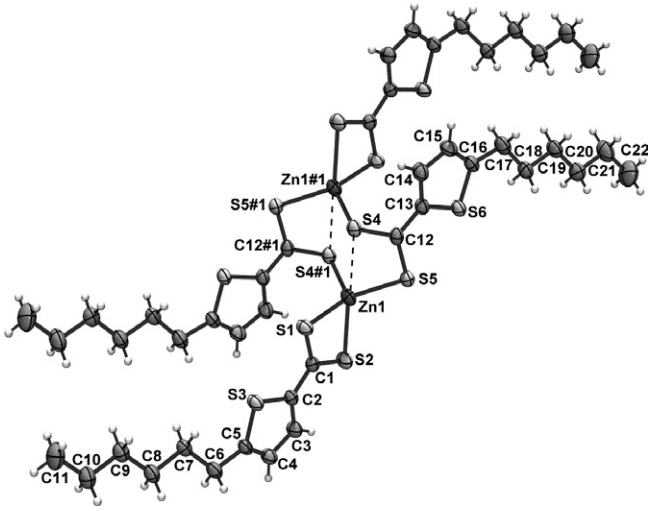

Fig. 1. An ORTEP + POV-Ray plot of the geometry of **2**. Displacement ellipsoids are set at 50% probability.

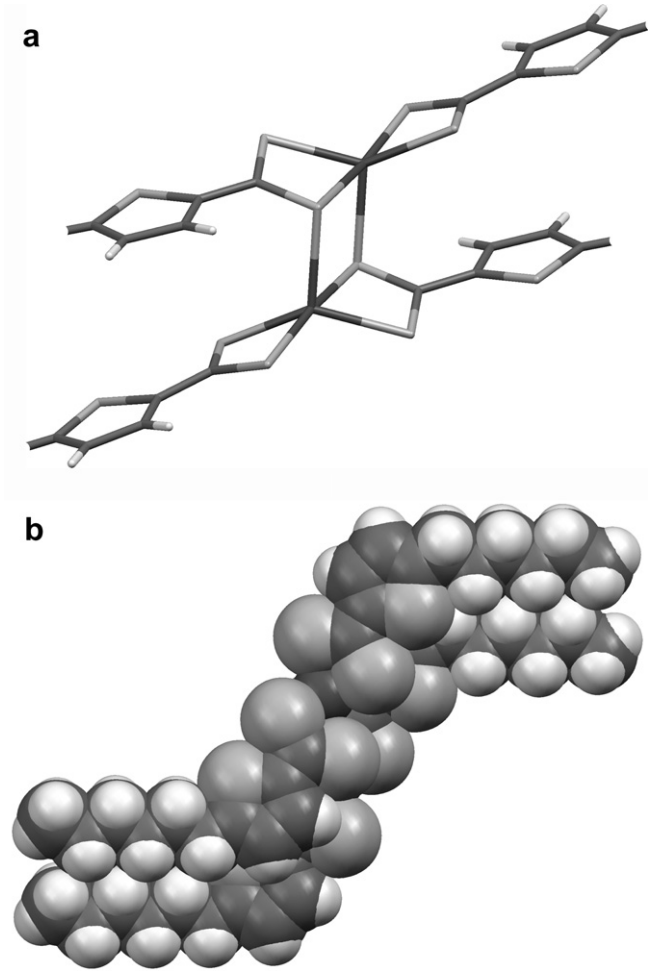

Fig. 2. View of molecule showing (a) the distorted trigonal bipyramidal arrangement of sulfur atoms around the zinc atoms and (b) a side-on view showing the "step-rod" assembly of atoms as a result of the five-member thiophene rings.

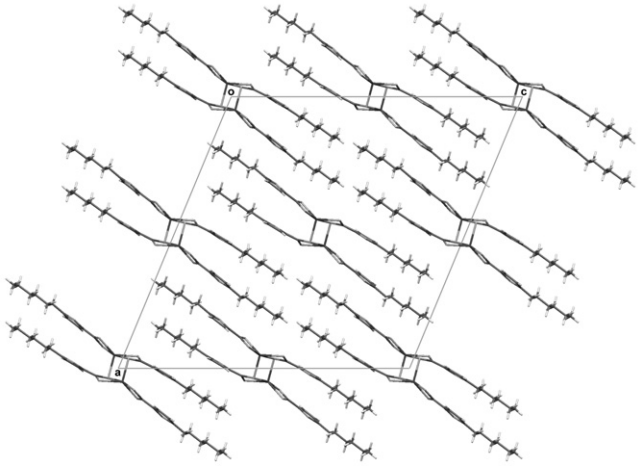

Fig. 3. Packing pattern of **2**.

Table 2
Selected bond lengths and bond angles for **2** and thiophene[a]

Bond length (Å)			
Zn1–S1	2.3697(7)	C1–C2	1.444(3)
Zn1–S2	2.4540(8)	C2–C3	1.371(4)
Zn1–S4	2.8840(8)	C3–C4	1.388(4)
Zn1–S4#1	2.3924(8)	C4–C5	1.362(4)
Zn1–S5	2.3543(8)	S6–C13	1.729(3)
S1–C1	1.701(3)	S6–C16	1.715(3)
S2–C1	1.690(3)	C12–C13	1.435(4)
S3–C2	1.727(3)	C13–C14	1.379(4)
S3–C5	1.721(3)	C14–C15	1.391(4)
S4–C12	1.723(3)	C15–C16	1.366(4)
S5–C12	1.683(3)		
Bond angle (°)			
S(1)–Zn(1)–S(2)	74.74(3)	S(5)–Zn(1)–S(2)	111.59(3)
S(1)–Zn(1)–S(4)	96.96(3)	S(5)–Zn(1)–S(4)#1	102.78(3)
S(1)–Zn(1)–S(4)	117.86(3)	C(5)–S(3)–C(2)	92.31(13)
S(2)–Zn(1)–S(4)	167.72(3)	C(1)–S(1)–Zn(1)	83.99(9)
S(4)#1–Zn(1)–S(2)	109.35(3)	C(1)–S(2)–Zn(1)	81.59(9)
S(4)–Zn(1)–S(4)	82.43(3)	C(12)–S(4)–Zn(1)	98.94(9)
S(5)–Zn(1)–S(1)	134.47(3)	C(12)–S(5)–Zn(1)	93.72(9)
S(5)–Zn(1)–S(4)	67.62(2)		

[a] The corresponding bond lengths and angles in thiophene are C2–S/C5–S 1.714(1) Å, C2–C3/C4–C5 1.370(2) Å, C3–C4 1.423(2) Å; C2–S–C5 = 92.2(1)°, S–C2–C3/S–C5–C4 = 111.5(3)°, C2–C3–C4/C5–C4–C3 = 112.5(3)° [26].

2.8840(8) Å (compared to an average value of 2.3926(8) Å for the other four Zn–S distances) in **2**. The geometry of sulfur atoms surrounding the zinc atom resembles a distorted trigonal bipyramidal rather than a square pyramidal structure (Fig. 2a). This is evident from three equidistant Zn–S bond distances (Zn–S1, Zn–S4#1 and Zn–S5) representing the equatorial plane of the trigonal bipyramid and the two longer Zn–S distances (Zn–S2 and Zn1–S4) for the sulfur atoms in the axial positions. As a result of the strain caused by the four-membered dithiocarboxylate chelate rings, the sulfur atoms are one in the axial and the other in an equatorial position. In the monomeric structure of $[Zn(S_2CPh)_2]$ the S–Zn–S′ angle of a chelate ring was 77°, giving a highly distorted tetrahedral geometry. The S2–Zn1–S4 angle in **2** is 167.7° and those in the equatorial plane 102.8°, 117.8° and 134.5° compared to a value of 172.4° and values of 102.5°, 115.3° and 140.5°, respectively, for the axial and equatorial positions in $[Zn_2(4\text{-bdtb})_4]$ (bdtb = butyloxydithiobenzoato) [9].

The C–S distance, C12–S4, of the bridging sulfur atoms of the dimeric structure in **2** is significantly longer than the other C–S distances which are comparable with the C–S distances in monomeric $[Zn(S_2CPh)_2]$ [4]. Important differences are observed in the bond distances of the thiophene rings compared to thiophene [26] and can be explained by electron delocalization outwards towards the coordinating CS_2-moiety compared to delocalization within the unsubstituted thiophene ring. Whereas the C–S distances and those of the double bonds in the rings are the same, the C3–C4 as well as the C14–C15 bond distances are significantly shorter in **2** compared to the corresponding distance in thiophene (1.423(2) Å).

The main structural difference between **2** and the linear, rod-like structures of the 1,4-substituted dithiobenzoates is the orientation of the alkyl chains with respect to the thiophene–metal–thiophene core that emerges for **2** as a consequence of the 2,5-disubstituted five-membered thiophene rings. This causes a step in the chain of the ligand and is shown in Fig. 2b. The packing pattern (Fig. 3) shows the appearance of ordered rods in the solid state.

3.2. Thermal behaviour

The thermal properties of the complexes were preliminarily examined by differential scanning calorimeter (DSC). Mesophases and liquid crystal phases can be inferred from DSC measurements by detecting the enthalpy change that is associated with a phase transition. Complexes **1**, **2** and **5** showed sharp single endothermic peaks whereas **3** and **4** showed two broad peaks, one small and one medium endothermic peak during melting.

The thermogram of $[Zn_2(S_2CTC_8H_{17})_4]$ (**3**) showed two endothermic peaks, at 69 °C and 102 °C. The first peak at 69 °C is regarded as a crystal–crystal transition. The peak at 102 °C is ascribed to the melting point of the complex. Sometimes multiple endothermic events might represent transitions from one crystalline state to another crystalline state, which occur when the substance exist in different molecular packing in the solid state at different temperatures [27]. Complex **4** showed two endothermic peaks. The melting points of **1**–**5** from DSC are given in Table 3.

Table 3
Melting points of **1**–**5** and analogue $[Zn(S_2CC_6H_4OR)_2]$ complexes[a]

Complex	Chain length	Melting point (°C)	$[Zn(S_2CC_6H_4OR)_2]$ R	Melting point[b] (°C)
1	C_4H_9	132	C_4H_9	172, (201)
2	C_6H_{13}	119	C_6H_{13}	155, (194)
3	C_8H_{17}	102	C_8H_{17}	147, (184), 140(N-SmC)
4	$C_{12}H_{25}$	84		
5	$C_{16}H_{33}$	52		

[a] See reference [9].
[b] The first value represents K-N and the values in brackets N-I phases unless stated otherwise.

The trend in the melting points is a steady linear decrease as the alkyl chain length of the complexes increased. We ascribe the decrease in melting point with increasing chain length to greater disorder resulting from less favourable interactions of longer alkyl chains in the packing of the rods in the solid state. Similar results have been reported earlier for metal alkanoates [28]. It is of interest to note that the alkyloxy dithiobenzoate complexes have higher melting points compared to the alkyl thiophene dithiocarboxylate complexes [9].

Two complexes, **5** that displayed a sharp endothermic peak and **4** that gave two broad endothermic peaks, were also examined by Hot-stage Polarising Optical microscopy. Complex **5** directly melted to the isotropic liquid without showing any mesophases. Complex **4**, when looking at the sample between crossed polarizers, gave an impression that there was a mesophase present above 80 °C. However, careful examination revealed that the birefringence observed was not due to a mesophase but due to tiny crystals floating in an isotropic melt. Cooling of the samples resulted in simple crystallization without forming any mesophases. Therefore complexes **4** and **5** are not liquid crystalline. By contrast, most alkyloxydithiobenzoate complexes of zinc(II) displayed a nematic phase while a smectic phase only appeared for the C_8 to C_{10} homologues [9].

Acknowledgements

Professor Koen Binnemans for POM measurements and helpful discussions. The National Research Foundation of South Africa under Grant No. 2047221 supported this project.

Appendix A. Supplementary material

DSC thermogram for **3**. Crystallographic data (excluding structure factors) for the structure reported in this

paper have been deposited with Cambridge Crystallographic Data Center as supplementary crystallographic data for **2**, CCDC-606946 and can be obtained free of charge via www.ccdc.cam.ac.uk/conts/retrieving.html (or from Cambridge Crystallographic Data Center, 12 Union Road, Cambridge CB21EZ, UK; fax: +44 1223 336 033; or deposit@ccdc.cam.ac.uk). Supplementary data associated with this article can be found, in the online version, at doi:10.1016/j.poly.2006.07.003.

References

[1] (a) M. Vašák, J.H.R. Kägi, B. Holmquist, B.L. Vallee, Biochemistry 20 (1981) 6659;
(b) C.D. Garner, S.S. Hasain, I. Bremner, J. Bordas, J. Inorg. Biochem. 16 (1982) 253.

[2] P.A. Cotton, G. Wilkinson, Advanced Inorganic Chemistry, fifth ed., Wiley, New York, 1988, p. 608.

[3] (a) S.A. Hudson, P.M. Maitlis, Chem. Rev. 93 (1993) 861;
(b) P. Espinet, M.A. Esterualas, L.A. Oro, J.L. Serrano, E. Sola, Coord. Chem. (1992) 215;
(c) A.-M. Giroud-Godquin, P.M. Maitlis, Angew. Chem., Int. Ed. Engl. 30 (1991) 375.

[4] M. Bonamico, G. Dessy, V. Fares, L. Scaramuzza, J. Chem. Soc., Dalton Trans. (1972) 2515.

[5] H. Adams, N.A. Bailey, D.C. Bruce, S.E. Hunt, E. Lalinde, A.A. Maggs, R. Orr, P. Styring, M.S. Wragg, P.M. Maitlis, Polyhedron 7 (1988) 1861.

[6] N. Hoshino, R. Hayakawa, T. Shibuya, Y. Matsunaga, Inorg. Chem. 29 (1990) 5129.

[7] (a) K. Ohta, G.J. Jiang, M. Yokoyama, S. Kusabayashi, H. Mikawa, Mol. Cryst. Liq. Cryst. 66 (1981) 283;
(b) D.W. Bruce, D.A. Dunmur, L.S. Santa, M.A. Wali, J. Mater. Chem. 2 (1992) 363.

[8] (a) D. Guillon, A. Skoulios, C. Piechocki, J. Simon, P. Weber, Mol. Cryst. Liq. Cryst. 100 (1983) 275;
(b) L.M. Severs, A.E. Underhill, D. Edwards, P. Wight, D. Thetford, Mol. Cryst. Liq. Cryst. (1988) 234.

[9] H. Adams, A.C. Albeniz, N.A. Bailey, D.W. Bruce, A.S. Cherodian, R. Dhillon, D.A. Dunmur, P. Espinet, J.L. Feijoo, E. Lalinde, P.M. Maitlis, R.M. Richardson, G. Ungar, J. Mater. Chem. 1 (1991) 843.

[10] M. Motevalli, P. O'Brien, J.R. Walsh, I.M. Watson, Polyhedron 15 (1996) 2801.

[11] R. Gimenez, A.B. Manrique, S. Uriel, J. Barbera, J.L. Serrano, Chem. Commun. (2004) 2064.

[12] G. Barberio, A. Bellusci, A. Crispini, M. Ghedini, A. Golemme, P. Prus, D. Pucci, Eur. J. Inorg. Chem. (2005) 181.

[13] M.B. Ros, J.L. Serrano, M.R. de la Fuente, C.L. Folcia, J. Mater. Chem. 15 (2005) 5093, and references therein.

[14] (a) I.A. Levitsky, K. Kishikawa, S.H. Eichhorn, T.M. Swager, J. Am. Chem. Soc. 122 (2000) 2474;
(b) M. Gharbia, A. Gharbi, H.T. Nguyen, J. Malthête, Curr. Opin. Colloid Interface Sci. 7 (2002) 312.

[15] (a) Y.M. Terblans, H.M. Roos, S. Lotz, J. Organomet. Chem. 566 (1998) 133;
(b) M. Landman, H. Görls, S. Lotz, Eur. J. Inorg. Chem. (2001) 233;
(c) M. Landman, H. Görls, S. Lotz, J. Organomet. Chem. 617–618 (2001) 280.

[16] G.H. Spies, R.J. Angelici, Organometallics 6 (1987) 1902.

[17] L. Brandsma, H.D. Verkruijsse, Preparative Polar Organometallic Chemistry, vol. 1, Springer Verlag, Heidelberg, 1987, p. 124.

[18] SMART (Version 5.054), SAINT (Version 6.45), SADABS (Version 2.10), SHELXTL (Version 6.12), Bruker AXS Inc., Madison, WI, USA, 2001.

[19] G.M. Sheldrick, SHELX-97, University of Göttingen, Germany, 1997.

[20] L.J. Farrugia, J. Appl. Crystallogr. 30 (1997) 565.

[21] The POV-Ray Team, POV-Ray 2004, URL: <http://www.pov-ray.org./download/>.

[22] Mercury, version 1.4.1. I.J. Bruno, J.C. Cole, P.R. Edgington, M.K. Kessler, C.F. Macrae, P. McCabe, J. Pearson, R. Taylor, Acta Crystallogr. B58 (2002) 389.

[23] R.J. Abraham, J. Fischer, P. Lottus, Introduction to NMR Spectroscopy, Wiley, New York, 1998, and references therein.

[24] (a) M.L. Shankaranarayana, C.C. Patel, Can. J. Chem. 39 (1961) 1633;
(b) J.M. Burke, J.P. Fackler Jr., Inorg. Chem. 11 (1972) 3000.

[25] M. Bonamico, G. Dessy, J. Chem. Soc. A (1971) 264.

[26] R.J. Angelici, Coord. Chem. Rev. 105 (1990) 61, and references therein.

[27] T. Seshadri, H.–J. Haupt, J. Mater. Chem. 8 (1998) 1345.

[28] (a) L. Jongen, K. Binnemans, D. Hinz, G. Meyer, Mater. Sci. Eng. C18 (2001) 199;
(b) K. Binnemans, L. Jongen, C. Bromant, D. Hinz, G. Meyer, Inorg. Chem. 39 (2000) 5938.

determined the chemistry of the copper(I) octa-nuclear cluster compounds has now also become biologically relevant [3]. However, due to difficulties in producing single crystals and often to inabilities in distinguishing similar clusters by conventional spectroscopic methods only one structure for each of the first two classes of clusters have been crystallographically characterized, $\{Cu_4[S_2P(O^iPr)_2]_4\}$ [4] and $\{Cu_6[S_2P(OEt)_2]_6\}$ [5], and a limited number of octameric structures, $\{Cu_8[S_2P(OR)_2]_6(\mu_8\text{-}X)\}$, R = Et, ^{n}Pr and ^{i}Pr, $X = S^{2-}$, Cl^- and Br^-, have been reported [5,6].

We have previously shown that solid-state NMR (^{31}P CP/MAS and static ^{65}Cu) in combination with copper K-edge EXAFS studies can be successfully used for characterizing the polycrystalline poly-nuclear copper(I) *O,O′*-dialkyldithiophosphate cluster compounds [6c,7]. The EXAFS data for the polycrystalline compounds, $\{Cu_8[S_2P(OR)_2]_6(\mu_8\text{-}S)\}$ with R = Et, ^{n}Pr, ^{i}Pr, ^{n}Bu, ^{i}Bu and ^{i}Am, have shown that copper cores are 'equally distorted' and the $[Cu_8(S_2P)_6(S_{centre})]$ units in these structures are independent of the size and the branching in the alkyl chains of the ligands [6c,7b]. The actual number of different copper sites in the octanuclear clusters with R = ^{n}Bu and ^{i}Bu has been revealed by the ^{65}Cu NMR studies, showing the presence of two different copper sites [7b,7c]. Possible intra-molecular motions were discussed in terms of the size and branching of the hydrocarbon chains, as reasons for the different ^{65}Cu NMR responses of the systems with R = Et, ^{n}Pr and ^{n}Bu [6c,7c].

The dithiophosphate ligand shells in the octanuclear clusters were found to contain three chemically different phosphorus sites in the cases of R = ^{n}Bu and ^{i}Bu while only one site was observed in the ^{31}P CP/MAS NMR spectra for the compounds with shorter hydrocarbon chains, R = Et, ^{n}Pr [6c,7b,7c].

As we have previously described, ^{31}P chemical shift tensor parameters (estimated from the intensities of the spinning sidebands in ^{31}P CP/MAS NMR spectra) can also be used for the assignment of the coordination mode (bridging or terminal) of *O,O′*-dialkyldithiophosphate ligands adsorbed on the surface of synthetic sphalerite, galena and chalcocite [8,7d]. In previous studies of chalcocite we have shown that the adsorption of potassium *O,O′*-dialkyldithiophosphate ligands (alkyl = Et or ^{i}Bu) leads to the formation of surface compounds such as Cu_6L_6 with $L = [S_2P(OEt)_2]$ [7d] or a mixture of $Cu_8L_6(S)$ and Cu_6L_6 with $L = [S_2P(O^iBu)_2]$ [7b] and a possible role of the disulfide (of the dithiophosphate) at the mineral surfaces has been discussed.

In the early 1970s Fuerstenau et al. showed that when a disulfide is added as a collector (instead of a dithiophosphate salt), chalcocite floated completely even at pH 13.4 [9] but the chemistry of the processes was not investigated. Recently, it has been suggested that copper(II) ions at a chalcocite surface may react with disulfide molecules forming hydrophobic copper(I) *O,O′*-dialkyldithiophosphate species which promote the flotation processes [7b,10].

Herein, we report the solid-state ^{31}P CP/MAS- and static ^{65}Cu NMR data for polycrystalline octa-nuclear dithiophosphate cluster compounds with R = ^{i}Pr and ^{i}Am and show differences and similarities to the NMR data for other *alkyl*-analogues, with particular reference to R = ^{n}Bu and ^{i}Bu. The ^{65}Cu transverse relaxation time, T_2, which indicated significant differences in the motions present, was determined at ambient temperature. The second part of the paper comprises the copper K-edge EXAFS and ^{31}P NMR data for $\{Cu_4[S_2P(O^iPr)_2]_4\}$ and $\{Cu_8[S_2P(O^iPr)_2]_6(\mu_8\text{-}S)\}$ in acetone and CH_2Cl_2 solutions, comparing for the first time the structures in the liquid- and solid-state for these types of clusters. In addition, we show the ^{31}P NMR responses of synthetic chalcocite surfaces treated independently with a potassium *O,O′*-di-iso-amyldithiophosphate collector, $K[S_2P(O^iAm)_2]$, and the corresponding disulfide-$[S_2P(O^iAm)_2]_2$, and discuss the formation of the copper(I)-di-*i*-amyldithiophosphate species on the mineral surfaces.

2. Experimental

2.1. Materials

Potassium *O,O′*-dialkyldithiophosphate ligands: $K[S_2P(O^iPr)_2]$ and $K[S_2P(O^iAm)_2]$, the commercial collectors *Danafloat 245K* and *656K*, respectively, were provided by CHEMINOVA AGRO A/S and used as received. Synthetic chalcocite, Cu_2S, was obtained from STREM CHEMICALS. The structural identity of the chalcocite was confirmed using X-ray powder diffraction data.

2.1.1. Synthesis and characterization of the polycrystalline copper(I) O,O′-dialkyldithiophosphate cluster compounds

$\{Cu_4[S_2P(O^iPr)_2]_4\}$, $\{Cu_8[S_2P(O^iPr)_2]_6(\mu_8\text{-}S)\}$ and $\{Cu_8[S_2P(O^iAm)_2]_6(\mu_8\text{-}S)\}$. The polycrystalline cluster compounds were obtained by following the methods of Kokotailo et al. [4] and Matsumato et al. [6b], respectively, and were characterized as reported elsewhere [7b].

$[S_2P(O^iAm)_2]_2$ was isolated using the following procedure: a concentrated alcoholic solution of iodine was added dropwise to a concentrated aqueous solution of potassium *O,O′*-di-*i*-amyldithiophosphate salt, $K[S_2P(O^iAm)_2]$, until a pale-yellow oil was obtained. The two phases were separated and the organic one was characterized by $^{31}P\{^1H\}$ NMR. No additional ^{31}P signals were observed in the ^{31}P NMR spectrum, showing that no secondary synthesis products were formed. Details about the preparation of the disulfide have been reported elsewhere [11].

2.1.2. Surface formed compounds

(a) One gram of synthetic chalcocite (Cu_2S) powder was immersed in an aqueous solution (50 ml) of $K[S_2P(O^iAm)_2]$ at pH 9.2 (borate buffer) and kept, under stirring, for 30 min. The ligand was dissolved in deionized water and after conditioning the samples were centrifuged at 4000 rpm for 5 min, rinsed with deionized water, centrifuged once more, and dried

in a vacuum desiccator. In this study, a 10 mmol dm^{-3} $K[S_2P(O^iAm)_2]$ aqueous solution was used. The procedure was repeated using a dilute aqueous solution of KOH to adjust the pH to 9.2 (instead of the borate buffer) and no change in the ^{31}P CP/MAS NMR spectra was observed. The synthetic chalcocite had a specific surface area of about 1 m^2/g.

(b) One gram of synthetic chalcocite (Cu_2S) powder was mixed with a droplet (0.0137 g) of $[S_2P(O^iAm)_2]_2$ and carefully stirred for about 5 min and then transferred to a rotor for subsequent NMR measurements.

3. Methods

All experiments were performed at ambient temperature (298 K).

3.1. ^{31}P CP/MAS NMR

Solid-state ^{31}P magic-angle-spinning (MAS) NMR spectra were recorded at 145.73 MHz on a Varian/Chemagnetics InfinityPlus CMX-360 ($B_0 = 8.46$ T) spectrometer with cross-polarization (CP) from the protons and proton decoupling [12]. The CP mixing time was 3 ms. The ^1H 90° pulse width was 5 μs. 32 (for the pure compounds) and 12 000–20 000 signal transients (for the surface compounds) were accumulated with 3 s relaxation delays. The samples were packed in standard ZrO_2 rotors: 4 mm for the pure cluster compounds and 7.5 mm for the surface compounds. To increase the reliability of the simulations of the chemical shift anisotropy parameters, the ^{31}P NMR spectra were obtained at three different spinning frequencies (in the range 3–6 kHz).

The compounds were additionally studied using a single pulse experiment with a proton-decoupled acquisition. The ^1H 90° pulse width was 5 μs and 6 s relaxation delays were used. No changes in the spectra in comparison to the ^{31}P CP/MAS NMR data were observed.

By analyzing the intensities of the spinning sidebands in the ^{31}P spectral patterns, the CSA parameters, δ_{aniso} and η, for the copper(I) *O*,*O*′-dialkyldithiophosphate cluster compounds were estimated. A simulation program in the Mathematica front-end was used for this purpose. The calculations involved the integrated intensities of the spinning sidebands, the Larmor resonance frequency, the spinning frequency and the noise level variance [13].

The liquid-state ^{31}P NMR spectra were recorded on the same spectrometer using a 10 mm broadband 'liquid' probe and a single-pulse experiment with and without proton decoupling. The ^1H 90° pulse width was 15 μs and 512 signal transients were accumulated with a 2 s relaxation delay. The samples were dissolved either in acetone or CH_2Cl_2.

All solid/liquid state ^{31}P NMR data were externally/internally referenced to 85.5% H_3PO_4 [14].

3.2. Static ^{65}Cu NMR

The ^{63}Cu and ^{65}Cu isotopes both have spin $I = 3/2$ and large quadrupole moments. Despite the lower natural abundance of the ^{65}Cu-isotope, it was preferred in this study since its resonance frequency falls in a spectral window that is relatively free from signals for isotopes of other elements and the effects of quadrupolar interactions are slightly smaller. Excitation at a single frequency was insufficient to excite whole central-transition spectra because of the width of the powder line-shapes, and they were therefore acquired by repeatedly stepping the carrier frequency by 100 kHz, retuning the probe and acquiring a new set of data, before finally adding all the sub-spectra together [15].

The solid-state ^{65}Cu NMR spectra of the compounds were recorded for three applied magnetic field strengths: 7.05, 9.4 and 14.1 T, using Bruker CXP-300, Bruker MSL-400 and Chemagnetics Infinity CMX-600 spectrometers with reference frequencies of 85.20, 113.62 and 170.40 MHz, respectively. The spectra were acquired using Bruker 5 (at 14.1 T) and 7 mm static probes, and spin-echo pulse-sequence experiments. At 7.05 T, the radio-frequency field strength, B_1, was 125 kHz, the pulse timings were (1.0 μs – τ – 1.0 μs, $\tau = 20$ μs) with 0.5 s relaxation delays, and 40 960 transients were averaged per resonance offset. At 9.4 T, B_1 was 116 kHz, and the same experimental timings and number of transients as those for 7.05 T were used. At 14.1 T, B_1 was 125 kHz, the pulse timings were (1.1 μs – τ – 1.1 μs, $\tau = 15$ μs) with a pulse delay of 40 ms, and 50 000 transients were averaged per resonance offset. The energy-level splittings that are utilized in NMR are smaller at lower magnetic field strengths, and the resulting weaker signal strengths are reduced further by the broader width of spectra such as those studied here. The range of transmitter frequencies used at the two lower field strengths was therefore limited to those in the region of line-shapes with smaller quadrupolar coupling constants and therefore narrower widths. All ^{65}Cu NMR spectra were externally referenced to a secondary standard of powdered CuCl at 0 ppm [16].

The NMR data were processed with the FID data left-shifted to the echo maximum prior to FT (giving a half echo). The second-order quadrupolar line-shapes for the central transition of ^{65}Cu nuclei, including chemical shift anisotropy (CSA) contributions where necessary, were simulated using the DMfit program [17]. The errors were estimated by changing a parameter's value when all of the other parameter values were kept constant. Furthermore, the ^{65}Cu NMR spectra were simulated using the SIMPSON simulation program [18] to confirm independently the NMR parameters obtained by DMFit.

The spin–spin transverse-relaxation time T_2 was measured at 14.1 T using a carrier frequency of 170.40 MHz and the relevant experimental conditions described above, by varying the value of τ.

3.3. EXAFS

About 20 mg of each compound, $\{Cu_4[S_2P(O^iPr)_2]_4\}$ and $\{Cu_8[S_2P(O^iPr)_2]_6(\mu_8\text{-}S)\}$, were dissolved in 2 cm^3 dry acetone to give an edge step in the transition mode of approximately one unit in the logarithmic intensity ratio. The copper K-edge EXAFS measurements were performed at the wiggler beam line I811 at the MAXII Synchrotron, the MAX Laboratory, Lund University, Sweden. The EXAFS station was equipped with a Si[1 1 1] double crystal monochromator and higher-order harmonics were reduced by detuning the second monochromator crystal to reflect 50% of the maximum intensity at the end of the scans. The internal energy calibration was made with a copper metal foil with the first inflection point assigned to 8980.3 eV [19]. Two scans (with a recording time of 90 min for each scan) were averaged to give good data quality in the k range 2–14 $Å^{-1}$ (k^3-weighted data). Calculated model functions using ab initio calculated phase and amplitude parameters obtained by the FEFF7 and GNXAS programs were curve-fitted in k-space [20].

The EXAFSPAK and GNXAS program packages were used for the data treatment. The final data analyses were performed by means of the GNXAS code in order to obtain the best possible splines [21,22]. The GNXAS code is based on the calculation of the EXAFS signal and a subsequent refinement of the structural parameters [22]. The GNXAS method accounts for multiple scattering (MS) paths, with correct treatment of the configurational average of all the MS signals to allow the fitting of correlated distances and bond distance variances (Debye–Waller factors). A correct description of the first coordination sphere of a studied compound has to account for asymmetry in the distribution of the ion–solvent distances [23]. Therefore the Cu–S two-body signals associated with the first coordination shells were modelled with Γ-like distribution functions that depend on four parameters, namely, the coordination number N, the average distance R, the mean-square variation σ, and the skewness β. The β term is related to the third cumulant C_3 through the relation $C_3 = \sigma^3\beta$. However, the β term was negligible for all distances of importance in this study. R is the first moment of the function $[4\pi/g(r)^2]dr$.

The standard deviations given for the refined parameters in Table 4 were obtained from k^2-weighted least squares refinements of the EXAFS function $\chi(k)$, and do not include systematic errors in the measurements. These statistical error estimates provide a measure of the precision of the results and allow various reasonable comparisons, including the significance of relative shifts in the distances. However, the variations in the refined parameters, including the shift in the E_0 value (for which $k = 0$), using different models and data ranges, indicate that the absolute accuracy of the distances given for the separate complexes is within ±0.01 to 0.02 Å for well-defined interactions. The 'standard deviations' given in the Table 4 have been increased accordingly to include the estimated additional effects of systematic errors.

3.4. Surface-area determination

A chalcocite sample was degassed at 575 K overnight and nitrogen adsorption measurements were performed on a Micromeritics ASAP 2010 instrument. The specific surface area was calculated using the BET equation [24].

4. Results and discussion

4.1. Solid-state studies on copper(I) O,O′-dialkyldithiophosphate cluster compounds (alkyl = ^{i}Pr and ^{i}Am)

4.1.1. ^{31}P CP/MAS NMR studies

The ^{31}P CP/MAS NMR spectra of the octa-nuclear copper(I) di-*iso*-propyl- and di-*iso*-amyldithiophosphate cluster compounds, $\{Cu_8[S_2P(OR)_2]_6(\mu_8\text{-}S)\}$ where R = ^{i}Pr and ^{i}Am, **1** and **2**, are shown in Figs. 1 and 2a, respectively. Both compounds display three ^{31}P NMR centre-band resonance lines with isotropic shifts at 103.8, 94.5, 93.2, for **1**, and 100.6, 98.3 and 96.7 ppm for **2** (see insets),

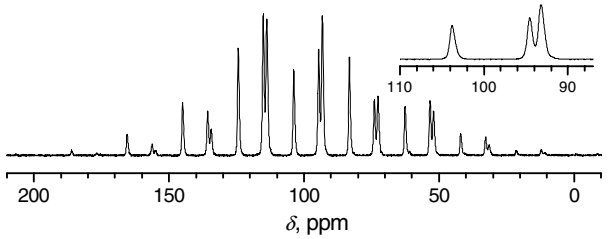

Fig. 1. ^{31}P CP/MAS NMR spectrum (at 8.46 T) of the polycrystalline $\{Cu_8[S_2P(O^iPr)_2]_6(\mu_8\text{-}S)\}$ (**1**); 32 signal transients. 3 kHz spinning frequency. The expanded centre-band region is shown in the inset.

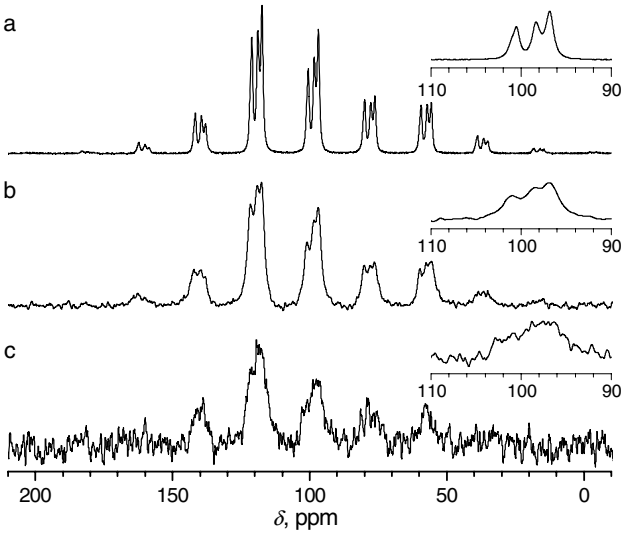

Fig. 2. ^{31}P CP/MAS NMR spectrum (at 8.46 T) of the polycrystalline $\{Cu_8[S_2P(O^iAm)_2]_6(\mu_8\text{-}S)\}$ (**2**), 32 signal transients (a); a chalcocite sample treated with a 10 mmol dm^{-3} aqueous solution of $K[S_2P(O^iAm)_2]$, 20 000 signal transients (b); and a chalcocite sample treated with the $[S_2P(O^iAm)_2]_2$, 12 000 signal transients (c); 3 kHz spinning frequency. The expanded centre-band regions are shown in the insets.

and relative integrated intensities of all sidebands close to 1:1:1 (for both cases). This indicates that the PO_2S_2 tetrahedra in the ligands are additionally distorted by different orientations of the hydrocarbon chains, and that the phosphorus sites in both clusters are chemically equivalent in pairs.

The symmetry of the electronic environments around each P-site can be estimated from the ^{31}P chemical shift anisotropy (CSA) parameters, δ_{aniso} and η, using the definitions: $\delta_{aniso} = \delta_{zz} - \delta_{iso}$; $\delta_{iso} = (\delta_{xx} + \delta_{yy} + \delta_{zz})/3$, where δ_{xx}, δ_{yy} and δ_{zz} are the principal values of the chemical shift tensor, $|\delta_{zz} - \delta_{iso}| \geqslant |\delta_{xx} - \delta_{iso}| \geqslant |\delta_{yy} - \delta_{iso}|$ and $\eta = (\delta_{yy} - \delta_{xx})/\delta_{aniso}$. The ^{31}P CSA parameters for these clusters were estimated from the intensities of the spinning sidebands, which flank the centre-bands at $\delta_{iso} \pm k(\nu_r/\nu_0) \times 10^6$ ppm, (ν_0 is the Larmor resonance frequency for the ^{31}P nuclei, ν_r is the sample spinning frequency and $k = 1,2,3\ldots$) and are shown in Tables 1 and 2, respectively.

In the known single crystal structure of the *iso*-propyl cluster, $\{Cu_8[S_2P(O^iPr)_2]_6(\mu_8\text{-}S)\} \cdot CH_2Cl_2$ [5], there are three crystallographically different P sites and indeed three phosphorus sites were observed in the ^{31}P CP/MAS NMR spectrum of **1**. Three isotropic resonance lines have also been observed for the octa-nuclear copper(I) clusters with R = ^{i}Bu [7b] and ^{n}Bu [7c]. Therefore, three isotropic resonances were also expected for the cluster compound with R = ^{i}Am, **2**, as the chemically similar octameric compounds with bulky alkyl groups are likely to show similar ^{31}P NMR responses.

The most de-shielded ^{31}P-resonances in **1** (103.8 ppm) have an asymmetric chemical shift tensor with η close to one. An interesting fact is that the isotropic chemical shift of these phosphorus sites in **1** coincides with that of the least de-shielded phosphorus sites in the corresponding potassium salt (see Table 1), but the results of the deconvolution procedure and the following ^{31}P CSA calculations revealed very different ^{31}P CSA parameters. Therefore, isotropic chemical shifts alone must be used with a precaution in assignments of the solid-state ^{31}P NMR spectra of dialkyldithiophosphate compounds.

Recent ab initio calculations of ^{31}P chemical shift tensors in a model fragment, $[PO_2S_2]^-$, have shown that negative

Table 1
^{31}P chemical shift and chemical shift anisotropy data (with 68.3% confidence limit) for the polycrystalline $\{Cu_8[S_2P(O^iPr)_2]_6(\mu_8\text{-}S)\}$ (**1**), $\{Cu_4[S_2P(O^iPr)_2]_4\}$ and the corresponding potassium salt

Compound	δ_{iso} (ppm) ± 0.1		δ_{aniso} (ppm)	η	δ_{xx}	δ_{yy}	δ_{zz}	Reference
$\{Cu_8[S_2P(O^iPr)_2]_6(\mu_8\text{-}S)\}$	103.8	mean	−66.4 ± 1.0	0.94 ± 0.02	168.2 ± 1.2	105.8 ± 2.0	37.4 ± 1.0	this work
	94.5	value	−66.9 ± 0.8	0.42 ± 0.04	142.0 ± 1.5	113.9 ± 3.0	27.5 ± 0.8	
	93.2	97.2	−56.5 ± 0.5	0.31 ± 0.05	130.2 ± 1.5	112.7 ± 3.0	36.7 ± 0.7	
	97.4[a]							
	98.6[b]							
$\{Cu_4[S_2P(O^iPr)_2]_4\}$	102.1	mean	−77.3 ± 1.2	0.28 ± 0.06	151.6 ± 2.4	129.9 ± 5.3	24.8 ± 1.2	[7a]
	100.8	value	−75.2 ± 1.1	0.32 ± 0.05	150.4 ± 2.0	126.4 ± 4.3	25.6 ± 1.1	
	95.7	98.0	−77.5 ± 0.7	0.53 ± 0.02	154.9 ± 0.9	113.9 ± 1.9	18.2 ± 0.7	
	93.5		−75.0 ± 0.6	0.40 ± 0.02	146.0 ± 1.9	116.0 ± 4.2	18.5 ± 0.6	
	97.4[a,c]							this work
	98.6[b]							
$K[S_2P(O^iPr)_2]$	111.7		−104.7 ± 1.3	0.32 ± 0.03	180.6 ± 1.8	148 ± 4	7.0 ± 1.3	[25]
	103.8		−116.7 ± 1.1	0.1 ± 0.1	166 ± 4	158 ± 9	−12.9 ± 1.1	

[a] In CH_2Cl_2.
[b] In acetone.
[c] In $CDCl_3$, $\delta_{iso} = 96.7$ ppm (Ref. [5]).

Table 2
^{31}P chemical shift and chemical shift anisotropy data (with 68.3% confidence limit) for the polycrystalline $\{Cu_8[S_2P(O^iAm)_2]_6(\mu_8\text{-}S)\}$ (**2**), the corresponding surface compounds, disulfide and potassium salt

Compound	δ_{iso} (ppm)	δ_{aniso} (ppm)	η	δ_{xx}	δ_{yy}	δ_{zz}	Reference
$\{Cu_8[S_2P(O^iAm)_2]_6(\mu_8\text{-}S)\}$	100.6 ± 0.2	−69.5 ± 1.3	0.52 ± 0.04	153.7 ± 1.7	117.6 ± 3.3	31.4 ± 1.3	this work
	98.3 ± 0.1	−63.4 ± 0.9	0.37 ± 0.06	141.5 ± 2.0	118.1 ± 4.3	34.7 ± 0.9	
	96.7 ± 0.2	−61.5 ± 0.3	0.20 ± 0.04	130.8 ± 1.3	121.5 ± 2.7	35.4 ± 0.3	
Surface compound when chalcocite treated with $K[S_2P(O^iAm)_2]$[a]	101.1 ± 0.3	−72 ± 3	0.45 ± 0.09	153.3 ± 3.9	120.9 ± 7.7	29.1 ± 3.0	
	98.7 ± 0.3	−67 ± 2	0.1 ± 0.1	135.6 ± 3.5	128.8 ± 7.6	31.7 ± 2.0	
	96.8 ± 0.3	−62.5 ± 0.8	0.1 ± 0.1	131.2 ± 3.2	124.9 ± 7.0	34.3 ± 0.9	
Surface compound when chalcocite treated with $[S_2P(O^iAm)_2]_2$[b]	98.0 ± 0.5	−69.9 ± 4.1	0.41 ± 0.15	147.3 ± 6.0	118.6 ± 12.2	28.1 ± 4.1	
$[S_2P(O^iAm)_2]_2$	85.0 ± 0.1						[25]
$K[S_2P(O^iAm)_2]$	108.8 ± 0.1	−120 ± 2	0.1 ± 0.1	174 ± 6	164 ± 13	−11 ± 2	

[a] De-convolution was made using a set of three peaks.
[b] De-convolution was made using a single peak due to the poor S/N ratio.

values of δ_{aniso} (and $0 < \eta < 1$) correspond to similar relatively large S-P-S bond angles, which are characteristic of bridging-type bonding, while positive values of δ_{aniso} reveal a terminal-type bonding [25]. These conclusions were also confirmed by ^{31}P CSA experimental data for mononuclear nickel(II)-, bi- and tetranuclear zinc(II)-, polynuclear Pb(II)- and Cd(II)-, and for the copper(I) tetra-, hexa- and octa-nuclear *O*,*O*′-dithiophosphate cluster compounds [7,25,26]. The ^{31}P CSA parameters for the phosphorus sites in the ionic potassium salts (δ_{aniso} larger than −100 ppm and $\eta \sim 0$) are very different from the ^{31}P CSA for the P sites in the two octa-nuclear copper(I) cluster compounds (δ_{aniso} varies between −56 and −69 ppm and $0.2 < \eta < 0.9$), which is an indication that the phosphorus sites belong to bridging-type ligands in the cluster compounds. It is notable that the most de-shielded phosphorus sites in both cluster compounds are characterized by the most asymmetric chemical shift tensors (observed in the values of the η-parameter). A similar trend was observed in the ^{31}P CP/MAS NMR spectra of other octanuclear copper(I) cluster compounds with R = ^{n}Bu and ^{i}Bu [7b,7c].

4.1.2. Static ^{65}Cu NMR studies

The static ^{65}Cu NMR spectra of **1** and **2** obtained at 7.05, 9.4 and 14.1 T are shown in Figs. 3 and 4, respectively, together with simulations. Table 3 summarizes the

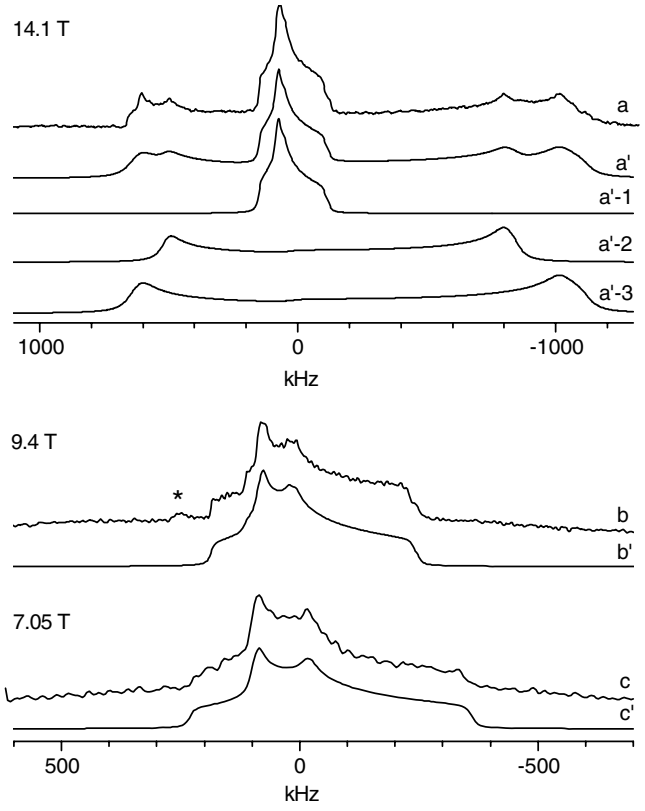

Fig. 3. Solid-state static ^{65}Cu NMR spectra (at 14.1, 9.4 and 7.05 T) of the polycrystalline $\{Cu_8[S_2P(O^iPr)_2]_6(\mu_8\text{-}S)\}$ (a-c), together with simulations (a′-c′); a′-1, a′-2 and a′-3 show the individual line-shapes used in a′. The broad components were not visible at 9.4 and 7.05 T. The probe background (at 9.4 T) is denoted with an asterisk.

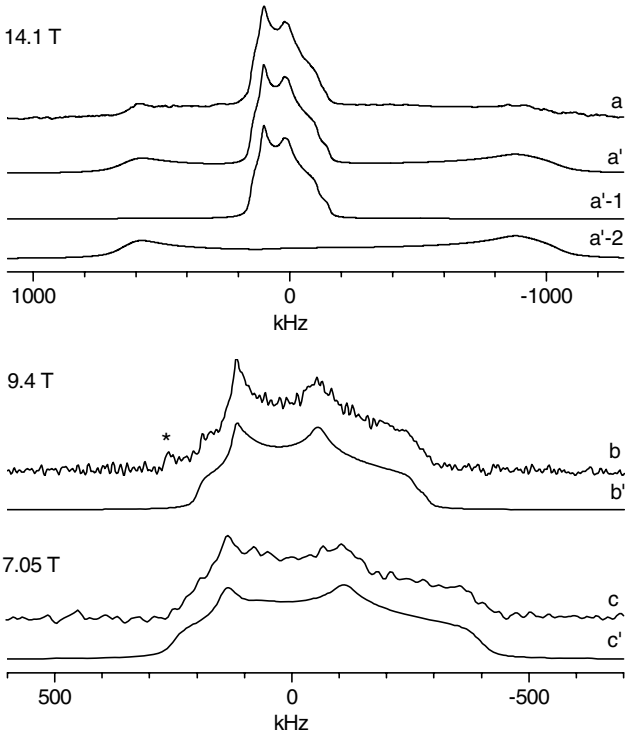

Fig. 4. Solid-state static ^{65}Cu NMR spectra (at 14.1, 9.4 and 7.05 T) of the polycrystalline $\{Cu_8[S_2P(O^iAm)_2]_6(\mu_8\text{-}S)\}$ (a-c), together with simulations (a′-c′); a′-1 and a′-2 show the individual line-shapes used in a′. The broad component was not visible at 9.4 and 7.05 T. The probe background (at 9.4 T) is denoted with an asterisk.

NMR parameters that were used to simulate the static ^{65}Cu NMR spectra of these two compounds and those for the ^{i}Bu-analogue, $\{Cu_8[S_2P(O^iBu)_2]_6(\mu_8\text{-}S)\}$, previously reported [7b]. These parameters describe two interaction tensors: the quadrupolar interaction (described by the quadrupolar coupling constant, $C_Q = e^2Qq/h$, and its asymmetry parameter, $\eta_Q = (V_{XX} - V_{YY})/V_{ZZ}$, where eQ is the nuclear electric quadrupolar moment, $eq = V_{ZZ}$, and $|V_{XX}| \leqslant |V_{YY}| \leqslant |V_{ZZ}|$ are the elements of the diagonalised EFG tensor) and the ^{65}Cu chemical shift (with an isotropic term δ_{iso}, and anisotropic terms δ_{CS} and η_{CS}). The spectra at 14.1 T for both compounds reveal the presence of more than one quadrupolar line-shape, which are substantially overlapped since the differences in isotropic chemical shift are much smaller than the quadrupolar line-widths, as expected. The relative orientations of the two interaction tensors for **1** and **2** are reflected in the angle parameters used in the simulations (see Table 3).

The static ^{65}Cu NMR spectrum of **1** at 14.1 T reveals three quadrupolar line-shapes with relative integrated intensities close to 1:1:2 (Fig. 3a and Table 3). The presence of such line-shapes with different characteristics (see Table 3) is an indication of the presence of at least three copper sites with different electric field gradients (EFG), although similarities in the local geometries for all copper sites, $[CuS_3\cdots S_{centre}]$, were expected to result in similar line-shapes and therefore similar EFG's. The line-shape for the copper sites with $\delta_{iso} = 460$ ppm has a noticeable

Table 3
^{65}Cu NMR parameters for the polycrystalline $\{Cu_8[S_2P(OR)_2]_6(\mu_8\text{-}S)\}$ (R = ^{i}Pr, ^{i}Am (**1** and **2**) and ^{i}Bu)

Cluster compound	δ_{iso} (ppm)	C_Q (MHz)	$\eta_Q \pm 0.02$	δ_{CS} (ppm)	$\eta_{CS} \pm 0.02$	ϕ (°)	X (°)	Ψ (°)	Integrated intensity	Reference
1	460 ± 30	15.7 ± 0.2	0.70	380 ± 50	0.00	–	9 ± 3	40 ± 10	0.18	this work
	170 ± 50	41.8 ± 0.2	0.03	nd	nd	–	–	–	0.26	
	100 ± 50	47.1 ± 0.2	0.05	nd	nd	–	–	–	0.56	
2	450 ± 50	17.6 ± 0.2	0.47	400 ± 50	0.00	–	14 ± 3	70 ± 10	0.48	
	300 ± 50	45.5 ± 0.2	0.08	nd	nd	–	–	–	0.52	
R = ^{i}Bu	410 ± 20	19.3 ± 0.1	0.40	450 ± 30	0.00	–	10 ± 1	65 ± 5	0.48	[7b]
	120 ± 50	46.0 ± 0.2	0.05	nd	nd	–	–	–	0.52	

nd – not detected.
– does not affect the line shape.

^{65}Cu CSA contribution and cannot be simulated exclusively by a quadrupolar interaction tensor, while for the copper sites with $\delta_{iso} = 170$ and 100 ppm, where the electric field gradient is very large, the simulations do not require such a combination of interactions.

In the crystal structure of $\{Cu_8[S_2P(O^iPr)_2]_6(\mu_8\text{-}S)\} \cdot CH_2Cl_2$ [5] there are four structurally non-equivalent copper sites in tetrahedral arrangements of the $[CuS_3\cdots S]$-type. However, singularities of only three second-order quadrupolar line-shapes are well delineated (Fig. 3a) in spite of the expected overlap of four similar quadrupolar patterns. The corresponding integrated intensities in the simulations of these sites, however, allow the spectrum to be considered as a superposition of the central transitions of the four copper sites ($CuS_3\cdots S$). Furthermore, data show that very small differences in the local geometry of the copper sites in **1** are producing large differences in the quadrupolar parameters (with a change in C_Q from 15.7 to 47.1 MHz), with corresponding differences in the electronic charge distribution.

The data presented in Fig. 3 for **1** are a useful illustration of the importance of studies involving multiple magnetic field strengths. Simulations of the smaller C_Q line-shape using the high-field data alone would not only provide an inaccurate value for C_Q but also an η_Q close to unity. The lower-field data show quite different line-shapes that are characteristic of tensors where $\eta_Q < 1$. At lower field-strengths, the chemical shift interaction is weaker but the second-order quadrupolar interaction terms are stronger. Such data therefore tends to provide useful information on quadrupolar interactions, with higher-field data being more useful for determining chemical shift tensors. The accuracy of the parameters used to describe the narrower line-shapes (of **1** and **2**) is increased by comparing powder spectra obtained at multiple magnetic field strengths and a fit for all three fields for both compounds cannot be achieved without including the CSA component. This component, however, is expected to be less significant for the broad line-shapes and therefore it was not included in their simulations. The sloping background intensities visible in the spectra acquired at lower magnetic field strengths are caused by these broad line-shapes and to a lesser extent the quadrupolar satellites, and are an effect of the limited sweep range.

The ^{65}Cu NMR spectrum of **2** reveals only two quadrupolar line-shapes with relative integrated intensities close to 1:1 (see Fig. 4a and Table 3) suggesting the existence of two types of site with equal-sized populations. Similar to the ^{65}Cu NMR data of $\{Cu_8[S_2P(OR)_2]_6(\mu_8\text{-}S)\}$ with R = ^{i}Bu and ^{n}Bu [7b,7c], the two quadrupolar line-shapes in the ^{65}Cu NMR spectrum of $\{Cu_8[S_2P(O^iAm)_2]_6(\mu_8\text{-}S)\}$ cluster are substantially overlapped and the narrower line-shape is again additionally perturbed by a considerable ^{65}Cu CSA contribution ($\delta_{CS} = 400$ ppm).

It is somewhat surprising that the copper sites in these copper clusters, all of which have an almost 'rigid' closest chemical environment of the $CuS_3\cdots S$-type, display different numbers of copper sites that are also characterized by very different quadrupolar parameters. Such differences are caused by different EFG's at the copper nuclei that are determined by differences in the local charge distributions, and are therefore sensitive to the bonding characteristics. The large differences in C_Q described above are indicative of significant differences in the bonding or bond-strengths at the different sites, which result in such differences in the ^{65}Cu spectra of these chemically very similar copper sites.

4.1.3. ^{65}Cu spin-echo decay constants, T_2, for the copper(I) O,O′-di-i-propyl- and O,O′-di-i-amyldithiophosphate cluster compounds

An NMR study of the dynamical behaviour of a system can be performed by measuring the spin-echo peak

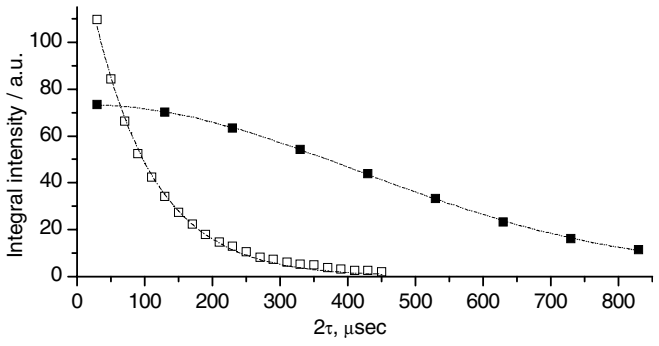

Fig. 5. ^{65}Cu NMR transverse relaxation decays (T_2) for the polycrystalline $\{Cu_8[S_2P(O^iPr)_2]_6(\mu_8\text{-}S)\}$ (filled squares) and $\{Cu_8[S_2P(O^iAm)_2]_6(\mu_8\text{-}S)\}$ (open squares) measured using a spin-echo pulse sequence. Broken lines are fits with T_2 of 590 (Gaussian) and 90 μs (exponential).

intensity, since the spin-echo experiment refocuses the effects of inhomogeneous broadening [27]. Fig. 5 shows the intensities of the ^{65}Cu NMR spin-echo signals of **1** and **2** at 14.1 T (at the carrier frequency of powdered CuCl, at 0 ppm) plotted versus the spin-echo delay time, τ. The magnetization decay is Gaussian (Eq. (1)) for **1** with $T_2 = 590 \pm 10$ μs and exponential (Eq. (2)) for **2** with $T_2 = 90 \pm 10$ μs:

$$M = M_0 \exp\left(\frac{-(2\tau)^2}{(T_2)^2}\right); \quad (1)$$

$$M = M_0 \exp\left(\frac{-2\tau}{T_2}\right) \quad (2)$$

In general, the decay of the spin echo intensity of a nucleus is a complex, many-site variable that involves couplings between neighbouring sites and fluctuations in the interactions affecting the precession frequency of the nucleus. In other words, it contains information about the surroundings of the nuclei of interest and through the T_2 value (its nature and magnitude) can reveal the nature of the dynamic processes in the system. (We use the characteristic decay in the magnetization measured using the spin-echo experiment as an operational definition of T_2 although there are both secular and non-secular terms which can contribute to the measured time and not all the secular terms will necessarily be refocussed by the pulse used here [28]. The sources of the decay cannot usually be determined, but some studies chose to define T_2 as the decay resulting from effects of homonuclear coupling, and use T_2' for the overall decay caused by the different contributing effects [29].) Whilst a full variable temperature study is needed to assure the details of the relaxation behaviour in the systems discussed here, the different functions describing the decay in **1** and **2** clearly indicate different dynamics (motions) in the two samples. A Gaussian T_2 decay (predominantly due to the dipole–dipole broadening [30]) is usually observed in cases with no motion on the NMR time scale that affect the resonance signal [30]. When there are motions (vibrational or/and rotational, and/or inhomogeneous spin fluctuations) present the T_2 undergoes a crossover from Gaussian to exponential. Although T_2 is short for compounds **1** and **2**, the substantially shorter T_2 for **2** indicates that there is motion in **2** that is causing additional relaxation, probably longitudinal relaxation (characterized by a time constant, T_1) and, since $T_1 \geqslant T_2$, [30] T_2 is considerably reduced.

We have recently reported (in the case of ^{65}Cu in the $\{Cu_8[S_2P(O^nBu)_2]_6(\mu_8\text{-}S)\}$ cluster compound) that a type of movement/motion of the structure, originating in the ligand tails, is most likely to be the reason for the observed exponential decay (with $T_2 = 160$ μs) and for the relatively weak spin-echo signal [7c].

For octa-nuclear copper(I) *O*,*O*′-dialkyldithiophosphate structures, it has been proposed that the main factors determining the overall motions/vibrations are the number of methylene groups (CH_2) (giving more flexibility of the structures and hence producing motions in the ligand tails) and the positional vibrations of the S_{centre} (due to the available 'free space' in the copper core cavities) [7c]. The T_2 value of 590 μs for **1** and the observed Gaussian decay indicate that some of the intra-molecular dynamic processes, present in the octa-nuclear cluster with R = ^{i}Am, **2**, are less effective or absent in the octa-nuclear cluster with R = ^{i}Pr (i.e. **1**). It is most likely that the absence of CH_2-groups in the ligand hydrocarbon chains of **1** is the reason for the more 'rigid environments' of the copper atoms in the cube. Therefore, considerably weaker fluctuations in the EFG's at the copper positions are expected, and hence a slower decay of the magnetization of the ^{65}Cu NMR echo signals is observed (and a Gaussian T_2 of 590 μs is determined).

For the case of **2**, the T_2 value of 90 μs and the observed exponential decay of the magnetization, indicate that different dynamic processes are dominating. The presence of two CH_2-groups in the hydrocarbon chains (none for R = ^{i}Pr) would allow a certain flexibility in the structure, and therefore fluctuations in the EFG's could arise, decreasing the value of T_2. Similar effects that could shorten further the relaxation time are intermolecular motions (together with intra-molecular motions). These are fairly likely to exist in **2**, due to its considerably larger ligands (in comparison to those in **1**) and the possible geometric positions in which the 12 hydrocarbon chains could exist. There is a possibility that some motions are hindered or enhanced in **2** by steric factors rather than electronic effects, but this could only be confirmed by low-temperature experiments.

It is worth noting that although the EXAFS data for the two compounds, have shown that the mean Cu–S, Cu···S_{centre} and Cu···Cu distances for both compounds are 2.285, 2.64 and 2.99 Å (which means that the two copper cores are very similar), this method only provides information about the average distances. There is therefore a possibility that the local surroundings of the copper sites in the two compounds are slightly dissimilar and that the observed shortening of T_2 is due to fluctuating EFG's (which are causing T_1 (and T_2) relaxation) that are experienced by some of the copper sites in the cubes more strongly than by others, and hence dominate the overall decay of the echo intensity in **1** and **2**.

4.2. Liquid-state EXAFS and ^{31}P NMR studies on copper(I) O,O′-di-iso-propyldithiophosphate cluster compounds with different nuclearity

There is very little known about the structures of the poly-nuclear copper(I) dialkyldithiophosphate compounds in solution, while numerous data for the mononuclear copper(II) dialkyldithiophosphate complexes have been reported [31]. In principle, it is accepted that the structures in the solid-state will be the same as those in solutions if there are no specific interactions with the solvents and no chemical decomposition occurs. $^{31}P\{^1H\}$ NMR data only for $\{Cu_4[S_2P(O^iPr)_2]_4\}$ and $\{Cu_6[S_2P(OEt)_2]_6\}$ compounds in $CDCl_3$ have been briefly reported together with the single crystal data for these compounds [5]. It is known that

$Zn_4L_6(Se)$ ($L = [Se_2P(OPr)_2]$) decomposes in solution to a monomer and a dimer, which are themselves in a dynamic equilibrium [32a]. The octanuclear copper(I) cluster with a similar ligand ($L = [Se_2P(O^iPr)_2]$) in a CH_2Cl_2 solution has shown only one resonance line in the $^{31}P\{^1H\}$ NMR [32b]. In this study we use EXAFS spectroscopy to investigate the structures of $\{Cu_4[S_2P(O^iPr)_2]_4\}$ and $\{Cu_8[S_2P(O^iPr)_2]_6(\mu_8\text{-}S)\}$ in solution, comparing the results to the EXAFS data for these compounds in the solid-state.

EXAFS is a lattice-independent structure method, which provides information about the structure around the absorbing atom in the sample (in this case, copper) and a correct description of the first coordination sphere of the studied compound is obtained when the distribution of the ion–solvent distances is taken into account. The raw EXAFS data for **1** and $\{Cu_4[S_2P(O^iPr)_2]_4\}$ in acetone solutions and in the solid-state are shown in Fig. 6a, the fitted Fourier transforms in Fig. 6b, and the refined structure parameters are summarized in Table 4. Solid-state EXAFS data are shown for comparison in Table 4 and the individual fits for all data are provided in the Supporting information. The cluster compounds in the solid-state display similar EXAFS functions with small differences between the two types of structures.

The average Cu···Cu, Cu–S, Cu···S_{centre} bond distances for **1** in an acetone solution and in the solid-state are almost identical (within the error limits). The mean Cu–S bond distance is 2.285 Å for the solid-state and 2.289 Å for the acetone solution. The mean Cu···Cu distances are 2.99 Å and 3.01 Å, respectively. Such a similarity between the solid- and liquid-state data is also observed in the mean Cu···Cu and Cu–S bond distances for the tetrameric copper(I) structure with the same ligand: the mean Cu–S bond distances are 2.265 and 2.262 Å, respectively, while the corresponding Cu···Cu bond distances are 2.82 and 2.84 Å. This shows that the structures around the copper(I) ions in both poly-nuclear cluster compounds, $\{Cu_4[S_2P(O^iPr)_2]_4\}$ and $\{Cu_8[S_2P(O^iPr)_2]_6(\mu_8\text{-}S)\}$, are principally identical in the solid- and liquid-states. Interactions with this solvent did not lead to any initiation of a decomposition process or formation of other copper(I) dithiophosphate species. If such products were formed then the structural parameters obtained would not be similar to those found for the compounds in the solid-state.

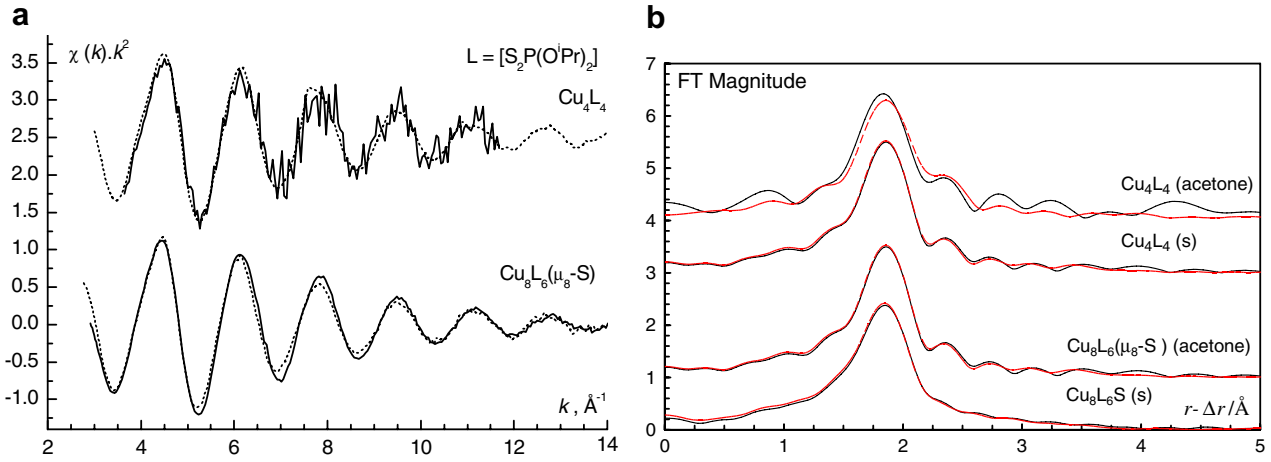

Fig. 6. (a) Raw copper K-edge EXAFS data of $\{Cu_8[S_2P(O^iPr)_2]_6(\mu_8\text{-}S)\}$ in the solid-state and in an acetone solution (no offset) and of $\{Cu_4[S_2P(O^iPr)_2]_4\}$ in the solid-state and an acetone solution (offset +2.5), broken lines – solid-state and solid lines – acetone solutions; (b) fitted Fourier transforms of $\{Cu_8[S_2P(O^iPr)_2]_6(\mu_8\text{-}S)\}$ in the solid-state (no offset) and in an acetone solution (offset +1.0) and of $\{Cu_4[S_2P(O^iPr)_2]_4\}$ in the solid-state (offset +3.0) and in an acetone solution (offset +4.0), solid black lines – experimental data and broken red lines – model; (s) indicates data in the solid-state.

Table 4
EXAFS mean bond distances, *d*/Å, Debye-Waller coefficient, σ^2 and number of distances, *N*, of the polycrystalline copper(I) *O*,*O*′-di-*i*-propyldithiophosphate cluster compounds in the solid-state and in acetone solutions

Cluster compound, $L = [S_2P(O^iPr)_2]$	Mean Cu···Cu distance			Mean Cu–S distance			Mean Cu···S_{centre} distance		
	EXAFS *d*/Å	σ^2	*N*	EXAFS *d*/Å	σ^2	*N*	EXAFS *d*/Å	σ^2	*N*
$\{Cu_8L_6(\mu_8\text{-}S)\}$									
Solid-state[a]	2.99(3)	0.044(3)	3	2.285(3)	0.0086(4)	3	2.64(2)	0.015(3)	1
Acetone	3.01(3)	0.049(3)	3	2.289(3)	0.0070(4)	3	2.67(2)	0.035(4)	1
$\{Cu_4L_4\}$									
Solid-state[a]	2.82(2)	0.023(3)	3	2.265(3)	0.0044(4)	3			
Acetone	2.84(3)	0.024(3)	3	2.262(5)	0.0055(5)	3			

[a] Data are taken from Ref. [6c].

The two acetone solutions were further studied by ^{31}P NMR and the data are shown in Table 1. Both compounds display a single ^{31}P NMR resonance line with isotropic shifts at 98.6 ppm. An isotropic chemical shift of 97.4 ppm was recorded for both when the samples were dissolved in CH_2Cl_2. The effect of the concentration was studied by taking several measurements with different sample concentrations in both solvents, and no differences in the aforementioned ^{31}P isotropic shifts were detected. It has been reported that in the absence of acid–base interactions between a solvent and a solute (which cause a change in the connectivity at the phosphorus), solvent effects (due to some inter-molecular interactions between the solute and the solvent) [27]) on phosphorus chemical shifts in the M-*O*,*O*′-dialkyldithiophosphate compounds (M = Zn, Hg, Pb, As, Sb and Bi) are small, typically from 1 to 2.2 ppm [33]. Therefore, the slightly different chemical shifts observed for the compounds in the two different solvents used clearly show that the PO_2S_2 tetrahedra in the two different clusters have very similar characteristics, and show ^{31}P NMR spectra that are averaged by the molecular tumbling to a single resonance line at the same chemical shift.

These results are not surprising when the ^{31}P CP/MAS NMR is considered in more detail with the crystallographic data for the systems. The corresponding isotropic ^{31}P chemical shifts for the two compounds in the solid-state together with their mean value for each compound are also shown in Table 1. These averages (97.2 and 98.0 ppm) are very close to the positions of the lines found in the liquid-state ^{31}P NMR spectrum and are therefore good indicators of the shifts in those spectra. In previous studies, we have reported ^{31}P NMR data for monomeric and dimeric zinc(II) *O*,*O*′-dialkyldithiophosphate complexes (in the solid-state, in acetone and chloroform solutions, and in melts) and differences of about 2–3 ppm between the expected isotropic chemical shifts (based on the solid-state data) and isotropic chemical shifts in the liquid-state (or melts) were observed [26a]. Therefore, the above difference of 0.8 ppm in the chemical shifts is likely to result in very similar or identical isotropic chemical shifts in liquid-state ^{31}P NMR spectra of these systems even though the exact value(s) cannot be predicted. When the crystal structures of the corresponding solid cluster compounds were analysed (by averaging all P–O and P–S bond distances and corresponding bond angles in the PO_2S_2 tetrahedra in each structure) it was found that the average bond distances in the P-tetrahedra differ by less than 0.01 Å for the two clusters and the differences in the corresponding average bond angles are less than 0.4°. These data are therefore very similar and are unlikely to cause the occurrence of two different isotropic chemical shifts in a ^{31}P NMR spectrum (where the accuracy of the data is limited to 0.1 ppm).

All of our attempts to record $^{63/65}Cu$ NMR spectra of the compounds in acetone or CH_2Cl_2, were unsuccessful, probably due to significantly distorted tetrahedral configurations of the copper sites [34].

4.3. Characterization of synthetic chalcocite surfaces when treated with K[S$_2$P(O^{i}Am)$_2$] and [S$_2$P(O^{i}Am)$_2$]$_2$: ^{31}P NMR studies

The ^{31}P CP/MAS NMR spectra of synthetic chalcocite samples treated with a 10 mM aqueous solution of the collector, $K[S_2P(O^iAm)_2]$ and with the oxidized collector, $[S_2P(O^iAm)_2]_2$, are shown in Figs. 2b and c, respectively. In both cases, a broad (about 8 ppm) centre-band resonance at about 100 ppm, flanked by the spinning sidebands is observed. No changes in the spectra were observed when a single pulse ^{31}P NMR experiment was conducted on these samples and no resonance lines corresponding to the phosphorus sites in the disulfide (at 85.0 ppm, see Table 2) were detected.

The spinning sideband patterns for the two samples are very similar and also resemble that for the pure cluster compound **2** (compare to Fig. 2a). Results of a de-convolution procedure and the following CSA simulations reveal that the ^{31}P CSA parameters (together with δ_{iso}) are similar (within the confidence limits) to those for **2**. The phosphorus sites on the collector-treated chalcocite surface and on the disulfide-treated surface show negative values of δ_{aniso} between −62 and −72 ppm and both correlate with the values of δ_{aniso} between −62 and −70 ppm for **2**, discussed above. This confirms the presence of only bridging-type coordination in the di-*i*-amyldithiophosphate species formed on the mineral surface. Furthermore, it can be concluded that treatments with a collector or an oxidized collector (disulfide in this case) both result in the formation of the same type of copper(I) *O*,*O*′-dithiophosphate species on the surface of synthetic chalcocite, and in the case of the *O*,*O*′-di-*i*-amyldithiophosphate derivative the dominant species have the $\{Cu_8[S_2P(O^iAm)_2]_6(\mu_8\text{-}S)\}$ type structure. These data correlate well with our previous studies of chalcocite surfaces (treated with $K[S_2P(O^iBu)_2]$ as a collector) where a mixture of $\{Cu_8L_6(S)\}$ and $\{Cu_6L_6\}$ species ($L = [S_2P(O^iBu)_2]$) on the mineral surface was detected [7b].

The fact that no traces of disulfides were observed in the ^{31}P NMR spectra of any of the collector treated Cu_2S samples in our previous and current studies, and that the disulfide-treated surfaces do not show the presence of adsorbed disulfide, show that the disulfide is quantitatively reduced and complex bound by copper ions to the corresponding copper(I) dithiophosphate cluster species formed at the chalcocite surface. However, such a reduction process must be accompanied by a corresponding oxidation process. Our preliminary adsorption studies of disulfide on synthetic sphalerite (ZnS) activated by copper(II), and Cu_2O surfaces, show that the corresponding copper(I)–dithiophosphate species are formed on the sphalerite surface and that the disulfide remains almost un-altered on the Cu_2O surface. The observations indicate that the model of interaction of the collector with the mineral surface should be re-considered with respect to the properties of the metal-sulfur containing mineral surfaces.

An interesting vibration spectroscopy study of the interaction between some sulfide minerals and *O*,*O*′-diethyldithiophosphate ions (DTP) in aqueous solutions was reported in 1994 [35]. The formation of disulfide at the mineral surfaces is ascribed as a result of a red-ox process between the *O*,*O*′-diethyldithiophosphate ions and highly oxidizing species such as $S_2O_8^{2-}$ and/or $S_2O_7^{2-}$, which are likely to exist on the surfaces of sulfide minerals that are characterized by short S···S distances (less that 3.6 Å) [35]. A relationship between the shortest S···S distance in the sulfide mineral and the type of product formed at the mineral surface (metal–dithiophosphate complex or disulfide) was proposed and for the surface of chalcocite (which has a longer S···S distance of 3.71 Å [36]) only the formation of ''CuDTP''-species was predicted and detected. This fact can also explain the absence of disulfide on the chalcocite surface (as reported in this study), based on the crystallographic characteristics of the mineral.

As the formation of $S_2O_8^{2-}$ and or $S_2O_7^{2-}$ ions at the chalcocite surface is very unlikely, a possible explanation of the disulfide–surface interactions at the mineral surface is that a process of involving the simultaneous oxidation of the sulfide ions at the surface occurs when the disulfide at the chalcocite surfaces is reduced to dithiophosphate ions. This can also be considered for the copper(II)-activated sphalerite surface even though the exact distribution of copper atoms at the surface is not known. The disulfide is not strong enough to oxidize the S^{2-} to SO_3^{2-} or SO_4^{2-} ions but poly-sulfur ions can probably still be formed. Similar oxidation processes on the surface of Cu_2O are not expected due to the chemical properties of O^{2-} ions. If only the copper ions were involved in the red-ox reaction between the disulfide and the chalcocite surface then the ''Cu-DTP'' species would have been formed at the surface of the Cu_2O treated with disulfide. More detailed studies involving different concentrations of the disulfide and further studies on the adsorption processes at different surfaces are, indeed, needed to reveal the actual interaction process between the collector and/or disulfide, and the chalcocite.

5. Conclusions

The polycrystalline $\{Cu_8[S_2P(O^iPr)_2]_6(\mu_8\text{-}S)\}$ and $\{Cu_8[S_2P(O^iAm)_2]_6(\mu_8\text{-}S)\}$ cluster compounds were synthesized and characterized by solid-state ^{31}P CP/MAS and static ^{65}Cu (at multiple magnetic field strengths) NMR. The ^{31}P and ^{65}Cu isotropic and anisotropic chemical shifts and ^{65}Cu quadrupolar interaction parameters for the cluster compounds were estimated by simulating the experimental NMR spectra. Three different quadrupolar line-shapes were detected in the solid-state static ^{65}Cu NMR spectrum of $\{Cu_8[S_2P(O^iPr)_2]_6(\mu_8\text{-}S)\}$ while only two were distinguishable in the case of $\{Cu_8[S_2P(O^iAm)_2]_6(\mu_8\text{-}S)\}$. The dithiophosphate ligand shells show a chemical equivalence in pairs of the six phosphorus sites (in both cases). Significantly different short transverse relaxation time constants, T_2, of 590 μs (Gaussian) and 90 μs (exponential), were determined for the octanuclear copper(I) cluster compounds, $\{Cu_8[S_2P(O^iPr)_2]_6(\mu_8\text{-}S)\}$ and $\{Cu_8[S_2P(O^iAm)_2]_6(\mu_8\text{-}S)\}$, respectively. The difference was ascribed to effects originating in the alkyl chains, despite the chemically identical local environment for all the copper sites, $[CuS_3\ldots S_{centre}]$.

The structural appearances of poly-nuclear cluster compounds $\{Cu_4L_4\}$ and $\{Cu_8L_6(S)\}$ ($L = S_2P(OR)_2$ with $R = {}^iPr$) in acetone solutions were examined by copper K-edge EXAFS and liquid-state ^{31}P NMR. It was determined that these structures are in principle the same in the solid-state and in the acetone solutions, and show identical ^{31}P isotropic chemical shifts in the liquid-state (acetone and CH_2Cl_2).

The adsorption mechanism of potassium *O*,*O*′-di-*iso*-amyldithiophosphate and of the corresponding disulfide on synthetic chalcocite surfaces were examined by means of solid-state ^{31}P NMR. From these data, it is concluded that which species are formed at the mineral surfaces is independent of the form of the dithio-ligand (a potassium salt or a disulfide). The ^{31}P chemical shift data (both isotropic chemical shifts and CSA's) for the species formed on the synthetic chalcocite surfaces were used to assign these species to a phase with a $\{Cu_8L_6(S)\}$ type structure, $L = S_2P(O^iAm)_2$.

Acknowledgements

The work was financed by Agricola Research Centre at Luleå University of Technology. The Varian/Chemagnetics Infinity CMX-360 spectrometer was purchased with a grant from the Swedish Council for Planning and Coordination of Research (FRN) and further upgraded with a grant from The Foundation to the memory of J.C. and S.M. Kempe. ^{65}Cu NMR measurements were initiated during a Framework 5 Marie Curie Training program at the University of Warwick, UK. The EXAFS data were carried out at MAXLab, University of Lund, and supported by The Swedish Research Council and The Wallenberg Foundation. The MAXLab, Lund University, is gratefully acknowledged for allocation of beam-time and putting laboratory facilities at our disposal. MAXLab is supported by The Swedish Research Council and The Knut and Alice Wallenbergs Stiftelse, and additional support was made by The Crafoordska Stiftelse and The Faculty of Science & Technology, Norwegian University of Science & Technology. We are grateful to Marshall Hughes, Organic Mass Spectroscopy Facility in the CSL at University of Tasmania, for the FAB-mass measurements of the cluster compounds. The authors also acknowledge *CHEMINOVA AGRO A/S* for dithiophosphate reagents. RD thanks the Leverhulme Trust for support. We thank Dr. Andy Howes, University of Warwick, UK for discussions and we are grateful for the support from Dr. Stefan Carlson at the MAXLab.

Appendix A. Supporting information

Supplementary data associated with this article can be found, in the online version, at doi:10.1016/j.poly.2006.07.013.

References

[1] (a) T. Colclough, Ind. Eng. Chem. Res. 26 (1987) 1888;
(b) K. Othmer, Encyclopedia of Chemical Technology, vol. 10, Wiley, New York, 1980, p. 523;
(c) X. Wang, W. Liu, F. Yan, Z. Zhang, B. Xu, Chem. Lett. 33 (2004) 196.

[2] (a) I. Haiduc, D.B. Snowerby, S.-F. Lu, Polyhedron 14 (1995) 3389;
(b) I. Haiduc, L.Y. Goh, Coord. Chem. Rev. 224 (2002) 151.

[3] G.N. George, J. Byrd, D.R. Winge, J. Biol. Chem. 263 (1988) 8199.

[4] S.L. Lawton, W.J. Rohrbaugh, G.T. Kokotailo, Inorg. Chem. 11 (1972) 612.

[5] C.W. Liu, T. Stubbs, J.P. Fackler Jr., J. Am. Chem. Soc. 117 (1995) 9778.

[6] (a) D. Wu, J.Q. Huang, Y. Lin, J.L. Huang, Sci. Sin. Ser. B, Engl. Ed. 31 (1988) 800;
(b) K. Matsumato, R. Shimomira, Y. Nakao, Inorg. Chim. Acta 304 (2000) 293;
(c) D. Rusanova, K.E. Christensen, I. Persson, K.J. Pike, O.N. Antzutkin, X. Zou, R. Dupree, W. Forsling, J. Coord. Chem., in press;
(d) C.W. Liu, M.D. Irwin, A.A. Mohamed, J.P. Fackler Jr., Inorg. Chim. Acta 357 (2004) 3950;
(e) Y.-B. Chen, Z.-J. Li, Y.-Y. Qin, Y. Kang, J.-K. Cheng, R.-F. Hu, Y.-H. Wen, Y.-G. Yao, Inorg. Chem. Commun. 6 (2003) 405.

[7] (a) D. Rusanova, W. Forsling, O.N. Antzutkin, K.J. Pike, R. Dupree, J. Magn. Reson. 179 (2006) 140;
(b) D. Rusanova, K.J. Pike, I. Persson, J.V. Hanna, R. Dupree, W. Forsling, O.N. Antzutkin, Chem. Eur. J. 12 (2006) 5282;
(c) D. Rusanova, K.J. Pike, R. Dupree, J.V. Hanna, O.N. Antzutkin, I. Persson, W. Forsling, Inorg. Chim. Acta 359 (2006) 3903;
(d) D. Rusanova, W. Forsling, O.N. Antzutkin, K.J. Pike, R. Dupree, Langmuir 21 (2005) 4420.

[8] (a) A.V. Ivanov, O.N. Antzutkin, A.-C. Larsson, M. Kritikos, W. Forsling, Inorg. Chim. Acta 315 (2001) 26;
(b) A.-C. Larsson, O.N. Antzutkin, A.V. Ivanov, W. Forsling, Proceedings Centenary of Flotation Symposium, The Australasian Institute of Mining and Metallurgy, Melbourne, 2005, p. 497.

[9] M.C. Fuerstenau, J.L. Huiatt, M.C. Kuhn, Trans. AIME 250 (1971) 227.

[10] A.N. Buckley, S.W. Goh, R.N. Lamb, R. Woods, Int. J. Miner. Process. 72 (2003) 163.

[11] (a) I. Haiduc, L.Y. Goh, Coord. Chem. Rev. 224 (2002) 151, and references therein;
(b) N.D. Yordanov, K. Ranguelova, Spectrochim. Acta, Part A 58 (2002) 1171.

[12] A. Pines, M.G. Gibby, J.S. Waugh, J. Chem. Phys. 56 (1972) 1776.

[13] O.N. Antzutkin, Y.K. Lee, M.H. Levitt, J. Magn. Reson. 135 (1998) 144.

[14] R.K. Harris, Encyclopedia of Nuclear Magnetic Resonance, vol. 6, Wiley, New York, 1996, p. 3612.

[15] T.J. Bastow, M.E. Smith, Solid State Nucl. Mag. 1 (1992) 165.

[16] K.J.D. Mackenzie, M.E. Smith, K.J.E. Dunn, Multinuclear Solid-State Nuclear Magnetic Resonance of Inorganic Materials, Pergamon Press, Amsterdam, 2002.

[17] D. Massiot, F. Fayon, M. Capron, I. King, S. Le Calvé, B. Alonso, J.-O. Durand, B. Bujoli, Z. Gan, G. Hoatson, Magn. Reson. Chem. 40 (2002) 70, DMfit program available at http://crmht-europe.cnrs-orleans.fr.

[18] M. Bak, J.T. Rasmussen, N.C. Nielsen, J. Magn. Reson. 147 (2000) 296. http://nmr.imsb.au.dk/bionmr/software/simpson.php.

[19] A. Thompson, D. Attwood, E. Gullikson, M. Howells, K.-J. Kim, J. Kirz, J. Kortright, I. Lindau, P. Pianatta, A. Robinson, J. Scofield, J. Underwood, D. Vaughan, G. Williams, H. Winick, X-ray Data Booklet, LBNL/PUB-490 Rev. 2, Lawrence Berkeley National Laboratory, Berkeley, CA 94720, 2001.

[20] (a) S.I. Zabinsky, J.J. Rehr, A. Ankudinov, R.C. Albers, M.J. Eller, Phys. Rev. B 52 (1995) 2995;
(b) A.L. Ankudinov, J.J. Rehr, Phys. Rev. B 56 (1997) R1712.

[21] G.N. George, I.J. Pickering, *EXAFSPAK* – A Suite of Computer Programs for Analysis of X-ray Absorption spectra, SSRL, Stanford University, CA, USA, 1993, The FEFF program available at http://feff.phys.washington.edu/feff.

[22] A. Filipponi, A. Di Cicco, Phys. Rev. A 52 (1995) 1072.

[23] (a) A. Filipponi, J. Phys.: Condens. Matter. 6 (1994) 8415;
(b) L. Hedin, B.I. Lundqvist, J. Phys. C: Solid State Phys. 4 (1971) 2064.

[24] S.J. Gregg, K.S.W. Sing, Adsorption, Surface Area and Porosity, Academic Press, London, 1982.

[25] A-.C. Larsson, A.V. Ivanov, W. Forsling, O.N. Antzutkin, A.E. Abraham, A.C. de Dios, J. Am. Chem. Soc. 127 (2005) 2218.

[26] (a) A.V. Ivanov, O.N. Antzutkin, A-.C. Larsson, M. Kritikos, W. Forsling, Inorg. Chim. Acta 315 (2001) 26;
(b) A-.C. Larsson, A.V. Ivanov, O.N. Antzutkin, A.V. Gerasimenko, W. Forsling, Inorg. Chim. Acta 357 (2004) 2510;
(c) A.V. Ivanov, A.V. Gerasimenko, O.N. Antzutkin, W. Forsling, Inorg. Chim. Acta 358 (2005) 2585;
(d) A-.C. Larsson, A.V. Ivanov, K.J. Pike, W. Forsling, O.N. Antzutkin, J. Magn. Reson. 177 (2005) 56.

[27] H. Günther, NMR Spectroscopy-basic Principles, Concepts, and Application in Chemistry, second ed., Wiley, Chichester, 1995.

[28] C.P. Slichter, Principles of Magnetic Resonance, Springer, Berlin, 1989.

[29] A. Lesage, M. Bardet, L. Emsley, J.Am. Chem. Soc. 121 (1999) 10987.

[30] A. Abragam, The Principles of Nuclear Magnetism, O.U.P., Oxford, 1961.

[31] N.D. Yordanov, Trans. Met. Chem. 22 (1997) 200, and references therein.

[32] (a) B.K. Santra, C.-M. Hung, B.-J. Liaw, J.-C. Wang, C.W. Liu, Inorg. Chem. 43 (2004) 7570;
(b) C.W. Liu, H.-C. Chen, J.-C. Wang, T.-C. Keng, Chem. Commun. (1981) 1831.

[33] C. Glidwell, Inorg. Chim. Acta 25 (1977) 159.

[34] K.B. Nilsson, I. Persson, Dalton Trans. (2004) 1312.

[35] M. Valli, B. Malmensten, I. Persson, Coll. Surf. A 83 (1994) 227.

[36] M.G. Buerger, B.J. Wuensh, Science 141 (1963) 276.

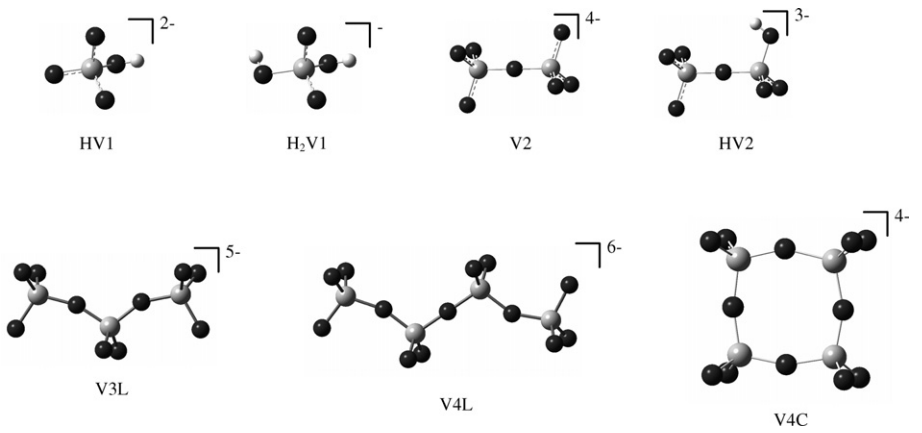

Fig. 1. Schematic structures of the main species in vanadate aqueous solutions (adapted from Refs. [3,4]) HVO_4^{2-} (HV1), $H_2VO_4^-$ (H_2V1), $V_2O_7^{4-}$ (V2), $HV_2O_7^{3-}$ (HV2), $V_3O_{10}^{5-}$ (V3L), $V_4O_{13}^{6-}$ (V4L) and $V_4O_{12}^{4-}$ (V4C).

it should be emphasized that not only hydrophobic interactions will lead to an association between a guest molecules and CD. Ionic solutes, such as non-associated inorganic salts, can also be involved in these complexes [13–15].

The present paper intends to fill this gap, and report conductance measurements and diffusion coefficients for vanadium (V) in aqueous solutions of β-cyclodextrin (β-CD) at 298.15 K. These studies are complemented and supported by nuclear magnetic resonance (NMR) spectroscopic studies in order to identify the dominant species involved in the diffusion and conductivity processes. To obtain a better understanding of the structure of the chemical species formed, we have complemented these studies using molecular mechanics calculations. Finally, a model to calculate the association constant between vanadium (V) and β-CD has been developed and the association constant estimated.

2. Experimental

2.1. Reagents

Ammonium monovanadate (Merck, *pro analysi*, >99%) was used without further purification. β-CD was purchased from Sigma (*pro analysi* >99%), and had a water content 13.1% as verified from thermal analysis.

Aqueous solutions were prepared using bi-distilled (diffusion measurements) or Millipore-Q (conductance measurements) water, and D_2O (NMR spectroscopy).

All solutions were freshly prepared before each experiment.

2.2. Diffusion measurements

Diffusion coefficients were measured with an open-ended capillary cell. The apparatus assembled for use with the open-ended capillary cell in this laboratory is essentially the same as previously reported [16]. The cell has two vertical capillaries, each closed at one end by a platinum electrode and positioned one above the other with the open ends separated by a distance of about 14 mm.

The upper and lower tubes, initially filled with solutions of concentrations $0.75c$ and $1.25c$, respectively, were surrounded with a solution of concentration c. This ambient solution was contained in a glass tank ($200 \times 140 \times 60$) mm immersed in a thermostat at 298.15 K. The tank was divided internally by Perspex sheets and a glass stirrer created a slow lateral flow of ambient solution across the open ends of the capillaries. Experimental conditions were such that the concentration at each of the open ends was equal to the ambient solution value c. That is the physical length of the capillary tube coincided with the diffusion path, such that the boundary conditions described in the literature [16] to solve Fick's second law of diffusion are applicable. As a consequence, the so-called Δl-effect [16] is reduced to negligible proportions. In contrast to a manual apparatus, where diffusion is followed by measuring the ratio of resistances of the top and bottom tubes, $w = R_t/R_b$, by an alternating current transformer bridge, in our automatic apparatus w was measured by a Solartron digital voltmeter (DVM) 7061 with 6 1/2 digits. A Bradley Electronics Model 232 power source supplied a 30 V sinusoidal signal of 4 kHz (stable up to 0.1 mV) to a potential divider that applied a 250 mV signal to the platinum electrodes at the top and bottom capillaries. By rapidly (<1 s) measuring the voltages V' and V'' from top and bottom electrodes to the central electrode at ground potential, the value $w = R_t/R_b$ was then calculated from the DVM reading.

To measure the differential diffusion coefficient, D, at a given concentration c, a "top" solution of concentration $0.75c$ and a "bottom" solution of concentration $1.25c$ were prepared, each in a 2 L volumetric flask. The "bulk" solution of concentration c was produced by mixing accurately measured volumes of 1 L of "top" solution with 1 L of "bottom" solution. The ammonium monovanadate solutions were prepared by heating to 353.15 K and then allowing them to cool to 298.15 K. The glass tank and the two capillaries were filled with solution c, immersed in the

thermostat, and were allowed to come to thermal equilibrium. The quantity $TR_{inf} = 10^4/(1 + w)$ was then measured very accurately. Here $w = R_t/R_b$ is the electrical resistance (R) ratio for solutions of concentration c of the top (t) and bottom (b) diffusion capillaries at infinite time. $TR = 10^4/(1 + w)$ is the equivalent at any time t.

The capillaries were filled with "top" and "bottom" solutions, which were allowed to diffuse into the "bulk" solution. Resistance ratio readings were taken at recorded times, beginning 1000 min after the start of each experiment. The diffusion coefficient was evaluated using a linear least-squares procedure to fit the data, followed by an iterative process which uses 20 terms of the expansion series of the solution of Fick's second law for the present boundary conditions. The theory developed for this cell has been described previously [16].

2.3. Conductance measurements

Solution electrical resistances were measured with a Wayne-Kerr model 4265 Automatic LCR meter at 1 kHz. A Shedlovsky-type conductance cell was used. Cell constants ($\approx$0.1417 ($\pm$0.0001) cm^{-1}) were determined from measurements with KCl (reagent grade, recrystallized, and dried) using the procedure and data of Barthel et al. [17]. Measurements were made at 298.15 ± 0.01 K. Solutions were always used within 12 h after preparation.

In a typical experiment a vanadium (V) solution (of concentration around 5 mM) was placed in the conductivity cell; then, aliquots of the β-CD solution (dissolved in ammonium monovanadate solution of the same concentration as that in the conductivity cell, to maintain a constant NH_4VO_3 concentration throughout the experiment) were added in a stepwise manner using a micropipette. The concentration of β-CD was varied from 0 to 8 mM. The conductance of the solution was measured after each addition. All solutions were freshly prepared just before each experiment.

2.4. NMR measurements

The ^1H, ^{13}C and ^{51}V NMR spectra were obtained on a Varian UNITY-500 NMR spectrometer (at 499.824, 125.692 and 131.404 MHz, respectively). The ^1H NMR spectra were recorded using spectral widths of 5000 Hz, acquisition times of 5 s, pulse delays of 5 s and about 320 pulses. The residual water signal was reduced by using the Presat sequence. The ^{13}C NMR spectra were obtained using proton-decoupling techniques taking advantage of the nuclear Overhauser effect due to the low intensity of the signals as a consequence of the bound ligand; spectral widths of 30000 Hz, acquisition times of 1 s, pulse delays of 10 s and about 5000 pulses were employed. The methyl signal of *tert*-butyl alcohol was used as internal reference for ^1H ($\delta = 1.3$) and ^{13}C ($\delta = 31.2$) relative to TMS. The ^{51}V NMR spectra were obtained using $VOCl_3$ ($\delta = 0$) as external reference, typically with spectral widths of 80000 Hz, acquisition times of 0.04 s, pulse delays of 0.02 s and about 16000 pulses. Slow exchange is confirmed in this system since in the ^1H and ^{13}C NMR spectra distinct signals appear for bound and free ligand.

2.5. Molecular mechanics studies (MM2)

Molecular mechanic studies are a valuable tool to interpret atom or ion dynamics of solute/solvent interactions in molecular systems involving large numbers of molecules or ions [18]. The calculations presented in this study were performed using the MM+ molecular mechanics force field, with a Polak–Ribiere algorithm having a convergence limit o 0.2 kJ/A mol, performed on a 3.2 MHz Pentium 4 workstation with HyperChem v6.

3. Results and discussion

3.1. NMR spectra of NH_4VO_3 in aqueous solutions of β-cyclodextrin

The ^{51}V NMR spectrum of a D_2O solution of NH_4VO_3 5×10^{-3} M (pH $\approx$ 7.5) shows four signals that can be assigned to tetrahedral monovanadate, divanadate, tetravanadate and pentavanadate [19]. In the presence of β-cyclodextrin (1×10^{-3} M), the slow equilibrium between oligomeric species is slightly changed and in the ^{51}V NMR spectra of solutions of NH_4VO_3/β-cyclodextrin (pH $\approx$ 7.5) in D_2O, in addition to the tetrahedral monovanadate (V_1), divanadate (V_2), tetravanadate (V_4) and pentavanadate (V_5) ions, it is possible to identify one additional signal ($\delta = -542$ ppm), that can be assigned to complex species formed between vanadate (V) and β-cyclodextrin. These species are also detected in the ^1H NMR spectra and in the ^{13}C NMR spectra for solutions with higher β-cyclodextrin concentrations.

When β-cyclodextrin is added to the vanadate solution, the signals due to oligomeric species V_1 and V_2 and V_4 decrease in intensity, and the spectra indicate the formation of the complex species. ^{51}V chemical shifts of complexes detected with β-cyclodextrin, suggest the presence of octahedral metal centres [3,19–21] in the complex (Fig. 2 and Table 1).

Mixtures of ammonium vanadate and β-cyclodextrin, in aqueous solution, show two additional sets of ^1H and ^{13}C signals, whose intensities depend on concentration and molar ratios, which are assigned to the complexed forms, in addition to those of the free ligand which is always present in excess.

Regarding the ^{13}C NMR spectra, the high frequency shifts relative to the free ligand observed upon binding ($\Delta\delta$) for carbinol carbon nuclei C-2 and C-3 are characteristic of the involvement of OH-2 and OH-3 groups in complexation as follows: for C-1, C-2, C-3 and C-5 two signals for bound ligand are detected in each case, which $\Delta\delta$ are 2.22 and 0.22 ppm, 8.79/11.26 and 7.89 ppm and 11.74, 10.23/7.75 ppm, and 1.55 and 0.38 ppm, respectively. For

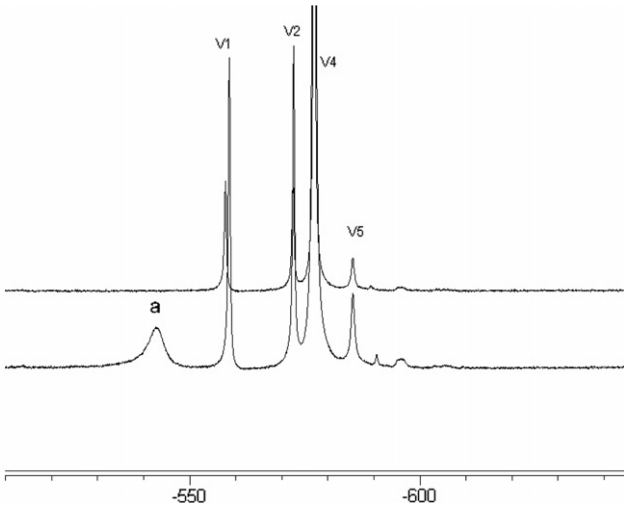

Fig. 2. ^{51}V NMR spectra (131.404 MHz) of a 5 mM solution of NH_4VO_3 (top) and a 5 mM:1 mM solution of NH_4VO_3/β-CD (bottom), pH ≈ 7.5, 298.15 K.

Table 1
Concentrations of vanadate species[a,b] obtained from ^{51}V NMR at 298.15 K

	V_1	V_2	V_4	V_5	CD2V
NH_4VO_3[c]	0.48	0.53	3.69	0.30	0.0
NH_4VO_3/β-cyclodextrin[d]	0.47	0.52	3.28	0.26	0.47
NH_4VO_3/β-cyclodextrin[e]	0.40	0.49	1.87	0.06	2.17
NH_4VO_3/β-cyclodextrin[f]	0.32	0.30	1.00	0.05	3.33
NH_4VO_3/β-cyclodextrin[g]	0.36	0.25	0.84	0.03	3.52

[a] The concentration of all the vanadate species are shown as vanadium atom concentration in millimolar dm^{-3} units and are obtained the ^{51}V integrals. Ionic strength was not controlled.

[b] V_1, monomeric vanadate; V_2, dimeric vanadate; V_4, tetrameric vanadate; V_5, pentameric vanadate; CD2V complex possessing octahedral centres.

[c] 5 mmol dm^{-3} solution, pH ≈ 7.5.

[d] 5.0:1.0 mmol dm^{-3} solution, pH ≈ 7.5.

[e] 5.0:5.6 mmol dm^{-3} solution, pH ≈ 7.5.

[f] 5.0:10.0 mmol dm^{-3} solution, pH ≈ 7.5.

[g] 5.0:13.0 mmol dm^{-3} solution, pH ≈ 7.5.

C-4 and C-6 only one signal is detected for bound ligand in each case, for which $\Delta\delta$ values are 0.15 and 0.56 ppm, respectively, presumably due to the superposition of the remaining signals with those of the free ligand. Similarly, in the ^1H NMR spectra, the protons H-2 and H-3 undergo a significant chemical shift, which is to high frequencies. Although the two signals relative to bound ligand are not observed for H-2, due to superposition with those of the free ligand, two signals for bound ligand are detected for H-3 ($\Delta\delta$ 0.67 and 0.52 ppm).

Thus, the coordination sites of the ligand should involve the (2,3)-diol group of two glucose moieties from different β-CD units, since the diol coordination requirements for an octahedral complex can only be fulfilled with four hydroxyl groups and the cyclic structure of the β-cyclodextrin does not allow four coordination sites in the same cyclodextrin molecule.

All these findings, associated with the fact that the two ligand molecules are magnetically equivalent, points to the conclusion that the two sets of bound ligand detected in the ^1H and ^{13}C NMR spectra are due to two 2:1 (ligand: metal) diastereoisomers (CD2V) differing in the relative configuration of O-2 and O-3 around the octahedral metal centre. Complexes have been characterized of Mo(VI) and W(VI) with α-hydroxyacids and sugar acids in aqueous solution having similar geometry [22,23].

3.2. Molecular mechanics analysis

From molecular mechanics, vanadium (V) coordination through oxygen 2 and 3 of a glucose residue from both β-CD rings with vanadium (V) induces just small conformational reorientation in all glucose rings of both β-CD molecules, but the main effect appears to be the tilting of one β-CD molecule relative to the other. Starting with both β-CD in a "in plane" situation, the MM+ geometry minimization always leads to a perfect octahedral coordination in vanadium (V) with the two β-CD molecules displaced by 45° (Fig. 3).

The energy variations before and after the vanadium coordination also support the 2:1 ratio of β-cyclodextrin/octahedral vanadium. The sum of the vacuum energies calculated for an isolated set of two β-cyclodextrin and an octahedral vanadium ($V(=O)_2(OH)_4$) is 890.2 kJ/mol and the calculated energy for the two β-cyclodextrin coordinated with an octahedral vanadium is 874.5 kJ/mol, showing a very small beneficial effect in the final coordination compound. The perfect octahedral coordination at vanadium

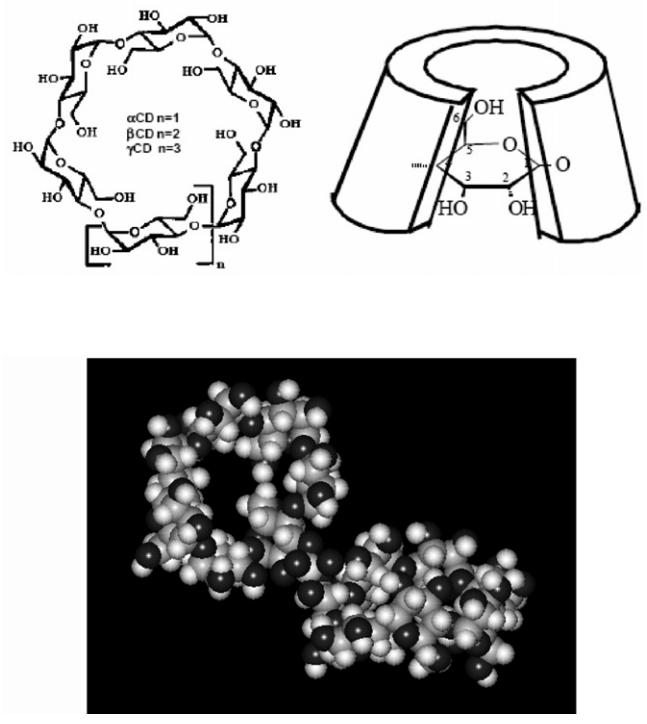

Fig. 3. 3D minimized structure of the 2:1 β-CD/vanadium complex.

and the energy calculations both point to 2:1 ratio β-cyclodextrin/octahedral vanadium (V) complexation, in agreement with the NMR data.

3.3. Electrical conductivity

Fig. 4 shows the effect of the β-CD on the molar conductivity of aqueous solutions of NH_4VO_3 at 298.15 K. The molar conductivity (Λ) was calculated using

$$\Lambda = (\kappa - \kappa_0)/(c \times 1000) \quad (1)$$

where κ and κ_0 are specific conductances of solution and water, respectively, and c is the ammonium vanadate concentration. The molar conductivity of the ammonium vanadate solution decreases with the addition of β-CD, providing further evidence for complexation between the NH_4VO_3 and β-CD. As a consequence, an appreciable fraction of the transport of NH_4VO_3 may occur via these larger aggregates, which will lead to high resistance to motion through the liquid and, consequently, a lower mobility and a decrease in the conductivity, as found; that is, the complexes are less effective as charge carriers (the ion mobility is decreased upon complexation). From the analysis of Fig. 4, it is also possible to conclude that no plateau of molar conductivity as a function of [β-CD] is reached at $[\beta\text{-CD}]/[NH_4VO_3] < 2$, which is a further evidence that no 1:1 complexation is occurring.

3.4. Diffusion coefficients of NH_4VO_3 in aqueous solutions of β-cyclodextrin

Tables 2 and 3 show the experimental diffusion coefficients with ammonium monovanadate solutions of concentrations from 1×10^{-3} to 5×10^{-2} M at 298.15 K alone, and in the presence of β-cyclodextrin. These results are the average of three experiments performed on consecutive days. Good reproducibility was observed, as seen by the small standard deviations of the mean, S_{Dav}. Previous papers [24,25] reporting data obtained with our conductivity cell have shown that the inaccuracy of our results should be close to the imprecision, giving therefore an experimental uncertainty 1–2%.

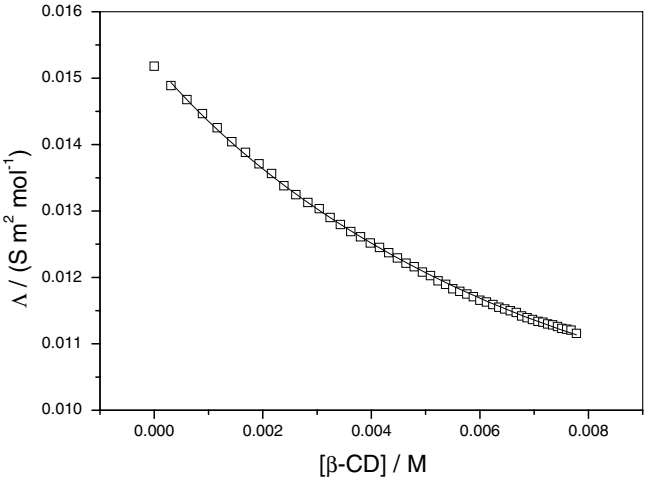

Fig. 4. Dependence of the molar conductivity of the NH_4VO_3 (4.907 mM) on the β-cyclodextrin concentration, at 298.15 K. Solid lines represent molar conductivities predicted by Eq. (9) using the parameters shown in Section 3.5.

Table 2
Diffusion coefficients, D, of NH_4VO_3 in aqueous solutions at 298.15 K at different concentrations, c (see Ref. [3])

c (M)	D (10^{-9} m^2 s^{-1})[a]	TR_{inf}[b]	S_{Dav} (10^{-9} m^2 s^{-1})[c]
0.001	1.264	5 000.5	0.018
0.003	1.203	4 999.8	0.009
0.005	1.174	5 000.0	0.003
0.008	1.147	5 000.1	0.006
0.010	1.135	5 000.2	0.010
0.020	1.116	5 010.0	0.008
0.030	1.110	5 011.1	0.007
0.050	1.090	4 995.5	0.008

[a] Mean value of D_{exp} in three experiments.
[b] $TR_{inf} = 10^4/(1 + w)$, where $w = R_t/R_b$ is the resistance ratio of top and bottom capillaries.
[c] S_{Dav} is the standard deviation of the mean of three experiments.

Table 3
Diffusion coefficients, D[a], of NH_4VO_3 in aqueous solutions of β-cyclodextrin (0.001 M) at different concentrations, c, and the standard deviations of the means, S_{Dav}

c (mol dm^{-3})	$T = 298.15$ K		
	D (10^{-9} m^2 s^{-1})[a]	S_{Dav} (10^{-9} m^2 s^{-1})[b]	$\Delta D/D$ (%)[c]
0.001	1.046	0.003	−17.2
0.01	1.058	0.002	−6.8
0.02	1.072	0.005	−3.9
0.05	1.112	0.001	+2.0

[a] D is the mean diffusion coefficient for three experiments.
[b] S_{Dav} is the standard deviation of that mean.
[c] $\Delta D/D$ represent the relative deviations between the diffusion coefficients of NH_4VO_3 at the specified concentration in 0.001 M β-cyclodextrin, D, and that of the NH_4VO_3 in water, D (Table 2).

From Table 2, the decrease of the diffusion coefficient of ammonium monovanadate in aqueous solutions with increasing concentration strongly suggests the presence of new species (e.g., $V_4O_{12}^{4-}$) resulting from condensation of the salt. The decrease of D with concentration may be explained by assuming those species have a lower mobility than other anions because of their size. The eventual onset and formation of ion pairs upon increasing concentration may also contribute to the decrease of D with concentration [24].

The β-cyclodextrin molecules exert a significant influence on the diffusion of ammonium monovanadate in the various aqueous solutions ($c \leqslant 0.05$ M). Under the present experimental conditions, i.e., $[NH_4VO_3]/$[carbohydrate] ratio values $\geqslant 1$ and dilute solutions, the motion of the solvent and the change of parameters such as viscosity, dielectric constant and degree of hydration with concentration, can be neglected. With a concentration gradient in a solution with exactly the same salt

concentration as that in the above solution of NH_4VO_3 but now with identical concentrations of β-cyclodextrin, we observe that the diffusion coefficient D is lower. Assuming that D [25] is a product of kinetic (molar mobility coefficient of a diffusing substance, U_m) and thermodynamic factors ($c\partial\mu/\partial c$, where μ represents the chemical potential), we suggest that both factors decrease, when we pass from a solution of pure NH_4VO_3 to a mixed solution having both NH_4VO_3 and β-cyclodextrin. In fact, the decrease of the kinetic factor is confirmed by the conductance results at 298.15 K (Table 3). Thus, two different effects can control the diffusion process: the ionic mobility and the gradient of the chemical potential. Based on these measurements, in conjunction with the conductance measurements, we conclude that, over the concentration range studied (Table 3), the diffusion of NH_4VO_3 in aqueous solutions at 298.15 K appears to be affected by complexation or aggregate formation between vanadate ions and β-cyclodextrin. This supports the above NMR, conductance, and MM2 studies. For the same concentrations, the observed deviations in diffusion coefficients for NH_4VO_3 in the presence and absence of β-cyclodextrin, are lower than obtained for conductance. Possibly, the slight decrease of the gradient of the chemical potential with concentration can explain this behaviour. These considerations should be taken into account when studying the corrosion of dental alloys containing vanadium.

3.5. Determination of association constants

According to the discussion of the NMR experimental results (see Section 3.1), the interaction between NH_4VO_3 (V) and β-cyclodextrin (CD) leads to a 2:1 (CD:V) complex, CD_2V. Assuming that such complexation occurs in a two-step model, the equilibrium equations can be written as:

$$CD + V \rightleftharpoons CDV \quad (2)$$

$$CDV + CD \rightleftharpoons CD_2V \quad (3)$$

The stability of the association complexes, CDV and CD_2V, can be described in terms of association constant, K_{11} and K_{21}, respectively.

$$K_{11} = C_{CDV}/(C_{CD,f} \cdot C_{V,f}) \quad (4)$$

$$K_{21} = C_{CD2V}/(C_{CD,f} \cdot C_{CDV}) \quad (5)$$

According to the law of conservation of mass:

$$C_{V,f} = C_{V,t} - C_{CDV} - C_{CD2V} \quad (6)$$

and

$$C_{CD,f} = C_{CD,t} - C_{CDV} - 2C_{CD2V} \quad (7)$$

where $C_{V,t}$ and $C_{CD,t}$, and $C_{V,f}$ and $C_{CD,f}$ represent the total (t) and free (f) concentrations of V and β-CD, and C_{CDV} and C_{CD2V} are the concentrations of 1:1 and 2:1 associate species, respectively.

Considering the CD concentration range where the free vanadium, $C_{V,f}$, and the free β-cyclodextrin, $C_{CD,f}$, are in equilibrium with the complexes, CDV and CD_2V, the observed specific conductance, κ, can be expressed as:

$$\kappa = \kappa_V + \kappa_{CDV} + \kappa_{CD2V} \quad (8)$$

where κ_V, κ_{CDV} and κ_{CD2V} are ammonium monovanadate and the associate compounds (1:1 and 2:1) specific conductances.

Taking into account the definition of molar conductivity, $\Lambda = \kappa/(C \cdot 1000)$ and from combination of Eqs. (4)–(8) gives, after some algebra, the following expression for the observed molar conductivity:

$$\Lambda = \frac{\Lambda_V + \Lambda_{CDV}K_{11}C_{CD,f} + \Lambda_{CD2V}K_{11}K_{21}C_{CD,f}^2}{1 + K_{11}C_{CD,f} + K_{11}K_{21}C_{CD,f}^2} \quad (9)$$

where Λ is the observed molar conductivity.

Least-square fits were performed using in-house written soft-ware based on the Gnuplot®. The fitting results are: $K_{11} = 98\ (\pm 2)\ M^{-1}$, $K_{21} = 440\ (\pm 5)\ M^{-1}$, $\Lambda_V = 0.0152\ (0.002)\ S\ m^2\ mol^{-1}$, $\Lambda_{CDV} \to 0$, $\Lambda_{CD2V} = 0.0112\ (0.003)\ S\ m^2\ mol^{-1}$ and $R = 2.20 \times 10^{-8}\ S^2\ m^4\ mol^{-2}$. The application of the model (Eq. (9)) to the experimental results shows that: (a) $K_{11} < K_{21}$, indicating that the formation of 2:1 stoichiometric complexes predominates rather than the 1:1, and (b) the fitting is independent of Λ_{CDV} when this value is lower than $1 \times 10^{-6}\ S\ m^2\ mol^{-1}$ and approaches to zero. This latter result suggests that the concentration of CD-V complexes affecting specific conductance, κ_{CDV}, can be neglected; that is, the concentration of CD-V species can also be neglected, which is in agreement with the results presented in (a) and the NMR results where no complex 1:1 is detected.

4. Conclusions

We have measured diffusion coefficients, electrical conductivity, obtained NMR spectral data for ammonium monovanadate in aqueous solutions of β-cyclodextrin, and have complemented these studies with molecular mechanics calculations. In the presence of this carbohydrate, the diffusion behaviour of ammonium monovanadate can be explained by formation of complexes in small concentrations. These species are suggested to be responsible by the decrease of the free energy gradient driving the diffusion process and the mobility factor. From the conductivity data, the presence of this carbohydrate decreases the mobility of the ammonium monovanadate.

Acknowledgements

We are grateful to Fundação para a Ciência e a Tecnologia, FEDER and POCI for funding through the Centro de Química (A.C.F.R., A.J.M.V., V.M.M.L., A.J.F.N.S., and H.D.B) and Unidade Espectroscopia RMN (M.L.R).

References

[1] D.M. Facchini, V.G. Yueng, M.L. Battell, J.H. McNeill, M.D. Grynpas, Bone 38 (2006) 368.
[2] Y. Hasegawa, M. Morioka, S. Hasegawa, J. Matsumoto, T. Kawano, Y. Kai, S. Yano, K. Fukunaga, J.I. Kuratsu, J. Pharmacol. Exp. Ther. 317 (2006) 875.
[3] A.C.F. Ribeiro, A.J.M. Valente, V.M.M. Lobo, E.F.G. Azevedo, A.M. Amado, A.M. Amorim da Costa, M.L. Ramos, H.D. Burrows, J. Mol. Struct. 703 (2004) 93.
[4] K. Uekama, F. Hirayama, T. Irie, Chem. Rev. 98 (1998) 2045.
[5] S. Li, W.C. Purdy, Chem. Rev. 92 (1992) 1457.
[6] W.R. Saenger, J. Jacob, K. Gessler, T. Steiner, D. Hoffmann, H. Sanbe, K. Koizumi, S.M. Smith, T. Takaha, Chem. Rev. 98 (1998) 1787.
[7] A.C.F. Ribeiro, M.A. Esteso, V.M.M. Lobo, A.J.M. Valente, S.M.N. Simões, A.J.F.N. Sobral, M.L. Ramos, H.D. Burrows, A.M. Amado, A.M. Amorim da Costa, J. Carbohydr. Chem. 25 (2006) 173.
[8] I. Tabushi, Chem. Res. 15 (1982) 66.
[9] S. Anderson, T.D.W. Claridge, H.L. Anderson, Angew. Chem., Int. Ed. Engl. 36 (1997) 1310.
[10] A.J.M. Valente, M. Nilsson, O. Söderman, J. Colloid Interface Sci. 281 (2005) 218.
[11] C. Cabaleiro-Lago, M. Nilsson, O. Söderman, Langmuir 21 (2005) 11637.
[12] J.A. Fernandes, S.S. Braga, M. Pillinger, R.A.S. Ferreira, L.D. Carlos, A. Hazell, P.R. Claro, I.S. Gonçalves, Polyhedron 25 (2006) 1471.
[13] A. Buvari, L. Barcza, Inorg. Chim. Acta 33 (1979) L179.
[14] A. Buvari, L. Barcza, J. Incl. Phenom. Macrocycl. Chem. 7 (1989) 379.
[15] E. Norkus, G. Grinciene, R. Vaitkus, Carbohydr. Res. 337 (2002) 1657.
[16] J.N. Agar, V.M.M. Lobo, J. Chem. Soc., Faraday Trans. I 71 (1975) 1659.
[17] J. Barthel, F. Feuerlein, R. Neuder, R. Wachter, J. Solution Chem. 9 (1980) 209.
[18] U. Burkert, N.L. Allinger, Molecular Mechanics, ACS Monograph 177, American Chemical Society, Washington, DC, 1982.
[19] C.F.G.C. Geraldes, M.M.C.A. Castro, J. Inorg. Biochem. 35 (1989) 79.
[20] J.-F. Verchère, S. Chapelle, F. Xin, D.C. Crans, Prog. Inorg. Chem. 47 (1998) 837.
[21] D. Rehder, Coord. Chem. Rev. 182 (1999) 297.
[22] M.L. Ramos, M.M. Pereira, A.M. Beja, M.R. Silva, JA. Paixão, V.M.S. Gil, J. Chem. Soc., Dalton Trans. 10 (2002) 2126.
[23] M.L. Ramos, V.M.S. Gil, Carbohydr. Res. 339 (2004) 2225, and references therein.
[24] A.C.F. Ribeiro, V.M.M. Lobo, E.F.G. Azevedo, J. Solution Chem. 30 (2002) 1111.
[25] L. Onsager, R.M. Fuoss, J. Phys. Chem. 36 (1932) 26.

2. Experimental

2.1. General methods

Microanalytical (C, H, N) data were obtained with a FLASH EA 1112 Series CHNS Analyzer. A SHIMADZU 3101- PC UV/VIS/NIR spectrophotometer was used to record the electronic spectra. Infrared spectra were recorded on KBr pellets with a JASCO-5300 FT-IR spectrophotometer. The variable temperature (90–305 K) magnetic susceptibility measurements were performed using the Faraday technique with a setup comprising a George Associates Lewis Coil force magnetometer, a CAHN microbalance, and an Air Products cryostat. $Hg[Co(NCS)_4]$ was used as the standard. Diamagnetic correction (-630×10^{-6} cgsu) for $[Cu_4(C_{54}H_{46}N_4O_{14})(OH)_2]$ calculated from Pascal's constants [12] was used to obtain the molar paramagnetic susceptibilities.

2.2. Materials

2,6-Diformyl-4-methylphenol (dfp) was prepared according to the reported procedure [13]. L-Tyrosine and sodium hydroxide were procured from Acros India and used as received. Solvents were purified by standard methods. All other chemicals used were of analytical reagent grade and used without further purifications.

2.3. Synthesis of $[Cu_4(C_{54}H_{46}N_4O_{14})(OH)_2]\cdot 10H_2O$ (1)

To a solution of L-tyrosine (0.18 g, 1 mmol) in ethanol–water mixture (3:1, 40 mL) was added NaOH (0.04 g, 1 mmol) and 2,6-diformyl-4-methylphenol (0.082 g, 0.5 mmol). The reaction mixture was stirred for 1 h at room temperature. To the resulting Schiff-base (H_3L), formed *in situ*, was added $CuSO_4\cdot 5H_2O$ (0.25 g, 1 mmol), and stirred again for another 12 h at room temperature. The resulting dark green solution was filtered and the filtrate on slow evaporation yielded green crystals of **1**. The crystals lose water molecules on exposure to atmosphere (taken out from mother liquor) at room temperature (as is evidenced from TGA studies and loss of single-crystallinity). Yield after water loss 55%. IR (KBr, cm^{-1}): 3391, 1641, 1552, 1516, 1452, 1367, 1321, 1242, 1084, 1045, 885, 858, 810, 765, 542. *Anal*. Calc. for $C_{54}H_{48}N_4O_{16}Cu_4$ (after water loss): C, 51.35; H, 3.83; N, 4.44. Found: C, 50.98; H, 3.95; N, 4.18%. UV/Vis [*N*,*N*-dimethylformamide; λ_{max}/nm (ε)]: 652 (348), 378 (14,951).

2.4. X-ray crystallography

Since the crystals of compound $[Cu_4(C_{54}H_{46}N_4O_{14})(OH)_2]\cdot 10H_2O$ (**1**) lose water molecules once out of mother liquor at ambient conditions, the crystals of **1** were cooled immediately to 100(2) K after removing from the mother liquor. The data were collected on a Bruker SMART APEX CCD area detector system [λ(Mo–Kα) = 0.71073 Å], graphite monochromator, 2400 frames were recorded with an ω scan width of 0.3°, each for 20 s, crystal-detector distance 60 mm, collimator 0.5 mm. The data were reduced using SAINTPLUS [14] and a multi-scan absorption correction using SADABS [14] was performed. The structure was solved by direct methods; structure solution and refinement were done using the programs of SHELX-97 [15]. All non-hydrogen atoms were refined anisotropically. One of the water molecules (O(11)) shows disorder over two positions with equal occupancy. Water hydrogen atoms (except that of O(11)) were located in the differential Fourier maps and their positions were refined using isotropic thermal parameters. Additional details of the data collection parameters and refinement are collected in Table 1. The final Fourier difference synthesis showed minimum and maximum peaks of −0.363 and +0.774 e Å^{-3}.

Table 1
Crystal data and structure refinement for **1**

Empirical formula	$C_{54}H_{68}Cu_4N_4O_{26}$
Formula weight	1443.28
Temperature (K)	100(2)
Crystal system	triclinic
Space group	$P\bar{1}$
a (Å)	10.7136(8)
b (Å)	10.7365(8)
c (Å)	13.7677(10)
α (°)	67.6070(10)
β (°)	87.3940(10)
γ (°)	82.0860(10)
Volume (Å^3)	1450.24(19)
Z	1
D_{calc} (Mg/m^3)	1.653
Absorption coefficient (mm^{-1})	1.538
F(000)	744
Crystal size (mm)	$0.22\times0.17\times0.08$
θ Range for data collection (°)	1.60–28.28
Reflections collected/unique (R_{int})	16998/6813 (0.0275)
Data/restraints/parameters	6813/11/436
Goodness-of-fit on F^2	0.983
Final R indices [$I > 2\sigma(I)$]	$R_1 = 0.0396$, $wR_2 = 0.1030$
R indices (all data)	$R_1 = 0.0534$, $wR_2 = 0.1109$
Largest difference in peak and hole (e Å^{-3})	0.774 and −0.363

3. Results and discussion

3.1. Synthesis

The ligand H_3L, formed *in situ*, by Schiff base condensation (Scheme 1), was reacted with copper(II) sulfate pentahydrate and NaOH at room temperature in ethanol–water mixture to afford the tetra-nuclear complex $[Cu^{II}_4L_2(OH)_2]\cdot 10H_2O$ (**1**) in moderate yield. The two OH^- groups, that act as bridging ligands per tetra-nuclear complex, seems to originate from the sodium hydroxide used in this synthesis. Deprotonation of the Schiff base ligand (removal of three protons per ligand) can also be caused by the added hydroxide ions.

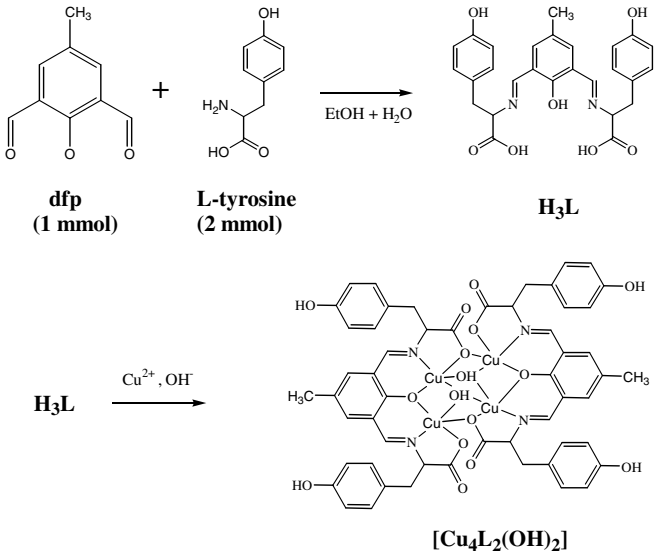

Scheme 1.

3.2. Description of the structure

The complex $[Cu_4(C_{54}H_{46}N_4O_{14})(OH)_2]$ can be formulated as $\{[Cu_2(C_{27}H_{23}N_2O_7)(OH)]\}_2$ in **1**; the centrosymmetric molecule being formed by two binuclear units, one of which is the crystallographic asymmetric unit (along with 5 water molecules). The crystal structure of the tetra-nuclear complex $[Cu_4(C_{54}H_{46}N_4O_{14})(OH)_2]$ in $[Cu_4(C_{54}H_{46}N_4O_{14})(OH)_2]\cdot 10H_2O$ (**1**) with the atom numbering scheme is shown in Fig. 1. Two binuclear units related by the center of symmetry are bridged by two hydroxide oxygen atoms O(8) and O(8)#1 (#1 $= -x+2, -y+1, -z+1$) and as a result form a tetranuclear structure. In the binuclear unit, the two copper centers are also bridged by endogenous phenolic oxygen. The coordination geometries of Cu(1) and Cu(2) in the crystallographically unique unit are slightly different. The coordination geometry of Cu(1) is square pyramidal with the basal co-ordination plane provided by O(1), O(2)and N(1) of the same binuclear unit and O(8)#1 from the adjacent binuclear unit. The axial co-ordination site is occupied by an hydroxide oxygen O(8). {Cu(1)–O(8) 2.3484(19) Å}. Atom Cu(1) deviates by 0.1074(10) Å toward the axial ligand O(8) from the equatorial co-ordination plane. The geometry of Cu(2) can also be described as distorted square pyramidal although the axial bond length is large compared to that of Cu(1). The oxygen atom O(2)#1 of the carboxylate group of the adjacent binuclear unit satisfies the fifth coordination of Cu(2) with a long axial distance of Cu(2)–O(2)#1 2.711(2) Å. The small difference in co-ordination geometries around Cu(1) and Cu(2) is also reflected in the respective bond distances. For example, Cu(2)–O(1) [1.9216(17) Å] is shorter than Cu(1)–O(1) [1.9442(17) Å].

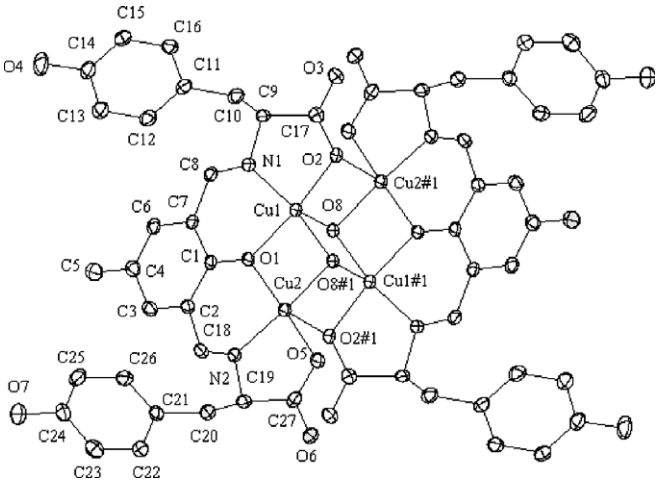

Fig. 1. Thermal ellipsoid plot of the structure of $[Cu_4(C_{54}H_{46}N_4O_{14})(OH)_2]$ in **1**. Hydrogen atoms have been omitted for clarity. Atoms with additional label #1 are related to each other by symmetry operations: #1 $-x+2, -y+1, -z+1$.

Although we have used a chiral amino acid L-tyrosine as starting material, it has undergone racemization under the reaction conditions. As a result, both the chiral carbons present in a particular dimer have opposite absolute configurations and the compound crystallizes in an achiral space group $P\bar{1}$ (C(9) and C(19)#1-(S) and C(19) and C(9)#1-(R)). Similar racemization phenomena have been reported previously [16].

The geometry of the centro-symmetric Cu_4O_4 central core of the molecule can be described as a 'double-open' face shared dicubane with two missing vertices (Fig. 1). One of the two cubanes may be outlined by three four-membered rings: (a) O(1)–Cu(1)–O(8)#1–Cu(2), (b) Cu(2)–O(8)#1–Cu(1)#1–O(2)#1 (c) Cu(1)–O(8)#1–Cu(1)#1–(O8) (#1 $= -x+2, -y+1, -z+1$). The two open cubanes are related by a crystallographic centre of symmetry located at the centroid of the face (c). A Cu_4N_6 defective dicubane-type motif with two missing vertices has been reported in the case of azido bridged 1D molecular railroad copper complex [17].

The most striking feature of the crystal structure of **1** is that, all five crystal water molecules, located in the asymmetric unit, are involved in forming a supramolecular acyclic water nonamer $(H_2O)_9$. This can be described as an "S" shaped water hexamer $(H_2O)_6$ connecting a near linear water trimer $(H_2O)_3$ as shown in Fig. 2 (left). Water nonamer is formed from the water molecules O(9)–O(13), located in the asymmetric unit. The O(11) water is disordered over two symmetry related positions (O(11) and O(11)#8), (#8 $-x, -y+2, -z+1$).

Infantes and Motherwell reported the patterns of water clusters within the Cambridge Structural Database (CSD) and classified them as discrete rings and chains, infinite chains and tapes, and layer structures [18]. According to their CSD search, there was only one discrete quasi-planar cyclic water nonamer known until 2002 [18]. Later, in 2005, Ghosh and Bharadwaj described a discrete open zig-zag water nonamer in an inorganic molecular crystalline hydrate [19]. Extended chain-like arrangement based on a $(H_2O)_9$ cluster is not known (CSD search until 2003)

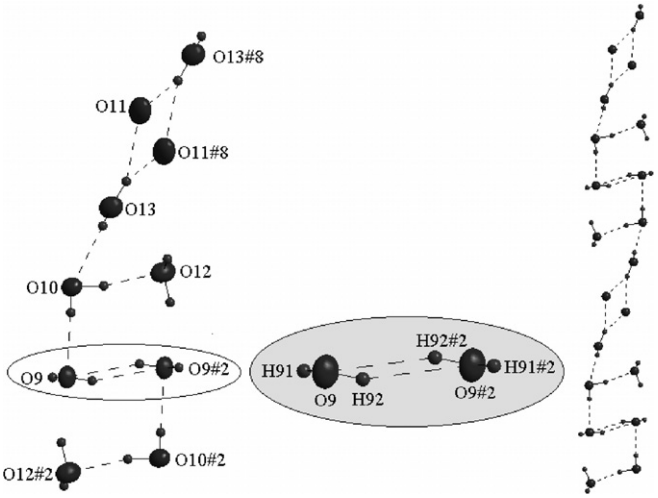

Fig. 2. Left: Water nonamer cluster consisting of a near linear water trimer and an "S" shaped water hexamer that incorporates a cyclic water dimer (highlighted in an ellipsoid). O(11) water is disordered over two positions. Middle: cyclic water dimer is highlighted separately. Right: water nonamer undergoes further hydrogen bond linking to a chainlike structure. Atoms with additional labels #2 and #8 are related to each other by symmetry operations: #2 $-x$, $2-y$, $2-z$; #8 $-x$, $2-y$, $1-z$.

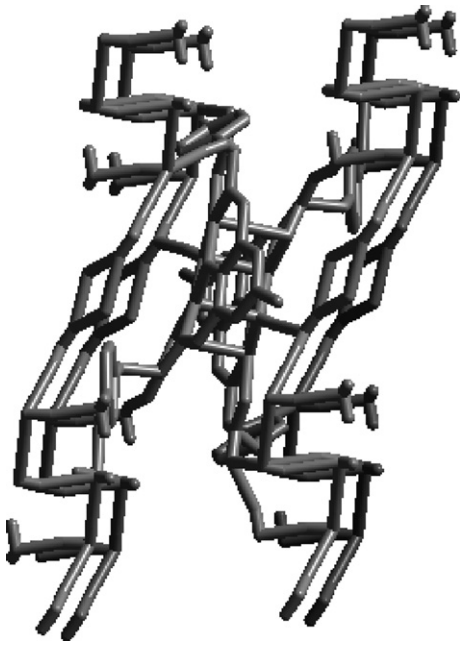

Fig. 3. $[Cu_4(C_{54}H_{46}N_4O_{14})(OH)_2]$ complex exhibiting its hydrogen bonding interactions with four surrounding water chains of $(H_2O)_9$ clusters.

[20]. The water nonamer, in the present study, undergoes hydrogen bond linking into an infinite chain through out the crystal lattice that extends along crystallographic *c* axis (Fig. 2, right). Very recently, Mascal et al. have published an essay on water oligomers in crystalline hydrates by choosing 17 random recent publications that describe unprecedented assemblies of water molecules and compared these structures against those already in the CSD [21]. However, the context of water nonamer is not discussed in this article.

The water nonamer, in the present case, features an inbuilt "cyclic" water dimer (O(9) and O(9)#2, Fig. 2, highlighted) of locally C_i symmetry. This dimer is formed by two O(9) water molecules which are related by a symmetry operation.

The stabilization of such $(H_2O)_9$ and $(H_2O)_2$ clusters in a molecular crystalline host is facilitated by suitable hydrogen bonding environment around the water structure. Indeed, the water chains are supported/anchored by the tetra-nuclear copper complex $[Cu_4(C_{54}H_{46}N_4O_{14})(OH)_2]$ in the crystal of **1** via O–H···O type hydrogen bonding interactions. Each $\{Cu_4\}$ complex connects four different water chains as shown in Fig. 3. Similarly, each water nonamer is anchored by six surrounding $\{Cu_4\}$ complexes (see Supplementary material). The hydrogen bonding parameters for the water nonamer are described in Table 2 and its interactions with the host (copper complex) are provided as Supplementary material (S-Table 3).

Table 2
Geometrical parameters of hydrogen-bonds (Å, °) in water nonamer (see Fig. 2)

D–H···A	*d*(D···H)	*d*(H···A)	*d*(D···A)	L(DHA)
O10–H101···O12	0.94(5)	1.74(4)	2.669(4)	167(3)
O10–H102···O9	0.82(4)	2.03(4)	2.848(3)	178(5)
O13–H132···O10	0.84(4)	2.10(5)	2.901(4)	158(9)
O13–H131···O11	0.89(4)	2.01(6)	2.822(6)	150(9)
O13–H131···O11#8	0.89(4)	2.16(7)	2.931(7)	144(9)
O9–H92···O9#2	0.70(3)	2.08(3)	2.747(5)	160(4)

Atoms with additional labels #2 and #8 are related to each other by symmetry operations specified in the caption of Fig. 2.

3.3. Magnetic studies

To evaluate the singlet–triplet energy separation ($-2J$), variable temperature magnetic study of the complex **1** (after solvent loss) was performed in the temperature range of 90–305 K. Despite the tetranuclear structure, the experimental magnetic susceptibility values were fitted [22] to the Bleaney–Bower's equation with a Curie type of impurity of $S = 0.5$ as shown in Fig. 4. The best fit of the magnetic data to this equation yielded $2J = -217\ cm^{-1}$, $g = 2.019$ and a TIP value of $60 \times 10^{-6}\ cm^3\ mol^{-1}$ (see Supplementary materials for magnetic details). This result may be interpreted in terms of a predominant magnetic interaction through the endogenous phenolic oxygen atom O(1) (and O(1)#1), the intra- and inter-dimer magnetic interactions through the exogenous hydroxide oxygen atom contributing little to the magnetic susceptibility (see also Fig. 1). The phenolic oxygen atom O(1) is bound to three atoms and has lone-pair electrons. On the other hand, the exogenous hydroxide oxygen atom is bound to four atoms and therefore has no lone-pair of electrons. It is likely that each bond involving the bridging oxygen with sp^3-hybridized orbitals is almost perfectly localized so that no spin-exchange interaction is operative.

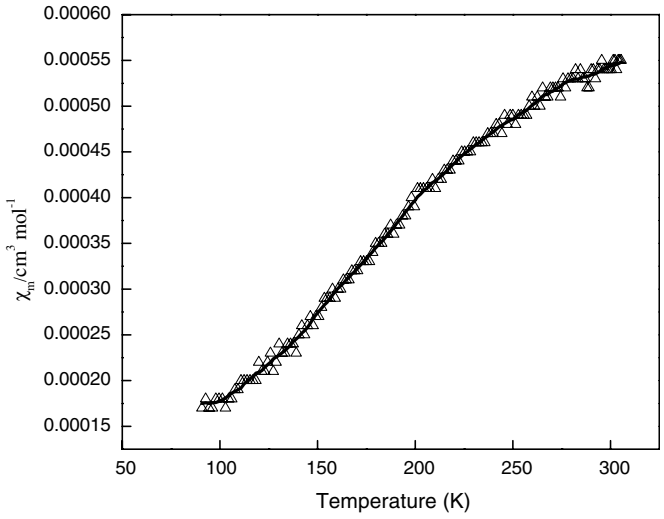

Fig. 4. Magnetic susceptibility data plotted in the form of χ_M (Δ) vs. T for complex **1** in the temperature range 90–305 K. The theoretical fit to the experimental data is shown by solid line.

3.4. TGA studies

Compound $[Cu_4(C_{54}H_{46}N_4O_{14})(OH)_2]\cdot 10H_2O$ (**1**) looses all ten lattice water molecules once the relevant crystals are taken out from mother liquor at room temperature (298 K). This is consistent with elemental analysis of the crystals dried at room temperature (see Synthesis of **1**). This why, the TGA curve shows almost flat feature upto ~200 °C. The loss of crystal water molecules at ambient conditions (once the crystals are removed from mother liquor) could be due to the fact that all these crystal water molecules (O(9) through O(13), see S-Figs. 2–4 in Supplementary section) are involved in forming a high energy form of water cluster. At ~250 °C, the curve show a sharp loss that corresponds to the loss of two OH^- groups of the complex $[Cu_4(C_{54}H_{46}N_4O_{14})(OH)_2]$ (for TGA curve, see S-Fig. 10 in Supplementary section).

4. Conclusions

We have described synthesis and characterization of a new tetra-nuclear copper(II) complex $[Cu_4(C_{54}H_{46}N_4O_{14})(OH)_2]\cdot 10H_2O$ (**1**) that features an unusual form of water nonamer, which in turn, congregates to a chainlike extended structure through-out the crystal. This is rare example of an extended water structure based on an odd numbered water cluster. The hydrogen bonding donor/acceptor sites of the copper complex in the crystal lattice provide a surrounding that stabilizes such high energy form of water nonamer inscribing a "transition state" water dimer.

Acknowledgements

We thank DST, Government of India, for financial support (Project No.: SR/S1/IC-18/2002). The National X-ray Diffractometer facility at University of Hyderabad by the Department of Science and Technology, Government of India, is gratefully acknowledged. We are grateful to UGC, New Delhi, for providing infrastructure facility at University of Hyderabad under UPE grant. We thank Professor M.V. Rajasekharan for helpful discussions. We are grateful to Professor A.R. Chakravarty of IISc. Bangalore for providing the variable temperature magnetic susceptibility data. C.P.P. and S.S. thank UGC, New Delhi for their fellowships.

Appendix A. Supplementary material

Crystallographic data for the structural analysis have been deposited with the Cambridge Crystallographic Data Centre, CCDC No. 286027 for compound **1**. Copies of this information may be obtained free of charge from the Director, CCDC, 12 Union Road, Cambridge CB2 1EZ, UK (fax: +44 1223 336033; e-mail: deposit@ccdc.cam.ac.uk or www: http://www.ccdc.cam.ac.uk). Supplementary data associated with this article can be found, in the online version, at doi:10.1016/j.poly.2006.07.008.

References

[1] B.J. Hathaway, in: G. Wilkinson, R.D. Gillard, J.A. McCleverty (Eds.), Comprehensive Coordination Chemistry, vol. 5, Pergamon, Oxford, 1987.
[2] O. Kahn, Molecular Magnetism, VCH, Weinheim, Germany, 1993.
[3] G. Preaux, C. Gielens, in: R. Lontie (Ed.), Copper Proteins and Copper Enzymes, vol. 2, CRC Press, Boca Raton, FL, 1984.
[4] E.I. Solomon, in: T.G. Spiro (Ed.), Metal Ions in Biology, vol. 3, Wiley Interscience, New York, 1981.
[5] J.L. Cole, P.A. Clark, E.I. Solomon, J. Am. Chem. Soc. 112 (1990) 9534.
[6] J.L. Cole, L. Avigliao, L. Morpugno, E.I. Solomon, J. Am. Chem. Soc. 113 (1991) 9080.
[7] J. Reim, B. Krebs, Angew. Chem. Int. Ed. Engl. 33 (1994) 1969.
[8] E. Colacio, M. Ghazi, R. Kivekäs, J.M. Moreno, Inorg. Chem. 39 (2000) 2882.
[9] P.E. Kruger, B. Moubaraki, G.D. Fallon, K.S. Murray, J. Chem. Soc. Dalton Trans. (2000) 713.
[10] A. Mukherjee, M.K. Saha, I. Rudra, S. Ramasesha, M. Nethaji, A.R. Chakravarty, Inorg. Chim. Acta 357 (2004) 1077, and references therein.
[11] S.K. Dey, B. Bag, K.M.A. Malik, M.S. El Fallah, J. Ribas, Inorg. Chem. 42 (2003) 4029.
[12] W.E. Hatfield, in: E.A. Boudreaux, L.N. Mulay (Eds.), Theory and Applications of Molecular Paramagnetism, Wiley, New York, 1976.
[13] R.R. Gagne, C.L. Spiro, T.J. Smith, C.A. Hamann, W.R. Thies, A.K. Shiemke, J. Am. Chem. Soc. 103 (1981) 4073.
[14] Bruker SADABS, SMART, SAINTPLUS and SHELXTL, Bruker AXS Inc., Madison, Wisconsin, USA, 2003.
[15] G.M. Sheldrick, SHELX-97, Programs for Crystal Structure Solution and Refinement, University of Göttingen, Germany, 1997.
[16] R.D. Gillard, P. O'Brien, J. Chem. Soc. Dalton Trans. (1978) 1444.
[17] L. Zhang, L.-F. Tang, Z.-H. Wang, M. Du, M. Julve, F. Lloret, J.-T. Wang, Inorg. Chem. 40 (2001) 3619.
[18] L. Infantes, S. Motherwell, CrystEngComm 4 (2002) 454.
[19] S.K. Ghosh, P.K. Bharadwaj, Inorg. Chem. 44 (2005) 5553.
[20] L. Infantes, J. Chisholm, S. Motherwell, CrystEngComm 5 (2003) 480.
[21] M. Mascal, L. Infantes, J. Chisholm, Angew. Chem. Int. Ed. 45 (2006) 32.
[22] G.V.R. Chandramouli, C. Balagopalakrishna, M.V. Rajasekharan, P.T. Manoharan, Comput. Chem. 20 (1996) 353.

properties of some fluoro-substituted Pcs. In the case of electron-withdrawing peripheral fluorine substituents, Pcs can be dissolved even in polar aprotic solvents and become good electron donors for use as chemical sensors [9,10,12].

In this paper, we report the preparation of some new bis(pentafluorophenyl)methoxyl substituted Pc derivatives, and their spectral, electrochemical, spectroelectrochemical and electrical properties (Scheme 1).

2. Experimental

The starting material 4-nitrophthalonitrile **2** was synthesized by the methods described previously in the literature [13]. Bis(pentafluorophenyl)methanol **1** was used as supplied commercially. Routine IR and UV–vis spectra were recorded on a Shimadzu FTIR-8300 spectrophotometer as KBr pellets and a Shimadzu UV-1601 UV–vis spectrophotometer, respectively. Elemental analyses were performed by the LECO CHNS 932. Mass spectra of 4-[bis(pentafluorophenyl)methoxy]phthalonitrile **3** and Pc derivatives **4–6** were obtained by using the Agilent LC/MSD-TOF spectrometer and Micromass Quattro LC–MS/MS spectrophotometer respectively. ^{1}H NMR and ^{19}F NMR spectra were obtained on a Varian Mercury-V × 400 MHz spectrophotometer.

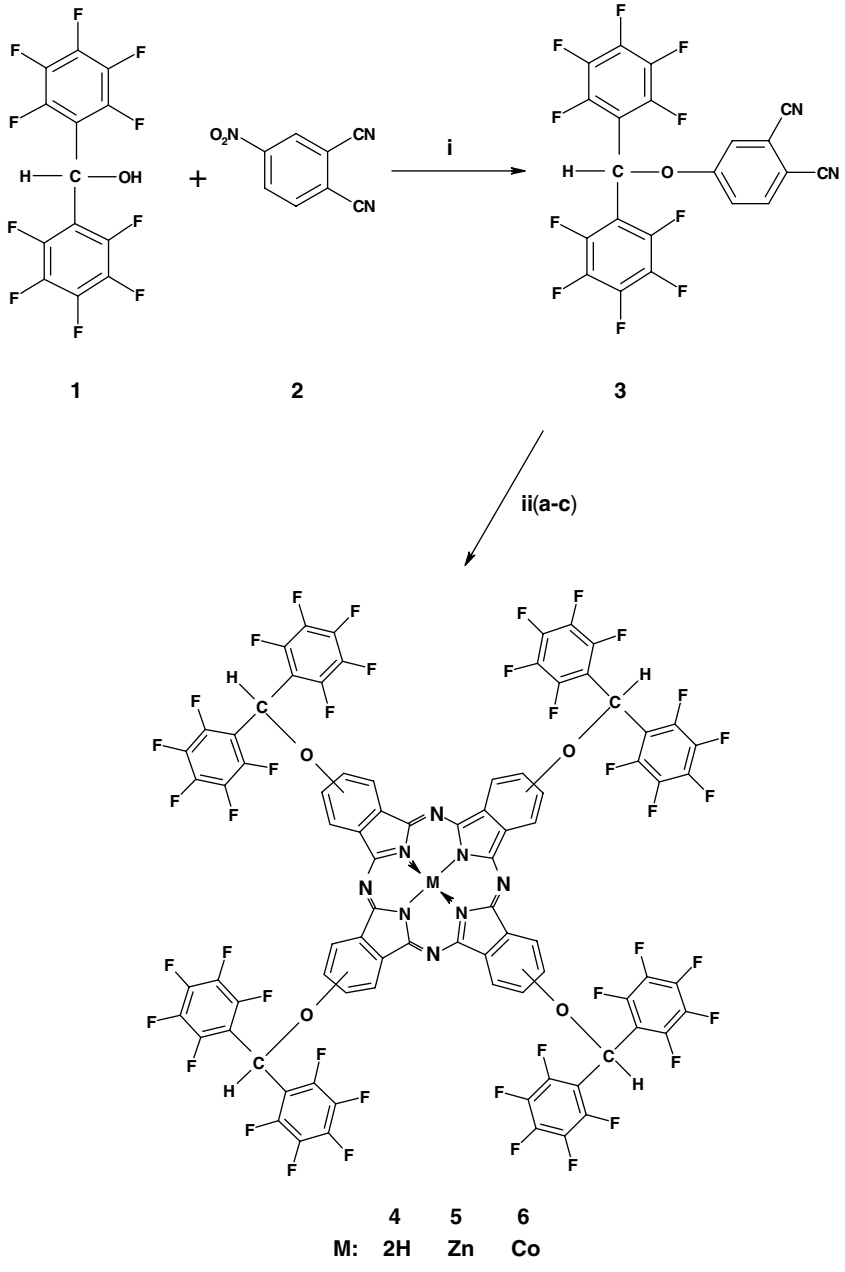

Scheme 1. (i) K_2CO_3, CH_3CN; (ii) a: Li, pentan-1-ol; b: $Zn(CH_3COO)_2 \cdot 2H_2O$, DMAE; c: $Co(CH_3COO)_2 \cdot 4H_2O$, DMAE.

2.1. Synthesis

2.1.1. 4-[Bis(pentafluorophenyl)methoxy]phthalonitrile (3)

A mixture of bis(pentafluorophenyl)methanol **1** (1.00 g, 2.74 mmol), 4-nitrophthalonitrile **2** (0.47 g, 2.74 mmol) and K_2CO_3 (1.14 g, 8.24 mmol) was heated for 24 h, refluxing in dry acetonitrile (40 mL) under argon. The cooled reaction mixture was filtered off and the filtrate evaporated to dryness under vacuum in a rotary evaporator. After being dried under vacuum, the yellowish viscous product was isolated with column chromatography over silica gel using chloroform as the eluent. The second fraction, which is targeted, was eluted with $CHCl_3$. On evaporation of the solvent, a white product was obtained (Scheme 1). The compound **3** is readily soluble in $CHCl_3$, CH_2Cl_2, acetone, THF, MeOH and EtOH. Yield: 0.822 g (61%), m.p. 128 °C. *Anal*. Calc. for $C_{21}H_4F_{10}N_2O$: C, 51.45; H, 0.82; N, 5.71. Found: C, 51.71; H, 0.81; N, 5.69%. MS (LC/MSD-TOF, APCI), *m/z*: 490 $[M]^+$, IR (KBr pellet) *ν*, cm^{-1}: 3090 (Ar–H), 2923–2854 (alkyl ≻CH), 2233 (C≡N), 1242 (C–O–C); ^1H NMR (*d*-$CDCl_3$): $\delta = 6.94$ (s, 1H, ≻CH), 7.24 (d, 1H, Ar–H), 7.33 (d, 1H, Ar–H), 7.76 (d, 1H, Ar–H). ^{19}F NMR (*d*-$CDCl_3$): δ (ppm) = −141.2 (d, *o*-fluoro), −149.9 (t, *p*-fluoro), −159.6 (q, *m*-fluoro).

2.1.2. Tetrakis[bis(pentafluorophenyl)methoxy]-2H-phthalocyanine (4)

Compound **3** (0.245 g, 0.5 mmol) was added to 5 mL pentan-1-ol and heated to dissolve. An excess of Li wire was subsequently added to the solution. As the Li was added, a large quantity of gas was evolved and the reaction mixture turned to dark green. The mixture was heated at reflux under nitrogen for 5 h [10]. On cooling, 30 mL of AcOH/H_2O (1:1-v/v) was added to the mixture and stirred for 20 min at the room temperature. The resulting waxy green Pc phase was separated from the mixture. The Pc product which remained in the flask was washed with water three times, and the residue was dried under vacuum to give tarry green Pc (Scheme 1). The crude Pc **4** was treated with three portions of 30 mL of ($CHCl_3$/H_2O – 3:1) (v/v) mixture. After the separation of the $CHCl_3$ phases, the $CHCl_3$ extracts were then combined, dried with anhydrous Na_2SO_4, and the total volume was evaporated to dryness using a rotary evaporator. The purification of the aimed Pc was carried out on silica gel column with $CHCl_3$. Compound **4** is soluble in $CHCl_3$, CH_2Cl_2, THF, EtOH, MeOH, DMSO and DMF. Yield: 0.085 g (34%). *Anal*. Calc. for $C_{84}H_{18}F_{40}N_8O_4$: C, 51.39; H, 0.92; N, 5.71. Found: C, 52.02; H, 0.89; N, 5.83%. MS(LC–MS/MS, ES+) *m/z*: 1963 $[M]^+$, IR (KBr pellet) *ν*, cm^{-1}: 3297 (NH), 3073 (Ar–H), 2948–2893 (alkyl ≻CH), 1236 (C–O–C). UV–vis (DMSO) *λ*, nm (log *ε*): 700(4.72), 674(4.75), 650(4.67), 326(5.03); ^1H NMR (*d*-$CDCl_3$) *δ*: 7.41–7.96 (m, 3H, Ar–H), 6.99 (s,1H, ≻CH), −8.2 (br s, 2H, NH).

2.1.3. Tetrakis[bis(pentafluorophenyl)methoxy]-phthalocyaninato zinc(II) (5)

Compound **3** (196 mg, 0.4 mmol) and $Zn(CH_3COO)_2 \cdot 2H_2O$ (22 mg, 0.10 mmol) were mixed in dry 2-*N*-*N*-dimethylaminoethanol (DMAE) (1 mL) in a glass tube. After being degassed with a vacuum, the mixture was sealed, and heated at 150–160 °C for 5 h to give a symmetrical substituted Pc (Scheme 1). After being cooled, the reaction mixture was poured into 100 mL of ethanol and the dark green precipitate was separated by centrifuging. The product was dissolved in DMF and precipitated with a mixture of $CHCl_3$ and acetone. After filtration, the precipitate was washed successively with boiling acetic acid, water and ether, and dried under vacuum. Compound **5** is soluble in DMSO and DMF, and partly soluble in acetone, MeOH and EtOH. Yield: 0.065 g (32%). *Anal*. Calc. for $C_{84}H_{16}F_{40}N_8O_4Zn$: C, 49.79; H, 0.80; N, 5.53. Found: C, 50.56; H, 0.83; N, 5.49%. MS(LC–MS/MS, ES+) *m/z*: 2026 $[M]^+$, IR (KBr pellet) *ν*, cm^{-1}: 3087 (Ar–H), 2925–2883 (alkyl ≻CH), 1242 (C–O–C); UV–vis (DMSO) *λ*, nm (log *ε*): 698(4.84), 641(4.35), 356(4.78); ^1H NMR (DMSO-d_6): $\delta = 7.94$–7.63 (m, 3H, Ar–H), 6.81 (s, 1H, ≻CH). ^{19}F NMR (DMSO-d_6): δ(ppm) = −143.2 (d, *o*-fluoro), −156.5 (t, *p*-fluoro), −163.2 (q, *m*-fluoro).

2.1.4. Tetrakis[bis(pentafluorophenyl)methoxy]-phthalocyaninato cobalt(II) (6)

A mixture of compound **3** (0.089 g, 0.18), $Co(CH_3COO)_2 \cdot 4H_2O$ (0.011 g, 0.045 mmol) and DMAE (0.5 mL) was heated and stirred at 150–160 °C for 6 h in a sealed glass tube under argon to afford symmetrical Pc (Scheme 1). After cooling to room temperature, the reaction mixture was treated with ethanol and a dark blue precipitate was separated by centrifuging. The product was dissolved in DMF and precipitated with a mixture of $CHCl_3$ and acetone. After filtration, the precipitate was washed several times with boiling AcOH, water and EtOH to obtain the targeted Pc. The dark blue product was dried under vacuum. Compound **6** is soluble in DMSO and DMF. Yield: 0.014 g (16%). *Anal*. Calc. for $C_{84}H_{16}F_{40}N_8O_4Co$: C, 49.95; H, 0.80; N, 5.55. Found: C, 49.08; H, 0.83; N, 5.62%. MS(LC–MS/MS, ES+) *m/z*: 2021 $[M + 1]^+$, IR (KBr pellet) *ν*, cm^{-1}: 3085 (Ar–H), 2927–2884 (alkyl ≻CH), 1244 (C–O–C); UV–vis (DMSO) *λ*, nm (log *ε*): 675(4.77), 320(4.99).

2.2. Electrochemical and spectroelectrochemical measurements

The cyclic voltammetry (CV) and controlled potential coulometry (CPC) measurements were carried out with a Princeton Applied Research Model VersaStat II potentiostat/galvanostat controlled by an external PC and utilizing a three-electrode configuration at 25 °C. The working electrode was a Pt plate with a surface area of 0.10 cm^2. The surface of the working electrode was polished with a H_2O

suspension of Al_2O_3 before each run. The last polishing was done with a particle size of 50 nm. A Pt wire served as the counter electrode. A saturated calomel electrode (SCE) was employed as the reference electrode and was separated from the bulk of the solution by a double bridge. The ferrocene/ferrocenium couple (Fc/Fc^+) was also used as an internal standard. Electrochemical grade tetrabutylammonium perchlorate (TBAP) in extra pure dimethylsulfoxide (DMSO) was employed as the supporting electrolyte at a concentration of 0.10 mol dm^{-3}. High purity N_2 was used for deoxygenating the solution for at least 20 min prior to each run and to maintain a nitrogen blanket during the measurements. For controlled potential chronocoulometry (CPC) studies, a Pt gauze working electrode (10.5 cm^2 surface area), Pt wire counter electrode separated by a glass bridge, and a SCE as a reference electrode were used. The spectroelectrochemical measurements were carried out with an Agilent Model 8453 diode array spectrophotometer equipped with a potentiostat/galvanostat and utilizing a three-electrode configuration of a thin layer quartz spectroelectrochemical cell at 25 °C. The working electrode was transparent Pt gauze. A Pt wire counter electrode separated by a glass bridge and a SCE reference electrode, separated from the bulk of the solution by a double bridge, were used.

2.3. Dc and impedance spectral measurements

Spin coated thin films of the compounds were prepared on a glass substrate fitted with interdigitated (IDT) gold electrodes for electrical characterization. Before vacuum evaporation, the glass substrates were thoroughly cleaned ultrasonically and then coated with 100 Å of chromium followed by 1200 Å of gold in a Leybold Univex 450 coater system. The film was patterned photolithographically and etched to provide 10 fingers pairs of electrodes having a width of 100 μm, spaced 100 μm from the adjacent electrodes. The finger overlap distance was 5 mm. DMF was used as the solvent. The reason for using DMF as the solvent is the good solubility of the compounds in DMF. The compounds were dissolved in DMF at concentrations of 5×10^{-3} M for all compounds. Twenty microlitres of such solutions were added with a glass pipette onto the IDT structure held on a spinner (Speciality Coatings Systems Inc., Model P6700 Series). The substrate was spun at 2000 rpm for 20 s and then the films were dried at 60 °C under vacuum for 2 h to evaporate the solvent. Dc conductivity measurements were performed between 290 K and 440 K using a Keithley 617 electrometer. Impedance spectroscopy measurements were carried out with a Keithley 3330 LCZ meter in the frequency range 40–10^5 Hz, and in the temperature range 290–440 K. A close cycle liquid helium cryostat was used to allow electrical characteristics to be measured over a wide temperature range. The temperature of the samples was controlled with a Leybold LTC 60 temperature controller during the measurements. The conductivity data were recorded using an IEEE 488 data acquisition system incorporated into a personal computer.

3. Results and discussion

3.1. Synthesis

The main precursor, molecule **3**, for the synthesis of bis(pentafluorophenyl)methoxyl substituted Pcs was obtained by a nitro displacement reaction [3,14] of 4-nitrophthalonitrile (**2**) and bis(pentafluorophenyl)methanol (**1**). The peripherally substituted Pc derivatives were prepared from the phthalonitrile derivative **3** with Li in pentan-1-ol [10] or with metal acetates [$Zn(OAc)_2 \cdot 2H_2O$ or $Co(OAc)_2 \cdot 4H_2O$] in DMAE by a cyclotetramerization reaction.

The central metal ions and the peripheral substituents on the Pc ring effect the solubility of the MPcs. Perfluoro-substituted compounds have a tendency for high solubility in polar solvents. This situation may be interpreted with the extreme electronegativity of the fluorine atom. Both the metal-free **4** and Zn(II) Pc **5** were soluble in strong and medium polar solvents such as DMSO, DMF, EtOH and MeOH, while the Co(II)-Pc (**6**) was soluble only in strong solvents, e.g. DMSO and DMF. On the contrary to Pcs **5** and (**6**), the metal-free one **4** also showed solubility in less polar solvents such as $CHCl_3$, CH_2Cl_2 and THF.

The IR spectra were derived from potassium bromide disks. The existence of C≡N groups was apparent from a single peak at 2233 cm^{-1} in the spectrum of **3**. The formation of phthalocyanines from the dinitrile derivative was verified by the disappearance of the C≡N stretching vibration band at 2233 cm^{-1}. The IR spectra of **4**–**6** showed similar characteristics, except for metal-free **4** which showed a peak at 3297 cm^{-1}, assigned to NH groups of the inner core.

The UV–vis spectra of **4**–**6** in DMSO show characteristic absorptions between 700 and 675 nm in the Q-band region. As expected, no splitting of the Q-band in the spectra of the MPcs (M: Zn, Co) was observed while the metal-free Pc **4** showed the expected Q band splitting. The Q band observed for all Pc compounds was attributed to the $\pi \rightarrow \pi^*$ transition from the highest occupied molecular orbital (HOMO) to the lowest unoccupied molecular orbital (LUMO) of the Pc ring. The λ_{max} value of the fluorinated compounds were slightly shifted to shorter wavelengths [8–10]. The other bands in the UV region at 326 nm for **4**, 356 nm for **5** and 320 nm for **6** were observed due to transitions from the deeper π levels to the LUMO (Fig. 1).

The ^1H NMR spectra are also consistent with the proposed structures. The ^1H NMR spectrum of **3** in *d*-$CDCl_3$ exhibited signals for the aromatic protons around 7.24–7.76 ppm as three doublets, and a peak for the >CH proton of the aliphatic group at 6.94 ppm as a singlet. However, the aromatic and aliphatic protons in Pcs **4** and **5** appeared as multiplets at 7.96–7.41, 7.94–7.63 ppm, and as singlets at

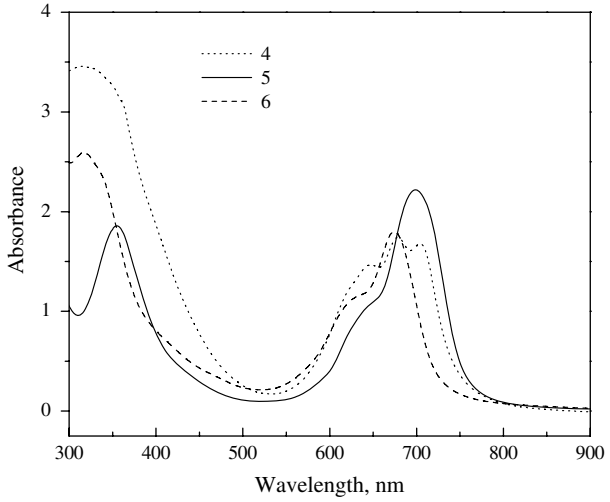

Fig. 1. UV–vis spectra of **4**–**6** in DMSO.

6.99, 6.81 ppm, respectively. The internal NH protons of metal-free Pc **4** were confirmed as a broad signal at −8.2 ppm.

A close investigation of the ^{19}F NMR spectra of compounds **3** and **5** confirmed the proposed structures. These compounds displayed signals due to $F_{2,6}$, F_4 and $F_{3,5}$ at δ: −141.2, −149.9 and −159.6 ppm, and −143.2, −156.5 and −163.2 ppm, respectively. The F_4 signal appeared as a triplet due to $F_{3,5}$ coupling, the $F_{2,6}$ signals appeared as a doublet and the $F_{3,5}$ signals as a quartet in both compound. Thus, the ^{19}F NMR measurements provided additional support for the structures of the fluorinated compounds **3** and **5** [15].

In addition to these supportive results for the structures, the mass spectra of compounds **3**–**6** gave the characteristic molecular ion peaks at *m/z*: 490 $[M]^+$, 1963 $[M]^+$, 2026 $[M]^+$ and 2021 $[M+1]^+$, respectively, from which the proposed structures were confirmed.

3.2. Electrochemistry and spectroelectrochemistry

Cyclic voltammetry of **4**–**6** was carried out on a platinum working electrode in DMSO. Controlled-potential coulometry studies showed that the redox processes monitored for these compounds generally involves the transfer of one electron. Voltammetric data of the compounds are presented in Table 1. It should be noted that as the third reductions occurred at very negative potentials, it was not possible to determine correctly the number of electrons transferred. However, on the basis of the studies reported previously for mono Pcs [16], it can be assumed that the third reduction for each compound involves the transfer of one electron.

Compound **4** displayed three quasi-reversible reduction waves at $E_{1/2} = -0.53$ V, $E_{1/2} = -0.93$ V and $E_{1/2} = -1.89$ V versus SCE, with considerably high anodic to cathodic peak separations (Fig. 2). These Pc ring-based redox processes were examined as a function of potential

Table 1
Voltammetric data for **4**–**6**

Compound	Redox couple	$E_{1/2}$[a] (V) vs. SCE and Fc/Fc^{+}[b]	ΔE_p[c] (V)
4	Pc(-2)/Pc(-3)	−0.53 (−1.03)	0.30
	Pc(-3)/Pc(-4)	−0.93 (−1.43)	0.42
	Pc(-4)/Pc(-5)	−1.89 (−2.39)	0.18
5	Pc(-2)/Pc(-3)	−0.67 (−1.17)	0.30
	Pc(-3)/Pc(-4)	−1.04 (−1.54)	0.44
	Pc(-4)/Pc(-5)	−1.94 (−2.44)	0.12
6	Co(III)/Co(II)	0.43 (−0.07)	0.06
	Co(II)/Co(I)	−0.43 (−0.93)	0.30
	Pc(-2)/Pc(-3)	−0.83 (−1.33)	0.54
	Pc(-3)/Pc(-4)	−1.39 (−1.89)	0.06

[a] $E_{1/2} = (E_{pa} + E_{pc})/2$ at 0.100 V s^{-1}.
[b] The values in parenthesis indicate the potentials vs. Fc/Fc^{+}.
[c] $\Delta E_p = E_{pa} - E_{pc}$ at 0.100 V s^{-1}.

scan rate in order to determine the mode of mass transport. The peak currents for the processes Ic, IIc and IIIc increased in direct proportion to the square root of the scan rate between 0.025 and 1.00 V/s, thus suggesting that the relevant reactions are controlled by diffusion. Compound **5** shows similar voltammetric behaviour to **4**. It also showed three one-electron, quasi-reversible reduction waves at $E_{1/2} = -0.67$ V, $E_{1/2} = -1.04$ V and $E_{1/2} = -1.94$ V versus SCE (Fig. 3). These reduction processes are probably ligand based since zinc is not redox active in Pc complexes. The first reduction processes of **4** occur at potentials slightly less negative than those of **5**. This can be attributed to the difference in the polarizing power of central metal and the hydrogens. The first two ring reduction processes for main group Pcs are generally separated by about 0.4–0.5 V. The third reduction occurs 0.8 V more negative than the second reduction. The separation between the second and the third reductions is smaller with more polarizing ions such as Zn(II) [16]. The redox potentials measured for **4** and **5** are consistent with the general

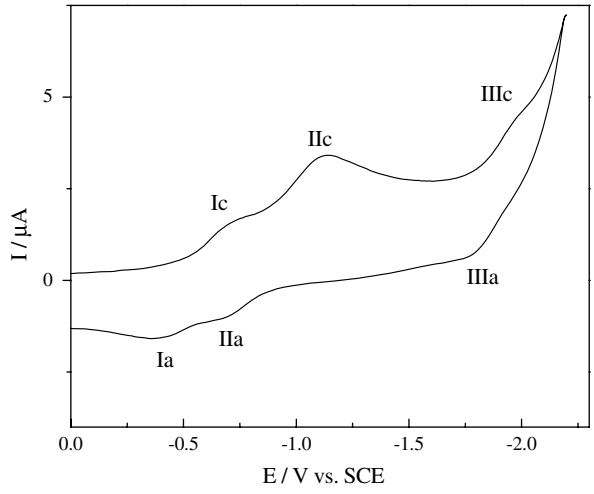

Fig. 2. Cyclic voltammogram of **4** at 0.100 V s^{-1} in DMSO/TBAP solution.

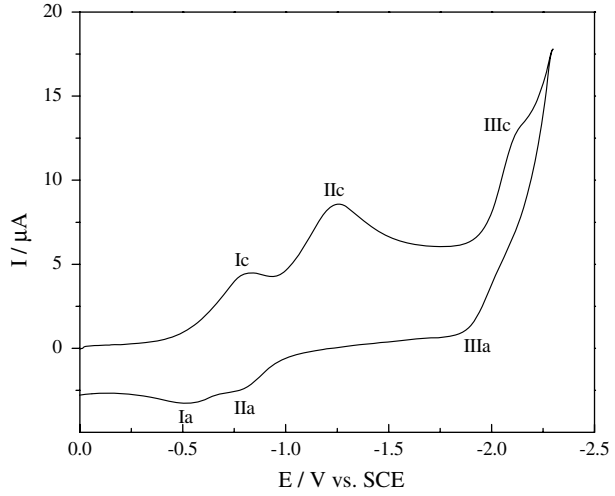

Fig. 3. Cyclic voltammogram of **5** at 0.100 V s^{-1} in DMSO/TBAP solution.

redox characteristics reported previously for similar Pcs. The first ring reduction potentials of **4** and **5** are less negative as compared with those given for unsubstituted Pcs in the literature [16]. This positive potential shift can be attributed to the electron withdrawing effect of the fluorine atoms in **4** and **5**. Therefore, it was possible to observe the third reductions for **4** and **5**, which cannot be monitored generally. On the other hand, the first oxidation could not be observed for **4** and **5**, probably for the same reason, positively shifted potentials.

A typical voltammogram for **6** is shown in Fig. 4. The voltammetric behaviour of **6** is different from those of **4** and **5**. It indicates three one-electron reduction processes at $E_{1/2} = -0.43$ V, $E_{1/2} = -0.83$ V and $E_{1/2} = -1.39$ V versus SCE, and a one-electron oxidation process at $E_{1/2} = 0.43$ V versus SCE. If the transition metal ion concerned has no accessible d orbital levels lying between the HOMO and LUMO gap of a Pc species, then its redox chemistry will appear very much like that of a main group Pc species. Nickel, copper, zinc and some other MPcs behave in this fashion, with the M(II) central ion being unchanged as the MPc unit is either oxidized or reduced. However, some species vary their electrochemical behaviour according to their environment, i.e., the oxidation of Co(II)Pc(-2) can lead to $[Co(III)Pc(-2)]^+$ or $[Co(II)Pc(-1)]^+$ depending on whether there are any available suitable coordinating species that would stabilize the Co(II) center. Such electrochemistry, especially of Co(II)Pc(-2) and Fe(II)Pc(-2) is split into two sections, that referring to donor solvents and that referring to non-donor solvents. The main difference lies in whether the metal or the ring is oxidized first. Donor solvents strongly favor Co(III)Pc(-2) by coordinating along the axis to form six coordinate species. If such donor solvents are absent, then oxidation to Co(III) is inhibited and ring oxidation occurs first. Thus, the first oxidation and the first reduction processes of **6** are probably metal based and correspond to Co(II)Pc(-2)/$[Co(III)Pc(-2)]^+$ and Co(II)Pc(-2)/$[Co(I)Pc(-2)]^-$, respectively, while the second and third reductions are ring based, since the voltammetric measurements were carried out in DMSO/TBAP.

In order to provide additional support for the identification of the redox processes of **5** and **6**, spectroelectrochemistry of these complexes was also studied. Typical absorption spectra for the neutral **5** and its electrochemically generated species are shown in Fig. 5. Fig. 6a shows the UV–vis spectral changes of complex **5** during the controlled potential reduction of the complex at −0.87 V versus SCE. Upon reduction, a decrease in the absorption of the Q band centered at 700 nm and its broadening towards the red region is observed. This is accompanied by an increase in absorption at the region, 500–600 nm. Isosbestic points are observed at 337, 372, 606 and 732 nm. These spectral changes are characteristic for the formation of Zn(II)Pc(-3) species [17,18]. The well-defined spectral

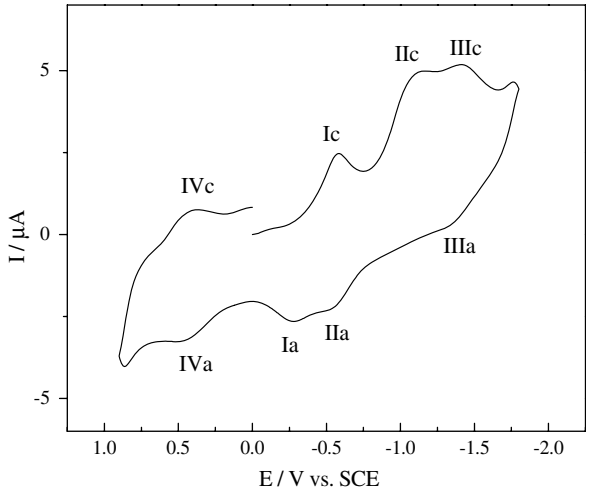

Fig. 4. Cyclic voltammogram of **6** at 0.100 V s^{-1} in DMSO/TBAP solution.

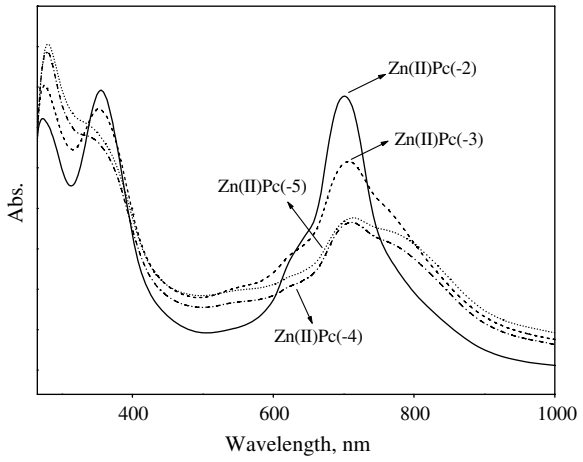

Fig. 5. UV–vis spectra of **5** and its electrochemically generated reduced species.

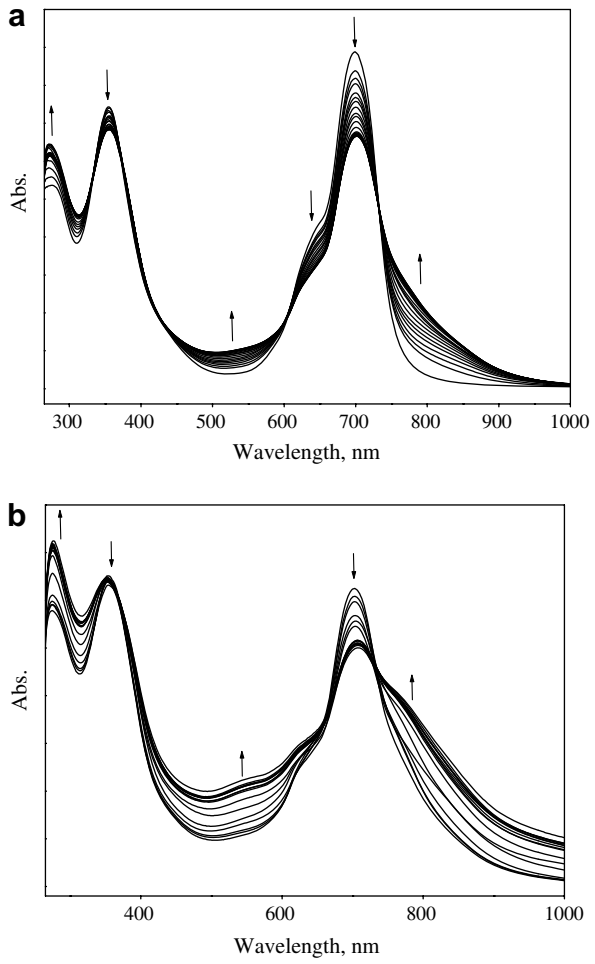

Fig. 6. UV–vis spectral changes during (a) the first reduction; (b) the second reduction of **5**.

changes during the second reduction of **5** with an applied potential of −1.40 V versus SCE are shown in Fig. 6b. Similar spectral changes continue with the formation of well-defined isosbestic points at 374, 666 and 730 nm. The appearance of a new broad absorption band with low intensity at 544 nm is also characteristic for ring reduction. The first and second reduction processes were chemically reversible on the spectroelectrochemical time scale and the nearly original spectrum of the neutral compound **5** was obtained upon reoxidation. It could be concluded that the species produced during the first and second reduction processes remained stable throughout the measurement. The final spectra obtained after the controlled potential electrolysis of **5** at −2.10 V versus SCE is given in Fig. 5. Unfortunately, the third reduction process was not chemically reversible on the spectroelectrochemical time scale although it was quasi-reversible during the cyclic voltammetric measurement. Reoxidation of the triply reduced species did not generate compound **5** with its original spectrum. This is probably due to the fact that the third reduction process occurs at considerably negative potentials, and decomposition of the complex may occur when the potential is held constant at a considerably negative potential.

Fig. 7 represents the UV–vis spectra of the neutral **6** and its electro-generated species. Fig. 8a shows the UV–vis spectral changes of **6** during its first reduction at −0.70 V versus SCE. The Q band absorption at 673 nm and the intensity of the shoulder at 623 nm decrease, while a new intense band at 480 nm appears and the absorption at the red region of the Q band increases during the controlled-potential electrolysis. This reduction process has well-defined isosbestic points at 393, 568 and 703 nm. The new band at 480 nm is typical for Co(I)Pc(-2) species, and thus suggests that the first reduction of **6** occurs at the metal center [19,20]. Upon reduction at −1.2 V versus SCE, the Q band absorption goes on decreasing without shift, and the absorption of the new band also decreases (Fig. 8b). These spectral changes are accompanied by an increase in the absorption at the red region of the Q band with isosbestic point at 396, 570 and 701 nm, which is characteristic for Pc ring reduction [21]. The spectral changes observed during the third reduction process corresponding to couple III were also typical for ring reduction. The final spectra of the species electrochemically generated after third reduction is shown in Fig. 7. Although the first and second reduction, and the first oxidation processes were chemically reversible, the third reduction process was not reversible on the spectroelectrochemical timescale, and the original species could not be obtained upon reoxidation of the triply reduced species. This is also probably due to decomposition after reduction. Fig. 8c shows the spectral changes during oxidation of **6**. The original Q band absorption at 673 nm increases with a clear shift to 683 nm while the absorption of the shoulder at 623 nm decreases slightly and the absorption in the 500–600 nm region increases. These spectral changes result in isosbestic points at 418, 612 and 728 nm, typical of a Co(II)Pc(-2)/Co(III)Pc(-2) redox process [20].

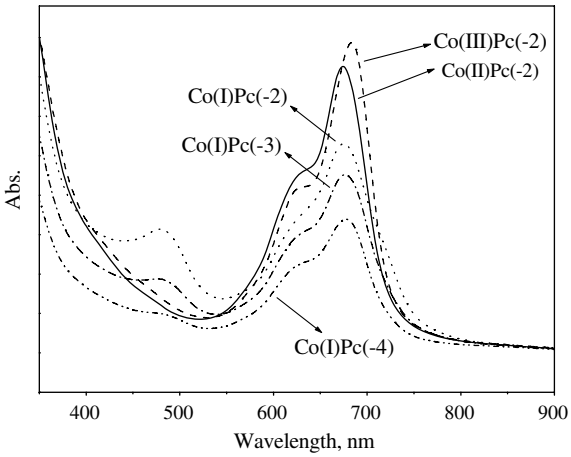

Fig. 7. UV–vis spectra of **6** and its electrochemically generated reduced and oxidized species.

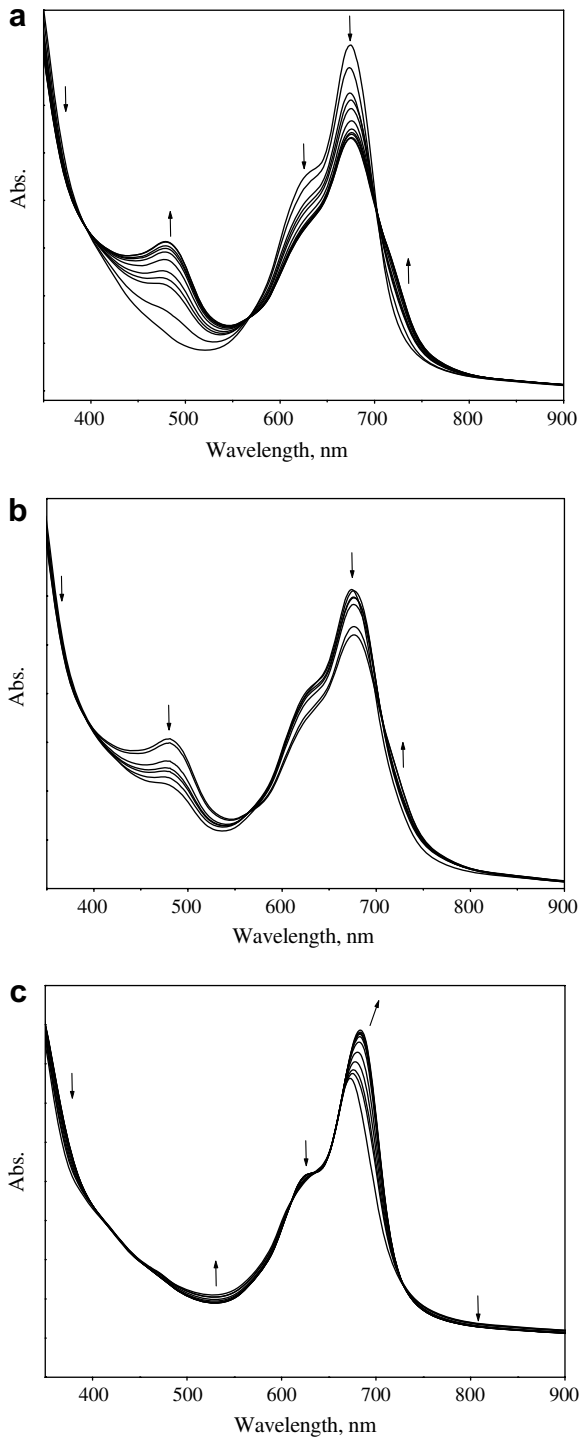

Fig. 8. UV–vis spectral changes during (a) the first reduction; (b) the second reduction; (c) the first oxidation of **6**.

3.3. Dc and impedance spectral measurements

To gain more valuable information on the processes taking place in the films, the temperature dependence of the direct current conductivity was examined during heating and cooling processes. Measurements were carried out in an ambient vacuum ($<10^{-3}$ mbar). In the current–voltage (I–V) measurements symmetrical currents at positive and negative polarization as well as an ohmic contact behaviour were found. The conductivity values of the films were calculated from the slopes of the measured I–V characteristics. It was found that the conductivity of the films were reversible for temperature cycling. The measured dc conductivity data of the prepared films were plotted as $\ln\sigma(T)$ versus $1/T$. This plot indicated that the compounds are semiconducting in nature. A linear relationship in conductivity variations are observed for **4**–**6** in the temperature range 290–440 K. The slopes of these plots are determined and used to evaluate the activation energies and the data are presented in Table 2. The general trend, for the order of electrical conductivities, observed in the whole temperature range for these compounds are $\sigma_{dc}(2H) > \sigma_{dc}(Co) \approx \sigma_{dc}(Zn)$. The observed electrical conductivities of the compounds are found to be $\sim 10^2$ times higher compared to their parent Pcs. Differences in the order of the electrical conductivities in this case are mainly due to the electron withdrawing effect of fluorine atoms. The electron withdrawing bis(pentafluorophenyl) substituents decreases the separation distance between the Pc macrocycles. The smaller interplanar spacing between the molecules as well as favorable intermolecular stacking are expected to lead to greater overlap between the π-electron orbitals of both macrocycles. This result is significant because it strongly suggests that the overlap of π-electron orbitals plays a major role in the electrical conduction behaviour. The highest conductivity in metal free Pc **4** indicates that the transport of charge carriers is through the ligands, and not through the metal ions.

The trend observed in the ac electrical conductivity was the same as the dc conductivity ($\sigma_{ac}(2H) > \sigma_{ac}(Co) \approx \sigma_{ac}(Zn)$). Fig. 9 shows the dependence of ac conductivity on frequency for the compounds at 350 K. As can be seen from Fig. 9, the frequency has a pronounced effect on the measured ac conductivity. The frequency dependence of the conductivity follow a universal power law for all the compounds [22],

$$\sigma_{ac}(\omega) = A\omega^s \quad (1)$$

where ω is the angular frequency, A and the frequency exponent s are material dependent constants. In general, ac conductivities are not equal to dc conductivities. Several mechanisms can be operative for ac conduction in molecular materials. In the case of ac conductivity, the measured conductivity depends not only the conductivity of the material, but also on capacitance. When the impedance of the sample becomes purely resistive the ac conductivity equals the dc conductivity. The interpretation of the

Table 2
The dc conductivity and activation energy values of the compounds

Compound	σ_{dc290} (S/cm)	σ_{dc400} (S/cm)	E_a (eV)
4	4.4×10^{-8}	1.3×10^{-4}	0.81
5	1.6×10^{-9}	5.1×10^{-5}	0.77
6	1.2×10^{-9}	4.0×10^{-5}	0.78

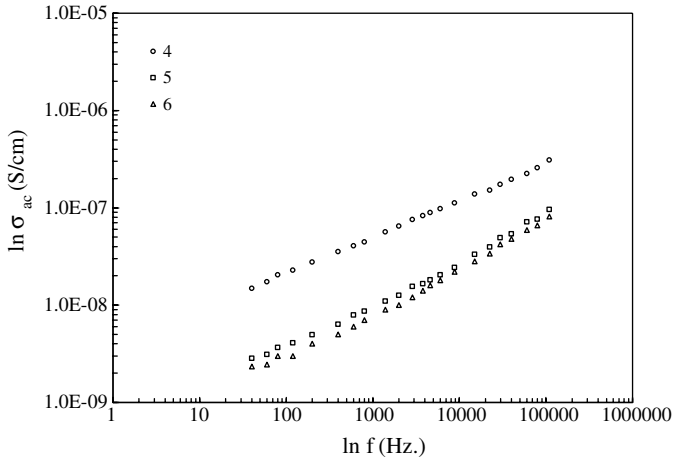

Fig. 9. The dependence of ac conductivity on frequency for **4**–**6** at 350 K.

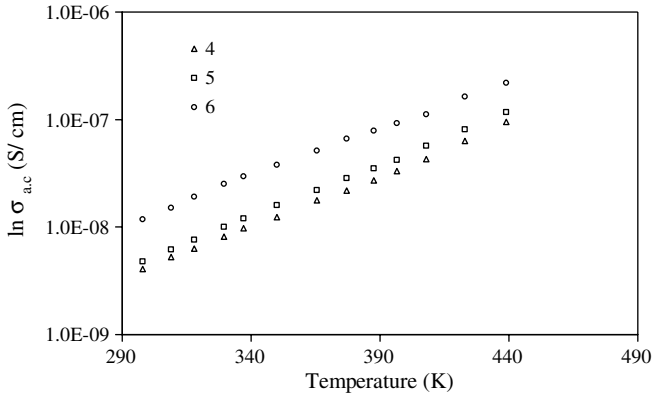

Fig. 10. The temperature dependence of the ac conductivity at a constant frequency of 15 kHz for **4**–**6**.

measured ac conductivity data should be focused on the hopping processes. The hopping model, which was developed by Eliot, assumes that charge carriers hop between sites over the potential barrier separating them, rather than tunnelling through the barrier [23]. This model gives an ac conductivity which can be expressed to a first-order approximation as

$$\sigma_{ac}(\omega, T) = \frac{n\pi^3 N^2 \varepsilon\varepsilon_0 \omega}{24} R_\omega^6 \quad (2)$$

where ε is the dielectric constant of the material, ε_0 that of free space, N is the spatial density of defect states, $n = 1$ for a single electron $n = 2$ for hopping of two electrons and R_ω is the hopping distance. The temperature dependent frequency exponent s for this model is given by,

$$s = 1 - \beta = 1 - 6k_B T/W_M \quad (3)$$

where W_M is the optical band gap, k_B is the Boltzman's constant and T is temperature. The variation of frequency exponent, s, with temperature gives information on the specific mechanism involved. The values of s have been calculated from the slope of $\ln \sigma_{ac}(\omega)$ versus $\ln \omega$ graphs. Our calculations showed that s is definitely a function of temperature for all compounds. The comparison of the experimentally determined s values with the prediction from the hopping model suggest that the dependence of exponent s on temperature is in agreement with the prediction of the hopping model for these compounds. However, the decrease in frequency exponent s with increasing temperature is not evident for the hopping model. In addition to the behaviour of s, the temperature dependence of the measured ac conductivity has to be considered. Eq. (2) can be rewritten in the form

$$\sigma_{ac}(\omega, T) = BC^{T/Q} \quad (4)$$

where $C = 1/\omega\tau_0$, B denotes all other temperature-independent parameters and $Q = W_M/6k_B$. According to Eq. (4), since C and Q are independent of the temperature, the slope of the $\ln \sigma_{ac}(\omega, T)$ versus T graph should be constant. Fig. 10 shows the temperature dependence of the measured ac conductivity at constant frequency (15 kHz). The linear relationship between σ_{ac} and T confirms that the charge carrier transport occurs via hopping processes.

Acknowledgements

This work was supported partly by the Turkish Academy of Sciences (TUBA), The Research Fund of Marmara University (SCIENCE-YYP-290506-0130 and SCIENCE-107/020603) and Scientific and Technical Research Council of Turkey (TUBITAK) [TBAG-HD/50 (105T262)].

References

[1] M.J. Cook, J. Mater. Chem. 6 (1996) 677.
[2] Ö. Bekaroğlu, Appl. Organomet. Chem. 10 (1996) 605, and literature references given therein.
[3] M. Özer, A. Altindal, A.R. Özkaya, M. Bulut, Ö. Bekaroğlu, Synth. Met. 155 (2005) 222.
[4] H. Yanagi, N. Tamura, S. Taira, H. Furuta, S. Douko, G. Schnurpfeil, D. Wohrle, Mol. Cryst. Liq. Cryst. 267 (1995) 435.
[5] T. Manaka, M. Iwamoto, Thin Solid Films 438–439 (2003) 157.
[6] Z. Bao, A.J. Lovinger, J. Brown, J. Am. Chem. Soc. 20 (1998) 207.
[7] S. Hiller, D. Schlettwein, N.R. Armstrong, D. Wöhrle, J. Mater. Chem. 8 (4) (1998) 945.
[8] S. Wie, D. Huang, L. Li, Q. Meng, Dyes Pigments 56 (2003) 1.
[9] L. Gao, X. Qian, Dyes Pigments 51 (2001) 51.
[10] T. Sugimori, S. Honike, M. Handa, K. Kasuga, Inorg. Chim. Acta 278 (1998) 253.
[11] C.C. Leznoff, J.L.S. Sanchez, Chem. Commun. (2004) 338.
[12] G. Winter, H. Heckmann, P. Haisch, W. Eberhardt, M. Hanack, L. Luer, H.J. Egelhaaf, D. Oelkrug, J. Am. Chem. Soc. 120 (1998) 11663.
[13] J.G. Young, W. Onyebuago, J. Org. Chem. 55 (1990) 2155.
[14] D. Wöhrle, G. Knothe, Synth. Commun. 19 (1989) 3231.
[15] S.K. Shukla, A. Ranjan, A.K. Saxena, Polyhedron 25 (2006) 1415.
[16] A.B.P. Lever, E.R. Milaeva, G. Speier, in: C.C. Leznoff, A.B.P. Lever (Eds.), Phthalocyanines: Properties and Applications, vol. 3, VCH Publishers, Weinheim, 1993, p. 1.
[17] J. Obirai, T. Nyokong, Electrochim. Acta 50 (2005) 3296.
[18] K. Hesse, D. Schlettwein, J. Electroanal. Chem. 476 (1999) 148.

[19] J. Obirai, N.P. Rodrigues, F. Bedioui, T. Nyokong, J. Porphyr. Phthalocya. 7 (2003) 508.
[20] M.J. Stillman, T. Nyokong, in: C.C. Leznoff, A.B.P. Lever (Eds.), Phthalocyanines: Properties and Applications, vol.1, VCH Publishers, Weinheim, 1993, Chapter 3.
[21] K.J. Balkus, A.G. Gabriclov, S.I. Bell, F. Bedioui, L. Roue, J. Deevynck, Inorg. Chem. 33 (1994) 67.
[22] N.F. Mott, E.A. Davis, Electronic Processes in Non-Crystalline Materials, 2nd ed., Clarendon Press, Oxford, 1979.
[23] S.R. Elliot, Adv. In. Phys. 36 (1987) 135.

antifungal effect of copper ions has been known for many years since the Bordeaux mixture was first used at the end of 19th century for the treatment of downy mildew of vines [19]. In this connection it is of interest to study various aspects of copper (II) coordination chemistry of SHD derivatives and its antifungal activities.

Recently, we have studied the interaction of a series of SHD derivatives with silver (I), copper (II), cobalt (II) and nickel (II) ions in aqueous ethanol solutions [20–25]. In these studies, the experimental data on the quantitative aspects of complexation equilibrium for metal ions forming complexes with the above-stated ligands in aqueous ethanol solutions were obtained by potentiometric titration. Potentiometric investigation of the equilibria in the systems containing metal (II) ions and SHD derivatives allowed us to recognize that complexes were formed, and to find out their composition and stability, thus allowing one to select optimal conditions for synthesizing the complexes. Continuing with our research program concerning the coordination chemistry and biological activity of SHD derivatives, we report herein the synthesis and characterization of Cu (II) complexes with 3,5-di(*tert*-butyl)-1,2-benzenediol (**I**), 4,6-di(*tert*-butyl)-1,2,3-benzentriol (**II**) and sulfur-containing SHD derivatives such as 4,6-di(*tert*-butyl)-3-(2-hydroxyethylsulfanyl)-1,2-benzenediol (**III**) and 2-[4,6-di(*tert*-butyl)-2,3-dihydroxyphenylsulfanyl]-acetic acid (**IV**):

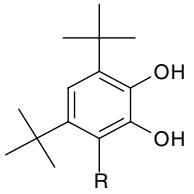

I – R=H

II – R=OH

III – R=SCH_2CH_2OH

IV – R=SCH_2COOH

We have also reported the synthesis of an Ag (I) complex with one of the ligands, 2-[4,6-di(*tert*-butyl)-2,3-dihydroxyphenylsulfanyl]acetic acid, which acts as a potentially antimicrobial substance [20]. Since our earlier work had revealed that Ag (I) complexation leads to enhancement of the antifungal activity of this ligand, we were motivated to explore whether there is a similar trend in the case of the Cu (II) complexes of the SHD derivatives.

In deciding on the subjects of our investigation, we also took into account that one of the key factors leading to a broad spectrum of antimicrobial activities of some transition metal complexes with *O*-coordinated ligands may be related to a direct interaction or complexation of the metal ion with biological ligands due to the ability of the *O*-coordinated ligand in this complex to be readily substituted by an *S*-coordinated bioligand [26,27]. Most bioligands contain the potential target sites for the inhibition of microbial growth by these metal complexes that reportedly might be the *S*-containing residues of proteins. In this connection it is of interest to study the structure–activity correlation in antifungal activities of the Cu (II) complexes with the aforesaid SHD ligands.

The solid Cu (II) complexes were characterized by means of elemental analysis, XRD, TG/DTA, FT-IR, ESR and XPS. However, a full structural analysis could not be performed because no single crystals suitable for X-ray diffraction studies were obtained. A special investigation showed that most of the metal complexes formed with the sterically hindered *o*-diphenol derivatives containing one or two *tert*-butyl groups were hard to crystallize [20–25,28]. Therefore, our notion of the coordination modes of the Cu (II) complexes reported here was formed on the basis of findings provided by other physico-chemical methods.

We also estimated the antifungal activities of the Cu (II) complexes as compared with those of the respective free ligands. Among the test microorganisms there were two plant pathogenic fungi (*Fusarium sp.*, *Botrytis cinerea*).

2. Experimental

2.1. Materials and methods

Chemicals were purchased from commercial sources and were used without further purification. The SHD derivatives were prepared according to [5,7,29–32]. The preparation of the Cu (II) complexes is described later.

Infrared spectra of the solids (the ligands **I**–**IV** and the synthesized Cu (II) complexes) were recorded with a Spectrum 1000 spectrophotometer in the wavelength range 4000–400 cm^{-1} at room temperature, using nujol mulls of the ligands and the complexes, and polyethylene windows.

Thermal analysis was performed with a derivatograph OD-103 MOM. TG/DTA measurements were run in the air between 20 and 450 °C (5 °C min^{-1}).

Elemental analyses were carried out according to standard methods by the Microanalytical Laboratory, Bioorganic Chemistry Institute, National Academy of Sciences, Belarus. Copper and sulfur determinations were carried out using an atomic emission spectrometer with an inductively coupled plasma excitation source (Spectroflame Modula). A sample of a Cu (II) complex was decomposed on treatment with $HNO_3 + H_2O_2$ using a Milestone mls 1200 mega microwave digestion system. After the complex had been decomposed, the contents of metal and sulfur in the resulting solution were determined.

XRD studies were made with an HZG 4A diffractometer ($Co_{K\alpha}$ radiation, MnO_2-filter). An XPS study was performed with an ES-2401 spectrometer. Sample surface etching with Ar^+ was employed. Core level energies were calibrated by the C 1s line with $E_B = 284.6$ eV.

ESR spectra of polycrystalline samples were measured on ERS-220 X-band spectrometer (9.45 GHz) at room temperature and at 77 K, using 100-kHz field modulation; *g* factors were quoted relative to the standard marker DPPH ($g = 2.0036$).

The molar conductances of 10^{-3} M solutions of the Cu (II) complexes in acetonitrile were measured at 20 °C using a TESLA BMS91 conductometer (cell constant 1.0).

2.2. Synthesis of the Cu (II) complexes with sterically hindered o-diphenol derivatives

Based on our previous findings [21–25], the conditions were created to purposefully provide the preferential formation of a complex with a Cu (II):L ratio of 1:2. A solution of the Cu (II) salt was added in small portions to the ligand solution under continuous stirring, so that the complexation always took place with an excess of ligand present. The preparation followed a common procedure. A solution of 0.050 mmol $Cu(CH_3COO)_2 \cdot H_2O$ in 10 ml of water was added dropwise to a colorless solution of 0.100 mmol of **I**–**IV** dissolved in 10 ml of ethanol (molar ratio Cu (II):L = 1:2). It must to be taken into account that these ligands are redox active when producing their complexes with transition metal ions, especially with copper (II), in order to prevent the production of the oxidized forms of the ligands (in particular, *o*-semiquinones, as was shown in [28,33]). Because of this, argon was bubbled through the solutions (pH $\leqslant$ 6) during the synthesis to ensure the absence of oxygen. The reaction vessel was shielded from light. Colored precipitates of the Cu (II) complexes formed instantaneously. After 1.5 h stirring, they were collected on membrane filters (JG 0.2 μm), washed with ethanol and water, and dried *in vacuo* (yield > 70%).

Cu(L^{I})$_2$. Dark blue. *Anal.* Calc. for $C_{28}H_{42}O_4Cu$: C, 66.50; H, 8.30; Cu, 12.55. Found: C, 66.47; H, 8.28; Cu, 12.49%.

Cu(L^{II})$_2$. Cherry-brown. *Anal.* Calc. for $C_{28}H_{42}O_6Cu$: C, 62.54; H, 7.81; Cu, 11.80. Found: C, 62.51; H, 7.78; Cu, 11.76%.

Cu(L^{III})$_2$. Brown. *Anal.* Calc. for $C_{32}H_{50}S_2O_6Cu$: C, 58.42; H, 7.59; S, 9.75; Cu, 9.64. Found: C, 58.40; H, 7.51; S, 9.72; Cu, 9.61%.

Cu(L^{IV})$_2$. Green-brown. *Anal.* Calc. for $C_{32}H_{46}S_2O_8Cu$: C, 56.03; H, 6.71; S, 9.36; Cu, 9.25. Found: C, 55.98; H, 6.68; S, 9.34; Cu, 9.22%.

2.3. Antifungal activities

Antifungal activities of the compounds were tested according to a method reported elsewhere [34]. The following test microorganisms (collection of Department of Microbiology, Belarusian State University) were used: *Aspergillus niger*, *Fusarium sp.*, *Penicillium lividum*, *Mucor sp.*, *B. cinerea*. The compounds were dissolved in DMSO and diluted in Sabouraud liquid medium to yield working solutions of the test complexes of concentration 100 μg mL^{-1}. The complexes, which were insoluble in DMSO, were ground to a fine powder and then suspended in the solvent. A solution of the compound was thoroughly mixed with the sterilized medium, and the mixture poured on glass Petri dishes. After solidification of the medium, the plates were inoculated with a small piece of micelial block of each test fungus cut out from the outer margin of the culture grown on a basal medium. The inoculated plates were incubated at 25 °C whereupon the linear growth of the fungal colony was measured in two directions at right angles to each other after 72 h, and the average of three replicates was taken as the diameter of the colony in millimeters. The concentration of DMSO in the medium did not affect the fungal growth. The degree of inhibition of radial growth (RI) was calculated as follows [35]: RI=100(C–T)/C (%), where T is the mean value of the diameter of the fungal colonies in the presence of a given concentration of each compound, and C is the mean value of the diameter of the fungal colonies in the absence of the same compound, measured under the same conditions. The results were confirmed in three independent experiments.

3. Results and discussion

All the complexes were characterized by X-ray patterns of their own, differing significantly from that of the respective ligands. The elemental analyses data for the complexes Cu (II) with **I**–**IV** are in agreement with the general formula $Cu(L)_2$.

The low solubility of most of these complexes in common organic solvents hinders their study in solution. All the complexes were insoluble in water, ethanol, diethyl ether, nitromethane and chloroform, and only $Cu(L^I)_2$ and $Cu(L^{III})_2$ were soluble in acetonitrile. The low values of the molar conductivity in acetonitrile for the complexes $Cu(L^I)_2$ (Λ_{mol}=8.9 Ω^{-1} cm^2 mol^{-1}) and $Cu(L^{III})_2$ (Λ_{mol}=4.5 Ω^{-1} cm^2 mol^{-1}) indicate them being essentially non-electrolytes in this solvent [36]. Thus, the conductivity data suggest that the ligands, in particular **I** and **III**, may be coordinated to the Cu (II) ion as uninegatively charged ligands.

3.1. Thermal studies

Thermal analyses in air flow with identification of the final products by X-ray powder diffraction has shown all the complexes to be anhydrous and unsolvated, because their DTA curves lack any endothermic peaks over a wide range from 60 to 150 °C. A summary of the results is given in Table 1.

Most of the complexes behaved very similarly on thermal analysis and generally showed two stages of decomposition, except for $Cu(L^{IV})_2$ (three stages). These stages correspond to the maximal weight losses. Taking the $Cu(L^I)_2$ complex as an example, the TGA curve shows that

Table 1
TG/DTA data for decomposition of the Cu (II) complexes to form CuO

Complex	Temperature (°C)	Process	% Weight loss	
			Found	Calc.
$Cu(L^I)_2$	160–390	exothermic	83.42	84.27
$Cu(L^{II})_2$	180–310	exothermic	84.13	85.21
$Cu(L^{III})_2$	170–390	exothermic	87.06	87.91
$Cu(L^{IV})_2$	190–410	exothermic	87.58	88.41

the maximal two-stage weight loss of 83.42% from 160 to 390 °C corresponds to the loss of two ligand molecules in the $Cu(L^I)_2$ complex (Calc. 84.27%): $Cu(L)_2 \rightarrow CuO$. The agreement between the experimental and theoretical weight losses for the above processes confirms the formulas of the Cu (II) complexes.

3.2. Infrared spectra

To specify the coordination modes in the Cu (II) complexes, we used IR spectroscopy (Table 2).

In the spectra of **I** and **II** there are two bands at 3200–3550 cm^{-1}, indicating the presence of intermolecular hydrogen bonds involving hydroxyl groups [37]. As for the spectra of $Cu(L^I)_2$ and $Cu(L^{II})_2$, there is only one broad band in that region, which allows one to suggest that **I** and **II** coordinate as κ^2O,O-ligands in the singly deprotonated form. The bands at 1200–1050 cm^{-1} in the spectra of **I** and **II**, assigned to the vibrations of the C–O band, are shifted towards lower frequencies in the spectra of $Cu(L^I)_2$ and $Cu(L^{II})_2$, indicating Cu (II) being coordinated with the hydroxyls of **I** and **II**. The strong band at 1463 cm^{-1} in the $Cu(L^{II})_2$ spectrum may be due to the radical-anionic ligand form being present [38].

IR spectral assignments of ligands **III** and **IV** and their Cu (II) complexes in the regions 3200–3550 cm^{-1} and 1200–1020 cm^{-1} are in much the same fashion as above mentioned. The shift of the bands at 1000–760 cm^{-1}, assigned to C–S bond vibrations, to the short-wave region in the spectrum of this complex suggests that the sulfur is involved in the complexation. In the spectrum of **IV** the band corresponding to the stretching vibrations of C=O in the carboxyl group is observed at 1690 cm^{-1}. It is absent in the spectrum of $Cu(L^{IV})_2$, but new bands at 1550 and 1600 cm^{-1} appear, which are characteristic of $-COO^-$ group vibrations [37]. The shift of the stretching vibration frequencies for the carboxylic group is indicative of the hydrogen ions therein being substituted by Cu (II) in the two coordinated ligand molecules.

It should be noted that in the spectra of all the complexes under study there are bands in the region of 470–580 cm^{-1} which may be assigned to the stretching vibrations of the Cu–O bond. As Cu–S stretching vibration frequencies are usually below 400 cm^{-1}, they could not be registered with the instrument employed here to register IR spectra.

Table 2
IR spectral assignments (cm^{-1}) of the ligands and the Cu (II) complexes

Compound	ν(–OH)	ν(C–S)	ν(COO^-)	ν(C–O)	ν(Cu–O)
L^I	3461			1105	
	3264				
$Cu(L^I)_2$	3484			1091	510
L^{II}	3540			1182	
	3440			1053	
$Cu(L^{II})_2$	3387			1097	489
				1023	
L^{III}	3536	857		1062	
	3339	848		1004	
$Cu(L^{III})_2$	3399	826		1064	477
		770		1010	
L^{IV}	3545	1030		1163	
	3447	775		1117	
	3349			1027	
$Cu(L^{IV})_2$	3377	1000	1602	1159	488
		767	1574		

3.3. ESR spectra

The ESR parameters of the Cu (II) complexes are presented in Table 3. The ESR spectra of complexes $Cu(L^I)_2$ and $Cu(L^{II})_2$ at room temperature were not observed, but all the complexes are characterized by the spectra at 77 K.

The ESR spectra of $Cu(L^I)_2$, $Cu(L^{II})_2$ and $Cu(L^{III})_2$ compounds in the polycrystalline state (77 K) are typical axial spectra (Fig. 1) with $g_\parallel$ and $g_\perp$ features at about 2.28–2.30 and 2.03–2.04. The geometric parameter G, which is a measure of the exchange interaction between the copper (II) centers in the polycrystalline compound, is calculated using the equation $G = (g_\parallel - 2.0023)/(g_\perp - 2.0023)$ [39]. The geometric parameter G for the complexes $Cu(L^I)_2$, $Cu(L^{II})_2$ and $Cu(L^{III})_2$ appears to be greater than 4, which shows that there are no magnetic exchange interactions between the copper (II) centers [40]. The solid state ESR spectra of all these complexes at 77 K are quite similar

Table 3
ESR parameters of Cu (II) complexes

Complex	$A_\parallel$	$g_\parallel$	$g_\perp$	$g(R^\cdot)$	g_1	g_2	g_3	G
$Cu(L^I)_2$	178	2.285	2.0278					11.09
$Cu(L^{II})_2$	171	2.278	2.0331	2.0043				8.95
$Cu(L^{III})_2$	145	2.297	2.0407					7.67
$Cu(L^{IV})_2$					2.230	2.111	2.0228	

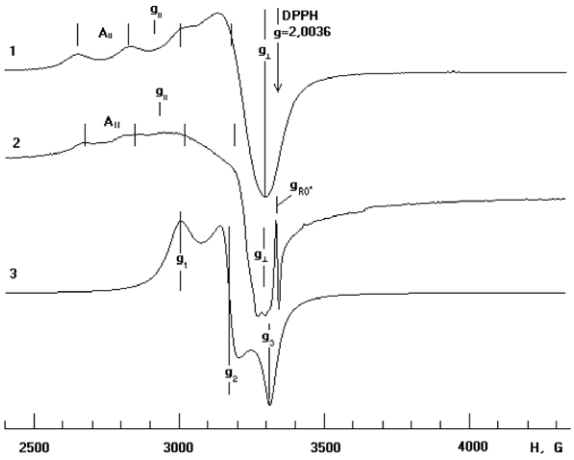

Fig. 1. ESR spectra of compounds $Cu(L^I)_2$ (**1**), $Cu(L^{II})_2$ (**2**) and $Cu(L^{IV})_2$ (**3**) in the polycrystalline state at 77 K.

and exhibit axially symmetric g-tensor parameters with $g_{\|} > g_{\perp} > 2.0023$. These data indicate that the copper site has a $d_{x^2-y^2}$ ground state, characteristic of square planar stereochemistry [41,42]. This structure of the complex agrees with the data of the elemental analysis for the aforesaid Cu (II) complexes.

The ESR spectrum of the $Cu(L^{IV})_2$ complex apparently shows rhombic symmetry ($g_1 = 2.230$; $g_2 = 2.111$; $g_3 = 2.0228$), which indicates the existence of partial mixing of the d_{z^2} orbital into the $d_{x^2-y^2}$ magnetic orbital [43]. Although it is impossible to obtain accurate molecular values from polycrystalline ESR spectra, it is possible to distinguish unambiguously between $d_{x^2-y^2}$ and d_{z^2} as ground states. Thus, the observed g-values ($g_{\|} > g_{\perp} > 0$) and the value of $R=(g_2 - g_1)/(g_3 - g_2)$ of 0.74 suggest a predominantly $d_{x^2-y^2}$ ground state [40].

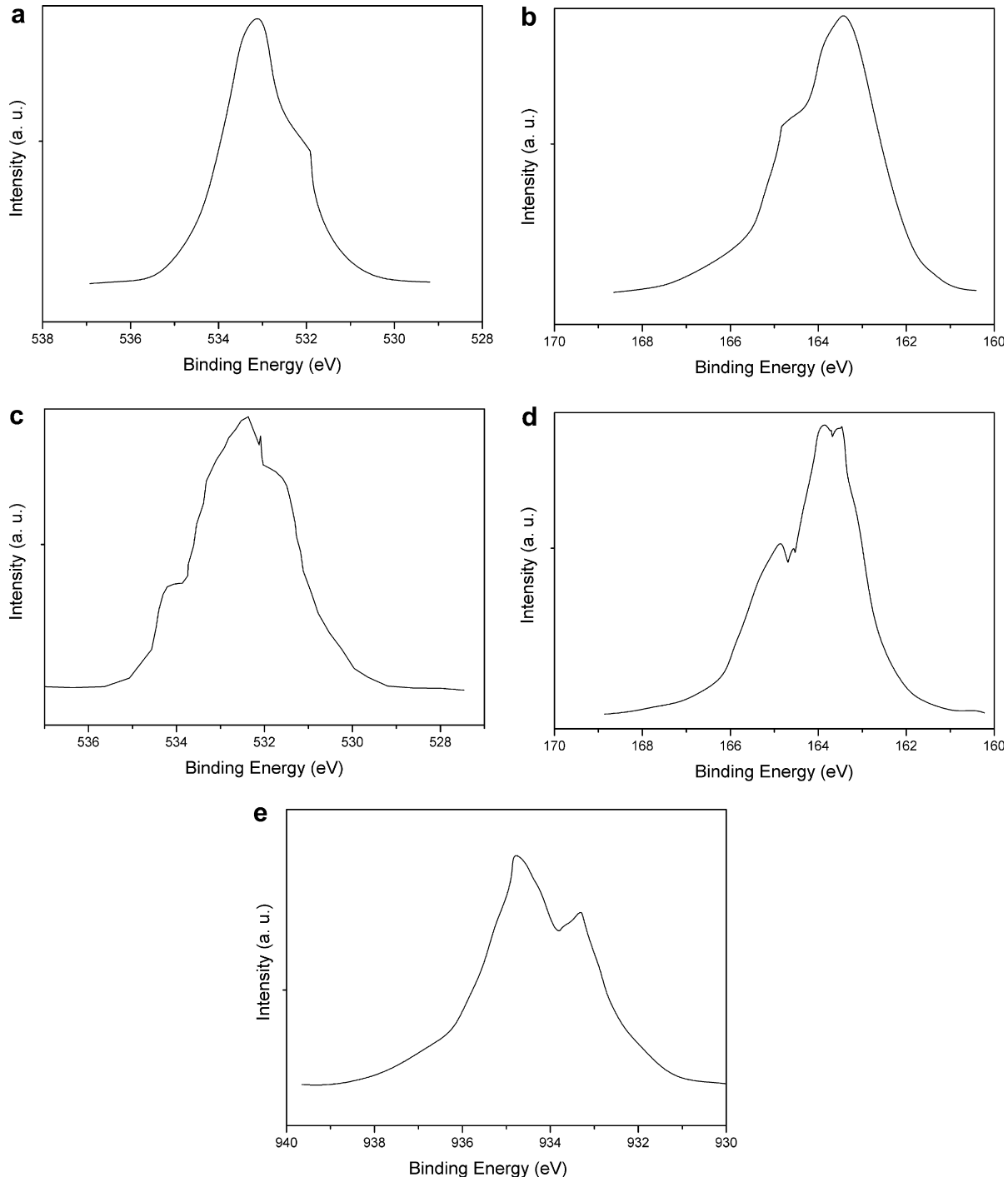

Fig. 2. The X-ray photoelectron spectra: (a) O 1 s core level spectrum of free **III** ligand; (b) S 2p core level spectrum of free **III** ligand; (c) O 1 s core level spectrum of $Cu(L^{III})_2$; (d) S 2p core level spectrum of $Cu(L^{III})_2$; (e) Cu 2p core level spectrum of $Cu(L^{III})_2$.

According to [44], $g_{\|}$ values less than 2.3 indicate considerable covalent character of M–L bonds (Table 3). The smaller $A_{\|}$ value for complex $Cu(L^{III})_2$ has been attributed to the high covalency of the Cu–S bonding [45].

It should be noted that the ESR spectrum of the $Cu(L^{II})_2$ complexes differ from those of $Cu(L^{I})_2$, $Cu(L^{III})_2$ and $Cu(L^{IV})_2$ by the presence of narrow singlet signals with a *g*-factor near 2 (Table 3). On the basis of the *g*-factor values (respectively, 2.0043 and 2.0045), it may be suggested that these radicals are phenoxyl ones. In the free crystalline ligands no stabilized radicals are registered. Concentration of phenoxyl radicals in the $Cu(L^{II})_2$ complex is about 4–8×10^{15} g^{-1}, thus they may be assumed to form during the synthesis of the complexes. No stabilized radicals being present in the $Cu(L^{I})_2$, $Cu(L^{III})_2$ and $Cu(L^{IV})_2$ complexes is evidence of the possibility of redox reactions on complexation, apparently depending on the ligand nature and on the conditions in which the complexation takes place [33].

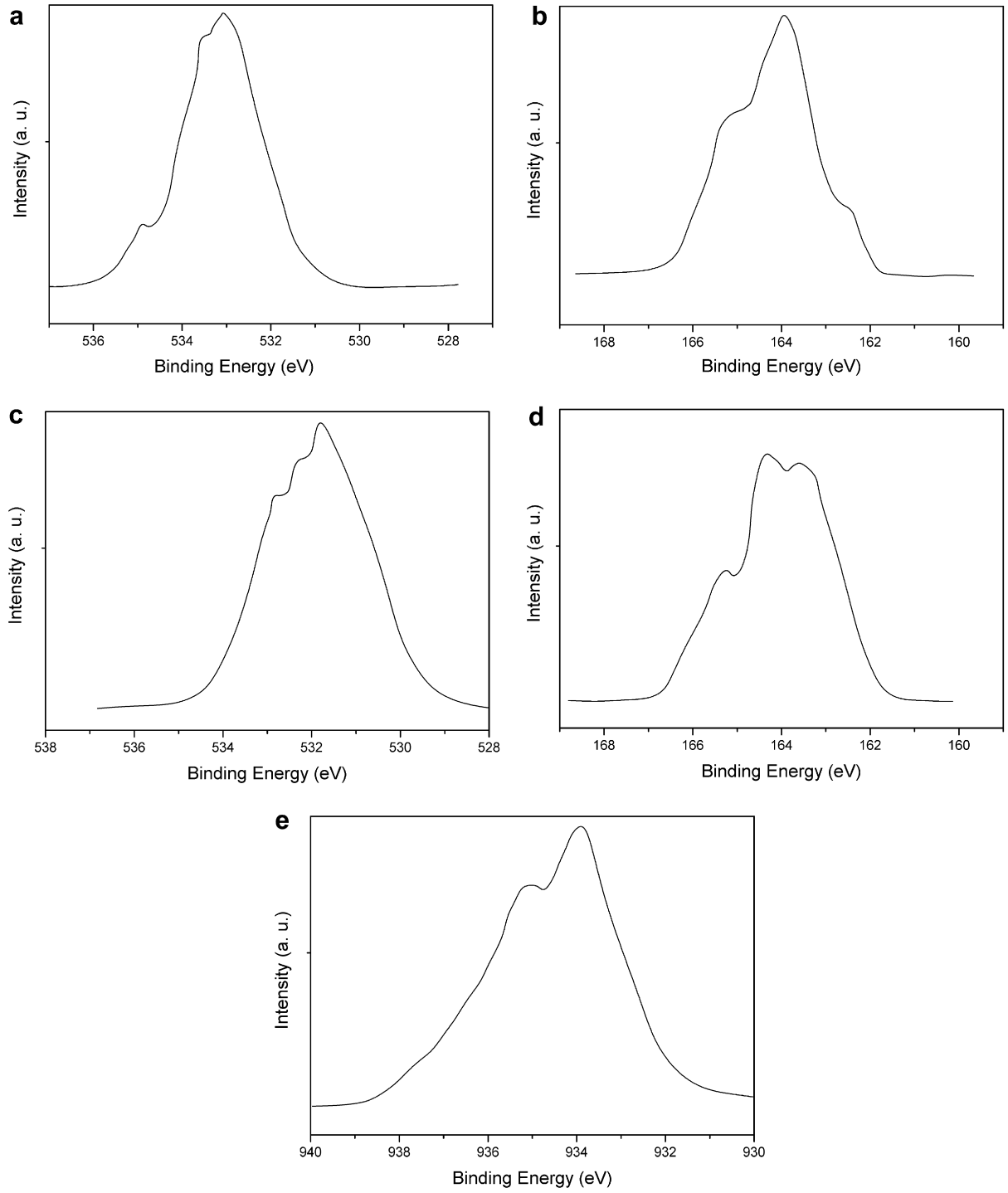

Fig. 3. The X-ray photoelectron spectra: (a) O 1 s core level spectrum of free **IV** ligand; (b) S 2p core level spectrum of free **IV** ligand; (c) O 1 s core level spectrum of $Cu(L^{IV})_2$; (d) S 2p core level spectrum of $Cu(L^{IV})_2$; (e) Cu 2p core level spectrum of $Cu(L^{IV})_2$.

Table 4
Antifungal activities of the free ligands **I**–**IV** and their Cu (II) complexes expressed as radial inhibition of mycelial growth (RI, %)

Compound	RI (%)				
	Aspergillus niger	*Fusarium sp.*	*Mucor sp.*	*Penicillium lividum*	*Botrytis cinerea*
L^{I}	65	100	100	80	100
$Cu(L^{I})_2$	35	80	0	75	50
L^{II}	100	100	100	75	100
$Cu(L^{II})_2$	75	80	100	60	100
L^{III}	50	60	0	60	100
$Cu(L^{III})_2$	75	95	25	75	100
L^{IV}	80	100	0	75	100
$Cu(L^{IV})_2$	80	100	50	80	100
Nystatin	80	90	100	90	60
Terbinafine	100	80	25	40	60

3.4. X-ray photoelectron spectra

Unfortunately, we failed to register the spectra of polycrystalline samples of $Cu(L^{I})_2$ and $Cu(L^{II})_2$ complexes, because the latter undergo decomposition under the conditions in which the spectra are registered.

In the case of $Cu(L^{III})_2$ and $Cu(L^{IV})_2$, the Cu 2p core level spectra are spin split into two peaks, respectively, at 934.7, 933.3 eV (Fig. 2e) and at 935.4, 934.4 eV (Fig. 3e). In the Cu (II) compounds, the Cu 2p energy is 934–935.5 eV, and for Cu (I) it is 932.1 eV [46]. Thus, the copper energy state in these complexes is Cu(II).

The S 2p core level spectra of $Cu(L^{III})_2$ and $Cu(L^{IV})_2$ have three distinct peaks each (respectively, Figs. 2d and 3d). The increased binding energies of S 2p and decreased electron density in the Cu(II) complexes in comparison with the parent ligands (respectively, Figs. 2b and 3b) may be indicative of the S atom being involved in forming the coordination core in the Cu(II) complexes.

The increased binding energies of O 1 s in the Cu(II) complexes (Figs. 2c and 3c) in comparison with the parent ligands (Figs. 2a and 3a) suggest the electron donating properties of the hydroxyl group and its coordination to Cu (II). The binding energy being decreased from 534.9 to 533.3 eV and from 533.6 to 532.7 eV may be related to the carboxylate anion being formed in $Cu(L^{IV})_2$ complex (Fig. 3a and c) [46].

3.5. Antifungal activities

Inhibition values of the free ligands and their Cu (II) complexes are listed in Table 4. It should be emphasized that antifungal tests of these compounds were first performed here. Commonly used antifungal drugs Nystatin and Terbinafine were tested as positive controls.

Most of the compounds (both the free ligands and the complexes) exert pronounced antifungal activities ($RI \geqslant 70\%$), which in a number of cases were comparable with those of Nystatin and Terbinafine or even higher. Except for the $Cu(L^{II})_2$ complex, all of them have the highest inhibitory properties ($RI = 100\%$) against *B. cinerea*.

The highest activity ($RI = 100\%$) is characteristic of both ligand **II** against *A. niger* and ligands **I, II**, **IV** and the $Cu(L^{IV})_2$ complex against *Fusarium sp*. Ligands **I**, **II** and $Cu(L^{II})_2$ complex are the best antifungal agents against *Mucor sp.* The most active compounds against *P. lividum* are ligand **I** and $Cu(L^{IV})_2$ complex.

$Cu(L^{I})_2$ and $Cu(L^{II})_2$ complexes, formed by κ^2O,O-ligands, exhibit inhibitory activity comparable to or lower than that of the free ligands. In spite of the activity becoming somewhat lower, the results obtained merit notice, because it is known that the presence of Cu (II) ions may substantially decrease the toxic effect of the ligands [17,18]. According to [47,48], ligands may be more reactive with the microelements necessary for fungal nutrition. Along with this explanation, the authors [49–51] suppose that the reduced activity of the compounds against fungi can be attributed to their inability to form hydrogen bonds through the *O*-donor groups with the active centres of the cell constituents.

It is evident that $Cu(L^{III})_2$ and $Cu(L^{IV})_2$ complexes, formed, respectively, by κ^2O,S- and κ^2O,O,S-ligands, exhibit inhibitory activity comparable to or higher than that of the free ligands. $Cu(L^{III})_2$ is more potent than the parent ligand towards *A. niger* and *Fusarium sp.*, as well as $Cu(L^{III})_2$ and $Cu(L^{IV})_2$, which show higher antifungal potency than the parent ligands towards *P. lividum* and *Mucor sp.* It is common knowledge that chelation could enhance the lipophilic character of central metal atoms which subsequently favours its penetration through the lipid layers of the cell membrane.

4. Conclusion

During the past decade the importance of *o*-diphenol-based (or catechol-based) metal complexes in biology has become evident. Because these ligands are redox active, it must be taken into account when producing their complexes with transition metal ions, especially with copper (II), in order to prevent the production of the oxidized forms of ligands (in particular, *o*-semiquinones, as was shown in [28,33]). We have synthesized several Cu (II) complexes with some SHD derivatives, which seem to be promising for the study of their antifungal activities. Our investigation shows that we have managed to avoid oxidation of the ligands **I**, **III** and **IV** on their complexation with

Cu (II) ions, and it was only for ligand **II** that stabilized phenoxyl radicals were found to be present in a very small amount. It should be noted that their presence in $Cu(L^{II})_2$ had no marked enhancing effect on the antifungal activities of the latter compared with that of the parent ligand **II**. In general, most of the compounds tested show a broad spectra of antifungal activities, which in a number of cases were comparable with those of Nystatin and Terbinafine, or were even higher. These facts may be of interest in the design of new effective drugs and agents against plant pathogenic fungi.

References

[1] K. Asai, N. Tsuchimori, K. Okonogi, J.R. Perfect, O. Gotoh, Y. Yoshida, Antimicrob. Agents Chemother. 43 (1999) 1163.
[2] O.I. Shadyro, G.K. Glushonok, T.G. Glushonok, I.P. Edimecheva, A.G. Moroz, A.A. Sosnovskaya, I.L. Yurkova, G.I. Polozov, Free Radical Res. 36 (2002) 859.
[3] O.I. Shadyro, I.P. Edimecheva, G.K. Glushonok, N.I. Ostrovskaya, G.I. Polozov, H. Murase, T. Kagiya, Free Radical Res. 37 (2003) 1087.
[4] G.N. Shilov, A.I. Balakleevskii, O.I. Shadyro, V.A. Timoshchuk, Russ. 182759, Ofits. Bull. Rossiiskogo agentstva po patentam I tovarnym znakam 26 (1993) (In Russian).
[5] D.K. Petrikevch, V.A. Timoshchuk, O.I. Shadyro, O.T. Andreeva, V.I. Votyakov, V.E. Zhelobkovich, Khim.-farm. zhurn. 12 (1995) 32, In Russian.
[6] T.A. Mikhas'ko, B.V. Dubovik, O.I. Shadyro, G.I. Polozov, Meditsinskie novosti 4 (2002) 81, In Russian.
[7] O.I. Shadyro, V.A. Timoshchuk, G.I. Polozov, V.N. Povalishev, O.T. Andreeva, V.E. Zhelobkovich, Khim.-farm. zhurn. 7 (1999) 25, In Russian.
[8] M.J. Laughton, B. Halliwell, P.J. Evans, J.R.S. Hoult, Biochem. Pharmacol. 38 (1989) 2859.
[9] G. Cao, E. Sofic, R. Prior, Free Radical Biol. Med. 22 (1997) 749.
[10] D. Metodiewa, A.K. Jaiswal, N. Cenas, E. Dickancaité, J. Segura-Aguilar, Free Radical Biol. Med. 26 (1999) 107.
[11] N. Yamashita, H. Tanemura, S. Kawanishi, Mutat. Res. 425 (1999) 107.
[12] I. Morel, G. Lescoat, O. Cogrel, O. Sergent, N. Pasdeloup, P. Brissot, P. Cillard, J. Cillard, Biochem. Pharmacol. 45 (1993) 13.
[13] F. Blasko, L. Perelló, J. Latorre, J. Borrás, S. Garciá-Granda, J. Inorg. Biochem. 61 (1996) 143.
[14] M. Ruiz, L. Perelló, J. Server-Carrió, R. Ortiz, S. Garciá-Granda, M.R. Diaz, E. Cantón, J. Inorg. Biochem. 69 (1998) 231.
[15] B. Simó, L. Perelló, R. Ortiz, A. Castińeiras, J. Lattore, E. Cantón, J. Inorg. Biochem. 81 (2000) 275.
[16] M.C. Linder, C.A. Goode, Biochemistry of Copper, Plenum, New York, 1991.
[17] J.R.J. Sorenson, Inflammatory Diseases and Copper, Humana Press, Clifton, 1982.
[18] I. Haiduc, C. Silvestru (Eds.), Organometallics in Cancer Chemotherapy, vol. II, CRS Press, Boston, 1989.
[19] P. Singleton, D. Sainsbury, Dictionary of Microbiology and Molecular Biology, 2nd ed., Wiley, New York, 1987.
[20] N.V. Loginova, A.A. Chernyavskaya, G.I. Polozov, T.V. Koval'chuk, E.V. Bondarenko, N.P. Osipovich, A.A. Sheryakov, O.I. Shadyro, Polyhedron 24 (2005) 611.
[21] T.V. Koval'chuk, N.V. Loginova, G.I. Polozov, G.A. Ksendzova, V.L. Sorokin, in: Proceedings of the Ninth International Conference on Physico-Chemical Processes in Inorganic Materials, vol. 2, Kemerovo, 2004, p. 46 (In Russian).
[22] T.V. Koval'chuk, N.V. Loginova, G.I. Polozov, G.A. Ksendzova, V.L. Sorokin, in: Proceedings of the Ninth International Conference on Problems of Solvation and Complex Formation in Solutions, Plyos, 2004, p. 258 (In Russian).
[23] T.V. Koval'chuk, N.V. Loginova, A.A. Chernyavskaya, N.P. Osipovich, G.I. Polozov, G.A. Ksendzova, V.L. Sorokin, in: Proceedings of the fifteenth Russian International Conference on Chemical Thermodinamics, RCCT 2005, vol. 2, Moscow, 2005, p. 92.
[24] T.V. Koval'chuk, N.V. Loginova, G.I. Polozov, R.A. Zheldakova, N.P. Osipovich, G.K. Glushonok, G.A. Ksendzova, N.V. Ushakov, V.L. Sorokin, in: Proceedings of the Twenty-second Chugaev International Conference on Coord. Chem., Kishinev, 2005, p. 383 (In Russian).
[25] A.A. Chernyavskaya, N.V. Loginova, G.I. Polozov, N.P. Osipovich, I.V. Paribok, V.N. Povalishev, in: Sviridov Readings, Issue 2, Minsk, 2005, p. 177 (In Russian).
[26] K. Nomiya, A. Yoshizawa, K. Tsukagoshi, N.C. Kasuga, S. Hirakawa, J. Watanabe, J. Inorg. Biochem. 98 (2004) 46.
[27] A.M. Lee, S.F. Singleton, J. Inorg. Biochem. 98 (2004) 1981.
[28] C.N. Verani, PhD Thesis, Ruhr-Universität Bochum, 2000.
[29] L.A. Maslovskaya, D.K. Petrikevch, V.A. Timoshchuk, O.I. Shadyro, Zhurn. obshchei khimii 66 (1996) 1893, In Russian.
[30] L.A. Maslovskaya, D.K. Petrikevch, V.A. Timoshchuk, O.I. Shadyro, Zhurn. obshchei khimii 66 (1996) 1899, In Russian.
[31] H. Schulze, W. Flaig, Liebigs Ann. Chem. 575 (1959) 231.
[32] I.S. Belostotskaya, N.L. Komissarova, E.V. Dzhuaryan, V.V. Ershov, Izv. AN SSSR, Ser. Chim. (1971) 2871, In Russian.
[33] J.S. Thompson, J.C. Calabrese, J. Am. Chem. Soc. 108 (1986) 1903.
[34] V.I. Bilai, Metody experimental'noi mikologii, Nauk. dumka, Kiev, 1982 (In Russian).
[35] D.J. Royse, S.M. Ries, Phytopathology 68 (1978) 603.
[36] W.J. Geary, Coord. Chem. Rev. 7 (1971) 81.
[37] K. Nakamoto, Infrared and Raman Spectra of Inorganic and Coordination Compounds, Wiley Inc., New York, 1986.
[38] A.I. Poddel'sky, V.K. Cherkasov, G.K. Fukin, M.P. Bubnov, L.G. Abakumova, G.A. Abakumov, Inorg. Chem. Acta 357 (2004) 3632.
[39] A.A. Tak, F. Arjmand, S. Tabassum, Transit. Met. Chem. 27 (2002) 741.
[40] B.J. Hathaway, D.E. Billing, Coord. Chem. Rev. 5 (1970) 143.
[41] M. Ruf, B. Noll, M. Groner, G.T. Yee, C.G. Pierpont, Inorg. Chem. 36 (1997) 4860.
[42] G. Speier, J. Csihony, A.M. Whalen, C.G. Pierpont, Inorg. Chem. 35 (1996) 3519.
[43] S. Katawa, S. Kitagawa, H. Kumagai, Ch. Kudo, M. Katada, Inorg. Chem. 35 (1996) 4449.
[44] D. Kivelson, R. Neiman, J. Chem. Phys. 35 (1961) 149.
[45] S. Mandal, G. Das, R. Singh, R. Shukla, P.K. Bharadwaj, Coord. Chem. Rev. 160 (1997) 191.
[46] V.I. Nefedov, Rentgenoelektronnaya spektroskopiya khimicheskikh soedinenii, Spravochnik, Khimiya, Moskwa, 1984 (In Russian).
[47] W.Q. Zhou, K. Sh. Leng, Y. Zhang, L.D. Lu, J. Mol. Struct. 657 (2003) 215.
[48] M. Devereux, M. McCann, V. Leon, M. Geraghty, V. McKee, J. Wikaira, Polyhedron 19 (2000) 1205.
[49] N. Dharmaraj, P. Viswanathamurthi, K. Natarajan, Transit. Metal Chem. 26 (2001) 105.
[50] R. Kurtaran, L.T. Yildirim, A.D. Azaz, H. Namli, O. Atakol, J. Inorg. Biochem. 99 (2005) 1937.
[51] R.P. John, A. Sreekanth, V. Rajakannan, T.A. Ajith, M.R. Prathapachandra Kurup, Polyhedron 23 (2004) 2549.

a methylene chloride/*n*-hexane mixture and compound **2** has been isolated as colourless crystals. Yield: 0.51 g (65%). M.p. 218 °C.

Path c: A suspension of anhydrous K_2CO_3 (1.10 g, 8 mmol), 18-crown-6 (0.1 g, 0.38 mmol as a catalyst) and bis-thiourea **1** (0.94 g, 1.6 mmol) in benzene solution (70 mL) was stirred at room temperature for 15 min. To the resulting potassium salt, a benzene (30 mL) solution of $ClCH_2C(O)OCH_3$ (0.35 g, 3.2 mmol) was added dropwise whilst stirring vigorously. The mixture was stirred at room temperature for a further 2 h, then the K_2CO_3 precipitate was filtered off and the solvent was removed in vacuo. The residue was recrystallized from a benzene/*n*-hexane mixture and compound **2** was isolated as colourless crystals. Yield: 0.30 g (59%). M.p. 218 °C. ^{1}H NMR ($CDCl_3$): $\delta = 1.25$ (d, $^3J_{H,H} = 5.1$ Hz, 6H, CH_3), 1.38 (d, $^3J_{H,H} = 5.1$ Hz, 6H, CH_3), 4.81 (d. sept, $^3J_{POCH} = 11.2$ Hz, $^3J_{H,H} = 5.1$ Hz, 2H, OCH), 7.15 (m, 2H, AA′ of AA′XX′, C_6H_4), 7.36 (m, 2H, XX′ of AA′XX′, C_6H_4), 11.97 (s, 2H, NH) ppm. $^{31}P\{^1H\}$ NMR ($CDCl_3$): 64.8 (t, $^3J_{POCH} = 11.2$ Hz) ppm. IR: $\tilde{\nu} = 3240$ (NH), 1648 (C=N), 1020, 980, 945 (POC), 648, 620 (P=S) cm^{-1}. *Anal.* Calc. for $C_{13}H_{20}N_3O_2PS$ (313.36): C, 49.83; H, 6.43. Found: C, 49.89; H, 6.56%.

2.2. Synthesis of [K(18-crown-6)L] (5)

A suspension of **2** (0.16 g, 0.5 mmol), 18-crown-6 (0.16 g, 0.6 mmol) and KOH (0.08 g, 1.5 mmol) in acetone solution (15 mL) was stirred at room temperature for 15 min, then the precipitate was filtered off. The solvent was removed in vacuo. The residue was recrystallized from a methylene chloride/*n*-hexane mixture and compound **5** was isolated as a colourless powder. Yield: 0.19 g (63%). M.p. 218 °C. ^{1}H NMR ($CDCl_3$): 1.25 (d, $^3J_{H,H} = 6.2$ Hz, 6H, CH_3), 1.30 (d, $^3J_{H,H} = 6.2$ Hz, 6H, CH_3), 3.62 (s, 24H, OCH_2), 4.77 (d. sept, $^3J_{POCH} = 9.7$ Hz, $^3J_{H,H} = 6.1$ Hz, 2H, OCH), 6.99 (m, 2H, AA′ of AA′XX′, C_6H_4), 7.20 (m, 2H, XX′ of AA′XX′, C_6H_4) ppm. ^{1}H NMR (d_6-acetone): 1.22 (d. d, $^3J_{H,H} = 6.1$ Hz, 12H, CH_3), 3.66 (s, 24H, OCH_2), 4.69 (d. sept, $^3J_{POCH} = 11.3$ Hz, $^3J_{H,H} = 6.1$ Hz, 2H, OCH), 6.76 (m, 2H, AA′ of AA′XX′, C_6H_4), 7.13 (m, 2H, XX′ of AA′XX′, C_6H_4) ppm. $^{31}P\{^1H\}$ NMR ($CDCl_3$): 62.1 (t, $^3J_{POCH} = 9.7$ Hz) ppm. $^{31}P\{^1H\}$ NMR (d_6-acetone): 61.6 (d. t, $^3J_{POCH} = 10.8$ Hz, $^2J_{PNH} = 8.0$ Hz) ppm. IR: $\tilde{\nu} = 3288$ (NH), 1624 (C=N), 1108 (COC), 992, 964, 948 (POC), 618, 584 (P=S) cm^{-1}. *Anal.* Calc. for $C_{25}H_{43}KN_3O_8PS$ (615.21): C, 48.76; H, 7.04; N, 6.82. Found: C, 48.73; H, 7.07; N, 6.79%.

2.3. Synthesis of O,O′-diisopropyl-(1-{[(diisopropoxyphosphorothio) amino]carbonothioyl}imidazolidine-2-ylidene)amidothiophosphate (8)

A suspension of anhydrous K_2CO_3 (1.38 g, 10 mmol), 18-crown-6 (0.1 g, 0.38 mmol as a catalyst) and bis-thiourea **6** (1.35 g, 2.5 mmol) in acetonitrile solution (50 mL) was stirred at room temperature for 4 h, then the K_2CO_3 precipitate was filtered off. To the filtrate, containing potassium salt **7**, (δ_P 66.0 ppm, CH_3CN), an acetonitrile (50 mL) solution of iodine (0.64 g, 2.5 mmol) was added dropwise whilst stirring vigorously. The mixture was stirred at room temperature for a further 3 h, then the formed white precipitate was filtered off and the solvent was removed in vacuo. The residue was recrystallized from a methylene chloride/*n*-hexane mixture and compound **8** was isolated as colourless crystals. Yield: 0.69 g (55%). M.p. 95 °C. ^{1}H NMR (C_6D_6): 1.43-1.50 (m, 24H, CH_3), 3.23 (m, 2H, AA′ of AA′XX′, NCH_2), 4.10 (m, 2H, XX′ of AA′XX′, NCH_2), 4.84 (d. sept, $^3J_{POCH} = 10.8$ Hz, $^3J_{H,H} = 6.2$ Hz, 2H, OCH), 5.06 (d. sept, $^3J_{POCH} = 10.8$ Hz, $^3J_{H,H} = 6.2$ Hz, 2H, OCH), 8.64 (s, 1H, N*H*CH_2), 12.65 (d, $^3J_{PNH} = 12.2$ Hz, 1H, NHP) ppm. ^{31}P NMR (C_6D_6): 59.2 (d. trip, $^3J_{POCH} = 10.6$ Hz, $^2J_{PNH} = 11.5$ Hz, 1P), 62.0 (t, $^3J_{POCH} = 10.8$ Hz, 1P) ppm. IR: $\tilde{\nu} = 3250$ (NH), 1650 (C=N), 1020, 1000, 975 (POC), 610 (P=S) cm^{-1}. *Anal.* Calc. for $C_{16}H_{34}N_4O_4P_2S_3$ (504.61): C, 38.09; H, 6.79. Found: C, 38.04; H, 6.77%.

2.4. Physical measurements

Infrared spectra (Nujol) were recorded on a Specord M-80 spectrometer in the range 400–3600 cm^{-1}. NMR spectra were obtained on a Varian Unity-300 NMR spectrometer at 25°C. ^{1}H, ^{31}P and $^{31}P\{^1H\}$ spectra were recorded at 299.948 and 121.420 MHz, respectively. Chemical shifts are reported with reference to $SiMe_4$ (^{1}H) and H_3PO_4 (^{31}P). Elemental analyses were performed on a Perkin–Elmer 2400 CHN microanalyser. *N*-Thiophosphorylated thioureas **1** and **6** were prepared according to the previously described methods [2,10].

2.5. Crystal structure determination and refinement

The X-ray diffraction data for the crystals of **2** and **8** were collected on a Enraf-Nonius CAD4 automatic diffractometer using graphite monochromated Mo Kα ($\lambda = 0.71073$ Å) radiation ($T = 293(2)$ K). The stability of the crystals and the experimental conditions were checked every 2 h using three control reflections, while the orientation was monitored every 200 reflections by centering two standards. The structures were solved by direct method using the SIR [12] program and refined by full-matrix least-squares using the program SHELXL-97 [13]. All non-hydrogen atoms were refined anisotropically. The hydrogen atoms were calculated and refined as riding atoms. All calculations were performed on a PC using the WinGX [14] program. Cell parameters, data collection and data reduction were performed on an Alpha Station 200 computer using the MOLEN [15] program. All figures were made using the program PLATON [16].

Some crystal data of **2**: $C_{13}H_{20}N_3O_2PS$; $M = 313.35$; space group $P2_1/n$ (No. 14); dimensions $0.40 \times 0.35 \times 0.30$ mm, $a = 11.245(2)$ Å, $b = 9.564(1)$ Å, $c = 15.243(2)$ Å;

$\beta = 92.69(6)°$; $V = 1637.5(4)$ Å^3, $D_{calc} = 1.27$ Mg m^{-3}, $Z = 4$, μ(Mo Kα) = 0.3 mm^{-1}; $F(000) = 664$, $\theta_{max} = 26.3°$. A total of 3429 unique reflections were measured, of which 2276 were with $I > 2\sigma(I)$. The structure converged with $R = 0.0382$, $R_w = 0.0968$. Some crystal data of **8**: $C_{16}H_{34}N_4O_4P_2S_3$; $M = 504.62$; space group $P2_1/n$ (No. 14); dimensions $0.40 \times 0.40 \times 0.35$ mm, $a = 10.418(5)$ Å, $b = 8.734(3)$ Å, $c = 29.616(7)$ Å; $\beta = 96.20(2)°$; $V = 2679(2)$ Å^3, $D_{calc} = 1.25$ Mg m^{-3}, $Z = 4$, μ(Mo Kα) = 0.420 mm^{-1}; $F(000) = 1072$, $\theta_{max} = 26.3$. A total of 4533 unique reflections were measured, of which 2463 were with $I > 2\sigma(I)$. The structure converged with $R = 0.0690$, $R_w = 0.1905$.

3. Results and discussion

3.1. Synthesis

Earlier it has been shown by us [11] that thiophosphorylated bis-thiourea (**1**) oxidation (Scheme 1, path a), leads to elimination of the thiophosphoric acid isothiocyanate molecule and to thiophosphorylated imine formation (**2**). In the present work we have established that thiourea **1** interaction with bases in benzene solution brings similar results (Scheme 1, path b). However, in the latter case 2–3 days are required for completion of the process.

It is known that the reactions of chloranhydrides, amides and monochloracetic acid ethers with *N*-thiophosphorylated thioureas lead to iminothiazolidine-4-on *N*-(thio)phosphorylated derivatives [3]. Bis-thiourea **1**, under similar conditions, does not form cyclic *S*-alkylation products, only imine **2** and isothiocyanate were isolated from the reaction mixture.

As a possible scheme of processes, one can assume reactive carbodiimide formation with subsequent intramolecular cyclization and isothiocyanate molecule elimination.

An electron acceptor effect of a thiophosphoryl substituent in combination with an opportunity of negative charge delocalization within the N–C=N fragment and the benzimidazolic cycle gives acidic properties. The reaction of **2** with KOH in acetone solution in the presence of 18-crown-6 has allowed the isolation of the potassium salt with $[K^+(18\text{-crown-6})L^-]$ composition as a colourless fine-crystalline solid, insoluble in water. Based on data of IR, ^{1}H and ^{31}P NMR spectroscopy and microanalysis, the structure **5** was ascribed to this salt (Scheme 2).

Bis-thiourea (**6**), containing an ethylenediamine fragment, behaves in the oxidation reaction differently: under KOH treatment it converts into salt (**7**), which does not experience any further transformations. In the IR spectrum of compound **7** there are no absorption bands in the range which is characteristic for the C=N bond. The NMR ^{31}P{^{1}H} spectrum of the salt **7** contains a signal with a chemical shift of 66.0 ppm, that is typical for such a kind of structure. Under iodine treatment on a salt **7** solution, an imidazolidine cycle (**8**) forms, but the process proceeds without isothiocyanate molecule elimination (Scheme 3).

Thiourea fragment preservation in the molecule of **8** is explained by the greater nucleophility of the imidazolidine fragment nitrogen atom in comparison with the benzo-analogue **2**. Electronic density delocalization in the conjugated

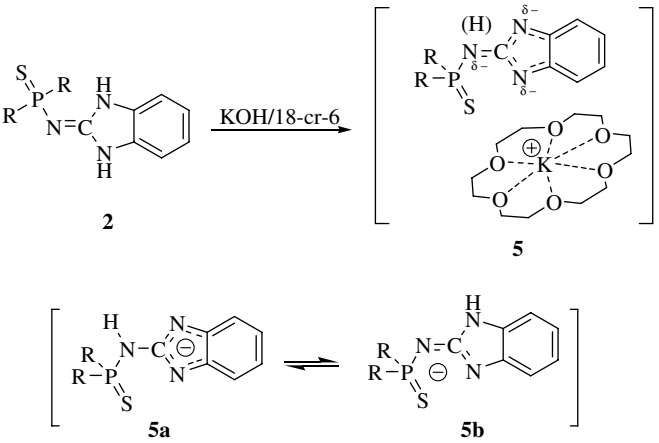

Scheme 2.

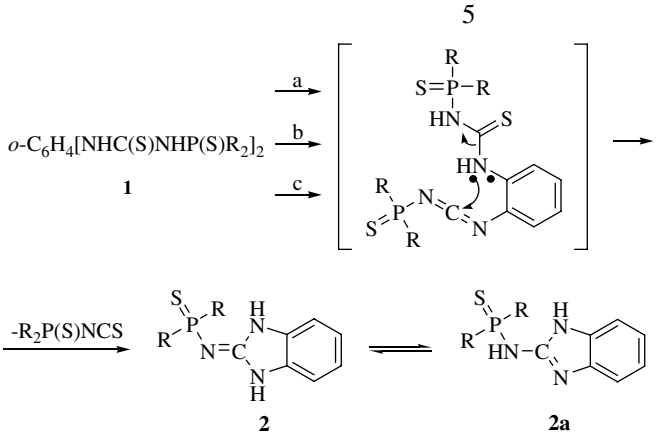

Scheme 1. R = O*i*-Pr. Reagents: (a) I_2, $2NEt_3$ (–[S], $–2NEt_3 \cdot HI$); (b) K_2CO_3/18-crown-6 ($–K_2S$); (c) $ClCH_2C(O)OCH_3$, $1/2(K_2CO_3$/18-crown-6) ($–HSCH_2C(O)OCH_3$, –KCl).

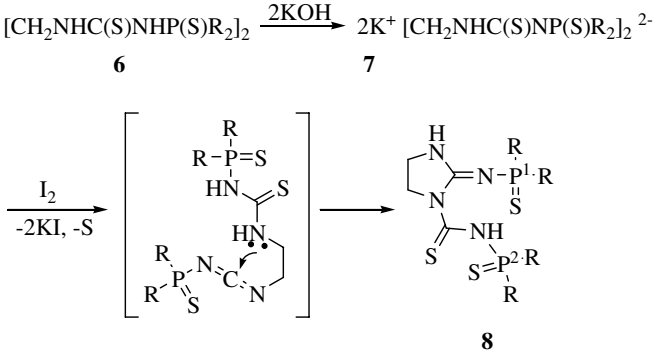

Scheme 3.

benzimidazolimine cycle makes the existence of a product of isocyanate addition to compound **2** unfavorable.

3.2. IR and NMR spectroscopy

The IR spectrum of **2** contains an absorption band for a C=N group at 1648 cm^{-1}. There are triplets at 64.8 ppm ($CDCl_3$) ($^3J_{POCH}$ 11.2 Hz) and 63.6 ppm (d_6-acetone) ($^3J_{POCH}$ 11.1 Hz) in the ^{31}P NMR spectrum, corresponding to the imidothiophosphate environment of phosphorus. Thus, in contrast with the phosphoryl analog reported in [6], the phosphorylimido form **2** is the major prototropic form both in the crystal and in solution. There are no spectral signs of the phosphorylamido form **2a** found in NMR spectra.

In the ^1H NMR spectrum of the benzimidazole **2**, the C_6H_4 moiety gives a AA′XX′ system which corresponds to symmetrical substitutions in the benzene ring. Protons of the NH-groups show up in the ^1H NMR spectrum as a singlet at 11.97 ppm, due to the deshielding effect of the benzene ring and H bond formation. The isothiocyanate (*i*-PrO)$_2$P(S)NCS has been found in the reaction mixture by IR and ^{31}P NMR spectroscopy (δ_P 43.0 ppm; ν(N=C=S) 2000 cm^{-1}).

The ^1H NMR spectrum of the salt **5** in $CDCl_3$ contains a singlet signal of 18-crown-6 OCH_2 groups at 3.62 ppm, with the intensity corresponding to 24 protons in comparison with signals of O*i*-Pr and C_6H_4 moieties. Low-frequency shift of the C=N band in the IR spectrum of compound **5** confirms the conjugated anion formation.

For the anion there are two possible prototropic forms, which differ from one another by the mode of negative charge delocalization (Scheme 2). In the form **5a** the negative charge is delocalized within the conjugated bicyclic system, whilst in the form **5b** the exocyclic CNPS fragment takes part in the delocalization.

^1H NMR spectra recorded for $CDCl_3$ and d_6-acetone solutions do not show the resonance of the NH proton. It could be due to fast proton exchange in solution between the forms **5a** and **5b**. In the ^{31}P NMR spectrum, recorded in d_6-acetone, a phosphorus signal has the shape of a doublet of triplets with $^2J_{PH}$ 8.0 Hz, which also confirms the formation of the form **5a** in solution (Scheme 2). The ^{31}P NMR spectrum recorded in $CDCl_3$ shows a triplet signal for the phosphorus atom with a characteristic constant $^3J_{POCH}$ of 9.7 Hz. The fact that the signal is not split by the proton of the neighbouring NHP group is a consequence of increasing of proton exchange rate in $CDCl_3$ media and of partial equilibrium shift to the form **5b**. In the ^1H NMR spectra of the salt **5** the C_6H_4 moiety gives a AA′XX′ spin system regardless of the solvent nature.

Another confirmation of **5a** form prevalence is the high-field shift of the phosphorus atom signal in ^{31}P NMR spectra, at 2.7 ppm ($CDCl_3$) and 3.2 ppm (d_6-acetone) with respect to neutral benzimidazole **2**. Quite contrary to that, the deprotonated forms of the *N*-acylamidophosphates $[RC(X)NP(Y)(OR')_2]^-$ (X, Y = O, S) have significant low-field shift of the signals in ^{31}P spectra due to delocalization of the negative charge in the XCNPS moiety [1].

The $^{31}P\{^1H\}$ NMR spectrum of **8** contains two singlet signals of equal intensity, with chemical shifts of 62.0 and 59.2 ppm, corresponding phosphorus atoms in imidothiophosphate (P^1) and amidothiophosphate (P^2) environments, respectively. In the NMR ^{31}P spectrum, without decoupling from protons, they represent a triplet and a doublet of triplets with characteristic $^3J_{POCH}$ and $^2J_{PNH}$ constants. A shift of the signal of the P^2NH group proton up to 12.65 ppm in the NMR ^1H spectrum specifies the preservation of the $N^4H\cdots N^3$ hydrogen bond in solution. The ^1H NMR spectrum of **8** contains a double set of isopropoxyl group signals; NCH_2 protons of the imidazolidine cycle exhibit an AA′XX′ system.

3.3. Crystal structure of 2

According to the X-ray data (Fig. 1), the five-membered $N^1C^2N^3C^4C^5$ cycle in a molecule of **2** is planar with maximal deviation of atoms from this plane with distances which do not exceed the experimental error (0.01(2) Å). It is an interesting fact that the P=S bond is practically in the covered eclipsed conformation with the rather double N=C bond. The molecule of **2** in a crystal forms two types of hydrogen bonds: intramolecular and intermolecular. The intramolecular hydrogen bond is formed by a proton of the NH-group and a sulfur atom. Parameters of the intramolecular hydrogen bond are as followed: $d(N^4–H^4)$ 0.80(2) Å, $d(H^2\cdots S^1)$ 2.52(3) Å, $d(N^4\cdots S^1)$ 3.151(2) Å, $\angle(N^3–H^3–S^1)$ 136(2)°. As a result of this bonding a six-membered cycle $S^1P^1N^2C^3N^3H^3$ having the "envelope" conformation forms: the $P^1N^2C^2N^3H^3$ moiety is planar with a maximal deviation for atom N^2 of 0.033(2) Å, atom S^1 is deviated from this plane with a distance of 0.5509(9) Å. Intermolecular hydrogen bonds $N^1–H^1\cdots N^{2'}$ $(1-x, 1-y, -z)$ lead to centrosymmetric dimer formation in the crystal. The bonds have the following parameters: $d(N^1–H^1)$ 0.81(2) Å, $d(H^1\cdots N^{2'})$ 2.12(2) Å, $d(N^1\cdots N^{2'})$ 2.922(2) Å, $\angle(N^1–H^1\cdots N^{2'})$ 173(3)°.

3.4. Crystal structure of 8

In the crystal of compound **8** (Fig. 2) there is an imidazolidine-2-imine planar fragment. Bonds at the C^3 atom in a cycle are not equivalent. The lone-pair of electrons of the N^2 nitrogen atom is in conjugation only with the C=N bond, while the N^1 atom is under thiocarbonylic group acceptor influence. The five-membered cycle $C^1C^2N^1C^3N^2$ in a molecule of **8** is planar with maximal deviation of atoms from this plane with distances 0.016(7) Å. As in **2**, the thiophosphoryl group is coplanar with the five-membered cycle. Deviations of sulfur, phosphorus and imine nitrogen atoms from the $C^1–C^2–N^1–C^3–N^2$ plane are 0.166(2), −0.166(1) and 0.028(4) Å, respectively. An exocyclic *N*-thiophosphorylthioamide fragment is in a conformation with a *syn*-arrangement of $S^3–C^4$ and $N^4–P^2$ bonds,

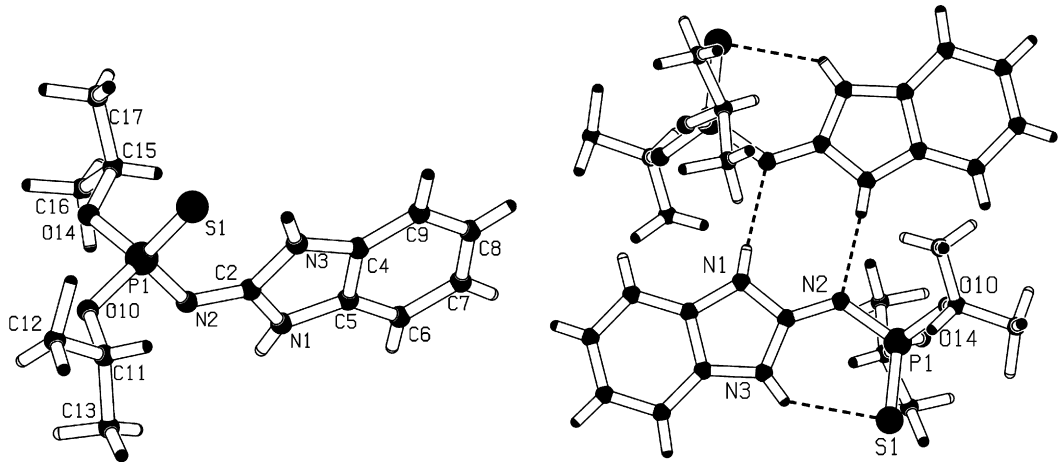

Fig. 1. Molecular drawing of **2** (left); hydrogen bonding between two molecules (right). Selected bond distances (Å), bond angles (°) and torsion angles (°) of **2**: S^1–P^1 1.9400(9), P^1–N^2 1.622(2), N^2–$C^3$1.317(3), N^1–C^3 1.352(3), N^4–C^3 1.361(3), P^1–N^2–C^2 126.8(2), S^1–P^1–N^2–C^3 −24.7(2), P^1–N^2–C^3–N^4 7.3(4).

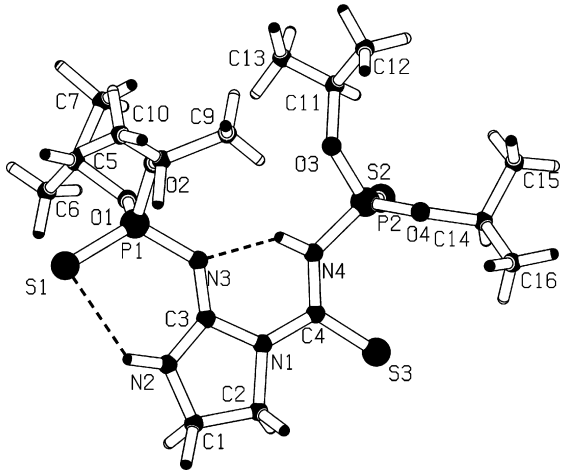

Fig. 2. Molecular drawing of **8**. Selected bond distances (Å), bond angles (°) and torsion angles (°) of **8**: S^1–P^1 1.938(2), P^1–N^3 1.626(5), N^3–C^3 1 1.294(6) N^1–C^3 1.402(4), N^2–C^3 1.397(6), N^2–C^1 1.438(8), N^1–C^2 1.471(6), N^1–C^4 1.399(5), S^2–P^2 1.918(2), P^2–N^4 1.680(3), N^4–C^4 1.351(6), S^4–C^4 1.651(5), $S^1P^1N^3$ 118.7(2), $S^2P^2N^4$ 116.2(1), $P^1N^3C^3$ 128.1(4), $P^2N^4C^4$ 127.8(3), $P^2N^4C^4$–S^4 8.7(7), $S^1P^1N^3C^3$ 21.9(5), $S^2P^2N^4C^4$ 63.3(5), $P^1N^3C^3N^2$ −9.4(8).

typical for such compounds [1]. The fragment S^3–C^4–N^4–P^2 belongs to the five-membered cycle plane. Maximal deviation from the C^1–C^2–N^1–C^3–N^2 plane for the phosphorus atom is −0.122(1) Å.

There are intramolecular hydrogen bonds, $N^2H\cdots S^1$ and $N^4H\cdots N^3$, in molecule **8**. Parameters of the intramolecular hydrogen bonds are as followed: $d(N^2$–$H^2)$ 0.86 Å, $d(H^2\cdots S^1)$ 2.60 Å, $d(N^2\cdots S^1)$ 3.224(6) Å, $\angle(N^2$–H^2–$S^1)$ 134.8° and $d(N^4$–$H^4)$ 0.86 Å, $d(H^4\cdots N^3)$ 1.91 Å, $d(N^4\cdots N^3)$ 2.616(6) Å, $\angle(N^4$–H^4–$N^3)$ 138.2°. These result in the formation of two six-membered cycles $N^3C^3N^1C^4N^4H^4$ and $S^1P^1N^3C^3N^2H^2$. Both of them have the "envelope" conformation, as in structure **2**. The $N^3C^3N^1C^4N^4$ fragment is planar with the maximum deviation of atom C^4 with a distance of 0.033(5) Å, and atom H^4 is deviated from this plane with a distance of 0.20 Å. The $S^1H^2N^2C^3N^3$ fragment is also planar within the limits of 0.038 Å (the maximum deviation of the H^2 atom), P^1 is deviated with a distance 0.302(1) Å.

4. Conclusion

It has been established that the bis-thiourea *o*-$C_6H_4[NHC(S)NHP(S)(O\textit{i}\text{-}Pr)_2]_2$ (**1**) undergoes cyclization with elimination of a molecule of diisopropylthiophosphoric acid isothiocyanate and with formation of a derivative of phosphorylated benzimidazole **2**. The cyclization process accelerates significantly upon using oxidants or alkylation agents. In contrast to the analogue with a phenylene bridging fragment, the bis-thiourea $[CH_2NHC(S)NHP(S)(O\textit{i}\text{-}Pr)_2]_2$, upon treatment with a base, converts into a salt, which oxidation with iodine affords the iminoimidazolidine **8**, containing the *N*-thiophosphorylthiourea fragment. Thiophosphoryl isothiocyanate elimination does not occur whilst cyclization is the case.

The synthesized compounds **2** and **8** contain neighbouring PS, CN, CS groups and acidic NH protons. All these make them interesting as polyfunctional ligands, capable of forming chelate complexes with d-metal cations.

Acknowledgements

We thank the joint program of CRDF and the Russian Ministry of Education (BHRE 2004 Y2-C-07-02, Grant REC-007) and the Russian Foundation for Basic Research (Grants # 03-03-32372-a, 03-03-96225-r2003tatarstan_a) for financial support.

Appendix A. Supplementary material

Crystallographic data of **2** and **8** have been deposited with the Cambridge Crystallographic Data Centre as supplementary Publication Nos. CCDC-295916 and CCDC-

295917, respectively. Copies of the data can be obtained free of charge on application to CCDC, 12 Union Road, Cambridge CB2 1EZ, UK (fax: +44 1223 336 033; e-mail: deposit@ccdc.cam.ac.uk). Supplementary data associated with this article can be found, in the online version, at doi:10.1016/j.poly.2006.07.016.

References

[1] F.D. Sokolov, V.V. Brusko, N.G. Zabirov, R.A. Cherkasov, Curr. Org. Chem. 10 (2006) 27.
[2] N.G. Zabirov, V.V. Brusko, A.Yu. Verat, D.B. Krivolapov, I.A. Litvinov, R.A. Cherkasov, Polyhedron 23 (2004) 2243.
[3] R.M. Kamalov, N.A. Khailova, M.A. Pudovik, A.N. Pudovik, Zh. Obshch. Khim. 59 (1989) 2666.
[4] R.M. Kamalov, M.G. Zimin, A.N. Pudovik, Usp. Khim. 54 (1985) 2044.
[5] A.N. Pudovik, V.K. Khairullin, R.M. Kamalov, M.A. Vasyanina, I.A. Litvinov, O.N. Kataeva, Zh. Obshch. Khim. 60 (1990) 1700.
[6] R.J. Anderson, D.J. Bendelt, M. Hooper, D. Cairns, S.P. Mackay, S.P. Hiremath, A.S. Jivanagi, S. Badami, J.S. Biradar, S. Townson, J. Pharm. Pharmacol. 53 (2001) 89.
[7] (a) P.J. Bailey, S. Pace, Coord. Chem. Rev. 214 (2001) 91;
(b) S.E. Castillo-Blum, N. Barba-Behrens, Coord. Chem. Rev. 196 (2000) 3.
[8] C.A. Tellez, E. Hollauer, J. Felcman, D.C.N. Lopez, R.A. Cattapan, Spectrochim. Acta A 58 (2002) 1853.
[9] A.E. Ceniceros-Gomez, N.B. Behrens, S. Bernes, H. Noeth, S.E. Castillo-Blum, Inorg. Chim. Acta 304 (2000) 230.
[10] N. Andrade-Lopez, A. Ariza-Castolo, R. Contreras, A. Vazquez-Olmos, N.B. Behrens, H. Tlahuext, Heteroat. Chem. 8 (1997) 397.
[11] F.D. Sokolov, V.V. Brusko, N.G. Zabirov, R.A. Cherkasov, Russ. J. Gen. Chem. 69 (1999) 1006.
[12] A. Altomare, G. Cascarano, C. Giacovazzo, D. Viterbo, Acta Crystallogr., Sect. A 47 (1991) 744.
[13] G.M. Sheldrick, SHELXS-97: Program for the Solution of Crystal Structure, University of Göttingen, Göttingen, Germany, 1997.
[14] L.J. Farrugia WinGX 1.64.05: an integrated system of Windows programs for the solution, refinement and analysis of single crystal X-ray diffraction data, J. Appl. Crystallogr. 32 (1999) 837.
[15] L.H. Straver, A.J. Schierbeek, MOLEN: Structure Determination System, Nonius B.V., Delft, The Netherlands, 1994, 1, 2.
[16] A.L. Spek, Acta Crystallogr., Sect. A 46 (1990) C-34.

We have been interested in the design, synthesis and investigation of polynuclear manganese complexes, especially based on pivalic acid [19–21]. In this paper, we report the synthesis, crystal structures and characterization of two new manganese pivalates, namely homo-valent $[Mn_3^{III}O\text{-}(O_2CCMe_3)_6(Im)_3](Me_3CCO_2)\cdot 0.5Me_3CCO_2H$ (**1**) and mixed-valent $[Mn_2^{III}Mn^{II}O(O_2CCMe_3)_6(1\text{-MeIm})_3]$ (**2**) (where Im = imidazole, 1-MeIm = 1-methylimidazole) complexes.

2. Experimental

2.1. Materials and methods

Starting materials were purchased from commercial sources and used without further purification. $[Mn_6O_2(O_2CCMe_3)_{10}(Me_3CCO_2H)_4]$ was prepared by the reported procedure [22]. The infrared spectra were recorded on a Perkin–Elmer Spectrum One spectrometer using KBr pellets in the region 4000–400 cm^{-1}. TG analyses were carried out on a Mettler-Toledo TA 50 in dry nitrogen (60 ml min^{-1}) at a heating rate of 5 °C min^{-1}.

2.2. Synthesis of complexes

2.2.1. Synthesis of $[Mn_3O(O_2CCMe_3)_6(Im)_3](Me_3CCO_2)\cdot 0.5Me_3CCO_2H$ (1)

Imidazole (1.25 g, 18.36 mmol) and pivalic acid (5.4 g, 52.89 mmol) were dissolved in water (4 ml) and stirred. Then, to this solution was added $MnCl_2\cdot 4H_2O$ (0.8 g, 4.06 mmol) followed by adding solid $KMnO_4$ (0.25 g, 1.58 mmol) in small portions to give a brown homogeneous solution. Finally, this solution was heated at 60 °C for 1 h and then was left to stand overnight at r.t. The microcrystalline precipitate was filtered off, washed with hexane and dried in air. Single crystals suitable for X-ray analysis were obtained by recrystallization of **1** from MeCN. Yield (after recrystallization): 0.36 g (30%). *Anal.* Calc. for $C_{93}H_{160}Mn_6N_{12}O_{32}$: C, 48.82; H, 7.05; N, 7.35. Found: C, 48.65; H, 7.04; N, 7.38%. IR (KBr, cm^{-1}) 3159m, 3067m, 2960m, 2872m, 1609vs, 1570m, 1547m, 1510m, 1482s, 1458m, 1405s, 1370s, 1358s, 1329m, 1224s, 1148w, 1098w, 1069m, 958w, 938w, 895w, 836w, 786m, 751m, 655m, 625m, 598m, 562w.

2.2.2. Synthesis of $[Mn_3O(O_2CCMe_3)_6(1\text{-MeIm})_3]$ (2)

Complex $[Mn_6O_2(O_2CCMe_3)_{10}(Me_3CCO_2H)_4]$ (0.5 g, 0.28 mmol) and $KMnO_4$ (0.05 g, 0.31 mmol) were dissolved in 1-MeIm (2 ml). The mixture was heated at 90 °C for an hour and then the reaction was allowed to cool. After two days this mixture was extracted with diethyl ether. On the next day, from the diethyl ether extracts, crystals suitable for X-ray analysis formed. The crystals were filtered off and washed with cold diethyl ether. Yield: 0.27 g (31.03%). *Anal.* Calc. for $C_{84}H_{144}Mn_6N_{12}O_{26}$: C, 48.79; H, 7.02; N, 8.13. Found: C, 47.78; H, 6.80; N, 8.15%. IR (KBr, cm^{-1}) 3129m, 2958s, 2926sh, 2869sh, 1608br.vs, 1538m, 1526m, 1482s, 1457m, 1411vs, 1370s, 1358s, 1286w, 1227s, 1110s, 1024w, 956w, 932w, 893w, 831m, 788m, 762w, 733w, 695m, 656m, 615m, 599m.

2.3. X-ray crystallography

Diffraction data were collected at 153 K for **1** and **2** with a Stoe Mark II Imaging Plate Diffractometer using Mo Kα graphite-monochromated radiation. Crystallographic data and details of the refinement process are summarized in Table 1. The structures were solved by direct methods using the program SHELXS-97 [23]. Refinement and all further calculations were carried out using SHELXL-97 [24]. H-atoms were located from Fourier difference maps and refined isotropically; their thermal parameters were kept fixed with $U_{iso} = 1.5U_{eq}$ of their carrier O and N atoms. In both structures some of methyl groups in the pivalate fragments are disordered over two positions with occupancies 0.50 ± 0.10. Non-hydrogen atoms were refined anisotropically, using weighted full-matrix least-squares on F^2.

2.4. Magnetic measurements

Magnetic susceptibility and magnetization data of powdered samples of compounds **1** and **2** were collected on a MPMS Quantum Design SQUID magnetometer (XL-5) in the temperature range of 300–1.8 K and at applied magnetic fields up to 5 T. The samples were placed in a saran foil bag for compound **1** and in a gelatine capsule for compound **2**. A straw was used as the sample holder. Data were corrected for the experimentally determined diamagnetism of the sample holder and the diamagnetic contributions of the samples, which were estimated from Pascal's constants. The Levenberg–Marquardt least-squares fitting algorithm, in combination with MAGPACK [25], was used to model the experimental magnetic susceptibility and magnetization data.

3. Results and discussion

3.1. Synthesis and preliminary characterization

The reaction of manganese(II) chloride with $KMnO_4$, imidazole and an excess of pivalic acid in a small amount of water leads to the formation of $[Mn_3O(O_2CCMe_3)_6(Im)_3](Me_3CCO_2)\cdot 0.5Me_3CCO_2H$ (**1**). This method of preparing oxo-bridged manganese complexes by the oxidation of Mn(II) ions using MnO_4^- ions in the presence of carboxylate ligands and aromatic amines was first used by Lis for the synthesis of a dodecanuclear complex [26] and then largely developed by Christou et al. [6,27]; it is a very useful synthetic route to design Mn complexes with higher oxidation states (Mn^{III}, Mn^{IV}). Moreover, the largest manganese carboxylate cluster, a Mn_{30} complex [28], was also obtained from this type of comproportionation reaction. The synthesis of the mixed-valence compound $[Mn_3O(O_2CCMe_3)_6(1\text{-MeIm})_3]$ (**2**) was performed by the

Table 1
Crystal data and details of structure determination

	1	2
Empirical formula	$C_{93}H_{160}Mn_6N_{12}O_{32}$	$C_{42}H_{72}Mn_3N_6O_{13}$
Formula weight	2287.97	1033.87
Temperature (K)	153(2)	153(2)
Wavelength (Å)	0.71073	0.71073
Crystal size (mm)	$0.30 \times 0.30 \times 0.20$	$0.40 \times 0.20 \times 0.15$
Crystal system	monoclinic	monoclinic
Space group	$P2_1/n$	$P2_1$
a (Å)	13.6326(5)	19.685(2)
b (Å)	46.1720(16)	19.7203(12)
c (Å)	19.6917(8)	13.5507(13)
β (°)	100.175(3)	90.792(12)
V (Å^3)	12199.9(8)	5259.8(8)
Z	4	4
D_{calc} (g/cm^3)	1.246	1.306
μ (mm^{-1})	0.674	0.770
$F(000)$	4832	2180
θ Range for data collections (°)	1.14–25.10	2.07–25.96
Index ranges	$-16 \leqslant h \leqslant 16$, $-53 \leqslant k \leqslant 55$, $-23 \leqslant l \leqslant 23$	$-24 \leqslant h \leqslant 24$, $-24 \leqslant k \leqslant 23$, $-16 \leqslant l \leqslant 16$
Reflections measured	98816	41579
Independent reflections [R_{int}]	21524 [0.0757]	19412 [0.1037]
Data/restraints/parameters	21524/0/1557	19412/1/1211
Goodness-of-fit on F^2	0.884	0.745
Final R indices [$I > 2\sigma(I)$]	$R_1 = 0.0471$, $wR_2 = 0.1098$	$R_1 = 0.0509$, $wR_2 = 0.0856$
R indices (all data)	$R_1 = 0.0876$, $wR_2 = 0.1246$	$R_1 = 0.1238$, $wR_2 = 0.1019$
Largest difference peak and hole (e Å^{-3})	0.355 and −0.312	0.477 and −0.528

interaction of the hexanuclear mixed-valent $[Mn^{II}_4Mn^{III}_2O_2(O_2CCMe_3)_{10}(Me_3CCO_2H)_4]$ cluster with $KMnO_4$ in 1-methylimidazole.

The IR spectra of complexes **1** and **2** have strong and broad bands in the 1609–1546 and 1369–1357 cm^{-1} region, which are due to asymmetric and symmetric vibrations, respectively, of the coordinated carboxylate groups [29,30] of the pivalate ligand. The broad bands with medium intensity in the 3159–3067 cm^{-1} region can be ascribed to the absorption frequencies of the N–H vibration of Im and O–H vibration of solvate pivalic molecules in compound **1**.

Thermal analysis of **1** and **2** has been performed in a nitrogen atmosphere in the temperature range 25–600 °C. For **1** the first weight loss of 19.05% from 110 to 210 °C corresponds to the loss of a half molecule (per formula unit) of solvate pivalic acid, one molecule of the uncoordinated pivalic anion and one imidazole molecule (calculated 19.25%). On further heating, the decomposition of remaining organic ligands takes place in two unidentified steps with total weight loss of 61.08% and is completed below 500 °C to give the expected oxide (observed 19.95%, calculated 20.00%). It is interesting to note that the mixed-valent oxo-centered trinuclear compound **2** decomposes to the final products below 275 °C, a much lower temperature compared to the above mentioned homo-valent compound **1**. The first weight loss of about 4.54% occurred at 110 °C, which corresponds to the loss of a half molecule (per formula unit) of 1-MeIm (calculated 3.97%). A further weight loss of 30.25% occurred between 130 and 210 °C, which agrees with calculated values of 29.62% for the release of the remaining 1-MeIm molecules and one molecule of pivalate ligand. The decomposition of the pivalate ligands was completed at ca. 275 °C (the weight loss is 40.55%) with the observed remaining weight percentage of 24.58%.

3.2. Crystal structures

3.2.1. The structure of $[Mn_3O(O_2CCMe_3)_6(Im)_3](Me_3CCO_2)\cdot 0.5Me_3CCO_2H$ (1)

The crystal structure of **1** consists of two independent $[Mn_3O(O_2CCMe_3)_6(Im)_3]^+$ cations (molecules **A** and **B**), two $Me_3CCO_2^-$ anions and a neutral Me_3CCO_2H molecule (Fig. 1). The structure of cation **A** is shown in Fig. 2. Selected bond distances and angles for **1** are listed in Table 2. Three Mn(III) atoms form a nearly equilateral triangle with an oxygen atom in the center. The Mn···Mn distances within the triangle are all very similar (3.260 ± 0.006 Å). The central μ_3-oxygen atom is slightly displaced from the Mn_3 triangular plane (0.015(2) Å for molecule **A** and 0.019(2) Å for molecule **B**). The Mn–(μ_3-O) bond distances are in the range of 1.879(2)–1.890(2) Å (Table 2). Four oxygen atoms from the bridging carboxylate groups and a terminal imidazole nitrogen atom additionally complete coordination at each Mn(III) atom. The Mn–O_{carb} bond distances range from 1.923(2) to 2.186(3) Å, and the Mn–N bond distances lie in the range of 2.011(3)–2.026(3) Å. Thus, the manganese coordination geometry can be regarded as a slightly distorted octahedron. The configuration, bond distances and bond angles of molecules **A** and **B**

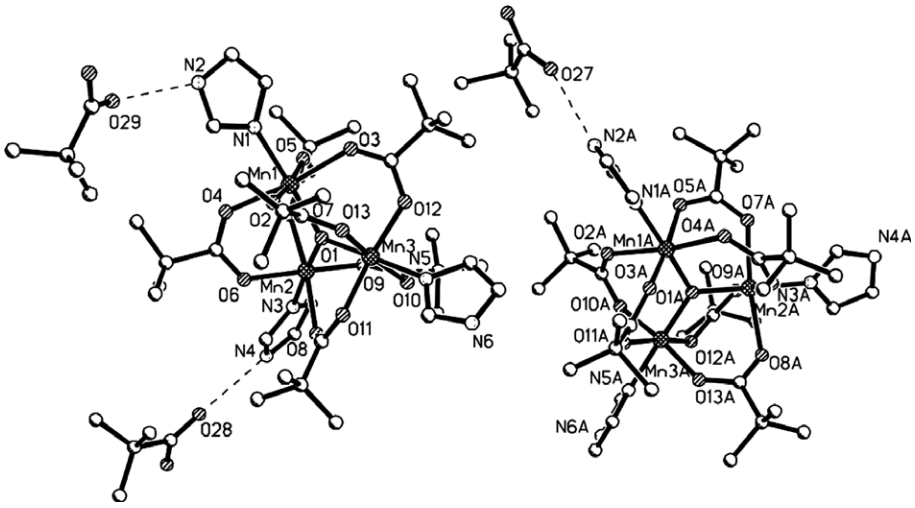

Fig. 1. View of the structure of complex **1** (molecule **A**, left; molecule **B**, right). Hydrogen bonds are shown as dashed lines. Hydrogen atoms are omitted for clarity.

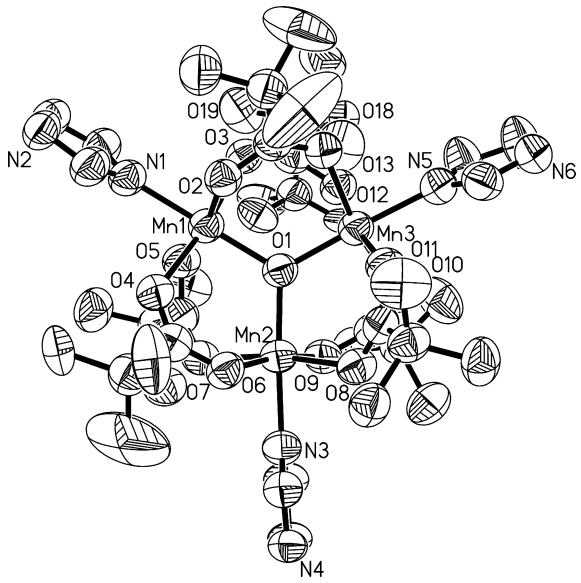

Fig. 2. View of the structure of molecule **A** in compound **1.** Hydrogen atoms are omitted for clarity.

are in a good agreement with the data in earlier investigated structures of oxo-centered trinuclear manganese(III) carboxylate complexes [13–15] (Table 3).

The presence of the uncoordinated carboxylic group of pivalic acid and the solvate acid molecule as well as of the N–H group of imidazole ligand results in an extensive hydrogen-bonded network in complex **1**. It is interesting to note that in this crystal structure the formation of centrosymmetric motifs consisting of four trinuclear clusters is observed. The packing of molecules in the crystal structure along the [0 0 1] direction is shown in Fig. 3a. In addition, these centrosymmetric motives are connected by hydrogen bonds N–H···O (2.636(4)–2.866(4) Å) between carboxyl oxygen atoms of pivalic acid and nitrogen atoms of Im, as well as by hydrogen bonds O–H···O of 2.556(4) Å, forming zig-zag chains (Fig. 3b). Finally, a 3D supramolecular architecture is formed in compound **1**. The parameters of all intermolecular hydrogen bonds are listed in Table 4.

3.2.2. The structure of $[Mn_3O(O_2CCMe_3)_6(1\text{-}MeIm)_3]$ (**2**)

X-ray diffraction analysis revealed that complex **2** consists of two independent molecules (**A** and **B**) of the trinuclear oxo-centered $[Mn_3O(O_2CCMe_3)_6(1\text{-}MeIm)_3]$ cluster in the unit cell. The structure of molecule **B** is shown in Fig. 4. Selected bond distances and angles for **2** are listed in Table 5. Each Mn atom adopts a slightly distorted octahedral geometry and is coordinated by an oxygen atom of the central triangle, four oxygen atoms from bridging pivalate ligands, and a terminal 1-MeIm nitrogen atom. The central μ_3-oxygen atom is slightly displaced from the Mn_3 triangular plane (0.029(2) Å for molecule **A** and 0.028(2) Å for molecule **B**). The Mn···Mn distances are in the range of 3.220(2)–3.408(2) Å, and the Mn(2)···Mn(3) distances of 3.220(2) and 3.312(2) Å for **A** and **B** molecules, respectively, are significantly shorter than the Mn(1)···Mn(2) (average value 3.391 Å) and Mn(1)···Mn(3) (average value 3.406 Å) distances. Based on the neutral charge of the $[Mn_3O(O_2CCMe_3)_6(1\text{-}MeIm)_3]$ cluster, the Mn oxidation states in this complex are given as $[Mn^{III}_2Mn^{II}O]^{6+}$. As expected for its lower oxidation state, the position of the Mn(II) atom can be assigned on the basis of its longer metal–μ-oxygen and metal–ligand bond distances compared with the Mn(III) atoms (Table 3). From these data Mn(1) is readily assigned as the Mn^{II} center, whereas Mn(2) and Mn(3) atoms are Mn^{III} centers. The Mn^{III}–O(1) bond distances are in the range 1.800(4)–1.848(4) Å, which is in agreement with the common basic carboxylate type seen for the above mentioned trinuclear manganese(III) complex **1** and other trinuclear manganese(III) carboxylate complexes (Table 3). For manganese(II) atoms these distances are significantly longer and

Table 2
Selected bond distances (Å) and angles (°) for compound **1**

Molecule	A	B	Molecule	A	B
Mn(1)–O(1)	1.885(2)	1.887(2)	Mn(2)–O(8)	2.182(2)	2.162(3)
Mn(1)–O(2)	1.944(2)	2.175(3)	Mn(2)–O(9)	1.935(2)	1.945(3)
Mn(1)–O(3)	2.173(2)	1.923(2)	Mn(2)–N(3)	2.011(3)	2.020(3)
Mn(1)–O(4)	2.165(2)	2.158(2)	Mn(3)–O(1)	1.890(2)	1.883(2)
Mn(1)–O(5)	1.925(2)	1.940(2)	Mn(3)–O(10)	2.171(2)	2.186(3)
Mn(1)–N(1)	2.013(3)	2.026(3)	Mn(3)–O(11)	1.931(2)	1.929(3)
Mn(2)–O(1)	1.879(2)	1.880(2)	Mn(3)–O(12)	1.927(2)	2.146(3)
Mn(2)–O(6)	1.947(2)	1.947(2)	Mn(3)–O(13)	2.143(2)	1.931(3)
Mn(2)–O(7)	2.174(2)	2.159(2)	Mn(3)–N(5)	2.023(3)	2.017(3)
O(1)–Mn(1)–O(2)	93.84(9)	92.49(9)	O(1)–Mn(2)–O(8)	92.06(9)	94.60(10)
O(1)–Mn(1)–O(5)	94.47(10)	94.58(10)	O(9)–Mn(2)–O(8)	98.75(9)	93.05(11)
O(5)–Mn(1)–O(2)	171.41(10)	84.82(9)	O(6)–Mn(2)–O(8)	84.51(9)	87.57(10)
O(1)–Mn(1)–N(1)	178.47(12)	178.15(11)	N(3)–Mn(2)–O(8)	85.39(10)	86.21(11)
O(5)–Mn(1)–N(1)	86.91(11)	86.06(11)	O(7)–Mn(2)–O(8)	172.21(9)	171.54(10)
O(2)–Mn(1)–N(1)	84.81(10)	85.84(11)	O(1)–Mn(3)–O(12)	94.07(9)	93.74(10)
O(1)–Mn(1)–O(4)	93.50(9)	94.53(9)	O(1)–Mn(3)–O(11)	93.82(9)	93.64(10)
O(5)–Mn(1)–O(4)	94.13(10)	92.14(10)	O(12)–Mn(3)–O(11)	172.08(10)	85.89(11)
O(2)–Mn(1)–O(4)	87.52(9)	172.55(9)	O(1)–Mn(3)–N(5)	177.70(10)	178.68(12)
N(1)–Mn(1)–O(4)	85.73(10)	87.17(11)	O(12)–Mn(3)–N(5)	86.28(11)	86.16(12)
O(1)–Mn(1)–O(3)	93.53(9)	94.40(10)	O(11)–Mn(3)–N(5)	85.86(11)	85.04(12)
O(5)–Mn(1)–O(3)	85.33(9)	170.81(10)	O(1)–Mn(3)–O(13)	94.80(9)	93.97(10)
O(2)–Mn(1)–O(3)	92.00(9)	96.74(10)	O(12)–Mn(3)–O(13)	91.61(9)	94.16(11)
N(1)–Mn(1)–O(3)	87.25(11)	85.02(11)	O(11)–Mn(3)–O(13)	87.07(9)	172.37(11)
O(4)–Mn(1)–O(3)	172.98(9)	85.21(10)	N(5)–Mn(3)–O(13)	87.46(10)	87.35(12)
O(1)–Mn(2)–O(9)	93.49(9)	93.71(10)	O(1)–Mn(3)–O(10)	93.27(9)	93.57(10)
O(1)–Mn(2)–O(6)	95.86(9)	94.14(10)	O(12)–Mn(3)–O(10)	85.70(9)	172.49(10)
O(9)–Mn(2)–O(6)	169.98(10)	172.06(10)	O(11)–Mn(3)–O(10)	94.51(9)	95.35(11)
O(1)–Mn(2)–N(3)	176.85(11)	179.16(11)	N(5)–Mn(3)–O(10)	84.48(10)	86.57(12)
O(9)–Mn(2)–N(3)	85.09(10)	85.99(11)	O(13)–Mn(3)–O(10)	171.67(9)	83.62(11)
O(6)–Mn(2)–N(3)	85.75(10)	86.15(11)	Mn(2)–O(1)–Mn(1)	120.01(11)	120.24(11)
O(1)–Mn(2)–O(7)	94.46(9)	93.73(9)	Mn(2)–O(1)–Mn(3)	120.18(11)	119.67(12)
O(9)–Mn(2)–O(7)	85.11(10)	87.88(10)	Mn(1)–O(1)–Mn(3)	119.79(11)	120.06(12)
O(6)–Mn(2)–O(7)	90.55(9)	90.36(10)			
N(3)–Mn(2)–O(7)	88.22(10)	85.47(10)			

equal to 2.128(5) Å for Mn(1)–O(1) and 2.170(4) Å for Mn(1A)–O(1A). The four Mn–O_{carb} distances around manganese(III) atoms are in the range of 1.947(5)–2.174(5) Å, and the Mn^{III}–N distances (2.060(6)–2.064(5) Å) are quite similar to those found in **1**. As expected for a typical manganese(II) atom, Mn–O_{carb} bond distances are found in the range of 2.129(5)–2.207(5) Å, which is slightly longer than those for Mn^{III} atoms. The Mn^{II}–N distance of 2.251(6) Å at Mn(1) and Mn(1A) is also longer than that for the trivalent manganese atom (2.256(6) Å). The Mn–O(1)–Mn angles range from 116.6(2)° up to 125.4(2)° and differ slightly from the analogous angles which were found in a Mn_3O cluster with imposed C_2 symmetry [9].

In contrast to **1**, in which an extensive network of hydrogen-bonding interactions is observed due to the presence of the uncoordinated carboxyl group of pivalic acid and the NH group of imidazole, aromatic C–H$\cdots\pi$ interactions [31–33] embracing 1-methylimidazole rings enhance the structural stability in compound **2**. Because the 1-MeIm heterocycles are not all parallel with each other, the aromatic–aromatic interactions in compound **2** are either edge-to-face interactions or T-shaped orientations. In addition to the aromatic C–H$\cdots\pi$ interactions, five 1-MeIm heterocycles from six heterocycles (heterocycles are marked as follows: N1 ∩ N2 is cycle N1C1N2C2C3, N3 ∩ N4–N3C5N4C6C7, etc.) exhibit five contacts, each between aliphatic C–H of the methyl group and the π-cycle of another molecule (Table 6). Note that all six 1-MeIm heterocycles are involved in such interactions forming a 3D network in compound **2** (Fig. 5). The heterocycle N5A ∩ N6A forms with the N1A ∩ N2A heterocycle two types of C–H$\cdots\pi$ contacts, one exhibiting aromatic–aromatic edge-to-face interaction having a centroid–centroid distance of 4.468 Å and plane angle of 24.47° between the aromatic heterocycles, and the other being an aliphatic–aromatic interaction between the hydrogen (H12E) of the methyl group (C12) and imidazole cycle (N1A ∩ N2A) with the shortest interatomic distance of 2.835 Å. Further, the cycle N1A ∩ N2A interacts with N1 ∩ N2 forming an edge-to-face contact with the centroid–centroid distance of 4.242 Å (plane angle 31.69°) and the aliphatic–aromatic interaction of 3.032 Å (a typical aliphatic–aromatic interaction is in the range of 2.79–3.05 Å [32]). The third edge-to-face interaction is found between cycles N1 ∩ N2 and N5 ∩ N6 (centroid–centroid distance 4.374 Å, plane angle 24.22°) and there is

Table 3
Selected average bond distances (Å) in $[Mn_3O(O_2CCR)(L)_3]^{0,1+}$

Compound	Mn–μ-O	$Mn–O_{carb}$	Mn–L	Ref.
Mn^{III}_3O				
$[Mn_3O(O_2CCMe_3)_6(Py)_3]ClO_4 \cdot MeCN$	1.891	2.033	2.084 (Mn–N)	[13]
$[Mn_3O(O_2CMe)_6(3\text{-}MePy)_3]ClO_4$	1.900	2.002	2.101 (Mn–N)	[14]
$[Mn_3O(O_2CC_2H_5)_6(3\text{-}MePy)_3]ClO_4$	1.888	1.990	2.062 (Mn–N)	[14]
$[Mn_3O(O_2CC_3H_7)_6(Py)_3]ClO_4$	1.893	2.025	2.15 (Mn–N)	[15]
$[Mn_3O(O_2CCMe_3)_6(Im)_3](Me_3CCO_2) \cdot 0.5Me_3CCO_2H$	1.884	2.051	2.018 (Mn–N)	this work
$Mn^{III}_2Mn^{II}O$				
$[Mn_3O(O_2CMe)_6(Py)_3] \cdot Py$	1.936	2.105	2.167	[4,6]
$[Mn_3O(O_2CMe)_6(3\text{-}ClPy)_3]$	2.034 (Mn^{II})	2.114 (Mn^{II})	2.280 (Mn^{II}–N)	[5]
	1.863 (Mn^{III})	2.072 (Mn^{III})	2.143 (Mn^{III}–N)	
$[Mn_3O(O_2CPh)_6(Py)_2(H_2O)] \cdot 0.5MeCN$	2.135 (Mn^{II})	2.166 (Mn^{II})	2.237 (Mn^{II}–O)	[6]
	1.816 (Mn^{III})	2.072 (Mn^{III})	2.088 (Mn^{III}–N)	
$[Mn_3O(O_2CPh)_6(Py)_3] \cdot 2MeCN$	1.972 and 1.966 (Mn^{II} and Mn^{III})*	2.108 and 2.129 (Mn^{II} and Mn^{III})*	2.194 and 2.199 (Mn^{II} and Mn^{III})*	[12]
	1.819 (Mn^{III})	2.066 (Mn^{III})	2.077 (Mn^{III}–N)	
$[Mn_3O(O_2CPh\text{-}2F)_6(Py)_3] \cdot 2MeCN$	1.990 (Mn^{II})	2.109 (Mn^{II})	2.234 (Mn^{II}–N)	[11]
	1.871 (Mn^{III})	2.048 (Mn^{III})	2.118 (Mn^{III}–N)	
$[Mn_3O(O_2CPh\text{-}3Cl)_6(Py)_2(H_2O)] \cdot 0.5H_2O$	2.064 (Mn^{II})	2.054 (Mn^{II})	2.123 (Mn^{II}–O)	[11]
	1.833 (Mn^{III})	2.016 (Mn^{III})	2.061 (Mn^{III}–N)	
$[Mn_3O(O_2CPh\text{-}3Br)_6(Py)_2(H_2O)] \cdot \frac{1}{4}H_2O$	2.066 (Mn^{II})	2.036 (Mn^{II})	2.140 (Mn^{II}–O)	[11]
	1.827 (Mn^{III})	2.077 (Mn^{III})	2.083 (Mn^{III}–N)	
$[Mn_3O(O_2CCH_2Cl)_6(Py)_2(H_2O)] \cdot 0.5MeCN$	2.136 (Mn^{II})	2.171 (Mn^{II})	2.222 (Mn^{II}–O)	[17]
	1.805 (Mn^{III})	2.073 (Mn^{III})	2.064 (Mn^{III}–N)	
$[Mn_3O(O_2CCCl_3)_6(H_2O)_3]$	1.924	2.055		[18]
$[Mn_3O(O_2CCMe_3)_6(Py)_3]$	2.171 (Mn^{II})	2.172 (Mn^{II})	2.339 (Mn^{II}–N)	[13]
	1.830 (Mn^{III})	2.088 (Mn^{III})	2.107 (Mn^{III}–N)	
$[Mn_3O(O_2CCMe_3)_6(Py)_3]$	2.114 (Mn^{II})	2.165 (Mn^{II})	2.289 (Mn^{II}–N)	[19]
	1.818 (Mn^{III})	2.056 (Mn^{III})	2.099 (Mn^{III}–N)	
$[Mn_3O(O_2CCMe_3)_6(1\text{-}MeIm)_3]$	2.149 (Mn^{II})	2.163 (Mn^{II})	2.254 (Mn^{II}–N)	this work
	1.816 (Mn^{III})	2.056 (Mn^{III})	2.062 (Mn^{III}–N)	

a contact with 2.848 Å distance formed by the C–H of the methyl group (C12) and the π-cycle (Table 6). The next C–H···π interactions consisting of the edge-to-face contact (centroid–centroid distance 4.250 Å, plane angle 18.11°) and aliphatic–aromatic contact (2.952 Å) are found between N5 ∩ N6 and N3 ∩ N4 heterocycles. There is further close C–H···π contact with distance of 2.999 Å between heterocycle N3 ∩ N4 (C6) and N3A ∩ N4A (C7–H7A), which is probably more of a T-shaped interaction based on the interplane angle of 68.64°. It is noted that there is only the aliphatic–aromatic C–H···π interaction of 2.986 Å between the heterocycle N3A ∩ N4A and the neighboring heterocycle N5A ∩ N6A (the centroid–centroid distance is 5.953 Å and plane 86.72°).

3.3. Magnetic properties

The magnetic susceptibility χ_{Mol} between 1.9 and 300 K of the trinuclear, μ_3-oxo-bridged manganese(III) compound **1** was determined. In Fig. 6, the temperature dependence of the inverse molar susceptibility χ^{-1}_{Mol} is depicted. Above 55 K, the data can be fitted to the Curie–Weiss expression with a Weiss constant $\theta = -147$ K which is indicative of antiferromagnetic exchange interactions. The thermal dependence of the molar susceptibility, plotted as $\chi_{Mol}T$ versus T is shown in Fig. 7. The $\chi_{Mol}T$ value at 300 K is 8.14 emu K mol^{-1}, which is a little below the calculated value of 9 emu K mol^{-1} for three non-interacting manganese(III) ions ($S = 2$, $g = 2$). The decrease of $\chi_{Mol}T$ with decreasing temperature suggests overall antiferromagnetic exchange interactions. A simulation based on the model proposed by Borrás-Almenar et al. [25] using the isotropic Heisenberg–Dirac–Van Vleck term, $\widehat{H}_O = -2\Sigma_{i,f}J_{if}\widehat{S}_i\widehat{S}_f$, as the leading part of the exchange spin Hamiltonian, was applied. Thereby and in correspondence with the structural data, the compound is regarded as an isosceles triangle and consequently, two different exchange coupling constants are considered: J between Mn(3)–Mn(1) and Mn(3)–Mn(2) and J^* between Mn(1) and Mn(2). However, as shown in a theoretical study by Brechin et al. [34], there is a high density of different energy levels close to the ground state and also the total S value of the ground state depends strongly on the ratio J/J^*, hence it is a quite complex situation. Taking the data of the temperature dependence of the magnetic susceptibility and the magnetization data which are measured at 1.85 K (Figs. 7 and S1), a simulation of the experimental data revealed the following parameters: $J = -7.5$ cm^{-1}, $J^* = -5.2$ cm^{-1}, $D = 15.5$ cm^{-1} and $g = 2.1$. With these parameters, the $\chi_{Mol}T$ versus T data can be simulated fairly well. On the basis of the same parameter set, also the magnetization data can be approached reasonably well,

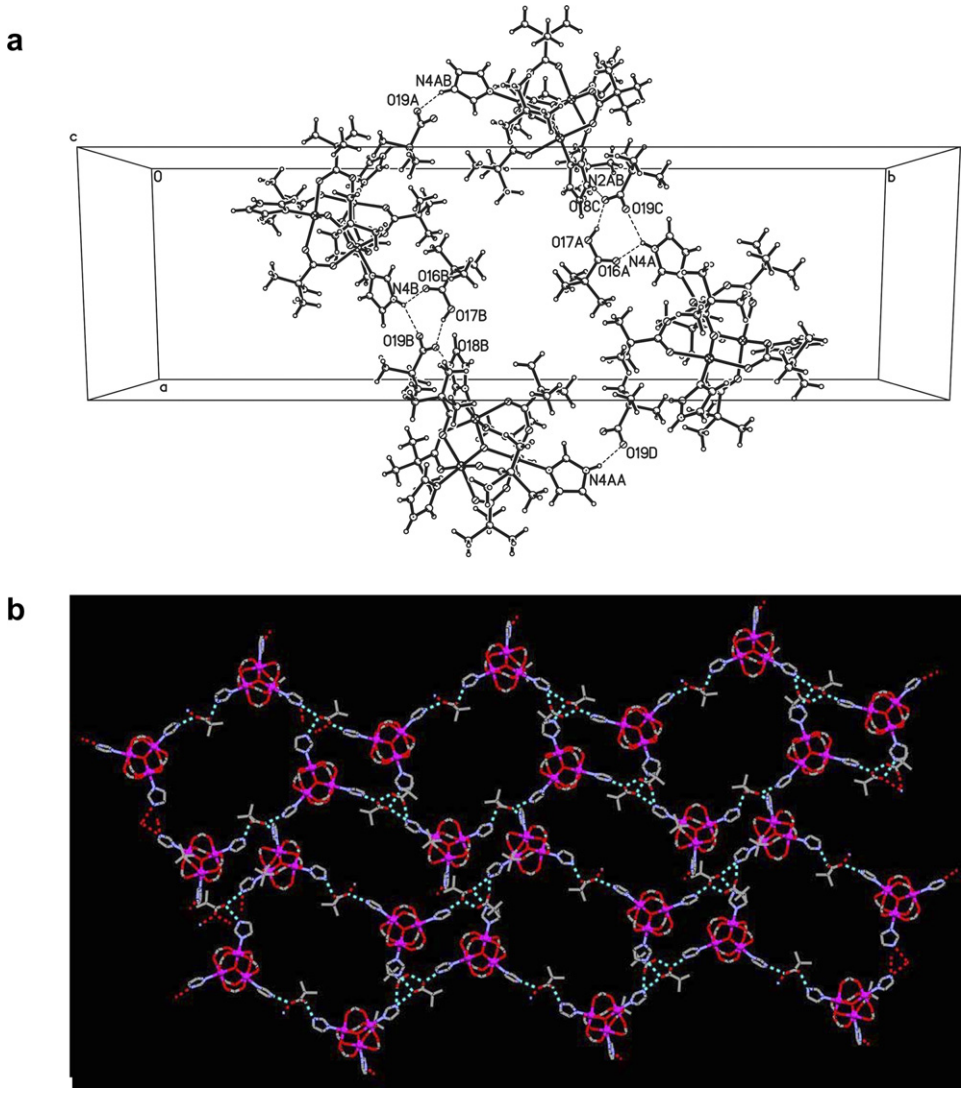

Fig. 3. (a) A fragment of the crystal structure in compound **1.** Hydrogen bonds are shown as dashed lines. (b) Perspective view of the crystal structure along the *b* axis. Hydrogen bonds are shown as dashed lines, the methyl groups of the coordinated pivalic acid are omitted for clarity.

especially if one notes the complex configuration of multiple states lying close to the ground-state. Overall, a ground state with $S = 0$ but with energetically close lying states with $S = 1$ and $S = 2$ can be anticipated.

Table 4
Hydrogen bonding interactions in compound **1**

D–H...A	*d*(D–H) (Å)	*d*(H...A) (Å)	*d*(D...A) (Å)	∠(DHA)
N(2)–H(2)...O(14)	0.88	1.96	2.685(5)	139.3
N(2A)–H(2A)...O(18)[1]	0.88	1.86	2.730(4)	169.4
N(4)–H(4)...O(19)[2]	0.88	2.13	2.779(4)	130.3
N(4)–H(4)...O(16)	0.88	2.22	2.866(4)	130.4
N(4A)–H(4A)...O(19)[3]	0.88	1.90	2.733(4)	156.2
N(6)–H(6)...O(15)[2]	0.88	1.80	2.655(4)	164.2
N(6A)–H(6A)...O(15)[2]	0.88	1.78	2.636(4)	164.1
O(17)–H(17)...O(18)[2]	0.84	1.75	2.556(4)	159.0

Symmetry transformations: [1]$x - 1, y, z$; [2]$x + 1/2, -y + 1/2, z + 1/2$; [3]$-x + 1, -y + 1, -z + 1$.

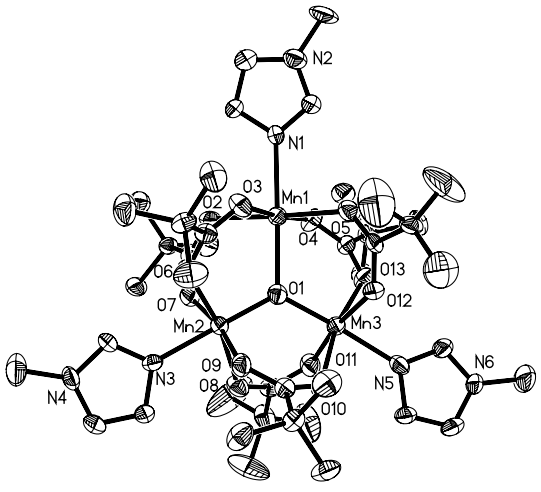

Fig. 4. View of the structure of molecule **B** in compound **2**. Hydrogen atoms are omitted for clarity.

Table 5
Selected bond distances (Å) and angles (°) for compound **2**

Molecule	A	B	Molecule	A	B
Mn(1)–O(1)	2.128(5)	2.170(4)	Mn(2)–O(8)	2.174(5)	2.090(5)
Mn(1)–O(2)	2.174(4)	2.178(5)	Mn(2)–O(9)	1.968(5)	2.030(5)
Mn(1)–O(3)	2.143(5)	2.149(5)	Mn(2)–N(3)	2.064(5)	2.063(6)
Mn(1)–O(4)	2.129(5)	2.143(5)	Mn(3)–O(1)	1.848(4)	1.813(4)
Mn(1)–O(5)	2.178(5)	2.207(5)	Mn(3)–O(10)	2.173(4)	2.110(5)
Mn(1)–N(1)	2.251(6)	2.256(6)	Mn(3)–O(11)	1.985(5)	2.000(5)
Mn(2)–O(1)	1.803(5)	1.800(4)	Mn(3)–O(12)	2.003(4)	2.047(5)
Mn(2)–O(6)	2.133(5)	1.998(5)	Mn(3)–O(13)	2.136(5)	2.015(5)
Mn(2)–O(7)	1.947(5)	2.082(6)	Mn(3)–N(5)	2.061(6)	2.060(6)
O(1)–Mn(1)–O(2)	91.13(17)	94.05(17)	O(1)–Mn(2)–O(8)	95.47(19)	94.15(19)
O(1)–Mn(1)–O(5)	90.92(17)	91.51(18)	O(9)–Mn(2)–O(8)	90.01(18)	92.3(2)
O(2)–Mn(1)–O(5)	177.60(17)	174.36(19)	O(6)–Mn(2)–O(8)	168.50(17)	86.4(2)
O(1)–Mn(1)–N(1)	176.90(17)	174.01(18)	N(3)–Mn(2)–O(8)	84.25(19)	86.0(2)
O(1)–Mn(1)–O(3)	92.47(17)	89.70(17)	O(7)–Mn(2)–O(8)	86.98(18)	170.24(19)
O(5)–Mn(1)–N(1)	91.40(19)	84.2(2)	O(1)–Mn(3)–O(12)	94.2(2)	96.69(19)
O(4)–Mn(1)–O(1)	91.90(18)	94.35(18)	O(1)–Mn(3)–O(11)	94.7(2)	95.00(19)
O(4)–Mn(1)–O(5)	90.95(19)	93.9(2)	O(11)–Mn(3)–O(12)	171.0(2)	88.9(2)
O(4)–Mn(1)–O(2)	87.73(18)	84.8(2)	O(1)–Mn(3)–N(5)	176.0(2)	178.8(2)
O(4)–Mn(1)–N(1)	86.0(2)	90.1(2)	O(12)–Mn(3)–N(5)	86.0(2)	84.5(2)
O(3)–Mn(1)–O(5)	88.22(18)	88.1(2)	O(11)–Mn(3)–N(5)	85.1(2)	85.3(2)
O(3)–Mn(1)–O(2)	92.94(18)	92.9(2)	O(1)–Mn(3)–O(13)	99.00(18)	95.6(2)
O(3)–Mn(1)–N(1)	89.7(2)	86.0(2)	O(12)–Mn(3)–O(13)	91.63(18)	92.2(2)
O(2)–Mn(1)–N(1)	86.51(18)	90.4(2)	O(11)–Mn(3)–O(13)	88.70(18)	169.1(2)
O(4)–Mn(1)–O(3)	175.57(19)	175.5(2)	N(5)–Mn(3)–O(13)	85.02(19)	84.0(2)
O(1)–Mn(2)–O(9)	94.89(19)	94.33(19)	O(1)–Mn(3)–O(10)	92.87(18)	94.4(2)
O(1)–Mn(2)–O(6)	95.97(19)	95.81(19)	O(12)–Mn(3)–O(10)	86.72(17)	168.8(2)
O(9)–Mn(2)–O(6)	87.90(18)	169.84(18)	O(11)–Mn(3)–O(10)	91.10(18)	89.1(2)
O(1)–Mn(2)–N(3)	179.5(2)	179.8(2)	N(5)–Mn(3)–O(10)	83.12(19)	84.4(2)
O(9)–Mn(2)–N(3)	84.65(19)	85.6(2)	O(13)–Mn(3)–O(10)	168.11(18)	87.6(2)
N(3)–Mn(2)–O(6)	84.30(19)	84.30(19)			
O(1)–Mn(2)–O(7)	95.06(19)	95.50(19)	Mn(2)–O(1)–Mn(1)	118.4(2)	117.9(2)
O(7)–Mn(2)–O(9)	169.83(18)	85.6(2)	Mn(2)–O(1)–Mn(3)	124.1(3)	125.4(2)
O(7)–Mn(2)–O(6)	93.12(18)	94.1(2)	Mn(3)–O(1)–Mn(1)	117.4(2)	116.6(2)
O(7)–Mn(2)–N(3)	85.38(19)	84.4(2)			

Table 6
CH···π contacts in compound **2**

Heterocycle···heterocycle[a]	Aliphatic CH···π (Å) (θ(HCC′), °)		Aromatic CH···π (Å) (θ (HCC′), °)		Centroid–centroid distance (Å) (plane angle, °)
N5A ∩ N6A···N1A ∩ N2A	C12A–H12E···C3A[b]	2.835 (36.25)			4.468 (24.47)
N1A ∩ N2A···N1 ∩ N2	C4–H4A···C3A[c]	3.032 (41.42)	C2A–H2A···C1[g]	2.917 (55.92)	4.242 (31.69)
N1 ∩ N2···N5 ∩ N6	C12–H12A···C3[d]	2.848 (29.68)			4.374 (24.22)
N5 ∩ N6···N3 ∩ N4	C8–H8A···C11[e]	2.952 (29.34)			4.250 (18.11)
N3 ∩ N4···N3A ∩ N4A			C7A–H7A···C6[h]	2.999 (45.85)	4.873 (68.64)
N3A ∩ N4A···N5A ∩ N6A	C8A–H8D···C9A[f]	2.986 (21.53)			

[a] Heterocycle N1 ∩ N2 (N1, C1, N2, C2, C3); N3 ∩ N4 (N3, C5, N4, C6, C7); N5 ∩ N6 (N5, C9, N6, C10, C11); N1A ∩ N2A (N1A, C1A, N2A, C2A, C3A); N3A ∩ N4A (N3A, C5A, N4A, C6A, C7A); N5A ∩ N6A (N5A, C9A, N6A, C10A, C11A).
[b] $1-x, 1/2+y, 1-z$.
[c] $1-x, y, z$.
[d] $-x, 1/2+y, 1-z$.
[e] $-x, -1/2+y, 2-z$.
[f] $1-x, -3/2+y, -z$.
[g] $1+x, y, z$.
[h] $x, y, -1+z$.

For the trinuclear mixed-valence compound **2**, the temperature dependence of the inverse molar susceptibility χ_{Mol}^{-1} between 1.9 and 300 K is depicted in Fig. 8. A fit above 55 K of the data to the Curie–Weiss expression gives a Weiss constant $\theta = -140$ K, which is indicative of antiferromagnetic exchange interactions. In Fig. 9 the thermal dependence of the molar susceptibility, plotted as $\chi_{\mathrm{Mol}}T$ versus T, is shown. The experimentally determined room

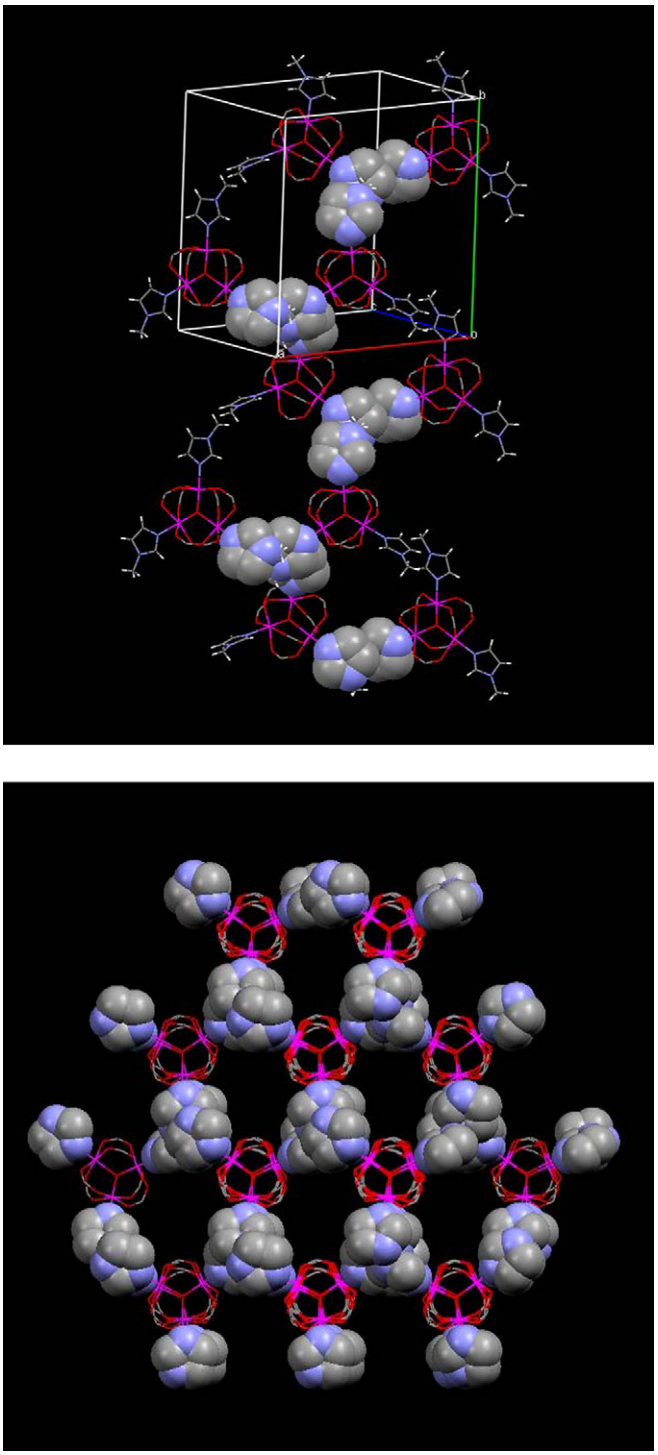

Fig. 5. Molecular packing and aromatic–aromatic interactions of compound **2**. The edge-to-face contacts are highlighted with the space-filled 1-MeIm heterocycle. The methyl groups of pivalic acid are omitted for clarity.

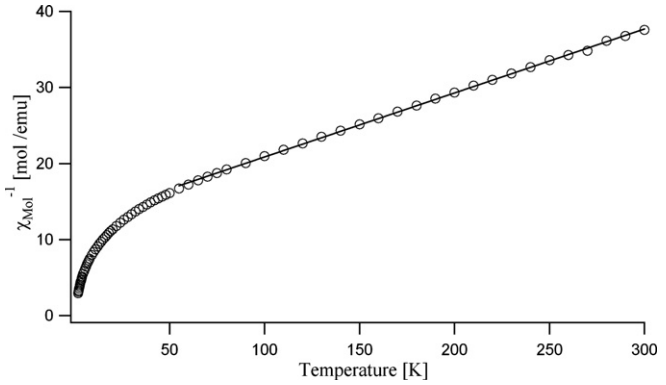

Fig. 6. The inverse molar susceptibility χ_{Mol}^{-1} vs. T for compound **1**. The solid line represents a linear fit to the data from 55 to 300 K, giving a Weiss constant $\theta = -147$ K.

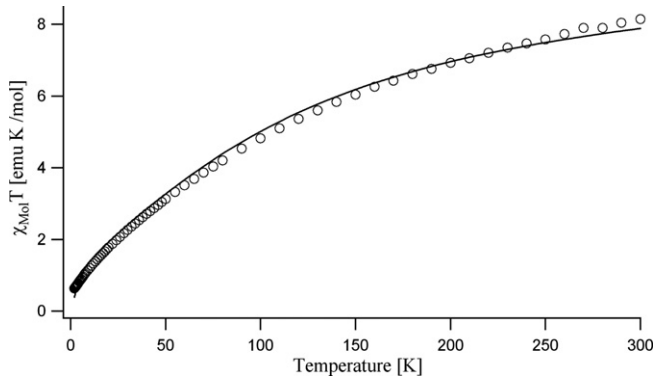

Fig. 7. Plot of the $\chi_{Mol}T$ product vs. T of compound **1** in an applied field of 1 kG. The solid curve represents a simulation from 2 to 300 K with the parameters $J = -7.5\ cm^{-1}$, $J^* = -5.2\ cm^{-1}$, $D = 15.5\ cm^{-1}$ and $g = 2.1$ (see text).

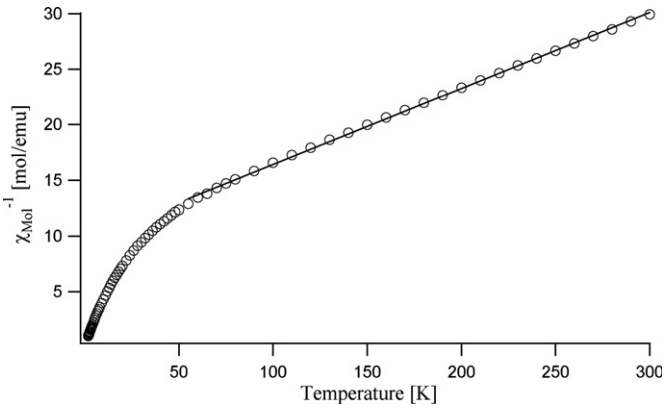

Fig. 8. The inverse molar susceptibility χ_{Mol}^{-1} vs. T for compound **2**. The solid line represents a linear fit to the data from 55 to 300 K, giving a Weiss constant $\theta = -140$ K.

temperature value $\chi_{Mol}T$ of 10.0 emu K mol^{-1} is in good agreement with a calculated value of 10.38 emu K mol^{-1} for the non-interacting two manganese(III) ions ($S = 2$, $g = 2$) and one manganese(II) ion ($S = 5/2$, $g = 2$). With decreasing temperature the $\chi_{Mol}T$ values drop slowly, which suggests overall antiferromagnetic exchange interactions. For the simulation of the data [25], two different exchange interactions have been considered: J between the Mn(II) ($S = 5/2$) and the two Mn(III) ($S = 2$) centers, and J^* between the two Mn(III) centers. The parameters found for the best simulation of the experimental data

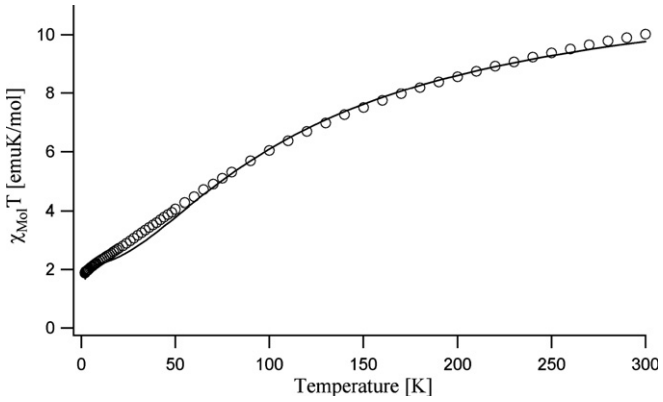

Fig. 9. Plot of the $\chi_{Mol}T$ product vs. T of compound **2** in an applied field of 1 kG. The solid curve represents the fit from 2 to 300 K with the parameters $J = -7.0\ cm^{-1}$, $J^* = -1.6\ cm^{-1}$, $D = -1.6\ cm^{-1}$ and $g = 2.2$ (see text).

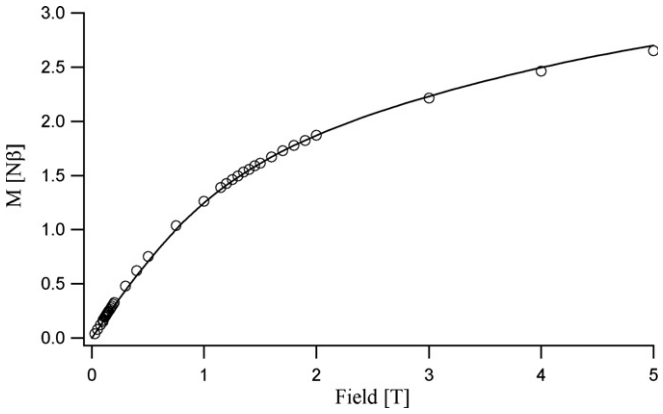

Fig. 10. Field dependence of the magnetization of compound **2** measured at $T = 1.85$ K. The solid curve represents the fit with the parameters $J = -7.0\ cm^{-1}$, $J^* = -1.6\ cm^{-1}$, $D = -1.6\ cm^{-1}$ and $g = 2.2$ (see text).

are: $J = -7.0\ cm^{-1}$, $J^* = -1.6\ cm^{-1}$, $D = -1.6\ cm^{-1}$ and $g = 2.2$. Moreover, with the same parameter set, a fairly good simulation of the magnetization data, measured at 1.85 K (see Fig. 10), has been obtained. At a magnetic field of 5 T, M_{sat} is not yet reached but a value close to 3 Nβ can be estimated. Accordingly, this would be consistent with a total ground state spin value of $S = 3/2$. This result is in accordance with a related detailed study by Ribas et al. [11].

4. Conclusions

In summary, we have synthesized and structurally characterized two new μ-oxo trinuclear manganese carboxylate complexes with imidazole and 1-methylimidazole ligands. One of them, complex $[Mn_3O(O_2CCMe_3)_6(Im)_3](Me_3CCO_2) \cdot 0.5Me_3CCO_2H$ (**1**) is a homo-valent Mn^{III}_3O cluster, which has been synthesized by comproportionation reaction of manganese(II) chloride with $KMnO_4$, imidazole and an excess of pivalic acid, whereas complex $[Mn_3O(O_2CCMe_3)_6(1\text{-}MeIm)_3]$ (**2**), which is a mixed-valent $Mn^{III}_2Mn^{II}O$ cluster, was isolated by the reaction of hexanuclear mixed-valent $[Mn^{III}_4Mn^{III}_2O_2(O_2CCMe_3)_{10}(Me_3CCO_2H)_4]$ with $KMnO_4$ in 1-methylimidazole. The trinuclear nature of these complexes has been compared to that of the previously reported μ-oxo trinuclear manganese carboxylates. The magnetic properties of **1** and **2** were studied by variable-temperature susceptibility measurements. The results reveal that both compounds are antiferromagnetically coupled, spin-frustrated triangular systems exhibiting weak to moderate exchange coupling constants.

Acknowledgment

This work was supported by the Swiss National Science Foundation (SCOPES 7MDPJ065712.01/1 and IB7320-110976/1).

Appendix A. Supplementary data

Crystallographic data have been deposited with the Cambridge Crystallographic Data Centre, CCDC Nos. 295955 (**1**), 295956 (**2**). Copies of this information may be obtained from The Director, CCDC, 12 Union Road, Cambridge, CB2 1EZ, UK (fax: +44 1233 336 033; e-mail: deposit@ccdc.cam.ac.uk or www: http://www.ccdc.cam.ac.uk). Supplementary data associated with this article can be found, in the online version, at doi:10.1016/j.poly.2006.07.014.

References

[1] (a) W. Wernsdorfer, N.E. Chakov, G. Christou, Phys. Rev. B 70 (2004) 132413;
(b) A.J. Tasiopoulos, W. Wernsdorfer, K.A. Abboud, G. Christou, Angew. Chem. Int. Ed. 43 (2004) 6338;
(c) A.J. Tasiopoulos, A. Vinslava, W. Wernsdorfer, K.A. Abboud, G. Christou, Angew. Chem. Int. Ed. 43 (2004) 2117;
(d) N. Aliaga-Alcalde, R.S. Edwards, S.O. Hill, W. Wernsdorfer, K. Folting, G. Christou, J. Am. Chem. Soc. 126 (2004) 12503;
(e) G. Rajaraman, M. Murugesu, E.C. Sañudo, M. Soler, W. Wernsdorfer, M. Helliwell, C. Muryn, J. Raftery, S.J. Teat, G. Christou, E.K. Brechin, J. Am. Chem. Soc. 47 (2004) 15445;
(f) M. Murugesu, J. Raftery, W. Wernsdorfer, G. Christou, E.K. Brechin, Inorg. Chem. 43 (2004) 4203;
(g) M. Murugesu, M. Habrych, W. Wernsdorfer, K.A. Abboud, G. Christou, J. Am. Chem. Soc. 126 (2004) 4766;
(h) G. Christou, Polyhedron 24 (2005) 2065.
[2] (a) L. Que Jr., A.E. True, Prog. Inorg. Chem. 38 (1990) 97;
(b) V.L. Pecoraro, Manganese Redox Enzymes, VCH Publishers Inc., New York, 1992;
(c) G.C. Dismukes, Chem. Rev. 96 (1996) 2909;
(d) G. Christou, Acc. Chem. Res. 22 (1989) 328.
[3] S. Uemura, A. Spencer, G. Wilkinson, J. Chem. Soc., Dalton Trans. (1973) 2565.
[4] A.R.E. Baikie, M.B. Hursthouse, D.B. New, P. Thornton, J. Chem. Soc., Chem. Commun. (1978) 62.
[5] A.R.E. Baikie, M.B. Hursthouse, L. New, P. Thornton, R.G. White, J. Chem. Soc., Chem. Commun. (1980) 684.
[6] J.B. Vincent, H.R. Chang, K. Folting, J.C. Huffman, G. Christou, D.N. Hendrickson, J. Am. Chem. Soc. 109 (1987) 5703.
[7] H.G. Jang, J.B. Vincent, M. Nakano, J.C. Huffman, G. Christou, M. Sorai, R.J. Wittebort, D.N. Hendrickson, J. Am. Chem. Soc. 111 (1989) 7778.

[8] M. Nakano, M. Sorai, J.B. Vincent, G. Christou, H.G. Jang, D.N. Hendrickson, Inorg. Chem. 28 (1989) 4608.
[9] J.K. Mccusker, H.G. Jang, S. Wang, G. Christou, D.N. Hendrickson, Inorg. Chem. 31 (1992) 1874.
[10] S.W. Zhang, Y.G. Wei, Q. Liu, M.C. Shao, Polyhedron 15 (1996) 1014.
[11] J. Ribas, B. Albela, H. Stoeckli-Evans, G. Christou, Inorg. Chem. 36 (1997) 2352.
[12] Z.J. Zhong, J.-Q. Tao, H. Li, X.-Z. You, T.C.W. Mak, Polyhedron 16 (1997) 1719.
[13] R.W. Wu, M. Poyraz, F.E. Sowrey, C.E. Anson, S. Wocadle, A.K. Powell, U.A. Jayasooriya, R.D. Cannon, T. Nakamoto, M. Katada, H. Sano, Inorg. Chem. 37 (1998) 1913.
[14] J. An, Z.-D. Chen, J. Bian, X.-L. Jin, S.-X. Wang, G.-X. Xu, Inorg. Chim. Acta 287 (1999) 82.
[15] J. Li, S. Yang, F. Zhang, Z. Tang, S. Ma, Q. Shi, Q. Wu, Z. Huang, Inorg. Chim. Acta 294 (1999) 109.
[16] C. Canada-Vilalta, J.C. Huffman, W.E. Streib, E.R. Davidson, G. Christou, Polyhedron 20 (2001) 1375.
[17] J. Li, F. Zhang, Q. Shi, J. Wang, Yu. Wang, Z. Zhou, Inorg. Chem. Commun. 5 (2002) 51.
[18] J. Kim, H. Cho, Inorg. Chem. Commun. 7 (2004) 122.
[19] N.V. Gerbeleu, G.A. Timco, O.S. Manole, Y.T. Struchkov, A.S. Batsanov, S.V. Grebenco, Russ. J. Coord. Chem. 20 (1994) 357.
[20] N.V. Gerbeleu, A.S. Batsanov, G.A. Timco, Yu.T. Struchkov, K.M. Indrichan, G.A. Popovici, Dokl. Akad. Nauk SSSR 294 (1987) 878.
[21] A.S. Batsanov, Y.T. Struchkov, G.A. Timco, N.V. Gerbeleu, O.S. Manole, S.V. Grebenco, Russ. J. Coord. Chem. 20 (1994) 604.
[22] A.R.E. Baikie, A.J. Howes, M.B. Hursthouse, A.B. Quick, P. Thornton, J. Chem. Soc., Chem. Commun. 4 (1986) 1587.
[23] G.M. Sheldrick, Acta Crystallogr., Sect. A 46 (1998) 467.
[24] G.M. Sheldrick, SHELXS-97, University of Göttingen, Germany, 1999.
[25] J.J. Borrás-Almenar, J.M. Clemente-Juan, E. Coronado, B.S. Tsukerblat, Inorg. Chem. 38 (1999) 6081.
[26] T. Lis, Acta Crystallogr., Sect. B 36 (1980) 2042.
[27] G. Aromi, S.M.J. Aubin, M.A. Bolcar, G. Christou, H.J. Eppley, K. Folting, D.N. Hendrickson, J.C. Huffman, R.C. Squire, H.-L. Tsai, S. Wang, M.W. Wemple, Polyhedron 17 (1998) 3005.
[28] (a) M. Soler, E. Rumberger, K. Folting, D.N. Hendrickson, G. Christou, Polyhedron 20 (2001) 1365;
(b) M. Soler, W. Wernsdorfer, K. Folting, M. Pink, G. Christou, J. Am. Chem. Soc. 126 (2004) 2156.
[29] K. Nakamoto, Infrared and Raman Spectra of Inorganic and Coordination Compounds, Wiley, New York, 1986, p. 230.
[30] R.C. Mehrota, R. Bohra, Metal Carboxylates, Academic Press, New York, 1983, p. 47.
[31] C.A. Hunter, K.R. Lawson, J. Perkins, C.J. Urch, J. Chem. Soc., Perkin Trans. 2 (2001) 651.
[32] H. Suezawa, T. Yoshida, M. Hirota, H. Takahashi, Y. Umezawa, K. Honda, S. Tsuboyama, M. Nishio, J. Chem. Soc., Perkin Trans. 2 (2001) 2053.
[33] M. Nishio, Cryst. Eng. Commun. 6 (2004) 130.
[34] L.F. Jones, G. Rajaraman, J. Brockman, M. Murugesu, E.C. Sanudo, J. Raftery, S.J. Teat, W. Wernsdorfer, G. Christou, E.K. Brechin, D. Collison, Chem. Eur. J. 10 (2004) 5180.

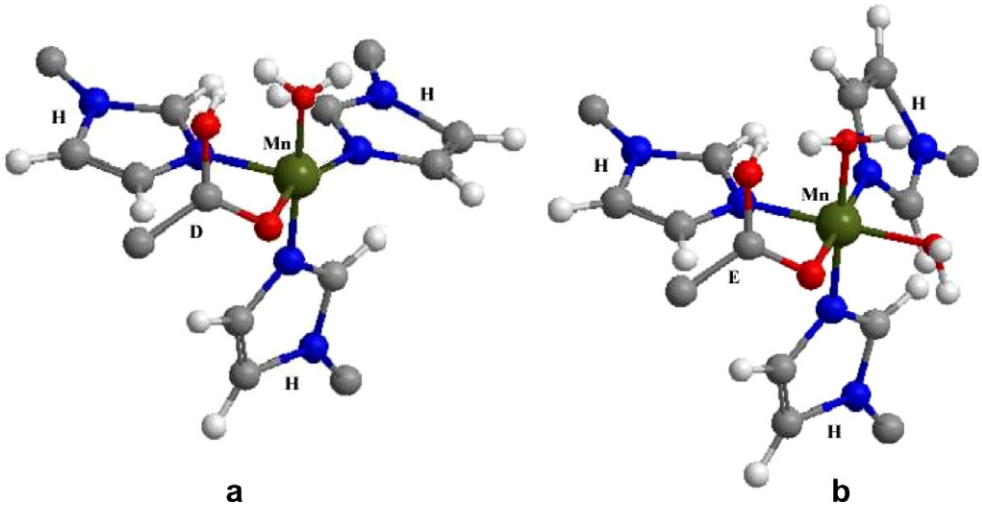

Fig. 1. Active site structure for Mn–SOD (a) and Mn(II)oxlate-oxidase (b).

molecules. The active site structures for other mononuclear manganese enzymes are not known with certainty, but based on their analogous iron enzymes, a square-pyramidal arrangement of two histidines, a glutamate and two water molecules has been proposed for Mn(II)dioxygenase [11] and an active site structure similar to the iron-containing soybean lipoxygenase has been proposed for the manganese lipoxygenase enzyme [12]. According to Minor et al. [13], the iron in iron-lipoxygenase, is coordinated to three nitrogens of histidine residues, one oxygen of a monodentate isoleucine and one oxygen of a weakly coordinated asparagine. A water molecule forming a hydrogen bond with the non-coordinated carboxylate oxygen of isoleucine, completes the distorted octahedral coordination sphere. A common structural feature found in most of the above proteins and enzymes is the presence of one or more carboxylate derived from aspartate/glutamate/isoleucine or asparagine side chains of the protein. These carboxylates act as a bridge between metal ions present in the binuclear manganese containing enzyme and also are suggested to play an important role for structural holding and proton transfer via hydrogen-bonding interactions in proteins [14]. The role of hydrogen bonding in the stabilization of structures as well as in the functions of various metalloproteins is well known in biochemistry [15].

There are several examples of mononuclear and binuclear manganese carboxylate complexes where the hydrogen atoms of the ligand alcohol groups, the bridging aqua or the lattice water molecules form inter/intramolecular hydrogen bonds with coordinated carboxylate groups available in the literature [16], but manganese carboxylate complexes with hydrogen bonds involving pyrazole groups are limited in number. In light of the importance of hydrogen bonded carboxylate and the limited examples of manganese carboxylate complexes with hydrogen bonded pyrazole, we have undertaken the synthesis, structural and SOD activity studies of some manganese carboxylate complexes in the present paper.

2. Experimental

2.1. Materials

All manipulations were carried out under nitrogen atmosphere using standard Schlenk tube techniques unless otherwise stated. The required organic solvents were carefully purified and distilled under nitrogen prior to use, by the literature method [17]. $MnCl_2 \cdot 4H_2O$ (reagent grade) was purchased from E. Merck. Other reagents were of the highest grade commercially available and were used without further purification. 3,5-*i*-Pr_2pzH [$Pz^{iPr2}H$] (**1**), KHB(3,5-*i*-$Pr_2pz)_3$ [Tp^{iPr2}] (**2**), [18] KHB(3-Ph,5-$Mepz)_3$ [$Tp^{Ph,Me}$] (**3**) [19] and Tp^{iPr2}MnCl (**4**) [20] were synthesized by the literature methods.

2.2. Physical methods

IR spectra were obtained on a Thermo Nikolet Nexus FT-IR spectrometer in KBr and FD-MS spectra were obtained on a Hitachi M-80 mass spectrometer. Room temperature magnetic susceptibility measurements were done on a Cahn Faraday magnetic susceptibility balance. The X-ray data collection and processing for **5** and **6** were performed on a Rigaku RAXIS-IV imaging plate area detector with Mo Kα radiation ($\lambda = 0.71070$ Å). In the reduction of data, Lorentz and polarization corrections, and empirical absorptions were made [21]. The structure analysis was performed on an IRIS O2 (Silicon Graphics) using the teXsan structure solving program system obtained from the Rigaku Corp., Tokyo, Japan [22]. Neutral scattering factors were obtained from the standard source [23]. The structures were solved by a combination of direct methods (SHELXS-86) [24] and Fourier synthesis (DIRDIF 94) [25]. Least-squares refinements were carried out using SHELXS-97 [24] linked to teXsan. All non-hydrogen atoms were refined anisotropically. Diffraction data for complex **7** were recorded at −80 °C with a Bruker

Smart CCD diffractometer. Emperical absorption corrections were applied. The structure was solved by Patterson methods and refined anisotropically with the SHELX program suite. Hydrogen atoms involved in hydrogen bonding were obtained by refinement, not by fixing the position. Single crystal diffraction studies for **8** and **10** were carried out on a Bruker Smart CCD diffractometer with Mo Kα radiation ($\lambda = 0.71073$ Å) in a sealed tube at 25 °C. Crystal structures were solved by direct methods and in anisotropic approximation refined using the SHELX TL package [26,27]. Hydrogen atoms were constrained by the rigid model.

2.3. Synthesis of complexes

2.3.1. *[(Pz^{iPr2}H)$_4$Mn(NO$_2$–OBz)$_2$] (**5**)*

(0.197 g, 1.00 mmol) $MnCl_2 \cdot 4H_2O$ and (0.604 g, 4.00 mmol) Pz^{iPr2}H were stirred in 25 mL CH_2Cl_2 and 5 mL CH_3OH for 1 h. To this solution was added a 5 mL acetonitrile solution of sodium *p*-nitrobenzoate (0.378 g, 2.00 mmol) and the reaction mixture was stirred for 12 h at room temperature. The mixture was filtered over celite and the solvent was evaporated to dryness. The compound was dissolved in 5 mL CH_3CN and colorless crystals were obtained at −20 °C (yield 84%). *Anal.* Calc. (%) for $C_{50}H_{72}N_{10}O_8Mn$: C, 60.26; H, 7.28; N, 14.06. Found: C, 60.09; H, 7.31; N, 13.72%. IR (KBr, cm^{-1}), *ν*(NH of pyrazole) 3211, ν_{as}(COO) 1576, ν_s(COO) 1473, $\mu_{eff} = 5.75$ BM at 295 K.

2.3.2. *[(Pz^{iPr2}H)$_4$Mn(F–OBz)$_2$] (**6**)*

(0.197 g, 1.00 mmol) $MnCl_2 \cdot 4H_2O$ and (0.604 g, 4.00 mmol) Pz^{iPr2}H were stirred in 30 mL CH_2Cl_2 and 5 mL CH_3OH for 1 h. A 5 mL acetonitrile solution of sodium *p*-fluorobenzoate (0.324 g, 2.00 mmol) was added to this solution and stirred for 12 h. The mixture was filtered over celite and the solvent was evaporated to dryness. The compound was dissolved in 5 mL acetonitrile and colorless crystals were obtained by slow cooling at −20 °C (Yield 80%). *Anal.* Calc. (%) for $C_{50}H_{72}N_8O_4F_2Mn$: C, 63.72; H, 7.70; N, 11.89. Found: C, 63.49; H, 7.67; N, 11.44%. IR (KBr, cm^{-1}) *ν* (NH of pyrazole) 3297, ν_{as}(COO) 1570, ν_s(COO) 1442, $\mu_{eff} = 5.78$ BM at 295 K.

2.3.3. *[Tp^{Ph,Me}Mn(OAc)Pz^{Ph,Me}H] (**7**)*

KTp^{Ph,Me} (0.521 g, 1.00 mmol) was stirred with $Mn(OAc)_2 \cdot 4H_2O$ (0.245 g, 1.00 mmol) and 1.0 equivalent of Pz^{Ph,Me}H (0.158 g, 1.00 mmol) in 25 mL dichloromethane and 5 mL methanol for 2 h. The mixture was filtered through celite and the filtrate was dried under vacuum. The colorless powder was dissolved in a mixture of dichloromethane and acetonitrile (1:1 ratio) and crystals were obtained by cooling the solution at −20 °C (Yield 65%). *Anal.* Calc. (%) for $C_{42}H_{41}BMnN_8O_2$: C, 66.76; H, 5.47; N, 14.83. Found: C, 66.56; H, 5.39; N, 14.90%. IR (KBr, cm^{-1}), *ν*(BH) 2539, ν_{as}(COO) 1572, ν_s(COO) 1435, $\mu_{eff} = 5.68$ BM at 295 K.

2.3.4. *[Tp^{iPr2}Mn(Cl)Pz^{iPr2}H] (**8**)*

$MnCl_2 \cdot 4H_2O$ (0.197 g, 1.00 mmol), KTp^{iPr2} (0.504 g, 1.00 mmol) and Pz^{iPr2}H (0.761 g, 5.00 mmol) were stirred in 25 mL CH_2Cl_2 and 5 mL CH_3OH for 1 h. The mixture was filtered over celite and the solvent was evaporated to dryness under vacuum. The compound was dissolved in 5.0 mL pentane and 3.0 mL ether. Colorless crystals were obtained from the filtrate at −20 °C in 85% yield. *Anal.* Calc. for $C_{36}H_{62}N_8BClMn$: C, 61.05; H, 8.82; N, 15.82; Cl, 5.00. Found: C, 61.12; H, 8.83; N, 15.97; Cl, 4.80%. IR (KBr, cm^{-1}) *ν*(BH) 2548, *ν*(NH of pyrazole) 3292, *ν*(CN of pyrazole) 1560, $\mu_{eff} = 5.70$ BM at 295 K.

2.3.5. *[Tp^{iPr2}Mn(F–OBz)] (**9**)*

To a 30 mL toluene solution of **4** (0.489 g, 0.882 mmol), was added a 10 mL acetonitrile solution of sodium *p*-fluorobenzoate (0.143 g, 0.882 mmol) and the reaction mixture was stirred for 16 h. The mixture was filtered over celite and the solvent was evaporated under vacuum. A colorless microcrystalline solid was obtained by slow cooling of an acetonitrile solution at −20 °C in 45% yield. *Anal.* Calc. (%) for $C_{34}H_{51}N_6BFO_2Mn$: C, 61.82; H, 7.78; N, 12.27. Found: C, 61.65; H, 7.90; N, 12.07%. IR (KBr, cm^{-1}), *ν*(BH) 2541, ν_{as}(COO) 1600, ν_s(COO) 1469, $\mu_{eff} = 5.83$ BM at 295 K, FD–MS (*m*/*z*) = 660.

2.3.6. *[Tp^{iPr2}Mn$_2$(μ-FOBz)$_3$(Pz^{iPr2}H)$_2$] (**10**)*

$MnCl_2 \cdot 4H_2O$ (0.168 g, 0.855 mmol), complex **4** (0.474 g, 0.855 mmol), sodium *p*-fluorobenzoate (0.419 g, 2.57 mmol) and Pz^{iPr2}H (0.260 g, 1.71 mmol) in a mixture of toluene and acetonitrile (1:1) were stirred for 12 h at room temperature. The mixture was filtered over celite and the solvent was evaporated to dryness. Colorless crystals were obtained by slow cooling of acetonitrile solution at −20 °C in 65% yield. *Anal.* Calc. (%) $C_{66}H_{90}N_{10}BF_3O_6Mn_2$; C, 61.11; H, 6.99; N, 10.79. Found: C, 60.85; H, 6.95; N, 10.85%. IR(KBr, cm^{-1}), *ν*(BH) 2538, ν_{as}(COO) 1594, ν_s(COO) 1469, $\mu_{eff} = 5.90/Mn^{2+}$ BM at 295 K.

3. Results and discussion

The reaction of $MnCl_2 \cdot 4H_2O$ with four equivalents of pyrazole **1** and two equivalent of sodium *p*-nitrobenzoate/sodium *p*-fluorobenzoate gave six coordinated mononuclear

$$MnCl_2.4H_2O + 4\ \text{eq. Pz}^{iPr2}\text{H} + 2\ \text{eq. NaOBzX} \longrightarrow (\text{Pz}^{iPr2}\text{H})_4\text{Mn(X-OBz)}_2$$

(X= NO_2, **5**)
(X= F, **6**)

Scheme 1.

manganese high spin complexes **5** $\{C_{50}H_{72}N_{10}O_8Mn\}$ and **6** $\{C_{50}H_{72}N_8O_4F_2Mn\}$ (Scheme 1). Selected bond distances and bond angles are listed in Table 1 and crystallographic data in Table 2. The Thermal ellipsoid view of the crystal structures for complexes **5** and **6** are given in Figs. 2 and 3, whereas the structure showing intramolecular hydrogen bonding and CH_3–π interactions for these complexes are given in Figs. 4 and 5, respectively. The coordination environment and geometry in complexes **5** and **6** are very similar. As shown in the X-ray structures, both complexes are six coordinated with a distorted octahedral geometry. The manganese–nitrogen and manganese–oxygen bond distances (Table 1) for **5** and **6** are nearly the same. The Mn–N bond distances are slightly longer than the Mn–N bond distances in Mn–Tp^{iPr2} complexes [28]. Also the Mn–O bond distances of coordinated *p*-nitrobenzoate/*p*-fluorobenzoate are slightly longer than the reported manganese carboxylate complexes having the Tp^{ipr2} ligand [28]. In both these complexes, the pyrazole as well as the benzoate groups are behaving as monodentate ligands; the *p*-nitrobenzoate/*p*-fluorobenzoate are coordinated to manganese by only one oxygen atom. The uncoordinated oxygen atom of each benzoate group forms intramolecular hydrogen bonds with two N–H hydrogen atoms attached to the pyrazole rings of $Pz^{iPr2}H$. The different values of the N–O bond distances (O2–N12, 2.833 (3); O2–N22 is 2.873(3) Å in **5** and O2–N12, 2.803 (2); O2–N22 is 2.831(3) Å in **6**), clearly indicate that the hydrogen bonding is stronger in complex **6** than in complex **5**. Besides the existence of intramolecular hydrogen bonding, both of these complexes exhibit a CH_3–π interaction between the CH_3 group of $Pz^{iPr2}H$ and the benzene ring of *p*-nitrobenzoate/*p*-fluorobenzoate as can be judged from the distances between the hydrogen and the centroid of the ring, 3.022 Å in **5** and 3.217 Å in **6** (Figs. 4 and 5). The presence of CH_3–π as well as the π–π stacking interaction is not uncommon in metal complexes [16h]. Several manganese benzoate complexes having Tp ligands have been reported [28], but mononuclear six coordinated manganese carboxylate complexes with intramolecular hydrogen bonding are not very common, except for some octahedral manganese (II) carboxylate complexes [29]. The presence of intramolecular hydrogen bonding as well as a CH_3–π interaction may be responsible for the stability of these complexes, as both are stable under air in the solid as well as in solution state, and they do not react with O_2 or CO_2.

When $Mn(OAc)_2 \cdot 4H_2O$ was allowed to react with $Tp^{Ph,Me}$ in the presence of pyrazole ($Pz^{Ph,Me}H$) (Scheme 2), a five coordinated intramolecular hydrogen bonded manganese (II) complex **7** $\{C_{42}H_{41}BMnN_8O_2\}$ was isolated. As shown in Fig. 6 (Thermal ellipsoid view), the manganese is coordinated with three nitrogen of the $Tp^{Ph,Me}$ ligand. The Mn–N bond distances in complex **7** (Table 1) are very similar to the Mn–N bond distances present in the mononuclear benzoate complex of manganese with Tp^{iPr2} (Mn1–N1, 2.195(4) Å; Mn1–N2, 2.277(4) Å; Mn1–N3, 2.161(3) Å) [28b] but longer than the Fe–N bond distances

Table 1
Selected bond lengths (Å) and angles (°) for $[(Pz^{iPr2}H)_4Mn(NO_2\text{–}OBz)_2]$ (**5**), $[(Pz^{iPr2}H)_4Mn(F\text{–}OBz)_2]$ (**6**), $[Tp^{Ph,Me}Mn(OAc)Pz^{Ph,Me}H]$ (**7**), $[Tp^{iPr2}Mn(Cl)Pz^{iPr2}H]$ (**8**) and $[Tp^{iPr2}Mn_2(\mu\text{-}FOBz)_3(Pz^{iPr2}H)_2] \cdot CH_3CN$ (**10** · CH_3CN)

$[(Pz^{iPr2}H)_4Mn(NO_2\text{–}OBz)_2]$			
Bond lengths (Å)			
Mn1–N11	2.327(1)	Mn1–N21	2.312(2)
Mn1–O1	2.174(2)	O1–C1	1.268(3)
O2–C1	1.249(3)		
Bond angles (°)			
O1–Mn1–O1	180.00(1)	O1–Mn1–N11	87.84(6)
O1–Mn1–N11	92.16(6)	O1–Mn1–N21	89.25(7)
O1–Mn1–N21	90.75(7)	N11–Mn–N11	180.00(0)
N21–Mn1–N21	180.00(0)		
$[(Pz^{iPr2}H)_4Mn(F\text{–}OBz)_2]$			
Bond lengths (Å)			
Mn1–N11	2.329(2)	Mn1–N21	2.327(2)
Mn1–O1	2.175(1)	O1–C1	1.251(2)
O2–C1	1.263(3)		
Bond angles (°)			
O1–Mn1–O1	180.00(0)	O1–Mn1–N11	90.92(6)
O1–Mn1–N11	89.08(6)	O1–Mn1–N21	90.68(6)
O1–Mn1–N21	89.32(6)	N11–Mn–N11	180.00(0)
N21–Mn1–N21	180.00(0)		
$[Tp^{Ph,Me}Mn(OAc)Pz^{Ph,Me}H]$			
Bond lengths (Å)			
Mn1–O1	2.024 (16)	Mn1–N4	2.149(18)
Mn1–N6	2.199(18)	Mn1–N7	2.233(18)
Mn1–N2	2.282(17)		
Bond angles (°)			
O1–Mn1–N4	118.91(7)	O1–Mn1–N6	146.99(7)
N4–Mn1–N6	93.36(7)	O1–Mn1–N7	95.65(7)
N4–Mn1–N7	94.20(7)	N6–Mn1–N7	88.18(6)
O1–Mn1–N2	93.25(7)	N4–Mn1–N2	84.81(6)
N6–Mn1–N2	82.27(6)	N7–Mn1–N2	170.32(6)
$[Tp^{iPr2}Mn(Cl)Pz^{iPr2}H]$			
Bond lengths (Å)			
Mn1–N3	2.151 (19)	Mn1–N5	2.164(2)
Mn1–N1	2.243(19)	Mn1–N7	2.306(2)
Mn1–Cl1	2.419(8)		
Bond angles (°)			
N3–Mn1–N5	95.61(7)	N3–Mn1–N1	82.08(7)
N5–Mn1–N1	80.64(7)	N3–Mn1–N7	90.56(7)
N5–Mn1–N7	89.16(7)	N3–Mn1–Cl1	125.15(5)
N5–Mn1–Cl1	139.15(5)	N1–Mn1–Cl1	105.37(5)
N7–Mn1–Cl1	87.89(5)	N5–Mn1–Cl1	89.16(7)
N2–N1–Mn1	114.89(13)		
$[Tp^{iPr2}Mn_2(\mu\text{-}FOBz)_3(Pz^{iPr2}H)_2] \cdot CH_3CN$			
Bond lengths (Å)			
Mn1–O2	2.133(3)	Mn1–O4	2.193(3)
Mn1–N3	2.238(3)	Mn1–N5	2.240(3)
Mn1–O6	2.255(3)	Mn1–N1	2.293(3)
Mn2–O3	2.096(3)	Mn2–O1	2.107(3)
Mn2–N7	2.216(3)	Mn2–O5	2.271(3)
Mn2–N9	2.272(3)		
Bond angles (°)			
O2–Mn1–O4	88.80(7)	O2–Mn1–O6	91.69(7)
O4–Mn1–O6	93.10(7)	N3–Mn1–O6	169.71(8)
N5–Mn1–O6	87.31(8)	O2–Mn1–N1	94.40(8)

(*continued on next page*)

Table 1 (*continued*)

$[Tp^{iPr2}Mn_2(\mu\text{-}FOBz)_3(Pz^{iPr2}H)_2]\cdot CH_3CN$			
Bond angles (°)			
O4–Mn1–N1	174.02(8)	O3–Mn2–N7	91.82(9)
O1–Mn2–N7	88.63(9)	N7–Mn2–O5	113.94(8)
O3–Mn2–N9	96.62(8)	O5–Mn2–N9	81.00(7)
O1–Mn2–N9	171.62(8)	N7–Mn2–N9	88.06(9)
O5–Mn2–N9	81.00(7)		

(Fe1–N1, 2.2626(15) Å; Fe1–N2, 2.0745(15) Å; Fe1–N3, 2.0855(16) Å) in a mononuclear iron acetate complex with Tp^{Ph2} [30]. The Mn–N bond distance of the coordinated $Pz^{Ph,Me}H$ (Mn1–N7, 2.234 (18) Å) is similar to the Fe–N bond distance with 3,5-diphenylpyrazole (Fe1–N4, 2.2347 (17) Å), but shorter than the Mn–N bond distance with $Pz^{iPr2}H$ coordination (Mn1–N4, 2.304 (4) Å). The acetate behaves as a monodendate ligand in **7** where one oxygen atom is bonded with the manganese center and the other oxygen atom forms a hydrogen bond with the proton lying on the nitrogen of $Pz^{PhMe}H$ coordinated at the apical position to the manganese ion. The carboxylate oxygen from asparate in Mn–SOD is also bound to the manganese unidentately as is the acetate anion in complex **7**. The existence of a hydrogen bond in complex **7** is clearly established on the basis of the location of the hydrogen bond with mean bond distances of Ha–O2, 1.909 Å and Ha–N8, 0.859 Å. The presence of a hydrogen bond also affects the appearance of the ν(NH) band in the IR spectrum of the complex as the free $Pz^{PhMe}H$ gives the band at 3180 cm^{-1}. The short distance of the carbonyl oxygen (O_2) of the acetate anion from the nitrogen of neutral pyr-

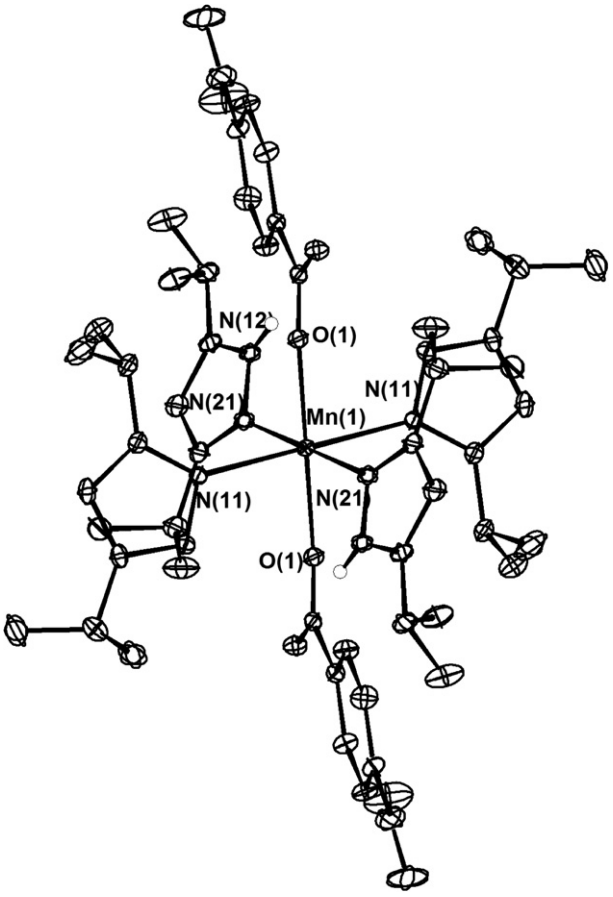

Fig. 2. Thermal ellipsoid view of complex **5** drawn at the 30% probability level. All hydrogen atoms have been omitted for clarity.

Table 2
Crystallographic data for $[(Pz^{iPr2}H)_4Mn(NO_2\text{–}OBz)_2]$ (**5**), $[(Pz^{iPr2}H)_4Mn(F\text{–}OBz)_2]$ (**6**), $[Tp^{Ph,Me}Mn(OAc)\ Pz^{Ph,Me}H]$ (**7**), $[Tp^{iPr2}Mn(Cl)Pz^{iPr2}H]$ (**8**) and $[Tp^{iPr2}Mn_2(\mu\text{-}FOBz)_3(Pz^{iPr2}H)_2]\cdot CH_3CN$ (**10** · CH_3CN)

	5	**6**	**7**	**8**	**10** · CH_3CN
Empirical formula	$C_{50}H_{72}N_{10}O_8Mn$	$C_{50}H_{72}N_8O_4F_2Mn$	$C_{42}H_{41}BMnN_8O_2$	$C_{36}H_{62}BClMnN_8$	$C_{68}H_{90}BF_3Mn_2N_{11}O_6$
Formula weight	996.12	942.10	755.58	708.14	1335.20
Crystal system	triclinic	monoclinic	triclinic	monoclinic	triclinic
Space group	$P\bar{1}$	$P2_1/n$	$P\bar{1}$	$P2_1/c$	$P\bar{1}$ (no. 2)
Lattice parameters					
a (Å)	10.715(6)	10.948(2)	11.7003(19)	13.312(2)	12.3069(16)
b (Å)	11.344(4)	12.663(3)	11.7630(19)	16.941(3)	13.4695(18)
c (Å)	12.747(8)	18.695(3)	15.425(3)	17.528(3)	24.205(3)
α (°)	100.33(3)	90.00(0)	86.927(3)	90.00(0)	81.3(0)
β (°)	107.16(2)	96.035(9)	87.581(3)	92.428(3)	80.22(0)
γ (°)	105.97(3)	90.00(0)	64.696(2)	90.00(0)	64.15(0)
V (Å^3)	1364(1)	2577.5(9)	1916.1(5)	3949.5(12)	3544.87(80)
Z	1	2	2	4	2
D_{calc} (g/cm^3)	1.212	1.214	1.310	1.191	1.251
Data collection					
μ(Mo Kα) (cm^{-1})	0.300	0.313	0.392	0.437	0.420
θ_{max} (°)	27.4	27.5	28.79	28.28	28.02
Number of measured reflections	5582	5613	17275	7344	26591
Number of observed reflections	4752	4352	6410	6922	10845
Number of parameters refined	329	311	491	442	841
R	0.0625	0.0588	0.0442	0.0514	0.0579
R_w	0.1756	0.1664	0.1313	0.1335	0.1591

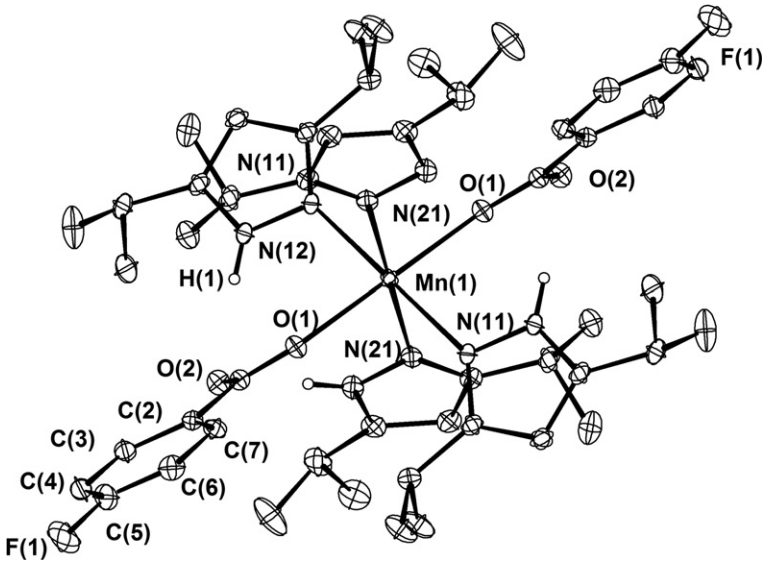

Fig. 3. Thermal ellipsoid view of complex **6** drawn at the 30% probability level. All hydrogen atoms have been omitted for clarity.

azole (N8) (O2–N8 bond, 2.76 Å), also suggest the presence of hydrogen bonding in **7**.

The Mn–O bond distance (Mn1–O1, 2.0240 (16) Å) is very similar to the Mn–O bond distance in a mononuclear hydrogen bonded manganese benzoate complex (Mn1–O1, 2.043(4) Å) [28b] but larger than the Fe–O1 bond distance in a mononuclear hydrogen bonded iron acetato complex (Fe–O1, 1.9634 (14) Å) [30]. The geometry of this complex is trigonal bipyramidal with one nitrogen (N2) from Tp^{PhMe} and N7 of the neutral pyrazole in apical positions.

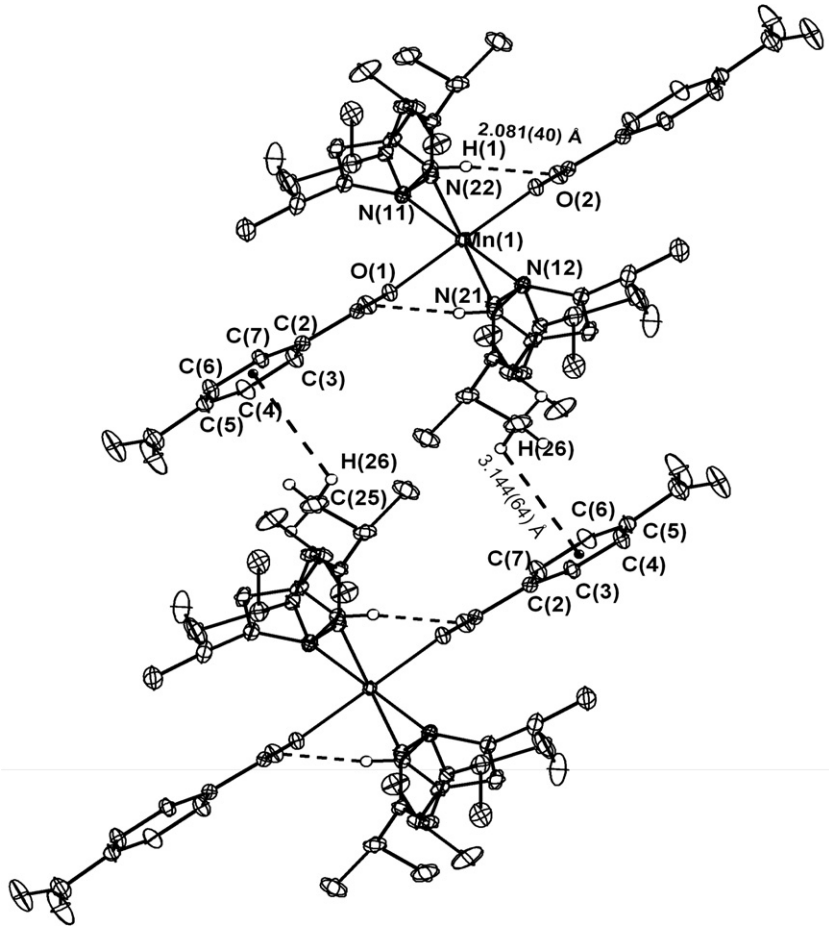

Fig. 4. Molecular structure showing intramolecular hydrogen bonding and CH_3–π interactions in complex **5**.

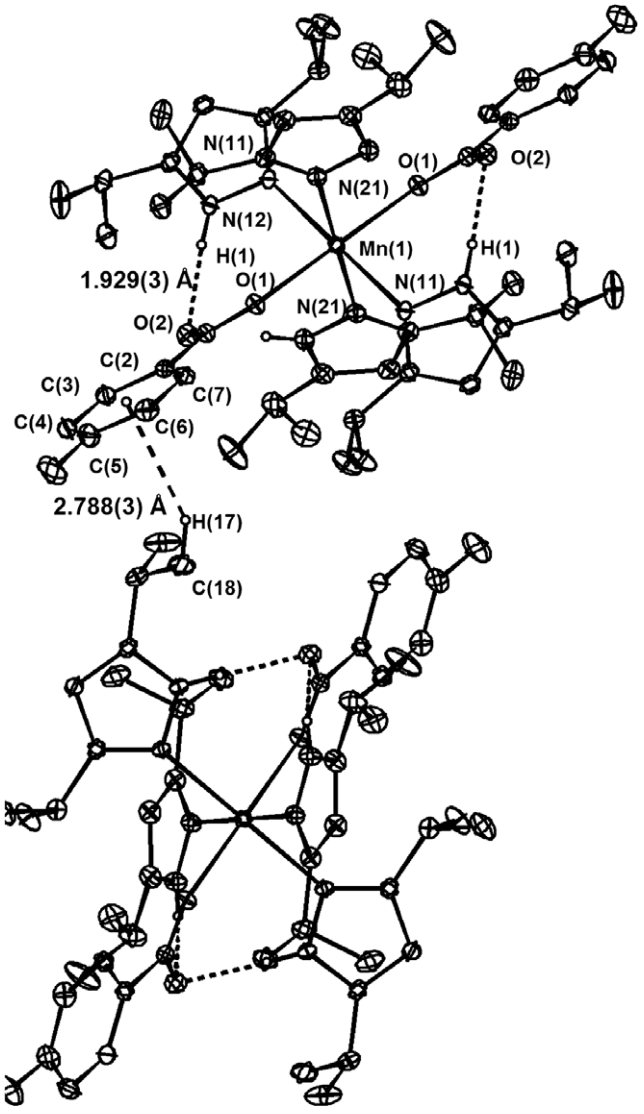

Fig. 5. Molecular structure showing intramolecular hydrogen bonding and CH_3–π interactions in complex **6**.

In another set of experiments, we have prepared $Tp^{iPr2}MnClPz^{iPr2}H$, $\{C_{36}H_{62}N_8BClMn\}$ (**8**) as a starting material for the preparation of other various manganese complexes. Complex **8** was prepared by the reaction of $MnCl_2 \cdot 4H_2O$ with KTp^{iPr2} in the presence of 1.5 equivalents of $Pz^{iPr2}H$, as shown in Scheme 3. Complex **8** is a mononuclear high spin manganese (II) species. As shown in the crystal structure (Fig. 7), it is five coordinate having a N_4Cl ligand donor set with a distorted geometry. The Mn1–Cl1 bond distance is 2.4193 Å, which is longer than the Mn–Cl bond distance in $Mn_2Cl_4(O{-}C_6H_4{-}p\text{-}CH_3)_2^{-2}$ (2.32 Å) [31] and [MnTPPCl](K222)] (2.364 Å) [31c], but similar to the Mn–Cl terminal bond distance in LMn_2Cl_2Br (2.411 Å) [31b]. The distances between manganese and nitrogens of the coordinated Tp^{iPr2} slightly differ from each other (Mn1–N1, 2.2425 (19) Å; Mn1–N3, 2.1507 Å; Mn1–N5, 2.164 (2) Å) and are considerably longer than the distances reported for $[Mn(HB(3,5\text{-}Mepz)_3)]^{+2}$ (1.96–1.98 Å) [32] and 2.05–2.23 Å in $[Mn_2O(O_2(CH_3)_2)(HB(pz)_3)_2] \cdot CH_3CN$ [33].

Using the literature method [20] we have prepared the complex $Tp^{iPr2}MnCl$, $\{C_{34}H_{51}N_6BFO_2Mn\}$ (**4**) by reacting $MnCl_2 \cdot 4H_2O$ and KTp^{iPr2} in a 1:1 ratio, to act as a starting material for the synthesis of complexes **9** $\{C_{34}H_{51}N_6BFO_2Mn\}$ and **10** $\{C_{66}H_{90}N_{10}BF_3O_6Mn_2\}$. Complex **9** was prepared by the reaction of **4** with one equivalent of sodium *p*-fluorobenzoate (Scheme 4). The spectroscopic characterization revealed that the benzoate group coordinates in a bidentate fashion. Although the crystal structure of **9** could not be determined, based on other spectroscopic data and the X-ray structure of a five coordinate cobalt fluorobenzoate complex with Tp^{iPr2} [34], we infer that **9** is also a monomeric five coordinate Mn(II) complex.

We have also succeeded in synthesizing an unsymmetrical fluorobenzoate bridged binuclear manganese (II) complex. The reaction of **4** with **1**, $MnCl_2 \cdot 4H_2O$ and sodium

$$Mn(OAc)_2.4H_2O + KTp^{Ph,Me} + Pz^{Ph,Me}H \longrightarrow Tp^{Ph,Me}Mn(OAc)Pz^{Ph,Me}H$$

7

Scheme 2.

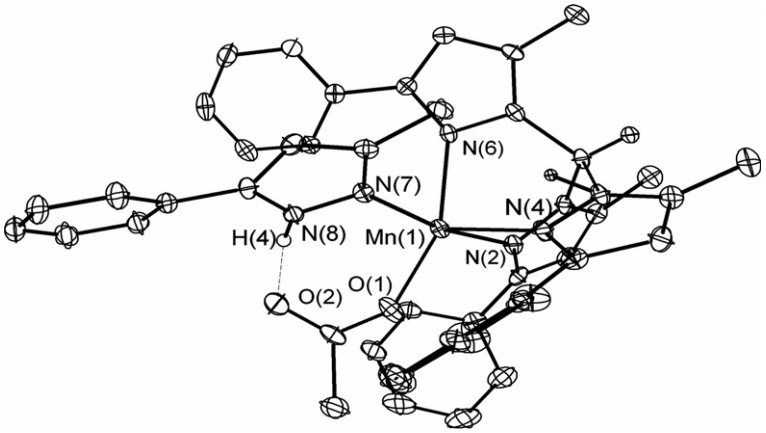

Fig. 6. Thermal ellipsoid view of complex **7**. All hydrogen atoms have been omitted for clarity.

$$MnCl_2.4H_2O + KTp^{iPr2} + Pz^{iPr2}H \longrightarrow Tp^{iPr2}Mn(Cl)Pz^{iPr2}H$$

8

Scheme 3.

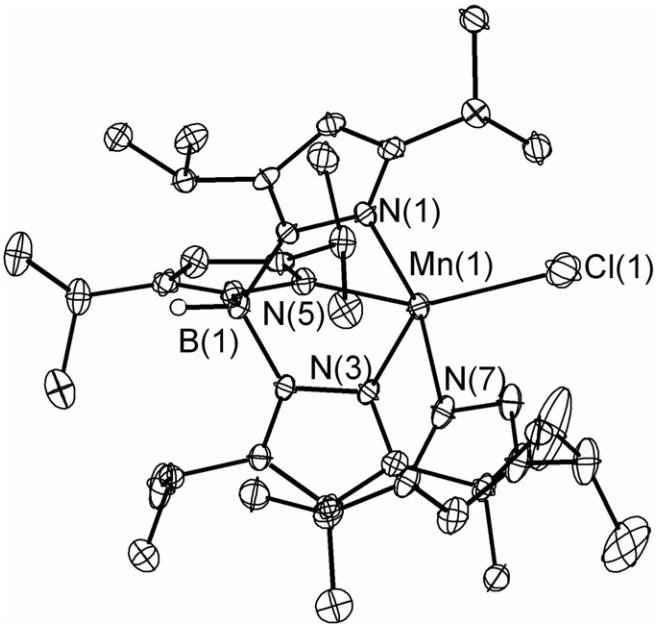

Fig. 7. Thermal ellipsoid view of complex **8** drawn at the 30% probability level. All hydrogen atoms have been omitted for clarity.

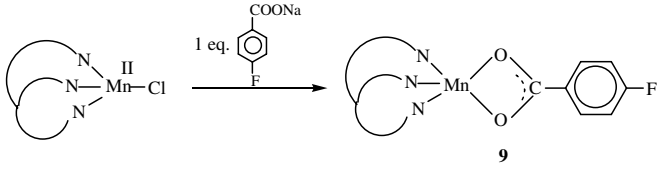

9

Scheme 4.

p-fluorobenzoate in mixed solvent (toluene:acetonitrile in a 1:1 ratio) gave complex **10** (Scheme 5). The presence of an IR band at 3297 cm^{-1} (due to the *v*N–H stretching band) in the IR spectrum of this complex suggested the existence of pyrazole in the protonated form. The molecular structure of **10** was determined by X-ray crystallography and its Thermal ellipsoid view is given in Fig. 8. As shown in Fig. 8, both manganese (II) ions are in the same environment. The two manganese (II) ions are bridged with three fluorobenzoate groups in an unsymmetrical manner with a Mn–Mn separation of 3.732(4) Å. Like the previously reported benzoate bridged binuclear manganese complex by Osawa et al. [35], in complex **10** both manganese ions are also in an octahedral environment and two of the μ-fluorobenzoate groups are symmetrically bridging, whereas the third one adopts a unique coordination mode i.e., only one oxygen from the carboxylate serves as a bridging ligand, while the other one binds to Mn2 terminally. A structurally similar (μ-carboxylato)$_3$ unit has been reported in a linear trinuclear manganese(II) carboxylato complex [36]. The Mn–Mn separation found in complex **10** is 3.732(4) Å, which is close to 3.739(2) Å [37] and 3.612(2) Å [38] in (μ-aqua)(bis(μ-carboxylato)dimanganese(II)) complexes but shorter than 4.034(2) Å in a symmetrical tris(μ-carboxylato)$_3$ complex [39]. The short metal–metal distance in **10** reflects the unusual nature of the tris(μ-fluorobenzoato)$_3$ unit with one oxygen atom from a fluorobenzoate group acting as a bridging ligand. The magnetic susceptibility of the powdered sample is 8.34 BM per mol. Efforts were also made for the successful removal of one bridging fluorobenzoate without disturbing the manganese bimetallic core, but the reaction of **10** with one equivalent of NaOH in toluene resulted in the formation of a mononuclear manganese (II) fluorobenzoate complex similar to **9**, in contrast to the pyrazole adduct as reported by Osawa et al. [35]. The resultant complex is five coordinated with a N_3O_2 ligand donor set and the fluorobenzoate group is coordinated to the manganese bidentately.

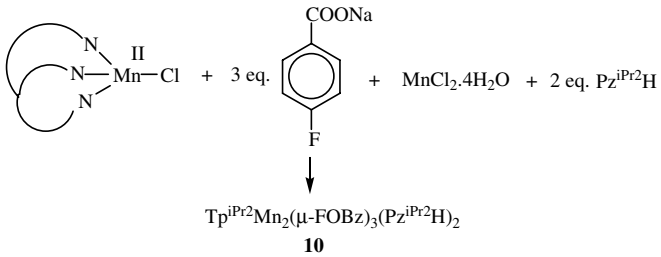

10

Scheme 5.

3.1. Superoxide dismutase activity studies

The complexes **5**–**8** and **10** were tested for their SOD activity using xanthine–xanthine oxidase–nitro blue tetrazolium (NBT) methods [40], as the coordination number around manganese in these complexes is close to the coordination number around the manganese in manganese-containing SOD enzyme [1] and also they have intramolecular hydrogen bonding, except in complexes **8** and **10**. The test was performed separately in duplicate for each compound in 3 ml of 50 mM potassium phosphate buffer (pH 7.4) at 25 °C in the absence of EDTA. The reaction mixture was prepared as follows:

Fifty micromoles of NBT, 50 μM xanthine, 1000 U/ml catalase and 0.04 U/ml xanthine oxidase were used to produce superoxide ions in solution. The formation of diformazan was monitored at 560 nm wavelength. The IC_{50} value in Fig. 9 means the concentration of the complex which exerts SOD activity equivalent to one unit of native SOD. Out of these tested complexes only complex **7** exhibited IC_{50} values

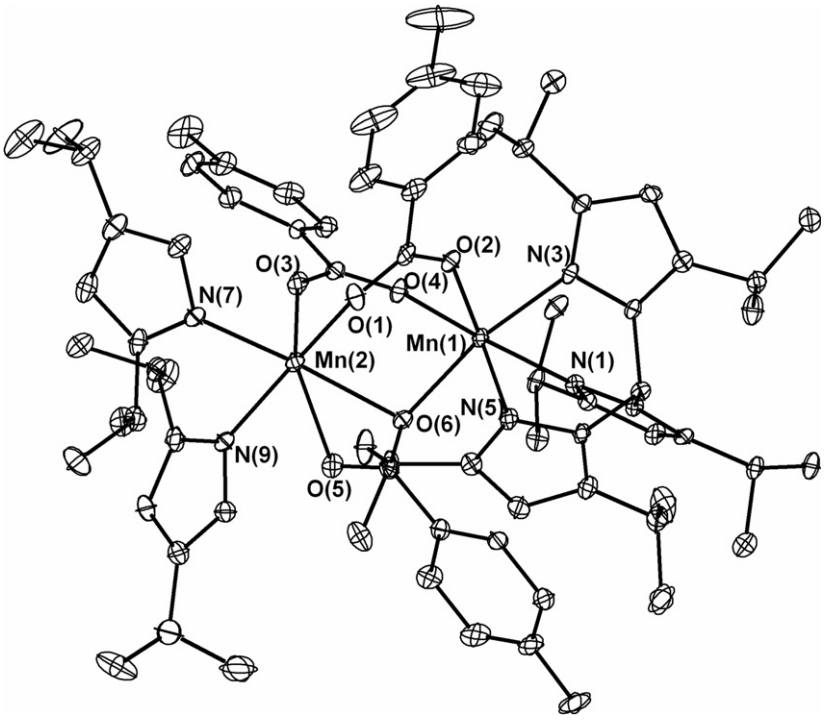

Fig. 8. Thermal ellipsoid view of complex **10** drawn at the 50% probability level. All hydrogen atoms have been omitted for clarity.

at 3.5 μM concentration (Fig. 9), clearly indicating that this may be a suitable model for a SOD mimic. The SOD activity value for **7** is much better than the previously reported SOD model complexes screened by the NBT method under the same conditions [41], but lower than the SOD model complex reported by Kitajima et al. [28b]. Also the ability of complex **7** to disproportionate O_2^- is comparatively better than the most active systems based on salen or porphyrin ligands reported by several workers [42]. The better SOD activities of complex **7** may be attributable to the very close structural similarities of this complex with the active site of native Mn–SOD.

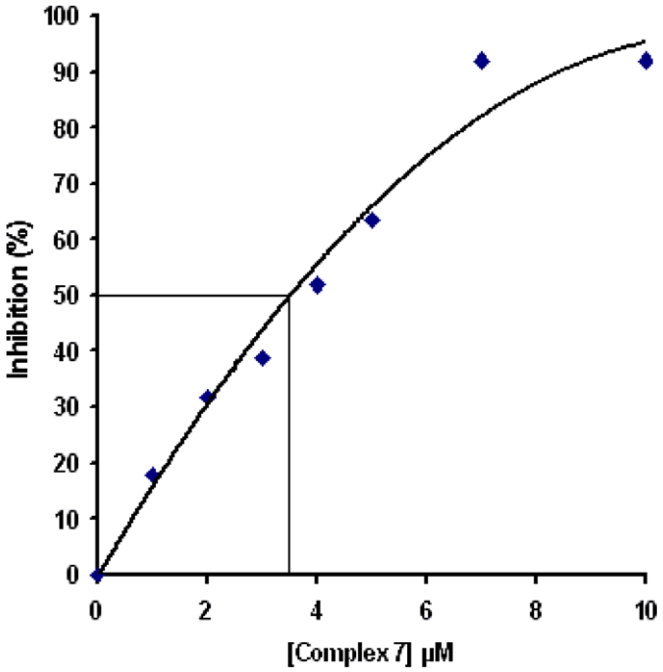

Fig. 9. SOD activity of complex **7** in xanthene oxidase-NBT assay.

4. Conclusion

We have reported several manganese carboxylate complexes, both with hydrogen as well as non-hydrogen binding, having five and six coordination numbers. The results presented in this paper demonstrated that different coordination modes of the carboxylate groups are possible simply by changing the supporting nitrogen donor ligands. It is possible to get the hydrogen bonded carboxylate complexes simply by adding the corresponding pyrazole to the reaction mixture as demonstrated in the formation of complex **7**, or by using pyrazole as a supporting ligand in the reaction as shown by the preparation of complexes **5** and **6**. The reaction of $Pz^{iPr2}H$ with $MnCl_2 \cdot 4H_2O$ and sodium *p*-nitrobenzoate/sodium *p*-fluorbenzoate resulted in the formation of octahedral complexes with intramolecular hydrogen bonding and CH_3–π interactions. The SOD activity studies on complexes **5**–**8** and **10** suggested that complex **7** seems to be a good model mimic of the native Mn–SOD enzyme as complex **7** has a suitable active site structure as well as intermolecular hydrogen bonding.

5. Supporting data

The crystallographic data have been deposited with the CCDC. Supplementary data are available from the CCDC, 12 Union Road, Cambridge CB2 1EZ, UK on requesting,

quoting the deposition numbers CCDC 293641–293644 and CCDC 293653, e-mail: deposit@ccdc.cam.ac.uk or www: http://www.ccdc.cam.ac.uk.

Acknowledgements

This work was supported by the Department of Science and Technology, Government of India. The authors are grateful to Prof. M. Akita (Tokyo Institute of Technology, Tokyo, Japan) and Prof. A. Ramanan (Indian Institute of Technology Delhi, India) for X-ray measurements.

References

[1] W.C. Stallings, K.A. Pattridge, R.K. Strong, M.L. Ludwig, J. Biol. Chem. 260 (1985) 16424.
[2] H. Wariishi, V. Khadar, M.H. Gold, Biochemistry 28 (1989) 6017.
[3] R. Cammack, A. Chapman, W.P. Lu, A. Karagouni, D.P. Kelly, FEBS Lett. 253 (1989) 239.
[4] (a) Y. Kono, I. Fridovich, J. Biol. Chem. 258 (1983) 6015;
(b) V.V. Barynin, A.A. Vagin, V.R. Melik-Adamyn, I. Grebenko, S.V. Khangulov, A.N. Popov, M.E. Andrianova, B.K. Vainshtein, Dokl. Akad. Nauk. SSSR (Crystallogr.) 288 (1986) 877.
[5] (a) P. Nordlund, B.M. Sjoberg, H. Eklund, Nature 345 (1990) 593;
(b) M. Atta, P. Nordlund, A. Aberg, H. Eklund, M. Fontecave, J. Biol. Chem. 267 (1992) 20684.
[6] (a) Y. Sugiura, H. Kawabe, H. Tanaka, S. Fujimoto, A. Ohara, J. Biol. Chem. 256 (1981) 10664;
(b) Y. Sugiura, H. Kawabe, H. Tanaka, S. Fujimoto, A. Ohara, J. Am. Chem. Soc. 103 (1981) 963.
[7] (a) G.C. Dismukes, Photochem. Photobiol. 43 (1986) 99;
(b) V. L Pecoraro, Photochem. Photobiol. 48 (1988) 249.
[8] C. Su, E.H. Oliw, J. Biol. Chem. 273 (1998) 13072.
[9] (a) E.J. Woo, J.M. Dunwell, P.W. Goodenough, A.C. Marvier, R.W. Pickersgill, Nat. Struct. Biol. 7 (2000) 1036;
(b) L. Requena, S. Bornemann, Biochem. J. 343 (1999) 185.
[10] (a) T. Takabatake, M. Hasegawa, T. Nagano, M. Hirobe, Chem. Pharm. Bull. 39 (1991) 1352;
(b) T. Takabatake, M. Hasegawa, T. Nagano, M. Hirobe, J. Biol. Chem. 267 (1992) 4613.
[11] S. Han, L.D. Eltis, K.N. Timmis, S.W. Muchmore, J.T. Bolin, Science 270 (1995) 976.
[12] C. Su, M. Sahlin, E.H. Oliw, J. Biol. Chem. 275 (2000) 18830.
[13] W. Minor, J. Steczko, B. Stec, Z. Otwinowski, J.T. Bolin, R. Walter, B. Axelrod, Biochemistry 35 (1996) 10687.
[14] (a) S.J. Lippard, J.M. Berg, Principles of Bioinorganic Chemistry, University Science Books, Hill Valley, CA 94941, 1994;
(b) R.H. Holm, P. Kennepohl, E.I. Solomon, Chem. Rev. 96 (1996) 2239.
[15] (a) R.A. Edwards, H.M. Baker, M.M. Whittaker, J.W. Whittaker, G.B. Jameson, E.N. Baker, J. Biol. Inog. Chem. 3 (1998) 161;
(b) V.V. Barynin, M.M. Whittaker, S.V. Antonyuk, V.S. Lamzin, P.M. Harrison, P.J. Artymiuk, W. Whittaker, Structure 9 (2001) 725;
(c) K. Hakansson, M. Carlsson, L.A. Svensson, A. Liljas, J. Mol. Biol. 227 (1992) 1192;
(d) E. Skrzypczak-Jankun, R.A. Bross, R.T. Carroll, W.R. Dunhan, M.O. Funk Jr., J. Am. Chem. Soc. 123 (2001) 10814.
[16] (a) Some recent references on manganese carboxylate complexes with hydrogen bonding – S.R. Fan, L.G. Zhu, H.P. Xiao, S.W. Ng, Acta Crystallogr. Sec E 61 (2005) 377;
(b) L.M. Wittick, K.S. Murray, B. Moubaraki, S.R. Batten, L. Spiccia, K.J. Berry, J. Chem. Soc., Dalton Trans. (2004) 1003;
(c) S. Konar, S.C. Manna, E. Zangrando, T. Mallah, J. Ribas, N.R. Chaudhuri, Eur. J. Inorg. Chem. (2004) 4202;
(d) J.C. Goodwin, D.J. Price, S.L. Heath, J. Chem. Soc., Dalton Trans. (2004) 2833;
(e) J.-M. Shi, W. Xu, C.-J. Wu, W.-T. Yu, Trans. Met. Chem. 28 (2003) 308;
(f) S.T. Warzeska, F. Micciche, M.C. Mimmi, E. Bouwman, H. Kooijman, A.L. Spek, J. Reedijk, J. Chem. Soc., Dalton Trans. (2001) 3507;
(g) B. Paluchowska, J.K. Maurin, J. Leciejewicz, J. Coord. Chem. 51 (2000) 335;
(h) M.R. Bermejo, M. Fondo, A. Garcia-Deibe, A.M. Gonzälez, A. Sousa, J. Sanmartin, C.A. McAuliffe, R.G. Pritchard, M. Watkinson, V. Lukov, Inorg. Chim. Acta 293 (1999) 210.
[17] D.D. Perrin, W.L. Armarego, D.R. Perrin, Purification of laboratory chemicals, second ed., Pergamon, New York, 1980.
[18] N. Kitajima, K. Fujisawa, C. Fujimoto, Y. Moro-oka, S. Hashimoto, T. Kitagawa, K. Toriumi, K. Tatsumi, A. Nakamura, J. Am. Chem. Soc. 114 (1992) 1277.
[19] S. Imai, K. Fujisawa, T. Kobayashi, N. Shirasawa, H. Fujii, T. Yoshimura, N. Kitajima, Y. Moro-oka, Inorg. Chem. 37 (1998) 3066.
[20] N. Kitajima, U.P. Singh, H. Amagai, M. Osawa, Y. Moro-oka, J. Am. Chem. Soc. 113 (1991) 7757.
[21] T. Higashi, Program for absorption correction, Rigaku Corp., Tokyo, Japan, 1995.
[22] TeXsan, Crystal structure analysis package, Ver. I:II; Rigaku Corp., Tokyo, Japan, 2000.
[23] International tables for X-ray crystallography, Kynoch Press, Birmingham, 1975, p. 4.
[24] (a) G.M. Sheldrick, SHELXS-86: program for crystal structure determination, University of Göttingen, Göttingen, Germany, 1986;
(b) G.M. Sheldrick, SHELXS-97: program for crystal structure determination, University of Göttingen, Göttingen, Germany, 1997.
[25] P.T. Beurskens, G. Admiral, G. Beurskens, W.P. Bosman, S. Garcia-Grands, R.O. Gould, J.M.M. Smits, C. Smykalla, The DIRDIF program system, Technical report of the crystallography laboratory, University of Nimegen, Nimegen, Netherland, 1992.
[26] G.M. Sheldrick, Acta Crystallogr. Sec. A 46 (1990) 467.
[27] G.M. Sheldrick, SHELXTL – NT 2000 version 6.12 reference manual, University of Göttingen, Göttingen, Germany.
[28] (a) U.P. Singh, R. Singh, S. Hikichi, M. Akita, Y. Moro-oka, Inorg. Chim. Acta 162 (2000) 273;
(b) N. Kitajima, M. Osawa, N. Tamura, Y. Moro-oka, T. Hirano, M. Hirobe, T. Nagano, Inorg. Chem. 32 (1993) 1879.
[29] M.A.S. Goher, A.A. Youssef, Z.Y. Zhou, T.C.W. Mak, Polyhedron 12 (1993) 1871.
[30] M.P. Mehn, K. Fujisawa, E.L. Hegg, L. Que Jr., J. Am. Chem. Soc. 125 (2003) 7828.
[31] (a) D. Cocouvanis, K. Greiwe, A. Salifoglou, P. Challen, A. Simopoulos, A. Kostikas, Inorg. Chem. 27 (1988) 593;
(b) H. Diril, H.-R. Chang, X. Zhang, S.K. Larsen, J.A. Potenza, C.G. Pierpont, H.J. Schugar, S.S. Isied, D.N. Hendrickson, J. Am. Chem. Soc. 109 (1987) 6207;
(c) R.B. Vanatta, C.E. Strouse, L.K. Hanson, J.S. Valentine, J. Am. Chem. Soc. 109 (1987) 1425.
[32] M.K. Chan, W.H. Armstrong, Inorg. Chem. 28 (1989) 3777.
[33] J.E. Sheats, R.S. Czernuszewicz, G.C. Dismukes, A.L. Rheingold, V. Petrouleas, J. Stubbe, W.H. Armstrong, R.H. Beer, S.J. Lippard, J. Am. Chem. Soc. 109 (1987) 1435.
[34] U.P. Singh, V. Aggarwal, A.K. Sharma, Inorg. Chim. Acta, 2006, submitted for publication.
[35] M. Osawa, U.P. Singh, M. Tanaka, Y. Moro-oka, N. Kitajima, J. Chem. Soc., Chem. Commun. (1993) 310.
[36] R.L. Rardin, P. Poganiuch, A. Bino, D.P. Goldberg, W.B. Tolman, S. Liu, S.J. Lippard, J. Am. Chem. Soc. 114 (1992) 5240.
[37] A. Caneschi, F. Ferraro, D. Gatteschi, M.C. Melandri, P. Rey, R. Sessoli, Angew. Chem., Int. Ed. Eng. 28 (1989) 1365.

[38] S.-B. Yu, S.J. Lippard, I. Shweky, A. Bino, Inorg. Chem. 31 (1992) 3502.
[39] K. Wieghardt, U. Bossek, B. Nuber, J. Weiss, J. Bonovoisn, M. Corbella, S.E. Vitols, J.J. Girerd, J. Am. Chem. Soc. 110 (1988) 7398.
[40] (a) J.M. McCord, I. Fridovich, J. Biol. Chem. 244 (1969) 6049;
(b) C. Beauchamp, I. Fridovich, Anal. Biochem. 44 (1971) 276.
[41] K. Yamaguchi, L. Spencer, D.T. Sawyer, FEBS Lett. 197 (1986) 249.
[42] (a) A. Deroche, I. Morgenstern-Badarau, M. Cesario, J. Guilhem, B. Keita, L. Nadjo, C. Houee-Levin, J. Am. Chem. Soc. 118 (1996) 4567;
(b) E.A. Lewis, H.H. Khodr, R.C. Hider, J.R.L. Smith, P.H. Walton, J. Chem. Soc., Dalton Trans. (2004) 187;
(c) R. Kachadourian, I.B. Haberle, I. Fridovich, Inorg. Chem. 38 (1999) 391;
(d) D.P. Riley, S.L. Henke, P.J. Lennon, R.H. Weiss, W.L. Neumann, W.J. Rivers, K.W. Aston, K.R. Sample, H. Rahman, C.S. Ling, J.J. Shieh, D.H. Busch, W. Szulbinski, Inorg. Chem. 35 (1996) 5213;
(e) D.P. Riley, Chem. Rev. 99 (1999) 2573;
(f) D. Salvemini, D.P. Riley, S. Cuzzocrea, Nat. Rev. Drug Discovery 1 (2002) 367;
(g) R. Krämer, Angew. Chem., Int. Ed. 39 (2000) 4469;
(h) M.J. Burkitt, B.C. Gilbert, Free Radical Res. Commun. 10 (1990) 265;
(i) D. Salvemini, Z.-Q. Wang, J. Zweier, A. Samouilov, H. Macarthur, T. Misko, M. Currie, S. Cuzzocrea, J. Sikorski, D.P. Riley, Science 286 (1999) 304;
(j) K. Aston, N. Rath, A. Naik, U. Slomczynska, O.F. Schall, D.P. Riley, Inorg. Chem. 40 (2001) 1779;
(k) S. Melov, J. Ravenscroft, S. Malik, M.S. Gill, D.W. Walker, P.E. Clayton, D.C. Wallace, B. Malfroy, S.R. Doctrow, G.J. Lithgow, Science 289 (2000) 1567;
(l) W. Musleh, A. Bruce, B. Malfroy, M. Baudry, Neuropharmacology 33 (1994) 929.

of two or more phthalonitrile derivatives with different substituents, isolation of each isomer is hardly possible, and the yield of the desired product could be very low [1,13,14]. Some unsymmetrical structures have been acquired by making use of boron subphtalocyanines [15].

Many binuclear phthalocyanines have been synthesized and various properties have been reported in last decade [16]. In our previous study, starting from a tetracyano compound with 12-membered dioxa-dithia macrocycles, in which oxygen and sulfur atoms are diagonally positioned, it has been possible to prepare either polymeric or dimeric phthalocyanines over iminoisoindoline compounds with subphthalocyanine [17] using the statistically mixed method [18]. In applications phthalocyanines are usually prepared by depositing the phthalocyanine molecules as thin films onto an appropriate substrate, using different methods (LB technique, high vacuum evaporation, spin coating, etc.). While the phthalocyanine thin films are used for the fabrication of practical devices, their electrical (d.c. and a.c.) properties must be taken into account. For example, to produce any device whose active layer is made of phthalocyanine films, we need to know the effect of the temperature on both a.c. and d.c. electrical properties of the film, so as to carry out an accurate design. The aim of this study is to synthesize binuclear octaphthalocyanine and dimeric phthalocyanine with six ferrocenyl groups. For this purpose, nitro-substituted dimeric phthalocyanine **3** was reacted with unsymmetric **4**, NaOH solution and activated zinc powder in THF to obtain **5**. In the second step, using hydrazine hydrate as a reductant, amine-substituted dimeric phthalocyanine **6** was synthesized from nitro-substituted dimeric phthalocyanine **3**. Finally, using ferrocenylaldehyde, **7** was prepared. The electrical properties of **3**, **5** and **6** were examined.

2. Experimental

2.1. Synthesis

All chemicals used were of reagent grade. All solvents were dried and purified as described by Perrin and Armarego [19]. The solvents were stored over molecular sieves. Soluble derivatives with eight alkylthio substituents have been synthesized through cyclotetramerization of 4,5-bis(hexylthio)phththalonitrile which has been prepared directly from the 4,5-dichloro compound with hexanethiol [20]. 4-Nitrophthalonitrile **2** was synthesized by the method described previously in the literature [21]. The progress of the reactions was monitored by thin layer chromatography (TLC). Column chromatography was used for purification of the complexes.

Elemental analyses were performed on a LECO CHNS 932 instrument. ^{1}H NMR spectra were determined with a Varian UNITY INOVA 500 MHz NMR spectrometer. IR spectra were recorded as KBr disks in the range of 400–4000 cm^{-1} on a SHIMADZU FTIR-8300 spectrometer. The electronic absorption spectra were measured in $CHCl_3$ for compounds **4**, **5** and DMSO for **3**, **6** with a UNICAM UV2-100 UV/VISIBLE spectrometer. Zinc, cobalt and iron contents in the digested mixture were determined on a Thermo X-Series/X7 ICP-MS. Before the ICP-MS measurements, compound **5** and **7** were digested with HNO_3.

2.2. [5′-6′-Bis(17′,25′,32′-trinitro-phthalocyaninyl)-(1,4,7,10-tetrathia-12-crown)dicobalt(II)] (3)

A mixture of **1** (0.062 g, 0.142 mmol), 4-nitrophthalonitrile **2** (0.150 g, 0.853 mmol) and $CoCl_2 \cdot 6H_2O$ (0.067 g, 0.284 mmol) was refluxed in amyl alcohol under argon for 6 h. The reaction mixture was cooled down to room temperature and precipitated by adding methanol. After filtration, the product was washed with methanol, chloroform and acetone. This compound was soluble in tetrahydrofuran (THF), dimethylformamide (DMF) and dimethylsulfoxide (DMSO). Yield: 75 mg (33%). UV–Vis (DMSO, λ_{max}/nm ($\log\varepsilon$)): 337 (5.090), 430(sh) (4.080), 642(sh) (4.610) and 682 (4.77). IR (KBr pellet) ν/cm^{-1}: 3060, 2983, 2923, 2858, 1620, 1523, 1344, 1260, 1090, 902, 742. *Anal*. Calc. for $C_{68}H_{30}N_{22}S_4O_{12}Co_2$: C, 51.56; H, 1.84; N, 19.55; S, 8.04. Found: C, 51.72; H, 1.70; N, 19.49; S, 7.95%.

2.3. [3-Nitro-9,10,16,17,23,24-hexakis(hexylthio)-phthalocyaninato Zn(II)] (4)

A well-powdered mixture of **2** (0.173 g, 1 mmol) and 4,5-bis(hexylthio) phthalonitrile (1.442 g, 4 mmol) were dissolved in dry DMF (3 mL) in a tube. Zinc(II) acetate (0.878 g, 4 mmol) was added to this solution and the mixture was sealed and heated at 170–180 °C for 6 h. to give an unsymmetrical substituted Pc. The reaction mixture was cooled down to room temperature and precipitated by adding methanol. After filtration, the dark green product was washed with methanol and purified by column chromatography (silica gel) with $CHCl_3$. Yield: 514 mg (39%). UV–Vis ($CHCl_3$, λ_{max}/nm ($\log\varepsilon$)): 337 (4.780), 363 (4.860), 440 (4.263), 638 (4.613) and 710 (5.269). IR (KBr pellet) ν/cm^{-1}: 3058, 2983, 2923, 2858, 1618, 1265, 902, 742; ^{1}H NMR (500 MHz, $CDCl_3$) δ: 0.88 (s, 18H, –CH_3), 1.92–2.16 (m, 36H, –CCH_2), 2.22 (br, 12H, SCH_2), 2.62 (br s, 12H, –$SCCH_2$), 6.70–8.20 (m, 9H, Ar-H). *Anal*. Calc. for $C_{68}H_{87}N_9S_6O_2Zn$: C, 61.86; H, 6.64; N, 9.55. Found: C, 61.58; H, 6.77; N, 9.39%.

2.4. {17,25,32,17′,25′,32′-Hexakisazo-69,69′-hexakis[74′,75′,81′,82′,88′,89′(hexylthio)-phthalocyaninyl-hexazinc(II)]-[bis-phthalocyaninatodicobalt(II)]} (5)

Compound **3** (0.064 g, 0.040 mmol) and compound **4** (0.320 g, 0.243 mmol) were dissolved in THF. A solution of NaOH (1 mL, 0.268 M) and activated zinc powder were added to the reaction mixture and refluxed for 24 h, after which time the solvent was evaporated under

reduced pressure (Scheme 1). After filtration, the dark green product was washed with methanol and purified by column chromatography (silica gel) with $CHCl_3$. Compound **5** is soluble in chloroform, dichloromethane, dimethylformamide and dimethylsulfoxide. Yield: 10 mg (28%). UV–Vis (DMSO, λ_{max}/nm ($\log\varepsilon$)): 290 (5.039), 364 (4.473) and 700 (4.968). IR (KBr pellet) ν/cm^{-1}: 3058, 2983, 2923, 2858, 1610, 1575, 1440, 1265, 1090, 902, 742 *Anal*. Calc. for $C_{476}H_{552}N_{76}S_{40}Co_2Zn_6$: C, 61.79; H, 6.93; N, 7.69; S, 17.58. Found: C, 62.05; H, 7.13; N, 7.18; S, 17.19%. ICP-MS (Zn, Co): *Anal*. Calc. for $C_{476}H_{552}N_{76}S_{40}Co_2Zn_6$: Zn, 4.21; Co, 1.31. Found: Zn, 4.25; Co, 1.36%.

2.5. [5,6,5′,6′-Bis(17′,25′,32′-trisamino-phthalocyaninyl)-(1,4,7,10-tetrathia-12-crown) dicobalt(II)] (6)

A mixture of **3** (0.030 g, 0.019 mmol), hydrazine hydrate (8 mL) and a catalytic amount of 10% Pd/C was refluxed in dry dioxan (30 mL) under an argon atmosphere for 24 h (Scheme 2). The reaction mixture was cooled and quickly suction filtered. The filtrate was evaporated to dryness

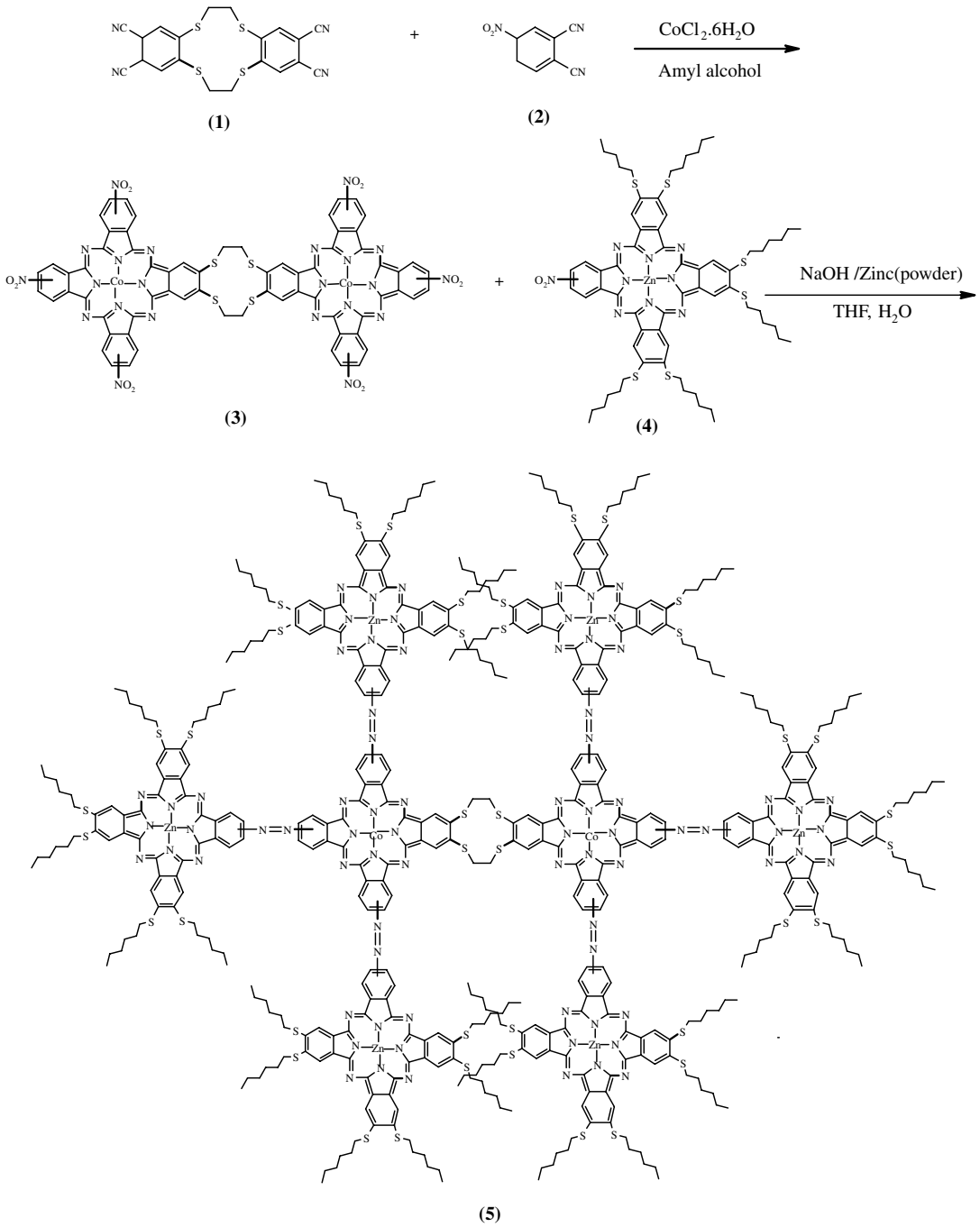

Scheme 1. Synthesis of Co(II) and Zn(II) binuclear octaphthalocyanine **5**.

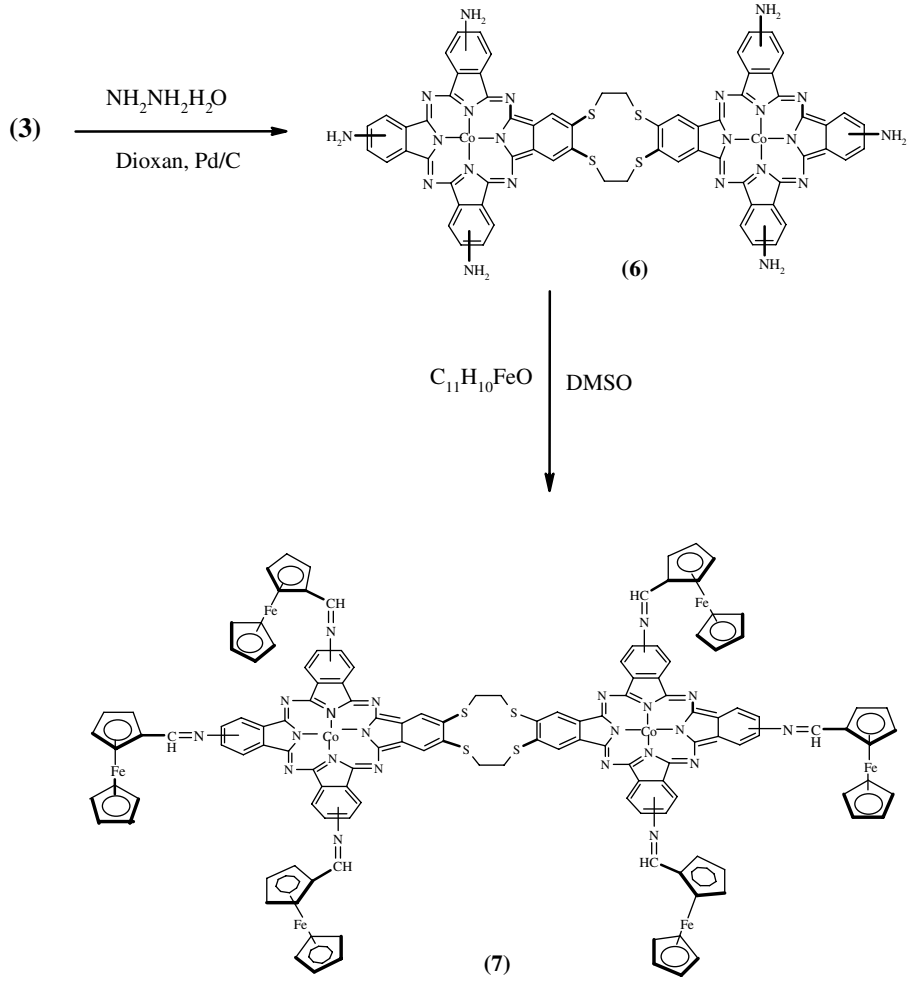

Scheme 2. Synthesis of dimeric phthalocyanine with six ferrocenyl groups **7**.

under vacuum and washed with methanol, THF and acetone. The dark green product was dried in vacuum. This compound is soluble in DMF and DMSO. Yield: 21.2 mg (79%). UV–Vis (DMSO, λ_{max}/nm ($\log\varepsilon$)): 358 (4.952), 643 (4.710) and 716 (4.897). IR (KBr pellet) ν/cm^{-1}: 3447, 3417, 3060, 2983, 2923, 2858, 1620, 1560, 1540, 1420, 1344, 1260, 1090, 902, 742. *Anal*. Calc. for $C_{68}H_{42}N_{22}S_4Co_2$: C, 57.79; H, 2.97; N, 21.81; S, 8.36. Found: C, 58.01; H, 2.79; N, 21.60; S, 9.18%.

2.6. [5,6,5′,6′-Bis(17′,25′-32′-tris-ferrocenylimin-phthalocyaninyl)(1,4,7,10-tetrathia-12-crown)dicobalt(II)] (7)

Compound **6** (0.015 g, 0.011 mmol) was dissolved in dry DMSO (0.022 g, 0.106 mmol) of ferrocenylaldehyde and a catalytic amount of *p*-toluene sulfonic acid were added to this solution and refluxed for 12 h (Scheme 2). The reaction mixture was cooled down to room temperature and methanol (20 mL) was added. After filtration, the dark green product was washed with methanol, DMF and acetone. This compound was insoluble in any solvent. Yield: 21.35 mg (75%). IR (KBr pellet) ν/cm^{-1}: 3050, 2923, 2858, 1602, 1569, 1460, 1420, 1390, 1340, 1265, 1090, 902, 820, 742. *Anal*. Calc. for $C_{134}H_{90}N_{22}S_4Fe_6Co_2$: C, 62.13; H, 3.48; N, 11.90; S, 4.95. Found: C, 62.28; H, 3.55; N, 11.62; S, 4.70%. ICP-MS (Fe, Co): *Anal*. Calc. for $C_{134}H_{90}N_{22}S_4Fe_6Co_2$: Fe, 12.98; Co, 4.56. Found: Fe, 12.90; Co, 4.65%.

2.7. Electrical characterization

For the electrical characterization, an interdigital comb structure with 100 μm gap on glass substrate was used. Thin films of compounds were obtained by the spin-coating method. A close-cycle liquid helium cryostat was used to allow electrical characteristics to be measured over a wide temperature range. DC conductivity measurements were performed between 295 and 400 K by using a Keithley 617 electrometer. AC conductivity measurements were carried out with a Keithley 3330 LCZ meter in the frequency range 40 Hz–100 kHz. in the temperature range from 295 to 400 K. During the measurement the temperature of the sample was controlled with a Leybold LTC 60 temperature controller. All the measurements were performed under 10^{-3} mbar in the dark. Both the d.c. and a.c. conductivity data were recorded using an IEEE-488 data acquisition system incorporated to a personal computer.

3. Results and discussion

3.1. Synthesis and characterization

Initial compounds **1**, **2** and 4,5-bis(hexylthio)phthalonitrile were available from an earlier study. Before the synthesis of **5**, the nitro-substituted dimeric Co(II) phthalocyanine **3** was prepared by reaction of **1**, **2** and cobalt(II) chloride in amyl alcohol.

In the second step, **2** was reacted with 4,5-bis(hexylthio)-1,2-dicyanobenzene and zinc(II) acetate in DMF to obtain unsymmetric Zn(II) phthalocyanine **4** [22]. This compound was purified by column chromatography (silica gel) with $CHCl_3$. The new compound **5** was prepared by the reaction of **3** and **4** with NaOH solution and activated zinc powder in THF. This compound was purified by column chromatography (silica gel) with $CHCl_3$. Peripheral nitro substituents on the Pc offer a number of possibilities to obtain reactive binding sites, such as reduction to an amine. For this purpose, hydrazine hydrate was used as the reductant. In order to demonstrate the reactivity of the amino groups in the hexaamino substituted dimeric Pc **6**, its condensation with ferrocenylaldehyde was carried out to furnish a new Pc with six ferrocenyl groups, **7**. Since this compound was insoluble, its structure was determined by elemental analysis, ICP-MS and IR spectroscopy.

The IR spectra of **3**, **4** and **5** were taken as KBr pellets. The stretching peaks at 2983 and 2858 cm^{-1} confirmed the presence of –CH and $–CH_3$ groups, respectively, for compounds **3**, **4** and **5**. The stretching peaks at around 1523–1344 cm^{-1} in the spectrum of **3** indicated the presence of a $–NO_2$ group that disappeared in the case of the amine-substituted Pc **6**. The presence of $–NH_2–$ in the structure of **6** was observed at 3447–3417 cm^{-1}. The C–S–C ether chain was characterized by an absorption at 1090 cm^{-1} for all the dimeric compounds. The stretching peaks at 1620–1575 cm^{-1} confirmed the presence of N=N groups for **5**. Comparison of the IR spectral data of compound **6** and **7** clearly indicates the conversion of the NH_2 groups to ferrocenylaldehyde groups by the disappearance of the NH_2 band at 3447–3417 cm^{-1} and the appearance of a new bands at 1569 and 1602 cm^{-1} in **7**.

The ^1H NMR data were taken in *d*-chloroform. In the ^1H NMR analysis of **4** aromatic protons appeared as multiplets at 6.70–8.20 ppm. The protons of $–CH_3$ groups at the end of the aliphatic chain appeared at 0.88 ppm for **4**. In the spectra of **4**, the $–CCH_2C–$ protons in the long aliphatic chain are at 1.92–2.16 ppm and the $–SCH_2$ group protons neighbouring an aromatic ring appear at 2.22–2.62 ppm. The UV–Vis absorption spectra of the phthalocyanine system exhibited characteristic Q and B bands. All of them showed typical electronic spectra with two strong absorption regions, one in the UV region at about 330 nm (B band), which is attributed to transitions from the deeper π levels to the LUMO. The other band was observed in the visible region at 670–720 nm (Q band) with a weaker satellite band around 600–650 nm [23] which indicated the aggregation. The characteristic Q band for all the compounds was ascribed to the $\pi–\pi^*$ transition from the highest occupied molecular orbital (HUMO) to the lowest unoccupied molecular orbital (LUMO). The band broadening that accompanied the exciton (or Davydon coupling) effects changes the visible region [24]. In the spectra of **3** and **6**, the Q bands shift from 682 to 716 nm. This is because of the electron-donating ability of the amino group [25]. A significant absorption for **3** was observed at 430 nm, corresponding to the electron-donor capacity of the nitro group, while the absorption disappeared at this position for **5** (Fig. 1).

Since compound **7** was insoluble, the UV–Vis spectra of this compound could not be taken. The ICP-MS measurements were done to determinate of the quantities of metals (Zn, Co and Fe) in the phthalocyanine structures for **5** and **7**. The results are given in Section 2. ICP-MS measurements provided additional support for the molecular structure of **5** and **7**.

3.2. DC conductivity measurement

The temperature dependence of the dark d.c. conductivity was obtained by the rapid cooling method which allows the avoidance of the influence of a sorption-desorption process. The measurements of direct current (d.c.) conductivity for **3**, **5** and **6** were carried out in the temperature range 290–400 K in a vacuum ($\leqslant 10^{-3}$ mbar). The variations of d.c. conductivity with temperature for the three compounds are plotted in Fig. 2. The plots indicated that **3**, **5** and **6** are semiconducting in nature. A good linear relationship in conductivity variations is observed (a region ascribed to a different activation energy corresponding to a different dominant excitation in the Arrehenius plots

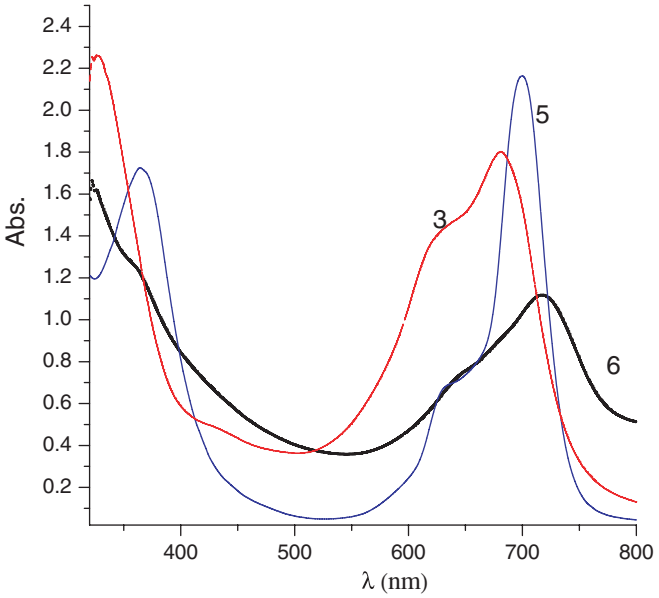

Fig. 1. UV–Vis spectra of **3** (3.06×10^{-5} M in DMSO), **5** (2.33×10^{-5} M in $CHCl_3$) and **6** (4.70×10^{-6} M in DMSO).

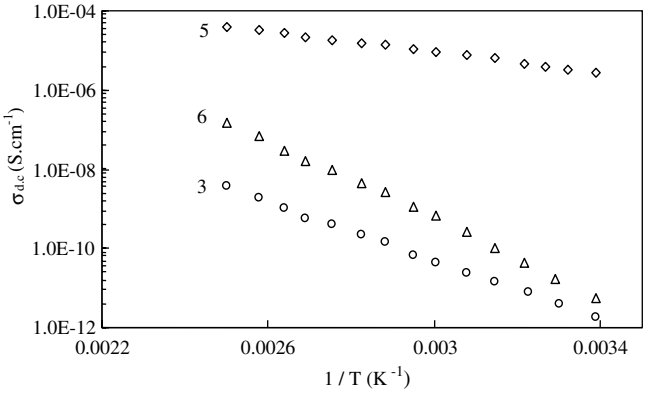

Fig. 2. Dependence of d.c. conductivity on the inverse of temperature for spin coated films of compounds **3**, **5** and **6**.

was not observed). In this case, the variation of the measured conductivity for the **3**, **6** and **5** films exhibit an exponential dependence on temperature and can be expressed as follows:

$$\sigma_{\mathrm{d.c.}} = \sigma_0 \exp(-E_A/kT) \quad (1)$$

where E_A is the activation energy, T is temperature, k is Boltzmann's constant and σ_0 is a constant of proportionality. The value of the activation energy was derived from the slope of the $\log \sigma_{\mathrm{d.c.}}$ versus $1/T$ graph and is 0.74 eV for compound **3**, 0.95 eV for compound **6** and 0.26 eV for compound **5**. Fig. 2 also shows that conductivity values at room temperature as well as at higher temperatures are different. The observed electrical conductivity values for **3**, **5** and **6** are 1.8×10^{-12} S/cm, 2.8×10^{-6} S/cm and 5.6×10^{-12} S/cm, respectively. The reduction of the electron withdrawing $-NO_2$ groups to electron donor $-NH_2$ groups was found to increase 3 times the electrical conductivity of the nitro substituted dimeric Co(II) phthalocyanine **3**. Whereas the azo coupling was found to increase the electrical conductivity by 10^6 times in comparison to dimeric Co(II) phthalocyanine **3**. A possible reason for the observed semiconducting property and improved electrical conductivity in **6** compared to **3** could be due to the smaller size of the amino group with respect to the nitro group. The smaller size of the amino group leads to stacking of the molecule with a smaller intermolecular distance resulting in greater π-electron interactions between the phthalocyanine molecules, thus providing a pathway for charge carriers. The higher conductivity of **5** can be expected due to the nature of the azo coupling and differences in the stacking arrangement of phthalocyanine molecules. This difference in arrangement may result in altering the interaction of π electron systems between the different molecules, which may affect the electrical conductivity of the phthalocyanine. Achar and Lokesh [26] studied the electrical properties of metal (II) tetranitro phthalocyanines of cobalt, nickel and copper. They found that an amine group substituent on the peripheral benzene ring of phthalocyanine molecule causes an increase in the electrical conductivity.

3.3. AC conductivity and impedance measurements

The ac conductivity and impedance spectral measurements were performed in the temperature range of 295–400 K and frequencies between 40 and 10^5 Hz.

Fig. 3 shows the frequency dependence of the imaginary part of impedance, loss spectra, for the films at different temperatures.

While a monotonic decrease in $Z''(f)$ can be noticed without any peak at low temperatures, with an increase of temperature, the spectra exhibits peaks at unique frequencies. A monotonic decrease in the loss spectra without any peaks up to 350 K means there is no current dissipation in this temperature region. The appearance of peaks at certain frequencies indicates the presence of an electrical

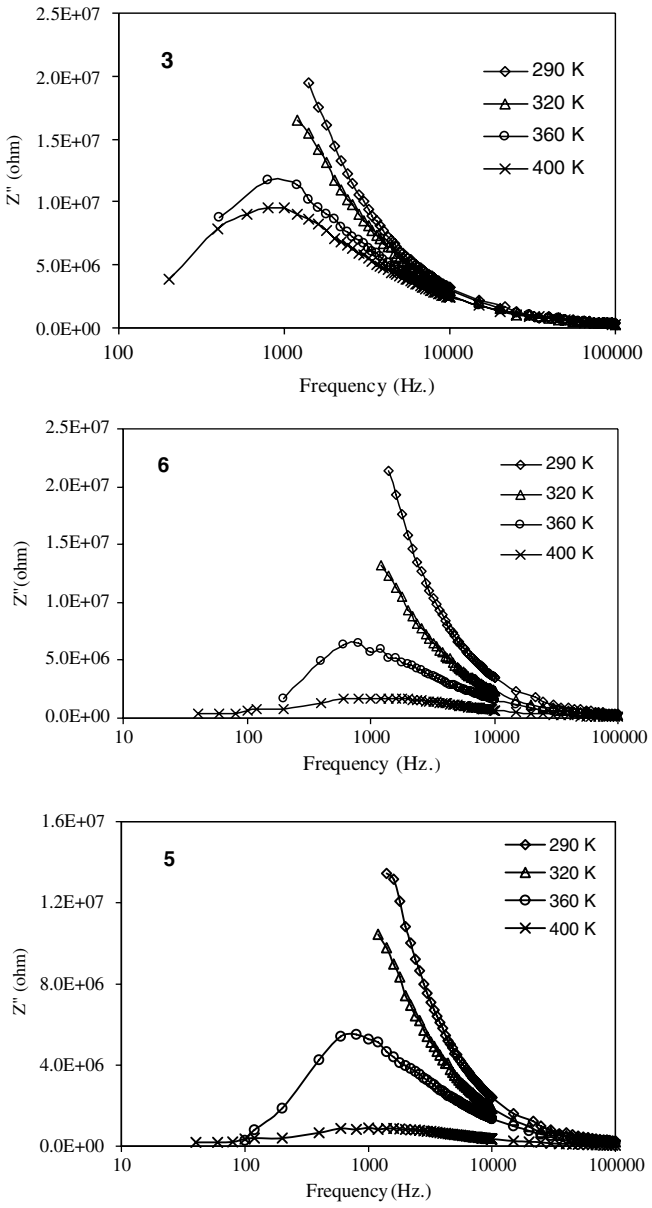

Fig. 3. Plot of the imaginary part of impedance with frequency for the films of **3**, **5** and **6**.

relaxation phenomenon in the films. It is noticed that the broadening of the $Z''(f)$ peaks is very obvious at higher temperatures. The observed broadening of the peaks with an increase in temperature suggests the presence of an electrical processes with a spread of relaxation time. The relaxation processes in the film may possibly be due to the presence of electron/immobile species at low temperatures and defects at higher temperatures. Further, the magnitude of $Z''(f)$ decreases gradually and it merges finally in the high frequency region. This behaviour can be attributed to the accumulation of space charge in the materials.

A considerable number of experimental results concerning the frequency dependent conductivity of a large variety of phthalocyanine materials can be found in the literature [27,28]. Room temperature a.c. behaviour of the compounds in the frequency range, 40–10^5 Hz is shown in Fig. 4. The effect of the reduction the nitro group to amines and azo coupling on the alternating current electrical conductivity can be seen clearly. The order of ac conductivities observed for these compounds are **5** > **6** > **3** for all frequencies investigated. These results for ac conductivity are in agreement with the observed d.c. conductivity. Fig. 4 also reveals that frequency has a pronounced effect on the measured ac conductivity for **3** and **6**. The frequency dependence of the conductivity follows a universal power law for compounds **3** and **6**, Fig. 4

$$\sigma_{\text{a.c.}}(\omega) = A\omega^s \tag{2}$$

where ω is the angular frequency, A and the frequency exponent s are material dependent constants. This type of a.c. conduction has been explained on the basis of two distinct mechanisms for carrier conduction.

One of them is quantum mechanical tunnelling (QMT) model. According to this model the conduction occurs by means of thermally assisted QMT. The other model, which is also known as correlated barrier hopping (CBH) model, is based on the concept of charged defects and in this bipolarons hop between two charged defect states D^+ and D^- over the barrier separating them, rather than tunnelling through the barrier. In these two models, the frequency exponent s is found to have two different trends with temperature and frequency [29]. The QMT model predicts a temperature independent s with a constant value around 0.8 which is given by

$$s = 1 - \frac{4}{\ln(\omega\tau_0)} \tag{3}$$

where ω is the angular frequency and τ_0 the characteristic relaxation time of the carrier. The values of s have been calculated from the slope of $\ln\sigma_{\text{ac}}(\omega)$ versus $\ln\omega$ graphs. Our calculations showed that s is definitely a function of temperature for compounds **3** and **6** and shows a general tendency to increase with decreasing temperature. The decrease in s with temperature is in contradiction with the QMT model. Therefore, it is apparent from the derived values of the index s that the conduction mechanism in **3** and **6** cannot be explained by the QMT model. In the case of **3** and **6** the hopping conduction process, which was developed by Elliot [29], is applicable. According to this model, the charge carriers hop between sites over the potential barrier separating them rather tunnelling through the barrier. The CBH model gives an ac conductivity which can be expressed to a first-order approximation as

$$\sigma_{\text{ac}}(\omega) = \frac{\pi^2 N^2 \varepsilon}{24}\left(\frac{8q^2}{\varepsilon W_{\text{OB}}}\right)^6 \frac{\omega^s}{\tau_0^\beta} \tag{4}$$

where ε is the dielectric constant, W_{OB} the optical band gap, τ_0 a characteristic relaxation time, q the electronic charge, k_{B} the Boltzmann's constant and N is the spatial density of defect states. The frequency exponent s for this model is evaluated as

$$s = 1 - \beta = 1 - 6k_{\text{B}}T/W_{\text{OB}} \tag{5}$$

The CBH model, in contrary to the QMT model, predicts a temperature-dependent s value which increases with decreasing temperature. The comparison of the experimentally determined s values with the prediction of the CBH model suggests that the dependence of the exponent s on temperature is in agreement with the prediction of the CBH model for compounds **3** and **6**.

A completely different frequency dependence was observed for compound **5**. The frequency dependence of a.c. conductivity at selected temperatures is shown in Fig. 5. It is clear from Fig. 5 that the a.c. conductivity for the spin coated film of compound **5** is frequency independent for all the temperature investigated.

Results indicate that the interpretation of the measured a.c. conductivity of compound **5** involves a number of difficulties; one of these is the contribution of the d.c. part. All the classical models based on the pair approximation deal only with pure a.c. conductivity, whereas the measured values include the d.c. limit. Therefore, any interpretation which is based on a model derived from the pair approximation has to exclude the d.c. limit somehow from the measured quantities. Conclusion of this topic is out of scope of this work.

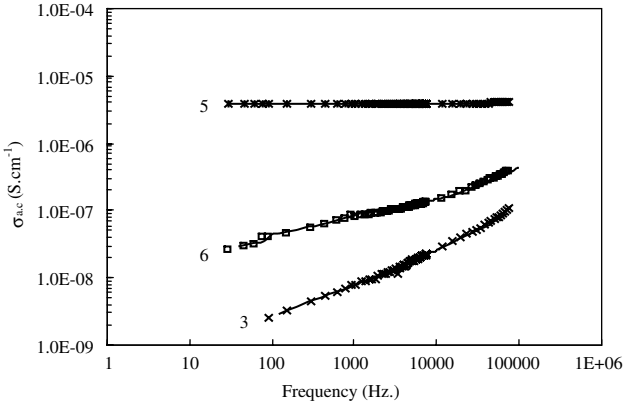

Fig. 4. Frequency dependent conductivity of the spin coated **3**, **5** and **6** films at room temperature.

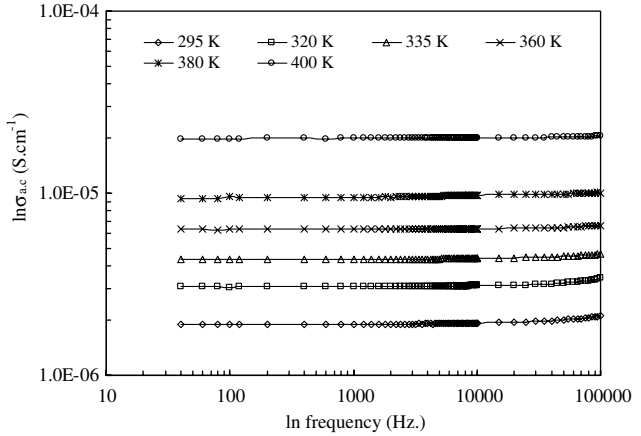

Fig. 5. Frequency dependence of a.c. conductivity of the spin coated film of **5** at the indicated temperatures.

4. Conclusions

In this study a new octaphthalocyanine **3** and a dimeric phthalocyanine with six ferrocenyl groups, **7**, were synthesized. The structures of these compounds were determined by elemental analysis, ICP-MS, IR, UV–Vis and ^{1}H NMR spectroscopy. Alternative current and direct current conductivity in thin films of compounds **3**, **5** and **6** at temperatures between 295 and 400 K were investigated. Well defined straight lines were obtained from the $\ln \sigma_{\mathrm{d.c.}}$ versus $1/T$ plots suggesting the presence of only one conduction mechanism in the whole temperature range for all compounds. While the frequency dependence of conductivity of the films of **3** and **6** is represented by the form ω^s, a frequency independent conductivity was observed for compound **5** above room temperature. A detailed analysis of the behaviour of **5** will be presented in a future paper.

Acknowledgements

This work was supported in part by The Turkish Academy of Sciences (TUBA) and The Research Fund of Marmara University (SCIENCE-077/081004 and SCIENCE-YYP-080805-0179).

References

[1] M.M. Nicholson, in: C.C. Leznoff, A.B.P. Lever (Eds.), The Phthalocyanines Properties and Applications, vol. 3, VCH, New York, 1993, pp. 76–117.
[2] H. Schultz, H. Lehman, M. Rein, M. Hanack, Struct. Bond. 74 (1991) 41.
[3] W.E. Ford, B.D. Rither, M.E. Kennedy, M.A.J. Rodgers, Photochem. Photobiol. 50 (1989) 277.
[4] C. Piechocki, J. Simon, New J. Chem. 9 (1985) 159.
[5] N. Toshima, S. Kawamura, T. Tominaga, Chem. Lett. (1993) 1299.
[6] (a) M. Rack, B. Hauschel, M. Hanack, Chem. Ber. 129 (1996) 237; (b) D. Guez, D. Markovitsi, M. Sommerauer, M. Hanack, Chem. Phys. Lett. 249 (1996) 309; (c) N. Koboyashi, in: C.C. Leznoff, A.B.P. Lever (Eds.), The Phthalocyanines Properties and Applications, Springer, New York, 1993, p. 2 (Chapter 3).
[7] (a) A.R. Koray, V. Ahsen, Ö. Bekaroğlu, J. Chem. Soc., Chem. Commun. (1986) 932; (b) V. Ahsen, E. Yılmazer, M. Ertaş, Ö. Bekaroğlu, J. Chem. Soc., Dalton Trans. (1988) 401; (c) V. Ahsen, A. Gürek, E. Musluoğlu, A. Gül, Ö. Bekaroğlu, Helv. Chim. Acta 73 (1990) 174.
[8] (a) M. Koçak, A. Cihan, A.İ. Okur, Ö. Bekaroğlu, J. Chem. Soc., Chem. Commun. (1991) 578; (b) A. Gürek, V. Ahsen, A. Gül, Ö. Bekaroğlu, J. Chem. Soc., Dalton Trans. (1991) 3367.
[9] G. Gümüş, Z. Öztürk, V. Ahsen, A. Gül, Ö. Bekaroğlu, J. Chem. Soc., Dalton Trans. (1992) 2495.
[10] I. Yılmaz, Ö. Bekaroğlu, Chem. Ber. 129 (1996) 967.
[11] M. Koçak, A.I. Okur, Ö. Bekaroğlu, J. Chem. Soc., Dalton Trans. (1994) 323.
[12] A. Gürek, Ö. Bekaroğlu, Helv. Chim. Acta 77 (1994) 1616.
[13] C.C. Leznoff, C.R. McArthur, Y. Qin, Can. J. Chem. 71 (1993) 1319.
[14] C. Piechoki, J. Simon, J. Chem. Soc., Chem. Commun. (1985) 259.
[15] (a) E. Musluoğlu, A. Gürek, V. Ahsen, A. Gül, Ö. Bekaroğlu, Chem. Ber. 125 (1992) 2337; (b) S. Dabak, A. Gül, Ö. Bekaroğlu, Chem. Ber. 127 (1994) 2009.
[16] Y.J. Zhang, Y. Li, Q. Liu, J. Jin, B. Ding, Y. Song, L. Jiang, X. Du, Y. Zhao, T.J. Li, Synth. Met. 128 (2002) 43.
[17] (a) A.G. Gürek, Ö. Bekaroğlu, J. Porphyr. Phthalocya. 1 (1997) 67; (b) A.G. Gürek, Ö. Bekaroğlu, J. Porphyr. Phthalocya. 1 (1997) 227.
[18] (a) Ş. Abdurrahmanoğlu, A. Altındal, A.R. Özkaya, M. Bulut, Ö. Bekaroğlu, Chem. Commun. (2004) 2096; (b) Ş. Abdurrahmanoğlu, A.R. Özkaya, M. Bulut, Ö. Bekaroğlu, J. Chem. Soc., Dalton Trans. 23 (2004) 4022.
[19] D.D. Perrin, W.L.F. Armarego, Purification of Laboratory Chemicals, 2nd ed., Pregamon Press, Oxford, 1980.
[20] S. Dabak, Ö. Bekaroğlu, New J. Chem. 21 (1997) 269.
[21] J.G. Young, W. Onyebuago, J. Org. Chem. 55 (1990) 2155.
[22] N. Ozan, O. Bekaroglu, Polyhedron 22 (2003) 819.
[23] S. Seelan, M.S. Srinivas, S. Sivasenker, J. Mol. Catal. A 168 (2001) 61.
[24] M.J. Stillman, T. Nyokong, in: C.C. Leznoff, A.B.P. Lever (Eds.), The Phthalocyanines Properties and Applications, vol.1, VCH, New York, 1993, p. 184.
[25] Y. Pan, W. Chen, S. Lu, Y. Zhang, Dyes Pigments 66 (2005) 115.
[26] B.N. Achar, K.S. Lokesh, J. Organomet. Chem. 689 (2004) 3357.
[27] A. Altındal, Ş. Abdurrahmanoğlu, M. Bulut, Ö. Bekaroğlu, Synt. Met. 18 (2005) 150.
[28] A.M. Saleh, A.O. Abu-Hilal, R.D. Gould, Curr. Appl. Phys. 3 (2003) 345.
[29] S.R. Elliot, Adv. Phys. 36 (1987) 135.

trinuclear [(bpy)Co(μ-OOCMe)$_3$Co(μ-OOCMe)$_3$Co(bpy)] [10], tetranuclear [Co$_4$(μ$_2$-OOCCF$_3$)$_2$(μ$_3$-OH)$_4$(bpy)$_4$] [17], binuclear compounds [Co$_2$(μ-Cl)$_2$(phen)$_2$](PF$_6$)$_2$ · 2Et$_2$O [18], [(phen)$_2$Co(μ-Cl)$_2$CoCl$_2$] · Et$_2$O [19] and [Co$_2$-(μ-N$_3$)$_2$(N$_3$)$_2$(dmph)$_2$] (dmph = 2,9-dimethyl-1,10-phenanthroline) [20]. In these compounds the Co–Co distances are relatively short, generally in the range 3.0–3.5 Å. Much longer distances were found in complexes with polycarboxylato bridging ligands: OOCRCOO (R = alkylene, arylene), e.g.: [Co$_2$\{μ-C$_6$H$_2$(COO)$_4$-1,2,4,5\}(N–N)$_4$] (N–N= bpy, phen and their derivatives) [21], [Co\{μ-C$_6$H$_2$(COO)$_2$-(COOH)$_2$-1,2,3,4,5\}(phen)(H$_2$O)]$_n$ [22], [Co$_2$\{μ-OOCCH=CHCOO\}$_2$(phen)$_2$]$_n$ [23]. In this paper, we present the X-ray structure, electronic, IR and ^{1}H NMR spectra and magnetic properties of a dinuclear Co(II) acetate complex [Co$_2$(μ-OAc)$_2$(OAc)$_2$(μ-H$_2$O)(phen)$_2$] with a structure similar to that of metalloenzymes.

2. Experimental

Reagents and solvents (pro analysis) were purchased from the Polish company POCH and were used as received. Infrared spectra (KBr pellets) were recorded with a Bruker IFS 113v, ^{1}H NMR spectra on a Bruker AMX 300 and a Bruker Avance 500. The temperature dependence of the magnetic susceptibility was measured with a Quantum Design MPMS-XL-5 SQUID susceptometer operating at a magnetic field of 0.5 T in the temperature range 2.5–300 K. The susceptibilities were corrected for the diamagnetism of the constituent atoms using Pascal's constants [24]. Elemental analysis was performed with a Vario EL3 CHN analyzer.

2.1. Synthesis and characterization of [Co$_2$(μ-OAc)$_2$(OAc)$_2$(μ-H$_2$O)(phen)$_2$]

To a hot solution of Co(CH$_3$COO)$_2$ · 4H$_2$O (0.04882 g, 2 mmol) in water (1.0 cm^3) was added a solution of 1,10-phenanthroline C$_{12}$H$_8$N$_2$ · H$_2$O (0.3964 g, 2 mmol) in DMF (1.5 cm^3). The reaction mixture was stirred at 75 °C for 15 min. The orange solution was cooled to room temperature and left for 3 h. The orange product was isolated and recrystallized from methylene chloride and vacuum dried. Yield: 0.5933 g (81%). *Anal.* Calc. for C$_{32}$H$_{30}$Co$_2$N$_4$O$_9$: C, 52.47; H, 4.13; N, 7.65; found. C, 52.33; H, 4.25; N, 7.28%.

IR (in KBr, cm^{-1}): 3432 vs (ν_{OH}), 3053 w (ν_{CH}), 3003 w (ν_{CH}), 2928 w (ν_{CH}), 2851 vw (ν_{CH}), 2086 w, 1993 w, 1955 w, 1619 vs ($\nu^{as}_{COOH} + \nu_{OH}$), 1537 sh, 1515 m, 1419 vs (ν^{s}_{COOH}), 1348 m, 1335 m, 1222 w 1209 vw, 1140 m, 1115 vw, 1103 m, 1045 w, 1015 w, 916 w, 894 w, 868 m, 849 m, 841 m, 775 w, 727 s, 653 s, 641 w, 614 w, 556 vw, 493 vw, 423 vw. UV–Vis [reflectance spectrum, cm^{-1}]: 8750, 16600, 19500, 21400, 26000, 38000. ^{1}H NMR [CD$_2$Cl$_2$, ppm] 64.23 (4H, ^{2,9}H), 38.61 (4H, ^{3,8}H), 22.18 (4H, ^{5,6}H), 7.62 (4H, ^{4,7}H), 1.24 (2H, H$_2$O), −0.52 (12H, CH$_3$).

2.2. X-ray crystallography study

All measurements of the crystal were performed at low temperature using an Oxford Cryosystem device on a Kuma KM4CCD κ-axis diffractometer with graphite-monochromated Mo Kα radiation. Accurate cell parameters were determined and refined by a least-squares fit of the strongest reflections. The data were corrected for Lorentz and polarization effects. No absorption correction was applied. Data reduction and analysis were carried out with the Oxford Diffraction, Poland (formerly Kuma Diffraction Wroclaw, Poland) programs. The structure was solved by direct methods (program SHELXS97 [25]) and refined by the full-matrix least-squares method on all F^2 data using the SHELXL97 [26] programs. Non-hydrogen atoms were refined with anisotropic vibrational parameters; hydrogen atoms of organic ligands were included from the geometry of the molecules and H atoms of aqua ligands were located from difference density maps and were refined with isotropic vibrational parameters.

3. Results and discussion

Complex [Co$_2$(μ-OOCCH$_3$)$_2$(OOCCH$_3$)$_2$(phen)$_2$(μ-OH$_2$)] (**1**), crystallizes in the monoclinic crystal system, $P2(1)/c$ space group. Crystallographic data are given in Table 1 and selected bond distances and angles are listed in Table 2.

Data on hydrogen bonds are presented in Table 3, an ORTEP plot of the complex is depicted in Fig. 1 and the stacking of the 1,10-phenanthroline ligands in the solid is

Table 1
Crystal data and structure refinement for complex [Co$_2$(μ-OOCCH$_3$)$_2$(OOCCH$_3$)$_2$(phen)$_2$(μ-OH$_2$)] (**1**)

Formula	C$_{32}$H$_{30}$Co$_2$N$_4$O$_9$
M	732.48
T (K)	100
λ (Å)	0.71073
Crystal system	monoclinic
Space group	$P2(1)/c$
a (Å)	8.9954(5)
b (Å)	15.1835(9)
c (Å)	23.7816(2)
β (°)	108.66(2)
V (Å^3)	3077.3(3)
Z	4
D_{calc} (Mg m^{-3})	1.581
μ (mm^{-1})	1.141
F(000)	1504
Crystal size (mm)	0.10 × 0.08 × 0.08
Diffractometer	Kuma KM4CCD
Θ (°)	3.27–28.47
Ranges of h, k, l	−10 ⩾ 11, −20 ⩾ 20, −30 ⩾ 24
Reflections collected	25553
Independent reflections (R_{int})	7209 (0.0751)
Data/parameters	7209/436
Goodness-of-fit on (F^2)	1.128
Final R_1/wR_2 indices [$I > 2\sigma$(I)]	0.0610/0.0923
Largest difference peak/hole (e Å^{-3})	0.362/−0.379

Table 2
Bond lengths (Å) and angles (°) for complex $[Co_2(\mu\text{-}OOCCH_3)_2(OOCCH_3)_2(phen)_2(\mu\text{-}OH_2)]$ (**1**)

Co(1)–O(1)	2.055(2)	O(1)–Co(1)–O(5)	93.39(9)
Co(1)–O(5)	2.070(2)	O(1)–Co(1)–O(6)	91.83(9)
Co(1)–O(6)	2.110(2)	O(5)–Co(1)–O(6)	174.74(9)
Co(1)–O(3)	2.134(2)	O(1)–Co(1)–O(3)	95.73(9)
Co(1)–N(1)	2.149(3)	O(5)–Co(1)–O(3)	91.81(9)
Co(1)–N(2)	2.174(3)	O(5)–Co(1)–N(1)	95.54(9)
Co(2)–O(2)	2.053(2)	O(6)–Co(1)–N(1)	85.32(9)
Co(2)–O(4)	2.069(2)	O(1)–Co(1)–N(2)	164.01(10)
Co(2)–O(9)	2.109(2)	O(5)–Co(1)–N(2)	83.61(9)
Co(2)–N(4)	2.118(3)	O(6)–Co(1)–N(2)	91.55(9)
Co(2)–O(3)	2.127(2)	O(3)–Co(1)–N(2)	100.05(9)
Co(2)–N(3)	2.178(3)	N(1)–Co(1)–N(2)	76.86(10)
O(6)–C(44)	1.262(4)	O(3)–Co(1)–N(1)	171.63(9)
O(1)–C(40)	1.257(4)	N(4)–Co(2)–O(3)	175.28(10)
O(2)–C(40)	1.264(4)	Co(2)–O(3)–Co(1)	114.01(10)
O(3)–H(1A)	0.923(18)	C(40)–O(1)–Co(1)	137.0(2)
O(3)–H(2A)	0.938(19)	C(44)–O(6)–Co(1)	131.1(2)

shown in Fig. 2. The ^1H NMR spectra of complex were investigated in CD_2Cl_2 in the range 223–298 K and in D_2O at 298 K. The ^1H NMR spectrum at 233 K is shown in Fig. 3. The magnetic susceptibility of complex **1** was measured in the temperature range 2.5–300 K. The temperature dependencies of the magnetic susceptibilities and effective magnetic moments of $[Co_2(\mu\text{-}OOCCH_3)_2(OOCCH_3)_2(phen)_2(\mu\text{-}OH_2)]$ are shown in Fig. 4.

Compound **1** was prepared by the reaction of cobalt(II) acetate with 1,10-phenanthroline in organic solvents (dimethylformamide, 1,4-dioxane). It is soluble in polar organic solvents and water. The X-ray structure shows that complex **1** has a structure similar to that of other dinuclear cobalt(II) compounds with carboxylato and nitrogen ligands. The Co(II) central atoms are bridged by two acetate anions and a water molecule and have octahedral coordination. The other coordination sites are occupied by terminal acetato ligands and 1,10-phenanthroline molecules, which are coordinated in nearly perpendicular planes. The nitrogen atoms are bound with the central atoms in trans positions to the bridging acetato ligands and water molecule. The structure of complex **1** is stabilized by strong hydrogen bonds formed by the water molecule with uncoordinated oxygen atoms of acetato ligands (d(O3–O7) = 2.566(3) Å and d(O3–O8) = 2.542(3) Å) and by weak C–H···O intra- and intermolecular hydrogen bonds (Table 3). The crystal structure of compound **1** is also stabilized by stacking of 1,10-phenanthroline ligands. The shortest distances between carbon atoms of two phenanthroline ligands vary in the range 3.34–3.70 Å (Fig. 2). The Co1–Co2 distance is equal to 3.574 Å, thus it is considerably greater than that in dicobalt methane monooxygenase hydroxylase (3.1 and 3.0 Å for protomers 1 and 2), but similar to the Fe–Fe distance (3.3 Å) in the reduced methane monooxygenase hydroxylase protomers and nearly the same as in dimanganese protomer 1 (3.5 Å) [3].

The presence of strong hydrogen bonds as well as bridging bidentate and terminal monodentate acetato ligands in the solid state was confirmed by the IR spectra of the complex in KBr and nujol mull. The monodentate CH_3COO ligands form such strong hydrogen bonds with the bridging

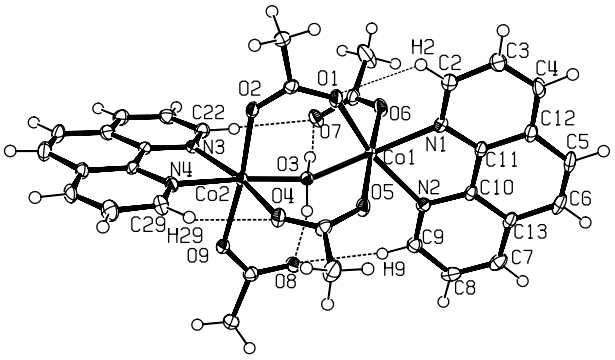

Fig. 1. ORTEP representation of complex **1** and hydrogen bonds in the solid state.

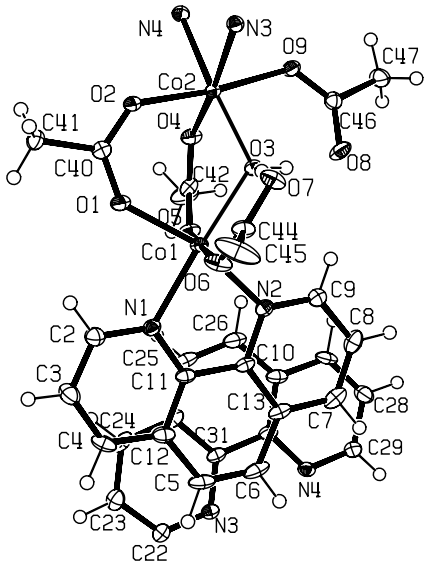

Fig. 2. The stacking of the phen ligand domains of **1**.

Table 3
Lengths (Å) and angles (°) of the hydrogen bonds for complex $[Co_2(\mu\text{-}OOCCH_3)_2(OOCCH_3)_2(phen)_2(\mu\text{-}OH_2)]$ (**1**)

D–H···A	D–H	H···A	D···A	∠D–H···A
O(3)–H(1A)···O(7)	0.92	1.65(4)	2.566(3)	177
O(3)–H(2A)···O(8)	0.93	1.63(4)	2.542(3)	166
C(2)–H(2)···O(1)	0.95	2.50(2)	3.046(4)	116
C(6)–H(6)···O(2)	0.95	2.48(4)	3.365(4)	154
C(9)–H(9)···O(8)	0.95	2.51(3)	3.443(4)	165
C(22)–H(22)···O(7)	0.95	2.38(2)	3.300(4)	163
C(27)–H(27)···O(6)	0.95	2.36(4)	3.277(4)	160
C(29)–H(29)···O(4)	0.95	2.59(4)	3.145(4)	117

Symmetry transformations used to generate equivalent atoms: $1 + x$, $-1/2 - y$, $1/2 + z$ and x, $-1/2 - y$, $-1/2 + z$.

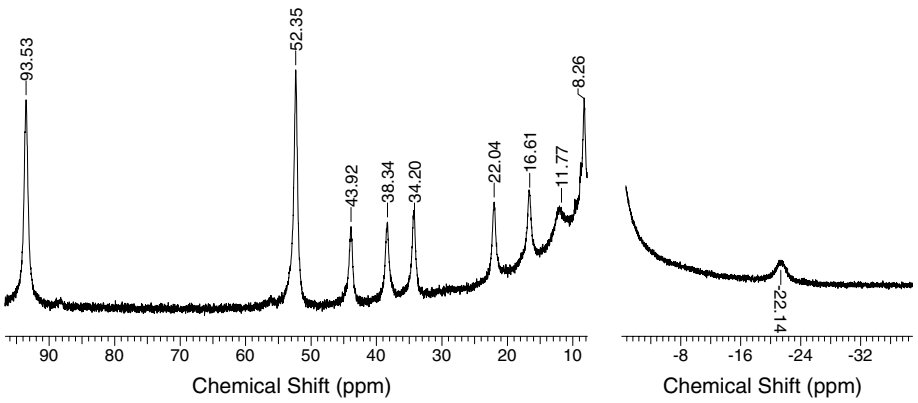

Fig. 3. The ^{1}H NMR spectrum of $[Co_2(\mu\text{-}OOCCH_3)_2(OOCCH_3)_2(phen)_2(\mu\text{-}OH_2)]$ in CD_2Cl_2 at 233 K.

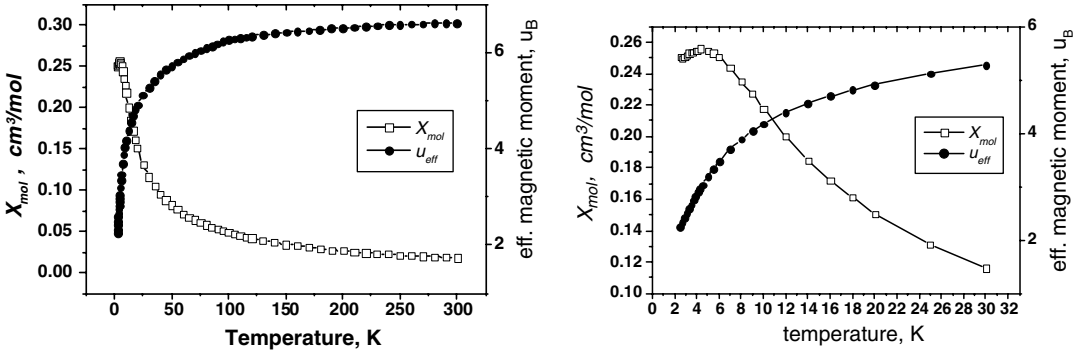

Fig. 4. Susceptibility and effective magnetic moment per dimer vs. temperature of complex $[Co_2(\mu\text{-}OOCCH_3)_2(OOCCH_3)_2(phen)_2(\mu\text{-}OH_2)]$.

H_2O ligand that the difference between the symmetrical and asymmetrical stretching vibration of the carboxylate group $\Delta\nu = \nu_{as}(COO) - \nu_s(COO) = 200\ cm^{-1}$ is approximately the same as for the bidentate bridging CH_3COO ligand. Therefore, only one broad $\nu_{as}(COO)$ and one $\nu_s(COO)$ band is observed in the IR spectrum of $[Co_2(\mu\text{-}OOCCH_3)_2(OOCCH_3)_2(phen)_2(\mu\text{-}OH_2)]$. The $\delta(OH)$ band is present at the same frequency as $\nu_{as}(COO)$, 1619 cm^{-1}.

In the reflectance electronic spectrum of the complex the $^4T_{2g} \leftarrow {}^4T_{1g}$ transition is observed at 8750 cm^{-1}. This band is symmetrical, thus the ^4T terms are not split owing to the lowering of the symmetry of the complex from O_h to C_{2v} for the $[CoN_2O_4]$ chromophore. However, the splitting of the term $^4T_{1g}(P)$ is observed because in the region of the transition $^4T_{1g}(P) \leftarrow {}^4T_{1g}$, 18 500–21 700 cm^{-1}, two bands are present, at 19 500 cm^{-1} and 21 400 cm^{-1}. Shoulders observed at 16 600 cm^{-1} and 18 800 cm^{-1} are most probably caused by spin forbidden $^2T_{1g}$, $^2T_{2g} \leftarrow {}^4T_{1g}$ and spin allowed $^4A_{2g} \leftarrow {}^4T_{1g}$ transitions, respectively.

The proton NMR spectra of the complex in CD_2Cl_2 were investigated in the temperature range 223–298 K. In the spectrum at 298 K, only five signals (assigned to the acetate and phen ligands) were found. Thus, at room temperature all the acetate groups are equivalent and both phenanthroline ligands become symmetrically coordinated with the Co(II) atoms, because the bridging and terminal acetate ligands interchange rapidly. The signals observed at 64.23, 38.61, 22.18, 7.62 and −0.52 ppm are assigned to the methyl groups of the acetato ligands and to the ^{2,9}H, ^{3,8}H, ^{5,6}H and ^{4,7}H protons of the bpy molecule, respectively. At lower temperatures the signals first broaden, then coalesce into three broad peaks. At 233 K and lower temperatures, separate resonances are observed: 2 for the methyl groups of acetate (at 93.53 pm – bridging and 52.35 pm – terminal) and 8 for the asymmetrically coordinated 1,10-phenanthroline ligands (at 43.92, 38.34, 34.20, 22.04, 16.61, 11.77, 8.26 and −22.14 ppm) with a ratio of methyl:methyl:aromatic signals equal to 3:3:1 (Fig. 3). Thus, at low temperatures the complex in CD_2Cl_2 solution has the same structure as in the solid state.

The relatively sharp signal at 298 K observed at 1.24 ppm is probably caused by a small amount of water contained in CD_2Cl_2. The resonance of coordinated water should be observed in the region where signals of solvent and its impurities are present. Therefore, it was not possible to determine the proton chemical shift of the aqua ligand. It is probable that at room temperature a fast exchange of protons between the aqua ligand and free water proceeds.

The ^{1}H NMR spectrum of the complex in D_2O solution shows the presence of three cobalt complexes with phenanthroline, namely complexes with Co:phen ratios equal to 1:1, 1:2 and 1:3. Phenanthroline signals for the 1:1 complex were observed at 76.76 (^{2,9}H), 41.05 (^{3,8}H), 34.11 (^{5,6}H) and

18.96 (^{4,7}H) ppm, for the 1:2 compound at 85.00 (^{2,9}H), 43.85 (^{3,8}H), 32.89 (^{5,6}H) and 16.72 (^{4,7}H) ppm and for the 1:3 complex at 106.15 (^{2,9}H), 50.15 (^{3,8}H), 33.52 (^{5,6}H) and 17.48 (^{4,7}H) ppm. The chemical shift for these complexes are nearly the same as for the appropriate 1,10-phenanthroline complexes with a chloride counter ion in D_2O. Thus, most likely, they form aqua complexes, although coordination of acetate ligands cannot be excluded. The methyl groups signal in D_2O was observed at 2.56 ppm The Co(phen)$_3$:Co(phen)$_2$:Co(phen):Co ratio in a solution of $[Co_2(OAc)_4(phen)_2(H_2O)]$ in D_2O is approximately equal to 1:4:15:6. These data indicate that in water solutions cobalt(II) complexes with Co:N–N ratios of 1:1 and 1:2 (N–N = phen, bpy and their derivatives) are labile and the heteroligand $[Co(N–N)_2X_2]^{m+}$ and $[Co(N–N)X_4{}^{n+}]$ as well as the homoligand $[Co(N–N)_2{}^{2+}]$ complexes are at equilibrium.

The dependences of magnetic susceptibility and effective magnetic moment of a polycrystalline sample of complex $[Co_2(OAc)_4(phen)_2(H_2O)]$ on temperature are shown in Fig. 4. Each Co(II) ion in this compound is octahedrally coordinated but the symmetry is axial due to rather strong distortions of the coordination spheres. The lowering of the symmetry is strong enough to remove the orbital degeneracy of the $^4T_{1g}$ ground state. Similar properties are shown by analogous Co(II) complexes containing *N*,*N*,*N*′,*N*′-tetramethylethane-1,2-diamine instead of 1,10-phenanthroline and other dinuclear Co(II) compounds: $[Co_2(\mu\text{-}OOCMe)_2(OOCMe)_2(\mu\text{-}H_2O)(Me_2NCH_2CH_2NMe_2)_2]$, $[Co_2(\mu\text{-}OOCCH_3)_3\{OC(NH_2)_2\}(Me_2NCH_2CH_2NMe_2)_2]^+$, $[Co_2(\mu\text{-}OOCCH_3)_2\{\mu\text{-}ONHC(=O)CH_3\}\{OC(NH_2)_2\}(Me_2NCH_2CH_2NMe_2)_2]^+$, $[Co_2(\mu\text{-}OOCCH_3)\{\mu\text{-}ONC(=O)CH_3\}_2(Me_2NCH_2CH_2NMe_2)_2]^+$ and $[Co_2(\mu\text{-}OOCR)_2(\mu\text{-}bhmp)]^+$ [2,5–9]. Therefore, the magnetic properties of the complex $[Co_2(OAc)_4(phen)_2(H_2O)]$ (**1**) can be explained assuming that the isotropic Heisenberg Hamiltonian is appropriate in this case [24,27]. The influence of the angular momentum is incorporated into the *g* tensors. Complex **1** shows a distinct maximum in χ_M at 4.5 K.

Calculations of χ_M were performed according to the method described in [24,27]. Satisfactory agreement of the calculated susceptibility with experimental data were obtained for average value $g = 2.1$ and $J = -2.1\ cm^{-1}$. These data exhibit that an antiferromagnetic interaction in this complex is stronger than in the dinuclear Co(II) complexes with three carboxylato bridges [2,5]. Thus, the antiferromagnetic interaction via three atoms of the carboxylic group is weak. This indicates that a considerably stronger antiferromagnetic interaction takes place via the O atom of the bridging water molecule. The effective magnetic moment of complex **1** (per dimer) at 300 K is equal to 6.62 μ_B and is somewhat lower than the spin-only value and considerably lower than the magnetic moments of compounds $[Co_2(\mu\text{-}OOCMe)_2(OOCMe)_2(\mu\text{-}H_2O)(Me_2NCH_2CH_2NMe_2)_2]$ and $[Co_2(\mu\text{-}OOCCH_3)_2\{\mu\text{-}ONHC(=O)CH_3\}\{OC(NH_2)_2\}(Me_2NCH_2CH_2NMe_2)_2]^+$ [2,5]. It decreases with diminishing temperature to 2.02 μ_B at 2 K.

4. Conclusions

Reaction of $Co(OOCCH_3)_2 \cdot 4H_2O$ with 1,10 phenanthroline in organic solvents gives the dinuclear complex $[Co_2(\mu\text{-}OAc)_2(OAc)_2(\mu\text{-}H_2O)(phen)_2]$ (**1**). Its structure and physicochemical properties have been investigated. The compound crystallizes in the monoclinic space group $P2(1)/c$. The Co–Co distance (3.574 Å) is similar to the Fe–Fe distance in the reduced methane monooxygenase hydroxylase and almost the same as in manganese monooxygenase. The Co(II) central atoms have an octahedral coordination, they are bridged by two acetate anions and a water molecule. The other coordination sites are occupied by terminal acetato ligands and 1,10-phenanthroline molecules, which are coordinated in nearly perpendicular planes. The structure of the complex is stabilized by strong hydrogen bonds formed by the water molecule with uncoordinated oxygen atoms of the acetato ligands and by weak C–H···O intra-and intermolecular hydrogen bonds. The crystal structure of compound **1** is also stabilized by stacking of the 1,10-phenanthroline ligands. The shortest C–C distances between two phenanthroline ligands vary in the range 3.34–3.70 Å. The complex exhibits antiferromagnetic exchange, the maximum in χ_M is observed at 4.5 K. The calculated value of the isotropic exchange parameter $J = -2.1\ cm^{-1}$. The proton NMR spectrum indicates that the structure of the complex in CD_2Cl_2 solution at low temperatures (223–243 K) is the same as in the solid state with symmetrically coordinated 1,10-phenanthroline ligands, however, at room temperature the bridging and terminal acetate ligands fast interchange. In water solution, the complex dissociates giving compounds with different Co:phen ratios.

5. Supplementary material

Crystallographic data for the structure reported in this paper (excluding structure factors) have been deposited at the Cambridge Crystallographic Data Centre and allocated the deposition number CCDC 604443. Copies of this information may be obtained free of charge from the Director, CCDC, 12 Union Road, Cambridge, CB2 1EZ. UK (fax: +44 1223 336 033; e-mail: deposit@ccdc.cam.ac.uk or http://www.ccdc.cam.ac.uk).

Acknowledgements

The authors are grateful to the Ministry of Science and Higher Education for support of this work (Grant No. 3 T09A 010 29).

References

[1] M. McCann, M. Geraghty, M. Devereux, D. O'Shea, J. Mason, L. O'Sullivan, Metal-Based Drugs 7 (2000) 185.
[2] D.A. Brown, W. Errington, W.K. Glass, W. Haase, T.J. Kemp, H. Nimir, S.M. Ostrovsky, R. Werner, Inorg. Chem. 40 (2001) 5962.

[3] M.H. Sazinsky, M. Merkx, E. Cadieux, S. Tang, S.J. Lippard, Biochemistry 43 (2004) 16263.
[4] H. Chao, L.-N. Ji, in: M. Gielen, E.R.T. Tiekink (Eds.), Metallotherapeutic Drugs and Metal-Based Diagnostic Agents, Wiley, Chichester, 2005 (Chapter 11).
[5] S.M. Ostrovsky, R. Werner, D.A. Brown, W. Haase, Chem. Phys. Lett. 353 (2002) 290.
[6] N.Dj. Lazarov, V. Spasojevic, V. Kusigerski, V.M. Matić, M. Milić, J. Magn. Magn. Mater. 272–276 (2004) 1065.
[7] D.A. Brown, W.K. Glass, N.J. Fitzpatrick, T.J. Kemp, W. Errington, G.J. Clarkson, W. Haase, F. Karsten, A.H. Mahdy, Inorg. Chim. Acta 357 (2004) 1411.
[8] Md.J. Hossain, M. Yamasaki, M. Mikuriya, A. Kuribayashi, H. Sakiyama, Inorg. Chem. 41 (2002) 4058.
[9] P.W. Ball, A.B. Blake, J. Chem. Soc., Dalton Trans. (1974) 852.
[10] B.-H. Ye, X.-M. Chen, F. Xue, L.N. Ji, T.C.W. Mak, Inorg. Chim. Acta 299 (2000) 1.
[11] D.A. Brown, W.K. Glass, N.J. Fitzpatrick, T.J. Kemp, W. Errington, H. Müller-Bunz, A.J. Hussein, H. Nimir, Inorg. Chim. Acta 358 (2005) 2755.
[12] A.P. Gylya, S.G. Shova, G.V. Novitskii, M.D. Mazus, Koord. Khim. 20 (1994) 111.
[13] Q. Miao, M.L. Hu, F. Chen, Acta Crystallogr. Sect. E 60 (2004) m1314.
[14] L.-L. Kong, L.-H. Huo, S. Gao, J.-G. Zhao, Acta Crystallogr. Sect. E 61 (2005) m2485.
[15] M.N. Hughes, in: G. Wilkinson, R.D. Gillard, J.A. McCleverty (Eds.), Comprehensive Coordination Chemistry, Pergamon Press, Oxford, 1987 (Chapter 62.1).
[16] S.J. Lippard, J.M. Berg, Principles of Bioinorganic Chemistry, University Science Books, Mill Valley, 1984.
[17] H. Zhao, J. Bacsa, K.R. Dunbar, Acta Crystallogr. Sect. E 60 (2004) m637.
[18] B. Brewer, N.R. Brooks, S. Abdul-Halim, A.G. Sykes, J. Chem. Cryst. 33 (2003) 651.
[19] B. Brewer, N.R. Brooks, A.G. Sykes, J. Chem. Cryst. 33 (2003) 663.
[20] T.-F. Liu, D. Fu, Y.-Z. Zhang, H.-L. Sun, G. Su, Y.-J. Liu, J. Am. Chem. Soc. 125 (2003) 13976.
[21] Y.-T. Li, C.-W. Yan, X.-H. Kong, Polish J. Chem. 73 (1999) 1665.
[22] M.-L. Hu, H.-P. Xiao, J.-X. Yuan, Acta Crystallogr. Sect. C 60 (2004) m112.
[23] J.-F. Ma, J. Yang, J.-F. Liu, Acta Crystallogr. Sect. C 59 (2003) m304.
[24] O. Khan, Molecular Magnetism, VCH Publishers, New York, 1993.
[25] G.M. Sheldrick, SHELXS97, Program for Solution of Crystal Structures, University of Göttingen, Göttingen, Germany, 1997.
[26] G.M. Sheldrick, SHELXL97, Program for Ccrystal Structure Refinement, University of Göttingen, Göttingen, Germany, 1997.
[27] W. Wojciechowski, Inorg. Chim. Acta 1 (1967) 319.

wide variety of conditions. Different routes can be found for the synthesis of cycles, however previous studies suggest thiosemicarbazones are typical substrates to undergo ring closure processes to afford the corresponding formation of 1,2,4-triazole (I) and 1,3,4-thiadiazole (II) derivatives, normally in the presence of a metallic salt (see Scheme 1) [13].

1,2,4-Triazol-3-thiones, as well as their corresponding thiosemicarbazones, can present in solution a *thione-thiol* tautomerism, whereas in the solid state they are present only in the thione form. The latter are very versatile, being able to form mono-, di- and polynuclear metal complexes as a result of two different coordination modes: as a monodentated ligand through the sulfur atom or as a bidentate bridge through the sulfur and a nitrogen atoms [14]. The presence of the soft thione donor group allows the stabilization of metal ions in low oxidation states such as Cu^{+}, Ag^{+}, Au^{+}. In addition, the pharmaceutical and industrial applications of some thiosemicarbazones increase the interest in this research field.

We have previously reported complexes containing thiosemicarbazone derivatives of 2-pyridinformamide and some transition and non-transition metals [15], nevertheless there are only a few reports on thiosemicarbazones complexes with Ag(I) [16,17]. Unexpectedly, there have been no X-ray structure determinations of Ag(I) thiosemicarbazone complexes until recently, with the publication of $[Ag_6(L^1H)_6]$ (L^1 = thiosemicarbazone of salicylaldehide) [18]. In order to extend our studies, in this work we described the preparation of a new silver(I) complex, $[Ag(E124tazt)]_6$ (**1**) (HE124tazt = 4-ethyl-5-pyridin-2-yl-2,4-dihydro-[1,2,4]triazol-3-thione), resulting from the cyclization 2-pyridinformamide *N*-4-ethylthio semicarbazone, HAm4E (Fig. 1), in the presence of Ag(I).

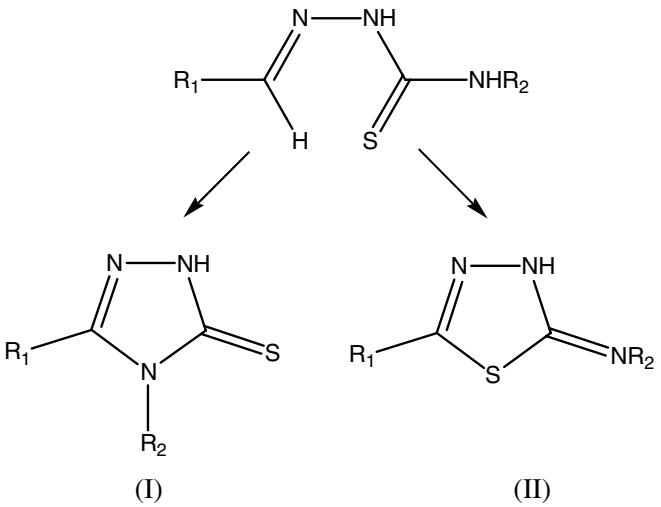

Scheme 1. Cyclization process of a thiosemicarbazone.

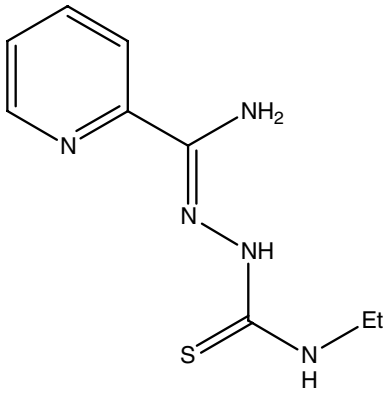

Fig. 1. Structure of 2-pyridinformamide *N*-4-ethylthiosemicarbazone, HAm4E.

2. Results and discussion

2.1. Synthesis

The reaction of $AgNO_3$ in H_2O/MeOH with the 2-pyridinformamide *N*-4-ethylthiosemicarbazone, HAm4E, led to the formation of $[Ag(E124tazt)]_6$ (**1**) (HE124tazt = 4-ethyl-5-pyridin-2-yl-2,4-dihydro-[1,2,4]triazol-3-thione), the structure of which contains a heterocyclic ring formed during the reaction. The formation of this kind of heterocyclic ring depends on the structure of the starting thiosemicarbazone, thus 1,2,4-triazole and 1,3,4-thiadiazole heterocyclic rings can both be formed from 2-pyridinformamide thiosemicarbazones derivatives. In particular HAm4E (Fig. 1) forms a 1,2,4-triazol-3-thione, the presence of a substituent on the N(4) nitrogen atom being a decisive factor for the regiochemistry of the cyclization.

The proposed cyclization mechanism suggests nucleophilic attack of the N5 thioamide on the azomethine carbon, with the elimination of a molecule of NH_3 (see Scheme 2) [14].

The preparation of HAm4E was carried out by reducing 2-cyanopyridine in the presence of *N*-4-ethylthiosemicarbazide, as described previously [15]. In the presence of silver(I) ions, HAm4E undergoes a cyclization process (see Scheme 3) to give a silver complex containing the deprotonated 4-ethyl-5-pyridin-2-yl-2,4-dihydro-[1,2,4]triazol-3-thiolato, E124tazt. The final compound is stable at room temperature, is not light sensitive and is insoluble in water or commonly used organic solvents.

2.2. Crystal structure of *1*

Single-crystal X-ray diffraction analysis indicates that the silver complex crystallizes in the trigonal space group $R\bar{3}c$. The crystal structure determination reveals that the asymmetric unit contains a silver(I) ion bonded to an E124tazt molecule through its sulfur atom. The space group symmetry generates a hexanuclear cluster, whose structure consists of six silver atoms and six deprotonated triazole-3-thione ligands. The deprotonation of the ligands

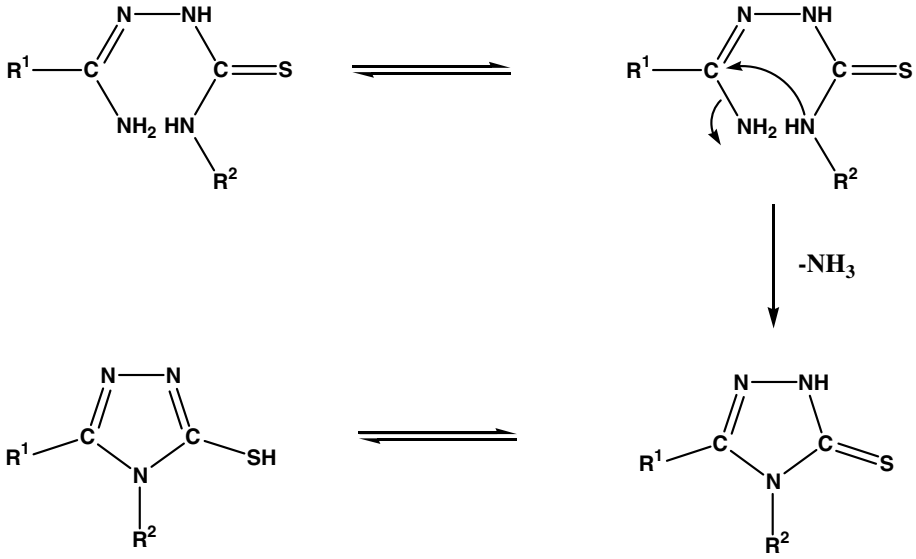

Scheme 2. Cyclization mechanism for 2-pyridinformamide thiosemicarbazones derivatives.

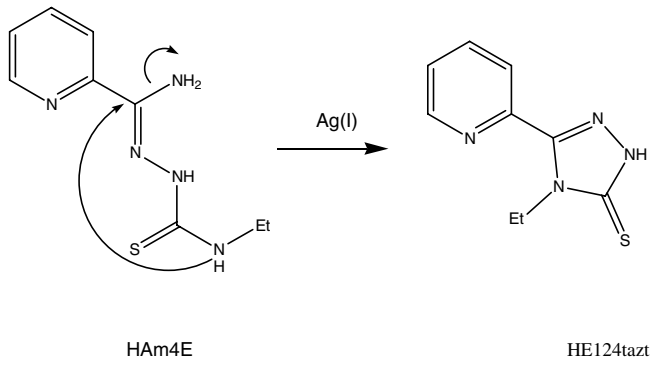

HAm4E HE124tazt

Scheme 3. Proposed cyclization mechanism for HAm4E to give HE124tazt.

on coordination is evident in the observed C–S bond distance of 1.726(5) Å instead the typical value of 1.671 Å for C=S [19]. Fig. 2 shows the molecular structure of the silver complex. Relevant interatomic bond distances and angles are given in Table 1.

The Ag_6S_6 central core is formed by two six-membered Ag_3S_3 rings linked together by 6 alternating NCS and SCN bridges (Fig. 3). The two six-membered Ag_3S_3 rings adopt a chair configuration, the silver atoms being coordinated to a triazole nitrogen and two sulfur atoms. The Ag–N bond distance is 2.225(4) Å, similar to those found in the complexes of Ag(I) and nitrogen-containing heterocyclic ligands [20,21]. Each thiolate sulfur atom bridges asymmetrically two silver atoms with Ag–S bond lengths of 2.4296(13) and 2.5984(14) Å, in the same range as other polynuclear silver complexes [18,22–24].

In both Ag_3S_3 rings, Ag(I) shows a trigonal planar coordination geometry (S1–Ag1–$S1^b$, 105.36; S1–Ag1–$N13^e$, 106.48; $N13^e$–Ag1–$S1^b$, 147.64°) with the metal atom lying 0.091(2) Å out of the NS_2 plane. However if the Ag···Ag interaction between rings (2.9996 Å) is considered, the resulting coordination polyhedron can be described as a highly distorted tetrahedron (S1–Ag1–$S1^b$, 105.36, $Ag1^e$–Ag1–$N1^e$, 83.94°) or, alternatively, as a trigonal pyramid.

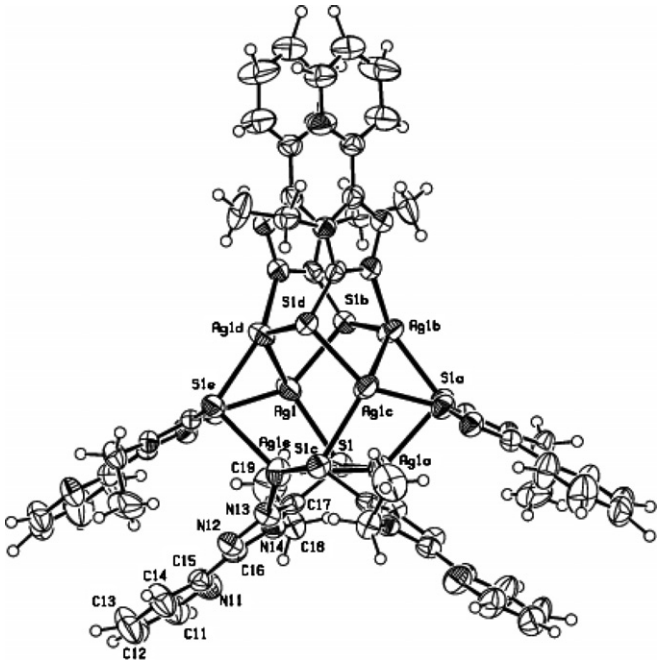

Fig. 2. Perspective view of **1**, showing 50% probability ellipsoids for the non-hydrogen atoms and the numbering scheme of the atoms in the molecule. Symmetry codes are given in Table 1.

In the Ag_6S_6 central core, the six silver atoms build a distorted octahedron formed by two parallel Ag_3 triangles, which adopt a staggered conformation [Ag···Ag distance of 3.8931(8) Å] and inter-ring distances of 3.6190(9) and 2.9996(9) Å. The Ag···Ag separation of 2.9996(9) Å is very close to that in metallic silver [2.889(6) Å], shorter than the sum of the van der Waals radii of two silver atoms (3.44 Å), suggesting the existence of some interaction between the

Table 1
Selected interatomic distances (Å) and angles (°) for **1** as observed experimentally and as calculated using DFT methods

Distances	Exp.	Calc.	Angles	Exp.	Calc.
Ag1–N13^{e}	2.225(4)	2.216	N13^{e}–Ag1–S1^{b}	147.65(11)	150.1
Ag1–S1^{b}	2.4296(13)	2.439	N13^{e}–Ag1–S1	106.48(11)	105.8
Ag1–S1	2.5984(14)	2.673	S1^{b}–Ag1–S1	105.35(6)	104.2
Ag1–Ag1^{d}	2.9996(9)	2.995	Ag1^{a}–S1–Ag1	101.43(5)	102.2
Ag1–Ag1^{e}	3.8931(8)	3.968	Ag^{d}–Ag1–N13^{e}	83.96(6)	83.9
Ag1–Ag1^{a}	3.6190(9)	3.716	C16–N12–N13	105.8(4)	107.2
C17–S1	1.726(5)	1.733	C17–N13–N12	109.0(4)	109.1
N12–C16	1.321(6)	1.330	C17–N14–C16	105.5(4)	105.5
N12–N13	1.379(5)	1.363	N12–C16–N14	110.6(4)	109.8
N13–C17	1.323(6)	1.344	N13–C17–N14	109.0(4)	108.3
N14–C17	1.354(6)	1.374	N13–C17–S1	126.2(4)	127.0
N14–C16	1.371(6)	1.385	N14–C17–S1	124.7(4)	124.7

Symmetry transformations used to generate equivalent atoms: (a) $-y$, $x-y$, z; (b) $-x+y$, $-x$, z; (c) y, x, $1/2-z$; (d) $-x$, $-x+y$, $-z+1/2$; (e) $x-y$, $-y$, $-z+1/2$.

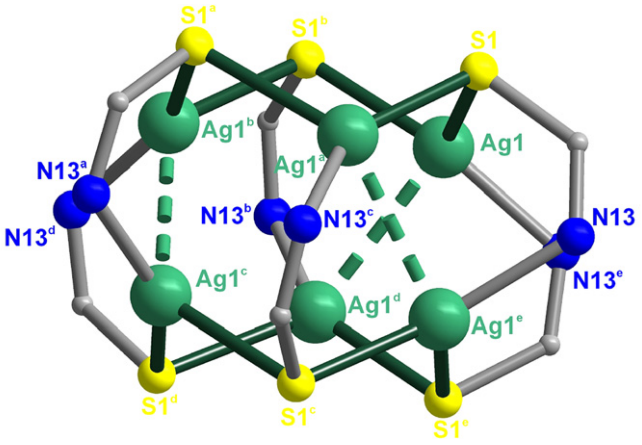

Fig. 3. Perspective view of the Ag_6S_6 central core illustrating the coordination geometry around the silver atoms. Symmetry codes are given in Table 1. Ag_3S_3 units are emphasized by black bonds.

silver atoms. Although the closed d^{10} configuration of silver(I) appears to prevent any intermetallic bonding in silver(I) complexes for Ag···Ag distances longer than 2.705(1) Å [25], many complexes with definitive Ag···Ag attractive forces, known as argentophilic interactions, have been reported [26–28].

The bond distances within the ligand are similar to those of other triazole-3-thione and 2-pyridyl derivatives, although the intra-triazole ring bond distances suggest some multiple bond character and delocalization of electronic density. These ligands are almost planar with an angle of 5.2 (3)° between the pyridine and triazole rings. In **1**, both ligands show an antiparallel arrangement, displaying intramolecular π–π stacking interactions between the triazole- and pyridine rings, with centroid–centroid separations of 3.593 and 3.959 Å, respectively (Table 2). Intermolecular π–π stacking interactions are also responsible of the formation of 2D polymers. These two-dimensional nets

Table 2
Parameters of the π–π interaction (Å, °)

Cg(I)···Cg(J)	d[Cg(I)···Cg(J)]	d[Cg(J)···⊥P(I)]	α	β	γ
Cg(4)···Cg(4)^{e}	3.5933	3.438	0.00	16.90	0.00
Cg(8)···Cg(8)^{e}	3.9595	3.760	0.00	18.27	0.00
Cg(4)···Cg(8)^{f}	4.1479	3.678	5.23	27.55	31.39
Cg(8)···Cg(4)^{f}	4.1479	3.541	5.23	31.39	27.55

(e) $x-y$, $-y$,$1/2-z$; (f) $2/3-x$, $1/3-y$, $1/3-z$; centroids: Cg(4): N(12)/N(13)/C(17)/N(14)/C(16)/C(26); Cg(8): N(11)/(11)/(12)/(13)/C(14)/C(15).

are stacked together along the crystallographic c axis generating hexameric parallel channels with crystallographic symmetry 3 (Fig. 4).

2.3. DFT calculations

In order to explore the nature of the Ag···Ag interactions from a theoretical point of view, quantum chemical investigations have been carried out using DFT methods. The structure optimization resulted in an excellent reproduction of the experimentally observed structural parameters (see Table 1). Therefore, the contribution of atomic orbitals (AOs) to molecular orbitals (MOs) has subsequently been studied by means of a Mulliken population analysis. The result, illustrated as the calculated density of states for all atoms versus silver atoms only, is given in Fig. 5.

The Ag valence orbitals (essentially 3d) are active between the energy level of the highest occupied molecular orbital (HOMO, at −3.7 eV) and −9.5 eV, which refers to about 100 occupied MOs. The maximum contribution of Ag, approx. 50% of the total DOS for all atoms, is observed for HOMO-41 (at −6.9 eV, i.e. 3.2 eV below the HOMO level). All MOs involving Ag d-orbitals have been analyzed with respect to the metal–metal contacts. This procedure revealed an essentially non-bonding (or weakly

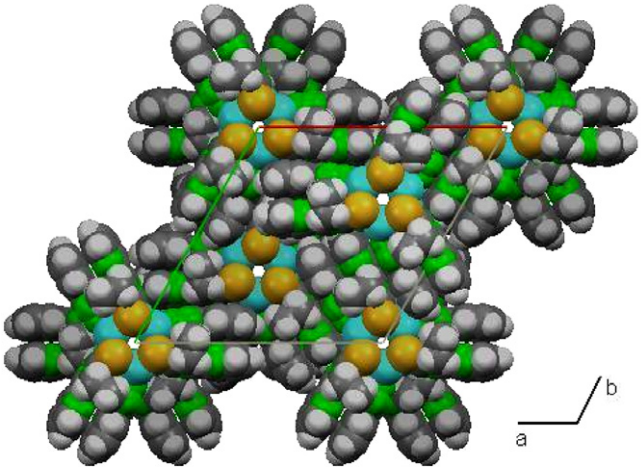

Fig. 4. The drawing of the packing diagram reveals the pattern of the array in the *ab* plane of **1**. Symmetry codes are given in Table 2.

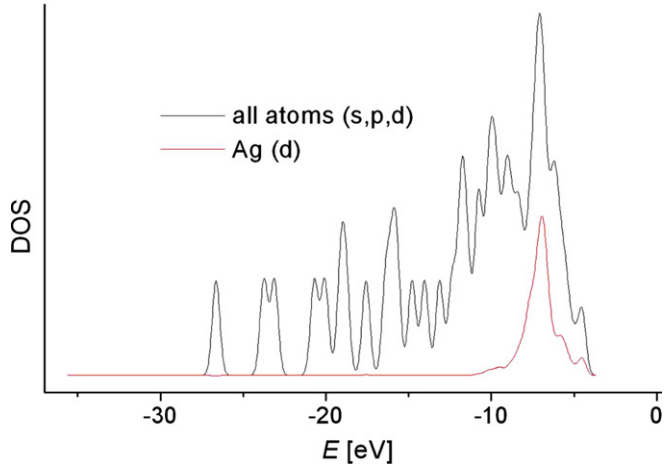

Fig. 5. Density of states (DOS) of the valence shell MOs (i.e. with contributions from C, N: 2s,2p; S: 3s,3p; Ag: 3d,4s) for the calculated $[Ag(E124tazt)]_6$. The solid line shows DOS considering all atoms, the dashed line refers only to the Ag d-orbital contribution; the latter represents essentially both the whole Ag valence orbital contribution (4s negligible) and the whole d-orbital contribution of all atoms (C, N, S d-contribution negligible).

antibonding) Ag···Ag situation for most of the respective MOs, with the exception of one MO (HOMO-56 at −7.3 eV, 36% Ag d-contribution) that clearly represents σ-bonds between Ag $d_{x^2-y^2}$ orbitals along all of the three short Ag···Ag contacts. Two further MOs (HOMO-63 and HOMO-64, both at −7.3 eV, 36% or 37% Ag d-contribution) show two or one such binding contacts involving d_{z^2} orbitals, besides one weakly antibonding or two weakly bonding ones, respectively. The quoted MOs are visualized in Fig. 6.

Preliminary neglecting the participation of orbitals of further atoms at the three MOs, one counts two electrons in each of these MOs to contribute to the binding Ag–Ag interactions. This denotes 2/3 e^- per Ag–Ag contact in HOMO-56, 1 e^- for each of the two binding Ag–Ag contacts in HOMO-64 and 2 e^- for one binding Ag–Ag contact in HOMO-63. The total number of two electrons per Ag–Ag contact which results from this crude estimation has to be reduced to an amount of ca. 2/3 electrons (36…37% of 2) per Ag–Ag contact according to the population analyses.

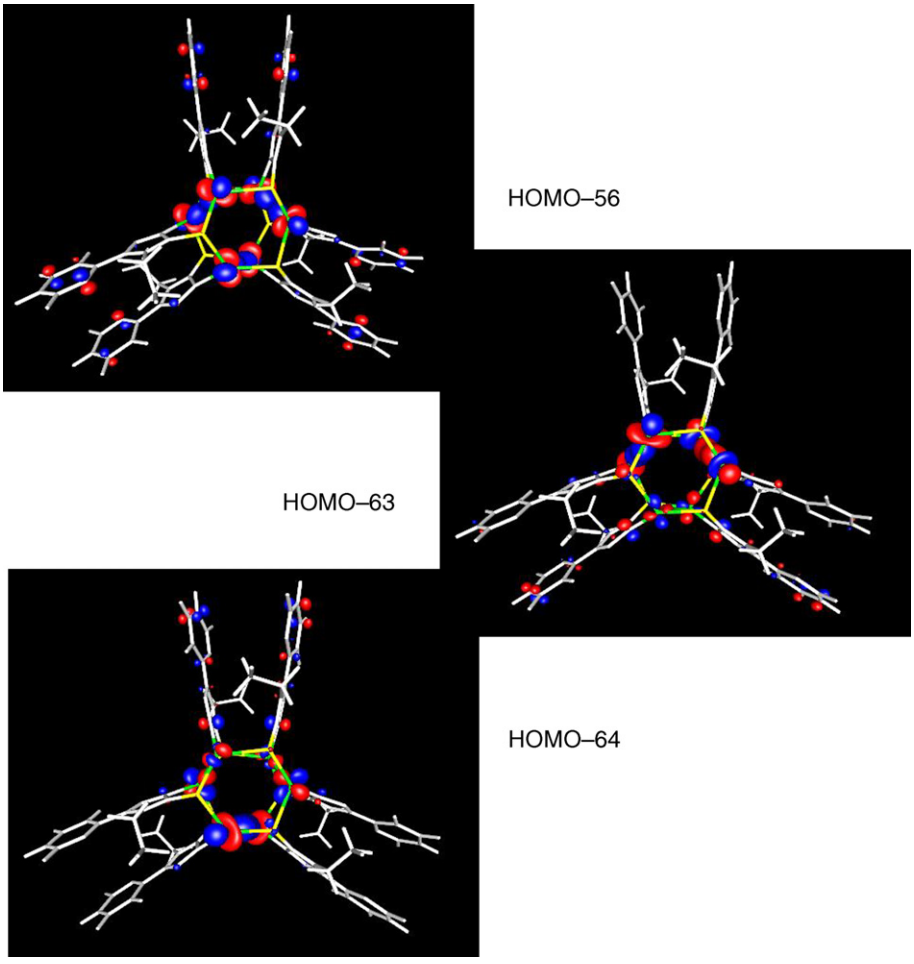

Fig. 6. Stick representation of the calculated $[Ag(E124tazt)]_6$ with visualization of the three MOs that show $d_{x^2-y^2}$–$d_{x^2-y^2}$ binding interactions between adjacent Ag atoms. For clarity, only Ag atoms (black) and S atoms (medium grey) are represented darker. Electron densities are drawn to 0.25 e^- Å^3.

2.4. Spectroscopic characterization

The IR spectrum of **1** shows absorption bands at 1588, 995 and 789 cm^{-1}, assigned to ν(C=N), ν(NN) and ν(CS), respectively. The absence of bands in the 3500–3000 cm^{-1} region due to NH stretching modes, supports the suggested cyclization of HAm4E, with elimination of NH_3 (Scheme 2) and deprotonation of the ligand in the thiol form. The bands at 346 and 304 cm^{-1} can be assigned to the vibrations ν(Ag–N) and ν(Ag–S), indicating the involvement of these atoms in the coordination [17].

The poor solubility of the complex only allows a ^1H NMR spectrum to be recorded. The spectrum shows signals assigned to the pyridine ring in the range of 8.71–7.50 ppm. The disappearance of the signal of the NH_2 group is in agreement with the cyclization of the thiosemicarbazone and the absence of an NH signal indicates the deprotonation of HE124tazt. The peaks corresponding to the ethyl group at 4.61 and 3.39 ppm are slightly shielded compared to those from HAm4E due to formation of the triazol group [15].

2.5. Luminescence measurements

It is known that most luminescence silver(I) compounds show their luminescence properties at low temperature, whereas only few of them are luminescent at room temperature [29]. Preliminary luminescence experiments on **1** as a nujol mull at room temperature are shown in Fig. 7.

Although the free ligand shows no luminescence, the spectra of **1** show two broad emission signals with shoulders at ~425 (shoulder at ~393 nm) and ~390 nm (shoulder at ~447 nm) upon excitation at 250 (curve a) and 350 nm (curve c), respectively. An unusual emission formed by two components at ~388 and ~410 nm was found upon excitation at 275 nm (curve b). This kind of dual emission could suggest the presence of different weakly coupled relaxation channels in **1**, as found in other compounds containing d^{10} metal centres [30,31]. Further investigations are being carried out to clarify this question.

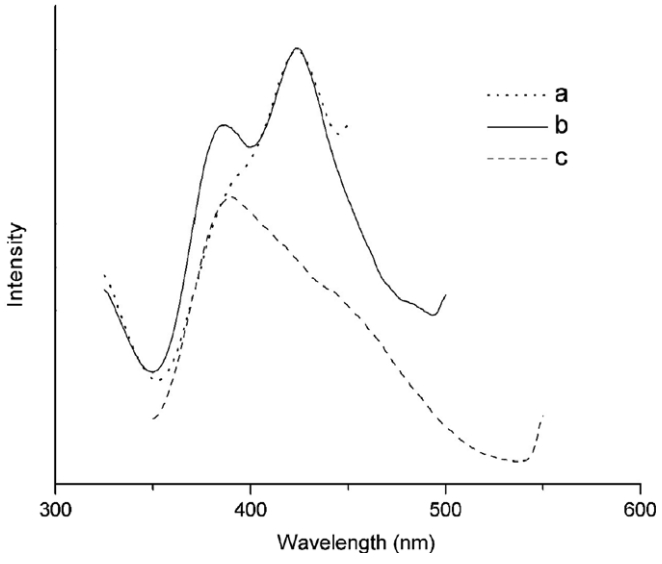

Fig. 7. Emission spectra of **1** as nujol mulls at room temperature. $\lambda_{exc} = 250$ nm (a); $\lambda_{exc} = 275$ nm (b); $\lambda_{exc} = 350$ nm (c).

3. Conclusions

A new air-stable silver triazol-3-thiolato complex, **1**, was synthesized and fully characterized, including X-ray crystal structure determination. The formation of **1** occurs through an oxidative cyclization of 2-pyridine *N*-4-ethyl thiosemicarbazone to 4-ethyl-5-pyridin-2-yl-2,4-dihydro-[1,2,4]triazol-thione, promoted by the presence of silver(I) ions. The X-ray crystal structure studies show the stabilization of the whole structure by π–π stacking interactions. DFT calculations that were carried out to study the nature of the Ag–Ag interaction, reveal that three of the MOs with Ag atomic orbital contributions clearly show d–d–σ-bonding. The approximate number of electrons involved in these Ag–Ag interactions is two. Preliminary luminescence experiments show fluorescence emission for **1** at room temperature. Upon excitation at 275 nm an unusual emission with two components is found, suggesting weak coupled relaxation channels. Further work on this subject is in progress.

4. Experimental

All commercials reagents were used as supplied. HAm4E was prepared according to the literature [15].

4.1. Synthesis of *1*

A solution of $AgNO_3$ (17 mg, 0.1 mmol) in H_2O (3 ml) was added to a solution of HAm4E (22 mg, 0.1 mmol) in MeOH (7 ml) and stirred for 30 min. The final clear yellow solution was kept in the dark and allowed to evaporate to give an orange product which was dissolved in DMF and overlayed with diethyl ether. Colourless single crystals suitable for a X-ray analysis of **1** were obtained.

Elemental analysis: *Anal.* Calc. for $C_{54}H_{54}Ag_6N_{24}S_6$: C, 34.5; H, 2.9; N, 17.9; S, 10.2. Found: C, 35.0; H, 3.2; N, 18.1; S, 9.7%. IR (ν_{max}/cm^{-1}): 1588 ν(C=N), 995 ν(NN), 789 ν(CS), 346 ν(Ag–N), 304 ν(Ag–S).

^1H NMR (DMSO-d_6, ppm): 8.71 (1H, d, H1); 7.98 (1H, m, H3); 7.93 (1H, d, H4); 7.50 (1H, m, H2); 4.61 (2H, s, CH_2), 3.39 (3H, s, CH_3).

4.2. Physical methods

Elemental analyses were performed with a Carlos Erba 1108 microanalyzer. NMR spectra were obtained from d^6-DMSO solutions with a Bruker AMX 300 spectrometer. Chemical shifts are reported in parts per million downfield from Me_4Si. IR spectra were recorded as KBr disks (4000–400 cm^{-1}) or polyethylene-sandwiched Nujol mulls (500–

100 cm^{-1}) with a Bruker IFS-66v spectrometer. Luminescence spectra were recorded at room temperature as Nujol mulls between quartz plates with a Varian Cary Eclipse Fluorescence Spectrophotometer.

4.3. X-ray crystallography

Crystals of **1**, grown in a mixture DMF/Et_2O, were mounted on glass fibers and were used for data collection. Reflections were obtained with a Bruker SMART CCD 1000 diffractometer. The data were processed with SAINT [32] and corrected for absorption using SADABS [33]. The structures were solved by direct methods [34], which revealed the position of all non-hydrogen atoms. They were refined on F^2 by a full-matrix least-squares procedure using anisotropic displacement parameters [35]. The hydrogen atoms were located from difference syntheses in their calculated positions, and were refined using a riding model. Atom scattering factors were taken from the International Table for X-ray Crystallography [36]. Crystal and refinement data are listed in Table 3.

4.4. Methods of the DFT investigations

The calculations using density functional theory (DFT) methods [37] were performed with the program system TURBOMOLE [38] (RIDFT program [39], Becke–Perdew functional (B–P-86) [40]). Basis sets were of TZVPP quality (triple zeta valence plus multiple polarization functions) [39b]. Relativistically corrected effective core potentials (ECP) were used for the Ag atoms (ECP-28) [41]. All geometry optimizations were performed without symmetry restrictions (C_1 symmetry), therefore convergence into local minimum structures can be assumed and is confirmed by an excellent agreement of the structural parameters with the experimentally observed data. Values given in Table 1 are average values of the slightly varying structural parameters, resulting without symmetry restrictions.

Table 3
Crystal data and structure refinement for **1**

Empirical formula	$C_{54}H_{54}Ag_6N_{24}S_6$
Colour, habit	colourless, prism
Formula weight	1878.79
Temperature (K)	293(2)
Crystal size (mm)	$0.14 \times 0.11 \times 0.10$
Crystal system	trigonal
Space group	$R\bar{3}c$ (no. 167)
Unit cell dimensions	
a (Å)	22.8293(14)
b (Å)	22.8293(14)
c (Å)	23.294(3)
α (°)	90(0)
β (°)	90(0)
γ (°)	120(0)
Volume (Å^3)	10513.8(16)
Z	6
Density (Mg/m^3)	1.780
Absorption coefficient (mm^{-1})	1.876
θ Range for data collection (°)	1.78–26.41
Index ranges	$-24 \leqslant h \leqslant 0$
	$0 \leqslant k \leqslant 28$
	$0 \leqslant l \leqslant 28$
Reflections collected	40437
Independent reflections (R_{int})	2412, 0.0391
Data/parameters	2412/136
Final R indices [$I > 2\sigma(I)$]	$R_1 = 0.0392$
	$wR_2 = 0.0917$
R indices (all data)	$R_1 = 0.0856$
	$wR_2 = 0.1009$
Goodness-of-fit	0.890
Largest diffraction peak/hole (e Å^{-3})	0.454/−0.960

Acknowledgement

We thank the Xunta de Galicia (Project PGIDIT03-PXIC20302PN) for continued financial support.

Appendix A. Supplementary material

Crystallographic data for the structure reported in this paper (excluding structure factors) have been deposited with the Cambridge Crystallographic Data Centre as Supplementary Publication No. CCDC-605304. Copies of the data can be obtained free of charge on application to CCDC, 12 Union Road, Cambridge CB2 1EZ, UK (fax: +44 1223/336 033. E-mail: deposit@ccdc.cam.ac.uk). Supplementary data associated with this article can be found, in the online version, at doi:10.1016/j.poly.2006.07.028.

References

[1] (a) S.R. Batten, R. Robson, Angew. Chem. 110 (1998) 1558;
(b) Angew. Chem., Int. Ed. 37 (1998) 1460;
(c) P.J. Stang, Chem. Eur. J. 4 (1998) 19;
(d) A.J. Blake, N.R. Champness, P. Hubberstey, W-S. Li, M. Schröder, M.A. Withersby, Coord. Chem. Rev. 183 (1999) 117.
[2] M.L. Tong, X.M. Chen, B.H. Ye, L.N. Ji, Angew. Chem. 111 (1999) 2376.
[3] M.L. Tong, X.M. Chen, B.H. Ye, L.N. Ji, Angew. Chem., Int. Ed. 38 (1999) 2237.
[4] C.M. Che, Z. Mao, V.M. Miskowski, M.C. Tse, C.K. Chan, K.K. Cheung Phillips, D.L. Leung, Angew. Chem. 112 (2000) 4250.
[5] C.M. Che, Z. Mao, V.M. Miskowski, M.C. Tse, C.K. Chan, K.K. Cheung Phillips, D.L. Leung, Angew. Chem., Int. Ed. 39 (2000) 4084.
[6] S.Q. Liu, T. Kuroda-Sowa, H. Konaka, Y. Suenaga, M. Maekawa, T. Mizutani, G.L. Ning, M. Munakata, Inorg. Chem. 44 (2005) 1031.
[7] (a) A.J. Blake, N.R. Champness, P.A. Cooke, J.E.B. Nicolson, Chem. Commun. (2000) 665;
(b) Y. Zheng, M. Cu, J-R. Zhang, X.-H. Bu, J. Chem. Soc., Dalton Trans. (2003) 1509;
(c) M.N. Huda, A.K. Ray, Phys. Rev. A 67 (2003) 013201-1;
(d) Q-M. Wang, T.C.W. Mak, J. Am. Chem. Soc. 123 (2001) 7594;
(e) M. Schmidt, Ph. Cahuzac, C. Bréchignac, H.-P. Cheng, J. Chem. Phys. 118 (2003) 10956;
(f) R. Fournier, J. Chem. Phys. 115 (2001) 2165.
[8] G.M. Koretsky, M.B. Knicelbein, J. Chem. Phys. 107 (1997) 10555.
[9] R.S. Eachus, A.P. Marchetti, A.A. Muenter, Annu. Rev. Phys. Chem. 50 (1999) 117.
[10] S.-H. Kin, G. Gedeiros-Ribeiro, D.A.A. Ohlberg, R. Stanley Willians, J.R. Heath, J. Phys. Chem. 103 (1999) 10341.
[11] A.A. Bagaur'yants, A.A. Safonow, H. Stoll, H.-J. Werner, J. Chem. Phys. 109 (1998) 3096.

[12] J.S. Casas, M.S. García-Tasende, J. Sordo, Coord. Chem. Rev. 209 (2000) 197.
[13] (a) P. Lo Meo, M. Gruttadauria, R. Noto, Arkivoc (2005) 114;
(b) M.A. Shaban, M.A. Mostafa, A.Z. Nasr, Pharmazie 58 (2003) 367;
(c) M.A. Martins Alho, R. Baggio, M.T. Garland, N.B. D'Accorso, O. Varela, Carbohydr. Res. 337 (2002) 1397;
(d) S. Buscemi, M. Gruttadauri, Tetrahedron 56 (2000) 999;
(e) R. Noto, P. Lo Meo, M. Gruttadauria, G. Werber, J. Heterocycl. Chem. 36 (1999) 667;
(f) S.A. Salim, K. Saleem, M.A. Khan, Indian J. Chem. 36B (1997) 617;
(g) R. Noto, P. Lo Meo, M. Gruttadauria, G. Werber, J. Heterocycl. Chem. 33 (1996) 863;
(h) R. Noto, F. Buccheri, G. Cusmano, M. Gruttadauria, G. Werber, J. Heterocycl. Chem. 28 (1991) 1421;
(i) M. Gruttadauria, F. Buccheri, S. Buscemi, G. Cusmano, R. Noto, G. Werber, J. Heterocycl. Chem. 29 (1992) 233;
(j) S. Kubota, Y. Ueda, K. Fujikane, K. Toyooka, M. Shibuya, J. Org. Chem. 45 (1980) 1473.
[14] I. García-Santos, Ph.D. Thesis. Univ. Santiago de Compostela, 2001.
[15] (a) E. Bermejo, A. Castiñeiras, L. Fostiak, I. García Santos, K. Swearingen, D.X. West, Polyhedron 23 (2004) 2303;
(b) E. Bermejo, A. Castiñeiras, I. García-Santos, L.M. Fostiak, J.K. Swearingen, D.X. West, Z. Anorg. Allg. Chem. 631 (2005) 728.
[16] K.K. Aravindakshan, C.G.R. Nair, Indian J. Chem. 20A (1981) 684.
[17] N.S. Youssef, K.H. Hegab, Synth. React. Inorg., Met.-Org. Nano-Met. Chem. 35 (2005) 391.
[18] L.J. Ashfield, A.R. Cowley, J.R. Dilworth, P.S. Donnelly, Inorg. Chem. 43 (2004) 4121.
[19] H.-B. Bürg, J.D. Dunitz (Eds.), Structure Correlations, VCH, Weinheim, Germany, 1994, p. 780.
[20] Y. Zheng, Acta Crystallogr. C 60 (2004) m471.
[21] Y.-B. Dong, H.-Y. Wang, J.-P. Ma, D.-Z. Shen, R.-Q. Huang, Inorg. Chem. 44 (2005) 4679.
[22] M. Cingi Biagini, M. Laufranchi, L. Marchiò, M.A. Pellinghelli, Inorg. Chim. Acta 305 (2000) 95.
[23] M. Yazdanbakhsh, M. Hakimi, M.M. Heravi, M. Ghassemzadeh, B. Neumüller, Z. Anorg. Allg. Chem. 631 (2005) 924.
[24] F. Adhami, M. Ghassemzadeh, M.M. Heravi, A. Taeb, Z. Anorg. Allg. Chem. 625 (1999) 1411.
[25] P. Pyykkö, Chem. Rev. 97 (1997) 597.
[26] L. Han, Z. Chen, J. Luo, M. Hong, R. Cao, Acta Crystallogr. E 58 (2002) m383.
[27] R.-F. Song, Y.-B. Xie, J.-R. Li, X.-H. Bu, J. Chem. Soc., Dalton Trans. (2003) 4742.
[28] S. Hamamci, V.T. Yilmaz, W.T.A. Harrison, Struct. Chem. 16 (2005) 379.
[29] (a) M.-L-. Tong, X.-M. Cheng, B.-H. Ye, L.-N. Ji, Angew. Chem. 111 (1999) 2376;
(b) Angew. Chem., Int. Ed. 38 (1999) 2237;
(c) Y.-Q. Wei, K.-C. Wu, B.-T. Zhuang, Z.-T. Zhou, M.-X. Zhang, C.-P. Liu, Z. Anorg. Allg. Chem. 631 (2005) 1532, and references therein.
[30] P. Sevillano, O. Fuhr, M. Kattannek, P. Nava, O. Hampe, S. Lebedkin, R. Ahlrichs, D. Fenske, M.M. Kappes, Angew. Chem. 118 (2006) 3785.
[31] P. Sevillano, O. Fuhr, M. Kattannek, P. Nava, O. Hampe, S. Lebedkin, R. Ahlrichs, D. Fenske, M.M. Kappes, Angew. Chem., Int. Ed. 45 (2006) 3702.
[32] Bruker, SMART and SAINT, Area Detector Control Integration Softhware, Bruker Analytical X-ray Instruments, Inc., Madison, WI, USA, 1999.
[33] G.M. Sheldrick, SADABS, Program for Empirical Absorption Correction of Area Detector Data, University of Göttingen, Germany, 1997.
[34] G.M. Sheldrick, Acta Crystallogr. A 46 (1990) 467.
[35] G.M. Sheldrick, SHELX-97, Program for the Refinement of Crystal Structures, University of Göttingen, Germany, 1997.
[36] International Tables for Crystallography, vol. C, Kluwer Academic Publishers, Dordrecht, The Netherlands, 1995.
[37] (a) R.G. Parr, W. Yang, Density Functional Theory of Atoms and Molecules, Oxford University Press, New York, 1988;
(b) T. Ziegler, Chem. Rev. 91 (1991) 651.
[38] (a) R. Ahlrichs, M. Bär, M. Häser, H. Horn, C. Kölmel, Chem. Phys. Lett. 162 (1989) 165;
(b) O. Treutler, R. Ahlrichs, J. Chem. Phys. 102 (1995) 346;
(c) M.v. Arnim, R. Ahlrichs, J. Chem. Phys. 111 (1999) 9183.
[39] (a) K. Eichkorn, O. Treutler, H. Öhm, M. Häser, R. Ahlrichs, Chem. Phys. Lett. 242 (1995) 652;
(b) K. Eichkorn, F. Weigend, O. Treutler, R. Ahlrichs, Theor. Chim. Acta 97 (1997) 119.
[40] (a) A.D. Becke, Phys. Rev. A 38 (1988) 3098;
(b) S.H. Vosko, L. Wilk, M. Nusair, Can. J. Phys. 58 (1980) 1200;
(c) J.P. Perdew, Phys. Rev. B 33 (1986) 8822.
[41] D. Andrae, U. Haeussermann, M. Dolg, H. Stoll, H. Preuss, Theor. Chim. Acta 77 (1990) 123.

Available online at www.sciencedirect.com
ScienceDirect
Polyhedron 25 (2006) 3661–3673
POLYHEDRON
www.elsevier.com/locate/poly

Author Index to Volume 25

Abarkan, I., 1763
Abbasi, A.R., 1915
Abboud, K.A., 613, 2605
Abdurrahmanoğlu, Ş., 3639
Abrahams, I., 241, 996
Abram, U., 3343
Abrutis, A., 293
Abu-Youssef, M.A.M., 1187
Adams, H., 869
Adhikary, B., 1681
Adhikary, C., 2191
Adrio, L.A., 1449, 2848
Afzaal, M., 864
Ağın, F.D., 3165
Ahmad, S., 1633, 2629
Ahn, K.H., 3025
Ainscough, E.W., 2341
Airoldi, C., 2880
Akba, O., 3133
Akbar Ali, M., 3245, 3337
Akilan, P., 2623
Akitsu, T., 1089, 2655
Al-Arfaj, A.R., 1633
Albert, J., 793
Ali, M.S., 2065
Ali, S., 1633
Alizadeh, M.H., 1567, 1921
Allain, M., 3201
Allan, G.M., 695
Almeida, M., 1209
Alonso, F.J.G., 105
Altındal, A., 737, 3593, 3639
Ambrus, C., 1613, 3617
Amim Jr., J., 2119
Amini, M.M., 3231
Amirnasr, M., 671, 1967
Andaç, Ö., 1279
Anderson, P.A., 568
Andrews, C.D., 853
Andrews, P.C., 1625
Angélica, R.S., 2880
Annibale, G., 1979
Anson, C.E., 530
Antelo, J.M., 1449, 2848
Antzutkin, O.N., 3569
Aoki, K., 2929
Aravindan, P.G., 2859
Argitis, P., 3427
Arif, A.M., 876
Arnold, D.P., 1195
Aromí, G., 325, 2791
Arora, M., 627
Aroz, R., 3066
Arslan, M., 3526
Arumugham, M.N., 1507, 3253
Arunachalam, S., 1507, 3113, 3253
Asali, K.J., 1695
Ashraf, W., 2629
Aslanoğlu, M., 1133
Aydın, A., 1279

Baca, S.G., 869, 1215, 3617
Backov, R.V., 2605
Baggio, R., 2072, 2277
Baggio, R.F., 9
Bahramian, B., 2904
Bai, S.-Q., 2778
Bai, Y.-G., 3209
Bakhtiari, A., 1893
Balakrishna, M.S., 815, 3215
Balamurugan, R., 1077
Balashova, T.V., 1105
Balde, L., 2229
Baldwin, M.J., 3145
Bali, S., 1033
Bandyopadhyay, P., 1177, 2149
Banerjee, A., 2284
Banerjee, D., 1299, 3077
Banerjee, P., 3138
Banerjee, R., 1367
Banthia, S., 2269
Bao, M., 1195
Baral, M., 722
Baran, E.J., 2597
Baranowska, K., 1555
Barba-Behrens, N., 2363
Barbazán, P., 3343
Barceló-Oliver, M., 71
Barloy, L., 3349
Barooah, N., 17
Barros-García, F.J., 43, 52
Bartole-Scott, A., 429
Bartyzel, A., 687
Baruah, J.B., 17, 2525
Basavaraj, T., 2976
Basson, S.S., 2415
Basta, R., 876
Bastida, R., 783
Basu, S., 1263
Basu Baul, T.S., 3441
Bataille, T., 3543
Batista, A.A., 1543
Batsanov, A.S., 17, 300
Bawa, G., 2897
Bayır, Z.A., 39
Becker, B., 1555, 2142

doi:10.1016/S0277-5387(06)00691-7

Beckett, M.A., 1011
Bedford, R.B., 1003
Beja, A.M., 2021
Bekaroğlu, Ö., 737, 3593, 3639
Bekiari, V., 2869
Belai, N., 2015
Belaj, F., 1893
Bellú, S., 1483
Belo, D., 1209
Beloso, I., 2673
Ben Dhia, M.T., 3299
Benito, A., 1585
Ben Nasr, C., 2953
Benoit, D.M., 996
Bensch, W., 3269
Bera, M., 2791
Beran, M., 1292
Bermejo, M.R., 1714
Bernalte-García, A., 52, 1399
Bernès, S., 1549
Bernhardt, P.V., 1811, 3245, 3337
Berrettini, F., 834
Berridge, R., 989
Berthet, J.-C., 1700
Berto, S., 2815
Beşli, S., 963
Betham, M., 1003
Beurer, E., 1514
Bharadwaj, P.K., 1491
Bharathi, K.S., 2859
Bhat, S.G., 61
Bhattacharyya, S., 550
Bhawmick, R., 1177
Bi, W.-H., 1239
Białońska, A., 3222
Bianchini, C., 1607
Bilgin, A., 3165
Bingham, A.L., 945, 3238
Binions, R., 3032
Binyamin, I., 3387
Biswas, A.N., 2149
Biswas, S., 1681
Blackman, A.G., 373
Blackman, C., 334
Blake, A.J., 591, 599
Blindauer, C.A., 513
Bobyljov, A.P., 2401
Boča, R., 1823, 3261
Bochkarev, M.N., 1105
Bochmann, M., 387, 843
Bogdanović, G.A., 1096
Bohra, R., 654
Bontchev, P.R., 2254
Bontchev, R.P., 2254
Borah, R., 3501
Bortoluzzi, M., 1979, 2698
Bose, D., 645, 663, 1477
Bott, R.K.J., 387
Bouachir, F., 1142
Boudalis, A.K., 1391
Bouet, G.M., 3201
Bouhmaida, N., 2229
Bouwman, E., 2967
Bozzuto, D., 776
Bradley, D.C., 821
Braga, S.S., 1471
Brechin, E.K., 325
Brennessel, W.W., 286
Breza, M., 2559
Bricklebank, N., 989
Bridgewater, B.M., 499
Brito, F., 3366
Brito, H.F., 3488
Brodie, A.M., 2341
Brooks, N.R., 3285
Bruce King, R., 3183
Bruce, D.W., 307
Brusko, V.V., 1433, 3330, 3611
Bujang, F.H., 3245
Bulak, E., 2577
Bulut, A., 1133
Bulut, M., 3593, 3639
Burrows, H.D., 3581
Bursten, B.E., 575
Butcher, R.E., 2093
Butcher, R.J., 87, 747, 2755, 2897, 3159
Büyükgüngör, O., 1279, 2829, 2985

Cachapa, A., 3366
Cahill, C.L., 776
Cai, J., 3045
Čajan, M., 1421
Calleja, S., 1625
Caneschi, A., 2175
Cano, J., 325
Cao, R., 1239
Carballo, R., 3343
Carlos, L.D., 1471, 2471
Carmalt, C.J., 3032
Carr, M.J., 1069
Carriedo, G.A., 105
Casabó, J., 801
Casellas, H., 2959
Castellano, E.E., 1543, 2597, 2920
Castiñeiras, A., 3653
Castro, J., 2673
Caudron, A., 2215
Caulton, K.G., 459
Cavaglioni, A., 834
Cerchiaro, G., 2055
Černák, J., 2935
Černík, M., 1292
Cerrada, E., 2785, 3066
Ceyhan, T., 737
Chafaa, S., 3201
Chaichit, N., 2198, 2710
Chakraborty, J., 3006, 3138
Chakravarty, A.R., 2135
Chan, Z.-K., 2325
Chand, B.G., 2333
Chang, T.M., 1287
Charan, S., 747
Chattopadhyay, N., 1753
Chattopadhyay, P., 1939
Chattopadhyay, S., 2241, 2513, 2637
Chaudhuri, S., 2191
Chauhan, A.K.S., 747
Chauhan, H.P.S., 2841
Chauvin, A.-S., 2261
Chawla, S.K., 627
Chen, C., 1307
Chen, C.-H., 2407
Chen, J.-D., 1307, 2325
Chen, J.-H., 1864, 2207
Chen, J.-S., 1359
Chen, T.-M., 1167

Chen, X.-T., 2426
Chen, Y., 3053
Cheng, C.-W., 1864
Cheng, R.-M., 2426
Cheng, S.-C., 3393
Cheng, Y.-X., 2153
Cherkasov, R.A., 3330
Chernyavskaya, A.A., 1723, 3603
Chiang, M.Y., 1125
Chimatadar, S.A., 2976
Chinea, E., 3366
Chingsubam, P., 2929
Chisholm, M.H., 827
Cho, J.H., 1811
Cho, K.-Y., 1864, 2207
Chojnacki, J., 1555, 2142
Chopra, D., 25, 2284
Choudhury, C.R., 1271
Chow, H.S., 1831
Christou, G., 203, 613, 1737
Churchill, D.G., 499, 1519
Ciesielski, A., 2643
Çiftçi, G.Y., 953
Çil, E., 3526
Cingolani, A., 124
Cini, R., 834
Ciullo, L., 1483
Ciunik, Z., 1994, 3222
Clarkson, A.J., 373
Clegg, W., 300, 1043, 2433, 3285
Clérac, R., 530
Cole-Hamilton, D.J., 853
Coles, M.P., 1247
Coles, S.J., 953, 963, 989, 1003, 1011
Collison, D., 325
Constable, E.C., 421, 437, 1831, 1844
Contreras, R., 1662, 2363
Conway, S.L.J., 406
Copley, R.C.B., 300
Cornard, J.-P., 2215
Coronado, E., 2433
Corsini, M., 834
Cortés, S., 2072
Cortez, L., 9
Costa-Filho, A.J., 2597
Cotton, F.A., 219
Cotton, S.A., 1057
Coutsolelos, A.G., 3427
Cowley, A.H., 259, 983
Cremona, M., 3488
Cronin, L., 3474
Cui, X.-L., 3305
Cunha, A.C., 2055
Curran, R., 1771
Curtis, N.F., 1204, 1313, 1579, 1601

Da Costa Ferreira, A.M., 2055
d'Angelo, J., 2229
Daniel, S.D., 205
Daniele, P.G., 2815
Danopoulos, A.A., 859
Dantsker, I.A., 2401
Daro, N., 1271
Das, D., 2333
Das, P., 1177, 2149
Das, S., 2289
Das, S.K., 3588
Datta, P., 2503, 3435
Dattelbaum, A.M., 349
Davar, F., 2127
Davie, M.E., 923
Davies, D.B., 953, 963
Davies, E.S., 591
Davies, M.J., 397
Davis, M.F., 930
Dawid, U., 3647
Day, P., 2583
de Andrade, R.P., 2119
De Bellis, V.M., 2119
de Faria Franca, E., 2119
de Galarreta, C.M.R., 3366
de Gelder, R., 2967
De Giovani, W.F., 1457
de Jesús, F., 3127
de la Calle, R.B., 3495
de Lima, A.A., 1457
de Meijere, A., 219
de Moraes Silva, A., 1319
de Sá, G.F., 3488
De Silva, C.R., 3449
de Silva, S.A., 2593
Deacon, G.B., 379
Decurtins, S., 1514, 1613, 3617
Defazio, S., 834
Dehnen, S., 3653
Deka, K., 2525
del Carmen Fernández-Fernández, M., 783
Demetriou, D.Z., 996
Depree, C.V., 2341
Desplanches, C., 1271
Devereux, M., 1771
Dey, G.K., 2383
Dey, S., 87, 2383
Dhar, B.B., 1367
Dhara, P.K., 1939
Dhia, M.T.B., 1373
Dhuri, S.N., 3269
Dias, H.V.R., 1655
Diaz, C., 2241, 3084
Dinda, J., 1125, 1791, 2333, 2503, 3053
Dinda, R., 2375
Diógenes, I.C.N., 1543
Divband, B., 1915
Diyabalanage, H.V.K., 1655
Dlháň, L., 1823, 3261
Do, Y., 1519
Dogan, A., 2577
Dolder, S., 1514
Doležal, K., 1421
Domínguez, S., 3366
Donnio, B., 307
Douadi, T., 3201
Doussineau, T., 1763
Douvas, A.M., 3427
Doyle, R.P., 3457
Drake, J.E., 945, 1033, 2915, 3238, 3481
Drew, M.G.B., 753, 888, 1939, 2241, 3084
Driessen, W.L., 599
Drożdżyński, J., 2083
Drylie, E.A., 853
Duarte, M.T., 1209
Duesler, E.N., 3387
Duimstra, J.A., 2705
Dupree, R., 3569
Durap, F., 3133

Eaton, R.J., 953, 963
Eberlin, M.N., 2055
Edwards, A.J., 211
Edwards, P.P., 568
Efremova, O.A., 1233
Eggert, J.P.W., 910
Eichhorn, B., 521
Einaga, Y., 1089, 2655
Eisenstein, O., 339
Eisler, D.J., 266
Ejau, W.B., 3337
Elango, S., 1864, 2207
El Fallah, M.S., 25, 2737, 2764, 3006
Elgin, J.D., 2616
Eliav, Y., 2593
El-Kaderi, H.M., 224
El-khateeb, M., 1386, 1695, 3413
Ellena, J., 1543, 2119, 2597
Ellern, A., 3474
Ellis, D., 915
Ely, T.O., 2065
Eng, G., 3441
Ephritikhine, M., 1537, 1700, 2439
Erbil, M.K., 737
Ernst, R.D., 876
Ertem, B., 3165
Escriche, L., 801
Esenturk, E.N., 521
Eshtiagh-hossieni, H., 1921
Espinosa, E., 2295
Essalah, K., 3299
Ettireddy, P.R., 1147
Eusébio, E., 2021
Eusébio, T., 1209
Evans, W.J., 484, 1105, 2691
Exley, C., 1707, 3399

Facchin, G., 2597
Fagin, A.A., 1105
Falvello, L.R., 1967, 2375
Fang, C.-J., 2778
Farías, L., 9
Faustino, W.M., 3488
Fawcett, J., 1182
Fedorov, V.E., 1233
Fedutik, Yu.A., 1723
Felcman, J., 1319
Felinto, M.C.F.C., 3488
Félix, V., 753
Feliz, M., 3366
Feng, S.-H., 2565, 3071
Fernandes, J.A., 1471
Fernández, J.J., 1449, 2848
Ferreira, V.F., 2055
Ferri-Mendoza, M.G., 1971
Fettinger, J., 521
Fettouhi, M., 2629
Field, L.D., 1498
Fielden, J., 3474
Figuerola, A., 2241, 3084
Filippova, I.G., 1215
Filoti, G., 2175
Findlater, M., 983
Fiol, J.J., 71, 2295
Fischer, L., 1011
Flood, K., 1313, 1579, 1601
Flores-Parra, A., 1662, 2363
Foerster, T., 923
Foguet-Albiol, D., 1737
Fondo, M., 1714
Font-Bardia, M., 793
Foreman, M.R.St.J., 888
Forsling, W., 3569
Forsyth, M., 379
Fox, J., 3387
Fox, M.A., 300
Franckevicius, V., 1057
Franken, A., 1069
Fraser, C.S.A., 266
Frost, R.L., 3379
Fu, R.-B., 1618
Fu, W., 2571
Fuess, H., 1823, 3261
Fun, H.-K., 1408

Gądek, A., 1441
Gahlot, P., 759
Gale, P.A., 901
Gallardo, G., 3366
Gallucci, J.C., 827
Gameson, I., 568
Gamez, P., 2959
Gan, X.-m., 3387
Gan, Y.-H., 3555
Gao, E.-Q., 2778
Gao, R.-Q., 2530, 3305
Gao, S., 1256
Gao, W., 2565
García, S., 1483
García-Deibe, A.M., 1714
García-Hernández, Z., 1662
García-Raso, A., 71, 2295
García-Santos, I., 3653
García-Vázquez, J.A., 2673
Gardiner, S., 1017
Garland, M.T., 9, 2277
Garner, C.D., 591
Garrioch, R.M., 915
Gayen, P., 3435
Gayoso, E., 1449
Gdaniec, M., 1215, 2175, 3417
Ge, H.-Y., 1875
Geist, A., 888
Gelbrich, T., 937
Geng, F.-Y., 2530, 3305
Geng, J., 585
George, P.P., 3215
George, T.A., 2721
Gerbeleu, N., 1215, 3617
Getova, V.T., 2254
Ghames, A., 3201
Ghermani, N.E., 2229
Gholivand, K., 711
Ghosh, A., 2241, 3084
Ghosh, B.K., 645, 663, 1477, 3104
Ghosh, R., 645, 3104
Ghosh, S., 2375
Ghosh, S.K., 1263
Giambastiani, G., 1607
Gich, M., 113
Gili, P., 3366
Gill, W.R., 300
Gladfelter, W.L., 279
Glenny, M.W., 599
Glowiak, T., 1561
Glukhova, T.A., 1105

Glushonok, G.K., 3603
Goddard, R., 1215
Goher, M.A.S., 1531
Gök, Y., 3165
Goldcamp, M.J., 3145
Golobič, A., 1161, 2824
Gómez, K., 3509
Gómez-García, C.J., 2433
Gonçalves, I.S., 1471
González, G., 3509
González, J.C., 1483
González-Baró, A.C., 2920
Görgülü, A.O., 3526
Gradinaru, J., 3417
Gramlich, V., 3006
Grandjean, F., 2616
Granell, J., 793
Granifo, J., 2277
Green, M.L.H., 406
Gregoliński, J., 2745
Gren, C.K., 286
Grevy, J.M., 1662
Grimditch, R.S., 300
Grover, R., 759
Guerfel, T., 1142
Guerra, D.L., 2880
Guerrero, J., 9
Guilardi, S., 2119
Guillon, D., 307
Gümgüm, B., 3133
Gundla, V.L.N., 3312
Gunjima, N., 3519
Gunning, P.T., 3474
Gupta, A., 654
Gusmeroli, D., 421
Gyepes, R., 2491

Haffar, D., 3201
Hagel, J., 3183
Halcrow, M.A., 235, 1077
Halliwell, M., 864
Hamaker, C.G., 119
Hamid, M.H.S.A., 3245
Hamilton, E.J.M., 1901
Hammud, H.H., 2721
Han, J., 2483, 3519
Han, L.-M., 3209
Han, Y.-W., 3405
Hanmungtum, P., 2710
Hanna, J.V., 3569
Hanusa, T.P., 286
Harrington, R.W., 2433
Harrison, J.A., 1729
Harrison, W.T.A., 2829
Harrowfield, J.M., 910, 1811
Hartinger, C.G., 1971
Harverson, P., 437
Havel, J., 1884
Hazarika, P., 3501
Hazell, A., 1471
He, J.-R., 1239
He, T., 1498
He, Z., 2778
Hearshaw, M.A., 853
Heeg, M.J., 224, 2109
Helliwell, M., 325
Henriques, R.T., 1209
Hermann, P., 1884
Hernández-Molina, R., 3366
Herrera, J.-M., 869
Hey-Hawkins, E., 1607
Hibbert, T.G., 300
Hill, N.J., 983
Hitchcock, P.B., 1247
Hoffman, D.M., 205
Hollandsworth, C.B., 827
Holman, K.T., 1567
Holmes, A.L., 271, 881
Hong, F.-E., 3555
Hope, E.G., 1182
Horton, P.N., 307, 989, 1003, 2583
Hossain, G.M.G., 95
Hossaini Sadr, M., 3285
Housecroft, C.E., 421, 437, 1831, 1844
Howard, J.A.K., 300
Howell, J.A.S., 2993
Howie, R.A., 695
Hsieh, H.-Y., 1864, 2207
Hsu, G.-Y., 3393
Hsu, S.-F., 1167
Hu, S.-M., 1
Huang, D., 459
Huang, J.-H., 559
Huang, W., 1379
Huang, W.L., 2160
Huang, X.-H., 1618
Hubert-Pfalzgraf, L.G., 293
Huch, V., 2841
Huck, D.M., 307
Huck, W.T.S., 585
Hudson, M.J., 888
Huffman, J.C., 550
Hughes, D.L., 387, 843
Humphrey, P., 1498
Humphrey, S.M., 1946
Hung, C.-H., 645, 2325
Hunter, A.D., 2755
Hursthouse, M.B., 307, 2583, 2915, 3238, 3481
Huth, S., 937
Hwang, I.-C., 3025
Hwang, L.-P., 2207
Hwang, W.-S., 1791, 3053

Ibañez, A., 2072
Incarvito, C.D., 1873
İrişli, S., 1333
Isab, A.A., 1633, 2629
Isber, S., 2721
Isihara, H., 2483
Islam, N.S., 3501
Isolani, P.C., 2447
Ivaniková, R., 1823, 3261

Jackson, W.G., 1955
Jaganyi, D., 2730
Jain, A.K., 654
Jain, V.K., 87, 2383, 3159
Jana, A.D., 1125
Janczak, J., 3319
Jankowska, A., 1348, 2663
Jarry, E., 3399
Jasimuddin, Sk., 1299, 1571
Jaworska, M., 1111, 2519, 2537
Jensen, P., 360
Jeong, J.H., 1787
Jezierska, J., 678

Jia, C., 1613
Jiang, J., 1195
Jiang, Y.-S., 1359
Jimenez-Rodriguez, C., 853
Jin, L.-P., 1327, 3017
Jin, R., 2530, 3305
Jing, S.-Y., 3053
Johnson, B.F.G., 585
Jones, C., 1592
Jones, J.N., 259
Jones, L.F., 325, 360
Jones, M.O., 568
Jones, R.A., 271, 881
Jones, R.M., 3145
Joniaková, D., 2491
Joseph, M., 61, 1408
Joshi, A., 2183
Jun, M.-J., 2318, 2717
Junk, P.C., 379, 1592

Kabir, S.E., 95
Kahrović, E., 2459
Kaim, W., 2577
Kakkar, R., 759
Kalita, D., 3501
Kalkan, A., 39
Kan, Y.-H., 635
Kandaswamy, M., 2623
Kang, H.C., 2318
Kang, Y.S., 3025
Kannan, S., 3095
Kannappan, R., 1646
Kanungo, B.K., 722
Kapoor, P., 31
Kapoor, R., 31
Karakaya, H., 2829
Karaliota, A., 1337
Karbowiak, M., 2083
Karslıoğlu, S., 3165
Kasumov, V.T., 1133
Kavanagh, K., 1771
Kawajiri, R., 2650
Kazak, C., 1133
Ke, J.L., 2160
Kedarnath, G., 2383
Kefi, R., 2953
Kemp, S., 2433
Kennedy, J.D., 1069
Keppler, B.K., 1971
Kessler, V.G., 2401
Khaddar, M.R., 1373, 3299
Khalaji, A.D., 1967
Khan, A.U., 2929
Khan, M.A., 3201
Khan, S.N., 2929
Khandar, A.A., 1893
Khanna, S., 2755
Khlebnikov, A.I., 2683
Khokhar, A.R., 2065
Khoshnavazi, R., 1921
Kılıç, A., 953, 963
Kilner, C.A., 235
Kim, J.Y., 1811
Kim, Y., 1811
Kisała, J., 3222
Kishore, A., 61
Kitiphaisalnont, P., 2710
Kivekäs, R., 801
Kłak, J., 1348, 2537, 2663
Klanicová, A., 1421
Klinowski, J., 2471
Kloth, M., 1592
Kneifel, A.N., 1271
Ko, J., 2318, 2717
Kochel, A., 2745, 3647
Kögerler, P., 3474
Kojić-Prodić, B., 2459
Köksal, F., 1133
Koman, M., 1561
Koner, R., 2007
Koner, S., 2191
Kong, C.W., 3118
Konitz, A., 1555
Korecz, L., 1483
Korp, J.D., 205
Kotek, J., 1884
Koval'chuk, T.V., 1723, 3603
Kozimor, S.A., 484
Kožíšek, J., 2559
Kozlevčar, B., 1161, 2824
Kozlova, S.G., 1233
Krause, J.A., 3145
Kremer, E., 2597
Krishna, H., 3189
Krishnamurthy, S.S., 3189
Krivolapov, D.B., 1433, 3330, 3611
Kroczewska, D., 678
Kropidłowska, A., 2142
Kruszynski, R., 1111, 1348, 1985, 2519, 2537, 2663
Kubicki, M., 2643
Kucera, B.E., 279
Kuiper, D.S., 251
Kulatilleke, C.P., 2593
Kulikova, T.I., 1105
Kumar, A., 747
Kumar, R., 3238
Kumar, R.S., 3113
Kumaraguru, N., 1507, 2452, 3253
Kumbhare, L.B., 3159
Kuncser, V., 2175
Kundu, P., 2007
Kundu, S., 1263
Kurek, S., 3222
Kuriakose, M., 61
Kuroda-Sowa, T., 2483, 3519
Kurskii, Y.A., 1105
Kurup, M.R.P., 61, 1408, 1931
Kurzak, B., 678
Kusyaev, D.M., 1105
Kwak, J., 1519
Kwiatkowski, E., 2809
Kwiatkowski, M., 2809
Kwon, S.J., 1519
Kwong, H.-K., 1256
Kyritsakas, N., 3349

Labat, G., 1613
Laguna, M., 2785, 3066
Lai, R.J., 881
Lancaster, S.J., 387
Landee, C.P., 2093
Landman, M., 3562
Lang, H., 3413
Langer, V., 1187
Lappert, M.F., 397
Lardiés, N., 2785

Laskar, I.R., 1167
Laskar, M., 2525
Lataifeh, A., 1695
Lath, H., 989
Latorre, R.O., 2026
Lau, T.-C., 1256
Leary, S.G., 379
Lee, C.-S., 1791, 3053
Lee, G.-b., 2318
Lee, G.-H., 2207
Lee, H.-T., 2944
Lee, J., 1519
Lee, J.-C., 3555
Lee, N.-k., 2318
Lee, T.-Y., 559
Lefebvre, F., 2953
Lehn, J.-M., 2643
Lehn, J.-S.M., 205
Lehtonen, A., 767
Lemoine, P., 2007
Lemos, V.P., 2880
Lemus, L., 9
Leong, W.K., 2392
Leovac, V.M., 1096
Levason, W., 930
Lewis, J., 211
Li, B.-L., 1875
Li, C.-K., 211
Li, F.-A., 2153
Li, G.-H., 1359, 2565, 3071
Li, H., 585
Li, L.-C., 3017
Li, Y.-J., 2530, 3305
Li, Y.-M., 1, 1618
Li, Y.-Z., 2426
Lian, Z.-X., 3045
Liang, G., 2571
Lianos, P., 2869
Liao, D.-Z., 2153
Liao, F.-L., 1864, 2207
Liao, Z.-L., 1359
Liaw, B.-J., 2897
Light, M.E., 901, 945, 1011, 1033, 2915, 3238, 3481
Liles, D.C., 3562
Lin, C.M., 1287
Lin, C.-N., 3104
Lin, J., 1909
Linarić, M.R., 2353
Lindberg, M., 3569
Lindemann, R.H., 2119
Linden, A., 3441
Liou, J.-C.-C., 1299
Lipkowski, J., 2175
Lis, T., 2083
Lisowski, J., 2745
Lissner, F., 2577
Litos, C., 1337
Litvinenko, A.S., 2465
Litvinov, I.A., 1433, 3330, 3611
Liu, C.W., 2897
Liu, J., 1901
Liu, P., 3045, 3533
Liu, Q., 1195
Liu, S.-X., 1514, 1613
Llusar, R., 3366
Lo, W.-K., 271
Lobana, T.S., 2755, 2897
Lobkovsky, E.B., 251
Lobo, V.M.M., 3581
Lodge, M.T.J., 568
Loginova, N.V., 1723, 3603
Long, D.-L., 3474
Long, G.J., 2616
Longoria Jr., E., 2065
Lönnecke, P., 1607
Lopes, E.B., 1209
Lopes, L.G.F., 1543
López-Sáez, M.-J., 1003
López-Torres, E., 1464
López-Zafra, A., 2295
Lorenz, I.-P., 654
Lotz, S., 3562
Lough, A.J., 429
Low, D.M., 325
Low, J.N., 695
Lozano, M.C., 3127
Lozano, R., 3127
Lozano-Vila, A.M., 1399
Lu, T.-H., 1125, 1299, 1571, 2503, 2764, 3077, 3104
Lubal, P., 1884
Lucas, C.R., 1681
Luckay, R.C., 3330
Luna-Giles, F., 43, 52, 1399
Luneau, D., 293, 2737
Lüning, U., 910
Luo, B., 279
Luque, A., 793

Ma, C., 1195
Ma, C.-L., 3405
Ma, H.-R., 195
Ma, J.-F., 635
MacBride, J.A.H., 300
Macdonald, C.L.B., 259
Machura, B., 1111, 1348, 1985, 2537, 2663
Macías, A., 783, 3495
Macías, R., 1069
Maekawa, M., 2483, 3519
Magalhães, H.M., 2055
Mague, J.T., 3215
Maguire, M., 1625
Mahon, M.F., 1057
Maiti, N., 1519
Majumder, A., 1753, 2550
Mak, T.C.W., 975, 2375
Makarenko, N.P., 1105
Mal, D., 2191
Malaestean, I., 3617
Malaisé, G., 3349
Maldonado-Rogado, M.A., 43, 52
Maldotti, A., 3427
Maleček, J., 1884
Małecki, J.G., 2519
Malik, M.A., 241, 864
Malinovskii, S., 3417
Malinovskii, S.T., 3617
Mallah, T., 325
Mallick, A., 1753
Mal'arová, M., 2935
Malta, O.L., 3488
Man, S.P., 1017
Mandal, D., 702
Mangrich, A.S., 1319
Manke, D.R., 493
Manna, S.C., 1779
Manners, I., 429

Manning, T.D., 334
Marangoni, G., 1979
Marchetti, F., 124
Marek, J., 2491
Mariño, M., 1449
Marken, F., 888
Martin, J.D., 349
Martínez, J., 2848
Martínez, M., 3509
Martínez-Máñez, R., 1585
Martínez-Sánchez, J.M., 3495
Mašlejová, A., 1823, 3261
Massera, C., 2959
Massoud, S.S., 1673
Masters, A.F., 1498
Mata, I., 2295
Mathur, S., 2841
Mathur, T., 2503
Matos, M.J., 1209
Matsushita, T., 3006
Mautner, F.A., 1531, 1673
Mayer, P., 654
Mayer-Figge, H., 3138
Mazur, M., 1561
McCann, M., 1771
Mcinnes, E.J.L., 325
McKee, V., 1771
McLauchlan, C.C., 119
McMaster, J., 591
Meade, T.J., 2705
Mech, A., 2083
Mederos, A., 3366
Medjidov, A.A., 1279
Meghdadi, S., 671
Mehandjiev, D.R., 2254
Melnik, M., 1561
Mena, A., 9
Mendiola, M.A., 1464
Mendoza, C., 3509
Mendoza, O., 2101
Mercê, A.L.R., 1319
Mereacre, V., 2175
Merlin, J.-C., 2215
Messerle, L., 559
Meyer, E., 1543
Meyers, E.A., 1901
Mhiri, T., 3543
Micera, G., 3173
Mička, Z., 2491
Mikloš, D., 1561, 1823
Miličević, A., 2800
Milios, C.J., 134
Miller, J.S., 1157, 1927
Mirkhani, V., 2904
Mironov, Y.V., 1233
Mironova, E.V., 3611
Mirza, A.H., 3245, 3337
Mirzaee, M., 3231
Mirzaei, M., 1567
Mirzaei, P., 3231
Mishra, A., 613
Mishra, D., 1681
Misra, P., 3393
Mitani, T., 2650
Mitewa, M., 2261
Mitiaev, A.S., 2401
Mitra, K., 1681
Mitra, S., 1271, 1753, 2550, 2737, 3006
Miyamoto, S., 2439
Moghadam, M., 2904
Mohamadou, A., 2236
Mohanta, S., 2007, 3393
Mohanty, S., 815
Mohr, F., 3066
Molčanov, K., 2459
Molins, E., 71, 113, 2295
Moncol, J., 1561
Mondal, A., 25, 2284
Mondal, T., 1125
Moore, J.A., 259
Moreira, I.S., 1543
Morewood, C.A., 211
Morgant, G., 2229
Morris, R.E., 853
Morshedi, M., 671
Mostafa, G., 645, 663, 1477, 1571, 2503, 2764
Motevalli, M., 241, 1017
Mottalib, Md.A., 95
Moubaraki, B., 360
Moxey, G.J., 379
Mrázová, V., 3261
Mroziński, J., 1348, 2537, 2663
Mtshali, T.N., 2415
Mu, Y., 2565, 3071
Mukherjee, A., 2135
Mukherjee, R., 1367
Mukkamala, S.B., 530
Munakata, M., 2483, 3519
Muns, V., 801
Murillo, C.A., 219
Murray, K.S., 360
Murugesu, M., 613
Mustarde, K., 996
Mutikainen, I., 81, 1646, 2236, 3278
Mzinyati, A., 2730

Nabei, A., 2483, 3519
Naik, S.G., 2135
Naïli, H., 3543
Nanda, P.K., 702, 2791
Nandibewoor, S.T., 2976
Narayanan, V., 2859
Nasrullayeva, T.M., 1279
Nastopoulos, V., 539
Natarajan, K., 2223
Nath, S., 1263
Näther, C., 3269
Nättinen, K., 627
Naumov, D.Y., 1233
Nayak, M., 2007
Nazarov, A.A., 1971
Necas, M., 809
Nedelko, N., 113
Neels, A., 1613
Nejati, K., 1915
Neogi, D.N., 1177, 2149
Neogi, S., 1491
Nethaji, M., 87, 1931, 2135, 3189
Neuburger, M., 421, 1831, 1844
Ng, C.H., 1287, 3118
Ng, S.W., 1287, 3118
Nguyen, H.L., 307
Nguyen, Q.T., 1787
Nichol, G.S., 1043
Nielson, A.J., 1729, 2039
Nirwan, M., 945

Niu, J.-Y., 2153
Nocera, D.G., 493
Nogueira, H.I.S., 753, 2471
Nordlander, E., 95, 437
Norman, V., 888
Novaković, S.B., 1096
Novio, F., 1714
Nowicki, W., 2809
Nsangou, M., 1373
Nutley, M., 3474
Nyokong, T., 1802

Oakley, S.H., 1247
O'Brien, P., 241, 864
Ocampo, N., 1714
O'Dea, L., 360
Odlazek, D., 1161
Offermann, D.A., 360
Ogawa, T., 1379
Okamoto, K.-I., 2191
Okubo, T., 2650
Oliveira, M.R.L., 2119
Olivera, M.S., 1483
Ölmez, H., 2985
Olmstead, M.M., 477
Olsson, J., 437
Olszewska, E., 687
Ong, H.K.A., 3118
Ooi, L.L., 1057
Orchin, M., 1147
Osipovich, N.P., 1723, 3603
Ősz, K., 3173
Otter, C.A., 2341
Ouahab, L., 1514
Ouellette, W., 3457
Oye, M.M., 271, 881
Özer, M., 3593
Özkar, S., 3133
Özkaya, A.R., 3593

Pai, C.C., 2160
Paine, R.T., 3387
Paixão, J.A., 2021
Pakawatchai, C., 2198
Pal, S., 1689
Pal, T., 1263
Palaniandavar, M., 1077
Palmer, E.J., 575
Palmer, S., 3379
Pampillón, C., 2101
Panda, B.K., 2289
Pang, K., 499
Panigrahi, S., 1263
Paolucci, G., 1979
Papánková, B., 1823
Parajón-Costa, B.S., 2920
Paredes-García, V., 2026, 2072
Parfenova, M.S., 1723
Park, Y.J., 2318
Parkin, G., 499
Parkin, I.P., 334, 3032
Parsons, S., 513, 923
Parveen, S., 2929
Pascu, S.I., 406
Pasko, S., 293
Pastor, C.J., 1464
Patel, R.N., 3312
Pathak, A., 31
Patra, D., 2637
Patrarakorn, S., 2710
Patrickios, C.S., 1737
Patroniak, V., 2643
Pattanayak, P., 2637
Pavlović, G., 2353
Paz, F.A.A., 2471
Peake, H.O., 406
Pedrero-Marín, R., 1399
Peña, O., 2072
Peña-Hueso, A., 2363
Peng, S.-M., 195, 3533
Pereira, L.J., 2392
Pereira, M.T., 2848
Pereiras-Gabián, G., 3343
Pérez-Lourido, P., 783, 2673, 3495
Perlepes, S.P., 134, 539, 1737, 2869
Perpétuo, G.J., 3319
Persson, I., 3569
Petrova, R., 2261
Pettinari, C., 124
Pettinari, R., 124
Pevec, A., 1161
Pfeffer, M., 3349
Phadnis, P.P., 87
Philip, V., 1931
Phuengphai, P., 2198
Pietryga, J.M., 259
Pike, K.J., 3569
Pike, R.D., 776
Pilet, G., 2550
Pillinger, M., 1471
Pink, M., 550
Pinkas, J., 809
Piro, O.E., 2597, 2920
Pis-Diez, R., 2920
Pitteri, B., 1979, 2698
Plater, M.J., 2433
Pokhodnya, K.I., 1927
Polamo, M., 3039
Polozov, G.I., 1723, 3603
Popa, I., 1421
Pope, M.T., 1921, 2015
Popović, Z., 2353
Porter, R.M., 859
Potapov, A.S., 2683
Pourayoubi, M., 711
Povalishev, V.N., 3603
Powell, A.K., 530
Power, P.P., 477
Prabhakaran, R., 2223
Pradeep, C.P., 3588
Praharaj, S., 1263
Pratihar, J.l., 2513, 2637
Prenesti, E., 2815
Příhoda, J., 1292
Proctor, K.M., 1592
Prodius, D., 2175
Pruchnik, F.P., 1994, 2773, 3647
Psycharis, V., 1391, 2869
Puddephatt, R.J., 266
Pulham, C., 923
Punji, B., 815
Purcell, W., 2415
Puschmann, H., 1204

Quesada, M., 2198
Quesada, R., 901
Quintal, S.M.O., 753

Quintanilla, A., 9
Qureshi, U., 334

Raftery, J., 325
Raghunathan, R., 2135
Rahaman, S.H., 645, 3104
Rahiman, A.K., 2859
Rahman, R.N.Z.R.A., 3118
Raithby, P.R., 211, 821, 1057
Rajak, K.K., 25, 2284
Rajesh, K., 2859
Rajeswaran, M., 1747, 2033
Rakhmatullin, A.I., 1433
Rakovský, E., 2491
Ramasesha, S., 2135
Ramesh, R., 3095
Ramos, M.L., 3581
Ramos-Organillo, Á., 1662
Ranjan, A., 1415
Rankin, D.W.H., 923
Raos, N., 2800
Rapko, B.M., 3387
Raptopoulou, C., 1337
Raptopoulou, C.P., 539, 1391, 1737, 2869
Rarig Jr., R.S., 3457
Ratnani, R., 945, 3238
Rauch, K., 219
Ray Chaudhuri, N., 1779
Ray, D., 702, 2791
Ray, M.S., 2241, 3084
Ray, U., 1299, 2764
Ray, U.S., 3077
Razavi, H., 1567
Razi, M.T., 513
Rebbouh, L., 2616
Redshaw, C., 1946
Reedijk, J., 81, 599, 1646, 2198, 2236, 2959, 2967, 3278
Reetz, M.T., 1215
Reger, D.L., 2616
Rego, D.B., 2691
Reid, G., 930
Rekik, W., 3543
Renkema, K.B., 459
Rezvani, Z., 1915
Rheingold, A.L., 1873
Ribas, J., 25, 645, 1779, 2284, 2737, 3006
Ribeiro, A.C.F., 3581
Ribeiro-Claro, P., 1471
Richards, A.F., 477
Rintoul, L., 1195
Riordan, C.G., 1873
Rissanen, K., 627
Robertson, S.D., 823
Robinson, W.T., 1313, 1579, 1601
Rockembauer, A., 1483
Rodrigues, C., 1209
Rodrigues, J.V., 1209
Rodríguez, E., 113
Rodríguez, M.L., 3366
Rodriguez, M.T.G., 2550
Roig, A., 113
Romanowski, G., 2809
Romero, J., 2673
Rontoyianni, A., 1337
Ros-Lis, J.V., 1585
Rosair, G.M., 915, 1753, 3006
Rosenberg, E., 95
Rosenfeld, D.C., 251
Rowan, R., 1771
Rubinger, M.M.M., 2119
Rüffer, T., 3413
Rusanova, D., 3569
Rzączyńska, Z., 687
Rzaigui, M., 2953

Sá Ferreira, R.A., 1471, 2471
Sadler, P.J., 513
Safin, D.A., 3330, 3611
Sahoo, S.K., 722
Said, M., 843
Sala, L.F., 1483
Salavati-Niasari, M., 2127
Salmon, L., 1537, 2439
Samanta, A., 2269
Samanta, B., 3006
Sanakis, Y., 1391
Sang, R.-L., 2167
Sanhoury, M.A.M.K., 1373, 3299
Sanmartín, J., 1714
Sanna, D., 3173
Santhakumar, K., 1507, 2452, 3253
Santiago, M.O., 1543
Santos, I.C., 1209
Santos, L.S., 2055
Santos, R.H.A., 3488
Sardroodi, J.J., 3285
Sarkar, A., 1689
Sarkar, B., 3084
Sarkar, S., 25, 2284
Sarker, K.K., 2333, 2764
Sarma, R.J., 17
Sarmah, S., 3501
Sarper, O., 2577
Sawka-Dobrowolska, W., 687
Saxena, A.K., 1415
Schaefer III, H.F., 2465
Schaffner, S., 421, 1831
Schenk, K.J., 671
Schleid, T., 2577
Schmitt, C.X., 1844
Schönherr, T., 3463
Schormann, M., 387
Schrock, R.R., 469
Schröder, M., 599
Schwendt, P., 2491
Scopelliti, R., 2261
Sebe, E., 2109
Seeger, E., 937
Segarra, A.M., 1607
Šegedin, P., 1161
Segla, P., 1561
Seichter, W., 3463
Sen, S., 1271, 2737
Senapoti, S., 1125, 1571
Sevillano, P., 3653
Shaabani, B., 1893
Shadyro, O.I., 3603
Shaik, N.M., 2841
Shakir, M., 2929
Shankar, R., 2183
Sharbatdaran, M., 3231
Shariatinia, Z., 711
Sharma, A.K., 3628
Shaw, R.A., 953, 963
Sheahan, A.M., 1771
Shee, B., 2513, 2637

Sheldrick, W.S., 3138
Shen, C., 1729, 2039
Sheng, T.-L., 1618
Shenkov, S., 2261
Shevchenko, G.P., 1723
Shi, Q.-Z., 195, 3533
Shields, G.P., 211
Shil, W.-Z., 1864
Shova, S., 2175
Shtyrlin, V.G., 1433
Shukla, S.K., 1415
Sienra, B., 3509
Sillanpää, R., 767, 801, 1223
Silva, M.R., 2021
Silva, S., 1209
Simões, S.M.N., 3581
Simonov, Y.A., 1215, 2175
Simpson, S.J., 2303
Singh, A.K., 1033, 2915, 3481
Singh, G., 2915, 3481
Singh, K.S., 3441
Singh, N., 3312
Singh, R.K., 3628
Singh, U.P., 2841, 3628
Sinha, C., 1125, 1299, 1571, 2333, 2503, 2764, 3077, 3435
Sinyashin, O.G., 1607
Siripaisarnpipat, S., 2710
Skabara, P.J., 989
Skakle, J.M.S., 695, 2055
Skelton, B.W., 124, 910
Slawin, A., 853
Slawin, A.M.Z., 823
Ślawska-Waniewska, A., 113
Smaïhi, M., 1763
Smart, B.A., 923
Smith, M.D., 2616
Soares-Santos, P.C.R., 2471
Sobral, A.J.F.N., 3581
Sokolov, F.D., 3330, 3611
Solans, X., 793
Solans-Monfort, X., 339
Soler, T., 1967
Somers, N., 124
Son, J.-H., 3025
Song, X., 3441
Song, Y., 2426, 3285
Sopo, H., 1223
Soria, D.B., 1247
Sorokin, V.L., 3603
Sortais, J.-B., 3349
Soto, J., 1585
Sousa, A., 2673
Sousa, J.R., 1543
Sóvágó, I., 3173
Soylu, M.S., 2985
Spichal, Z., 809
Spodine, E., 2026, 2072
Sreedaran, S., 2859
Sreekanth, A., 1408
Srinivasan, B.R., 3269
Srivastava, R.C., 747
Stamatatos, T.C., 134, 1737
Stanciu, C., 477
Starikova, Z.A., 2401
Starosta, R., 1994
Stasch, A., 1592
Stender, M., 477
Stern, C.L., 2705
Stiefvater-Thomas, B.M., 1011
Stoeckli-Evans, H., 25, 3617
Strauch, P., 1161, 2824
Strekopytov, S., 1707, 3399
Strohfeldt, K., 2101
Stuart, A.M., 1182
Su, B.-Y., 3289
Su, Q., 2565
Su, Z.-M., 635
Suen, M.-C., 2325, 2944
Suenaga, Y., 2483, 3519
Sujandi, 1811
Sukanya, D., 2223
Süli-Vargha, H., 3173
Sullivan, A., 1017
Sun, C.-Y., 1327, 3017
Sun, I.-W., 2407
Sun, Y., 2571
Suni, V., 1931
Suo, Q.-L., 3209
Supriya, S., 3588
Suresh, D., 3215
Suresh, E., 61
Sussuchi, E.M., 1457
Sutter, J.-P., 1271
Sviili, J., 1223
Svoboda, I., 1823, 3261
Sweeney, N.J., 2101
Swenson, D.C., 559
Szeto, L., 1256
Szewczyk, A., 113
Szilágyi, O., 3173
Szymańska-Buzar, T., 1441

Tacke, M., 2101
Talham, D.R., 2605
Talja, M., 3039
Tallon, T., 1771
Talukder, P., 1271
Tamasi, G., 834
Tan, K.W., 3118
Tanase, S., 1646, 2236, 2967
Tangestaninejad, S., 2904
Tao, R.-J., 2153
Tarbraue, C., 3366
Tasada, A., 71, 2295
Taşcıoğlu, S., 1279
Tashev, E., 2261
Tasiopoulos, A.J., 1737
Tau, P., 1802
Tazeev, D.I., 1607
Teat, S.J., 1057
Teixeira, A.B., 2055
Téllez, F., 2363
Téllez Souto, C.A., 1319
Teoh, S.G., 1287
Teotonio, E.E.S., 3488
Terrón, A., 71
Terzis, A., 539, 1337, 1391, 1737
Thiakou, K.A., 539, 2869
Thirumavalavan, M., 2623
Thohinung, S., 2710
Thomas, M.S., 3562
Thorn, A., 2891
Thorum, M.S., 1927
Threlfall, T.L., 937
Thuéry, P., 1537, 1700, 1811, 2439
Tiburcio, J., 1549

Tiekink, E.R.T., 3066
Timoshkin, A.Y., 2465
Titiš, J., 3261
Tomás, M., 2375
Tonzetich, Z.J., 469
Torre, M.H., 2597
Torrens, H., 1549
Tosheva, T., 2261
Toso, S., 2815
Touati, N., 293
Trávníček, Z., 1421, 2935
Trindade, T., 2471
Tsai, K.-R., 1909
Tseng, M.C., 2160
Tung, J.-Y., 1864, 2207
Tunney, J.M., 591
Turki, T., 1142
Turnbow, L., 1157
Turner, P., 1498
Turova, N.Y., 2401
Turpeinen, U., 81, 1646, 2236, 3278
Turta, C., 2175
Tušek-Božić, L., 2459
Twamley, B., 2093, 2891
Tyagi, P., 3628

Uçar, İ., 1133
Ülkü, D., 3133
Umeda, K., 2447
Upreti, S., 2183, 3628

Valencia, L., 783
Valencia Matarranz, L., 3495
Valente, A.J.M., 3581
Valenzuela, C.D., 105
Valenzuela, M.L., 105
Valko, M., 1561
Valkonen, A., 1223
van Albada, G.A., 81, 2198, 2236, 2967, 3278
van de Water, L.G.A., 599
van der Merwe, E.M., 3562
van Son, M., 2967
Varbanov, S., 2261
Varghese, B., 2383
Varma, K.S., 1011
Várnagy, K., 3173
Vázquez-López, E.M., 3343
Velmurugan, D., 2859
Venegas-Yazigi, D., 2026, 2072
Venugopalan, P., 31
Verat, A.Y., 3611
Vere, J.M., 599
Vicente, R., 1673
Videva, V., 2261
Viertler, H., 3488
Vikić-Topić, D., 2353
Vila, J.M., 1449, 2848
Vinković, M., 2353
Viñuelas-Zahínos, E., 43, 52
Viola, N.A., 3457
Visser, H.G., 2415
Voo, J.K., 1873
Vordemvenne, E., 996

Wade, K., 300
Waheed, A., 881
Wałęsa, M., 2643
Wallis, J.D., 2583
Walsh, R.D.B., 663, 1477
Wan, L., 3305
Wang, C.-J., 195, 3533
Wang, H., 195
Wang, H.-X., 2530, 3305
Wang, J.-C., 2325, 2944
Wang, L.-S., 1
Wang, Q.-L., 2153
Wang, R., 1195, 3449
Wang, S., 2583
Wang, S.-S., 1864, 2207
Wang, S.P., 2160
Wang, Y.-B., 3209
Wang, Y.-H., 2944
Wang, Y.-L., 1239
Wang, Y.-Q., 1239
Wang, Y.-Y., 195, 3533
Ward, M.D., 869
Wardell, J.L., 695, 2055
Wardell, S.M.S.V., 695, 2055
Wasberg, M., 767
Waters, J.M., 1729, 2039
Wazeer, M.I.M., 2629
Weber, E., 3463
Weberski Jr., M.P., 119
Webster, M., 930
Wei, H.-H., 2007, 3393
Weigl, M., 888
Welch, A.J., 821, 915
Weng, L.-H., 3209
Wernsdorfer, W., 325, 613
West, A.J., 1182
Westerhausen, M., 1271
Whitcomb, D.R., 1747, 2033
White, A.H., 124, 910
Whitmire, K.H., 2065
Wiles, A.B., 776
Willett, R.D., 2093, 2891
Wilson, C., 591, 599
Wilson, J., 1017
Winter, C.H., 224, 2109
Wojnowski, W., 1555
Wolczanski, P.T., 251
Wołowiec, S., 3222
Wong, D.M., 2303
Wong, W.-K., 271
Wong, W.-T., 1256
Woo, H.K., 2318
Woodward, J.D., 2605
Woollins, J.D., 823
Wu, C.-Y., 1791, 3053
Wu, H.-F., 2530, 3305
Wu, J.-S., 3077
Wu, Q., 271
Wu, Q.-L., 2565
Wu, W.-P., 3533
Wu, X.-T., 1, 1618
Wu, Y.-J., 3305
Wu, Y.-P., 3533

Xiang, S.-C., 1, 1618
Xu, H.-B., 635
Xu, J., 2530
Xu, J.-S., 3071
Xu, L., 2167

Yakhvarov, D.G., 1607
Yalçın, B., 1279

Yamato, T., 2439
Yamin, B.M., 3118
Yan, C.-H., 2778
Yan, W.-B., 1909
Yanar, S., 1333
Yang, C.-H., 2407
Yang, F.-A., 2207
Yang, X., 271, 881
Yang, X.-L., 3305
Yap, G.P.A., 1873
Yap, S.Y., 1287
Yeh, C.-W., 1307
Yeşilel, O.Z., 2985
Yeung, W.-F., 1256
Yıldırım, L.T., 3133
Yilmaz, F., 2829
Yilmaz, V.T., 2829
Yoon, D.C., 1811
You, X.-Z., 2426
Youm, K.-T., 2318, 2717
Youngme, S., 2198
Youssef, A.A., 1531
Yu, R., 219
Yu, Z., 2426
Yu, Z.-T., 1359
Yuan, D.-Q., 1618
Yue, S.-M., 635
Yue, Y.-F., 2778

Zabirov, N.G., 1433, 3330, 3611
Zacharias, P.S., 3588
Žák, Z., 1292
Zaleski, J.M., 550
Zang, S.-Q., 2153
Zangrando, E., 1779
Zare, D., 3285
Zaworotko, M.J., 663, 1477
Zbořil, R., 2935
Zdrahal, Z., 809
Zecchin, S., 3417
Zeller, M., 2755
Zhang, H., 1909
Zhang, H.-J., 635
Zhang, J.-J., 1, 1618
Zhang, R.-F., 3405
Zhang, W.-Q., 2530
Zhang, Y., 1875
Zhang, Y.-M., 1875
Zhang, Y.-T., 3071
Zhao, J.-S., 3289
Zhao, X.-L., 975
Zheldakova, R.A., 3603
Zheng, Z., 3449
Zhou, D., 585
Zhou, H.-C., 2530
Zhou, J.-H., 2426
Zhou, Z.-H., 1909
Zhu, G., 499
Zhu, N., 3209
Zhu, X., 1875
Ziller, J.W., 484, 2691
Zuber, M., 2773
Zukerman-Schpector, J., 2447
Žúrková, L'., 2491

Available online at www.sciencedirect.com
ScienceDirect
Polyhedron 25 (2006) 3675–3682
POLYHEDRON
www.elsevier.com/locate/poly

Subject Index to Volume 25

ab initio computations, 2465
Absorption, 2160, 3449
Acetamide, 1287
Acetylacetone, 2683
Acetylenediide, 975
2-Acyl-1,3-indandionate, 3488
4-Acyl-5-pyrazolones, 124
Adducts, 2065, 3127
Adsorption, 3569
AFM, 1723
Ag-catechol, 2033
Ag-complex, 2033
Aggregation, 493
α-Agostic interactions, 339
β-alanine, 1279
L-Alanine, 1287
Al_{13}, 2880
Al(III) complexation, 2215
Alendronate, 1017
Alkali metal bis(fluorosulfuryl)imides, 1292
Alkali metal complexes, 1043
Alkaline-earth metals, 2175
Alkaline tartrates, 937
Alkoxide, 205, 827
Alkoxide and amido complexes, 575
Alkoxide complexes, 767
Alkyl, 251
Alkyl amine, 3045
1-Alkyl-2-(arylazo)imidazoles, 2764
Alkylation, 1105
Alkylidene complexes, 339
Alkyltriphenylstannane, 695
Alkyne, 211, 421, 793, 3066
Allene complex, 559
Allyl, 286
^{27}Al NMR, 3231
Aluminate, 293
Aluminium, 1592, 1625, 1707, 3399
Aluminium alkoxide, 3231
Aluminium complex, 3231
Aluminium complexes, 654
Aluminium hydroxide, 1707
Ambident ligands, 1147
Amide, 205, 279
Amidinate, 259
Amidinates, 983, 1592
Amido, 279
Amidopyridine, 3039
Amido titanium, 859
Amine complexes, 923
Amine–imine ligands, 1601
Amines, 2303
Amino acid binding, 3474
Amino acids, 71, 379, 1319, 2800
2-Aminobenzothiazole, 2363
2-Aminobenzothiazole phosphorus amides, 1662
2-Aminomethylpyridine (structure-directing), 2953
Aminohydroxamic acids, 678
Aminohydroxyakylidenebisphosphonates, 1017
Aminophosphine, 3133
Aminophosphines, 3215
4-Aminophthalimide, 2269
Aminopyridinato, 3039
3-Aminosalicylic acid, 753
Ammonium salts, 1555
Amorphous, 1707
Anilines, 1979
Anion, 2318
Anion control, 3474
Anion role, 1875
Anionic complexes, 747
Ansa, 963
Ansa metallocene, 499
Ansa-metallocenes, 406
Antenna effect, 2869
Anthranilates, 379
Anti-bacterial, 1771
Anti-cancer drug, 2101
Anti-fungal, 1771
Antibacterial activity, 3095
Anticancer compound, 1971
Antiferromagnetic, 2433
Antiferromagnetic exchange, 2175
Antiferromagnetic interaction, 3647
Antiferromagnetic interactions, 1613
Antiferromagnetism, 2191
Antifungal activity, 3603
Antimicrobial activity, 61, 2829, 2841, 3138
Antimony, 1415
Antimony oxide, 3032
APCVD, 3032
Apjohnite, 3379
Aqua complexes, 1187
Aquation kinetics, 1955
Aqueous solution, 113
Arachno, 1901
Argentophilic, 1747
Aromatic, 349
Arsine ligands, 1111
Arsine oxide, 930
1-Arylazo-2-ethyl sulfanyl benzene, 2513
Arylazopyrimidine, 1571
Aryloxide, 477
Aryloxides, 1946
Ascorbate, 1367
Asymmetric Henry reaction, 1787
Atom transfer, 251
ATP, 1319
Autocatalysis, 2976
Axial amine ligand, 1893
Axial co-ordination, 2815
Aza, 599
2-Azacyclononanone, 2447
Azamacrocycle compounds, 1204, 1313
Azide, 25, 1531, 2284, 3006, 3077, 3104
Azide bridged, 2241
Azido, 1187
Azine, 3053
Azo, 1915

B3LYP, 1373, 3145
Barbital, 2829
Barium, 224
Barium alkoxide hydrolysis, 2401
Bedt-ttf, 1209
^{9}Be NMR, 1373
Benzaldehyde thiosemicarbazone, 2897
Benzenedicarboxylic acid, 3017
Benzotriazole, 360
Benzoylation, 2525
2-Benzoylpyridine, 61, 1408
Benzyl, 945
Bergman cyclization, 550
Beryllium complexes, 1373
BF_2^+ cappe, 3165
Bidentate ligand of DHA, 3095
Bidentate polypyridyl ligands, 3312
Biimidazole, 2167
Bimetallic, 484, 663
Bimetallic complexes, 843
BINAP, 1182
Binuclear complex, 1279
Binuclear complexes, 809, 1681
Binuclear helicate, 2778
Biogeochemistry, 3399
Bioinorganic chemistry, 3399
Biomimetic, 2904
Biphasic systems, 3427
Biphenylcarboxylic acid, 39
2,2′-bipyridine, 1125, 3113
2,2′-Bipyridyl, 627, 2683
Bipyridine coordination polymers, 2605
Biquinoline ligand, 9
bis-(2-aminobenzothiazolium) tetrachloro-diphenyl plumbate, 1662
1,4-Bis(3-pyridyl)-2,3-diaza-1,3-butadiene, 2277
1,4-Bis(4-pyridyl)-2,3-diaza-1,3-butadiene, 2277
2,6-Bis(benzimidazol-2yl)-pyridine, 635
Bis(bidentate) diazine ligands, 2778
Bis(diazacrown ethers), 3165

doi:10.1016/S0277-5387(06)00692-9

Bis(diphenylphosphino)butane dioxide, 809
Bis(imidazolyl)group, 3173
Bis(pentafluorophenyl)methoxyl, 3593
Bis(pyrazol-1-yl)methane complexes, 2683
Bis(tetradentate), 702
Bis(thienyl)tellurium(IV) chloride, 3481
Bis-1,2,4-triazine-3-yl-pyridines, 888
Bis(triazole) ligand, 1875
Bis(tridentate) ligand, 2643
Bis-tridentate ligand, 1271
Bisbidentate ligand behaviour, 1714
Bismuth antiulcer, 1633
Bisphosphonate, 1017
Bisthienylethene, 2483
Blue copper protein model compounds, 2559
Bond valence, 2519
Bonding, 759
Borane, 2730
Borane cluster, 1069
Boron, 397, 983
Boroxinate anions, 1011
Boroxines, 1011
Borylamides, 493
Bridged thiocyanato, 1673
Bromide oxidant, 3501
Bulky salicylaldiminato-Cu(II) complexes, 1133

C–H activation, 2848
C–H agostic interaction, 559
C–H bond activation, 2773
C–H···O hydrogen bonds, 1043
C–H···O/π interactions, 881
C–N coupling reaction, 1571
ca_2en Schiff base, 1967
Cadmium, 513, 1017, 2593
Cadmium(II), 645, 1187, 3045
Cadmium(II) complex, 43, 52
Cadmium bromide salt, 2891
Cadmium complexes, 2353
Cadmium selenolate, 2383
Caffeic acid, 2215
Cage compounds, 2318
Calcium, 224
Calix[4]arene, 2261
Calix[*n*]arenes, 2439
Calixarenes, 910
Calorimetry, 3127
Capillary electrophoresis, 1884
Carbamato, 241
2-Carbethoxy-6-iminopyridine, 3289
Carbodiimide, 983
Carbohydrates, 3581
Carbonate, 373
Carbonyl, 3413
Carbonyl complexes, 105
Carborane, 300
Carboxycinnamic acid, 3017
Carboxylate, 1747, 1779
Carboxylate bridges, 1681
Carboxylate bridging ligands, 2026
Carboxylate complexes, 3617
Carboxylate ligand, 3628
Carboxylates, 2277, 3441
Catalysis, 815, 1215, 1263, 2525, 2976
Catalytic activity, 2223
Catalytic amination, 859
Catechol, 2033
Catechol oxidation, 2623
Cation, 1700
Cation coordination, 1585
Cation sensor, 2593
Cation template, 2929
CBH, 737
CdSe, 2383
Cerium, 205
1D chain, 2191
Chain, 2944
Chain structure, 3562
Chalcocite, 3569
Chalcogen, 1233
Chalcogenide ligands, 1333
Chalcogenolato, 864
Characterization, 3481
Charge transfer salts, 2583
Charge-transfer complex, 1514
Charge-transfer salt, 1613
Chelate, 1695, 3349
Chelate complexes, 2577
Chelate ligands, 387
Chelates, 1433
Chelating, 1946
Chelation, 2142, 2415
Chemical exchange, 1433, 2392
Chemical redox behaviors, 1133
Chemical reduction, 1142
Chemical synthesis, 3543
Chemical vapour deposition, 585
Chemisorption, 349
Chemosensors, 1585
Chiral amines, 1625
Chiral ligand, 3349
Chiral metal complex, 484
Chiral solvating agent, 953
Chiral tetradentate Cu(II) complex, 1787
Chirality, 2303
Chloride, 1367
Chlorine, 1901
Chlorodiphenylphosphine, 3133
Chlorothionoformates, 1386
Chromium, 530
Chromogenic sensing, 1585
cis, 2824
cis-dbe, 2483
Cis-platin, 2101
Cl_2-oxidation, 2503
Cluster, 3066
Cluster carbonyl, 211
Cluster compounds, 1
Cluster molecule, 585
Clusters, 134, 325, 1233, 1901
CMC, 1507, 2452, 3253
Co(II) and Ni(II) complexes, 3017
Co(II) complexes, 3077
Co(III), 373
Co-ordination compounds, 3463
Cobaloxime complexes, 3417
Cobalt, 39, 585, 1017, 1279, 1519, 2967, 3253, 3647
Cobalt(II), 2341, 3006
Cobalt(III), 1507, 1955, 2935
Cobalt 1,1-cyclobutanedicarboxylate, 687
Cobalt Aluminate, 568
Cobalt carbonyl, 421
Cobalt complex, 1875, 2710, 3113
Cobalt complexes, 1096, 2673, 3509
Cobalt(II) chelates, 3330
Cobalt (II) complex, 52
Cobalt(II) complex, 1215, 1399
Cobalt(II) complexes, 31, 1421
Cobalt(III) complex, 3165
Cobalt(III) complexes, 1531, 1893
Colloids, 1763
Competitive coordination, 1147
Complex, 635, 776, 823, 2915
3d–4f Complex, 271, 881
3d–4f Complexes, 2655
Complex formation, 2815
Complexes, 259, 1386, 1695, 1971, 2142, 2809, 3201
Computational study, 286, 3138
Concave reagent, 910
Conductance, 2452
Conductivity, 1507, 3581
Connectivity indices, 2800
Constrained geometry catalysts, 3071
Cooperative multiple hydrogen bonds, 1662
Coordination, 437, 1043
Coordination chemistry, 134, 834
Coordination compounds, 530, 2363, 2503
Coordination modes, 2471, 2829
Coordination modes of 3-hydroxypyridine-2-carboxylic acid, 2353
Coordination network, 869
Coordination networks, 360, 937
Coordination pockets, 2039
Coordination polymer, 71, 1561, 2153, 2717, 2944, 3017
Coordination polymers, 134, 1215, 2277, 2325, 2705, 2829
Copper, 81, 119, 124, 513, 550, 627, 776, 1161, 1233, 1307, 1519, 2153, 2643, 2824, 2915, 2944, 2993, 3278, 3463, 3481
Copper(I), 349
Copper(II), 1287, 1579, 1931, 2198, 3045
Copper(II) and nickel(II) complexes, 3245
Copper(II)-azide, 2764
Copper (II) azido complex, 2191
Copper(II)benzoate complex, 2525
Copper(II)/cadmium(II), 1477
Copper(II) chelates, 2800
Copper(I) cluster compounds, 3569
Copper complex, 2055
Copper(II) complex, 1215, 1399
Copper complexes, 759, 1319, 1884, 1915, 3285
Copper(I) complexes, 2269
Copper(II) complexes, 61, 195, 1077, 1089, 1561, 1673, 2683, 3173
Copper (II) complexes, 3603
Copper(II) compounds, 1204
Copper 1,1-cyclobutanedicarboxylate, 687
Copper(II) dithiocarbamates, 3366
Copper halide dimers, 2093
Copper(II)-imidazolylazothioether complexes, 1299
Copper(II) ion, 2815
Copper(II) macrocycles, 2072
Copper(II)/manganese(II), 663
Copper nanorod, 1263
Copper(II), nickel(II) complexes, 1271
Copper(II)nitrate, 2525
Copper trimers, 3084
Copper–phenanthroline oxovanadates, 2491
Copper(II)–N-salicylideneserinato, 2295
Corrole, 1519

Coumarin, 2593
Counteranions, 2072
CP MAS NMR studies, 2629
Cr(VI), 1483
Crown, 599
18-Crown-6, 2691
Crown-ether, 3611
Crystal, 1747, 2530, 3305
Crystal engineering, 901, 2007, 3474
Crystal structure, 25, 61, 195, 235, 241, 300, 687, 702, 753, 767, 859, 910, 923, 963, 983, 996, 1033, 1204, 1223, 1239, 1247, 1313, 1337, 1408, 1449, 1514, 1519, 1531, 1537, 1543, 1561, 1571, 1646, 1673, 1681, 1779, 1787, 1823, 1875, 1893, 1939, 2033, 2065, 2083, 2119, 2135, 2149, 2175, 2191, 2223, 2229, 2261, 2269, 2333, 2383, 2415, 2459, 2629, 2705, 2721, 2745, 2791, 2848, 2859, 2891, 3118, 3133, 3201, 3261, 3289, 3319, 3330, 3349, 3417, 3441, 3533, 3543, 3562, 3588, 3617, 3628
Crystal-structure, 1167
Crystal structures, 43, 87, 95, 119, 124, 360, 613, 671, 869, 888, 901, 1057, 1089, 1215, 1271, 1359, 1379, 1399, 1601, 1689, 1729, 1737, 1753, 1811, 1946, 2039, 2153, 2167, 2198, 2439, 2471, 2491, 2655, 2673, 2737, 2778, 3039, 3138, 3449, 3463, 3611
Crystal to crystal transition, 1491
Crystalline phase, 2483, 3519
Cu complexes, 2318
Cu(II) complexes, 2254, 2597, 3519, 3533
Cu^{II} complexes, 2241
Cubane-like, 1618
CV, 2160
CVD, 334
Cyanide, 869
Cyanide-bridged, 2655
Cyanides, 2705
4-Cyanobenzoic acid, 975
Cyanometallate, 2007
Cyclam derivatives, 3463
Cycles, 300
Cyclic, 2993
Cyclic amine–imine, 1579
Cyclic amine–imine compounds, 1313
Cyclic voltammetry, 1514, 1519, 1646, 1802, 2026, 2623, 3201, 3312, 3593
Cyclization, 3653
β-Cyclodextrin, 3581
Cyclodextrins, 1471
Cyclometalated, 1167
Cyclometallated complexes, 2160
Cyclometallation, 1177, 1449, 2149, 2848, 3053
Cyclooctatetraenyl, 484
Cyclopentadienyl, 484, 1177, 3413
Cyclopentadienyl-monophenoxides, 1729
Cyclophosphazene derivatives, 953
Cyclophosphazenes, 963
Cycloplatination, 2530
Cyclotriphosphazene, 2341
Cytokinins, 1421
Cytosine, 2295
Cytotoxicity, 1421

3D architecture, 2717
Dacarbazine, 1971
d-block metal, 1327
Decameric water aggregate, 2135
Dechlorination, 3427
Dehydration, 2935
Dendrimer, 421
Density Functional, 834
Density functional calculations, 2577, 2920
Density functional theory, 575, 827, 996, 3145
Denticity, 513
Detection of chlorinated pollutants, 3427
DFT, 339, 759, 1373, 1979, 2993
DFT/B3LYP, 3299
DFT calculations, 1111, 1348, 1421, 1985, 2537, 2663, 3653
DFT method, 2559
DFT studies, 195
1,2-Diaminoethanes, 2800
Di-2-pyridylketone, 1618
Di-2-pyridyl ketone, 1931
Di-2-pyridyl ketone-based ligands, 539, 2869
Di-tin linkers, 2015
Diarylethene, 3519
Diastereomers, 1625, 2303
Diazoketiminato species, 2637
1,5-Diazonia-9-aza-nonane, 3269
1,7-Diazonia-4-aza-heptane, 3269
Dicarbaborane, 1069
Dicarboxylates, 901
Dicobalt model hydrolase, 3647
Dicopper, 2791
Dicyanamide, 360, 2236, 2550, 3393
Differential scanning calorimetry, 1707
Diffusion, 3581
Diglyme, 2691
Dihalogen adducts, 989
Dihydroxybenzoic acids, 1337
α-Diimine, 1142
Diiminedioxime, 2710
(μ-oxo)diiron(III,III), 1367
β-Diketonate, 1471, 3488
Dimer, 279
Dimeric, 3639
Dimethylcyclohexadienyl complex, 876
Dimethylformamide, 1700
Dimethylsulfoxide, 3238
Dimolybdenum compounds, 219
Dinuclear-di-μ-oxo-complexes, 2459
Dinuclear, 81, 559, 1161, 2426, 3278, 3393
Dinuclear complex, 3647
Dinuclear complexes, 1673, 1714
Dinuclear heptadentate Cd(II), 1753
Dinuclear iron(III) complexes, 1391
Dinuclear lanthanide(III) nitrate complexes, 2869
Dinuclear mononuclear complexes, 1549
Dinuclear peroxotungstate, 3501
Dioxouranium (VI) complexes, 1921
Dipeptides, 2597
μ_2-Diphenoxo bridged complexes, 1753
Diphenyl(2-pyridyl)phosphine, 2663
Diphenylphosphine, 95
(Diphenylphosphino)ethylenediamines, 3133
1,3-Diphenylpropane 1,3-dionato, 2447
Diphosphine, 95, 1333
Dipicolinic acid, 2223
Dipyridyl and diamine-bridged compound, 2375
Diradical, 550
Dirhodium(II) complexes, 1994
Disilaalkanes, 2183
Disulfide, 3569
1,3-Dithia-2-stibacyclopentane, 2841
1,4-Dithiane, 1543
Dithiocarbamate, 3238
Dithiocarbamate derivative, 2650
Dithiocarbimate complexes, 2119
Dithiocarbonate, 1695, 3238
Dithiolate, 1157
Dithiolene, 591
Dithiophosphates, 945, 2841
Divalent metal ions, 1714
DNA, 3113
DNA cleavage, 1287, 3118
DNA helix, 2929
Dodecahedral coordination geometry, 539
Dodecahedral geometry, 52
π-donation, 575
Donor–acceptor complexes, 2465
1D open channel, 3533
1D polymer, 2721
DOTA, 3457
Double chain, 3393
DSC measurements, 2021
Dynamic NMR, 1864, 2207

Early transition metal complexes, 2109
Eelectron spin resonance, 2433
2-{(*E*)-4-hydroxy-3-[(*E*)-4-(aryl)iminomethyl]-phenyldiazenyl}benzoic acid, 3441
Electrical conductivity, 3319
Electrocatalysis, 1457
Electrochemical property, 3209
Electrochemical synthesis, 2673
Electrochemistry, 397, 1125, 1133, 1299, 1543, 1571, 1607, 1681, 1893, 2223, 2503, 2859, 3077, 3435
Electrocrystallization, 2583
Electroluminescence, 1167, 2407
Electron paramagnetic resonance spectra, 1408
Electronic coupling, 219
Electronic structure, 1348, 2663
Electronic structures, 759
Electrospray mass spectrometry, 809
Electrostatic binding, 3113
Δ and Λ enantiomeric pair, 1379
Enantiomerically pure crystals, 1379
'End-off' ligand, 2859
Epoxidation, 2904
EPR, 61, 81, 119, 1161, 1561, 1646, 2223, 2597, 2824, 2967, 3278
EPR and NMR spectroscopy, 2055
EPR parameters, 1319
EPR pattern, 1483
EPR radicals, 1209
EPR spectra, 1077, 1689
Equilibria, 678
Er(III) isothiocyanate complexes, 539
ESI mass spectrometry, 2055
Ethoxy-oxo(TPP)Mo(V) porphyrin, 3427
Ethylene, 1607
(*N*,*N*′-ethylenediaminediacetato)metal(II), 3118
Ethylene polymerization, 3071
Ethylene polymerization/oligomerization catalyst, 3289
1-(Ethylthio)-2-(diphenylphosphino) ethane, 2915
1-Ethylthio-2-[2-thienyltelluro]ethane, 3481

Europium, 1471, 3488
Europium complexes, 3449
EXAFS, 3569
Exchange phenomena, 2072
Extended chainlike structure of water nonamer, 3588
Extended halometallate lattice, 2891
Extraction, 3165

f–f spectra, 539
FAB mass, 1415
Fe_8, 113
{Fe_2MO} core, 2175
^{57}Fe Mössbauer spectroscopy, 2026
Ferric complex, 2717
Ferricyanide reduction, 2007
Ferrocene, 387
Ferrocene derivatives, 3343
Ferrocenophane, 429
Ferrocenylacetylene, 3209
Ferrocenylamines, 2530, 3305
Ferrocyanide, 2007
Ferromagnetic, 25, 2284
First row transition metal complexes, 17
Five-coordinate complexes, 678
Five-membered chelate rings, 1096
Five-membered N-donors, 2698
Fluorescence, 1239, 1753, 2269, 2289, 3435
Fluorescence spectroscopy, 2215
Fluorescent sensor, 2593
Fluorocarbons, 459
^{19}F NMR, 3299
Formation constant, 2721
Formation constants, 722
Framework, 2944
Fulvene, 2101
Functionalized phosphines, 1994
Furan, 499

Gadolinium, 722, 869
Gallium, 286, 1592, 1625, 1864, 3457
Gas sensor, 3032
Gd(III), 1779
GGA-PBE, 759
GIAO, 339
Glucose, 1263
Glycine, 71
Gold, 591, 2993
Gold antiarthritic, 1633
Gold bisdithiolate, 1209
Gold complexes, 2577
Grid-type complexes, 2643
Group 13, 286
Group 2 elements, 224
Guanidine, 983, 1247

$H_{\perp 1}$, 1161
Hafnium, 293, 469
Half unit ligand, 671
Halides, 1415
Halotrichite, 3379
Heptanuclear trigonal prism, 1
Heterobimetallic derivatives, 124
Heterobinuclear complexes, 2623
Heterocarboxylate, 1161
Heterocycles, 2698, 3611
Heterocyclic bases, 2142
Heterocyclic N,N ligands, 2289
Heterocyclic nitrogen ligand, 9
Heteroleptic, 484
Heteroleptic dithiolenes, 2785
Heteroligand diperoxotungsten(VI), 3501
Heterometallates, 2655
Heterometallic alkoxide, 293
Heterometallic complexes, 2392
Heteronuclear NMR, 1979
Heterotrinuclear, 1477
Heterotrinuclear carboxylates, 2175
Hexaazacyclotetradecane, 2127
Hexachlorocyclotriphosphazene, 3526
Hexacyanoferrates(III), 2935
Hexadentate, 702
Hexadentate Schiff base, 3104
Hexafluoroacetylacetonate, 2691
Hexameric, 3639
Hexameric water clusters, 3533
High κ dielectrics, 293
Hmt, 3006
^{1}H NMR, 2791
Homoleptic double-decker, 1195
Homologous series, 695
Homophthalate, 1239
Hybrid inorganic–organic compounds, 2491
Hybrid organic–inorganic salt, 2891
Hydrates, 2083
Hydrazido, 259
Hydrazido ligands, 2109
Hydrazone complexes, 3343
Hydride, 1441
Hybrid organotellurium ligands, 1033
Hydrides, 1592
Hydrobromination, 853
Hydrodenitrogenation, 499
Hydrodesulfurization, 499
Hydrogen bond, 266, 1247, 1307, 1327, 2167, 2710, 2717, 3025
1D and 2D hydrogen bonded and coordination network, 3138
Hydrogen bonded 3D supramolecular architecture, 2229
Hydrogen bonding, 17, 1043, 1555, 1909, 2325, 3133
Hydrogen bonding interactions, 2550, 3269
Hydrogen bonds, 901, 937, 2021
Hydrogen peroxide, 3118
Hydrogencarbonate bridged, 2791
Hydrogenphosphate, 2198
Hydrolysis, 373
Hydrosilylation, 1441, 2183
Hydrothermal reaction, 1327
Hydrothermal synthesis, 2571, 3006, 3387
Hydroxamic acids, 759
Hydroxide, 2401
Hydroxo-bridged aggregates, 530
Hydroxyaluminosilicate, 1707, 3399
3-Hydroxyanthranilic acid, 753
4-(Hydroxymethyl)pyridine metal complexes, 1737
Hydroxylation, 2904
Hydroxymethyl substituents, 1811
8-Hydroxyquinoline, 3231
Hysteresis, 613

Icosahedron, 521
IGLO, 339
Imidazole, 975, 1994
Imidazole complexes, 1823
Imidazole ligands, 2577
Imidazoles, 1771
Imidazolidine ring hydrolysis, 702
Imido-bis(sulfuric acid) difluoride, 1292
Imine σ and π-bonding, 3053
Impedance spectra, 3593, 3639
Inclusion complex, 975
Inclusion compounds, 1471
Indazole, 43, 52
Indium, 864, 1592
Inert pair effect, 996
Infinite chains, 493
Infrared, 776
Infrared and NMR spectra, 1147
Infrared and Raman spectroscopy, 3379
Infrared spectroscopy, 3145
Inner-sphere, 1367
Inorganic synthesis, 1955
Inorganic–organic compounds, 1359
Insertion, 793, 983
Insertion reaction, 3215
Intermolecular interactions, 923
Intramolecular coordination, 747
Intramolecular hydrogen bonding, 2929
Iodide, 1700
Iodine, 1514
Iodine interactions, 71
Iodo-derivatives, 2683
Ion-exchange, 568
IR, 1187, 2353, 2841
IR spectra, 31, 687, 2491
Iridium(III) complex, 2407
Iridium-complexes, 1167
Iron, 235, 325, 613, 1247, 1386, 1646, 1695, 2967
Iron(II), 2616
Iron carbonyl complex, 3053
Iron(III) carboxylate chemistry, 1391
Iron(II) complexes, 801
Isocytosine, 2295
Isomerisation mechanisms, 915
Isomerization, 1884
Isomers, 1433
Isonitriles, 2303
Isostructural anions and cations, 1069
Isostructurality, 937
Isothiosemicarbazide, 1096

Jahn–Teller distortion, 2824
Jahn–Teller effect, 3543
Jarosite, 3379

Keggin, 1567
Ketohexoses, 1483
Kinetics, 373, 1367, 1483, 1884, 2415, 2698, 2730, 3127, 3509
Kinetic studies, 2859

Ladder structure, 2605
Lanthanide, 613
Lanthanide complexes, 910, 2471, 2745
Lanthanides, 1, 809, 1491, 1700
Lanthanoids, 1057
Lanthanum, 722
Layered compounds, 2953
Layered structures, 2401
Lead, 2593, 2691

Lifetime, 2160
Ligand, 373
Ligand effects, 3127
Ligand metallation, 2773
Liquid crystal, 307
Liquid crystals, 3562
Lithium amides, 493
Lithium bis(fluorosulfuryl)imide, 1292
Lithium phosphinoamide, 843
LLC-PK, 2101
L–M–L type co-ordination polymers, 3006
Low oxidation state, 1592
Luminescence, 271, 635, 1471, 2333, 2471, 3104, 3231, 3488, 3653
Luminescence property, 3138
Lutetium, 722

M_4O_4, 1618
M(0)-carbonyl (M=Cr,Mo), 3435
Macrobicyclic complexes, 2623
Macrocycle, 2127
Macrocycles, 599, 2745
Macrocyclic ligand, 3495
Macrocyclic ligands, 3463
Macrocyclic ring size, 2623
Magnesium, 387
Magnetic behavior, 1779
Magnetic exchange, 2093
Magnetic measurements, 235
Magnetic ordering, 1927
Magnetic properties, 530, 1256, 1391, 2135, 2153, 2241, 2616, 2721, 2764, 2791, 2967, 3084, 3319, 3393, 3617
Magnetic property, 2426
Magnetic studies, 2737, 3588
Magnetic study, 1271
Magnetic susceptibility, 1209
Magnetism, 81, 360, 1823, 2072, 2198, 2236, 2778, 3278
Magneto-structural correlation, 3261
Magnetochemical properties, 2254
Magnetochemistry, 1681, 1737
Manganese, 613, 1017, 1247, 1256, 2142, 2236, 2643, 3628
Manganese(II), 2737, 3393
Manganese(III), 1681
Manganese benzoate chemistry, 1737
Manganese(II) complex, 1408
Manganese complexes, 1147, 3617
Manganese(III) complexes, 2737
Manganese salophen, 2904
Mannich aminomethylation, 1287
Mannich condensation, 1204
Mass spectrometry, 1971
Mechanism, 1483, 3305
Mechanisms, 459, 3509
Melamine, 776, 1307
14-Membered, 2127
Mercuration, 3305
Mercury, 1033, 2915
Mercury(I), 2976
Mercury complexes, 1464
Mercury(II) complexes, 2629
Metal, 2303
Metal complex, 783
Metal complexes, 1033, 3481, 3495
Metal coordination, 937
Metal-directed reactivity, 437
Metal halides, 349
Metal-organic framework, 1491
Metallaboranes oxidation state, 3183
Metallacarborane, 915
Metallacycles, 1147
Metallocene catalyst, 2565
Metallocenes, 3071
Metalloenediynes, 550
Metallomacrocycle, 1033, 1831, 1844
Metallomesogen, 307, 1915
Metallosurfactants, 1507, 2452, 3253
Metal–metal bonds, 827
Metaloxylation, 1177
Methane elimination, 406
Methanol as ligand, 2142
Methanol solvates, 2401
Methoxide, 95
Methoxycarbonylation, 853
4-Methylimidazole, 2985
Methylmercury complexes, 1464
Mg(II), Zn(II), Co(II) and Ni(II) complexes, 2229
Micelles, 1507, 3253
Micellization, 2452
Microemulsion, 1763
Microstructure, 1763
Mixed ligand, 3017
Mixed-ligand complexes, 678, 2683, 3253
Mixed valence, 2439
Mixed-valence complex, 1279
Mixed-valence dinuclear iron(II,III) complexes, 2026
Mixed-valence manganese clusters, 1737
Mixed-valence system, 2650
Mo, 339
MOCVD, 293
Model compounds, 3285
Modified electrodes, 1457
Modular assembly, 2167
Molecular ion, 663, 1477
Molecular magnetism, 134, 2705
Molecular mechanics and semi-empirical method, 722
Molecular orbital theory, 575
Molecular polygon, 1844
Molecular spectrophotometry, 2815
Molecular square, 1256
Molecule-based magnets, 1157
Molybdate, 1909
Molybdenum, 499, 767, 1142, 1909, 3222, 3238, 3413
Molybdenum(V), 2459
Molybdenum (II) diazadiene complexes, 1142
Molybdenum(VI) dimer, 2375
Mono and binuclear metal complexes, 2859
Mono- and binuclear palladium(II) complexes, 3138
Monocarbaboranes, 1069
Monodentate ligand, 3312
Mononuclear Ni(II), 1753
MonoPhos, 1182
Mössbauer, 3441
Mössbauer spectroscopy, 1391, 2616, 2935
MSDA, 2824
Murine macrophages, 3366

N-adamantylacetamide, 2447
N-alkylated amino acids, 2800
N-alkylation, 783
N-benzoyl 3,5-dimethylpyrazole, 2525
N-benzoylimidazole, 2525
N,*O* ligands, 2471
N-phthaloylglycine, 17
1*N*-(2-pyridyl-2-methyl)-2-arylazo aniline, 2637
N-(2-Thienylmethylidene)-2-pyridylamine derivatives, 1791
N-Thioacylamido(thio)phosphates, 3330
N,*N*,*N*′,*N*′-tetraethylpyridine-2,6-dicarboxamide, 31
N amide donor, 1714
N ligands, 1607, 2109, 2616
N—N bond activation, 3053
N,N,N donor tridentate Schiff base, 2241
N,O ligand, 2791
N-heterocyclic ligands, 3261
N-Ligands, 224, 1592
N-oxide, 2207
Nanoparticles, 585, 1763, 2383
2-Naphthol, 1263
Naphthylamine Schiff base, 2333
Naphthylazoimidazole, 2333
Naphthylazoimidazoles, 3435
Naphthylazomidazole, 1125, 3077
Neodymium, 3387
Neodymium diiodide, 1105
Neutral N_3S_2 thiosemicarbazone, 3337
Nickel, 1, 25, 843, 945, 1017, 1247, 1256, 1433, 2284, 2705, 2785, 2967, 3145
Nickel(II), 645, 671, 2127, 2341, 2426
Nickel complex, 2710
Nickel complexes, 1607, 2119
Nickel(II) complexes, 1823, 3261
Nickel compounds, 1313, 1601
Nickel(II) *p*-aminobenzoate complex, 2721
Niobium, 2109
Nitrate, 1057
Nitric oxide, 3366
Nitrido complex, 2415
Nitrile reduction, 2730
Nitrilotriacetate, 1909
Nitrilotriacetic acid, 1909
Nitrito, 1673
Nitro compounds, 1313
Nitrogen donor ligands, 815
Nitrogen heterocycle, 1844
Nitrogen ligands, 2318, 2717
5-Nitrosalicylic acid ligand, 2229
NMR, 87, 953, 2745, 2773, 3133, 3159, 3222, 3441, 3581
NMR spectra, 2841
NMR spectroscopy, 513, 711, 915, 1415, 1901, 2015, 2353, 2730, 2953, 3189
NMR spin–spin J_{C-H} coupling constant, 339
Nonaboranes, 1901
Non-covalent forces, 2959
Nonlinear optical properties, 3285
Novel ligand, 195
Nuclear expanding reaction, 3209
Nucleobase, 2065
Nucleolytic efficiency, 3118
Nucleophilicity, 2698
Nucleoside, 2065

Octahedral, 1167
Octahedral Cd(II), 2550
Octahedral geometry, 52

o-(Diphenylphosphino)benzoic acid, 87
o-, *m*-, *p*-tolyl, 945
[O–H···O] interacting unit, 2284
Olefin, 349, 469
Oligomerization, 1607
Oligopyridine, 437
One-dimensional, 3393
One-dimensional polymer complex, 1791
Optical isomers, 2745
Optical properties, 2021
Optimal geometry, 2559
Organic halides, 1607
Organic light-emitting diode, 2407
Organic–inorganic, 1567
Organic–inorganic hybrid materials, 2198
Organically templated, 2571
Organoditantalum, 559
Organoelement analogues of β-dicarbonyl ligands, 3330
Organohalides, 1105
Organometallic, 459, 1625
Organometallics, 406, 575
Organotin, 2015
Organotin(IV), 3405
Organotin(IV) complex, 711
Orotate complexes, 2985
Orthometallation, 1003, 1994, 2513, 3555
Ortho-metallation, 3305
Osmium, 211, 459, 2392
Osmium carbonyl, 95
Oxazoline, 3025
Oxetanes, 1811
Oxidation, 2976
Oxidation of alcohols, 3095
Oximate group, 134
Oxime, 2710, 3145, 3526
Oxime derivatives, 3526
Oxime group, 134
Oxime-phosphazenes, 3526
Oxo, 251
Oxo complexes, 1457
Oxobridged peroxotungstate, 3501
Oxomolybdenum, 1337
Oxotransfer property, 2375
Oxovanadium(IV), 1689
Oxoverdazyl, 2433
Oxygen insertion, 864, 1177

p-Block, 286
Packing phenomena, 2072
Palladacycle, 793, 1003
Palladium, 550, 753, 1003, 1033, 1177, 1449, 2785, 2848, 3481
Palladium(II), 2976, 3159
Palladium (II), 87
Palladium and platinum complexes, 3215
Palladium(II)–C(naphthyl) bond, 2149
Palladium complex, 815
Palladium complexes, 1333
Palladium dimer, 3555
Partially oxidized diphthalocyanine, 3319
Pb(II) halides, 996
p-Carboxycinnamic acid, 1327
Penta-coordination, 1096
Pentacyclic aromatic system, 2363
Pentadentate thiosemicarbazone, 3337
Pentadienyl titanium(III) structure, 876
Pentadienyl zirconium(IV) structure, 876
Pentafluorophenyl, 1415
Pentagonal bipyramid, 3039
Pentagonal bipyramidal Mn(II), 2550
Pentagonal-bipyramidal zinc(II) and cadmium-(II) complexes, 3337
Peptide containing peroxotungstate, 3501
Perchlorate bridged, 2241
Periodate, 2904
Peri-palladate, 2149
Peroxidative bromination, 3501
Phase transition, 2021, 3543
1,10-Phenanthroline, 3238
Phenanthroline, 2537
Phenolate ligands, 767
Phenoxo complexes, 1223
Phenoxo ligands, 2039
Phenoxy, 1802
1,2-Phenylenedioxoborylcyclopentadienes, 397
Phosphanes, 2392
Phosphate hydrolysis, 2623, 3509
Phosphathiamacrocycles, 801
Phosphazene, 3526
Phosphine, 1333, 1543, 3066
Phosphine complexes, 843
Phosphine ligands, 1457, 1985
Phosphine oxide, 930
Phosphine sulphide, 1333
Phosphines, 1449, 1549
Phosphite, 1003
Phosphoamide modification, 2261
Phosphocreatine, 1319
Phosphonate complexes, 1884
Phosphonic acid derivatives, 3387
Phosphoramidate, 711
Phosphorescence, 2160
Phosphorus ligands, 3189
Phosphoryl ligands, 1373, 3299
Phosphorylated derivatives, 3611
Photoassisted ligand exchange reactions, 3427
Photochromism, 2483, 3519
Photoinduced electron transfer, 2593
Photoluminescence, 1167, 2407, 3449
Photoluminescence studies of europium(III) and terbium(III) complexes, 2869
Photoluminescent properties, 1359
Phthalate compounds, 1215
Phthalocyanine, 39, 737, 1195, 3593
Phthalocyanines, 1802, 3639
Pickingerite, 3379
Picoline, 2519
Pigment, 568
Pillared clay, 2880
Pivalic acid, 2426
Platinum, 266, 753, 843, 1033, 1256, 1979, 2065, 2698, 3481
Platinum (II), 87, 2513
Platinum(II), 1571, 1844, 3159
Platinum (IV), 2513
Platinum complexes, 901
Platinum metals, 1182
Plumbane, 429
^{31}P NMR, 1373, 3299
Podand, 1491
Polyalkyne, 421
Polyamine macrocycles, 1811
Polyamines, 678
Polycatenar, 307
Polyethyleneimine, 3113
Polygermanide, 521
Polymer, 266, 1747
Polymeric chain, 3533
Polymerisation catalysis, 387
Polymerization, 469
Polymers, 645
Polynuclear, 437
Polynuclear assemblage, 1537
Polynuclear copper complex, 2650
Polyoxometallate, 1567
Polyoxotungstates, 2015
Polyphosphazenes, 105
Polypyrazolylborate, 3222, 3285
Polypyridine, 801
Polypyridine complexes, 2277
Polypyridyl ligand, 1457
Polytungstoarsenates, 1921
Potentiometry, 3173
Precursors of ceramic materials, 2401
Pressure resolved XRD, 349
Proline, 1567
Propafenone, 2254
Protonation constants, 722
Pseudohalides, 1967
Pyrazine, 1514
Pyrazinecarboxylate, 2967
Pyrazolate, 1655
Pyrazole, 1111, 1399, 1994
Pyrazole and pyrazine, 1348
Pyrazole derivatives, 2055
Pyrazole ligand, 3628
Pyrazolylborates, 2616
Pyridine *N*-oxide derivatives, 3387
Pyridine-2-carbaldehyde thiosemicarbazone, 2897
Pyridine-2-carboxylato anion, 2415
Pyridine dicarboxylic acid, 1531, 2920
3-Pyridinepropionic acid, 2944
Pyridines, 1979
2-(2-Pyridyl)-benzimidazole, 635
2-(2-Pyridyl)-imidazole, 635
Pyridyl ligand, 2325
Pyridyl macrocyclic ligand, 783
Pyridyl oximes, 134
Pyridylazoimidazoles, 2503
3-Pyridylmethanol, 1561
Pyridylthioazophenolates, 1939
Pyrimidine, 2295
Pyrimidine manganese complexes, 1737

Quadruple bond, 219
Quinazoline, 1187
Quinoline-4-carboxylate, 1187
2-Quinoline carboxaldehyde Schiff base, 3245
Quinoliniumdichromate, 2976

Radical, 2433
Raman, 1195
Raman spectroscopy, 3145
Rare earth, 1195
Rare earths, 379
Re, 339
Reaction kinetics, 815
Reaction mechanisms, 3127
Redox potentials, 888
Red phosphorescent, 2407
Red shift, 2815
Redox properties, 591, 1077, 1939

Reduced Schiff base, 25
Reducing ligands, 2109
Reduction, 1105, 1483, 2577
Reductive methylation, 2530
Reorganization energy, 2559
Rh – bipyridine, 2773
Rhenium, 753, 1233
Rhenium complexes, 3343
Rhenium nitrosyl complexes, 1985
Rhenium oxo complexes, 1111, 2537
Rhodium, 834
Rhodium (III) complex, 3349
Rhenium(III) complexes, 2663
Rhenium(IV) complexes, 1348
Rhodium(II), 2483
Rhodium complexes, 1549
Ring-opening polymerization, 429
Ring-strain, 429
Ru(0)-azoimine-carbonyl, 2503
Ruthenium, 211, 437, 459, 869, 1379, 1543, 2303, 2392, 2705, 2915
Ruthenium(II), 1125, 1831, 2897, 3215
Ruthenium arene complexes, 2519
Ruthenium complexes, 9, 1457
Ruthenium (III) complexes, 1939
Ruthenium(III) complexes, 2223
Ruthenium(III) Schiff base complexes, 3095

S ligands, 1433
S···H–Ar, S···S, S···P and S···Cl sulfur donor and acceptor interactions, 1662
Salicylaldiminato-N,O chelates, 654
Salicylaldimine, 1915
Salicylaldimine complexes, 654
Sandwich complex, 1195
Schiff base, 271, 793, 1089, 1279, 1537, 2135, 2459, 2583, 2809, 3084, 3201, 3312
Schiff base complexes, 671
Schiff base ligands, 654, 1714, 2737
Schiff base metal complexes, 2026
Schiff bases, 1915
Schiff bases derived from *S*-methyldithiocarbazate, 3245
Schiff-base, 702, 1893
Schiff-base ligand, 3588
Schiff-base ligands, 1646
Secondary interaction, 747
Seleneophen, 499
Selenido, 3159
Selenium, 1386
Selenothiocarbonate, 1386
Self-assembly, 266, 1689, 1831, 2318, 2643, 2929, 3066, 3533
Selones, 2629
Sensing, 3427
Seven membered rings, 2897
Short contacts, 2583
Si–H activation, 1441
Silane, 1441
Silanethiol, 1555
Silanethiolates, 2142
Silica, 1763
Silicic acid, 1707, 3399
Siloxide, 1247
Silsesquioxanes, 853
Silver, 71, 307, 1655, 1747, 2643, 2829, 2944, 2993, 3066, 3481
Silver(I), 1771
Silver(I) cluster complex, 3653
Silver (I) complex, 975, 1723, 3349
Silver(I) complexes, 1967, 3189
Silver antimicrobial, 1633
Silver co-ordination, 2033
Silver nanoparticles, 1723
Single crystal structure, 2915, 3481
Single-crystal analysis, 1921
Single crystal X-ray analysis, 2841
Single-crystal X-ray crystallography, 2869
Single-molecule magnet, 113, 613
Single-molecule magnets, 325
Single-stranded helicate, 2929
Single-walled carbon nanotubes, 585
S-methyldithiocarbazate, 3245
Smectic C, 1915
Smectite, 2880
^{119}Sn NMR, 3299
^{119}Sn–^{31}P coupling constants, 3299
Sn(II) halides, 996
SOD, 3312, 3628
Sodium complexes, 2261
Sodium tetrachloropalladate, 2637
Sol–gel, 1763
Solid solution, 2809
Solid–gas reaction, 3045
Solid–vapor reaction, 3045
Solid-state ^{31}P and ^{65}Cu NMR spectroscopy, 3569
Solid-state structures, 1233
Solvent, 1089
Solvent effect, 2452
Solvothermal synthesis, 1239
Sorptive reconstruction, 349
Speciation, 3366
Spectra, 1299, 1531, 3435
Spectroelectrochemistry, 1802, 3593
Spectroscopic studies, 678, 2597
Spectroscopic study, 3603
Spectroscopy, 1133
Spectrum–structure correlation, 2815
Spin crossover, 2616
Spiro, 963
Spontaneous resolution, 1379
Square grid, 2007
Square pyramidal Zn(II), 2550
Stability, 2269, 2745
Stability constant, 3173
Stability constants, 910, 1319, 3366
Stacking, 71
π–π Stacking, 2229
Stereochemistry, 1955
Stereoelectronic properties, 1549
Stereogenicity, 953
Stereoselectivity, 2530
Steric effects, 477
Steric influences, 1729
Sterically hindered *o*-diphenols, 3603
Stilbazole, 307
Strain energy, 2559
Strontium, 224
Structural characterization, 2055
Structure, 81, 279, 293, 591, 945, 1386, 1625, 1747, 2236, 2571, 3222, 3278
Structures, 530, 2550
Structure analysis, 937
Structure prediction, 996
Styrene polymerization, 2565
Substitution, 2415
Substitution reaction, 1
Sulfonamide, 2119
Sulfonamide ligands, 2673
Sulfonate, 3045
Sulfur, 300, 823, 1695, 3413
Sulfur and selenium derivatives, 3215
Sulphate, 3379
Supramolecular architectures, 2550
Supramolecular arrangements, 2363
Supramolecular assemblies, 881
Supramolecular assembly, 975, 1491, 2135
Supramolecular association, 747
Supramolecular chemistry, 71, 663, 989, 1477, 3653
Supramolecular complex, 2167
Supramolecular compounds, 195
Supramolecular hydrogen bonding network, 3588
Supramolecular materials, 2959
Supramolecular motif, 2183
Supramolecular network, 1327
Supramolecular networks, 901
Supramolecular self-assembly, 2778
Supramolecule, 3639
Supramolecules, 645
Surfactantless, 1263
Susceptibility, 2433
Suzuki-cross-coupling reactions, 815
Suzuki reaction, 3555
Syndiotactic polystyrene, 2565
Synthesis, 568, 864, 915, 1033, 1415, 2083, 3209, 3289, 3449, 3481, 3593
Synthetic methods, 599

Ta, 339
Tantalum, 559, 2109, 3039
TCNE, 1927
TDDFT method, 2519
Te–C bond cleavage, 747
TEM, 1723, 2383
Template effect, 3165
Template synthesis, 2127, 2318
Terathiotungstate, 3269
Terminal ligand, 1
Ternary complexes, 1319, 1689
Terphenyl, 477
2,2′:6′,2″-Terpyridine, 1831
tert-Butyl lithium, 2101
tert-Butylphenoxy, 1802
Tetraamine, 373
1,4,8,11-Tetraazacyclotetradecane-1, 8-bis(methylphosphonic acid), 1884
Tetraazacyclotetradecadiene, 1579
Tetraazamacrocycle, 1579
Tetrachlorozincate salts, 1601
Tetracopper(II) complex, 2135
Tetracyanonickelate(II) compound, 1579
Tetradentate ligand, 3025
Tetradentate ligands, 1601
Tetrafluorobutane-1,4-dioxy derivatives, 963
Tetranuclear, 2764
Tetranuclear copper(I) complex, 1791
Tetra-nuclear copper(II) complex, 3588
Tetraorganodistannoxanes, 87
Tetrathiafulvalene, 1613, 2583
TFA ligands, 1864
TGA, 3457

TGA/DTA analysis, 2353
TG-FTIR analysis, 687
Thallium, 1864, 2207
Thallium amides, 493
Therapeutic agents, 1633
Thermal analysis, 687, 2721
Thermal behaviour, 3543
Thermal decomposition, 2985
Thermochemistry, 17
Thermocyclization, 3071
Thermodynamic, 1433
Thermodynamic parameters, 2721
Thermodynamic properties, 1507, 2452, 2465, 3253
Thermogravimetric analysis, 1707
Thermogravimetry, 776
Thermolysis, 2465
Thiazine, 52
Thiazoline, 43, 1399
Thienyl-substitution, 1519
Thiocarbamate, 864
Thiocarbamato, 241
Thiocarboxylate, 3413
Thiocyanate, 627, 3006, 3104
Thioether, 550, 599
Thiolate, 2993
Thiolates, 823, 1555
Thiometallate, 3285
Thionyl chloride, 300
Thiophene, 499, 1844, 3562
Thiophosphinato, 241
Thiopyrimidine, 834
Thiosemicarbazide, 627
Thiosemicarbazone, 61, 1408, 1931, 3653
Thiosemicarbazones, 1449, 2848
Thioureas, 3611
Three coordinate complex, 2915
Ti(IV), 1729, 2039
Tin(IV) fluoride, 930
Tin tetrachloride, 3299
TIP, 2072
Titanium, 259, 387, 397, 823, 923, 1802
Titanium complex, 2565
Titanium complexes, 3071
Titanocene, 2101, 2565
Torsion angle, 2207
TPPO, 3488
(±)*trans*-2-Aminocyclohexylammonium, 3269
trans-1,2-Bis(4-pyridyl)ethylene, 975
trans-1,2-Diaminocyclohexane, 2007
Transition metal, 3289, 3543
Transition metals, 888
Transition metal complexes, 339
Transition-metal containing phosphine ligand, 3555
Transparent, 568
2,4,6-Tri-α-pyridyl-1,3,5-triazine, 1057
Tri- and pentadentate ligands, 1077
Triazine, 1464
1,2,4-Triazol-3-thione, 3653
1,2,4-Triazole, 2426
1,3,5-Triazine, 2959
Tribenzyltin, 3441
Tricapped trigonal prismatic geometry, 539
Tricarbonylrhenium(I) complexes, 2289
Tricyanomethanide, 360
Tridentate, 279
Tridentate ONO donor ligand, 2375
Tridentate Schiff base, 2191
Tridentate Schiff base ligand, 1753
Triflate ion, 3417
2,4,5-Trifluoro-3-methoxybenzoic acid, 3405
2,4,6-Tri(2-pyridyl)-1,3,5-triazine, 3449
Trigonal bipyramidal geometry, 2717
Trimethylsilanes, 1105
Trinuclear Ag(I) complexes, 1655
Trinuclear complex, 1279
Trinuclear complexes, 3159
Trinuclear compound tetracyanonickelate(II)-bridged compound, 1579
Trinuclear Zn(II), 1753
Tripeptide, 3173
Triphenylphosphine, 627
Triphenylphosphine oxide, 2447
Triphos, 1979
Triplet energy, 2407
Tripodal amine, 645
Tripodal polycatechol-amine ligand, 722
Tris(2-aminoethylamine), 663, 1477
tris-Cyclopentadienyl, 575
Trishomobarrelene-1,5-dicarboxylate, 219
TTF, 1514
Tungsten, 105, 251, 767, 827, 1441, 1946
Tungsten(V) complexes, 3127
Two-dimensional polymer complex, 1791

Uracil, 1043
Uracil-5-carboxylic acid, 1043
Uranium, 484, 1537, 1700, 2439
Uranium(III), 2083
Uranyl, 2447
Uranyl compounds, 1359
Uranyl ion, 1223
Uranyl ion extraction, 1223
UV–Vis, 1319
UV–Vis absorbance spectra, 1723
UV–vis spectra, 31, 3330, 3593
UV–Vis spectroscopy, 2215

Vanadium, 119, 2920, 3581
Vanadium(V), 2809
Vanadium antidiabetic, 1633
Vanadium phosphites, 2571
Vanadyl, 119
Vanillic acid, 1161
Vanillin, 2824
Variable range hopping, 737
Variable-temperature magnetic susceptibility studies, 2026
Vibrational spectroscopy, 2920
vic-Dioxime, 3165
Visible absorption spectra, 2815
VOC sensing, 737
Volatility, 2691

Water cluster, 1491
Wavenumber-linear scaling, 3145
Weak hydrogen bonding, 3405
Werner complexes, 1955
Wide bite angle, 3349
^{183}W NMR, 1921

Xanthene dibenzofuran, 859
X-band e.p.r, 3312
XPS, 2655
X-ray, 513, 776, 2303, 2401
X-ray analysis, 687, 1096, 1464
X-ray crystal structure, 211, 1133, 1700, 1931, 2375, 2503
X-ray crystal structures, 31, 379, 1391, 1909, 3495
X-ray crystallography, 271, 711, 809, 834, 881, 915, 953, 989, 2015, 3189
X-ray data, 2254
X-ray diffraction, 853, 1864, 1901, 2207, 2353, 2953
X-ray structure, 71, 783, 823, 1069, 1077, 1111, 1125, 1182, 1187, 1299, 1307, 1348, 1543, 1555, 1695, 1967, 1985, 2241, 2289, 2295, 2519, 2537, 2597, 2663, 2920, 2935, 3077, 3084, 3413, 3457
X-ray structure analysis, 1333
X-ray structures, 259, 695, 1011, 1017, 1256, 1421, 1655, 1771, 2341
X-ray studies, 2093

Zeolite, 568
Zero-field splitting, 1823, 3261
Zinc, 39, 241, 279, 513, 1017, 1247, 2333, 2593, 2944
Zinc(II), 2341, 3104
Zinc(II) and cadmium(II) complexes, 2959
Zinc(II) clusters, 2277
Zinc complex, 3474
Zinc(II) complexes, 3173
Zinc coordination polymers, 2605
Zinc 1,1-cyclobutanedicarboxylate, 687
Zinc dithiocarboxylate complexes, 3562
Zinc-lanthanide, 271
Zinc oxide, 241
Zinc salts, 2325
Zink, 1233
Zintl, 521
Zirconium, 387, 397, 469
Zirconium(IV), 349
Zirconium diphthalocyanine, 3319
Zirconocene, 429
Zn(II) complex, 3025
Zwitter ionic complexes, 1223

POLYHEDRON

The International Journal for Inorganic and Organometallic Chemistry

Executive Editors

The Americas
G. Christou
Department of Chemistry, University of Florida,
Gainesville, FL 32611-7200, USA
E-mail: christou@chem.ufl.edu

Rest of the world
C.E. Housecroft
Department of Chemistry, University of Basel,
Spitalstrasse 51, CH-4056 Basel, Switzerland
E-mail: poly-chemie@unibas.ch

Associate Regional Editor for China
T.C.W. Mak
Department of Chemistry, University Science Centre,
The Chinese University of Hong Kong,
Shatin NT, Hong Kong, People's Republic of China
E-mail: tcwmak@cuhk.edu.hk

Polyhedron Reports
Editor
G. Christou *(Gainesville, FL, USA)*

Symposia-in-print
Editor
G. Parkin *(New York, NY, USA)*

Editorial Board
N.Y. Barba-Behrens *(Mexico, DF, Mexico)*
A.G. Blackman *(Dunedin, New Zealand)*
D.C. Bradley *(London, UK)*
D. Braga *(Bologna, Italy)*
A. Brodie *(Palmerston North, New Zealand)*
A. Castiñeiras *(Santiago de Compostela, Spain)*
M.H. Chisholm *(Columbus, OH, USA)*
E.C. Constable *(Basel, Switzerland)*
E. Coronado *(Valencia, Spain)*
W.J. Evans *(Irvine, CA, USA)*
L.H. Gade *(Heidelberg, Germany)*
M.B. Hursthouse *(Southampton, UK)*
C. Kepert *(NSW, Australia)*
T. Kiss *(Szeged, Hungary)*
L. Manners *(Bristol, UK)*
S. Perlepes *(Patras, Greece)*
P.P. Power *(Davis, CA, USA)*
T.B. Rauchfuss *(Urbana, IL, USA)*
J. Reedijk *(Leiden, The Netherlands)*
A.L. Rheingold *(Newark, DE, USA)*
A.G. Sykes *(Newcastle upon Tyne, UK)*
L.K. Thompson *(St John's, NF, Canada)*
M.D. Ward *(Sheffield, UK)*
R.E.P. Winpenny *(Manchester, UK)*
M. Yamashita *(Sendai, Japan)*
M. Zaworotko *(Tampa, FL, USA)*

Aims and Scope

Polyhedron will publish original, fundamental, experimental and theoretical work of the highest quality in all the major areas of inorganic chemistry. These include synthetic chemistry, coordination chemistry, organometallic chemistry, bioinorganic chemistry, and solid-state and materials chemistry. Papers should be complete pieces of work, and the inclusion of results from spectroscopic and/or physical techniques is encouraged. Papers merely reporting the preparation and X-ray structural characterization of only a single compound will not be considered appropriate unless the compound and its structure are particularly interesting.

Similarly, papers concerned solely with stability constants determined by potentiometric titration data unsupported by other e.g. spectroscopic techniques will not be acceptable nor will solvent extraction data unless supported by other data of interest to inorganic chemists. Unnecessary fragmentation of work is not acceptable.

In addition Polyhedron publishes specially commissioned review articles (Polyhedron Reports) and collections of original research papers (Polyhedron Symposia-in-Print) of appropriate timeliness.

Publication Information: Polyhedron (ISSN 0277-5387). For 2006, volume 25 is scheduled for publication. Subscription prices are available upon request from the Publisher or from the Regional Sales Office nearest you or from this journal's website (http://www.elsevier.com/locate/poly). Further information is available on this journal and other Elsevier products through Elsevier's website (http://www.elsevier.com). Subscriptions are accepted on a prepaid basis only and are entered on a calendar year basis. Issues are sent by standard mail (surface within Europe, air delivery outside Europe). Priority rates are available upon request. Claims for missing issues should be made within six months of the date of dispatch.

Orders, Claims and Journal Enquiries

(no manuscript enquiries)

Please contact the Customer Support Department at the Regional Sales Office nearest you:

Orlando
Elsevier
Customer Service Department
6277 Sea Harbor Drive
Orlando, FL 32887-4800
USA
Tel.: (877) 8397126 or (800) 6542452 [toll free numbers for US customers];
(+1) (407) 3454020 or
(+1) (407) 3454000 [customers outside US]
Fax: (+1) (407) 3631354 or
(+1) (407) 3639661
E-mail: usjcs@elsevier.com or elspcs@elsevier.com

Amsterdam
Elsevier
Customer Service Department
P.O. Box 211
1000 AE Amsterdam
The Netherlands
Tel.: (+31) 20-485-3757
Fax: (+31) 20-485-3432
E-mail: nlinfo-f@elsevier.com

Tokyo
Elsevier K.K.
Customer Service Department
4F Higashi-Azabu, 1-Chome Bldg
1-9-15 Higashi-Azabu
Minato-ku, Tokyo 106-0044
Japan
Tel.: (+81) 3-5561-5037
Fax: (+81) 3-5561-5047
E-mail: jp.info@elsevier.com

Singapore
Elsevier
Customer Service Department
3 Killiney Road
#08-01 Winsland House 1
Singapore 239519
Tel.: (+65) 6349-0222
Fax: (+65) 6733-1510
E-mail: asiainfo@elsevier.com

USA mailing notice: *Polyhedron* (ISSN 0277-5387) is published triweekly by Elsevier Ltd. (P.O. Box 211, 1000 AE Amsterdam, The Netherlands). Annual subscription price in the USA US$ 7049.00 (valid in North, Central and South America), including air speed delivery. Periodical postage rate is paid at Jamaica, NY 11431.
USA POSTMASTER: Send change of address to *Polyhedron*, Elsevier, 6277 Sea Harbor Drive, Orlando, FL 32887-4800.
AIRFREIGHT AND MAILING in the USA by Publications Expediting Inc., 200 Meacham Avenue, Elmont, NY 11003.

Advertising Information

Advertising orders and enquiries can be sent to: **South America:** Mr Tino DeCarlo, The Advertising Department, Elsevier Inc., 360 Park Avenue South, New York, NY 10010-1710, USA; tel.: (+1) (212) 633 3815; fax: (+1) (212) 633 3820; e-mail: t.decarlo@elsevier.com. **Europe, USA, Canada and ROW:** Miss Katrina Barton, Commercial Sales, Elsevier, 84 Theobald's Road, London, WCIX 8RR, UK; phone: (+44) (0) 20 7611 4117; fax: (+44) (0) 20 7611 4463; e-mail: commercialsales@elsevier.com

POLYHEDRON

The International Journal for Inorganic and Organometallic Chemistry

Executive Editors

The Americas
G. Christou
Department of Chemistry, University of Florida,
Gainesville, FL 32611-7200, USA
E-mail: christou@chem.ufl.edu

Rest of the world
C.E. Housecroft
Department of Chemistry, University of Basel,
Spitalstrasse 51, CH-4056 Basel, Switzerland
E-mail: poly-chemie@unibas.ch

Associate Regional Editor for China
T.C.W. Mak
Department of Chemistry, University Science Centre,
The Chinese University of Hong Kong,
Shatin NT, Hong Kong, People's Republic of China
E-mail: tcwmak@cuhk.edu.hk

Polyhedron Reports
Editor
G. Christou *(Gainesville, FL, USA)*

Symposia-in-print
Editor
G. Parkin *(New York, NY, USA)*

Editorial Board
N.Y. Barba-Behrens *(Mexico, DF, Mexico)*
A.G. Blackman *(Dunedin, New Zealand)*
D.C. Bradley *(London, UK)*
D. Braga *(Bologna, Italy)*
A. Brodie *(Palmerston North, New Zealand)*
A. Castiñeiras *(Santiago de Compostela, Spain)*
M.H. Chisholm *(Columbus, OH, USA)*
E.C. Constable *(Basel, Switzerland)*
E. Coronado *(Valencia, Spain)*
L. Cronin *(Glasgow, UK)*
W.J. Evans *(Irvine, CA, USA)*
L.H. Gade *(Heidelberg, Germany)*
L. Hubert-Pfalzgraf *(Villeurbanne, France)*
M.B. Hursthouse *(Southampton, UK)*
C. Kepert *(NSW, Australia)*
T. Kiss *(Szeged, Hungary)*
L. Manners *(Bristol, UK)*
S. Perlepes *(Patras, Greece)*
P.P. Power *(Davis, CA, USA)*
T.B. Rauchfuss *(Urbana, IL, USA)*
J. Reedijk *(Leiden, The Netherlands)*
A.L. Rheingold *(Newark, DE, USA)*
A.M.Z. Slawin *(Fife, UK)*
A.G. Sykes *(Newcastle upon Tyne, UK)*
L.K. Thompson *(St John's, NF, Canada)*
M.D. Ward *(Sheffield, UK)*
R.E.P. Winpenny *(Manchester, UK)*
M. Yamashita *(Sendai, Japan)*
M. Zaworotko *(Tampa, FL, USA)*

Aims and Scope

Polyhedron will publish original, fundamental, experimental and theoretical work of the highest quality in all the major areas of inorganic chemistry. These include synthetic chemistry, coordination chemistry, organometallic chemistry, bioinorganic chemistry, and solid-state and materials chemistry. Papers should be complete pieces of work, and the inclusion of results from spectroscopic and/or physical techniques is encouraged. Papers merely reporting the preparation and X-ray structural characterization of only a single compound will not be considered appropriate unless the compound and its structure are particularly interesting.

Similarly, papers concerned solely with stability constants determined by potentiometric titration data unsupported by other e.g. spectroscopic techniques will not be acceptable nor will solvent extraction data unless supported by other data of interest to inorganic chemists. Unnecessary fragmentation of work is not acceptable.

In addition Polyhedron publishes specially commissioned review articles (Polyhedron Reports) and collections of original research papers (Polyhedron Symposia-in-Print) of appropriate timeliness.

Publication Information: Polyhedron (ISSN 0277-5387). For 2006, volume 25 is scheduled for publication. Subscription prices are available upon request from the Publisher or from the Regional Sales Office nearest you or from this journal's website (http://www.elsevier.com/locate/poly). Further information is available on this journal and other Elsevier products through Elsevier's website (http://www.elsevier.com). Subscriptions are accepted on a prepaid basis only and are entered on a calendar year basis. Issues are sent by standard mail (surface within Europe, air delivery outside Europe). Priority rates are available upon request. Claims for missing issues should be made within six months of the date of dispatch.

Orders, Claims and Journal Enquiries

(no manuscript enquiries)

Please contact the Customer Support Department at the Regional Sales Office nearest you:

Orlando
Elsevier
Customer Service Department
6277 Sea Harbor Drive
Orlando, FL 32887-4800
USA
Tel.: (877) 8397126 or (800) 6542452 [toll free numbers for US customers];
(+1) (407) 3454020 or
(+1) (407) 3454000 [customers outside US]
Fax: (+1) (407) 3631354 or
(+1) (407) 3639661
E-mail: usjcs@elsevier.com or elspcs@elsevier.com

Amsterdam
Elsevier
Customer Service Department
P.O. Box 211
1000 AE Amsterdam
The Netherlands
Tel.: (+31) 20-485-3757
Fax: (+31) 20-485-3432
E-mail: nlinfo-f@elsevier.com

Tokyo
Elsevier K.K.
Customer Service Department
4F Higashi-Azabu, 1-Chome Bldg
1-9-15 Higashi-Azabu
Minato-ku, Tokyo 106-0044
Japan
Tel.: (+81) 3-5561-5037
Fax: (+81) 3-5561-5047
E-mail: jp.info@elsevier.com

Singapore
Elsevier
Customer Service Department
3 Killiney Road
#08-01 Winsland House 1
Singapore 239519
Tel.: (+65) 6349-0222
Fax: (+65) 6733-1510
E-mail: asiainfo@elsevier.com

USA mailing notice: *Polyhedron* (ISSN 0277-5387) is published triweekly by Elsevier Ltd. (P.O. Box 211, 1000 AE Amsterdam, The Netherlands). Annual subscription price in the USA US$ 7049.00 (valid in North, Central and South America), including air speed delivery. Periodical postage rate is paid at Jamaica, NY 11431.
USA POSTMASTER: Send change of address to *Polyhedron*, Elsevier, 6277 Sea Harbor Drive, Orlando, FL 32887-4800.
AIRFREIGHT AND MAILING in the USA by Publications Expediting Inc., 200 Meacham Avenue, Elmont, NY 11003.

Advertising Information

Advertising orders and enquiries can be sent to: **South America:** Mr Tino DeCarlo, The Advertising Department, Elsevier Inc., 360 Park Avenue South, New York, NY 10010-1710, USA; tel.: (+1) (212) 633 3815; fax: (+1) (212) 633 3820; e-mail: t.decarlo@elsevier.com. **Europe, USA, Canada and ROW:** Miss Katrina Barton, Commercial Sales, Elsevier, 84 Theobald's Road, London, WCIX 8RR, UK; phone: (+44) (0) 20 7611 4117; fax: (+44) (0) 20 7611 4463; e-mail: commercialsales@elsevier.com

POLYHEDRON

The International Journal for Inorganic and Organometallic Chemistry

Executive Editors

The Americas
G. Christou
Department of Chemistry, University of Florida,
Gainesville, FL 32611-7200, USA
E-mail: christou@chem.ufl.edu

Rest of the world
C.E. Housecroft
Department of Chemistry, University of Basel,
Spitalstrasse 51, CH-4056 Basel, Switzerland
E-mail: poly-chemie@unibas.ch

Associate Regional Editor for China
T.C.W. Mak
Department of Chemistry, University Science Centre,
The Chinese University of Hong Kong,
Shatin NT, Hong Kong, People's Republic of China
E-mail: tcwmak@cuhk.edu.hk

Polyhedron Reports
Editor
G. Christou *(Gainesville, FL, USA)*

Symposia-in-print
Editor
G. Parkin *(New York, NY, USA)*

Editorial Board

N.Y. Barba-Behrens *(Mexico, DF, Mexico)*
A.G. Blackman *(Dunedin, New Zealand)*
D.C. Bradley *(London, UK)*
D. Braga *(Bologna, Italy)*
A. Brodie *(Palmerston North, New Zealand)*
A. Castiñeiras *(Santiago de Compostela, Spain)*
M.H. Chisholm *(Columbus, OH, USA)*
E.C. Constable *(Basel, Switzerland)*
E. Coronado *(Valencia, Spain)*
L. Cronin *(Glasgow, UK)*
W.J. Evans *(Irvine, CA, USA)*
L.H. Gade *(Heidelberg, Germany)*
L. Hubert-Pfalzgraf *(Villeurbanne, France)*
M.B. Hursthouse *(Southampton, UK)*
T. Kiss *(Szeged, Hungary)*
L. Manners *(Bristol, UK)*
S. Perlepes *(Patras, Greece)*
P.P. Power *(Davis, CA, USA)*
T.B. Rauchfuss *(Urbana, IL, USA)*
J. Reedijk *(Leiden, The Netherlands)*
A.L. Rheingold *(Newark, DE, USA)*
A.M.Z. Slawin *(Fife, UK)*
A.G. Sykes *(Newcastle upon Tyne, UK)*
L.K. Thompson *(St John's, NF, Canada)*
M.D. Ward *(Sheffield, UK)*
R.E.P. Winpenny *(Manchester, UK)*
M. Yamashita *(Sendai, Japan)*
M. Zaworotko *(Tampa, FL, USA)*

Aims and Scope

Polyhedron will publish original, fundamental, experimental and theoretical work of the highest quality in all the major areas of inorganic chemistry. These include synthetic chemistry, coordination chemistry, organometallic chemistry, bioinorganic chemistry, and solid-state and materials chemistry. Papers should be complete pieces of work, and the inclusion of results from spectroscopic and/or physical techniques is encouraged. Papers merely reporting the preparation and X-ray structural characterization of only a single compound will not be considered appropriate unless the compound and its structure are particularly interesting.

Similarly, papers concerned solely with stability constants determined by potentiometric titration data unsupported by other e.g. spectroscopic techniques will not be acceptable nor will solvent extraction data unless supported by other data of interest to inorganic chemists. Unnecessary fragmentation of work is not acceptable.

In addition Polyhedron publishes specially commissioned review articles (Polyhedron Reports) and collections of original research papers (Polyhedron Symposia-in-Print) of appropriate timeliness.

Publication Information: Polyhedron (ISSN 0277-5387). For 2006, volume 25 is scheduled for publication. Subscription prices are available upon request from the Publisher or from the Regional Sales Office nearest you or from this journal's website (http://www.elsevier.com/locate/poly). Further information is available on this journal and other Elsevier products through Elsevier's website (http://www.elsevier.com). Subscriptions are accepted on a prepaid basis only and are entered on a calendar year basis. Issues are sent by standard mail (surface within Europe, air delivery outside Europe). Priority rates are available upon request. Claims for missing issues should be made within six months of the date of dispatch.

Orders, Claims and Journal Enquiries

(no manuscript enquiries)

Please contact the Customer Support Department at the Regional Sales Office nearest you:

Orlando
Elsevier
Customer Service Department
6277 Sea Harbor Drive
Orlando, FL 32887-4800
USA
Tel.: (877) 8397126 or (800) 6542452 [toll free numbers for US customers];
(+1) (407) 3454020 or
(+1) (407) 3454000 [customers outside US]
Fax: (+1) (407) 3631354 or
(+1) (407) 3639661
E-mail: usjcs@elsevier.com or elspcs@elsevier.com

Amsterdam
Elsevier
Customer Service Department
P.O. Box 211
1000 AE Amsterdam
The Netherlands
Tel.: (+31) 20-485-3757
Fax: (+31) 20-485-3432
E-mail: nlinfo-f@elsevier.com

Tokyo
Elsevier K.K.
Customer Service Department
4F Higashi-Azabu, 1-Chome Bldg
1-9-15 Higashi-Azabu
Minato-ku, Tokyo 106-0044
Japan
Tel.: (+81) 3-5561-5037
Fax: (+81) 3-5561-5047
E-mail: jp.info@elsevier.com

Singapore
Elsevier
Customer Service Department
3 Killiney Road
#08-01 Winsland House 1
Singapore 239519
Tel.: (+65) 6349-0222
Fax: (+65) 6733-1510
E-mail: asiainfo@elsevier.com

USA mailing notice: *Polyhedron* (ISSN 0277-5387) is published triweekly by Elsevier Ltd. (P.O. Box 211, 1000 AE Amsterdam, The Netherlands). Annual subscription price in the USA US$ 7049.00 (valid in North, Central and South America), including air speed delivery. Periodical postage rate is paid at Jamaica, NY 11431.
USA POSTMASTER: Send change of address to *Polyhedron*, Elsevier, 6277 Sea Harbor Drive, Orlando, FL 32887-4800.
AIRFREIGHT AND MAILING in the USA by Publications Expediting Inc., 200 Meacham Avenue, Elmont, NY 11003.

Advertising Information

Advertising orders and enquiries can be sent to: **South America:** Mr Tino DeCarlo, The Advertising Department, Elsevier Inc., 360 Park Avenue South, New York, NY 10010-1710, USA; tel.: (+1) (212) 633 3815; fax: (+1) (212) 633 3820; e-mail: t.decarlo@elsevier.com. **Europe, USA, Canada and ROW:** Miss Katrina Barton, Commercial Sales, Elsevier, 84 Theobald's Road, London, WCIX 8RR, UK; phone: (+44) (0) 20 7611 4117; fax: (+44) (0) 20 7611 4463; e-mail: commercialsales@elsevier.com

POLYHEDRON

The International Journal for Inorganic and Organometallic Chemistry

Executive Editors

The Americas
G. Christou
Department of Chemistry, University of Florida,
Gainesville, FL 32611-7200, USA
E-mail: christou@chem.ufl.edu

Rest of the world
C.E. Housecroft
Department of Chemistry, University of Basel,
Spitalstrasse 51, CH-4056 Basel, Switzerland
E-mail: poly-chemie@unibas.ch

Associate Regional Editor for China
T.C.W. Mak
Department of Chemistry, University Science Centre,
The Chinese University of Hong Kong,
Shatin NT, Hong Kong, People's Republic of China
E-mail: tcwmak@cuhk.edu.hk

Polyhedron Reports
Editor
G. Christou *(Gainesville, FL, USA)*

Symposia-in-print
Editor
G. Parkin *(New York, NY, USA)*

Editorial Board

N.Y. Barba-Behrens *(Mexico, DF, Mexico)*
A.G. Blackman *(Dunedin, New Zealand)*
D.C. Bradley *(London, UK)*
D. Braga *(Bologna, Italy)*
A. Brodie *(Palmerston North, New Zealand)*
A. Castiñeiras *(Santiago de Compostela, Spain)*
M.H. Chisholm *(Columbus, OH, USA)*
E.C. Constable *(Basel, Switzerland)*
E. Coronado *(Valencia, Spain)*
L. Cronin *(Glasgow, UK)*
W.J. Evans *(Irvine, CA, USA)*
L.H. Gade *(Heidelberg, Germany)*
L. Hubert-Pfalzgraf *(Villeurbanne, France)*
M.B. Hursthouse *(Southampton, UK)*
T. Kiss *(Szeged, Hungary)*
L. Manners *(Bristol, UK)*
S. Perlepes *(Patras, Greece)*
P.P. Power *(Davis, CA, USA)*
T.B. Rauchfuss *(Urbana, IL, USA)*
J. Reedijk *(Leiden, The Netherlands)*
A.L. Rheingold *(Newark, DE, USA)*
A.M.Z. Slawin *(Fife, UK)*
A.G. Sykes *(Newcastle upon Tyne, UK)*
L.K. Thompson *(St John's, NF, Canada)*
M.D. Ward *(Sheffield, UK)*
R.E.P. Winpenny *(Manchester, UK)*
M. Yamashita *(Sendai, Japan)*
M. Zaworotko *(Tampa, FL, USA)*

Aims and Scope

Polyhedron will publish original, fundamental, experimental and theoretical work of the highest quality in all the major areas of inorganic chemistry. These include synthetic chemistry, coordination chemistry, organometallic chemistry, bioinorganic chemistry, and solid-state and materials chemistry. Papers should be complete pieces of work, and the inclusion of results from spectroscopic and/or physical techniques is encouraged. Papers merely reporting the preparation and X-ray structural characterization of only a single compound will not be considered appropriate unless the compound and its structure are particularly interesting.

Similarly, papers concerned solely with stability constants determined by potentiometric titration data unsupported by other e.g. spectroscopic techniques will not be acceptable nor will solvent extraction data unless supported by other data of interest to inorganic chemists. Unnecessary fragmentation of work is not acceptable.

In addition Polyhedron publishes specially commissioned review articles (Polyhedron Reports) and collections of original research papers (Polyhedron Symposia-in-Print) of appropriate timeliness.

Publication Information: Polyhedron (ISSN 0277-5387). For 2006, volume 25 is scheduled for publication. Subscription prices are available upon request from the Publisher or from the Regional Sales Office nearest you or from this journal's website (http://www.elsevier.com/locate/poly). Further information is available on this journal and other Elsevier products through Elsevier's website (http://www.elsevier.com). Subscriptions are accepted on a prepaid basis only and are entered on a calendar year basis. Issues are sent by standard mail (surface within Europe, air delivery outside Europe). Priority rates are available upon request. Claims for missing issues should be made within six months of the date of dispatch.

Orders, Claims and Journal Enquiries

(no manuscript enquiries)

Please contact the Customer Support Department at the Regional Sales Office nearest you:

Orlando
Elsevier
Customer Service Department
6277 Sea Harbor Drive
Orlando, FL 32887-4800
USA
Tel.: (877) 8397126 or (800) 6542452 [toll free numbers for US customers];
(+1) (407) 3454020 or
(+1) (407) 3454000 [customers outside US]
Fax: (+1) (407) 3631354 or
(+1) (407) 3639661
E-mail: usjcs@elsevier.com or elspcs@elsevier.com

Amsterdam
Elsevier
Customer Service Department
P.O. Box 211
1000 AE Amsterdam
The Netherlands
Tel.: (+31) 20-485-3757
Fax: (+31) 20-485-3432
E-mail: nlinfo-f@elsevier.com

Tokyo
Elsevier K.K.
Customer Service Department
4F Higashi-Azabu, 1-Chome Bldg
1-9-15 Higashi-Azabu
Minato-ku, Tokyo 106-0044
Japan
Tel.: (+81) 3-5561-5037
Fax: (+81) 3-5561-5047
E-mail: jp.info@elsevier.com

Singapore
Elsevier
Customer Service Department
3 Killiney Road
#08-01 Winsland House 1
Singapore 239519
Tel.: (+65) 6349-0222
Fax: (+65) 6733-1510
E-mail: asiainfo@elsevier.com

USA mailing notice: *Polyhedron* (ISSN 0277-5387) is published triweekly by Elsevier Ltd. (P.O. Box 211, 1000 AE Amsterdam, The Netherlands). Annual subscription price in the USA US$ 7049.00 (valid in North, Central and South America), including air speed delivery. Periodical postage rate is paid at Jamaica, NY 11431.
USA POSTMASTER: Send change of address to *Polyhedron*, Elsevier, 6277 Sea Harbor Drive, Orlando, FL 32887-4800.
AIRFREIGHT AND MAILING in the USA by Publications Expediting Inc., 200 Meacham Avenue, Elmont, NY 11003.

Advertising Information

Advertising orders and enquiries can be sent to: **South America:** Mr Tino DeCarlo, The Advertising Department, Elsevier Inc., 360 Park Avenue South, New York, NY 10010-1710, USA; tel.: (+1) (212) 633 3815; fax: (+1) (212) 633 3820; e-mail: t.decarlo@elsevier.com. **Europe, USA, Canada and ROW:** Miss Katrina Barton, Commercial Sales, Elsevier, 84 Theobald's Road, London, WCIX 8RR, UK; phone: (+44) (0) 20 7611 4117; fax: (+44) (0) 20 7611 4463; e-mail: commercialsales@elsevier.com

POLYHEDRON

The International Journal for Inorganic and Organometallic Chemistry

Executive Editors

The Americas
G. Christou
Department of Chemistry, University of Florida,
Gainesville, FL 32611-7200, USA
E-mail: christou@chem.ufl.edu

Rest of the world
C.E. Housecroft
Department of Chemistry, University of Basel,
Spitalstrasse 51, CH-4056 Basel, Switzerland
E-mail: poly-chemie@unibas.ch

Associate Regional Editor for China
T.C.W. Mak
Department of Chemistry, University Science Centre,
The Chinese University of Hong Kong,
Shatin NT, Hong Kong, People's Republic of China
E-mail: tcwmak@cuhk.edu.hk

Polyhedron Reports
Editor
G. Christou *(Gainesville, FL, USA)*

Symposia-in-print
Editor
G. Parkin *(New York, NY, USA)*

Editorial Board
N.Y. Barba-Behrens *(Mexico, DF, Mexico)*
A.G. Blackman *(Dunedin, New Zealand)*
D.C. Bradley *(London, UK)*
D. Braga *(Bologna, Italy)*
A. Brodie *(Palmerston North, New Zealand)*
A. Castiñeiras *(Santiago de Compostela, Spain)*
M.H. Chisholm *(Columbus, OH, USA)*
E.C. Constable *(Basel, Switzerland)*
E. Coronado *(Valencia, Spain)*
L. Cronin *(Glasgow, UK)*
W.J. Evans *(Irvine, CA, USA)*
L.H. Gade *(Heidelberg, Germany)*
L. Hubert-Pfalzgraf *(Villeurbanne, France)*
M.B. Hursthouse *(Southampton, UK)*
T. Kiss *(Szeged, Hungary)*
L. Manners *(Bristol, UK)*
S. Perlepes *(Patras, Greece)*
P.P. Power *(Davis, CA, USA)*
T.B. Rauchfuss *(Urbana, IL, USA)*
J. Reedijk *(Leiden, The Netherlands)*
A.L. Rheingold *(Newark, DE, USA)*
A.M.Z. Slawin *(Fife, UK)*
A.G. Sykes *(Newcastle upon Tyne, UK)*
L.K. Thompson *(St John's, NF, Canada)*
M.D. Ward *(Sheffield, UK)*
R.E.P. Winpenny *(Manchester, UK)*
M. Yamashita *(Sendai, Japan)*
M. Zaworotko *(Tampa, FL, USA)*

Aims and Scope

Polyhedron will publish original, fundamental, experimental and theoretical work of the highest quality in all the major areas of inorganic chemistry. These include synthetic chemistry, coordination chemistry, organometallic chemistry, bioinorganic chemistry, and solid-state and materials chemistry. Papers should be complete pieces of work, and the inclusion of results from spectroscopic and/or physical techniques is encouraged. Papers merely reporting the preparation and X-ray structural characterization of only a single compound will not be considered appropriate unless the compound and its structure are particularly interesting.

Similarly, papers concerned solely with stability constants determined by potentiometric titration data unsupported by other e.g. spectroscopic techniques will not be acceptable nor will solvent extraction data unless supported by other data of interest to inorganic chemists. Unnecessary fragmentation of work is not acceptable.

In addition Polyhedron publishes specially commissioned review articles (Polyhedron Reports) and collections of original research papers (Polyhedron Symposia-in-Print) of appropriate timeliness.

Publication Information: Polyhedron (ISSN 0277-5387). For 2006, volume 25 is scheduled for publication. Subscription prices are available upon request from the Publisher or from the Regional Sales Office nearest you or from this journal's website (http://www.elsevier.com/locate/poly). Further information is available on this journal and other Elsevier products through Elsevier's website (http://www.elsevier.com). Subscriptions are accepted on a prepaid basis only and are entered on a calendar year basis. Issues are sent by standard mail (surface within Europe, air delivery outside Europe). Priority rates are available upon request. Claims for missing issues should be made within six months of the date of dispatch.

Orders, Claims and Journal Enquiries

(no manuscript enquiries)

Please contact the Customer Support Department at the Regional Sales Office nearest you:

Orlando
Elsevier
Customer Service Department
6277 Sea Harbor Drive
Orlando, FL 32887-4800
USA
Tel.: (877) 8397126 or (800) 6542452 [toll free numbers for US customers];
(+1) (407) 3454020 or
(+1) (407) 3454000 [customers outside US]
Fax: (+1) (407) 3631354 or
(+1) (407) 3639661
E-mail: usjcs@elsevier.com or elspcs@elsevier.com

Amsterdam
Elsevier
Customer Service Department
P.O. Box 211
1000 AE Amsterdam
The Netherlands
Tel.: (+31) 20-485-3757
Fax: (+31) 20-485-3432
E-mail: nlinfo-f@elsevier.com

Tokyo
Elsevier K.K.
Customer Service Department
4F Higashi-Azabu, 1-Chome Bldg
1-9-15 Higashi-Azabu
Minato-ku, Tokyo 106-0044
Japan
Tel.: (+81) 3-5561-5037
Fax: (+81) 3-5561-5047
E-mail: jp.info@elsevier.com

Singapore
Elsevier
Customer Service Department
3 Killiney Road
#08-01 Winsland House 1
Singapore 239519
Tel.: (+65) 6349-0222
Fax: (+65) 6733-1510
E-mail: asiainfo@elsevier.com

USA mailing notice: *Polyhedron* (ISSN 0277-5387) is published triweekly by Elsevier Ltd. (P.O. Box 211, 1000 AE Amsterdam, The Netherlands). Annual subscription price in the USA US$ 7049.00 (valid in North, Central and South America), including air speed delivery. Periodical postage rate is paid at Jamaica, NY 11431.
USA POSTMASTER: Send change of address to *Polyhedron*, Elsevier, 6277 Sea Harbor Drive, Orlando, FL 32887-4800.
AIRFREIGHT AND MAILING in the USA by Publications Expediting Inc., 200 Meacham Avenue, Elmont, NY 11003.

Advertising Information

Advertising orders and enquiries can be sent to: **South America:** Mr Tino DeCarlo, The Advertising Department, Elsevier Inc., 360 Park Avenue South, New York, NY 10010-1710, USA; tel.: (+1) (212) 633 3815; fax: (+1) (212) 633 3820; e-mail: t.decarlo@elsevier.com. **Europe, USA, Canada and ROW:** Miss Katrina Barton, Commercial Sales, Elsevier, 84 Theobald's Road, London, WCIX 8RR, UK; phone: (+44) (0) 20 7611 4117; fax: (+44) (0) 20 7611 4463; e-mail: commercialsales@elsevier.com

POLYHEDRON

The International Journal for Inorganic and Organometallic Chemistry

Executive Editors

The Americas
G. Christou
Department of Chemistry, University of Florida,
Gainesville, FL 32611-7200, USA
E-mail: christou@chem.ufl.edu

Rest of the world
C.E. Housecroft
Department of Chemistry, University of Basel,
Spitalstrasse 51, CH-4056 Basel, Switzerland
E-mail: poly-chemie@unibas.ch

Associate Regional Editor for China
T.C.W. Mak
Department of Chemistry, University Science Centre,
The Chinese University of Hong Kong,
Shatin NT, Hong Kong, People's Republic of China
E-mail: tcwmak@cuhk.edu.hk

Polyhedron Reports
Editor
G. Christou *(Gainesville, FL, USA)*

Symposia-in-print
Editor
G. Parkin *(New York, NY, USA)*

Editorial Board

N.Y. Barba-Behrens *(Mexico, DF, Mexico)*
A.G. Blackman *(Dunedin, New Zealand)*
D.C. Bradley *(London, UK)*
D. Braga *(Bologna, Italy)*
A. Brodie *(Palmerston North, New Zealand)*
A. Castiñeiras *(Santiago de Compostela, Spain)*
M.H. Chisholm *(Columbus, OH, USA)*
E.C. Constable *(Basel, Switzerland)*
E. Coronado *(Valencia, Spain)*
L. Cronin *(Glasgow, UK)*
W.J. Evans *(Irvine, CA, USA)*
L.H. Gade *(Heidelberg, Germany)*
L. Hubert-Pfalzgraf *(Villeurbanne, France)*
M.B. Hursthouse *(Southampton, UK)*
T. Kiss *(Szeged, Hungary)*
L. Manners *(Bristol, UK)*
S. Perlepes *(Patras, Greece)*
P.P. Power *(Davis, CA, USA)*
T.B. Rauchfuss *(Urbana, IL, USA)*
J. Reedijk *(Leiden, The Netherlands)*
A.L. Rheingold *(Newark, DE, USA)*
A.M.Z. Slawin *(Fife, UK)*
A.G. Sykes *(Newcastle upon Tyne, UK)*
L.K. Thompson *(St John's, NF, Canada)*
M.D. Ward *(Sheffield, UK)*
R.E.P. Winpenny *(Manchester, UK)*
M. Yamashita *(Sendai, Japan)*
M. Zaworotko *(Tampa, FL, USA)*

Aims and Scope

Polyhedron will publish original, fundamental, experimental and theoretical work of the highest quality in all the major areas of inorganic chemistry. These include synthetic chemistry, coordination chemistry, organometallic chemistry, bioinorganic chemistry, and solid-state and materials chemistry. Papers should be complete pieces of work, and the inclusion of results from spectroscopic and/or physical techniques is encouraged. Papers merely reporting the preparation and X-ray structural characterization of only a single compound will not be considered appropriate unless the compound and its structure are particularly interesting.

Similarly, papers concerned solely with stability constants determined by potentiometric titration data unsupported by other e.g. spectroscopic techniques will not be acceptable nor will solvent extraction data unless supported by other data of interest to inorganic chemists. Unnecessary fragmentation of work is not acceptable.

In addition Polyhedron publishes specially commissioned review articles (Polyhedron Reports) and collections of original research papers (Polyhedron Symposia-in-Print) of appropriate timeliness.

Publication Information: Polyhedron (ISSN 0277-5387). For 2006, volume 25 is scheduled for publication. Subscription prices are available upon request from the Publisher or from the Regional Sales Office nearest you or from this journal's website (http://www.elsevier.com/locate/poly). Further information is available on this journal and other Elsevier products through Elsevier's website (http://www.elsevier.com). Subscriptions are accepted on a prepaid basis only and are entered on a calendar year basis. Issues are sent by standard mail (surface within Europe, air delivery outside Europe). Priority rates are available upon request. Claims for missing issues should be made within six months of the date of dispatch.

Orders, Claims and Journal Enquiries

(no manuscript enquiries)

Please contact the Customer Support Department at the Regional Sales Office nearest you:

Orlando
Elsevier
Customer Service Department
6277 Sea Harbor Drive
Orlando, FL 32887-4800
USA
Tel.: (877) 8397126 or (800) 6542452 [toll free numbers for US customers];
(+1) (407) 3454020 or
(+1) (407) 3454000 [customers outside US]
Fax: (+1) (407) 3631354 or
(+1) (407) 3639661
E-mail: usjcs@elsevier.com or elspcs@elsevier.com

Amsterdam
Elsevier
Customer Service Department
P.O. Box 211
1000 AE Amsterdam
The Netherlands
Tel.: (+31) 20-485-3757
Fax: (+31) 20-485-3432
E-mail: nlinfo-f@elsevier.com

Tokyo
Elsevier K.K.
Customer Service Department
4F Higashi-Azabu, 1-Chome Bldg
1-9-15 Higashi-Azabu
Minato-ku, Tokyo 106-0044
Japan
Tel.: (+81) 3-5561-5037
Fax: (+81) 3-5561-5047
E-mail: jp.info@elsevier.com

Singapore
Elsevier
Customer Service Department
3 Killiney Road
#08-01 Winsland House 1
Singapore 239519
Tel.: (+65) 6349-0222
Fax: (+65) 6733-1510
E-mail: asiainfo@elsevier.com

USA mailing notice: *Polyhedron* (ISSN 0277-5387) is published triweekly by Elsevier Ltd. (P.O. Box 211, 1000 AE Amsterdam, The Netherlands). Annual subscription price in the USA US$ 7049.00 (valid in North, Central and South America), including air speed delivery. Periodical postage rate is paid at Jamaica, NY 11431.
USA POSTMASTER: Send change of address to *Polyhedron*, Elsevier, 6277 Sea Harbor Drive, Orlando, FL 32887-4800.
AIRFREIGHT AND MAILING in the USA by Publications Expediting Inc., 200 Meacham Avenue, Elmont, NY 11003.

Advertising Information

Advertising orders and enquiries can be sent to: **South America:** Mr Tino DeCarlo, The Advertising Department, Elsevier Inc., 360 Park Avenue South, New York, NY 10010-1710, USA; tel.: (+1) (212) 633 3815; fax: (+1) (212) 633 3820; e-mail: t.decarlo@elsevier.com. **Europe, USA, Canada and ROW:** Miss Katrina Barton, Commercial Sales, Elsevier, 84 Theobald's Road, London, WCIX 8RR, UK; phone: (+44) (0) 20 7611 4117; fax: (+44) (0) 20 7611 4463; e-mail: commercialsales@elsevier.com

POLYHEDRON

The International Journal for Inorganic and Organometallic Chemistry

Executive Editors

The Americas
G. Christou
Department of Chemistry, University of Florida,
Gainesville, FL 32611-7200, USA
E-mail: christou@chem.ufl.edu

Rest of the world
C.E. Housecroft
Department of Chemistry, University of Basel,
Spitalstrasse 51, CH-4056 Basel, Switzerland
E-mail: poly-chemie@unibas.ch

Associate Regional Editor for China
T.C.W. Mak
Department of Chemistry, University Science Centre,
The Chinese University of Hong Kong,
Shatin NT, Hong Kong, People's Republic of China
E-mail: tcwmak@cuhk.edu.hk

Polyhedron Reports
Editor
G. Christou *(Gainesville, FL, USA)*

Symposia-in-print
Editor
G. Parkin *(New York, NY, USA)*

Editorial Board
N.Y. Barba-Behrens *(Mexico, DF, Mexico)*
A.G. Blackman *(Dunedin, New Zealand)*
D.C. Bradley *(London, UK)*
D. Braga *(Bologna, Italy)*
A. Brodie *(Palmerston North, New Zealand)*
A. Castiñeiras *(Santiago de Compostela, Spain)*
M.H. Chisholm *(Columbus, OH, USA)*
E.C. Constable *(Basel, Switzerland)*
E. Coronado *(Valencia, Spain)*
L. Cronin *(Glasgow, UK)*
W.J. Evans *(Irvine, CA, USA)*
L.H. Gade *(Heidelberg, Germany)*
L. Hubert-Pfalzgraf *(Villeurbanne, France)*
M.B. Hursthouse *(Southampton, UK)*
T. Kiss *(Szeged, Hungary)*
L. Manners *(Bristol, UK)*
S. Perlepes *(Patras, Greece)*
P.P. Power *(Davis, CA, USA)*
T.B. Rauchfuss *(Urbana, IL, USA)*
J. Reedijk *(Leiden, The Netherlands)*
A.L. Rheingold *(Newark, DE, USA)*
A.M.Z. Slawin *(Fife, UK)*
A.G. Sykes *(Newcastle upon Tyne, UK)*
L.K. Thompson *(St John's, NF, Canada)*
M.D. Ward *(Sheffield, UK)*
R.E.P. Winpenny *(Manchester, UK)*
M. Yamashita *(Sendai, Japan)*
M. Zaworotko *(Tampa, FL, USA)*

Aims and Scope

Polyhedron will publish original, fundamental, experimental and theoretical work of the highest quality in all the major areas of inorganic chemistry. These include synthetic chemistry, coordination chemistry, organometallic chemistry, bioinorganic chemistry, and solid-state and materials chemistry. Papers should be complete pieces of work, and the inclusion of results from spectroscopic and/or physical techniques is encouraged. Papers merely reporting the preparation and X-ray structural characterization of only a single compound will not be considered appropriate unless the compound and its structure are particularly interesting.

Similarly, papers concerned solely with stability constants determined by potentiometric titration data unsupported by other e.g. spectroscopic techniques will not be acceptable nor will solvent extraction data unless supported by other data of interest to inorganic chemists. Unnecessary fragmentation of work is not acceptable.

In addition Polyhedron publishes specially commissioned review articles (Polyhedron Reports) and collections of original research papers (Polyhedron Symposia-in-Print) of appropriate timeliness.

Publication Information: Polyhedron (ISSN 0277-5387). For 2006, volume 25 is scheduled for publication. Subscription prices are available upon request from the Publisher or from the Regional Sales Office nearest you or from this journal's website (http://www.elsevier.com/locate/poly). Further information is available on this journal and other Elsevier products through Elsevier's website (http://www.elsevier.com). Subscriptions are accepted on a prepaid basis only and are entered on a calendar year basis. Issues are sent by standard mail (surface within Europe, air delivery outside Europe). Priority rates are available upon request. Claims for missing issues should be made within six months of the date of dispatch.

Orders, Claims and Journal Enquiries

(no manuscript enquiries)

Please contact the Customer Support Department at the Regional Sales Office nearest you:

Orlando
Elsevier
Customer Service Department
6277 Sea Harbor Drive
Orlando, FL 32887-4800
USA
Tel.: (877) 8397126 or (800) 6542452 [toll free numbers for US customers];
(+1) (407) 3454020 or
(+1) (407) 3454000 [customers outside US]
Fax: (+1) (407) 3631354 or
(+1) (407) 3639661
E-mail: usjcs@elsevier.com or elspcs@elsevier.com

Amsterdam
Elsevier
Customer Service Department
P.O. Box 211
1000 AE Amsterdam
The Netherlands
Tel.: (+31) 20-485-3757
Fax: (+31) 20-485-3432
E-mail: nlinfo-f@elsevier.com

Tokyo
Elsevier K.K.
Customer Service Department
4F Higashi-Azabu, 1-Chome Bldg
1-9-15 Higashi-Azabu
Minato-ku, Tokyo 106-0044
Japan
Tel.: (+81) 3-5561-5037
Fax: (+81) 3-5561-5047
E-mail: jp.info@elsevier.com

Singapore
Elsevier
Customer Service Department
3 Killiney Road
#08-01 Winsland House 1
Singapore 239519
Tel.: (+65) 6349-0222
Fax: (+65) 6733-1510
E-mail: asiainfo@elsevier.com

USA mailing notice: *Polyhedron* (ISSN 0277-5387) is published triweekly by Elsevier Ltd. (P.O. Box 211, 1000 AE Amsterdam, The Netherlands). Annual subscription price in the USA US$ 7049.00 (valid in North, Central and South America), including air speed delivery. Periodical postage rate is paid at Jamaica, NY 11431.
USA POSTMASTER: Send change of address to *Polyhedron*, Elsevier, 6277 Sea Harbor Drive, Orlando, FL 32887-4800.
AIRFREIGHT AND MAILING in the USA by Publications Expediting Inc., 200 Meacham Avenue, Elmont, NY 11003.

Advertising Information

Advertising orders and enquiries can be sent to: **South America:** Mr Tino DeCarlo, The Advertising Department, Elsevier Inc., 360 Park Avenue South, New York, NY 10010-1710, USA; tel.: (+1) (212) 633 3815; fax: (+1) (212) 633 3820; e-mail: t.decarlo@elsevier.com. **Europe, USA, Canada and ROW:** Miss Katrina Barton, Commercial Sales, Elsevier, 84 Theobald's Road, London, WCIX 8RR, UK; phone: (+44) (0) 20 7611 4117; fax: (+44) (0) 20 7611 4463; e-mail: commercialsales@elsevier.com

POLYHEDRON

The International Journal for Inorganic and Organometallic Chemistry

Executive Editors

The Americas
G. Christou
Department of Chemistry, University of Florida,
Gainesville, FL 32611-7200, USA
E-mail: christou@chem.ufl.edu

Rest of the world
C.E. Housecroft
Department of Chemistry, University of Basel,
Spitalstrasse 51, CH-4056 Basel, Switzerland
E-mail: poly-chemie@unibas.ch

Associate Regional Editor for China
T.C.W. Mak
Department of Chemistry, University Science Centre,
The Chinese University of Hong Kong,
Shatin NT, Hong Kong, People's Republic of China
E-mail: tcwmak@cuhk.edu.hk

Polyhedron Reports
Editor
G. Christou *(Gainesville, FL, USA)*

Symposia-in-print
Editor
G. Parkin *(New York, NY, USA)*

Editorial Board
N.Y. Barba-Behrens *(Mexico, DF, Mexico)*
A.G. Blackman *(Dunedin, New Zealand)*
D.C. Bradley *(London, UK)*
D. Braga *(Bologna, Italy)*
A. Brodie *(Palmerston North, New Zealand)*
A. Castiñeiras *(Santiago de Compostela, Spain)*
M.H. Chisholm *(Columbus, OH, USA)*
E.C. Constable *(Basel, Switzerland)*
E. Coronado *(Valencia, Spain)*
L. Cronin *(Glasgow, UK)*
W.J. Evans *(Irvine, CA, USA)*
L.H. Gade *(Heidelberg, Germany)*
L. Hubert-Pfalzgraf *(Villeurbanne, France)*
M.B. Hursthouse *(Southampton, UK)*
T. Kiss *(Szeged, Hungary)*
L. Manners *(Bristol, UK)*
S. Perlepes *(Patras, Greece)*
P.P. Power *(Davis, CA, USA)*
T.B. Rauchfuss *(Urbana, IL, USA)*
J. Reedijk *(Leiden, The Netherlands)*
A.L. Rheingold *(Newark, DE, USA)*
A.M.Z. Slawin *(Fife, UK)*
A.G. Sykes *(Newcastle upon Tyne, UK)*
L.K. Thompson *(St John's, NF, Canada)*
M.D. Ward *(Sheffield, UK)*
R.E.P. Winpenny *(Manchester, UK)*
M. Yamashita *(Sendai, Japan)*
M. Zaworotko *(Tampa, FL, USA)*

Aims and Scope

Polyhedron will publish original, fundamental, experimental and theoretical work of the highest quality in all the major areas of inorganic chemistry. These include synthetic chemistry, coordination chemistry, organometallic chemistry, bioinorganic chemistry, and solid-state and materials chemistry. Papers should be complete pieces of work, and the inclusion of results from spectroscopic and/or physical techniques is encouraged. Papers merely reporting the preparation and X-ray structural characterization of only a single compound will not be considered appropriate unless the compound and its structure are particularly interesting.

Similarly, papers concerned solely with stability constants determined by potentiometric titration data unsupported by other e.g. spectroscopic techniques will not be acceptable nor will solvent extraction data unless supported by other data of interest to inorganic chemists. Unnecessary fragmentation of work is not acceptable.

In addition Polyhedron publishes specially commissioned review articles (Polyhedron Reports) and collections of original research papers (Polyhedron Symposia-in-Print) of appropriate timeliness.

Publication Information: Polyhedron (ISSN 0277-5387). For 2006, volume 25 is scheduled for publication. Subscription prices are available upon request from the Publisher or from the Regional Sales Office nearest you or from this journal's website (http://www.elsevier.com/locate/poly). Further information is available on this journal and other Elsevier products through Elsevier's website (http://www.elsevier.com). Subscriptions are accepted on a prepaid basis only and are entered on a calendar year basis. Issues are sent by standard mail (surface within Europe, air delivery outside Europe). Priority rates are available upon request. Claims for missing issues should be made within six months of the date of dispatch.

Orders, Claims and Journal Enquiries

(no manuscript enquiries)
Please contact the Customer Support Department at the Regional Sales Office nearest you:

Orlando
Elsevier
Customer Service Department
6277 Sea Harbor Drive
Orlando, FL 32887-4800
USA
Tel.: (877) 8397126 or (800) 6542452 [toll free numbers for US customers];
(+1) (407) 3454020 or
(+1) (407) 3454000 [customers outside US]
Fax: (+1) (407) 3631354 or
(+1) (407) 3639661
E-mail: usjcs@elsevier.com or elspcs@elsevier.com

Amsterdam
Elsevier
Customer Service Department
P.O. Box 211
1000 AE Amsterdam
The Netherlands
Tel.: (+31) 20-485-3757
Fax: (+31) 20-485-3432
E-mail: nlinfo-f@elsevier.com

Tokyo
Elsevier K.K.
Customer Service Department
4F Higashi-Azabu, 1-Chome Bldg
1-9-15 Higashi-Azabu
Minato-ku, Tokyo 106-0044
Japan
Tel.: (+81) 3-5561-5037
Fax: (+81) 3-5561-5047
E-mail: jp.info@elsevier.com

Singapore
Elsevier
Customer Service Department
3 Killiney Road
#08-01 Winsland House 1
Singapore 239519
Tel.: (+65) 6349-0222
Fax: (+65) 6733-1510
E-mail: asiainfo@elsevier.com

USA mailing notice: *Polyhedron* (ISSN 0277-5387) is published triweekly by Elsevier Ltd. (P.O. Box 211, 1000 AE Amsterdam, The Netherlands). Annual subscription price in the USA US$ 7049.00 (valid in North, Central and South America), including air speed delivery. Periodical postage rate is paid at Jamaica, NY 11431.
USA POSTMASTER: Send change of address to *Polyhedron*, Elsevier, 6277 Sea Harbor Drive, Orlando, FL 32887-4800.
AIRFREIGHT AND MAILING in the USA by Publications Expediting Inc., 200 Meacham Avenue, Elmont, NY 11003.

Advertising Information

Advertising orders and enquiries can be sent to: **South America:** Mr Tino DeCarlo, The Advertising Department, Elsevier Inc., 360 Park Avenue South, New York, NY 10010-1710, USA; tel.: (+1) (212) 633 3815; fax: (+1) (212) 633 3820; e-mail: t.decarlo@elsevier.com. **Europe, USA, Canada and ROW:** Miss Katrina Barton, Commercial Sales, Elsevier, 84 Theobald's Road, London, WCIX 8RR, UK; phone: (+44) (0) 20 7611 4117; fax: (+44) (0) 20 7611 4463; e-mail: commercialsales@elsevier.com

POLYHEDRON

The International Journal for Inorganic and Organometallic Chemistry

Executive Editors

The Americas
G. Christou
Department of Chemistry, University of Florida,
Gainesville, FL 32611-7200, USA
E-mail: christou@chem.ufl.edu

Rest of the world
C.E. Housecroft
Department of Chemistry, University of Basel,
Spitalstrasse 51, CH-4056 Basel, Switzerland
E-mail: poly-chemie@unibas.ch

Associate Regional Editor for China
T.C.W. Mak
Department of Chemistry, University Science Centre,
The Chinese University of Hong Kong,
Shatin NT, Hong Kong, People's Republic of China
E-mail: tcwmak@cuhk.edu.hk

Polyhedron Reports
Editor
G. Christou *(Gainesville, FL, USA)*

Symposia-in-print
Editor
G. Parkin *(New York, NY, USA)*

Editorial Board
N.Y. Barba-Behrens *(Mexico, DF, Mexico)*
A.G. Blackman *(Dunedin, New Zealand)*
D.C. Bradley *(London, UK)*
D. Braga *(Bologna, Italy)*
A. Brodie *(Palmerston North, New Zealand)*
A. Castiñeiras *(Santiago de Compostela, Spain)*
M.H. Chisholm *(Columbus, OH, USA)*
E.C. Constable *(Basel, Switzerland)*
E. Coronado *(Valencia, Spain)*
L. Cronin *(Glasgow, UK)*
W.J. Evans *(Irvine, CA, USA)*
L.H. Gade *(Heidelberg, Germany)*
L. Hubert-Pfalzgraf *(Villeurbanne, France)*
M.B. Hursthouse *(Southampton, UK)*
T. Kiss *(Szeged, Hungary)*
L. Manners *(Bristol, UK)*
S. Perlepes *(Patras, Greece)*
P.P. Power *(Davis, CA, USA)*
T.B. Rauchfuss *(Urbana, IL, USA)*
J. Reedijk *(Leiden, The Netherlands)*
A.L. Rheingold *(Newark, DE, USA)*
A.M.Z. Slawin *(Fife, UK)*
A.G. Sykes *(Newcastle upon Tyne, UK)*
L.K. Thompson *(St John's, NF, Canada)*
M.D. Ward *(Sheffield, UK)*
R.E.P. Winpenny *(Manchester, UK)*
M. Yamashita *(Sendai, Japan)*
M. Zaworotko *(Tampa, FL, USA)*

Aims and Scope

Polyhedron will publish original, fundamental, experimental and theoretical work of the highest quality in all the major areas of inorganic chemistry. These include synthetic chemistry, coordination chemistry, organometallic chemistry, bioinorganic chemistry, and solid-state and materials chemistry. Papers should be complete pieces of work, and the inclusion of results from spectroscopic and/or physical techniques is encouraged. Papers merely reporting the preparation and X-ray structural characterization of only a single compound will not be considered appropriate unless the compound and its structure are particularly interesting.

Similarly, papers concerned solely with stability constants determined by potentiometric titration data unsupported by other e.g. spectroscopic techniques will not be acceptable nor will solvent extraction data unless supported by other data of interest to inorganic chemists. Unnecessary fragmentation of work is not acceptable.

In addition Polyhedron publishes specially commissioned review articles (Polyhedron Reports) and collections of original research papers (Polyhedron Symposia-in-Print) of appropriate timeliness.

Publication Information: Polyhedron (ISSN 0277-5387). For 2006, volume 25 is scheduled for publication. Subscription prices are available upon request from the Publisher or from the Regional Sales Office nearest you or from this journal's website (http://www.elsevier.com/locate/poly). Further information is available on this journal and other Elsevier products through Elsevier's website (http://www.elsevier.com). Subscriptions are accepted on a prepaid basis only and are entered on a calendar year basis. Issues are sent by standard mail (surface within Europe, air delivery outside Europe). Priority rates are available upon request. Claims for missing issues should be made within six months of the date of dispatch.

Orders, Claims and Journal Enquiries

(no manuscript enquiries)

Please contact the Customer Support Department at the Regional Sales Office nearest you:

Orlando
Elsevier
Customer Service Department
6277 Sea Harbor Drive
Orlando, FL 32887-4800
USA
Tel.: (877) 8397126 or (800) 6542452 [toll free numbers for US customers];
(+1) (407) 3454020 or
(+1) (407) 3454000 [customers outside US]
Fax: (+1) (407) 3631354 or
(+1) (407) 3639661
E-mail: usjcs@elsevier.com or elspcs@elsevier.com

Amsterdam
Elsevier
Customer Service Department
P.O. Box 211
1000 AE Amsterdam
The Netherlands
Tel.: (+31) 20-485-3757
Fax: (+31) 20-485-3432
E-mail: nlinfo-f@elsevier.com

Tokyo
Elsevier K.K.
Customer Service Department
4F Higashi-Azabu, 1-Chome Bldg
1-9-15 Higashi-Azabu
Minato-ku, Tokyo 106-0044
Japan
Tel.: (+81) 3-5561-5037
Fax: (+81) 3-5561-5047
E-mail: jp.info@elsevier.com

Singapore
Elsevier
Customer Service Department
3 Killiney Road
#08-01 Winsland House 1
Singapore 239519
Tel.: (+65) 6349-0222
Fax: (+65) 6733-1510
E-mail: asiainfo@elsevier.com

USA mailing notice: *Polyhedron* (ISSN 0277-5387) is published triweekly by Elsevier Ltd. (P.O. Box 211, 1000 AE Amsterdam, The Netherlands). Annual subscription price in the USA US$ 7049.00 (valid in North, Central and South America), including air speed delivery. Periodical postage rate is paid at Jamaica, NY 11431.
USA POSTMASTER: Send change of address to *Polyhedron*, Elsevier, 6277 Sea Harbor Drive, Orlando, FL 32887-4800.
AIRFREIGHT AND MAILING in the USA by Publications Expediting Inc., 200 Meacham Avenue, Elmont, NY 11003.

Advertising Information

Advertising orders and enquiries can be sent to: **South America:** Mr Tino DeCarlo, The Advertising Department, Elsevier Inc., 360 Park Avenue South, New York, NY 10010-1710, USA; tel.: (+1) (212) 633 3815; fax: (+1) (212) 633 3820; e-mail: t.decarlo@elsevier.com. **Europe, USA, Canada and ROW:** Miss Katrina Barton, Commercial Sales, Elsevier, 84 Theobald's Road, London, WCIX 8RR, UK; phone: (+44) (0) 20 7611 4117; fax: (+44) (0) 20 7611 4463; e-mail: commercialsales@elsevier.com

POLYHEDRON

The International Journal for Inorganic and Organometallic Chemistry

Executive Editors

The Americas
G. Christou
Department of Chemistry, University of Florida,
Gainesville, FL 32611-7200, USA
E-mail: christou@chem.ufl.edu

Rest of the world
C.E. Housecroft
Department of Chemistry, University of Basel,
Spitalstrasse 51, CH-4056 Basel, Switzerland
E-mail: poly-chemie@unibas.ch

Associate Regional Editor for China
T.C.W. Mak
Department of Chemistry, University Science Centre,
The Chinese University of Hong Kong,
Shatin NT, Hong Kong, People's Republic of China
E-mail: tcwmak@cuhk.edu.hk

Polyhedron Reports
Editor
G. Christou *(Gainesville, FL, USA)*

Symposia-in-print
Editor
G. Parkin *(New York, NY, USA)*

Editorial Board
N.Y. Barba-Behrens *(Mexico, DF, Mexico)*
A.G. Blackman *(Dunedin, New Zealand)*
D.C. Bradley *(London, UK)*
D. Braga *(Bologna, Italy)*
A. Brodie *(Palmerston North, New Zealand)*
A. Castiñeiras *(Santiago de Compostela, Spain)*
M.H. Chisholm *(Columbus, OH, USA)*
E.C. Constable *(Basel, Switzerland)*
E. Coronado *(Valencia, Spain)*
L. Cronin *(Glasgow, UK)*
W.J. Evans *(Irvine, CA, USA)*
L.H. Gade *(Heidelberg, Germany)*
L. Hubert-Pfalzgraf *(Villeurbanne, France)*
M.B. Hursthouse *(Southampton, UK)*
T. Kiss *(Szeged, Hungary)*
L. Manners *(Bristol, UK)*
S. Perlepes *(Patras, Greece)*
P.P. Power *(Davis, CA, USA)*
T.B. Rauchfuss *(Urbana, IL, USA)*
J. Reedijk *(Leiden, The Netherlands)*
A.L. Rheingold *(Newark, DE, USA)*
A.M.Z. Slawin *(Fife, UK)*
A.G. Sykes *(Newcastle upon Tyne, UK)*
L.K. Thompson *(St John's, NF, Canada)*
M.D. Ward *(Sheffield, UK)*
R.E.P. Winpenny *(Manchester, UK)*
M. Yamashita *(Sendai, Japan)*
M. Zaworotko *(Tampa, FL, USA)*

Aims and Scope

Polyhedron will publish original, fundamental, experimental and theoretical work of the highest quality in all the major areas of inorganic chemistry. These include synthetic chemistry, coordination chemistry, organometallic chemistry, bioinorganic chemistry, and solid-state and materials chemistry. Papers should be complete pieces of work, and the inclusion of results from spectroscopic and/or physical techniques is encouraged. Papers merely reporting the preparation and X-ray structural characterization of only a single compound will not be considered appropriate unless the compound and its structure are particularly interesting.

Similarly, papers concerned solely with stability constants determined by potentiometric titration data unsupported by other e.g. spectroscopic techniques will not be acceptable nor will solvent extraction data unless supported by other data of interest to inorganic chemists. Unnecessary fragmentation of work is not acceptable.

In addition Polyhedron publishes specially commissioned review articles (Polyhedron Reports) and collections of original research papers (Polyhedron Symposia-in-Print) of appropriate timeliness.

Publication Information: Polyhedron (ISSN 0277-5387). For 2006, volume 25 is scheduled for publication. Subscription prices are available upon request from the Publisher or from the Regional Sales Office nearest you or from this journal's website (http://www.elsevier.com/locate/poly). Further information is available on this journal and other Elsevier products through Elsevier's website (http://www.elsevier.com). Subscriptions are accepted on a prepaid basis only and are entered on a calendar year basis. Issues are sent by standard mail (surface within Europe, air delivery outside Europe). Priority rates are available upon request. Claims for missing issues should be made within six months of the date of dispatch.

Orders, Claims and Journal Enquiries

(no manuscript enquiries)
Please contact the Customer Support Department at the Regional Sales Office nearest you:

Orlando
Elsevier
Customer Service Department
6277 Sea Harbor Drive
Orlando, FL 32887-4800
USA
Tel.: (877) 8397126 or (800) 6542452 [toll free numbers for US customers];
(+1) (407) 3454020 or
(+1) (407) 3454000 [customers outside US]
Fax: (+1) (407) 3631354 or
(+1) (407) 3639661
E-mail: usjcs@elsevier.com or elspcs@elsevier.com

Amsterdam
Elsevier
Customer Service Department
P.O. Box 211
1000 AE Amsterdam
The Netherlands
Tel.: (+31) 20-485-3757
Fax: (+31) 20-485-3432
E-mail: nlinfo-f@elsevier.com

Tokyo
Elsevier K.K.
Customer Service Department
4F Higashi-Azabu, 1-Chome Bldg
1-9-15 Higashi-Azabu
Minato-ku, Tokyo 106-0044
Japan
Tel.: (+81) 3-5561-5037
Fax: (+81) 3-5561-5047
E-mail: jp.info@elsevier.com

Singapore
Elsevier
Customer Service Department
3 Killiney Road
#08-01 Winsland House 1
Singapore 239519
Tel.: (+65) 6349-0222
Fax: (+65) 6733-1510
E-mail: asiainfo@elsevier.com

USA mailing notice: *Polyhedron* (ISSN 0277-5387) is published triweekly by Elsevier Ltd. (P.O. Box 211, 1000 AE Amsterdam, The Netherlands). Annual subscription price in the USA US$ 7049.00 (valid in North, Central and South America), including air speed delivery. Periodical postage rate is paid at Jamaica, NY 11431.
USA POSTMASTER: Send change of address to *Polyhedron*, Elsevier, 6277 Sea Harbor Drive, Orlando, FL 32887-4800.
AIRFREIGHT AND MAILING in the USA by Publications Expediting Inc., 200 Meacham Avenue, Elmont, NY 11003.

Advertising Information

Advertising orders and enquiries can be sent to: **South America:** Mr Tino DeCarlo, The Advertising Department, Elsevier Inc., 360 Park Avenue South, New York, NY 10010-1710, USA; tel.: (+1) (212) 633 3815; fax: (+1) (212) 633 3820; e-mail: t.decarlo@elsevier.com. **Europe, USA, Canada and ROW:** Miss Katrina Barton, Commercial Sales, Elsevier, 84 Theobald's Road, London, WCIX 8RR, UK; phone: (+44) (0) 20 7611 4117; fax: (+44) (0) 20 7611 4463; e-mail: commercialsales@elsevier.com

POLYHEDRON

The International Journal for Inorganic and Organometallic Chemistry

Executive Editors

The Americas
G. Christou
Department of Chemistry, University of Florida,
Gainesville, FL 32611-7200, USA
E-mail: christou@chem.ufl.edu

Rest of the world
C.E. Housecroft
Department of Chemistry, University of Basel,
Spitalstrasse 51, CH-4056 Basel, Switzerland
E-mail: poly-chemie@unibas.ch

Associate Regional Editor for China
T.C.W. Mak
Department of Chemistry, University Science Centre,
The Chinese University of Hong Kong,
Shatin NT, Hong Kong, People's Republic of China
E-mail: tcwmak@cuhk.edu.hk

Polyhedron Reports
Editor
G. Christou *(Gainesville, FL, USA)*

Symposia-in-print
Editor
G. Parkin *(New York, NY, USA)*

Editorial Board

N.Y. Barba-Behrens *(Mexico, DF, Mexico)*
A.G. Blackman *(Dunedin, New Zealand)*
D.C. Bradley *(London, UK)*
D. Braga *(Bologna, Italy)*
A. Brodie *(Palmerston North, New Zealand)*
A. Castiñeiras *(Santiago de Compostela, Spain)*
M.H. Chisholm *(Columbus, OH, USA)*
E.C. Constable *(Basel, Switzerland)*
E. Coronado *(Valencia, Spain)*
L. Cronin *(Glasgow, UK)*
W.J. Evans *(Irvine, CA, USA)*
L.H. Gade *(Heidelberg, Germany)*
L. Hubert-Pfalzgraf *(Villeurbanne, France)*
M.B. Hursthouse *(Southampton, UK)*
T. Kiss *(Szeged, Hungary)*
L. Manners *(Bristol, UK)*
S. Perlepes *(Patras, Greece)*
P.P. Power *(Davis, CA, USA)*
T.B. Rauchfuss *(Urbana, IL, USA)*
J. Reedijk *(Leiden, The Netherlands)*
A.L. Rheingold *(Newark, DE, USA)*
A.M.Z. Slawin *(Fife, UK)*
A.G. Sykes *(Newcastle upon Tyne, UK)*
L.K. Thompson *(St John's, NF, Canada)*
M.D. Ward *(Sheffield, UK)*
R.E.P. Winpenny *(Manchester, UK)*
M. Yamashita *(Sendai, Japan)*
M. Zaworotko *(Tampa, FL, USA)*

Aims and Scope

Polyhedron will publish original, fundamental, experimental and theoretical work of the highest quality in all the major areas of inorganic chemistry. These include synthetic chemistry, coordination chemistry, organometallic chemistry, bioinorganic chemistry, and solid-state and materials chemistry. Papers should be complete pieces of work, and the inclusion of results from spectroscopic and/or physical techniques is encouraged. Papers merely reporting the preparation and X-ray structural characterization of only a single compound will not be considered appropriate unless the compound and its structure are particularly interesting.

Similarly, papers concerned solely with stability constants determined by potentiometric titration data unsupported by other e.g. spectroscopic techniques will not be acceptable nor will solvent extraction data unless supported by other data of interest to inorganic chemists. Unnecessary fragmentation of work is not acceptable.

In addition Polyhedron publishes specially commissioned review articles (Polyhedron Reports) and collections of original research papers (Polyhedron Symposia-in-Print) of appropriate timeliness.

Publication Information: Polyhedron (ISSN 0277-5387). For 2006, volume 25 is scheduled for publication. Subscription prices are available upon request from the Publisher or from the Regional Sales Office nearest you or from this journal's website (http://www.elsevier.com/locate/poly). Further information is available on this journal and other Elsevier products through Elsevier's website (http://www.elsevier.com). Subscriptions are accepted on a prepaid basis only and are entered on a calendar year basis. Issues are sent by standard mail (surface within Europe, air delivery outside Europe). Priority rates are available upon request. Claims for missing issues should be made within six months of the date of dispatch.

Orders, Claims and Journal Enquiries

(no manuscript enquiries)

Please contact the Customer Support Department at the Regional Sales Office nearest you:

Orlando
Elsevier
Customer Service Department
6277 Sea Harbor Drive
Orlando, FL 32887-4800
USA

Tel.: (877) 8397126 or (800) 6542452 [toll free numbers for US customers];
(+1) (407) 3454020 or
(+1) (407) 3454000 [customers outside US]
Fax: (+1) (407) 3631354 or
(+1) (407) 3639661
E-mail: usjcs@elsevier.com or elspcs@elsevier.com

Amsterdam
Elsevier
Customer Service Department
P.O. Box 211
1000 AE Amsterdam
The Netherlands
Tel.: (+31) 20-485-3757
Fax: (+31) 20-485-3432
E-mail: nlinfo-f@elsevier.com

Tokyo
Elsevier K.K.
Customer Service Department
4F Higashi-Azabu, 1-Chome Bldg
1-9-15 Higashi-Azabu
Minato-ku, Tokyo 106-0044
Japan
Tel.: (+81) 3-5561-5037
Fax: (+81) 3-5561-5047
E-mail: jp.info@elsevier.com

Singapore
Elsevier
Customer Service Department
3 Killiney Road
#08-01 Winsland House 1
Singapore 239519
Tel.: (+65) 6349-0222
Fax: (+65) 6733-1510
E-mail: asiainfo@elsevier.com

USA mailing notice: *Polyhedron* (ISSN 0277-5387) is published triweekly by Elsevier Ltd. (P.O. Box 211, 1000 AE Amsterdam, The Netherlands). Annual subscription price in the USA US$ 7049.00 (valid in North, Central and South America), including air speed delivery. Periodical postage rate is paid at Jamaica, NY 11431.
USA POSTMASTER: Send change of address to *Polyhedron*, Elsevier, 6277 Sea Harbor Drive, Orlando, FL 32887-4800.
AIRFREIGHT AND MAILING in the USA by Publications Expediting Inc., 200 Meacham Avenue, Elmont, NY 11003.

Advertising Information

Advertising orders and enquiries can be sent to: **South America:** Mr Tino DeCarlo, The Advertising Department, Elsevier Inc., 360 Park Avenue South, New York, NY 10010-1710, USA; tel.: (+1) (212) 633 3815; fax: (+1) (212) 633 3820; e-mail: t.decarlo@elsevier.com. **Europe, USA, Canada and ROW:** Miss Katrina Barton, Commercial Sales, Elsevier, 84 Theobald's Road, London, WCIX 8RR, UK; phone: (+44) (0) 20 7611 4117; fax: (+44) (0) 20 7611 4463; e-mail: commercialsales@elsevier.com

POLYHEDRON

The International Journal for Inorganic and Organometallic Chemistry

Executive Editors

The Americas
G. Christou
Department of Chemistry, University of Florida,
Gainesville, FL 32611-7200, USA
E-mail: christou@chem.ufl.edu

Rest of the world
C.E. Housecroft
Department of Chemistry, University of Basel,
Spitalstrasse 51, CH-4056 Basel, Switzerland
E-mail: poly-chemie@unibas.ch

Associate Regional Editor for China
T.C.W. Mak
Department of Chemistry, University Science Centre,
The Chinese University of Hong Kong,
Shatin NT, Hong Kong, People's Republic of China
E-mail: tcwmak@cuhk.edu.hk

Polyhedron Reports
Editor
G. Christou *(Gainesville, FL, USA)*

Symposia-in-print
Editor
G. Parkin *(New York, NY, USA)*

Editorial Board
N.Y. Barba-Behrens *(Mexico, DF, Mexico)*
A.G. Blackman *(Dunedin, New Zealand)*
D.C. Bradley *(London, UK)*
D. Braga *(Bologna, Italy)*
A. Brodie *(Palmerston North, New Zealand)*
A. Castiñeiras *(Santiago de Compostela, Spain)*
M.H. Chisholm *(Columbus, OH, USA)*
E.C. Constable *(Basel, Switzerland)*
E. Coronado *(Valencia, Spain)*
L. Cronin *(Glasgow, UK)*
W.J. Evans *(Irvine, CA, USA)*
L.H. Gade *(Heidelberg, Germany)*
L. Hubert-Pfalzgraf *(Villeurbanne, France)*
M.B. Hursthouse *(Southampton, UK)*
T. Kiss *(Szeged, Hungary)*
L. Manners *(Bristol, UK)*
S. Perlepes *(Patras, Greece)*
P.P. Power *(Davis, CA, USA)*
T.B. Rauchfuss *(Urbana, IL, USA)*
J. Reedijk *(Leiden, The Netherlands)*
A.L. Rheingold *(Newark, DE, USA)*
A.M.Z. Slawin *(Fife, UK)*
A.G. Sykes *(Newcastle upon Tyne, UK)*
L.K. Thompson *(St John's, NF, Canada)*
M.D. Ward *(Sheffield, UK)*
R.E.P. Winpenny *(Manchester, UK)*
M. Yamashita *(Sendai, Japan)*
M. Zaworotko *(Tampa, FL, USA)*

Aims and Scope

Polyhedron will publish original, fundamental, experimental and theoretical work of the highest quality in all the major areas of inorganic chemistry. These include synthetic chemistry, coordination chemistry, organometallic chemistry, bioinorganic chemistry, and solid-state and materials chemistry. Papers should be complete pieces of work, and the inclusion of results from spectroscopic and/or physical techniques is encouraged. Papers merely reporting the preparation and X-ray structural characterization of only a single compound will not be considered appropriate unless the compound and its structure are particularly interesting.

Similarly, papers concerned solely with stability constants determined by potentiometric titration data unsupported by other e.g. spectroscopic techniques will not be acceptable nor will solvent extraction data unless supported by other data of interest to inorganic chemists. Unnecessary fragmentation of work is not acceptable.

In addition Polyhedron publishes specially commissioned review articles (Polyhedron Reports) and collections of original research papers (Polyhedron Symposia-in-Print) of appropriate timeliness.

Publication Information: Polyhedron (ISSN 0277-5387). For 2006, volume 25 is scheduled for publication. Subscription prices are available upon request from the Publisher or from the Regional Sales Office nearest you or from this journal's website (http://www.elsevier.com/locate/poly). Further information is available on this journal and other Elsevier products through Elsevier's website (http://www.elsevier.com). Subscriptions are accepted on a prepaid basis only and are entered on a calendar year basis. Issues are sent by standard mail (surface within Europe, air delivery outside Europe). Priority rates are available upon request. Claims for missing issues should be made within six months of the date of dispatch.

Orders, Claims and Journal Enquiries

(no manuscript enquiries)

Please contact the Customer Support Department at the Regional Sales Office nearest you:

Orlando
Elsevier
Customer Service Department
6277 Sea Harbor Drive
Orlando, FL 32887-4800
USA
Tel.: (877) 8397126 or (800) 6542452 [toll free numbers for US customers];
(+1) (407) 3454020 or
(+1) (407) 3454000 [customers outside US]
Fax: (+1) (407) 3631354 or
(+1) (407) 3639661
E-mail: usjcs@elsevier.com or elspcs@elsevier.com

Amsterdam
Elsevier
Customer Service Department
P.O. Box 211
1000 AE Amsterdam
The Netherlands
Tel.: (+31) 20-485-3757
Fax: (+31) 20-485-3432
E-mail: nlinfo-f@elsevier.com

Tokyo
Elsevier K.K.
Customer Service Department
4F Higashi-Azabu, 1-Chome Bldg
1-9-15 Higashi-Azabu
Minato-ku, Tokyo 106-0044
Japan
Tel.: (+81) 3-5561-5037
Fax: (+81) 3-5561-5047
E-mail: jp.info@elsevier.com

Singapore
Elsevier
Customer Service Department
3 Killiney Road
#08-01 Winsland House 1
Singapore 239519
Tel.: (+65) 6349-0222
Fax: (+65) 6733-1510
E-mail: asiainfo@elsevier.com

USA mailing notice: *Polyhedron* (ISSN 0277-5387) is published triweekly by Elsevier Ltd. (P.O. Box 211, 1000 AE Amsterdam, The Netherlands). Annual subscription price in the USA US$ 7049.00 (valid in North, Central and South America), including air speed delivery. Periodical postage rate is paid at Jamaica, NY 11431.
USA POSTMASTER: Send change of address to *Polyhedron*, Elsevier, 6277 Sea Harbor Drive, Orlando, FL 32887-4800.
AIRFREIGHT AND MAILING in the USA by Publications Expediting Inc., 200 Meacham Avenue, Elmont, NY 11003.

Advertising Information

Advertising orders and enquiries can be sent to: **South America:** Mr Tino DeCarlo, The Advertising Department, Elsevier Inc., 360 Park Avenue South, New York, NY 10010-1710, USA; tel.: (+1) (212) 633 3815; fax: (+1) (212) 633 3820; e-mail: t.decarlo@elsevier.com. **Europe, USA, Canada and ROW:** Miss Katrina Barton, Commercial Sales, Elsevier, 84 Theobald's Road, London, WCIX 8RR, UK; phone: (+44) (0) 20 7611 4117; fax: (+44) (0) 20 7611 4463; e-mail: commercialsales@elsevier.com

POLYHEDRON

The International Journal for Inorganic and Organometallic Chemistry

Executive Editors

The Americas
G. Christou
Department of Chemistry, University of Florida,
Gainesville, FL 32611-7200, USA
E-mail: christou@chem.ufl.edu

Rest of the world
C.E. Housecroft
Department of Chemistry, University of Basel,
Spitalstrasse 51, CH-4056 Basel, Switzerland
E-mail: poly-chemie@unibas.ch

Associate Regional Editor for China
T.C.W. Mak
Department of Chemistry, University Science Centre,
The Chinese University of Hong Kong,
Shatin NT, Hong Kong, People's Republic of China
E-mail: tcwmak@cuhk.edu.hk

Polyhedron Reports
Editor
G. Christou *(Gainesville, FL, USA)*

Symposia-in-print
Editor
G. Parkin *(New York, NY, USA)*

Editorial Board
N.Y. Barba-Behrens *(Mexico, DF, Mexico)*
A.G. Blackman *(Dunedin, New Zealand)*
D.C. Bradley *(London, UK)*
D. Braga *(Bologna, Italy)*
A. Brodie *(Palmerston North, New Zealand)*
A. Castiñeiras *(Santiago de Compostela, Spain)*
M.H. Chisholm *(Columbus, OH, USA)*
E.C. Constable *(Basel, Switzerland)*
E. Coronado *(Valencia, Spain)*
L. Cronin *(Glasgow, UK)*
W.J. Evans *(Irvine, CA, USA)*
L.H. Gade *(Heidelberg, Germany)*
L. Hubert-Pfalzgraf *(Villeurbanne, France)*
M.B. Hursthouse *(Southampton, UK)*
T. Kiss *(Szeged, Hungary)*
L. Manners *(Bristol, UK)*
S. Perlepes *(Patras, Greece)*
P.P. Power *(Davis, CA, USA)*
T.B. Rauchfuss *(Urbana, IL, USA)*
J. Reedijk *(Leiden, The Netherlands)*
A.L. Rheingold *(Newark, DE, USA)*
A.M.Z. Slawin *(Fife, UK)*
A.G. Sykes *(Newcastle upon Tyne, UK)*
L.K. Thompson *(St John's, NF, Canada)*
M.D. Ward *(Sheffield, UK)*
R.E.P. Winpenny *(Manchester, UK)*
M. Yamashita *(Sendai, Japan)*
M. Zaworotko *(Tampa, FL, USA)*

Aims and Scope

Polyhedron will publish original, fundamental, experimental and theoretical work of the highest quality in all the major areas of inorganic chemistry. These include synthetic chemistry, coordination chemistry, organometallic chemistry, bioinorganic chemistry, and solid-state and materials chemistry. Papers should be complete pieces of work, and the inclusion of results from spectroscopic and/or physical techniques is encouraged. Papers merely reporting the preparation and X-ray structural characterization of only a single compound will not be considered appropriate unless the compound and its structure are particularly interesting.

Similarly, papers concerned solely with stability constants determined by potentiometric titration data unsupported by other e.g. spectroscopic techniques will not be acceptable nor will solvent extraction data unless supported by other data of interest to inorganic chemists. Unnecessary fragmentation of work is not acceptable.

In addition Polyhedron publishes specially commissioned review articles (Polyhedron Reports) and collections of original research papers (Polyhedron Symposia-in-Print) of appropriate timeliness.

Publication Information: Polyhedron (ISSN 0277-5387). For 2006, volume 25 is scheduled for publication. Subscription prices are available upon request from the Publisher or from the Regional Sales Office nearest you or from this journal's website (http://www.elsevier.com/locate/poly). Further information is available on this journal and other Elsevier products through Elsevier's website (http://www.elsevier.com). Subscriptions are accepted on a prepaid basis only and are entered on a calendar year basis. Issues are sent by standard mail (surface within Europe, air delivery outside Europe). Priority rates are available upon request. Claims for missing issues should be made within six months of the date of dispatch.

Orders, Claims and Journal Enquiries

(no manuscript enquiries)
Please contact the Customer Support Department at the Regional Sales Office nearest you:

Orlando
Elsevier
Customer Service Department
6277 Sea Harbor Drive
Orlando, FL 32887-4800
USA
Tel.: (877) 8397126 or (800) 6542452 [toll free numbers for US customers];
(+1) (407) 3454020 or
(+1) (407) 3454000 [customers outside US]
Fax: (+1) (407) 3631354 or
(+1) (407) 3639661
E-mail: usjcs@elsevier.com or elspcs@elsevier.com

Amsterdam
Elsevier
Customer Service Department
P.O. Box 211
1000 AE Amsterdam
The Netherlands
Tel.: (+31) 20-485-3757
Fax: (+31) 20-485-3432
E-mail: nlinfo-f@elsevier.com

Tokyo
Elsevier K.K.
Customer Service Department
4F Higashi-Azabu, 1-Chome Bldg
1-9-15 Higashi-Azabu
Minato-ku, Tokyo 106-0044
Japan
Tel.: (+81) 3-5561-5037
Fax: (+81) 3-5561-5047
E-mail: jp.info@elsevier.com

Singapore
Elsevier
Customer Service Department
3 Killiney Road
#08-01 Winsland House 1
Singapore 239519
Tel.: (+65) 6349-0222
Fax: (+65) 6733-1510
E-mail: asiainfo@elsevier.com

USA mailing notice: *Polyhedron* (ISSN 0277-5387) is published triweekly by Elsevier Ltd. (P.O. Box 211, 1000 AE Amsterdam, The Netherlands). Annual subscription price in the USA US$ 7049.00 (valid in North, Central and South America), including air speed delivery. Periodical postage rate is paid at Jamaica, NY 11431.
USA POSTMASTER: Send change of address to *Polyhedron*, Elsevier, 6277 Sea Harbor Drive, Orlando, FL 32887-4800.
AIRFREIGHT AND MAILING in the USA by Publications Expediting Inc., 200 Meacham Avenue, Elmont, NY 11003.

Advertising Information

Advertising orders and enquiries can be sent to: **South America:** Mr Tino DeCarlo, The Advertising Department, Elsevier Inc., 360 Park Avenue South, New York, NY 10010-1710, USA; tel.: (+1) (212) 633 3815; fax: (+1) (212) 633 3820; e-mail: t.decarlo@elsevier.com. **Europe, USA, Canada and ROW:** Miss Katrina Barton, Commercial Sales, Elsevier, 84 Theobald's Road, London, WCIX 8RR, UK; phone: (+44) (0) 20 7611 4117; fax: (+44) (0) 20 7611 4463; e-mail: commercialsales@elsevier.com

POLYHEDRON

The International Journal for Inorganic and Organometallic Chemistry

Executive Editors

The Americas
G. Christou
Department of Chemistry, University of Florida,
Gainesville, FL 32611-7200, USA
E-mail: christou@chem.ufl.edu

Rest of the world
C.E. Housecroft
Department of Chemistry, University of Basel,
Spitalstrasse 51, CH-4056 Basel, Switzerland
E-mail: poly-chemie@unibas.ch

Associate Regional Editor for China
T.C.W. Mak
Department of Chemistry, University Science Centre,
The Chinese University of Hong Kong,
Shatin NT, Hong Kong, People's Republic of China
E-mail: tcwmak@cuhk.edu.hk

Polyhedron Reports
Editor
G. Christou *(Gainesville, FL, USA)*

Symposia-in-print
Editor
G. Parkin *(New York, NY, USA)*

Editorial Board
N.Y. Barba-Behrens *(Mexico, DF, Mexico)*
A.G. Blackman *(Dunedin, New Zealand)*
D.C. Bradley *(London, UK)*
D. Braga *(Bologna, Italy)*
A. Brodie *(Palmerston North, New Zealand)*
A. Castiñeiras *(Santiago de Compostela, Spain)*
M.H. Chisholm *(Columbus, OH, USA)*
E.C. Constable *(Basel, Switzerland)*
E. Coronado *(Valencia, Spain)*
L. Cronin *(Glasgow, UK)*
W.J. Evans *(Irvine, CA, USA)*
L.H. Gade *(Heidelberg, Germany)*
L. Hubert-Pfalzgraf *(Villeurbanne, France)*
M.B. Hursthouse *(Southampton, UK)*
T. Kiss *(Szeged, Hungary)*
S. Perlepes *(Patras, Greece)*
P.P. Power *(Davis, CA, USA)*
T.B. Rauchfuss *(Urbana, IL, USA)*
J. Reedijk *(Leiden, The Netherlands)*
A.L. Rheingold *(Newark, DE, USA)*
A.M.Z. Slawin *(Fife, UK)*
F.G.A. Stone *(Waco, TX, USA)*
A.G. Sykes *(Newcastle upon Tyne, UK)*
L.K. Thompson *(St John's, NF, Canada)*
M.D. Ward *(Sheffield, UK)*
R.E.P. Winpenny *(Manchester, UK)*
M. Yamashita *(Sendai, Japan)*
M. Zaworotko *(Tampa, FL, USA)*

Aims and Scope

Polyhedron will publish original, fundamental, experimental and theoretical work of the highest quality in all the major areas of inorganic chemistry. These include synthetic chemistry, coordination chemistry, organometallic chemistry, bioinorganic chemistry, and solid-state and materials chemistry. Papers should be complete pieces of work, and the inclusion of results from spectroscopic and/or physical techniques is encouraged. Papers merely reporting the preparation and X-ray structural characterization of only a single compound will not be considered appropriate unless the compound and its structure are particularly interesting.

Similarly, papers concerned solely with stability constants determined by potentiometric titration data unsupported by other e.g. spectroscopic techniques will not be acceptable nor will solvent extraction data unless supported by other data of interest to inorganic chemists. Unnecessary fragmentation of work is not acceptable.

In addition Polyhedron publishes specially commissioned review articles (Polyhedron Reports) and collections of original research papers (Polyhedron Symposia-in-Print) of appropriate timeliness.

Publication Information: Polyhedron (ISSN 0277-5387). For 2006, volume 25 is scheduled for publication. Subscription prices are available upon request from the Publisher or from the Regional Sales Office nearest you or from this journal's website (http://www.elsevier.com/locate/poly). Further information is available on this journal and other Elsevier products through Elsevier's website (http://www.elsevier.com). Subscriptions are accepted on a prepaid basis only and are entered on a calendar year basis. Issues are sent by standard mail (surface within Europe, air delivery outside Europe). Priority rates are available upon request. Claims for missing issues should be made within six months of the date of dispatch.

Orders, Claims and Journal Enquiries

(no manuscript enquiries)

Please contact the Customer Support Department at the Regional Sales Office nearest you:

Orlando
Elsevier
Customer Service Department
6277 Sea Harbor Drive
Orlando, FL 32887-4800
USA
Tel.: (877) 8397126 or (800) 6542452 [toll free numbers for US customers];
(+1) (407) 3454020 or
(+1) (407) 3454000 [customers outside US]
Fax: (+1) (407) 3631354 or
(+1) (407) 3639661
E-mail: usjcs@elsevier.com or elspcs@elsevier.com

Amsterdam
Elsevier
Customer Service Department
P.O. Box 211
1000 AE Amsterdam
The Netherlands
Tel.: (+31) 20-485-3757
Fax: (+31) 20-485-3432
E-mail: nlinfo-f@elsevier.com

Tokyo
Elsevier K.K.
Customer Service Department
4F Higashi-Azabu, 1-Chome Bldg
1-9-15 Higashi-Azabu
Minato-ku, Tokyo 106-0044
Japan
Tel.: (+81) 3-5561-5037
Fax: (+81) 3-5561-5047
E-mail: jp.info@elsevier.com

Singapore
Elsevier
Customer Service Department
3 Killiney Road
#08-01 Winsland House 1
Singapore 239519
Tel.: (+65) 6349-0222
Fax: (+65) 6733-1510
E-mail: asiainfo@elsevier.com

USA mailing notice: *Polyhedron* (ISSN 0277-5387) is published triweekly by Elsevier Ltd. (P.O. Box 211, 1000 AE Amsterdam, The Netherlands). Annual subscription price in the USA US$ 7049.00 (valid in North, Central and South America), including air speed delivery. Periodical postage rate is paid at Jamaica, NY 11431.
USA POSTMASTER: Send change of address to *Polyhedron*, Elsevier, 6277 Sea Harbor Drive, Orlando, FL 32887-4800.
AIRFREIGHT AND MAILING in the USA by Publications Expediting Inc., 200 Meacham Avenue, Elmont, NY 11003.

Advertising Information

Advertising orders and enquiries can be sent to: **South America:** Mr Tino DeCarlo, The Advertising Department, Elsevier Inc., 360 Park Avenue South, New York, NY 10010-1710, USA; tel.: (+1) (212) 633 3815; fax: (+1) (212) 633 3820; e-mail: t.decarlo@elsevier.com. **Europe, USA, Canada and ROW:** Miss Katrina Barton, Commercial Sales, Elsevier, 84 Theobald's Road, London, WCIX 8RR, UK; phone: (+44) (0) 20 7611 4117; fax: (+44) (0) 20 7611 4463; e-mail: commercialsales@elsevier.com

POLYHEDRON

The International Journal for Inorganic and Organometallic Chemistry

Executive Editors

The Americas
G. Christou
Department of Chemistry, University of Florida,
Gainesville, FL 32611-7200, USA
E-mail: christou@chem.ufl.edu

Rest of the world
C.E. Housecroft
Department of Chemistry, University of Basel,
Spitalstrasse 51, CH-4056 Basel, Switzerland
E-mail: poly-chemie@unibas.ch

Associate Regional Editor for China
T.C.W. Mak
Department of Chemistry, University Science Centre,
The Chinese University of Hong Kong,
Shatin NT, Hong Kong, People's Republic of China
E-mail: tcwmak@cuhk.edu.hk

Polyhedron Reports
Editor
G. Christou *(Gainesville, FL, USA)*

Symposia-in-print
Editor
G. Parkin *(New York, NY, USA)*

Editorial Board
N.Y. Barba-Behrens *(Mexico, DF, Mexico)*
A.G. Blackman *(Dunedin, New Zealand)*
D.C. Bradley *(London, UK)*
D. Braga *(Bologna, Italy)*
A. Brodie *(Palmerston North, New Zealand)*
A. Castiñeiras *(Santiago de Compostela, Spain)*
M.H. Chisholm *(Columbus, OH, USA)*
E.C. Constable *(Basel, Switzerland)*
E. Coronado *(Valencia, Spain)*
L. Cronin *(Glasgow, UK)*
W.J. Evans *(Irvine, CA, USA)*
L.H. Gade *(Heidelberg, Germany)*
L. Hubert-Pfalzgraf *(Villeurbanne, France)*
M.B. Hursthouse *(Southampton, UK)*
T. Kiss *(Szeged, Hungary)*
P.P. Power *(Davis, CA, USA)*
T.B. Rauchfuss *(Urbana, IL, USA)*
J. Reedijk *(Leiden, The Netherlands)*
A.L. Rheingold *(Newark, DE, USA)*
A.M.Z. Slawin *(Fife, UK)*
F.G.A. Stone *(Waco, TX, USA)*
A.G. Sykes *(Newcastle upon Tyne, UK)*
L.K. Thompson *(St John's, NF, Canada)*
M.D. Ward *(Sheffield, UK)*
R.E.P. Winpenny *(Manchester, UK)*
M. Zaworotko *(Tampa, FL, USA)*

Aims and Scope

Polyhedron will publish original, fundamental, experimental and theoretical work of the highest quality in all the major areas of inorganic chemistry. These include synthetic chemistry, coordination chemistry, organometallic chemistry, bioinorganic chemistry, and solid-state and materials chemistry. Papers should be complete pieces of work, and the inclusion of results from spectroscopic and/or physical techniques is encouraged. Papers merely reporting the preparation and X-ray structural characterization of only a single compound will not be considered appropriate unless the compound and its structure are particularly interesting.

Similarly, papers concerned solely with stability constants determined by potentiometric titration data unsupported by other e.g. spectroscopic techniques will not be acceptable nor will solvent extraction data unless supported by other data of interest to inorganic chemists. Unnecessary fragmentation of work is not acceptable.

In addition Polyhedron publishes specially commissioned review articles (Polyhedron Reports) and collections of original research papers (Polyhedron Symposia-in-Print) of appropriate timeliness.

Publication Information: Polyhedron (ISSN 0277-5387). For 2006, volume 25 is scheduled for publication. Subscription prices are available upon request from the Publisher or from the Regional Sales Office nearest you or from this journal's website (http://www.elsevier.com/locate/poly). Further information is available on this journal and other Elsevier products through Elsevier's website (http://www.elsevier.com). Subscriptions are accepted on a prepaid basis only and are entered on a calendar year basis. Issues are sent by standard mail (surface within Europe, air delivery outside Europe). Priority rates are available upon request. Claims for missing issues should be made within six months of the date of dispatch.

Orders, Claims and Journal Enquiries

(no manuscript enquiries)

Please contact the Customer Support Department at the Regional Sales Office nearest you:

Orlando
Elsevier
Customer Service Department
6277 Sea Harbor Drive
Orlando, FL 32887-4800
USA
Tel.: (877) 8397126 or (800) 6542452 [toll free numbers for US customers];
(+1) (407) 3454020 or
(+1) (407) 3454000 [customers outside US]
Fax: (+1) (407) 3631354 or
(+1) (407) 3639661
E-mail: usjcs@elsevier.com or elspcs@elsevier.com

Amsterdam
Elsevier
Customer Service Department
P.O. Box 211
1000 AE Amsterdam
The Netherlands
Tel.: (+31) 20-485-3757
Fax: (+31) 20-485-3432
E-mail: nlinfo-f@elsevier.com

Tokyo
Elsevier K.K.
Customer Service Department
4F Higashi-Azabu, 1-Chome Bldg
1-9-15 Higashi-Azabu
Minato-ku, Tokyo 106-0044
Japan
Tel.: (+81) 3-5561-5037
Fax: (+81) 3-5561-5047
E-mail: jp.info@elsevier.com

Singapore
Elsevier
Customer Service Department
3 Killiney Road
#08-01 Winsland House 1
Singapore 239519
Tel.: (+65) 6349-0222
Fax: (+65) 6733-1510
E-mail: asiainfo@elsevier.com

USA mailing notice: *Polyhedron* (ISSN 0277-5387) is published triweekly by Elsevier Ltd. (P.O. Box 211, 1000 AE Amsterdam, The Netherlands). Annual subscription price in the USA US$ 7049.00 (valid in North, Central and South America), including air speed delivery. Periodical postage rate is paid at Jamaica, NY 11431.
USA POSTMASTER: Send change of address to *Polyhedron*, Elsevier, 6277 Sea Harbor Drive, Orlando, FL 32887-4800.
AIRFREIGHT AND MAILING in the USA by Publications Expediting Inc., 200 Meacham Avenue, Elmont, NY 11003.

Advertising Information

Advertising orders and enquiries can be sent to: **South America:** Mr Tino DeCarlo, The Advertising Department, Elsevier Inc., 360 Park Avenue South, New York, NY 10010-1710, USA; tel.: (+1) (212) 633 3815; fax: (+1) (212) 633 3820; e-mail: t.decarlo@elsevier.com. **Europe, USA, Canada and ROW:** Miss Katrina Barton, Commercial Sales, Elsevier, 84 Theobald's Road, London, WCIX 8RR, UK; phone: (+44) (0) 20 7611 4117; fax: (+44) (0) 20 7611 4463; e-mail: commercialsales@elsevier.com

POLYHEDRON

The International Journal for Inorganic and Organometallic Chemistry

Executive Editors

The Americas
G. Christou
Department of Chemistry, University of Florida,
Gainesville, FL 32611-7200, USA
E-mail: christou@chem.ufl.edu

Rest of the world
C.E. Housecroft
Department of Chemistry, University of Basel,
Spitalstrasse 51, CH-4056 Basel, Switzerland
E-mail: poly-chemie@unibas.ch

Associate Regional Editor for China
T.C.W. Mak
Department of Chemistry, University Science Centre,
The Chinese University of Hong Kong,
Shatin NT, Hong Kong, People's Republic of China
E-mail: tcwmak@cuhk.edu.hk

Polyhedron Reports
Editor
G. Christou *(Gainesville, FL, USA)*

Symposia-in-print
Editor
G. Parkin *(New York, NY, USA)*

Editorial Board
N.Y. Barba-Behrens *(Mexico, DF, Mexico)*
A.G. Blackman *(Dunedin, New Zealand)*
D.C. Bradley *(London, UK)*
D. Braga *(Bologna, Italy)*
A. Brodie *(Palmerston North, New Zealand)*
A. Castiñeiras *(Santiago de Compostela, Spain)*
M.H. Chisholm *(Columbus, OH, USA)*
E.C. Constable *(Basel, Switzerland)*
E. Coronado *(Valencia, Spain)*
L. Cronin *(Glasgow, UK)*
W.J. Evans *(Irvine, CA, USA)*
L.H. Gade *(Heidelberg, Germany)*
L. Hubert-Pfalzgraf *(Villeurbanne, France)*
M.B. Hursthouse *(Southampton, UK)*
T. Kiss *(Szeged, Hungary)*
P.P. Power *(Davis, CA, USA)*
T.B. Rauchfuss *(Urbana, IL, USA)*
J. Reedijk *(Leiden, The Netherlands)*
A.L. Rheingold *(Newark, DE, USA)*
A.M.Z. Slawin *(Fife, UK)*
F.G.A. Stone *(Waco, TX, USA)*
A.G. Sykes *(Newcastle upon Tyne, UK)*
L.K. Thompson *(St John's, NF, Canada)*
M.D. Ward *(Sheffield, UK)*
R.E.P. Winpenny *(Manchester, UK)*
M. Zaworotko *(Tampa, FL, USA)*

Aims and Scope

Polyhedron will publish original, fundamental, experimental and theoretical work of the highest quality in all the major areas of inorganic chemistry. These include synthetic chemistry, coordination chemistry, organometallic chemistry, bioinorganic chemistry, and solid-state and materials chemistry. Papers should be complete pieces of work, and the inclusion of results from spectroscopic and/or physical techniques is encouraged. Papers merely reporting the preparation and X-ray structural characterization of only a single compound will not be considered appropriate unless the compound and its structure are particularly interesting.

Similarly, papers concerned solely with stability constants determined by potentiometric titration data unsupported by other e.g. spectroscopic techniques will not be acceptable nor will solvent extraction data unless supported by other data of interest to inorganic chemists. Unnecessary fragmentation of work is not acceptable.

In addition Polyhedron publishes specially commissioned review articles (Polyhedron Reports) and collections of original research papers (Polyhedron Symposia-in-Print) of appropriate timeliness.

Publication Information: Polyhedron (ISSN 0277-5387). For 2006, volume 25 is scheduled for publication. Subscription prices are available upon request from the Publisher or from the Regional Sales Office nearest you or from this journal's website (http://www.elsevier.com/locate/poly). Further information is available on this journal and other Elsevier products through Elsevier's website (http://www.elsevier.com). Subscriptions are accepted on a prepaid basis only and are entered on a calendar year basis. Issues are sent by standard mail (surface within Europe, air delivery outside Europe). Priority rates are available upon request. Claims for missing issues should be made within six months of the date of dispatch.

Orders, Claims and Journal Enquiries

(no manuscript enquiries)
Please contact the Customer Support Department at the Regional Sales Office nearest you:

Orlando
Elsevier
Customer Service Department
6277 Sea Harbor Drive
Orlando, FL 32887-4800
USA
Tel.: (877) 8397126 or (800) 6542452 [toll free numbers for US customers];
(+1) (407) 3454020 or
(+1) (407) 3454000 [customers outside US]
Fax: (+1) (407) 3631354 or
(+1) (407) 3639661
E-mail: usjcs@elsevier.com or elspcs@elsevier.com

Amsterdam
Elsevier
Customer Service Department
P.O. Box 211
1000 AE Amsterdam
The Netherlands
Tel.: (+31) 20-485-3757
Fax: (+31) 20-485-3432
E-mail: nlinfo-f@elsevier.com

Tokyo
Elsevier K.K.
Customer Service Department
4F Higashi-Azabu, 1-Chome Bldg
1-9-15 Higashi-Azabu
Minato-ku, Tokyo 106-0044
Japan
Tel.: (+81) 3-5561-5037
Fax: (+81) 3-5561-5047
E-mail: jp.info@elsevier.com

Singapore
Elsevier
Customer Service Department
3 Killiney Road
#08-01 Winsland House 1
Singapore 239519
Tel.: (+65) 6349-0222
Fax: (+65) 6733-1510
E-mail: asiainfo@elsevier.com

USA mailing notice: *Polyhedron* (ISSN 0277-5387) is published triweekly by Elsevier Ltd. (P.O. Box 211, 1000 AE Amsterdam, The Netherlands). Annual subscription price in the USA US$ 7049.00 (valid in North, Central and South America), including air speed delivery. Periodical postage rate is paid at Jamaica, NY 11431.
USA POSTMASTER: Send change of address to *Polyhedron*, Elsevier, 6277 Sea Harbor Drive, Orlando, FL 32887-4800.
AIRFREIGHT AND MAILING in the USA by Publications Expediting Inc., 200 Meacham Avenue, Elmont, NY 11003.

Advertising Information

Advertising orders and enquiries can be sent to: **South America:** Mr Tino DeCarlo, The Advertising Department, Elsevier Inc., 360 Park Avenue South, New York, NY 10010-1710, USA; tel.: (+1) (212) 633 3815; fax: (+1) (212) 633 3820; e-mail: t.decarlo@elsevier.com. **Europe, USA, Canada and ROW:** Miss Katrina Barton, Commercial Sales, Elsevier, 84 Theobald's Road, London, WCIX 8RR, UK; phone: (+44) (0) 20 7611 4117; fax: (+44) (0) 20 7611 4463; e-mail: commercialsales@elsevier.com

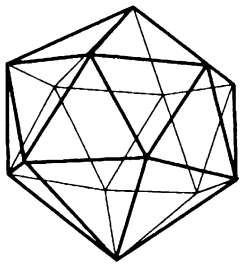

POLYHEDRON

The International Journal for Inorganic and Organometallic Chemistry

Founding Editor: **Sir Geoffrey Wilkinson**✠

Executive Editors

The Americas

G. Christou
Department of Chemistry, University of Florida, Gainesville, FL 32611-7200, USA
E-mail: christou@chem.ufl.edu

Rest of the world

C.E. Housecroft
Department of Chemistry, University of Basel, Spitalstrasse 51, CH-4056 Basel, Switzerland
E-mail: poly-chemie@unibas.ch

Associate Regional Editor for China

T.C.W. Mak
Department of Chemistry, University Science Centre, The Chinese University of Hong Kong, Shatin NT, Hong Kong, People's Republic of China
E-mail: tcwmak@cuhk.hk

Polyhedron Reports

G. Christou
Department of Chemistry, University of Florida, Gainesville, FL 32611-7200, USA
E-mail: christou@chem.ufl.edu

Symposia-in-print

G. Parkin
Department of Chemistry (Box 3115), Columbia University, 3000 Broadway, New York, NY 10027, USA
E-mail: parkin@chem.columbia.edu

Editorial Board

N.Y. Barba-Behrens *(Mexico, DF, Mexico)*
A. Blackman *(Dunedin, New Zealand)*
D.C. Bradley *(London, UK)*
D. Braga *(Bologna, Italy)*
A. Brodie *(Palmerston North, New Zealand)*
A. Castiñeiras *(Santiago de Compostela, Spain)*
M.H. Chisholm *(Columbus, OH, USA)*
E.C. Constable *(Basel, Switzerland)*
E. Coronado *(Valencia, Spain)*
W.J. Evans *(Irvine, CA, USA)*
L.H. Gade *(Heidelberg, Germany)*
J.F. Harrod *(Montreal, Que., Canada)*
L. Hubert-Pfalzgraf *(Villeurbanne, France)*
M.B. Hursthouse *(Southampton, UK)*
T. Kiss *(Szeged, Hungary)*
P.P. Power *(Davis, CA, USA)*
T.B. Rauchfuss *(Urbana, IL, USA)*
J. Reedijk *(Leiden, The Netherlands)*
A.L. Rheingold *(La Jolla, CA, USA)*
F.G.A. Stone *(Waco, TX, USA)*
A.G. Sykes *(Newcastle upon Tyne, UK)*
L.K. Thompson *(St John's, NF, Canada)*
M.D. Ward *(Bristol, UK)*
R.E.P. Winpenny *(Manchester, UK)*

ELSEVIER

Amsterdam — Boston — Jena — London — New York — Oxford — Paris — Philadelphia — San Diego — St Louis

Available online at www.sciencedirect.com
ScienceDirect
Polyhedron 25, issue 18, 25 December 2006
POLYHEDRON
www.elsevier.com/locate/poly

Contents

Papers

Nerissa A. Viola, Randy S. Rarig Jr., Wayne Ouellette, Robert P. Doyle

Polyhedron 25 (2006) 3457

Synthesis, structure and thermal analysis of the gallium complex of 1,4,7,10-tetraazacyclododecane-*N*,*N*′,*N*″,*N*‴-tetraacetic acid (DOTA)

The reaction of gallium chloride with DOTA at room temperature in aqueous solution affords the complex [Ga(HDOTA) · 5.5H_2O] (**1**), which is characterized by single-crystal X-ray spectroscopy, electrospray mass spectrometry and thermal gravimetric analysis. Gallium displays 6-coordinate distorted octahedral geometry within a puckered macrocyclic DOTA framework. The equatorial plane comprises two nitrogens of the DOTA ring and two oxygens from two of the four pendant carboxylic acid groups. The axial positions are comprised of the remaining two transannular nitrogens of the DOTA ring.

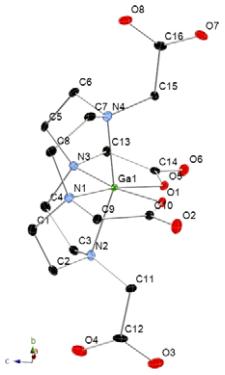

Thomas Schönherr, Wilhelm Seichter, Edwin Weber

Polyhedron 25 (2006) 3463

Complexes of pendant-armed cyclam derivatives with copper(II) perchlorate: Synthesis and crystal structures

Preparation and X-ray crystal structures of a designed series of cyclam type macrocyclic ligands that feature a different degree of saturation and number of functional appendages of the macroring, including corresponding complexes with Cu(II) perchlorate are reported and comparatively discussed. Dependent on the nature of the compound, transanular, pendant arm and anion involving conventional and weaker H bond contacts are shown to be operating in the formation of the crystal structures.

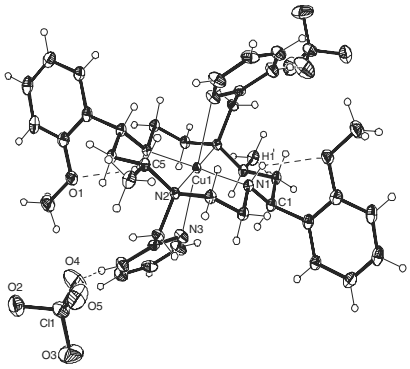

John Fielden, Patrick T. Gunning, De-Liang Long, Margaret Nutley, Arkady Ellern, Paul Kögerler, Leroy Cronin

Polyhedron 25 (2006) 3474

Anion control of isomerism, crystal packing and binding properties in a mononuclear zinc complex

Mononuclear zinc(II) complexes of the tetradentate pyridyl N-donor ligand *cis*-3,5-*bis*-[2-pyridinyleneamin]-*trans*-hydroxycyclohexane (DDOP) have been synthesised with nitrate and triflate counterions. The nature of the anion is seen to exert a significant influence on the arrangement of the axial ligands, construction of the solid state hydrogen bonded networks, and the ability to bind amino acid substrates.

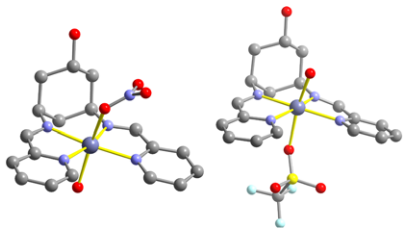

Garima Singh, Ajai K. Singh, John E. Drake, Michael B. Hursthouse, Mark E. Light

Polyhedron 25 (2006) 3481

1-Ethylthio-2-[2-thienyltelluro]ethane (**L**) a new (Te, S) ligand: Synthesis and complexation with Ag(I), Cu(I), Pd(II) and Pt(II) – Single crystal structures of [$PdCl_2$(**L**)] and bis(thienyl) tellurium(IV) chloride

1-Ethylthio-2-[2-thienyltelluro]ethane(**L**) and its complexes [$PdCl_2$(**L**)] (**1**), [$PtCl_2$(**L**)] (**2**), [Ag(**L**)$_2$][ClO_4] (**3**) and [CuBr(**L**)]$_2$ (**4**) were synthesized. [$HgCl_2$(**L**)] on crystallization decomposes giving Th_2TeCl_2 (**5**) [Th = 2-thienyl]. **L** and **1**–**4** exhibit characteristic ^{1}H and ^{13}C NMR spectra. Single crystal structures of **1** and **5** were solved. The Pd–Te, Pd–S and Pd–Cl bond lengths are 2.5040(4), 2.273(1) and 2.322(1)/2.380(1) Å, respectively, in square planar **1**. Intermolecular weak interactions exist in **1** between Te/S and Cl [Te–Cl/S–Cl 3.401/3.488 Å]. Complex **5** has a saw-horse type structure [Te–Cl, 2.480(1) Å].

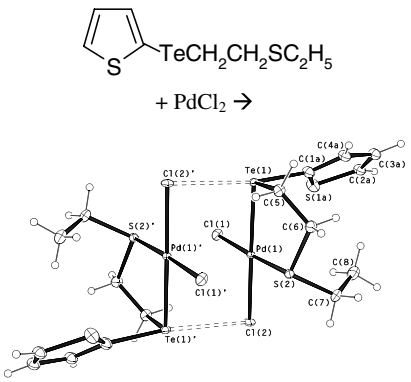

Ercules E.S. Teotonio, Hermi F. Brito, Hans Viertler, Wagner M. Faustino, Oscar L. Malta, Gilberto F. de Sá, Maria Cláudia F.C. Felinto, Regina H.A. Santos, Marco Cremona

Polyhedron 25 (2006) 3488

Synthesis and luminescent properties of Eu^{3+}-complexes with 2-acyl-1,3-indandionates (ACIND) and TPPO ligands: The first X-ray structure of Eu–ACIND complex

Europium complexes presenting general formulas [Eu(ACIND)$_3$(H_2O)$_2$] and [Eu(ACIND)$_3$(TPPO)$_2$] have been synthesized and characterized. In these formulas ACIND stands for the 2-acyl-1,3-indandionate ligands. The [Eu(ISOVIND)$_3$(H_2O)(EtOH)] complex was also prepared and its structure determined by single crystal X-ray analysis. Photoluminescence properties suggest an efficient ligand-to-metal intramolecular energy transfer process.

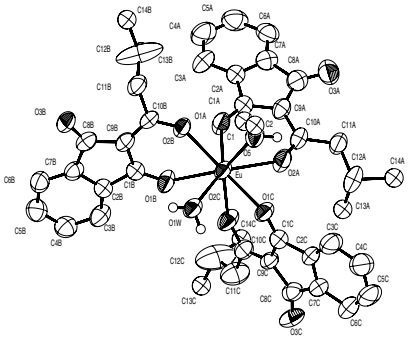

Jesús M[a] Martínez-Sánchez, Rufina Bastida de la Calle, Alejandro Macías, Paulo Pérez-Lourido, Laura Valencia Matarranz

Polyhedron 25 (2006) 3495

Co(II), Ni(II) and Cu(II) metal complexes with a N_8 azamacrocyclic ligand

Hydrated nitrate and perchlorate salts of the transitional metal ions Co^{2+}, Ni^{2+} and Cu^{2+} have been used to investigate the coordination capability of the octaaza macrocycle L derived from 2,6-diformylpyridine and diethylenetriamine. The synthesis of the metal complexes was carried out in 1:1 and 2:1 metal:ligand molar ratios, but dinuclear complexes were obtained in all cases. The complexes have been characterized by elemental analysis, molar conductivity, mass spectrometry, IR spectroscopy, diffuse reflectance and magnetic measurements. The crystal structures of [$Ni_2L(NO_3)_2$](NO_3)$_2$, [$Cu_2L(NO_3)_4$] and [$Cu_2L(ClO_4)_4$] have been determined.

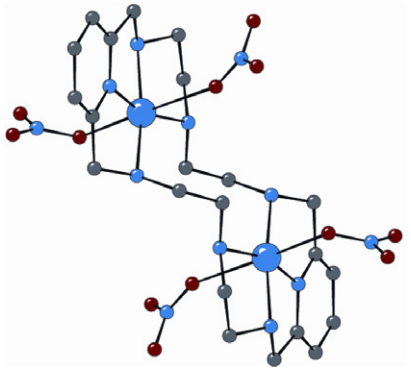

Pankaj Hazarika, Diganta Kalita, Swapnalee Sarmah, Ruli Borah, Nashreen S. Islam

Polyhedron 25 (2006) 3501

New oxo-bridged dinuclear peroxotungsten(VI) complexes: Synthesis, stability and activity in bromoperoxidation

Two new dinuclear oxo-bridged tetraperoxo complexes of tungsten with coordinated dipeptides of the type, $Na_2[W_2O_3(O_2)_4$(dipeptide)$_2] \cdot 3H_2O$ (dipeptide = gly-gly or gly-leu) have been synthesized. Distinctive features of the complexes include their high stability in solutions of a wide range of pH values and their ability to oxidize bromide to a bromination competent intermediate at physiological pH.

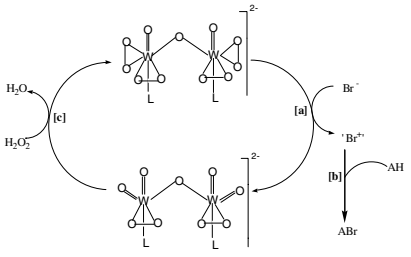

Kerman Gómez, Gabriel González, Manuel Martínez, Carolina Mendoza, Beatriz Sienra

Polyhedron 25 (2006) 3509

Absence of phosphate hydrolysis in the nucleotide substitution reaction on *cis*-$[Co(H_2O)_2(cyclen)]^{3+}$ at physiological pH: Importance of hydrogen-bonding and conjugate base-catalysis

cis-$[Co(Cl)_2(tetraamine)]^+$ complexes are in the chloroaqua/chlorohydroxo forms under physiological conditions. Substitution studies with nucleotides indicate that the processes correspond to a simple reaction, producing final stable mixtures of monodentate *O*-phosphato and chelate *O*-phosphato-*N*-nucleotide forms. No hydrolytic cleavage of the phosphato-nucleoside bond has been observed.

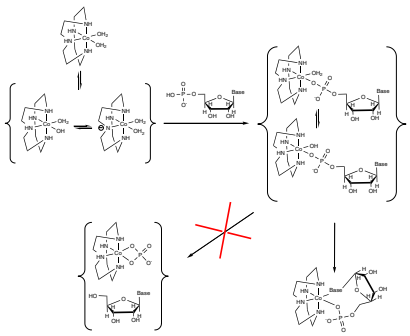

Megumu Munakata, Jing Han, Atsuhiro Nabei, Takayoshi Kuroda-Sowa, Masahiko Maekawa, Yusaku Suenaga, Nozomu Gunjima

Polyhedron 25 (2006) 3519

Syntheses, structures and photochromism of two novel copper(II) complexes with 1,2-bis(2′-methyl-5′-(2″-pyridyl)-3′-thienyl)perfluorocyclopentene

Two novel Cu(II) complexes with photochromic BM-2-PTP or closed-BM-2-PTP were prepared and characterized. Both complexes displayed reversible photochromism in the crystalline phase upon appropriate photoirradiation. [Cu(closed-BM-2-PTP)Cl_2] (**2**) was revealed to exist as a mixture of two photoactive conformers by X-ray crystallographic analysis and displayed distinct absorption changes from [Cu(BM-2-PTP)Cl_2] (**1**) during its photoreaction.

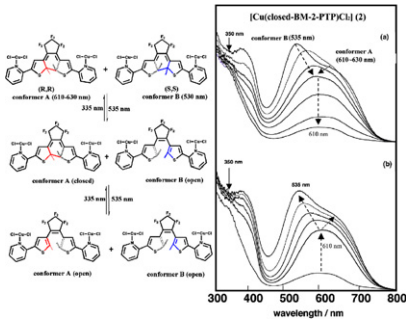

E. Çil, M. Arslan, A.O. Görgülü

Polyhedron 25 (2006) 3526

Synthesis and characterization of benzyl and benzoyl substituted oxime-phosphazenes

Two oxime-cyclophosphazenes (**3** and **8**) were prepared. The reactions of these oximes with alkyl and acyl halides were studied. Hexa, penta and trisubstituted compounds were obtained from these reactions. However, the oxime groups on **3** rearranged to nitrile in the reaction of **3** with benzenesulfanoyl chloride and 1-napthalenesulfanoyl chloride. All products were generally obtained in high yields.

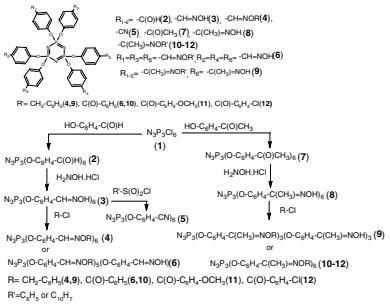

Ya-Pan Wu, Cui-Juan Wang, Yao-Yu Wang, Ping Liu, Wei-Ping Wu, Qi-Zhen Shi, Shie-Ming Peng

Polyhedron 25 (2006) 3533

Three copper(II) complexes constructed from a new 1,3,5-triazine derivative ligand

Three new complexes $\{[Cu(dpdapt)(Hhbd)] \cdot 6H_2O\}_n$ (**1**), $[Cu(dpdapt)(SO_4)] \cdot 2H_2O$ (**2**) and $[Cu(dpdapt)(oxa)] \cdot H_2O$ (**3**) have been synthesized from a new 1,3,5-triazine derivative ligand and copper salts. The molecular structures of **1**, **2** and **3** have been established by single-crystal X-ray diffraction studies. The UV/vis, IR spectra, fluorescence and TG analysis are also discussed.

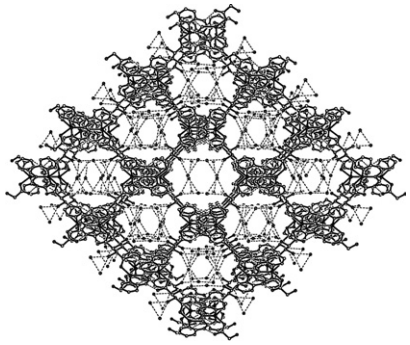

H. Naïli, W. Rekik, T. Bataille, T. Mhiri

Polyhedron 25 (2006) 3543

Crystal structure, phase transition and thermal behaviour of dabcodiium hexaaquacopper(II) bis(sulfate), $(C_6H_{14}N_2)[Cu(H_2O)_6](SO_4)_2$

A new transition metal sulfate in the presence of dabco amine, $(C_6H_{14}N_2)[Cu(H_2O)_6](SO_4)_2$, has been prepared and characterized. The structural arrangement is pointed out, in which dabco plays a templating role. A structural phase transition is highlighted at low temperature and the thermal decomposition of the precursor, at high temperature, is discussed.

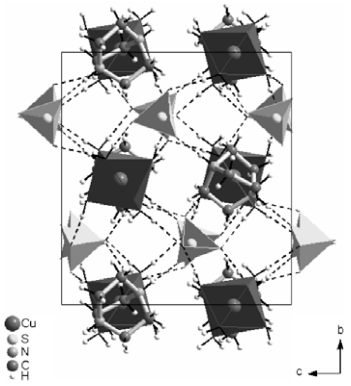

Ya-Huei Gan, Jian-Cheng Lee, Fung-E. Hong

Polyhedron 25 (2006) 3555

Preparation of a palladium dimer with a cobalt-containing bulky phosphine ligand: Its application in palladium catalyzed Suzuki reactions

A palladium dimer with a cobalt-containing phosphine ligand, $\{(\mu\text{-}PPh_2CH_2PPh_2)Co_2(CO)_4(\mu,\eta\text{-}(t\text{Bu})_2PC{\equiv}CC_6H_4\text{-}\kappa C^1)Pd(\mu\text{-}Cl)\}_2$ (**3**), was prepared from the reaction of its monomer precursor, $(\mu\text{-}PPh_2CH_2PPh_2)Co_2(CO)_4(\mu,\eta\text{-}(t\text{Bu})_2PC{\equiv}CC_6H_4\text{-}\kappa C^1)Pd(\mu\text{-}OAc)$ (**2**), with LiCl. Suzuki coupling reactions were carried out catalytically using **2** and **3** as catalyst precursors.

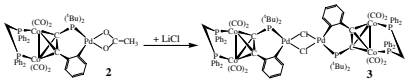

Mary S. Thomas, David C. Liles, Marilé Landman, Elizabeth M. van der Merwe, Simon Lotz

Polyhedron 25 (2006) 3562

The synthesis, structural features and thermal behaviour of thiophene-containing dithiocarboxylate complexes of zinc(II)

The complexes $[Zn_2(S_2CTR)_4]$ (T = 2,5-disubstituted thiophene, R = C_4H_9, C_6H_{13}, C_8H_{17}, $C_{12}H_{25}$ and $C_{16}H_{33}$) have been synthesized, their structural features investigated and their thermal behaviour studied.

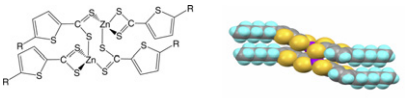

Daniela Rusanova, Kevin J. Pike, Ingmar Persson, Ray Dupree, Mats Lindberg, John V. Hanna, Oleg N. Antzutkin, Willis Forsling

Polyhedron 25 (2006) 3569

Solid-state static ^{65}Cu and ^{31}P CP/MAS NMR, and liquid-state EXAFS studies on copper(I) *O,O′*-dialkyldithiophosphate cluster compounds: Formation of the copper(I) *O,O′*-di-*iso*-amyldithiophosphate cluster compound on the surface of synthetic chalcocite

The ^{65}Cu transverse relaxation in $Cu_8L_6(S)$ [L = $S_2P(OR)_2$, R = ^{i}Pr or ^{i}Am] is found to be very different for different R. EXAFS data for $Cu_4L_4/Cu_8L_6(S)$ in solid-state and in solution are provided. Adsorption of KL or L_2 (L = $S_2P(O^iAm)_2$) on chalcocite surfaces is probed and a phase with a $\{Cu_8L_6(S)\}$ type structure is detected for both cases.

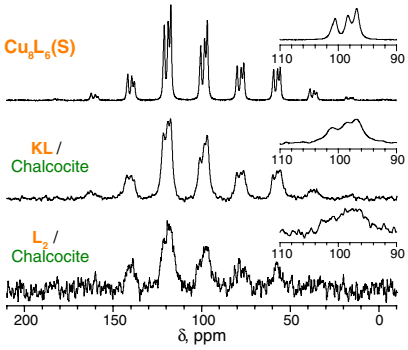

A.C.F. Ribeiro, V.M.M. Lobo, A.J.M. Valente, S.M.N. Simões, A.J.F.N. Sobral, M.L. Ramos, H.D. Burrows

Polyhedron 25 (2006) 3581

Association between ammonium monovanadate and β-cyclodextrin as seen by NMR and transport techniques

The paper presents data concerning NMR and transport data of association between β-cyclodextrin (β-CD) and ammonium monovanadate. These properties are markedly influenced by the presence of β-CD. Data from NMR spectroscopy and molecular mechanics calculations show that these effects are due to strong interactions between this carbohydrate and vanadate (2:1 complexes).

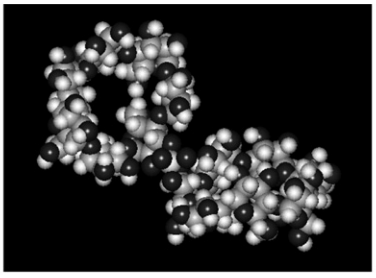

3D minimized structure of the 2:1 - β-CD/vanadium complex

Chullikkattil P. Pradeep, Sabbani Supriya, Panthapally S. Zacharias, Samar K. Das

Polyhedron 25 (2006) 3588

A tetra-nuclear copper(II) complex stabilizes an extended structure of a water nonamer: Synthesis and characterization of $[Cu_4(C_{54}H_{46}N_4O_{14})(OH)_2] \cdot 10H_2O$

An unusual form of water nonamer, consisting of an "S"-shaped water hexamer and a near-linear water trimer, has been identified in a crystalline hydrate of a tetra-nuclear copper(II) complex. The water nonamer, in turn, self assembles to an extended water structure that is anchored by the (host) copper complex through non-covalent supramolecular interactions.

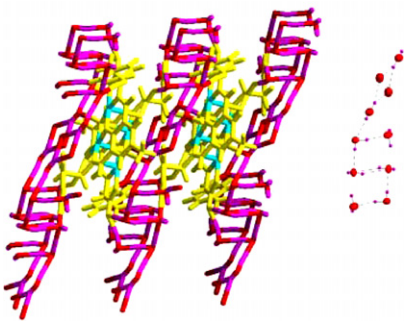

Metin Özer, Ahmet Altındal, Ali Rıza Özkaya, Mustafa Bulut, Özer. Bekaroğlu

Polyhedron 25 (2006) 3593

Synthesis, characterization and some properties of novel bis(pentafluorophenyl)methoxyl substituted metal free and metallophthalocyanines

The preparation of some new tetrakis[bis(pentafluorophenyl)methoxy] metal free and metallophthalocyanine complexes were achieved by the tetramerization of 4-[bis(pentafluorophenyl)methoxy]phthalonitrile with Li metal in pentan-1-ol or metal [Co(II) or Zn(II)] acetates in DMAE, respectively. The electrical, electrochemical and spectroelectrochemical properties of the complexes were also studied.

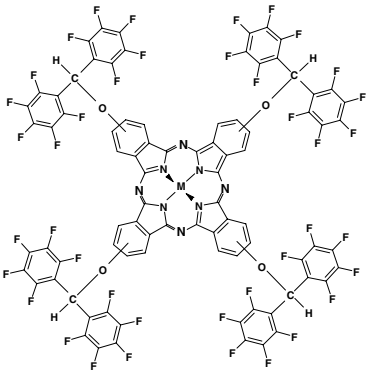

N.V. Loginova, T.V. Koval'chuk, R.A. Zheldakova, A.A. Chernyavskaya, N.P. Osipovich, G.K. Glushonok, G.I. Polozov, V.N. Povalishev, V.L. Sorokin, O.I. Shadyro

Polyhedron 25 (2006) 3603

Synthesis, characterization and antifungal activity of copper (II) complexes of sterically hindered *o*-diphenol derivatives

Cu(II) complexes with sterically hindered *o*-diphenol derivatives have been synthesized and characterized by means of elemental analysis and various physico-chemical techniques. The antifungal activities of all the compounds were tested against *Aspergillus niger*, *Fusarium sp.*, *Penicillium lividum*, *Mucor sp.* and *Botrytis cinerea*.

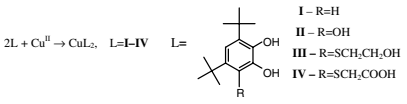

Felix D. Sokolov, Damir A. Safin, Nail G. Zabirov, Alexander Yu. Verat, Vasiliy V. Brusko, Dmitry B. Krivolapov, Ekaterina V. Mironova, Igor A. Litvinov

Polyhedron 25 (2006) 3611

Synthesis, structure and properties of novel *N*-thiophosphorylated derivatives of 1,3-dihydro-2*H*-benzimidazol-2-imine and imidazolidine-2-imine

N-Thiophosphorylated thioureas are of interest as complexing agents and precursors for the synthesis of heterocycles containing exocyclic phosphorylic groups. Thus a number of reactions with their participation, leading to phosphor-containing iminothiazolidines, iminooxazolidines and thiophosphoryl-(phosphonyl)aminothiozoles formation have been reported. With the presence of two thiourea fragments occupying α,β positions in a molecule, it is reasonable to expect interesting transformations leading to cyclic structures.

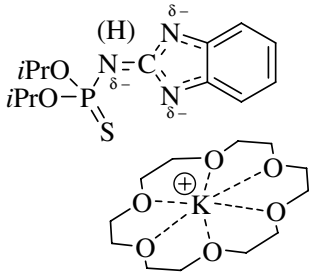

Svetlana G. Baca, Helen Stoeckli-Evans, Christina Ambrus, Stanislav T. Malinovskii, Iurii Malaestean, Nicolae Gerbeleu, Silvio Decurtins

Polyhedron 25 (2006) 3617

Synthesis, crystal structures and magnetic properties of trinuclear oxo-centered homo- and mixed-valence manganese pivalate complexes with imidazole (Im) and 1-methylimidazole (1-MeIm): $[Mn_3^{III}O(O_2CCMe_3)_6(Im)_3](Me_3CCO_2) \cdot 0.5Me_3CCO_2H$ and $[Mn_2^{III}Mn^{II}O(O_2CCMe_3)_6(1\text{-}MeIm)_3]$

Two new μ_3-oxo-centered trinuclear manganese complexes, one of them a homo-valence $[Mn_3^{III}O(O_2CCMe_3)_6(Im)_3](Me_3CCO_2) \cdot 0.5Me_3CCO_2H$ (**1**) pivalate complex and the other a mixed-valence $[Mn_2^{III}Mn^{II}O(O_2CCMe_3)_6(1\text{-}MeIm)_3]$ (**2**) pivalate complex (where Im = imidazole, 1-MeIm = 1-methylimidazole), have been synthesized and characterized by IR spectroscopy, thermogravimetric analysis, X-ray crystallography. Magnetic studies reveal that both compounds represent antiferromagnetically coupled, spin-frustrated triangular systems exhibiting weak to moderate exchange coupling constants.

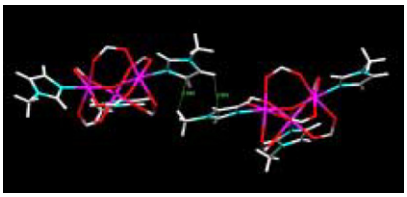

Udai P. Singh, Asish K. Sharma, Pooja Tyagi, Shailesh Upreti, Raj K. Singh

Polyhedron 25 (2006) 3628

Mononuclear manganese carboxylate complexes: Synthesis and structural studies

Several manganese carboxylates complexes having different pyrazoles/hydrotris (pyrazolyl)borate ligands have been synthesised and structurally characterized. Out of all synthesized complexes, only complex **7** has SOD activity as its structure is very much similar to the active site structure of the native Mn–SOD enzyme.

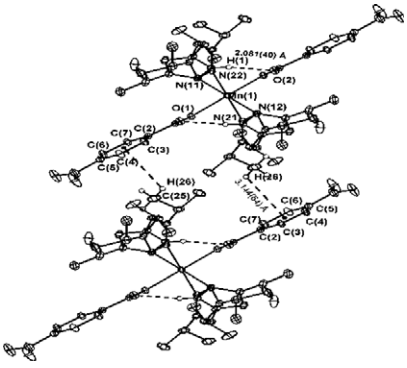

S. Abdurrahmanoğlu, Ahmet Altındal, Mustafa Bulut, Özer. Bekaroğlu

Polyhedron 25 (2006) 3639

Synthesis and electrical properties of novel supramolecular octa-phthalocyaninato-dicobalt(II)-hexazinc(II) and dicobalt(II)-dimeric-phthalocyanine with six ferrocenylimin pendant groups

The titled compound was prepared by nitro coupling dimeric cobalt and six asymmetric nitro phthalocyanine and was characterized by ICP-MS, UV–Vis, IR and elemental analyses. DC conductivity and impedance measurements have also been performed.

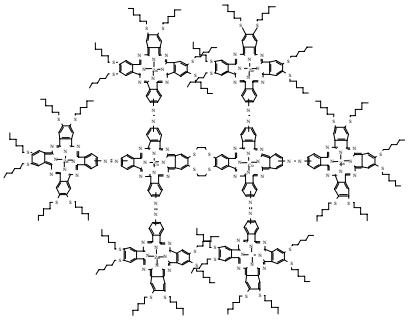

Florian P. Pruchnik, Urszula Dawid, Andrzej Kochel

Polyhedron 25 (2006) 3647

Structure and properties of the dinuclear complex $[Co_2(\mu\text{-}OAc)_2(OAc)_2(\mu\text{-}H_2O)(phen)_2]$

The dinuclear complex $[Co_2(\mu\text{-}OAc)_2(OAc)_2(\mu\text{-}H_2O)(phen)_2]$ has a structure analogous to that of metalloenzymes, Co(II) atoms are bridged by two acetato and an aqua ligand. The complex exhibits antiferromagnetic exchange, $T_N = 4.5$ K, with an isotropic exchange parameter $J = -2.1$ cm^{-1}. The crystal structure of compound **1** is stabilized by O–H···O hydrogen bonds and stacking of 1,10-phenanthroline ligands. The proton NMR spectrum indicates that the structure of the complex in CD_2Cl_2 solution is the same as in the solid state.

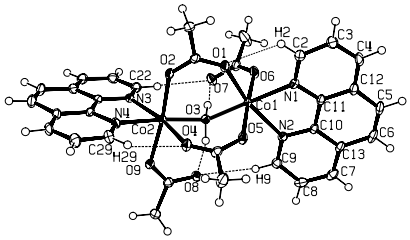

Alfonso Castiñeiras, Isabel García-Santos, Stefanie Dehnen, Paloma Sevillano

Polyhedron 25 (2006) 3653

Synthesis, characterization and DFT calculations of a novel hexanuclear silver(I) cluster-complex containing 4-ethyl-5-pyridin-2-yl-2,4-dihydro-[1,2,4]triazol-3-thione as a result from the cyclization of 2-pyridinformamide *N*-4-ethylthiosemicarbazone

A new hexanuclear silver triazol-3-thiolato complex, **1**, was synthesized and fully characterized, including X-ray crystal structure determination, that show the stabilization of the whole structure by π–π stacking interactions. DFT calculations reveal that three of the MOs with Ag atomic orbital contributions clearly show d-d-σ-bonding. Luminescence experiments show an unusual fluorescence emission with two components, suggesting weak coupled relaxation channels.

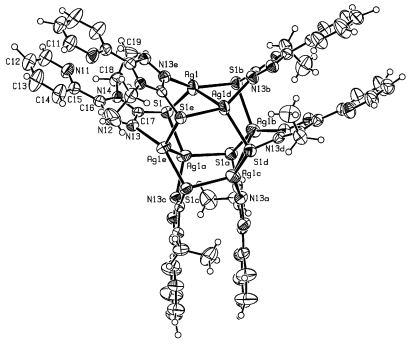

Author Index to Volume 25 3661

Subject Index to Volume 25 3675

The Publisher encourages the submission of articles in electronic form thus saving time and avoiding rekeying errors. For detailed instructions on the preparation of manuscripts and of electronic artwork, consult the Author Gateway for Elsevier at http://authors.elsevier.com

ScienceDirect

Full text of this journal is available, on-line from **ScienceDirect**. Visit **www.sciencedirect.com** for more information.

Available online at www.sciencedirect.com
ScienceDirect
Polyhedron 25, issue 13, 11 September 2006
POLYHEDRON
www.elsevier.com/locate/poly

Contents

Papers

Jing Han, Atsuhiro Nabei, Yusaku Suenaga, Masahiko Maekawa, Hiromichi Isihara, Takayoshi Kuroda-Sowa, Megumu Munakata

Polyhedron 25 (2006) 2483

Photochromic Rh(II) complexes based on 1,2-dicyano-1,2-bis(2,4,5-trimethyl-3-thienyl)-ethene

Three novel dirhodium pivalate complexes with *cis*-dbe, *trans*-dbe and closed-dbe were synthesized and characterized. Complex **3**, of which closed-dbe bridges two different di-rhodium pivalate moieties through one cyano and one thienyl group, was transferred to the ring-open isomer when excited with 529 nm light in the crystalline phase.

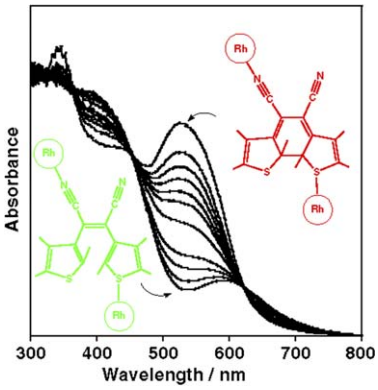

D. Joniaková, R. Gyepes, E. Rakovský, P. Schwendt, Ľ. Žúrková, J. Marek, Z. Mička

Polyhedron 25 (2006) 2491

Structural variability of copper-1,10-phenanthroline–oxovanadate hybrid inorganic–organic compounds

The single crystal X-ray diffraction of seven new compounds, $[Cu_2(H_2O)_2(OH)_2(phen)_2][Cu_2(OH)_2(phen)_2(V_4O_{12})] \cdot 6H_2O$, $[Cu_2(phen)_4(V_4O_{12})] \cdot 4H_2O$, $[Cu_2(phen)_4(V_4O_{12})] \cdot 6H_2O$, $[Cu_2(phen)_4(VO_3)_4] \cdot 10H_2O$, $[Cu(phen)_3]_2V_4O_{12} \cdot phen \cdot 22H_2O$, $[Cu(phen)(VO_3)_2]$ and $[Cu_2(phen)_4(V_4O_{12})] \cdot 4H_2O$, revealed a variability in mutual bonding interactions between the cationic and anionic units.

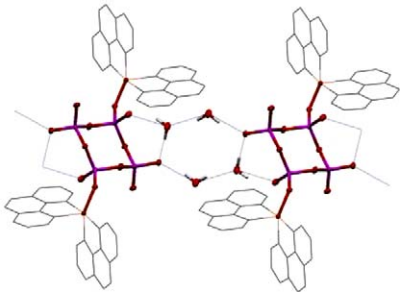

T. Mathur, J. Dinda, P. Datta, G. Mostafa, T.-H. Lu, C. Sinha

Polyhedron 25 (2006) 2503

Ru(0)-azoimine-carbonyl and Ru(II)-pyridyl-azo-imidazole complexes

Ruthenium(II) and ruthenium(0) carbonyl complexes of pyridyl-azo-imidazoles are described. The ligand is an unsymmetric biheterocyclic azo system having an azoimine function. The structure of Ru(CO)-ligand is confirmed by a single crystal X-ray diffraction study in one case along with other spectral data. The Ru(II) complexes exist in two isomeric forms. The redox properties of the complexes are examined by cyclic voltammetry.

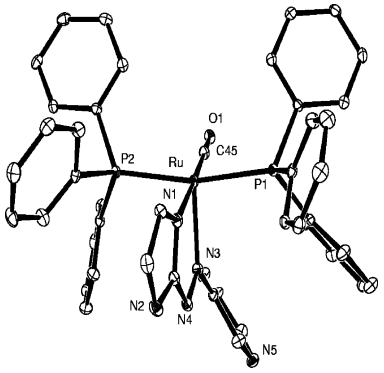

Biswaranjan Shee, Jahar lal Pratihar, Surajit Chattopadhyay

Polyhedron 25 (2006) 2513

Synthesis and characterization of new Pt(II) and Pt(IV) orthometallated complexes incorporating 1-arylazo-2-ethyl sulfanyl benzene

Reaction of 1-arylazo-2-ethyl sulfanyl benezene (LH) with K_2PtCl_4 and K_2PtI_4 has been studied. In both the cases orthoplatinated compounds were isolated and characterized. K_2PtCl_4 afforded Pt(II) complexes, Pt(L)Cl, while K_2PtI_4 produced the Pt(IV) compounds, $Pt(L)I_3$. The oxidations of Pt in the case of $Pt(L)I_3$ have been believed to occur as a result of unusual oxidative addition of LH.

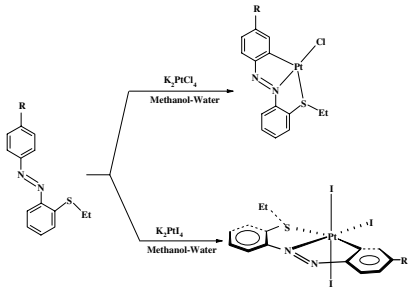

J.G. Małecki, M. Jaworska, R. Kruszynski

Polyhedron 25 (2006) 2519

Synthesis, molecular, crystal and electronic structure of $[(C_6H_6)RuCl_2(picoline)]$

$[(C_6H_6)RuCl_2(picoline)]$ complexes have been synthesized by the reaction of $[(C_6H_6)RuCl_2]_2$ with α-, β- and γ-picoline in methanolic solution. The prepared complexes have been studied by IR, UV–Vis and ^1H NMR spectroscopy. The crystal structure of the complex with α-picoline has been determined by X-ray crystallography. The electronic spectra of the compounds have been calculated by the TDDFT method.

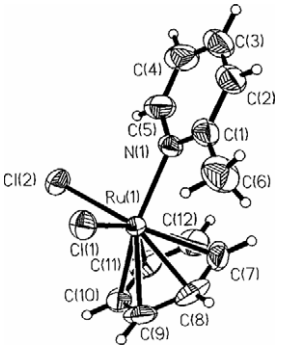

Kaustavmoni Deka, Moitree Laskar, Jubaraj B. Baruah

Polyhedron 25 (2006) 2525

Carbon–nitrogen bond cleavage by copper(II) complexes

N-benzoylimidazole reacts with copper(II) nitrate to give tetra(imidazole)copper(II) nitrate, whereas copper(II) nitrate trihydrate hydrolytically degrades *N*-benzoyl 3,5-dimethylpyrazole to give an adduct of copper complexes having the composition *cis*-$(pz)_2Cu(OBz)_2 \cdot$ *trans*-$(pz)_2Cu(OBz)_2H_2O$ (where pz = 3,5-dimethylpyrazole and OBz = benzoate anion).

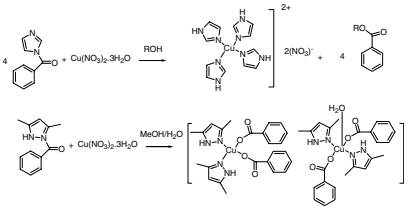

Hong-Xing Wang, Hong-Fei Wu, Hui-Chao Zhou, Rong Jin, Ren-Qing Gao, Feng-Ying Geng, Jian Xu, Ying-Jie Li, Wen-Qin Zhang

Polyhedron 25 (2006) 2530

Activation of the C—H bond in $[(\eta^5\text{-}C_5H_5)\text{-}Fe(\eta^5\text{-}C_5H_4CH_2N(CH_3)CH_2C_6H_4R\text{-}4)]$ induced by platinum (II): Crystal structure of σ-$Pt[(\eta^5\text{-}C_5H_5)Fe(\eta^5\text{-}C_5H_3CH_2N(CH_3)\text{-}CH_2C_6H_4OCH_3\text{-}4)]Cl(DMSO)$

Treatment of $[(\eta^5\text{-}C_5H_5)Fe(\eta^5\text{-}C_5H_4CH_2N\text{-}(CH_3)CH_2C_6H_4R\text{-}4)]$ **5a–e** (R = CH_3O(**a**), CH_3(**b**), H(**c**), Cl(**d**), NO_2(**e**)) with *cis*-$[Pt(DMSO)_2Cl_2]$ in methanol produced predominately σ-$Pt[(\eta^5\text{-}C_5H_5)Fe(\eta^5\text{-}C_5H_3CH_2N\text{-}(CH_3)CH_2C_6H_4R\text{-}4)]Cl(DMSO)$ **6** (R = same as before) in which the configurations consisted of R_NR_P and S_NS_P. The structure of **6a** was determined by X-ray single crystal diffraction. The possible mechanism for the formation of **6** was discussed.

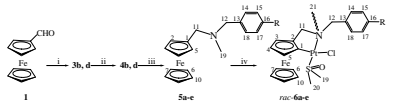

B. Machura, R. Kruszynski, M. Jaworska, J. Kłak, J. Mroziński

Polyhedron 25 (2006) 2537

Synthesis, crystal, molecular and electronic structure of $[ReOCl_3(phen)]$ and $[ReCl_2(phen)(PPh_3)_2](ReO_4)$ complexes

The reactions of $[ReOCl_3(OAsPh_3)(AsPh_3)]$ and $[ReOCl_3(PPh_3)_2]$ with 1,10-phenanthroline (phen) have been examined and the $[ReOCl_3(phen)]$ (**1**) and $[ReCl_2(phen)(PPh_3)_2](ReO_4)$ (**2**) complexes have been obtained. The compounds have been studied by IR, UV–Vis spectroscopy and X-ray crystallography. The electronic structures of **1** and **2** have been calculated with the density functional theory (DFT) method. The spin-allowed electronic transitions have been calculated with the time-dependent DFT method for $[ReOCl_3(phen)]$, $[ReCl_2(phen)(PPh_3)_2]^+$ cation and ReO_4^- anion, and the UV-Vis spectra of the title compounds have been discussed on this basis.

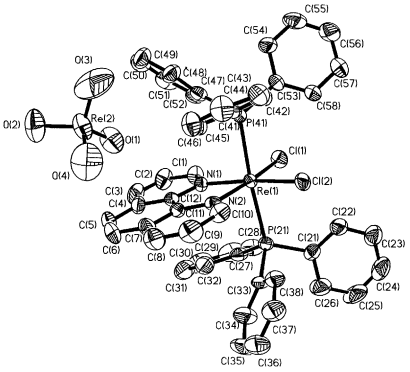

Arpi Majumder, Guillaume Pilet, María Teresa Garland Rodriguez, Samiran Mitra

Polyhedron 25 (2006) 2550

Synthesis and structural characterisation of three dicyanamide complexes with Mn(II), Zn(II) and Cd(II): Supramolecular architectures stabilised by hydrogen bonding

Three new dicyanamide complexes with Mn(II), Zn(II) and Cd(II) have been synthesised at ambient temperature. Complexes **1** and **2** are mononuclear and **3** is a dicyanamide bridged dinuclear species, which is rare in the literature. All three structures exhibit supramolecular frameworks resulting from the numerous hydrogen bonding interactions involving the constituent materials.

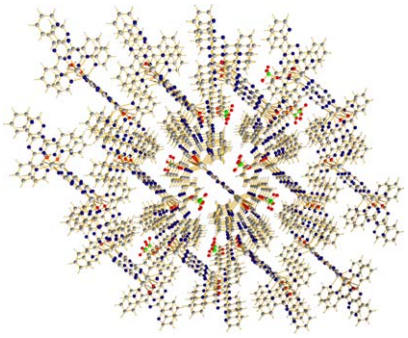

Martin Breza, Jozef Kožíšek

Polyhedron 25 (2006) 2559

DFT studies of copper complexes with biphenyldiimino dithioether II. Mechanical strain

The geometries of tetrahedral and square-planar Cu(bite)^q complexes, q = +1 or +2, and of the free bite ligand, bite = tetrabenz[a,e,g,k]-15,18-dithia-9,24-diazacyclohexadeca-9,23-diene, have been optimized using the DFT method. The reorganization and strain energy values are evaluated.

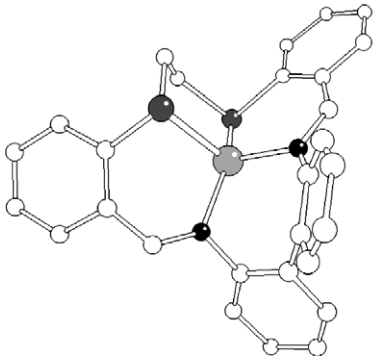

Qiao-Lin Wu, Qing Su, Guang-Hua Li, Wei Gao, Ying Mu, Shou-Hua Feng

Polyhedron 25 (2006) 2565

Diphenyl substituted cyclopentadienyl titanium trichloride derivatives: Synthesis, crystal structure and properties as catalysts for styrene polymerization

1,2-Diphenyl-4-R-1,3-cyclopentadienyl titanium trichloride (R = Me (4), *n*-Bu(5), Ph(6)) have been synthesized by modified literature procedures. The molecular structure of **4** was characterized by spectroscopy and X-ray crystallography. All of the complexes exhibit high catalytic activities and syndiospecificities for the polymerization of styrene in the presence of methylaluminoxane (MAO).

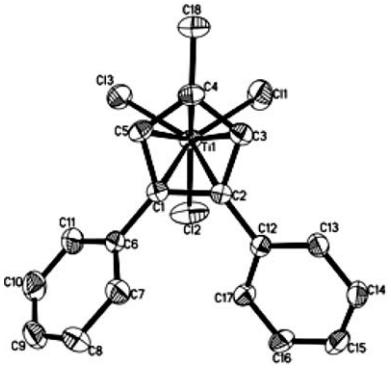

Wensheng Fu, Guoming Liang, Yuyang Sun

Polyhedron 25 (2006) 2571

Hydrothermal synthesis and characterization of organically templated vanadium phosphite with two-dimensional structures, $(C_6H_{16}N_2)$-$[V^{III}(OH)_2(V^{IV}O)_2(HPO_3)_4] \cdot H_3O$

A novel open-framework vanadium phosphite $(C_6H_{16}N_2)[V^{III}(OH)_2(V^{IV}O)_2(HPO_3)_4] \cdot H_3O$ was obtained as good quality single crystals by the hydrothermal method, templated by the *N*,*N*′-dimethylpiperazine cation. This organically templated vanadium phosphite possesses alternating inorganic and organic layers, formed by four- and eight-membered rings. The *N*,*N*′-dimethylpiperazine cation, as a template for directing, is occupied between two vanadium phosphite layers and interacts with the layers though N—H···O hydrogen bonds.

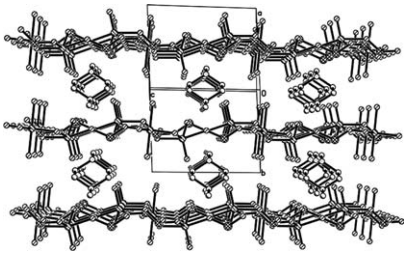

Ece Bulak, Orkan Sarper, Akbey Dogan, Falk Lissner, Thomas Schleid, Wolfgang Kaim

Polyhedron 25 (2006) 2577

Dichlorogold(III) complexes of bis(1-methyl-2-imidazolyl)ketone and related ligands: Geometrical and electronic structures

Complexes of the title ligands with $[AuCl_2]^+$ show metal binding to the imine nitrogen atoms of the imidazole groups to yield six-membered chelate ring structures. A comparison of the complexes with the now structurally characterized "bik" ligand shows no unusual coordination effects, the electrochemical reduction of the complex ion $[(bik)AuCl_2]^+$ is Au/Cl centered in agreement with DFT calculation results.

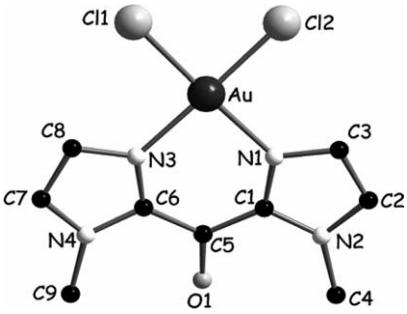

Shi Wang, Peter Day, John D. Wallis, Peter N. Horton, Michael B. Hursthouse

Polyhedron 25 (2006) 2583

Synthesis, crystal structures and magnetic properties of charge transfer salts with anions containing Schiff base ligands

Charge transfer salts of the electron donors TTF and BEDT-TTF with anions of the type $[M(Schiff\ base)(NCS)_2]^-$ have been synthesised for the first time, where M = Cr, Fe. Their crystal structures and bulk magnetic properties are reported.

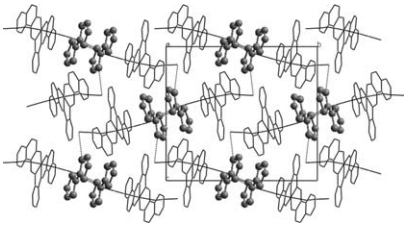

Chandrika P. Kulatilleke, Saliya A. de Silva, Yair Eliav

Polyhedron 25 (2006) 2593

A coumarin based fluorescent photoinduced electron transfer cation sensor

We wish to report 4-[(Bis(pyridin-2-ylmethyl)-amino)methyl]-7-methoxychromen-2-one, **1**, as a fluorescent photoinduced electron transfer cation sensor that is capable of indicating the presence of Zn^{2+}, Cd^{2+} and Pb^{2+} ions via a fluorescence signal. Log binding constants, β, for these metal ions have been measured, and were found to be 6.10 ± 0.4, 6.37 ± 0.3, and 5.67 ± 0.3, respectively.

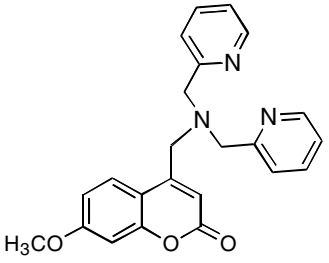

1

Gianella Facchin, Eduardo Kremer, Enrique J. Baran, Eduardo E. Castellano, Oscar E. Piro, Javier Ellena, Antonio J. Costa-Filho, María H. Torre

Polyhedron 25 (2006) 2597

Structural characterization of a series of new Cu-dipeptide complexes in solid state and in solution

Four new Cu(II)-dipeptide complexes were synthesized and studied in solid state and in solution. They were characterized by infrared, electronic and EPR spectroscopic techniques. The crystal structure of $[Cu(gly\text{-}val)] \cdot \frac{1}{2}H_2O$, [Cu(val-gly)], [Cu(val-phe)] and [Cu(phe-phe)] was determined by X-ray diffraction methods.

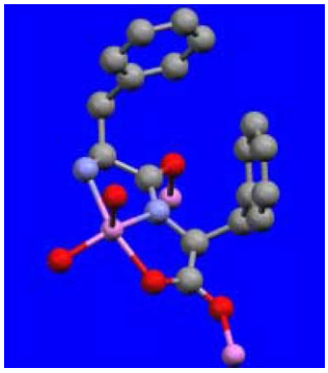

Jonathan D. Woodward, Rénal V. Backov, Khalil A. Abboud, Daniel R. Talham

Polyhedron 25 (2006) 2605

Monomers, chains, ladders, and two-dimensional sheets: Structural diversity in six new compounds of Zn(II) with 4,4′-bipyridine

Six new zinc(II)–4,4′-bipyridine coordination polymers with diverse structural topologies are reported. The versatility of bipy as a spacer ligand when assembling transition metal ions into coordination polymers is illustrated, providing examples of monomeric, linear chain, zig-zag chain, ladder, and two-dimensional network structures.

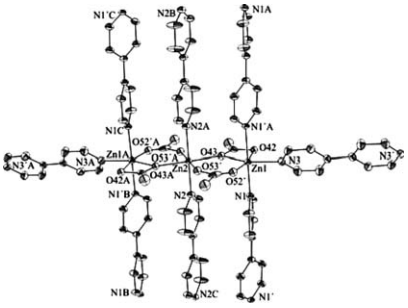

Daniel L. Reger, J. Derek Elgin, Mark D. Smith, Fernande Grandjean, Leila Rebbouh, Gary J. Long

Polyhedron 25 (2006) 2616

Structural identification of the factors that prevent an electronic spin-state crossover in $Fe[(C_6H_5)B(3\text{-}Mepz)_3]_2$ (pz = pyrazolyl ring)

In contrast to other $Fe[(p\text{-}R\text{-}C_6H_4)\text{-}B(3\text{-}Mepz)_3]_2$ (R = I, —C≡C—H, —C≡C—$SiMe_3$, or —C≡C—C_6H_5) derivatives, magnetic, Mössbauer spectral, and X-ray crystallographic studies clearly demonstrate that $Fe[(C_6H_5)B(3\text{-}Mepz)_3]_2$ remains high spin down to 4 K. Analysis of the data indicate that the degree of twisting of the pyrazolyl rings from ideal C_{3v} coordination symmetry (see figure) explains the lack of the spin-state crossover for $Fe[(C_6H_5)B(3\text{-}Mepz)_3]_2$.

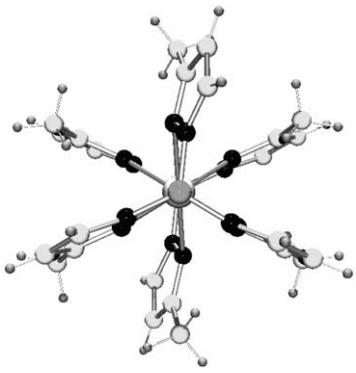

M. Thirumavalavan, P. Akilan, M. Kandaswamy

Polyhedron 25 (2006) 2623

Synthesis of heterobinuclear Cu(II)—Zn(II) complexes derived from lateral macrobicyclic tricompartmental ligands: Spectral, electrochemical and kinetic studies

Spectral, electrochemical and kinetic studies of heterobinuclear Cu(II)—Zn(II) complexes were carried out and compared with homobinuclear Cu(II) complexes. Cyclic voltammetric studies show quasireversible one electron reduction wave due to the reduction of Cu(II) to Cu(I) and Zn(II) ion does not undergo reduction. The catalytic activities of the complexes increase with increase in macrocyclic ring size. Macrocyclic ring size influences the spectral, electrochemical and catalytic properties of the complexes.

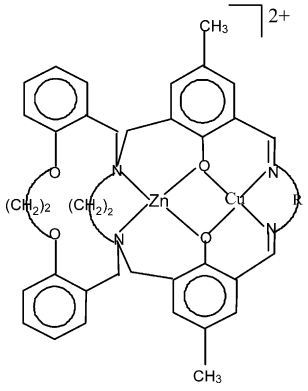

Anvarhusein A. Isab, Mohammed I.M. Wazeer, Mohammed Fettouhi, Saeed Ahmad, Waqar Ashraf

Polyhedron 25 (2006) 2629

Synthesis and characterization of mercury(II) complexes of selones: X-ray structures, CP MAS and solution NMR studies

Mercury(II) complexes of selones (L) having the general formulae, $[L_2HgCl_2]$, $[L_3HgCl]Cl$ and $[L_4Hg]Cl_2$ have been prepared and characterized by elemental analysis, IR and NMR (^1H, ^{13}C, ^{15}N, ^{77}Se, ^{199}Hg) spectroscopy. The complex of dichloro-bis(*N-isopropyl*-imidazolidine-2-selone-S)mercury(II), has been characterized by X-ray crystal analysis. The principal components of the ^{77}Se and ^{199}Hg shielding tensors were determined from solid-state NMR data.

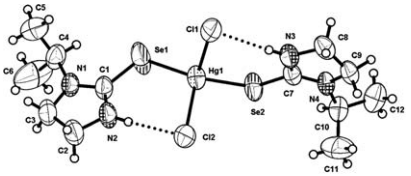

Molecular structure of dichloro-bis(N-*isopropyl*-imidazolidine-2-selone-S)mercury(II)

Debprasad Patra, Jahar lal Pratihar, Biswaranjan Shee, Poulami Pattanayak, Surajit Chattopadhyay

Polyhedron 25 (2006) 2637

Syntheses, characterisation and structure of new diazoketiminato chelates of palladium(II) incorporating a tridentate (*N*,*N*,*N*) azo ligand

Transition metal complexes incorporating polydentate azo ligands are demonstrated to possess interesting electron transfer behaviour and photophysical properties due to the presence of a low lying azo-π^* orbital. This work describes the synthesis and structure of new Pd(II) complexes of a delocalised tridentate (*N*,*N*,*N*) ligand forming a six membered diazoketiminato chelate.

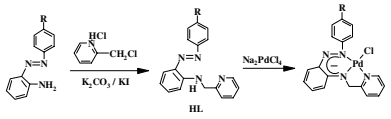

Violetta Patroniak, Jean-Marie Lehn, Maciej Kubicki, Artur Ciesielski, Monika Wałęsa

Polyhedron 25 (2006) 2643

Chameleonic ligand in self-assembly and synthesis of polymeric manganese(II), and grid-type copper(I) and silver(I) complexes

The complexation of ligand **L**, comprising N,N,O donor atoms units, with manganese(II) ions, whose tendency to form polymeric complexes is well-known, yielded a new zigzag polymeric chain: $[MnL]_n$. With tetrahedrally coordinated metal ions such as Cu(I) and Ag(I) ligand **L** is adequate for the generation of [2 × 2] grids.

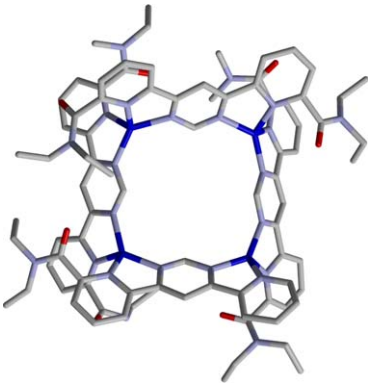

Ryo Kawajiri, Takashi Okubo, Tadaoki Mitani

Polyhedron 25 (2006) 2650

Structural and magnetic studies on a new mixed-valence Cu(I)–Cu(II) octanuclear cluster with a dithiocarbamate derivative

A new mixed-valence Cu(I)–Cu(II) octanuclear cluster, $[Cu^{I}Cu^{II}(n\text{-}Pr_2dtc)Cl_2]_2$-$[Cu^{II}_2(n\text{-}Pr_2dtc)_2Cl_2]_2$ (**1**), was synthesized with a dithiocarbamate derivative (n-Pr_2dtc^- = di-*n*-propyl-dithiocarbamate), and was structurally and magnetically characterized. Complex **1** has infinite one-dimensional assembly structure consists of a mixed-valence Cu(I)–Cu(II) tetranuclear unit and two chloride-bridged Cu(II) dinuclear units. The magnetic study indicates the existence of a strong antiferromagnetic interaction (J = −35.6 cm^{-1}).

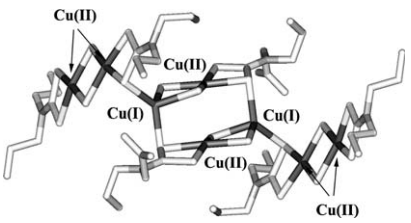

Takashiro Akitsu, Yasuaki Einaga

Polyhedron 25 (2006) 2655

Structures and XPS studies of several 3d–4f cyano-bridged Ln^{III}–Fe^{III}/Co^{III} heterometallic complexes

We have newly carried out the crystal structure determination of several 3d–4f cyano-bridged bimetallic assemblies, $Ln(DMF)_4(H_2O)_3Co(CN)_6 \cdot H_2O$ (DMF = *N*,*N*′-dimethylformamide; Ln = Tb, Dy, Ho and Er) and X-ray photoelectron spectroscopy (XPS) studies of several analogous 3d–4f complexes, $Ln(DMF)_4(H_2O)_3M(CN)_6 \cdot H_2O$ (Ln = Ce, Nd, Sm, Gd, Tb, Dy, Ho and Er; M = Co and Fe) systematically. The results revealed that the reasons for photo-induced magnetization of Nd^{III}–Fe^{III} or Co^{III} complexes could be attributed to characteristic bent structures around cyano-bridges and gradual shifts of binding energies of Ln $4d_{3/2}$ peaks being closed to mixed-valence states.

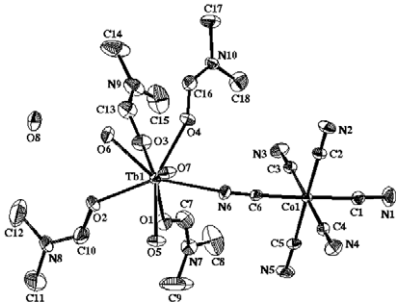

The Publisher encourages the submission of articles in electronic form thus saving time and avoiding rekeying errors. For detailed instructions on the preparation of manuscripts and of electronic artwork, consult the Author Gateway for Elsevier at http://authors.elsevier.com

ScienceDirect

Full text of this journal is available, on-line from **ScienceDirect**. Visit **www.sciencedirect.com** for more information.

Available online at www.sciencedirect.com
SCIENCE DIRECT®
Polyhedron 25, issue 5, 27 March 2006
POLYHEDRON
www.elsevier.com/locate/poly

Contents

Papers

Ramalingam Balamurugan, Mallayan Palaniandavar, Malcolm A. Halcrow

Polyhedron 25 (2006) 1077

Copper(II) complexes of sterically hindered Schiff base ligands: Synthesis, structure, spectra and electrochemistry

The synthesis, structure and spectral and redox behaviour of copper(II) complexes of sterically constrained N_3, N_3S_2 and N_2S_2 ligands are described. In the crystal structure of one of the complexes the CuN_3Cl_2 chromophore possesses a distorted square pyramidal coordination geometry. The replacement of isopropyl groups in this complex by the less sterically demanding methyl groups leads to a decreased geometric distortion. The interesting electrochemical behavior of the complexes has been explained based on a square scheme.

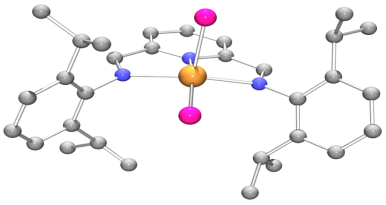

Takashiro Akitsu, Yasuaki Einaga

Polyhedron 25 (2006) 1089

Synthesis and crystal structures of the flexible Schiff base complex bis(*N*-1,2-diphenylethylsalicydenaminato-κ^2N,O)copper(II) (methanol): A rare case of solvent-induced distortion

We report a new mononuclear Schiff base copper(II) complex, bis(*N*-1,2-diphenylethylsalicydenaminato-κ^2N,O)copper(II) (green form, **1**) and its co-crystal containing methanol solvent molecules (brown form, **2**), which take different conformations in the solid state. We also discuss their absorption spectra in various solvents in view of dipole moment and transitions.

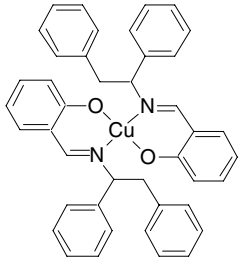

1

2 = **1** • CH_3OH

Sladjana B. Novaković, Goran A. Bogdanović, Vukadin M. Leovac

Polyhedron 25 (2006) 1096

Transition metal complexes with thiosemicarbazide-based ligands. Part L. Synthesis, physicochemical properties and crystal structures of Co(II) complexes with acetone *S*-methylisothiosemicarbazone

The analyses of the geometries of five-coordinated bis(bidentate)–Co complexes containing five-membered chelate rings suggest that if there is no steric hindrance between the ligands in the basal plane complexes rather adopt square-pyramidal than trigonal-bipyramidal ligand arrangement.

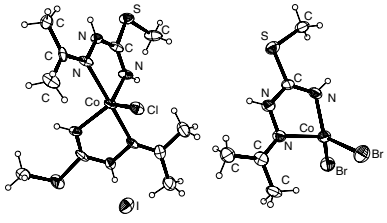

Anatolii A. Fagin, Tatyana V. Balashova, Dmitrii M. Kusyaev, Tatyana I. Kulikova, Tatyana A. Glukhova, Natalya P. Makarenko, Yurii A. Kurskii, William J. Evans, Mikhail N. Bochkarev

Polyhedron 25 (2006) 1105

Reactions of neodymium(II) iodide with organohalides

The reactions of NdI_2 with organohalides PhX, $C_7H_{15}X$, *cyclo*-$C_6H_{11}X$, *t*-BuX (X = Cl, Br, I) in THF afford mainly the respective hydrocarbons R–H. Chlorotrimethylsilane is converted into Me_3SiH, $Me_3SiSiMe_3$ and $Me_3SiO(CH_2)_4CH_3$. The interactions of NdI_2 with alkyl halides in benzene result in alkylation of the solvent to give the mono- and disubstituted products R-Ph and $R_2C_6H_4$. Treatment of benzyl chloride by NdI_2 without solvent causes the oligomer $PhCH_2$-(p-$C_6H_4CH_2)_{28}C_6H_4CH_2Cl$ formation.

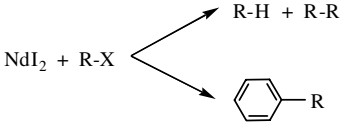

B. Machura, R. Kruszynski, M. Jaworska

Polyhedron 25 (2006) 1111

Synthesis, crystal, molecular and electronic structure of the $[ReOCl_2(pzH)_2(OAsPh_3)]$-($ReO_4$) and $[\{ReCl_2(pzH)_2\}_2(\mu\text{-}O)]$ complexes

The reactions of the $[ReOCl_3(AsPh_3)(OAsPh_3)]$ and $[ReOCl_3(PPh_3)_2]$ complexes with pyrazole (pzH) have been examined and two novel oxo compounds – $[ReOCl_2(pzH)_2(OAsPh_3)](ReO_4)$ (**1**) and $[\{ReCl_2(pzH)_2\}_2(\mu\text{-}O)]$ (**2**) have been obtained. The crystal, molecular and electronic structures of **1** and **2** have been determined. The geometric parameters of **1** and **2** have been examined using the density functional theory (DFT) method. The spin-allowed singlet–singlet electronic transitions have been calculated with the time-dependent DFT method for the $[ReOCl_2(pzH)_2(OAsPh_3)]^+$ cation, ReO_4^- anion and $[\{ReCl_2(pzH)_2\}_2(\mu\text{-}O)]$ complex, and the UV–Vis spectra of the title compounds have been discussed on this basis.

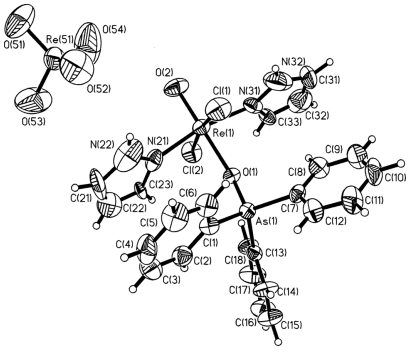

J. Dinda, S. Senapoti, T. Mondal, A.D. Jana, M.Y. Chiang, T.-H. Lu, C. Sinha

Polyhedron 25 (2006) 1125

Synthesis, spectral characterisation, and electrochemistry of bis-(2,2′-bipyridine)(1-alkyl-2-(naphthylazo)imidazole)ruthenium(II) complexes: X-ray crystal structure of [bis-(2, 2′-bipyridine)-{1-ethyl-2-(naphthyl-α-azo)imidazole}ruthenium(II) perchlorate

Title compounds have been synthesized by Ag-assisted route to remove Cl from $Ru(bpy)_2Cl_2$ followed by chelation with NaiR (1-alkyl-2-(naphthyl-α/β-azo) imidazole). The structure has been established by X-ray crystallography. Redox property gives Ru(III)/Ru(II) couple and ligand reductions.

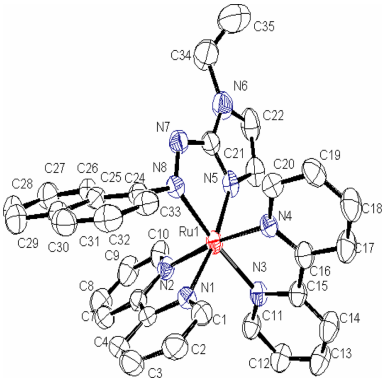

Veli T. Kasumov, Ahmet Bulut, Fevzi Köksal, Mehmet Aslanoğlu, İbrahim Uçar, Canan Kazak

Polyhedron 25 (2006) 1133

Synthesis, structure, spectroscopic and redox properties of copper(II)-*N*-3, 5-Bu^t_2phenylsalicylaldinine complexes: Crystal and molecular structure of bis(*N*-3, 5-Bu^t_2-phenylsalicylaldininato)copper(II)

The synthesis, spectroscopic (NMR, IR, UV/Vis, ESR) and electrochemical properties and redox behaviors of new bis(*N*-3, 5-Bu^t_2-R-salicylaldiminato)copper(II) complexes are described. Oxidation of some complexes with $(NH_4)_2Ce(NO_3)_6$ results in the generation of Cu(II)-phenoxyl radicals. As confirmed by X-ray crystallography complex **1** (R = H) has a slightly distorted *cis*-CuN_2O_2 coordination polyhedron.

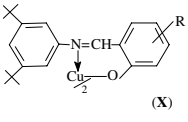

(**X**)

R = H (**L_1H**), **X = 1**
R = 3-OCH_3 (**L_2H**), **X = 2**
R = 4-OCH_3 (**L_3H**), **X = 3**
R = 3- OH (**L_4H**), **X = 4**
R = 4 - OH (**L_5H**), **X = 5**
R = 3,5-Bu^t_2 (**L_6H**), **X = 6**

Thouraya Turki, Taha Guerfel, Faouzi Bouachir

Polyhedron 25 (2006) 1142

Synthesis and crystal structure of tetracoordinated molybdenum (II) complexes containing rigid α-diimine ligands

Six new molybdenum complexes of formulae (dad)$MoCl_2$ [**3ai**, **3bi**, **3c**] (dad = R′N═C(R)–C(R)═NR′) have been synthesized and characterized by various physicochemical methods. The X-ray structure determination of **3a2** reveals a relatively tetrahedral coordination geometry.

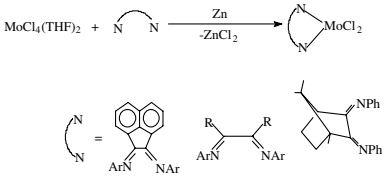

Padmanabha R. Ettireddy, Milton Orchin

Polyhedron 25 (2006) 1147

$[(CO)_3(dppe)Mn(OH_2)]BF_4$ (**1**). A synthetically versatile compound and its use as a probe for determining the preferred site of coordination on ambident ligands

The aqua ligand in the titled compound, **1**, is readily replaced by many other neutral or anionic ligands. Polydentate ligands react at every coordination site. Ambident ligands react selectively. ^1H NMR and IR spectra indicate which atom of the K^1 complexed ambident ligand is attached to the Mn atom.

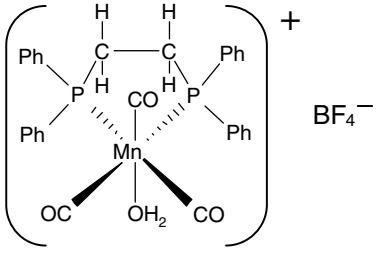

fac-$[(CO)_3(dppe)Mn(OH_2)]BF_4$, 1

Laura Turnbow, Joel S. Miller

Polyhedron 25 (2006) 1157

The quest for magnets based upon S = 1/2 bis(maleonitriledithiolato)nickelate(III), $\{Ni[S_2C_2(CN)_2]_2\}^{\cdot-}$, and bis(maleonitriledithiolato)metallate(IV), $\{M[S_2C_2(CN)_2]_2\}^{2-}$ (M = Co, Cu)

$V\{Ni[S_2C_2(CN)_2]_2\}_2$ an analog the room temperature $V[TCNE]_x$ magnet exhibits antiferromagnetic coupling ($\theta \sim -400$ K) and does not magnetically order.

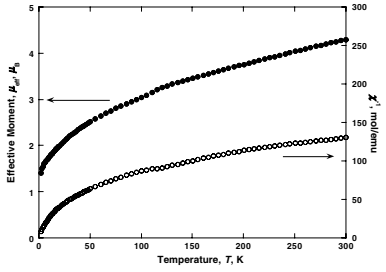

Bojan Kozlevčar, Darja Odlazek, Amalija Golobič, Andrej Pevec, Peter Strauch, Primož Šegedin

Polyhedron 25 (2006) 1161

Complexes with lignin model compound vanillic acid. Two different carboxylate ligands in the same dinuclear tetracarboxylate complex $[Cu_2(C_8H_7O_4)_2(O_2CCH_3)_2(CH_3OH)_2]$

Two different carboxylate anions were found in the dinuclear copper(II) tetracarboxylate $[Cu_2(C_8H_7O_4)_2(O_2CCH_3)_2(CH_3OH)_2]$ (heterocarboxylate). The compound decomposes outside mother-liquid, by replacement of methanol with water molecules. EPR spectra and $\mu_{eff} < 1.73$ BM confirm the dinuclear cage structure of the decomposed complex. The compound is compared to a related homocarboxylate complex $[Cu_2(C_8H_7O_3)_4(H_2O)_2]$. In the EPR spectra of this complex, six signals of the triplet state $S = 1$ (H_{z1}, H_1 (H_{x1}, H_{y1}), H_2 (H_{x2}, H_{y2}), H_{z2}) are observed.

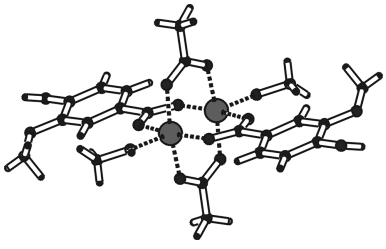

Inamur R. Laskar, Shih-Feng Hsu, Teng-Ming Chen

Polyhedron 25 (2006) 1167

Investigating photoluminescence and electroluminescence of iridium(III)-based blue-emitting phosphors

The syntheses of new blue-emitting phosphorescent iridium(III) based complexes were carried out. The maximum emission wavelengths were tuned with respect to the electronic properties of the substituents. The photoluminescence behavior of picolinates versus acetylacetonates was investigated. One of the substituted complex dopants was applied in organic light emitting devices and compared with its unsubstituted analogue.

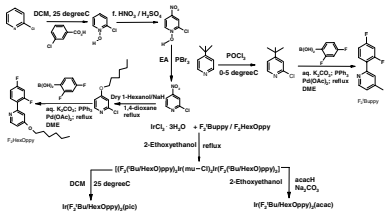

Rupa Bhawmick, Purak Das, Debatra Narayan Neogi, Pinaki Bandyopadhyay

Polyhedron 25 (2006) 1177

Metaloxylation of cyclopalladated 1-(1′-naphthylazo)naphthalene complexes by *m*-chloroperbenzoic acid: Oxygen insertion into metal–carbon(naphthyl) bond

The cyclopalladation of symmetrical 1-(1′-naphthylazo)naphthalene(HL) affords dimeric complexes of the type $[Pd_2(L)_2X_2]$ **1** (where X represents Cl or OAc). Complexes **1** undergo regiospecific metaloxylation (M–C → M–O–C) reaction with *m*-chloroperbenzoic acid (*m*-CPBA) at C2 and produce complexes $[Pd_2(LO)_2X_2]$ **3** where LOH is 1-(1′-naphthylazo)-2-hydroxynaphthalene.

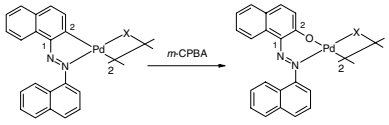

John Fawcett, Eric G. Hope, Alison M. Stuart, Andrew J. West

Polyhedron 25 (2006) 1182

Rhodium, palladium and platinum coordination complexes of fluoroalkylated-BINAP and -MonoPhos ligands

The coordination chemistry of fluoroalkylated-BINAP and -MonoPhos ligands to rhodium, palladium and platinum is described, including a single-crystal X-ray structural determination of $[Cp^*RhCl_2((R)\text{-MonoPhos})]$.

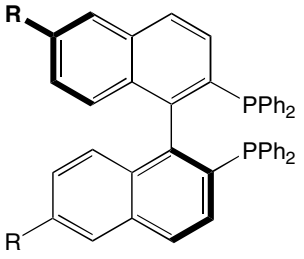

R = C_6F_{13} (**I**), $CH{=}CHC_6F_{13}$ (**II**), $CH_2CH_2C_6F_{13}$ (**III**)

Morsy A.M. Abu-Youssef, Vratislav Langer

Polyhedron 25 (2006) 1187

1D, 2D and 3D cadmium(II) polymeric complexes with quinoline-4-carboxylato anion, quinazoline and 2,5-dimethylpyrazine

Three new complexes $[Cd(Qux)_2(H_2O)]_n$ (**1**), $[Cd(Quz)_2(N_3)_2]_n$ (**2**) and $[Cd(dmpz)(N_3)_2]_n$ (**3**) (Qux = quinoline-4-carboxylato anion, Quz = quinazoline, dmpz = 2,5-dimethylpyrazine) have been synthesized and found by X-ray crystallography to have 1D, 2D and 3D topologies, respectively. Compound (**1**) polymerizes through μ-aqua molecules and di-μ-O,O′-bridging quinoline-4-carboxylato anions, compound (**2**) polymerizes through chairlike bridging di(EE) azido ligands while compound (**3**) contains bridging μ-*N*,*N*′-dimethylpyrazine and di(EE) azido ligands.

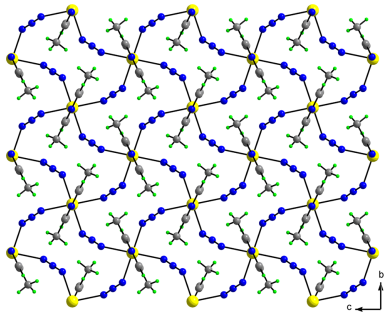

Meng Bao, Rongming Wang, Llew Rintoul, Qingyun Liu, Dennis P. Arnold, Changqin Ma, Jianzhuang Jiang

Polyhedron 25 (2006) 1195

Vibrational spectroscopy of phthalocyanine and naphthalocyanine in sandwich-type (na)phthalocyaninato and porphyrinato rare earth complexes. Part 13. The Raman characteristics of phthalocyanine in unsubstituted and peripherally octa(octyloxy)-substituted homoleptic bis(phthalocyaninato) rare earth complexes

The solid state Raman spectra of the series of double-decker sandwich complexes $M(Pc)_2$ and $M[Pc(OC_8H_{17})_8]_2$ were recorded with excitation at 633 and 785 nm. The energies and relative intensities of various characteristic bands vary systematically with the ionic radius of the rare earth ion.

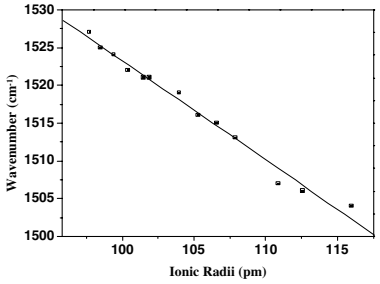

Neil F. Curtis, Horst Puschmann

Polyhedron 25 (2006) 1204

Copper(II) compounds of some nitro-substituted imine-triamine macrocycles: The structure of (aqua κ^1-*O*)-(13-ethyl-5,7,7-trimethyl-13-nitro-1,4,8,11-tetraazacyclotetradec-4-ene κ^4-$N^{1,4,8,11}$)copper(II) perchlorate

Reactions of (4,6,6-trimethyl-3,7-diazanon-3-ene-1,9-diamine)copper(II) perchlorate with methanal and nitroethane, or nitropropane, yield the nitro-substituted imine-triamine azamacrocyclic compounds (5,7,7,13-tetramethyl-13-nitro-1,4,8,11-tetraazacyclotetradec-4-ene) copper(II) perchlorate or the 13-ethyl-5,7,7-trimethyl-homologue.

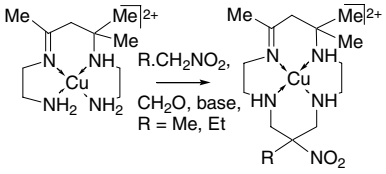

Dulce Belo, César Rodrigues, Isabel C. Santos, Susana Silva, Teresa Eusébio, Elsa B. Lopes, João V. Rodrigues, Manuel J. Matos, Manuel Almeida, M. Teresa Duarte, Rui T. Henriques

Polyhedron 25 (2006) 1209

Synthesis, crystal structure and magnetic properties of bis(3,4;3′,4′-ethylenedithio)-2,2′,5,5′-tetrathiafulvalene-bis(cyanoimidodithiocarbonate)aurate(III), (bedt-ttf)[Au(cdc)$_2$]

The new compound, (bedt-ttf)[Au(cdc)$_2$], where bedt-ttf stands for bis(3,4;3′,4′-ethylene-dithio)-2,2′,5,5′-tetrathiafulvalene and cdc for cyanodithiocarbimate, was synthesised. Its structure is monoclinic, space group $P2_1/n$ and consists in alternated stacking of donor and acceptor moieties along *c*. This compound is a semiconductor with a room temperature resistivity of 6.5×10^3 Ω cm. The anisotropy and thermal dependence of the ESR signal, only due to the bedt-ttf cations, was studied in the range 4–300 K. The static and EPR spin susceptibilities indicate an almost temperature independent value of 2.5×10^{-4} emu/mol ascribed to a three-dimensional network of antiferromagnetic interactions.

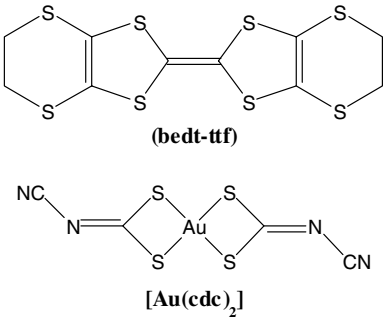

Svetlana G. Baca, Manfred T. Reetz, Richard Goddard, Irina G. Filippova, Yurii A. Simonov, Maria Gdaniec, Nicolae Gerbeleu

Polyhedron 25 (2006) 1215

Coordination polymers constructed from *o*-phthalic acid and diamines: Syntheses and crystal structures of the phthalate-imidazole complexes $\{[Cu(Pht)(Im)_2] \cdot 1.5H_2O\}_n$ and $[Co(Pht)(Im)_2]_n$ and their application in oxidation catalysis

Two new Cu(II) and Co(II) coordination polymers, $\{[Cu(Pht)(Im)_2] \cdot 1.5H_2O\}_n$ (**1**) and $[Co(Pht)(Im)_2]_n$ (**2**) (where Pht^{2-} = dianion of *o*-phthalic acid; Im = imidazole) have been synthesized and their crystal structures determined by X-ray crystallography. The structures of **1** and **2** comprise, respectively, $[Cu(Im)_2]$ and $[Co(Im)_2]$ units linked by bridging 1,6-phthalate ions to form infinite chains. Extended hydrogen bonding networks stabilize the three-dimensional structures in both complexes. Preliminary results show that **1** and **2** exhibit catalytic activity on the oxidation of cyclohexene using hydrogen peroxide as oxidant under aerobic conditions at ambient temperature.

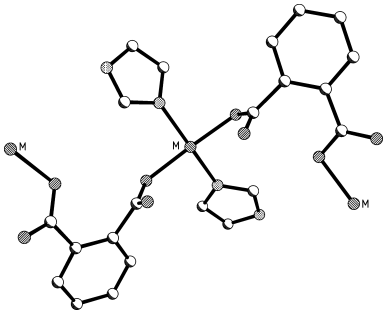

Harri Sopo, Jukka Sviili, Arto Valkonen, Reijo Sillanpää

Polyhedron 25 (2006) 1223

Uranyl ion complexes with aminoalcohol-bis(phenolate) [O,N,O′] donor ligands

The reaction between uranyl nitrate hexahydrate and phenolic ligand precursor *N*,*N*-bis-(2-hydroxy-3,5-dimethylbenzyl)-2-aminoethanol (H_3L1) in acetonitrile without base affords the dinuclear uranyl complex $[(UO_2)_2(H_2L1)_2(NO_3)_2]$ (**1**); in the presence of base, the mononuclear complex $[UO_2(H_2L1)_2] \cdot 2H_2O$ (**2**) is formed. Ligands (H_3L2–H_3L4), similar to H_3L1, formed only the complexes of the type **2**. Extraction studies of the uranyl ion from water to dichloromethane with these ligands are also presented.

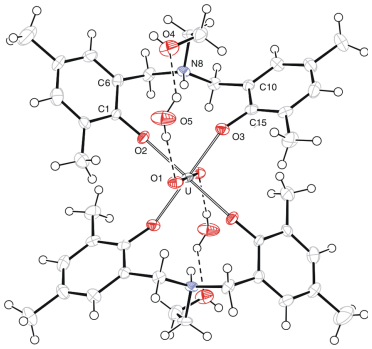

Olga A. Efremova, Yuri V. Mironov, Dmitry Yu. Naumov, Svetlana G. Kozlova, Vladimir E. Fedorov

Polyhedron 25 (2006) 1233

Cyano-bridged chalcocyanide complexes based on the cubane-like cluster with mixed cluster core $\{Re_4S_{4-x}Te_x\}$

Three new tetrahedral chalcocyanide cluster compounds $[\{Cu(en)_2\}_2Re_4S_{3.83}Te_{0.17}(CN)_{12}] \cdot H_2O$ (**1**), $[\{Zn(en)_2\}_2Re_4S_{3.60}Te_{0.41}(CN)_{12}] \cdot 3.75H_2O$ (**2**), and $[\{Cu(dien)(NH_3)\}_2Re_4S_{3.45}Te_{0.55}(CN)_{12}] \cdot 3H_2O$ (en = ethylenediamine, dien = diethylenetriamine) have been synthesized. All compounds have been characterized by single-crystal X-ray diffraction analysis. In structures of all three compounds, the Te atom positions of cluster cores are ordered, and metal cations are coordinated by CN groups which are the closest to tellurium atom position.

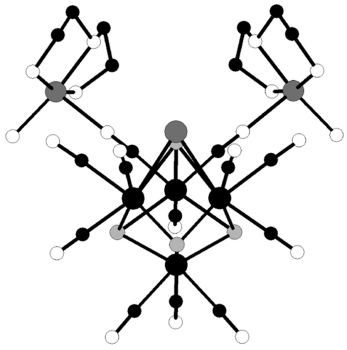

Jin-Run He, Yu-Ling Wang, Wen-Hua Bi, Yan-Qin Wang, Rong Cao

Polyhedron 25 (2006) 1239

Four new cadmium(II) homophthalate diimine complexes: Syntheses, structures and fluorescence

Four new complexes $[Cd(hpht)(phen)]_n$ (**1**), $[Cd(hpht)(2,2'\text{-bpy})]_n$ (**2**), $[Cd(hpht)(2,2'\text{-bpy})(H_2O)]_n \cdot 2nH_2O$ (**3**), and $[Cd(hpht)(4,4'\text{-bpy})]_n \cdot nH_2O$ (**4**) were solvothermally synthesized by reactions of homophthalic acid and $Cd(NO_3)_2 \cdot 4H_2O$ with different diimine auxiliary ligands, respectively. Complexes **1**–**3** feature interesting chain structures, and **4** is 2-D network. Complexes **1**–**4** exhibit specific photoluminescence properties and may be potential candidates for photoactive materials.

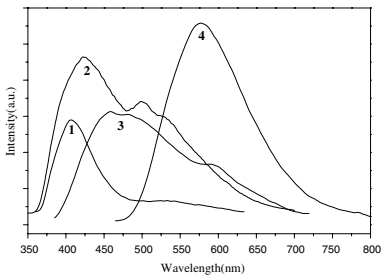

Sarah H. Oakley, Delia B. Soria, Martyn P. Coles, Peter B. Hitchcock

Polyhedron 25 (2006) 1247

Intramolecular hydrogen bonding in complexes containing bicyclic guanidine ligands

A series of complexes with formula $MX_2(hppH)_2$ [hppH 1,3,4,6,7,8-hexahydro-2Hpyrimido[1,2-a]pyrimidine have been structurally characterized revealing a tetrahedral metal centre, with intramolecular hydrogen bonding to the halide; the lithiated siloxide, $[Ph_3SiOLi(hppH)(THF)]_2$ is dimeric with intramolecular N*H*···O interactions.

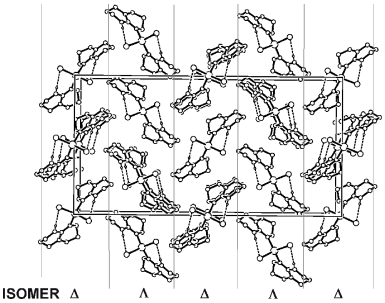

Wai-Fun Yeung, Hoi-Ki Kwong, Tai-Chu Lau, Song Gao, Lap Szeto, Wing-Tak Wong

Polyhedron 25 (2006) 1256

Cyano-bridged molecular squares: Synthesis and structures of $[Ni(cyclen)]_2[Pt(CN)_4]_2 \cdot 6H_2O$, $[Ni(cyclen)]_2[Ni(CN)_4]_2 \cdot 6H_2O$ and $[Mn(cyclen)]_2[Ni(CN)_4]_2 \cdot 6H_2O$

Three cyano-bridged molecular squares, $[Ni(cyclen)]_2[Pt(CN)_4]_2 \cdot 6H_2O$ (**1**), $[Ni(cyclen)]_2[Ni(CN)_4]_2 \cdot 6H_2O$ (**2**) and $[Mn(cyclen)]_2[Ni(CN)_4]_2 \cdot 6H_2O$ (**3**) (cyclen = 1,4,7,10-tetraazacyclododecane) have been synthesized and characterized by X-ray crystallography. The magnetic data suggest that there is very weak ferromagnetic intradimer interaction and an even weaker interdimer antiferromagnetic coupling in (**1**) and (**2**).

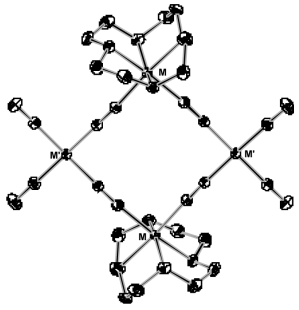

Sudipa Panigrahi, Subrata Kundu, Sujit Kumar Ghosh, Sudip Nath, Snigdhamayee Praharaj, Soumen Basu, Tarasankar Pal

Polyhedron 25 (2006) 1263

Selective one-pot synthesis of copper nanorods under surfactantless condition

Selective evolution of copper nanorods has been achieved from alkaline $CuSO_4$ solution using a specific concentration of glucose but spherical particles become the sole product above or below the critical concentration.

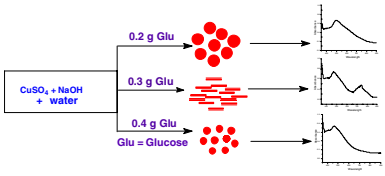

The Publisher encourages the submission of articles in electronic form thus saving time and avoiding rekeying errors. For detailed instructions on the preparation of manuscripts and of electronic artwork, consult the Author Gateway for Elsevier at http://authors.elsevier.com

SCIENCE DIRECT®

Full text of this journal is available, on-line from **ScienceDirect**. Visit **www.sciencedirect.com** for more information.

Available online at www.sciencedirect.com
SCIENCE DIRECT®
Polyhedron 25, issue 12, 21 August 2006
POLYHEDRON
www.elsevier.com/locate/poly

Contents

Papers

Zora Popović, Gordana Pavlović, Marijana Vinković, Dražen Vikić-Topić, Maša Rajić Linarić

Polyhedron 25 (2006) 2353

Coordination modes of 3-hydroxypicolinic acid (OH-picH): Synthesis and characterization of cadmium(II) complexes. Crystal and molecular structures of $[CdX(OH\text{-}pic)(OH\text{-}picH)(H_2O)]_2$ X = Cl^-, Br^-

The cadmium(II) chloride and bromide react almost instantaneously with 3-hydroxypicolinic acid in water solution giving isostructural dinuclear complexes of general formula $[CdX(OH\text{-}pic)(OH\text{-}picH)(H_2O)]_2$; X = Cl^-, Br^- which is established by the X-ray structural analysis and also supported by the thermal analysis. These compounds are not stable in solutions and NMR spectral analysis revealed the presence of cadmium(II) 3-hydroxypicolinate as the only cadmium(II) compound in solution. Although, the synthesis conditions permit also a formation $Cd(OHpic)_2$, apparently the packing forces in the solid state yield to the title complexes.

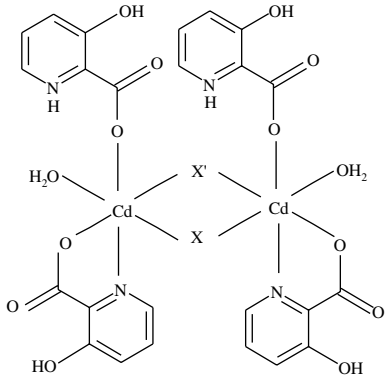

Fabiola Téllez, Adrian Peña-Hueso, Noráh Barba-Behrens, Rosalinda Contreras, Angelina Flores-Parra

Polyhedron 25 (2006) 2363

Coordination compounds in a pentacyclic aromatic system from 2-aminobenzothiazole derivatives and transition metal ions

The syntheses and structural analyses of coordination compounds derived from 2-(2-benzothiazolylamino)benzothiazole (**1**), 2-(2-aminobenzothiazolylamino)benzoxazole (**2**) and 2-(2-benzothiazolylamino)benzimidazole (**3**) with Co(II), Ni(II), and Zn(II) acetates and ligand **1** with Hg(II) acetate are reported. Three different geometries for the metal atoms were found: a distorted tetrahedron (for ML_2 Co, Ni, Zn and Hg), a square pyramid [for Co and Ni in $NiL_2(MeOH)$] and an octahedron for $Ni(L)(OAc)(MeOH)_2$.

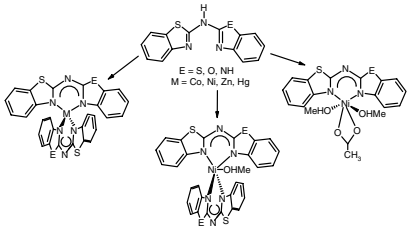

Rupam Dinda, Saktiprosad Ghosh, Larry R. Falvello, Milagros Tomás, Thomas C.W. Mak

Polyhedron 25 (2006) 2375

Synthesis, structure, and reactivity of some new dipyridyl and diamine-bridged dinuclear oxomolybdenum(VI) complexes

Some new diimine and diamine-bridged dinuclear Mo(VI) complexes of the general formula $[(MoO_2L)_2(\mu\text{-}N\text{–}N)]$ along with their common mononuclear precursor $[MoO_2L(C_2H_5OH)]$ have been synthesized and structurally characterized by X-ray crystallography. The ONO donor ligand (LH_2) is 2-hydroxy benzoylhydrazone of 2-hydroxybenzaldehyde and the bridging (μ-N–N) ligands are 4, 4′-bipyridine(4,4′-bpy), *trans*-1,2-bis(4-pyridyl) ethene (bpe), *trans*-1,2-bis(4-pyridyl) ethane (bpa) and *p*-phenylenediamine (ppda).

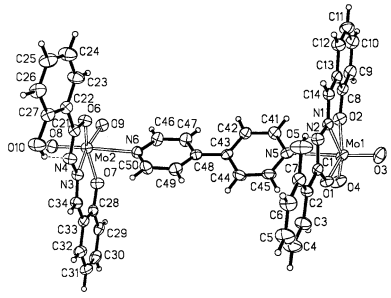

G. Kedarnath, Sandip Dey, Vimal K. Jain, Gautam K. Dey, Babu Varghese

Polyhedron 25 (2006) 2383

2-(*N*,*N*-Dimethylamino)ethylselenolates of cadmium(II): Syntheses, structure of $[Cd_3(OAc)_2(SeCH_2CH_2NMe_2)_4]$ and their use as single source precursors for the preparation of CdSe nanoparticles

Cadmium selenolates, $[Cd(SeCH_2CH_2NMe_2)_2]$ and $[Cd_3(OAc)_2(SeCH_2CH_2NMe_2)_4]$, have been prepared and characterized. The structure of the latter has been established by X-ray crystallography. Thermolysis of $[Cd(SeCH_2CH_2NMe_2)_2]$ in a mixture of solvents (HDA/TOPO) or in a furnace gave CdSe nanoparticles which were characterized by UV–Vis, photoluminescence, X-ray diffraction and electron microscopy.

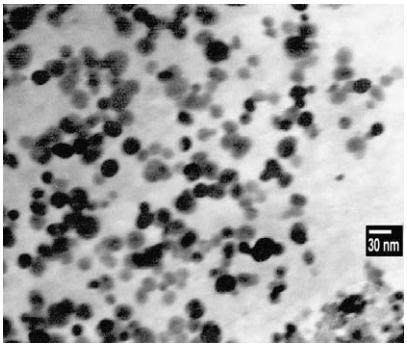

Leonard Joachim Pereira, Weng Kee Leong

Polyhedron 25 (2006) 2392

Substitution derivatives of the heteronuclear cluster $RuOs_3(\mu\text{-}H)_2(CO)_{13}$: Disubstituted group 15 derivatives

The structures in the solid state and solution state of tertiary group 15 ligand disubstituted derivatives of the heteronuclear cluster $RuOs_3(\mu\text{-}H)_2(CO)_{13}$ are examined. A number of isomeric structural types have been identified. In solution, most of these isomers are rapidly interconverting via hydride migrations. Substitution appears to be directed electronically to the ruthenium vertex, although steric hindrance appears to drive subsequent isomerisation via migration of the second group 15 ligand.

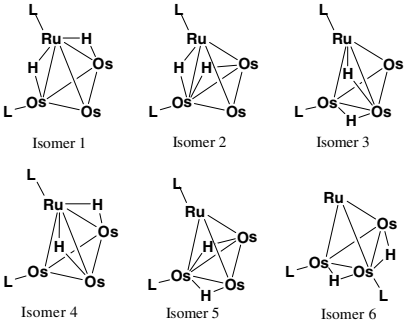

Zoya A. Starikova, Vadim G. Kessler, Nataliya Ya. Turova, Ilya A. Dantsker, Alexandr P. Bobyljov, Alexander S. Mitiaev

Polyhedron 25 (2006) 2401

Interaction of barium oxide and hydroxide with methanol: X-ray single crystal study of $Ba(OH)_2$ methanol solvates

Dissolution of barium oxide or hydroxide in methanol or hydrolysis of barium methoxide results in the formation of crystalline products identified as methanol solvates of barium hydroxide, $[Ba(OH)_2(H_2O)_2](MeOH)_2$ (**1**) and $[Ba(OH)_2(MeOH)_2](MeOH)$ (**2**).

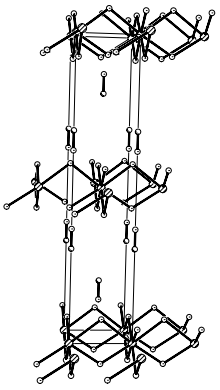

Cheng-Hsien Yang, Chun-Hung Chen, I-Wen Sun

Polyhedron 25 (2006) 2407

Bathochromic effect of trifluoromethyl-substituted 2-naphthalen-1-yl-pyridine ligands in color tuning of iridium complexes

The iridium complexes, $(4\text{-fnapy})_2Ir(acac)$ and $(5\text{-fnapy})_2Ir(acac)$, were prepared and their X-ray crystal structures were determined. Compared to $Ir(napy)_2(acac)$, the introduction of trifluoromethyl-substituted ligands resulted in remarkable bathochromic effect. The trifluoromethyl group has a stronger influence on lowering the LUMO levels.

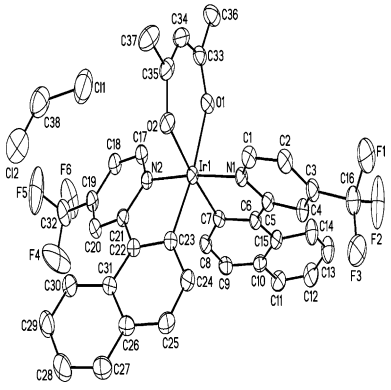

Thato N. Mtshali, Walter Purcell, Hendrik G. Visser, Stephen S. Basson

Polyhedron 25 (2006) 2415

A crystallographic and kinetic study of the formation of the tricyanonitrido(pyridine-2-carboxylato-κN,κO)rhenate(V) ion, [ReN-(η^2-pic)$(CN)_3]^{2-}$

The substitution reaction between [ReN-$(H_2O)(CN)_4]^{2-}$ and pic$^-$ (pyridine-2-carboxylato anion) resulted in the substitution of the aqua and cyano ligands to form the [ReN-(η^2-pic)$(CN)_3]^{2-}$ complex. The two consecutive reactions were kinetically investigated with the fast aqua substitution resulting in a rate constant of $1.92(5) \times 10^{-1}$ M^{-1} s^{-1} at 40.3 °C. A rate constant of $1.84(2) \times 10^{-2}$ s^{-1} at 80 °C was obtained for the second, slower cyano substitution. The negative entropy of activation of −133.4(3) J K^{-1} mol^{-1} for the slow reaction points to associative activation.

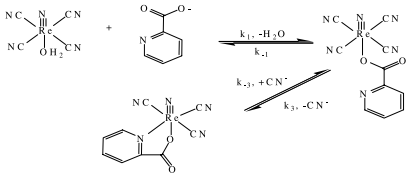

Jian-Hao Zhou, Ru-Mei Cheng, You Song, Yi-Zhi Li, Zhi Yu, Xue-Tai Chen, Xiao-Zeng You

Polyhedron 25 (2006) 2426

Syntheses, structures and magnetic properties of two new water bridged dinuclear nickel(II) complexes containing derivatives of 1,2,4-triazole and pivalate ligands

Two new water bridged dinuclear nickel(II) complexes **1** · $13H_2O$ and **2** · $3H_2O$ containing derivatives of 1,2,4-trizaole and pivalate ligands have been synthesized and structurally characterized. Magnetic susceptibility measurements on the powder samples of **1** and **2** at 1.8–300 K revealed that the overall weak antiferromagnetic coupling occur among nickel(II) ions.

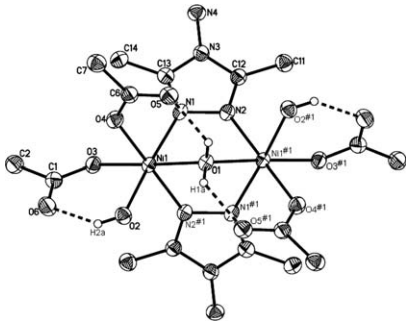

M. John Plater, Steven Kemp, Eugenio Coronado, Carlos J. Gómez-García, Ross W. Harrington, W. Clegg

Polyhedron 25 (2006) 2433

A stable oxoverdazyl free radical: Structural and magnetic characterization

Stable red crystals of **1** were too small for standard X-ray single-crystal structure determination so synchrotron radiation was used to solve the structure. Data were collected on a sample of the radical that had been accidentally set aside in a sample vial for five years. Susceptibility measurements showed that weak anti-ferromagnetism exists between the radicals. ESR spectroscopy shows the spin distribution in this stable radical.

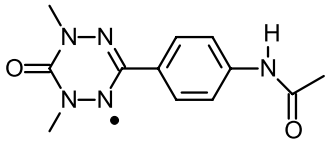

Lionel Salmon, Pierre Thuéry, Shinpei Miyamoto, Takehiko Yamato, Michel Ephritikhine

Polyhedron 25 (2006) 2439

Uranium(V) and uranium(IV/V) mixed valence complexes with *p-tert*-butylhomocalix-[*n*]arenes (*n* = 4, 6)

UCl_4 reacts with homocalixarenes comprising four or six phenolic units to give either a mononuclear U^V complex with the smaller macrocycle or, with the larger one, a tetranuclear U^{IV}/U^V mixed valence species built from two macrocycles, two μ_3-oxo and two bridging chlorine atoms. In both cases, all the phenoxide groups are metal-bound. The mononuclear species assembles to form a dimeric capsule through weak interactions with the counter-ions.

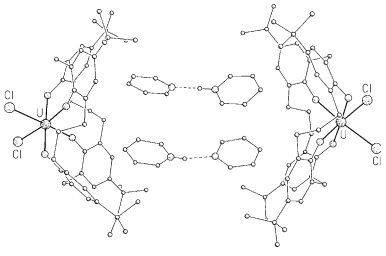

K. Umeda, J. Zukerman-Schpector, P.C. Isolani

Polyhedron 25 (2006) 2447

Uranyl (1,3-diphenylpropane-1,3-dionato) complexes with *N*-adamantylacetamide and azacyclononanone: Synthesis, spectroscopy, luminescence and crystal structures

The synthesis and characterization of uranyl 1,3-diphenylpropane-1,3-dionato (benzoylacetonate, ba) complexes with *N*-adamantylacetamide, 2-azacyclononanone and triphenylphosphine oxide, with general formula $UO_2(ba)_2L$ are described. They were characterized by infrared, Raman and emission spectroscopies. All complexes are luminescent, presenting the characteristic uranyl vibronic spectrum. The crystal structures of the *N*-adamantylacetamide and 2-azacyclononanone were determined. All complexes are heptacoordinated and all neutral ligands bond through an oxygen atom. In the case of the *N*-adamantylacetamide complex there are two independent molecules in the asymmetric unit cell. Both structures are reported.

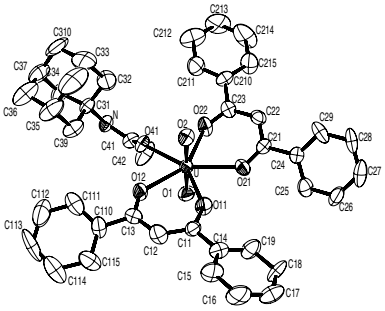

N. Kumaraguru, K. Santhakumar

Polyhedron 25 (2006) 2452

Studies on solvophobic interactions and micelle formation of some surface active Cr(III) complexes in non-aqueous solvents

The critical micelle concentration (cmc) of three kinds of metallosurfactants of the type *cis*-halogeno(dedocylamine)bis(ethylenediamine)chromium(III) have been studied in *n*-alcohol and formamide mixtures at different temperatures by the electrical conductivity method. Specific conductivity data (at 293–313 K) served for the evaluation of temperature dependent cmc values and thermodynamic parameters such as ΔG^0_m, ΔH^0_m and ΔS^0_m.

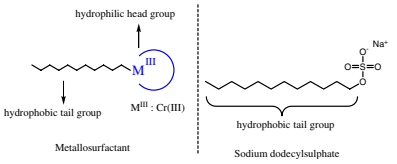

Emira Kahrović, Krešimir Molčanov, Ljerka Tušek-Božić, Biserka Kojić-Prodić

Polyhedron 25 (2006) 2459

New complexes of Mo(V) with Schiff bases: Crystal structure of butylammonium di-μ-oxo-μ-acetato-bis[(*N*-butylsalicylideniminato-*N*,*O*)-oxomolybdenum(V)] benzene, acetic acid solvate

Mo(V) Schiff base complexes derived from alkylamines and salycilaldehide were prepared and characterised by chemical analysis, IR and UV/Vis spectroscopy. The title complex $C_4H_9NH_3[Mo_2O_4(N\text{-}C_4H_9\text{-salim})_2OCOCH_3] \cdot C_6H_6 \cdot CH_3COOH$ is characterised by X-ray structure analysis. The structure is composed of a dinuclear di-μ-oxo-μ-acetato-bis[(*N*-butylsalicylideniminato-*N*,*O*)oxomolybdenum(V)] anion, butylammonium cation and two solvent molecules: benzene and acetic acid.

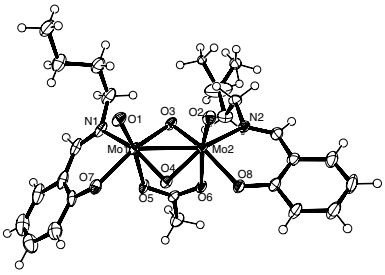

Anna S. Litvinenko, Alexey Y. Timoshkin, Henry F. Schaefer III

Polyhedron 25 (2006) 2465

Thermodynamics of thermal decomposition of group 13 metal trihalide adducts with piperidine: A combined theoretical and experimental study

Three major decomposition pathways of complexes formed by MX_3 (M = Al, Ga; X = Cl, I) and piperidine (pip) have been theoretically considered at the B3LYP/LANL2DZ(d,p) level of theory. Hydrogen gas elimination with formation of gaseous $MX_3 \cdot$ pyridine complexes becomes thermodynamically favorable above 500 K and is expected as a primary thermolysis product of $MX_3 \cdot$ pip. Alternative routes, which include dissociation into components or hydrogen halide elimination, require much higher temperatures. This theoretical conclusion is in qualitative agreement with present experimental thermolysis study of the $GaCl_3 \cdot$ pip complex.

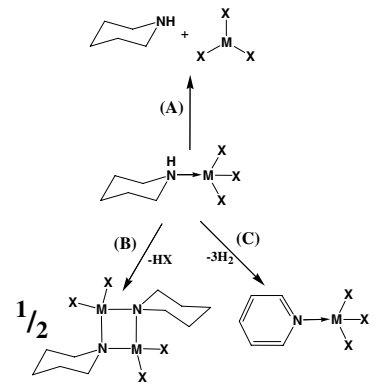

Paula C.R. Soares-Santos, Filipe A. Almeida Paz, Rute A. Sá Ferreira, Jacek Klinowski, Luís D. Carlos, Tito Trindade, Helena I.S. Nogueira

Polyhedron 25 (2006) 2471

Coordination modes of pyridine-carboxylic acid derivatives in samarium (III) complexes

Coordination modes of picolinic, 3-hydroxypicolinic and 2-hydroxynicotinic acids in samarium (III) complexes were investigated, showing *N*,*O*- or *O*,*O*-chelation in one-dimensional chains. These complexes show room-temperature photoluminescence.

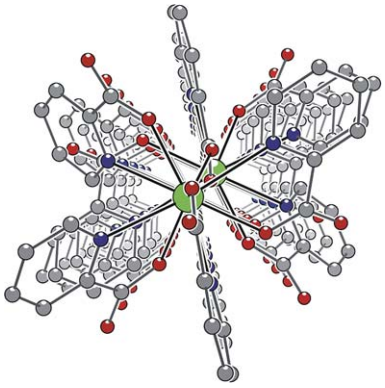

The Publisher encourages the submission of articles in electronic form thus saving time and avoiding rekeying errors. For detailed instructions on the preparation of manuscripts and of electronic artwork, consult the Author Gateway for Elsevier at http://authors.elsevier.com

SCIENCE DIRECT®

Full text of this journal is available, on-line from **ScienceDirect**. Visit **www.sciencedirect.com** for more information.

Available online at www.sciencedirect.com
SCIENCE DIRECT®
Polyhedron 25, issue 10, 10 July 2006
POLYHEDRON
www.elsevier.com/locate/poly

Contents

Papers

Alastair J. Nielson, Chaohong Shen, Joyce M. Waters

Polyhedron 25 (2006) 2039

Molecular engineering of coordination pockets in chloro-tris-phenoxo complexes of titanium(IV)

The preparation and characterisation of chloro-tris-phenoxo complexes of titanium(IV) in which coordination pockets are produced by varying the substituent in the 2-position of the phenoxo ligand phenyl ring is described. Collapse of the pockets in these complexes and some nitrogen tied-back anologues is determined using bipyridyl and pyridine ligands.

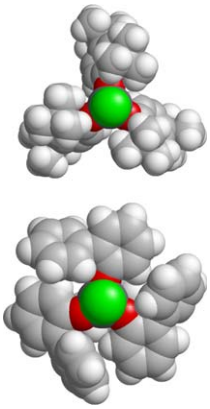

Giselle Cerchiaro, Ana M. Da Costa Ferreira, Aline B. Teixeira, Hugo M. Magalhães, Anna C. Cunha, Vitor F. Ferreira, Leonardo S. Santos, Marcos N. Eberlin, Janet M.S. Skakle, Solange M.S.V. Wardell, James L. Wardell

Polyhedron 25 (2006) 2055

Synthesis and crystal structure of 2,4-dihydro-4-[(5-hydroxy-3-methyl-1-phenyl-1H-pyrazol-4-yl)imino]-5-methyl-2-phenyl-3H-pyrazol-3-one and its copper(II) complex

A new method for preparing 2,4-dihydro-4-[(5-hydroxy-3-methyl-1-phenyl-1H-pyrazol-4-yl)-imino]-5-methyl-2-phenyl-3H-pyrazol-3-one (**3**), in an one-step diazo-transfer process, and its corresponding crystal structure are reported. Reaction of **3** with copper(II) ions at stoichiometric ratio gave complex **4** involving tautomeric forms.

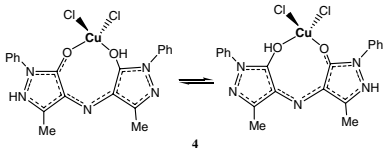

4

Mohammad S. Ali, Edio Longoria Jr., Teyeb Ould Ely, Kenton H. Whitmire, Abdul R. Khokhar

Polyhedron 25 (2006) 2065

Homopiperazine Pt(II) adducts with DNA bases and nucleosides: Crystal structure of $[Pt^{II}(homopiperazine)(9\text{-ethylguanine}_2](NO_3)_2$

A series of homopiperazine-Pt(II) mono and diadducts with purine and pyrimidines nucleobases and nucleosides have been synthesized and characterized by ^{1}H, ^{13}C, ^{195}Pt NMR. The crystal structure of one of these complexes $[Pt^{II}(homopiperazine)(9\text{-EtGua})_2](NO_3)_2$ is also reported here.

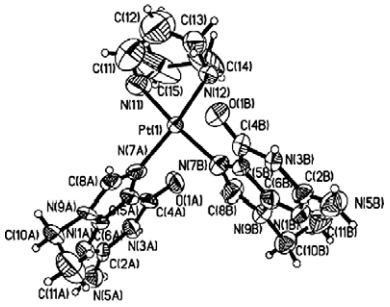

Diego Venegas-Yazigi, Susana Cortés, Verónica Paredes-García, Octavio Peña, Andrés Ibañez, Ricardo Baggio, Evgenia Spodine

Polyhedron 25 (2006) 2072

Modulating magnetic properties of a macrocyclic dinuclear copper(II) complex: Influence of counteranions on the crystal structure

The influence of the counteranions on the structure and magnetic properties of binuclear copper(II) complexes with the macrocyclic ligand, derived from 4-methyl-2,6-diformylphenol and 1,3-diamine-2-propanol, have been studied. Bulk magnetic properties are strongly affected by the nature of the anion.

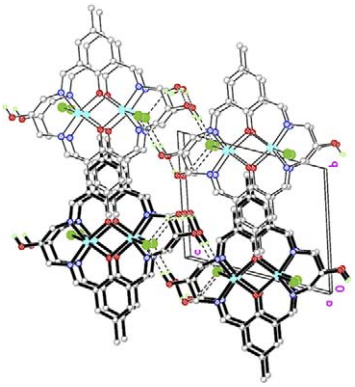

A. Mech, M. Karbowiak, T. Lis, J. Drożdżyński

Polyhedron 25 (2006) 2083

Monomeric, dimeric and polymeric structure of the uranium trichloride hydrates

Three different uranium trichloride hydrates have been isolated and their crystal and molecular structures have been determined. $UCl_3 \cdot 2H_2O \cdot 2CH_3CN$ crystallizes in the triclinic system forming infinitive zigzag chains, $UCl_3 \cdot 6H_2O$ crystallizes in the monoclinic system with a monomeric structure, while the characteristic feature of $UCl_3 \cdot 7H_2O$ structure are $[(H_2O)_7UCl_2U(H_2O)_7]^{4+}$ dimers.

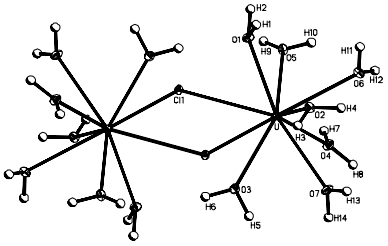

Roger D. Willett, Robert E. Butcher, Christopher P. Landee, Brendan Twamley

Polyhedron 25 (2006) 2093

Two halide exchange in copper(II) halide dimers: (4,4′-bipyridinium)$Cu_2Cl_{6-x}Br_x$

The presence of N–H···X and C–H···X hydrogen bonding interactions between the 4,4′-bipyridinium dications and $Cu_2X_6^{2-}$ dimers force short X···X contacts between the dimers with X···X distances of 3.645–3.690 Å. In this manner, alternating AFM magnetic chains are formed with alternating exchange pathways: the intradimer exchange coupling, J_2, and the X···X pathway, J_1. Magnetic studies indicate that these systems behave as chains with quite strong coupling, with $|J_1| > |J_2|$. The AFM coupling increases monotonically as the bromide content increases.

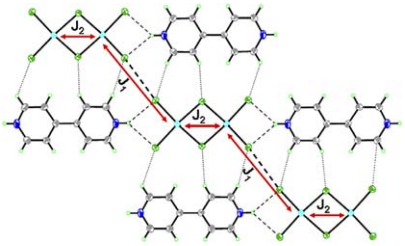

Clara Pampillón, Oscar Mendoza, Nigel J. Sweeney, Katja Strohfeldt, Matthias Tacke

Polyhedron 25 (2006) 2101

Diarylmethyl substituted titanocenes: Promising anti-cancer drugs

Bis-[di-(*p*-*N*,*N*-dimethylaminophenyl)methylcyclopentadienyl] titanium(IV) dichloride is a promising candidate for an anti-cancer drug and was synthesised starting from 6-(*p*-*N*,*N*-dimethylanilinyl)fulvene and 4-lithio-*N*,*N*-dimethylaniline. Herein, we present the synthesis and DFT structure of the titanocene and two further derivatives followed by MTT-based cytotoxicity tests on pig kidney carcinoma (LLC-PK) cells.

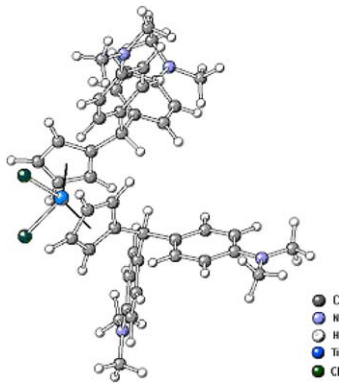

Elena Sebe, Mary Jane Heeg, Charles H. Winter

Polyhedron 25 (2006) 2109

Niobium and tantalum complexes containing 1,1-dialkylhydrazine-derived ligands

Niobium and tantalum complexes of the formula $[M(NNMe_2)Cl_2(NH_2NMe_2)(TMEDA)]Cl \cdot CH_2Cl_2$, $[M(NN(CH_2)_5)Cl_2(NH_2N(CH_2)_5)(TMEDA)]Cl \cdot CH_2Cl_2$ and $[M(NN(CH_2)_5)Cl_2(NH_2N(CH_2)_5)_2]Cl \cdot [(CH_2Cl_2)(C_6H_{14})_{0.5}]$ were prepared by treatment of the corresponding metal pentachloride with a trimethylsilylhydrazine derivative in the presence of TMEDA or the parent hydrazine. The new complexes were characterized by NMR spectroscopy and X-ray crystallography.

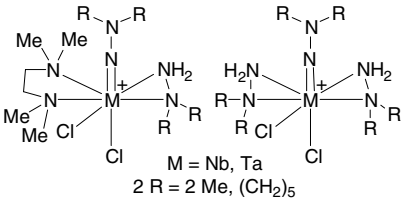

Eduardo de Faria Franca, Marcelo R.L. Oliveira, Silvana Guilardi, Renato Pereira de Andrade, Renata Hernandez Lindemann, Jorge Amim Jr., Javier Ellena, Vito M. De Bellis, Mayura M.M. Rubinger

Polyhedron 25 (2006) 2119

Preparation, crystal structure and spectroscopic characterization of nickel(II) complexes with dithiocarbimate derivated of sulfonamides

Three new *N*-R-sulfonyldithiocarbimate nickel(II) complexes with the formula $(Ph_4P)_2[Ni\text{-}(RSO_2NCS_2)_2]$ have been obtained in crystalline form by the reaction of appropriate potassium *N*-R-sulfonyldithiocarbimate salts and nickel(II) chloride hexahydrate. The compounds were characterized by single crystal X-ray diffraction technique and by IR and NMR spectroscopy.

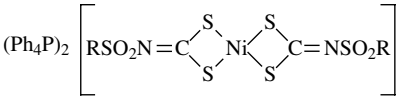

R = C_2H_5 (**1**), 4-IC_6H_4 (**2**) and 2,5-$Cl_2C_6H_3$ (**3**)

Masoud Salavati-Niasari, Fatemeh Davar

Polyhedron 25 (2006) 2127

Synthesis and characterization of nickel(II) complexes of 14-membered hexaaza macrocyclic ligands ''3,10-dialkyl-dibenzo-1,3,5,8,10,12-hexaazacyclotetradecane'' produced by the in situ one-pot template reaction of formaldehyde and 1,2-phenylenediamine with alkyl or benzyl amine in the presence of the nickel(II) ion

New square-planar Ni(II) complexes of 14-membered hexaaza macrocyclic ligands ''dibenzo-3,5,9,10,12,14-hexaazacyclotetradecane, $[Ni(R_2Bzo_2[14]aneN_6)]^{2+}$ (R = H, Me, Et, Bu, Benzyl)'' have been prepared by the in situ one-pot template synthesis (IOPTS) of formaldehyde and 1,2-phenylenediamine with alkyl amine or benzyl amine in the presence of the nickel(II) ion. The complexes of the hexaaza macrocycles have been characterized by elemental analyses, IR, FAB, UV–Vis and ^1H NMR spectroscopy, conductometric and magnetic measurements. The spectra of all the complexes show that the four secondary nitrogen atoms are coordinated to the nickel(II) ion.

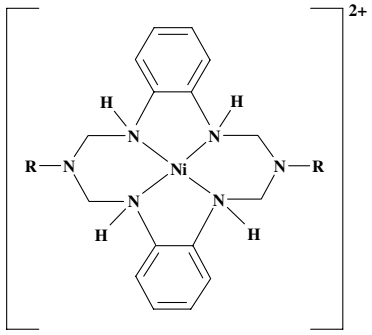

R= H, Me, Et, Bu, Benzyl

Sunil G. Naik, Arindam Mukherjee, Rajamani Raghunathan, Munirathinam Nethaji, Suryanarayanasastry Ramasesha, Akhil R. Chakravarty

Polyhedron 25 (2006) 2135

Magneto-structural study on a tetracopper(II) Schiff base complex stabilizing a decanuclear water aggregate

An antiferromagnetically spin-coupled tetranuclear copper(II) Schiff base complex $[Cu_4L_2(3\text{-}ppz)_2]$ (**1**) containing the 3-phenylpyrazole ligand has been prepared and structurally characterized. The crystal structure of $\mathbf{1} \cdot 6H_2O$ shows the formation of a decameric water cluster having two dimeric and one cyclic chair hexameric water aggregate anchored onto two complex units through hydrogen bonding interactions.

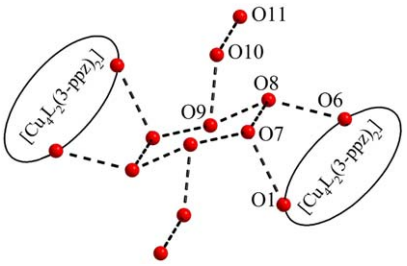

Anna Kropidłowska, Jarosław Chojnacki, Barbara Becker

Polyhedron 25 (2006) 2142

Tri-*tert*-butoxysilanethiolate complexes of manganese(II) with chelating heterocyclic bases – Structure of compounds with a $MnN_2O_2S_2$ or MnN_2OS_2 kernel and MeOH within the coordination sphere

Three stable $[Mn\{SSi(OBu^t)_3\}_2(N–N)]$ complexes have been described, where N–N = 2,2′-bipyridine, 1,10-phenanthroline and 2,9-dimethyl-1,10-phenanthroline. For the first time one of these manganese(II) thiolate complexes have been shown to bind and release a methanol molecule.

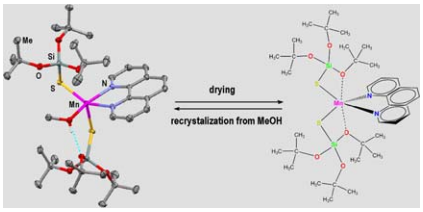

Debatra Narayan Neogi, Purak Das, Achintesh Narayan Biswas, Pinaki Bandyopadhyay

Polyhedron 25 (2006) 2149

Regiospecific cyclometallation: Synthesis, spectral properties and crystal structure of *peri*-palladate

At room temperature naphthylazophenol undergoes regiospecific palladation at the *peri*-position of the naphthyl ring and binds palladium(II) as a dianionic terdentate ligand. The spectral properties and crystal structure of the *peri*-palladate have been described.

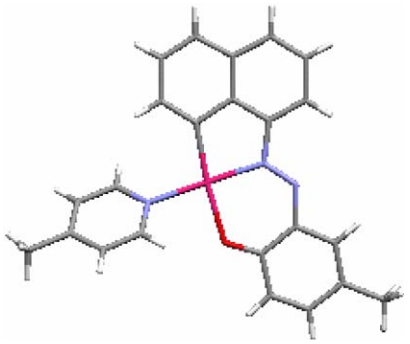

Ruo-Jie Tao, Fu-An Li, Shuang-Quan Zang, Yan-Xiang Cheng, Qing-Lun Wang, Jing-Yang Niu, Dai-Zheng Liao

Polyhedron 25 (2006) 2153

Syntheses, crystal structures and magnetic properties of two heterometallic coordination polymers

Two heterometallic coordination polymers with the chemical formula $\{[Cu_2Mn_2L_2(CH_3OH)(H_2O)] \cdot 0.5CH_3OH \cdot 0.5CH_3CH_2OH\}_n$ (**1**) and $\{[Cu_2Co_2L_2(H_2O)_2] \cdot H_2O\}_n$ (**2**) have been synthesized and characterized by IR, UV spectroscopy and single-crystal X-ray structural analysis, where H_4L = 2-hydroxy-3-[(E)-({2-[(2-hydroxybenzoyl)amino]ethyl}-imino)methyl] benzoic acid. The magnetic measurements showed that two compounds exhibit antiferromagnetic coupling exchange interactions, and satisfactory fittings to the observed magnetic susceptibility data were obtained by assuming a linear four-spin arrangement with two isotropic magnetic exchange interactions.

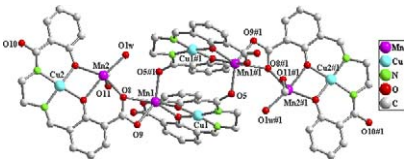

Mei Ching Tseng, Jin Lian Ke, Chang Chi Pai, Shao Pin Wang, Wen Liang Huang

Polyhedron 25 (2006) 2160

Photophysical and electrochemical studies of heteroleptic cyclometallated complexes of rhodium(III) containing 2-benzoylpyridine

Two heteroleptic cyclometallated complexes, *cis*-[Rh(bzpy)(bipy)Cl_2] (**1**) and *cis*-[Rh(bzpy)-(phen)Cl_2] (**2**) have been synthesized (bzpy = 2-(2-pyridylcarbonyl)phenyl, bipy = 2,2′-bipyridine and phen = 1,10-phenanthroline). The coordinated bzpy ligand is *N*,*C* coordinated with Rh(III) based on IR and NMR data. At 77 K, **1** and **2** in EtOH/MeOH (9:1, v/v), each show a broad, symmetric and structureless red emission assigned as dd^* phosphorescence. Analysis of voltammetric data also provides evidence in support of this assignment.

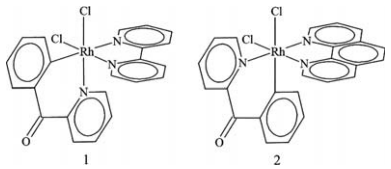

Rui-Li Sang, Li Xu

Polyhedron 25 (2006) 2167

Supramolecular architectures built of biimidazole complexes and sulfate or nitrate anions

The strong affinity of coordinated biimidazole for inorganic counter-anions (sulfate or nitrate) via N–H…O hydrogen bonding has been used as a strategy to build up four different modular assemblies, $[Zn(H_2biim)_3]SO_4$, $[Cu(H_2biim)_2(H_2O)]SO_4 \cdot 3H_2O$, $[Cd(H_2biim)_2(NO_3)(H_2O)]_4(NO_3)_4$ and $[Zn(H_2biim)_2(H_2O)](NO_3)_2$. An unusual four-membered water hexamer has been found in **2**.

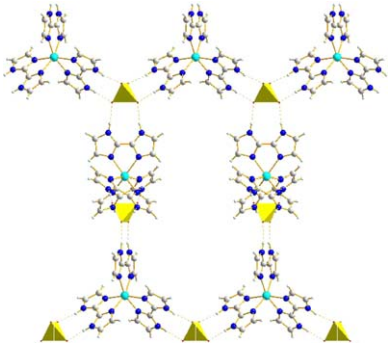

Denis Prodius, Constantin Turta, Valeriu Mereacre, Sergiu Shova, Maria Gdaniec, Yurii Simonov, Janusz Lipkowski, Victor Kuncser, George Filoti, Andrea Caneschi

Polyhedron 25 (2006) 2175

Synthesis, structure and properties of heterotrinuclear carboxylate complexes $[Fe_2M(Ca, Sr, Ba)O(CCl_3COO)_6(THF)_n]$

Three novel μ_3-oxo trinuclear carboxylates $[Fe_2CaO(CCl_3COO)_6(THF)_4] \cdot THF$ (**1**), $[Fe_2SrO(CCl_3COO)_6(THF)_6] \cdot 0.5H_2O \cdot 0.5THF$ (**2**) and $[Fe_2BaO(CCl_3COO)_6(THF)_6] \cdot 0.5H_2O \cdot 0.5THF$ (**3**) have been synthesised and characterised by X-ray structure analysis, TG-, IR-spectroscopy and magnetochemistry. Compounds **1** and **3** are molecular complexes with s- and d-metals displayed in the apices of isosceles triangles with a triply bridging oxygen atom at its centre.

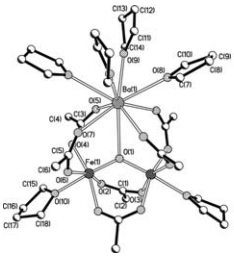

Ravi Shankar, Arti Joshi, Shailesh Upreti

Polyhedron 25 (2006) 2183

Preparation and characterization of functional disilaalkanes: Supramolecular motifs in the crystal structures of $Ph_3SiCH_2CH_2SiRR'_2$ [R = Me, R′ = Cl; R = R′ = Ph] mediated by C–H···Cl and/or C–H···π interactions

The syntheses of the disilaalkanes $Ph_3SiCH_2CH_2SiRR'_2$ [R = Me, R′ = Cl (**1**); R = Ph, R′ = Cl (**2**); R = R′ = Cl (**3**), Ph (**4**), OEt (**5**), H (**6**)] along with the crystal structures of **1** and **4** are described.

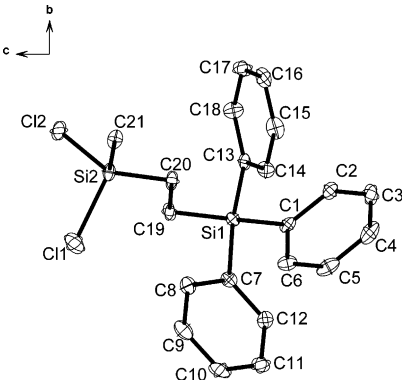

The Publisher encourages the submission of articles in electronic form thus saving time and avoiding rekeying errors. For detailed instructions on the preparation of manuscripts and of electronic artwork, consult the Author Gateway for Elsevier at http://authors.elsevier.com

SCIENCE DIRECT®

Full text of this journal is available, on-line from **ScienceDirect**. Visit **www.sciencedirect.com** for more information.

Available online at www.sciencedirect.com
ScienceDirect
Polyhedron 25, issue 16, 13 November 2006
POLYHEDRON
www.elsevier.com/locate/poly

Contents

Papers

D. Banerjee, U.S. Ray, J.-S. Wu, T.-H. Lu, C. Sinha

Polyhedron 25 (2006) 3077

Naphthylazoimidazole complexes of cobalt(II): Synthesis structure and electrochemistry

The title complexes have been synthesized and characterized by X-ray structure determination in one case. Cyclic voltammetry shows a high potential Co(III)/Co(II) redox response along with azo reductions. The tris-chelated complexes are unstable to moisture.

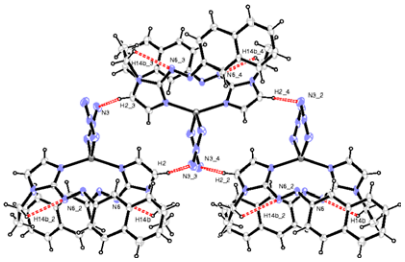

Biswarup Sarkar, Mau Sinha Ray, Michael G.B. Drew, Albert Figuerola, Carmen Diaz, Ashutosh Ghosh

Polyhedron 25 (2006) 3084

Trinuclear Cu(II) complexes containing peripheral ketonic oxygen bridges and a μ_3-OH core: Steric influence on their structures and existence

Two trinuclear copper(II) complexes, $[(CuL^1)_3(\mu_3\text{-fOH})](ClO_4)_2$ (**1**) and $[(CuL^2)_3(\mu_3\text{-OH})](ClO_4)_2 \cdot 0.75H_2O$ (**2**), where HL^1 and HL^2 are two tridentate Schiff base ligands derived from mono condensation of 1-benzoylacetone with 1,2-ethanediamine and 1,2-propanediamine, respectively, and a mononuclear complex, $[Cu(bn)(pn)]ClO_4$ (**3**), where bn = 1-benzoylacetonato and pn = 1,3-propanediamine, have been synthesized and structurally characterized. Variable-temperature magnetic susceptibility measurements reveal antiferromagnetic coupling in complexes **1** and **2**.

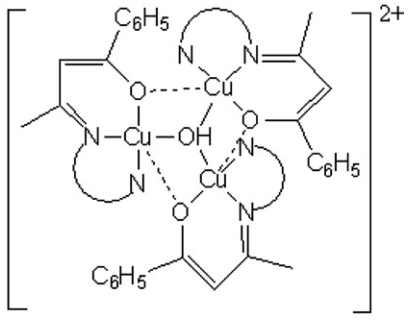

Sethuraman Kannan, Rengan Ramesh

Polyhedron 25 (2006) 3095

Synthesis, characterization, catalytic oxidation and biological activity of ruthenium(III) Schiff base complexes derived from 3-acetyl-6-methyl-2H-pyran-2,4(3H)-dione

A series of paramagnetic low spin Ru(III) complexes of the type $[RuX_2(EPh_3)_2(L)]$ (where X = Cl or Br; E = P or As; L = monobasic bidentate Schiff base ligands) have been synthesized and characterized. The catalytic efficiency of one of the ruthenium complexes (**10**) was determined in the case of oxidation of primary and secondary alcohols into their corresponding aldehydes and ketones in the presence of *N*-methylmorpholine-*N*-oxide(NMO) as co-oxidant. Further, the in vitro toxicity of these complexes was tested against the growth of bacterial species viz., *Staphylococcus aureus* (209p) and *Escherichia Coli* ESS (2231).

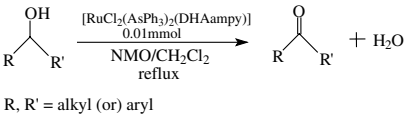

R, R' = alkyl (or) aryl

Rajarshi Ghosh, Sk Hafijur Rahaman, Chun-Nan Lin, Tian-Huey Lu, Barindra K. Ghosh

Polyhedron 25 (2006) 3104

Coordination behaviour of symmetrical hexadentate N-donor Schiff bases towards zinc(II)pseudohalides: Syntheses, crystal structures and luminescence

Two series of zinc(II) pseudohalide complexes of dinuclear type $[Zn_2(L^1/L^2)(X)_4]$ (**1a**–**1d**) (L^1:X = N_3^-, **1a** and X = NCS^-, **1b**; L^2:X = N_3^-, **1c** and X = NCS^-, **1d**) and molecular ion-pair type $[Zn(L^1/L^2)][Zn(X)_4]$ (**2a**–**2d**) (L^1:X = N_3^-, **2a** and X = NCS^-, **2b**; L^2:X = N_3^-, **2c** and X = NCS^-, **2d**) [*N*-(1-pyridin-2-ylformylidene)-*N*′-[2-({2-[(1-pyridin-2-ylformylidene)amino]ethyl}amino)ethyl]-ethane-1,2-diamine (L^1) and *N*-(1-pyridin-2-ylformylidene)-*N*′-[2-(4-{2-[(1-pyridin-2ylformylidene)amino]ethyl}piperazin-1-yl)ethyl]amine (L^2)] have been prepared. Single crystal X-ray diffraction studies confirm the structures of the two representative members, $[Zn_2(L^2)(N_3)_4]$ (**1c**) and $[Zn(L^1)][Zn(NCS)_4]$ (**2b**).

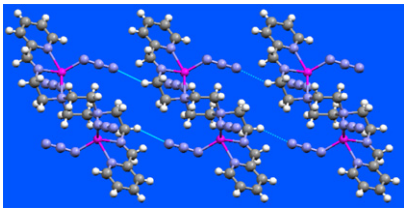

R. Senthil Kumar, S. Arunachalam

Polyhedron 25 (2006) 3113

Synthesis, characterization and DNA binding studies of a polymer-cobalt(III) complex containing the 2,2′-bipyridyl ligand

A polymer-cobalt(III) complex containing the 2,2′-bipyridyl ligand was prepared by the ligand substitution method and characterized. DNA binding studies of this polymer-cobalt(III) complex have been examined by absorption spectroscopy, fluorescence spectroscopy and gel electrophoresis.

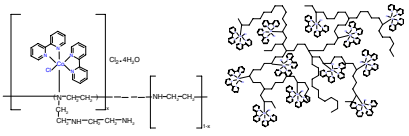

Chew Hee Ng, Han Kiat Alan Ong, Chiak Wu Kong, Kong Wai Tan, Raja Noor Zaliha Raja Abd. Rahman, Bohari M. Yamin, Seik Weng Ng

Polyhedron 25 (2006) 3118

Factors affecting the nucleolytic cleavage of DNA by (*N*,*N*′-ethylenendiaminediacetato)-metal(II) complexes, M(edda). Crystal structure of Co(edda)

Metal(II) complexes of a tetradentate amino acid: structural studies, binding to DNA and nucleolytic properties.

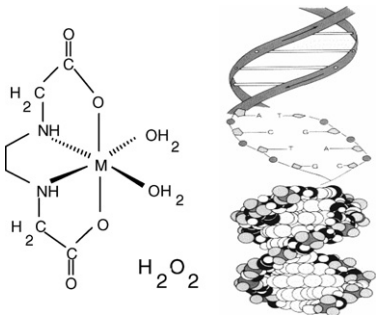

R. Lozano, F. de Jesús, M.C. Lozano

Polyhedron 25 (2006) 3127

Synthesis, spectral, thermal and kinetic studies on the adducts with pyridines of tungsten(V) binuclear thiocomplexes with di-isopropyldithiocarbamate

When the thermal decomposition of di-μ-sulfido-bis-(sulfido *N*,*N*,di-*i*-propyldithiocarbamate)di-tungsten(V) adducts with pyridines was investigated, the DSC curves of all the compounds showed a first endothermic peak over 115–162 °C. The mass loss accompanying this transition corresponds on the TG curves to the loss of two moles of coordinated base.

Bahattin Gümgüm, Osman Akba, Feyyaz Durap, Leyla Tatar Yıldırım, Dinçer Ülkü, Saim Özkar

Polyhedron 25 (2006) 3133

Synthesis, characterization, crystal and molecular structure of diphenyloxophosphinoethylenediamines

Bis-, tris- and tetrakis(diphenyloxophosphino)- ethylenediamine compounds can be synthesized starting with ethylenediamine and diphenylchlorophosphine.

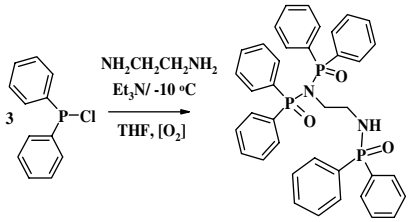

Jishnunil Chakraborty, Heike Mayer-Figge, William S. Sheldrick, Pradyot Banerjee

Polyhedron 25 (2006) 3138

Structure and property of unsymmetrical binuclear [(3,5-dimethylpyrazole)$_2$Pd$_2$(μ-3,5-dimethylpyrazolate)$_2$(2,6-dipicolinate)] and mononuclear [Na$_2$(H$_2$O)$_4$Pd(2,6-dipicolinate)$_2$] complexes

The syntheses, structures and properties of two palladium(II) complexes, [(3,5-Hdmpz)$_2$Pd$_2$(μ-3,5-dmpz)$_2$(2,6-dipic)] (**1**) and [Na$_2$(H$_2$O)$_4$-Pd(2,6-dipic)$_2$] (**2**), are reported. Complex **1** forms a hydrogen bonded 1D network while **2** forms an extended 2D coordination network. A detailed quantum-chemical calculation on the Na-chain has been performed utilizing the crystal data of **2**.

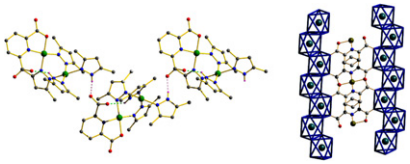

Rebecca M. Jones, Michael J. Goldcamp, Jeanette A. Krause, Michael J. Baldwin

Polyhedron 25 (2006) 3145

Theoretical, structural, and spectroscopic studies of a series of Ni^{II}(TRISOXH$_3$)X$_2$ complexes

Geometries of nickel tris(oxime)amine complexes optimized by density functional theory show small average deviations when compared to experimental data. Vibrational modes observed by Raman and infrared spectroscopy were assigned using a linear scaling procedure, resulting in 2- to 3-fold improvement in the agreement between experimental and theoretical wavenumbers.

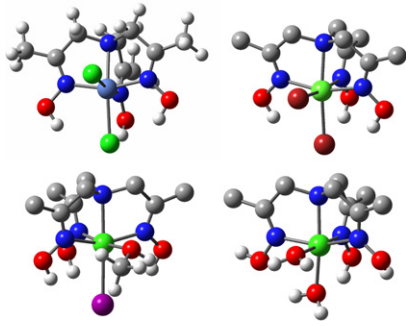

Liladhar B. Kumbhare, Vimal K. Jain, Ray J. Butcher

Polyhedron 25 (2006) 3159

Unprecedented formation of selenido-bridged tri-nuclear palladium(II) and platinum(II) complexes, [M$_3$(μ$_3$-Se)$_2$(P$^\frown$P)$_3$]$^{2+}$, via C–Se bond cleavage

Trinuclear selenido-bridged complexes, [M$_3$-(μ$_3$-Se)$_2$(P$^\frown$P)$_3$][BPh$_4$]$_2$ are formed in good yields via unprecedented cleavage of C–Se linkage of selenocarboxylate in a reaction of [M(SeCOC$_6$H$_4$Me-4)$_2$(P$^\frown$P)] with MCl$_2$(P$^\frown$P) in the presence of NaBPh$_4$.

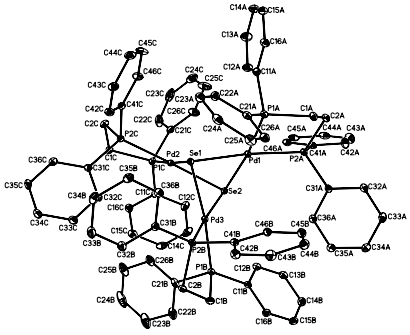

Ahmet Bilgin, Beytullah Ertem, Fatma Dinç Ağın, Yaşar Gök, Selami Karslıoğlu

Polyhedron 25 (2006) 3165

Synthesis, characterization and extraction studies of a new *vic*-dioxime and its complexes containing bis(diazacrown ether) moieties

A *vic*-dioxime ligand containing bis(diaza-12-crown-4) units and its complexes were synthesized from the appropriate starting materials. Additionally, their cation-binding abilities were evaluated for alkali and heavy metal picrates using a solvent extraction technique. The novel compounds have been characterized by physical and spectroscopic techniques.

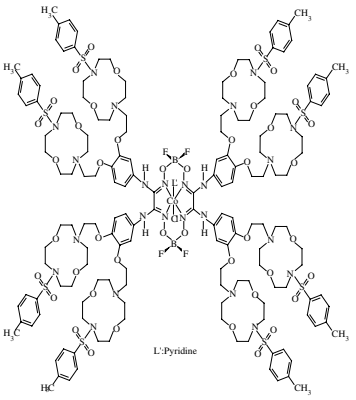

Olga Szilágyi, Katalin Ősz, Katalin Várnagy, Daniele Sanna, Helga Süli-Vargha, Imre Sóvágó, Giovanni Micera

Polyhedron 25 (2006) 3173

Potentiometric and spectroscopic studies on the copper(II) and zinc(II) complexes of bis(imidazol-2-yl) derivatives of tripeptides

Copper(II) and zinc(II) complexes of the tripeptides containing chelating bis(imidazol-2-yl)methyl agents at the C-termini were studied. The formation of stable ML and ML_2 complexes was detected with a tridentate coordination of the ligands resulting in macrochelates. For GlyIleGly-BIMA and GlyGlyHis-BIMA polynuclear species exist in basic solution.

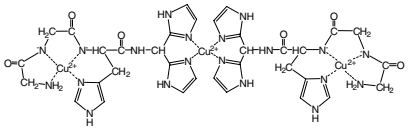

R. Bruce King, John Hagel

Polyhedron 25 (2006) 3183

The role of the metal formal oxidation state in metallaborane structures relating to *closo*/*isocloso* and *nido*/*isonido* pairs

The metal formal oxidation state increases by two units in a *closo* → *isocloso* or *nido* → *isonido* structural transformation, generally involving diamond–square–diamond processes relating to internal metal oxidative addition reactions. More exotic "*isoiso*" structures are found for metallaboranes containing metals exhibiting relatively high oxidation states such as molybdenum, tungsten, and rhenium.

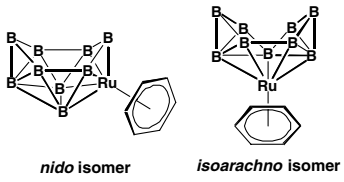

Heera Krishna, Setharampattu S. Krishnamurthy, Munirathinam Nethaji

Polyhedron 25 (2006) 3189

An unexpected entry into the silver(I) chemistry of diphosphazane ligands: Crystal and molecular structures of $[Ag\{Ph_2PN(Pr^i)PPh_2\}(CF_3SO_3)]_2$, $[Ag\{Ph_2PN(Pr^i)PPh(OC_6H_3Me_2\text{-}2,6)\}_2]PF_6$, and $[Ag_3(\mu\text{-}Cl)_2\{Ph_2PN(R)PPh_2\}_3]PF_6$ (R = H, Pr^i)

The reactions of AgX (X = Cl, NO_3 or CF_3SO_3) with diphosphazane ligands of the type $X_2PN(R)PXY$ give mononuclear, binuclear and trinuclear silver(I) complexes which exhibit different coordination numbers and geometries as revealed by single crystal X-ray diffraction studies.

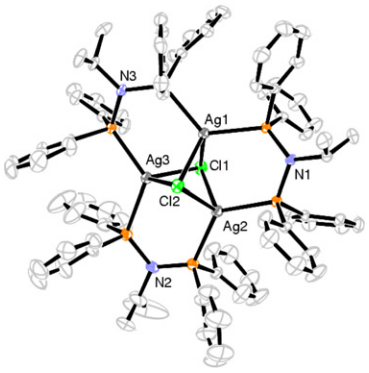

Amel Ghames, Tahar Douadi, Djahida Haffar, Salah Chafaa, Magali Allain, Mustayeen A. Khan, Gilles M. Bouet

Polyhedron 25 (2006) 3201

Structural and electrochemical studies of Co(II), Ni(II), Cu(II) and Cd(II) complexes with a new symmetrical N_2O_2 Schiff base: Crystal structure of the ligand 1,2-di[4-(2-imino 4-oxo pentane)phenyl]ethane

The crystal structure of 1,2-di[4-(2-imino 4-oxo pentane)phenyl]ethane (H_2L) is described. This new tetradentate Schiff base gives complexes with cobalt(II), nickel(II), copper(II) and cadmium(II). These new complex species are formulated as $[CoL] \cdot (H_2O)_3$, $[(NiCl_2)_2(H_2L)]$, $[CuCl_2(H_2L)]$ and $[CdCl_2(H_2L)]$, respectively. The coordination occurs through the N_2O_2 system, using various tautomers. In addition, their cyclic voltammograms are discussed.

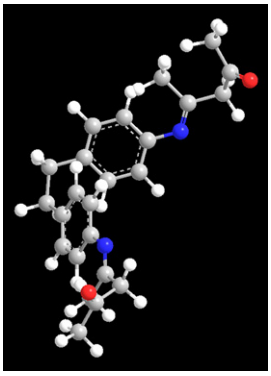

Quan-Ling Suo, Ning Zhu, Li-Min Han, Yi-Bing Wang, Yue-Guang Bai, Lin-Hong Weng

Polyhedron 25 (2006) 3209

Studies on the synthesis of novel 2,2′-bis-(ferrocenyl)propane derivatives and their reactivity with metal carbonyl clusters

A new ligand, $HC{\equiv}C(C_5H_5FeC_5H_3)C(CH_3)_2Fc'C{\equiv}CH$, and its cluster $[HC{\equiv}C(C_5H_5FeC_5H_3)C(CH_3)_2Fc'C{\equiv}CH][Co_2(CO)_6]_2$ (**5**) have been synthesized, and novel complex $[FcC(CH_3)_2Fc'CH{\equiv}C]FeCo_2(CO)_9$ (**6**) was obtained by using an nuclear enlarging reaction of complex $[FcC(CH_3)_2Fc'C{\equiv}CH]Co_2(CO)_6$ with $Fe_2(CO)_9$. The molecular structures of the compounds were determined by element analysis, FT-IR, ^1H (^{13}C) NMR, MS or X-ray crystallography.

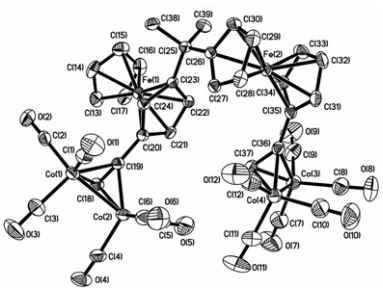

Maravanji S. Balakrishna, D. Suresh, Paulose P. George, Joel T. Mague

Polyhedron 25 (2006) 3215

Aminophosphines derived from morpholine and *N*-methylpiperazine: Synthesis, oxidation reactions and transition metal complexes

The synthesis, derivatization and metal complexes of morpholine and *N*-methylpiperazine derived tertiary phosphines are described.

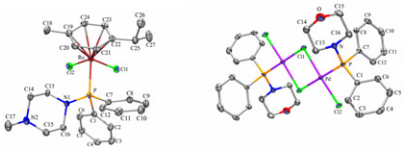

Joanna Kisała, Agata Białońska, Zbigniew Ciunik, Stefan Kurek, Stanisław Wołowiec

Polyhedron 25 (2006) 3222

Complexes of heteroscorpionate trispyrazolylborate ligands. Part XIII: Molybdenum complexes of hydrobis(5-methyl-3-phenylpyrazolyl)(3-methyl-5-phenylpyrazolyl)borate, hydrotris(3-(2-thienyl)-5-methylpyrazolyl)borate and tetranuclear molybdenum(V) complex of hydrotris(3,5-dimethylpyrazolyl)borate

The hydrotris(3-(2-thienyl)-5-methylpyrazolyl)-borate (Tp′) coordinates to molybdenum in κ^3 fashion in $[Et_4N][Tp'Mo(CO)_3]$ and $Tp'Mo(CO)_3(allyl)$ complexes. The aerial oxidation of $Tp^*Mo(CO)_2(I)$ led to the unique tetranuclear linear complex of molybdenum(V) with two Tp^* terminal ligands and terminal oxo as well as bridging oxo donors. The molybdenum(0) and (II) complexes were also synthesized and studied by the ^1H NMR spectroscopy and electrochemical measurements.

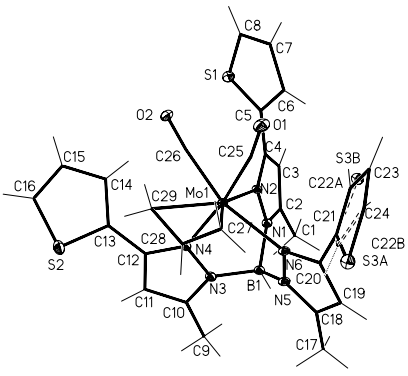

The Publisher encourages the submission of articles in electronic form thus saving time and avoiding rekeying errors. For detailed instructions on the preparation of manuscripts and of electronic artwork, consult the Author Gateway for Elsevier at http://authors.elsevier.com

Full text of this journal is available, on-line from **ScienceDirect**. Visit **www.sciencedirect.com** for more information.

Available online at www.sciencedirect.com
ScienceDirect
Polyhedron 25, issue 14, 23 October 2006
POLYHEDRON
www.elsevier.com/locate/poly

Contents

Papers

B. Machura, A. Jankowska, R. Kruszynski, J. Kłak, J. Mroziński

Polyhedron 25 (2006) 2663

Structural and spectroscopic studies on rhenium(III) diphenyl(2-pyridyl)phosphine oxide complexes

The reactions of the complexes [Re$OX_3(PPh_3)_2$] (X = Cl, Br) with diphenyl-(2-pyridyl)phosphine (PPh_2py) have been examined and two novel Re(III) compounds – [$ReCl_3(PPh_3)(OPPh_2py$-O,N)] (**1**) and [$ReBr_3(PPh_3)(OPPh_2py$-O,N)] (**2**) – have been obtained. The compounds have been studied by IR, UV–Vis spectroscopy, magnetic measurements and X-ray crystallography. The electronic structure of **1** has been calculated with the density functional theory (DFT) method. The spin-allowed triplet–triplet electronic transitions of **1** have been calculated with the time-dependent DFT method, and the UV–Vis spectra of the title compounds have been discussed on this basis.

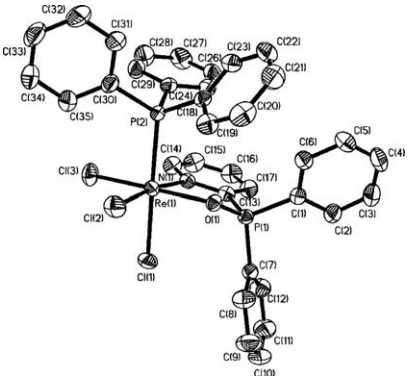

Inmaculada Beloso, Jesús Castro, José A. García-Vázquez, Paulo Pérez-Lourido, Jaime Romero, Antonio Sousa

Polyhedron 25 (2006) 2673

Electrochemical synthesis and structural characterization of heteroleptic cobalt(II) complexes of N-2-pyridyl sulfonamide ligands

The complexes [CoL_2L'] (L′ = 2,2′-bipyridine or 1,10-phenanthroline) have been synthesized by the electrochemical oxidation of anodic metal in acetonitrile solutions of the appropriate methyl-substituted N-2-pyridylsulfonamide ligand (HL) ligand and the corresponding coligand L′. The crystal structures of the compounds show the metal in a distorted octahedral geometry, [N6] or [N4O2], that depends on the position of the substituent on the pyridine ring.

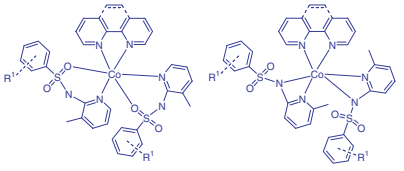

Andrei S. Potapov, Andrei I. Khlebnikov

Polyhedron 25 (2006) 2683

Synthesis of mixed-ligand copper(II) complexes containing bis(pyrazol-1-yl)methane ligands

Complexes of copper(II) nitrate and chloride with several bis(pyrazol-1-yl)methane derivatives were prepared and characterized by spectroscopic and electrochemical techniques. The complexes obtained were reacted with bidentate (2,2′-bipyridyl and acetylacetone) and monodentate (triphenylphosphine, 1*H*-benzimidazole, 1*H*-benzotriazole, 3,5-dimethyl-1*H*-pyrazole) ligands forming mixed-ligand complexes.

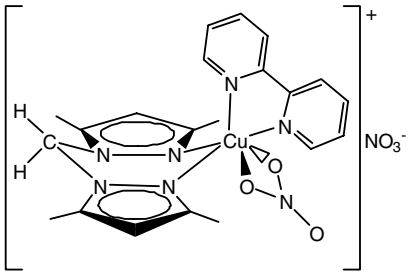

William J. Evans, Daniel B. Rego, Joseph W. Ziller

Polyhedron 25 (2006) 2691

Synthesis and structure of the diglyme-bridged lead hexafluoroacetylacetonate complex $[Pb(hfac)_2(\mu\text{-}\eta^3\text{:}\eta^1\text{-diglyme})]_2$

The title complex is readily made from PbO and Hhfac in the presence of diglyme. The volatile complex exists as enantiomeric pairs linked by bridging oxygens, as shown here.

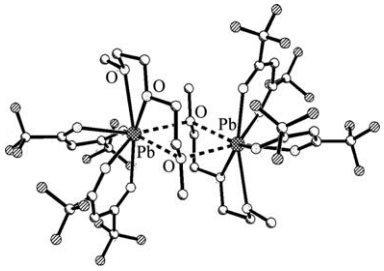

Bruno Pitteri, Marco Bortoluzzi

Polyhedron 25 (2006) 2698

Reactivity of neutral nitrogen donors in square-planar d^8 metal complexes: The system chloro(2,2′:6′,2″-terpyridine)platinum(II) cation with five-membered N-donor heterocycles in methanol

The kinetics of the reversible displacement of chloride from the square-planar $[Pt(terpy)Cl]^+$ cation (terpy = 2,2′:6′,2″-terpyridine) by five-membered N-donor heterocycles (thiazoles, oxazole, isoxazole, imidazole and pyrazoles) have been studied spectrophotometrically in MeOH. The reactivity of the considered nucleophiles has been related to their electronic and steric characteristics.

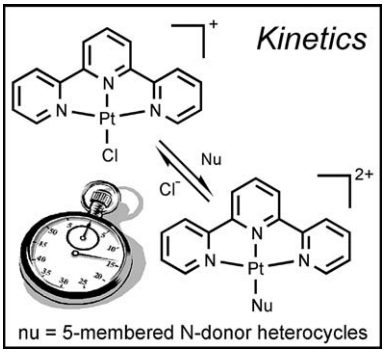

Joseph A. Duimstra, Charlotte L. Stern, Thomas J. Meade

Polyhedron 25 (2006) 2705

Magnetic and structural properties of a cyano-bridged 1D ruthenium(III)–nickel(II) coordination polymer

Reaction of $[Ni(cyclam)](ClO_4)_2$ with $Na[Ru(salen)(CN)_2]$ generated a 1D coordination polymer whose structural composition consisted of alternating Ni(II) and Ru(III) ions bridged by cyanide ligands and whose magnetic properties indicated ferromagnetic coupling between Ni(II) and Ru(III).

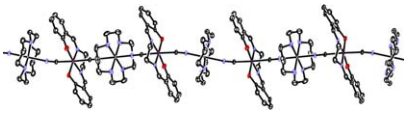

Panana Kitiphaisalnont, Santi Thohinung, Prapaipim Hanmungtum, Narongsuk Chaichit, Surapol Patrarakorn, Sutatip Siripaisarnpipat

Polyhedron 25 (2006) 2710

Effect of metal ions and length of alkylene bridge on the strength of hydrogen bonds in diiminedioxime cobalt(III) and nickel(II) complexes

Comparison of crystal structures for diiminedioxime (BnH_2 and EnH_2) complexes of Co(III) and Ni(II) indicates that introduction of a propylene bridge opposite the hydrogen bond imposes no significant constraint but the ethylene bridge impose significant constraint. Hence the O—O distance of $[Co(EnH)Cl_2]$ is much longer than those for $[Co(BnH)(NO_3)_2]$ and $[Co(BnH)Cl_2]$.

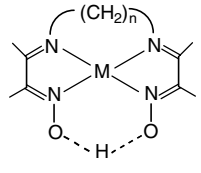

M	n	O-O distance (Å)	
Co^{3+}	2	2.708	
Co^{3+}	4	2.434	$[Co(BnH)(NO_2)_2]$
		2.423	$[Co(BnH)Cl_2]$
Ni^{4+}	4	2.432	

Kyoung-Tae Youm, Jaejung Ko, Moo-Jin Jun

Polyhedron 25 (2006) 2717

Non-classical hydrogen bonds (C–H···X, X = Cl and N) induced 3D architecture: Trigonal bipyramidal ferric complex, $[Fe(btp)Cl_3]_n$ (btp = 2,6-bis(*N*1-1,2,4-triazolyl)-pyridine)

The reaction of $FeCl_3 \cdot 6H_2O$ with btp afforded the trigonal bipyramidal ferric complex, $[Fe(btp)Cl_3]_n$ (**1**) consisting of three chloride ligands and two nitrogen atoms of btp. Interestingly, in **1**, a 3D architecture is induced by non-classical C–H···Cl and C–H···N hydrogen bonds between 1D zigzag chains in which btp ligands bind ferric ions through coordination bonds.

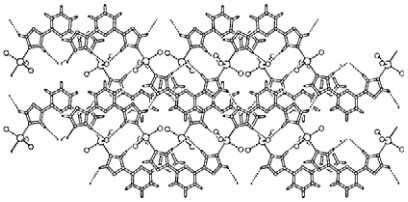

T. Adrian George, Hassan H. Hammud, Samih Isber

Polyhedron 25 (2006) 2721

Structure, thermal analysis and magnetism of the doubly bridged linear polymer $[Ni(4\text{-}NH_2\text{-}C_6H_4CO_2)_2(CH_3OH)_2] \cdot CH_3OH$

The title compound $[Ni(4\text{-}NH_2\text{-}C_6H_4CO_2)_2(CH_3OH)_2] \cdot CH_3OH$ (**1**) consists of Ni(II) atoms doubly bridged by *p*-aminobenzoate ligands (PAB) into 1D chains which are further connected into a 3D framework by methanol molecules through hydrogen bonding. Intrachain π–π interactions are observed between the aromatic rings of doubly bridging PAB. The magnetic data of compound **1** for the temperature range 300–3 K is indicative of ferromagnetically coupled nickel species. Thermogravimetric analysis of **1** indicates a sharp weight loss of one PAB ligand and two coordinated methanol molecules. The formation constant and thermodynamic parameters of complexation of Ni(II) with *p*-aminobenzoic acid have been evaluated.

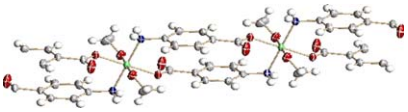

D. Jaganyi, A. Mzinyati

Polyhedron 25 (2006) 2730

An ^{11}B NMR spectroscopy investigation of the mechanism of the reduction of nitriles by $BH_3 \cdot SMe_2$

The reduction of acrylonitrile at 25 °C was monitored by ^{11}B NMR spectroscopy to the vinyliminoborane and exhibited simple second-order kinetics.

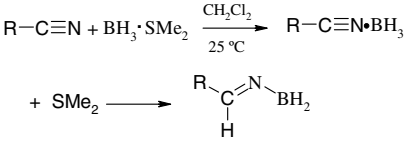

Soma Sen, Samiran Mitra, Dominique Luneau, M. Salah El Fallah, Joan Ribas

Polyhedron 25 (2006) 2737

Synthesis, crystal structure and magnetic properties of two new manganese Schiff base complexes $[Mn_2(L^1)_2(NCS)_2]$ and $[Mn(L^2)(N_3)(H_2O)]$ $[\{L^1H = C_{13}H_{10}N_2O_2\}; \{L^2H_2 = C_{19}H_{22}N_2O_4\}]$

A μ_2-dicarboxylato bridged dinuclear manganese(II) Schiff base complex $[Mn_2(L^1)_2(NCS)_2]$ (**1**), {L1=C13H9N2O2-} and a mononuclear manganese(III) Schiff base complex $[Mn(L^2)(N_3)(H_2O)]$ (**2**), $\{L^2=C_{19}H_{22}N_2O_4^{-2}\}$ have been synthesised and characterised by elemental analysis, IR and UV–Vis spectra. Structures of both complexes have been established by single crystal X-ray analysis. Complex **1** shows a very weak antiferromagnetic interaction. Complex **2** forms a dimer through a H-bonding interaction.

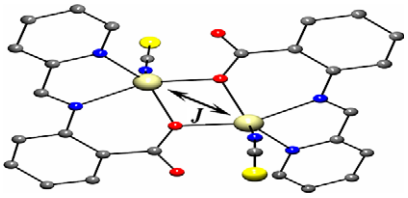

Janusz Gregoliński, Andrzej Kochel, Jerzy Lisowski

Polyhedron 25 (2006) 2745

Lanthanide complexes of 2 + 2 meso-type macrocycle derived from *trans*-1,2-diaminocyclohexane and 2,6-diformylpyridine: X-ray crystal structures of La(III) and Sm(III) complexes

The title complexes have been synthesised and characterized by spectroscopic methods. The X-ray crystal structures of the isomorphic La(III) and Sm(III) complexes have been determined. The properties and stability of the lanthanide(III) complexes of the ligand L have been compared with those of the isomeric chiral ligand L1 derived from enantiopure (1*R*,2*R*)-*trans*-1,2-diaminocyclohexane.

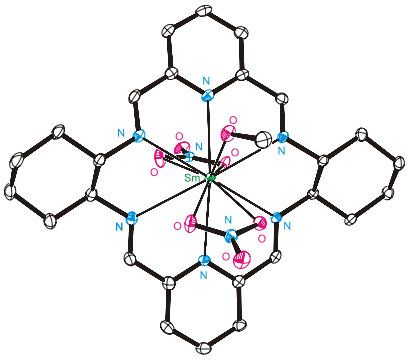

Tarlok S. Lobana, Sonia Khanna, Ray J. Butcher, A.D. Hunter, M. Zeller

Polyhedron 25 (2006) 2755

Synthesis, crystal structures and multinuclear NMR spectroscopy of copper(I) complexes with benzophenone thiosemicarbazone

Benzophenone thiosemicarbazone has yielded tetrahedral complexes with copper(I) chloride/bromide in presence of PPh_3 (**1** and **2**), and a trigonal planar with copper(I) iodide (**3**).

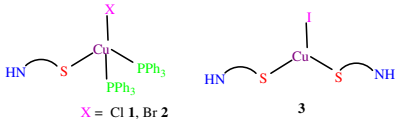

Umasankar Ray, Kamal Krishna Sarker, Golam Mostafa, Tian-Huey Lu, M. Salah El Fallah, Chittaranjan Sinha

Polyhedron 25 (2006) 2764

Copper(II) azide complexes of 1-alkyl-2-(arylazo)imidazoles: Structure and magnetism

Tetranuclear Cu(II)-azido complexes of composition $[Cu(RaaiR')(N_3)_2]_4$ have been synthesized and one of them has been characterized by X-ray crystallography. Variable temperature magnetic measurement indicates ferromagnetic and antiferromagnetic interactions, with $J_1 = +25.3\ cm^{-1}$ and $J_2 = -4.7\ cm^{-1}$.

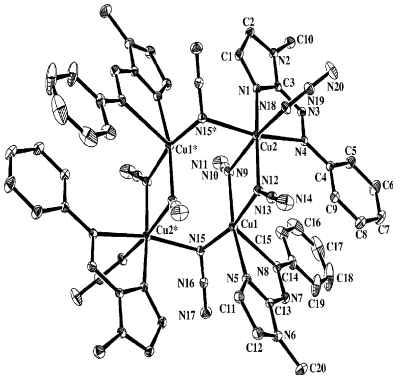

M. Zuber, F.P. Pruchnik

Polyhedron 25 (2006) 2773

Hydridobipyridine rhodium complexes as a result of the C–H bond activation in coordinated ligand, NMR studies

2,2′-Bipyridine ligand in Rh(I) complexes undergoes **H3,3′–D3,3′** exchange in basic solution CD_3ONa/CD_3OD. The hydride resonances in the range −14 to −28 ppm are observed although the only hydrogen source is bpy ligand. This strongly suggests that oxidative addition of C3-H to rhodium takes place in the exchange process.

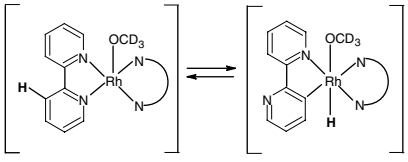

Yan-Feng Yue, En-Qing Gao, Chen-Jie Fang, Zheng He, Shi-Qiang Bai, Chun-Hua Yan

Polyhedron 25 (2006) 2778

Crystal structures and magnetic properties of triple helical binuclear complexes with bis-(bidentate) diazine ligands

Three triple helical binuclear complexes, with two metal ions wrapped by three bis(bidentate) diazine bridging ligands in a spiral conformation, are structurally and magnetically characterized.

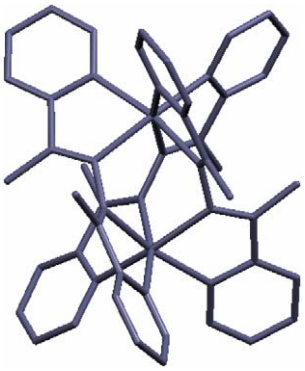

Nora Lardiés, Elena Cerrada, Mariano Laguna

Polyhedron 25 (2006) 2785

Synthesis of heteroleptic nickel(II) and palladium(II) dithiolenes

Reaction of 4-(*p*-cyanophenyl)-1,3-dithiole-2-thione, 4-(2-thienyl)-1,3-dithiole-2-one (**1**) and 4-(3-thienyl)-1,3-dithiole-2-one (**2**) with a base and the subsequent addition of nickel(II) and palladium(II) complexes give the formation of heteroleptic dithiolenes with 1,2-bis(diphenylphosphino)ethane as an ancillary ligand.

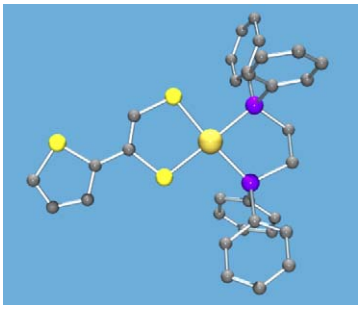

Prasant Kumar Nanda, Manindranath Bera, Guillem Aromí, Debashis Ray

Polyhedron 25 (2006) 2791

Atmospheric CO_2 fixation leads to a unique $\eta^2 : \mu\text{-}HCO_3^-$ bridged $[Cu_2^{II}]$ complex and coordination induced ligand hydrolysis to a $[Cu^{II}]$ complex

Atmospheric CO_2 fixation in basic medium leads to a novel hydrogencarbonate single oxygen bridged dicopper(II) complex $[Cu_2^{II}(L)(HCO_3)] \cdot 4H_2O(1 \cdot 4H_2O)$ from the dinucleating ligand H_3L, whereas in neutral medium the monocopper(II) complex $[Cu^{II}(HL^1)] \cdot 2ClO_4$ (**2**) of the zwitterionic ligand (HL^1), is obtained following 2-(2′-hydroxyphenyl)imidazolidine ring and terminal (2-hydroxyphenyl)methylimine hydrolysis.

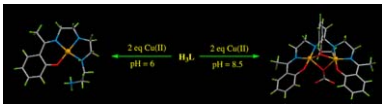

Ante Miličević, Nenad Raos

Polyhedron 25 (2006) 2800

Estimation of stability of coordination compounds by using topological indices

Stability constants of copper(II) chelates with amino acids and diaminoethanes were correlated to the 3rd valence connectivity indices, $^3\chi^v$, of the corresponding complexes. The first and second stability constants were fairly well reproduced, yielding an error of the estimate around 0.3 log *K* units.

$$^3\chi^v = \sum_{\text{path}} \{\delta(i)\delta(j)\delta(k)\delta(l)\}^{-0.5}$$

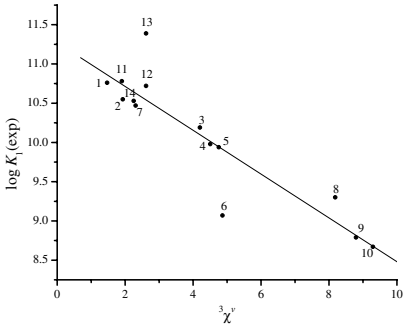

The Publisher encourages the submission of articles in electronic form thus saving time and avoiding rekeying errors. For detailed instructions on the preparation of manuscripts and of electronic artwork, consult the Author Gateway for Elsevier at http://authors.elsevier.com

Full text of this journal is available, on-line from **ScienceDirect**. Visit **www.sciencedirect.com** for more information.

Available online at www.sciencedirect.com
SCIENCE DIRECT®
Polyhedron 25, issue 11, 31 July 2006
POLYHEDRON
www.elsevier.com/locate/poly

Contents

Papers

Chandan Adhikary, Dasarath Mal, Ken-Ichi Okamoto, Siddhartha Chaudhuri, Subratanath Koner

Polyhedron 25 (2006) 2191

Synthesis, characterization, X-ray structure and magnetic study of the azido adducts of tridentate (NNO) Schiff base copper (II) complexes

Simple variation of the substitution in the ligand affords different molecular architectures. While the ethyl substituted diamine gives a monomeric species, methyl substitution affords an infinite 1D chain involving copper (II) linked by μ-1,3-azido bridges. Consequently, the two complexes exhibit different magnetic properties.

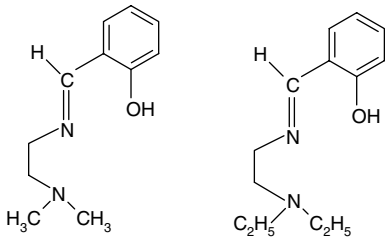

Pongthipun Phuengphai, Sujittra Youngme, Narongsak Chaichit, Chaveng Pakawatchai, Gerard A. van Albada, Manuel Quesada, Jan Reedijk

Polyhedron 25 (2006) 2198

Crystal structures and magnetic properties of two new phosphate-metal complexes: $[Cu_2(bpy)_2(\mu,\eta^2\text{-}HPO_4)(\mu,\eta^1\text{-}H_2PO_4)(\mu,\eta^2\text{-}H_2PO_4)]_n$ and $[Cu_4(phen)_4(\mu_3,\eta^2\text{-}HPO_4)_2(\mu,\eta^2\text{-}H_2PO_4)_2(H_2PO_4)_2](H_2O)_4$

Two novel dinuclear-based polynuclear and tetranuclear Cu(II) compounds with mixed $H_xPO_4^{(3-x)-}$ bridges (x = 1, 2), $[Cu_2(bpy)_2(\mu,\eta^2\text{-}HPO_4)(\mu,\eta^1\text{-}H_2PO_4)(\mu,\eta^2\text{-}H_2PO_4)]_n$ (**1**) and $[Cu_4(phen)_4(\mu_3,\eta^2\text{-}HPO_4)_2(\mu,\eta^2\text{-}H_2PO_4)_2(H_2PO_4)_2](H_2O)_4$ (**2**) have been synthesized and characterized as well as the magnetic properties discussed. Both Cu(II) ions in a dimeric unit in **1** are in a distorted square pyramidal environment and linked by $\mu,\eta^2\text{-}HPO_4$ and $\mu,\eta^1\text{-}H_2PO_4$ ligands. In case of **2**, each Cu(II) ion displays a distorted square-pyramidal geometry, with two $\mu_3,\eta^2\text{-}HPO_4$ groups and two $\mu,\eta^2\text{-}H_2PO_4$ groups bridging, and two non-bridging H_2PO_4 groups.

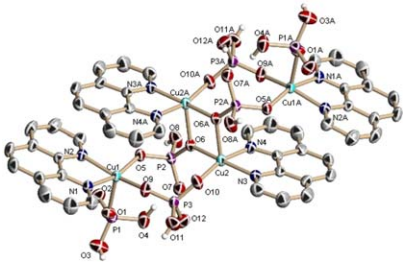

Fuh-An Yang, Kuan-Yu Cho, Jyh-Horung Chen, Shin-Shin Wang, Jo-Yu Tung, Hsi-Ying Hsieh, Feng-Ling Liao, Gene-Hsiang Lee, Lian-Pin Hwang, Shanmugam Elango

Polyhedron 25 (2006) 2207

Thallium complexes of tetraphenylporphyrin: Tl(tpp-*N*-O)(OAc) and *cis*-acetato-N-*p*-*tert*-butylbenzensulfonylimido-*meso*-tetraphenylporphyrinatothallium(III) Tl(N-*p*-$NSO_2C_6H_4$-^{t}Bu-tpp)(OAc)

The crystal structures of Tl(tpp-*N*-O)(OAc) (**3**) was determined and the coordination sphere around Tl^{3+} in **3** is described as a distorted square-based pyramid in which the apical site is occupied by a bidentate chelating OAc^- group.

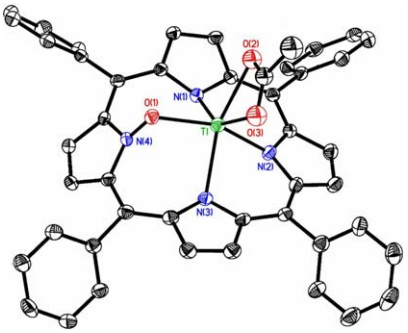

Elsevier Ltd.

Jean-Paul Cornard, Alexandra Caudron, Jean-Claude Merlin

Polyhedron 25 (2006) 2215

UV–visible and synchronous fluorescence spectroscopic investigations of the complexation of Al(III) with caffeic acid, in aqueous low acidic medium

The interactions between aluminium (III) ions and caffeic acid in aqueous solution, at pH 5 and 6.5 were investigated. The complexes were characterized by electronic absorption and synchronous fluorescence spectroscopies combined with chemometrics methods. The stoichiometry composition and stability constants of complexes have been determined.

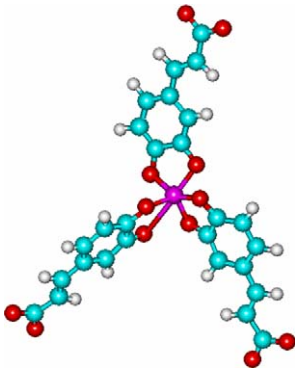

Duraiswamy Sukanya, Rathinasabapathi Prabhakaran, Karuppannan Natarajan

Polyhedron 25 (2006) 2223

Ruthenium(III) complexes of dipicolinic acid with PPh_3/$AsPh_3$ as co-ligand: Synthesis and structural characterization

New hexa-coordinated Ru(III) complexes of the type $[Ru(dipic)(EPh_3)_2X]$ have been synthesized by reacting 2,6-pyridinedicarboxylic acid (dipicolinic acid, H_2dipic) with the appropriate starting complexes $[RuX_3(EPh_3)_3]$ (where X = Cl, Br; E = P, As). The ligand behaves as tridentate dibasic chelate. Single-crystal X-ray analysis of the complex $[Ru(dipic)(PPh_3)_2Cl]$ revealed that the coordination environment around ruthenium metal consists of an NO_2P_2Cl octahedron with dipicolinic acid occupying equatorial plane.

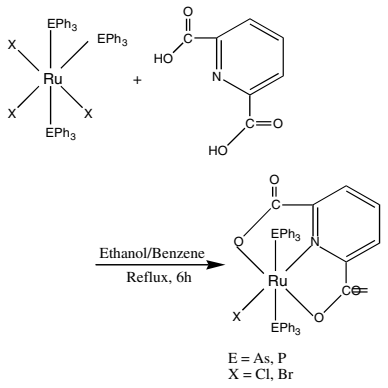

Georges Morgant, Nouzha Bouhmaida, Lamine Balde, Nour Eddine Ghermani, Jean d'Angelo

Polyhedron 25 (2006) 2229

Low-temperature (100 K) crystal structures of pentaaqua(5-nitrosalicylato) complexes of magnesium(II), zinc(II), cobalt(II) and nickel(II): A π–π stacked and hydrogen bonded 3D supramolecular architecture

Reactions of metal chloride or sulfate and the sodium salt of 5-nitrosalicylic acid (5-nsa) in aqueous solution result in isomorphous complexes of type $[M(H_2O)_5(5\text{-nsa})]^+$ $(5\text{-nsa})^- \cdot H_2O$ [M = Mg (**1**), Zn (**2**), Co (**3**), Ni (**4**)] in the solid state. The metal-bonded cationic moiety and the non-ligating anionic one are engaged in π-stacking interactions. The anchoring of the individual ionic subunits through π–π stacking and extensive hydrogen bonding results in a 3D supramolecular architecture.

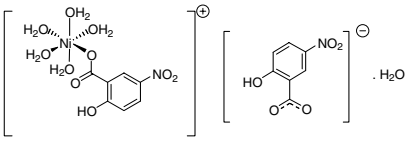

Gerard A. van Albada, Stefania Tanase, Aminou Mohamadou, Ilpo Mutikainen, Urho Turpeinen, Jan Reedijk

Polyhedron 25 (2006) 2236

Synthesis, structure and magnetism of two new polymeric double dicyanamido-bridged Mn(II) compounds

Two new 1D polymeric Mn(II) compounds with the general formula $[Mn(II)(dca)_2(L)_2]_n$ (L = C_2H_5OH and 2-aminopyrimidine, dca = dicyanamide) are reported. The Mn(II) ions in the polymeric compounds are connected via doubly bridged $\mu_{1,5}$-dca molecules.

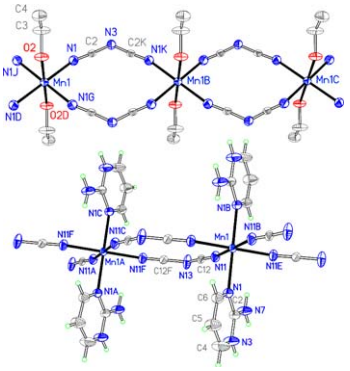

Shouvik Chattopadhyay, Mau Sinha Ray, Michael G.B. Drew, Albert Figuerola, Carmen Diaz, Ashutosh Ghosh

Polyhedron 25 (2006) 2241

Facile synthesis of Cu(II) complexes of mono-condensed N,N,N donor Schiff base ligands: Crystal structure, spectroscopic and magnetic properties

Four new copper(II) complexes of the general formula $CuLN_3ClO_4$, where L represents four similar tridentate N,N,N donor Schiff base ligands, have been synthesized in a very convenient way and structurally characterized. Two of the complexes consist of double basal–apical end-on (EO) azide bridged dinuclear Cu^{II} complexes and are antiferromagnetically coupled through the azido bridges. The third one is a perchlorate bridged one-dimensional Cu^{II} chain; two such chains are connected by hydrogen bonds. It shows two different magnetic interactions through the two kinds of hydrogen bonds; one is antiferromagnetic and the other is ferromagnetic. The fourth compound consists of 1-D chains in which the Cu^{II} ions are alternately bridged by single EO and end-to-end (EE) azido ligands. From a magnetic point of view it is a ferromagnetic dinuclear complex coupled through the EO bridge only.

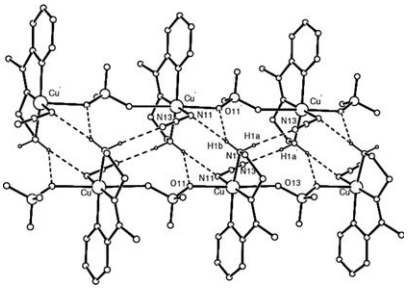

V.T. Getova, R.P. Bontchev, D.R. Mehandjiev, P.R. Bontchev

Polyhedron 25 (2006) 2254

Complexes of 1-[2-[2-hydroxy-3-(propylamino)propoxy]phenyl]-3-phenyl-1-propanone (propafenone) with copper(II): Crystal structure of the mononuclear Cu(II) complex with propafenone

Two new copper(II) complexes – mono- and binuclear ones, of the aminoalcohol drug propafenone were synthesized and studied by spectral (UV–Vis, IR, EPR, NMR), thermogravimetric and magnetochemical methods. The structure of the mononuclear complex was determined using X-ray diffraction of monocrystals.

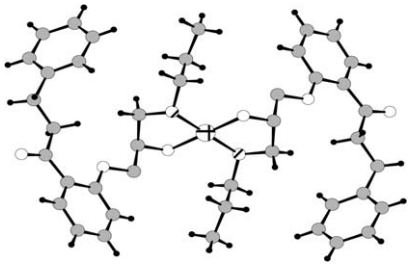

Vladimira Videva, Tania Tosheva, Anne-Sophie Chauvin, Stoycho Shenkov, Rosica Petrova, Rosario Scopelliti, Emil Tashev, Sabi Varbanov, Mariana Mitewa

Polyhedron 25 (2006) 2261

Phosphoamide – modified *p-tert*-butyl calix[4]-arene and its sodium complexes. Synthesis, coordination ability and structure

The X-ray structure of the complex $[Na_2L_2](ClO_4)_2 \cdot 4CH_3OH$ comprises of 2 calix[4]arene ligands, $2Na^+$, $2(ClO_4)^-$ and $4CH_3OH$. Each of the calix[4]arene ligands participate in the complex, being bonded to Na^+ by only one of the P=O groups. Both Na^+ cations are placed outside of the ligand cavities. Each cation is coordinated to one ClO_4^- (Na^+ is directly bonded to one oxygen of the perchlorate), one terminal and two bridging CH_3OH molecules.

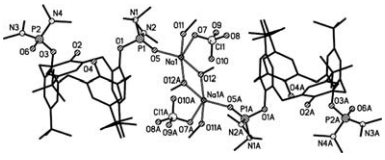

Sandip Banthia, Anunay Samanta

Polyhedron 25 (2006) 2269

Synthesis and structure of unusually stable linear copper(I) complexes with blue fluorescence

A two-coordinate linear complex of copper(I) based on the fluorescent 4-aminophthalimide platform has been synthesized by the in situ reduction of copper(II). This complex, which has been characterized by X-ray crystallography, reveals weak Cu···O interactions and strong intermolecular hydrogen bonding leading to interesting structural features and unusual stability towards oxidation both in the solid state as well as in coordinating or protic solvents.

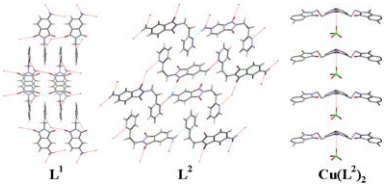

Juan Granifo, María T. Garland, Ricardo Baggio

Polyhedron 25 (2006) 2277

The effect in the assembly and node nuclearity of the long and rigid character of bis-pyridyl *exo*-bidentate spacers when react with zinc acetate: Crystal structures of the high nuclearity coordination polymers $[Zn_7(\mu_4\text{-}O)_2(OAc)_{10}(3pdb)]_n$ (3pdb = 1,4-bis(3-pyridyl)-2,3-diaza-1,3-butadiene) and $[Zn_7(\mu_4\text{-}O)_2(OAc)_{10}(4pdb)]_n$ (4pdb = 1,4-bis(4-pyridyl)-2,3-diaza-1,3-butadiene)

Two new coordination polymers $[Zn_7(\mu_4\text{-}O)_2(OAc)_{10}(3pdb)]_n$ (3pdb = 1,4-bis(3-pyridyl)-2,3-diaza-1,3-butadiene) and $[Zn_7(\mu_4\text{-}O)_2(OAc)_{10}(4pdb)]_n$ (4pdb = 1,4-bis(4-pyridyl)-2,3-diaza-1,3-butadiene) have been isolated which contain heptanuclear cluster as nodes.

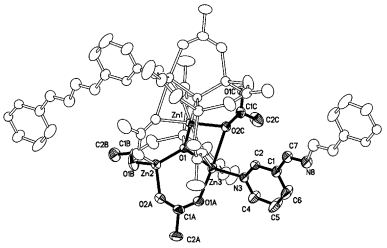

Sumana Sarkar, Amrita Mondal, Atanu Banerjee, Deepak Chopra, Joan Ribas, Kajal Krishna Rajak

Polyhedron 25 (2006) 2284

Binuclear $\mu_{1,1}$-N_3 and O–H···O bridged nickel(II) complex with a N_3O chelating agent: Synthesis, structure and magnetic properties

The reaction of $Ni(ClO_4)_2 \cdot 6H_2O$ with a NNNO-coordinating tripodal ligand in methanol in the presence of excess sodium azide afforded a $\mu_{1,1}$-N_3 bridged binuclear nickel(II) complex in excellent yield. Variable temperature magnetic susceptibility measurements confirm the ferromagnetic behavior in the solid state.

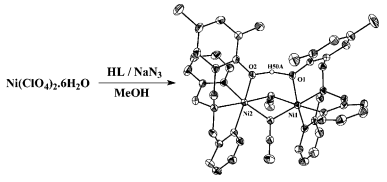

Samir Das, Bikash Kumar Panda

Polyhedron 25 (2006) 2289

Synthesis and structure of luminescent $Re^I(CO)_3Cl$ complexes incorporating pyridyltriazine, pyrazinyltriazine and triazolopyridine chelation

The reaction of $Re^I(CO)_5Cl$ with pyridyltriazine (L^1), pyrazinyltriazine (L^2) and triazolopyridine (L^3) (general abbreviation L) has furnished complexes of the type $Re^I(CO)_3Cl(L)$, **A**, in excellent yield. The X-ray structures of complexes incorporating the L^1 and L^3 ligands have been determined. The tricarbonylrhenium(I) complex of the triazolopyridine ligand is strongly fluorescent (**A**) whereas complexes with pyridyltriazine and pyrazinyltriazine ligands exhibit weak fluorescence in solution.

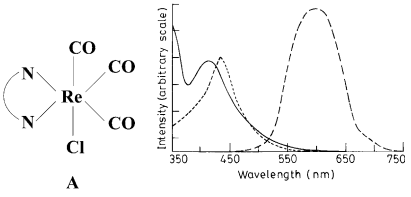

Angel García-Raso, Juan J. Fiol, Adela López-Zafra, Andrés Tasada, Ignasi Mata, Enrique Espinosa, Elies Molins

Polyhedron 25 (2006) 2295

Different ways of interaction between binary copper(II)-Schiff bases (Cu–N-salicylideneserinato) and pyrimidine derivatives

Five ternary complexes of Cu(II)–(N-salicylideneserinato) with different pyrimidine ligands have been prepared and the crystal structures determined. Different ways of interaction between binary copper(II)–N-salicylideneserinato and cytosine or isocytosine derivatives have found. Cytosine derivatives interact via N(3), isocytosine yields a N(1) complex and the 6-aminoisocytosine ligand is coordinated via the exocyclic oxygen O(4).

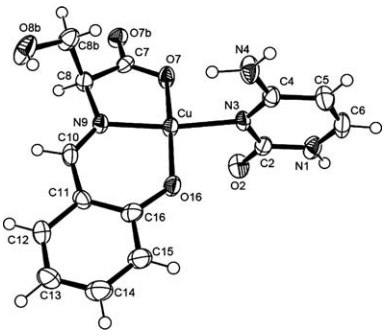

Dawn M. Wong, Stephen J. Simpson

Polyhedron 25 (2006) 2303

Preparation of the chiral amine salts $[(\eta^5\text{-}C_5H_5)Ru(PPh_3)(CN^tBu)(NH_2R)]PF_6$, RNH_2 = α-methylbenzylamine, 1-cyclohexylethylamine, and 1-(1-naphthyl)ethylamine: X-ray single crystal structures of the diastereomeric salts $(S_{Ru}R_C)$- and $(R_{Ru}R_C)$-$[(\eta^5\text{-}C_5H_5)Ru(PPh_3)(CN^tBu)\{NH_2CH(Me)(Ph)\}]PF_6$

The structure of diastereomeric salts containing a chiral amine and a metal centre has been investigated by single crystal X-ray crystallography and by observing diamagnetic anisotropy effects in NMR spectroscopy. Attempts to remove the amine ligand to produce homochiral at metal products are reported.

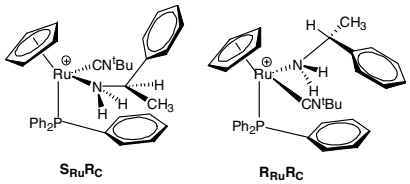

Kyoung-Tae Youm, Hyuk Chae Kang, Gun-bong Lee, Hyun Kyung Woo, Young Jun Park, Nam-kyu Lee, Jaejung Ko, Moo-Jin Jun

Polyhedron 25 (2006) 2318

Anion-templating self-assembly of $[Cu_2(OMe)_2]^{2+}$ SBUs depending on the size of the anion in the solid state

The $[Cu_2(OMe)_2]^{2+}$ secondary building units (SBUs) are self-assembled into 3D cages or an infinite 1D coordination polymer depending on whether the counter-anion exerts a size-templating effect or not. Small anions of $[BF_4]^-$ and $[ClO_4]^-$ make two SBUs interconnect each other with four btp (=2,6-bis(*N*1-1,2,4-triazolyl)pyridine), leading the anion-encapsulated 3D cages. Meanwhile the triflate anion ($[OTf]^-$) does not induce a cage structure, leading instead to an infinite 1D coordination polymer.

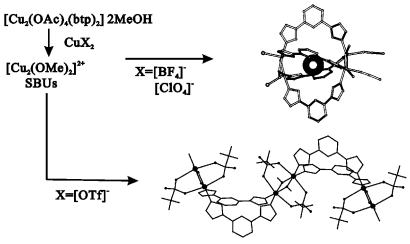

Maw-Cherng Suen, Zhi-Kai Chan, Jhy-Der Chen, Ju-Chun Wang, Chen-Hsiung Hung

Polyhedron 25 (2006) 2325

Syntheses and structures of three new coordination polymers generated from the flexible 1,3-bis(4-pyridyl)propane ligand and zinc salts

The synthesis and structures of three new coordination polymers, $[Zn_7(O_2CCH_3)_{10}(\mu_4\text{-}O_2)(bpp)\cdot 4H_2O]_n$ (bpp = 1,3-bis(4-pyridyl)-propane) (**1**), $[Zn(SiF_6)(bpp)_2\cdot 4H_2O\cdot 2CH_3\text{-}OH]_n$ (**2**), and $[Zn(bpp)(SO_4)\cdot CH_3OH]_n$ (**3**), are reported.Complex **1** exhibits heptanuclear clusters which are bridged by the bpp ligands to form 1-D zig–zag chains, while complexes **2** and **3** show 2-D grid and 3-D porous structures.

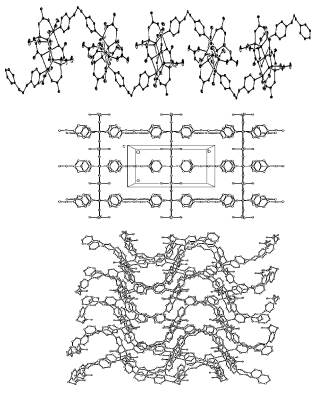

D. Das, B.G. Chand, K.K. Sarker, J. Dinda, C. Sinha

Polyhedron 25 (2006) 2333

Zn(II)-azide complexes of diimine and azoimine functions: Synthesis, spectra and X-ray structures

Two series of Zn(II)-azido complexes of diimine (—N=C—C=N—) and azoimine (—N=N—C=N—) are described. The ligands belong to α/β-naphthyl-(2-pyridylmethylene)-amine (diimine) and 1-alkyl-2-(naphthyl-α/β-azo)imidazoles (azoimine). The complexes are structurally characterized. The diimine system has end-on azido bridged ligands and the azoimine system gives terminal azido bridged complexes. They exhibit high intense ligand centered emissions.

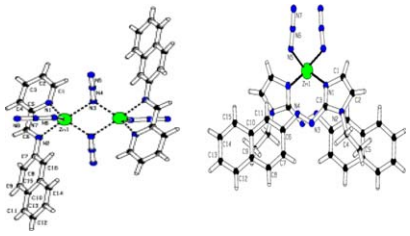

Eric W. Ainscough, Andrew M. Brodie, Craig V. Depree, Carl A. Otter

Polyhedron 25 (2006) 2341

Divalent cobalt, nickel and zinc halide complexes with multimodal ligands based on the cyclotriphosphazene platform: A structural study

The reaction of the divalent halides of cobalt, nickel and zinc with two cyclotriphosphazenes with pyridyloxy pendant arms affords a rich variety of mono- and dimetallic complexes which have been characterised by X-ray crystallography.

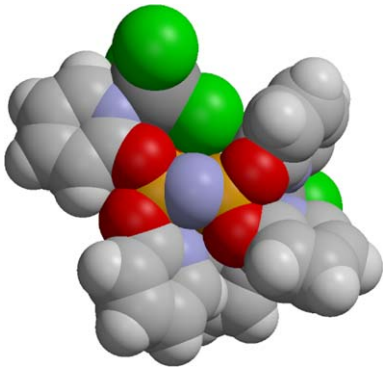

The Publisher encourages the submission of articles in electronic form thus saving time and avoiding rekeying errors. For detailed instructions on the preparation of manuscripts and of electronic artwork, consult the Author Gateway for Elsevier at http://authors.elsevier.com

SCIENCE DIRECT®

Full text of this journal is available, on-line from **ScienceDirect**. Visit **www.sciencedirect.com** for more information.

Available online at www.sciencedirect.com
SCIENCE DIRECT®
Polyhedron 25, issue 9, 19 June 2006
POLYHEDRON
www.elsevier.com/locate/poly

Contents

Papers

Xia Zhu, Hai-Yan Ge, Yu-Mei Zhang, Bao-Long Li, Yong Zhang

Polyhedron 25 (2006) 1875

Self-assembly of five cobalt(II) coordination polymers from 1,2-bis(1,2,4-triazol-1-yl)ethane

There are three motifs (2D (4,4) network, single chain and double-stranded chain) in five complexes: 2D (4,4) network (**1**), single chain (**2**), double-stranded chain (**3** and **4**), and a combination of two motifs (single chain + double-stranded chain) (**5**).

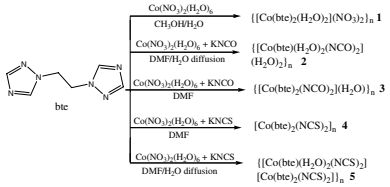

P. Lubal, J. Maleček, P. Hermann, J. Kotek, J. Havel

Polyhedron 25 (2006) 1884

Capillary electrophoretic separation and kinetic study of inert copper(II) complexes of 1,8-bis(methylphosphonate) derivative of cyclam

Pentacoodinated *pc*-$[Cu(L)]^{2-}$ and octahedral *hx*-$[Cu(L)]^{2-}$ complexes and the free ligand dianion $(H_2L)^{2-}$ were successfully separated by means of CE. The method was used for evaluation of isomerization kinetics of the pentacoordinated isomer to the octahedral species. The isomerization was proved to be a highly energetically inconvenient process.

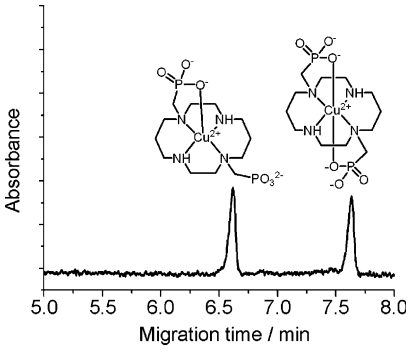

Ali Akbar Khandar, Behrouz Shaabani, Ferdinand Belaj, Akbar Bakhtiari

Polyhedron 25 (2006) 1893

Synthesis, characterization and spectroscopic and electrochemical studies of new axially coordinated cobalt(III) salen (salen=*N*,*N*′-bis-(salicylidene)-1,2-ethylenediamine) complexes. The crystal structure of $[Co^{III}(salen)(aniline)_2]$-$ClO_4$

Cobalt(III) complexes with some potentially tetradentate salen Schiff-bases as equatorial ligands and with different axial amine ligands were synthesized in situ and characterized by IR, ^1H NMR and elemental analysis. Electronic structure calculations indicate metal–ligand charge transfer transitions between 420 and 440 nm. The cyclic voltammetry of the complexes show that the axial amine ligands affect reduction potentials of Co(III) in the order of changes of their pK_a. In the crystal structure of $[Co(salen)(aniline)_2]ClO_4$ cobalt(III) center is six coordinated surrounded by an equatorial tetradentate salen ligand and two aniline axial ligands and ClO_4^- acts as a counter ion.

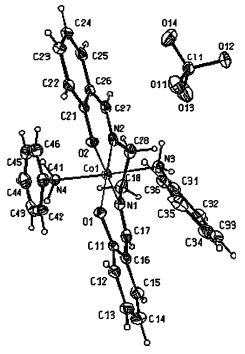

Ewan J.M. Hamilton, Jianping Liu, Edward A. Meyers

Polyhedron 25 (2006) 1901

The reactions of *arachno*-$[B_9H_{14}]^-$ and *nido*-$[B_9H_{12}]^-$ with acids: Preparation and structures of chlorononaborates

The unidentified product from the hydride abstraction reaction between $[B_9H_{14}]^-$ and BCl_3 that produces $B_{10}H_{14}$, $[HBCl_3]^-$, and H_2 was previously thought to possess a polymeric structure, but has been shown to consist of a mixture of singly-, doubly- and triply-chlorinated analogues of *arachno*-$[B_9H_{14}]^-$. X-ray diffraction analyses indicate that these species co-crystallize in the solid state. These problems of disorder prompted us to prepare the analogous singly-substituted cluster $[B_9H_{13}Cl]^-$ by a different route. This species was obtained from the reaction between *nido*-$[B_9H_{12}]^-$ and anhydrous HCl, and its structure was also determined by X-ray analysis.

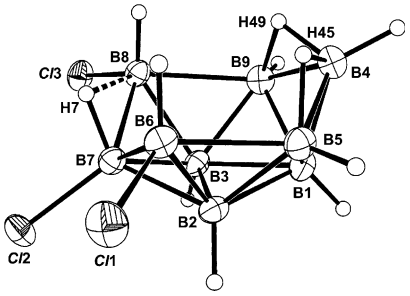

Zhao-Hui Zhou, Jing Lin, Wen-Bin Yan, Hui Zhang, Khi-Rui Tsai

Polyhedron 25 (2006) 1909

pH dependent transformation of nitrilotriacetato molybdates (VI) – Synthesis, spectral and structural characterization

Very strong hydrogen bonds are found to exist in two hydrogen nitrilotriacetato molybdates (VI), which obviously decompose into the free ligand, based on ^{13}C NMR observations.

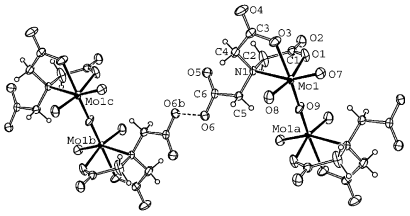

Zolfaghar Rezvani, Baharak Divband, Amir Reza Abbasi, Kamellia Nejati

Polyhedron 25 (2006) 1915

Liquid crystalline properties of copper(II) complexes derived from azo-containing salicylaldimine ligands

Bis[5-((4-*n*alkoxyphenyl)azo)-*N*-ethanol salicylaldiminato]copper(II) complex homologues have been synthesized. The liquid crystalline character of these complexes has been examined by using differential scanning calorimetry (DSC) and a polarizing microscope equipped with a heating and cooling stage. All complexes form the enantioptropic Smectic C mesophase.

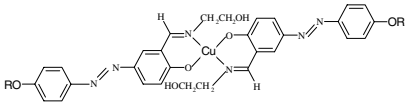

R. Khoshnavazi, H. Eshtiagh-hossieni, M.H. Alizadeh, M.T. Pope

Polyhedron 25 (2006) 1921

Syntheses and structures determination of new polytungstoarsenates $[Na_2As_2W_{18}U_2O_{72}]^{12-}$ and $[MAs_2W_{18}U_2O_{72}]^{13-}$ ($M = NH_4^+$ and K^+)

New sandwiched type tungstoarsenates of $[Na_2As_2W_{18}U_2O_{72}]^{12-}$ and $[MAs_2W_{18}U_2O_{72}]^{13-}$ ($M = NH_4^+, K^+$) have been synthesized by the self-assembly reaction of tungstate, arsenate and uranyl ions in a stoichiometric ratio and characterized by spectroscopy tools and single crystal structure analysis.

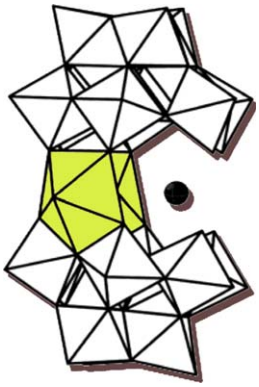

Matthew S. Thorum, Konstantin I. Pokhodnya, Joel S. Miller

Polyhedron 25 (2006) 1927

Solvent enhancement of the magnetic ordering temperature (T_c) of the room temperature V[TCNE]$_x$ · S (S = solvent, TCNE = tetracyanoethylene; $x \sim 2$) magnet

The reaction of TCNE and $V(CO)_6$ and several solvents (S) form an immediate black precipitate of V(TCNE)$_x$ · yS (S = solvent; $x \sim 2$; $y \sim 0.5$), which have a magnetic ordering onset temperature in the range of 385–390 K. When S = $PhCF_3$ in addition to the onset temperature being enhanced it exhibits greater thermal stability.

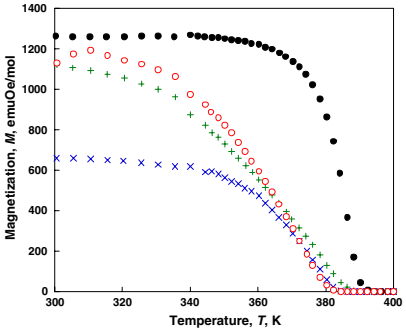

Varughese Philip, V. Suni, Maliyeckal R. Prathapachandra Kurup, Munirathinam Nethaji

Polyhedron 25 (2006) 1931

Copper(II) complexes derived from di-2-pyridyl ketone *N*(4),*N*(4)-(butane-1,4-diyl)-thiosemicarbazone: Crystal structure and spectral studies

Neutral copper(II) complexes with a tetradentate NNNS Schiff base have been synthesized using the ligand, di-2-pyridyl ketone *N*(4),*N*(4)-(butane-1,4-diyl)thiosemicarbazone (HL). A series of five binuclear complexes of HL with the general stoichiometry *CuLX* [*X* = Cl (**1**), Br (**2**), NO_3 (**3**), N_3 (**4**) and SCN (**5**)], a dinuclear complex [$Cu_2L^1Cl_3$] (**6**) with copper(II) chloride, and a tetranuclear complex [$Cu_4L^1_4(SO_4)_2$] (**7**) with copper(II) sulfate were also synthesized. The crystal structure of [$Cu_2L_2(SO_4)$] · $3H_2O$ has been determined by X-ray diffraction studies. Crystal analysis shows that the complex is tetranuclear with five coordinated copper centers.

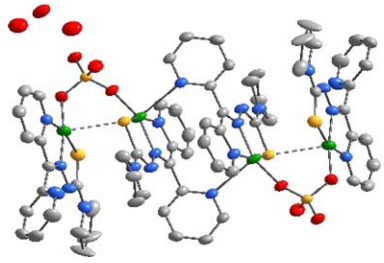

Pulak K. Dhara, Michael G.B. Drew, Pabitra Chattopadhyay

Polyhedron 25 (2006) 1939

Ruthenium (III) complexes of tetradentate NSNO pyridylthioazophenolates: Synthesis, spectral studies, crystal structure and redox properties

A family of monomeric low-spin octahedral ruthenium (III) complexes of tetradentate monobasic NSNO donor chelators (HL) have been synthesized and isolated in their pure form. Dark brown colored *trans*-dichloro and *cis*-dichloro ruthenium (III) complexes of pyridylthioazophenolates, having the general formula [Ru(L)Cl_2], were separated chromatographically. The structure of one of the complexes, *trans*-[Ru(L1)Cl_2] (**2a**), has been confirmed by single-crystal X-ray analysis. The reactivity of the *cis*-[Ru(L)Cl_2] complexes (**1**) with the bidentate bipyridyl ligand in the presence of $AgNO_3$ produces [Ru(L)(bpy)$_2$](PF_6)$_2$ (**3**).

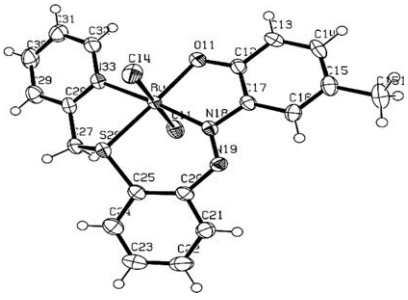

Carl Redshaw, Simon M. Humphrey

Polyhedron 25 (2006) 1946

Complexes of tungsten(IV,VI) derived from linked aryloxide ligands

A series of tungsten complexes containing either bi- or tridentate aryloxides have been prepared and characterized. Six of these complexes have been the subject of single crystal X-ray diffraction studies.

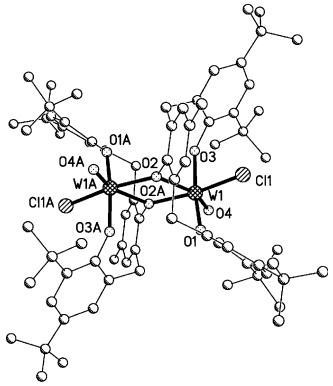

W. Gregory Jackson

Polyhedron 25 (2006) 1955

Classic coordination complexes: The kinetics and stereochemistry of acid hydrolysis of *cis*- and *trans*-$[Co(NH_3)_4Cl_2]^+$

Through the isolation of pure *trans*- and *cis*-$[Co(NH_3)_4(OH_2)Cl]^{2+}$, the steric course of acid hydrolysis of the classic Werner complexes has been determined spectrophotometrically and confirmed by a ^1H NMR study; the $[Co(NH_3)_4(OH_2)Cl]^{2+}$ equilibrium is 88% *cis* and 12% *trans* isomer.

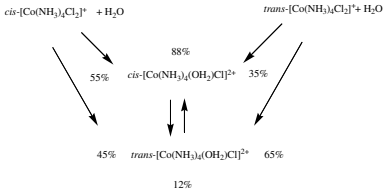

Mehdi Amirnasr, Aliakbar Dehno Khalaji, Larry R. Falvello, Tatiana Soler

Polyhedron 25 (2006) 1967

Synthesis, characterization, and crystal structures of $[Ag(ca_2en)(PPh_3)(X)]$ (X = N_3, SCN) complexes

The synthesis and characterization of two Ag(I) complexes with the Schiff base ligand ca_2en are reported. The crystal and molecular structures of $[Ag(ca_2en)(PPh_3)(X)]$ (X = N3 (**1**), SCN (**2**)) were determined by X-ray crystallography from single crystal data. The coordination polyhedron about the silver(I) center is best described as a distorted tetrahedron. Unlike its copper analogue, the SCN is coordinated through the S atom in (**2**).

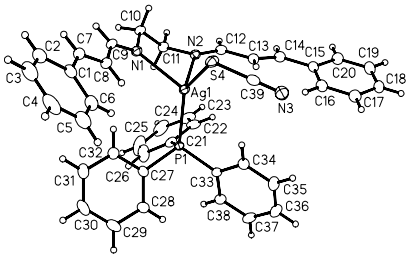

Christian G. Hartinger, Maria G. Ferri-Mendoza, Alexey A. Nazarov, Bernhard K. Keppler

Polyhedron 25 (2006) 1971

Electrospray ionization mass spectrometric study on the coordination behavior of dacarbazine towards transition metal ions

The complexation properties of the antitumor drug dacarbazine were studied by comparison of electrospray ionization mass spectra of isolated transition metal complexes and in situ-formed ones.

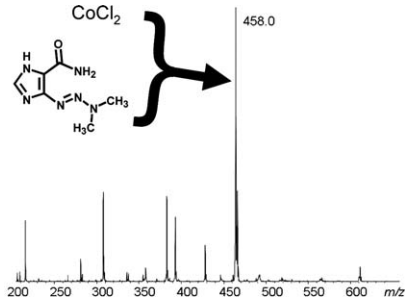

Marco Bortoluzzi, Giuliano Annibale, Giampaolo Marangoni, Gino Paolucci, Bruno Pitteri

Polyhedron 25 (2006) 1979

^{31}P NMR and DFT studies on square-planar bis(diphenylphosphinoethyl)phenylphosphine (triphos) complexes of Pt(II) with pyridines and anilines

The complexes $[Pt(triphos)(4\text{-R-py})](ClO_4)_2$ and $[Pt(triphos)(4\text{-R-an})](ClO_4)_2$ {4-R-py = *para*-substituted pyridines; 4-R-an = *para*-substituted anilines} were prepared starting from $[PtCl(triphos)]ClO_4$. The correlations between the pK_a of the pyridines and anilines and the $^1J_{Pt-P}$ couplings of the complexes are pointed out and informations about the structural and electronic properties of some of these derivatives, obtained with DFT calculations, are reported.

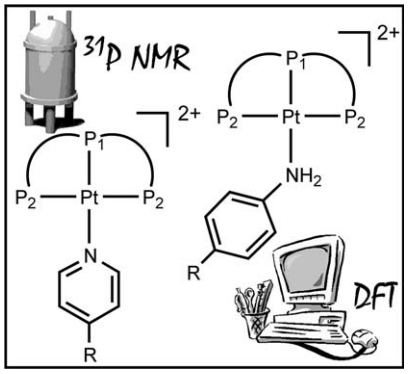

B. Machura, R. Kruszynski

Polyhedron 25 (2006) 1985

Synthesis, crystal, molecular and electronic structure of the $[Re(NO)Cl_2(PPh_3)(PPh_2py\text{-}P,N)]$ complex

The reaction of the $[ReCl_3(NO)(PPh_3)(OPPh_3)]$ complex with diphenyl(2-pyridyl)phosphine (PPh_2py) has been examined and a novel $\{ReNO\}^6$ rhenium nitrosyl – $[Re(NO)Cl_2(PPh_3)(PPh_2py\text{-}P,N)]$ has been obtained. The compound has been studied by IR, UV–Vis spectroscopy and X-ray crystallography. The molecular orbital diagram of $[Re(NO)Cl_2(PPh_3)(PPh_2py\text{-}P,N)]$ has been calculated with the density functional theory (DFT) method. The spin-allowed singlet–singlet electronic transitions of $[Re(NO)Cl_2(PPh_3)(PPh_2py\text{-}P,N)]$ have been calculated with the time-dependent DFT method, and the UV–Vis spectrum of the title compound has been discussed on this basis.

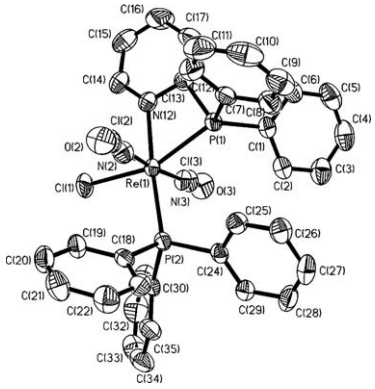

Radosław Starosta, Florian P. Pruchnik, Zbigniew Ciunik

Polyhedron 25 (2006) 1994

Carboxylatodirhodium(II) complexes with orthometallated tris(*p*-methoxyphenyl)phosphine and their reactions with pyrazole and imidazole

Exchange reactions of the acetato bridges in $[cis\text{-}Rh_2(\mu\text{-}OAc)_2\{\mu\text{-}(C_6H_3\text{-}4\text{-}OMe)P(C_6H_4\text{-}4\text{-}OMe)_2\}_2(HOAc)_2]$ give the new complexes: $[cis\text{-}Rh_2(\mu\text{-}O_2CCF_3)_2\{\mu\text{-}(C_6H_3\text{-}4\text{-}OMe)P(C_6H_4\text{-}4\text{-}OMe)_2\}_2(HO_2CCF_3)_2]$ and $[cis\text{-}Rh_2(\mu\text{-}O_2CCH_2CH_3)_2\{\mu\text{-}(C_6H_3\text{-}4\text{-}OMe)P(C_6H_4\text{-}4\text{-}OMe)_2\}_2(HO_2CCH_2CH_3)_2]\cdot HO_2CCH_2CH_3$. Molecular structures of these complexes were established spectroscopically and with X-ray methods. Reactions of all complexes with pyrazole and imidazole were investigated spectroscopically. X-ray structures of $[cis\text{-}Rh_2(\mu\text{-}O_2CCF_3)_2\{\mu\text{-}(C_6H_3\text{-}4\text{-}OMe)P(C_6H_4\text{-}4\text{-}OMe)_2\}_2(Hpz)_2]$ and $[cis\text{-}Rh_2(\mu\text{-}O_2CCH_2CH_3)_2\{\mu\text{-}(C_6H_3\text{-}4\text{-}OMe)P(C_6H_4\text{-}4\text{-}OMe)_2\}_2(Hpz)_2]$ have been determined.

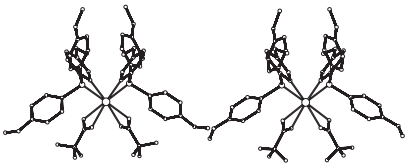

Malabika Nayak, Parimal Kundu, Pascale Lemoine, Rajesh Koner, Ho-Hsiang Wei, Sasankasekhar Mohanta

Polyhedron 25 (2006) 2007

Crystal engineering and magnetic properties of a 2D cyano-bridged $Ni^{II}Fe^{II}$ network formed through reduction of ferricyanide

Reaction of potassium ferricyanide with a mixture of nickel(II) chloride and *trans*-1,2-diaminocyclohexane (L) produces both a ferrocyanide ($[Ni^{II}L_2]_2[Fe^{II}(CN)_6]\cdot 5H_2O$ (**1**)) and a ferricyanide ($[Ni^{II}(L)_2]_3[Fe^{III}\text{-}(CN)_6]_2\cdot 2H_2O$ (**2**)) compound. From spectrophotometric titration, it has been established that the diamine is responsible for the reduction of ferricyanide to ferrocyanide. The factors that affect the formation of the two compounds as well as crystal engineering and magnetic properties of the ferrocyanide analogue, **1**, have been described. The structure of **1** consists of a two-dimensional cyano-bridged square grid network which is self-assembled into three-dimensions due to hydrogen bonding interactions.

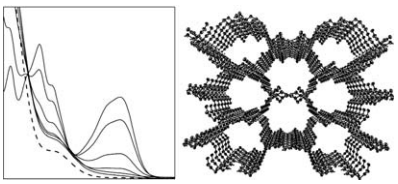

Nebebech Belai, Michael T. Pope

Polyhedron 25 (2006) 2015

Synthesis and structural characterization of new organotin derivatives of polyoxotungstates via transmetallation and coupling reactions

Insertion of $\{RSn\}^{3+}$ into polyoxoytungstate structures by displacement of transition metal centers has been demonstrated with the chiral Tourné–Zonnevijlle anions and with $[Ce(W_5O_{18})_2]^{9-}$. Robust coupling of polyoxotungstates is achieved by the use of $\{Sn(CH_2)_nSn\}^{6+}$ as linkers.

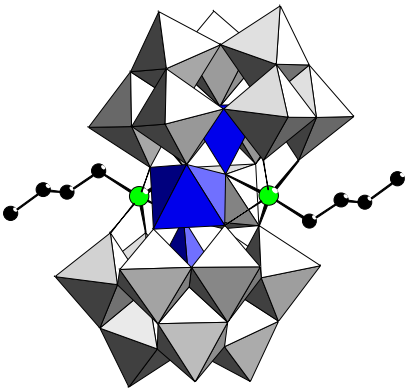

José António Paixão, Manuela Ramos Silva, Ana Matos Beja, Ermelinda Eusébio

Polyhedron 25 (2006) 2021

Crystal structure and properties of L-tryptophanium hydrogen selenite

Structure characterisation of L-tryptophanium hydrogen selenite at low and room temperature. A disordered hydrogen atom shared between the carboxylic group of the cation and one of the oxygen atoms of the anion is found to order at low temperature.

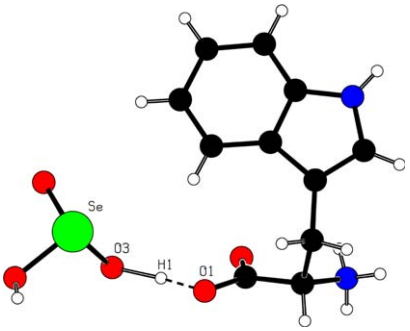

V. Paredes-García, D. Venegas-Yazigi, R.O. Latorre, E. Spodine

Polyhedron 25 (2006) 2026

Electronic properties of mixed valence iron(II,III) dinuclear complexes with carboxylate bridges

Two mixed valence dinuclear iron(II,III) complexes with carboxylate bridges of the type $[Fe_2L_2(H_2O)_4](NO_3)(H_2O)_3$, where L = Schiff base derived from an α-amino acid (glycine or L-isoleucine) and 5-bromosalicylaldehyde have been prepared and characterised by different spectroscopic techniques, magnetic susceptibility, conductivity, and electrochemical measurements. The existence of the mixed valence species was corroborated by Mössbauer spectroscopy and electrochemical measurements. Temperature dependence of the reciprocal molar susceptibility indicates a weakly antiferromagnetically coupled system ($-J \sim 0.17$ and 0.14 cm^{-1}). The conproportionation constant values, at 298 K, are approximately 3.7×10^4 and 5.4×10^4. The obtained values are in agreement with a moderate electron coupling between the redox sites.

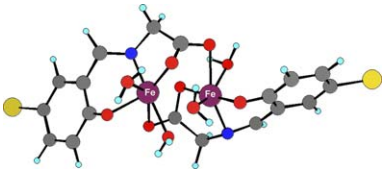

D.R. Whitcomb, M. Rajeswaran

Polyhedron 25 (2006) 2033

The first silver catechol complexes: Crystal structures of triphenylphosphine stabilized silver tetra-bromo and tetra-chloro-catechols

The solid-state structures of the first verifiable silver complexes containing bound catechol ligands, $Ag(Br_4C_6(OH)O)(Ph_3P)_2$ and $Ag(Cl_4C_6(OH)O)(Ph_3P)_2$, are reported. In both complexes, only one of the catechol oxygens is coordinated to the silver along with the *ortho*-halogen, which forms the chelate ring with the metal. Additional hydrogen bonding is observed between the catechol groups to form a dimeric species in the solid state.

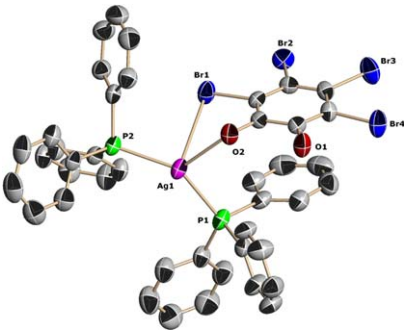

The Publisher encourages the submission of articles in electronic form thus saving time and avoiding rekeying errors. For detailed instructions on the preparation of manuscripts and of electronic artwork, consult the Author Gateway for Elsevier at http://authors.elsevier.com

SCIENCE DIRECT®

Full text of this journal is available, on-line from **ScienceDirect**. Visit **www.sciencedirect.com** for more information.

Available online at www.sciencedirect.com
SCIENCE DIRECT®
Polyhedron 25, issue 3, 13 February 2006
POLYHEDRON
www.elsevier.com/locate/poly

Contents

Papers

S.K. Chawla, M. Arora, K. Nättinen, K. Rissanen

Polyhedron 25 (2006) 627

Unique copper ion catalyzed hydrolytic cleavage of C–N(2) bond of thiosemicarbazide

An unusual hydrolysis of C–N(2) bond of thiosemicarbazide is reported by $[Cu(2,2'\text{-bpy})X_2] \cdot xH_2O$ and $[Cu(\phi_3P)_2(CH_3CN)_2]ClO_4$ complexes. Thiocyanate, the hydrolytic product coordinates to Cu ion, $[Cu(2,2'\text{-bpy})(NCS)_2]$ and $[Cu(\phi_3P)_2(NCS)]_2$ are formed, respectively.

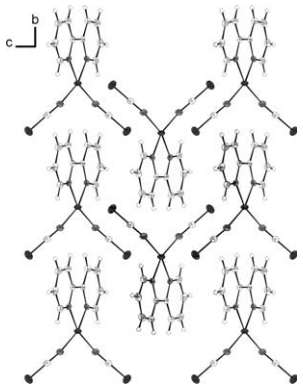

Shu-Mei Yue, Hong-Bin Xu, Jian-Fang Ma, Zhong-Min Su, Yu-He Kan, Heng-Jun Zhang

Polyhedron 25 (2006) 635

Design and syntheses of blue luminescent zinc(II) and cadmium(II) complexes with bidentate or tridentate pyridyl-imidazole ligands

A series of luminescent Zn(II) and Cd(II) complexes have been prepared based on three differently π-conjugated ligands, 2-(2-pyridyl)-imidazole (HL1), 2-(2-pyridyl)-benzimidazole (HL2) and 2,6-bis(benzimidazol-2yl)-pyridine (H_2L3). The spectra of the complexes with the ligands show the same rule. The structures of $Zn(L2)_2 \cdot H_2O$, $[Cd(L2)_2 \cdot (H_2O)_2] \cdot 2DMSO$, $Zn(HL2)_2$ and $Cd(HL3)_2$ have been established by X-ray crystallography. They display a blue luminescence and have high luminescence quantum efficiency. A theoretical study is consistent with the experimental results.

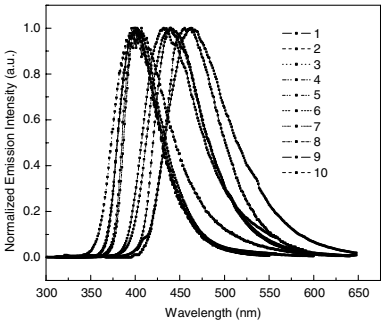

Doyel Bose, Sk Hafijur Rahaman, Rajarshi Ghosh, Golam Mostafa, Joan Ribas, Chen-Hsiung Hung, Barindra K. Ghosh

Polyhedron 25 (2006) 645

Architectures in two crystalline homo and hetero two-dimensional polymers of the type $[Cd_3(tren)_2(NCS)_6]_n$ and $[Ni_2Cd(tren)_2(NCS)_6]_n$ [tren = Tris(2-aminoethyl)amine] through molecular ion bridges

2D polymeric networks in homonuclear $[Cd_3(tren)_2(NCS)_6]_n$ and heteronuclear $[Ni_2Cd(tren)_2(NCS)_6]_n$ containing $[Cd(NCS)_6]^{4-}$ as a molecular ion bridge and a M(II) (M = Cd or Ni) malleable template, and the orientation of the tripod in the crystalline state controlling hydrogen bonding in the superstructures are described.

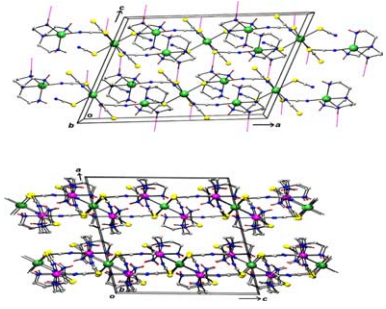

Amit K. Jain, Anjali Gupta, Rakesh Bohra, Ingo-Peter Lorenz, Peter Mayer

Polyhedron 25 (2006) 654

Synthesis and molecular elucidation of some novel aluminium(III) complexes with Schiff bases: Crystal and molecular structure of $[Al\{O(C_6H_4)CH{=}NC_6H_5\}_2\{HO(C_6H_4)CH{=}NC_6H_5\}_2]Br$

Reaction of $Et_3Al \cdot Et_2O/Et_2AlBr$ with bidentate Schiff base ligands (LH) in different molar ratios yield Et_2AlL, $EtAlL_2$ and $[Al\{O(C_6H_4)CH{=}NC_6H_5\}_2\{HO(C_6H_4)CH{=}NC_6H_5\}_2]Br$ (**9**). These are characterized by elemental analyses, FAB mass, IR and NMR spectral studies. The crystal structure of **9**, indicates the presence of hexa coordination around central aluminium(III) atom.

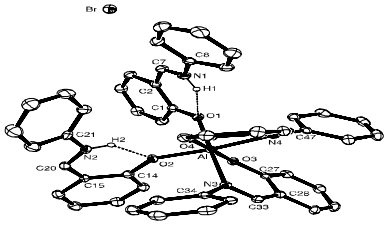

Doyel Bose, Golam Mostafa, Rosa D. Bailey Walsh, Michael J. Zaworotko, Barindra K. Ghosh

Polyhedron 25 (2006) 663

Bimetallic complex of the type $[Cu(tren)(NCS)]_4[Mn(NCS)_6]$: A hydrogen bonded network structure

The crystal structure of $[Cu(tren)(NCS)]_4[Mn(NCS)_6]$ displays three-dimensional hydrogen bonded network of $[Cu(tren)(NCS)]^+$ and $[Mn(NCS)_6]^{4-}$ ions. Four copper(II) units are hydrogen bonded to form a hydrogen bonded tetramer. Each manganese(II) in turn is further engaged in hydrogen bonding to four such tetramers leading to the 3D network.

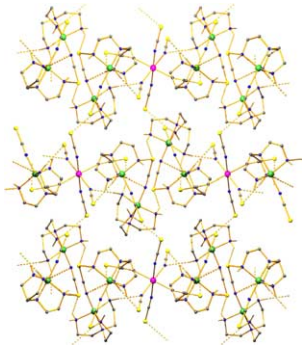

Mehdi Amirnasr, Kurt J. Schenk, Soraia Meghdadi, Mahbod Morshedi

Polyhedron 25 (2006) 671

Synthesis, characterization and X-ray crystal structures of $[Ni(Me\text{-}sal)_2dpt]$ and [Ni(Me-sal)dpt]Cl

The synthesis, characterization, and single-crystal X-ray diffraction studies for two new Ni(II) complexes, $[Ni(Me\text{-}sal)_2dpt]$ (**1**) and [Ni(Me-sal)dpt]Cl (**2**), with penta- and tetradentate ligands $H_2(Me\text{-}sal)_2dpt$ and H(Me-sal)dpt containing N_3O_2 and N_3O donor sets, respectively, are reported. The coordination polyhedron about the Ni(II) center in complex (**1**) is best described as distorted trigonal bipyramidal and that of complex (**2**) as distorted square planar containing a "half unit" ligand, (Me-sal)dpt.

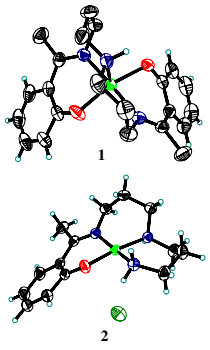

Danuta Kroczewska, Barbara Kurzak, Julia Jezierska

Polyhedron 25 (2006) 678

The role of the carboxylic group in the copper(II) mixed-ligand complexes of DL-aspartic acid-β-hydroxamic acid and polyamines

Stability of the mixed-ligand complexes with tridentate amines as a primary ligand and DL-aspartic acid-β-hydroxamic acid as a secondary ligand, their absorption and EPR spectra indicate a five-coordinate structure of the formed complexes. H-Asp-β-ha coordinates to $[Cu(A)]^{2+}$ by the carboxylate group in addition to the amino nitrogen (glycine-like coordination) in acidic and neutral pH. At higher pH the hydroxamate ligand is coordinated by N_{amino} and $N_{hydrox.}$ donor atoms.

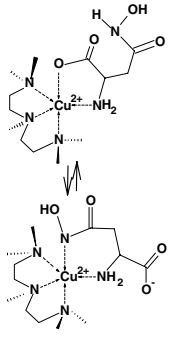

Zofia Rzączyńska, Agata Bartyzel, Elżbieta Olszewska, Wanda Sawka-Dobrowolska

Polyhedron 25 (2006) 687

Synthesis and characterization of Co(II), Cu(II) and Zn(II) complexes with 1,1-cyclobutanedicarboxylic acid

Polycrystalline complexes of $Co(C_6H_6O_4) \cdot 2H_2O$, $Cu(C_6H_6O_4)$, and $Zn_2(C_6H_6O_4)_2 \cdot 3H_2O$ were synthesized. The complexes were characterized by elemental analysis, IR spectroscopy, thermal analysis (TG, DSC/DTA, and TG-FTIR) and X-ray analysis. During recrystallization, single crystals of $[Co_2(C_6H_6O_4)_2(H_2O)_3]$ and $[Cu(C_6H_6O_4)H_2O]$ were obtained.

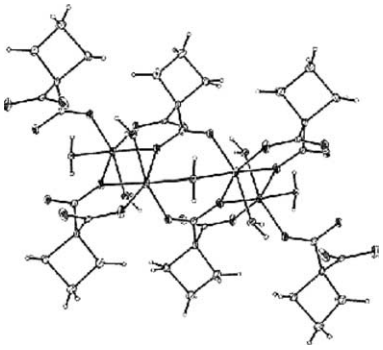

Gillian M. Allan, R. Alan Howie, John N. Low, Janet M.S. Skakle, James L. Wardell, Solange M.S.V. Wardell

Polyhedron 25 (2006) 695

Structural relationships in the homologous series of alkyltriphenylstannane compounds of formula $Ph_3Sn(CH_2)_{n-1}CH_3$, with *n* even and in the range 4–14 and 18

The solid state structures of several compounds in the homologous series of alkyltriphenylstannanes of general formula $Ph_3Sn(CH_2)_{n-1}CH_3$ have been determined. For *n* in the range 4–10 the structures are monoclinic with space group $P2_1/c$. For *n* greater than 10 they are, instead, triclinic with space group $P\bar{1}$. The structural difference between the two classes is attributable to a change in the degree of control over the packing of the molecules exerted by the triphenylstannyl entity on the one hand and the alkyl chain on the other.

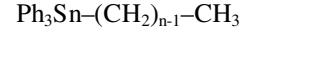

Prasant Kumar Nanda, Debashree Mandal, Debashis Ray

Polyhedron 25 (2006) 702

Coordination induced 2-(2′-hydroxyphenyl) imidazolidine ring hydrolysis of dinucleating amine–imine–phenol ligands: X-ray structures of hardness-matched mononuclear cobalt(III) complexes as end products having isomeric N_4O_2 coordination spheres

Two dinucleating ligands having pendant imidazolidine rings have been reacted with cobalt salts in aqueous methanol at room temperature to obtain the mononuclear complexes $[Co^{III}L_1]Cl \cdot 2H_2O$ (**1** · $2H_2O$) and $[Co^{III}L_2]ClO_4 \cdot H_2O$ (**2** · H_2O) of hydrolyzed ligands. Anticipated dicobalt(II/II or III/III) complexes were not obtained due to a coordination driven hydrolytic cleavage of the substituted central imidazolidine rings of the ligands. Structurally characterized hardnessmatched complexes **1** · $2H_2O$ and **2** · H_2O, show *mer*- and *fac*-ON_2 binding modes of the two tridentate halves of the parent hexadentate ligands.

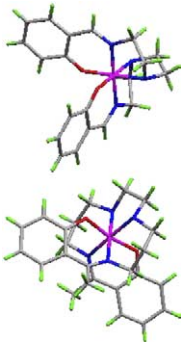

Khodayar Gholivand, Zahra Shariatinia, Mehrdad Pourayoubi

Polyhedron 25 (2006) 711

Syntheses, spectroscopic characterization and crystal structures of some new phosphoramidates and an organotin(IV) complex of *N*-(4-fluorobenzoyl)-*N*′,*N*″-bis(piperidinyl)-phosphoric triamide

Some new phosphoramidates were synthesized. The reaction of 4-F-$C_6H_4C(O)N(H)P(O)(NC_5H_{10})_2$ (**2**) with $SnCl_2(CH_3)_2$ leads to an octahedral organotin(IV) complex (**8**) with equal ligands in *trans* positions. Compound **2** exists as four symmetrically independent molecules in the crystalline lattice. Compounds **1**, **2**, **4**, **5** and **8** form intermolecular –P=O···H–N– hydrogen bonds in the crystals.

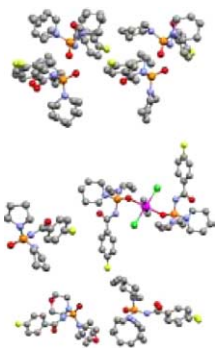

Suban K. Sahoo, Minati Baral, B.K. Kanungo

Polyhedron 25 (2006) 722

Potentiometric, spectrophotometric, theoretical studies and binding properties of a novel tripodal polycatechol-amine ligand with lanthanide(III) ions

A new tripodal ligand *cis*,*cis*-1,3,5-tris[(2,3-dihydroxybenzylamino)aminomethyl] cyclohexane (TMACHCAT), bearing three catechol units attached to a tris-methylaminocyclohexane (TMACH) ring has been synthesized and characterized by elemental analyses, UV–VIS, IR and ^{1}H NMR spectral data. The complexation behaviour of the ligand with H^+, La(III), Gd(III) and Lu(III) was studied by potentiometric and spectrophotometric methods.

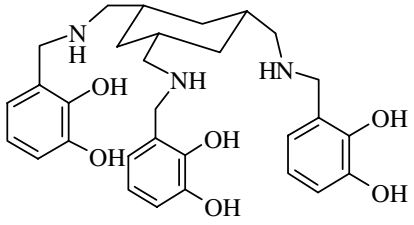

Tanju Ceyhan, Ahmet Altındal, Mehmet K. Erbil, Özer Bekaroğlu

Polyhedron 25 (2006) 737

Synthesis, characterization, conduction and gas sensing properties of novel multinuclear metallo phthalocyanines (Zn, Co) with alkylthio substituents

Novel multinuclear metallo phthalocyanines (Zn, Co) with alkylthio substituents have been synthesized and their electrical conductance (a.c and d.c) and sensitivity to several volatile organic compounds are investigated by conductivity measurements.

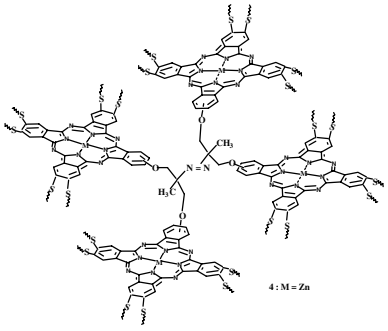

Ashok K.S. Chauhan, Arun Kumar, Shobhit Charan, Ramesh C. Srivastava, Ray J. Butcher

Polyhedron 25 (2006) 747

Role of electronic factors in the formation of anionic complexes of tellurium(IV): Crystal structure of bis(4-methylbenzoylmethyltriphenylphosphonium) hexabromotellurate(IV)

Interaction of $(4\text{-}XC_6H_4COCH_2)_2TeBr_2$ with $(4\text{-}XC_6H_4COCH_2)Ph_3PBr$ gives the 1:1 adduct $[(4\text{-}XC_6H_4COCH_2)Ph_3P]^+[(4\text{-}XC_6H_4COCH_2)_2\text{-}TeBr_3]^-$ in the initial step when X = H or Me. A methoxy substituent (X = MeO) in any of the reactants, however, promotes the cleavage of Te–C bonds and bis(4-substitutedbenzoylmethyltriphenylphosphonium) hexabromotellurates(IV) are isolated. The crystal structure of $[(4\text{-}MeC_6H_4COCH_2)Ph_3P]_2[TeBr_6] \cdot CH_2Cl_2$ shows close C–H···Br/Cl contacts among the ions and solvated molecules, and supramolecular extended arrays of ionic molecular units formed by means of solvated head-to-tail linkers are identified.

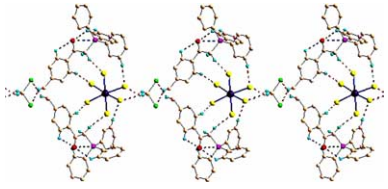

Susana M.O. Quintal, Vitor Félix, Michael G.B. Drew, Helena I.S. Nogueira

Polyhedron 25 (2006) 753

Coordination modes of 3-aminosalicylic and 3-hydroxyanthranilic acids in palladium(II), platinum(II) and rhenium(V) complexes. The crystal structure of *cis*-$[Pt(HsalNH)(PPh_3)_2] \cdot 0.25C_2H_5OH$

A comparative study was performed on the coordination modes of Pd(II), Pt(II) and Re(V) in complexes with 3-aminosalicylic and 3-hydroxyantranilic acids. The crystal structure of the Pt(II) complex with 3-aminosalicylic acid shows coordination through the nitrogen and oxygen atoms of the amino and phenolate groups (*N*,*O*-chelating mode), respectively.

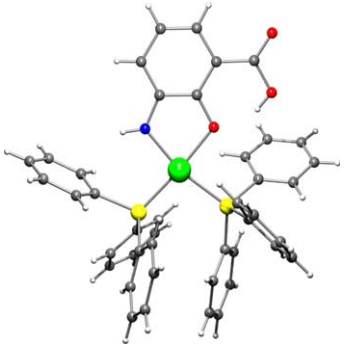

Rita Kakkar, Rajni Grover, Pragya Gahlot

Polyhedron 25 (2006) 759

Density functional study of the properties of isomeric aminophenylhydroxamic acids and their copper (II) complexes

The three isomeric aminophenylhydroxamic acids and their copper (II) complexes have been investigated by the density functional theory using different potentials. A comparison is made of the electronic structures of the acids to understand why they form different types of complexes.

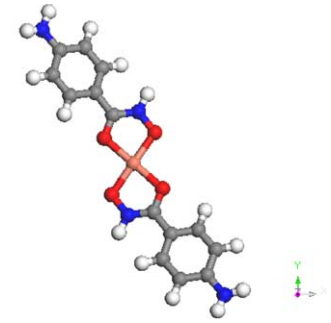

Cu(II) complex of 4-Aminophenylhydroxamic acid

Ari Lehtonen, Mikael Wasberg, Reijo Sillanpää

Polyhedron 25 (2006) 767

Dioxomolybdenum(VI) and -tungsten(VI) complexes with tetradentate aminobis(phenol)s

Aminobis(phenol) ligands (H_2L^n) carrying either a dimethylamino, a pyridyl or a methoxy sidearm donor react with [W(eg)$_3$] (eg = 1,2-ethanediolate dianion) or [MoO_2(acac)$_2$] to yield mononuclear dioxometal(VI) complexes of type [$MO_2(L^n)$].

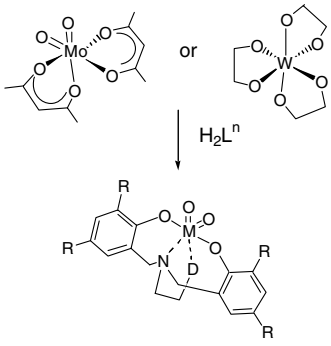

Austin B. Wiles, Daniel Bozzuto, Christopher L. Cahill, Robert D. Pike

Polyhedron 25 (2006) 776

Copper (I) and (II) complexes of melamine

Coordination of copper (I) and (II) salts to melamine (Mel) produces [CuX(Mel)] (X = Br, I, NO_3), [CuCl(Mel)$_{1.1}$], [CuX_2(Mel)$_2$] · S (X = Cl, S = H_2O; X = Cl, S = 2 MeOH; X = Br, S = 1/2H_2O; X = OAc, S = none), and [Cu(OAc)$_2$(Mel)]. The chemical identity of the complexes has been confirmed by elemental analysis, X-ray powder diffraction, thermogravimetry, and infrared analysis.

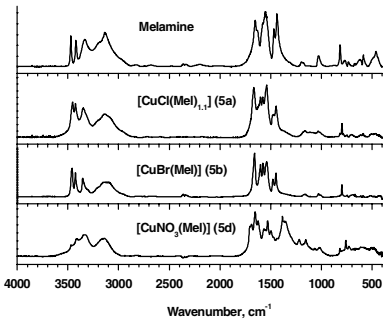

M[a] del Carmen Fernández-Fernández, Rufina Bastida, Alejandro Macías, Laura Valencia, Paulo Pérez-Lourido

Polyhedron 25 (2006) 783

Different nuclearities of M(II) nitrate complexes (M = Co, Ni, Cu and Cd) with a tetrapyridyl pendant-armed hexaazamacrocyclic ligand

A new series of nitrate M(II) (M = Co, Ni, Cu and Cd) complexes with a tetrapyridyl pendant-armed hexaazamacrocyclic ligand (L) has been synthesized. [$Co_2L(NO_3)_4$] · 2H_2O and [$Cu_2L(H_2O)_4$](NO_3)$_4$, show the metal atoms exocyclically coordinated in a distorted square pyramid [N4O] and distorted octahedral geometry [N4O2], respectively. In [$Cd_2L(NO_3)2$]-(NO_3)$_2$ · 5H_2O · CH_3CN the metal atoms are in a [N5O2] core in a distorted capped octahedral geometry. Finally, the structure of [CdL]-(NO_3)$_2$ · 6H_2O shows the metal centre in a distorted octahedral geometry [N6].

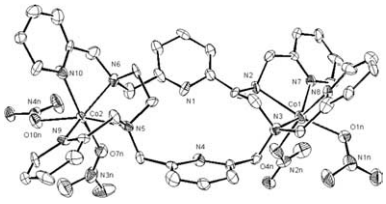

Joan Albert, Jaume Granell, Ana Luque, Mercè Font-Bardia, Xavier Solans

Polyhedron 25 (2006) 793

Monoinsertion of but-2-ynedioic acid dimethyl ester into palladium–carbon σ bonds of cyclopalladated compounds derived from biphenyl-2-ylamine: X-ray molecular structure of biphenyl-2-yl-(2,4,6-trimethoxy-benzylidene)-amine

The synthesis and characterization of the organopalladium compounds shown below are reported.

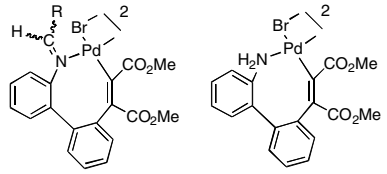

2a (R = 2,4,6-trimethoxyphenyl) **2d**
2b (R = 2,6-dichlorophenyl)
2c (R = 2,6-difluorophenyl)

Lluis Escriche, Jaume Casabó, Vicens Muns, Raikko Kivekäs, Reijo Sillanpää

Polyhedron 25 (2006) 801

New phosphathiamacrocycles containing polypypiridine units

The first example of phosphathiamacrocycles containing polypyridine units L and Lox are reported. Their reaction in front of Fe(II) gives in both cases octahedral complexes with a low-spin configuration for L and high-spin for Lox.

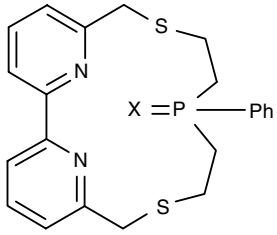

X = lone pair, **L**
X = O, **Lox**

Zdenek Spichal, Marek Necas, Jiri Pinkas, Zbynek Zdrahal

Polyhedron 25 (2006) 809

Binuclear complexes of lanthanides with 1,4-bis(diphenylphosphino)butane dioxide

A series of binuclear complexes were prepared by the solvothermal reactions of $Ph_2P(O)$–$(CH_2)_4$–$P(O)Ph_2$ (dppbO_2) with lanthanide cations (Pr, Nd, Sm, Dy, Lu). The compounds were characterized by mass spectrometry with electrospray ionization, and their molecular structures were determined by single crystal X-ray diffraction.

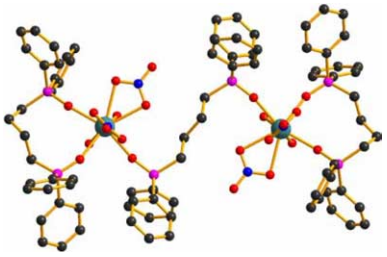

Sasmita Mohanty, Benudhar Punji, Maravanji S. Balakrishna

Polyhedron 25 (2006) 815

Synthesis and reaction kinetics of Pd(1,5-cyclooctadiene)Cl_2 with *N*,*N*′-methylene-bis-(2-aminopyridyl): An efficient catalyst for Suzuki-cross-coupling reactions

The rate constants of the reaction of Pd^{2+} complex with ligand *N*,*N*′-methylene-bis-(2-aminopyridyl) are determined and the application of complex (**2**) for Suzuki-cross-coupling reactions is studied.

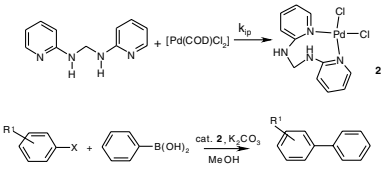

The Publisher encourages the submission of articles in electronic form thus saving time and avoiding rekeying errors. For detailed instructions on the preparation of manuscripts and of electronic artwork, consult the Author Gateway for Elsevier at http://authors.elsevier.com

SCIENCE DIRECT®

Full text of this journal is available, on-line from **ScienceDirect**. Visit **www.sciencedirect.com** for more information.

CONTENTS Direct

This journal is part of **ContentsDirect,** the ***free*** alerting service which sends tables of contents by e-mail for Elsevier books and journals. You can register for **ContentsDirect** online at: **http://contentsdirect.elsevier.com**

Available online at www.sciencedirect.com
ScienceDirect
Polyhedron 25, issue 17, 4 December 2006
POLYHEDRON
www.elsevier.com/locate/poly

Contents

Papers

Mostafa M. Amini, Massomeh Sharbatdaran, Mehdi Mirzaee, Payman Mirzaei

Polyhedron 25 (2006) 3231

Synthesis, structure and luminescence study of a binuclear aluminium complex: A novel structure containing six coordinated aluminium atoms in two distinct coordination geometries

The reaction of 8-hydroxyquinoline with aluminium 2-methoxyethoxide and aluminium 2-ethoxyethoxide in refluxing benzene leads to the formation of luminescent complexes $[Al(C_9H_6NO)_2(\mu\text{-}OCH_2CH_2O\text{–}CH_3)]_2$ and $[Al(C_9H_6NO)_2(\mu\text{-}OCH_2CH_2O\text{–}CH_2CH_3)]_2$. X-ray structure analysis reveals two distinct coordination geometries for the aluminium atoms in the binuclear complex.

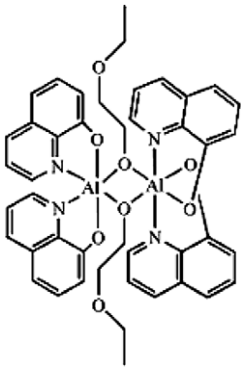

Ann L. Bingham, John E. Drake, Michael B. Hursthouse, Mark E. Light, Ravindra Kumar, Raju Ratnani

Polyhedron 25 (2006) 3238

Synthesis, spectroscopic characterization and structural studies of bromodioxodimethylsulfoxide (*N*,*N*′-dialkyldithiocarbamates and *O*-alkyl dithiocarbonate)molybdenum(VI) complexes: Crystal structures of $MoO_2Br_2(OSMe_2)_2$ and $MoO_2Br_2(C_{12}H_8N_2)\cdot CH_2Cl_2$

Reactions of dibromodioxobis(dimethylsulfoxide)molybdenum(VI) with sodium/potassium salts of *N*,*N*′-dialkyl dithiocarbamates or *O*-alkyl dithiocarbonates yield bromodioxomolybdenum(VI) complexes of the type, $MoO_2Br(S_2CNR_2)(OSMe_2)$ or $MoO_2Br(S_2COR)(OSMe_2)$. Crystals of $MoO_2Br_2(OSMe_2)_2$ and $MoO_2Br_2(C_{12}H_8N_2)\cdot CH_2Cl_2$ have distorted octahedral environments around molybdenum with two *cis*-oxygen atoms and two *trans*-bromine atoms in both along with two *cis*-dimethylsulfoxide moieties in the former and 1,10-phenanthroline in the latter.

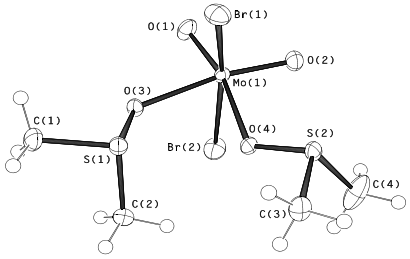

M. Akbar Ali, A.H. Mirza, Fatriah Hj Bujang, Malai Haniti S.A. Hamid, Paul V. Bernhardt

Polyhedron 25 (2006) 3245

Synthesis, characterization and X-ray crystallographic structural study of copper(II) and nickel(II) complexes of the 2-quinoline carboxaldehyde Schiff base of *S*-methyldithiocarbazate (Hqaldsme)

The complexes, $[Cu(qaldsme)(X)(CH_3OH)_n]$ and $[Ni(qaldsme)_2]\cdot 0.5CH_3CCN$ (qaldsme = anionic form of the quinoline-2-carboxaldehyde Schiff base of *S*-methyldi-thiocarbazate; X = NCS^-, I^-, NO_3^-; n = 0, 1) have been prepared and characterized. X-ray analysis shows that $[Cu(qaldsme)(CH_3OH)(NO_3)]$ is monomeric and five-coordinate, $[Cu(qaldsme)(NCS)]_2$ is a dimer and $[Ni(qaldsme)_2]\cdot 0.5CH_3CN$ has a distorted octahedral geometry.

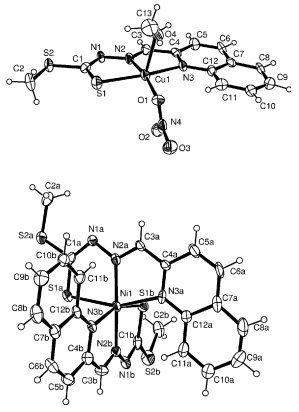

N. Kumaraguru, K. Santhakumar, S. Arunachalam, M.N. Arumugham

Polyhedron 25 (2006) 3253

Synthesis, characterization and micellization behaviour of some surface active mixed-ligand complexes of cobalt(III)

A number of mixed ligand cobalt(III)–surfactant coordination complexes were synthesized from the corresponding dihalogeno complexes by the ligand substitution method. These compounds form a foam in aqueous solution when shaken. The critical micelle concentration (CMC) values of these surfactant metal complexes in aqueous solution were obtained from conductance measurements. Specific conductivity data (at 303, 308 and 313 K) served for the evaluation of the temperature-dependent critical micelle concentration (CMC) and the thermodynamics of micellization (ΔG^0_m, ΔH^0_m and ΔS^0_m) are discussed.

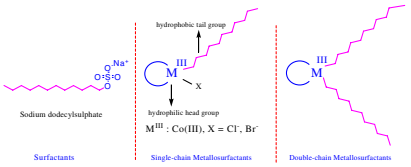

R. Ivaniková, R. Boča, L. Dlháň, H. Fuess, A. Mašlejová, V. Mrázová, I. Svoboda, J. Titiš

Polyhedron 25 (2006) 3261

Heteroleptic nickel(II) complexes formed from N-donor bases, carboxylic acids and water: Magnetostructural correlations

Four nickel(II) complexes with the general formula $[Ni(L^1)_2(L^2)_2(H_2O)_2]$, where L^1 = 2-methylimidazole, 1,2-dimethylimidazole, *iso*-quinoline and furo[3,2-*c*]pyridine, L^2 = formate and acetate, have been prepared and their structures determined by single-crystal X-ray diffraction techniques. All complexes show magnetic behavior typical for zero-field splitting systems. The axial parameter of the zero-field splitting, *D*, adopts moderately negative values and it correlates with the axial distortion of the coordination polyhedron.

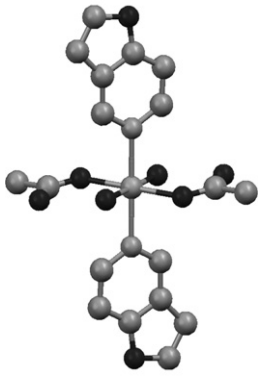

Bikshandarkoil R. Srinivasan, Christian Näther, Sunder N. Dhuri, Wolfgang Bensch

Polyhedron 25 (2006) 3269

Cation–anion interactions in bis(±)*trans*-2-aminocyclohexylammonium tetrathiotungstate, 1,7-diazonia-4-aza-heptane tetrathiotungstate and 1,5-diazonia-9-aza-nonane tetrathiotungstate

The structures of the title complexes consist of tetrahedral tetrathiotungstate anions which are linked to the partially protonated organic ammonium cations with the aid of weak hydrogen bonding interactions. A comparative study of the structural features of several tetrathiotungstates is presented and the interactions between the organic ammonium cation and the tetrathiotungstate anion are discussed in terms of the magnitude of Δ, the difference between the longest and the shortest W–S bond distances.

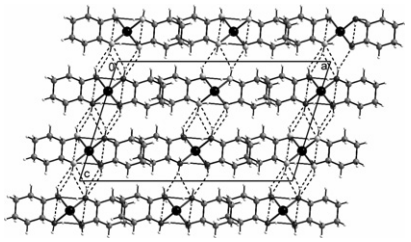

Gerard A. van Albada, Ilpo Mutikainen, Urho Turpeinen, Jan Reedijk

Polyhedron 25 (2006) 3278

Crystal structure, magnetism and spectroscopy of two strongly antiferromagnetically coupled dinuclear Cu(II) paddlewheel-like compounds with 4-azabenzimidazole as a ligand

Two paddlewheel-like dinuclear compounds, $[Cu_2(azab)_4Cl_2]Cl_2(CH_3OH)_3$ (**1**) and $[Cu_2(azab)_4Br_2]Br_2(H_2O)_{1/2}$ (**2**) (in which azab = 4-azabenzimidazole), have been synthesized. Characterization is done by X-ray crystallography, infrared spectroscopy and EPR. Also the magnetic susceptibility of both compounds are investigated and obtained a strong antiferromagnetic interaction between the Cu(II) ions.

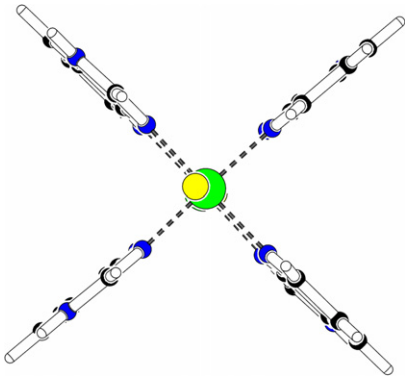

Moayad Hossaini Sadr, Jaber Jahanbin Sardroodi, Davood Zare, Neil R. Brooks, William Clegg, Yinglin Song

Polyhedron 25 (2006) 3285

Nonlinear optical properties and crystal structure determination of a pentanuclear copper(I) cluster $(NEt_4)_2[MoS_4(CuBp)_4]$ (Bp = H_2B-(pyrazolyl)$_2$)

The bis(tetraethylammonium) salt of this molybdenum–copper cluster anion, with tetrahedral coordination of both Mo and Cu, shows non-linear optical activity as a potential optical limiter.

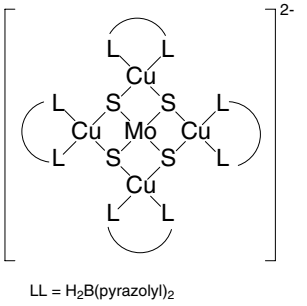

Bi-Yun Su, Jian-She Zhao

Polyhedron 25 (2006) 3289

Preparation, structure and ethylene polymerization/oligomerization behavior of 2-carbethoxy-6-iminopyridine-based transition metal complexes

The synthesis, characterization and ethylene polymerization/oligomerization of a series of transition metal complexes with the formula {2-carbethoxy-6-[1-[(2,6-dimethylphenyl)imino]-ethyl]pyridine}$_n$$MCl_2$ [M = Mn(II) (**8**), Fe(II) (**9**), Co(II) (**10**), Cu(II) (**11**), Zn(II) (**12**), n = 1; Ni(II) (**13**), n = 2]; {2-carbethoxy-6-[1-[(2,4,6-trimethylphenyl)imino]ethyl]pyridine}-MCl_2 [M = Fe(II) (**14**), Co(II) (**15**), Ni(II) (**16**)]; {2-carbethoxy-6-[1-[(2,6-diethylphenyl)-imino]ethyl]pyridine}MCl_2 [M = Fe(II) (**17**), Co(II) (**18**), Ni(II) (**19**)] have been reported. The systematic studies are focused on the relationship between the catalytic activity of these complexes for ethylene polymerization/oligomerization and the electronic property of central metal, the ligand structure, as well as the reaction conditions.

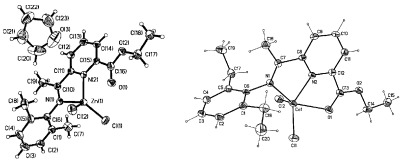

M.A.M.K. Sanhoury, M.T. Ben Dhia, K. Essalah, M.R. Khaddar

Polyhedron 25 (2006) 3299

Phosphoramidic difluoride complexes of tin(IV) chloride: A multinuclear (^{119}Sn, ^{31}P, ^{19}F and ^{1}H) NMR characterisation in solution

Two new octahedral complexes of the type $SnCl_4 \cdot 2(O)PF_2NR_2$ (R = Me (**1**) or Et (**2**)) were prepared and characterised by multinuclear NMR spectroscopy, showing that the two ligands are in a *cis* position. Additionally, DFT/ B3LYP calculations have been carried out to support the interpretations of NMR data.

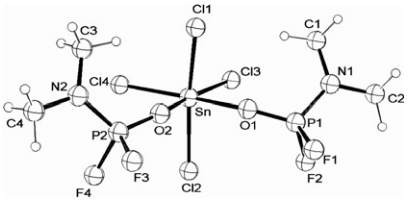

Hong-Xing Wang, Ying-Jie Li, Hong-Fei Wu, Ren-Qing Gao, Feng-Ying Geng, Xiao-Li Yang, Li Wan, Rong Jin, Xiu-Ling Cui, Yang-Jie Wu

Polyhedron 25 (2006) 3305

Ortho-mercurated [({*N*-methyl-*N*-arylamino}-methyl)ferrocenes] and their transpalladation. Crystal structures of $[(\eta^5\text{-}C_5H_5)Fe\{\eta^5\text{-}C_5H_3\text{-}(HgCl)CH_2N(CH_3)C_6H_4OCH_3\text{-}4\}]_2$, $[(\eta^5\text{-}C_5H_5)\text{-}Fe\{\eta^5\text{-}C_5H_3(HgCl)CH_2N(CH_3)C_6H_4Cl\text{-}3\}]$ and $[(\eta^5\text{-}C_5H_4HgCl)Fe\{\eta^5\text{-}C_5H_4CH_2N(CH_3)\text{-}C_6H_4Cl\text{-}4\}]$

Treatment of ferrocenylamines $[(\eta^5\text{-}C_5H_5)\text{-}Fe(\eta^5\text{-}C_5H_4CH_2N(CH_3)C_6H_4\text{-}R)]$ (**4**) with $Hg(OAc)_2$/LiCl resulted in predominately the *ortho*-mercurated complexes **6**. The preferable intermolecular over intramolecular N–Hg interaction was observed and rationalized. Transpalladation of **6** gave the cyclopalladated complexes in low yields. The structures of **6a**, **e**, and **7** were determined by X-ray single crystal diffraction.

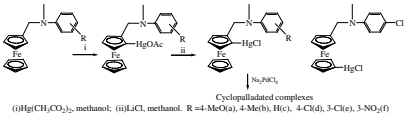

R.N. Patel, Nripendra Singh, V.L.N. Gundla

Polyhedron 25 (2006) 3312

Synthesis, structure and properties of ternary copper(II) complexes of ONO donor Schiff base, imidazole, 2,2′-bipyridine and 1,10-phenanthroline

Three new complexes [Cu(SAA)(ImH)] (**1**), [Cu(SAA)(bipy)] CH_3CN (**2**), [Cu(SAA)(phen)] (**3**) were characterized by elemental analysis, magnetic susceptibility, X-band e.p.r., electronic spectroscopy and cyclic voltammetry. Single crystal X-ray analysis of (**1**) has revealed the presence of a distorted square planar geometry (N_2O_2) and (**2**) has revealed the presence of a distorted square pyramidal (4+1) geometry. In both structures the ONO Schiff base occupies the basal plane. Magnetic susceptibility measurements at room temperature were in the range 1.79 ± 0.01 BM. Superoxide dismutase (SOD) activity of the present complexes were also measured and discussed.

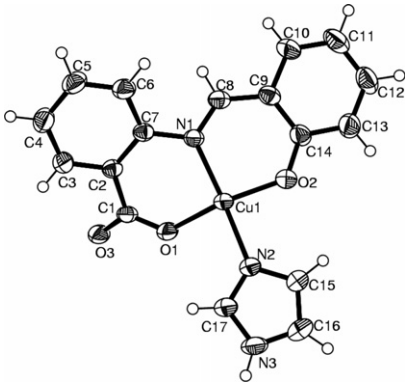

Jan Janczak, Genivaldo J. Perpétuo

Polyhedron 25 (2006) 3319

Synthesis, crystal structure and charge transport properties of one-electron oxidized zirconium diphthalocyanine, $[ZrPc_2]IBr_2$

Crystals of $[ZrPc_2]IBr_2$ were obtained by cyclic tetramerization of phthalonitrile in the presence of powdered zirconium under oxidative conditions of IBr. Single crystal X-ray analysis supported by Raman and EPR spectroscopies shows a one-dimensional arrangement of one-electron oxidized $[ZrPc_2]^+$ units. Single-crystal conductivity experiments show its non-metallic character ($d\sigma/dT > 0$) and anisotropy.

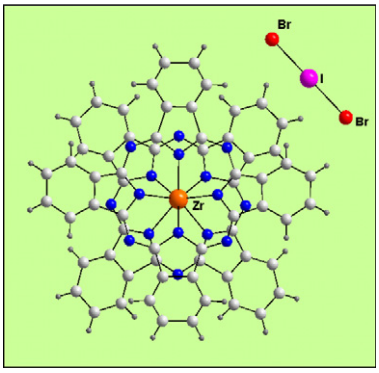

Damir A. Safin, Felix D. Sokolov, Nail G. Zabirov, Vasiliy V. Brusko, Dmitry B. Krivolapov, Igor A. Litvinov, Robert C. Luckay, Rafael A. Cherkasov

Polyhedron 25 (2006) 3330

Studies on cobalt(II) complexes with *N*-thioacylamido(thio)phosphates: X-ray crystal structure of the $Co[PhC(S)NP(S)(OPr^i)_2]_2$

Unsaturation of CoO_2S_2 coordination environment opens opportunities for wide number of heteroligand complexes synthesis. It can be reached by interaction of such complexes with various donor agents. As donors, both monodentate ligands and chelating agents might be used. A variety of donors structure opens wide prospects for supramolecular units with in advance set properties synthesis. 2,2′-Bipyridine and 1,10-phenanthroline were used in our work as donor ligands.

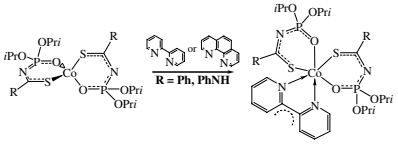

Mohammad Akbar Ali, Aminul H. Mirza, William Bin Ejau, Paul V. Bernhardt

Polyhedron 25 (2006) 3337

Preparation and characterization of pentagonal-bipyramidal zinc(II) and cadmium(II) complexes of a neutral N_3S_2 thiosemicarbazone derived from ^{2}N-methylthiosemicarbazide and the X-ray crystal and molecular structures of the free ligand and its cadmium(II) complex, $Cd(dap\text{-}^2NMetsc)(NO_3)_2$

The complexes, $[M(dap\text{-}^2NMetsc)(NO_3)_2]$-(dap-^{2}NMetsc = 2,6-didacetylpyridine bis-(^{2}N-methylthiosemicarbazone); M = Zn^{2+}, Cd^{2+}) have been prepared and characterized. The structures of the free ligand and its Cd(II) complex, $[Cd(dap\text{-}^2NMetsc)(NO_3)_2]$ have been determined by X-ray diffraction. The complex, $[Cd(dap\text{-}^2NMetsc)(NO_3)_2]$ has a distorted pentagonal-bipyramidal geometry with the ligand coordinated to the cadmium atom as a pentadentate chelating agent *via* the pyridine nitrogen, the azomethine nitrogen and the thione sulfur atoms. The two nitrate anions are coordinated as monodentate ligands occupying axial positions.

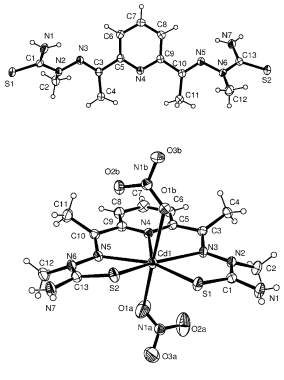

Paula Barbazán, Rosa Carballo, Ulrich Abram, Gumersindo Pereiras-Gabián, Ezequiel M. Vázquez-López

Polyhedron 25 (2006) 3343

Synthesis and characterization of ferrocenylcarbaldehyde benzoylhydrazone and its rhenium(I) complex

The ferrocenylcarbaldehyde hydrazide ligand $H(Fe)L^1$ and its rhenium(I) complex $[Re-Br(CO)_3\{H(Fe)L^1\}]$ have been obtained. Both compounds have been characterized by elemental analysis, MS, IR, UV–Vis and ^1H NMR spectroscopic methods and their structures elucidated by X-ray diffraction. The hydrazide group is O,N-bidentate affording a five-membered chelate ring in the rhenium complex.

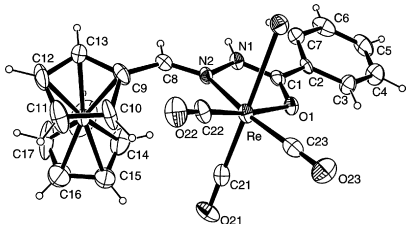

Grégory Malaisé, Jean-Baptiste Sortais, Laurent Barloy, Michel Pfeffer, Nathalie Kyritsakas

Polyhedron 25 (2006) 3349

Nitrogen-containing xanthene-based chiral ligands: Synthesis, NMR and X-ray analyses, and catalytic applications of their palladium, silver and rhodium complexes

Chiral ligands with a rigid xanthene backbone and phosphorus and/or nitrogen donor atoms were synthesized and characterized. They behaved as bidentate ligands in silver (I) complexes, whereas a tridentate coordination mode was observed in a rhodium (III) complex.

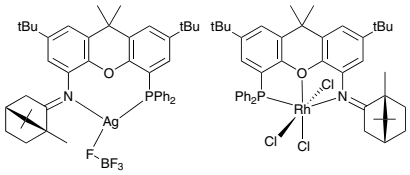

Agostinho Cachapa, Alfredo Mederos, Pedro Gili, Rita Hernández-Molina, Sixto Domínguez, Erasmo Chinea, Matías López Rodríguez, Marta Feliz, Rosa Llusar, Felipe Brito, Carlos M. Ruiz de Galarreta, Carlos Tarbraue, Germán Gallardo

Polyhedron 25 (2006) 3366

Studies of the interaction between bis(dithiocarbamato)copper(II) complexes with nitric oxide in aqueous solution and biological applications

Three new bis di(thiocarbamato)copper(II) complexes, CuL_2, have been prepared and characterized. The interaction of three CuL_2 complexes soluble in water with nitric oxide at pH 7.4 and 20 °C was spectrophotometrically studied, and the stability constants of the complexes $CuL_2(NO)$ and $CuL_2(NO)_2$ were determined. These CuL_2 complexes decrease the NO produced by NPS and cultured murine macrophages J774.

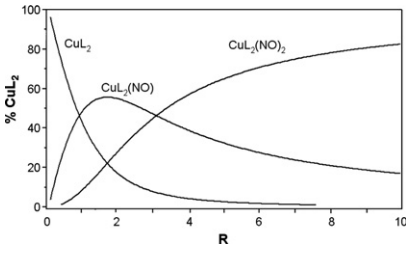

Sara Palmer, Ray L. Frost

Polyhedron 25 (2006) 3379

Synthesis and spectroscopic characterization of apjohnite and pickingerite

Raman and infrared spectroscopy at 298 K has been used to characterise synthetic and natural halotrichites.

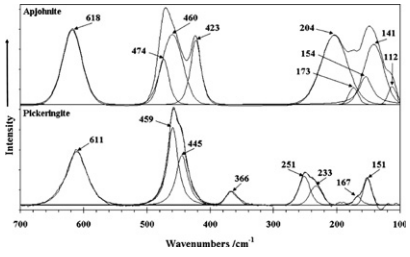

Xin-min Gan, Iris Binyamin, Brian M. Rapko, Jesse Fox, Eileen N. Duesler, Robert T. Paine

Polyhedron 25 (2006) 3387

Formation of a 1-D chain structure from Nd(III) and 2,6-bis(methylphosphonic acid)-pyridine *N*-oxide

The facile synthesis of the multifunctional phosphonic acid ligand shown here is reported along with the hydrothermal synthesis of a complex with Nd(III). Single crystal X-ray diffraction analysis reveals that the asymmetric unit $Nd(L\text{-}H_2^{2-})(L\text{-}H^{1-}) \cdot 4/3H_2O$ forms spiral chains through Nd–O–P bridges involving the $(L\text{-}H_2^{2-})$ ligand fragment and both $L\text{-}H_2^{2-}$ and $L\text{-}H^{1-}$ act as tridentate chelates on the central Nd(III) ion.

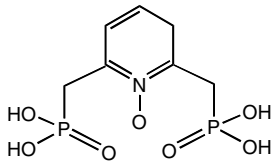

Guang-Yuan Hsu, Phalguni Misra, Sheng-Chuan Cheng, Ho-Hsiang Wei, Sasankasekhar Mohanta

Polyhedron 25 (2006) 3393

Syntheses, structures, and magnetic properties of dicyanamide bridged one-dimensional double chain and discrete dinuclear complexes of manganese(II) derived from 6,7-dimethyl-2,3-di(2-pyridyl)quinoxaline or 2,4,6-tri(2-pyridyl)-1,3,5-triazine

Syntheses, structures, and variable-temperature magnetic studies of a dicyanamide (dca) bridged one-dimensional double chain compound, $[Mn^{II}(DMeDPQ)(\mu_{1,5}\text{-dca})_2]_n$, and a discrete dinuclear complex, $[Mn_2^{II}(TPT)_2(\mu_{1,5}\text{-dca})_2(H_2O)_2](ClO_4)_2$, have been described (DMeDPQ = 6,7-dimethyl-2,3-di(2-pyridyl)-quinoxaline; TPT = 2,4,6-tri(2-pyridyl)-1,3,5-triazine).

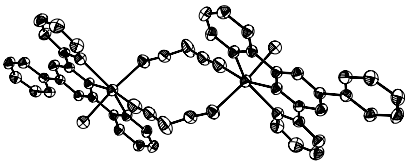

Stanislav Strekopytov, Eve Jarry, Christopher Exley

Polyhedron 25 (2006) 3399

Further insight into the mechanism of formation of hydroxyaluminosilicates

When the kinetics of formation of hydroxyaluminosilicates (HAS) were investigated we obtained the first direct experimental evidence that the formation of HAS_A, an HAS with a Si:Al ratio of 0.5, was a prerequisite to the formation of HAS_B, an HAS with a Si:Al ratio of 1.0. We also found that the interconversions between $Al(OH)_{3(s)}$, HAS_A and HAS_B were critically dependent upon the concentration of silicic acid ($Si(OH)_4$) with the rapid formation of HAS_A being favoured when $[Si(OH)_4] = [Al]$ and the rapid formation of HAS_B being favoured when $[Si(OH)_4] \gg [Al]$.

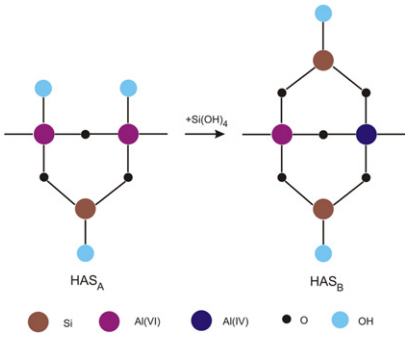

Chun-Lin Ma, Ya-Wen Han, Ru-Fen Zhang

Polyhedron 25 (2006) 3405

Syntheses and crystal structures of di- and triorganotin(IV) derivatives with 2,4,5-trifluoro-3-methoxybenzoic acid

Eight new organotin(IV) complexes with 2,4,5-trifluoro-3-methoxybenzoic acid $R_nSn(O_2CC_6HF_3OCH_3)_{4-n}$ (n = 3: R = Ph (**1**), $PhCH_2$ (**2**), Me (**3**), *n*-Bu (**4**); n = 2: R = Ph (**5**), $PhCH_2$ (**6**), Me (**7**), *n*-Bu (**8**)) have been synthesized. All complexes were characterized by elemental, IR, ^1H and ^{13}C NMR spectra analyses, and the structures of complexes **1**, **3**, **7** and **8** were also determined by X-ray crystallography. The geometries at the tin atoms of **1** and **3** are five-coordinated and those of complexes **7** and **8** are six-coordinated. The structures of complexes **1**, **3**, **7** and **8** have been found to consist of 1D chains built up by intermolecular C–H···F weak hydrogen bonding. Intermolecular C–F···F weak non-hydrogen interactions in the crystal lattice of **3** link the molecules into a 2D network.

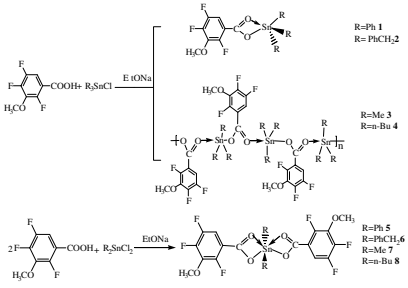

Mohammad El-khateeb, Tobias Rüffer, Heinrich Lang

Polyhedron 25 (2006) 3413

Molybdenum S-bonded mono-thiocarboxylate complexes $CpMo(CO)_3SCOR$: Structure of $CpMo(CO)_3SCOPh$

Monothiocarboxylate complexes of molybdenum of the type $CpMo(CO)_3SCOR$ [R = Me (**1**), CH_2Cl (**2**), Ph (**3**), 4-$C_6H_4NO_2$ (**4**), 3,5-$C_6H_3(NO_2)_2$ (**5**)] have been obtained by the reaction of the hydrosulfido complex, $CpMo(CO)_3SH$, with acid chlorides. Complexes **1**–**5** have been characterized by IR and ^{1}H-NMR spectroscopy, elemental analyses and by the X-ray diffraction method for **3**.

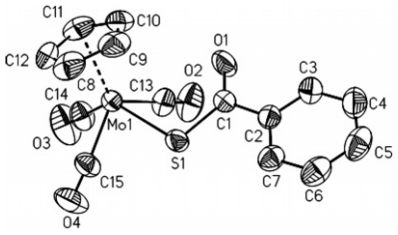

Julieta Gradinaru, Stanislav Malinovskii, Maria Gdaniec, Sandro Zecchin

Polyhedron 25 (2006) 3417

Trinuclear tris-Co(II) and *trans*-cobaloxime type Co(III) complexes prepared from Co(II) triflate precursor: Synthesis, structure and properties

Three new coordination compounds, one trinuclear tris Co(II):$[Co_3(DH)_6] \cdot 24H_2O$ (**I**), and two mononuclear *trans*: $[Co(DH)_2Tu_2]$-CF_3SO_3 (**II**) and $[Co(DH)_2Py_2]CF_3SO_3$ (**III**) (where DH^- = monoanion of dimethylglyoxime, Py = pyridine, Tu = thiourea), were synthesized starting from $Co(CF_3SO_3)_2 \cdot 6H_2O$. The complexes were characterized by X-ray crystallography, spectroscopic methods (IR, UV–Vis, ^{1}H and ^{13}C NMR, MS) and magnetochemistry.

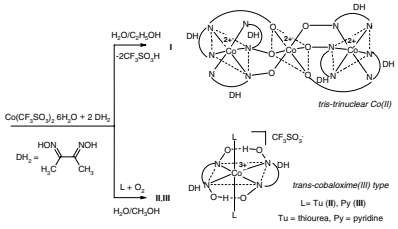

Antonios M. Douvas, Panagiotis Argitis, Andrea Maldotti, Athanassios G. Coutsolelos

Polyhedron 25 (2006) 3427

Photochemically-induced ligand exchange reactions of ethoxy-oxo-molybdenum(V) tetraphenylporphyrin in chlorinated solvents

The photoassisted ligand exchange reactions of oxomolybdenum(V) porphyrins in view of possible technological applications and especially in the area of sensing devices or pollutant dechlorination, have been investigated. We report on the photochemically-induced ligand exchange reactions of the ethoxy-oxo(TPP)Mo(V) complex, mainly in chlorinated solvents and secondarily in non-chlorinated solvents.

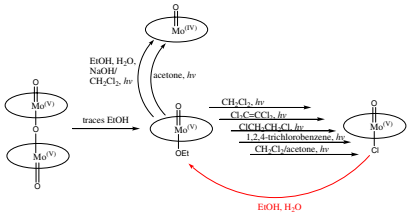

P. Datta, P. Gayen, C. Sinha

Polyhedron 25 (2006) 3435

Naphthylazoimidazole complexes of tetracarbonylchromium and molybdenum: Synthesis, spectra, electrochemistry and photophysical studies

Cis-$[M(CO)_4(\alpha/\beta\text{-NaiR}')]$ (M = Cr(0), Mo(0) and α/β-NaiR′ = 1-alkyl-2-(naphthyl-α/β-azo)-imidazoles) are described in this work. Fluorescence shows a π–π^* emission. Cyclic voltammetry gives two metal centred oxidations, M^+/M^0 and M^{2+}/M^+, and two ligand centred reductions, azo/azo$^-$ and azo$^-$/azo$^{=}$.

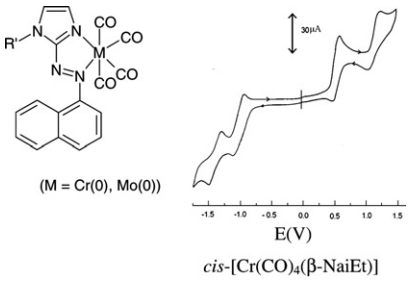

Tushar S. Basu Baul, Keisham Surjit Singh, Anthony Linden, Xueqing Song, George Eng

Polyhedron 25 (2006) 3441

Synthesis, spectroscopic characterization of tribenzyltin(IV) complexes of polyaromatic carboxylic acid ligands: Crystal and molecular structures of $Bz_3Sn[O_2CC_6H_4\{N{=}N(C_6H_3\text{-}4\text{-}OH(C(H){=}NC_6H_4X\text{-}4))\}\text{-}o](OH_2)$ (X = –Cl, $–OCH_3$)

The tribenzyltin(IV) complexes of 2-[(*E*)-2-(3-formyl-4-hydroxyphenyl)-1-diazenyl]benzoic acid and 2-{(*E*)-4-hydroxy-3-[(*E*)-4-(aryl)-iminomethyl]phenyldiazenyl}benzoic acids (aryls = 4-CH_3, 4-Br, 4-Cl, 4-OCH_3) have been synthesized and characterized by ^{1}H, ^{13}C, ^{119}Sn NMR, IR and ^{119m}Sn Mössbauer spectroscopic techniques in combination with elemental analysis. The crystal structures of two tribenzyltin(IV) complexes, $Bz_3Sn[O_2CC_6H_4\{N{=}N(C_6H_3\text{-}4\text{-}OH(C(H){=}NC_6H_4X\text{-}4))\}\text{-}o](OH_2)$ (X = –Cl and $–OCH_3$) are reported.

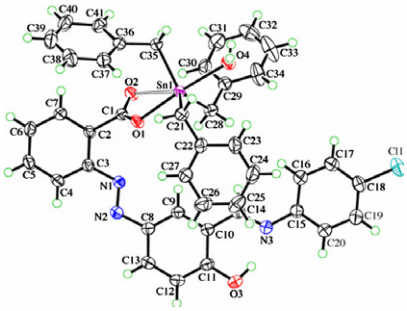

Channa R. De Silva, Ruiyao Wang, Zhiping Zheng

Polyhedron 25 (2006) 3449

Highly luminescent Eu(III) complexes with 2,4,6-tri(2-pyridyl)-1,3,5-triazine ligand: Synthesis, structural characterization, and photoluminescence studies

Two new Eu(III) complexes featuring 1,1,1,5,5,5-hexafluoro-2,4-pentanedionate and a Lewis base ligand 2,4,6-tri(2-pyridyl)-1,3,5-triazine were synthesized, and structurally characterized using single crystal X-ray diffraction. Both complexes display red emission characteristic of Eu(III) ion with high quantum yields upon UV excitation.

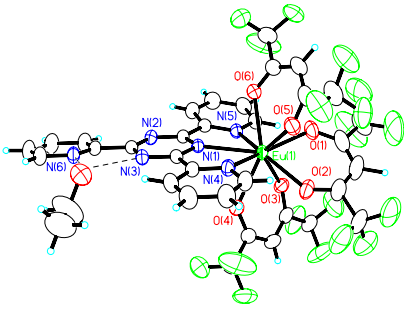

The Publisher encourages the submission of articles in electronic form thus saving time and avoiding rekeying errors. For detailed instructions on the preparation of manuscripts and of electronic artwork, consult the Author Gateway for Elsevier at http://authors.elsevier.com

ScienceDirect

Full text of this journal is available, on-line from **ScienceDirect**. Visit **www.sciencedirect.com** for more information.

Available online at www.sciencedirect.com
SCIENCE DIRECT®
Polyhedron 25, issue 7, 8 May 2006
POLYHEDRON
www.elsevier.com/locate/poly

Contents

Papers

Subhadip Neogi, Parimal K. Bharadwaj

Polyhedron 25 (2006) 1491

Metal-organic frameworks of lanthanide (III) ions with a podand bearing terminal carboxylates: Identification of water clusters of different nuclearity

Hydrothermally synthesized porous 3D MOF structures look like a continuous array of metallomacrocycles. Water clusters of different nuclearity are present in the large voids. The La(III)-bound acyclic water tetramer moves away from the metal upon heating keeping the crystallinity intact.

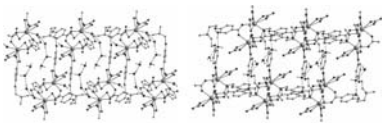

Leslie D. Field, Taian He, Paul Humphrey, Anthony F. Masters, Peter Turner

Polyhedron 25 (2006) 1498

Manganese complexes of the pentaphenylcyclopentadienyl ligand

The complexes, $[Mn(C_5Ar_5)(CO)_2L]$ (Ar = Ph, *p*-tol; L = CO, PMe_2Ph), of the bulky cylopentadienyl ligands, pentaphenylcyclopentadienyl and penta(*p*-tolyl)cyclopentadienyl have been prepared and characterised. The crystal structures of two derivatives are reported. The reversible cyclic voltammetric oxidations of the compounds $[Mn(C_5Ar_5)(CO)_3]$ indicate that the *p*-tolyl substituents confer thermodynamic stability on higher oxidation state complexes of these ligands.

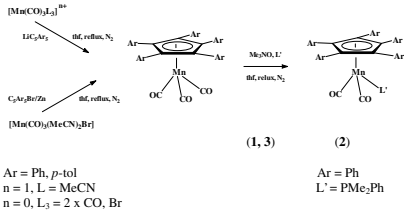

K. Santhakumar, N. Kumaraguru, M.N. Arumugham, S. Arunachalam

Polyhedron 25 (2006) 1507

Metallomicelles of Co(III) coordination complexes – Synthesis, characterization and determination of CMC values

A number of mixed ligand cobalt(III)-surfactant coordination complexes, of the type *cis*-$[Co(en)_2(A)X]^{2+}$ and *cis*-α-$[Co(trien)(A)X]^{2+}$ (A = Dodecyl or Cetylamine, X = Cl^-, Br^-, NO_2) were synthesized from the corresponding dihalogeno complexes by ligand substitution method. These compounds form foam in aqueous solution when shaken. The critical micelle concentration (CMC) values of these surfactant metal complexes in aqueous solution were obtained from conductance measurements. Specific conductivity data (at 303, 308 and 313 K) served for the evaluation of the temperature-dependent critical micelle concentration (CMC) and the thermodynamics of micellization (ΔG^0_m, ΔH^0_m and ΔS^0_m).

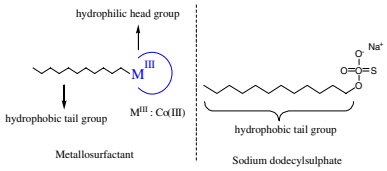

Stefan Dolder, Shi-Xia Liu, Eva Beurer, Lahcène Ouahab, Silvio Decurtins

Polyhedron 25 (2006) 1514

Synthesis and characterization of a new pyrazine functionalized TTF derivative and crystal structure of its charge-transfer complex with iodine

The unique crystal structure of a charge transfer complex of new donor **1** with I_2 shows that the radical cation forms π-dimers embedded in layers of a 2D iodide network.

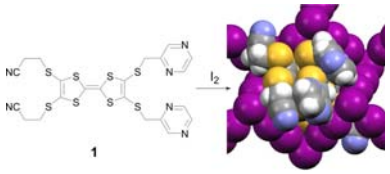

Nilkamal Maiti, Junseong Lee, Seong Jung Kwon, Juhyoun Kwak, Youngkyu Do, David G. Churchill

Polyhedron 25 (2006) 1519

Synthetic, crystallographic and electrochemical studies of thienyl-substituted corrole complexes of copper and cobalt

Novel thienyl *meso*-substituted 5,10,15-tris-(2-thienyl)corrole and 5,10,15-tris(3-thienyl)-corrole and their copper and cobalt complexes have been prepared and fully characterized. Single-crystal X-ray diffraction studies for copper(5,10,15-tris(2-thienyl)corrole) and both cobalt(5,10,15-tris(thienyl)corrole)$(Py)_2$ isomers were obtained. CV data supports monomer redox, devoid of dinuclear products arising from intermolecular C–C coupling observed in related systems.

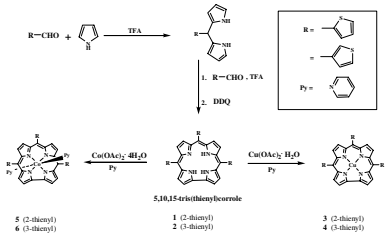

Mohamed A.S. Goher, Adel A. Youssef, Franz A. Mautner

Polyhedron 25 (2006) 1531

Synthesis and structural characterization of two new anionic cobalt(III) azide complexes of 2,3- and 2,5-pyridine dicarboxylic acids

Two new anionic cobalt(III) azide complexes of 2,3- and 2,5-pyridine dicarboxylic acid have been prepared and structurally characterized.

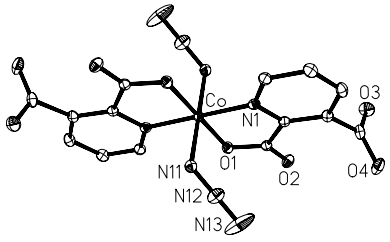

Lionel Salmon, Pierre Thuéry, Michel Ephritikhine

Polyhedron 25 (2006) 1537

Polynuclear uranium(IV) compounds with $(\mu_3\text{-oxo})U_3$ or $(\mu_4\text{-oxo})U_4$ cores and compartmental Schiff base ligands

Polynuclear complexes of uranium(IV) with the Schiff bases *N*,*N*′-bis(3-hydroxysalicylidene)-2-methyl-1,2-propanediamine (H_4L^1) and *N*,*N*′-bis(3-hydroxysalicylidene)-2,2-dimethyl-l,3-propanediamine (H_4L^2) contain U_3 or U_4 cores held by central μ_3- or μ_4-oxo atoms, respectively. Different Schiff base conformations and uranium environments are present in these trianionic $[U_3L^1Cl_9O]^{3-}$ and dicationic $[U_4(L^2)_2(H_2L^2)_2(py)_2O]^{2+}$ species.

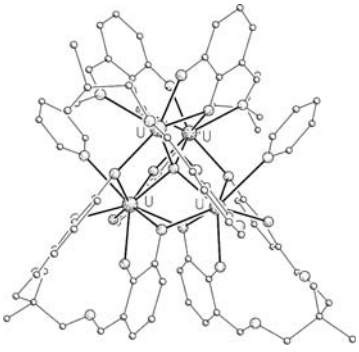

Marcelo O. Santiago, Jackson R. Sousa, Izaura C.N. Diógenes, Luiz Gonzaga F. Lopes, Emerson Meyer, Eduardo E. Castellano, Javier Ellena, Alzir A. Batista, Icaro S. Moreira

Polyhedron 25 (2006) 1543

The versatility of the 1,4-dithiane ligand towards the coordination chemistry of ruthenium-phosphine complexes

The *trans*-[$RuCl_2$(dppb)(1,4-dt)], *mer*-[$RuCl_3$(dppb)(1,4-dt)] and [{$RuCl_3$(dppb)}$_2$-(μ-(1,4-dt))] complexes were synthesized and characterized by spectroscopic and electrochemical techniques. The [$RuCl_2$(dppb)] moiety is the first example of a metallic system that form complexes with the 1,4-dithiane molecule acting as bidentate, monodentate and bridged ligand.

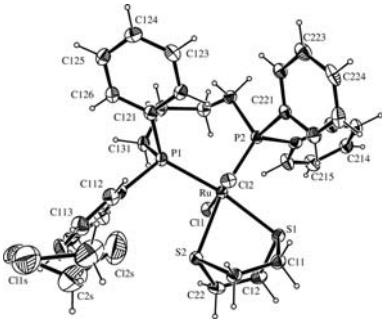

Jorge Tiburcio, Sylvain Bernès, Hugo Torrens

Polyhedron 25 (2006) 1549

Electronic and steric effects of triaryl phosphines on the synthesis, structure and spectroscopical properties of mononuclear rhodium(I)–chloride complexes

A systematic study of the reaction between the dinuclear complex [{Rh(μ-Cl)(η^4-COD)}$_2$], with 14 different triarylphosphines is presented. A chemical equilibrium in solution was observed between the dinuclear and mononuclear species, with the formation of the latter being disfavoured by the use of bulky and electron poor phosphines. The complex with the extremely bulky phosphine R = 2-$CH_3C_6H_5$, was undetected in solution by NMR, however could be crystallized and its molecular structure determined by X-ray diffraction.

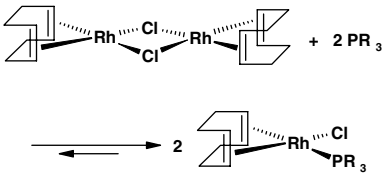

Katarzyna Baranowska, Jaroslaw Chojnacki, Antoni Konitz, Wieslaw Wojnowski, Barbara Becker

Polyhedron 25 (2006) 1555

New examples of $N^{(+)}$–H···$^{(-)}$S hydrogen bonds: Synthesis and X-ray study of selected secondary ammonium tri-*tert*-butoxysilane thiolates

Anionic sulfur atom, from tri-*tert*-butoxysilanethiolate anion, was utilised as an acceptor in charge-assisted hydrogen bonding of the $N^{(+)}$–H···$S^{(-)}$ type. Hydrogen bonds form an eight-membered ring with four donor and two acceptor atoms in all ammonium salts studied.

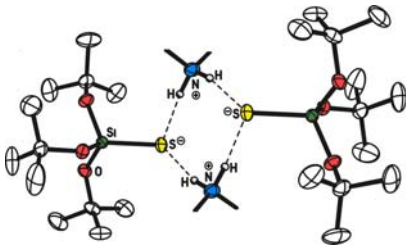

Jan Moncol, Peter Segla, Dusan Miklos, Milan Mazur, Milan Melnik, Tadeusz Glowiak, Marian Valko, Marian Koman

Polyhedron 25 (2006) 1561

Structural diversity of coordination polymers with bridging 3-pyridylmethanol ligand: New type of coordination polymer with different stereochemistry of copper(II) atom

New coordination polymers based by copper(II) benzoate and pyridinecarboxylate compounds with bridged by 3-pyridylmethanol, [CuX_2-(3PM)$_2$]$_n$ (where X = 2-methyltionicotinate (2-MeSnic) or 2-chlorobenzooate (2-Clbz) and [Cu_3(2-Clnic)$_6$(μ-3PM)$_4$ (3PM)$_2$]$_n$ (2-Clnic = 2-chloronicotinate) have been prepared and spectroscopic studied. Both the [CuX_2(3PM)$_2$]$_n$ compounds seem to possess octahedral copper(II) stereochemistry with differing tetragonal distortions. The copper(II) atoms of [Cu_3-(2-Clnic)$_6$(μ-3PM)$_4$(3PM)$_2$]$_n$ are tetragonal bipyramidal and tetragonal pyramidal.

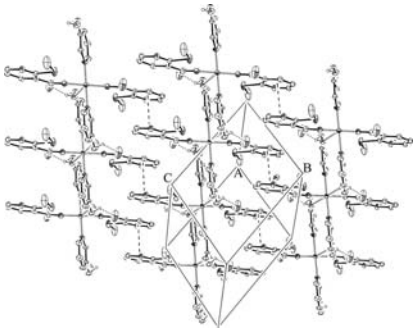

M.H. Alizadeh, K. Travis Holman, M. Mirzaei, H. Razavi

Polyhedron 25 (2006) 1567

Triprolinium 12-phosphomolybdate: Synthesis, crystal structure and properties of $[C_5H_{10}NO_2]_3[PMo_{12}O_{40}] \cdot 4.5H_2O$

This new organic–inorganic salt, hereafter **I**, has been synthesized and characterized by means of elemental analyses, IR spectrum, PNMR, ^{13}C NMR and single-crystal X-ray diffraction. The crystal structure consists of $[PMo_{12}O_{40}]^{3-}$ units linked together with $C_5H_{10}NO_2^{1+}$ cations and hydrogen bonded waters. The L-prolines retain their chirality and the zig-zag arrangement of the Keggin units bears some resemblance to the DNA strands.

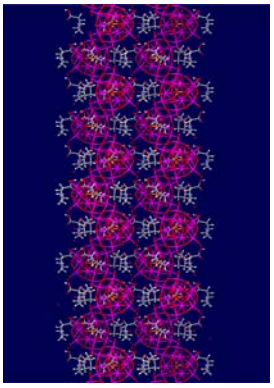

S. Senapoti, Sk. Jasimuddin, G. Mostafa, T.-H. Lu, C. Sinha

Polyhedron 25 (2006) 1571

Coupling of arylamine with coordinated arylazopyrimidine in platinum(II) complexes. Single crystal X-ray structure, spectra and electrochemistry

Dichloro platinum(II) complexes of 2-(arylazo)pyrimidine and their reaction with aromatic amines are described in this work. One of the reaction products has been confirmed by X-ray diffraction study. The spectral and electrochemical results have been correlated with MO calculation.

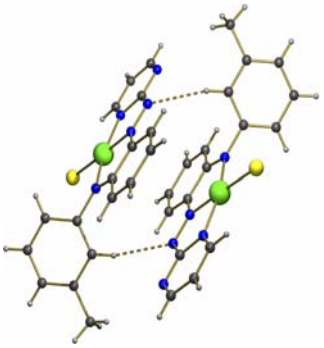

Neil F. Curtis, Kelly Flood, Ward T. Robinson

Polyhedron 25 (2006) 1579

N-rac-(5,7,7,12,12,14-hexamethyl-1,4,8,11-tetraazacyclotetradeca-4,14(1)-diene)copper(II): Structures of the perchlorate salt and a trinuclear tetracyanonickelato-bridged compound

The cation of *N-rac*-(5,7,7,12,12,14-hexamethyl-1,4,8,11-tetraazacyclotetradeca-4,14(1)-diene)copper(II) perchlorate has twofold symmetry with $Cu–N_{amine}$ = 1.994(1) and $Cu–N_{imine}$ = 1.969(1) Å, and with weak off-axis interactions with perchlorate oxygen atoms, Cu–O = 3.017(1) Å. The structure is compared with those of homologues with 14–18 ring-members. The tetracyanonickelate(II) compound has a trinuclear tetracyanonickelate-bridged cation with mean $Cu–N_{amine}$ = 2.009(3), mean $Cu–N_{imine}$ = 1.974(3), $Cu–N_{cyano}$ = 2.298(2) Å and $Cu–N_{cyano}{=}C$ = 142.1(2)°.

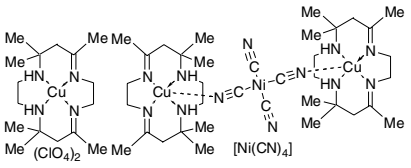

Jose V. Ros-Lis, Ramón Martínez-Máñez, Angel Benito, Juan Soto

Polyhedron 25 (2006) 1585

Naphthoquinone derivatives as receptors for the chromogenic sensing of metal cations and anions

The use of two naphthoquinone derivatives as cation and anion chromogenic chemosensors is reported.

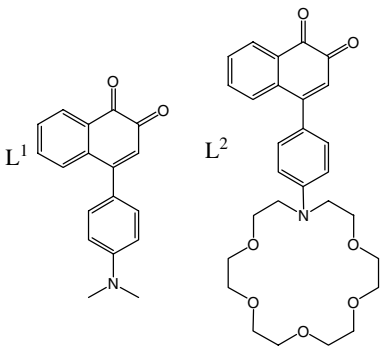

Cameron Jones, Peter C. Junk, Marc Kloth, Kathryn M. Proctor, Andreas Stasch

Polyhedron 25 (2006) 1592

Bulky amidinato complexes and amidine adducts of Al, Ga and In halides

The reactions of several bulky amidinate salts with group 13 metal(I), (II) and (III) halides have been carried out. These have led to a variety of amidinato-metal(II) or (III) halide complexes (e.g., see picture) which have been structurally characterised.

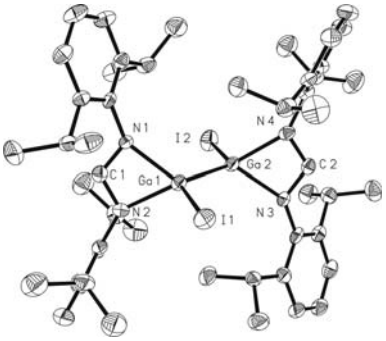

Neil F. Curtis, Kelly Flood, Ward T. Robinson

Polyhedron 25 (2006) 1601

Some nickel(II) and copper(II) compounds with β-amino-imine ligands; the structures of {4,5-dimethyl- (and 4,6-diethyl-6-methyl-) -3,7-diazanon-3-ene-1,9-diamine}nickel(II) tetrachlorozincate

Reaction of tris(ethane-1,2-diamine)nickel(II) or bis(ethane-1,2-diamine)copper(II) tetrachlorozincate with butanone yields (4,6-diethyl-6-methyl-3,7-diazanon-3-ene-1,9-diamine)-nickel or -copper(II) tetrachlorozincate while the reaction in the presence of paraformaldehyde yields (4,5-dimethyl-3,7-diazanon-3-ene-1,9-diamine)-nickel or -copper(II) tetrachlorozincate. The structures of the nickel(II) compounds are reported.

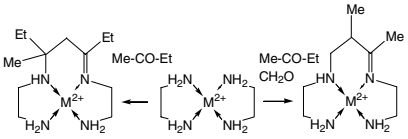

Dmitry G. Yakhvarov, Damir I. Tazeev, Oleg G. Sinyashin, Giuliano Giambastiani, Claudio Bianchini, Anna M. Segarra, Peter Lönnecke, Evamarie Hey-Hawkins

Polyhedron 25 (2006) 1607

Electrochemical synthesis of the σ-aryl complex [NiBr(Mes)(bpy)] and its use as catalyst precursor for the oligomerization of ethylene (Mes = 2,4,6-trimethylphenyl, bpy = 2,2′-bipyridine)

An efficient catalyst precursor for the oligomerization of ethylene to even-numbered olefins in the C_4–C_{26} range with a Schulz–Flory distribution – the organonickel σ-aryl complex [NiBr(Mes)(bpy)] (Mes = 2,4,6-trimethylphenyl, bpy = 2,2′-bipyridine) – was prepared in high-yield by oxidative addition of mesityl bromide either to electrochemically generated [Ni(bpy)] or to [Ni(COD)$_2$] (COD = 1,5-cyclooctadiene) in the presence of 2,2′-bipyridine.

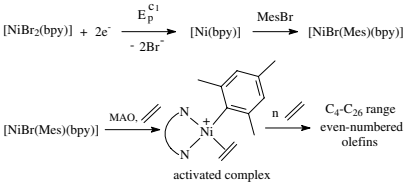

Chunyang Jia, Shi-Xia Liu, Christina Ambrus, Gäel Labat, Antonia Neels, Silvio Decurtins

Polyhedron 25 (2006) 1613

An organic charge transfer salt (TCN-DBTTF)[Fe(H_2O)$_6$][$FeBr_4$]$_3$: Synthesis, crystal structure and physical properties

A charge transfer salt (TCN-DBTTF)-[Fe(H_2O)$_6$][$FeBr_4$]$_3$ was synthesized by electrocrystallization and structurally characterized. As a result of the specific crystal packing, the compound shows a low electrical conductivity in the order of 10^{-7} S cm^{-1} and the magnetic measurements exhibit overall antiferromagnetic exchange interactions among the three different spin carriers.

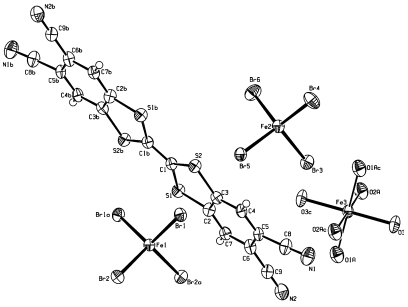

Ya-Min Li, Jian-Jun Zhang, Rui-Biao Fu, Sheng-Chang Xiang, Tian-Lu Sheng, Da-Qiang Yuan, Xi-He Huang, Xin-Tao Wu

Polyhedron 25 (2006) 1618

Three new cubane-like transition metal complexes of di-2-pyridyl ketone in gem-diol form: Syntheses, crystal structures and properties

Three new complexes, $[\{Cu_4(dpd\text{-}H)_4(ClO_4)_2(H_2O)_2\}(ClO_4)_2 \cdot 2H_2O]$ (**1**), $[\{Ni_4(dpd\text{-}H)_4(H_2O)_4\}(ClO_4)_4 \cdot 4H_2O]$ (**2**) and $[\{Ni_4(dpd\text{-}H)_4(OAc)_2(H_2O)_2\}(ClO_4)_2]$ (**3**) have been synthesized and characterized. Single crystal X-ray analysis shows all of them have the same M_4O_4 (M = Cu, Ni) cubane-like centers.

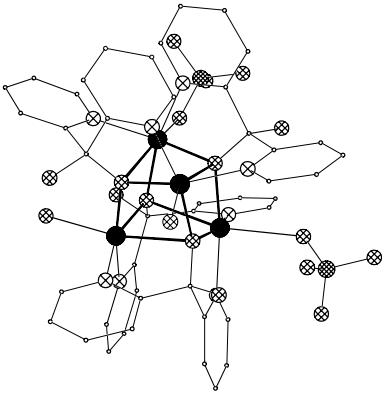

Philip C. Andrews, Simone Calleja, Melissa Maguire

Polyhedron 25 (2006) 1625

Crystal structures and unusual solution behaviour of diastereomeric aluminium and gallium complexes of chiral amines $[Me_3M \cdot RR^*NH]$

Six highly air and moisture sensitive diastereomeric adducts of trimethylaluminium and gallium have been formed from reaction with the three commonly used chiral secondary amines; ((*S*)-Ph(Me)CH)(PhCH$_2$)NH, (*R*,*R*)-Ph(Me)CH$_2$NH and (*S*)-Ph(Me)CH(CH$_2$CH=CH$_2$)NH, and their structures determined by single crystal X-ray diffraction. They were all found to be four coordinate monomers crystallising in the space group $P2_12_12_1$. Investigation of their solution structures by multinuclear and variable temperature NMR indicated that in contrast to the others (*S*,*R*)-$[Me_3Al \cdot HN(CHMePh)(CH_2Ph)]$ appeared to form two different isomers in toluene solution.

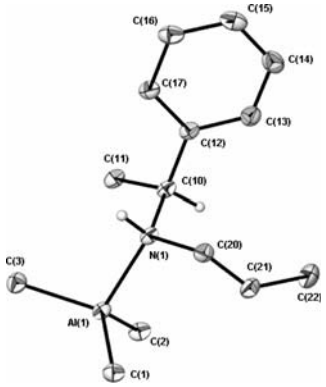

Saeed Ahmad, Anvarhusein A. Isab, Saqib Ali, Abdul Rahman Al-Arfaj

Polyhedron 25 (2006) 1633

Perspectives in bioinorganic chemistry of some metal based therapeutic agents

The use of metals in therapeutic drugs have become increasingly important over the last couple of decades resulting in a variety of exciting and valuable drugs such as cisplatin and auranofin. In this review, biocoordination chemistry of several metallodrugs (gold antiarthritic, silver antibacterial, vanadium antidiabetic and bismuth antiulcer, drugs) and their possible mechanism of action has been described. Various structure–activity relationships and biochemical aspects of metal binding to cellular targets have been explained.

Ramu Kannappan, Stefania Tanase, Ilpo Mutikainen, Urho Turpeinen, Jan Reedijk

Polyhedron 25 (2006) 1646

Low-spin iron(III) Schiff-base complexes with symmetric hexadentate ligands: Synthesis, crystal structure, spectroscopic and magnetic properties

The paper describes the synthesis and characterization of four new iron(III) complexes with two hexadentate Schiff-base ligands having N_4O_2 donor sets. In all cases, the molecular structure is built up by complex cations $[Fe(L)]^+$ and counter anions, ClO_4^- or BF_4^-. The mononuclear entities are organized into infinite 1D chains as a result of the hydrogen-bonding interactions established between the secondary amine functions of the Schiff-base ligand and counterions. Spectroscopic studies as well as temperature dependent magnetic properties indicate that all four iron(III) complexes are in low-spin electronic configuration.

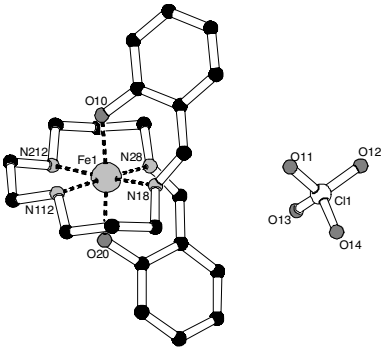

H.V. Rasika Dias, Himashinie V.K. Diyabalanage

Polyhedron 25 (2006) 1655

Trimeric silver(I) pyrazolates with isopropyl, bromo, and nitro substituents: Synthesis and characterization of $\{[3,5\text{-}(i\text{-}Pr)_2Pz]Ag\}_3$, $\{[3,5\text{-}(i\text{-}Pr)_2,4\text{-}(Br)Pz]Ag\}_3$, and $\{[3,5\text{-}(i\text{-}Pr)_2,4\text{-}(NO_2)Pz]Ag\}_3$

Trimeric Ag(I) complexes of 3,5-di(isopropyl)-pyrazolate, 3,5-di(isopropyl),4-bromopyrazolate, and 3,5-di(isopropyl),4-nitropyrazolate ligands have been isolated. Both $\{[3,5\text{-}(i\text{-}Pr)_2Pz]Ag\}_3$ and $\{[3,5\text{-}(i\text{-}Pr)_2,4\text{-}(Br)Pz]Ag\}_3$ exist as pairs of trimers with weak Ag···Ag contacts, whereas $\{[3,5\text{-}(i\text{-}Pr)_2,4\text{-}(NO_2)Pz]Ag\}_3$ exists as isolated trimers in the solid state.

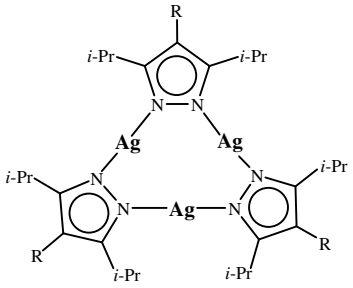

$\{[3,5\text{-}(i\text{-}Pr)_2,4\text{-}(R)Pz]Ag\}_3$

R = H, Br, NO_2

Zureima García-Hernández, Angelina Flores-Parra, Jean Michel Grevy, Ángel Ramos-Organillo, Rosalinda Contreras

Polyhedron 25 (2006) 1662

2-Aminobenzothiazole phosphorus amides: Molecular and supramolecular structures, hydrogen bonds and sulfur donor–acceptor interactions

Nine phosphorus amides derived from 2-amino-benzothiazole (**1**): 2-aminobenzothiazole-diphenyl-phosphane (**2**), 2-aminobenzothiazole-diethylphos-phite (**3**), and lithium 2-aminobenzothiazolide-diphe-nylphosphane (**9**) and their corresponding oxidated compounds **4**–**8** and **10** are reported. In solution, preferred tautomers and conformers of **2**–**10** have been identified using NMR spectroscopy. Oxidation of **2** and **3** produces **4**–**8** associated with migration of the anilinic proton to the endocyclic nitrogen leading a delocalized dienyl system. Migration of phenyl groups from **2** and chlorides from $NHEt_3Cl$ to $Pb(NO_3)_2$ afforded *bis*-(2-aminobenzothiazolium) tetrachloro-diphenyl plumbate (**11**). Analysis of the X-ray dif-fraction structures of **2**, **7**, **10** and **11** showed S···H–Ar, S···S, S···P, and S···Cl donor acceptor interactions in the solid state, and that compounds **2** and **7** form dimers by **6** and **4** intermolecular cooperative hydrogen bonds.

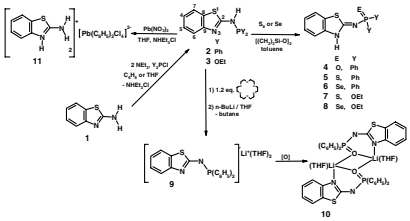

Franz A. Mautner, Ramon Vicente, Salah S. Massoud

Polyhedron 25 (2006) 1673

Structure determination of nitrito- and thio-cyanato-copper(II) complexes: X-ray struc-tures of $[Cu(Medpt)(ONO)(H_2O)]ClO_4$ (**1**), $[Cu(dien)(ONO)]ClO_4$ (**2**) and $[Cu_2(Medpt)_2(\mu_{N,S}\text{-}NCS)_2](ClO_4)_2$ (**3**) (Medpt = 3,3′-diamino-*N*-methyldipropylamine and dien = diethylenetriamine)

The synthesis, characterization and X-ray structures of the mononomeric nitrite complexes $[Cu(Medpt)(ONO)(H_2O)]ClO_4$ (**1**), $[Cu(dien)(ONO)]ClO_4$ (**2**), and the dinuclear bridged thiocyanato complex $[Cu_2(Medpt)_2(\mu_{N,S}\text{-}NCS)_2](ClO_4)_2$ (**3**) are described.

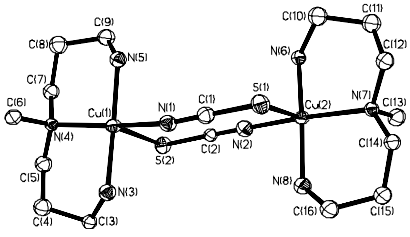

Kamala Mitra, Dipankar Mishra, Subhendu Biswas, C. Robert Lucas, Bibhutosh Adhikary

Polyhedron 25 (2006) 1681

Binuclear manganese(III) complexes with car-boxylate bridges: Synthesis, structure, electro-chemistry and magnetic properties

A series of μ-oxo, μ-carboxylato binuclear manganese(III) complexes derived from bipy, phen and different carboxylate ligands have been synthesized.

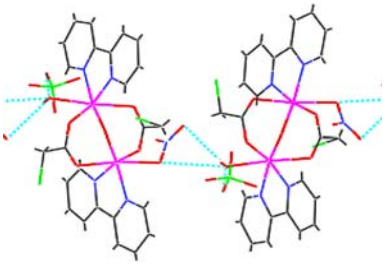

Anindita Sarkar, Samudranil Pal

Polyhedron 25 (2006) 1689

Some ternary complexes of oxovanadium(IV) with acetylacetone and *N*-(2-pyridyl)-*N*′-(salicylidene)hydrazine and its derivatives

Synthesis and physical properties of a series of ternary oxovanadium(IV) complexes having the formula [VO(phsalR)(acac)] (HphsalR = *N*-(2-pyridyl)-*N*′-(5-R-salicylidene)hydrazine and Hacac = acetylacetone) have been described. X-ray structures reveal distorted octahedral N_2O_4 coordination sphere around the metal centre and intermolecular N–H···O=V hydrogen bond assisted self-assembly to one-dimensional ordering in the crystal lattice.

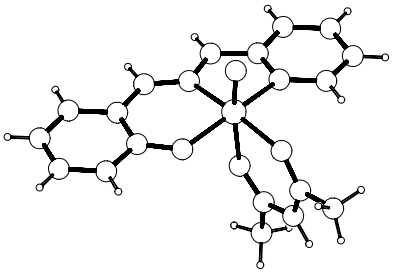

Mohammad El-khateeb, Khalil J. Asali, Anas Lataifeh

Polyhedron 25 (2006) 1695

Iron dithiocarbonate complexes: Structure of $CpFe(CO)_2SC(S)O\text{-}4\text{-}C_6H_4Cl$

The complexes $CpFe(CO)_2S\text{-}C(S)OAr$ (**1**) were prepared by the reaction of $(\mu\text{-}S_x)[CpFe(CO)_2]_2$ with aryl-chlorothionoformates (Ar = Ph (**1a**), $4\text{-}C_6H_4Cl$ (**1b**), $4\text{-}C_6H_4F$ (**1c**), C_6F_5 (**1d**), $4\text{-}C_6H_4CH_3$ (**1e**)). The conversion of **1** into $CpFe(CO)(\kappa^2S,S\text{-}SC(S)OAr)$ (**2**), in which the dithiocarbonate ligand is bonded to the iron through the two S-atoms, can be achieved photolytically. The structure of $CpFe(CO)_2SC(S)O\text{-}4\text{-}C_6H_4Cl$ (**1b**) is reported.

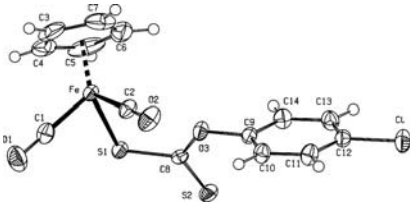

Jean-Claude Berthet, Pierre Thuéry, Michel Ephritikhine

Polyhedron 25 (2006) 1700

First characterization of an uranium(III) complex with a carbonyl-containing ligand: Syntheses and X-ray crystal structures of the homoleptic dimethylformamide complexes $[M(dmf)_n]I_3$ (M = Ce, Nd and n = 8; M = La, Ce, U and n = 9)

Crystals of the title compounds were deposited from dmf solutions of LnI_3 (Ln = La, Ce, Nd) and $[UI_3(py)_4]$. The crystal structures show the differences in the M–O distances to reflect the variation in the ionic radii of the metals.

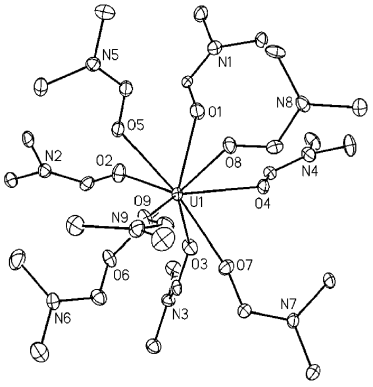

The Publisher encourages the submission of articles in electronic form thus saving time and avoiding rekeying errors. For detailed instructions on the preparation of manuscripts and of electronic artwork, consult the Author Gateway for Elsevier at http://authors.elsevier.com

SCIENCE DIRECT®

Full text of this journal is available, on-line from **ScienceDirect**. Visit **www.sciencedirect.com** for more information.

Available online at www.sciencedirect.com
SCIENCE DIRECT®
Polyhedron 25, issue 6, 17 April 2006
POLYHEDRON
www.elsevier.com/locate/poly

Contents

Papers

Soma Sen, Chirantan Roy Choudhury, Pritha Talukder, Samiran Mitra, Matthias Westerhausen, Alexander Nikolai Kneifel, Cédric Desplanches, Nathalie Daro, Jean-Pascal Sutter

Polyhedron 25 (2006) 1271

A novel polymeric Cu(II) assemblage and a monomeric Ni(II) complex from a new easy-to-prepare flexible polytopic ligand: Synthesis, structural and magnetic studies

The difference in coordination behavior of one new flexible polytopic ligand $\mathbf{H_2L}$ ($\mathbf{L} = C_{16}H_{14}N_6O_2$) has been examined with Cu(II) and Ni(II) acetate. It leads to the formation of a polynuclear pentacoordinated Cu(II) assemblage and a mononuclear four coordinated Ni(II) complex. The polynuclear copper complex exhibits strong antiferromagnetic behavior at low temperature with $J = -327\ cm^{-1}$.

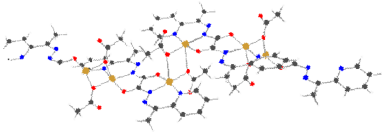

Sülin Taşcıoğlu, Bahattin Yalçın, Tarana M. Nasrullayeva, Ömer Andaç, Orhan Büyükgüngör, Adnan Aydın, Ajdar Akber Medjidov

Polyhedron 25 (2006) 1279

The syntheses, structure and properties of cobalt complexes with β-alanine derivatives

Cobalt(II) reacts with *N*-(2-hydroxynaphtalidene)-β-alanine to give binuclear (Co^{II}–Co^{II}) complex **III** and trinuclear mixed-valence (Co^{III}–Co^{II}–Co^{III}) complex **IV**. X-ray and magnetic data along with the spectral data indicated the weak distorted octahedric environment around Co(III) of **IV**. Binuclear complex is oxidized by oxygen to give trinuclear complex in the presence of Co(II) and is reduced by $NaBH_4$ to give the Co(II) complex of reduced form of the Schiff base, for which kinetic data have been evaluated. Trinuclear complex **IV** could not be reduced.

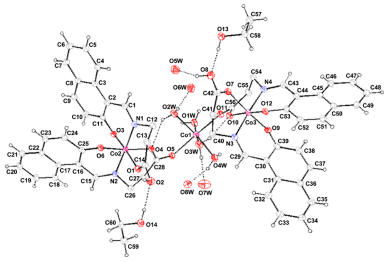

Chew Hee Ng, Chia Meow Lin, Ti Mei Chang, Siang Guan Teoh, Siaw Yang Yap, Seik Weng Ng

Polyhedron 25 (2006) 1287

Mono- and di-*N*-acetamidomethylated derivatives of *bis*(L-alaninato)copper(II): Characterization and nucleolytic property. Crystal structure of *bis*[*N*,*N*-di-(*N*′-methylacetamido)-L-alaninato]copper(II)

Mono- and di-*N*-acetamidomethylated derivatives of Cu(L-ala)$_2$. Crystal structure determination of the latter ($R_1 = R_2 = CH_2NH(C{=}O)CH_3$) shows intra- and intermolecular hydrogen bonding of the *N*-methylacetamido substituents. The former derivative ($R_1 = H$; $R_2 = CH_2NH(C{=}O)CH_3$), which dissolves readily in water, cleaves DNA more efficiently than Cu(L-ala)$_2$. Both complexes are additionally characterized by electron impact mass spectrometry.

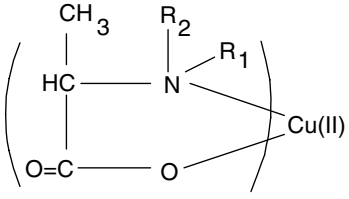

Martin Beran, Jiří Příhoda, Zdirad Žák, Miloš Černík

Polyhedron 25 (2006) 1292

A new route to the syntheses of alkali metal bis(fluorosulfuryl)imides: Crystal structure of $LiN(SO_2F)_2$

A new route to the syntheses of alkali metal bis(fluorosulfuryl)imides was developed. The crystal structure of lithium bis(fluorosulfuryl) imide was determined.

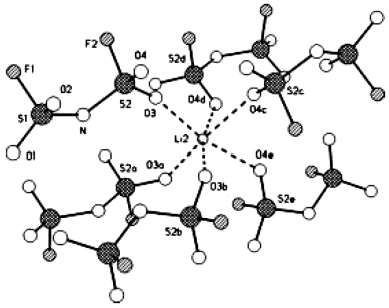

Debasis Banerjee, Umasankar Ray, Sk. Jasimuddin, Jian-Cheng. Liou, Tian-Huey Lu, Chittaranjan Sinha

Polyhedron 25 (2006) 1299

Copper(II) complexes of thioether containing an azoimidazolyl system. X-ray structure of $Cu(SEtaaiNEt)Cl_2$ (SEtaaiNEt = 1-ethyl-2-{(*o*-thioethyl)phenylazo}imidazole)

A new series of tridentate NN′S ligands has been synthesized by coupling of the thioalkylaryldiazonium ion with imidazole and subsequent alkylation. Copper(II) complexes $Cu(NN'S)Cl_2$ are synthesized and structurally characterized. Ternary complexes are also reported.

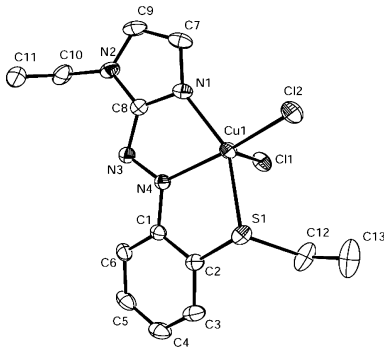

Chi Chen, Chun-Wei Yeh, Jhy-Der Chen

Polyhedron 25 (2006) 1307

Syntheses, structures and thermal properties of two new copper(II) melamine complexes

The reactions of melamine with $CuCl_2 \cdot 2H_2O$ and $Cu(OAc)_2 \cdot H_2O$ in boiling methanol afforded the complexes $Cu_2Cl_2\mu\text{-}Cl)(\mu\text{-}OCH_3)\text{-}(CH_3OH)_2(MA)_2 \cdot 2Et_2O$ (MA = melamine), **1**, and $[Cu(\eta^1\text{-}OAc)(\mu\text{-}OCH_3)(MA)]_2 \cdot 0.33\text{-}H_2O$, **2**, respectively. The molecules of these two complexes are interlinked by the N–H···N self-complementary hydrogen bonds and N–H···X (X = Cl or O) interactions to form 2-D molecular sheets and a 3-D porous structure, respectively. Complex **2** shows both hexagonal and triangular pores constrained by the N–H···N self-complementary hydrogen bonds.

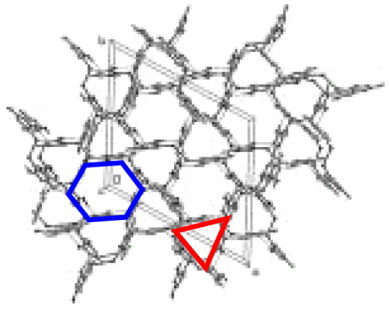

Neil F. Curtis, Kelly Flood, Ward T. Robinson

Polyhedron 25 (2006) 1313

Nickel(II) compounds of some nitro-substituted imine–triamine macrocycles; the structure of (5,7,7,13 tetramethyl-13-nitro-1,4,8,11-tetraazacyclotetradec-4-ene κ^4 $N^{1,4,8,11}$)-nickel(II) tetrachlorozincate(II)

Reactions of (4,6,6-trimethyl-3,7-diazanon-3-ene-1,9-diamine)nickel(II) with methanal and nitroethane (or nitropropane) yield (5,7,7,13-tetramethyl-13-nitro-1,4,8,11-tetraazacyclotetradec-4-ene)nickel(II) {or (13-ethyl-5,7,7-trimethyl-13-nitro-1,4,8,11-tetraazacyclotetradec-4-ene)nickel(II)}. The structure of (5,7,7,13-tetramethyl-13-nitro-1,4,8,11-tetraazacyclotetradec-4-ene) nickel(II) tetrachlorozincate is reported.

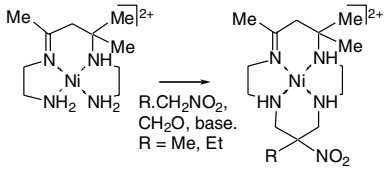

Andréa de Moraes Silva, Ana Lucia Ramalho Mercê, Antonio Sálvio Mangrich, Cláudio A. Téllez Souto, Judith Felcman

Polyhedron 25 (2006) 1319

Potentiometric and spectroscopic study of mixed copper(II) complexes with amino acids and either adenosine 5′ triphosphate or phosphocreatine

The present paper reports the results of aqueous solution equilibria and spectral studies of binary and ternary copper(II) ion complexes with adenosine 5′ triphosphate or phosphocreatine with the amino acids glycine, serine, tyrosine and threonine.

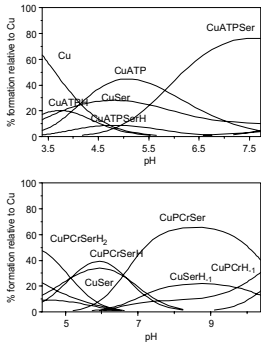

Chang-Yan Sun, Lin-Pei Jin

Polyhedron 25 (2006) 1327

Supramolecular architecture constructed by *p*-carboxycinnamic acid and d-block metal ions

The structures of four new supramolecular complexes of *p*-carboxycinnamic acid and d-block metal ions are reported. Their supramolecular networks are constructed by coordination bonds, hydrogen bonds and π–π stacking interactions.

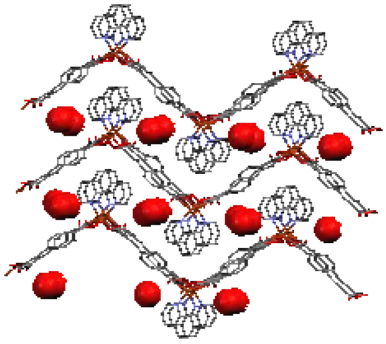

Sevil İrişli, Selmin Yanar

Polyhedron 25 (2006) 1333

Synthesis and crystallographic characterization of cationic Pd(II) complexes containing bis(diphenylthiophosphinyl)methane

The reactions of $PdCl_2(L\text{-}L)$ [L-L = $Ph_2PCH_2PPh_2$ (dppm), $Ph_2PCH_2CH_2PPh_2$ (dppe) and $Ph_2PCH_2CH_2CH_2PPh_2$ (dppp)] with an equivalent amount of $Ph_2P(S)CH_2P(S)Ph_2$ ($dppmS_2$) gave the cationic complexes $[Pd(L\text{-}L)(dppmS_2)]^{2+}$ which were isolated as perchlorate salts [dppm (**1**), dppe (**2**) and dppp (**3**)]. The complexes **1** and **3** were crystallographically characterized.

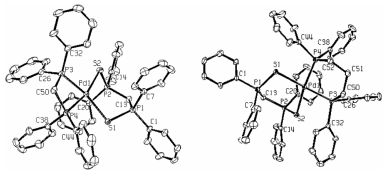

Charalambos Litos, Aris Terzis, Catherine Raptopoulou, Aliki Rontoyianni, Alexandra Karaliota

Polyhedron 25 (2006) 1337

Polynuclear oxomolybdenum(VI) complexes of dihydroxybenzoic acids: Synthesis, spectroscopic and structure characterization of a tetranuclear catecholato-type coordinated 2,3-dihydroxybenzoate and a novel tridentate salicylato-type coordinated 2,5-dihydroxybenzoate trinuclear complex

The synthesis and the single-crystal X-ray structural characterization of two novel complexes of molybdenum with 2,3- and 2,5-dihydroxybenzoic acids are reported. The tetranuclear complex with 2,3-DHBA has two μ_3-OCH_3 bridges and intramolecular hydrogen bonding of the carboxylic group. The unusual trinuclear complex with 2,5-DHBA demonstrates a unique binding mode of the ligand. The spectroscopic properties in solid state and in solution have been studied and interpreted.

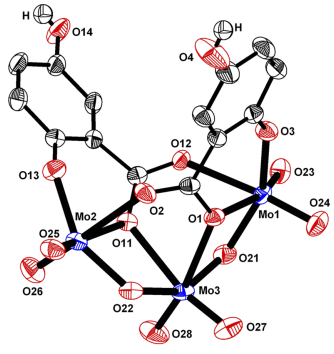

B. Machura, A. Jankowska, R. Kruszynski, J. Kłak, J. Mroziński

Polyhedron 25 (2006) 1348

Synthesis, crystal, molecular and electronic structure of the $[ReCl_4(pzH)(PPh_3)]$ and $[ReCl_4(pyz)(PPh_3)]$ complexes

The reactions of the $[ReCl_4(PPh_3)_2]$ complex with pyrazole (pzH) and pyrazine (pyz) have been examined and two novel Re(IV) compounds – $[ReCl_4(pzH)(PPh_3)]$ (**1**) and $[ReCl_4(pyz)(PPh_3)]$ (**2**) – have been obtained. The compounds have been studied by IR, UV–Vis spectroscopy and X-ray crystallography. The electronic structures of **1** and **2** have been calculated with the density functional theory (DFT) method. The spin-allowed quartet–quartet electronic transitions of **1** and **2** have been calculated with the time-dependent DFT method, and the UV–Vis spectra of the title compounds have been discussed on this basis. From magnetic studies a small, negative value of *J* obtained confirms the occurrence of weak antiferromagnetic interactions between the rhenium centers in the crystal lattice.

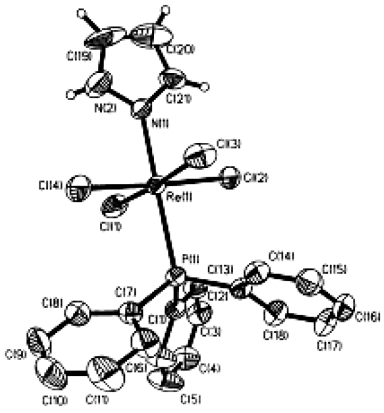

Yu-Sheng Jiang, Zhen-Tao Yu, Zuo-Lei Liao, Guang-Hua Li, Jie-Sheng Chen

Polyhedron 25 (2006) 1359

Syntheses and photoluminescent properties of two uranyl-containing compounds with extended structures

Two new uranyl-containing compounds were synthesized hydrothermally and they exhibited intense yellow light under the excitation of UV rays. The structures of the two compounds were analyzed by single-crystal X-ray diffraction.

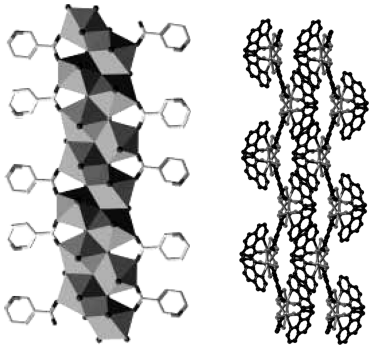

Ritam Mukherjee, Basab Bijayi Dhar, Rupendranath Banerjee

Polyhedron 25 (2006) 1367

Electron transfer between ascorbic acid and a (μ-oxo) diiron(III,III) complex: An example of chloride inhibition

The complex ion $[Fe_2^{III}(\mu\text{-}O)(phen)_4(H_2O)_2]^{4+}$ (**1**) and each of its H_2O acid dissociated derivatives **1a** and **2a** react with one ascorbate ion in presence of excess phenanthroline in an inner sphere pathway to produce $[Fe(phen)_3]^{2+}$.

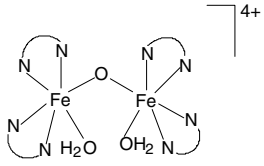

(**1**)

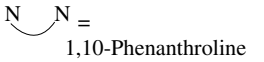

1,10-Phenanthroline

M.A.M. Khouna Sanhoury, M.T. Ben Dhia, M. Nsangou, M.R. Khaddar

Polyhedron 25 (2006) 1373

Beryllium(II) complexes with $(R_2N)_2P(O)F$ (R = Me or Et): Synthesis and characterisation by multinuclear (^{31}P, ^{19}F and ^{9}Be) NMR in solution

Two complexes of the type $Be[(R_2N)_2P(O)F]_4(ClO_4)_2$ (R = Me (**1**) and R = Et (**2**)) were prepared from beryllium perchlorates and the ligands $(R_2N)_2P(O)F$. They were characterised in solution by multinuclear (^{31}P, ^{19}F and ^{9}Be) NMR spectroscopy. DFT calculations were carried out to complement the NMR data.

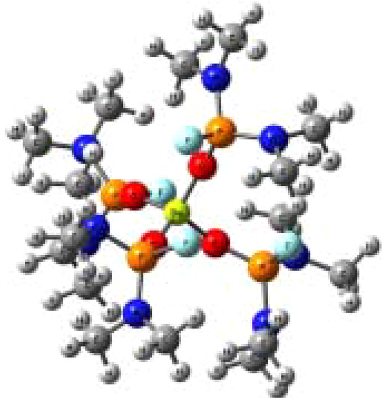

Wei Huang, Takuji Ogawa

Polyhedron 25 (2006) 1379

Spontaneous resolution of Δ and Λ enantiomeric pair of $[Ru(phen)(bpy)_2](PF_6)_2$ (phen = 1,10-phenanthroline, bpy = 2,2′-bipyridine) by conglomerate crystallization

Spontaneous resolution is achieved for the Δ and Λ enantiomeric pair of ruthenium(II) complexes obtained by conglomerate crystallization from alcohol–water solutions, which is uncommon for six-coordinate Ru(II) complexes. The enantiomerically pure crystals pack into the chiral $P4_1$ and $P4_3$ space groups, respectively. A ligand exchange reaction is found between phen and bpy ligands for these Ru(II) complexes, but racemization is accompanied which has been proved by the single-crystal structure of the product.

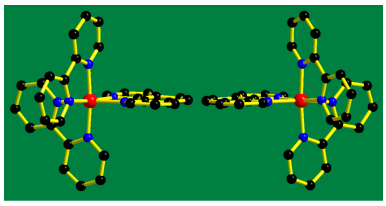

Δ (left) and Λ (right) enantiomeric pair of ruthenium(II) complexes

Mohammad El-khateeb

Polyhedron 25 (2006) 1386

Selenothiocarbonate complexes of iron: Structure of $CpFe(CO)_2SeC(S)O\text{-}4\text{-}C_6H_4Cl$

Stable complexes of general formula $CpFe(CO)_2SeC(S)OR$, were prepared by the reaction of $(\mu\text{-}Se)[CpFe(CO)_2]_2$ with ROC(S)Cl at room temperature. When a THF solution of **1** was photolyzed the chelate complexes $CpFe(CO)(\kappa^2 Se,S\text{-}SeC(S)OR)$ (**2**) were obtained in good yields. The structure of $CpFe(CO)_2SeC(S)O\text{-}4\text{-}C_6H_4Cl$ (**1b**) is reported.

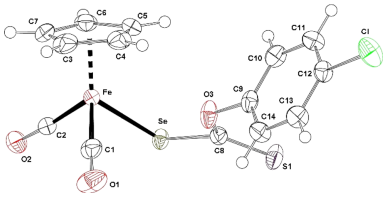

Athanassios K. Boudalis, Yiannis Sanakis, Catherine P. Raptopoulou, Vassilios Psycharis, Aris Terzis

Polyhedron 25 (2006) 1391

Further investigations on the $Fe(ClO_4)_3/RCO_2^-$/phen reaction system: Syntheses, structural and physical characterization of complexes $[Fe_2O(O_2CCCl_3)_2(phen)_2(H_2O)_2](ClO_4)_2$ and $[Fe_2O(O_2CCMe_3)_2(phen)_2(H_2O)_2](ClO_4)_2$

Two dinuclear complexes containing the $\{Fe_2O(O_2CR)_2\}_{2+}$ core have been synthesized and characterized structurally and spectroscopically by IR and ^{57}Fe Mössbauer spectroscopies. Magnetic susceptibility and EPR studies have been carried out on one of them.

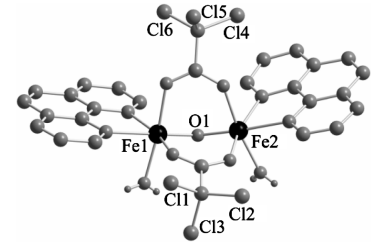

A. Bernalte-García, A.M. Lozano-Vila, F. Luna-Giles, R. Pedrero-Marín

Polyhedron 25 (2006) 1399

Structural characterization of a thiazoline-pyrazole ligand and its complexes with cobalt(II) and copper(II)

The thiazoline derivative 2-(pyrazol-1-yl)-2-thiazoline (PyTn) yields two novel complexes, $[CoCl_2(PyTn)_2] \cdot 2H_2O$ and $[\{CuCl(PyTn)\}_2(\mu\text{-}Cl)_2]$, by reaction with $CoCl_2 \cdot 6H_2O$ and $CuCl_2 \cdot 2H_2O$, respectively, in ethanol-water solution. The crystal structure of the cobalt(II) complex reveals a distorted octahedral geometry around cobalt(II) ion, whereas the copper(II) complex presents a structure consisting of two square pyramids linked by one edge.

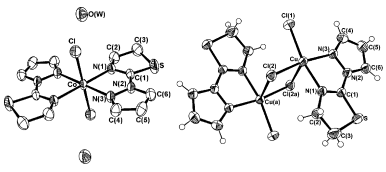

A. Sreekanth, Marthakutty Joseph, H.-K. Fun, M.R. Prathapachandra Kurup

Polyhedron 25 (2006) 1408

Formation of manganese(II) complexes of substituted thiosemicarbazones derived from 2-benzoylpyridine: Structural and spectroscopic studies

Three manganese(II) complexes of 2-benzoylpyridine-3-tetramethyleneiminyl thiosemicarbazone (HBpypTsc), 2-benzoylpyridine *N*(4)-cyclohexyl thiosemicarbazone (HBpychTsc) and 2-benzoylpyridine *N*(4)-phenylthiosemicarbazone (HBpyphTsc) were synthesized and physico-chemically characterized by means of partial elemental analyses, molar conductance measurements, magnetic measurements, electronic, infrared and EPR spectral studies. The three complexes were given the formulae as $[Mn(BpypTsc)_2]$ (**1**), $[Mn(BpychTsc)_2] \cdot H_2O$ (**2**), $[Mn(BpyphTsc)_2]$ (**3**). The structure of the compound **1** has been solved by single crystal X-ray crystallography and was found to be distorted octahedral.

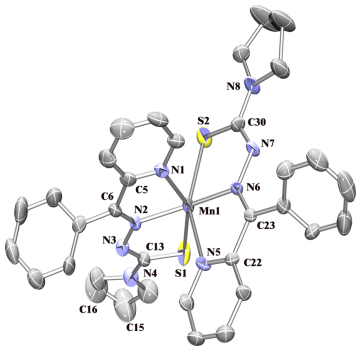

Sanjeev K. Shukla, A. Ranjan, A.K. Saxena

Polyhedron 25 (2006) 1415

Synthesis and characterization of some new mixed pentafluorophenyl organoantimony-(III and V) derivatives

Compounds of the type $(C_6F_5)_nSb(III)R_{3-n}$ [R = CH_3, $C_6H_4CH_3$-*p*, C_6H_5] have been synthesized by using grignard reactions and their oxidative addition reactions with Cl_2 or Br_2 carried out, which afford corresponding $(C_6F_5)_nSb(V)R_{3-n}X_2$ [X = Cl or Br] derivatives. The compounds were characterized by the micro-analysis, IR, NMR (^1H, ^{13}C and ^{19}F) and FAB mass analysis.

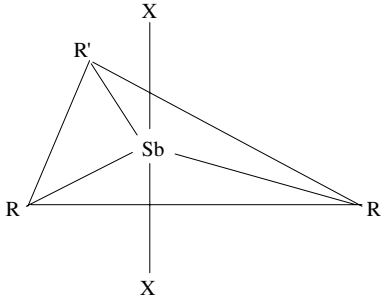

Alena Klanicová, Zdeněk Trávníček, Igor Popa, Michal Čajan, Karel Doležal

Polyhedron 25 (2006) 1421

Synthesis, characterization and in vitro cytotoxicity of Co(II) complexes with *N*6-substituted adenine derivatives: X-ray structures of 6-(4-chlorobenzylamino)purin-di-ium diperchlorate dihydrate and $[Co_6(\mu\text{-}L_6)_4Cl_8\text{-}(DMSO)_{10}] \cdot 4DMSO$

New mononuclear tetrahedral high-spin Co(II) complexes with 6-benzylaminopurine derivatives have been synthesized. The coordination via the *N9* atom of the adenine moiety has been confirmed by NMR data and DFT calculations. In vitro cytotoxicity of the complexes against human melanoma, sarcoma, leukaemia and carcinoma cell lines has been determined.

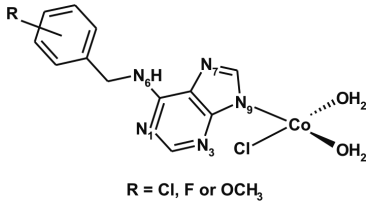

Vasiliy V. Brusko, Aydar I. Rakhmatullin, Valery G. Shtyrlin, Dmitry B. Krivolapov, Igor A. Litvinov, Nail G. Zabirov

Polyhedron 25 (2006) 1433

Crystal structure and dynamic behavior of $[Ni\{PhNHC(S)NP(S)(OPr^i)_2\text{-}S,S\}_2]$ complex in dichloromethane solution

The title complex has been found in crystal to be *trans* square-planar isomer with C_i symmetry (**C**). In solution three diamagnetic square-planar isomers – *trans*-chair–boat (**A**), *cis*-boat–boat (**B**), and *trans*-boat–boat (**C**) – are in slow exchange equilibria and undergo rather fast chemical exchange with minor (unobserved) paramagnetic pseudo-tetrahedral isomers ($\mathbf{A_T}$, $\mathbf{B_T}$, and $\mathbf{C_T}$). The thermodynamic constants, rate constants and activation parameters of these equilibria were calculated.

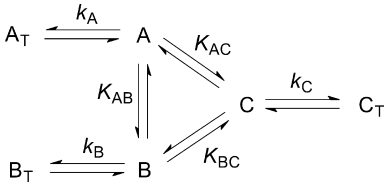

Agnieszka Gądek, Teresa Szymańska-Buzar

Polyhedron 25 (2006) 1441

Activation of the Si—H bond of silanes in photochemical reactions with $W(CO)_6$: Hydrosilylation of ketones and dehydrosilylation of alcohol by H_2SiPh_2

Photolysis of $W(CO)_6$ in the presence of hydrosilanes in *n*-heptane solution leads to Si—H bond activation and to the formation of a W—H bond. The photochemical activation of $W(CO)_6$ has been found effective for both the hydrosilylation of ketones as well as the dehydrosilylation of 2-propanol and water by H_2SiPh_2.

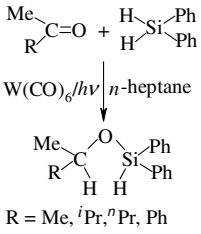

Marta Mariño, Eduardo Gayoso, José M. Antelo, Luis A. Adrio, Jesús J. Fernández, José M. Vila

Polyhedron 25 (2006) 1449

Synthesis and crystal structure analysis of ferrocenylthiosemicarbazone complexes of palladium(II): Unusual σPd–C bond cleavage

The thiosemicarbazone ligands $(\eta^5\text{-}C_5H_5)\text{-}Fe(\eta^5\text{-}C_5H_4)C(H)=NNHC(=S)NHR$ (R = H, Me) reacted with potassium tetrachloropalladate to give cyclometallated compounds with the organic ligand as terdentate [C, N, S], from which novel di- and tetranuclear species were obtained by reaction with the tertiary mono-, PPh_3, PPh_2Et, $P(C_6D_5)_3$, and diphosphines, $Ph_2PCH_2PPh_2$ (dppm) and $Ph_2P(CH_2)_4PPh_2$ (dppb), respectively.

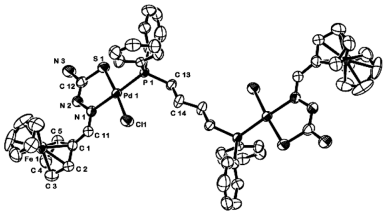

Eliana M. Sussuchi, Andréia A. de Lima, Wagner F. De Giovani

Polyhedron 25 (2006) 1457

Synthesis and electrochemical, spectral and catalytic properties of diphosphine–polypyridyl ruthenium complexes

The complexes $[Ru(L)(totpy)(H_2O)](PF_6)_2$ (L = 1,2-bis(dimethylphosphino)ethane and 1,2-bis(dichlorophosphino)ethane; totpy = 4′-(4-tolyl)-2,2′:6′,2″-terpyridine) were synthesized. Their electrochemical behaviour in function of pH was studied. The complexes were used as catalysts in electrochemical oxidations of benzyl alcohol, cyclohexanol, cyclohexene, ethylbenzene, 1,2-butanediol and 1, 4-butanediol, in solution and immobilized in carbon paste and ITO/Nafion® electrodes.

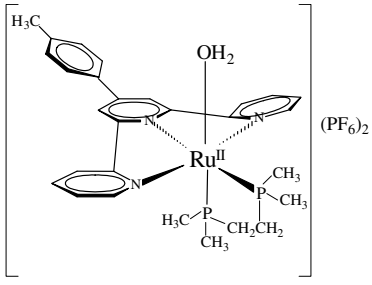

Elena López-Torres, Mª Antonia Mendiola, César J. Pastor

Polyhedron 25 (2006) 1464

Mercury and methylmercury complexes with a triazine-3-thione ligand

A new complex derived from 5-methoxy-5,6-diphenyl-4,5-dihydro-2H-[1,2,4]triazine-3-thione (LH_2OCH_3) with methylmercury chloride was synthesised and characterised. Its crystal structure, as well as those of the mercury nitrate derivative, shows that the ligand L is only bonded through the sulphur atom, coordination mode that is nor usual in this kind of ligands, giving a linear geometry around the mercury ion in both complexes.

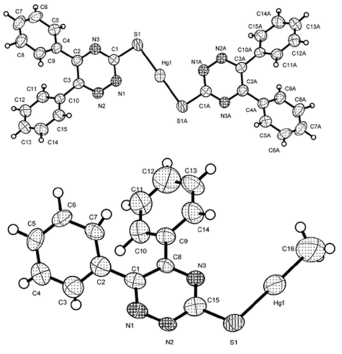

José A. Fernandes, Susana S. Braga, Martyn Pillinger, Rute A. Sá Ferreira, Luís D. Carlos, Alan Hazell, Paulo Ribeiro-Claro, Isabel S. Gonçalves

Polyhedron 25 (2006) 1471

β-Cyclodextrin inclusion of europium(III) tris(β-diketonate)-bipyridine

The crystal structure of the compound Eu(NTA)$_3$ · bipy · 0.44CHCl$_3$ was determined by X-ray diffraction and compared with previously reported structures containing the adduct Eu(NTA)$_3$ · bipy. Encapsulation of Eu(NTA)$_3$ · bipy in β-cyclodextrin gave an inclusion compound which exhibited photoluminescence and excitation spectra different from those of the non-included complex, revealing, in particular, an enhancement of the Eu^{3+} sensitized process.

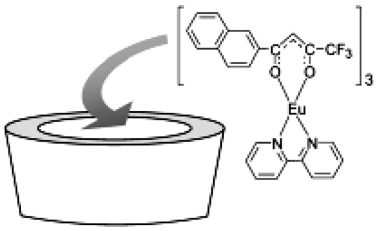

Doyel Bose, Golam Mostafa, Rosa D. Bailey Walsh, Michael J. Zaworotko, Barindra K. Ghosh

Polyhedron 25 (2006) 1477

Synthesis, structure and properties of a trinuclear compound $[Cu_2Cd(tren)_2(NCS)_6]$: Example of dynamic molecular ion, $[Cd(NCS)_{6-n}(SCN)_n]^{4-}$ (n = 0–6)

A 1:2:2:6 molar ratio of Cd(NO$_3$)$_2$ · 4H$_2$O, Cu(NO$_3$)$_2$ · 3H$_2$O, tren and NH$_4$NCS in aqueous solution affords a trinuclear complex of the type $[Cu_2Cd(tren)_2(NCS)_6]$ (**1**). The crystal structure of **1** displays three-dimensional hydrogen bonded network of the trinuclear units.

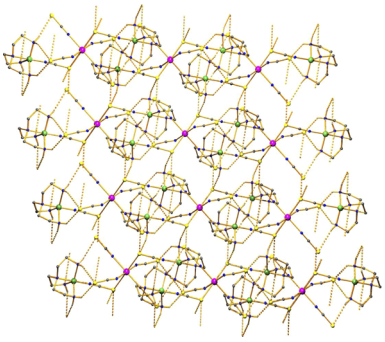

Silvia García, Laura Ciullo, María Silvina Olivera, Juan Carlos González, Sebastián Bellú, Antal Rockembauer, Lazlo Korecz, Luis F. Sala

Polyhedron 25 (2006) 1483

Kinetics and mechanism of the reduction of chromium(VI) by D-fructose

The reduction of chromium(VI) to chromium(III) by D-fructose in $HClO_4$ takes places through a complex multistep mechanism.

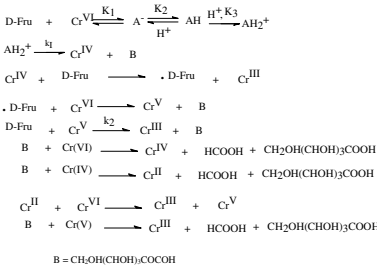

The Publisher encourages the submission of articles in electronic form thus saving time and avoiding rekeying errors. For detailed instructions on the preparation of manuscripts and of electronic artwork, consult the Author Gateway for Elsevier at http://authors.elsevier.com

SCIENCE DIRECT®

Full text of this journal is available, on-line from **ScienceDirect**. Visit **www.sciencedirect.com** for more information.

Available online at www.sciencedirect.com
ScienceDirect
Polyhedron 25, issue 15, 3 November 2006
POLYHEDRON
www.elsevier.com/locate/poly

Contents

Papers

Edmund Kwiatkowski, Grzegorz Romanowski, Waldemar Nowicki, Marek Kwiatkowski

Polyhedron 25 (2006) 2809

Dioxovanadium(V) complexes of Schiff bases derived from *S*-(+)-2-(aminomethyl)pyrrolidine and aromatic *o*-hydroxycarbonyl compounds: Synthesis, characterization and structure

Two diastereomers, which differ in absolute configurations of chiral centres and in conformation of five-membered rings, in one crystal of *N*-(7-methylsalicylidene)-(*S*)-(2-pyrrolidynylmethyl)amine dioxovanadium(V).

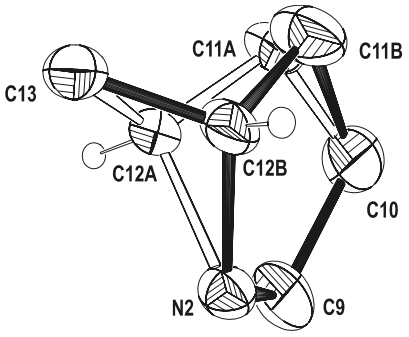

Enrico Prenesti, Pier Giuseppe Daniele, Silvia Berto, Simona Toso

Polyhedron 25 (2006) 2815

Spectrum–structure correlation for visible absorption spectra of copper(II) complexes showing axial co-ordination in aqueous solution

Structure proposed for the complexes: (a) Cu(bipy); (b) $Cu(bipy)_2$; and (c) $Cu(bipy)_3$. The ligand is schematised for sake of simplicity.

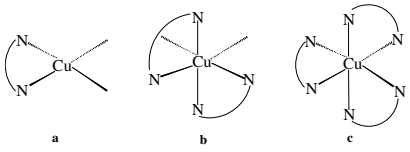

Bojan Kozlevčar, Amalija Golobič, Peter Strauch

Polyhedron 25 (2006) 2824

Dynamic pseudo Jahn–Teller distortion in a compressed octahedral CuO_6 complex

The coordination sphere of *cis*-$[Cu(C_8H_7O_3)_2(H_2O)_2]$ at 115 K, with three rhombic coordination axes, differs importantly from the room temperature one, where compressed axial axes were determined. The MSDA analysis confirms the vibrational disorder in the structure at high temperature, and its gradual freezing by decreasing temperature. These results are in agreement with the EPR data that also show the reversibility of this change. Based on the EPR data, a $\{d_{z^2}\}^1$ ground state is proposed, although the room temperature spectrum suggests a $\{d_{x^2-y^2}\}^1$ ground state, but with a small g_3 value (close to g_e).

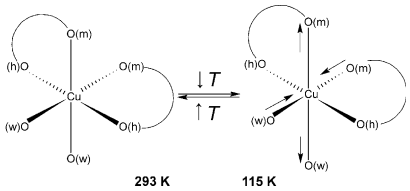

Veysel T. Yilmaz, Fatih Yilmaz, Haydar Karakaya, Orhan Büyükgüngör, William T.A. Harrison

Polyhedron 25 (2006) 2829

Silver(I)-barbital based frameworks: Syntheses, crystal structures, spectroscopic, thermal and antimicrobial activity studies

Three Ag^{I}-barb coordination polymers have been reported. $Na_3[Ag_3(\mu\text{-barb})_6]$ is a 3D mixed-metal complex, while $\{[Ag_2(\mu\text{-barb})_2][Ag_2(\mu\text{-en})_2] \cdot 5H_2O\}_n$ contains the barb dianion and features 2D grid-type layers, which are further connected by extensive hydrogen bonds resulting in a 3D framework with open channels. $[Ag(barb)(\mu\text{-bpe})]_n$ consists of 1D helical chains connected by hydrogen bonds between barb ligands to form 2D supramolecular sheets, which are further linked by aromatic π–π stacking interactions into a 3D network. The barb ligand has been shown to be able to exhibit different coordination modes. Different coordination modes of barb are seen in $Na_3[Ag_3(\mu\text{-barb})_6]$ and $\{[Ag_2(\mu\text{-barb})_2][Ag_2(\mu\text{-en})_2] \cdot 5H_2O\}_n$. Antimicrobial studies of the title complexes were also performed. While barb and the other coligands did not show any significant antimicrobial activity, complexes **1**–**3** exhibited a wide spectrum of antimicrobial activity against selected bacteria and fungi.

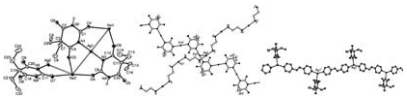

H.P.S. Chauhan, U.P. Singh, N.M. Shaik, S. Mathur, V. Huch

Polyhedron 25 (2006) 2841

Synthetic, spectroscopic, X-ray structural and antimicrobial studies of 1,3-dithia-2-stibacyclopentane derivatives of phosphorus based dithiolato ligands

Mixed 1,3-dithia-2-stibacyclopentane derivatives with phosphorus based dithiolato ligands of the types $\overline{SCH_2CH_2SSbS(S)POGO}$ {where G = —CH(Me)—CH(Me)— and —$C(Me)_2$—$C(Me)_2$—} and $\overline{SCH_2CH_2SSbS(S)P(OR)_2}$ {where R = Pr^n, Bu^n and Ph} have been synthesized and characterized by physicochemical and spectral [UV, IR, NMR (^1H, ^{13}C and ^{31}P)] methods. The antimicrobial activities of these complexes were found in vitro against a number of microorganisms by the disc diffusion method and they were found to be better antimicrobial agents than the tested standard antibiotics (chloroamphenicol and terbinafin). The single crystal X-ray diffraction analysis of 1,3-dithia-2-stibacyclopentane 2, 3-butylenedithiophosphate revealed a monodentate mode of bonding of the dithiophosphate ligand in the complex.

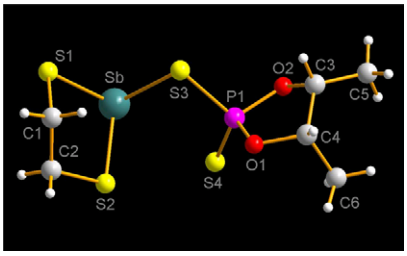

Javier Martínez, Luis A. Adrio, José M. Antelo, M[a] Teresa Pereira, Jesús J. Fernández, José M. Vila

Polyhedron 25 (2006) 2848

New thiosemicarbazone palladacycles with chelating bis(diphenylphosphino)methane

The reaction of tetranuclear cyclometallated palladium thiosemicarbazone compounds with $Ph_2PCH_2PPh_2$ and hydrochloric acid affords mononuclear palladacycles with a chelated diphosphine as 1:1 electrolytes.

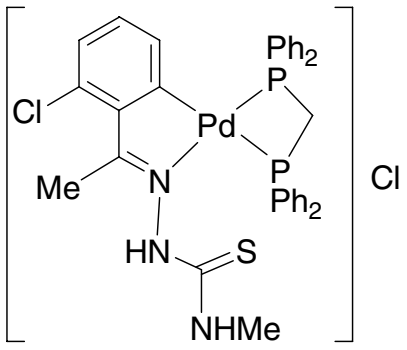

K. Shanmuga Bharathi, A. Kalilur Rahiman, K. Rajesh, S. Sreedaran, P.G. Aravindan, D. Velmurugan, V. Narayanan

Polyhedron 25 (2006) 2859

Synthesis of new 'end-off' μ-phenoxo and bis-μ-acetato tri-bridged copper(II), nickel(II) and zinc(II) complexes: Spectral, magnetic, electrochemical and catalytic studies

A new end-off type acyclic ligand with two *N*-methyl piperazine arms, 2,6-bis[(4-methylpiperazin-1-yl)]-4-formylphenol [L] has been synthesized by a simple Mannich reaction. L crystallises in the triclinic space group $P\bar{1}$. The mono and binuclear complexes of Cu(II), Ni(II) and Zn(II) have been prepared. Spectral, magnetic, electrochemical and catalytic studies on the complexes have been carried out.

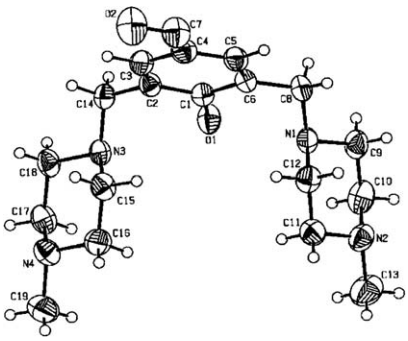

Katerina A. Thiakou, Vlasoula Bekiari, Catherine P. Raptopoulou, Vassilis Psycharis, Panagiotis Lianos, Spyros P. Perlepes

Polyhedron 25 (2006) 2869

Dinuclear lanthanide(III) complexes from the use of di-2-pyridyl ketone: Preparation, structural characterization and spectroscopic studies

The reactions between $Ln(NO_3)_3 \cdot xH_2O$ (Ln = Pr, Eu, Tb, Er) and di-2-pyridyl ketone in a mixture of MeOH and EtOH give dinuclear nitrate complexes containing the monoanions of both the *gem*-diol and hemiacetal derivatives of the ketone as ligands. The ligands adopt the three shown coordination modes in every complex. The Eu(III) and Tb(III) complexes display an intense red and green emission, respectively, in the solid state, the photoluminescence being achieved by an indirect process (antenna effect).

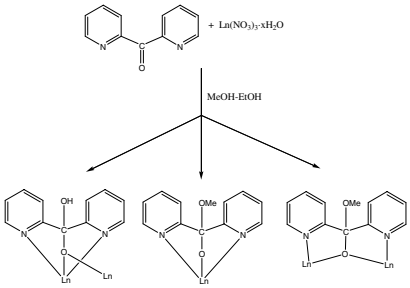

Denis Lima Guerra, Vanda Porpino Lemos, Claudio Airoldi, Rômulo Simões Angélica

Polyhedron 25 (2006) 2880

Influence of the acid activation of pillared smectites from Amazon (Brazil) in adsorption process with butylamine

The pillared interlayered clays are prepared through charge-compensating cations exchange present in the interlayer space of the swelling clays with aluminum cations polymer. On calcining, the inserted cations polymers yield rigid, thermally stable oxide species, named pillars.

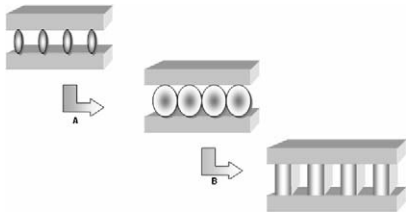

Adrienne Thorn, Roger D. Willett, Brendan Twamley

Polyhedron 25 (2006) 2891

Crystal structure of $[(C_2H_5)_2NH_2]_2$-$[Cd_3Br_8(CdBr_2)] \cdot H_2O$: An augmented ribbon structure

The decorated $[Cd_3Br_8]_n^{2n-}$ ribbons in this structure consist of triple chains of edge-shared $CdBr_6$ octahedra fringed with tetrahedral $CdBr_4$ groups. The triple chains can be viewed as being excised from the parent hexagonal $CdBr_2$ lattice by the action of the diethylammonium 'molecular scissors'.

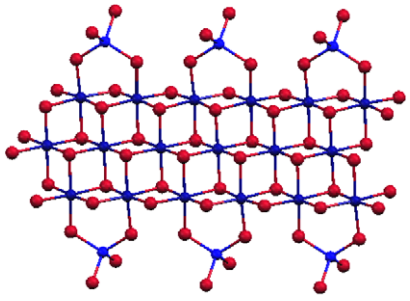

Tarlok S. Lobana, Gagandeep Bawa, Ray J. Butcher, Ben-Jie Liaw, Chen W. Liu

Polyhedron 25 (2006) 2897

Thiosemicarbazonates of ruthenium(II): Crystal structures of [bis(diphenylphosphino)-butane][bis(pyridine-2-carbaldehydethiosemicarbazonato)] ruthenium(II) and [bis-(triphenylphosphine)][bis(benzaldehydethiosemicarbazonato)] ruthenium(II)

The first example of a ruthenium(II) complex **(1)** with a chelating diphosphine forming a stable seven membered P,P-chelate ring in the presence of a potentially tridentate pyridine-2-carbaldehyde thiosemicarbazonate anion coordinating via N^2, S-donor atoms is described.

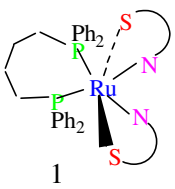

1

Valiollah Mirkhani, Majid Moghadam, Shahram Tangestaninejad, Bahram Bahramian

Polyhedron 25 (2006) 2904

Polystyrene-bound 1,4-phenylenediamine as a heterogeneous axial ligand for Mn-(salophen)Cl and its use as biomimetic alkene epoxidation and alkane hydroxylation catalyst with sodium periodate

Efficient alkene epoxidation and alkane hydroxylation with sodium periodate catalyzed by Mn(salophen) supported on polystyrene-bound 1,4-phenylenediamine is reported.

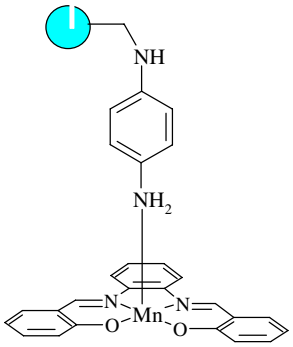

Garima Singh, Ajai K. Singh, John E. Drake, Michael B. Hursthouse, Mark E. Light

Polyhedron 25 (2006) 2915

Synthesis and single crystal structure of a three coordinate complex of mercury(II) with 1-(ethylthio)-2-(diphenylphosphino) ethane (**L**) prepared by a new simple method

The (P, S) ligand 1-(ethylthio)-2-(diphenylphosphino) ethane (**L**) is synthesized in good yield by reacting Ph_2PLi with CH_3CH_2-SCH_2CH_2Cl. Its complexation with Cu(I), Hg(II) and organometallic species of Ru(II) are explored. The single crystal structure of Hg(II) complex of **L** has been determined. It is found to be a three coordinate species. The geometry of Hg can be best described as trigonal planar. The Hg(1)–P(1) bond length is 2.415(1) Å and the Hg–Br bond lengths are 2.5152(6) and 2.5952(6) Å. There exists a weak secondary interaction between Hg and the S donor site of the ligand.

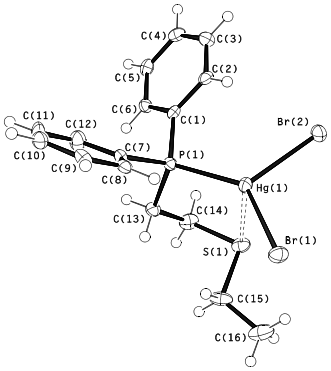

Beatriz S. Parajón-Costa, Oscar E. Piro, Reinaldo Pis-Diez, Eduardo E. Castellano, Ana C. González-Baró

Polyhedron 25 (2006) 2920

Crystal structures, spectroscopic characterization and theoretical calculations of the guanidinium and ammonium salts of the insulin-enhancing anion $[VO_2(dipic)]^-$

The guanidinium and ammonium salts of the bisoxodipicolinatevanadate(V) anion were synthesized and characterized by single-crystal X-ray diffraction and spectroscopic techniques. The optimized geometry of $[VO_2$-$(dipic)]^-$ and its corresponding harmonic vibrational frequencies were calculated using methods of the density functional theory. Hydrogen bonding interactions appear to be relevant in stabilizing their crystal structures.

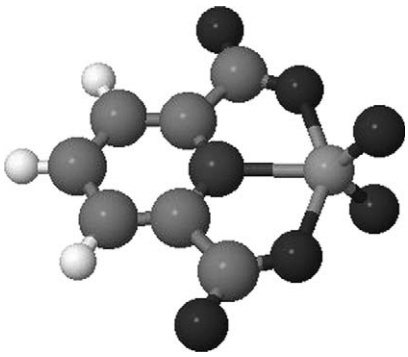

Mohammad Shakir, Shama Parveen, Poonam Chingsubam, Katsuyuki Aoki, Shahper N Khan, Asad U Khan

Polyhedron 25 (2006) 2929

Cation supported self-assembly of coordination polymers, $[(H_2en)(ntpMCl_2)]_n$ ($M = Zn^{II}$, Cd^{II}, Hg^{II}) involving the tripodal acid, ntp: X-ray crystal structure and DNA binding studies on zinc helicate

A first report on the self-assembly of novel coordination polymers of the type, $[(H_2en)(ntpMCl_2)]_n$ [$M = Zn^{II}$, Cd^{II}, Hg^{II}] resulting due to deprotonation of ntp, present as the zwitterion $[NH^+(CH_2CH_2COOH)_2$-$(CH_2CH_2COO)^-]$ in aqueous medium, by en leading to the formation of the ditopic anion ntp^{2-}, suggesting that H_2en^{2+} acts as a cation template. The coordination polymers thus resulted involve $[ntpMCl_2]^{2-}$ as building units stabilized via hydrogen bonding interactions. X-ray analyses on $[(H_2en)(ntpZnCl_2)]_n$ features four coordinate Zn^{2+} defined by two oxygen donors from ntp^{2-} ligands and two chloride anions.

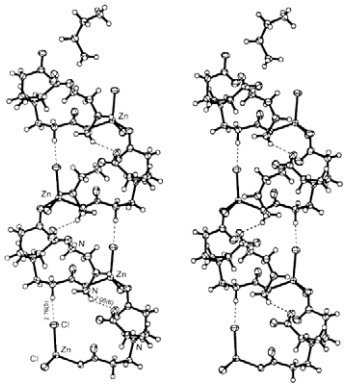

Miroslava Maľarová, Zdeněk Trávníček, Radek Zbořil, Juraj Černák

Polyhedron 25 (2006) 2935

$[Co(en)_3][Fe(CN)_6] \cdot H_2O$ and $[Co(en)_3][Fe(CN)_6]$: A dehydration process investigated by single crystal X-ray analysis, thermal analysis and Mössbauer spectroscopy

Single crystals of $[Co(en)_3][Fe(CN)_6] \cdot H_2O$ (**1**) have been transformed to an anhydrous complex of $[Co(en)_3][Fe(CN)_6]$ (**2**) by dynamic heating of (**1**) up to 150 °C in the solid state. X-ray structures have been determined in both cases.

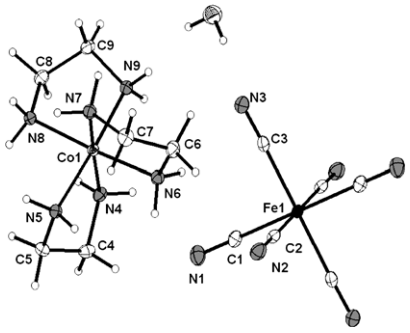

Yueh-Hua Wang, Maw-Cherng Suen, Hsun-Tsing Lee, Ju-Chun Wang

Polyhedron 25 (2006) 2944

Syntheses and structural characterization of three new coordination polymers of $[Ag(PPIA) \cdot H_2O]_n$, $[Cu(PPIA)_2 \cdot 2H_2O]_n$ and $[Zn(PPIA)_2(H_2O)_2]_n$; PPIA = 3-pyridinepropionic acid

The syntheses and crystal structures of three new coordination polymers of the type $[Ag(PPIA) \cdot H_2O]_n$ (PPIA = 3-pyridinepropionic acid) (**1**), $[Cu(PPIA)_2 \cdot 2H_2O]_n$ (**2**), and $[Zn(PPIA)_2(H_2O)_2]_n$ (**3**), are reported. Interestingly, the one-dimensional chain complex of **1** or the two-dimensional frameworks of **2** and **3** are also linked to form three-dimensional networks through hydrogen bonds.

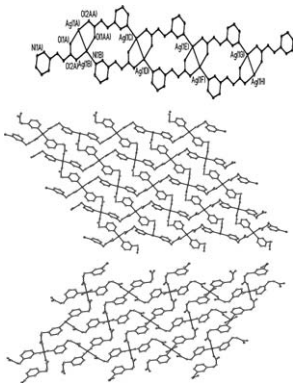

R. Kefi, C. Ben Nasr, F. Lefebvre, M. Rzaigui

Polyhedron 25 (2006) 2953

Hydrothermal synthesis and characterization of a new zinc phosphate $[Zn_{2.5}(HPO_4)_2(PO_4)][C_6H_{10}N_2] \cdot 5H_2O$

A novel two-dimensional zinc phosphate, $[Zn_{2.5}(HPO_4)_2(PO_4)][C_6N_2H_{10}] \cdot 5H_2O$ has been hydrothermally synthesized. The structure of this compound, determined by single crystal X-ray diffraction, represents the first one with a Zn/P ratio of 5/6. Solid-state ^{13}C and ^{31}P MAS NMR spectroscopies agree perfectly with the X-ray structure. Ab initio calculations allow the attribution of phosphorus and carbon signals to the independent crystallographic sites and to the various atoms of the organic groups.

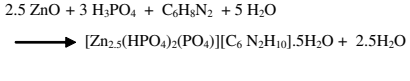

Hélène Casellas, Patrick Gamez, Jan Reedijk, Chiara Massera

Polyhedron 25 (2006) 2959

Solvent control in the synthesis of Zn(II) and Cd(II) supramolecular compounds with *N*,*N*′-{2,4-di-[(di-pyridin-2-yl)amine]-1,3,5-triazine}-ethylenediamine

The reactions of $Zn(NO_3)_2$ or $Cd(NO_3)_2$ with the ligand *N*,*N*′-{2,4-di-[(di-pyridin-2-yl)-amine]-1,3,5-triazine}-ethylenediamine yield mono or trinuclear coordination compounds under the same experimental procedure, depending on the nature of the solvent used, namely methanol or acetonitrile.

Stefania Tanase, Martin van Son, Gerard A. van Albada, René de Gelder, Elisabeth Bouwman, Jan Reedijk

Polyhedron 25 (2006) 2967

Self-assembly of extended structures through non-coordination intermolecular forces: Synthesis, crystal structures, and properties of metal complexes with 5-methyl-2-pyrazinecarboxylate

The present paper describes the synthesis and characterization of several metal complexes with the ligand 5-methyl-2-pyrazinecarboxylate: $[Co(mpca)_2(H_2O)_2]$, $[Ni(mpca)_2(H_2O)_2]$, $[Cu(mpca)_2(H_2O)] \cdot 3H_2O$ and $[Fe(mpca)_2(OH)_2] \cdot 2H_2O$. In all cases, the X-ray crystal structure analysis reveals extended structures formed by non-covalent intermolecular forces, such as hydrogen-bonding and/or π–π stacking interactions.

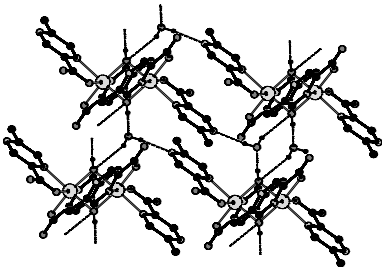

S.A. Chimatadar, T. Basavaraj, S.T. Nandibewoor

Polyhedron 25 (2006) 2976

Mechanistic study of quinoliniumdichromate (QDC) oxidation of mercury(I) in aqueous sulfuric acid in the presence of micro amounts of palladium(II) – Autocatalysis in catalysis

The kinetics of oxidation of mercury(I) with quinoliniumdichromate (QDC) in the presence of micro amounts of palladium(II) catalyst in aqueous sulfuric acid medium has been studied. The active species of oxidant, reductant and catalyst in the reaction medium were understood to be $HCrO_4^-$, $[Hg_2(SO_4)HSO_4]^-$ and $PdCl^+$, respectively. The autocatalysis by one of the products, chromium(III), was observed.

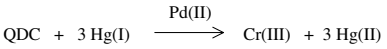

Okan Zafer Yeşilel, Mustafa Serkan Soylu, Halis Ölmez, Orhan Büyükgüngör

Polyhedron 25 (2006) 2985

Synthesis and spectrothermal studies of vitamin B13 complexes of cobalt(II) and nickel(II) with 4-methylimidazole: Crystal structure of $[Ni(HOr)(H_2O)(4\text{-}Meim)_3]_2 \cdot 5H_2O$

The aquatris(4-methylimidazole)orotatocobalt(II), $[Co(HOr)(H_2O)(4\text{-}Meim)_3]$, and bis[aquatris(4-methylimidazole)orotatonickel(II)] pentahydrate, $[Ni(HOr)(H_2O)(4\text{-}Meim)_3]_2 \cdot 5H_2O$, have been synthesized and characterized by means of elemental analysis, thermal analysis, IR, UV–Vis and mass spectroscopic studies. The crystal structure of **2** was also determined by single crystal X-ray diffraction. The Co(II) and Ni(II) ions in $[M(C_5H_2N_2O_4)(H_2O)(C_4H_6N_2)_3]$ are chelated to the deprotonated N3 pyrimidine atom and to the carboxylate oxygen atom of the bidentate orotate dianion, and to the three nitrogen atoms of the 4-Meim ligands, and their octahedral geometries are completed by an aqua ligand. The thermal decomposition pathway of the complexes has been predicted with the help of thermal analysis (TG, DTG and DTA) and mass spectroscopic data.

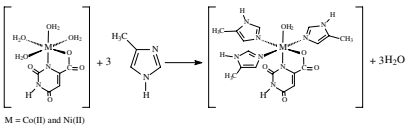

James A.S. Howell

Polyhedron 25 (2006) 2993

Structure and bonding in cyclic thiolate complexes of copper, silver and gold

The structure and bonding of cyclic thiolate complexes of copper, silver and gold has been examined by DFT calculation

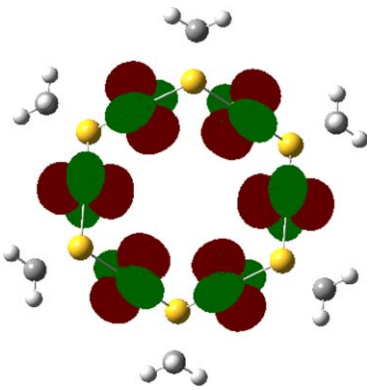

Joy Chakraborty, Brajagopal Samanta, G. Rosair, Volker Gramlich, M. Salah El Fallah, Joan Ribas, T. Matsushita, Samiran Mitra

Polyhedron 25 (2006) 3006

Two new hydrothermally synthesised L–M–L type cobalt(II) hydrogen bonded co-ordination complexes with mixed ligands: Characterisation and magneto-structural correlation

Two new hydrogen bonded 2-D polymeric L–M–L type Co(II) metal coordination complexes have been synthesised under controlled hydrothermal condition and spectroscopically characterised. X-ray study reveals the presence of weak covalent and extensive inter/intra molecular H-bonding interactions within the chains responsible for polymeric network. Both the complexes are found to be weakly antiferromagnetic in nature corroborating well with their structures.

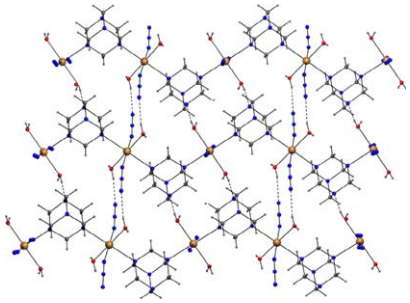

Chang-Yan Sun, Li-Cun Li, Lin-Pei Jin

Polyhedron 25 (2006) 3017

Dicarboxylate anion-dependent assembly of Co(II) and Ni(II) coordination polymers with 1,2-bis(4-pyridyl)ethane

Using mixed ligands, five new coordination polymers were obtained. Complexes **1**–**4** possess different complicated 3D metal-organic frameworks, while complex **5** is of (4,4) 2D grid-like layers. These results show that the position of carboxylate groups greatly affects the structure of the complexes.

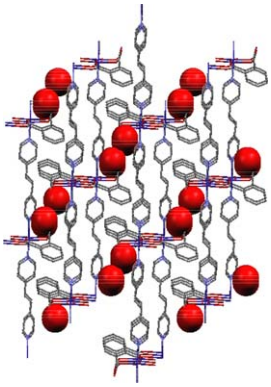

Young Soon Kang, Jeong-Ho Son, In-Chul Hwang, Kyo Han Ahn

Polyhedron 25 (2006) 3025

Synthesis of a bis(oxazoline)-*N*-carboxylate ligand and its Zn(II) complex that shows C–H···Cl hydrogen bonding

A novel N_3O-type chelate and its Zn(II) complex are synthesized. The chelate is a branched type N_3O ligand, (*S*,*S*)-[Bis{(4-isopropyl-4,5-dihydrooxazol-2-yl)methyl}amino]acetic acid sodium salt, which was synthesized through a stepwise introduction of the oxazoline rings. The Zn(II) complex shows C–H···Cl–Zn hydrogen bonding both in the solid and solution states. A single crystal X-ray analysis of the Zn(II) complex supports the C–H···Cl–Zn hydrogen bonding, showing a microchannel structure.

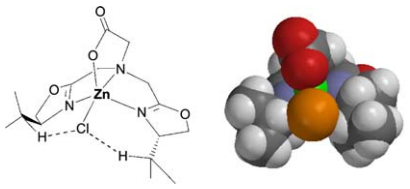

C-H---Cl Hydrogen bonding both in the solid and solution states

Russell Binions, Claire J. Carmalt, Ivan P. Parkin

Polyhedron 25 (2006) 3032

Antimony oxide thin films from the atmospheric pressure chemical vapour deposition reaction of antimony pentachloride and ethyl acetate

The reaction of antimony pentachloride and ethyl acetate under atmospheric pressure chemical vapour deposition conditions leads to the production of antimony (III) oxide thin films on glass and gas sensor substrates. Scanning electron microscopy (SEM) indicated that an island growth mechanism predominated. X-ray photoelectron spectroscopy (XPS) revealed binding energy shifts of 20.6 eV for O 2s and 35.4 eV for Sb 4d. The films were X-ray amorphous. Energy dispersive X-ray analysis (EDXA) and electron probe microanalysis (EPMA) gave coherent elemental compositions indicating that single phase Sb_2O_3 was made, with negligible impurity levels. The films showed little optical reflectance (~10%) and 65–75% total transmission from 400 to 800 nm. Gas sensing experiments indicated that the films responded best to a reducing gas at 400 °C.

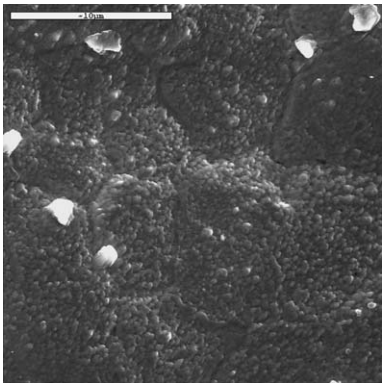

Markku Talja, Mika Polamo

Polyhedron 25 (2006) 3039

Configurational isomerism in crystalline bis-(amidopyridine)trichloro complexes of tantalum(V)

The structures of tantalum amidopyridine complexes were studied by X-ray diffraction. The seven-coordinated mononuclear bis-(amidopyridine) complexes displayed configurational isomerism in the crystalline state. Distortions in the coordination polyhedra around the Ta center were evaluated.

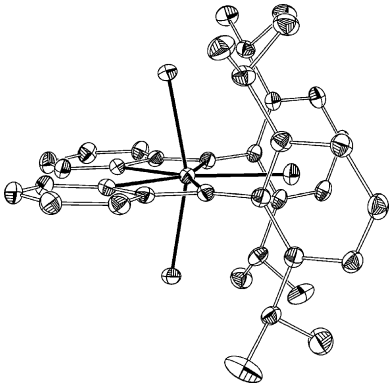

Ping Liu, Zhao-Xun Lian, Jiwen Cai

Polyhedron 25 (2006) 3045

Solid–vapor reaction properties of copper(II) and cadmium(II) sulfonates with amines

Copper(II) and cadmium(II) sulfonates react with amine vapors and form stable mono-amine-coordinated complexes. Single crystals can grow in situ via the solid–vapor reaction process.

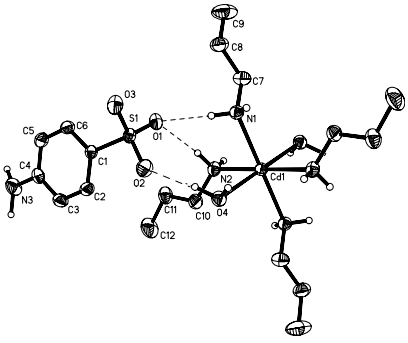

Chih-Yu Wu, Yi Chen, Shiau-Yi Jing, Chen-Shiang Lee, Joydev Dinda, Wen-Shu Hwang

Polyhedron 25 (2006) 3053

Reactions of diiron nonacarbonyl with pyrrolyl-, pyridyl- and thienyl-substituted azines: N—N bond cleavage, cyclometallation and C=N σ and π-bonding

The reactions of pyrrolyl, pyridyl and thienyl azines with $Fe_2(CO)_9$ yielded various types of diironhexacarbonyl complexes with different coordination modes, which resulted from (1) N—N bond cleavage, (2) cyclometallation, (3) diaza-bridge coordination, (4) σ- and π-imine bridge coordination and (5) π-imine bridge coordination of the ligand.

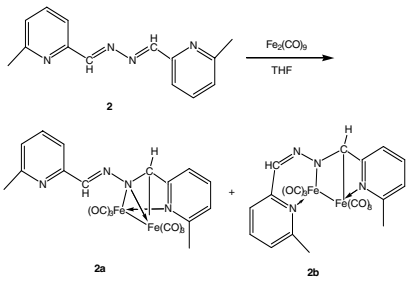

Raquel Aroz, Fabian Mohr, Elena Cerrada, Edward R.T. Tiekink, Mariano Laguna

Polyhedron 25 (2006) 3066

One-pot self-assembly of trinuclear silver(I) clusters containing propargyl alcohols and bis(diphenylphosphino)methane (dppm) ligands

A simple, safe and high yielding one-pot procedure for the synthesis of trinuclear silver(I) acetylide clusters containing propargyl alcohols HC≡CCRR′OH (R = R′ = H, Me; R = Me, R′ = Et) and dppm ligands is presented. The X-ray crystal structure of *rac*-$[Ag_3\{\mu_3\text{-}\eta^1\text{-}C{\equiv}CC(Me)(Et)OH\}(\mu\text{-dppm})_3](NO_3)_2 \cdot CH_2Cl_2$ was determined and the luminescence properties of the complexes were studied.

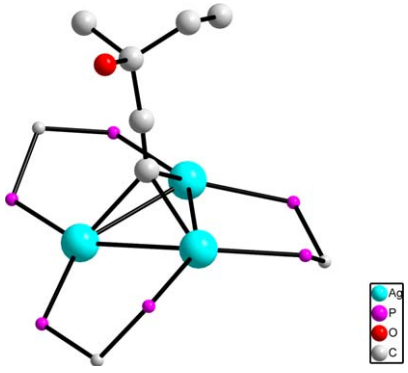

Jian-Sheng Xu, Yue-Tao Zhang, Guang-Hua Li, Ying Mu, Shou-Hua Feng

Polyhedron 25 (2006) 3071

Constrained geometry tetramethylcyclopentadienyl-phenoxy titanium complexes: Synthesis, structures and catalytic properties for ethylene polymerization

The synthesis of a new bidentate ligand, 1-(2-methoxyphenyl)-2,3,4,5-tetramethyl-cyclopentadiene (**1**), as well as its corresponding constrained geometry titanium complex, 2-tetramethylcyclopentadienyl-phenoxytitanium dichloride [(TCP)$TiCl_2$, **2**], was described. Complex **2** was synthesized by reaction of $TiCl_4$ with the lithium salt of **1**, followed by CH_3Cl elimination at 65 °C. Molecular structures of **2** and a known complex, 2-tetramethylcyclopentadienyl-6-methyl-phenoxytitanium dichloride [(TCMP)$TiCl_2$, **IVd**], were determined by single-crystal X-ray diffraction. When activated with Al^tBu_3 and $Ph_3C^+B(C_6F_5)_4^-$, complex **2** exhibits moderate catalytic properties for ethylene polymerization.

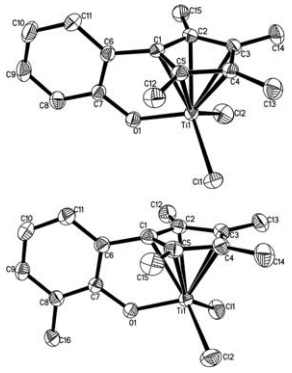

The Publisher encourages the submission of articles in electronic form thus saving time and avoiding rekeying errors. For detailed instructions on the preparation of manuscripts and of electronic artwork, consult the Author Gateway for Elsevier at http://authors.elsevier.com

ScienceDirect

Full text of this journal is available, on-line from **ScienceDirect**. Visit **www.sciencedirect.com** for more information.

Available online at www.sciencedirect.com
SCIENCE DIRECT®
Polyhedron 25, issue 4, 6 March 2006
POLYHEDRON
www.elsevier.com/locate/poly

Contents

Preface 821

Papers

Stuart D. Robertson, Alexandra M.Z. Slawin, J. Derek Woollins

Polyhedron 25 (2006) 823

The preparation and characterisation of a series of group IV metallocene dithiolato complexes containing a naphthalene backbone

Metathesis reactions lead to $(Cp)^{*}_{2}MS_2C_{10}H_6$ [M = Ti, Zr, Hf] which are isomorphous allowing a comparison of the structural parameters.

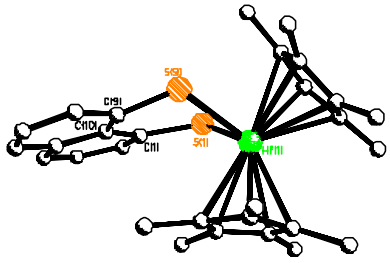

Malcolm H. Chisholm, Judith C. Gallucci, Carl B. Hollandsworth

Polyhedron 25 (2006) 827

Crystal and molecular structure of $W_2(OBu^t)_6$ and electronic structure calculations on various conformers of $W_2(OMe)_6$

The X-ray crystal structure of $W_2(OBu^t)_6$ is reported. The structure reveals 1.5 dimers in the asymmetric unit. One of the dinuclear molecules is highly disordered with respect to the W–W vectors. The alkoxide ligands are found in the common one distal, two proximal arrangement. DFT (ADF 2003.02) computational studies on several conformers of the model compound $W_2(OMe)_6$ reveal that there is little energetic difference between conformers of different proximality in the gas phase.

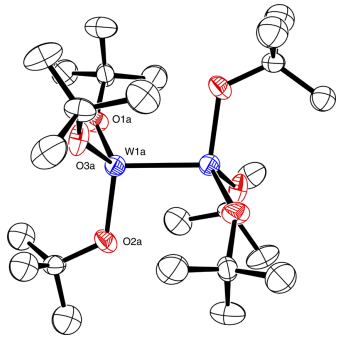

Renzo Cini, Gabriella Tamasi, Sandra Defazio, Maddalena Corsini, Francesco Berrettini, Alessandro Cavaglioni

Polyhedron 25 (2006) 834

Unusual hetero-atomic RhSCNSb(Rh) coordination ring: Synthesis and X-ray structure of [Rh($\underline{N}^1$,$\underline{S}^2$-2-thiopyrimidinato)$_2$($\underline{N}^1$(Sb),$\underline{S}^2$-(Rh)-2-thiopyrimidinato){Sb(C_6H_5)$_3$}] and long time sought structure of *mer*-[$RhCl_3$-{Sb(C_6H_5)$_3$}$_3$]

The reaction of [$RhCl_3(SbPh_3)_3$] with 2-thio-1,3-pyrimidine (Htpym) in ethanol produces crystalline [$Rh(tpym)_3(SbPh_3)$] that contains two $tpym^-$ N,S-chelating anions and a $tpym^-$ S-monodentate anion; this latter donates via a N atom to the Sb atom. The X-ray structure of [$RhCl_3(SbPh_3)_3$] shows that the chloride anion *trans* to Sb is significantly activated towards dissociation, an event that gives a rationale to the formation of [$RhCl_2(Ph)(SbPh_3)_3$] previously reported from this laboratory.

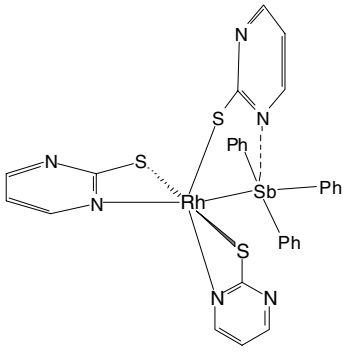

Musa Said, David L. Hughes, Manfred Bochmann

Polyhedron 25 (2006) 843

Synthesis and structures of diphosphinoamide complexes of nickel, palladium and platinum

The syntheses and single-crystal X-ray structures of bimetallic Ni–Li, Ni–Sn, Ni–Si, Pt–Li and Pt–Si complexes are described, based on the [amidobis(phosphine)]$^-$ anion as bridging ligand. The structures are based on MP_2N four-membered rings, the geometric parameters of which proved rather insensitive to changes in the N-main group element bond.

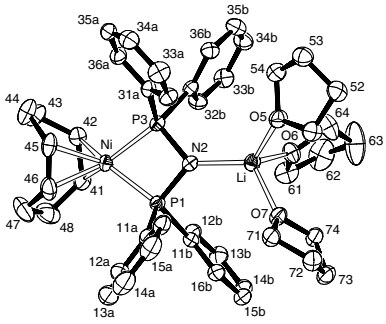

Ewan A. Drylie, Christopher D. Andrews, Meredith A. Hearshaw, Cristina Jimenez-Rodriguez, Alexandra Slawin, David J. Cole-Hamilton, Russell E. Morris

Polyhedron 25 (2006) 853

Synthesis and crystal structures of bromo- and ester-functionalised polyhedral silsesquioxanes

Two new functionalised octasilsesquioxanes have been prepared using octavinylsiloxane as the starting material. 1,3,5,7,9,11,13,15-octakis[ethylbromide]octasiloxane has been prepared by radical-initiated addition of HBr across the vinyl group and 1,3,5,7,9,11,13,15-octakis[methylpropanoate]octasiloxane has been prepared by direct methoxycarbonylation using a Pd(0) catalyst. Crystal structures of both compounds have been determined.

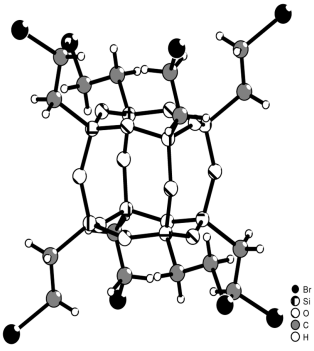

Robin M. Porter, Andreas A. Danopoulos

Polyhedron 25 (2006) 859

Dimethylxanthene- and dibenzofuran-diamido complexes of titanium

Tridentate dialkylamido- and diarylamido-ligands based on the dimethylxanthene and dibenzofuran backbones have been synthesised and used to prepare titanium dialkylamides and alkyls.

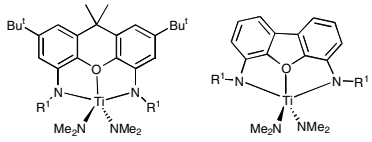

Mohammad A. Malik, Mohammad Afzaal, Paul O'Brien, Madeleine Halliwell

Polyhedron 25 (2006) 864

Synthesis of novel mixed indium(III) chalcogenolato complexes: Potential precursors for indium chalcogenides

Three new mixed chalcogenolato indium compounds have been synthesised and their structures determined by X-ray crystallographic method.

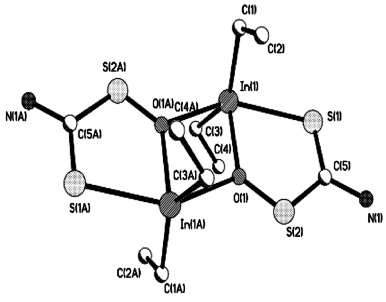

Juan-Manuel Herrera, Svetlana G. Baca, Harry Adams, Michael D. Ward

Polyhedron 25 (2006) 869

Syntheses and structures of two- and three-dimensional cyanide-bridged coordination networks derived from crystallization of diimine-tetracyanoruthenate anions with gadolinium(III) cations

Crystallisation of the cyanometallate complexes $[Ru(phen)(CN)_4]^{2-}$ and $[\{Ru(CN)_4\}_2(\mu\text{-bpym})]^{4-}$ (phen = 1,10-phenanthroline; bpym = 2,2′-bipyrimidine) with Gd(III) species affords two-dimensional or three-dimensional coordination networks based on Ru–CN–Gd bridges.

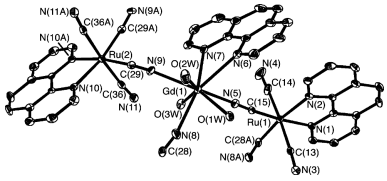

Atta M. Arif, Rehan Basta, Richard D. Ernst

Polyhedron 25 (2006) 876

Syntheses and characterization of mono-(6,6-dimethylcyclohexadienyl) complexes of titanium and zirconium

The reaction of $Ti(6,6\text{-dmch})_2$ with 1,2-$C_2H_4Cl_2$ led to the formation of the one-dimensional chloride-bridged polymer, $[Ti(6,6\text{-dmch})Cl_2]_n$, with a four-legged piano stool geometry (dmch = dimethylcyclohexadienyl). A mono(6,6-dmch) complex of zirconium, $Zr(6,6\text{-dmch})Br_3(dmpe)$, was isolated from the reaction of $Zr(6,6\text{-dmch})_2Br_2$ with dmpe (1,2-dimethylphosphinoethane).

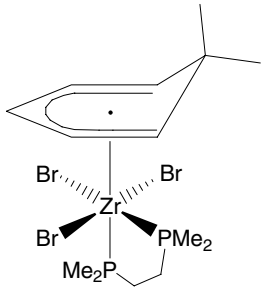

Xiaoping Yang, Richard A. Jones, Rachel J. Lai, Abdul Waheed, Michael M. Oye, Archie L. Holmes

Polyhedron 25 (2006) 881

Supramolecular assembly of nanometer-sized heterobimetallic 3d–4f complexes formed with benzimidazole based N,O-donor ligands

New heterobimetallic Cu–Ln complexes formed with benzoimidazole based N,O-donor ligands exhibit supramolecular 3D-networks via C–H··· O and CH···π interactions.

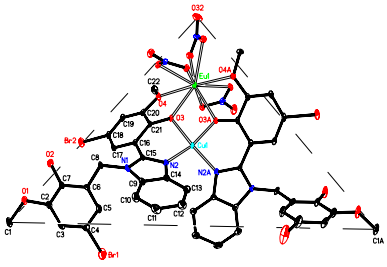

Michael G.B. Drew, Mark R.St.J. Foreman, Andreas Geist, Michael J. Hudson, Frank Marken, Virginia Norman, Michael Weigl

Polyhedron 25 (2006) 888

Synthesis, structure, and redox states of homoleptic d-block metal complexes with bis-1,2,4-triazin-3-yl-pyridine and 1,2,4-triazin-3-yl-bipyridine extractants

Cobalt(II), copper(II), iron(II), manganese(II), nickel(II) and zinc(II) form six-coordinate octahedral 1:2 complexes with triazinyl bipyridines. These metal complexes have been studied by crystallographic, electrochemical and theoretical methods.

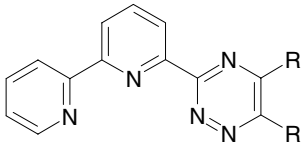

Philip A. Gale, Mark E. Light, Roberto Quesada

Polyhedron 25 (2006) 901

Formation and X-ray crystal structures of neutral 3D networks by charge-assisted hydrogen bonds between tetrakis(thiourea)-platinum(II) complexes and dicarboxylates

Complex salts of the tetrakis(thiourea)-platinum(II) cation and dicarboxylates are shown to be adequate molecular building blocks for the synthesis of three dimensional networks through charge-assisted hydrogen bonds.

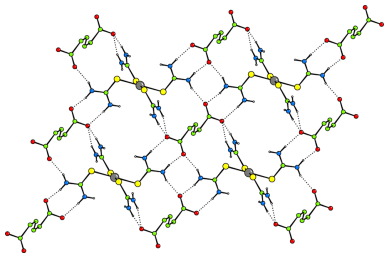

Jan P.W. Eggert, Jack M. Harrowfield, Ulrich Lüning, Brian W. Skelton, Allan H. White

Polyhedron 25 (2006) 910

Lanthanide(III) ion coordination by a concave reagent

Structural characterisation of the Yb(III) complex of a phenanthroline-bridged calix[6]-arene shows the ligand cavity to act as a receptor for another complex molecule rather than a bound ligand.

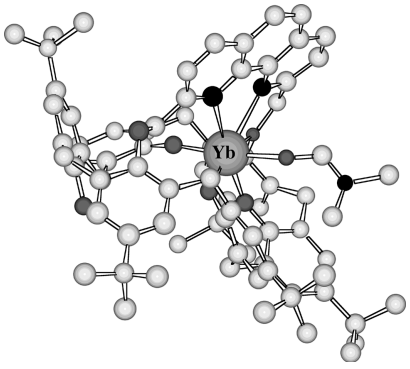

David Ellis, Rhona M. Garrioch, Georgina M. Rosair, Alan J. Welch

Polyhedron 25 (2006) 915

Isomerisation following the platination of $[7,8\text{-}Ph_2\text{-}9,11\text{-}I_2\text{-}7,8\text{-}\textit{nido}\text{-}C_2B_9H_7]^{2-}$

9-substituted- and 9,11-disubstituted-7,8-nido-diphenylcarboranes have been prepared and the latter platinated to afford three C atom isomerised species.

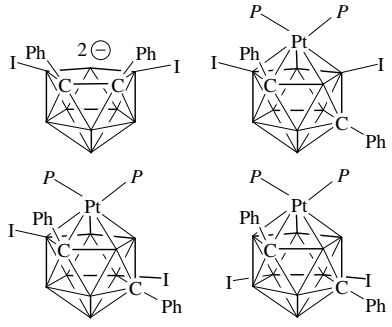

Morag E. Davie, Thomas Foerster, Simon Parsons, Colin Pulham, David W.H. Rankin, Bruce A. Smart

Polyhedron 25 (2006) 923

The crystal structure of tetrakis(dimethyl-amino)titanium(IV)

Although $Ti(NMe_2)_4$ has S_4 symmetry in the gas phase, in the solid state it has C_1 symmetry in order to avoid the formation of short methyl–methyl contacts.

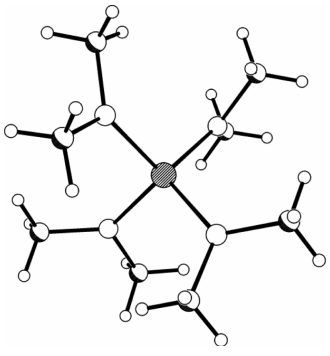

Martin F. Davis, William Levason, Gillian Reid, Michael Webster

Polyhedron 25 (2006) 930

Synthesis and characterisation of tin(IV) fluoride complexes of phosphine and arsine oxide ligands

The pseudooctahedral complexes $[SnF_4L_2]$ (L = Ph_3PO, Ph_3AsO, Me_3PO, Me_3AsO) and $[SnF_4(L–L)]$ (L–L = $Ph_2P(O)CH_2P(O)Ph_2$, *o*-$C_6H_4(P(O)Ph_2)_2$, *o*-$C_6H_4(P(O)Me_2)_2$) have been prepared and the X-ray crystal structures of *trans*-$[SnF_4(OPMe_3)_2]$, $[SnF_4\{o\text{-}C_6H_4(P(O)Ph_2)_2\}] \cdot CH_2Cl_2 \cdot H_2O$ and $[o\text{-}C_6H_4(P(O)Ph_2)_2] \cdot CH_2Cl_2$ have been determined. The structural and NMR spectroscopic data on $[SnX_4L_2]$ (X = F, Cl, Br or I) show that SnF_4 is the strongest Lewis acid in the series towards hard Lewis bases.

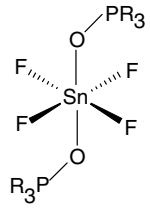

Thomas Gelbrich, Terence L. Threlfall, Susanne Huth, Eva Seeger

Polyhedron 25 (2006) 937

Structures of racemic lithium tartrate hydrates

A systematic study of the structures of LiM tartrate hydrates (M = Li, Na, K, Rb, Cs, NH_4) shows the occurrence of two- or three-dimensional coordination or hydrogen-bonded networks. Their similarities and differences are highlighted.

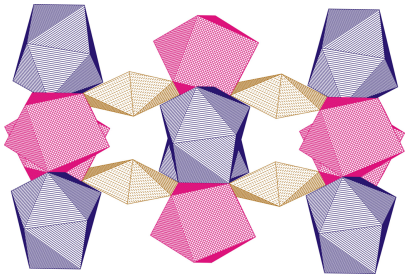

Ann L. Bingham, John E. Drake, Mark E. Light, Manisha Nirwan, Raju Ratnani

Polyhedron 25 (2006) 945

Synthesis, spectroscopic characterization and structural studies of nickel complexes of *O*,*O*′-diaryl(dibenzyl) dithiophosphates: Crystal structures of $Ni[S_2P(OC_6H_4CH_3\text{-}o)_2]_2$, $Ni[S_2P(OC_6H_4CH_3\text{-}m)_2]_2$ and $Ni[S_2P(OCH_2Ph)_2]_2$

Purple-coloured, tetra-coordinated Ni(II) complexes, $Ni[S_2P(OR)_2]_2$ (R = *o*-, *m*-, *p*-OC_6H_4Me, Ph and CH_2Ph) have been obtained by reaction of $NiCl_2$ with salts of corresponding *O*,*O*′-diaryl(dibenzyl) dithiophosphates and characterized by elemental analysis, UV, IR, ^1H, and ^{31}P NMR spectroscopy. The crystal structures of $Ni[S_2P(OC_6H_4Me\text{-}o)_2]_2$, $Ni[S_2P(OC_6H_4Me\text{-}m)_2]_2$ and $Ni[S_2P(OCH_2Ph)_2]_2$ are also described.

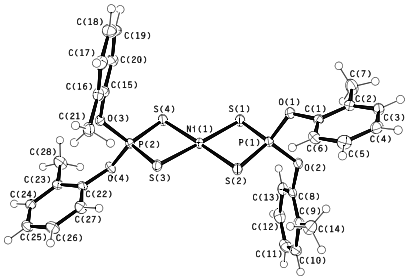

Simon J. Coles, David B. Davies, Robert J. Eaton, Adem Kılıç, Robert A. Shaw, Gönül Yenilmez Çiftçi

Polyhedron 25 (2006) 953

Structural and stereogenic properties of spiro- and ansa-substituted 1,3-propanedioxy derivatives of a spermine-bridged cyclotriphosphazene

Reaction of the achiral spermine-bridged cyclotriphosphazene compound (A-Z = Cl) with 1,3-propanediol at different molar ratios in THF gives various spiro- and ansa-derivatives with different stereogenic properties, i.e., racemates for unsymmetrically-substituted derivatives and meso, diastereoisomeric or achiral forms for symmetrical substitution.

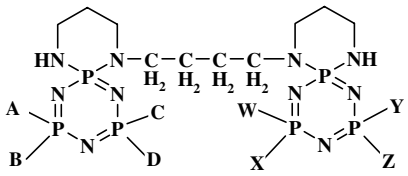

Serap Beşli, Simon J. Coles, David B. Davies, Robert J. Eaton, Adem Kılıç, Robert A. Shaw

Polyhedron 25 (2006) 963

Competitive formation of spiro and ansa derivatives in the reactions of tetrafluorobutane-1,4-diol with hexachlorocyclotriphosphazene: A comparison with butane-1,4-diol

Six products were isolated from the reaction of the sodium derivative of $HOCH_2CF_2CF_2CH_2OH$ with $N_3P_3Cl_6$: the mono-spiro compound, $N_3P_3Cl_4(OCH_2CF_2CF_2CH_2O)$ and its ansa isomer, the di-spiro derivative, $N_3P_3Cl_2(OCH_2CF_2CF_2CH_2O)_2$ and its spiro–ansa and ansa–ansa isomers (displayed) and a tri-spiro compound $N_3P_3(OCH_2CF_2CF_2CH_2O)_3$.

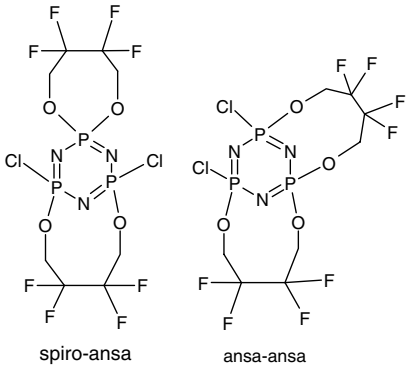

Xiao-Li Zhao, Thomas C.W. Mak

Polyhedron 25 (2006) 975

Supramolecular assembly of some polynuclear silver(I) complexes with encapsulated acetylenediide dianion and potentially exo-bidentate ligands

Five new $C_2@Ag_n$-containing complexes (bpe-$H_2 \cdot 2H_2O)[Ag_8(C_2)(CF_3CO_2)_8(H_2O)_2] \cdot 2H_2O$ (**1**), $[Ag_{14}(C_2)_2(C_2F_5CO_2)_{10}(H_2O)_4(bpe)] \cdot H_2O$ (**2**), $[Ag_7(C_2)(CF_3CO_2)_2(cba)_3]$ (**3**), $[Ag_7(C_2)$-$(C_2F_5CO_2)_5(cbaH)(H_2O)_2]$ (**4**) and $(imH)_3$-$[Ag_8(C_2)(CF_3CO_2)_9] \cdot H_2O$ (**5**) have been shown to exhibit a variety of supramolecular structures. Complex **1** provides the first example of a layer-type inclusion complex constructed with $C_2@Ag_n$ polyhedra.

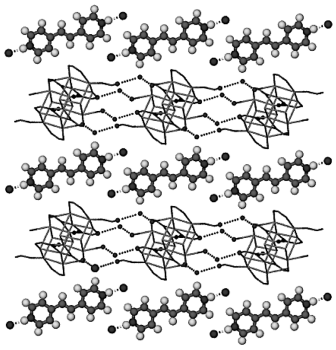

Michael Findlater, Nicholas J. Hill, Alan H. Cowley

Polyhedron 25 (2006) 983

Amidinate-substituted boron halides: Synthesis and structure

The synthesis and molecular structures of novel boron-substituted amidinates are reported. The unprecedented carbodiimide insertion into a boron–nitrogen bond is also discussed.

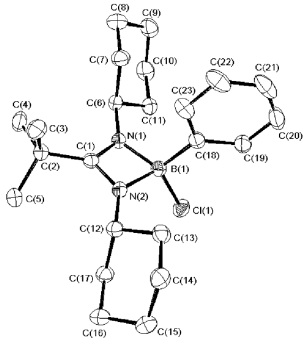

Peter J. Skabara, Rory Berridge, Neil Bricklebank, Helena Lath, Simon J. Coles, Peter N. Horton

Polyhedron 25 (2006) 989

Self-assembly of halogen adducts of ester and carboxylic acid functionalised 1,3-dithiole-2-thiones

New halogen adducts of 1,3-dithiole-2-thione-4-carboxylic acid and dimethyl 1,3-dithiole-2-thione-4,5-dicarboxylate have been prepared and characterised by X-ray crystallographic studies. The adducts feature an array of intramolecular and intermolecular close contacts involving chalcogen–chalcogen, chalcogen–halogen and halogen–halogen interactions.

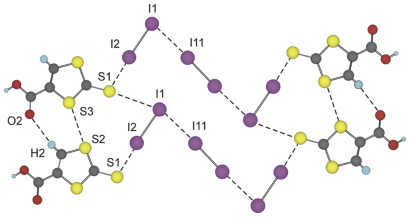

I. Abrahams, D.Z. Demetriou, E. Vordemvenne, K. Mustarde, D.M. Benoit

Polyhedron 25 (2006) 996

Lone pair effects in trihalo-stannate and -plumbate anions in the crystal structures of $Sr(MX_3)_2 \cdot 5H_2O$ (M = Sn, X = Cl, Br; M = Pb, X = Br): A joint crystallographic and electronic structure calculation approach

Electronic structure calculations in combination with X-ray crystallography have been used to examine valence electron pair distribution in $Sr(MX_3)_2 \cdot 5H_2O$ (M = Sn, X = Cl, Br; M = Pb, X = Br) and total energy minimisation methods used to predict the structure of $Sr(PbCl_3)_2 \cdot 5H_2O$.

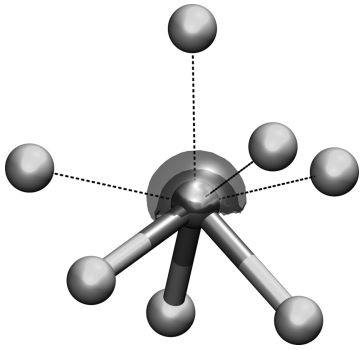

Robin B. Bedford, Michael Betham, Simon J. Coles, Peter N. Horton, María-José López-Sáez

Polyhedron 25 (2006) 1003

The influence of steric bulk on the geometry of triarylphosphite-based palladacycles and their tricyclohexylphosphine adducts

An exploration of the role of steric bulk on the synthesis and geometries of both simple triarylphosphite palladium (II) complexes (**A**) and their dimeric orthometallated counterparts (**B**).

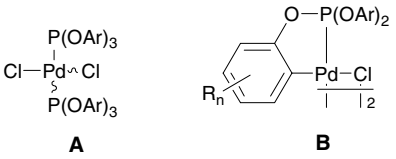

Michael A. Beckett, Simon J. Coles, Mark E. Light, Lars Fischer, Ben M. Stiefvater-Thomas, K. Sukuma Varma

Polyhedron 25 (2006) 1011

Synthesis and X-ray characterization of the organotriboroxinate salts $[Me_3NCH_2CH_2OH][Ph_4B_3O_3]$ and $[NEt_3H][Ph_3B_3O_3(OH)]$, and the X-ray structure of the triarylboroxine, $(4\text{-}MeOC_6H_4)_3B_3O_3$

The synthesis and characterization of the organotriboroxinate salts $[Me_3NCH_2CH_2OH][B_3O_4Ph_4]$ and $[NEt_3H][B_3O_3Ph_3(OH)]$ are reported. The latter contains the first example of a hybrid inorganic/organic triboroxinate anion, and exists in the solid-state as a dimer with H-bond ion-pair interactions between anions and cations and additional anion-anion H-bond interactions.

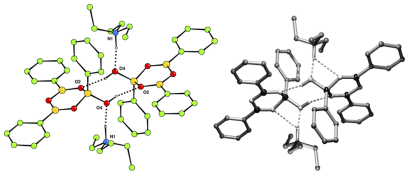

Siud Pui Man, Majid Motevalli, Stuart Gardiner, Alice Sullivan, John Wilson

Polyhedron 25 (2006) 1017

Structural studies on new metal derivatives of osteoporosis therapeutic aminohydroxyalkylidenebisphosphonic acids with C_4 and C_6 aminoalkyl chains

Hydrothermal reactions between the bisphosphonic acid 6-amino-1-hydroxy-1,1-hexylidene bisphosphonic acid and divalent hydrated metal nitrates of cobalt, nickel or zinc, afforded mononuclear dichelate products. Similar reactions using manganese or cadmium gave dinuclear products with chelate bridging as well as chelate terminal bisphosphonate ligands. The reaction between 4-amino-1-hydroxy-1,1-butylidene bisphosphonic acid and hydrated cobalt nitrate gave a dinuclear product. The C_6 alkylammonium chains in dinuclear compounds display supramolecular structure directing effects which are different from those in related compounds with C_4 alkylammonium chains.

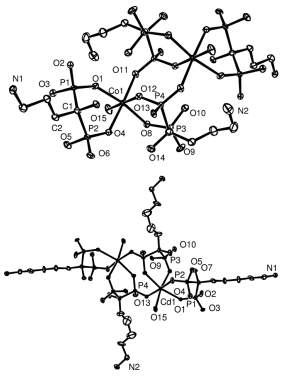

Sumit Bali, Ajai K. Singh, John. E. Drake, Mark. E. Light

Polyhedron 25 (2006) 1033

Multidentate hybrid organotellurium ligands 1-(4-methoxyphenyltelluro)-2-[3-(6-methyl-2-pyridyl)propoxy]ethane ($\mathbf{L}^1$) 2-methyl-6-{3-[2-({2-[3-(6-methyl-2-pyridyl)propoxy]ethyl}telluranyl)ethoxy]propyl}pyridine ($\mathbf{L}^2$) and their metal complexes: Formation of 20-membered metallomacrocycle by $\mathbf{L}^1$

1-(4-Methoxyphenyl-telluro)-2-[3-(6-methyl-2-pyridyl)propoxy]ethane ($\mathbf{L}^1$) 2-methyl-6-{3-[2-({2-[3-(6-methyl-2-pyridyl)propoxy]ethyl}-telluranyl)ethoxy]propyl}pyridine ($\mathbf{L}^2$) and their complexes $[PdCl_2(\mathbf{L}^1)]_2$ (**1**), $[PtCl_2(\mathbf{L}^1)]_2$ (**2**), $[HgBr_2(\mathbf{L}^1)]$ (**3**), $[PdCl_2\ (\mathbf{L}^2)]_2$ (**6**), $[PtCl_2(\mathbf{L}^2)]_2$ (**7**) and $[(PdCl_2)_3(\mathbf{L}^2)_2]$ (**8**) have been synthesized and characterized by IR, ^1H and ^{13}C NMR spectra. **3** on crystallization from acetone:hexane (2:1) mixture gives $MeOC_6H_4HgBr$ (**4**) and $[RTe^+–HgBr_2]Br^-$ (R = $–CH_2CH_2OCH_2CH_2CH_2$-(2-(6-CH_3–C_5H_3N))) (**5**).The crystal structures of **1**, **2** and **4** are solved. **1** and **2** are 20-membered metallomacrocycles and do not dissociate in solution. The crystals of **1** and **2** have chloroform and benzene, respectively, in the lattice whereas **4** is a linear ArHgBr type species. The Pd/Pt in **1** and **2** has square planar geometry. The Pd–Te and Pd–N bond lengths in **1** are 2.530(1)/2.5313(9) and 2.097(4) and 2.101(4) Å, respectively.

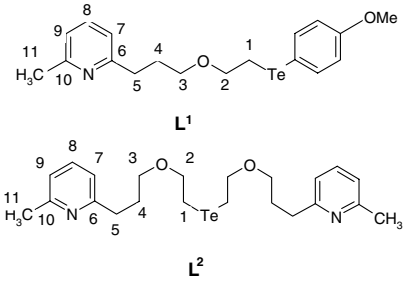

Gary S. Nichol, William Clegg

Polyhedron 25 (2006) 1043

Classical hydrogen bonding and weaker C–H···O interactions in complexes of uracil-5-carboxylic acid with the alkali metals Na–Cs

Five alkali metal complexes of the organic acid uracil-5-carboxylic acid, all synthesised from aqueous solution, are presented. Crystal structure analysis showed that hydrogen bonding is important in all compounds, with chain, sheet and tape motifs being formed. C–H···O hydrogen bonding, although weaker, also has a major role to play in most of the structures.

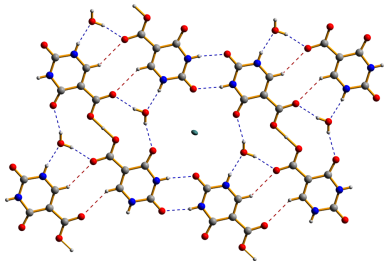

Simon A. Cotton, Vilius Franckevicius, Mary F. Mahon, Li Ling Ooi, Paul R. Raithby, Simon J. Teat

Polyhedron 25 (2006) 1057

Structures of 2,4,6-tri-α-pyridyl-1,3,5-triazine complexes of the lanthanoid nitrates: A study in the lanthanoid contraction

The structures of 20 new lanthanoid complexes all containing the 2,4,6-tri-α-puridyl-1,3,5-triazine ligand have been determined crystallographically. The majority of the complexes have the formula $[Ln(tptz)(NO)_3(H_2O)] \cdot 2EtOH$, with the two ethanol molecules hydrogen bonded to the complex. The lanthanoid ions are 10 co-ordinate and an analysis of the metal–ligand bond lengths is consistent with the lanthanide contraction across the series.

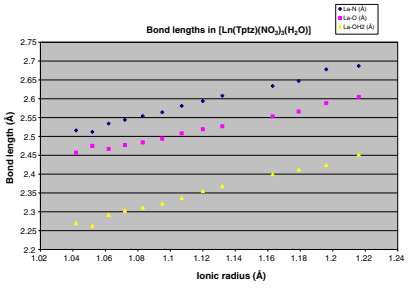

Michael J. Carr, Andreas Franken, Ramón Macías, John D. Kennedy

Polyhedron 25 (2006) 1069

Twelve-vertex polyhedral carbaborane chemistry. Isostructural cations and anions: The 'globule–globule' salt $[H_3NCH_2C_2B_{10}H_{11}]$-$[H_3CCH_2CB_{11}H_{11}]$

Chemistry associated with attempts to synthesise the salt $[H_3NCH_2C_2B_{10}H_{11}]^+$ $[H_3CCH_2CB_{11}H_{11}]^-$, of which the anions and cations are isostructural, are described.

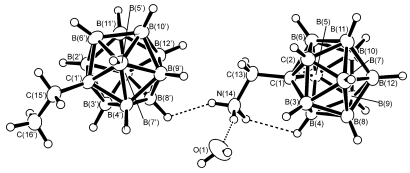

The Publisher encourages the submission of articles in electronic form thus saving time and avoiding rekeying errors. For detailed instructions on the preparation of manuscripts and of electronic artwork, consult the Author Gateway for Elsevier at http://authors.elsevier.com

SCIENCE DIRECT®

Full text of this journal is available, on-line from **ScienceDirect**. Visit **www.sciencedirect.com** for more information.

CONTENTS direct

This journal is part of **ContentsDirect,** the ***free*** alerting service which sends tables of contents by e-mail for Elsevier books and journals. You can register for **ContentsDirect** online at: **http://contentsdirect.elsevier.com**

Available online at www.sciencedirect.com
SCIENCE DIRECT®
Polyhedron 25, issue 2, 23 January 2006
POLYHEDRON
www.elsevier.com/locate/poly

Contents

Preface 203

Papers

Sherrika D. Daniel, Jean-Sébastien M. Lehn, James D. Korp, David M. Hoffman

Polyhedron 25 (2006) 205–210

Syntheses and X-ray structures of cerium amide complexes

The complexes $Ce(TMP)_3$ (TMP-H = 2,2,6,6-tetramethylpiperidine), $[Ce(\mu\text{-}OCH{=}CH_2)(TMP)_2]_2$, and $Ce[N\text{-}t\text{-}Bu(SiMe_3)]_3$ were synthesized. The alkoxide ligand in $[Ce(\mu\text{-}OCH{=}CH_2)(TMP)_2]_2$ originated from the THF solvent. There is evidence to suggest the presence of a weak Ce–vinyl group interaction in the structure of $[Ce(\mu\text{-}OCH{=}CH_2)(TMP)_2]_2$. $Ce(TMP)_3$ and $Ce[N\text{-}t\text{-}Bu(SiMe_3)]_3$ are trigonal planar monomers in the solid state.

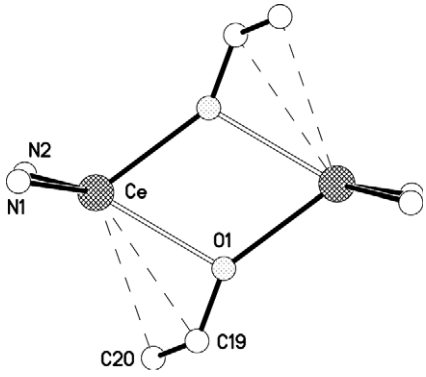

Andrew J. Edwards, Jack Lewis, Chi-Keung Li, Catherine A. Morewood, Paul R. Raithby, Gregory P. Shields

Polyhedron 25 (2006) 211–218

Synthesis and molecular structure of mixed alkyne-cyclopentadienyl clusters via the ionic coupling of $[Os_3(CO)_9(R_2C_2)]^{2-}$ with $[Ru(\eta^5\text{-}C_5H_5)(MeCN)_3]^+$ and the reaction $[Os_3RuH(\eta^5\text{-}C_5H_5)(CO)_{10}(MeCN)]$ with alkynes (R_2C_2) (R = Me, Ph)

The coupling reaction of the dianion $[Os_3(CO)_9(R_2C_2)]$ (R = Me, Ph) with two equivalents of the monocation $[Ru(\eta^5\text{-}C_5H_5)(CH_3CN)_3]^+$ affords the neutral clusters $[Os_3Ru_2(CO)_9(R_2C_2)(\eta^5\text{-}C_5H_5)_2]$. These clusters exhibit a capped pseudo-octahedral $Os_3Ru_2C_2$ core, with the alkyne bonded parallel to the hinge bond of the capped butterfly metal geometry in a $\mu_4\text{-}\eta^2$ manner. Similarly, reaction of the activated cluster $[Os_3RuH(\eta^5C_5H_5)(CO)_{10}(MeCN)]$ with RCCR (R = Me, Ph) affords the related clusters $[Os_3RuH(CO)_9(\eta^5\text{-}C_5H_5)(R_2C_2)]$.

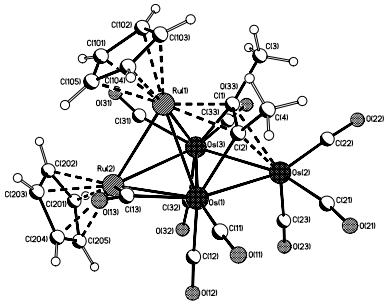

F. Albert Cotton, Armin de Meijere, Carlos A. Murillo, Karsten Rauch, Rongmin Yu

Polyhedron 25 (2006) 219–223

Trishomobarrelenedicarboxylate dianion as a bridge between dimolybdenum units: Comparison to similar compounds

The structure of a new molecular pair, $[Mo_2(DAniF)_3]_2(O_2CC_{11}H_{12}CO_2)$, is described along with its ^1H NMR and UV–Vis spectra. The comparison of its electrochemistry with analogous compounds is discussed.

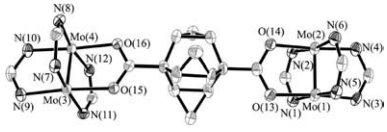

Hani M. El-Kaderi, Mary Jane Heeg, Charles H. Winter

Polyhedron 25 (2006) 224–234

Complexes of the heavier alkaline earth metals containing β-diketiminato and iodide ligand sets

A series of mixed ligand complexes of calcium, strontium, and barium containing β-diketiminato and iodide ligands has been synthesized and characterized. Dimers or tetramers were obtained, which were connected through bridging iodide ligands. Depending on the steric bulk of the nitrogen atom substituents and the metal ion, η^5-, η^2-, or μ-η^2:η^5-β-diketiminato ligand coordination modes were observed. The combined results suggest that β-diketiminato ligands are strongly coordinating for group 2 metal ions, and are effective at stabilizing mixed ligand complexes toward redistribution equilibria.

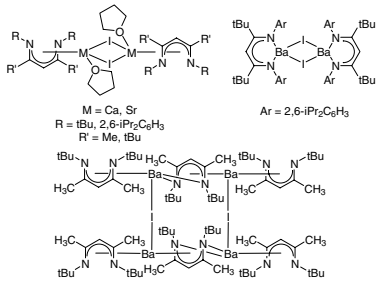

Colin A. Kilner, Malcolm A. Halcrow

Polyhedron 25 (2006) 235–240

An iron(II) complex of 2,6-di(pyrazol-1-yl)-pyrazine that crystallises in three forms, two of which exhibit an unusual angular Jahn–Teller distortion

Slow diffusion of Et_2O vapour into a solution of bis[2,6-di(pyrazol-1-yl)pyrazine]iron(II) dihexafluoroantimonate **1[SbF$_6$]$_2$** in CH_3NO_2 yielded three different single crystalline phases. Solvent-free **1[SbF$_6$]$_2$** and solvated **1[SbF$_6$]$_2$** · $2CH_3NO_2$ are both high-spin, and have undergone an unusual angular Jahn–Teller distortion to different extents. In contrast **1[SbF$_6$]$_2$** · $3CH_3NO_2$ is low-spin at room temperature and has a regular six-coordinate geometry.

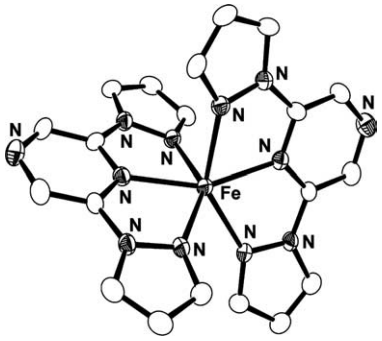

Mohammad Azad Malik, Paul O'Brien, Majid Motevalli, Isaac Abrahams

Polyhedron 25 (2006) 241–250

The adoption of the beryllium acetate structural motif in zinc oxycarbamates, oxythiocarbamates and oxythiophosphinates

Zn_4OL_6(L = S_2CNEt_2, S_2PEt_2 and $OCNEt_2$) complexes are readily formed by hydrolysis of the mixed alkylzinc-carbamato, thiophophinato or thiocabamato (RZnL) compounds. These oxyzinc complexes all adapt a basic beryllium-acetate-like tetrahedral (μ_4-O)Zn_4 core.

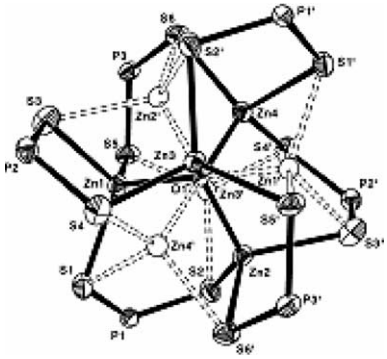

Devon C. Rosenfeld, David S. Kuiper, Emil B. Lobkovsky, Peter T. Wolczanski

Polyhedron 25 (2006) 251–258

Synthesis and reactivity of (silox)$_2$R$_2$WO (R = Cl, Me, Et, ^{n}Pr and ^{n}Bu; silox = OSi^{t}Bu$_3$) and (silox)$_2$MO$_2$ (M = Mo and W)

The lack of oxygen atom transfer from (silox)$_2$R$_2$WO (**4**-R, R = Me, Et,^{n}Pr, ^{n}Bu; R = Cl, **3**) and (silox)$_2$M(O)$_2$ (M = Mo, **6**; W, **7**) may be a consequence of orbital symmetry constraints.

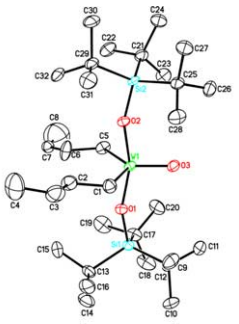
(silox)$_2$(^{n}Bu)$_2$WO (**4**-^{n}Bu)

Jeffrey M. Pietryga, Jamie N. Jones, Charles L.B. Macdonald, Jennifer A. Moore, Alan H. Cowley

Polyhedron 25 (2006) 259–265

Titanium(IV) complexes with amidinate and/or hydrazido ligands

Two new titanium(IV) complexes have been synthesized and characterized by X-ray diffraction. The first complex, $[Ti_2Cl_4(NNMe_2)_2(py)_3]$, is dimeric and features two η^2-dimethyl-hydrazido bridges. The second complex, $[TiCl(PhC\{N(SiMe_3)_2\}_2)_2(MeNN\text{-}Me_2)]$, is mononuclear and the coordination sphere comprises two η^2-bonded amidinate ligands, one chloride and one η^2-bonded trimethylhydrazide.

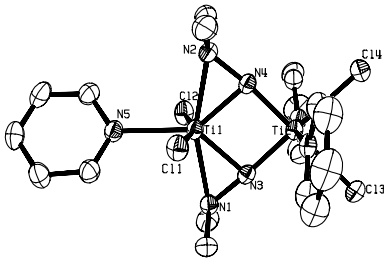

Christopher S.A. Fraser, Dana J. Eisler, Richard J. Puddephatt

Polyhedron 25 (2006) 266–270

Self-assembly of organometallic polymers through hydrogen bonding: A diplatinum(IV) complex with a single bridging halide ligand

The binuclear platinum(IV) complex $[\{PtMe_2(CH_2C_6H_4CO_2H)(bu_2bipy)\}_2(\mu\text{-}Br)][PF_6]$ contains an unsupported bridging bromide ligand and forms a self-assembled polymer through intermolecular hydrogen bonding between pairs of carboxylic acid groups.

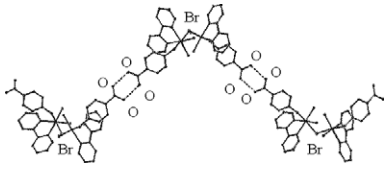

Xiaoping Yang, Richard A. Jones, Qiaoyin Wu, Michael M. Oye, Wing-Kit Lo, Wai-Kwok Wong, Archie L. Holmes

Polyhedron 25 (2006) 271–278

Synthesis, crystal structures and antenna-like sensitization of visible and near infrared emission in heterobimetallic Zn–Eu and Zn–Nd Schiff base compounds

Visible and near infrared (NIR) luminescence are observed in heterobimetallic 3d–4f Schiff base complexes $[ZnLEu(OAc)(NO_3)_2] \cdot EtOH \cdot H_2O$ (**2**) and $[ZnLNd(OAc)(NO_3)_2(H_2O)] \cdot EtOH$ (**3**), respectively.

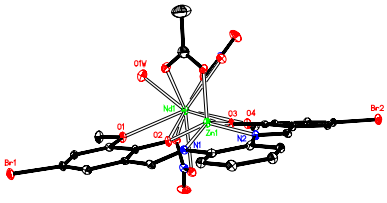

Bing Luo, Benjamin E. Kucera, Wayne L. Gladfelter

Polyhedron 25 (2006) 279–285

Syntheses and X-ray crystal structures of zinc complexes with an amido-diamine ligand

Zinc complexes with an amido-diamine ligand, $LZnN(CH_2CH_2NMe_2)_2$ (L = Cl, Et, $N(CH_2CH_2NMe_2)_2$ and N^iBu_2), were synthesized and characterized. Mass spectral, NMR and X-ray structural analyses indicated that these compounds were dimeric with bridging $N(CH_2CH_2NMe_2)_2$ ligands.

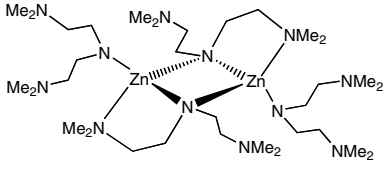

Cameron K. Gren, Timothy P. Hanusa, William W. Brennessel

Polyhedron 25 (2006) 286–292

Allyl complexes of heavy group 13 elements: Structure and bonding in $[1,3\text{-}(SiMe_3)_2C_3H_3]_3$-Ga

The first structurally characterized example of a gallium allyl complex, $[1,3\text{-}(SiMe_3)_2C_3H_3]_3Ga$, has been synthesized from $GaCl_3$ and $K[1,3\text{-}(SiMe_3)_2C_3H_3]$. The complex is fluxional on the NMR timescale, and X-ray crystal data reveals a σ-bonded structure, confirmed as the most stable geometry by density functional theory calculations.

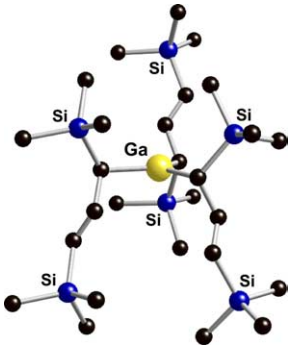

Liliane G. Hubert-Pfalzgraf, Adulfas Abrutis, Sergej Pasko, Nadia Touati, Dominique Luneau

Polyhedron 25 (2006) 293–299

Synthesis and characterization of Hf–Al heterometallic aminoalkoxides as single-source MOCVD precursors for hafnium aluminate films

The first Hf–Al aminoalkoxide $HfAl_2(\mu\text{-}OPr^i)_2(\mu,\eta^2\text{-}OC_2H_4NMe_2)_2(OPr^i)_6$ has been structurally characterized. It is an attractive single-source precursor for liquid-injection MOCVD of $(HfO_2)_x(Al_2O_3)_{1-x}$ films. These were characterized by XRD, AFM and XPS.

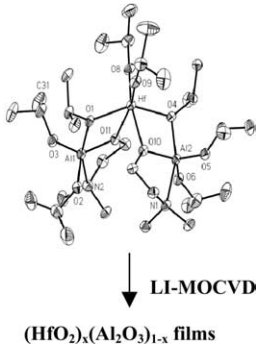

Andrei S. Batsanov, William Clegg, Royston C.B. Copley, Mark A. Fox, Wendy R. Gill, Rachel S. Grimditch, Thomas G. Hibbert, Judith A.K. Howard, J.A. Hugh MacBride, Kenneth Wade

Polyhedron 25 (2006) 300–306

Preparative and structural studies on sulfur-linked carborane icosahedra: 2-Phenyl-*ortho*-carboranyl-sulfur systems $(2\text{-Ph-}1,2\text{-}C_2B_{10}H_{10})_2X$ (X = S, S_2 or SO), and *ortho*-carboran-di-yl systems $(1,2\text{-}C_2B_{10}H_{10}Y)_2$ (Y = S or SO)

The new carborane derivatives $(PhCb°)_2X$, where PhCb° = 2-Ph-1,2-$C_2B_{10}H_{10}$ and X = S or SO, were prepared from PhCb°Li and SCl_2 or $SOCl_2$, respectively. Attempts to prepare cyclic systems $(Cb°Y)_2$, in which two *ortho*-carboran-di-yl residues Cb° are linked through two bridging units Y (S, SO) are also reported.

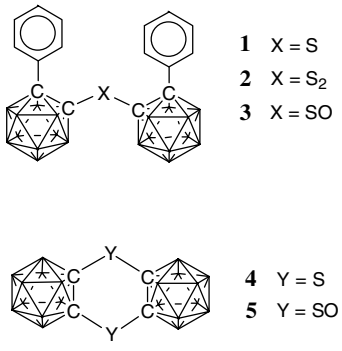

Deborah M. Huck, H. Loc Nguyen, Peter N. Horton, Michael B. Hursthouse, Daniel Guillon, Bertrand Donnio, Duncan W. Bruce

Polyhedron 25 (2006) 307–324

Mesomorphic silver(I) complexes of polycatenar 2′- and 3′-stilbazoles. Crystal and molecular structure of 3,4-dimethoxy-3′-stilbazole and of two silver triflate complexes

Di- and tri-alkoxy-2′ and 3′-stilbazoles were synthesised using a Siegrist methodology. None of these ligands was mesomorphic, but their complexes with silver(I) dodecylsulphate and triflate les to complexes showing columnar mesophases as characterised by optical microscopy and X-ray diffraction. Single crystal structures of one ligand and two triflate complexes are reported.

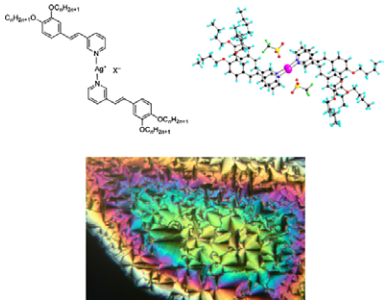

Leigh F. Jones, David M. Low, Madeleine Helliwell, James Raftery, David Collison, Guillem Aromí, Joan Cano, Talal Mallah, Wolfgang Wernsdorfer, Euan K. Brechin, Eric J.L. Mcinnes

Polyhedron 25 (2006) 325–333

Fe(III) clusters built with tripodal alcohol ligands

Use of the tripodal ligand H_3thme has led to the isolation of a number of new Fe(III) clusters ranging in nuclearity from 4 to 16. Magnetic studies reveal that the [Fe_{11}] complex shown is a single-molecule magnet.

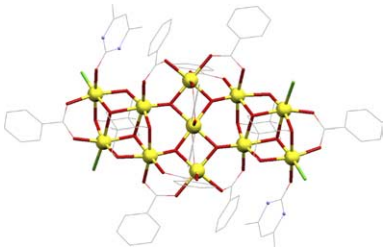

Uzma Qureshi, Troy D. Manning, Christopher Blackman, Ivan P. Parkin

Polyhedron 25 (2006) 334–338

Composite thermochromic thin films: (TiO_2)–(VO_2) prepared from titanium isopropoxide, $VOCl_3$ and water

Atmospheric chemical vapour deposition (APCVD) was used to deposit composite TiO_2–VO_2 films on glass. The films were characterised by X-ray photoelectron spectroscopy, X-ray diffraction, Raman, energy dispersive X-ray analysis and scanning electron microscopy. These composite films exhibited photo-induced hydrophilicity, photocatalysis and a thermochromic switching temperature of 54 °C.

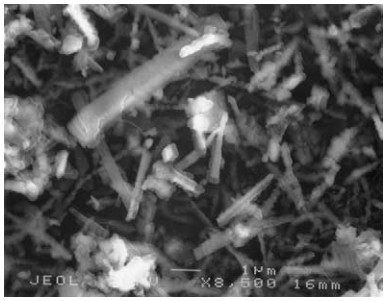

Xavier Solans-Monfort, Odile Eisenstein

Polyhedron 25 (2006) 339–348

DFT calculations of NMR $J_{C–H}$ coupling constants: An additional tool to characterize the α-agostic interaction in high oxidation state M-alkylidene complexes (M = Re, Mo and Ta)

DFT calculations have been used to calculate the spin–spin $J_{C–H}$ coupling constants for the C–H alkylidene bond in Re(≡CR)(=CHR)(X)(Y), Mo(=NR′)(=CHR)(X)(Y) and Ta($C_5R'_5$)(=CHR)(X)(Y), where the experiment suggests a weak agostic interaction for Re and Mo and a strong agostic interaction for Ta. The calculated $J_{C–H}$ are in good agreement with the experiment when the IGLO basis sets are used. The calculations reproduce that $J_{C–H}$ is lower for the *syn* than for the *anti* isomer. They also show that $J_{C–H}$ depends on the metal even in the absence of agostic interaction.

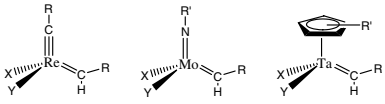

J_{C-H} from DFT calculations ?

Andrew M. Dattelbaum, James D. Martin

Polyhedron 25 (2006) 349–359

Benzene and ethylene binding to copper(I)–ziconium(IV) chloride materials: The crystal structure and solid-state reactivity of $((bz)_2Cu)_2Zr_2Cl_{10} \cdot bz$

$((bz)_2Cu)_2Zr_2Cl_{10} \cdot bz$ (**1**) was synthesized by solvothermal methods. The title compound looses benzene in a stepwise fashion to yield $((bz)Cu)_2Zr_2Cl_{10}$ (**2**) which exhibits brilliant luminescence from a metal-to-ligand charge transfer state, and $Cu_2Zr_2Cl_{10}$ (**3**) proposed to have a clay-type structure. Both **2** and **3** reversibly sorb ethylene at modest pressure.

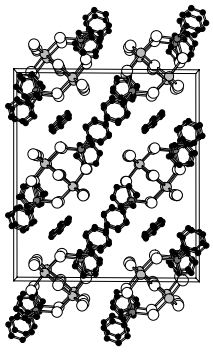

Leigh F. Jones, Laura O'Dea, Daniel A. Offermann, Paul Jensen, Boujemaa Moubaraki, Keith S. Murray

Polyhedron 25 (2006) 360–372

Benzotriazole based 1-D, 2-D and 3-D metal dicyanamide and tricyanomethanide coordination networks

The synthesis, structure and magnetism of benzotriazole based 1-D, 2-D and 3-D metal dicyanamide and tricyanomethanide coordination networks are described.

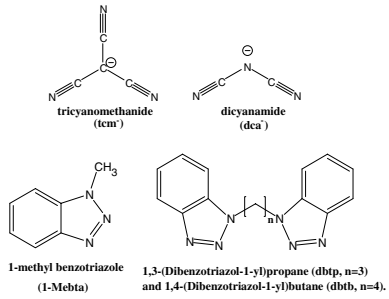

Andrea J. Clarkson, Allan G. Blackman

Polyhedron 25 (2006) 373–378

Synthesis and Co(III) complexes of the new tetradentate mixed-donor tetraamine ligand *N*-{2-[(2-pyridin-2-ylethyl)amino]ethyl}ethane-1,2-diamine (peda)

The syntheses of the new linear tetradentate tetraamine ligand *N*-{2-[(2-pyridin-2-ylethyl)-amino]ethyl}ethane-1,2-diamine (peda) and some Co(III) complexes of this ligand are reported. An X-ray crystal structure of $[Co(peda)O_2CO]I \cdot H_2O$ and kinetic data for the acid hydrolysis of $[Co(peda)(O_2CO)]ClO_4 \cdot H_2O$ are detailed.

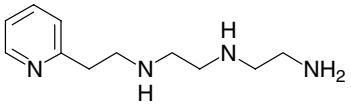

Glen B. Deacon, Maria Forsyth, Peter C. Junk, Stuart G. Leary, Graeme J. Moxey

Polyhedron 25 (2006) 379–386

Synthesis and structural diversity of rare earth anthranilate complexes

Four structural classes have been established for rare earth anthranilates, which have been prepared from the lanthanoid chloride or triflate and anthranilic acid followed by pH adjustment to 4. Polymeric structures are observed for lanthanum and ytterbium, a dimeric complex for erbium, and a monomer for neodymium (pictured). The anthranilate ligands exhibit a diverse range of binding modes within the four structural classes.

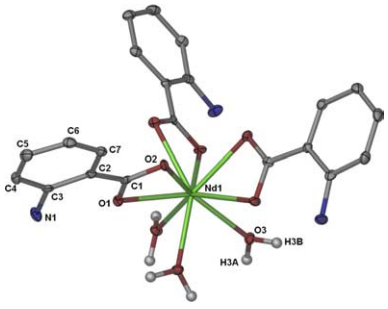

Robyn K.J. Bott, Mark Schormann, David L. Hughes, Simon J. Lancaster, Manfred Bochmann

Polyhedron 25 (2006) 387–396

Synthesis and structures of ferrocenyl-substituted salicylaldiminato complexes of magnesium, titanium and zirconium

The preparation and structures of the *N*-ferrocenyl salicylaldiminato complexes $(FcPI)_2Mg(THF)_2$, $CpTiCl_2(FcPI) \cdot CH_2Cl_2$, $CpZrCl(FcPI)_2$, $CpZrCl_2(FcPI)$, and $(FcPI)_2ZrCl_2 \cdot CH_2Cl_2$ is described. They are electrochemically active, with redox potentials close to ferrocene. On activation with methylaluminoxane, the Ti complex polymerises ethylene, while $(FcPI)_2ZrCl_2$ is a highly active ethylene oligomerisation catalyst.

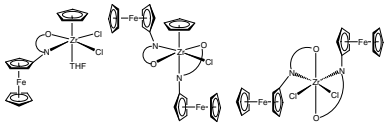

Michael J. Davies, Michael F. Lappert

Polyhedron 25 (2006) 397–405

Studies on 1,2-phenylenedioxoborylcyclopentadienes and some of their metal (Ti, Zr, Fe) complexes

17 Compounds, including **2a**, **3a** and **9** have been studied with respect to (i) (modest) catalytic activity for C_2H_4 or C_3H_6 polymerisation, and (ii) the electronic effect of the boryl substituent (using ^{11}B NMR spectroscopy, cyclic voltammetry and EPR spectra of reduced species). (BCAT = $BO_2C_6H_4$-1,2, $BCAT^t$ = the 4-^{t}Bu analogue).

$Ti(\eta^5\text{-}C_5H_4BCAT)Cl_3]$
2a

$Zr(\eta^5\text{-}C_5H_4BCAT)_2Cl_2]$
3a

$Fe(\eta^5\text{-}C_5H_4BCAT^t)_2]$
3a

Stephen L.J. Conway, Malcolm L.H. Green, Sofia I. Pascu, Henry O. Peake

Polyhedron 25 (2006) 406–420

Structure–reactivity correlations in new W(IV) and Nb(IV) silicon-bridged *ansa*-metallocene hydrides

New W(IV) and Nb(IV) derivatives: [W(L1)MeI] (**1**), [W(L1)MeH] (**2**) and [W(L1)O] (**3**), $[W(L2)Cl_2]$ (**4**), $[W(L2)H_2]$ (**5**), $[W(L2)H_3][BF_4]$ (**6**), $[Nb(L2)Cl_2]$ (**7**) and $[Nb(L2)(\eta^2\text{-}BH_4)]$ (**8**) (where **L1** = $[(\eta\text{-}C_5H_4)_2SiMe_2]^{2-}$ and **L2** = $[(\eta\text{-}C_5H_3TMS)_2SiMe_2]^{2-}$) have been prepared and their structural and dynamic properties have been investigated.

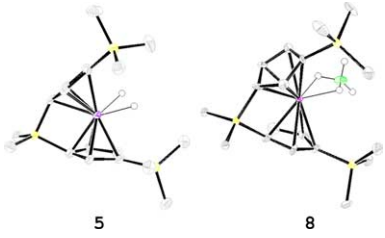

Edwin C. Constable, Deborah Gusmeroli, Catherine E. Housecroft, Markus Neuburger, Silvia Schaffner

Polyhedron 25 (2006) 421–428

Cobalt decorated metallostars and metallodendrimers: Synthetic strategies and spectroscopic correlations

A series of compounds containing polyalkyne frameworks decorated with dicobalt carbonyl clusters has been prepared, and spectroscopic data have been analyzed to provide correlations to assist in the characterization of cobaltadendrimers.

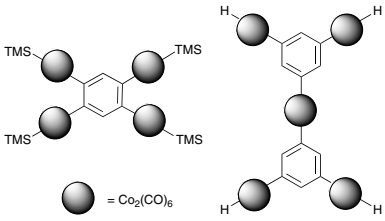

Alexandra Bartole-Scott, Alan J. Lough, Ian Manners

Polyhedron 25 (2006) 429–436

Synthesis and reactivity of [2]ferrocenophanes containing C–Pb and C–Zr bridges

The synthesis and reactivity of a carboplumba[2]ferrocenophane and a carbozircona[2]ferrocenophane are reported and X-ray characterization of the latter species demonstrated moderate tilting away from the bridging elements. Attempts to induce ring-opening polymerization were unsuccessful, however these compounds underwent stoichiometric ring-opening reactions.

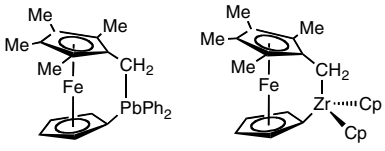

Cp = (η-C_5H_5)

Edwin C. Constable, Peter Harverson, Catherine E. Housecroft, Ebbe Nordlander, Jerry Olsson

Polyhedron 25 (2006) 437–458

Conventional and metal-directed synthesis of homodinuclear and heterotrinuclear complexes of homoditopic and heteroditopic ligands incorporating bpy and tpy metal-binding domains

Strategies for the preparation of multinuclear complexes containing homoditopic and heteroditopic ligands based upon 2,2′-bipyridine (bpy) and 2,2′:6′,2″-terpyridine metal binding domains are presented. Both conventional approaches based upon preparation of a free ligand and subsequent coordination and metal-directed reactions of coordinated ligands are utilized in the various strategies.

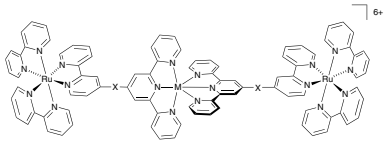

Dejian Huang, Kenton B. Renkema, Kenneth G. Caulton

Polyhedron 25 (2006) 459–468

Cleavage of F–C(sp^2) bonds by MHR(CO)-(P^tBu_2Me)$_2$ (M = Os and Ru; R = H, CH_3 or Aryl): Product dependence on M and R

The very different products of vinyl C–F bonds reacting with unsaturated Ru vs. Os Hydride compounds are explained in terms of the lifetimes of the adducts of metal complex with fluoro-olefin.

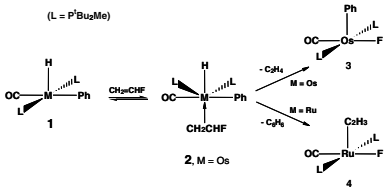

Zachary J. Tonzetich, Richard R. Schrock

Polyhedron 25 (2006) 469–476

Potential Group IV olefin polymerization catalysts that contain a diamido ligand substituted with hexaisopropylterphenyl groups

The diamido ligand, $[HIPTN_2]^{2-}$ ($HIPTN_2$ = (*N*-hexa-*iso*-propyl-3,5-terphenyl)diaminobinaphthalene), has been prepared and shown to support a variety of Group IV complexes. Several Zr and Hf alkyls of the ligand have been synthesized as potential olefin polymerization catalysts. Activation of $[HIPTN_2]$-$ZrMe_2$ with a variety of Lewis acids gives rise to different species depending on the nature of the activator employed.

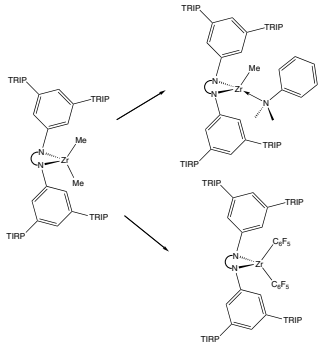

Corneliu Stanciu, Anne F. Richards, Matthias Stender, Marilyn M. Olmstead, Philip P. Power

Polyhedron 25 (2006) 477–483

New terphenylphenoxides of group 13 and 14 elements

Sterically encumbering terphenoxide ligands have been used to isolate aluminum and gallium alkyl derivatives as well as low coordinate germanium and tin divalent compounds.

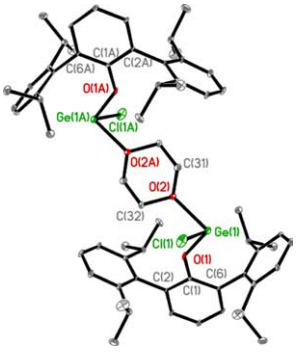

William J. Evans, Stosh A. Kozimor, Joseph W. Ziller

Polyhedron 25 (2006) 484–492

Synthesis of heteroleptic uranium compounds including an asymmetric, sterically unsaturated, bimetallic, organouranium(IV) halide: $(C_5Me_5)(C_8H_8)ClU(\mu\text{-}Cl)U(C_8H_8)(C_5Me_5)$

The synthesis of $(C_5Me_5)(C_8H_8)ClU(\mu\text{-}Cl)U(C_8H_8)(C_5Me_5)$ via an unusual $(C_5Me_5)^{1-}$ displacement reaction is described as well as its structure and reactivity. It readily adds a base, e.g. with ε-caprolactam, to form a complex containing four different ligands, $(C_5Me_5)(C_8H_8)U(Cl)[OCNH(CH_2)_5]$. It can also be used as a precursor to $(C_5Me_5)(C_8H_8)U[N(SiMe_3)_2]$.

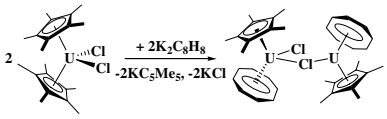

David R. Manke, Daniel G. Nocera

Polyhedron 25 (2006) 493–498

Solid state aggregation of lithium and thallium(I) bis(alkylamido)phenylboranes

Lithium and thallium(I) complexes of bis(alkylamido)phenylborane ligands, $[RN\text{–}B^{Ph}\text{–}NR]M_2$ (R = ^{t}Bu,Pr; M = Li, Tl), have been prepared and characterized by ^1H and ^{11}B NMR spectroscopy. Single crystal X-ray structure analysis demonstrates interesting aggregation in the solid state. The bis(*tert*-butylamido)phenylborane complex of thallium(I) is shown.

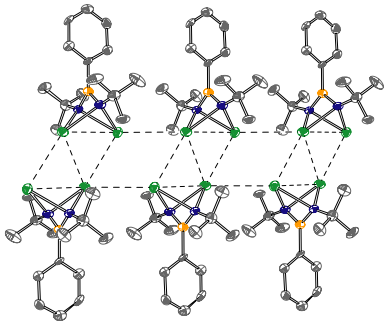

David G. Churchill, Brian M. Bridgewater, Guang Zhu, Keliang Pang, Gerard Parkin

Polyhedron 25 (2006) 499–512

Carbon–hydrogen versus carbon–chalcogen bond cleavage of furan, thiophene and selenophene by *ansa* molybdenocene complexes

$[Me_2Si(C_5Me_4)_2]MoH_2$ reacts with furan to yield a product resulting from C–H bond cleavage, namely $[Me_2Si(C_5Me_4)_2]Mo(\eta^1\text{-}C\text{-}C_4H_3O)H$, whereas the corresponding reactions of thiophene and selenophene yield products resulting from C–S and C–Se bond cleavage, namely $[Me_2Si(C_5Me_4)_2]Mo(\eta^2\text{-}C,S\text{-}SC_4H_4)$ and $[Me_2Si(C_5Me_4)_2]Mo(\eta^2\text{-}C,Se\text{-}SeC_4H_4)$.

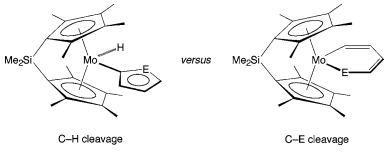

Claudia A. Blindauer, M. Tahir Razi, Simon Parsons, Peter J. Sadler

Polyhedron 25 (2006) 513–520

Metal complexes of *N*,*N*,*N*′,*N*′-tetrakis(2-pyridylmethyl)ethylenediamine (TPEN): Variable coordination numbers and geometries

Interesting variations in the structures of Cu(II), Zn(II) and other metal complexes of *N*,*N*,*N*′,*N*′-tetrakis(2-pyridylmethyl)ethylenediamine (TPEN) are described.

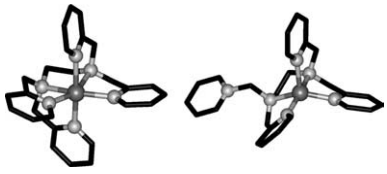

Emren N. Esenturk, James Fettinger, Bryan Eichhorn

Polyhedron 25 (2006) 521–529

Synthesis and characterization of the $[Ni_6Ge_{13}(CO)_5]^{4-}$ and $[Ge_9Ni_2(PPh_3)]^{2-}$ Zintl ion clusters

Reactions between K_4Ge_9, $Ni(CO)_2(PPh_3)_2$, and 2,2,2-crypt in ethylenediamine solutions give the $[Ni_6Ge_{13}(CO)_5]^{4-}$ ion (see structure) at low temperatures (~40 °C) and the $[Ge_9Ni_2(PPh_3)]^{2-}$ ion at higher temperatures (~118 °C). The biicosahedral structure of the $[Ni_6Ge_{13}(CO)_5]$ ion is unique in Zintl cluster chemistry.

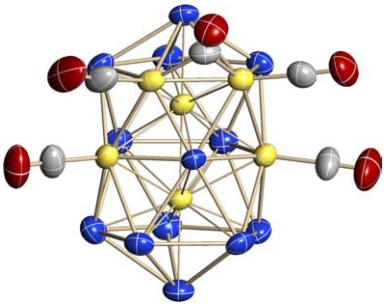

Saratchandra B. Mukkamala, Rodolphe Clérac, Christopher E. Anson, Annie K. Powell

Polyhedron 25 (2006) 530–538

Structures and magnetic behaviour of hydroxo-bridged Cr^{III} aggregates: $[Cr_4(\mu\text{-}OH)_4(hpdta)_2]^{2-}$ and $[Cr_6(\mu\text{-}OH)_8(hpdta)_2(en)_2]$

Hydroxo-bridged Cr(III) tetranuclear and hexanuclear aggregates show antiferromagnetic coupling which can be modelled relatively easily. The parallels to the structures and properties of the related Fe(III) and Al(III) compounds are discussed.

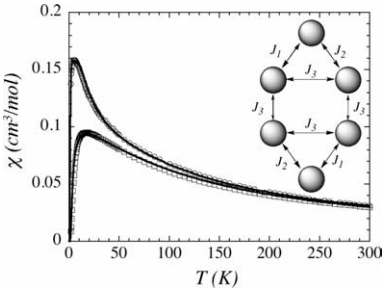

Katerina A. Thiakou, Vassilios Nastopoulos, Aris Terzis, Catherine P. Raptopoulou, Spyros P. Perlepes

Polyhedron 25 (2006) 539–549

Di-2-pyridyl ketone in lanthanide(III) chemistry: Mononuclear and dinuclear erbium(III) complexes

The reaction between $Er(NCS)_3$ and di-2-pyridyl ketone in alcohols gives mononuclear and dinuclear isothiocyanate complexes depending on the OH^- concentration in the reaction system. In the mononuclear complexes the neutral hemiacetal form of the ligand adopts the coordination mode **A**, while in the dinuclear complex the hemiacetal form of the ligand is anionic bridging two Er^{III} atoms (coordination mode **B**).

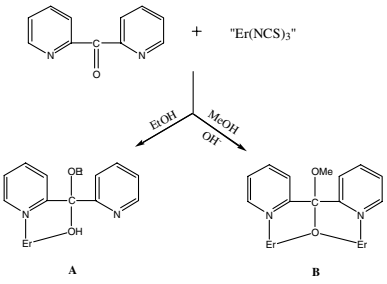

Sibaprasad Bhattacharyya, Maren Pink, John C. Huffman, Jeffrey M. Zaleski

Polyhedron 25 (2006) 550–558

Thioether coordinated metalloenediynes: Syntheses, structures and thermal reactivity comparison

The d^{10} species of these novel thioether coordinated metalloenediynes have distorted but near tetrahedral geometries with weak thioether coordination, while the d^9 and d^8 species are likely *trans* tetragonal and square planar, respectively. Remarkably, the latter structures exhibit Bergman cyclization temperatures ~25 °C *lower* than their tetrahedral counterparts, and on the order of 50–100 °C lower than that expected for complexes with *trans* geometries. This chemical behavior derives from the fluxionality of the thioether linkage and an unusual *trans* to pseudo *cis* conformational change during upon heating.

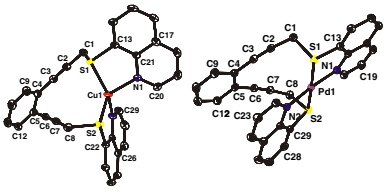

Jui-Hsien Huang, Ting-Yu Lee, Dale C. Swenson, Louis Messerle

Polyhedron 25 (2006) 559–567

Dinuclear coordination of a novel four-electron reduced μ-η^1,η^3-allene ligand with β-agostic C–H···Ta interaction: Direct addition of allene to $(C_5Me_5)_2Ta_2(\mu\text{-}X)_4$ (X = Cl, Br), and molecular structure of $(C_5Me_5)_2Ta_2(\mu\text{-}\eta^1,\eta^3\text{-}C_3H_4)(\mu\text{-}Cl)Cl_3$

The d^2–d^2 organoditantalum(III) compound $(C_5Me_5)_2Ta_2(\mu\text{-}X)_4$ (X = Cl, Br) coordinates allene in an unusual alkylidene-diyl fashion to give the fluxional $(C_5Me_5)_2Ta_2(\mu\text{-}\eta^1,\eta^3\text{-}C_3H_4)(\mu\text{-}Cl)Cl_3$ with an agostic interaction of one hydrogen from the formally four electron reduced allene ligand.

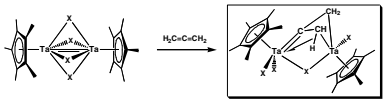

Matthew Thomas Jamie Lodge, Peter P. Edwards, Paul A. Anderson, Martin O. Jones, Ian Gameson

Polyhedron 25 (2006) 568–574

Synthesis of micro-crystals of transparent cobalt aluminate, shrouded in siliceous material, from Co(II)-exchanged zeolite X

We report the synthesis and characterisation of cobalt aluminate spinel micro-crystals, formed by the heat-induced collapse of cobalt ion-exchanged zeolite X precursors; the resulting transparent blue micro-crystals are covered in a siliceous coating which may reduce the potential environmental impact of the included cobalt compounds.

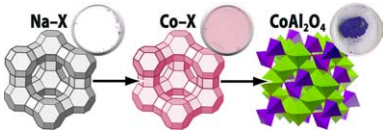

Erick J. Palmer, Bruce E. Bursten

Polyhedron 25 (2006) 575–584

Theoretical studies of π-loading and structural diversity in Cp_3MX (M = Zr, Hf; X = H, CH_3, OR, NR_2) compounds

DFT calculations have been used to explore the bonding and geometric preferences of Cp_3MX (M = Zr, Hf; X=H, CH_3, OR, NR_2) compounds containing σ-donor and π-donor X ligands. The compounds with a σ-only X ligand were found to be more stable as the "**3-5**" isomer, while the compounds with a π-donor X ligand were more stable as the "**2-5,1-1**" isomer. This stability difference is explained using molecular orbital theory.

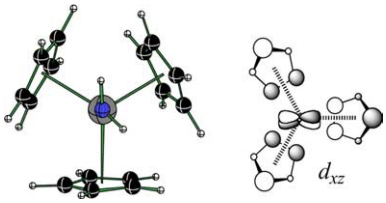

Junfeng Geng, Hongwei Li, Dejian Zhou, Wilhelm T.S. Huck, Brian F.G. Johnson

Polyhedron 25 (2006) 585–590

A dendrimer-based Co_{32} nanocluster: Synthesis and application in diameter-controlled growth of single-walled carbon nanotubes

We report the synthesis and characterization of a dendrimer-based Co_{32} nanocluster molecule and its use as uniform-size catalytic seed for diameter-controlled growth of single-walled carbon nanotubes.

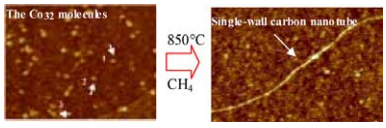

Josephine M. Tunney, Alexander J. Blake, E. Stephen Davies, Jonathan McMaster, Claire Wilson, C. David Garner

Polyhedron 25 (2006) 591–598

Synthesis and structure of gold(III) complexes of asymmetric dithiolene ligands

Four square planar $[Au(dithiolene)_2]^-$ complexes have been synthesized and characterized; they comprise Au(III) bound to two asymmetrically substituted ene-1,2-dithiolates and both *cis* and *trans* isomers are present in solution. Each complex undergoes an oxidation and a reduction, the potentials of which correlate with the electron withdrawing nature of the dithiolene.

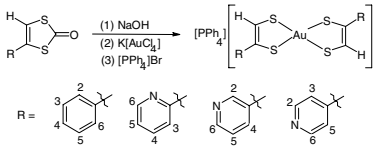

Mark W. Glenny, Leon G.A. van de Water, Joanna M. Vere, Alexander J. Blake, Claire Wilson, Willem L. Driessen, Jan Reedijk, Martin Schröder

Polyhedron 25 (2006) 599–612

Improved synthetic methods to mixed-donor thiacrown ethers

A series of azathia- and azaoxathiacrown ether macrocycles have been prepared in good yields via the use of *N*-boc-bis(2-chloroethyl)amine as a precursor; this route minimises undesirable side reactions and facilitates subsequent deprotection to the free cyclic amine.

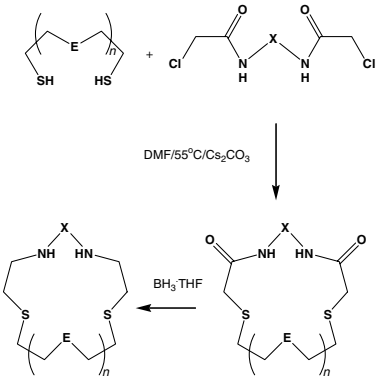

Muralee Murugesu, Abhudaya Mishra, Wolfgang Wernsdorfer, Khalil A. Abboud, George Christou

Polyhedron 25 (2006) 613–625

Mixed 3d/4d and 3d/4f metal clusters: Tetranuclear $Fe^{III}_2M^{III}_2$ (M^{III} = Ln, Y) and $Mn^{IV}_2M^{III}_2$ (M = Yb, Y) complexes, and the first Fe/4f single-molecule magnets

Mixed 3d/4d and 3d/4f tetranuclear complexes have been synthesized, comprising Fe_2Ln_2, Fe_2Y_2, Mn_2Yb_2 and Mn_2Y_2 clusters. The compounds were prepared by using triethanolamine, pyridine-2,6-dimethanol, or methanolysis conditions. The Fe_2Ln_2 (Ln = Ho^{III}, Dy^{III}) were found to be single-molecule magnets (SMMs) by low temperature, single crystal hysteresis studies, and these complexes thus represent the first mixed-metal Fe/Ln SMMs to be discovered.

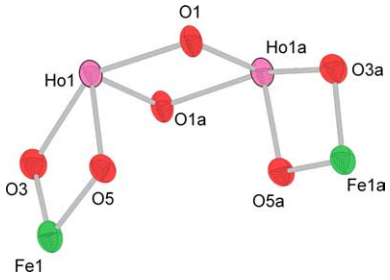

The Publisher encourages the submission of articles in electronic form thus saving time and avoiding rekeying errors. For detailed instructions on the preparation of manuscripts and of electronic artwork, consult the Author Gateway for Elsevier at http://authors.elsevier.com

SCIENCE DIRECT®

Full text of this journal is available, on-line from **ScienceDirect**. Visit **www.sciencedirect.com** for more information.

CONTENTS Direct

This journal is part of **ContentsDirect,** the ***free*** alerting service which sends tables of contents by e-mail for Elsevier books and journals. You can register for **ContentsDirect** online at: **http://contentsdirect.elsevier.com**

Available online at www.sciencedirect.com
SCIENCE DIRECT®
Polyhedron 25, issue 1, 2 January 2006
POLYHEDRON
www.elsevier.com/locate/poly

Contents

Papers

Jian-Jun Zhang, Sheng-Min Hu, Sheng-Chang Xiang, Xin-Tao Wu, Long-Sheng Wang, Ya-Min Li

Polyhedron 25 (2006) 1

Syntheses and characterization of two novel heptanuclear trigonal prismatic $LnNi_6$ clusters with different terminal ligands

Two novel heptanuclear trigonal prismatic $LnNi_6$ clusters with the same $[LnNi_6(Gly)_6(\mu_3\text{-}OH)_3]$ core but different terminal aromatic ligands were prepared.

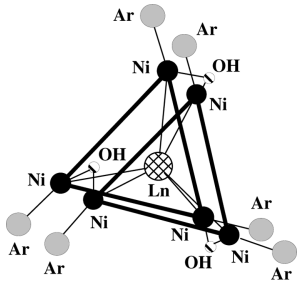

Juan Guerrero, Liliana Farías, Luis Lemus, Africa Quintanilla, Alex Mena, Luis Cortez, Ricardo F. Baggio, María T. Garland

Polyhedron 25 (2006) 9

The new $Ru(NBD)Cl_2$(substituted-2,2′-biquinoline) complexes. Synthesis and characterization

The syntheses of three complexes having the general formula $Ru(NBD)Cl_2L$ (with L = 2,2′-biquinoline derivative) are described. Their spectroscopic properties are analyzed showing slight dependence with the complexes conformation, which is modulated, by the 3,3′-substitued position on the 2,2′-biquinoline ligand.

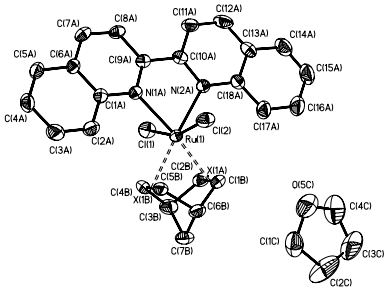

Nilotpal Barooah, Rupam J. Sarma, Andrei S. Batsanov, Jubaraj B. Baruah

Polyhedron 25 (2006) 17

N-phthaloylglycinato complexes of cobalt, nickel, copper and zinc

Cobalt(II), zinc(II), copper(II) and nickel(II) complexes of *N*-phthaloylglycinato (Nphgly) ligands are synthesised and characterised. The cobalt and zinc complexes have composition $[M(Nphgly)_2(H_2O)_4]2H_2O$ and are iso-structural with octahedral geometry around the metal. A copper complex with composition $[Cu(Nphgly)_2(py)_3]$ where (py = pyridine) has a square pyramidal structure. Similar nickel complex has composition of $[Ni(Nphgly)_2(py)_3\text{-}1.3H_2O]$ has a trimeric H-bonded network.

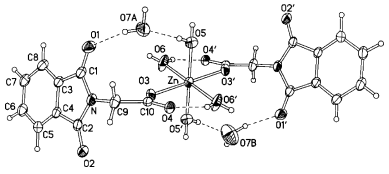

Sumana Sarkar, Amrita Mondal, Mohamed Salah El Fallah, Joan Ribas, Deepak Chopra, Helen Stoeckli-Evans, Kajal Krishna Rajak

Polyhedron 25 (2006) 25

Synthesis, structure and magnetic properties of two end-on double azido bridged nickel(II) dinuclear entities incorporating *N*,*N*,*N*-coordinating tridentate reduced Schiff base ligands

The reaction of $Ni(NO_3)_2 \cdot 6H_2O$ with *N*,*N*,*N*-coordinating reduced Schiff base ligands in methanol in the presence of excess azide afforded $\mu_{1,1}$-N_3 bridged dinuclear nickel(II) complexes in excellent yields. Variable temperature magnetic susceptibility measurements confirm the ferromagnetic behavior of the complexes.

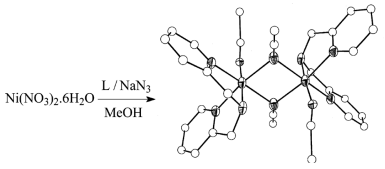

Ramesh Kapoor, Anuradha Pathak, Pratibha Kapoor, Paloth Venugopalan

Polyhedron 25 (2006) 31

Studies on cobalt(II) complexes with *N*,*N*,*N*′,*N*′-tetraethylpyridine-2,6-dicarboxamide(L^1) containing PF_6^-, BF_4^-, ClO_4^- and NO_3^- anions: X-ray crystal structures of $[Co(L^1)_2(CH_3CN)](PF_6)_2$ and $[Co(L^1)_2(H_2O)_2](X)_2 \cdot H_2O$ ($X = PF_6^-, ClO_4^-$)

Octahedral cobalt(II) complexes $[Co(L^1)_2(CH_3CN)](PF_6)_2$ (**1**) and $[Co(L^1)_2(H_2O)_2](X)_2$ ($X = PF_6^-$ (**2**), BF_4^- (**3**), ClO_4^-, (**4**), NO_3^- (**5**)) have been prepared; the composition of the product is dependent upon the reaction medium. The ligands use either ONO or ON donor atoms depending upon the steric demands. Compounds **2** and **4** are structurally similar and the lattice water is involved in the formation of chains by hydrogen bonding between different structural units.

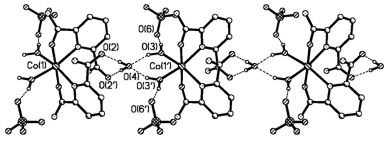

Ayfer Kalkan, Zehra Altunta Bayır

Polyhedron 25 (2006) 39

Phthalocyanines with rigid carboxylic acid containing pendant arms

We report on synthesis and characterisation of metal-free and metallophthalocyanines (M = Zn, Co) substituted with four carboxybiphenyloxy groups on the peripheral positions.

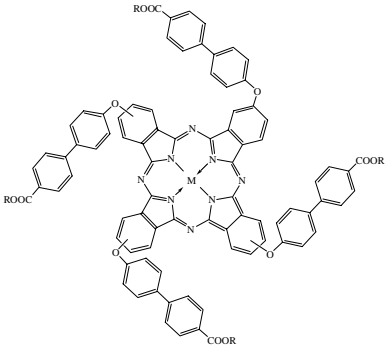

F.J. Barros-García, F. Luna-Giles, M.A. Maldonado-Rogado, E. Viñuelas-Zahínos

Polyhedron 25 (2006) 43

The coordination behaviour of two structural isomeric ligands towards cadmium (II): Synthesis, spectroscopic characterization and crystal structures

Two thiazoline/indazole derivative ligands, 2-(indazol-1-yl)-2-thiazoline (TnInA) and 2-(indazol-2-yl)-2-thiazoline (TnInL) and their Cd(II) complexes were synthesized and characterized by physical measurements. The X-ray crystal structures of TnInA, TnInL, $[Cd(NO_3)_2(TnInA)_2]$ and $[Cd(NO_3)_2(TnInL)_2]$ have also been determined. The geometry around the cadmium atoms can be described as a triangulated dodecahedron.

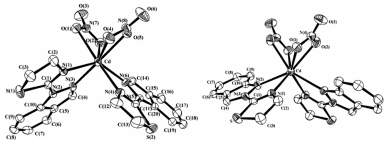

F.J. Barros-García, A. Bernalte-García, F. Luna-Giles, M.A. Maldonado-Rogado, E. Viñuelas-Zahínos

Polyhedron 25 (2006) 52

Synthesis, characterization and crystal structures of a bidentate indazole–thiazine derivative ligand and its cobalt (II) and cadmium (II) metal complexes

A novel thiazine/indazole derivative ligand *N*-(5,6-dihydro-4H-1,3-thiazin-2-yl)indazole (InTz) and its cobalt (II) and cadmium (II) complexes were synthesized and characterized by physical measurements. The X-ray crystal structures of InTz, cobalt complex and cadmium complex have also been determined. The geometry around the metallic atoms can be described as a distorted octahedron for cobalt complex and as a distorted dodecahedron for cadmium complex.

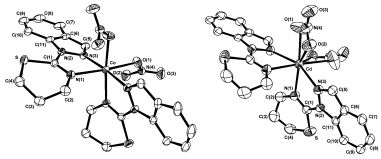

Marthakutty Joseph, Mini Kuriakose, M.R. Prathapachandra Kurup, E. Suresh, Archana Kishore, Sarita G. Bhat

Polyhedron 25 (2006) 61

Structural, antimicrobial and spectral studies of copper(II) complexes of 2-benzoylpyridine *N*(4)-phenyl thiosemicarbazone

A series of five Cu(II) complexes of 2-benzoylpyridine *N*(4)-phenyl thiosemicarbazone (HL) with a general formula [CuLX], except the perchlorate complex were prepared. The complexes were characterized by means of spectroscopic methods. The antimicrobial studies shows that the copper complexes were active against *Vibrio cholerae* O1 and *Salmonella paratyphi*. Single crystal XRD studies revealed the chloro complex to be a chlorine bridged dimer and the thiocyanato complex with a distorted square planar geometry.

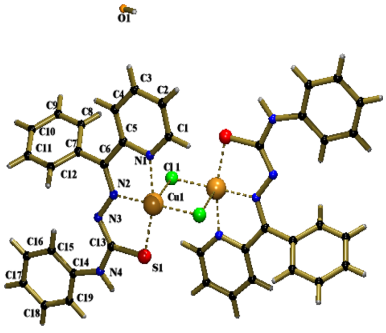

Miquel Barceló-Oliver, Andrés Tasada, Juan J. Fiol, Angel García-Raso, Angel Terrón, Elies Molins

Polyhedron 25 (2006) 71

Molecular architecture by means of interactions between Ag(I) and glycine derivatives

Two different types of tubular channels in $[Ag(pyr\text{-}gly)] \cdot 0.5H_2O$.

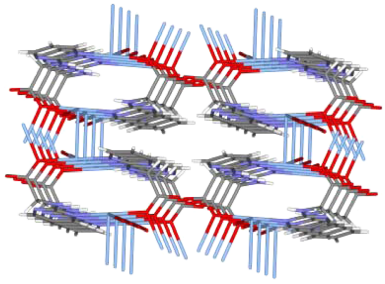

Gerard A. van Albada, Ilpo Mutikainen, Urho Turpeinen, Jan Reedijk

Polyhedron 25 (2006) 81

Crystal structure, magnetism and spectroscopy of a dinuclear Cu(II) compound with a chiral ligand; $Cu_2(SL)(\mu\text{-}Cl)(Cl)_2(CH_3OH)$ (HSL = *S*-1,2-bis(benzimidazol-2-yl)-1-hydroxyethane)

A new dinuclear Cu(II) compound with a chiral ligand, $Cu_2(SL)(\mu\text{-}Cl)(Cl)_2(CH_3OH)$ (in which HSL = *S*-1,2-bis(benzimidazol-2-yl)-1-hydroxyethane) displaying a strong antiferromagnetism of $J = -348$ cmis reported.

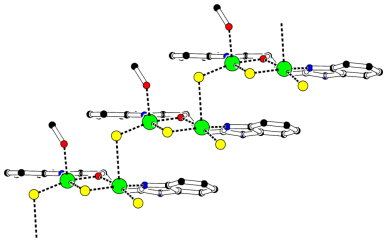

Prasad P. Phadnis, Sandip Dey, Vimal K. Jain, M. Nethaji, Ray J. Butcher

Polyhedron 25 (2006) 87

Synthesis, spectroscopy and structures of *o*-diphenylphosphinobenzoic acid complexes of diorganotin (IV), palladium (II) and platinum (II)

The reactions of diorganotin oxides and palladium (II) and platinum (II) precursors with *o*-diphenylphosphinobenzoic acid ([PPh_2-(o-C_6H_4COOH)], LH) have been investigated and a variety of complexes have been isolated and characterized by elemental analyses, IR, NMR (H, $^{13}C\{^1H\}$, $^{31}P\{^1H\}$ and $^{119}Sn\{^1H\}$) and UV–Vis spectroscopy. The stereochemistry of these complexes has been deduced from spectroscopic data. The structures of $[\{Bu_2Sn(OOC\text{-}C_6H_4PPh_2)\}_2O]_2$ and $[Pt(O_2CC_6H_4PPh_2)_2]$ have been established by X-ray crystallography.

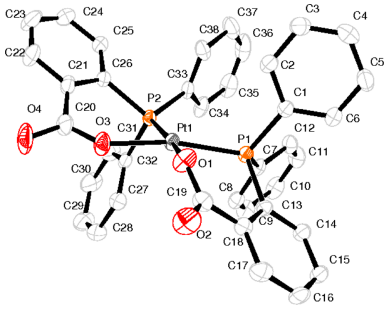

Shariff E. Kabir, Md. Abdul Mottalib, G.M. Golzar Hossain, Ebbe Nordlander, Edward Rosenberg

Polyhedron 25 (2006) 95

Reactions of $[(\mu\text{-}H)Os_3(CO)_{10}(\mu\text{-}OMe)]$ and $[(\mu\text{-}H)Os_3(CO)_9(\mu\text{-}OMe)(MeCN)]$ with dppm, dppe, dppp, and PPh_2H: X-ray crystal structures of $[(\mu\text{-}H)Os_3(CO)_8(\mu\text{-}OMe)(\mu_2\text{-}\eta^2\text{-}dppm)]$ and $[(\mu\text{-}H)Os_3(CO)_9(\mu\text{-}OMe)(PPh_2H)]$

The reactions of $[(\mu\text{-}H)Os_3(CO)_{10}(\mu\text{-}OMe)]$ (**1**) and its monoacetonitrile derivative $[(\mu\text{-}H)Os_3(CO)_9(\mu\text{-}OMe)(MeCN)]$ with diphosphines (dppm, dppe and dppp) and monophosphine (PPh_2H) are described. The structures of the products formed depend on the phosphine used. The crystal structures of two new compounds are reported.

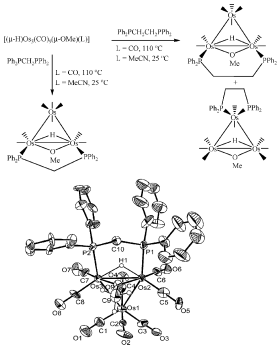

Gabino A. Carriedo, F.J. Garcia Alonso, Carlos Diaz Valenzuela, Maria Luisa Valenzuela

Polyhedron 25 (2006) 105

Synthesis and thermal decarbonylation of $W(CO)_5$ complexes supported by nitrile, pyridine or phosphine ligands to poly-spirophosphazene random copolymers carrying O–C_6H_5–CO_2Pr groups

Phosphazene copolymers carrying nitrile, pyridine and phosphine ligands have been synthesized by sequential substitution from $[NPCl_2]_n$. Their reactions with $[W(MeOH)(CO)_5]$ gives the corresponding tungsten carbonyl complexes, that undergo a complete decarbonylation below 300 °C forming metal containing species that have a stabilizing effect on the polymeric matrices.

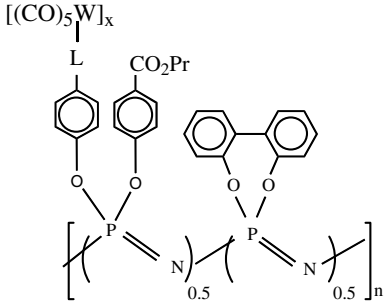

Elisenda Rodríguez, Martí Gich, Anna Roig, Elies Molins, Nataliya Nedelko, Anna Ślawska-Waniewska, Andrzej Szewczyk

Polyhedron 25 (2006) 113

Investigations of the stability of $\{[(tacn)_6Fe_8(\mu_3\text{-}O)_2(\mu_2\text{-}OH)_{12}]Br_7(H_2O)\}Br \cdot 8H_2O$ (Fe_8) cluster in aqueous solution by spectroscopic and magnetic methods

We report on the characterization of the single molecular magnet (SMM) $\{[(tacn)_6Fe_8\mu_3\text{-}O_2(\mu_2\text{-}OH)_{12}]Br_7(H_2O)]\}Br \cdot 8H_2O$, tacn = 1,4,7-triazacyclononane in aqueous solution. Spectroscopic and magnetic measurements evidence the lack of stability of the complex in aqueous solution.

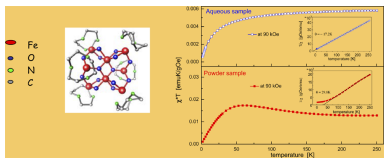

Michael P. Weberski Jr., Craig C. McLauchlan, Christopher G. Hamaker

Polyhedron 25 (2006) 119

Synthesis and X-ray structural characterization of M(3,5-^{t}Bu$_2$-salophen) (M = Cu, VO)

The synthesis, spectroscopic properties, and X-ray crystal structures of the copper (II) and vanadyl complexes of *N*,*N*′-phenylenebis(3,5-di-*tert*-butylsalicylideneimine) are reported.

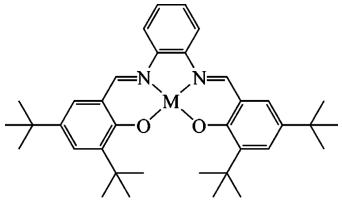

M = Cu^{2+}, $[VO]^{2+}$

Augusto Cingolani, Fabio Marchetti, Claudio Pettinari, Riccardo Pettinari, Brian W. Skelton, Neil Somers, Allan H. White

Polyhedron 25 (2006) 124

Copper(I) monophosphine complexes with functionalized acylpyrazolonate ligands: Syntheses of heterobimetallic Cu–Zn and Cu–Ru adducts

New phosphino–copper(I) acylpyrazolonate derivatives have been synthesized and characterized in the solid state and solution. They are monomeric compounds where the acylpyrazolonates act as O_2- or N_2-donor ligands depending on their substituents. In the latter case, the ligand is also able to coordinate other metal centres through the carbonyl arms, affording heterobimetallic derivatives.

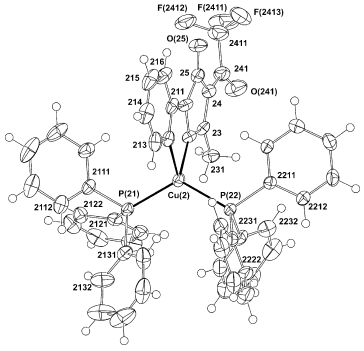

Constantinos J. Milios, Theocharis C. Stamatatos, Spyros P. Perlepes

Polyhedron 25 (2006) 134

The coordination chemistry of pyridyl oximes

This paper reviews the coordination chemistry of pyridyl oximes. The immense structural diversity of the pyridyloximate complexes stems from the ability of these ligands to exhibit a great variety of coordination modes. The products range from simple mononuclear metal complexes to heterometallic clusters and polymeric metallosupramolecular arrays. Aspects of the activation of 2-pyridyl oximes by 3d-metal centers are also detailed.

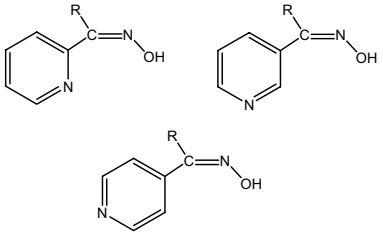

Cui-Juan Wang, Yao-Yu Wang, Hai-Rui Ma, Hui Wang, Qi-Zhen Shi, Shie-Ming Peng

Polyhedron 25 (2006) 195

A novel ligand *N*,*N*′-di(2-pyridyl)-2,4-diamino-6-phenyl-1,3,5-triazine (dpdapt) and its complexes: $[Cu(dpdapt)Cl_2]$ and $[Cu(dpdapt)(NO_3)(H_2O)] \cdot NO_3 \cdot H_2O$

A new ligand, dpdapt, and two crystalline polymorphic forms, $[Cu(dpdapt)Cl_2]$ (**1**) and $[Cu(dpdapt)(NO_3)(H_2O)] \cdot NO_3 \cdot H_2O$ (**2**), have been synthesized. The molecular structures of **1** and **2** were established by single-crystal X-ray diffraction studies. DFT calculations have been used to gain some insight about the coordination behavior of dpdapt and complex **1**.

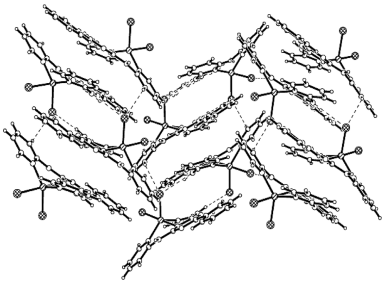

The Publisher encourages the submission of articles in electronic form thus saving time and avoiding rekeying errors. For detailed instructions on the preparation of manuscripts and of electronic artwork, consult the Author Gateway for Elsevier at http://authors.elsevier.com

SCIENCE DIRECT®

Full text of this journal is available, on-line from **ScienceDirect**. Visit **www.sciencedirect.com** for more information.

CONTENTS Direct

This journal is part of **ContentsDirect,** the ***free*** alerting service which sends tables of contents by e-mail for Elsevier books and journals. You can register for **ContentsDirect** online at: **http://contentsdirect.elsevier.com**